Russian Chemical Reviews, Volume 70 (2001)

Contents of Volume

Number 1

Correlation analysis in the chemistry of free radicals 1
A R Cherkasov, M Jonsson, V I Galkin, R A Cherkasov

Rotaxanes and polyrotaxanes. Their synthesis and the supramolecular devices based on them 23
I G Panova, I N Topchieva

Mechanochemical synthesis of intermetallic compounds 45
T F Grigorieva, A P Barinova, N Z Lyakhov

Chemical modification and blending of polymers in an extruder reactor 65
E V Prut, A N Zelenetskii

Rigid-rod poly(benzobisazoles) and molecular composites based on them 81
L G Komarova, A L Rusanov

Number 2

Modern chemistry of nitrous oxide 91
A V Leont'ev, O A Fomicheva, M V Proskurnina, N S Zefirov

Organic hydrotrioxides 105
V V Shereshovets, S L Khursan, V D Komissarov, G A Tolstikov

Hydrogen-containing carbon nanostructures: synthesis and properties 131
B P Tarasov, N F Goldshleger, A P Moravsky

Metallic nanosystems in catalysis 147
V I Bukhtiyarov, M G Slin'ko

Electrochemically active species and multielectron processes in ionic melts 161
V I Shapoval, V V Solov'ev, V V Malyshev

Number 3

Nanoclusters and nanocluster systems. Assembling, interactions and properties 177
I P Suzdalev, P I Suzdalev

Nitrosonium complexes of organic compounds. Structure and reactivity 211
G I Borodkin, V G Shubin

Chemistry of xenon derivatives. Synthesis and chemical properties 231
V K Brel, N Sh Pirkuliev, N S Zefirov

Number 4

Size effects in chemistry of heterogeneous systems 265
N F Uvarov, V V Boldyrev

Size effects in electrochemistry 285
O A Petrii, G A Tsirlina

Pyridopyridines 299
V P Litvinov, S V Roman, V D Dyachenko

Mechanism of thermal decomposition of silanes 321
A A Onischuk, V N Panfilov

Physiologically active compounds interacting with serotonin (5-hydroxytryptamine) receptors 333
O N Zefirova, N S Zefirov

Number 5

Chemical chromaticity: potential of the method, application areas and future prospects 357
V M Ivanov, O V Kuznetsova

X-Ray synchrotron radiation in physicochemical studies 373
Ya V Zubavichus, Yu L Slovokhotov

Regio- and stereochemistry of 1,3-dipolar cycloaddition of nitrile oxides to alkenes 405
R P Litvinovskaya, V A Khripach

Problems of control of the reactivity of macroradicals and the growth of polymer chains 425
D F Grishin, L L Semyonycheva

Number 6

Femtochemistry 449
O M Sarkisov, S Ya Umanskii

Ultrafast nonradiative transitions between higher excited states in organic molecules 471
V L Ermolaev

Design of site-specific RNA-cleaving reagents 491
V N Silnikov, V V Vlassov

Affinity sorbents containing nucleic acids and their fragments 509
I G Shishkina, A S Levina, V F Zarytova

Number 7

Paramagnetic resonance and detection of a single electron spin 535
A L Buchachenko, F I Dalidchik, S A Kovalevskii, B R Shub

Electrochemical reactions of alkenes induced by anodic oxidation and their applications in organic synthesis 543
Yu N Ogibin, G I Nikishin

Spectral properties of porphyrins and their precursors and derivatives 577
N Zh Mamardashvili, O A Golubchikov

Detonation synthesis ultradispersed diamonds: properties and applications 607
V Yu Dolmatov

Number 8

Scanning tunnelling vibrational spectroscopy of single surface complexes and detection of single electron spins 627
F I Dalidchik, S A Kovalevskii, B R Shub

1,3-Dipolar cycloaddition reactions of nitrile oxides in the synthesis of natural compounds and their analogues 641
A I Kotyatkina, V N Zhabinsky, V A Khripach

Sulfur ylides in the synthesis of heterocyclic and carbocyclic compounds 655
S N Lakeev, I O Maydanova, F Z Galin, G A Tolstikov

Marine polar steroids 673
V A Stonik

Number 9

Superconducting MgB_2 and related compounds: synthesis, properties and electronic structure 717
A L Ivanovskii

Synthetic methodologies for carbo-substituted conjugated dienes 735
A A Vasil'ev, E P Serebryakov

Magnetic properties of complex oxides $LiMO_2$ (M = Sc–Ni) with different types of cationic ordering 777
D G Kellerman

Characteristic features of heterophase polymerisation of styrene with simultaneous formation of surfactants at the interface 791
N I Prokopov, I A Gritskova

Anion-conducting fluoride and oxyfluoride glasses 801
N I Sorokin

Number 10

Nanochemistry of metals 809
G B Sergeev

The chemistry and application of carbon nanotubes 827
E G Rakov

State-of-the-art coordination chemistry of radioactive elements 865
B I Kharisov, M A Mendez-Rojas

Recent trends in the chemistry of sulfur-containing reducing agents 885
S V Makarov

Number 11

Oleg Matveevich Nefedov

Rearrangements of sulfoxides and sulfones in the total synthesis of natural compounds 897
E N Prilezhaeva

(Het)aroylpyruvic acids and their derivatives as promising building blocks for organic synthesis 921
S G Perevalov, Ya V Burgart, V I Saloutin, O N Chupakhin

Synthetic molecular systems based on porphyrins as models for the study of energy transfer in photosynthesis 939
N V Konovalova, R P Evstigneeva, V N Luzgina

Silica gel in organic synthesis 971
A K Banerjee, M S Laya, W J Vera

Number 12

Organic molecules with abnormal geometric parameters 991
I V Komarov

Fluorescent and photochromic chemosensors 1017
V A Bren

Structural and configurational relationships 'metal complex–substrate–product' in asymmetric catalytic hydrogenation, hydrosilylation and cross-coupling reactions 1037
V A Pavlov

© 2008, No Rights Reserved.

Russian Chemical Reviews **70** (1) 1 – 22 (2001) © 2001 Russian Academy of Sciences and Turpion Ltd

DOI 10.1070/RC2001v070n01ABEH000574

Correlation analysis in the chemistry of free radicals

A R Cherkasov, M Jonsson, V I Galkin, R A Cherkasov

Contents

I.	Introduction	1
II.	Correlation analysis for reactions involving free radicals	2
III.	The use of r^{-2} analysis in free-radical chemistry	11
IV.	Conclusion	20

Abstract. Published data now available on the use of correlation analysis in free-radical chemistry are discussed systematically. The scales of 'radical' σ-constants of substituents proposed previously are analysed. It is shown that none of them is applicable as a general scale because almost in all cases, it is impossible to separate correctly the proper radical and polar contributions to the overall effect of substituents. A new approach to the quantitative estimation of the relationship between the structure and reactivity of molecules in free-radical processes called r^{-2}-analysis is proposed. The bibliography includes 238 references.

I. Introduction

Correlation analysis is a widely used mathematical formalisation of the chemical similarity principle.

The foundations of the analysis were laid by Hammett, who discovered a correlation between the rate constants (k) or equilibrium constants (K) of reactions involving benzene derivatives and the ionisation constants of benzoic acids [1]

$$\log\frac{k_X}{k_H} = \rho\log\frac{K_X}{K_H} = \rho\sigma,$$

where the subscripts X and H refer to substituted and unsubstituted derivatives and ρ is the reaction constant for the given series. The reaction series of dissociation of benzoic acids in aqueous solutions at 25 °C was chosen as the reference series, described by $\rho = 1$, and the ratio

$$\log\frac{K_X}{K_H},$$

was introduced as the σ-constant, reflecting the influence of the substituent X in a set of similar reaction series. This empirical approach, which is also known as $\sigma\rho$-analysis, became one of the first quantitative methods for describing the structure – reactivity relationship for compounds and has served as the basis for the subsequent development of the general formal theory of the influence of substituents.

The principles of linear free energy (LFE) and polylinearity (PL) provide the physical grounds for this approach, according to which the increment of the Gibbs energy change (ΔG) in a reaction or of the activation energy caused by the introduction of a substituent is represented as the additive sum

$$\delta\Delta G = \delta\Delta G_I + \delta\Delta G_S + \delta\Delta G_R,$$

each of the terms reflecting a particular type of substituent effects, namely, inductive (I), steric (S) or resonance (R) effect. The multitude of inductive, steric and resonance constants determined from diverse experimental sources, together with some specific constants (for example, 'phosphorus' or 'silicon' constants) form dozens of scales which are widely used to describe the influence of substituents on the reactivity at the group level of additivity.

Various aspects of the determination and versatile practical application of steric and inductive constants of groups and the concept of electronegativity tightly connected to them have been described in detail in our previous reviews.[2–5] It should only be noted that modern correlation analysis has long overstepped the limits of a purely empirical approach. The group constants of substituents have provided the experimental basis for the physical interpretation and for the development of various quantitative models describing the steric and electronic effects.

Certainly, some key problems of the formal theory of interaction and correlation analysis are still to be ultimately solved. For example, the nature of the inductive effect and the mechanism of its transfer remain one of the most debatable and topical problems of physical chemistry [2] (the state-of-the-art in this line of research has been discussed comprehensively in recent review publications [5–8]). Nevertheless, it can be stated with confidence that the theoretical grounds of modern correlation analysis provide in general a clear picture and give good grounds for the extensive use of the substituent constants for description of the structure – property relationships in the chemistry of organic and heteroorganic compounds. Perhaps, the only field of chemistry in which the use of correlation analysis has not yet provided good results is free-radical chemistry. The application of LFE and PL principles in this field of chemistry is still limited to a rather narrow range of compounds (mainly, aromatics).

In this review, the current state of the use of correlation analysis for radical reactions is considered for the first time. In addition, we thought it necessary to present the generalising results obtained by the new approach to the estimation of the structure – reactivity relationship in free-radical reactions which we have developed and called 'r^{-2} analysis'.

A R Cherkasov, V I Galkin, R A Cherkasov Department of Chemistry, Kazan State University, ul. Kremlevskaya 18, 420008 Kazan, Russian Federation. Fax (7-843) 231 54 16. Tel. (7-843) 231 54 16.
E-mail: vladimir.galkin@ksu.ru (V I Galkin);
rafael.cherkasov@ksu.ru (R A Cherkasov)
M Jonsson Department of Chemistry, Royal Institute of Technology, Teknikringen 56, S-100 44 Stockholm, Sweden. Fax (46-8) 790 87 72. Tel. (46-8) 790 91 23. E-mail: matsj@nuchem.kth.se

Received 2 February 2000
Uspekhi Khimii **70** (1) 3 – 27 (2001); translated by Z P Bobkova

II. Correlation analysis for reactions involving free radicals

1. Methods for the description of the effects of substituents in homolytic processes based on kinetic parameters. $\sigma^{\cdot}$-Scales

Despite the fact that the applicability of the Hammett equation to homolytic processes is sometimes debated,[9] there exist quite a few examples of successful use of various polar constants for the description of free-radical reactions.[10–28]

In addition to the proper Hammett σ-constants,[18–29] which reflect the overall effect of substituents in aromatic systems, so-called dual σ^+ and σ^- parameters of substituents, which imply direct polar (mesomeric) interaction of $^+$M or $^-$M substituents with the reaction centre, are also actively used in the analysis of homolytic processes.

The scale of σ^+-constants proposed by Brown and Okamoto,[30] which is based on the rates of solvolysis of *para*- and *meta*-substituted cumyl chlorides, is believed to be more adequate in describing the properties of aromatic radicals than the scale of Hammett σ-constants.[31] In our opinion, the use of σ^+-constants is really more effective as far as the properties of radical cations are concerned but this is not that obvious for neutral radicals. Nevertheless, radical bromination of substituted toluenes with bromine,[24] *N*-bromosuccinimide [24] and bromotrichloromethane [32] as well as the quantitative interpretation of abstraction of a hydrogen atom by alkoxy radicals,[11,12,33] chlorine atoms,[34] and peroxy radicals [34] have become classical examples of successful use of the σ^+ constants in free-radical chemistry. Experimental results obtained by one of the authors of this review have confirmed the exceptionally high efficiency of the σ^+ constants in correlations with single-electron reduction potentials of various aromatic molecules and radicals.[35–40]

Other researchers [18,41] have also considered the Brown–Okamoto scale to be the most suitable scale for the description of properties of free radicals; it is the scale of σ^+ constants that has served as the base for the introduction of several specific radical constants of substituents $\sigma^{\cdot}$ (they will be considered in detail in the subsequent sections of this review).

The σ^--constants found from the pK values for ionisation of substituted anilines, *N*,*N*-dimethylanilines and phenols [42,43] have also been used successfully to describe a number of radical processes.[29,44] However, polar constants are finding fairly limited application in free-radical chemistry. The scope of application of particular scales to the description of properties of free radicals remains obscure, identification of statistically significant correlations in each successful case being rather a matter of luck than of a systematic approach. Additional difficulties arise when the correlation analysis technique is employed to describe the properties of non-aromatic free radicals.

The main problem in the quantitative estimation of the effects of substituents in homolytic processes is, undoubtedly, the necessity of adequate description of their ability to delocalise the unpaired electron. Currently, this is one of the most topical and ambiguous problems in free-radical chemistry (see, for example, a monograph [45] and references therein).

There is a common opinion that both donors and acceptors are capable of stabilising a radical centre;[45] this is often used as an argument in favour of the introduction of special radical $\sigma^{\cdot}$ constants of substituents, which are expected to describe quantitatively the ability of substituents to delocalise spin density. The methods of determination of $\sigma^{\cdot}$-constants can be classified into three main types. The first type includes methods based on the use of kinetic parameters of homolytic processes; the second type comprises physicochemical methods which provide direct information on the spin density distribution in radicals; and thermodynamic approaches operating with energy characteristics belong to the third type. Below we consider the existing approaches in accordance with this classification.

The methods based on the kinetic parameters of homolytic processes are used most widely in determining the $\sigma^{\cdot}$-constants of substituents and are modifications of the classical correlation analysis, based on the use of the extended Hammett equation

$$\log\frac{k}{k_0} = \rho_1\sigma^{X} + \rho_2\sigma^{\cdot}. \qquad (1)$$

The essence of this approach is to separate the contribution of the proper radical stabilisation ($\sigma^{\cdot}$) from the polar effect (σ^{X}); hence, it requires selecting a model reaction series in which the latter contribution would be small and could be determined reliably in terms of polar constants. The most widely used reactions involving free radicals include electron transfer, free-radical transfer of a hydrogen atom and radical addition.

The kinetic approach to the description of the effects of substituents in radical reactions was first employed by Alfrey and Price [46] in a study of the reactivity of vinylic monomers in copolymerisation. The researchers [46] did not use the classical logarithmic form of Eqn (1); however, the capacity of substituents for stabilisation of radicals was estimated quantitatively for the first time in terms of group constants Q, whereas the polar component was taken into account by the parameter e (the Q constants are given in Table 1)

$$\frac{k_1}{k_2} = \frac{Q_1}{Q_2}\exp\left[-e_1(e_1 - e_2)\right]. \qquad (2)$$

A substantial disadvantage of this approach is the fact that the calculation of Q is based on the analysis of a set of data on copolymerisation, and introduction of new individual values requires a consistent procedure for recalculation of the whole array of Q.

Walling *et al.*[59] have critisised the theoretical substantiation of the Alfrey–Price approach, which ignores the possibility of resonance stabilisation of a radical transition state.

Later, the group parameters E_R have been introduced using the relative reactivity of monomers ($1/r$) in the radical copolymerisation of aryl-substituted methacrylates [47,48,60]

$$\log\frac{1}{r} = \rho\sigma + \gamma E_R\,, \qquad (3)$$

where the γ coefficient was taken to be 1, and the parameter E_R was interpreted as the resonance component of the substituent effect in free-radical processes. Subsequently,[49] this approach was subjected to severe criticism, the legitimacy of the E_R and γ values being prejudiced. The researchers [49] believed that the nature of E_R is rather complex; therefore they proposed adjusted values, E_R^n, free from the contribution of heterolytic resonance (see Table 1).

A similar scale of resonance constants E_D has been developed to describe the effects of *para*-substituents in the addition of trichloromethyl radical to substituted styrenes [53]

$$\log\frac{k_p}{k_H} = \rho\sigma_p^{+}(\rho\sigma_p) + E_D\,; \qquad (4)$$

in this case, the polar effect was taken into account by both the Brown–Okamoto constants and the Hammett σ_p-constants. Correspondingly, two sets of E_D parameters for *para*-substituents (MeO, Cl, CN, NO_2) in styrenes were obtained [$E_D(\sigma)$ and $E_D(\sigma^+)$ in Table 1]. The E_D constants of these substituents found using the σ^+ parameters are in good agreement with the Alfrey–Price Q constants.

A similar approach was used [54] to develop the τ scale, which reflects the conjugation effects in radical arylation of substituted benzenes

$$\log\frac{k_p}{k} = \rho\sigma_p + \tau_p\,, \qquad (5)$$

where k_p are the rate constants for the arylation into the *para*-position expressed in terms of the Hammett constants of *para*-substituents (σ_p) and the group parameters τ_p, which reflect the additional delocalisation effects of *para*-substituents. The ρ-constant appearing in Eqn (5) was determined on the basis of a similar reaction series of *meta*-arylation, the influence of substituents

Table 1. Constants characterising the radical-stabilisation properties of substituents (data of kinetic studies).

Substituent	log$Q$	$E_R(p)$	$E_R(m)$	E_R^n	$E_D(\sigma)$	$E_D(\sigma^+)$	τ_p	τ_o	$\sigma^{\cdot}_{FM}$	$\sigma^{\cdot}_J$	$\frac{\lvert\sigma^{\pm}-\sigma\rvert}{n}$	$\sigma^{\cdot}_C(p)$	$\sigma^{\cdot}_C(m)$	$\sigma^{\cdot}_{JJ}(p)$	$\sigma^{\cdot}_{JJ}(m)$
	see [a]	see [b]	see [b]	see [c]	see [d]	see [d]	see [e]	see [e]	see [f]	see [g]	see [h]	see [i]	see [i]	see [j]	see [j]
H	0.00	0.00	0.00	0.000	0.00	0.00	0.00	0.00	0.00	0.00	0.000	0.00	0.00	0.00	0.00
Me	0.04	0.03	–	−0.020	0.16	0.11	0.09	0.50	−0.02	0.38(0.39)	0.170	0.11	−0.02(0.03)	0.15	0.00
OMe	0.13	0.11	–	−0.008	0.40	0.19	0.14	–	−0.12	0.31(0.42)	0.250	0.24	−0.02	0.23	0.10
NO_2	0.21	0.41	0.35	0.410	0.27	0.27	0.90	0.88	0.27	0.73(0.76)	0.440	0.57	−0.11	0.36	0.001
CN	0.27	0.24	–	0.230	0.33	0.32	–	–	0.34	(0.41)	0.260	0.46	−0.12	0.42	0.11
F	–	–	–	–	–	–	–	–	−0.25	0.07(0.12)	0.065	−0.08	−0.05	−0.02	0.03
Cl	0.01	0.10	0.08	0.062	0.12	0.07	0.16	0.48	0.08	0.06(0.18)	0.065	0.12	−0.04	0.22	−0.05
Br	0.04	0.12	–	0.072	–	–	–	–	0.17	(0.20)	0.055	0.13	–	0.23	0.12
I	0.07	0.12	–	0.037	–	–	–	–	0.16	–	0.075	0.41	0.10	–	–
OH	–	0.21	–	–	–	–	–	0.57	–	–	–	–	–	–	–
C(O)Me	–	–	–	0.240	–	–	–	–	0.53	–	–	–	–	0.54	–
$P(O)(OEt)_2$	–	–	–	–	–	–	–	–	–	–	–	0.18	−0.11	–	–
$P(S)(OEt)_2$	–	–	–	–	–	–	–	–	–	–	–	0.29	−0.06	–	–
Ph	–	–	–	–	–	–	–	–	0.12	0.39(0.42)	0.230	0.46	–	0.47	–
SMe	–	–	–	–	–	–	–	–	–	(0.49)	–	0.43	−0.03	0.62	–
SPh	–	–	–	–	–	–	–	–	–	–	–	–	–	–	–
CF_3	–	–	–	–	–	–	–	–	–	–	–	0.08	−0.07	−0.01	−0.07
OPh	–	0.13	–	−0.147	–	–	–	–	–	–	–	–	–	–	–
CO_2Et	–	–	–	–	–	–	–	–	–	–	–	0.39	–	–	–
CO_2Me	–	–	–	–	–	–	–	–	–	–	–	0.35	–	0.33	0.10
C(O)Ph	–	–	–	–	–	–	–	–	–	–	–	–	–	–	–
Bu^t	–	0.03	–	0.014	–	–	–	–	–	–	–	0.13	–	0.26	0.11
Et	–	–	–	–	–	–	–	–	–	–	–	–	–	0.15	–
Pr^i	–	0.03	–	0.034	–	–	–	–	–	–	–	–	–	–	–
SOMe	–	–	–	–	–	–	–	–	–	–	–	0.18	0.01	0.50	–
SC(O)Me	–	–	–	–	–	–	–	–	–	–	–	–	–	–	–
S(O)OMe	–	–	–	–	–	–	–	–	–	–	–	0.18	−0.07	0.38	–
SO_2Ph	–	–	–	–	–	–	–	–	–	–	–	–	–	–	–
S(O)Ph	–	–	–	–	–	–	–	–	–	–	–	–	–	–	–
SO_3Me	–	–	–	–	–	–	–	–	–	–	–	–	–	–	–
OC(O)Me	–	–	–	–	–	–	–	–	–	–	–	–	–	−0.11	−0.10
OC(O)Ph	–	–	–	–	–	–	–	–	–	–	–	–	–	–	–
N = NPh	–	–	–	–	–	–	0.90	–	0.33	–	–	1.08	–	–	–
NH_2	–	–	–	–	–	–	–	–	–	–	–	0.69	–	–	–
NMe_2	–	0.24	–	−0.110	–	–	–	–	–	–	0.535	0.90	–	1.00	–
$SiMe_3$	–	–	–	–	–	–	–	–	–	–	–	0.17	–	0.31	–
$CH = CH_2$	–	–	–	–	–	–	–	–	–	–	–	0.67	–	–	–

Note. The values which vary in original publications are given in parentheses.

[a] From Ref. 46; [b] from Refs 47, 48; [c] from Refs 49 – 52; [d] from Ref. 53; [e] from Ref. 54; [f] from Ref. 55; [g] from Refs 50 – 52; [h] from Ref. 56; [i] from Ref. 57; [j] from Ref. 58.

being entirely ascribed to the polar interaction. The parameters τ_o for *ortho*-substitution were introduced by a similar procedure. The 4-$XC_6H_4\dot{C}H_2$ radicals, where X = H, NO_2, Cl, Me, MeO, were investigated (regardless the nature of the attacking agent); in this case, the τ_p and τ_o constants decreased in the series $PhNO_2 \gg$ PhCl, PhOMe > PhMe (see Table 1). This model series has an important advantage: the measured kinetic parameters vary over a broad range due to the direct conjugation of para-substituents with a cyclohexadienyl radical.

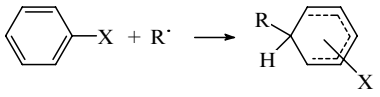

However, it cannot be ruled out that, within the framework of the given reaction series, fairly reactive phenyl radicals would be involved with high probability in side homolytic properties.

The methodology of the above approaches is evidently similar to that used in the classical equations of correlation analysis, which determine the inductive and resonance constituents of the polar effect of substituents in terms of Taft,[42,61–63] Exner,[64–66] Yukawa–Tsuno,[67,68] Swain–Lupton,[69] Dewar–Grisdale,[70] Charton [71] and Palm [72,73] approaches. In all the studies described above, except for the study by Alfrey and Price,[46] the researchers dealt only with aromatic systems. Therefore, the radical constants τ, E_R and E_D are believed to contain a component due to the polar effect.

Fisher *et al.*[55,74,75] used radical bromination of 4-substituted 3-cyanotoluenes with *N*-bromosuccinimide as the model reaction to determine the 'extra-resonance' (this name was proposed by the authors), *i.e.*, the proper radical contribution (the polar contribution is minimised). When considering the possible canonical forms of the transition state of hydrogen abstraction *via* the reaction

$$YH + Z^{\cdot} \longrightarrow \left[\dot{Y}\,\dot{H}\,\dot{Z} \longleftrightarrow \underset{\mathbf{1a}}{Y^{+}\,\dot{H}\,Z^{-}} \longleftrightarrow \underset{\mathbf{1b}}{Y^{-}\,\dot{H}\,Z^{+}} \quad \underset{\mathbf{1c}}{}\right],$$

the researchers suggested that the high electronegativity of the attacking bromine atom Z precludes a substantial contribution of structure **1c**. In order to destabilise the polar form **1b** to decrease its contribution, the electron-withdrawing CN group was introduced in the *meta*-position relative to the methyl group (substrate YH) of the substituted toluene. The radical intermediate **1a** is stabilised additionally due to direct resonance. Assuming that the polar effects in the model system were thus minimised, Fisher *et al.*[55,74,75] proposed a scale of $\sigma^{\cdot}$ radical constants within the framework of a two-parameter equation including the Brown–Okamoto constant σ^{+}

$$\log\frac{k}{k_0} = \rho\sigma^{+} + \sigma^{\cdot}, \qquad (6)$$

in which the parameter ρ was determined on the basis of a similar reaction series of 4-substituted toluenes.

Fisher and Meierhoefer [55] did not use a series of *meta*-substituted toluenes as the standard for determining ρ on the ground that the corresponding parameter in Eqn (6) reflects, in their opinion, both the resonance and inductive polar effects. Thus, the differences between the effects of substituents in the free radical bromination of monosubstituted and 3-cyano-4-substituted toluenes by *N*-bromosuccinimide were attributed to the stabilisation of the structure **1a**; they were proposed as characteristics of the radical effects of *para*-substituents. In accordance with the results of this study, the ability of substituents to stabilise free radicals increases in the series F < OMe < Me < H < Cl < Ph < I < Br < NO_2 < N=NPh < CN < Ac, the $\sigma^{\cdot}$ constants for F and MeO being negative [$\sigma^{\cdot}$(F) = −0.25, $\sigma^{\cdot}$(MeO) = −0.12], which implies that these groups destabilise the radical reaction center (see Table 1).[55]

Meanwhile, it is obvious that the resonance stabilisatoion of substituted benzyl radicals by electron-withdrawing substituents (structures **2a** and **2b**) is similar to resonance delocalisation of the negative charge. This accounts for the most pronounced radical-stabilisation properties of substituents such as Ac, CN, N=NPh and NO_2, which also exhibit a negative mesomeric effect.

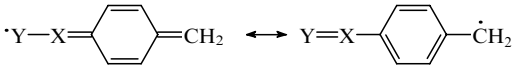

2a **2b**

In the case of stabilisation of the benzyl radical by the donor mesomeric effect of some substituents such as halogens (except for F), the researchers cited [55] discussed the formation of three contributing structures **2c**, **2d** and **2e**.

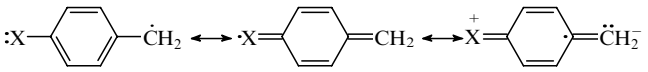

2c **2d** **2e**

Structure **2e** is characterised by substantial charge separation, which makes it energetically less favourable. The electrically neutral structure **2d** implies delocalisation of the unpaired electron because it has been added to the electron octet of the X atom. As Tsuno *et al.*[68] rightly noted, elements of Period II, O and F, are incapable of this type of interaction, which accounts for the negative values of the corresponding radical constants.

The presence of negative $\sigma^{\cdot}$ values in the Fisher–Meierhoefer scale hampers its quantitative comparison with other known scales, in most of which the radical constants can be only positive, implying that the radical reaction centres are stabilised by both donors and acceptors. It should also be noted that in the model system of disubstituted toluenes proposed, the possibility of resonance effect of *para*-substituents is retained, despite the minimisation of polar effects.

The search for standard reaction series with a clear-cut radical character of the transition state, which rules out a noticeable influence of polar interactions, has led Jackson *et al.*[50,51,56,76,77] to consideration of the thermal dissociation of dibenzylmercury derivatives in solution.

$$ArCH_2HgCH_2Ar \longrightarrow Ar\dot{C}H_2 + \dot{H}gCH_2Ar$$

$$\dot{H}gCH_2Ar \longrightarrow Hg + Ar\dot{C}H_2\,.$$

It was found that homolysis occurs in two stages. The first, rate-determining stage is generation of benzyl and benzylmercurio radicals;[52,78,79] it was suggested that in the transition state, one C–Hg bond has been cleaved almost completely, which corresponds to the formation of a nearly free benzyl radical.

The conventional $\sigma\rho$-analysis, which makes use of the first-order rate constants for the reaction under consideration and the Hammett σ-constants (subsequently, the σ^0 parameters were used), identified a linear correlation for *meta*-derivatives, whereas *para*-substituents of both electron-donating and electron-withdrawing nature accelerate homolysis, due to an additional stabilisation of benzyl radicals. In the equation

$$\log\frac{k}{k_0} = \rho\sigma + \rho^{\cdot}\sigma^{\cdot} \qquad (7)$$

resulting from the correlation procedure, the parameter $\rho^{\cdot}$ was taken to be unity for reactions giving rise to free benzyl radicals in the rate-determining step. In terms of the regression analysis performed, the constants which were later designated by $\sigma_J^{\cdot}$ (see Ref. 45) and which reflect the stabilising effect of substituents in the *para*-position of the benzyl radicals were determined from the deviations from the *meta*-correlation (see Table 1). The $\sigma_J^{\cdot}$ values were found to be in good agreement with the Q, τ, E_D and E_R scales (the correlation coefficients r varied from 0.83 to 0.92); as regards the Fisher–Meierhoefer constant ($\sigma_{FM}^{\cdot}$), only some qualitative correspondence was found in this case (r = 0.63).

It has been proposed [56] to use the $|\sigma^{\pm} - \sigma|/n$ scale, where $\sigma^{\pm}$ is the σ^{+} or σ^{-} constant, as a measure of radical stabilisation; for substituents containing a lone electron pair n = 2, while for groups with a multiple bond or any other π-system, n = 1. This

scale correlates well with the $\sigma_J^{\cdot}$ values. As drawbacks of this approach, the authors note the difficulty of preparing a broad range of dibenzylmercury derivatives and the limited solubility of these compounds in octanol, used as the reaction medium.

An attempt to select a perfect free-radical transition state is also the central point in Creary's approach,[57, 80–84] in which thermal rearrangement of 3-aryl-2,2-dimethylmethylenecyclopropanes **4** has been used as a standard reaction series to introduce the scale of radical constants $\sigma_C^{\cdot}$.

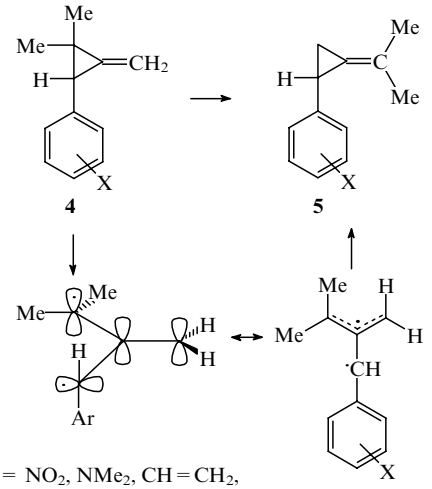

X = NO_2, NMe_2, $CH=CH_2$, $C(Me)=CH_2$, Ph, cyclo-C_3H_5, CH_2SiMe_3, $SiMe_3$, $SnMe_3$, HgCl, $B(OCH_2CH_2O)$.

The transition state of the rearrangement is of biradical nature; this has been confirmed in a series of studies.[85–94] Proceeding from the assumption that the biradical nature of the transition state rules out the possibility of substantial charge separation in it, Creary suggested using the logarithm of the relative rate constant for the reaction, k_{rel}, as a measure for the ability of substituents to stabilise the benzylic radical centre

$$\sigma_C^{\cdot} = \log k_{rel} . \quad (8)$$

The kinetic parameters of thermal rearrangement of 2-aryl-3,3-dimethylmethylenecyclopropanes **4** into 2-arylisopropylidenecyclopropanes **5** can be easily determined by gas chromatography or NMR; this permits determination of radical constants for *meta*- and *para*-substituents of the aromatic ring within the framework of this approach. It is also possible to evaluate the stabilising influence on the radical centre of heteroorganic substituents.[45]

It was found [57, 84] that electronegative substituents in the *meta*-position retard the rearrangement, which might point to an electron-deficient character of the biradical transition state. Most *para*-substituents, both electron-donating and electron-withdrawing ones have positive values of $\sigma_C^{\cdot}$ constants. An exception is F, for which $\sigma_C^{\cdot} = -0.08$ (see Table 1); this was explained by the destabilising influence of F caused by the enhanced inductive effect. The influence of the *para*-methoxy group was regarded as stabilisation ($\sigma_C^{\cdot} = 0.24$), caused by the contribution of the canonical forms **7a**,**b**.

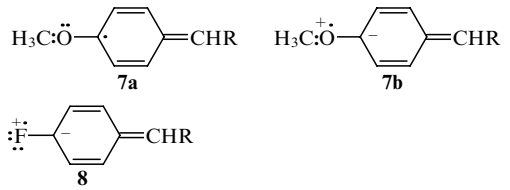

A similar structure for the *para*-fluorine-substituted system appears less favourable because of the high electronegativity of fluorine. From the molecular-orbital standpoint, the stabilising effect of the *para*-methoxy group can be due to the interaction of the radical centre with the filled non-bonding orbital of oxygen; however, the low energy of the filled 2*p* orbital of fluorine precludes manifestation of the effects of this type.

As has been noted in a monograph,[45] synthesis of a broad range of methylenecyclopropanes **4** is quite difficult; therefore, the reaction series proposed by Creary has no advantages in this respect over thermal dissociation of mercury dibenzyl derivatives. In addition, it is not quite clear to what extent the centre in the transition state **6** is a radical centre. Nevertheless, this approach has been successfully developed; it was shown in a recent publication [94] that the introduction of nitrogen-containing substituents into the *para*-position of the substrate **4** provides considerable radical stabilisation. Moreover, some substituents, for example, $CH=NNMe_2$, $N=NPh$, $N=N(O)Bu^t$ and $CH=N(O)Bu^t$ ($\sigma_C^{\cdot}$ = 0.92, 1.08, 1.08 and 1.13, respectively), displayed extraordinary radical-stabilisation capacity; they were called super-stabilisers.

A free-radical transition state in aliphatic systems [45, 95–100] has been modelled by pyrolysis of substituted azopropanes **9**.

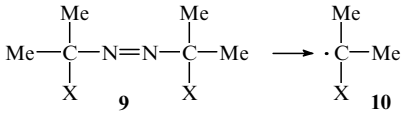

According to the researcher's assumption, this reaction series is characterised by slight steric and inductive interactions; therefore, the pronounced difference between the reaction rates (the range of variation of the rate constants is 10^9) is interpreted as being due exclusively to resonance stabilisation. Later, the kinetic characteristics of pyrolysis of the azopropanes **9** were found to be well correlated with the Creary radical constants $\sigma_C^{\cdot}$, despite the substantial difference between the structures of the radical substrates **6** and **10** and the fact that the extents of influence of substituents on the radical centres are difficult to compare.[83]

The series of model aryl-substituted azoalkanes has been markedly extended [101] by the inclusion of polycyclic azoalkane derivatives,[102] symmetrical azopropanes,[103, 104] azoethanes,[105, 106] azomethanes,[98] azoneopentanes [107] and 3,5-diaryl-1-pyrazolines,[98, 108] for which the kinetic parameters of pyrolysis have been found. It is worth mentioning that, only in terms of two-parameter correlations including polar constants σ, was it possible to attain satisfactory relationships between the experimental relative rate constants for the thermolysis of azo derivatives and the corresponding Creary parameters $\sigma_C^{\cdot}$.[84]

The equilibrium constant of the dissociation of substituted hexaarylethanes to triarylmethyl radicals has been used successfully as a measure of radical-stabilising capacity of substituents.[109]

An association reaction, namely, thermal [2 + 2]-cycloaddition of substituted α,β,β-trifluorostyrenes **11** [58] has been used as a model series for determination of spin-delocalisation group constants $\sigma_{JJ}^{\cdot}$ (see Table 1).

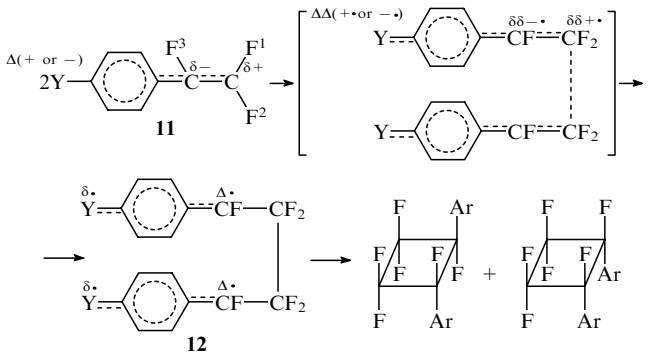

An advantage of this model reaction is that no side radical processes are involved. In addition, charge distribution in the transition state **12** is symmetric, which eliminates additional polar effects. Study of the kinetics of this reaction gave a two-parameter correlation equation

$$\log\frac{k_Y}{k_H} = \rho_{mb}\sigma_{mb} + \rho^{\cdot}\sigma^{\cdot}_{JJ}, \quad (9)$$

which was employed for the introduction of spin-delocalisation constants of substituents $\sigma^{\cdot}_{JJ}$. The σ_{mb} parameter in Eqn (9) is identical to the group constant proposed previously, which is determined on the basis of fluorine chemical shifts in the ^{19}F NMR spectra of compounds **11**.[58,110–113] The mb (multiple bond) subscript reflects the hypothetical additional repulsive component of interaction between the double bond and the electron lone pair or π-electrons in the Y substituent in the compound **11** (Jiang *et al.*[113] consider this to be a fundamental feature distinguishing the scale of σ_{mb} constants from the Brown–Okamoto σ^+ constants). Equation (9) provided the possibility of determining the $\sigma^{\cdot}_{JJ}$ constants for 32 substituents (see Table 1) at five different temperatures; this allowed the researchers to verify the adequacy of the correlation parameters proposed and to introduce an averaged scale.

By the use of the $\sigma^{\cdot}_{JJ}$ scale, together with the σ^+ parameters, the kinetic data underlying other scales of $\sigma^{\cdot}$ radical constants have been reproduced with rather high accuracy within the framework of a two-parameter equation. Assuming that the $\sigma^{\cdot}_{JJ}$ parameters reflect the real ability of substituents to delocalise spin density, Dust and Arnold[114] used the ratio of the coefficients of the two-parameter equations $\left|\frac{\rho}{\rho^{\cdot}}\right|$ as a measure of the relative contributions of radical effects in the corresponding model series. Thus it was shown that the ratio $\left|\frac{\rho}{\rho^{\cdot}}\right|$ for the reaction series of monosubstituted toluenes used by Fisher and Meierhoefer[55] to determine polar effects amounts to 4.8, whereas an analogous model series of substituted toluenes containing a cyano group in the *meta*-position is described by a ratio of polar to resonance effect equal to 1 : 1.51; in addition, the accuracy to which each contribution has been determined does not provide the possibility of their correct separation.

It should be noted that many researchers[4,52,77,114,115] proposed their own scales of $\sigma^{\cdot}$ constants which they considered to be the most suitable for estimating the radical character of transition states. For instance, Jackson *et al.*[56] used the $\sigma^{\cdot}_{J}$ scale and demonstrated that in the transition states of the model homolytic reactions that underlay the Fisher–Meierhoefer radical constants $\sigma^{\cdot}_{FM}$ and the E_R and E_D parameters, the fraction of structures corresponding to the proper benzyl radicals is not more than 50%.

The authors of most of the approaches discussed above have attempted to formulate the requirements to an ideal model system to be used for kinetic determination of radical constants.

1. The substituents should interact directly with the radical centre.

2. The mechanism of the model reaction should be as clear as possible.

3. Side reactions should be minimised.

4. Model systems should be preferred in which substituents have a strong influence on the reaction rate and for which accessible and precise methods for the determination of relevant kinetic parameters exist.

5. The polar effects should be either absent or minimised, or be reliably separated from the effect of radical stabilisation.

6. The model compounds should be readily available and should contain diverse substituents of both electron-donating and electron-withdrawing natures.

7. The role of other external and internal factors, for example, the solvent and the steric effect, should be minimised.

8. One of the most important features required for a free-radical reaction to be used as a model to describe the radical effects of substituents is that the nature of the transition state should be as radical as possible.

According to the Hammond postulate,[116] the last-mentioned condition (this is very important to emphasise) implies a late transition state of the process, which corresponds to a more endothermic generation of free radicals. This, in turn, stipulates a higher selectivity of the reaction.[117] Therefore, the radical effects of substituents (in particular, the captodative effect† of radical stabilisation) are often considered in the context of selectivity of free-radical processes (see, for example, Refs 45, 118).

It should be noted that in none of the above-listed approaches, the transition state can be considered completely radical — in any case, one should suggest the presence of charge separation and polar interactions. Therefore, the topicality of the question of to what extent a particular scale of radical constants is free from the polar constituent is beyond doubt. Apparently, the polar constituent can hardly be ruled out completely.

2. Spectroscopic determination of the capacity of substituents for delocalisation of spin density in free radicals

Physicochemical methods such as EPR spectroscopy permit direct investigation of the properties of free radicals.

According to the McConnel equation

$$a_H = Q\rho^{\pi}_C,$$

the hyperfine splitting (HFS) constants a_H in the EPR spectra are directly proportional to ρ.[118]

For a number of compounds, the relative HFS constants have been found[119,120] to correlate with the σ and σ^- polar constants; it was concluded[119] that delocalisation of an electron pair is a more substantial stabilising factor than spin density delocalisation. A non-kinetic scale of the stability of alkyl radicals based on HFS constants of β-protons has been composed.[121]

The approach proposed by Arnold *et al.*[122–126] is best known of all; according to this approach, the HFS constants of α-protons are used as a measure of stabilisation energy, determined by delocalisation of spin density in substituted benzyl radicals **13** with respect to $PhC\dot{H}_2$.

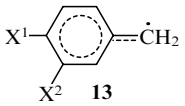

13

This method has obvious advantages, which include the absence of side radical reactions and the relative ease of generation of the required free radicals.[45] In addition, the radical constants $\sigma^{\cdot}_{\alpha}$, defined by the equation

$$\sigma^{\cdot}_{\alpha} = 1 - \frac{a(H_X)}{a(H_0)}, \quad (10)$$

where $a(H_X)$ and $a(H_0)$ are the HFS constants of the α-protons in the substituted and unsubstituted radicals, respectively, can be considered to be free from the polar effects characteristic of radical-like transition states and do not correlate with the substituent effects in the corresponding diamagnetic initial compounds. The researchers[122] assumed that other factors which can potentially influence the HFS constants (hybridisation of the orbital bearing the unpaired electron, interaction with β-substituents, steric effects reflected in the geometry of benzyl radicals[118]) are insensitive to the substitution in the aromatic ring.

The $\sigma^{\cdot}_{\alpha}$ values thus obtained (Table 2) confirmed that the *meta*-substituents in the aromatic ring decrease delocalisation of the unpaired electron. The correlation established between the constants of *meta*-substituted benzyl radicals and the corresponding Hammett *meta*-constants (σ_m) made it possible to relate the destabilising effect of *meta*-substituents to their inductive electron-withdrawing effect.[45] However, it is not entirely clear why electronegative *meta*-substituents hamper delocalisation of spin density on the methylene carbon atom in the benzyl system.[124]

† Captodative effect is a joint influence of electron-donating and electron-withdrawing substituents on a radical reaction centre, resulting in a stabilisation greater than the sum of the two stabilising effects in the corresponding monosubstituted radicals.[45]

Table 2. Constants characterising the radical-stabilisation properties of substituents (from EPR data and bond energies).

Substituent	$\sigma^{\cdot}_{\alpha}(p)$ see [a]	$\sigma^{\cdot}_{\alpha}(m)$ see [a]	ΔD_p see [b]	ΔD_m see [b]	E_d see [c]	$\sigma^{\cdot}_{av}$ see [d]	RRS_X see [c]
H	0.000	0.000	0.00	0.00	104.4	0.00	0.0
Me	0.015	−0.001(0.002)	0.02	−0.09	100.3	0.23	2.3
OMe	0.034(0.018)	−0.001	−0.05	−0.15	93.3	0.35	4.5
NO_2	–	–	0.90	−0.06	–	0.76	9.4
CN	0.043(0.040)	−0.039(−0.026)	0.54	−0.14	92.9	0.63	8.6
F	−0.011	−0.018(−0.009)	−0.17	–	101.0	−0.03	−1.4
Cl	0.017(0.011)	−0.001(−0.007)	0.09	−0.08	99.2	0.18	2.4
Br	–	–	0.05	–	102.5	0.23	0.9
I	–	–	0.04	−0.09	103.4	–	0.2
OH	–	–	−0.05	−0.22	95.0	–	3.1
C(O)Me	0.066 (0.060)	–	–	–	–	0.58	10.2
$P(O)(OEt)_2$	–	–	–	–	–	–	–
$P(S)(OEt)_2$	–	–	–	–	–	–	–
Ph	–	–	–	–	87.9	0.59	11.2
SMe	0.063	–	–	–	–	0.55	10.7
SPh	0.058	–	–	–	–	–	10.7
CF_3	0.001(−0.009)	−0.014(−0.017)	0.11	−0.04	106.7	0.09	−0.3
OPh	0.018	−0.013(−0.002)	–	–	–	–	4.9
CO_2Et	–	–	–	–	–	–	–
CO_2Me	0.048(0.043)	−0.004	0.53	–	–	0.54	7.9
C(O)Ph	0.064(0.055)	–	–	–	–	0.65	9.3
Bu^t	0.036(0.008)	–	–	–	93.9	0.13	3.0
Et	0.012	–	–	–	99.7	–	1.5
Pr^i	0.009	–	–	–	–	–	–
SOMe	0.006(0.018)	–	–	–	–	–	4.1
SC(O)Me	0.029	–	–	–	–	–	6.7
S(O)OMe	0.016(0.005)	–	–	–	–	–	3.6
SO_2Ph	0.018	–	–	–	–	–	4.5
S(O)Ph	0.026	–	–	–	–	–	5.9
SO_3Me	0.003(0.013)	–	–	–	–	–	2.9
OC(O)Me	0.001(−0.005)	−0.014	–	–	–	–	0.9
OC(O)Ph	0.000	–	–	–	–	–	0.0
N=NPh	–	–	–	–	–	–	–
NH_2	–	–	0.30	−0.19	94.0	–	8.4
NMe_2	–	–	–	–	84.0	–	8.9
$SiMe_3$	–	–	–	–	–	–	3.5
$CH=CH_2$	–	–	–	–	86.7	–	12.8

Note. E_d is the energy of homolytic dissociation of the C−X bond in substituted methanes.
[a] From Refs 114, 125; [b] from Ref. 127; [c] from Ref. 45; [d] from Ref. 115.

Presumably,[124, 128] a decrease in the electron density by the inductive mechanism prevents the effective overlap of the interacting sites, *i.e.*, of the orbital carrying the unpaired electron with the π-system of the benzene ring, or, in other words, it decreases the energy of the π-system and thus weakens the interaction between the CH_2-group carbon and the aromatic ring.

The effects of the OC(O)Me, CF_3 and F groups located in the *para*-position were found to destabilise the radical centre, whereas other *para*-substituents, according to the data obtained from EPR, favour spin density delocalisation.

It has been suggested that a decrease in the spin density in the α-position of the benzyl radical would result in an increase in the π-resonance binding of the aromatic system with the methylene group and, correspondingly, in an increase in the barrier to rotation around the $C_{arom}-CH_2$ bond.[45, 124] The π-component of the stabilisation energy (E_s) of the π-radical was expressed *via* the rotation barriers of the CH_2 group in the $Z\dot{C}H_2$ radicals with or without spin density delocalisation

$$E_s = V_2(\dot{C}H_2) - V_2^*,$$

where the corresponding rotation barriers (V_2 and V_2^*) can be determined from EPR data.

Jackson [129, 130] has noted that the range of HFS constants considered by Arnold *et al.*[122–126] is rather narrow and some individual values were determined with substantial errors. Therefore, he developed a new approach that provided more accurate determination of the HFS constants $a(CH_2)$ in the EPR spectra of benzyl radicals.[116] The results [129, 130] are generally consistent with the $\sigma^{\cdot}_{\alpha}$ scale.

Yet another example of using quantitative parameters of EPR spectra is a study by Adam *et al.*,[127, 131–135] who made use of the electronic spin–spin splitting parameters *D*. The parameter *D* is a sensitive function of the averaged distance between the unpaired electrons in a biradical ($D \propto 1/r^3$) which is proportional to the product of local spin densities in the triplet biradicals **14** and **15**, chosen as the reference species to determine the capacity of the substituent X for spin density delocalisation.[130–132]

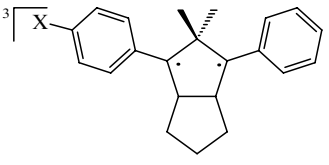

14

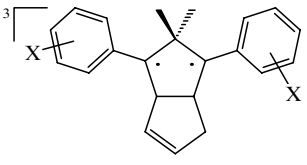

15

Proceeding from the assumption that specific electronic effects (captodative stabilisation, spin polarisation, *etc.*) are relatively insignificant in 1,3-biradicals,[136] Adam *et al.*[127, 132–134] proposed the scale of $\Delta D = D_H - D_X$ values (where H corresponds to the unsubstituted radical), which reflects delocalisation of the unpaired electron by the aryl group. Negative ΔD values, which should correspond to electron-donating groups, were found for all *meta*-substituents (including charged ones, *viz.*, NH_3^+, O^-) and for *para*-substituents such as F, OMe, OC(O)Me and OH. The *para*-substituents NO_2, CN, C(O)OMe, NH_2 and CF_3 exhibit the highest capacity for spin density delocalisation (see Table 1).

The additivity of ΔD values found for monosubstituted and symmetrically disubstituted triplet biradicals **14** and **15** served as the basis for the assumption that each of them can be represented as composed of two fixed fragments of the cumyl radical. Hence, the researchers suggested[127, 132] that the ΔD scale could also be used for adequate description of benzyl monoradicals. This suggestion is supported by the fact that the parameters D for triplet biradicals are correlated with the α-spin densities and the energies of resonance stabilisation of the corresponding cumyl radicals.[127, 132–134]

Comparison of the ΔD scale with known radical constants based on the properties of benzyl radicals revealed a relatively good correlation of this scale with the Fisher data (the correlation coefficient squared is $r^2 = 0.92$); however, the discrepancies with the $\sigma_J^{\cdot}$, $\sigma_C^{\cdot}$, and $\sigma_{JJ}^{\cdot}$ arrays are quite substantial ($r^2 = 0.33–0.60$). Subsequently, this approach has been extended to heteroaromatic π-systems such as pyridine and furan derivatives and some other.[135]

3. Thermodynamic approaches to the estimation of radical stabilisation. Bond energy as a measure of radical stabilisation

Study of the effects of substituents in free radicals is tightly connected with the problem of quantitative evaluation of the energies of dissociation of chemical bonds.

The energy of an R–R′ bond is known[136] to be determined by the enthalpy ΔH_1^0 of homolytic dissociation of this bond, giving rise to free radicals R$^{\cdot}$ and $\dot{R}'$

$$R-R' \longrightarrow \dot{R} + \dot{R}'.$$

In turn, the ΔH_1^0 value is determined by the standard enthalpies of formation of RR′, R$^{\cdot}$ and $\dot{R}'$

$$\Delta H_1^0 = \Delta H^0(\dot{R}) + \Delta H^0(\dot{R}') - \Delta H^0(RR').$$

Thus, the relative energies of the homolytic dissociation of bonds can serve as a measure of radicals stabilisation. On the basis of the foregoing, Benson and O'Neal[137, 138] have proposed estimating the stabilisation energy for π-resonance delocalised radicals R(π-$\dot{C}H_2$) as the difference between the dissociation energies E_d of the corresponding derivatives

$$E_s[R(\pi\text{-}\dot{C}H_2)] = E_d[R(CH_2-H)] - E_d[R(\pi\text{-}CH_2-H)].$$

Subsequently, the C–H bond energies have been widely used to estimate the stabilisation energies for carbon-centred radicals. For example, the resonance stabilisation energy of the benzyl radical can be represented as the difference between the energy of the benzylic bond in toluene and the energy of the C–H bond in ethane.[45, 139, 140] The enthalpy of dissociation of the C–H bond in the methane molecule $E_d(CH_3-H) = 439$ kJ mol^{-1} is used most often as the reference value.[140–145]

In one of the first studies dealing with this topic, the enthalpy of the isodesmic reaction (*i.e.*, a reaction in which the number and character of bonds do not change on passing from the initial compounds to the products)[146]

$$R^{\cdot} + CH_4 \longrightarrow RH + {}^{\cdot}CH_3$$

was identified as the stabilisation energy E_R of the R$^{\cdot}$ radicals[146]

$$E_R(R^{\cdot}) = \Delta H_2^0 = E_d(CH_3-H) - E_d(R-H).$$

Subsequently, stabilisation energies of radicals expressed in terms of E_d, *i.e.*, $E_s(R^{\cdot}) = E_d(CH_3-H) - E_d(R-H)$, have been widely used for various correlations.[138–145]

Bordwell *et al.*[147, 148] have proposed a scale of redox potentials I_{AO}, which is also actually based on the relative energies of dissociation of bonds in substituted fluorenes.

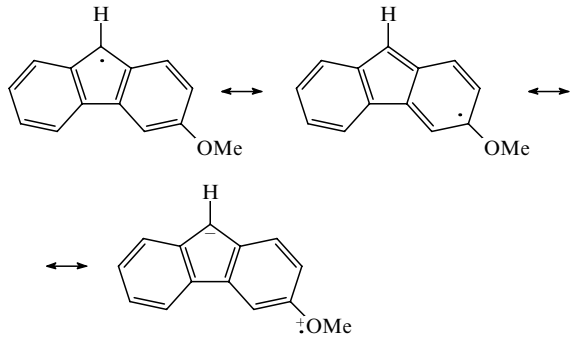

The potentials were determined using the thermodynamic cycle

HA	⟶	$H^+ + A^-$	(pK_a)
A^-	⟶	$A^{\cdot} + e^-$	(E^{ox})
$H^+ + e^-$	⟶	$H^{\cdot}$	(E^{red})
HA	⟶	$H^{\cdot} + A^{\cdot}$	(E_d),

in which the proton reduction potential E^{red} is a constant and the sum $pK_{HA} + E^{ox} = I_{AO}$ can be regarded as a measure of relative radical stability of the radical A$^{\cdot}$.

The oxidation potentials E^{ox} of substituted fluorenide ions were determined experimentally in DMSO solutions, and the pK values of the conjugate acids were established on the basis of their correlation with E^{ox}; this gave rise to a scale of I_{AO} values for a number of substituents at the 2-, 4- and 7-positions expressed in kJ mol^{-1} and reflecting the ability of these substituents to delocalise the unpaired electron in fluorenes.

The application of this approach to 9-substituted fluorenes and to 3- and 4-substituted phenylacetonitriles has made it possible to analyse a wide spectrum of radical-stabilisation and -destabilisation effects.[149, 150] Comparison of the I_{AO} values for 4-substituted arylacetonitriles with the $\sigma_{JJ}^{\cdot}$ constants within the framework of a two-parameter equation containing the σ^+-parameter showed that the contributions of the polar and radical constituents to I_{AO} are approximately equal.[58]

It has been proposed to use the E^{ox} oxidation potentials of 3- and 9-substituted fluorenes[150, 151] and of α-substituted acetone and acetophenone derivatives[152] in DMSO as the basis for determination of the stabilisation energies E_{RS} of the corresponding radicals

$$\Delta E_d = 1.37\Delta pK_{HA} + 23.1\Delta E^{ox}(A^-) = E_{RS}.$$

The resulting values point to a stabilising effect of substituents at the 3-position in substituted fluorenyl radicals, except for F and $PhSO_2$. Substitution into the 9-position both by donors and by acceptors results, as a rule, in system stabilisation. Most of 4-substituents (except for F and CF_3) also exhibit pronounced stabilising properties.[148] In general, it was concluded[150] that the majority of substituents play a dual role in the stabilisation of a free radical: they destabilise the radical due to the electron-acceptor influence and stabilise it due to delocalisation.

In some studies, the radical-stabilisation energy of substituent X was set identical to the covalent component of the dissociation energy of the XR–Z bond, where R is a permanent molecular fragment (for example, the aromatic ring), while R–Z is the 'indicator' bond.[140, 153–156] The notion 'indicator' bond was introduced back in Pauling's studies;[151] the stabilisation energy E_{RS} was defined *via* the relative dissociation energies of bonds in symmetrically substituted molecules

$$E_{RS} = 0.5\,E_d(XR-RX) - 0.5\,E_d(HR-RH).$$

A similar approach has been proposed by Leroy,[157, 158] who used the enthalpies of atomisation ΔH_a together with the standard bond energy E_{AB} to define the stabilisation energy E_s

$$E_s = \Delta H_a - \Sigma N_{AB} E_{AB},$$

where N_{AB} is the number of AB bonds. This procedure was applied successfully both to free radicals and to diamagnetic molecules.

Thermochemical and kinetic investigations of the rupture of the C—C bond have been employed to define the parameter E_{RS}, introduced to reflect the difference between the stabilities of the hydrocarbon radical **16a** and the corresponding substituted radical **16b**.[117, 156, 159–161]

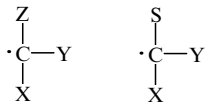

16a **16b**

X, Y, Z are hydrogen atoms or alkyl substituents and S is a functional group.

A substantial drawback of the approaches in which the radical stabilisation is defined in terms of the relative bond energies and the reason why these approaches are severely criticised is the fact that the energy of homolytic dissociation of a bond is a relative value, *i.e.*, the difference between the energies of the molecule and the corresponding radicals; therefore, the substituent effect cannot be attributed to the properties of the free radical alone.[117, 143, 162, 163] It is well known that the dissociation energies of bonds depend on steric effects [116] and on polar effects;[164] the presence of numerous correlations between E_d(CH) and the 'ionic' constants of substituents σ^+ (see publications [23, 147, 165]) is common knowledge. In our opinion, this virtually rules out a legitimate separation of the polar and radical effects in this type of approach. Moreover, it was shown that in some cases, the effect of substituents can even prevail in the ground state; then the corresponding ΔE_d values reflect destabilisation of the molecule rather than stabilisation of the free radical.[163] It has been clearly demonstrated [143] using, among other reasons, vast literature data that relative bond energies cannot be related directly to the stability of radicals.

4. Calculation of the energies of stabilisation of radical centres

Apart from experimental methods, there also exist theoretical methods for the determination of group parameters of substituents reflecting their capacity for stabilisation of radical centres.

Modern quantum-chemical approximations permit direct calculation of quantitative characteristics of radicals such as the total energy, the standard enthalpy of formation, the energy of the orbital with the unpaired electron and the spin and charge density, which make it possible to judge the stabilising influence of substituents. Many quantitative parameters employed to determine the radical-stabilisation effects in terms of the experimental approaches described above such as the kinetic parameters of free-radical reactions and the overall thermodynamic characteristics, spin densities and rotation barriers in free radicals can be calculated quite reliably by quantum-chemical methods. Certainly, any general description of theoretical approaches requires separate consideration. Within the framework of this review, we shall dwell only on those of them that have served as the base for the introduction of sets (scales) of energetic parameters of substituents reflecting their radical-stabilisation influence and implying consistent utilisation of the LFE principle.

In studies by Pasto *et al.*,[166, 167] the change in the total energy of species participating in the free-radical transfer of a hydrogen atom has been identified with the stabilisation energy E_{RS} of the corresponding substituted methyl radical. The E_{RS} values were calculated for a large number of substituents. The captodative effect of radical stabilisation and the influence of the substituents attached to the reaction centre containing an unpaired electron were analysed from the additivity standpoint.[166] The comparison of the calculated E_{RS} values with the known scales demonstrated a relatively good quantitative agreement with the I_{AO} parameters for 3- and 9-substituted fluorenes and 4-substituted phenylacetonitriles,[148] with the relative constant of the thermal rearrangement of 3-aryl-2,2-dimethylmethylenecyclopropanes [57, 82, 83] and α-spin density in 4-substituted benzyl radicals.[114] Within the framework of this approach, it was found that the radical-stabilisation effect markedly increases on passing from F- to O- and N-containing substituents. In the series Cl, S, P, the capability for spin density delocalisation increases due to the decrease in the energy gap between the vacant MO of the methyl radical and the MO occupied by the unpaired electron. Study of the effects of substitution with charged ($^+NR_3$, $^+SR_2$, $^+PR_3$) or electronegative non-charged (CF_3, SOR, SO_2R) groups showed that they destabilised the radical. In addition, it was found that the energies of stabilisation of the radical centre calculated in terms of the approach proposed are exceptionally sensitive to the conformation of the free radical and the corresponding diamagnetic molecule.

Isodesmic reactions (see Section II.3) proved convenient for the calculation of $E_{RS}(R^{\cdot})$.[44, 144, 168–173] The enthalpy of hydrogen atom detachment in these reactions is a measure of the energy of stabilisation of the radical centre; the use of this value decreases the errors related to the basis set chosen and to electron correlation effects.[174]

The stabilisation energies of the radical centre E_{RS} correlated with the barriers to rotation around the C—C bond in benzyl radicals were calculated by quantum-chemical methods, as well as the difference between the energies of the conformers corresponding to angles of rotation around the σ-bond equal to 90° and 0°.[175–177]

$$E_{RS} = \Delta H_f(90) - \Delta H_f(0).$$

The E_{RS} values thus obtained are well correlated with the parameters D of the biradicals **14** and **15** determined experimentally by EPR.[127]

5. Critical analysis of the existing approaches

The attempts at systematisation of the existing radical scales of substituents made previously can be classified, in our opinion, into two main types, namely, the choice of the $\sigma^{\cdot}$-scale describing most accurately the standard homolytic reaction series and the development of a quantitative approach integrating the accumulated arrays of 'radical' constants and combining them into some universal scale.

We have already mentioned that the authors of many of the studies presented in the previous Sections proposed their own standard series; the corresponding arrays of the group parameters were regarded as most suitable for developing a scale that could be used as the reference in analogous approaches. However, the search for this optimal scale did not reveal obvious advantages of any of the known sets of radical parameters; therefore, in some cases, it was concluded [9] that development of universal radical constants $\sigma^{\cdot}$ is impossible in principle. The attempts to find multiparameter correlations with the use of various combinations of polar and radical scales did not produce a satisfactory general result either. Moreover, the methodology of using the extended Hammett equation for the description of radical-stabilisation effects has been criticised.[49]

In view of the difficulty of using group radical constants to describe homolytic processes, Hansch and Leo [178] proposed that the polar parameters σ should be used for this purpose whenever possible. Exner [179] also suggested that the σ_p^+ and $\sigma_{m,p}$ constants suffice for interpretation of the free-radical reactivity. In another study,[180] radical-stabilisation effects of substituents are described in terms of the quadratic function σ^2; this, in principle, contradicts the LFE formalism.

Several prominent researchers attempted, in a joint review,[45] to devise a universal scale of relative radical stabilisation (RRS), based on averaging of the above-mentioned scales of the Creary ($\sigma^{\cdot}_{C}$),[57,80–84] Jackson ($\sigma^{\cdot}_{J}$)[51,52,56,76–79] and Arnold ($\sigma^{\cdot}_{\alpha}$) constants,[114,122–125] the kinetic parameters of radical fragmentation of bis-azo derivatives[96–100] and a number of other analogous characteristics of free-radical reactions.[45,180–184] It was suggested that statistical averaging would eliminate the errors inherent in each of basic experimental approaches. In addition, the average group RRS parameters are expected to reflect the degree of additivity of the group influences upon multiple substitution at the carbon radical centre and to describe the effect of captodative radical stabilisation.

Positive averaged RRS_X values (see Table 2), which imply radical-stabilisation properties, were found for a large number of diverse substituents. The only exceptions were F and CF_3, for which the RRS_X(F) values were -1.4 and -0.3, respectively.

By means of the scale of averaged RRS_X, the researchers[45] were able to identify a number of interesting correlations which point, in particular, to underestimation of the radical-stabilisation properties of electron-withdrawing substituents and overestimation of the role of electron donors in terms of some $\sigma^{\cdot}$-approaches.

The averaged radical $\sigma^{\cdot}_{av}$ scale was based[115] on two sets of EPR characteristics of benzyl radicals taken from the literature[115,124] and on three 'kinetic' arrays, namely, scales of the $\sigma^{\cdot}_{C}$ (see Refs 57, 80–84) and $\sigma^{\cdot}_{J}$ (see Refs 50–52, 56, 76–79) constants and kinetic data taken from the literature.[101] The $\sigma^{\cdot}_{av}$ values (see Table 1) confirmed the radical-stabilisation properties of the vast majority of *para*-substituents including CF_3. Only the averaged constant for *p*-F was found to be negative ($\sigma^{\cdot}_{av} = -0.02$). This deviation was explained by assuming that, under the action of the electronegative F atom, hybridisation of the carbon atom at the 4-position changes somewhat towards sp^3; this disturbs the aromaticity of the benzene ring and, hence, destabilises the radical centre.

Each of the definitions of the radical $\sigma^{\cdot}$ constants characterised in this Section suffers from its own specific disadvantages. They were noted above whenever appropriate. In addition, the methods of description of the radical effects of substituent can be subjected to a common criticism. It is expedient to arrange critical remarks in accordance with the above classification.

1. Kinetic methods. It is known that the classical σ-constants of electron-withdrawing substituents, which stabilise an electron-enriched reaction centre, are positive, whereas electron-donating groups, which stabilise electron-deficient systems, have negative polar constants. In turn, the sign of the parameter ρ of the correlation equation reflects the character (either electrophilic or nucleophilic) of the reaction, while the magnitude of ρ shows the degree of charge separation in the transition state. It is commonly known that the polar constants of substituents correlate equally adequately with the properties of the transition state and the ground state (numerous polar scales are based on the physicochemical, for example spectroscopic, properties of neutral molecules). Thus, successful description of energy characteristics of heterolytic processes in terms of group constants is normally explained by assuming either that the substituent effects in the transition and ground states are correlated or that the latter can be neglected. The kinetic methods of determination of substituent effects in homolytic processes also deal with the difference between the energy of the ground and radical-like transition states. However, a significant specific feature of free-radical reactions is that the natures of the initial species (or products) and the transition state in any homolytic process are fundamentally different because of the presence of an unpaired electron; the effects of substituents on the energies of the ground and transition states differ not merely quantitatively, as in the case of heterolytic processes, but also qualitatively. Furthermore, the numerous examples cited in the preceding Sections point to the importance of substituent effects in the ground state of homolytic processes, which precludes the possibility of neglecting them. In addition, even if the polar interactions in the ground state are assumed to be proportional to those in the radical-like state, their role in delocalisation of the proper unpaired electron still remains obscure.

Strictly speaking, the magnitudes of radical $\sigma^{\cdot}$ parameters established by kinetic methods often reflect the differences between the influence of substituents on the initial and transition states of a particular reaction but not the effectiveness of delocalisation of the unpaired electron by one or another substituent. In this connection, the numerous examples of successful use of polar constants alone for the description of free-radical processes seem quite obvious and the lack of correlation between radical scales is quite logical. Thus, reasonable separation of the effects related to charge stabilisation and to delocalisation of the unpaired electron within the framework of kinetic approaches appears unlikely, if achievable at all.

It is also worthy of note that the role of other factors (steric effects and, especially, solvent effects) has been interpreted fairly arbitrarily in most of the approaches considered. As a rule, the authors assumed that the homolytic mechanism of the standard reaction allows the solvent effects to be completely neglected. However, as has already been noted, in reality, none of the kinetic approaches allows complete elimination of the influence of polar interactions (which can depend substantially on the properties of the medium); this casts doubt on the proper methodology of determination of many $\sigma^{\cdot}$-scales.

2. Spectroscopic methods. Methods based on the use of EPR for determination of the spin density distribution are free from the drawbacks associated with the substituent effects in the corresponding molecules. Meanwhile, the question of whether spin density delocalisation follows a linear correlation with the stabilisation energy of a free radical remains relevant. In addition, it is unclear to what degree the spin density distribution is governed by the delocalisation contribution and to what degree, by the spin-polarisation contribution.[45] And, finally, what is the role of polar effects (for example, resonance effects) in the spin density distribution? Is it proper to consider them insignificant and related exclusively to charge stabilisation?

In our opinion, the following circumstance is also rather important. Let us assume that the spectral $\sigma^{\cdot}$-constants do actually reflect the capacity of substituents for delocalisation of the unpaired electron. Then it is clear that valid considerations about the mechanisms of delocalisation of an unpaired electron by substituents can be constructed on their basis and the $\sigma^{\cdot}$ values can be used to verify the adequacy of similar approaches to the solution of problems for which the correlation analysis methods are meant. However, the scope of applicability of these spectral radical scales still remains vague, while their predictive capacity and practical application hardly possess considerable advantages. In any case, when describing real homolytic reaction series, the presence of polar interactions (which are always quite probable, as we have repeatedly emphasised above) implies the use of a two-parameter correlation equation containing both radical and polar constants. One or another polar scale can be preferred and the relationship between the polar and radical components of the stabilisation effect can be identified only on the basis of a statistical selection procedure. From a practical point of view, this brackets the $\sigma^{\cdot}$ constants obtained by spectroscopic methods with those determined by kinetic methods.

3. Thermodynamic methods. The approaches based on the use of thermodynamic methods are criticised especially vigorously. As has been mentioned above, determination of radical-stabilisation effects in terms of thermodynamic parameters (bond energies) corresponding to diamagnetic substrates does not permit one to rule out the substituent effects related to the molecules or to distinguish the proper radical stabilisation from polar or steric factors. Strictly speaking, these approaches are rather suitable for discussing the relative effects of substituents on the energies of covalent bonds; this, in itself, is a complex problem not ultimately solved. It is also noteworthy that, within the framework of

thermodynamic approaches, the radical stabilisation effect is largely replaced by the notion of radical stability. Strictly speaking, this is not the same; below we shall consider this point in more detail.

To conclude this section, it can be stated that none of the existing methods of $\sigma\rho$-description of substituent effects in free-radical processes is free from serious drawbacks and, as a rule, each method operates within a narrow reaction series. The lack of correspondence between radical scales and the different in kind interpretations of the radical-stabilisation properties of the same substituents in terms of different approaches make difficult the understanding of the physical meaning of radical constants and preclude the possibility of their joint application.

It cannot be ruled out that the correlation analysis formalism cannot, in principle, be applied in full measure to the description of homolytic processes because the additivity of group interactions is there violated. An especially clear example is the captodative stabilisation effect, or push – pull effect, repeatedly mentioned above.

4. Captodative effect. The existence of an extra-stabilisation effect peculiar to bifunctional radicals was first assumed by Dewar.[185] A quantitative proof of the unusual stability of these radicals was later presented in studies by Balaban *et al.*,[186, 187] who used the term 'push – pull resonance.' Later, Katritzky *et al.*[188 – 190] arrived at the conclusion that radical centres bearing simultaneously an electron-donating and an electron-withdrawing group are subject to an extra-stabilisation effect, which was called merostabilisation (later, captodative effect).[45,191 – 194]

A simple substantiation of the captodative stabilisation can be derived from the numbers of contributing structures [in the example presented below, there are two structures for the amino- (**17**) or the cyano-derivative (**18**)] corresponding to monosubstituted radicals and to a disubstituted radical containing both electron-donating and electron-withdrawing groups [five contributing structures are presented for the amino-cyano-substituted radicals **19**].

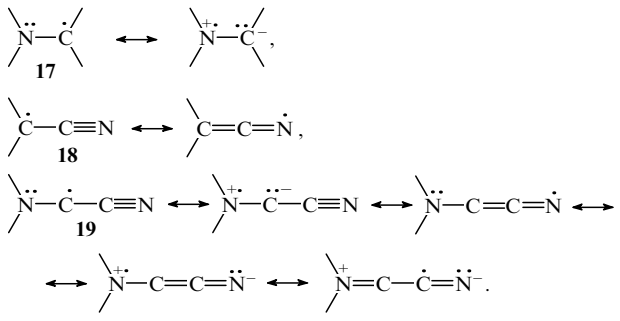

For disubstituted radicals containing either only amino- (**20**) or only cyano groups (**21**), three contributing structures can be proposed

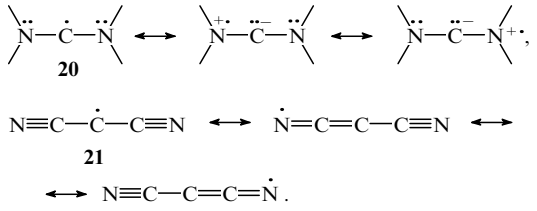

Thus, stabilisation of these species due to delocalisation would be somewhat weaker than is expected based on the sum of the substituent effects in the monosubstituted analogues.

The over-additive stabilisation effect in radical species containing both electron-donating and electron-withdrawing groups has been repeatedly confirmed experimentally. The enhanced reactivity of captodative alkenes has been noted in radical [193 – 199] and [2 + 2]-cycloaddition [45, 199 – 202] reactions. The captodative acceleration was considered to be the reason explaining the results obtained in studies of cyclisation of 6-substituted hex-5-en-1-yl radical,[203] homosolvolysis of some alkyl bromides on treatment with di-*tert*-butylnitroxide,[204] thermal rearrangement of substituted 2-arylmethylenecyclopropanes,[205] isomerisation of diastereomeric substituted cyclopropanes [206, 207] and thermal homolysis of the C – C bond in hexa-1,5-dienes [207] and dibenzyls.[208, 209]

EPR data for substituted benzyl radicals point to enhanced stabilisation of those radicals that contain both electron-donating and electron-withdrawing substituents, whereas two identical substituents decrease radical stabilisation.[114] Analysis of the barriers to internal rotation and the energy barriers to *E*,*Z*-isomerisation of substituted allylic radicals determined from EPR data also attests in favour of captodative interactions.[210] Study of the barriers to rotation around the C – N bond in substituted aminoalkyl radicals has led to similar conclusions.[211] In several publications,[161, 212, 213] the captodative effect was substantiated from the standpoint of orbital views. Calculations of the stabilisation effects in free radicals also predict an enhanced stabilisation of captodatively substituted derivatives.[45, 163, 214, 215]

However, a number of experimental and theoretical studies have not elucidated any significant distinctive features of captodatively substituted radicals and demonstrated strictly additive influence of the corresponding substituents at a radical reaction centre.[216 – 219] Moreover, some researchers cast doubt on the existence of an additional captodative stabilisation. Within the context of the present consideration, we would only like to mention that, under the assumption of the existence of captodative stabilisation of free radicals, the use of additive correlation equations based on LFE and polylinearity principles to describe homolytic processes should be subject to certain, perhaps quite substantial, constraints.

Thus, analysis of the published data available to date provides grounds for the following conclusions.

1. The classical polar constants σ are not fully applicable to the description of free-radical processes and do not reflect the radical-stabilisation effects of substituents. In all probability, one can speak about a disproportion of substituent effects in heterolytic and homolytic processes. Although quite a few examples of successful use of polar constants in free-radical chemistry have been reported, the existing scales of specific radical constants $\sigma^{\cdot}$ are not general. The lack of correspondence between the scales and vagueness of their physical meaning might be due to the constrains inherent in the use of the LFE principles and correlation analysis in free-radical chemistry and violation of the additvity of the group influence in paramagnetic systems rather than to the drawbacks of the methods of their determination.

2. It is obvious that an approach, new in principle, to the description of substituent effects in free-radical systems needs to be developed. It is important that this approach should possess predictive capacity and provide a quantitative estimate of the character of interaction of substituents with the radical reaction centre. However, it is quite probable that the physical nature of this interaction would not be clarified completely but it would be possible to obtain a satisfactory quantitative description of the structure – reactivity relationship as applied to the chemistry of free radicals.

III. The use of r^{-2} analysis in free-radical chemistry

1. Modelling of inductive and steric effects

Previously, we have developed quantitative procedures for determination of the steric and inductive effects of substituents in terms of discrete atomic contributions. Detailed description and theoretical substantiation of the models proposed, aspects of their practical use and the inductive electronegativity concept based on them have been presented in our previous reviews.[2 – 6] In the context of this review, we considered it pertinent to mention the main theses of these approaches.

Steric interactions were determined in terms of the model of frontal steric effect in which the steric effect of a substituent is represented as a result of mechanical shielding of the reaction centre by the surrounding atoms

$$R'_S = \sum_{i=1}^{n} \frac{R_i^2}{4r_i^2}, \tag{11}$$

where R'_S is the steric constant, n is the number of atoms in the substituent, R_i is the radius of an ith atom and r_i is the distance from the ith atom to the reaction centre.

It should be emphasised that in terms of this approach, the steric effect of any substituent at any reaction centre can be predicted with high accuracy on the basis of only fundamental parameters (the size and the distance to the reaction centre) of the atoms forming the substituent. The R'_S parameters calculated for a broad range of the most frequently encountered groups follow a good correlation with the Taft steric constants ($N = 35$, $R = 0.9854$, $S = 0.141$).

In the model of inductive effect, the inductive constant σ^* of an n-atomic substituent was represented at the atomic additivity level

$$\sigma^* = \sum_{i=1}^{n} \frac{\sigma_{A(i)}}{r_i^2}, \tag{12}$$

where σ_A is an empirical constant introduced in the model of inductive effect and reflecting the ability of an atom to exhibit the inductive effect, which depends on the nature and valence state of the atom. The σ_A values have been established for a wide range of elements; the inductive constants calculated theoretically using these values (altogether 426 substituents) have formed a high-quality correlation with the corresponding experimental data ($N = 426$, $R = 0.9910$, $S = 0.190$).

The practical use of this additive approach in the description of reactivity and investigation of the mechanisms of reactions involving organic and heteroorganic compounds proved fairly successful. This has also contributed to the solution of a number of important theoretical problems related to inductive interactions such as the inductive effect of alkyl substituents, the presence or absence of linearity in the inductive effects of substituents on carbon and heteroatom reaction centres and some others. The models developed make it possible to describe quantitatively only the inductive and steric effects; no approach based on the modelling principle for estimation of resonance interactions has been devised yet. Nevertheless, as shown in our study,[4] the additive model of inductive effect describes rather adequately the electronic interactions in various conjugated systems and only some of them, subjected to the influence of direct polar conjugation, can provide exceptions.

2. Combinational approach. r^{-2}-Analysis. Ionisation energies of amines

The new topological approach developed on the basis of the above models, which allows the substituent effect to be expressed in terms of discrete atomic contributions, was first reported in our publication and called r^{-2}-analysis.[220]

Since both the steric and inductive constants were expressed in Eqns (11) and (12) as functions of $1/r^{-2}$, the two-parameter Taft equation

$$Y = \rho \sum_i \sigma^* + \delta \sum_i E_s \tag{13}$$

can be represented in terms of discrete atomic contributions

$$Y - Y^0 = \sum_{i \neq rc}^{N-1} \frac{e_i}{r_{rc-i}^2}, \tag{14}$$

where N is the number of atoms in the molecule, rc is the atom chosen as the reaction centre, r_{rc-i} is the distance between atom i and the reaction centre. The dependent parameter Y can be represented by any physical value which is used in terms of a general correlation equation (13) (the logarithm of the rate or equilibrium constant, the reaction or activation energy, *etc.*), Y^0 is the same parameter for a compound chosen as the standard in this reaction series, and e is a parameter reflecting the capacity of an atom of a definite type for exhibiting intramolecular effects determining the Y values.

The approximation we used permits one, first of all, to verify whether it is possible, in principle, to introduce the operational atomic constants e_i corresponding to atoms of different types and depending on the nature and the valence state. The next step is to determine their physical meaning. The formalism of this approach implies that each atom encountered in all the molecules of the reaction series can, in principle, be regarded as a hypothetical reaction centre. In this case, for each molecule contained in the reaction series, the other $N-1$ atoms are treated as a single sub-substituent.

After the reaction centre for a given series has been chosen, the matrix of sums

$$\sum_k \frac{1}{r_{rc-m_k}^2},$$

corresponding to the types of atoms present should be composed. A table should be made up, containing N vertical matrix elements (rows), where N is the number of molecules in the reaction series, and M horizontal elements (columns),where M is determined by the types of atoms represented in the molecules of the series. The k value in the matrix of sums corresponds to the number of atoms of type m in molecule n, and $r_{rc-m_k}^2$ are the distances between type m atoms and the reaction centre rc in molecule n. If no type m atoms are present in molecule n, the corresponding matrix element is taken to be zero. As an example, Table 3 gives the r^{-2}-matrix for the reaction series including the $MeH_2C^{\cdot}$, $ClH_2C^{\cdot}$, and $Me(NH_2)HC^{\cdot}$ radicals in which the carbon bearing the unpaired electron is chosen as the reaction centre. In real calculations, the number of horizontal elements should exceed the number of vertical elements; then the columns of this matrix can be regarded as sets of independent arguments and the $Y - Y^0$ array can be regarded as an array of dependent values of multiparameter linear regression (14).

Table 3. r^{-2}-Matrix for the reaction series containing the $MeH_2C^{\cdot}$, $ClH_2C^{\cdot}$ and $Me(NH_2)HC^{\cdot}$ radicals.

Radical	Type of atom			
	H	C(sp^3)	Cl	N(sp^3)
$MeH_2\dot{C}$	$\frac{2}{1.09^2} + \frac{3}{2.16^2}$	$\frac{1}{1.54^2}$	0	0
$ClH_2\dot{C}$	$\frac{2}{1.09^2}$	0	$\frac{1}{1.76^2}$	0
$Me(NH_2)H\dot{C}$	$\frac{1}{1.09^2} + \frac{3}{2.16^2} + \frac{2}{2.04^2}$	$\frac{1}{1.54^2}$	0	$\frac{1}{1.46^2}$

Thus, if the corresponding multiparameter correlation can be established with a satisfactory accuracy, its linear coefficients are the operational atomic constants e_i corresponding to particular types of atoms. It is clear that this scheme should be effective in the description of those reaction series that can be analysed quantitatively using inductive and steric group constants.

The method developed for the description of substituent effects has several obvious advantages over classical correlation analysis. First, it is free from the restrictions associated with the choice of an appropriate scale of substituents because it deals directly with interatomic distances and is conformationally sensitive. Second, the use of a simple mathematical apparatus allows one to analyse quickly and effectively indefinitely large sets of

parameters. Third, within the framework of this model, it becomes possible to consider all the potential reaction centres of the series, which can provide additional information on the mechanism of the process under study. This is important in those cases where interpretation of the mechanism does not appear unambiguous and variation of the reaction centre could permit decision in favour of one of the most probable mechanisms.

We implemented the algorithm outlined above as a product called RMATRIX, which was developed on the basis of the MATLAB program.[221] The RMATRIX program allows importing of intramolecular distances from HyperChem or from similar files containing data on the spatial structure of the molecules of a reaction series; then it composes the r^{-2}-matrix corresponding to the reaction centre chosen for each molecular series, and, finally, it establishes statistically the operational atomic increments e for the series.

3. The physical meaning of the operational atomic parameters

A drawback of r^{-2}-analysis is that it does not allow direct consideration of resonance interactions because they cannot be described certainly by any distance function. However, a more substantial problem is that the physical meaning of the operational atomic parameters e_i, defined by Eqn (14), remains vague and does not provide the possibility of resolving the substituent effects into the inductive and steric components. The analysis of the e_i values presented below is pertinent in this connection. The correlations established previously in terms of the steric and inductive models can serve as the basis for this consideration.

Thus it has been found[4] that the σ_A constants for a broad range of elements are correlated with the difference between Pauling's electronegativities $\Delta\chi_{i-rc}$ of a given element A and the atomic reaction centre (rc) (this difference reflects the ability of atom A to displace electron density) and with the squared covalent radius of the A atom (which reflects its capacity for charge delocalisation)[4, 5, 222]

$$\sigma_A = 7.84\Delta\chi_{i-rc}R_i^2 .$$

The back calculation of the χ values using this relation makes it possible to introduce a new scale of 'inductive' electronegativities, which is purely empirical because it is based on the inductive constants describing a huge array of reaction series.[4, 5] This scale is, by definition, in good agreement with Pauling's electronegativities, except that for carbon. According to the 'inductive' scale, the electronegativity of carbon is 2.1. This value appears to be more plausible than $\chi^P = 2.55$ proposed in the Pauling scale.[2, 223, 224] The latter value implies that carbon should be more electronegative than, say, phosphorus ($\chi^P = 2.2$) or iodine ($\chi^P = 2.4$), which is not the case in reality. The low polarity of the C—H bond also indicates that the Pauling χ^P value for carbon is overestimated. Subsequently, a scale of group inductive electronegativities and the concept of inductive chemical hardness, which interpret a number of widely used reactivity indices using simple geometrical characteristics of bonded atoms, have been developed in terms of this approach.[2] These concepts were considered in detail in our review [2] and in a number of publications.[223–231]

On the basis of established correlations, the Taft inductive constant can be expressed in terms of fundamental characteristics of the atoms of substituents and the reaction centre, namely, electronegativities, radii and interatomic distances

$$\sigma^* = 7.84\sum_i \frac{\Delta\chi R_i^2}{r_i^2} . \qquad (15)$$

By superposition of Eqns (11)–(14), the atomic parameters e_i can be represented as the sum of inductive and steric constituents

$$e_i = a\Delta\chi_{i-rc}R_i^2 + bR_i^2 . \qquad (16)$$

Evidently, if a satisfactory correlation of type (16) has been established, it becomes possible not only to calculate the unknown e_i values on its basis but also to express the dependent parameters Y in terms of inductive and steric Taft constants as an ordinary two-parameter equation (13). If the 'inductive' electronegativity of the reaction centre atom is unknown, the e value can be found using the two-parameter correlation

$$e_i = a'\chi_i R_i^2 + b'R_i^2 , \qquad (17)$$

where the coefficient b' includes the χ_{rc} value.

It should be emphasised that correct separation of the inductive and steric effects requires that the nature (electronegativity) of the reaction centre be known exactly and, in any case, it implies certain assumptions. Nevertheless, the corresponding atomic operational constants e_i still can be employed to predict the unknown Y values for related molecular systems consisting of atoms with known e_i even in those cases where correlations (15) and (16) cannot be established.

Except for the inapplicability for the description of the resonance effect, the method under discussion does not have any serious limitations and can be used successfully even in those cases where the standard empirical scales are ineffective. The quantitative description of the vertical and adiabatic ionisation potentials of amines performed in our study exemplifies the practical application of the r^{-2}-scheme.[221]

Previously, the dependence of the ionisation potentials of a limited range of amines on their structure has been interpreted with utilisation of a large number of independent parameters both those reflecting particular inductive, resonance and polarisation effects and those chosen rather arbitrarily.[232]

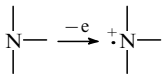

We attempted to consider the ionisation potentials of amines in terms of the unified approach developed and composed the corresponding r^{-2}-matrix in which the nitrogen atom was chosen as the reaction centre. The adiabatic and vertical ionisation potentials (I^{ad}, I^{vert}) of amines in the gas phase, taken from a publication,[233] were analysed in terms of the parameters of the basic equation (14). As a result, reliable multiparameter correlations were established for the sets of adiabatic and vertical potentials

$$I^{vert}_{R_3N} = \sum_i^{N-1} \frac{i_i^{vert}}{r_i^2} + \text{const}_1 \ (R = 0.954, S = 0.331, N = 287), \qquad (18)$$

$$I^{ad}_{R_3N} = \sum_{i=1}^{N-1} \frac{i_i^{ad}}{r_i^2} + \text{const}_2 \ (R = 0.960, S = 0.341, N = 231), \qquad (19)$$

where N is the number of atoms in the amine molecule and i_i^{vert} and i_i^{ad} are the operational atomic parameters reflecting the capacity of the atom of a definite type for participation in intramolecular interactions, which determine the I^{vert} and I^{ad} values, respectively.

The following fact attracts attention: although we analysed arrays of the absolute values of I^{ad} and I^{vert} not referred to any standard, the free terms of multiparameter correlations (18) and (19) determined statistically actually reproduced the corresponding ionisation potentials of the ammonia molecule.

The values of the $i^{ad/vert}$ parameters were then analysed using Eqn (16); the following correlations were identified:

$$i^{ad} = 4.55(\chi - 2.79)R^2, \qquad (20)$$

$$i^{vert} = 4.38(\chi - 2.98)R^2. \qquad (21)$$

Thus, the correlations found allow the calculation of the unknown parameters $i^{ad/vert}$ and, hence, the previously unknown ionisation potentials of amines from atom electronegativities and covalent radii. Moreover, if the role of steric effect during electron transfer is assumed to be insignificant (which appears quite reasonable), values of 2.79±0.7 and 2.98±0.7 found using these

relations are in a fairly good agreement with the inductive electronegativity of nitrogen (2.56, see Ref. 223).

4. Ionisation energies of free radicals

The possibility of quantitative determination of the energies of oxidation of amines to the corresponding radical cations using the approach we developed points to its adequacy and applicability to free-radical processes. As noted above, the examples of quantitative interpretation of the reactivity of free radicals currently available are limited, as a rule, to aromatic systems.

We attempted to apply the r^{-2}-analysis to electron transfer, which is one of the least studied homolytic reactions from the standpoint of 'radical' effects of substituents. We did not restrict ourselves to narrow series of aromatic compounds but considered single-electron processes involving diverse C-, N-, S- and O-centred radicals both belonging to aromatic and aliphatic series.[233, 234] The single-electron ionisation potentials of free radicals in the gas phase were taken from a database [235] and analysed in terms of our approach.

a. Carbon-centred radicals

In accordance with the approach developed, the ionisation potentials (I) and electron affinities (A_e) of carbon-centred radicals were analysed using the equations

$$I_{R^\cdot} - I_{Me^\cdot} = \sum_{i \subset R} \frac{e_i^+}{r_i^2} \text{ and} \tag{22}$$

$$A_e(R^\cdot) - A_e(Me^\cdot) = \sum_{i \subset R} \frac{e_i^-}{r_i^2}, \tag{23}$$

in which the I and A_e values for the methyl radical are included as reference values provided that the carbon atom bearing the unpaired electron is taken to be the reaction centre.

The multiparameter correlations (22) and (23) were established with high accuracy. The operational parameters e^+ and e^- found from relations (22) and (23) are presented in Tables 4 and 5 together with the corresponding values for the inductive electronegativities and the covalent radii of atoms. By comparing them in terms of a type (17) relation, we expressed the e^+ parameters in the form

$$e_i^+ = (1.09 \pm 0.33)\chi_i R_i^2 - (5.49 \pm 0.97) R_i^2 \tag{24}$$

(the O, N and S atoms were not included in the correlation) or

$$e_i^+ = 1.09(\chi_i - 5.04) R_i^2 .$$

Thus, the ionisation potentials of C-centred radicals in the gas phase can be expressed in terms of fundamental parameters of atoms

$$I = I_{Me^\cdot} + 1.09 \sum_{i=1}^{N} \frac{(\chi_i - 5.04) R_i^2}{r_i^2} . \tag{25}$$

Relations (24) and (25) demonstrate that the vast majority of atoms [except highly electronegative ones such as *sp*-hybridised N atom ($\chi = 6.76$)] introduced in the environment of the C$^\cdot$ reaction centre decrease the corresponding ionisation energy relative to that of the methyl radical. The deviation of the atomic parameters e^+ for O, N and S atoms from the general pattern of dependence is apparently due to the resonance effect, which cannot be described from the standpoint of the given approach, as has been repeatedly mentioned above. To elucidate the reasons for this deviation, a special detailed analysis is required; we plan to perform it subsequently. In addition, analysis of the predicted ionisation potentials demonstrates a substantial deviation of the I_{pred} value for the methyl radical, which is a typical problem for this type of approach. Since the methyl radical was chosen as the reference species ($\Delta I = 0$), its e^+ parameter should, by definition, be equal

Table 4. Operational atomic parameters e^+_{emp} found from experimental ionisation potentials and the corresponding e^+_{calc} values calculated using correlation (17).

Radical centre	Atom	χ_i	R^2	e^+_{emp}	e^+_{calc}	$e^+_{emp} - e^+_{calc}$
C$^\cdot$	C	2.10	0.593	−1.86±0.11	−1.90	0.04
	H	2.10	0.090	−0.25±0.04	−0.29	0.04
	C(arom.)	2.45	0.449	−1.45±0.14	−1.27	−0.18
	C(sp^2)	2.25	0.449	−1.78±0.14	−1.37	−0.41
	C(*sp*)	2.65	0.390	−0.80±0.39	−0.55	−0.25
	Cl	3.09	0.980	−1.91±0.19	−2.09	0.18
	Br	2.97	1.299	−2.73±0.23	−2.94	0.21
	F	3.93	0.409	−0.78±0.10	−0.50	−0.28
	S	2.67	1.082	−6.61±0.58	−2.78	−3.83
	O	3.05	0.436	−3.77±0.27	−0.95	−2.82
	N	2.56	0.490	−6.15±0.26	−1.33	−4.82
	N(*sp*)	6.76	0.3025	5.888	0.562	5.326
N$^\cdot$	C	2.10	0.593	−6.202±1.361	−5.70	−0.502
	H	2.10	0.090	−0.217±0.485	−0.87	0.653
	N	2.56	0.490	−5.996±2.652	−4.46	−1.536
	C(arom.)	2.45	0.449	−1.934±1.088	−4.14	2.206
O$^\cdot$	C	2.10	0.593	−5.407±0.534	−6.22	0.813
	H	2.10	0.090	0.022±0.327	−0.94	0.962
	O	3.05	0.436	−3.663±0.799	−2.93	−0.733
	Cl	3.09	0.980	−6.307±1.052	−6.45	0.143
	F	3.93	0.410	−0.498±0.748	−1.34	0.842
	Br	2.97	1.300	−8.942±1.244	−9.17	0.228
	I	2.80	1.769	−14.25±1.51	−13.66	−0.59
	C(arom.)	2.45	0.449	−4.071±0.348	−4.09	0.019
S$^\cdot$	C	2.10	0.593	−3.370±1.831	−4.57	1.2
	H	2.10	0.090	0.003±1.089	−0.69	0.693
	S	2.67	1.082	−8.680±2.598	−7.25	−1.43
	F	3.93	0.410	−0.814±1.848	−1.88	1.066
	C(arom.)	2.45	0.449	−2.429±0.972	−3.19	0.761

Table 5. Operational atomic parameters e^-_{emp} found from experimental electron affinities and the corresponding e^-_{calc} values calculated using correlation (17).

Radical centre	Atom	χ_i	R^2	e^-_{emp}	e^-_{calc}	$e^-_{emp} - e^-_{calc}$
C˙	C	2.10	0.593	−0.26±0.14	0.17	−0.43
	H	2.10	0.090	−0.01±0.04	0.03	−0.04
	C(arom.)	2.45	0.449	0.60±0.06	0.38	0.22
	C(sp^2)	2.25	0.449	0.51±0.37	0.24	0.27
	Cl	3.09	0.980	2.22±0.17	1.87	0.35
	Br	2.97	1.299	2.08±0.23	2.22	−0.14
	F	3.93	0.409	1.04±0.08	1.35	−0.31
	O	3.05	0.436	−0.16±0.44	0.80	−0.96
N˙	C	2.10	0.593	−0.396±0.255	−0.39	−0.006
	H	2.10	0.090	−0.008±0.093	−0.059	0.051
	C(arom.)	2.45	0.449	0.687±0.091	0.69	−0.003
O˙	C	2.10	0.593	−0.104±0.155	0.19	−0.294
	H	2.10	0.090	0.025±0.098	0.029	−0.004
	O	3.05	0.436	−1.654±0.257	0.66	−2.314
	Cl	3.09	0.980	1.328±0.340	1.527	−0.199
	F	3.93	0.410	0.936±0.242	1.07	−0.134
	Br	2.97	1.300	1.839±0.402	1.83	0.009
	I	2.80	1.769	2.338±0.488	2.11	0.228
	C(arom.)	2.45	0.449	0.379±0.111	0.34	0.039
S˙	C	2.10	0.593	−0.41±0.386	−0.008	−0.403
	H	2.10	0.090	−0.12±0.261	−0.001	−0.121
	S	2.67	1.082	−1.84±0.457	−2.09	0.263
	O	3.05	0.436	−1.95±0.482	−1.36	−0.596
	C(arom.)	2.45	0.449	−0.02±0.236	−0.52	0.500

or nearly equal to zero, which is not always fulfilled. The e^+(H) value found statistically is markedly smaller than zero, as well as the calculated $\Delta I(CH_3)$ value.

Taft [236] was faced with similar difficulties when using the methyl group as the reference for the scale of inductive constants σ^*. There are also other factors determining the so pronounced difference between the experimental and calculated ionisation potentials of methyl radicals in the construction of a scale of radical constants. Detailed analysis of these factors is beyond the scope of this review.

When considering the e^- parameters found from the electron affinities of carbon-centred radicals, the following correlation was established:

$$e_i^- = (1.64 \pm 0.43)\chi_i R_i^2 - (3.17 \pm 1.26)R_i^2 \quad (26)$$

or

$$e_i^- = 1.64(\chi_i - 1.93)R_i^2.$$

As for ionisation potentials, this correlation permits the electron affinity parameters of carbon-centred radicals to be expressed at the atomic level on the basis of fundamental atomic characteristics, namely, electronegativities, sizes and interatomic distances

$$A_e = A_e(Me^{\cdot}) + 1.64\sum_{i=1}^{N}\frac{(\chi_i - 1.93)R_i^2}{r_i^2}. \quad (27)$$

The ionisation potentials and electron affinities of carbon-centred radicals calculated from the atomic inductive electronegativities and covalent radii are listed in Tables 6 and 7; the statistical parameters of correlations are presented in Table 8, and the operational parameters e^+ and e^- are given in Tables 4, 5.

b. Deviations from the general dependence

As noted above, the presence of substantial resonance interactions in radicals can result in deviation of their characteristics predicted in terms of the additive scheme in question from the corresponding experimental values. An alternative and, perhaps preferable, explanation of most of the deviations observed in the description of redox properties of carbon-centred radicals is that in some radicals, the carbon atom bearing the unpaired electron is not the ionisation centre.

For example, in the case of ionisation potentials, the operational atomic parameters e^+ for S, N and O atoms deviate from the linear dependence (24), and the effects of the corresponding substituents observed experimentally exceed those predicted based on the e^+ values. The experimental values of the ionisation potential I_{exp} might correspond to the I value of a heteroatom (S, N, O) present in the carbon-centred radicals and having a lone electron pair rather than to the I value of the radical centre. A similar deviation from the linear dependence has been observed in a study of the single-electron reduction potentials of arylmethylchalcogenide radical cations in aqueous solutions.[40] In addition, electron-withdrawing substituents (NO_2, CN, Hal) are able to enter into reduction processes and, hence, only for some of the carbon-centred radicals considered, do the A_e values correspond completely to the ionisation of the radical centre. For some strong electron acceptors, a saturation effect also cannot be ruled out.

Thus, most of the observed deviations of the predicted ionisation potentials and electron affinities of substituted carbon-centred radicals are most likely due to non-homogeneity of the data arrays considered. It should also be borne in mind that the ionisation potentials and the electron affinities of radicals match the energy differences between the radical and the corresponding cation in the former case and between the anion and the radical in the latter case. Hence, the energy effects of substituents described by Eqns (22) and (23) can refer both to the radical and to the corresponding ion. The positive values of e^+ and e^- imply that the radical is stabilised by the substituent in question more efficiently than the cation as compared with the $\dot{C}H_3/CH_3^+$ pair (for ionisation potentials), and that the anion is stabilised by the given substituent more efficiently than the radical, compared with the $CH_3^-/\dot{C}H_3$ system (in the case of electron affinity). Note that, the use of the notion of relative stabilisation can also imply lesser

Table 6. Ionisation potentials (in eV) of C-, S-, N- and O-centred radicals determined experimentally (I_{exp}), predicted (I_{pred}) using relation (14) and calculated (I_{calc}) from Eqns (25), (28), (30), (32).

Radical	I_{exp}	I_{pred}	$I_{exp} - I_{pred}$	I_{calc}	$I_{exp} - I_{calc}$
$MeNH\dot{C}H_2$	5.9	6.1	−0.20	8.23	−2.33
$Me(NH_2)\dot{C}H$	5.7	5.72	−0.02	7.86	−2.16
$Me_2N\dot{C}H_2$	5.7	5.74	−0.04	7.86	−2.16
$Me_2(NH_2)\dot{C}$	5.4	4.98	0.42	7.11	−1.71
$(H_2C=CH)_2\dot{C}H$	7.25	7.3	−0.05	7.73	−0.48
$Me_2(HC\equiv C)\dot{C}$	7.44	7.44	0	7.51	−0.07
(cyclo-C_5H_9)$^{\cdot}$	7	7.22	−0.22	7.38	−0.38
$HS\dot{C}H_2$	7.54	7.32	0.22	8.44	−0.91
$MeS\dot{C}H_2$	6.85	7.07	−0.22	8.19	−1.34
$H_3C^{\cdot}$	9.84	9.21	0.63	9.11	0.73
$Me_3C^{\cdot}$	6.7	7	−0.3	6.88	−0.18
$MeEt\dot{C}H$	7.25	7.41	−0.16	7.28	−0.03
$Pr^n\dot{C}H_2$	8.02	8	0.02	7.88	0.14
$Pr^i\dot{C}H_2$	7.93	7.81	0.12	7.68	0.25
$Me\dot{C}H_2$	8.12	8.47	−0.36	8.37	−0.25
$Me_2\dot{C}H$	7.37	7.74	−0.37	7.62	−0.25
$Et\dot{C}H_2$	8.09	8.14	−0.05	8.03	0.06
$HO\dot{C}H_2$	7.56	7.51	0.05	8.82	−1.25
$Me(HO)\dot{C}H$	6.85	6.77	0.08	8.07	−1.22
$MeO\dot{C}H_2$	6.9	7.13	−0.23	8.43	−1.53
$Me(MeO)\dot{C}H$	6.5	6.4	0.1	7.68	−1.18
$NC\dot{C}H_2$	9.9	9.9	0	9.18	0.72
$H_2N\dot{C}H_2$	6.29	6.45	−0.16	8.6	−2.31
$Cl_3\dot{C}$	8.06	7.99	0.07	7.82	0.24
$Cl_2H\dot{C}$	8.32	8.4	−0.08	8.25	0.07
$ClH_2\dot{C}$	8.75	8.8	−0.05	8.68	0.07
$F_3\dot{C}$	8.76	8.57	0.19	9.03	−0.27
$F_2H\dot{C}$	8.78	8.79	−0.01	9.06	−0.28
$FH_2\dot{C}$	9.04	9	0.04	9.08	−0.04
$Br_3\dot{C}$	7.5	7.59	−0.09	7.42	0.08
$Br_2H\dot{C}$	8.3	8.13	0.17	7.99	0.31
$BrH_2\dot{C}$	8.61	8.67	−0.06	8.55	0.06
$Me\dot{C}F_2$	7.92	8.05	−0.13	8.31	−0.39
$Me\dot{C}HF$	7.93	8.26	−0.33	8.34	−0.41
$H_2C=CH\dot{C}H_2$	8.18	8.25	−0.07	8.42	−0.24
(cyclo-C_3H_5)$^{\cdot}$	8.18	7.87	0.31	7.77	0.41
$CH_2=C(Me)\dot{C}H_2$	7.9	7.95	−0.05	8.11	−0.21
$(H_2C=CH)Me\dot{C}H$	7.49	7.52	−0.03	7.67	−0.18
(cyclo-C_4H_7)$^{\cdot}$	7.54	7.41	0.13	7.29	0.25
$H_2C=CHCH_2\dot{C}H_2$	8.04	8.05	−0.01	8.04	0
(cyclo-C_5H_9)$^{\cdot}$	7.21	7.11	0.1	6.98	0.23
$H_2C=CH\dot{C}Me_2$	7.13	6.78	0.35	6.93	0.2
$H_2C=CH\dot{C}HEt$	7.3	7.19	0.11	7.33	−0.03
$MeCH=CH\dot{C}HMe$	7.07	7.39	−0.32	7.54	−0.47
$H_2C=CHCH(Me)\dot{C}H_2$	8	7.71	0.29	7.69	0.31
$H_2C=C(Et)\dot{C}H_2$	7.9	7.66	0.24	7.81	0.09
$(C_6H_5)^{\cdot}$	8.32	8.31	0.01	8.46	−0.14
$Ph\dot{C}H_2$	7.24	7.24	−0.01	7.42	−0.19
$HO^{\cdot}$ (*ref*) [a]	13.017	13.04	−0.02	11.99	1.024
$HOO^{\cdot}$	11.35	11.35	0	11.45	−0.095
$ClO^{\cdot}$	10.885	10.89	0	10.84	0.048
$FO^{\cdot}$	12.78	12.78	0	12.38	0.399
$BrO^{\cdot}$	10.46	10.46	0	10.4	0.064
$IO^{\cdot}$	9.66	9.66	0	9.8	−0.137
$MeO^{\cdot}$	10.72	10.39	0.33	9.31	1.406
$EtO^{\cdot}$	9.11	9.47	−0.36	8.13	0.978
$Pr^nO^{\cdot}$	9.2	9.1	0.11	7.62	1.581
$PhO^{\cdot}$	8.56	8.56	0	8.14	0.425
$HS^{\cdot}$ (*ref*) [a]	10.429	10.43	0	10.04	0.386
$MeSS^{\cdot}$	8	8	0	8.05	−0.052
$FS^{\cdot}$	10.16	10.16	0	9.81	0.35
$MeS^{\cdot}$	9.262	9.38	−0.12	8.64	0.625
$EtS^{\cdot}$	9.6	8.92	0.68	7.93	1.673
$Pr^nS^{\cdot}$	8.2	8.73	−0.53	7.61	0.594

Table 6 (continued).

Radical	I_{exp}	I_{pred}	$I_{exp} - I_{pred}$	I_{calc}	$I_{exp} - I_{calc}$
PhS˙	8.63	8.63	0	7.82	0.81
H_2N˙ (*ref*) [a]	10.78	10.36	0.43	9.08	1.698
MeṄH	6.7	7.55	−0.85	6.7	−0.003
Me_2N˙	5.17	4.75	0.43	4.32	0.846
PhṄH	8.26	8.26	0	4.82	3.442
$H_2N-\dot{N}H$	7.61	7.61	0	7.39	0.222

[a] The reference species in the corresponding reaction series.

Table 7. Electron affinities (in eV) of C-, S-, N- and O-centred radicals determined experimentally [A_e(exp)], predicted [A_e(pred)] using relation (14) and calculated [A_e(calc)] from Eqns (27), (29), (31) and (33).

Radical	A_e(exp)	A_e(pred)	A_e(exp) − A_e(pred)	A_e(calc)	A_e(exp) − A_e(calc)
H_3C˙	0.08	0.05	0.03	0.14	−0.06
$MeC\dot{H}_2$	−0.26	−0.05	−0.21	0.21	−0.47
$MeCH_2C\dot{H}_2$	−0.07	−0.09	0.02	0.24	−0.31
$Me_2C\dot{H}$	−0.32	−0.16	−0.16	0.27	−0.59
MeEtC̈H	−0.12	−0.2	0.08	0.30	−0.42
Me_3C˙	−0.16	−0.27	0.11	0.34	−0.50
$H_2C=CHC\dot{H}_2$	0.36	0.36	0.00	0.27	0.09
$PhC\dot{H}_2$	0.91	0.62	0.29	0.49	0.42
$Ph_2C\dot{H}$	1.36	1.2	0.16	0.84	0.52
Ph_3C˙	1.56	1.77	−0.21	1.19	0.37
F_3C˙	1.84	1.76	0.08	2.27	−0.43
F_2HC˙	1.21	1.19	0.02	1.56	−0.35
FH_2C˙	0.20	0.62	−0.42	0.85	−0.65
Cl_3C˙	2.17	2.23	−0.06	1.89	0.28
Cl_2HC˙	1.58	1.5	0.08	1.31	0.27
ClH_2C˙	0.80	0.78	0.02	0.73	0.07
Br_3C˙	1.73	1.79	−0.06	1.91	−0.18
BrH_2C˙	0.82	0.63	0.19	0.73	0.09
$CF_3C\dot{F}_2$	1.81	1.76	0.05	2.26	−0.45
$MeOC\dot{H}_2$	−0.02	−0.02	0.00	0.52	−0.54
HO˙ (*ref*)	1.83	1.83	0.00	1.86	−0.03
HOO˙	1.08	1.08	0.00	2.14	−1.06
ClO˙	2.28	2.28	0.00	2.34	−0.07
FO˙	2.27	2.27	0.00	2.34	−0.06
BrO˙	2.35	2.35	0.00	2.35	0.00
IO˙	2.38	2.38	0.00	2.33	0.05
MeO˙	1.62	1.62	0.00	1.94	−0.32
EtO˙	1.72	1.72	0.00	1.98	−0.26
Pr^nO˙	1.79	1.79	0.00	1.99	−0.20
PhO˙	2.25	2.25	0.00	2.21	0.04
Pr^iO˙	1.84	1.84	0.00	2.01	−0.17
Bu^tO˙	1.91	1.91	0.00	1.96	−0.05
HS˙ (*ref*)	2.31	2.25	0.07	2.32	0.00
MeSS˙	1.75	1.80	−0.05	1.81	−0.06
MeS˙	1.87	2.12	−0.25	2.31	−0.45
EtS˙	1.95	2.05	−0.10	2.31	−0.36
Pr^nS˙	2.00	2.02	−0.02	2.31	−0.32
PhS˙	2.26	2.26	0.00	1.93	0.32
HSS˙	1.90	1.86	0.05	1.81	0.09
HOS˙	1.65	1.65	0.00	1.87	−0.22
Pr^iS˙	2.02	1.98	0.04	2.31	−0.30
Bu^tS˙	2.07	1.90	0.16	2.31	−0.24
H_2N˙ (*ref*)	0.78	0.77	0.01	0.66	0.12
MeṄH	0.45	0.60	−0.15	0.50	−0.05
Me_2N˙	0.38	0.43	−0.05	0.34	0.04
PhṄH	1.70	1.57	0.13	1.48	0.22
PhMeN˙	1.65	1.40	0.25	1.32	0.33
Ph_2N˙	2.18	2.37	−0.19	2.30	−0.12

Table 8. Statistical parameters for correlations of type (14) determined for various classes of free radicals.

Type of radicals	Series	N	R	S/ eV
C-centred	I	48	0.9768	0.2345
	A_e	20	0.9816	0.1995
S-centred	I	7	0.9278	0.6105
	A_e	10	0.8390	0.1491
O-centred	I	10	0.9938	0.3557
	A_e	12	0.9836	0.1150
N-centred	I	5	0.968	1.041
	A_e	6	0.9744	0.2179

destabilisation. In a published discussion[9–11] dealing with the influence of substituents on bond energies, similar considerations are presented concerning the situation where the effects observed can be attributed both to the RX molecule and the R˙ radical.

Equation (25) indicates that a substituent atom should have an abnormally high electronegativity ($\chi > 5.04$) to stabilise a radical more effectively than the corresponding cation. In turn, relation (27) illustrates the fact that for most of atoms ($\chi > 1.93$), stabilisation of anions predominates. Thus, it can be concluded that the described substituent effects which determine the electron potentials of free radicals refer to stabilisation of the corresponding ions. The role of steric interactions can be elucidated by comparing the adiabatic ionisation potentials, studied within the framework of the approach under discussion, with the corresponding vertical ionisation potentials.

The adiabatic potentials reflect the difference between the energies of the radicals and the cation having the most favourable (equilibrium) spatial structure, whereas vertical potentials imply identical geometries of these species. Thus, the difference between the adiabatic and vertical potentials can be attributed to structural reorganisation of a free radical caused by its oxidation.

The adiabatic and vertical potentials of the methyl radical are known to be equal. This is apparently due to the fact that both the radical and the cation are planar. The other primary, secondary and tertiary carbon-centred radicals are non-planar, unlike the corresponding cations. The difference between their adiabatic and vertical potentials remains approximately constant (0.3–0.4 eV) and does not change significantly on passing from primary to secondary or tertiary radicals, *i.e.*, the steric contribution to the adiabatic ionisation potentials is insignificant but they do contain a constant component due to the energy of spatial reorganisation. The absence of this component in the case of the methyl radical can be the main reason for the observed difference between the predicted and experimental $I(\dot{C}H_3)$ values.

The foregoing attests that steric interactions have no influence on the ionisation potentials and electron affinities of free radicals and the corresponding effect of substituents has a purely inductive nature.

It is common knowledge that cations are stabilised by electron-donating substituents and anions are stabilised by electron-withdrawing substituents. According to Eqn (15), the atomic inductive effect is proportional to the difference between the electronegativities of the given atom and the reaction centre. Hence, it is reasonable to assume that the electronegativity of the central atom (carbon) increases in the series anion < radical < cation, while the inductive effect of the substituent atoms switches from electron-withdrawing to electron-donating influence, and only in extreme cases [for example, for N(*sp*), which has $\chi_{ind} = 6.76$], is the effect of the atom adjacent to the cationic centre maintained as the electron-withdrawing influence. Thus, parameters of 5.04 and 1.93 in Eqns (24) and (26) can actually be taken as the inductive electronegativity of the reaction centre, *i.e.*, of positively and negatively charged carbon, respectively.

c. The group σ_+^C and σ_-^C scales

The empirical operational parameters e^+ and e^- established have also been used to introduce group scales called σ_+^C and σ_-^C, which make it possible to calculate the I and A_e values for carbon-centred radicals in terms of an additive scheme.[233]

$$I = I_0 + \sum \sigma_+^C$$

$$A_e = A_e^0 + \sum \sigma_-^C$$

These parameters were calculated for the most frequently encountered organic substituents with the assumption of the standard geometries and using the e^+ and e^- values for atoms contained in these substituents. These radical scales, based on electron transfer reactions and considering the substitution effect at the group level of additivity, reflect, as do the Hammett σ-constants, the overall influence of substituents on a radical reaction centre without separation of the inductive, resonance, and steric constituents. The use of group σ_+^C and σ_-^C scales simplifies the procedure of calculation of the ionisation energies of radicals and eliminates the necessity of determining interatomic distances.

Similarly, we calculated the ionisation energies of O-, S- and N-centred radicals in terms of the basic equation (14). The atomic operational parameters e^+ and e^- found in this way were then analysed using relation (16). The corresponding equations for radicals of various types are presented below in the same order which was accepted for carbon-centred radicals.[234]

d. Oxygen-centred radicals

For oxygen-centred radicals, the operational parameters e^+, which determine the relative contributions of atoms to the ionisation energy of the system, are described with high accuracy by means of atomic electronegativities and the covalent radii in accordance with Eqn (16)

$$e_i^+ = (3.94 \pm 1.01)\chi_i R_i^2 - (18.77 \pm 2.93)R_i^2$$

or

$$e_i^+ = 3.94(\chi_i - 4.76)R_i^2.$$

The corresponding atomic parameters e^- are determined in a similar way

$$e_i^- = (1.25 \pm 0.27)\chi_i R_i^2 - (2.31 \pm 0.79)R_i^2$$

or

$$e_i^- = 1.25(\chi_i - 1.84)R_i^2.$$

Thus, the ionisation energy of the alkoxy radicals $I(RO^{\cdot})$ can be presented by the relation

$$I(RO^{\cdot}) = I(HO^{\cdot}) + 3.94\sum_{i=1}^{N}\frac{(\chi_i - 4.76)R_i^2}{r_i^2}, \qquad (28)$$

and the electron affinity of oxygen-centred radicals is determined in terms of atomic parameters

$$A_e(RO^{\cdot}) = A_e(HO^{\cdot}) + 1.25\sum_{i=1}^{N}\frac{(\chi_i - 1.84)R_i^2}{r_i^2}. \qquad (29)$$

e. Sulfur-centred radicals

The atomic operational constants e^+ and e^- of sulfur-centred radicals determined from the ionisation potentials and the electron affinity correlate with the atomic electronegativities and atomic radii with a lower accuracy

$$e_i^+ = (1.71 \pm 2.19)\chi_i R_i^2 - (11.29 \pm 5.93)R_i^2$$

or

$$e_i^+ = 1.71(\chi_i - 6.61)R_i^2,$$

$$e_i^- = (-3.27 \pm 1.41)\chi_i R_i^2 + (6.84 \pm 3.68)R_i^2$$

or

$$e_i^- = -3.27(\chi_i - 2.09)R_i^2.$$

Nevertheless, the expressions obtained which relate the ionisation energies of sulfur-centred radicals to parameters of the atoms forming them appear well substantiated

$$I(\mathrm{RS}^{\cdot}) = I(\mathrm{HS}^{\cdot}) + 1.71\sum_{i=1}^{N}\frac{(\chi_i - 6.61)R_i^2}{r_i^2}. \quad (30)$$

The electron affinity of sulfur-centred radicals is found from the relation

$$A_e(\mathrm{RS}^{\cdot}) = A_e(\mathrm{HS}^{\cdot}) - 3.27\sum_{i=1}^{N}\frac{(\chi_i - 2.09)R_i^2}{r_i^2}. \quad (31)$$

f. Nitrogen-centred radicals

A similar correlation obtained for nitrogen-centred radicals is unsatisfactory because of the deficiency and great inaccuracy of the corresponding experimental data; therefore, the available data on the ionisation of N-centred radicals cannot serve as the base for discussion. Nevertheless, we thought it fit to present the relations determining the e^+ and e^- parameters for atoms making up N-centred radicals. As in the above cases, the electronegativities and the sizes of atoms forming the corresponding N-centred radical were used.

$$e_i^+ = (1.14 \pm 10.70)\chi_i R_i^2 - (12.01 \pm 24.9)R_i^2$$

or

$$e_i^+ = 1.14(\chi_i - 10.55)R_i^2,$$

$$e_i^- = (6.24 \pm 0.41)\chi_i R_i^2 + (13.76 \pm 0.92)R_i^2,$$

or

$$e_i^- = 6.24(\chi_i - 2.20)R_i^2.$$

The ionisation energies and electron affinities of nitrogen-centred radicals can be written as follows:

$$I(\mathrm{R_2N}^{\cdot}) = I(\mathrm{H_2N}^{\cdot}) + 1.14\sum_{i=1}^{N}\frac{(\chi_i - 10.55)R_i^2}{r_i^2}, \quad (32)$$

$$A_e(\mathrm{R_2N}^{\cdot}) = A_e(\mathrm{H_2N}^{\cdot}) + 6.24\sum_{i=1}^{N}\frac{(\chi_i - 2.20)R_i^2}{r_i^2}. \quad (33)$$

The ionisation potentials and the electron affinities of S-, N- and O-centred radicals calculated on the basis of the atomic inductive electronegativities and covalent radii are given in Tables 6 and 7. The electronegativities of ionic forms of the C, S, N and O atoms considered as reaction centres, obtained in accordance with the proposed procedure, are given in Table 9.

Table 9. Electronegativities and statistical parameters for correlations of type (16) determined for various types of free radicals.

Type of radicals	Parameter	χ_{rc}	N	R	S/ eV
C-centred	e^+	5.04	8 [a]	0.9509	0.266
	e^-	1.93	7 [b]	0.9502	0.328
S-centred	e^+	6.61	5	0.9368	1.3768
	e^-	2.09	5	0.8739	0.5329
O-centred	e^+	4.76	8	0.9891	0.7342
	e^-	1.84	7 [b]	0.9808	0.1975
N-centred	e^+	10.55	4	0.8393	1.9877
	e^-	2.20	3	0.9977	1.041

[a] Except for parameters for the O, N, S and N(sp) atoms; [b] except for parameters for the O atom.

The same Table contains the statistical parameters of the corresponding correlations of type (16) found for the the operational atomic parameters e^+ and e^- of the series studied.

5. The stability of free radicals in redox processes

We have already noted that the problem of radical stability, especially within the framework of the thermodynamic approaches proposed here, largely overlaps the problem of radical reactivity and is considered from the standpoint of the influence of substituents.

The stability of free radicals itself in terms of the relative energies of covalent bonds in the corresponding systems with filled electron shells is normally considered separately from the known effect of steric shielding of the unpaired electron by the molecular environment, decreasing the reactivity of the radical.[45, 114, 237] In our opinion, the concept of radical stability (reactivity) should be supplemented by one more type, namely, stability of free radicals in redox processes (subsequently referred to as redox stability).

As has already been noted, single-electron transfer is one of the most frequently encountered types of reaction in homolytic chemistry. Meanwhile, neither kinetic nor thermodynamic methods for the description of the radical effects of substituents take into account the redox stability of free radicals or provide the possibility of quantitative interpretation of the corresponding single-electron potentials. However, it is absolutely clear that the lower the ionisation potential and the higher the electron affinity of a free radical, the more easily it would enter into single-electron transfer reactions.

Thus, the redox stability of a free radical can be matched to its absolute chemical hardness (η)

$$\eta = \frac{I - A_e}{2},$$

where I and A_e are the single-electron ionisation potential and the electron affinity of the radical in the gas phase determined experimentally.

Let us consider carbon-centred radicals. Using relations (25) and (26), we express the relative chemical hardness of a carbon-centered radical (η) in terms of fundamental atomic characteristics used to describe its single-electron potentials

$$\eta(\mathrm{R}^{\cdot}) = \eta(\mathrm{Me}^{\cdot}) - 0.28\sum_{i=1}^{N}\frac{(\chi_i - 4.22)R_i^2}{r_i^2}.$$

This relation reflects the trend of the redox stability of C-centred radicals to decrease under the influence of the vast majority of atoms present in the environment of a carbon reaction centre; only the most electronegative elements increase the $\eta(\mathrm{R}^{\cdot})$ value with respect to the chemical hardness of the methyl radical $\eta(\mathrm{Me}^{\cdot})$.

As noted above, the stability of carbon-centred radicals is often expressed as a derivative of the dissociation energy of the C–H bonds. A lower energy implies higher radical stabillity. However, a low bond energy often corresponds to a low chemical hardness of the corresponding radical. In conformity with our approach, this, conversely, implies a lower redox stability of the radical. Hence, the criteria used to describe radical stability should be chosen with caution.

6. Energies of dissociation of C–H bonds

An attractive aspect of our approach is, in our opinion, the possibility of using it successfully to describe dissociation energies of bonds E_d. We demonstrated this taking carbon–hydrogen bonds as an example.[238]

We obtained a large array of E_d(CH) values using the following relation

$$E_d(\mathrm{R_3CH}) - E_d(\mathrm{CH_4}) = \sum_i \frac{d_i}{r_{\mathrm{C}-i}^2}. \quad (34)$$

Here $E_d(CH_4)$ is the energy of the C–H bond in the methane molecule, $E_d(R_3CH)$ is the energy of the C–H bond in the corresponding derivative; the correlation parameters are: $N = 72$, $R = 0.9773$, $S = 8.484$ kJ mol^{-1}.

Equation (34) allowed high-accuracy determination of atomic constants which were designated by d and corresponded to the operational parameters e_i in the base equation (14). We were unable to determine the parameters d using the inductive and steric constituents and a correlation of type (15). Thus, the relationship between the redox and thermodynamic [expressed in terms of relative $E_d(CH)$] stabilities of free radicals remains uncertain. Nevertheless, the operational values d can be used successfully to calculate unknown energies of the C–H bonds.

IV. Conclusion

To summarise, it can be stated that the use of polar constants for the description of the reactivity and physicochemical properties of free radicals is rather limited, although in some cases, it is quite successful. The scales of specific radical constants $\sigma^{\cdot}$ are not general either. The absence of coordination between them and the ambiguity of the physical meaning of the $\sigma^{\cdot}$ radical constants might be due not only to the drawbacks of methods of their determination but rather to the limitations of principle inherent in the application of the linear methodology of correlation analysis to the free-radical chemistry and to the violation of additivity of the group influence in paramagnetic systems.

Thus, the problem of using correlation analysis in the chemistry of free radicals is far from being solved; in this respect 'homolytic' chemistry is markedly inferior to the 'heterolytic' chemistry of organic compounds. The new approaches to the quantitative description of the structure–reactivity (property) relationships for the participants of homolytic processes which we propose give hope for elimination of this objectively formed unbalance and make the quantitative organic chemistry more harmonious in some respect.

The model we developed, based on the consideration of discrete contributions of atoms, depending on the remoteness, to the substituent effects makes it possible to predict with high accuracy the quantitative characteristics of free radicals obtained experimentally. The method implies taking account of the influence of the molecular environment on the reaction centre without preliminary resolution of the effect into electronic and steric constituents. This approach provides the possibility of analysing efficiently diverse experimental results, irrespective of the nature of reaction centres.

Within the framework of our approach, we have considered only one of the three main types of free-radical processes. The quantitative description of the ionisation potentials and the electron affinities of diverse C-, N-, S- and O-centred radicals and the ionisation energies of aliphatic and aromatic amines permitted us to identify the physical nature of the corresponding substituent effects and to demonstrate the versatility of this approach in interpretation of the results of quantitative investigations in the chemistry of organic and heteroorganic free radicals.

In our opinion, of fundamental importance is the established fact that the substituent effects determining the electronic potentials of free C-, N-, O- and S-centred radicals are correlated with the stability of the corresponding ions and can be regarded as purely inductive. Nevertheless, correct quantitative determination of these values requires that the electronegativities of the ionic forms of C, N, O and S acting as the reaction centres be established.

The σ_+^C and σ_-^C scales introduced on the basis of atomic operational parameters e^+ and e^-, which determine the overall effects of substituents in single-electron transfer reactions involving C-centred radicals, exhibit high predictive capacity, although they do not clarify the physical nature of the corresponding interactions.

The approaches that we developed provide the possibility of describing a large array of dissociation energies of the C–H bonds and of determining operational atomic constants d, which are applicable for predicting unknown $E_d(CH)$ values. The notion 'redox stability of free radicals' also appears useful. It interprets this type of stability in terms of absolute hardness, without resorting to the approach according to which the relative bond energies are used as a measure of radical stability and which is criticised in the literature.

Successful use of the developed approaches for the quantitative interpretation of the ionisation energies of free radicals and molecules with closed electron shells gives hope that they would also be employed to describe the effects of substituents in other types of free-radical processes.

References

1. L P Hammett *J. Am. Chem. Soc.* **59** 96 (1937)
2. A R Cherkasov, V I Galkin, E M Zueva, R A Cherkasov *Usp. Khim.* **67** 423 (1998) [*Russ. Chem. Rev.* **67** 375 (1998)]
3. V I Galkin, R D Sayakhov, R A Cherkasov *Usp. Khim.* **60** 1617 (1991) [*Russ. Chem. Rev.* **60** 815 (1991)]
4. A R Cherkasov, V I Galkin, R A Cherkasov *Usp. Khim.* **65** 695 (1996) [*Russ. Chem. Rev.* **65** 641 (1996)]
5. V I Galkin *J. Phys. Org. Chem.* **12** 283 (1999)
6. O Exner, M Charton, V Galkin *J. Phys. Org. Chem.* **12** 289 (1999)
7. O Exner *J. Phys. Org. Chem.* **12** 265 (1999)
8. M Charton *J. Phys. Org. Chem.* **12** 275 (1999)
9. K Herberger *J. Phys. Org. Chem.* **7** 244 (1994)
10. K M Johnston, G H Williams. *J. Chem. Soc.* 1446 (1960)
11. R D Gilliom, B F Ward Jr *J. Am. Chem. Soc.* **87** 3944 (1965)
12. B R Kennedy, K U Ingold *Can. J. Chem.* **44** 2381 (1966)
13. H Sakurai, A Hosomi *J. Am. Chem. Soc.* **89** 458 (1967)
14. H Sakurai, K Tokumaru (Eds) *Chemistry of Free Radicals* (Tokyo: Nankodo, 1967) Ch. 17
15. C Walling, J A McGuinness *J. Am. Chem. Soc.* **91** 2053 (1969)
16. D A Pratt, J S Wright, K U Ingold *J. Am. Chem. Soc.* **121** 4877 (1999)
17. J A Howard, J H B Chenier *J. Am. Chem. Soc.* **95** 3054 (1973)
18. W A Pryor, W H Davis Jr, J P Stanley *J. Am. Chem. Soc.* **95** 4754 (1973)
19. W A Pryor, T H Lin, J P Stanley, R W Henderson *J. Am. Chem. Soc.* **95** 6993 (1973)
20. W H Davis Jr, W A Pryor *J. Am. Chem. Soc.* **99** 6365 (1977)
21. I B Afanas'ev *Int. J. Chem. Kinet.* **13** 173 (1981)
22. H R Dutsch, T H Fisher *Int. J. Chem. Kinet.* **14** 195 (1982)
23. W A Pryor, F Y Tang, R H Tang, D F Church *J. Am. Chem. Soc.* **104** 2885 (1982)
24. R E Pearson, J C Martin *J. Am. Chem. Soc.* **85** 354 (1963)
25. R W Henderson *J. Am. Chem. Soc.* **97** 213 (1975)
26. E V Blackburn, D D Tanner. *J. Am. Chem. Soc.* **102** 692 (1980)
27. A Streitwieser Jr, C Perrin *J. Am. Chem. Soc.* **86** 4938 (1964)
28. D D Tanner, J A Plambeck, D W Reed, T W Mojelsky *J. Org. Chem.* **45** 5177 (1980)
29. C Hansch, H Gao *Chem. Rev.* **97** 2995 (1997)
30. H C Brown, Y Okamoto *J. Am. Chem. Soc.* **80** 4979 (1958)
31. C Hansch, A Leo, R W Taft *Chem. Rev.* **91** 165 (1991)
32. E S Huyser *J. Am. Chem. Soc.* **82** 394 (1960)
33. C Walling, B B Jacknow *J. Am. Chem. Soc.* **82** 6113 (1960)
34. G A Russell, R C Williamson Jr *J. Am. Chem. Soc.* **86** 2357 (1964)
35. M Jonsson, J Lind, G Merenyi, T E Eriksen *J. Chem. Soc., Perkin Trans. 2* 2149 (1994)
36. M Jonsson, J Lind, T E Eriksen, G Merenyi *J. Chem. Soc., Perkin Trans. 2* 1567 (1993)
37. M Jonsson, J Lind, T Reitberger, T E Eriksen, G Merenyi *J. Phys. Chem.* **97** 11 278 (1993)
38. M Jonsson, J Lind, T E Eriksen, G Merenyi *J. Am. Chem. Soc.* **116** 1423 (1994)
39. M Jonsson, J Lind, G Merenyi, T E Eriksen *J. Chem. Soc., Perkin Trans. 2* 61 (1995)
40. M Jonsson, J Lind, G Merenyi, T E Eriksen *J. Chem. Soc., Perkin Trans. 2* 67 (1995)

41. M J Jones, G Moad, E Rizzardo, D H Solomon *J. Org. Chem.* **54** 1607 (1989)
42. S Eherson, R T C Brownlee, R W Taft *Prog. Phys. Org. Chem.* **10** 1 (1973)
43. P R Wells *Chem. Rev.* **63** 171 (1963)
44. A Zavitsas, J A Pinto *J. Am. Chem. Soc.* **94** 7390 (1972)
45. H G Viehe, Z Janousek, R D Merenyi (Eds) *Substituent Effects in Radical Chemistry (NATO SAD Ser.)* (Dordrecht; Boston; Lancaster; Tokyo: Reidel, 1986)
46. T Alfrey Jr, C C Price *J. Polym. Sci.* **2** 101 (1947)
47. T Otsu, T Ito, Y Fujii, M Imoto *Bull. Chem. Soc. Jpn.* **41** 204 (1968)
48. T Yamamoto, T Otsu *Chem. Ind.* 787 (1967)
49. A P G Kieboom *Tetrahedron* **28** 1325 (1972)
50. S Dinctmrk, R A Jackson, M Townson *J. Chem. Soc., Chem. Commun.* 172 (1979)
51. S Dinctmrk, R A Jackson, M Townson, H Agirbas, N C Brillingham, G March *J. Chem. Soc., Perkin Trans. 2* 1121 (1981)
52. H Agirbas, R A Jackson *J. Chem. Soc., Perkin Trans. 2* 739 (1983)
53. H Sakurai, S-i Hayasaki, A Hosomi *Bull. Chem. Soc. Jpn.* **44** 1945 (1971)
54. R Ito, T Migita, N Morikawa, O Simamura *Tetrahedron* **21** 955 (1965)
55. T H Fisher, A W Meierhoefer *J. Org. Chem.* **43** 224 (1978)
56. S Dinctmrk, R A Jackson *J. Chem. Soc., Perkin Trans. 2* 1127 (1981)
57. X Creary *J. Org. Chem.* **45** 280 (1980)
58. X-K Jiang, G-Z Ji *J. Org. Chem.* **57** 6051 (1992)
59. C Walling, E R Briggs, K B Wolfstirn, F R Mayo *J. Am. Chem. Soc.* **70** 1537 (1948)
60. T Otsu, T Yamamoto *J. Soc. Org. Synth. Chem. Jpn.* **23** 643 (1965)
61. R W Taft Jr, I C Lewis *J. Am.Chem. Soc.* **80** 2436 (1958)
62. R W Taft Jr, I C Lewis *J. Am. Chem. Soc.* **81** 5343 (1959)
63. R W Taft Jr *J. Phys. Chem.* **64** 1805 (1960)
64. O Exner *Tetrahedron Lett.* 815 (1963)
65. O Exner, J Lakomy *Collect. Czeh. Chem. Commun.* **35** 1371 (1970)
66. K Kalfus, M Vecera, O Exner *Collect. Czeh. Chem. Commun.* **35** 1195 (1970)
67. Y Yukawa, Y Tsuno *Bull. Chem. Soc. Jpn.* **32** 971 (1959)
68. Y Tsuno, M Sawada, T Fujii, Y Yukawa *Bull. Chem. Soc. Jpn.* **48** 3347 (1975)
69. C G Swain, E C Lupton Jr *J. Am. Chem. Soc.* **90** 4328 (1968)
70. M J S Dewar, P J Grisdale *J. Am. Chem. Soc.* **84** 3539 (1962)
71. M Charton *J. Am. Chem. Soc.* **97** 1552 (1975)
72. V A Palm *Osnovy Kolichestvennoi Teorii Organicheskikh Reaktsii* (Foundations of the Quantitative Theory of Organic Reactions) (Leningrad: Khimiya, 1977)
73. V A Palm, A V Tuulmets, in *Reaktsionnaya Sposobnost' Organicheskikh Soedinenii* (Reactivity of Organic Compounds) (Tartu: Tartu State University, 1964) Vol. 1, No. 1, p. 33
74. T H Fisher, A W Meierhoefer *Tetrahedron* **31** 2019 (1975)
75. T H Fisher, S M Dershem, M Lynn Prewitt *J. Org. Chem.* **55** 1040 (1990)
76. R A Jackson, F Malek *J. Chem. Soc., Perkin Trans. 1,* 1207 (1980)
77. N M K El-Durini, R A Jackson *J. Organomet. Chem.* **232** 117 (1982)
78. R A Jackson, D W O'Neill *J. Chem. Soc., Perkin Trans. 2* 509 (1978)
79. R A Jackson *J. Organomet. Chem.* **437** 77 (1992)
80. X Creary, C C Geiger, K Hilton *J. Am. Chem. Soc.* **105** 2851 (1983)
81. X Creary *Acc. Chem. Res.* **18** 3 (1985)
82. X Creary, B Benage, M E Mehrsheikh-Mohammadi, J P Bays *Tetrahedron Lett.* **26** 2383 (1985)
83. X Creary, M E Mehrsheikh-Mohammadi *J. Org. Chem.* **51** 1110 (1986)
84. X Creary, M E Mehrsheikh-Mohammadi, S McDonald *J. Org. Chem.* **52** 3254 (1987)
85. J P Chesick *J. Am. Chem. Soc.* **85** 2720 (1970)
86. T C Shields, B A Shoulders, J F Krause, C L Osborn, P D Gardner *J. Am. Chem. Soc.* **87** 3026 (1965)
87. J J Gajewski *J. Am. Chem. Soc.* **90** 7178 (1968)
88. R Noyari, H Takaya, Y Nakanisi, H Nozaki *Can. J. Chem.* **47** 1242 (1969)
89. J C Gilbert, J R Butler *J. Am. Chem. Soc.* **92** 2168 (1970)
90. W von E Doering, H D Roth *Tetrahedron,* **26** 2825 (1970)
91. J J Gajewski *J. Am. Chem. Soc.* **93** 4450 (1971)
92. W Kirmse, H-R Murawski *J. Chem. Soc., Chem. Commun.* 122 (1977)
93. X Creary *J. Org. Chem.* **43** 1777 (1978)
94. X Creary, P S Engel, N Kavaluskas, L Pan, A Wolf *J. Org. Chem.* **64** 5634 (1999)
95. J C Martin, J W Timberlake *J. Am. Chem. Soc.* **92** 978 (1970)
96. J W Timberlake, M L Hodges *Tetrahedron Lett.* 4147 (1970)
97. J W Timberlake, A W Garner, M L Hodges *Tetrahedron Lett.* 309 (1973)
98. B K Bandlish, A W Garner, M L Hodges, J W Timberlake *J. Am. Chem. Soc.* **97** 5856 (1975)
99. M F Dube, J W Timberlake *Tetrahedron,* **36** 1753 (1980)
100. A E Luedtke, J W Timberlake *J. Org. Chem.* **50** 268 (1985)
101. W M Nau, H M Harrer, W Adam *J. Am. Chem. Soc.* **116** 10 972 (1994)
102. W Adam, H M Harrer, W M Nau, K Peters *J. Org. Chem.* **59** 3786 (1994)
103. J R Shelton, C K Liang, P Kovacic *J. Am. Chem. Soc.* **90** 354 (1968)
104. P Kovacic, R R Flynn, J F Gormish, A H Kappelman, J R Shelton *J. Org. Chem.* **34** 3312 (1969)
105. J R Shelton, C K Liang *Synthesis* 204 (1971)
106. J R Shelton , C K Liang *J. Org. Chem.* **38** 2301 (1973)
107. A Peyman, E Hickl, H-D Beckhaus *Chem. Ber.* **120** 713 (1987)
108. J W Timberlake, B K Bandlish *Tetrahedron Lett.* 1393 (1971)
109. W P Neumann, A Penenory, U Stewen, M Lehnig *J. Am. Chem. Soc.* **111** 5845 (1989)
110. G-Z Ji, X-K Jiang, Y-H Zhang, S-G Yuan, C-X Yu, Y-Q Shi, X-L Zhang, W-T Shi *J. Phys. Org. Chem.* **3** 643 (1990)
111. X K Jiang, G-Z Ji, C-X Yu *Acta Chim. Sin., Engl. Ed.* 369 (1985)
112. X-K Jiang, G-Z Ji, C-X Yu *Acta Chim. Sin., Engl. Ed.* 82 (1984)
113. X-K Jiang, C-J Wu, X-X Wu *Acta Chim. Sin., Engl. Ed.* 42 (1983)
114. J M Dust, D R Arnold *J. Am. Chem. Soc.* **105** 1221 (1983)
115. R A Jackson, M Sharifi *J. Chem. Soc., Perkin Trans. 2* 775 (1996)
116. G S Hammond *J. Am. Chem. Soc.* **77** 334 (1955)
117. C Rüchardt *Angew. Chem., Int. Ed. Engl.* **9** 830 (1970)
118. J E Wertz, J R Bolton *Electron Spin Resonance* (New York: McGraw-Hill, 1972) Ch. 6
119. R I Walter *J. Am. Chem. Soc.* **88** 1923 (1966)
120. E G Janzen *Acc. Chem. Res.* **2** 279 (1969)
121. I B Afanas'v *Int. J. Chem. Kinet.* **7** 856 (1975)
122. J M Dust, D R Arnold *J. Am. Chem. Soc.* **105** 6531 (1983)
123. W J Leigh, D R Arnold, R W R Humphreys, P C Wong *Can. J. Chem.* **58** 2537 (1980)
124. D D M Wayner, D R Arnold *Can. J. Chem.* **63** 2378 (1985)
125. D D M Wayner, D R Arnold *Can. J. Chem.* **62** 1164 (1984)
126. A M de P Nicholas, D R Arnold *Can. J. Chem.* **64** 270 (1986)
127. W Adam, H M Harrer, F Kita, W M Nau *Pure Appl. Chem.* **69** 91 (1997)
128. A Pross, L Radom *Prog. Phys. Org. Chem.* **13** 1 (1981)
129. R A Jackson *J. Chem. Soc., Perkin Trans. 2* 523 (1983)
130. R A Jackson *J. Chem. Soc., Perkin Trans. 2* 1991 (1993)
131. W Adam, L Fröhlich, W M Nau, H-G Korth, R Sustmann *Angew. Chem., Int. Ed. Engl.* **32** 1339 (1993)
132. W Adam, F Kita, H M Harrer, W M Nau, R Zipf *J. Org. Chem.* **61** 7056 (1996)
133. W Adam, C van Barneveld, O Emmert, H M Harrer, F Kita, A S Kumar, W Maas, W M Nau, S H K Reddy, J Wirz *Pure Appl. Chem.* **69** 735 (1997)
134. W Adam, H M Harrer *An. Quim. Int. Ed.* **93** 271 (1997)
135. W Adam, O Emmert, T Heidenfelder *J. Org. Chem.* **64** 3417 (1999)
136. D A Dougherty *Acc. Chem. Res.* **24** 88 (1991)
137. S W Benson *J. Chem. Educ.* **42** 502 (1965)
138. H E O'Neal, S W Benson, in *Free Radicals* Vol. 2 (Ed. J K Kochi) (New York: Wiley, 1973)
139. M Rossi, D M Golden *J. Am. Chem. Soc.* **101** 1230 (1979)
140. D J DeFrees, R T McIver Jr, W J Hehre *J. Am. Chem. Soc.* **102** 3334 (1980)
141. D F McMillen, D M Golden *Annu. Rev. Phys. Chem.* **33** 493 (1982)
142. D C Nonhebel, J C Walton *J. Chem. Soc., Chem. Commun.* 731 (1984)
143. A M de P Nicholas, D R Arnold *Can. J. Chem.* **62** 1850 (1984)
144. D D M Wayner, K B Clark, A Rauk, D Yu, D R Armstrong *J. Am. Chem. Soc.* **119** 8925 (1997)
145. J Berkowitz, G B Ellison, D Gutman *J. Phys. Chem.* **98** 2744 (1994)
146. M Szwarc *J. Chem. Phys.* **16** 128 (1948)
147. X-M Zhang, F G Bordwell, J E Bares, J-P Cheng, B C Petrie *J. Org. Chem.* **58** 3051 (1993)

148. F G Bordwell, M J Bausch *J. Am. Chem. Soc.* **108** 1979 (1986)
149. F G Bordwell, X-M Zhang, R Filler *J. Org. Chem.* **58** 6067 (1993)
150. F G Bordwell, X-M Zhang *Acc. Chem. Res.* **26** 510 (1993)
151. L Pauling *The Nature of Chemical Bond* (Ithaca, NY: Cornell University Press, 1960)
152. F G Bordwell, M J Bausch *J. Am. Chem. Soc.* **108** 1985 (1986)
153. W M Nau *J. Org. Chem.* **61** 8312 (1996)
154. W M Nau *J. Phys. Org. Chem.* **10** 445 (1997)
155. G Leroy, M Sana, C Wilante *J. Mol. Struct. (Theochem)* **205** 97 (1990)
156. C Ruchardt, H-D Beckhaus *Top. Curr. Chem.* **130** 1 (1986)
157. G Leroy *Int. J. Quantum Chem.* **23** 271 (1983)
158. G Leroy *J. Mol. Struct. (Theochem)* **93** 175 (1983)
159. F M Welle, S P Verevkin, H-D Beckhaus, C Rüchardt *Liebigs Ann. Chem.* 155 (1997)
160. C Rüchardt *Angew. Chem.* **82** 845 (1970)
161. F M Welle, H-D Beckhaus, C Rüchardt *J. Org. Chem.* **62** 552 (1997)
162. A M de P Nicholas, D R Arnold *Can. J. Chem.* **62** 1860 (1984)
163. K B Clark, D D M Wayner *J. Am. Chem. Soc.* **113** 9363 (1991)
164. A A Zavitsas, C C Chatgilialoglu *J. Am. Chem. Soc.* **117** 10 645 (1995)
165. W A Pryor, D F Church, F Y Tang, R H Tang, in *Frontiers in Free Radical Chemistry* (Ed. W A Pryor) (New York: Academic Press, 1980) p. 335
166. D J Pasto *J. Am. Chem. Soc.* **110** 8164 (1988)
167. D J Pasto, R Krasnansky, C Zercher *J. Org. Chem.* **52** 3062 (1987)
168. W J Hehre, L Radom P von R Schleyer, J A Pople *Ab Initio Molecular Orbital Theory* (New York: Wiley-Interscience, 1986)
169. M J S Dewar, M A Fox, D J Nelson *J. Organomet. Chem.* **185** 157 (1980)
170. M Lehd, F Jensen *J. Org. Chem.* **56** 884 (1991)
171. J D Goddard *Can. J. Chem.* **60** 1250 (1982)
172. B S Jursic, J W Timberlake, P S Engel *Tetrahedron Lett.* **37** 6473 (1996)
173. Y-D Wu, C-L Wong, K W K Chan, G-Z Ji, X-K Jiang *J. Org. Chem.* **61** 746 (1996)
174. W J Hehre, R Ditchfield, L Radom, J A Pople *J. Am. Chem. Soc.* **92** 4796 (1970)
175. A E Dorigo, Y Li, K N Houk *J. Am. Chem. Soc.* **111** 6942 (1989)
176. F G Bordwell, X-M Zhang, M S Alnajjar *J. Am. Chem. Soc.* **114** 7623 (1992)
177. D A Hrovat, W T Borden *J. Phys. Chem.* **98** 10460 (1994)
178. C Hansch, A Leo *Substituent Constants for Correlation Analysis in Chemistry and Biology* (New York: Wiley, 1979)
179. O Exner *Advances in Linear Free Energy Relationships* (Eds N B Chapman, J Shorter) (London: Plenum, 1971) p. 1
180. A Cammarata, S J Yau *J. Polym. Sci., A1* **8** 1303 (1970)
181. L Sylvander, L Stella, H-G Korth, R Sustmann *Tetrahedron Lett.* **26** 749 (1985)
182. M C Flowers, H M Frey *Proc. R. Soc. London, A Math. Phys. Sci.,* **257** 122 (1960)
183. M Arai, R J Crawford *Can. J. Chem.* **50** 2158 (1972)
184. W Kirmse, M Zeppenfeldt *J. Chem. Soc., Chem. Commun.* 124 (1977)
185. M J S Dewar *J. Am. Chem. Soc.* **74** 3353 (1952)
186. A T Balaban *Rev. Roum. Chim.* **16** 725 (1971)
187. A T Balaban, M T Caproiu, N Negoita, B Baican *Tetrahedron* **33** 2249 (1977)
188. R W Baldock, P Hudson, A R Katritzky, F Soti *Heterocycles* **1** 67 (1973)
189. R W Baldock, P Hudson, A R Katritzky, F Soti *J. Chem. Soc., Perkin Trans. 1* 1422 (1974)
190. A R Katritzky, F Soti *J. Chem. Soc., Perkin Trans. 1* 1427 (1974)
191. L Stella, Z Janousek, R Merenyi, H G Viehe *Angew. Chem., Int. Ed. Engl.* **17** 691 (1978)
192. H G Viehe, R Merenyi, L Stella, Z Janousek *Angew. Chem., Int. Ed. Engl.* **18** 917 (1979)
193. S Mignani, M Beaujean, Z Janousek, R Merenyi, H G Viehe *Tetrahedron* **37** (Suppl. 1) 111 (1981)
194. S Mignani, R Merenyi, Z Janousek, H G Viehe *Bull. Soc. Chim. Belg.* **93** 991 (1984)
195. S Mignani, Z Janousek, R Merenyi, H G Viehe *Bull. Soc. Chim. Fr.* 1267 (1985)
196. S Mignani, R Merenyi, Z Janousek, H G Viehe *Tetrahedron* **41** 769 (1985)
197. S Mignani, Z Janousek, R Merenyi, H G Viehe, J Riga, J Verbist *Tetrahedron Lett.* **25** 1571 (1984)
198. F Lahousse, R Merenyi, J R Desmurs, H Allaime, A Borghese, H G Viehe *Tetrahedron Lett.* **25** 3823 (1984)
199. C De Cock, S Piettre, F Lahousse, Z Janousek, R Merenyi, H G Viehe *Tetrahedron* **41** 4183 (1985)
200. K D Gundermann, E Rohrl *Liebigs Ann. Chem.* 1661 (1974)
201. R M Moriarty, C R Romain, I L Karle, J Karle *J. Am. Chem. Soc.* **87** 3251 (1965)
202. H K Hall Jr *Angew. Chem.* **95** 448 (1983)
203. S-U Park, S-K Chung, M Newcomb *J. Am. Chem. Soc.* **108** 240 (1986)
204. H Singh, J M Tedder *J. Chem. Soc., Chem. Commun.* 1095 (1980)
205. X Creary, Z Jiang, M Butchko, K McLean *Tetrahedron Lett.* **37** 579 (1996)
206. A De Mesmaeker, L Vertommen, R Merenyi, H G Viehe *Tetrahedron Lett.* **23** 69 (1982)
207. R Merenyi, A De Mesmaeker, H G Viehe *Tetrahedron Lett.* **24** 2765 (1983)
208. M van Hoecke, A Borghese, J Penelle, R Merenyi, H G Viehe *Tetrahedron Lett.* **27** 4569 (1986)
209. R Merenyi, V Daffe, J Klein, W Masamba, H G Viehe *Bull. Soc. Chim. Belg.* **91** 456 (1982)
210. H-G Korth, P Lommes, W Sicking, R Sustmann *J. Am. Chem. Soc.* **106** 663 (1984)
211. I MacInnes, J C Walton, D C Nonhebel *J. Chem. Soc., Chem. Commun.* 712 (1985)
212. H G Viehe, Z Janousek, R Merenyi, L Stella *Acc. Chem. Res.* **18** 148 (1985)
213. M Klessinger *Angew. Chem., Int. Ed. Engl.* **19** 908 (1980)
214. G Leroy, D Peeters *J. Mol. Struct. (Theochem)* **85** 133 (1981)
215. A R Katritzky, M C Zerner, M M Karelson *J. Am. Chem. Soc.* **108** 7213 (1986)
216. H-G Korth, P Lommes, W Sicking, R Sustmann *Chem. Ber.* **188** 4627 (1985)
217. H-G Korth, R Sustmann, R Merenyi, H G Viehe *J. Chem. Soc., Perkin Trans. 2* 67 (1983)
218. M Zamkanei, J H Kaiser, H Birkhofer, H-D Beckhaus, C Rüchardt *Chem. Ber.* **116** 3216 (1983)
219. H Birkhofer, J Hädrich, H-D Beckhaus, C Rüchardt *Angew. Chem., Int. Ed. Engl.* **26** 573 (1987)
220. A Cherkasov, M Jonsson, V I Galkin *J. Mol. Graph. Model.* **17** 28 (1999)
221. *MATLAB The Language of Technical Computing* 5.2.0.3084, The MathWorks Inc., 1998
222. A R Cherkasov, V I Galkin, R A Cherkasov *J. Phys. Org. Chem.* **11** 437 (1998)
223. A R Cherkasov, V I Galkin, E M Zueva, R A Cherkasov *Zh. Obshch. Khim.* **66** 877 (1996) [a]
224. V I Galkin, A R Cherkasov, R D Sayakhov, R A Cherkasov *Zh. Obshch. Khim.* **65** 458 (1995) [a]
225. A R Cherkasov, V I Galkin, E M Zueva, R A Cherkasov *Zh. Obshch. Khim.* **66** 411 (1996) [a]
226. A R Cherkasov, V I Galkin, E M Zueva, R A Cherkasov *Zh. Obshch. Khim.* **67** 92 (1997) [a]
227. A R Cherkasov, V I Galkin, R A Cherkasov *Zh. Org. Khim.* **35** 163 (1999) [b]
228. A R Cherkasov, V I Galkin, R A Cherkasov *J. Mol. Struct. (Theochem)* **489** 43 (1999)
229. A R Cherkasov, V I Galkin, R A Cherkasov *J. Mol. Struct. (Theochem),* **497** 115 (2000)
230. V I Galkin, A R Cherkasov, R A Cherkasov *Phosphorus Sulfur Silicon Relat. Elem.* **144–146** 329 (1999)
231. A R Cherkasov, V I Galkin, R A Cherkasov *Phosphorus Sulfur Silicon Relat. Elem.* **144–146** 775 (1999)
232. I A Koppel, U H Molder, R I Pikver *Org. React.* **18** 380 (1981)
233. A Cherkasov, M Jonsson *J. Chem. Inf. Comput. Sci.* **38** 1151 (1998)
234. A Cherkasov, M Jonsson *J. Chem. Inf. Comput. Sci.* **39** 1057 (1999)
235. *NIST Standard Reference Database* No. 69, November 1998, Release
236. R W Taft Jr *J. Am. Chem. Soc.* **75** 4538 (1953)
237. D Griller, K U Ingold *Acc. Chem. Res.* **9** 13 (1976)
238. A Cherkasov, M Jonsson *J. Chem. Inf. Comput. Sci.* **40** 1222 (2000)

[a] — *Russ. J. Gen. Chem. (Engl. Transl.)*
[b] — *Russ. J. Org. Chem. (Engl. Transl.)*

Russian Chemical Reviews **70** (1) 23 – 44 (2001) © 2001 Russian Academy of Sciences and Turpion Ltd

DOI 10.1070/RC2001v070n01ABEH000608

Rotaxanes and polyrotaxanes. Their synthesis and the supramolecular devices based on them

I G Panova, I N Topchieva

Contents

I.	Introduction	23
II.	Rotaxanes	23
III.	Polyrotaxanes	30
IV.	Supramolecular devices based on rotaxanes and polyrotaxanes	41

Abstract. Various approaches to the synthesis of rotaxanes and polyrotaxanes are considered. The principles employed in the design of highly organised structures comprising rod-shaped polymeric molecules, *viz*., macromolecular inclusion complexes, are discussed. In addition to the conventional (step-by-step) methodology which consists of polymerisation of monomers in the presence of macrocycles, molecular self-assembly is gaining an ever increasing significance. The main emphasis is laid on the preparation and characterisation of inclusion complexes which are based on cyclodextrins and linear synthetic polymers. The bibliography includes 138 references.

I. Introduction

Supramolecular chemistry as a new line of research has evolved and has developed intensively in the past few years. This interdisciplinary science encompasses the chemistry of noncovalent interactions, molecular physics and molecular biology. Its main attention is focussed on the systems which are capable of self-organisation, *i.e*., spontaneous production of definite structures by self-assembly of constituents into supramolecular assemblies. The synthesis of such structures is based on the molecular recognition principle and is effected by the cooperation of various non-covalent interactions, *e.g*., electrostatic, hydrophobic, hydrogen bonding, *etc*.

The principle of molecular recognition can be exemplified in the formation of complexes of the 'host – guest' type. The role of 'hosts', *i.e*., receptors, is played by cyclic molecules, *e.g*., cryptands, crown ethers, cyclodextrins and calixarenes. The chemical nature of 'guests' is extremely diverse, they include both small particles (*e.g*., inert gas atoms, metal ions, *etc*.) and complex bulky molecules of the fullerene type. In the past few years, supramolecular chemistry has been enriched by systems with polymers as the 'guest' molecules, which underlies the supramolecular chemistry of polymers.

This approach has made it possible to obtain such compounds as polyrotaxanes, catenanes, 'molecular necklaces', dendrimers, *etc*., which possess novel, previously unknown structures and remarkable properties. This review is devoted to one type of polymeric supramolecular assemblies, *viz*., polyrotaxanes. In the latter, the macrocycles are 'threaded' onto a polymeric molecule with bulky terminal groups. In addition to polyrotaxanes, their topological analogues, *viz*., pseudopolyrotaxanes including 'molecular necklaces', are reviewed. Since these structures are synthesised using essentially the same procedures as for rotaxanes, the strategy of rotaxane synthesis is also discussed.

I G Panova, I N Topchieva Department of Chemistry, M V Lomonosov Moscow State University, Leninskie Gory, 119899 Moscow, Russian Federation. Fax (7-095) 939 01 74. Tel. (7-095) 939 31 27.
E-mail: vspan@redline.ru (I G Panova); kurganov@gagarinclub.ru (I N Topchieva)

Received 2 June 2000
Uspekhi Khimii **70** (1) 28 – 51 (2001); translated by R L Birnova

II. Rotaxanes

Rotaxanes (Rt) represent complexes comprising cyclic molecules (C) threaded onto linear molecules (L). Their characteristic feature is the lack of covalent binding between the components C and L. In order to prevent the dissociation of the complex into constituents, the 'stoppers' (S), *i.e*., bulky molecules which are covalently linked to the ends of linear molecules, are used (Fig. 1 *a*, *b*). Similar structures in which the molecules S are absent are called pseudorotaxanes (pseudo-Rt) (Fig. 1 *c*). The nomenclature used to describe such compounds takes account of the number of components involved in the complexation. Thus [2]-Rt (see Fig. 1 *a*) contains one L and one C molecule; [3]-Rt is comprised of one L and two C molecules (see Fig. 1 *b*), *etc*.

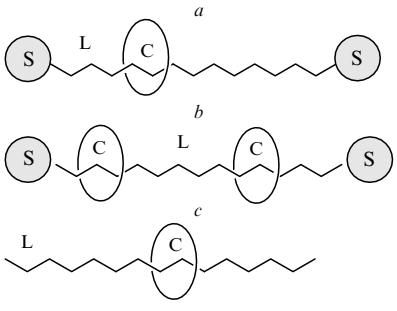

Figure 1. A schematic representation of rotaxanes: (*a*) [2]-Rt, (*b*) [3]-Rt, (*c*) pseudo-Rt.

1. General approaches to the rotaxane synthesis

It should be noted that the threading of cyclic molecules onto linear components, which forms the basis for all the strategies of the rotaxane synthesis (Fig. 2), is a reversible process which is described by the equilibrium constant $K_{eq} = [Rt]/[L][C]$.

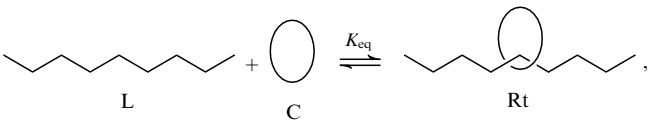

Therefore, the creation of conditions where the equilibrium of the reaction is shifted towards complex formation is the key event in the assembly of rotaxane molecules. Quantitatively, this process can be described by standard thermodynamic equations:

$$RT\ln K_{eq} = -\Delta G = -(\Delta H - T\Delta S), \quad (1)$$

$$\ln K_{eq} = -\frac{\Delta H}{RT} + \frac{\Delta S}{R}. \quad (2)$$

As can be seen from Eqn (2), two extreme cases are thermodynamically possible. First, the so-called statistical threading, *i.e.*, a random collision and interaction of molecules of different nature (*e.g.*, L and C). The enthalpy of such a reaction, ΔH, is close to zero or is positive, *i.e.*, the threading is determined by the entropy factor. Second, template-directed threading, which is based on the principle of molecular self-assembly where the reaction is energetically favourable due to the existence of specific non-covalent interactions between the particles L and C ($\Delta H < 0$).

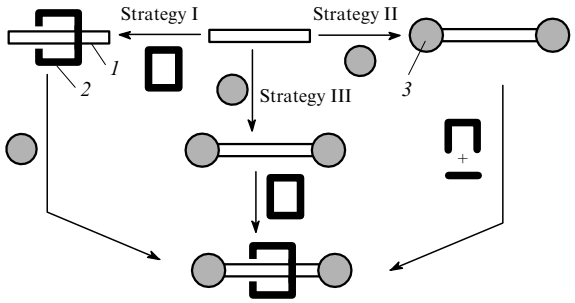

Figure 2. The strategies of the chemical synthesis of rotaxanes: (*1*) rod molecule, (*2*) macrocycle, (*3*) 'stopper'.

When considering the strategies of chemical synthesis of rotaxanes (see Fig. 2), one can distinguish three general approaches: [1]

(1) threading of a macrocycle onto a rod molecule and subsequent interaction of the complex formed with the blocking reagents (strategy I);

(2) cyclisation in the presence of compounds having a dumbbell-like structure (strategy II);

(3) temperature-induced 'slipping' of the macrocycle onto bulky terminal groups of the dumbbell-shaped molecule (strategy III).

2. The statistical approach to the rotaxane synthesis

The first attempts to synthesise rotaxanes were based on statistical threading of a cyclic component onto linear molecules. The first report on a successful synthesis of such complexes,[2] which consisted of random threading of a macrocyclic acyloin onto decane-1,10-diol using bulky trityl groups as stoppers, was published in 1967. After a 70-fold passage of the reaction mixture containing components L and S through a column with an immobilised cyclic component (C) and subsequent chromatographic separation of the eluate, the yield of rotaxane was as low as 6%. Further experiments [3,4] were aimed at establishing a correlation between the efficiency of statistical threading, the properties of the reactants C, L and S and reaction conditions.

The synthesis of rotaxanes from various dibenzocrown ethers, ethylene oxide oligomers (EOO) and trityl chloride by their joint fusion has been described.[4] In this case, the efficiency of threading depended on the size of the ring, the L : C ratio, the length of the chains of the L-molecules and the total volume of the reaction mixture, whereas temperature had no effect on the course of the reaction. The maximum degree of threading was achieved when a mixture of an ethylene oxide oligomer having a molecular mass (MM) of 1000 and crown ethers (on average, dibenzo-58.2-crown-19.4) is used. Mixing of EOO (MM = 400) with dibenzo-58.2-crown-19.4 at 130 °C and subsequent addition of triphenylchloromethane gave the corresponding [2]-Rt in 15% yield. The introduction of bromomethyl substituents into each phenyl group of the blocking reagent and the reaction in the presence of the Zn/Cu couple in DMF resulted in [4]-Rt in 8% yield.[5]

The experiments [3] with statistical threading of cyclic hydrocarbons onto 1,10-bis(triphenylmethoxy)decane at 120 °C revealed that only rotaxanes comprising C_{29} rings were more or less stable at this temperature, although their yields did not exceed 1.6%.

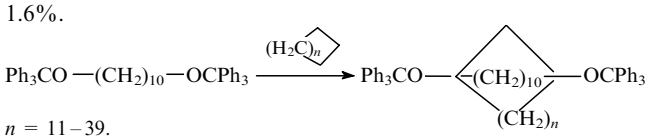

$n = 11-39$.

Later, it was found [4] that a macrocycle which has to be threaded onto the methylene groups should contain no less than 22 carbon atoms. It was shown also that terminal trityl groups can hold the rings which contained no more than 29 carbon atoms. Bulkier tris(*p*-butylphenyl)methyl groups prevent the dissociation of the rings containing 42 carbon atoms.

Thus, the statistical approach affords a mixture of starting compounds and rotaxanes; the isolation of the latter often presents a problem.[2–5] The efficiency of threading and the yields are controlled by varying the concentrations of the reactant and their molar ratios and by matching the geometric parameters of the molecules L, C and S. It is noteworthy that this approach gives relatively low yields of reaction products which at best do not exceed 15%. On the other hand, one of the benefits of the statistical approach to the rotaxane synthesis is the possibility of using a vast diversity of linear and cyclic molecules of different chemical nature which significantly expand the range of the structures that can be synthesised by this method.

3. Template synthesis of rotaxanes

Yet another approach to the rotaxane synthesis is based on the use of the fundamental principle of supramolecular chemistry, namely, the self-organisation of molecules due to specific non-covalent interactions. This approach is named template or directed synthesis, since in this case the process is directed by molecular recognition between two or more complementary fragments of the interacting molecules. Depending on the type of bonding, the following main routes to the rotaxane synthesis may be distinguished: (1) the formation of metal–ligand coordination bonds; (2) donor–acceptor interactions; (3) combined interactions which are observed in the formation of inclusion complexes based on cyclodextrins.

a. The synthesis of rotaxanes using transition metal ions

This strategy is based on the assembling and 'orientational' properties of transition metals. The complexation of two 2,9-disubstituted 1,10-phenanthrolines **1a**,**b** with the copper(I) ion was

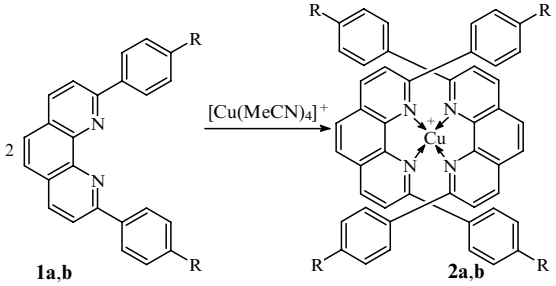

R = OMe (**a**), OH (**b**).

Scheme 1

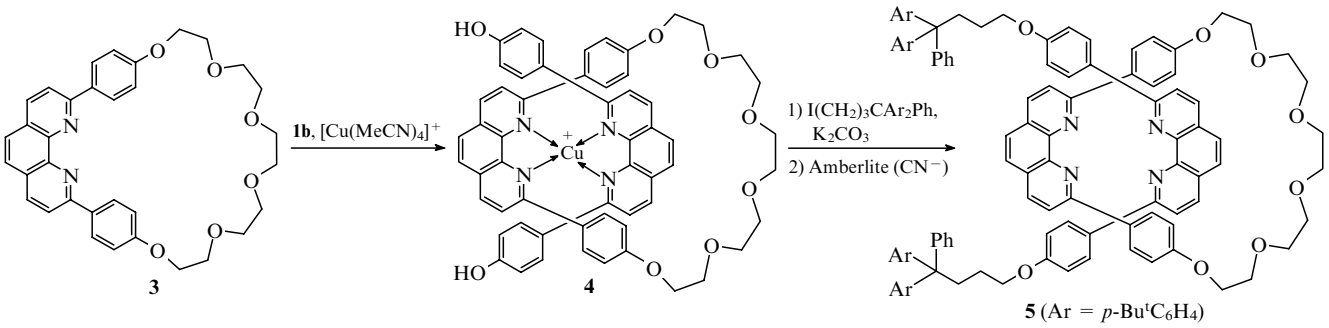

first proposed as the template-based reaction.[6] The complexes **2a**,**b** formed have an ideal spatial structure for the synthesis of rotaxanes based on them.

The synthesis of the macrocycle **3** incorporating one bidentate centre has been described.[7] The reaction of compound **3** with $[Cu(MeCN)_4]^+[BF_4]^-$ and 2,9-bis(4-hydroxyphenyl)phenanthroline **1b** affords the pseudorotaxane **4** (Scheme 1).[7] Reactive phenolic groups can react with different stoppers. Modification of the terminal groups of the complex **4** with alkyl iodide containing the bulky triarylmethyl group has led to [2]-Rt **5**.[8] In order to remove Cu^I, the complex formed was passed through an ion-exchange resin. The structure of the individual [2]-Rt **5** isolated in 21% yield was confirmed by ^1H NMR spectroscopy and mass spectrometry.

Later, data on the synthesis of porphyrin-containing rotaxanes have been documented (Scheme 2).[9–12] Initially, compound

Scheme 2

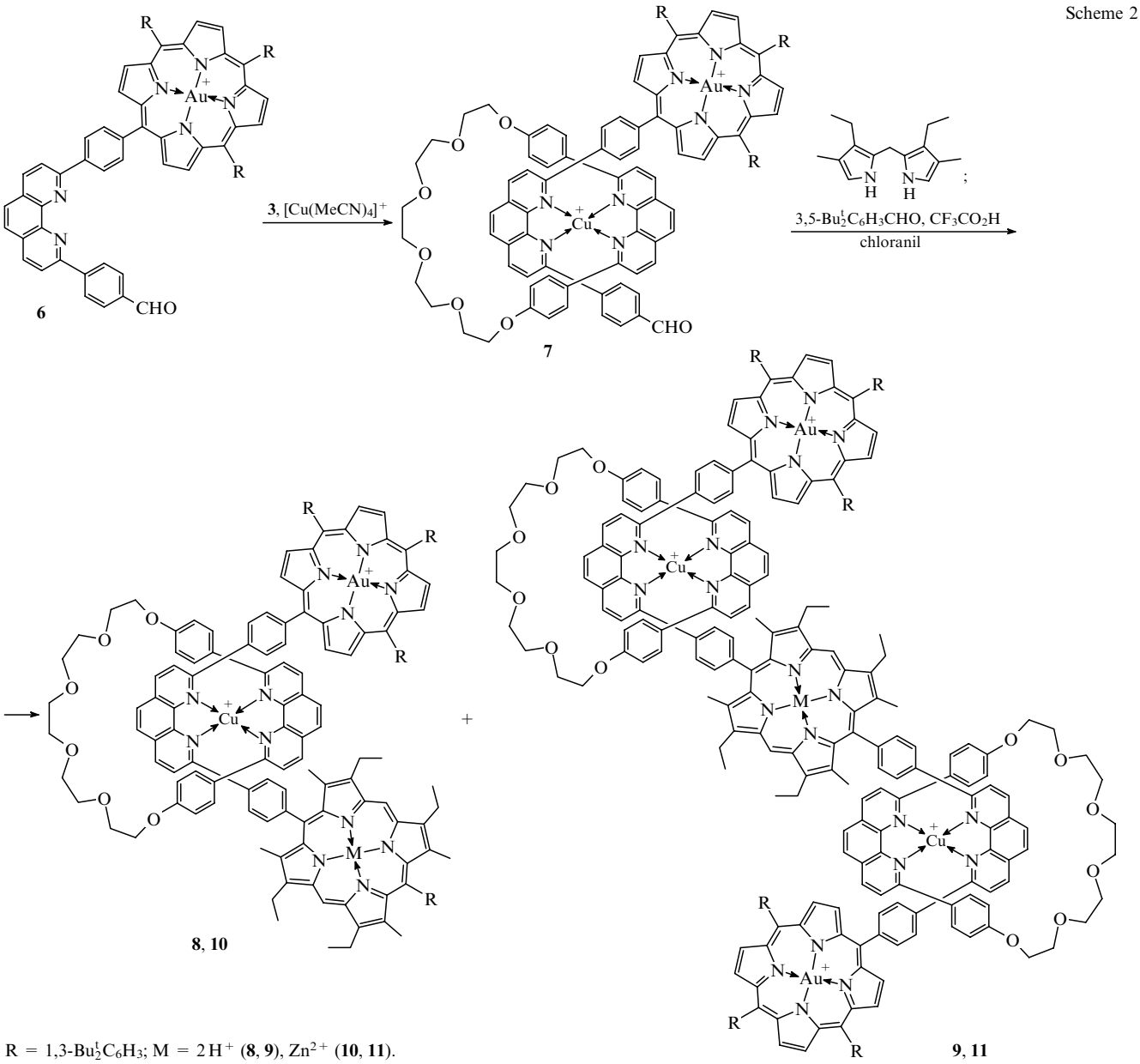

R = 1,3-$Bu^t_2C_6H_3$; M = $2H^+$ (**8**, **9**), Zn^{2+} (**10**, **11**).

Scheme 3

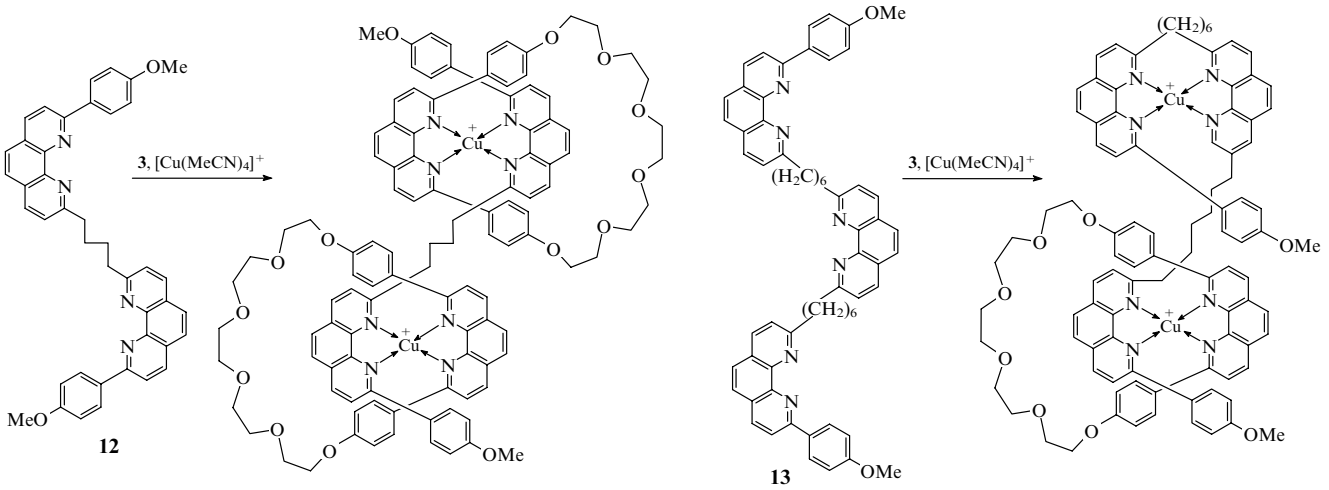

6 which contained a porphyrin–gold(III) complex as a stopper was prepared. This complex was added to the macrocycle **3** in the presence of a copper(I) complex. The intermediate product **7** formed reacted with 3,5-di-*tert*-butylbenzaldehyde and bis-(3-ethyl-4-methylpyrrol-2-yl)methane in the presence of trifluoroacetic acid. The intermediate porphyrinogen was oxidised with chloranil. Chromatographic separation gave [2]-Rt (**8**) and [3]-Rt (**9**) in 25% and 32% yields, respectively.[11] The rotaxanes **8** and **9** were converted into their Zn-analogues **10** and **11** by treatment with $Zn(OAc)_2 \cdot 2H_2O$. A ^1H NMR spectroscopic study showed that demetallation of the phenanthroline moiety of [2]-Rt by ion exchange with KCN changes its structure so that the phenanthroline fragment of the macrocycle lies outside the 'cleft' formed by the porphyrin fragments.[12]

Several modifications of this synthetic procedure are known. In one of them, the blocking groups are represented by fullerenes.[13]

It was suggested [14] to use linear molecules incorporating two (**12**) or three (**13**) 1,10-phenanthroline fragments for the synthesis of structurally more elaborate rotaxanes. Their interactions with the macrocycle **3** in the presence of $[Cu(MeCN)_4]^+ [BF_4]^-$ have been studied (Scheme 3). It was shown that [3]-pseudo-Rt formed on the basis of compound **12** has the composition $L : Cu^I : C = 1 : 2 : 2$. Compound **13**, which contains three phenanthroline fragments, yields a complex with the composition $L : Cu^I : C = 1 : 2 : 1$, *i.e.*, [2]-Rt in which two phenanthroline fragments of the rod molecule interact both with each other and with Cu^I, rather than the expected complex with a $L : Cu^I : C$ ratio of 1 : 3 : 3. This phenomenon was attributed to the flexibility of the stretched rod molecule. The ability for self-complexation must be taken into consideration in the synthesis of [3]- and [4]-Rt by this method.

b. Rotaxane syntheses based on donor-acceptor interactions of L and C molecules

This method consists in the interaction of electron-donor and electron-acceptor molecules or their fragments and results in π-bonding. Cyclobis(paraquat-*p*-phenylene) **14**,[15] which reacts with a variety of aromatic electron-donor substrates, and bis-*p*-phenylene-34-crown-10 (**15**),[16] which forms a complex with paraquat bis(hexafluorophosphate), have received especially wide acceptance as receptors. Using X-ray diffraction analysis, it was shown [17,18] that the complexes prepared on the basis of these compounds and the corresponding ligands have ordered structures both in solution and in the solid phase and represent pseudorotaxanes. The aromatic rings of the 'guest' molecules are accommodated inside the 'host' molecules between the rings of the receptor, which are stacked parallel to one another. The complexes have box-like structures, which are ideal for their conversion into rotaxanes.

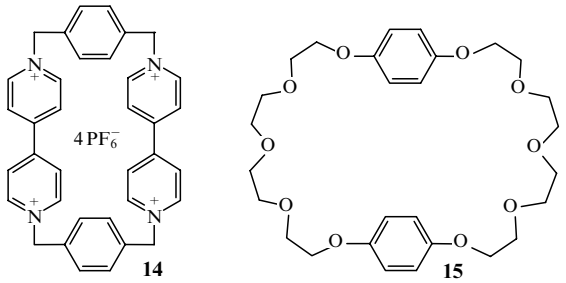

The interaction of compounds **16** and **17** (Scheme 4) with the macrocycle **14** in acetonitrile followed by a reaction with triisopropylsilyl triflate was studied.[19] After purification of the reaction mixture by column chromatography on silica gel, [2]-Rt **16′** and **17′** were isolated in equal yields (22%).

A similar compound, *viz.*, [2]-Rt **17′**, was obtained in 14% yield using strategy II (see Scheme 2, Fig. 2).[20] It was noted [19] that the reduction in the length of the oligoethylene oxide fragments of the rod molecules changes the arrangement of the *p*-dioxyphenylene fragments relative to the plane of cyclophane and results in the increase in the distance between the complementary aromatic fragments of the L and C molecules.

An increase in the number of electron-donor fragments in the rod molecule not only increases the yields due to the self-organisation of rotaxanes, but also enables the synthesis of the so-called molecular shuttles,[21–27] *viz.*, the complexes in which the macrocycle can migrate from one part of the rod molecule to another (the so-called translocation isomers). For the first time, such rotaxanes were synthesised in 1991 [21] by the reaction of the tetracationic cyclophane **14** with the dumbbell-shaped compound **18** (Scheme 5) containing two *p*-dioxyphenylene fragments. The corresponding rotaxane was obtained in 32% yield. A ^1H NMR spectroscopic study revealed that the cyclophane migrated between the two aromatic fragments of the L molecule at a rate of 500 s^{-1}. The activation free energy of the migration observed (ΔG) is $\sim$ 13 kcal mol^{-1}.

Strategy II was also used for the synthesis of a series of [2]-Rt **19–22** (yields 1%, 25%, 29% and 40%, respectively).[22] It is remarkable that in neither case [3]-Rt was obtained. Of the four rotaxanes isolated, only complex **22** exists in the form of two translocation isomers. Similar 'molecular shuttles' were obtained by substitution of electron-donor (*e.g.*, tetrathiofulvalene,[23–25] 4,4′-bisphenol, benzidine [26,27]) fragments for one of the *p*-dioxyphenylene fragments of the rod molecule; the yields of the isolated rotaxanes did not exceed 9%. Presumably, this can be attributed

Scheme 4

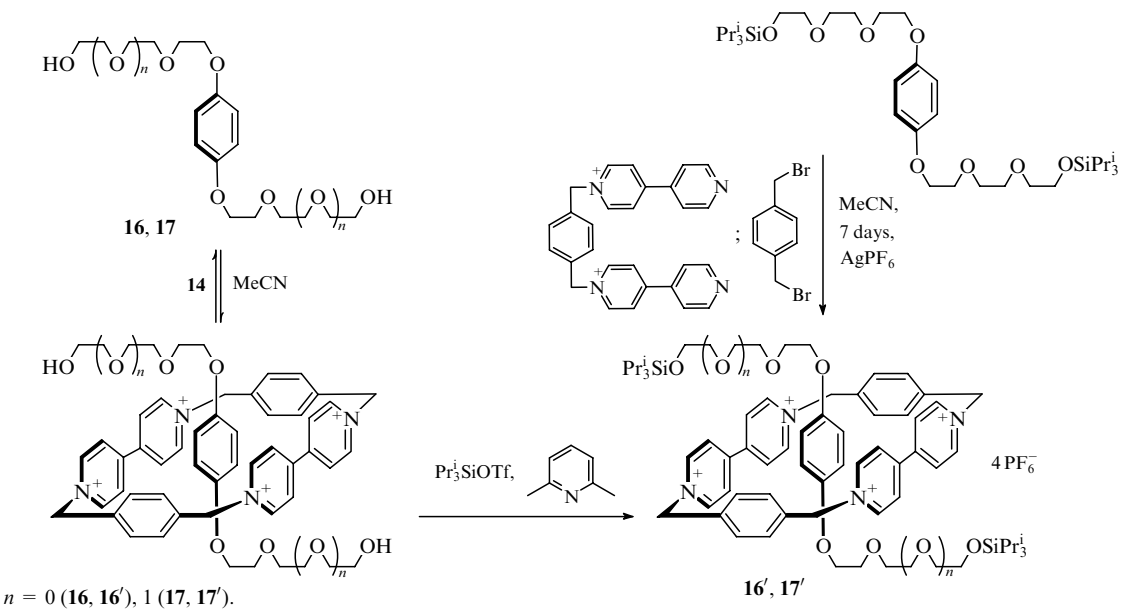

n = 0 (**16**, **16′**), 1 (**17**, **17′**).

Scheme 5

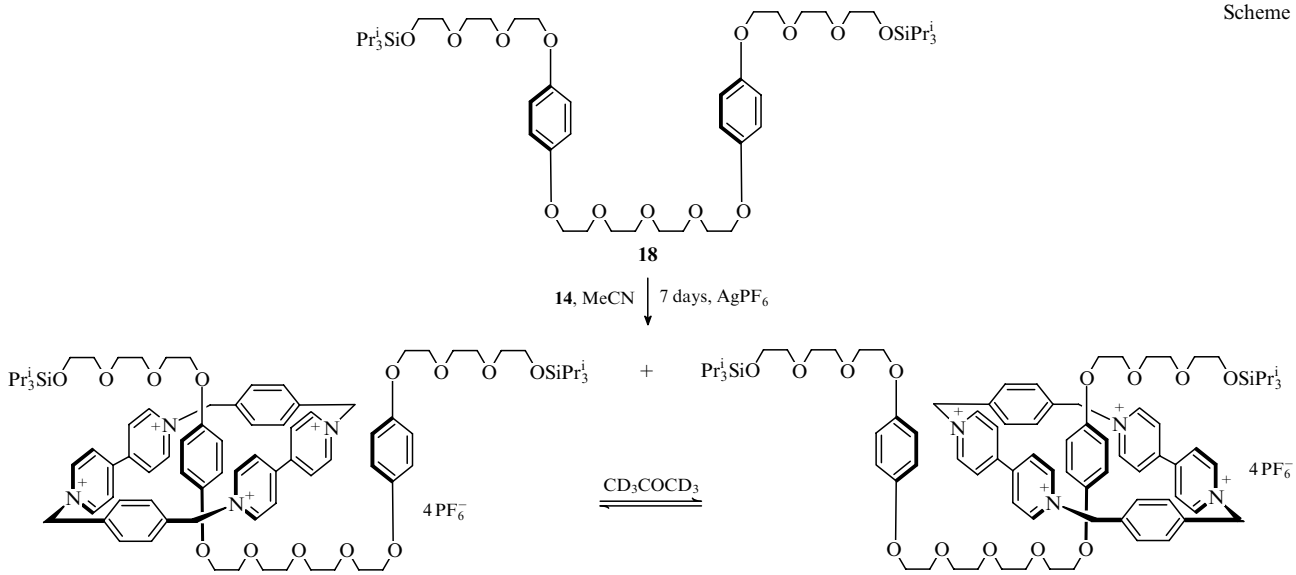

to the fact that in these cases the complexation largely involves one binding centre of the rod molecule.

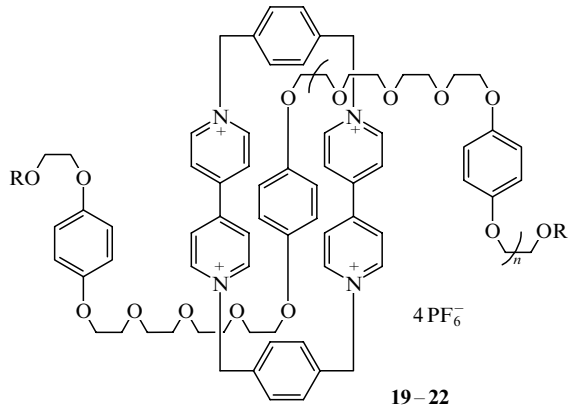

R = 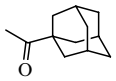 ; n = 0 (**19**), 1 (**20**), 2 (**21**), 3 (**22**).

The synthesis of rotaxanes based on crown ether **15** was carried out using strategies I and III.[28] Thus the reaction of the dication **23** with the bulky blocking reagent **24** in the presence of an equimolar amount of the macrocycle **15** under high pressure (strategy I) (Scheme 6) has been described. The yield of the target product, *viz*., [2]-Rt, was 23%. Noteworthy, the rate of the translocation of the macrocycle between the two dications in this complex is $\sim 300\,000\ s^{-1}$, which markedly exceeds that of rotaxanes based on cyclobis(paraquat-*p*-phenylene).

By varying the size of the blocking group in the dumbbell-shaped molecule **25** (Scheme 7), it became possible to synthesise rotaxanes using thermodynamically more favourable slipping of the macromolecule **15** onto the bulky terminal groups of compound **25** (strategy III, see Fig. 2). Compound **25** in which the terminal *tert*-butyl groups were replaced severally by isopropyl, ethyl and methyl groups as well as by hydrogen atoms were heated in acetonitrile with four equivalents of the macrocycle **15** at 60 °C.[29] This resulted in the self-organisation of [2]-Rt of the type **26** (see Scheme 7) in 47%, 45% and 51% yields for R = Et, Me and H, respectively. The isopropyl groups appeared to be too bulky for the slipping of the macrocycle. All the rotaxanes thus prepared were stable at room temperature.

Strategy III was also employed in the synthesis of [2]- and [3]-Rt containing two bipyridine fragments.[30] It should be noted that such rotaxanes cannot be synthesised using strategies I and II,

Scheme 6

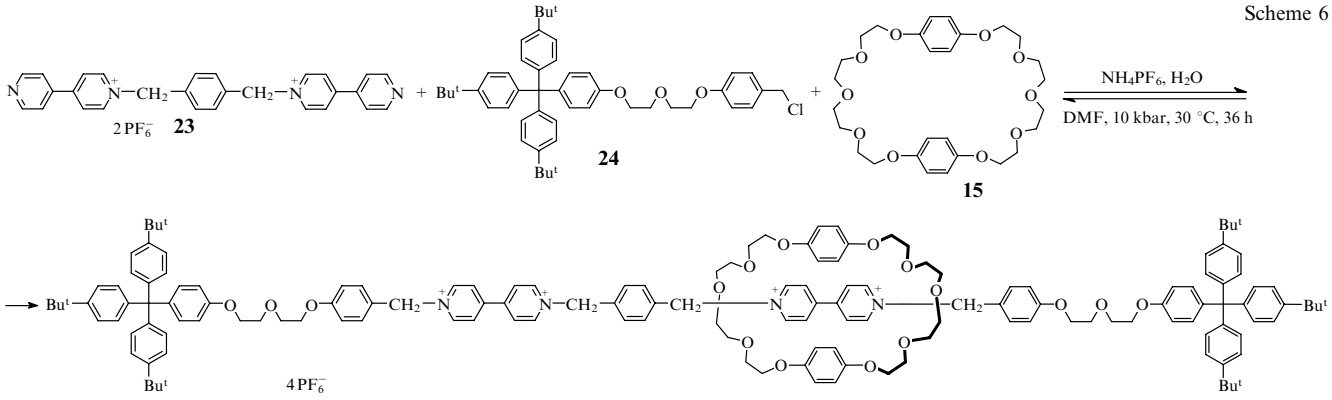

Scheme 7

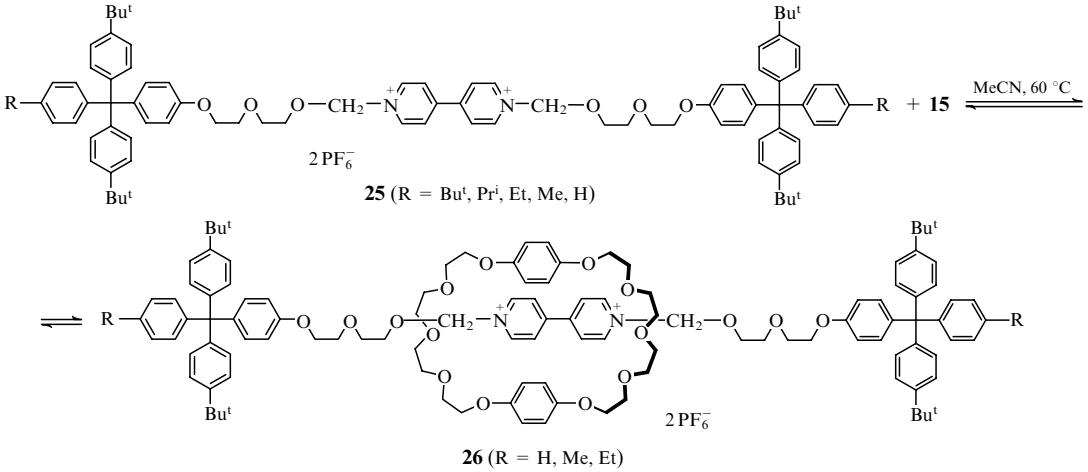

whereas slipping allows one to obtain them in 20% and 55% yields, respectively.

An illustrative example of a successful application of strategy III has been described.[31] Heating of a mixture containing compound **27** and the macrocycle **15** affords [2]-Rt **28** (yield 19%), [3]-Rt **29** (yield 41%) and [4]-Rt **30** (yield 22%) (Fig. 3). Such branched supramolecular assemblies are the first examples of dendritic rotaxanes.

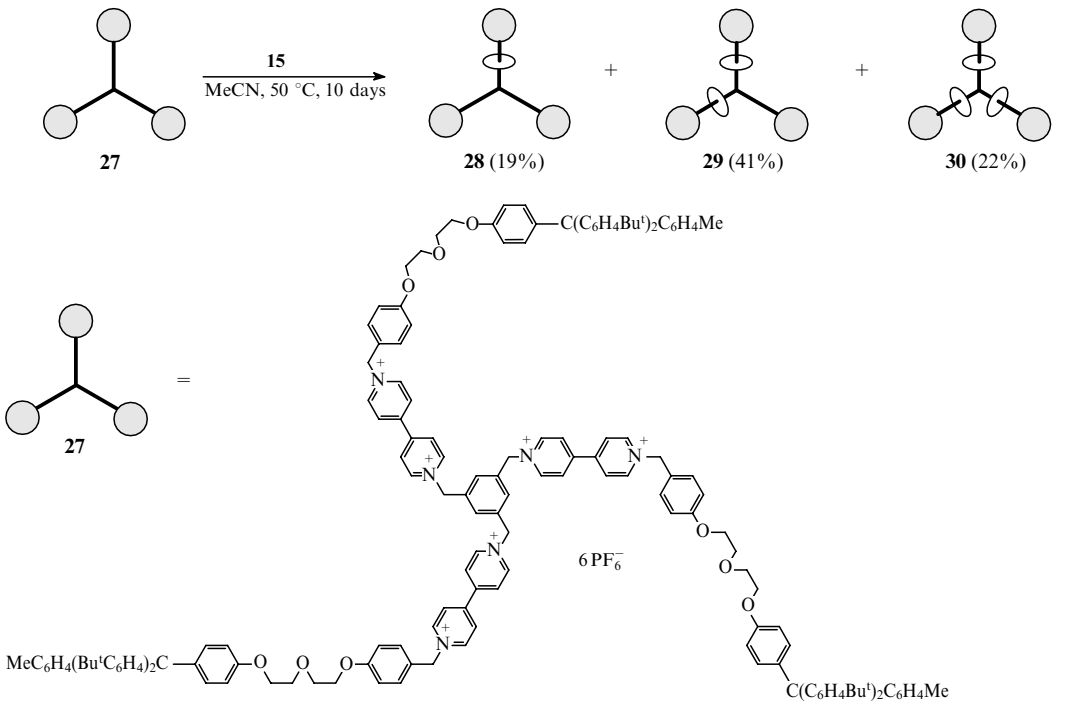

Figure 3. The synthesis of dendrimeric rotaxanes using strategy III.[31]

c. The synthesis of cyclodextrin-containing rotaxanes

The use of cyclodextrins (CD) as cyclic components has marked a new step in the synthesis of rotaxanes. These compounds were first discovered in 1891 [32] and represent cyclic oligosaccharides built up of D-glucopyranose units linked together by α-1,4-glucoside bonds. The shape of the cyclodextrin molecules resembles a torus. The structure of α-, β- and γ-cyclodextrins is schematically represented in Fig. 4. The presence of a cylindrical hydrophobic cavity determines the ability of cyclodextrins to form inclusion complexes with molecules of different chemical nature in aqueous solutions. The synthesis and characteristics of such complexes have been outlined in numerous reviews and monographs.[33–39] Suffice it to say that the driving forces of this complexation are Coulombic, dipole–dipole, hydrophobic and van der Waals interactions as well as hydrogen bonds between the CD and 'guest' molecules. Matching of the geometrical characteristics of the cyclodextrin cavity and those of the 'guest' molecule is an important prerequisite for the formation and stability of the inclusion complexes. The unique capacity of cyclodextrins to interact selectively with the substrate molecules which are complementary in size makes them attractive subjects of the supramolecular chemistry.

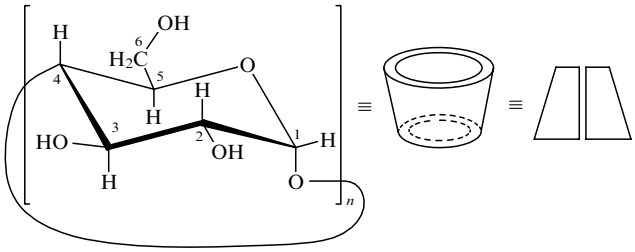

Figure 4. The structural formula of α- (n = 6), β- (n = 7) and γ-cyclodextrins (n = 8).

Initially, syntheses of cyclodextrin-containing rotaxanes were based on the ability of CD molecules to be threaded onto polymethylene chains. It should be noted that the cavity of one macrocycle accommodates approximately five methylene units. The blocking groups were introduced into pseudorotaxanes by the reaction with the terminal functional groups of the rod molecules. The role of stoppers was played by transition metal complexes. This approach was used in the synthesis of [2]-Rt **31**–**33** based on α- and β-CD.[40] The maximum yield of the rotaxanes (19%) was obtained for the systems comprising α-cyclodextrin and linear molecules whose alkyl chains contained 12 carbon atoms (n = 12). Similarly, [2]-Rt **34** was prepared by the reaction of the α-CD–1,1′-nonamethylenebis(4,4′-bipyridine) complex with cyanoferrate(II) in an aqueous solution.[41] The rotaxane formed was kinetically labile, so it could not be isolated from the solution.

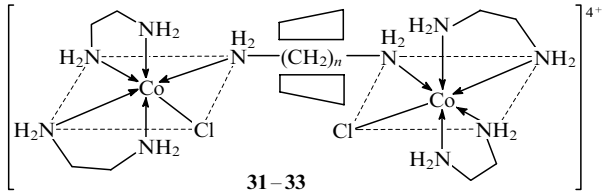

31–**33**

n = 8 (**31**), 10 (**32**), 12 (**33**); = α-CD, β-CD.

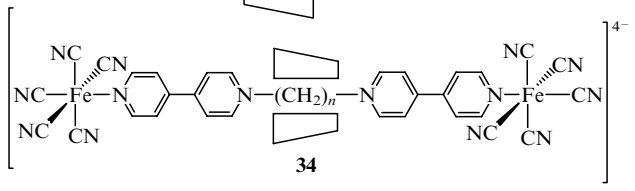

34

Ion-to-ion interactions were used to stabilise cyclodextrin-containing pseudorotaxanes.[42] The role of the thread was played by molecules carrying terminal ammonium groups, heptakis(2,6-di-*O*-methyl)-β-cyclodextrin (DM-β-CD) was used as the cyclic component. Pseudorotaxane **35** was precipitated from the solution by addition of tetraphenylborate; after isolation and purification, its yield was 71%. [3]-Rt **36** which can be regarded as an analogue of heme-containing proteins was synthesised in a similar way.[43]

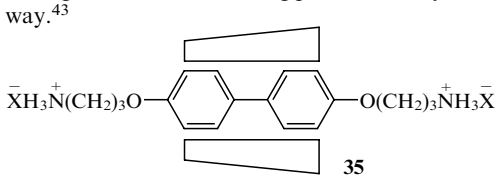

35

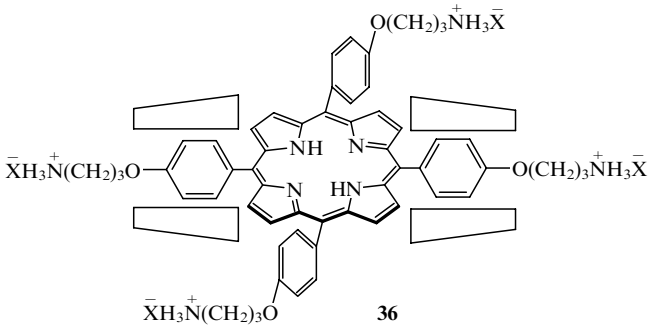

36

X = Ph_4B^-; = DM-β-CD.

Stable rotaxanes can only be obtained in those cases where stoppers are covalently bound to the termini of the 'guest' molecule. The main difficulty is related to the choice of a solvent which must serve as a suitable medium for the chemical reaction of the terminal groups of the pseudorotaxane and simultaneously ensure stabilities of the inclusion complexes. Water, which is the best solvent for the interaction of cyclodextrins with the substrate, is most often inappropriate for the introduction of terminal groups, since these reagents are usually poorly soluble in water or undergo hydrolysis. To overcome this problem, it was suggested [44] to use strong nucleophiles (*e.g.*, NH_2) as the functional groups of the stoppers and aliphatic carboxylic acid derivatives as the rod molecules.

This approach was used in the synthesis of two [2]-Rt, *viz.*, **37a**,**b**, and their orientational isomers **38a**,**b** in 15% yield.[45]

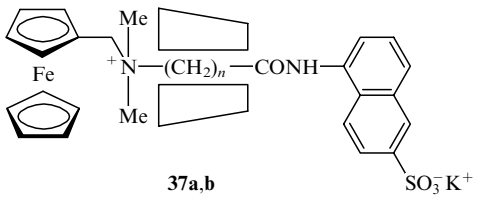

37a,**b**

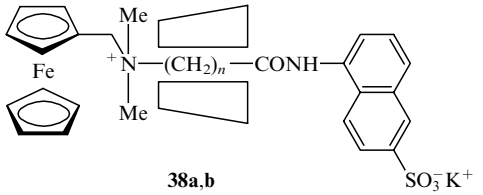

38a,**b**

n = 7 (**a**), 11 (**b**).

It is remarkable that the isomer **37a** remained stable, whereas the complex **38a** dissociated into constituents. This example illustrates the strong dependence of the stability of the rotaxanes on the spatial orientation of the CD molecules threaded onto the 'guest' molecules. A similar strategy of the rotaxane synthesis in aqueous solutions on the basis of rod molecules carrying terminal NH_2 groups and di-*O*-methyl- and tri-*O*-methyl-α-cyclodextrins

was used by Harada and Kamachi.[46] In this study, 1,12-diaminododecane complexes with methylated cyclodextrins reacted with an aqueous solution of trinitrobenzenesulfonic acid, which resulted in the corresponding rotaxanes isolated in 42% and 48% yields.

The formation of inclusion complexes based on cyclodextrins is often used for stabilisation of photosensitive compounds.[34–36] The conversion of such complexes into rotaxanes is a logical sequel of these studies. Thus an azo dye was synthesised from a bisdiazonium salt and a β-naphthol derivative in the presence of various cyclodextrins.[47] Rotaxanes **39a**,**b** were prepared from α- and β-CD in 12% and 15% yields, respectively. The formation of such water-soluble rotaxanes illustrates the possibility of an increase in the stabilities and solubilities of practically important synthetic dyes using this simple approach. It has thus been demonstrated that molecular self-assembly is an efficient tool for the design of new structures.

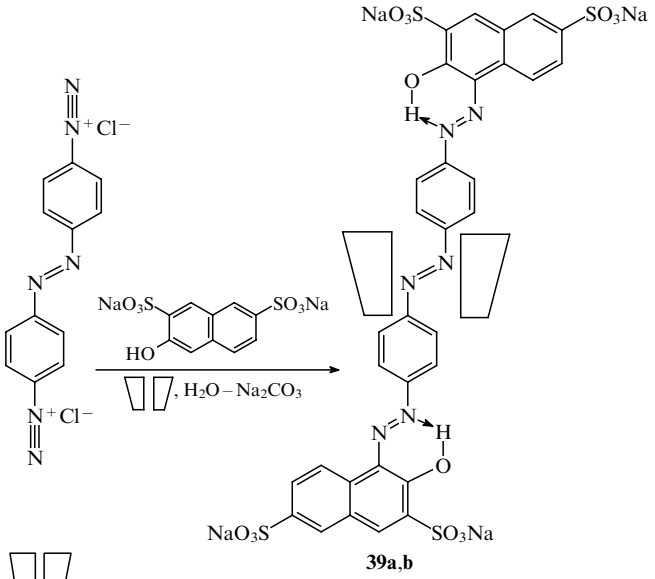

III. Polyrotaxanes

The strategies of rotaxane synthesis can also be applied to the development of procedures for the preparation of structurally more elaborate compounds, *viz*., polyrotaxanes (PRt or [*n*]-Rt) which represent supramolecular assemblies where multiple macrocycles are non-covalently bound with the polymeric chains. Two main types of such complexes are distinguished, *viz*., linear polyrotaxanes where the macrocycles are threaded onto the main chain (Fig. 5 *a*) and comb-like polyrotaxanes (Fig. 5 *b*).

There are several main approaches to the synthesis of polyrotaxanes, namely, the formation of a polymer in the presence of a macrocycle (method 1); the formation of a ring in the presence of a macromolecule (method 2); polymerisation or polycondensation of a stable pseudorotaxane (method 3); self-organisation of a pseudopolyrotaxane (pseudo-PRt) due to specific non-covalent interactions (method 4) and temperature-induced slipping of the macrocycles onto the stoppers, *viz*., terminal groups or those pertaining to the main chain (method 5). It should be noted that cyclisation is usually performed in dilute solutions. However, if polyrotaxanes are synthesised by the method 2, the Le Chatelier principle requires that the polymer was used as a solvent or was taken in excess. This results in a significant increase in the viscosity of the reaction mixture and, correspondingly, in a decrease in the rate of the reaction. For this reason, method 2 is virtually inapplicable to the synthesis of polyrotaxanes. The role of macrocycles is usually played by synthetic or natural cyclic molecules, *e.g*., crown ethers [48–59] or cyclodextrins.[60–117]

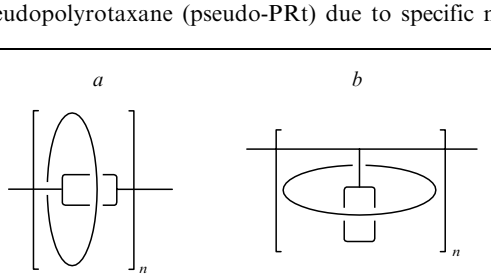

Figure 5. A schematic representation of polyrotaxanes: (*a*) linear, (*b*) comb-like.

1. Linear polyrotaxanes based on crown ethers

The procedures used for the synthesis of polyrotaxanes which incorporate crown ethers have been studied in sufficiently great detail.[48–59] They are based on the statistical threading of macrocycles onto the rod molecule in the course of polymerisation (method 1). The possibility of the use of virtually all (as regards their chemical nature) linear molecules for the rotaxane synthesis allows the design of a great diversity of pseudopolyrotaxanes. 36-Crown-12, 42-crown-14, 48-crown-16 and 60-crown-20 are usually used as crown ethers.

Radical polymerisation was used for the synthesis of pseudopolyrotaxanes **40** based on polyacrylonitrile.[48,49,59] Polystyrene-based polyrotaxanes **41** were synthesised by anionic polymerisation of styrene in the presence of 36-crown-12 and 42-crown-14.[50] Pseudopolyrotaxanes and polyrotaxanes based on various polyesters (compound **42**) and polyurethanes (compounds **43** and **44**) were obtained by polycondensation and polyesterification.[51–58]

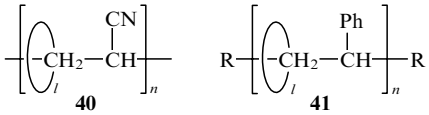

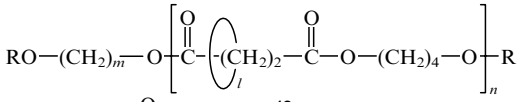

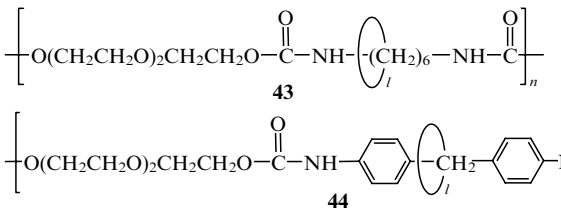

— 30-crown-10, 42-crown-14, 48-crown-16, 60-crown-20.

The isolation and purification of the polymers thus formed were carried out by multiple precipitation of the macrocycles using selective solvents. To ensure invariable composition, it is sufficient to repeat the procedure once or twice even in the case of pseudopolyrotaxanes. This suggests that the folded conformation of the macromolecules prevents the dissociation of the complex into the constituents. The properties of the polymers synthesised were studied by NMR spectroscopy, gel permeation chromatography (GPC), viscosimetry and differential scanning calorimetry (DSC). It was found that the molecular mass of the polyrotaxane formed and the degree of threading of the crown ether increase with an increase in the concentration of the macrocycle and depend on the ratio of the components in the original mixture. The maximum efficiency of threading of crown ethers is achieved where the latter are used as solvents or co-solvents for monomers in the course of polymerisation.

Scheme 8

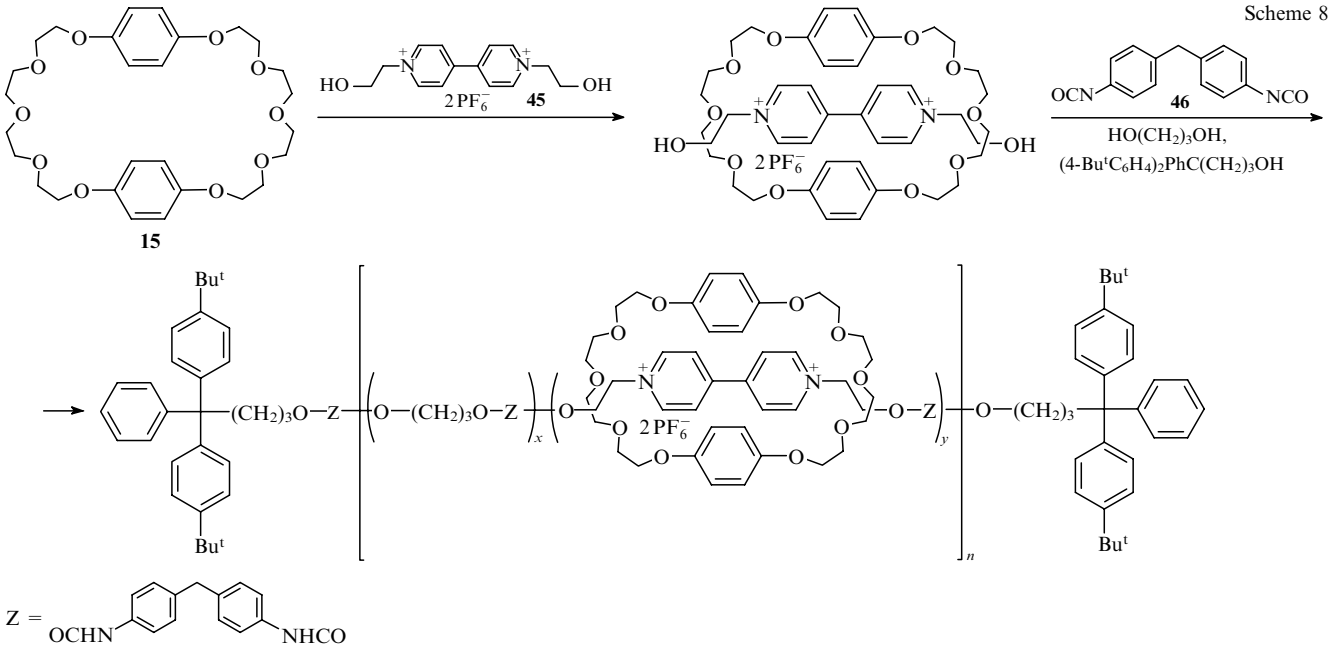

The possibility of a template synthesis of polyrotaxanes was also studied using crown ether **15** as a template. Co-polymerisation of *N*,*N*′-bis(2-hydroxyethyl)-4,4′-bipyridinium bis(hexafluorophosphate) (**45**) with bis(*p*-isocyanatophenyl)methane (**46**) in the presence of the macrocycle **15** (Scheme 8) afforded a polyrotaxane with a high (54%) content of cyclic molecules.[51, 55] To increase the flexibility of the synthetic polymer, small amounts of an ethylene oxide oligomer were added to the reaction mixture. It was found that the molecular mass and the amount of the macrocycle in polyrotaxane depend on the ratio of the starting components as well as by the amount of the stopper added.

The incorporation of macrocycles into polymers causes significant changes in the physicochemical properties (*e.g.*, solubility, thermal and mechanical characteristics) of the rotaxanes formed in comparison with the starting compounds. Some authors [48–59] consider crown-ether-based polyrotaxanes as specific copolymers of the cyclic and linear components. The solubilities of polyurethane- and polyester-based rotaxanes depend on their composition as well as on the nature and size of the macrocycle. For example, the incorporation of 60-crown-20 increases the polarities of polyurethane-based rotaxanes so that these compounds, contrary to the original polymers, become soluble in polar solvents. In some cases, synthetic polyrotaxanes were water-soluble producing micellar structures.[55, 56] Treatment of polyurethane-based rotaxanes with solvents which are selective with respect to the incorporated polymer was accompanied by the aggregation and even crystallisation of the cyclic component which was attributed [55, 56] to the free migration of the crown ethers along the rod molecule.

Studies of the thermal characteristics of polyrotaxanes by DSC revealed that phase-transition temperatures strongly depend on the nature of the interacting components and the composition of the supermolecules formed. For example, the polymer based on poly(butane-1,4-diyl sebaceate) and 60-crown-20 produced two endothermal peaks at 40 and 60 °C, which corresponded to the melting of the cyclic and linear components, respectively. These values are several degrees lower than those for the corresponding individual crown ethers and the polyester, which suggests a decrease in the crystallinity of each of the polyrotaxane components.[53] The glass transition of polyurethane-based rotaxanes is also observed at a lower temperature range in comparison with the glass transition temperatures for the original components.[59]

According to Gibson *et al.*,[48–59] the properties of polyrotaxanes formed by polymerisation of monomers can be changed directionally by varying their compositions. The feasibility of incorporation of crown ethers into polymers as plasticisers was also considered.[56]

2. Linear polyrotaxanes based on cyclodextrins

The procedure for the preparation of cyclodextrin-containing polyrotaxanes by the method 1 included polycondensation of 1,4-bis(ω-hydroxyhexyloxy)benzene (**47**) and 4,4′-methylenediphenylisocyanate (**48**) (Scheme 9) in the presence of permethylated α- and β-cyclodextrins (PM-α-CD and PM-β-CD).[60] This approach was used to synthesise a series of polyurethane-based pseudopolyrotaxanes in high yields (85% – 92%) with the starting components taken at different ratios. It was found that the compositions of the synthetic polymers depend on the PM-CD : monomer ratio. The maximum content of the macrocycles for PM-α-CD and PM-β-CD is one molecule of a cyclodextrin per four and five repeating fragments of the polymer, respectively. A ^{1}H NMR spectroscopic study revealed that in the polymers synthesised PM-α-CD fragments are accommodated on the polymethylene groups, whereas PM-β-CD, which has a larger cavity, is predominantly localised on the aromatic groups of the

Scheme 9

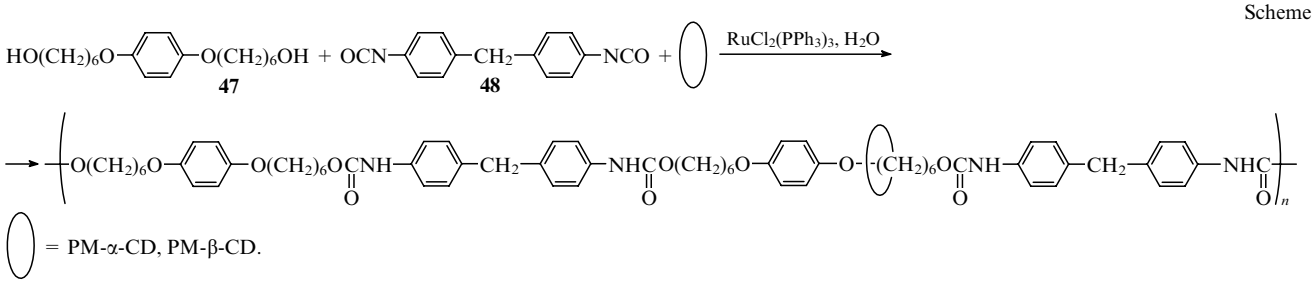

rod macromolecule. As in the case of the polyrotaxanes containing crown ethers, the glass transition temperature of cyclodextrin-based polyurethane pseudopolyrotaxanes was lower than that of the native polymer. This is attributed to partial destruction of polyurethane-specific intramolecular hydrogen bonds as a result of shielding of polar NH-groups of the polymer by the cyclic macromolecule.

A similar strategy was used in the polycondensation of monomers which contained either binding centres or blocking groups in the presence of a macrocycle.[61] It was shown that catalytic oxidative polycondensation of compounds **49** and **50** in the presence of α-CD resulted in the formation of irregular polyrotaxanes which comprised block copolymers incorporating the structural fragments A and B in a 16 : 84 ratio.

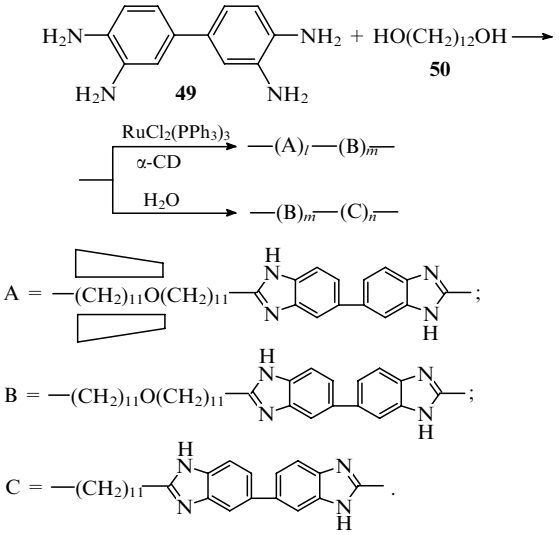

It is of note that the polyrotaxanes synthesised contain no structural fragments of the C type, whereas in the absence of cyclodextrin the polycondensation affords a polymer which contains ~ 20% of such blocks.

An alternative strategy of the polyrotaxane synthesis consisted in preliminary synthesis of inclusion complexes of a series of diamines with β-cyclodextrin and their subsequent polycondensation with isophthaloyl or terephthaloyl chlorides[62] (method 3). The conclusion concerning the formation of the macromolecular cyclodextrin – polymer complex was made on the basis of the results of elemental and differential thermal analyses. Radical polymerisation was used in the synthesis of cyclodextrin-containing homopolymers and copolymers based on inclusion complexes of β-CD with vinylidene chloride, allyl chloride, styrene and methyl methacrylate.[63] In this case, the reaction was accompanied by the chain transfer to cyclodextrin. The attempts to characterise unambiguously the compositions and structures of the resulting complexes failed owing to their poor solubilities and the presence of by-products.[62, 63] For this reason, the synthesis of supramolecular structures incorporating polymers and cyclodextrin from the inclusion complexes of the corresponding monomers did not acquire popularity.

a. Water-insoluble cyclodextrin-containing polyrotaxanes

Two independent groups of investigators[64–85] demonstrated the possibility of applying the molecular self-assembly principle (method 4) to the synthesis of polyrotaxanes. This method consists in the direct interaction of cyclodextrin and polymers in aqueous solutions.

A group of Japanese investigators[64–80] carried out a detailed study of interactions of poly(ethylene oxides) (PEO) with α-cyclodextrin. It was shown that mixing of aqueous solutions of the polymer and CD resulted in the precipitation of a weakly soluble product. It was assumed that in this case 'self-organisation' of the inclusion complex occurred in which cyclodextrin molecules are threaded onto the polymeric chain. This type of complexes have acquired the name of 'molecular necklaces' (MN). As a matter of fact, these structures represent pseudopolyrotaxanes which can be converted into polyrotaxanes by modification of their terminal groups.

Studies of complexation of poly(ethylene oxides) with α-cyclodextrin by the nephelometric method revealed that the lowest molecular mass of a polymer necessary for the formation of insoluble complexes is 300. However, in a more recent publication by these authors it was shown that 'molecular necklaces' can be prepared from tetra(oxyethylene) dibromide (MM = 176).[78] The rate of complexation reaches a maximum at the average molecular mass (M_n) of 1000 and shows a tendency to decrease with a further increase in M_n.[68] This result is attributed to a decrease in the number of terminal groups with an increase in the molecular mass of the polymer, which in its turn is due to the inclusion nature of the complexes. Evidence for the formation of MN can be obtained from the results of elemental and thermogravimetric studies as well as from ^{1}H and ^{13}C NMR spectroscopy and X-ray diffraction data. Thus ^{1}H NMR spectroscopy was used to determine the compositions of the complexes synthesised. Irrespective of the molecular mass of PEO and the molar ratios of the reagents, the complexes formed had strictly stoichiometric compositions where one molecule of α-cyclodextrin corresponded to two ethylene oxide units. Molecular simulation revealed that the diameter of the PEO chain matches perfectly the width of the inner cavity of α-CD, whereas the length of two ethylene oxide fragments is practically equal to the height of the cyclodextrin cone. Additional evidence in favour of MN formation can be derived from the fact that in the case where PEO molecules contained bulky terminal groups (2,4-dinitrophenyl or 3,5-dinitrobenzoyl groups), the sizes of which exceed that of the inner cavity of α-CD, cyclodextrin loses its ability to be threaded onto the polymeric chain and no inclusion complex is formed. It was suggested that the driving force of self-organisation of the complexes are hydrophobic interactions between the cyclodextrin cavity and the polymer fragments as well as the formation of hydrogen bonds between the OH groups of the neighbouring CD molecules.

Further studies showed that similar complexes could be prepared with other cyclodextrin – polymer pairs (Table 1). These data suggest that hydrophobic polymers can be used for complexation along with hydrophilic ones. Although the formation of complexes based on hydrophobic polymers takes much more time and requires preliminary sonication of the reaction mixture, the pseudopolyrotaxanes produced possess strictly stoichiometric compositions and they can be obtained in sufficiently high yields. It should be noted that the dependences of the yields of MN on the molecular mass of the polymer differ substantially for the complexes prepared from hydrophilic or hydrophobic polymers and cyclodextrin. Thus for the α-CD – PEO complex, this dependence is described by a curve which consists of two parts. First, the yield of the polymer increases with an increase in the molecular mass and then is independent of the molecular mass. For hydrophobic polymers, this dependence is bell-shaped;[65, 71, 74] in some cases, *e.g.*, for poly(isobutylene),[73] the product yield decreases monotonically. The observed regularities can be explained as follows. In aqueous solutions, hydrophobic polymers exist in an aggregated state. Since the tendency for aggregation increases with an increase in the molecular mass, the accessibility of the terminal groups of the polymer for the interaction with cyclodextrin is expected to decrease; therefore, only part of the macromolecules can find their 'partners'. Some polymers, *e.g.*, poly(oxytrimethylene), form pseudopolyrotaxanes with both α- and β-cyclodextrins (see Table 1), which was attributed[72] to different conformations of the polymer incorporated.

It was shown with the help of ^{1}H NMR spectroscopy and other analytical methods that the stoichiometric compositions of the complexes are usually independent of the molecular masses of the polymers in the MM range studied and are consistent with the results of molecular simulation studies.[64–68] Violations of this

Table 1. Pseuropolyrotaxanes based on α- and β-cyclodextrins and polymers.

Polymer	MM	Yields of products (%) (number of monomeric units : number of CD molecules)			Ref.
		α-CD	β-CD	γ-CD	
Poly(ethylene oxide)	300	22 (2 : 1)	none	traces	68
	400	83	"	"	
	600	89	"	"	
	1000	91	"	"	
	1500	93	"	"	
	2000	94	"	"	
	5000	21	"	"	
Poly(propylene oxide)	400	none	1 (2 : 1)	76 (2 : 1)	71
	425	"	27	74	
	725	"	84	77	
	1000	"	96	80	
	2000	"	50	31	
	3000	"	32	20	
	4000	"	27	15	
Poly(methyl vinyl ether)	20 000	none	none	67 (3 : 1)	68
Poly(oligoethylene)	702	67 (3 : 1)	"	none	70
Poly(isobutylene)	100	none	67 (3 : 1)	"	73
	500	"	18	64 (3 : 1)	
	800	"	8	90	
	1350	"	4	96	
	2700	"	5	87	
Poly(oxytrimethylene)	700	87 (1.5 – 2.0 : 1.0)	52 (2.0 – 2.5 : 1.0)	–	72
	1200	90 (1.5 – 2.0 : 1.0)	67 (2.0 – 2.5 : 1.0)	–	
	3100	34 (5 : 1)	55 (4 : 1)	–	
Poly(oxytetramethylene)	250	82 (1.5 : 1.0)	–	–	72
	1000	–	–	100 (2.8 : 1.0)	
Poly(ε-caprolactam)	530	82 (1 : 1)	–	–	74

regularity were observed only for the interaction of α- and β-cyclodextrins with poly(oxytrimethylene).[72] When polymers with MM $\leqslant$ 2000 were used, the compositions of MN remained constant and corresponded to one molecule of cyclodextrin per 1.5 – 2 or 2 – 2.5 monomeric units of the polymer for α- and β-CD, respectively. However, with an increase in the molecular mass of the rod macromolecule, the stoichiometry of the complex formed changed (see Table 1). Presumably, the increase in the hydrophobicity with an increase in MM prevents the diffusion of the polymer in the aqueous medium and the involvement of all of the macromolecules in the complex formation.[72] Probably, the precipitation of the complex is accompanied by co-precipitation of the free polymer; therefore, the composition of the pseudopolyrotaxane cannot be calculated exactly.

It was shown [69] that γ-cyclodextrin forms no stable complexes with unmodified PEO, although, like β-cyclodextrin, it forms a 2 : 1 complex with poly(propylene oxide) (PPO) (see Table 1). It was also found that poly(ethylene oxide) which contained bulky terminal substituents, *e.g.*, the 3,5-dinitrobenzoyl substituent, interacted with γ-cyclodextrin to form crystalline complexes in very high yields.[70] A ^{1}H NMR spectroscopic study revealed that the cavity of γ-CD accommodates four oxyethylene fragments, which suggests that γ-cyclodextrin is threaded simultaneously onto two polymeric chains. To corroborate this hypothesis, Harada *et al.*[69] obtained a fluorescently labelled polymer, *viz.*, bis(2-naphthylacetyl)poly(ethylene oxide). The MN prepared on the basis of this compound and γ-cyclodextrin also had a stoichiometric composition 1 : 4. Fluorescence spectroscopic studies revealed the presence of excimers, which suggests close contacts between the naphthyl residues and corroborates the hypothesis that the γ-cyclodextrin molecule incorporates two PEO chains (Fig. 6). Similar crystalline double-stranded inclusion complexes based on γ-cyclodextrin and PEO (MM = 1500) were obtained in high (~ 80%) yields;[86] in this case the complexation did not necessitate blocking of the chain termini by bulky substituents.

Later, a group of Japanese investigators synthesised a polyrotaxane **51** based on the molecular necklaces by the reaction of terminal amino groups of bisaminopoly(ethylene oxide) incorporated into α-cyclodextrin with fluoro-2,4-dinitrobenzene.[66] The yield of the reaction product after isolation and purification by GPC was 60%. Subsequent modifications of the polyrotaxane **51** allowed the authors to synthesise oligomers containing cross-linked cyclodextrins, the so-called 'polymeric tubes' (Fig. 7).[80] These compounds were synthesised by treatment of the polymer **51** in 10% NaOH with epichlorohydrin. Using GPC, it was shown that epichlorohydrin cross-linked CD molecules along the polymeric chain with the formation of hydroxypropylene bridges. The blocking groups were removed by hydrolytic cleavage with 25% NaOH which resulted in the release of the polymer enclosed inside the tube. The final product (yield 92%) represented a hollow tube which consisted of about 15 cross-linked cyclodextrin molecules (MM = 20 000) (**52**, see Fig. 7). Probably, such structures can be used for selective separation of substances.

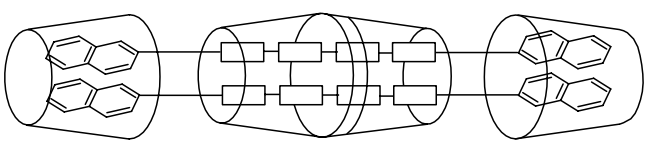

Figure 6. A schematic representation of an inclusion complex of γ-cyclodextrin with bis(2-naphthylacetyl)poly(ethylene oxide).[69]

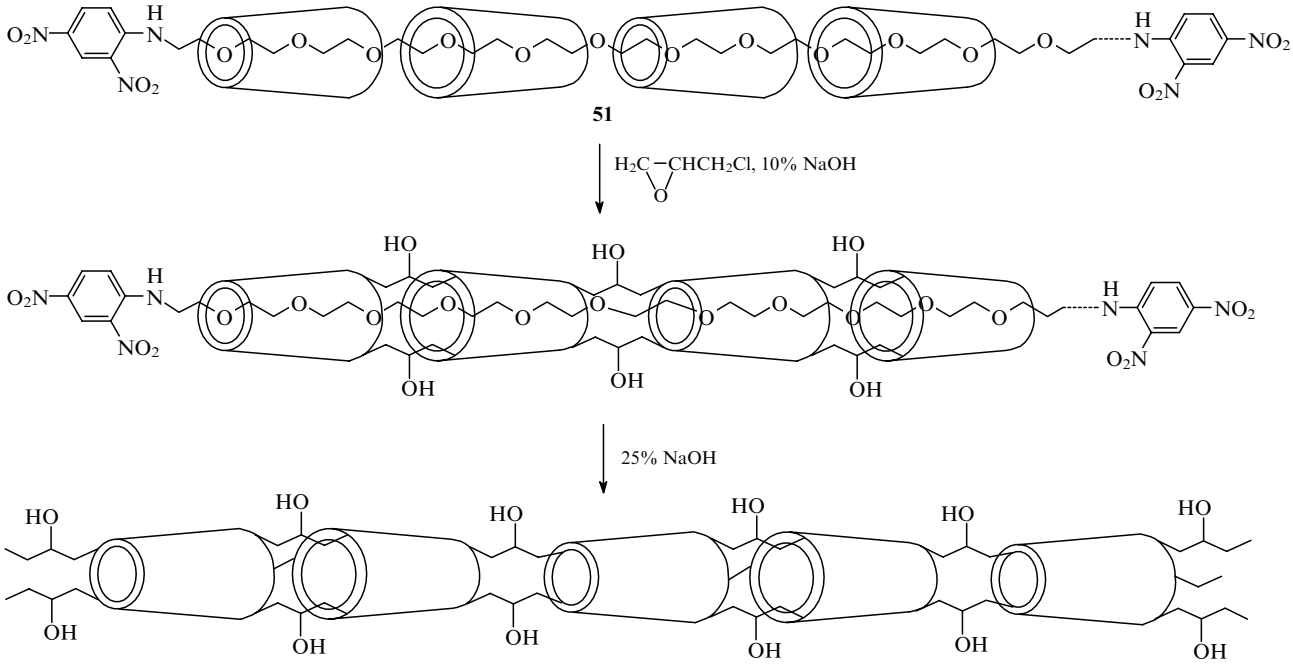

Figure 7. A scheme of synthesis of polymeric tubes from polyrotaxanes based on bisaminopoly(ethylene oxide) and α-cyclodextrin.[85]

It was shown[87] that the reaction of cyclodextrin with the conjugated conducting polymer **53** (polyaniline), which contains emeraldine bases,

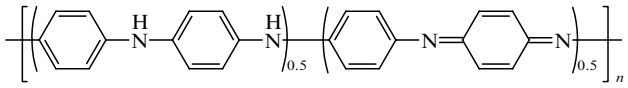

53

afforded a pseudopolyrotaxane in which the polymer was incorporated inside the cavity of the non-conducting cyclic molecules. These structures have been termed as 'insulating molecular wires'. This system was used to demonstrate that cyclodextrins prevent chemical oxidation of the rod macromolecule, *e.g.*, on doping of polyaniline with iodine.

The use of modified CD (particularly, of methylated macrocycles) as 'hosts' allows one to compare processes of molecular recognition involving native CD and their derivatives. Using ^{1}H NMR spectroscopy, it was shown than none of the methylated cyclodextrins form complexes with PEO as can be evidenced from the fact that no precipitation occurred even after 2-months' storage of their mixture. A different situation is observed in the interaction of these cyclodextrins with hydrophobic polymers. Complexes of PPO and poly(tetrahydrofuran) (PTHF) with heptakis- and hexakis-(2,6-di-*O*-methyl)cyclodextrins (DM-CD) as well as with heptakis- and hexakis-(2,3,6-tri-*O*-methyl)cyclodextrins (TM-CD) have been described in the literature.[79] It was shown that the addition of DM-β-CD first increases significantly the solubility of PPO in water and then a crystalline complex is formed. However, TM-α-CD, TM-β-CD and DM-α-CD neither favour the solubilisation of PPO in water nor form inclusion complexes. The solubility of PTHF in water increases in the presence of low concentrations of DM-β-CD and DM-α-CD. At high concentrations of these cyclodextrins, the solubility of PTHF decreases and inclusion complexes are precipitated. TM-β-CD also forms inclusion complexes with PTHF. The yields of PTHF – DM-β-CD complexes increase with an increase in the weight-average molecular mass (M_w), it is a maximum at $M_w = 1000$. The stoichiometric composition of PTHF – DM-β-CD complexes corresponds to one molecule of the macrocycle per 1.0 – 1.5 monomeric units of the rod macromolecule. Taking into account the number of atoms in the repeating fragment of the polymer per one CD molecule, it appears that the composition of the PTHF – DM-β-CD complex is consistent with the stoichiometric composition of the corresponding MN based on α-CD. The experimental data altogether suggest that hydrophobic interactions between methylated cyclodextrins and hydrophobic polymers make a weighty contribution to the process of molecular recognition.

Based on the geometrical correspondence of the CD molecules to polymeric 'guests', one can postulate the existence of ternary complexes which represent MN with low-molecular-weight 'guests' incorporated into them. Such complexes were obtained in PEO-β-CD – aromatic compound systems.[88] Benzene, its mono-, di- and tri-substituted derivatives were used as aromatic compounds. After mixing of these three components, a complex precipitated from the aqueous solution. Radiolabelled ^{3}H-PEO was used for quantitative determination of poly(ethylene oxide) content in the complexes. The content of β-CD was determined polarimetrically, while that of the aromatic compound was established by UV spectroscopy. The composition of the complexes corresponds to one β-CD molecule per two units of PEO and one molecule of the aromatic compound. The ternary complexes precipitate with benzene, benzoic acid and *p*-nitrophenol but do not precipitate in the presence of *o*-nitrophenol and 2,4-dinitrophenol. X-Ray diffraction studies have shown that the structures of the ternary complexes are identical with that of MN. Simulation of the ternary complexes demonstrated that the regular orientation of CD in MN is not disturbed upon incorporation of benzene and its monosubstituted derivatives into their cavities.

The molecular dynamics of MN based on α-CD – PEO[89] and β-CD – PPO[90] complexes has been studied. It was shown that the main driving force of molecular recognition are the van der Waals interactions. Hydrogen bonds provide arrangement of the CD rings in a 'head-to-head' and 'tail-to-tail' fashion. Cyclodextrins in polyrotaxanes exist in a more symmetrical and a less rigid conformation than in the individual state. The formation of polyrotaxanes is accompanied by the transition of the polymers to the stretched conformation due to an increase in the proportion

of *trans*-conformers in comparison with the state of the isolated polymeric chains. The structure- and energy-related reasons for the non-statistical distribution of CD in MN prepared on the basis of PEO – PPO block copolymers were established using the dynamic Monte Carlo method.[91] It was found that the stability of the complexes is determined by both hydrophobic interactions between the 'host' cavity and the 'guest' molecule and the hydrogen bonds between the cyclodextrin molecules.

It should be noted that the interest in MN is generated largely by fundamental problems. According to Tonelli *et al.*,[92–94] the polymeric inclusion complexes are convenient subjects for studying the behaviour of ordered and isolated polymeric chains, which simulates the state of oriented polymers in the crystalline phase.

It was also shown that macromolecular inclusion complexes can be used for the preparation of high-strength oriented fibres. Removal of cyclic molecules from the complexes was carried out by treatment of the polymers with a solvent which is selective with respect to cyclic compounds.[92] The selectivity of formation of crystalline polymeric inclusion complexes incorporating cyclodextrins served as a basis for the development of a new procedure for purification of polymeric materials under laboratory conditions, the so-called extractive crystallisation.[94]

b. Pseudopolyrotaxanes based on block copolymers

Considerable progress in the synthesis of supramolecular structures based on CD and polymers is associated with the use of block copolymers (BC) of ethylene oxide and propylene oxide (pluronics) as the 'guest' molecules. Pluronics differ in their compositions, number of blocks and mutual arrangements, which permits the synthesis of MN having different structures and properties. By varying the length of the free component of the complex based on a BC and cyclodextrin, one can obtain both water-insoluble [95–99] and water-soluble [100] polymeric inclusion complexes. For steric reasons, α-CD cannot interact with a poly(ethylene oxide) component of BC of the PPO – PEO – PPO type.

A systematic study of the reactions of α-, β- and γ-CD with different types of PEO – PPO block copolymers [95–99] has been carried out. Their characteristics are listed in Table 2. The interaction of α- and β-CD with BC I and BC II built up of poly(ethylene oxide) and poly(propylene oxide) blocks of virtually equal lengths has been studied.[95] It was found that the addition of solutions of block copolymers to aqueous solutions of the corresponding macrocycles results in the precipitation of water-insoluble complexes. Using the α-CD – BC I system as an example, it was shown that with an increase in the pluronic concentration the mass of the isolated complex increases at first and after reaching a certain maximum remains unchanged, which suggests the formation of a stoichiometric complex. Polarimetric and IR spectroscopic studies of these complexes as well as molecular simulation studies revealed that different pluronic blocks become involved in this process depending on the type of the cyclodextrin (α- or β-CD, which differ in the diameter of their inner cavity) used for the complexation. Thus, the interaction with α-CD involves

Table 2. Some characteristics of the block copolymers based on poly(ethylene oxide) (PEO) and poly(propylene oxide) (PPO) used in the synthesis of pseudopolyrotaxanes.[95–99]

Block copolymer	Type of copolymer	MM	Content of PPO (%)	Degree of polymerisation	
				PEO	PPO
I	PEO – PPO	3000	50	30	28
II	PEO – PPO	2000	60	18	20
III	PEO – PPO – PEO	2700	45	18 [a]	19
IV	PEO – PPO – PEO	6000	23	52 [a]	24
V	PPO – PEO – PPO	3000	40	40	10 [a]

[a] The degree of polymerisation of one block.

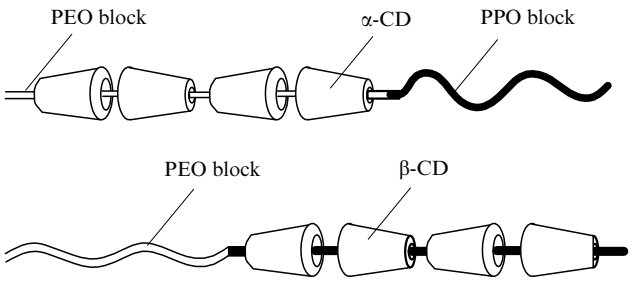

Figure 8. A schematic representation of α- and β-cyclodextrin complexes with ethylene oxide and propylene oxide diblock copolymers.[95]

only the PEO block, while the interaction with β-CD, only the PPO block. The stoichiometric compositions of the complexes are similar to those of MN based on homopolymers, *viz*., two monomeric units of ethylene oxide or propylene oxide per one α- or β-CD molecule, respectively. Thus the interactions of α- and β-CD with the PEO – PPO diblock copolymers result in the formation of new BC (Fig. 8) which consist of a rigid block, *viz*., a MN, and a free flexible poly(alkylene oxide).

A study of the interactions of cyclodextrins with PEO – PPO triblock copolymers III – V (see Table 2) revealed that the compositions of the crystalline complexes depend on the position of the interacting block and the reaction conditions.[96–98] If CD is threaded onto the inner block of the copolymer, the complex formed (**54**, Fig. 9) has a stoichiometric composition which is characteristic of cyclodextrin complexes with homopolymers and diblock copolymers. In those cases where CD is threaded onto the peripheral blocks, two types of block structures can be formed depending on the reaction conditions, *viz*., BC with a symmetrical position of MN (Fig. 9, complexes **55** and **56**) and non-symmetrical BC which are composed of three different blocks, one of them being MN (Fig. 9, complexes **57** and **58**). This depends on the concentration of the reagents in the solution. Thus in saturated solutions where the rate of complexation is comparable with the rate of crystallisation, it is the non-symmetrical complexes with one filled block that are formed. In dilute cyclodextrin solutions, *i.e*., under conditions where the rate of crystallisation is much lower than the rate of threading of CD onto the polymeric chains, both peripheral blocks of the complexes represent MN.

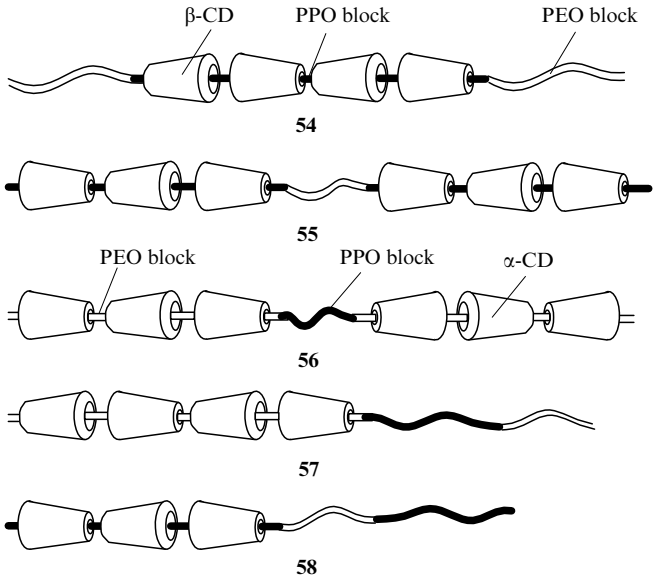

Figure 9. A schematic representation of α- and β-cyclodextrin complexes with ethylene oxide and propylene oxide triblock copolymers.

As has been noted above, two types of inclusion complexes of γ-cyclodextrin with poly(alkylene oxides) are possible. These comprise either one PPO chain or two PEO chains. The use of PEO–PPO block copolymers as 'guests' makes it possible to elucidate to which of these blocks γ-CD manifests higher affinity. To answer this question, the complexation of γ-CD with PEO–PPO diblock copolymers was studied where PEO and PPO blocks are sterically equally accessible for the interaction with cyclodextrin.[96–98] An analysis of the compositions of the complexes formed shed some light on the localisation of γ-cyclodextrins, since the number of γ-CD molecules that are threaded onto PEO and PPO blocks differs significantly for the given BC (I or II). It was shown experimentally that the number of γ-CD molecules per one copolymer molecule (r_{exp}) represents an intermediate value between the r_{theor} values calculated in the assumption that either PEO or PPO blocks take part in the complexation. This finding suggests that the interaction of γ-CD with PEO and PPO is nonselective.

The use of the γ-cyclodextrin–triblock copolymer couple opens up an opportunity for preparing new non-linear BC. Complexation of γ-CD with pluronics of the PEO–PPO–PEO type which contain peripheral ethylene-oxide blocks affords double-stranded inclusion complexes. It was found[97] that in saturated solutions the composition of the complex formed remains unchanged at any value of the γ-CD : BC IV ratio. This suggests that the interaction of γ-CD with the above block copolymer results in a stoichiometric complex, namely, a double-stranded inclusion complex in which two strands of PEO which belong to different copolymer molecules appear to be incorporated into the channel formed by the macrocycles. Taking account of different accessibility of the PEO blocks with respect to α-CD, it was demonstrated that the interaction of γ-CD with a triblock copolymer of the PEO–PPO–PEO type yields compound **59** (Fig. 10) which is characterised by nonsymmetrical distribution of the free PEO blocks. In dilute solutions, the complexation of γ-CD with the PEO–PPO–PEO copolymer results in pseudopolyrotaxane **60** in which both PEO blocks are coated with the CD molecules (see Fig. 10). Thus, the vast potentials in the design of pluronics and the ability of cyclodextrins to interact selectively with PEO and PPO blocks enable one to use them as a basis for the synthesis of inclusion complexes of different compositions and molecular architecture.

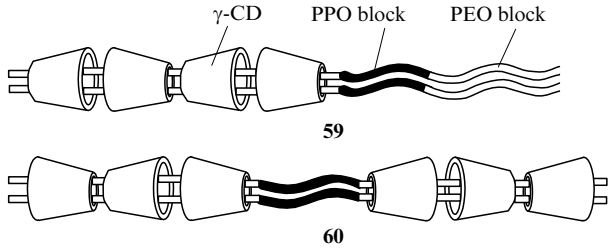

Figure 10. A schematic representation of γ-cyclodextrin complexes with the triblock copolymer IV.

c. The complexes of nonionic surfactants with cyclodextrins

Poly(ethylene oxide)-containing surfactants can be regarded as particular BC which comprise hydrophilic poly(ethylene oxide) blocks, whereas the hydrocarbon fragments play the role of their hydrophobic 'tails'. PEO surfactants of different chemical nature, *viz*., octylphenyl PEO ethers [Triton X-45 (**61a**) and Triton X-100 (**61b**)], polyethylene glycol-1000 monostearate (**62**) and dodecyl poly(ethylene oxide) ether (**63**) were used as 'guests'.[97, 99, 101, 102]

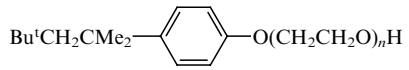

61a,**b**

n = 5 (**a**), 10 (**b**)

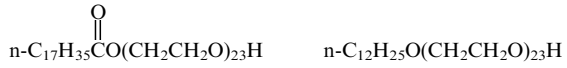

62

63

Mixing of saturated aqueous solutions of poly(alkylene oxides) and α-CD resulted in the formation of a crystalline precipitate the structure of which is similar to that of MN based on PEO. The determination of the compositions of the complexes showed that one CD molecule corresponds to two monomeric units; thus, the α-CD molecules are selectively threaded onto the PEO fragments of surfactants. Important information about the type of interaction of PEO surfactants with cyclodextrins in dilute solutions can be derived from an analysis of colloidal and chemical properties of the surfactants, primarily, from the effect of CD on the critical micelle concentration (CMC). The dependences of CMC on the CD : surfactant molar ratio represent curves with saturation, which allows one to determine the stoichiometric compositions of inclusion complexes in solution. It is worth noting that the compositions of such complexes are identical both in solution and in the solid phase. The complexes formed by the interaction of the same surfactant with α-, β- and γ-CD differ drastically both in the structures and their colloidal and chemical properties.[101, 102] The chemical nature of the group linking together the hydrophilic and hydrophobic fragments of surfactants was found to affect critically the localisation and possible migration of CD molecules along the surfactant chains.

The covalent binding of poly(ethylene oxide) fragments to cyclodextrin molecules results in the formation of PEO–CD conjugates which represent bouquet-like structures endowed with amphiphilic properties (Fig. 11).[103–105] The conjugates have molecular masses of 3000–5500 and are characterised by narrow molecular mass distributions; the average degree of substitution is 8 to 12 ethylene oxide units per one glucose residue. A study of the complexation of the conjugates with Triton X-100 (**61b**) revealed that the pseudopolyrotaxanes formed have a stoichiometric composition, *i.e*., one molecule of the conjugate is threaded onto each hydrophilic fragment of the surfactant. These pseudopolyrotaxanes can form micellar structures in aqueous solutions. The architecture of the spherical molecular assemblies consisting of highly branched structural elements resembles that of dendrimers (Fig. 12).

Branched structures of yet another type were obtained[99, 106] as a result of interactions of star-shaped conjugates of PEO and PEO–PPO diblock copolymers with proteins, *e.g*., α-chymotrypsin (ChT). Such conjugates are formed as a result of one-point covalent attachment of the monofunctional derivatives of the polymers to the amino groups of the protein. Mixing of these compounds with cyclodextrin (PEO–ChT–CD and

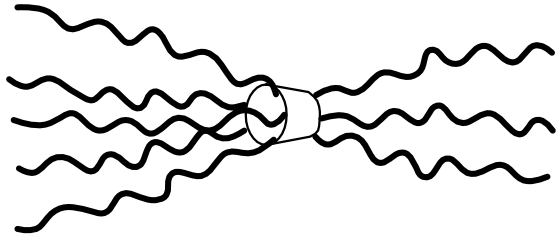

Figure 11. The structure of the poly(ethylene oxide)–cyclodextrin conjugate.[104]

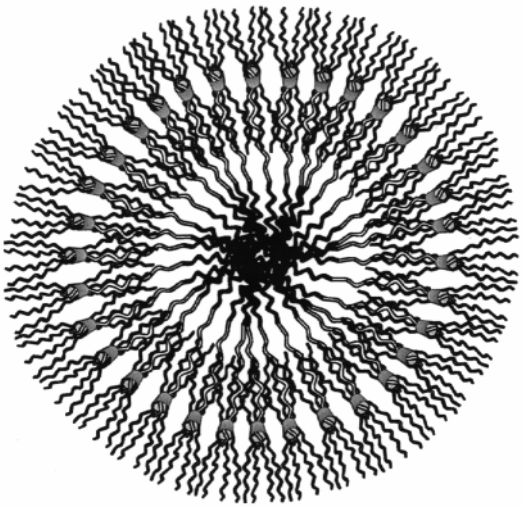

Figure 12. The hypothetical dendrimer-like structure based on the poly(ethylene oxide)–cyclodextrin conjugate and a micelle of Triton X-45.[105]

BC–ChT–CD conjugates) results in the formation of precipitates. The determination of their compositions revealed that they are similar to those of the complexes based on linear polymers and the corresponding CD. This implies that all the polymeric chains within the conjugates are accessible for the interaction with the CD. The crystalline structures of the resulting complexes are identical to those of MN. A decrease in the solubility of the complexes in water in comparison with the original polymer–protein conjugates or non-covalent polymer–protein adducts limits their application in biotechnology. The PEO–CD conjugates were used to confer solubility onto the complexes prepared on the basis of polymer–protein adducts and CD.[107, 108] The complexation between PEO chains, which are the components of covalent and non-covalent PEO–ChT and PEO–CD adducts, was studied using a kinetic method based on the analysis of enzymic properties of novel supramolecular structures incorporating these components.[107] For this purpose, the rate constants of thermoinactivation of ChT (k) in the adducts of PEO–ChT with PEO–β-CD were determined. A decrease in k suggests that complexation of the constituents occurs. The stoichiometric compositions of the complexes formed were determined from the dependence of k on the PEO–β-CD : $PEO_{(ad)}$ molar ratio, where $PEO_{(ad)}$ is the poly(ethylene oxide) that is involved in the adducts. It was shown that each of the polymeric chains of the PEO–ChT conjugates forms an inclusion complex with PEO–β-CD, whereas in the case of non-covalent PEO–ChT complexes only a half of the polymeric chains of $PEO_{(ad)}$ take part in the formation of the supramolecular structures. The hypothetical structures of supramolecular dendritic assemblies are depicted in Fig. 13.

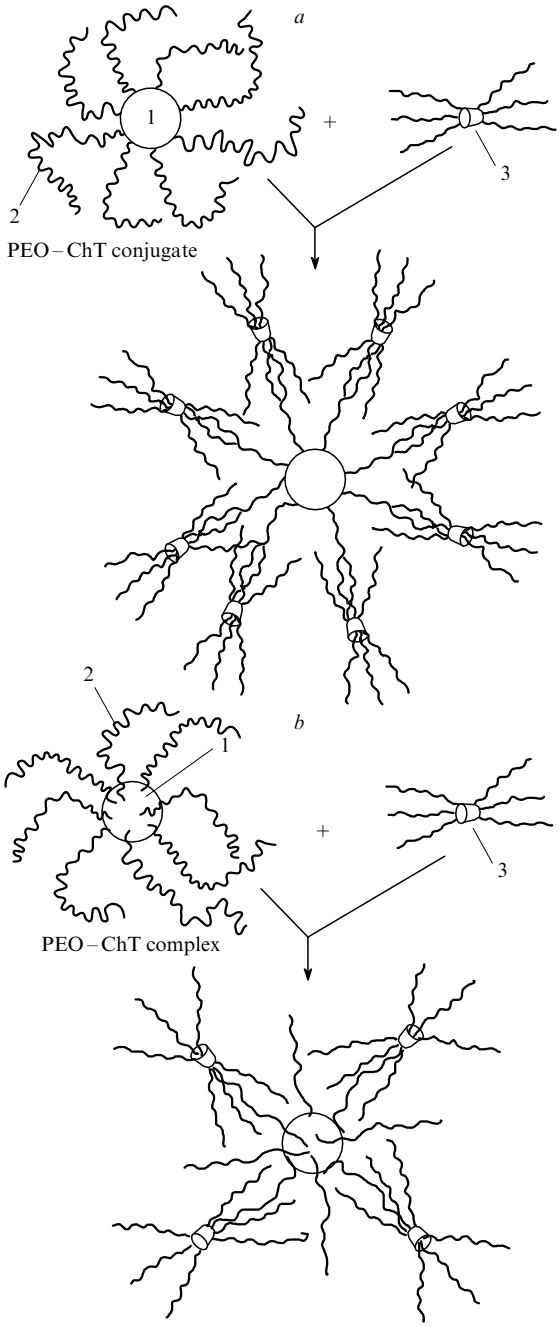

Figure 13. The hypothetical dendrimer-like structures of the complexes formed by the covalent (*a*) and non-covalent (*b*) adducts of PEO–ChT and the β-CD–PEO conjugate;
(*1*) α-chymotrypsin, (*2*) poly(ethylene oxide), (*3*) covalent adduct based on PEO and β-cyclodextrin (β-CD–PEO).[107]

d. Studies of the structural organisation of crystalline pseudopolyrotaxanes based on cyclodextrins

Supramolecular assemblies can be characterised both by the type of the intermolecular interactions which hold together their constituents and by their spatial configuration, *viz*., their architecture or 'suprastructure'. The phase state and the organisation of macromolecular inclusion complexes are studied using TGA, DSC, X-ray diffraction analysis as well as by optical, scanning electron and scanning tunnelling microscopy.

An X-ray diffraction analysis showed that the precipitates formed by poly(alkylene oxide)–cyclodextrin complexes have crystalline structures and differ from one another and from the original components in the type of the crystal lattice. It should be noted that the method which is commonly employed for the description of the structural organisation of 'molecular necklaces' is based on comparison of the diffractograms of MN and the complexes of the corresponding CD with various low-molecular-weight compounds. According to Saenger's classification,[34] the structures of the CD-based complexes can be divided into two main types, *viz*., cage-type structures in which cyclic molecules form brick network patterns and channel-type structures where the macrocycles are stacked sequentially in a pillar-like fashion. A comparative analysis of the diffractograms revealed [68, 71, 72] that MN belong to channel-like structures. However, this approach discloses only the qualitative differences but cannot provide quantitative evaluation of the parameters of the crystal lattices of macromolecular inclusion complexes.

Harada *et al*.[76, 77] have succeeded in growing single crystals of α-CD complexes with tetra- and hexa(ethylene oxide) and β-CD with poly(propylene oxide) (MM = 425), which mimic MN, and

the β-CD – poly(oxytrimethylene) complex (MM = 1400) and carried out their detailed X-ray diffraction analysis. It was found that in all these cases the macrocycles are arranged in a 'head-to-head' and 'tail-to-tail' fashion to form hydrogen bonds between all the secondary hydroxy groups of the large bases of the cyclodextrin torus. Water molecules are localised within the structure of α-CD-based [4]-Rt between the minor bases of the macrocycles. The β-CD dimers are shifted relative to one another due to the presence of only one hydrogen bond between the primary OH groups. Rod-like macromolecules are localised inside the narrow channels formed by cyclodextrins and exist in a *trans*-conformation.

The use of single crystals for the disclosure of the structural organisation of rotaxanes allows one to estimate, with a high degree of accuracy, the unit cell parameters, to determine the coordinates of all the atoms within the composition of the complex and to characterise the intermolecular contacts. However, this method has not received wide acceptance in structural studies of high-molecular-weight compounds because of the difficulty and sometimes impossibility of obtaining suitable large-sized single crystals. An approach to the description of the structural organisation of polymeric crystals consists in the use of oriented samples and in the recording and interpretation of X-ray fibre patterns. It was shown [86, 109] that in contrast to ordinary polymers whose orientation demands preliminary treatment, the formation of MN is accompanied by spontaneous formation of oriented structures. An X-ray diffraction analysis which includes a comparison of X-ray fibre patterns and diffractograms enables one to index the observed reflections, to determine the parameters of crystal lattices of the complexes formed and thus to characterise the structure of polymeric inclusion complexes at the molecular level. The results obtained suggest that crystallisation of MN results in the formation of structures in which cyclodextrin molecules are arranged one after another along a common symmetry axis. X-Ray diffraction data suggest the hexagonal, monoclinic and tetragonal packing of MN based on α-, β- and γ-cyclodextrins, respectively.

In order to obtain the information about the morphology of the crystallites formed by MN and the nature of their mutual packing in the course of precipitation, cyclodextrin complexes with poly(alkylene oxides) were studied by optical microscopy and scanning electron microscopy.[86, 109] The crystals of the β-CD – PPO complexes have the shape of sharply edged parallelograms, whereas those of the γ-CD – PEO complexes have the shape of rectangular parallelipipeds with an average facet size of the order of several microns, which is consistent with the results of an X-ray diffraction analysis of the symmetry of the crystal lattices of the complexes. The precipitates of cyclodextrin – poly(alkylene oxide) complexes represent lamellar structures the MN in which are located at right angles to the planes of the lamellae.

Isolated MN were visualised by scanning tunnelling microscopy. Japanese investigators [75, 87] have succeeded in photographing α-CD – PEO and β-CD – polyaniline complexes containing discernible rod-like structures. Their lengths correspond to the lengths of the extended molecule of the polymeric 'guest', while their widths match the diameter of the macrocycle.

These results are of fundamental importance for the understanding of the mechanism of the self-assembly of the supramolecular structures formed by polymeric inclusion complexes at different levels of their structural organisation. Three main stages in the formation of the nanostructures in such complexes can be distinguished. The first step consists in the threading of the macrocycles onto the polymeric chains. The driving forces of this process are the cooperation of the hydrophobic interactions between the nonpolar cavity of the cyclic molecule and the fragments of the polymeric 'guest' and the formation of hydrogen bonds between the hydroxy groups of the cyclodextrins. The second step is the crystallisation of MN and the formation of lamellar crystallites the inclusion complexes in which are located at right angles to the planes of the lamellae. In the third step, individual crystallites of the complex are aggregated to form an oriented precipitate. In the precipitation, the lamellae are aligned in parallel to the plane of the support to form an axial pattern of the precipitated material. Thus, polymeric cyclodextrin – poly(alkylene oxide) inclusion complexes can serve as a basis for the design of well-organised supramolecular assemblies.

e. Water-soluble polyrotaxanes

Cyclodextrin-containing water-soluble pseudopolyrotaxanes were first synthesised by the interaction of CD with polyelectrolytes.[81 – 85] Self-assembly method was used to obtain inclusion complexes of the so-called poly(iminooligomethylenes) (**64a – c**),[81] *viz*., the polymers containing oligomethylene and quaternary ammonium fragments (**65**,[82] **66**,[83] **67a**,**b**[84, 85]), with α-cyclodextrin. In this case, the threading of CD molecules occurs by virtue of cooperation of hydrophobic and van der Waals interactions between the cyclodextrin cavity and the aliphatic sites of the polymers.

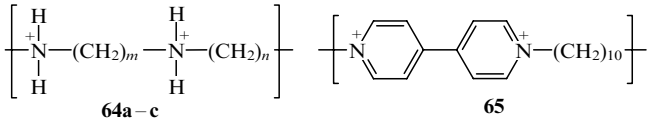

64a – c **65**

$m = n = 6$ (**a**); 11 (**b**); $m = 10$, $n = 3$ (**c**).

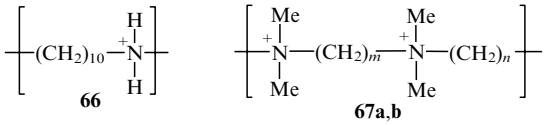

66 **67a**,**b**

$m = n = 10$ (**a**); $m = 6$, $n = 10$ (**b**).

Using ^{1}H NMR spectroscopy, it was shown that α-CD molecules are localised on oligomethylene fragments containing no less than 10 units. Therefore, the short-chain polymer **64a** does not form any complex with α-CD. In contrast with poorly soluble MN, soluble complexes are formed at a very low rate at room temperature, this takes from several hours to several months and even years (in the case of compound **66**). Such a kinetics is attributed to the low rate of migration of CD molecules along the polymeric chain which in turn is due to steric hindrances created by bulky hydrate shells around the charged amino groups. At higher temperatures, slipping of the macrocycles over these 'barriers' occurs (method 5, Section III) resulting in a significant increase in the threading rate.[85]

Polyrotaxanes **68a**,**b** which are also readily soluble in water were prepared on the basis of MN consisting of polymers **64b**,**c** and α-CD, respectively.[81]

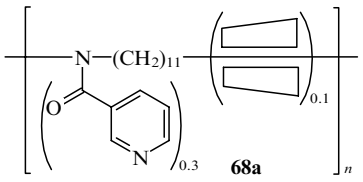

68a

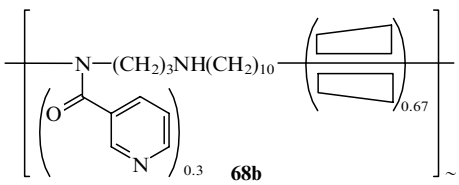

68b

The binding of α-CD molecules to definite sites of the polymeric chain was achieved by acylation of the imino groups by nicotinyl chloride. Using polymers **64c** and **66** as examples, it was demonstrated that β-CD which has a larger cavity does not form any stable inclusion complexes. However, the use of an α- and β-CD mixture made it possible to prepare polyrotaxanes containing 60% β-CD and 7.5% α-CD in which β-CD was

blocked at the ends by α-CD molecules which slip off the chain at a very low rate.[83]

The possibility of formation of a water-soluble pseudopolyrotaxane was also demonstrated for the β-CD – triblock copolymer PEO – PPO – PEO.[100] It was found that the interaction of β-CD with block copolymers of the $PEO_n - PPO_m - PEO_n$ type gives either a crystalline precipitate ($n \ll m$) or a water-soluble complex ($n \gg m$) depending on the composition of the polymer used. The addition of cyclodextrin induces an upfield shift of the methyl and methylene proton signals in the ^1H NMR spectra. This suggests the complexation with block copolymers incorporated into the cavity of CD.

Amphiphilic DM-β-CD as a macrocycle and an analogous PEO – PPO – PEO copolymer with blocks of approximately equal sizes ($n \approx m$) were used to study the interactions of cyclodextrin with polymers in a monolayer. This study showed [100, 110] that the polymer passes from the coil to the rod-like conformation during complexation. Hence, one of the approaches to the synthesis of water-soluble MN consists in the introduction, into the starting polymer, of hydrophilic fragments which are not involved in the complexation.

Yet another approach to confer water solubility onto polymeric complexes is based on chemical modification of CD molecules in polyrotaxanes. The synthesis of water-soluble biodegradable polyrotaxanes was carried out by Ooya *et al.*[111–114] These authors used bis[aminopoly(ethylene oxide)] as the polymer and α-cyclodextrin as the cyclic compound. The terminal groups were blocked by an excess of L-phenylalanine (L-Phe) derivatives. The polyrotaxane formed was treated with propylene oxide which alkylated the OH groups of CD. The enhanced solubility of MN in water seems to be due to the destruction of hydrogen bonds. A three-step synthesis including removal of protective groups from the fragment of the stopper is depicted in Scheme 10. The results of light scattering studies [112, 113] suggest that the polyrotaxanes based on hydroxypropylated α-CD and PEO (MM = 2000 for **69a** and 4000 for **69b**) aggregate in aqueous solutions; the degree of aggregation of polyrotaxanes is much lower than that of the original PEO containing the same terminal fragments and is equal to 16 – 23 and 2 for the complexes **69a**,**b**, respectively. It was noted also that these polyrotaxanes preserve their rod-like conformation in solutions. It was found [112, 113] that enzymic hydrolysis of peptide bonds with papain which resulted in the cleavage of the stoppers brought about simultaneous supramolecular destruction of polyrotaxanes **69a**,**b**. This leads to complete dissociation of these polyrotaxanes into constituents irrespective of the degree of their aggregation (Fig. 14).

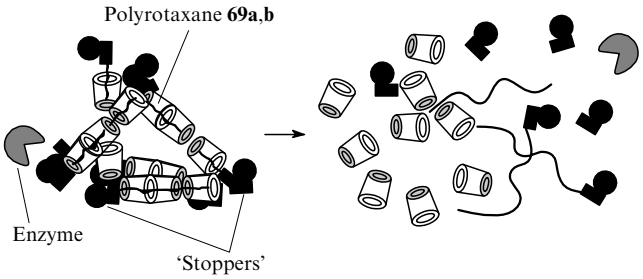

Figure 14. The destruction of the polyrotaxanes **69a**,**b** caused by enzymic hydrolysis of terminal L-Phe groups.[113]

It was shown [116, 117] that polyrotaxanes of the type **69a**,**b** can be used in pharmacology and medicine as drug carriers and drug permeation enhancers. The interaction of these polyrotaxanes with blood cells was studied in detail; it was found that hydroxypropylated polyrotaxanes increase the fluidity of membranes and control the level of calcium by inhibiting platelet-induced elevation of Ca^{2+}.

The same group of investigators proposed to use this principle in the design of drug conjugates on the basis of polyrotaxanes and were the first to attempt to prepare such conjugates with insulin [112] and theophylline [115] which are covalently linked to CD molecules (Fig. 15).

Scheme 10

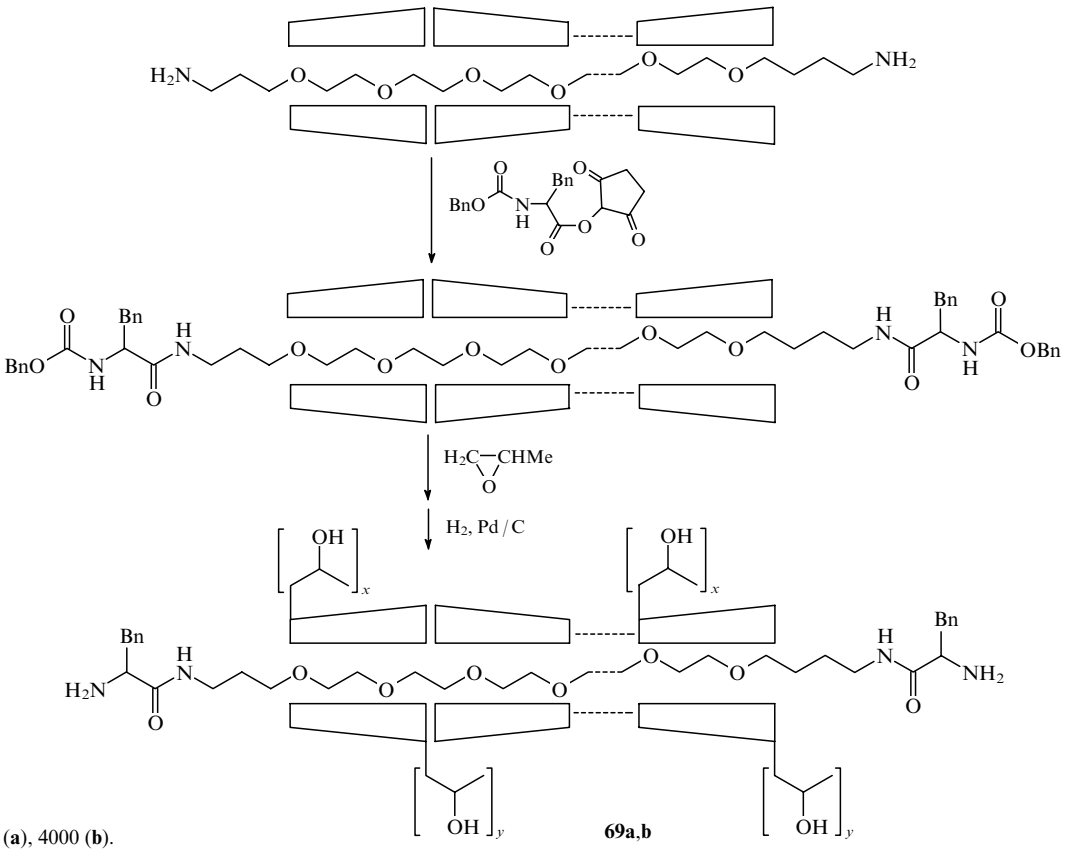

MM = 2000 (**a**), 4000 (**b**).

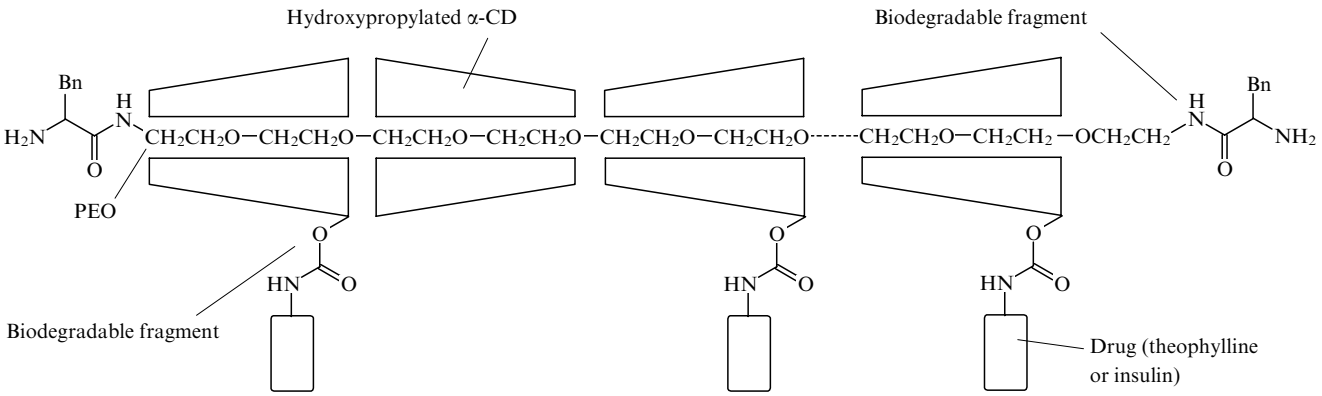

Figure 15. The drug–polyrotaxane complex prepared on the basis of poly(ethylene oxide) blocked by L-phenylalanine and hydroxypropylated α-cyclodextrin.

3. Comb-like polyrotaxanes

Non-covalent interactions of cyclodextrins with lateral fragments of comb-like polymers is yet another interesting example of molecular recognition. The determination of rate constants for the complexation of cyclodextrin with a series of copolymers of acrylamide with alkyl methacrylates (Table 3)[118] demonstrated the possibility of selective interaction of CD with comb-like polymers resulting in the formation of pseudopolyrotaxanes. In order to design true polyrotaxanes, Ritter *et al.*[119,120] proposed to use the strategy of covalent attachment of preformed pseudorotaxane **70** which is blocked at one end to the activated side fragments of the polymer (Scheme 11).

Table 3. The constants of complexation (K) of cyclodextrins and aliphatic fragments of water-soluble copolymers of acrylamide with alkyl methacrylates.[118]

Alkyl in alkyl methacrylate	K /litre mol^{-1}		
	α-CD	β-CD	γ-CD
Bu^n	55	–	–
Bu^t	–	340	57
Bu^i	36	–	–
n-C_6H_{13}	290	110	–
iso-C_8H_{17}	303	294	51
n-$C_{12}H_{25}$	990	660	245

A series of polyrotaxanes incorporating DM-β-CD have been synthesised.[119–123] It was found that these polyrotaxanes are less viscous than the starting polymers, apparently due to destruction of the hydrogen bonds between the fragments in the rod macromolecule.

The same group of investigators made an attempt to synthesise comb-like polyrotaxanes by radical polymerisation in aqueous solutions of the corresponding pseudorotaxanes based on β-CD, DM-β-CD and *N*-methacryloyl-11-aminodecanoic acid (method 2). However, this attempt was unsuccessful, since polymerisation was accompanied by elimination of the macrocycle from the side fragments of the polymer being formed.[124]

Alkylation of NH groups of poly(benzoimidazoles) with $Br(CH_2)_{12}OC(O)CH_2CPh_3$ in the presence of TM-β-CD resulted in comb-like polyrotaxane **71a–d**.[125]

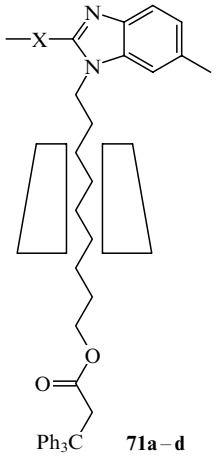

71a–d

X = *p*-C_6H_4 (**a**),
$(CH_2)_8$ (**b**),
$(CH_2)_{11}O(CH_2)_{11}$ (**c**),
$(CH_2)_{11}$ (**d**);

= TM-β-CD.

It was found that the degree of *N*-alkylation and the amount of the macrocycles incorporated depend on the lengths of the 'spacers' between the benzoimidazole fragments.

Scheme 11

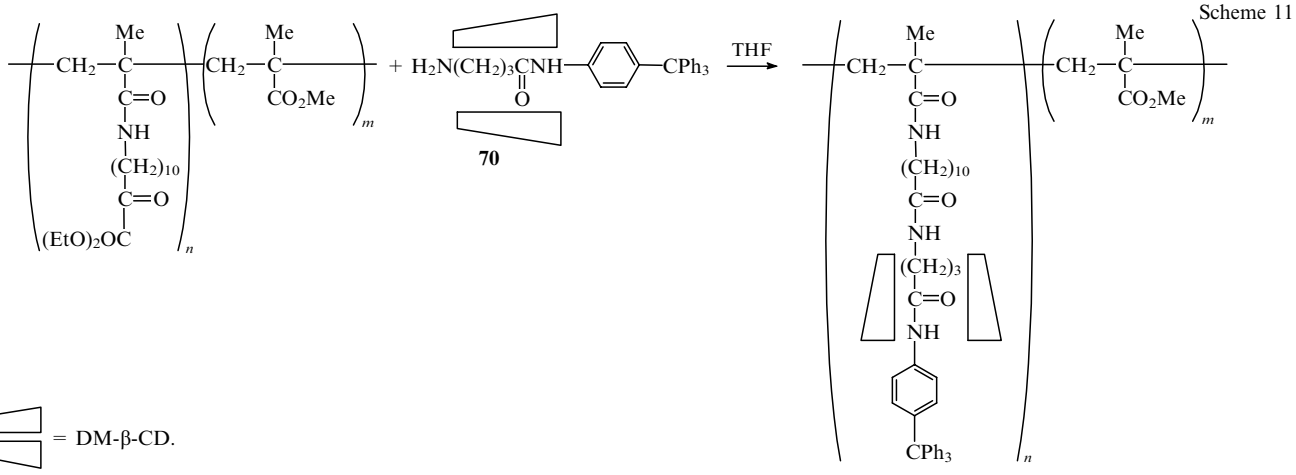

IV. Supramolecular devices based on rotaxanes and polyrotaxanes

Characteristic physicochemical properties of rotaxane-like structures are determined by both the unusual topology and the nature of their constituents. In the recent years, rotaxanes as molecular assemblies are considered as promising candidates for the construction of supramolecular devices which represent functional, structurally organised systems.[126–128] The feasibility of using rotaxanes in this area is due primarily to the ease of control over molecular directionality which determines the specific spatial configuration of their constituents. The introduction of photo-, electro- or ion-active groups into rotaxane molecules will allow the transfer of energy, electrons or ions as well as the transmission of signals and the storage of information.[12, 126–128]

Rotaxanes [2]-Rt which incorporate two different porphyrins as stoppers can serve as examples. The photophysical properties of [2]-Rt **10** and **72a**,**b** were studied [12, 129–131] and the rates of a photoinduced intramolecular electron transfer from the excited Zn-porphyrin to Au-porphyrin (1, 22 and 34 ps for complexes **10**, **72a** and **72b**, respectively) were compared to that in the dumbbell-shaped bisporphyrin **73** (55 ps). It was found that in the case of rotaxanes, the rate of the electron transfer increases significantly, the maximum increase being observed for complex **10**. This finding was attributed to the presence of copper(I) ions which play the role of mediators and to changes in the energy of the orbitals in the supermolecule under effect of the coordination centre.[129–131]

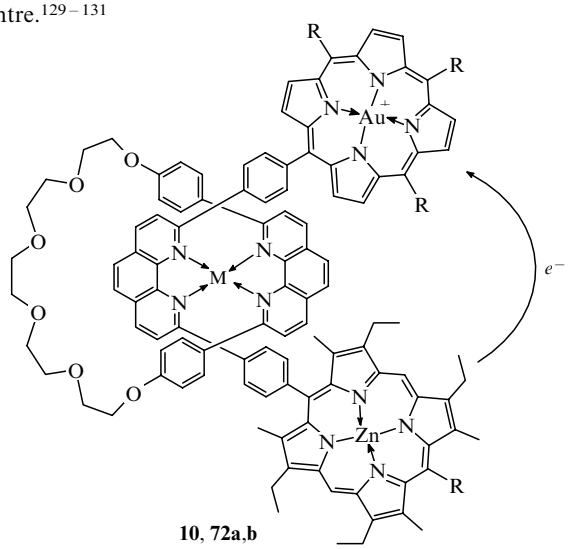

10, **72a**,**b**

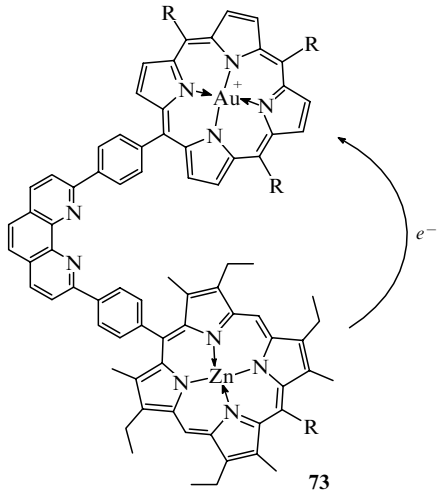

73

M = Cu^+ (**10**), Zn^{2+} (**72a**), none (**72b**); R = 1,3-$Bu^t_2C_6H_3$.

The photosensitive rotaxane **74** was prepared on the basis of the naphthalene derivative of α-cyclodextrin (N-α-CD) and poly(ethylene oxide) with dansyl groups as stoppers.[132]

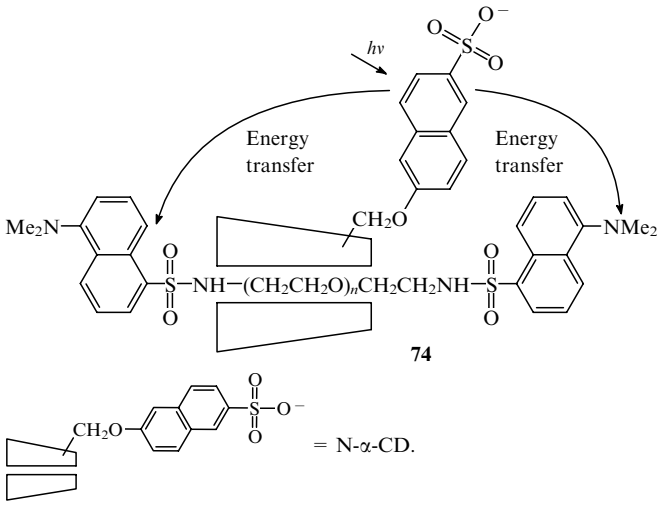

The fluorescence spectra of rotaxane **74** displayed a significant decrease in the intensity of signals elicited by the naphthalene fragments in comparison with the original N-α-CD which is due to the transfer of energy from the excited naphthalene groups of modified CD to the terminal dansyl groups of the rod molecule of PEO. The results of these studies are of interest for the construction of photochemical supramolecular devices which are able to effect directed transfer of electrons and energy.

Yet another promising line of investigations is the preparation of controlled 'molecular switches' (or 'shuttles' according to Stoddart). Molecular switch-on/off processes represent reversible transitions of one of the components between the two positions which differ either in structure or in conformation. The recently synthesised [2]-Rt **75** (Scheme 12) can serve as an example of an electrochemical (or chemical) 'molecular shuttle'.[127, 133] In this case, the migration of the macrocycle **14** occurs as a result of a redox reaction or protonation–deprotonation.

The synthesis of a photoreactive molecular switch prepared on the basis of CD-containing [2]-Rt **76** has been carried out (Fig. 16).[134] Here, azobenzene was used as a rod molecule, while 2,4-dinitrophenyl groups were used as stoppers. Irradiation of an aqueous solution of the complex **76** with UV light (λ = 360 nm) induced *trans*–*cis*-isomerisation of the azobenzene fragment. This reaction is reversible which was confirmed by the reverse reaction occurring upon irradiation of the solution in the visible region of the spectrum (λ = 430 nm). These changes in the configuration of the rod molecule induce the migration of the cyclodextrin molecule from one binding centre to another. A pH-sensitive 'molecular shuttle' was synthesised by self-organisation of aliphatic diamines and a triamine ligand.[135, 136]

Studies with polyrotaxanes based on β-CD and the PEO–PPO–PEO triblock copolymer showed that these polymers also manifest the properties of 'molecular switches'.[137, 138] The transition of polyrotaxanes from the insoluble into the soluble state can occur either upon a rise in the temperature or upon an increase in a pH above 12 due to the destruction of the hydrogen bonds between the CD molecules. As a result, the macrocycles migrate along the rod macromolecule. ^{1}H NMR studies of polyrotaxane solutions in 0.1 M NaOH showed that at room temperature CD molecules are distributed statistically along the whole polymeric chain, whereas upon heating the macrocycles are predominantly localised on PPO fragments (Fig. 17). Apparently, by changing such parameters as temperature and permittivity of the medium, one can govern the solubility of polyrotaxanes and the distribution of the CD molecules.

The design of photonic, electroninc and ionic switching devices based on molecular components and their incorporation

Scheme 12

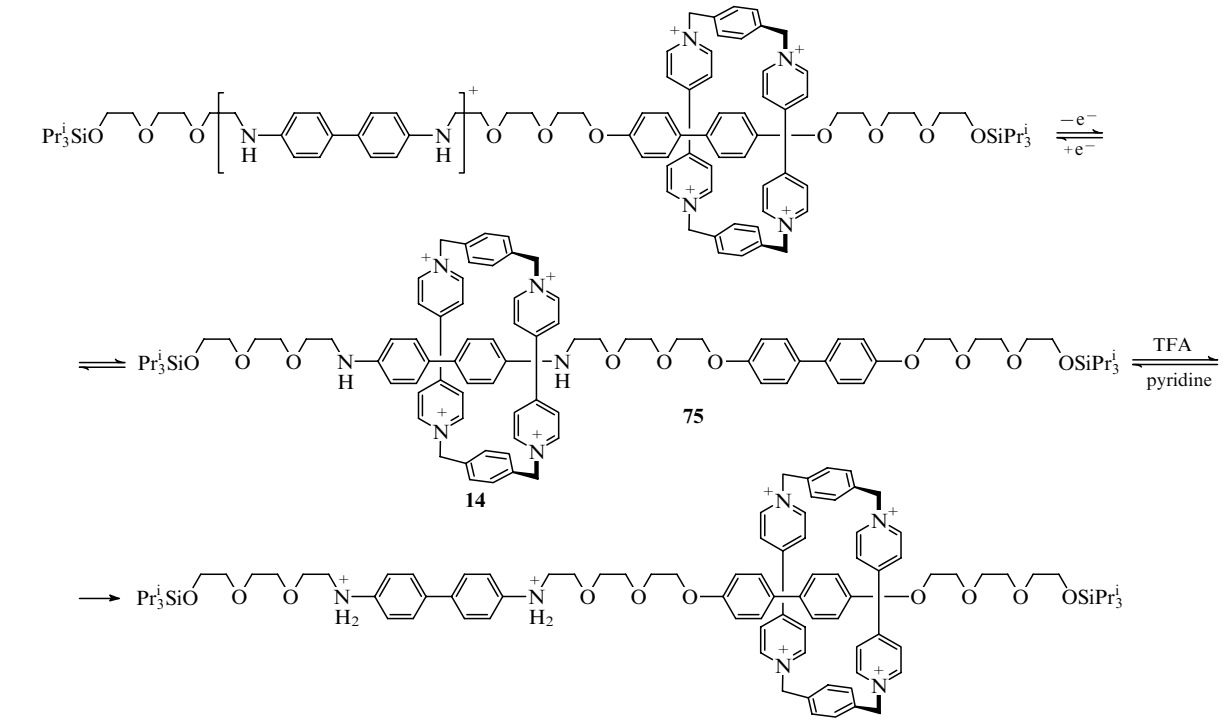

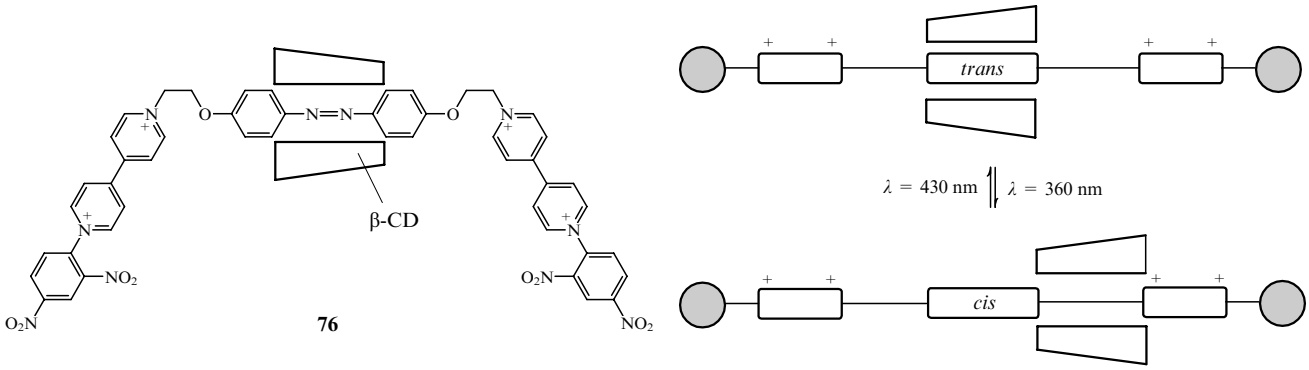

Figure 16. A photosensitive 'molecular switch' based on β-cyclodextrin.

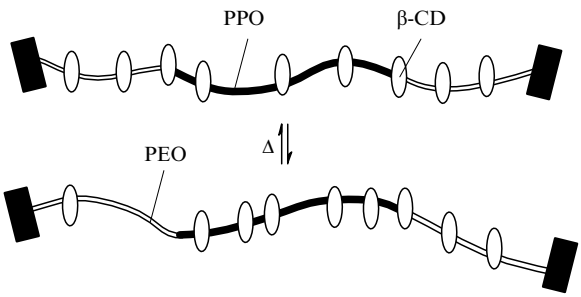

Figure 17. A mechanical 'molecular switch' based on polyrotaxane.

into well-organised assemblies is the next step in the development of functional materials on a nanoscale. Further studies in this field will inevitably culminate in the construction on their basis of multifunctional chemical 'machines' as the basis for the development of chemical informatics and an analysis of functioning of these devices in close conjunction with related biological processes.[126]

* * *

Thus, we are witnessing a revival of interest in rotaxane-like structures. New papers are being published and these are devoted to a search for their practical application. The literature data concerning polyrotaxanes consider them as a new type of regulatory polyfunctional rigid-chain polymers. It is these properties that determine the area of their further applications. New opportunities are emerging for the construction of complex polymeric structures which combine the blocks of 'molecular necklaces' with the flexible blocks of free polymers. Therefore, the fundamental problems related to the development of methods of synthesis of new supramolecular assemblies and investigation into their structural organisation and properties still remain in the focus of attention.

This review has been written with the financial support of the Russian Foundation for Basic Research (Project No. 00-03-32770).

References

1. D B Amabilino, J F Stoddart *Chem. Rev.* **95** 2725 (1995)
2. I T Harrison, S Harrison *J. Am. Chem. Soc.* **89** 5723 (1967)
3. I T Harrison *J. Chem. Soc., Chem. Commun.* 231 (1972)
4. G Agam, D Graiver, A Zilkha *J. Am. Chem. Soc.* **98** 5206 (1976)
5. G Agam, A Zilkha *J. Am. Chem. Soc.* **98** 5214 (1976)

6. C O Dietrich-Buchecker, P A Marnot, J-P Sauvage *Tetrahedron Lett*. **23** 5291 (1982)
7. C O Dietrich-Buchecker, J-P Sauvage *Tetrahedron Lett*. **24** 5091 (1983)
8. C Wu, P R Lecavalier, Y X Shen, H Gibson *Chem. Mater*. **3** 569 (1991)
9. C Dietrich-Buchecker, J-P Sauvage *Tetrahedron* **46** 503 (1990)
10. J-C Chambron, V Heitz, J-P Sauvage *J. Chem. Soc., Chem. Commun*. 1131 (1992)
11. J-C Chambron, A Harriman, V Heitz, J-P Sauvage *J. Am. Chem. Soc*. **115** 6109 (1993)
12. J-C Chambron, V Heitz, J-P Sauvage *J. Am. Chem. Soc*. **115** 12 378 (1993)
13. F Diederich, C O Dietrich-Buchecker, J-F Nierengarten, J-P Sauvage *J. Chem. Soc., Chem. Commun*. 781 (1995)
14. J-C Chambron, C O Dietrich-Buchecker, J-F Nierengarten, J-P Sauvage *J. Chem. Soc., Chem. Commun*. 801 (1993)
15. B Odell, M V Reddington, A M Z Slawin, N Spenser, J F Stoddart, D J Williams *Angew. Chem*. **100** 1605 (1988)
16. R C Helgeson, T L Tarnowski, J M Timko, D J Cram *J. Am. Chem. Soc*. **99** 6411 (1977)
17. P R Ashton, A M Z Slawin, N Spenser, J F Stoddart, D J Williams *J. Chem. Soc., Chem. Commun*. 1066 (1987)
18. Y A Shen, P T Engen, M A Berg, J P Merola, K P Parry, A M Slawin, J F Stoddart *Macromolecules* **25** 2768 (1992)
19. P L Aneli, P R Ashton, R Ballardini, V Balzani, M Delgado, M T Gandolfi, T T Goodnow, A E Kaifer, D Philp, M Pietraszkiewicz, L Prodi, M V Reddington, A M Z Slawin, N Spenser, J F Stoddart, C Vicent, D J Williams *J. Am. Chem. Soc*. **114** 193 (1992)
20. P R Ashton, M Grognuz, A M Z Slawin, J F Stoddart, D J Williams *Tetrahedron Lett*. **32** 6235 (1991)
21. P L Aneli, N Spenser, J F Stoddart *J. Am. Chem. Soc*. **113** 5131 (1991)
22. X Sun, D B Amabilino, J W Parsons, J F Stoddart *Polym. Prepr. (Am. Chem. Soc., Div. Polym. Chem.)* **34** 104 (1993)
23. D Philp, A M Z Slawin, N Spenser, J F Stoddart, D J Williams *J. Chem. Soc., Chem. Commun*. 1584 (1991)
24. P R Ashton, R A Bissell, N Spencer, J F Stoddart, M S Tolley *Synlett* 923 (1992)
25. V Balzani, A Credi, G Mattersteig, O A Matthews, F M Raymo, J F Stoddart, M Venturi, A J P White, D J Williams *J. Org. Chem*. **65** 1924 (2000)
26. E Cordova, R A Bissell, N Spenser, J F Stoddart, A E Kaifer *J. Org. Chem*. **58** 6550 (1993)
27. M Asakawa, G L Brown, S Menzer, F M Raymo, J F Stoddart, D J Williams *J. Am. Chem. Soc*. **119** 2614 (1997)
28. P R Ashton, D Philp, N Spencer, J F Stoddart *J. Chem. Soc., Chem. Commun*. 1124 (1992)
29. R R Ashton, M Belohradsky, D Philp, J F Stoddart *J. Chem. Soc., Chem. Commun*. 1269 (1993)
30. M Asakawa P R Ashton, R Ballardini, V Balzani, M Belohradsky, M T Gardolfi, O Kocian, L Prodi, F M Raymo, J F Stoddart, M Venturi *J. Am. Chem. Soc*. **119** 302 (1997)
31. D B Amabilino, P R Ashton, M Belohradsky, F M Raymo, J F Stoddart *J. Chem. Soc., Chem. Commun*. 751 (1995)
32. A Villers *C.R. Hebd. Seances Acad. Sci*. **112** 536 (1891)
33. J Szejtli *Cyclodextrins and Their Inclusion Complexes* (Budapest: Academia Kiado, 1982)
34. W Saenger, in *Inclusion Compounds* (Eds J L Atwood, J E D Davies, D D MacNicols) (London: Academic Press, 1984)
35. J Szejtli, in *Topics in Inclusion Science* (Ed. J E D Davies) (Dordrecht: Kluwer Academic 1988) p. 26
36. H-J Schneider *Angew. Chem., Int. Ed. Engl*. **30** 1417 (1991)
37. A K Chatjigakis, C Donze, A W Coleman, P Cardot *Anal. Chem*. **64** 1632 (1992)
38. G Wenz *Angew. Chem., Int. Ed. Engl*. **33** 803 (1994)
39. C A Nepogodiev, J F Stoddart *Chem. Rev*. **98** 1969 (1998)
40. H Ogino *J. Am. Chem. Soc*. **103** 1303 (1981)
41. R S Wylie, D H Macartney *J. Am. Chem. Soc*. **114** 3136 (1992)
42. T V S Rao, D S Lawrence *J. Am. Chem. Soc*. **112** 3614 (1990)
43. J S Manka, D S Lawrence *J. Am. Chem. Soc*. **112** 2440 (1990)
44. R Isnin, A E Kaifer *J. Am. Chem. Soc*. **113** 8188 (1991)
45. J F Stoddart *Angew. Chem., Int. Ed. Engl*. **31** 846 (1992)
46. A Harada, M Kamachi *Chem. Commun*. 1413 (1997)
47. S Anderson, T D W Claridge, N L Anderson *Angew. Chem., Int. Ed. Engl*. **36** 1310 (1997)
48. P T Engen, H W Gibson *New J. Chem*. **17** 723 (1993)
49. H Marand, A Prasad, C Wu, M Bheda, H W Gibson *Polym. Prepr. (Am. Chem. Soc., Div. Polym. Chem.)* **32** 639 (1991)
50. H W Gibson, P T Engen, S-H Lee, S Liu, H Marand *Polym. Prepr. (Am. Chem. Soc., Div. Polym. Chem.)* **32** 64 (1991)
51. H W Gibson, C Wu, Y X Shen, M Bheda, J Sze, P Engen, A Prasad, H Marad, D Loveday, G Wilkes *Polym. Prepr. (Am. Chem. Soc., Div. Polym. Chem.)* **32** 593 (1991)
52. H W Gibson, C Wu, Y X Shen, M Bheda, J Sze, P Engen, A Prasad, H Marad, D Loveday, G Wilkes *Polym. Prepr. (Am. Chem. Soc., Div. Polym. Chem.)* **32** 637 (1991)
53. Y X Shen, H W Gibson *Macromolecules* **25** 2058 (1992)
54. X Shen, P T Engen, M Berg, J S Merola, H W Gibson *Macromolecules* **25** 2786 (1992)
55. Y X Shen, D Xie, H W Gibson *J. Am. Chem. Soc*. **116** 537 (1994)
56. H W Gibson, S Liu, P Lecavalier, C Wu, Y X Shen *J. Am. Chem. Soc*. **117** 852 (1995)
57. H W Gibson, D Nagvekar, N Yamaguchi, W S Bryant, S Battacharjee *Polym. Prepr. (Am. Chem. Soc., Div. Polym. Chem.)* **38** 64 (1997)
58. H W Gibson, D Nagvekar, W S Bryant, J Powell, S S Battacharjee *Polym. Prepr. (Am. Chem. Soc., Div. Polym. Chem.)* **38** 115 (1997)
59. P E Mason, W S Bryant, H W Gibson *Macromolecules* **32** 1559 (1999)
60. I Yamaguchi, Y Takenaka, K Osakada, T Yamamoto *Macromolecules* **32** 2051 (1999)
61. I Yamaguchi, K Osakada, T Yamamoto *J. Am. Chem. Soc*. **118** 1811 (1996)
62. N Ogata, K Sanui, J Wada *J. Polym. Sci., Polym. Lett*. **14** 459 (1976)
63. M Maciejewski *J. Macromol. Sci., Chem*. **13A** 77 (1979)
64. A Harada, M Kamachi *Macromolecules* **23** 2821 (1990)
65. A Harada, M Kamachi *J. Chem. Soc., Chem. Commun*. 1322 (1990)
66. A Harada, J Li, M Kamachi *Nature (London)* **356** 325 (1992)
67. A Harada, J Li, M Kamachi *Macromolecules* **26** 5698 (1993)
68. A Harada, J Li, S Suzuki, M Kamachi *Macromolecules* **26** 5267 (1993)
69. A Harada, J Li, M Kamachi *Nature (London)* **370** 126 (1994)
70. J Li, A Harada, M Kamachi *Bull. Chem. Soc. Jpn*. **67** 2808 (1994)
71. A Harada, M Okada, J Li, M Kamachi *Macromolecules* **28** 8406 (1995)
72. A Harada, M Okada, J Li *Acta Polym*. **46** 453 (1995)
73. A Harada, S Suzuki, M Okada, M Kamachi *Macromolecules* **29** 5611 (1996)
74. A Harada, Y Kawaguchi, T Nishiyama, M Kamachi *Macromol. Rapid. Commun*. **18** 535 (1997)
75. A Harada, in *Abstracts of Reports of the 9th International Symposium on Cyclodextrins, Santiago de Compostela, 1998* 2-O-2
76. A Harada, J Li, M Kamachi, M Kitagawa, Y Katsube *Carbohydr. Res*. **305** 127 (1998)
77. S Kamitori, O Matsuzaka, S Kondo, S Muraoka, K Okuyama, K Noguchi, M Okada, A Harada *Macromolecules* **33** 1500 (2000)
78. A Harada, M Okada, Y Kawaguchi, M Kamachi *Polym. Adv. Technol*. **10** 3 (1999)
79. M Okada, M Kamachi, A Harada *Macromolecules* **32** 7202 (1999)
80. A Harada, J Li, M Kamachi *Nature (London)* **364** 516 (1993)
81. G Wenz, B Keller *Angew. Chem., Int. Ed. Engl*. **31** 197 (1992)
82. B Keller, G Wenz, in *Abstracts of Reports of the 6th International Symposium on Cyclodextrins* (Ed. A R Hedges) (Paris: Editions de Sante, 1992) p. 192
83. G Wenz, B Keller *Polym. Prepr. (Am. Chem. Soc., Div. Polym. Chem.)* **34** (1) 62 (1993)
84. G Wenz, F Wolf, M Wagner, S Kubik *New J. Chem*. **17** 729 (1993)
85. W Herrmann, B Keller, G Wenz *Macromolecules* **30** 4966 (1997)
86. I G Panova, V I Gerasimov, F A Kalashnikov, I N Topchieva *Vysokomol. Soedin., Ser. B* **40** 2077 (1998) [a]
87. K Yoshida, T Shimomura, K Ito, R Hayakawa *Langmuir* **15** 910 (1999)
88. I N Topchieva, E I Popova, F A Kalashnikov, I G Panova, V G Avakyan, A L Ksenofontov, V I Gerasimov *Dokl. Akad. Nauk* **357** 648 (1997) [b]
89. J Pozuelo, F Mendicuti, W L Mattice *Macromolecules* **30** 3685 (1997)
90. J Pozuelo, F Mendicuti, W Mattice *Polym. J*. **30** 479 (1998)
91. B Mayer, C T Klein, I N Topchieva, G Köhler *J. Comput.-Aided Mol. Design* **13** 373 (1999)

92. A E Tonelli *Polym. Int*. **43** 295 (1997)
93. A E Tonelli, S Nojima *Macromolecules* **27** 7220 (1994)
94. L Huang, A E Tonelli *J. Macromol. Sci., Rev. Macromol. Chem. Phys*. **38C** 781 (1998)
95. I G Panova, V I Gerasimov, T E Grokhovskaya, I N Topchieva *Dokl. Akad. Nauk* **347** 61 (1996) [b]
96. I N Topchieva, I G Panova, V I Gerasimov in *Preprints of the 8th International Cyclodextrin Symposium, Budapest, 1996* p. 31
97. I G Panova, V I Gerasimov, V N Tashlitskii, I N Topchieva, V A Kabanov *Vysokomol. Soedin., Ser. A* **39** 663 (1997) [a]
98. I N Topchieva, I G Panova, V I Gerasimov, K I Karezin, V A Kabanov *Polym. Prepr. (Am. Chem. Soc., Div. Polym. Chem.)* **38** 589 (1997)
99. I N Topchieva, V I Gerasimov, I G Panova, K I Karezin, N V Efremova *Vysokomol. Soedin., Ser. A* **40** 310 (1998) [a]
100. I N Topchieva, A L Blyumenfel'd, A A Klyamkin, V A Polyakov, V A Kabanov *Vysokomol. Soedin., Ser. A* **36** 271 (1994) [a]
101. I N Topchieva, K I Karezin, I G Panova, V I Gerasimov *Dokl. Akad. Nauk* **355** 357 (1997) [b]
102. I N Topchieva, K I Karezin *J. Colloid Interface Sci*. **213** 29 (1999)
103. I N Topchieva, V A Polyakov, S V Elezkaya, G V Bystryzky, K I Karezin *Polym. Bull*. **38** 359 (1997)
104. I N Topchieva, P Mishnik, G Kyun, K I Karezin, S V Eletskaya *Dokl Akad. Nauk* **360** (1998) [b]
105. I N Topchieva, P Mischnick, G Kuehn, V A Polyakov, S V Elezkaya, G I Bystryzky, K I Karezin *Bioconjugate Chem*. **9** 676 (1998)
106. I N Topchieva, N V Efremova, B I Kurganov *Usp. Khim*. **64** 293 (1995) [*Russ. Chem. Rev*. **64** 277 (1995)]
107. I N Topchieva, E M Sorokina, E M Medvedeva, N V Efremova, B I Kurganov *Bioorg. Khim*. **25** 520 (1999) [c]
108. I Topchieva, E Sorokina, N Efremova, A Ksenofontov, B Kurganov *Bioconjugate Chem*. **11** 22 (2000)
109. I G Panova, V I Gerasimov, F A Kalashnikov, I N Topchieva *Dokl. Akad. Nauk* **355** 641 (1997) [b]
110. A A Klyamkin, I N Topchieva, S Yu Zaitsev, V P Zubov *Biol. Membr*. **13** 313 (1996) [d]
111. T Ooya, H Mori, M Terano, N Yui *Macromol. Rapid. Commun*. **16** 259 (1995)
112. T Ooya, N Yui *Adv. Polym. Biomater. Sci*. 283 (1997)
113. H Fujita, T Ooya, N Yui *Macromol. Chem. Phys*. **199** 2311 (1998)
114. J Watanabe, T Ooya, N Yui *Chem. Lett*. 1031 (1998)
115. T Ooya, N Yui *J. Control. Rel*. **58** 251 (1999)
116. W Kamimura, T Ooya, N Yui *J. Control. Rel*. **44** 295 (1997)
117. N Yui, T Ooya, T Kumeno *Bioconjugate Chem*. **9** 118 (1998)
118. M Born, H Ritter *Macromol. Chem. Rapid. Commun*. **12** 471 (1991)
119. H Ritter *Makromol. Symp*. **77** 73 (1994)
120. M Born, T Koch, H Ritter *Acta Polym*. **45** 68 (1994)
121. M Born, T Koch, H Ritter *Macromol. Chem. Phys*. **196** 1761 (1995)
122. M Born, H Ritter *Angew. Chem., Int. Ed. Engl*. **35** 309 (1995)
123. M Born, H Ritter *Adv. Mater*. **8**149 (1996)
124. J Jeromin, H Ritter *Macromolecules* **32** 5236 (1999)
125. I Yamaguchi, K Osakada, T Yamamoto *Macromolecules* **30** 4288 (1997)
126. J-M Lehn *Supramolecular Chemistry* (Weinheim: VCH, 1995)
127. V Balzani, M Gómez-López, J F Stoddart *Acc. Chem. Res*. **31** 405 (1998)
128. N Armaroli, V Balzani, J-P Collin, P Gavina, J-P Sauvage, B Ventura *J. Am. Chem. Soc*. **121** 4397 (1999)
129. J-C Chambron, A Harriman, V Heitz, J-P Sauvage *J. Am. Chem. Soc*. **115** 6109 (1993)
130. E David, R Born, E Kaganer, E Joselevich, H Dürr, J Willner *J. Am. Chem. Soc*. **119** 7778 (1997)
131. S S Zhu, P J Carroll, T M Swager *J. Am. Chem. Soc*. **118** 8713 (1996)
132. M Tamura, D Gao, A Uen, in *Abstracts of Reports of the 9th International Symposium on Cyclodextrins, Santiago de Compostela, 1998* 4-P-9
133. R A Bissell, E Cordova, A E Kaifer, J F Stoddart *Nature (London)* **369** 133 (1994)
134. M-V Martinez-Diaz, N Spenser, J F Stoddart *Angew. Chem., Int. Ed. Engl*. **36** 1904 (1997)
135. D A Leigh, A Murphy, J P Smart, A M Z Slawin *Angew. Chem., Int. Ed. Engl*. **36** 728 (1997)
136. A S Lane, D A Leigh, A Murphy *J. Am. Chem. Soc*. **119** 11 092 (1997)
137. H Fujita, T Ooya, M Kurisawa, H Mori, M Terano, N Yui *Macromol. Rapid. Commun*. **17** 509 (1996)
138. H Fujita, T Ooya, M Kurisawa, N Yui. *Adv. Polym. Biomater. Sci*. 649 (1997)

[a] — *Polym. Sci. (Engl. Transl.)*
[b] — *Dokl. Chem. Technol., Dokl. Chem. (Engl. Transl.)*
[c] — *Russ. J. Bioorg. Chem. (Engl. Transl.)*
[d] — *Biol. Membr. (Engl. Transl.)*

Russian Chemical Reviews **70** (1) 45 – 63 (2001) © 2001 Russian Academy of Sciences and Turpion Ltd

DOI 10.1070/RC2001v070n01ABEH000598

Mechanochemical synthesis of intermetallic compounds

T F Grigorieva, A P Barinova, N Z Lyakhov

Contents

I.	Introduction	45
II.	Mechanochemical synthesis of intermetallic compounds and solid solutions at concentration limits of binary equilibrium diagrams	46
III.	Mechanochemical synthesis of non-equilibrium phases in bimetallic systems with negative mixing enthalpies	47
IV.	Mechanochemical synthesis of supersaturated solid solutions in systems with positive mixing enthalpies	50
V.	Quasicrystals and amorphous alloys	52
VI.	Phase and structural transformations in the mechanochemical synthesis of intermetallic compounds	53

Abstract. The current state of studies on the mechanochemical synthesis of binary metallic systems is considered. It is shown that this method is suitable for the preparation of intermetallic compounds and solid solutions in concentration limits of equilibrium diagrams of many binary systems. The mechanochemical approach is demonstrated to exhibit the most promise for preparing intermetallic compounds in systems characterised by large differences in the melting points and in the densities of the initial components as well as phases with nanometer grain sizes and metastable phases. The major factors, which influence the concentration limits of existence of non-equilibrium solid solutions prepared by the mechanochemical method, are revealed. Using numerous examples, it is demonstrated that the formation of solid solutions may involve several stages. At the first stage, nanosized layered composite structures are formed with simultaneous dispersion of the initial components (the formation of a large contact area). The second stage involves the synthesis of intermetallic compounds in nanosized layered composites. At the third step, the intermetallic compounds are dissolved in a metal solvent to give a solid solution. The bibliography includes 397 references.

I. Introduction

Intermetallic compounds can exist only in the crystalline state. Individual molecules cannot be distinguished in these compounds and they cannot be melted or dissolved without the loss of individuality and do not exist in the gaseous phase. In addition, the physicochemical properties of intermetallic compounds differ substantially from those of their components.[1–3] Intermetallides with a particular composition differ in the chemical properties not only from the constituent metals, but also from intermetallides, which are characterised by the same elemental composition, and yet contain the components in a different ratio.[4,5]

T F Grigorieva, A P Barinova, N Z Lyakhov Institute of Solid State Chemistry and Mechanochemistry, Siberian Branch of the Russian Academy of Sciences, ul. Kutateladze 18, 630128 Novosibirsk, Russian Federation. Fax (7-383) 232 28 47. Tel. (7-383) 217 09 58.
E-mail: root@solid.nsk.su (T F Grigorieva).
Tel. (7-383) 232 86 83. E-mail: lyakhov@solid.nsk.su (N Z Lyakhov)

Received 24 April 2000
Uspekhi Khimii **70** (1) 52 – 71 (2001); translated by T N Safonova

Presently, a general theory, which would allow one to reveal factors stabilising particular intermetallic compounds, is lacking. A search for these factors was performed as follows. A group of systems in which the stability of intermetallic phases can be related to the effect of a particular factor was established after which the effect of this factor in other systems in which it was less evident was analysed. Three factors were revealed, *viz*., the ratio of the total number of valence electrons (e) to the total number of atoms per unit cell (a), the tendency for the maximum filling of space (*i.e*., for the formation of closest packing or structures with high coordination numbers) and the difference between the electronegativities of the components. The latter factor is of minor importance and is clearly manifested only in a small group of Zintl phases,[6] *viz*., in compounds of active metals (alkali metals, alkaline-earth metals, magnesium and aluminium) with germanium, tin, lead and bismuth.[7,8]

Hume-Rothery demonstrated[9] that phases with the same electron concentration (e/a) have similar crystal structures. In different systems, one of the following three types of structures is characteristic of phases with an electron concentration of 3/2, the so-called β phases: body-centred cubic (BCC) structures (the Cu – Zn, Cu – Al and Cu – Sn systems), structures of the β-Mn type (Cu – Si, Ag – Al and Au – Al) or hexagonal structures (Ag – Zn, Cu – Si and Ag – Sn). Phases with an electron concentration of 21/13 have complex cubic structures of γ-brass. In the case of $e/a = 7/4$, ε phases with hexagonal close-packed (HCP) structures are formed. The β, γ and ε phases have come to be known as electron compounds. In the case of a favourable dimension factor (more exactly, the number of electrons per unit cell), the electron concentration is of primary importance in the formation and stability of a particular crystal structure.

Compounds belonging to the $MgZn_2$, $MgCu_2$ and $MgNi_2$ structural types (the so-called Laves phases) are the most widespread intermetallides. For these compounds, the ratios between the atomic radii of the components (in addition to the above-mentioned stabilising factors) are also of great importance. The characteristic feature of Laves phases is that the smaller atoms (Zn, Cu and Ni) are grouped together to form tetrahedra linked to each other. The $MgZn_2$, $MgCu_2$ and $MgNi_2$ structures differ in the mode of arrangement of the tetrahedra. The bulkier magnesium atoms occupy the holes in the network of tetrahedra. As a result, very close packed structures are formed, the coordination number of the bulkier atoms being equal to 16. This value is larger than the coordination number (12) corresponding to the maximum density of packing of spheres of the same size. The

coordination numbers of the smaller atoms in these structure are equal to 12.[6]

The above-mentioned factors are responsible for the stability of solid solutions as one of the types of intermetallic compounds.[7] In the case of similar electronegativities of the elements and a favourable dimension factor, the electron concentration is the major factor affecting the limiting solubility. The quantitative theory of solubility of polyvalent elements in metals of the copper group is based on the concept of filling of the first Brillouin zone with electrons in the face-centred cubic (FCC) crystal structure.[8] Theoretically (taking into account the electron concentration), a solid solution can exist over wide concentration limits. However, the preparation of such solutions in these limits is determined primarily by the dimension factor. It was empirically established that if the atomic diameter of the element dissolved differs from the atomic diameter of the solvent by more than 14% – 15%, the dimension factor is unfavourable and the region of existence of the solid solution is limited.[9] No reliable theoretical explanation has been provided for the threshold value of 15%. Quantitative calculations were carried out within the framework of an elastic-sphere model. King [10] calculated the dimension factors for 469 substitution solid solutions and confirmed the above threshold value.

Therefore, the major factors influencing the formation and thermodynamic stability of intermetallic phases at equilibrium were revealed empirically.

Main procedures for the preparation of equilibrium intermetallic compounds involve alloying followed by homogenisation and sintering. Intermetallides with high formation enthalpies are generally prepared by the self-propagating high-temperature synthesis. Yet another procedure for the synthesis of intermetallic compounds, *viz*., the mechanochemical method, has been developed intensively in recent years. This method is promising in the synthesis of equilibrium and metastable phases, supersaturated solid solutions and amorphous phases and allows the preparation of intermetallides from components possessing high melting and boiling points (for example, $MoSi_2$) as well as from components characterised by large differences between these points (for example, the boiling point of magnesium in the Mg – Ti system is lower than the melting point of titanium). The mechanochemical procedure can be used for the introduction of the third component into a binary system to impart special properties to intermetallides.

Compounds prepared by the mechanochemical method are characterised by high dispersity (in most cases, nanosized particles are obtained), which affects the physicochemical properties of these compounds. Currently, one of the major problems with which researchers are faced in dealing with mechanochemical synthesis is to reveal the factors governing the formation and stability of phases prepared by this method.

In the present review, the experimental data on the problems of the mechanochemical synthesis in metallic systems published over the last 15 years are systematised. Earlier data, as a rule, are cited in the discussion of the general problems of metal deformation and mass transfer in the solid body.

II. Mechanochemical synthesis of intermetallic compounds and solid solutions at concentration limits of binary equilibrium diagrams

Analysis of the published data demonstrated that the mechanochemical method can be used for the synthesis of all major groups of intermetallic compounds, *viz*., of the following electron compounds: ε and β phases in the Zn – Ag [11] and Cu – Zn [12] systems, γ phases in the Cu – Zn system,[13] ε and η phases in the Cu – Sn system,[14] η (Cu_2Sb) and δ ($Cu_{4.5}Sb$) phases in the Cu – Sb system [15] and the Laves phases Fe_2Ti,[16] Mg_2Ni,[17–19] Mg_2Cu,[19] $MgZn_2$ [19] and Fe_2Tb.[20] The mechanochemical procedure for the synthesis of intermetallic compounds is most promising when the use of conventional metallurgical methods presents difficulties, in particular, in the synthesis of silicides of refractory metals. For example, the melting point of molybdenum (2620 °C) is virtually equal to the boiling point of silicon (2600 °C), whereas the densities of these elements differ by a factor of more than four (10.2 and 2.308 g cm^{-3}, respectively). In the case of silicon and tungsten, the difference between these parameters is even larger [T_{melt}(W) ≈ 3400 °C; ρ(W) = 19.35 g cm^{-3}]. Reactions of these elements can occur only through reactive diffusion at very high temperatures over a long period. However, it is very difficult to prepare monophase systems even under these conditions.[4]

Silicides of molybdenum,[21–27] tungsten [28] and tantalum [22,29,30] were synthesised by the mechanochemical method. The stoichiometric intermetallide $NbSi_2$ was prepared according to this method after continuous activation for 65 min.[31,32] The use of the mechanochemical method substantially simplified the preparation of iron silicides.[26,27,33,34] The boiling points of the first metals in the Mg – Ni, Mg – Ti, Mg – Si, Al – Nb, Al – Ru, Sn – Nb and Te – Cu binary systems are lower than the melting points of the second metals, but the mechanochemical approach allowed the preparation of the intermetallides Mg_2Si,[17,35,36] Mg_2Ni,[37] $NbAl_3$,[38] Nb_3Sn, Nb_6Sn_5,[39] AlRu [40] and Cu_2Te.[41]

Even more so, the synthesis of intermetallides according to conventional procedures presents technological problems due to a large difference between the melting points of the initial components. Hence, such intermetallides as FeSn, $FeSn_2$,[42–44] Ti_3Al,[38,45,46] TiAl,[45–51] $TiAl_3$,[41,45,46,52] AlPd,[53] Nb_3Ge, Nb_5Ge_2, $NbGe_2$,[39,54] ZrAl,[55] Ni_3Sn_2,[56] Ni_3Sn,[56] Ni_2Al_3,[57] NiAl,[57–65] VAl_3, V_5Al_8, V_4Al_2 and VAl_{10} [66] were prepared by the mechanochemical method.

The intermetallide Cu_7Hg_6, which is of practical importance, was prepared by mechanical alloying of copper with mercury.[67,68] These metals differ substantially in melting points. In addition, the vapour pressure of mercury at elevated temperature is very high.

Relushko *et al*.[69] studied the mechanochemical synthesis of iron aluminides in the Fe – Al system and revealed the sequence of formation of the Fe_2Al_5 and FeAl phases, *i.e*., the authors followed the stages of the synthesis of the intermetallides. The formation of the intermetallides in this system was also considered in more recent studies. Thus, Bonetti *et al*.[70] investigated Fe_3Al and FeAl and Morris and Morris [71] studied $FeAl_3$.

However, attempts to bring the mechanochemical synthesis to completion are not necessarily successful. In some cases, prolonged (during many hours) mechanochemical activation is required. It was found that mechanochemical treatment can substantially decrease the temperature of the subsequent thermal synthesis. Thus, preliminary mechanochemical activation of molybdenum and silicon powders for 2 h allowed the preparation of the intermetallide $MoSi_2$ at 800 °C.[72,73] After mechanochemical treatment of tungsten and silicon powders, the temperature of the synthesis of WSi_2 was 950 °C.[28] In the synthesis of β-$FeSi_2$, the duration of preliminary activation was decreased (50 h) by using brief mechanochemical treatment followed by annealing at 700 °C.[74] Conventional procedures for the synthesis required prolonged annealing at 982 °C;[75] however, the desired homogeneity of β-$FeSi_2$ was not achieved even in this case. Brief annealing of non-equilibrium systems obtained upon mechanochemical activation also afforded intermetallides, for example, Fe_3Al, FeAl, $FeAl_3$,[76] Fe_2Al_5,[76,77] γ-TiAl, $TiAl_3$ [51,52] and the corresponding compounds in the Co – Ti system.[78]

Systems characterised by large heats of formation of intermetallic compounds are worthy of particular consideration. Preliminary mechanochemical activation of these systems favours the subsequent self-propagating high-temperature synthesis. The new approach involving mechanochemical activation and self-propagating high-temperature synthesis extends the range of systems in which the latter can be performed,[79,80] expands the concentration limits of the synthesis and allows one to accelerate substantially the synthesis and to perform it in the solid-phase mode.[79,81] This approach was used for the preparation of the intermetallides NiTi,

NiAl, Ni_3Al, NiGe,[79–81] Ni_3Si,[82] $FeSi_2$,[75] $NbAl_3$,[83] FeAl[84–87] and $MoSi_2$.[86,88,89]

The mechanochemical method was employed for the synthesis of equilibrium solid solutions in systems characterised by continuous and very wide solubility ranges. Thus, Pavluykhin *et al.*[90] investigated the conditions of accelerated diffusion in binary metallic systems upon mechanochemical activation in centrifugal planetary mills and obtained solid solutions in the Fe–Cr system. Davis and Koch[91] were the first to examine the possibility of mechanical alloying of solid solutions consisting of fragile components. In the cited study, mechanical alloying of germanium with silicon (compositions containing 72 at.% and 50 at.% of Si) was investigated. Silicon and germanium are isomorphous and their unit cell parameters depend almost linearly on the concentration of the second element. The measured unit cell parameter of germanium was larger than that expected based on the Vegard rule, but this deviation virtually disappears in the case of specimens containing more than 72 at.% of Si. At lower concentrations of silicon, the deviation of the unit cell parameter persists even after annealing.

Yurchikov *et al.*[92,93] studied the formation of intermetallic compounds and solid solutions in the Fe–Cr and Fe–Si systems under high pressure on doubled Bridgman anvils with a rotating central part. Neverov *et al.*[94,95] prepared a large number of solid solutions on Bridgman anvils.

In the Fe–Co system, solid solutions with body-centred cubic structures were formed on mechanical alloying of mixtures containing less than 80 at.% of Co, whereas solid solutions with face-centred cubic structures were formed in the case of 90 at.% of Co.[96–99] In this system, the sizes of blocks of the body-centred cubic and face-centred cubic phases were 10–30 and 40–70 nm, respectively. Monophase solid solutions were obtained in the Fe–Ni system with the use of a planetary ball mill.[100]

All phase compositions in the Fe–Mn system were obtained in a high-energy ball mill. However, the concentration limits of the regions of solid solutions were substantially extended compared to those observed in the equilibrium diagram. The particle sizes were 20–80 nm.[101]

The mechanochemical synthesis of nanocrystalline solid solutions with body-centred cubic structures using high-energy mills was reported.[102–106] It was suggested that a solid solution of aluminium in iron became partially ordered on prolonged activation. Nanocrystalline solid solutions of iron containing 4 mass % (8 at.%) of Al were prepared in a high-energy SPEX 8000 ball mill (USA) during intervals from 10 to 60 min.[107]

Therefore, analysis of the published data demonstrated that the mechanochemical synthesis of equilibrium intermetallic compounds is most efficient in the cases of large differences between the melting points and between the densities of the initial components, high temperatures of the synthesis and, if required, in the preparation of phases with nanosized grains.† This method is used more widely in preparation for the subsequent thermal synthesis or for the self-propagating high-temperature synthesis.

III. Mechanochemical synthesis of non-equilibrium phases in bimetallic systems with negative mixing enthalpies

The mechanochemical synthesis of non-equilibrium phases can successfully compete with such methods for their preparation as superfast quenching and precipitation from the gaseous phase. Practical interest in metastable compounds (*i.e.*, in systems with an excessive free energy) arises from their high reactivities. These phases find wide application. It is evident that chemical activity of metastable phases depends substantially on crystal structure imperfection, which, in turn, is determined by the degree to which the phase is in non-equilibrium. Therefore, the major problem of the preparation of metastable phases is to achieve the maximum concentration deviation from the equilibrium state with retention of the crystal structure of the initial phase. As mentioned above, in equilibrium systems, the maximum concentration of an alloying (dissolved) element in solid solutions is determined by the electron concentration and the difference between the atomic radii, which should be no higher than 15%. Analysis of the published data demonstrated that mechanochemical synthesis leads to changes of priorities and variations in the above parameters. First, the mutual correlation between the crystal structures of the components assumes great importance. Second, the dimension factor is shifted to the region of 15%–28% to attain substantial concentration deviations.

Binary metallic systems in which the course of mechanochemical synthesis of non-equilibrium phases is governed by the difference between the atomic radii are listed in Table 1. It can be seen that metastable solid solutions characterised by a substantial deviation of the concentration form the equilibrium state can be synthesised by the mechanochemical method in systems in which the solubility of one element in another is limited by the dimension factor and in which the difference between the atomic radii is 15%–25%. The concentrations of such solid solutions are higher than both the low-temperature (in all the cases under consideration) and high-temperature (Cu–Hg, Ni–Sn and Fe–Sn) equilibrium limits. For the Cu–Sn system, these concentrations are also higher than the concentrations of solid solutions prepared by fast quenching, (in the latter case, these values amount to only 8 at.% of Sn; Fig. 1). Tianen and Schwarz[56] prepared supersaturated solid solutions of tin based on α-nickel with the lattice parameter $a = 0.3699$ nm, which is 5% larger than that of pure nickel.

Table 1. Differences between the atomic radii (ΔR) and the concentrations of equilibrium (C) and supersaturated solid solutions (c) prepared by the mechanochemical method in different systems.

System	ΔR (%)	C (at.% of the second element)		c (at.% of the second element)	Ref.
		I	II		
Cu–Sn	19	11.25 (852°C)	~0	10	108–111
Cu–Hg	20	5 (657°C)	0	17	111–113
Cu–In	23	10.8 (574°C)	>1	11	114–116
Ni–Sn	21	10.4 (1130°C)	0	17.7	117–119
Ni–In	25	14.5 (908°C)	0	14.5	117–119
Fe–Sn	20	9.8 (900°C)	>2	32	120–124
Ni–Bi	30	0.5 (>500°C)	0	3	125, 126

Note. The following notations are used: I is the concentration at high temperatures and II is the concentration at room temperature.

The limiting non-equilibrium concentration decreases as the difference between the atomic radii increases further. In the Ni–Bi system in which the difference between the atomic radii is 30%, the enthalpy of formation of solid solutions calculated by the Miedema method[127–129] has a small negative value. According to the equilibrium diagram,[108] this system contained two intermetallic compounds with the bismuth contents of 78.08 mass % (NiBi) and 91.44 mass % ($NiBi_3$), the solubility of bismuth in solid nickel being no higher than 0.5 at.%.[125] Solid solutions of bismuth in nickel with bismuth concentrations of up to 3 at.% were synthesised by the mechanochemical method.[126]

In systems in which the limiting solubility is determined by the electron concentration, the content of the alloying element exceeding the value allowed in this crystal structure is very difficult to achieve. In the Cu–Al system, the difference between the atomic radii is 11%. Taking into account the electron concentration under equilibrium conditions at room temperature, the limiting

† The term 'nanosized grain' used in many modern publications is generally related to the sizes of coherent-scattering regions.

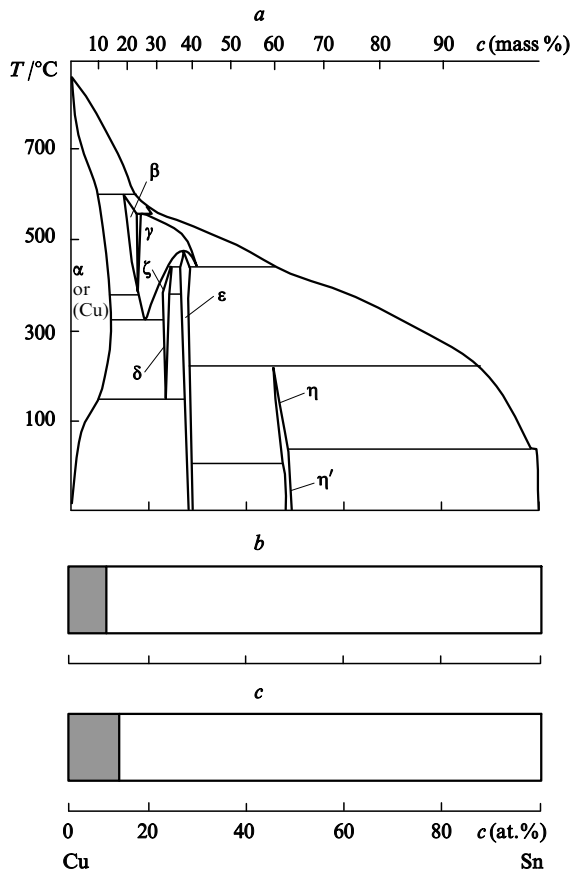

Figure 1. Equilibrium diagram of the Cu – Sn system (*a*) and the limiting concentrations of the solid solution prepared by fast quenching (*b*) and the mechanochemical method (*c*).

aluminium content in copper can be as high as 20 at.%. Solid solutions with a maximum aluminium content of up to 23 at.% were also prepared by the mechanochemical method.[111, 130, 131]

If there is structural compatibility between the metal serving as the solvent and the closest intermetallide and there is a favourable dimension factor, the resulting solid solutions are characterised by a very broad concentration range of supersaturation. In the Ni – Al system, the intermetallic compound Ni_3Al is structurally similar to nickel serving as the solvent.[132] According to the equilibrium diagram, the limiting solubility of aluminium in nickel is 13.5 at.% and 3.85 at.% at 1100 and 500 °C, respectively. At room temperature, the solubility is insignificant. The homogeneity region of the intermetallic compound Ni_3Al varies from 23 at.% to 27.5 at.% of Al.[108] Solid solutions of aluminium in nickel containing up to 28 at.% of Al were synthesised by the mechanochemical method.[111, 133]

The Ni – Ga system is characterised by an electron concentration identical to that observed in the Ni – Al system and by the favourable dimension factor ($\Delta R \simeq 10\%$).[134] The maximum gallium content in the equilibrium solid solution of gallium in nickel is 24.3 at.%. At the peritectic temperature of 1210 °C, the α' phase (Ni_3Ga) was formed. The solubility of gallium in nickel depends substantially on the temperature. For example, the solubility at 700 °C decreases to 15 at.% of Ga.[135] The system contained the β phase, *viz.*, the solid solution based on the intermetallide NiGa. The homogeneity region of the β phase falls in the concentration ranges of gallium from 36 at.% to 60 at.% and from 48.3 at.% to 53.3 at.% at high and low temperatures, respectively. At 1204 °C and a concentration of gallium of 29.4 at.%, the α' and β phases formed an eutectic. At 940 and 685 °C , two peritectoid reactions proceeded giving rise to new phases, *viz.*, γ and δ, respectively. The low-temperature γ' phase formed from the γ phases below 685 °C has the Ni_3Ga_2 composition and is characterised by a narrow homogeneity region. The Ni_3Ga phase (the Cu_3Au structural type) is structurally similar to β-nickel (the face-centred cubic structure). The succeeding Ni_3Ga_2 phase crystallises in the γ-Mn structural type, which can be described as a deformed structure of β-nickel, whereas the NiGa phase crystallises in the CsCl structural type (the body-centred cubic structure).[132] The mechanochemical method was used for the preparation of solid solutions of gallium in nickel with a Ga concentration of up to 50 at.%,[117, 133] *i.e.*, including the concentration range of existence of both structurally similar phases.

In the Ni – Ge system, the difference between the atomic radii of the metals is small,[134] but the region of existence of the solid solution, which is determined by the electron concentration, is noticeably narrower than that in the Ni – Ga system. According to the equilibrium diagram, the limiting solubility of germanium in nickel is 13.8 at.% at 1161 °C.[125] The solid solution is followed by the β phase, which is a solid solution based on the intermetallide Ni_3Ge. The β phase is homogeneous in the concentration range from 22.9 at.% to 24.8 at.% of Ge and has the cubic structure of the Cu_3Au type similar to that of β-nickel. The following ε phase is a solid solution based on Ni_2Ge with the hexagonal structure of the nickel-arsenide type, which differs substantially from the structure of the preceding phase. The mechanochemical method was used for the synthesis of non-equilibrium solid solutions whose homogeneity region extends to a concentration of 25 at.% of Ge.[133]

It is known that a solid solution of aluminium in α-iron was formed in the Fe – Al system at concentrations of aluminium varying from 0 at.% to 25 at.% (quenched alloys).[132] The further addition of aluminium led to a gradual ordering of the solid solution. Under favourable conditions, for example, upon annealing, ordering started even at 18 at.% of Al. At 25 at.% and 50 at.% of Al, the intermetallides Fe_3Al and FeAl, respectively, were formed. Solid solutions of aluminium in iron with an aluminium content of up to 50 at.% were prepared by the mechanochemical method.[136 – 138]

Therefore, the mechanochemical method enables one to extend substantially the concentration range of existence of solid solutions toward the non-equilibrium region if the intermetallic compounds closest to the metal, which serves as the solvent, are structurally similar.

Metastable solid solutions can be prepared by the mechanochemical method from powders of metals in different systems among which are systems characterised by large differences between the melting points and between the densities of the initial components, by high melting points of the resulting intermetallic compounds and by narrow homogeneity regions of the equilibrium chemical compound. In the synthesis of supersaturated solid solutions, as in the synthesis of intermetallides, systems with very large differences between the melting points of the initial components attract particular attention. Among these are systems containing tungsten ($T_{melt} \approx 3400$ °C) and tantalum ($T_{melt} = 3015$ °C) whose melting points are higher than boiling points of many metals.

In the Ni – W system, the boiling point of nickel (2900 °C) is lower than the melting point of tungsten and hence compounds are difficult to prepare from these elements by conventional procedures. According to the equilibrium diagram, this system contained (*a*) the α phase, *viz.*, a solid solution of tungsten in nickel with a homogeneity regions from 0 at.% to 35 at.% of W at 900 °C and from 0 at.% to 41.5 at.% of W at temperatures from 1000 °C to the melting point, (*b*) the β phase, *viz.*, the intermetallic compound Ni_4W, and (*c*) the γ phase, *viz.*, a solid solution of nickel in tungsten containing ~4 at.% of Ni.[125] Solid solutions of tungsten in nickel were synthesised from a mixture of these metals by the mechanochemical method.[139]

An analogous ratio between the melting points of the initial components is observed in the Fe – W system. According to the

equilibrium diagram, the system contained two intermetallides, *viz*., Fe_2W and Fe_3W_2. At 1520 °C and at room temperature, the solubility of tungsten in iron is 33 mass % (13 at.%) and 8 mass % (3 at.%), respectively. At 1640 °C, the solubility of iron in tungsten in the solid state is only 0.8 mass % (2.6 at.%).[125] The solid-phase synthesis in this system was carried out by the mechanochemical method to produce solid solutions.[140]

In the Cu – Ta system, the mixing enthalpy is close to zero, the difference between the atomic radii is large (~ 25%), the initial components belong to different structural types, and the boiling point of copper is almost 600 °C lower than the melting point of tantalum. According to the published data,[108, 141] the solid-phase solubility of tantalum in copper is virtually absent. At 1200 °C, only 0.009 at.% of Ta was dissolved in copper and no other metallic compounds were formed. Supersaturated solid solutions of tantalum in copper were prepared by the mechanochemical method.[142]

In the Cu – Nb system, the difference between the melting points of the initial components is also large. According to the equilibrium diagram, the system contained only two phases, *viz*., solid solutions based on copper (α) and niobium (β). The solubility of niobium in copper at 1100 and 20 °C is 1.66 mass % (1.14 at.%) and 0.2 mass % (0.13 at.%), respectively. The solubility of copper in niobium at high temperatures and at 700 °C amounts to ~2 at.% and 0.07 at.%, respectively.[141] Solid solutions with concentrations of each component up to 10 mass % (7.05 at.%) were prepared by the mechanochemical method.[143, 144]

The limiting solubilities (~10 at.%) both of niobium in a solid solution of nickel (a face-centred cubic structure) and of nickel in a solid solution of niobium (a body-centred cubic structure) were achieved in the Ni – Nb system by the mechanochemical method.[145] For comparison, is should be noted that the equilibrium solubilities are 4.2 at.% of Nb (at 987 °C) and 3.5 at.% of Ni (at 1000 °C).[146]

Solid solutions of aluminium based on different metals are of particular interest in materials technology. These compounds differ sharply from the starting compounds in chemical properties. The concentration of aluminium introduced has a pronounced effect on the properties. Gerasimov *et al*.[147] observed the formation of supersaturated solid solutions based on α-titanium for the compositions $Ti_{100-x}Al_x$ ($x < 60$ at.%). The solutions were formed even if the equilibrium phases Ti_3Al and TiAl were used as the starting components. The authors believed that the intermetallides can decompose and tribochemical equilibrium was established in the course of mechanical alloying giving rise to metastable phases. Solid solutions in the Ti – Al system were prepared in a planetary ball mill using the Ti_xAl_{100-x} compositions (x = 75 at.%, 50 at.% and 35 at.%). In none of the compositions examined did amorphisation occur. In all cases, the formation of solid solutions was observed, *viz*., the hexagonal Ti(Al) solid solution in the cases of $Ti_{75}Al_{25}$ and $Ti_{50}Al_{50}$ and a mixture of hexagonal Ti(Al) and cubic Al(Ti) solid solutions in the case of $Ti_{35}Al_{65}$. Variations in the conditions of activation led to a change in the quantitative ratio between the hexagonal and cubic phases.[148]

It is known that the equilibrium concentration of aluminium in niobium is less than 10 at.% at 1000 °C.[149] The use of the mechanochemical method allowed an increase in the concentration to 30 at.%.[150]

Supersaturated solutions were formed in the Zr – Al system containing up to 15 at.% of Al, the lattice parameters a and c of zirconium being decreased from 0.3235 to 0.3200 and from 0.5196 to 0.5148 nm, respectively.‡ After mechanochemical activation for 12 h, the particle size was ~ 12 nm.[55]

‡ Here, the first and second values correspond to the lattice parameters of zirconium and of the solid solution of aluminium in zirconium, respectively.

Solid solutions with an Al content of up to 50 at.% were formed in the Al – Pd system in which the equilibrium solubility of aluminium in palladium is 15 at.%.[53]

The mechanochemical method was used for the synthesis of solid solutions Al – 10 at.% of X (X = Ti, Zr or Hf) from powders of the metals.[151] Supersaturated solid solutions containing up to 13 at.% of Sb with a grain size of 10 nm were obtained in the Cu – Sb system.[152] The maximum concentration of 2.1 at.% of Sb was achieved in the Fe – Sb system.[153] In the Fe – Tb system, the mechanochemical method made it possible to attain a solubility of 36 at.% of Tb.[20] Metastable solid solutions W – 25 mass % (25 at.%) of Re with nanosized grains were also prepared by this method.[154]

Systems in which the absence of solubility of one element in another one is associated neither with the difference between the atomic radii nor with the difference in the structural type, but is most probably determined by the electron concentration are a special case. For example, the difference between the atomic radii in the Ge – Sn system is ~ 12%.[134] The face-centred cubic structure of germanium is similar to the tetragonal structure of β-Sn.[125] However, the equilibrium concentration of germanium in solid tin falls in the concentration range of 0.001% – 0.1% (see Ref. 125) and the formation of intermetallides was not observed. Solid solutions with a substantial deviation from the equilibrium state containing 12 at.% – 24 at.% of Sn were synthesised by the mechanochemical method.[155] These concentrations of tin are substantially higher than its concentrations in solid solutions prepared by fast quenching.[156] The non-equilibrium solubility of germanium in tin is achieved if the particle sizes of germanium are no larger than 10 nm.

In the Ge – Al system in which the initial elements belong to the same structural type and the difference between the atomic radii is very small (only ~3%), no intermetallides are formed. At 424 °C and 54 mass % (30.3 at.%) of Ge, the eutectic consisting of two solid solutions appeared. The germanium content in a solid solution based on aluminium decreased from 5.1 mass % (~2 at.%) at the eutectic temperature to 0.3 mass % (> 0.1 at.%) at 20 °C.[125] Metastable intermetallic compounds were obtained by quenching from the liquid state.[42, 157] Structurally similar metastable intermetallides were also synthesised by the mechanochemical method.[158, 159]

Analysis of the experimental data demonstrated that systems in which the atomic radius of the alloying element is larger than that of the metal serving as the solvent are characterised by higher equilibrium solubilities than those observed in systems with other ratios between the atomic radii. For example, the solubilities of aluminium (R = 0.143 nm) in nickel (R = 0.124 nm), iron (R = 0.126 nm) and copper (R = 0.128 nm) amount to tens of atomic percent, whereas the solubilities of iron, nickel and copper in aluminium are close to zero. The use of the mechanochemical method allowed a substantial extension of the region of existence of such solid solutions. Thus, metastable solid solutions based on aluminium with Cu and Fe contents of up to 33 at.% (see Ref. 160) and 10 at.%, respectively, were prepared.[161 – 163] Pekala and Oleszak[164] prepared a solid solution with composition $Fe_{10}Al_{90}$ in a horizontal low-energy ball mill after activation for 200 h. The average size of crystallites of the solid solution was ~7 nm. It was found that the mechanochemical formation of the solid solution in the course of activation was preceded by the short-duration formation of the intermetallide $FeAl_3$ from powders of iron and aluminium. Dunlap *et al*.[165] compared the microstructures of supersaturated solid solutions of iron in aluminium synthesised by the mechanochemical method and fast quenching and demonstrated that alloys with composition $Al_{98}Fe_2$ prepared by fast quenching occurred as monophase supersaturated solid solutions. In the initial stage of the mechanochemical synthesis, a supersaturated solid solution whose microstructural properties are similar to those of quenched alloys was formed. Further activation led to a decrease in the grain size and gave rise to an amorphous phase.

Supersaturated solutions with a magnesium content of up to 45 at.% were synthesised in the Al – Mg system by the mechanochemical method. The particle sizes were in the range of 2 – 10 nm.[166]

In the case of intermetallides with low enthalpies of formation or with enthalpies close to mixing enthalpies, supersaturated solid solutions can be prepared not only by mechanochemical synthesis from powders of the initial elements, but also on mechanochemical activation of intermetallides resulting in disordering of the equilibrium intermetallic phases synthesised by other methods. For example, the intermetallides Nb_3Al,[167] V_3Ga,[168] Nb_3Au,[169 – 171] Ni_3V,[172, 173] $Cr_{53}Fe$ [174] and Fe_3Ge [176] were transformed into solid solutions with body-centred cubic structures, whereas $NbAl_2$ (see Ref. 172) and $TiAl_3$ (see Ref. 175) were transformed into solid solutions with face-centred cubic structures upon mechanochemical activation. As a result of disordering of equilibrium intermetallides, solid solutions also formed in the Ni – Al system.[177]

Supersaturated solid solutions of tin in iron characterised by a substantial deviation from the equilibrium state can be prepared using mechanochemical activation both of a monophase intermetallide and a mixture of intermetallic compounds.[178 – 180]

Therefore, the mechanochemical method allows the preparation of supersaturated solutions in systems with negative enthalpies of mixing of the components. For most systems, the degree of supersaturation depends on the difference between the atomic radii of the initial elements, their structural compatibility and the electron concentration.

IV. Mechanochemical synthesis of supersaturated solid solutions in systems with positive mixing enthalpies

Of systems with positive mixing enthalpies, the Fe – Cu system has received the most study. If the concentrations of the components are equal to 50 at.% each, the mixing enthalpy calculated by the Miedema method [127 – 129] is 22 kJ mol^{-1}. It is believed that one of the reasons for the immiscibility of these metals in the solid state is the difference in their structural types. Thus, copper has the face-centred cubic (FCC) lattice and α-iron has the body-centred cubic (BCC) lattice. However, it is known that the structural type of iron changes as the temperature is increased: α-Fe (BCC) → β-Fe (BCC) at 770 °C → γ-Fe (FCC) at 920 °C. Hence, the possibility of dissolution is higher at high temperatures. At 1094 °C, the equilibrium solubilities of iron in copper and copper in γ-iron are 3.8 mass % (4.2 at.%) and ~8 mass % (~7.1 at.%), respectively.[108, 125] Solid solutions, which are non-equilibrium at room temperature, can be prepared by quenching from vapour or liquid phases. For example, solid solutions based on iron (BCC lattice) in the concentration range of up to 15 mass % (13.5 at.%) of Cu and based on copper (FCC lattice) in the concentration range of up to 20 mass % (22 at.%) of Fe were obtained from melts by quenching.[181] Supersaturated solid solutions in a wider concentration range were prepared by precipitation from the vapour phase *in vacuo* on a support at room temperature. It was demonstrated [182] that solutions had BCC structures if the copper content was lower than 50 mass % (47 at.%) and FCC structures if the copper content was higher than 70 mass % (68 at.%). Solutions with concentrations of copper in the range of 50 mass % – 70 mass % were not prepared. Supersaturated solid solutions in a wide concentration range were also synthesised by quenching from the vapour phase. Solid solutions based on iron existed up to 40 mass % (37 at.%) of Cu. Solid solutions based on copper with a FCC structure occurred up to 60 mass % (57 at.%) of Cu.[183]

Benjamin [184] was the first to report the results of mechanochemical alloying of the components in the Fe – Cu system. He obtained the homogeneous mixtures 80 mass % (82 at.%) of Fe – 20 mass % (18 at.%) of Cu and 50 mass % (24 at.%) of Pb – 50 mass % (76 at.%) of Cu in a high-energy laboratory mill. Metallographic studies of a specimen of the Cu – Fe system confirmed its homogeneity. It was also noted that the colour changed from red (the colour of copper) to grey (the colour of steel). Neverov *et al.*[94, 185] obtained solid solutions on a Bridgman anvil. The concentrations of copper in iron and iron in copper reached 40 mass % and 10 mass %, respectively. Gusev [186] demonstrated that solid solutions based on copper (FCC lattice) with compositions up to $Cu_{40}Fe_{60}$ and solid solutions based on iron (BCC lattice) with compositions up to $Cu_{30}Fe_{70}$ can be obtained in a centrifugal planetary ball mill. Kaloshkin *et al.*[187, 188] prepared supersaturated solid solutions $Fe_{100-x}Cu_x$ ($x = 20 – 80$) from powders of iron and copper in a planetary ball mill. The mechanochemical formation of solid solutions was completed in 30 min. It was also established that the FCC phase of the solid solution, the BCC phase of the solid solution and a mixture of these phases were formed at $x = 40$ at.% – 80 at.% of Cu, $x = 20$ at.% of Cu and $x = 30$ at.% of Cu, respectively. In studies of structural changes occurring in the course of mechanical alloying, Barro *et al.*[189] observed the formation of solid solutions in the Fe_xCu_{100-x} system ($x = 5$, 10 and 20). Uenishi *et al.*[190] performed mechanical alloying of the solid solution $Fe_{1-x}Cu_x$ and prepared also monophase compositions with BCC (if $x < 40$ at.%) and FCC (if $x > 40$ at.%) structures. Yavari *et al.*[191] confirmed that the lattice parameters in these compositions were increased. Eckert *et al.*[192, 193] prepared solid solutions Fe_xCu_{100-x} in a SPEX 8000 ball mill. It was demonstrated that monophases with FCC and BCC structures exist at $x \leqslant 60$ and $x \geqslant 80$, respectively, whereas solid solutions with FCC and BCC structures coexist in the range of $60 \leqslant x \leqslant 80$. The formation of solid solutions starts when grains reach nanometer sizes.

Jiang *et al.*[194, 195] also observed the formation of solid solutions in the Cu – Fe system and detected small amounts of γ-Fe (a FCC structure) in all specimens subjected to mechanochemical treatment for more than 10 h. Supersaturated solid solutions in the Cu – Fe system were also prepared in SPEX 8000 ball mills in more recent studies (see, for example, Refs 196 – 206). It was established by different methods that monophase supersaturated solid solutions were formed in mixtures containing more than 80 mass % or less than 60 mass % of copper, whereas two phases coexisted in the region with a copper content from 50 mass % – 60 mass % to 80 mass %.

Therefore, the mechanochemical method allows the preparation of supersaturated solid solutions throughout the concentration range of existence of a binary system with a high positive heat of mixing of the initial components (Fig. 2).

The Cu – Co system also has a positive mixing enthalpy (~20 kJ mol^{-1} for the equiatomic composition). According to the data reported by different researchers, the concentration of cobalt in a solid solution based on copper (β phase) at 1100 °C changes from 5.2 mass % to 8 mass % (from 5.6 at.% to 8.5 at.%) and the concentration of copper in a solid solution based on cobalt at the same temperature changes from 12 mass % to 14 mass % (from 11.2 at.% to 13.1 at.%). At temperatures below 500 °C, the mutual solubility of one element in another is no higher than 0.1%.[108] The low mutual solubility is attributable to the difference in the structural types of these elements. However, it is known that α-Co (the hexagonal close-packed structure) is transformed into β-Co at 350 – 470 °C. The latter, like copper, has a FCC structure. The high mutual solubility of these elements is quite possible due to the insignificant difference between their atomic radii. Fast quenching made it possible to dissolve up to 20 mass % of Co and less than 25 mass % of Cu in cobalt. The mechanochemical method was used for the preparation of solid solutions with FCC structures throughout the concentration range of existence of this binary system.[197, 199, 207 – 213] In a number of studies, it was found that phase transformations of cobalt occurred upon mechanochemical activation in ball mills.[214 – 216]

The Cu – Cr system is also characterised by a positive mixing enthalpy (~20 kJ mol^{-1} for the equiatomic composition). In this

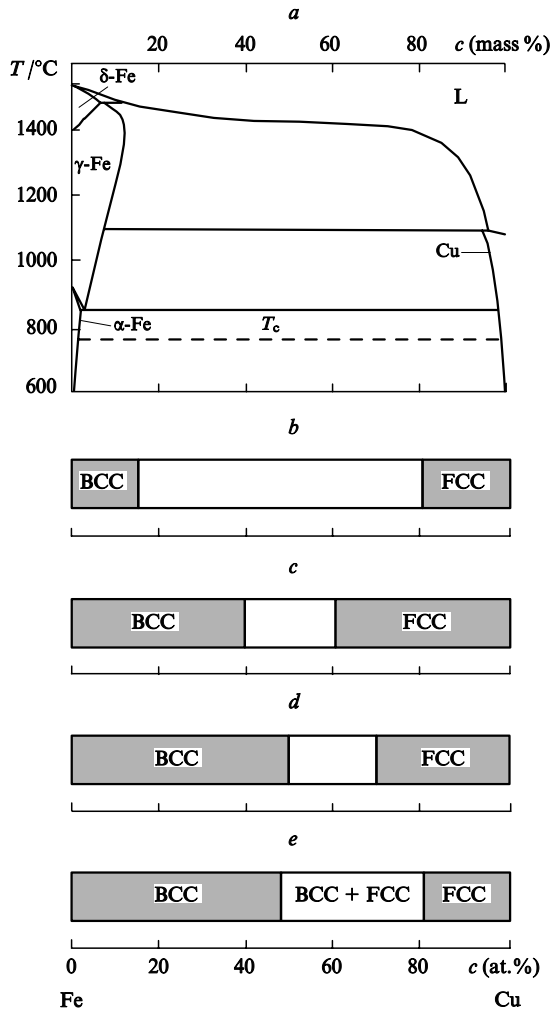

Figure 2. Equilibrium diagram of the Fe – Cu system (*a*) and the regions of existence of solid solutions synthesised by quenching from a melt (*b*), quenching from the vapour phase (*c*), precipitation from the vapour phase (*d*) and the mechanochemical method (*e*).

system, as in the above-considered one, the difference between the atomic radii of the initial metals is insignificant, but their structural types differ substantially (BCC and FCC structures, respectively). The solubility of chromium in copper varies from 1.25 mass % to 0.5 mass % (from 1.5 at.% to 0.6 at.%) at 1050 °C and it is less than 0.03 mass % at 400 °C. The solubility of copper in chromium is 0.16 at.% and 0.085 at.% at 1300 °C and 1150 °C, respectively.[141] Chromium has several crystal modifications, *viz*., α-Cr (BCC structure), β-Cr and γ-Cr. Supersaturated solid solutions characterised by substantial deviations from the equilibrium state were prepared by the mechanochemical method.[217–220]

In the Cu – V system, the atomic radii of the initial metals have close values, whereas their structural types are different (FCC and BCC structures, respectively). According to the equilibrium diagram, solid solutions based on copper (α) and vanadium (β) are formed in the system. The maximum solubility of vanadium in copper is 0.8 at.% at 1120 °C (0.1 at.% at 20 °C) and the maximum solubility of copper in vanadium is 8 at.% at 1530 °C.[141] A wide range was found in which the components in the liquid state were immiscible (the range from 4.0 at.% to 84.6 at.% of V). Solid solutions both with BCC and FCC structures were prepared on mechanochemical activation.[218,221] It was demonstrated [221] that the particle sizes of the components should be no larger than 30 nm for solid solutions to be prepared.

In the Cu – Ag system, both components have FCC lattices, the difference between the atomic radii is ~11% and the melting points of the components have close values. However, according to the equilibrium diagram of this system, the components have limited solubilities in the solid state at the eutectic temperature (~780 °C). At this temperature, the solubility of silver in copper is 8.0 mass % (4.9 at.%) and the solubility of copper in silver is 8.8 mass % (14.1 at.%). Quenching at a rate of cooling of 10^7 deg s^{-1} afforded a continuous series of solid solutions. On cooling at lower rates, a continuous series of solid solutions was not detected. Depending on the conditions, solid solutions with different contents of the second element can be synthesised by the mechanochemical method throughout the concentration range of this system.[42,186,222–225]

In the Pb – Al system, both elements also have FCC structures, the difference between their atomic radii is ~18% and both metals are rather low-melting. However, the system is characterised by a positive mixing enthalpy. The metals do not form intermetallides and mutual solubility is absent. Supersaturated solid solutions were prepared in this system by the mechanochemical method.[226]

The Fe – Ag system is characterised by a very high positive mixing enthalpy, the initial elements have different structural types (BCC and FCC, respectively) and the mutual solubility of the components is limited even in the liquid state. The solubility of silver in solid iron is no higher than 0.01% and the solubility of iron in solid silver is 0.0006%.[125] Solid solutions are difficult to synthesise by the mechanochemical method.[227–230] Only very thin dispersions of iron in a silver matrix were obtained; the average radius of iron particles was equal to several nanometers.[230]

In systems with positive mixing enthalpies, a low mutual solubility of one component in another may be associated with a large difference between the atomic radii of the initial elements. For example, this difference in the Cu – Bi system is ~30% and the solubility of bismuth in copper in the solid state is only 0.003 at.% at 800 °C, the solubility of copper in bismuth being insignificant.[231] The formation of the metastable intermetallide with composition Cu_5Bi_2 was observed in this system.[232] The mechanochemical method was used for the preparation of supersaturated solid solutions of bismuth in copper with a concentration of bismuth of up to 4 at.%; the average grain size was ~10 nm.[233]

The Fe – In system is also characterised by a positive mixing enthalpy and the difference between the atomic radii of ~23%. In the equilibrium state mutual solubility is completely absent. Solid solutions of indium in iron with rather low concentrations of indium were prepared by the mechanochemical method.[234]

In solid solutions prepared by the mechanochemical method in systems characterised by positive mixing enthalpies and large differences between the atomic radii, the maximum solubilities of one element in another are rather low compared to those in systems in which the differences between the atomic radii of the initial elements are smaller and the elements can adopt similar structures due to phase transitions on mechanochemical activation.

The use of the mechanochemical synthesis for the preparation of intermetallides and solid solutions in immiscible systems with a large difference between the melting points of the initial components, in particular, in systems in which the melting point of one component is higher than the boiling point of another one, is of most practical interest. For example, the Mg – Ti system is characterised by a positive mixing enthalpy (12 kJ mol^{-1}). In this system, the difference between the atomic radii is ~9%, the components belong to the same structural type and the melting point of titanium is ~500 °C higher than the boiling point of magnesium. Hence, solid solutions are difficult to prepare by conventional methods (probably, they can be synthesised by precipitation from the vapour phase). Solid solutions of titanium in magnesium with concentrations of up to 20 mass % of Ti were synthesised by the mechanochemical method.[235] Moritaka *et al*.[236] examined the Ti – *x*Mg system (*x* = 10 at.%, 20 at.%,

30 at.%, 40 at.%, 50 at.%, 60 at.%, 70 at.%, 80 at.% and 95 at.%). Mechanical alloying was carried out in a Frich ball mill (P-7 type). Supersaturated solid solutions were detected at a magnesium content of $\geqslant 60$ at.%. In the range from 70 at.% to 80 at.% of Mg, the coexistence of solid solutions based both on titanium and magnesium was observed. The sizes of crystallites were larger and nonuniform distortions of the lattices of solid solutions based on magnesium were more substantial than those observed in the case of nanocrystalline solid solutions based on titanium.

The Cu–W system is characterised by a very high positive mixing enthalpy (35 kJ mol^{-1}). In this system, the difference between the atomic radii is $\sim 8\%$, the structural types of the initial metals are different (FCC and BCC, respectively) and the boiling point of copper is lower than the melting point of tungsten. Solid solutions were synthesised in this system by the mechanochemical method.[237,238] Raghu *et al.*[239] performed mechanical alloying in the systems Cu–5 mass % (1.9 at.%) of W and Cu–15 mass % (5.2 at.%) of W and demonstrated that nonequilibrium solubilities both of copper in tungsten and tungsten in copper occurred.

Therefore, the use of mechanochemical synthesis in systems which are immiscible in the equilibrium state allows the preparation both of metastable intermetallic compounds and non-equilibrium solid solutions. In systems in which the atomic radii of the initial components have close values and their structural types become similar due to phase transitions, the concentration ranges of existence of supersaturated solid solutions prepared by the mechanochemical method are extended most significantly compared to those of analogous solutions prepared by quenching. If the immiscibility in the equilibrium state is dictated by the difference between the atomic radii of the initial components, a substantially lower solubility is attained. In the latter case, rarely, if ever, can supersaturated solid solutions be prepared by quenching, whereas a particular solubility is achieved using the mechanochemical method, but this solubility is substantially lower than that in systems in which the difference between the atomic radii is small.

V. Quasicrystals and amorphous alloys

Follstaedt and Knapp[240] were the first to use solid-phase diffusion for the synthesis of icosahedral phases in the Al–Ru and Al–Mn systems. The melting point of ruthenium is substantially higher than that of aluminium and an alloy of these elements is difficult to prepare by quenching. Hence, the search for new procedures for the synthesis of these alloys is a topical problem. The formation of an icosahedral phase in experiments on heterophase diffusion signifies that nuclei of this phase are formed and grow more rapidly than the crystalline phase with the corresponding composition and a lower free energy in the solid state. This may be due to the fact that the fragments characterised by the short-range icosahedral order are more ordered in the crystal structure. Taking into account the results of experimental investigation of heterodiffusion and assuming that the mechanism of formation of amorphous alloys and supersaturated solid solutions on mechanical alloying is also associated with the process of heterodiffusion, Follstaedt and Knapp suggested that an icosahedral phase can also be prepared by mechanochemical alloying. Independently, Ivanov *et al.*[241] were the first to synthesise the icosahedral phases $Mg_{32}(Zn, Al)_{49}$ and $Mg_{32}(Cu, Al)_{49}$ from elements by the mechanochemical method and performed structural transformations of the corresponding Frank–Casper cubic phases into icosahedral phases by mechanochemical activation. The synthesis of the icosahedral phase $Mg_{32}(Zn, Al)_{49}$ from the elements involved an intermediate step giving rise to an amorphous phase. Apparently, clusters possessing short-range icosahedarl order were formed in this step. Then an icosahedral phase arose. This phase appeared to be rather stable and remained unchanged in the course of further treatment in a ball mill. The authors demonstrated that the synthesis of the icosahedral phase on mechanical alloying of metallic powders was accompanied by intermediate formation of an amorphous phase. Mechanochemical treatment of the cubic phase led to gradual broadening and then disappearance of a series of X-ray diffraction reflections belonging to this phase, whereas the remaining reflections were shifted so that they corresponded to the icosahedral phase. The X-ray diffraction reflections of the final product are broadened compared to those of quenched specimens. The metastable icosahedral phase was transformed into the cubic phase upon heating. According to the data of differential scanning calorimetry, this transformation was accompanied by three exothermic effects. The first of these effects most probably corresponds to annealing of defects in the icosahedral phase, which is confirmed by the fact that the X-ray diffraction reflections corresponding to this phase were narrowed after annealing of a specimen at the temperature of the first exothermic peak.

Eckert *et al.*[242] synthesised quasicrystals of $Al_{65}Cu_{20}Mn_{15}$ from the elements by mechanochemical activation in a planetary ball mill for 90 h. This phase also appeared to be stable to mechanochemical treatment. Thus, the X-ray diffraction pattern remained virtually unchanged in the course of grinding during 160 h. Unlike the authors of the above-considered study, Eckert *et al.* did not observe the formation of an intermediate amorphous phase and suggested that the formation of the icosahedral phase proceeded by a mechanism of heterodiffusion at the expense of heat, which was released upon dissipation of the kinetic energy of colliding balls. More recently (see, for example, Ref. 243), the icosahedral phase $Al_{70}Cu_{20}Fe_{10}$ has been synthesised from a mixture of metallic powders by the mechanochemical method. Local icosahedral symmetry was observed in alloys of aluminium with molybdenum after their mechanical grinding.[244]

The investigation performed by Schwarz and Johnson,[245] who demonstrated that amorphous alloys can be formed through heterodiffusion in a layered composite, has stimulated increased interest in the preparation of amorphous alloys in solid-phase processes. More recently, Schultz[246] has prepared a voluminous amorphous nickel–zirconium alloy by the annealing of a repeatedly rolled layered specimen. These facts suggested that the preparation of amorphous alloys by mechanical alloying occurred as a solid-phase process. During the last decade, a rich variety of amorphous alloys both in binary and multicomponent metallic systems, including systems characterised by large differences in the melting points and in the densities of the initial components, have been synthesised by mechanical alloying of powders of elements. For example, it was demonstrated that amorphous alloys can be prepared in the Ni–Mg system by the mechanochemical method (this process depends substantially on the blend composition). In addition, the formation of an amorphous alloy in magnesium-rich compositions was preceded by the formation of the intermetallic compound Mg_2Ni, whereas amorphous alloys were formed immediately from metallic powders in compositions with high nickel contents in spite of the fact that, according to the equilibrium diagram, the intermetallide Ni_2Mg existed in this concentration range.[247]

Nanosized amorphous alloys were also prepared in the Cu–Zr system.[248] The amorphous alloys Al_x-Zr_{100-x},[249] $Fe_{50}-Ta_{50}$,[250] Ni_xTa_{100-x},[251] Cu–Ti,[252] $Fe_{75}Zr_{25}$[253] and $Fe_{66.7}Zr_{33.3}$[254] were synthesised. In the Ti–Fe system, the formation of amorphous alloys was preceded by the formation of the supersaturated solid solutions β-Ti(Fe) and α-Fe(Ti) and the intermetallides FeTi and Fe_2Ti.[255] Amorphous phases were prepared in the systems Fe–6 mass % (11.3 at.%) of Si (see Ref. 256) and Se–As.[257] In the Fe–Cr system, amorphous alloys containing only 28 mass % (26.5 at.%) and 45 mass % (43 at.%) of Fe were prepared.[258] Multicomponent systems containing boron, phosphorus, silicon, carbon and other elements, for example, $Ni_{50}Pd_{40}Si_{10}$ (see Ref. 259) and YNi_2B_2C,[260] have received much consideration. In the latter system, the formation of nanocrystalline or amorphous phases is determined to a large extent by the

activation parameters (an amorphous phase appeared only after prolonged activation). Amorphous phases with composition $Cu_{86-x}Sn_xP_{14}$ ($x = 2-15$) can be prepared from powders of the initial elements, the time of the preparation of the amorphous phase depending on the tin content in the mixture. Thus, the duration of activation was 28, 20, 12 and 32 h at $x = 4, 5, 8$ and 10, respectively.[261] The alloy $Fe_{39}Ni_{39}Si_{10}B_{12}$ can be prepared both in the amorphous and nanocrystalline states.[262] An amorphous alloy with composition $(Zr_{0.65}Al_{0.075}Cu_{0.175}Ni_{0.1})_{100-x}Fe_x$ ($x \leqslant 20$) was synthesised from powders of the initial elements.[263]

Ermakov *et al.*[264–267] were the first to perform amorphisation of intermetallic compounds by the mechanochemical method. They carried out the structural transformation of the intermetallic compounds X–M, where X = Y, Gd or Tb and M = Fe or Co, from the crystalline to amorphous state in a wide concentration range by mechanical grinding. In the late 1980s, investigations of this process have been started by many researchers.[268–272] Amorphisation of intermetallides was examined in the Sn–Nb, Ge–Nb,[39,269] Cr–Ti, Cu–Ti, Fe–Ti, Mn–Ti, Co–Ti, Ni–Ti, Cu–Cr, Ni–Zr, Mn–Si[270] and Ni–Al[271,272] systems. Koch[13] was the first to initiate the process of amorphisation of intermetallides and called it 'mechanical grinding' rather than 'mechanical alloying' from the initial elements. In the last decade, this process has been studied intensively. Amorphisation of the Laves phases Fe_2Sc and Fe_2Y was investigated.[273,274] It was demonstrated that vigorous mechanical grinding of the intermetallide Fe_2Sc led initially to partial chemical disordering followed by amorphisation, whereas Fe_2Y was transformed into the amorphous state without preliminary disordering. Amorphisation of the intermetallides $Ni_{10}Zr_7$ and $NiZr_2$ was also studied.[275–277] Skakov *et al.*[278] investigated the process of amorphisation in the Ni–Nb system. An amorphous phase with composition $Fe_{78}P_{22}$ was prepared by mechanical grinding.[279] Poon *et al.*[280] succeeded in transforming supersaturated solid solutions based on titanium into amorphous phases.

For some systems, amorphisation upon mechanical grinding occurred as a cyclic process. For example, investigations of the structural evolution of powders of elements upon mechanical grinding of the $Co_{75}Ti_{25}$ and $Co_{50}Ti_{50}$ mixtures[281–283] demonstrated that the formation of amorphous alloys with these compositions occurred rather rapidly, but these alloys were transformed into Co_3Ti and CoTi (both compounds have BCC structures) on further mechanical treatment. These intermetallides were thermally stable and were not transformed into other phases upon heating to 1300 K. However, further grinding again afforded the amorphous compositions $Co_{75}Ti_{25}$ and $Co_{50}Ti_{50}$. Surinach *et al.*[284] observed the transformation of an amorphous phase into a nanocrystalline phase in the $Fe_{77.5}Cu_1Nb_3Si_{9.5}B_9$ system and determined the activation energy of the nanocrystalline transformation.

Amorphous structures can also be prepared according to the mechanochemical method by grinding intermetallides together with metallic powders. Thus, an amorphous phase in the Cu–Cd system was prepared by grinding the equilibrium δ phase together with a copper powder.[285] It should be noted that attempts to obtain an amorphous structure in this system either by mechanical alloying of powders of copper and cadmium or by grinding of the single δ phase failed.

Amorphous phases in the Mg–Ni and Mg–Ni–V systems were synthesised upon mechanical grinding of the Mg_2Ni alloy with powders of nickel and vanadium, respectively.[286] An amorphous phase was formed by mechanical grinding of the intermetallide $EuFe_2$ as well as by its grinding with powders of europium and iron.[287] More complex amorphous phases were also synthesised in such a manner. The amorphous compositions $Mg_2Ni_1M_{0.1}$ (where M = Ni, Ca, La, Y, Al, Si, Cu or Mn) can be prepared by mechanochemical grinding of the binary system of the intermetallide $Mg_2Ni_{0.9}M_{0.1}$ and a powder of nickel.[288]

The regions of existence of amorphous alloys synthesised by the mechanochemical method were calculated and determined experimentally in a large number of studies (see, for example, Refs 289–295).

VI. Phase and structural transformations in the mechanochemical synthesis of intermetallic compounds

Benjamin[184,296,297] considered mechanical alloying of metallic powders in attritors as a repeated process of cold welding under pressure and grinding. He believed that a metal particle is flattened upon its initial collision with balls, *i.e.*, the ratio of the surface area of the particle to its volume increases, surface films of adsorbed impurities being disrupted. Flattened metal particles contact with each other through the freshly formed surfaces giving rise to a layered composite of powdered particles (Fig. 3). The layers in this composite become thinner as welding and grinding are continued. The formation of layered composites was detected in many systems.[13,230,247,298,299] There are five typical stages of evolution of a mixture of powders of two plastic metals (Fig. 4).

The formation of layered composites from mixtures of metallic powders is accompanied by their intensive dispersion as evidenced by the results of investigations on deformation of metals. Initially, the so-called elementary structure of slip bands appears upon deformation of pure metals even without the use of activators and mills.[300] This band consists of thin slip lines, which

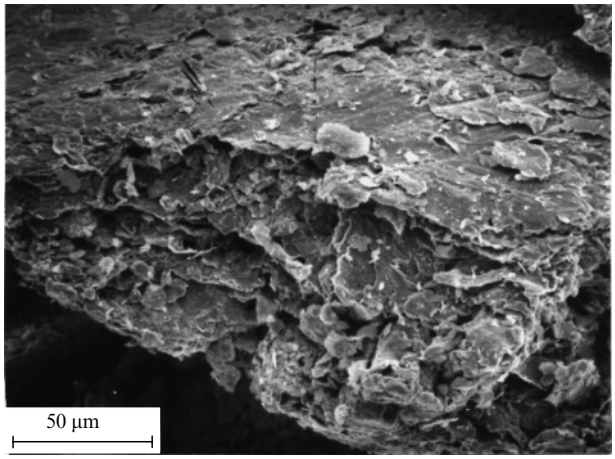

Figure 3. Microphotograph of a cross-cut cleavage of the layered composite (the system Ni–14 at.% of Al, mechanochemical activation for 30 s).[80]

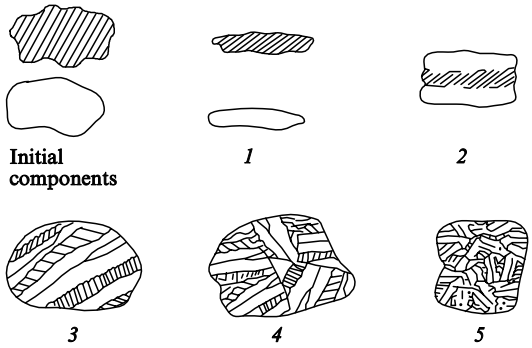

Figure 4. Typical stages of evolution of plastic powders in the course of mechanochemical activation;[84]
(*1*) plastic deformation of the initial particles (flattening), (*2*) the formation of new contacts between the initial elements, (*3*) accumulation of dislocations and breakage of layers into blocks, (*4*) and (*5*) subsequent stages of mixing and diffusion giving rise to the product.

cover the crystal surface uniformly. As plastic deformation is developed, packets of slip bands arise and deformation is distributed less uniformly throughout the bulk of the crystal. More in-depth investigation demonstrated that crystals were broken up into blocks, which were slightly disordered with respect to each other, even in the initial stage of deformation. At this stage, the appearance of dislocation networks was observed in studies of a thin foil by electron microscopy. Further development of plastic deformation led to roughening of the dislocation network to form an irregular cellular structure, the density of dislocations at the interface of the cells being substantially higher than the average density throughout the bulk. At this stage, the growth of disordered blocks was observed.[300] The mechanism of formation of the cellular structure is not entirely known. However, it is assumed that processes of polygonisation associated with dislocation climb and rearrangement are of great importance in this mechanism. Since dislocation climb can occur only under the action of very large stresses or through diffusion inflow of point defects,[301] the formation of the cellular structure is estimated taking into account these factors. At rather high temperatures (close to the temperature of recrystallisation), the formation of a cellular structure is promoted by a high rate of migration of vacancies. The concentration of vacancies in plastically deformed metal is also high. Thus, it is believed that this concentration and the equilibrium concentration of point defects at temperatures close to the melting point are of the same order of magnitude. According to van Bueren,[302] after low-temperature deformation, which leads to a change in the linear dimensions of the specimen by only 10%, the concentration of point defects reaches $10^{19}-10^{20}$ cm^{-3}. Apparently, the high concentration of point defects upon low-temperature deformation is responsible for the formation of a cellular structure. In addition, low-temperature deformation is favourable for a decrease in the cell dimensions.[303] Rapid deformation also influences the cell dimensions, *viz*., it causes the formation of extremely small cells.[303, 304] The formation of cellular structures characterised by the disordered arrangement of the adjacent cells and substantial deformations were observed for chromium,[303] iron,[305] copper,[306] tantalum,[307] molybdenum and its alloys [308–312] and for a number of other metals and alloys.[313–316]

Therefore, domains of the crystal lattice are rearranged in the course of plastic deformation. This effect was revealed both for metals and their alloys in wide ranges of temperature, stresses and rates of deformation. The fragment-boundary angles depend on the degree of deformation and can be as large as several tens of degrees. The boundaries are either small-angle walls and networks or grain boundaries of a deformation nature.

Plastic deformation arising under the joint action of high pressure and shear on mixtures of metals leads to a decrease in the dimensions of coherent-scattering regions compared to the analogous regions for individual compounds treated analogously.[317–321] Positron studies of structural defects in metals subjected to high pressure and shear deformations demonstrated that vacancy clusters with sizes of up to 0.5 nm were formed in these specimens. In addition, specimens were intensively saturated with dislocations as the degree of deformation increased.[319]

Therefore, plastic deformation leads to the formation of non-equilibrium point defects and their clusters and to a high density of dislocations. As the degree of deformation increases, a cellular structure is developed followed by fragmentation. In the case of plastic deformation of heterogeneous mixtures, blocks become smaller and interactions at the boundaries of dissimilar blocks occur.

Processes of grinding and formation of layered composites occur more vigorously in planetary ball mills because rapid shear deformations are realised on collisions in such mills. The dynamics of grinding, the microstructure and the sizes of the particles formed depend both on the conditions of mechanical treatment and on the properties of metals as exemplified by copper, nickel, iron and germanium.[320–326]

The process leading to a decrease in the grain size in ball mills involves three steps.[326]

1. Initially, deformation is localised in slip bands consisting of a series of high-density dislocations.

2. When a particular degree of deformation is achieved, annihilation and recombination of these dislocations take place within small-angle grain boundaries separating individual grains. The grain sizes thus obtained are 20–30 nm.

3. The orientation of individual crystalline grains with respect to the adjacent grains becomes totally random.

These stages are typical of deformation processes, which involve metals with BCC lattices and intermetallic compounds and which occur at high rates of deformation.

Eckert *et al*.[327] found that the minimum grain size of nanocrystalline metals (generally, 6–22 nm) is achieved if two competitive process take place, *viz*., substantial plastic deformation caused by mechanical treatment in a ball mill and relaxation of the material. Moreover, it was found that the minimum grain size of metals with FCC lattices is in inverse proportion to the melting point.[328, 329] Fecht *et al*.[328] demonstrated that the average grain sizes of metals with BCC lattices and hexagonal close-packed lattices are decreased to 9 and 13 nm, respectively.

The initial step of the mechanical synthesis in metallic systems involves the formation of layered composite structures accompanied by simultaneous dispersion of the initial components to nanosized grains. The formation of such layered composites results in an increase in the contact area between the initial components. It is known that heterogeneous solid-phase reactions can proceed only at the regions of tight contacts of the reacting phases. At these regions, a layer of the product arises and the further course of the reaction depends on the mechanism of diffusion of the reacting compounds through this layer. Solid-phase compounds are transferred primarily through diffusion whose rate depends on the mobility of lattice defects (their mobility is particularly high at the crystal surface even at low temperature).[330]

Pavlyukhin *et al*.[90] studied the formation of solid solutions in the Fe–Cr system and demonstrated that accelerated diffusion can proceed in binary metallic mixtures upon their mechanical activation in centrifugal planetary mills. Based on the results of Mössbauer spectroscopy, the authors estimated the diffusion coefficient (D) for the system containing spherical particles of radius R under conditions of activation. The determined value $D \simeq 10^{-5}-10^{-7}$ cm^2 s^{-1} is seven orders of magnitude larger than the diffusion coefficient of chromium in iron at 1600 K ($10^{-12}-10^{-14}$ cm^2 s^{-1}). A change in the microstructure of the alloy, which is generally observed in the initial step of mechanical alloying, was ignored in calculations. However, since the thickness of layers changes substantially in the course of mechanical alloying, the radius of the initial species is not the only factor determining the diffusion path.

In the case of plastic deformation of metals, diffusion can be substantially accelerated due to destruction and generation of dislocations [331] along which the rate of diffusion in metals is several orders of magnitude larger than along other directions.[332–339] In addition, it was demonstrated [340–345] that the diffusion coefficient is linearly proportional to the rate of deformation. Therefore, solid-phase dissolution of elements can be substantially accelerated on rapid plastic deformation. If this process is accompanied by the formation of layered composites, mass transfer can be promoted, on the one hand, due to short diffusion distances, and, on the other hand, due to acceleration of diffusion upon rapid plastic deformation.

Clemens [346] found parallels between mechanochemical synthesis and solid-phase transformations in layered film systems. He believed that the role of mechanical activation consists in the formation of a composite from disperse particles of the initial components and promotion of diffuse mixing due to generation of non-equilibrium defects.

Hellstern and Schultz[347] considered phase formation taking into account solid-phase diffusion. In the cited study, mechanical mixing of pure powders of iron and chromium was performed in a ball mill under argon. The authors believed that mechanical treatment afforded a layered microstructure consisting of two elements and the layers became thinner in the course of treatment. Since this system possesses a substantial chemical driving force, which favours diffusion between layers, the process occurs through the mechanism of a solid-phase diffusion reaction. An analogous viewpoint was also followed in a more recent study.[348] In the latter study, it was demonstrated that particles with a typical layered structure were formed in Ni–Zr and Fe–Zr systems at the initial stage of mechanical treatment of initially crystalline powders in a mill. Further mechanical treatment afforded composites consisting of ultrathin layers in which solid-phase diffusion proceeded. Samwer suggested[349,350] that amorphous alloys are formed in the course of solid-phase diffusion and this process occurs at low temperature due to rapid diffusion of one component into another one. As a result of mechanical treatment, particles of the components adopt a 'multilayer-sandwich' form and a negative heat of mixing is the driving force for the process. Koch *et al.*[271] also believed that mechanochemical reactions are accompanied by the formation of ultradisperse composite particles, solid-phase diffusion occurs in these particles and a negative mixing enthalpy is the driving force for diffusion.

Most researchers attributed fast mass transfer in mechanochemical reactions characterised by negative mixing enthalpies to a large contact area and a high rate of solid-phase diffusion at high rates of plastic deformation of metals.

A large number of experimental studies of spontaneous diffusion arising when particles of the initial components (which are in intimate contact) become nanosized, have been carried out in recent years.

In many systems, non-equilibrium solid-phase solubility of one element in another one is readily realised when grains become nanosized. It was found that extremely high diffusion rates are characteristic of highly disperse nanosized particles.[351–353] It was found that copper immediately dissolved in nanosized gold particles at room and lower temperatures.[354] Fast spontaneous alloying afforded the intermetallides $AuSb_2$, InSb and AlSb.[355–357] It was demonstrated that every pair of elements is characterised by its own critical grain (particle) size at which spontaneous alloying starts at room temperature. The critical size of the initial particles increases as the heat of alloy formation increases. In the Au–Cu,[358] Au–Zn[353] and Au–Al[359] systems, the mixing enthalpies are negative and spontaneous alloying takes place even in the case of a rather large critical particle size. In the Au–Ni system, the enthalpy is positive and spontaneous alloying at room temperature occurs only if grains are very small. In the In–Al system, the mixing enthalpy is substantially larger than zero and hence, spontaneous alloying was not achieved (Fig. 5). Phase diagrams for systems consisting of nanosized particles differ substantially from standard diagrams and the solid-phase solubility of one element in another increases essentially (reaches several tens of percent) even if the elements virtually do not form solid solutions.[361] It was assumed that relaxation of lattice distortions, which may be caused by a dissolved atom, proceeds much more readily in nanosized particles than in bulkier particles because the lattice becomes more mobile (Fig. 6).[362,363]

Therefore, mass transfer in layered composite structures containing nanosized grains, which are formed in the first step in metallic systems with negative mixing enthalpies, proceeds through spontaneous diffusion. This diffusion can take place at room temperature because the critical grain size at which it starts depends on the mixing enthalpy, *viz.*, the larger the (negative) mixing enthalpy the larger the appropriate grain size. In systems in which intermetallides with high heats of formation (or, at least, in which the heats of formation of intermetallic compounds are substantially larger than the heats of mixing of solid solutions), these intermetallic compounds are formed first. Examination of

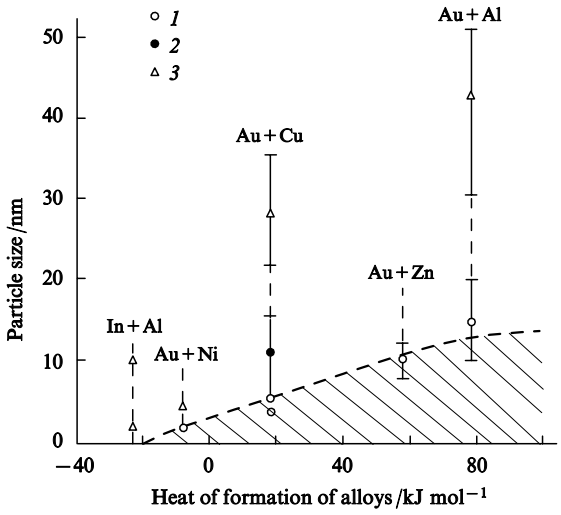

Figure 5. Dependence of the critical sizes of the initial particles on the heat of formation of alloys in different systems at 300 K;[360] (*1*) complete spontaneous alloying at 300 K, (*2*) partial spontaneous alloying, (*3*) alloying does not occur.

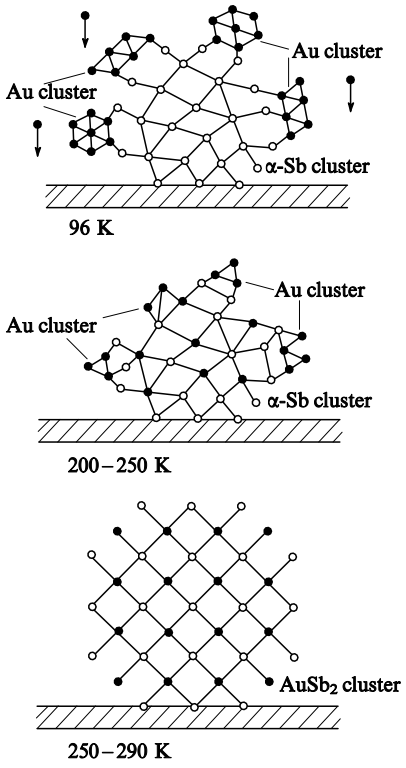

Figure 6. Scheme of spontaneous alloying of gold and antimony particles.

the mechanochemical synthesis of solid solutions demonstrated that in layered composites, intermetallides are actually formed first. In the second step of the mechanochemical synthesis, intermetallides characterised by a high heat of formation and a high content of the alloying element arise in the Ni–Ge, Ni–Al, Ni–Si, Ni–Bi, Ni–Sn, Ni–In, Ni–Ga, Cu–Sn, Cu–In, Cu–Ga and Fe–Sn systems.[111,113,115–119,121–124,126,132,364] X-Ray diffraction data corresponding to the phase formation in the course of the mechanochemical synthesis of solid solutions of bismuth in nickel are shown in Fig. 7. In this system, two intermetallic compounds, *viz.*, NiBi (78.8 mass % Bi) and $NiBi_3$

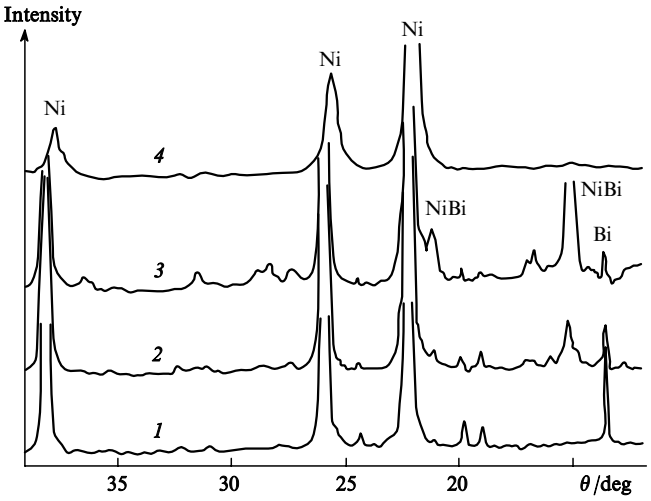

Figure 7. X-Ray diffraction patterns of the products of mechanical alloying of nickel with 10 mass % of bismuth. The activation time (min): (*1*) 1, (*2*) 3, (*3*) 10, (*4*) 90.[126]

(91.44 mass % Bi), exist.[108] The enthalpies of formation of these compounds calculated by the Miedema method[127–129] are approximately -4 kJ mol^{-1} for NiBi and -2 kJ mol^{-1} for $NiBi_3$. In the course of the mechanochemical synthesis of solid solutions in this system, the formation of layered composites is followed by the formation of the intermetallide NiBi (see Fig. 7). It is worthy of note that the above-mentioned phase can be formed under equilibrium conditions only if the bismuth content is 78 mass % and the mixture subjected to mechanical activation contains only 10 mass % of Bi. As the time of activation was increased, the intensities of reflections of the NiBi phase increased (see Fig. 7, curves *2* and *3*), the lattice parameter of nickel remaining the same. The growth of the NiBi phase proceeded until the bismuth was completely consumed. Only further activation of the resulting intermetallide with unconsumed nickel led to a decrease in the intensities of reflections of the intermetallide NiBi, broadening of the diffraction peaks of nickel and their shift to the small-angle region (see Fig. 7, curve *4*), which is indicative of the formation of a solid solution. Analogous changes in the diffraction patterns were observed for other systems. The dynamics of changes in the phase composition of the mixture can be followed using the Fe–Sn system as an example (Fig. 8). Thus, the amount of the intermetallic compound $FeSn_2$ increased and then decreased upon mechanochemical dissolution of $FeSn_2$ in iron to form a solid α-solution of tin in iron. Mechanochemical activation led to a decrease in the grain size of α-Fe to 10–20 nm and the resulting intermetallide $FeSn_2$ also contained nanosized particles (Fig. 8 *b*). It should be noted that the intensive formation of the solid solution α-Fe(Sn) was observed only if the grain sizes of the phases α-Fe and $FeSn_2$ reached 3–8 nm. These values agree well with other data on the mechanochemical synthesis of solid solutions in this system.[122]

Investigations demonstrated that the dynamics of formation of intermediate intermetallic compounds in the second step of the mechanochemical synthesis of solid solutions in metallic systems characterised by negative enthalpies of formation correlates with the enthalpies of formation of equilibrium intermetallic compounds.[365–368]

Comparative studies of mechanochemical synthesis from a mixture of metallic powders and from a mixture of a metal serving as the solvent and intermetallic compounds, whose phase compositions are identical to those of substances which are formed in the intermediate stage of the mechanochemical reaction of the metallic powders, demonstrated that the dynamics of formation of the solid solution is virtually the same in both cases.[369]

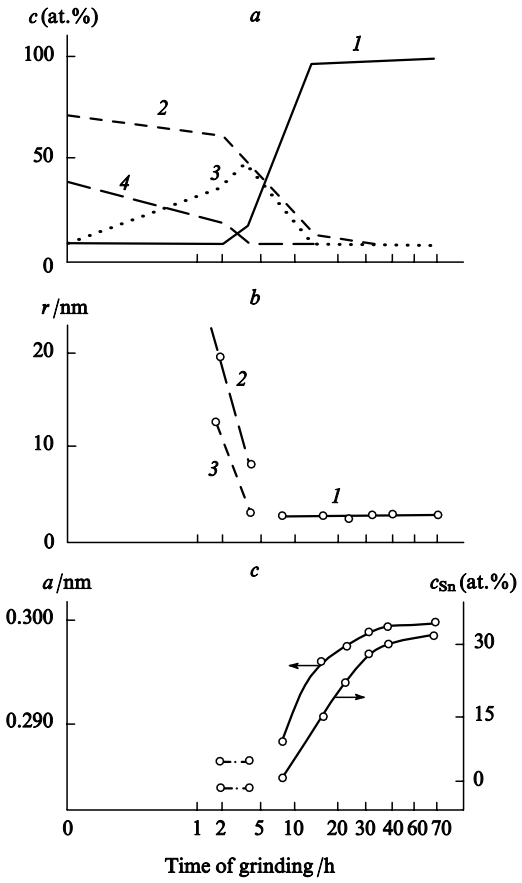

Figure 8. Dependences of the phase composition (*a*), the average size of crystallites (*b*), the lattice parameter of the resulting BCC phase and the concentration of tin (*c*) on the time of grinding in a Pulverizette-5 mill;[123] (*1*) α-Fe(Sn), (*2*) α-Fe, (*3*) $FeSn_2$, (*4*) β-Sn.

Therefore, the synthesis of solid solutions in metallic systems characterised by negative mixing enthalpies may involve the following stages.

1. The formation of layered composite structures with simultaneous dispersion of the initial components to nanosized particles (a sharp increase in the contact area between the initial components).

2. The formation of intermetallic compounds in nanosized layered composites.

3. Dissolution of intermetallic compounds in the metal acting as the solvent to form a solid solution.

Most of researchers assumed that the process of formation of amorphous alloys from metallic powders involves two steps. In the first step, layered composites containing nanosized grains are formed. The formation of an amorphous alloy in the second step proceeds through diffusion in a heated specimen. It is believed that the specimen is heated at the expense of the energy of collision of balls and the temperature increases to hundreds of degrees, but it does remain inadequate to attain crystallisation of an amorphous alloy. This point of view was confirmed by Petzoldt *et al.*[370] The authors observed amorphous interlayers between layers of nickel and niobium by electron microscopy. These interlayers are analogous to those between layers of nickel and zirconium observed by Meng *et al.*[371] in experiments on annealing of sputtered films.

In a number of studies, the formation of intermetallic phases before amorphisation was detected. This fact seems to be quite reliable because amorphous alloys in many systems were prepared by mechanical grinding of intermetallides. The formation of intermetallic compounds involves, most probably, two steps

because intermetallides can arise immediately in layered composite structures.

In layered composite structures, which are formed in metallic systems, spontaneous diffusion of the initial compounds can proceed at room temperature due to the thermodynamic driving force for the process. In analogous layered composites formed in systems characterised by a positive mixing enthalpy, this driving force is absent. It can be suggested that the formation of solid solutions under conditions of mechanochemical activation proceeds, most probably, through quenching from the liquid state because, first, the temperatures of phase transitions, including the solid phase → liquid phase transition, sharply decrease compared to those in a bulky material as the sizes of the initial particles decrease to several nanometers,[372–376] and, second, sharp local increases in temperature and pressure can take place in activators.

Bowden *et al.*[377–379] gained experimental evidence for the existence of local heating and revealed their sites, which arise at the contacts between particles of solid compounds on their mechanical treatment. The authors established that the area of heating sites is, on the average, 10^{-2} cm^2, the time of their existence is 10^{-5}–10^{-3} s and the temperature jumps at the sites of heating can be as large as 800–1000 K and sometimes even larger. According to the hypothesis proposed by Dubnov, Sukhikh and Tomashevich,[380] individual dislocation pairs with antiparallel Burgers vectors in the regions of intensive shear can annihilate with restoration of a perfect structure and liberation of the dislocation energy, which, according to estimates made by Cottrell,[381] is ~1 eV. Since the atomic forces act only through very short distances, the region of energy liberation is limited to a radius of about one interatomic distance. In this case, local heating is $\sim 10^3$ K.

Avvakumov[321] also concluded that local sites of heating limited by the melting point of particles being treated can arise in the mechanochemical processes.

Urakaev and Avvakumov[382] calculated the thickness of the molten zone. They believed that this value can reach 5×10^{-7} cm if the size of rubbing particles is $\sim 10^{-4}$ cm and the sites of local heating (taking into account the possibility of melting of particles treated) are limited by their melting points. Kopylov *et al.*[383] suggested that intermetallic compounds can be synthesised in a planetary mill due to short-period local heating on friction of the particles. Based on the results of calculations, it was concluded[384–387] that high local temperatures and pressures can arise in the course of mechanochemical activation.

Dannik[388] solved the problem of collision of two particles taking into account frictional forces on interaction of rigid bodies. Based on Dannik's equations, Urakaev[389] calculated the temperatures at the contacts between inorganic particles rubbed in drums of centrifugal planetary mills. The maximum local temperature at the rubbing surface of the particles is ~1030 K and the lifetime of this temperature is 10^{-9} s.

Ermakov, Yurchikov and Barinov[390] also considered the problem of the effect of the temperature on processes occurring in mechanochemical activators. They believed that substantially heated and rapidly cooled local regions (hot spots) can appear at the surface of the particles. The lifetime of hot regions of sizes 1–10 nm 'heated' almost to the melting point is 10^{-3}–10^{-6} s. The authors also estimated the rate of cooling of these regions at 10^6–10^9 deg s^{-1}. The appearance of hot sites has also been observed in more recent studies. For example, the intermetallide SnTe was synthesised at room temperature by repeated cold pressing of granulated tin and powdered tellurium.[391] The system consisted of the initial elements until the pressing action provided an adequate mechanical energy. Hot regions of diameter 1–2 nm were observed at the metal surface with particle sizes of 10–15 nm. In these regions, 0.25%–0.35% of the total deformation energy was accumulated after 30-fold pressing (1.25 g of a mixture of Sn and Te, 343 MPa).

Eckert *et al.*[392] also calculated the high local temperatures arising at contact sites. The experiments were carried out using a 'Pulverizette-5' planetary ball mill (Frich, Germany) at the ball rates of 2.5, 3.6 and 4.7 m s^{-1}. The temperatures at the contact sites, which are shifted with respect to each other due to deformation caused by colliding balls, were calculated as described by Schwarz and Koch.[393] The following values were obtained: at the rate of 2.5 m s^{-1}, $\Delta T = 80$ deg; at the rate of 3.6 m s^{-1}, $\Delta T = 167$ deg; at the rate of 4.7 m s^{-1}, $\Delta T = 287$ deg. The authors believed that the average temperature of the drum, which was 50, 80 and 120 °C, respectively, in the case of the above-mentioned rates, should be added to the temperature developed due to collisions.

Zalkin[394] concluded that molten zones can arise at temperatures, which are substantially lower than the melting point of a low-melting element; in this case, diffusion has virtually no effect on the onset of melting.

Experimental investigations aimed at direct measurement of local temperatures are many fewer in number compared to studies in which local temperatures were calculated. Changes in the temperature are sometimes determined on vibrating mills with the use of thermocouples. A thermocouple is attached to the outer wall of the drum and the temperature can be monitored throughout the process. In this case, it is assumed that the temperatures of the drum, balls and the material under treatment are equal or differ insignificantly. Kimura *et al.*[395] used this procedure for the measurements of the temperature of the drum wall depending on the rate of the stirrer of the attritor and demonstrated that the temperature of powders reached 573 K.

The AGO planetary ball mills are characterised by very high energies and the input power of ~1 W per cm^3 of the drum volume.[396] The temperature of balls can amount to 500 °C increasing very rapidly.[397] Hence, not only dispersion of the initial components, but also substantial temperature jumps, which arise upon contact of the material treated with balls, should be taken into account in mechanochemical synthesis in high-energy mills.

Analysis of the published data demonstrated that mechanochemical synthesis of non-equilibrium solid solutions in metallic systems characterised by a positive mixing enthalpy involves two steps. In the first step, layered composite structures containing nanosized grains of the initial components are formed. In the second step, solid solutions arise. The second step can proceed through quenching of the liquid phase in which, apparently, mixing of the components occurs. The liquid phase is formed both due to a sharp decrease in the temperature of phase transition to the liquid state when grains become nanosized and due to local temperature jumps in the contact region at the instant grinding particles collide.

In the case of metallic systems with a positive mixing enthalpy, it seems reasonable to speak about mechanical alloying rather than about the mechanochemical synthesis of non-equilibrium solid solutions. Unfortunately, the term 'mechanical alloying' is assigned in the literature both to systems in which chemical reactions proceed and to systems in which components are only mixed.

The formation of intermetallic compounds upon liquid-phase contact interaction in metallic systems, which are characterised by a negative mixing enthalpy and which contain a low-melting component, should also be taken into account. The presence of layered composites in metallic systems containing nanosized grains in which the melting temperature is sharply decreased with simultaneous existence of rather high temperature jumps at sites of contacts with grinding particles can ensure contact melting of the components and their chemical reaction in the liquid phase.

Presently, there is no agreement regarding the nature of mechanochemical synthesis, *viz.*, the question of whether it is a solid-phase process or it proceeds in the liquid phase remains open. A large number of calculations and experimental studies available in the literature indicate that substantial temperature jumps can occur in activators. However, the direct mechanochemical synthesis from components with high melting temperatures and the fact that mechanochemical synthesis can be performed on

Bridgman anvils and in low-energy ball mills in which high temperatures are difficult to attain provide evidence in favour of the solid-phase nature of the processes.

In the present review, various opinions as to the mechanisms of processes occurring in mechanochemical synthesis in metallic systems are surveyed. It should be noted that most researchers consider the preparation of amorphous alloys and supersaturated solid solutions by the mechanochemical method as the process of disordering of equilibrium phases.

References

1. S P Yatsenko *Indii. Svoistva i Primenenie* (Indium. Properties and Applications) (Moscow: Nauka, 1987)
2. G V Samsonov, V N Bondarev *Germanidy* (Germanides) (Moscow: Metallurgiya, 1968)
3. E I Gil'debrand, A B Fasman *Skeletnye Katalizatory v Organicheskoi Khimii* (Skeletal Catalysts in Organic Chemistry) (Alma-Ata: Nauka, 1982)
4. G V Samsonov, L A Dvorina, B M Rud' *Silitsidy* (Silicides) (Moscow: Metallurgiya, 1979)
5. A E Vol, *Stroenie i Svoistva Dvoinykh Metallicheskikh Sistem* (Structure and Properties of Binary Metallic Systems) (Moscow: Fizmatgiz, 1959) Vol. 1
6. E M Sokolovskaya, L S Guzei *Metallokhimiya* (Metallochemistry) (Moscow: Moscow State University, 1986)
7. C S Barrett, T B Massalski *Structure of Metals* (Oxford: Pergamon Press, 1980)
8. Ya S Umanskii, Yu A Skakov *Fizika Metallov* (The Physics of Metals) (Moscow: Atomizdat, 1978)
9. W Hume-Rothery *Elements of Structural Metallurgy* (London: Institute of Metals, 1961)
10. H W King *J. Mater. Sci.* **1** 79 (1964)
11. V V Neverov, P P Zhitnikov *Fiz. Met. Metalloved.* (11) 143 (1990) [a]
12. B T McDermott, C C Koch *Scr. Metall.* **20** 669 (1986)
13. C C Koch *Annu. Rev. Mater. Sci.* **19** 121 (1989)
14. Y Z Yang, Y L Zhu, Q S Li, X M Ma, Y D Dong, Y Z Chuang *Mater. Sci. Technol.* **14** 551 (1998)
15. M Kis-Varga, D L Beke *Mater. Sci. Forum* **225**–**227** 465 (1996)
16. S Enzo, P Macri, P Rose, N Cowlam, in *Proceedings of the 2nd International Conference on Structural Applications of Mechanical Alloying, Vancouver, 1993* p. 101
17. Z T Liu, O N C Uwakweh *J. Mater. Synth. Proc.* **5** (2) 135 (1997)
18. S Ordonez, G Garcia, D Serafini, A San Martin U *Mater. Sci. Forum* **299**–**300** 478 (1999)
19. H Enoki, D Sun, E Akiba, F Gindl *J. Alloys Compd.* **285** 279 (1999)
20. P Ruuskanen *Mater. Sci. Forum* **269**–**272** 139 (1998)
21. B B Bokhonov, I G Konstanchuk, V V Boldyrev *J. Alloys Compd.* **218** 190 (1995)
22. E Belyaev, O Lomovsky, G Golubkova *Mater. Sci. Forum* **179**–**181** 403 (1995)
23. E Yu Belyaev, O I Lomovsky, A I Ancharov, B P Tolochko *Nucl. Instrum. Methods Phys. Res., A* **405** 435 (1998)
24. B K Yen, T Aizawa, J Kihara *Mater. Sci. Eng., A* **220** 8 (1996)
25. S N Patankar, S-Q Xiao, J J Lewandovski, A H Heuer *J. Mater. Res.* **8** 1311 (1993)
26. E Yu Belyaev, O I Lomovskii, in *Khimiya Tverdogo Tela i Novye Materialy (Sb. Dokl. Vseros. Konf.), Ekaterinburg, 1996* [The Chemistry of Solids and New Materials (Collection of Reports of All-Russian Conference), Ekaterinburg, 1996] Vol. 1, p. 212
27. N Iwamoto, S Uesaka *Mater. Sci. Forum* **88**–**90** 763 (1992)
28. E Ivanov, in *Proceedings of the 2nd International Conference on Structural Applications of Mechanical Alloying, Vancouver, 1993* p. 415
29. A A Popovich, V N Vasilenko, in *Mekhanokhimicheskii Sintez v Neorganicheskoi Khimii* (Mechanochemical Synthesis in Inorganic Chemistry) (Novosibirsk: Nauka, 1991) p. 168
30. A A Popovich, V N Vasilenko, V P Reva *Poroshk. Metall.* (11) 22 (1992)
31. L Liu, F Padella, W Guo, M Magini *Acta Metall. Mater.* **43** 3755 (1995)
32. T Lou, G Fan, B Ding, Z Hu *J. Mater. Res.* **12** 1172 (1997)
33. D Oleszak, M Jachimovich, H Matyja *Mater. Sci. Forum* **179**–**181** 215 (1995)
34. M Umemoto, S Shiga, K Raviprasad, I Okane *Mater. Sci. Forum* **179**–**181** 165 (1995)
35. L Lu, M O Lai, M L Hoe *Nanostruct. Mater.* **10** 551 (1998)
36. M Riffel, J Schilz *J. Mater. Sci.* **33** 3427 (1998)
37. L Zaluski, A Zaluska, J O Strom-Olsen *J. Alloys Compd.* **217** 245 (1995)
38. D Oleszak, M Burzynska-Szyszko, H Matyja *J. Mater. Sci. Lett.* **12** 3 (1995)
39. C C Koch, M S Kim *J. Phys.* **46** 5731 (1985)
40. E Hellsten, H J Fecht, C C Garland, W L Johnson *Proc. MRS Symp.* **132** 137 (1989)
41. K Chattopadhaya, K Sridhar *J. Alloys Compd.* **264** 293 (1998)
42. K B Gerasimov, V V Boldyrev *Mater. Res. Bull.* **31** 1297 (1996)
43. G Le Gaër, P Mattezzi, B Fultz *J. Mater. Res.* **7** 1387 (1992)
44. V A Varnek, L A Strugova, E G Avvakumov *Fiz. Tv. Tela* **16** (6) 1816 (1974) [b]
45. D K Nukhopadhaya, S Suryanarayana, F H Froes, in *Proceedings of the 2nd International Conference on Structural Applications of Mechanical Alloying, Vancouver, 1993* p. 131
46. S Ghosh, D Linch, E C Baburaj, F H Froes, in *Proceedings of Symposium on Synthesis of Lightweight Metals. III, San-Diego, 1999* p. 43
47. J H Ahn, K R Lee, H K Cho *Mater. Sci. Forum* **179**–**181** 153 (1995)
48. J S C Jang, C C Koch *J. Mater. Res.* **5** 498 (1990)
49. M Qi, M Zhu, G B Li, D Z Yang *J. Mater. Sci. Lett.* **11** 1147 (1992)
50. P S Goodwin, T M T Hinder, A Wisbey, C M Ward-Close *Mater. Sci. Forum* **269**–**272** 53 (1998)
51. St Lauer, Z Guan, H Wolf, Th Wichert *Mater. Sci. Forum* **269**–**272** 485 (1998)
52. R C Benn, P K Mirchandani, A S Watwe, in *Modern Development in Powder Metallurgy* No. 4 (Princton: Metal Powder Industries Federation, 1988) p. 479
53. A Calka, A P Radlinski *Scr. Metall.* **23** 1497 (1989)
54. E A Kenik, R J Bayuzick, M S Kim, C C Koch *Scr. Metall.* **21** 1137 (1987)
55. H J Fecht, G Han, Z Fu, W L Johnson *J. Appl. Phys.* **67** 1744 (1990)
56. T J Tianen, R B Schwarz *J. Less-Common Met.* **140** 99 (1988)
57. E Ivanov, T Grigorieva, V Boldyrev, A Fasman, S Mihkailenko, O Kalinina *Mater. Lett.* **7** 51 (1988)
58. E Ivanov, S Makhlouf, K Sumiyama, K Suzuki, H Yamauchi, in *Proceedings of the 2nd International Conference on Structural Applications of Mechanical Alloying, Vancouver, 1993* p. 177
59. C Kuhrth, H Schropf, L Schultz, E Arztz, in *Proceedings of the 2nd International Conference on Structural Applications of Mechanical Alloying, Vancouver, 1993* p. 269
60. E Hellsten, H J Fecht, Z Fu, W L Johnson *J. Mater. Res.* **5** 498 (1990)
61. B L Huang, J Vallone, M J Luton *Nanostruct. Mater.* **5** 411 (1995)
62. I Borner, J Eckert *Mater. Sci. Forum* **225**–**227** 377 (1996)
63. E Ivanov, S Makhlouf, K Sumiyama, H Yamauchi, K Suzuki, G Golubkova *J. Alloys Compd.* **185** 28 (1992)
64. S Makhlouf, K Sumiyama, K Suzuki *J. Alloys Compd.* **199** 119 (1992)
65. T Chen, J M Hampikian, N N Thadhani *Acta Mater.* **47** 2567 (1990)
66. F Cardellini, V Contini, G Mazzone *Philos. Mag., A* **78** 1021 (1998)
67. T F Grigorieva, E Yu Ivanov, G V Golubkova, E I Petrachkov, T G Marenina, in *Mekhanokhimicheskii Sintez v Neorganicheskoi Khimii* (Mechanochemical Synthesis in Inorganic Chemistry) (Novosibirsk: Nauka, 1991) p. 214
68. T F Grigorieva, E Yu Ivanov, V V Boldyrev, E I Petrachkov, T I Samsonova, V P Chuev *Izv. Sib. Otd. Akad. Nauk, Ser. Khim. Nauk* **3** 73 (1989)
69. P F Relushko, I P Berestnitskaya, V V Moskvin, L I Trusov, V I Novikov, P Yu Butyagin, in *X Vsesoyuz. Soveshch. po Kinetike i Mekhanizmu Khimicheskikh Reaktsii v Tverdom Tele (Tez. Dokl.), Chernogolovka, 1989* [The Xth All-Union Meeting on Kinetics and Mechanism of Chemical Reactions in Solids (Abstracts of Reports), Chernogolovka, 1989] p. 187
70. E Bonetti, G Scipione, S Enzo, R Frattini, L Schiffini *Nanostruct. Mater.* **6** 397 (1995)
71. M A Morris, D G Morris *Mater. Sci. Forum* **88**–**90** 529 (1992)
72. E Gaffet, N Malhouroux-Gaffet *J. Alloys Compd.* **205** 27 (1994)
73. N Malhouroux-Gaffet, E Gaffet *J. Alloys Compd.* **198** 143 (1993)
74. M Umemoto, S Shiga, K Raviprasad *Mater. Sci. Forum* **225**–**227** 841 (1996)

75. C Gras, E Gaffet, F Bernard, J C Niepce *Mater. Sci. Eng., A* **264** 94 (1999)
76. F Cardellini, V Contini, R Gupta, G Mazzone, A Montone, A Perin, G Principi *J. Mater. Sci.* **33** 2519 (1998)
77. M Meyer, L Mendoza-Zelis, F H Sanchez *Mater. Sci. Forum* **225**–**227** 441 (1996)
78. R Martinez-Sanchez, J G Cabanas-Moreno, H A Calderon, M Umemoto *Mater. Sci. Forum* **225**–**227** 435 (1996)
79. M A Korchagin, T F Grigorieva, A P Barinova, N Z Lyakhov *Int. J. SHS* (3) (2000)
80. T F Grigorieva, M A Korchagin, A P Barinova, N Z Lyakhov *Dokl. Akad. Nauk* **369** 345 (1999) [c]
81. M A Korchagin, T F Grigorieva, A P Barinova, N Z Lyakhov *Dokl. Akad. Nauk* **372** 40 (2000) [c]
82. J Lagerbom, T Tianen, M Lehtonen, P Lintula *J. Mater. Sci.* **34** 657 (1999)
83. V Gauthier, C Josse, F Bernard, E Gaffet, J P Larpin *Mater. Sci. Eng., A* **265** 117 (1999)
84. F Charlot, E Gaffet, B Zeghmati, F Bernard, J C Niepce *Mater. Sci. Eng., A* **262** 279 (1999)
85. D Klein, J C Niepce, F Charlot, E Gaffet F Bernard *Acta Mater.* **47** 619 (1990)
86. F Charlot, C Gras, M Gramond, E Gaffet, F Bernard, J C Niepce *J. Phys. IV, Colloq.* **8** (P5) 497 (1998)
87. E Gaffet, F Charlot, D Klein, F Bernard, J-C Niepce *Mater. Sci. Forum* **269**–**272** 379 (1998)
88. F Charlot, C Gras, F Bernard, J C Niepce, E Gaffet *Acta Mater.* **47** 2113 (1999)
89. C Gras, E Gaffet, F Bernard, D Vrel, J C Niepce in *Book of Abstracts of the Vth International Symposium on SHS, Moscow, 1999* p. 38
90. Yu T Pavlyukhin, Yu E Manzanov, E G Avvakumov, V V Boldyrev *Izv. Sib. Otd. Akad. Nauk, Ser. Khim. Nauk* **6** 84 (1981)
91. R M Davis, C C Koch *Scr. Metall.* **21** 305 (1987)
92. E E Yurchikov, V P Pilyugin, R I Kuznetsov, in *IV Vsesoyuz. Seminar 'Struktura Dislokatsii i Mekhanicheskie Svoistva Metallov i Splavov' (Tez. Dokl.), Sverdlovsk, 1987* [The IVth All-Union Meeting 'Structure of Dislocation and Mechanical Properties of Metals and Alloys' (Abstracts of Reports), Sverdlovsk, 1987] p. 80
93. E E Yurchikov, V P Pilyugin, V A Barinov, in *IV Vsesoyuz. Seminar 'Struktura Dislokatsii i Mekhanicheskie Svoistva Metallov i Splavov' (Tez. Dokl.), Sverdlovsk, 1987* [The IVth All-Union Meeting 'Structure of Dislocation and Mechanical Properties of Metals and Alloys' (Abstracts of Reports), Sverdlovsk, 1987] p. 185
94. V V Neverov, Doctoral Thesis in Physicomathematical Sciences, Novokuznetsk Pedagogical Institute, Novokuznetsk, 1995
95. V V Neverov, V N Burov *Izv. Sib. Otd. Akad. Nauk, Ser. Khim. Nauk* **9** 3 (1979)
96. R Brüning, K Samwer, C Kuhrt, L Schultz *J. Appl. Phys.* **72** 2978 (1992)
97. C Kuhrt, L Schultz *J. Appl. Phys.* **71** 1896 (1992)
98. C Kuhrt, L Schultz *J. Appl. Phys.* **73** 6588 (1993)
99. V V Cherdyntsev, S D Kaloshkin, Yu V Baldokhin, I A Tomilin, E V Shelekhov *Fiz. Met. Metalloved.* **84** (4) 154 (1997) [a]
100. V V Cherdyntsev, S D Kaloshkin, I A Tomilin, E V Shelekhov, Yu V Baldokhin *Nanostruct. Mater.* **12** 139 (1999)
101. V V Tcherdyntsev, S D Kaloshkin, I A Tomilin, E V Shelekhov, Yu V Baldokhin *Mater. Sci. Forum* **269**–**272** 145 (1998)
102. V I Fadeeva, A V Leonov, L N Khodina *Mater. Sci. Forum* **179**–**181** 397 (1994)
103. K Wolski, G Le Caer, P Delcroix, R Fillit, F Thevenot, J Le Core *Mater. Sci. Eng., A* **207** 97 (1996)
104. E Bonetti, G Scipione, G Valdre, G Cocco, R Frattini, P P Marci *J. Appl. Phys.* **74** 2053 (1993)
105. S Surinach, X Amils, S Gialanella, L Lutterotti, M D Baro *Mater. Sci. Forum* **235**–**238** 415 (1997)
106. V I Fadeeva, V K Portnoy, Yu V Baldokhin, G A Kochetov, H Matyja *Nanostruct. Mater.* **12** 625 (1998)
107. H G Jiang, R J Perez, M L Lau, E J Lavernia *J. Mater. Res.* **12** 1429 (1997)
108. M Hansen, K Anderko *Constitution of Binary Alloys)* (New York: McGraw-Hill, 1961)
109. V V Chervyakova, A A Presnyakov *Slozhnye Latuni i Bronzy* (Complex Brasses and Bronzes) (Alma-Ata: Nauka, 1974)
110. I S Miroshnichenko *Zakalka iz Zhidkogo Sostoyaniya* (Hardening from the Liquid State) (Moscow: Metallurgiya, 1982)
111. T F Grigorieva, Candidate Thesis in Chemical Sciences, Institute of Solid State Chemistry and Mechanosynthesis, Siberian Branch of the Academy of Sciences of the USSR, Novosibirsk, 1988
112. E Lugscheider, G Yang *Z. Met.kd.* **62** 548 (1971)
113. E Ivanov *Mater. Sci. Forum* **88**–**90** 475 (1992)
114. A E Vol, I Kagan, *Stroenie i Svoistva Dvoinykh Metallicheskikh Sistem* (Structure and Properties of Binary Metallic Systems) (Moscow: Fizmatgiz, 1976) Vol. 3
115. T F Grigorieva, V V Boldyrev *Dokl. Akad. Nauk* **340** 329 (1995) [c]
116. T F Grigorieva, A P Barinova, V V Boldyrev *Neorg. Mater.* **32** 41 (1996) [d]
117. T F Grigorieva, A P Barinova, V V Boldyrev *Neorg. Mater.* **31** 1551 (1995) [d]
118. T F Grigorieva, A P Barinova, V D Belykh, E Yu Ivanov, V V Boldyrev, in *Proceedings of the 5th European Conference on Advanced Materials, Processes and Applications (EUROMAT'97), Maastricht, 1997* V. 1, p. 447
119. T F Grigorieva, V V Boldyrev *Dokl. Akad. Nauk* **340** 195 (1995) [c]
120. O Kubashewski *Iron Binary Diagrams* (Berlin: Springer, 1982)
121. A F Cabrera, F H Sanchez, L Mendoza-Zelis *Mater. Sci. Forum* **179**–**181** 231 (1995)
122. G Le Caer, P Delcroix, M O Kientz, B Malaman *Mater. Sci. Forum* **179**–**181** 469 (1995)
123. E P Elsukov, G A Dorofeev, G N Konygin, A L Ul'yanov, V A Barinov, T F Grigorieva, V V Boldyrev *Khim. Interes. Ustoich. Razvit.* **6** 131 (1998) [e]
124. E P Yelsukov, G A Dorofeev, V A Barinov, T F Grigorieva, V V Boldyrev *Mater. Sci., Forum.* **269**–**272** 151 (1998)
125. A E Vol, I Kagan, *Stroenie i Svoistva Dvoinykh Metallicheskikh Sistem* (Structure and Properties of Binary Metallic Systems) (Moscow: Fizmatgiz, 1962) Vol. 2
126. T F Grigorieva, V V Boldyrev, T I Samsonova *Dokl. Akad. Nauk* **340** 495 (1995) [c]
127. A R Miedema, R Boom, F R de Boer *J. Less-Common Met.* **41** 283 (1975)
128. A R Miedema *J. Less-Common Met.* **46** 67 (1976)
129. A R Miedema, P F de Chatel, F R de Boer *Physica B* **100** 1 (1980)
130. T F Grigorieva, E Yu Ivanov, V V Boldyrev, S V Vos'merikov, T I Samsonova *Izv. Sib. Otd. Akad. Nauk SSSR, Ser. Kkhim. Nauk* (5) 91 (1989)
131. T F Grigorieva, E Yu Ivanov, in *XVI Vsesoyuzn. Nauchn.-Tekhnich. Konf. 'Poroshkovaya Metallurgiya' (Tez. Dokl.), Sverdlovsk, 1989* [The XVIth All-Union Scientific and Technical Conference 'Powder Metallurgy' (Abstracts of Reports), Sverdlovsk, 1989] Part 1, p. 61
132. G B Bokii *Vvedenie v Kristallokhimiyu* (Introduction in Crystal Chemistry) (Moscow: Moscow State University, 1954)
133. T F Grigorieva, A P Barinova, V V Boldyrev, E Yu Ivanov *Solid State Ion.* **101**–**103** 17 (1997)
134. M P Shaskol'skaya *Kristallografiya* (Crystallography) (Moscow: Vysshaya Shkola, 1984)
135. S P Yatsenko *Gallii. Vzaimodeistvie s Metallami* (Gallium. Interaction with Metals) (Moscow: Nauka, 1974)
136. T F Grigorieva, G V Golubkova, E Yu Ivanov, in *XVI Vsesoyuz. Nauch.-Tekhnich. Konf. 'Poroshkovaya metallurgiya' (Tez. Dokl.), Sverdlovsk, 1989* [The XVIth All-Union Scientific and Technical Conference 'Powder Metallurgy' (Abstracts of Reports), Sverdlovsk, 1989] Part 1, p. 108
137. S Enzo, G Mulas, R Frattini *Mater. Sci. Forum* **269**–**272** 385 (1998)
138. D Oleszak, P H Shingu *Mater. Sci. Eng., A* **181**/**182** 1217 (1994)
139. T G Popova, P Y Butyagin, A N Streletski, V K Portnoy *Colloid J.* **59** 737 (1997)
140. X S Huang, T Mashimo *J. Mater. Process. Technol.* **85** 135 (1999)
141. *Dvoinye i Mnogokomponentnye Sistemy na Osnove Medi. Spravochnik* (Binary and Multi-Component System Based on Copper. Handbook) (Moscow: Nauka, 1979)
142. J H He, E Ma *Proc. MRS Symp.* **481** 637 (1998)
143. A H Advani, N N Thadhani *Metall. Mater. Trans. A, Phys. Metall. Mater. Sci.* **30** 1367 (1999)

144. D G Morris, M A Morris, A Benghalem, C Bisell, in *Proceedings of the 2nd International Conference on Structural Applications of Mechanical Alloying, Vancouver, 1993* p. 353
145. P Y Lee, C C Koch *J. Non-Cryst. Solids* **94** 88 (1987)
146. I J Duerden, W Hume-Rothery *J. Less-Common Met.* **11** 381 (1966)
147. K B Gerasimov, V V Kolpakov, A A Gusev, E Yu Ivanov, in *Proceedings of the 2nd International Symposium on the Solid State Chemistry, Pardubice, 1989* p. 9
148. A V Leonov, E Szewczak, O E Gladilina, H Matya, V I Fadeeva *Mater. Sci. Forum* **225–227** 277 (1996)
149. C E Lundin, A S Yamamoto *Trans. AIME* **236** 863 (1966)
150. E Hellstern, L Schultz, R Bormann, D Lee *Appl. Phys. Lett.* **53** 1399 (1988)
151. R B Schwarz, P B Desch, S R Srinivasan, in *Proceedings of the 2nd International Conference on Structural Applications of Mechanical Alloying, Vancouver, 1993* p. 227
152. M Kis-Varga, D L Beke *Mater. Sci. Forum* **225–227** 465 (1996)
153. M Kis-Varga, D L Beke, S Meszaros, K Vad, Gy Kerekes, L Daroczi *Mater. Sci. Forum* **269–272** 961 (1998)
154. E Yu Ivanov, B D Bryskin *Mater. Sci. Forum* **269–272** 111 (1998)
155. P Boolchand, C C Koch *J. Mater. Res.* **7** 2876 (1992)
156. R N Kuzmin, S V Nikitina *Sov. Phys.-Solid State* **13** 3151 (1972)
157. H Jones *Rep. Prog. Phys.* **36** 1425 (1973)
158. P Ramachandrarao, M G Scott, G A Chadwick *Philos. Mag., B* **25** 961 (1972)
159. P J Yvon, R B Schwarz, in *Proceedings of the 2nd International Conference on Structural Applications of Mechanical Alloying, Vancouver, 1993* p. 393
160. F Li, K N Ishihara, P H Shingu *Metall. Trans. A, Phys. Metall. Mater. Sci.* **22** 2849 (1991)
161. P H Shingu, B Huang, S R Nishitani, S Nasu *J. Jpn. Inst. Met., Suppl.* **29** 3 (1988)
162. P H Shingu, B Huang, J Kuyama, K N Ishihara, S Nasu, in *New Materials by Mechanical Alloying Technique* (Eds E Artz, L Schultz) (Oberursel, Germany: DGM Informationgeselschaft, 1989) p. 319
163. B Huang, N Tokizane, K N Ishihara, P H Shingu, S Nasu *J. Non-Cryst. Solids* **117/118** 688 (1990)
164. M Pekala, D Oleszak *Mater. Sci. Forum* **235–238** 547 (1997)
165. R A Dunlap, J R Dahn, D A Eelman, G R Mackay *Hyperfine Interact.* **116** 117 (1998)
166. A Calka, W Kaczmarek, J S Williams *J. Mater. Sci.* **28** 15 (1993)
167. M Oering, R Bormann *J. Phys. Colloq.* **51** C4-169 (1990)
168. L M Di, H Bakker *J. Phys., Condens. Matter* **3** 3427 (1991)
169. L M Di, H Bakker *J. Appl. Phys.* **71** 5650 (1992)
170. L M Di, H Bakker *J. Phys., Condens. Matter* **3** 9319 (1991)
171. L M Di, H Bakker, P Barczy, Z Gacsi *Acta Metall. Mater.* **41** 2923 (1993)
172. H Bakker, L M Di *Mater. Sci. Forum* **88–90** 27 (1992)
173. H Yang, H Bakker, in *Proceedings of the 2nd International Conference on Structural Applications of Mechanical Alloying, Vancouver, 1993* p. 401
174. H Yang, L M Di, H Bakker *Intermetallics* **1** 29 (1993)
175. G F Zhou, H Bakker *Europhys. Lett.* **30** 433 (1995)
176. M Oering, Z H Yan, T Klassen, R Bormann *Phys. Status Solidi, A* **131** 671 (1992)
177. T F Grigorieva, M A Korchagin, A P Barinova, N Z Lyakhov *Metally* (4) 64 (2000)
178. E P Elsukov, V V Yakovlev, V A Barinov *Fiz. Met. Metalloved.* **77** (4) 131 (1994) [a]
179. E P Elsukov, V V Yakovlev, E V Voronina, V A Barinov, in *Dokl. Mezhdunar. Nauch. Seminara 'Mekhanokhimiya i Mekhanicheskaya Aktivatsiya', Sankt-Peterburg, 1995* (Proceedings of International Scientific Seminar 'Mechanochemistry and Mechanical Activation', St-Petersburg, 1995) p. 67
180. E P Yelsukov, E V Voronina, G N Konygin, V A Barinov, S K Gogovnikov, G A Dorofeev, A V Zagainov *J. Magn. Magn. Mater.* **166** 334 (1997)
181. P H Duwer R H Willens, W Klement Jr *J. Appl. Phys.* **31** 1136 (1960)
182. E F Kneller *J. Appl. Phys.* **35** 2210 (1965)
183. K Sumiyama, T Yoshitake, Y Nakamura *Acta Metall.* **33** 1791 (1985)
184. J S Benjamin *Sci. Am.* **234** 40 (1976)
185. V V Neverov, V N Burov, P P Zhitnikov *Izv. Sib. Otd. Akad. Nauk, Ser. Khim. Nauk* (5) 54 (1983)
186. A A Gusev, Candidate Thesis in Chemical Sciences, Institute of Solid State Chemistry and Mechanosynthesis, Siberian Branch of the Russian Academy of Sciences, Novosibirsk, 1993
187. S D Kaloshkin, I A Tomilin, G Andrianov, Yu V Baldokhin, E V Shelehkov *Mater. Sci. Forum* **225–227** 331 (1996)
188. S D Kaloshkin, I A Tomilin, E V Shelekhov, V V Cherdyntsev, G A Andrianov, Yu V Baldokhin *Fiz. Met. Metalloved.* **84** (3) 68 (1997) [a]
189. M J Barro, E Navarro, P Agudo, A Hernando, P Crespo, A Garsia Escorial *Mater. Sci. Forum* **235–238** 553 (1997)
190. K Uenishi, K F Kobayashi, S Nasu, H Hatano, K N Ishihara, P H Shingu *Z. Met.kd.* **83** 132 (1992)
191. A R Yavari, P J Desre, T Benameur *Phys. Rev. Lett.* **68** 2235 (1992)
192. J Eckert, J C Holzer, W L Johnson *J. Appl. Phys.* **73** 131 (1993)
193. J Eckert, J C Holzer, C E Krill, W L Johnson *J. Appl. Phys.* **73** 2794 (1993)
194. J Z Jiang, U Gonser, C Gente, R Bormann *Appl. Phys. Lett.* **63** 2768 (1993)
195. J Z Jiang, U Gonser, C Gente, R Bormann *Appl. Phys. Lett.* **63** 1056 (1993)
196. P P Macri, P Rose, R Frattini, S Enzo, G Principi, W X Hu, N Cowlam *J. Appl. Phys.* **76** 4061 (1994)
197. P P Macri, S Enzo, N Cowlam, R Frattini, G Principi, W X Hu *Philos. Mag., B* **71** 249 (1995)
198. P P Macri, P Rose, D E Banda, N Cowlam, G Principi, S Enzo *Mater. Sci. Forum* **179–181** 249 (1995)
199. R Elkalkouli, P Chartier, J -F Dinhut *Mater. Sci. Forum* **179–181** 267 (1995)
200. K Tokumitsu *Mater. Sci. Forum* **269–272** 467 (1998)
201. F Cardellini, V Contini, G D'Agostino, A Filipponi *Mater. Sci. Forum* **269–272** 473 (1998)
202. P Gorria, P Crespo, J M Barandiaran, A Hernando, J S Garitaonandia, J L Hodeau, E Dooryhee *Mater. Sci. Forum* **269–272** 479 (1998)
203. S Q Wei, H Oyanadi, C Wen, Y Z Yang, W H Lui *J. Phys. Condens. Matter* **9** 11077 (1997)
204. T Mashimo, X S Huang *J. Alloys Compd.* **288** 299 (1999)
205. P J Schilling, J H He, R C Tittsworth, E Ma *Acta Mater.* **47** 25 (1999)
206. R A Dunlap, D A Felman, G R Mackay *J. Mater. Sci. Lett.* **17** 437 (1998)
207. J G Cabanas-Moreno, V M Lopez-Hirata, H A Calderon, J C Rendon-Angeles *Scr. Metall. Mater.* **28** 645 (1993)
208. J G Cabanas-Moreno, H Dorantes, V M Lopez-Hirata, H A Calderon, J M Hallen-Lopez *Mater. Sci. Forum* **179–181** 243 (1995)
209. F W Gayle, F S Biancaniello *Nanostruct. Mater.* **6** 429 (1995)
210. A Ye Yermakov, M A Uimin, A V Shangurov, A V Zarubin, Y V Chechetkin, A K Shtolz, V V Kondratyev, G N Konygin, E P Yelsukov, S Enzo, P P Macri, R Frattini, N Cowlam *Mater. Sci. Forum* **225–227** 147 (1996)
211. S W Mahon, X Song, M A Howson, B J Hickey, R F Cochrane *Mater. Sci. Forum* **225–227** 157 (1996)
212. C Gente, M Oering, R Bormann *Phys. Rev. B, Condens. Matter* **48** 13 244 (1993)
213. J X Huang, Y K Wu, A Q He, H Q He *Nanostruct. Mater.* **4** 293 (1994)
214. F Cardellini, G Mazzone *Philos. Mag., A* **67** 1289 (1993)
215. J Y Huang, Y K Wu, H Q He *Appl. Phys. Lett.* **66** 308 (1995)
216. J Y Huang, Y K Wu, H Q He *Acta Mater.* **44** 120 (1996)
217. Y Ogino, T Yamasaki, S Myrayama, R Sakai *J. Non-Cryst. Solids* **117/118** 737 (1990)
218. D G Morris, M A Morris *Scr. Metall. Mater.* **24** 1701 (1990)
219. M A Morris, D G Morris *Mater. Sci. Eng., A* **111** 115 (1989)
220. D G Morris, M A Morris *Mater. Sci. Eng., A* **104** 201 (1989)
221. M Baricco, L Battezzati, S Enzo, I Soletta, G Cocco *Spectrochim. Acta, Part A* **49** 1331 (1993)
222. K Uenishi, K F Kobayashi, K N Ishihara, P H Shingu *Mater. Sci. Eng., A* **134** 1342 (1991)
223. S D De la Torre, A Yamamoto, K N Ishihara, P H Shingu, T Hirano, Y Awakura *Mater. Sci. Forum* **179–181** 237 (1995)
224. T G Richards, G P Johari *Philos. Mag., B* **58** 445 (1998)
225. R Najafabadi, D J Srolovitz, E Ma, M Atzmon *J. Appl. Phys.* **74** 3144 (1993)

226. M Zhu, X Z Che, Z X Li, J K L Lai, M Qi *J. Mater. Sci.* **33** 5873 (1998)
227. Q A Pankhurst, N S Cohen, M Odlyha *J. Phys., Condens. Matter* **10** 1665 (1998)
228. N S Cohen, Q A Pankhurst, L F Bardin *J. Phys., Condens. Matter* **11** 8839 (1999)
229. P H Shingu, K N Ishihara, K Uenishi, J Kuyama, S Nasu in *Solid State Powder Processing* (Eds A H Clauer, J J de Barbadillo) (Cincinnatti: The Minerals Metals and Materials Society, 1990) p. 21
230. M Angiolini, A Deriu, F Malizia, G Mazzone, A Montone, F Roncone, M Vittori-Antisari, J S Pedersen *Mater. Sci. Forum* **269–272** 397 (1998)
231. D J Chakrabarti, D E Laughloh *Binary Alloy Phase Diagr.* **5** 732 (1984)
232. A K Covington, K Groenwolt, B W Howlett *J. Inst. Met.* **89** 291 (1961)
233. R Birringer, H Hahn, H Hofler, J Karch, H Gleiter *Defects Diffus. Forum* **59** 17 (1988)
234. P A I Smith, J M D Coey *J. Magn. Magn. Mater.* **197** 199 (1999)
235. S B Dodd, S Morris, M Wardclose, in *Symposium of Synthesis of Lightweight Metals. III, San Diego, 1999* p.177
236. H Moritaka, K Asai, Y Takemoto, A Sakakibara *Mater. Sci. Forum* **235–238** 187 (1997)
237. E Gaffet, C Louison, M Harmelin, F Faudot *Mater. Sci. Eng., A* **134** 1380 (1991)
238. T Aboud, B-Z Weiss, R Chaim *Nanostruct. Mater.* **6** 405 (1995)
239. T Raghu, R Sundaresan, T R R Mohan, P Ramakrishnan *Mater. Sci. Forum* **225–227** 397 (1996)
240. D M Follstaedt, J A Knapp *J. Less-Common Met.* **140** 375 (1988)
241. E Ivanov, I Konstanchuk, B Bokhonov, V Boldyrev *React. Solids* **7** 167 (1989)
242. J Eckert, L Schultz, K Urban *Appl. Phys. Lett.* **55** 117 (1989)
243. P Barua, V Srinivas, B C Murty *Philos. Mag., A* **80** 1207 (2000)
244. M Monagheddu, F Delogu, L Schiffini, R Frattini, S Enzo *Nanostruct. Mater.* **11** 1253 (1999)
245. R B Schwarz, W L Johnson *Phys. Rev. Lett.* **51** 415 (1983)
246. L Schultz, in *Proceedings of WRS European Meeting on Amorphous Metals and Non-Eequilibrium Processing, Strasbourg, 1984* p. 135
247. S J Ji, J C Sun, Z W Yu, Z K Hei, L Yan *Int. J. Hydrog. Energy* **24** (1) 59 (1999)
248. N Q Wu, L Z Su, M Y Yuan, J M Wu, Z Z Li *Mater. Sci. Eng., A* **257** 357 (1998)
249. H W Sheng, K Lu, E Ma *Proc. MRS Symp.* **481** 433 (1998)
250. C K Lin, P Y Lee, J L Yang, C Y Tung, N F Cheng, Y K Hwu *J. Non-Cryst. Solids* **234** 520 (1998)
251. P Y Lee, J L Yang, H M Lin *J. Mater. Sci.* **33** 235 (1998)
252. A A Savin, V A Chaika *Poroshk. Metall.* (7–8) 118 (1998)
253. R Pizarro, J M Barandiaran, F Plazaola, A Gutierrez *J. Magn. Magn. Mater.* **203** 143 (1999)
254. M Bionducci, G Navarra, R Bellisent, G Concas, F Congiu *J. Non-Cryst. Solids* **252** 605 (1999)
255. A A Novakova, O V Agladze, B P Tarasov, G V Sidorova, R A Andrievsky *Mater. Sci. Forum* **269–272** 127 (1998)
256. Y Xu, C S Kiminami, A F Filho, C Bolfarini *Scr. Mater.* **42** 213 (1999)
257. T Fukunaga, S Kajikawa *J. Non-Cryst. Solids* **250** 384 (1999)
258. S K Xia, F C Rizzo Assuncao, E Baggio-Saitovich *Mater. Sci. Forum* **225–227** 459 (1996)
259. H F Zhang, J Li, Q H Song, Z Q Hu *J. Mater. Res.* **13** 2779 (1998)
260. L Ledig, D Hough, C G Oertel, J Eckert, W Skrotzki *J. Alloys Compd.* **285** 27 (1999)
261. B W Zhang, H W Xie, S Z Liao *J. Mater. Process. Technol.* **90** 378 (1999)
262. J J Sunol *Mater. Sci. Forum* **269–272** 503 (1998)
263. R Lin, M Seidel, J Z Jiang, J Eckert *Mater. Sci. Forum* **269–272** 461 (1998)
264. A E Ermakov, V V Serikov, V A Barinov, Ya S Shchur *Fiz. Met. Metalloved.* **42** (2) 408 (1976) [a]
265. A E Ermakov, E E Yurchikov, V A Barinov, in *Fizicheskie Svoistva Magnitnykh Materialov* (Physical Properties of Magnetic Materials) (Sverdlovsk: Urals Scientific Centre, Academy of Sciences of the USSR, 1982) p. 82
266. A E Ermakov, E E Yurchikov, V A Barinov *Fiz. Met. Metalloved.* **53** (2) 302 (1982) [a]
267. A E Ermakov, V A Barinov, E E Yurchikov *Fiz. Met. Metalloved.* **54** (5) 935 (1982) [a]
268. V A Barinov, Candidate Thesis in Chemical Sciences, Institute of Physics of Metals, Urals Branch of Academy of Sciences of the USSR, Sverdlovsk, 1986
269. M S Kim, Ph.D Thesis, North Caroline State University, North Caroline, 1987
270. P Y Lee, J Jang, C C Koch *J. Less-Common Met.* **140** 73 (1988)
271. C C Koch, J Jang, P Y Lee, in *Proceedings of DGM Conference on New Materials by Mechanical Alloying Technique, Calw-Hirsau, 1988* p. 101
272. E Ivanov, T Grigorieva, G Golubkova, in *Proceedings of the 2nd Japan-Soviet Symposium on Mechanochemistry, Tokyo, 1988* p. 219
273. C Larica, K M B Alves, E Baggio-Saitovich, A P Guimaraes *J. Magn. Magn. Mater.* **145** 306 (1995)
274. S K Xia, C Larica, V A Rodriguez, F C Rizzo Assuncao, E Baggio-Saitovich *Mater. Sci. Forum* **225–227** 389 (1996)
275. M Abdellaoui, E Gaffet *J. Alloys Compd.* **209** 351 (1994)
276. Y Chen, M Bibole, R Hazif, G Martin *Phys. Rev. B, Condens. Matter* **48** 14 (1993)
277. L Chaffron, S Poissonet *Mater. Sci. Forum* **225–227** 217 (1996)
278. Yu A Skakov, N P Djakonova, T A Sviridova, E V Shelekhov *Mater. Sci. Forum* **269–272** 595 (1998)
279. E P Yelsukov, G N Konygin, A V Zagainov, V A Barinov *J. Magn. Magn. Mater.* **195** 601 (1999)
280. S J Poon, K J Doherty, A J Akerman, G J Shiffet, D J Li *Scr. Mater.* **38** 603 (1998)
281. K Aoki, M S El-Eskandarany, K Sumiyama, K Suzuki *Mater. Sci. Forum* **269–272** 119 (1998)
282. M Sherif El-Eskandarany, K Aoki, K Sumiyama, K Suzuki *Appl. Phys. Lett.* **70** 1679 (1997)
283. M Sherif El-Eskandarany, K Aoki, K Sumiyama, K Suzuki *Scr. Mater.* **36** 1001 (1997)
284. S Surinach, M Enrech, A Khalladi, J S Munoz, M D Baro *Mater. Sci. Forum* **225–227** 347 (1996)
285. D L Zhang, T B Massalski *Metall. Mater. Trans. A, Phys. Metall. Mater. Sci.* **29** 2425 (1998)
286. L Sun, G X Wang, H K Liu, D H Bradhurst, S N Don *Electrochem. Solid State Lett.* **3** (3) 121 (2000)
287. E Passamani, C Larica, W R Santos, K M B Alves, A Boindo, E Nunes *J. Phys., Condens. Matter* **11** 1147 (1999)
288. N Terashita, M Takahasi, K Kobayashi, T Sasai, E Akiba *J. Alloys Compd.* **295** 541 (1999)
289. C J Van der Kolk, A R Miedema, A K Nilssen *J. Less-Common Met.* **145** 1 (1988)
290. A W Weeber, P I Loeff, H Bakker *J. Less-Common Met.* **145** 293 (1988)
291. A W Weeber, H Bakker *Physica B* **135** 93 (1988)
292. R Bormann, F Gartner, K Zoltzer *J. Less-Common Met.* **145** 19 (1988)
293. E Hellstern, L Schultz, J Eckert *J. Less-Common Met.* **140** 93 (1988)
294. J Eckert, L Schultz, K Urban *J. Less-Common Met.* **145** 283 (1988)
295. L Schultz, E Helstern, in *Glass Formation by Mechanical Alloying in Science and Technology of Rapidly Quenched Alloys* (Eds M Tenhover, L E Tanner, W L Johnson) (Boston: Material Research Society 1989) Pap. G 1.1, p. 4
296. P S Gilman, J S Benjamin *Annu. Rev. Mater. Sci.* **13** 279 (1983)
297. J S Benjamin *Metall. Trans. A* **1** 2943 (1970)
298. E Ivanov, I Konstanchuk, A Stepanov, V V Boldyrev *J. Less-Common Met.* **131** 25 (1987)
299. E Yu Ivanov, Doctoral Thesis in Chemical Sciences, Institute of Solid State Chemistry and Mechanochemistry, Siberian Branch of the Academy of Sciences of the USSR, Novosibirsk, 1990
300. V A Pavlov *Fizicheskie Osnovy Plasticheskoi Deformatsii Metallov* (Physical Foundations of Plastic Deformation of Metals) (Moscow: Academy of Sciences of the USSR, 1962)
301. J Friedel *Dislocations* (Oxford: Pergamon Press, 1964)
302. H G Van Bueren *Imperfections in Crystals* (Amsterdam: North-Holland, 1960)
303. Yu E Zubets, V A Manilov, G F Sazhin *Fiz. Met. Metalloved.* **28** (6) 1055 (1969) [a]
304. O A Kaibyshev, G A Kaibysheva, Ya S Umanskii, G M Epshtein *Fiz. Met. Metalloved.* **24** (3) 505 (1967) [a]

305. A S Ke, in *Pryamoe Nablyudenie Nesovershenstv v Kristallakh* (Direct Study of Imperfections in Crystals) (Moscow: Metallurgizdat, 1964) p. 160
306. N A Koneva, E V Kozlov, N A Ponova, Yu F Ivanov, L N Ignatenko, in *International Symposiums on Metastable Mechanically Alloyed and Nanocrystalline Materials, Rome, 1966* p. D21
307. W Spitzig, T E Mitchell *Acta Metall.* **14** 1311 (1966)
308. E V Belik, S N Kaverina, V N Minakov, V I Trefilov *Fiz. Met. Metalloved.* **24** (3) 535 (1967) [a]
309. V A Wilox, A Gillbert *Acta Metall.* **15** 601 (1967)
310. S V Konetskii, G I Kulesko, N N Nasikhanova *Fiz. Khim. Obrab. Mater.* (3) 73 (1971)
311. Z V Vrublevskaya, G A Ivanova, L G Orlov *Fiz. Met. Metalloved.* **20** (3) 448 (1965) [a]
312. E D Martynov, V I Trofimov, S A Firstov *Dokl. Akad. Nauk SSSR* **176** 1276 (1967) [c]
313. V A Likhachev, M M Myshlyaev, O N Sen'kov, in *IV Vsesoyuz. Seminar 'Struktura Dislokatsii i Mekhanicheskie Svoistva Metallov i Splavov' (Tez. Dokl.), Sverdlovsk, 1987* [The IVth All-Union Meeting 'Structure of Dislocation and Mechanical Properties of Metals and Alloys' (Abstracts of Reports), Sverdlovsk, 1987] p. 168
314. N D Zemtsova, in *IV Vsesoyuz. Seminar 'Struktura Dislokatsii i Mekhanicheskie Svoistva Metallov i Splavov' (Tez. Dokl.), Sverdlovsk, 1987* [The IVth All-Union Meeting 'Structure of Dislocation and Mechanical Properties of Metals and Alloys' (Abstracts of Reports), Sverdlovsk, 1987] p. 61
315. L G Chernykh, V A Starenchenko, in *IV Vsesoyuz. Seminar 'Struktura Dislokatsii i Mekhanicheskie Svoistva Metallov i Splavov' (Tez. Dokl.), Sverdlovsk, 1987* [The IVth All-Union Meeting 'Structure of Dislocation and Mechanical Properties of Metals and Alloys' (Abstracts of Reports), Sverdlovsk, 1987] p. 63
316. L A Kornienko, G L Balach, B F Dudarev, in *IV Vsesoyuz. Seminar 'Struktura Dislokatsii i Mekhanicheskie Svoistva Metallov i Splavov' (Tez. Dokl.), Sverdlovsk, 1987* [The IVth All-Union Meeting 'Structure of Dislocation and Mechanical Properties of Metals and Alloys' (Abstracts of Reports), Sverdlovsk, 1987] p. 65
317. V A Zhorin, D P Shashkin, N S Enikolopyan *Dokl. Akad. Nauk SSSR* **278** 144 (1984) [b]
318. V A Zhorin, V B Fedorov, V D Khakimova *Dokl. Akad. Nauk SSSR* **275** 1447 (1984) [c]
319. I B Kevdina, V A Zhorin, V P Shantarovich *Dokl. Akad. Nauk SSSR* **280** 394 (1985) [c]
320. P Le Brun, E Gaffet, L Froyen, L Delaey *Scr. Metall. Mater.* **26** 1743 (1992)
321. E G Avvakumov *Mekhanicheskie Metody Aktivatsii Khimicheskikh Protsessov* (Mechanical Methods for the Activation of Chemical Processes) (Novosibirsk: Nauka, 1986)
322. I Barker, B Ralph, N Hansen, in *Proceedings of the 8th International Conference on Strength in Metals and Alloys (ICSMA-8), Tampere, 1988* Vol. 1, p. 277
323. A L Windgrove *J. Inst. Met.* **100** 313 (1972)
324. H H Hausner, M Kumar Mal, in *Handbook of Powder Metallurgy* (New York: Chemical Publishing Company, 1982) p. 542
325. T F Grigorieva, M A Korchagin, A P Barinova, N Z Lyakhov *Khim. Inter. Ustoich. Razvit.* **8** 685 (2000) [e]
326. H-J Fecht *Nanostruct. Mater.* **6** 33 (1995)
327. J Eckert, J C Holzer, C E Krill, W L Johnson *J. Mater. Res.* **7** 1751 (1992)
328. H-J Fecht, E Hellstern, Z Fu, W L Johnson *Adv. Powder Metall.* **1** 111 (1989)
329. T G Nich, J Wadsworth *Scr. Metall.* **25** 955 (1991)
330. W E Garner *Chemistry of the Solid State* (London: Butterworth, 1955)
331. M Ya Bernshtein, V A Zaimovskii *Mekhanicheskie Svoistva Metallov* (Mechanical Properties of Metals) (Moscow: Metallurgiya, 1979)
332. R W Balluffi, in *Termicheski Aktivirovannye Protsessy v Kristallakh* (Thermally Activated Processes in Crystals) (Translation into Russian; Moscow: Mir, 1973) p. 42
333. R W Balluffi, A L Ruoff *J. Appl. Phys.* **34** 1634 (1963)
334. A L Ruoff, R W Balluffi *J. Appl. Phys.* **34** 1848 (1963)
335. R W Balluffi *Phys. Status Solidi* **42** 11 (1970)
336. S M Klotsman, A N Timofeev, I Sh Trakhtenberg *Fiz. Met. Metalloved.* **23** (2) 257 (1967) [a]
337. P V Pavlov, L V Maiorov, V V Panteleev *Fiz. Tv. Tela* **6** (2) 382 (1964) [b]
338. C H Lee, R Maddin *J. Appl. Phys.* **32** 1848 (1961)
339. E W Hart *Acta Metall.* **5** 597 (1957)
340. L M Shestopalov, Yu P Romashkin *Fiz. Tv. Tela* **2** (12) 2998 (1960) [b]
341. Yu P Romashkin *Fiz. Tv. Tela* **2** (12) 3050 (1960) [b]
342. S V Zemskii, N E Fomin, G K Mal'tseva *Fiz. Khim. Obrab. Mater.* (4) 91 (1974)
343. S V Zemskii, P L Gruzin, A S Tikhonov *Fiz. Khim. Obrab. Mater.* (5) 83 (1971)
344. M A Krishtan, R I Dubrovskii, O V Stepanova *Fiz. Khim. Obrab. Mater.* (6) 88 (1973)
345. L N Larikov, A M Makara, A T Nazarchuk, V M Fal'chenko *Fiz. Khim. Obrab. Mater.* (4) 113 (1971)
346. B M Clemens *Phys. Rev. B, Condens. Matter* **33** (11) 7615 (1986)
347. E Hellstern, L Schultz *Appl. Phys. Lett.* **49** 1163 (1986)
348. L Schultz *J. Less-Common Met.* **145** 233 (1988)
349. K Samwer, in *Hydrogen in Disordered and Amorphous Solids* (New York: Plenum, 1986) p. 173
350. K Samwer *J. Less-Common Met.* **140** 25 (1988)
351. Y Huang, J Z Jiang, H Yasuda, H Mori *Phys. Rev. B, Condens. Matter* **58** R 11817 (1998)
352. H Mori, M Komatsu, K Takeda, H Fujita *Philos. Mag. Lett.* **63** 173 (1991)
353. H Yasuda, H Mori *Phys. Rev. Lett.* **69** 3747 (1992)
354. H Yasuda, H Mori, M Komatsu, K Takeda *Appl. Phys. Lett.* **61** 2173 (1992)
355. H Mori, H Yasuda *Intermetallics* **1** 35 (1993)
356. H Yasuda, H Mori, T Muraki, T Sakata *Z. Phys. D, At. Mol. Clusters* **31** 209 (1994)
357. H Yasuda, H Mori *Mater. Sci. Eng., A* **217**/**218** 249 (1996)
358. H Yasuda, H Mori *Z. Phys. D, At. Mol. Clusters* **31** 131 (1994)
359. H Mori, H Yasuda *J. Microsc.* **180** 33 (1995)
360. H Mori, H Yasuda *Mater. Sci. Forum* **269**–**272** 327 (1998)
361. H Yasuda, H Mori *Mater. Sci. Forum* **269**–**272** 333 (1998)
362. J Harada, K Ohshima *Surf. Sci.* **106** 51 (1981)
363. T Matsubara, Y Iwase, A Momokita *Prog. Theor. Phys.* **58** 1102 (1977)
364. T F Grigorieva, A P Barinova, V V Boldyrev, E Yu Ivanov *Dokl. Akad. Nauk* **345** 343 (1995) [c]
365. T F Grigorieva, A P Barinova, E Yu Ivanov, V V Boldyrev *Dokl. Akad. Nauk* **350** 59 (1996) [c]
366. T F Grigorieva, A P Barinova, E Yu Ivanov, V V Boldyrev *Mater. Sci. Forum* **235**–**238** 577 (1997)
367. V V Boldyrev, S V Tsybulya, S V Cherepanova, G N Kryukova, T F Grigorieva, E Yu Ivanov *Dokl. Akad. Nauk* **361** 784 (1998) [c]
368. T F Grigorieva, S V Tsybulya, S V Cherepanova, G N Kryukova, A P Barinova, V D Belykh, V V Boldyrev *Neorg. Mater.* **36** 194 (2000) [d]
369. T F Grigorieva, M A Korchagin, A P Barinova, V V Boldyrev *Khim. Inter. Ustoich. Razvit.* **7** 505 (1999) [e]
370. F Petzoldt, B Scholz, H-D Kunze *Mater. Lett.* **5** 280 (1987)
371. W L Meng, C W Nieh, W L Johnson *Appl. Phys. Lett.* **51** 1693 (1987)
372. M Takagi *J. Phys. Soc. Jpn.* **9** 359 (1951)
373. J Sambles *Proc. R. Soc. London A, Math. Phys. Sci.* **324** 339 (1971)
374. G L Allen, R A Bayles, W W Gile, W A Jesser *Thin Solid Films* **144** 297 (1986)
375. T Castro, R Reinfenberger, E Choi, R P Andres *Phys. Rev. B, Condens. Matter* **42** 8548 (1990)
376. H Yasuda, H Mori *Z. Phys. D, At. Mol. Clustors* **37** 181 (1996)
377. F P Bowden, D Tabor *The Friction and Lubrication of Solids* (Oxford: Clarendon Press, 1958)
378. F P Bowden, F P S Thomas *Proc. R. Soc. London, A, Math. Phys. Sci.* **223** 29 (1954)
379. F P Bowden, P A Persson *Proc. R. Soc. London, A, Math. Phys. Sci.* **260** 433 (1961)
380. A V Dubnov, V A Sukhikh, I I Tomashevich *Fiz. Goren. Vzryv.* **7** (1) 147 (1972)
381. A H Cottrell *Dislocations and Plastic Flow in Crystals* (Oxford: Clarendon Press, 1953)
382. F Kh Urakaev, E G Avvakumov *Izv. Sib. Otd. Akad. Nauk, Ser. Khim. Nauk* **7** 10 (1978)
383. A V Kopylov, E G Avvakumov, F Kh Urakaev *Izv. Sib. Otd. Akad. Nauk, Ser. Khim. Nauk* **4** 8 (1979)

384. F Kh Urakaev, in *Trenie i Iznos* (Friction and Wear) (Minsk: Nauka i Tekhnika, 1980) Vol. 1, No. 6, p. 1078
385. F Kh Urakaev, E G Avvakumov, Kh Iost *Izv. Sib. Otd. Akad. Nauk SSSR, Ser. Khim. Nauk* **3** 9 (1982)
386. F Kh Urakaev, I L Zhogin, E L Gol'dberg *Izv. Sib. Otd. Akad. Nauk, Ser. Khim. Nauk* **3** 124 (1985)
387. F Kh Urakaev *Izv. Sib. Otd. Akad. Nauk, Ser. Khim. Nauk* **7** 5 (1978)
388. A N Dannik *Izbrannye Trudy* (Selected Proceedings) (Kiev: Academy of Sciences of Ukr. SSR, 1952) Vol. 1
389. F Kh Urakaev, Candidate Thesis in Chemical Sciences, Institute of Solid State Chemistry and Mechanosynthesis, Siberian Branch of the Academy of Sciences of the USSR, Novosibirsk, 1978
390. A E Ermakov, E E Yurchikov, V A Barinov *Fiz. Met. Metalloved.* **52** (6) 1184 (1981) [a]
391. S D De La Torre, K N Tshihara, P H Shingu *Mater. Sci. Eng. A* **266** 37 (1999)
392. J Eckert, L Schultz, E Hellstern, K Urban *J. Appl. Phys.* **64** 3224 (1988)
393. R B Schwarz, C C Koch *J. Appl. Phys. Lett.* **49** 146 (1986)
394. V M Zalkin *Priroda Evtekticheskikh Splavov i Effekt Kontaktnogo Plavleniya* (Nature of Eutectic Alloys and Contact Melting Effect) (Moscow: Metallurgiya, 1987)
395. H Kimura, M Y Kimura, F Takada *J. Less-Common Met.* **140** 113 (1988)
396. USSR P. 975 068; *Byull. Izobret.* (43) 23 (1982)
397. K B Gerasimov, A A Gusev, V V Kolpakov, E Yu Ivanov *Sib. Khim. Zh.* (3) 140 (1990)

[a] — *Phys. Met. Metall. (Engl. Transl.)*
[b] — *Phys. Solid. State (Engl. Transl.)*
[c] — *Dokl. Chem. Technol., Dokl. Chem. (Engl. Transl.)*
[d] — *Inorg. Mater. (Engl. Transl.)*
[e] — *Chem. Sustain. Dev. (Engl. Transl.)*

Russian Chemical Reviews **70** (1) 65 – 79 (2001) © 2001 Russian Academy of Sciences and Turpion Ltd

DOI 10.1070/RC2001v070n01ABEH000624

Chemical modification and blending of polymers in an extruder reactor

E V Prut, A N Zelenetskii

Contents

I.	Introduction	65
II.	Characteristic features of reactive blending processes	65
III.	Grafting of low-molecular-mass compounds onto polymers	67
IV.	Reactions between terminal groups of polymers	70
V.	Transesterification reactions and interchange processes	71
VI.	Preparation of thermoplastic elastomers by dynamic vulcanisation	71
VII.	Solid-phase reactions in an extruder reactor	75

Abstract. Chemical modification and blending of polymers in an extruder reactor are discussed. Relationships between the parameters affecting the reaction kinetics, *viz*., mixing time, duration of a chemical reaction and the residence time of the system in the extruder reactor, and the structure of the materials produced are analysed. The mechanisms of (i) grafting of low-molecular-mass compounds onto polymers; (ii) reactions between terminal groups of different polymers and (iii) transesterification and interchange reactions are considered. The factors affecting the mechanism of dynamic vulcanisation and the properties of thermoplastic elastomers are identified. Solid-phase reactions of polysaccharides in an extruder are discussed. The priority aspects of studies on the chemical modification and blending of polymers are noted. The bibliography includes 90 references.

I. Introduction

Polymeric composites are currently widely used and actively studied. Particular interest has been shown in multicomponent polymer blends and alloys. The creation of such polymeric materials entails the possibility of combining attractive qualities of each component of the polymer blend in the end product.[1–3] Useful properties of polymer blends are affected by such characteristics as the nature of the dispersed and dispersion phases, the volume ratio of the phases, the sizes and size distributions of the particles of the dispersed phase, and interfacial adhesion.

Much attention is paid by investigators to the processes of preparation of materials by blending components in which chemical reactions proceed.[4,5] Such processes are called 'reactive blending' or 'reactive extrusion'. Only a few polymers are thermodynamically compatible and form blends with homogeneous morphology at a molecular level. The majority of polymers exhibit limited compatibility or are incompatible and their blends possess heterogeneous morphologies.

Reactive blending extends the possibilities of controlling the phase structures of multicomponent polymeric materials. Not only does the technology for reactive blending of polymers open new ways for the employment of polymeric products already available but also permits the creation of blends, the preparation of which by other methods has been economically unfavourable. Application of methods of organic chemistry and reactive blending allows preparation of diverse modified polymers and polymer blends based on a a small number of industrially produced polymers.[4]

II. Characteristic features of reactive blending processes

1. Blending condition

Blending of polymers is an intricate physicochemical process, which proceeds under the action of mechanical and temperature fields. If blending of polymers is accompanied by chemical reactions, their rates are determined by the character of blending, temperature gradients and by diffusion of the reagents and products. These characteristics can be controlled if reactive blending is carried out in extruder reactors.

Currently, continuous extruder reactors (Fig. 1) are available. Extrusion is used for the preparation of products or semifinished items of desired shape by forcing polymer melts through an exit (a shape-forming orifice).[6–8] Extrusion processing of plastics is effected by using mainly single-screw and twin-screw extruders. Technologies with employment of extruder reactors combine the processes that are usually separated, *e.g*., blending, chemical reactions and moulding. Here, new problems arise associated with, *e.g*., changes in the viscosity during the reaction or heat removal. Some lines of attacking such problems, as applied to polymerisation reactions, have been considered.[5,9] It was found that in the case of chemically reacting systems twin-screw extruders are preferable to single-screw extruders owing to more efficient mixing and heat removal. However, the complexity of chemical and physical processes proceeding in an extruder reactor hampers the choice of the moulding parameters and equipment.

This requires experimental and theoretical studies on the evolution of the structure and properties of polymers during the preparation of materials using extruder reactors.[10–13] However, experimental investigation of the polymer structure is a complicated multiparameter problem. On the other hand, only a few

E V Prut N N Semenov Institute of Chemical Physics, Russian Academy of Sciences, ul. Kosygina 4, 117977 Moscow, Russian Federation. Fax (7-095) 938 21 56. Tel. (7-095) 939 71 55.
E-mail: evprut@center.chph.ras.ru
A N Zelenetskii N S Enikolopov Institute of Synthetic Polymer Materials, Russian Academy of Sciences, ul. Profsoyuznaya 70, 117393 Moscow, Russian Federation. Fax (7-095) 420 22 29. Tel. (7-095) 332 58 45.
E-mail: anzel@icpm.ru

Received 4 September 2000
Uspekhi Khimii **70** (1) 72 – 87 (2001); translated by A M Raevsky

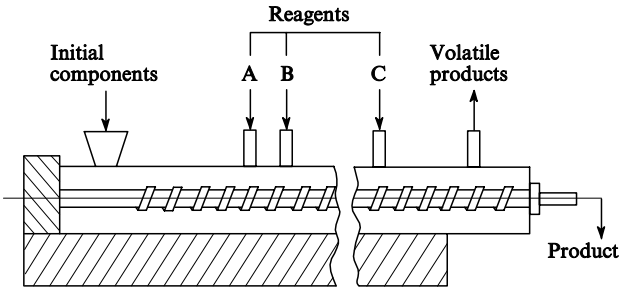

Figure 1. A scheme of an extruder reactor.

theories which allow qualitative description of the changes in the polymer structures after completion of the chemical reactions in the system have been developed.[14–16] This can be illustrated as follows. If a reaction proceeds in the melt, the reaction rate can be strongly affected by diffusion. Changes in the blend composition during the reaction can in turn affect the diffusion processes. Therefore, a theory is required which describes the evolution of the structure of a polymer blend taking into account the mutual influence of the chemical reaction and diffusion.[17]

Changes in the structure of a model heterogeneous blend, in which the copolymer AB is an intermediate of a polymeranalogous reaction A → B have been considered.[18] It was shown that diffusional mixing has a pronounced effect on the reaction kinetics. This effect manifests itself if the characteristic time of the chemical reaction,

$$\tau_r = \frac{1}{k},$$

(k is the rate constant of the chemical reaction) is shorter than, or comparable with, the mixing time τ_m. The mixing can be considered efficient if

$$\tau_m < \tau_r. \qquad (1)$$

This condition holds well for the alcoholysis of poly(ethylene-*co*-vinyl acetate) with aliphatic alcohols (octan-1-ol, 2-ethylhexan-1-ol, 3-phenylpropan-1-ol) in the bulk and in solution (dodecan-1-ol) with dibutyltin dilaurate as catalyst.[19] The bulk reaction was carried out in a Haake Rheochord mixer (Germany).

It was shown [19] that the reaction in solution and in the bulk follows the same mechanism, which is independent of the nature of the alcohol. The equilibrium constants of the reactions in solution and in the bulk were equal. The reaction rates were of the second order with respect to the concentrations of reagents. The viscosities of the systems in solution and in the bulk differed by five orders of magnitude. Based on the results of analysis of the kinetic data, it was suggested that (i) the reaction rate is substantially lower than the diffusion rate and (ii) mechanical mixing is necessary only for the homogenisation of the reaction system in the initial stage of the reaction (once this is achieved, mixing is of no significance during the reaction).

However, the differences between the limiting degrees of conversion have not been discussed.[19] From the plots reported in this study it follows that the limiting degree of conversion in the bulk at 180 °C is ~ 65% while that in solution at 170 °C is ~ 90%. This is most likely due to the change in the viscosity of the reaction system.

Usually, the viscosity of the medium increases during the reaction, thus hampering homogenisation of the reaction system and leading to the formation of structurally inhomogeneous material. Changes in the viscosity during the ionic and radical polymerisation reactions have been analysed [9, 20] and a theoretical approach to quantitative estimation of these changes has been considered.

During the reaction, the system can become heterogeneous and the reaction kinetics can in turn change. The kinetics of the chemical reactions in homogeneous and heterogeneous polymer melts have been analysed taking the esterification reaction between 1-naphthylacetic acid (NAA) and a random ethylene/ethyl acrylate/glycidyl methacrylate (E–EA–GMA) terpolymer as an example.[21] Being initially homogeneous, the system NAA–E–EA–GMA became heterogeneous upon addition of an inert polymer, *viz*., polystyrene (PS). Polystyrene and E–EA–GMA are immiscible, whereas NAA can be mixed with both polymers in the concentration and temperature ranges studied. It was shown that the mechanisms of these reactions are identical and that the rate of NAA diffusion is much higher than the reaction rates in both systems.

Thus, preparation of materials with homogeneous distribution of submicroscopic particles of the dispersed phase requires that the condition (1) be met.

2. Effect of the residence time of a system in an extruder reactor

The reaction in an extruder reactor goes to completion if

$$\tau_r \ll \tau_f, \qquad (2)$$

where τ_f is the mean residence time of the reaction system in the extruder reactor (hereafter, the residence time). This time depends on the ratio of the extruder length, l, to the longitudinal component of the flow rate, V,

$$\tau_f = \frac{l}{V}. \qquad (3)$$

Generally, the residence time is determined by some distribution function.[22] The distribution functions, f(τ), for a ZSK-30 co-rotating twin-screw extruder (Werner and Pfleiderer, Germany; screw length-to-diameter ratio, $l/d = 42$) are shown in Fig. 2*a*. Proceeding to the dimensionless time

$$\theta = \frac{\tau}{\tau_f},$$

where τ is the current residence time of the reaction system in the extruder reactor, gives the residence time distribution function, f(θ), shown in Fig. 2*b*. As can be seen, the f(θ) curves are shifted to a short-time domain when the feed rate Q and screw speed N increase, *i.e*., τ_f shortens and the f(θ) curves match one another. It is believed that the mechanical mixing intensity does not vary much upon varying Q and N at a constant Q/N ratio. On the other hand, the residence time distribution function, which characterises macromixing, changes. The ratio between the convection mass transfer in a flow and free molecule diffusion is characterised by the Peclet number (criterion), Pe (Ref. 24)

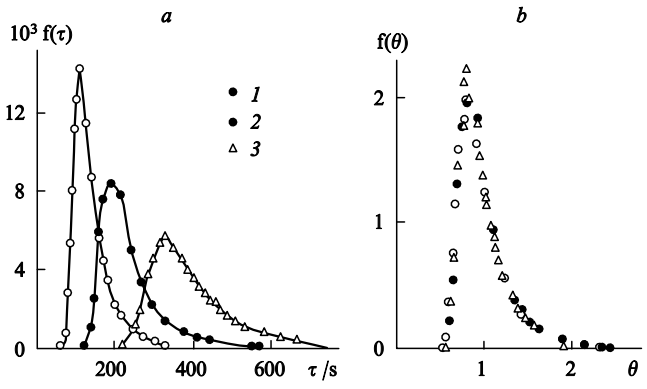

Figure 2. Residence time distribution function in dimensional (*a*) and dimensionless form (*b*) as a function of the feed rate Q and screw speed N at a constant Q/N value of 1/43 kg min h^{-1} rev^{-1};
(*1*) Q = 5.6 kg h^{-1}, N = 240 rev min^{-1}; (*2*) Q = 3.5 kg h^{-1}, N = 150 rev min^{-1}; (*3*) Q = 2.1 kg h^{-1}, N = 90 rev min^{-1}.[24]

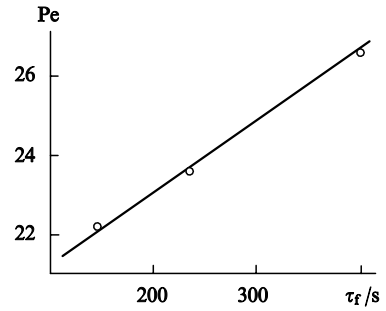

Figure 3. Dependence of the Peclet number on the residence time.

$$\mathrm{Pe} = \frac{Vl}{D},$$

where D is the diffusion coefficient. The dependence of the Peclet number on τ_f is shown in Fig. 3. As can be seen, the Pe number increases as τ_f increases. This plot was constructed using the results obtained by Sun *et al.*[23] Unfortunately, they reported no numerical data for the calculation of the Peclet numbers. At small Pe values, free molecule diffusion predominates, while convection mass transfer is predominant at large Pe values. Hence, the contribution of the convection mass transfer increases with lengthening of the residence time τ_f, (*i.e.*, with a decrease in the feed rate Q and screw speed N).

The residence time was found to be the main parameter which controls the degree of grafting (q) of, *e.g.*, GMA onto polypropylene (PP). As Q and N decrease, τ_f and q (Fig. 4) increase. On the other hand, the degree of grafting decreases with increase in the energy supplied per unit mass of the reacting system U (Fig. 5).

Thus, the degree of grafting is mainly determined by the mixing mechanism rather than energy expenditure.

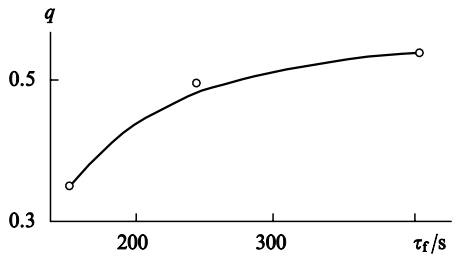

Figure 4. Dependence of the degree of grafting of GMA onto PP (q) on the residence time at $l/d = 42$, $Q/N = 1/43$ kg min h^{-1} rev^{-1}.

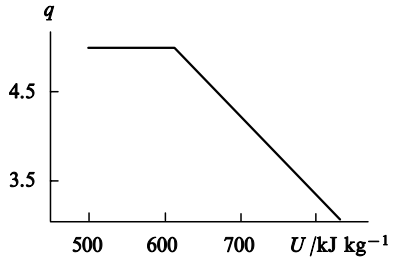

Figure 5. Dependence of the degree of grafting on the energy supplied per unit mass of the reaction system at $Q/N = 1/43$ kg min h^{-1} rev^{-1} (see Ref. 24).

III. Grafting of low-molecular-mass compounds onto polymers

1. Grafting onto polypropylene

Modification of polymers is carried out for compatibilisation of polymer blends. This is achieved by using block and graft copolymers.[25] Preparation of diverse polymer blends by reactive blending has been reported.[4] The synthesis of graft copolymers of polyalkenes by reactive extrusion has been reviewed [26] and the mechanisms of grafting and structures of graft copolymers depending on the reaction conditions have been analysed.

Polypropylene is one of the intensively studied polymers. Grafting of GMA onto PP proceeds by a radical mechanism. The limiting degree of grafting increases with increase in the peroxide concentration [23] as well as upon introduction of styrene as the second monomer. In the latter case, $\overline{M}_w$ increases from 220 000 in the absence of styrene to 350 000 in the presence of styrene.

The stage that follows grafting is blending of polymers. Here, reactions of graft polymers with other blend components take place. These reactions result in improvement of interfacial adhesion. Problems arising where two processes, *viz.*, functionalisation and chemical mixing, are carried out in one extrusion step have been considered.[27, 28]

In situ compatibilisation of PP and poly(butylene terephthalate) (PBT) blends (PP : PBT = 70 : 30) was carried out by one-step reactive extrusion in a ZSK-30 co-rotating twin-screw extruder (Werner and Pfleiderer, Germany) ($d = 30$ mm, $l/d = 42$).[27] Possible screw configurations are schematically represented in Fig. 6.[28] The extruder is divided into two functional zones: grafting of GMA onto PP is carried out in the first part of the extruder and the reaction between the GMA-*g*-PP and the carboxy group of the PBT is carried out in the second part of the extruder.

It was found that changes in the compatibility of the PP – PBT blend are accompanied by changes in its morphology. In the mechanical blend of the initial components, the particle size of the dispersed phase (PBT) was larger than in the blend of grafted PP and PBT. In the latter case, the interfacial adhesion was also improved.

The plot of the residence time distribution function in the reaction of PP with PBT [27] is similar to that considered above (see Fig. 2 *a*). As the feed rate Q and screw speed N increase, the residence time distribution function curve is shifted to the short-

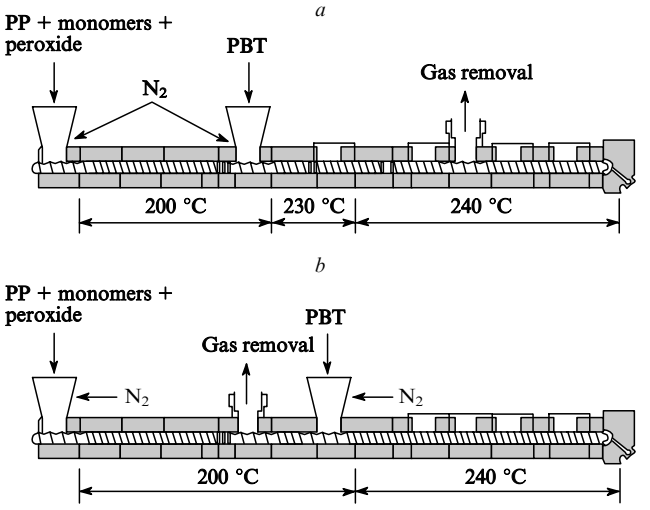

Figure 6. Examples of screw configurations for combining the modification of PP and its blending with PBT.[28]

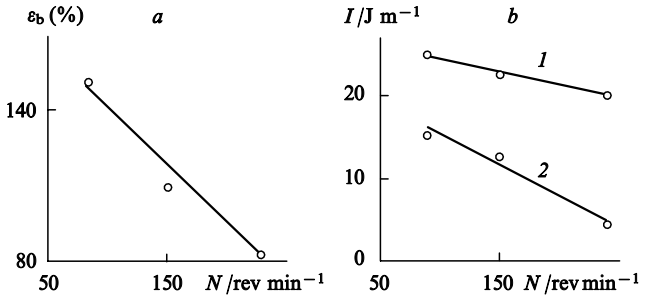

Figure 7. Dependence of the elongation at break (*a*) and impact strength (*b*) on the screw speed at $Q/N = 1/30$ kg min h^{-1} rev^{-1} (see Ref. 27). Temperature: (*1*) 0 and (*2*) 720 °C.

time domain. In dimensionless coordinates, the plots of these functions match one another (see Fig. 2*b*).[24] The elongation at break and the impact strength depend on the residence time of the system in the extruder. With a decrease in Q and N, the residence time lengthens and, correspondingly, the elongation at break (ε_b) and the impact strength (I) increase (Fig. 7).

The effects of the chemical nature and concentration of compounds subject to grafting onto PP, the concentration of the initiator (peroxide) and some other parameters on PP modification have been studied.[28] Among the three compounds studied, namely, acrylic acid (AA), maleic anhydride (MA) and GMA, the last-named compound was found to be the most efficient for the modification of PP–PBT blends. After optimisation of the reaction conditions, the elongation at break and impact strength of the modified PP–PBT blend (PP : PBT = 70 : 30) increased 15- to 20-fold as compared with the corresponding parameters for the mechanical blend. Further increase in the PBT concentration leads to a decrease in the elongation at break and impact strength of the modified PP–PBT blend. This is probably due to cross-linking reactions.

Comparison of the properties of the polymer blends prepared by one-step reactive extrusion[27] and by conventional two-step technique showed that the elongations at break and impact strengths of the blends prepared by the former method are higher.[8]

Numerous studies have been concerned with grafting of MA onto PP.[29–34] It was shown[29] that if the reaction was carried out with 2,5-dimethyl-2,5-bis(*tert*-butylperoxy)hexane as the initiator, the dependence of the degree of grafting on the MA concentration passes through a maximum. This is due to the fact that the PP–MA system becomes a two-phase system with an increase in the MA concentration and, hence, the effective concentrations of the MA and peroxide decrease. In this case, the grafting reaction was carried out in a batch mixer at 215–220 °C at a rotor speed of 64 rev min^{-1} over a period of 15 min. If grafting is carried out in a twin-screw extruder (200 °C, $\tau_f = 3$ min, screw speed = 75 rev min^{-1}), the degree of grafting increases; however, intense degradation of the extrudate is observed.

Modification of PP is accompanied by its degradation. An important problem is to reduce the degree of polymer degradation during the grafting. It was found[23] that introduction of an electron-donor monomer (*e.g.*, styrene) causes an increase in the degree of grafting of MA onto PP and substantially inhibits degradation.

Similar results were obtained by Bettini and Agnelli[30,31] who studied the effect of content of MA and a 46.5% concentrate of 2,5-dimethyl-2,5-bis(*tert*-butylperoxy)hexane in $CaCO_3$, the rotor speed and duration of the reaction on the degree of grafting of MA onto PP and on changes in the molecular mass (MM). Blending was carried out in a System 90 torque rheometer (Haake, Germany) equipped with a Rheomix 600 mixer. It was found that an increase in the peroxide concentration leads to an increase in the degree of grafting and to a decrease in the MM. The dependence of the degree of grafting on the MA concentration passes through a maximum, the position of which is determined by the rotor speed and duration of the reaction. Degradation of PP is a complex function of the MA concentration: at high MA concentration, the melt flow index (MFI) decreases, *i.e.*, the degradation of PP is retarded.

Grafting of MA onto PP of different stereoregularity in melt and in solution in the presence of dicumyl peroxide has been compared.[32–34] Similarly to the reactions discussed above, the dependence of the degree of grafting on the MA and peroxide concentrations was also found to pass through an extremum. The degree of grafting in the melt was higher than that in solution (with xylene and decalin as solvents). The maximum degree of grafting onto atactic PP was found to be higher than onto isotactic PP. However, the modified atactic PP was more compositionally heterogeneous.

Different types of peroxides were used as radical initiators of the grafting reactions. Naturally, the question arises: how does the chemical nature of the peroxide affect the grafting kinetics?

A number of functional peroxides (peroxy esters) has been studied.[35] The structures of functional nonsymmetric peroxides and the corresponding trade names are shown below.

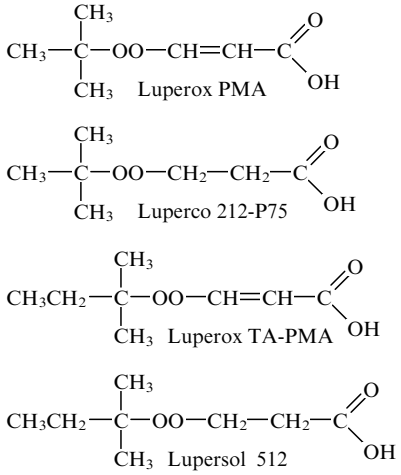

Blending of PP and peroxides was carried out in a Rheochord 90 counter-rotating, twin-screw extruder (Haake, Germany). The screw speed was 15 rev min^{-1}, which corresponded to a residence time of ~ 7 min. The reactions were carried out in a N_2 atmosphere. It was assumed that the residence time is sufficient for the peroxides to decompose completely.

The degree of grafting of a carboxylic acid onto PP and degradation of PP has been studied.[35] Grafting reactions carried out in the presence of peroxides which decompose to give methyl radicals were found to be more efficient than those in the presence of peroxides which decompose to give ethyl radicals. The increase in the concentration of polymeric radicals leads to an increase in the degree of grafting and to greater degradation of PP. A similar effect was also observed upon the formation of radicals with double bonds.

Thus, varying the molecular structure of the peroxide allows the degree of grafting of functional groups onto PP to be changed.

Grafting of MA onto PP can also be carried out using not only radical reactions accompanied by intense degradation of PP but also other types of reactions. The degradation upon radical modification of PP can be reduced and the process becomes controllable if a 'specific' functionalisation, *viz.*, the reaction of the terminal vinylidene groups with various compounds, is carried out. Among possible reactions, the Alder ene addition seems to be the most convenient to be performed in an extruder reactor.[36] The reaction rate depends on the acidity and basicity of the ene moiety and enophilic fragments and on the reaction conditions; it increases in the presence of Lewis acids.

Grafting of MA onto PP in the presence of Lewis acids ($SnCl_2$, $RuCl_2$) in an LSM 30.34 co-rotating twin-screw extruder (Leistritz, Germany; $d = 34$ mm; $l/d = 42$) has been studied.[36]

Grafting of MA onto PP using the Alder ene reaction was shown [36] to proceed without considerable degradation of PP. An increase in the reaction temperature and the MA concentration leads to an increase in the degree of grafting, which also increases with improved mixing. For this reaction, $RuCl_2$ was found to be a more efficient catalyst than $SnCl_2$.

2. Grafting onto polyethylene

Polyethylene (PE) is yet another polymer which is widely used in polymer blends. The number of different types of PE is larger than that of PP. Therefore, it is of interest to analyse the effect of grafting onto PE as function of its structure. Grafting of diethyl maleate (DEM) onto high-density polyethylene (HDPE) and linear low-density polyethylene (LLDPE) in two co-rotating twin-screw extruders, namely, a ZSK-30 extruder (Werner and Pfleiderer, Germany) and a ECS-2E25 extruder (Berstorff, Germany) has been studied.[37] Screw configurations, extrusion conditions and the order of introduction of the components into the extruder were varied. The effects of different parameters on the residence time distribution function were analysed. As for PP, the efficiency of grafting was determined by the residence time. When the transport delay time and the mean residence time exceeded certain critical values, the concentration of free radicals decreased owing to secondary reactions (*e.g.*, thermal oxidation, mechanochemical degradation and/or chain branching, *i.e.*, the formation of long branches for LLDPE), which resulted in a decrease in the degree of grafting.

An increase in the degree of grafting with increase in the initiator concentration was independent of the screw configuration and extruder type. The molecular mass distribution (MMD) of the DEM graft LLDPE was virtually the same as that of the initial sample. However, $\bar{M}_w$ of the DEM graft HDPE decreased and the MMD became narrower. Hence, the degree of grafting onto PE is determined by the residence time of the system in the extruder while the MMD is determined by the type of the PE.

Rosales *et al.*[37] also studied the influence of chemical nature of the peroxide by comparing the effects of a 90% solution of 2,5-dimethyl-2,5-bis(*tert*-butylperoxy)hexane and dicumyl peroxide. The second initiator was found to be less efficient.

A study of the effect of the degree of grafting on the rheological and thermal properties has been reported.[38] It was shown that the rheological properties are more sensitive to the changes due to grafting than the structural parameters determined from the measurements of thermal behaviour. An increase in the dynamic viscosity with increase in the degree of grafting was observed at low frequencies of strain sweep. Mention was made that the blends obtained possess enhanced compatibility with polyamides and polyesters.

Compared to the molecular structure characteristics, the rheological properties of the modified LLDPE are also more sensitive to the changes due to reactions at low peroxide concentrations.[39, 40] LLDPE was extruded in the presence of the initiator, 2,5-dimethyl-2,5-bis(*tert*-butylperoxy)hexane, in a co-rotating twin-screw extruder (Leistritz, Germany; $d = 34$ mm, $l/d = 35$). The screw configuration was varied. The peroxide concentration was low in order to prevent cross-linking. In this case, the MMD broadened owing to an increase in the percentage of the high-molecular-mass fraction, which increased with increase in the peroxide concentration.

The proportion and lengths of the side groups were determined by different methods (size-exclusion liquid chromatography, nuclear magnetic resonance, differential scanning calorimetry). It was found that the proportion of unsaturated terminal units in the modified LLDPE diminished. Based on the results obtained, a reaction mechanism was proposed.

The authors established that an increase in the complex viscosity at low frequencies of strain sweep is due to the formation of a small number of long-chain branches. Changes in the molecular parameters of the modified LLDPE affected not only the shear characteristics of the flow but also the flow characteristics in the longitudinal direction. The modified LLDPE had higher viscosity in the longitudinal direction. However, this was accompanied by a decrease in the tensile deformability. Swelling of the extrudate decreased with increase in the peroxide concentration. The efficiency of the LLDPE modification in the extrusion strongly depended on the temperature and quality of mixing.

The influence of extrusion on the cross-linking and degradation of PE has been studied.[41] Cross-linking of HDPE in the presence of a peroxide, 1,3-bis(*tert*-butylperoxyisopropyl)benzene (system 1), and mixtures of this peroxide with coagents, *viz.*, trimethylolpropane triacrylate (TMPTA) (system 2) and *para*-benzoquinone (PBQ) (system 3), in the extrusion in a twin-screw extruder ($d = 25$ mm; $l/d = 30$) at 230 °C has been studied.

It was shown that the MFI decreased rapidly as the peroxide concentration increased in system 1, more smoothly in system 2 and showed a slight increase in system 3. The last-named effect was probably due to degradation of HDPE.

Thermal properties of the modified HDPE depend on the peroxide concentration in a complex manner. The melting temperature, T_m, and the crystallisation temperature, T_{cr}, increase with increase in the peroxide concentration. On the other hand, T_m decreases while T_{cr} increases as the concentration of the peroxide–TMPTA initiator increases. Initially, the heat of melting increases and then decreases with increase in the concentration of the initiator.

The effect of the peroxide and TMPTA concentrations on the mechanical properties can be followed from the data listed in Table 1. As can be seen, the impact strength increases by ~ 7-fold as compared to that of the initial HDPE.

Table 1. The effect of the peroxide and TMPTA concentrations on the mechanical properties of cross-linked HDPE.

[Peroxide] [a]	[TMPTA] [a]	MFI /g/10 min	D	I	E	σ_y	ε_b
–	–	4.74	61	148	1290	27.5	600
0.05	–	1.62	62	576	1290	30.0	20
–	0.3	0.95	62	1084	1400	37.5	30
0.05	0.3	0.037	64	770	1440	42.0	30
0.01	0.1	1.78	62	908	1340	35.0	30
0.01	0.2	0.98	63	1032	1410	39.0	20
0.02	0.1	0.49	61	1011	1340	35.5	20
0.02	0.2	0.13	62	1016	1420	38.5	20

Note. The following notations are used here and in Tables 2–5: D is the hardness (arbitrary units), I is the notched Izod impact strength (J m^{-1}), E is the flexural modulus (MPa), σ_y is the yield stress (MPa) and ε_b is the elongation at break (%).

[a] The concentrations of peroxide and TMPTA are given in mass parts per 100 mass parts of HDPE.

3. Grafting onto an ethylene/propylene terpolymer and polylactide

Grafting of MA onto ethylene/propylene/ethylidenenorbornene terpolymer (EPDM, with ethylene and ethylidenenorbornene concentrations of 56 mass % and 5.7 mass %, respectively) in a Rheomix 750 mixer (Haake-Buchler, Germany) at ~ 160 °C with dicumyl peroxide as the initiator has been studied.[42] It was shown that the amount of the gel fraction initially increases up to 4 mass % with an increase in the MA concentration and then decreases. On the other hand, the amount of the gel fraction increases monotonically with increase in the peroxide concentration.

As in the case of polyalkenes, the dependence of the degree of grafting onto EPDM on the MA concentration increases as the MA concentration increases up to 3 mass % and then decreases, thus passing through an extremum. The degree of grafting

increases with increase in the peroxide concentration. The reaction is accompanied by cross-linking and degradation of the terpolymer.

Introduction of an electron donor (*e.g.*, stearamide) into the reaction system inhibits side reactions, *viz.*, cross-linking and degradation. The optimum content of stearamide was found to be $\sim$ 20 mass %.

Grafting of MA onto other types of polymers has also been studied. In particular, a study on the grafting of MA onto polylactide in a co-rotating twin-screw extruder (Baker Perkins, United Kingdom) with 2,5-dimethyl-2,5-bis(*tert*-butylperoxy)-hexane as the initiator has been reported.[43] Polylactide is a biodegradable polymer widely used in medicine. It was shown that the degree of grafting increases with increase in the initiator concentration, while MM decreases (the MFI increases). The ratio of the weight-average molecular mass to the number-average molecular mass, $\bar{M}_w/\bar{M}_n$, remained virtually constant. It was found that even a small amount of the MA graft onto polylactide essentially improves the interfacial adhesion in the polylactide-based blends and composites.

IV. Reactions between terminal groups of polymers

Chain extension in PBT owing to the reactions of the epoxy groups of diglycidyl tetrahydrophthalate with the terminal hydroxy and carboxy groups of PBT has been studied.[44]

The synthesis of high-molecular-mass PBT is a rather complicated problem. Industrially, PBT with an MFI greater than 20 g/10 min can be produced, while the PBT with relatively low MM possesses poor mechanical properties. Therefore, the problem of chain extension is topical. One of the possible ways of solving this problem is to carry out reactions of bifunctional compounds with terminal groups of PBT. Guo and Chan[44] carried out the reaction of epoxy groups with the carboxy and hydroxy groups of PBT in a Rheomix 600 mixer (Haake, Germany). The rotor speed was varied from 30 to 120 rev min^{-1} and the temperature was varied from 230 to 280 °C. As the temperature was raised and the rate of shear increased, the duration of the reaction of the terminal groups of PBT with the epoxy groups decreased owing to an increase in the rate of diffusion of the epoxy groups. The duration of the reaction was found to be $\sim$ 3 min at 260 °C. Therefore, this reaction can be performed in both single-screw and twin-screw extruders.

The results of mechanical and rheological tests of the PBT thus obtained are listed in Table 2. As can be seen, the MFI value decreases rapidly with increase in the concentration of epoxy groups, while the notched Izod impact strength and the elongation at break increase. The PBT thus obtained was found to be more thermally stable.

Table 2. The effect of the concentration of epoxy groups [E] on the mechanical properties of PBT.[41]

[E] (mass %)	σ_b /MPa	ε (%)	σ_{bn} /MPA	I /J m^{-1}	MFI /g/10 min
0	53.7	50.2	88.6	19.9	35.4
0.4	54.4	62.3	91.2	20.2	29.8
0.5	53.9	76.9	91.7	22.9	23.5
0.7	52.3	101.8	93.2	23.2	17.8
0.8	52.6	130.4	89.3	24.1	15.4
0.9	52.3	267.7	93.3	25.7	13.1
1.0	53.5	262.5	92.1	26.3	10.3
1.2	53.0	278.5	92.5	34.4	8.4
1.3	53.0	329.2	93.0	39.2	5.0
1.4	52.9	360.1	92.4	51.9	3.6
1.6	52.1	360.0	92.2	49.5	2.6

Note. The following notations are used: σ_b is the tensile strength and σ_{bn} is the bending strength.

On the other hand, the reaction considered above can be accompanied by cross-linking; the longer the chain the higher the degree of cross-linking. Cross-linking begins as the concentration of epoxy groups exceeds 1.2 mass %; the amount of the gel fraction was 7.97 mass % at an epoxy group concentration of 1.4 mass %.

Compatibilisation of PP and a liquid-crystal copolyester Vectra A900 (LCC) following the reactions between the epoxy groups of poly(ethylene-*co*-GMA) (EGMA) containing 12% GMA with the hydroxy and/or carboxy groups has been studied.[45] It was found that the EGMA graft LCC is formed at the PP – LCC interface and the surface tension decreases. Blending was carried out in a co-rotating twin-screw extruder (d = 30 mm) in the temperature range 265 – 290 °C. The PP – LCC blends thus obtained possessed higher elongations at break and impact strengths. The LCC domains were found to be of smaller size and the crystallinity of the modified PP was lower than that of the blends prepared by conventional (mechanical) technique. The use of ethyltriphenylphosphonium bromide as a catalyst improves the blend compatibility owing to grafting.

A broad class of polymer blends based on polyamides (PA) was obtained.[1] Compatibilisation by the strengthening of the interaction between the blend components is a major way of modification of toughened materials.

Kudva *et al.*[46] studied blends of Nylon-6 with acrylonitrile/butadiene/styrene terpolymer (ABS) and poly(styrene-*co*-acrylonitrile) (SAN) using copolymers of GMA with methyl methacrylate (MMA) as compatibilisators. The GMA molecules contain epoxy groups which can react with the terminal groups of PA, while poly(methyl methacrylate) (PMMA) can be mixed with the SAN phase of ABS at any concentration of acrylonitrile. Blends were prepared in a Killion single-screw extruder (Germany) (d = 25.4 mm; l/d = 30) at 240 °C and a screw speed of 40 rev min^{-1} or in a Baker-Perkins co-rotating twin-screw extruder at 240 °C and a screw speed of 170 rev min^{-1}.

The dependence of the mass-average size of the SAN particles ($\bar{d}_w$) on the GMA concentration in poly(GMA-*co*-MMA) is shown in Fig. 8. The complex shape of the curve describing the variation of $\bar{d}_w$ is due to chemical reactions between the epoxy groups and the amino and carboxy terminal groups of Nylon-6 at the interface (Fig. 9). Owing to the nature of the PA, the interdomain space is filled with loop-like and bridging structures.

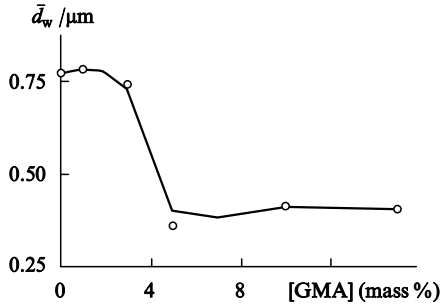

Figure 8. Dependence of the mass-average size of SAN particles on the GMA content in poly(GMA-*co*-MMA).
The blend ratio was Nylon-6 : SAN : poly(GMA-*co*-MMA) = 75 : 20 : 5. The SAN copolymer contained 25% of acrylonitrile. In the absence of poly(GMA-*co*-MMA), a blend with the ratio Nylon-6 : SAN = 75 : 25 was studied.[43]

It was found that the notched Izod impact strength decreases upon introduction of the copolymer containing 3 mass % of GMA (Fig. 10). When the GMA content was 5 mass % and 10 mass %, the impact strength increased. More intense mixing using a twin-screw extruder resulted in a substantial decrease in

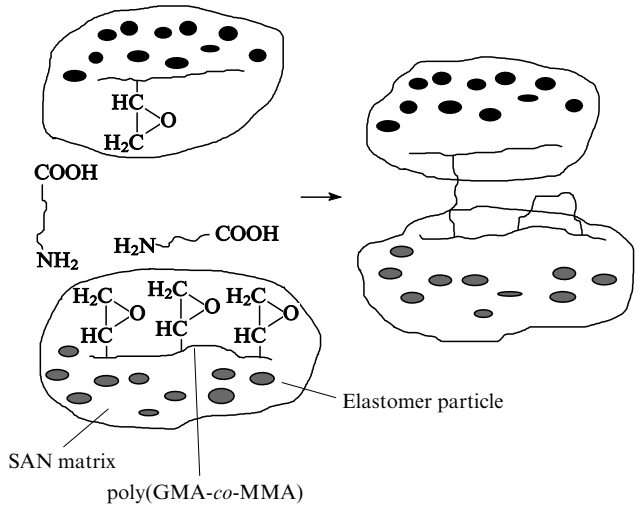

Figure 9. A scheme of the reaction between Nylon-6 and poly(GMA-*co*-MMA) in the Nylon-6 – ABS – poly(GMA-*co*-MMA) blend.[43]

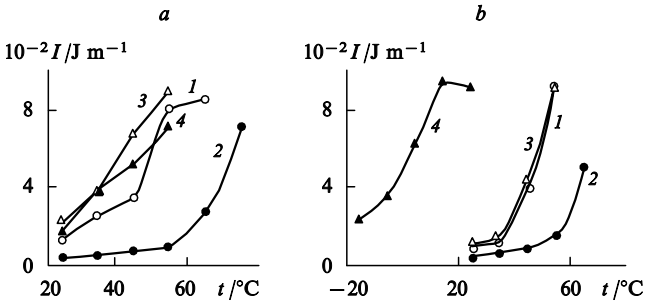

Figure 10. Temperature dependences of the notched Izod impact strength for Nylon-6 – ABS blend (*1*) and ternary blends Nylon-6 : ABS : (GMA – MMA) = 47.5 : 47.5 : 5.0 at a GMA content of 3% (*2*), 5% (*3*) and 10% (*4*) in single-screw (*a*) and twin-screw (*b*) extruders.[43]

the domains of the dispersed phase and in an increase in the impact strength.

V. Transesterification reactions and interchange processes

The kinetics of the transesterification reaction between poly(ethylene terephthalate) (PETP) and co[poly(PETP – *p*-hydroxybenzoate)] copolyesters (PHB – PETP) at blend ratios of 85 : 15, 70 : 30 and 50 : 50 in a Brabender Plasticorder mixer (Germany) at 275, 285 and 293 °C has been studied taking two types of the PHB – PETP copolyesters, with a PHB : PETP ratio of 40 : 60 (P46) and 60 : 40 (P64), as examples.[47] It was shown that the reaction is described by a second-order kinetic equation and the effective rate constant of the reaction depends on the blend ratio and temperature.

Yet another type of reaction, namely, interchange processes between a polyhydroxyether of bisphenol A and a segmented copolyetherester Hytrel, has been studied.[48] The copolyester is a thermoplastic elastomer comprising rigid crystallisable tetramethylene terephthalate blocks and flexible polytetramethylene – ether glycol – terephthalate blocks. Mixing of the components was carried out in a Brabender Plasticorder mixer. The kinetics of the interchange reactions was studied by tracing the torque variations. After mixing for 15 min, the interchange processes are completed to yield mainly branched and cross-linked products. The induction period was independent of the blend ratio and always exceeded 15 min at 240 °C.

Owing to specific interactions, the components of this blend are miscible at any ratios. Because of this, only one glass transition temperature is observed.

VI. Preparation of thermoplastic elastomers by dynamic vulcanisation

Among reactive blending processes in an extruder reactor, dynamic vulcanisation is the most promising for industrial use.[49] Thermoplastic elastomers (TPE), prepared from polymer blends by dynamic vulcanisation, are a specific class of materials which, on the one hand, can be processed in the molten state as thermoplastic polymers and, on the other hand, possess the properties of vulcanised elastomers at operating temperatures. Since they are quite competitive with conventional rubbers in the market, interest in these materials is currently increasing.[50]

The merit of TPE is their ability to be reprocessed. The properties of TPE do not change essentially upon reprocessing. This allows complete recycling and waste utilisation. Creation of polymer blends which can be non-waste processed is an important ecological problem due to the increasing accumulation of plastics waste and environmental protection demands.[51]

The history of the creation of different types of TPE up to the year 1987 has been considered in a comprehensive review by Legge.[52] Technological fundamentals of the preparation of modern types of TPE have been developed by Coran.[49] An *in situ* dynamic vulcanisation technique has been proposed, where vulcanisation of an elastomer proceeds simultaneously with its mixing with a thermoplastic polymer. This allows the preparation of blends with unique morphology characterised by 'dispersion' of the particles of the vulcanised elastomer in a continuous thermoplastic matrix. This technique permits the production of materials with excellent operating characteristics and these materials can be readily non-waste reprocessed.[53]

Polymeric compositions based on 11 different elastomers and 9 thermoplastic polymers have been considered.[49] Combining these elastomers and plastics allowed the preparation of more than 75 types of TPE.

1. The mechanism of dynamic vulcanisation

The properties of TPE depend on many parameters such as blend composition, the nature of vulcanising agents, blending conditions, temperature – time superposition during the formation of network structure of the elastomer, *etc.*

The preparation of TPE with improved mechanical properties requires mixing of dispersions of submicron sizes.[49, 50, 53] In particular, the tensile strength and elongation at break of the PP – EPDM-based blends (PP : EPDM = 40 : 60) increase with the decrease in the domain size (Fig. 11). In this case, mixing is superimposed on the cross-linking reaction which causes changes

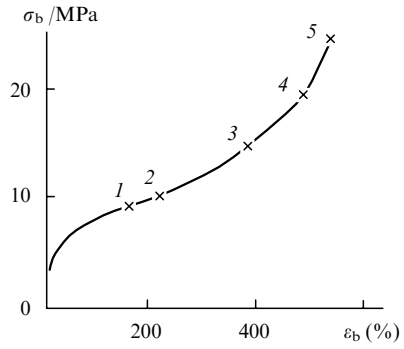

Figure 11. 'Stress – strain' diagrams for PP – EPDM blends (PP : EPDM = 40 : 60) with different domain size of the elastomer phase (× denotes a break).[49]
Number-average domain size /μm: (*1*) 72, (*2*) 39, (*3*) 17, (*4*) 5.4, (*5*) 1 – 1.5.

in the morphology of the elastomer phase, thus resulting in an increase in the viscosity of the medium and hampering the blend homogenisation. Therefore, efficient blending leading to a material with homogeneous submicroscopic distribution of the particles of the dispersed phase requires that the condition (1) be met.

The plots shown in Fig. 12 illustrate the effect of the density of cross-links, v_e, on the tensile strength σ_b and tension set ε_∞ of TPE. As can be seen, σ_b monotonically increases with increasing v_e, whereas ε decreases rapidly even at small v_e values. It is noteworthy that the rigidity of the material varies only slightly in this case.

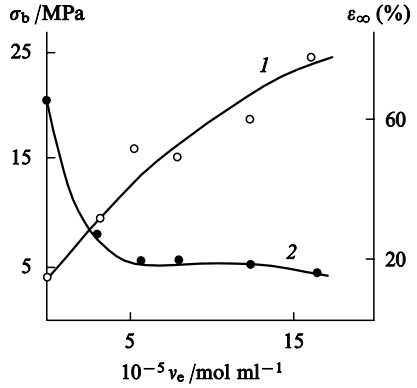

Figure 12. The effect of the density of cross-links v_e on the tensile strength σ_b (*1*) and tension set ε_∞ (*2*).[47]

Polypropylene-based TPE are usually prepared at temperatures above 180 °C. Degradation of TPE, which occurs at this temperature, detracts from the properties of the PP and elastomer phase.[54] If peroxides are used as vulcanising agents, degradation is accompanied by cross-linking. Therefore, the preparation of TPE with optimum properties requires knowledge of the parameters of temperature – time superposition during the formation of a network structure of the elastomer in the blend. Additionally, if the process is performed in the presence of peroxides, one should know the kinetics of (i) degradation and cross-linking of PP and (ii) the formation of interfacial polymer – elastomer links.

Regularities in the cross-linking and degradation of a polyisoprene elastomer SKI-3℗ at 190 °C have been reported.[55] The content of the sol fraction and its MMD was studied as function of the duration of vulcanisation at different concentrations of tetramethylthiuram disulfide (TMTD) and sulfenamide C (SA) used as vulcanising agents. Figure 13 presents typical gel chromatograms of the sol fractions of the SKI-3℗ elastomer cross-linked at different TMTD : SA ratios. After heating the main peak on the chromatogram of the elastomer is shifted towards the low MM region due to the depletion of the rubber fractions with the highest molecular masses. As can be seen, the rates of vulcanisation and degradation depend on the ratio of the components of the vulcanising system. For instance, for the same vulcanisation time of 3.5 min the system with the ratio TMTD : SA = 2 : 0 exhibits a bimodal distribution (Fig. 13 *a*), the system with the ratio TMTD : SA = 1 : 1 exhibits a shoulder (Fig. 13 *b*) while the system with the ratio TMTD : SA = 0 : 2 exhibits a broad unimodal distribution, which also covers the region of the initial molecular masses (Fig. 13 *c*). The existence of the limiting MM value of the sol fraction of the cross-linked elastomer was established [55] and it was found that this value remains virtually the same at any ratio of the vulcanising agents in the system. A similar picture was also observed in the case of prolonged vulcanisation carried out for 14 min (see Fig. 13, curves *3*).

The kinetics and mechanism of degradation of an elastomer – polymer blend can be significantly different. It was shown [56] that the induction period for the oxidation of PP – EPDM blends at

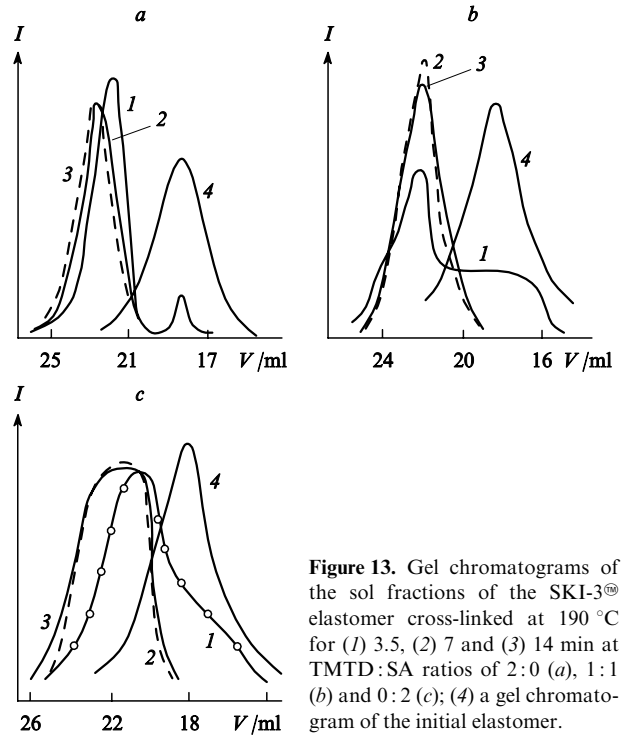

Figure 13. Gel chromatograms of the sol fractions of the SKI-3℗ elastomer cross-linked at 190 °C for (*1*) 3.5, (*2*) 7 and (*3*) 14 min at TMTD : SA ratios of 2 : 0 (*a*), 1 : 1 (*b*) and 0 : 2 (*c*); (*4*) a gel chromatogram of the initial elastomer.

110 °C is longer than that for the oxidation of the initial PP and can even be longer than the induction period for the oxidation of EPDM at a particular blend ratio. Upon introduction of vulcanising agents the oxidation resistance of the material increases and depends on the type of the vulcanising system of the rubber. Degradation products changes the blend morphology, thus changing the properties of TPE. This effect was particularly pronounced in the case of dynamic vulcanisation of ternary PE – PP – EPDM blends in the presence of peroxide as the vulcanising agent.[57,58] It was found that the tensile strength σ_b and modulus of elasticity E decrease with increase in the peroxide concentration in the blends with high PP content, whereas in the blends with high EPDM content these parameters increase under the same conditions. George *et al.*[59] showed that the cross-linking reaction dominates over degradation in the PP – nitrile elastomer blend in the presence of dicumyl peroxide.

The effect of the chemical nature and concentration of the vulcanising system on the properties of an EPDM – HDPE blend was studied.[60] The vulcanising systems investigated exhibited different induction periods and rates of EPDM vulcanisation. The sulfur-containing vulcanising system exhibited the shortest induction period and the highest rate of vulcanisation, whereas the resin-based system exhibited the longest induction period and the lowest rate of vulcanisation.

Studies on the kinetics of vulcanisation of systems with different concentrations of vulcanising agents showed that the rates of vulcanisation remain virtually constant irrespective of the chemical nature of the vulcanising system as the concentrations of these agents is doubled or halved. On the other hand, the induction period lengthens as the concentration of the sulfur-based vulcanising system decreases and remains the same if the resin-based system is used.

It was shown [61] that the dependence of the density of cross-links in the ethylene/propylene/vinylnorbornene terpolymer on the peroxide concentration passes through an extremum.

Vulcanised EPDM samples exhibited the greatest tensile strength in the presence of the sulfur-containing system, while the largest elongation at break and tension set were attained if the resin-based system was used as the vulcanising agent. The tensile strength increased to some extent with increasing concentration of activators (the sulfur-containing system). A decrease in the con-

centration of the vulcanising agents caused some deterioration of the stress–strain properties and an increase in the elongation at break and tension set. Mechanical properties of the vulcanisates remained virtually unchanged in the presence of the resin-based system.

For TPE samples, the concentration of vulcanising agents had almost no effect on the rebound elasticity and hardness. The strain–strength properties of TPE improved with the increase in the concentration of the sulfur-containing system and deteriorated as the concentration of the resin-based system increased. A decrease in the concentration of the vulcanising agents caused a decrease in the tensile strength, while the elongation at break and tension set at break increased.

The effect of the chemical nature of the vulcanising system on the physical properties of the TPE based on the EPDM–PP blends can be followed from the data listed in Table 3.[62] As can be seen, TPE prepared with the use of the phenolic system exhibit better characteristics (especially, swelling in oil and tension set at compression).

Table 3. The effect of the chemical nature of the vulcanising system on the properties of TPE based on SKEPT℗–PP blends [EPDM : PP = 60 : 40 (mass %)].[62]

Property	Vulcanising agent		
	sulfur-containing system	dimethylol-alkylphenol	peroxide
D (arbitrary units)	43	44	39
σ_b /MPA	24.3	25.6	15.9
$\sigma_{\varepsilon = 100\%}$ /MPa	8.00	9.72	8.07
ε_b (%)	530	350	450
H (%)	194	109	225
ε'_∞ (%)	43	24	32

Note. The following notations are used: D is the Shore hardness; $\sigma_{\varepsilon = 100\%}$ is the stress at 100% elongation; H is the swelling in oil and ε'_∞ is the tension set upon compression (22 h, 100 °C).

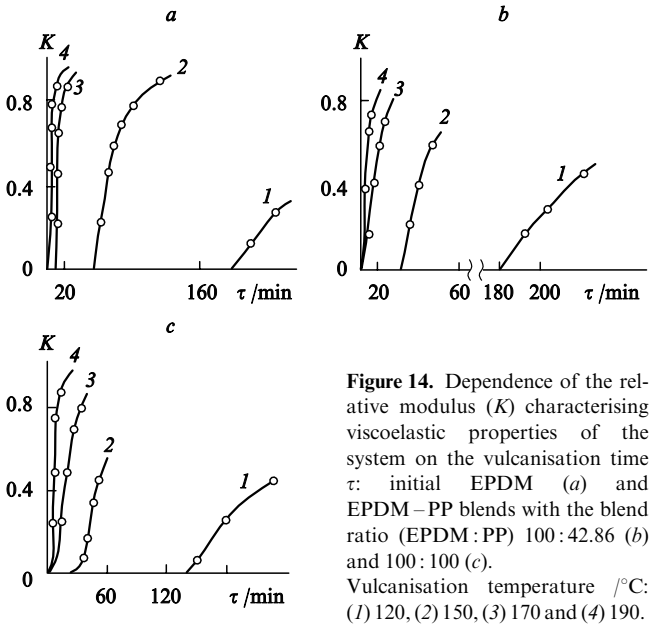

Figure 14. Dependence of the relative modulus (K) characterising viscoelastic properties of the system on the vulcanisation time τ: initial EPDM (*a*) and EPDM–PP blends with the blend ratio (EPDM : PP) 100 : 42.86 (*b*) and 100 : 100 (*c*).
Vulcanisation temperature /°C: (*1*) 120, (*2*) 150, (*3*) 170 and (*4*) 190.

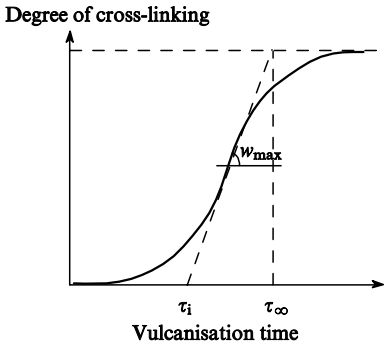

Figure 15. A schematic representation of the vulcanisation curve.

Does the thermoplastic polymer affect the kinetics of vulcanisation of the elastomer? Sengupta and Konar[63] studied this problem taking the vulcanisation of EPDM–PP blends in the presence of a sulfur-containing vulcanisation accelerator in the temperature range from 120 to 190 °C as an example. The blend ratio was varied from EPDM : PP = 100 : 0 to EPDM : PP = 100 : 100. Analysis of the vulcanisation curves revealed three time intervals corresponding to the main stages of vulcanisation (Fig. 14), *viz*., the induction period of the vulcanisation, the network formation period and the reversion period, respectively. The effective activation energy of vulcanisation varies only slightly, being equal to 8.85 kcal mol^{-1} for the initial elastomer and lying between 7.11 and 11.17 kcal mol^{-1} for the EPDM–PP blends. On the other hand, the induction period and the rate constant of the vulcanisation change.

Figure 15 presents a general pattern of a vulcanisation curve. In the second stage of vulcanisation, the degree of cross-linking, q, can be to a first approximation written as the following linear relation:[64]

$$q = w_{max}(\tau - \tau_i), \tag{4}$$

where w_{max} is the maximum vulcanising rate, τ is the vulcanising time and τ_i is the induction period. Preparation of a material with homogeneous submicroscopic distribution of the particles of the dispersed phase requires that the following condition [see the inequality (1) above] be met

$$\tau_m < \tau_i . \tag{5}$$

The time taken to reach the limiting degree of cross-linking (τ_∞) can be determined from the relation (4)

$$\tau_\infty = \tau_i + \frac{q_\infty}{w_{max}}, \tag{6}$$

where q_∞ is the limiting degree of cross-linking.

As to degradation, it has no pronounced effect on the material structure if

$$\tau_f < \tau_d , \tag{7}$$

where τ_d is the induction period of degradation.

The limiting degree of cross-linking should be reached during the time τ_f, therefore

$$\tau_\infty \ll \tau_f . \tag{8}$$

Based on the inequalities (5)–(8), a criterion for the choice of optimum temperature–time superposition during dynamic vulcanisation can be written as follows:

$$\tau_m \leqslant \tau_i \leqslant \tau_\infty \ll \tau_f < \tau_d . \tag{9}$$

The vulcanising agents and temperature-time superposition during the formation of TPE are chosen taking into account relations (9) and the criteria (10a)–(10c)

$$\tau_i \geqslant \frac{R^2}{6D}, \tag{10a}$$

$$w_{max} \geqslant \frac{1}{l/V - \tau_i} \quad (10b)$$

or

$$w_{max} \geqslant \frac{1}{\tau_d - \tau_i}, \quad (10c)$$

where R is the radius of the extruder and D is the effective diffusion coefficient.[64] These conditions hold if the vulcanising agents are introduced into the initial elastomer prior to blending.

The problem of the order in which the blend components are fed into the extruder reactor is also topical. For instance, by varying the order of the introduction of carbon black in TPE one can change the resistivity of the end product from 3.7×10^{13} to 2.5 Ω cm.

The knowledge of the order in which the components are fed into the extruder reactor and employment of the criteria (10a)–(10c) allowed the development of one-step dynamic vulcanisation.[65]

2. Structure and properties of thermoplastic elastomers

Thermoplastic elastomers represent two-phase systems in which cross-linked elastomer particles of size ~1 to 2 μm are uniformly distributed in the polymer matrix.[49, 50, 53]

Dynamic vulcanisation has been carried out in either a Brabender mixer or a Berstorff twin-screw extruder.[65] The temperature-time superposition as well as the type and order of feeding the blend components into the extruder were chosen with account taken of the criteria for the formation of TPE [relationships (10a)–(10c)]. Table 4 lists the results of mechanical and rheological tests of the TPE obtained upon varying the blend ratio. As can be seen, the rigidity and tension set of the TPE increase with the increase in the PP content, *i.e.*, the elastomeric properties of the TPE diminish. On the other hand, the rheological properties of the TPE are improved (the MFI increases). As the oil content increases, the rheological characteristics are also improved, while the strength characteristics deteriorate. Similar results have also been reported by Coran.[49]

Table 4. Effect of the TPE composition on their mechanical and rheological properties.

TPE composition			E_0 /MPa	E_{100} /MPa	σ_b /MPa	ε_b (%)	MFI[a]	D	ε_∞ (%)
[PP] (vol.%)	[EPDM] (vol.%)	M							
40	60	100	67	4.5	5.7	270	20.2	86	20
35	65	100	55	3.8	5.9	345	17.5	80	15
30	70	100	42	3.6	6.2	380	11.1	69	7
25	75	100	36	3.4	7.8	452	2.3	65	5
30	70	20	58	4.4	12.8	685	0.8	80	16
30	70	30	52	4.2	9.7	500	4.3	72	9
30	70	40	47	3.9	8.2	446	6.2	69	7

Note. The following notations are used: M is the oil content (in mass parts per 100 mass parts of the elastomer), E_0 is the initial modulus of elasticity, E_{100} is the modulus of elasticity at 100% elongation, D is the Shore hardness (in arbitrary units) and ε_∞ is the tension set.
[a] In g/10 min.

3. Deformation of thermoplastic elastomers

Deformation mechanisms of TPE have been poorly studied as yet.[66] It is unclear so far why the mechanical properties of TPE at room temperature are determined by the properties of the dispersed phase rather than of the matrix.[67, 68]

Figure 16 presents the stress–tensile strain diagrams of TPE in the coordinates $\sigma-\varepsilon$ at a tensile strain rate of 2.4×10^{-4} s^{-1} and different temperatures.[66] Similar patterns of the stress–tensile strain diagrams were also observed for other tensile strain rates. No 'neck' formation was observed in all cases. At $\varepsilon > 3\%$, the $\sigma-\varepsilon$ diagrams are well linearised in the coordinates $\sigma-(\lambda-\lambda^{-2})$, where $\lambda = 1 + \varepsilon$ (Fig. 16 *b*). At small elongations ($\varepsilon < 3\%$), a rapid increase in σ (a jump) was observed. The results obtained can be described by the following equation

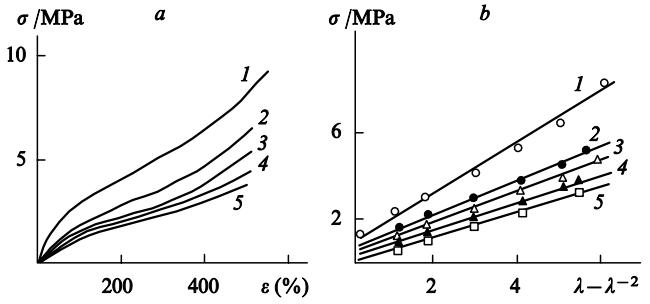

Figure 16. Stress–tensile strain diagrams $\sigma-\varepsilon$ (*a*) and $\sigma-(\lambda-\lambda^{-2})$ (*b*). The λ values at a tensile strain rate of 2.4×10^{-4} s^{-1} are given for 20 (*1*), 50 (*2*), 75 (*3*), 100 (*4*) and 125 °C (*5*).

$$\sigma = \sigma_0 + G(\lambda-\lambda^{-2}), \quad (11)$$

where σ_0 is the jump magnitude and G is the modulus determined from the slope of the straight line.

Thus, the overall stress is determined by the sum of two contributions, *viz.*, the stress which rapidly increases with the tensile strain and reaches the σ_0 value and the stress which linearly depends on $\lambda-\lambda^{-2}$. It was found that the jump magnitude, σ_0, decreases linearly with the increase in the temperature and is independent of the tensile strain rate (Fig. 17). At $T \to 145$ °C, $\sigma_0 \to 0$. This temperature corresponds to the onset of the melting of PP. Therefore, it was assumed that σ_0 is determined by the tensile strain of PP. The modulus G increases as the tensile strain rate increases and decreases with the increase in temperature.†

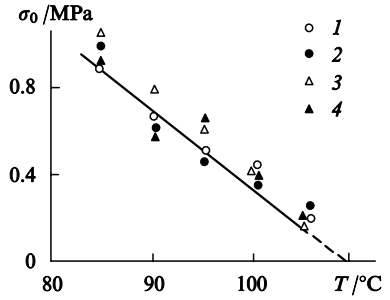

Figure 17. Temperature dependences of the σ_0 jump at tensile strain rates of 2.4×10^{-4} (*1*), 2.4×10^{-3} (*2*), 2.4×10^{-2} (*3*) and 9.5×10^{-2} s^{-1} (*4*).

The dependences of the tensile strength σ_b and elongation at break ε_b on the tensile strain rate $\dot{\varepsilon}$ and temperature are shown in Fig. 18. As can be seen, ε_b is temperature independent. As $\dot{\varepsilon}$ increases, the elongation at break decreases rapidly and then varies only slightly. The tensile strength, σ_b, is a linear function of $\log\dot{\varepsilon}$. The straight lines obtained for different temperatures are parallel to one another. The slope of the straight lines $\sigma_b - \log\dot{\varepsilon}$ is very small, which means that σ_b depends only slightly on the tensile strain rate.

Based on the results obtained, a structural model and a deformation mechanism were proposed for TPE.[66] At high PP

† Similar results for other types of TPE were recently obtained by S I Volfson, R R Grabdrashitov and K S Minsker *Russ. Polym. News* **5** (3) 1 (2000).

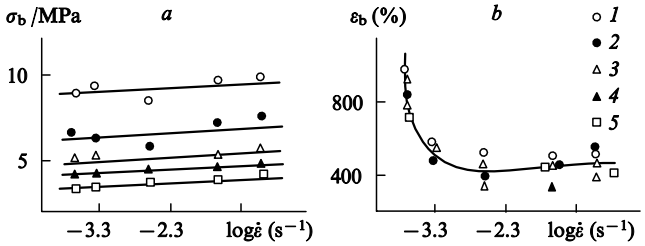

Figure 18. Dependences of the tensile strain (*a*) and elongation at break (*b*) on $\log\dot{\varepsilon}$ at 20 (*1*), 50 (*2*), 75 (*3*), 100 (*4*) and 125 °C (*5*).

content in the blend, the cross-linked EPDM domains are linked by the PP chains; at high EPDM content, they are linked by the elastomer chains. The space between the EPDM domains and the links is filled with oil and PP spherolites (Fig. 19). Initially, only the PP matrix undergoes deformation, thus being responsible for the initial jump, σ_0. In further stages, deformation of the PP matrix occurs simultaneously with that of the dispersed EPDM phase.

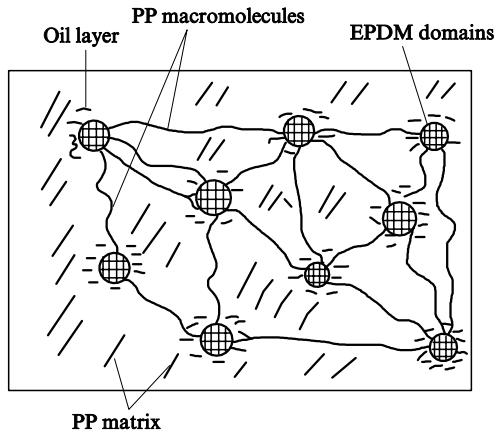

Figure 19. A scheme of the TPE structure.

4. Processing of thermoplastic elastomers

The processability of TPE depends on their rheological properties. Chung *et al.* showed [69] that in the molten state thermoplastic elastomers behave like the melts of filled polymers or rubber-modified plastics.

The properties of TPE allow their processing in the same manner as thermoplastic polymers, *i.e.*, by compression moulding, blow moulding, extrusion welding, calendering and thermoforming. Comparison of the production processes designed for rubbers and TPE (Scheme 1) reveals the major advantages of TPE, namely, easy processing, the possibility of re-moulding, multiple waste recycling, *etc*.

In the case of TPE, the process parameters are determined by the composition of the TPE and preparation conditions. The structure of the TPE specimens obtained by injection moulding has been studied [70] as a function of the radii of the specimens. It was found that the surface layers are highly oriented. A decrease in the process temperature leads to the formation of a disordered smectic structure in several TPE specimens and to a change in the EPDM : PP ratio in the layers owing to the orientation of the PP phase.

Yet another advantage of TPE as compared to the initial component (PP) is an increase in the highest operating temperature. It was shown [71] that at 280 °C the thermo-oxidative stabilities of the blends of PP with rubbers of different nature are higher and the mass losses are ~5 to 20 times smaller than those

Scheme 1

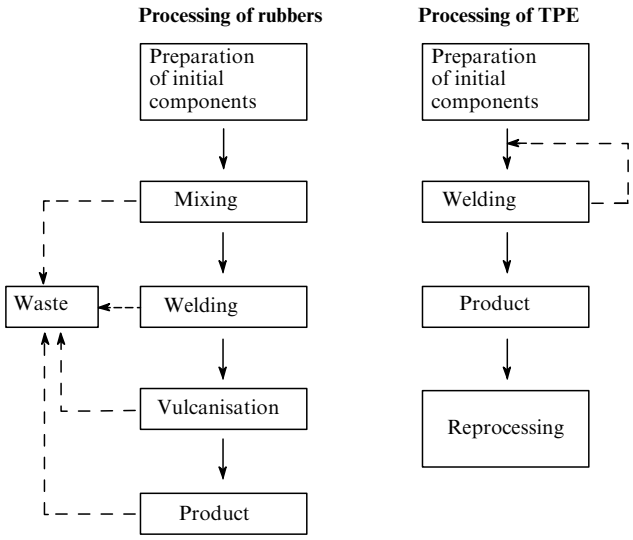

of the virgin PP (Fig. 20). Thermal stability of the polymer blends is independent of the blend ratio and is not determined by the thermal stability of the initial rubber (polyisoprene rubber SKI-3™, butadiene–nitrile rubber SKN-40™ or EPDM). It was also found that the thermal stability increases in the order PP–SKN-40™ < PP–SKI-3™ < PP–EPDM and is independent of the degree of vulcanisation of the elastomer.

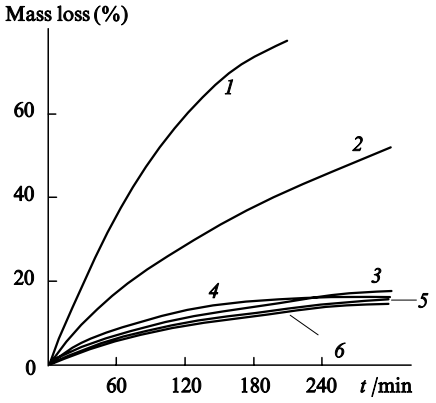

Figure 20. Isothermal TGA curves obtained at 280 °C in air for PP (*1*), EPDM (*4*) and PP–EPDM blends of compositions (PP : EPDM) (mass %) 95 : 5 (*2*), 20 : 80 (*3*), 50 : 50 (*5*) and 80 : 20 (*6*).

Replacement of traditionally used rubbers by TPE will make it possible to reduce the environmental pollution during their processing. These materials seem to be among the most promising materials to be used in the XXIst century and the areas of application of TPE are intensively expanded.

VII. Solid-phase reactions in an extruder reactor

Investigations into the solid-phase reactions in extruder reactors date back to the studies carried out by Academician N S Yenikolopyan at the N N Semenov Institute of Chemical Physics.[72] Solid-phase modification of polymers has an advantage over conventional modification techniques because it is more efficient and ecologically safe and permits substantial reduction of the cost of the end product.

1. Modification of polyalkenes

In studies on the solid-phase modification of isotactic PP and low-density polyethylene (LDPE) in the presence of maleic acid and its derivatives (maleic anhydride and sodium maleate) in an extruder reactor it was found that grafting depended only slightly on the presence of a radical initiator, *viz*., azoisobutyronitrile (AIBN).[73–77] The amount of the graft compound was found to be dependent on the intensity of mechanical treatment and the total mechanical energy supplied. The best result ($\sim$1.5 mass %) was obtained using the extruder reactor equipped with a set of cams which permitted the highest compression and shear stress of the materials. During processing, the particles of the PP phase undergo plastic deformation and breakdown.[78]

Mechanical properties of the solid-phase modified polyalkenes are much the same as those of the initial polymers. The modified polyalkenes exhibit adhesion to aluminium foil, which is more than an order of magnitude higher even at low degree of grafting (0.1 mass % to 0.2 mass %).[79,80] Degradation of the solid-phase modified polyalkenes is reduced as compared to the melt modified polyalkenes.

2. Modification of polysaccharides

The interest in natural polymers (in particular, polysaccharides) is due to the need for rational use of these materials and to the design of new ecologically safe processes. The most abundant natural polysaccharides are cellulose and chitin containing in the shells of crustacean and insects and in mushrooms.

Natural cellulose is widely used in the production of artificial fibres and films and in the textile industry.

Chitin and its deacetylated derivative, chitosan, are of considerable interest because they possess film-forming and fibre-forming properties and are biologically active compounds. Chitin and its derivatives are thought to be promising materials for biotechnological processes that use immobilised enzymes, for the creation of ion-exchange membranes for ultrafiltration and dialysis and for use as sorbents and ion-exchange resins. The complex-forming abilities of these polymers and their derivatives containing ionogenic groups can be used for selective extraction of metals from sea water.

Systematic studies on the solid-phase modification of natural polysaccharides under the joint action of high pressure and shear strain using different types of equipment[81] showed that under such conditions the polymers pass to the plastic flow state, which is accompanied by changes in their morphologies. This leads to a substantial enhancement of the reactivities of the polymers. These conditions have been employed to prepare three most abundant cellulose derivatives (alkali cellulose, carboxymethyl cellulose and cellulose acetate), chitosan (from chitin) and a number of its derivatives.

3. Modification of cellulose

The formation of alkali cellulose under the action of concentrated NaOH solutions on cellulose (mercerisation of cellulose) is one of the main stages of the process of viscose fibre production. Industrially, cellulose sheets are treated with a large excess of 18% aqueous NaOH (usually, the ratio of the volume of the liquid to the mass of cellulose varies from 20 to 40). This ratio is dictated by the necessity of complete and uniform swelling of cellulose. The large amount of waste water substantially detracts from the ecological characteristics of this process.

If mercerisation of cellulose is carried out in an extruder reactor, cellulose sheets are preliminarily milled and then the milled cellulose is treated with alkali solutions at a minimum volume of water. Depending on the initial concentration of alkali, the alkali cellulose thus formed differs in the degree of substitution of hydroxy groups, degree of polymerisation and some other characteristics.

Using the joint effect of shear strain and pressure on a mixture of cellulose with alkali allows the preparation of alkali cellulose with preset characteristics and improved properties, which is due to higher homogeneity of the product. Since in this case the amount of liquid is minimal, the process does not include the stage of removal of excess alkali solution. Here, water consumption reduces by an order of magnitude while alkali consumption reduces threefold as compared to the corresponding parameters of conventional procedures for the modification of cellulose. This to a great extent improves the ecological characteristics of the process.

Carboxymethyl cellulose (CMC) is one of numerous and valuable cellulose derivatives. Water-soluble CMC is widely used in the food, cosmetic and petroleum refining industry and in pharmacy.

Usually, CMC is obtained by treatment of cellulose with monochloroacetic acid (MCAA) in the presence of NaOH in an aqueous or aqueous-organic medium. However, this is accompanied by a side reaction (alkaline hydrolysis of MCAA) which nearly halves the efficiency of the procedure employed.

The ratio of the contributions of these reactions to the overall process can be changed by excluding water or any other dispersion medium from the reaction volume, *i.e*., by carrying out a solid-phase reaction under the conditions of shear strain.[82]

The yield of CMC increases with increase in the initial concentrations of MCAA and alkali in the blend. The degree of substitution varies in parallel and can be as high as 0.94. The efficiency of MCAA increases (up to 60% to 70%, *cf*. 50% for the conventional process); however, it decreases with increase in the MCAA concentration in the initial blend. Finely milled cellulose is much more reactive than coarsely milled cellulose and the CMC obtained from the former possesses a higher degree of substitution and solubility.

Cellulose acetates are used in the manufacture of artificial fibres, film, lacquers and plastics, so production quantities of cellulose acetates are rather large. Usually, acetylation of cellulose is carried out with acetic anhydride as the acetylating agent and with an acid (*e.g*., sulfuric acid) as the catalyst at 35–40 °C over a period of 4 to 6 h. It is known that cellulose acetates with a high degree of substitution cannot be obtained by treatment of cellulose with acetic acid. Strong intermolecular interaction in solid cellulose due to the formation of hydrogen bonds is the main factor precluding the esterification of the hydroxy groups of cellulose by acetic acid.

Figure 21 presents the dependences of the degree of substitution of hydroxy groups on the concentration of H_2SO_4 in the blend in the acetylation of cellulose by different acetylating agents under normal conditions and under the conditions of joint action of high pressure and shear strain. Acetylation by acetic acid under normal conditions results in the formation of cellulose acetates with a low

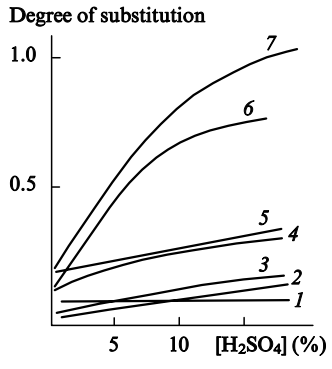

Figure 21. Effect of the concentration of H_2SO_4 on the degree of substitution of the hydroxy groups of cellulose in acetylation under normal conditions (the duration of the acetylation reaction was 4 h, at 20 °C) (*1–3*) and under plastic flow conditions (p = 1 GPa) (*4–7*).
(*1*, *5*) Cellulose : CH_3COOH = 1 : 3, (*2*, *7*) cellulose : CH_3COOH (glacial) = 1 : 3, (*3*, *6*) cellulose : $(CH_3CO)_2O$ = 1 : 1.5, (*4*) cellulose : : CH_3COOH (glacial) = 1 : 1.5.

degree of substitution. Treatment of cellulose with acetic anhydride yields cellulose acetates with higher degrees of substitution.[83]

If the process is performed under the conditions of plastic flow and high pressure, the degrees of substitution for all acetylating agents are higher than those observed under normal conditions.

4. Delignification of wood

Wood is a multicomponent polymeric system. The existing technologies for chemical processing of wood with the aim of cellulose production have some drawbacks. The loss of the wood content in the course of processing is nearly 50% and the amounts of toxic wastes and waste gases are large. Purification of these wastes presents severe difficulties. Modification of the technologies for wood processing to obtain wood pulp in such a way that the yield of the end product be 90% to 95% would allow substantial reduction of toxic waste and waste gases.[84]

A study on the model processes of delignification of wood and mercerisation of cellulose using Bridgman anvils has been reported.[85] The specimens were exposed to the joint action of high pressure and shear strain. It was found that under these conditions the above-mentioned processes proceed without an activation barrier. The activation energy for the delignification of wood by means of alkali cooking was found to be 32 kcal mol^{-1}.[86]

Delignification of wood in an extruder reactor resulted in products with fibrous structures. The reason is that the plastic flow of wood under the joint action of pressure and shear strain occurs mainly along the boundaries of strong, rigid fibres. This results in cleavage of the inter-fibre links and, correspondingly, in degradation of the wood. The fibrous products obtained in the extruder reactor exhibited improved mechanical properties as compared to those of the products prepared by conventional methods.

5. Preparation of chitosan and its derivatives

Chitin is less reactive than cellulose. This is due to specific features of its molecular and supramolecular structure, strong hydrogen bonding and a less active surface.

Chitosan is usually obtained by long-term treatment of chitin with concentrated NaOH solution at elevated temperatures. The existing technology for the production of chitosan is rather inefficient and requires high energy expenditures, the use of a large excess of aqueous alkali solutions and subsequent utilisation of alkali waste and waste water. It was shown [87] that the grinding of chitin and chitosan in a solvent in an extruder reactor leads to partial breakdown of the crystal structure. This appreciably enhances their reactivities towards etherification and leads to some decrease in MM.

Deacetylation of chitin in the temperature range 25 – 200 °C has been studied.[88] An increase in the excess of NaOH favours an increase in both the degree of deacetylation and solubility of the products obtained. The preparation of nearly completely deacetylated product with a solubility of 90% requires only a fivefold molar excess of NaOH, whereas conventional procedures for the preparation of chitosan require at least 10 moles of NaOH per 1 mole of chitin. Both the degree of deacetylation and solubility of the product can be increased by lengthening the residence time of the reaction system in the extruder reactor. Experimental studies showed that raising the temperature from 25 to 200 °C at the mole ratio chitosan : alkali = 1 : 5 results in an increase in the degree of deacetylation from 0.33 to 0.98 and in a substantial decrease in MM.

Conventional procedures for the preparation of chitin and chitosan carboxymethyl ethers are inconvenient since they are time-consuming, proceed as multistage reactions and require large consumption of reagents.[89]

A recently developed solid-phase method [90] for the preparation of these compounds allows improvement of ecological characteristics of the process owing to the absence of solvents and shortening of the reaction time from several hours to several minutes. The reaction was carried out in a Berstorff twin-screw extruder reactor. In the first stage, a mixture of chitin and solid NaOH was extruded at different ratios of the components. Alkali chitosan thus obtained was mixed with an alkylating agent (*e.g.*, MCAA dissolved in isopropyl alcohol or solid sodium monochloroacetate) and again fed into the extruder reactor (stage 2). The residence time in the extruder reactor was 3 to 5 min.

The effect of the reaction conditions on the properties of the reaction products can be followed from the data listed in Table 5. As can be seen, an increase in the concentration of MCAA and alkali leads to an increase in the degree of substitution, which reaches a maximum value of 1.4.

Table 5. Effect of the reaction conditions on the properties of the reaction products.

Specimen number	A	T_{react} /°C		P	$10^{-3} M$ (see note [a])	$x_1 + x_2$	z
		stage 1	stage 2				
1	1 : 4.25 : 2.0	absent	80	48	–	0.90	0.10
2	1 : 2.60 : 2.3	absent	80	20	47	0.40	0.62
3	1 : 4.80 : 2.3	180	120	30	5	0.51	0.32
4	1 : 5.25 : 2.5	100	100	70	82	0.70	0.35
5	1 : 5.25 : 2.5	200	100	68	6	0.68	0.29
6	1 : 8.40 : 2.9	120	120	65	70	1.02	0.25
7	1 : 8.40 : 4.0	80	60	70	90	1.40	0.20
8	1 : 2.60 : 2.3	100	100	46	62	0.65	0.45
9	1 : 4.40 : 4.0	100	100	58	45	0.87	0.27

Note. The following notations are used: A denotes the chitin : NaOH : MCAA mole ratio; P is the solubility in water (in mass %); x_1, x_2 and z are the degrees of substitution as regards the *O*-carboxymethyl, *N*-carboxymethyl and *N*-acetyl groups, respectively. Specimen 1 was obtained from chitosan and specimens 2 – 9 were obtained from chitin. Specimens 4 – 7 were obtained using a 40% solution of MCAA in isopropyl alcohol and specimens 8 and 9 were obtained using solid sodium monochloroacetate as the alkylating agent.

[a] The molecular mass of the soluble fraction of the end product.

The specimen prepared from chitosan in one extrusion step (see Table 5, specimen 1) exhibited a relatively high degree of carboxymethylation (0.9) at smaller consumption of MCAA. The molecular mass decreased dramatically as the temperature increased. This feature is common to solid-phase extrusion-modified polymers.

Solid-phase reactions of chitosan with a higher fatty acid (stearic acid) and with dicarboxylic acids (oxalic, malonic and succinic acids) in a twin-screw extruder have been studied.[82] The residence time of the reaction system in the extruder was 3 to 5 min.

Reaction products of chitosan with higher fatty acids combine the properties of polymeric substances (film-forming, fibre-forming, thickening properties, *etc.*) and surfactants. They can be of interest as amphiphilic materials for the preparation of solid and hydrogel membranes. Modification of chitosan by lipophilic compounds with the aim of enhancement of both the surfactant properties and the ability not only to thicken but also stabilise the food and cosmetic compositions containing oils and lipids is also topical.

The addition of stearic acid to chitosan proceeds mainly by an ionic mechanism. Reactions of chitosan with dicarboxylic acids occur as both the ionic and covalent linking. Studies on the reactions of chitosan with phthalic, succinic and maleic anhydrides showed [89] that these compounds react mainly with the amino groups of chitosan and that the degree of conversion increases with increase in temperature.

This work has been written with the financial support by the Russian Foundation for Basic Research (Project No. 00-03-33099).

References

1. D R Paul, S Newman (Eds) *Polymer Blends* (New York: Academic Press, 1978)
2. V N Kuleznev *Smesi Polimerov* (Polymer Blends) (Moscow: Khimiya, 1980)
3. L A Utracki *Polymer Alloys and Blends: Thermodynamics and Rheology* (Munich, Vienna, New York: Hanser Publishers, 1989)
4. A O Baranov, A V Kotova, A N Zelenetskii, E V Prut *Usp. Khim.* **66** 972 (1997) [*Russ. Chem. Rev.* **66** 877 (1997)]
5. M Xanthos (Ed.) *Reactive Extrusion: Principles and Practice* (Munich: Hanser Publishers, 1992)
6. V E Gul', M S Akutin *Osnovy Pererabotki Plastmass* (The Foundations of Plastic Processing) (Moscow: Khimiya, 1985)
7. R V Torner *Teoreticheskie Osnovy Pererabotki Polimerov* (Theoretical Foundations of Polymer Processing) (Moscow: Khimiya, 1977)
8. Z Tadmor, C G Gogos *Principles of Polymer Processing* (New York: Wiley, 1979)
9. A Ya Malkin, V P Begishev *Khimicheskoe Formovanie Polimerov* (Chemical Moulding of Polymers) (Moscow: Khimiya, 1991)
10. N A Plate, A D Litmanovich, V V Yashin, I V Ermakov, Ya V Kudryavtsev, E N Govorun *Vysokomol. Soedin., Ser A*. **39** 8 (1997) [a]
11. N A Plate, A D Litmanovich, O V Noa *Makromolekulyarnye Reaktsii* (Macromolecular Reactions) (Moscow: Khimiya, 1977)
12. A D Litmanovich *Dokl. Akad. Nauk SSSR* **240** 111 (1978) [b]
13. A D Litmanovich *Eur. Polym. J.* **16** 269 (1980)
14. A D Litmanovich, V O Cherkezyan *Eur. Polym. J.* **20** 1041 (1984)
15. A D Litmanovich, V O Cherkezyan *Vysokomol. Soedin., Ser. A* **27** 1865 (1985) [a]
16. V O Cherkezyan, A D Litmanovich *Vysokomol. Soedin., Ser. A* **28** 820 (1986) [a]
17. E N Govorun, Candidate Thesis in Physicomathematical Sciences, Moscow State University, Moscow, 1997
18. L V Kudryavtsev, Candidate Thesis in Physicomathematical Sciences, Moscow State University, Moscow, 1997
19. G-H Hu, J T Lindt, M Lambla *J. Appl. Polym. Sci.* **46** 1039 (1992)
20. A Ya Malkin *Polym. Eng. Sci.* **20** 1035 (1980)
21. G-H Hu, S Triouleyre, M Lambla *Polymer* **38** 545 (1997)
22. H Kramers, K Westerterp *Elements of Chemical Reactor — Design and Operation* (Amsterdam: Netherlands University Press, 1963)
23. Y-J Sun, G-H Hu, M Lambla *J. Appl. Polym. Sci.* **57** 1043 (1995)
24. D A Frank-Kamenetskii *Diffuziya i Teploperedacha v Khimicheskoi Kinetike* (Diffusion and Heat Transfer in Chemical Kinetics) (Moscow: Nauka, 1967)
25. J A Manson, L H Sperling *Polymer Blends and Composites* (Moscow: Khimiya, 1979)
26. G Moad *Prog. Polym. Sci.* **24** 81 (1999)
27. G-H Hu, Y-J Sun, M Lambla *J. Appl. Polym. Sci.* **61** 1039 (1996)
28. Y-J Sun, G-H Hu, M Lambla, H K Kotlar *Polymer* **37** 4119 (1996)
29. G-H Hu, J-J Flat, M Lambla *Makromol. Chem., Macromol. Symp.* **75** 135 (1993)
30. S H P Bettini, J A M Agnelli *J. Appl. Polym. Sci.* **74** 247 (1999)
31. S H P Bettini, J A M Agnelli *J. Appl. Polym. Sci.* **74** 256 (1999)
32. J Garcia-Martinez, O Laguna, E Collar *J. Appl. Polym. Sci.* **68** 483 (1998)
33. J Garcia-Martinez, A Cofrades, S Areso, O Laguna, O Collar *J. Appl. Polym. Sci.* **69** 931 (1998)
34. J Garcia-Martinez, O Laguna, S Areso, O Collar *J. Appl. Polym. Sci.* **73** 2837 (1999)
35. L Assoun, S C Manning, R B Moore *Polymer* **39** 2571 (1998)
36. M R Thompson, C Tzoganakis, G L Rempel *J. Appl. Polym. Sci.* **71** 503 (1999)
37. C Rosales, R Perera, M Ichazo, J Conzalez, H Rojas, A Sanchez, A Diaz Barrios *J. Appl. Polym. Sci.* **70** 161 (1998)
38. C Rosales, R Perera, J Conzalez, M Ichazo, H Rojas, A Sanchez *J. Appl. Polym. Sci.* **73** 2549 (1999)
39. M G Lachtermacher, A Rudin *J. Appl. Polym. Sci.* **58** 2077 (1995)
40. M G Lachtermacher, A Rudin *J. Appl. Polym. Sci.* **58** 2433 (1995)
41. K J Kim, B K Kim *J. Appl. Polym. Sci.* **48** 981 (1993)
42. M Mehrabzadeh, S Kasali, M Khosravi *J. Appl. Polym. Sci.* **70** 1 (1998)
43. D Carlson, L Nie, R Narayan, P Dybois *J. Appl. Polym. Sci.* **72** 477 (1999)
44. B Guo, C-M Chan *J. Appl. Polym. Sci.* **77** 1827 (1999)
45. J-P Chiou, K-C Chiou, F-C Chang *Polymer* **37** 4099 (1996)
46. R A Kudva, H Keskkula, D R Paul *Polymer* **39** 2447 (1998)
47. C F Ou, M S Chao, S L Huang *J. Appl. Polym. Sci.* **73** 2727 (1999)
48. M Gaztelumendi, J Nazabal *J. Appl. Polym. Sci.* **70** 185 (1998)
49. A Y Coran, in *Thermoplastic Elastomers: A Comprehensive Review* (Eds N R Legge, G Holden, H G Schroeder) (Munich, Vienna, New York: Hanser Publishers, 1987) p. 133
50. J Karger-Kocsis, in *Polymer Blends and Alloys* (Eds G O Shonaike, G P Simon) (New York: Marcel Dekker, 1999) p. 125
51. E V Prut *Vysokomol. Soedin., Ser. A* **36** 601 (1994) [a]
52. N R Legge *Rubber Chem. Technol.* **62** 529 (1989)
53. E V Prut, in *IV Sessiya Mezhdunarodnoi Shkoly Povysheniya Kvalifikatsii 'Inzhenerno-Khimicheskaya Nauka dlya Peredovykh Tekhnologii'* (The IVth Session of International Training School 'Engineering and Chemical Science for Progressive Technologies') (Moscow: L Ya Karpov Institute of Physical Chemistry, 1998) p. 94
54. N Grassie, G Scott *Polymer Degradation and Stabilisation* (London: Cambridge University Press, 1985)
55. O P Kuznetsova, L M Chepel', G M Trofimova, D D Novikov, A N Zelenetskii, E V Prut *Vysokomol. Soedin., Ser. B* **39** 1706 (1997) [a]
56. L S Shibryaeva, A A Veretennikova, A A Popov, T A Gugueva, A A Kanauzova *Vysokomol. Soedin., Ser. A* **41** 695 (1999) [a]
57. C S Ha, S C Kim *J. Appl. Polym. Sci.* **35** 2211 (1988)
58. C S Ha, S C Kim *J. Appl. Polym. Sci.* **37** 317 (1989)
59. S George, N R Neelakantan, K T Varughese, S Thomas *J. Polym. Sci., Part B, Polym.-Phys.* **35** 2309 (1997)
60. T A Gugueva, A A Kanauzova, S V Reznichenko *Kauchuk Rezina* (4) 7 (1998)
61. M D Ellul, P S Ravishankar *PMSE Symp., ACS Meeting* **79** 90 (1998)
62. S Abdou-Sabet *PMSE Symp., ACS Meeting* **79** 86 (1998)
63. A Sengupta, B B Konar *J. Appl. Polym. Sci.* **66** 1231 (1997)
64. E V Prut *Khim. Fiz.* **17** (9) 67 (1998) [c]
65. Russ. P. 2 069 217; *Byull. Isobr.* (32) 168 (1996)
66. L V Kompaniets, N A Erina, L M Chepel', A N Zelenetskii, E V Prut *Vysokomol. Soedin., Ser. A* **39** 1219 (1997) [a]
67. S Kawabata, S Kitawaki, H Arisawa, Y Yamashita, X Guo *J. Appl. Polym. Sci., Appl. Polym. Symp.* **50** 245 (1992)
68. Y Kikuchi, T Fukui, T Okada, T Inoue *J. Appl. Polym. Sci., Appl. Polym. Symp.* **50** 261 (1992)
69. O Chung, A J Coran, J L White *SPE ANTEC Tech. Pap.* **43** 3455 (1997)
70. M Cakmak, S Cronin *PMSE Symp., ACS Meeting* **79** 113 (1998)
71. V K Skachkova, N A Erina, E V Prut *Vysokomol. Soedin., Ser. A* **42** 1563 (2000) [a]
72. N S Enikolopyan *Dokl. Akad. Nauk SSSR* **283** 897 (1985) [b]
73. N S Enikolopov, M D Sizova, L O Bunina, S N Zelenetskii, V P Volkov, N Yu Artem'eva *Vysokomol. Soedin., Ser. A* **36** 608 (1994) [a]
74. V P Volkov, L O Bunina, M D Sizova, S N Zelenetskii, N Yu Artem'eva, N A Egorova, V P Nikol'skaya, E S Obolonkova, A B Gil'man, S L Kotova *Plast. Massy* (3) 25 (1997)
75. A N Zelenetskii, L O Bunina, E S Obolonkova, V P Volkov *Plast. Massy* (7) 19 (1999)
76. L O Bunina, V P Volkov, E S Obolonkova *Plast. Massy* (7) 13 (1999)
77. L O Bunina, V P Volkov, E S Obolonkova *Plast. Massy* (7) 22 (1999)
78. A N Zelenetskii, M D Sizova, V P Volkov, N Yu Artem'eva, N A Egorova, V P Nikol'skaya *Vysokomol. Soedin., Ser. A* **41** 798 (1999) [a]
79. V P Volkov, A N Zelenetskii, M D Sizova, N Yu Artem'eva, N A Egorova, V P Nikol'skaya, in *The 1st International Conference 'Polymer Modification, Degradation and Stabilisation'* (Palermo, Italy: University Palermo, 2000) p. 7
80. V P Volkov, A N Zelenetskii, M D Sizova, L O Bunina, L V Vladimirov, N A Egorova, in *Vtoroi Vserossiiskii Karginskii Simpozium 'Khimiya i Fizika Polimerov v Nachale XXI Veka'* (The Second All-Russian Kargin Symposium 'Chemistry and Physics in the Beginning of the XXIth Century') (Chernogolovka: Institute of Problems of Chemical Physics, 2000) p. Ts4

81. S Z Rogovina, T A Akopova *Vysokomol. Soedin., Ser. A* **36** 593 (1994) [a]
82. T A Akopova, G A Vikhoreva, S Z Rogovina, V A Zhorin, L S Gal'braikh, N S Enikolopyan *Vysokomol. Soedin., Ser. B* **32** 182 (1990) [a]
83. S Z Rogovina, L S Sakhonenko, V A Zhorin, M A Trunova *Vysokomol. Soedin., Ser. B* **31** 127 (1989) [a]
84. S Z Rogovina, T A Akopova, G A Vikhoreva, I N Gorbacheva, S N Zelenetskii *Vysokomol. Soedin., Ser. B* **40** 1389 (1998) [a]
85. E A Balashova, Candidate Thesis in Chemical Sciences, Institute of Chemical Physics, Academy of Sciences of the USSR, Moscow, 1988
86. E A Balashova, L S Sakhonenko, S Z Rogovina, N S Enikolopyan *Dokl. Akad. Nauk SSSR* **302** 1134 (1988) [b]
87. S Z Rogovina, V A Zhorin, D P Shashkin *Vysokomol. Soedin., Ser. A* **31** 1255 (1989) [a]
88. T A Akopova, S Z Rogovina, G A Vikhoreva, S N Zelenetskii, L S Gal'braikh, N S Enikolopyan *Vysokomol. Soedin., Ser. B* **33** 735 (1991) [a]
89. S Z Rogovina, G A Vikhoreva, T A Akopova, I N Gorbacheva, S N Zelenetskii *Vysokomol. Soedin., Ser. A* **39** 941 (1997) [a]
90. T A Akopova, S Z Rogovina, G A Vikhoreva, S N Zelenetskii *Vysokomol. Soedin., Ser. B* **37** 1797 (1995) [a]

[a] — *Polym. Sci. (Engl. Transl.)*
[b] — *Dokl. Chem. Technol., Dokl. Chem. (Engl. Transl.)*
[c] — *Chem. Phys. Rep. (Engl. Transl.)*

Russian Chemical Reviews **70** (1) 81 – 90 (2001) © 2001 Russian Academy of Sciences and Turpion Ltd

DOI 10.1070/RC2001v070n01ABEH000578

Rigid-rod poly(benzobisazoles) and molecular composites based on them

L G Komarova, A L Rusanov

Contents

I.	Introduction	81
II.	Rigid-rod poly(benzazoles)	81
III.	Molecular composites	86
IV.	Conclusion	88

Abstract. The results of studies in the field of rigid-rod poly(benzobisazoles) and molecular composites based on them are analysed and generalised. Poly(benzobisazoles) are most promising candidates for high-strength and high-modulus polymeric materials, while the molecular composites based on them can be employed in the synthesis of polymeric materials with a broad spectrum of mechanical properties. The bibliography includes 101 references.

I. Introduction

Rigid-rod polymers began to attract the keen attention of investigators after two main hypotheses had been put forward,[1] namely:

1. Those materials which possess high rigidity manifest the highest deformation strengths. In terms of their moduli of elasticity (E) the polymers, all the macromolecules in which are straightened in the same direction, can be equivalent to steel.

2. The polymers with relatively low densities possess high mechanical characteristics. This suggests that the values of specific moduli of rupture and deformation strengths of the straightened macromolecules can be very high.[2]

These statements have predetermined the increased interest of synthetic chemists in the construction of macromolecules which display maximum thermodynamic rigidities.[3]

High deformation strengths and rigidities of polymers are provided by covalent bonds between the macromolecules which should manifest high levels of straightness and contain predominantly aromatic rings. These properties also determine the thermal stabilities of the polymers.[3,4]

High levels of molecular straightness are more effectively achieved in fibres than in bulk products; therefore, special attention to the design of high-strength fibres for composite materials was given.[3–5]

The first steps in these investigations were aimed predominantly at the preparation of fibres based on aromatic polyamides devoid of non-symmetrical fragments and 'hinge' groups, *e.g.*, poly(*p*-benzamide) and poly(*p*-phenyleneterephthalamide).[6–12]

L G Komarova, A L Rusanov A N Nesmeyanov Institute of Organoelement Compounds, Russian Academy of Sciences, ul. Vavilova 28, 117813 Moscow, Russian Federation. Fax (7-095) 135 50 85. Tel. (7-095) 135 93 27. E-mail: komarova@ineos.ac.ru (L G Komarova). Tel. (7-095) 135 63 72. E-mail: alrus@ineos.ac.ru (A L Rusanov)

Received 2 February 2000
Uspekhi Khimii **70** (1) 88 – 98 (2001); translated by R L Birnova

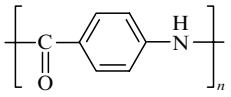

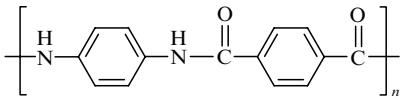

The latter polymer, which is commonly known under the commercial name Kevlar, and its different modifications are used as the basis for the preparation of high-modulus and high-strength polymeric materials.

In addition to aromatic polyamides synthesised from carbocyclic diamines and dicarboxylic acids, polyamides based on heterocyclic monomers, *e.g.*, poly[(2-phenylbenzoimidazole-5,4′-diyl)terephthalamide], are of considerable interest.[10]

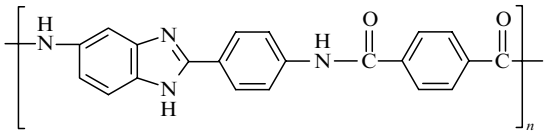

It should be noted however that the presence of amide groups in the macromolecules of these polymers limits their thermal and thermohydrolytic stabilities. Hence, in the second step of investigations in this field, the main attention was focused on rigid-rod polymers which contain only aromatic carbo- and heterocycles,[13–18] the so-called rigid-rod poly(heteroarylenes).

II. Rigid-rod poly(benzazoles)

In the series of rigid-rod polyheteroarylenes, the poly(benzoazoles) (PBAz) **1** and **2** and, particularly, poly(benzobisazoles) (PBBAz) **3a–c** or isomeric structures have been studied in especially great detail.[17–23]

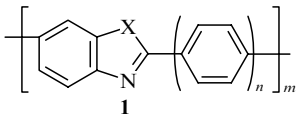

1

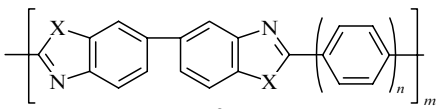

2

X = NH, NPh, O; n = 1, 2.

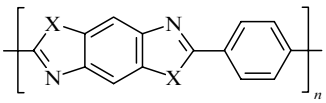

3a–c

X = NH (**a**), O (**b**), S (**c**).

High-temperature polycyclocondensation of 1,2,4,5-tetraaminobenzene-,[26] 4,6-diaminodihydroxybenzene-[27] and 2,5-diaminobenzene-1,4-dithiol hydrochlorides[28,29] with terephthalic acid in polyphosphoric acid (PPA)[23–25] is the most popular procedure for the synthesis of the polymers **3a–c**.

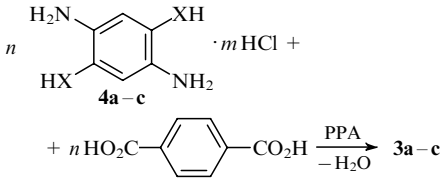

4a–c

m = 4, X = NH (**a**); *m* = 2: X = O (**b**), S (**c**).

If the synthesis is performed at polymer concentrations which are high enough for the formation of anisotropic solutions, the resulting polymeric solutions can be used directly for the preparation of high-modulus fibres[29,30] and films.[31]

Because of high oxidisability of the tetrafunctional nucleophilic monomers **4a–c**, these are used in the form of hydrochlorides or other salts rather than as free bases. The process is performed in two steps. In the first step which is carried out at 60–80 °C, the nucleophilic monomers are subjected to dehydrochlorination; in the second step, terephthalic acid is added, the mixture is slowly heated to 190–200 °C and stirred at this temperature for 8–10 h.

In the course of polycyclocondensation, the content of P_2O_5 in PPA decreases, and its properties as the solvent, catalyst and cyclodehydrating agent deteriorate. The addition of P_2O_5 to the solutions results in both acceleration of the polycyclodehydration reaction and an increase in the molecular mass of the target polymers.[32–35] In addition to dicarboxylic acids, the respective acid chlorides are also used for the synthesis of PBBAz in a PPA medium.[36] Since the glass transition temperatures of PBBAz often exceed their decomposition temperatures,[14] the fibres and films are usually prepared directly from the solutions of these polymers.

Poly(benzobisazoles) are soluble in strong acids, *e.g.*, PPA, methanesulfonic acid, chlorosulfonic acid, 100% H_2SO_4 and Lewis acids (*e.g.*, $BiCl_3$ or $SbCl_3$). Recently,[37] it was shown that poly(benzobisthiazole) (PBBT **3c**) forms liquid-crystalline solutions in nitromethane containing $AlCl_3$ or $GaCl_3$. Liquid-crystalline solutions of PBBAz yield high-strength and high-modulus films and fibres. Very often, the deformation strength characteristics of PBBAz fibres even surpass those of Kevlar polyamide fibres which is attributed, in particular, to the greater values of the Kuhn segments in PBBAz (see Table 1 and Fig. 1).[38–45]

Table 1. The ultimate rupture strength (σ), the modulus of elasticity (E), the elongation at rupture (ε) and values of the Kuhn segment (A) of fibres based on rigid-rod polymers.

Polymer	σ/GPa	E/GPa	ε(%)	A/Å	Ref.
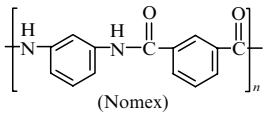 (Nomex)	0.70	17.3	22	47	9
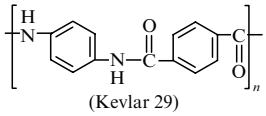 (Kevlar 29)	2.64	58.9	4	300	38
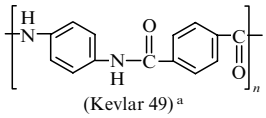 (Kevlar 49)[a]	2.64	127.5	2.4	300	39
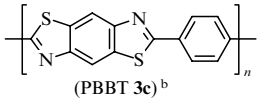 (PBBT **3c**)[b]	0.5–2.2	50–76	4.5	1060	40, 41
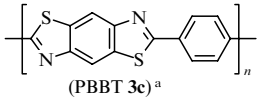 (PBBT **3c**)[a]	0.8–2.5 (4.2)	76–265 (< 300)	1.0–1.5	1060	42
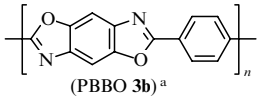 (PBBO **3b**)[a]	2.8–3.4	467		–	34, 44

[a] Heat-treated; [b] freshly formed.

The films with controlled planar orientation based on PBBT and PBBO have specific strengths of 2 GPa and moduli of elasticity of 270 GPa.

Poly(benzobisazoles) are distinguished by extremely high thermal stabilities, *viz.*, under conditions of a dynamic thermogravimetric analysis in air (ΔT = 10 deg min^{-1}), they begin to lose weight at temperatures above 600 °C (Fig. 2).[18] Under conditions of an isothermal analysis in circulating air at 371 °C, their thermal characteristics markedly exceed those of poly(*p*-benzamide), PBBT **3c** being much more resistant to heating than PBBO **3b** (Fig. 3).[46]

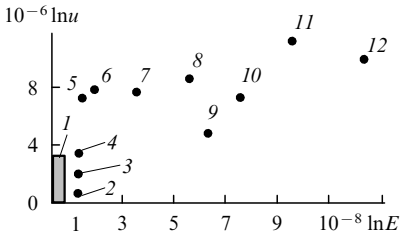

Figure 1. The specific moduli of elasticity (E) and the specific strains (u) of some materials;[45]
(*1*) organic compounds, (*2*) aluminium, (*3*) steel, (*4*) 'E'-glass, (*5*) 'S'-glass, (*6*) Kevlar 29, (*7*) Kevlar 49, (*8*) freshly formed poly(benzobisoxazole) (PBBO **3b**) fibre, (*9*) boron fibre, (*10*) freshly formed poly(benzobisthiazole) (PBBT **3c**) fibre, (*11*) heat-treated PBBT **3c** fibre, (*12*) heat-treated PBBO **3b** fibre.

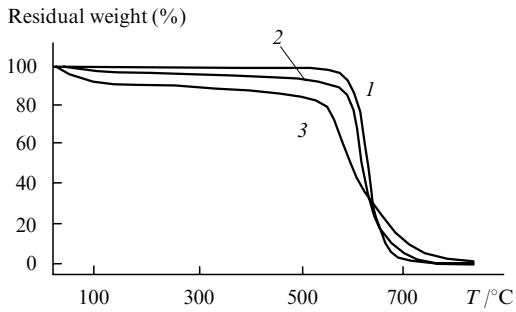

Figure 2. Thermogravimetric analysis of PBBAz in air (the rate of heating is 10 deg min^{-1});[18] (*1*) PBBT, (*2*) PBBO, (*3*) poly(benzobisimidazole) (PBBI **3a**).

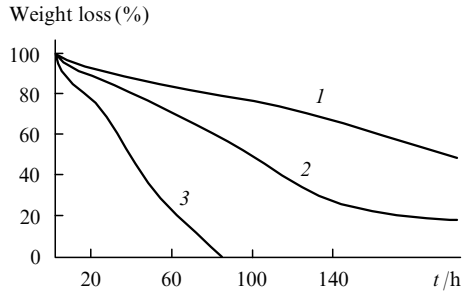

Figure 3. Isothermal ageing in circulating air at 371 °C; (*1*) PBBT **3c**, (*2*) PBBO **3b**, (*3*) poly(benzamide).

A significant disadvantage of all PBBAz is their low compression strength. Modification of the basic chains of their macromolecules and the introduction of bulky substituents into macromolecules were undertaken in order to enhance this parameter, to improve the solubility of PBBAz and to impart specific properties to these systems.

Thus the *p*-phenylene residues of terephthalic acid in the basic chains of PBBAz were replaced by thiophene-2,5-diyl,[47–49] fluorene-2,7-diyl,[50] adamantanediyl,[51] bicyclo[2.2.2]octanediyl [52,53] and 2,2′-bipyridinediyl [54] fragments. In particular, the reaction of the 2,5-diaminobenzene-1,4-dithiol dihydrochloride (**4c**) with thiophene- (**5a**), bithiophene- (**5b**) and terthiophenedicarbonyl (**5c**) dichlorides afforded PBBT **6** soluble in methanesulfonic and sulfuric acids.[47]

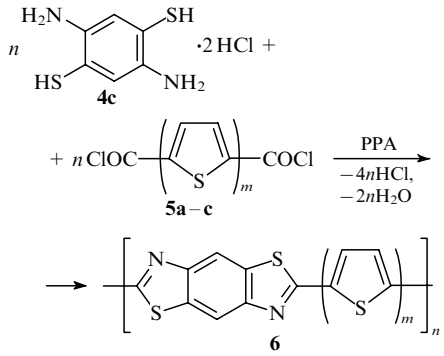

m = 1 (**5a**), 2 (**5b**), 3 (**5c**).

A similar approach was used for the synthesis of a thiophene-containing PBBO.[49] Although PBBT and PBBO are characterised by much lower values of the Kuhn segment than those of the analogous polymers based on terephthalic acid, the majority of their solutions in various acids manifest liquid-crystalline properties.

A certain deviation from a strictly straightened chain was also observed in the case of PBBT **7** prepared from the dihydrochloride **4c** in PPA after partial substitution of fluorene-2,7-dicarbonyl dichloride for the terephthaloyl dichloride (Scheme 1).[50]

Polycyclocondensation at 165 °C results in the formation of high-molecular-weight polymers which are completely soluble in methanesulfonic and sulfuric acids. At higher temperatures, this reaction is accompanied by the formation of insoluble polymers which can be due to the five-membered ring opening in the fluorene fragment.

The colourless PBBT **8** was obtained by the reaction of the dihydrochloride **4c** with bicyclo[2.2.2]octane-1,4-dicarboxylic acid (**9a**), its dimethyl ester (**9b**) or the dichloride (**9c**) in PPA.[52,53]

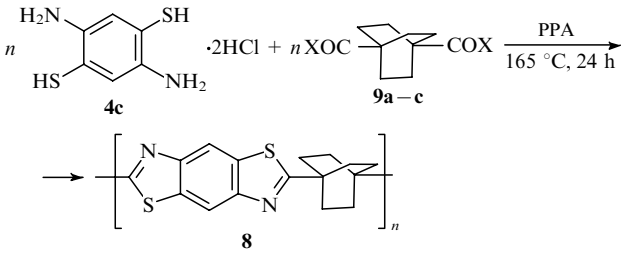

X = OH (**9a**), OMe (**9b**), Cl (**9c**).

The resulting polymer is soluble in methanesulfonic and sulfuric acids. In terms of thermal stability, the rupture strength and modulus of elasticity, the polymer **8** ranks below PBBT **3** based on terephthalic acid but considerably surpasses it in compression strength.

Poly(benzobisoxazoles) and poly(benzobisthiazoles) containing 2,2′-bipyridinediyl residues were obtained by the reaction of 2,2′-bipyridine-4,4′- or -5,5′-dicarboxylic acids with various mononuclear diaminodiols and diaminodithiols (Scheme 2).[54]

The 4,4′-substituted PBBAz **11** and **12** are soluble in methanesulfonic, sulfuric, trifluoroacetic and formic acids as well as in a mixture of nitromethane with $AlCl_3$. They form strong films. The 5,5′-substituted polybenzazoles **13** and **14** are soluble only in methanesulfonic acid and in a mixture of nitromethane with $AlCl_3$. The solutions of PBBAz **14** form lyotropic mesophases in methanesulfonic acid.

The poly(benzobisazoles) **12a**,**b** and **13a**,**b** manifest extremely high thermal stabilities in inert media and in air (Table 2).

Table 2. Some characteristics of the PBBAz **12** and **13**.[54]

Compound	η_{log} (see [a])	T_{destr} /°C		Yield (%)
		in air	in N_2 atmosphere	
13b	3.1	591	668	82
13c	3.7	537	585	83
12b	1.7	586	648	86
12c	2.1	569	597	87

[a] $MeSO_3H$, 30 °C, c = 0.25 g dl^{-1}.

The synthesis of the phenyl-substituted poly[benzo(*N*-phenyl)bisimidazole] **15** [55,56] was carried out in two steps. In the first step, 4,6-dianilinobenzene-1,3-diamine **16** reacted with terephthaloyl dichloride in *N*-methylpyrrolidone (NMP); in the second step, the poly(dianilino)amide **17** formed is cyclodehydrated in PPA to PBBAz **15**.

Poly[benzo(*N*-phenyl)bisimidazole] **15** is one of the first rigid-rod PBBAz. It is soluble in methanesulfonic, sulfuric and formic

Scheme 1

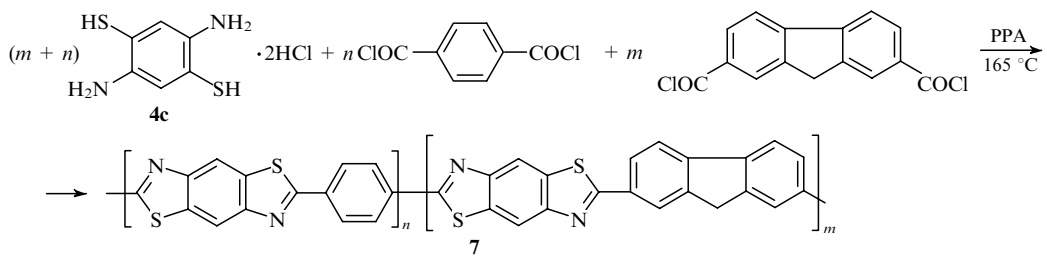

Scheme 2

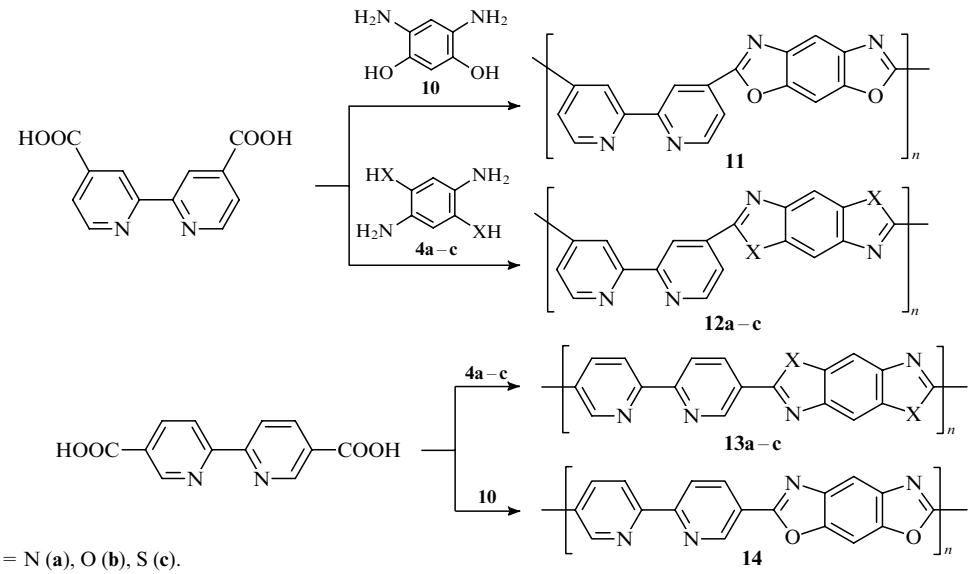

X = N (**a**), O (**b**), S (**c**).

acids as well as in a tetrachloroethane – phenol mixture (3 : 1). This corroborates the hypothesis [57] that the phenyl substituents in the heterocyclic fragment improve the solubility of polyheteroarylenes.[57]

The polymer **15** has a specific viscosity of 9.9 dl g^{-1} and a glass transition temperature (T_g) at 380 °C; at 450 °C, it loses 5% of its mass. Casting of the polymeric solutions was used to obtain films with a rupture strength of 135 MPa.

It should be noted that in contrast to other PBBAz, poly-[benzo(*N*-phenyl)bisimidazole] **15** is not formed by direct reaction of 4,6-dianilinobenzene-1,3-diamine **16** with terephthalic acid or its dichloride in PPA.

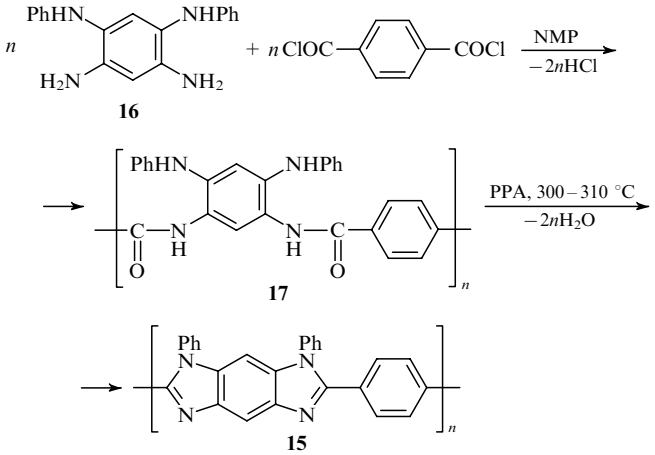

Much attention has been given to the synthesis of PBBAz with bulky substituents in the carbocyclic fragments of the macromolecules. Such structures are usually synthesised by polycyclocondensation of dicarboxylic acids or their derivatives containing the corresponding substituents.

Wolfe and Arnold [27] were among the first who have synthesised PBBO **18a** – **c** based on di-, tri- and tetraphenyl-*p*-terphenyldicarboxylic acids.

The solubilities of the phenyl-substituted polymers **18a** – **c** exceeds markedly that of the unsubstituted PBBO. In addition to methanesulfonic and chlorosulfonic acids, they are soluble in benzenesulfonic acid and a 7 : 3 mixture of *m*-cresol with dichloroacetic acid as well as in a 9 : 1 mixture of dichloroacetic acid with methanesulfonic acid.

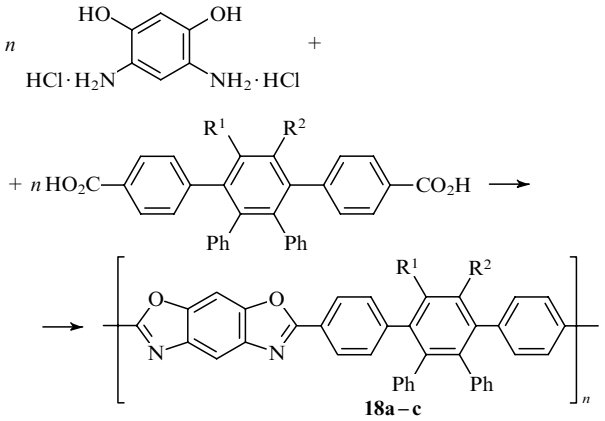

$R^1 = R^2 = H$ (**a**), $R^1 = H$, $R^2 = Ph$ (**b**), $R^1 = R^2 = Ph$ (**c**).

An analysis of the thermal stabilities of PBBO **3b** and the polymer **18b** containing a triphenyl-substituted central fragment revealed that the latter is more resistant to isothermal ageing at 316 °C than PBBO **3b**, but is decomposed more rapidly at 371 °C (Fig. 4) due to the splitting of the phenyl groups.

The poly(benzobisoxazoles), poly(benzobisthiazoles) and poly(benzobisimidazoles) **19a** – **f** containing benzooxazol-2-yl or benzothiazol-2-yl substituents in the phenyl fragment were obtained using the corresponding substituted terephthalic acids **20**.[58 – 61]

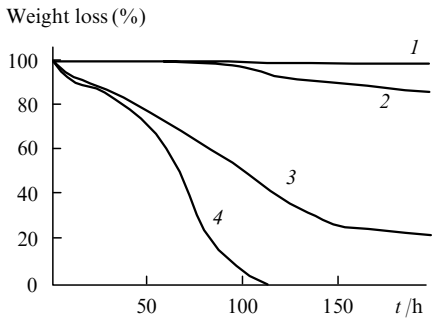

Figure 4. Isothermal ageing of PBBO **3b** and the polymer **18b** powders in circulating air;[27] (*1*) polymer **18b** at 316 °C, (*2*) PBBO **3b** at 316 °C, (*3*) PBBO **3b** at 371 °C, (*4*) polymer **18b** at 371 °C.

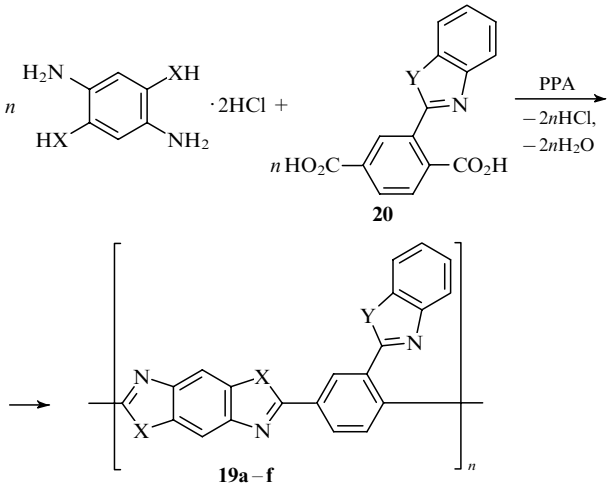

20

19a – f

X = Y = O (**19a**); X = O, Y = S (**19b**); X = Y = S (**19c**);
X = S, Y = O (**19d**); X = NH, Y = O (**19e**); X = NH, Y = S (**19f**).

The PBBAz **19a – f** thus formed were soluble in sulfuric and methanesulfonic acids; the specific viscosities of their solutions in methanesulfonic acid varied from 4 to 19 dl g^{-1}. The anisotropic polymeric solutions (10%, w/w) were used to obtain fibres. The fibres from PBBT **19c** manifested the most valuable properties, *viz*., stability of 2.4 GPa and specific modulus of elasticity of 172 – 207 GPa. Their compression strengths (380 MPa) exceed that of the unsubstituted PBBT **3c**.

2,5-Di(benzothiazolyl)terephthalic acid was used together with 2-benzoazolylterephthalic acids **20** in the synthesis of PBBAz, which afforded PBBAz **21**.[61]

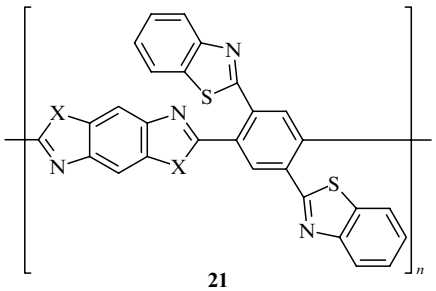

21

Dicarboxylic acids **22a – d** were used as acid components in the synthesis of PBBT and PBBO in order to achieve an even greater disturbance of the close packing of PBBAz and to increase the compression strength.[62, 63]

It should be noted that high-molecular-weight PBBAz **23a – d** were obtained only in those cases where polycyclocondensation was carried out at very low concentrations of the monomers in PPA ($\leqslant$ 1%), whereas with an increase in their concentration to 10% only low-molecular-weight oligomers could be isolated from their solutions (Scheme 3).[62]

The poly(benzobisazoles) **23a – d** are soluble in sulfuric, methanesulfonic and trifluoromethanesulfonic acids. The intrinsic viscosities, [η], of the polymers **23a – d** measured in methanesulfonic acid at 30 °C were equal to 12.0, 7.7, 11.4 and 8.7 dl g^{-1}, respectively.

The presence of extended side groups in the PBBAz synthesised prevents the straightening of the basic chains of the macromolecules and the formation of anisotropic solutions as a result of which the attempt to prepare high-quality fibres based on them failed.

The introduction of insignificant amounts (1 mol.% – 2 mol.%) of benzothiazolylphenyl-substituted *p*-terphenyldicar-

Scheme 3

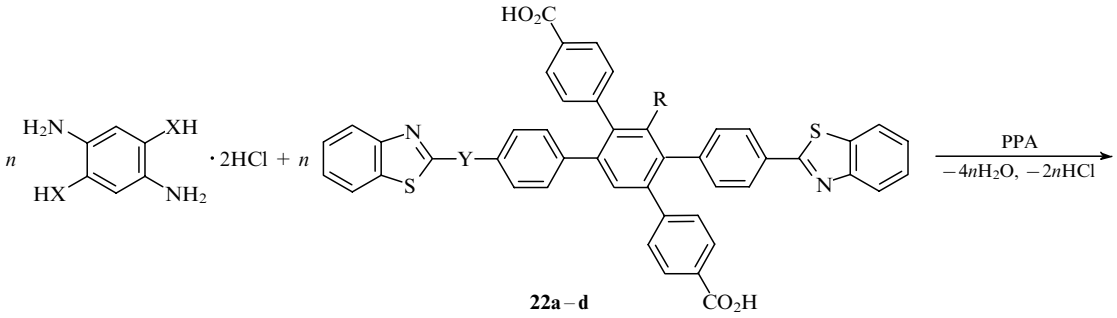

22a – d

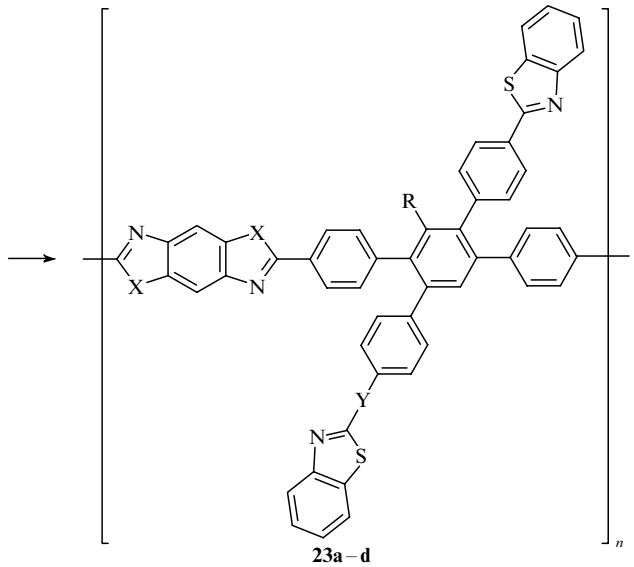

23a – d

Compound **23**	X	R	Y
a	S	Ph	absent
b	O	Ph	"
c	S	H	O–
d	O	H	O–

boxylic acid as a co-monomer to terephthalic acid results in the copolymers **24**.[64]

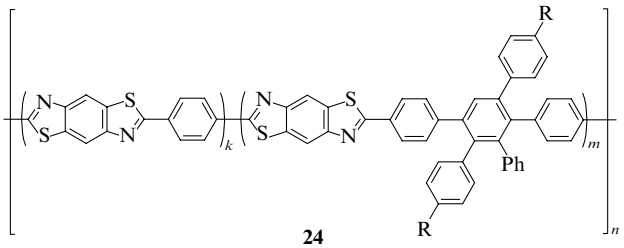

24

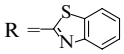

The polycyclocondensation at the concentrations of 10% (w/w) yielded copolymers with intrinsic viscosities of 20 to 28 dl g^{-1}. The fibres prepared from the copolymers **24** manifested a specific strength of 2.5 GPa, a modulus of elasticity of 193–283 GPa and compression strengths of 344 to 482 MPa.

The poly(benzobisazoles), *e.g.*, **25** and **26**, with aryloxide and arylthio substituents were obtained[65] by the reactions of 4,6-diaminoresorcinol, 2,5-diaminohydroquinone-, 4,6-diaminobenzene-1,3-dithiol and 2,5-diaminobenzene-1,4-dithiol hydrochlorides with 4,8-diaryloxy(arylthio)naphthalene-2,6-dicarboxylic acids in PPA.[65]

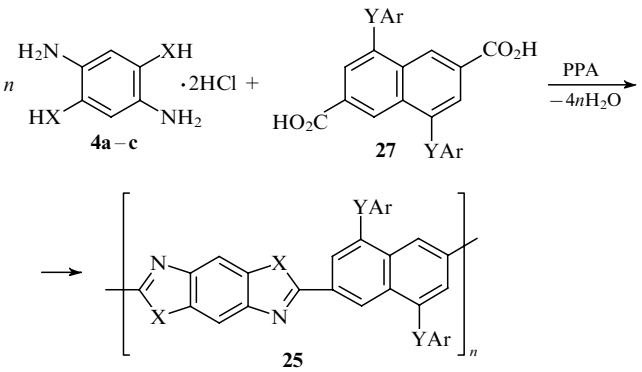

4a–c **27** **25**

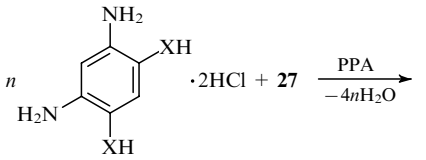

26

X = O, S, NH; Ar = 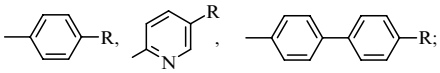

R = H, Me, Et, Pr^n, Pr^i; Y = O, S.

In addition to a single-step synthesis of PBBAz in PPA, two-step synthetic procedures have been developed which yield prepolymers in the first stage under mild conditions. Their subsequent solid-phase cyclisation yields poly(benzobisazoles).

Thus the polymers **28** which are soluble in mixtures of dichloromethane chloride with methanesulfonic and trifluoroacetic acids have been synthesised from the silyl derivatives **29** and aryloxy-substituted terephthaloyl dichlorides by Kricheldorf *et al.*[66–70]

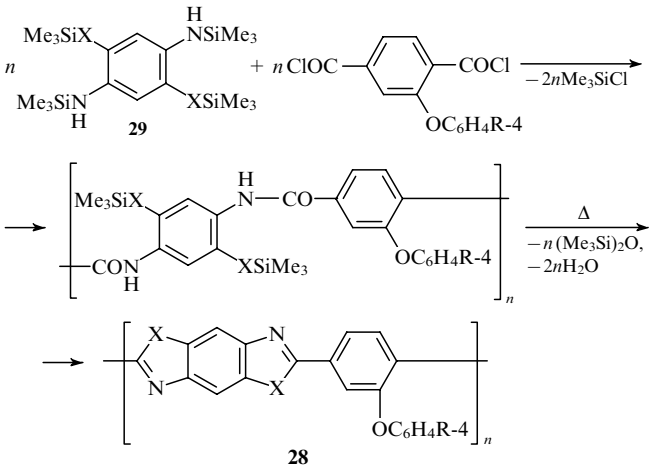

29 **28**

X = O, S; R = Ph, OPh, Bu^t, Cl, Br.

The use of silylated monomers makes it possible to increase the nucleophilicity of the nitrogen atom, as a result of which the reaction with acid chlorides proceeds more selectively and does not affect the trimethylsilyloxy(thio) groups.[71–74]

Kimura *et al.*[75] used a stepwise procedure for the synthesis of the alkoxy-substituted PBBT **30**.

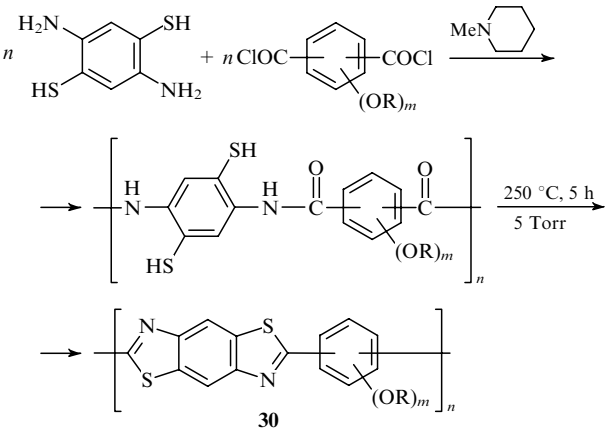

30

R = Bu^n, n-C_6H_{13}, n-C_8H_{17}, n-$C_{10}H_{21}$, n-$C_{12}H_{25}$; m = 1, 2.

Nearly all the PBBT **30** were able to form anisotropic melts in the temperature range from 280 to 450 °C.

On the whole, it should be noted that most PBBAz can successfully be used for the preparation of high-quality fibres and films; however, bulk products can hardly be obtained, since their glass transition temperatures exceed their decomposition temperatures. This problem was solved, to a large extent, within the framework of a new concept in materials technology, namely, the construction of molecular composites.[76]

III. Molecular composites

The term molecular composites is usually applied to describe systems which consist of rigid-rod molecules dispersed in matrices of flexible-rod molecules at the molecular level; in this case, rigid-rod molecules play the role of reinforcing elements.

Molecular composites can be prepared both by mixing rigid- and flexible-rod polymers at the molecular level and by synthesising block and graft copolymers containing rigid- and flexible-rod fragments.

Among the first molecular composites were those based on PBBT **3c** as a rigid-rod component and polybenzoimidazole (**31**, ABPBI) as a flexible-rod component.[77–79]

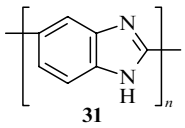

31

Poly(benzoimidazole) (**31**) was obtained by homocondensation of 3,4-diaminobenzoic acid in PPA.[80,81]

Mixtures of these polymers at the molecular level were prepared from solutions with concentrations below those required for precipitation.[78,79] The mechanical properties of PBBT – ABPBI molecular composites (both as fibres and as films) are listed in Table 3. As can be seen from the Table 3, the introduction of 30% PBBT into the matrices of ABPBI enhances significantly the deformation strength characteristics of the material. The results of morphological studies of these mixtures, *viz*., low- and wide-angle X-ray scattering, optical microscopy and scanning electron microscopy suggest the absence of phase separation.[77,82,83]

Table 3. Mechanical characteristics of fibres and films based on the PBBT – ABPBI molecular composites.

Composite	Product	E/GPa	σ/MPa	ε(%)	Ref.
PBBT	fibre	300	3000	1.1	82
ABPBI [a]	"	16.8	675	29	77
ABPBI [b]	"	36.0	1110	5.2	82
PBBT – ABPBI					
(30 : 70) [a]	"	16.8	1161	7.2	77
see [c]	"	71.7	1215	2.5	77
see [d]	"	109.7	1283	1.8	77
PBBT – ABPBI					
(30 : 70) [a]	film	30.4	690	55	83
see [e]	"	88.2	918	2.4	83

[a] Freshly formed; [b] heat-treated; [c] heat-treated at 427 °C; [d] heat-treated at 525 °C; [e] heat-treated at 540 °C.

The processability of molecular composites could be improved using thermoplastic polymers, *e.g*., amorphous and partially crystalline polyamides,[84,85] poly(phenylquinoxalines)[86] and poly(ether ether ketones)[87] as flexible-rod matrices. The mechanical characteristics of the molecular composites based on thermoplastic polymers and PBBT are listed in Table 4. Thus the mechanical properties of the PBBT – Nylon system exceed those of a monoaxially oriented fibrous composite with identical composition by 50% – 300%.

As well as the construction of composites at the molecular level, the design of molecular composites by the synthesis of block and graft copolymers has become a very popular approach. Whereas in the molecular composites prepared by mechanical mixing of flexible- and rigid-rod components the reinforcing

Table 4. Mechanical characteristics of PBBT – thermoplastic molecular composites.

Thermoplastics	Composition (w/w)	Product	E/GPa	σ/MPa	Ref.
Poly(phenylquinoxaline)	30 : 70	fibre	17.5	355	86
Nylon	30 : 70	"	36.0	345	86
Poly(ether ether ketone)	50 : 50	film	11.0	248	87
		block	15.8	105	87
Nylon-6,6	50 : 50	"	20.8	183	85

macromolecules are bound to the matrices exclusively due to physical interactions, in block copolymer-based molecular composites the flexible- and rigid-rod fragments are linked by covalent bonds. As a result, the transfer of strains from the rigid-rod fragments to the flexible-rod matrices occurs more effectively, hence, the block copolymer-based molecular composites manifest higher deformation strengths and dimensional stabilities.

The block copolymers **32** of the ABA type[88] which contain rigid-rod blocks B and flexible-rod blocks A[88] were synthesised as model systems. Macromolecules of PBBT **33** with carboxy terminal groups ($[\eta] = 10-24$ dl g^{-1}) used as rigid-rod blocks were introduced into co-polycondensation with 3,4-diaminobenzoic acid hydrochloride, which resulted in the formation of benzoimidazole rings and simultaneous binding of the individual blocks (Scheme 4).

The compositions of the blocks were varied by changing the content of 3,4-diaminobenzoic acid used for co-polycondensation. As can be seen from Table 5, the moduli of elasticity of the block-copolymeric molecular composites are comparable with those of the dynamic mixtures; their magnitudes depend on the ratios of the rigid- and flexible-rod components. The values of the moduli suggest that the reinforcement does not necessarily require highly extended macromolecules of PBBT **32**. Comparison of the breaking strengths (see Table 5) points to a much higher (up to

Table 5. Some characteristics of the block copolymers and mixed molecular composites.[88]

Ratios [a]	$[\eta]$/dl g^{-1}		E/GPa	σ/MPa	ε(%)
	PBBT **32**	copolymer			
30 : 70	10.7	8.5	102.7	1696	2.3
25 : 75	12.9	10.7	94.5	1566	2.5
30 : 70	17.7	7.3	115.8	1600	1.4
30 : 70	see [b]	see [b]	116.5	1268	1.4

[a] The PBBT **32** : ABPBI **31** ratios for the copolymer; [b] a physical mixture comprising 30% (w/w) PBBT **32** ($[\eta] = 31$ dl g^{-1}) and 70% (w/w) ABPBI **31** ($[\eta] = 17.6$ dl g^{-1}).

Scheme 4

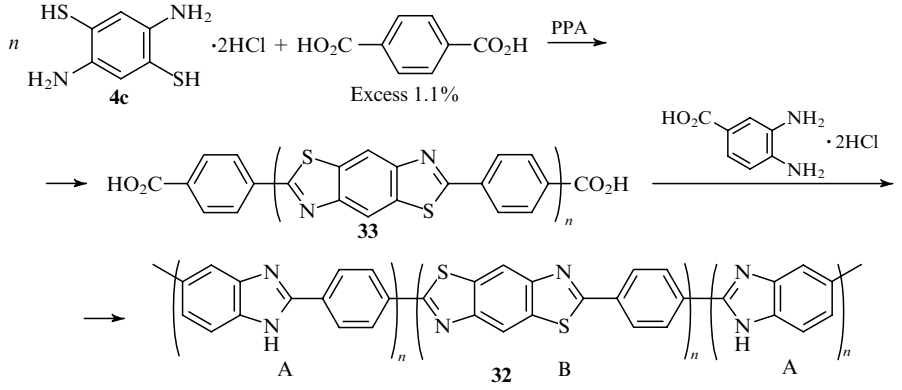

33%) deformation strength of the block-copolymeric molecular composites compared with the materials prepared from mechanical mixtures.

The polybenzobisthiazoles carrying terminal carboxy groups were introduced into the Friedel–Crafts polycondensation reaction with *m*-phenoxybenzoic acid in a P_2O_5–$MeSO_3H$ mixture.[89] This reaction yielded block copolymers of the ABA type which contained flexible-rod polyether ketone blocks and rigid-rod PBBT blocks.

In addition to block-copolymeric molecular composites, much attention has been given to the synthesis of molecular composites based on graft copolymers containing rigid- and flexible-rod macromolecules. In particular, benzothiazol-2-yl-substituted PBBI **34** was metallated using NaH in DMSO with subsequent treatment with acrylamide[90] or, which is especially important, with propylene oxide.[90–92]

The grafted copolymer **35** is soluble in methanesulfonic, 97% formic and trifluoroacetic acids much more easily than PBBI **34**.

Although the softening of these polymers could not be detected by differential scanning calorimetry, their solid melts could be obtained by compaction at 190–232 °C. The introduction of polypropylene oxide side chains is accompanied by a significant decrease in their thermal stabilities in comparison with that of the starting compound, *viz*., PBBI **34**.

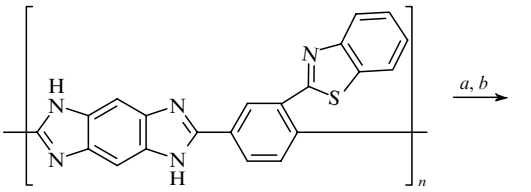

34

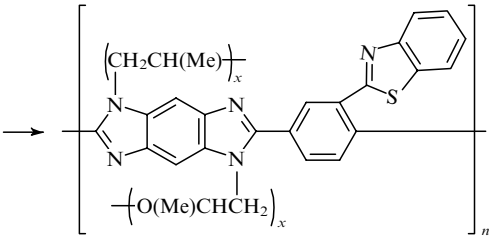

35

(*a*) NaH, DMSO, (*b*) Me–CH(O)–CH_2.

Of special interest is the synthesis of molecular composites based on grafted copolymers with heat-resistant side chains. Since rigid-rod PBBAz are soluble only in acidic solvents, the set of reactions used for the grafting is rather limited. Evers *et al*.[93,94] used the Friedel–Crafts reaction of *m*-phenoxybenzoic acid with poly(benzobisthiazole) in $MeSO_3H$–P_2O_5 (10 : 1, w/w) for the synthesis of grafted copolymers of the AB type. Thus the reaction of the polybenzobisthiazole copolymer **36** containing 4,4′-(*o*-diphenoxyphenylene) groups which are distributed statistically among the fragments of the rigid-rod PBBT with *m*-phenoxybenzoic acid afforded the copolymer **37** (Scheme 5).[95]

Compaction at high temperatures and pressures (285 °C, 6.9 MPa) is employed for the preparation of bulk products possessing isotropic properties. The main disadvantage of this approach is the low elasticity of the grafted fragments.

An alternative approach is based on the use of polybenzobisthiazole copolymers containing 2,6-dimethylphenoxide side groups as the basic macromolecular chains.[96,97] Treatment of these systems with *m*-phenoxybenzoic acid in P_2O_5–$MeSO_3H$ was accompanied by the formation of the grafted copolymers **38** (Scheme 6).

According to the dynamic mechanical analysis data, the softening of the grafted copolymers **38** occurs at 180–265 °C depending on the value of y.[98] Their secondary processing into bulk products is carried out at pressures up to 40 MPa and at temperatures which are 40 to 50 °C higher than the softening temperature. A specimen containing 46% (w/w) of PBBT **3c** and 54% (w/w) of the copolymer **38** manifests a rupture strength of 40 MPa and modulus of elasticity of 9.7 GPa.

IV. Conclusion

Rigid-rod PBBAz are the most promising materials in those fields where small weight, high deformation strength, rigidity, thermal and chemical stability as well as radiotransparency are the critical factors. The latter property is especially important, and in this respect PBBAz fibres have an indisputable advantage over graphite fibres. PBBAz fibres manifest greater elongation at rupture in comparison with graphite fibres and possess higher thermal and thermooxidative stabilities in comparison with Kevlar fibres. This altogether demonstrates their usefulness for aeronautical, aerospace and electronic engineering. Yet another field of application in which PBBAz have obvious advantages over glass, Kevlar fibres and coal plastics are thermostable membranes and filters. Further progress in this area will largely depend on the cost of the monomers and the 'cost–property' ratios of these systems.

The main drawback of the materials based on PBBAz is their low compression stability. This review considers the individual approaches to the solution of this problem which are based on structural modifications of these polymers. In recent years, increasing attention has been given to the construction of

Scheme 5

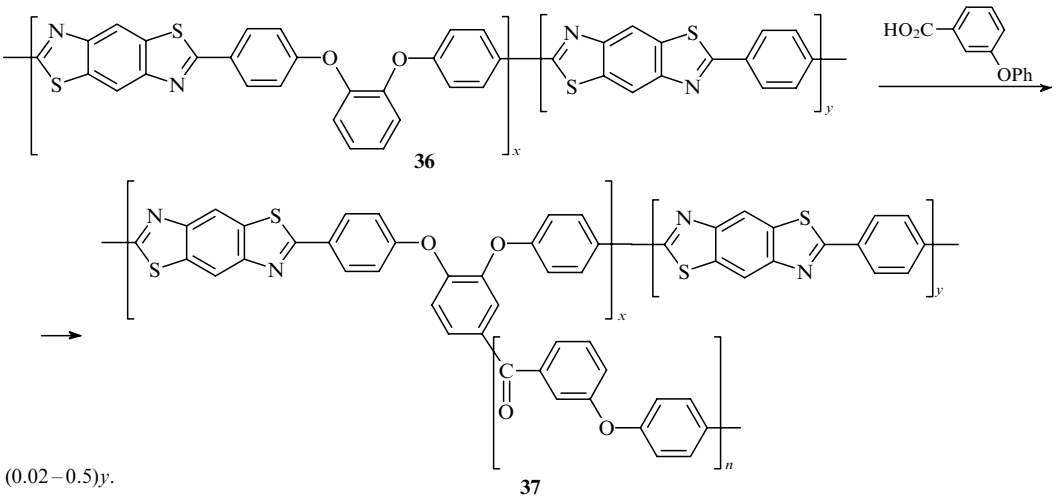

36

37

$x = (0.02–0.5)y$.

Scheme 6

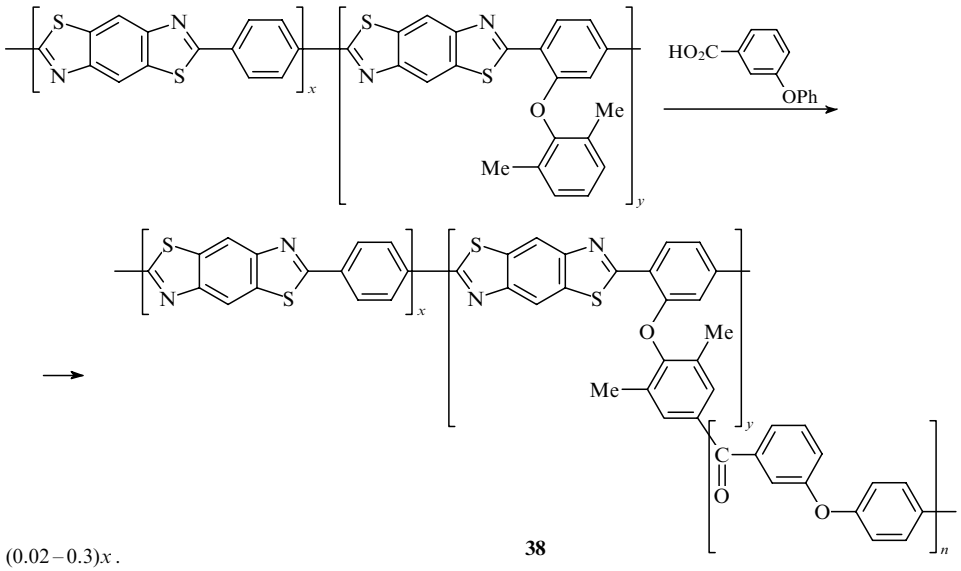

$y = (0.02-0.3)x$.

38

PBBAz that can be cross-linked to form three-dimensional structures.[99–101] Further developments in this field will obviously be aimed at the construction of systems whose solidification is not accompanied by the evolution of volatile by-products.

References

1. F C Frank *Proc. R. Soc. London, A Math. Phys. Sci.* **319** 127 (1970)
2. A J Kinlock, P R Young *Fracture Behaviour of Polymers* (London: Applied Science Publishers, 1983)
3. R T Read *Polym. Paint Colour J.* **178** 664 (1988)
4. R T Read *Spec. Chem.* **9** 30 (1989); *Ref. Zh. Khim.* **13** 4 (1989)
5. D Hall *Introduction to Composite Materials* (Cambridge: Cambridge University Press, 1981)
6. A Ciferri, I Ward (Eds) *Ultra-High Modulus Polymers* (London: Interscience, 1979)
7. A J Owen, in *Developments in Orient Polymers* Vol. 2 (London; New York: Applied Science Publishers, 1987) p. 237
8. A A Konkin (Ed.) *Termo-Zharostoikie i Negoryuchie Volokna* (Thermostable, Heat-Resistant and Non-Combustible Fibres) (Moscow: Khimiya, 1978) p. 422
9. M G Dobb, J E McIntyre *Adv. Polym. Sci.* **60**/**61** 61 (1984)
10. A V Volokhina, G I Kudryavtsev, in *Zhidkokristallicheskie Polimery* (Mesomorphic Polymers) (Ed. N A Plate) (Moscow: Khimiya, 1988) p. 37
11. BRD P. 1 929 713A; *Chem. Abstr.* **72** 122 796 (1970)
12. J Preston, in *Encyclopedia of Polymer Science and Engineering* Vol. 11 (Eds H F Mark, N M Bikales, C G Overberger, G Menges) (New York: Wiley, 1988) p. 381
13. J P Critchley *Angew. Makromol. Chem.* **B109**/**110** 41 (1982)
14. J F Wolfe, in *International Symposium on Materials. Approaches to Property Limits in Polymers, Princeton, 1986* p. 12
15. V N Odnoralova, in *Itogi Nauki i Tekhniki. Khimiya i Tekhnologiya Vysokomolekulyarnykh Soedinenii* [The Chemistry and Technology of High-Molecular Compounds (Advances in Sciences and Engineering Series)] (Moscow: Izd. VINITI, 1988) Vol. 25, p. 85
16. Y Imai *Bull. Jpn. Inst. Met.* **25** 772 (1986)
17. J P Critchley *Prog. Polym. Sci.* **2** 51 (1970)
18. F E Arnold Jr , F E Arnold *Adv. Polym. Sci.* **117** 257 (1994)
19. A A Izyneev, M M Teplyakov, V G Samsonova, A D Maksimov *Usp. Khim.* **36** 2090 (1967) [*Russ. Chem. Rev.* **36** 912 (1967)]
20. V V Korshak, M M Teplyakov *J. Macromol. Sci., Rev. Macromol. Chem.* **5** 409 (1971)
21. C S Marvel *J. Macromol. Sci., Rev. Macromol. Chem.* **13C** 219 (1975)
22. V V Korshak, G V Kazakova, A L Rusanov *Vysokomol. Soedin., Ser. A* **31** 5 (1989) [a]
23. E S Krongauz, A L Rusanov, T L Renard *Usp. Khim.* **39** 1591 (1970) [*Russ. Chem. Rev.* **39** 747 (1970)]
24. N Yoda, M Kurihara *J. Polym. Sci., Part D, Macromol. Rev.* **5** 109 (1971)
25. N Yoda, M Kurihara, M Dokoshi *Prog. Polym. Sci. Jpn.* **4** 1 (1972)
26. R F Kovar, F E Arnold *J. Polym. Sci., Polym. Chem. Ed.* **14** 2807 (1976)
27. J F Wolfe, F E Arnold *Macromolecules* **14** 909 (1981)
28. J F Wolfe, B H Loo, F E Arnold *Macromolecules* **14** 915 (1981)
29. S R Allen, A G Filippov, R J Farris, E L Thomas, C-P Wong, G C Berry, E C Chenevey *Macromolecules* **14** 1135 (1981)
30. US P. 4 606 875; *Chem. Abstr.* **106** 6348 (1987)
31. L Feldman, R J Farris, E L Thomas *J. Mater. Sci.* **20** 2719 (1985)
32. A W Chow, J F Somdell, J F Wolfe *Polymer* **29** 1307 (1987)
33. J F Wolf, in *Encyclopedia of Polymer Science and Engineering* Vol. 11 (Eds H F Mark, N M Bikales, C G Overberger, G Menges) (New York: Wiley, 1988) p. 601
34. WO PCT 8 401 160; *Chem. Abstr.* **101** 56 435 (1984)
35. US P. 4 533 724; *Chem. Abstr.* **101** 131 731 (1984)
36. E W Choe, S N Kim *Macromolecules* **14** 920 (1981)
37. S A Jenekhe, P O Johnson *Macromolecules* **23** 4419 (1990)
38. V N Tsvetkov *Zhestkotsepnye Polimernye Molekuly* (Rigid-Rod Polymer Molecules) (Leningrad: Nauka 1986)
39. A E Zachariadis, R E Porter (Eds) *High Modulus Polymers — Approaches to Design and Development* (New York: Marcel Dekker, 1987) p. 523
40. A Feldblum, Y W Park, A J Heeger, A G MacDiarmid, G Wnek, F E Karasz, J C W Chien *J. Polym. Sci., Polym. Phys. Ed.* **19** 173 (1981)
41. S-G Chu, S Venkatraman, G C Berry, Y Einaga *Macromolecules* **14** 939 (1981)
42. M Lipovics *Chem. Eng.* **91** 147 (1984)
43. *Mater. Eng.* **103** 39 (1986)
44. S J Krause, T B Haddock, D L Vezie, P G Lenhert, W F Hwang, G E Price, T E Helminiak, J F O'Brien, W W Adams *Polymer* **29** 1354 (1988)
45. Y-H So, J P Heeschen, B Bell, P Bonk, M Briggs, R De Caire *Macromolecules* **31** 5229 (1998)
46. US P. 4 225 700; *Chem. Abstr.* **94** 4410 (1980)
47. M Dotrong, R C Tomlinson, M Sinsky, R C Evers *Polym. Prepr. (Am. Chem. Soc., Div. Polym. Chem.)* **32** (1) 85 (1991)
48. J H Promislov, E T Samulski, J Preston *Polym. Prepr. (Am. Chem. Soc., Div. Polym. Chem.)* **32** (2) 211 (1991)
49. J H Promislov, J Preston, E T Samulski *Macromolecules* **26** 1793 (1993)
50. M Dotrong, R C Evers *J. Polym. Sci., Part A, Polym. Chem.* **28** 3241 (1990)
51. T D Dong, T G Archibald, A A Malik, F O Bonsu, K Baum, L S Tan, F E Arnold *Polym. Prepr. (Am. Chem. Soc., Div. Polym. Chem.)* **32** (1) 199 (1991)
52. M Dotrong, M H Dotrong, G J Moore, R C Evers *Polym. Prepr. (Am. Chem. Soc., Div. Polym. Chem.)* **32** (1) 201 (1991)

53. M Dotrong, M H Dotrong, C S Wang, H Song, G J Moore, R C Evers *J. Polym. Sci., Part A, Polym. Chem.* **32** 2953 (1994)
54. Sze Chit Yu, Xiong Gong, Wai Kin Chan *Macromolecules* **31** 5639 (1998)
55. D S Tugushi, V V Korshak, A L Rusanov, V G Danilov, G M Cherkasova, G M Tseitlin *Vysokomol. Soedin., Ser. A* **15** 969 (1973) [a]
56. V V Korshak, A L Rusanov, D S Tugushi, G M Cherkasova *Macromolecules* **5** 807 (1972)
57. V V Korshak, A L Rusanov *Usp. Khim.* **52** 812 (1983) [*Russ. Chem. Rev.* **52** 459 (1983)]
58. T-t Tsai, F E Arnold *Polym. Prepr. Am. Chem. Soc., Div. Polym. Chem.* **27** (2) 221 (1986)
59. US Appl. 84 784; *Chem. Abstr.* **109** 171 065 (1988)
60. US Appl. 85 094; *Chem. Abstr.* **109** 171 120 (1988)
61. T-t Tsai, F E Arnold *High Perform. Polym.* **3** 179 (1989)
62. J Burkett, F E Arnold *Polym. Prepr. (Am. Chem. Soc., Div. Polym. Chem.)* **28** (2) 278 (1987)
63. F E Arnold *Mater. Res. Soc. Symp. Proc.* **134** 117 (1989)
64. C S Wang, J Burkett, S Bhattacharya, H-H Chuah, F E Arnold *Polym. Mater. Sci. Eng.* **60** 767 (1989)
65. US P. 4 762 908; *Chem. Abstr.* **106** 85 274 (1987)
66. H R Kricheldorf, J Engelhardt *Makromol. Chem. B, Makromol. Chem. Phys.* **190** 2939 (1989)
67. BRD P. 3 940 792; *Chem. Abstr.* **115** 208 889 (1991)
68. H R Kricheldorf, in *Silicon in Polymer Chemistry* (Ed. H R Kricheldorf) (Berlin: Springer, 1996) p. 321
69. H R Kricheldorf, J Engelhardt *Makromol. Chem. B, Makromol. Chem. Phys.* **191** 2017 (1990)
70. H R Kricheldorf, A Domschke *Polymer* **35** 198 (1994)
71. Y Imai, Y Oishi *Prog. Polym. Sci.* **14** 173 (1989)
72. A L Rusanov *Usp. Khim.* **59** 1492 (1990) [*Russ. Chem. Rev.* **59** 868 (1990)]
73. R D Katsarava, Ya S Vygodskii *Usp. Khim.* **61** 1142 (1992) [*Russ. Chem. Rev.* **61** 629 (1992)]
74. H R Kricheldorf, in *Silicon in Polymer Chemistry* (Ed. H R Kricheldorf) (Berlin: Springer, 1996) p. 288
75. K Kimura, D L Meurer, R F Hutzler, P E Cassidy, J W Fitch *Macromolecules* **27** 1303 (1994)
76. S Jenkins, K I Jacob, M B Polk, S Kumar, T D Dang, F E Arnold *Macromolecules* **33** 8731 (2000)
77. W F Hwang, C L Benner, D R Wiff, T E Helminiak *J. Macromol. Sci. Phys.* **B22** 231 (1983)
78. W F Hwang, C L Benner, D R Wiff, T E Helminiak, in *Proceedings of the 28th IUPAC Macromolecular Symposium, Dayton, 1982* B27
79. W F Hwang, D R Wiff, C Verschoore *Polym. Eng. Sci.* **23** 789 (1983)
80. Y Imai, I Taoka, K Uno, Y Iwakura *Makromol. Chem. B, Makromol. Chem. Phys.* **83** 167 (1965)
81. A W Chow, S P Bitler, P E Penwell, D J Osborn, J F Wolfe *Macromolecules* **22** 3514 (1989)
82. S J Krause, T B Haddock, G E Price, P G Lenhert, J F O'Brien, T E Helminiak, W W Adams *J. Polym. Sci., Part B, Polym. Phys.* **24** 1991 (1986)
83. M Wellman, G Husman, A K Kulshreshta, T E Helminiak, D R Wiff, C L Benner, W F Hwang *Org. Coat. Plast. Chem.* **43** 783 (1980)
84. T Kyu, T E Helminiak *Polymer* **28** 2810 (1987)
85. C S Wang, I J Goldfarb, T E Helminiak *Polymer* **29** 825 (1988)
86. W F Hwang, D R Wiff, C Verschoore, G E Price, T E Helminiak, W W Adams *Polym. Eng. Sci.* **23** 784 (1983)
87. C A Gabriel, R J Farris, M F Malone, in *Nonwavence Conference, New York, 1986* p. 255
88. T-t Tsai, F E Arnold, W F Hwang *J. Polym. Sci., Part A, Polym. Chem.* **27** 2839 (1989)
89. K L Cooper, F E Arnold *Polym. Prepr. Am. Chem. Soc., Div. Polym. Chem.* **33** (1) 1006 (1992)
90. US P. 5 008 346; *Chem. Abstr.* **115** 115 354 (1991)
91. R C Evers, T D Dang D Moore *Polym. Prepr. (Am. Chem. Soc., Div. Polym. Chem.)* **29** (1) 244 (1988)
92. R C Evers, T D Dang, D R Moore *J. Polym. Sci., Part A, Polym. Chem.* **29** 121 (1991)
93. S J Bai, M Dotrong, E J Soloski, R C Evers *J. Polym. Sci., Part B, Polym. Phys.* **29** 119 (1991)
94. M Dotrong, M H Dotrong, S J Bai, R C Evers *Sci. Adv. Mater. Proc. Eng. Tech. Symp. Ser.* **37** 1004 (1992)
95. M Dotrong, M H Dotrong, R C Evers *Polymer* **34** 726 (1993)
96. M Dotrong, M H Dotrong, R C Evers *Polym. Mater. Sci. Eng.* **65** 38 (1991)
97. M Dotrong, M H Dotrong, R C Evers *Polym. Prepr. (Am. Chem. Soc., Div. Polym. Chem.)* **33** 477 (1992)
98. U M Vakil, C S Wang, C Y-C Lee, M H Dotrong, M Dotrong, R C Evers *Polym. Prepr. (Am. Chem. Soc., Div. Polym. Chem.)* **33** (1) 479 (1992)
99. T-t Tsai, F E Arnold *Polym. Prepr. (Am. Chem. Soc., Div. Polym. Chem.)* **29** (2) 324 (1988)
100. H H Chuah, T-t Tsai, K H Wei, C S Wang, F E Arnold *Polym. Mater. Sci. Eng.* **60** 517 (1989)
101. W Sweeny *J. Polym. Sci., Part A, Polym. Chem.* **30** 1111 (1992)

[a] — *Polym. Sci. (Engl. Transl.)*

Russian Chemical Reviews **70** (2) 91 – 104 (2001) © 2001 Russian Academy of Sciences and Turpion Ltd

DOI 10.1070/RC2001v070n02ABEH000631

Modern chemistry of nitrous oxide

A V Leont'ev, O A Fomicheva, M V Proskurnina, N S Zefirov

Contents

I.	Introduction	91
II.	Atmospheric nitrous oxide	91
III.	Structure and properties	92
IV.	Decomposition of nitrous oxide	93
V.	Chemistry of nitrous oxide	94
VI.	Applied aspects of the chemistry of nitrous oxide	99
VII.	Conclusion	101

Abstract. Modern trends of the chemistry of nitrous oxide are discussed. Data on its structure, physical properties and reactivity are generalised. The effect of N_2O on the environment and the possibility of its utilisation are considered. Attention is focused on the processes in which the oxidising potential of nitrous oxide can be employed. The bibliography includes 329 references.

I. Introduction

Nitrous oxide was discovered by J Priestley in 1772. After experiments performed by H Davy in 1799, N_2O received the name 'laughing gas' from its action. In the mid-nineteenth century, N_2O assumed importance and found wide application as a soft anaesthetic. Presently, nitrous oxide is used in medicine primarily in mixtures with other more powerful inhalation anaesthetics.[1] Since nitrous oxide is non-toxic and readily soluble in lipophilic media, it finds use in food industry as a foaming agent. Nitrous oxide is one of three compounds containing N–O bonds which were discovered in interstellar space.[2]

In the last two decades, the chemistry of nitrous oxide has been substantially developed. In one aspect or another, N_2O was mentioned in a large body of research. In the present review, the abundant data on nitrous oxide are surveyed. Particular attention is given to studies in which N_2O was described as the reagent. The role of N_2O in the destruction of the ozone layer giving rise to the so-called 'greenhouse' effect is also considered.

A V Leont'ev, O A Fomicheva, M V Proskurnina Department of Chemistry, M V Lomonosov Moscow State University, Leninskie Gory, 119899 Moscow, Russian Federation. Fax (7-095) 939 02 90. Tel. (7-095) 939 50 59 (A V Leont'ev, O A Fomicheva), (7-095) 939 16 20 (M V Proskurnina). E-mail: alexandr@org.chem.msu.ru (A V Leont'ev), marina@org.chem.msu.ru (M V Proskurnina)
N S Zefirov Department of Chemistry, M V Lomonosov Moscow State University, Leninskie Gory, 119899 Moscow, Russian Federation, Institute of Physiologically Active Compounds, Russian Academy of Sciences, 142432 Chernogolovka, Moscow Region, Russian Federation. Fax (7-095) 913 21 13. Tel. (7-095) 939 16 20. E-mail: zefirov@org.chem.msu.ru

Received 23 October 2000
Uspekhi Khimii **70** (2) 107 – 122 (2001); translated by T N Safonova

II. Atmospheric nitrous oxide

1. Sources of atmospheric N_2O and its environmental effects

The environmental effects of nitrous oxide have been the subject of much attention of ecologists over the last several decades. This interest is primarily associated with the fact that the role of 'laughing gas' (previously, it had been thought that this gas was quite harmless) in the atmospheric processes is beginning to emerge. It was realised that nitrous oxide plays a role in destruction of the ozone layer and gives rise to the greenhouse effect.

It was demonstrated that the average residence time of nitrous oxide in the lower layers of the atmosphere is about 120 years due to the lack of processes necessary for chemical conversions of N_2O.[3] Nitrous oxide gradually diffuses from the troposphere to the stratosphere, where it decomposes partly through photolysis and partly in reactions with reactive O and $^{\bullet}OH$ species formed upon photolysis.[4]

$$N_2O \xrightarrow{h\nu} N_2 + O(^1D),$$

$$N_2O + O(^1D) \longrightarrow 2\,NO,$$

$$N_2O + O(^1D) \longrightarrow N_2 + O_2,$$

$$N_2O + {}^{\bullet}OH \longrightarrow N_2 + HO_2^{\bullet}.$$

Nitric oxide (NO), in turn, reacts with ozone to form O_2 and NO_2. The latter undergoes disproportionation to give NO and O under the action of solar radiation, this process occurring repeatedly.[5]

Nitrous oxide is the third most abundant minor component of the atmosphere, exceeded in amount only by carbon dioxide and methane. It is believed that these gases along with ozone and Freons are of importance in processes providing thermal balance of the Earth. Their molecules adsorb heat given up by the Earth as infrared radiation resulting finally in a noticeable increase in the temperature of the troposphere and the greenhouse effect.[6, 7] Although the contribution of N_2O to the total greenhouse effect is evaluated at 6%, the 'greenhouse-forming' power of nitrous oxide is approximately 260 times larger than that of carbon dioxide.[4, 5] Taking into account the residence time of nitrous oxide in the atmosphere and the fact that its discharge to the atmosphere from anthropogenic sources cannot be terminated immediately, ecologists have expressed serious concern over the contribution of N_2O to the greenhouse effect.

Analysis of air samples taken from cavities in land ice in Greenland demonstrated that the nitrous oxide content of the

atmosphere remained rather constant ($\sim$ 280 ppb) over the last thousand years.[8] Beginning in the mid-eighteenth century, the growth in industry was accompanied by a progressive increase in the N_2O content in the atmosphere. Presently, the concentration of N_2O in the Northern Hemisphere reaches $\sim$ 314 ppb and continues to increase at a rate of $\sim 0.5-0.9$ ppb per annum. Thus, the nitrous oxide content of the atmosphere increases by 0.2% – 0.3% annually. The same trends are true for the Southern Hemisphere.

Identification of all sources of discharge of nitrous oxide to the atmosphere and quantitative estimation of the contributions of these sources are stubborn problems. For various reasons, the scatter in the data obtained by different researchers is very wide.[4,9] However, the available models are steadily improved with the aim of gaining reliable information on the processes influencing the total balance of emission of N_2O to the atmosphere and its decomposition.[10]

In 1990, emission of nitrous oxide to the atmosphere was $\sim$ 12.7 million tons [11] of which about 35 percent were of anthropogenic origin. Processes of nitrification and denitrification in soils of tropical and temperate regions and in oceanic waters are the major natural contributors of N_2O. It is assumed with a rather low accuracy that these processes are responsible for 45%, 25% and 30% of all natural emission of N_2O, respectively. Heating and power plants,[12,13] motor transport (18%),[14,15] some industrial chemical processes (12%) [16] and agriculture (70%) [17] are recognised to be the major sources of N_2O of anthropogenic origin.

One cannot say that no efforts are being undertaken to decrease the discharge of nitrous oxide to the atmosphere. Thus, the largest world's manufacturers of adipic acid ($\sim$ 5% – 8% of the total anthropogenic emission of N_2O) concluded an agreement [18] and committed themselves to supply plants with special technological cycles and to reduce the amount of N_2O exhausted into the atmosphere by more than 90% by 2000. New catalysts and catalytic processes for decomposition of N_2O are being developed.[19,20] However, agriculture remains the major contributor of nitrous oxide. The amount of nitrous oxide can be reduced by decreasing the use of nitrogen-containing fertilisers and by reducing flooded areas under rice crops where anaerobic processes of N_2O formation occur. However, it is difficult to accomplish this goal because the growth of population generates a need for the solution of food problems, while modern highly productive agricultural crops require the intensive use of nitrogen fertilisers.

Therefore, it was predicted that the N_2O content in the atmosphere will be increased by 0.2% – 0.3% annually in the coming years, as has been observed in recent years.[11,21]

2. Catalytic purification of waste gases from N_2O

Presently, a number of catalytic processes for the neutralisation of pollutants are available and successfully used.[22] Purification of waste gases from N_2O is one of the steps aimed at reducing its discharge to the atmosphere. Apparently, the optimum procedure involves catalytic decomposition of nitrous oxide.

For a long time, investigations in this field were carried out from the standpoint of fundamental science.[19] The available systems often did not satisfy strict requirements imposed upon industrial catalysts for gas purification. More recently, many available catalytic systems have been reinvestigated under 'pseudoindustrial' conditions, *viz*., in the presence of complex gas mixtures, at temperature modes typical of heating furnaces and at high flow rates.[23,24] The world's large manufacturers of adipic acid, for example, DuPont (the catalyst is $CoO-NiO/ZrO_2$), BASF and Asahi (the catalyst is Cu/Al_2O_3), developed new technologies for the utilisation of N_2O.[25,26] However, the available catalytic compositions are far short of optimum. In addition, a wide variety of industrial sources of N_2O emission as well as operating conditions varying over a wide range call for a search for new more perfect catalysts. In addition, it was established that installations used for the neutralisation of NO and NO_2 can serve as sources of nitrous oxide.[25] Denitrification of waste gases in industrial scrubbers is generally performed using selective high-temperature reduction of nitrogen oxides NO_x with ammonia or hydrocarbons in the presence of a catalyst.[27] The conditions and parameters of the reactions of N_2O with reducing agents [RH,[28–33] NH_3 (see Refs 34 and 35) or CO [36–38]] have also been studied extensively. Since the maximum conversions of NO and N_2O into N_2 are achieved at different temperatures, the possibility of the simultaneous removal of these gases is an important criterion for the estimation of the efficiency of catalysts used for the purification of waste gases from nitrogen oxides.[39–41]

It should be mentioned that catalytic procedures for the purification of waste gases from nitrogen oxides are generally more favourable both from the economical standpoint and from the viewpoint of the efficiency of a reduction in the amount of NO_x to the maximum permissible concentrations. The adsorption methods can also be employed for the solution of this problem. Thus Centi *et al.* [42] demonstrated that Ba – ZSM-5 zeolites can be used for the selective removal of nitrous oxide from gas flows containing 0.1% – 0.2% of N_2O, and mixtures enriched with nitrous oxide (5%) can be either utilised as an oxidant or directed to refineries for subsequent decomposition.

III. Structure and properties

1. Structure of the nitrous oxide molecule

Generally, the structure of the nitrous oxide molecule (the symmetry group $C_{\infty v}$) is described by the resonance forms **A** and **B**.

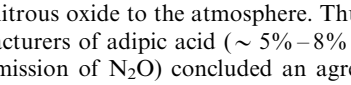

A **B**

It is believed that the *N*-oxide form **A** makes the major contribution to the geometric and electronic structure of the molecule. The total effective charges on the atoms in the form **A** are given below:

Calculation procedure	q_N	$q_{N(O)}$	q_O	Ref.
CNDO/2	−0.14	0.47	−0.33	43
4-31G	−0.07	0.62	−0.55	44
MP3	−0.11	0.44	−0.33	45

The opposite charge distribution in the resonance forms **A** and **B** accounts for the relatively low dipole moment of the molecule (0.161 D).[46] The N – N bond (1.128 Å) in nitrous oxide is substantially shorter than the standard N = N bond (1.24 Å, MeN = NMe) and is only insignificantly longer than the N ≡ N bond (1.10 Å, N_2). The N – O bond (1.184 Å, N_2O) is quite similar to the standard N = O double bond (1.21 Å, MeN = O).[47] Therefore, the N – N and N – O bond orders in nitrous oxide are estimated at 2.73 and 1.61, respectively.[48]

It is easy to see that the representation of the N_2O molecule by the resonance forms **A** and **B** formally assumes the presence of ambidentate properties, which can be manifested in the reactions of nitrous oxide both with electrophilic [49] and nucleophilic [50] agents.

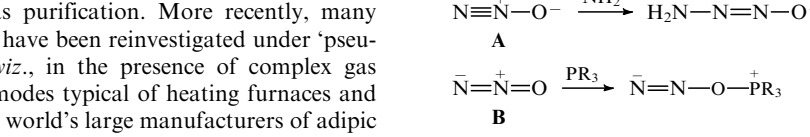

The zwitterionic resonance forms **A** and **B** can be supplemented with the form **C** (1,3-dipole)

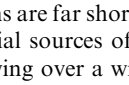

C

which can be involved in cycloaddition.

Data on the formation of stable five-membered rings in the reactions of N_2O with dipolarophiles are lacking. The theoretical possibility of this cycloaddition was discussed.[51,52] Bridson-Jones *et al.*[53] suggested that dihydro-1,2,3-oxadiazoles can be formed as intermediates in high-temperature oxidation of alkenes with nitrous oxide.

It should be noted that the non-classical representation of the nitrous oxide molecule as a biradical **D**[47,54] also allows an adequate description of the behaviour of N_2O in chemical reactions.

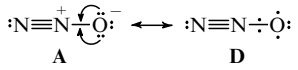

A **D**

Within the framework of the molecular orbital method, this description implies that one-electron delocalisation of the $2p\pi_x$ and $2p\pi_y$ orbitals of O^- results in the fact that electrons occupy the π_x and π_y bonding molecular orbitals which form one-electron π_x(NO) and π_y(NO) bonds and weak partial π_x(NN) and π_y(NN) bonds.

2. Brønsted basicity

Based on the data on the equilibrium constants of several tens gas-phase reactions

$$B_1H^+ + B_2 \rightleftharpoons B_2H^+ + B_1$$

the absolute gas-phase basicity scale for a wide range of compounds from N_2 to *tert*-butylamine was proposed.[55] According to this scale, the proton affinity of nitrous oxide (137.8 kcal mol^{-1}) is comparable with those of methane (130.2 kcal mol^{-1}) and carbon monoxide (141.9 kcal mol^{-1}). Olah *et al.*[44] prepared (and characterised) $MeON_2^+$ by the reaction

$$N_2O + MeF \xrightarrow[-80\ ^\circ C]{SO_2F_2,\ SbF_5} MeON_2^+SbF_6^-,$$

However, the authors did not detect the hydroxydiazonium ion $NNOH^+$ in the reaction of N_2O with superacids.

The protonated form of nitrous oxide in the gas phase was detected by IR spectroscopy.[56] The spectral characteristics were not unambiguously assigned to particular isomers, *viz.*, to $NNOH^+$ or ^+HNNO. Calculations[57,58] demonstrated that protonation of the oxygen atom is more favourable than protonation of the nitrogen atom. However, the results of these calculations depend substantially on the electron correlation methods applied.[59]

3. Physical properties

Nitrous oxide is a colourless diamagnetic gas with a weak pleasant odour and sweetish flavour. It is incombustible but can maintain burning. The nitrous oxide molecule is very stable. In the absence of a catalyst at 400–530 °C, thermal decomposition of N_2O is insignificant (0.22%–0.23%)[60]

$$2N_2O \longrightarrow 2N_2 + O_2.$$

The activation energy E_a of this non-adiabatic spin-forbidden process is ~ 59 kcal mol^{-1}.[61]

Nitrous oxide possesses a high critical temperature. At room temperature under high pressure (50.1 atm, 21 °C), it can exist as a liquid and can be stored in steel cylinders. In laboratory conditions, N_2O is generally prepared either by thermal decomposition of ammonium nitrate or by the reaction of potassium nitrosyl sulfate with sulfuric acid.[61] The physical properties of nitrous oxide are given below.[62–64]

Melting point /°C	−90.86
Boiling point /°C	−88.48
Critical pressure /atm	71.7
Critical temperature /°C	36.5
Critical density /g cm^{-3}	0.452
Density of N_2O (liq) at −88.48 °C /g cm^{-3}	1.226
Density of N_2O (g) at 0 °C /mg cm^{-3}	1.997
Enthalpy of formation ($\Delta_fH^0_{298}$) /kcal mol^{-1}	19.6
Free energy of formation ($\Delta_fG^0_{298}$) /kcal mol^{-1}	24.6
Entropy (S^0) /cal K^{-1} mol^{-1}	52.52
Thermal capacity (C^0_p) /cal K^{-1} mol^{-1}	9.19

IV. Decomposition of nitrous oxide

1. Thermal decomposition

Homogeneous thermal decomposition of nitrous oxide is one of the most extensively studied chemical reactions.[65,66] This process is often used as a model for testing new theories and experimental systems[67] and it is also widely employed for the preparation of atomic oxygen $O(^3P)$.[68]

The following most important elementary stages resulting in decomposition of N_2O are distinguished:

$$N_2O + M \longrightarrow N_2 + O + M, \quad (1)$$

$$N_2O + O \longrightarrow N_2 + O_2, \quad (2)$$

$$N_2O + O \longrightarrow NO + NO, \quad (3)$$

$$N_2O + H \longrightarrow N_2 + {}^{\bullet}OH, \quad (4)$$

$$N_2O + {}^{\bullet}OH \longrightarrow N_2 + HO_2^{\bullet}. \quad (5)$$

From the above-listed equations it can be seen that decomposition of nitrous oxide can occur either as a result of collisions with the third body M [reaction (1)] or through secondary reactions with the oxygen atom or with radical species [reactions (2)–(5)]. The nature of the species M and the character and concentrations of the radical species have an essential effect on this process.

In most of the early investigations, the kinetics of decomposition of nitrous oxide was examined in the presence of argon or nitrogen at 850–1300 °C. However, the formation of nitrous oxide in industrial apparatuses used for denitrification of waste gases and in heating and power plants, which are important anthropogenic contributors of N_2O,[9] occurs at moderately high temperatures (600–900 °C) in complex gas mixtures. The necessity of gaining an insight into the kinetics of these processes gave impetus to investigations of thermal decomposition of N_2O at 600–900 °C in the presence of carbon dioxide, water vapour, hydrogen, methane, oxygen and other gases.[69–71]

2. Heterogeneous catalytic decomposition

A search for new alternative oxidants, on the one hand, and the necessity of the environmental protection aimed at reducing industrial discharge of nitrous oxide to the atmosphere, on the other hand, gave impetus to the development of efficient procedures for catalytic decomposition of nitrous oxide. These procedures were devised primarily by large manufacturers of adipic acid. Thus the BASF, Bayer, DuPont and Asahi companies use catalytic systems for decomposition of N_2O in waste gases,[72] whereas the Solutia company employs recirculation of N_2O to the technological cycle and utilises it as an oxidant for the direct preparation of phenol from benzene.[73]

Problems of a search for efficient catalysts of decomposition of nitrous oxide were covered in an excellent review[25] in which the data on decomposition of N_2O with the use of different heterogeneous catalysts published up to 1996 inclusive have been surveyed and analysed. In the cited review, the mechanism and kinetics of decomposition of N_2O were considered, the role of different oxygen forms occurring on the surface of catalysts was discussed and the problem of catalyst poisoning was touched on. However, a body of the published data in this field increases very rapidly and we believe that it is necessary to survey the data published in 1997–2000 (Table 1).[74–106]

The discovery of isothermal oscillation of concentrations of N_2O, N_2 and O_2 upon decomposition of nitrous oxide on the

Table 1. Catalytic systems for decomposition of nitrous oxide.

Catalyst	Support	Ref.
Catalysts fixed on inert supports		
Cu, Co, Ni, K, Mg, Mn, Ba	C	74–79
Rh, Ru	ZrO_2	81, 82
CuO, Ru, RuO_2	Al_2O_3	88–91
Cu	C, Al_2O_3, SiO_2, ZSM-5	92
Rh	USY, NaY, Al_2O_3, ZrO_2, FSM-16, CeO_2, La_2O_3	96–98
CuO, CoO, Fe_2O_3	SiO_2, MgO, CaO	105
Zeolite catalysts		
[Fe], [Al]–ZSM-22		80
Co, Cu, Fe–ZSM-5		83–87
Oxide catalysts		
CaO, MgO		93–95
Ex-hydrotalcites		
Mg, Co, Ti, Al, La, Rh		99–104
Spinels		
$(Mg_xCo_{1-x})Co_2O_4$		106

Cu–ZSM-5 zeolite catalyst [107] was mentioned in a review.[25] Later, a mechanism was proposed according to which the concentrations of the components change in a wave-like fashion due to cyclic oxidation–reduction of active copper(I) centres responsible for decomposition of N_2O.[108–110] Recently, oscillation of nitrous oxide on the Rh/ZrO_2 (Ref. 111) and Fe–ZSM-5 (Ref. 112) catalysts was observed.

3. Photochemical decomposition

Photochemical decomposition of nitrous oxide affords N_2, O_2, NO and NO_2.[113] Spin-forbidden primary processes (6) and (7) occurring under exposure to light ($\lambda \approx 250$ and 200 nm, respectively) are convenient procedures for the preparation of atomic oxygen in investigations of the kinetics of different reactions in the gas phase.[114, 115]

$$N_2O \xrightarrow{h\nu} N_2 + O(^3P) \quad (6)$$

$$N_2O \xrightarrow{h\nu} N_2 + O(^1D) \quad (7)$$

In recent years, considerable attention has been paid to electronic, vibrational and rotational states of both photofragments, *viz*., N_2 and O,[116, 117] with the aim of giving a comprehensive description of N_2O photolysis.

Great interest was also expressed in photochemical reactions of nitrous oxide in the atmosphere [4] because photolytic decomposition of N_2O is the key process in the conversion of nitrous oxide in the stratosphere.

4. Photocatalytic decomposition

Presently, photocatalysis is the most vigorously evolving line of photochemistry,[118, 119] and this method can be successfully used for decomposition of nitrous oxide. Thus photodecomposition of N_2O under irradiation with UV light ($\lambda < 300$ nm) at room temperature readily proceeds on the surfaces of ZnO,[120] TiO_2,[25] Pt/TiO_2 [121] or Cu–ZSM-5.[122] Copper(I) compounds applied to inert supports,[123] Ag, Cu/TiO_2 [124] or ions of different transition metals in zeolite matrices [125] exhibit high catalytic activities. Possible mechanisms of decomposition, in particular, on zeolites ZSM-5, were discussed.[126, 127] Based on the data from IR and UV spectroscopy, it was concluded [127] that the reaction of N_2O with the Ag^+–ZSM-5 system afforded the Ag^+–N_2O complex whose photoactivation resulted in decomposition of nitrous oxide into N_2 and O_2.

Photodissociation of nitrous oxide on heterogeneous catalysts may be very useful not only in denitrification but also in oxidation or destruction of organic compounds. Photocatalytic degradation of salicylic acid [128] in saturated aqueous solutions of N_2O in the presence of ZnO or ZnO/TiO_2 is an example.

V. Chemistry of nitrous oxide

1. Thermodynamical analysis of the use of N_2O as an oxidant

A change in the Gibbs free energy Δ_rG^0 can be used as a criterion for the possibility of a particular reaction occurring. Thus the reactions can take place and proceed spontaneously if Δ_rG^0 (in kcal mol^{-1}) < 0, whereas in the range of 0–10 kcal mol^{-1}, the reactions are unlikely. This situation calls for further investigation. If $\Delta_rG^0 > 10$ kcal mol^{-1}, the reactions cannot proceed; however, special conditions can help in performing these processes. The Δ_rG^0 value at which the reaction under consideration cannot be carried out depends on many factors and the above-mentioned values can be considered only as a very rough estimate.

The thermochemical data for hypothetical and actual reactions of N_2O with the reagents X or HX, which were calculated as differences between the total changes of the enthalpies ($\Delta_fH^0_{298}$) or the Gibbs free energies ($\Delta_fG^0_{298}$) of formation of the final and starting compounds, are given in Tables 2–5.

$$X + N_2O\,(g) \longrightarrow XO + N_2\,(g),$$

$$2XH + 3N_2O\,(g) \longrightarrow 2XO + 3N_2\,(g) + H_2O\,(g).$$

The required thermodynamical properties of individual compounds were taken from handbooks.[129–133] It should be emphasised once again that the data in Tables 2–5 serve only as a qualitative estimate of the possibility for the reaction to occur. In addition, the above-mentioned data should be compared with each other with caution because the compounds exist in different

Table 2. Changes in the Gibbs free energy of the reactions of nitrous oxide with inorganic compounds.

Substrate (X or HX)	Reaction product (XO)	$\Delta_rH^\circ_{298}$	$\Delta_rG^\circ_{298}$
PCl_3 (g)	$POCl_3$ (g)	−88	−87
CO (g)	CO_2 (g)	−89	−86
SO_2 (g)	SO_3 (g)	−43	−42
NH_3 (g)	NH_2OH (sol)	−34	–
NH_3 (g)	N_2 (g)	−210	−230
H_2O (g)	H_2O_2 (g)	6	5
H_2 (g)	H_2O (g)	−77	−80
Cu (sol)	CuO (sol)	−57	−55

Note. Hereinafter, the values are given in kcal mol^{-1}.

Table 3. Changes in the Gibbs free energy of the reactions of nitrous oxide with some classes of organic compounds.

Substrate (X)	Reaction product (XO)	$\Delta_rH^\circ_{298}$	$\Delta_rG^\circ_{298}$
PhSH (liq)	PhSSPh (liq)	−57	–
Me_2S (g)	Me_2SO (liq)	−58	−50
Me_2SO (liq)	Me_2SO_2 (sol)	−80	−73
MeNC (g)	MeNCO (liq)	−77	–
PhN=NPh (sol)	PhN(O)=NPh (sol)	−42	–
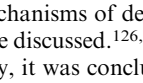	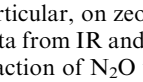	−35	−47

Table 4. Changes in the Gibbs free energy of the reactions of nitrous oxide with aliphatic and aromatic hydrocarbons.

Substrate (X)	Reaction product (XO)	$\Delta_r H^\circ_{298}$	$\Delta_r G^\circ_{298}$
CH_4 (g)	MeOH (g)	−50	−51
MeOH (g)	HCOH (g)	−57	−68
HCOH (g)	HCO_2H (g)	−82	−81
n-C_3H_8 (g)	MeCH(OH)Me (g)	−61	−61
MeCH(OH)Me (g)	$Me_2C(O)$ (g)	−63	−74
Me_3CH (g)	Me_3COH (liq)	−73	−64
Me_3COH (liq)	Me_3COOH (liq)	−4	–
$H_2C=CH_2$ (g)	(g)	−47	−54
$CH_2=CHMe$ (g)	$CH_2=CHCH_2OH$ (g)	−56	−57
$CH_2=CHCH_2OH$ (g)	$CH_2=CHCHO$ (g)	−64	−73
$CH_2=CHCHO$ (g)	$CH_2=CHCO_2H$ (g)	−82	−82
PhH (g)	PhOH (g)	−62	−64
PhMe (liq)	$PhCH_2OH$ (liq)	−61	−59
$PhCH_2OH$ (liq)	PhCHO (liq)	−76	–
PhCHO (liq)	$PhCO_2H$ (sol)	−94	–
$PhCO_2H$ (sol)	$PhCO_3H$ (sol)	−15	–
PhEt (liq)	PhCOMe (liq)	−128	−137
(liq)	(sol)	−82	–
(liq)	(liq)	−59	–

Table 5. Changes in the Gibbs free energy of some reactions involving nitrous oxide.

Reaction type	$\Delta_r H^\circ_{298}$	$\Delta_r G^\circ_{298}$
$4\,Na\,(sol) + 3\,N_2O\,(g) + NH_3\,(g) \rightarrow$ $\rightarrow NaN_3\,(sol) + 3\,NaOH\,(sol) + 2\,N_2\,(g)$	−349	−322
$2\,NaNH_2\,(sol) + N_2O\,(g) \rightarrow$ $\rightarrow NaN_3\,(sol) + NaOH\,(sol) + NH_3\,(g)$	−71	−70
$C_6H_{11}NH_2\,(g) + N_2O\,(g) \rightarrow C_6H_{11}N_3\,(liq) + H_2O\,(liq)$	−27	–
$2\,NH_3\,(sol) + N_2O\,(g) \rightarrow NH_4N_3\,(sol) + H_2O\,(liq)$	−38	−8
$2\,Na_2O\,(sol) + N_2O\,(g) + NH_3\,(g) \rightarrow$ $\rightarrow NaN_3\,(sol) + 3\,NaOH\,(sol)$	−112	–

physical states and the determined Gibbs energies and enthalpies of the initial and final compounds may be inexact.

Therefore, N_2O is potentially a powerful oxidant. However, only the data on high-temperature oxidation of organic substrates on heterogeneous catalysts and several examples of oxidation of some substrates in homogeneous reactions catalysed by transition-metal complexes are available in the literature. Evidently, this inertness is associated with the high activation energy of decomposition of nitrous oxide. Apparently, this problem can be solved by searching for suitable catalysts.

2. The use of N_2O in oxidative catalysis

Considerable progress has been achieved in oxidative catalysis over the latter part of the twentieth century;[134] however, the advances in oxidative hydroxylation of paraffins and aromatic compounds are still poor. Generally, the reactions using atmospheric or molecular oxygen as an oxidant proceed with low selectivity (sometimes these reactions lead to complete oxidation of the substrate). Presently, several major approaches to the solution of this problem are available, *viz*., the employment of membrane-type reactors,[135, 136] the separate performance of reduction and reoxidation of catalyst's surface (two-step process) [137] or the use of alternative oxidants. In the latter case, major hopes are placed on the use of hydrogen peroxide on titanium silicate catalysts [138] and nitrous oxide on ZSM-5 zeolite catalysts.[139]

Two main lines of investigation, *viz*., selective oxidation of aliphatic (aromatic) hydrocarbons and oxidative condensation of lower alkanes, were mentioned in reviews [139, 140] devoted to the employment of N_2O as an oxidant under conditions of heterogeneous catalysis. However, in spite of a large number of studies,[141–151] the latter reaction is, in Krylov's opinion,[152] substantially less useful than other oxidative conversions of hydrocarbons. Actually, direct oxidation reactions of benzene to phenol or of methane to methanol are of importance. Phenol is still prepared by the oxidation of cumene, and methanol is prepared by the conversion of the synthesis gas. A multitude of catalytic systems, including those involving N_2O as an oxidant, *viz*., various metal oxides (mixed solid solutions doped with ions of other metals fixed on inert supports), heteropolyacids and their salts, zeolites, *etc*., were examined in direct oxidation reactions of benzene and methane.[139, 140] Some catalysts of hydroxylation of methane and benzene with nitrous oxide are listed in Table 6. However, attempts to perform the selective conversion of methane to methanol failed.

Table 6. Catalysts of oxidative hydroxylation with the use of nitrous oxide.

Hydrocarbon	Catalytic system	Ref.
Benzene	Fe–Si, $FePO_4$, H–Ga–FER	153, 154
	H, Na, H–[Al], Fe–ZSM-5	156–159
Methane	Fe–Si, $FePO_4$, H–Ga–FER	155
	H, Na, H–[Al], Fe–ZSM-5	160–162
	Sr- or Ca-hydroxyapatites	163, 164
	Mo/SiO_2	165
	12-phosphomolybdic acid	166

The major progress has been achieved in performing the oxidation of benzene to phenol.[167] A new procedure for the synthesis of phenol, which is based on the use of Fe-containing ZSM-5 zeolites and is characterised by high selectivity with respect to both phenol (97%–98%) and nitrous oxide (85%), was developed by researchers from the G K Boreskov Institute of Catalysis of the Siberian Branch of the Russian Academy of Sciences in cooperation with the Solutia company (USA). Successful tests of a pilot plant were performed and the construction of the industrial plant (Pensacola, Florida) rated at 140 thousand tons of phenol per annum is being brought to completion.[168] It should be noted that the results of many investigations in this field were covered by patents.[169–176]

The nature of high catalytic activity of zeolites in oxidation of benzene is the matter of vivid debates. Presently, two major hypotheses are available. One of them is based on a conventional view of zeolites as acid catalysts whose activity is associated with Lewis [156, 159, 177] and (or) Brønsted [178, 179] acidic centres. However, a special investigation [180] did not confirm the hypothesis based on the concept of Brønsted centres.

The second hypothesis was proposed by Panov *et al*.[139, 181] These authors believed that the interaction of N_2O with the surface of Fe-ZSM-5 zeolites afforded a special form of surface oxygen arbitrarily called α-oxygen. In its properties, α-oxygen differs substantially from the known surface forms of oxygen.[182, 183] α-Oxygen cannot be formed upon adsorption of molecular O_2. It was assumed that α-oxygen resembles somewhat active oxygen of monooxygenases for which hydroxylation of C–H bonds is a typical reaction. Quantum-chemical calculations

of the thermodynamical and geometric parameters of the formation of α-oxygen and its successive reactions with benzene or methane were performed.[184, 185]

It was demonstrated[162] that CH_4 reacted virtually quantitatively with the α-form of oxygen, which arose as a result of decomposition of N_2O on Fe-ZSM-5 zeolite, at room temperature. However, the resulting methanol was strongly bound to the zeolite surface and its desorption into the gas phase did not occur. An increase in the temperature to 250–300 °C led to vigorous CO evolution due to secondary conversion of the product.

A search for possible catalysts of selective oxidation of hydrocarbons is not restricted to zeolites. Different research groups made efforts to search for a means of activation of C–H bonds.[186] Wang *et al.*[187] succeeded in performing oxidative carbonylation of methane on $Rh/FePO_4$ at 300–400 °C in the presence of CO and nitrous oxide to form MeOH, $MeCO_2H$ and $MeCO_2Me$. Partial oxidation of methane with nitrous oxide under conditions of plasma discharge[188] gave rise to HCHO and MeOH in a total yield of 10%, which is comparable with the results obtained with the use of the best catalytic systems.

On the whole, the problem of direct oxidation of methane to form methanol, in spite of efforts made, is still far from solution.

3. Oxidation reactions involving N_2O

As mentioned above, nitrous oxide is a potentially strong oxidant, but it is very inert for kinetic reasons. Under mild conditions, N_2O reacts only with highly reactive compounds, such as organoboranes,[189] silaethenes[190] or disilenes.[191]

$$BEt_3 + N_2O \xrightarrow[-15\ ^\circ C]{C_6H_{14}} N_2 + (Et_2B)_2O + C_2H_4 + H_2O$$

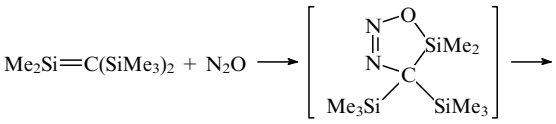

$$\longrightarrow (Me_2SiO)_n + (Me_3Si)_2CN_2$$

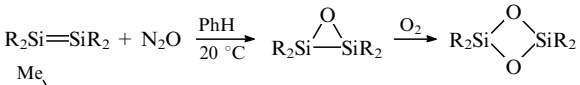

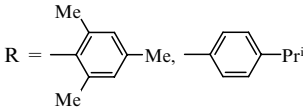

In the absence of a catalyst, N_2O does not react with alkanes, arenes, amines, esters and aliphatic alcohols even at 200–300 °C and 100–500 atm.[53] Under these conditions, alkenes and alkynes form predominantly carbonyl compounds.[192, 193]

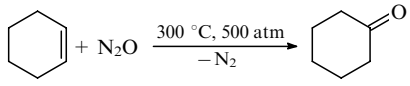

The reactions of nitrous oxide with a solution of triethyl phosphite or cyclohexyl isocyanide in benzene (20 atm, 130 °C) afforded triethyl phosphate (80%) or cyclohexyl isocyanate (20%), respectively.[194] A series of oxides of tertiary phosphines were prepared in quantitative yields[195] with the use of nitrous oxide in the supercritical state (100–140 atm, 60–100 °C).

The reaction of N_2O with nitrogen trifluoride in the presence of an excess of SbF_5 gave rise to $NF_2O^+Sb_2F_{11}^-$ whose vacuum pyrolysis afforded NF_3O.[196] Until recently, procedures for the preparation of NF_3O by direct chemical oxo transfer from an O-donor to NF_3 were lacking.

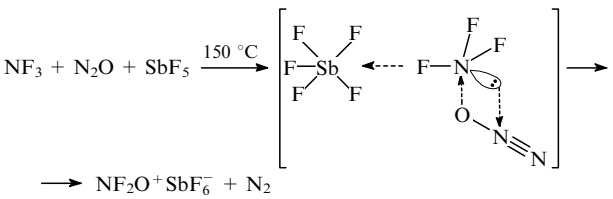

Oxidation of aqueous solutions of alcohols, amines and ethers with nitrous oxide in the presence of Pt or Pd black proceeds according to a radical mechanism.[197] It is assumed that reductive decomposition of N_2O adsorbed on platinum gives rise to N_2 and the $Pt(^{\bullet}OH)$ radicals, which are strong electrophilic oxidants.

$$Me_2CHOH + Pt(^{\bullet}OH) \longrightarrow Me_2\dot{C}OH + H_2O + Pt,$$

$$Pt(N_2O) + Me_2\dot{C}OH \longrightarrow N_2 + Me_2CO + Pt(^{\bullet}OH).$$

On the whole, activation of N_2O is generally a necessary condition for its involvement in oxidation as the oxo donor.

4. Reactions with nucleophilic reagents

The reactions of N_2O with melts of amides of alkali metals and alkaline-earth metals giving rise to the corresponding azides are among the most important reactions of nitrous oxide with nucleophilic reagents.[50] Since sodium azide is rather stable, it serves as the starting compound for the preparation of other azides, and this reaction provides the basis for the industrial production of NaN_3.[198]

$$2NaNH_2 + N_2O \longrightarrow NaN_3 + NaOH + NH_3.$$

Sodium azide is also formed in the reaction of N_2O either with Na in liquid ammonia

$$4Na + 3N_2O + NH_3 \longrightarrow NaN_3 + 3NaOH + 2N_2,$$

or with sodium oxide[61]

$$2Na_2O + N_2O + NH_3 \xrightarrow{110-190\ ^\circ C} NaN_3 + 3NaOH.$$

The reaction of N_2O with ammonia over the $Ni-Al_2O_3$ catalyst afforded ammonium azide[63]

$$2NH_3 + N_2O \xrightarrow{Ni-Al_2O_3} NH_4N_3 + H_2O.$$

Diazo transfer from nitrous oxide to anions of different anilines was carried out (2–5 atm, 20 °C)[199] and the corresponding aryl azides were isolated (10%–35%).

The reaction of N_2O with the monolithium derivative of 1,1-dibenzylhydrazine (**1**) proceeded successively through the formation of *N*-azidoamine **2** and *N*-nitrene **3**.[200]

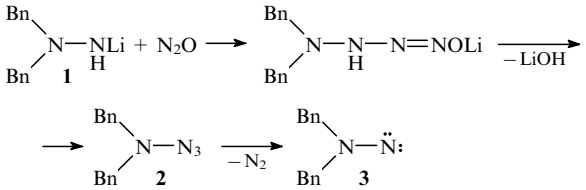

1,2-Diphenylethane (12%) and *N*,*N*-dibenzylbenzalhydrazone (11%) were identified as the major products of the above reaction.

The reactions of N_2O with phosphorus ylide $Ph_3P^+CH_2^-$ (see Ref. 201) or with MeLi[202] gave rise to diazomethane (in 25% or 70% yields, respectively). It should be noted that, with rare exceptions, the reactions of nitrous oxide with anions of organolithium compounds afforded mixtures of *N*- and *O*-products due to the ambidentate character of the former. In addition, the possibility of direct oxidation of organometallic compounds with nitrous oxide must not be ruled out. Based on the results of investigations into the reactions of N_2O with different organolithium compounds, two pathways were proposed.

Pathway *a* (see Ref. 203)

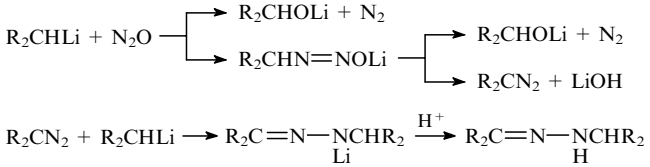

Pathway *b* (see Refs 204, 205)

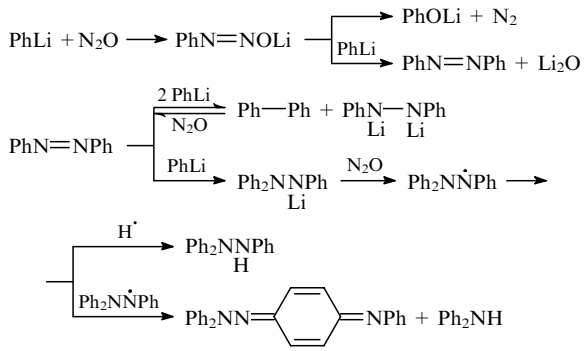

To our knowledge, the procedure for the preparation of diazoferrocene (**4**) (the yield was 25%) developed by Nesmeyanov *et al.*[206] is the only example of the successful application (from the synthetic standpoint) of diazo transfer involving nitrous oxide.

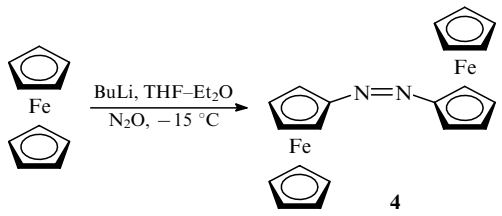

4

Recently, this procedure was used for the preparation of N=N-bonded ferrocene oligomers.[207, 208]

Grignard reagents, unlike organolithium compounds, do not react with nitrous oxide.[203] However, it was demonstrated [209] that the reaction of PhMgBr with N_2O in the presence of CuCl (10 mol.%) afforded small amounts of PhN=NPh (2%) and Ph_2NH (1%). Previously, it has been found [210] that organocalcium analogues of Grignard reagents, for example, PhCaI, reacted with N_2O to yield azobenzene (8%), biphenyl (10%) and traces of benzidine, phenol and hydrazobenzene.

The potential of this reaction as a new procedure for the formation of C–N bonds was examined. [211] It appeared that the yields and the ratio of the reaction products depend substantially on the solvent and the type of substitution in the benzene ring. The maximum yield of azobenzene (60%) was achieved in dimethoxyethane. However, substantial amounts of biphenyl obtained as a by-product impair the synthetic significance of this reaction. The reaction of N_2O with Ph_2Ca afforded azobenzene as the major product (10%).[211] This provides evidence that PhN=NPh can be formed by the direct insertion of N_2O at the R–M–R bond, and not just by the reaction of diazotate R–N=N–OM with the second R–M molecule, as has been suggested previously.[210]

5. Reactions with metal-complex compounds

Nitrous oxide can act as the oxo donor in reactions with metal-complex compounds. The pioneering studies in this field were performed by Bottomley *et al.*[212–218] The authors used N_2O as an oxidant for the synthesis of a series of oxometallocenes with terminal and(or) bridging oxygen atoms, such as oxocyclopentadienyl derivatives of titanium,[213, 214] chromium [215, 216] and vanadium.[217, 218]

Generally, the reactions of low-valence cyclopentadienyl derivatives of transition metals with N_2O afford oxometallocenes containing the central metal atom in an intermediate oxidation state, whereas the reactions with O_2 give rise to oxo clusters containing the metal atoms in the highest oxidation state.[212] Thus oxidation of dicyclopentadienylchromium with oxygen [212] or nitrous oxide [216] afforded two different derivatives, *viz.*, **5** and **6**, respectively.

$$2(\eta\text{-}C_5Me_5)_2Cr + 2O_2 \longrightarrow [(\eta\text{-}C_5Me_5)Cr(O)(\mu\text{-}O)]_2 + (C_5Me_5)_2,$$

5

$$4(\eta\text{-}C_5Me_5)_2Cr + 4N_2O \longrightarrow [(\eta\text{-}C_5Me_5)Cr(\mu_3\text{-}O)]_4 + 4N_2 + 2(C_5Me_5)_2.$$

6

From Bottomley's standpoint [212] this fact cannot be explained only by thermodynamical reasons [the energy of the N–O (D^0_{298}) bond in N_2O is ~ 40 kcal mol^{-1} and the energy of the O–O bond in O_2 is 119 kcal mol^{-1}].[133] The difference in the structures of oxometallocenes should be determined by the reaction mechanisms, which are poorly understood so far because of their complexity. The reactions of titanocene and vanadocene [219] with nitrous oxide proceeded through the formation of the monomers $[(\eta\text{-}C_5Me_5)_2]M(O)$ (M = Ti or V) whose decomposition afforded the oxo clusters $[(\eta\text{-}C_5Me_5)M_4(\mu\text{-}O)_6]$.

More recently, many researchers used nitrous oxide along with conventional oxo donors (PyO, $OPPh_3$, Me_2SO or O_2) for the preparation of different terminal (bridging) oxo metal complexes. Thus the reactions of N_2O with the tetraaza[14]annulene–Sn(II) complex,[220] $U(OC_6H_3Bu^t_2\text{-}2,6)_3$ (see Ref. 221) and $V[(Me_3SiNCH_2CH_2)_3N]$ [222] were reported. Cyclopentadienyl derivatives of uranium,[223] samarium,[224] zirconium [225, 226] and hafnium [227] also reacted with nitrous oxide to give oxo compounds. The heterobinuclear zirconium–iridium oxo complex **7** was prepared.[228]

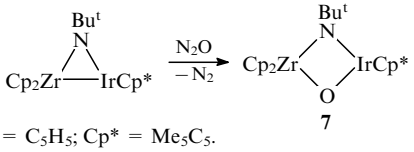

7

Cp = C_5H_5; Cp* = Me_5C_5.

The reactions of N_2O with metal complexes can be accompanied by insertion of the former at the $(L_n)M-R$ bond. Generally, these reactions afford compounds of the $(L_n)MOR$ type as the final products. However, intermediate complexes **8** containing the nitrous oxide molecule were isolated and characterised in the case of titano- [229] and zirconocene [230, 231] systems.

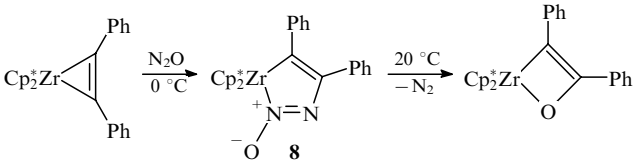

8

Nickel compounds reacted with N_2O to form stable alkyl(aryl)oxy complexes **9** and **10**.[232–234]

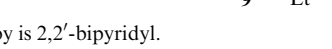

9

bipy is 2,2′-bipyridyl.

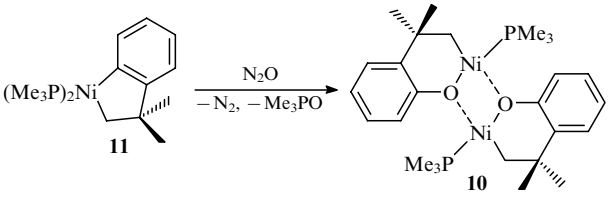

11 **10**

It was proposed [232] that the reaction with nickel complex **11** proceeded *via* intermediates analogous to the zirconium complexes **8**.

The insertion of N_2O at the $(L_n)M-R$ bond giving rise to the $(L_n)MOR$ compounds was described for the complexes of Hf [235] and Ru.[236, 237]

The reactions of nitrous oxide with some metal complexes proceed according to unique mechanisms. Thus the molybdenum complex **12** is the only known metal complex, which can cleave the N–N bond in the N_2O molecule.[238]

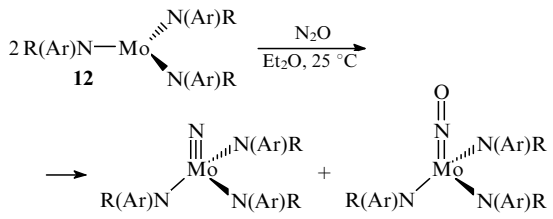

R = $C(CD_3)_2Me$; Ar = $C_6H_3Me_2$-3,5.

Based on the results of calculations, it was suggested [239] that the reactions of this complex with N_2O and N_2 proceed by different mechanisms, *viz*., by bimolecular and monomolecular mechanisms in the cases of nitrous oxide and N_2, respectively.

Two different complexes were obtained in the reactions of iridabenzenes **13a**,**b**, which differ by the substituents in the phosphine ligands.[240]

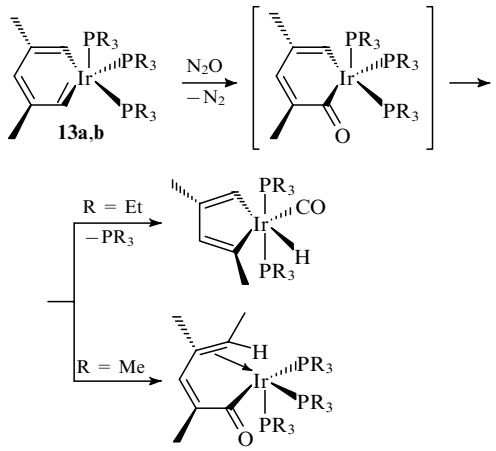

R = Et (**a**), Me (**b**).

It was found [241] that the reactions of the $[Cr(OCP)Li_2(THF)_4]$ complex (OCP is octaalkylcalix[4]pyrrole) with N_2O gave rise to two different oxygen-containing products depending on the solvent used.

6. Metal-complex catalysis of oxo transfer

Apparently, the high activation energy of decomposition of N_2O (E_a = 59 kcal mol^{-1}) [61]

$$N_2O\,(g) \longrightarrow N_2\,(g) + O\,(g)\,(^1D), \quad \Delta H^\circ = 85 \text{ kcal mol}^{-1},$$

$$N_2O\,(g) \longrightarrow N_2\,(g) + O\,(g)\,(^3P), \quad \Delta H^\circ = 40 \text{ kcal mol}^{-1},$$

is the only factor that prevents the wide use of nitrous oxide as an oxo donor. Powerful inexpensive nitrous oxide, which can be readily removed from the reaction medium and does not introduce impurities, could be a valuable oxidant. A search for suitable catalysts of N_2O decomposition seems to be the most promising way of solving this problem. Oxo transfer from the reagent to the substrate under the action of metal-complex catalysts is used in various reactions.[242] Acyl(alkyl) peroxides, molecular oxygen, amine *N*-oxides, hydrogen peroxide and aryliodoso compounds are most popular oxo donors. Attempts to use nitrous oxide have also been undertaken, but no noticeable success has been achieved. Generally, elimination of the O atom from N_2O either gives rise to oxo derivatives of complexes which cannot participate in the catalytic cycle for various reasons, or leads to the oxidation of ligands involved in the coordination sphere about the metal atom.

Thus the use of N_2O in the catalytic cycle of oxidation of PPh_3 to form Ph_3PO in the presence of $HCo(N_2)(PPh_3)_3$ was reported.[243] The following reaction scheme was proposed:

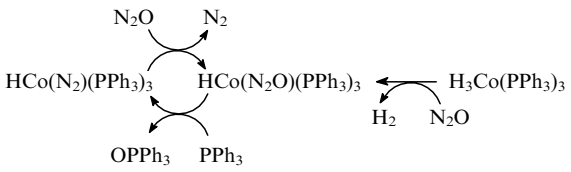

Oxidation of carbon monoxide is catalysed by carbonyl complexes of Rh,[244] Ru, Os or Fe.[245]

$$N_2O + CO \xrightarrow{cat} N_2 + CO_2.$$

It was suggested [245] that the reactions in the [Rh]–CO–N_2O and [Fe]–CO–N_2O systems proceeded through different mechanisms. In the case of rhodium complexes, the catalytic cycle involves one-electron transfer from $[Rh(CO)]^-$ to N_2O yielding $N_2O^{-\bullet}$, its capture by the $[Rh_4(CO)_{11}]^{2-}$ anion and subsequent elimination of N_2 and CO_2 (the fragment **A** of the resulting cluster **14** is shown).

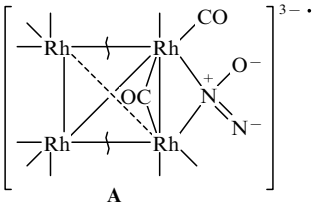

A

$$[Rh(CO)_4] + N_2O \rightleftharpoons [Rh(CO)_4]^\bullet + N_2O^{-\bullet}$$

$$[Rh_4(CO)_{11}]^{2-} + N_2O^{-\bullet} \longrightarrow [Rh_4(CO)_{11}(N_2O)]^{3-\bullet} \longrightarrow$$

14

$$\longrightarrow [Rh_4(CO)_{10}]^{3-\bullet} + N_2 + CO_2$$

In the presence of iron carbonyls, the nucleophilic attack of N_2O on the reactive intermediates occurs giving rise to an intermediate adduct **15**.

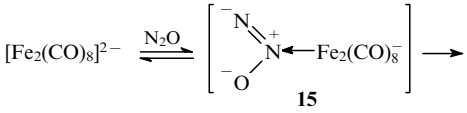

15

$$\longrightarrow [Fe_2(CO)_7]^{2-} + CO_2 + N_2$$

It should be mentioned that molecules which are incorporated into complexes and can regenerate these complexes in the catalytic cycle serve as substrates in the above-considered oxidation reactions involving N_2O. These reactions are not versatile, which impairs their practical significance. Oxidation of CO [246, 247] and PR_3,[248] which are incorporated into metal complexes, with nitrous oxide beyond the catalytic cycle is also documented. The reactions of nitrous oxide with cyclopentadienyl complexes of cobalt at 130 °C resulted in their decomposition to form the corresponding furans and but-2-ene-1,4-dials.[249]

Oxo transfer from N_2O to triphenylphosphine in the presence of $[(CN)_5Mo(O)](PPh_4)_3$ proceeded through the formation of $[(CN)_4Mo(O)_2]^{2-}$ (**16**), the latter serving as an oxidant.[250]

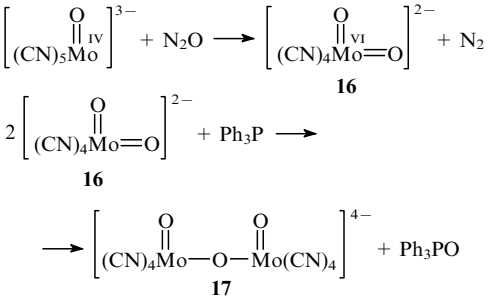

16

17

However, the reaction of the dioxo complex **16** with the substrate afforded compound **17**, which cannot be involved in subsequent reactions, and these reaction cannot be performed in the catalytic mode. Triphenylphosphine was oxidised with nitrous oxide in an autoclave at 80 °C in the presence of phthalocyanine complexes of Al and Cu.[251]

In the studies cited, the possibility of the use of N_2O as the oxo donor in reactions catalysed by metal complexes was merely mentioned. However, a series of investigations in which N_2O was used in the catalytic cycle were published in recent years. Thus it was demonstrated [252] that Ru(II)(TMP)$(THF)_2$ (TMP is tetramesitylporphyrin) reacted with nitrous oxide under mild conditions. The reaction of the resulting complex, *viz.*, of *trans*-Ru(VI)$(O)_2$(TMP), with styrene afforded finally the starting Ru(II) complex and oxirane, thus closing the catalytic cycle. Yamada *et al.*[253] examined the possibility of activation of nitrous oxide with some low-valent transition-metal complexes. Oxidation of PPh_3 was used as the model reaction in the presence of acetylacetonates of the corresponding metals as precatalysts. It was found that Co- and Ni-containing compounds exhibit high activities. The reactions were carried out in the presence of 20 mol.% of metal acetylacetonate and 40 mol.% of diisobutylaluminium hydride under atmospheric pressure of N_2O.

$$Ph_3P \xrightarrow[N_2O,\ 20\ ^\circ C,\ PhMe]{M(acac)_n,\ Bu^i_2AlH} Ph_3PO$$

$M(acac)_n$	$Co(acac)_2$	$Ru(acac)_3$	$Fe(acac)_3$	$Pd(acac)_2$	$Ni(acac)_2$
Yield Ph_3PO (%)	98	43	18	0	89

VI. Applied aspects of the chemistry of nitrous oxide

1. Reduction in protic media

Reduction of nitrous oxide with a copper-containing enzyme, *viz.*, N_2O reductase, is one of the stages of microbiological denitrification [254]

$$NO_3^- \longrightarrow NO_2^- \longrightarrow NO \longrightarrow N_2O \longrightarrow N_2,$$

which, in turn, together with nitrogen fixation and nitrification comprise the global biogeochemical cycle of nitrogen in nature. At the same time, nitrous oxide can serve as a substrate both for natural nitrogenases [255,256] and for synthetic protic nitrogen-fixing systems.[257]

$$N_2O + 2e^- + 2H^+ \longrightarrow N_2 + H_2O.$$

It was demonstrated [258] that N_2O reacts also with aprotic synthetic nitrogen-fixing compositions.

$$Li-Me_3SiCl-MCl_n + N_2O \xrightarrow[-LiCl]{THF,\ 20\ ^\circ C,\ 24\ h} \longrightarrow [M{-}N(SiMe_3)_n] + (Me_3Si)_3N + Me_3SiOSiMe_3$$

M = Cr, Fe, Co, Ti.

A number of other metal-containing enzymes (CO dehydrogenase [259] and methionine synthetase [260]) also react with nitrous oxide.

Aqueous solutions of strong reductants, such as $CrCl_2$, can also reduce nitrous oxide [261] although this reduction proceeds very slowly. The rate constant of this reaction increases more than 10^8 times if nitrous oxide is present as a ligand in the $[Ru(NH_3)_5(N_2O)]^{2+}$ complex.[262] This complex, which was isolated in its individual state as salts with PF_6^- or BF_4^-,[263] is presently the only known stable metal complex containing N_2O as a ligand. The mode of coordination of nitrous oxide in this complex is not finally established;[264] however, according to calculations,[265] the Ru–NNO mode of bonding is preferential.

The reactions of N_2O with solutions of some transition-metal compounds were investigated.[266] In particular, it was demonstrated that the reduction of N_2O in aqueous solutions with potassium borohydride was catalysed by cobalt complexes $Co(bipy)_3(ClO_4)_3$ and $Co(DMG)_2PyCl$ (DMG is dimethylglyoxime) and by vitamin B_{12}.

$$Co(I) + N_2O \longrightarrow Co(II) + N_2.$$

In the absence of a reductant, vitamin B_{12} is oxidised by N_2O according to the following scheme

$$Cob(I)alamin + N_2O + H_2O \longrightarrow Cob(III)alamin + N_2 + 2OH^-,$$

$$Cob(I)alamin + Cob(III)alamin \longrightarrow 2Cob(II)alamin.$$

The discovery of this reaction, which proceeds both *in vitro* and *in vivo*, was of importance for anaesthetics and hematology.[267]

Tetraaza[14]annulene compounds of Ni(I) and Cu(I) also proved to be capable of reducing N_2O in the two-electron mode.[268] The Ni(II)Ann complex (Ann is tetraaza[14]annulene) was subsequently used as a catalyst of electrochemical reduction of nitrous oxide and showed high efficiency and chemical stability.[269]

Reduction of N_2O in aqueous solutions is a thermodynamically favourable process. However, in most cases the reactions in the absence of a catalyst proceed very slowly for kinetic reasons.

2. Electrocatalytic reduction

Presently, electrochemical processes are successfully used both in the synthesis of a great variety of compounds and in environmentally safe technological processes.[270,271] It is known that N_2O along with Freons plays a crucial role in the destruction of stratospheric ozone and hence maximum effort is expended to decrease its discharge to the atmosphere. As mentioned above, high-temperature catalytic processes are most often used for the neutralisation of nitrogen oxides. However, electrochemical reduction of nitrous oxide has advantages over thermal destruction because the former process is not accompanied by the formation of by-products, *viz.*, NO_x. Reduction of N_2O to molecular nitrogen is thermodynamically favourable.

$$N_2O + 2H^+ + 2e^- \longrightarrow N_2 + H_2O,\ E^\circ = +1.77\ V.$$

The kinetics of electrochemical reduction on platinum electrodes in alkaline [272] and acidic [273,274] solutions was examined by cyclic voltammetry. A model was proposed [273,274] according to which adsorbed hydrogen plays the key role in reduction of N_2O.

$$N_2O\ (ads) + H\ (ads) \longrightarrow N_2\ (g) + OH\ (ads).$$

On the other hand, Ahmadi *et al.*[275] believed that decomposition of adsorbed nitrous oxide is the limiting stage of this process.

$$Pt-N_2O\ (ads) \longrightarrow N_2\ (g) + Pt-O.$$

The stage of subsequent reduction on the electrode, on the contrary, proceeds very rapidly.

$$Pt-O + 2H^+ + 2e^- \longrightarrow Pt + H_2O.$$

Electrochemical reduction of N_2O on other metal [276,277] and semiconducting oxide [278,279] electrodes was investigated. With Au, Pd, Cu, Ag, ZnO or In_2O_3, high current efficiency was achieved.

Tetraaza[14]annulene-nickel complexes,[269,280] cobalt porphyrins,[281,282] myoglobin [283] and iron–molybdenum complexes [284] fixed on graphite electrodes can be used as catalysts of electrochemical reduction of nitrous oxide.

A possibility of performing the destruction of NO_x on a cathode under conditions of a gas diffusion electrode seems to be promising. Both platinum [285] (or modified platinum [286,287]) electrodes and electrodes prepared from other transition metals [288] are employed as cathodes. In all cases, reduction of N_2O to N_2

proceeds smoothly without the formation of by-products. In addition, it was demonstrated [285] that N_2O-H_2 (1 M KOH) fuel cells can be used as chemical sources of electrical current.

Catalytic reduction of N_2O with atomic hydrogen was successfully carried out in a special electrochemical membrane-type reactor.[289] Reduction of nitrous oxide with carbon monoxide was also performed in an electrolytic cell supplied with a solid oxide electrolyte.[290]

Considerable attention is given to the development of electrochemical methods for the analysis of nitrous oxide in liquids.[291, 292] These methods, unlike chromatographic methods, allow one to monitor changes in the N_2O content on-line. Undoubtedly, these gas analysers will find wide use in medicine, food industry and systems of environmental monitoring.

3. Radiation-induced reactions in aqueous media

Ionising radiation in water induces processes giving rise to radicals, ions and stable species:[293]

Product of water radiolysis	$^{\bullet}OH$	$^{\bullet}H$	e^-_{aq}	H_2	H_2O_2	H_3O^+
Radiochemical yield G /μmol J^{-1}	0.29	0.06	0.29	0.04	0.08	–

In aqueous solutions saturated with N_2O, solvated electrons e^-_{aq} react with nitrous oxide to give the $^{\bullet}OH$ radicals, the total radiochemical yield [$G(^{\bullet}OH)$] of the latter being increased to ~ 0.58 μmol J^{-1}.

$$N_2O + e^-_{aq} \longrightarrow {}^{\bullet}OH + N_2 + OH^-.$$

This procedure for the generation of hydroxyl radicals, which are powerful electrophilic oxidants, is rather widely used in the laboratory practice.[294, 295] In addition, the ability of N_2O to react with solvated electrons attracts attention of researchers engaged in the application of ionising radiation to purification of sewage. It is well known that radiation treatment (cathode-ray or gamma radiation) in combination with other chemical or biological methods for the purification of liquid waste often proves to be convenient for the decomposition of harmful impurities.[296] The efficiency of this purification can be improved by introducing compounds which transform water radiolysis products to radicals acting as reductants (oxidants).[297, 298] Bubbling of nitrous oxide through sewage may improve the efficiency of the purification process.[299] However, the presence of N_2O sometimes substantially impairs the efficiency of this process.[298]

Not only gamma radiators or cathode-ray accelerators, but also ultrasonic probes and UV lamps can be employed as sources of ionising radiation. Thus photoinduced oxidation of aqueous solutions of Am(III),[300] Np(IV), Pu(IV),[301] aliphatic alcohols [302] and amino acids [303] saturated with nitrous oxide was reported. Shilov *et al.*[304] demonstrated that $\sim 35\%$ of Np(V) existing as a suspension of its hydroxide in 1 M LiOH solution saturated with N_2O was converted into Np(VII) upon sonication (44 KHz) for 40 min.

Oxidation of organic substrates with nitrous oxide under the action of ionising radiation can occur both in the gas phase [305] and in non-aqueous media.[306]

4. Nitrous oxide oligomers as potential high-energy materials

Semiempirical calculation procedures are finding increasing application in the search for new high-energy fuels and explosives. Before proceeding to the development of procedures for the synthesis of this type of compound, calculations are performed to elucidate whether conditions necessary for the preparation of the desired high-energy compound are fulfilled.

In a series of studies, calculations for hypothetical nitrous oxide oligomers were performed. Thus, Vol'pin *et al.*[307] examined the possibility of the existence of the cyclic trimer $(N_2O)_3$ (**18**). The heats of its formation (ΔH_0) calculated by different methods are given in Table 7.

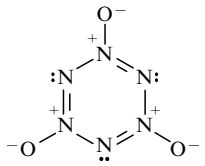

18

The potential barrier to the $(N_2O)_3 \rightarrow 3\,N_2O$ decomposition reaction of the benzene-like molecule **18** (the ΔE_a value varies from 33 to 85 kcal mol^{-1}) is rather high, and it could exist due to kinetic stability.

Selected geometric and thermodynamical parameters (see Table 7) of the hypothetical cyclic structure N_4O_2 (**19**) were discussed.[308, 309]

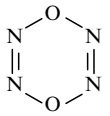

19

Jones [308] believed that the N_4O_2 molecule is planar (the symmetry group D_{2h}). However, Manaa and Chabalowski [309] reasoned that this conformation is only intermediate one between two equivalent boat conformations (the symmetry C_{2v}). According to the calculations performed by these authors, the potential barrier to this transformation is approximately 7–10 kcal mol^{-1}.

Table 7. Heat of formation ΔH_0 of nitrous oxide cyclic oligomers.

Oligomer	ΔH_0 /kcal mol^{-1}						Ref.
	MINDO/3	MNDO	AM1	DZPSCF	MP_2	QCSISD	
18	−17	−48	−155				307
19	−48.5	−3.2	−82.0				308
				−86.3	−100.5	−78.5	309

The assumed structures and properties of open-chain,[310] crown-like [311] and $(NO)_3$-grafted [312] nitrous oxide oligomers were considered with the use of *ab initio* calculations. Jones and Csizmadia [310–312] believed that the occurrence of such metastable compounds is quite possible. The authors reasoned that high pressures, which have become accessible in recent years, can provide a decrease in the activation energy necessary for polymerisation of nitrous oxide and favour the formation of these unusual structures.

It should be noted that the $(N_2O)_n$ polymers in the form of ionic clusters [313, 314] or weakly bound complexes [315, 316] have long been known. However, these systems are of no interest as high-energy compounds. Thus the trimer of nitrous oxide, which has been observed in a molecular beam by IR spectroscopy,[315] exists as a non-planar acyclic weakly bound molecular complex characterised by the energy of dissociation into monomers equal to ~ 3.5 kcal mol^{-1}.

5. Nitrous oxide in the supercritical state

In the late 1980's, liquids in the supercritical state rekindled interest owing to their unique properties and unusual sensitivity with respect to small changes in the state parameters. The major fields of their application are supercritical liquid extraction,[317] chromatography [318] and synthetic chemistry.[319, 320]

Nitrous oxide in the supercritical state [N_2O(sc)] is more polar than CO_2(sc), which allows one to use the former with greater success both for extraction of different organic compounds [321, 322] and as a mobile phase in chromatography.[323, 324] In the synthetic chemistry, N_2O(sc) can be employed either as a reagent [195] or as a solvent.[325] Oxidation of tertiary phosphines with N_2O(sc) or with

the $N_2O(sc)/CO_2(sc)$ mixture was performed.[195] However, attempts to oxidise other classes of organic compounds, including compounds sensitive to oxidation by atmospheric oxygen, such as aldehydes, failed.[195] Poh *et al*.[195] reported that secondary alcohols can be oxidised under analogous conditions in the presence of palladium black. In addition, in some cases[326, 327] the use of $N_2O(sc)$ in the presence of rather low concentrations of organic compounds led to explosions. This is a serious obstacle to the wide application of $N_2O(sc)$ as a reagent. However, it is believed that the use of co-solvents, two-phase systems or carefully selected conditions can make these reactions less dangerous.

VII. Conclusion

Analysis of the data published over the last fifteen years demonstrated that the majority of studies concerned in one way or another with nitrous oxide have been carried out within the framework of either the environmental chemistry or heterogeneous catalysis. It should be noted that these lines of investigation are closely related.

On the one hand, there is a need to diminish the emission of nitrous oxide by 70% – 80% to stop an increase of its content in the atmosphere. This aim should be aided by employing new selective catalysts of decomposition of nitrous oxide in motor vehicles, heating and power plants and industrial processes. On the other hand, there are grounds to believe that N_2O will be used as one of the major oxidants in industry. Presently, procedures for the preparation of nitrous oxide by direct oxidation of ammonia over a catalyst are being developed.[167, 328, 329]

In our opinion, in the coming years the major efforts will go into the solution of problems associated with catalytic activation (destruction) of N_2O and ecological monitoring of nitrous oxide in the atmosphere.

References

1. J O'Connor *Can. J. Anaesth.* **37** 603 (1990)
2. L M Ziurys, A J Apponi, J M Hollis, L E Snyder *Astrophys. J.* **436** L181 (1994)
3. G Fellenberg *Chemie der Umweltbelastung* (Stuttgart: B G Teubner, 1990)
4. S S Prasad *J. Geophys. Res., Sect. D, Atmos.* **102** 21527 (1997)
5. B Festy *Ann. Pharm. Fr.* **55** 143 (1997)
6. W R Moomaw *Energy Policy* **24** 951 (1996)
7. G C Hegerl, U Cubasch *Environ. Sci. Pollut. Res.* **3** 99 (1996)
8. J Flückiger, A Dällenbach, T Blunier, B Stauffer, T F Stocker, D Raynaud, J-M Barnola *Science* **285** 227 (1999)
9. J C Kramlich, W P Linak *Prog. Energ. Combust. Sci.* **20** 149 (1994)
10. T Rahn, M Wahlen *Glob. Biogeochem. Cycles* **14** 537 (2000)
11. C Kroeze *Sci. Total Environ.* **143** 193 (1994)
12. K Svoboda, J Cermak, M Hartman *Chem. Pap., Chem. Zvesti* **54** 118 (2000)
13. M A Wojtowicz, J R Pels, J A Moulijn *Fuel Process. Technol.* **34** 1 (1993)
14. K H Becker, J C Lörzer, R Kurtenbach, P Wiesen, T E Jensen, T J Wallington *Environ. Sci. Technol.* **33** 4134 (1999)
15. J M Dasch *J. Air Waste Manage. Assoc.* **42** 63 (1992)
16. G De Soete *Rev. Inst. Fr. Petrol.* **48** 413 (1993)
17. A Kasimir, L Klemedtsson, K Berglund, P Martikainen, J Silvola, O Oenema *Soil Use Manag.* **13** 245 (1997)
18. R A Reimer, C S Slaten, M Seapan, M W Lower, P E Tomlinson *Environ. Prog.* **13** 134 (1994)
19. B W Riley, J R Richmond *Catal. Today* **17** 277 (1993)
20. G Centi, S Perathoner, F Vazzana *Chemtech* **29** (12) 48 (1999)
21. R E Dickinson, R J Cicerone *Nature (London)* **319** 109 (1986)
22. J N Armor *Appl. Catal. B* **1** 221 (1992)
23. A J S Mascarenhas, H M C Andrade *React. Kinet. Catal. Lett.* **64** 215 (1998)
24. T W Dann, K H Schulz, M Mann, M Collings *Appl. Catal. B* **6** 1 (1995)
25. F Kapteijn, J Rodriguez-Mirasol, J Moulijn *Appl. Catal. B* **9** 25 (1996)
26. R M Heck *Catal. Today* **53** 519 (1999)
27. R I Kuz'mina, V P Sevost'yanov *Ros. Khim. Zh.* **44** 71 (2000) [a]
28. J Perez-Ramirez, A R Vaccaro, F Kapteijn, J A Moulijn *Chem. Eng. Technol.* **23** 721 (2000)
29. K Yamada, S Kondo, K Segawa *Micropor. Mesopor. Mat.* **35 – 36** 227 (2000)
30. G Centi, F Vazzana *Catal. Today* **53** 683 (1999)
31. K Yamada, C Pophal, K Segawa *Micropor. Mesopor. Mat.* **21** 549 (1998)
32. C Pophal, T Yogo, K Yamada, K Segawa *Appl. Catal. B* **16** 177 (1998)
33. R Burch, P J Millington *Catal. Today* **26** 185 (1995)
34. M Mauvezin, G Delahay, B Coq, S Kieger *Appl. Catal. B* **23** L79 (1999)
35. M Mauvezin, G Delahay, F Kisslich, B Coq, S Kieger *Catal. Lett.* **62** 41 (1999)
36. R Sundararajan, V Srinivasan *Appl. Catal. A* **141** 45 (1996)
37. R R Sadhankar, D T Lynch *J. Catal.* **149** 278 (1994)
38. R R Sadhankar, J Ye, D T Lynch *J. Catal.* **146** 511 (1994)
39. B Coq, M Mauvezin, G Delahay, J-B Butet, S Kieger *Appl. Catal. B* **27** 193 (2000)
40. M Kögel, R Mönnig, W Schwieger, A Tissler, T Turek *J. Catal.* **182** 470 (1999)
41. M Kögel, V H Sandoval, W Schwieger, A Tissler, T Turek *Catal. Lett.* **51** 23 (1998)
42. G Centi, P Generali, L dall'Olio, S Perathoner, Z Rak *Ind. Eng. Chem. Res.* **39** 131 (2000)
43. K N Houk, J Sims, R E Duke Jr , R W Strozier, J K George *J. Am. Chem. Soc.* **95** 7287 (1973)
44. G A Olah, R Herges, K Laali, G A Segal *J. Am Chem. Soc.* **108** 2054 (1986)
45. G M Chaban, N M Klimenko, O P Charkin *Izv. Akad. Nauk SSSR, Ser. Khim.* 126 (1992) [b]
46. K Mogi, T Komine, K Hirao *J. Chem. Phys.* **95** 8999 (1991)
47. R D Harcourt, A Schulz *J. Phys. Chem. A* **104** 6510 (2000)
48. N N Greenwood, A Earnshaw *Chemistry of the Elements* (New York: Pergamon Press, 1984) p. 510
49. H Staudinger, E Hauser *Helv. Chim. Acta* **4** 861 (1921)
50. K Clusius, H Schumacher *Helv. Chim. Acta* **41** 972 (1958)
51. M Su, H Liao, W Chung, S Chu *J. Org. Chem.* **64** 6710 (1999)
52. K N Houk, J Sims, C R Watts, L J Luskus *J. Am. Chem. Soc.* **95** 7301 (1973)
53. F S Bridson-Jones, G D Buckley, L H Cross, A P Driver *J. Chem. Soc.* 2999 (1951)
54. R D Harcourt, N Hall *J. Mol. Struct. (Theochem)* **342** 59 (1995)
55. J E Szulejko, T B McMahon *J. Am. Chem. Soc.* **115** 7839 (1993)
56. T Amano *Chem. Phys. Lett.* **127** 101 (1986)
57. J M L Martin, T J Lee *J. Chem. Phys.* **98** 7951 (1993)
58. J E Rice, T J Lee, H F Schaefer *Chem. Phys. Lett.* **130** 333 (1986)
59. S P Ekern, A J Illies, M L McKee *Mol. Phys.* **78** 263 (1993)
60. G J Hutchings, H Comninos, R G Copperthwaite, L J van Rensburg, R Hunter, T Themistocleous *J. Chem. Soc., Faraday Trans. 1* **85** 633 (1989)
61. F M Rapoport, A A Il'inskaya. in *Laboratornye Metody Polucheniya Chistykh Gazov* (Laboratory Methods of Preparation of Pure Gases) (Moscow: Goskhimizdat, 1963) p. 185
62. *Mellors Comprehensive Treatise on Inorganic and Theoretical Chemistry* Suppl. II, Vol. 8 (London: Longmans, 1957) p. 382
63. K Jones, in *Comprehensive Inorganic Chemistry* Vol. 2 (Eds J C Bailar, H J Emeleus, R Nuholm, A F Trotman-Dickenson) (Oxford: Pergamon Press, 1973)
64. W C Trogler *Coord. Chem. Rev.* **187** 303 (1999)
65. W C Gardiner Jr (Ed.) *Combustion Chemistry* (New York: Springer, 1984)
66. W Tsang, J T Herron *J. Phys. Chem. Ref. Data* **20** 609 (1991)
67. H Nakamura, S Kato *J. Chem. Phys.* **110** 9937 (1999)
68. R G Hynes, J C Mackie, A R Masri *J. Phys. Chem. A* **103** 5967 (1999)
69. G Löffler, V J Wargadalam, F Winter, H Hofbauer *Combust. Flame* **120** 427 (2000)
70. M T Allen, R A Yetter, F L Dryer *Int. J. Chem. Kinet.* **27** 883 (1995)
71. P Glarborg, J E Johnsson, K Dam-Johansen *Combust. Flame* **99** 523 (1994)
72. A Scott *Chem. Week* **160** 37 (1998)
73. M S Reisch *Chem. Eng. News* **76** 19 (1998)

74. J Ma, N M Rodriguez, M A Vannice, R T K Baker *Top. Catal.* **10** 27 (2000)
75. A Dandekar, R T K Baker, M A Vannice *J. Catal.* **183** 131 (1999)
76. Z Zhu, G Q M Lu, Y Zhuang, D Shen *Energ. Fuel* **13** 763 (1999)
77. Z Zhu, S Wang, G Q Lu, D-K Zhang *Catal. Today* **53** 669 (1999)
78. Z Zhu, G Q Lu *J. Catal.* **187** 262 (1999)
79. S A Carabineiro, F B Fernandes, J S Vital, A M Ramos, I F Silva *Catal. Today* **54** 559 (1999)
80. M Kasture, J Krysciak, L Matachowski, T Machej, M Derewinski *Stud. Surf. Sci. Catal.* **125** 579 (1999)
81. G Centi, L Dall'Olio, S Perathoner *Appl. Catal. A* **194 – 195** 79 (2000)
82. F Pinna, M Scarpa, G Strukul, E Guglielminotti, F Boccuzzi, M Manzoli *J. Catal.* **192** 158 (2000)
83. M Rauscher, K Kesore, R Mlnnig, W Schwieger, A Tissler, T Turek *Appl. Catal. A* **184** 249 (1999)
84. M Kögel, V H Sandoval, W Schwieger, A Tissler, T Turek *Chem. Eng. Technol.* **21** 655 (1998)
85. J Wang, N Mizuno, M Misono *Bull. Chem. Soc. Jpn.* **71** 947 (1998)
86. R S da Cruz, A J S Mascarenhas, H M C Andrade *Appl. Catal. B* **18** 223 (1998)
87. F Kapteijn, G Marbán, J Rodriguez-Mirasol, J A Moulijn *J. Catal.* **167** 256 (1997)
88. K W Yao, S Jaenicke, J Y Lin, K L Tan *Appl. Catal. B* **16** 291 (1998)
89. X F Wang, H C Zeng *Appl. Catal. B* **17** 89 (1998)
90. H C Zeng, X Y Pang *Appl. Catal. B* **13** 113 (1997)
91. K Li, X F Wang, H C Zeng *Chem. Eng. Res. Design* **75** 807 (1997)
92. A Dandekar, M A Vannice *Appl. Catal. B* **22** 179 (1999)
93. A Satsuma, R Akahori, M Kato, S Komai, H Yoshida, T Hattori *J. Mol. Catal. A* **155** 81 (2000)
94. A Snis, H Miettinen *J. Phys. Chem. B* **102** 2555 (1998)
95. X Lu, X Xu, N Wang, Q Zhang *J. Phys. Chem. B* **103** 3373 (1999)
96. K Yuzaki, T Yarimizu, K Aoyagi, S Ito, K Kunimori *Catal. Today* **45** 129 (1998)
97. G Centi, A Galli, B Montanari, S Perathoner, A Vaccari *Catal. Today* **35** 113 (1997)
98. J Oi, A Obuchi, G R Bamwenda, A Ogata, H Yagita, S Kushiyama, K Mizuno. *Appl. Catal. B* **12** 277 (1997)
99. J Perez-Ramirez, J Overeijnder, F Kapteijn, J A Moulijn *Appl. Catal. B* **23** 59 (1999)
100. J Perez-Ramirez, F Kapteijn, J A Moulijn *Catal. Lett.* **60** 133 (1999)
101. S Kannan *Appl. Clay Sci.* **13** 347 (1998)
102. J Oi, A Obuchi, A Ogata, G R Bamwenda, R Tanaka, T Hibino, S Kushiyama *Appl. Catal. B* **13** 197 (1997)
103. S Kannan, C S Swamy *Catal. Today* **53** 725 (1999)
104. H Dandl, G Emig *Appl. Catal. A* **168** 261 (1998)
105. R S Drago, K Jurczyk, N Kob *Appl. Catal. B* **13** 69 (1997)
106. U Chellam, Z P Xu, H C Zeng *Chem. Mater.* **12** 650 (2000)
107. H-G Lintz, T Turek *Catal. Lett.* **30** 313 (1995)
108. T Ochs, T Turek *Chem. Eng. Sci.* **54** 4513 (1999)
109. T Turek *J. Catal.* **174** 98 (1998)
110. P Ciambelli, A Di Benedetto, E Garufi, R Pirone, G Russo *J. Catal.* **175** 161 (1998)
111. G Centi, L Dall'Olio, S Perathoner *J. Catal.* **192** 224 (2000)
112. El-M El-Malki, R A van Santen, W M H Sachtler *Micropor. Mesopor. Mat.* **35 – 36** 235 (2000)
113. H Okabe *Photochemistry of Small Molecules* (New York: Wiley, 1978)
114. M Brouard, H M Lambert, J Short, J P Simons *J. Phys. Chem.* **99** 13571 (1995)
115. A J Alexander, F J Aoiz, M Brouard, I Burak, Y Fujimura, J Short, J P Simons *Chem. Phys. Lett.* **262** 589 (1996)
116. D W Neyer, A J R Heck, D W Chandler, J M Teule, M H M Janssen *J. Phys. Chem. A* **103** 10388 (1999)
117. D W Neyer, A J R Heck, D W Chandler *J. Chem. Phys.* **110** 3411 (1999)
118. S C Ameta, R Ameta, J Vardia, R Ameta, Z Ali *J. Indian Chem. Soc.* **76** 281 (1999)
119. M I Litter *Appl. Catal. B* **23** 89 (1999)
120. A A Glebovskii, A A Lisachenko, I F Moiseenko *Zh. Fiz. Khim.* **58** 1116 (1984) [c]
121. A Kudo, T Sakata *Chem. Lett.* 2381 (1992)
122. K Ebitani, M Morokuma, J-H Kim, A Morikawa *J. Chem. Soc., Faraday Trans.* **90** 377 (1994)
123. M Matsuoka, W-S Ju, K Takahashi, H Yamashita, M Anpo *J. Phys. Chem. B* **104** 4911 (2000)
124. A Kudo, H Nagayoshi *Catal. Lett.* **52** 109 (1998)
125. K Ebitani, Y Hirano, A Morikawa *J. Catal.* **157** 262 (1995)
126. K Ebitani, M Morokuma, A Morikawa *Stud. Surf. Sci. Catal.* **84** 1501 (1994)
127. M Matsuoka, W-S Ju, M Anpo *Chem. Lett.* 626 (2000)
128. V Sukharev, R Kershaw *J. Photochem. Photobiol. A* **98** 165 (1996)
129. *Spravochnik Khimika* (Handbook for Chemist) Vol. 1 (Leningrad: Khimiya, 1971)
130. D R Stull, E F Westrum, G C Sinke *The Chemical Thermodynamics of Organic Compounds* (New York: Wiley, 1969)
131. M Kh Karapet'yants, M L Karapet'yants *Osnovnye Termodinamicheskie Konstanty Neorganicheskikh i Organicheskikh Veshchestv* (The Main Thermodynamic Constants of Inorganic and Organic Substances) (Moscow: Khimiya, 1968)
132. J B Pedley, R D Naylor, S P Kirby *Thermochemical Data of Organic Compounds* (London: Chapman and Hall, 1986)
133. D R Lide (Ed.) *CRC Handbook of Chemistry and Physics* (Boca Raton, FL: CRC Press, 1992 – 1993)
134. J M Thomas, K I Zamaraev (Eds) *Perspectives in Catalysis* (Oxford: Blackwell, 1992)
135. K K Sirkar, P V Shanbhag, A S Kovvali *Ind. Eng. Chem. Res.* **38** 3715 (1999)
136. M A Pena, J P Gomez, J L G Fierro *Appl. Catal. A* **144** 7 (1996)
137. L Weismantel, J Stöckel, G Emig *Appl. Catal. A* **137** 129 (1996)
138. J Mlochowski, S B Said *Pol. J. Chem.* **71** 149 (1997)
139. A S Kharitonov, V I Sobolev, G I Panov *Usp. Khim.* **61** 2062 (1992) [*Russ. Chem. Rev.* **61** 1130 (1992)]
140. A Reitzmann, M Häfele, G Emig *Trends Chem. Eng.* **3** 63 (1996)
141. M Bajus, M H Back *Stud. Surf. Sci. Catal.* **119** 289 (1998)
142. A G Anshits, E V Kondratenko, E N Voskresenskaya, L I Kurteeva, N I Pavlenko *Catal. Today* **46** 211 (1998)
143. Y Matsumura, S Sugiyama, H Hayashi, J B Moffat *J. Solid State Chem.* **114** 138 (1995)
144. E N Voskresenskaya, L I Kurteeva, G G Pervyshina, A G Anshits *Catal. Today* **24** 277 (1995)
145. G M Pajonk, T Manzalji *Appl. Catal. A* **108** 41 (1994)
146. A G Anshits, E V Kondratenko, N G Maksimov *Catal. Today* **21** 281 (1994)
147. A G Anshits, V G Roguleva, E V Kondratenko *Stud. Surf. Sci. Catal.* **82** 337 (1994)
148. H Yamamoto, H Y Chu, M T Xu, C L Shi, J H Lunsford *J. Catal.* **142** 325 (1993)
149. C Shi, M Xu, M P Rosynek, J H Lunsford *J. Phys. Chem.* **97** 216 (1993)
150. V G Roguleva, M A Nikiphorova, N G Maksimov, A G Anshits *Catal. Today* **13** 219 (1992)
151. N I Il'chenko, L N Raevskaya, A I Bostan, G I Golodets *Kinet. Katal.* **32** 880 (1991) [d]
152. O V Krylov *Usp. Khim.* **61** 2040 (1992) [*Russ. Chem. Rev.* **61** 1118 (1992)]
153. E Selli, A Isernia, L Forni *Phys. Chem. Chem. Phys.* **2** 3301 (2000)
154. S S Shevade, B S Rao *Catal. Lett.* **66** 99 (2000)
155. Y Wang, K Otsuka *J. Catal.* **171** 106 (1997)
156. M Hifele, A Reitzmann, D Roppelt, G Emig *Appl. Catal. A* **150** 153 (1997)
157. W F Hoelderich *Appl. Catal. A* **194 – 195** 487 (2000)
158. J L Motz, H Heinichen, W F Hölderich *J. Mol. Catal. A* **136** 175 (1998)
159. L M Kustov, A L Tarasov, V I Bogdan, A A Tyrlov, J W Fulmer *Catal. Today* **61** 123 (2000)
160. T Ono, H Kudo, M Anpo *Appl. Catal. A* **194 – 195** 71 (2000)
161. S N Vereshchagin, N P Kirik, N N Shishkina, A G Anshits *Catal. Lett.* **56** 145 (1998)
162. K A Dubkov, V I Sobolev, G I Panov *Kinet. Katal.* **39** 79 (1998) [d]
163. S Sugiyama, K Abe, H Hayashi, Y Matsumura, J B Moffat *J. Mol. Catal. A* **144** 347 (1999)
164. S Sugiyama, K Abe, H Hayashi, J B Moffat *Appl. Catal. A* **183** 135 (1999)
165. A W Sexton, E M Coda, B K Hodnett *Catal. Today* **46** 127 (1998)
166. S S Hong, J B Moffat *Catal. Lett.* **40** 1 (1996)

167. G I Panov, A S Kharitonov *Ros. Khim. Zh.* **44** 7 (2000) [a]
168. A M Thayer *Chem. Eng. News* **76** 21 (1998)
169. US P. 6 156 938 (2000)
170. Eur. P. 889 018; *Chem. Abstr.* **130** 97 164 (1999)
171. US P. 5 892 132; *Chem. Abstr.* **128** 155 809 (1998)
172. US P. 5 874 646 ; *Chem. Abstr.* **128** 142 330 (1998)
173. US P. 5 874 647; *Chem. Abstr.* **128** 155 819 (1998)
174. US P. 5 977 008; *Chem. Abstr.* **128** 155 820 (1998)
175. US P. 5 672 777; *Chem. Abstr.* **127** 320 210 (1997)
176. US P. 5 756 861; *Chem. Abstr.* **124** 120 759 (1996)
177. J L Motz, H Heinichen, W F Hölderich *Stud. Surf. Sci. Catal.* **105** 1053 (1997)
178. R Burch, C Howitt *Appl. Catal. A* **103** 135 (1993)
179. R Burch, C Howitt *Appl. Catal. A* **86** 139 (1992)
180. V I Sobolev, K A Dubkov, E A Paukshtis, L V Pirutko, M A Rodkin, A S Kharitonov, G I Panov *Appl. Catal. A* **141** 185 (1996)
181. V I Sobolev, G I Panov, A S Kharitonov, V N Romannikov, A M Volodin *Kinet. Katal.* **34** 887 (1993) [d]
182. G I Panov, A K Uriarte, M A Rodkin, V I Sobolev *Catal. Today* **41** 365 (1998)
183. G I Panov, V I Sobolev, A S Kharitonov, E A Paukshtis, in *Catalysis of Organic Reactions* (Eds M G Scaros, M L Prunier) (New York: Marcel Dekker, 1995) p. 525
184. K Yoshizawa, T Yumura, Y Shiota, T Yamabe *Bull. Chem. Soc. Jpn.* **73** 29 (2000)
185. K Yoshizawa, Y Shiota, T Yumura, T Yamabe *J. Phys. Chem. B* **104** 734 (2000)
186. A E Shilov, G B Shul'pin *Aktivatsiya i Kataliticheskie Reaktsii Uglevodorodov* (Activation and Catalytic Reactions of Hydrocarbons) (Moscow: Nauka, 1995)
187. Y Wang, M Katagiri, K Otsuka *Chem. Commun.* 1187 (1997)
188. S Tanabe, K Egashira, K Okitsu, H Matsumoto *Chem. Lett.* 871 (1999)
189. P Paetzold, G Schimmel *Z. Naturforsch. B, Chem. Sci.* **35** 568 (1980)
190. N Wiberg, G Preiner, K Schurz *Chem. Ber.* **121** 1407 (1988)
191. H B Yokelson, A J Millevolte, G R Gillette, R West *J. Am. Chem. Soc.* **109** 6865 (1987)
192. F S Bridson-Jones, G D Buckley *J. Chem. Soc.* 3009 (1951)
193. G D Buckley, W J Levy *J. Chem. Soc.* 3016 (1951)
194. T Saegusa, S Kobayashi, Y Ito *Bull. Chem. Soc. Jpn.* **43** 275 (1970)
195. S Poh, R Hernandez, M Inagaki, P G Jessop *Org. Lett.* **1** 583 (1999)
196. K O Christe *J. Am. Chem. Soc.* **117** 6136 (1995)
197. B Ohtani, S-i Takamiya, Y Hirai, M Sudoh, S-i Nishimoto, T Kagiya *J. Chem. Soc., Perkin Trans. 2* 175 (1992)
198. In *Ullmann's Encyclopedia of Industrial Chemistry* Vol. A13 (Weinheim: VCH, 1989) p.194
199. G Koga, J-P Anselme *J. Chem. Soc., Chem. Commun.* 446 (1968)
200. G Koga, J-P Anselme *J. Org. Chem.* **35** 960 (1970)
201. W Rundel, P Kästner *Liebigs Ann.* **686** 88 (1965)
202. E Müller, W Rundel *Chem. Ber.* **90** 1302 (1957)
203. F M Beringer, J A Farr Jr, S Sands *J. Am. Chem. Soc.* **75** 3984 (1953)
204. R Meier *Chem. Ber.* **86** 1483 (1953)
205. R Meier, W Frank *Chem. Ber.* **89** 2747 (1956)
206. A N Nesmeyanov, E G Perevalova, T V Nikitina *Dokl. Akad. Nauk SSSR* **138** 1118 (1961) [e]
207. M Kurihara, M Kurosawa, T Matsuda, H Nishihara *Synth. Met.* **102** 1517 (1999)
208. M Kurosawa, T Nankawa, T Matsuda, K Kubo, M Kurihara, H Nishihara *Inorg. Chem.* **38** 5113 (1999)
209. A V Leont'ev, in *Lomonosov-97 (Tez. Dokl. Mezhdunarod. Konf. Studentov i Aspirantov po Fundamental'nym Naukam. Sektsiya Khimicheskaya), Moskva, 1997*, in [Lomonosov-97 (Abstracts of Reports of International Conference of Students and Post-Graduates on Fundamental Sciences. Chemical Section), Moscow, 1997] p. 160
210. R Meier, K Rappold *Angew. Chem.* **65** 560 (1953)
211. M L Hays, T P Hanusa *Tetrahedron Lett.* **36** 2435 (1995)
212. F Bottomley *Polyhedron* **11** 1707 (1992)
213. F Bottomley, H H Brintzinger *J. Chem. Soc., Chem. Commun.* 234 (1978)
214. F Bottomley, G O Egharevba, I J B Lin, P S White *Organometallics* **4** 550 (1985)
215. F Bottomley, D E Paez, P S White *J. Am. Chem. Soc.* **103** 5581 (1981)
216. F Bottomley, J Chen, S M MacIntosh, R C Thompson *Organometallics* **10** 906 (1991)
217. F Bottomley, D E Paez, P S White *J. Am. Chem. Soc.* **104** 5651 (1982)
218. F Bottomley, C P Magill, B Zhao *Organometallics* **10** 1946 (1991)
219. M R Smith III, P T Matsunaga, R A Andersen *J. Am. Chem. Soc.* **115** 7049 (1993)
220. M C Kuchta, T Hascall, G Parkin *Chem. Commun.* 751 (1998)
221. L R Avens, D M Barnhart, C J Burns, S D McKee, W H Smith *Inorg. Chem.* **33** 4245 (1994)
222. C C Cummins, R R Schrock, W M Davis *Inorg. Chem.* **33** 1448 (1994)
223. J-C Berthet, J-F Le Maréchal, M Nierlich, M Lance, J Vigner, M Ephritikhine *J. Organomet. Chem.* **408** 335 (1991)
224. W J Evans, J W Grate, I Bloom, W E Hunter, J L Atwood *J. Am. Chem. Soc.* **107** 405 (1985)
225. W A Howard, T M Trnka, M Waters, G Parkin *J. Organomet. Chem.* **528** 95 (1997)
226. K McNeill, R G Bergman *J. Am. Chem. Soc.* **121** 8260 (1999)
227. W A Howard, G Parkin *J. Organomet. Chem.* **472** C1 (1994)
228. A M Baranger, T A Hanna, R G Bergman *J. Am. Chem. Soc.* **117** 10041 (1995)
229. G A Vaughan, C D Sofield, G L Hillhouse *J. Am. Chem. Soc.* **111** 5491 (1989)
230. A K List, K Koo, A L Rheingold, G L Hillhouse *Inorg. Chim. Acta* **270** 399 (1998)
231. G A Vaughan, G L Hillhouse, A L Rheingold *J. Am. Chem. Soc.* **112** 7994 (1990)
232. K Koo, G L Hillhouse, A L Rheingold *Organometallics* **14** 456 (1995)
233. P T Matsunaga, J C Mavropoulos, G L Hillhouse *Polyhedron* **14** 175 (1995)
234. K Koo, G L Hillhouse *Organometallics* **17** 2924 (1998)
235. G A Vaughan, P B Rupert, G L Hillhouse *J. Am. Chem. Soc.* **109** 5538 (1987)
236. A W Kaplan, R G Bergman *Organometallics* **17** 5072 (1998)
237. A W Kaplan, R G Bergman *Organometallics* **16** 1106 (1997)
238. A R Johnson, W M Davis, C C Cummins, S Serron, S P Nolan, D G Musaev, K Morokuma *J. Am. Chem. Soc.* **120** 2071 (1998)
239. D V Khoroshun, D G Musaev, K Morokuma *Organometallics* **18** 5653 (1999)
240. J R Bleeke, R Behm *J. Am. Chem. Soc.* **119** 8503 (1997)
241. M Dionne, J Jubb, H Jenkins, S Wong, S Gambarotta *Inorg. Chem.* **35** 1874 (1996)
242. W J Mijs, C R H I deJonge (Eds) *Organic Syntheses by Oxidation with Metal Compounds* (New York: Plenum, 1986)
243. A Yamamoto, S Kitazume, L S Pu, S Ikeda *J. Am. Chem. Soc.* **93** 371 (1971)
244. J-D Lee, W-P Fang, C-S Li, C-H Cheng *J. Chem. Soc., Dalton Trans.* 1923 (1991)
245. C-S Li, K-S Sun, C-H Cheng *J. Chem. Soc., Dalton Trans.* 1025 (1992)
246. C Barrientos, C K Ghosh, W A G Graham, M J Thomas *J. Organomet. Chem.* **394** C31 (1990)
247. F Bottomley, J Darkwa *J. Chem. Soc., Dalton Trans.* 2505 (1988)
248. K A Hall, J M Mayer *J. Am. Chem. Soc.* **114** 10402 (1992)
249. A V Leont'ev, O A Fomicheva, M V Proskurnina, N S Zefirov *Zh. Org. Khim.* **34** 1864 (1998) [f]
250. H Arzoumanian, D Nuel, J Sanchez *J. Mol. Catal.* **65** L9 (1991)
251. A V Leont'ev, O A Fomicheva, M V Proskurnina, N S Zefirov, in *Khimicheskie Reaktivy. Reagenty i Protsessy Malotonnazhnoi Khimii. (Reaktiv-2000) (Tez. Dokl. XIII Mezhdunarod. Nauchno-Tekhnicheskoi Konf.), Tula, 2000* [Chemical Reagents. Reagents and Processes of Low-Tonnage Chemistry (Agent-2000) (Abstracts of Reports of the XIIIth International Scientific and Engineering Conference), Tula, 2000] p. 176
252. J T Groves, J S Roman *J. Am. Chem. Soc.* **117** 5594 (1995)
253. T Yamada, K Suzuki, K Hashimoto, T Ikeno *Chem. Lett.* 1043 (1999)
254. W G Zumft *Microbiol. Mol. Biol. Rev.* **61** 533 (1997)

255. R W F Hardy, F Bottomley, R H Burns (Eds) *A Treatise on Dinitrogen Fixation* (New York: Wiley, 1979)
256. B B Jensen, R H Burris *Biochemistry* **25** 1083 (1986)
257. L A Nikonova, N I Pershikova *Izv. Akad. Nauk SSSR, Ser. Khim.* 711 (1983) [b]
258. O A Mironov, A V Leont'ev, in *Lomonosov-97 (Tez. Dokl. Mezhdunarod. Konf. Studentov i Aspirantov po Fundamental'nym Naukam. Sektsiya Khimicheskaya), Moskva, 1997*, in [Lomonosov-97 (Abstracts of Reports of International Conference of Students and Post-Graduates on Fundamental Sciences. Chemical Section), Moscow, 1997] p. 134
259. W-P Lu, S W Ragsdale *J. Biol. Chem.* **266** 3554 (1991)
260. J T Drummond, R G Matthews *Biochemistry* **33** 3732 (1994)
261. M L Nichols, I A Derbigny *J. Phys. Chem.* **30** 491 (1926)
262. J N Armor, H Taube *J. Am. Chem. Soc.* **93** 6476 (1971)
263. A A Diamantis, G J Sparrow, M R Snow, T R Norman *Aust. J. Chem.* **28** 1231 (1975)
264. F Bottomley, W V F Brooks *Inorg. Chem.* **16** 501 (1977)
265. D F-T Tuan, R Hoffmann *Inorg. Chem.* **24** 871 (1985)
266. R G S Banks, R J Henderson, J M Pratt *J. Chem. Soc., A* 2886 (1968)
267. E Eger (Ed.) *Nitrous Oxide/N_2O* (New York: Elsevier, 1985)
268. A M Tait, M Z Hoffman, E Hayon *Inorg. Chem.* **15** 934 (1976)
269. I Taniguchi, T Shimpuku, K Yamashita, H Ohtaki *J. Chem. Soc., Chem. Commun.* 915 (1990)
270. K Jüttner, U Galla, H Schmieder *Electrochim. Acta* **45** 2575 (2000)
271. S Trasatti *Int. J. Hydrogen Energ.* **20** 835 (1995)
272. K E Johnson, D T Sawyer *J. Electroanal. Chem.* **49** 95 (1974)
273. H Ebert, R Parsons, G Ritzoulis, T VanderNoot *J. Electroanal. Chem.* **264** 181 (1989)
274. G Ritzoulis *J. Electroanal. Chem.* **327** 209 (1992)
275. A Ahmadi, E Bracey, R W Evans, G Attard *J. Electroanal. Chem.* **350** 297 (1993)
276. A Kudo, A Mine *J. Electroanal. Chem.* **408** 267 (1996)
277. G A Attard, A Ahmadi *J. Electroanal. Chem.* **389** 175 (1995)
278. A Kudo, A Mine *Appl. Surf. Sci.* **121**/**122** 538 (1997)
279. A Kudo, A Mine *J. Electroanal. Chem.* **426** 1 (1997)
280. Z U Bae, Y C Park, J H Lee, H Y Chang, S H Lee *Bull. Korean Chem. Soc.* **21** 749 (2000)
281. M Tezuka, M Iwasaki *Chem. Lett.* 1017 (1998)
282. J P Collman, M Marrocco, C M Elliott, M L'Her *J. Electroanal. Chem.* **124** 113 (1981)
283. M Bayachou, L Elkbir, P J Farmer *Inorg. Chem.* **39** 289 (2000)
284. S Kuwabata, S Uezumi, K Tanaka, T Tanaka *Inorg. Chem.* **25** 3018 (1986)
285. N Furuya, H Yoshiba *J. Electroanal. Chem.* **303** 271 (1991)
286. N Furuya, H Yoshiba, M Shibata *Denki Kagaku* **66** 811 (1998); *Chem. Abstr.* **129** 181 371 (1998)
287. N Konishi, K Hara, A Kudo, T Sakata *Bull. Chem. Soc. Jpn.* **69** 2159 (1996)
288. M Shibata, K Murase, N Furuya *Denki Kagaku* **65** 1039 (1997); *Chem. Abstr.* **128** 120 881 (1998)
289. Y Yoshida, S Ogata, S Nakamatsu, H Inoue, C Iwakura *Electrochim. Acta* **44** 3585 (1999)
290. V D Belyaev, T I Politova, V A Sobyanin *Catal. Lett.* **57** 43 (1999)
291. B Wang, X Li *Anal. Chem.* **70** 2181 (1998)
292. H McPeak, C E W Hahn *J. Electroanal. Chem.* **427** 179 (1997)
293. A K Pikaev *Sovremennaya Radiatsionnaya Khimiya. Radioliz Gazov i Zhidkostei* (Modern Radiation Chemistry. Radiolysis of Gases and Liquids) (Moscow: Nauka, 1986)
294. M Ali, I Zilbermann, H Cohen, A I Shames, D Meyerstein *Inorg. Chem.* **35** 5127 (1996)
295. M Lal *Radiat. Phys. Chem.* **43** 595 (1994)
296. A K Pikaev *Khim. Vys. Energ.* **34** 83 (2000) [g]
297. D C Schmelling, K A Gray, P V Kamat *Environ. Sci. Technol.* **32** 971 (1998)
298. M Al-Sheikhly, J Silverman, P Neta, L Karam *Environ. Sci. Technol.* **31** 2473 (1997)
299. K Vinodgopal, P V Kamat, in *Environmental Applications of Ionizing Radiation* (Eds W J Cooper, R D Curry, K E O'Shea) (New York: Wiley, 1998) p. 587
300. V P Shilov, A B Yusov *Radiokhimiya* **35** 38 (1993) [h]
301. V P Shilov, L N Astafurova, A B Yusov *Radiokhimiya* **37** 509 (1995) [h]
302. M Sacher, N Getoff *Z. Phys. Chem.* **99** 59 (1976)
303. H Gorner, D N Nikogosyan *J. Photochem. Photobiol. B* **39** 84 (1997)
304. M V Nikonov, K V Kuranov, V P Shilov *Izv. Akad. Nauk SSSR, Ser. Khim.* 717 (1988) [b]
305. Y Shimizu, S Nagai *Appl. Radiat. Isot.* **41** 457 (1990)
306. H Karasawa, R Yugeta, S Sato *Bull. Chem. Soc. Jpn.* **53** 1479 (1980)
307. I V Stankevich, A L Chistyakov, V B Shur, M E Vol'pin *Dokl. Akad. Nauk SSSR* **313** 118 (1990) [e]
308. W H Jones *J. Phys. Chem.* **96** 5184 (1992)
309. M R Manaa, C F Chabalowski *J. Phys. Chem.* **100** 611 (1996)
310. W H Jones *J. Phys. Chem.* **96** 594 (1992)
311. W H Jones *J. Mol. Struct. (Theochem)* **103** 299 (1993)
312. W H Jones, I G Csizmadia *Z. Phys. D* **32** 145 (1994)
313. J B Kim, P G Wenthold, W C Lineberger *J. Chem. Phys.* **108** 830 (1998)
314. B R Cameron, C G Aitken, P W Harland *J. Chem. Soc., Faraday Trans.* **90** 935 (1994)
315. R E Miller, L Pedersen *J. Chem. Phys.* **108** 436 (1998)
316. R E Miller, L Pedersen *Chem. Phys. Lett.* **275** 307 (1997)
317. X Chaudot, A Tambute, M Caude *Analusis* **25** 81 (1997)
318. M Perrut *J. Chromatogr.* **658** 293 (1994)
319. P G Jessop, W Leitner (Eds) *Chemical Synthesis Using Supercritical Fluids* (Weinheim: VCH; Wiley, 1999)
320. P G Jessop, T Ikariya, R Noyori *Chem. Rev.* **99** 475 (1999)
321. V Vandana, A S Teja, L H Zalkow *Fluid Phase Equilib.* **116** 162 (1996)
322. T S Oostdyk, R L Grob, J L Snyder, M E McNally *Anal. Chem.* **65** 596 (1993)
323. M B Baastoe, E Lundanes *J. Chromatogr.* **558** 458 (1991)
324. L Karlsson, L Mathiasson, J Akesson, J A Jonsson *J. Chromatogr.* **557** 99 (1991)
325. S N Wang, W Bonrath, H Pauling, F Kienzle *J. Supercrit. Fluid.* **17** 135 (2000)
326. D E Raynie *Anal. Chem.* **65** 3127 (1993)
327. R E Sievers, B Hansen *Chem. Eng. News* **69** 2 (1991)
328. A O Koryabkina, A S Noskov, E M Slavinskaya, in *Student i Nauchno-Tekhnicheskii Progress (Tez. Dokl. XXXVII Mezhdunarod. Nauchnoi Studencheskoi Konf. Sektsiya Khimicheskaya), Novosibirsk, 1999* [Student and Scientific and Engineering Progress (Abstracts of Reports of the XXXVIIth International Scientific Student Conference. Chemical Section), Novosibirsk, 1999] p. 84
329. US P. 5 849 257; *Chem. Abstr.* **127** 320 504 (1997)

[a] — *Mendeleev Chem. J. (Engl. Transl.)*
[b] — *Russ. Chem. Bull. (Engl. Transl.)*
[c] — *Russ. J. Phys. Chem. (Engl. Transl.)*
[d] — *Kinet. Catal. (Engl. Transl.)*
[e] — *Dokl. Chem. Technol., Dokl. Chem. (Engl. Transl.)*
[f] — *Russ. J. Org. Chem. (Engl. Transl.)*
[g] — *High Energ. Chem. (Engl. Transl.)*
[h] — *Radiochemistry (Engl. Transl.)*

Russian Chemical Reviews **70** (2) 105 – 129 (2001) © 2001 Russian Academy of Sciences and Turpion Ltd

DOI 10.1070/RC2001v070n02ABEH000622

Organic hydrotrioxides

V V Shereshovets (deceased), S L Khursan, V D Komissarov, G A Tolstikov

Contents

I.	Introduction	105
II.	Synthesis of hydrotrioxides	107
III.	The structure, thermochemistry and spectroscopy	107
IV.	The mechanism of formation of organic hydrotrioxides	112
V.	Decomposition of hydrotrioxides	114
VI.	The mechanism of thermal decomposition of hydrotrioxides	121
VII.	Organic hydrotrioxides as oxidants	123

Abstract. The results of studies on the synthesis, structure, thermochemistry and oxidising capacity of organic hydrotrioxides are generalised. Particular emphasis is placed on the analysis of thermal and catalytic decomposition of ROOOH and on generation of free radicals and singlet molecular oxygen. Problems concerning the mechanisms of formation and decomposition of organic hydrotrioxides are also considered. The bibliography includes 154 references.

I. Introduction

The chemistry of trioxides, *viz*., compounds with a $-O-O-O-$ fragment, has been a matter of considerable interest during recent decades.[1–5] The family of trioxides comprises hydrogen trioxide HOOOH, organic hydrotrioxides ROOOH, dialkyl- and diaryltrioxides ROOOR. Primary ozonides (1,2,3-trioxolanes) and transannular ozonides can be considered as cyclic analogues of dialkyl- and diaryltrioxides. Phosphite ozonides [*e.g*., $(RO)_3PO_3$], ozone–arene complexes $ArX \cdot O_3$ as well as alkali metal and ammonium ozonides also belong to trioxides.

The nomenclature of compounds with the general formula RO_nR' has not been settled yet. For $n = 2$, this formula corresponds to the class of peroxides, the simplest representative of which is hydrogen peroxide (or hydrogen dioxide), HOOH. Extension of the oxygen chain by an O atom gives compound HOOOH, which by analogy should be named 'hydrogen trioxide'. Replacement of H atoms by organic radicals leads to 'hydrotrioxides' (HTO), ROOOH, and 'trioxides', ROOOR. 'Tetraoxides' RO_4R are formed in the radical-chain oxidation of organic compounds, in the stage of quadratic termination of the oxidation chain induced by peroxyl radicals $ROO^{\bullet}$. Hydrotrioxides of different classes of organic compounds have the general formula ROOOH and should probably be named by analogy with hydroperoxides ROOH. For instance, the term 'acylhydrotrioxides' refers to aldehyde hydrotrioxides.

In this review, we analyse the publications devoted to the synthesis, structure and decomposition of HTO and their use as oxidants of various organic compounds. The latest review concerning this topic was published by Plesničar in 1992.[4] Since then, numerous papers dealing with various aspects of the chemistry of HTO have appeared and a considerable body of new information on their structures and reactivity has been obtained. Progress in the studies of HTO necessitates generalisation of these data, refinement or even revision of some statements in Plesničar's review [4] concerning, *e.g*., the efficiency of generation of $^1O_2$ in the decomposition of HTO. In addition, the kinetics of the synthesis of ROOOH, the synthesis of ROOOH on surfaces, thermochemistry of HTO and related compounds, radical and catalytic decomposition of HTO, the use of HTO as oxidants of unsaturated, organophosphorus, nitrogen- and sulfur-containing organic compounds are considered in detail in the present review. We also present comprehensive information on the kinetics of thermal decomposition of HTO and report a critical analysis of the data on the efficiency of generation of singlet molecular oxygen in the thermal decomposition of ROOOH. In his review,[4] Plesničar did not dwell on these problems or only briefly outlined them.

Finally, it should be noted that studies carried out by the researchers from the Russian Federation have been incompletely covered in that review.[4] Therefore, we deemed it our duty to consider in the present review not only the results of studies carried out during the last eight years but also those reported before 1992.

For a rather long time, HTO were thought of only as hypothetic labile intermediates in the studies of the mechanisms of ozonisation of saturated organic compounds. However, once the fact that hydrotrioxides are stable at low temperatures had been revealed, the chemistry of HTO has progressed rapidly. Methods for the synthesis of HTO have been developed which allow the preparation of HTO at concentrations as high as ~ 1 mol litre^{-1}. Organic HTO appeared to be both efficient oxidants in reactions with various organic substrates and convenient chemical sources of singlet molecular oxygen in organic media.

V V Shereshovets Institute of Organic Chemistry, Ufa Scientific Centre of the Russian Academy of Sciences, prosp. Oktyabrya 71, 450054 Ufa, Russian Federation
S L Khursan, V D Komissarov Bashkir State University, ul. Frunze 32, 450074 Ufa, Russian Federation. Fax (7-347) 235 60 66. Tel. (7-347) 223 67 27. E-mail: khursanSL@bsu.bashedu.ru (S L Khursan)
G A Tolstikov N N Vorozhtsov Novosibirsk Institute of Organic Chemistry, Siberian Branch of the Russian Academy of Sciences, prosp. Akad. Lavrent'eva 9, 630090 Novosibirsk, Russian Federation. Fax (7-383) 335 47 52. Tel. (7-383) 234 38 50. E-mail: gtolstik@nioch.nsc.ru

Received 28 September 2000
Uspekhi Khimii **70** (2) 123 – 148 (2001); translated by A M Raevsky

A hypothesis that hydrotrioxides are formed as intermediates in the ozonisation of certain organic compounds RH was first put forward independently by Price and Tumolo [6] and by White and Bailey [7] to rationalise the results obtained in studies of the reactions of ozone with ethers [6] and aromatic aldehydes.[7] Rapidly, this hypothesis has gained acceptance and was nearly simultaneously used by different authors in their studies on ozonisation of saturated hydrocarbons,[8–10] alcohols,[9] acetals [11] and silanes.[12]

Murray *et al.*[13–15] were the first who have provided strong experimental evidence for the existence of HTO. They have shown that unstable peroxide compounds **1a**, **2** and **3a** (Table 1) accumulated in the reaction medium during the low-temperature ozonisation of benzaldehyde, 2-methyltetrahydrofuran and isopropyl methyl ether, respectively. A signal at δ 13.1 was present in the ^{1}H NMR spectra of compounds **1a**, **2** and **3a**, which was tentatively assigned to the OOOH proton.

In further studies, ^{1}H NMR spectroscopy has become the basic method for identification and quantification of HTO in solution. Table 1 lists hydrotrioxides derived from aromatic aldehydes, ethers, linear and cyclic acetals, alcohols and ketones and Table 2 presents hydrotrioxides derived from hydrocarbons known to date. Organic compounds of other carbon subgroup elements also form hydrotrioxides upon oxidation by ozone. Hydrotrioxides of organosilicon and organogermanium com-

Table 1. Hydrotrioxides derived from aromatic aldehydes, ethers, linear and cyclic acetals, alcohols and ketones.

Formula	Compound	R^1	R^2	Ref.
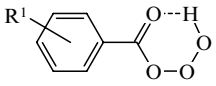	**1a**	H		15, 16
	1b	2-Cl		16
	1c	3-Cl		16
	1d	4-Cl		16
	1e	2-F		16
	1f	4-OMe		16
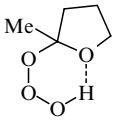	**2**			15
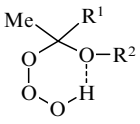	**3a**	Me	Me	13
	3b	Ph	Me	17
	3c	4-MeC_6H_4	Me	17
	3d	4-$MeOC_6H_4$	Me	17
	3e	4-FC_6H_4	Me	17
	3f	4-ClC_6H_4	Me	17
	3g	4-BrC_6H_4	Me	17
	3h	H	Et	18
	3i	Ph	Et	17
	3j	4-MeC_6H_4	Et	17
	3k	4-ClC_6H_4	Et	17
	3l	4-BrC_6H_4	Et	17
	3m	Me	Pr^i	16
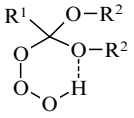	**4a**	Me	Me	19, 20
	4b	Ph	Me	19, 20
	4c	3-MeC_6H_4	Me	19, 20
	4d	4-$MeOC_6H_4$	Me	19, 20
	4e	4-FC_6H_4	Me	19, 20
	4f	4-ClC_6H_4	Me	19, 20
	4g	4-BrC_6H_4	Me	19, 20
	4h	Me	Et	19–21
	4i	Ph	Et	19, 20
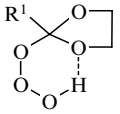	**5a**	H		22, 23
	5b	Me		23
	5c	Pr^n		18
	5d	Ph		19, 20, 22
	5e	4-MeC_6H_4		19, 20
	5f	3-ClC_6H_4		19, 20
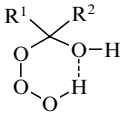	**6a**	H	H	18
	6b	Me	H	18, 24, 25
	6c	CH_2Cl	H	26
	6d	Et	H	26
	6e	Pr^n	H	26
	6f	Me	Me	18, 26
	6g	CH_2OH	Me	26
	6h	Et	Me	26
	6i	MeCHOH	Me	26
	6j	CH_2CH_2OH	Me	26
	6k	Ph	Me	17
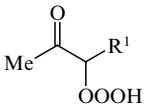	**7a**	Me		27
	7b	Pr^n		27

Table 2. Hydrotrioxides derived from hydrocarbons.

Formula	Compound	Ref.
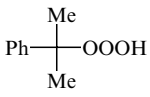	**8**	28, 29
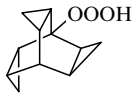	**9**	30
	10a	30
	10b	30
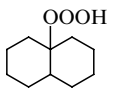	**11**	18, 31
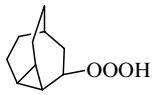	**12**	30
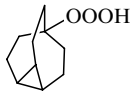	**13**	30
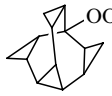	**14**	30
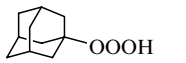	**15**	18, 31, 32
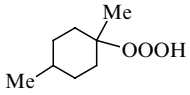	**16**	18, 31
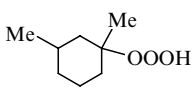	**17**	18, 31
Ph_3COOOH	**18**	18, 31
$EtMe_2COOOH$	**19**	18, 31

pounds have been detected (Table 3). Presumably, HTO represent labile intermediates in the ozonisation of stannanes,[36] though their formation from organotin compounds has not been reported so far.

Table 3. Hydrotrioxides derived from organoelement compounds.

Formula	Compound	R	Ref.
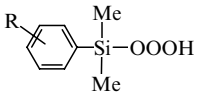	**20a**	H	33, 34
	20b	4-Me	33
	20c	4-MeO	33
	20d	4-Cl	33
$R_3SiOOOH$	**21a**	Et	35, 36
	21b	Bu^n	37
$Et_3GeOOOH$	**22**		36

II. Synthesis of hydrotrioxides

It was only recently that the methods for the synthesis of the simplest trioxide, HOOOH (**23**), have been proposed. Hydrogen trioxide **23** is formed upon oxidation of 9,10-dihydroxyanthracene, 2-ethyl-9,10-dihydroxyanthracene or hydrazobenzene by ozone (−78 °C, acetone-d_6 or methyl acetate).[34]

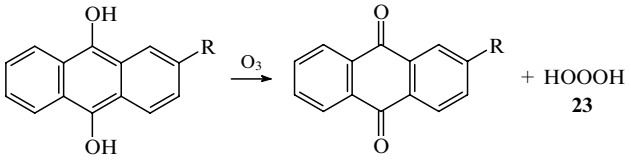

R = H, Et.

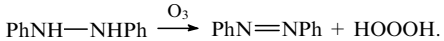

Hydrogen trioxide **23** is also formed in the decomposition of silane hydrotrioxides.[33, 34]

All HTO listed in Tables 1–3 can be synthesised using a rather simple and virtually identical procedure consisting of bubbling a cooled O_3-O_2 or O_3-N_2 gas mixture through a liquid substrate RH or its solution at reduced temperature (−20 to −78 °C). After completion of the reaction, the unconsumed ozone is removed by blowing air or (if necessary) an inert gas and then the concentration of HTO in the solution is determined by NMR spectroscopy. The yield of ROOOH with respect to the consumed RH depends on the substrate structure and varies from 1%–2% for cumene hydrotrioxide **8** to 70%–90% for acetal, alcohol and silane hydrotrioxides.

A modified procedure for the synthesis of HTO involves ozonisation of organic compounds on the surface of silica gel (the so-called 'dry' ozonisation).[18, 31, 32, 38, 39] It was used to obtain the hydrotrioxides **11** and **15**–**19**, which could not be prepared in the liquid-phase ozonisation.[18, 31, 32] Highly polar silica gel surface stabilises the ionic intermediates of the ozonisation reaction, thus favouring the formation of ROOOH even from non-activated hydrocarbons. It can be hypothesised that 'dry' ozonisation will also be convenient for the synthesis of other HTO which cannot be obtained by liquid-phase ozonisation.

The kinetics of formation of compounds **3m**,[16] **4h**,[21] **6d**,[25] **6f**[16] and **7b**[27] have been studied. At sufficiently low temperatures where thermal decomposition of HTO can be ignored the kinetic curves of accumulation of HTO have the shape of saturation curves, which means that the yield of ROOOH (α) calculated with respect to the ozone consumed decreases with an increase in conversion. The extent of the reaction is related to the amount of the ozone absorbed $\Delta(O_3)$ and the yield of ROOOH is calculated by the formula

$$\alpha = \frac{[ROOOH]}{\Delta(O_3)}.$$

The yield calculated with respect to the ozone consumed (α_0) is obtained by extrapolating the value of α to the zero time [$\Delta(O_3) = 0$].

The α_0 values for a number of HTO are listed in Table 4. The decrease in the yield with the increase in the extent of the reaction is explained by consumption of the HTO in the reactions with ozone.

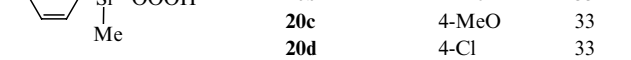

The rate constants for the first (k_1) and second (k_2) stages of ozonisation of 1,1-diethoxyethane at −60 and −80 °C are $k_1 = 6.8 \times 10^{-4}$ and 2.5×10^{-5} litre mol^{-1} s^{-1} and $k_2 = 3.0 \times 10^{-3}$ and 1.2×10^{-4} litre mol^{-1} s^{-1}, respectively.[21]

Table 4. Yields of hydrotrioxides (α_0) calculated with respect to the consumed ozone.

Compound	Temperature /°C	α_0 /mol mol^{-1}	Ref.
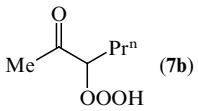 (**7b**)	−60	0.5	27
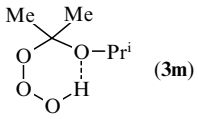 (**3m**)	−78	0.45	16
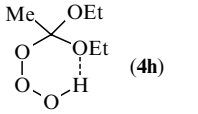 (**4h**)	−78	0.51	21
	−60	0.45	21
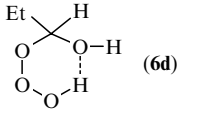 (**6d**)	−98	0.90	25
	−78	0.80	25
	−50	0.20	25
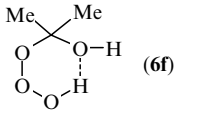 (**6f**)	−78	0.98	16
	−40	0.80	16

III. The structure, thermochemistry and spectroscopy

1. The structure

a. Equilibrium molecular geometry of hydrotrioxides

Experimental data on the spatial structure of HTO are lacking and this was established only from the results of semiempirical (EHT, CNDO/2, MINDO/3, AM1)[40–43] and *ab initio* quantum-chemical calculations.[33, 44–54]

Ab initio calculations of the equilibrium molecular geometry of HOOOH have been carried out at different levels of theory, from simple calculations in the one-determinant approximation with the STO-2G basis set to sophisticated calculations with different TZP basis sets augmented with diffuse functions and intensive treatment of electron correlation. Both partial[44–48, 50] and full optimisation of the molecular geometry[33, 49, 51, 52, 54] were employed. Tables 5 and 6 present the results of *ab initio* calcu-

Table 5. Results of *ab initio* calculations of the equilibrium geometries and total energies of HOOOH.

Basis set	r(HO) /Å	r(OO) /Å	θ(HOO) /deg	θ(OOO) /deg	φ /deg	E_{total}	Ref.
RHF/STO-3G	1.002	1.392	102.5	105.9	84.2	−222.58049	49
RHF/4-31G	0.959	1.437	103.6	106.0	83.5	−225.21862	49
RHF/6-31G	0.958	1.432	104.1	106.5	83.9	−225.44304	33
RHF/6-31G*	0.953	1.373	103.2	107.2	80.1	−225.53362	49
RHF/6-31G**	0.949	1.373	103.5	107.4	80.8	−225.54584	51
MP2/4-31G	0.992	1.539	99.6	104.4	78.3	−225.62077	49
MP2/6-31G*	0.980	1.442	100.3	106.1	78.5	−226.09075	49
MP2/6-31++G*	0.982	1.445	100.8	106.4	79.6	−226.10273	52
MP2/6-31G**	0.972	1.441	100.2	106.2	78.7	−226.11275	51

Note. Hereafter, the E_{total} are given in hartree.

Table 6. Results of *ab initio* calculations [54] of the equilibrium geometries and total energies of hydrotrioxides H_3COOOH and $H_3SiOOOH$.

Basis set	r(XO) /Å	r(XOO) /Å	r(OOH) /Å	r(OH) /Å	θ(OOH) /deg	θ(OOO) /deg	θ(XOO) /deg	φ(HXOO) /deg	φ(XOOO) /deg	φ(OOOH) /deg	E_{total}
Compound H_3COOOH											
RHF/STO-3G	1.453	1.396	1.392	1.003	102.4	105.9	106.5	179.1	87.8	83.5	−261.16718
RHF/4-31G	1.438	1.436	1.440	0.958	103.4	106.1	107.7	179.0	85.8	82.4	−264.18963
RHF/6-31G	1.439	1.430	1.433	0.957	103.9	106.5	108.1	179.0	86.0	82.6	−264.45417
Compound $H_3SiOOOH$											
RHF/6-31G	1.771	1.441	1.429	0.958	103.9	106.2	109.6	180.2	84.1	79.3	−515.49701

lations [53] of the molecular structures of HOOOH, H_3COOOH and $H_3SiOOOH$ with full geometry optimisation.

The data listed in Tables 5 and 6 reveal salient features of the molecular geometry of hydrotrioxides.

1. The r(O−O) distances in trioxides are close to those in peroxides. Blint and Newton [46] found that the O−O bond length can be calculated with a reasonable accuracy using the empirical Pauling equation

$$r_e = r_e^s - \alpha \ln(n), \quad (1)$$

where r_e is the equilibrium bond length (Å); r_e^s is the equilibrium length of a bond with the order of unity; $\alpha = 0.351$ Å is the empirical constant; and n is the bond order. According to calculations with the 4-31G basis set, r(O−O) ≈ 1.41 – 1.44 Å in polyoxides. The O−O bond in HOOOH is 0.03 to 0.04 Å shorter than in HOOH. A similar tendency of changes in the O−O bond length is observed for the pairs H_3COOOH/H_3COOH and $H_3SiOOOH/H_3SiOOH$,[54] which seems to be a general feature.

2. The torsion (dihedral) angle φ in the HTO molecules characterises the positions of the substituent atoms with respect to the plane passing through three O atoms. According to the most sophisticated calculations,[49, 54] $\varphi \approx 75 – 80°$. The calculations revealed two stable conformations, *anti* (**A**) and *syn* (**B**), for the hydrogen trioxide molecule, which differ in positions of the H atoms with respect to the trioxide plane.

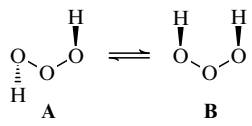

A **B**

The assumption of the existence of stable *anti* and *syn* conformations of hydrogen trioxide molecule (**23**) is indirectly confirmed by the results of IR and microwave spectroscopic studies of hydrogen trisulfide, a close analogue of HOOOH.[55] According to the results of quantum-chemical calculations carried out at the MP2/TZ+P and QCISD/TZ+P levels of theory, the *anti* conformation of HSSSH molecule is 0.25 kcal mol^{-1} (87 cm^{-1}) more stable than the *syn* conformation.

For the HOOOH molecule, conformation **A** is more energetically favourable (by 3.5±1.0 kcal mol^{-1}) than conformation **B** (see Refs 43, 44, 46, 49). This gives a rationale of the low stability of 1,2,3-trioxolanes, which are intermediates of the ozonolysis of alkenes, compared to linear trioxides. The molecule of primary ozonide (1,2,3-trioxolane **24**) adopts an 'envelope' conformation [56, 57] in which the positions of methylene groups formally correspond to the *syn* conformation of the trioxide.

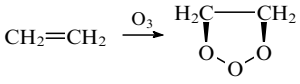

24

Hence, the energy of conformational transition and strain energy in the five-membered ring [∼6 kcal mol^{-1} (see Ref. 58)] contribute to the destabilisation of the primary ozonide. As a consequence, the activation energy of further transformations of compound **24** is ∼10 kcal mol^{-1} lower than those of thermal decomposition of dialkyl trioxides.[5]

Hydrotrioxides derived from alcohols, ethers and acetals can form intramolecularly hydrogen-bonded structures only if these molecules adopt the *syn* conformation.[13, 14, 16, 17, 19, 20, 24]

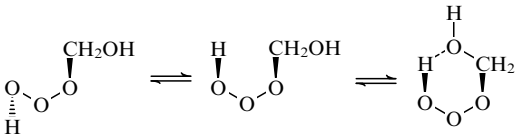

Hence, the enthalpy of formation of a hydrogen bond, $\Delta H°$, includes the *anti*–*syn* interconversion energy.[18] Radical decomposition of the cyclic intermediate removes the conformational strain, thus decreasing the activation energy for this process.

3. The H−O−O and C−O−O bond angles (see Tables 5 and 6, respectively) in hydrotrioxide molecules are somewhat larger than in the corresponding hydroperoxides. The O−O−O bond angles in different HTO (104 – 107°) are in good agreement with the IR spectroscopic estimate.[59]

4. Conformational analysis of the HOOOH molecule has been carried out.[49] The potential energy surface for simultaneous

rotation of the OH groups about the O—O axes in the molecule was calculated. Analogous semiempirical AM1 calculations were carried out for hydrogen trioxide and tetraoxide.[43] The nature of the barriers to rotation was interpreted based on the results of the Fourier analysis of the conformational potential of the polyoxides. The conformational behaviour of polyoxides is dominated by the repulsion between the lone electron pairs of the neighbouring oxygen atoms and by stabilisation of the hydropolyoxide owing to delocalisation of the lone electron pair (n_O) over the σ*-antibonding orbital of the neighbouring O—O bond (or O—C and O—H bonds).[18, 54] The latter effect provides an explanation for the shortening of the r(O—O) distance in trioxides compared to peroxides, since the stabilising effect of hyperconjugation $n_O - \sigma^*_{O-O}$ on the trioxide molecule is more pronounced than that of hyperconjugation $n_O - \sigma^*_{O-OH}$ on the peroxide molecule, thus favouring a decrease in the O—O bond length.[54]

Analysis of the potential surface for internal rotation of hydrogen trioxide suggests that the most favourable conversional process between two global energy minima (**A**[1] and **A**[2]) for the *anti* conformation of HOOOH involves a two-step flip-flop rotation rather than simultaneous rotation of the OH groups.[43, 49]

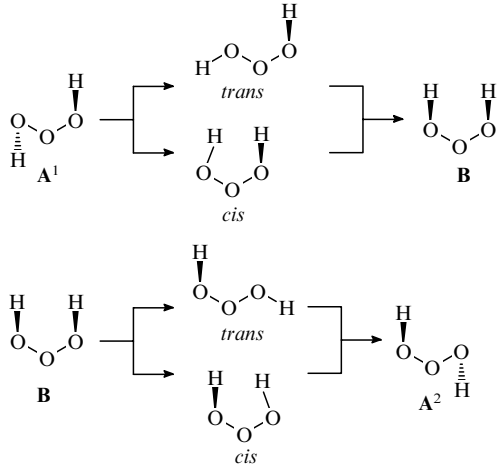

b. Association of hydrotrioxides

The binding energies of the intermolecularly hydrogen-bonded dimers were calculated taking dimerisations of HOOOH, H_3COOOH and $H_3SiOOOH$ as examples.[33, 53]

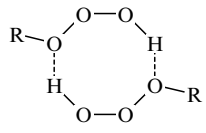

R = H, CH_3, SiH_3.

Relatively high binding energies (E = 6–8 kcal mol^{-1} per O—H bond) are close to the hydrogen bond energy in cyclic dimers of carboxylic acids.[60, 61] This confirms the assumption that self-association is a salient feature of HTO molecules. It should be noted, however, that the computational method (RHF/6-31G) employed by Plesničar *et al.*[33, 53] overestimates the energies of hydrogen bonds. Indeed, augmentation of the basis set with *p*-polarisation functions for hydrogen and *d*-polarisation functions for other atoms leads to more realistic results, *viz*., the binding energy of H_3COOOH in the eight-membered dimer is 4.5 kcal mol^{-1} per hydrogen bond.[18]

The effect of water on the decomposition of HOOOH has been studied.[52, 54] The water molecule acts as a bifunctional catalyst, thus facilitating the decomposition of hydrogen trioxide into H_2O and $^1O_2$. This reaction is preceded by the formation of a six-centred hydrogen-bonded complex. The binding energy in this complex is 1.5 kcal mol^{-1} lower than in the cyclic dimer of HOOOH. The calculated height of the potential barrier to decomposition of hydrogen trioxide (15.1 kcal mol^{-1} relative to noninteracting reagents) is in good agreement with the experimentally found effective activation energies for the decomposition of HOOOH.[34, 52, 62]

Ab initio calculations of intramolecularly hydrogen-bonded structures ROOOH have been carried out taking methanol hydrotrioxide (**6a**) as an example.[18] The most stable conformers of the molecule are the *anti* (**C**) and *syn* (**D**) conformers with nearly equal energies.

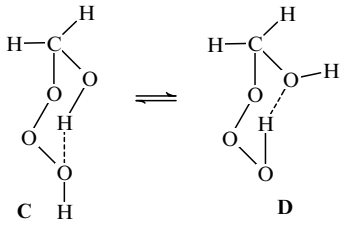

The *anti* conformer **C** is stabilised by the hydrogen bond between the H atom of the alcoholic hydroxy group and the most distant (from the carbon atom) O atom of the trioxide fragment. The *syn* conformation **D** favours the formation of a hydrogen bond between the OOOH hydrogen and alcoholic O atom. The binding energies of structures **C** and **D** calculated at the MP2//RHF/6-31G** level of theory are 2.2 and 5.4 kcal mol^{-1}, respectively.

In conclusion, mention should be made that HTO can form associates with carbonyl compounds.[18] In addition to the signal at δ = 13, the ^{1}H NMR spectrum of 1,4-dimethylcyclohexyl hydrotrioxide (**16**) in acetone exhibits two peaks at δ = 4.15 and 4.35 which disappear irreversibly upon heating. It is well known that hydrogen peroxide[63] and hydroperoxides[64, 65] readily react with aliphatic and alicyclic ketones to give α-hydroxy hydroperoxides and α-hydroxy peroxides. Presumably, a similar reversible reaction occurs in the system HTO **16** – acetone resulting in a derivative of 2-R-trioxy-2-hydroxypropane **25**.[18] Compound **25** exists in two forms, which accounts for the presence of two OH proton resonance peaks in its ^{1}H NMR spectrum.

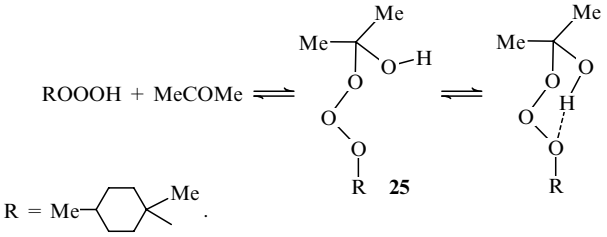

2. Thermochemistry

In this Section, we outline briefly the possibilities of estimation of the enthalpies of formation and bond dissociation energies in hydrotrioxides. For more detailed data, see a recent review.[66]

The experimentally determined thermodynamic characteristics of HTO (enthalpies of formation and of phase transitions, entropies, *etc*.) are lacking. Therefore, thermochemical calculations of the thermal effects of the reactions involving ROOOH were carried out using approximate computational schemes, in particular, the approach of additivity of thermochemical increments developed by Benson *et al.*[58, 67, 68] In the framework of Benson's scheme, the enthalpies of formation of hydropolyoxides are related by simple relationships

$$\Delta_f H^\circ(\text{ROOOH}) = \Delta_f H^\circ(\text{ROOH}) + \Delta_f H^\circ[\text{O}-(\text{O})_2], \quad (2)$$

$$\Delta_f H^\circ(\text{ROOOOH}) = \Delta_f H^\circ(\text{ROOOH}) + \Delta_f H^\circ[\text{O}-(\text{O})_2], \quad (3)$$

where the second term in the right side of Eqns (2) and (3) is the polyoxide group increment, which characterises the enthalpy contribution of the central O atom of the trioxide fragment. As will be shown below, the assumption that the enthalpy of formation changes linearly in the order ROOH—ROOOH—

ROOOOH is rough and leads to substantial discrepancies between the results of thermochemical studies carried out by different authors.

Practically, the most convenient way of calculating the $\Delta_f H^\circ$(ROOOH) values is to use Eqn (2). A number of experimentally determined enthalpies of formation of hydroperoxides has been reported.[69] Good agreement with experimental $\Delta_f H^\circ$(ROOH) values is also observed when using the method of isodesmic reactions as well as *ab initio* calculations with extended basis sets and inclusion of electron correlation (CI or perturbation theory).[70, 71] Unfortunately, high computational cost of real-time calculations of $\Delta_f H^\circ$(ROOH) allows them to be carried out only for the simplest substituents R. Thermochemistry of peroxides has been analysed using a large body of experimental data on the enthalpies of formation (see Ref. 72 and references cited theirein), increments for calculating $\Delta_f H^\circ$(ROOH) in both the gas phase and condensed phase were proposed.

The polyoxide group increment, $\Delta_f H^\circ[O-(O)_2]$, which plays the key role in calculations of the enthalpies of formation of hydrotrioxides, cannot be calculated from the available experimental data on $\Delta_f H^\circ$ and bond dissociation energies in related compounds. Since the accuracy of indirect estimates is insufficient, the numerical value of $\Delta_f H^\circ[O-(O)_2]$ has been the subject of systematic revisions.[70, 73–77]

a. Comparison of the enthalpies of formation

The first estimates of $\Delta_f H^\circ[O-(O)_2]$ (25±6 and 19±4 kcal mol^{-1}, see Refs 73 and 74, respectively) were made based on the assumption that thermodynamic properties change linearly in the order $ROR'-ROOR'-ROOOR'$ and from comparison of the enthalpies of formation for pairs of compounds H_2O and H_2O_2,[73, 74] MeOH and MeOOH and MeOMe and MeOOMe.[74] This approach was found to be very rough. In particular, the results obtained suggested that tetraoxides can be synthesised at temperatures below 80–100 K.[74] Later, it has been shown[78–80] that tetraoxides ROOOOR (R = *tert*-Alk, ArAlk) are rather stable at $T \leqslant 170$ K, which indicated overestimation of the $\Delta_f H^\circ[O-(O)_2]$ value reported in earlier studies.[73, 74]

b. Comparison of thermal effects of reactions

Another procedure for the calculation of the polyoxide group increment was used by Nangia and Benson.[75] Based on the reaction equations

$$Bu^tOOOOBu^t \longrightarrow 2\,Bu^tOO, \quad (4)$$

$$Bu^tOOOBu^t \longrightarrow Bu^tO + Bu^tOO, \quad (5)$$

$$Bu^tOOBu^t \longrightarrow 2\,Bu^tO \quad (6)$$

with the known thermal effects $\Delta H^\circ(4) = 9.0\pm1.5$[78, 79] and $\Delta H^\circ(6) = 38.0\pm1.0$ kcal mol^{-1} (see Ref. 81) and using the additivity rule, according to which

$$\Delta H^\circ(5) = 0.5[\Delta H^\circ(4) + \Delta H^\circ(6)],$$

they found that $\Delta H^\circ(5) = 23.5\pm0.8$ kcal mol^{-1} and $\Delta H^\circ(6) - \Delta H^\circ(5) = \Delta H^\circ(5) - \Delta H^\circ(4) = 14.5\pm0.8$ kcal mol^{-1}. By representing the enthalpies of formation of the molecules under study as the sums of the enthalpies of formation of the thermochemical groups, one can readily obtain the expression for the calculation of the polyoxide group increment

$$\Delta H^\circ(6) - \Delta H^\circ(5) = \Delta_f H^\circ(RO) - \Delta_f H^\circ(ROO) + \Delta_f H^\circ[O-(O)_2]. \quad (7)$$

Using the known values of the enthalpies of formation of the $MeO^\bullet$ and $MeOO^\bullet$ radicals, the new polyoxide group increment $\Delta_f H^\circ[O-(O)_2]$ was found to be 16.8±2.2 kcal mol^{-1} (see Ref. 75). A year later, Nangia and Benson corrected this estimate and reported that $\Delta_f H^\circ[O-(O)_2] = 14.8$ kcal mol^{-1}.[76] This approach has a drawback consisting of the assumption of linear changes in the ΔH° of the reactions (4)–(6). Recent experiments showed that $\Delta H^\circ(5) = 20-21$ kcal mol^{-1} (see Refs 18, 82, 83). Mention has been made of the nonlinear character of changes in the enthalpies of formation in the order 'peroxide–trioxide–tetraoxide'.[84]

c. Quantum-chemical calculations of the enthalpies of formation

The use of quantum-chemical methods has opened new possibilities for the thermochemical analysis of the reactions of HTO and higher polyoxides.[44, 46, 50, 70, 71, 77, 82, 84–87] However, direct calculations of the enthalpies of formation of polyoxides can lead to large errors owing to incomplete inclusion of electron correlation in the *ab initio* computational schemes and inadequate parametrisation of semiempirical methods. This can be illustrated as follows. The enthalpy of formation of MeOOOH obtained from MP4SDTQ/6-31G*//MP2/6-31G* calculations is −22.2 kcal mol^{-1} and must correspond to the energy of dissociation of the weakest O–O bond, D(MeO–OOH); however, D(MeO–OOH) = 35.8 kcal mol^{-1} (see Ref. 70). The value cannot be regarded as realistic despite the high level of quantum-chemical calculations. It is only 2 to 3 kcal mol^{-1} lower than the corresponding bond dissociation energies in peroxides. However, the temperature intervals of stability of these compounds are not comparable: peroxides are rather stable at room temperature, while the lifetimes of HTO under these conditions are within several minutes. Therefore, the numerical estimates of the polyoxide group increment obtained from both semiempirical MNDO[77] and *ab initio*[70] calculations of $\Delta_f H^\circ$ of polyoxides {$\Delta_f H^\circ[O-(O)_2]$ = 13.1±1.5 and 9.6±0.1, respectively} should be used with caution.

d. Quantum-chemical calculations of bond dissociation energies

The best results can be obtained from calculations of bond dissociation energies (strengths). This is due to mutual cancellation of the errors of calculations of $\Delta_f H^\circ$ for polyoxide and its decomposition products. Systematic studies of the O–O and O–H bond dissociation energies in organic polyoxides (see Table 7) have been carried out.[18, 82, 84–86] This allowed calculations of the enthalpies of formation for a number of peroxides, trioxides and tetraoxides. It was found that the difference $\Delta_f H^\circ(ROOR') - \Delta_f H^\circ(ROR')$ is 5 to 8 kcal mol^{-1} larger than $\Delta_f H^\circ(ROOOOR') - \Delta_f H^\circ(ROOOR')$. The reason for this discrepancy was explained based on the results of analysis of the conformational potentials of polyoxide compounds H_2O_x (x = 2,

Table 7. Bond strengths D (kcal mol^{-1}) in organic hydropolyoxides.

Bond type	D	Ref.
R–OOOH [a]	63.6 ± 1.2	18
RO–OOH [b]	20.4 ± 1.0 (MNDO)	86
	20.8 ± 1.1 (AM1)	86
	23.4 [c]	88
ROO–OH [b]	(25.5 ± 0.6) + (1.97 ± 0.49)·σ*(R) (MNDO)	86
	(23.8 ± 0.6) + (1.38 ± 0.49)·σ*(R) (AM1)	86
	30.1 [c]	88
HO–OOH	24.8 (CI(SDQ))	50
	25.0 (MNDO)	86
	25.2 (AM1)	86
HOOO–H	82.6	70
ROOO–H [d]	80.8 ± 0.8	18
R–OOOOH [a]	63.6 ± 1.2	18
RO–OOOH [a]	20.8 ± 1.4	18
ROO–OOH [a]	8.7 ± 1.2	84
HOO–OOH	7.1 (MNDO)	82
	12.1 (MNDO)	77
ROOO–OH [a]	25.1 ± 0.5	18
ROOOO–H [a]	80.8 ± 0.8	18

[a] R = Alk. [b] R is unsubstituted, halo-, hydroxy- or alkoxy-substituted alkyl. [c] R = Me. [d] R is unsubstituted, halo-, hydroxy- or alkoxy-substituted alkyl, H, HCO or MeCO.

3, 4).[43] It was shown that the enthalpies of formation in the series 'peroxide – trioxide – tetraoxide' do not change linearly as it would follow from the additivity method owing to additional stabilisation of peroxides by the dipole – dipole interaction between the alkoxy groups. Therefore, the $\Delta_f H^\circ[O-(O)_2]$ group increment can be calculated as the difference between the enthalpies of formation of a trioxide and tetraoxide with the same substituents. Calculations of the enthalpies of formation of trioxides from the corresponding peroxides should be carried out with inclusion of the energy of conformational rearrangement of the molecule (~ 5 kcal mol^{-1}).

For practical calculations of $\Delta_f H^\circ$ values in polyoxides we recommend the following relationships

$$\Delta_f H^\circ(\mathrm{ROOOR}') = \quad (8)$$
$$= \Delta_f H^\circ(\mathrm{ROOR}') + (17.6 \pm 1.6) \text{ kcal mol}^{-1},$$
$$\Delta_f H^\circ(\mathrm{ROOOOR}') = \quad (9)$$
$$= \Delta_f H^\circ(\mathrm{ROOOR}') + (11.1 \pm 1.0) \text{ kcal mol}^{-1}.$$

Calculations using Eqns (8) and (9) allow correct reproduction of the intervals of thermal stability of trioxides and tetraoxides and give the bond dissociation energies that are close to the activation energies for decomposition of polyoxides (provided that E_a is corrected for the normal value of the pre-exponential factor).

3. Spectroscopic studies

a. UV, IR and Raman spectra

Scarce experimental data indicate that the electronic spectra of HTO are similar to those of related peroxide compounds. The optical spectrum of HOOOH obtained in the pulse radiolysis experiments is similar to that of hydrogen peroxide and exhibits a somewhat larger molar extinction, $\varepsilon \approx 100$ litre mol^{-1} cm^{-1} ($\lambda = 240$ nm).[62] Weak absorption at $\lambda > 320$ nm in the spectrum of benzaldehyde hydrotrioxide (**1a**) can be assigned to the S_1 ($\pi^*_{O-O} \rightarrow \sigma^*_{O-O}$) transition. The position and spectral features of this signal are similar to those of aromatic endoperoxides.[89] Thus, the UV spectra of HTO exhibit no characteristic bands suitable for identification and determination of the concentration of ROOOH. Since almost any reaction of the synthesis or decomposition of HTO proceeds to give peroxides as side or major products, one can conclude that investigations into the chemical nature of organic HTO based on the UV spectra is hardly probable.

Specific features of the IR spectra of hydrogen and deuterium trioxides and tetraoxides allowed Giguere and Herman [59] to relate the observed frequencies to vibrations of the zigzag chain of the O atoms linked by single bond. They estimated the O – O bond length at ~ 1.5 Å and the O – O – O bond angle at 100 to 120 ° and concluded that internal rotation of the OH groups in free molecules is only weakly hindered, whereas in the solid state their orientation will be strongly dependent on the possibility of hydrogen bonding, as in hydrogen peroxide. More recently,[90] normal coordinate analyses for HOOOH and HOOOOH molecules were performed. Nonplanar hydrogen polyoxide structures exhibited fairly good correspondence between the calculated frequencies and experimental IR spectrum and the existence of several spatial isomers was suggested. Further quantum-chemical studies have confirmed in general the above-mentioned conclusions [59, 90] (see Table 3).

Raman spectra of hydrogen polyoxides have been studied.[91, 92] The fundamental skeletal vibrations of the HOOOH and HOOOOH molecules and their deuterated analogues were identified and interpreted (Table 8). The frequencies observed are consistent with the C_2 symmetry of the molecular structure in the form of a skew chain of O atoms linked by single bonds.

Vibrational spectra of organic hydroperoxides have not been studied as yet.

Table 8. Vibrational spectra of hydrogen polyoxides.[92]

Compound	Frequencies /cm^{-1}		Assignment
	Raman	IR	
HOOOH	~ 855	~ 855	ν_s(O – O)
	500	–	δ(O – O – O)
	755	755	ν_{as}(O – O)
DOOOD	~ 857	~ 857	ν_s(O – O)
	497	–	δ(O – O – O)
	760	760	ν_{as}(O – O)
HO(1)O(2)O(3)O(4)H	~ 855	–	ν_s(O – O)
	~ 764	–	ν[O(2) – O(3)]
	450	–	δ_s(O – O – O)
	~ 98	–	δ_{tors}[O(2) – O(3)]
	~ 823	~ 823	ν_{as}(O – O)
	–	435	δ_{as}(O – O – O)
DO(1)O(2)O(3)O(4)D	~ 857	–	ν_s(O – O)
	~ 768	–	ν[O(2) – O(3)]
	~ 440	–	δ_s(O – O – O)
	~ 98	–	δ_{tors}[O(2) – O(3)]
	~ 828	~ 828	ν_{as}(O – O)
	–	~ 430	δ_{as}(O – O – O)

b. NMR studies

Organic HTO can be conveniently identified by NMR spectroscopy owing to the presence of characteristic signals of the hydrotrioxide fragment. Resonance absorptions of other groups are less characteristic. The chemical shifts of the ^{1}H, ^{13}C and ^{29}Si nuclei in the NMR spectra of a number of HTO and related compounds [17, 29, 33] are listed in Tables 9 and 10.

Typical of HTO is the signal of the OOOH proton at $\delta \sim 13$ in the ^{1}H NMR spectra, the position of the signal being virtually independent of the nature of ROOOH.[13 – 17, 19 – 21, 23 – 30, 33, 34, 36, 37] In the series ROH – ROOH – ROOOH, the chemical shift of H increases from δ 0.5 – 5.5 for ROH to δ 7.6 – 9.2 for ROOH [93] and δ 12 – 14 for ROOOH. Unlike alcohols and hydroperoxides,[93] dilution of HTO solutions has little effect on the chemical shift of the trioxide proton. Based on these observations, it was concluded that hydrotrioxides form strong intramolecularly hydrogen-bonded complexes.[13, 14]

A peculiarity of the ^{1}H NMR spectra of hydrotrioxides is the appearance, in some cases, of the splitting of the OOOH proton signal into two signals.[14, 16, 17, 19, 20, 24] The chemical shifts of these signals also show little change with dilution. Heating of the samples results in broadening and coalescence of the lines. The coalescence temperature depends on the chemical nature of both ROOOH and the solvent. For instance, two peaks in the ^{1}H NMR spectrum of 2-methyltetrahydrofuran hydrotrioxide (**2**) coalesce at -27 °C.[14] For hydrotrioxide **3b** obtained from methyl α-methylbenzyl ether in Freon 11/12, two peaks appear in its ^{1}H NMR spectrum only at -50 °C and lower temperatures, whereas no peak coalescence is observed in diethyl ether, acetone-d_6 and ethyl acetate even at -10 °C.[17] The origin of two resonance signals for the OOOH proton is still to be clarified. This can be due to either the 'chair – boat' conformational transition of the six-membered ring resulting from the formation of intramolecular hydrogen bond or the presence of two conformations with the R group at the O atom in either axial or equatorial position. Hydrotrioxides derived from cyclic acetals [19, 20] can form various complexes owing to nonequivalence of the two acetal O atoms with respect to the OOOH group.

Studies of the ^{1}H NMR spectra of hydrotrioxides in different solvents [17] showed that though the chemical shifts of two peaks vary insignificantly, their relative intensities can vary over a rather wide range (see Table 9). In diethyl ether, the more intense low-field peak of the hydrotrioxide **3b** disappears upon heating with a somewhat higher rate compared with the high-field signal. The

Table 9. Chemical shifts and multiplicities of signals in the ^1H and ^{13}C NMR spectra of organic hydrotrioxides and related compounds.

Compound	X	δ ^1H	δ ^{13}C			
			C(1)	C(2)	C(Me)	other C atoms
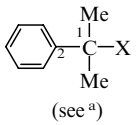 (see [a])	H	1.17 d (Me)	34.6	148.8	24.3	–
	OH	1.50 (Me), 5.18 (OH)	72.1	150.7	32.3	–
	OOH	1.52 (Me), 10.95 (OOH)	84.0	145.5	26.6	–
	OOOH (**8**)	1.64 (Me), 13.67 (OOOH)	104.3	134.5	–	–
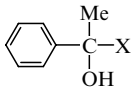	H	1.33 d (Me), 4.65 q (H), 5.3 (OH)	69.9	147.3	25.1	–
	OOOH (**6k**)	13.20, 13.23 (1.2 : 1) (OH, OOOH)	105.26	–	–	–
	OOOH [b] (**6k**)	12.95, 13.12 (1 : 1) (OH, OOOH)	105.15	–	–	–
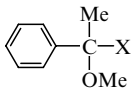	H	–	79.7	144.4	24.7	56.2
	H [c]	1.35 d (Me), 3.05 (OMe), 4.12 q (H)	79.7	143.9	24.0	56.1
	OOH	10.6 (OOH)	106.4	142.5	25.4	49.7
	OOH [c]	1.65 (Me), 3.35 (OMe), 8.85 (OOH)	106.7	140.5	24.6	49.9
	OOOH (**3b**)	1.60 (Me), 3.25 (OMe), 13.19, 13.54 (1 : 1.2)	108.1	134.3	26.0	–
	OOOH [b] (**3b**)	1.80 (Me), 12.81, 13.04 [1 : (7 – 10)] (OOOH)	103.2, 104.1	–	–	–
	OOOH [d] (**3b**)	1.57 (Me), 12.90, 13.15 (1 : 1.2) (OOOH)	108.1	–	–	–

Note. The spectra were measured in $(CD_3)_2CO$ at −60 °C, the chemical shifts are given in ppm relative to tetramethylsilane; the signals in the ^1H NMR spectra are singlets unless otherwise specified; the ratios of the signal intensities are given in parentheses.
[a] At −73 °C. [b] In Et_2O. [c] In $CDCl_3$. [d] In $MeCO_2Et$.

Table 10. Chemical shifts of signals in the ^1H, ^{13}C and ^{29}Si NMR spectra of hydrotrioxides derived from organosilicon compounds and related compounds.

Compound	X	δ ^1H	δ ^{13}C		δ $^{29}Si(1)$
			C(1)	C(Me)	
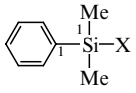	H	0.30 (Me), 4.40 (H)	140.6	−1.1	−16.95
	OH	0.32 (Me), 4.5 – 5.5 (OH)	143.5	3.1	3.30
	OOH	0.43 (Me), 11.2 (OOH)	139.6	2.8	14.31
	OOOH (**20a**)	0.55 (Me), 13.96 (OOOH)	138.5	2.7	17.31
	OOOH (**20a**) [a]	13.64 (OOOH)	–	–	–
	OOOH (**20a**) [b]	13.40 (OOOH)	–	–	–
	$OSiMe_2Ph$	0.33 (Me)	143.1	3.9	−0.96
	$OOSiMe_2Ph$	0.40 (Me)	139.5	2.8	16.6

Note. The spectra were measured in $(CD_3)_2CO$ at −78 °C; the chemical shifts are given in ppm relative to tetramethylsilane.
[a] In $MeCO_2Et$. [b] In Me_2O.

possibility of assigning the weaker signal to the ROOOH formed from the solvent was rejected.[17]

Based on the results of the concentration dependence and temperature variation studies, Plesničar *et al.*[17] concluded that HTO can form either intramolecularly hydrogen-bonded structures or rather strong eight-membered intermolecular associates.

In conclusion mention may be made of the first identification of isopropyl alcohol hydrotrioxide (**6f**) and hydrogen trioxide (**23**) by ^{17}O NMR spectroscopy.[94,95] The experimental results are in reasonable agreement with those of the *ab initio* GIAO/MP2/6-311++G** calculations of the ^{17}O chemical shifts. For HO(1)O(2)O(3)H (**23**), the experimental and calculated chemical shifts for the O(2) atom are 421 and 433 ppm, respectively, while δ[O(1,3)] = 305 (*cf.* the calculated value δ = 306). Hydrotrioxide $Me_2C(OH)$[O(1)O(2)O(3)H] (**6f**) is characterised by δ[O(1)] = 368, δ[O(2)] = 445 and δ[O(3)] = 305 (relative to $H_2{}^{17}O$). Probably, ^{17}O NMR spectroscopy of hydrotrioxides would serve as the basis for a breakthrough in understanding of the structure of organic HTO in the condensed phase.

IV. The mechanism of formation of organic hydrotrioxides

1. Experimental results

The reactions of ozone with C–H bonds of organic compounds leading to hydrotrioxides have been proposed to follow three main mechanisms, *viz*., a concerted 1,3-dipolar insertion of ozone (route *a*),[6,8,11,96,97] homolytic abstraction of an H atom by ozone followed by cage recombination of the radical pair (route *b*)[9,10,96,98] and ionic (molecular) mechanism (route *c*).[10,11,76,98]

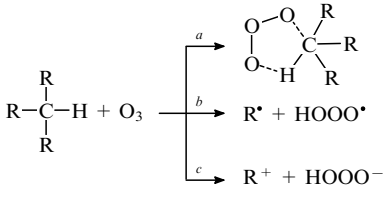

Obviously, the variety of transformations of organic compounds in the reactions with ozone to give HTO cannot be described by a common mechanism. In this connection, the

study by Giamalva, Church and Pryor[99] is remarkable. They proposed that the reactions of O_3 with a number of cage hydrocarbons proceed by the insertion mechanism (route *a*) with the feasible transition states considered to be a set of resonance structures including both the radical (route *b*) and ionic (route *c*) mechanisms as the limiting cases.

The dominating reaction mechanism depends on the nature of the substrate and oxidation conditions. Let us consider the experimental grounds that serve as the basis for inferences about the most plausible mechanism of the ozone reaction with the C–H bond.

a. Reaction kinetics

The pre-exponential factors for the reaction RH + O_3 (Table 11) are 2 to 3 orders of magnitude lower than those of typical radical abstraction reactions of the H atom.[101] The estimate $\log A \approx 6.5$ obtained for the 1,3-addition reaction (route *a*) (see Ref. 76) is close to the activation parameters listed in Table 11; however, the experimental activation energies are incompatible with the energies of formation of pentacoordinated carbon. Taking into account the strain energy in the five-membered ring in the transition state of the 1,3-addition reaction, the expected E_a value must lie between 20 and 26 kcal mol^{-1} (see Ref. 76).

Table 11. Activation parameters of the reactions of organic compounds with ozone.[100]

Substrate	Solvent	$\log A$ /litre mol^{-1} s^{-1}	E_a /kcal mol^{-1}
cyclo-C_6H_{12}	cyclo-C_6H_{12}	7.71	13.7
$PhPr^i$	$PhPr^i$	6.4	8.7
EtOH	EtOH	4.88	7.3
	MeCOOH	6.15	9.1
	CCl_4	6.81	10.0
cyclo-$C_6H_{11}OH$	CCl_4	6.26	7.9
MeCOEt	CCl_4	10.7	18.5

b. Kinetic isotope effect

Relatively high k_H/k_D values (see Table 12) indicate substantial weakening of the C–H bond in the transition state of the reaction RH + O_3. A large kinetic isotope effect is evidence for the linear transfer of a proton and its symmetric localisation in the transition state.[102] This conclusion contradicts the mechanism of 1,3-cycloaddition and precludes linear arrangement of the C, H and O atoms.

Table 12. Kinetic isotope effect in the oxidation of organic compounds by ozone.[10, 96, 100]

Substrate	Solvent	T/K	k_H/k_D
cyclo-C_6D_{12}	cyclo-C_6H_{12}–cyclo-C_5H_{10}	295	4.1–4.5
$PhCD_2OCMe_3$	Freon 11	273	3.8–4.1
$MeCD_2OCMe_3$	Me_2CO	273	2.4–4.5
$MeCD_2OH$	CCl_4	293	5.9

c. Relative reactivity

Ozone exhibits a much higher selectivity toward primary, secondary and tertiary C–H bonds (0.003 : 1 : 87) as compared to alkoxyl (0.08 : 1 : 33.7) and peroxyl (0.024 : 1 : 10) radicals.[4]

d. Structure of a substrate

It is remarkable that compounds used as substrates in the liquid-phase ozonisation to give HTO, *viz*., oxygen-containing compounds (acetals, ethers, alcohols), hydrocarbons (cumene, cage compounds, including those containing the cyclopropane fragment) and silanes exhibit a common feature consisting of the possibility of effective stabilisation of the derived carbocation. Ozone was found to react with the benzylic C–H bond of fluorene at a much lower rate than with the analogous bond in diphenylmethane and 9,10-dihydroanthracene derivatives.[103] The low reactivity of fluorene is due to the fact that the formation of a carbocation from fluorene is less energetically favourable than from the other two compounds.[103]

Studies within the same class of compounds showed that electron-donor substituents accelerate the reaction of the RH + O_3 type and that the apparent rate constant for the reaction series for substituted toluenes ($\rho = -2.07$) substantially differs from the ρ values for peroxyl (-0.76) and alkoxyl (-0.34) radicals.[4]

e. Solvent effect

The yields of HTO in the oxidation of aliphatic and aromatic acetals by ozone in polar solvents (acetone, diethyl ether) are much higher than in dichloromethane and pentane.[4, 19, 20]

f. Formation of charge-transfer complexes

Taking into account the high electron affinity of ozone, one can assume that the reaction with the appropriate substrate will proceed with partial transfer of the electron density to the O_3 molecule. Indeed, the reaction of ozone with alkylaromatic compounds (*e.g*., cumene) results in a charge-transfer complex, which was proved by spectroscopic methods.[104–107] Further nonradical transformation of the complex results in the hydrotrioxide. This is confirmed by a substantial increase in the yield of the hydrotrioxide **8** upon irradiation of the reaction mixture by light in the spectral region corresponding to absorption of the charge-transfer complex;[28, 29] the absence of kinetic isotope effect in the reaction of ozone complex with toluene-d_8[108] and by acceleration of the decomposition of ozone–arene complexes in polar solvents.[109]

2. Thermochemical analysis of the mechanisms of formation of ROOOH

Thermochemistry of the reactions of ozone with the C–H bonds was investigated taking the reaction with ethanol as an example. Detailed kinetic studies[24, 100] of the reaction revealed its first order with respect to both reagents, the rate constants were determined over a wide temperature range (see Table 11) and the dependence of the rate constant on the chemical nature of solvent was investigated.

At $T = 293$ K, the rate constant for the gas-phase reaction EtOH + O_3 is 0.72±0.06 litre mol^{-1} s^{-1}.

Let us consider a feasible mechanism for this reaction. α-Hydroxyethyl hydrotrioxide **6b** was reliably established[24, 100] to be the major product. As mentioned above, the mechanism of 1,3-dipolar insertion (route *a*), for which $\log A \approx 6.5$ and $E_a \approx 20-26$ kcal mol^{-1}, is inconsistent with the observed Arrhenius parameters (see Table 11).

The enthalpies of the reactions proceeding by routes *b* and *c* can be calculated using the following values (in kcal mol^{-1}): $\Delta_f H^\circ$(EtOH) = −56.1,[110] $\Delta_f H^\circ(O_3)$ = 34.0,[110] $\Delta_f H^\circ$(MeĊHOH) = −14.5±3,[111] $\Delta_f H^\circ$(MeC$^+$HOH) = 139±3[111] and $\Delta_f H^\circ$(HOOO$^\bullet$) = 15.3.[18] The $\Delta_f H^\circ$(HOOO$^-$) value can be found using the gas-phase acidity of HOOOH (352 kcal mol^{-1} obtained from the *ab initio* MP4//MP2/6-31++G* calculations[52]) and $\Delta_f H^\circ$(HOOOH) = −12.2 kcal mol^{-1} (see Ref. 18). Thus we get $\Delta_f H^\circ$(HOOO$^-$) = −25.9 kcal mol^{-1}.

The activation energy of the gas-phase reaction of ethanol with ozone was estimated using the experimental rate constant $k = 0.72$ litre mol^{-1} s^{-1} provided that $A = 1 \times 10^8$ litre mol^{-1} s^{-1} (see Ref. 112); this gives $E_a = 10.9$ kcal mol^{-1}.

The enthalpy of a reaction proceeding by the radical route *b* is

$$\Delta H^\circ(b) = \Delta_f H^\circ(\mathrm{MeC\dot{H}OH}) + \Delta_f H^\circ(\mathrm{HOO\dot{O}}) - \\ - \Delta_f H^\circ(\mathrm{EtOH}) - \Delta_f H^\circ(\mathrm{O_3}) = \\ = 15.3 - 14.5 - 34.0 + 56.1 = 22.9 \text{ kcal mol}^{-1}.$$

Comparison of the $\Delta H^\circ(b)$ and E_a values suggests that the homolytic mechanism for the formation of the hydrotrioxide **6b** is energetically unfavourable. In addition, both thermochemical estimates [18, 66] and quantum-chemical calculations [70, 71, 113] predict that the radical $HOOO^\bullet$ is less stable compared to its decomposition products ($HO^\bullet$ and O_2) and decomposes almost barrierlessly. This reduces the role of the radical $HOOO^\bullet$ in the formation of HTO from saturated organic compounds to a minimum. Thus, the homolytic mechanism (route *b*) is inconsistent with thermochemical estimates.

The enthalpy of the gas-phase reaction of the hydride ion transfer (route *c*) can be calculated using the following equation

$$\Delta H^\circ(c) = \Delta_f H^\circ(\mathrm{MeC^+HOH}) + \Delta_f H^\circ(\mathrm{HOOO^-}) - \\ - \Delta_f H^\circ(\mathrm{EtOH}) - \Delta_f H^\circ(\mathrm{O_3}) + E_q\,.$$

Here, E_q is the energy of the Coulomb interaction within the ion pair ($-e^2/r$), where r is the inter-charge separation. Assuming that $r = 2.65 \pm 0.05$ Å,[76] we get

$$\Delta H^\circ(c) = 139 - 25.9 - 34.0 + 56.1 - 125 = 10.2 \text{ kcal mol}^{-1}.$$

As can be seen, the calculated E_a value is in good agreement with $\Delta H^\circ(c)$.

Calculations of $\Delta H^\circ(c)$ values for liquid-phase reactions face considerable difficulties owing to the lack of reliable methods for calculating the solvation energies of reactants, $\Delta H^\circ(\mathrm{solv})$. A qualitative estimate, $\Delta H^\circ(\mathrm{solv}) < 0$, can be obtained by simply reasoning that the ionic character of the transition state will favour its solvation compared to the electrically neutral EtOH and O_3. It is also clear that $\Delta S_0(\mathrm{solv}) < 0$. Therefore, the $\log A$ and E_a values for the liquid phase will be smaller than those obtained for the gas phase, which is consistent with the experimental results (see Table 11). Nangia and Benson [76] used the Kirkwood formula for calculating the change in the Gibbs free energy of solvation. However, it was noted [100] that this approach *a priori* implies too strong a dependence of the rate constant for the reaction on the dielectric constant of the medium. We believe that a consistent explanation is that the actual transition state is not purely ionic but includes to a great extent the contribution of charge transfer from MeC^+HOH to $HOOO^-$.

3. Formation of hydrotrioxides in the ozonisation of hydrocarbons

Experiments show that the most plausible mechanism for the reaction of ozone with the C–H bonds of organic compounds involves a hydride transfer of hydrogen to ozone followed by cage recombination of the ion pair (route *c*). The reaction is favoured by some factors responsible for the stabilisation of the carbocation formed: the structure of the substrate, polar substituents in the substrate, the presence of electron-donor substituents at the reaction centre.

In the absence of these factors the most plausible mechanism for the reaction $RH + O_3$ involves a homolytic abstraction of a H atom by the ozone molecule. The energy profiles of the reactions of ozone with the C–H bonds of methane, ethane, propane and isobutane have been studied.[113] In the transition state, the H atom is nearly orthogonal to the plane passing through three oxygen atoms, which indicates the involvement of the π-MO of ozone in the formation of a new bond. The C–H–O angle is rather large (167 to 174°) and the C–H and H–O distances are close (1.28 and 1.25 Å for methane and 1.27 and 1.34 Å for isobutane, respectively). This is consistent with the results obtained in studies of the kinetic isotope effect (see Section IV.1). According to quantum-chemical calculations, all the localised transition states have large contributions of biradical structures. The radical $HOOO^\bullet$ formed in the reaction is extremely unstable and decomposes into the oxygen molecule and the hydroxyl radical

$$RH + O_3 \longrightarrow R^\bullet + HOOO^\bullet \longrightarrow R^\bullet + O_2 + {}^\bullet OH.$$

Thus, the probability of the homolytic mechanism of the ozonisation of hydrocarbons containing non-activated C–H bonds in the gas phase (or in non-polar solvents) is very low.

On the other hand, the contribution of radical structures to the transition state decreases as the number of alkyl substituents in the α-position relative to the C–H bond involved in the reaction increases.[113] Hence under specific conditions (*e.g.*, with appropriate substituents and medium) the ionic mechanism can become even more energetically favourable. This can occur in the ozonisation of alkanes in superacidic solutions at −78 °C.[114, 115] The reaction proceeds *via* a transition state with the 3c-2e bond between the protonated ozone, $HOOO^+$, and the C–H bond. The pentacoordinated carbonium ion either undergoes further decomposition or loses a proton to give the corresponding hydrotrioxide:

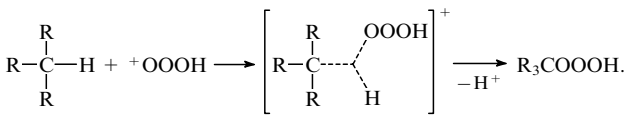

Yet another specific procedure for the preparation of hydrotrioxides of non-activated organic compounds is 'dry' ozonisation, *i.e.*, the reaction of ozone with hydrocarbons adsorbed on a polar surface. The synthesis of HTO **11** and **15**–**19** by 'dry' ozonisation of aliphatic, alicyclic and alkylaromatic hydrocarbons on silica gel has been reported.[18, 31, 32]

$$RH \xrightarrow[-70\ ^\circ C]{O_3,\ SiO_2} \underset{\mathbf{11,\ 15-19}}{ROOOH}.$$

It was also noted in these studies that hydrotrioxides **11** and **15**–**19** cannot be obtained by conventional liquid-phase oxidation.

Triphenylmethylhydrotrioxide **18** can be prepared not only by 'dry' ozonisation but also in solution. However, low solubility of triphenylmethane at temperatures near −70 °C precludes the synthesis of Ph_3COOOH in solution. In addition, this synthesis requires thermal activation or photoactivation of the intermediate complex $ArH \cdot O_3$, as in the case of cumyl hydrotrioxide.[28, 29] In 'dry' ozonisation, the polar surface acts as an activator.

We can distinguish several factors responsible for the differences between the low-temperature ozonisation of hydrocarbons on the surface and the ozonisation in solution. First, the concentrations of reagents on the surface of the adsorbent can be very high, which cannot be achieved in solution at low temperature. As a result, ozonisation on the surface proceeds much faster.[116] Second, low mobility of the adsorbed reagents, intermediates and products reduces the probability of side reactions and, hence, increases selectivity of the process. Finally, the surface of silica gel is a highly polar anisotropic medium, which stabilises the ionic intermediates. Thus, the formation of hydrotrioxides ROOOH by 'dry' ozonisation is yet another argument in favour of the ionic mechanism of the reactions of ozone with the C–H bonds of saturated organic compounds.

V. Decomposition of hydrotrioxides

1. Reaction products. Chemiluminescence

The thermolysis products of hydrotrioxides **1a**, **2**, **3d**, **3m**, **4h**, **5a**,**b**, **8** and **20a** are presented in Table 13. It should be noted that with a few exceptions (see notes to Table 13) the decomposition products were analysed together with the products formed in the synthesis of ROOOH; because of this, the yields of each of the products were calculated with respect to ozone consumed to give the

Table 13. Thermal decomposition products of ROOOH.

ROOOH	Solvent	Product	Yield [a] /mol mol^{-1}	Ref.
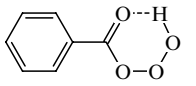 (**1a**)	RH	$PhCO_2H$	0.96	14
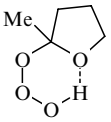 (**2**)	RH	$MeCOCH_2CH_2CH_2OH$	0.70 [b]	14
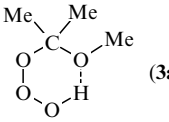 (**3a**)	CD_3COCD_3	Me_2CO MeOH HOOH $Me_2C(OMe)OOH$	0.32 0.29 0.05 0.03	95
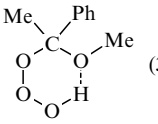 (**3b**)	Me_2CO $MeCO_2Et$	PhCOMe MeOH $PhCO_2Me$ $PhCO_2H$	0.50 0.14 0.20 0.05	17
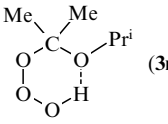 (**3m**)	RH	$Me_2CO : Me_2CHOH : MeCO_2Pr^i = 1 : 1.3 : 2.7$		96
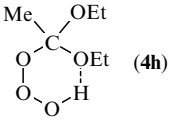 (**4h**)	RH	$MeCO_2Et$ EtOH	0.80 – 0.85 0.75 – 0.80	20
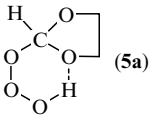 (**5a**)	RH	$HCOOCH_2CH_2OH$	1.0	23
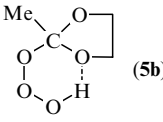 (**5b**)	RH	$MeCO_2CH_2CH_2OH$	1.0	23
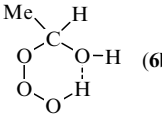 (**6b**)	RH	MeCHO $MeCO_2H$ HCOOH HOOH	0.31 0.56 0.12 0.58	25, 100
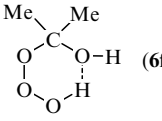 (**6f**)	Bu^tCOMe	Me_2CO $MeCO_2H$ HOOH	0.37 0.39 0.11	95
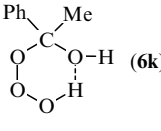 (**6k**)	Me_2CO $MeCO_2Et$	PhCOMe $PhCO_2H$	0.65 0.05	17
$PhMe_2COOOH$ (**8**)	CD_3COCD_3	$PhMe_2COH$ PhCOMe	0.8 – 0.9 [c] 0.1 – 0.2 [d]	29
$PhMe_2SiOOOH$ (**20a**)	CD_3COCD_3	$PhMe_2SiOH$ $PhMe_2SiOSiMe_2Ph$ H_2O_2 $PhMe_2SiOOH$	0.9 [c] 0.08 0.09 0.05	33

Note. Hydrotrioxides ROOOH were obtained by oxidation of the corresponding substrates RH. [a] The yields are given with respect to ozone consumed in the reactions, $\Delta(O_3)$. [b] The product undergoes further cyclisation and dehydration to give 2-methyl-4,5-dihydrofuran. [c] The yields are given with respect to HTO. [d] The yield is given with respect to Δ[ROOOH]; decomposition of the hydrotrioxide **8** in the presence of ionol results in $PhMe_2COH$ as the only reaction product.

particular product, $\Delta[P]/\Delta(O_3)$. All the reactions are accompanied by evolution of molecular oxygen including $^1O_2$.

According to the data listed in Table 13 thermal decomposition reactions of the hydrotrioxides derived from benzaldehyde (**1a**), acetals (**4h**, **5a**,**b**), cumene (**8**) and dimethylphenylsilane (**20a**) in which the reaction products are formed in nearly 100% yields exhibit the highest selectivities. As was mentioned above, silane-derived hydrotrioxides decompose to give, in particular, HOOOH.[33,34] Taking hydrotrioxide **6b** as an example, it was shown that the yields of the major decomposition products, *viz*., $\Delta[P]/\Delta(O_3) = 0.30\pm0.04$ for MeCHO, 0.56 ± 0.03 for MeCOOH, 0.11 ± 0.03 for HCOOH and 0.57 ± 0.03 for H_2O_2, are virtually independent of temperature in the range between -78 and 0 °C.[25]

Decomposition of HTO is accompanied by chemiluminescence in the visible spectral region.[16,21,27,117–119] The chemiluminescence spectra of compounds **8**, **6d**, **6f**, **6e**, **7a**, **3m** and **1** exhibit maxima (λ) at 425, 425, 405, 405, 405, 405 and 515 nm, respectively. No chemiluminescence was observed in the thermolysis of the hydrotrioxide **6b**. Based on comparison of both the fluorescence and phosphorescence spectra of the carbonyl compounds which resulted from decomposition of ROOOH and the chemiluminescence spectra in the visible spectral region it was concluded that the emitters of chemiluminescence are excited carbonyl groups ($>C=O^*$).

One of the most interesting and important properties of hydrotrioxides is their ability to generate $^1O_2$ during thermal decomposition.[13,14,16,17,19–21,27,31–33,35,52,89,117,118,120–122] The formation of singlet molecular oxygen was proved by carrying out specific reactions of singlet oxygenation of unsaturated organic compounds (see Section VII.1). Yet another convincing proof of the formation of $^1O_2$ is intense chemiluminescence in the IR spectral region with a maximum at $\sim$1270 nm, which is typical of O_2 ($^1\Delta_g$).[123]

Chemiluminescence in the visible and IR spectral regions has also been observed in the decomposition of adamantyl hydrotrioxide **15** on the surfaces of silica gel and alumina.[32,39] Spectral characteristics of chemiluminescence were found to be identical with those observed in the liquid phase. The yield of singlet molecular oxygen was determined by three methods.

The first method involved measurements of the amount of the $^1O_2$ acceptor consumed (1,3-diphenylisobenzofuran, 1,2-dimethylcyclohexene or tetraphenylcyclopentadienone).[13–15,17,19,20,28,29,35] The yield of singlet molecular oxygen ($\Phi_0 = \Delta[^1O_2]/\Delta[ROOOH]$ /mol mol^{-1}) was calculated based on the assumption that the amount of $^1O_2$ that evolved in the reaction ($\Delta[^1O_2]$) is equal to the amount of acceptor consumed ($\Delta[A]$). However, this approach provides only semiquantitative data on the yield of $^1O_2$,[124] so it is not surprising that the results obtained in the experiments with different $^1O_2$ acceptors differ substantially. For instance, the $\Delta[^1O_2]/\Delta[ROOOH]$ values for 1,1-diethoxyethane-derived hydrotrioxide (**4h**) found using tetraphenylcyclopentadienone and 1,3-diphenylisobenzofuran were $20\pm5\%$ and $54\pm5\%$, respectively.[20] Quantitative determination of the yield of $^1O_2$ requires a kinetic approach based on rigorous analysis of all possible consumption channels for the $^1O_2$ acceptor, hydrotrioxide and singlet molecular oxygen. The drawback of this method is that the acceptor of singlet molecular oxygen can be oxidised by the hydrotrioxide, which leads to overestimation of the results of measurements of the Φ_0 values.

Generation of $^1O_2$ in the decomposition of ROOOH, its deactivation and quenching by acceptors A was found [16] to follow a mechanism similar to that of the thermolysis of organic phosphite ozonides [124]

$$ROOOH \xrightarrow{k_0} P_0 + O_2,\ ^1O_2,$$

$$^1O_2 \xrightarrow{k_d} O_2, h\nu,$$

$$^1O_2 + A \xrightarrow{k_r} AO_2,$$

$$^1O_2 + A \xrightarrow{k_q} A + O_2,$$

where k_0, k_d, k_r and k_q are the rate constants for thermal decomposition of the hydrotrioxide, radiative deactivation of singlet molecular oxygen and chemical and physical quenching of $^1O_2$ by the acceptor A, respectively; and P_0 is the decomposition product of the hydrotrioxide.

Based on this mechanism, for the steady state we get

$$\ln\left(\frac{I_0}{I_t}\right) = k_0 t, \tag{10}$$

$$\frac{I_0}{I_A} = 1 + k\tau_d[A], \tag{11}$$

$$\frac{[A]_0 - [A]_\infty}{[ROOOH]_0} = \Phi_0\Phi_r - (k\tau_d)^{-1}\left\{\frac{\ln([A]_0/[A]_\infty)}{[ROOOH]_0}\right\}. \tag{12}$$

Here I_0 and I_A are the initial intensities of chemiluminescence in the absence and in the presence of the acceptor A, respectively; I_t is the current intensity of chemiluminescence in the absence of the acceptor; t is time; $k = k_r + k_q$; $\tau_d = 1/k_d$ is the lifetime of $^1O_2$ in the solvent specified; $[A]_\infty$ is the concentration of the acceptor in the reaction mixture after complete decomposition of ROOOH ($t \to \infty$); and $\Phi_r = k_r/(k_q + k_r)$.

Equation (10) can be used to follow the kinetics of the overall decomposition of ROOOH in the absence of the acceptor A. The Stern–Volmer equation (11) allows determination of the parameter $k\tau_d$ and calculation of the overall rate constant for quenching of singlet molecular oxygen by the substrate A provided that τ_d is known. This approach was used [120–122] for calculations of the k values for quenching of $^1O_2$ that evolved during the decomposition of hydrotrioxides **4h**, **6b**,**f** and **7b** by alkenes, dienes, phenols, glycosides and flavonoids.

The yield of $^1O_2$ can be determined from Eqn (12) using the Φ_r and $(k\tau_d)^{-1}$ values that can be found experimentally. Preference should be given to those acceptors which are characterised by high k_r values and $\Phi_r \approx 1$ (*e.g.*, 1,3-diphenylisobenzofuran). The results obtained by this method for hydrotrioxides **3m**, **4h** and **6b**,**f** are listed in Table 14. This approach is appropriate in the case of systems with relatively low concentrations of the acceptor (10^{-5} to 10^{-3} mol litre^{-1}). If the initial concentrations of the acceptor ($[A]_0$) are high, account must be taken of the reaction of the acceptor with HTO.

Yet another procedure for the determination of Φ_0 involves measurements and comparison of total light emissions for the reactions of thermal decomposition of ROOOH under study and a standard source of $^1O_2$ (*e.g.*, triphenyl phosphite ozonide).[18] This method has been employed for the determination of Φ_0 in the recombination of peroxyl radicals [125] and decomposition of di(*tert*-butyl) trioxide in various solvents.[126] The Φ_0 values were calculated using Eqn (13)

$$\Phi_0 = \Phi_{st}\frac{S_{ROOOH}}{S_{st}}\frac{k_d}{k_d^{st}}\frac{k_r^{st}}{k_r}\frac{[(PhO)_3PO_3]_0}{[ROOOH]_0}, \tag{13}$$

where Φ_0 is the yield of singlet molecular oxygen per 1 mol of HTO decomposed; $\Phi_{st} = 1$ (see Ref. 124) is the yield of singlet molecular oxygen in the decomposition of the standard source of $^1O_2$ (triphenyl phosphite ozonide); and S_{ROOOH} and S_{st} are the areas under the chemiluminescence decay curves for the decomposition of ROOOH and the standard source of $^1O_2$, respectively.

The Φ_0 values for a number of HTO are listed in Table 14. In all cases, except for hydrotrioxide **6f** in propan-2-ol, methods A and D give close Φ_0 values which are much smaller than the yields of $^1O_2$ calculated by methods B and C. This suggests that HTO are efficient sources of singlet molecular oxygen, though their efficiency has sometimes been overestimated.

Table 14. The yield of singlet molecular oxygen upon thermolysis of hydrotrioxides.[14, 16, 18, 20, 89]

Hydrotrioxide	Solvent	T /°C	Φ_0 (%)	Method of determination of Φ_0 [a]
1a	CH_2Cl_2	4.5	0.04	A
	Et_2O	−30	0.02	see [b]
	RH	⩾ −50	96	B
2	RH	⩾ −70	80	B
3a	RH	⩾ −23	30	B
3b	Me_2CO	–	45	B
	Me_2CO	–	22	C
3h	CH_2Cl_2	3.0	10.1	A
3m	CH_2Cl_2	6.0	5.0	A
	RH	−10	1.7	D
4h	CH_2Cl_2	7.5	19.0	A
	RH	−58	7.3	D
	RH	−45	5.2	D
	RH	⩾ −50	54	B
	RH	⩾ −50	20	C
5c	CH_2Cl_2	5.0	0.5	A
6a	CH_2Cl_2	6.0	2.5	A
6b	CH_2Cl_2	6.5	13.6	A
	RH	−20	10.3	D
6f	CH_2Cl_2	8.0	8.0	A
	PhCl	0	7.0	D
	RH	−29	78	D
	RH	−20	70	D
	RH	−10	55	D
	RH	−2.5	48	D
6k	Me_2CO	–	60	B
	Me_2CO	–	25	C
7a	CH_2Cl_2	6.0	3.0	A
11	CH_2Cl_2	6.0	1.2	A
15	CH_2Cl_2	−3.0	7.2	A
	CH_2Cl_2	12.0	6.4	A
16	CH_2Cl_2	15.0	15.0	A
18	CH_2Cl_2	5.0	2.6	A
19	CH_2Cl_2	12.0	5.2	A
	CH_2Cl_2	6.0	5.6	A
20a	CD_3COCD_3	⩾ −78	65	B
	CD_3COCD_3	⩾ −78	25	C

Note. Hydrotrioxides ROOOH were obtained by oxidation of the corresponding substrates RH. [a] For methods A and D, the yield of $^1O_2$ was determined from Eqn (10) and Eqn (12), respectively; for methods B and C, the Φ_0 value was determined by following the consumption of the acceptors of singlet molecular oxygen, *viz*., 1,3-diphenylisobenzofuran (B) and tetraphenylcyclopentadienone (C). [b] The HTO was decomposed by a light pulse (λ = 266 nm), the Φ_0 value was determined from the relative intensity of chemiluminescence at λ = 1270 nm.

The influence of the reaction conditions on the yield of singlet molecular oxygen has been studied.[16, 18] It was found that the Φ_0 value decreases as the initial concentration of hydrotrioxide **3m** ([**3m**]$_0$) increases. This effect was explained by an increase in the contribution of 'blank' decomposition (without production of $^1O_2$) of ROOOH induced by free radicals with an increase in [**3m**]$_0$.[18] Taking hydrotrioxides **6f** [16] and **6b** [18] as examples, it was shown that the increase in temperature leads to a decrease in Φ_0. For compound **6b**, the temperature dependence of Φ_0 is satisfactorily described by the Bagdasaryan equation.[127] It seems likely that singlet molecular oxygen can be produced either by molecular conversion of ROOOH or as a result of disproportionation of the solvent-caged radical pair, [RO$^{\bullet}$ $^{\bullet}$OOH]. In a recent study,[18] preference has been given to the latter mechanism for the formation of ROOOH.

Table 15. Effect of solvents on the rate constant for decomposition and on the yield of singlet molecular oxygen in thermolysis of the hydrotrioxide **6b** {5 °C, [MeCH(OH)OOOH] = 0.011 mol litre^{-1}}.

Solvent	$10^3 k$ /s^{-1}	Φ_0 (%)	Solvent	$10^3 k$ /s^{-1}	Φ_0 (%)
$CFCl_3$	47.7	18.1	$C_6D_5CD_3$	21.4	13.6
CCl_4	57.4	10.1	$PhCH_2Cl$	10.6	10.4
$CHCl_3$	42.5	15.2	$PhCH_2OH$	40.0	1.6
CH_2Cl_2	31.5	13.3	PhEt	22.6	7.6
$C_2H_4Cl_2$	22.7	11.6	$PhPr^i$	32.8	5.6
PhH	28.9	8.0	Me_2CO	3.6	14.6
PhCl	34.0	6.4	MeCN	9.0	12.7
PhMe	24.4	13.0	$MeNO_2$	22.0	0.9

Solvent has a pronounced effect on Φ_0 in the case of thermal decomposition of the hydrotrioxide **6b** (Table 15). Using the Koppel – Palm correlation equation, the yield of $^1O_2$ was analysed as the function of the properties of the solvent and it was found that the yield of singlet molecular oxygen, Φ_0, increases as the solvent polarity increases, whereas enhancement of specific solvation in the transition state leads to a decrease in Φ_0.[18]

2. The kinetics of overall decomposition of hydrotrioxides

The kinetics of overall decomposition of HTO is studied by ^{1}H NMR spectroscopy (as the basic method) and chemiluminescence technique. Within the limits of experimental errors, both methods give usually the same results. Decomposition of ROOOH proceeds as a first-order reaction [14 – 21, 23, 24, 26 – 29, 31, 33, 35, 89, 119, 128]

$$-\frac{d[ROOOH]}{dt} = k_0[ROOOH].$$

The available rate constants k_0 and activation parameters of the reaction are collected in Table 16. The $\log A_0$ and E_0 values are related by a linear dependence (the compensation effect):

$$\log A_0 = -3.5 + 0.95\,E_0\,.$$

This dependence holds for a very broad range of changes in E_0 (from 1.7 to 25.1) and $\log A_0$ (from 0.2 to 21.6). It covers almost all available experimental data (Fig. 1) and suggests a common mechanism for the decomposition of ROOOH. The linear dependence between $\log A_0$ and E_0 indicates that the linear free energy relationship and the correlation equations based on it which relate the reactivity of HTO to their structure and to the physicochemical properties of the medium should also hold in the case of thermal decomposition of ROOOH in the liquid phase.

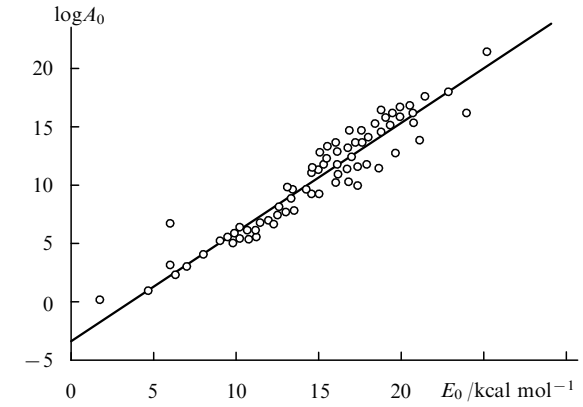

Figure 1. Compensation effect in the thermal decomposition of hydrotrioxides.

Table 16. Kinetic parameters of the overall decomposition of hydrotrioxides.

Compound	Solvent	Temperature /°C	$\log A_0$ ($\log k_0$)	E_a /kcal mol^{-1}	$\Delta G^{\neq}$ /kcal mol^{-1}	$\Delta H^{\neq}$ /kcal mol^{-1}	$\Delta S^{\neq}$ /cal mol^{-1} K^{-1}	Ref.
1a	RH	−34 – 12	5.4	10.7	19.2	10.2	−35.5	14
	RH : Et_2O = 21.3 : 78.7 (mass %)	−39 to −19	11.1	16.4	18.3	15.9	−9.4	14
	Et_2O	–	10.1	17.2	20.3	16.7	−14.1	89
	RH	0	(−3.16)	–	–	–	–	129
1b	CH_2Cl_2 : MeOH = 1 : 1 (vol.%)	−50 – 30	7.7	13.0	–	–	–	16
1c	CH_2Cl_2 : MeOH = 1 : 1 (vol.%)	−50 – 30	5.45	10.1	–	–	–	16
1d	CH_2Cl_2 : MeOH = 1 : 1 (vol.%)	−50 – 30	2.3	6.3	–	–	–	16
1e	CH_2Cl_2 : MeOH = 1 : 1 (vol.%)	−50 – 30	5.45	10.3	–	–	–	16
1f	CH_2Cl_2 : MeOH = 1 : 1 (vol.%)	−50 – 30	5.7	11.2	–	–	–	16
2	RH	−68 to −6	4.1	8.0	18.0	7.5	−41.4	14
	RH : Et_2O = 15.4 : 84.6 (mass %)	−33 to −11	11.7	17.4	18.6	16.9	−6.6	14
3a	RH	−38 to −9	11.5	16.6	18.0	16.1	−7.6	14
3b	Me_2CO	−30 to −10	16.0	19.9	16.1	19.4	13.0	17
	$MeCO_2Et$	−25 to −15	14.2	18.0	16.3	17.5	4.8	17
	$MeCO_2Et$ [a]	−25 to −15	15.3	19.3	16.3	18.8	9.8	17
	Freon 11/12	−20	(−1.73)	–	–	–	–	17
	Freon 11/12	−25	(−1.98)	–	–	–	–	17
	Et_2O	−45 to −35	12.9	15.1	16.4	14.6	7.2	17
	Me_2CO [a]	−30 to −15	16.4	20.6	16.3	20.1	14.8	17
	Et_2O [a]	−45 to −35	13.3	15.5	14.8	15.0	0.7	17
3c	Me_2CO	−30 to −10	13.8	17.6	16.4	17.1	3.0	17
	$MeCO_2Et$	−30 to −15	11.8	15.3	16.4	14.8	−6.2	17
	Et_2O	−50 to −35	16.4	18.8	14.9	18.3	13.4	17
3d	Et_2O	−45 to −30	13.7	16.0	14.9	15.5	2.5	17
3e	$MeCO_2Et$	−25	(−1.73)	–	–	–	–	17
	$MeCO_2Et$	−20	(−1.42)	–	–	–	–	17
	Et_2O	−45 to −35	13.2	15.5	15.0	15.0	0.2	17
3f	Et_2O	−55 to −40	14.8	16.8	15.1	16.3	4.9	17
3g	Me_2CO	−30 to −20	16.8	20.4	15.7	19.9	16.7	17
	$MeCO_2Et$	−20 to −10	11.5	14.8	16.2	14.3	−7.6	17
	Et_2O	−55 to −35	14.7	16.9	15.9	16.4	2.1	17
3i	Et_2O	−40 to −25	12.3	15.4	15.9	14.9	−3.9	17
3j	Et_2O	−40 to −30	11.6	14.6	15.9	14.1	−7.1	17
3k	Et_2O	−50 to −35	16.4	19.2	14.9	18.7	14.9	17
3l	Et_2O	−50 to −35	14.8	17.6	15.2	17.1	7.5	17
3m	RH	−50 – 30	11.0	16.2	–	–	–	16
4a	RH	−20 to −10	15.6	20.7	17.4	20.2	11.2	20
	RH : CH_2Cl_2 = 3 : 7 (mass %)	−10	(−1.40)	–	–	–	–	20
	RH : Et_2O = 3 : 7 (mass %)	−20 to −10	11.8	16.1	17.2	15.6	−6.2	20
4b	RH : Et_2O = 3 : 7 (mass %)	−40 to −30	15.9	19.0	15.3	18.5	12.6	20
4c	RH : Et_2O = 3 : 7 (mass %)	−35 to −20	17.8	21.4	15.5	20.9	21.3	20
4d	RH : Et_2O = 3 : 7 (mass %)	−35 to −25	13.7	17.2	16.1	16.7	2.5	20
4e	RH : Et_2O = 3 : 7 (mass %)	−40 to −30	16.4	19.5	15.2	19.0	14.9	20
4f	RH : Et_2O = 3 : 7 (mass %)	−40 to −35	15.4	18.4	15.3	17.9	10.3	20
4g	RH : Et_2O = 3 : 7 (mass %)	−35 to −25	21.6	25.1	15.7	24.6	35.1	20
4h	RH	−20 to −10	11.1	14.5	16.4	14.0	−9.4	20
	RH : Et_2O = 3 : 7 (mass %)	−20 to −10	9.8	13.2	16.6	12.7	−15.3	20
	RH [b]	−50 to −10	18.2	22.8	16.5	22.3	23.1	21
4i	RH : Et_2O = 3 : 7 (mass %)	−40 to −30	16.7	19.8	15.2	19.3	16.2	20
5a	RH	−30	(−4.15)	–	–	–	–	23
5b	RH	−30	(−3.85)	–	–	–	–	23
5d	RH : CH_2Cl_2 = 3 : 7 (mass %)	−30 to −20	16.6	20.5	16.0	20.0	15.8	20
	RH : Et_2O = 3 : 7 (mass %)	−40 to −30	13.1	15.9	15.5	15.4	−2.4	20
4n	CH_2Cl_2	−30 to −20	14.7	18.7	16.4	18.2	7.1	20
	RH : Et_2O = 3 : 7 (mass %)	−40	(−1.96)	–	–	–	–	20
5f	RH : Et_2O = 3 : 7 (mass %)	−40	(−1.57)	–	–	–	–	20
6b	RH	−70 to −30	3.08	7.0	18.2	6.5	−46.1	24
	CH_2Cl_2	−15 – 18	8.1	12.6	–	–	–	18
6c	CH_2Cl_2	−20	(−2.12)	–	–	–	–	26
6d	RH	−30 – 8	12.6	17.0	17.1	16.5	−2.5	26
	CH_2Cl_2	−20	(−1.43)	–	–	–	–	26
6e	RH	−20	(−1.51)	–	–	–	–	26
	CH_2Cl_2	−20	(−1.59)	–	–	–	–	26

Table 16 (continued).

Compound	Solvent	Temperature /°C	$\log A_0$ ($\log k_0$)	E_a /kcal mol^{-1}	$\Delta G^{\neq}$ /kcal mol^{-1}	$\Delta H^{\neq}$ /kcal mol^{-1}	$\Delta S^{\neq}$ /cal mol^{-1} K^{-1}	Ref.
6f	RH	−30 – 8	7.93	13.4	19.0	12.9	−23.9	26
6f	CH_2Cl_2	−20	(−2.55)	–	–	–	–	26
	$CHCl_3$	−20 – 5	11.9	17.8	18.8	17.3	−5.7	26
	CCl_4	−10 – 5	6.37	10.2	17.6	9.7	−31.0	26
	n-C_6H_{14}	−30 – 0	6.17	11.2	18.78	10.7	−31.9	26
	MeCN	−20 – 6	0.16	1.72	16.3	1.2	−59.5	26
	EtOH : H_2O = 4 : 1 (vol.%)	−20 – 8	5.32	9.0	17.6	8.5	−35.9	26
	EtOH : H_2O = 1 : 4 (vol.%)	0	(−2.27)	–	–	–	–	26
	Et_2O [b]	−20 – 0	10.32	16.8	19.6	16.3	−13.0	26
6g	Pr^iOH	−30 – 8	9.73	14.3	17.8	13.8	−15.7	26
6h	RH	−30 – 8	6.19	10.7	18.3	10.2	−31.9	26
	CH_2Cl_2	−20	(−2.29)	–	–	–	–	26
6i	CH_2Cl_2	−30 – 8	9.69	13.4	16.9	12.9	−15.9	26
6j	CH_2Cl_2	−30 – 8	3.15	6.0	17.1	5.5	−45.8	26
6k	Me_2CO	−35 to −15	13.4	16.9	16.1	16.4	1.1	17
	$MeCO_2Et$	−40 to −15	13.6	17.0	16.0	16.5	2.1	17
	EtO	−30 to −20	13.3	16.8	16.1	16.3	0.7	17
7b	RH	−31 – 0	6.92	11.4	18.1	10.9	−28.5	27
8	$(CD_3)_2CO$	−33 to −12	10.4	16.0	18.7	15.5	−12.6	29
	$(CD_3)_2CO$ [c]	−18 to −3	16.4	23.9	19.6	23.4	14.9	29
11	CH_2Cl_2 [d]	6 – 26	9.2	15.0	–	–	–	18
	CH_2Cl_2 [d]	5 – 30	10.2	16.0	–	–	–	18
15	CH_2Cl_2 [d]	0 – 27	9.5	15.0	–	–	–	18
	CH_2Cl_2 [d]	1 – 20	14.0	21.0	–	–	–	18
	CH_2Cl_2 [d]	0 – 27	9.3	14.6	–	–	–	18
	Me_2CO [d]	4 – 18	12.9	19.6	–	–	–	18
16	CH_2Cl_2 [d]	−7 – 17	7.0	11.9	–	–	–	18
	CH_2Cl_2 [d]	6 – 27	7.1	11.9	–	–	–	18
	Me_2CO [d]	5 – 27	5.1	9.8	–	–	–	18
18	CH_2Cl_2	−2 – 20	9.0	13.3	–	–	–	18
19	CH_2Cl_2 [d]	7 – 27	11.5	18.6	–	–	–	18
	CH_2Cl_2 [d]	7 – 27	6.8	12.2	–	–	–	18
20a	$(CD_3)_2CO$	−80 to −65	1.0	4.7	18.3	4.2	−55.6	33
	$(CD_3)_2CO$ [b]	−60 to −20	5.5	9.5	17.9	9.0	−35.0	33
	Me_2O	−60 to −30	8.2	12.6	17.8	12.1	−22.7	33
	$MeCO_2Me$	−70 to −20	5.9	10.0	17.9	9.5	−33.2	33
21a	CH_2Cl_2	−60	(−2.33) [e]	–	–	–	–	35
	CS_2	−60	(−1.16) [e]	–	–	–	–	35
	$(CD_3)_2CO$	−54 to −40	–	–	~17 [f]	17.2	1.6	36
21b	RH	−70 to −50	6.84	6.0	–	–	–	37
22	$(CD_3)_2CO$	−50 to −35	–	–	~17 [f]	13.3	−17	36
23	$(CD_3)_2CO$	−50 – 10	6.1	11.0	18.7	10.5	−32.3	34
	$(CD_3)_2CO$	−20 – 10	7.7	13.0	18.8	12.5	−25.0	34
	$MeCO_2Me$	−20 – 10	7.5	12.5	18.5	12.0	−25.9	34
	$(CD_3)_2CO$ [c]	−20 – 10	6.1	11.3	19.0	10.8	−32.3	34
	$(CD_3)_2CO$ [c]	−20 – 10	5.8	11.2	19.2	10.7	−33.6	34
	$MeCO_2Me$ [c]	−20 – 10	5.8	10.8	18.8	10.3	−33.6	34

Note. The A_0 and k_0 values are given in s^{-1}; the $\Delta G^{\neq}$, $\Delta H^{\neq}$ and $\Delta S^{\neq}$ values were calculated using the data taken from the corresponding references (−20 °C). Hydrotrioxides ROOOH were obtained by oxidation of the corresponding substrates RH. [a] In the presence of 2,6-di-*tert*-butyl-4-methylphenol. [b] The addition of 2,6-di-*tert*-butyl-4-methylphenol has no effect on k_0. [c] In the presence of 2,6-di-*tert*-butyl-4-methylphenol. [d] The rate constant depends on the initial concentration of hydrotrioxide which was varied between 2×10^{-3} and 8×10^{-3} mol litre^{-1}. [e] Calculated from $\tau_{1/2}$. [f] The thermodynamic parameters are given for $T = -50$ °C.

Indeed, analysis of the kinetics of decomposition of hydrotrioxides derived from benzaldehydes **1b**–**f**, acetals **4b**–**g**, benzyl methyl ethers **3b**–**g**, alcohols **6b**–**j** and silanes **20a**–**d** using the Hammett – Taft equation shows that the rate constant for thermal decomposition of ROOOH increases as the electron-acceptor properties of substituent R become stronger [16, 17, 20, 33] and its polarity increases.[26]

The effect of the solvent nature on the rate constant of the overall decomposition has been studied taking hydrotrioxides **6b**,**f** (see Table 16) as examples.[26] Both dependences can be described using the Koppel – Palm correlation equation:

$$\log k_0 = \log k_0^0 + yY + pP + eE + bB,$$

where Y, P, E, B are empirical parameters which describe the polarity, polarisability, specific electrophilic solvation ability and specific nucleophilic solvation ability of the solvent, respectively.

However, the regression coefficients at the parameters Y, P, E and B differ appreciably for the two structurally similar HTO.

Presumably, this points to a formal type of description of the dependence of the rate constant for thermal decomposition of ROOOH on the chemical nature of the solvent rather than a real influence of different solvation mechanisms on the reactivity of HTO.

The activation parameters of the overall decomposition of ROOOH in the presence of inhibitors of radical-chain processes are listed in Table 16. The rate constant for decomposition of the hydrotrioxide **8** substantially decreases in the presence of ionol.[28,29] In other cases, inhibitors have little or even no effect on the rate constant.

3. Radical decomposition of hydrotrioxides

ESR studies showed that free radicals are generated only in the decomposition of cumyl hydrotrioxide (**8**).[29] The ESR spectrum is a single line with $g = 2.0151$, which is typical of peroxyl radicals. Some other examples of detection and identification of free radicals in the presence of spin traps have been reported.[130] Decomposition of HTO synthesised from methyl oleate, 2-methyl-1,3-dioxolane, propan-2-ol, 1,1-diethoxyethane, diisopropyl ether, benzaldehyde, methyl α-methylbenzyl ether and dimethylphenylsilane was studied and the spin traps used were 2-methyl-2-nitrosopropane, *C*-phenyl-*N*-*tert*-butylnitrone and methyl-*N*-(2,3,5,6-tetramethylphenyl)nitrone. Spin trap technique has also been used to identify alkyl, acyl, alkoxyl and peroxyl radicals.[17,21,22,131]

It should be noted that this method does not allow unambiguous inference about the initial products of radical decomposition of HTO. First, spin trap technique allows detection of only those radicals which form stable adducts. Second, not only the primary reaction products but also the radicals formed in the secondary reactions (reaction with the solvent, transformation of an adduct into another one[130]) are trapped in this case. Third, the spin trap is often oxidised by the hydrotrioxide to give a paramagnetic adduct.

The ratio of the radical and non-radical routes of decomposition of ROOOH was determined[21,128,129] taking the decomposition of HTO in the presence of di(*p*-methoxyphenyl)nitroxyl (an acceptor of free radicals) as an example (Table 17). The contribution of radical decomposition, k_r/k_0, varies from 0 (**6f**, EtOH : H_2O = 1 : 4) to ~23% (**1a**, PhCHO). The contribution of homolytic decomposition of ROOOH depends on the structure of HTO and temperature. For the hydrotrioxide **6f**, $\log k_r = (16.7\pm0.9)-(25.2\pm2.5)/\theta$ ($\theta = 2.303RT$/kcal mol^{-1}).

The nature of the solvent has a pronounced effect on the rate constant for radical decomposition. However, the ratio of radical and non-radical routes of decomposition remains virtually constant (see Table 17).

Table 17. Kinetic parameters of the radical decomposition of hydrotrioxides.[21,129]

Hydrotrioxide	Solvent	T/°C	$10^5 k_r$/s^{-1}	$10^2(k_r/k_0)$
1a	PhCHO	−20	1.90	12.7
	PhCHO	0	15.7	22.8
3m	Pr^i_2CO	0	0.125	0.007
4h	$MeCH(OEt)_2$	−45	1.26	0.59
6f	Pr^iOH	−30	0.019	0.25
	Pr^iOH	−10	2.10	3.48
	Pr^iOH	0	5.75	3.89
	$CHCl_3$	0	13.20	3.47
	n-C_6H_{14}	0	1.65	0.81
	Et_2O	0	0.605	0.39
	EtOH : H_2O (4 : 1)	0	3.02	0.19
	MeCN	0	1.19	0.04
	EtOH : H_2O (4 : 1)	0	0	0

4. Catalytic decomposition of hydrotrioxides

Acid- and amine-catalysed decomposition of HTO is of interest since it allows both extension of the temperature range in which these compounds can be used for generation of singlet molecular oxygen (Section V.1) and free radicals (Section V.3) and controllability of the rate of these reactions. Catalytic effect of organic acids and amines on the decomposition of HTO has been studied.[132,133] Catalytic effects of strong mineral acids (H_2SO_4 and $HClO_4$) on the decomposition of HOOOH[134] and of *N*,*N*-dimethylacetamide on the decomposition of hydrotrioxides derived from alkyl α-methylbenzyl ethers[17] have also been reported.

a. Amine-catalysed overall decomposition of organic hydrotrioxides

The kinetics of decomposition of hydrotrioxides **1a**, **3m**, **4h** and **6f** in the presence of amines (triethylamine; pyridine; 2-methylpyridine; 3-methylpyridine; 4-methylpyridine; 2-bromopyridine; 2,4-dimethylpyridine; 2,6-dimethylpyridine and quinoline) has been studied by ^{1}H NMR spectroscopy and chemiluminescence method.[132]

In the presence of amines, the rate constant for the decomposition of the hydrotrioxide **6f** increases. A similar effect is also observed upon addition of triethylamine and pyridine to benzaldehyde-derived hydrotrioxide (**1a**). However, the addition of pyridine [$(4-50)\times10^{-3}$ mol litre^{-1}] to hydrotrioxides **3m** and **4h** has no catalytic effect on their decomposition.

Catalytic decomposition in the presence of amines seems to follow a complex mechanism. On the other hand, the main channels of consumption of the ROOOH and amine can be described by a simple scheme:

$$\mathrm{ROOOH} \xrightarrow{k_0} \mathrm{P_0}\,,$$

$$\mathrm{ROOOH} + \mathrm{Am} \xrightarrow{k_{1.1}} N\text{-oxide} + \mathrm{P_{1.1}}\,,$$

$$\mathrm{ROOOH} + \mathrm{Am} \xrightarrow{k_{1.2}} \mathrm{P_{1.2}}\,,$$

where k_0, $k_{1.1}$, $k_{1.2}$ are the rate constants for the overall thermal decomposition, formation of *N*-oxide and catalytic decomposition of ROOOH, respectively; Am is amine; and P_0, $P_{1.1}$ and $P_{1.2}$ are the reaction products.

According to this scheme, the overall rate constant for the consumption of ROOOH is given by the formula

$$k = k_0 + (k_{1.1} + k_{1.2})[\mathrm{Am}]_0\,. \qquad (14)$$

Almost no *N*-oxides are formed at low concentrations of amine. This allows determination of k_0 and $k_{1.2}$ using Eqn (14) (Table 18). The temperature dependence of the rate constant for pyridine-catalysed decomposition of the hydrotrioxide **6f** is described as follows

$$\log k_{1.2} = (12.6\pm1.1) - (15.9\pm2.0)/\theta,$$

where $\theta = 2.303RT$ kcal mol^{-1}.

Linear correlation between the $\log k_{1.2}$ values and pK_a of amines is in good agreement with the Brønsted relationship for the general acid-base catalysis.[135] Thus, the kinetic data provide

Table 18. Kinetic parameters of decomposition of the hydrotrioxide **6f** in the presence of amines in isopropyl alcohol.

Amine	T/°C	$10^3 k_0$/s^{-1}	$k_{1.2}$/litre mol^{-1} s^{-1}
Pyridine	−26	0.177	0.03
	−14	0.417	0.16
	−1	1.45	0.69
2-Bromopyridine	−2	1.32	0.0005
Quinoline	−2	1.32	0.33
2-Methylpyridine	−2	1.32	0.93
3-Methylpyridine	−2	1.32	0.95
4-Methylpyridine	−1	1.45	1.34

an explanation for low yields of *N*-oxide in the oxidation of amines by hydrotrioxides (see Section VII.2): ROOOH is not only consumed in the oxidation reaction but also undergoes conversion following other routes, *e.g.*, thermal and amine-catalysed decomposition. As the amine basicity increases, the rate of catalytic process also increases with concomitant decrease in the yield of the corresponding *N*-oxide.

b. Acid catalysis of the overall decomposition of organic hydrotrioxides

Formic, acetic, monochloroacetic, trichloroacetic, trifluoroacetic and butyric acids were found to accelerate the decomposition of hydrotrioxides **3m** and **6f**.[133]

Acid-catalysed decomposition of hydrotrioxides is described by a first-order equation, the effective rate constant being proportional to the concentration of the acid (HA)

$$k = k_0 + k_{cat}[HA].$$

The rate constants for noncatalytic (k_0) and catalytic (k_{cat}) reactions are listed in Table 19.

Table 19. Kinetic parameters for the overall decomposition of the hydrotrioxide **6f** catalysed by carboxylic acids (in isopropyl alcohol).

Acid	T /°C	$10^3 k_0$ /s^{-1}	$10^2 k_{cat}$ /litre mol^{-1} s^{-1}
HCOOH	0	1.29	1.76
$MeCO_2H$	0	1.44	1.90
$ClCH_2CO_2H$	0	1.34	4.00
Cl_3CCO_2H	0	1.89	11.00
F_3CCO_2H	0	1.70	14.60
	−10	0.74	11.00
	−20	0.16	5.40
	−32	0.09	1.90
	0	11.18 [a]	11.50 [a]
$BuCO_2H$	0	1.27	2.15

[a] The data for the hydrotrioxide **3m** in diisopropyl ether.

The temperature dependences of the rate constants k_0 and k_{cat} for decomposition of the hydrotrioxide **6f** catalysed by CF_3CO_2H are as follows:

$$\log k_0 = (7.3 \pm 1.7) - (12.6 \pm 2.0)/\theta,$$

$$\log k_{cat} = (6.1 \pm 0.9) - (8.6 \pm 1.0)/\theta,$$

where $\theta = 2.303RT$ kcal mol^{-1}.

As for amines, the $\log k_{cat}$ values and the pK_a of the acids are related by a linear dependence, which is in agreement with the Brønsted relationship for acid catalysis.[135]

We cannot perform a detailed analysis of the mechanism of consumption of ROOOH in the presence of acids based on the knowledge of the formal kinetics of the process. It can be assumed that the decomposition of the hydrotrioxides can be accelerated owing to, in particular, the formation of associates ROOOH···HA, which leads to polarisation of the O−O bond, thus facilitating thermolysis of ROOOH. Such a 'through-the-H-bond' association followed by decomposition of the associates with cleavage of the O−O bond was found in the hydroperoxide–carboxylic acid system.[136, 137]

VI. The mechanism of thermal decomposition of hydrotrioxides

Thermal decomposition of HTO can follow several routes:

$$ROOOH \longrightarrow RO^{\bullet} + {}^{\bullet}OOH, \quad (15)$$

$$ROOOH \longrightarrow ROO^{\bullet} + {}^{\bullet}OH, \quad (16)$$

$$ROOOH + X^{\bullet} \longrightarrow ROOO^{\bullet} + XH \longrightarrow RO^{\bullet} + O_2 + XH, \quad (17)$$

$$ROOOH \longrightarrow \text{molecular products}. \quad (18)$$

In reaction (17), X represents a radical which escaped from the solvent cage, thus initiating induced decomposition of HTO.

The thermal effects of reactions (15) and (16) are equal to the dissociation energies of the corresponding O−O bonds. By substituting the data listed in Table 7 we get $\Delta H^{\circ}(15) \approx 20-21$ kcal mol^{-1} and $\Delta H^{\circ}(16) \approx 26-27$ kcal mol^{-1}. Therefore, it seems likely that reaction (16) can be ignored in the case of homolytic decomposition of ROOOH. The exothermicity of reaction (17) is equal to the difference between the dissociation energies of the ROOO−H (see Table 7) and X−H bonds. If X = ROO, the reaction (17) can be considered thermally neutral since $\Delta H^{\circ}(17) \approx -5 \pm 3$ kcal mol^{-1}. If X = RO, the reaction (17) is exothermic [$\Delta H^{\circ}(17) \approx 20$ to 25 kcal mol^{-1}].

The enthalpy of the reaction of molecular decomposition of ROOOH depends on the chemical nature of both R and products formed but, as a rule, it is much less than zero. For instance, decomposition of cyclohexyl hydrotrioxide into cyclohexanol and singlet molecular oxygen is characterised by $\Delta H^{\circ}(18) = -55$ kcal mol^{-1} and the formation of cyclohexanol and hydrogen peroxide is characterised by $\Delta H^{\circ}(18) = -75.5$ kcal mol^{-1}.

Taking into account the experimental activation energies of thermal decomposition of ROOOH (see Table 16), we can conclude that virtually all mechanisms for the decomposition of ROOOH, *viz.*, reactions (15), (17) and (18), are possible. Large values of the pre-exponential factors for the rate constant of thermal decomposition of several HTO often make the radical mechanism preferable. Solvation of polar transition state can change the log A and E values in the 'compensating' manner. The fact that this dependence holds for almost all compounds ROOOH (see Fig. 1) suggests a common mechanism of the decomposition of HTO with different structures.

Our thermochemical analysis of possible channels of the decomposition of ROOOH is consistent with the experimental results. The particular route of thermal decomposition is determined by the structure of HTO and reaction conditions. This is illustrated below taking different classes of hydrotrioxides as examples.

1. Silane-derived hydrotrioxides

Plesničar *et al.*[33] reported a detailed study of the mechanism of decomposition of silane-derived hydrotrioxides taking dimethylphenylsilyl hydrotrioxide (**20a**) as an example. They determined the kinetic and activation parameters of the reaction (in particular, large negative entropy of activation), revealed a pronounced substituent effect, found that the rate constant for decomposition depends on the solvent polarity and showed that the radical inhibitor, 2,6-di-*tert*-butyl-4-methylphenol (ionol), has no effect on the kinetics of decomposition. Based on these results, the authors suggested the molecular route as the major channel of decomposition of silane-derived hydrotrioxides.[33]

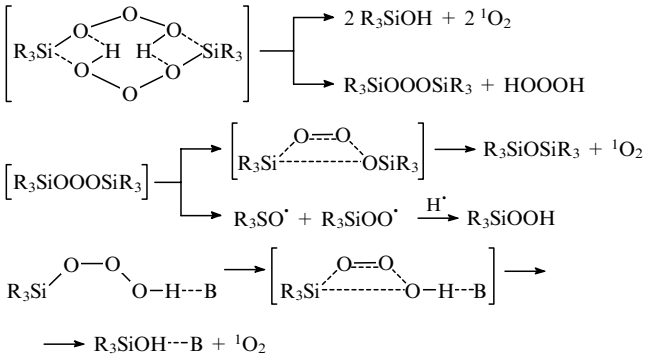

The formation of dimethylphenylsilyl hydroperoxide at $T > -50$ °C indicates some contribution of the radical reaction to the overall mechanism; however, Plesničar *et al.*[33] concluded that homolytic processes are a minor channel (< 10%) under the conditions investigated.

2. Cumyl hydrotrioxide

Cumyl hydrotrioxide (**8**) is a carbon analogue of dimethylphenylsilyl hydrotrioxide; the kinetics of its decomposition have been studied by ^{1}H NMR spectroscopy.[28,29] It was found that thermal decomposition of **8** at $T > -40$ °C (E_a = 16.0±0.1 kcal mol^{-1} and log A = 10.4±0.1) is substantially retarded in the presence of ionol. Correspondingly, the activation parameters of the reaction change (E_a = 23.9±0.1 kcal mol^{-1} and log A = 16.4±0.1). In the absence of the inhibitor, the reaction results in 2-phenylpropan-2-ol (the major product), acetophenone and cumyl hydroperoxide.

$$PhCMe_2OOOH \longrightarrow PhCMe_2O^{\bullet} + {}^{\bullet}OOH,$$

$$PhCMe_2O^{\bullet} ({}^{\bullet}OOH) + PhCMe_2OOOH \longrightarrow$$
$$\longrightarrow PhCMe_2OH\ (HOOH) + PhCMe_2OO^{\bullet},$$

$$PhCMe_2OO^{\bullet} \longrightarrow PhCMe_2O^{\bullet} + O_2,$$

$$PhCMe_2O^{\bullet} \longrightarrow PhCOMe + Me^{\bullet},$$

$$PhCMe_2O^{\bullet} + PhCHMe_2 \longrightarrow PhCMe_2OH + Ph\dot{C}Me_2,$$

$$Ph\dot{C}Me_2 + O_2 \longrightarrow PhCMe_2OO^{\bullet},$$

$$PhCMe_2OO^{\bullet} + PhCHMe_2 \longrightarrow PhCMe_2OOH + Ph\dot{C}Me_2.$$

In the presence of ionol, induced decomposition is inhibited and 2-phenylpropan-2-ol is virtually the only organic reaction product.[28,29]

$$PhCMe_2O^{\bullet} ({}^{\bullet}OOH) + ArOH \longrightarrow PhCMe_2OH\ (HOOH) + ArO^{\bullet},$$

$$PhCMe_2O^{\bullet} ({}^{\bullet}OOH) + ArO^{\bullet} \longrightarrow \text{non-radical products}.$$

3. Hydrotrioxides derived from oxygen-containing compounds

The kinetic parameters of thermal decomposition of hydrotrioxides derived from oxygen-containing compounds are listed in Table 16 and the reaction products are presented in Table 13.

We will consider the decomposition derived from hydrotrioxides of oxygen-containing compounds taking ethanol-derived hydrotrioxide (**6b**) as an example. Despite the fact that HTO derived from alcohols, ethers, acetals, *etc*., can form intramolecularly hydrogen-bonded structures [based on this, the molecular route of decomposition (Scheme 1, route *a*) was proposed [13]], the experimental results are altogether in better agreement with the radical mechanism for decomposition of ROOOH, the first stage of which involves homolysis of the RO–OOH bond (Scheme 1, route *b*).

Low yields of radicals escaped from the solvent cage are due to self-association of ROOOH and the formation of intermolecular hydrogen bonds (HTO dimers, association with the solvent molecules).[128,129] Yet another factor which stabilises the transition state of the reaction that follows route *b* is an increase in the proton acidity and, hence, strengthening of the hydrogen bond [pK_a(HOOOH) ≈ 9.5,[62] whereas pK_a of the decomposition product, *i.e*., the hydroperoxyl radical, is 4.4 [134]].

The hydrotrioxide **6b** decomposes into acetaldehyde, water, acetic acid and hydrogen peroxide (see Table 13). The first pair of products is formed as a result of disproportionation of the radical pair **A** (Scheme 1, route *c*). The second pair, $MeCO_2H$ and H_2O_2, are formed [76] owing to rotation about the C–O bond in the oxyl radical **A** followed by disproportionation of the radical pair **B** (Scheme 1, route *d*).

The formation of small amounts of organic peroxide products is due to homolytic oxidation reactions which proceed involving free radicals escaped from the solvent cage into the bulk.

4. Factors responsible for the mechanism of thermolysis

As was shown above, thermal decomposition of ROOOH can follow several pathways. The contribution of each mechanism (radical, induced or molecular decomposition) can vary depending on the experimental conditions. A number of factors determining the direction of decomposition of hydrotrioxides can be distinguished.

1. The nature of the atom bonded to the hydrotrioxide group. The larger the difference between the electronegativities of the X and O atoms in the hydrotrioxide $R^1R^2R^3XOOOH$ the more polar the X–O bond. Because of this, one should expect a larger contribution of the molecular channel of the reaction for silane-derived hydrotrioxides (X = Si). Comparison of the mechanisms for decomposition of hydrotrioxides **8** and **20a** which differ only in the nature of the atom X (see Sections VI.1 and VI.2) confirms this assumption. Koenig *et al.*[36] suggested that in the case of hydrotrioxides derived from organogermanium and organotin compounds (X = Ge, Sn) the molecular mechanism for decomposition is even more pronounced.

2. Temperature. Hydrotrioxides are typical peroxide compounds. By analogy with the latter, the increase in temperature causes a relative increase in the contribution of radical processes characterised by higher activation energies and pre-exponential factors. At low temperatures, polar rearrangements without formation of radical intermediates are more probable. This is confirmed by the results obtained by Plesničar *et al.*[33] who have found that $PhCMe_2OOH$, a typical product of radical transformation, is formed only at relatively high (as regards decomposition of dimethylphenylsilyl hydrotrioxide **20a**) temperatures ($T > -50$ °C) under conditions of fast warmup procedure.

3. Solvent. As was shown in Section V.2, the rate constant for decomposition of hydrotrioxides is affected by both specific and non-specific solvation of HTO and the transition states.[18,26] Polar solvents accelerate the molecular decomposition of ROOOH. For the hydrotrioxide **20a**, the effect of solvent decreases in the order: acetone-d_6 > methyl acetate > dimethyl ether.[33] The solvent polarity has a less pronounced effect on homolysis of the O–O

Scheme 1

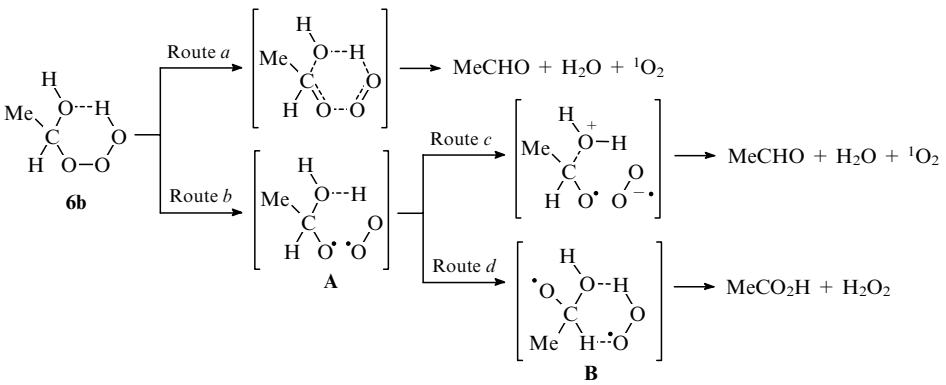

bond: hydrotrioxides **3b** and **6k** decompose in acetone, ethyl acetate and diethyl ether with nearly the same rate.[17] Specific interactions (*e.g.*, the formation of hydrogen bonds) cause an increase in the viscosity of HTO solutions and in the degree of association of HTO molecules in solution.

Correspondingly, the amount of radicals escaping from the solvent cage decreases. As a result, the radical mechanism becomes a 'hidden-radical' one, which is virtually indistinguishable from the molecular mechanism under the experimental conditions. We believe that 'hidden-radical' processes make a rather large contribution to the decomposition of HTO of oxygen-containing organic compounds and, hence, the initiating ability of ROOOH is low[129] owing to large cage effect and despite the formally radical type of decomposition.

4. The presence of a heteroatom in the ROOOH molecule. On the one hand, the O atom in α-position relative to the hydrotrioxide group stabilises the positive charge on the carbon atom in the formation of ROOOH (see Section IV.1). On the other hand, this structure of the oxygen-containing compound is extremely favourable for the formation of an intramolecular hydrogen bond. Self-association of ROOOH molecules also decreases the yield of radicals into the bulk, which manifests itself in low initiating ability and the absence of the effect of radical inhibitors on the kinetics of thermal decomposition. This type of HTO decomposes following a non-chain radical route. If the ROOOH molecules contain no heteroatom appropriate for the formation of hydrogen bond, they decompose to give high yields of radicals that initiate an induced decomposition of the HTO.[29]

5. Formation of electronically excited products

As was shown above (Section V.1), decomposition of ROOOH is accompanied by chemiluminescence in the visible and IR spectral regions. The radical mechanism for the decomposition of HTO provides better explanation for the appearance of chemiluminescence in the visible spectral region.

$$ROOOH \longrightarrow RO^{\bullet} + {}^{\bullet}OOH,$$

$$RO^{\bullet}({}^{\bullet}OOH) + RH\,(SolvH) \longrightarrow R^{\bullet}(Solv^{\bullet}) + ROH\,(HOOH),$$

$$R^{\bullet}(Solv^{\bullet}) + O_2 \longrightarrow ROO^{\bullet}(SolvOO^{\bullet}),$$

$$ROO^{\bullet} + ROO^{\bullet}(SolvOO^{\bullet} + SolvOO^{\bullet}) \longrightarrow \rangle C{=}O^{*} + \ldots$$

Solv — solvent.

Emitters of the chemiluminescence are the excited carbonyl compounds that are formed in the recombination of peroxyl radicals.[138] It is believed that the source of peroxyl radicals is the solvent SolvH (or RH if hydrotrioxides are synthesised in the bulk).

An increase in the cage effect makes the role of free-radical processes less significant and reduces the probability of the formation of triplet excited carbonyl compounds. Indeed, thermal decomposition of hydrotrioxide **6b** proceeds without formation of free radicals[128] and is not accompanied by luminescence in the visible spectral region.

Luminescence in the IR spectral region is caused by singlet oxygen $^1\Delta_g$. The mechanism for its formation has been less studied. The yield of $^1O_2$ determined using polyaromatic acceptors of singlet molecular oxygen was found to be nearly equal for both silane-derived hydrotrioxide **20a** (25% – 60%)[33] which decomposes following the molecular route and the hydrotrioxide **3b** (25% – 45%)[17] which mainly undergoes homolytic decomposition. A drawback of this procedure for the determination of the yield of $^1O_2$ is that the acceptor can be simply oxidised by the hydrotrioxide, which can introduce large errors into the results of measurements. However, the yield of $^1O_2$ in both processes is nearly the same. Thermochemically, the formation of singlet molecular oxygen in the reaction

$$ROOOH \longrightarrow ROH + O_2$$

is quite possible. It is known[69] that the enthalpies of formation of alcohols ROH and corresponding hydroperoxides are related by a simple relationship

$$\Delta_f H^{\circ}(ROOH) = \Delta_f H^{\circ}(ROH) + 19.2 \text{ kcal mol}^{-1}. \quad (19)$$

Taking into account Eqn (11), we get

$$\Delta_f H^{\circ}(ROOOH) = \Delta_f H^{\circ}(ROH) + 36.8 \text{ kcal mol}^{-1}. \quad (20)$$

Thus, according to Eqn (20), the thermal effect of the reaction of decomposition of ROOOH into ROH and O_2 molecule (the barrier height is $\sim 10 + 36.8$ kcal mol^{-1}) is sufficient for populating the $^1\Delta_g$ singlet level of molecular oxygen (22.5 kcal mol^{-1}). It is reasonable that singlet molecular oxygen can also be efficiently generated following the radical mechanism to give the same products (however, in this case the activation energy is higher).

It should be noted that, despite the absence of free radicals and chemiluminescence in the visible spectral region, decomposition of the hydrotrioxide **6b** is accompanied by bright chemiluminescence in the IR spectral region.[16, 18] This indicates the formation of $^1O_2$ in the 'hidden-radical' reactions.

It seems likely that generation of singlet molecular oxygen can proceed by several mechanisms simultaneously.

Route *a* (molecular)

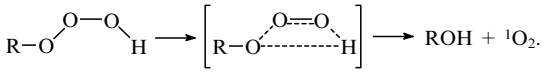

Route *b* ('hidden-radical')

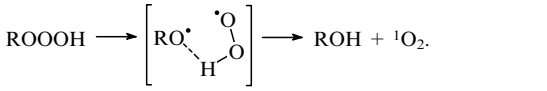

Route *c* (radical-chain)

$$ROOOH \longrightarrow RO^{\bullet} + {}^{\bullet}OOH,$$

$$RO^{\bullet}({}^{\bullet}OOH) + RH\,(SolvH) \longrightarrow R^{\bullet}(Solv^{\bullet}) + ROH\,(HOOH),$$

$$R^{\bullet}(Solv^{\bullet}) + O_2 \longrightarrow ROO^{\bullet}(SolvOO^{\bullet}),$$

$$ROO^{\bullet} + ROO^{\bullet}(SolvOO^{\bullet} + SolvOO^{\bullet}) \longrightarrow {}^1O_2 + \ldots$$

Undoubtedly, the mechanisms of the formation of singlet molecular oxygen in the thermal decomposition of HTO are still unclear and deserve further investigation.

VII. Organic hydrotrioxides as oxidants

It is well known that peracids and hydroperoxides ROOH (R is alkyl, aryl, acyl) containing active oxygen are highly reactive compounds.[139, 140] Hydrotrioxides containing two active oxygen atoms are highly active oxidants of unsaturated (alkenes, dienes, acenes) and heteroorganic compounds (amines, phosphines, phosphites, sulfides, sulfoxides, sulfur ylides). A salient feature of hydrotrioxides is that both the ROOOH molecule and singlet molecular oxygen generated in the decomposition of ROOOH can act as the oxidants.

1. Oxidation of unsaturated compounds

Depending on the structure of the substrate, the reactions of ROOOH with unsaturated compounds can result in epoxides, hydroperoxides, endoperoxides, 1,2-dioxetanes (or products of their transformations in the reaction medium).

a. Preparation of epoxides

Epoxidation of alkenes at -50 °C in $CHCl_3$ under the action of ROOOH has been studied taking the reactions of 4-trimethylsilylcyclohexene with hydrotrioxides **1a** and **6f**,**h** as examples (the yields of 4-trimethylsilyl-1,2-epoxycyclohexane calculated with respect to Δ[ROOOH] were ~60%, 13% and 6%, respectively).[141]

It seems likely that epoxidation by hydrotrioxide **1a** proceeds analogously to the Prilezhaev reaction.[139] In addition, since the radical mechanism contributes largely to the overall decomposition of the hydrotrioxide **1a** (see Table 17), one cannot rule out the contribution of the corresponding channel to the overall reaction of the synthesis of epoxide.[137, 142]

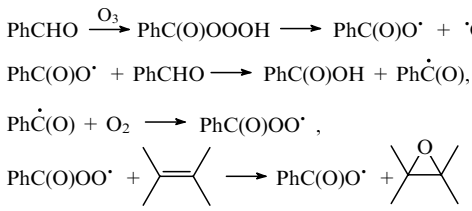

b. Preparation of hydroperoxides

Hydroperoxides can be prepared by oxidation of unsaturated compounds by singlet molecular oxygen generated in the decomposition of hydrotrioxides. Treatment of hydroperoxides with reducing agents results in the corresponding alcohols. This procedure is employed in the synthesis of natural compounds. The oxidation of tetramethylethylene by hydrotrioxides **3m**[13] and **21a**[35] and the oxidation of 1,2-dimethylcyclohexene by hydrotrioxides **1a** and **2** follow this pathway (Scheme 2).[14]

Scheme 2

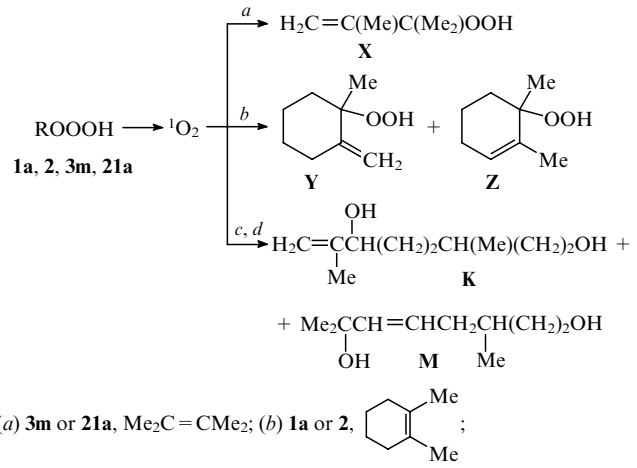

(*a*) **3m** or **21a**, $Me_2C=CMe_2$; (*b*) **1a** or **2**, ;

(*c*) **21a**, $Me_2CH=CH(CH_2)_2CH(Me)(CH_2)_2OH$; (*d*) $NaBH_4$, EtOH.

The yields of compounds **X**, **Y**, **Z**, **K** and **M** are presented in Table 20. It should be noted that in both cases the oxidation of 1,2-dimethylcyclohexene results in the products **Y** and **Z** in the ratio ~9 : 1, which is typical of the oxidation of this substrate by singlet molecular oxygen.[143] If hydroperoxides obtained upon oxidation of citronellol by hydrotrioxide **21a** are reduced by sodium borohydride (Scheme 2), a 1 : 1 mixture of diols **K** and **M** is formed (see Table 20).[35]

Table 20. The yields of compounds **X**, **Y**, **Z**, **K**, **M**.

Reagent	T /°C	Solvent	Yield (%)				Ref.
			X	**Y**	**Z**	**K**, **M**	
3m	−10 – 5	CH_2Cl_2	61 [a]				13
21a	−78	CH_2Cl_2	40 [b]				35
1a	23	RH	51.3 [a]	51.3 [a]	5.8 [a]		14
2	23	RH		39.7 [a]	3.5 [a]		14
21a	−78	CH_2Cl_2				25 [b, c]	35

[a] Calculated with respect to $\Delta[O_3]$. [b] Calculated with respect to Δ[A]. [c] The ratio **K** : **M** was 1 : 1.

c. Synthesis of endoperoxides

The reaction proceeds by the mechanism of [4 + 2]-cycloaddition of the singlet molecular oxygen generated to conjugated carbo- and heterodienes.

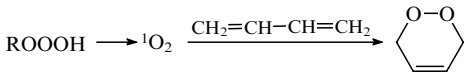

This reaction has been studied in most detail. The corresponding results are presented in Table 21.

d. Synthesis of 1,2-dioxetanes

Oxidation of 2-(trimethylsilyloxy)bicyclo[2.2.1]hept-2-ene into the corresponding dioxetane under the action of hydrotrioxide **21a** (−78 °C, CH_2Cl_2) also follows the mechanism of [2 + 2]-cycloaddition of singlet molecular oxygen evolved in the decomposition of ROOOH to the C = C bond of the substrate. The yield calculated with respect to Δ[A] is 50%.[35]

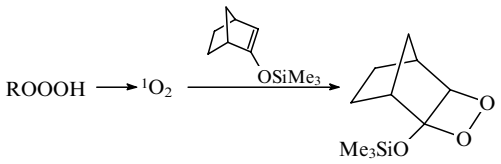

The reactions of adamantylideneadamantane with hydrotrioxides **1a**, **3m**, **4h** or **6f** in the $RH-CHCl_3$ medium at −78 °C proceed to give a mixture of the epoxide **L** and the 1,2-dioxetane **Q**.

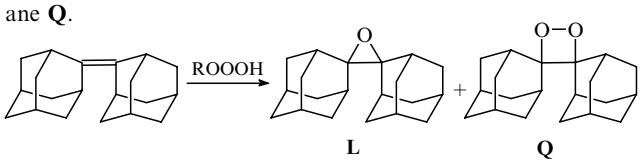

This reaction is an interesting example of dual reactivity of hydrotrioxides. Here, the role of oxidants is played by both the HTO which reacts to give the epoxide **L** and the singlet molecular oxygen which enters into the [2 + 2]-cycloaddition reaction to give the dioxetane **Q**.

Depending on the structure of the hydrotrioxide and composition of the reaction mixture, the reaction can be shifted towards the formation of either the epoxide **L** or the 1,2-dioxetane **Q**. The highest yield of dioxetane **Q** (~85% with respect to Δ[A]) was attained with the hydrotrioxide **4h** taken in the equimolar ratio to the substrate. The most efficient epoxidising agents are hydrotrioxides **1a** and **3m**; if the substrate and oxidant are taken in 1 : 10 ratio, the yield of the epoxide **L** calculated with respect to Δ[A] is 84% for **1a** and 88% for **3m**.[118, 144]

2. Oxidation of nitrogen-containing compounds

a. Secondary amines

Reactions of hydrotrioxides **1a**, **4h**, **6b**,**f** with diphenylamine or 2,2,6,6-tetramethylpiperidine (−20 °C, the substrate : oxidant ratio is 20 : 1) result in diphenylnitroxyl and 2,2,6,6-tetramethylpiperidin-1-oxyl, respectively.[145]

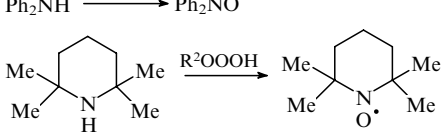

R^2OOOH = **1a**, **4h**, **6b**,**f**.

The yield of nitroxyl radicals calculated with respect to the hydrotrioxide consumed is low (~2%). This is likely due to either a fast reaction of the radicals with the HTO [129] or amine-catalysed decomposition of the HTO that proceeds concurrently (see Section V.4.a).

Table 21. Oxidation products of conjugated carbo- and heterocyclic dienes by hydrotrioxides.

Substrate	Reaction product	Hydrotrioxide	Temperature /°C	Solvent	Yield (%)	Ref.
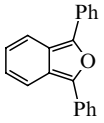	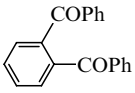	**1a**	−50	$RH-CH_2Cl_2$	96 [a]	14
		2	−70	$RH-Me_2CO$	80 [a]	14
		3a	−23	RH	30 [a]	14
		3b	−40 to −10	Me_2CO	45 [a]	17
				$MeCO_2Et$	–	17
		4f	−50 to −40	$MeCO_2Et$	55 [a]	20
		4h	−50 to −40	RH	54 [a]	20
		5a	−50 to −40	$MeCO_2Et$	46 [a]	20
		5d	−50 to −40	$MeCO_2Et$	85 [a]	20
		6k	−40 to −10	Me_2CO	60 [a]	17
				$MeCO_2Et$	60 [a]	17
		20a	−70 to −40	CD_3COCD_3	65 [a]	33
		21a	−78	CH_2Cl_2	45 [a], 91 [b]	35
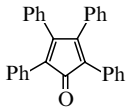	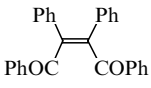	**3m**	−10–5	$RH-CH_2Cl_2$	38 [a]	13
		21a	−78	CH_2Cl_2	62 [b]	35
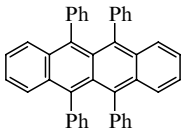	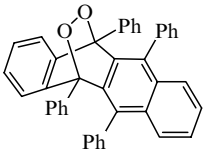	**3m**	−10–5	$RH-CH_2Cl_2$	47 [a]	13
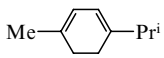	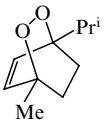	**21a**	−78	CH_2Cl_2	90 [b]	35
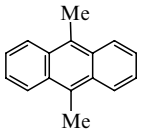	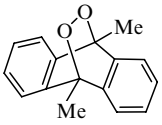	**21a**	−78	CH_2Cl_2	92 [b]	35
	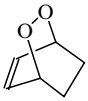	**21a**	−78	CH_2Cl_2	46 [b]	35

[a] Calculated with respect to the amount of ozone [$\Delta(O_3)$] consumed in the synthesis of ROOOH. [b] Calculated with respect to the substrate.

b. Tertiary amines

At −80 to −50 °C, tertiary amines undergo selective oxidation to give the corresponding *N*-oxides.[132, 146]

$$R^1_3N \xrightarrow{R^2OOOH} R^1_3N{\rightarrow}O$$

R^1_3N R^1_3 — pyridine, 2-methylpyridine, 2,4-dimethylpyridine, 2,6-dimethylpyridine, quinoline, 7-nitroquinoline;

R^2OOOH = **4h**, **6b**,**f**.

The yields of *N*-oxides calculated with respect to $\Delta[R^2OOOH]$ increase as the ratio $[R^1_3N]_0 : [R^2OOOH]_0$ increases. For instance, the yield of pyridine *N*-oxide in the oxidation of pyridine by the hydrotrioxide **6f** is ~27% if the reagents are taken in ~2 : 1 ratio and 60% if this ratio is 20 : 1. The nature of the HTO has little effect on the yield of *N*-oxides. As the basicity of the amine increases, the ratio $\Delta R^1_3[NO]/\Delta[R^2OOOH]$ decreases, which is due to the amine-catalysed decomposition of the hydrotrioxide (see Section V.4.a).

3. Oxidation of phosphorus-containing compounds

a. Phosphines

At −78 °C, hydrotrioxides **6b**,**f** oxidise triphenylphosphine into triphenylphosphine oxide nearly quantitatively, the reaction being completed during the mixing time of the reactants.[147] As the ratio of the initial concentrations, $[Ph_3P]_0 : [ROOOH]_0$, changes from 1 : 1 to 1 : ⩾ 2, the ratio $\Delta[Ph_3P] : \Delta[ROOOH]$ increases from 1 to 2. The change in the stoichiometric coefficient is thought to be due to the reduction of a hydroperoxide by triphenylphosphine.

$$ROOOH \xrightarrow{Ph_3P} ROOH \xrightarrow{Ph_3P} ROH.$$

Fast and nearly quantitative reduction of HTO with an excess of triphenylphosphine serves as the basis for the method for quantitative determination of HTO by analysing the unconsumed Ph_3P.[147]

Pryor *et al.*[29] used the reaction of Ph_3P with the hydrotrioxide **8** in acetone at −73 °C for identification of the HTO **8**.

b. Phosphites

Hydrotrioxides **1a**, **4a**,**h**, **5a**, **6b**,**d**,**f** oxidise phosphites into the corresponding phosphates (at −78 to −50 °C) in nearly quantitative yields.[148–150]

$$(R^1O)_3P \xrightarrow{R^2OOOH} (R^1O)_3P{=}O$$

R^1 = Me, Et, Pr^i, Bu^n, $CH_2{=}CHCH_2$, Ph, 2-MeC_6H_4;

R^2OOOH = **1a**, **4a**,**h**, **5a**, **6b**,**d**,**f**.

Aromatic phosphites are oxidised somewhat slower than the aliphatic phosphites.[149] The reactivities of phosphites towards the hydrotrioxide **6f** have been studied by the method of competing reactions (at −50 °C in propan-2-ol) with $(EtO)_3P$ as the reference compound:

$$n_r(R^1O)_3P + R^2OOOH \xrightarrow{k_r} n_r(R^1O)_3PO,$$

$$n_0(EtO)_3P + R^2OOOH \xrightarrow{k_0} n_0(EtO)_3PO,$$

where k_r and k_0 are the rate constants for the oxidation of the phosphite under study and triethyl phosphite, respectively, and n_r and n_0 are the stoichiometric coefficients of the corresponding reactions.

If $[R^2OOOH]_0 \ll [(R^1O)_3P] = [(EtO)_3P]_0$ and the stoichiometric coefficients $n_r \approx n_0 \approx 2$, for the relative rate constant we get

$$k_r/k_0 = [(R^1O)_3PO]/[(EtO)_3PO].$$

A correlation was found between the $\log(k_r/k_0)$ value and the sum of the Kabachnik constants ($\Sigma\sigma^{\Phi}$) of the substituents at the phosphorus atom

$$\log(k_r/k_0) = -0.87 - 0.96\,\Sigma\sigma^{\Phi}.$$

At low $[(R^1O)_3P]_0/[R^2OOOH]_0$ ratios, the stoichiometric coefficient $\Delta[(R^1O)_3P]/\Delta[R^2OOOH] \approx 1$. As the phosphite concentration increases, this coefficient also increases approaching a value of 2. It seems likely that here, as in the preceding case, not only the hydrotrioxide but also the hydroperoxide acts as the oxidant. Probably, the reactions of phosphites with hydroperoxides occur during the warmup of the reaction mixtures.

Chemical polarisation of ^{31}P nuclei in $(PhO)_3PO$ observed in the *in situ* reaction of triphenyl phosphite with the hydrotrioxide **6f** carried out in an NMR tube (in propan-2-ol at ~40 °C) indicates the presence of radical species.[149] It is essential that the ^{31}P nuclei in the major product, phosphate, are strongly polarised. This system differs from the phosphite–hydroperoxide system in which the atomic nuclei in the molecules of the minor products are strongly polarised whereas a very weak or even no chemical polarisation is observed for the major product, *viz*., phosphate.[151] The addition of styrene (a free radical acceptor) does not lead to disappearance of chemical polarisation. It thus follows that the polarised phosphate molecules are formed as a result of recombination of the geminate radical pair without exit of the radicals into the bulk.

Taking the oxidation of triphenyl phosphite by hydrotrioxides **1a**, **4h** and **6f** (−26 °C, CH_2Cl_2) as an example, it was found that the reactions are accompanied by chemiluminescence in the visible and IR spectral regions.[144] Maxima in the spectra of chemiluminescence in the visible spectral region are observed at $\lambda = 460\pm20$ nm. It is assumed [144] that the emitter of chemiluminescence is the triplet excited phosphate (the phosphorescence spectrum of triphenyl phosphate exhibits a maximum at $\lambda = 465$ nm), as in the case of the oxidation of phosphites by hydroperoxides. The emitter of luminescence in the IR spectral region is the singlet molecular oxygen generated in the thermal decomposition of ROOOH that proceeds in parallel.

4. Oxidation of sulfur-containing compounds

a. Sulfoxides

Oxidation of dimethyl sulfoxide and dibutyl sulfoxide by hydrotrioxides **1**, **3m**, **4h** and **6b**,**f** (−78 to −50 °C, $[R^2OOOH]_0:[R^1SOR^1]_0 \approx 1-10$, 10–12 h) results in the corresponding sulfones in nearly 100% yields.[152]

$$R^1SOR^1 \xrightarrow{R^2OOOH} R^1SO_2R^1$$

R^1 = Me, Bu^n; R^2OOOH = **1a**, **3m**, **4h**, **6b**,**f**.

The most efficient oxidants are hydrotrioxides **1a** and **6f**. Complete conversion of sulfoxides into sulfones requires a threefold to fivefold excess of these reagents.

The yields of sulfones calculated with respect to $\Delta[R^2OOOH]$ are, as a rule, 5% to 30%; the higher the thermal stability of the HTO the higher the yield of the sulfone. Thus, the oxidation of sulfoxides is accompanied by thermal decomposition of the hydrotrioxide which proceeds concurrently at a rather high rate; singlet molecular oxygen thus formed is inactive in the reaction with sulfoxides under these conditions. Otherwise, one would expect an increase in the yield of sulfones with the increase in the rate of decomposition of such an efficient source of $^1O_2$, as, *e.g*., the hydrotrioxide **6f**.

It was shown [33] that the transfer of oxygen from the hydrotrioxide **20a** to the substrates, $4\text{-}XC_6H_4S(O)Me$ (X = MeO, Me, H, Cl), follows the electrophilic mechanism ($\rho = -1.1$, −78 °C, Me_2CO).

b. Sulfides

Depending on the composition of the initial reaction mixture and the reaction time, sulfides undergo selective oxidation into either sulfoxides or sulfones (at T from −78 to −40 °C).[23, 144, 153]

$$R^1SR^1 \xrightarrow{R^2OOOH} R^1SOR^1,$$

$$R^1SR^1 \xrightarrow{R^2OOOH} R^1SO_2R^1$$

R^1 = Me, Pr^n, Bu^n, n-C_6H_{13}, n-C_7H_{15}; R^2OOOH = **1a**, **4h**, **5a**,**b**, **6b**,**f**,**h**.

The first reaction proceeds at the ratio of the initial concentrations $[R^2OOOH]_0:[R^1SR^1]_0 \leqslant 1$ (the reaction goes to completion within 15 to 30 min).[144, 153] The yields of sulfoxides calculated with respect to sulfides consumed are close to 100%. If hydrotrioxides **1a** and **6f** are used, the yields calculated with respect to the HTO consumed in the reaction are also close to 100%. On the other hand, if $[\mathbf{6f}]_0:[R^1SR^1]_0 = 2$, the yields of sulfoxides decrease down to 50%, which indicates that the reaction is accompanied by thermal decomposition of the excess HTO which proceeds concurrently and that $^1O_2$ evolved in the reaction with the sulfide is inactive.

Oxidation of R^1SR^1 into $R^1SO_2R^1$, which seems to proceed *via* the corresponding sulfoxide R^1SOR^1, is observed if the HTO is taken in large excess and the reaction takes a long time. This indicates a relatively low reactivity of sulfoxides towards hydrotrioxides. For instance, a nearly quantitative conversion of dibutyl sulfide into dibutyl sulfone under the action of hydrotrioxides **1a** or **6f** requires that the following conditions be met for the ratios of the initial concentrations, $[\mathbf{1a}]_0:[R^1SR^1]_0 \geqslant 15$ or $[\mathbf{6f}]_0:[R^1SR^1]_0 \geqslant 4$; the yields of the sulfones calculated with respect to $\Delta[R^2OOOH]$ were ~7% and 25%, respectively.

The oxidation of sulfides $4\text{-}XC_6H_4SMe$ (X = MeO, Me, H, Cl) by hydrotrioxides **20a**,**b** and **23** in acetone, methyl acetate and n-pentane at −78 °C has been studied.[33, 34] The reactions resulted in the corresponding sulfoxides as the major products (the yields are 70% to 80%); sulfones are not formed in large amounts, since the reactivities of the sulfides are much higher than those of the sulfoxides. The Hammett ρ constants for the oxidation of these aryl methyl sulfides by hydrotrioxides **20a**,**b** and **23** in different solvents are listed in Table 22. An electrophilic nature of the oxidant was revealed.

Table 22. The Hammett ρ constants for the oxidation of aryl methyl sulfides by hydrotrioxides.

Hydrotrioxide	Solvent	ρ	Ref.
20a	Me_2CO	−1.99	33
	$MeCO_2Me$	−1.59	33
	n-C_5H_{14}	−1.65	33
20b	Me_2CO	−1.83	33
	$MeCO_2Me$	−1.77	33
	n-C_5H_{14}	−1.53	33
23	MeCOMe	−1.9	34
	$MeCO_2Me$	−1.9	34

c. Sulfur ylides

Oxidation of the ylide $Me_2\overset{+}{S}-\overset{-}{C}HCO_2Et$ by the excess of the hydrotrioxide **6f** results in a mixture of the oxidation and decomposition products, *viz*., $Me_2S(O)CHCO_2Et$, $EtOC(O)CHO$, Me_2SO and Me_2SO_2, in 2.1 : 4.5 : 1.8 : 1.0 ratio (−78 to −60 °C, $[ROOOH]_0 : [ylide]_0 \approx 4.5$).[154]

* * *

Summing up, mention may be made that hydrotrioxides have found wide use in organic synthesis. They can be used as oxidants, sources of singlet molecular oxygen and initiators of free-radical reactions. Reactions of organic HTO proceed under mild conditions, which extends the possibilities for the synthesis of many valuable compounds. It is hoped that as new experimental information will be available, the use of organic hydrotrioxides will rank high among other synthetic methods.

References

1. P S Bailey *Ozonation in Organic Chemistry* Vol. 1 (New York; San Francisco; London: Academic Press, 1978)
2. V Karnojitzky *Double Liasion-Chim. Peint*. **30** 14 (1983)
3. B Plesničar, in *The Chemistry of Peroxides* Vol. 16 (Ed. S Patai) (Chichester: Wiley, 1983) p. 483
4. B Plesničar, in *Organic Polyoxides* (Ed. W Ando) (New York: Wiley, 1992) p. 479
5. A F Khalizov, S L Khursan, V V Shereshovets *Kinet. Katal*. **40** 216 (1999) [a]
6. C C Price, A L Tumolo *J. Am. Chem. Soc*. **86** 4691 (1964)
7. H M White, P S Bailey *J. Org. Chem*. **30** 3037 (1965)
8. J F Batterbee, P S Bailey *J. Org. Chem*. **32** 3899 (1967)
9. M C Whiting, A J N Bolt, J H Parish *Adv. Chem. Ser*. (77) 4 (1968)
10. G A Hamilton, B S Ribner, T M Hellman *Adv. Chem. Ser*. (77) 15 (1968)
11. P Deslongchamps, C Moreau *Can. J. Chem*. **49** 2465 (1971)
12. J D Austin, L Spialter *Adv. Chem. Ser*. (77) 26 (1968)
13. R W Murray, W C Lumma, J W-P Lin *J. Am. Chem. Soc*. **92** 3205 (1970)
14. F E Stary, D E Emge, R W Murray *J. Am. Chem. Soc*. **98** 1880 (1976)
15. F E Stary, D E Emge, R W Murray *J. Am. Chem. Soc*. **96** 5671 (1974)
16. N N Kabal'nova, Candidate Thesis in Chemical Science, Institute of Chemistry of Bashkir Scientific Centre, Urals Branch of Academy of Sciences of the USSR, Ufa, 1988
17. B Plesničar, F Kovač, M Schara *J. Am. Chem. Soc*. **110** 214 (1988)
18. S L Khursan, Doctoral Thesis in Chemical Sciences, Institute Organic Chemistry Urals Scientific Centre, Russian Academy of Sciences, Ufa, 1999
19. F Kovač, B Plesničar *J. Chem. Soc., Chem. Commun*. 122 (1978)
20. F Kovač, B Plesničar *J. Am. Chem. Soc*. **101** 2677 (1979)
21. V V Shereshovets, F A Galieva, N N Kabal'nova, N M Shishlov, R A Sadykov, V D Komissarov, G A Tolstikov *Izv. Akad. Nauk SSSR, Ser. Khim*. 317 (1986) [b]
22. W A Pryor, in *Oxygen and Oxy-Radicals in Chemistry and Biology* (Eds M A Rodgers, E L Powers) (New York: Academic Press, 1981) p. 133
23. E M Kuramshin, L G Kulak, S S Zlotskii, D L Rakhmankulov *Zh. Org. Khim*. **22** 1986 (1986) [c]
24. N Ya Shafikov, R A Sadykov, V V Shereshovets, A A Panasenko, V D Komissarov *Izv. Akad. Nauk SSSR, Ser. Khim*. 1923 (1981) [b]
25. N Ya Shafikov, Candidate Thesis in Chemical Sciences, Institute of Chemistry of Bashkir Branch, Academy of Sciences of the USSR, Ufa, 1985
26. V V Shereshovets, F A Galieva, V D Komissarov *Izv. Akad. Nauk SSSR, Ser. Khim*. 304 (1988) [b]
27. V V Shereshovets, N N Kabal'nova, V D Komissarov, G A Tolstikov *Izv. Akad. Nauk SSSR, Ser. Khim*. 1660 (1985) [b]
28. W A Pryor, N Ohto, D F Church *J. Am. Chem. Soc*. **104** 5813 (1982)
29. W A Pryor, N Ohto, D F Church *J. Am. Chem. Soc*. **105** 3614 (1983)
30. M Zarth, A de Meijere *Chem. Ber*. **118** 2429 (1985)
31. E V Avzyanova, Q K Timerghazin, A F Khalizov, S L Khursan, L V Spirikhin, V V Shereshovets *J. Phys. Org. Chem*. **13** 87 (2000)
32. E V Avzyanova, Q K Timerghazin, A F Khalizov, S L Khursan, L V Spirikhin, V V Shereshovets *Mendeleev Commun*. 227 (1997)
33. B Plesničar, J Cerkovnik, J Koller, F Kovač *J. Am. Chem. Soc*. **113** 4946 (1991)
34. J Cerkovnik, B Plesničar *J. Am. Chem. Soc*. **115** 12169 (1993)
35. E J Corey, M M Mehrotra, A U Khan *J. Am. Chem. Soc*. **108** 2472 (1986)
36. M Koenig, J Barrau, N Ben-Hamida *J. Organomet. Chem*. **356** 133 (1988)
37. B I Tarunin, V N Tarunina, Yu A Kurskii *Zh. Obshch. Khim*. **58** 1060 (1988) [d]
38. E V Avzyanova, N N Kabal'nova, V V Shereshovets *Izv. Akad. Nauk, Ser. Khim*. 375 (1996) [b]
39. Q K Timerghazin, N M Shishlov, N N Kabalnova, S L Khursan, V V Shereshovets *Mendeleev Commun*. 231 (1997)
40. T V Yagodovskaya, D Yu Zhogin, L I Nekrasov *Zh. Fiz. Khim*. **49** 2683 (1975) [e]
41. G A Shchembelov, T V Yagodovskaya, L I Nekrasov *Zh. Fiz. Khim*. **50** 772 (1976) [e]
42. M R Khadzhi-Ogly, I P Gloriozov, T V Yagodovskaya, L I Nekrasov *Zh. Fiz. Khim*. **57** 1910 (1983) [e]
43. S L Khursan, V V Shereshovets *Izv. Akad. Nauk, Ser. Khim*. 1356 (1996) [b]
44. L Radom, W J Hehre, J A Pople *J. Am. Chem. Soc*. **93** 289 (1971)
45. L Radom, W J Hehre, J A Pople *J. Am. Chem. Soc*. **94** 2371 (1972)
46. R J Blint, M D Newton *J. Chem. Phys*. **59** 6220 (1973)
47. B Plesničar, S Kaiser, A Ažman *J. Am. Chem. Soc*. **95** 5476 (1973)
48. B Plesničar, D Kocjan, S Murovec, A Ažman *J. Am. Chem. Soc*. **98** 3143 (1976)
49. D Cremer *J. Chem. Phys*. **69** 4456 (1978)
50. C F Jackels, D H Phillips *J. Chem. Phys*. **84** 5013 (1986)
51. C Gonzalez, J Theisen, L Zhu, H B Schlegel, W L Hase, E W Kaiser *J. Phys. Chem*. **95** 6784 (1991)
52. J Koller, B Plesničar *J. Am. Chem. Soc*. **118** 2470 (1996)
53. J Koller, M Hodošček, B Plesničar *J. Am. Chem. Soc*. **112** 2124 (1990)
54. D J Mckay, J S Wright *J. Am. Chem. Soc*. **120** 1003 (1998)
55. M Liedtke, A H Saleck, K M T Yamada, G Winnewisser, D Cremer, E Kraka, A Dolgner, J Hahn, S Dobos *J. Phys. Chem*. **97** 11204 (1993)
56. D Cremer *J. Chem. Phys*. **70** 1898 (1979)
57. D Cremer *J. Chem. Phys*. **70** 1911 (1979)
58. S W Benson *Thermochemical Kinetics* (New York: Wiley, 1976)
59. P A Giguere, K Herman *Can. J. Chem*. **48** 3473 (1970)
60. G Pimentel, A L McClellan *The Hydrogen Bond* (San Francisco: Freeman, 1960)
61. N D Sokolov *Vodorodnaya Svyaz'* (The Hydrogen Bond) (Moscow: Nauka, 1981)
62. B H J Bielski, H A Schwarz *J. Phys. Chem*. **72** 3836 (1968)
63. M C V Sauer, J O Edwards *J. Phys. Chem*. **75** 3004 (1971)
64. V L Antonovskii, V A Terent'ev, in *Uspekhi Khimii Organicheskikh Perekisnykh Soedinenii i Autookisleniya* (Advances in the Chemistry of Organic Peroxide Compounds and Autooxidation) (Eds N M Emanuel, K I Ivanov, G A Razuvaev, T I Yurzhenko, V A Shushunov, A T Menyailo, B V Erofeev, A I Yurzhenko) (Moscow: Khimiya, 1969) p. 442
65. V V Lipes, G A Kurkchi, E A Bakova, N M Grushina, T N Timrot, G N Koshel', V L Antonovskii *Kinet. Katal*. **26** 560 (1985) [a]
66. S L Khursan, V V Shereshovets *Kinet. Katal*. **40** 167 (1999) [a]
67. S W Benson, J H Buss *J. Chem. Phys*. **29** 546 (1958)
68. S W Benson, R Shaw, in *Organic Peroxides* Vol. 1 (Ed. D Swern) (New York: Wiley-Interscience, 1970) p. 105
69. E T Denisov, T G Denisova *Zh. Fiz. Khim*. **62** 304 (1988) [e]
70. T H Lay, J W Bozzelli *J. Phys. Chem. A* **101** 9505 (1997)
71. T P W Jungkamp, J H Seinfeld *Chem. Phys. Lett*. **257** 15 (1996)
72. Yu Ya Van Chin Syan, N S Kachurina *Vestn. Nizhegorodsk. Gos. Univ. im. N I Lobachevskogo* 29 1996
73. S W Benson *J. Chem. Phys*. **33** 306 (1960)
74. S W Benson *J. Am. Chem. Soc*. **86** 3922 (1964)
75. P S Nangia, S W Benson *J. Phys. Chem*. **83** 1138 (1979)
76. P S Nangia, S W Benson *J. Am. Chem. Soc*. **102** 3105 (1980)
77. J S Francisco, I H Williams *Int. J. Chem. Kinet*. **20** 455 (1988)
78. K Adamic, J A Howard, K U Ingold *Can. J. Chem*. **47** 3803 (1969)
79. J E Bennett, D M Brown, B Mile *Trans. Faraday Soc*. **66** 397 (1970)

80. S L Khursan, V V Shereshovets, N M Shishlov, A F Khalizov, V D Komissarov *React. Kinet. Catal. Lett.* **52** 249 (1994)
81. E G Kiparisova, I B Rabinovich *Dokl. Akad. Nauk SSSR* **199** 1075 (1971) [f]
82. S L Khursan, V V Shereshovets, A F Khalizov, A I Voloshin, V D Komissarov, V P Kazakov *Izv. Akad. Nauk, Ser. Khim.* 2056 (1993 [b]
83. A F Khalizov, S L Khursan, V V Shereshovets *Izv. Akad. Nauk, Ser. Khim.* 61 (1999) [b]
84. S L Khursan, V V Shereshovets *Izv. Akad. Nauk, Ser. Khim.* 2190 (1996) [b]
85. S L Khursan, V V Shereshovets *Izv. Akad. Nauk, Ser. Khim.* 327 (1996) [b]
86. S L Khursan, V V Shereshovets *Izv. Akad. Nauk, Ser. Khim.* 1129 (1996) [b]
87. T P W Jungkamp, J H Seinfeld *Chem. Phys. Lett.* **263** 371 (1996)
88. S W Benson *Oxid. Commun.* **2** 169 (1982)
89. P T Chou, M L Martinez, S L Studer *Chem. Phys. Lett.* **174** 46 (1990)
90. T V Yagodovskaya, L I Nekrasov *Zh. Fiz. Khim.* **51** 2434 (1977) [e]
91. X Deglise, P A Giguere *Can. J. Chem.* **49** 2242 (1971)
92. J L Arnau, P A Giguere *J. Chem. Phys.* **60** 270 (1974)
93. D Swern, A H Clements, T M Luong *Anal. Chem.* **41** 412 (1969)
94. B Plesničar, J Cerkovnik, T Tekavec, J Koller *J. Am. Chem. Soc.* **120** 8005 (1998)
95. B Plesničar, J Cerkovnik, T Tekavec, J Koller *Chem. Eur. J.* **6** 809 (2000)
96. R E Erickson, R T Hansen, J Harkins *J. Am. Chem. Soc.* **90** 6777 (1968)
97. D Tal, E Keinan, Y Mazur *J. Am. Chem. Soc.* **101** 502 (1979)
98. T M Hellman, G A Hamilton *J. Am. Chem. Soc.* **96** 1530 (1974)
99. D H Giamalva, D F Church, W A Pryor *J. Org. Chem.* **53** 3429 (1988)
100. V D Komissarov, Doctoral Thesis in Chemical Science, Institute of Chemistry of Bashkir Scientific Centre, Urals Branch of Academy of Sciences of the USSR, Ufa, 1990
101. D G Hendry, T Mill, L Piszkiewicz, J A Howard, H K Eigenmann *J. Phys. Chem. Ref. Data* **3** 937 (1974)
102. L Melander, W H Saunders *Reaction Rates of Isotopic Molecules* (New York: Wiley, 1980)
103. W A Pryor, G J Gleicher, D F Church *J. Org. Chem.* **49** 2574 (1984)
104. P S Bailey, J W Ward, T P Carter, E Nieh, C M Fischer, A I Y Khashab *J. Am. Chem. Soc.* **96** 6136 (1974)
105. V V Shereshovets, V D Komissarov, L G Galimova *Izv. Akad. Nauk SSSR, Ser. Khim.* 2632 (1980) [b]
106. V V Shereshovets, L G Galimova, V D Komissarov *Izv. Akad. Nauk SSSR, Ser. Khim.* 2488 (1981) [b]
107. V V Shereshovets, N M Korotaeva, V D Komissarov *Izv. Akad. Nauk SSSR, Ser. Khim.* 1684 (1985) [b]
108. V V Shereshovets, R K Yanbaev, V D Komissarov *React. Kinet. Catal. Lett.* **46** 7 (1992)
109. R K Yanbaev, V V Shereshovets, V D Komissarov *React. Kinet. Catal. Lett.* **48** 255 (1992)
110. D R Stull, E F Westrum, G C Sinke *The Chemical Thermodynamics of Organic Compounds* (New York: Wiley, 1969)
111. J L Holmes, F P Lossing, P M Mayer *J. Am. Chem. Soc.* **113** 9723 (1991)
112. E T Denicov, T G Denicova *Kinet. Katal.* **37** 51 (1996) [a]
113. Q K Timerghazin, S L Khursan, V V Shereshovets *J. Mol. Struct. (Theochem)* **489** 87 (1999)
114. N Yoneda, G A Olah *J. Am. Chem. Soc.* **99** 3113 (1977)
115. G A Olah, N Yoneda, D G Parker *J. Am. Chem. Soc.* **98** 5261 (1976)
116. A L J Beckwith, C L Bodkin, T Duong *Aust. J. Chem.* **30** 2177 (1977)
117. G L Sharipov, V V Shereshovets, V P Kazakov, V D Komissarov, G A Tolstikov *Izv. Akad. Nauk SSSR, Ser. Khim.* 1216 (1985) [b]
118. V V Shereshovets, G L Sharipov, N N Kabal'nova, V P Kazakov, V D Komissarov, G A Tolstikov *Zh. Org. Khim.* **22** 2549 (1986) [c]
119. V V Shereshovets, V D Komissarov, S I Maslennikov, N N Kabal'nova *Izv. Akad. Nauk SSSR, Ser. Khim.* 2631 (1982) [b]
120. V V Shereshovets, N N Kabalnova, V D Komissarov, V K Mavrodiev, B M Lerman, T A Belogaeva, G A Tolstikov *React. Kinet. Catal. Lett.* **41** 251 (1990)
121. N N Kabal'nova, V V Shereshovets, A S Vorob'ev, I A Rusakov, A A Furlei, Yu I Murinov *Izv. Akad. Nauk, Ser. Khim.* 2132 (1993) [b]
122. N N Kabal'nova, V V Shereshovets, Yu I Murinov, D V Kazakov, G R Abuzarova, G A Tolstikov *Izv. Akad. Nauk, Ser. Khim.* 57 (1996) [b]
123. A A Krasnovskii *Zh. Prikl. Spektrosk.* **32** 852 (1980) [g]
124. A M Caminade, F ElKhatib, M Koenig, J M Aubry *Can. J. Chem.* **63** 3203 (1985)
125. Q J Niu, G D Mendenhall *J. Am. Chem. Soc.* **114** 165 (1992)
126. A F Khalizov, Candidate Thesis in Chemical Sciences, Institute of Organic Chemistry, Ufa Scientific Centre of the Russian Academy of Sciences, Ufa, 1997
127. Kh S Bagdasar'yan *Usp. Khim.* **53** 1073 (1984) [*Russ. Chem. Rev.* **53** 623 (1984)]
128. V V Shereshovets, F A Galieva, V D Komissarov *Izv. Akad. Nauk SSSR, Ser. Khim.* 1668 (1984) [b]
129. V V Shereshovets, F A Galieva, R A Sadykov, V D Komissarov, G A Tolstikov *Izv. Akad. Nauk SSSR, Ser. Khim.* 2208 (1989) [b]
130. V E Zubarev, V N Belevskii, L T Bugaenko *Usp. Khim.* **48** 1361 (1979) [*Russ. Chem. Rev.* **48** 729 (1979)]
131. W A Pryor, D G Prier, D F Church *J. Am. Chem. Soc.* **105** 2883 (1983)
132. V V Shereshovets, L A Bachanova, U M Dzhemilev, V D Komissarov, G A Tolstikov *Izv. Akad. Nauk SSSR, Ser. Khim.* 2447 (1985) [b]
133. V V Shereshovets, N N Kabalnova, N M Korotaeva, V D Komissarov *React. Kinet. Catal. Lett.* **34** 231 (1987)
134. G Czapski, B H J Bielski *J. Phys. Chem.* **67** 2180 (1963)
135. E T Denisov *Kinetika Gomogennykh Khimicheskikh Reaktsii* (Kinetics of Homogeneous Chemical Reactions) (Moscow: Vysshaya Shkola, 1978)
136. E T Denisov *Kinetika i Kataliz. Mekhanizmy Gomoliticheskogo Raspada Molekul v Zhidkoi Faze (Itogi Nauki i Tekhniki)* [Kinetics and Catalysis. Mechanisms of Homolytic Degradation of Molecules in the Liquid Phase (Advances in Science and Engineering Series)] (Moscow: Izd. VINITI, 1981) Vol. 9
137. E T Denisov, V V Azatyan *Ingibirovanie Tsepnykh Reaktsii* (Inhibition of Chain Reactions) (Chernogolovka: Institute of Chemical Physics in Chernogolovka, Russian Academy of Sciences, 1997)
138. V Ya Shlyapintokh, A A Kefeli, V I Gol'denberg, S D Razumovskii *Dokl. Akad. Nauk SSSR* **186** 1132 (1969) [f]
139. E N Prilezhaeva *Reaktsiya Prilezhaeva. Elektrofil'noe Okislenie* (Prilezhaev Reaction. Electrophilic Oxidation) (Moscow: Nauka, 1974)
140. G A Tolstikov *Reaktsii Gidroperekisnogo Okisleniya* (Reactions of Hydroperoxide Oxidation) (Moscow: Nauka, 1976)
141. V V Shereshovets, V D Komissarov, L A Bachanova, I A Gailyunas, G A Tolstikov *Izv. Akad. Nauk SSSR, Ser. Khim.* 1929 (1981) [b]
142. E T Denisov, N I Mitskevich, V E Agabekov *Mekhanizm Zhidkofaznogo Okisleniya Kislorodsoderzhashchikh Soedinenii* (Mechanism of Liquid-Phase Oxidation of Oxygen-Containing Compounds) (Minsk: Nauka i Tekhnika, 1975)
143. C S Foote *Acc. Chem. Res.* **1** 104 (1968)
144. V V Shereshovets, Doctoral Thesis in Chemical Sciences, Institute of Organic Chemistry, Urals Branch of the Russian Academy of Sciences, Ufa, 1992
145. V V Shereshovets, R A Sadykov, L A Bachanova, A A Panasenko, V D Komissarov, G A Tolstikov *Izv. Akad. Nauk SSSR, Ser. Khim.* 1675 (1982) [b]
146. V V Shereshovets, L A Bachanova, V D Komissarov, N S Vostrikov, G A Tolstikov *Izv. Akad. Nauk SSSR, Ser. Khim.* 1922 (1982) [b]
147. V V Shereshovets, F A Galieva, N Ya Shafikov, R A Sadykov, A A Panasenko, V D Komissarov *Izv. Akad. Nauk SSSR, Ser. Khim.* 1177 (1982) [b]
148. V V Shereshovets, V D Komissarov, L A Bachanova, R Sh Burkhanova, G A Tolstikov *Zh. Org. Khim.* **19** 892 (1983) [c]
149. V V Shereshovets, L A Bachanova, V D Komissarov *React. Kinet. Catal. Lett.* **25** 313 (1984)
150. E I Gol'dfarb, V V Shereshovets, R K Yanbaev, O A Cherkasova, V D Komissarov, N A Mukmeneva, G A Tolstikov *Izv. Akad. Nauk SSSR, Ser. Khim.* 493 (1988) [b]

151. A D Pershin, D G Pobedimskii, V A Kurbatov, A L Buchachenko *Izv. Akad. Nauk SSSR, Ser. Khim.* 581 (1975) [b]
152. V V Shereshovets, L A Bachanova, V D Komissarov, G A Tolstikov *Zh. Org. Khim.* **21** 482 (1985) [c]
153. V V Shereshovets, V D Komissarov, N Ya Shafikov, L A Bachanova, V S Kolosnitsyn, Yu E Nikitin, G A Tolstikov *Zh. Org. Khim.* **19** 225 (1983) [c]
154. V V Shereshovets, F Z Galin, A A Elichev, N M Korotaeva, V D Komissarov, G A Tolstikov *Izv. Akad. Nauk SSSR, Ser. Khim.* 718 (1988) [b]

[a] — *Kinet. Catal. (Engl. Transl.)*
[b] — *Russ. Chem. Bull. (Engl. Transl.)*
[c] — *Russ. J. Org. Chem. (Engl. Transl.)*
[d] — *Russ. J. Gen. Chem. (Engl. Transl.)*
[e] — *Russ. J. Phys. Chem. (Engl. Transl.)*
[f] — *Dokl. Chem. Technol., Dokl. Chem. (Engl. Transl.)*
[g] — *J. Appl. Spectroscop. (Engl. Transl.)*

Russian Chemical Reviews **70** (2) 131 – 146 (2001) © 2001 Russian Academy of Sciences and Turpion Ltd

DOI 10.1070/RC2001v070n02000621

Hydrogen-containing carbon nanostructures: synthesis and properties

B P Tarasov, N F Goldshleger, A P Moravsky

Contents

I. Introduction 131
II. Synthesis of hydrofullerenes 131
III. Properties of hydrofullerenes 135
IV. Sorption of hydrogen by carbon nanotubes and graphite nanofibres 138
V. Conclusion 143

Abstract. Data on the interaction of carbon nanomaterials (fullerenes, carbon nanotubes, graphite nanofibres and their metal-doped modifications) with hydrogen are surveyed. New results on the preparation and properties of hydrofullerenes are presented. The prospects for the use of carbon nanomaterials as reversible hydrogen sorbents are discussed. The bibliography includes 183 references.

I. Introduction

Hydrogen has indisputable advantages over other energy carriers as it is a versatile, highly efficient and environmentally safe energy carrier. This provides good prospects for its wide application in power engineering, especially as a fuel for vehicles transport.[1] However, there is a very serious problem hampering the use of hydrogen as a fuel, namely, hydrogen storage and transportation. None of the currently available methods for the storage of hydrogen (in the gas state under high pressure, in the liquid state, as metal hydrides and hydrides of intermetallic compounds, or in the adsorbed state at low temperatures, see Table 1) meets the requirements imposed on hydrogen storage systems, *e.g.*, by the US Department of Energy (DOE) Hydrogen Plan (content of hydrogen $\geqslant 6.5$ mass % or $\geqslant 63$ kg m^{-3})[2] and by the International Energy Agency (content of hydrogen $\geqslant 5$ mass %, release of hydrogen at temperatures below 373 K).[3] Therefore, the development of new, more efficient methods for the storage and transportation of hydrogen is still an important task the success of which will determine, in many respects, further progress in the development of the 'hydrogen' technology and power engineering.

Hydrogen accumulation based on the reversible sorption of hydrogen is one of the most promising and popular methods for the storage of hydrogen. The most popular sorbents include hydride-forming metals and intermetallic compounds[4,5] as well as active carbons prepared by various methods.[6–9] Fullerenes and their derivatives, carbon nanofibres and nanotubes have been suggested repeatedly over recent years as hydrogen-accumulating substrates.[2,6,10,11] In the present review, we consider the data on the interaction of molecular hydrogen with these carbon nanomaterials (NM) and the prospects for their application as reversible sorbents for the storage of hydrogen.

Table 1. Traditional hydrogen storage methods.[3]

Method and conditions for hydrogen storage	Hydrogen content in the sorbent (mass %)	Hydrogen volume content /kg m^{-3}	Drawbacks of the method
Gaseous H_2 (300 K, 10 MPa)	100	7.7	heavy containers, small volume capacity
Liquid H_2 (20 K)	100	71	high losses, high cost
Metal-hydride			
TiH_2	4.0	150	insufficient
MgH_2	7.6	120	capacity; necessity
$LaNi_5H_{6.7}$	1.4	85	of heating;
$TiFeH_2$	1.9	95	sensitivity
Mg_2NiH_4	3.7	80	to admixtures
Cryoadsorption activated carbon (155 K, 6.9 MPa)	0.05 – 2	~1 – 2	necessity of cooling and compression

II. Synthesis of hydrofullerenes

The presently known methods for the preparation of hydrofullerenes,† such as the Birch – Hückel reduction of fullerenes, hydroboration, catalytic hydrogenation of fullerenes, reduction of fullerenes based on non-catalytic transfer of hydrogen from a donor to an acceptor, *etc.*, have been surveyed in detail in several reviews.[12–14] However, the rapid development of studies in this field requires a continuous analysis of the newly appearing methods for the synthesis of hydrofullerenes, especially because no ideal procedure for the preparation of hydrofullerenes with reliably controlled composition is yet available.

B P Tarasov, N F Goldshleger, A P Moravsky Institute of Problems of Chemical Physics, Russian Academy of Sciences, 142432 Chernogolovka, Moscow Region, Russian Federation. Fax (7-096) 576 40 09. Tel. (7-095) 913 21 09. E-mail: btarasov@icp.ac.ru (B P Tarasov), gold@cat.icp.ac.ru (N F Goldshleger), moralex@icp.ac.ru (A P Moravsky)

Received 18 August 2000
Uspekhi Khimii **70** (2) 149 – 166 (2001); translated by S S Veselyi

† Hydrofullerenes are also called fullerene hydrides or hydrogen-containing fullerene compounds; sometimes they are also called hydrofullerites in order to emphasise the solid state of the product.

1. Hydrogenation of fullerites and metal fullerides with molecular hydrogen

Chemical transformations occurring in mechanical mixtures of powders of a fullerite (C_{60}, C_{60}/C_{70}) and hydrogen-sorbing metals and intermetallic compounds (Pd, V, $LaNi_5$, $LaNi_{4.65}Mn_{0.35}$, $CeCo_3$) under the action of molecular hydrogen or deuterium have been studied in a wide pressure and temperature range.[15–19] It has been found that hydrogenation at 1.0–5.0 MPa and 573–673 K results in mixtures of metal hydrides MH_y and hydrofullerenes $C_{60}H_x$:

$$\{C_{60} + M\} + H_2 \longrightarrow \{C_{60}H_x + MH_y\}.$$

Heating of the resulting mixture $\{C_{60}H_x + MH_y\}$ in an inert atmosphere results first in dehydrogenation of the metal hydride and then (at 800 K) dehydrogenation of the hydrofullerene to give hydrogen and fullerene–metal compositions.‡

$$\{C_{60}H_x + MH_y\} \xrightarrow[-H_2]{<600\ K} \{C_{60}H_x + M\} \xrightarrow[-H_2]{\sim 800\ K} \{C_{60} + M\}.$$

Hence, we are dealing with a system which can accumulate hydrogen under certain conditions and release it under other conditions. This reaction cycle can be repeated many times, but the side reactions, such as polymerisation and carbide formation, restrict the prospects of application of these systems for hydrogen accumulation.

Depending on the temperature, the reaction of the pre-synthesised fullerides $C_{60}Pt$ and $C_{60}Pd_{4.9}$ with hydrogen (the H_2 pressure being 1–3 MPa) results either in hydrogen compounds of metallofullerides $<C_{60}MH_x>$ or in mixtures of hydrofullerenes $C_{60}H_x$ ($x = 2–26$) with Pt or PdH_y, respectively.

$$C_{60}Pt + H_2 \xrightarrow{400–550\ K} <C_{60}PtH_x>$$
$$C_{60}Pt + H_2 \xrightarrow{600–700\ K} C_{60}H_x + Pt$$

$$C_{60}Pd_{4.9} + H_2 \xrightarrow{400–550\ K} <C_{60}Pd_{4.9}H_x>$$
$$C_{60}Pd_{4.9} + H_2 \xrightarrow{600–700\ K} C_{60}H_x + PdH_y$$

Upon heating to 800 K, almost all the hydrogen is evolved from the reaction products, and the resulting mixture of the fullerite with the metal (Pd, Pt) can be hydrogenated again in the temperature range from 400 to 700 K to give mixtures of the hydrofullerene with PdH_y or Pt.[20–22]

The source of gaseous hydrogen and its purity affect considerably the hydrogenation of solid fullerenes and the state of the reaction products. For example, the hydrogenation of crystalline fullerene (fullerite) with hydrogen evolved upon the decomposition of hydrides of intermetallic compounds results in crystalline hydrofullerenes containing from 10 to 30 hydrogen atoms per fullerene molecule.[23,24] The content of hydrogen in the product increases with the number of the 'heating to 673 K–cooling to 300 K' cycles. The thermal cyclic hydrogenation mode not only provides a deeper process but also gives samples with a more homogeneous distribution of the components over the volume. The IR spectra of the resulting hydro- or deuteriofullerenes show intense absorption bands in the regions of C–H (2800–3000 cm^{-1}) and C–D (2050–2200 cm^{-1}) stretching vibrations. The relative intensities of the absorption bands of the starting C_{60} decrease abruptly (Fig. 1).

X-Ray diffraction analysis of the reduction product shows that hydrofullerene $C_{60}H_x$ (or deuteriofullerene $C_{60}D_x$) retains the crystal structure of the parent fullerite; the a_0 parameter of the face-centred cubic (FCC) lattice increases monotonically with the amount of hydrogen (or deuterium) in the hydrofullerene (Fig. 2).§

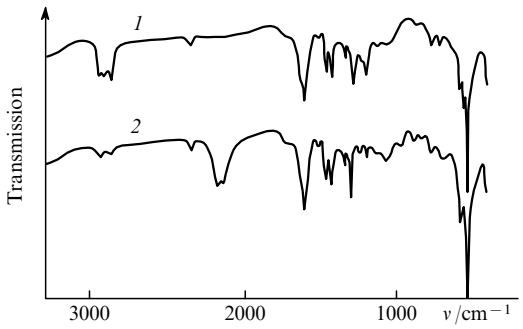

Figure 1. IR spectra of hydro- (*1*) and deuteriofullerenes (*2*) $C_{60}H(D)_{18–24}$.[24]

Heating of the hydrides synthesised by this method to 800 K results in intense evolution of hydrogen. The IR spectrum of the solid product of the thermal decomposition of hydrofullerene manifests bands corresponding to C_{60} and a series of bands the positions of which are close to those of the photo- or thermobarically polymerised C_{60} with the cyclobutane rings between the fullerene molecules,[26] which indicates that thermal dehydrogenation is accompanied by polymerisation of the fullerene cages.

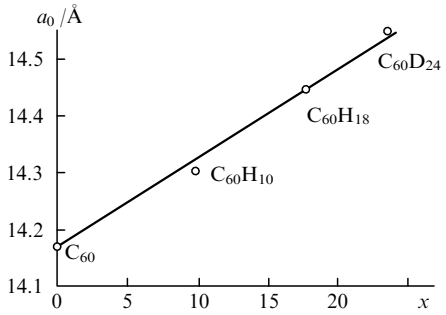

Figure 2. Dependence of the FCC lattice parameter a_0 of hydro- and deuteriofullerenes $C_{60}H(D)_x$ on the number of hydrogen and deuterium atoms.[25]

The samples dehydrogenated at 800 K can be hydrogenated again, but repeated 'hydrogenation–dehydrogenation' cycles result in the accumulation of polymerised fullerene.[25] The addition of NH_3, HI or C_2H_5I (5 mass %–10 mass %) to the hydrogen evolved from a metal-hydride accumulator accelerates considerably the hydrogenation of the fullerite but also increases the degree of polymerisation of the fullerene molecules formed upon the dehydrogenation of the hydrofullerene.[3]

Studies of the magnetic properties of hydrofullerenes prepared by hydrogenation of fullerene with hydrogen liberated from an accumulator based on hydrides of intermetallic compounds of nickel and rare-earth metals [23] showed that the samples contained ferromagnetic particles; this was explained by the gas-phase transfer into the reactor of traces of metal or metal hydride particles by hydrogen which has evolved from the accumulator. One could assume that fine particles of nickel and/or nickel–rare-earth metal intermetallides act as catalysts of the solid-phase hydrogenation of fullerene. The use of a nickel catalyst for hydrogenation of solid fullerite, *e.g.*, by controlled addition of volatile nickel compounds to the gas fed into the reactor, could

‡ In certain cases, heating above 950 K results in irreversible formation of metal carbides.

§ According to the reported data,[25] the lattice parameters for $C_{60}H_x$ and $C_{60}D_x$ are similar for equal x values.

provide more efficient reversible systems for hydrogen accumulation.

The solid-phase hydrogenation of fullerenes continues to attract the attention of scientists from the viewpoint of both practical application (hydrogen storage) and synthesis of individual hydrofullerenes. For example, solid-phase deuteration of C_{60} at 373–773 K and p_{D_2} = 15 MPa gave deuterides with the compositions $C_{60}D_8$, $C_{60}D_{18}$ and $C_{60}D_{36}$ (FCC structure, a_0 = 1.423, 1.448 and 1.500 nm, respectively).[27] Controlled doping of fullerene with palladium decreases (down to 373 K) the temperature of hydrogen or deuterium sorption relative to that for the undoped C_{60} sample at a gas (H_2 or D_2) pressure of 100 MPa.[28] A neutron diffraction study of palladium-doped fullerene showed no characteristic peaks of metallic Pd. Similarly, these peaks were not observed in the samples treated with hydrogen. Treatment of fullerene-containing carbon black by hydrogen plasma gives hydrofullerenes with low hydrogen content (x = 1–6).[29] Prolonged treatment does not increase the amount of sorbed hydrogen.

Progress is also observed in the field of liquid-phase hydrogenation of fullerenes. Cheaper heterogeneous catalysts have been developed and methods for more selective and extensive hydrogenation have been found. For example, the hydrogenation of C_{60} on the Ni/Al_2O_3 catalyst[30] occurs under milder conditions (toluene, 423–523 K, 2.5–7.5 MPa) than the hydrogenation on the Ru/C catalyst.[31] The reaction occurs selectively to give $C_{60}H_{36}$. The reaction selectivity can primarily be accounted for by the high dispersion of nickel deposited onto Al_2O_3.¶ A decrease in the reaction temperature decreases the selectivity (similarly to the reduction of C_{60} with dihydroanthracene in the presence of an organic catalyst[32]).

Liquid-phase hydrogenation of C_{60} with hydrogen (at atmospheric pressure, in the presence of 4% Pd/SiO_2, 5% Ru/Al_2O_3 or 5% Rh/Al_2O_3) or with hydrogen donors (cyclohexane, decalin, *etc.*) at 323–343 and 348–433 K, respectively, results in hydrofullerenes $C_{60}H_x$.[33] In some experiments, Pd/SiO_2 was used as the catalyst for the hydrogenation of fullerene by hydrogen transfer from a donor (cyclohexane, cyclohexene) to the acceptor (C_{60}). Titration of the hydrogen peroxide formed due to the oxidation of $C_{60}H_x$ with 2-ethylanthraquinone in the presence of O_2, chemical determination of hydrogen in $C_{60}H_x$, as well as IR and NMR spectra indicate that the C_{60} reduction products have the composition $C_{60}H_{42-46}$.[33] Unfortunately, the results of mass spectrometric determination of the hydrofullerenes formed have not been reported; this might provide direct information on the composition of $C_{60}H_x$.[33]

In a search for systems for the hydrogenation of fullerenes and dehydrogenation of hydrofullerenes which would comply with the requirements for the practically applicable hydrogen accumulators, Loutfy *et al.*[34] have examined whether soluble catalysts could be employed for hydrogenation of the C=C bonds and if salt melts could be used as the reaction media for hydrogenation. They also studied the effect of modification of the fullerene electronic structure on the hydrogenation process. This approach was based on the achievements in studies of the activation of the C–H bonds by metal complexes,[35] on the one hand, and on the data on the efficient catalytic hydrogenation of the C=C bonds with hydrogen in the presence of Cs_6C_{70},[36] on the other hand. Alkoxy compounds of the Group IV metals were found to be efficient as the soluble catalysts for fullerite hydrogenation and hydrofullerite dehydrogenation. This study[34] has shown that the use of certain soluble catalysts made it possible to decrease considerably the activation energy of hydrogenation and the temperature of the process. For example, the dehydrogenation of $(C_{60}/C_{70})H_{36}$ occurred at 573 K (6 h) to give $(C_{60}/C_{70})H_{22}$ (the loss of 1.74 mass % H_2), while the repeated hydrogenation of $(C_{60}/C_{70})H_{22}$ occurred at 423 K (12 h, 3.6 MPa) to give $(C_{60}/C_{70})H_{\sim 45}$. It has also been shown that doping of fullerene by an alkali metal facilitated markedly the fullerene hydrogenation. The dehydrogenation in this system occurs at considerably lower temperatures than the non-catalytic dehydrogenation of solid hydrofullerites.

The use of operating temperatures below 400 K is important for hydrogen-accumulating systems, hence these results[34] demonstrate that an almost acceptable temperature range can be achieved.

2. Reduction of fullerenes in the 'metal–hydrogen donor' system

The reduction of fullerenes is carried out using many traditional methods of organometallic chemistry (see, *e.g.*, the review[37]). For example, lithium in liquid ammonia in the presence of Bu^tOH was used for the reduction of C_{60}.[38]

$$C_{60} \xrightarrow{Li,\ NH_3\,(liq),\ Bu^tOH} C_{60}H_{2n}\,.$$

The process stopped in the step of the formation of $C_{60}H_{32-36}$ (see Refs 12 and 13). The products with a lower hydrogen content, *e.g.*, $C_{60}H_{32}$, were probably formed during the analysis or storage of the samples. The composition $C_{60}H_{36}$ of the reduction product of C_{60} fullerene with lithium in liquid ammonia has also been confirmed by other researchers.[39]

Polyfullerenes obtained by photo-induced and radical polymerisation of C_{60} cages (the radical polymerisation is preferable for the synthesis of polyfullerenes) are also reduced according to the Birch–Hückel method to give hydropolyfullerenes with a mean hydrogen content of ~3.5 mass % (for $C_{60}H_{36}$, 4.76 mass % H_2).[40] Hydropolyfullerenes, unlike monomeric hydrofullerenes with an equal hydrogen content, are almost insoluble in CS_2. This implies that the reduction at low temperatures does not involve cleavage of the C–C bonds between the fullerene cages in the polymers; this has been confirmed by gel-permeation chromatography. The IR spectra of hydropolyfullerenes contain intense bands in the region of C–H stretching vibrations. The ^1H and ^{13}C NMR spectra indicate structural similarity between polymeric and monomeric hydrofullerenes (the positions of the hydrogen atoms in the fullerene cage). The use of polyfullerenes does not increase the degree of hydrogenation of the fullerene cage, and hence, the amount of stored hydrogen. Thus, polyfullerenes are not superior to C_{60} molecules in hydrogenation and dehydrogenation reactions.

The reaction of C_{60} with $EtAlCl_2$ and activated magnesium [C_{60} : Al : Mg = 1 : (50–150) : (30–50); 293–295 K] in a THF–toluene mixture in the presence of Cp_2TiCl_2 (1 mol.%–3 mol.%) results in fullerene-containing aluminacyclopropane (yield 75%–90%), hydrolysis of which in D_2O results in a partially deuterated fullerene derivative.[41] Metallation of C_{60} with an excess of Et_3Al in the presence of Cp_2ZrCl_2 gives 2,3-fullerenoaluminacyclopentanes, hydrolysis of which results in mixtures of hydrogen-containing ethylfullerenes of the type $H_mC_{60}Et_m$ (m = 1–12).[42]

The reduction of C_{60} and C_{70} in the 'metal (M)–proton donor' system, where M = Zn (E° = −0.76 V), Ti (E° = −1.63 V), Al (E° = −1.66 V) or Mg (E° = −2.37 V), was also studied.[43–46] It was shown that the reaction of C_{60} with the Zn/Cu redox couple and a proton donor in toluene , unlike the reaction of C_{60} with Zn dust,[43] results in a more efficient fullerene reduction which occurs *via* the consecutive formation of $C_{60}H_2$, $C_{60}H_4$, and finally, $C_{60}H_6$; the target compounds can be isolated in each step.[44–47] Prolonged heating of a C_{60}–Zn/Cu–H_2O mixture in toluene results in two $C_{60}H_6$ isomers in the ratio 6 : 1, these amount to 30%–40% with respect to the starting C_{60}. The ^1H and ^{13}C NMR data show 1,2,33,41,42,50-$C_{60}H_6$ to be the main reaction product.[44,45]

¶ The results obtained[30] agree with the conclusion on the possible involvement of highly-dispersed nickel particles in the solid-phase hydrogenation of C_{60}.[23,24]

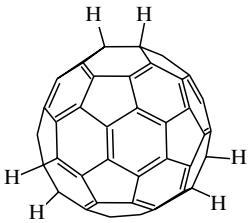

The hydrogen atoms in 1,2,33,41,42,50-$C_{60}H_6$ are not exchanged with deuterium atoms from D_2O on the NMR time scale, *i.e.*, the pK_a of $C_{60}H_6$ is much higher than that of $Bu^tC_{60}H$, which rapidly exchanges protons with the medium.[48] An attempt to isomerise 1,2,33,41,42,50-$C_{60}H_6$ in the presence of a Pd/C or Pt/C catalyst (as has been done for 7,8-$C_{70}H_2$, *cf.* Ref 49) resulted in rapid dehydrogenation of hydrofullerene instead of the expected reaction.[44]

The reaction in the $C_{70}-Zn/Cu-H_2O$ system under certain conditions results in preferential formation of $C_{70}H_{10}$, 7,8,19,26,33,37,45,49,53,63-$C_{70}H_{10}$ being the major isomer.[50] For various reasons (the presence of an oxide film, difficult separation of the products from the reaction mixture, *etc.*), efficient and selective reduction of fullerenes in the presence of other metals (Ti, Al, Mg)[44,46] was found to be impossible.

Water is the most suitable proton donor for the preparation of reduced fullerene derivatives in the $C_n-Zn/Cu-H_2O$ systems (n = 60, 70). Hydrofullerenes with low hydrogen content, *viz.*, $C_{60}H_2$, $C_{60}H_4$, $C_{60}H_6$ and $C_{70}H_{10}$, were obtained in good yields.[44,50] The isomer distribution is controlled by the reduction kinetics. The use of strong acids as proton donors for the reduction of fullerenes gives hydrofullerenes with higher hydrogen content.[51]

In toluene, the reduction of the fullerene cage in the $C_{61}H_2$ fulleroid in the presence of Zn/Cu occurs more slowly than that of fullerene,[52] but the reaction in *o*-dichlorobenzene occurs quite efficiently to give three isomeric compounds $C_{61}H_4$ which are light- and air-sensitive even at low temperatures. The reaction of sodium naphthalenide with C_{60} in THF gives 1,1′,2,2′-tetrahydro-bi[60]fulleren-1-yl $C_{120}H_2$ together with other products (including 1,2-dihydrofullerene).[53] Compound $C_{120}H_2$ is also formed upon hydrolysis of the salt $(Me_2NC_6H_4)_3C^+[C_{60}]^{-\bullet}$ obtained by the reduction of C_{60} with the crystal violet radical.[54]

The reaction of C_{60} with dilithiumacetylenide results in bis(hydrofullerenyl)acetylene $C_{122}H_2$ (yield 6.6%).[53] It should be noted that deprotonation of $C_{120}H_2$ is accompanied by fast dissociation of the transient C_{120}^{2-} dianion to the C_{60}^{-} monoanion, whereas deprotonation of $C_{122}H_2$ results in the C_{122}^{2-} dianion.[53]

3. Reduction of fullerenes by organic compounds

The reduction of fullerenes based on non-catalytic hydrogen transfer from a donor (*e.g.*, dihydroanthracene) to an acceptor (*e.g.*, C_{60} fullerene) results in selective formation of $C_{60}H_{36}$ † or $C_{60}H_{18}$, depending on the reaction conditions.[55,56]

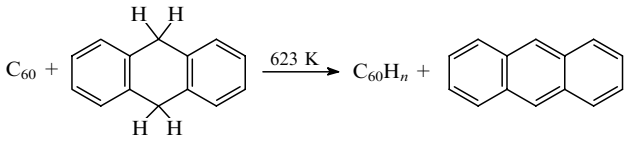

The hydrogenation of C_{70} with dihydroanthracene results in a series of hydrofullerenes $C_{70}H_n$ (n = 36–46), $C_{70}H_{36}$ being the major product.

Anhydrous hydrazine in benzene reduces C_{60} and the endohedral compound $^3He@C_{60}$ into the lower hydrides $C_{60}H_2-C_{60}H_8$ and $^3He@C_{60}H_2-{}^3He@C_{60}H_8$; their compositions and structures were determined using ^1H and ^3He NMR spectroscopy (in the case of $^3He@C_{60}$). At high hydrazine concentrations, the reaction mixture also contained higher hydrofullerenes, *viz.*, $C_{60}H_{18}$ and $C_{60}H_{36}$.[57]

Photoinduced electron transfer (PET) plays an important role in the reduction and oxidation of fullerenes. Since the one-electron oxidation potential of the triplet-excited state of C_{60} is 1.14 V (relative to the saturated calomel electrode),[58] electron donors having less positive oxidation potentials can be used for the photoreduction of C_{60}. For example, the photoreduction of C_{60} with allyltributyltin in the presence of CF_3COOH results in the selective formation of 1-allyl-1,2-dihydrofullerene, C_{60}-1,2-(H)C_3H_5,[59] while the reaction of C_{60} with tributyltin hydride in benzene occurs (under irradiation[59] or at elevated temperatures[60]) to give C_{60}-1,2-(H)$SnBu_3$. If 10-methyl-9,10-dihydroacridine is used as a hydrogen donor in the presence of $PhCN-CF_3COOH$ in photoreduction of C_{60} (λ > 540 nm), fullerene is reduced selectively to give 1,2-$C_{60}H_2$ (70%).[59]

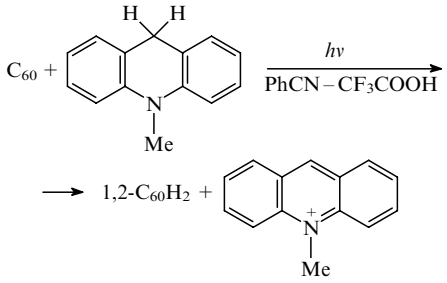

This photoreduction reaction of C_{60} is superior to, *e.g.*, the hydroboration of C_{60} (see Ref. 61) because of its selectivity and because mild reducing agents are used. However, in the absence of irradiation this reaction does not occur even at 373 K.

The bimolecular rate constant for quenching of the triplet-excited C_{60} ($^3C_{60}$) by 10-methyl-9,10-dihydroacridine (k_q = 4.3×10^9 litre mol^{-1} s^{-1}) and the mechanism of the photoreduction of C_{60} have been determined.[62]

Similarly to the two-electron reduction of C_{60} in the presence of 10-methyl-9,10-dihydroacridine, the one-electron reduction of C_{60} involving 1-benzyl-1,4-dihydronicotinamide and its dimer occurs through photoinduced electron transfer from the electron donor to $^3C_{60}$.[63,64] The difference between the redox and acid-base properties of the radical cations formed upon PET can define the reaction pathway.

Heating (100 °C, toluene) or pulse photolysis (Nd^{3+} : YAG laser, λ = 532 nm, benzonitrile) of a mixture of C_{60} with the Hantzsch ester (diethyl 2,6-dimethyl-1,4-dihydropyridine-3,5-dicarboxylate) under anaerobic conditions result in fullerene hydrogenation products and diethyl 2,6-dimethylpyridine-3,5-dicarboxylate (the dehydrogenation product of the Hantzsch ester).

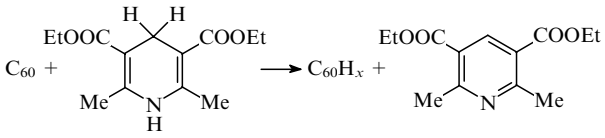

The progress of the dehydrogenation of the Hantzsch ester with the fullerene was monitored by ^1H NMR spectroscopy and a signal at δ 5.93 characteristic of 1,2-$C_{60}H_2$ could be detected if the reaction was carried out at room temperature. Heating of the reaction mixture in the presence of excess Hantzsch ester results in hydrofullerenes with the composition $C_{60}H_x$ (x = 2, 4, 6) identified by mass spectrometry.[65,66]

Illumination of the same mixture by visible light under aerobic conditions (room temperature), in agreement with the known data[67] on the sensitising effect of C_{60}, completely converted the Hantzsch ester in the presence of fullerenes to give the correspond-

† Lobach *et al.*[56] paid much attention to standardisation of the conditions for the preparation of $C_{60}H_{36}$ because the synthetic procedure affects considerably the properties and structures of hydrofullerenes.

ing pyridine derivative; the concentration of C_{60} remained unchanged.[65]

Tertiary amines are widely used in the photoreduction of fullerenes. Prolonged irradiation (λ = 350 nm, N_2) of a mixture of C_{60} with tertiary amines $RNMe_2$ (R = Ph, Me) gives 1,2-$C_{60}H_2$ along with a pyrrolidine derivative of C_{60} (fullereno[C_{60}]pyrrolidine).[68]

The ESR method was used to study many photoreduction reactions of C_{60}. For example, it was found that the $C_{60}^{-\bullet}$ radical anion is formed in the presence of photo-activated TiO_2[69] or triethylamine[70] in a mixture of organic solvents[69,70] and in an aqueous solution.[71] The photochemical reduction of C_{60} in the presence of TiO_2 or ascorbic acid was studied.[72] It was found that the C_{60} fullerene is reduced photochemically by triethylamine to give $C_{60}^{-\bullet}$. Prolonged irradiation of the reaction mixture results in $C_{60}H^-$ (the C_{60}^{2-} protonation product) which is decomposed to $C_{60}^{-\bullet}$ in a dark reaction.[73]

Irradiation of C_{60} in the presence of certain acceptor-type photosensitisers (9,10-dicyanoanthracene, 1,4-dicyanonaphthalene, *N*-methylacridinium and 2,4,6-triphenylpyrylium hexafluorophosphates) results in 1-substituted 1,2-dihydro[60]fullerenes following introduction of proton donors such as *N*,*N*-dimethylformamide, 1,3-dioxolane, phenylacetaldehyde, methyl formate, *tert*-butyl alcohol, propionic acid, *etc*.[74,75]

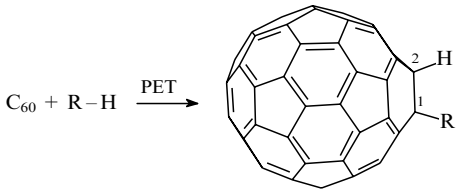

Co-sensitisers, *e.g*., biphenyl, are used in order to increase the yield of the products. The $C_{60}^{+\bullet}$ radical cation formed was shown to possess electrophilic character.

$$C_{60} \xrightarrow[\text{PET}]{h\nu} C_{60}^{+\bullet},$$

$$C_{60}^{+\bullet} + RH \longrightarrow H-C_{60}^{+} + R^{\bullet},$$

$$H-C_{60}^{+} + R^{\bullet} + e^- \longrightarrow H-C_{60}-R.$$

4. Other methods for the preparation of hydrogen-containing fullerene derivatives

Dihydrofullerene $C_{60}H_2$ was obtained in low yield upon sonication of C_{60} solutions in decahydronaphthalene.[76] The formation of dihydrofullerene $C_{60}H_2$ upon electrochemical hydrogenation of C_{60} in 30% aqueous KOH was also reported.[77] The electrolytic hydrogenation of C_{60} and dehydrogenation of $C_{60}H_2$ are reversible.[77]

$$C_{60} + xH_2O + x\,e^- \rightleftharpoons C_{60}H_x + xOH^-.$$

Mechanochemical reactions involving fullerenes and graphite have been studied.[78–81] Mechanochemical treatment of graphite in an atmosphere of hydrogen (1 MPa) at room temperature results in nano-structured graphite which adsorbs hydrogen both physically and chemically.[81] The method of 'high-speed vibration milling' (under these conditions, crystalline C_{60} is pulverised into particles with sizes smaller than 1 μm) was found to be highly efficient for the supramolecular complexation of fullerenes and their derivatives with γ-cyclodextrin and sulfocalixarene.[79] The yields of [4 + 2]-cycloaddition products of fused aromatic compounds (anthracene, tetracene, pentacene and naphtho[2,3-*a*]pyrene) to C_{60} obtained according to this procedure are higher than the yields of the same products obtained by heating the components in solution.[80] The solid-phase reaction of C_{60} with KCN, unlike the homogeneous reaction, gives the C_{120} dimer.[82] This reaction also occurs in the presence of other salts (K_2CO_3, AcOK), metals (Li, Na, K, Mg, Al and Zn) and organic bases (4-dimethylamino- and 4-aminopyridine).[82] It is probable that the mechanochemical method can also be applied for the synthesis of hydrogenated fullerene derivatives ‡ (similarly to the hydrogenation of organic compounds with hydrogen[84]).

III. Properties of hydrofullerenes

1. The state of hydrogen in solid hydrofullerenes

In the majority of experiments on the reduction of C_{60} and C_{70}, mixtures of fullerene hydrides are obtained. Solid samples of hydrofullerenes with the same molecular formula but prepared by different methods differ strongly in their solubilities, light and air resistances, abilities to withstand prolonged storage and in other properties (see, *e.g*., Refs 13, 51, 85).

Of hydrofullerenes, $C_{60}H_{36}$ has been studied most thoroughly. Electron-impact and field-desorption mass spectrometric analysis showed that $C_{60}H_{18}$ is the first stable thermal decomposition product of $C_{60}H_{36}$ prepared under the conditions of non-catalytic transfer of hydrogen from a donor to an acceptor.[56] The intermediate hydrides $C_{60}H_n$ (n = 33–35) are much less stable than $C_{60}H_{36}$. Intense peaks of $C_{60}H_{18}$ and C_{60} appearing in the mass spectrum of a sample of $C_{60}H_{36}$ after its prolonged storage indicate that $C_{60}H_{36}$ undergoes decomposition; the presence of the C_{60} peak is evidence of possible reversible addition of hydrogen to fullerene. The formation of $C_{60}H_{36}$ as the only reduction product of C_{60} under non-catalytic hydrogen transfer conditions is also confirmed by the spectra obtained using matrix-assisted laser desorption ionisation mass spectrometry (MALDI-MS): the most abundant peak is that of $C_{60}H_{35}^+$, the fragmentation is insignificant, the intensities of the satellite peaks corresponding to the oxidation products $C_{60}H_xO^+$ are much lower than in the case of the $C_{60}H_{36}$ obtained by the Birch reduction.[39]

As noted above, solid hydrofullerenes decompose at temperatures above 800 K in an inert or in a hydrogen atmosphere to give hydrogen and fullerenes.[23,86] The thermal decomposition product of crystalline $C_{60}D_{24}$ at 823 K mainly consists of fullerene (Fig. 3)

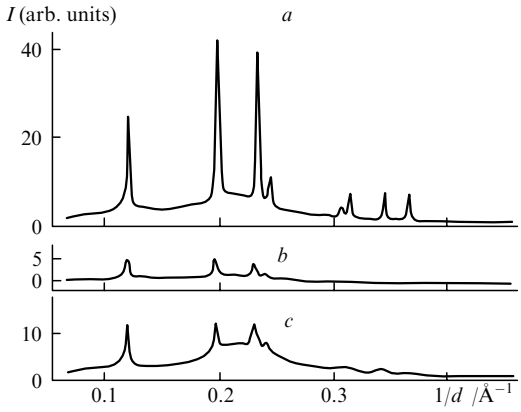

Figure 3. Diffractograms of the parent fullerene (*a*), fullerene deuteride $C_{60}D_{24}$ (*b*) and the product of thermodecomposition of the deuteride (*c*).[25]

with the distance between the C_{60} molecules considerably exceeding that in the parent fullerene (the a_0 constants of the FCC lattice of the decomposition product and C_{60} are 1.452 and 1.417 nm, respectively). Presumably, the increase in the fullerene crystal lattice constant resulting from hydrofullerene decomposition can be useful in the synthesis of alkali metal fullerides with superconducting properties.[86] The position of the C1*s* peak maximum in the X-ray photoelectron spectrum of the $C_{60}D_{24}$ deuteride is shifted towards lower bond energies in comparison with that of C_{60}, which makes it possible to conclude that a small positive charge exists on the deuterium atoms. The peak becomes narrower

‡ Apparently, the microwave irradiation method[83] can also be used for the preparation of hydrogenated fullerene derivatives.

as the deuteride undergoes thermal decomposition, and its 'centre of gravity' shifts to higher bond energies.[86]

Particular interest in the fundamental and applied aspects is felt in the synthesis of hydrofullerenes in which the hydrogen atoms are located both outside and inside the fullerene cage. This is a way to increase the hydrogen capacity of fullerenes. Therefore, studies of the properties of individual hydrogen molecules located in a closed space are also of interest. For example, it was found that compounds $C_{60}H_{52}$ and $C_{60}H_{48}$ fluoresce in the long-wave region. This phenomenon was interpreted taking account of the possibility of penetration of hydrogen molecules into a closed hydrofullerene cavity.[87] Hydrofullerites obtained under ultrahigh hydrogen pressures, $p_{H_2} = 0.6$ and 3.0 GPa, were studied by inelastic neutron scattering (INS) spectroscopy.[88] The spectra showed that the synthesis of $C_{60}H_x$ ($p_{H_2} = 0.6$ and 3.0 GPa, 620 K, 24 h) followed by cooling the sample to 77 K under a high pressure of H_2 is accompanied by the formation of a solid solution of hydrogen in the $C_{60}H_x$ lattice ($x \approx 24$ and 32–46 for $p_{H_2} = 0.6$ and 3.0 GPa, respectively).[88,89] The main features of the INS spectrum of $C_{60}H_{32}$ obtained at $p_{H_2} = 3.0$ GPa [90] are similar to those for $C_{60}H_{\sim 23}$ obtained at $p_{H_2} = 0.6$ GPa.[91] Presumably, a considerable fraction of hydrogen (~ 3 H_2 molecules per C_{60} molecule) are located as H_2 molecules in the interstices of the $C_{60}H_x$ lattices. Upon heating to 293 K, the H_2 molecules leave the sample with heat evolution. Dissolved molecular hydrogen is detected by the rotational transition peaks in the H_2 molecule (~ 15 and 30 meV) in the difference INS spectra between the 'quenched' (H_2-containing) and heated (H_2-free) products. The possibility of polymeric binding of the $C_{60}H_{32}$ hydrofullerite at high H_2 pressure (3.0 GPa) is suggested by the presence of a peak near 13 meV in its INS spectrum. The low-energy part of the INS spectrum (< 9 meV) for $C_{60}H_{32}$ is believed to indicate [88,89] the presence of an endohedral hydrogen atom unbound with carbon.

Hydrofullerites obtained at $p_{H_2} = 0.6$ and 3.0 GPa and $T = 520$–620 K and then quenched at $T < 120$ K exhibited ferromagnetic properties up to $T \approx 300$ K. Their magnetisation was as high as $M = 1.2$ emu g^{-1} at $H = 1$ T.[92] According to analytical data, the concentration of ferromagnetic admixtures in hydrofullerenes is insignificant. Magnetisation which disappears upon heating of the samples above 340 K or upon prolonged storage at room temperature is a property inherent in hydrofullerites obtained by various methods.[92,93] Probably, their magnetisation is caused by the presence of unstable transient radical-type electronic states. The penetration of hydrogen inside the cage, polymerisation of the fullerene cages upon dehydrogenation and other high-energy transformations of the C–C and C–H bonds in sterically hindered fullerene lattices could be the reasons for the generation of quasistable carbon atoms with unsaturated valence or delocalised unpaired electrons.

2. Thermodynamic analysis of the dehydrogenation of hydrofullerenes

The thermodynamic properties of the $C_{60}H_{36}$ hydrofullerene obtained by non-catalytic hydrogen transfer [56] have been studied in the temperature range from 4.8 to 340 K.[94,95] The following values of thermal capacity, enthalpy, entropy and Gibbs free energy were found for the hydrofullerene obtained at $T = 298.15$ K and $p = 101.325$ kPa:

$$C_p^\circ(298.15) = 690 \text{ J K}^{-1} \text{ mol}^{-1};$$

$$H^\circ(298.15) - H^\circ(0) = 84.94 \text{ kJ mol}^{-1};$$

$$S^\circ(298.15) = 506 \text{ J K}^{-1} \text{ mol}^{-1};$$

$$-[G^\circ(298.15) - H^\circ(0)] = 66.17 \text{ kJ mol}^{-1}.$$

High temperature is required for the dehydrogenation of hydrogen-containing fullerene derivatives. Quantum-chemical calculations of the C–H bond energy in fullerene hydrides performed by the semi-empirical AM1 method gave the values of 306.27, 298.32, 295.80 and 293.72 kJ mol^{-1} for $C_{60}H_{12}$ (T_h), $C_{60}H_{18}$ (C_3) and $C_{60}H_{36}$ (T and T_h), respectively.[96] Heating of $C_{60}H_{36}$ under isothermal conditions (594 and 610 K, 20 h) results in dehydrogenation of the sample and evolution of gaseous H_2. In this case, the composition of the solid residue is '$C_{60}H_6$': $C_{60}H_{36} \rightarrow C_{60}H_{18} \rightarrow$ '$C_{60}H_6$'. The dehydrogenation occurs stepwise [97] and is accompanied by sublimation of $C_{60}H_{36}$ and $C_{60}H_{18}$. The estimated saturated vapour pressures of $C_{60}H_{36}$ and $C_{60}H_{18}$ at 594 K are 9.8×10^{-9} and 5.4×10^{-9} MPa, respectively.

3. Specific features of hydrofullerene structures

The $C_{60}D_{24}$ deuteride obtained by deuteration of crystalline fullerene with gaseous D_2 is a crystalline powder with an FCC lattice ($a_0 = 1.455$ nm) [23] and a crystallite size of 51–56 nm.[25] The synthesis of $C_{60}D_{36}$ with an FCC lattice ($a_0 = 1.500$ nm) has been reported.[27] On the other hand, $C_{60}H_{36}$ samples obtained by hydrogenation under high pressure [98] or in the presence of iodine [99] have body-centred cubic (BCC) lattices.[100]

Theoretical and experimental studies of the structures of the most stable (T, T_h, S_6 and two D_{3d}) isomers of the $C_{60}H_{36}$ hydrofullerene have been carried out.[99–103] Comparison of the experimental ^1H and ^{13}C NMR spectra of the solid $C_{60}H_{36}$ (see Ref. 99) with the calculated ones [104] made it possible to assume a structure with the T symmetry [105] for $C_{60}H_{36}$ obtained by non-catalytic hydrogen transfer.[56] According to X-ray emission and photoelectron spectral data, quantum-chemical calculations and electrochemical behaviour, the most probable structure for the $C_{60}H_{36}$ hydrofullerene is that with the T symmetry and with four isolated benzenoid (non-hydrogenated) rings located on the surface of the $C_{60}H_{36}$ hydrofullerene in the vertices of an imaginary tetrahedron (Fig. 4).[103,106,107]

Comparison of the CK_α spectra of C_{60}, $C_{60}H_{36}$ and C_6H_6 prompts the conclusion that the π-electron systems of hydrofullerenes and benzene are similar; the localisation of the HOMO electron density of the $C_{60}H_{36}$ hydrofullerene on the benzenoid rings allows one to assume that η^6 metal complexes based on $C_{60}H_{36}$ can be synthesised.[106,108] Studies of the electrochemical behaviour of the $C_{60}H_{36}$ hydrofullerene indicates that $C_{60}H_{36}$ is a rather 'hard' molecule with low reactivity in redox reactions. The electrochemical electronegativity decreases in the series $C_{60} > C_{60}H_2 > C_{60}H_{36} \approx C_6H_6$. The approximate equivalence of the electronegativities of the two latter compounds can also be evidence in favour of the T-symmetrical structure of $C_{60}H_{36}$.[107]

The presence of a large number of reaction centres in the fullerene molecules results in a large number of possible isomers of hydro- and fluorofullerenes. Based on a combination of the MO LCAO method with molecular mechanics, Breslavskaya and D'yachkov [109] predicted the structures of the most stable C_nX_k

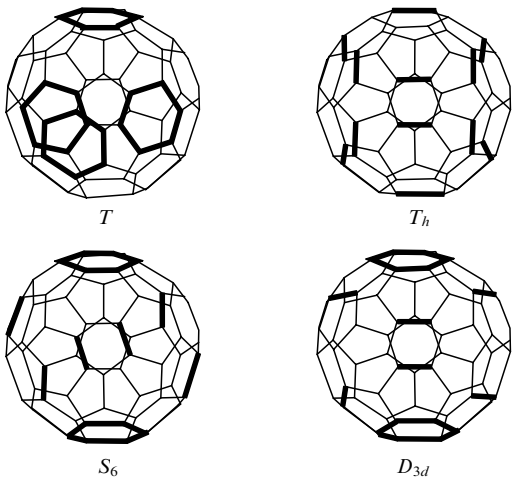

Figure 4. The most stable $C_{60}H_{36}$ isomers (one of the two D_{3d} is shown).[103] The thick lines denote the non-hydrogenated C–C bonds.

isomers with high hydrogen and fluorine contents (X = H, F; n = 76, 78, 84) and compared the theoretical data with the available experimental results. According to the neutron diffraction structural data[110] for $C_{60}D_{36}$ prepared according to a reported method[99] by deuteration of C_{60} at 623 K and a D_2 pressure of 3.4 MPa in the presence of iodine as a promoter, the structure with the T symmetry is most stable for this deuteriofullerene as well [a structure with the T symmetry has been suggested previously[99] as the most stable one for $C_{60}H_{36}$ (IR and ^{13}C NMR spectral data)].

Billups *et al.*[111] studied the ^3He spectra of $^3He@C_{60}H_{36}$ samples prepared by reduction of $^3He@C_{60}$ with lithium in liquid ammonia[38] and by non-catalytic hydrogen transfer.[55] The ^3He NMR spectra of both $^3He@C_{60}H_{36}$ samples contain peaks at δ −7.7 and −7.8; the third peak at δ −16.45 was assigned to the chemical shift of the $^3He@C_{60}H_{18}$ hydrofullerene. Comparison of the experimental spectra[111] with the calculated chemical shifts for the most stable $^3He@C_{60}H_{36}$ isomers [δ −10.8 (T), −7.7 ($D_{3d'}$), −6.1 (S_6), −3.4 (T_h) and −5.6 (D_{3d})][104] makes it possible to assume that the $D_{3d'}$ isomer is formed in both cases. In addition, based on the ^3He NMR spectra of the sample prepared by reduction of $^3He@C_{60}$ with lithium in liquid ammonia, the conclusion was made as to the low probability of the formation of the isomer with the T_h symmetry which had previously been suggested[38] for a $^3He@C_{60}H_{36}$ sample. According to the reported data,[112] the isomer with the S_6 symmetry (see Fig. 4) is the most stable $C_{60}H_{36}$ hydride, though the difference between the energies of the ten most stable isomers is less than 62.76 kJ mol^{-1}. In the previous studies by the same authors, isomers with the T and D_{3d} symmetries were noted as the most stable ones of the large number of possible structures suggested for the $C_{60}H_{36}$ fullerene hydride.[101]

Thus, it has been shown for $C_{60}H_{36}$ that not only different chemical methods can result in isomers with different symmetries, but also products with different isomer compositions can be formed within a single procedure (see, *e.g.*, Refs 85 and 106). In the case of the $C_{60}H_{36}$ molecule, the problem of the most stable structure remains open and requires more accurate theoretical calculations. It is quite possible that certain methods for the synthesis of $C_{60}H_{36}$ can produce thermodynamically unstable isomers (*e.g.*, due to kinetic factors). In order to verify the validity of this assumption, one has to perform in-depth experimental and theoretical studies, including the isomerisation of $C_{60}H_{36}$. A reliable determination of the $C_{60}H_{36}$ structure is also interesting from the practical respect. For instance, the knowledge of its exact structure is very useful when one plans the syntheses based on this hydrofullerene.

4. The reactivities of hydrofullerenes

According to the reported data,[113] a hydride with the net composition $C_{60}H_{18.7}$ with a_0 = 1.476 nm is stable up to 703 K in an Ar atmosphere. Further increase in the temperature results in hydrogen evolution and is accompanied by decomposition of part of the fullerene molecules and formation of graphite platelets and methane.§ The use of catalytic amounts of ruthenium or platinum did not decrease the temperature of hydrofullerene dehydrogenation.

The dehydrogenation of $C_{60}H_{36}$ on treatment with a strong hydrogen acceptor, *viz.*, 2,3-dichloro-5,6-dicyano-1,4-benzoquinone, which is widely used in the analysis of hydrofullerenes, was found to be non-quantitative, since in addition to C_{60}, its derivatives were also formed.[56] Thermogravimetric (TG) and differential thermogravimetric (DTG) studies of $C_{60}H_{36}$ in the presence of oxygen were carried out.[30] It was found that $C_{60}H_{36}$ is partially oxidised at 550 K to give $C_{60}H_{36}O_x$ ($x \approx 4.8$) and that its combustion occurs at 745 K. As it might have been expected, these temperatures are much lower than the temperatures of partial oxidation and combustion of C_{60} (705 and 888 K, respectively).[30] Complexes of polyaromatic compounds and fullerene with platinum immobilised on silica exist in the temperature range 323–373 K and can be repeatedly hydrogenated and dehydrogenated.[114] It is these properties that are required for practically usable systems for the storage of hydrogen: good reproducibility of hydrogenation–dehydrogenation cycles in a temperature range as low as possible.

Deprotonation of 1,2-$C_{60}H_2$ in the presence of Bu_4NOH (benzonitrile, anaerobic conditions) is accompanied by the formation of the C_{60}^{2-} dianion which quickly reacts with a number of alkyl halides to give mono- and dialkylfullerenes.[115]

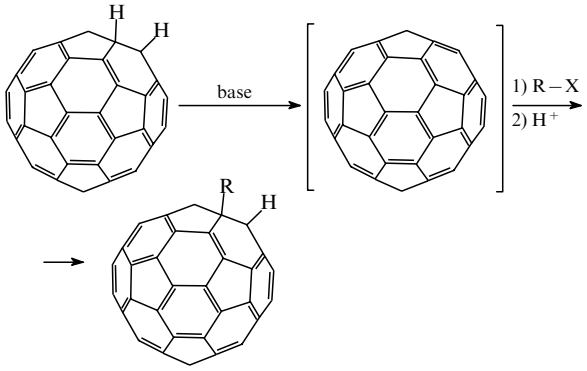

Ph_2CHBr, $PhCH_2Br$, MeI, propargyl bromide and allyl bromide are used as the alkylating reagents. However, attempts at alkylation of the C_{60}^{2-} formed with octyl bromide failed. Analysis of the absorption spectra for mono- and dialkylated C_{60} derivatives shows that the sp^3 carbon atoms in the monoalkyl derivative are in the 1,2-position, while in dialkyl-C_{60} derivatives, they are in the 1,4-position. Fukuzumi *et al.*[116] studied the mechanisms of formation of R_2C_{60} and $R(R')C_{60}$ dialkylfullerenes from chemically obtained C_{60}^{2-} and various alkyl halides (RX and R′X) differing both in the nature of the R and R′ radicals and of the halogen atom. In the first step, transfer of one electron from the C_{60}^{2-} dianion to an alkyl halide occurs to give RC_{60}^-, which is transformed to R_2C_{60} or $R(R')C_{60}$ according to the S_N2 mechanism.

It was shown that protonation of $Bu^tC_{60}^-$ with trifluoroacetic acid initially gives 1,4-$Bu^tC_{60}H$; the latter is then quickly transformed to 1,2-$Bu^tC_{60}H$ which is more stable thermodynamically. Photoinduced transfer of an electron from a soft reducing agent, 1-benzyl-4-*tert*-butyl-1,4-dihydronicotinamide, to triplet-excited C_{60} results eventually in selective two-electron reduction of C_{60} to give $Bu^tC_{60}^-$, which reacts with $PhCH_2Br$ or Bu^tI in the next step to give 1,4-$Bu^t(PhCH_2)C_{60}$ (see Ref. 63) or $Bu^t_2C_{60}$ (see Ref. 117), respectively. Photoalkylation of C_{70} occurs similarly to give $Bu^tC_{70}^-$ (and $Bu^tC_{70}H$ after protonation); the formation of five regioisomers is possible for $Bu^tC_{70}^-$, unlike $AlkC_{60}^-$ which gives only one product.[118]

The reactivities of the $C_{60}^{-\bullet}$ radical anion or the C_{60}^{2-} dianion manifest themselves not only in reactions with alkyl halides. The higher C–H bond strength in lower hydrofullerenes in comparison with the higher ones results in the possibility of the transfer of a hydrogen atom onto these anions from higher hydrofullerenes. It was shown by cyclic voltammetry that the reaction between C_{60} and $C_{60}H_{36}$ in a propylene carbonate–toluene mixture is induced by electron transfer and eventually involves transfer of a hydrogen atom from $C_{60}H_{36}$ to the fullerene.[119] The pathway according to which the $C_{60}^{-\bullet}$ radical anion and the C_{60}^{2-} dianion electrogenerated from C_{60} react with $C_{60}H_{36}$ was considered as the most probable variant of the transformation; this reaction involves the transfer of a hydrogen atom from $C_{60}H_{36}$ and results in $C_{60}H_2$ (proton transfer is impossible since the calculated[120] pK_1 for $C_{60}H_{36}$ is 31.35 and $C_{60}H_2$ is a rather strong acid[121,122] with pK_1 = 4.7 and pK_2 = 16). In order to estimate the possibility of formation of

§ Presumably, the character of thermal decomposition and the crystal lattice parameters of hydrofullerenes depend considerably on the conditions of fullerene hydrogenation.

$C_{60}H_2$ from C_{60} and $C_{60}H_{36}$, Tkachenko *et al.*[119] calculated the mean C–H bond energies in hydrofullerenes $C_{60}H_2$ and $C_{60}H_{36}$, which were found to be 295 and 279 kJ mol^{-1}, respectively. Thus, cleavage of a C–H bond in $C_{60}H_{36}$ with subsequent formation of a C–H bond in $C_{60}H_2$ is energetically favourable.

The relatively week C–H bond strength in higher hydrofullerenes enables its homolytic cleavage by other relatively weak acceptors as well. Elimination of a hydrogen atom from $C_{60}H_{36}$ under mild conditions can also be carried out by treatment with the 2-(*p*-fluorophenyl)hexafluoroisopropyl radical.[123] Heating (353 K) of hydrofullerenes $C_{60}H_x$ ($x = 6-18$) with $Hg[N(SiMe_3)_2]_2$, $Ti[N(SiMe_3)_2](NEt_2)_3$ and other metal complexes also results in elimination of a hydrogen atom from $C_{60}H_x$ and formation of fullerene-containing oligomers, *e.g.*, $-[(C_{60}H_n)Hg_2]_m-$.[124]

$$mC_{60}H_x + 2mHg[N(SiMe_3)_2]_2 \longrightarrow$$
$$\longrightarrow -[(C_{60}H_n)Hg_2]_m- + 2mHN(SiMe_3)_2.$$

IV. Sorption of hydrogen by carbon nanotubes and graphite nanofibres

Much attention has been given recently to the sorption of hydrogen by such carbon nanostructures as carbon nanotubes, graphite nanofibres and their metal-doped modifications.

Carbon nanotubes (NT) with low-defect structures were found in 1991 in the products of electric-arc evaporation of graphite.[125] However, long before that, similar NT¶ with a high content of structural defects have repeatedly been detected in solid products of hydrocarbon pyrolysis on metal catalysts.[126] Owing to its high efficiency, the catalytic pyrolysis of hydrocarbons is still widely used for the practical production of long (up to millimetres) carbon nanostructures, including NT and the so-called vapour-grown carbon fibres (VGCF).

A graphene sheet rolled in a seamless cylinder is the main element of carbon NT. Multi-walled nanotubes (MWNT) consisting of graphene sheets rolled as a cylindrical spiral also exist.

Vapour-grown carbon nanofibres can consist of parallel-sided graphene platelets perpendicular to the fibre axis (platelet-type VGCF), of nested graphene cones (herring-bone VGCF), of truncated cones (conical layer nanotubes, CLNT), *etc*.

Single-walled nanotubes (SWNT) are closed networks built of quasi-sp^2-hybridised carbon atoms. The network consists of hexagonal cells on the side surface of the cylinder. Open and closed SWNT exist; in the latter, the cylinder ends are closed by hemispheres ('fullerene halves') consisting of hexagonal and pentagonal cells. The SWNT diameter ranges within 0.8–5 nm (most often, 1–2 nm) and its length is 1–500 μm (most often, 5–50 μm). Carbon SWNT have a rather narrow diameter distribution, in contrast to activated carbons in which the sizes of macro-, meso- and micropores differ by a factor of several hundred.[127]

A typical feature of SWNT is the formation of rather strong molecular aggregates (named as bundles, strands, ropes, braids, *etc*.), in which the axes of separate SWNT are parallel to each other. The shortest distance between the carbon skeletons of the adjacent SWNT in the bundles is 0.32 nm. This value is close to the size of the van der Waals distance between graphene layers in graphite and can be changed by introduction of inorganic or organic intercalants, surfactants or by chemical modification of the cylindrical surface of the NT.

Ideal (defect-free) multi-walled nanotubes (MWNT) are built of SWNT inserted one into another. Ideal MWNT are formed in a carbon arc if no metal catalyst is added to the graphite to be vaporised. The distances between the layers in MWNT are close to the interlayer distance in graphite. The outer diameters of electric-arc MWNT are 5–40 nm (most often 15 nm), the inner diameters are 0.8–5.0 nm (mostly 1–2 nm), and the lengths are 0.5–70 μm.

¶ These nanotubes were called tubular graphite fibres.

The synthesis of SWNT and MWNT is accompanied by the formation of other carbon modifications: fullerenes, multilayer polyhedral nanoparticles, graphite microcrystals and amorphous carbon. Furthermore, mixtures of products obtained by the catalytic method contain metal particles. The content of carbon NT in the synthesis products does not exceed 20%–70% (for different methods), therefore in all cases purification from admixtures is the most laborious stage in the preparation of pure carbon NT.

Many publications (see, *e.g.*, the corresponding reviews[128–133]) report the state-of-the-art of the methods for the preparation and study of the properties of carbon nanostructures and their use.

1. Sorption of hydrogen by single-walled carbon nanotubes

The carbon material obtained by the electric-arc method and containing single-walled carbon NT (in the form of bundles containing 7–14 NT), amorphous carbon and particles of a catalyst (for example, Co) adsorbs 5 mass %–10 mass % H_2 (with respect to the pure SWNT) at 273 K and 300 Torr followed by cooling to 90 K.[134] According to the temperature-programmed desorption (TPD) data,[134] hydrogen is desorbed from nanotubes and activated carbon at 133 K. However, if a sample containing SWNT is preliminarily subjected to a treatment which opens the 'plugs' at the tube ends, a second peak almost at room temperature (290 K) appears on the TPD curve. This peak is explained by the evolution of hydrogen adsorbed inside the SWNT due to the penetration of H_2 molecules through the open tube ends. No high-temperature peak of this type is observed in the desorption of hydrogen from activated carbon samples or from fullerene soot obtained in the absence of a catalyst. It is believed[134] that in the carbon material obtained by the electric-arc method, the 'high-temperature' hydrogen is mainly located in the SWNT channels, whereas the 'low-temperature' hydrogen is adsorbed on amorphous carbon, on the outer surface of the SWNT and/or in the intertube space of the SWNT bundles.

The amount of adsorbed hydrogen (99.9999% purity) for relatively pure carbon SWNT obtained by the laser method (see Refs 135 and 136) exceeds 8 mass % H_2 at 10–12 MPa and 80 K.[137] In this case, the mean diameter and the specific surface of a separate SWNT are ~ 1.3 nm and 1300 $m^2\ g^{-1}$, respectively. The diameters of the SWNT bundles are ~ 6–12 nm. The outer specific surface of the bundles measured by the BET method is 285±5 $m^2\ g^{-1}$. The amount of adsorbed hydrogen depends on the number of 'sorption–desorption' cycles. For freshly prepared samples of pure SWNT, the C : H ratio of ≈ 1 (~ 8.25 mass % H_2) is achieved at 80 K and 7 MPa of H_2 (Fig. 5, curve *1*).

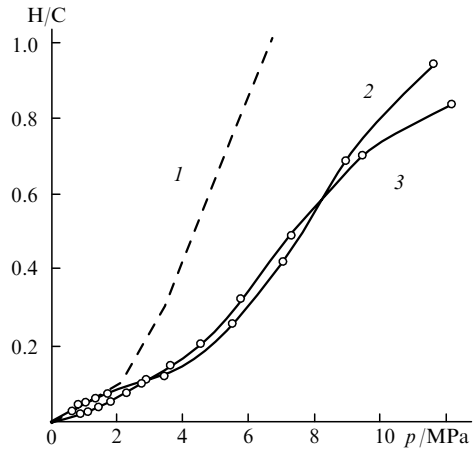

Figure 5. Dependence of the amount of hydrogen adsorbed by an SWNT at 80 K on pressure in the first (*1*) and subsequent cycles (*2* and *3*).[137]

Hydrogen is initially adsorbed on the outer surface of an SWNT bundle. An increase in pressure to 12 MPa during subsequent cycles increases the amount of absorbed H_2, which is attributed to the penetration of H_2 molecules into the intertube space of the bundles. As a result, the intertube space increases and the bundle breaks into separate SWNT; the outer SWNT surfaces are completely covered and the inner surfaces are partially covered by H_2 molecules (Fig. 5). The increase in the intertube distance inside the SWNT bundle can be detected by X-ray diffraction and NMR spectroscopy.[138] It has been shown that an SWNT bundle expands after immersing a carbon SWNT sample in a nitric acid solution and shrinks to the original configuration after deintercalation of HNO_3, *i.e.*, this change is reversible.

Liu *et al.*[139] synthesised carbon SWNT by the electric arc method (the production rate of SWNT was 2 g per hour) in the presence of hydrogen [a nickel–cobalt–iron powder (Ni : Co : Fe = 3 : 0.75 : 0.75) was used as the catalyst, and FeS was used as the SWNT growth accelerator]. The content of SWNT in the carbon material obtained by this method was ~ 60%, the mean SWNT size was 1.85 nm, the diameter of the SWNT bundles was about 20 nm. Upon treatment of the SWNT samples, which included, in particular, heating at 770 K, the amount of adsorbed hydrogen (room temperature, 10 MPa) reached 4.2 mass %, which corresponded to the ratio H : C = 0.52. Up to 78% of the adsorbed hydrogen desorbed under standard conditions. The remaining hydrogen (from 0.52 mass % to 0.95 mass % H_2 for different SWNT specimens) desorbed on heating the sample to 423 K.

Studies of the hydrogen-sorbing properties of a carbon material obtained by the electric-arc method [140] and containing ~ 70 mass % SWNT showed that it adsorbs about 3.5 mass % H_2 at 10 MPa and with multiple repetition of the cycles 'cooling to 77 K – heating to 300 K'.[3, 6] Interesting results were reported [141] that up to 6.5 mass % – 7.0 mass % of hydrogen was absorbed by an SWNT at room temperature and 0.1 MPa.

The specific surface and the gas-sorbing capacity of carbon materials depend considerably on the preliminary thermal treatment. It was shown [142] that heating of an SWNT sample, which has preliminarily been acid-etched, above 600 K *in vacuo* results in the liberation of different gases (CH_4, CO, CO_2 and H_2). After thermal pretreatment, SWNT adsorb a considerably greater amount of xenon at 95 K: the SWNT samples annealed at 1073 K absorbed 20 times more Xe than the samples heated to 623 K. The increase in the adsorption capacity of SWNT was explained by the effect of high-temperature annealing, which removes the carboxyl groups blocking the ends and defects of the NT walls (Fig. 6). Apparently, such a thermal treatment should also affect the hydrogen adsorption capacity of NT.

Hydrogen can also be stored in SWNT using an electrochemical process which is reversible. The relatively low but quite reliably measured hydrogen capacity in the process

$$HT + x\,H_2O + x\,e^- \xrightarrow{\text{charge}} (HT + x\,H) + x\,OH^-$$

is about 0.4 mass % for a number of SWNT specimens. In this case, SWNT/Au is the negative electrode, Ni is the positive electrode, $Hg/HgO/OH^-$ is the reference electrode, and 6 M KOH is the electrolyte. The capacity decreases by only 30% after 100 charge–discharge cycles.[143]

The maximum content of hydrogen in carbon NT specimens reduced with dihydroanthracene at 623 K or with lithium under modified Birch conditions corresponds to the '$C_9H-C_{10}H$' and 'C_8H' compositions, respectively;[144, 145] this is several times less than in the systems using physical hydrogen adsorption at high pressures. The desorption of hydrogen from such hydrogen-containing nanotube derivatives occurs only at 773 K, which implies that hydrogen is chemically bound.[145]

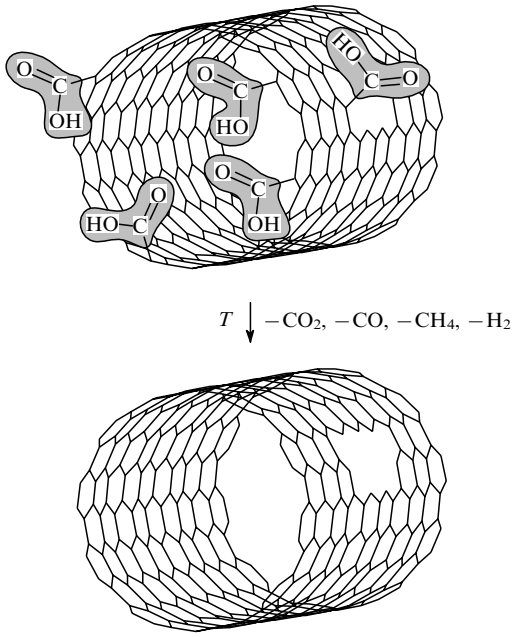

Figure 6. Schematic drawing of chemically treated single-walled NT before and after heating above 600 K.[142]

2. Sorption of hydrogen by graphite nanofibres

Inconsistent data on the hydrogen-sorbing properties have been reported for vapour-grown carbon fibres (VGCF). The highest hydrogen-sorbing capacity of VGCF (11 mass % – 67 mass % H_2) has been reported by Chambers *et al.*[146] The graphite nanofibres were obtained by catalytic pyrolysis of carbon-containing gases on the nanoparticles of a metal catalyst containing iron, nickel and copper, and then purified from the catalyst particles. The VGCF with a length of 10 – 100 μm and a diameter of 3 – 50 nm obtained by this method can be assigned to the platelet-type or conical layered structures.[146] In a favourable conformation, the distance between the graphene sheets is 0.337 nm, while the gas-kinetic molecular diameter of hydrogen is 0.289 nm. The sorption of hydrogen at 12 MPa and 298 K was studied on a Sieverts-type apparatus.

In a series of studies,[147, 148] attention was drawn to the necessity of careful preparation of the samples intended for the H_2 sorption capacity measurements. It was noted that VGCF having developed systems of slit-shaped nanopores with a great number of open edges have a perfect configuration for hydrogen adsorption. Owing to this unique VGCF structure, the hydrogen molecules interact not only with the graphene sheet surface but also with the adjacent H_2 molecules; it is believed that this may result in the capillary condensation of hydrogen at anomalously high temperatures.[146] Moreover, the sorption of H_2 is accompanied by the expansion of pores (crevices), which can also result in polymolecular sorption of hydrogen. Comparison of X-ray diffraction spectra of VGCF samples before and after hydrogen adsorption indicates that the interlayer distance d between separate graphene sheets increases to 0.347 nm after H_2 adsorption (d = 0.340 nm for the initial VGCF). As the adsorbed H_2 is removed from the sample, the parameter d returns to the original value (0.340 nm).[147, 148]

The results on the hydrogen sorption by VGCF reported by Chambers *et al.*[146] have evoked both much interest and many critical comments,† as all attempts to reproduce this experiment failed.[6, 149, 150] Moreover, the reported high values of H_2 absorption considerably exceed even the highest theoretical estimates.[2, 151]

† It may well be that an error was made in the evaluation of the amount of hydrogen adsorbed by the VGCF. For example, the same study [146] reported data on the sorption of hydrogen by palladium and intermetallic compounds which were much higher than the generally accepted values.

Stöbel *et al.*[150] studied the adsorption of hydrogen on two types of carbon materials: on various specimens of amorphous high-porosity activated carbon and on VGCF synthesised in the presence of a catalyst. The adsorption of H_2 by activated carbon measured at 296 K and an H_2 pressure of 12 MPa was 1.6 mass %, which is in good conformity with calculations on the physical adsorption of hydrogen. Under these conditions, the adsorption of H_2 by VGCF did not exceed 1.2 mass %. The authors [150] did not obtain high H_2 absorption on carbon nanofibres with parallel-laminated structure prepared by them; however, they noted an unusual behaviour of the material in a hydrogen atmosphere, which may be due to the fibre nanostructure.

The hydrogen-sorbing properties of a lithium- and potassium-doped carbon material prepared by catalytic decomposition of methane have been studied. After removal of the catalyst, the material contained up to 90% VGCF ‡ with an outer diameter of 25–35 nm, with mainly platelet or conical-layered structures.[152] Doping with lithium or potassium [Li(K) : C ≈ 1 : 15] occurred under conditions of the solid-phase reaction between VGCF and Li(K)-containing compounds such as carbonates and nitrates. Hydrogen uptake reaches 20 mass % for the Li-containing VGCF at 653 K and 14 mass % for the K-containing VGCF at room temperature, which amounts to ~ 160 and 112 kg (H_2) m^{-3}, respectively.[152] Multiple repetition of the H_2 absorption–desorption process results in an insignificant (~ 10%) loss of the sorption capacity of the material. The specimens doped with lithium had higher chemical stabilities under ordinary conditions than those doped with potassium. The high sorption capacity of Li(K)-doped VGCF is attributed to the layered VGCF structure with large interlayer clearance (0.347 and 0.335 nm for VGCF and graphite, respectively) between the small-size (50 nm and less) graphene sheets in the VGCF, as well as to the presence of an alkali metal. Without alkali doping, the absorption of H_2 by the VGCF decreases abruptly.

Chen *et al.*[152] have also obtained anomalously high values of H_2 sorption by graphite doped with Li and K [up to 35%–70% of the sorption capacity of Li(K)-VGCF at 473–673 K and p_{H_2} = 0.1 MPa]. The high hydrogen sorption by VGCF doped with alkali metals was explained by possible dissociative hydrogenation of the carbon sorbent, in which the alkali metal is a catalytic active centre. This hypothesis is supported by the fact that a band characteristic of the Li–H bond vibrations (~ 1420 cm^{-1}) appears in the IR spectrum of a Li-doped VGCF specimen upon treatment with H_2. In the temperature range from 473 to 673 K, the intensity of the Li–H vibrations correlates with the hydrogen absorption. Subsequently, the hydrogen atoms are transferred to the carbon network and add to carbon atoms. The appearance of an absorption band in the region of the C–H stretching vibrations confirms the dissociative mechanism of VGCF interaction with hydrogen. An increase in temperature causes the desorption of hydrogen and, correspondingly, disappearance of the bands assigned to vibrations of the C–H bond. Thus, systems based on Li(K)-VGCF can store hydrogen at elevated temperatures.

While recognising the validity of the qualitative dependences of hydrogen sorption by carbon nanomaterials doped with alkali metals,[152] Yang [153] assumed that these results might have been affected by the presence of moisture in the hydrogen used. Comparative experiments on the absorption of extremely pure (99.999%) absolutely dry and moist hydrogen by the lithium-doped VGCF obtained using the above technique [152] have shown that the adsorption was 2 mass % and 12 mass % H_2, respectively. It was assumed [153] that the anomalously high hydrogen sorption (up to 20 mass %) by the VGCF doped by Li and K [152] can be due to the formation of alkali metal hydroxides and hydrates in a humid atmosphere.

The graphite nanofibres obtained by pyrolysis of CO in the presence of Co/La_2O_3 also absorb H_2;[154] preheating of the samples at 1173 K is necessary in order to provide a high sorption efficiency (see also Ref. 148). The samples preheated at 673 K absorbed much less H_2, whereas graphite was found to be completely inert under identical conditions.

The effect of thermal treatment of a carbon material surface on the adsorption of hydrogen is shown by the data listed in Table 2. It was found that etching followed by treatment of carbon nanostructures increased their specific surfaces and the hydrogen-sorbing capacities, which resulted in the stable absorption of 5 mass % H_2 by the samples treated with a NaOH solution.[155] The VGCF-containing carbon soot obtained by catalytic pyrolysis of ethylene on nickel at 900 K adsorbs about 2.5 mass % of hydrogen at 5–7 MPa and with repetition of the cycles 'cooling to 77 K – heating to 300 K'.[3, 6]

Table 2. Effect of pretreatment of carbon nanotubes on hydrogen adsorption at p_{H_2} = 10 MPa and T = 293 K.[155]

Conditions of NT pretreatment	H_2 (mass %)
Mechanochemical treatment (30 min), etching (65% HNO_3, 72 h)	2.67
Mechanochemical treatment (30 min), etching (65% HNO_3, boiling)	1.16
Heating with NaOH (3 mol $litre^{-1}$, 1 h), washing with H_2O, drying at 373 K (2 h), calcination at 823 K (1 h), treatment with H_2SO_4 (15%, 1.5 h), heating at 373 K (10 min), washing with H_2O, drying at 373 K	5.15

Catalytic decomposition of acetylene at 1173 K in the presence of Co/SiO_2 results in the formation of carbon nanofibres.[156, 157] The sorption capacities of such metal-free carbon fibres at 10 MPa hydrogen pressure is ~ 1 mass % H_2. Although the structure of the carbon material obtained by Klyamkin *et al.*[156, 157] is similar to that of the VGCF obtained by Chambers *et al.*,[146] their sorption capacities differ strongly (1 mass % H_2 [156] and 67 mass % H_2 [146]), despite the similar behaviour of the specimens in the stage of hydrogen desorption. According to the reported data,[158] multi-walled carbon NT absorb up to 1 mass % H_2 at 10 MPa and 298 K. The amount of adsorbed H_2 increases with an increase in pressure in the range of 10–200 MPa.

The $CO : H_2$ ratio affects the specific surface of the nanocarbon fibre obtained upon pyrolysis of CO in the presence of a Fe–Ni–Cr alloy and its sorption capacity with respect to H_2: the hydrogen uptake by the VGCF decreases with an increase in the H_2 content in the starting mixture.[159]

High-precision calorimetric methods [160] were used to study the adsorption capacity of a number of carbon materials, including VGCF obtained according to the reported technique,[161] and commercial SWNT. The materials studied were found to be poor H_2 adsorbents under the experimental conditions (H_2 adsorption at 303 K, H_2 desorption at 373 K), and their adsorption capacities did not exceed that of activated carbon, which disagrees with other reported data.[146]

Ozaki *et al.*[162] compared the adsorption of hydrogen on platinum-coated carbon fibres prepared by two methods. The first method involved the preparation of a homogeneous mixture of a polymer with a metal complex followed by high-temperature carbonisation of the specimen. High-temperature activation of this specimen in water vapour or in CO_2 resulted in the migration of the metal particles to the outer surface of the carbon carrier. The second method employed a mixture of polymers, *viz.*, one

‡ Chen *et al.*[152] relate this material, which contains layered truncated graphene cones, to carbon nanotubes. In accordance with the terminology accepted by Dresselhaus [2] and by us, it should be attributed to graphite nanofibres.

which underwent pyrolysis and one which underwent carbonisation. The addition of a metal (Pt) compound to the pyrolysable polymer made it possible to deposit the metal on the walls of the pores formed upon pyrolysis. The H_2 adsorption for the material obtained according to the second method depends on the amount of platinum added: a small amount of platinum favours H_2 spillover and higher H : Pt ratios. A decrease in the H : Pt ratio with increase in the platinum concentration is due to an increase in the metal particle sizes.[162]

It was shown that thermal treatment of carbon nanofibres prepared by pyrolysis of ethylene in the presence of a Fe—Ni—Cu alloy (Fe : Ni : Cu = 85 : 10 : 5) in argon at 1273 K resulted in a noticeable increase in the amount of the stored hydrogen (up to 6.5 mass % H_2).[163] The importance of pretreatment of a specimen before hydrogen sorption has also been noted in other studies [148, 154] where the necessity of a special thermal treatment of VGCF in order to remove the chemisorbed gases has been shown. By analogy with NT (see Refs 142, 155), it may be surmised that chemical treatment of VGCF and their subsequent high-temperature annealing increase the specific surface of a VGCF and its activity with respect to H_2 adsorption. After an appropriate treatment, VGCF and NT obtained under catalytic pyrolysis conditions (carbon source: benzene or methane; precursor of the catalytically active species: ferrocene) can adsorb up to 4.0 mass % – 5.7 mass % H_2.[164] The absorption of pure hydrogen (99.999%) by graphite fibre with a parallel-laminated structure (98% of VGCF in the mixture) starts immediately without an induction period to reach 10 mass % – 13 mass % H_2 in the first cycle (Table 3). The H_2 adsorption and desorption rates are high.[166] Upon repeated adsorption – desorption cycles, the sorption capacity of the material decreases to approximately 70% of the original value, which is thought to be due to the destruction of the graphite fibre structure. The graphite nanofibre obtained by pyrolysis of acetylene and ethylene at 873 K in the presence of Ni adsorbs up to 10 mass % H_2 following keeping for 16 h at room temperature at 12 MPa. After a decrease in pressure, almost all hydrogen is released (Fig. 7).[166]

Table 3. Effect of pretreatment of a graphite nanofibre on hydrogen adsorption at p_{H_2} = 11 MPa and T = 373 K.[165]

Mean VGCF diameter /nm	Conditions of VGCF pretreatment	H_2 (mass %)
80	evacuation, 5 h, 373 K	12.38
90	treatment with 37% HCl, washing with H_2O, evacuation, 5 h, 373 K	12.82
100	dispersion in ethanol, treatment with 37% HCl, washing with H_2O, evacuation, 5 h, 373 K	10.03
125	dispersion in ethanol, treatment with 37% HCl, washing with H_2O, evacuation, 5 h, 373 K	10.1

Note. The graphite nanofibre was obtained by pyrolysis of benzene at 1373 – 1473 K in the presence of Fe and S.

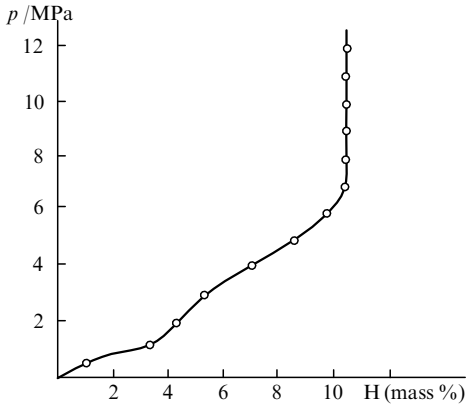

Figure 7. Hydrogen desorption isotherm at 300 K.[166]

Despite the observed discrepancies in the available experimental data (*cf.*, *e.g.*, Refs 148, 150, 158, 165), it is obvious that NT and VGCF are actually characterised by high capacities with respect to hydrogen.

3. Sorption of hydrogen by nanostructured graphite

The sorption of hydrogen on activated carbons at 133 K and p_{H_2} = 2 MPa is 0.5 g H_2 per 1 kg of C (Ref. 8) and 2 mass % at 155 K and p_{H_2} = 6.9 MPa.[150] A uniquely high, though hard to explain, hydrogen-sorbing capacity was observed for carbon of AX-21 grade with 3000 $m^2\ g^{-1}$ overall material surface and 700 – 1800 $m^2\ g^{-1}$ micropore surface; the mass and volume densities of H_2 at 77 K and 5.0 MPa were 100 g H_2 per 1 kg of the adsorbent and 32 kg H_2 per 1 m^3, respectively.[9]

The relationship between the sorption capacity and the volume of micropores has been analysed for a series of activated carbons. It has been found that a pore size optimal for the adsorption of hydrogen exists.[167]

Thermal desorption spectroscopy was used to study the sorption of hydrogen by nanoporous carbon (NPC).[168] It was shown that the maximum amount of H_2 that can be adsorbed by NPC is 15.6 at.% at 266 MPa and 773 K. Mechanochemical treatment of graphite in an extra-pure hydrogen atmosphere (99.9999%) at room temperature and starting hydrogen pressure of 1.0 MPa results in nanostructured graphite which adsorbs H_2 well.[81] After milling for 80 h, the maximum amount of adsorbed H_2 for such a sample is 7.4 mass % ($CH_{0.95}$). This value is comparable to the values of H_2 absorption reached for nanotubes and superactive carbon at temperatures below 100 K and H_2 pressures of about 5 MPa.

Enoki *et al.*[169] studied the properties of nanostructured graphite and its intercalated compounds. The composites prepared by mechanical grinding of Mg and graphite in the presence of organic additives (THF, cyclohexane, benzene) were found to be efficient hydrogen-adsorbing materials.[170, 171] The introduction of an organic additive is necessary for the composite structure to form and its hydrogen-adsorbing properties to appear.

4. Theoretical calculations of hydrogen adsorption by carbon nanomaterials

The mechanism of the uniquely high hydrogen sorption by carbon NM has not yet been clarified. Different variants have been considered: physical adsorption and chemisorption of H_2 molecules on the graphene sheet surface; the arrangement of more than one layer of H_2 molecules between the graphene planes; capillary condensation of hydrogen inside the nanotubes and in the space between the graphene sheets at anomalously high temperatures; the charge state of hydrogen in carbon nanomaterials. Therefore, the calculated maximum hydrogen capacities of NM differ strongly as well.

The Monte-Carlo method was used [172] to calculate the adsorption capacities of carbon materials with crevice-shaped and cylindrical pores with respect to gaseous H_2 at various temperatures and pressures. The calculated values of H_2 sorption were compared to the experimental results obtained for the specially prepared microporous activated carbon (AC). A linear relationship between the adsorption capacity of hydrogen and the specific surface of AC was found. The best AC samples had a specific surface of 2290 $m^2\ g^{-1}$; the corresponding maximum amount of adsorbed H_2 was 0.6 mass %. This value is in good agreement with the calculated value of 0.7 mass % H_2 for ideal slit-shaped pores with S = 2600 $m^2\ g^{-1}$ at 300 K and p_{H_2} = 6 MPa.

According to the reported data,[172] carbon materials with slit-shaped pores ($d = 0.7$ nm) are the optimum H_2 adsorbents at room temperature and $p_{H_2} = 10$ MPa. The highest calculated H_2 volume density is equal to 14 kg m^{-3} (mass content equal to 1.3 mass % H_2). According to the data of Rzepka *et al.*,[172] the sorption capacities of carbon materials with slit-shaped pores are higher than those of materials with cylindrical pores over practically the entire temperature and pressure range studied. It was noted that polymolecular (two-layer) sorption of hydrogen can be observed at 77 K in pores with $d = 1.0$ nm even at low H_2 pressures; this corresponds to the gravimetric capacity of the carbon material equal to ~ 2.0 mass % and 5.5 mass % H_2 for cylindrical and slit-shaped pores, respectively. Therefore, the observed high values of H_2 uptake by single-walled nanotubes (5 mass % – 10 mass % H_2 at room temperature)[134] cannot be explained by pure physical adsorption occurring in SWNT due to strong capillary forces.

Calculations[172] of physical H_2 adsorption at room temperature and $p_{H_2} = 11$ MPa on carbon material with slit-shaped pores with $d = 0.34$ nm corresponding to the interlayer distance in VGCF[146] imply that hydrogen cannot be adsorbed by this material. Since under these conditions the gravimetric capacity of a microporous carbon material with $d = 0.7$ nm is as low as 1.3%, the increase in d observed for VGCF in the course of hydrogen adsorption cannot result in adsorption equal to 11% – 67% reported in Ref. 146. Using the model of VGCF structure with sorbed hydrogen shown in Fig. 8 for the calculation of H_2 adsorption, it has been shown[173] that the distance of 0.34 nm between the graphene layers is insufficient for the incorporation of hydrogen molecules. Moreover, a graphite nanofibre with $d = 0.9$ nm can adsorb as low as 0.46 mass % – 1.6 mass % H_2 at 298 K and $p_{H_2} = 5 – 11.2$ MPa.

Analysis of H_2 adsorption on a graphite surface taking into account the real sorption conditions and the geometric parameters of the hydrogen molecule and the graphite layer gives the value of ~ 2.8 mass % H_2 for one H_2 layer adsorbed on a separate graphene sheet.[2] In real systems, the intermolecular forces, the interaction of the H_2 molecules with the material surface and the presence of surface defects can result in the formation of additional sites for H_2 adsorption. Considering the possible formation of the second hydrogen layer, the value of H_2 sorption on the carbon surface was assessed to be ~ 4.1 mass %.

Doping of graphite with K, Rb and Cs increases slightly its sorption capacity with respect to H_2; the H_2 content due to chemisorption corresponds to the $C_8KH_{2/3}$ composition, and the H_2 content due to physical adsorption corresponds to the $C_{24}KH_2$ composition. However, the hydrogen content is small in both cases (see Ref. 2 and the references therein). On the other hand, for VGCF doped by a metal, high H_2 absorption was obtained even at a low metal : carbon ratio (1 : 15), apparently because of partial reduction of carbon in the graphite layer due to the catalytic effect of alkali metals.[152] However, other researchers are skeptical about the high values of H_2 adsorption obtained[152] (see, for example, Refs 153 and 174), despite the elegant hypothesis put forward by Chen *et al.*[152] for the explanation of the absorption of hydrogen by nanomaterials doped by alkali metals.

Two geometrical models have been suggested for hydrogen sorption by carbon NT bundles.[2] In the first one, hydrogen is considered as a liquid capable of filling the free space unoccupied by the carbon atoms of the nanotube. The use of density values of 0.071 and 2.26 g cm^{-3} for liquid hydrogen and carbon atoms, respectively, results in the H_2 adsorption equal to 2.3 mass %. According to the second model which accounts for the adsorption of hydrogen molecules with a gas kinetics diameter of 0.289 nm both inside the SWNT and in the inter-tube space of SWNT bundles (Fig. 9), the overall H_2 adsorption for a (10,10)NT bundle§ (the NT diameter being 1.38 nm) was found to be 4.0 mass % H_2. Of these, 3.3 mass % H_2 corresponds to the adsorption inside the tubes and 0.7 mass % H_2, to adsorption between the NT in the bundle. Under high-pressure conditions, the compressibility of hydrogen and intermolecular interaction might result in a denser packing of the hydrogen molecules and hence in an increase in its adsorption on carbon NT. In order to confirm this assumption, a detailed calculation has been carried out[175] which has shown that the density of hydrogen in this case can be, in fact, higher than follows from purely geometrical considerations.

Computer simulation of hydrogen adsorption by SWNT and a carbon material with idealised slit-shaped pores has also been carried out.[151] The hydrogen – hydrogen and hydrogen – carbon interactions were simulated using the Silvera – Goldman and Crowell – Brown potentials, respectively; quantum effects were also taken into account. Adsorption of hydrogen inside the NT, between the tubes in the bundles and on the outer SWNT surface was assumed in the calculations. The computer simulation of hydrogen absorption by SWNT and activated coal is in favour of SWNT but does not confirm the high values of hydrogen adsorption for SWNT and VGCF found experimentally.[134, 146]

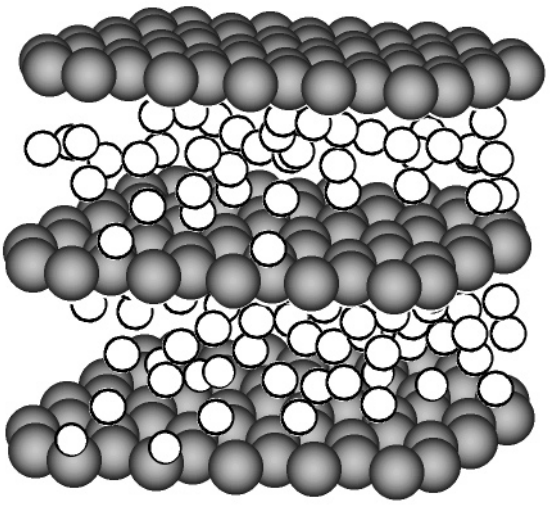

Figure 8. Cell model for the calculation of hydrogen adsorption by a platelet-type graphite nanofibre (pore diameter 0.9 nm). The dark and light circles indicate the carbon atoms and hydrogen molecules, respectively.[173]

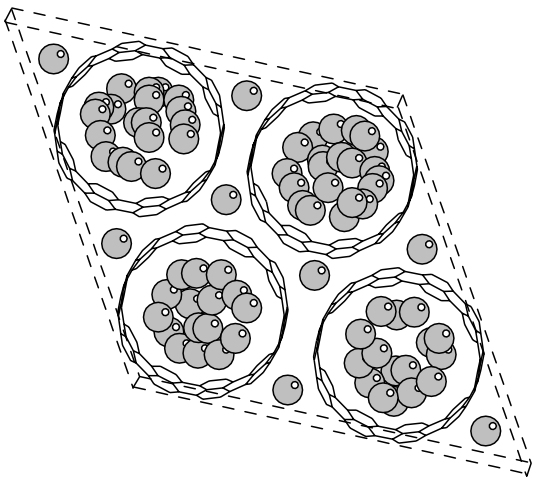

Figure 9. A typical arrangement of H_2 molecules adsorbed on triangularily packed carbon nanotubes.[2]

§ The numbers in parentheses indicate the indices used for the description of the nanotube structures; they are related directly to the NT diameter and the chiral angle.

Calculations of H_2 adsorption in SWNT bundles show [151] that the dense packing of SWNT results in lower gravimetric and volume densities of hydrogen even at sufficiently high adsorption potentials. Low adsorption can result from the surface inaccessibility in dense SWNT bundles.

The results of calculations using the Monte-Carlo method carried out for bundles of parallel SWNT demonstrate a strong dependence of the gravimetric adsorption of hydrogen on the bundle diameter, *i.e.* on its specific surface.[176] At 77 K and p_{H_2} = 10 MPa, the adsorption of H_2 for isolated (10,10)NT and for bundles consisting of three and seven (10,10)NT were 9.6 mass %, 7.0 mass % and 5.5 mass %, respectively. A dependence of the gravimetric capacity of NT on the inter-tube distance in a bundle was also noted.

The increase [138] in the inter-tube distance inside the SWNT bundles observed upon their treatment with nitric acid allows one to assume that the parameter $g = a - d$ (where g is the van der Waals gap, a is the lattice spacing, d is the NT diameter) used in the calculations of H_2 adsorption can be optimised.[177] Optimisation of the packing geometry (the g parameter) for SWNT has been carried out in order to obtain the maximum hydrogen adsorption on SWNT at 298 and 77 K. With this purpose, a series of NT have been studied, *viz*., (9,9)NT with d = 1.22 nm, (12,12)NT with d = 1.63 nm and (18,18)NT with d = 2.44 nm. It has been found that the optimum g value is a function of temperature and equals 0.6 and 0.9 nm at 298 and 77 K, respectively.

It has been shown that none of the SWNT packing geometries studied (the triangular and square ones) can provide high hydrogen adsorption at room temperature. Hydrogen adsorption capacity approximating that recommended by the International Power Agency can be obtained on carbon NT with d = 1.22 nm and g = 0.9 nm only at 77 K and $p_{H_2} > 5$ MPa.

Calculations for charged carbon NT by the Monte-Carlo method have confirmed their somewhat higher ability to adsorb H_2 in comparison with uncharged NT: the presence of a charge results in an increase in H_2 adsorption by 10% – 20% and 15% – 30% for 298 and 77 K, respectively.[178] However, the hydrogen mass and volume densities at 298 K are still too small even for charged tubes.

Calculations using the density functional theory performed in order to search the optimum conditions of hydrogen sorption by SWNT showed that there are two types of H_2 chemisorption sites on the outer and inner NT surfaces.[179] Hydrogen is sorbed in the atomic state on the outer and inner SWNT surfaces, and also in the molecular form ¶ inside the SWNT channel.[181] The emergence of a new absorption band at 4226 cm^{-1} in the Raman spectrum of NT samples after their electrochemical charging (for gaseous H_2, 4161 cm^{-1}) assigned to the absorption of molecular hydrogen was considered as proof of the presence of adsorbed hydrogen. The H_2 capacity of cylindrical channels of carbon SWNT increases linearly with the NT diameter in accordance with the expression: c_{H_2}(mass %) $\geqslant 14.3(d/d_0)$ [where 14.3 is the amount of H_2 (in mass %) adsorbed by (10,10)NT, d_0 is the diameter of (10,10)NT]. The maximum H_2 storage capacity of carbon NT is limited by the energies of intermolecular repulsion between hydrogen molecules located in the inner SWNT cavity and those between H_2 molecules and SWNT walls.

Lee *et al*.[181] calculated the sorption of hydrogen by multilayer carbon nanotubes. Hydrogen atoms were found to be preferentially adsorbed on the outer NT surface and the sorption capacities of MWNT with respect to H_2 were found to be independent of their diameters.[181] The maximum capacities of (5,5)@(10,10)MWNT and (10,10)SWNT are 7.7 mass % and 14.3 mass % H_2, respectively.[179, 181]

¶ The inelastic neutron scattering spectra of SWNT after hydrogen adsorption on them display a peak at *ca.* 14.5 meV corresponding to rotational transitions in the H_2 molecule. The presence of this peak indicates that physical adsorption of H_2 occurs under the experimental conditions; the peak intensity decreases with a temperature increase in the range of 25 – 40 K.[180]

V. Conclusion

Carbon nanomaterials attract interest as promising materials for the development of hydrogen accumulators.

Theoretically, fullerene can be hydrogenated to $C_{60}H_{60}$ without destruction of the fullerene skeleton; this corresponds to 7.7 mass % H_2 (0.92 m^3 of H_2 per 1 kg of $C_{60}H_{60}$). However, attempts at synthesis and characterisation of the hydrofullerene with this composition have failed so far. Compound $C_{60}H_{60}$ should be extremely unstable; the excessive strain of this molecule stems from the appreciable deviation of the configuration of bonds between the carbon atoms from the most stable tetrahedral configuration. According to molecular mechanics calculations, the strain in the $C_{60}H_{60}$ molecule can be decreased if at least ten hydrogen atoms in the $C_{60}H_{60}$ molecule are bound endohedrally (this is the most stable conformation for the $C_{60}H_{60}$ composition).[182]

The methods used in practice for the reduction of fullerenes give $C_{60}H_x$ compounds with 4.5 mass % – 6.0 mass % H_2. Their preparation requires high temperatures and H_2 pressures or reactive reducing agents (see, *e.g*., Refs 12 and 13). Analysis of numerous studies on the synthesis, structures and reactivities of hydrofullerenes shows that the practical applications of fullerenes and their metal derivatives as hydrogen sorbents require that the actual sorption capacities are increased, the hydrogenation is accelerated, the dehydrogenation temperature is decreased and the hydrogenation – dehydrogenation reversibility is ensured. In addition, side reactions should be eliminated.[3] Nevertheless, $C_{60}H_x$ and $C_{70}H_x$ hydrofullerenes have already been suggested, for example, as modifying additives for the carbon anodes of reversible Li-batteries.[183]

Other carbon nanostructures, such as single-walled carbon nanotubes and vapour-grown carbon fibres, as well as their metal-doped modifications, are quite promising as hydrogen-storage media. This is evident from Table 4 which shows generalised data on the hydrogen-sorption capacities of SWNT and VGCF, which in certain cases exceed considerably the values required for mobile hydrogen-storage systems. However, the data on the amount of hydrogen accumulated by carbon NM obtained by different authors differ considerably. The reasons for the discrepancies lie in the absence of reliable methods for the preparation of pure SWNT and VGCF and the absence of generally accepted techniques for their certification, for example, with respect to purity, degree of their 'openness', nanotube diameter and interlayer distances, and the amount of metal catalysts. In addition, the

Table 4. Sorption characteristics of various carbon nanomaterials.

Material	Maximum capacity (mass %)	T /K	p_{H_2} /MPa	Ref.
SWNT	8.25	80	7.18	137
SWNT	5 – 10	90	0.04	134
SWNT	4.2	300	10 – 12	2, 139
SWNT	6.5 – 7	300	0.1	141
SWNT	1.1 – 5.2	293	10	155
SWNT	3.5	77 ↔ 300 [a]	5 – 10	3
VGCF	11 – 67	300	11	146
VGCF	0.4	298 – 773	0.1	152
VGCF	10 – 12	373	11	166
VGCF	2.5	77 ↔ 300 [a]	5 – 10	3
Li-VGCF	20	473 – 673	0.1	152
K-VGCF	14	473 – 673	0.1	152
VGCF	10	300	12	167

[a] 'Cooling to 77 K ↔ heating to 300 K' process.

hydrogen-sorbing capacity depends crucially on the pretreatment of carbon nanomaterials and the purity of hydrogen used. Therefore, the results obtained in the studies on hydrogen sorption characterise only a particular material and cannot as yet be used for comparison of the efficiencies of different types of carbon NM. The mechanism of the uniquely high hydrogen sorption by carbon nanomaterials is not clear, either. Nevertheless, the existence of high hydrogen capacities in nanocarbon materials is obvious. This allows one to hope that nanocarbon materials (provided that they are accessible) can be used in actual hydrogen-storage systems.

The experimental and theoretical materials presented in this review testify to a significant increase in the scope of research on the synthesis and hydrogen-sorbing properties of carbon nanostructures aimed both at the solution of fundamental scientific problems and at the development of mobile hydrogen-storage systems. This is also evident from presentations submitted at various conferences on carbon nanomaterials, hydrides and hydrogen power engineering.

This review was financially supported by the Russian Foundation for Basic Research (Project Nos 99-03-32647 and 00-03-32018) and the Russian Scientific and Technical Programme (Project No. 99005).

References

1. D Yu Gamburg, V P Semenov, N F Dubovkin, L N Smirnova *Vodorod. Svoistva, Poluchenie, Khranenie, Transportirovanie, Primenenie. Spravochnoe Izdanie* (Hydrogen. Properties, Preparation, Storage, Transportation, Applications. Handbook) (Eds D Yu Gamburg, N F Dubovkin) (Moscow: Khimiya, 1989)
2. M S Dresselhaus, K A Williams, P A C Eklund *MRS Bull.* **45** (1999)
3. B P Tarasov, in *Fullereny i Fullerenopodobnye Struktury v Kondensirovannykh Sredakh* (Fullerenes and Fullerene-Like Structures in Condensed Media) (Minsk: Belorussian State University, 2000) p. 113
4. B P Tarasov, S P Shilkin *Zh. Prikl. Khim.* **68** 21 (1995) [a]
5. B A Kolachev, A A Shalin, A A Il'in, in *Splavy — Nakopiteli Vodoroda* (Alloys as Hydrogen Accumulators) (Moscow: Metallurgiya, 1995) p. 384
6. B P Tarasov *Int. Sci. J. Altern. Energy Ecology* (1) 168 (2000)
7. B P Tarasov, O N Efimov *Nauka Proizvodstvu* (10) 47 (2000)
8. J Jagiello, T J Bandosz, K Putyera, J A Schwarz *J. Chem. Soc., Faraday Trans.* **91** 2929 (1995)
9. R Chahine, T K Bose *Int. J. Hydrog. Energy* **19** 161 (1994)
10. J Withers, R Loutfy, T Love *Fullerene Sci. Technol.* **5** 1 (1997)
11. M Terrones, H W Kuang, H W Kroto, D R M Walton *Top. Curr. Chem.* **199** 189 (1999)
12. A Hirsch *Chemistry of Fullerenes* Ch. 5 (Stuttgart: Georg Thieme, 1994) p. 117
13. N F Goldshleger, A P Moravsky *Usp. Khim.* **66** 353 (1997) [*Russ. Chem. Rev.* **66** 323 (1997)]
14. A Hirsch *Top. Curr. Chem.* **199** 1 (1999)
15. B P Tarasov, V N Fokin, A P Moravsky, Yu M Shul'ga *Izv. Akad. Nauk, Ser. Khim.* 679 (1997) [b]
16. B P Tarasov, V N Fokin, A P Moravsky, Yu M Shul'ga, V A Yartys' *J. Alloys Compd.* **253–254** 25 (1997)
17. B P Tarasov, V N Fokin, A P Moravsky, Yu M Shul'ga *Zh. Neorg. Khim.* **42** 920 (1997) [c]
18. B P Tarasov *Zh. Obshch. Khim.* **68** 1245 (1998) [d]
19. B P Tarasov, V N Fokin, A P Moravsky, Yu M Shul'ga, V A Yartys', D V Schur, in *Proceedings of the 12th World Hydrogen Energy Conference, Buenos Aires, Argentina, 1998* Vol. 2, p. 1221
20. A S Lobach, B P Tarasov, Yu M Shul'ga, A A Perov, A N Stepanov *Izv. Akad. Nauk, Ser. Khim.* 483 (1996) [b]
21. N F Goldshleger, B P Tarasov, Yu M Shul'ga, A A Perov, O S Roschupkina, A P Moravsky *Izv. Akad. Nauk, Ser. Khim.* 999 (1999) [b]
22. N F Goldshleger, B P Tarasov, Yu M Shul'ga, O S Roschupkina, A A Perov, A P Moravsky, in *Fullerenes. Recent Advances in the Chemistry and Physics of Fullerenes and Related Materials* Vol. 7 (Eds K M.Kadish, P V Kamat, D Guldi) (Pennington, NJ: The Electrochemical Society, 1999) p. 647
23. B P Tarasov, V N Fokin, E E Fokina, Z A Rumynskaya, L S Volkova, A P Moravsky, Yu M Shul'ga *Zh. Obshch. Khim.* **68** 1585 (1998) [d]
24. B P Tarasov, V N Fokin, A P Moravsky, Yu M Shul'ga *Izv. Akad. Nauk, Ser. Khim.* 2093 (1998) [b]
25. Yu M Shul'ga, B P Tarasov, V N Fokin, N Yu Shul'ga, V N Vasilets *Fiz. Tv. Tela* **41** 1520 (1999) [e]
26. A M Rao, P C Eklund, U D Venkateswaran, J Tucker, M A Dunkan, G M Bendele, P W Stephens, J-L Hodeau, L Marques, M Nunez-Regueiro, I O Bashkin, E G Ponyatovsky, A P Moravsky *Appl. Phys. A, Solids Surf.* **64** 231 (1997)
27. V N Bezmelnitsyn, V P Glazkov, V P Zhukov, V A Somenkov, S Sh Shilstein, in *The 4th Biennial International Workshop in Russia 'Fullerene and Atomic Clusters' (Abstracts of Reports), St. Petersburg, 1999* p. 70
28. V P Glazkov, V P Zhukov, V A Somenkov, T N Ivanova, in *The 4th Biennial International Workshop in Russia 'Fullerene and Atomic Clusters' (Abstracts of Reports), St. Petersburg, 1999* p. 71
29. T S Ugnovenok, Yu P Udalov, I B Gavrilenko *Zh. Prikl. Khim.* **72** 1728 (1999) [a]
30. T Osaki, T Tanaka, Y Tai *Phys. Chem. Chem. Phys.* **1** 2361 (1999)
31. K Shigematsu, K Abe, M Mitani, K Tanaka *Chem. Express* **8** 37 (1993)
32. M Gerst, H-D Beckhaus, C Rüchardt, E E B Campbell, R Tellgmann *Tetrahedron Lett.* **34** 7729 (1993)
33. A Drelinkiewicz, P Byszewski, A Bielanski *React. Kinet. Catal. Lett.* **59** 19 (1996)
34. R O Loutfy, E M Veksler, A P Moravsky, in *The 4th Biennial International Workshop in Russia 'Fullerene and Atomic Clusters' (Abstracts of Reports), St. Petersburg, 1999* p. 153
35. A E Shilov, G B Shul'pin *Chem. Rev.* **97** 2879 (1997)
36. S Serizawa, I Gabrielova, T Fujimoto, T Shido, M Ichikawa *J. Chem. Soc., Chem. Commun.* 799 (1994)
37. N G Connelly, W E Geiger *Chem. Rev.* **96** 877 (1996)
38. R E Haufler, J Conceicao, L P F Chibante, Y Chai, N E Byrne, S Flanagan, M M Haley, S C O' Brien, C Pan, Z Xiao, W E Billups, M A Ciufolini, R H Hauge, J L Margrave, L J Wilson, R F Curl, R E Smalley *J. Phys. Chem.* **94** 8634 (1990)
39. Yu Vasil'ev, D Wallis, M Nüchter, B Ondruschka, A Lobach, T Drewello *Chem. Commun.* 1233 (2000)
40. G E Lawson, B Ma, H R Rollins, A M Hajduk, Y-P Sun *Res. Chem. Intermed.* **23** 549 (1997)
41. U M Dzhemilev, A G Ibragimov, L O Khafizova, L M Khalilov, Yu V Tomilov, O M Nefedov, in *The 4th Biennial International Workshop in Russia 'Fullerene and Atomic Clusters' (Abstracts of Reports), St. Petersburg, 1999* p. 31
42. U M Dzhemilev, A G Ibragimov, L O Khafizova, L M Khalilov, Yu V Vasil'ev, R F Tuktarov, Yu V Tomilov, O M Nefedov *Izv. Akad. Nauk, Ser. Khim.* 572 (1999) [b]
43. M S Meier, P K Corbin, V K Vance, M Clayton, M Mollman, M Poplawska *Tetrahedron. Lett.* **35** 5789 (1994)
44. R G Bergosh, M S Meier, J A Laske Cooke, H P Spielmann, B R Weedon *J. Org. Chem.* **62** 7667 (1997)
45. M S Meier, B R Weedon, H P Spielmann *J. Am. Chem. Soc.* **118** 11682 (1996)
46. M S Meier, J A Laske Cooke, B R Weedon, H P Spielmann, in *Fullerenes. Recent Advances in the Chemistry and Physics of Fullerenes and Related Materials* Vol. 3 (Eds K M Kadish, R S Ruoff) (Pennington, NJ: The Electrochemical Society, 1996) p. 1193
47. R G Bergosh, M S Meier, H P Spielmann, G-W Wang, B R Weedon, in *Fullerenes. Recent Advances in the Chemistry and Physics of Fullerenes and Related Materials* Vol. 4 (Eds K M Kadish, R S Ruoff) (Pennington, NJ: The Electrochemical Society, 1997) p. 241
48. P J Fagan, P J Krusic, D H Evans, S A Lerke, E Johnston *J. Am. Chem. Soc.* **114** 9697 (1992)
49. C C Henderson, C M Rohlfing, K T Gillen, P A Cahill *Science* **264** 397 (1994)
50. H P Spielmann, B R Weedon, M S Meier *J. Org. Chem.* **65** 2755 (2000)
51. A D Darwish, A K Abdul-Sada, J Langley, H W Kroto, R Taylor, D R M Walton *J. Chem. Soc., Perkin Trans. 2* 2359 (1995)
52. B R Weedon, M S Meier, H P Spielmann, in *Fullerenes. Recent Advances in the Chemistry and Physics of Fullerenes and Related Materials* Vol. 6 (Eds K M Kadish, R S Ruoff) (Pennington, NJ: The Electrochemical Society, 1998) p. 1094

53. T Tanaka, K Komatsu *J. Chem. Soc., Perkin Trans. 1* 1671 (1999)
54. T Kitagawa, Y Lee, K Takeuchi *Chem. Commun.* 1529 (1999)
55. C Rüchardt, M Gerst, J Ebenhoch, H-D Beckhaus, E E B Campbell, R Tellgmann, H Schwarz, T Weiske, S Pitter *Angew. Chem., Int. Ed. Engl.* **32** 584 (1993)
56. A S Lobach, A A Perov, A I Rebrov, O S Roshchupkina, V A Tkacheva, A N Stepanov *Izv. Akad. Nauk, Ser. Khim.* 671 (1997) [b]
57. W E Billups, W Luo, A Gonzalez, D Arguello, L B Alemany, T Marriott, M Saunders, H A Jiménez-Vázquez, A Khong *Tetrahedron Lett.* **38** 171 (1997)
58. J W Argobast, C S Foote, M Kao *J. Am. Chem. Soc.* **114** 2277 (1992)
59. S Fukuzumi, T Suenobu, S Kawamura, A Ishida, S Takamuku, S Matsumoto, K Mikami, in *The 189th Electrochemical Society Meeting (Abstracts of Reports), Los Angeles, 1996* No. 566
60. A Hirsch, T Grösser, A Skiebe, A Soi *Chem. Ber.* **126** 1047 (1993)
61. C C Henderson, P A Cahill *Science* **259** 1885 (1993)
62. S Fukuzumi, T Suenobu, S Kawamura, A Ishida, K Mikami *Chem. Commun.* 291 (1997)
63. S Fukuzumi, T Suenobu, M Patz, T Hirasaka, S Itoh, M Fujitsuka, O Ito *J. Am. Chem. Soc.* **120** 8060 (1998)
64. S Fukuzumi, M Patz, T Suenobu, A Ishida, K Mikami, in *Fullerenes. Recent Advances in the Chemistry and Physics of Fullerenes and Related Materials* Vol. 4 (Eds K M Kadish, R S Ruoff) (Pennington, NJ: The Electrochemical Society, 1997) p. 45
65. N F Goldshleger, A S Astakhova, A S Lobach, G N Boiko, N N Denisov, V A Nadtochenko, O S Roshchupkina, Yu M Shul'ga *Izv. Akad. Nauk, Ser. Khim.* 2531 (1996) [b]
66. N F Goldshleger, G N Boiko, N N Denisov, V A Nadtochenko, M G Kaplunov, A V Kulikov, in *Sb. Dokl. VII Vseros. Konf. po Metalloorganicheskoi Khimii, Moskva, 1999* (Abstracts of Reports of the VIIth All-Russian Conference on Organometallic Chemistry, Moscow, 1999) Vol. 2, p. 122
67. C S Foote *Top. Curr. Chem.* **169** 347 (1994)
68. K-F Liou, C-H Cheng *Chem. Commun.* 1423 (1996)
69. A Staško, V Brezová, S Biskupič, K-P Dinse, P Schweitzer, M Baumgarten *J. Phys. Chem.* **99** 8782 (1995)
70. V Brezová, A Staško, P Rapta, G Domschke, A Bartl, L Dunsch *J. Phys. Chem.* **99** 16234 (1995)
71. A Staško, V Brezová, P Rapta, K-D Asmus, D M Guldi *Chem. Phys. Lett.* **262** 233 (1996)
72. V Brezová, A Staško, D Dvoranová, K-D Asmus, D M Guldi *Chem. Phys. Lett.* **300** 667 (1999)
73. A Staško, V Brezová, S Biskupič, A Neudeck, A Bartl, L Dunsch, in *Fullerenes. Recent Advances in the Chemistry and Physics of Fullerenes and Related Materials* Vol. 6 (Eds K M Kadish, R S Ruoff) (Pennington, NJ: The Electrochemical Society, 1998) p. 310
74. C Siedschlag, H Luftmann, C Wolff, J Mattey *Tetrahedron* **53** 3587 (1997)
75. C Siedschlag, H Luftmann, C Wolff, J Mattey *Tetrahedron* **55** 7805 (1999)
76. D Mandrus, M Kele, R L Hettich, G Guiochon, B C Sales, L A Boatner *J. Phys. Chem. B* **101** 123 (1997)
77. R Nozu, O Matsumoto *J. Electrochem. Soc.* **143** 1919 (1996)
78. K Komatsu, Y Murata, G-W Wang, T Tanaka, N Kato, K Fujiwara *Fullerene Sci. Technol.* **7** 609 (1999)
79. K Komatsu, K Fujiwara, Y Murata, T Braun *J. Chem. Soc., Perkin Trans. 1* 2963 (1999)
80. Y Murata, N Kato, K Fujiwara, K Komatsu *J. Org. Chem.* **64** 3483 (1999)
81. S Orimo, G Majer, T Fukunaga, A Züttel, L Schlapbach, H Fujii *Appl. Phys. Lett.* **75** 3093 (1999)
82. K Komatsu, G-W Wang, Y Murata, T Tanaka, K Fujiwara, K Yamamoto, M Saunders *J. Org. Chem.* **63** 9358 (1998)
83. R S Varma *Clean Prod. Process.* **1** 132 (1999)
84. L D Field, S Sternhell, H V Wilton *Tetrahedron Lett.* **39** 115 (1998)
85. R V Bensasson, T J Hill, E J Land, S Leach, D J McGarvey, T G Truscott, J Ebenhoch, M Gerst, C Rüchardt *Chem. Phys.* **215** 111 (1997)
86. Yu M Shul'ga, B P Tarasov *Pis'ma Zh. Eksp. Teor. Fiz.* **68** 239 (1998) [f]
87. A D M Darwish, R Taylor, R Loutfy, in *Proceedings of the 197th Meeting of Electrochemical Society, Toronto, 2000* No. 693
88. I O Bashkin, V E Antonov, A I Kolesnikov, E G Ponyatovsky, J Mayers, S F Parker, J Tomkinson, A P Moravsky, Yu M Shul'ga *Mol. Mater.* **13** 251 (2000)
89. I O Bashkin, V E Antonov, O V Boltalina, I V Gol'd, A F Gurov, A I Kolesnikov, E P Krinichnaya, A P Moravsky, S S Khasanov, Yu M Shul'ga, E G Ponyatovsky *Int. Sci. J. Alternative Energy Ecology* (1) 134 (2000)
90. A I Kolesnikov, V E Antonov, I O Bashkin, J C Li, A P Moravsky, E G Ponyatovsky, J Tomkinson *Physica B* **263–264** 436 (1999)
91. A I Kolesnikov, V E Antonov, I O Bashkin, G Grosse, A P Moravsky, A Yu Muzychka, E G Ponyatovsky, F E Wagner *J. Phys., Condens. Matter* **9** 2831 (1997)
92. I O Bashkin, V E Antonov, Yu A Ossipyan, E G Ponyatovsky, A P Moravsky, Yu M Shul'ga, Yu G Morozov *Mol. Mater.* **13** 263 (2000)
93. Yu M Shul'ga, A S Lobach, Yu G Morozov, V N Spektor, A A Ovchinnikov *Zh. Fiz. Khim.* **72** 115 (1998) [g]
94. B V Lebedev, T A Bukova, A S Lobach, in *The 4th Biennial International Workshop in Russia 'Fullerene and Atomic Clusters' (Abstracts of Reports), St. Petersburg, 1999* p. 184
95. B V Lebedev, T A Bykova, A S Lobach *Dokl. Akad. Nauk* **368** 629 (1999) [h]
96. A Rathna, J Chandrasekhar *Chem. Phys. Lett.* **206** 217 (1993)
97. P A Dorozhko, A S Lobach, A A Popov, V M Senyavin, V V Yushenko, M V Korobov, in *The 4th Biennial International Workshop in Russia 'Fullerene and Atomic Clusters' (Abstracts of Reports), St. Petersburg, 1999* p. 183
98. C Jin, R Hettich, R Compton, D Joyce, J Blencoe, T Burch *J. Phys. Chem.* **98** 4215 (1994)
99. M I Attalla, A M Vassallo, B N Tattam, J V Hanna *J. Phys. Chem.* **97** 6329 (1993)
100. L E Hall, D R McKenzie, M I Attalla, A M Vassallo, R L Davis, J B Dunlop, D J H Cockayne *J. Phys. Chem.* **97** 5741 (1993)
101. D L Kepert, B W Clare *Coord. Chem. Rev.* **155** 1 (1996)
102. L D Book, G E Scuseria *J. Phys. Chem.* **98** 4283 (1994)
103. B I Dunlap, D W Brenner, G W Schriver *J. Phys. Chem.* **98** 1756 (1994)
104. M Bühl, W Thiel, U Schneider *J. Am. Chem. Soc.* **117** 4623 (1995)
105. A S Lobach, Yu M Shul'ga, A I Rebrov, A A Perov, Yu G Morozov, in *Fullerenes. Recent Advances in the Chemistry and Physics of Fullerenes and Related Materials* Vol. 4 (Eds K M Kadish, R S Ruoff) (Pennington, NJ: The Electrochemical Society, 1997) p. 246
106. A V Okotrub, L G Bulusheva, I P Asanov, A S Lobach, Yu M Shulga *J. Phys. Chem. A* **103** 716 (1999)
107. A S Lobach, V V Strelets *Izv. Akad. Nauk, Ser. Khim.* 2083 (1999) [b]
108. A V Okotrub, L G Bulusheva, I P Asanov, A S Lobach, Yu M Shul'ga *Zh. Neorg. Khim.* **45** 523 (2000) [c]
109. N N Breslavskaya, P N D'yachkov *Zh. Neorg. Khim.* **45** 499 (2000) [c]
110. L E Hall, D R McKenzie, R L Davis, M I Attalla, A M Vassallo *Acta Crystallogr., Sect. B, Struct. Sci.* **54** 345 (1998)
111. W E Billups, A Gonzalez, C Gesenberg, W Luo, T Marriott, L B Alemany, M Saunders, H A Jiménez-Vázquez, A Khong *Tetrahedron Lett.* **38** 175 (1997)
112. B W Clare, D L Kepert *J. Mol. Struct. (Theochem)* **177** 466 (1999)
113. E L Brosha, J Davey, F H Garzon, S Gottesfeld *J. Mater. Res.* **14** 2138 (1999)
114. V Ya Davydov, N Sheppard, E Osava *Int. Sci. J. Alternative Energy Ecology* (1) 183 (2000)
115. M S Meier, R G Bergosh, in *Fullerenes. Recent Advances in the Chemistry and Physics of Fullerenes and Related Materials* Vol. 6 (Eds K M Kadish, R S Ruoff) (Pennington, NJ: The Electrochemical Society, 1998) p. 1103
116. S Fukuzumi, T Suenobu, T Hirasaka, R Arakawa, K M Kadish *J. Am. Chem. Soc.* **120** 9220 (1998)
117. S Fukuzumi, T Hirasaka, T Suenobu, X Gao, K M Kadish, in *The 195th Electrochemical Society Meeting (Abstracts of Reports), Seattle, USA, 1999* No. 652
118. S Fukuzumi, T Hirasaka, T Suenobu, O Ito, M Fujisuka, X Gao, K M Kadish, in *The 195th Electrochemical Society Meeting (Abstracts of Reports), Seattle, USA, 1999* No. 729
119. L I Tkachenko, A S Lobach, V V Strelets *Izv. Akad. Nauk, Ser. Khim.* 1136 (1998) [b]
120. K Choho, G van Lier, G Van de Woude, P Geerlings *J. Chem. Soc., Perkin Trans. 2* 1723 (1996)

121. M E Niyazymbetov, D E Evans, S A Lerke, P A Cahill, C C Herderson *J. Phys. Chem.* **98** 13093 (1994)
122. D E Cliffel, A J Bard *J. Phys. Chem.* **98** 8140 (1994)
123. B L Tumanskii, O G Kalina, V V Bashilov, A V Usatov, E A Shilova, Yu I Lyakhovetskii, S P Solodovnikov, N N Bubnov, Yu N Novikov, A S Lobach, V I Sokolov *Izv. Akad. Nauk, Ser. Khim.* 1119 (1999) [b]
124. G A Domrachev, S N Titova, G V Markin, S Yu Khorshev, L V Kalutskaya, E V Ivanova, B S Kaverin, A I Kirillov, V L Karnatchevich, Yu A Kurskii, A S Shavyrin, in *Mezhdunar. Konf. 'Metalloorganicheskie Soedineniya — Materialy Budushchego Tysyacheletiya' (III Razuvaevskie Chteniya) (Tez. Dokl.), N Novgorod, 2000* [International Conference 'Organometallic Compounds are Materials of the Future Millennium (IIIrd Razuvaev Lectures) (Abstracts of Reports), N Novgorod, 2000] p. 28
125. S Iijima *Nature (London)* **354** 56 (1991)
126. R A Buyanov, in *Zakoksovanie Katalizatorov* (Coking of Catalysts) (Novosibirsk: Nauka, 1983) p. 109
127. A S Fialkov *Uglerod. Mezhsloevye Soedineniya i Kompozity na Ego Osnove* (Carbon. Interstitial Compounds and Composites Based on It) (Moscow: Aspekt-Press, 1997)
128. D Tomanek, R J Enbody (Eds) *Science and Application of Nanotubes* (New York: Kluwer Academic, Plenum, 2000)
129. A L Ivanovskii *Usp. Khim.* **68** 119 (1999) [*Russ. Chem. Rev.* **68** 103 (1999)]
130. E G Rakov *Usp. Khim.* **69** 41 (2000) [*Russ. Chem. Rev.* **69** 53 (2000)]
131. J Hu, T W Odom, C M Lieber *Acc. Chem. Res.* **32** 435 (1999)
132. P M Ajayan *Chem. Rev.* **99** 1787 (1999)
133. E G Rakov *Zh. Neorg. Khim.* **44** 1827 (1999) [c]
134. A C Dillon, K M Jones, T A Bekkedahl, C H Kiang, D S Bethune, M J Heben *Nature (London)* **386** 377 (1997)
135. A G Rinzler, J Liu, H Dai, P Nikolaev, C B Huffman, F J Rodriquez-Macias, P J Boul, A H Lu, D Heymann, D T Colbert, R S Leu, J E Fischer, A M Rao, P C Eklund, R E Smalley *Appl. Phys. A, Solids Surf.* **67** 29 (1998)
136. J Liu, A G Rinzler, H J Dai, J H Hafner, R K Bradly, P J Boul, A Lu, T Iverson, K Shelimov, C B Huffman, F J Rodriquez-Macias, Y S Shon, T R Lee, D T Golbert, R E Smalley *Science* **280** 1253 (1998)
137. Y Ye, C C Ahn, C Witham, B Fultz, J Liu, A G Rinzler, D Colbert, K A Smith, R E Smalley *Appl. Phys. Lett.* **74** 2307 (1999)
138. C Bower, A Kleinhammes, Y Wu, O Zhou *Chem. Phys. Lett.* **288** 481 (1998)
139. C Liu, Y Y Fan, M Liu, H T Cong, H M Cheng, M S Dresselhaus *Science* **286** 1127 (1999)
140. Yu M Shul'ga, B P Tarasov, E P Krinichnaya, V E Muradyan, Yu G Morozov, N Yu Shul'ga, in *Fullereny i Fullerenopodobnye Struktury v Kondensirovannykh Sredakh* (Fullerenes and Fullerene-Like Structures in Condensed Media) (Minsk: Belorussian State University, 2000) p. 41
141. M J Heben, A C Dillon, T Genett, J L Alleman, K M Jones, P K Parilla, in *International Symposium on Metal–Hydrogen Systems (Abstracts of Reports), Noosa, Australia, 2000* Vol. 2, p. 2
142. A Kuznetsova, D B Mawhinney, V Naumenko, J T Yates Jr, J Liu, R E Smalley *Chem. Phys. Lett.* **321** 292 (2000)
143. C Nützenadel, A Züttel, D Chartouni, L Schlapbach *Electrochem. Solid-State Lett.* **2** 30 (1999)
144. A S Lobach, A S Astakhova, N G Spitsyna, in *Vseros. Seminar 'Nanochastitsy i Nanokhimiya' (Tez. Dokl.), Chernogolovka, 2000* [All-Russian Seminar 'Nanoparticles and Nanochemistry (Abstracts of Reports) , Chernogolovka, 2000] p. 65
145. S Pekker, J-P Salvetat, E Jakab, J-M Bonnard, L Forro, in *Proceedings of the XIIIth International Winterschool 'Electronic Properties of Novel Materials — Science and Technology of Molecular Nanostructures', Melville, NY, 1999* (Eds H Kuzmany, J Fink, M Mehring, S Roth) p. 474
146. A Chambers, C Park, R T K Baker, N M Rodriguez *J. Phys. Chem. B* **102** 4253 (1998)
147. C D Tan, P E Anderson, N M Rodriguez, in *The 195th Electrochemical Society Meeting (Abstracts of Reports), Seattle, USA, 1999* No. 541
148. C Park, P E Anderson, A Chambers, C D Tan, R Hidalgo, N M Rodriguez *J. Phys. Chem. B* **103** 10572 (1999)
149. C C Ahn, Y Ye, B V Ratnakumar, C Witham, R C Bowman Jr, B Fultz *Appl. Phys. Lett.* **73** 3378 (1998)
150. R Ströbel, L Jörissen, T Schliermann, V Trapp, W Schütz, K Bohmhammel, G Wolf, J Garche *J. Power Sources* **84** 221 (1999)
151. Q Wang, J K Johnson *J. Chem. Phys.* **110** 577 (1999)
152. P Chen, X Wu, J Lin, K L Tan *Science* **285** 91 (1999)
153. R T Yang *Carbon* **38** 623 (2000)
154. X B Wu, P Chen, J Lin, K L Tan *Int. J. Hydrogen Energy* **25** 261 (2000)
155. H W Zhu, A Chen, Z Q Mao, C L Xu, X Xiao, B Q Wei, J Liang, D H Wu *J. Mater. Sci. Lett.* **19** 1237 (2000)
156. S N Klyamkin, K Metenier, D E Sklovsky, S Bonnamy, F Beguin, in *Carbon'99. The 24th Biennial Conference on Carbon (Abstracts of Reports), Charlestone, SC, 1999* p. 628
157. S N Klyamkin, D E Sklovsky, K Metenier, S Bonnamy, F Beguin *Mol. Mater.* **13** 367 (2000)
158. S N Klyamkin, K Metenier, D E Sklovsky, S Bonnamy, F Beguin, in *Carbon'99. The 24th Biennial Conference on Carbon (Abstracts of Reports), Charlestone, SC, 1999* p. 94
159. I M Mellor, R J Mortimer, M Turpin, in *Carbon'99. The 24th Biennial Conference on Carbon (Abstracts of Reports), Charlestone, SC, 1999* p. 622
160. T D Jarvi, J Sun, L F Conopask, S Satyapal, in *The 195th Electrochemical Society Meeting (Abstracts of Reports), Seattle, USA, 1999* No. 542
161. N M Rodriguez *J. Mater. Res.* **8** 3233 (1992)
162. J Ozaki, W Ohizumi, A Oya, M J Illan-Gomez, M C Roman-Martinez, A Linares-Solano *Carbon* **38** 778 (2000)
163. D J Browning, M L Gerrard, J B Lakeman, I M Mellor, R J Mortimer, M C Turpin, in *Proceedings of the 39th Power Source Conference-2000, Sagamor, USA, 2000* p. 192
164. S M Cheng, C Liu, Y Y Fan, F Li, G Su, H T Cong, L L He, M Liu *Z. Met.kd.* **91** 306 (2000)
165. Y Y Fan, B Liao, M Liu, Y L Wei, M Q Lu, H M Cheng *Carbon* **37** 1649 (1999)
166. B K Gupta, O N Srivastava *Int. J. Hydrog. Energy* **25** 825 (2000)
167. M A de la Casa-Lillo, D Cazorla-Amorus, A Linares-Solano, P Malbrunot, D Vidal, in *Carbon'99. The 24th Biennial Conference on Carbon (Abstracts of Reports), Charlestone, SC, 1999* p. 780
168. E A Evard, I E Gabis, S K Gordeev, in *Fullereny i Fullerenopodobnye Struktury v Kondensirovannykh Sredakh* (Fullerenes and Fullerene-Like Structures in Condensed Media) (Minsk: Belorussian State University, 2000) p. 34
169. T Enoki, Y Shibayama, B L V Plasad, H Sato *Mol. Mater.* **13** 31 (2000)
170. H Imamura, Y Takesue, T Akimoto, S Tabana *J. Alloys Compd.* **293–295** 564 (1999)
171. H Imamura, Y Takesue, S Tabata, N Shigetoni, Y Sakata, S Tsuchiya *Chem. Commun.* 2277 (1999)
172. M Rzepka, P Lamp, M A de la Casa-Lillo *J. Phys. Chem. B* **102** 10894 (1998)
173. Q Wang, J K Johnson *J. Phys. Chem. B* **103** 277 (1999)
174. F E Pinkerton, B G Wicke, C H Olk, G G Tibbetts, G P Meisner, M S Meyer, J F Herbst *J. Phys. Chem. B* **104** 9460 (2000)
175. G Stan, M W Cole *Surf. Sci.* **395** 280 (1998)
176. K A Willams, P C Eklund *Chem. Phys. Lett.* **320** 352 (2000)
177. Q Wang, J K Johnson *J. Phys. Chem. B* **103** 4809 (1999)
178. V V Simonyan, P Diep, J K Johnson *J. Chem. Phys.* **111** 9778 (1999)
179. S M Lee, Y H Lee *Appl. Phys. Lett.* **76** 2877 (2000)
180. J E Fisher *Chem. Innov.* **30** 21 (2000)
181. S M Lee, K S Park, Y C Choi, Y S Park, J M Bok, D J Bae, K S Nahm, Y G Choi, S C Yu, N-g Kim, T Frauenheim, Y H Lee *Synth. Met.* **113** 209 (2000)
182. M Saunders *Science* **253** 330 (1991)
183. US P. 6 146 791 (2000)

[a] — *Russ. J. Appl. Chem. (Engl. Transl.)*
[b] — *Russ. Chem. Bull. (Engl. Transl.)*
[c] — *Russ. J. Inorg. Chem. (Engl. Transl.)*
[d] — *Russ. J. Gen. Chem. (Engl. Transl.)*
[e] — *Phys. Solid State (Engl. Transl.)*
[f] — *J. Exp. Theor. Phys. Lett. (Engl. Transl.)*
[g] — *Russ. J. Phys. Chem. (Engl. Transl.)*
[h] — *Dokl. Chem. Technol.*, *Dokl. Chem. (Engl. Transl.)*

Russian Chemical Reviews **70** (2) 147 – 159 (2001) © 2001 Russian Academy of Sciences and Turpion Ltd

DOI 10.1070/RC2001v070n02ABEH000637

Metallic nanosystems in catalysis

V I Bukhtiyarov, M G Slin'ko

Contents

I.	Introduction	147
II.	Physicochemical properties of nanostructures	147
III.	Reactivities and catalytic properties of nanostructures	150
IV.	The prospects for the application of nanostructures in catalytic processes	154
V.	Conclusion	157

Abstract. The reactivities of metallic nanosystems in catalytic processes are considered. The activities of nanoparticles in catalysis are due to their unique microstructures, electronic properties and high specific surfaces of the active centres. The problems of increasing the selectivities of catalytic processes are discussed using several nanosystems as examples. The mutual effects of components of bimetallic nanoparticles are discussed. The prospects for theoretical and experimental investigations into catalytic nanosystems and the construction of industrial catalysts based on them are evaluated. The bibliography includes 207 references.

I. Introduction

Metallic catalysts supported on various carriers (*e.g.*, SiO_2, α- and γ-Al_2O_3, zeolites, magnesium and chromium oxides, carbonaceous materials, *etc*.) are widely employed in chemical, petrochemical and oil-refining industries as well as for purification of gaseous industrial wastes and motor transport exhausts from toxic components. The production of efficient industrial catalysts includes selection of inert carriers of definite porous structures, their coating with particles of active metals of predetermined compositions, sizes and structures and the most efficient unimodal distribution of these particles over the carrier surface.

Catalytic reactions occurring on the catalyst's surface consist in adsorption of molecules of the starting compounds, their migrations, chemical conversions of adsorbed substances and subsequent desorption of the products formed. The gas-phase components are dissolved in the near-surface layers of the catalyst thus changing its reactivity. In some cases where a certain degree of coating of the catalyst's surface with the adsorbed molecules is achieved, its spontaneous and adsorption-induced reconstruction takes place. The energies of lateral interactions of the adsorbed species, their mobilities and the energies of binding of the interacting molecules to the catalyst are the crucial factors which determine the rates of the elementary catalytic steps mentioned above. The efficiency of a catalyst depends on how fast and concertedly do the active sites on the catalyst's surface adsorb the reacting species, retain them during the chemical conversions and liberate the reaction products to be recovered for the next catalytic cycle. The maximum reaction rate is reached when the adsorption, reaction and desorption possess the optimum energies of binding of molecules to the catalyst (the Sabatier – Balandin principle).

The rates of individual elementary stages depend differently on the size of the active metal particles; hence, the total rate of the reaction varies with a change in the particle size. The knowledge of the structure and properties of the active sites and their distribution over the catalyst's surface is of primary importance for establishing a correlation between the structure and properties of the catalyst's surface and the particle size. It is also desirable to establish the number of adsorbed reacting species and metal atoms involved in an elementary catalytic act.

II. Physicochemical properties of nanostructures

The intermediate position occupied by nanoparticles between the metals in bulk and individual atoms predetermines the deviation of their physicochemical properties from those of bulk metals, on the one hand, and those of isolated atoms, on the other hand. Such characteristics of nanoparticles with the sizes ranging from several tens to units of nanometres are affected as the electronic, magnetic, optical properties and many others. The changes in the surface structures and electronic properties of metallic nanoparticles present the greatest interest for specialists in catalysis, because these characteristics determine primarily specific interactions of the reactants with the surface of the active component, the nature and reactivities of the adsorbed species and eventually the activities and selectivities of the nanosystems in heterogeneous catalysis.

1. The structure and geometry of the surface

The atoms inside bulk crystals have optimum chemical bonds with all adjacent atoms. If the number of metal atoms in the particle (N) is less than 13, it has a close packing in which each atom represents a surface atom. For $N \geqslant 13$, two kinds of atoms exist, *viz*., the inner and surface ones. The proportion of surface atoms in a cluster † depends on the total number of atoms.

† Many investigators believe that in contrast to particles, clusters comprise a strictly definite number of atoms and thus represent nearly monodisperse structures with sizes less than 10 nm.

V I Bukhtiyarov G K Boreskov Institute of Catalysis, Siberian Branch of the Russian Academy of Sciences, prosp. Akad. Lavrent'eva 5, 630090 Novosibirsk, Russian Federation. Fax (7-383) 234 37 66. Tel. (7-383) 234 17 71. E-mail: vib@catalysis.nsk.su
M G Slin'ko State Scientific Centre of the Russian Federation 'L Ya Karpov Institute of Physical Chemistry', ul. Vorontsovo Pole 10, 103004 Moscow, Russian Federation. Fax (7-095) 975 24 50. Tel. (7-095) 917 78 70. E-mail: slinko@polymer.chph.ras.ru

Received 20 November 2000
Uspekhi Khimii **70** (2) 167 – 181 (2001); translated by R L Birnova

Number of atoms in a cluster	13	55	147	349	561
Proportion of surface atoms (%)	92	76	63	52	45

These data refer to clusters with 'shell' structures which are characterised by close packing of their metal atoms (see below). For $N = 13$, such clusters have only one inner layer (consisting of only one atom, whereas for $N = 55$ and $N = 147$, these have two and three inner layers of atoms, respectively. Then, the particle size increases from 0.8 to 2 nm. In particles with sizes of 2–10 nm, the numbers of surface and inner atoms are comparable, whereas in particles with sizes > 30 nm the fraction of surface atoms is less than 2%. Hence, the proportion of surface atoms decreases with an increase in the particle size, their coordination properties with respect to the reactants change too. Small particles form many different faces; their number and parameters depend on the method used for their preparation. The properties of the particles approach those of bulk crystals with an increase in the particle size.

The surface structures of metallic particles are studied by theoretical and experimental methods.[1–4] The theoretical approach is based on the analysis of the equilibrium form of crystals [1] determined by the minimum value of Gibbs' free energy. The total energy depends on the thermodynamic properties of the bulk phases, the contribution of the planar surface and the plane intersection energy, which corresponds to the contribution of curved or rough surfaces. Obviously, the surface structures of nanoparticles are determined by the ratio of contributions of planar and rough surfaces, which in turn depends on the particle size. For large particles, the contribution of rough surfaces is insignificant and the equilibrium form of a crystal is determined by the minimum surface energy. The contribution of the curved surface increases with a decrease in the particle size. Hence, the surface of nanoparticles contains predominantly planar, planar and rough or predominantly rough areas depending on their sizes.

Experimental studies of surface structures are complicated, since the methods employed should ensure resolution at the atomic level. Transmission electron microscopy (TEM) is one such method. Studies of nanoparticles using TEM corroborated the presence of planar and rough surface areas and made it possible to follow their alterations with a change in the nanoparticle size.[3,4] Thus a combination of TEM with computer simulation of surface structures showed that the surface of platinum particles (~ 8 nm) consists of (111) faces (~ 37%), (100) faces (28%) and rough areas (35%).[4] It is noteworthy that the rough areas contain faces with higher Miller's indices, *e.g.*, (001), (113), (012) and (133) faces. The results of computer simulation studies of rough areas and of platinum particles as a whole are presented in Fig. 1.

In recent years, scanning tunnelling microscopy (STM), which ensures resolution at the atomic level, has been widely used for the study of surface structures of metallic nanoparticles.[5–9] It was found that surface structures of small (1–2 nm) metallic particles are determined by their shapes which in turn strongly depend on the nature of the support. At the same time, such low coordinated sites as edges and kinks strongly affect the interaction of a surface with adsorbed species. The use of STM for the analysis of surface structures of metallic nanoparticles seems promising, since in contrast to TEM this method allows *in situ* analysis of surface structures, *i.e.*, in the course of a catalytic reaction.

An alternative procedure is based on the adsorption of molecules the spectral characteristics of which are sensitive to the structure of the adsorption centre. Successful application of this method entails the choice of a suitable molecular probe and measurements of its spectral characteristics in the adsorption on single crystals with different surface structures. Like STM, this method permits one to obtain information *in situ*, which is extremely important in studies of catalytic reactions, especially those where the molecular probe is one of reactants. NMR and IR spectroscopic studies of CO adsorption on platinum and palladium clusters supported on SiO_2 is an example.[10–12] It was shown

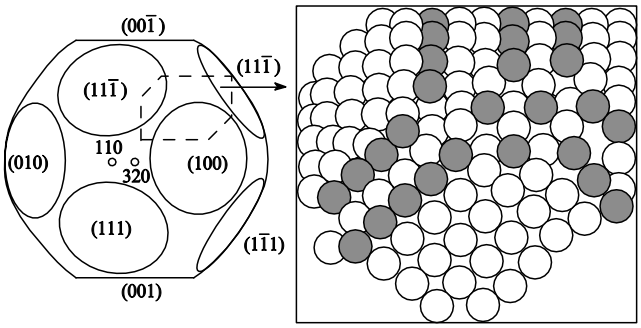

Figure 1. The types of faces on the surface of a platinum particle (8 nm) and a structural model of a site marked by a dashed line.[4] The light and dark circles designate the atoms localised at different levels.

that part of the ^{13}CO is adsorbed on platinum catalysts in a linear rather than a bridge-like form, the proportion of the linear fraction being increased with an increase in the degree of platinum dispersion from 16%–19% to 56%.[10] This effect was attributed to the fact that the surfaces of smaller platinum particles contain more low-coordinated sites. A similar conclusion was made by Xu *et al.*[11] who showed that the major part of the CO is adsorbed on small palladium particles in a linear rather than in a bridge-like form. This points to a higher concentration of defect/edge sites in small nanoparticles in comparison with large ones.

An analysis of spectra of the O 1*s* core level recorded after low-temperature adsorption of O_2 was proposed by us for investigation of surface structures of supported silver. This approach is based on the previously established regularity, *viz.*, the greater the number of defects on the silver surface the lower the minimum temperature needed for dissociation of oxygen molecules.[13–15] In other words, the amount of atomic oxygen after low-temperature adsorption correlates with surface defects of the supported silver particles. Studies of low-temperature ($T = 140$ K) adsorption of O_2 on silver particles deposited onto a graphite surface revealed that the form (atomic or molecular) of the chemisorbed oxygen depends on the sizes of the silver particles. The molecular form is absent in the case of small (< 10 nm) particles which suggests a high degree of defectiveness of their surface structures, while this is present with an increase in the particle sizes to 20–40 nm. The latter circumstance points to the formation of (111) and (110) low-index faces. It is worth noting that the dimension-dependent effect is manifested in the epoxidation of ethylene on silver catalysts in the range of particle size from 40 to 50 nm.

These data altogether suggest that the surfaces of small clusters do not exclusively contain low-index faces, such as (111), (110) or (100) faces. The greater part of the surface, which increases with a decrease in the nanoparticle size, is occupied by curved areas. This circumstance is of crucial importance for the catalysis by nanoparticles, since the adsorption properties of rough surface defects (*e.g.*, angles, steps, edges, *etc.*) differ from those of flat surfaces. Therefore, simple extrapolation of experimental data obtained for single crystals to real catalytic systems is impossible. In this connection, studies of reactivities of metallic nanoparticles become especially urgent.

2. Electronic properties

As the number of atoms in nanoparticles is limited, their electronic structures occupy an intermediate position between the discrete energy levels of free atoms and continuous energy bands of the bulk metal. The dependence of electronic structures of metallic particles on their sizes was studied in particular by Kubo,[16] who suggested that the spectrum of the energy levels of nanometre particles should resemble that of a large molecule rather than that of a bulky solid. The electronic levels of atoms in a large metallic particle are close to one another and eventually overlap to form energy bands. The expression:

$$h = \frac{E_F}{N}, \quad (1)$$

where E_F is the Fermi level energy and N is the number of atoms in a metallic particle, was proposed to evaluate the distance between the neighbouring energy levels (h). Estimation of the maximum size of a particle where changes in its electronic properties can occur as calculated by this simple formula gives the value of ~ 2 nm. Presumably, this is the threshold size where significant changes in the electronic properties of supported metallic nanoparticles are observed. This hypothesis was confirmed by experimental data. It was found that the properties of nanoparticles change so drastically in the size range of 2–5 nm that a 'metal–non-metal' transition becomes very likely. This conclusion is based on the increase in the binding energy of electrons (E_b) at core levels [16] [the binding energy was measured by X-ray photoelectron spectroscopy (XPS)] with a decrease in the sizes of metallic nanoparticles.

In the general case, the changes in ΔE_b are due to the contribution of the following terms:

$$\Delta E_b = \Delta E + \Delta E_R + \Delta E_F, \quad (2)$$

where ΔE is the 'true chemical shift' equal to the difference between the energies of different initial states of the element under study,‡ ΔE_R is the change in the relaxation energy and ΔE_F is the difference between the Fermi level energies.

The last two terms in equation (2) are determined by the effects of the final state as a result of photoelectron emission, *viz*., the ΔE_R value reflects the changes in the relaxation energy upon the screening of photoelectron vacancies caused by redistribution of electrons in the solid, whereas ΔE_F reflects possible changes in the Fermi level of a sample relative to that of the spectrometer.§ If the conductivity of the sample is high enough, an electrochemical equilibrium is established between the sample and the spectrometer. In this case, the positive charge induced by photoelectron emission is neutralised due to the transition of electrons from the 'earth' to the sample and the contribution of ΔE_F to the total change in ΔE_b will be insignificant. If the electronic conductivity of the sample is not high enough to compensate for the charge due to photoemission, the positive charge is accumulated on the surface of the sample. The electrons passing through this positively charged layer lose their kinetic energies, which results in the overestimation of the apparent binding energy. This suggests that the Fermi levels of the sample and the spectrometer are no longer at equilibrium, which results in the charging effect due to accumulation of unknown surface potential.

The subdivision into terms proved to be useful for establishing the reasons for the change in ΔE_b with a decrease in the metallic nanoparticle sizes. It was suggested (see, *e.g*., Refs 17 and 18) that it is the relaxation effect that underlies the positive shift of the binding energy in small metallic nanoparticles (2–3 nm) by 0.5–1.0 eV in comparison with the binding energy of the bulk metal. However, studies of alloys [19,20] and those employing isochromatic spectroscopy [21,22] revealed that the observed shift in the binding energy cannot be attributed to the relaxation effect alone. It was concluded that the changes in the initial state of atoms in metal clusters with particle sizes of less than 2–3 nm are due to the 'metal–non-metal' transition. This conclusion is of fundamental importance, since the changes in the initial states of atoms in small clusters should influence (and they do influence, as will be shown below) their reactivities with respect to the gases to be adsorbed. It is evident that the catalytic properties of clusters cannot remain unchanged under these conditions.

In contrast to the initial-state and relaxation effects, the contribution of the charging effect to total changes in ΔE_b was not taken into consideration by the majority of authors who dealt with studies of electronic properties of metal clusters. Such an approach is justified with respect to homogeneous insulator specimens where the magnitude of the charging potential is identical for all inner levels and can be easily taken into consideration in the analysis of XPS spectra by the internal standard method. The situation is more complicated in heterogeneous systems where different phases are characterised by different conductivities. In this case, the surface charges are different in individual phases of the specimen, which generates the so-called differential charging of the more conducting phase in comparison with the less conducting one. Apparently, this situation is quite realistic in the case of heterogeneous catalysts which contain metallic nanoparticles supported onto the surface of dielectric substrates (Al_2O_3, SiO_2, *etc*.). Indeed, it was demonstrated [23,24] that metallic crystallites with the sizes ranging from five to several tens of nanometres manifest the properties of conducting metals by providing more efficient compensation of the surface charge in comparison with the surface of insulating substrates. As a result, the charge potential on metallic particles is lower than that of the dielectric substrate, and the corresponding lines of the substrate in the XPS spectra manifest a greater shift in the binding energy (ΔE_b) than those of the supported metal. Then, the shift of the spectra by a value equal to the charge of the substrate, the lines of which are generally used as internal standards in calibration of XPS spectra, will produce an apparent negative shift in the lines of the corresponding spectra of the metals.

The latter effect is manifested exclusively upon photoemission; however, it can be of tremendous importance for characterisation of reactivities of various particles including silver particles. The hypothetical role of the conductivity electrons in the formation of chemical bonds between the metal surface and chemisorbed molecules which was put forward as early as 1937,[25] was corroborated later by quantum-chemical calculations.[26] The role of the conductivity electrons in the formation of chemical bonds was confirmed experimentally by the presence of the Knight shift in the ^{13}C NMR spectra of carbon oxide adsorbed on supported metallic particles.[27,28]

The effects of differential charging can be taken into account with the help of those parameters of XPS spectra which do not depend on the surface charge. One of them is the modified Auger parameter α, which represents the sum of the binding energies of the most intense line in the XPS spectrum of the element under study and the kinetic energy of the corresponding Auger peak.[29] Since the charge potential increases the binding energy of the core level and decreases the corresponding kinetic energy of the Auger peak by the same value, their sum is not changed with changes in the charge. With the use of the Auger parameter we have demonstrated that it is the differential charging of supported nickel and silver particles that is responsible for the changes in the binding energies of their core levels ($2p_{3/2}$ and $3d_{5/2}$, respectively) in catalysts (both fresh and treated with the reaction mixture) for butadiene hydrogenation (Ni/C) and ethylene epoxidation (Ag/Al_2O_3).[30–32]

Treatment of nickel particles supported onto carbon filaments with the reaction mixture causes a shift in the overall Ni spectrum ($2p_{3/2}$) by 1.1 eV towards higher values of E_b with a simultaneous decrease in the Ni : C ratio.[30] The constancy of the parameter α and the absence of a shake-up satellite in the Ni $2p_{3/2}$ spectrum indicate that both fresh and treated samples contain metallic nickel, whereas the shift in the Ni spectrum $2p_{3/2}$ is due to the differential charging.

Studies of Ag/Al_2O_3 catalysts where the sizes of silver particles vary from 10 to 100 nm revealed a negative shift in the Ag $3d_{5/2}$ spectra by 0.3–0.4 eV for particles with the sizes above 50 nm.[31,32] In this case, the parameter α was constant for all

‡ The XPS method owes its second name which is widely used by researchers *viz*., 'electron spectroscopy for chemical analysis' (ESCA), to the term ΔE.

§ 'The Fermi level of spectrometer' is a popular term used to define the Fermi level of the material (mostly, gold) of which the energy analyser of the spectrometer is made.

specimens and equal to 726.2 eV. Comparison of this parameter with the known values of α for metallic silver (726.0 – 726.3 eV) and silver oxides (724.0 – 724.5 eV) suggests that the samples under study contain particles of metallic silver. This conclusion was confirmed by the results of an X-ray phase analysis and scanning tunnelling microscopy, which have demonstrated the presence of the α-Al_2O_3 phase and metallic silver in the specimens.[33]

The observed change in E_b(Ag $3d_{5/2}$) is determined by the effect of a differential charging of the supported silver, which in turn is due to the inner conductivity of large silver particles and the lack of conductivity of the surface of the non-conducting substrate.[31] This conclusion is in good agreement with the results of NMR studies of silver catalysts[34,35] according to which the Knight shift of the ^{147}Ag signal disappears if the size of silver particles is less than 50 nm. Since the Knight shift is determined by hyperfine interactions of silver nuclei with the conductivity electrons, it is clear that the size of several tens of nanometres is critical with respect to the conductivities of supported silver particles. The great importance of such changes in the properties of silver conductivity electrons for catalysis is illustrated in Fig. 2. As can be seen, the rate of ethylene epoxidation decreases more than 10-fold with a decrease in the sizes of silver particles below 50 nm. It will be shown below that this correlation depends on the form of oxygen adsorbed on silver.

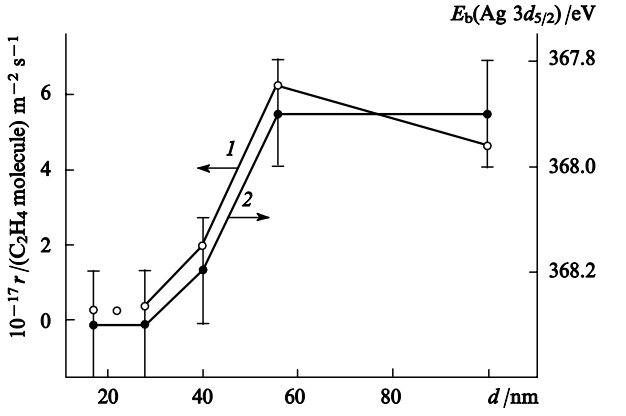

Figure 2. The dependence of the rate of ethylene epoxidation (*1*) and the binding energy E_b(Ag $3d_{5/2}$) (*2*) on the average size of silver particles in non-promoted Ag/Al_2O_3 catalysts.

A correlation was also found[36–38] between the deviation of electronic properties of supported nanoparticles from those of bulk metals and the catalytic activities of nanoparticles.

III. Reactivities and catalytic properties of nanostructures

The existence of size effects in electronic and structural properties of nanostructures implies that their reactivities with respect to gaseous molecules also differ from those of bulk metals, this difference being more pronounced in smaller particles. The first evidence for such dependence was obtained in catalytic studies which demonstrated that the rates of numerous reactions catalysed by metallic nanoparticles vary in the same range[39] as their electronic and structural properties.[10–12,19–21,40–42] Catalytic reactions usually occur on the catalyst's surface. Therefore, the activities of catalysts are conventionally referred to unit surface area. This quantity, which is termed 'specific catalytic activity' (SCA), is determined by the chemical composition, sizes of crystallites, structures of surface faces, structural irregularities and miscellaneous defects. Therefore, the knowledge of changes in the catalytic properties of the catalyst's surface caused by changes in both the sizes of crystallites and surface structures of their faces is of fundamental importance for the theory and practice of catalysis. Although the structures of nanocrystals can differ from those of macroscopic crystals due to exposure of other types of faces on their surface,[43] we thought it appropriate to analyse, at least briefly, the results of investigations of applied single crystals with different surface orientations as the subjects. This is especially important, because the results of such studies are very often used as references for illustrating the dependence of reactivities of metallic nanoparticles on their sizes, as will be shown below.

1. The reactivities and catalytic properties of single crystal faces

The properties of atoms in the crystal lattices of metals are determined by their specific atomic environment, *i.e.*, the number of adjacent and more remote neighbours, and the sizes of the corresponding coordination zones. Therefore, the reactivity of a surface depends essentially on the localisation of atoms on one or another crystallographic face and the parameters of their atomic environment. A correlation between the orientation of the crystal faces and their catalytic activities was established by A A Balandin as early as 1929.[44] In the past years, the number of investigations of this kind has increased manifold.

The rates of carbon monoxide oxidation on (111), (100), (410) and (210) faces of the single crystal $Pt_{0.25}Rh_{0.75}$ at different temperatures, total pressure of 2×10^{-7} mbar and the $CO:O_2$ ratio of 2 : 1 differ markedly.[45] On heating, the reaction rates on different planes increase rapidly but differently in the range of 400 – 500 K and then decrease slowly after reaching a certain maximum. The higher the strength of lateral interactions of the CO molecules, the higher the temperature at which the maximum rate is achieved. The oxidation of CO on the faces of Pt, Pd, Ir, Rh and Ru crystals proceeds in a similar way.

The catalytic activity of the (111) face of iron in the synthesis of ammonia from nitrogen and hydrogen is about 430 times higher than that of the closely packed (110) face and 13 times higher than that of the (100) face.[46] It is also known that aromatisation and cyclisation of hydrocarbons occur on the (111) face of platinum, whereas the (100) face is responsible for their isomerisation and hydrogenolysis. The presence of curved areas, *e.g.*, (10 8 7) favours the formation of undesired products, such as propane and ethane.

The atoms in the surface layer can be at equilibrium with the atoms in the second layer. Since the bonds of the surface atoms are not compensated, their equilibrium positions can differ from their positions in the bulk. Such 'surface reconstruction' was observed in the CO oxidation catalysed by platinum and some other metals. For example, the reaction occurring on the (110) face of platinum single crystals is accompanied by spontaneous reconstruction of the surface from the (1×1) state into the (1×2) state. Surface rearrangements are due to interactions between the platinum atoms, CO molecules and oxygen atoms.[47–49] The higher reactivity of the (110) face of platinum in comparison with other faces can be the reason for autooscillations of the reaction rate.[48–54] On this face, spatial-temporal self-organisation in the form of progressive spiral and stationary reaction waves and chaotic regimes were observed in the nano- and micrometre ranges. On the other hand, the oxidation of carbon monoxide by oxygen on the (111) face of platinum at low partial pressures of CO and O_2 and at 300 – 700 K was unaccompanied by changes in the surface structure and, correspondingly, by autooscillations of the reaction rate.

The activation energy of a catalytic reaction depends on the coverage of the catalytic surface with oxygen and carbon monoxide.[47] The adsorbed oxygen atoms increase the reaction rate, while adjacent CO molecules decrease it. The distribution of atoms and molecules adsorbed on the surface of a catalytic species influences substantially the dependence of the rates of elementary stages of the catalytic reaction on the degree of coverage of the catalytic surface.

Spatial-temporal self-organisation was also observed in a nanometre range in the interaction of NO and H_2 on the (110) face of rhodium single crystals at partial pressures of nitrogen

oxide and hydrogen of 10^{-6}–10^{-4} mbar and at temperatures on the catalyst's surface of 300–800 K.[55–58] Phase transitions of the 'order–disorder' type and various superstructures of adsorbed hydrogen atoms were found. The nitrogen atoms initiated the rearrangement of the original surface resulting in the appearance of the (3×1)–N superstructure recorded by low energy electron diffraction. This was transformed into the (2×1)–N superstructure with an increase in the degree of coverage of the catalyst's surface with the adsorbed nitrogen.[59] Lateral interactions of adsorbed particles and their mobilities exert a crucial effect on the formation of structures on a nanometre range. The NO + H_2 system on Rh(110) was also characterised by anisotropy of the near-surface layer and the presence of unusual reaction autowaves of different shapes. Non-linear phenomena, *e.g.*, spatial-temporal self-organisation in nanosized particles, significantly influence both the spatial structure of the reaction autowaves at the meso level and the rate of the catalytic reaction.

The effects of the structural factor on SCA can also be explained by assuming that the surface of small metallic clusters contains many more low-coordinated atoms than that of bulk metals.[60] Indeed, the proportion of surface atoms, particularly those localised in the apices as well as on the boundaries and faces and characterised by lower coordination numbers than atoms localised inside the crystals, increases essentially in crystallites the sizes of which exceed 5 nm. If this is true, SCA will depend on the changes in the crystallite sizes in the range of not more than 1–5 nm, whereas the catalytic activities of larger crystallites will be determined by the structures of the faces exposed on the surface of the nanoparticles.

2. The reactivities and catalytic activities of nanostructures

The first attempts to establish a correlation between the rate of a catalytic reaction and the particle size of the active component were undertaken by Kobozev in the late 1930's.[61] These investigations were continued in the early 1950's by Boreskov *et. al.*[62, 63] who have formulated a rule of relative stability of SCA of catalysts having identical chemical compositions. A similar conclusion was made later by Boudart *et al.*[64, 65] who have named this kind of reaction 'structure-insensitive reactions'. However, the rates of many reactions do depend on the degree of dispersion of the active component, and these reactions have been named 'structure-sensitive reactions'. Further studies of the dependence of catalytic activities of metals on the particle size have revealed [66–76] that all metal-catalysed reactions can be classified into four main groups, *viz.*,

(a) SCA depends only weakly on the size of the supported metal particles (structure-insensitive reactions);

(b) SCA drops with a decrease in the particle size (the so-called negative size effect);

(c) SCA increases with a decrease in the particle size (the positive size effect);

(d) maximum SCA is characteristic of particles of intermediate sizes.

Seemingly, in the case of structural insensitivity or a positive dimensional effect the sizes of nanoparticles of the active component in certain systems can be minimised, thus affecting favourably the economical parameters of the industrial process. Unfortunately, this assumption was refuted by some examples.[77, 78] It was shown [77] that the rate of even such structure-insensitive reactions as the hydrogenation of hydrocarbons decreases by more than two orders of magnitude in those cases where iridium nanoclusters ($d \approx 2$–3 nm) supported on MgO were used instead of conventional Ir/MgO catalysts, whereas the tenfold increase in the activity of the Ir_n/γ-Al_2O_3 catalyst in the hydrogenation of toluene is explained [78] by the formation of iridium agglomerates during the annealing of fresh samples in hydrogen at 573 K.[78]

Obviously, such drastic differences in the behaviour of SCA as a function of the particle size are due to changes in the reactivities of the particles with respect to the participants of the catalytic reaction. This accounts for a great number of publications devoted to the analysis of reactivities of nanoparticles. However, real specimens used in catalytic studies appeared to be unsuitable subjects for establishing an exact correlation between the changes in the catalytic properties and reactivities. Progress in this field could be achieved, if model systems were used. These were prepared by covering flat samples of a substrate with metal particles using physical (*e.g.*, deposition of bulk metals in high vacuum) or chemical methods (*e.g.*, introduction of chemical compounds of a metal followed by reduction and/or calcination).

For the first time, the reactivities of metallic clusters were studied in detail using the oxidation of CO on platinum metals as an example.[79–82] This choice has been made owing to the large body of experimental material obtained in precision studies of this reaction on bulk metals.[83–86] These results could be used for the analysis of reactivities of nanostructures supported on metals.

Thus the earlier established mechanism of this reaction carried out on the (111) face of palladium [83] was used to explain the peculiarities of CO oxidation on palladium clusters supported on α-Al_2O_3.[79, 80] The threefold increase in the rate of CO_2 formation at temperatures > 500 K upon a decrease in the sizes of palladium clusters from 4.9 to 1.5 nm was attributed to the increased coefficient of CO adhesion to edge and corner palladium atoms the number of which increases with a decrease in the particle size.[79] This explanation was corroborated by experiments [87] in which the reactivities of palladium clusters with respect to CO were studied by temperature-programmed desorption (TPD). It was shown that the TPD spectra of CO molecules adsorbed on palladium with the particle size of 27 nm and on the (111) face of palladium single crystals coincide, whereas the corresponding spectra of desorption of CO with a particle size of 2.5 nm display an additional peak at lower temperatures. Similar TPD spectra were recorded by following the CO desorption from palladium with a particle size of < 5 nm supported on mica. This suggests that the formation of weakly bound forms of carbon monoxide is characteristic of small palladium particles and does not depend on the nature of the substrate.[88] Presumably, it is the appearance of a weakly bound adsorbed form of CO that is responsible for the increased rate of CO_2 formation with a decrease in the sizes of palladium nanoparticles.[79, 80]

Quite opposite regularities were observed by following the temperature-programmed desorption of CO molecules from platinum particles supported on Al_2O_3 (Ref. 89) and mica (Ref. 90), *viz.*, the intensity of the low-temperature peak of the CO desorption decreased with a decrease in the size of the platinum particles (> 4 nm). It was thus concluded that CO molecules are more strongly adsorbed on small particles, which can account for the decrease in the rate of CO oxidation on small (< 2.5 nm) platinum particles.[81]

Comparison of CO adsorption on supported platinum and rhodium particles revealed that the ratio of low- and high-temperature components in the TPD spectra of rhodium particles (in contrast to the corresponding parameters in the TPD spectra of platinum particles), only weakly depends on the size of the metal particles.[91] Presumably, this peculiarity of CO adsorption on rhodium is the reason for the structure-insensitivity of the CO oxidation on Rh-containing catalysts.[82]

These data suggest that a correlation exists between catalytic activity in the CO oxidation on various platinum metals and the strength of the CO–metal bond despite significant differences in the manifestations of the size effect. The fact that the structure-insensitivity of the CO oxidation on rhodium, its negative sensitivity on palladium and its positive sensitivity on platinum could be explained on the basis of 'single crystal data' gave impetus to the studies of the behaviour of nanoparticles in other catalytic systems.[82, 92, 93] For example, the results of TPD studies of NO molecules [92] provided an explanation for the 45-fold decrease in the rate of the CO + NO reaction with a decrease in the size of rhodium particles on Rh/α-Al_2O_3 from ~ 70 to 1 nm (see Ref. 82). According to these data, the major part of the nitrogen

is desorbed from large particles at 463 K and only a small part is desorbed at 553 K. The amount of nitrogen adsorbed at high temperatures increases with decrease in the particle size. Stronger adsorption of nitrogen on the surface of small rhodium particles can be responsible for the structure-sensitivity of the CO + NO reaction on rhodium.[82] It is of note that the nature of the support (α-Al_2O_3, θ-Al_2O_3, SiO_2) has practically no effect on the activity of rhodium particles in this reaction.

Yet another example is the $CH_4 + O_2$ reaction and O_2 adsorption on Pt/Al_2O_3 catalysts with average sizes of platinum particles of < 2 and 20 nm.[94] It was found that the catalysts with larger particle sizes are ninefold more active in the methane oxidation, these are characterised by lower heats of oxygen adsorption (250 kJ mol^{-1} instead of 280 kJ mol^{-1} for smaller particles) and the oxygen adsorbed on them is more reactive with respect to hydrogen. The latter assumption is based on the fact that the oxygen adsorbed on a platinum catalyst with a particle size of 20 nm is totally desorbed by hydrogen at 195 K, whereas in the case of smaller platinum particles it does not react with hydrogen at temperatures up to 276 K. These findings point to a weakening of the bond between the platinum surface and the adsorbed oxygen with an increase in the particle size and a concomitant increase in the reaction rate.[94]

Studies aimed at establishing a relationship between the changes in the reactivities of nanoparticles and their electronic and structural properties are of fundamental importance.

The discovery of a dependence of the heat of desorption of CO on the crystallographic orientation of platinum faces[95–97] aroused debates concerning the effect of the structural factor on the heat of CO adsorption with changes in the particle size.[94] It is known that the spectra of the temperature-programmed desorption of carbon monoxide from the closely packed (111) face of platinum have the main peak at 400 K,[95] whereas its desorption from the more open (110) face of platinum or from platinum foil is accompanied by the appearance of an additional peak at 510 K, the relative intensity of the high-temperature peak being increased with an increase in the densities of the monoatomic steps.[96,97]

Comparison of spectra of temperature-programmed desorption of CO molecules from platinum single crystals and Pt/Al_2O_3 particles revealed that the weakening of the CO–Pt bond on large particles is due to predominant localisation on their surface of terraces the structure of which is identical with that of the (111) face, whereas small particles contain a large number of coordinatively unsaturated sites, which favours strengthening of this bond.[89] The presence of such low-coordinated sites was related to possible dissociation of the CO molecules on small platinum particles.[87] Their structure was simulated as a (100) step separating the (111) terraces. It was suggested that the repulsion of carbon atoms adsorbed on such sites from the CO molecules adsorbed on the (111) face of platinum weakens the CO–metal bond.[89]

The expediency of the structural approach is also confirmed by the fact that the shape of TPD spectra of the CO molecules did not depend on the orientation of the faces of Rh single crystals,[98,99] which is in complete agreement with the structure-insensitivity of the $CO + O_2$ reaction on rhodium-containing catalysts. The decrease in the heat of adsorption of oxygen and the corresponding increase in its reactivity with an increase in the size of platinum nanoparticles supported on alumina was attributed to the increased number of smooth areas on the catalyst's surface.

The electronic approach to rationalise unusual reactivities of metallic clusters was largely developed in studies with the use of methods suitable for the analysis of the nature of adsorbed particles together with the electronic properties of metal atoms.[10,100–103] Studies of CO adsorption on palladium, copper and nickel clusters supported on graphite revealed that a 'metal–dielectric' transition and strengthening of the CO–M bond with a decrease in the cluster size are observed within the same range of particle sizes.[103] It was found that in small particles the decrease in the intensity of the C 1*s* signal which is associated with the adsorbed CO (E_b = 285.9 eV) occurs at higher temperatures. Moreover, the strengthening of the CO–M bond on nickel particles results in the dissociation of CO as can be evidenced from the appearance, in the TPD spectrum, of a C 1*s* signal with E_b = 284.2 eV characteristic of elemental carbon, after heating of the sample to 300 K. It was assumed that the observed increase in the reactivities of small nickel particles with respect to the CO oxidation is accounted for by closeness of the 3*d*-levels of Ni and the $2\pi^*$-orbital of CO.

If the sizes of palladium and nickel nanoparticles are less than 3 nm, their metallic properties are weakened, which correlates with an increase in their reactivities towards oxygen[101] and hydrogen sulfide,[102] respectively. The conclusion about the strengthening of the O–Pd bond was based on data from microcalorimetry according to which the heat of adsorption of O_2 remains unchanged ($Q \approx 210$ kJ mol^{-1}) for particle sizes ranging from 1000 to 3 nm, but increases drastically (up to 335 kJ mol^{-1}) for smaller particles.[101] The nature of the support does not influence the heat of adsorption of O_2 on palladium particles sprayed over SiO_2, η-Al_2O_3 and SiO_2–Al_2O_3. The conclusion about enhanced dissociation of H_2S on smaller nickel clusters is based on the increase in the relative intensity of the S 2*p* line (E_b = 162.0 eV) characteristic of S^{2-} ions in comparison with the line (E_b = 164.5 eV) related to hydrogen sulfide adsorbed as a molecule with a decrease in the particle size.[102]

One should not rule out the possibility that the proportion of rough surfaces in particles with sizes varying from 3 to 5 nm is greater, since they contain a large number of low-coordinated atoms on the steps, in the edges, *etc*. Apparently, the electronic and structural factors are closely interrelated and their effects on the reactivities of metallic clusters cannot be differentiated. The correctness of this statement can be illustrated by the results of experiments carried out by Zilm *et al*.[10] Comparison of ^{13}C NMR spectra of adsorbed CO molecules recorded with and without magic angle spinning allowed the authors to suggest that the significant decrease in the diffusion rates of carbon monoxide on the surface of small palladium particles is due to stronger binding of CO to these particles. It was concluded that strongly bound CO with a lowered ability for diffusion is linearly adsorbed on edge and corner palladium atoms the proportion of which increases with a decrease in the particle size. Moreover, comparison of the Knight shift for the linear and bridge-like forms of CO demonstrated that these low-coordinated sites are characterised by electron deficiency resulting from changes in their Fermi levels relative to those of the bulk metal.

It is worth noting that the differences in the properties of the conductivity electrons of supported nickel[30] and silver[31,32] particles, on the one hand, and those of the corresponding bulk metals, on the other hand, also correlate with changes in the surface structures of the particles, which become more defective after their treatment with the reaction medium. In the case of Ni–C catalysts for butadiene hydrogenation, this conclusion was based on TEM data, whereas for silver particles active in ethylene epoxidation it was based on the disappearance, from the XPS spectra, of the O 1*s* line characteristic of the adsorbed oxygen.

The variations in the routes of NO decomposition and the CO + NO reaction with a decrease in the size of palladium particles supported on silica was explained by the effect of low-coordinated sites, with lower electron density on the NO adsorption.[103] The strengthening of the NO–Pd bond in such low-coordinated sites the existence of which was confirmed by comparison of infrared absorption spectra of CO molecules adsorbed on palladium particles and on (111) and (110) faces of palladium single crystals,[104,105] favours the dissociation of NO into nitrogen and oxygen atoms. In the absence of NO adsorbed as molecules on the surface of small palladium particles, N_2O cannot be formed as was demonstrated using the temperature-programmed reaction (TPR).

As mentioned above, the number of papers which attribute the changes in selectivity caused by a decrease in the size of metallic

nanoparticles to changes in the chemical nature of their surface adsorption in comparison with adsorption on bulk metals will unquestionably be increasing. The above-cited NMR studies of CO adsorption on palladium supported on SiO_2 represent a first step in this direction.[10] It was shown that two types of CO molecules on the surfaces of small palladium particles differ in the degree of mixing of their electronic levels with the electronic zones of the metal.

The correlation between the nature of the adsorbed molecules and the catalytic properties (in the first place, selectivities) of supported nickel and silver particles has been demonstrated.[30, 31, 106] The TPD spectra of hydrogen following its adsorption for 2 min on two catalysts of selective hydrogenation of butadiene differing in their Ni : C ratios are depicted in Fig. 3. The selectivity of butadiene hydrogenation to butene on a catalyst with a low carbon content (Ni : C ratio of 0.4) was 45%, whereas that on a catalyst with a higher carbon content (Ni : C ratio of 0.1) reached 95%.[30] As can be seen from Fig. 3, the more selective catalyst gives one TPD peak at 320 K, whereas the TPD spectrum of the less selective specimen contains a weakly expressed additional peak corresponding to more strongly bound hydrogen (at 360 K). These peaks were assigned based on the TPD data and work function measurements of hydrogen adsorption on specimens of bulk nickel (single crystals and foil) obtained in earlier studies.[107, 108] In experiments where hydrogen exposure varied, it was established that hydrogen in a high-temperature form is initially adsorbed on the nickel surface and the work function increases markedly. The TPD peak at 360 K was ascribed to the negatively charged hydrogen ions, H^-. The intensity of the high-temperature peak becomes constant with an increase in the hydrogen exposure, whereas the 320 K peak continues to increase gradually. The work function did not change in the studied range of coverage of the nickel surface with hydrogen, which points to the absence of a charge on the low-temperature form of hydrogen.[107] High reactivity of hydride ions is a possible reason for non-selective hydrogenation of butadiene on specimens with high Ni : C ratios (~ 0.4). The lack of this form in specimens with the Ni : C ratio of ≈ 0.1 (see Fig. 3) is the reason for increased selectivity. Unfortunately, these conclusions cannot be corroborated by XPS, since hydrogen does not generate a photoelectron spectrum.

This approach is quite useful in studies of different forms of oxygen adsorption on silver. The screening of O 1*s* signals from the adsorbed oxygen by the oxygen of the substrate (α-Al_2O_3) used in industrial catalysts of ethylene epoxidation was eliminated by replacing the latter with a model substrate (graphite).[106] The oxygen adsorbed on the surface of silver particles with the sizes of 10 nm produces one peak with $E_b = 530.5$ eV, while larger particles produce an additional peak with $E_b = 528.5$ eV. Comparison of these values with the E_b values for oxygen adsorbed on bulk silver specimens prompted a conclusion about the formation

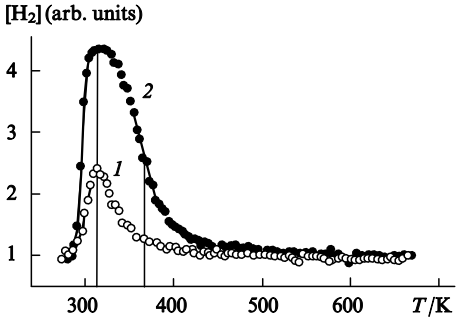

Figure 3. The TPD spectra of hydrogen after its 2-min adsorption at $P = 10$ Pa and $T = 270$ K on Ni–C catalysts with the Ni : C ratio of 0.1 (*1*) and 0.4 (*2*).

of two forms of oxygen adsorbed as atoms, *viz*., the peak with a lower binding energy is related to nucleophilic oxygen (O^{2-}), while the second peak is related to the electrophilic form ($O^{\delta-}$). It was shown [109, 110] that the formation of ethylene oxide requires the co-existence of these two forms of the adsorbed oxygen on the silver surface: the electrophilic oxygen participates in the formation of ethylene oxide directly by reacting with ethylene, while the nucleophilic oxygen serves as a source of surface Ag^+ ions (surface silver oxide), which are the sites of adsorption of ethylene molecules. The key step of the ethylene epoxidation can be presented as follows:

$$O^{\delta-}_{ads} + C_2H_{4\,ads}(Ag^+) \longrightarrow C_2H_4O.$$

With account taken of the sharp drop in the concentration of nucleophilic oxygen with a decrease in the size of the silver particles in the range of 50–20 nm, the mechanism proposed provides an explanation for the sharp decrease in the rate of epoxidation on silver catalysts with a particle size of less than 50 nm.[76] The reaction rate decreases as a result of less effective adsorption of ethylene on small particles which contain no Ag^+ sites. Since the nucleophilic oxygen is active exclusively in complete oxidation of ethylene, its disappearance due to a decrease in the size of the catalyst's nanoparticles will increase the selectivity of ethylene oxide formation. This suggestion has been confirmed experimentally by Verykios *et al.*[111] who have observed a continuous increase in the selectivity with a decrease in the size of silver particles from 50 to 20 nm. These data and the results of other investigations [109, 110] suggest that this size range is an optimum for particles of highly reactive and highly selective silver catalysts for ethylene epoxidation.

Studies of the dependence of selectivities of chemical reactions on the average sizes of coated nanoparticles of the active components revealed both positive and negative effects and, in some cases, their independence of the particle size (see, *e.g.*, Refs 112–114). We shall consider only the results of several experiments which are promising for use in practical catalysis.

The dependence of selectivities of the synthesis of higher hydrocarbons from CO and H_2 on Co–MgO and Co–ZnO catalysts on the sizes of coated cobalt particles was established.[115] The smaller the average sizes of cobalt nanoparticles, the higher the selectivity expressed by the Anderson–Schulz–Flory distribution coefficient (α). It was suggested that the amount of dissolved hydrogen responsible for complete hydrogenation of hydrocarbon intermediates decreases with a decrease in the particle size, eventually resulting in the formation of heavier hydrocarbons. The selectivity of hydrodesulfurisation of thiophene increased with a decrease in the sizes of ruthenium nanoparticles supported on alumina.[116] Comparison of Co/Al_2O_3 catalysts accelerating steam conversion of ethanol and prepared from different Co-containing precursors revealed that the selectivity of this reaction decreases in the following order: Co (carbonyl) > Co (chloride) > Co (acetate) > Co (nitrate).[117] Since the sizes of metal particles increase in the reverse order, the observed decrease in selectivity was attributed to the enlargement of cobalt nanoparticles. And, finally, it was found [118] that the selectivity of n-pentane hydrogenolysis on Pt/Y-zeolite catalysts increases linearly with decrease in the size of the metallic nanoparticles.

Even these few examples illustrate the remarkable effects of the average sizes of active metal nanoparticles on the relative rates of individual steps of multiroute catalytic reactions which influences the selectivities of formation of the reaction products. The catalytic activities manifested by nanosystems in reactions in which bulk specimens or even supported large crystallites are virtually inactive corroborate this statement. Gold nanoparticles which, in contrast with the bulk metal, manifest catalytic activity in certain reactions including those promising for industrial use, provide an illustrative example. In the 1980's, Japanese investigators succeeded in demonstrating that Au nanoparticles supported on Fe_2O_3 or Co_3O_4 represent active catalysts for low-temperature oxidation of CO.[119] This finding has stimulated the

appearance of numerous publications devoted to the analysis of the catalytic properties of these systems. The dependence of their catalytic properties on the nature of the substrate, size of gold particles and further treatment of freshly prepared specimens was studied.[120–125] It was shown that the size of gold nanoparticles is the key factor which determines the activity of a catalyst in CO oxidation; this activity changes 2–3-fold with different substrates (TiO_2, Al_2O_3, SiO_2), whereas the reaction rate increased by one and even two orders of magnitude with a decrease in the gold particle sizes below 4 nm.[120–122] The maximum catalytic activity was observed in particles with a size of 3.2 nm.[123] It is of note that gold-containing catalysts manifest high activity even at low temperatures (250–270 K), whereas such a catalytically active metal as platinum is inactive at these temperatures due to the blocking of its surface by adsorbed CO molecules.[126]

The range of reactions catalysed by gold nanoparticles appeared to be rather broad. It was demonstrated that impregnated Au/SiO_2 and Au/Al_2O_3 catalysts manifest high selectivities in the hydrogenation of buta-1,3-diene to butene.[127] The selectivity of hydrogenation of diene mixtures into alkenes on Au/ZrO_2 catalysts reached 100%.[128] Studies into hydrogenation of CO_2 on Cu-, Ag- and Au-containing catalysts supported on ZrO_2 revealed that these metals are catalytically active in methanol synthesis.[129] Gold nanoparticles used as catalysts for low-temperature reduction of NO with propene have certain advantages.[130] Unlike Rh-,[131] Pt-[132] and Pd-containing[133] catalysts with which N_2 is formed instead of N_2O at temperatures above 570 K, the formation of nitrogen on Au/Al_2O_3 proceeds efficiently even at 370 K.

The use of gold nanoparticles as catalysts of propene epoxidation provides a more interesting example. The gas-phase oxidation of propene by an oxygen–hydrogen mixture on Au/TiO_2 catalysts ensures nearly 100% selectivity of propene oxide formation at a 1% conversion of C_3H_6.[134] A detailed study of various factors revealed that the selectivity of this reaction depends critically both on the nature of the substrate and the size of gold nanoparticles. If the particle size is less than 2 nm, the reaction performed on gold catalysts changes its route in such a way that propane is formed with nearly 100% selectivity.[135] This finding is in good agreement with the high activity of the low-percentage Au/SiO_2 catalyst in the hydrogenation of alkenes.[136] It may thus be concluded that gold nanoparticles with sizes ranging from 2 to 4 nm catalyse propene epoxidation, whereas smaller particles catalyse its hydrogenation. It was found that the selectivity of formation of some industrially important products increases considerably with a decrease in the particle size.[137,138] For example, Pt_n clusters within the structure of the zeolite LTL provided a nearly 100% selectivity of dehydrogenation of n-hexane to benzene.[137]

A vast variety of physical instrumental methods, such as molecular beam technique, low energy electron diffraction, electronic Auger spectroscopy, photoelectron X-ray spectroscopy, vacuum tunnelling microscopy, nuclear magnetic resonance, electron spin resonance, Raman spectroscopy, calorimetry, TPR, TPD, infrared spectroscopy, EXAFS, Mössbauer spectroscopy, *etc*., came into use in the last decades of the XXth century for studying surfaces of heterogeneous catalysts at the molecular level. However, despite the high precision achieved in the techniques for measuring and the control of the state of the catalytic surfaces, the 'cognitive' potential of the experimental results is rather limited because these measurements are usually indirect and the information derived from them demands quantitative processing and interpretation. This can be done only with the use of mathematical models. It is clear that successful interpretation of the results obtained requires that the mathematical models and the methods employed for their analysis provide an accurate description of the whole body of experimental results.[139–146]

The lattice gas model is an example. The main difference between ordinary and lattice gases is that in the former case a particle can have any coordinates, whereas molecules of lattice gases occupy definite positions in space, *viz*., those in the knots of a certain regular lattice where elementary processes can occur. These processes are described either by computational methods conventionally used in statistical physics (*e.g*., the Monte-Carlo and cellular automaton methods) or by using cluster approximations, which allow simple estimation of thermodynamic parameters of a system and the rates of elementary surface acts based on the classical transition state theory developed by M I Temkin for heterogeneous catalysis.

Sequential implementation of a series of elementary steps results in changes in the state of the lattice cells and the evolution of the system. The Monte-Carlo method considers evolution as a random Markovian chain of elementary events occurring in the lattice cells. The cellular automaton approach also represents an effective tool for simulating the dynamics of elaborate spatially distributed systems based on the analysis of their local behaviour. To obvious disadvantages of stochastic methods, one can relate the large body of calculations, whereas their main advantage is the possibility of precise control over the position of a particle on the surface of a catalyst. The deterministic approach entails the solution of systems of nonlinear differential equations derived from the main kinetic equation using certain approximations.

The energy of lateral interactions of the adsorbed species involved in reactions and their mobilities are the main parameters which characterise their surface layer. The latter represents an open, non-ideal, non-linear system which exchanges mass and energy with the environment. The use of the non-linear dynamics method made it possible to gain considerable experience in mathematical simulation of catalytic systems starting at the molecular level.[143–146] Non-linear events, such as self-organisation, the appearance of chemical turbulence, *etc*., have also been studied. However, the attempts to simulate the effects of the particle size on such events have not been undertaken yet.

IV. The prospects for the application of nanostructures in catalytic processes

1. Ligand-stabilised transition metal clusters

The catalytic properties of supported particles can differ essentially from those of bulk metals; therefore, new routes of catalytic processes should not be ruled out. It can thus be assumed that the advantages of nanostructures prepared by conventional methods as highly selective catalysts cannot always be realised due to the broad size distribution of particles and their sintering in the course of the catalyst's operation. In supported metallic catalysts obtained by industrial synthesis, which includes impregnation of substrate granules with solutions of active metal compounds followed by calcination and/or reduction, strong interactions between metallic nanoparticles and the substrate surface are usually absent, which results in the statistical distribution of particles according to their sizes and also facilitates their sintering.

There are several ways to solve this problem, namely, modification of the support aimed at generating a sufficient number of centres for nucleation of metallic particles,[147] the choice of materials (a substrate and an active component) providing the epitaxial growth of nanoparticles owing to the structural matching of parameters of crystal lattices,[148] the use of novel substrates with an original geometry of the pore volume,[149] *etc*. The size homogeneity of nanostructures can be achieved through the use of ligand-stabilised metallic clusters.[150,151] Isolated transition metal nanoclusters which are the most commonly used as active components of supported metal catalysts, are prepared by the following techniques: (1) reduction of transition metal salts; (2) reduction and removal of ligands from organometallic compounds; (3) electrochemical synthesis.[151] Studies into the kinetics of growth of nanoclusters revealed that clusters containing the so-called magic number of atoms are characterised by regular geometry of the outer surface and manifest enhanced stabilities. The other name of these clusters, *viz*., 'full-shell clusters', reflects the presence of fully packed layers surrounding the central metal atom. The number of

the metal atoms (N) in the nth-layer is determined by the equation:[151]

$$N = 10n^2 + 2 \ (n > 0). \quad (3)$$

Thus, full-shell clusters contain 13 (1 + 12); 55 (13 + 42); 147 (55 + 92); 309 (147 + 162), *etc*., atoms (see Section II.I). The enhanced stabilities of these clusters stem from their closely packed structures which ensure the formation of the maximum number of metal–metal bonds and, as a consequence, the minimum surface energy.

An excellent survey of growth mechanisms of nanoclusters has been given in reviews.[152–154] It was shown that the formation of iridium nanoclusters stabilised by the $P_2W_{15}Nb_3O_{62}^{9-}$ polyoxoanion follows an autocatalytic surface growth mechanism, which provides an explanation for the formation of isolated full-shell clusters in a kinetically controlled regime of synthesis. Experimental evidence for these conclusions can be derived from the formation of nearly monodisperse rhodium nanoclusters ($d = 4\pm0.6$ nm) in the reduction of polyoxoanionic Rh(I) complexes with hydrogen in acetone.[154]

The nature of nanoclusters stabilised by ligands entails the possibility of their additional stabilisation by electrostatic and steric interactions. Electrostatic or inorganic stabilisation is achieved by adsorption of ions on the electrophilic surface of a metal.[155] Such adsorption results in the appearance, on the surface of nanoclusters, of a double electrical layer which provides Coulombic repulsion of like-charged individual species. Steric or organic stabilisation is provided by the surrounding of the metal centre of the nanocluster with a layer of bulky structures,[155] such as polymeric units[156] or surfactants.[157] The geometric sizes of these adsorbates favour the formation of a steric barrier which prevents the contacts between the metal centres of nanoclusters. It is evident that some of the stabilising agents, *e.g*., polyoxoanions, combine electrostatic and steric functions.[151, 158] Stabilisation of nanoclusters with ligands presents substantial interest as regards the synthesis of supported catalysts characterised by enhanced stabilities and homogeneous size distribution of metal particles. In addition, this makes the use of metallic nanoclusters promising for homogeneous catalysis, as will be shown below.

The catalytic properties of metallic nanoclusters have been studied by several groups of investigators (for a review see Ref. 151). In 1981, Schmid *et al*.[159] succeeded in synthesising a cluster with the composition $Au_{55}(PPh_3)_{12}Cl_6$ by passing B_2H_6 through a solution of PPh_3AuCl in benzene. Later, $Rh_{55}(PPh_3)_{12}Cl_6$, $Ru_{55}(PBu^t_3)_{12}Cl_{20}$, $Pt_{55}(AsBu^t_3)_{12}Cl_{20}$ clusters were synthesised using diborane as the reductant.[160, 161] Substitution of hydrogen for diborane made possible the synthesis of $Pt_{\sim309}phen_{\sim36}O_{\sim30\pm10}$ and $Pt_{\sim561}phen_{\sim36}O_{\sim190-200}$ clusters.[162, 163] As can be seen, all these clusters are 'magic' ones, which provides additional evidence in favour of enhanced stabilities of the full-shell nanostructures cited above. First attempts at using Ru clusters as catalysts in homogeneous hydrogenation reactions were unsuccessful because of their rapid decomposition.[163] Therefore, further efforts of this research group were directed to the use of nanoclusters for the synthesis of supported heterogeneous catalysts. It was shown that palladium clusters with sizes of 3–4 nm stabilised by ligands manifest high activities and selectivities in the hydrogenation of hex-2-yne into *cis*-hex-2-ene. It was shown that the activity of a catalytic system depends on the nature of the stabilising ligands, while the selectivity is always equal to 100%. Rhodium and palladium nanoclusters supported on TiO_2 and Al_2O_3 appeared to be highly efficient catalysts of hydroformylation[164] and hydrogenation[165] reactions.

Unlike the authors of the above-cited papers, in the early 1980's Vargaftik, Moiseev *et al*.[166] carried out a successful synthesis of ligand-stabilised clusters which are active and stable in homogeneous catalysis. The $Pd_{\sim561}phen_{\sim60}(OAc)_{\sim180}$ and $Pd_{\sim561}phen_{\sim60}O_{\sim60}(PF_6)_{\sim60}$ clusters catalysed oxidative acetoxylation of a series of light organic compounds, *e.g*., of ethylene into vinyl acetate, of propene into allyl acetate and of toluene into benzyl acetate, with 95%–98% selectivity. Moreover, these catalysts effected the oxidation of primary alcohols into ethers and aldehydes and of secondary alcohols into ketones.[166] Yet another example of a successful application of metallic nanoclusters in homogeneous catalysis is the use of rhodium clusters stabilised by polyoxoanions, which manifested high selectivities in the hydrogenation of cyclohexene.[154] This was ascribed to the double stabilisation (both electrostatic and steric) of the clusters by polyoxoanions.[167]

Notwithstanding, the majority of successful applications of metallic nanoclusters as catalysts is connected with the use of systems fixed or immobilised on the surface of porous and non-porous supports, *e.g*., SiO_2, Al_2O_3 or TiO_2. It was shown, in particular, that 5% colloidal rhodium supported on activated charcoal with a narrow size distribution of clusters (1.2–2.2 nm) was nearly 3 times more active in the hydrogenation of butyronitrile than the corresponding industrial catalyst which also contains 5% Rh on activated charcoal with a greater scatter of particle sizes (1–5 nm).[168] In catalysts stabilised by ligands, the size of rhodium particles varies from 1.2 to 2.0 nm, whereas standard catalysts contain predominantly large crystallites, while the fraction of small particles (1–5 nm) is small. A representative list of reactions which are efficiently catalysed by clusters stabilised by ligands is given in a review.[151] This list includes various reactions of enantioselective hydrogenation,[169] hydrosilylation,[170] hydropyrolysis and hydrogenolysis,[171] CO and CO + H_2 oxidation,[172] cycloaddition reactions,[173] *etc*.

This can be supplemented with examples of enhanced stabilities of catalysts based on clusters stabilised by ligands under conditions of a catalytic reaction. Thus the 'lifetime' of a catalyst containing palladium nanoclusters in the reaction of cyclooctene hydrogenation was 96 000 turnovers, whereas that of an industrial catalyst (*e.g*., palladium on activated charcoal) was 38 000 turnovers.[168] The $Ir_{\sim300}$ nanoclusters did not change their activities after 3200 ± 1000 hydrogenation turnovers, which is comparable with the corresponding value (3950 ± 1000 turnovers) for the industrial catalyst (7.9% Ir/γ-Al_2O_3) and markedly exceeds the 'lifetime' of Ir/η-Al_2O_3 ('Exxon', USA) equal to 1740 ± 250 turnovers.

Ligand-stabilised metallic clusters are extremely interesting subjects for the development of fundamental concepts of catalysis by nanostructures, since it allows one to control precisely the size distribution of nanoparticles, to establish relationships between their sizes and catalytic properties and even to govern the activities and selectivities of catalysts based on them. However, the high cost of such catalysts in comparison with ordinary specimens is an obstacle to their wide industrial application. Only electrochemical synthesis makes it possible to prepare relatively large (*e.g*., hundreds of milligrams) amounts of catalysts based on metal clusters stabilised by ligands. Therefore, industrial applications of such nanoclusters in large-scale catalytic processes is hardly probable. However, their use in fine organic syntheses where high selectivity of formation of the target product is the main requirement imposed on a catalyst can be of considerable practical interest. It is anticipated that the attainment of 100% selectivity will become one of the main challenges to catalytic science in the next few decades.[174] This can be exemplified by successful recent applications of clusters stabilised by ligands in various hydrogenation reactions including enantioselective hydrogenation.[175, 176]

2. Bimetallic clusters: molecular design of active centres

Studies into bimetallic systems have the same long history as studies of individual metals. This is primarily due to the search for the ways of increasing the activities, selectivities and stabilities of monometallic catalysts. The first patents which suggested the use of Pd–Au catalysts for hydrocarbon conversions instead of palladium ones appeared in the 1960's.[177] In the past years, the number of investigations (including those having industrial applications) which demonstrate the advantages of bimetallic catalysts

over monometallic ones has increased manifold.[178–184] Most of these studies dealt with the dependences of catalytic activities related to the surface metal atoms and their selectivities on the ratios of metals. For example, the maximum activity of Pt–Re/SiO_2 catalysts containing 75% rhenium exceeds those of individual platinum and rhenium supported on SiO_2 by more than two orders of magnitude.[180] Rubidium, palladium or platinum additives increased the activities of nickel-containing zeolites in butyronitrile hydrogenation in both gas and liquid phases.[181] The steady-state activity of Pd–Re/Al_2O_3 catalysts in the hydrogenolysis of 2,2-dimethylpropane passes through an obvious maximum at a rhenium content of 50 at.%.[182] Examples of enhanced selectivity in the formation of various products through multiroute catalytic reactions are even more impressive. The above-cited patent[177] claims that the selectivity of n-heptane isomerisation increases from 66.9% to 81.3% with a change in the Pd : Au ratio of Pd–Au/Al_2O_3 catalysts from 6 : 1 to 1 : 2 (mass %). The selectivity of monometallic palladium and gold catalysts is equal to 50% and ~ 25%, respectively. The selectivity of 1% Ru/SiO_2, which is a catalyst of cyclohexane dehydrogenation to benzene, increases, following introduction of inactive copper and silver (1 mass %), from 76% to 94% and 87.9%, respectively.[183] The enhanced selectivity of nitrogen formation and decreased yields of ammonia were observed in the reduction of NO with hydrogen with an increase in the rhenium content in bimetallic Pt–Re/SiO_2 catalysts.[184] Modification of platinum nanoparticles on silica with tungsten made it possible to reach 99.2% selectivity of methanol formation in the reaction of CO_2 with hydrogen, the conversion being 2.6%.[185] It is of note that platinum alone catalyses the formation of CO with nearly 100% selectivity, whereas tungsten is inactive in this reaction. It was shown[181] that all M–Cu/NaY catalysts (M = Ru, Rh, Pd, Pt) manifest high selectivities in the formation of tertiary amines from acetonitrile.

The unusual properties of bimetallic catalysts gave impetus to the studies of their surface using model systems and sensitive physical methods. The experimental results have been generalised in the reviews.[186, 187] It was found that the introduction of a second metal influences the catalytic properties of the first metal through the following mechanisms:

(1) by changing the electronic properties of the first metal atoms (as has been shown previously, the electronic properties of metals influence the nature and reactivities of adsorbed particles);

(2) by changing the number of identical atoms within the structure of the adsorption centre (as is known, adsorption of molecules from the gas phase often requires a combination of specifically arranged atoms rather than a single 'landing' site).

In the first case, we deal with an electronic (ligand-associated) effect, whereas in the second case the multiplet ensemble effect is manifested.[178, 186, 187] With regard to real catalysts, this is, most probably, artificial, therefore, the existence of such effects has been demonstrated using only model systems.

Direct evidence for the electronic effect was obtained in experiments with adsorption of simple gases on the surface of a metal single crystal covered with a monolayer of atoms of another metal. Concrete systems for such experiments were selected on the basis of structural matching of this monolayer and the plane of a metal substrate.[188–191] For example, a palladium monolayer was deposited onto the (110) face of tungsten the hexagonal structure of which ensured a practically complete coincidence of Pd–Pd distances in the monolayer (0.2740 nm) and onto the (111) face of the bulk Pd single crystal (0.2751 nm).[188] The activation energy of desorption of CO molecules from the surface of Pd/W(110) appeared to be by 85 kJ mol^{-1} smaller than that from the surface of the Pd(111) single crystal. In addition, the preexponential factor in the equation of CO desorption rate increased by five orders of magnitude. Combined use of both factors caused a decrease in the desorption temperature from 510 K on Pd(111) to 330 K on the monolayer of Pd/W(110) in the case of a low degree of coverage by CO. A similar effect was observed when palladium was deposited onto the surface of the Re(0001) hexagonal face.[189] An analysis of UV photoelectron spectra of the palladium monolayer on the (110) faces of tantalum[190] or niobium[191] revealed that the densities of filled electronic states of palladium near the Fermi levels in these systems are significantly decreased in comparison with that on Pd(111). As a result, the electronic structure of the surface layer of palladium becomes similar to that of the Group IA metals characterised by weak chemosorption bonds with CO. This can be explained by the formation of covalent bonds between palladium and niobium due to rehybridisation of *d*- and *sp*-orbitals, although a small charge transfer can also take place. Alloys with high negative enthalpies of formation are related to the systems in which the electronic effect plays a crucial role.[187]

Depending on the strength of the interaction between the main and incorporated metals, the ensemble effects are conventionally divided into simple and mixed ones.[186, 187] Simple effects are largely manifested in systems where a reactive metal is mixed with an inert one. For example, the multibound state of CO on platinum and nickel is not realised following their fusion with copper.[192, 193] The triply bound form of NO which predominates on the (111) face of platinum is not detected on the surface of the (3×3)-$SnPt_2$/Pt(111) alloy where triatomic platinum multiplets are completely absent.[194] Decisive evidence for the existence of a mixed ensemble effect was obtained in the study of a copper monolayer deposited onto the (111) face of nickel single crystals.[195, 196] Despite the higher strength of binding of the bridge-like form of CO to the nickel surface in comparison with the linear form, the latter was exclusively formed at low coverage of carbon monoxide. This was inferred from the results of high-resolution electron energy loss spectroscopy (HREELS) which point to the absence of Ni—Ni couples on the surface of this bimetallic system. However, a bridge-like form was also detected at higher degrees of CO coating, which is due to the presence of Ni—Cu couples.[196]

The mutual effects of individual components are characteristic of many bimetallic systems. Therefore, several attempts have been undertaken to use these regularities for the directed synthesis of bimetallic catalysts with predetermined properties. Thus Besenbacher *et al.*[197] proposed to introduce atoms of gold into a nickel-containing catalyst of the steam conversion of methane in order to reduce the rate of its coking. The choice of gold was based on the results of fundamental investigations of single crystals and porous specimens of the catalyst using physical methods and quantum-chemical calculations of activation energies of the abstraction of the first hydrogen atom from the methane molecule and carbon atom adsorption on pure and modified nickel surfaces. The conditions for gold introduction were also established. This resulted in the synthesis of an Au—Ni bimetallic catalyst, which, in contrast to the nickel catalyst, preserved its activity in n-butane conversion due to the absence of graphite deposits on its surface.

The most remarkable achievements in the design of bimetallic catalysts can be expected from the use of nanoclusters which allows molecular design of active centres. There exist several synthetic routes which ensure control over the composition and properties of the nanostructures formed,[198] *viz.*, combined or sequential reduction of metal salts, electrochemical synthesis and reduction of double complexes. Studies of synthetic nanoclusters by physical methods aimed at elucidating their structures acquires special importance, since in addition to the crystal structure of the bulk alloy, bimetallic nanoclusters contain unusual structures which have no analogues among bulk materials. These include two types of structures, *viz.*, 'core–shell' and 'cluster-in-cluster' types.

Core–shell structures were detected in Pd—Pt clusters stabilised by poly(*N*-vinyl-2-pyrrolidone) (PVP) with a Pd : Pt ratio of 4 : 1; they were prepared by the reduction of a H_2PtCl_6—$PdCl_2$ mixture.[199–201] Elucidation of exact structures of these nanoclusters required the use of a combination of methods, *e.g.*, X-ray phase analysis, TEM, XPS, UV-visible absorption spectroscopy (UV-Vis) and EXAFS. Analysis of the UV-Vis spectra and X-ray diffractograms confirmed the formation of bimetallic nanoclus-

ters. Using the TEM approach, it was shown that the Pd–Pt clusters formed are homogenous according to their sizes (the mean size was 1.5 nm) and belong to 'magic' clusters with $N = 55$.[169] A conclusion about the saturation of the nanocluster surface with palladium was inferred from the quantitative XPS data.[202] And, finally, the coordination numbers for palladium and platinum were determined using EXAFS. Comparison of experimental results with the values calculated for two models, *viz*., a model with inner platinum nuclei and a statistical distribution model, revealed that the former best fits the experimental results.[199] The experimental data altogether allowed one to propose a structural model of a Pd–Pt nanocluster in which a monolayer of 42 palladium atoms covers a nucleus consisting of 13 platinum atoms.[198] Later, bimetallic nanoclusters containing core–shell structures could successfully be obtained by stabilisation of Pd–Au, Pt–Au and Rh–Pt systems by polyvinylpyrrolidone.[203, 204]

In bimetallic nanosystems of the 'cluster-in-cluster' type, the atoms of one component form a cluster, whereas the atoms of the other component cover only some of its planes (not necessarily as a monolayer) to form an intertwining structure. The fact that such structures are formed in Pd–Au clusters with a change in the Pd : Au ratio from 4 : 1 to 1 : 1,[203] implies that it can represent a modified structure with an inner nucleus. Additional evidence in favour of this suggestion can be derived from the transformation of Pd–Pt nanoclusters with inner nuclei into 'cluster-in-cluster' structures in their application onto inorganic materials.[205] Without going into details about the similarities and differences of these two structures, it should be noted that the surface of nanoclusters of the 'cluster-in-cluster' type contains some centres which consist of two kinds of atoms, *i.e*., the ensemble effect is possible, whereas only the electronic (ligand) effect is *a priori* possible in structures with inner nuclei.

It is the ligand effect that is responsible for the enhanced catalytic activities of PVP-stabilised Pd–Pt clusters in the hydrogenation of cycloocta-1,3-diene into cyclooctene. Indeed, the maximum increase in activity (more than twofold in comparison with pure palladium) was observed for the Pd : Pt ratio of 4 : 1,[200] *i.e*., under conditions where palladium atoms completely covered the inner platinum nucleus. A similar dependence was observed in the case of Pd–Au nanoclusters.[203] The fourfold increase in the catalyst's activity in comparison with those of individual components was observed in the hydrogenation of cyclopentadiene into cyclopentene on Pd–Rh nanoclusters.[198]

Yet another example of the ensemble effect is the reaction of selective hydration of acrylonitrile to acrylamide:

$$CH_2=CH-CN + H_2O \longrightarrow CH_2=CH-CONH_2$$

on bimetallic Cu–Pd nanoclusters stabilised by PVP.[206] It was found that this reaction occurs on two adjacent palladium and copper atoms: the coordination of the C=C bond takes place on the palladium atom, which brings the C≡N bond close to the adjacent copper atom which effects hydration. This results in the enhancement of activity and nearly 100% selectivity of the amide synthesis. It was shown also that the supported Pd–Mo/SiO_2 catalyst based on a bimetallic precursor manifests higher activity in the CO + NO + O_2 reaction than analogous specimens synthesised from individual organometallic complexes.[207]

V. Conclusion

The fundamental knowledge of catalytic properties of nanosystems at the molecular level and practical application of their peculiarities largely determine progress in industrial catalysis and, correspondingly, the economic potential of certain branches of the chemical industry and the environmental situation.

The unique microstructures of nanosystems in comparison with ordinary metals and chemical compounds confer novel properties on them. The characteristic features of nano- and microgeometry of nanosystems and their high specific surfaces open up new opportunities for the design of highly selective and highly reactive perfect catalysts. Some of these features can be synergistic, *e.g*., in bimetallic clusters where one component influences the properties of the adjacent component. Detailed investigations into such interactions will allow the synthesis of novel selective catalysts with predetermined properties. It is the selectivity that is the key problem in the theory and practice of catalysis. And if the problems of sizes and compositions of nanoclusters which ensure their optimum selectivity, detailed electronic structures of cluster complexes, *etc*., are solved, surface reactivity will be put under control.

Nanosystems are a 'natural bridge' between homogeneous and heterogeneous catalysis. Many metals, especially Group VIII metals, which manifest the highest activity as heterogeneous catalysts form numerous cluster compounds endowed with unique catalytic properties. The chemistry of these elements has been studied in sufficiently great detail and the dependence of physicochemical properties of the corresponding clusters on their sizes has been established. However, in more general terms the state-of-the-art in the studies of catalytic activities of nanosystems can be characterised as 'abundance without order'. The main task for the next few years is to combine experimental studies aimed at the construction of new active catalysts based on nanosystems with theoretical (including quantum-mechanical) calculations and more extensive use of physical (both instrumental and diagnostic) methods as well as kinetic studies and mathematical simulation.

This review has been written with the financial support of the Russian Foundation for Basic Research (Project Nos 96-03-33891 and 00-15-99-335).

References

1. W L Winterbottom *Acta Metall.* **15** 303 (1967)
2. T Wang, C Lee, L D Schmidt *Surf. Sci.* **163** 181 (1985)
3. M Drechsler *Surf. Sci.* **162** 755 (1985)
4. M Drechsler, J M Dominguez *Surf. Sci.* **217** L406 (1989)
5. K Hayek, M Fuchs, B Klotzer, W Reichl, G Rupprechter *Top. Catal.* **13** 55 (2000)
6. A Piednoir, E Perrot, S Granjeaud, A Humbert, C Chapon, C R Henry *Surf. Sci.* **391** 19 (1997)
7. X Lai, T P St Clair, M Valden, D W Goodman *Prog. Surf. Sci.* **59** 25 (1998)
8. K H Hansen, T Worren, S Stempel, E Lœgsgaard, M Bäumer, H-J Freund, F Besenbacher, I Stensgaard *Phys. Rev. Lett.* **83** 4120 (1999)
9. M Bäumer, H-J Freund *Prog. Surf. Sci.* **61** 127 (1999)
10. K W Zilm, L Bonneviot, G L Haller, O H Han, M Kermarec *J. Phys. Chem.* **94** 8495 (1990)
11. X Xu, J Szanyi, Q Xu, D W Goodman *Catal. Today* **21** 57 (1994)
12. D W Goodman *Surf. Sci.* **299**/**300** 837 (1994)
13. C Backx, C P M de Groot, P Biloen, W M H Sachtler *Surf. Sci.* **128** 81 (1981)
14. C T Campbell *Surf. Sci.* **143** 517 (1984)
15. C T Campbell *Surf. Sci.* **157** 43 (1985)
16. R Kubo *J. Phys. Soc. Jpn.* **17** 975 (1962)
17. W F Egelhoff, G G Tibbetts *Solid State Commun.* **29** 53 (1979)
18. M K Bahl, S C Tsai, Y W Chung *Phys. Rev. B, Condens. Matter* **21** 1344 (1980)
19. M G Mason *Phys. Rev. B, Condens. Matter* **27** 748 (1983)
20. M G Mason, in *Cluster Model for Surface and Bulk Phenomena* (New York: Plenum, 1992)
21. V Vijayakrishnan, A Chainani, D D Sarma, C N R Rao *J. Phys. Chem.* **96** 8679 (1992)
22. C N R Rao, V Vijayakrishnan, H N Aiyer, G U Kulkarni, G N Subbanna *J. Phys. Chem.* **97** 11 157 (1993)
23. T L Barr *J. Vac. Sci. Technol. A, Vac. Surf. Films* **7** 1677 (1989)
24. T L Barr *Crit. Rev. Anal. Chem.* **22** 229 (1991)
25. J E Lennard-Jones, R T Goodwin *Proc. R. Soc. London A, Math. Phys. Sci.* **163** 101 (1937)
26. D M Newns *Surf. Sci.* **171** 600 (1986)

27. J-P Ansermet, P-K Wang, C P Slichter, J H Sinfelt *Phys. Rev. B, Condens. Matter* **37** 1417 (1988)
28. S L Rudas, J-P Ansermet, P-K Wang, C P Slichter, J H Sinfelt *Phys. Rev. Lett.* **54** 71 (1985)
29. C D Wagner, in *Practical Surface Analysis* (Eds D Briggs, M P Seach) (New York: Wiley, 1990) p. 595
30. V V Molchanov, V V Chesnokov, R A Buyanov, N A Zaitseva, V N Zaikovskii, L M Plyasova, V N Bukhtiyarov, I P Prosvirin, B N Novgorodov *Kinet. Katal.* **39** 416 (1998) [a]
31. V I Bukhtiyarov, I P Prosvirin, R I Kvon *J. Electron. Spectrosc. Relat. Phenom.* **77** 7 (1996)
32. V I Bukhtiyarov, I P Prosvirin, R I Kvon, S N Goncharova, B S Balzhinimaev *J. Chem. Soc., Faraday Trans.* **93** 2323 (1997)
33. S V Tsybulya, G N Kryukova, S N Goncharova, A N Shmakov, B S Balzhinimaev *J. Catal.* **154** 194 (1995)
34. V M Mastikhin, S N Goncharova, V M Tapilin, V V Terskikh, B S Balzhinimaev *J. Mol. Catal. A, Chem.* **96** 175 (1995)
35. J K Plischke, A J Benesi, M A Vannice *J. Phys. Chem.* **96** 3799 (1992)
36. L V Nosova, M V Stenin, Yu N Nogin, Yu A Ryndin *Appl. Surf. Sci.* **55** 43 (1992)
37. Y Takasu, N Ohashi, X-G Zhang, Y Murakami, H Minagawa, S Sato, K Yahikozawa *Electrochim. Acta* **41** 2595 (1996)
38. M Valden, X Lai, D W Goodman *Science* **281** 1647 (1998)
39. M Che, C O Bennett *Adv. Catal.* **36** 55 (1989)
40. A F Carley, M K Rajumon, M W Roberts *J. Solid State Chem.* **106** 156 (1993)
41. G K Wertheim *Z. Phys. B, Condens. Matter* **66** 53 (1987)
42. G K Wertheim, S B Dicenzo, D N E Buchnan *Phys. Rev. B, Condens. Matter.* **33** 5384 (1986)
43. J J Burton *Catal. Rev. Sci. Eng.* **9** 209 (1974)
44. A A Balandin *Zh. Rus. Fiz.-Khim. O-va* **61** 909 (1929)
45. J Siera, F Rutten, B E Nieuwenhuys *Catal. Today* **10** 353 (1991)
46. M Grunze, in *Fundamental Studies of Heterogeneous Catalysis. The Chemical Physics of Solid Surfaces and Heterogeneous Catalysis* Vol. 4 (Amsterdam: Elsevier, 1982) p. 27
47. F Zaera, J Liu, G Xu, H Kuiper, J Segner *J. Chem. Phys.* **106** 4204 (1997)
48. G L Kellogg *Phys. Rev. Lett.* **55** 2168 (1985)
49. G L Kellogg *Surf. Sci.* **290** 295 (1993)
50. M Eiswirth, G Ertl *Surf. Sci.* **177** 90 (1986)
51. M Sander, R Imbihl, G Ertl *J. Chem. Phys.* **97** 5193 (1992)
52. K Kischer, M Eiswirth, G Ertl *J. Chem. Phys.* **96** 9161 (1992)
53. K Kischer, M Eiswirth, G Ertl *J. Chem. Phys.* **97** 307 (1992)
54. M M Slinko, N I Jaeger *Oscillating Heterogeneous Catalytic Systems* Vol. 86 (Amsterdam: Elsevier, 1994) p. 393
55. N Gottschalk, F Mertens, M Bar, M Eiswirth, R Imbihl *Phys. Rev. Lett.* **73** 3483 (1994)
56. F Mertens, N Cottschalk, M Bar, M Eiswirth, A Mikhailov *Phys. Rev. A, Gen. Phys., Ser. 3* **51** R5193 (1995)
57. F Mertens, R Imbihl *Surf. Sci.* **347** 355 (1996)
58. F Mertens, S Schwegmann, R Imbihl *J. Chem. Phys.* **106** 4319 (1997)
59. P W Murray, G Thornton, M Bowker, V R Dhanak, A Baraldi, R Rosei, M Kiskinova *Phys. Rev. Lett.* **71** 4369 (1993)
60. O M Poltorak *Lektsii po Teorii Geterogennogo Kataliza* (Lectures on the Theory of Heterogeneous Catalysis) (Moscow: Moscow State University, 1968)
61. N I Kobozev *Zh. Fiz. Khim.* **13** 1 (1939) [b]
62. G K Boreskov *Geterogennyi Kataliz v Khimicheskoi Promyshlennosti* (Heterogeneous Catalysis in Chemical Industry) (Moscow: Goskhimizdat, 1955) p. 5
63. V S Chesalova, G K Boreskov *Zh. Fiz. Khim.* **30** 2560 (1956) [b]
64. M Boudart, A Aldag, J E Benson, N A Dougharty, C Girvin *J. Catal.* **6** 92 (1966)
65. M Boudart *Adv. Catal.* **20** 153 (1969)
66. O M Poltorak, V S Boronin *Zh. Fiz. Khim.* **40** 2671 (1966) [b]
67. R van Hardeveld, F Hartog *Surf. Sci.* **15** 189 (1969)
68. R van Hardeveld, F Hartog *Adv. Catal.* **22** 75 (1972)
69. G C Bond, in *Proceedings of the 4th International Congress on Catalysis, Moscow, 1968* Vol. 2, p. 266
70. J F Hamilton, P C Logel *J. Catal.* **29** 253 (1973)
71. J F Hamilton, R C Baetzold *Science* **205** 1213 (1979)
72. G C Bond *Surf. Sci.* **156** 966 (1985)
73. V Ponec *Adv. Catal.* **32** 149 (1983)
74. R Burch *Catalysis* **7** 149 (1985)
75. *Proceedings of International Symposium on the Physics and Chemistry of Finite Systems: from Clusters to Crystals, Richmond, 1991* 105 p.
76. S N Goncharova, E A Paukshtis, B S Balzhinimaev *Appl. Catal.* **126** 67 (1995)
77. Z Xu, F-S Xiao, S K Purnell, O Alexeev, S Kawi, S E Deutsch, B C Gates *Nature (London)* **372** 346 (1994)
78. S Kawi, J-R Chang, B C Gates *J. Phys. Chem.* **98** 12 978 (1994)
79. S Ladas, H Poppa, M Boudart *Surf. Sci.* **102** 151 (1981)
80. F Rumpf, H Poppa, M Boudart *Langmuir* **4** 722 (1988)
81. M Herskowitz, R Holliday, M B Cutlip, C N Kenney *J. Catal.* **74** 408 (1982)
82. S H Oh, C C Eickel *J. Catal.* **128** 526 (1991)
83. T Engel, G Ertl *J. Chem. Phys.* **69** 1267 (1978)
84. T Engel, G Ertl *Adv. Catal.* **22** 2 (1979)
85. V I Savchenko *Usp. Khim.* **55** 462 (1986) [*Russ. Chem. Rev.* **55** 222 (1986)]
86. C T Campbell, S-K Shi, J M White *Appl. Surf. Sci.* **2** 382 (1979)
87. I Stara, V Matolin *Surf. Sci.* **313** 99 (1994)
88. E Gillet, S Channakhone, V Matolin, M Gillet *Surf. Sci.* **152**/**153** 603 (1985)
89. E I Altman, R J Gorte *Surf. Sci.* **172** 71 (1986)
90. D L Doering, H Poppa, J T Dickinson *J. Vac. Sci. Technol.* **20** 827 (1982)
91. E I Altman, R J Gorte *Surf. Sci.* **195** 392 (1988)
92. E I Altman, R J Gorte *J. Catal.* **113** 185 (1988)
93. B Tardy, C Noupa, C Leclercq, J C Bertolini, A Hoareau, M Treilleux, J P Faure, G Nihoul *J. Catal.* **129** 1 (1991)
94. P Briot, A Auroux, D Jones, M Primet *Appl. Catal.* **59** 141 (1990)
95. R W McCabe, L D Schmidt *Surf. Sci.* **66** 101 (1977)
96. P Hofman, S R Bare, D A King *Surf. Sci.* **117** 245 (1982)
97. C S Ko, R J Gorte *J. Catal.* **90** 59 (1984)
98. R J Baird, R C Ku, P Wynblatt *Surf. Sci.* **97** 346 (1980)
99. T W Root, L D Shmidt, G B Fisher *Surf. Sci.* **150** 173 (1985)
100. A K Santra, S Ghosh, C N R Rao *Langmuir* **10** 3937 (1994)
101. P Chou, M A Vannice *J. Catal.* **105** 342 (1987)
102. C N R Rao, V Vijayakrishnan, A K Santra, M W J Prins *Angew. Chem., Int. Ed. Engl.* **31** 1062 (1992)
103. X Xu, D W Goodman *Catal. Lett.* **24** 31 (1994)
104. W K Kuhn, J Szanyi, D W Goodman *Surf. Sci.* **274** L611 (1992)
105. A Ortega, F M Hoffman, A M Bradshaw *Surf. Sci.* **119** 79 (1982)
106. V I Bukhtiyarov, A F Carley, L A Dollard, M W Roberts *Surf. Sci.* **381** L605 (1997)
107. V I Savchenko, G K Boreskov *Kinet. Katal.* **9** 142 (1968) [a]
108. K Christmann, O Schober, G Ertl, M Neumann *J. Chem. Phys.* **60** 4528 (1974)
109. V I Bukhtiyarov, A I Boronin, I P Prosvirin, V I Savchenko *J. Catal.* **150** 262 (1994)
110. V I Bukhtiyarov, I P Prosvirin, R I Kvon *Surf. Sci.* **320** L47 (1994)
111. X E Verykios, F P Stein, R W Coughlin *J. Catal.* **66** 368 (1980)
112. T Mallat, S Frauchiger, P J Kooyman, M Schürch, A Baiker *Catal. Lett.* **63** 121 (1999)
113. A Feller, M Claeys, E van Steen *J. Catal.* **185** 120 (1999)
114. P Denton, A Giroir-Fendler, H Praliaud, M Primet *J. Catal.* **189** 410 (2000)
115. A A Khassin, T M Yurieva, V N Parmon *React. Kinet. Catal. Lett.* **64** 55 (1998)
116. M Nagai, K Koizumi, S Omi *Sekiyu Gakkaishi* **42** 12 (1999)
117. F Haga, T Nakajima, K Yamashita, S Mishima *Nippon Kagaku Kaishi* (11) 758 (1997)
118. D C Koningsberger, J de Graaf, B L Mojet, D E Ramaker, J T Miller *Appl. Catal. A* **191** 205 (2000)
119. M Haruta, N Yamada, T Kobayashi, S Iijima *J. Catal.* **115** 301 (1989)
120. F Boccuzzi, A C Chiorino, S Tsubota, M Haruta *Catal. Lett.* **29** 225 (1994)
121. M Haruta *Catal. Today* **36** 153 (1997)
122. M Okumura, S Nakamura, S Tsubota, T Nakamura, M Azuma, M Haruta *Catal. Lett.* **51** 53 (1998)
123. M Valden, S Pak, X Lai, D W Goodman *Catal. Lett.* **56** 7 (1998)
124. J-D Grunwaldt, C Kiener, C Wögerbauer, A Baiker *J. Catal.* **181** 223 (1999)
125. J -D Grunwaldt, M Maciejewski, O S Becker, P Fabrizioli, A Baiker *J. Catal.* **186** 458 (1999)

126. K Ruth, M Hayes, R Burch, S Tsubota, M Haruta *Appl. Catal. B* **24** L133 (2000)
127. P A Sermon, G C Bond *J. Chem. Soc., Faraday Trans. 1* **74** 385 (1978)
128. M Shibata, N Kawata, T Masumoto, M Kimura, in *Proceedings of Japanese-France Seminar on Catalysis, Tokyo, 1987* p. 98
129. A Baiker, M Kilo, M Maciejewski, S Menzi, A Wokaun, in *New Frontiers in Catalysis* (Amsterdam: Elsevier, 1993) p. 1257
130. A Ueda, M Haruta *Appl. Catal. B* **18** 115 (1998)
131. J J M Schwartz, L D Schmidt *J. Catal.* **148** 22 (1994)
132. A Torncrona, M Skoglundh, P Thormahlen, E Fridell, E Jobson *Appl. Catal. B* **14** 131 (1997)
133. A E Hamdaoui, G Bergeret, J Massardier, M Primet, A Renouprez *J. Catal.* **148** 47 (1994)
134. T Hayashi, M Haruta *Shokubai* **37** 72 (1995)
135. T Hayashi, K Tanaka, M Haruta *J. Catal.* **178** 566 (1998)
136. S Naito, M Tanimoto *J. Chem. Soc., Chem. Commun.* 832 (1988)
137. G C Lane, F S Madica, J T Miller *J. Catal.* **129** 145 (1991)
138. E Mielczarski, S B Hong, R J Davis, M E Davis *J. Catal.* **134** 359 (1992)
139. M G Slin'ko *Modelirovanie Khimicheskikh Reaktorov* (Modelling of Chemical Reactors) (Moscow: Nauka, 1968)
140. *Plenarnye Lektsii Konferentsii po Khimicheskim Reaktoram* (Plenary Lectures of the Conference on Chemical Reactors) (Novosibirsk: Institute of Catalysis, Siberian Branch of the Russian Academy of Sciences, 1996) 179 p.
141. M G Slin'ko, G G Elenin *Khim. Promst* (4) 243 (1989)
142. G G Elenin, M G Slin'ko *Matematicheskoe Modelirovanie Yavlenii na Poverkhnosti (Ser. Matematika i Kibernetika)* [Mathematical Modelling of Surface Phenomena (Mathematics and Cybernetics Series)] (Moscow: Znanie, 1988) No. 8
143. A A Samarskii, M G Slin'ko *Izv. Akad. Nauk, Ser. Khim.* 1895 (1998) [c]
144. T I Zelenyak, M G Slin'ko *Kinet. Katal.* **18** 1235 (1977) [a]
145. T I Zelenyak, M G Slin'ko *Kinet. Katal.* **18** 1548 (1977) [a]
146. M G Slin'ko, T I Zelenyak, T A Akramov, M M Lavrent'ev Jr., V S Sheplev *Matemat. Model.* **9** 87 (1997)
147. L Furuoga, T Shirasaki *Sekiyu Gakkaishi* **13** 1 (1971)
148. Y Wakayama, S-I Tanaka *Surf. Sci.* **420** 190 (1999)
149. P Ehrburger *Adv. Colloid Interface Sci.* **21** 275 (1984)
150. G Schmid *Endeavour, New Ser.* **14** 172 (1990)
151. J D Aiken III, R G Finke *J. Mol. Catal. A* **145** 1 (1999)
152. M A Watzky, R G Finke *Chem. Mater.* **9** 3083 (1997)
153. M A Watzky, R G Finke *J. Am. Chem. Soc.* **119** 10382 (1997)
154. J D Aiken, R G Finke *Chem. Mater.* **11** 1035 (1999)
155. R J Hunter *Foundations of Colloid Science* Vol. 1 (London: Oxford University Press, 198)7
156. A J Bard, L R Faulkner *Electrochemical Methods* (New York: Wiley, 1980)
157. D H Napper *Polymeric Stabilisation of Colloidal Dispersions* (London: Academic Press, 1983)
158. Y Lin, R G Finke *J. Am. Chem. Soc.* **116** 8335 (1994)
159. G Schmid, R Boese, R Pfeil, F Bandermann, S Meyer, G H M Calis, J A W van der Velden *Chem. Ber.* **114** 3634 (1981)
160. G Schmid *Struct. Bonding* **62** 51 (1985)
161. G Schmid *Polyhedron* **7** 2321 (1988)
162. G Schmid, B Morum, J-O Malm *Angew. Chem., Int. Ed. Engl.* **28** 778 (1989)
163. G Schmid *Mater. Chem. Phys.* **29** 133 (1991)
164. G Schmid *Chem. Rev.* **92** 1709 (1992)
165. G Schmid, V Maihack, F Lantermann, S Peschel *J. Chem. Soc., Dalton Trans.* 589 (1996)
166. M N Vargaftik, V P Zagorodnikov, I P Stolyarov, I I Moiseev, V A Likholobov, D I Kochubey, A L Chuvilin, V I Zaikovsky, K I Zamaraev, G I Timofeeva *J. Chem. Soc., Chem. Commun.* 937 (1985)
167. Y Lin, R G Finke *Inorg. Chem.* **33** 4891 (1994)
168. H Bönnemann, G Braun, W Brijoux, R Brinkmann, A S Tilling, K Seevogel, K Siepen *J. Organomet. Chem.* **520** 143 (1996)
169. H Bönnemann, G A Braun *Angew. Chem., Int. Ed. Engl.* **35** 1992 (1996)
170. J Stein, L N Lewis, Y Gao, R A Scott *J. Am. Chem. Soc.* **121** 3693 (1999)
171. J P Wilcoxon, T Martino, E Klavetter, A P Sylwester *Nanophase Mater.* 771 (1994)
172. T J Scmidt, M Noeske, H A Gasteiger, R J Behm, P Britz, W Brijoux, H Bönnemann *Langmuir* **13** 2591 (1997)
173. M T Reetz, R Breinbauer, P Wedemann, P Binger *Tetrahedron* **54** 1233 (1998)
174. Vision 2020 Catalysis Report; http://www ccrhq org/vision
175. H Bönnemann, W Brijoux, A S Tilling, K Siepen *Top. Catal.* **4** 217 (1997)
176. H Bönnemann, G A Braun *Chem. Eur. J.* **3** 1200 (1997)
177. US P. 3 442 973 (1969)
178. J H Sinfelt *Bimetallic Catalysts. Discoveries, Concepts and Applications* (New York: Wiley, 1983)
179. W M H Sachtler *Le vide* **163** 19 (1979)
180. S N Augustine, W M H Sachtler *J. Phys. Chem.* **91** 5953 (1987)
181. Y Y Huang, W M H Sachtler *J. Catal.* **188** 215 (1999)
182. M Bonarowska, A Malinowski, Z Karpiński *Appl. Catal. A* **188** 145 (1999)
183. US P. 3 617 518 (1971)
184. G Diaz, A Gomezcortes, M Benaisa *Catal. Lett.* **38** 63 (1996)
185. C P Shao, L Fan, K Fujimoto, Y Iwasawa *Appl. Catal. A* **128** L1 (1995)
186. C T Campbell, in *Handbook of Heterogeneous Catalysis* Vol. 2 (Eds G Ertl, H Knozinger, J Weitkamp) (Weinheim: VCH, 1997) p. 814
187. W M H Sachtler, in *Handbook of Heterogeneous Catalysis* Vol. 3 (Eds G Ertl, H Knozinger, J Weitkamp) (Weinheim: VCH, 1997) p. 1077
188. H-W Yang, J C Lin, T Engel *Surf. Sci.* **289** 267 (1993)
189. J A Rodrigues, R A Campbell, D W Goodman *J. Vac. Sci. Technol. A, Vac. Surf. Films* **10** 2540 (1992)
190. A Sellidj, B E Koel *Surf. Sci.* **284** 139 (1993)
191. M W Ruckman, M Strongin *Phys. Rev. Lett.* **29** 7105 (1984)
192. U Schneider, H Busse, R Linke, G R Castro, K Wandelt *J. Vac. Sci. Technol. A, Vac. Surf. Films* **12** 2069 (1994)
193. G R Castro, U Schneider, H Busse, T Janssens, K Wandelt *Surf. Sci.* **269**/**270** 321 (1992)
194. C Xu, B E Koel *Surf. Sci.* **310** 198 (1994)
195. E Garfunkel, M Yu, S Yang, X Feng *J. Vac. Sci. Technol. A, Vac. Surf. Films* **7** 1579 (1989)
196. X H Feng, M R Yu, S Yang, G Meigs, E Garfunkel *J. Chem. Phys.* **90** 7516 (1989)
197. F Besenbacher, I Chorkendorff, B S Clausen, B Hammer, A M Molenbroek, J K Nørskov, I Stensgaard *Science* **279** 1913 (1998)
198. N Toshima, T Yonezawa *New J. Chem.* 1179 (1998)
199. N Toshima, M Harada, T Yonezawa, K Kushihashi, K Asakura *J. Phys. Chem.* **95** 7448 (1991)
200. N Toshima, K Kushihashi, T Yonezawa, H Hirai *Chem. Lett.* 1769 (1989)
201. N Toshima, T Yonezawa, M Harada, K Asakura, Y Iwasawa *Chem. Lett.* 815 (1990)
202. T Yonezawa, N Toshima *J. Chem. Soc., Faraday Trans.* **91** 4111 (1995)
203. N Toshima, M Harada, Y Yamazaki, K Asakura *J. Phys. Chem.* **96** 9927 (1992)
204. M Harada, K Asakura, N Toshima *J. Phys. Chem.* **98** 2653 (1994)
205. K Asakura, Y Yamazaki, H Kuroda, M Harada, N Toshima *Jpn. J. Appl. Phys.* **32** 448 (1993)
206. N Toshima, Y Wang *Adv. Mater.* **6** 245 (1994)
207. T E Hoost, G W Graham, M Shefel, O Alexeev, B C Gates *Catal. Lett.* **38** 57 (1996)

[a] — *Kinet. Catal. (Engl. Transl.)*
[b] — *Russ. J. Phys. Chem. (Engl. Transl.)*
[c] — *Russ. Chem. Bull. (Engl. Transl.)*

Russian Chemical Reviews **70** (2) 161 – 176 (2001) © 2001 Russian Academy of Sciences and Turpion Ltd

DOI 10.1070/RC2001v070n02ABEH000619

Electrochemically active species and multielectron processes in ionic melts

V I Shapoval (deceased), V V Solov'ev, V V Malyshev

Contents

I.	Introduction	161
II.	Model concepts on the structures of ionic melts	162
III.	Structures, chemical and electrochemical properties of titanium-containing fluoride melts	164
IV.	Structures, chemical and electrochemical properties of boron-containing fluoride melts	165
V.	Effect of cations on the mechanisms of chemical and electrochemical reactions in ionic melts	166
VI.	Theoretical and experimental studies of cation – anion interactions in nitrate- and carbonate-containing melts	167
VII.	Multielectron electrochemical reduction of oxoanions of high-melting metals and non-metals in ionic melts	169

Abstract. The model concepts for the mechanisms of formation of electrochemically active species and multielectron processes in ionic nitrate-, carbonate-, boron- and titanium-containing fluoride melts are generalised. The fundamental importance of the acid-base properties of a melt in the mechanism of formation of electrochemically active species is shown for nitrate- and carbonate-containing melts. This fact is confirmed by electrochemical measurements and by calculations of force constants for oxyanions. The optimum form of electrochemically active species has been established; their reduction abilities depend on the cationic composition of a melt, the adsorption properties of the electrode surface and the electric field strength. The bibliography includes 218 references.

I. Introduction

Complex multicomponent systems containing ions of polyvalent metals are used as reaction media in the preparation of inorganic and organic compounds by high-temperature electrochemical synthesis, for the implementation of processes in high-temperature current sources, in electrometallurgy, in electroplating and other areas where a specific approach to the control of chemical processes in melts is required. Molten salts are widely used in practice, that is why the study on their structures, chemical and electrochemical properties is an issue of current interest.[1–3]

This review covers the state-of-the-art of a fundamental problem of electrochemistry of ionic melts, *viz*., determination of the nature of electrochemically active species (EAS) involved in electrochemical reactions and the conditions required for multielectron transformations at electrode – electrolyte interfaces. The electrochemically active species are groups of ions formed in a melt due to acid-base interactions and possessing the highest abilities to accept electrons in the double electric layer. To date, this problem got both the theoretical background and was confirmed comprehensively by experiment for not-too-complicated electrochemical systems with simple one-element ions. If the components of a system arise from complexes, the electrode reactions are supposed to involve multiple-charged ions with complex compositions. Such systems can exist both in aqueous electrolytes and in ionic melts. The problem of theoretical description of multielectron electrochemical reactions in ionic melts has not been solved unambiguously so far. In order to describe experimental results on multielectron transformations at interfaces of electrochemical systems, one mainly uses the concepts on acid-base equilibria and the concepts on electron density redistribution mechanisms during the formation of new chemical bonds or under the influence of the outer-sphere cations and anions on the intracomplex bonds.

The concepts of the mechanism of formation of electrochemically active species in ionic melts based on the analysis of thermodynamic and kinetic parameters are phenomenological. The lack of systematic studies on the relationship between chemical reactions of EAS formation in the bulk melt and their electrochemical reduction and on the effect of the adsorption properties of electrode surfaces and the external electric field on the acid-base interactions in ionic melts not only predetermines the existence of controversial results in the interpretation of the relationships obtained experimentally but also prevents the formulation of basic principles of EAS formation and control of electrochemical processes. The most abundant information on the interaction between the species in a melt and on the processes of their electrochemical reduction can be obtained from data on the changes in the electronic state of the species.[4–7] Therefore, it seems expedient to use the results of both theoretical and modern experimental research methods for the substantiation of EAS formation mechanisms in ionic melts. Once this mechanism has been established, it will be possible to develop a theoretical basis for creating the general principles for control over multielectron processes.

In ionic liquids (ionic melts), the acid-base interactions manifest themselves explicitly,[8,9] but it is difficult to conceive their mechanisms because of their complexity. A cation – anion interaction model is used for the description of this mechanism. In accordance with this model, the acid-base properties of a medium with respect to a particular anion are changed by addition of different types of cations to a dilute solution. Let us consider how this model 'operates' for such anions as NO_3^-, CO_3^{2-}, TiF_6^{2-}, BF_4^-, WO_4^{2-} and MoO_4^{2-} (hard bases) and such cations as Cs^+, Rb^+,

V I Shapoval, V V Malyshev V I Vernadsky Institute of General and Inorganic Chemistry, National Academy of Sciences of Ukraine, prosp. Palladina 32/34, 252680 Kiev, Ukraine. Fax (38-044) 444 30 70. Tel. (38-044) 444 14 62. E-mail: synthesis@ionc.kar.net (V V Malyshev)
V V Solov'ev Yu Kondratyuk Poltava State Technical University, Pervomaiskii prosp. 24, 36601 Poltava, Ukraine. Fax (38-053) 256 18 96. Tel. (38-053) 227 46 48

Received 15 August 2000
Uspekhi Khimii **70** (2) 182 – 199 (2001); translated by S S Veselyi

K^+, Na^+, Li^+, Pb^{2+}, Ba^{2+}, Sr^{2+}, Ca^{2+}, Mg^{2+}, Be^{2+} (hard acids) in nitrate-, carbonate-, boron- and titanium-containing fluoride melts that are widely used in practice.[2–4]

II. Model concepts on the structures of ionic melts

The physicochemical properties of ionic melts containing polycoordinated anions, *viz*., NO_3^- and CO_3^{2-}, are determined by the electronic structures of the oxygen-containing anions and the character of their interactions with the melt cations. There is only the near-range order in ionic liquids, which creates problems both for the interpretation of the experimental relationships and for the theoretical descriptions of the melt structures. This can explain the existence of various model concepts as to the structures of ionic melts.

Studies on the changes in the intra-anion bonds depending on the cationic environment (changes in the force constants of the bonds and in bond angles were analysed) in melts of monovalent metal nitrates have led to the conclusion that contact cation–anion pairs exist in these melts.[10, 11] Based on this conclusion, a model of an ion pair was built. This model has been used, *e.g*., for the explanation of the features of IR and Raman spectra of $LiNO_3$ and alkaline-earth nitrate melts, namely, the low-frequency component of the spectrum resulting from the M–O vibrations and splitting of one of the frequencies in the NO_3^- spectrum.

The quasi-lattice model of the melt structure accounts for the concerted vibrational movement of the ions. Considering the mean statistical distribution of the inter-ion potential, the existence of two sublattices, namely, cationic and anionic, was assumed.[12, 13] This model denies the existence of ion pairs due to the comparability of lifetimes of the vibrational levels and the diffusional migration of species. Based on this quasi-lattice model, the existence of $[M(NO_3)_4]^{3-}$ complexes was assumed;[14] this was confirmed by spectroscopic data.[15]

The Kucharski–Flengas quasi-chemical model[16] and the three-sphere Ferland model[17] account for the statistical exchange of cations in sublattices of mixed nitrate melts. Complex ions existing in the melt are regarded as fragments of the ionic structure rather than isolated species of an anionic sublattice.[16] The asymmetry of the cation-anionic environment and the existence of independent kinetic species are explained[18] by effects of various cations, in agreement with the assumptions made elsewhere.[10, 11]

For objective reasons, the above models cannot claim to provide full description of the structures of ionic melts, but each of them states unambiguously that the structure depends significantly on the cationic compositions. This dependence has been confirmed by spectroscopic data for systems with polycoordinate anions, *viz*., complexation products. In fact, the geometries and types of complex species in melts containing insignificant amounts of transition metal salts as well as in melts with oxygen-containing anions have been established based on spectroscopic data.[19] Analysis of the spectra of sulfate melts revealed a considerable contribution of π-interactions to the chemical bonds of the metal complexes studied.[15] The characteristic vibration frequencies were found to depend on the cationic composition for individual and mixed melts containing molecular ions as the starting structural elements. In many cases, C–O and S–O vibration frequency shifts for outer-sphere cations $Cs^+ > K^+ > Na^+ > Li^+$, accompanied by band broadening due to the polarising effect of the cations, were observed in carbonate- and sulfate-containing solutions.[15]

However, the reasons for the frequency shifts in the spectra of melts were explained either qualitatively[20, 21] or on the basis of various model assumptions on the melt structures (the quasi-lattice model,[13] the ion-pair model,[10, 11] *etc*.). In addition, mutually exclusive interpretations of the same data can be found as well.

The use of spectroscopic methods for the study on dilute oxygen-containing melts encounters considerable difficulties in the interpretation of the bands because of their low intensities. On the other hand, information on the acid-base interactions in ionic liquids can be obtained by studying electrode processes. Let us consider certain specific features of electrode processes in melts, in particular those containing nitrate and carbonate ions.

Neglecting of the role of acid-base properties of the medium has traditionally led researchers to mutually exclusive conclusions in the explanation of the same features of electrode processes. For example, Delimarskii *et al*.[22, 23] showed that a cathodic process with a 100% yield of carbon was possible in the electrolysis of a molten equimolar mixture of lithium and potassium carbonates. They noted a specific feature of the voltammetric curves, *viz*., the existence of a region with a distinct limiting current at potentials 0.4–0.5 V, and considered that this region corresponded to the evolution of carbon preceding that of the alkali metal.[23] The existence of limiting currents in voltammograms has also been reported in other studies on cathodic processes in molten carbonates (see, *e.g*., Refs 24–27), but these features have been interpreted differently by different authors. Studies on the possibility of carbon evolution preceding the discharge of alkali metal cations[28, 29] showed that cathodic carbon evolution depends on the electrolyte cationic composition and can occur not only from carbonates but also from chlorides, either supplemented with thermally unstable carbonates or saturated with gaseous CO_2. The dependence of the amount of carbon evolved on the cationic composition of the carbonate electrolyte showed the dominating role of the reducing ability of CO_2 formed in the redox reaction

$$(2/m)\,M^{m+} + CO_3^{2-} \rightleftharpoons M_{2/m}O + CO_2\,. \qquad (1)$$

As in the case of carbonate-containing melts, the development of concepts on the mechanism of formation of electrochemically active species in nitrate-containing melts was facilitated by the existence of many different interpretations of the features of cathodic processes. In fact, the nature of the electrode process preceding the electrochemical reduction of alkali metals, which has first been reported by Lyalikov and Karamzin,[30] was interpreted in different manners. Rust and Duke,[31] who studied acid-base equilibria, assumed that it is the dissociation product of the anion, *viz*., the nitronium ion NO_2^+, that is reduced in electrochemical and chemical reactions. A similar conclusion was reached by Delimarskii *et al*.[32] However, no direct measurements could prove the existence of NO_2^+ in nitrate melts. It was also found[33] that noticeable amounts of NO_2^+ cannot be formed in the presence of strong acids; instead, a compound is formed the properties of which coincide with those of NO_2. This subsequently undergoes one-electron reduction into nitrite. Usanovich[34] believes that $[H_2NO_3]^+$ ions rather than NO_2^+ exist in aqueous melts.

A different viewpoint regarding the nature of the electrode process preceding the alkali metal evolution was given by Delimarskii *et al*.:[35] this process results from direct NO_3^- reduction, irrespective of the electrolyte cationic composition. A similar interpretation has been given in other studies,[36–38] but the reasons for the direct electrochemical nitrate ion reduction have not been explained.

The currently available experimental results on electrode processes in molten salts, particularly in nitrate melts, are used as a base for the simulation of various schemes of formation of electrochemically active species and the corresponding electrode processes. Let us consider some of the models.

Tkalenko *et al*. applied the regularities of the electrochemical reduction of NO_3^- in aqueous solutions[39] to melts;[40–43] this allowed them to propose a model scheme of the cathodic process in concentrated nitrate melts. According to this scheme, the NO_3^- ion in the bulk melt is an ellipsoid with the negative charge distributed over the periphery. Near the electrode surface, the ion is subjected to a combined effect of the cation and electrode fields, therefore its state differs from that in the bulk. It is believed that at negative potentials (cathodic polarisation) the NO_3^- ions are polarised additionally by the electrode force field in such a way that the positively charged nitrogen atom is displaced towards the

electrode relative to the oxygen atoms. The nitrate ion polarised by the electrode field is regarded as an activated complex. Species that form activated complexes under the action of both the electrode field and cation field in the double electric layer are considered electrochemically active.[43] It is the NO_3^- ions that undergo discharge upon cathodic polarisation, hence they can be regarded as electrochemically active species.

We feel that the above scheme of the formation of electrochemically active species has a number of drawbacks. First, though the authors do not deny the effect of the electrolyte cationic composition, they believe that the cation–anion interaction is limited to indirect anion polarisation (through variation of the field potential). They rule out the formation of metal complexes as electrochemically active species; this disagrees with the concept on the chemical interaction of species in melts. In addition, this assumption contradicts the results of studies on the electrochemical reduction of oxygen-containing anions [4, 44, 45] and spectroscopic data.[15, 19, 46] Second, the unreasonable overestimation of the electrode field effect requires a thorough consideration. And, finally, while noting the possible effect of both the electrode field and cations, the authors do not estimate the contributions of each of the effects to the formation of the activated complex.

A different model of the formation of electrochemically active species in melts has been proposed by Chernukhin *et al.*[47, 48] The model is based on the concept on inter-species interactions in condensed media. It was suggested [48] that inter-species interactions result in concerted groups of ions consisting of one anion and surrounding cations. The anion can be transformed to the activated state and undergo electrochemical transformation. In their study on electrode processes in ternary mixtures, Chernukhin *et al.* assumed that the inter-species interactions in the double electric layer and in the melt bulk have similar natures.

Within the framework of the concept that melts are dynamic systems † and based on the results reported by Belen'kaya *et al.*[50] (see footnote ‡), it was assumed [48] that the state of an anion depends on the concerted action of the ionic environment. The activation of anion discharge was explained by the polarising action of the electrode field resulting in a definite anion orientation and, subsequently, localisation of its pairwise inter-species interactions, preferably with cations having the strongest polarising effect. This enhances the non-equivalence of the N–O bonds and prolongs considerably the life-time of the group consisting of the anion and the first-sphere cations. Such a group has been called the activated complex.[48] For example, the formation of an activated complex is given by the following scheme for a binary melt containing potassium and calcium:

$$K^+_{n-x}Ca^{2+}_{x-1}\{Ca^{2+}[ONO_2]^-\} \xrightarrow{-E} K^+_{n-x}Ca^{2+}_{x-1}\{Ca^{2+}...O...[(NO_2]^+\}, \quad (2)$$

where n is the coordination number (c.n.) of the anion during discharge, which is constant irrespective of the cationic composition; $K^+_{n-x}Ca^{2+}_{x-1}\{Ca^{2+}[ONO_2]^-\}$ is the binary melt formula which emphasises the polarising effect of the cation on the NO_3^- anion by designating the anion as $[ONO_2]^-$. Within the scope of Scheme (2), the electrode reaction has the form:

$$Ca^{2+} + NO_3^- \xrightarrow{-E} \{Ca^{2+}...O...[NO_2]^+\} \xrightarrow{2e^-} CaO + NO_2^- . \quad (3)$$

For similar lithium-containing melts, an intermediate compound LiO^- can be formed:

$$Li^+ + NO_3^- \xrightarrow{-E} \{Li^+...O...[NO_2]^+\} \xrightarrow{2e^-} LiO^- + NO_2^- . \quad (4)$$

Based on the above model for the formation of electrochemically active species, the appearance of additional cathodic waves in the voltammograms upon addition of strongly polarising cations, *e.g.*, in melts of sodium and potassium nitrates, can be explained by an increase in anion asymmetry. The shift of the reduction wave upon addition of strongly polarising cations to the melt occurs due to the gradual replacement of the background cations in the nitrate ion environment by cations with a higher polarising strength. This scheme, unlike that proposed by Tkalenko,[43] is generally consistent with the concept on the chemical interactions between species in melts and with the data of numerous spectroscopic studies on concentrated nitrate melts. However, certain aspects of the mechanism discussed above are debatable.

Shapoval *et al.*[4, 44] generalised their own results and other data and explained some features of the electrochemical reduction of oxygen-containing anions. It was assumed that electrode processes in molten salts with oxygen-containing anions are limited by a preceding chemical reaction. For example, the formation of electrochemically active species in the reduction of the carbonate ion in lithium-containing melts was represented by the scheme:

$$n\,Li^+ + CO_3^{2-} \rightleftharpoons [Li_nCO_3]^{n-2} \rightleftharpoons Li_nO^{n-2} + CO_2 . \quad (5)$$

A similar scheme of the preceding acid-base reaction has been proposed for nitrate-containing melts based on data for NO_3^- reduction in a KCl–LiCl eutectic as the background:[45]

$$2\,Li^+ + NO_3^- \rightleftharpoons [Li_2NO_3]^+ \rightleftharpoons Li_2O + NO_2^+ . \quad (6)$$

As follows from Eqns (5) and (6), it is not anions but their reaction products with cations of the molten media that are electrochemically active species.

The proposed anion–cation interaction scheme agrees most closely with the concepts on the chemical reactions of species in ionic melts, but this has a phenomenological character.[51] The anion–cation interaction mechanism can be comprehended more precisely by studying it at an electronic level with the use of quantum-chemical calculations and by comparing them with experimental data. The CO_3^{2-} and NO_3^- anions which are most sensitive to variations of the acid-base properties of a melt are most convenient for the comparison of the electrochemical reduction characteristics.

The scheme for the formation of electrochemically active species in oxygen-containing melts proposed by Shapoval *et al.*[4, 44] does not account fully for the function of cations as acids which, like protons in aqueous media, can add to anions and thus accelerate electrochemical reduction. The complex nature of interaction between species in ionic media creates difficulties for their theoretical description. Therefore, it is expedient to consider a model scheme of cation–anion interaction which makes it possible to change the acid-base properties of the medium with respect to a selected anion by gradual accumulation of cations in the anion's first solvation shell (cationised anion).[52] The cation–anion interaction for carbonate- and nitrate-containing melts can be represented as follows:

$$n\,M^{m+} + CO_3^{2-} \rightleftharpoons \begin{matrix} \{M_n^{m+}[CO_3]^{2-}\}^{(mn-2)+} \\ \rightleftharpoons \\ M_{2/m}O + CO_2 + (n-2/m)M^{m+} \end{matrix} , \quad (7)$$

$$n\,M^{m+} + NO_3^- \rightleftharpoons \begin{matrix} \{M_n^{m+}[NO_3]^-\}^{(mn-1)+} \\ \rightleftharpoons \\ M_{2/m}O + NO_2^+ + (n-2/m)M^{m+} \end{matrix} , \quad (8)$$

where m is the cation charge, n is the reaction order with respect to the cation (coordination number). Thus, cation–anion interaction can result either in cationised anions (metal complexes) or in anion dissociation (both under direct influence of cations and *via* intermediate formation of 'short-lived' metal complexes).

Earlier quantum-chemical calculations [53] and electrochemical data [51, 54] showed that cation–anion interactions in nitrate-containing melts result mostly in nitrate metal complexes, whereas in carbonate-containing melts, two mechanisms of the EAS formation in accordance with Scheme (7) are equally probable. On the

† These views have later been generalised by Delimarskii *et al.*[49]

‡ Belen'kaya *et al.*[50] used Raman spectroscopy to study the changes in the geometry and the potential function of nitrate ion in molten alkali nitrates. It was shown that the bond lengths and strengths in molecular ions can be changed with strengthening of inter-species interactions in the melt. Therefore, the reactivities of species in molten media can be controlled directly by varying their compositions.

other hand, the model proposed, which is valid in dilute melts as the background, does not account for the effects of the electrode surface adsorption properties and the electric field on the character of acid-base interactions and on the charge transfer elementary act.

A calculation of the total energies, charges and populations for carbonate ions showed [55] that the presence of uncharged electrode surface atoms (this surface was simulated by a linear cluster of three carbon atoms) favours the electron density redistribution in an isolated CO_3^{2-} anion according to the σ,π-mechanism (where the σ-component predominates), which, in turn, weakens the intra-anion bonds. Estimates of contributions from the electrode surface and from the cation field to the changes in the C–O bond energy showed that the latter contribution predominates, *i.e.*, the electrode surface does not affect in principle the mechanism of the EAS formation within this model. This mechanism is primarily determined by the melt cationic composition.

The cation–anion interactions are affected considerably not only by the adsorption effects but also by electric fields.[56] Comparison of the energy characteristics and atomic charges and orbital populations in an isolated CO_3^{2-} anion and in an anion located near the electrode surface under the effect of the cation field and an external electric field ($E = 2 \times 10^{10}$ V m^{-1}) showed that cleavage of C–O bonds occurs with formation of CO_2. It is believed [57] that the effect of the electrode surface lowers the activation barriers for two- and four-electron CO_3^{2-} reduction in comparison with the similar magnitudes for an isolated anion. The additional effect of the electric field increases the effect discovered (by a factor of ~2) and favours the direct discharge of the CO_2 molecule

$$CO_2 + 4e^- \longrightarrow C + 2O^{2-} . \quad (9)$$

The geometric sizes of metal complexes resulting from cation–anion interactions in nitrate-containing melts are much larger than that of the linear cluster of three carbon atoms mentioned above. This fact prompted a search for new clusters simulating the electrode surface.[58] The optimum four-cluster variant selected is an aromatic system of 12 carbon atoms (48 basis orbitals) which ensures an adequate representation of the donor-acceptor properties of an uncharged electrode surface. Interaction of a surface cluster with an NO_3^- anion initiates the electron density redistribution in it according to the σ,π-mechanism (with the σ-component predominating) which weakens the intra-anion bonds. An additional influence of the field from the melt cations, *e.g.*, Li^+ and Be^{2+}, on the NO_3^- anion results in a considerable (three- to fourfold) increase in the N–O bond energies. In this case, the π-component predominates in the σ,π-mechanism. Both of these factors increase the N–O bond energy. The trend towards strengthening the N–O bonds is preserved as the c.n. of the cation is increased. Solov'ev *et al.*[59] emphasised that the overall effect of the electrode surface and melt cations on the EAS formation mechanism is determined by competition of two opposite trends in electron density redistribution in NO_3^- and concluded that the electrode surface effect on the mechanism of formation of EAS, such as metal complexes $\{M_n^{m+}[NO_3]^-\}^{(mn-1)+}$, is insignificant within the framework of Scheme (8).

Calculations carried out by Solov'ev *et al.*[60] showed that the external electric field (2×10^{10} V m^{-1}) imposed on a cationised nitrate ion located near the electrode surface virtually does not change the energy of N–O intra-anion bonds against the background of the rather strong interaction of NO_3^- with Li^+ or Be^{2+}. It was found that the contributions of both electric field and electrode surface do not greatly affect the cation–anion interaction.

It has been found [58] (from activation barrier calculations) that the effect of the electrode surface increases considerably the reactivity of metal complexes with respect to two-electron reduction. This effect increases with increase in the cation specific charge and coordination number. The trend towards lowering of activation barriers is preserved under an external electric field. An estimate of the electrode surface effects, the cation field and the external electric field on the elementary charge transfer act showed that the adsorption properties of the electrode surface play the most significant role in these processes. The optimum coordination numbers were found to be 2 for NO_3^- surrounded by Li^+ cations and 3 for the same anion surrounded by Be^{2+} cations. Taking electrochemical measurement data into account,[61] electrochemical reduction can be represented as follows

$$\{M_n^{m+}[NO_3]^-\}^{(mn-1)+} + 2e^- \longrightarrow NO_2^- + n M_{2/m}O + (n-2/m) M^{m+} . \quad (10)$$

Experimental studies [62] not only confirm the formation of EAS according to Scheme (8) but also suggest unambiguously the catalytic nature (caused by the depolariser regeneration) of nitrate reduction waves in the presence of strongly polarising cations. An excess of the latter is believed to result in regeneration of the original EAS

$$3NO_2^- \xrightarrow{M^{m+},\ -E} NO_3^- + 2NO + O^{2-} . \quad (11)$$

The possible realisation of Scheme (11) follows from quantum-chemical calculations of interactions between $M_n^{m+} \cdots NO_2^-$ ($M = Li^+, Be^{2+}$) in an electric field with a strength of $E = 0$; 0.2; 2×10^{10} V m^{-1} (see Ref. 55). Similar calculations showed the priority of cation–anion interactions in the EAS formation in ionic melts. This fact was confirmed in IR and Raman spectroscopic studies on the effect of the melt cationic composition on the force constants of the N–O, C–O, W–O and Mo–O bonds in NO_3^-, CO_3^{2-}, WO_4^{2-} and MoO_4^{2-} anions. The force constants calculated for the $[MNO_3]^0$ and $[M_2CO_3]^0$ systems ($M = Cs^+$, Rb^+, K^+, Na^+, Li^+) suggest [53, 62] a trend towards an increase in the stretching force constants of the N–O and C–O bonds compared with the same bonds in isolated NO_3^- and CO_3^{2-} anions as the cation specific charge increases in the series from Cs^+ to Li^+. The observed effect of the increase in the N–O bond strength due to anion cationisation was confirmed by quantum-chemical calculations and by analysis of electronic absorption spectra.[15, 19] In carbonate melts containing the Cs^+, Rb^+ and K^+ cations, the C–O force constants tend to increase, which also agrees with quantum-chemical calculations.

Calculations of force constants for $[MEO_4]^0$ systems ($M = Na_2^+, Li_2^+, Pb^{2+}, Ba^{2+}, Sr^{2+}, Ca^{2+}$; E = W, Mo) showed [61] that the E–O bond stretching force constants and the deformation force constants in EO_4^{2-} increase with the increase in the cation specific charge. The increase in the force constants of these interactions is believed to result from an increase in the degree of delocalisation of the valence electrons of the EO_4^{2-} anion on the cation orbital. In turn, this stabilises the electronic energy levels of the inner shells in EO_4^{2-}.

III. Structures, chemical and electrochemical properties of titanium-containing fluoride melts

To date, data on the structure of dilute titanium-containing melts in fluoride–chloride systems are very scarce, therefore even the simplest models of the structures of these melts are unavailable. However, there are a number of publications devoted to the studies of these melts.

Analysis of the electronic absorption spectra of the fluoride-containing system KCl–NaCl–NaF with the use of the ligand field theory [63] revealed transient coordination forms of the Ti^{3+} ion resulting from mixed coordination with Cl^- and F^- anions. In the presence of a 100-fold excess of F^- with respect to TiF_3, the formation of a trigonally distorted complex was detected. Complexation of lower titanium compounds with fluoride ions in KCl–NaCl melts was reported [64–66] and it was noted that the c.n. with respect to the F^- ligand in the complexes formed is 3–4.

The existence of $[TiF_4Cl_2]^{2-}$ complexes, presumably with distorted octahedral symmetry, in K_2TiF_6–NaF melts was stated.[67] The possible formation of titanium tetrafluoride in these melts was also reported by Rolin.[68] The formation of poorly soluble compounds $MTiF_4$ in titanium-containing melts cannot be ruled out.[69, 70]

Thus, based on the results of the few studies on the structure of titanium-containing fluoride–chloride melts, one can assume that they contain the mixed $[TiF_4Cl_2]^{2-}$ complex and that the interaction mechanism of the melt species, which results in the compounds $MTiF_4$, depends considerably on the cationic composition.

The electrochemical reduction of titanium-containing fluorides in the presence of chlorides was studied by Smirnov *et al.*[70] The steady-state polarisation curve method was used to study the reduction of Ti^{4+} in the 0.14 K_2TiF_6–0.86 NaCl melt at 1033 K. The titanium deposition mechanism was studied by recording the potentiometric voltammetric characteristics of electrochemical reduction on steel, graphite and titanium electrodes (tetravalent titanium ions were assumed to be the EAS). A polarographic study on the electrochemical reduction of K_2TiF_6 with a KCl–NaCl melt as the background was first carried out by Vitlaci and Nechel[71] who have established the two-electron nature of the charge transfer to the TiF_4^{2-} anion.

Analysis of results reported in these studies[70, 71] suggests unambiguously the possibility of formation of new titanium-containing species upon dissociation of the original complex, *viz.*, chloride–fluoride titanium complexes with titanium in various valent states and cationised titanium-containing anions. These species can react with the melt components. In such cases, a multistep electrode process is observed, and the transfer act can involve several species.

A higher level of experimental data interpretation (with calculation of diagnostic criteria of electrochemical reduction) distinguishes a series of studies[65, 66, 72] which served as a basis for the assumption on the formation of TiF_4 molecules from the original species TiF_6^{2-} and the cationised anion $\{M_n^{m+}[TiF_6]^{2-}\}^{(mn-2)+}$. However, the studies discussed above and those by Juman and White[73] do not report any quantitative data on the electrochemical reduction kinetics and merely suggest the electrode reaction mechanisms.

The most comprehensive data on the electrochemical properties of titanium-containing fluoride melts have been obtained in the studies on the electrochemical reduction of the TiF_6^{2-} anion with a KCl–NaCl melt as the background.[74–76] The possible formation of new EAS, *viz.*, dissociation products of the original complex, was also reported in these studies. Three reduction waves were found in the cathodic polarisation curves. The first wave was interpreted as a result of charge transfer to the dissociation product, *i.e.*, the TiF_4 molecule, and the second one, as a result of four-electron charge transfer directly to the complex anion. The third wave could not be interpreted on the basis of the experimental data.

The authors of the majority of studies discussed above did not relate the results obtained to the effect of the melt cationic composition on the EAS formation mechanism. It seems most reasonable to study this mechanism with the use of quantum-chemical methods which enable the simulation of EAS formation at the electronic level by relating it to electron transfer during electrochemical reduction.

The successful application of the cation–anion interaction model to the studies on carbonate- and nitrate-containing melts stimulated the use of this model for the study on melts containing complex anions. A scheme of the cation–anion interaction in titanium-containing fluoride melts was represented as follows:[77]

$$n\mathrm{M}^{m+} + \mathrm{TiF}_6^{2-} \rightleftharpoons \{\mathrm{M}_n^{m+}[\mathrm{TiF}_6]^{2-}\}^{(mn-2)+} \rightleftharpoons \mathrm{TiF}_4 + 2\mathrm{F}^- + n\,\mathrm{M}^{m+}. \quad (12)$$

According to this scheme, the cation–anion interaction can involve the formation of cationised anions (metal complexes) $\{M_n^{m+}[TiF_6]^{2-}\}^{(mn-2)+}$ or dissociation of the TiF_6^{2-} anion to give titanium tetrafluoride.

Calculations showed[78] that dissociation of an isolated TiF_6^{2-} anion is impossible for energetic reasons: comparative analysis of atomic orbital populations in an isolated TiF_6^{2-} anion and that in cationic environment showed that electron density redistribution cannot result in cleavage of the Ti–F bond in this anion. Reactions of the Na^+ or Li^+ cations with the TiF_6^{2-} anion yield metal complexes with coordination numbers equal to 2, 4 and 6. The Ti–F bond energies decrease with the increase in the c.n. under the influence of cations, whereas the energies of the cation–anion bonds increase. The interaction between Mg^{2+} cations and TiF_6^{2-} at c.n. = 2 results in cleavage of two Ti–F bonds. Further increase in the number of Mg^{2+} cations in the first solvate shell results in further dissociation of the TiF_6^{2-} anion.

Weakening of Ti–F bonds due to the cation–anion interaction results from electron density redistribution in the TiF_6^{2-} anion according to the σ,π-mechanism. The electron density redistribution increases with the increase in both c.n. and the cation specific charge.

It was noted[79] that the cation–anion interaction lowers the activation barriers for two- and four-electron reduction of metal complexes of the TiF_6^{2-} anions and titanium tetrafluoride molecular associates in comparison with the corresponding values for isolated TiF_6^{2-} and TiF_4. Predominance of four-electron reduction was established for metal complexes; on the contrary, two-electron charge transfer predominates for isolated TiF_4.

Volkov[80] does not rule out that the EAS formation mechanism is affected by chloride anions of the background electrolyte. The existence of stable ion-molecular associates $\{Cl_2^-[TiF_4]^0\}^{2-}$ in the melt bulk is probable. This follows from an estimate (based on quantum-chemical calculations) of the interaction of Cl^- ions with the TiF_4 molecule. The activation barriers for two- and four-electron reduction of TiF_4 increase considerably in the presence of chloride anions. Hence, anionic environments (unlike cationic ones) do not increase the reducing ability of EAS.

It has been shown[81] that the electrode surface effect results in electron density redistribution in cationised TiF_6^{2-} anions and in TiF_4 molecular associates, as well as in isolated TiF_4, according to the σ,π-mechanism with predominance of the σ-component. Hence, the electrode surface does not affect considerably the EAS formation mechanism but only enhances the cation–anion interaction effect. Comparative analysis of atomic charges and atomic orbital populations[82] showed that the electric field initiates electron density redistribution in the TiF_6^{2-} anion with predominance of the σ-component and in TiF_4 with predominance of the π-component. The combined effect of the electrode surface and the electric field results in considerable lowering of the activation barrier for EAS four-electron reduction. A TiF_6^{2-} anion surrounded by six cations and a TiF_4 molecule surrounded by four alkali metal cations have the optimum reducing ability. In our opinion, these results are in full compliance with the idea of outer-sphere cationisation in melts containing anions with complex compositions[3, 44, 45] confirmed by electrochemical studies on tungstate- and molybdate-containing systems.[83]

IV. Structures, chemical and electrochemical properties of boron-containing fluoride melts

Much less data are currently available on the structures and properties of boron-containing fluoride melts than on titanium-containing fluoride melts; these data have almost not been interpreted.

Raman spectroscopic studies on the $NaBF_4$ and $NaF–NaBF_4$ melts[84] showed that the structure of the BF_4^- anion remains unchanged at temperatures up to 880 K. A similar conclusion was made by Prostakov *et al.*[85] who also noted that various complex associates can exist in $KBF_4–KF–CsF$ melts. Pirina and

Prostakov[86] used data on the specific densities and electric conductivities of the $KBF_4-KF-CsF$ system to calculate the stabilisation energies of these complex associates. They also stated that complex anions $[M(BF_4)_4]^{3-}$ with tetrahedral configurations were formed predominantly and noted that mixing of salts having the same cation resulted in gradual substitution of anions to give mixed complexes of the types $[MF_4]^{3-}$, $[M_4F]^{3+}$, $[M(BF_4)_4]^{3-}$, $[M(BF_4)_6]^{3-}$, $[M(BF_4)_3F]^{3-}$ and $[M(BF_4)_2F_2]^{3-}$.

A study on solubility of BF_3 in $KCl-KF$ melts at 870–970 K showed[87] that after dilution of the melt with respect to fluoride or after addition of strongly polarising cations (Li^+, Mg^{2+}, Ba^{2+}, Ca^{2+}), the system contains (in addition to the BF_4^- species) mixed fluoride–chloride boron complexes and BF_3 molecules in equilibrium with halide ions. Based on data on boron equilibrium potentials in $KCl-KF-KBF_4$ melts,[88,89] it was concluded that the majority of boron ions exist as higher fluoride and fluoride–choride complexes, *viz*., $[BF_4]^-$ and $[BF_3Cl]^-$, respectively. It was assumed[90] taking account of viscosity and specific density data for $NaCl-NaBF_4$ and $NaCl-RbBF_4$ melts that the structures of tetrafluoroborate melts comply with the model of 'solids' (with retention of the short order arrangement of species).

The ambiguous interpretation and scantiness of data on the structures and physicochemical properties of boron-containing melts often result in conflicting concepts on the electrochemical reduction processes in these melts. Studies on the cathodic process in the $LiF-KBF_4-KF$ system showed that reduction of the BF_4^- anion involves simultaneous transfer of three electrons.[91] It was assumed that diffusion of the BF_4^- anions from the melt bulk is not a limiting step of electrochemical reduction, and this is an indication of the process complexity. Myshalov[92] who studied the electrochemical reduction in boron-containing melts concluded that boron reduction follows a two-step mechanism. Vasil'eva *et al*.[93] studied the possibility of electrochemical preparation of boron from borax-containing melts; they detected several waves on the polarisation curves originating from the stepwise reduction of the oxygen-containing anion.

The reduction kinetics of boron compounds in fluoride-containing melts have been studied most thoroughly by Tsiklauri *et al*.[94–96] Analysis of reduction chronovoltammograms and interpretation of the spectral characteristics of the ternary molten system $KCl-NaCl-KBF_4$ suggest that the chloride–fluoride melt contains several boron-containing equilibrium forms. Reduction of three of them, *viz*., BF_4^-, BF_3Cl^- and BF_3, is believed to account for two waves in the voltammetric curves. This conclusion does not contradict the data by Zarutskii *et al*.[97] On the other hand, the EAS formation mechanism was not related to the melt cationic composition[98] which is important in EAS formation in the melt bulk.

The EAS formation scheme in fluoride boron-containing melts is represented as follows:[99]

$$n\,M^{m+} + BF_4^- \rightleftharpoons \begin{matrix} \{M_n^{m+}[BF_4]^-\}^{(mn-1)+} \\ BF_3 + F^- + n\,M^{m+} \end{matrix} \qquad (13)$$

Preliminary calculations showed that dissociation of an isolated BF_4^- anion is impossible for energetic reasons. It was found that the interaction of this anion with Na^+ and Mg^{2+} cations demonstrates a trend towards a decrease in the intra-anion bond energies, while the interaction with the Li^+ cations, the trend is towards their increase. Distribution of atomic charges and populations of the atomic orbitals of these systems indicates strengthening of the B–F bonds in metal complexes of the anion with Li^+ cations due to predominance of the π-component in the σ,π-mechanism of electron density redistribution in BF_4^-. In metal complexes with Na^+ and Mg^{2+} cations, the σ-component was found to predominate.

The possible dissociation of the BF_4^- anion upon cation–anion interaction cannot be ruled out. The interaction of one of the products of reaction (13), *viz*., the BF_3 molecule, with the melt cations has been studied.[100] Analysis of the interaction energies of BF_3 with Na^+ or Li^+ for the cases where the coordination numbers of these cations are equal to 1, 2 and 3 showed that cleavage of the B–F bonds does not occur, though they are weakened considerably. On the other hand, interaction of two Mg^{2+} cations with BF_3 results in decomposition of the BF_3 molecule; in this case, the formation of $\{Mg_2^{m+}[BF_3]^0\}^{2m+}$ associates in the melt bulk is possible.

It was noted[101] that the cationic environment lowers the activation barriers for two- and four-electron reduction of the products of reaction (13), *i.e*., metal complexes of the BF_4^- anion and associates of the BF_3 molecule, in comparison with the corresponding values for the isolated BF_4^- and BF_3 species. Predominance of two-electron reduction over four-electron reduction is observed both for cationised anions and for BF_3.

Spectroscopic studies on the molten ternary system $KCl-NaCl-KBF_4$ suggest that mixed chloride–fluoride complex ions $[BF_{4-x}Cl_x]^-$ exist in the melt.[102] Analysis of the effect of the background electrolyte chloride anions on the interaction of the BF_4^- species with one or two lithium cations (carried out by quantum-chemical calculations) showed the possible formation of both $[BF_{4-x}Cl_x]^-$ complexes and their associates in the cationic environment. The $\{[BF_3]^0Cl^-\}^-$ species is the most reduction-stable. The activation barrier for two-electron reduction of these associates is lower than that of the BF_4^- anion without the cationic environment. The maximum decrease is achieved for the $\{Li^+[BF_3Cl]^-\}^0$ system. However, though the effect of the activation barrier decrease for BF_4^- and BF_3 in a cationic environment is greater than that for the $\{Li^+[BF_3Cl]^-\}^0$ associate, one cannot rule out a possible decrease in the latter.

Solov'ev[103] assumed that the effect of the electrode surface in boron-containing fluoride melts causes electron density migration in EAS according to the σ-mechanism, resulting in an insignificant weakening of the B–F bonds. It was therefore concluded that, within the model scheme selected, the electrode surface does not affect greatly the EAS formation mechanism.

Imposed electric field ($E = 2\times10^{10}$ V m^{-1}) enhances the trend towards weakening of the B–F bonds in $\{M_n^{m+}[BF_4]^-\}^{(mn-1)+}$ and strengthens slightly these bonds in other EAS.[104] On the other hand, the decrease in the activation barriers for reduction due to the surface and electric field effects results in a considerable increase in the reducing ability of cation–anion interaction products. Taking this into consideration, the following EAS forms can be assumed: $\{M_4^{m+}[BF_4]^-\}^{(4m-1)+}$, $\{M_2^{m+}[BF_3]^0\}^{2m+}$, BF_3, $\{M^+[BF_3Cl]^-\}^0$. Thus, the EAS formation mechanism was complemented as follows:

$$n\,M^{m+} + BF_3 \rightleftharpoons \{M_n^{m+}[BF_3]^0\}^{mn+}, \qquad (14)$$

$$n\,M^{m+} + [BF_{4-x}Cl_x]^- \rightleftharpoons \{M_n^{m+}[BF_{4-x}Cl_x]^-\}^{(mn-1)+}. \qquad (15)$$

Analysis of electrochemical measurements of BF_4^- and BF_3 reduction with the $KCl-NaCl$ melt as the background has been carried out by Tsiklauri *et al*.[95,96] without interpretation of the EAS reduction waves. Based on the calculations, the existence of an additional EAS (besides BF_3 and associates of chloride–fluoride complexes) was assumed,[104] namely, $\{M_n^{m+}[BF_3]^0\}^{mn+}$; the probability of its reduction is higher than that of mixed chloride–fluoride associates.

V. Effect of cations on the mechanisms of chemical and electrochemical reactions in ionic melts

The effect of the solvent nature on the mechanism and rate of chemical reactions in ionic melts was first discovered by Rust and Duke[31] in a study on acid-base equilibria in nitrate-containing melts. It was shown that replacement of a solvent with weakly polarising cations by a solvent with strongly polarising cations accelerates the reactions. This effect was explained by activation of the reacting molecules by the cationic environment. In other studies, the role of the melt cationic composition was ignored. For example, in studies on the electrochemical reduction of oxygen-

containing anions [26, 35, 36] it was assumed that, irrespective of the electrolyte cationic composition, the anions themselves participate in the cathodic reaction. The specific features of the cathodic reduction of anions in the presence of cations were explained by various factors excluding the acid-base interaction.

Certain model concepts used in studies on aqueous solutions were applied to ionic melts. In an analysis of the possible direct discharge of the nitrate ion in aqueous solutions, Lopatin[105] used the 'cationic bridges' concept which makes it possible to explain the effect of the solution cations on the cathodic process. Having studied the anion discharge kinetics near the zero charge potential of the electrode, he explained the effect of cations on the discharge rate by a decrease in the negative reduction potential of the nitrate ion with increase in the concentration and the cation charge. The possibility of direct discharge of the nitrate ion has also been noted.[106] Kvaratskheliya [39] studied the effect of the cation nature on the shift of NO_3^- cathodic reduction waves in aqueous electrolyte solutions. In his opinion, one of the reasons for the effect of salts with polyvalent cations on the positive shift of the cathodic wave is the formation of cation–anion pairs in which one of the N—O bonds is weakened under the effect of the cationic environment.

In studies on electrode processes in melts of individual nitrates with various cationic compositions,[40–42] it was concluded that the activity of the nitrate ion is determined by its environment and hence depends on the acid-base properties of the melt. Differences in the positions of the NO_3^- electrochemical reduction wave were explained by the different charge densities of the cations whose force field affects both the NO_3^- anions and the O^{2-} ions formed in the cathodic process. Attempts were made to find an empirical relationship between the composition of a nitrate-containing melt and the reactivities of its components. For example, Fletcher *et al.*[107] reported an inverse dependence of the isobaric potential of activation of NO_3^- electrochemical reduction on the solvent cation radius.

In a study on the self-diffusion and charge transfer in carbonate- and nitrate-containing melts, the existence of metal complexes such as MCO_3^-, MNO_3^- and $M_2NO_3^+$ (the latter being most probable for the lithium cation) in the melt was assumed and the possibility of the following elementary chemical reactions in a melt was noted:[108]

$$M^{n+} + \text{base} \rightleftharpoons \text{acid}. \qquad (16)$$

Of interest are the studies by Shams El Din *et al.*[109, 110] reporting a comparative estimate of the acidities of alkali and alkaline-earth metal cations. According to these data, the acidity changes in the series of cations: $Ca^{2+} > Li^+ > Sr^{2+} > Ba^{2+} > Na^+, K^+$.

One of the first theoretical studies on the effect of the medium on the elementary act of chemical reactions in the condensed phase can be found in a series of works.[98, 111–113] They considered certain classes of chemical and electrochemical processes and calculated the kinetic parameters of the elementary act of charge transfer, the mechanism of which being dynamically affected by the macroscopic medium. In their opinion, the dynamic effect is determined by fluctuations or changes in the ionic environment surrounding the reacting species; chemical reactions are assumed to occur in a polar liquid and to be accompanied by a considerable charge density redistribution in the reacting species.[110] It was noted [111] that short-range effects predominate in reactions in ionic melts.

Proof that the cationic composition of the medium affects the mechanisms of electrochemical reactions in nitrate-containing melts was obtained in a series of studies [47–49] where a different scheme for the EAS formation mechanism in such melts was suggested (see Section II). However, we feel many statements of this scheme to be debatable because of the doubtful assumption that the nature of inter-species interactions in the electric double layer is the same as in the melt bulk. The electrochemical reaction mechanisms have also been found to be affected by cations for titanium-[66, 69, 70] and boron-containing [84–86, 97] halide melts. Unfortunately, the results obtained were not accompanied by conclusions or generalisations.

The results of experimental studies [28–30, 44, 45] on the kinetics of electrode processes with conjugate acid-base reactions in oxychloride molten salts demonstrate that the cationic composition of the melt affects the rate and mechanism of the reactions occurring in the melt. These studies are based on the idea that the electrochemical activities of oxygen-containing anions originate from the cation–anion mechanism of the EAS formation specific for molten salts (see Section II). This mechanism can be regarded as acid-base interaction where the decisive role belongs to the acid properties of the cations. The formation of EAS and their reactions in the near-electrode layer occur at a limited rate since these processes involve complete restructuring of the reacting species.

The assumption on the cation–anion interaction in molten electrolytes was confirmed in studies on the electrochemical reduction kinetics of oxygen-containing anions in chloride and oxide melts. Detailed studies on the electrochemical reduction of WO_4^{2-} with an equimolar KCl–NaCl melt as the background [4] and of a sodium tungstate melt [114] showed that the tungstate ion itself is not an electrochemically active species but it can generate such species. Owing to the cation–anion interaction, a sufficient excess of strongly polarising cations results in outer-sphere cationisation of the WO_4^{2-} anion to give symmetrically cationised species. Thus, the electrochemical reduction of oxygen-containing anions in the presence of molten chlorides as the background is preceded by a slow acid-base reaction which is the rate-determining step of the electrode process. The EAS are formed due to the interaction of the oxygen-containing anion with the molten electrolyte according to the cation–anion interaction mechanism determined by the acid-base properties of the medium.

VI. Theoretical and experimental studies of cation–anion interactions in nitrate- and carbonate-containing melts

The results of experimental studies discussed above [28–30, 39–42, 44–49, 108–110] suggest that the reduction of oxygen-containing anions depends on the cationic composition of the melt. Hence, it is necessary, first, to estimate the possibility of the formation of cationised anions (metal complexes) in principle and second, to study the effect of cations on the reducing abilities of anions. In application to nitrate- and carbonate-containing melts, the cation–anion interaction was represented by Schemes (7) and (8).

The CO_3^{2-} anion, the CO_2 molecule and their complexes with the lithium cations (up to five-coordinate complexes) were selected as model compounds for preliminary quantum-chemical calculations. A preliminary energy-based estimate of cation–anion interaction pathways for carbonate-containing melts based on a semiempirical calculation showed [115, 116] the possibility of formation of a broad spectrum of metal complexes of the CO_3^{2-} anion with lithium cations and the effect of the cation nature on the increase in the reducing ability of cation–anion interaction products.

Analysis of the energy profiles of potential surfaces of the interaction of NO_3^- and CO_3^{2-} with Li^+ or Be^{2+} showed that the interaction of cations preferentially occurs along the bisecting line of any bond angle of the anion; there are local energy minima in the monodentate position of the cation with respect to the anion.[117, 118] If interaction between cations and anions is sufficiently strong (it is more efficient in the case of Be^{2+}), the weakening of N—O intra-anion bonds under the effect of the cation was found to differ noticeably from that of C—O bonds. As calculations showed, bidentate interaction of an anion with a cation results in electron density migration from the $2s$, $2p_x$ and $2p_y$ orbitals of the O(1) and O(2) atoms to the corresponding

cation orbitals with formation of σ-bonds. As a result, an effective positive charge σ^+ is transferred to the oxygen atoms.

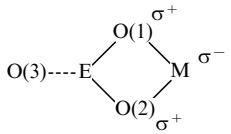

(17)

In turn, this favours the electron-donating effect of the $2p_2$ orbitals of O(3)

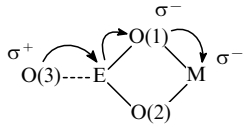

(18)

with formation of π-bonds.

In complexes formed by the nitrate ion, electron density redistribution along the π-bonds under the effect of cations occurs within the NO_3^- anion and causes strengthening of the N—O bond. On the contrary, the σ-mechanism of electron density redistribution predominates in the carbonate ion and in the corresponding complexes, resulting in a considerable weakening of the C—O bonds. Thus, the role of metal cations is to effect the polarisation of an anion as a whole according to the σ,π-interaction mechanism with predominance of one of the interaction types in the isoelectronic ions NO_3^- and CO_3^{2-} (see Refs 119, 120). The results of semiempirical and *ab initio* calculations coincided qualitatively, which afterwards permitted the use of semiempirical calculations which are less laborious.

The gradual increase in the number of the first solvate shell cations, results in the weakening of C—O bonds in CO_3^{2-} with an increase in the coordination number. For the coordination number equal to 2, cleavage of one C—O bond occurs. Conversely, a trend towards strengthening of the N—O bonds is observed for NO_3^-. This conclusion was confirmed by data on charge transfer and electron density migration within anions for the entire coordination number range and by spectroscopic data.[121]

Analysis of the energies of the frontier molecular orbitals showed that the ability of NO_3^- to undergo reduction is higher than that of CO_3^{2-}. Cationisation results in a decrease in the energy gap between the highest occupied and lowest unoccupied molecular orbitals in these anions, which suggests that the cation–anion interaction has a favourable effect on the ability of anions to undergo reduction.[122, 123] Comparison of the reduction activation barriers for NO_3^- and CO_3^{2-} and their metal complexes also indicates an increase in the ability of anions to undergo reduction due to the cation–anion interaction. This interaction decreases the reduction activation barriers for the entire series of complexes.[123]

Electric field is one of the most important factors affecting the reduction in melts. The results of quantum-chemical calculations were used to estimate the effect of the electric field on the acid-base interaction and on the elementary charge transfer act. A uniform electric field was simulated by a system of opposite charges located symmetrically at a long distance from the molecule. The calculations were carried out using a programme developed for this purpose.[124] It was shown[125] that a field which enhances the specificity of cation–anion interaction (predominantly, σ-type in carbonate ion and π-type in nitrate ion) affects considerably the reducing ability of the interaction products; specifically, it lowers the activation barrier.

Shapoval *et al.*[126] reported the results of an experimental examination of the acid-base interaction mechanism by determining a number of electrochemical parameters of the electrode process affected most strongly by the acidity of the melt. The model, Scheme (8), determined the choice of the starting system for the study on cation–anion interaction in melts. Studies on NO_3^- electrochemical reduction in a K, Na, Cs/Cl eutectics as the background (T = 793 K) showed that, like the K, Na, Rb/Cl eutectics, it is weakly acidic with respect to the NO_3^- anion and is suitable for studies on NO_3^- anions with strongly polarising cations. Introduction of Mg^{2+}, Ca^{2+} or Li^+ cations to a nitrate-containing chloride melt at concentrations no higher than a two-, four- and hundred-fold excess, respectively, with respect to NO_3^- shifted the electrochemical reduction wave towards negative potentials.[127–129] Further increase in the concentration of the added anions shifted the discharge potential to more positive region. Analysis of the chronovoltammograms for the NO_3^- anion in the presence of, *e.g.*, a strongly polarising Ca^{2+} cation suggested unambiguously the catalytic character of nitrate reduction waves in the presence of excess Ca^{2+}. It was shown[127, 129] that the excess of these cations is not only consumed in the formation of qualitatively new electrochemically active species, *viz.*, metal complexes, but also results in regeneration of the depolariser in agreement with the experimental Scheme (11).

The coordination number of the Ca^{2+} cations determined in the presence of a considerable excess of these cations equalled 2, while that in the case of excess magnesium cations equalled 3. Calculations of heterogeneous rate constants of charge transfer and regeneration of the original EAS indicate that introduction of cations to the melt catalyses the overall process,[127, 130] while the EAS formation during the electrochemical reduction of NO_3^- in the presence of Li^+, Ca^{2+}, Mg^{2+} occurs according to the cation–anion interaction mechanism in accordance with Scheme (8).

Experimental studies on the cation–anion interaction of CO_3^{2-} with strongly polarising cations[131–133] indicate that this can be described by Scheme (7).

Experimental studies confirmed certain regularities obtained from quantum-chemical calculations.[134] For example, an increase in the rate constants of charge transfer and regeneration of the original EAS with an increase in the specific charges and concentrations of cations in a melt corresponded to a decrease in the activation barrier for EAS reduction. The reduction potential shift by more than 0.6 V upon replacement of Na^+ by Mg^{2+} correlated with the calculated changes in the N—O bond energies in metal complexes formed by the nitrate ion. The absence of electrochemical activity in CO_3^{2-} in the presence of weakly polarising cations in a melt correlates with high activation barriers of two- and four-electron reduction. The experimentally found reduction of CO_3^{2-} in the same potential range in the presence of cations with various polarising strengths correlates with the calculated data, according to which CO_3^{2-} is characterised by a trend towards dissociation. Similar results were also obtained in other studies[51, 135] on the electrochemical reduction of CO_3^{2-} in tungstate melts with various cationic compositions.

The results of a theoretical and experimental study on the mechanism of cation–anion interaction in carbonate and nitrate-containing melts were reviewed by Solov'ev.[136] It is generally acknowledged that this mechanism includes the formation of cationised anions (metal complexes) $[M_nNO_3]^{(mn-1)+}$ and dissociation of CO_3^{2-} under the effect of cationic environment. However, this mechanism being applied to dilute melts did not account for the effect of the electrode surface and the electrical field on both the character of cation–anion interaction and the elementary charge transfer act.

The electrochemical reduction characteristics measured depend on a combination of various factors. The adsorption properties of the electrode surface (together with the temperature mode and the electrical field) affect strongly the character of electrochemical reduction in melts. Considering the surface of a solid electrode as possessing a discrete structure and the differences in the structures of the melt–electrode interfaces (at zero charge potential) caused by individual features of the electrode and melt surfaces, one should take into account the interaction of the surface atoms with adsorbed species of the melt. In accordance with the general physical concepts, this results in changes in the electronic properties of the interface. A preliminary estimate (quantum-chemical calculations) of the electrical field effect on the reactivity of cation–anion interaction products[125] agrees with

real processes of electrochemical reduction in melts. Such processes occur on electrode – melt interfaces where a certain potential gradient exists. Electrochemical reduction and cation – anion interaction are influenced not only by adsorption effects but also by the electrical field (external field and double layer field). Therefore, more detailed studies of the field effect on electrochemical reduction (on the energy parameters of cation – anion interaction products and on their reactivities) are necessary.

Thus, three basic factors should be taken into account in the analysis of the EAS formation mechanism and electrochemical reduction in nitrate- and carbonate-containing melts, *viz*., the acid-base properties of a melt, the electrode surface properties and the effect of the electric field.

VII. Multielectron electrochemical reduction of oxoanions of high-melting metals and non-metals in ionic melts

Multielectron electrochemical discharge – ionisation reactions can occur with simultaneous charge transfer or through a number of consecutive steps, with transfer of one or several electrons involved in each of the steps. It was noted [137–139] that the mechanisms of these reactions can be described by determining experimentally the effective transfer factors or the stoichiometric factors of the elementary steps. However, due to the diversity of ionic states in electrolytes and structures of cathodic deposits, it is unlikely that a general (common) mechanism for the electrochemical deposition of polyvalent metals and non-metals will ever be established.[140, 141] One can govern the reactivities, solubilities and electrochemical properties of the starting and transient forms by changing, *e.g*., the temperature and electrolytes.

There are several viewpoints on the mechanisms of electrochemical reduction of high-melting polyvalent metals from ionic melts. According to one of them (*cf.* Ref. 141), electrochemical reactions result in cathodic deposition of high-melting metals as solid oxygen-containing compounds (oxides and bronzes). A different viewpoint was expressed by Spitsyn *et al*.[142] who believe that the deposits in question consisted of products of electrochemically initiated polymerisation of high-melting metal ions. At the moment, it is hardly possible to prefer the involvement of one particular species over another in reduction. However, there is no doubt that after multicharged species obtain the first electrons, they become reactive and initiation of polymerisation of the species becomes possible. In this case, the situation resembles that observed in aqueous solutions.[141] It is believed that the alkali metal acts as the reduced state stabiliser in melts and in non-aqueous solutions; in aqueous solutions, this role is played by hydrogen. However, the mechanism suggested is questionable, especially in the case where solid oxygen-containing compounds are not formed on the cathode.

It was assumed in certain publications (see, *e.g*., Refs 143 and 144) that the discharge and ionisation of polyvalent metals in aqueous solutions occur *via* transient ions with intermediate valence, the kinetic and thermodynamic stabilities of which depend on the nature of the metal and the electrolyte. Many of the intermediates formed in the bulk of the near-electrode layer possess high reactivities; they react with each other (disproportionation) and with the solution components (redox reactions). As a consequence, the life-times of these ions are small. It is a matter of discussion whether these concepts can be applied to ionic melts.

Polyakov [145] analysed the studies on the electrochemical behaviour of niobium in chloride, oxochloride, chloride – fluoride, oxochloride – fluoride, chloride and oxofluoride melts. It was concluded that both multistep discharge (according to virtually every possible scheme for pentavalent metals, including the transient formation of clusters and intermediates) and single-step discharge of niobium-containing ions are possible. It is generally acknowledged that niobium is reduced in two or three steps in chloride – fluoride electrolytes. The number of steps of niobium reduction in oxochloride – fluoride melts depends on the O : Nb ratio (for $O : Nb \leqslant 1$, a single-step process is observed).

The diversity of niobium oxofluoride and fluoride complexes existing in melts based on NaCl – KCl and the variety of mechanisms of their electrochemical reduction have been noted in a number of studies.[146–151] To date, much remains unclear in the chemistry and electrochemistry of niobium in salt melts.[145] A general problem, as in studies on other metals, is the establishment of correlations between the data from physicochemical and spectroscopic studies and the results of electrochemical measurements obtained by linear voltammetry, chronopotentiometry and other related methods. In addition, discharge of different-ligand complexes and release of their anionic shells in the near-cathode layer can involve the formation of species with compositions other than those of species in the melt bulk.

The laws of electrochemical behaviour of tantalum resemble those of niobium in similar melts.[147]

In their surveys Kuznetsov *et al*.[152, 153] noted diverse views on the electrochemical reduction mechanism of zirconium in fluoride, chloride, fluoride – chloride and oxofluoride melts. Some researchers consider that discharge of ZrF_6^{2-} to give the metal is preceded by various intermediate steps (formation of complex fluorides $n\,MF \cdot ZrF_2$, poorly soluble complex salts $MZrF_4$, *etc*.). Others believe that the reduction of ZrF_6^{2-} is a multistep (involving two or even three steps) or a one-step process. The existing disagreement can be explained by differences in the experimental conditions and in techniques for the interpretation of results.[154, 155] It is presently believed [155, 156] that the electrochemical reduction of zirconium in chloride – fluoride melts occurs either according to the auto-inhibition scheme or with four-electron reversible single-step charge transfer, depending on the concentration of the F^- ion.

Of particular interest are theoretical studies on the stepwise character of charge transfer. For non-adiabatic reactions, the discharge of polyvalent ions is usually represented by a sequence of single-electron charge transfer steps with concomitant intervalent interactions, which are also considered to be one-electron processes.[157, 158] However, a series of studies on the features of electrochemical reduction of the elements in question did not reveal any steps in the discharge of the corresponding oxo, oxohalide and halide complexes. Studies on adiabatic electrochemical electron transfer reactions showed [157, 158] that at a certain ratio between the energy of environment reorganisation accompanying the electron transfer and the Coulombic interaction energy of valence electrons in the reagent, the consecutive single-electron discharge can become multi-electron discharge. In this case, the elementary charge transfer act can be compared to a continuous stream of electrons which cannot be separated into separate steps.

To date, the stepwise character of multielectron processes could not be detected by methods of electrochemical analysis. The use of quantum-chemical methods was suggested for this purpose.[57, 79, 101, 104] A specially developed technique was used for comparison of the activation barriers of multi- and single-step electrochemical EAS reduction with optimal compositions and forms in carbonate-, nitrate-, boron- and titanium-containing melts.[57, 104] For boron-containing melts it was found [57, 101] that the activation barriers for two-step reduction of BF_4^- anions and BF_3 molecules are lower than those for single-step reduction. This law is no longer valid in the case of boron-containing metal complexes. It was concluded for titanium-containing fluoride melts [57, 79] that single-step reduction is more favourable than multi-step reduction.

Thus, no common mechanism of electrochemical reduction of multivalent metals and non-metals has been established to date. Different states of the ions of these metals in electrolytes, structures of cathodic deposits and conditions of the process (temperature and the nature of the electrolyte) can favour one or another electrochemical reduction mechanism. The ambiguity

and diversity of electrochemical reduction mechanisms of EAS can also be due to differences in the melt compositions (different anionic and cationic compositions, admixtures) and in features of experimental techniques (for example, electrode polarisation rates, purity of reagents, materials of electrodes and atmosphere in voltammetry). The possible 'masking' of the apparent stepwise mechanism by autoinhibition should also be noted. Therefore, in each particular case of single-step electrochemical reduction, one should speak of a narrow potential range, which practically cannot be resolved by the existing methods.

The processes of electrochemical evolution of high-melting metals and non-metals from ionic melts underlie a new promising method for the preparation of carbides, borides and silicides of Group IV–VIA metals, *i.e.*, high-temperature electrochemical synthesis.[3, 159] It should be noted that there is as yet no generally accepted opinion on the mechanism of EAS formation involving these compounds. In this Section, we survey the results of experimental studies on the mechanisms of formation and structures of the EAS of high-melting metals.

1. MoO_4^{2-} and WO_4^{2-} anions with chloride melts as the background in the presence of strongly polarising cations

Systematic studies on the electrochemical behaviour of molybdate and tungstate ions in oxohalide electrolytes were carried out by many research groups. Electrochemists from the Sverdlovsk scientific school studied the electrochemical deposition from melts based on alkaline-earth metal chlorides. It was found[160] that anodic dissolution of molybdenum in $CaCl_2$–CaO melts produces MoO_4^{2-} ions; if an admixture of MoO_3 is present, the formation of $Mo_2O_7^{2-}$ ions is more probable. Depending on the melt temperature on the cathode, either molybdenum oxide Mo_2O_3 or metallic molybdenum are deposited.[161] Deposition of molybdenum occurs from electrolytes with acidic properties caused by the presence of calcium cations.[160–162]

It has been shown by electrochemists from the Kiev scientific school[163, 164] that EO_4^{2-} anions (E = Mo, W) in an equimolar KCl–NaCl melt as the background (973–1073 K) do not manifest electrochemical activity up to decomposition potentials of the background electrolyte. The equilibrium potential of molybdenum (tungsten) is not reached in these systems, as noticeable metallic corrosion occurs. The acidic character of alkali and alkaline-earth metal cations (Li^+, Ba^{2+}, Ca^{2+}, Mg^{2+}, Al^{3+}) was established.[165, 166] Introduction of cations with high polarising strength (Li^+, Ba^{2+}, Ca^{2+}) to melts containing EO_4^{2-} anions gives rise to a reduction wave at more positive potentials than the decomposition potential of the background electrolyte.[167, 168] Acidification of the melt results in a considerable increase in the reduction wave of molybdate (tugstate) ions and its displacement to the positive range of potentials. If the melt is acidified with a small concentration of Ca^{2+} cations, one wave is observed; two waves are observed at $[Ca^{2+}] \approx (4-5)\,[WO_4^{2-}]$: the first wave reaches a maximum, and a second wave appears at more negative potentials. Upon acidification with Li^+, Ba^{2+} or Ca^{2+} cations, the WO_4^{2-} reduction waves maintain their kinetic nature. This follows from the absence of a linear dependence of the limiting current on the cation concentration and from the activation energy of the limiting current (88.2 kJ mol^{-1} for $[Ca^{2+}] \to 0$). As the melt is acidified, the surface kinetic constant increases by an order of magnitude and reaches the values comparable to the diffusion constant, while the activation energy of the limiting current decreases to 12.4 kJ mol^{-1} (see Ref. 169).

If a 3.5–4.0-fold excess of Mg^{2+} cations with respect to EO_4^{2-} is introduced, an almost proportional relationship between the limiting current of the reduction waves and the concentration of these cations is observed.[170, 171] The maximum limiting current is reached at $[Mg^{2+}] \approx 4\,[EO_4^{2-}]$. Under these conditions, the mass transfer rate constant $[(1.5-2.0)\times 10^{-3}$ cm s$^{-1}]$ is comparable to the diffusion constant; this suggests the diffusion nature of the steady-state waves.

Introduction of Al^{3+} cation also resulted in a proportional dependence of the limiting current on the concentration of this cation. At $[AlCl_3] > 0.5\,[EO_4^{2-}]$, strong evolution of gases (chlorine, chlorine oxides) and a decrease in the limiting current were observed.

In a chloride melt as the background, the electrochemical reduction of MoO_4^{2-} and WO_4^{2-} anions to the metals in the presence of various cations (Li^+, Ba^{2+}, Ca^{2+}, Mg^{2+}, Al^{3+}) occurs at various potentials. On going from Li^+ to Al^{3+}, the reduction potentials are shifted in the positive direction by more than 1 V. The limiting current of MoO_4^{2-} and WO_4^{2-} electrochemical reduction is reached at a non-equivalent concentration of cations. The shift of the reduction half-wave potentials ($E_{1/2}$) upon a ten-fold increase in cation concentration is 0.2–0.4 V. Such a significant $E_{1/2}$ shift upon changing the concentration and the cation polarising strength results from the different compositions of the electrochemically active species due to changes in the acid-base properties of the melt. As Shapoval *et al.*[170, 171] report, this shows that, first, variations of the acid strength and the cation concentration change the acid-base reaction stoichiometry, which cannot be described by dissociation of the anion; second, it cannot be described by a reaction resulting in the complete loss of oxygen ions by the metal.

The EAS formation mechanism in melts with various cationic compositions can be presented by the following scheme:

$$xM^{z+} + EO_4^{2-} \rightleftarrows \begin{matrix} \{M_x^{z+}[EO_4^{2-}]\}^{zx-2} \\ \rightleftarrows \\ EO_{4-x}^{2(x-1)} + xM^{z+}O^{2-} \end{matrix}, \qquad (19)$$

where E = Mo, W; $M^{z+} = Li^+$, Ba^{2+}, Ca^{2+}, Mg^{2+}, Al^{3+}.

The direction of shift of equilibrium (19) is determined by the polarising strength and concentration of the cation and by the anion strength. In any case, the cation–anion interaction occurs through a step of the formation of metal complexes.

Acidification of a melt containing MoO_4^{2-} or WO_4^{2-} by Li^+, Ba^{2+}, Ca^{2+} or Mg^{2+} cations results in outer-sphere cationisation of anions giving metal complexes $\{M_x^{z+}[EO_4^{2-}]\}^{(xz-2)+}$. Acidification of the same melts by the Al^{3+} cation results in decomposition of the anions to give $EO_{4-x}^{2(x-1)-}$ species.

The outer-sphere cationisation of WO_4^{2-} anion by the Ca^{2+} cation was studied by IR emission spectroscopy.[172] It was shown that at $[Ca^{2+}] > [WO_4^{2-}]$, symmetric cationisation occurs to give the $\{Ca_4^{2+}[WO_4^{2-}]\}^{6+}$ species.

Shapoval *et al.*[170, 171] also observed an increase in the electron-accepting properties of molybdate and tungstate ions with increase in their degree of cationisation and increase in the acid strength of the cation. This indicates that multielectron processes might have occurred. Apparently, the specific features of multielectron processes are caused by the particular structure of the cationised EAS. For example, in the case of Ca^{2+} and Li^+ cations, two electrons are transferred in the electrode process

$$\{Ca_x[WO_4^{2-}]\}^{2(x-1)} + 2e^- \rightleftharpoons WO_2 + x\,CaO + (2-x)\,O^{2-}, \qquad (20)$$

where $1 \leqslant x \leqslant 2$.

For $x = 4$ in the presence of Mg^{2+}, Al^{3+} in the melt, transfer of six electrons occurs in a practically unresolvable range of potentials. The multielectron electrochemical processes are described by the following overall reactions:

$$\{Li_4^+[EO_4^{2-}]\}^{2+} + 6e^- \longrightarrow E + 2\,Li_2O + 2O^{2-}, \qquad (21)$$

$$\{Ca_4^{2+}[EO_4^{2-}]\}^{6+} + 6e^- \longrightarrow E + 4\,CaO, \qquad (22)$$

$$\{Mg_4^{2+}[EO_4^{2-}]\}^{6+} + 6e^- \longrightarrow E + 4\,MgO. \qquad (23)$$

In the case of acidification by the Al^{3+} cations

$$AlO_2Cl_{2+x}^x + 6e^- \rightleftharpoons Al + 2\,O^{2-} + (2+x)\,Cl^-. \qquad (24)$$

2. CO_3^{2-} anions with chloride and carbonate melts as the background

The cathodic evolution of carbon upon electrolysis of molten carbonates has first been reported by Haber and Tolloczko [173] who obtained carbon deposits from a $BaCl_2-BaCO_3$ melt at 853 K. Systematic studies on electrolysis and electrode processes involving carbonates have been carried out by electrochemists from the Kiev and Sverdlovsk scientific schools. Delimarskii *et al.*[22] have found that graphite powder is the only cathodic product in the electrolysis of an equimolar $Li_2CO_3-K_2CO_3$ mixture at 853–873 K (current efficiency ~100%); carbon dioxide and oxygen (in 2:1 ratio) are the anodic products. The cathodic process is believed [174, 175] to include the reaction

$$CO_3^{2-} \rightleftharpoons CO_2 + O^{2-} \quad (25)$$

and reaction (9), while the anodic process includes the reactions

$$CO_3^{2-} \longrightarrow CO_2 + (1/2)O_2 + 2e^- , \quad (26)$$

$$O^{2-} \longrightarrow (1/2)O_2 + 2e^- . \quad (27)$$

The ratio of the parallel reactions (26) and (27) is determined by the current density. It has been noted that carbon is not formed in the electrolysis of pure K_2CO_3. If this melt is saturated with CO_2 (under pressure), carbon is precipitated on the cathode. Shapoval *et al.*[176, 177] concluded that a certain CO_2 concentration is required for carbon deposition from molten chlorides; it can be achieved by addition of thermally unstable carbonates or by saturation of the melt with gaseous carbon dioxide.

Trunov and Stepanov [178, 179] showed that a platinum electrode which contacts with a mixed stream of carbon dioxide and oxygen is reversible with respect to a carbonate melt. They believe that an equilibrium (between carbonate ions and molecules of CO_2 and O_2) is established on the electrode. Smirnov *et al.*[180] studied the polarisation of platinum and nickel electrodes in a melt of alkali metal carbonates. It was shown that, depending on the current density, various electrode reactions occur resulting in formation of carbides, evolution of free carbon and carbon(II) oxide, as well as discharge of alkali metal cations. The polarisation depends on the concentration of carbonate ions and is due to their diffusion from the bulk melt to the surface. The mechanisms of anodic processes in chloride–carbonate melts in various atmospheres (He, CO, CO_2 or $2CO_2 + O_2$ mixture) have been studied in detail.[181]

Bartlett and Johnson [27, 182] calculated the decomposition potential of alkali and alkaline-earth metal carbonates and considered all possible variants in the reduction of carbonate ions. Based on the calculations, it was concluded that the precipitation of the alkali metal is energetically more favourable at all temperatures for K_2CO_3; for Na_2CO_3, the evolution of carbon is possible up to 1143 K, while that of sodium is possible above 1143 K. Reduction of lithium, calcium, magnesium and barium carbonates gives carbon.

In a series of studies,[183–187] the formation of new species upon dissolution of carbon dioxide in molten $Li_2CO_3-Na_2CO_3-K_2CO_3$ eutectics was reported. The formation of dicarbonate ions was confirmed by potentiometric titration, by structural studies on a melt and by determination of the free energy ($\Delta H = -142$ kJ mol^{-1}) of the reaction between CO_2 and CO_3^{2-} to give $C_2O_5^{2-}$ (see Ref. 183). The possible existence of such species as CO_4^{2-} (see Refs 184, 185), $C_2O_6^{2-}$ (see Ref. 184), $C_2O_4^{2-}$ (see Ref. 186) and CO_2^{2-} (see Ref. 187) was noted.

In K, Na, Rb/Cl melts as the background, the carbonate ion does not show electrochemical activity.[188] An increase in temperature to 700 °C does not favour the electrochemical reduction of CO_3^{2-} either. The addition of a 500-fold excess of LiCl with respect to CO_3^{2-} does not produce a wave on the voltammograms. As the Li^+ concentration is increased, a small wave of CO_3^{2-} electrochemical reduction stretched along the potential axis is observed in the potential range from 0.7 to 0.9 V. The Ca^{2+} cation affects the electrochemical reduction of CO_3^{2-} more strongly than Li^+ does. A noticeable wave is observed even with a 200-fold excess of Ca^{2+}. The waves in the presence of Ca^{2+} are also extended along the potential axis. The wave heights were not found to depend explicitly on the cation concentration. The effect of the Mg^{2+} cation was found to be most pronounced. A distinct wave appears even with a four-fold excess of Mg^{2+}. Further increase in the Mg^{2+} concentration increases the wave height, and it reaches a maximum with a 100-fold excess of Mg^{2+}. Evacuation of the system after reaching the maximum wave height decreases the latter. The addition of Mg^{2+} after evacuation increases the wave again.

It should be noted that the electrochemical reduction of CO_3^{2-} in molten chlorides as the background occurs in the same potential range, irrespective of the polarising force of the cation. Hence, the electrode processes in melts with different cationic compositions involve the same species, namely, CO_2. The electrochemical reduction of CO_3^{2-} under the action of strongly polarising cations occurs at much lower temperatures than the thermal decomposition temperatures of the corresponding carbonates. Hence, the formation of CO_2 does not result from thermal decomposition but is a consequence of the polarising effect of cations.

3. MoO_4^{2-}, WO_4^{2-} and CO_3^{2-} anions in oxide melts as the background in the presence of strongly polarising cations

It is known [189–192] that polytungstate and polymolybdate melts $Na_2EO_4-EO_3$ (E = Mo, W) can be considered as melts of eutectic mixtures $Na_2EO_4-Na_2E_2O_7$ containing the Na^+, EO_4^{2-} and $E_2O_7^{2-}$ ions. The ratio between the concentrations of EO_4^{2-} and $E_2O_7^{2-}$ ions is determined by the equilibrium

$$2\,EO_4^{2-} \rightleftharpoons E_2O_7^{2-} + O^{2-} . \quad (28)$$

Presumably, the introduction of Li_2WO_4 or $ZnWO_4$ as well as of WO_3 in a sodium tungstate melt complicates the structure of tungsten–oxygen groups, for example, owing to the reaction

$$2\,WO_4^{2-} + x\,Li^+ \longrightarrow Li_xO^{(2-x)-} + W_2O_7^{2-} . \quad (29)$$

However, if this concept is applied to molten $M^{I}EO_4-M^{II}EO_4$ mixtures (M^{I} = Li, Na, K; M^{II} = Ca, Zn, Ba, Sr, Mg, Al), some contradictions arise. First, if the equilibrium (28) took place upon introduction of tungstates of strongly polarising cations, *e.g.*, $CaWO_4$, in a sodium tungstate melt, this would have occurred in melts containing an excess of the Ca^{2+} cation with formation of the tungstate ion dimer. However, studies on the electrochemical behaviour of the $CaCl_2-CaWO_4-CaO$ system at high temperatures [152] and the IR spectra of a $KCl-NaCl-Na_2WO_4-CaCl_2$ melt (for $[Ca^{2+}] > [WO_4^{2-}]$) [14] indicate that the tungstate ion retains its tetrahedral structure. Second, the solubility of tungstates (molybdates) with strongly polarising cations in sodium or potassium tungstate (molybdate) decreases with the increase in the cation specific charge.[193] These facts can imply that the strength of $M^{z+}-EO_4^{2-}$ interaction increases with increase in the specific charge and that the concentration of oxygen ions in the molten mixtures decreases.

In our opinion, the cationic composition of tungstate and molybdate mixtures, like that of oxochloride melts, should affect considerably the EAS composition and the parameters of the electrode process. Kushkhov *et al.*[194, 195] studied the melts of $Na_2WO_4-MEO_4$ mixtures (M = Li, Ca, Zn, Ba, Sr, Mg, Al; E = Mo, W). The addition of tungstates and molybdates with strongly polarising cations shifts the oxygen electrode potential towards more positive values, *i.e.*, decreases the activity of the O^{2-} ion. An increase in the cation specific charge in the series Ba^{2+}, Sr^{2+}, Li^+, Mg^{2+}, Al^{3+} leads to a more significant shift. In the cases of addition of aluminium tungstate (molybdate) and tungsten (molybdenum) trioxide, the concentration dependences of the oxygen electrode potential practically coincide. It can thus be assumed that if a strongly polarising cation is present in a melt, an acid-base reaction of the molybdate (tungstate) ion with the Al^{3+} cation is possible

$$2\,Al^{3+} + 3\,EO_4^{2-} \longrightarrow 3\,EO_3 + Al_2O_3\,. \quad (30)$$

According to reactions (28) and (29), the parameters (potentials, rates) of electrochemical evolution of tungsten and molybdenum should be virtually identical in melts with identical acidities, irrespective of the cationic composition. However, an increase in the cation specific charge shifts the electrochemical reduction wave towards more positive potentials. For example, the shift upon transition from Na^+ to Al^{3+} is $\sim$1.0 V.

This fact cannot be explained using the viewpoint that EAS are formed in melts of sodium tungstate containing molybdates and tungstates of strongly polarising cations according to reaction (28). In melts with equal acidities, the specific charge on cations affects considerably the electrochemical reduction potential. In fact, the electrochemical reduction potentials of tungstate ion in the presence of barium, magnesium and aluminium cations are within 1.8–1.9, 1.5–1.7 and 1.0–1.2 V, respectively. A similar situation is observed for molybdate ion.

The acid-base (cation–anion) interactions occurring in a melt of sodium tungstate upon addition of the carbonate ion are judged by changes in the e.m.f. of a cell with oxygen electrodes.[135] Upon addition of carbonates, the oxygen electrode potential is shifted towards negative values, indicating an increase in the oxygen ion activity in the melt. The addition of lithium carbonate shifts the oxygen electrode potential much more strongly than that of sodium carbonate. This is due to the fact that the stability constant of sodium carbonate is higher than that of lithium carbonate.[196] For the same reasons, a melt of sodium tungstate containing lithium carbonate has a lower pCO_2.

The electrochemical reduction of carbonate ion in sodium tungstate as the background can be detected only upon addition of lithium carbonate. The absence of a linear dependence of the reduction wave current on the lithium carbonate concentration and the decrease in the diagnostic criterion $j_p/V^{1/2}$ (where j_p is the peak current density, V is the potential sweep rate) with an increase in the polarisation rate implies the kinetic nature of electrochemical reduction waves of carbonate ion. Electrochemically active CO_2 species are formed as a result of cation-anionic interaction of the strongly polarising Li^+ cation with the carbonate ion. The formation of CO_2 can be described by the above scheme [see Eqn (5)]. The addition of sodium carbonate increases pCO_2 considerably, therefore the CO_2 reduction wave is not observed in the voltammetric curves.

4. Effect of PO_3^- anions on the formation of electrochemically active species in the presence of MoO_4^{2-} and WO_4^{2-} anions

Introduction of PO_3^- in $KCl-NaCl-Na_2WO_4$ (Na_2MoO_4) melts gives two waves on the voltammograms.[197, 198] An increase in PO_3^- concentration within $0.01 < [PO_3^-]/[EO_3^{2-}] < 0.2$ increases the current of the second wave, whereas the potentials and currents of the first wave remain unchanged. The current of the second wave is proportional to the PO_3^- concentration. Potentiostatic electrolysis of molybdate (tungstate)-containing melts with the specified concentration ratio of molybdate (tungstate) and metaphosphate anions gives a deposit of the corresponding high-melting metal on the cathode.

Our assumption on the participation of the dimeric ionic forms of molybdenum and tungsten in the electrode processes in question is based on the following data. It has been shown [199] that introduction of sodium metaphosphate in a purely tungstate melt shifts the potential of the tungsten electrode from -1.8 to -1.0 V. It is at -1.0 V that discharge of $W_2O_7^{2-}$ ions occurs; the existence of these ions has been proven both electrochemically [200] and by high-temperature radiography.[201]

Based of voltammetric data,[197, 198] the effect of PO_3^- on the electrochemical reduction of MoO_4^{2-} and WO_4^{2-} can be interpreted as follows. The role of PO_3^- involves the formation of two EAS forms according to the scheme

$$PO_3^- + 2EO_4^{2-} \rightleftharpoons \begin{matrix} E_2O_7^{2-} + PO_4^{3-} \\ 2EO_3 + PO_4^{3-} + O^{2-}\,. \end{matrix} \quad (31)$$

The formation of ditungstate ions in a sodium tungstate melt in the presence of PO_3^- anions has also been reported by Malyshev.[202]

5. Effect of neutral MoO_3, WO_3 and B_2O_3 molecules on the formation of electrochemically active species in the presence of MoO_4^{2-} and WO_4^{2-} anions

The effect of tungsten trioxide on the electrode processes in tungstate melts has been studied in detail by a research group directed by Academician A N Baraboshkin.[189, 191, 200] Contradictory opinions on the ionic composition of tungstate melts exist at present. It has been noted above that the melts of the $Na_2WO_4-WO_3$ system can be regarded as melts of the $Na_2WO_4-Na_2W_2O_7$ eutectic mixture and that they mostly consist of a mixture of Na^+, WO_4^{2-} and $W_2O_7^{2-}$ ions.

The discharge of $W_2O_7^{2-}$ occurs more easily than that of the tungstate ion. This is evident from a thermodynamic calculation of the decomposition potentials of the corresponding compounds [203, 204] and from experimental data:[190, 191] introduction of small amounts of WO_3 increases abruptly the potential of tungsten evolution and decreases the decomposition potential of polytungstate melts.

The effect of MoO_3 on electrode processes in the sodium tungstate melt and the EAS formation mechanism were studied by potentiometric and voltammetric measurements (a cell with oxygen electrodes was used).[205, 206] Measurements of the equilibrium potentials of the oxygen electrode showed that in the presence of up to 2 mol.% – 3 mol.% MoO_3 in the sodium tungstate melt, the pre-logarithmic factor of the dependence of the oxygen electrode potential on MoO_3 concentration is 0.120 V. This means that in this concentration range molybdenum exists mainly as MoO_4^{2-} ions. The pre-logarithmic factor of this dependence at concentrations 7 mol.% – 20 mol.% is 0.112 V. Hence, molybdenum is present mainly as dimolybdate ions $Mo_2O_7^{2-}$ in this concentration range. The experimental dependences match the calculated ones, which confirms the validity of the chosen model of the ionic composition of the melt.

Measurements of the potential of a molybdenum electrode *versus* MoO_3 concentration showed the existence of two equilibria.[206, 207] At MoO_3 concentration up to 4 mol.% – 5 mol.%, metallic molybdenum is in equilibrium with a melt containing $Mo_2O_7^{2-}$ ions. The concentration dependence of the equilibrium potential is well described by the Nernst equation. The number of electrons per one electroactive species calculated from the slope of the plot of the molybdenum electrode potential against MoO_3 concentration, ($dE/d\log[MoO_3]$), equals 1.5. This value is consistent with the equilibrium

$$4\,Mo_2O_7^{2-} + 6\,e^- \rightleftharpoons Mo + 7\,MoO_4^{2-}\,. \quad (32)$$

At high MoO_3 concentrations (> 5 mol.%), the activity of $Mo_2O_7^{2-}$ increases, and a tungstate–molybdate melt is in equilibrium with the dioxide MoO_2 rather than with metallic molybdenum

$$2\,Mo_2O_7^{2-} + 2\,e^- \rightleftharpoons MoO_2 + 3\,MoO_4^{2-}\,. \quad (33)$$

The number of electrons per one electroactive species, also calculated from the slope $dE/d\log[MoO_3]$, equals 1. This value describes the equilibrium (33).

The formation of dimolybdate and ditungstate ions in tungstate–molybdate melts in the presence of B_2O_3 was noted.[208, 209]

6. Effect of fluoride and fluoroaluminate ions on the formation of electrochemically active species in the presence of CrO_3, MoO_3, WO_3, CrO_4^{2-}, MoO_4^{2-} and WO_4^{2-} in chloride–fluoride melts

Tungsten and molybdenum trioxides can be stabilised in chloride melts by binding them in oxofluoride complexes which are more

stable. Such complexes have been described in the literature; they are obtained by treatment of tungstates and molybdates with hydrofluoric acid. We were able to find data on the existence of these compounds in melts in only one publication.[210]

The composition range of oxohalide melts where tungsten and molybdenum exist as stable oxofluoride complexes was determined by studying $KCl-NaCl-NaF-EO_3$ melts (E = Mo W) with different [NaF]/[EO_3] concentration ratios.[211,212] Based on the results of these studies, the overall electrode process of electrochemical reduction of the oxofluorotungstate complex can be presented as follows:

$$[WO_2F_4]^{2-} + 6e^- \rightleftharpoons W + 2O^{2-} + 4F^- , \quad (34)$$

$$2O^{2-} + [WO_2F_4^-]^{2-} \rightleftharpoons WO_4^{2-} + 4F^- , \quad (35)$$

$$2[WO_2F_4]^{2-} + 6e^- \rightleftharpoons W + WO_4^{2-} + 8F^- . \quad (36)$$

As noted above, MoO_4^{2-} and WO_4^{2-} in melts of chlorides of weakly polarising cations (Na^+, K^+) as the background manifest no electrochemical activity up to decomposition potentials of the background electrolyte. The addition of fluoride ion to a sodium chloride melt containing molybdate and tungstate ions does not change the shapes of the voltammetric curves. The molybdate and tungstate ions are stable in NaCl–NaF melts; the O^{2-} is not replaced by F^- with the formation of oxofluoride complexes, and they do not manifest electrochemical activities up to decomposition potentials of the background electrolyte.[213,214]

It is known that aluminium fluoride complexes possess acceptor properties with respect to O^{2-} ions and hence can be used for controlling the acid-base properties. On introduction of AlF_6^{3-} in a sodium chloride melt containing MoO_4^{2-} and WO_4^{2-} anions, waves at 0.7–1.0 V appear on the voltammetric curves.[163,164] Acid-base interaction of EO_4^{2-} with AlF_6^{3-} is accompanied by replacement of F^- by O^{2-} in the aluminium environment to give $AlOF_x^{1-x}$ complexes ($x = 2-5$), while EO_4^{2-} is bound in oxofluoride complexes. For example, for $x = 2$

$$EO_4^{2-} + 2AlF_6^{3-} \longrightarrow EO_2F_4^{2-} + 2AlOF_2^- . \quad (37)$$

The proof that tungsten and molybdenum are evolved from oxofluoride complexes in the $NaCl-Na_3AlF_6-Na_2EO_4$ systems is as follows. First, the deposition potentials of tungsten and molybdenum from these systems correlate well with the deposition potentials of these elements from WO_2F_2, MoO_2F_2 relative the oxygen electrode calculated from thermodynamic data.[203,204] Second, the deposition potential of tungsten (molybdenum) from the system in question coincides with the deposition potential of tungsten (molybdenum) from the $NaCl-KCl-NaF-EO_3$ system, in which the high-melting metal exists as $EO_2F_4^{2-}$ (see Refs 215, 216). The formation of $EO_2F_4^{2-}$ and its subsequent electrochemical reduction to the metal in a $KF-MoO_3-B_2O_3$ melt was assumed by Japanese researchers.[213] The electrochemical reduction waves recorded for a $NaCl-Na_3AlF_6$ melt containing EO_3 and Na_2EO_4 both separately and simultaneously are virtually identical. Hence, the reaction between tungstate (molybdate) and fluoroaluminate ions results in $EO_2F_4^{2-}$ and $AlOF_x^{1-x}$.

Taking into account the linear dependences of the reduction wave peak current on the EO_3 (EO_4^{2-}) concentration and on the polarisation rate and using the mass transfer constant of $(5-6)\times10^{-3}$ cm s^{-1}, Malyshev *et al.*[214] reached a conclusion on the diffusion nature of the limiting current. The dependence of the potential of molybdenum or tungsten electrode in a $NaCl-Na_3AlF_6$ melt on the EO_3 or EO_4^{2-} concentration *vs.* the Pt, O_2/NaCl–0.05 Na_2MO_4 half-cell is well described by the Nernst equation. The number of electrons per one electroactive species calculated from the slope of plots of the metal electrode potential against the EO_3 (or EO_4^{2-}) concentration equals 5.8±0.2. For these melts, the polarisation curves of the molybdenum and tungsten electrodes are characterised by low overvoltage; the cathodic and anodic segments of polarisation curves are symmetric up to the overvoltage of 0.35 V. Based on the slopes of the polarisation curves in the current–overvoltage coordinates, the number of electrons participating in the electrode process was found to be 5.5–6.1. These data suggest the reversibility of the charge transfer step. The overall electrochemical reaction can be represented as follows:

$$EO_2F_4^{2-} + 2AlF_6^{3-} + 6e^- \rightleftharpoons E + 2AlOF_4^{3-} + 8F^- . \quad (38)$$

Several studies[214,217,218] deal with the effect of fluoride complexes AlF_6^{3-} and SiF_6^{2-}, manifesting acid properties with respect to O^{2-} ions on the electrochemical reduction of CrO_4^{2-} in K, Na/Cl, F melts as the background. The chromate ion in halide melts as the background with weakly polarising cations, such as Na^+ and K^+, does not manifest electrochemical activity up to the decomposition potentials of the support electrolyte. The formation of EAS can be represented by an equation analogous to Eqn (38). The Cr_2O_3 formation potential coincides with its evolution potential from $CrO_2F_4^{2-}$ *vs.* the oxygen electrode calculated from thermodynamic data.[203,204] The dependence of the chromium electrode potential in a $NaCl-Na_3AlF_6$ melt (50 mass % : 50 mass %) on CrO_4^{2-} concentration at 1173 K obeys well the Nernst equation with the number of electrons per EAS equal to 3.0±0.1. The electrochemical deposition of Cr_2O_3 occurs without a noticeable overvoltage; analysis of polarisation curves gives 5.7–6.1 electrons. These data suggest the reversibility of the charge transfer step. The overall electrochemical equilibrium can be expressed as follows:

$$2CrO_2F_4^{2-} + AlF_6^{3-} + 6e^- \rightleftharpoons Cr_2O_3 + AlOF_4^{3-} + 10F^- . \quad (39)$$

Studies on the electrochemical reduction of oxoanions of high-melting metals in the presence of chloride, chloride–fluoride and oxide melts with various acid-base properties made it possible to reveal three mechanisms of EAS formation:[3,4] anion cationisation with formation of $\{M_x^{z+}[EO_{n/2+1}]^{2-}\}^{(xz-2)+}$ species, oxoanion decomposition to give $\{EO_{[(n+2(1-x)]/2}Hal_{2(x-1)+y}\}^{y-}$ oxohalide complexes, formation of $[E_{(1+x)}O_{n(1+x)/2+1}]^{2-}$ dimer complexes where E = Cr, Mo, W, C; M = Li^+, Ba^{2+}, Sr^{2+}, Mg^{2+}, Zn^{2+}, Al^{3+}.

The direction of EAS formation is determined by the acid properties and the concentration of M^{z+}, EO_n, PO_3^-, F^- and the stability of the EO_n^{2-} anion.

One can create conditions enabling various multielectron electrochemical processes to favour a particular reduction mechanism in ionic melts, by constructing electrochemically active species with various structures and compositions (in other words, by controlling the cation–anion interactions).

References

1. A L Buchachenko *Usp. Khim.* **68** 99 (1999) [*Russ. Chem. Rev.* **68** 85 (1999)]
2. Yu K Delimarskii, L P Barchuk *Prikladnaya Khimiya Ionnykh Rasplavov* (Applied Chemistry of Ionic Melts) (Kiev: Naukova Dumka, 1988)
3. V I Shapoval, V V Malyshev, I A Novoselova, Kh B Kushkhov, V V Solov'ev *Usp. Khim.* **64** 133 (1995) [*Russ. Chem. Rev.* **64** 125 (1995)]
4. V I Shapoval, V V Malyshev, I A Novoselova, Kh B Kushkhov, V V Solov'ev *Ukr. Khim. Zh.* **60** 483 (1994)
5. R G Pearson *J. Chem. Educ.* **45** 581, 643 (1968)
6. K B Yatsimirskii *Teor. Eksp. Khim.* **6** 462 (1970) [a]
7. G Klopman *J. Am. Chem. Soc.* **90** 225 (1968)
8. V V Malyshev, I A Novoselova, V I Shapoval *Molt. Salts Bull. Sels Fond.* **63** 2 (1997)
9. V L Cherginets, E G Khailova, O V Demirskaya *Electrochim. Acta* **41** 463 (1996)
10. R E Hester, K Krishnan *J. Chem. Phys.* **47** 1747 (1967)
11. R E Hester, K Krishnan *J. Chem. Phys.* **46** 3405 (1967)
12. J P Devlin, P C Li, G Pollard *J. Chem. Phys.* **52** 2267 (1970)
13. G H Wegdam, R Bonn, I Vander Elsken *Chem. Phys. Lett.* **2** 182 (1968)

14. A A Farmakovskaya, I A Brovkina, M V Smirnov, V A Khokhlov, in *Fizicheskaya Khimiya i Elektrokhimiya Rasplavlennykh i Tverdykh Elektrolitov* (Physical Chemistry and Electrochemistry of Molten and Solid Electrolytes) (Sverdlovsk: Institute of Electrochemistry, Urals Scientific Centre, Academy of Sciences of the USSR, 1973) p. 30
15. S V Volkov, V F Grishchenko, Yu K Delimarskii *Koordinatsionnaya Khimiya Solevykh Rasplavov* (Coordination Chemistry of Salt Melts) (Kiev: Naukova Dumka, 1977)
16. A S Kucharski, S N Flengas *J. Electrochem. Soc.* **119** 1170 (1972)
17. B R Sundheim (Ed.) *Fused Salts* New York: McGraw-Hill, 1964)
18. R R Dogonadze, A M Kuznetsov, M A Vorotyntsev *Phys. Status Soc.* **54** 125 (1972)
19. S V Volkov, K B Yatsimirskii *Spektroskopiya Rasplavlennykh Solei* (Spectroscopy of Molten Salts) (Kiev: Naukova Dumka, 1977)
20. Ir W C Child, G M Begun, D H Smith *J. Chem. Soc., Faraday Trans.* **77** 2237 (1978)
21. Yu V Yurinov, Author's Abstract of the Candidate Thesis in Chemical Sciences, Institute of Electrochemistry, Urals Scientific Centre, Academy of Sciences of the USSR, Sverdlovsk, 1973
22. Yu K Delimarskii, A V Gorodyskii, V F Grishchenko *Dokl. Akad. Nauk SSSR* **156** 650 (1964) [b]
23. Yu K Delimarskii, V I Shapoval, V F Grishchenko *Dokl. Akad. Nauk SSSR* **183** 1332 (1968) [b]
24. V A Oleinikova, M V Smirnov, L A Tsiovkina *Tr. Inst. Elektrokhim. Ural. Nauchn. Tsentr. Akad. Nauk SSSR* **15** 135 (1970)
25. M V Smirnov, I Ya Lyubimtseva, L A Tsiovkina *Elektrokhimiya* **7** 566 (1971) [c]
26. M D Ingram, B Baron, G I Janz *Electrochim. Acta* **11** 1629 (1966)
27. H E Bartlett, K E Johnson *Can. J. Chem.* **44** 2119 (1966)
28. Yu K Delimarskii, V I Shapoval, V A Vasilenko *Elektrokhimiya* **7** 1301 (1971) [c]
29. USSR P. 361 675; *Byull. Izobret.* (35) 176 (1975)
30. Yu S Lyalikov, V I Karmazin *Zavod. Lab.* **14** 144 (1948)
31. R N Rust, F R Duke *J. Am. Chem. Soc.* **85** 3338 (1963)
32. Yu K Delimarskii, N Kh Tumanova, V L Kislenko *Elektrokhimiya* **9** 584 (1973) [c]
33. L E Topol, R A Osteryoung, J H Christie *J. Phys. Chem.* **70** 2857 (1966)
34. M I Usanovich *Zh. Obshch. Khim.* **9** 180 (1939) [d]
35. Yu K Delimarskii, D A Tkalenko, N A Chmilenko *Elektrokhimiya* **17** 155 (1981) [c]
36. D A Tkalenko, S A Kudrya, L I Antropov *Elektrokhimiya* **11** 1432 (1975) [c]
37. D A Tkalenko, S A Kudrya *Ukr. Khim. Zh.* **43** 1256 (1977)
38. M G Susteric, W E Triaca, A I Arvia *Electrochim. Acta* **19** 1 (1974)
39. R K Kvaratskheliya, Doctoral Thesis in Chemical Sciences, Institute of Organoelement Compounds, Academy of Sciences of the USSR, Moscow, 1977
40. D A Tkalenko, N A Chmilenko, Yu K Delimarskii *Elektrokhimiya* **15** 1740 (1979) [c]
41. D A Tkalenko, N A Chmilenko *Elektrokhimiya* **16** 880 (1980) [c]
42. N A Chmilenko, D A Tkalenko *Elektrokhimiya* **16** 1368 (1980) [c]
43. D A Tkalenko *Elektrokhimiya Nitratnykh Rasplavov* (Electrochemistry of Nitrate Melts) (Kiev: Naukova Dumka, 1983)
44. V I Shapoval, Yu K Delimarskii, V F Grishchenko, in *Ionnye Rasplavy* (Ionic Melts) (Kiev: Naukova Dumka, 1974) No. 1, p. 222
45. V I Shapoval, Doctoral Thesis in Chemical Sciences, Institute of Organic and Inorganic Chemistry, Academy of Sciences of Ukr. SSR Kiev, 1975
46. S V Volkov, N P Evtushenko, K B Yatsimirskii *Dokl. Akad. Nauk SSSR* **207** 348 (1972) [b]
47. S I Chernukhin, S A Kirillov, V D Prisyazhnyi, in *VI Vsesoyuz. Konf. po Elektrokhimii (Tez. Dokl.), Moskva, 1982* [The VIth All-Union Conference on Electrochemistry (Abstracts of Reports), Moscow, 1982] p. 286
48. S I Chernukhin, S A Kirillov, V D Prisyazhnyi, I M Safronov *Elektrokhimiya* **18** 916 (1982) [c]
49. Yu K Delimarskii, S A Kirillov, V D Prisyazhnyi, in *Ionnye Rasplavy* (Ionic Melts) (Kiev: Naukova Dumka, 1974) No. 1, p. 117
50. E N Belen'kaya, S A Kirillov, A I Agulyanskii *Teor. Eksp. Khim.* **13** 512 (1977) [a]
51. V V Malyshev *Rasplavy* (2) 42 (1999)
52. V V Solov'ev, V I Shapoval *Ukr. Khim. Zh.* **61** 100 (1995)
53. V V Solov'ev, V I Shapoval, Kh B Kushkhov, A G Korotkii *Ukr. Khim. Zh.* **57** 572 (1991)
54. V I Shapoval, Kh B Kushkhov, V V Malyshev *Ukr. Khim. Zh.* **54** 1155 (1988)
55. V I Shapoval, V V Solov'ev, E D Lavrinenko-Ometsinskaya, Kh B Kushkhov *Ukr. Khim. Zh.* **51** 951 (1985)
56. V V Solov'ev, L P Davidenko, V I Shapoval, Kh B Kushkhov, A E Kovalev *Ukr. Khim. Zh.* **56** 466 (1990)
57. V V Solov'ev, O V Kuz'mich, V I Shapoval *Ukr. Khim. Zh.* **62** (4) 94 (1996)
58. V V Solov'ev, Kh B Kushkhov, V I Shapoval *Ukr. Khim. Zh.* **59** 903 (1993)
59. V V Solov'ev, Kh B Kushkhov, V I Shapoval *Ukr. Khim. Zh.* **59** 828 (1993)
60. V V Solov'ev, Kh B Kushkhov, V I Shapoval *Ukr. Khim. Zh.* **55** 37 (1989)
61. V V Solov'ev, N F Kovalenko, Kh B Kushkhov, V I Shapoval *Teor. Eksp. Khim.* **27** 120 (1991) [a]
62. V I Shapoval, V V Solov'ev, N F Kovalenko, Kh B Kushkhov *Teor. Eksp. Khim.* **25** 230 (1989) [a]
63. S V Volkov, V I Shapoval, N I Buryak, V G Lutsenko *Zh. Neorg. Khim.* **25** 2993 (1980) [e]
64. V I Shapoval, V F Grishchenko, L I Zarubitskaya, V V Nerubashchenko *Ukr. Khim. Zh.* **46** 800 (1980)
65. V I Shapoval, I V Zarutskii, V V Malyshev, N N Uskova *Usp. Khim.* **68** 1015 (1999) [*Russ. Chem. Rev.* **68** 925 (1999)]
66. I V Zarutskii, V V Malyshev *Zh. Prikl. Khim.* **70** 1475 (1997) [f]
67. G J Janz, C T Brown, H J Gardner, C Solomons *J. Phys. Chem.* **62** 1479 (1958)
68. M Rolin *J. Four Electr. Ind. Electrochim.* **62** 83 (1953)
69. N A Loginov, M B Smirnov *Ukr. Khim. Zh.* **49** 501 (1983)
70. M V Smirnov, L A Tsiovkina, N A Loginov *Dokl. Akad. Nauk SSSR* **136** 1388 (1961) [b]
71. R Vitlaci, A Nechel *Metallurgia* **34** 538 (1980)
72. V I Taranenko, V I Shapoval, V V Nerubashchenko *Ukr. Khim. Zh.* **51** 1041 (1985)
73. D Juman, S H White *J. Appl. Electrochem.* **8** 375 (1978)
74. O G Tsiklauri, V I Shapoval, A Sh Avaliani, N V Dvali *Soobshch. Akad. Nauk Gruz. SSR* **97** 109 (1980)
75. O G Tsiklauri, V I Shapoval, N G Dvali *Elektrokhimiya* **22** 1426 (1986) [c]
76. V I Shapoval, I V Zarutskii, V V Malyshev *Elektrokhimiya* **34** 1107 (1998) [c]
77. V V Solov'ev, O G Tsiklauri, V I Shapoval, L P Davidenko *Ukr. Khim. Zh.* **58** 7 (1992)
78. V V Solov'ev, O G Tsiklauri, V I Shapoval, L P Davidenko *Ukr. Khim. Zh.* **58** 131 (1992)
79. V V Solov'ev, V I Shapoval, O V Kuz'mich *Ukr. Khim. Zh.* **62** (6) 106 (1996)
80. S V Volkov, in *Ionnye Rasplavy* (Ionic Melts) (Kiev: Naukova Dumka, 1974) No. 2, p. 109
81. V V Solov'ev, L P Davidenko, V I Shapoval *Ukr. Khim. Zh.* **61** (11) 30 (1995)
82. V V Solov'ev, O G Tsiklauri, V I Shapoval *Ukr. Khim. Zh.* **58** 199 (1992)
83. V V Malyshev *Chem. Pap.* **52** 96 (1998)
84. A S Quist, J B Bates, G E Boyd *J. Chem. Phys.* **54** 4896 (1971)
85. M E Prostakov, A I Kruglov, V I Pirina, in *III Ural'sk. Konf. po Vysokotemperaturnoi Fizicheskoi Khimii i Elektrokhimii (Tez. Dokl.), Sverdlovsk, 1981* [The Third Urals Conference on High-Temperature Physical Chemistry and Electrochemistry (Abstracts of Reports), Sverdlovsk, 1981] p. 77
86. V K Pirina, M E Prostakov *Zh. Fiz. Khim.* **50** 2671 (1976) [g]
87. M D Keller *J. Electrochem. Soc.* **120** 3288 (1973)
88. O V Chemezov, L E Ivanovskii, V N Batukhtin, in *III Ural'sk. Konf. po Vysokotemperaturnoi Fizicheskoi Khimii i Elektrokhimii (Tez. Dokl.), Sverdlovsk, 1981* [The Third Urals Conference on High-Temperature Physical Chemistry and Electrochemistry (Abstracts of Reports), Sverdlovsk, 1981] p. 143
89. L E Ivanovskii, O V Chemezov, V P Batukhtin, in *III Mezhdunarodnyi Simpozium po Boru, Boridam, Karbidam i Rodstvennym Soedineniyam (Tez. Dokl.), Tbilisi, 1984* [The Third International Symposium on Boron, Borides, Carbides and Related Compounds (Abstracts of Reports), Tbilisi, 1984] p. 6

90. R De Witt, J Witteuberg, S Cantor *Phys. Chem. Liq.* **2** 113 (1974)
91. M Makyta, K Matiasovsky, P Ellner *Electrochim. Acta* **29** 1653 (1984)
92. M V Myshalov, in *VII Vsesoyuz. Konf. po Fizicheskoi Khimii i Elektrokhimii Ionnykh Rasplavov i Tverdykh Elektrolitov (Tez. Dokl.), Sverdlovsk, 1976* [The VIIth All-Union Conference on Physical Chemistry and Electrochemistry of Ionic Melts and Solid Electrolytes (Abstracts of Reports), Sverdlovsk, 1976] p. 17
93. A I Vasil'eva, V S Tiunov, A G Morachevskii, in *IV Ural'sk. Konf. po Vysokotemperaturnoi Fizicheskoi Khimii i Elektrokhimii (Tez. Dokl.), Perm', 1985* [The IVth Urals Conference on High-Temperature Physical Chemistry and Electrochemistry (Abstracts of Reports), Perm', 1985] p. 178
94. L R Bezarashvili, N I Buryak, S V Volkov, O G Tsiklauri *Ukr. Khim. Zh.* **54** 769 (1988)
95. O G Tsiklauri, I A Bairamishvili, M N Kobalova, V D Dzhaparidze *Soobshch. Akad. Nauk Gruz. SSR* **134** 133 (1989)
96. O G Tsiklauri, G A Gelovani *Rasplavy* (5) 35 (1989)
97. I V Zarutskii, V V Malyshev, V I Shapoval *Rasplavy* (4) 83 (1999)
98. E D German, A V Gorodyskii, V G Dvali, R R Dogonadze *Elektrokhimiya* **11** 321 (1975) [c]
99. O G Tsiklauri, V V Solov'ev, V I Shapoval, A Yu Abramov *Ukr. Khim. Zh.* **56** 1123 (1990)
100. V V Solov'ev *Ukr. Khim. Zh.* **63** (4) 123 (1997)
101. V V Solov'ev, O V Kuz'mich, V I Shapoval *Ukr. Khim. Zh.* **62** (5) 11 (1996)
102. V V Solov'ev, O G Tsiklauri, V I Shapoval, A Yu Abramov *Ukr. Khim. Zh.* **62** (9) 21 (1996)
103. V V Solov'ev *Ukr. Khim. Zh.* **63** (5) 39 (1997)
104. V V Solov'ev *Ukr. Khim. Zh.* **63** (6) 110 (1997)
105. B A Lopatin *Teoreticheskie Osnovy Elektrokhimicheskikh Metodov Analiza* (Theoretical Foundations of Electrochemical Methods of Analysis) (Moscow: Vysshaya Shkola, 1975)
106. G G Hammes *Investigation of Rates and Mechanisms of Reactions* (New York: Wiley, 1975)
107. A N Fletcher, M N Miles, M L Chan *J. Electrochem. Soc.* **126** 1496 (1979)
108. F Lantelme, M Chemla *Electrochim. Acta* **10** 663 (1965)
109. A M Shams El Din, A A Hosary *J. Electroanal. Chem.* **16** 551 (1968)
110. A M Shams El Din, H D Taki El Din, A A El Hosary *Electrochim. Acta* **13** 407 (1968)
111. A V Gorodyskii, V G Dvali, R R Dogonadze, T A Marsagishvili *Ukr. Khim. Zh.* **45** 691 (1979)
112. R R Dogonadze, T A Marsachishvili, G M Chonishvili, in *Materialy Frumkinskikh Chtenii* (Materials of Frumkin Reading) (Tbilisi: Metsniereba, 1980) p. 16
113. V M Bernikov, R R Dogonadze *Teor. Eksp. Khim.* **17** 742 (1981) [a]
114. S V Devyatkin, V V Malyshev, in *Proceedings of the International Symposium on Molten Salts, Dresden, 1998* Vol. 11, p. 666
115. V I Shapoval, E D Lavrinenko-Ometsinskaya, V V Solov'ev, Kh B Kushkhov, in *Doklady Mezhdunarodnoi Shkoly po Fizike Ionnoi Sol'vatatsii* (Proceedings of the International School on the Physics of Ionic Solvation) (Kiev: Institute of Theoretic Physics, Academy of Sciences, Ukr. SSR, 1983) p. 69
116. V I Shapoval, E D Lavrinenko-Ometsinskaya, V V Solov'ev, Kh B Kushkhov, in *VIII Vsesoyuz. Konf. po Fizicheskoi Khimii i Elektrokhimii Ionnykh Rasplavov i Tverdykh Elektrolitov (Tez. Dokl.)* [The VIIIth All-Union Conference on Physical Chemistry and Electrochemistry of Ionic Melts and Solid Electrolytes (Abstracts of Reports)] (Leningrad: Nauka, 1983) Vol. 1, p. 136
117. A T Pilipenko, V A Zaets, L I Savranskii *Dokl. Akad. Nauk SSSR* **270** 915 (1983) [b]
118. V N Kolomiets, V V Solov'ev *Programma dlya Poluempiricheskikh Raschetov Molekul s Otkrytoi Obolochkoi* (The Program for Semiempirical Calculations of Open-Shell Molecules); articles deposited at the VINITI, No. 2929 (Moscow, 1980)
119. I B Bersuker *Stroenie i Svoistva Koordinatsionnykh Soedinenii* (Structure and Properties of Coordination Compounds) (Leningrad: Khimiya, 1971)
120. I B Bersuker *Zh. Neorg. Khim.* **9** 36 (1964) [e]
121. S V Volkov *Zh. Neorg. Khim.* **21** 1676 (1976) [e]
122. K Fukui, T Jonesawa, H Shingu *J. Chem. Phys.* **20** 722 (1952)
123. V I Shapoval, V V Solov'ev, Kh B Kushkhov, E D Lavrinenko-Ometsinskaya, in *XV Vsesoyuz. Soveshch. po Khimii Kompleksnykh Soedinenii (Tez. Dokl.), Kiev, 1985* [The XVth All-Union Meeting on the Chemistry of Complex Compounds (Abstracts of Reports), Kiev, 1985] Pt. 1, p. 276
124. V V Solov'ev, E D Lavrinenko-Ometsinskaya *Poluempiricheskii Raschet Ion-Molekulyarnykh Vzaimodeistvii vo Vneshnem Elektricheskom Pole* (Semiempirical Calculations of Ion-Molecular Interactions in External Electric Field); articles deposited at the Ukr. NII NTI, No. 1586 (Kiev, 1986)
125. V I Shapoval, V V Solov'ev, E D Lavrinenko-Ometsinskaya, Kh B Kushkhov, in *Ukrainskaya Respublikanskaya Konf. po Elektrokhimii (Tez. dokl.)* (Ukrainian Republican Conference on Electrochemistry (Abstracts of Reports)] (Kiev: Naukova Dumka, 1984) p. 158
126. V I Shapoval, Kh B Kushkhov, V V Solov'ev, in *VIII Vsesoyuz. Soveshch. po Polyarografii (Tez. Dokl.), Dnepropetrovsk, 1984* [The VIIIth All-Union Meeting on Polarography (Abstracts of Reports), Dnepropetrovsk, 1984] p. 99
127. V I Shapoval, Kh B Kushkhov, V V Solov'ev *Ukr. Khim. Zh.* **50** 1066 (1984)
128. V I Shapoval, Kh B Kushkhov, V V Solov'ev, V G Shevchuk *Ukr. Khim. Zh.* **50** 1184 (1984)
129. V I Shapoval, Kh B Kushkhov, V V Solov'ev, in *V Konf. Sots. Stran po Khimii Rasplavlennykh Solei (Tez. Dokl.)* [The Vth Conference of Socialist States on the Chemistry of Molten Salts (Abstracts of Reports)] (Kiev: Naukova Dumka, 1984) p. 48
130. A Ya Gokhshtein, Ya P Gokhshtein *Dokl. Akad. Nauk SSSR* **131** 601 (1960) [b]
131. V I Shapoval, K B Kushkhov, V V Solovjov, in *The 37th Meeting of the International Electrochemical Society (Abstracts of Reports), Vilnius, 1986* Vol. 3, p. 53
132. Yu K Delimarskii, V I Shapoval, V A Vasilenko *Ukr. Khim. Zh.* **39** 617 (1973)
133. V I Shapoval, Yu K Delimarskii *Teor. Eksp. Khim.* **9** 748 (1973) [a]
134. V I Shapoval, V V Solov'ev, Kh B Kushkhov, E D Lavrinenko-Ometsinskaya *Ukr. Khim. Zh.* **51** 493 (1985)
135. V V Malyshev, I A Novoselova, Kh B Kushkhov, V I Shapoval *Zh. Neorg. Khim.* **42** 540 (1997) [e]
136. V V Solov'ev, Candidate Thesis in Chemical Sciences, Institute of Organic and Inorganic Chemistry, Academy of Sciences of Ukr. SSR, Kiev, 1985
137. A L Rotinyan, K I Tikhonov, I A Shotina *Teoreticheskaya Elektrokhimiya* (Theoretical Electrochemistry) (Leningrad: Khimiya, 1981)
138. A N Frumkin *Izbrannye Trudy. Elektrodnye Protsessy* (Selected Transactions. Electrode Processes) (Moscow: Nauka, 1987)
139. B N Kabanov *Elektrokhimiya Metallov i Adsorbtsiya* (Electrochemistry of Metals and Adsorption) (Moscow: Nauka, 1966)
140. A V Gorodyskii *Sovershenstvovanie Vol'tampernykh Izmerenii* (Development of Voltammetric Measurements) (Kiev: Znanie, 1980)
141. A T Vas'ko, S K Kovach *Elektrokhimiya Tugoplavkikh Metallov* (Electrochemistry of High-Melting Metals) (Kiev: Tekhnika, 1983)
142. V I Spitsyn, T I Drobasheva, L P Kozanskii, in *Khimiya Soedinenii Mo(VI) i W(VI)* [The Chemistry of Mo(VI) anf W(VI) Compounds] (Novosibirsk: Nauka, 1979) p. 3
143. L F Kozin, in *Teoreticheskie Osnovy Elektrokhimicheskoi Kinetiki* (Theoretical Foundations of Electrochemical Kinetics) (Kiev: Naukova Dumka, 1984) p. 3
144. L F Kozin *Elektroosazhdenie i Rastvorenie Mnogovalentnykh Metallov* (Electrodeposition and Dissolution of Polyvalent Metals) (Kiev: Naukova Dumka, 1989)
145. E G Polyakov *Zh. Prikl. Khim.* **71** 181 (1998) [f]
146. L P Polyakova, Z A Kononova, V G Kremenetskii, E G Polyakov *Elektrokhimiya* **33** 1088 (1997) [c]
147. F Lantelme, J Barner, G Picard *J. Electrochem. Soc.* **142** 4097 (1995)
148. M Chemla, V Grinevitch *Bull. Soc. Chim. Fr.* **3** 853 (1973)
149. S A Kuznetsov, A L Glagolevskaya, V V Grinevich, P T Stangrit *Elektrokhimiya* **28** 1344 (1992) [c]
150. S A Kuznetsov, A L Glagolevskaya, V V Grinevich, S V Kuznetsova *Elektrokhimiya* **33** 259 (1997) [c]
151. S A Kuznetsov, S V Kuznetsova, S V Devyatkin, D Kaptai *Zh. Prikl. Khim.* **71** 74 (1998) [f]

152. S A Kuznetsov, L P Polyakova, E G Polyakov, P T Stangrit, in *Ionnye Rasplavy i Tverdye Elektrolity* (Ionic Melts and Solid Electrolytes) (Kiev: Naukova Dumka, 1987) No. 2, p. 71
153. S A Kuznetsov, S V Devyatkin, A L Glagolevskaya *Rasplavy* (2) 67 (1992)
154. L S Korobeinikov, S V Kuznetsova, S A Kuznetsov *Vysokochist. Veshch.* **4** 93 (1992)
155. V V Malyshev, A N Romanenko, N N Uskova, V I Shapoval *Ukr. Khim. Zh.* **61** (12) 115 (1995)
156. N N Uskova, S Yu Sarychev, V V Malyshev, V I Shapoval *Zh. Prikl. Khim.* **73** 1456 (2000) [f]
157. A I Karasevsky, R E Kris, E V Panov, A V Gorodyski *J. Electroanal. Chem.* **325** 45 (1992)
158. A I Karasevsky, I N Karnaukhov *J. Electroanal. Chem.* **348** 49 (1993)
159. V I Shapoval, V V Malyshev, I A Novoselova, Kh B Kushkhov *Zh. Prikl. Khim.* **67** 928 (1994) [f]
160. A F Shunailov, A N Baraboshkin, V A Martynov *Tr. Inst. Elektrokhim. Ural. Nauchn. Tsentr. Akad. Nauk SSSR* **13** 40 (1969)
161. A N Baraboshkin, A F Shunailov, V A Martynov *Tr. Inst. Elektrokhim. Ural. Nauchn. Tsentr. Akad. Nauk SSSR* **15** 44 (1970)
162. P V Smirnov, Candidate Thesis in Technical Sciences, Institute of Steel and Melts, Moscow, 1982
163. Kh B Kushkhov, V V Malyshev, V I Shapoval, S G Gasviani *Ukr. Khim. Zh.* **57** 375 (1991)
164. Kh B Kushkhov, V I Shapoval, A A Tishchenko, S G Gasviani *Elektrokhimiya* **28** 152 (1992) [c]
165. Yu K Delimarskii, V I Shapoval, N N Ovsyannikova *Ukr. Khim. Zh.* **43** 115 (1977)
166. N N Ovsyannikova, Yu F Rybkin *Ukr. Khim. Zh.* **42** 151 (1976)
167. V I Shapoval, Yu K Delimarskii, Kh B Kushkhov *Elektrokhimiya* **14** 1141 (1978) [c]
168. V I Shapoval, Kh B Kushkhov *Ukr. Khim. Zh.* **45** 392 (1979)
169. V I Shapoval, Kh B Kushkhov *Ukr. Khim. Zh.* **45** 698 (1979)
170. V I Shapoval, Kh B Kushkhov, V A Vasilenko *Ukr. Khim. Zh.* **45** 509 (1979)
171. Kh B Kushkhov, V I Shapoval, I A Novoselova *Elektrokhimiya* **24** 1496 (1988) [c]
172. V I Shapoval, S V Volkov, Kh B Kushkhov, P A Romanyk *Ukr. Khim. Zh.* **47** 344 (1981)
173. F Haber, S Toolloczko *Z. Anorg. Allg. Chem.* **41** 412 (1904)
174. Yu K Delimarskii, V F Grishchenko, A V Gorodyskii *Ukr. Khim. Zh.* **31** 32 (1965)
175. Yu K Delimarskii, V F Grishchenko, V A Vasilenko *Zh. Prikl. Khim.* **42** 224 (1969)
176. V I Shapoval, Yu K Delimarskii, G V Reznik, in *Ionnye Rasplavy* (Ionic Melts) (Kiev: Naukova Dumka, 1974) No. 2, p. 212
177. Yu K Delimarskii, V I Shapoval, V A Vasilenko *Zh. Prikl. Khim.* **43** 2634 (1970) [f]
178. A M Trunov, G K Stepanov *Tr. Inst. Elektrokhim. Ural. Nauchn. Tsentr. Akad. Nauk SSSR* **2** 102 (1961)
179. A M Trunov, G K Stepanov *Tr. Inst. Elektrokhim. Ural. Nauchn. Tsentr. Akad. Nauk SSSR* **3** 69 (1962)
180. M V Smirnov, L A Tsikovkina, V A Oleinikova *Tr. Inst. Elektrokhim. Ural. Nauchn. Tsentr. Akad. Nauk SSSR* **6** 69 (1965)
181. N M Barbin, V N Neckarov, O I Terentiev, A P Pekar *Refr. Met. Molt. Salts (NATO ASI Ser. 3)* **53** 173 (1998)
182. H E Bartlett, K E Jonson *J. Electrochem. Soc.* **114** 457 (1967)
183. D Moyaux, D Peeters P Claes, in *Proceedings of the International Symposium on Molten Salts, Dresden, 1998* Vols 5–6, p. 131
184. G B Dunks, D Stelman *Inorg. Chem.* **22** 2168 (1983)
185. D Moyaux, J Gilbert, P Claes *J. Electroanal. Chem.* **349** 415 (1993)
186. W M Vogel, L J Bregoli, S W Smith *J. Electrochem. Soc.* **127** 833 (1980)
187. A Borucka *J. Electrochem. Soc.* **124** 972 (1977)
188. V I Shapoval, Kh B Kushkhov, V V Solov'ev *Ukr. Khim. Zh.* **51** 1263 (1985)
189. A N Baraboshkin *Elektrokristallizatsiya Metallov iz Rasplavlennykh Solei* (Electrocrystallisation of Metals from Molten Salts) (Moscow: Nauka, 1976)
190. S M Zakhar'yash, Author's Abstract of Candidate Thesis in Chemical Sciences, Institute of Electrochemistry, Urals Scientific Centre of Academy of Sciences of the USSR, Sverdlovsk, 1982
191. A N Baraboshkin, V P Bychin *Elektrokhimiya* **20** 579 (1984) [c]
192. V K Perevozkin, A N Baraboshkin *Tr. Inst. Elektrokhim. Ural. Nauchn. Tsentr. Akad. Nauk SSSR* **27** 35 (1988)
193. M V Mokhosoev, F P Alekseev, V I Lutsyk *Diagrammy Sostoyaniya Molibdenovykh i Vol'framovykh Sistem* (State Diagrams of Molybdenum and Tungsten Systems) (Novosibirsk: Nauka, 1978)
194. Kh B Kushkhov, V V Malyshev, V I Shapoval *Elektrokhimiya* **26** 1115 (1990) [c]
195. Kh B Kushkhov, V V Malyshev, V I Shapoval *Ukr. Khim. Zh.* **58** 400 (1992)
196. B Andersen *Thermodynamic Properties of Molten Alkali Carbonates* (Lyngby: The Technical University of Denmark, 1985)
197. I A Novoselova, V V Malyshev, A E Finadorin, V I Shapoval *Zh. Neorg. Khim.* **40** 1438 (1995) [e]
198. V V Malyshev, I A Novoselova, A E Finadorin, V I Shapoval *Elektrokhimiya* **32** 754 (1996) [c]
199. V I Raksha, Author's Abstract of Candidate Thesis in Chemical Sciences, Institute of Electrochemistry, Urals Scientific Centre of Academy of Sciences of the USSR, Sverdlovsk, 1982
200. A Yu Khvatov, A N Baraboshkin, K P Tarasova *Elektrokhimiya* **21** 1657 (1985) [c]
201. H Miyake, K Okada, Sh Twai *J.Chem. Soc., Faraday Trans. 1* **84** 1141 (1988)
202. V V Malyshev *Ukr. Khim. Zh.* **63** (6) 115 (1997)
203. Kh B Kushkhov, I A Novoselova, V I Shapoval *Termodinamicheskoe Obosnovanie Vysokotemperaturnogo Elektrokhimicheskogo Sinteza Metallopodobnykh Tugoplavkikh Soedinenii* (Thermodynamic Basis of High-Temperature Electrochemical Synthesis of Metal-Like High-Melting Compounds); articles deposited at the VINITI, No. 147-V (Moscow, 1986)
204. I A Novoselova, V V Malyshev, V I Shapoval, Kh B Kushkhov, S V Devyatkin *Teor. Osn. Khim. Tekhnol.* **31** 286 (1997)
205. V I Shapoval, A N Baraboshkin, Kh B Kushkhov, V V Malyshev *Elektrokhimiya* **23** 942 (1987) [c]
206. V V Malyshev, I A Novoselova, V I Shapoval *Zh. Prikl. Khim.* **69** 1233 (1996) [f]
207. V V Malyshev, Kh B Kushkhov *Elektrokhimicheskoe Povedenie Platino-Kislorodnogo i Molibdenovogo Elektrodov v Vol'framatno-Molibdatnykh Rasplavakh* (Electrochemical Behaviour of Platinum–Oxygen and Molybdenum Electrodes in Tungstate–Molybdate Melts); articles deposited at the VINITI, No. 2319-V (Moscow, 1988)
208. V V Malyshev, N N Uskova S Yu Sarychev, V I Shapoval *Zashch. Met.* **32** 653 (1996)
209. V V Malyshev, N N Uskova, S Yu Sarychev, V I Shapoval *Ukr. Khim. Zh.* **62** (8) 112 (1996)
210. V A Pavlovskii, V A Reznichenko, in *Fiziko-Khimicheskie Svoistva Rasplavlennykh i Tverdykh Elektrolitov* (Physicochemical Properties of Molten and Solid Electrolytes) (Kiev: Naukova Dumka, 1979) p. 83
211. Kh B Kushkhov, I A Novoselova, D G Supatashvili, V I Shapoval *Elektrokhimiya* **26** 48 (1990) [c]
212. Kh B Kushkhov, D G Supatashvili, I A Novoselova, V I Shapoval *Elektrokhimiya* **26** 720 (1990) [c]
213. H Koichiro, O Jasuhiko, O Shinichiro, T Kazuo *Denki Kagaku* **52** 368 (1984)
214. V V Malyshev, Kh B Kushkhov, S G Gasviani, V I Shapoval *Ukr. Khim. Zh.* **59** 739 (1993)
215. W H Kruesi, D J Fray *Trans.Met. Soc.* **24** 605 (1993)
216. F Lantelme *J. Electroanal. Chem.* **196** 227 (1985)
217. V V Malyshev, Kh B Kushkhov, V I Shapoval *Poroshk. Metall.* (1) 34 (1994)
218. G R Stafford, B Grushko, R D Mc Michel *J. Alloys Compd.* **200** 107 (1993)

[a] — *Theor. Exp. Chem. (Engl. Transl.)*
[b] — *Dokl. Chem. Technol., Dokl. Chem. (Engl. Transl.)*
[c] — *Russ. J. Electrochem. (Engl. Transl.)*
[d] — *Russ. J. Gen. Chem. (Engl. Transl.)*
[e] — *Russ. J. Inorg. Chem. (Engl. Transl.)*
[f] — *Russ. J. Appl. Chem. (Engl. Transl.)*
[g] — *Russ. J. Phys. Chem. (Engl. Transl.)*

Russian Chemical Reviews **70** (3) 177 – 210 (2001) © 2001 Russian Academy of Sciences and Turpion Ltd

DOI 10.1070/RC2001v070n03ABEH000627

Nanoclusters and nanocluster systems. Assembling, interactions and properties

I P Suzdalev, P I Suzdalev

Contents

I.	Introduction	177
II.	Synthesis and classification of nanoclusters and nanocluster structures	177
III.	Properties of isolated nanoclusters	179
IV.	Cluster nanosystems and nanostructures	185
V.	Conclusion	206

Abstract. Data on the structures and properties of nanoclusters and nanocluster systems are analysed. A classification of nanoclusters and nanosystems based on the method of their preparation is proposed. Methods for assembling nanoclusters to give nanostructures, the main principles of assembling and the types of nanosystems are described. The appearance of new properties upon combination of nanoclusters into a nanosystem is noted. The bibliography includes 274 references.

I. Introduction

The properties of a material are known to change significantly on passing from macrostructures to the microstructures the size of which lies in the nanometer range. Thus the crystal lattice parameters, the heat capacity, the melting point and the electrical conductivity of nanoclusters in the condensed state differ from those of the corresponding macrocrystals. In addition, they acquire new optical, magnetic, and electronic characteristics; their reactivity and catalytic properties also change.[1–10] The properties of nanostructures are determined by not only the cluster size but also the mode of their organisation or self-organisation into a nanocluster structure in which the clusters act as separate atoms. Nanostructures, in turn, can form supramolecular structures.

The ways of assembly of nanoclusters into nanostructures depend not only on the properties of separate nanoclusters and intercluster interactions but also on the methods used to prepare nanoclusters. Thus, several main trends can be distinguished in research on nanoclusters and cluster nanosystems

— methods for the preparation and classification of nanoclusters;
— properties of isolated nanoclusters;
— ways of assembly (self-assembly) of cluster nanosystems;
— properties of nanocluster systems.

Great progress in studies of nanoclusters and nanostructures has been achieved in the last decade. An enormous number of publications have appeared, devoted both to fundamental research on nanoclusters and nanostructures and to the ways of using them in nanotechnologies (design of magnetic recording devices, nanodiodes, nanowires, and single-electron transfer devices tuned by changing the size of the nanolaser; production of new nanomaterials with specific mechanical, thermal, electronic, optical, and magnetic properties).

In this review, we present data on nanoclusters and nanostructures obtained both by methods of inorganic, physical, and solid-state chemistry and by methods of condensed-state physics and the physics of gases, using diverse calculation procedures and experimental equipment. We have not intended to give an exhaustive review on the published data concerning all the properties of nanoclusters, but considered only those of them that are of fundamental importance in the formation of cluster systems. Some of the problems considered in the review related to the interpretation of experimental facts and, especially, classification of clusters and nanoparticles are debatable. In addition, not all the cluster effects are considered. Nevertheless, we hope that the information we present would be of interest for researchers engaged in the chemistry or nanotechnologies and in physics.

II. Synthesis and classification of nanoclusters and nanocluster structures

As noted above, many properties of nanoclusters and nanosystems depend on the method used to prepare them. Therefore, we attempted to classify the clusters in terms of the method of synthesis. With this empirical approach, the diversity of properties of clusters and cluster systems can be represented on the basis of their origin. In terms of the preparation method, clusters can be classified into six groups: molecular, gas-phase, colloid, solid-state, matrix and film clusters. Isolated nanoclusters can be prepared by chemical reactions (molecular clusters), laser vaporisation (gas-phase clusters) or by matrix isolation (solid-state and colloid syntheses). Nanosystems are mainly formed in solid-state and colloid syntheses.

1. Molecular ligand metal clusters

Molecular metal clusters are multinuclear complex compounds the molecular structure of which is based on a core (cell) of metal atoms (their number should be greater than two) bound directly to one another and surrounded by ligands. The metal–metal distances in these clusters are usually shorter than those in the bulk metal.[11] The metal core consists of chains of different lengths and different branching types, rings or polyhedra or combinations of these structural units. Both homo- and heterometallic clusters are known.

I P Suzdalev, P I Suzdalev N N Semenov Institute of Chemichal Physics, Russian Academy of Sciences, ul. Kosygina 4, 117977 Moscow, Russian Federation. Fax (7-095) 137 83 18. Tel. (7-095) 939 71 01.
E-mail: suzdalev@chph.ras.ru

Received 9 October 2000
Uspekhi Khimii **70** (3) 203 – 240 (2001); translated by Z P Bobkova

Molecular ligand metal clusters are produced from metal complexes upon various chemical reactions. An enormous number of publications have been devoted to the synthesis, structure and properties of molecular metal clusters (see, for example, a monograph [11] and references therein).

2. Gaseous ligand-free clusters

Ligand-free clusters of metals or metal oxides can be prepared, for example, by laser vaporisation of metals from a substrate followed by separation according to size (or weight) in a time-of-flight mass-spectrometer. The clusters formed upon vaporisation are fixed in traps (or on substrates) and then their electronic, optical, and other properties are studied.[12] The clusters obtained in this way contain from several dozens to several hundreds of atoms. The synthesis of big nanoclusters ($\geqslant 100$ nm) is performed by heating and vaporisation of metals in a radio-frequency electromagnetic field *in vacuo* or under an inert gas followed by deposition of clusters onto a substrate or a filter.[13] The use of a substrate is necessary because nanoparticles are highly reactive and stick together upon collisions, while the substrate stabilises them.

Yet another method for the preparation of gas-phase metal clusters is vaporisation of metals in an inert gas followed by the formation of metal clusters in a low-temperature matrix (cryochemical method).[14]

Gas-phase methods of synthesis are also used for the preparation of carbon clusters (in particular, fullerenes). Thus C_{60} fullerene was prepared for the first time by laser vaporisation of graphite in 1985.[15] Fullerenes with the compositions C_{36}, C_{70}, C_{82}, C_{84}, C_{90} and C_{96} have also been synthesised.[16–19]

Among other gas-phase ligand-free clusters, van der Waals clusters of noble gases and water should be mentioned.

The evaporation–condensation technique allows the preparation of the purest metal particles; therefore, nowadays, this method is still finding application. However, when using this method, it is difficult to control the size of the resulting metal clusters. The clusters obtained in this way are characterised by broad size distributions.

3. Colloid clusters and nanosystems

Colloid solutions containing metal nanoclusters and their compounds have long been known; however, in connection with the task of preparing assembled nanostructures, it became necessary to synthesise monodisperse colloid systems with a controlled cluster size. Monodisperse colloid systems are usually synthesised using sol–gel technology,[20] which includes preparation of a sol and its transformation into a gel. Sols are prepared using dispersion and condensation (physical and chemical) methods. Thus hydrolysis of metal salts or metal alkoxides gives rise to sols of metal oxides or hydroxides characterised by high excess energy. Owing to the excess energy, aggregation of sols takes place in these systems, accompanied by the formation of a gel. This process affords nanostructures with a size of up to 100 nm.

In recent years, the use of microemulsion systems (direct and reverse micelles) for the preparation of nanoclusters with a narrow size distributions of particles has started.† Many metal clusters with particle size of 1 to 10 nm have been prepared in this way.[21,22]

4. Solid-state clusters

Solid-state clusters are formed as a result of diverse transformations of the solid phase: chemical reactions in the solid phase, crystallisation of an amorphous phase, mechanochemical transformations, *etc*.[23] Many chemical reactions in the solid state for example, thermal decomposition of metal salts and complexes are accompanied by the formation of metal or metal oxide nuclei, which then grow due to sintering. The size of nanoclusters thus formed varies over a very broad range — from one to hundreds of nanometers.

Crystallisation is employed to prepare nanoclusters from amorphous alloys. The crystallisation conditions are maintained in such a way as to generate as many crystallisation centres as possible; the growth of nanoclusters should occur at a low rate.

Solid-state nanoclusters can also be prepared *via* photochemical reactions, for example, those involving silver halides. These reactions, too, start with the formation of nuclei, which are then enlarged giving rise to nanoclusters with sizes ranging from tens to hundreds of nanometers.[7]

Apart from chemical reactions in solids, mechanochemical transformations can also be used to prepare solid-state clusters. Thus mechanical grinding of a bulk solid permits one to prepare nanoclusters the size of which does not exceed several nanometers. Due to the activation of the newly formed surface, new nanocluster compounds differing from the initial ones can arise.[6,8]

Yet another method for the preparation of solid-state nanoclusters consists in nanostructurisation of a material on exposure to pressure with shear.[6] By increasing pressure to 5 GPa and shear to 1000 °C, one can prepare nanoclusters with a grain size reaching several nanometers the properties of which differ sharply from those of the initial material. Nanoclusters are also produced when other methods of plastic yield are employed.

5. Matrix clusters

Methods for the preparation of nanoclusters which make use of various inorganic and organic matrices and matrix isolation constitute a self-dependent group, although they can include some features of the gas-phase, solid-state and other methods. The point is that nanoclusters prepared using matrix methods differ from those formed, for example, in solid-state chemical reactions because they are isolated from one another by the matrix and, therefore, heating of the whole nanosystem does not result in an increase in the cluster size due to sintering. The originality of this approach is that it provides the possibility of restricting size dispersion of the nanoclusters and of changing the intercluster interactions in a required manner. Thus microencapsulation of nanoclusters in inert gases at low temperatures is used to prepare gas-phase metal clusters.

Clusters and cluster systems are often prepared by chemical reactions in solution followed by precipitation of the resulting compounds in the pores of a solid. Nanoclusters and nanosystems can also be prepared by impregnating porous matrices with solutions and performing chemical reactions in the pore acting as a micro- or a nanoreactor. This procedure is used, for example, to prepare metal and metal oxide clusters in zeolites, the cluster size being determined by the size of zeolite cells (1–2 nm). In this case, aluminosilicates promote the formation of assembled cluster structures.

Broad opportunities for the variation of the size and composition of clusters are provided by using inorganic and organic sorbents (for example, silica gels and aluminogels, ion exchange resins and polysorbs).[3] In this case, the change in the cluster size and cluster organisation takes place due to both the change in the pore size and the variation of the surface hydrophilicity (or hydrophobicity), the concentration of initial components, temperature, *etc*.

6. Nanofilms

When nanoclusters are formed in nanofilms, the mechanism of nucleation and growth differs from those in the formation of solid-state clusters because the synthesis is related to the surface chemistry (the formation of two-dimensional structures). Epitaxial nanofilms on an oriented crystalline surface are prepared using laser vaporisation and molecular beams.[17]

In recent years, the CVD method has started to be widely used to apply nanocluster nanofilms on the surface.[24] According to this

† Procedures for the synthesis of ultradisperse particles based on the sol–gel method and microemulsion systems are described in the recent review by B D Summ, N I Ivanova *Usp. Khim.* **69** 995 (2000). [*Russ. Chem. Rev.* **69** 911 (2000)]

method, the initial substances are first evaporated and then transferred through the gas phase and deposited in a required proportion onto a chosen substrate.

To produce molecular layers with controlled composition and thickness, the method of molecular layering is used, the essence of which is to induce surface chemical reactions separated in space and time.[25–27] Nanofilms containing one to ten monolayers have been prepared in this way.

The technology of synthesis of Langmuir–Blodgett films, which has been developed in recent years, makes it possible to introduce metal ions and metal complexes into the surfactant film being formed on the surface of water and thus to prepare nanoclusters. The use of this approach results in the formation of Langmuir–Blodgett films with an ordered monolayer of clusters, which can then be applied onto a solid substrate using a special technique. This procedure can be repeated thus forming multilayer films and superstructures.[28]

III. Properties of isolated nanoclusters

Clusters occupy an intermediate position between separate molecules and macro-solids. Therefore, the properties of a single isolated cluster can be compared both with the properties of separate atoms or molecules and with the properties of a bulk solid.

The notion 'isolated cluster' is rather abstract because it is virtually impossible to obtain a cluster not interacting with the environment. In addition, when investigating the properties of isolated clusters, one should take into account their interaction with the measuring instrument, which can change the properties of the cluster during the measurements. This is especially true for contact techniques of measurement (for example, tunnelling microscopy). However, these changes are relatively insignificant and we shall not consider this type of interaction in this review. Since molecular metal clusters, van der Waals noble gas and water clusters, gas-phase metal clusters, and fullerenes are subject only to weak intercluster interactions, they can conventionally be considered as isolated clusters.

In this Section, we shall consider the structure, the atomic dynamics, and the electronic, optical, and magnetic properties of isolated clusters.

1. Molecular ligand clusters in solutions

Molecular clusters are important objects of coordination, inorganic and structural chemistry. The unusual features of their structures and properties caused by the presence of a core of metal atoms have stimulated the development of a separate branch of science — cluster chemistry — possessing its own calculation, synthesis and investigation methods. Since the number of metal atoms forming the cluster core can vary from a few to hundreds or even thousands, a specific approach to the choice of the investigation method for each particular cluster is required. The methods range from those designed for separate atoms (for example, atomic molecular spectroscopy), used in the case of small clusters, to those developed to study the collective and dynamic properties, which are used for big clusters.

In this Section we consider specific quantum-size properties of molecular clusters, which display themselves when the size of the metal core of the cluster ranges from 1 to 3 nm. The properties of bigger clusters (3 to 20 nm) are discussed in the Section devoted to colloid clusters.

The core of a molecular cluster is formed in accordance with the close-packing pattern of metal atoms, similarly to the bulk metal.[29,30] The number of metal atoms in a close-packed core constructed as a regular 12-vertex polyhedron (cubooctahedron, icosahedron, or anticubooctahedron) can be found from the formula

$$N = \frac{1}{3}(10n^3 + 15n^2 + 11n + 3),$$

where n is the number of layers around the central atom. Thus, the smallest close-packed core contains 13 atoms: one central atom and 12 first-layer atoms. This gives a set of 'magic' numbers $N = 13, 55, 147, 309, 561, 923, 1415, 2057, 2869$, *etc*. corresponding to the most stable cores of metal clusters. Indeed, the following clusters are known: 13-atomic (single-layer) clusters $[Au_{13}(diphos)_6](NO_3)_4$ (diphos is $PPh_2CH_2CH_2PPh_2$)[31] and $[Rh_{13}(CO)_{24}H_3]^{2-}$ (see Ref. 32) with icosahedral and cuboocta-hedral cores, respectively, 55-atomic (two-layer) clusters $Au_{55}(PPh_3)_{12}Cl_6$,[33,34] $Rh_{55}(PPh_3)_{12}Cl_6$, $Pt_{55}(AsBu^t_3)_{12}$,[35,36] $Ru_{55}(PBu^t_3)_{12}Cl_{20}$ (see Ref. 37) with cubooctahedral cores, a 309-atomic (four-layer) cluster $Pt_{309}Phen'_{36}O_{30\pm10}$ [Phen′ is the sodium salt of 4,7-bis(phenylsulfate)-1,10-phenanthroline] with a cubooctahedral core,[38] a 561-atomic (five-layer) cluster $Pd_{561}Phen_{60}(OAc)_{180}$ (Phen is phenanthroline) with an icosahedral core,[39,40] 1415-atomic (seven-layer) cluster $Pd_{1415}Phen_{60}O_{\sim1100}$ and a 2057-atomic (eight-layer) $Pd_{2057}Phen_{84}O_{\sim1600}$ cluster.[10] It should be noted that, in addition to stable clusters, with 'magic' numbers of metal atoms, intermediate clusters with other numbers of atoms are also inevitably formed.

For the Au_{55} and Pd_{561} clusters, electrical conductivity, heat capacity, and magnetic susceptibility were measured. These characteristics proved to differ substantially from those of the bulk metal. The electrons of the metal atoms forming the cluster core are not delocalised, unlike the collectivised electrons in a bulk metal sample; instead, they form discrete energy levels differing from molecular orbitals. On passing from the bulk metal to a cluster and then to a molecule, delocalised *s*- and *d*-electrons forming the conduction band in the bulk metal are replaced by non-delocalised electrons, which form discrete energy levels in a cluster, and then by molecular orbitals.

The appearance of discrete electron bands in metal clusters with a size ranging from 1 to 4 nm should be accompanied by the appearance of single-electron transitions. An efficient technique for observing effects of this type is tunnelling microscopy (TM), which provides voltammetric characteristics when the tip of the microscope is fixed on a molecular cluster. Upon transition from the cluster to the tip of the tunnelling microscope, an electron overcomes a Coulomb barrier the height of which is equal to the electrostatic energy $\Delta E = e^2/2C$ (C is the nanocluster capacity proportional to its size). For small clusters, the electrostatic energy of an electron becomes greater than its kinetic energy kT; therefore, steps corresponding to the single-electron transition appear on the voltammetric curve $U = f(I)$. Thus, a decrease in the cluster size and in the temperature of the single-electron transition results in violation of the linear dependence $U = f(I)$, typical of the bulk metal. A stepwise dependence has been observed for the $Au_{55}(PPh_3)_{12}Cl_6$ molecular cluster with a size of 1.4 nm even at room temperature.[41] As the temperature further decreases to 90 K, several Coulomb steps appear on the voltammetric curve (Fig. 1 *a*,*b*).

Quantum-size effects were observed in the measurements of the magnetic susceptibility and the heat capacity of the molecular clusters $Pd_{561}Phen_{60}(OAc)_{180}$, $Pd_{561}Phen_{36}O_{200}$, $Pd_{1415}Phen_{54}$. O_{1000} and $Pd_{2057}Phen_{78}O_{1600}$ (see Ref. 42) at ultralow temperatures. Bulk Pd exhibits Pauli paramagnetism, which is provided by electrons with an energy E_F near the Fermi energy; therefore, its magnetic susceptibility barely depends on the temperature down to the liquid-helium temperature.

Calculations show that on passing from Pd_{2057} to Pd_{561}, *i.e*., as the size of Pd clusters diminishes, the density of states near E_F decreases, resulting in a change in the magnetic susceptibility. The calculation predicts that upon a decrease in the temperature ($T \to 0$), the susceptibility should either drop to zero or increase to infinity for even and odd numbers of electrons, respectively. Since the study was performed for clusters containing an odd number of electrons, the magnetic susceptibility was actually found to increase. The increment is substantial for Pd_{561} (with a maximum at $T < 2$ K) and slight for Pd_{1415}. In the case of Pd_{2057}, virtually no temperature variation is observed, which is typical of

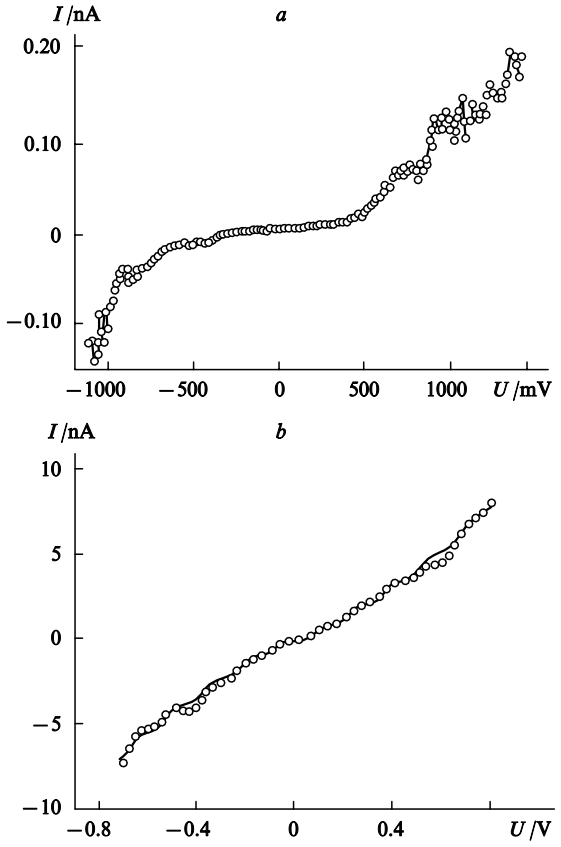

Figure 1. Voltammetric characteristics of the $Au_{55}(PPh_3)_{12}Cl_6$ cluster at $T = 300$ (*a*) and 90 K (*b*).[41]

bulk Pd, although, as noted above, the values of magnetic susceptibility found for Pd_{2057} are much lower than those for bulk Pd.

Heat capacity measurements for giant Pd molecular clusters have revealed equally interesting features. Bulk solids are characterised by a linear temperature dependence of electron heat capacity, $C \sim T$. The transition from the bulk solid to nanoclusters gives rise to quantum-size effects,[42] which are manifested as a deviation of the $C = f(T)$ plot from linearity following a decrease in the cluster size. Thus the greatest deviation from the linear dependence is observed for Pd_{561}. With a correction for the ligand dependence ($C \sim T^3$), a $C \sim T^2$ dependence was obtained for nanoclusters at ultralow temperatures $T < 1$ K. The heat capacity of a cluster is known to be $C = kT/\delta$ (δ is the mean distance between energy levels, $\delta = E_F/N$, where N is the number of electrons in the cluster). Calculations of the δ/k value carried out for Pd_{561}, Pd_{1415} and Pd_{2057}, and for the colloid Pd cluster with a size of $\sim$15 nm, gave values of 12, 4.5, 3.0 and 0.06 K, respectively. Thus, the unusual $C \sim T^2$ dependence in the region of $T < 1$ K indicates that quantum-size effects are involved. Note that the $C \sim T^2$ dependence is also typical of amorphous solids and is attributable to tunnelling effects.[43]

Quantum-size effects have also been observed in non-metal and metal oxide and chalcogenide ligand clusters.[44–46] The internal metallic core in the molecular cluster $[Mn_{12}(CH_3COO)_{16}.(H_2O)_4O_{12}]\cdot 2CH_3COOH\cdot 4H_2O$ (Mn^*_{12}) has a tetragonal two-layer structure: the Mn^{4+} atoms of the inner cubane structure of Mn_4O_4 have total spin $S = 3/2$, and the eight outer Mn^{3+} atoms have spin $S = 2$.[45] The exchange interactions within the cluster stabilise the ferromagnetic ground state with a collective spin $S = 10$ (parallel and antiparallel alignment of the individual spins of Mn^{4+} and Mn^{3+}). A single crystal constructed from Mn^*_{12} clusters was placed in an external magnetic field ($H = 5$ T) and its magnetisation at $T = 1.55 - 3.2$ K was measured.[45]

The Mn^*_{12} cluster with the spin $S = 10$ forms energy levels in an external magnetic field. Electronic transitions between these levels can be either induced by thermal fluctuations or occur *via* quantum tunnelling. A thermally activated transition can be due to superparamagnetism (superparamagnetic relaxation), when the total magnetic moment of the cluster fluctuates as a whole. In this case, the magnetisation curves vary smoothly. For a single crystal constructed from Mn^*_{12} clusters, unusual 'stepwise' hysteresis curves (Fig. 2) resembling single-electron conductivity curves have been obtained. A magnetisation curve has steps in the case where the quantum mechanism of tunnelling is involved. This effect takes place when the magnetic field strength is such that the energy levels coincide. At these H values, the relaxation by a tunnelling mechanism from one spin state to another is accelerated compared to the superparamagnetic relaxation. As a consequence, at low temperatures, discontinuous changes in the magnetisation by $H_{n+1} - H_n = \Delta H = 0.44$ T are observed in the region of H from 0 to 2.64 T, in accordance with quantisation of the spin levels in a magnetic field.

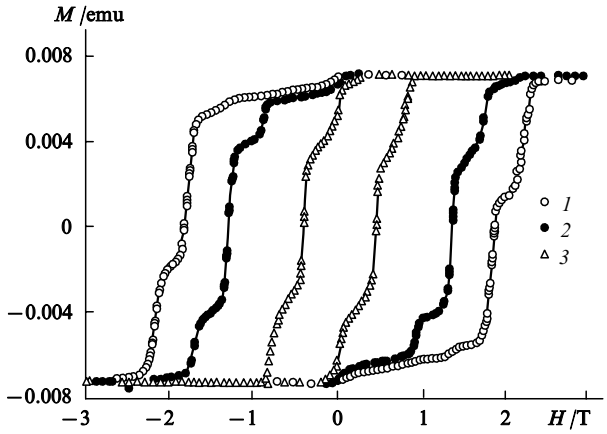

Figure 2. Magnetisation curves for a single crystal of the Mn^*_{12} acetate cluster at different temperatures.[45]
Temperature /K: 1.77 (*1*), 2.10 (*2*) and 2.64 (*3*).

Semiconductor molecular clusters also exhibit a number of remarkable properties. Since semiconductor clusters acquire discrete energy levels in the valence band and in the conduction band, and the energy gap between them increases (with respect to that in the bulk sample), the optical transitions between these levels are characterised by greater energies. The smaller the cluster, the greater the energy of optical transitions. This is the so-called blue shift of the radiation frequency observed upon a decrease in the cluster size. A similar effect has been observed for the $Cd_{32}S_{17}(SC_6H_5)_{36}(DMF)_4$ clusters with a semiconductor CdS nucleus having a size of $\sim$1.5 nm.[46] The increase in the radiation frequency is accompanied by an increase in the oscillator strength, which is now concentrated on several transitions.

A decrease in the cluster size also restricts the wavelength of carriers in semiconductors. The appearance of discrete levels in the clusters characterises them as quantum dots with zero dimensionality.

Examples of semiconductor clusters with specific optical properties will be considered in the Section devoted to colloid clusters.

Thus, the molecular ligand clusters of metals and metal oxides and chalcogenides possessing quantum-size properties can underlie the design of materials with new electronic, magnetic, and optical properties.

2. Gaseous ligand-free clusters

Ligand-free clusters are devoid of a ligand shell influencing the properties of the surface atoms of the core; in this respect, they

differ from molecular clusters. Ligand-free clusters have been obtained for almost each element of the Periodic System. Several groups of ligand-free clusters possessing characteristic properties can be distinguished: alkali metal clusters, carbon clusters, rare gas clusters and van der Waals clusters.

a. Alkali metal clusters

The properties of alkali metal clusters are well described in terms of the jellium model or, what is the same, the drop shell model. According to this model, a cluster is considered as two subsystems: positively charged ions forming the core and delocalised *s*-electrons, which can form shells similar to the electron shells in atoms. The electron shell in an atom is occupied by the numbers of electrons $n_e = 2, 8, 18, 20, 34, 40$, *etc*., which corresponds to the filling of 1*s*, 1*p*, 1*d*, 2*s*, 1*f*, 2*p*, *etc*. shells.[47,48] The number of metal atoms in a cluster that corresponds to the number of electrons in the filled shells is called the 'magic' number. The 'electronic magic numbers'‡ correspond to the most stable electronic configurations of clusters with filled shells. They were discovered experimentally during measurements of ionisation potentials and electron affinities.[49]

Calculations carried out in terms of the jellium model made it possible to explain the shell structure of the clusters. The classical expression for the electron work function in the jellium model (drop model) of the cluster[50]

$$W(R,z) = W_\infty + \frac{(z + 3/8)e^2}{R}, \qquad (1)$$

[W_∞ is the electron work function for the bulk metal, z is the charge of the cluster (spherical), and R is the cluster radius] predicts higher ionisation potentials for clusters compared to bulk solids. In the case of nanoclusters, a stepwise dependence of the ionisation potential on the number of atoms is observed (the steps occur at points corresponding to 'magic' numbers). The stability of charged clusters is determined by the dissociation energy. Thus the dissociation energies for Na_n^+ and K_n^+ pass through maxima at $n = 9$ and 21, which corresponds to filled shells containing 8 and 20 electrons.[51,52]

The quantum-size effects manifest themselves in the optical properties of clusters, which is expressed as the appearance of a discrete structure and broadening of spectral lines.[53] An interesting effect is giant resonance associated with oscillations and polarisability of the cluster electrons. Similar giant resonance effects have also been observed for atomic nuclei, in which they are related to the collective motion of protons relative to neutrons. The optical absorption in a cluster is calculated using the Mie equation,[54] derived for a spherical cluster. According to Mie, light absorption cross-section (σ) has a resonance form

$$\sigma = \frac{ne^2}{mc\Gamma\varepsilon_0} \frac{\omega^2}{\omega^2 - \omega_0^2 + (\omega\Gamma)^2}, \qquad (2)$$

where n is the number of electrons, e and m is the charge and the mass of an electron, c is the velocity of sound, Γ is the damping coefficient for the oscillation of electrons in an electromagnetic field (line width), ε_0 is polarisability in vacuum, ω is the oscillation frequency, and $\omega_0 = \omega_p/\sqrt{3}$ is the resonance oscillation frequency constituting a part of the plasmon frequency (ω_p) of electron oscillations in the bulk metal ($\omega_p = e^2/4\pi\varepsilon_0 V$, $V = 4/3\pi r_s^3$, r_s is the Wigner – Seitz radius).

Calculation of the cluster polarisability in terms of the jellium model predicts that the cluster polarisability $\alpha = (ne^2/m\varepsilon_0)\omega_0^2$ should be greater than that of a bulk sample, which is actually observed for Na and K clusters with $n \leqslant 40$.[55] Ellipsoidal clusters have two resonance frequencies, longitudinal and transverse ones; this makes it possible to estimate the cluster shape. Figure 3 shows

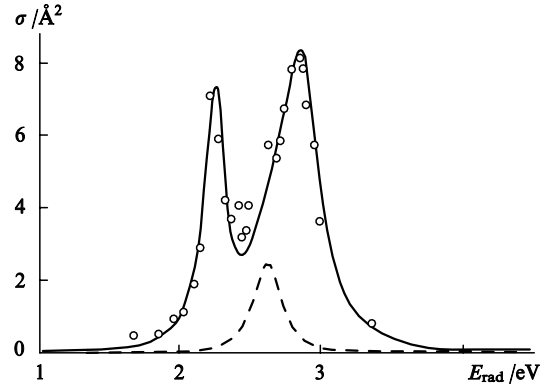

Figure 3. Giant resonance for ellipsoidal Na_{11}^+ clusters.[56] The lower-energy peak corresponds to vibrations along the ellipsoid axis and the higher-energy peak corresponds to perpendicular vibrations. The dashed line corresponds to spherical Na_9^+ clusters.

the resonance dependences of absorption cross-sections on the radiation energy for the ellipsoidal Na_{11}^+ and spherical Na_9^+ clusters.[56] The two resonance peaks on the curve for the ellipsoidal Na_{11}^+ cluster imply that the oscillation frequencies along (low energies) and across (high energies) the cluster axis are different.

A shell electronic structure was also found for noble metal clusters. Although the valence bands in Cu and Ag clusters are almost twice as wide as those in alkali metal clusters, their electronic structures are similar. Due to stronger bonding of Ag atoms, the shell effects are more pronounced in the Ag cluster. The shell structure of Ag_n^- clusters ($n = 3$ to 21) was studied by photoelectron spectroscopy.[57] The greatest Ag – Ag energy was found for the Ag_{17}^- cluster, which corresponds to a filled 18-electron shell. Quantum-mechanical calculations carried out in the same study demonstrated the legitimacy of using the shell model for virtually any Ag_n^- cluster, except for Ag_7^- and Ag_9^-, which might be due to the shape of these anions.

b. Transition metal clusters

In this Section, the attention is focused on the stability and reactivity of transition metal clusters and their magnetic properties. It has been noted previously that the stability and reactivity of clusters are due to two series of 'magic' numbers, one of them being related to the geometric factor (close packing), as in ligand metal clusters, and the other being related to the electronic shell structure, as in alkali metal clusters. The properties of most ligand-free clusters of transition metals are determined by both electronic and geometric factors. In addition, for ligand-free transition metal clusters, the ability of metal atoms to exist in different oxidation states becomes especially significant; therefore, the properties of these clusters cannot be characterised by the simple shell model, as were the properties of alkali metal clusters. Exceptions are provided by Cu, Ag and Au atoms in which the *d* shell is filled and compressed, so that only *s* electrons are involved in binding.

One of the important characteristics of metal nanoclusters is ionisation energy. According to the drop model, it should increase with a decrease in the cluster size according to the $1/R$ law. However, the ionisation energy of Fe_n, Co_n and Nb_n clusters calculated using this model proved to be markedly lower than the value obtained in experiments. In addition, for small clusters with $n < 25$, the ionisation energy was shown to vary irregularly with size: the ionisation energies for clusters with even numbers of atoms are greater than those for odd numbers of atoms. The deviation from the drop model points to a difference between the electron *d* bands formed during the variation of n (even or odd).[58,59]

Let us follow the variation of the properties of a cluster depending on its size and structure taking niobium clusters as

‡ Of course, the 'electronic magic numbers' do not coincide with the Kini 'magic' numbers[29] (see above).

examples. The reactivity of Nb_n clusters was studied in the reactions with N_2 and D_2.[60] Among niobium clusters with $n < 21$, Nb_8, Nb_{10} and Nb_{16} were the most stable, which correlates with minima of the ionisation potential. It was found that some Nb clusters can exist as several geometric isomers differing in reactivity.[61] The geometric structure influences most substantially the reactivity of Nb_n clusters with $n = 3-35$.[62] However, the reactivity of Nb_n clusters with $n = 2-20$ is still governed by the electronic structure. Thus the photoelectron spectra of Nb_n^- clusters ($n = 6-17$) with even numbers of electrons differ from the spectra of Nb_n^- clusters with odd numbers of electrons,[63] which is related to the occupation of the electron shells. The highest transition energies were found for Nb_8, Nb_{10} and Nb_{16}.

A number of ligand-free copper sulfide clusters $[Cu_nS_m]^-$ with $n = 6-45$ and $m = 4-23$ have been prepared by laser vaporisation.[64] Different reactivities of $[Cu_{10}S_6]^-$ and $[Cu_6S_4]^-$ were noted. The former cluster is inert in gas-phase reactions with RSH (R = H, Pr, Ph), while the latter reacts with them to give addition products.[64]

The stability of the clusters was also estimated from their trend to decompose, undergo fission or store energy. The Coulomb fission (induced by repulsion of two charged clusters) and vaporisation of the Sb_n^+ and Sb_n^{2+} clusters ($5 \leqslant n \leqslant 80$) have been studied.[65] The results were interpreted using two models — the drop model taking into account vaporisation of fragments and the Coulomb model. Decomposition of a cluster depended on its charge. For Sb_n^+ clusters with $5 \leqslant n \leqslant 8$, decomposition with vaporisation of neutral dimers was observed, while for Sb_n^+ clusters with $n \geqslant 8$, decomposition with vaporisation of Sb_4 took place. The fragmentation of Sb_n^{2+} clusters followed a different route: for Sb_n^{2+} with $26 \leqslant n \leqslant 36$, asymmetric fission with evolution of Sb_5^+ and Sb_7^+ occurred, whereas for Sb_n^{2+} with $n > 40$, the fission was more symmetric ($Sb_n^{2+} \rightarrow Sb_{n-p}^+ + Sb_p^+$), the masses of the fragments differing by less than 30%. The rate of fission of Sb_n^{2+} clusters with $n < 36$ depends on the type of decomposition and varies according to the $1/n$ pattern, which is in line with the drop model. For larger clusters with $n > 40$, the decrease in the fission rate no longer obeys the $1/n$ law, indicating a deviation from the drop model. In this case, fission occurs simultaneously with vaporisation of Sb_4 fragments.

The variation of the magnetic moment of a substance on passing from an atom to a solid has been followed in relation to gas-phase ligand-free clusters of transition and rare earth metals. The magnetic moment of an isolated transition metal atom differs from the value found for a bulk sample. This is due to the facts that the bulk metal has a *d* conduction band and that the *d* electrons in delocalised states undergo exchange interactions known as itinerant exchange interactions. Thus the magnetic moment of an iron atom in mono- and binuclear iron compounds amounts to $6\,\mu_B$, while the magnetic moment of an iron atom in a bulk ferromagnet is $2.2\,\mu_B$. The magnetic moments of metal atoms and the magnetic properties of a cluster depend on the number of metal atoms in the cluster and vary over a broad range. This may be due to the possible rearrangement of the crystal lattice consisting of clusters, which does not coincide with the crystal lattice of the bulk sample. The determination of magnetic properties during cluster formation can occur in accordance with either the geometric close-packing model, as in the case of molecular ligand clusters with the 'magic' numbers 13, 55, 147, 304, 561, *etc.*, or the structure of the electron shell, as in the case of alkali metal clusters.

For Fe, Co and Ni clusters, the magnetic moments of the metal atoms in the core were found to increase with respect to the values for the same atoms in the bulk sample.[66,67] Thus the Fe magnetic moment increased to $3.2\,\mu_B$; this was accompanied by fluctuations of the magnetic moment depending on the number of metal atoms in the cluster (Fig. 4*a*), which may be due to the geometric filling of close-packed layers. The value $\mu = 2.2\,\mu_B$, typical of Fe atoms in a bulk sample, is attained when the number of atoms (n) in the cluster has increased to 500. For Ni atoms, the lowest magnetic moments were found in the Ni_{13} and Ni_{55} clusters, which corresponds to the 'magic' numbers of close packing.[68] However, when measuring the magnetic properties, the electronic properties of the cluster and the itinerant magnetism should be taken into account. A decrease in the cluster size not only increases the magnetic moments of the atoms forming it but also gives rise to a magnetic moment of the cluster as a whole, which was observed for clusters of non-magnetic Rh (Fig. 4*b*).[69]

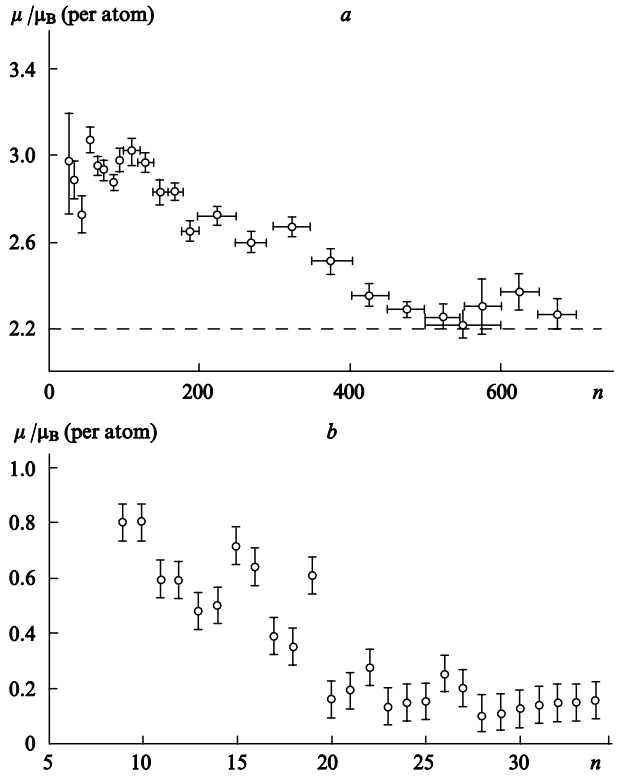

Figure 4. Magnetic moments (per atom) for Fe (*a*)[66] and Rh (*b*)[69] clusters of various sizes. The dashed line corresponds to the magnetic moment $\mu = 2.2\,\mu_B$ of bulk Fe; n is the number of metal atoms in the cluster.

c. Carbon clusters

Carbon atoms readily form clusters. They are usually prepared by laser vaporisation of a graphite target. Their mass distribution is normally studied using mass spectrometry. The mass spectrum of these species has a bimodal divergence. Among small carbon clusters with $n < 24$, clusters with odd 'magic' numbers (3, 7, 11, 19, 23) of carbon atoms were the most stable, while among big clusters (fullerenes), the most stable species are those with even numbers of carbon atoms.

Small carbon clusters display enhanced stabilities when $n = 7$, 11, 15, 19 and 23, which is related to 'magic' numbers corresponding to close packing of atoms.[70,71] The fragmentation of carbon clusters is accompanied by detachment of C_3 and C_5 fragments, pointing to high stability of these fragments. The reasons for the formation of stable carbon clusters include easy *sp*-hybridisation of carbon atoms and high strength of π-bonds.

Quantum-mechanical calculations for the molecular orbitals in carbon clusters indicate that clusters with $n \leqslant 10$ tend to have a linear structure. As the number of carbon atoms increases, the linear structure is replaced by a ring structure.[72] Thus both chain and ring species were found for the C_7^+ clusters.[70] However, the ring structure is subject to additional strain, which increases the total energy of the cluster; therefore, it is more favourable for big clusters. For C_{20}, a three-dimensional structure also becomes possible. Clusters with mixed structures were also detected. Small positively charged carbon clusters react with various diatomic molecules in the gas phase,[70,73] and also with small

hydrocarbon molecules such as C_2H_2 ($C_n^+ + C_2H_2 \rightarrow C_{n+2}H_2$)[74] and HCN ($C_n^+ + HCN \rightarrow HC_nCN^+$).[75]

The first representatives of big carbon clusters, C_{60} and C_{70} fullerenes, were discovered in 1985 based on the mass spectra;[15] as soon as 1990, the method of fullerene preparation by vaporisation of graphite electrodes in an electric arc was developed.[16] This technique was used to prepare diverse fullerenes, which triggered extensive studies on their physical and chemical properties.

The best studied fullerene is C_{60}, shaped like a truncated icosahedron in which the pentagonal cells are coupled with hexagonal ones. This fullerene is the most symmetrical among all the fullerenes prepared. The unique feature of C_{60} is that it is the only structure in which all the carbon atoms in the five- and six-membered rings are equivalent (*i.e.*, the strain is uniformly distributed). In addition, in this fullerene, the five-membered rings are all separated from one another.

How does the so well-organised and symmetrical molecule arise? Calculations using simple kinetic models[76] describing the nucleation and growth of carbon clusters from the carbon atoms produced upon laser-induced vaporisation of graphite electrodes showed that the formation of a linear chain is energetically the most favourable. These chains interact with one another in a plasma giving rise to aggregates of 20–30 carbon atoms. During aggregation, aromatic rings or graphene layers are formed as a result of fluctuations. If the density of carbon atoms is rather high, the rings become twisted to give carbon black particles. There exists, however, a large probability that the opposite edges of the rings would meet; this yields fullerene.

The symmetrical closed structure of C_{60} and C_{70} fullerenes produces an impression that they should have low reactivity. However, a tremendous number of fullerene compounds are known. Various atoms and molecules can be attached to the carbon atoms of the fullerene cage (exohedral fullerenes); foreign atoms and molecules can be introduced inside the fullerene cage (endohedral fullerenes); the carbon atoms in the cage can be replaced by other atoms (substitution fullerenes).

The following substitution fullerenes are known: $C_{59}B$, $C_{69}B$,[77] $C_{59}N$ and $(C_{59}N)_2$.[78] The cage can also incorporate silicon and niobium atoms.[79–82] Fullerenes containing transition metal atoms $C_{59}M$ and $C_{69}M$ (M = Fe, Co, Ni, Rh, Ir) have been synthesised.[83] This was done by mixing metal and fullerene vapours. The formation of $C_{59}M$ and $C_{69}M$ fullerenes was detected in the mass spectra after photoionisation of the clusters. Substitution fullerenes have also been obtained by photoionisation of the exohedral fullerenes $C_{60}M_x$ and $C_{70}M_x$ ($x = 0–30$) with metal atoms on the surface of the cluster. It was found that, after crossing the photoionisation threshold, the metal atoms passed from the cluster surface (exohedral position) into the fullerene cage (substitution fullerenes).

Among exohedral fullerenes, fluorinated fullerenes, $C_{60}F_{60}$, are the most interesting.[84] These clusters and materials based on them are suggested to act as 'molecular ball bearings' and superlubricants. The $C_{60}M_x$ and $C_{70}M_x$ fullerenes with exohedrally attached alkali metal atoms have found extensive use. Of considerable interest are not only the structure and reactivity of these compounds but also the high-temperature superconductivity arising in them. Thus C_{60} fullerenes with a Cs/Rb component ($T_c = 33$ K) and with a Rb/Tl component ($T_c = 43$ K) have been prepared.[85] It is expected that fullerenes with an I_2 component would have $T_c = 70$ K.

The first endohedral fullerene La@C_{60} has been synthesised simultaneously with the discovery of fullerenes themselves.[86] Endohedral fullerenes can be prepared either during the fullerene synthesis by vaporisation of graphite electrodes containing a particular metal or by introducing atoms of inert gases inside the fullerene cage at high pressures and temperatures.[87,88] The size of the fullerene inner cavity increases with an increase in the number of carbon atoms; a larger fullerene cavity can accommodate several metal atoms. For example, evidence for the insertion of the La_3 cluster inside C_n fullerenes with $n \geqslant 88$ has been obtained.[89] Study of the photofragmentation of fullerenes containing K and Cs atoms showed that the minimum C_n clusters whose cavity can accommodate K and Cs atoms are C_{44} and C_{48}, respectively.[88,90]

d. Van der Waals clusters of inert gases and other small molecules

The properties of clusters formed by atoms of inert gases are dictated by weak van der Waals interactions. The stability of these clusters, like that of molecular ligand metal clusters, is associated with the 'magic' numbers characterising the geometric close packing. Clusters of inert gases with $n = 3$ are shaped like triangles, those with $n = 4$ are tetrahedra, the clusters with $n = 7$ are pentagonal pyramids, and starting with $n = 13$, the icosahedral geometry appears. The next icosahedra are formed for $n = 55$, 147, 309, 561, *etc.*, that is, for n values equal to the 'magic' numbers. For clusters with $n > 800$, a face-centered cubic packing becomes favourable.[91,92]

For rare gas clusters, effects related to photoabsorption, fluorescence, photoionisation and photofragmentation thresholds, as well as to the formation and relaxation of excitons have been studied. Fluorescence was excited by synchroton radiation.

The exciton transitions in krypton clusters have been studied. Various Kr_n clusters, atomic Kr, and a bulk sample were used (Fig. 5).[93] The Kr atomic spectrum (Fig. 5 *a*) contains two narrow bands caused by the $4p^6 \rightarrow 4p^5 5s$ transition (spin–orbit splitting). The spectra of Kr_n clusters (Fig. 5 *b–e*) exhibit lines corresponding to exciton transitions. Excitation of an electron in the Kr atom gives rise to a positive charge (hole). The electron and the hole form a series of hydrogen-like states, which are manifested in the fluorescence spectra as broadening, displacement, and additional lines.

Apart from the differences between the spectra of atoms, clusters, and bulk materials, differences between the spectra of atoms located on the surface and inside the cluster are also observed. For example, the spectra of Xe_mAr_n clusters ($n = 1000$) were found to contain lines corresponding to the Xe atoms located on the surface and inside the Ar_n clusters and also incorporated in the cage made of Ar atoms.[94]

In charged rare gas clusters, the charge is not delocalised over the whole cluster, as, for example, in Na_n^+, but is located on a small structural fragment (dimer, trimer, or tetramer), the rest of the cluster remaining neutral, as, for example, in $(Ar_x^+)Ar_{n-x}$ ($x = 3$, 4).[95]

Van der Waals clusters formed by H_2O, CO_2, SF_6 and C_6H_6 molecules able to form weak van der Waals polarisation contacts and hydrogen bonds are also known. For example, for the $(CO_2)_n$, $(SF_6)_n$ and $(C_6H_6)_n$ clusters, the van der Waals bonding energy is lower than 0.1 eV; for $(HF)_n$, $(H_2O)_n$ and $(CH_3OH)_3$, this value is lower than 0.3 eV.[96] Clusters with relatively small numbers of molecules, $n < 5$, can have ring structures. Small clusters with $5 < n \leqslant 20$ are non-symmetrical because side chains are attached to the ring structure, the whole cluster looking like a fragment of an amorphous or liquid structure. This trend is retained until the cluster size reaches $n = 20$. Then switching to ordered structures typical of big clusters takes place. The structures of molecular clusters are characterised by fast dynamic transitions between various conformations. The changes in the widths and positions of bands in the IR spectra of these clusters attest to the change in the number of molecules forming the clusters.[97]

Of special interest are water clusters that constitute liquid water and ice. They also participate in the formation of clouds and rains. The progress in laser spectroscopy and molecular dynamics made it possible to determine a number of properties of water clusters caused by their dynamic structure. Data on the geometric structure and hydrogen bond tunnelling in water tri-, tetra-, penta- and hexamers have been obtained.[98] Calculations[99,100] predict a planar structure for the tri-, tetra- and pentamers and a three-dimensional structure for the heptamers and larger clusters of water. The optimal configuration is characterised by the maximum number of hydrogen bonds and the minimum geo-

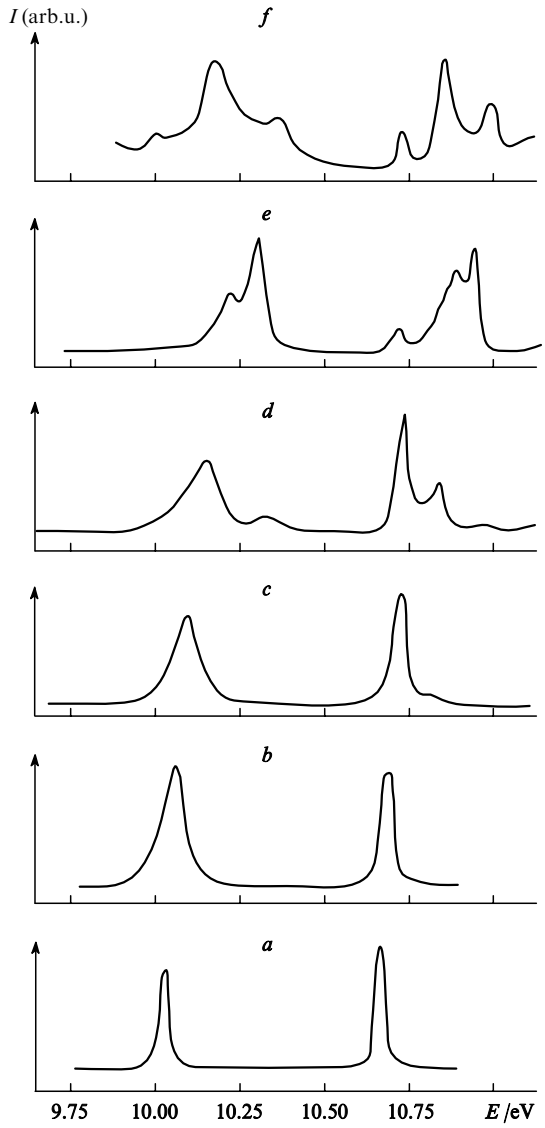

Figure 5. Fluorescence excitation spectra of atomic Kr (*a*), Kr_n clusters (*b*–*e*) with different numbers of Kr atoms, and a bulk sample (*f*).[93]
Number of krypton atoms in the cluster: 3 (*b*), 8 (*c*), 200 (*d*), 10^4 (*e*).

metric strain. IR-spectroscopic data confirm these assumptions.[98] Frequencies equal to 206, 304 and 658 cm^{-1} corresponding to the barriers to the rearrangement of the hydrogen bond configurations were found for three-, tetra- and pentamers, respectively. Water clusters are also formed upon hydration of gas-phase and colloid clusters, in particular, upon the hydration of macromolecules and proteins.

3. Colloid clusters

Colloid clusters are formed in solutions upon chemical reactions; their sizes range from 1 to 100 nm. They can exist in the liquid phase for long periods without being precipitated or coagulated, owing to weak intercluster interactions, charge repulsion and surface passivation. In terms of their behaviour towards the liquid medium, colloid clusters can be divided into two groups: lyophilic (hydrophilic) and lyophobic (hydrophobic) clusters.

Lyophilic clusters can sorb molecules from the environment and form strong solvation complexes with them. Clusters of this type are surrounded by a liquid shell, which is partially retained upon coagulation of separate clusters or on passing into a gel nanosystem. The most typical representatives of hydrophilic clusters are those formed by silicon and iron oxides and other metal oxides.

Lyophobic clusters do not adsorb solvent molecules on their surface. However, the surface can be modified by ions from solution, thus acquiring a positive or a negative charge. The giant Pd clusters the structure and the properties of which were considered in Section III.1 can be classified as colloid clusters in terms of the preparation method and the size (1.4–2.0 nm).

Normally, colloid clusters of metals are passivated with various ligands to prevent sticking together. Compounds suitable as these ligands are, for example, thiols, triphenylphosphine and its derivatives, phenanthroline.[101] Colloid clusters of semiconductors such as CdS, CdSe, CdTe, SnO_2, TiO_2, Fe_2O_3, MoS_2, HgS, InAs, GaP, GaAs, BiI_3, *etc* have been prepared.[7, 101, 102]

The weak intercluster interaction in solutions of colloid clusters does not preclude investigation of their individual properties. Among the optical properties peculiar to colloid clusters, the shift of the absorption frequency and the change in the oscillator strength following the change in the cluster size are the most impressive. As the size of the nanocluster decreases, the bands corresponding to the electronic excitation shift to higher energies and the oscillator strength is concentrated on several transitions. These effects are due to the replacement of the band spectrum corresponding to transitions between the conduction and valence bands in the bulk sample by the line spectrum of a cluster. It has also been reported that a decrease in the cluster size results in shorter lifetimes of excited states.

An expression for the calculation of the transition energy as $E \approx 1/R^2$ (R is the cluster radius) can be deduced from the quantum-size dependence $\Delta p \Delta x \geqslant h$ (p is the momentum, x is the coordinate) with the assumption that $\Delta x = R$. For semiconductors, the absorption and emission of energy are related to the formation and decomposition of the exciton (hydrogen-like bound state of a conduction electron and a hole); hence, the energy of exciton excitation is written in the form

$$E_n = \frac{h^2 n^2}{3R^2 m^*_{ef}},$$

where n is an integer, R is the cluster radius, m^*_{ef} is the effective mass of the exciton. Figure 6 shows the variation of the coefficient of light absorption by CdS colloid clusters with sizes from 6.4 to 48 nm *vs*. wavelength.[102] It can be seen that an increase in the

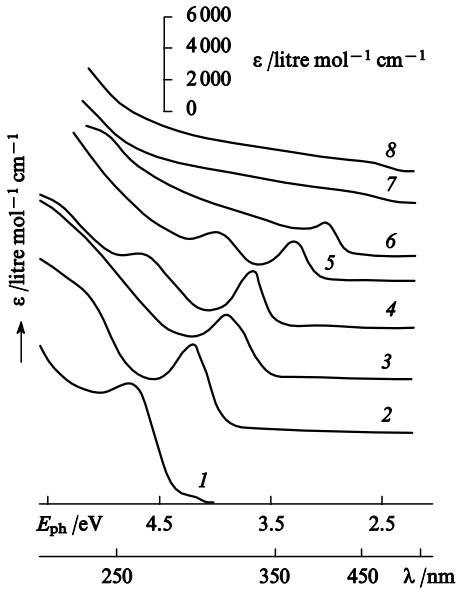

Figure 6. Absorption of light by CdS clusters *vs*. cluster size ('blue shift').[102]
Cluster size /nm: 6.4 (*1*), 7.2 (*2*), 8.0 (*3*), 9.3 (*4*), 11.6 (*5*), 19.4 (*6*), 28.0 (*7*), 48.0 (*8*). E_{ph} is the phonon energy.

cluster size entails a displacement of the absorption peak toward shorter wavelengths ('blue shift'). Similar shifts have also been observed for CdSe clusters.[103]

In the luminescence of nanoclusters caused by charge generation on exposure to light, a shift to shorter wavelengths following a decrease in the cluster size also takes place. Luminescence was observed for the ZnO, ZnS, CdS and CdSe clusters.[104–110] The change in the wavelength in the light absorption and emission spectra following a change in the cluster size can be employed in the design of frequency-tuned lasers on the basis of InAs and CdS.[111, 112]

The accumulation of the oscillator strength in several narrow bands or an increase in the oscillator strength normalised to the volume with a decrease in the cluster size should also be classified as quantum-size effects. This is caused by the increase in the overlap integral of the electron and hole wave functions. The oscillator strength corresponds to the radiation lifetime of the excited state at low temperature, while the oscillator strength normalised to the volume corresponds to the light absorption coefficient. For bulk semiconductors, the width of the exciton band is 0.15–0.3 eV; however, in clusters, the width of transitions decreases to 0.1–0.5 meV as a result of quantum restriction, which leads to the accumulation of the integral oscillator strength and to substantial growth of the exciton absorption of nanoclusters.[103, 113]

For clusters, the radiation lifetime of fluorescence was found to decrease with a decrease in the cluster size.[114] For instance, the lifetime of a Eu^{2+} tracer in clusters of alkali metal halides and chalcogenides[115, 116] and in ZnS[117] was found to decrease by almost five orders of magnitude with respect to the lifetime of Eu^{2+} in the bulk material. However, in another study,[118] no decrease in the lifetime was observed for Eu^{2+} in a 4-nm ZnS cluster. Thus, the data for the Eu^{2+} tracer lifetime in ZnS clusters are contradictory. This interesting phenomenon requires further studies and collection of experimental data both for the elucidation of the quantitative relationships between the cluster size and the optical characteristics and for the production of new optical materials.

IV. Cluster nanosystems and nanostructures

In this Section, we discuss the principles and approaches to the formation of nanosystems from clusters, from separate clusters and matrices, and from a bulk material. The properties of nanostructures to be considered include the intracluster, atomic, and intercluster dynamics, structural and mechanical properties, electrical conductivity, and optical and magnetic properties.

1. The formation of nanostructures. Assembly and self-assembly

Assembly and self-assembly of nanoclusters to nanostructures is an important problem the solution of which would contribute to the design of a new generation of materials with unique properties. The properties of materials can be changed in two ways: by changing the size of nanoclusters and by changing the intercluster interactions. The assembly of a nanostructure from nanoclusters follows the same laws as the formation of crystals from atoms; however, clusters differ substantially from atoms because they have a real surface and real cluster boundaries.§ Therefore, the formation of nanosystems from nanoclusters is accompanied by generation of numerous defects and stresses, resulting in fundamental changes in the properties of the nanosystem.

Nanostructures and nanosystems can be formed from clusters of any type. However, before proceeding to consideration of the processes of formation of nanosystems from solid-state and matrix clusters, it is necessary to consider the primary cluster nucleation processes because the properties and structure of these clusters depend markedly on their interaction with the matrices.

a. Nanosystems based on solid-state clusters

Let us consider the formation of nanosystems from solid-state nanoclusters using thermal decomposition of iron salts as an example. Decomposition of iron salts at a temperature above some critical (or threshold) value starts with the formation of a mobile active reaction medium in which nucleation of iron oxide nanoclusters occurs.[119] The process of cluster formation can be compared with seed formation in a confined space in a solution or in a melt (a cage or a pore). In this case, the role of this confinement can be played by diffusion restriction, which prevents the perturbation of the concentration of the mother medium caused by the change in the cluster size from migrating over the nucleation time (t_n) by a distance longer than $L \approx (Dt_n)^{1/2}$ (D is the diffusion coefficient). It is this distance that determines the size of the cage surrounding the cluster beyond which components of the mother medium cannot migrate. For a system of non-contacting clusters, the dependence of the Gibbs energy (ΔG_f) on the cluster radius (R) for one cluster is described by the formula ¶

$$\Delta G_f = 4\pi R^2\alpha - \frac{4}{3}\pi R^3\rho\Delta\mu, \tag{3}$$

where α is the density of the surface energy of the cluster (α = const), ρ is the substance density in the cluster (the number of atoms in 1 m^3), $\Delta\mu$ is the change in the chemical potential of the system caused by the transfer of a single iron atom from the medium to the cluster. If the cluster and the surrounding medium contain N atoms of any type of which n_0 are iron atoms (n iron atoms being contained in the cluster), then for $N \gg n_0 > n$

$$\Delta\mu = \Delta\mu^0 + \ln\frac{n_0 - n}{N}. \tag{4}$$

Here $\Delta\mu^0$ is the change in the standard chemical potential upon the transfer of one iron atom from the medium to the cluster structure expressed in kT units. At the initial stage, clusters do not contact one another. Since the volume of this cluster is $V_f = (4/3)\pi R^3$ and the surface area is $S_f = 4\pi R^2$, relation (3) can be written in the form

$$\Delta G_f = \alpha S_f - \left(\Delta\mu^0 + \ln\frac{n_0 - n}{N}\right)\rho V_f. \tag{5}$$

The function ΔG_f passes through a maximum at $R = R_{cr}$ (R_{cr} is the critical radius of seeds in the nucleation) and through a minimum at $R = R_{max}$ (R_{max} is the cluster radius corresponding to a stable equilibrium state of the system) (Fig. 7).

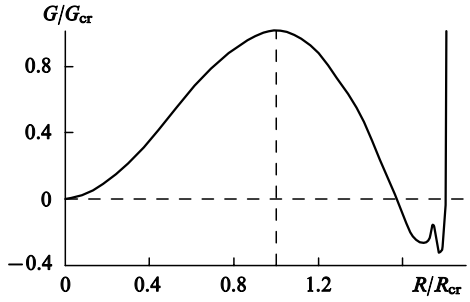

Figure 7. Change in the Gibbs energy G/G_{cr} upon nucleation, cluster growth and cluster sintering according to relations (5) and (7) in R/R_{cr} units.

§ The same boundaries appear on grinding of a bulk sample, for example, using mills or by plastic deformation.

¶ It should be noted that the thermodynamic approach is used in relation to ensembles of atoms or clusters which contain a large number of particles. However, this approach also proved effective (as will be shown below) for a limited number of particles.

Expression (5) characterises the stages of nucleation and the growth of a cluster in the system of weakly interacting non-contacting clusters. Upon further growth of clusters, they come into contact and the boundaries between them vanish (sintering). The onset of cluster sintering corresponds to a discrete transition from isolated clusters first, to weakly interacting and then, to strongly interacting clusters. If half of the distance R_t between the cluster centres at the stage of sintering is equal to R_t = const, the surface area (S_s) and the volume (V_s) of the cluster which has formed contacts with k neighbours can be calculated fairly accurately using the expressions

$$S_s = 4\pi R^2 + k2\pi R(R_t - R), \tag{6}$$

$$V_s = \frac{4}{3}\pi R^3 + k\frac{1}{3}\pi(-2R^3 + 3R^2R_t - R_t^3).$$

Correspondingly, the change in the Gibbs energy at the stage of sintering, *i.e.*, when $R > R_t$, is

$$\Delta G_s = \alpha S_s - \left(\Delta\mu^0 + \ln\frac{n_0 - n}{N}\right)\rho V_s. \tag{7}$$

Thus, the profile of the variation of free energy of the system per one cluster over the whole range of R is determined by relation (5) for $R < R_t$ and by relation (7) for $R > R_t$. As an example, Fig. 7 presents the $\Delta G(R/R_{cr})$ plot for $R_t = 1.75\,R_{cr}$. The curve given in the Figure has three minima separated by two maxima. The first minimum at the point $R = 0$ corresponds to the initial state of the mother medium; the second minimum at $R = R_{max}$ matches the first stable state, namely, the equilibrium state of the cluster having formed but not contacting (this is possible when $R_{max} < R_t$); the third minimum matches a system of sintering clusters each of them having k contacts. Correspondingly, the first maximum at $R = R_{cr}$ corresponds to the potential barrier to nucleation, while the second one corresponds to the potential barrier to sintering. Figure 8 shows the shape of the potential barrier to sintering for $k = 6$ and for different R_t. In a system densely populated by clusters, at $R_t \leqslant 1.7\,R_{cr}$, sintering occurs without a barrier; in a system less densely populated by clusters, at $R_t = 1.75R_{cr}$, the transfer to sintering requires overcoming a potential barrier, and in an even less densely populated system, at $R_t = 1.8R_{cr}$, sintering does not occur at all because in this case, this process is associated with an increase in the free energy.

The differential thermal analysis (DTA) and differential thermal gravimetry (DTG) curves recorded during thermal decomposition of iron oxalate $Fe_2(C_2O_4)_3 \cdot 5\,H_2O$ in air exhibit two minima at T_d = 200 and 260 °C.[120] The first minimum in both curves corresponds to dehydration of the iron complex with its partial decomposition giving rise to CO and CO_2. When $T_d > 200$ °C, a mobile medium starts to form, in which nucleation and growth of iron oxide clusters takes place. The second minimum is apparently due to further removal of CO and CO_2 and the onset of sintering of iron oxide clusters. The cluster size can be estimated from the specific surface area (BET) or using data of X-ray diffraction analysis, atomic force microscopy (AFM) and Mössbauer spectroscopy. The AFM images of iron oxide-based cluster systems formed at T_d = 265 °C are shown in Fig. 9 *a*,*b*. The contacting clusters which undergo sintering can be readily seen in Fig. 9 *a*.

Figure 10 shows how the thermodynamic model of nucleation and cluster growth and sintering (the upper section of the Figure)

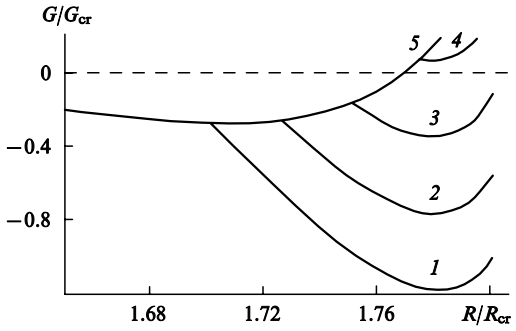

Figure 8. Change in the Gibbs energy G/G_{cr} in the region of the onset of cluster sintering *vs.* R/R_{cr} at different R_t values (which is half the distance between the cluster centers).
$R_t = 1.7R_{cr}$ (*1*), $1.73R_{cr}$ (*2*), $1.75R_{cr}$ (*3*), $1.77R_{cr}$ (*4*), $1.78R_{cr}$ (*5*).

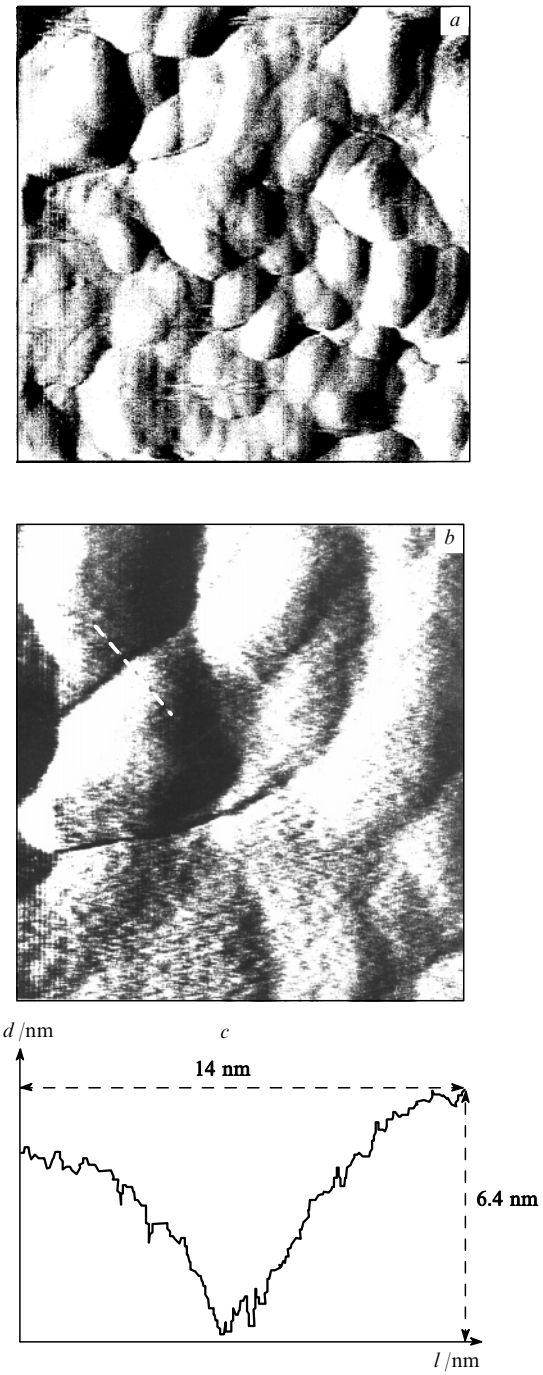

Figure 9. Computer images of a nanocluster system of strongly interacting iron oxide clusters obtained by an atomic-force microscope with a resolution of 500 (*a*) and 150 nm (*b*); and surface relief (*c*) along the dashed line drawn in the upper left section of Fig. 9 *b*. The line is 14 nm long; the maximum relief depth is 6.4 nm.

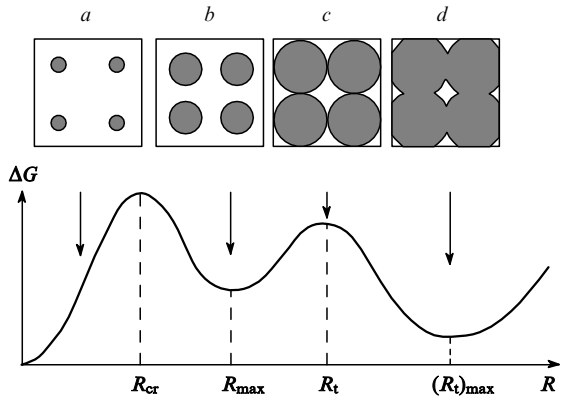

Figure 10. Scheme of cluster formation, growth and sintering; (*a*) formation of seeds, (*b*) maximum size (5–6 nm) of a stable cluster in a weakly interacting system of clusters, (*c*) onset of sintering; (*d*) formation of a system of strongly interacting clusters. The arrows match steps *a*–*d* to the curve for the change in the Gibbs energy obtained upon thermal decomposition of iron oxalate.

interprets the experimental data on iron oxalate thermolysis (the low section of the Figure). The subcritical range of cluster sizes ($R < R_{cr}$) corresponds to the stage of fluctuation nucleation of clusters; in this range, the function $\Delta G(R)$ increases (Fig. 10 *a*). In the region of $R > R_{cr}$, the enlargement of clusters is accompanied by a decrease in the free energy; it proceeds spontaneously and ends in the formation of a stable cluster with the size $R_{max} = 5-6$ nm and a nanosystem formed by weakly interacting clusters (Fig. 10 *b*). When the distance between the centres of neighbouring clusters ($2R_t$) approaches the value $2R$, sintering starts (Fig. 10 *c*). In the region of $R_{max} < R < R_t$, the function $\Delta G(R)$ increases, which forms a potential barrier to the sintering with a maximum at $R = R_t$. With further increase in R ($R > R_t$), sintering occurs spontaneously and is accompanied by a decrease in the Gibbs energy. The second potential well in the $\Delta G(R)$ curve corresponds to a system of strongly interacting clusters (Fig. 10 *d*). When $R > (R_t)_{max}$, the potential well disappears and further sintering becomes impossible because it would be accompanied by an increase in the Gibbs energy ($\Delta G > 0$). Since the R_{max} and R_t values are dictated by experimental conditions, the outcome of the topochemical reaction depends on the reactor temperature, duration of sintering and the previous history of the sample.

Thus, the formation of a nanosystem includes two main stages: first, a nanosystem of weakly interacting clusters is formed (this stage starts with nucleation and ends in cluster sintering) and subsequently it is converted into a nanosystem of strongly interacting clusters (this stage starts with cluster sintering). Figure 9 *a* corresponds to a nanosystem formed by strongly interacting clusters† with sizes of 20–50 nm. The appearance of strong intercluster interaction and the sintering bring about substantial interfacial stresses. These stresses (p) are generated by the 'neck' formed due to the surface tension (the region where the clusters are contacting):[121] $p = 2\alpha/x$ (α is the surface tension, x is the radius of the neck formed upon cluster sintering). Assuming that $\alpha = 1\ \mathrm{N\,m^{-1}}$ for iron oxide[122] and $x \approx 1$ nm, we obtain $p \approx 10^9-10^{10}$ Pa.

Excessive pressure also develops due to the presence of defects and dislocations at the interface; for ~10-nm clusters, it reaches 10^9 Pa.[6,123–125] The stress and pressure developing in a system of strongly interacting nanoclusters are important factors determining the formation and properties of the nanostructure.

A system of strongly interacting solid-state clusters can also arise upon mechanical treatment of bulk samples. Thus plastic deformation of Ni and Cu bulk samples gave nanosystems of Ni and Cu clusters with an average size of 100 and 50 nm, respectively.[126–128] Titanium nanoclusters with sizes of up to 30–40 nm[129] have been prepared by imposing pressure with shear on the titanium carbide $TiC_{0.62}$.

Crystallisation of multicomponent alloys is of considerable interest. Thus crystallisaton of amorphous Fe–Cu–Nb–Si–B alloys at 700–900 K affords a cluster system consisting of an amorphous matrix with 10-nm α-Fe clusters and ~1-nm Cu clusters uniformly distributed in the matrix.[130,131] Crystallisation conditions can be altered by preliminary treatment of the alloy. In this case, α-Fe clusters with sizes of up to 5 nm were obtained.[130,131] Crystallisation of rapidly solidifying amorphous alloys Al–Cr–Ce–M (M = Fe, Co, Ni, Cu) with Al concentrations of more than 90% yields icosahedral Al nanoclusters, which occur in an amorphous matrix.

b. Nanoclusters prepared using matrices

In this Section, we shall find out how a matrix influences the properties of nanoclusters formed in it. The formation of nanocluster seeds from a supercooled liquid or a supersaturated solution in an infinite space has been extensively studied and discussed, in particular, from the thermodynamic standpoint.[132–134]

The Gibbs energy for this process is calculated using an equation[132–134] similar to equation (3) introduced for solid-phase reactions

$$\Delta G = 4\pi\alpha R^2 - \frac{4}{3}\pi R^3 \rho \Delta\mu. \qquad (8)$$

For a solution with the finite concentration $c = n_0/N$ (n_0 is the number of atoms of a dissolved substance, *e.g.*, iron, N is the number of solvent atoms), the $\Delta\mu$ value is found from the relation

$$\Delta\mu = \Delta\mu^0 + \ln\frac{n_0}{N} = \Delta\mu_0\,. \qquad (9)$$

Thermodynamic estimation of the influence of a pore on the features of the formation of a nanocluster in it has been reported.[135] For a closed pore in which a cluster of n atoms is formed,

$$\Delta\mu = \Delta\mu^0 + \ln\frac{n_0 - n}{N}, \qquad (10)$$

where $\Delta\mu^0 = \mu_l - \mu_s$ is the difference between the chemical potentials of the liquid and solid standard states. Thus, the Gibbs energy for cluster formation in a closed pore can be written as

$$\Delta G = \frac{4}{3}\pi\rho R^3\left[\frac{3\alpha}{\rho R} - \left(\Delta\mu_0 + \ln\frac{n_0}{n_0 - n}\right)\right]. \qquad (11)$$

The pattern of the $\Delta G(n)$ dependences describing the formation of a cluster in an infinite space and in a closed pore is shown in Fig. 11. The curves describing the change in the Gibbs energy upon the formation of nanoclusters in an infinite space have a maximum at the points n_{min} corresponding to the critical volume of formation of a stable cluster seed (Fig. 11, curves *1*, *2*). For a supersaturated solution (Fig. 11, curve *1*) or a supercooled melt, the n_{min} value is found from Eqn (8). As the initial concentration n_0/N decreases, the n_{min} value shifts to greater n [$(n_{min})_2$ in curve *2*].

The formation of a cluster in a closed pore is illustrated by curves *3* and *4* (Fig. 11). The limited concentration of the solute inside the pore entails the existence of a limiting volume of the cluster n_{max}; after this volume has been reached, cluster growth becomes energetically unfavourable and ceases. One more important factor influencing cluster formation and growth in a pore is pore heterogeneity. Heterogeneity of a pore changes the condi-

† The change in the type of intercluster interaction changes many properties of the nanosystem; this will be discussed in the Section dealing with the properties of nanostructures.

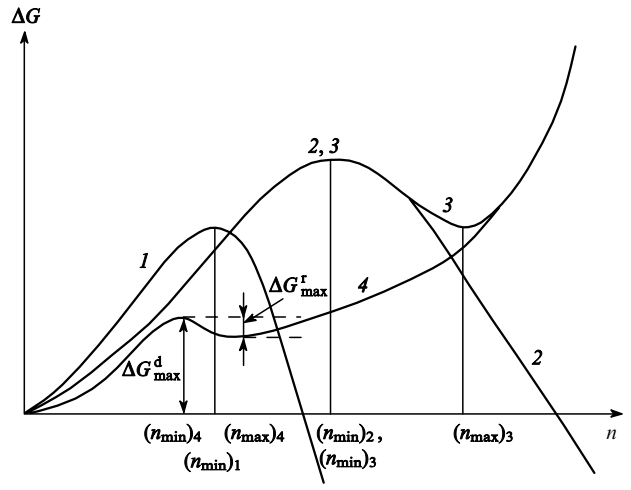

Figure 11. Funcion $\Delta G = f(n)$ characterising the growth of a cluster with an increase in n;
(*1*) in a supersaturated solution having a macrovolume, (*2*) in a solution with finite concentration c, (*3*) in a pore; (*4*) in a pore with allowance for the heterogeneity factor K.

tions of cluster formation and decreases the energy barrier to the formation of a stable seed of a cluster having the critical volume.[135]

Now we shall consider the variation of ΔG_{max} as a function of cluster size (n). In the region of $n \ll n_0$,

$$n_{min} = \frac{32\alpha^3}{3\rho^2\Delta\mu_0^3}. \quad (12)$$

It follows from Eqn (11) that an increase in the concentration n_0/N decreases the cluster critical volume (size). The height of the energy barrier to the formation of a stable cluster equals

$$\Delta G_{max} = \frac{16\pi\alpha^3}{3\rho^2\Delta\mu_0^2}. \quad (13)$$

However, in the region of $n_{min} \ll n < n_0$

$$n_{max} = n_0 \frac{\Delta\mu_0}{2 + \Delta\mu_0}. \quad (14)$$

Thus, the maximum size of the clusters (n_{max}) in a pore is always smaller than n_0 and, for a constant concentration, it increases with an increase in the pore size. When estimating n_{max}, one should take into account the influence of pore heterogeneity and the fact that the probability of formation of several clusters in one pore increases with an increase in the pore size from 10 to 100 nm and further; naturally, this results in smaller n_{max} (in large pores, $n_{max} \ll n_0$).

As noted above, pore heterogeneity decreases the energy barrier to cluster formation. The Gibbs energy of both the formation (ΔG^d_{max}) and decomposition (ΔG^r_{max}) of clusters can be considered. With allowance for the heterogeneity factor K ($K < 1$), which depends on the contact angle between the cluster and the pore surface,

$$\Delta G^d_{max} = \frac{16\pi\alpha^3 K}{3\rho^2\Delta\mu_0^2}. \quad (15)$$

The pore also influences the ΔG^r_{max} value, *viz*., decreases it. As a consequence, with a decrease in n_{max} (especially for pores of $\sim$10 nm), $\Delta G^r_{max} < \Delta G^d_{max}$.

The surface and the volume of a pore influence as well the rate of cluster formation, which increases due to a decrease in the energy barrier and the heterogeneity factor.[134, 135]

The nucleation and the formation of iron hydroxide clusters in organic sorbents — styrene and divinylbenzene copolymers (polysorbs) with a specific surface area of up to 1000 $m^2\ g^{-1}$ and a pore size of 7 to 50 – 100 nm have been investigated.[135, 136] The pore surface in polysorbs bears no functional groups; therefore, the influence of chemisorption on cluster formation can be neglected. Polysorbs were impregnated with ferric chloride solutions with different concentrations and purged with air containing an ammonia admixture (0.008% – 0.08%). As a result the irreversible chemical reaction

$$FeCl_3 + H_2O + NH_3 \longrightarrow Fe(OH)_3 + NH_4Cl + NH_4OH,$$

resulting in the formation of iron hydroxide took place in the polysorb pore. This changed the pH of the medium and induced the growth of insoluble iron clusters in the pore.

Changes in the intensity (ε) of spectral lines in the Mössbauer spectra of iron hydroxide clusters were used to investigate the influence of various parameters (pore size, concentration of ammonia in air, concentration of $FeCl_3 \cdot 6\,H_2O$) on the size of the resulting clusters. Figure 12 shows the dependence of ε on the size (d) of the pore in polysorb at different ammonia concentrations in air.[135] It was found that a decrease in the pore size results in a corresponding decrease in the cluster size [*e.g*., according to Eqn (14)] and, hence, in a decrease in the intensity of spectral lines. For large pores, a decrease in ε with an increase in the iron chloride concentration was also observed, which can be due to the formation of several smaller clusters within one pore. A substantial increase in the rate of cluster formation with respect to that in a macro-volume was noted, which is consistent with the heterogeneity factor and Eqn (15).

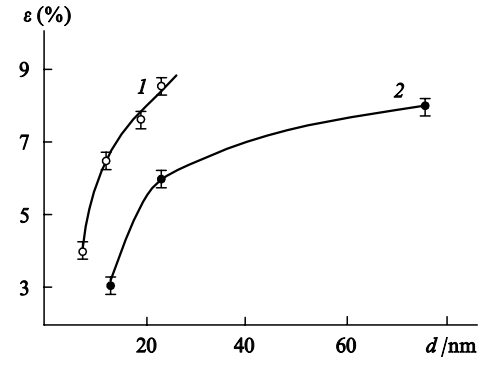

Figure 12. Line intensity in the Mössbauer spectrum of iron oxide clusters formed in the polysorb pores *vs*. pore diameter ($T = 300$ K) at an ammonia concentration in air of 0.08% (*1*) and 0.008% (*2*).

Yet another active matrix widely used to prepare nanoclusters is porous active carbon. The deposition of metal salts, for example, iron oxalate $Fe_2(C_2O_4)_3 \cdot 5\,H_2O$, on an active carbon substrate followed by annealing and reduction under a hydrogen atmosphere gives rise to a mixed heterogeneous system of Fe_3O_4, γ-Fe_2O_3 and metallic iron clusters on a carbon substrate. Depending on the duration of the reduction with hydrogen, the size of oxide clusters ranges from 7 to 12 nm, and the size of iron (α-Fe) clusters is 3 – 7 nm.[137] It is noteworthy that a nanosystem of these clusters possesses a self-forming property: the reduction by hydrogen is accompanied by hydrogenation (carbon burning) accompanied by an increase in the pore size. The size and composition of nanoclusters are also markedly affected by the nature of the carbon surface.[138, 139]

c. Colloid nanosystems

Nanostructures prepared from colloidal solutions and sols by sol – gel technology can be used in conductive systems, optics and catalysts. Systems consisting of zirconium, titanium or aluminium alkoxides [$Zr(OPr^i)_4$, $Ti(OBu^i)_4$, $Al(OPr^i)_3$] and iron or cobalt complexes are fairly promising.[140] Based on them, supported catalysts represented by nanocluster systems have been prepared, for example, FeO/ZrO_2, FeO/TiO_2, FeO/Al_2O_3. The cluster size was varied by changing the concentrations of components and the heating temperatures. However, clusters prepared by sol – gel technology are unsuitable for the design of assembled nanostructures because of the large scatter in the nanocluster size. It is more promising to assemble nanostructures from clusters prepared using direct and reverse micelles.[21, 22, 141, 142] These clusters are distinguished by narrow size distributions.

Since reverse microemulsions are characterised by high mobility and great interfacial surface area, they can act as a universal medium for numerous chemical syntheses including those giving rise to metal, metal sulfide and other clusters. In a microemulsion, drops constantly collide due to the Brownian motion, coalesce and again split, which results in the continuous exchange of their contents.

Thus Ag_2S clusters are prepared using mixtures of two types of reverse micelles, the aqueous phases of which contain Na_2S and Ag-surfactant, respectively. Upon collision, these micelles coalesce, which is accompanied by the exchange of the contents of the aqueous media. This exchange yields solid Ag_2S particles. The size of a new-phase particle is limited by the size of the drop. The size of Ag_2S clusters was found to increase from 3.0 to 5.8 nm with an increase in the size of water drops.[21] In this case, the model of nucleation in a pore considered in Section IV.1.b is also valid. To release the nanoclusters from the micelle, the micelle is destroyed by thiols, the resulting nanoclusters are dissolved in an appropriate solvent, the solution is filtered, and the solvent is evaporated. This procedure permits preparation of nanoclusters with a size of up to 10 nm passivated by thiols (*e.g.*, dodecanethiol). Two- and three-dimensional nanostructures are formed from these clusters on various substrates.

Characteristic features of the formation of nanostructures from Ag_2S clusters have been described.[141, 142] The researchers observed the self-assembly of clusters to give ordered two- and three-dimensional structures. Organised nanostructures have also been obtained from metallic Ag, Co, Au and semiconductor nanoclusters.[143 – 147] Alkanethiols, alkylphosphines and dithiols were used as nanocluster surface passivators.

Figure 13 presents two photomicrographs of the Ag_2S nanostructure prepared from passivated nanoclusters with a size of 5.8 nm. The photomicrograph shown in Fig. 13 *b* clearly demonstrates that the nanoclusters are strictly assembled to give a nanostructure rather than arranged randomly. Like conventional crystals, this structure can contain dislocations and defects (they are marked by arrows in photomicrograph 13 *a* obtained with a smaller magnification).

Two-dimensional nanostructures (2D structures) are closely packed monolayers, while 3D structures have a face-centred cubic (FCC) lattice.

The procedure for the preparation of monodisperse nanoclusters using microemulsion systems makes it possible to vary the size of the initial nanoclusters, a sort of 'atoms'. Figure 14 presents three photomicrographs of the nanostructures prepared from Ag_2S nanoclusters with a size of 3.0 (*a*, *b*), 4.0 (*c*, *d*) and 5.8 nm (*e*, *f*). Despite the difference in the shape of the aggregated nanostructures (Fig. 14 *a*,*c*,*e*), the type of organisation is the same

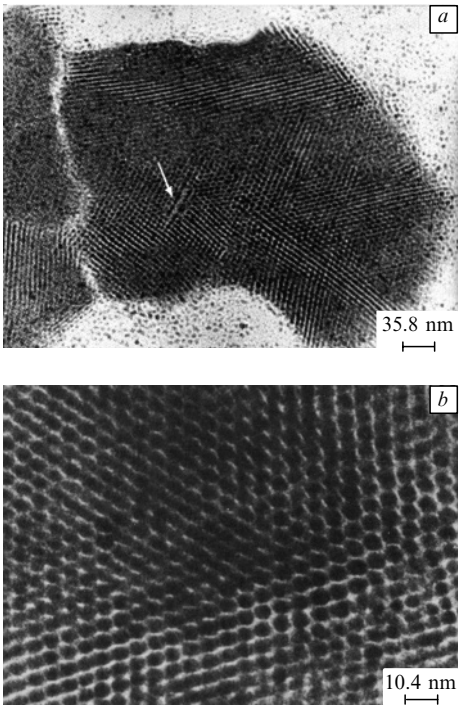

Figure 13. Photomicrographs of Ag_2S nanocluster structures with a resolution of 35.8 (*a*) and 10.4 nm (*b*). The white arrow marks a defect in the nanostructure 'crystallinity'.[21]

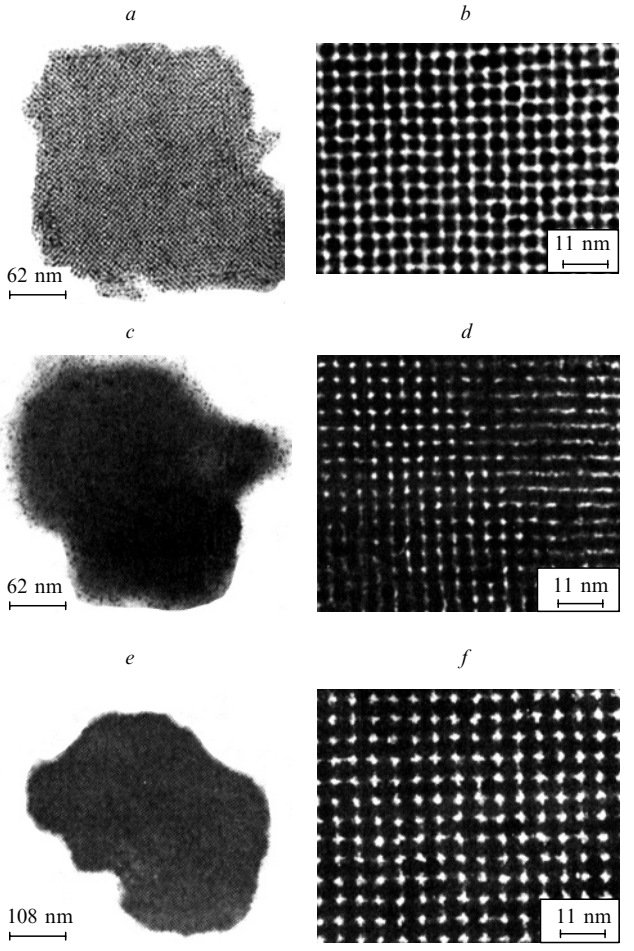

Figure 14. Photomicrographs of nanocluster structures formed from Ag_2S clusters with different sizes: 3.0 (*a*, *b*), 4.0 (*c*, *d*) and 5.8 nm (*e*, *f*).[21]

and corresponds to the body-centred cubic (BCC) lattice (Fig. 14 *b*,*d*,*f*).

In this case, assembly and self-assembly of nanoclusters to give a BCC crystal lattice is induced, apparently, by van der Waals forces acting between separate nanoclusters having a nearly spherical shape.

d. Assembling of fullerenes, fullerides, fullerene-like structures and nanotubes

Fullerenes are fairly convenient structural materials for the formation of nanostructures because they are perfectly monodisperse and spherical. The organisation and self-organisation of colloid and gas-phase fullerenes to nanostructures (fullerides) is induced by heating, pressing, *etc*. In aqueous solutions, the star hexaanion derivatives $C_{60}[(CH_2)_4SO_3]_6^-$ form spherical aggregates comprising four molecules.[148] The shape, the size and the structure of aggregates were studied by small-angle neutron and X-ray scattering. An unusual stability of these aggregates was noted: their volume and shape do not depend on the fullerene concentration or on the inter-aggregate interaction.

Larger aggregates were formed from colloid solutions of C_{60} fullerene in benzonitrile at C_{60} concentrations of more than 100 μmol litre^{-1} (at lower C_{60} concentrations, only separate fullerene molecules are present in the solution).[149] In this case, the average size of the aggregate reached $\sim$250 nm. These aggregates, existing as dynamic systems,‡ were detected using picosecond photolysis. No aggregates of this type are formed in benzene or decalin up to concentrations of 500 μmol litre^{-1}. Apparently, the formation of aggregates is influenced by solvent polarity and the symmetry of the molecules being joined. Indeed, the non-symmetrical C_{70} molecule does not form aggregates either in polar benzonitrile or in nonpolar benzene or decalin.

The preparation and study of the nanocrystals of fullerene fluorides $C_{60}F_x$, $C_{60}F_{36}$ and $C_{60}F_{48}$ present considerable interest.[84, 150, 151] It was found that at room temperature, the crystals of $C_{60}F_{36}$ have a BCC lattice, while those of $C_{60}F_{48}$ crystallise with a body-centred tetragonal lattice. The data of high-temperature (T = 353 K) X-ray diffraction *in situ* point to a phase transition in a $C_{60}F_{48}$ nanocrystal: the body-centred tetragonal lattice is transformed into a face-centred cubic lattice.

The parameters governing the formation of fullerene nanostructures (crystals) are the pressure and the temperature. Thus crystallisation of C_{60} fullerene at 1.56 GPa and 423 K affords a crystal lattice the structural elements of which are dumb-bell-shaped $C_{60}-C_{60}$ dimers.[152] (This reaction is similar to the mechanochemical reaction of C_{60} with KCN.[153]) An increase in the temperature induces decomposition of the dimers to give an orthorhombic polymeric structure of C_{60} molecules, which is converted into a polymeric tetragonal structure at $T \approx 723$ K.

Carbon nanotubes (NT) are also used for the formation of nanostructures. A nanotube is a graphene sheet rolled into a hollow cylinder. The chirality and the diameter of this tube can be characterised by the vector $\mathbf{c} = n\mathbf{a} + m\mathbf{b}$, ($\mathbf{a}$, $\mathbf{b}$ are the unit vectors of the hexagonal cell and m and n are integers). Depending on the mode of rolling, nanotubes can be either achiral zigzag-like (two sides of each hexagon are parallel to the NT axis, $m = 0$), or armchair-like (two sides of each hexagon are normal to the NT axis, $n = m$), or chiral helix-like (each pair of the hexagon sides is arranged at an angle other than 0 or 90 ° to the NT axis). The form of the nanotubes influences substantially the properties of nanostructures (metallic or semiconducting). By varying and combining two types of nanotubes, for example, zigzag and armchair nanotubes, one can create single-electron devices with different conductivities, for example, diodes.[154] The size (length) of nanotubes also influences the properties of nanostructures formed from them. Depending on the nanotube size, the properties of nanosystems vary from semiconductor properties with a real forbidden gap (quantum dots, 0D) to metallic properties for a unidimensional system (quantum wire, 1D). According to quantum-mechanical calculations, transition from (0D) to (1D) structures takes place if the nanotube becomes more than 10-nm long.

‡ Aggregates of C_{60} are unstable and undergo constant assembly and destruction of the type $nC_{60} \leftrightarrows (C_{60})_n$.

e. Nanofilms

Nanofilms are two-dimensional structures. There exist numerous expedients for film deposition or growth on metallic, oxide, chalcogenide and other substrates. The method used most widely to prepare organised films is deposition of atoms or molecules from the gas phase onto the surface of a single crystal and design of epitaxial or polycrystalline atomic or molecular layers from them.

Considerable progress has been attained in the synthesis of films from fullerenes on substrates of various materials including metals,[155, 156] semiconductors,[157–159] layered materials,[160, 161] insulators,[162] *etc*. However, the question of what factor dictates the type of the structure being formed (face-centred, hexagonal or close-packed) still remains open. It can only be concluded that weak interaction of the fullerene molecules with the substrate favours the formation of an ordered layer of C_{60} molecules, whereas strong chemisorption of C_{60} on the substrate surface gives rise to a disorganised, disordered structure. The structure of a thin film of fullerene molecules formed on the graphite surface has been studied.[163] It was shown by computer simulation that the C_{60} film supported on graphite has a hexagonal structure.

The films deposited on a substrate can also have a nonuniform, islet structure. The formation of films of gas-phase clusters on a substrate depends on the time, temperature and deposition velocity. The final state of the film is determined by the average size and density of the cluster islets: the larger the islets, the smaller the density.

The rate of atom diffusion is known to be low at low temperatures; therefore, relatively small clusters with high density are formed. The same considerations are valid for the formation of films from clusters. The formation of nanostructures from antimony clusters on the amorphous surface of carbon has been studied as a function of the number of Sb atoms in the cluster (n = 4–2200).[164] (The antimony clusters were prepared by condensation of antimony vapour in a helium cell cooled with liquid nitrogen.) The dependence of the average size (N) of the cluster islet structure on the average size (n) of the primary antimony cluster passes through a minimum at $n = 350 \pm 50$. This was interpreted as being due to the fact that the size distribution of the islet structure becomes narrower as the cluster size approaches the optimum value ($n = 350 \pm 50$). As the size of the primary antimony cluster increases, the rate of its diffusion over the substrate surface decreases; hence, the probability of coalescence of the primary clusters to an islet nanostructure also decreases. Each large primary cluster (from $n > 400$ to $n = 2200 \approx N$) is adsorbed on the surface and retained unchanged for some densities of the primary beam. From small clusters with $n < 350$, it is possible to form islet structures with large N (> 3000), owing to higher diffusion rates.

An effective method for the formation of nanofilms from clusters is deposition from plasma as well as chemical and physical vapour deposition (CVD and PVD).[8, 165] In plasma deposition, the film thickness and the size of crystallites are controlled by variation of the gas pressure and discharge parameters. Dudko *et al*.[166] and Barg [167] prepared chromium films on a copper substrate with an average size of crystallite clusters of $\sim$20 nm. The increase in the film thickness to 500 nm resulted in its crystallisation. The ion-plasma deposition of titanium carbide and nitride also results in the formation of nanocrystalline films.[165] The use of magnetron sputtering of the initial substances allows the substrate temperature to be decreased by 100–200 °C; this extends the scope of the preparation of nanotubes. This procedure was employed to produce Ni_3Al films with a crystallite size of 20 nm.[168]

The preparation of nanofilms from colloid solutions has been considered in the previous Section in relation to the formation of silver sulfide-based nanostructures.[21] It has been noted [21] that hexagonal ordering of clusters (3 – 5 nm) is observed even within a monolayer. Generally, to prepare assembled nanofilms from colloid solutions, it is necessary to have monodisperse nanoclusters, which are self-assembled into a film due to weak van der Waals intercluster interactions.

In recent years, a procedure has been developed for the formation of films on a liquid surface (Langmuir – Blodgett) and transferring them onto a solid surface. This method permits the formation of superlattices and nanometer layers of organic molecules with a specified pattern of layer alternation.

The organisation of nanofilms by chemical assembling and molecular layering methods has been described.[27] In the synthesis of highly organised structures by the chemical assembling method, the key role is played by the chemical reactions taking place between the functional groups located on the surface of a solid (substrate) and the adsorbed molecules with specified composition. This procedure is used, for example, to apply organised layers of metal oxide clusters.

f. Compacted nanosystems

Compacting of gas-phase, colloid or molecular clusters by pressing followed by the high-temperature sintering of nanoclusters gives rise to nanosystems.[169, 170] The most densely organised nanostructures are produced from the smallest monodisperse clusters. Thus a nanostructure based on titanium nitride were prepared by pressing nanoclusters with a size of 8 – 25 nm with subsequent sintering.[171] To preserve a small size of crystallites in nanosystems, low sintering temperatures and doping additives hampering the crystal growth are required. An example is provided by WC – Co nanocrystalline solid alloys, which consist of WC nanoclusters (50 nm) dissolved in a Co matrix.[172, 173] Tungsten carbide (up to 1 mass %) is added to retard the crystal growth.

A magnetic-pulse method is also used to compact nanosystems.[174] In this case, pressing occurs on exposure to pulse compression waves and is accompanied by local heating due to the fast energy evolution upon the friction of particles during packing. The magnetic-pulse pressing allows the generation of pulse compression waves with an amplitude of up to 5 GPa and a duration of several microseconds. The use of pulse pressures results in a higher compaction density compared to that reached by static pressing. Apparently, this is due to the generation of intercluster pressures, which enhance the intercluster interactions. The magnetic-pulse method was used, for example, to press Al_2O_3 [175] and TiN [176] nanoparticles. An increase in the temperature of magnetic-pulse pressing was found to be more efficient than an increase in the pressure (cold pressure). With a pulse pressure of 4.1 GPa and a temperature of 870 K, nanosystems with a grain size of 80 nm and a density of 83% of the theoretical one were prepared. Upon a decrease in the temperature to 720 K, the density decreased to 81%.

2. The properties of nanocluster systems

As noted above, isolated nanoclusters possess unique properties related to their nanometer size. However, in most cases, nanoclusters are interacting with one another; this can not only induce a quantitative change in their properties but also provoke the appearance of new properties. The assembly and self-assembly of clusters to give nanocluster systems changes many properties of the clusters. The most vivid properties of nanosystems such as structural phase transitions (in particular, in ferroelectrics and fullerenes) and optical, electric and magnetic (giant magnetoresistance, quantum magnetic tunnelling, magnetic phase transitions) properties are related to the atomic and cluster dynamics.

It is pertinent to consider both the intracluster atomic dynamics and the intercluster dynamics in a nanosystem where the cluster moves as a a single whole.

a. Intracluster atomic dynamics

The intracluster atomic mobility (in relation to the melting dynamics) is studied using microscopic and quantum-statistical methods as well as methods based on the use of thermodynamic models and computer simulation of motions (molecular dynamics and Monte Carlo method). The most important and characteristic parameters of motion are the mean square displacements of atoms in the cluster

$$\langle \bar{r}^2(t)\rangle = \frac{1}{N}\langle [x(t) - x(0)]^2\rangle \tag{16}$$

$\{\langle [x(t) - x(0)]^2\rangle$ is the mean-square displacement along the x axis in which the displacement is time averaged$\}$ and the diffusion coefficient

$$D = \frac{1}{6}\,\frac{\mathrm{d}\langle \bar{r}^2(t)\rangle}{\mathrm{d}t}\,.$$

At longer times, $\langle \bar{r}^2(t)\rangle = 6Dt$.

Before we proceed to the consideration of the microscopic approach, it is necessary to discuss two points: (i) whether the concept of phonons determining the dynamics of solids is applicable to clusters and (ii) what changes in the vibrational and rotational spectra would occur upon a decrease in the nanocluster size. The point is that in crystals constructed of nanoclusters, the lattice is not strictly periodical, unlike that in molecular crystals (because the substantial influence of the surface should be taken into account for clusters); therefore, phonons cannot be considered as plane waves with the energy E and momentum q. However, a cluster can be regarded as a single giant molecule with $3N$ degrees of freedom (N is the number of atoms in the cluster). All the natural frequencies ω corresponding to the vibrations of this 'molecule' and eigenvectors can be found. Thus, the vibrational states can be numbered in terms of frequencies ω_i rather than momenta. The mean square displacement of an atom can be found from the formula [119]

$$\langle r^2\rangle = \frac{\hbar}{NM}\sum_i \frac{\bar{n}_i + 1/2}{\omega_i}\,, \tag{17}$$

where M is the atom mass, $\bar{n}_i$ is the averaged number of vibrations.

For large clusters, the density of phonon states $\rho(\omega)$ should be introduced and the summation over frequencies should be replaced by integration. In this case, we obtain

$$\langle r^2\rangle = \frac{\hbar}{NM}\int\left(\frac{1}{2} + \frac{1}{\exp(\hbar\omega/kT) - 1}\right)\frac{\rho(\omega)}{\omega}\,\mathrm{d}\omega\,. \tag{18}$$

The form of the function $\rho(\omega)$ depends on the phonon spectra and on the model of the atomic cluster mobility chosen. In the case of the Debye model,

$$\rho(\omega) = \frac{9N\omega^2}{\omega_{\max}^3}$$

and

$$\langle r^2\rangle = \frac{9\hbar^2}{4Mk\theta_{\mathrm{D}}}\left(1 + \frac{4T^2}{\theta_{\mathrm{D}}^2}\int_0^{\theta_{\mathrm{D}}/T}\frac{u\,\mathrm{d}u}{\exp(u-1)}\right), \tag{19}$$

where θ_{D} is the Debye temperature, $u = \hbar\omega/kT$. At high temperatures, $T \gg \theta_{\mathrm{D}}$

$$\langle r^2\rangle = \frac{9kT}{M\omega^2}\,, \tag{20}$$

$$\langle x^2\rangle \approx \frac{3kT}{M\omega^2}\,.$$

For the Einstein model,

$$\rho(\omega) = 3N\delta(\omega - \omega_{\mathrm{E}})$$

(δ is the δ function, ω_{E} is the Einstein frequency) and

$$\langle x^2\rangle = \frac{\hbar}{2M\omega_t}\mathrm{cth}\left(\frac{\hbar\omega_E}{2kT}\right). \quad (21)$$

Before we consider the phonon spectra of small particles, it is necessary to calculate the density of states function $\rho(\omega)$ for the vibrations in clusters. Specific features of the spectra of clusters are due to the presence of a large number of surface atoms. It is known that atoms on the cluster surface are more weakly attached to the lattice and, hence, their vibration frequencies are lower. Therefore, the vibrational spectrum of the cluster exhibits a large number of low-energy vibrations, which results, in accordance with (18)–(21), in an increase in $\langle r^2\rangle$. However, clusters are characterised by limiting phonon wavelengths stipulated by the cluster size, *i.e.*, the phonon spectrum loses some of the low-frequency vibrations, and $\langle r^2\rangle$ decreases. Thus, the phonon spectrum of the cluster becomes discrete. However, if the Debye dependence is assumed for the contribution of the density of phonon states [$\rho(\omega) \sim \omega^2$], the effect of cutting of the phonon spectrum would be insignificant, and the overall effect for the isolated clusters would still be related to an increase in $\langle r^2\rangle$.

Even a simple model of the atomic cluster mobility predicts unusual cluster properties. If a cluster is regarded as a sphere consisting of two parts — the surface layer and the inner core — a characteristic Einstein frequency and the mean square displacement of atoms can be attributed to each part, $(\omega_E)_s$ and $\langle x^2\rangle_s$ for the surface and $(\omega_E)_i$ and $\langle x^2\rangle_i$ for the inner core. In this case,

$$\langle x^2\rangle_s = \frac{\hbar}{2M(\omega_E)_s}\mathrm{cth}\left[\frac{\hbar(\omega_E)_s}{2kT}\right]$$

and

$$\langle x^2\rangle_i = \frac{\hbar}{2M(\omega_E)_i}\mathrm{cth}\left[\frac{\hbar(\omega_E)_i}{2kT}\right].$$

According to the Lindemann criterion, melting of a substance starts when $\langle x^2\rangle_m \simeq 0.1a^2$ (a is the average distance between the atoms); the difference between melting of the surface layer and the inner core of the cluster should be taken into account because $\langle x^2\rangle_s$ is greater than $\langle x^2\rangle_i$ owing to the decrease in the number of atomic bonds for the surface atoms.[177] Figure 15 shows the temperature dependences of $\langle x^2\rangle_s$ (curve *1*) and $\langle x^2\rangle_i$ (curve *2*). Due to the difference between the $\langle x^2\rangle_s$ and $\langle x^2\rangle_i$ values, the $\langle x^2\rangle_m$ point where melting starts would be matched by different melting points for the surface $(T_m)_s$ and internal $(T_m)_i$ atoms. Moreover, apart from the regions corresponding to the solid and liquid states of the system, a transient region appears corresponding to the solid and liquid states existing simultaneously (see Fig. 15).

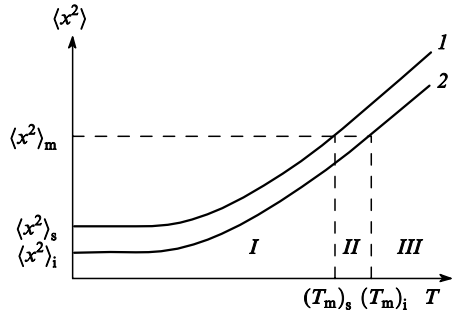

Figure 15. Temperature dependence of $\langle x^2\rangle$ for atoms on the cluster surface (*1*) and inside the cluster core (*2*). The subscripts s and i denote the surface and the cluster core, $\langle x^2\rangle_m$ are the mean-square displacements corresponding to the Lindemann criterion, $(T_m)_s$ and $(T_m)_i$ are the melting points of the surface layer and the cluster core; (*I*) is the region corresponding to the solid, (*II*) is the region corresponding to the solid–liquid transition state, (*III*) is the region corresponding to liquid.

Now we shall consider the quantum-statistical method for the investigation of the atomic mobility.

The change in the thermodynamic state of a cluster can be described by the free energy function $\Delta G = \Delta E - T\Delta S$ (E is the internal energy of states of the cluster, S is entropy). The entropy of the cluster can be calculated from the formula

$$S = -kT\ln Z,$$

where $Z = \sum g_i \exp(E_i/kT)$ is the function of distribution of states (here, g_i and E_i are the degeneracy and the energy of an ith level). Numerous studies have been devoted to the calculation of the Z value by quantum-statistical methods (see, for example, a number of studies [178–180]). The energy distribution of states for a solid cluster differs substantially from that for a liquid. At low temperatures, the density of states is greater for a solid than for a liquid; however, at high temperatures, the situation is reversed; as a consequence, the temperature of the equilibrium transition (T_{eq}) from the solid to the liquid state appears. Thus, at low temperatures, the energy change ΔE is determined by the vibrational and rotational energy levels of a solid. As the temperature increases, the entropy factor, *i.e.,* the disorder of motions, starts to play the crucial role, which is typical of a liquid. The T_{eq} value (or the melting point of the cluster) depends on the model chosen for the calculation of states for the solid and the liquid and on the number of states, *i.e.*, on the cluster size. When $T = T_{eq}$, the system contains both the solid and liquid phases.

The degree of disorder of the solid or liquid state can be characterised, for example, by the non-rigidity parameter (γ).[181] The variation of the Gibbs energy $G(T,\gamma)$ of a cluster system as a function of γ showed that the freezing point (T_f) and the melting point (T_m) of a cluster system do not coincide, *i.e.*, there is a region of coexistence of the solid and liquid states.

Yet another approach to the study of the dynamics of cluster melting is based on computer simulation of melting using Monte Carlo or molecular dynamics methods.[182–184] To determine the $\langle r^2\rangle$ and $\langle x^2\rangle$ parameters, one should solve a set of equations for the movement of clusters in a field with a specified attraction potential between atoms or molecules. The calculations can be carried out for a constant energy or temperature. In addition to the $\langle r^2\rangle$ and $\langle x^2\rangle$ parameters, this approach gives the time-averaged mean kinetic energy (temperature) over all the degrees of freedom of the cluster atoms

$$T = \frac{2\bar{E}}{(3N-6)k}$$

and the relative averaged change in the bond length (δ)

$$\delta = \frac{2}{N(N-1)}\sum_{ij}\frac{(\langle r_{ij}^2\rangle - \langle r_{ij}\rangle^2)^{1/2}}{\langle r_{ij}\rangle}.$$

By analysing these values, one can draw a conclusion about the cluster dynamics, in particular, about the melting–freezing phase transition. Figure 16 presents the computer simulation data for the Ar_{13} cluster.[185] The temperature at which δ sharply increases, which is interpreted as melting of the cluster in accordance with the Lindemann criterion, can be clearly seen in the Figure. The dependence of $\langle T\rangle$ on the system energy in the solid and liquid states indicates that the melting E_m and freezing E_f energies of the Ar_{13} cluster are different. The results of calculations of $\langle r^2\rangle$ for Ar_{13} also point to a substantial difference between the solid and liquid states. For the solid state, $\langle r^2\rangle$ reaches a flat plateau after 100 time intervals of simulation, whereas for the liquid state, $\langle r^2\rangle$ increases in accordance with the diffusion equation.

The organisation of the $(C_{60})_n$ structure on a graphite substrate and phase transitions in it have been studied by computer simulation.[163] A nanosystem in the ground state consists of hexagonal monolayers parallel to the substrate surface. The most stable structures were formed for n = 7, 19, 37, 61. Raising

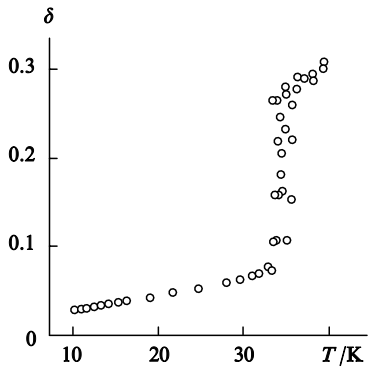

Figure 16. Temperature dependence of the mean-square change in the distance (δ) between the closest neighbours in the Ar_{13} cluster.[185]

the temperature had induced sublimation of C_{60} before the system passed into the state where the solid and the liquid phase coexisted. Study of the thermal stability of the $(C_{60})_{55}$ nanosystem near the graphite substrate demonstrated that, due to the low mobility of C_{60} clusters, this system did not undergo noticeable structural changes prior to the onset of sublimation.

Melting of clusters can also be considered within the framework of the thermodynamic formalism.[177, 186–191] The state of the clusters formed during solid-state reactions or from solutions and melts is determined by the free energy $G = f(\alpha,\mu,R)$ [see Eqns (3) and (8)]. The difference between the free energies of the cluster in the liquid and solid states is

$$\Delta G = 4\pi R^2\Delta\alpha + \frac{4}{3}\pi R^3\rho\Delta\mu, \tag{22}$$

where $\Delta\alpha = \alpha_l - \alpha_s$ is the difference between the surface energies, $\Delta\mu = \mu_l - \mu_s$ is the difference between the chemical potentials for the liquid and solid states of the cluster. It is obvious that for melting, $\Delta\alpha < 0$ and $\Delta\mu > 0$. The $\Delta G(R)$ curves are shown in Fig. 17. The critical cluster size corresponding to the transition from the solid to liquid state ($\Delta G = 0$) is calculated from the formula

$$R_{cr} = \frac{3\Delta\alpha}{\rho\Delta\mu}. \tag{23}$$

When $R < R_{cr}$, a cluster occurs in the liquid state. It follows from Eqn (23) that the solid–liquid transition state cannot be realised for separate atoms in a matrix (for $\Delta\alpha = 0$), when a cluster has not yet formed. Meanwhile the $\Delta\alpha$ value should be the greatest for a free cluster. Any intercluster interactions would decrease this

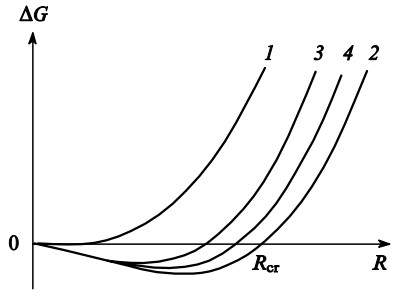

Figure 17. Change in the Gibbs energy for an ensemble of separate atoms in a solid (*1*), for an isolated cluster (*2*) and for a system of interacting clusters (*3*, *4*) occurring in the solid and liquid states *vs*. cluster size.
(*3*) Clusters interacting with one another, (*4*) clusters after treatment with surfactants.

value and, hence, the R_{cr} value, which determines the region of possible fluctuations of the solid and liquid states.

Cluster stability can be characterised by the change in the pressure $\delta p = p_0 - p$ or temperature $\delta T = T_0 - T$ which corresponds to a given difference between the chemical potentials $\Delta\mu = f(p,T)$ and brings the phases to equilibrium at a specified cluster size (p_0 and T_0 are the pressure in the medium and the melting point for the bulk material).

If the function $\Delta\mu = f(p,T)$ is replaced by its series expansion in terms of δp at the point p_0, then, with allowance for the fact that $\partial\mu_l/\partial p = V_l$, $\partial\mu_s/\partial p = V_s$ (V_l and V_s are the molecular volumes of the cluster in the liquid and solid states),[192] we have

$$\Delta\mu \approx -(V_l - V_s)\delta p. \tag{24}$$

Using the Clapeyron–Clausius formula

$$\frac{\delta p}{\delta T} = \frac{q}{T_0}(V_l - V_s),$$

where q is the latent heat of the phase transition, we obtain

$$\Delta\mu \approx -\frac{q\delta T}{T_0}. \tag{25}$$

Substitution of Eqn (25) into Eqn (23) gives a hyperbolic variation of the phase transition temperature for a cluster *vs*. its radius

$$\frac{\delta T}{T_0} \approx -\frac{3\Delta\alpha}{\rho q R}. \tag{26}$$

Dependence (26) indicates that the melting point of a cluster decreases with a decrease in the cluster size. Dependence (22) shown in Fig. 17 allows one to conclude that at a given temperature and pressure of the medium, the initially stable structure of the cluster ($\Delta\mu > 0$) becomes metastable with respect to the liquid phase at $R < R_{cr}$.

Analysis of the experimental data on the atomic dynamics of clusters attests mainly to an increase in the mean square displacements in the metal and oxide clusters compared with the displacements in bulk samples.[119] Thus a decrease in the probability of the Mössbauer effect and an increase in the mean square displacements of atoms $\langle r^2\rangle$ was observed for the W, β-Sn, Fe and α-Fe_2O_3 clusters.[119] An exception is provided by the Au clusters with a size of 6–20 nm for which the probability of the Mössbauer effect was found to increase and $\langle r^2\rangle$ was found to decrease with a decrease in the cluster size; this was explained by the long-wavelength restriction of the phonon spectrum. Study of thin oxide films on the surface of β-Sn and Fe clusters also points to an increase in $\langle x^2\rangle$ for atoms located on the surface.[119] Apart from the increase in the $\langle x^2\rangle$ values, an important feature of atomic dynamics on the surface is the anisotropy of the atomic vibrations. Anisotropy of the atomic vibrations along the surface and normal to the surface has been observed for iron and tin atoms deposited on the extensive surface of η-Al_2O_3, silica gels and zeolites.

A decrease in the melting point (down to room temperature) with a decrease in the cluster size has been observed for gold, tin and CdS nanoclusters.[193–195] An electron microscopy study of tin films[194] has also revealed the separation of the melting and freezing points and the existence of a specific solid ⇌ liquid state in which clusters possess an enhanced mobility in the transient temperature range.

In several publications, melting of iron oxide nanoclusters has been studied.[135, 190, 191] It was noted that melting of these clusters is accompanied by an increase in the mean square displacements of atoms. Figures 12 and 18 present the Mössbauer spectroscopy data for iron hydroxide clusters formed in polysorbs with pore diameters of 7.5 to 0.75 nm and for the nanosystem formed from the iron oxide clusters prepared by thermal decomposition of iron oxalate. For iron hydroxide clusters (see Fig. 12), the intensity of

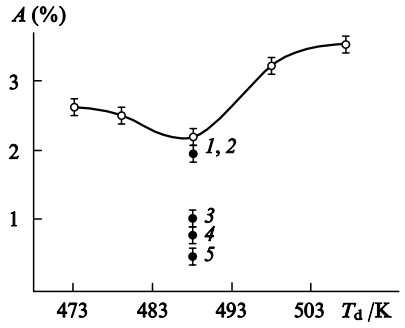

Figure 18. Spectral surface area of the Mössbauer spectrum of a nanosystem formed from iron oxide clusters prepared by decomposition of iron oxalate *vs*. temperature of thermal decomposition T_d.
The light dots are experimental data. The dark dots correspond to the surfactants: (*1*) ethanol, (*2*) isopropanol, (*3*) the surfactant Twin-65, (*4*) butanol, (*5*) SDS.

the spectral line sharply decreased upon an increase in the polysorb pore size. According to nucleation conditions [135] [see Eqn (13)–(15)], a decrease in the pore size leads to a decrease in the cluster size in the pore. The curve shown in Fig. 12 corresponds to the onset of cluster melting, which is attributable to an increase in the intracluster atomic mobility. For the γ-Fe_2O_3 nanocluster system, the dependence of the spectral surface area A on the temperature of thermal decomposition of iron oxalate (T_d) has a minimum at $T_d \approx 488$ K (Fig. 18). According to Mössbauer spectroscopy, the T_d value is related to the mean size of the γ-Fe_2O_3 cluster prepared by decomposition of iron oxalate. It was found that the cluster size increases from 2 to 4 nm as the temperature T_d changes from 488 to 508 K. The right-hand branch of the curve in Fig. 18 is related to a decrease in A (following an increase in T_d) and an increase in the atomic mobility in the γ-Fe_2O_3 cluster, similarly to the observed decrease in A in the iron hydroxide clusters formed in polysorb pores. It should be noted that the Mössbauer spectra of iron hydroxide and iron oxide clusters contain no 'broad component' corresponding to the movement of the cluster as a whole, which is due to the restricted diffusion of clusters in the pores. This will be discussed in the Section 'intercluster dynamics.' Thus, changes in the spectral surface area are associated with the change in the atom mobility within the cluster.

The left-hand ascending branch in the curve $A = f(T_d)$ (Fig. 18) is related to further decrease in T_d and, correspondingly, to a decrease in the size of clusters down to their disappearance to give separate atoms, dimers and trimers of Fe^{3+} (see Fig. 17, curve *1*). Thus, the minimum in the $A = f(T_d)$ curve observed at $T_d = 488$ K appears to be due to the onset of formation of an iron oxide cluster.

As noted above, the atomic cluster mobility is strongly influenced by the intercluster interactions. They decrease the surface energy. However, the intercluster interactions and strain can be reduced due to the action of surfactants or mechanochemical treatment. It can be seen from Fig. 18 that the spectral surface area markedly decreases after the action of surfactants. Thus, weakening of the intercluster interaction results in an increase in the intracluster atomic mobility and in a decrease in the melting point. Relation (26) can be used to estimate the R_{cr} value, corresponding to the onset of melting of γ-Fe_2O_3 clusters and to compare it with the $R(V)$ value observed experimentally from Mössbauer spectra. Using the values $\rho = 5.18 \times 10^6$ g m^{-3} (see Ref. 196), $\Delta\alpha \approx 1$ J m^{-2} (see Ref. 197) and $q \approx 2 \times 10^{-19}$ (see Ref. 136), we obtain

$$R = \frac{aT_0}{\delta T},$$

where $a = 0.1-1.0$ nm. As a result, for $T_m = 300$ K, we have $R \approx 0.1-1.2$ nm, which is in good agreement with the value $d = 2$ nm found from the Mössbauer spectrum.

It is also noteworthy that the existence of the specific solid–liquid transition state in which atoms possess enhanced mobility can provide an interpretation for the effect of adsorption decrease in the material strength (Rehbinder effect)[198] at the atomic-molecular level due to wetting and deformation of its surface under the action of a surfactant.

For nanosystems prepared by compacting, changes in $\langle r^2 \rangle$ and in the heat capacity were noted. Thus the low-temperature heat capacity in the region of T from 0.06 to 10 K for a compacted nanosystem of copper clusters with nanocluster sizes of 6.0 and 8.5 nm was 5–10 times higher than the heat capacity of bulk copper. An increase in the heat capacity of a nanostructured copper [199] is attributable to an increase in $\langle r^2 \rangle$ on the surface of nanoclusters.

Study of the phonon spectra of a compacted system of Ni clusters with a size of 10 nm prepared by neutron scattering showed an increase in the density of phonon states at low frequencies (below 14 MeV) [200] with respect to coarsely crystalline Ni. Calculation of the heat capacity based on these data demonstrated its increase (1.5–2-fold) for a nanosystem with respect to the bulk material. A Ni nanosystem formed from 70-nm clusters [130, 201] also has a higher heat capacity (by 10%–25%) up to 600 K, which is attributed to a decrease in the Debye temperature.

A model calculation of nanosystems with cluster sizes of 1.1, 2.0 and 2.8 nm using the Lennard-Jones potential showed [202] diffusion of the phonon spectrum to both high- and low-frequency regions, most of the additional vibrational modes being located at grain boundaries. The results point to a substantial increase in the heat capacity with a decrease in the cluster size in the region of $T \approx 100$ K, which is due to the predominant contribution of the low-frequency vibrations at grain boundaries.

Thus, joining of nanoclusters into a nanosystem smoothes only partially the dynamic characteristics of nanoclusters.

b. Intercluster dynamics

Convenient nanosystems for study of the movement of a cluster as a whole are represented by cation exchange resins, for example, styrene–divinylbenzene copolymers with different degrees of cross-linking (1%, 2% and 12% — samples A, B and C, respectively) and different sets of nanopores containing iron oxide nanoclusters with a size of 3 nm.[203–205] Due to the cross-links, which restrict the diffusion of iron hydroxide nanoclusters in the copolymer, nanoclusters are placed in cages with a varied size. The Mössbauer spectra of iron hydroxide clusters in polymeric systems with different degrees of cross-linking are presented in Fig. 19. These spectra in the velocity range of ± 100 mm s^{-1} exhibit a narrow component and a broad component.

The movement of iron hydroxide clusters can be described in terms of the model of limited diffusion of particles in the field of a potential. The form of the potential and the diffusion rate can be found from the temperature dependence of the surface area of the narrow component and from the shape of the broad component.[206] The Mössbauer spectrum consists of Lorentzian components with non-broadened (narrow) lines having the intensity

$$A_0 = z^{-2}\left|\int \exp(i\mathbf{k}^*\mathbf{R}) \exp\left(-\frac{U(\mathbf{R})}{kT}\right) d^3\mathbf{R}\right|^2.$$

Here $z = \int \exp(U(\mathbf{R})/kT) d^3\mathbf{R}$, $\mathbf{k}^*$ is the radiation wave vector, $\mathbf{R}$ is the cluster radius.

Analysis of the $A = f(T)$ function provides the possibility of reproducing the movement potential $U(\mathbf{R})$. Study of the temperature dependence $A_0 = f(T)$ for a sample with 2% cross-linking (sample B) gives $A_0 = 0.06$ ($T = 264-243$ K) and the potential form as a square (spherical) well with elastic walls (Fig. 20). If we

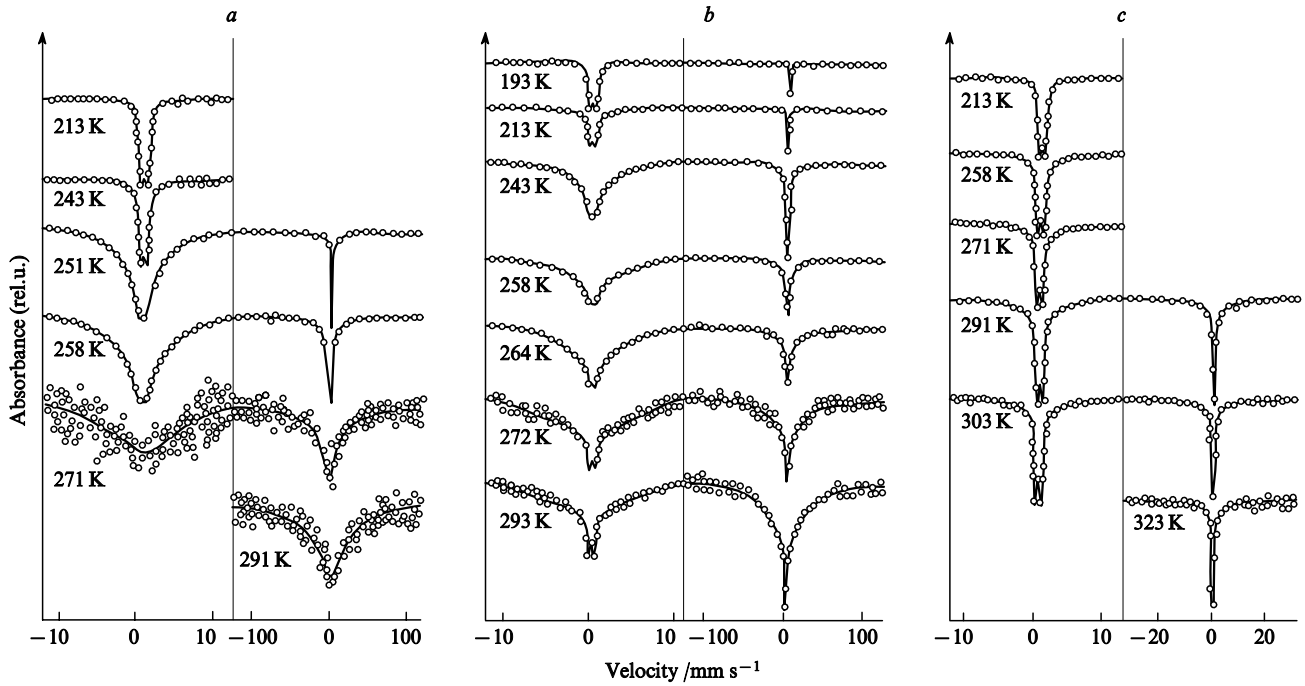

Figure 19. Mössbauer spectra of iron hydroxide in an ion exchange sulfo resin at different temperatures; (*a*) 1% (sample A), (*b*) 2% (sample B), (*c*) 12% of cross-linking (sample C).

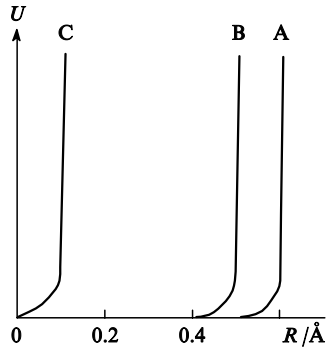

Figure 20. Shape of the potential well describing the movement of iron hydroxide clusters in samples A, B and C (see the notation to Fig. 19).

assume that in a spherical cage with radius b, only the diffusion coefficient is temperature-dependent, then

$$A_0 = \frac{g(\sin kb - kb\cos kb)^2}{(kb)^6}.$$

For $kb = 3.6$, the radius of the potential well is 0.5 Å. The spectrum calculated using these parameters is in good agreement with the experimental one.[203–205] An increase in the size of the cage (sample A) increases the well radius to 0.62 Å, while a decrease (sample C) arrests completely the cluster movement. Thus, the maximum clearance between the cluster and the network is equal to 0.62 Å. This type of motion with limited diffusion is observed for iron oxide hydroxide FeO(OH) clusters in an iron accumulating protein, ferritin.[206]

c. Structural features of nanosystems. The role of defects and stresses

Combination of clusters into a nanosystem gives rise to numerous phase boundaries and dislocations and a corresponding intercluster stress. The phase boundaries play a crucial role in considering many mechanical properties, heat conductivity, electrical conductivity and magnetic characteristics of nanostructures. The size effects and intercluster interactions also influence the structural phase transitions. The phase transitions related to the movement of atoms in a cluster were considered in the previous Section. Now we shall discuss the structural changes in a nanosystem induced by variations of the cluster size, intercluster interactions, defects and dislocations.

The intercluster interactions create stresses, excess energy and excess pressure at the cluster boundaries. The excess energy per dislocation is calculated from the formula [207]

$$E_d = \frac{Gb^2}{4\pi(1-v)}\ln\frac{r}{r_0}, \qquad (27)$$

where G is the shear modulus, b is the Burgers vector characterising the magnitude of the shift of an edge dislocation, $b = a_0/\sqrt{2}$ (a_0 is the lattice constant), v is the Poisson coefficient (usually 0.3), r is the maximum distance at which the influence of dislocations is still retained, r_0 is the minimum dislocation size. With the assumption that the concentration of dislocations in a cluster is determined by the ratio of the cluster surface area to the cluster volume, the excess energy density of the cluster ε_d is

$$\varepsilon_d = \frac{Gb^2}{4\pi(1-v)}\frac{1}{R}\ln\frac{r}{r_0}. \qquad (28)$$

Thus, the excess energy density decreases as the cluster size R increases and approaches zero for a bulk material. It should be noted that the applicability of this approach to small nanoclusters is restricted by the thickness of the surface layer of the cluster (a), *i.e.*, Eqn (28) can be used only to calculate the excess energy of clusters with $R > a$.

When considering the influence of defects and dislocations on the properties of nanosystems constructed from nanoclusters of arbitrary sizes, one should proceed from the thermodynamic concentration of defects and dislocations, which takes into account the chemical potential and the excess energy of the cluster surface. The excess energy gives rise to excess pressure, which is equal to $\sim 10^9$ Pa for 1-nm clusters. If the pressure drop between the cluster bulk and the cluster surface is neglected, the concen-

tration of defects in the cluster (c_s) can be calculated from the relation

$$c_s = \frac{a(3R^2 - 3aR + a^2)}{R^3}, \quad (29)$$

where a is the thickness of the surface layer. It can be assumed that in the absence of pressure drop, *i.e.*, when the influence of defects inside the cluster is counterbalanced by the influence of defects on its surface, the difference between the chemical potentials in the cluster and on the surface is equal to zero

$$\Delta\mu^0(0) + kT\ln\frac{c_s}{c_0} = 0, \quad (30)$$

where c_0 is the defect concentration on the surface.

Naturally, the allowance made for the pressure drop shifts the equilibrium by

$$\Delta\mu^0(\delta p) = \Delta\mu^0(0) + V\delta p, \quad (31)$$

where V is the volume of a defect, $\delta p = 2\alpha/R$ (α is the surface tension). In this case, the new equilibrium of the system is determined by the expression

$$\Delta\mu^0(0) + V\delta p + kT\ln\frac{c}{c_0} = 0. \quad (32)$$

By solving the set of equations (30) and (32), we obtain

$$c = c_s\exp\left(-\frac{2\alpha V/R}{kT}\right). \quad (33)$$

The dependence of c on the cluster size in the R/a units is shown in Fig. 21. The maximum in the $c = f(R/a)$ curves is located at $R/a = 25$, which corresponds to $R = 10-50$ nm. It is the 10–50-nm clusters, having the maximum defect concentration and the highest excess energy, that are involved in the formation of nanosystems. This is important for the understanding of the reasons for the appearance of new properties in nanosystems. In nanostructures formed by molecular clusters from CO_2, N_2 and SF_6, an increase in the stress with an increase in the cluster size was observed.[208] Numerous studies of nanosystems by X-ray diffraction methods point to the influence of the cluster size and interfacial stresses on the structure of a nanosystem.[209] Analysis of nanocrystalline Al, Ru, Cu and AlRu systems[210,211] showed that the mean square deformation of these systems is equal to 1%–3%, which is markedly greater than the deformation of coarse-grain metals. Meanwhile, by modelling X-ray diffraction of clusters of different size,[212] it was shown that small clusters do not contribute to the elastic distortions of the crystal lattice caused by dislocations at phase boundaries. The major contribution is made by larger nanoclusters. Thus, there exists a transient region of nanocluster sizes in which the effect of stresses at phase boundaries is a maximum; this complies with the conclusions based on the thermodynamic model for the influence of defects [see relations (29) and (33)].

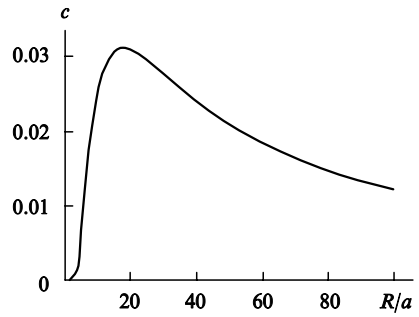

Figure 21. Density of defects c in the cluster *vs*. the cluster size (in the R/a units).

The excess stresses result in a change in the crystal lattice constant. In most cases, the lattice parameters decrease, which is attributed to the generation of additional energy at phase boundaries, to the change in the specific volume and to the appearance of excess pressure.[213–215]

Nanosystems are characterised by unusual mechanical properties: microhardness and superplasticity. At room temperature, microhardness of nanosystems is 2–7 times higher than that of the corresponding bulk materials. According to a publication,[216] the Vickers microhardness of a cluster

$$H_v \approx H_0 + k_0 d^{-1/2}$$

increases with a decrease in the cluster size. The results of microhardness measurements for nanosystems formed by Ag, Cu, Pd, Se, Fe and Ni metal clusters have been reported.[217] It was found that a decrease in the cluster size is accompanied by an increase in the nanosystem hardness. In addition, microhardness of a nanosystem depends on the conditions of its treatment. These conditions influence the structure of interfaces, cluster interactions and the cluster size. For example, relaxation and annealing of defects at the phase boundaries of the $Al_{98.5}Mg_{1.5}$ clusters, with the cluster size remaining invariant ($d \approx 150$ nm),[218] decrease the microhardness from 1.7 to 1.45 GPa. However, the cluster size is affected by annealing to a markedly greater extent. Thus annealing of a nanosystem formed by Pd clusters at 475–600 K brings about an increase in the cluster size and, hence, an almost threefold decrease in the system microhardness. Upon annealing of nanosystems of Ag ($d \approx 10$ nm) and MgO ($d \approx 10$ nm) clusters, their microhardness changed in different ways: the microhardness of the metallic nanosystem decreased[219] (apparently, due to an increase in the size of Ag clusters), while the microhardness of the oxide system remained constant up to 870 K.[220]

Yet another remarkable feature of nanosystems is superplasticity: upon stretching, the sizes of samples can increase by factors of dozens without fracture. For example, the Ni and Ni_3Al nanosystems were found to exhibit low-temperature superplasticity at $T_s = 470$ and 450 °C, respectively (these temperatures are almost three times as low as the melting point).[221] The superplasticity of oxides and ceramics presents considerable interest from both theoretical and practical standpoint. The results of a study[222] indicate that the superplasticity of nanosystems manifests itself for cluster sizes from 1 nm to 1 μm; the cluster size should not change on thermal treatment. For example, in two-phase systems, the growth of clusters of one phase caused by heat treatment is suppressed due to the presence of the other phase. It is also believed that the system superplasticity is affected by the presence of the amorphous phase.[223]

The high strength and the superplasticity of nanosystems can be explained by using the extremal dependence of the defect density and excess energy on the nanocluster size which we obtained. Indeed, nanosystems composed of small nanoclusters with sizes $d < 10$ nm contain few defects and dislocations and display exceptionally high hardness. Meanwhile, in nanosystems formed by clusters with intermediate size ($10 < d < 100$ nm), the number of dislocations is maximal, which ensures their record plasticity.

Thus, superhard materials can be produced by using nanosystems composed of nanoclusters with $d < 10$ nm, while manufacture of superplastic materials requires nanosystems composed of nanoclusters with $10 < d < 100$ nm.

The stresses arising at phase boundaries play one more important role — they act as growth stimulators for assembled nanosystems. The self-assembly and the growth of superlattices of the $Si_{0.84}Ge_{0.16}$ alloy under the action of stress induced by alternating absorption of layers of silicon and germanium atoms at the Si(001) plane at 380 °C has been considered.[224] Computer simulation using an elastic field of stress forces arising on the layer surfaces showed that the stresses are different for the layers formed by atoms differing in size. The superlattice $Si_{0.84}Ge_{0.16}$

formed under the action of stresses had equal distances between the layers (*i.e.*, a regular alternation of layers was observed) and a regular arrangement of atoms within a layer. The period of the $Si_{0.84}Ge_{0.16}$ superlattice was 3 nm.

Considerable interest is also aroused by structural phase transformations in nanosystems. It was found that the nanometer size results in stabilisation of many non-equilibrium structures. Thus nanoclusters with a size of several nanometers constructed from unstable Fe(C) and γ-Fe phases are known. They are stable even at room temperature, whereas in the bulk materials, these phases are stable only at temperatures of 800 and 1000 °C, respectively.[225] Stable CdS nanoclusters with the rock salt structure are also known, whereas bulk CdS can be stabilised only at high pressures.[226] The stabilisation of structures not equilibrated at a given temperature due to the formation of small clusters with $d < 10$ nm can be explained by the action of the surface energy and pressure created by the surface tension, which reaches a value of several Gigapascals for 1–2-nm clusters.

Non-equilibrium states of a cluster system can also be stabilised by external pressure. The phase transitions induced by high pressure (1.5 GPa) in the crystal of C_{60} (fullerite) but absent at normal pressure have been studied.[152] It was found that crystallisation of C_{60} at room temperature yields a crystal lattice with dumb-bell-shaped $(C_{60})_2$ dimers in the lattice points.§ An increase in the temperature (> 423 K) gives an orthorhombic C_{60} structure, which passes into a tetragonal structure at 723 K.

Now we shall consider one more example of phase transitions in nanocrystalline ferroelectrics. A ferroelectric transition accompanied by a first-order structural phase transition was observed in $BaTiO_3$ [227] and $PbTiO_3$ [228] crystals. This transition is characterised by a critical temperature T_C (similar to the Curie point for ferromagnets) above which the substance passes into the paraelectric state. Spontaneous polarisation in ferroelectrics results from first-order phase transitions, due to the tetragonal distortion of the crystal lattice (change in the $c:a$ ratio). At temperatures above T_C, the tetragonal crystal lattice is transformed into a cubic lattice; then $c:a \to 1$.¶

The influence of the cluster size on the ferroelectric transition was studied in relation to the $PbTiO_3$ nanosystem. This system was prepared by precipitation from a solution of clusters with sizes of 20–100 nm. For the $PbTiO_3$ crystal, the effect of the cluster size on the temperature and character of the phase transition was studied by X-ray diffraction analysis and differential scanning calorimetry (DSC). The X-ray diffraction study (Fig. 22 *a*) showed that the $c:a$ ratio changes upon phase transition. It was found that, as the cluster size decreases, the $c:a$ ratio decreases; however, even for the smallest of the clusters studied (with $d = 23$ nm), the $c:a$ ratio does not reach unity. The extrapolation $c:a \to 1$ gives the d_{cr} value, *i.e.*, the cluster size at which the spontaneous polarisability disappears, the lattice symmetry becomes cubic, and the nanosystem passes into a paraelectric state. The DSC data indicate that the phase transition temperature (T_C) decreases as the cluster size decreases from 80 to 30 nm (Fig. 22 *b*), the phase transition is gradually smeared and for clusters with $d = 26$ nm, no phase transition is observed. The decrease in T_C amounted to 20 °C. Despite the absence of obvious indications of the transition, in the case of the crystal consisting of clusters with $d = 26$ nm, one should still assume the presence of a residual smeared ferroelectric transition, which cannot be observed, apparently, due to the scatter of particles over sizes and the diffusion character of the transition itself.† It should be noted that the T_C value is also influenced by the intercluster interaction, which determines not only the T_C value but also its scatter.

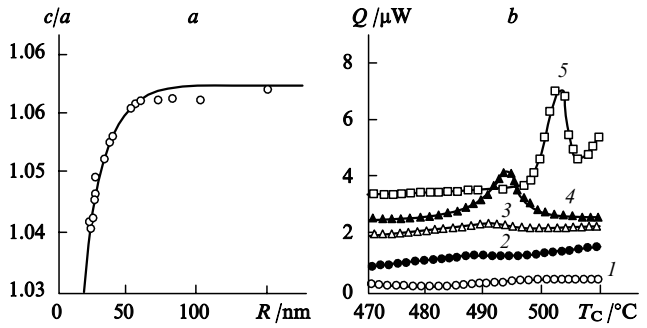

Figure 22. Ratio c/a (tetragonal distortion) (*a*) and temperature of phase transition (*b*) in the crystal of the $PbTiO_3$ ferroelectric *vs.* the cluster size.[228]
(*a*) X-Ray diifraction data; (*b*) differential scanning calorimetry data (scanning 5 K/min) obtained for clusters with $R = 26$ (*1*), 31 (*2*), 39 (*3*), 57 (*4*) and 81 nm (*5*).

The structure-magnetic properties of nanocluster systems depend largely on the presence of defects and dislocations. As noted above, the formation of a nanosystem is accompanied by the appearance of interfaces (or phase boundaries). Under some conditions, these phase boundaries can participate in the nucleation of nanoclusters. Thus the magnetic properties of cluster nitride phases arising upon nitriding of an iron catalyst in a flow of ammonia at 200–350 °C were studied by Mössbauer spectroscopy. When the nitrogen concentration in the cluster catalyst is 1 mass % – 2 mass %, phases of defect ε-iron nitride are formed in the catalyst. During low-temperature annealing (200 °C) in air, the nitrogen atoms are segregated at phase boundaries, resulting in a decrease in T_C of the nitride phase. Nitrogen is accumulated on the defects. An increase in the temperature of annealing to 400 °C results in normal gradient concentrational diffusion of the nitrogen atoms over the cluster, resulting in their uniform distribution and an increase in T_C. The equilibrium segregation of nitrogen atoms near the phase boundaries decreases the magnetic stability of the defect regions and serves as a peculiar method for 'magnetic decoration' of the stress fields by defects.[230]

Let us consider yet another example of the influence of phase boundaries and defects on the magnetic properties of the copper nanostructure with an admixture of iron atoms. Plastic deformation of the copper samples with iron dissolved therein [231] afforded copper clusters with a size of 130–150 nm and ~3-nm iron clusters.‡ The annealing of this system at a temperature of < 1000 K results in the diffusion of iron atoms along the grain boundaries and in enlargement of iron clusters; simultaneously, the magnetic properties of the system change. As the temperature rises (> 1000 K), the solubility of iron in copper increases, and normal concentrational diffusion starts; this results in vanishing of the clusters and uniform dissolution of iron atoms in copper.

The magnetic susceptibility of paramagnetics is influenced by the presence of vacancies in the crystal lattice. For nanocrystalline Pd prepared by plastic deformation (pressure with shear),[6] the magnetic susceptibility was found to increase, which was attributed to an increase in the density of electronic states at the Fermi level. This increase is possible due to the presence of vacancies in the lattice formed by palladium clusters.

d. Optical and electric properties of nanocluster systems

Specific optical and electric properties arise in nanocluster systems owing to the effects associated with the restriction of the electron

§ The same dimers are formed in the mechanochemical reaction.[153]

¶ As noted above, nanosystems composed of clusters with $d < 10$ nm contain fewer defects and dislocations. The minimisation of the crystal lattice energy with a decrease in the cluster size results in the transition from a crystal lattice with lower symmetry to a lattice with higher symmetry.[229]

† The residual smeared ferroelectric transition appears to occur also in the crystals formed from clusters smaller than 26 nm, down to 7 nm.

‡ Iron clusters can be located, for example, at grain boundary junctions.

free path (quantum restrictions) and with the appearance of discrete energy levels in the valence band and the conduction band, which changes the selection rules for optical transitions. It is possible to create one-electron nanocluster systems in which the number of discrete energy levels increases, as the cluster size decreases; in this case, the energy of electron transition from one electronic level to another increases according to the relation $e^2/2c$ ($c \approx d$). This energy can become greater than the kinetic energy of an electron (kT) and thus stimulate tunnel transitions. The development of these systems provides new potentialities for the manufacture of rectifier devices, diodes, *etc*.

It has already been noted that the nanocluster semiconductors CdS, CdSe and InP exhibit a 'blue shift' of frequency. For example, in the case of CdSe, the energy of electron transition changes from 1.7 eV (red region) to 2.4 eV (green region) as the cluster size diminishes from 20 to 2 nm.

The preparation of light-tunable diodes based on CdSe nanoclusters has been described.[232,233] In one study,[232] CdSe nanoclusters were assembled as a thin film on the surface of a luminescent polymer (poly-*p*-phenylenevinylene, PPV). The polymer was grown on an indium oxide–tin layer able to let carriers as holes pass through. In addition, a nanocrystalline CdSe layer was coated with a Mg–Ag film for electron injection. When a voltage was applied to this system, electroluminescence was observed. The electroluminescence wavelength can be changed by varying the size of nanoclusters.

An increase in the oscillator strength and a decrease in the de-excitation time typical of some nanoclusters may lead to the design of non-linear optical nanosystems, for example, optical switches which modulate a laser beam from a high-power laser by weak, non-resonant pulses.

Light absorption and emission by porous silicon is attributed to the appearance of new optical transitions. In bulk silicon, electronic transitions between the excited state of the conduction band and the ground state of the valence band are forbidden. Only non-radiative transitions involving phonons are possible. In nanocrystalline silicon, non-radiative transitions are also retained but their contribution is insignificant. Radiative electronic transitions are more characteristic in this case.[234,235]

In addition to the 'blue shift', a 'red shift' can also be observed in nanosystems. This occurs in semiconductors with a broad forbidden band. For example, a decrease in the absorption edge energy by 0.2 eV ('red shift') has been observed for the γ-Fe_2O_3 nanoclusters with $d \sim 8.5$ nm residing in the pores of a polymeric ion exchange sulfo resin.[236] The most probable reason for the 'red shift' is the appearance of strains and stresses on the surface of the clusters (due to surface tension) which form the lattice of the solid. Indeed, in a 5-nm γ-Fe_2O_3 cluster, the internal pressure ($p = 2\alpha/R$) equals 0.4 GPa.

X-Ray diffraction studies demonstrated a 0.35% decrease in the lattice volume for γ-Fe_2O_3 nanoclusters. If the compression modulus for γ-Fe_2O_3 is taken to be equal to that for Fe_3O_4, then a 0.35% compression of the γ-Fe_2O_3 lattice brings about an internal pressure of 0.35 GPa, which is in agreement with the calculated value, equal to 0.46 GPa, derived from the estimates of the influence of the surface tension. The action of pressure is known to induce a phase transition of a semiconductor to the conducting state. Thus, when magnetite Fe_3O_4 is kept under a pressure of 5 GPa, it passes to the conducting state. Since the forbidden gap (E_g) for γ-Fe_2O_3 is 2.1 eV and that for Fe_3O_4 is 2 eV, then the decrease in the width of the forbidden gap in γ-Fe_2O_3 induced by high pressure is 0.15 eV, which is in good agreement with the results obtained in the optical experiment.

The optical properties of a nanosystem depend on its organisation and on the intercluster interaction. Light absorption by silver nanoclusters prepared using reverse micelles has been studied.[142] This procedure yields nanoclusters with a very narrow size distribution (2 to 8 nm), the surface of which can be stabilised by thiols, and then they can be used for assembling two- and three-dimensional structures. Nanosystems incorporating silver nanoclusters with sizes of 4.5, 5.2 and 6.1 nm were prepared. Two- and three-dimensional systems were formed on a graphite substrate by applying a drop or several drops of a colloid solution of silver nanoparticles in hexane. It was found that coating of the surface of silver nanoclusters by dodecanethiols influences their optical properties: the absorption band of the plasmon peak shifts to lower energies (from 2.85 to 2.73 eV) and its width increases (from 0.9 to 1.3 eV). These data were interpreted on the basis of the model of light absorption by clusters proposed in a study.[54] The shift of the absorption band was attributed to the electronic plasmon absorption inside the cluster, while band broadening was ascribed to the change in the dielectric constant of the medium (intercluster absorption). Simulation of the absorption spectra of a 2D nanosystem showed that a decrease in the cluster size in an isolated medium (reverse micelle) results in a substantial increase in the width of the absorption band due to the restriction of the electron free path, while placing the clusters in media with different dielectric constants ε_m stimulates the shift of the absorption band, an increase in ε_m resulting in a substantial decrease in the absorption energy. Thus, the shift of the absorption band observed for silver nanoclusters can be explained by the increase in the dielectric constant upon the assembly of a 2D hexagonal network of silver clusters.

Optical investigations (Fig. 23) of the nanosystems formed show that their properties depend on the degree of structure perfection and the preparation procedure. Application of one drop of a colloid solution on the substrate gives rise to a 2D nanosystem with a hexagonal network of silver clusters (Fig. 23, curve *2*). The absorption spectrum of nanoclusters in this system differs from the spectrum of these clusters in solution: the plasmon absorption band shifts by 0.27 eV and its width increases from 0.8 eV (in solution) to 1.0 eV (in the nanosystem).

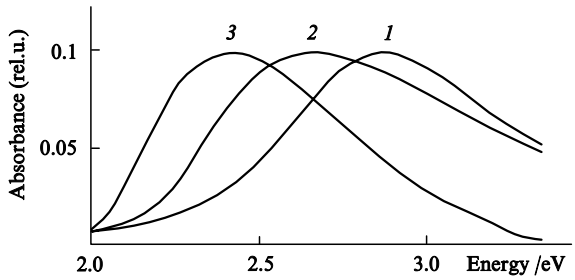

Figure 23. Variation of the plasmon absorption width and peak shift in a colloid solution and in nanosystems containing 4.5-nm silver clusters formed on a carbon substrate.[142]
(*1*) Initial colloid solution with $[Ag_n] = 2.5 \times 10^{-3}$ mol litre^{-1}; (*2*) two-dimensional cluster system formed on a substrate after deposition of one drop of a colloid solution; (*3*) three-dimensional cluster system formed after deposition of three drops of a colloid solution.

An increase in the concentration of nanoclusters in a colloid solution or deposition of several drops of the colloid solution on a graphite substrate afford a more perfect, three-dimensional, face-centred cubic structure.

For the 3D structure (Fig. 23, curve *3*), further shift (by 0.47 eV with respect to that in solution) of the absorption band toward lower energies is observed; however, the width of the plasmon peak diminishes to 0.7 eV. The narrowing down of the absorption band is a result of the increase in the electron free path. This implies that an electron penetrates the barrier between the nanoclusters (a ~2-nm thick coating). The possibility of electron tunnelling between metal surfaces by such a long distance[237] is an important feature for the design of new materials for lasers, optics and electronics.

The restriction of the electron free path in small clusters and the presence of intercluster boundaries impart new electric properties to nanosystems obtained on the basis of nanoclusters. For

example, metals or semiconductors pass into a non-conductive state. This transition is due, first, to a decrease in the carrier density as a result of the restriction of the electron wavelength and the appearance of discrete electronic levels and, second, to a decrease in the conductivity as a result of electron scattering at phase boundaries and generation of dielectric charges. Indeed, a 7–20-fold increase in the electric resistance was observed for nanocrystalline copper in the region of $T < 275$ K.[238] The high resistivity of cobalt films (2- to 50-nm thick) was mainly attributed [239] to the effects of electron localisation. The influence of the phase boundaries between nanoclusters on the electric properties of nanosystems may be due to long-range stress fields and to the dynamic state of the atoms.

In recent years, substantial progress in the fabrication of 3D, 2D and 1D electronic nanosystems (see, for example, Ref. 41) used to produce single-electron transitions, unidimensional nanowires, *etc.* has been made. The 3D organisation of nanoclusters is the most obvious. The 3D nanosystems are prepared by crystallisation of clusters (instead of atoms). For example, nanocrystalline copper was prepared in this way. However, the researchers were able to crystallise only large copper clusters (~40 nm) passivated by thiols.[143] Crystallisation of copper selenide clusters $Cu_{146}Se_{75}(PPh_3)_{10}$ was also performed.[240] The crystals thus obtained can be used in semiconductor devices. The idea of producing an organised 3D cluster structure from clusters linked by spacer molecules proved fruitful. The spacers allow one to control the distance between the clusters; this can be accompanied by spontaneous crystallisation. An advantage of this approach is that it provides the possibility of changing the energy barrier to passage of an electron through the cluster. Figure 24 shows the change in the Coulomb barrier between the Au_{55}^* clusters depending on the spacer length and nature.[41]

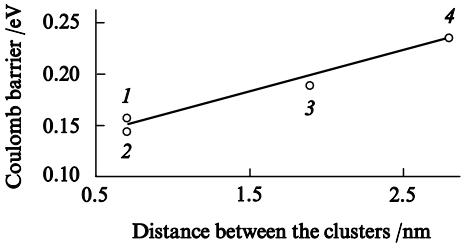

Figure 24. Coulomb barrier *vs.* distance between the clusters.[41]
The dots on the straight line correspond to the $Au_{55}(PPh_3)_{12}Cl_6$ (Au_{55}) (*1*) and $Au_{55}(PPh_2C_6H_4SO_3Na \cdot H_2O)_{12}Cl_6$ (Au_{55}^*) (*2*) clusters and the systems

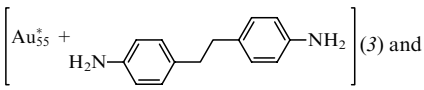

(*3*) and

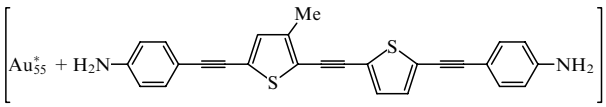

(4).

Two-dimensional cluster structures are usually assembled using molecular clusters stabilised by ligands. Perfect layers of gold clusters with alkanethiol coatings which virtually did not interact with the substrate and were self-assembled due to van der Waals forces have been prepared.[241] If the interaction of the clusters with the substrate is enhanced, the structure loses its perfection. However, 2D cluster structures cannot be used in conducting devices or in a tunnelling microscope without proper fixing on the substrate. Study of Au and Pd clusters on various substrates (gold, mica, glass, silicon) demonstrated that chemical fixing of clusters on the support can be easily attained, whereas a perfect organisation of the 2D structure is achieved with difficulty.[41] The point is that self-assembly requires that the building blocks be free and mobile; however, when the clusters are attached to the substrate surface, the mobility decreases. The binding between the adsorbed cluster and the substrate can be weakened by treating the substrate with a surfactant. Thus deposition of the $Au_{55}(Ph_2PC_6H_4SO_3H)_{12}Cl_6$ clusters onto a single-crystal Au(111) surface modified by aminothiols improved the ordering of the 2D layer.

The assembly of the 2D layers for electronic devices is performed in the presence of spacer molecules, which allow one to control the distances between the clusters. These nanostructures are prepared by dissolution of clusters with appropriate spacers in Langmuir–Blodgett films; the cluster ligands and the spacer molecules should be complementary.

Of great interest from the practical standpoint are unidimensional cluster structures, nanowires. They are formed as whiskers at atomic steps of the surfaces. A nanowire from gold clusters was prepared using porous membranes based on alumina with 7-nm channels in which clusters consisting of Au_{55} cores stabilised by ligands were placed.[242]

Nanowires are also prepared from carbon nanotubes. The conduction of nanotubes can be switched (from the metallic to the semiconductor type) by changing their helical structure.[154] Electronic devices are assembled by combining nanotubes with different structures. The combination of carbon nanotubes in pairs of 'armchair' (A) and 'zigzag' (Z) types was considered.[154] Calculation of the switching from the metallic type of conduction (A state) to the semiconductor type (Z state) showed an asymmetry along the tube axis, which provides a rectifier effect. This result is in line with experimental data [243] on the rectifying effect of nanotubes.

e. Magnetic properties

The magnetic properties of nanocluster systems are influenced by both size effects and intercluster interactions and the cluster organisation. One of the best known and well-studied phenomena is superparamagnetism, *i.e.*, the change in the direction of the magnetic moment of the cluster as a whole due to thermal fluctuations without losing the magnetic ordering. The formation of magnetic domains in cluster systems depends on both the individual properties of the clusters (magnetic anisotropy) and the intercluster interactions. Therefore, magnetisation processes in these systems depend appreciably on the defectiveness of the cluster structure and on phase boundaries.

The magnetic quantum tunnelling effects and giant magnetoresistance also present interest. The new effects include the first-order magnetic phase transitions in nanoclusters and nanocluster systems in which the magnetic ordering and magnetisation disappear by a jump upon an increase in the temperature or a decrease in the cluster size.

Superparamagnetism. The phenomenon of superparamagnetism consists in the generation of measurable thermal fluctuations of the magnetic moment of the cluster upon a decrease in the cluster size to 1–10 nm. The fluctuation time ($\tau = 10^{-9}$–10^{-10} s) can be calculated using a simple equation

$$\tau = \tau_0 \exp\left(\frac{K_a V}{kT}\right), \qquad (34)$$

where K_a is the magnetic anisotropy constant of the cluster, V is the cluster volume. The observation of superparamagnetism depends on the time of measurement (τ_{meas}) of the magnetic characteristics, namely, magnetisation and magnetic susceptibility. If $\tau < \tau_{meas}$, the system is referred to as a superparamagnetic system. If $\tau > \tau_{meas}$, the superparamagnetic state cannot be detected. In this connection, Mössbauer spectroscopy with a characteristic time of measurement $\tau_{meas} = 10^{-8}$ s (the time of Larmor precession of the ^{57}Fe nuclear spin in the magnetic field) has become a unique method for the investigation of superparamagnetism. The superparamagnetic relaxation of the magnetic moment with $\tau \approx 10^{-8}$–10^{-10} s causes line broadening in the Mössbauer spectra and disappearance of the magnetic hyperfine

structure. Mössbauer spectroscopy makes it possible to estimate the relaxation times in the range of $10^{-8}-10^{-10}$ s and cluster sizes in the range from several nanometers to tens of nanometers.

One more important characteristic of a nanosystem is the magnetic anisotropy constant. This value is related to the magnetic structure and the shape of the cluster. In addition, it characterises the state of the surface, defects and intercluster interactions. Thus for γ-Fe_2O_3 nanoclusters formed in the pores of a sulfo resin with a size of ~ 7 nm, the magnetic anisotropy [236] is 4.4×10^5 J m^{-3}, which is much higher than the value $K_a = 4.7\times10^3$ J m^{-3} for a bulk sample.

It is known that ferromagnets have a magnetic domain structure below the critical temperature. In the absence of an external magnetic field, a system formed from ferromagnetic clusters has a minimum magnetic energy (E_m), which consists of the exchange and dipole energies and the energy of magnetic anisotropy

$$E_m = E_{ex} + E_d + E_{an}\,.$$

The exchange interaction (E_{ex}) lines up the magnetic moments parallel to one another; it is responsible for the uniform magnetisation of domains, and the dipole interaction (E_d) induces antiparallel arrangement of the magnetisation vectors of neighbouring domains, thus decreasing E_m.

As the cluster size decreases below some critical value, the fragmentation of a cluster into domains becomes energetically unfavourable; in this case, a system of single-domain clusters with single-phase magnetisation is formed. Transition of a ferromagnetic cluster from the single-domain state with single-phase magnetisation into a multidomain state changes superparamagnetic properties.[244, 245] When the cluster size increases ($R > R_{cr}$), the energy of anisotropy $U = E_{an} = K_aV$ decreases to zero, which is accompanied by a corresponding decrease in the relaxation time τ and the change in the superparamagnetic properties.

A cluster having the critical size R_{cr} occurs in a state of uniform magnetisation, its magnetic moment being constant over the whole volume $\mathscr{M}(r,\theta,\varphi) = \mathscr{M}_0$ (r is the radial coordinate, θ and φ are the polar and azimuthal angles). When $R > R_{cr}$, the uniform magnetisation state is no longer energetically the most favourable, and rearrangement of $\mathscr{M}$ over the whole particle bulk takes place. It was found [244, 245] that

$$R_{cr} \simeq 2.085\sqrt{\frac{3I}{4\pi}}\,,$$

where I is the exchange integral. The height of the potential barrier was calculated [244] using the formula

$$U = \frac{K_a}{2}\int\left(\cos^4\omega - 3\cos^2\omega\sin^2\omega + \frac{3}{8}\sin^4\omega\right)\mathrm{d}V, \qquad (35)$$

where ω is the function $\omega(R,\theta)$, characterising the deviation of the magnetic moment of the cluster from the uniform magnetisation state. For a nanosystem with a cubic symmetry ($\omega \ll 1$),

$$U_{cub} = \frac{K_a}{2}\int(1-5\omega^2)\mathrm{d}V. \qquad (36)$$

If one compares expressions (35) and (36) with the relation for the calculation of the total moment of the cluster

$$\mathscr{M} = \mathscr{M}_0\int\cos\omega\;\mathrm{d}V \approx \mathscr{M}_0\int\left(1-\frac{\omega^2}{2}\right)\mathrm{d}V, \qquad (37)$$

it turns out that a minor deviation of $\mathscr{M}$ from $\mathscr{M}_0$ (by $\omega^2/2$) gives an order of magnitude higher change in the energy of the anisotropy of the potential barrier. Note that for clusters with a uniaxial symmetry, in which the magnetisation state deviates from the uniform state, the U value does not decrease sharply with the cluster size

$$U_{rel} = \frac{K_a}{2}\int\left(1-\frac{3}{2}\sin^2\omega\right)\mathrm{d}V. \qquad (38)$$

The superparamagnetic behaviour of a nanocluster system formed by Fe–Ni and Fe clusters with a size of 10–25 nm has been studied.[244, 245] To separate the clusters and to weaken the magnetic dipole interaction between them, clusters with a filler and with a content of iron clusters equal to 10% were studied. The data of Mössbauer spectroscopy indicate that the superparamagnetic relaxation time for 11.5-nm clusters is shorter than the relaxation time of 10.5-nm clusters; subsequently, τ increases in proportion with K_aV, which is consistent with the beginning of the deviation from uniform magnetisation.

Magnetisation and quantum magnetic tunnelling. The state of the cluster surface, cluster shape and intercluster interaction influence substantially the magnetisation curves of a nanosystem and the coercive force. Calculations of the relaxation time upon transition of the system into the state with uniform magnetisation show an increase in the energy of anisotropy and the related coercive force following a decrease in the cluster size.[244] The magnetic hysteresis curves for nanocrystalline Ni and Co [246] indicate that the coercive force H_c in cluster nanosystems subjected to plastic deformation is several times as great as H_c for bulk materials. Low-temperature annealing leads to a decrease in H_c with the cluster size remaining invariant, due to the annealing of defects, while high-temperature annealing results in lower H_c and larger clusters. Thus, the increased coercive force of nanocrystalline metals and alloys is related to the stresses and defects at the cluster boundaries and to the single-domain state of the clusters.

The influence of arrangement of Co nanoclusters on the magnetisation curves has been investigated.[22] The colloid Co clusters with sizes of 5.8–8.0 nm were arranged into a 2D hexagonal lattice on a graphite substrate. Studies of the superparamagnetic properties of this system demonstrated shifting of the blocking temperature § of the assembled structure ($T_b = 63$ K) towards higher values with respect to T_b for the colloid solution ($T_b = 58$ K). The increase in T_b is due to the increase in the energy barrier K_aV as a result of intercluster interactions. The total saturation magnetisation of the nanocrystalline system was found to decrease to $M_s = 80$ emu g^{-1} with respect to that of bulk cobalt ($M_s = 162$ emu g^{-1}). The decrease in M_s is due to the presence of the stabilising ligand layer around the Co clusters, which decreases the total magnetic moment of the cluster due to the exclusion of electrons of the Co atoms located on the surface. Attention is drawn to the difference between the magnetisation curves and hysteresis loops for colloid solutions of clusters and organised nanosystems (Fig. 25). Magnetic saturation is achieved for the fields $H = \sim 2$ T only in the case of the organised nanosystem, which implies collective rotation of the magnetic moments of nanoclusters.

The superparamagnetic behaviour of nanoclusters has been considered so far as a thermally activated process with an energy barrier of about K_aV. However, in organised nanosystems, quantum-tunnelling transitions accompanied by a discrete change in the magnetisation of the whole nanocluster system are also possible. These effects were observed for the $[Mn_{12}(CH_3COO)_{16}\cdot(H_2O)_4O_{12}]\cdot 2\,CH_3COOH\cdot 4\,H_2O$ single crystal, which is constructed from acetylacetonate manganese nanoclusters (Mn_{12}^*) with identical sizes.[45] This nanosystem exhibits unusual magnetisation and magnetic hysteresis curves (see Fig. 2). The hysteresis loop is stepwise and consists of vertical and flat sections. In the flat sections of the hysteresis loop, the relaxation time of the magnetic moment is longer than the time of the measurement ($\tau_{meas} \approx 600$ s). In the sloping sections, the relaxation time is close to the time of measurement, which gives rise to several

§ Blocking temperature is the temperature at which no thermal fluctuations take place over the period of magnetisation measurement.

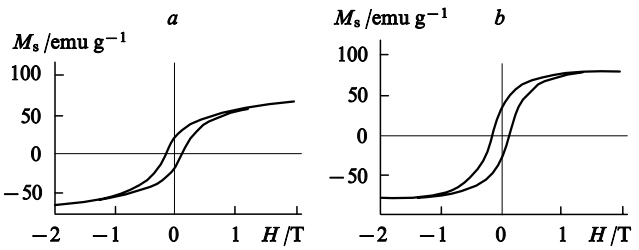

Figure 25. Magnetisation curves for Co nanoclusters with $d = 5.8$ nm; (*a*) a colloid solution in pyridine ($T = 3$ K), (*b*) a nanosystem organised on the graphite surface.[22]

minima in the curves for the dependence of τ on the external magnetic field (Fig. 26*a*). The dependence of $\Delta M/\Delta H$ on H provides exact magnitudes of the fields at which the relaxation times have a minimum. The relaxation time oscillates with respect to the applied field with a minimum corresponding to the steps in the hysteresis loop. Figure 26*b* gives the experimental τ values obtained at different temperatures for the H_0 values corresponding to the minima in the $\tau = f(H)$ curve (Fig. 26*a*): H_0 varies from 0 to 2.64 T with the step $H_{n+1} - H_n = \Delta H = 0.44$ T. At these points discontinuous change in τ is observed. They correspond to the sequence of intersection of electron levels with the spin $S = 10$. Calculation using the formula $\Delta H = D/g\mu_B = 0.44$ T (D is splitting of the level in the crystal field, g is the gyromagnetic ratio) gives $D = 0.60$ K, which coincides with the value $D = 0.61$ K,

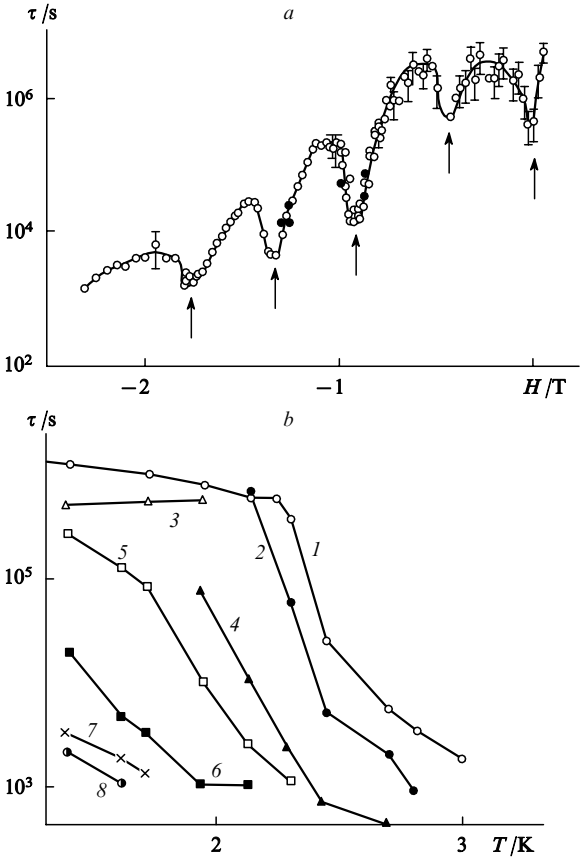

Figure 26. Relaxation time of the magnetic moment of the Mn_{12}^* cluster *vs.* the strength of the external magnetic field (*a*) and *vs.* temperature at different H_0 values (*b*).[45] The measurements were carried out at $T = 2.1$ K; (*a*) the arrows mark the H_0 values at which the steps are observed when the electron levels coincide; (*b*) H_0 values (in T): (*1*) 0, (*2*) 0.44, (*3*) 0.60, (*4*) 0.88, (*5*) 1.32, (*6*) 1.76, (*7*) 2.20, (*8*) 2.64.

reported in a study.[247] Thus, relaxation of the magnetic moment is accelerated when tuning by the magnetic field results in coincidence of the electron levels. This is indicative of quantum tunnelling in the magnetic cluster system, which is possible only when the levels of all clusters contained in the molecular crystal strictly coincide. The decrease in the relaxation time with an increase in temperature (Fig. 26*b*) is apparently due to the electron tunnelling through excited levels with lower Boltzmann occupancy. The probability of tunnelling depends on the width and the height of the barrier. Each minimum of the relaxation time corresponds to the resonance tunnelling from a given level with a time of the order of the measurement time.

An attempt has been made[248] to find out whether quantum tunnelling occurs in large clusters, for example in iron oxide hydroxide clusters, which constitute the core of the protein ferritin. The superparamagnetism phenomenon in such a large cluster (maximum size 6 nm) is usually observed at temperatures above 10 K (depending on the size of the ferritin core). Nevertheless, at low temperatures (5 and 12 K), the hysteresis curve for magnetisation of this cluster in the field with $H = 0$ also displays a step. It is obvious that for this system, coincidence of levels upon tuning by a magnetic field is impossible, which precludes quantum tunnelling. However, at one point ($H = 0$) with doubly degenerate levels, tunnelling is still possible. In addition, the blocking temperature of this system depends on the external magnetic field according to a non-trivial pattern. The temperature increases for low fields, passes through a maximum and decreases for high fields with $H > 0.3$ T. The increase in T_b for low fields is attributed to the violation of the quantum tunnelling condition at $H \neq 0$, while the decrease observed at high fields is ascribed to the decrease in the activation barrier to thermal fluctuations. It should be noted that in this experiment, the $\Delta M/\Delta H = f(H)$ curves have a standard shape, pointing to the absence of the quantum character of transitions.

Giant magnetoresistance effects. The giant magnetoresistance effect (GMR) in clusters is a great decrease in the resistance of the cluster material (by 1000%) when it has been inserted in a magnetic field, whereas the magnetoresistance of a bulk sample changes slightly (for example, the resistance of permalloy, 80% Ni–20% Fe, increases by 3% in a magnetic field). The GMR effects were observed in a study of the magnetic properties of various metallic[249–252] and oxide[253–257] nanosystems, the mechanisms of GMR origination for nanocrystalline metals and metal oxides being different.

Magnetic nanoclusters are prepared by dissolving one metal (for example, Fe or Co) in the matrix of another (conducting) metal (for example, Cu or Ag); these two components should be poorly soluble in each other. In a nanosystem consisting of a conducting metallic matrix and magnetic clusters, the conduction electrons of the matrix are scattered on the magnetic moments of the clusters. When a magnetic field is applied, the direction of the magnetic moments of the clusters changes; this changes their interaction with the conduction electrons of the metallic matrix and, hence, the conductivity. The magnitude of the GMR effect is determined by the ratio of the electron free path (l) to the distance between the neighbouring magnetic clusters, which depends on the concentration of the dissolved metal. When the free path is long, an electron undergoes numerous scattering events before it enters into interaction with the magnetic cluster (the direction of the cluster magnetic moment does not influence the electron scattering and no GMR is observed). If the free path is relatively short, magnetic clusters can be involved in the percolation processes of the matrix and can interact strongly with one another, which also eliminates GMR.

For a system consisting of Co clusters dissolved in an Ag matrix,[251] the change in the Co concentration from 10% to 50% is accompanied by a substantial change in the electric resistance of clusters in the magnetic field (Fig 27). The most pronounced effect is observed when the Co concentration is $\sim 20\%$, which is

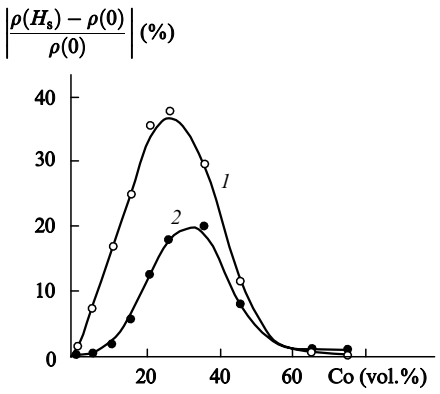

Figure 27. Giant magnetoresistance effect in the Co–Ag nanosystem *vs.* the Co concentration at $T = 5$ (*1*) and 300 K (*2*) in a 0.5-T magnetic field.[251]

attributed to the optimal size of the Co clusters in the Ag matrix. The GMR effect increases with a decrease in temperature.

To interpret the appearance of GMR, the two-current model is used. According to this model, electron scattering on the cluster magnetic moment in a disordered system is equivalent in two directions (for example, up and down). In a system ordered by a magnetic field, one direction, namely, that along the field, has a lower resistance than the other direction; this results in an overall decrease in the resistance. The change in the resistance ($\Delta\rho$) correlates with the change in the size of the magnetic cluster (d): $\Delta\rho \sim 1/d$.

Nanosystems that contain magnetic clusters are promising for controlling the magnetic field of conduction valves. A model system with epitaxially deposited Co(2.5 nm)–Cu(2.2 nm) nanofilms and with a Pb monolayer as an interlayer [252] demonstrated high sensitivity with respect to relatively weak fields (up to 0.05 T), which is of interest for practical purposes.

An even more pronounced effect (decrease of resistance by several orders of magnitude) was observed for perovskite structures of manganites.[253] These are ceramic samples, and, at first sight, in is difficult to distinguish a nanostructure in them. However, as will be shown below, the results of magnetic measurements in this type of system are interpreted resorting to cluster models. The results of studies of the $La_{0.67}Ca_{0.33}MnO_x$ films on $LaAlO_3$ substrates [253] are shown in Fig. 28. In the manganite,

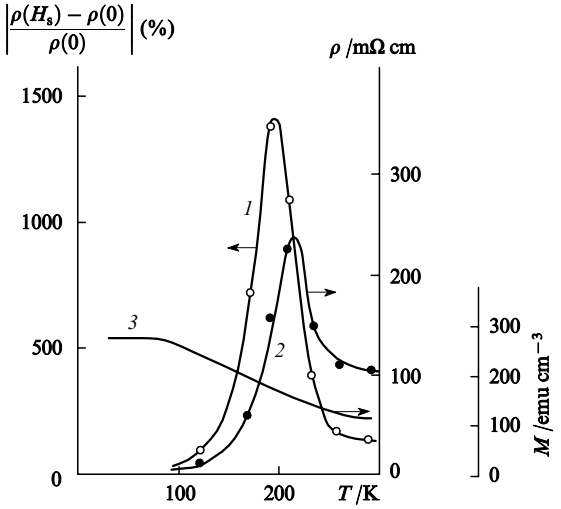

Figure 28. Temperature dependence of the giant magnetoresistance $|\rho(H_s)-\rho(0)/\rho(0)|$ (curve *1*), the resistance (ρ) (curve *2*) and magnetisation (M) (curve *3*) for $La_{0.67}Ca_{0.33}MnO_x$.

unlike metals or alloys, GMR does not cover the whole range of temperature measurement but occurs only in the vicinity of the phase transition from the semiconductor to metallic state (at $T = 220$ K). The most pronounced GMR effect induced by switching on a magnetic field with $H = 4-6$ T is achieved at $T \approx 190$ K, *i.e.*, near the point of transition to the metallic state. However, the temperature dependence of the magnetic moment of the manganite indicates that no sharp magnetic phase transition occurs at $T = 190-220$ K, magnetisation decreasing from the maximum value (saturation at $T = 100$ K) to $M \approx 100$ emu cm^{-3} (at room temperature). This indicates that the GMR is mainly influenced by the semiconductor–metal phase transition rather than the magnetic phase transition.

The GMR value is sensitive to the temperature of annealing and to the concentration of oxygen. Thus GMR measurements for a film prepared at 640 °C gave a smeared GMR peak with a maximum $\Delta\rho/\rho = 500\%$ at $T = 100$ K; for a film annealed at 700 °C in an O_2 atmosphere for 0.5 h, the peak $\Delta\rho/\rho = 1400\%$ was observed at $T \approx 200$ K; further increase in the annealing temperature to 900 °C resulted in a shift of the $\Delta\rho/\rho$ maximum to $T = 280$ K. The giant magnetoresistance observed in ceramics will undoubtedly find practical application.

The mechanism of the formation of GMR in ceramics differs apparently from that for metals. The spin dynamics in manganites of the $La_xCa_yMn_zO_3$ type in which the Mn atoms have been partly replaced by Fe has been studied by Mössbauer spectroscopy.[254–257] A $La_{0.75}Ca_{0.25}Mn_{0.98}Fe_{0.02}O_3$ sample prepared by sintering of salts and oxides was employed.[254] Figure 29 shows the Mössbauer spectra of this compound at different temperatures. Typically, in the region of GMR, the spectrum is separated into the paramagnetic central doublet and the magnetic HFS.[253] Broadening of the HFS lines points to a relaxation type of behaviour of the magnetic moment in the compound $La_{0.75}Ca_{0.25}Mg_{0.98}Fe_{0.02}O_3$, which is similar to the superparamagnetism observed for cluster nanosystems. However, ceramics consist of coarse grains, whose size is beyond the nanometer range.

Data on inelastic neutron scattering (INS) [258] attest that this compound is a ferromagnet at low temperatures; however, when the temperature rises, an inelastic component appears in the INS spectra. As the point of transition of the ceramics from the metallic to the paramagnetic state ($T_c = 250$ K) is approached, this component starts to predominate. This result suggests that in the region of transition of the ceramics from the semiconductor to metallic state, the GMR arises due to the appearance of fluctuating nano-sized regions, which possess ferromagnetic ordering. The size of these regions increases as the temperature decreases. An increase in the size of the region in which the ceramic passes from the paramagnetic to the metallic state is accompanied by an increase in the superparamagnetic relaxation time and the ultimate transition to the magnetically ordered, ferromagnetic state. The temperature range in which this magnetic transition takes place covers tens of degrees but it is in this region that the scattering of conduction electrons changes and the GMR effect arises due to the change in the relaxation time of the magnetic moment, the distances between the fluctuating clusters, and the cluster size (at temperatures below the phase transition temperature, there are no ferromagnetic nano-sized regions, whereas at high temperatures, there is no metallic electrical conductivity).

Magnetic phase transitions. In isolated nanoclusters and nanosystems, magnetic phase transitions are observed; usually, they are second-order phase transitions.¶ The magnetic phase transitions are characterised by Langevin dependences of magnetisation,[259] by disappearance of the magnetic order and spontaneous magnetisation at the Curie (T_C) and Neel (T_N) temperatures, respectively, and by smooth curves for the variation of the magnetisation with temperature. (Nanosystems can also possess superparamagnetism, resulting in an effective lowering of T_C and T_N.)

¶ These transitions are similar to those observed in bulk magnets.

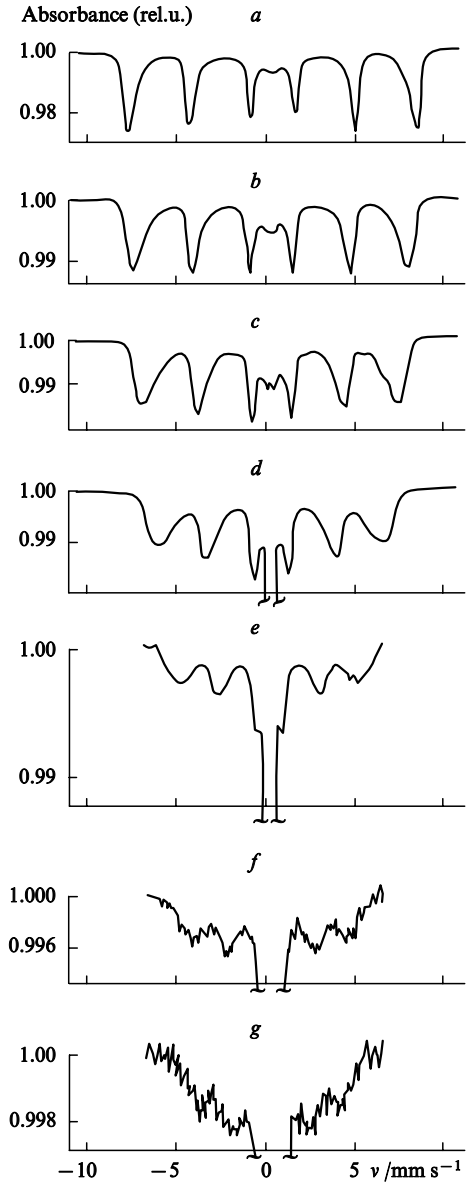

Figure 29. Mössbauer spectra ($a-g$) of a ceramic $La_{0.75}Ca_{0.25}Mn_{0.98}$-$Fe_{0.02}O_3$ sample at different temperatures.[254]
Temperature /K: 78 (*a*), 100 (*b*), 120 (*c*), 150 (*d*), 185 (*e*), 200 (*f*) 210 (*g*).

For several metal oxide clusters, in addition to second-order magnetic phase transitions, first-order magnetic phase transitions were also observed. In this case, a nanosystem lost abruptly the spontaneous magnetisation at some temperature T_{cc} or at some critical cluster size, below which the cluster passed into the paramagnetic state (not the superparamagnetic state). It is difficult to observe the first-order magnetic phase transitions in clusters by magnetisation measurements due to the scatter of clusters over sizes (this scatter results inevitably in smooth variations of the nanosystem magnetisation, and it is difficult to distinguish it from the superparamagnetic behaviour). However, Mössbauer spectroscopy can draw a distinction between the paramagnetic and magnetically ordered states; therefore, it is widely used to study the magnetic phase transitions.

The stepwise magnetic phase transitions were observed for iron oxide-based nanoclusters and nanosystems.[120,260–263] Note that first-order magnetic phase transitions also take place in some bulk transition metal and rare earth metal oxides and alloys.[259] They are interpreted using a thermodynamic model.[264]

A thermodynamic model for magnetic phase transitions in nanoclusters has been proposed.[261] A cluster is assumed to exhibit a pronounced magnetostriction effect, *i.e.*, to change its volume on passing from the magnetically ordered to the paramagnetic state. Meanwhile, the Curie point of a substance depends on its volume

$$T_C = T_0\left(1 + \beta\frac{V - V_0}{V_0}\right), \tag{39}$$

where β is the magnetostriction constant of a substance, V and V_0 are molecular volumes of a substance in the magnetically ordered and paramagnetic states. The change in the Gibbs energy density on passing from the magnetically ordered state to the paramagnetic state is written in the form

$$\Delta G_V = -\frac{1}{2}NkTm^2 + \frac{1}{2}\eta\left(\frac{V - V_0}{V_0}\right)^2 + 2\frac{\alpha}{R}\frac{V - V_0}{V_0} + \frac{1}{2}NkT\left(\ln\frac{1 - m^2}{4} + m\ln\frac{1 + m}{1 - m}\right), \tag{40}$$

where N is the number of atoms with the spin 1/2, $m = M/M_s$ is the relative magnetisation value (M_s is the saturation magnetisation), η is the volume compressibility, and α is the surface tension. The first term in Eqn (40) corresponds to the exchange energy density in the molecular field approximation, the second term reflects the deformation energy, the third term corresponds to the surface energy, and the fourth one matches the entropy term for the temperature dependence of magnetisation.

Minimisation of the free energy and solution of the set of equations $d\Delta G_V/dV = 0$, $d\Delta G_V/dm = 0$ gives

$$\frac{T}{T_{c0}} = m\left(\frac{1}{3}\gamma m^2 + 1\right)\left(\frac{1}{2}\ln\frac{1 + m}{1 - m}\right)^{-1}, \tag{41}$$

where $T_{c0} = T_0(1 - \beta\eta p)$ shows the change in T_0 due to pressure ($p = 2\alpha/R$), $\gamma = (3/2)NkT_0\eta\beta^2(1 - \beta\eta p)^{-1}$.

Figure 30 presents the temperature dependence $m = f(T/T_{c0})$ for different values of the parameter γ, which determines the character of the magnetic phase transition. For $\gamma < 1$, the phase transition corresponds to a second-order magnetic transition and when $\gamma \geqslant 1$, it is a first-order magnetic transition. The γ value can be represented as $\gamma = T_{cc}/T_{c0}$, where $T_{cc} = (3/2)NkT_0^2\eta\beta^2$. If the cluster size $R \leqslant R_{cr}$, then for $\gamma \geqslant 1$, the cluster passes from the magnetically ordered to the paramagnetic state upon a first-order phase transition.

$$R_{cr} = \frac{2\alpha\beta\eta}{1 - T_{cc}/T_{c0}}. \tag{42}$$

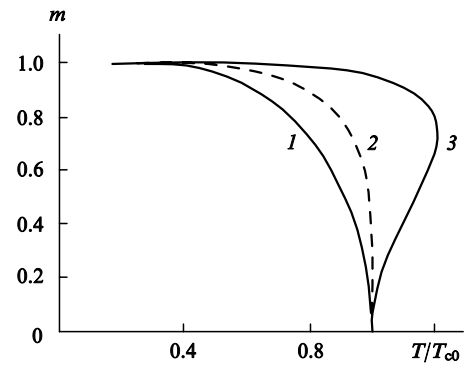

Figure 30. Temperature dependence of the cluster magnetisation for different γ (see the text).
(*1*) $\gamma < 1$, (*2*) $\gamma = 1$, (*3*) $\gamma > 1$.

For larger clusters, only the second-order phase transition can take place. It can also manifest itself as superparamagnetism at temperatures $kT > K_aV$.

The first- and second-order magnetic transitions were observed, for example, for the ferrihydrite $Fe_5HO_8 \cdot 4H_2O$ clusters formed in the polysorb pores.[261] The matrix method allows two cluster systems to be produced, namely, a system with isolated clusters and that with clusters interacting with one another (if several clusters occur in a pore). Figures 31 and 32 show the Mössbauer spectra of the ferrihydrite clusters obtained in 13- and 20-nm polysorb pores. The spectrum recorded at 4.2 K corresponds to a quadrupole doublet and consists of two parts — the central component and the magnetic hyperfine structure with relatively narrow lines (with allowance for the disorder of the cluster structure). As the temperature is raised, some of the HFS of the spectrum is converted into a paramagnetic doublet, without entering the intermediate states corresponding to the superparamagnetic behaviour. The results presented in Figs 31 and 32 suggest that a jumpwise first-order magnetic phase transition occurs in ferrihydrite clusters in the temperature range of 4.2–6 K. An increase in the iron concentration results in an increase in the cluster size; nevertheless, the spectral pattern at 4.2 and 6 K does not change.

In the spectra recorded at 10 K (Fig. 32 *c*) for large clusters ($c = 1.2 \times 10^{-3}$ mol litre^{-1}) formed in a 13-nm pore, the absorption line is broadened, which corresponds to the intermediate forms (between the quadrupole doublet and HFS), peculiar to superparamagnetism. Thus, at 10 K, a second-order magnetic transition is observed for large clusters, in addition to the first-order phase transition. For smaller clusters ($c = 1.2 \times 10^{-3}$ mol litre^{-1}, Fig. 31 *b*), line broadening is barely observed and the second-order magnetic transitions (superparamagnetism) do not show themselves. The appearance of superparamagnetism at 10 K made it possible to estimate the critical cluster size from the broadening of the HFS lines in the spectrum (Fig. 32 *c*), using relation (34): $R_{cr} \approx 2$ nm.

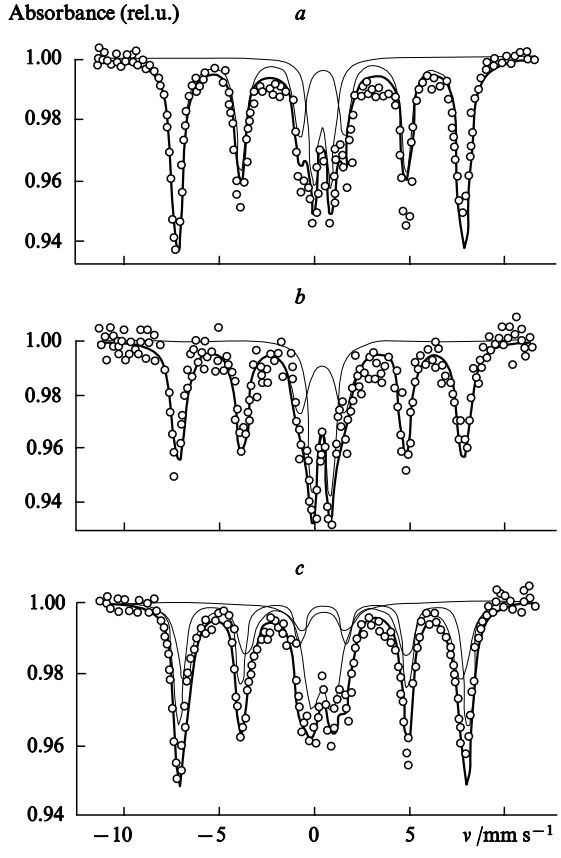

Figure 31. Mössbauer spectra of ferrihydrite clusters ($c = 1.2 \times 10^{-3}$ mol litre^{-1}) in polysorb pores with sizes of 13 (*a*, *b*) and 20 nm (*c*). Here and in Figs 32 and 33, the thick lines show the results of computer processing of the spectrum and the thin lines show its separation into components.
Temperature /K: (*a*) 4.2, (*b*) 10, (*c*) 42.

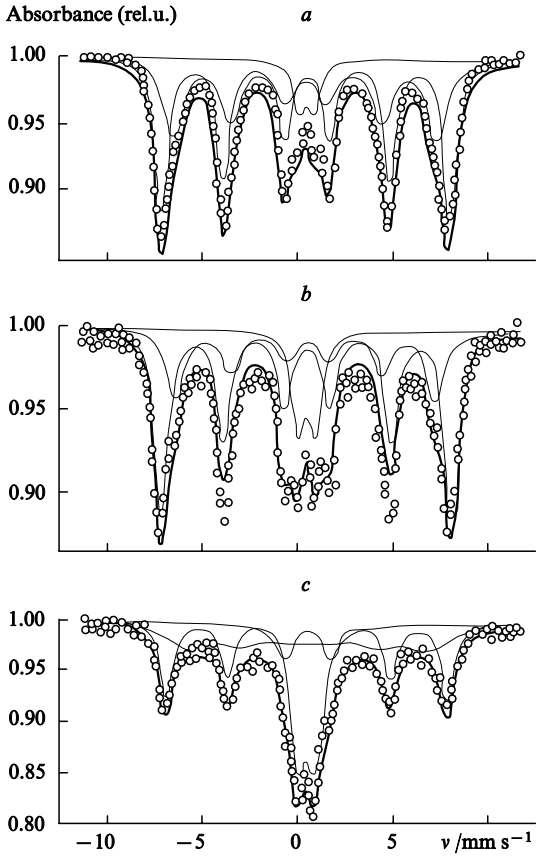

Figure 32. Mössbauer spectra of ferrihydrite clusters ($c = 1.2\,10^{-2}$ mol litre^{-1}) obtained in polysorb pores with a size of 13 nm at different temperatures.
Temperature /K: (*a*) 4.2, (*b*) 6, (*c*) 10.

Estimation of the size of the cluster formed in a pore from the concentration of iron atoms ($c = 1.2 \times 10^{-3}$ mol litre^{-1}) gives the value $R \approx 1-2$ nm (for an isolated cluster). Thus, these data and the data obtained on the basis of superparamagnetic relaxation can be used to estimate the R_{cr} value ($R_{cr} \approx 1.5-2$ nm).

Further growth of clusters and enhancement of their interactions is accompanied by appearance of second-order magnetic transitions: the HFS lines are markedly broadened and the first-order phase transition can no longer be distinguished against the background of the second-order transitions. Estimation of the R_{cr} size using relation (42) gives $R_{cr} \approx 1$ nm, which coincides in order of magnitude with the results obtained in experiments.

The effects similar to a first-order magnetic phase transition were also observed in the α-Fe_2O_3 nanoclusters,[265] in the α-FeOOH – α-Fe_2O_3 system,[266, 267] and in proteins, ferritin and hemosiderin, which include the magnetic core $(FeOOH)_8 \cdot (FeOOPO_3H)$.[268]

Yet another parameter determining the character of the magnetic phase transition is the external excess pressure. It has been noted above that the critical temperature of phase transition decreases upon an increase in pressure due to the change in the surface tension. A change in the external pressure by Δp entails a change in the magnetic transition temperature for the cluster by the value

$$\frac{\Delta T_{c0}}{T_0} = \frac{\Delta p}{2\alpha/R - 1/\beta\mu}. \quad (43)$$

Thus, a decrease in T_{c0} increases the probability of the first-order magnetic phase transition. A study of two nanosystems, namely, an ion exchange sulfo resin (sulfo cation exchange resin) incorporating iron hydroxide clusters with a size of 3 nm and a globular protein (ferritin) incorporating iron hydroxide clusters with a size of 6 nm has been reported.[262] In these systems, the interaction of clusters with the polymeric and biopolymeric networks changed due to hydration. The excess pressure on the cluster was determined from the deformation of the polymeric matrix [from the increase in the water volume which accompanied its crystallisation (freezing)]. This pressure is calculated from the expression

$$\Delta p = \frac{1}{\eta_m}\frac{\Delta V}{V}. \quad (44)$$

For $\Delta V/V = 0.09$ (for water) and $1/\eta_m = 5-10$ GPa,[196] it was found that $\Delta p = 0.45-0.9$ GPa, which is comparable in magnitude with the surface pressure in a 1.5-nm cluster (~ 1 GPa). Using relation (43), one can estimate the decrease in T_{c0} under the action of pressure. Assuming that $p = 1$ GPa, $\beta = 10^2$, $\mu = 10^{-11}$ m^2 J^{-1} and $1/N \sim 10^{-28}$ m^3 (the data were taken from publications [196, 261]), we have $\Delta T_{c0} = (0.1-1.0)T_{c0}$. Thus, ΔT_{c0} can reach a value of the order of T_{c0}.

The ΔT_{c0} value was estimated from the Mössbauer spectra of the sulfo cation exchange resin (in the range of $T = 4.2-30$ K) and ferritin (in the range of 4.2–78 K).[262] Hydration followed by freezing was found to be accompanied by a decrease in T_{c0}. This value was determined from spectra in which the paramagnetic state and the magnetic HFS of the spectra were equal. The following values were obtained: T_{c0}: 9–10 K for the hydrated sulfo cation exchange resin, 13–14 K for the dry cation exchanger, 30 K for hydrated ferritin, and 30–34 K for dry ferritin. Comparison of the T_{c0} values for the dry and hydrated samples provides the temperature shift $\Delta T_{c0} \approx 3-4$ K, which is in line with thermodynamic estimates.

The first-order magnetic phase transitions induced by intercluster stresses and defects can also arise in nanosystems containing larger nanoclusters (20–50 nm). These systems are formed in solid-phase chemical reactions (see Fig. 9),[263] for example, in cluster sintering, and are subject to substantial intercluster interactions. The phase transitions observed in these systems are similar to those in the ferrihydrite clusters (1–3 nm) in a polymeric matrix. Figure 33 shows the Mössbauer spectra of the α-Fe_2O_3–γ-Fe_2O_3 nanosystem. The spectra indicate that jumpwise magnetic transitions from the magnetically ordered state (magnetic HFS) to the paramagnetic state (central doublet) can take place in this system. These magnetic transitions take place at distributed critical temperatures $T_{c0} = 120-300$ K, which are lower than the temperatures T_{c0} for bulk samples of α- and γ-Fe_2O_3 (856 and 965 K, respectively). The decrease in T_{c0} cannot be due to superparamagnetism because of the large cluster size (see Fig. 9); therefore, the calculation using relation (34) affords relaxation times several orders of magnitude longer than τ_{meas}. As a consequence, magnetisation disappears abruptly, which is related to the transformation of the magnetic HFS of γ-Fe_2O_3 into a paramagnetic doublet (Figs 33 and 34 *a*).

The presence of the first-order magnetic phase transition in the α-Fe_2O_3–γ-Fe_2O_3 nanosystem is related to the strong intercluster interactions, which bring about substantial stress in the nanosystem. This stress results in the generation of enormous pressures (up to several Gigapascals). The pressures arise during sintering [121] of the α- and γ-Fe_2O_3 clusters, the unit cells of which have different specific volumes,† and under the action of defects

† The α-Fe_2O_3 clusters have an rhombohedral structure of the corundum type and γ-Fe_2O_3 has a spinel type cubic structure.

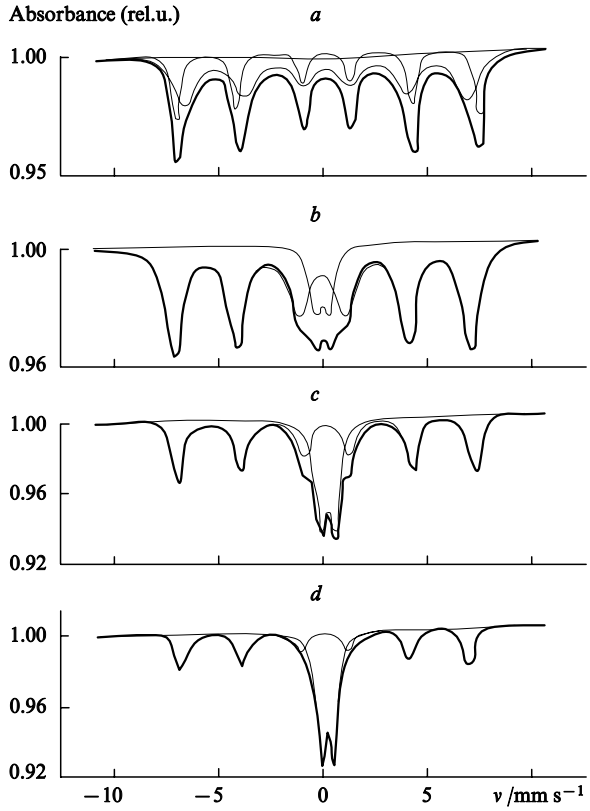

Figure 33. Mössbauer spectra of the α-Fe_2O_3–γ-Fe_2O_3 nanosystem (see Fig. 9) at different measurement temperatures.
Temperature /K: (*a*) 77, (*b*) 120, (*c*) 160, (*d*) 300.

and dislocations. As has been shown above (see Fig. 21), the density of defects has a maximum at a cluster size of exactly 20–30 nm. Further increase in the cluster size is accompanied by a decrease in the fraction of phase boundaries and defect density; thus, the cluster properties approach the properties of a bulk substance.

In addition to the first-order magnetic phase transition in this nanosystem, two more phase transitions were observed in this system, namely, a weak ferromagnetic–antiferromagnetic transition and a collective magnetic phase transition to give twined nanostructures.

Transitions from weak ferromagnetism (non-collinear antiferromagnetism) to antiferromagnetism (collinear antiferromagnetism) were observed for the α-Fe_2O_3 crystals. Weak ferromagnetism is also typical of $MnCO_3$, $CoCO_3$, MnF_2 and orthorhombic $MFeO_3$ crystals (M is a rare earth metal).[259] Weak ferromagnetism is found for antiferromagnetics with some small extent of non-collinearity of sublattice magnetisation. The non-collinearity of the magnetisation of sublattices in antiferromagnetic structures arises upon an increase in the temperature as a consequence of the instability of compensated antiferromagnetism.[269]

For bulk α-Fe_2O_3, a magnetic phase transition, known also as the Morin transition, takes place at $T_M \approx 260$ K; in this transition, the type of magnetic ordering changes jumpwise. When $T_M < 260$ K, collinear antiferromagnetism exists, while at $T > 260$ K, non-collinear antiferromagnetism (weak ferromagnetism) is observed. This transition is due to the internal symmetry of the crystal, which allows distortions in the crystal lattice at higher temperatures; this is accompanied by the rotation of spins through 90 °. The collinearity–non-collinearity phase transition for the magnetic moments of sublattices can be traced in the Mössbauer spectra as the change in the sign and the magnitude of the quadrupole splitting of the spectrum (ΔE_Q) possessing a magnetic HFS

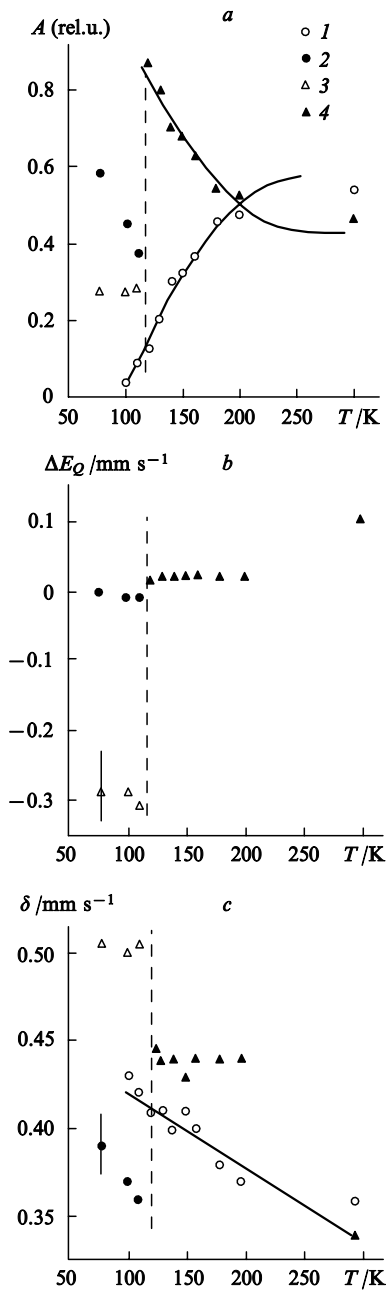

Figure 34. Results of computer simulation of the Mössbauer spectra of the α-Fe_2O_3–γ-Fe_2O_3 nanosystem: temperature dependences of the spectral surface areas (A) for various iron species (a), the quadrupole shift ΔE_Q of the magnetic HFS (b) and the isomer shift δ (c).
(1) Paramagnetic component (quadrupole doublet), (2) the magnetic component of γ-Fe_2O_3, (3) the magnetic component of α-Fe_2O_3, (4) the component corresponding to the twinning structure. The dashed line designates the region of the Morin phase transition.

$$\Delta E_Q = \frac{1}{8} e^2 q Q (3\cos^2\theta - 1),$$

where e is the electron charge, q is the crystal field gradient, Q is the quadrupole moment of the ^{57}Fe nucleus, θ is the angle between the directions of the atom spin and the electric field gradient on the nucleus. The high-temperature α-Fe_2O_3 phase is responsible for $\Delta E_Q = 0.2$ mm s^{-1}, and for the low-temperature phase, $\Delta E_Q = -0.3$ mm s^{-1}.

Now we shall consider specific features of this phase transition in the α-Fe_2O_3–γ-Fe_2O_3 nanosystem (Fig. 34 b). The low-temperature α-Fe_2O_3 phase ($\Delta E_Q = -0.3$ mm s^{-1}), exhibiting collinear antiferromagnetism at $T < 120$ K, passes into a state of non-collinear antiferromagnetism with $\Delta E_Q = 0-0.1$ mm s^{-1} at $T = 120$ K (high-temperature phase). Thus, in the nanosystem, the temperature of the Morin transition decreases to 120 K and the high-temperature phase has a lower ΔE_Q. The decrease in T_M is related to the magnetic dipole energy E_M and the exchange energy E_{exc} by a simple relation. As the cluster size decreases, the E_{exc} value decreases (because the T_{c0} value for Fe_2O_3 diminishes), and the probability of existence of the non-collinear antiferromagnetism increases. Similar examples of decrease in T_M following a decrease in the cluster size have been reported in other studies.[270, 271]

Yet another important circumstance should be mentioned. Despite the broad size distribution of nanoclusters, the phase transition in a nanosystem occurs at a fixed temperature $T_M = 120$ K. This attests to a collective transformation of the whole nanosystem, where the phase transition in one cluster initiates the phase transition in the whole sample. This type of phase transition with instantaneous collective phase transformations of the whole sample was also observed for the transformation of austenite into martensite in carbon steels (martensite transitions).[272]

Let us consider the temperature behaviour of the α-Fe_2O_3–γ-Fe_2O_3 nanosystem (from the Mössbauer spectroscopy data). At low temperatures ($T < 120$ K), both phases, α-Fe_2O_3 and γ-Fe_2O_3 exist in the system; at $T > 120$ K, the α-Fe_2O_3 and γ-Fe_2O_3 phases are converted into one common structure with the ΔE_α parameter corresponding to the α-phase, the crystal lattices of both phases being retained (X-ray diffraction data). The temperature dependence of the isomer shift δ (Fig. 34 c) demonstrates a sharp change in δ at 120 K: for the α-phase, δ decreases, while for the γ-phase, it increases jumpwise to an average value of 0.45 mm s^{-1}. These data point to collective transformations of the γ- and α-phases into an α-like phase; the retention of the crystal lattices of both phases can be explained by assuming the formation of a twinned nanostructure. Twinned structures are often formed upon crystallisation induced by mechanical deformations and during seed sintering. Twinning also occurs upon fast thermal expansion or compression and on heating of deformed crystals.[273, 274]

During the formation of the α-Fe_2O_3–γ-Fe_2O_3 nanosystem, sintering of iron oxide seeds takes place, resulting in the formation of strongly interacting clusters. It is strong intercluster interaction that appears to be responsible for the twin collective transitions in a nanosystem. As a consequence, the two-phase heterogeneous ($\alpha-\gamma$)-iron oxide nanosystem undergoes a sort of a phase temperature transition into a one-phase twinned nanostructure in which the γ-phase is attached to the α-phase. This transition is accompanied by the transfer of an electron from the γ-phase to the α-phase, which shows itself as an increase in the isomer shift.

This transition is a new feature of a heterogeneous nanosystem in which the generator of the transition, a cluster possessing a first-order collinear phase transition, induces the collective transition of the system to a twinned nanostructure. Indeed, the temperature of the twinning phase transition ($T_t = 120$ K) for this nanosystem coincides with the temperature of the antiferromagnetic–weak ferromagnetic phase transition ($T_M = 120$ K).

V. Conclusion

The unusual properties of nano-sized cluster systems have been attracting the attention of researchers for many years, and the interest in these systems has not abated. It is noteworthy that substantial progress in the study of nanoclusters and nanocluster systems has been achieved in recent years. This is due to the fact that the modern level of experiment permits not only the preparation of separate nanocluster particles but also investigation of their properties.

The main advances achieved in the design of new nanocluster systems are listed below:

— methods for the preparation of monodisperse nanoclusters and ordered nanosystems have been developed;

— ways of controlling cluster size, intercluster interaction and intercluster stress, permitting the formation and variation of the properties of nanosystems have been found;

— methods of stabilisation of nanocluster systems *via* passivation of isolated clusters have been proposed;

— methods for the production of ordered layers and superlattices using film and matrix relaxation and by the introduction of spacers have been developed.

Further progress in nanocluster chemistry would involve the synthesis of new nanostructures, creation and development of theoretical and experimental approaches to the study of mechanical, elastic, thermal, electronic, optical and magnetic properties of nanoclusters and nanosystems. The sequence nanocluster – nanosystem – nano-device should be adhered to.

The ordered systems and cluster nanocrystals manufactured on the basis of molecular clusters, fullerenes and colloid clusters can be used in nanotechnology for the design of single-electron devices, optical switches and non-linear systems, lasers with frequency tuned by changing the cluster size and quantum magnetics.

Fullerenes can be employed to manufacture unidimensional wires, rectifiers, diodes, electroluminescent light sources, field-emission cathodes and flat displays.

There appeared the possibility to produce superplastic materials by varying the mechanic properties.

The development of ordered nanolayers and superlattices opens the way to the development of single-electron devices, holographic images and superhigh-density magnetic recording.

The authors are grateful to Academician I I Moiseev, who initiated writing of this reviews and to Academicians V I Gol'dansky and L A Piruzyan, Doctors of Science V N Buravtsev and Yu M Maksimov for useful remarks.

This work was supported by the Russian Foundation for Basic Research (Project No. 00-03-3267).

References

1. I Prigogine, S Rice (Eds) *Evolution of Size Effect in Chemical Dynamics* Part 2 (New York: Wiley, 1988)
2. H Haberland (Ed.) *Clusters of Atoms and Molecules* (Berlin; Heidelberg: Springer, 1994)
3. A D Pomogailo, A S Rozenberg, I E Uflyand *Nanochastitsy Metallov v Klasterakh* (Metal Nanoparticles in Clusters) (Moscow: Khimiya, 2000)
4. I P Suzdalev *Vestn. RFFI* **1** (15) 24 (1999)
5. E L Nagaev *Usp. Fiz. Nauk* **162** (9) 49 (1992) [a]
6. A I Gusev *Usp. Fiz. Nauk* **168** (1) 55 (1998) [a]
7. R F Khairutdinov *Usp. Khim.* **67** 125 (1998) [*Russ. Chem. Rev.* **67** 109 (1998)]
8. R A Andrievskii *Usp. Khim.* **63** 431 (1994) [*Russ. Chem. Rev.* **63** 411 (1994)]
9. V I Sokolov *Izv. Akad. Nauk, Ser. Khim.* 1211 (1999) [b]
10. M N Vargaftik, N Yu Kozitsyna, N V Sherkashina, R I Rudy, D I Kochubey, I I Moiseev, in *Metal Clusters in Chemistry* Vol. 3 (Eds P Branstein, L A Oro, L A Raithly) (New York: VCH, 1999) p. 1363
11. S P Gubin *Khimiya Klasterov* (The Chemistry of Clusters) (Moscow: Nauka, 1987)
12. H Haberland, in *Clusters of Atoms and Molecules* (Ed. H Haberland) (Berlin; Heidelberg: Springer, 1994) p. 207
13. Yu I Petrov *Klastery i Malye Chastitsy* (Clusters and Small Particles) (Moscow: Nauka, 1986)
14. G B Sergeev *Vestn. Mosk. Univ., Ser. 2, Khim.* **40** 312 (1999) [c]
15. H W Kroto, J R Heath, S C O'Brien, R F Curl, R E Smalley *Nature (London)* **318** 162 (1985)
16. W Krätschmer, L D Lamb, K Fostiropoulos, D R Huffman *Nature (London)* **347** 354 (1990)
17. G Hammond, V Kuck (Eds) *The Fullerens* (Washington, DC: American Chemical Society, 1993)
18. R Taylor, D R M Walton *Nature (London)* **363** 685 (1993)
19. W E Billups, M A Cinfolini (Eds) *Buckminsterfullerenes* (New York: VCH, 1993)
20. O Lev, Z Wu, S Bharathi, V Glezer, A Modestov, J Gun, L Rabinovich, S Sampath *Chem. Mater.* **9** 2354 (1997)
21. L Motte, F Billoudet, E Lacaze, J Douin, M P Pileni *J. Phys. Chem. B* **101** 138 (1997)
22. C Petit, A Taleb, M P Pileni *J. Phys. Chem. B* **103** 1805 (1999)
23. J Evans *J. Chem. Soc., Dalton Trans* 555 (1996)
24. V G Syrkin *CVD-Metod. Khimicheskoe i Parofaznoe Okislenie* (CVD Method. Chemical and Vapour-Phase Oxidation) (Moscow: Nauka, 2000)
25. A A Chuiko, Yu I Gorlov *Khimiya Poverkhnosti Kremnezema* (The Chemistry of Silica Surface) (Kiev: Naukova Dumka, 1992)
26. G V Lisichkin, A Yu Fadeeva *Ross. Khim. Zh.* **40** 65 (1996) [d]
27. V B Aleskovskii *Khimiya Nadmolekulyarnykh Soedinenii* (The Chemistry of Supermolecular Compounds) (St. Petersburg: St. Petersburg State University, 1996)
28. V V Arslanov *Usp. Khim.* **63** 3 (1994) [*Russ. Chem. Rev.* **63** 1 (1994)]
29. P Chini *J. Organomet. Chem.* **200** 37 (1980)
30. B K Teo, N J A Sloane *Inorg. Chem.* **24** 4545 (1985)
31. J W A van der Velden, F A Vollenbroek, J J Bour, P T Beurkens, J M M Smits, W P Bosman *Recl. Trav. Chim. Pays-Bas* **100** 148 (1981)
32. V G Albano, A Ceriotti, P Chini, S Martinengo, W M Anker *J. Chem. Soc., Chem. Commun.* 859 (1975)
33. G Schmid, R Pfeil, R Boese, F Bandermann, S Meyer, G H M Calis, J W A van der Velden *Chem. Ber.* **114** 3634 (1981)
34. R G Wallenberg, J O Bovin, G Schmid *Surf. Sci.* **154** 256 (1985)
35. G Schmid *Chem. Rev.* **92** 1709 (1992)
36. R G Wallenberg, J O Bovin, A K Petford-Long, D J Smith *Ultramicroscopy* **20** 71 (1986)
37. J O Malm, J O Bovin, A K Petford-Long, D J Smith, G Schmid, N Klein *Angew. Chem., Int. Ed. Engl.* **27** 555 (1988)
38. G Schmid, B Morun, J O Malm *Angew. Chem.* **101** 772 (1989)
39. M N Vargaftik, V P Zagorodnikov, I P Stolarov, I I Moiseev, D I Kochubey, V A Liholobov, A L Chuvilin, K I Zamaraev *J. Mol. Catal.* **53** 315 (1989)
40. M N Vargaftik, I I Moiseev, D I Kochubey, K I Zamaraev *Faraday Discuss.* **92** 13 (1991)
41. G Schmid *J. Chem. Soc., Dalton Trans.* 1077 (1998)
42. Y Volokitin, J Sinzig, L J de Jough, G Schmid, M N Vargaftik, I I Moiseev *Nature (London)* **384** 621 (1996)
43. V I Gol'danskii, L I Trakhtenberg, V N Flerov *Tunnel'nye Yavleniya v Khimicheskoi Fizike* (Tunnel Effects in Chemical Physics) (Moscow: Nauka, 1986)
44. J R Friedman, U Voskoboynik, M P Sarachik *Phys. Rev. B, Condens. Matter* **56** 10793 (1997)
45. L Thomas, F Lionti, R Ballou, D Gatteschi, R Sessoli, B Barbara *Nature (London)* **383** 145 (1996)
46. N Herron, J C Calabrese, W E Farweth, Y Wang *Science* **259** 1426 (1993)
47. W Ekardt *Phys. Rev. B, Condens. Matter* **29** 1558 (1984)
48. W D Knight, K Clemenger, W A de Heer, W A Saunders, M Y Chou, M L Cohen *Phys. Rev. Lett.* **52** 2141 (1984)
49. M M Kappes, M Schar, U Rothlisberger, C Yeretzian, E Schumacher *Chem. Phys. Lett.* **143** 251 (1988)
50. D M Wood *Phys. Rev. Lett.* **46** 749 (1981)
51. C Bréchignac, Ph Cahuzac, F Carlier, M de Frutos, J Leygnier *J. Chem. Phys.* **93** 7449 (1990)
52. Z Penzar, W Ekardt *Z. Phys. D, At. Mol. Clusters* **17** 69 (1990)
53. D M Wood, N N Ashcroft *Phys. Rev. B, Condens. Matter* **25** 6255 (1982)
54. G Mie *Ann. Phys. (Germany)* **25** 377 (1908)
55. W D Knight, K Clemenger, W A de Heer, W A Saunders *Phys. Rev. B, Condens. Matter* **31** 2539 (1985)
56. C Bréchignac, Ph Cahuzac, F Carlier, M de Frutos, J Leygnier *Chem. Phys. Lett.* **189** 28 (1992)
57. H Handschuh, Chia Yen Cha, P S Bechthold, G Ganteför, W Eberhardt *J. Chem. Phys.* **102** 6406 (1995)
58. S Yang, M B Knickelbein *J. Chem. Phys.* **93** 1953 (1990)
59. M F Jarrold, in *Clusters of Atoms and Molecules* (Ed. H Haberland) (Berlin; Heidelberg: Springer, 1994) p. 315

60. A Berces, P A Hackett, L Lian, S A Mitchell, D M Rayner *J. Chem. Phys.* **108** 5476 (1998)
61. S K Nayak, B K Rao, S N Khanna, P Jena *Chem. Phys. Lett.* **259** 588 (1996)
62. S A Mitchell, L Lian, D M Rayner, P A Hackett *J. Chem. Phys.* **103** 5539 (1995)
63. H Kietzmann, J Morenzin, P S Bechthold, G Ganteför, W Eberhardt *J. Chem. Phys.* **109** 2275 (1998)
64. K Fisher, I Dance, G Willett, M Yi *J. Chem. Soc., Dalton Trans.* 709 (1996)
65. C Bréchignac, Ph Cahuzac, F Carlier, M de Frutos, J Leygnier, J Ph Roux *J. Chem. Phys.* **102** 763 (1995)
66. I M Billas, J A Becker, A Chatelain, W A de Heer *Phys. Rev. Lett.* **71** 4067 (1993)
67. I M L Billas, A Chatelain, W A de Heer *Science* **265** 1682 (1994)
68. J Shi, S Gider, K Babcock, D D Awschalom *Science* **271** 937 (1996)
69. A J Cox, J G Lounderback, S E Apsel, L A Bloomfield *Phys. Rev. B, Condens. Matter* **49** 12295 (1994)
70. S W McElvany, B I Dunlap, A O'Keefe *J. Chem. Phys.* **86** 715 (1986)
71. E A Rohlfing, D M Cox, A Kaldor *J. Chem. Phys.* **81** 3322 (1984)
72. G E Scuseria *Science* **271** 942 (1996)
73. P A Hintz, M B Sowa, S L Anderson *Chem. Phys. Lett.* **177** 146 (1991)
74. S W McElvany *J. Chem. Phys.* **89** 2063 (1988)
75. D C Parent, S W McElvany *J. Am. Chem. Soc.* **111** 2393 (1989)
76. W R Creasy *J. Chem. Phys.* **92** 7223 (1990)
77. A Muhr, R Nesper, B Schmyder, R Kotz *Chem. Phys. Lett.* **249** 399 (1996)
78. J C Hummelen, B Knight, J Pavlovich, R González, F Wudl *Science* **269** 1554 (1995)
79. K Kimura, T Sugai, H Shinohara *Chem. Phys. Lett.* **256** 269 (1996)
80. M Pellarin, C Ray, P Melinon, J Lerme, J L Vialle, P Keghelian, A Perez, M Broyer *Chem. Phys. Lett.* **277** 96 (1997)
81. D E Clemmer, J M Hunter, K B Shelimov, M F Jarrold *Nature (London)* **372** 248 (1994)
82. F Tast, N Malinowski, S Frank, M Heinebrodt, I M L Billas, T M Martin *Z. Phys. D, At. Mol. Clusters* **40** 351 (1997)
83. W Branz, I M L Billas, N Malinowski, F Tast, M Heinebrodt, T P Martin *J. Chem. Phys.* **109** 3425 (1998)
84. S Kawasaki, T Aketa, H Touhara, F Okino, O V Boltalina, I V Gol'dt, S I Troyanov, R Taylor *J. Phys. Chem. B* **103** 1223 (1999)
85. K Tanigaki, T W Ebbesen, S Saito, J Mizuki, J S Tsai, Y Kubo, S Kuroshima *Nature (London)* **352** 222 (1991)
86. J R Heath, S C O'Brien, Q Zhang, Y Liu, R F Curl, H W Kroto, F K Tittel, R E Smalley *J. Am. Chem. Soc.* **107** 7779 (1985)
87. M Saunders, H A Jiménez-Vázquez, R J Cross, S Mroczkowski, M L Gross, D E Giblin, R J Poreda *J. Am. Chem. Soc.* **116** 2193 (1994)
88. F D Weiss, J L Elkind, S C O'Brien, R F Curl, R E Smalley *J. Am. Chem. Soc.* **110** 4464 (1988)
89. Y Chai, T Guo, C Jin, R E Haufler, L P Chibante, J Fure, L Wong, J M Alford, R E Smalley *J. Phys. Chem.* **95** 7564 (1991)
90. B L Tumanskii, V V Bashilov, S P Solodovnikov, V I Sokolov, V P Bubnov, E E Laukhina,Yu I Estrin,V K Kol'tover, E B Yagubskii *Fullerene Sci. Technol.* **6** 445 (1998)
91. J A Northby *J. Chem.* 6166 (1987)
92. O Echt, O Kandler, T Leisner, W Miehle, E Recknagel *J. Chem. Soc., Faraday Trans.* 2411 (1990)
93. J Stapelfeldt, J Wormer, T Moller *Phys. Rev. Lett.* **62** 89 (1989)
94. D Scharf, J Jortner, U Landman *J. Chem. Phys.* **88** 4273 (1988)
95. W Miehle, O Kaundler, T Leisner, O Echt *J. Chem. Phys.* **91** 5940 (1989)
96. J Jortner, D Scharf, U Landman, in *Elemental and Molecular Clusters* (Eds G Benedek, T P Martin, G Pacchioni) (Berlin; Heidelberg: Springer, 1988) p. 148
97. U Buck, in *Clusters of Atoms and Molecules* (Ed. H Haberland) (Berlin Heidelberg: Springer, 1994) p. 396
98. K Liu, J D Cruzan, R J Saykally *Science* **271** 929 (1996)
99. J van Duijneveldt-van de Rijdt, F B van Duijneveldt *Chem. Phys.* **175** 271 (1993)
100. R Knochenmuss, S Leutwyler *J. Chem. Phys.* **96** 5233 (1992)
101. G Schmid, V Maihack, F Lantermann, S Peschel *J. Chem. Soc., Dalton Trans.* 589 (1996)
102. A P Alivisatos *Science* **271** 933 (1996)
103. M Mittleman, R W Schoeulein, J J Shiang, V L Colvin, A P Alivisatos, C V Shank *Phys. Rev. B, Condens. Matter* **49** 14435 (1994)
104. S Hotchandani, P V Kamat *J. Phys. Chem.* **96** 6834 (1992)
105. H C Youn, S Baral, J H Fendler *J. Phys. Chem.* **92** 6320 (1988)
106. M F Finlayson, K H Park, N Kakuta, A J Bard, A Campion, M A Fox, S E Weller, J M White *J. Lumin.* **39** 205 (1988)
107. K R Gopidas, P V Kamat *Proc. Indian Acad. Sci. Chem. Sci.* **105** 505 (1993)
108. A I Ekimov, I A Kudryavtsev, M G Ivanov, A L Efros *J. Lumin.* **46** 83 (1990)
109. T Rajh, O I Micic, D Lawless, N Serpone *J. Phys. Chem.* **96** 4633 (1992)
110. K R Gopidas, P V Kamat *Mater. Lett.* **9** 372 (1990)
111. M Grundemann *Phys. Rev. Lett.* **74** 4043 (1995)
112. T Vossmeyer, L Katsikas, M Giersig, I G Popovic, H Weller *J. Phys. Chem.* **98** 7665 (1994)
113. T Itoh, M Furumiya, T I Kehara *Solid State Commun.* **73** 272 (1990)
114. R W Schoeulein, D M Mitteman, J J Shiang, A P Alivisatos, P V Shank *Phys. Rev. Lett.* **70** 1014 (1993)
115. R L Fock, D W Taylor, K R German, A Kiel, E Buehler *Phys. Rev. Lett.* **32** 781 (1974)
116. R L Fock, D W Taylor *Phys. Rev. B, Condens. Matter* **19** 3365 (1979)
117. R N Bhargava, R N Gallagher, X Hong, A Nuemikko *Phys. Rev. Lett.* **72** 416 (1994)
118. N Murase, R Jagannathan, Y Kanematsu, M Watanabe, A Kurita, K Hirata, T Yazawa, T Kushida *J. Phys. Chem. B* **103** 754 (1999)
119. I P Suzdalev *Dinamicheskie Effekty v Gamma-Rezonansnoi Spektroskopii* (Dynamic Effects in Mössbauer Spectroscopy) (Moscow: Atomizdat, 1979)
120. I P Suzdalev, Yu V Maksimov, V N Buravtsev, V K Imshennik, A G Kazakevich, S V Novichikhin *Kolloid. Zh.* **62** 257 (2000) [e]
121. Ya G Geguzin *Fizika Spekaniya* (The Physics of Caking) (Moscow: Nauka, 1984)
122. N D Kingery, H K Bowen, D R Uhlmann *Introduction to Ceramic* (New York: Wiley, 1976)
123. A A Nazarov, A E Romana, R Z Valiev *Nanostruct. Mater.* **4** 1033 (1994)
124. R Z Valiev *Nanostruct. Mater.* **6** 73 (1995)
125. M Yu Gutkin, K N Mikaelzyan, I A Ovid'ko *Fiz. Tv. Tela* **37** 552 (1995) [f]
126. R Z Valiev, O A Kaibyshev, R I Kuznetsov, R Sh Musalimov, N K Tsenev *Dokl. Akad. Nauk SSSR* **301** 864 (1988) [g]
127. R Z Valiev, N A Krasilnikov, N K Tsenev *Mater. Sci. Eng. A, Struct. Mater.* **137** 35 (1991)
128. R Z Valiev, A V Korznikov, R R Mulyukov *Fiz. Met. Metalloved.* **73** 70 (1992) [h]
129. A V Rempel', A I Gusev, R R Mulyukov, in *Ul'tradispersnye Poroshki, Materialy i Nanostruktury* (Ultradispersed Powders, Materials and Nanostructures) (Ed. V E Red'kin) (Krasnoyarsk: Krasnoyarsk State Engineering University, 1996) p. 186
130. N I Noskova *Fiz. Met. Metalloved.* **73** 102 (1992) [h]
131. N I Noskova *Fiz. Met. Metalloved.* **76** 171 (1993) [h]
132. T Hill *Thermodynamics of Small Systems* (New York: Benjamin, 1964)
133. A W Adamson *Physical Chemistry of Surface* (New York: Wiley, 1976)
134. D W Oxtoby, in *Advances in Chemical Physics* Vol. 70 (New York: Wiley, 1988)
135. I P Suzdalev, V N Buravtsev, V K Imshennik, S V Novichikhin *Khim. Fiz.* **12** 555 (1993) [i]
136. I P Suzdalev, V K Imshennik, S V Novichikhin *Nucl. Instrum. Methods, Phys. Res. B* **76** 421 (1993)
137. V K Imshennik, I P Suzdalev, O N Stavinskaya, N I Shklovskaya, V Schuenemann, A X Trautwein, H Winkler *Microporous Mater.* **10** 225 (1997)
138. O N Stavinskaya, V K Imshennik, E I Oranskaya, I P Suzdalev, N I Shklovskaya *Zh. Fiz. Khim.* **72** 1269 (1998) [j]

139. O N Stavinskaya, V K Imshennik, S V Novichikhin, N I Shklovskaya, I P Suzdalev *Zh. Fiz. Khim.* **72** 1282 (1998) [j]
140. Yu V Maksimov, I P Suzdalev, M V Tsodikov, V Ya Kugel, O V Bukhtenko, E V Slivinskii, J A Navio *J. Mol. Catal. A, Chem.* **105** 167 (1996)
141. L Motte, F Billoudet, M P Pileni *J. Phys. Chem.* **99** 16425 (1995)
142. A Taleb, C Petit, M P Pileni *J. Phys. Chem. B* **102** 2214 (1998)
143. R L Whetten, J T Khoury, M M Alvarez, S Murthy, L Vezmar, Z L Wang, C Cleveland, W D Luedke, V Laudman *Adv. Mater.* **8** 428 (1996)
144. M Brust, D Bethell, D J Schiffrin, C J Kiely *Adv. Mater.* **7** 9071 (1995)
145. S A Harfenist, Z L Wang, M M Alvarez, I Vezmar, R I Whetten *J. Phys. Chem. B* **100** 13904 (1996)
146. J R Heath, C M Knobler, D V Leff *J. Phys. Chem. B* **101** 189 (1997)
147. S A Harfenist, Z L Wang, R L Whetten, I Vezmar, M M Alvarez *Adv. Mater.* **9** 817 (1997)
148. U-S S Jeng, T-L Lin, Ch-S Tsao, Ch-H Lee, T Canteenwala, L Y Wang, L Y Chiang, Ch C Han *J. Phys. Chem. B* **103** 1059 (1999)
149. S Nath, H Pal, D K Palit, A V Sapre, J P Mittal *J. Phys. Chem. B* **102** 10158 (1998)
150. E G Hope, J H Holloway *The Chemistry of Fullerenes* (Singapore: World Sci., 1995)
151. A A Gakh, A A Tuinman, J L Adcock *J. Am. Chem. Soc.* **116** 819 (1994)
152. V A Davydov, L S Kashevarova, A V Rakhmanina, V Agafonov, H Allouchi, R Céolin, A V Dzyabchenko, V M Senyavin, H Szwarc, T Tanaka, K Komatsu *J. Phys. Chem. B* **103** 1800 (1999)
153. G W Wang, K Komatsu, Y Murata, M Shiro *Nature (London)* **387** 583 (1997)
154. G Treboux, P Lapstun, K Silverbrook *J. Phys. Chem. B* **103** 1871 (1999)
155. Y Kuk, D K Kim, Y D Suh, K H Park, H P Noh, S J Oh, S K Kim *Phys. Rev. Lett.* **70** 1948 (1993)
156. T Hashizume, K Motai, X D Wang, H Shinohara, Y Saito, Y Makuyma, K Ohno, Y Kawazoe, Y Nishina, H W Pickering, Y Kuk, T Sakurai *Phys. Rev. Lett.* **71** 2959 (1993)
157. X D Wang, T Hashizume, H Shinohara, Y Saito, Y Nishina, T Sakurai *Phys. Rev. B, Condens. Matter* **47** 15923 (1993)
158. H Xu, D M Chen, W N Creager *Phys. Rev. Lett.* **70** 1850 (1993)
159. D Klyacko, D M Chen *Phys. Rev. Lett.* **75** 3693 (1995)
160. M Sakurai, H Tada, K Saiki, A Koma, H Funaska, Y Kishimoto *Chem. Phys. Lett.* **208** 425 (1993)
161. G Gensterblum, L M Yu, J J Pireaux, P A Thiry, R Caudano, J M Themblin, S Bouzidi, F Coletti, J H Debever *Appl. Phys.* **156** 175 (1993)
162. O Wada, Y Hanazato, M Miyamoto, S Suzuki, M Kataoka, S Isoda *Fullerene Sci. Technol.* **1** 393 (1993)
163. C Rey, J Garcia-Rodeja, L J Gallego *Phys. Rev. B, Condens. Matter* **55** 7190 (1997)
164. C Bréchignac, Ph Cahuzac, F Carlier, M de Frutos, A Masson, C Mory, C Colliex, B Yoon *Phys. Rev. B, Condens. Matter* **57** R2084 (1998)
165. R A Andrievskii *Usp. Khim.* **66** 57 (1997) [*Russ. Chem. Rev.* **66** 53 (1997)]
166. D A Dudko, V G Aleshin, A E Barg, N E Dubovitskaya, L N Larikov, A A Smekhnov *Dokl. Akad. Nauk SSSR* **285** 106 (1985) [g]
167. A E Barg *Metallofizika* **9** 118 (1995)
168. H van Swygenhoven *Nanostruct. Mater.* **6** 739 (1995)
169. R W Siegel, H Hahn, in *Current Trends in Physics of Materials* (Ed. M Yusouff) (Singapore: World Sci., 1987) p. 403
170. H Gleiter *Prog. Mater. Sci.* **33** 233 (1989)
171. T Rabe, R Wasche *Nanostruct. Mater.* **6** 357 (1995)
172. B H Kear, P R Strutt *Nanostruct. Mater.* **6** 827 (1995)
173. P Seegopaul, L E McCaudish, F M Shinneman *Int. J. Refract. Met. Hard Mater.* **15** 133 (1997)
174. G V Ivanov, N A Yavorovskii, Yu A Kotov, V I Davydovich, G A Mel'nikova *Dokl. Akad. Nauk SSSR* **275** 873 (1984) [g]
175. V V Ivanov, A N Vikhrev, A L Nozdrin *Fiz. Khim. Obrab. Mater.* **3** 67 (1997)
176. R A Andrievskii, A N Vikhrev, V V Ivanov, R I Kuznetsov, N I Noskova, V A Sazonova *Fiz. Met. Metalloved.* **81** 137 (1996) [h]
177. I P Suzdalev, V N Buravtsev, A V Volynskaya, V K Imshennik, V V Matveev *Khim. Fiz.* **14** 114 (1995) [i]
178. R M Lynden-Bell, D J Wales *J. Chem. Phys.* **101** 1460 (1994)
179. C L Cleveland, U Landman, W D Luedke *J. Phys. Chem.* **98** 6272 (1994)
180. R S Berry *J. Phys. Chem.* **98** 6910 (1994)
181. R S Berry, T L Beck, H L Davis, in *Evolution of Size Effect in Chemical Dynamics* (Eds I Prigogine, S Rice) (New York: Wiley, 1988) p. 75
182. S K Nayak, R Ramaswamy *J. Phys. Chem.* **98** 9260 (1994)
183. A Boutin, B Roussean, A H Fuchs *Chem. Phys. Lett.* **218** 128 (1994)
184. J Garcia-Rodeja, C Rey, L J Gallego, J A Alonso *Phys. Rev. B* **49** 8495 (1994)
185. R S Berry, in *Clusters of Atoms and Molecules* (Ed. H Haberland) (Berlin; Heidelberg: Springer, 1994) p. 201
186. I P Suzdalev, V N Buravtsev, V K Imshennik, Yu V Maksimov, V V Matveev, A V Volynskaya, A X Trautwein, H Winkler *Nuovo Cimento D* **18** 287 (1996)
187. I P Suzdalev, V N Buravtsev, Yu V Maksimov, A X Trautwein, H Winkler *Hyperfine Interact. (Netherlands)* **C1** 290 (1996)
188. I P Suzdalev, N I Shklovskaya *Colloid Surf. A* **108** 315 (1996)
189. I P Suzdalev *J. Radioanal. Nucl. Chem. Artic.* **190** 279 (1995)
190. I P Suzdalev, V K Imshennik, V V Matveev *Neorg. Mater.* **31** 807 (1995) [k]
191. I P Suzdalev, V N Buravtsev, V K Imshennik, Yu V Maksimov, V V Matveev, A V Volynskaya, A X Trautwein, H Winkler *Z. Phys. D, At. Mol. Clusters* **36** 163 (1996)
192. L D Landau, E M Lifshits *Statisticheskaya Fizika* (Statistic Physics) (Moscow: Nauka, 1951)
193. Ph Buffat, J P Borel *Phys. Rev. A, Gen. Phys., Ser. 3* **13** 22 (1976)
194. Y Osima, K Takaynagi *Z. Phys. D, At. Mol. Clusters* **27** 287 (1993)
195. A N Coldstein, C M Echer, A P Alivisatos *Science* **256** 1425 (1992)
196. I R Grigor'ev, U S Meilikhov (Eds) *Fizicheskie Velichiny. Spravochnik* (Physical Values. Handbook) (Moscow: Energoatomizdat, 1991)
197. B F Ormont *Dokl. Akad. Nauk SSSR* **124** 132 (1959) [g]
198. P A Rehbinder *Poverkhnostnye Yavleniya v Dispersnykh Sistemakh, Fiziko-Khimicheskaya Mekhanika* (Surface Effects in Dispersed Systems, Physicochemical Mechanics) (Moscow: Nauka, 1979) p. 142
199. G Goll, H Lohneyen *Nanostruct. Mater.* **6** 559 (1995)
200. J Trampenau *Nanostruct. Mater.* **6** 511 (1995)
201. R Z Valiev *Pis'ma Zh. Tekh. Fiz.* **15** 78 (1989) [l]
202. J Wang *Nanostruct. Mater.* **6** 747 (1995)
203. A S Plachinda, V E Sedov, V I Khromov, I P Suzdalev, V I Goldanskii, G U Nieuhaus, F Parak *Phys. Rev. B, Condens. Matter* **45** 7716 (1991)
204. A S Plachinda, V E Sedov, V I Khromov, L V Bashkaev, I P Suzdalev *Chem. Phys. Lett.* **175** 101 (1990)
205. V I Khromov, A S Plachinda, S I Kamyshanskii, I P Suzdalev *Izv. Akad. Nauk, Ser. Khim.* 886 (1996) [b]
206. I P Suzdalev, V I Goldanskii, Yu F Krupyanskii, I V Kurinov, A S Plachinda *Hyperfine Interact. (Netherlands)* **66** 177 (1991)
207. Ch Kittel *Introduction to Solid State Physics* (New York: Wiley, 1976)
208. J-B Maillet, A Boutin, S Battefey, F Calvo, A H Fuchs *J. Chem. Phys.* **109** 329 (1998)
209. I V Aleksandrov, R Z Valiev *Fiz. Met. Metalloved.* **77** 77 (1994) [h]
210. G W Neiman, J R Weertman, R W Siegel *J. Mater. Res.* **6** 1012 (1991)
211. J A Eastmen, M Fitzsimmons, L J Thompson *Philos. Mag. B* **66** 667 (1992)
212. I V Alexandrov, R Z Valiev *Philos. Mag. B* **73** 861 (1996)
213. H Muller, H G Fritsche, L Skala, in *Clusters of Atoms and Molecules* (Ed. H Haberland) (Berlin; Heidelbery: Springer, 1994) p. 114
214. X Y Qin, X Y Wu, I F Cheng *Nanostruct. Mater.* **2** 99 (1993)
215. M L Sui, K Lu *Mater. Sci. Eng. A, Struct. Mater.* **179–180** 541 (1994)
216. N J Petch *Iron Steel Int.* **174** 25 (1953)
217. R W Siegel, G E Fougere *Nanostruct. Mater.* **6** 205 (1995)
218. R Z Valiev, A V Korznikov, R R Mulyukov *Mater. Sci. Eng. A, Struct. Mater.* **168** 141 (1993)
219. Y Ishida *Nanostruct. Mater.* **6** 115 (1995)
220. T Kizuka *Philos. Mag. A* **69** 551 (1994)

221. S X McFadden, R S Mishra, R Z Valiev, A P Zhilyaev, A K Mukherjce *Nature (London)* **398** 684 (1999)
222. O D Sherby, O A Ruano, in *Superplastic Forming of Structural Alloys* (Eds E N Paton, C H Hamilton) (New York: The Metall. Soc. of AIME, 1982) p. 241
223. J G Wang, R J Raj *J. Am. Ceram. Soc.* **67** 385 (1984)
224. P Venezuela, J Tersoff, J A Floro, E Chason, D M Follstaedt, F Liu, M G Lagally *Nature (London)* **397** 678 (1999)
225. L H Schwartz, in *Application of Mössbauer Spectroscopy* Vol. 1 (Ed. R I Cohen) (New York: Academic Press, 1976) p. 37
226. J Lin, E Cates, P A Bianconi *J. Am. Chem. Soc.* **116** 4738 (1997)
227. K Uchino, E Sadanaga, T Hirose *J. Am. Ceram. Soc.* **72** 1555 (1989)
228. S Chettopadhyay, P Ayyub, V R Palkar, M Multani *Phys. Rev. B, Condens. Matter* **52** 13177 (1995)
229. P Ayyub, V R Palkar, S Chettopadhyay, M Multoni *Phys. Rev. B, Condens. Matter* **51** 6135 (1995)
230. Yu V Maksimov, I P Suzdalev, M Ya Kushnerev, R A Arents *Fiz. Met. Metalloved.* **37** 267 (1974) [h]
231. A A Rempel' *Dokl. Akad. Nauk* **347** 750 (1996) [g]
232. V L Colvin, M C Schlamp, A P Alivisatos *Nature (London)* **370** 354 (1994)
233. B O Dabbousi, M G Bawendi, O Onitsuka, M F Rubner *Appl. Phys. Lett.* **66** 1316 (1995)
234. L E Brus, P E Szajowski, W L Wilson, T D Harris, S Schuppler, P H Citrin *J. Am. Chem. Soc.* **117** 2915 (1995)
235. S H Tolbert, A B Herheld, C S Johnson, A P Alivisatos *Phys. Rev. Lett.* **73** 3266 (1994)
236. J K Vassiliou, V Mehrotra, M W Russell, E P Giannelis, R D McMichael, R D Shull, R Ziolo *J. Appl. Phys.* **73** 5109 (1993)
237. T Ung, M Giersig, D Dunstan, P Mulvaney *Langmuir* **13** 1773 (1997)
238. H Y Kai, Ph. D. Thesis, Netherland, Amsterdam Universiteit van Amsterdam, 1993
239. G I Frolov *Fiz. Tv. Tela* **38** 1208 (1996) [f]
240. D Fenske, in *Clusters and Colloids: From Theory to Application* (Ed. G Schmid) (Weinheim: VCH, 1994) p. 212
241. P Andres, J D Bielefeld, J I Heuderson, D B Yanes, V R Kolagunat, C P Kubiak, W J Mahoney, R G Osifchin *Science* **273** 1690 (1996)
242. G Hornyak, M Kröll, R Pugin, Th Sawitowski, G Schmid, J-O Bovin, G Karsson, H Hofmeister, S Hopfe *Chem. A, Eur. J.* 1951 (1997)
243. P G Collins, A Zettl, H Bando, A Thess, R E Smalley *Science* **278** 100 (1997)
244. A M Afanas'ev, I P Suzdalev, M Ya Gen, V I Gol'danskii, V P Korneev, E A Manykin *Zh. Eksp. Teor. Fiz.* **58** 115 (1970) [m]
245. A P Amulyavichus, I P Suzdalev *Zh. Eksp. Teor. Fiz.* **64** 1702 (1973) [m]
246. Kh Ya Mulyukov, G F Korznikova, R Z Valiev *Phys. Status Solidi A* **125** 609 (1991)
247. R Sessoli, D Gatteschi, A Caneschi, M A Novak *Nature (London)* **365** 141 (1993)
248. J R Friedman, M P Sarachik, J Tejoda, R Ziolo *Phys. Rev. Lett.* **56** 3830 (1996)
249. A E Berkowitz *Phys. Rev. Lett.* **68** 3745 (1992)
250. J Q Xiao, J S Jiang, C L Chien *Phys. Rev. Lett.* **68** 3749 (1992)
251. C L Chien *Annu. Rev. Mater. Sci.* **25** 129 (1995)
252. H D Chopka, B J Hockey, P J Chew, W F Egelhoff Jr, M Wuttig, S Z Hua *Phys. Rev. B, Condens. Matter* **95** 8340 (1997)
253. S Jin, T H Tiefel, M McCormack, R A Fastnacht, R Ramesh, L H Chen *Science* **264** 413 (1994)
254. M Pissas, G Kallias, E Devlin, A Simopoulos, D Niarchos *J. Appl. Phys.* **81** 5770 (1997)
255. Z W Li, A H Morrish, X Z Zhou, S Dai *J. Appl. Phys.* **83** 7198 (1998)
256. A Simopoulos, G Kallias, E Delvin, I Pangiotopoulos, M Pissas *J. Magn. Magn. Mater.* **171**–**181** 860 (1998)
257. A Tkachuk, K Rogucki, D E Brown, B Dabrowski, A J Fedro, C W Kimball, B Pyles, X Xiong, D Rosemann *Phys. Rev. B, Condens. Matter* **57** 8509 (1998)
258. J W Lynn, R W Erwin, J A Borchers, Q Huang, A Santoro, J L Peng, Z Y Li *Phys. Rev. Lett.* **76** 4046 (1996)
259. S V Vonsovskii *Magnetizm* (Magnetism) (Moscow: Nauka, 1971)
260. Yu F Krupyanskii, I P Suzdalev *Zh. Eksp. Teor. Fiz.* **67** 736 (1974) [m]
261. I P Suzdalev, V N Buravtsev, V K Imshennik, Yu V Maksimov, V V Matveev, S V Novichikhin, A X Trautwein, H Winkler *Z. Phys. D, At. Mol. Clusters* **37** 55 (1996)
262. I P Suzdalev, A S Plachinda, V N Buravtsev, Yu V Maksimov, S I Reiman, V I Khromov, D A Dmitriev *Khim. Fiz.* **17** 145 (1998) [g]
263. I P Suzdalev, Yu V Maksimov, S V Novichikhin, V N Buravtsev, V K Imshennik, V V Matveev *Khim. Fiz.* **19** 105 (2000) [i]
264. C V Bean, D S Rodbell *Phys. Rev.* **126** 104 (1962)
265. W Kundig, H Bommel, G Constabaris, R H Lindquist *Phys. Rev.* **142** 327 (1966)
266. A M van der Kraan, L I van Loef *Phys. Lett.* **20** 614 (1966)
267. T Shinjo *J. Phys. Soc. Jpn.* **21** 917 (1966)
268. S H Bell, H P Meir, D P E Dickson, J P Gibson, G A Sharp, T V Peters *Biochim. Biophys. Acta* **787** 227 (1984)
269. I E Dzyaloshinskii *Zh. Eksp. Teor. Fiz.* **33** 1454 (1957) [m]
270. Yu V Krupyanskii, I P Suzdalev *Fiz. Tv. Tela* **17** 588 (1975) [f]
271. A M van der Kraan *Mössbaur Effect Studies of Superparamagnetic α-FeOOH and α-Fe_2O_3* (Meppel: Krips Repro, 1972)
272. G E R Schulze *MetallPhysik* (Berlin: Academie-Verlag, 1967)
273. D P Hirth, J Lothe *Theory of Dislocations* (New York: McGraw-Hill, 1970)
274. J P Hirth *Acta Metall.* **22** 1023 (1971)

[a] — *Physics-Uspekhi (Engl. Transl.)*
[b] — *Russ. Chem. Bull. (Engl. Transl.)*
[c] — *Moscow Univ. Bull. (Engl. Transl.)*
[d] — *Mendeleev Chem. J. (Engl. Transl.)*
[e] — *Colloid J. (Engl. Transl.)*
[f] — *Phys. Solid State (Engl. Transl.)*
[g] — *Dokl. Chem. Technol., Dokl. Chem. (Engl. Transl.)*
[h] — *Phys. Met. Metall. (Engl. Transl.)*
[i] — *Chem. Phys. Rep. (Engl. Transl.)*
[j] — *Russ. J. Phys. Chem. (Engl. Transl.)*
[k] — *Inorg. Mater. (Engl. Transl.)*
[l] — *Techn. Phys. Lett. (Engl. Transl.)*
[m] — *J. Exp. Theor. Phys. (Engl. Transl.)*

Russian Chemical Reviews **70** (3) 211 – 230 (2001) © 2001 Russian Academy of Sciences and Turpion Ltd

DOI 10.1070/RC2001v070n03ABEH000634

Nitrosonium complexes of organic compounds. Structure and reactivity

G I Borodkin, V G Shubin

Contents

I.	Introduction	211
II.	Complexes of the nitrosonium ion with alkanes	211
III.	Complexes of the nitrosonium ion with alkenes	212
IV.	Nitrosonium complexes of aromatic compounds	214
V.	Complexes of the nitrosonium ion with nitrogen-containing organic compounds	223
VI.	Complexes of the nitrosonium ion with organic compounds containing Group VI elements	225
VII.	Complexes of the nitrosonium ion with halogen-containing organic compounds	228

Abstract. Data on the structures and reactivities of nitrosonium complexes of organic compounds are systematised and generalised. The characteristic features of the electronic structure of the NO^+ cation are responsible for a wide structural variety of nitrosonium complexes. Reactions of nitrosonium complexes are described. The bibliography includes 172 references.

I. Introduction

Nitrosonium complexes of organic compounds have been extensively studied over many years. The continuing interest in these complexes stems from the fact that they are intermediates in a series of reactions, including nitrosation of aromatic compounds,[1] nitrosohalogenation of alkenes,[2–4] *etc*.[5] Recently, interest in these complexes has increased due to the discovery of the unique role of the NO molecule in biochemical processes.[6–15] It is assumed that the nitrosonium cation and some molecules generating the nitrosonium ion are involved in processes of neurotoxic and neuroprotective actions of nitric oxide[16,17] (*cf*. Refs 18–20)† and participate in cross-linking of DNA.[21,22]

Investigations of the structures and reactivities of nitrosonium complexes are essential to the understanding of the role of the NO^+ cation in various chemical processes (from ionospheric[23,24] to biochemical[9,16–19]) giving rise to different classes of organic compounds.

In the present review, the data on the structures and reactivities of nitrosonium complexes published over the last 10–15 years are analysed and systematised. The results of earlier studies are cited if they are necessary for an understanding of the problem and for elucidation of new trends in this area of exploration.

† Hereinafter, the reader is referred to studies, which are either indirectly associated with the problem under consideration or even contradictory.

G I Borodkin, V G Shubin N N Vorozhtsov Novosibirsk Institute of Organic Chemistry, Siberian Branch of the Russian Academy of Sciences, prosp. Akad. Lavrent'eva 9, 630090 Novosibirsk, Russian Federation.
Fax (7-383) 234 47 52. Tel. (7-383) 234 43 86.
E-mail: gibor@nioch.nsc.ru (G I Borodkin).
Tel. (7-383) 234 26 51. E-mail: vshubin@nioch.nsc.ru (V G Shubin)

Received 10 November 2000
Uspekhi Khimii **70** (3) 241 – 261 (2001); translated by T N Safonova

II. Complexes of the nitrosonium ion with alkanes

Electrophilic substitution in the aliphatic series of compounds lies at the basis of one of the procedures for the functionalisation of alkanes.[25–27] Weak electrophiles, in particular NO^+, can be involved in electrophilic aliphatic substitution reactions along with strong electrophiles, such as H^+ and Alk^+. Nitrosonium salts react with adamantane in the presence of HF, oxygen or nitriles to form 1-fluoroadamantane,[28] 1-nitroadamantane[29] or *N*-(1-adamantyl)amides,[30] respectively. Generally, it is assumed that the attack of the electrophile E^+ in electrophilic aliphatic substitution reactions occurs at the C–H bond to give intermediates of the type **1** characterised by the two-electron three-centre mode of bonding of the E, H and C atoms (3X-2e-intermediates)[25–27] (*cf*. Ref. 31).

$$HCR_3 + E^+ \longrightarrow \underset{\mathbf{1}}{\overset{E^+}{H\cdots CR_3}} \longrightarrow CR_3E + H^+$$

According to high-level *ab initio* calculations for the reactions of the NO^+ cation with methane and ethane,[32,33] the mechanism of the reactions of the nitrosonium cation with alkanes might differ from that described above. Thus, the NO^+ cation attacks the methane molecule at the carbon atom to form complex **2** whose precursor is unstable complex **3** [$\Delta H_0 = -15.5$ kJ mol^{-1}, where ΔH_0 is the relative energy of the complex taking into account the zero-point energy; the results of calculations by the MP4SDTQ/6-31 + G(dp)/MP2/6-31 + G(dp) + ZPVE//MP2/6-31 + G(dp) method]. An alternative path involving the attack of the NO^+ cation at the C–H bond is less favourable (by 60.2 kJ mol^{-1}).

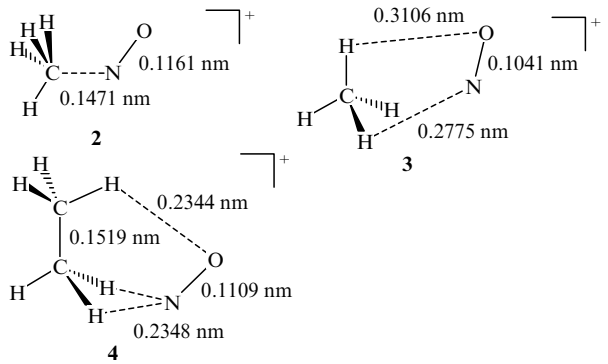

Analogously, unstable complex **4** {$\Delta H_0 = -16.7$ kJ mol^{-1}; calculations by the CISD + Q/TZP + //MP2/6-31G(dp) + ZPVE[MP2/6-31G(d)] method} is initially formed in the reaction with ethane. In the latter complex, the NO^+ cation is bound to the ethane molecules *via* polarisation and Coulomb interactions.[33] Subsequent conversions of this complex are shown in Scheme 1.

Scheme 1

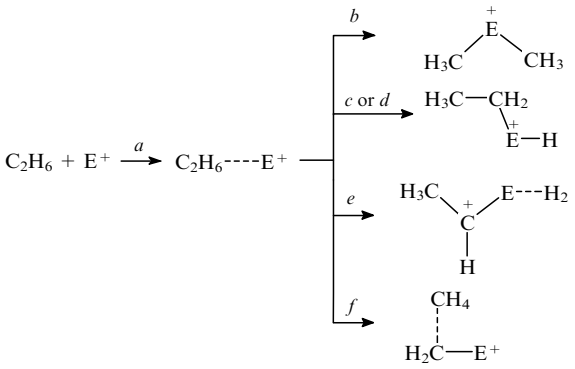

(*a*) $\Delta H_0 = -17.2$ kJ mol^{-1}; (*b*) insertion of E^+ at the C–C bond; $\Delta H_0 = -118.8$ kJ mol^{-1}; (*c*) insertion of E^+ at the C–H bond, $\Delta H_0 = -84.5$ kJ mol^{-1}; (*d*) elimination of H^-, addition of EH, $\Delta H_0 = -84.5$ kJ mol^{-1}; (*e*) elimination of H_2, $\Delta H_0 = 119.2$ kJ mol^{-1}; (*f*) elimination of CH_4, $\Delta H_0 = 39.7$ kJ mol^{-1}.

Although the attack of the NO^+ cation at the C–C bond is thermodynamically favourable (see Scheme 1), Schreiner *et al.*[33] believed that the attack on the C (to form a complex of the type **2**) and H atoms is kinetically more favourable. Elimination of the H_2 molecule is also unlikely because this path is thermodynamically unfavourable ($\Delta H_0 = 119.2$ kJ mol^{-1}). Attempts to isolate the transition states in these reactions failed. The activation barriers to elimination of methane and the hydride ion giving rise to nirosomethane and nirosoethane, respectively, have similar values (140.2 and 130.1 kJ mol^{-1}, respectively).

III. Complexes of the nitrosonium ion with alkenes

In a series of investigations, alkene–NO^+ complexes were proposed as intermediates of reactions of alkenes with nitrosyl halides[2–4] and $[NO]^+X^-$ salts (see Refs 34–37). These reactions are of importance in the synthesis of halonitroso- and halonitroorganic,[1–4,38] N,O-heterocyclic[34–36,39] and some other organic compounds.[37,40–42]

The energy profiles of fluoronitrosation of ethylenes were calculated by the MINDO/3 and UMINDO/3 quantum-chemical methods.[43] The facts that the NO^+ cation approaches the ethylene molecule at an angle to the symmetry plane of the latter and attacks the carbon atom to form σ-complex **5** are attributed to a strong $\pi_\sigma - \pi_\sigma$ interaction between the unoccupied e(π*)-MO of the NO^+ cation and HOMO of ethylene.

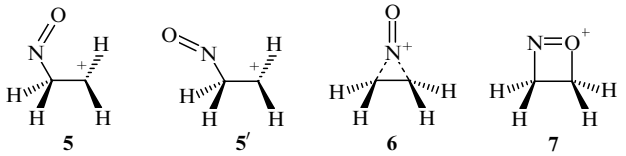

According to the results of MINDO/3 calculations, the isomeric form **5′** is less favourable than the structure **5** ($\Delta\Delta H_f = 22.2$ kJ mol^{-1}, where ΔH_f is the enthalpy of complex formation). The open cation **5** is rearranged into isomeric cyclic structures **6** and **7**, the activation energies (E_a) of these rearrangements being low ($E_a = 5.0$ and 14.2 kJ mol^{-1}, respectively). Among the structures **5**–**7**, the π-complex **6** is the most stable.

Ab initio calculations (the STO-3G basis set) predicted that the structure **7** should be the most stable.[43] Higher-level *ab initio* quantum-chemical calculations (MP4/6-31G + D) also provided evidence for higher stability of the structure **7** (Table 1).[44] In addition to the π-complex **6** in which the NO group is located in proximity to the ethylene fragment [the distance from the N atom to the C–C bond (*d*) is 0.1272 nm], more favourable (within the framework of the MP4 method) 'loose' π-complex **9** was found. In the latter, the distance *d* is substantially larger (0.1978 nm) and the NO group is located at an angle to the plane passing through the C, C and N atoms (Fig. 1, see Table 1).

Table 1. Relative energies (E_{rel} /kJ mol^{-1}) of the structures **7**–**10** obtained by *ab initio* quantum-chemical calculations.[44]

Structure	Basis set	E_{rel} [a] calculated by the method				
		HF	MP2	MP3	MP4	CCD + ST(4)
7	STO-3G	−335.6	–	–	–	–
	6-31G	−77.4	76.6	−36.8	43.1	–
	6-31G + D	−75.3	−16.3	−75.7	−33.1	–
8	STO-3G	−223.8	–	–	–	–
	6-31G	−89.1	31.0	−79.5	17.6	5.0
	6-31G + D	−35.1	−15.9	−60.7	−11.7	−13.8
9	STO-3G	−132.6	–	–	–	–
	6-31G	−65.7	−10.5	−76.1	−31.8	−38.1
	6-31G + D	−30.1	−41.4	−61.9	−49.4	−50.2
10	STO-3G	−139.7	–	–	–	–
	6-31G	−49.4	59.4	−27.2	22.2	13.4
	6-31G + D	5.4	33.1	−2.9	7.9	6.7

[a] The total energy of the C_2H_4 molecule and the NO^+ cation was taken equal to zero.

The σ-complex **10** is substantially less stable than the π-complexes **8** and **9** (see Table 1, Fig. 1). The C–N bond in the cation **10** is unusually long, which indicates that the C and N atoms are weakly bound together[44] (*cf.* Refs 37 and 43).

The structural and energy characteristics of the nitrosonium complexes with cyclobutadiene were calculated by the MINDO/3 and *ab initio* methods (the STO-3G basis set).[45] Qualitative analysis of orbital interactions revealed five structures with attractive interactions of the $\pi_\sigma - \pi_\sigma (p_\sigma - \pi_\sigma)$ type between the NO^+ cation and the ring. In the complexes **11** and **12**, the nitroso group is located parallel to the plane of the carbon ring above its centre and above one of the double bonds, respectively.

In the structures **13**–**15**, the NO group is perpendicular to the plane of the ring. Interactions between the orbitals of the nitroso group and the π orbitals of one of the double bonds occur in the isomers **13** and **15**, whereas interactions between the orbitals of the nitroso group and all π orbitals of the ring take place in the pyramidal structure **14**. The energy characteristics of the cations **11**–**13**, **15**, **17** and **18** are given in Table 2. According to calculations by the MINDO/3 method, the azapyrylium cation **18** is the most stable one in the above-mentioned series.

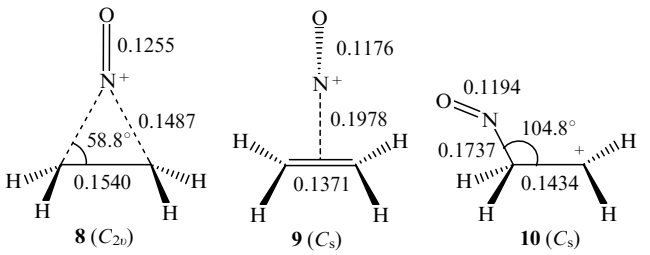

Figure 1. Geometric parameters of the π-complexes **8** and **9** and the σ-complex **10** obtained by *ab initio* calculations (the STO-3G basis set).[44] The bond lengths are expressed in nm; the symmetry is given in parentheses.

Table 2. Enthalpies of formation (ΔH_f), total energies (E_{tot}) and relative energies (E_{rel}) of the structures **11**–**13**, **15**, **17** and **18**.[45]

Parameter	**11**		**12**		**13**		**15**	**17**	**18**
	MINDO/3	STO-3G	MINDO/3	STO-3G	MINDO/3	STO-3G	MINDO/3		
ΔH_f /kJ mol^{-1}	1036.0	–	1016.3	–	1044.7	–	885.8	931.4	681.6
E_{tot} /a.u.[a]	–	−279.1292	–	−279.1439	–	−279.0593	–	–	–
E_{rel} /kJ mol^{-1}	354.4	38.6	334.7	0	363.1	222.1	204.2	249.8	0

[a] 1 a.u. = 2625.5 kJ mol^{-1}.

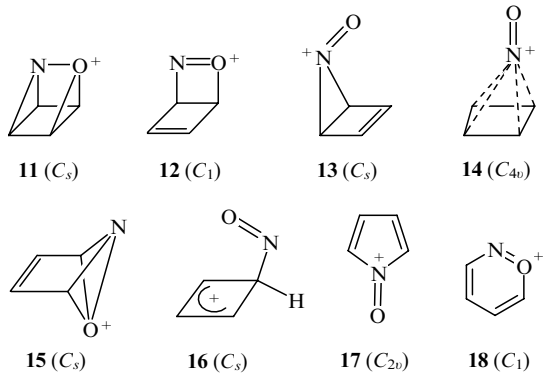

Ab initio calculations (the STO-3G basis set) for the structures **11**–**13** predicted the higher stability of the cation **12**. In the case of the pyramidal structure **14**, no minimum was found on the potential energy surface (PES).‡ The conversion of this structure into the structure **13** is barrierless, the latter being the only η^n structure ($n = 1-4$) corresponding to a local minimum. There is also no minimum on the potential energy surface corresponding to the σ-complex **16**. Minkin *et al.*[45] believe that attempts to generate the nitrosocyclobutenyl cation in the gas phase or in a weakly solvating solvent will fail.

Calculations by the MINDO/3 method for the structure **12** predicted that the nitroso group can either migrate parallel to the plane of the cyclobutadiene ring (Scheme 2, path *a*) or rotate about the C–O bond (Scheme 2, path *b*).[45]

Scheme 2

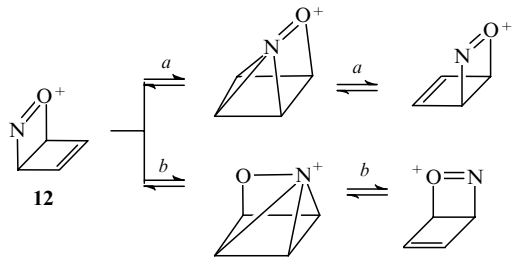

For the η^2-isomer **13**, the rotational-type rearrangement **13** ⇋ **13′** ⇋ **13″** with the low energy barrier (E_a = 46.9 kJ mol^{-1}) involving cation **16** as the transition state was revealed.[45]

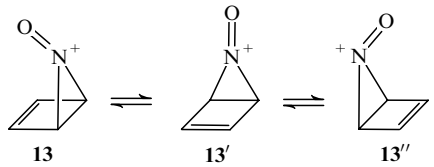

‡ *Ab initio* calculations taking into account the electron correlation (MP2/6-31G*+ZPE) also demonstrated that the structure **14** does not correspond to the minimum on the PES.[46]

It should be noted that the above-considered topomerisation reactions of the structures **12** (see Scheme 2) and **13** are, apparently, of only theoretical interest because these complexes are kinetically unstable and are converted into the structures **18** and **17**, respectively, with low energy barriers (E_a = 14.2 and 16.7 kJ mol^{-1}, respectively).[45]

Until recently, experimental data on π-complexes of alkenes with the nitrosonium cation were lacking in the literature. Attempts to synthesise complexes of this type by reactions of $[NO]^+[BF_4]^-$ with ethylene or 2,3-dimethylbut-2-ene failed. In the former case, the reaction did not proceed, whereas the latter reaction afforded exclusively polymeric products.[47] Olah *et al.*[47] believed that the reaction of $[NO]^+[BF_4]^-$ with adamantylideneadamantane gave rise to either a dynamical σ-complex or a π-complex. However, the authors failed to choose between these complexes. The first reliable data on the synthesis of an alkene–NO^+ complex were obtained in a study by Borodkin and coworkers.[48] According to the results of ^{1}H, ^{13}C and ^{27}Al NMR spectroscopy using the isotope perturbation method, the complex of 1,2,3,3,4,5,6,6-octamethylcyclohexa-1,4-diene with the NO^+ cation is a η^2-type π-complex (structure **19**).[48,49] It appeared that this complex underwent degenerate π,π-rearrangement **19** ⇋ **19′** (in the $SO_2-SO_2ClF-CD_2Cl_2$ system), rapid within the NMR time scale even at low temperature (−80 to −90 °C), the rate of intramolecular transfer of the NO^+ group being higher than the rate of intermolecular transfer.

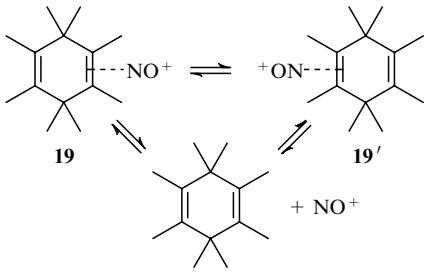

The rate of the intermolecular rearrangement increases on going from the $SO_2-SO_2ClF-CD_2Cl_2$ system to the $SO_2-CD_2Cl_2$ system.[48,49]

The results of quantum-chemical calculations for the nitrosonium complexes with cyclohexa-1,4-diene and 1,2,3,3,4,5,6,6-octamethylcyclohexa-1,4-diene by the MINDO/3 and MNDO/PM3 methods indicate that η^2-type π-complexes (**20** and **21**) are more stable than the corresponding σ-complexes (**22** and **23**) and η^4-type π-complexes (**24** and **25**)[48,49] through which intramolecular transfer of the nitroso group apparently proceeds.

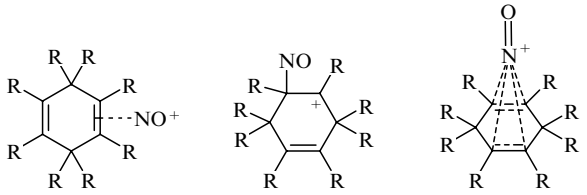

R = H (**20**, **22**, **24**), Me (**21**, **23**, **25**).

As mentioned above, *ab initio* calculations provided evidence for the existence of two types of ethylene complexes with the NO^+ cation (**8** and **9**). These complexes differ in geometry and, primarily, in the distance between the nitrogen atom and the C=C bond (d = 0.1272 and 0.1978 nm, respectively).[44] The structure of the nitrosonium complex with 2,3-dimethylbut-2-ene was analysed in detail by ^1H and ^{13}C NMR spectroscopy using the isotope perturbation method and by *ab initio* quantum-chemical (6-31G* basis set) and IGLO calculations.[50] As in the case of the ethylene–NO^+ isomers, the calculations predicted the existence of two types of complexes characterised by the symmetry C_{2v} (**26**) and the approximate symmetry C_s (**27**). In these complexes, the distances from the N atom to the C=C bond are 0.1225 and 0.2183 nm, respectively.

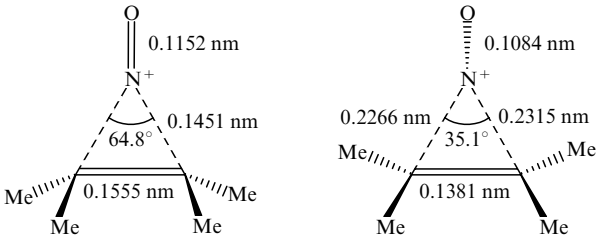

26 (C_{2v}) **27** ($\sim C_s$)

In the complexes **26** and **27**, the energies of binding of the nitrosonium cation with 2,3-dimethylbut-2-ene are 93.7 and 117.6 kJ mol^{-1}, respectively, which is indicative of higher stability of the complex **27**. The experimental chemical shifts of the C(2) and C(3) atoms (190.2 ppm) are substantially closer to those calculated by the IGLO(DZ) method for the complex **27** (δ_C 183.4 and 189.8, respectively) than to those for the complex **26** (δ_C 67.2). The equivalence of the C(2) and C(3) atoms and the equivalence of the carbon atoms of the methyl groups observed in the ^{13}C NMR spectrum of the complex **27** were attributed either to the inversion of the nitrogen atom or to the rotation of the NO group about the axis passing through the nitrogen atom perpendicular to the C(2)–C(3) bond as well as to the high rate of migration of this group.[50]

Complexes of different alkenes with the $[NO]^+[BF_4]^-$ and $[NO]^+[PF_6]^-$ salts and with other sources of the nitrosonium cation ($RONO-CF_3CO_2H$, $NOCl-CF_3CO_2H$ and $N_2O_4-SbF_5$) were investigated.[51] At low temperature, the electronic spectra of 2,3-dimethylbut-2-ene, 2,3,4-trimethylpent-2-ene and adamantylideneadamantane have charge-transfer bands. The reactions of other alkenes, such as 2,5-dimethylhex-2-ene, 2,4,4-trimethylpent-2-ene, 1-methylcyclohexene, cyclohexene, 2,3,3-trimethylbut-1-ene, norbornene, 3,3-dimethylbut-1-ene and hex-1-ene, with the above-mentioned salts either afforded slightly coloured solutions or did not give coloured solutions corresponding to the formation of charge-transfer complexes at all. These differences in the behaviour of alkenes containing the completely substituted C=C bond and those with the partially substituted C=C bond were attributed to the difference in the oxidation potentials (E_{ox}) of these alkenes.[51] Thus the oxidation potentials of 2,3-dimethylbut-2-ene and 2,3,4-trimethylpent-2-ene (E_{ox} = 1.6 V) are substantially smaller than those of 2-methylbut-2-ene and but-2-ene ($E_{ox} \approx$ 2.0 and 2.4 V, respectively). The thermal and photochemical behaviour of the alkene–NO^+ complexes is explained by the formation of charge-transfer complexes.

The photochemical activation of these complexes leads to generation of the corresponding radical cations. Thus irradiation of 2,3-dimethylbut-2-ene and N_2O_4 in a matrix at the frequency corresponding to the charge-transfer band (ν_{CT}) at 75 K afforded a pair of the type **28**.

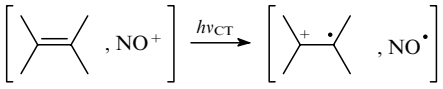

28

The subsequent reaction of the radical cation of 2,3-dimethylbut-2-ene with nitric oxide gave rise to the 1-nitroso-2,3-dimethylbut-2-yl cation, which reacted with the NO_3^- anion to form nitrosonitrate.[51,52]

The reaction of 1,2-bis(pentamethylphenyl)bicyclo[2.2.2]oct-2-ene (**29**) with the nitrosonium cation in CH_2Cl_2 at 25 °C afforded π-complex **30**. The characteristic feature of the latter complex is the fact that the NO group in this complex can interact with both the double bond and the aromatic rings (Scheme 3).[53]

Scheme 3

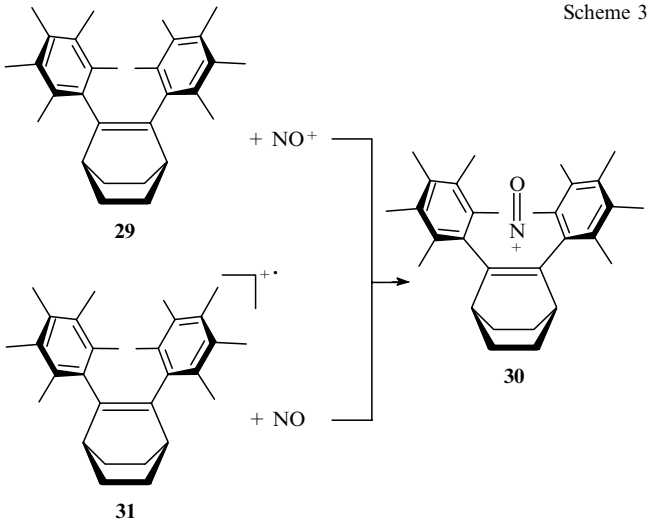

Electrochemical oxidation of the alkene **29** gave rise to the corresponding radical cation **31** whose reaction with gaseous nitric oxide afforded the same π-complex **30**[53] (*cf.* Ref. 54). X-Ray diffraction analysis of the π-complex **30** (with the $SbCl_6^-$ counterion) revealed the presence of noncovalent bonding of the NO^+ cation with the aromatic rings (the average distance to the plane of the rings is ~0.25 nm) and with the double bond, the positive charge being primarily localised at the aromatic and alkene carbon atoms, respectively.[53] The C(1)=C(2) bond length in the complex **30** (0.137 nm) is larger than that in the precursor **29** (0.133 nm) and is virtually identical to the above-mentioned C=C bond lengths in the complexes **9** and **27** determined by *ab initio* calculations. The strong bond between the NO^+ group and the unsaturated system in the complex **30** is consistent with its high formation constant ($> 3 \times 10^6$ litre mol^{-1}).[53]

IV. Nitrosonium complexes of aromatic compounds

Nitrosonium complexes of monocyclic aromatic compounds have been investigated in sufficient detail.[44,55–90] These complexes attract the attention of organic chemists primarily because they are analogues of intermediates of such important reactions as diazotisation, C-nitrosation and nitration proceeding through nitrosation of aromatic compounds[1,90–95] (*cf.* Ref. 96). In addition, it is known that the NO^+ cation catalyses bromination of aniline derivatives[97] and proton exchange in the *N*,*N*-dimethylanilinium ion,[98] which was assigned to the formation of the corresponding arene–NO^+ complexes.

The nitrosation of benzene was investigated by quantum-chemical methods.[70] Thus, the pathway of electrophilic replacement of the hydrogen atom in the benzene ring by the NO^+ cation was calculated by the MINDO/3 method. Initially, the electron is transferred from the frontier orbital of the benzene molecule to the π* orbital of the nitrosonium cation to form π-complexes **32** and **33**. The enthalpies of their formation are 1017.1 and 959.0 kJ mol^{-1}, respectively.

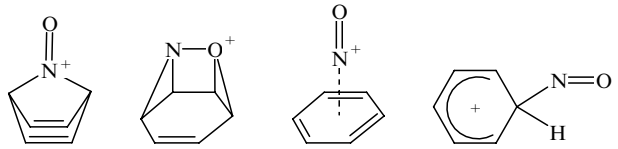

32 (C_{2v}) **33** (C_1) **34** (C_{6v}) **35** (C_s)

According to the rule of electron counting for pyramidal structures,[99–101] the π-complex **34** with the symmetry C_{6v} is unstable (ΔH_f = 1031.8 kJ mol^{-1}) and corresponds to a peak top on the potential energy surface. A shallow minimum on the PES (8.4 kJ mol^{-1}) corresponds to the structure of σ-complex **35** (ΔH_f = 928.8 kJ mol^{-1}), which indicates that it is not detectable experimentally.

Calculations for the π-complexes **32** and **33** provided evidence for the occurrence of a sixfold-degenerate rearrangement with a low energy barrier (E_a < 12.6 kJ mol^{-1}) caused by 'switching' of the C–N bond in the complex **32** and migration of the nitroso group over the plane of the ring in the structure **33**:

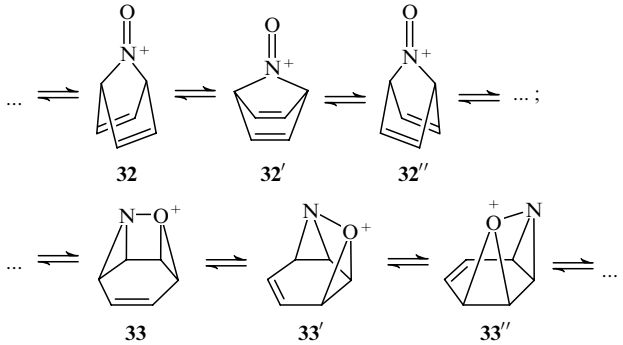

32 **32′** **32″**

33 **33′** **33″**

The $\Delta\Delta H_f$ value (relative to the C_6H_6–NO^+ system) found by higher-level quantum-chemical calculations (*ab initio*, MP2/6-31G+D)[44] for the centrosymmetrical structure **34** is −189.1 kJ mol^{-1}, which is close to the experimental value for the gas phase (−172±21 kJ mol^{-1}).[44,64] The corresponding σ-complex is substantially less stable ($\Delta\Delta H_f$ = −23.4 kJ mol^{-1}).

Ab initio B3LYP/6-31G(d) calculations revealed stable π-complex **36** with the symmetry C_1. The energy of its formation from benzene and the NO^+ cation is −220.5 kJ mol^{-1}.[89] In addition, the calculations gave local minima for the π-complexes **32** and **33** whose relative energies are 163 and 201 kJ mol^{-1}, respectively, smaller than that in the case of the π-complex **36**.

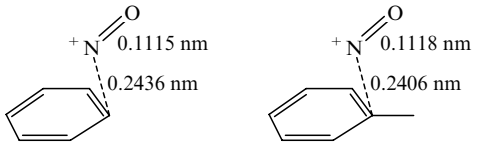

36 **37**

According to the results of quantum-chemical calculations, the π-complex of toluene with the NO^+ cation (**37**) is more stable than the π-complex **36** (ΔE_{rel} = 17.6 kJ mol^{-1}). The stretching vibration frequency of the NO group calculated for the complex **37** (2087 cm^{-1}) is smaller than that for the complex **36** (2110 cm^{-1}), which is indicative of a higher degree of electron density transfer from the aromatic ring to the NO group in the cation of the complex **37**.[89]

The first experimental data on the formation of ArH–NO^+ π-complexes were obtained by electronic spectroscopy of nitrosonium complexes of benzene and its derivatives.[58,59] Shortly thereafter, π-complexes of the NO^+ cation with benzene derivatives were investigated by Allan *et al.*[60,61] More recently, NMR spectroscopy along with electronic and IR spectroscopy were employed for studying cationic π-complexes. The available spectral data for the nitrosonium π-complexes of benzene and its derivatives are summarised in Tables 3–5. The formation of π-complexes leads to characteristic changes, in particular, to downfield shifts of the signals in the ^{1}H and ^{13}C NMR spectra (see Tables 3 and 4, respectively), to the appearance of charge-transfer bands in the electronic spectra and to a decrease in the stretching vibration frequency of the NO group in the complexes compared to those in $[NO]^+X^-$ salts (see Table 5). Apparently, all the above-mentioned changes are caused by the electron density transfer from the aromatic moiety of the complex to the nitroso group.

Table 3. ^{1}H NMR spectral data for the π-complexes of benzene and its derivatives with the nitrosonium cation (the molar ratio ArH : $[NO]^+X^-$ = 1 : 1).

Compound	Salt	Solvent	Chemical shifts (δ_H) [a]		Ref.
			CH_3	H_{arom}	
Benzene	$NOAlCl_4$	SO_2		8.03 (0.62)	72
	$NOGaCl_4$	SO_2		7.75 (0.34)	72
	$NOHSO_4$	H_2SO_4		7.89	64
	see [b]	see [c]		7.49 (0.11)	78
	$NOPF_6$	SO_2		> 7.34	73
	$NOSbCl_6$	SO_2		7.81	73
	$NOTiCl_4$	SO_2		7.60 (0.19)	72
Toluene	$NOAlCl_4$	SO_2	2.67 (0.37)	7.92 (0.72)	72
	see [b]	see [c]	2.52 (0.14)	7.57 (0.31)	78
	$NOPF_6$	SO_2	2.42 (0.12)	7.38, 7.45	73
	$NOSbCl_6$	SO_2	2.78 (0.48)	8.05 (0.85)	73
	$NOSbCl_6$ (see [d])	SO_2	2.47 (0.17)	7.46 (0.26)	73
	$(NO)_2SnCl_4F_2$	SO_2	2.56 (0.26)	7.65, 7.74	72
	$NOTaCl_6$	SO_2	2.57	7.70–7.82	74
p-Xylene	$NOAlCl_4$	SO_2	2.63 (0.35)	7.81 (0.70)	72
	$NONbCl_6$	SO_2	2.57	7.67	74
	$NONbF_6$	SO_2	2.45	7.43	74
	$NOPF_6$	SO_2	2.55 (0.27)	7.63 (0.52)	73
	$NOSbCl_6$	SO_2	2.58 (0.30)	7.67 (0.56)	73
	$(NO)_2SnCl_4F_2$	SO_2	2.67 (0.39)	7.83 (0.72)	72
	$NOTaCl_6$	SO_2	2.44	7.40	74
	$NOTiCl_6$	SO_2	2.38 (0.10)	7.30 (0.19)	72

Table 3 (continued).

Compound	Salt	Solvent	Chemical shifts (δ_H) [a]		Ref.
			CH_3	H_{arom}	
Mesitylene	$NOAlCl_4$	SO_2	2.58 (0.35)	7.58 (0.77)	72
	see [b]	see [c]	2.52 (0.24)	7.49 (0.66)	78
	$NONbCl_6$	SO_2	2.52	7.44	74
	$NONbF_6$	SO_2	2.41	7.18	74
	$NOPF_6$	SO_2	2.52 (0.29)	7.45 (0.64)	73
	$NOPF_6$	CD_3NO_2	2.51	7.50	76
	$(NO)_2SnCl_6$	SO_2	2.42 (0.19)	7.21 (0.40)	72
	$(NO)_2SnCl_4F_2$	SO_2	2.60 (0.37)	7.57 (0.76)	72
	$NOTaCl_6$	SO_2	2.58	7.57	74
	$NOTaF_6$	SO_2	2.51	7.40	74
Durene	see [b]	see [c]	2.48 (0.30)	7.67 (0.78)	78
	$NOPF_6$	CD_3NO_2 (see [e])	2.37 (0.19)	7.42 (0.54)	62
	$NOPF_6$	CD_3NO_2	2.43	7.56	76
tert-Butylbenzene	$NOSbl_6$	SO_2	1.47 (0.17)	7.89, 7.96, 8.05	73
Pentamethylbenzene	see [b]	see [c]	2.44 (0.28), 2.46 (0.26)	7.66 (0.87)	78
	$NOPF_6$	CD_3NO_2 (see [e])	2.38 (0.20), 2.44 (0.23)	7.52 (0.71)	62
	$NOPF_6$ (see [d])	CD_3NO_2 (see [e])	2.27 (0.09), 2.31 (0.10)	7.1 (0.29)	62
	$NOPF_6$	CD_3NO_2	2.44, 2.51	7.66	76
Hexamethylbenzene	$NOAlCl_4$	SO_2	2.48 (0.33)		72
	$NOAsF_6$	SO_2	2.39 (0.24)		73
	$NOBF_4$	SO_2	2.42 (0.27)		72
	$(NO)_2GeCl_2F_4$	SO_2	2.45 (0.30)		72
	$(NO)_2GeF_6$	SO_2	2.32 (0.17)		72
	$NOMoCl_6$	SO_2	2.21		74
	$NOMoF_6$	SO_2	2.40		74
	$NOMo_2O_2F_9$	SO_2	2.46		74
	$NONbCl_6$	SO_2	2.49		74
	$NONbF_6$	SO_2	2.46		74
	$NOPF_6$	SO_2	2.47 (0.32)		73
	$NOPF_6$	CD_3CN	2.48 (0.30)		78
	$NOPF_6$	CD_3CN	2.48		76
	$NOSbCl_6$	SO_2	2.47 (0.32)		73
	$NOSbF_6$	SO_2	2.48 (0.33)		73
	$(NO)_2SiF_6$	SO_2	2.42 (0.27)		72
	$(NO)_2SnCl_6$	SO_2	2.49 (0.34)		72
	$(NO)_2SnCl_4F_2$	SO_2	2.50 (0.35)		72
	$NOTaCl_6$	SO_2	2.48		74
	$NOTaF_6$	SO_2	2.47		74
	$(NO)_2TiCl_6$	SO_2	2.50 (0.35)		72
	$(NO)_2TiF_6$	SO_2	2.48 (0.33)		72
	$NOUF_6$	SO_2	2.34		74
	$NOUF_7$	SO_2	2.47		74
	$NOWCl_7$	SO_2	2.46		74
	$NOW_2O_2F_9$	SO_2	2.42		74
Chlorobenzene	$NOGaCl_4$	SO_2		7.38	72

[a] The differences between the chemical shifts of the signals for the protons in the spectra of the π-complex and its precursor are given in parentheses. [b] Either $NOBF_4$ or $NOPF_6$ was used as the salt. [c] Either CD_3CN or CD_3NO_2 was used as the solvent. [d] The ArH : $[NO]^+X^-$ molar ratio was 2 : 1. [e] The reaction temperature was 35 °C; in all other cases, the temperature was not reported.

Table 4. ^{13}C NMR spectral data for the π-complexes of benzene and its derivatives with the nitrosonium cation (the molar ratio ArH : $[NO]^+X^-$ = 1 : 1).

Compound	Salt	Solvent	Chemical shifts (δ_C) [a]		Ref.
			CH_3	C_{arom}	
Benzene	$NOAlCl_4$	SO_2		137.1 (7.9)	72
	see [b]	see [c]		131.0 (1.2)	78
	$NOGaCl_4$	SO_2		134.8 (5.6)	72
	$NOPF_6$	SO_2		> 129.1	73
	$NOTiCl_4$	SO_2		132.2 (3.0)	72
	$NOSbCl_6$	SO_2		136.7 (7.5)	73

Table 4 (continued).

Compound	Salt	Solvent	Chemical shifts (δ_C) [a]		Ref.
			CH_3	C_{arom}	
Toluene	see [b]	see [c]	21.7 (0)	132.5 (4.8), 135.1 (5.1), 136.1 (5.7), 147.6 (8.0)	78
	$NOPF_6$	SO_2	20.9 (0.1)	128.4, 131.3, 132.1, 142.0	73
	$NOSbCl_6$ (see [d])	SO_2	20.8	129.8, 132.6, 133.2, 144.3	73
	$(NO)_2SnCl_4F_2$	SO_2	21.3 (0.5)	132.6, 135.1, 136.0	72
	$NOTaCl_6$	SO_2	21.4	133.7, 136.1, 137.0, 149.3	74
p-Xylene	$NOPF_6$	SO_2	20.7	137.6, 147.6	73
	$NONbF_6$	SO_2	20.6	135.0 [e]	74
	$NOSbCl_6$	SO_2	20.8	137.8, 148.0	73
	$(NO)_2SnCl_4F_2$	SO_2	21.1	139.9, 151.1	72
	$NOTaF_6$	SO_2	20.6	134.3, 142.5	74
Mesitylene	$NOAlCl_4$	SO_2	see [f]	139.1 [e]	72
	see [b]	see [c]	21.6 (0.1)	137.8 (9.6), 151.8 (12.5)	78
	$NOPF_6$	SO_2	20.9	137.1, 151.1	73
	$NONbF_6$	SO_2	20.7	132.9, 145.5	74
	$NOTaCl_6$	SO_2	21.2	138.9, 153.4	74
	$NOTaF_6$	SO_2	20.9	136.1, 149.8	74
	$(NO)_2TiCl_6$	SO_2	20.9	135.2 (4.7) [e]	72
Durene	$NOAlCl_4$	CH_2Cl_2 (see [g])	19.8	142.0, 150.3	71
	see [b]	see [c]	19.7 (0.4)	142.9 (10.6), 151.3 (16.2),	78
	$NOAlCl_4$	see [g, h]	20.1	148.3, 154.5	71
tert-Butylbenzene	$NOSbCl_6$	SO_2	30.5, 36.5	134.3, 134.8, 136.9, 163.5	73
Pentamethylbenzene	see [b]	see [c]	21.1 (0.3), 17.3 (0.9), 16.9 (0.8)	141.5 (11.3), 151.0 (17.4), 151.5 (17.0), 152.8 (16.7)	78
Hexamethylbenzene	$NOAlCl_4$	CH_2Cl_2 (see [g])	17.5	147.7	71
	$NOAlCl_4$	SO_2	17.3 (1.6)	149.9 (18.9)	72
	$NOAlCl_4$	see [g, h]	18.6	142.1	71
	$NOAsF_6$	SO_2	17.1 (1.4)	149.1 (18.1)	73
	$(NO)_2GeF_6$	SO_2	16.7 (1.0)	142.1 (11.1)	72
	$NOMoCl_6$	SO_2	16.5	131.7	74
	$NOMoF_6$	SO_2	17.1 (1.4)	147.9 (16.9)	74
	$NOMo_2O_2F_9$	SO_2	17.1 (1.4)	148.6 (17.6)	74
	$NONbF_6$	SO_2	17.1 (1.4)	148.1 (17.1)	74
	$NOPF_6$	SO_2	17.1 (1.4)	149.8 (18.8)	73
	$NOPF_6$	CD_3NO_2	17.9 (0.9)	150.8 (17.6)	78
	$NOSbCl_6$	SO_2	18.2 (2.5)	150.2 (19.2)	73
	$NOSbCl_6$	see [h]	20.5	151.9	78
	$NOSbF_6$	SO_2	17.1 (1.4)	150.1 (19.1)	73
	$(NO)_2SiF_6$	SO_2	16.9 (1.2)	144.6 (13.6)	72
	$(NO)_2SnCl_4F_2$	SO_2	17.3 (1.6)	150.2 (19.2)	72
	$NOTaCl_6$	SO_2	17.5 (1.8)	150.3 (19.3)	74
	$NOTaF_6$	SO_2	17.2 (1.5)	149.8 (18.8)	74
	$(NO)_2TiCl_6$	SO_2	17.3 (1.6)	150.2 (19.2)	72
	$(NO)_2TiF_6$	SO_2	17.1 (1.4)	148.8 (17.8)	72
	$NOUF_6$	SO_2	17.2 (1.5)	143.7 (12.7)	74
	$NOUF_7$	SO_2	17.3 (1.6)	149.5 (18.5)	74
	$NOWCl_7$	SO_2	17.7 (2.0)	150.5 (19.5)	74
	$NOW_2O_2F_9$	SO_2	17.4 (1.7)	146.9 (15.9)	74

[a] The differences between the chemical shifts of the signals for the carbon atoms in the spectra of the π-complex and its precursor are given in parentheses. [b] Either $NOBF_4$ or $NOPF_6$ was used as the salt. [c] Either CD_3CN or CD_3NO_2 was used as the solvent. [d] The $ArH : [NO]^+X^-$ molar ratio was 2 : 1. [e] The chemical shift is given only for the CH fragment. [f] The chemical shift was not reported. [g] The reaction temperature was 20 °C; in all other cases, the temperature was not reported. [h] For the crystalline form.

Table 5. Data from IR (ν_{NO}) and electronic absorption spectroscopy (λ_{max}) of the π-complexes of benzene and its derivatives with the nitrosonium cation (the molar ratio $ArH : [NO]^+X^- = 1 : 1$).

Compound	Reagent	Solvent	ν_{NO} /cm^{-1}	λ_{max} /nm (ε)	Ref.
Benzene	$NOAlCl_4$	CH_2Cl_2	–	335	72
	$NOHSO_4$	H_2SO_4	–	332 (18 000)	64
	$NOBF_4$	MeCN	–	346 (780), 460 (60)	76, 78
	$NOGaCl_4$	CH_2Cl_2	–	335	72

Table 5 (continued).

Compound	Reagent	Solvent	ν_{NO} /cm^{-1}	λ_{max} /nm (ε)	Ref.
Benzene	$NOPF_6$	$MeNO_2$	2075	–	78
	$NOSbCl_6$	–	–	344	73
Toluene	$NOAlCl_4$	CH_2Cl_2	–	338 (11 000)	72
	$NOBF_4$	MeCN	–	342 (400)	76, 78
	$NOPF_6$	$MeNO_2$	2037	–	78
	$NOSbCl_6$	$MeNO_2$	2030	–	78
Toluene	$NOSbCl_6$	–	–	340 (10 600)	73
	$NOSbCl_6$	–	–	340 (5300) [a]	73
o-Xylene	$NOBF_4$	MeCN	–	338 (2200), 500 (180)	78
	$NOPF_6$	$MeNO_2$	2000	–	78
p-Xylene	$NOAlCl_4$	CH_2Cl_2	–	340	72
	$NOBF_4$	MeCN	–	336 (1300), 520 (81)	78
	$NOBF_4$	CH_2Cl_2	–	496 [b]	83
	N_2O_4	CH_2Cl_2	1964 [c]	–	83
	$N_2O_4(SbCl_6)$	CH_2Cl_2	–	506 [b]	83
	$NOPF_6$	$MeNO_2$	1998	–	78
	$NONbF_6$	see [d]	1810	–	74
	$NOTaF_6$	see [d]	1810	–	74
	$NOTaF_6$	CH_2Cl_2	–	274, 446	74
	$NOSbCl_6$	CH_2Cl_2	–	340 (10 000)	73
Mesitylene	$NOAlCl_4$	CH_2Cl_2	–	343	72
	$NOBF_4$	MeCN	–	345 (2080)	76
	$NOBF_4$	MeCN	–	345 (2100)	78
	$NOBF_4$	$MeNO_2$	2000 – 1950	–	62
	$NOBF_4$	CH_2Cl_2	–	486 [b]	83
	N_2O_4	CH_2Cl_2	1948 [c]	–	83
	$N_2O_4(SbCl_6)$	see [e]	1954	–	83
	$N_2O_4(SbCl_6)$	CH_2Cl_2	–	493 [b]	83
	$NONbF_6$	CH_2Cl_2	–	386	74
	$NOPF_6$	CH_2Cl_2	1967	335	76
	$NOPF_6$	$MeNO_2$	1975	–	78
	$NOPF_6$	see [f]	2016	–	76
	$NOSbCl_6$	$MeNO_2$	1964	–	78
	$(NO)_2SiF_6$	CH_2Cl_2	–	390	72
	$(NO)_2SnCl_4F_2$	CH_2Cl_2	–	391	72
	$NOTaF_6$	CH_2Cl_2	–	388	74
	$(NO)_2TiCl_6$	CH_2Cl_2	–	285	72
tert-Butylbenzene	$NOBF_4$	MeCN	–	340 (270), 460 (52)	78
	$NOSbCl_6$	–	–	339 (5000)	73
	$(NO)_2SnCl_6$	CH_2Cl_2	–	360	72
1,3,5-Tri-*tert*-butylbenzene	$NOBF_4$	MeCN	–	349 (1730)	76
	$NOBF_4$	MeCN	–	349 (1700)	78
	$NOPF_6$	$MeNO_2$	1964	–	78
Durene	$NOBF_4$	MeCN	–	336 (1100), 520 (40)	78
	$NOBF_4$	CH_2Cl_2	–	486 [b]	83
	N_2O_4	CH_2Cl_2	1948 [c]	–	83
	$N_2O_4(SbCl_6)$	see [e]	1880	–	83
	$N_2O_4(SbCl_6)$	CH_2Cl_2	–	489 [b]	83
	$NOPF_6$	$MeNO_2$	1933	–	62, 78
	$NOPF_6$	CH_2Cl_2	1929	335, ~500	76
	$NOPF_6$	MeCN	1930	–	62
	$NOPF_6$	$MeNO_2$	1930	–	62
	$NOPF_6$	MeCN or $MeNO_2$	–	335	62
	$NOPF_6$	see [f]	1986	–	76
Pentamethylbenzene	$NOBF_4$	MeCN	–	337 (2400)	76, 78
	$NOBF_4$	CH_2Cl_2	–	491 [b]	83
	N_2O_4	CH_2Cl_2	1896 [c]	–	83
	$N_2O_4(SbCl_6)$	CH_2Cl_2	–	490 [b]	83
	$NOPF_6$	MeCN or $MeNO_2$	–	340	62
	$NOPF_6$	CH_2Cl_2	1904	–	76
	$NOPF_6$	MeCN	1900	–	62
	$NOPF_6$	$MeNO_2$	1900	–	62
	$NOPF_6$	$MeNO_2$	1907	–	78
	$NOPF_6$	see [f]	1927	–	76

Table 5 (continued).

Compound	Reagent	Solvent	ν_{NO} /cm^{-1}	λ_{max} /nm (ε)	Ref.
Hexamethylbenzene	$NOAlCl_4$	see [d]	1853	–	71
	$NOAlCl_4$	CH_2Cl_2	–	334 (10 000)	72
	$NOAsF_6$	–	–	334 (47 000)	73
	$NOBF_4$	MeCN	–	337 (3000)	76
	$NOBF_4$	MeCN	–	337 (3100)	78
	$NOBF_4$	CH_2Cl_2	–	325 (7300), 499 [b]	72, 83
	$(NO)_2GeF_6$	CH_2Cl_2	–	338 (7100)	72
	$NOFeCl_4$	CH_2Cl_2	–	325, 360	74
	$NOMo_2O_2F_9$	CH_2Cl_2	–	323	74
	$NOMo_2O_2F_9$	see [d]	1870	–	74
	$NOMoF_6$	see [d]	1780	–	74
	N_2O_4	CH_2Cl_2	1862 [c]	495 [b]	83
	$N_2O_4(SbCl_6)$	see [e]	1850	–	83
	$N_2O_4(SbCl_6)$	CH_2Cl_2	–	499 [b]	83
	$NOPF_6$	CH_2Cl_2	1880	337, ~500	76
	$NOPF_6$	–	–	275 [g]	73
	$NOPF_6$	$MeNO_2$	1885	–	78
	$NOPF_6$	see [f]	1899	–	76
	$NONbF_6$	see [d]	1850	–	74
	$NONbF_6$	CH_2Cl_2	–	330	74
	$NOSbCl_6$	see [d]	1849	–	73
	$NOSbCl_6$	–	–	334 (8100)	73
	$NOSbCl_6$	$MeNO_2$	1885	–	78
	$NOSbF_6$	see [d]	1850	–	73
	$NOSbF_6$	CH_2Cl_2	–	330	55
	$NOSbF_6$	–	–	272	73
	$(NO)_2SiF_6$	CH_2Cl_2	–	338	72
	$(NO)_2SnCl_6$	CH_2Cl_2	–	336	72
	$(NO)_2SnCl_4F_2$	CH_2Cl_2	–	336	72
	$NOTaCl_6$	CH_2Cl_2	–	332	74
	$NOTaF_6$	see [d]	1800	–	74
	$NOTaF_6$	CH_2Cl_2	–	334	74
	$NOTiCl_6$	CH_2Cl_2	–	310	72
	$(NO)_2TiCl_4F_2$	CH_2Cl_2	–	340	72
	$(NO)_2TiF_6$	CH_2Cl_2	–	326	72
	$NOUF_6$	see [d]	1880	–	74
	$NOUF_6$	CH_2Cl_2	–	320	74
	$NOUF_7$	see [d]	1870	–	74
	$NOUF_7$	CH_2Cl_2	–	325	74
	$NOWCl_7$	CH_2Cl_2	–	358	74
	$NOW_2O_2F_9$	see [d]	1878	–	74
Hexaethylbenzene	$NOBF_4$	CH_2Cl_2	–	511 [b]	83
	$NOPF_6$	$MeNO_2$	1900	–	78
	N_2O_4	CH_2Cl_2	–	516 [b]	83
1,3-Dineopentyl-2,4,5,6-tetramethylbenzene	$NOPF_6$	$MeNO_2$	1884	–	78
1,4-Dineopentyl-2,3,5,6-tetramethylbenzene	$NOPF_6$	$MeNO_2$	1884	–	78
Anisole	$NOBF_4$	MeCN	–	344 (1000), 480 (635) [h]	84
Chlorobenzene	$NOBF_4$	MeCN	–	343 (110), 500 (6.4)	78
	$NOGaCl_4$	CH_2Cl_2	–	290 [g]	72
2-Methylanisole	$NOBF_4$	MeCN	–	346, 477 [h]	84
4-Methylanisole	$NOBF_4$	MeCN	–	346 (980), 506 (370) [h]	84
	$NOBF_4$	CH_2Cl_2	–	334	78
3,5-Dimethylanisole	$NOBF_4$	MeCN	–	355, 488 [h]	84
2-Bromoanisole	$NOBF_4$	MeCN	–	353, 463 [h]	84
4-Bromoanisole	$NOBF_4$	MeCN	–	340 (470), 500 (100) [h]	84
1,4-Dimethoxybenzene	$NOBF_4$	CH_2Cl_2	–	366 [c]	85

[a] The ArH : $[NO]^+X^-$ molar ratio was 2 : 1. [b] The λ_{max} value is given only for the long-wavelength band (at −78 °C). [c] At −78 °C. [d] In KBr pellets. [e] Mineral oil mull. [f] Spectra of the crystalline form. [g] Shoulder. [h] At −40 °C.

The degree of electron density transfer can be estimated from ^{13}C NMR spectral data. It is known that the chemical shifts of the sp^2-hybridised carbon atoms in charged π-electron systems correlate linearly with the π-charges on these atoms.[102, 103] Assuming that the degree of electron density transfer to the nitroso group in the π-complex depends on the ionisation potential of the aromatic substrate (I_p), one would expect a relationship between the positive π-charges (q_π^+) and the ionisation potentials of the aromatic donor.[78] Actually, a linear correlation between these characteristics takes place in the case of the nitrosonium π-complexes of benzene and alkylbenzenes [78] (Fig. 2) from which it can be seen that an increase in the donating ability of the aromatic substrate leads to an increase in the degree of charge transfer.

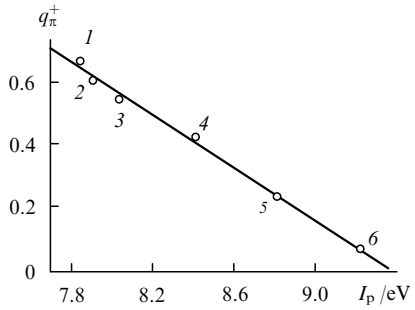

Figure 2. Correlation between the positive π-charges (q_π^+) on the aromatic fragments in the nitrosonium complexes with benzene and alkylbenzenes and the ionisation potentials (I_p) of the aromatic donors:[78] (*1*) hexamethylbenzene, (*2*) pentamethylbenzene, (*3*) durene, (*4*) mesitylene, (*5*) toluene, (*6*) benzene ($r = -0.998$). The q_π^+ values were calculated using the differences between the chemical shifts of the complexes and their precursors determined in the study;[78] the value of 160 ppm was taken per unit π-charge.

It was demonstrated[78] that the degree of charge transfer in π-complexes can be estimated by IR spectroscopy. Thus a linear correlation between the ionisation potentials of the aromatic substrate and the degree of charge transfer (Z) was found for benzene and its derivatives. The degree of charge transfer was determined from the following formula:

$$Z = (\nu_{NO^+}^2 - \nu_\pi^2)/(\nu_{NO^+}^2 - \nu_{NO}^2),$$

where ν_{NO^+}, ν_π and ν_{NO} are stretching vibration frequencies of the NO group in the NO^+ cation, the π-complex and nitric oxide, respectively (Fig. 3).[78]

X-Ray diffraction studies provide the most reliable information on the structures of cationic complexes. The first data on the structures of nitrosonium complexes of aromatic compounds obtained[68,69] for the complex of hexamethylbenzene with the NO^+ cation disclosed that the conventional view (*cf.* Refs 61 and 64) that π-complexes of aromatic compounds with electrophilic agents are highly symmetrical systems should be revised.[104] According to the X-ray diffraction data,[68,71] the normal (which passes through the nitrogen atom of the NO group) to the plane of the core of this complex is displaced from the centre of the aromatic ring and the nitroso group is located at an angle of ~50° (the structure **38**), the nitrogen atom being rather far removed from the ring (by 0.21 nm).

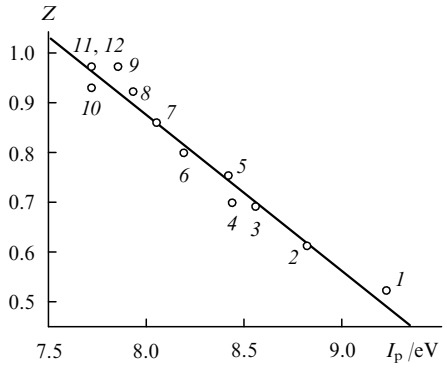

Figure 3. Correlation between the degree of electron transfer (Z) in nitrosonium complexes with benzene and alkylbenzenes and the ionisation potentials (I_p) of the aromatic donors: (*1*) benzene, (*2*) toluene, (*3*) 1,2-dimethylbenzene, (*4*) 1,4-dimethylbenzene, (*5*) 1,3,5-trimethylbenzene, (*6*) 1,3,5-tri(*tert*-butyl)benzene, (*7*) 1,2,4,5-tetramethylbenzene, (*8*) pentamethylbenzene, (*9*) hexamethylbenzene, (*10*) hexaethylbenzene, (*11*) 1,4-di(neopentyl)-2,4,5,6-tetramethylbenzene, (*12*) 1,3-di(neopentyl)-2,3,5,6-tetramethylbenzene ($r = -0.987$).[78]

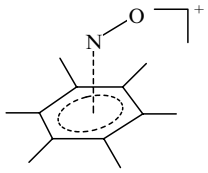

38

The nitrosonium complexes of toluene,[73] mesitylene,[78] durene,[71] hexaethylbenzene,[88] 2,3-dimethyl-2,3-diphenylbutane,[81] 1,2,3,4,5,6,7,8,9,10,11,12-dodecahydro-1,4;5,8;9,12-triethanotriphenylene[88] and octamethyl-9,10-dihydro-9,10-ethanoanthracene[105] have analogous structures. A comparison of the structures and geometric parameters of nitrosonium complexes of arenes and alkenes disclosed that these complexes are somewhat similar, *viz.*, the NO group is located at an angle to the plane of the core and the distances from the nitrogen atom to this plane have close values.

According to the results of CNDO/2 calculations with the use of the real geometry of the hexamethylbenzene complex with the nitrosonium cation, the positive charges on the aromatic carbon atoms of the same type differ substantially from those on the carbon atoms of the methyl groups.[71] Nevertheless, two rather narrow singlets are observed in the ^{13}C NMR spectra recorded both for solutions (in the HSO_3F-SO_2ClF mixture, −130 °C)[75] and for the solid phase,[71] which is attributable to the π,π-rearrangement, rapid within the NMR time scale.

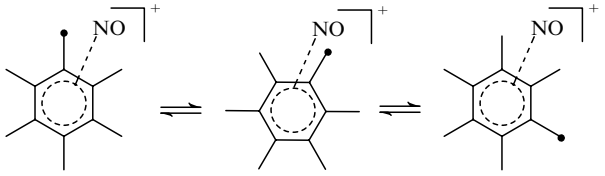

38 **38′** **38″**

The mechanism of this rearrangement involves either the migration of the NO group over the plane of the ring or the rotation of this ring about its 'normal' followed by 'switching' of the $C_{arom}-N$ bonds, the latter situation being more probable for the complex in the crystalline state.[71,75] The results of studies of the isotope effects of deuterium manifested in the ^{13}C NMR spectra of nitrosonium π-complexes with $C_6(CD_3)_m(CH_3)_{6-m}$ compounds do not contradict the conclusion that these complexes undergo rapid π,π-rearrangement in solutions.[80] The kinetic parameters of this rearrangement ($E_a = 42.7\pm2.5$ kJ mol^{-1}, $\log A = 13.9\pm0.3$) for the crystalline complex were determined by relaxation NMR spectroscopy.[75]

According to the ^1H and ^{13}C NMR spectral data, analogous π,π-rearrangements occur, apparently, in the nitrosonium complexes of benzene,[72,73,78] alkylbenzenes,[62,72–74,76,78] chlorobenzene,[72] anisole,[87] 2,3,5,6,8,9-hexahydro-1,2;3,4;5,6-tris(cyclopenta)benzene,[106] [2.2]paracyclophane[107] and triptycene.[107]

To reveal the contributions of the intermolecular and intramolecular mechanisms of rearrangements of nitrosonium complexes, it is important to elucidate the influence of the structure of the aromatic substrate on the formation constants of these complexes (K):

$$ArH + NO^+ \overset{K}{\rightleftharpoons} ArH-NO^+.$$

The quantitative data on the constants K for the π-complexes of benzene and its derivatives were obtained[76,78,81,84,88] by processing electronic absorption spectra using the Benesi–Hildebrand method. A linear correlation between the logarithms of the formation constants of the π-complexes and the ionisation potentials of the corresponding aromatic hydrocarbons was found[76] (Fig. 4). The point corresponding to 1,3,5-tri(*tert*-butyl)benzene deviates from the dependence presented in Fig. 4[76] due, appa-

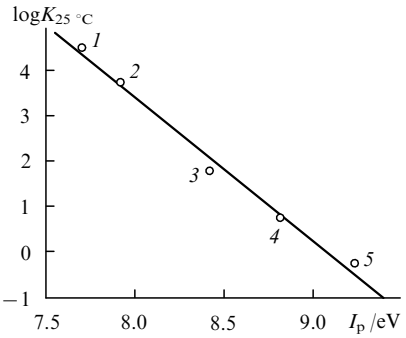

Figure 4. Dependence of the logarithms of the formation constants ($\log K$) of the $ArH-NO^+$ complexes (BF_4^- as the anion) in MeCN at 25 °C on the ionisation potentials (I_p) of the aromatic donors: (*1*) hexamethylbenzene (*2*) pentamethylbenzene (*3*) mesitylene (*4*) toluene (*5*) benzene ($r = -0.995$).[76]

rently, to steric inhibition of the donor-acceptor interaction between the aromatic substrate and the nitrosonium cation (*cf.* Ref. 88).

The high degree of charge transfer in the ground state of nitrosonium complexes of aromatic compounds containing donor substituents agrees well with the chemical behaviour of these complexes. The key stage of these reactions involves the transfer of one electron from the aromatic donor to the NO^+ group giving rise to a radical cation, which undergoes further transformations:

$$ArH + NO^+ \rightleftharpoons [ArH, NO^+],$$

$$[ArH, NO^+] \rightleftharpoons [ArH^{+\bullet}, NO^{\bullet}],$$

$$[ArH^{+\bullet}, NO^{\bullet}] \longrightarrow \text{products}.$$

This general scheme can be exemplified by the conversions of aromatic compounds **39**–**43** into products **44**–**50** (Scheme 4). In these processes, $ArH-NO^+$ π-complexes are, apparently, generated at the initial stage (see Refs 78 and 81).

All the above-considered calculated and experimental data provide evidence that the reactions of the nitrosonium cation with monocyclic aromatic compounds generally afford π-complexes rather than σ-complexes. In this connection, it is of interest that investigation of the kinetics of nitrosodeiodination of 4-iodoanisole by electronic absorption spectroscopy [63] provided evidence for the formation of the σ-complex, *viz.*, the 1-iodo-4-methoxy-1-nitrosobenzenonium ion (*cf.* Ref. 91). Recently, the nitrosonium σ-complexes with benzene, mesitylene, hexamethylbenzene and other aromatic compounds have been detected by this method using the femtosecond laser technique at low temperature.[90] However, it is known that information on the structures of cationic complexes of aromatic compounds obtained by electronic absorption spectroscopy is less reliable than that provided by NMR spectroscopy.[103] The more reliable NMR spectral data demonstrated that the reactions of anisole [87] and hexamethylbenzene [80] with $[NO]^+[AlCl_4]^-$ in the $SO_2-CD_2Cl_2$ system at low temperature afforded π-complexes (*cf.* Refs 68 and 71–76).

The nitrosonium cation is a strong oxidising agent [108, 109] (*cf.* Refs 55 and 56). Generally, its reactions with bi- and polycyclic arenes possessing, as a rule, low ionisation potentials [110] give rise to the corresponding radical cations or their reaction products.[55, 78, 109] Thus, the reactions of naphthalene with nitrosonium salts in trifluoroacetic acid at ~20 °C afforded initially a monomeric radical cation, followed by the formation of a dimeric radical cation and, finally, of a mixture of hydrocarbons $C_{10}H_7-(C_{10}H_6)_m-C_{10}H_7$.[109, 111, 112] Most likely, the transfer of one electron from the aromatic substrate to the NO^+ cation is preceded by the formation of the $ArH-NO^+$ π-complex. In spite of the importance of the data on the structures and reactivities of nitrosonium complexes with polycyclic aromatic compounds,

Scheme 4

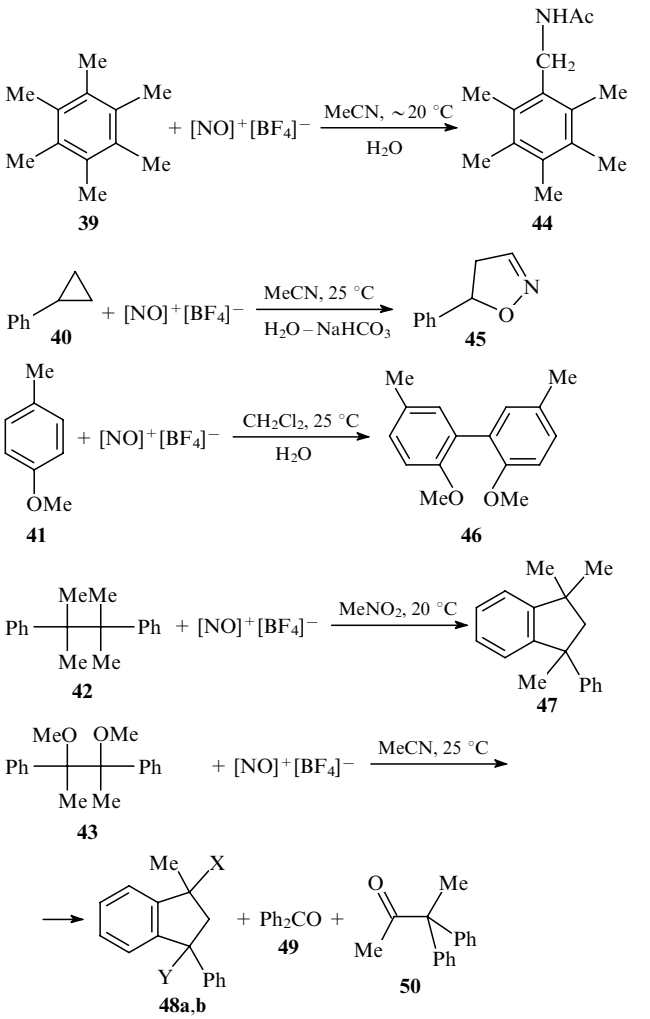

48a: X = OMe, Y = Me;
48b: X = Y = OMe.

attempts to generate these complexes have long been unsuccessful.[61, 76, 113–117]

The first data on the formation of nitrosonium π-complexes with fused arenes were obtained for derivatives of naphthalene,[113, 114] fluorene [113] and acenaphthylene [114] (*cf.* Refs 55 and 76). The reactions of $[NO]^+[AlCl_4]^-$ with methylnaphthalenes **51a**–**i** in SO_2 at low temperatures (from −70 to −80 °C) afforded cationic π-complexes **52a**–**i**, respectively.[115, 116]

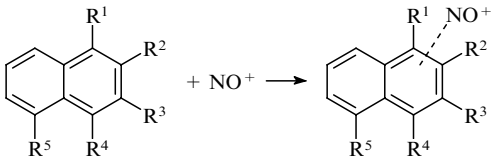

51a–**i** **52a**–**i**

Compounds **51**, **52**	R^1	R^2	R^3	R^4	R^5
a	H	H	H	H	H
b	Me	H	H	H	H
c	H	Me	H	H	H
d	Me	Me	H	H	H
e	Me	H	Me	H	H
f	Me	H	H	Me	H
g	Me	H	H	H	Me
h	H	H	H	Me	Me
i	H	Me	Me	H	H

Table 6. Parameters of the ^{13}C NMR spectra (δ_C) of the complexes **57a**,**c**–**f** [117, 119] and the charges q_π^+ on the C(3)–C(8b) atoms.

Complex	System or solvent	Temperature /°C	$\delta_{C(1)}$, $\delta_{C(2)}$ (see [a])	$\Delta\sum\delta_{C(3)-C(8b)}$ (see [b])	q_π^+ (see [c])
57a	HSO_3F-SO_2	−70	170.8	33.9	0.21
		−40	171.3	35.4	0.22
57c	SO_2-SO_2ClF	−95	153.6, 168.0	–	–
57d	SO_2	−80	150.6, 166.4	41.6	0.26
57e	CD_2Cl_2	−80	80.8	10.1	0.06
57f	HSO_3F-SO_2ClF	−50	98.3	17.4	0.11

[a] The chemical shifts are given relative to Me_4Si; CD_2Cl_2 was used as the internal standard (δ 52.9). [b] The difference between the total chemical shifts of the signals for the C(3)–C(8b) atoms in the spectra of the π-complex and its precursor. [c] In calculations, the value of 160 ppm was taken per unit π-charge.[102]

The structures of these complexes were confirmed by the results of ^1H, ^{13}C and ^{15}N NMR spectroscopy using the isotope perturbation method.[116] The equivalence of the methyl groups in the π-complexes **52f**–**i** observed in the ^1H NMR spectra was attributed [116] to the rapid (within the NMR time scale) intra- and(or) intermolecular migration of the NO group from one aromatic ring to another.

Apparently, analogous rearrangements occur in the nitrosonium complexes of fluorene (**53**),[113] [2.2]paracyclophane (**54**),[107] triptycene (**55**) [107] and corannulene (**56**) [118] (Scheme 5).

Unlike the complexes of the nitrosonium ion **52**–**56**, the nitrosonium complexes with 1-R-2-methylacenaphthylene (R = Me, CH_2D, CH_2Cl or Br) **57a**–**d** do not exhibit dynamical properties.[117]

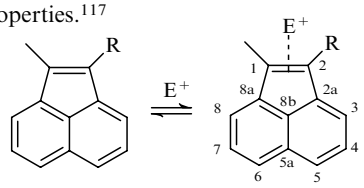

57a–**f**

Compound **57**	E	R
a	NO	Me
b	NO	CH_2D
c	NO	CH_2Cl
d	NO	Br
e	MeS	Me
f	PhS	Me

This is evidenced by the ^1H, ^{13}C and ^{15}N NMR spectral data and by the results obtained by the isotope perturbation method.[117] The fact that the signals for the C(1) and C(2) atoms in the π-complexes **57a**–**d** are shifted downfield compared to those of their analogues, *viz*., the episulfonium ions **57e**,**f** [119] (Table 6), was taken [117] as convinicng evidence for the preferential localisation of the NO group at the C(1)–C(2) bond assuming that the C(1) and C(2) atoms have nearly sp^2-hybridisation.

Substantial electron density transfer from the aromatic fragment to the NO^+ group is observed in the complexes of acenaphthylene and naphthalene derivatives (Table 7, see Table 6), as in nitrosonium complexes of monocyclic aromatic compounds containing donor substituents.[78] The greater the number of methyl groups in the rings of the complexes **52a**–**i**, the higher the degree of transfer.[116, 117] In addition, judging from the difference between the total chemical shifts of the signals for the C(1)–C(4) and C(5)–C(8) atoms in the ^{13}C NMR spectra of the π-complex and its precursor, the positive charge is localised predominantly at the methylated aromatic ring. Interestingly, an approximate linear correlation between the total positive π-charges on the core (q_π^+) and the oxidation potentials of the precursors ($E_{1/2}$) is observed for the nitrosonium complexes of naphthalene and its derivatives (Fig. 5, see Table 7). As expected, a decrease in the oxidation potential of the aromatic hydrocarbon leads to an increase in the positive π-charge on the aromatic fragment of the π-complex **52**.

Scheme 5

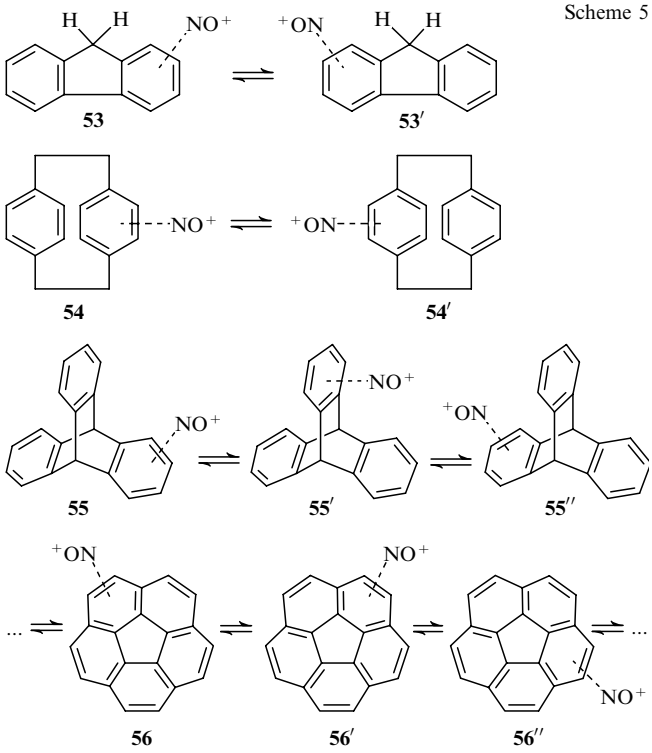

As mentioned above, naphthalene is oxidised by the nitrosonium cation at room temperature to form the corresponding

Table 7. Parameters of the ^{13}C NMR spectra of the complexes **52a**–**i** (SO_2, −70 °C) [116] and the oxidation potentials of their precursors **51a**–**c**, **e**–**i**.

Compounds **51** and **52**	$\Delta\sum\delta_{C(1)-C(4)}/\Delta\sum\delta_{C(5)-C(8)}$ [a]	q_π^+[C(1)–C(8a)] [b]	$E_{1/2}$ /V [c]
a	25.2 / 25.2	0.34	1.54
b	44.9 / 16.2	0.40	1.43
c	40.6 / 18.6	0.39	1.45
d	60.9 / 19.7	0.54	–
e	56.2 / 16.9	0.47	1.38
f	60.8 / 15.6	0.49	1.32
g	36.2 / 36.2 [d]	0.49	1.43
h	32.7 / 32.7 [e]	0.42	1.30
i	47.2 / 16.8	0.42	1.44

[a] The ratio of the differences between the total chemical shifts of the signals for the C(1)–C(4) and C(5)–C(8) atoms in the spectra of the complexes **52a**–**i** and their precursors. [b] In calculations, the value of 160 ppm was taken per unit π-charge.[102] [c] The data were reported in Ref. 120. [d] At −75 °C. [e] At −80 °C.

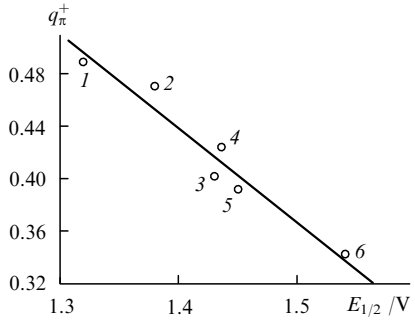

Figure 5. Correlation between the q_π^+ values for the π-complexes **52a**–**c**,**e**,**f**,**i** and the oxidation potentials ($E_{1/2}$) of their precursors **51a**–**c**,**e**,**f**,**i**:[120] (*1*) 1,4-dimethylnaphthalene, (*2*) 1,3-dimethylnaphthalene, (*3*) 1-methylnaphthalene, (*4*) 2,3-dimethylnaphthalene, (*5*) 2-methylnaphthalene, (*6*) naphthalene ($r = -0.970$). The data for the π-complexes **52g**,**h** were not taken into consideration because the q_π^+ values for the latter complexes were determined from ^{13}C NMR spectra measured at different temperatures.

radical cation.[109, 111, 112] In the case of methylnaphthalenes, an analogous process takes place at low temperature. As the temperature increases from −60 or −70 °C to −30 or −50 °C, the signals in the ^1H NMR spectra of the complexes **52a**–**i** become broader (up to their 'disappearance'), which was explained [116] by the one-electron transfer between the aromatic core of the complex and the NO group.

Dimerisation of the resulting radical cations is one of the possible conversions of these compounds.[116] Actually, storage of solutions of the complexes **52b**,**d**,**e**,**h** at −20 to −30 °C for 1–2 h followed by their treatment with water afforded 4,4′-dimethylbinaphthyl, 3,3′,4,4′-tetramethylbinaphthyl, 2,2′,4,4′-tetramethylbinaphthyl and 4,4′,5,5′-tetramethylbinaphthyl, respectively, in ~20% yields. Analogous reactions proceeded with the participation of 2-methyl-, 1-ethyl-, 2-ethyl-, 1,6-dimethyl-, 2,3-dimethyl-, 2,6-dimethyl-, 2,7-dimethyl-, 1-methoxy-, 2-methoxy-, 1-bromo- and 2-hydroxynaphthalenes (the yields of the dimeric products were 25%–95%).[121, 122]

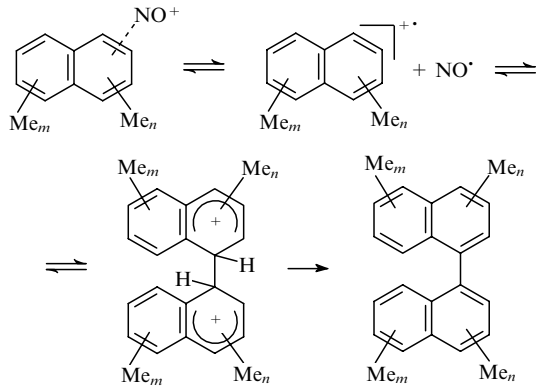

$m = 0, 1; n = 0–2$.

V. Complexes of the nitrosonium ion with nitrogen-containing organic compounds

In a number of studies it has been suggested that nitrosonium complexes of amines and N-heterocyclic compounds are intermediates in diazotisation,[1] nitrosation of amides [1] and N-heterocyclic compounds,[123, 124] the formation [1, 125] and denitrosation [126] of nitrosoamines and other reactions involving the nitrosonium cation.[1, 127–130]

According to the results of quantum-chemical calculations [131–133] and experimental data for the gas phase,[66, 134] N-bases possess high affinities for the NO^+ cation. Thus according to the results of *ab initio* calculations [HF/6-31 + G(d)], the energy of binding of the NO^+ cation with the methylamine molecule is 127.7 kJ mol^{-1} (*cf.* Ref. 133). The data on the binding energies (E_b) of the NO^+ cation with nitriles, pyridine and the derivatives of the latter [134] were obtained by ion-cyclotron resonance and in studies of the fragmentation of $L^1(NO^+)L^2$ dimers by kinetic methods (Table 8). A linear correlation between the E_b values for alkylnitriles RCN and Taft's σ*-constants of the substituents [135] was revealed (Fig. 6). Consequently, the inductive effect of the substituents R is the major factor responsible for the stability of the $RCN-NO^+$ complexes (*cf.* Ref. 66).

Table 8. Energies of binding (E_b) of the NO^+ cation with N-bases.[134]

Compound	E_b /kJ mol^{-1}	Compound	E_b /kJ mol^{-1}
$CH_2(CN)_2$	82.0	PhCN	121.3
MeCN	110.5	*o*-MeC_6H_4CN	123.4
EtCN	115.5	3-FC_5H_4N	156.1
Pr^nCN	117.2	4-ClC_5H_4N	162.3
Pr^iCN	118.8	C_5H_5N	167.8
Bu^tCN	121.3	3-MeC_5H_4N	172.0

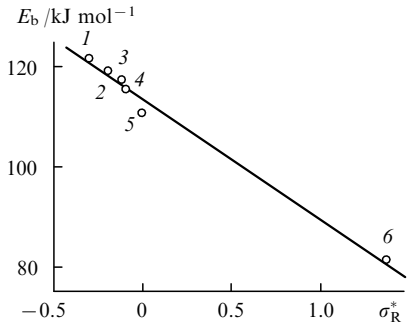

Figure 6. Correlation between the energies of binding (E_b) of the NO^+ cation with nitriles RCN [134] and the σ*-constants of the substituents R (σ_R^*),[135] where R = Bu^t (*1*), Pr^i (*2*), Pr^n (*3*), Et (*4*) or Me (*5*) and RCN = $CH_2(CN)_2$ (*6*) ($r = -0.995$).

A linear correlation between the E_b values [134] and the σ-constants of the substituents X [135] observed for pyridine and its derivatives XC_5H_4N (Fig. 7) indicates that both the inductive and resonance effects are of considerable importance.

The reaction of the $[NO]^+[BF_4]^-$ salt with pyridine in polar solvents (MeCN, $MeNO_2$, SO_2 or sulfolane) was examined by ^1H NMR and IR spectroscopy.[136] The results obtained in the

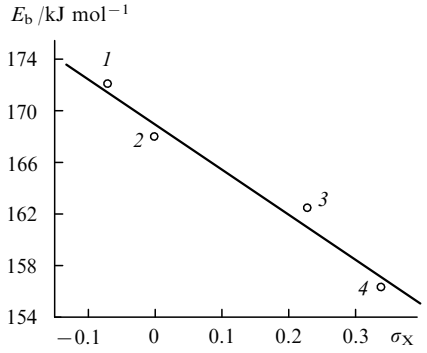

Figure 7. Correlation between the energies of binding (E_b) of the NO^+ cation with the XC_5H_4N compounds [134] and the σ-constants of the substituents X (σ_X),[135] where X = 3-Me (*1*), H (*2*), 4-Cl (*3*) or 3-F (*4*) ($r = -0.984$).

cited study provided evidence for the formation of the $C_5H_5N-NO^+$ *n*-complex (*cf.* Refs 76, 82 and 137). It should be noted that the transfer of the NO group from the nitrogen atom to the carbon atom of the ring was not observed even under the conditions of thermal decomposition of the $[C_5H_5N-NO]^+[BF_4]^-$ salt.[136]

The reactions of pyridine, its derivatives, quinoline and 1,10-phenanthroline with $[NO]^+[BF_4]^-$ in $(CD_3)_2SO$ at 20 °C or with $[NO]^+[AlCl_4]^-$ in SO_2 at −60 °C afforded complexes **58a–d**, **59** and **60** whose structures were confirmed by ^1H and ^{13}C NMR spectroscopy.[138,139]

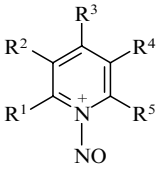

58a–d

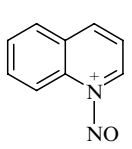

59

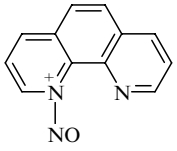

60

Compound **58**	R^1	R^2	R^3	R^4	R^5
a	H	H	H	H	H
b	H	Me	H	H	H
c	H	H	CHO	H	H
d	Me	H	Me	H	Me

The ^1H and ^{13}C NMR spectra of the complex **60** are indicative of a degenerate rearrangement rapid within the NMR time scale, which proceeds through the intra- and(or) intermolecular transfer of the NO group.

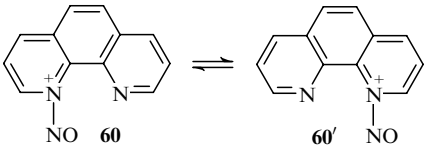

60 **60′**

Nitrosonium complexes of pyrimidine derivatives (**61** and **62**) undergo analogous rearrangements persisting even at −70 °C.[140]

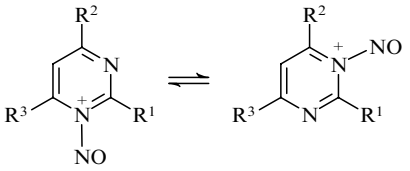

61, **62**

61: R^1 = Me, R^2 = R^3 = Ph; **62**: R^1 = PhO, R^2 = R^3 = Me.

According to the experimental data for the gas phase, pyridine derivatives and alkylbenzenes possess similar affinities for the NO^+ cation.[134] The formation constant of the 2,6-dimethylpyridine complex with the nitrosonium cation in MeCN was determined by the competitive method.[82] On gradual addition of 2,6-dimethylpyridine to a solution of the durene complex with $[NO]^+[BF_4]^-$ in acetonitrile, the intensity of the charge-transfer band for the durene–NO^+ complex decreases monotonically, while the intensity of the corresponding band for the nitrosonium complex with 2,6-dimethylpyridine increases due to the following reactions:

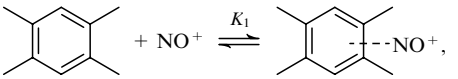

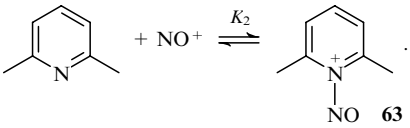

63

The equilibrium constant, K_2, of the reaction of NO^+ with 2,6-dimethylpyridine [$K_2 = (3\pm2)\times10^3$ litre mol^{-1}] was determined[82] from the equilibrium constant of the reaction of durene with the NO^+ cation (K_1 = 450 litre mol^{-1}) estimated previously. A somewhat different value was obtained for electrochemical reduction of complex **63**, ($K_2 \approx 500$ litre mol^{-1}). This difference in the constant determined by different methods is due partially to salt effects.[82]

Intensely coloured solutions of complexes of aromatic compounds with $C_5H_5N^+-NO$ ($PyNO^+$) in acetonitrile are decolourised in the presence of alkyl derivatives of benzene or naphthalene at room temperature in the dark, the rate of this process being decreased in the series 1,4-dimethylnaphthalene > hexamethylbenzene > durene ≫ *p*-xylene > toluene.[82] The chemical conversions responsible for decolouration of the complexes under the action of 1,4-dimethylnaphthalene, durene and hexamethylbenzene are shown in Scheme 6.[82]

Scheme 6

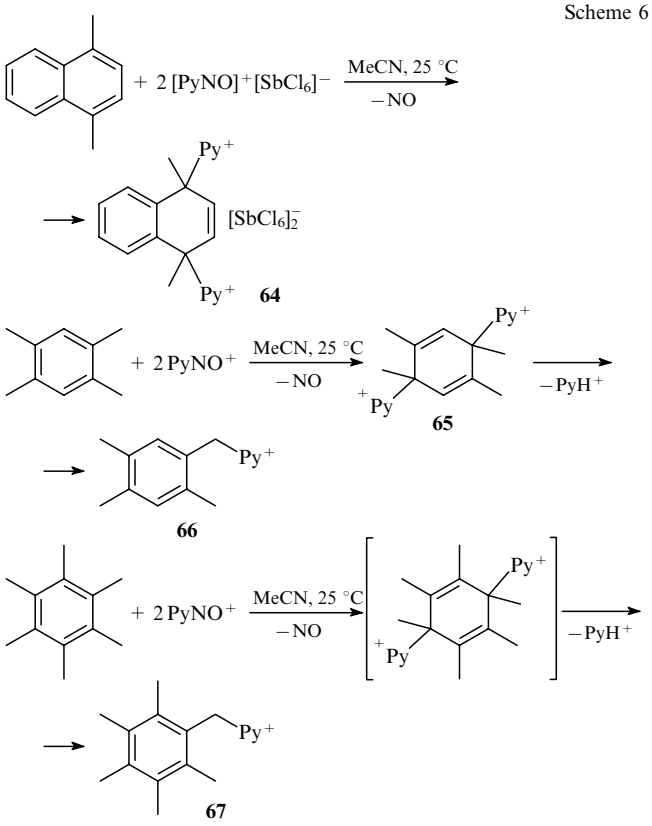

64

65

66

67

The structures of complexes **64–67** were established by ^1H NMR spectroscopy. The structure of the complex **65** (with the $SbCl_6^-$ anion) was additionally confirmed by X-ray diffraction analysis. Interestingly, the reaction of durene with the $[PyNO]^+[SbCl_6]^-$ salt afforded exclusively the *trans*-adduct **65**, while the reaction with the $[PyNO]^+[BF_4]^-$ salt gave rise to an equimolar mixture of the *trans*- and *cis*-adducts.[82]

N-Nitrosation reactions of secondary amines with complexes synthesised by the reactions of N_2O_4 with pyridine or triethylamine have been examined.[137]

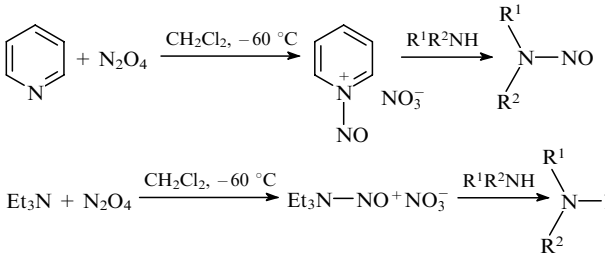

Analogous N-nitrosation reactions of amino acids containing secondary amine groups under the action of a mixture of nitro-

sonium tetrafluoroborate and pyridine have been described[141] (*cf.* Ref. 127). Apparently, the $[PyNO]^+[BF_4]^-$ complex served as an active nitrosating agent in these reactions.[141]

VI. Complexes of the nitrosonium ion with organic compounds containing Group VI elements

Complexes of the nitrosonium ion with compounds of the R^1ER^2 and $R^1R^2C=E$ types (E is the Group VI element) were considered as intermediates in many liquid-phase reactions of O-bases (alcohols,[1,142,143] ketones,[144–146] *etc.*[1,92–94]) and S-bases (desulfofluorination of thioesters,[147] conversions of thioketones and thioamides giving rise to ketones and amides of acids, respectively,[148] *etc.*[149–151]).

According to the results of quantum-chemical calculations[133,152–154] and experimental data for the gas phase obtained by the ion-cyclotron resonance[66,134] and kinetic methods,[134] O-bases possess rather high affinities for the NO^+ cation.

Calculations based on thermochemical data demonstrated that the energy of the nitrosonium complex with ethylene oxide (**68**) is 112.5 kJ mol^{-1} lower than those of the initial reagents.[152]

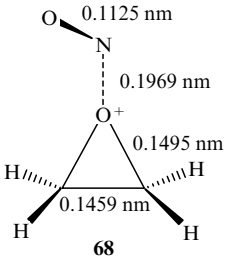

68

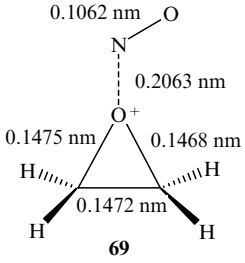

69

Ab initio calculations (SCF/MP2) demonstrated that the planar analogue of this complex (**69**) is somewhat energetically less favourable (ΔE_{rel} = 15.1 kJ mol^{-1}), the latter being a transitional structure between two equivalent forms **68**. According to the results of *ab initio* calculations (MP2/6-31+G*), the energy of the nitrosonium complex with acetaldehyde (**70**), which is isomeric with structure **68**, is 115.5 kJ mol^{-1} lower than those of the initial reagents, whereas the nitrosonium complex with the enol form of acetaldehyde (**71**) is energetically less favourable than the complex **70** (ΔE_{rel} = 105.0 kJ mol^{-1}).[152]

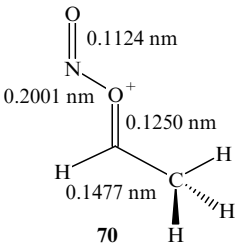

70

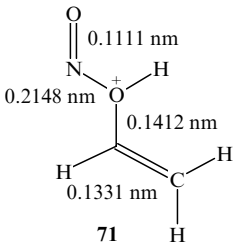

71

Analogously, *ab initio* calculations [HF/6-31+G(d)[133] and G2[154]] gave rather high affinities of the NO^+ cation for methanol (97.3 and 105.9 kJ mol^{-1}, respectively).

The *ab initio* energies of binding of the NO^+ cation with acetaldehyde and methanol are very close to the experimental values determined for the gas phase (Table 9).[134]

The energies of binding of the NO^+ cation with O-bases were analysed within the framework of Taft's equation.[66] Linear correlations were revealed for each class of compounds (MeCOR, where R = H, Me or Et; ROAc or RCHO, where R = Me, Et or Pr^i; and ROH, where R = Me, Et or Pr^i). Analogous relationships are true for the compounds of the $RONO_2$ and RNO_2 types (Fig. 8).

As mentioned above, nitrosonium complexes with O-bases were postulated for many liquid-phase reactions. However, the data on generation of these complexes in solutions are scarce.[77,155–159]

Table 9. Energies of binding (E_b) of the NO^+ cation with O-bases.[134]

Compound	E_b /kJ mol^{-1}	Compound	E_b /kJ mol^{-1}
H_2O	77.4	MeCHO	115.5
MeOH	97.5	Me_2CO	130.1
CH_2O	112.5	$MeCO_2Et$	131.4
$MeONO_2$	86.6	MeCOEt	134.3
$EtONO_2$	95.0	Et_2CO	136.8
Pr^iONO_2	101.7	Pr^iCOMe	138.1
$MeNO_2$	104.2	Bu^tCOMe	140.2
$EtNO_2$	112.5	Bu^t_2CO	141.0
Pr^nNO_2	115.9	Pr^i_2CO	142.3
Pr^iNO_2	118.0	PhCOMe	146.9
Bu^nNO_2	116.7	$(C_3H_5)_2CO$	152.7
Bu^tNO_2	123.4	Ph_2CO	160.2
$MeCOC(OMe)_2Me$	154.8	$(PhCH_2)_2CO$	165.3
$MeCO_2Bu^t$	141.0		

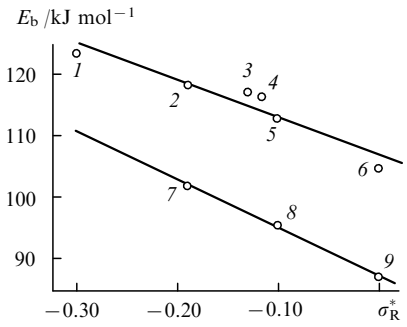

Figure 8. Correlation between the energies of binding (E_b) of the NO^+ cation with the RNO_2 (*1–6*) and $RONO_2$ compounds[134] (*7–9*) and the σ^*-constants of the substituents R (σ^*_R),[135] where R = Bu^t (*1*), Pr^i (*2*, *7*), Bu^n (*3*), Pr^n (*4*), Et (*5*, *8*) or Me (*6*, *9*) (r = −0.955 and −0.999, respectively).

Thus, the reactions of the $[NO]^+[BF_4]^-$ and $[NO]^+[PF_6]^-$ salts with 18-crown-6, 15-crown-5 and 12-crown-4 in dichloromethane, acetonitrile and nitromethane were studied by ^{1}H NMR and IR spectroscopy and conductometry.[155] The reactions of 18-crown-6 and 12-crown-4 with $[NO]^+X^-$ afforded the 1:1 and 2:1 complexes, respectively. In the case of 15-crown-5, the 1:1 stoichiometry was observed if the reaction was performed in MeCN or $MeNO_2$, whereas the 2:1 stoichiometry was achieved in CH_2Cl_2. The addition of the $[NO]^+X^-$ salt to a solution of a complex always leads to a downfield shift of the signal of the crown ether in the ^{1}H NMR spectrum, one narrow singlet being observed due to the rapid (within the NMR time scale) exchange between the free crown molecule and the molecule involved in the complex. New absorption bands at 1850–1852 and 1876 cm^{-1} appeared in the IR spectra of solutions of 18-crown-6, 15-crown-5 and 12-crown-4 in CH_2Cl_2 and MeCN, respectively, upon the addition of the $[NO]^+X^-$ salts, which indicates that the NO^+ cation is covalently bonded to the crown molecule.[155] It should be noted that the positions of the bands in the IR spectra are virtually independent of the nature of the counterion.[155]

The reaction of 18-crown-6 with the NO^+ cation (BF_4^- as the counterion) was examined by ^{1}H and ^{13}C NMR, IR and Raman spectroscopy.[156] The ^{1}H and ^{13}C NMR spectra of the 1:1 complex have singlets at δ 3.67 and 70.327, respectively. The ^{13}C chemical shift changes only slightly (by 0.428 ppm) on going from free 18-crown-6 to the ether involved in the complex. The IR spectrum of the [18-crown-6–NO]$^+[BF_4]^-$ salt (in hexachlorobutadiene) has an absorption band of the NO group at 2274 cm^{-1} the position of which differs substantially from those observed in the spectra of this complex in CH_2Cl_2 or MeCN (see above).

Analogous results were obtained in another study.[157] It was suggested that the band at 2250 cm^{-1} in the IR spectrum of a solution of the [18-crown-6–NO]$^+$[BF_4]$^-$ complex in CH_2Cl_2 and the charge-transfer band of this complex (λ_{max} = 300 nm) be used for the detection of an impurity of the [NO]$^+$[BF_4]$^-$ salt in the [NO_2]$^+$[BF_4]$^-$ specimen.[77] A polycrystalline specimen prepared by the reaction of N_2O_4 with 18-crown-6 was studied by Raman spectroscopy.[158] The Raman spectrum of the salt [18-crown-6–NO]$^+$H$^+$[NO_3^-]$_2$ has an intense band at 2270 cm^{-1} belonging to the stretching vibration of the NO^+ group bound to the crown ether. No explanation was provided for the above-mentioned differences in the stretching vibration frequency of the NO group.[156–158] Apparently, these differences are associated with a change in the mode of bonding of the NO^+ cation with 18-crown-6.

The complex of 18-crown-6 with [NO]$^+$[BF_4]$^-$ in MeCN was examined by cyclic voltammetry.[77] The complexation constant ($K > 10^4$ litre mol^{-1}) was estimated based on the oxidation and reduction potentials. Reduction of the complex **72** gave rise to the compound **73**. On oxidation of the latter, NO molecules were only partially converted into NO^+ cations and its complex with the crown ether.

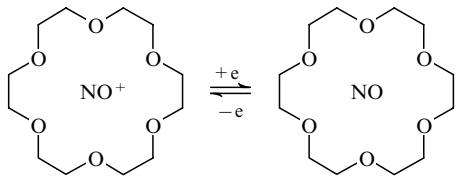

72 **73**

The reversible reduction potential of the complex **72** in MeCN ($E_{red} \approx 0.9$ B) is smaller than the E_{red} values determined for the hexamethylbenzene complex with the NO^+ cation (E_{red} = 1.02 V) and for NO^+ (E_{red} = 1.28 V).[77]

The reactivity of the nitrosonium cation changes substantially on the involvement of the [NO]$^+$[BF_4]$^-$ salt in the complex with 18-crown-6.[156] Thus the [18-crown-6–NO]$^+$[BF_4]$^-$ complex did not react with benzamide in MeCN at low temperature, whereas the amide was rapidly converted into acid under the action of [NO]$^+$[BF_4]$^-$ in the absence of the crown ether.[156]

The nitrosonium cation vigorously reacts with ketones in the gas phase[66, 134] to give the [R^1R^2C=ONO]$^+$ complexes (see Table 9). Analogous complexes were obtained in the reactions of the NO^+ cation with compounds of the ArN=O and R_2S=O types in the liquid phase.[93, 94, 159]

Kinetic studies of the mechanism of nitrosation of aromatic compounds provided evidence for the formation of [ArNO–NO]$^+$ complexes in which the nitrosonium cation is bound to the oxygen atom of the NO group in the ArNO molecule.[92–94] The formation constants of the complex of the NO^+ cation with 4-nitrosotoluene and 1,3-dimethyl-4-nitrosobenzene in trifluoroacetic acid are 58 000 and 38 000 litre mol^{-1}, respectively.[93]

Studies by ^{1}H, ^{13}C and ^{15}N NMR spectroscopy showed[159] that the reaction of [NO]$^+$[PF_6]$^-$ with dimethyl sulfoxide in SO_2 or the reaction of [NO_2]$^+$[PF_6]$^-$ with dimethyl sulfide in SO_2 at low temperature gave rise to nitrosonium complex **75** (existing in equilibrium with complex **74**).

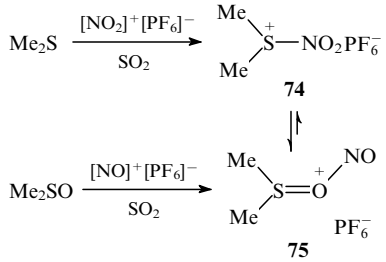

Analogously, the reaction of [NO_2]$^+$[PF_6]$^-$ with dimethyl selenide in SO_2 at −78 °C afforded nitrosonium complex **77** along with complex **76**.[159]

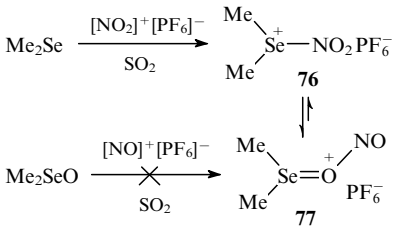

However, all attempts to generate the complex **77** by the reaction of [NO]$^+$[PF_6]$^-$ with dimethyl selenoxide failed because the latter readily underwent Pummerer fragmentation.[159]

The ambident reactivity of the NO_2^+ cation (the competitive O- or N-reactions) is manifested in its reactions with triphenylphosphine. In this case, as in the case of the S- and Se-analogues, the equilibrium **78** ⇋ **79** is shifted toward the nitritophosphonium complex **79**.[159]

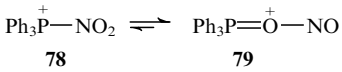

78 **79**

Investigations of the interaction of the NO^+ cation with O- and S-anions using perturbation theory demonstrated that the nitrosonium cation acts as a soft acid [160] (*cf.* Ref. 161). According to the Pearson concept,[162] the complexes of the NO^+ cation with S-bases should be more stable than those with O-bases. This statement can be exemplified by the fact that the reaction of thioanisole with [NO]$^+$[$AlCl_4$]$^-$ in the SO_2–CD_2Cl_2 system at −70 °C afforded an *n*-complex (**80**), whereas the reaction of anisole under these conditions gave rise to π-complex **81**, the oxygen atom of the anisole remaining unbound.[87]

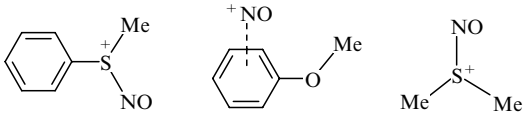

80 **81** **82**

The structures of these complexes were confirmed by ^{1}H, ^{13}C and ^{15}N NMR spectroscopy. In particular, the fact that the cation **80** belongs to an *n*-complex is witnessed by the close values of the corresponding chemical shifts in the ^{15}N NMR spectra of this complex and Me_2S^+–NO (**82**) [HSO_3F–SO_2, δ(−70 °C) 291.6 and 258.6, respectively].[87] The results of quantum-chemical calculations by the MINDO/3 method confirmed that of the *n*-, π- and σ-complexes, the *n*-complex of thioanisole and the π-complex of ansiole are more stable.[87]

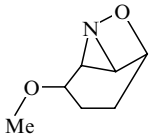

ΔH_f = 643.9 kJ mol^{-1}

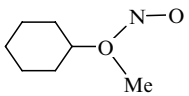

ΔH_f = 761.5 kJ mol^{-1}

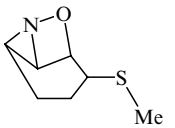

ΔH_f = 832.6 kJ mol^{-1}

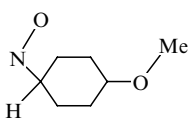

ΔH_f = 663.6 kJ mol^{-1}

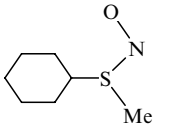

ΔH_f = 788.3 kJ mol^{-1}

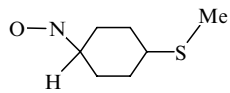

ΔH_f = 854.0 kJ mol^{-1}

The preferential binding of the NO^+ cation at the sulfur atom rather than at the oxygen atom in the PhEMe compounds (E = O or S) was attributed [87] to the lower electronegativity of the S atom and a greater *p*,π-conjugation of the aromatic fragment with the MeO group compared to that with the MeS group. It was suggested [163] that binding of the nitrosonium cation in the case of thioanisole, occurs preferentially at the S atom due to the fact that the HOMO of thioanisole has the highest coefficient at the sulfur atom.

Ab initio (the 4-31G basis set), CNDO and INDO quantum-chemical calculations were performed with the aim of studying the reaction of 2-(methylthio)ethylamine with the NO^+ cation.[164] The structures of the complexes **83a**,**b** and **84** optimised by the CNDO and INDO methods are shown in Fig. 9. Analysis within the framework of perturbation theory demonstrated that the NO^+ cation acts as a soft acid, *i.e.*, it is bound primarily to the sulfur atom rather than to the nitrogen atom, the energy of the N-complex **84** being 50 kJ mol^{-1} higher than the energy of the stable *syn*-complex **83a**.[164]

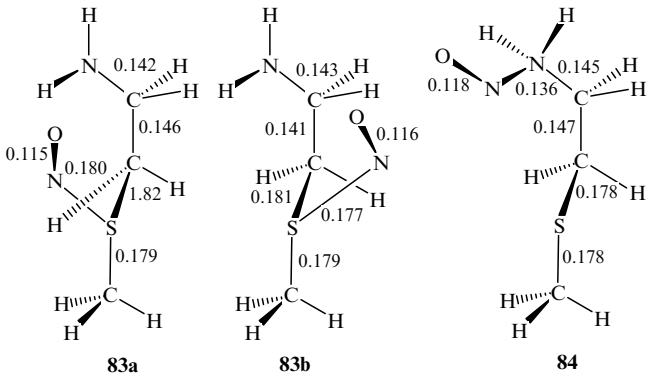

83a **83b** **84**

Figure 9. Geometric parameters of the *n*-complexes **83a**,**b** and **84** calculated by the CNDO and INDO methods.[164] The bond lengths are given in nm.

The reaction of 1,3-dimethylthiobenzene with $[NO]^+[AlCl_4]^-$ in the $SO_2-CD_2Cl_2$ system at −70 °C produced *n*-complex **85**, which underwent degenerate rearrangement, rapid within the NMR time scale (Scheme 7).[165]

Scheme 7

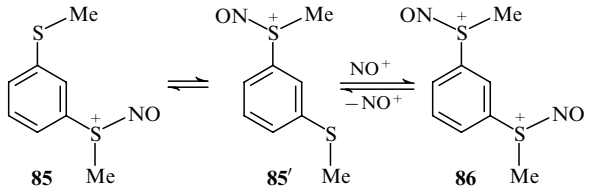

85 **85′** **86**

The structure of the complex **85** was confirmed by ^1H, ^{13}C and ^{15}N NMR spectroscopy. As expected, the ^{15}N chemical shift for the complex **85** (δ_N 267.1 relative to $MeNO_2$, −70 °C) is similar to that observed in the spectrum of the nitrosonium complex with thioanisole (δ_N 291.6 relative to $MeNO_2$, −70 °C).[87] The signals for the protons of the aromatic ring and methyl groups and the signals for the C(2), C(4), C(5) and C(6) atoms are shifted downfield as the 1,3-dimethylthiobenzene : $[NO]^+[AlCl_4]^-$ ratio changes from 1 : 1 to 1 : 2 due, apparently, to the shift of the equilibrium **85′** ⇌ **86** (see Scheme 7) to the dication **86**. A further increase in the amount of the salt (to 1 : 5) has no effect on the positions of the above-mentioned signals.

The complexes of dialkyl, alkylaryl and diaryl sulfides with $[NO]^+[BF_4]^-$ or N_2O_4 in CH_2Cl_2 were studied by electronic spectroscopy.[86] At low temperature, the spectra have charge-transfer bands whose positions depend only slightly on the nature of the counterion (NO_3^- or BF_4^-) (Table 10). It was demonstrated

Table 10. Parameters of electronic absorption spectra (λ_{CT} /nm) of the nitrosonium complexes with the R^1R^2E compounds (E = S or Se) in CH_2Cl_2 at −78 °C.[86, 166]

R^1	R^2	λ_{CT} (E = S)		λ_{CT} (E = Se)	
		A	B	A	B
Me	Me	390	393	–	–
Bu^n	Bu^n	400	400	–	–
Me	$PhCH_2$	406	406	426	424
Me	Bu^t	396	400	–	–
$(CH_2)_4$		387	386	–	–
Bu^t	$Me(CH_2)_{17}$	–	408	–	–
Me	Ph	502	500	494	498
Et	Ph	500	500	–	–
Pr^i	Ph	494	494	500	496
Me	*p*-ClC_6H_4	510	512	–	–
Me	*p*-MeC_6H_4	514	514	–	–
Me	*p*-$MeOC_6H_4$	542	542	–	–
Me	*p*-$Bu^tC_6H_4$	514	517	–	–
$PhCH_2$	$PhCH_2$	–	–	452	444
Ph	$PhCH_2$	506	–	508	506
Ph	Ph	558	563	–	–

Note. A and B are the complexes with the $[NO]^+[BF_4]^-$ salt and N_2O_4, respectively.

that low-temperature irradiation of the $[R^1R^2SNO]^+[NO_3]^-$ complexes at the frequency corresponding to the charge-transfer band afforded sulfoxides. The complexation constants for dialkyl and alkylaryl sulfides (K_1 and K_2, respectively) were estimated by the competitive method.

$$R_2S + [NO]^+[BF_4]^- \overset{K_1}{\rightleftharpoons} [R_2S, NO]^+[BF_4]^-$$

$$R_2S + [ArH, NO]^+[BF_4]^- \overset{K_2}{\rightleftharpoons} [R_2S, NO]^+[BF_4]^- + ArH$$

The complexation constant (K_1) for Bu^n_2S in CH_2Cl_2 at −78 °C is similar to that for hexamethylbenzene ($K_1 \approx 3 \times 10^4$ litre mol^{-1}), whereas ethylphenyl sulfide possesses a somewhat lower affinity for the NO^+ cation ($K_1 \leqslant 3 \times 10^3$ litre mol^{-1}).

Analogously, the reactions of dialkyl and alkylaryl selenides with $[NO]^+[BF_4]^-$ or N_2O_4 in CH_2Cl_2 at −78 °C gave rise to the nitrosonium complexes $R^1R^2SeNO^+$ (see Table 10).[166] As can be seen from Table 10, the positions of charge-transfer bands in the spectra of the nitrosonium complexes R^1R^2S and R^1R^2Se are rather close. Low-temperature irradiation of the complex $[PhMeSeNO]^+[NO_3]^-$ at the frequency ν_{CT} gave rise to the corresponding selenoxide PhSe(O)Me.[166]

The reactions of nitrosonium salts with diaryl tellurides, unlike those with S- and Se-containing aromatic compounds, did not produce nitrosonium complexes.[167] Thus treatment of bis(4-methylphenyl) telluride (**87**) with the $[NO]^+[BF_4]^-$ salt in the CH_2Cl_2-MeCN system at −40 °C under an atmosphere of argon afforded dication **88**.

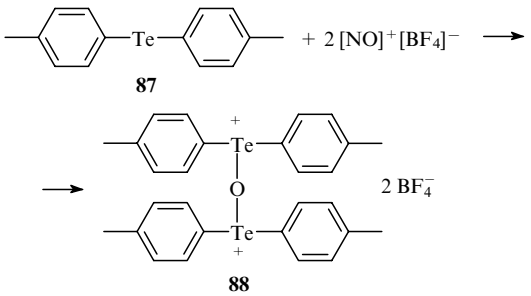

87 **88**

It was found that the oxygen atom in the dication **88** was derived from the nitrosonium salt.[167]

VII. Complexes of the nitrosonium ion with halogen-containing organic compounds

The reactions of the nitrosonium cation with organic halogen derivatives RX in the gas phase generate chemically active species, which can dissociate to form carbocations, nitrosyl halides and nitrosonium complexes of alkenes.[168]

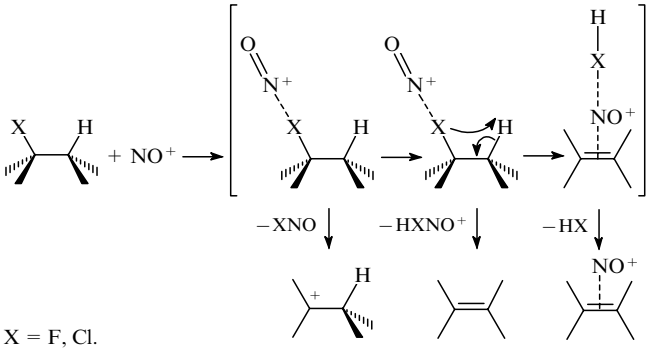

X = F, Cl.

The latter react with alkyl halides yielding halonitrosonium complexes. Thus the reactions involving Pr^iCl or Pr^iF proceeded as follows:[168]

$$(MeCH{=}CH_2)\cdot NO^+ + Pr^iX \longrightarrow Pr^iX\cdot NO^+ + C_3H_6$$

X = F, Cl.

It is assumed that analogous ion-molecular reactions take place upon interaction of the vibrationally excited NO^+ cation with different alkyl halides (see Ref. 169 and references cited therein).

The data on the energies of binding of the NO^+ cation with alkyl chlorides RCl (R = Me, Et or Pr^i; E_b = 77.4, 82.0 and 89.5 kJ mol^{-1}, respectively) were determined by the ion-cyclotron resonance and kinetic methods.[134] The following correlation between the E_b values for aryl chlorides and Taft's σ^*-constants was deduced: [135]

$$E_b = (76.8 \pm 1.3) - (63.4 \pm 10.7)\,\sigma^*,\ r = -0.986,\ s = 1.4.$$

To our knowledge, the data on generation of long-lived nitrosonium complexes of halogen-containing organic compounds in solutions are lacking. However, such complexes can be generated in different reactions of alkyl and aryl halides with salts of the nitrosonium cation.[170, 171] Thus, a new procedure was developed [170] for the preparation of amides by the reactions of alkyl or aryl halides with nitriles in the presence of the $[NO]^+X^-$ salts. The assumed mechanism involves the formation of a nitrosonium *n*-complex *via* the lone electron pairs of the halogen atom followed by nucleophilic substitution (of the S_N1 or S_N2 type) of nitrile for the XNO^+ group.[170]

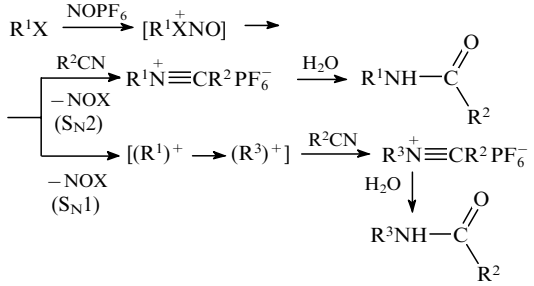

R^1 = Alk, $ArCR^2R^3$; R^2 = Me, Et, Pr, Ph, $PhCH_2$;
$(R^3)^+$ — isomer $(R^1)^+$; X = F, Cl, Br.

Analogous results were obtained in another study. [172]

* * *

To summarise, abundant data on the structures and reactivities of different classes of nitrosonium organic complexes have been accumulated due to the extensive use of modern physical and quantum-chemical methods. In the present review, we generalise the results of recent studies in this area. The necessity of summarising these data stems from the fact that investigations aimed at refining the theoretical notion of the processes, which involve nitrosonium complexes and include both classical organic and biochemical reactions, are progressing rapidly.

This review has been written with the financial support of the Russian Foundation for Basic Research (Project No. 99–03–32878).

References

1. D L H Williams *Nitrosation* (Cambridge: Cambridge University Press, 1988)
2. P P Kadzyauskas, N S Zefirov *Usp. Khim.* **37** 1243 (1968) [*Russ. Chem. Rev.* **37** 543 (1968)]
3. P B D de la Mare, R Bolton *Electrophilic Additions to Unsaturated Systems* (Amsterdam: Elsevier, 1982) p. 247
4. L F Fieser, M Fieser *Reagents for Organic Synthesis* (New York: Wiley, 1968)
5. G A Olah, K K Laali, Q Wang, G K S Prakash, in *Onium Ions* (New York: Wiley, 1998) p. 40
6. E Culotta, D E Koshland *Science* **258** 1862 (1992)
7. A R Butler, D L H Williams *Chem. Soc. Rev.* **22** 233 (1993)
8. M Fontecave, J-L Pierre *Bull. Soc. Chim. Fr.* **131** 620 (1994)
9. V P Reutov, in *Uspekhi Biologicheskoi Khimii* (Advances in Biological Chemistry) (Ed. B F Poglazov) (Pushchino: Izd. ONTI PNTs RAN, 1995) Vol. 35, p. 189
10. A R Butler *Chem. Ind.* 828 (1995)
11. J S Stamler, M Feelisch, in *Methods in Nitric Oxide Research* (Eds M Feelisch, J S Stamler) (Chichester: Wiley, 1996) p. 19
12. F Murad *Angew. Chem., Int. Ed. Engl.* **38** 1856 (1999)
13. R F Furchgott *Angew. Chem., Int. Ed. Engl.,* **38** 1870 (1999)
14. L J Ignarro *Angew. Chem., Int. Ed. Engl.* **38** 1882 (1999)
15. R P Patel, J McAndrew, H Sellak, C R White, H Jo, B A Freeman, V M Darley-Usmar *Biochim. Biophys. Acta* **1411** 385 (1999)
16. S A Lipton, Y-B Choi, Z-H Pan, S Z Lei, H-S V Chen, N J Sucher, J Loscalzo, D J Singel, J S Stamler *Nature (London)* **364** 626 (1993)
17. J S Stamler, D J Singel, J Loscalzo *Science* **258** 1898 (1992)
18. A R Butler, F W Flitney, D L H Williams *Trends Pharmacol. Sci.* **16** 18 (1995)
19. M A de Groote, T Testerman, Y Xu, G Stauffer, F C Fang *Science* **272** 414 (1996)
20. M N Hughes *Biochim. Biophys. Acta* **1411** 263 (1999)
21. J J Kirchner, S T Sigurdsson, P B Hopkins *J. Am. Chem. Soc.* **114** 4021 (1992)
22. A H Elcock, P D Lyne, A J Mulholland, A Nandra, W G Richards *J. Am. Chem. Soc.* **117** 4706 (1995)
23. P Mack, J M Dyke, T G Wright *Chem. Phys.,* **218** 243 (1997)
24. L Angel, A J Stace *J. Phys. Chem., A* **102** 3037 (1998)
25. G A Olah, O Farooq, G K S Prakash, in *Activation and Functionalization of Alkanes* (Ed. C L Hill) (New York: Wiley, 1989) p. 27
26. G A Olah, G K S Prakash, R E Williams, L D Field, K Wade *Hypercarbon Chemistry* (New York: Wiley-Interscience, 1987)
27. G A Olah, G K S Prakash, J Sommer *Superacids* (New York: Wiley-Interscience, 1985)
28. G A Olah, J G Shih, B P Singh, B G B Gupta *J. Org. Chem.* **48** 3356 (1983)
29. G A Olah, P Ramaiah, C B Rao, G Sandford, R Golam, N O Trivedi, J A Olah *J. Am. Chem. Soc.* **115** 7246 (1993)
30. G A Olah, B G B Gupta *J. Org. Chem.* **45** 3532 (1980)
31. A A Fokin, P A Gunchenko, S A Peleshanko, P von R Schleyer, P R Schreiner *Eur. J. Org. Chem.* 855 (1999)
32. P R Schreiner, P von R Schleyer, H F Schaefer III *J. Am. Chem. Soc.* **115** 9659 (1993)
33. P R Schreiner, P von R Schleyer, H F Schaefer III *J. Am. Chem. Soc.* **117** 453 (1995)
34. M L Scheinbaum, M B Dines *Tetrahedron Lett.* 2205 (1971)
35. G H Lee, J M Lee, W B Jeong, K Kim *Tetrahedron Lett.* **29** 4437 (1988)
36. R L Danheiser, D A Becker *Heterocycles* **25** 277 (1987)

37. H O Bertrand, J L Burgot *Phosphorus Sulfur Silicon Relat. Elem.* **97** 103 (1994)
38. A V Pankratov *Khimiya Ftoridov Azota* (The Chemistry of Nitrogen Fluorides) (Moscow: Khimiya, 1973)
39. Q B Broxterman, H Hogeveen, R F Kingma, F van Bolhuis *J. Am. Chem. Soc.* **107** 5722 (1985)
40. G A Olah, G Salem, J S Staral, T-L Ho *J. Org. Chem.* **43** 173 (1978)
41. V S Savostin, I I Krylov, A P Kutepov, A I Rapkin, A V Fokin *Izv. Akad. Nauk SSSR, Ser. Khim.* 1851 (1990) [a]
42. R Chang, K Kim *Bull. Korean Chem. Soc.* **16** 475 (1995)
43. R M Minyaev, M E Kletskii, V I Minkin *Zh. Org. Khim.* **23** 2508 (1987) [b]
44. K Raghavachari, W D Reents, Jr, R C Haddon *J. Comput. Chem.* **7** 265 (1986)
45. V I Minkin, I A Yudilevich, R M Minyaev *Zh. Org. Khim.* **23** 717 (1987) [b]
46. M N Glukhovtsev, P von R Schleyer, N J R von E Hommes, V I Minkin *Chem. Phys. Lett.* **205** 529 (1993)
47. G A Olah, P Schilling, P W Westerman, H C Lin *J. Am. Chem. Soc.* **96** 3581 (1974)
48. G I Borodkin, I R Elanov, V A Podryvanov, M M Shakirov, V G Shubin *J. Am. Chem. Soc.* **117** 12863 (1995)
49. G I Borodkin, I R Elanov, M M Shakirov, V G Shubin *Zh. Org. Khim.* **33** 363 (1997) [b]
50. G I Borodkin, I R Elanov, A M Genaev, M M Shakirov, V G Shubin *Mendeleev Commun.* 83 (1999)
51. E Bosch, J K Kochi *Res. Chem. Intermed.* **22** 209 (1996)
52. F Blatter, H Frei *J. Phys. Chem.* **97** 1178 (1993)
53. R Rathore, S V Lindeman, J K Kochi *Angew. Chem., Int. Ed. Engl.* **37** 1585 (1998)
54. S Sankararaman, W Lau, J K Kochi *J. Chem. Soc., Chem. Commun.* 396 (1991)
55. J K Kochi *Acta Chem. Scand.* **44** 409 (1990)
56. J K Kochi *Acc. Chem. Res.* **25** 39 (1992)
57. G I Borodkin, V G Shubin *Zh. Org. Khim.* **36** 479 (2000) [b]
58. D Dimitrov, F Fratev *Compt. Rend. Acad. Bulg. Sci.* **16** 729 (1963)
59. D Dimitrov, F Fratev *Compt. Rend. Acad. Bulg. Sci.* **16** 825 (1963)
60. Z J Allan, J Podstata, D Šnobl, J Jarkovský *Tetrahedron Lett.* 3565 (1965)
61. Z J Allan, J Podstata, D Šnobl, J Jarkovský *Collect. Czech. Chem. Commun.* **32** 1449 (1967)
62. E Hunziker, J R Penton, H Zollinger *Helv. Chim. Acta* **54** 2043 (1971)
63. A R Butler, A P Sanderson *J. Chem. Soc., Perkin Trans. 2* 1671 (1974)
64. W D Reents Jr, B S Freiser *J. Am. Chem. Soc.* **102** 271 (1980)
65. R Wolfschütz, H Schwarz. *Int. J. Mass Spectrom. Ion Phys.* **33** 291 (1980)
66. W D Reents Jr, B S Freiser *J. Am. Chem. Soc.* **103** 2791 (1981)
67. J A Stone, D E Splinter, S Y Kong *Can. J. Chem.* **60** 910 (1982)
68. V I Mamatyuk, A N Detsina, Sh M Nagi, Yu V Gatilov, G I Borodkin, I L Mudrakovskii, in *III Vsesoyuz. Soveshch. 'Spektroskopiya Koordinatsionnykh Soedinenii' (Tez. Dokl.), Krasnodar, 1984* [The IIIth All-Union Meeting 'Spectroscopy of Coordination Compounds' (Abstracts of Reports), Krasnodar, 1984] p. 55
69. S Brownstein, E Gabe, F Lee, L Tan *J. Chem. Soc., Chem. Commun.* 1566 (1984)
70. V I Minkin, R M Minyaev, I A Yudilevich, M E Kletskii *Zh. Org. Khim.* **21** 926 (1985) [b]
71. G I Borodkin, Sh M Nagi, Yu V Gatilov, V I Mamatyuk, I L Mudrakovskii, V G Shubin *Dokl. Akad. Nauk SSSR* **288** 1364 (1986) [c]
72. S Brownstein, A Morrison, L K Tan *Can. J. Chem.* **64** 265 (1986)
73. S Brownstein, E Gabe, F Lee, A Piotrowski *Can. J. Chem.* **64** 1661 (1986)
74. S Brownstein, E Gabe, B Irish, F Lee, B Louie, A Piotrowski *Can. J. Chem.* **65** 445 (1987)
75. A E Mefed, Sh M Nagi, G I Borodkin, V I Mamatyuk, V G Shubin *Dokl. Akad. Nauk SSSR* **297** 133 (1987) [c]
76. E K Kim, J K Kochi *J. Org. Chem.* **54** 1692 (1989)
77. K Y Lee, D J Kuchynka, J K Kochi *Inorg. Chem.* **29** 4196 (1990)
78. E K Kim, J K Kochi *J. Am. Chem. Soc.* **113** 4962 (1991)
79. T M Bockman, Z J Karpinski, S Sankararaman, J K Kochi *J. Am. Chem. Soc.* **114** 1970 (1992)
80. G I Borodkin, I R Elanov, M M Shakirov, V G Shubin *Izv. Akad. Nauk, Ser. Khim.* 2104 (1992) [a]
81. E K Kim, J K Kochi *J. Org. Chem.* **58** 786 (1993)
82. K Y Lee, J K Kochi *J. Chem. Soc., Perkin Trans. 2* 237 (1994)
83. E Bosch, J K Kochi *J. Org. Chem.* **59** 3314 (1994)
84. E Bosch, J K Kochi *J. Org. Chem.* **59** 5573 (1994)
85. R Rathore, E Bosch, J K Kochi *Tetrahedron* **50** 6727 (1994)
86. E Bosch, J K Kochi *J. Org. Chem.* **60** 3172 (1995)
87. G I Borodkin, V A Podryvanov, M M Shakirov, V G Shubin *J. Chem. Soc., Perkin Trans. 2* 1029 (1995)
88. R Rathore, S V Lindeman, J K Kochi *J. Am. Chem. Soc.* **119** 9393 (1997)
89. S Skokov, R A Wheeler *J. Phys. Chem. A,* **103** 4261 (1999)
90. S M Hubig, J K Kochi *J. Am. Chem. Soc.* **122** 8279 (2000)
91. A R Butler, A P Sanderson *J. Chem. Soc., Perkin Trans. 2* 989 (1972)
92. V L Lobachev, O B Savsunenko, E S Rudakov *Kinet. Katal.* **32** 17 (1991) [d]
93. J H Atherton, R B Moodie, D R Noble *J. Chem. Soc., Perkin Trans. 2* 699 (1999)
94. J H Atherton, R B Moodie, D R Noble *J. Chem. Soc., Perkin Trans. 2* 229 (2000)
95. M V Gorelik, V I Lomzakova, E A Khamidova, V Ya Shteiman, M G Kuznetsova *Zh. Org. Khim.* **31** 408 (1995) [b]
96. L R Dix, R B Moodie *J. Chem. Soc., Perkin Trans. 2* 1097 (1986)
97. M V Gorelik, V I Lomzakova, E A Khamidova, V Ya Shteiman, M G Kuznetsova, A M Andrievskii *Zh. Org. Khim.* **31** 553 (1995) [b]
98. D J Mills, J H Ridd *J. Chem. Soc., Perkin Trans. 2* 637 (1980)
99. V I Minkin, R M Minyaev *Zh. Org. Khim.* **15** 1569 (1979) [b]
100. R M Minyaev *Zh. Org. Khim.* **20** 897 (1984) [b]
101. V I Minkin, R M Minyaev *Neklassicheskie Struktury Organicheskikh Soedinenii* (Non-classical Structures of Organic Compounds) (Rostov-on-Don: Rostov State University, 1985)
102. J B Stothers *Carbon-13 NMR Spectroscopy* (New York: Academic Press, 1972)
103. V A Koptyug *Arenonievye Iony. Stroenie i Reaktsionnaya Sposobnost'* (Arenonium Ions. Structure and Reactivity) (Novosibirsk: Nauka, 1983)
104. V I Minkin, B Ya Simkin, R M Minyaev *Kvantovaya Khimiya Organicheskikh Soedinenii. Mekhanizmy Reaktsii* (Quantum Chemistry of Organic Compounds. Mechanisms of Reactions) (Moscow: Khimiya, 1986)
105. R Rathore, J K Kochi *J. Org. Chem.* **63** 8630 (1998)
106. V F Loktev, V G Shubin *Izv. Akad. Nauk SSSR, Ser. Khim.* 2276 (1987) [a]
107. G I Borodkin, I R Elanov, V G Shubin, in *Book of Abstracts of the 13th IUPAC Conference on Physical Organic Chemistry, Inchon, 1996* p. 243
108. L Eberson, F Radner *Acc. Chem. Res.* **20** 53 (1987)
109. A S Morkovnik *Usp. Khim.* **57** 254 (1988) [*Russ. Chem. Rev.* **57** 144 (1988)]
110. V N Kondrat'ev (Ed.) *Energii Razryva Khimicheskikh Svyazei. Potentsialy Ionizatsii i Srodstvo k Elektronu* (Energies of Rupture of Chemical Bonds. Ionisation Potentials and Electron Affinities) (Moscow: Nauka, 1974)
111. A S Morkovnik, O Yu Okhlobystin *Zh. Obshch. Khim.* **55** 692 (1985) [e]
112. A S Morkovnik, N M Dobaeva, O Yu Okhlobystin *Zh. Obshch. Khim.* **59** 921 (1989) [e]
113. G I Borodkin, I R Elanov, V G Shubin, in *Sovremennye Problemy Organicheskogo Sinteza (Tez. Dokl. Vsesoyuz. Konf. Molodykh Uchenykh), Irkutsk, 1988* [Topical Problems of Organic Synthesis (Abstracts of Reports of The All-Union Conference of Young Scientists), Irkutsk, 1988] p. 141
114. G I Borodkin, I R Elanov, M M Shakirov, V G Shubin, in *Tez. Dokl. Chetvertoi Vsesoyuz. Konf. po Khimii Nizkikh Temperatur, Moskva, 1988* (Abstracts of Reports of the Fourth All-Union Conference on the Chemistry of Low Temperatures, Moscow, 1988) p. 119
115. G I Borodkin, I R Elanov, M M Shakirov, V G Shubin *Izv. Akad. Nauk SSSR, Ser. Khim.* 206 (1989) [a]
116. G I Borodkin, I R Elanov, M M Shakirov, V G Shubin *J. Phys. Org. Chem.* **6** 153 (1993)

117. G I Borodkin, I R Elanov, M M Shakirov, V G Shubin *Zh. Org. Khim.* **27** 889 (1991) [b]
118. G I Borodkin, I R Elanov, P-C Cheng, L T Scott, V G Shubin, in *Book of Abstracts of the Sixth European Symposium on Organic Reactivity, Louvain-la-Neuve, 1997* p. 98
119. G I Borodkin, E I Chernyak, M M Shakirov, V G Shubin *Zh. Org. Khim.* **26** 785 (1990) [b]
120. N V Vasil'eva, V F Starichenko, V A Koptyug *Zh. Org. Khim.* **23** 1020 (1987) [b]
121. F Radner *J. Org. Chem.* **53** 702 (1988)
122. M Tanaka, H Nakashima, M Fujiwara, H Ando, Y Souma *J. Org. Chem.* **61** 788 (1996)
123. A Castro, E Iglesias, J R Leis, M E Peña, J V Tato, D L H Williams *J. Chem. Soc., Perkin Trans. 2* 1165 (1986)
124. R N Loeppky, W Cui *Tetrahedron Lett.* **39** 1845 (1998)
125. R N Loeppky, Y T Bao, J Bae, L Yu, G Shevlin, in *Nitrosamines and Related N-Nitroso Compounds. Chemistry and Biochemistry* (Eds R N Loeppky, C J Michejda) (Washington, DC: American Chemical Society, 1994) p. 52
126. D L H Williams, in *Nitrosamines and Related N-Nitroso Compounds. Chemistry and Biochemistry* (Eds R N Loeppky, C J Michejda) (Washington, DC: American Chemical Society, 1994) p. 66
127. M A Freitas, R A J O'Hair, J A R Schmidt, S E Tichy, B E Plashko, T D Williams *J. Mass Spectrom.* **31** 1086 (1996)
128. A S Morkovnik, L N Divaeva, O Yu Okhlobystin *Zh. Obshch. Khim.* **58** 2174 (1988) [e]
129. C York, G K S Prakash, Q Wang, G A Olah *Synlett* 425 (1994)
130. H Cai, J C Fishbein *J. Am. Chem. Soc.* **121** 1826 (1999)
131. S A Kulkarni, S S Pundlik *Chem. Phys. Lett.* **245** 143 (1995)
132. M Aschi, F Grandinetti *Chem. Phys. Lett.* **267** 98 (1997)
133. L L Torday, M B Santillán, G M Ciuffo, E A Jáuregui, J Pataricza, J G Papp, I G Csizmadia *J. Mol. Struct. (Theochem)* **465** 69 (1999)
134. F Cacace, G de Petris, F Pepi *Proc. Natl. Acad. Sci. USA* **94** 3507 (1997)
135. Yu A Zhdanov, V I Minkin *Korrelyatsionnyi Analiz v Organicheskoi Khimii* (Correlation Analysis in Organic Chemistry) (Rostov-on-Don: Rostov State University, 1966)
136. G A Olah, J A Olah, N A Overchuk *J. Org. Chem.* **30** 3373 (1965)
137. N N Makhova, G A Karpov, A N Mikhailyuk, A E Bova, L I Khmel'nitskii, S S Novikov *Izv. Akad. Nauk SSSR, Ser. Khim.* 226 (1978) [a]
138. G I Borodkin, V G Shubin, R V Andreev, in *Book of Abstracts of the International Conference on Reactive Intermediates and Reaction Mechanisms, Ascona, 1998* p. 38
139. R V Andreev, G I Borodkin, V G Shubin, in *Molodezhnaya Nauchnaya Shkola po Organicheskoi Khimii (Tez. Dokl.), Ekaterinburg, 1999* [Young Researchers' School on Organic Chemistry (Abstracts of Reports), Ekaterinburg, 1999] p. 65
140. G I Borodkin, R V Andreev, I R Elanov, V G Shubin, in *Book of Abstracts of the 7th European Symposium on Organic Reactivity, Ulm, 1999* p. 136
141. H T Nagasawa, P S Fraser, D L Yuzon *J. Med. Chem.* **16** 583 (1973)
142. M J Crookes, D L H Williams *J. Chem. Soc., Chem. Commun.* 571 (1988)
143. G A Olah, P Ramaiah *J. Org. Chem.* **58** 4639 (1993)
144. J R Leis, M E Peña, D L H Williams *J. Chem. Soc., Chem. Commun.* 45 (1987)
145. J R Leis, M E Peña, D L H Williams, S D Mawson *J. Chem. Soc., Perkin Trans. 2* 157 (1988)
146. A Castro, M González, F Meijide, M Mosquera *J. Chem. Soc., Perkin Trans. 2* 2021 (1988)
147. C York, G K S Prakash, G A Olah *Tetrahedron* **52** 9 (1996)
148. G A Olah, M Arvanaghi, L Onannesian, G K S Prakash *Synthesis* 785 (1984)
149. Y L Chow, K Iwai *J. Chem. Soc., Perkin Trans. 2* 931 (1980)
150. F Meijide, G Stedman *J. Chem. Soc., Perkin Trans. 2* 1087 (1988)
151. A Coello, F Meijide, J V Tato *J. Chem. Soc., Perkin Trans. 2* 1677 (1989)
152. F Cacace, G de Petris, F Pepi, I Rossi, A Venturini *J. Am. Chem. Soc.* **118** 12 719 (1996)
153. F Bernardi, M A Robb, I Rossi, A Venturini *J. Org. Chem.* **58** 7074 (1993)
154. M Aschi, F Grandinetti *Chem. Phys. Lett.* **258** 123 (1996)
155. G S Heo, P E Hillman, R A Bartsch *J. Heterocycl. Chem.* **19** 1099 (1982)
156. R Savoie, M Pigeon-Gosselin, A Rodrigue, R Chênevert *Can. J. Chem.* **61** 1248 (1983)
157. R L Elsenbaumer *J. Org. Chem.* **53** 437 (1988)
158. S Ricard, P Audet, R Savoie *J. Mol. Struct.*, **178** 135 (1988)
159. G A Olah, B G B Gupta, S C Narang *J. Am. Chem. Soc.* **101** 5317 (1979)
160. K A Jørgensen, M T M El-Wassimy, S-O Lawesson *Acta Chem. Scand., Ser. B* **37** 785 (1983)
161. K A Jørgensen, S-O Lawesson *J. Chem. Soc., Perkin Trans. 2* 231 (1985)
162. R G Pearson *Symmetry Rules for Chemical Reactions. Orbital Topology and Elementary Processes* (New York: Wiley, 1976)
163. O Dolgounitcheva, V G Zakrzewski, J V Ortiz, G V Ratovski *Int. J. Quantum Chem.* **70** 1037 (1998)
164. K A Jørgensen *J. Org. Chem.* **50** 4758 (1985)
165. G I Borodkin, E B Belikova, M M Shakirov, V G Shubin *Zh. Org. Khim.* **34** 1868 (1998) [b]
166. E Bosch, J K Kochi *J. Chem. Soc., Perkin Trans. 1* 2731 (1996)
167. K Kobayashi, N Deguchi, E Horn, N Furukawa *Angew. Chem., Int. Ed. Engl.* **37** 984 (1998)
168. A D Williamson, J L Beauchamp *J. Am. Chem. Soc.* **97** 5714 (1975)
169. T Wyttenbach, M T Bowers *J. Phys. Chem.* **96** 8920 (1992)
170. G A Olah, B G B Gupta, S C Narang *Synthesis* 274 (1979)
171. C Matt, A Wagner, C Mioskowski *J. Org. Chem.* **62** 234 (1997)
172. R D Bach, T H Taaffee, S J Rajan *J. Org. Chem.* **45** 165 (1980)

[a] — *Russ. Chem. Bull. (Engl. Transl.)*
[b] — *Russ. J. Org. Chem. (Engl. Transl.)*
[c] — *Dokl. Chem. Technol., Dokl. Chem. (Engl. Transl.)*
[d] — *Kinet. Catal. (Engl. Transl.)*
[e] — *Russ. J. Gen. Chem. (Engl. Transl.)*

Russian Chemical Reviews **70** (3) 231 – 264 (2001) © 2001 Russian Academy of Sciences and Turpion Ltd

DOI 10.1070/RC2001v070n03ABEH000626

Chemistry of xenon derivatives. Synthesis and chemical properties

V K Brel, N Sh Pirkuliev, N S Zefirov

Contents

I.	Introduction	231
II.	Synthesis and properties of xenon difluoride-based reagents	231
III.	Reactions of xenon difluoride and its derivatives with unsaturated compounds	233
IV.	Reactions of xenon derivatives with aromatic and polyfluoroaromatic compounds	236
V.	Reactions of xenon difluoride with organic acids and their derivatives	239
VI.	Organic xenon(II) compounds containing the C – Xe bond	242
VII.	Reactions of xenon difluoride with nitrogen-containing compounds	245
VIII.	Oxidative fluorination of organoelement compounds by xenon difluoride and its derivatives	248
IX.	Miscellaneous reactions	258

Abstract. The published data on the synthesis and chemical transformations of xenon derivatives are generalised and analysed. The bibliography includes 489 references.

I. Introduction

Xenon derivatives were obtained for the first time in 1962 by Bartlett [1] who used elementary xenon and PtF_6 as the oxidant to synthesise a xenon-containing salt.

$$Xe + PtF_6 \longrightarrow XePtF_6$$

Further studies showed that xenon compounds can be synthesised from elementary xenon and other oxidants. For example, the oxidation of elementary xenon by AgF_2 in anhydrous HF in the presence of BF_3 (see Ref. 2) results in XeF_2, whereas in the presence of AsF_5 the cation $Xe_2F_3^+$ is formed (see Refs 2 – 5).

$$2AgF_2 + 2BF_3 + Xe \xrightarrow{HF(liq)} 2AgBF_4 + XeF_2$$

$$4AgF_2 + 5AsF_5 + 2Xe \xrightarrow{HF(liq)} 4AgAsF_6 + Xe_2F_3^+AsF_6^-$$

Mass-spectrometric studies of the reaction of xenon with SiF_4 in the gas phase revealed the presence of the cation F_3SiXe^+ (see Ref. 6), whereas the formation of the cations $C_2H_4Xe^+$ and $C_2H_4XeF^+$ was established in reactions where the cations Xe_2F^+ or XeF_2^+ were generated in the presence of ethene (see Ref. 7). These reactions present substantial theoretical interest, since they illustrate the high synthetic potential of xenon.

At present xenon chemistry rests predominantly on fluorinated derivatives of xenon, such as xenon tetrafluoride and particularly xenon difluoride, the latter being produced by different manufacturers. The methods for the direct synthesis of XeF_2 and XeF_4 from fluorine and xenon at elevated temperatures were published in the early 1960's independently by several groups of investigators.[8,9] Further studies [10] were mostly directed at the elaboration of more convenient and simpler procedures for the preparation of xenon derivatives. A variety of inorganic xenon derivatives, both unstable and sufficiently stable in a broad temperature interval, were synthesised within a relatively short period of time. The first xenon derivatives containing Xe – N (see Ref. 11), Xe – B (see Ref. 12) and Xe – C bonds (see Ref. 13) were also prepared.

The interest in xenon chemistry stimulated the appearance of numerous reviews. Some of those [14 – 35] dealt with the discovery of noble gases, the chemistry of inorganic xenon derivatives and their applications in the fluorination of unsaturated and aromatic compounds. The physical and chemical properties of noble gas derivatives have been documented.[22 – 24] In some publications (see, *e.g.*, Refs 26, 27 and 32), xenon chemistry is considered in only a little detail and mostly in connection with other fields of chemistry, *e.g.*, the synthesis of organofluorine compounds, *etc.* All of these reviews generalised the literature data published before the early 1990's.

The aim of this review is to systematise, analyse and generalise the literature data concerning the synthesis and chemical properties of xenon derivatives with special emphasis on the chemistry of xenon difluoride and its derivatives.

II. Synthesis and properties of xenon difluoride-based reagents

At present, xenon difluoride is the only commercially available xenon derivative. A characteristic feature of this reagent is that it behaves as a radical fluorinating agent in the gas phase or under irradiation and as an electrophilic agent under other conditions. It is of note that the reactivity of XeF_2 increases dramatically in the presence of Lewis acids, apparently due to ionization of the XeF_2 molecule resulting in the formation of $XeF^+MF_n^-$ or $Xe_2F_3^+MF_n^-$ salts which are both strong oxidants.[35,36]

Some properties of xenon difluoride, *e.g.*, melting point, enthalpy of formation, critical parameters, solubility, maximum permissible concentrations, *etc.*, have been documented in earlier publications.[3,20 – 24,29,30,36 – 39]

V K Brel, N Sh Pirkuliev Institute of Physiologically Active Compounds, Russian Academy of Sciences, 142432 Chernogolovka, Moscow Region, Russian Federation. Fax (7-095) 913 21 13. Tel. (7-095) 913 21 13.
E-mail: brel@ipac.ac.ru (V K Brel).
Tel. (7-095) 939 51 55 (N Sh Pirkuliev)
N S Zefirov Department of Chemistry, M V Lomonosov Moscow State University, Leninskie Gory, 119899 Moscow, Russian Federation.
Fax (7-095) 932 88 46. Tel. (7-095) 939 16 20, (7-095) 524 50 62

Received 5 September 2000
Uspekhi Khimii **70** (3) 262 – 298 (2001); translated by R L Birnova

The methods used for the synthesis of inorganic xenon derivatives can arbitrarily be divided into two main groups, *viz*., reactions of elementary xenon with various oxidising systems and synthesis of fluorinated xenon derivatives directly from xenon and fluorine. Xenon difluoride, -tetrafluoride and -hexafluoride were obtained in good yields by varying xenon and fluorine ratios as well as by selecting appropriate reaction conditions (pressure, temperature).[40–43] A photochemical method was developed in addition to the thermal procedure. Thus UV irradiation of a xenon–fluorine mixture results in xenon fluorides in satisfactory yields.[44–48] By virtue of their simplicity, thermal and photochemical methods are especially popular. These methods allow the synthesis of xenon difluoride with 99% purity. Other fluorinating reagents (with the exception of elementary fluorine) can also be used for the fluorination of elementary xenon. Thus the more readily available and safe ClF_3 was successfully used in the synthesis of large amounts of xenon difluoride,[49] whereas O_2F_2 was used in the synthesis of xenon tetrafluoride and -hexafluoride.[50] Other examples of xenon fluoride synthesis by oxidation of elementary xenon [13–23], *e.g*., irradiation of crystalline xenon by a flux of fluorine atoms, thermocatalytic synthesis,[51,52] γ-irradiation of a fluorine–xenon mixture [53] and electrochemical fluorination, have also been described.[54]

Other xenon halides, *e.g*., xenon chlorides [55,56] and -bromides,[57] are also known, but these compounds are difficult to access due to their low stabilities and are therefore virtually noninvestigated.

Some xenon compounds are synthesised by substitution of ligands for fluorine in the corresponding fluorides. For example, the reaction of xenon fluorides with oxygen-containing substrates yields compounds containing covalent Xe–O or Xe=O bonds.[58] The formation of the Xe=O bond usually occurs upon hydrolysis of xenon fluorides. The hydrolysis of xenon difluoride which gives xenon and hydrogen peroxide has been studied in detail. The Appelman hypothesis [59] about the formation of the oxidising species Xe=O in the first step of hydrolysis was corroborated by other authors.[60–64]

Aqueous solutions of XeF_2 oxidise both inorganic [58–60] and organic compounds.[61–64] The reactions of xenon difluoride with alcohols give reactive alkoxyxenonium fluorides ROXeF which manifest pronounced electrophilic properties (see Section III).

Hydrolysis of xenon hexafluoride by two equivalents of water results in xenon oxytetrafluoride $XeOF_4$ (**1**);[65] the highly explosive xenon trioxide XeO_3 is formed in the presence of excess water, apparently, *via* xenon dioxydifluoride (**2**). Compound **2** reacts with AsF_5 to yield the cation $[XeO_2F]^+$ (compound **3**) or the bridged cationoid structure **4**.[66,67]

$$XeF_6 + 2H_2O \longrightarrow \underset{\mathbf{1}}{XeOF_4} + 2HF$$

$$\underset{\mathbf{2}}{XeO_2F_2} + AsF_5 \xrightarrow{HF} \underset{\mathbf{3}}{[XeO_2F]^+AsF_6^-}$$

$$\underset{\mathbf{2}}{2XeO_2F_2} + AsF_5 \xrightarrow{HF} \underset{\mathbf{4}}{[FO_2XeFXeO_2F]^+AsF_6^-}$$

Xenon oxytetrafluoride $XeOF_4$ (**1**) is formed upon reactions of xenon hexafluoride with SeO_2F_2,[68] $NaNO_3$ [69–71] and TcO_3F.[72] However, these methods have some limitations connected with the use of toxic reagents and the possibility of formation of the explosive xenon trioxide as a by-product. These problems can be overcome by carrying out the reaction with phosphorus oxyfluoride. This reaction proceeds with a nearly quantitative yield; XeO_3 is not formed.[73]

$$XeF_6 + POF_3 \longrightarrow \underset{\mathbf{1}}{XeOF_4} + PF_5$$

Xenon oxytetrafluoride (**1**) can form complexes with alkali metal fluorides [74,75] which are attractive as regards their structural parameters and salts of the $[XeOF_5]Y$ type, *e.g*., where $Y = NO^+$ (see Refs 76–80).

$$XeOF_4 + ONF \longrightarrow NO^+XeOF_5^-$$

Perxenonates pertaining to octavalent xenon derivatives can be obtained by the following scheme:[81]

$$XeF_6 \xrightarrow{HOPOF_2} XeO_3 \xrightarrow{NaOH} Na_4XeO_6 + Xe.$$

Perxenonates are the starting compounds in the preparation of perxenates [82,83] and hydroxenates.[84] Perxenates of virtually all alkali metals,[85] alkaline-earth metals and actinide elements have presently been synthesised.[35] All of them are potent oxidants.[86]

Xenon fluorides react with various oxo acids to give compounds rather stable at low temperatures.[87–95] These reactions have been especially well studied for XeF_2 which forms mono- (**5a–j**) or diesters (**6a–j**) depending on the reagent ratio (Scheme 1).

Scheme 1

$$XeF_2 \xrightarrow[-78\ ^\circ C]{CH_2Cl_2} \begin{cases} \xrightarrow{HOR} \underset{\mathbf{5a-j}}{FXeOR} + HF \\ \xrightarrow{2\,HOR} \underset{\mathbf{6a-j}}{Xe(OR)_2} + 2\,HF \end{cases}$$

Compounds **5** and **6**	R	Ref.
a	OSO_2F	87, 88
b	OSO_2CF_3	89
c	OSO_2Me	89
d	$OCOCF_3$	89–91
e	$OPOF_2$	92
f	$OIOF_4$	93, 94
g	$OClO_3$	87–89
h	$OSeF_5$	95, 96
i	$OTeF_5$	90, 97–99
j	ONO_2	88

The Xe–O bond can also be formed through insertion of XeF_2 into the E=O bond. This approach was used in the reaction of XeF_2 with SO_3 [100] and resulted in mono- (**5a**) or difluorosulfate (**6a**) depending on the reagent ratio.

$$XeF_2 \begin{cases} \xrightarrow{SO_3} \underset{\mathbf{5a}}{FXeOSO_2F} \\ \xrightarrow{2\,SO_3} \underset{\mathbf{6a}}{Xe(OSO_2F)_2} \end{cases}$$

XeF_2 or the monoesters **5a**,**f** react with iodine trifluorodioxide analogously.[94]

$$XeF_2 + IO_2F_3 \xrightarrow[BrF_5 \text{ or } CFCl_3]{SO_2ClF} \underset{\mathbf{5f}}{FXeOIOF_4}$$

$$\underset{\mathbf{5a,f}}{FXeR} + IO_2F_3 \xrightarrow[BrF_5 \text{ or } CFCl_3]{SO_2ClF} \underset{\mathbf{6f,k}}{RXeOIOF_4}$$

R = OSO_2F (**5a**, **6k**), $OIOF_4$ (**5f**, **6f**).

Exchange of ligands (other than fluorine) at the xenon atom is also possible, although this reaction has not been well studied yet.[94]

$$\underset{\mathbf{6i}}{Xe(OTeF_5)_2} + 2\,HOIOF_4 \xrightarrow{CFCl_3} \underset{\mathbf{6f}}{Xe(OIOF_4)_2} + 2\,HOTeF_5$$

In some cases, synthesis of bivalent xenon derivatives is accompanied by the formation of undesirable side products directly from acids and XeF_2. Hydrogen fluoride liberated can be bound by $(Me_3Si)_2NH$ or its formation can be prevented by boric anhydrides of the type $B(OR)_3$ (R = SO_2CF_3, $C(O)CF_3$).[101]

$$XeF_2 \begin{cases} \xrightarrow{B(OSO_2CF_3)_3} \underset{\mathbf{5b}}{FXeOSO_2CF_3} \\ \xrightarrow{2/3B(OC(O)CF_3)_3} \underset{\mathbf{6d}}{Xe(OCOCF_3)_2} + BF_3 \end{cases}$$

The ligands $OTeF_5$ and $OSeF_5$ manifesting pronounced electron-withdrawing properties and maximum stabilising effect in comparison with other known oxygen ligands are the most suitable for the synthesis of tetra- and hexavalent xenon derivatives containing covalent Xe–O bonds.[102,103] The Xe(IV) **7**[104–108] and Xe(VI) **8** and **9**[106–109] derivatives were obtained using $OTeF_5$ as the ligand.

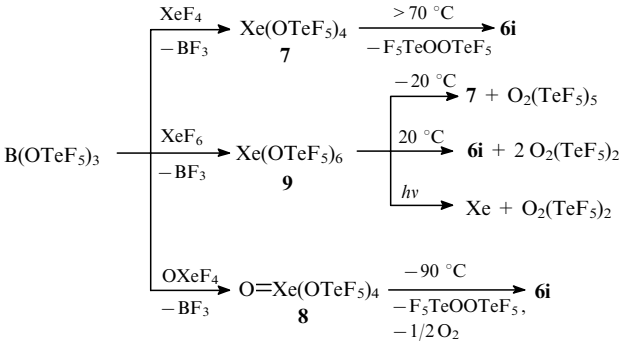

The synthesis of bis(pentafluorotellurium) xenonate (**10**) and tetrakis(pentafluorotellurium) xenonate (**8**) made use of the corresponding boric anhydride.[110]

$$3XeO_2F_2 + 2B(OTeF_5)_3 \longrightarrow 3(F_5TeO)_2XeO_2 + 2BF_3$$
2 **10**

$$3XeOF_4 + 4B(OTeF_5)_3 \longrightarrow 3OXe(OTeF_5)_4 + 4BF_3$$
8

The reaction of xenon with O_2BF_4 results in the evolution of O_2 and F_2 and the formation of white crystals with the composition $FXeBF_2$ (see Ref. 11). This is the only currently known compound containing a Xe–B bond. At 243 K, it decomposes to yield an equimolar mixture of Xe and BF_3.

$$Xe + O_2BF_4 \longrightarrow FXeBF_2 + O_2 + F_2$$

III. Reactions of xenon difluoride and its derivatives with unsaturated compounds

Reactions of XeF_2 with alkenes, alkynes and dienes have been described in detail in reviews.[20,30–33] In the general case, XeF_2 reacts with ethylene and terminal alkenes to afford mixtures of the addition products to the double bond and of the substitution products of fluorine for an alkene hydrogen atom.[111–113] This reaction occurs more selectively in the presence of HF, *viz.*, the addition products to the double bond are formed in up to 95% yields.[114–119] In addition to fluorine derivatives, the reaction of alkenes with XeF_2 in CF_3CO_2H also gives the corresponding trifluoroacetates.[120] 1-Phenyl-substituted cycloalkenes react with XeF_2 in the presence of HF to give a mixture of *cis*- and *trans*-difluorides (in up to 90% yields); the isomer ratio depends on the ring size.[121,122] Fluorohalogenation of the substrate occurs in the presence of a chlorine or a bromine source.[122] The reaction of XeF_2 with acenaphthylene, indene, 1,2- and 1,4-dihydronaphthalenes,[123,124] norbornene[125–130] and norbornadiene[125,130,131] results in the corresponding difluorides. The reaction of aliphatic 1,3-dienes with XeF_2 in the presence of $BF_3 \cdot Et_2O$ gives 1,2-addition products (75%–100%).[132] The reaction of enols with XeF_2 results in α-fluorocarbonyl compounds.[133–140] The reaction of diphenylacetylene with XeF_2 catalysed by trace amounts of HF gives 1,2-diphenyltetrafluoroethane in 50% yield.[141]

The fluorination of acetyl derivatives of D-fucal, D-glucal and D-galactal by XeF_2 has been described.[142–144]

Thus tri-*O*-acetyl-D-glucal reacts with XeF_2 in the presence of $BF_3 \cdot OEt_2$ to give a mixture of 2-fluoroglycosyl fluorides.[142]

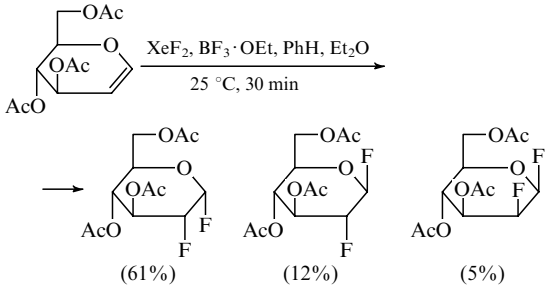

The fluorination of tri-*O*-acetyl-D-galactal by XeF_2 in $CFCl_3$ and subsequent hydrolysis of the reaction product with hydrochloric acid affords 2-deoxy-2-fluoro-D-galactose.[144]

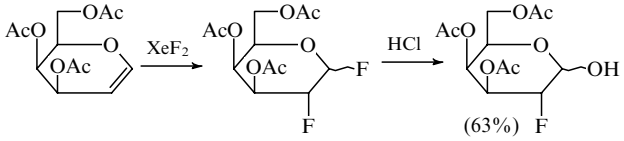

A versatile procedure for chemical doping of π-conjugated polymers, *e.g.*, polyacetylene and poly(*p*-phenylene), has been developed which allows introduction of various anions (A^-) into the polymer. The polymer is treated with xenon difluoride used as the oxidant and the corresponding acid, *e.g.*, HA (XeF_2 : HA = 1 : 2) in liquid HF or CH_2Cl_2.[145] Such a modification of polymers is not accompanied by incidental formation of degradation or fluorination products.

$$P + 1/2n\,XeF_2 + 1/n\,HA \longrightarrow P^{n+}(A^-)_n + 1/2n\,Xe + 1/n\,H$$

where P is the elementary unit of the polymer (CH or C_6H_4), *n* is the degree of doping, A = BF_4, AsF_6, SbF_6, OSO_2F, OSO_2Me or $OCOCF_3$.

The degree of doping of the polymers under study by the XeF_2–2HA system increases with increase in the reaction time and the reagent : polymer molar ratio. The doping ability of anions decreases in the following order: $SbF_6^- > AsF_6^- \geqslant BF_4^- \geqslant OSO_2F^- > OSO_2Me^- > OCOCF_3^-$, which correlates with the order of the relative withdrawing capacity of the corresponding acids in reactions with XeF_2.[22] The maximum degree of doping of poly(*p*-phenylene) (0.97) is achieved with the anion SbF_6^-. This is probably due to the generation of the active species XeF^+ [its electron affinity is 10.4 eV (see Ref. 3)] as a result of complete ionisation of the XeF_2–2HA complex and the formation of $XeF^+SbF_6^-$ (see Ref. 146). It should be noted that the oxidising system XeF_2–2 HA allows variations of the anion A in a broad range, which makes this system superior to oxidants of the AsF_5 and I_2 type.[145]

Reactions of alkenes of different structures with other xenon derivatives including fluoroxenon triflate (**5b**), fluorosulfate (**5a**) and nitrate (**5j**), have been studied.[147–150] These reagents appeared to be more reactive than XeF_2. Xenon bis(fluorosulfate) (**6a**) reacts explosively with ordinary unsaturated hydrocarbons even at low temperatures. On the other hand, electron-deficient alkenes (**11**) yield covalent bis(fluorosulfonates) **12**.[149]

$$Cl(R)C{=}C(R)Cl + Xe(OSO_2F)_2 \xrightarrow[-Xe]{\text{Freon 113, } -10\ ^\circ C} (FSO_2O)Cl(R)CC(R)Cl(OSO_2F)$$
11 **6a** **12**

R = H, Cl, F.

A one-step procedure for the preparation of fluorohalogenoalkenes using the reagent **5b** has recently been proposed.[151] Thus mixing of equimolar amounts of XeF_2 and CF_3CO_2H in anhydrous CH_2Cl_2 and subsequent addition of 1,1-dichloroalkene results in fluorodichloroalkenes **13a–c**, *viz.*, the products of formal substitution of fluorine for the vinylic hydrogen atom.[151] This approach is an alternative to the Swarts fluorination.[152]

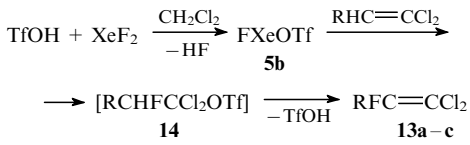

Tf = CF_3SO_2; R = H (**13a**, 65%), Me (**13b**, 66%), Et (**13c**, 63%).

The addition of the reagent **5b** follows the Markownikoff rule and yields the adducts **14**. Spontaneous elimination of trifluoromethanesulfonic acid from the adducts **14** can be attributed to the fact that the easily leaving triflate group and two electronegative chlorine atoms are localised at the same carbon atom.

cis-β-Fluorocyclohexyl fluorosulfate (**15**) was obtained as the main product in 50% yield in the reaction of xenon fluorosulfonate fluoride (**5a**) with cyclohexene; the reaction with tetrachloroethylene gave the adduct **16**, which was unstable at room temperature and could be identified as ethyl dichlorofluoroacetate (**17**).[150]

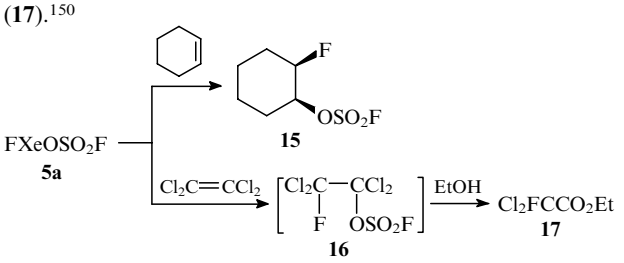

The reactions of compounds **5a**,**b**,**j** with hex-1-ene result in β-fluoroalkyl sulfonates or nitrates **18** and **19** with the predominance of the Markownikoff regioisomers **18a**,**b**,**j**.[148,149]

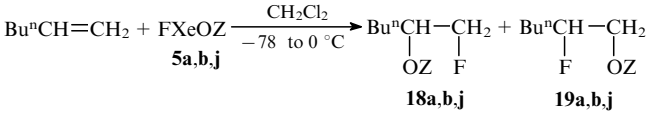

Reagent	Z	Yield (%)	
		18	**19**
5a	SO_2F	34	17
5b	Tf	48	15
5j	NO_2	18	9

Analogous reactions with cyclohexene yield predominantly *cis*-adducts. Thus *cis*-2-fluorocyclohexyl triflate **20b** is exclusively formed in 75% yield when the reagent **5b** is used. The reagent **5a** reacts with cyclohexene to give a mixture of the *cis*- and *trans*-isomers **20a** and **21a** in a 3 : 1 ratio (the total yield is 64%). The reaction of cyclohexene with the reagent **5j** gives a mixture of the isomers **20j** and **21j** in a total yield of 25%.[148,150]

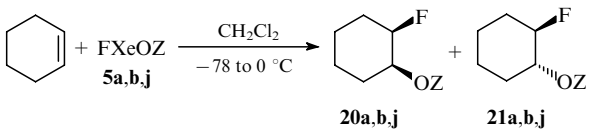

Z = OSO_2F (**a**), OTf (**h**), ONO_2 (**j**).

Earlier, it was assumed[20,30–34] that the addition of the reagents **5a**,**b**,**j** to alkenes occurs by a carbocationic mechanism involving the 'electrophilic' fluorine. However, the selective formation of *cis*-adducts in the reaction with cyclohexene cannot be rationalised within the framework of this mechanism. Based on the fact that the addition of triflates and perchlorates of trivalent iodine to alkenes also results in *cis*-adducts[153–162] and taking into account the isoelectronic nature of I(III) and Xe(II) derivatives, a reaction mechanism was proposed[148] which includes electrophilic addition of the reagents **5** to the double bond and the formation of the intermediate **22**.

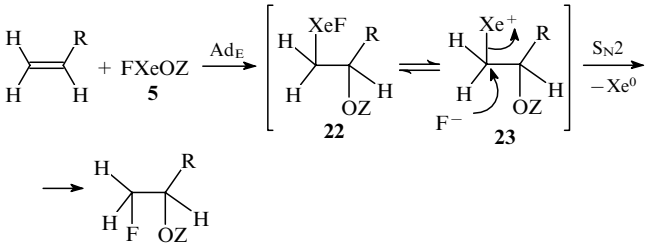

This reaction occurs in a *trans*-selective manner as in the case of trivalent iodine compounds.[153–162] Its second step includes stereospecific nucleophilic substitution of fluorine for xenon by the S_N2 mechanism, which is accompanied by an inversion of configuration and the formation of the *cis*-product.[163] Additional evidence in favour of the intermediate formation of the organoxenon compounds **22** and **23** containing the C–Xe bond in these reactions will be given in Section VI.

The reaction of XeF_2 with alkenes in the presence of aliphatic alcohols has been studied.[164–169] It was shown that methanolysis of XeF_2 yields an unstable electrophilic intermediate with hypothetical composition MeOXeF, which generates a potential electrophilic fluorine donor **24** in the presence of HX. MeOXeF reacts with boron trifluoride to give the positive oxygen electrophile **25**. The reaction of the intermediates **24** or **25** with alkenes results in carbocations containing F or OR in the α-position.[164]

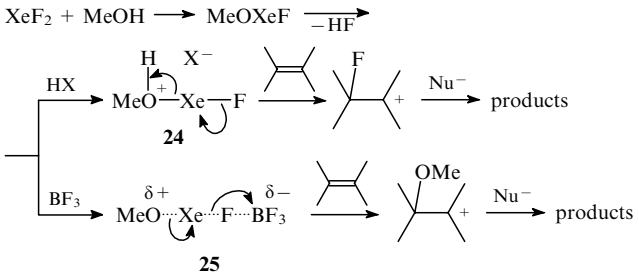

It was found[164] that the reaction of XeF_2 with alkenes in methanol involves MeOXeF rather than MeOF[170] the formation of which requires a stronger oxidant than XeF_2 (*e.g.*, F_2). In the absence of alkenes, MeOXeF disproportionates quantitatively with the formation of HF, Xe and CH_2O. The presence of an acid catalyst strongly affects the regioselectivity of the reaction. In the presence of hydrogen fluoride, MeOXeF reacts with *cis*- and *trans*-1-phenylpropenes **26** to give the final Markownikoff products **27** and **28**, whereas in the presence of BF_3 (in Et_2O or MeOH) the anti-Markownikoff products **29** predominate in the reaction mixture.[164,165]

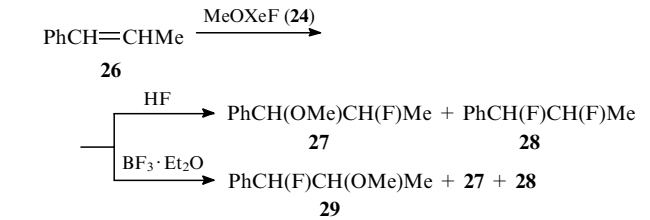

Catalyst	Yield of **27** (%)		Yield of **28** (%)		Yield of **29** (%)	
	erythro	*threo*	*erythro*	*threo*	*erythro*	*threo*
cis-**26** as the substrate						
HF	0	25	2	73	0	0
$BF_3 \cdot Et_2O$	0	1	3	26	27	43
trans-**26** as the substrate						
HF	0	2	2	96	0	0
$BF_3 \cdot Et_2O$	1	0	3	29	20	47

^1H and ^{13}C NMR spectroscopy and mass spectrometry were used to study the regio- and stereochemistry of reactions of indene

with the unstable intermediates **30a–j** formed upon the reaction of XeF_2 with the corresponding alcohols.[164–166, 169]

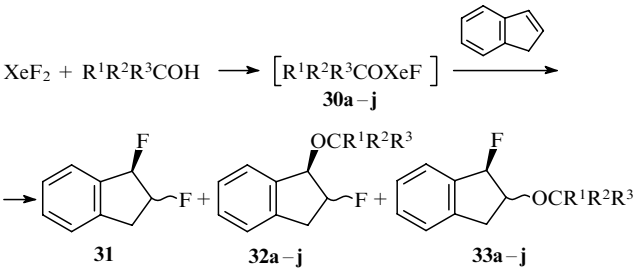

31 **32a–j** **33a–j**

$R^1 = R^2 = R^3 = H$ (**a**); $R^1 = R^2 = Me$, $R^3 = H$ (**b**); $R^1 = R^2 = R^3 = Me$ (**c**); $R^1 = ClCH_2$, $R^2 = R^3 = H$ (**d**); $R^1 = FCH_2$, $R^2 = R^3 = H$ (**e**); $R^1 = CF_3$, $R^2 = R^3 = H$ (**f**); $R^1 = R^2 = R^3 = CF_3$ (**g**); $R^1 = CF(NO_2)_2$, $R^2 = R^3 = H$ (**h**); $R^1 = C(NO_2)_3$, $R^2 = R^3 = H$ (**i**); $R^1 = MeC(NO_2)_2$, $R^2 = R^3 = H$ (**j**).

The reaction with xenon methoxyfluoride (**30a**) in the presence of HF (MeOH, 0–12 °C) gives predominantly a mixture of *cis*- and *trans*-isomers of the methoxy fluoride **32a** (52% and 46%, respectively); the yield of yet another reaction product, *viz*., the difluoride *cis*-**31**, is 2%.

The anti-Markownikoff adducts **33** (26% of the *cis*-isomer and 52% of the *trans*-isomer) are the main products of the reaction carried out in the presence of $BF_3 \cdot Et_2O$ (MeOH, 0 °C).[164, 165]

Alkoxyfluorides **32b**,**c** (*cis*- and *trans* isomers) are the main reaction products formed in the presence of protic catalysts (HF generated *in situ*) in Pr^iOH or Bu^tOH. Alkoxy fluorides **33b**,**c** (*cis*- and *trans*-isomers) are formed first in the presence of $BF_3 \cdot OEt_2$. In both cases, *cis*- and *trans*-difluoroindanes **31** are formed as admixtures. Compounds **33b**,**c** rearrange under the reaction conditions into the thermodynamically more stable adducts **32b**,**c**. In the absence of $BF_3 \cdot Et_2O$, the rearrangement occurs more slowly, *viz*., within several days. Reactions with alcohols containing electron-withdrawing substituents occur faster due to their higher acidities. The product yields in CF_3CO_2H decrease owing to the polymerisation of indene.[166, 169]

The nortricyclane derivatives **38** and **39** were also identified in reactions with norbornene along with the isomeric difluorides **34** and the methoxy fluorides **35**, **36** and **37**.[164, 165]

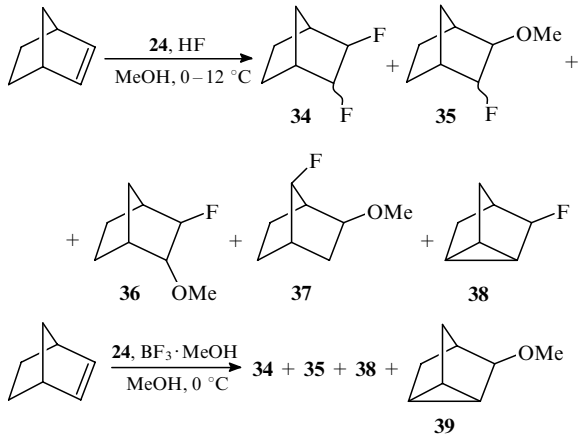

The reaction of 1,3-dimethylbuta-1,3-diene with XeF_2 in methanol in the presence of a catalyst (HF or $BF_3 \cdot MeOH$) affords a mixture of various 1,2- and 1,4-adducts, *viz*., difluorides and methoxy fluorides. The addition occurs both according to the Markownikoff rule and against it.[165]

In the absence of a catalyst, dihydropyrane (**40**) reacts with XeF_2 and MeOH to give *cis*- and *trans*-isomers of the adduct **41**.[165]

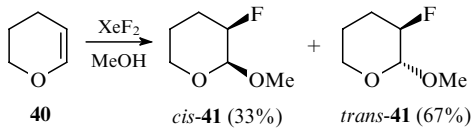

40 *cis*-**41** (33%) *trans*-**41** (67%)

It is of note that hex-1-ene, buta-1,3-diene and methyl crotonate do not react with MeOXeF; in this case, the latter rapidly disproportionates to afford formaldehyde quantitatively.[165]

Shellhamer *et al*.[166] studied the mechanism of the reaction of alkenes with XeF_2 in the presence of alcohols using indene as an example.

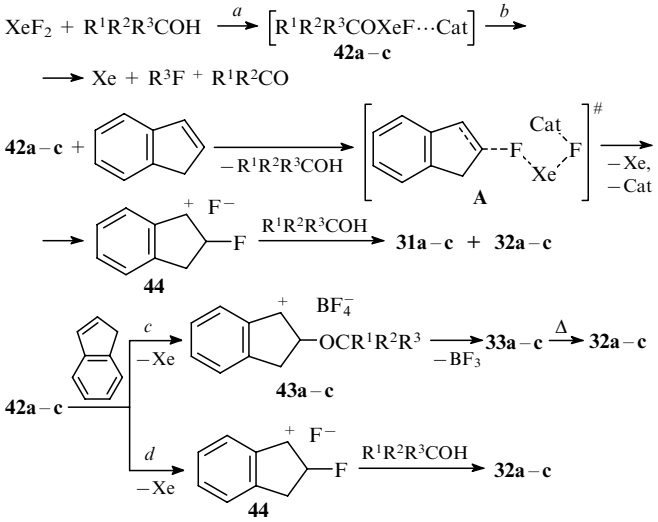

(*a*) Cat, slow step; (*b*) fast step; (*c*) BF_3, fast step; (*d*) HF, fast step.

In the absence of alkenes or in the case of their low reactivities, alcohols undergo oxidation into aldehydes or ketones with the concomitant formation of alkyl fluorides and evolution of elementary xenon (routes *a* and *b*). It is believed that the complexes **42a–c** of xenon alkoxy fluorides **30a–c** with the catalyst are the intermediate products of this reaction. The intermediates **42a–c** are trapped by highly reactive alkenes (*e.g*., indene) to give complexes **A**; further conversions depend on the nature of the alcohol and the catalyst. In the presence of BF_3, xenon alkoxy fluorides **30a–c** react with indene as positive oxygen electrophiles to give, after elimination of xenon, 2-alkoxyindan-1-ylium tetrafluoroborates (**43a–c**). Their stabilisation is accompanied by the liberation of BF_3 and the formation of compounds **33a–c** (route *c*). The latter rearrange into more stable isomers **32a–c**. The intermediates **42a–c** act as electrophilic fluorine donors in the reaction with protic catalysts (HF); after the intermediate 2-fluoroindan-1-ylium fluoride **44** has been formed, they give compounds **32a–c** (route *d*).[166] The dependence of the direction of the reaction on the nature of the alcohols used (*e.g*., their acidity) is explained in the following way. In the presence of alkoxy substituents containing electron-withdrawing groups (CF_3CH_2, CF_3) in the intermediates **42**, they react as open ions (route *d*), whereas in the presence of electron-donor groups in alkoxy substituents they react with indene to afford the soft bridged intermediates **45a–c**. The reaction of these intermediates with the tetrafluoroborate anion results in the predominant formation of the *trans*-adducts **33a–c** which are transformed into compounds **32a–c** under the reaction conditions.[166]

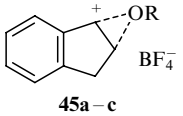

45a–c

R = Me (**a**), Pr^i (**b**), Bu^t (**c**).

The reaction of 2-methylpent-1-ene with XeF_2 in CF_3CH_2OH at 0–25 °C yields the alkoxy fluorides **46** (route *c*) and **47** (route *d*) in a total yield of 76% and in a *ca.* 1 : 1 ratio (these compounds were isolated by preparative GLC). Only the difluorides **48** and **49** could be prepared from hex-1-ene under analogous conditions, which corresponds to direct fluorination (route *d*).

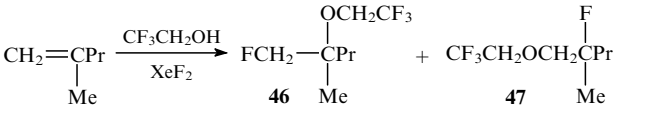

tert-Butyl hypochlorite and XeF_2 react with cyclohexene in CCl_4 to give a complex mixture of compounds with *trans*-1-chloro-2-fluorocyclohexane (**50**) as the main product.[171]

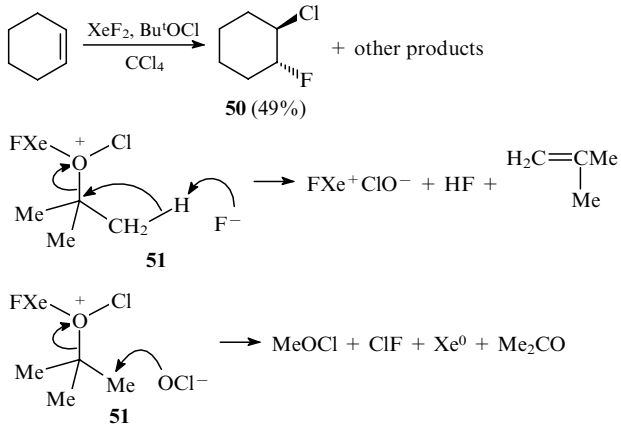

In this case, the lack of selectivity is attributed[171] to the formation of an intermediate complex of xenon fluoride with ButOCl (**51**), which generates various reactive species upon decomposition. It should be noted that *tert*-butyl hypochlorite and XeF_2 do not react with cyclohexene when used separately.[171]

This reaction was extended to other hypohalites (MeOX, ButOX, where X = Cl, Br).[171,172] It is assumed that the reaction of hypohalites with XeF_2 gives the corresponding interhalides HalX (Hal = Br, Cl), which are weaker electrophilic reagents than Cl_2 or BrCl. Therefore, they react more selectively with electron-enriched unsaturated and aromatic compounds to give the corresponding difluorides in high yields. Cyclohexene, methylenecyclohexane, hex-1-ene, hept-1-ene, hex-3-yne, 3,4-dihydro-2*H*-pyran, anisole, *etc*., were used as substrates.[171,172]

The fluorination of the phenyl-substituted alkenes **52a–e** with XeF_2 in the presence of 0.1–0.2 equiv. of anhydrous HF results in the difluorides **53a–e**.[173]

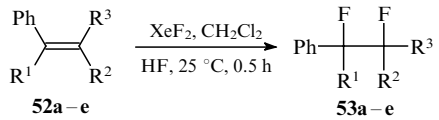

52a–e **53a–e**

$R^1 = R^2 = R^3 = H$ (**a**); R^1 = Me, $R^2 = R^3 = H$ (**b**); R^2 = Me, $R^1 = R^3 = H$ (**c**); R^1 = Ph, $R^2 = R^3 = H$ (**d**); R^1 = Ph, R^2 = Me, $R^3 = H$ (**e**).

The reaction of XeF_2 with 3-phenyl-1*H*-indene (**54a**) affords 3-phenyl-2-fluoro-1*H*-indene (**55a**) as a result of addition–elimination. The fluorination of 4-phenyl-1,2-dihydronaphthalene (**54b**) and 9-phenyl-6,7-dihydro-5*H*-benzocycloheptene (**54c**) by XeF_2 yields diastereomeric pairs of the vicinal difluorides **56a**,**b** and **57a**,**b**. They are unstable on heating and eliminate HF at 200 °C, being converted into 3-fluoro-4-phenyl-1,2-dihydronaphthalene (**55b**) and 8-fluoro-9-phenyl-6,7-dihydro-5*H*-benzocycloheptene (**55c**).[173]

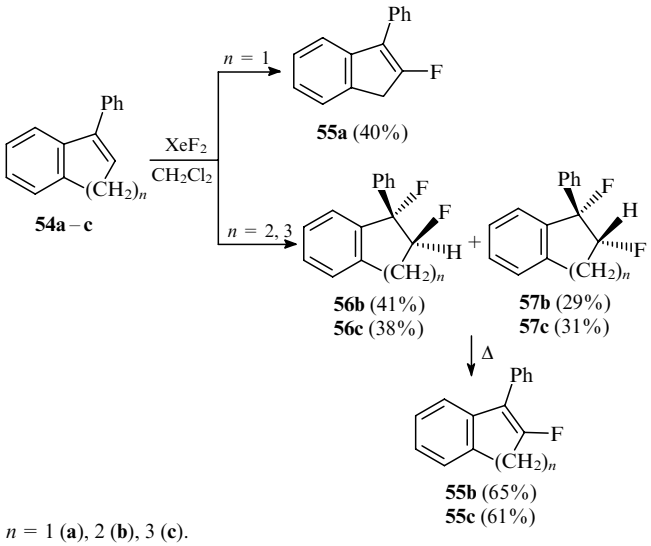

n = 1 (**a**), 2 (**b**), 3 (**c**).

The reaction of enol trimethylsilyl ethers with XeF_2 has recently been studied.[174] Thus 1-trimethylsilyloxycyclohexene (**58**) reacts with XeF_2 to give α-fluorocyclohexanone (**59**) in a quantitative yield. In the case of XeF^+, this reaction gives a mixture of three products (**59**–**61**); their formation is interpreted in terms of a single-electron transfer mechanism.[174]

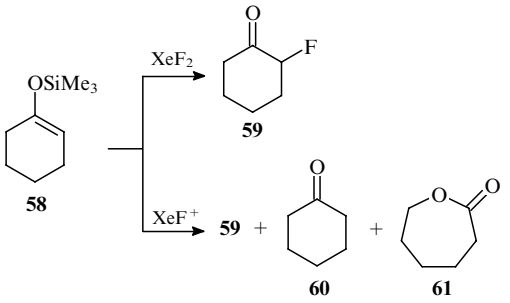

IV. Reactions of xenon derivatives with aromatic and polyfluoroaromatic compounds

Xenon difluoride is a convenient fluorinating agent for the preparation of fluorine-containing mono- and polycyclic aromatic compounds. The reaction of aromatic and polyfluoroaromatic hydrocarbons with XeF_2 has been described in detail in reviews,[20,30–33] therefore, in Table 1 we shall cite only the most common reactions. Special attention will be given only to those papers which have not been surveyed in the literature.

Several papers are devoted to the reactions of functional derivatives of aromatic hydrocarbons with XeF_2. Thus the reaction of XeF_2 with anisole and 1,2-dimethoxybenzene gives 4-fluoroanisole and 4-fluoro-1,2-dimethoxybenzene (yields 72% and 37%, respectively).[198] The reaction of phenol with XeF_2 in CH_2Cl_2 yields a mixture or isomeric fluorophenols (47%);[198] in water, phenol is oxidised into *p*-benzoquinone.[63,199,200] Hydroquinone and 4-*tert*-butylcatechol are oxidised by XeF_2 into benzoquinone derivatives,[201] whereas catechol affords 4-fluorocatechol in 38% yield.[198] The initially proposed structure of the reaction product of pentafluorophenol with XeF_2 ($C_6F_5OOC_6F_5$)[202] was later refuted;[203] it was shown that this reaction yielded perfluoro-4-phenoxycyclohexa-2,5-dienone and perfluorocyclohexa-2,5-dienone. The reaction of (perfluoroaryl)-trimethylsilanes (Ar_F = C_6F_5, 4-$CF_3C_6H_4$, 4-C_5F_4N) with XeF_2 results in desilylation and formation of perfluorobiaryls.[204,205]

The fluorination of the aromatic nucleus of L-3-methoxy-4-hydroxyphenylalanine[206,207] used in the synthesis of L-6-fluorodihydroxyphenylalanine-[^{18}F] occurs smoothly.[207]

Table 1. The reaction products of aromatic compounds with xenon difluoride.

Starting compound	T/°C	Solvent	Catalyst	Reaction products	Yield (%)	Ref.
PhH	165			mixture of mono-, di and trifluorobenzenes		175
	145			the same		175
	25	CCl_4	HF	C_6H_5F	68	176 – 178
PhMe	25	CCl_4	HF	C_6H_4FMe (mixture of *o*-, *m*- and *p*-isomers)	32	177, 179, 180
PhCl	25	CCl_4	HF	C_6H_4FCl (mixture of *o*-, *m*- and *p*-isomers)	65	177, 179, 180
PhF	25	CCl_4	HF	$C_6H_4F_2$ (mixture of *o*-, *m*- and *p*-isomers)	47	177, 179, 180
$PhCF_3$	25	CCl_4	HF	$C_6H_4FCF_3$ (mixture of *o*-, *m*- and *p*-isomers)	75	177, 179, 180
PhOMe	20	CCl_4	HF	$C_6H_4(OMe)F$ (mixture of *o*-, *m*- and *p*-isomers)	65	177, 179, 180
$PhNO_2$	120			mixture of *o*-, *m*- and *p*-nitrofluorobenzenes		175
	167			the same	81	177, 179, 180
1,4-$F_2C_6H_4$	100			1,2,4-$C_6H_3F_3$: 1,2,4,5-$C_6H_2F_4$ = 8 : 1		175
1,2-$F_2C_6H_4$	100			1,2,4-$C_6H_3F_3$: 1,2,4,5-$C_6H_2F_4$ = 42 : 1		175
1,2,3-$C_6H_3Me_3$	25	CH_2Cl_2	HF	1,4-F_2-3,4,5-C_6HMe_3 : 1-F-2,3,4-$C_6H_2Me_3$ = 1 : 2	38	181
C_6Me_6	25	CH_2Cl_2	HF	$C_6Me_5CH_2F$	72	182
	25	CH_2Cl_2	CF_3CO_2H	$C_6Me_5CH_2OCOCF_3$	68	182
Indan	25	CH_2Cl_2	HF	5-fluoroindan	60	183
5-Fluoroindan	25	CH_2Cl_2	HF	5,6-difluorindan	62	183
Tetralin	25	CH_2Cl_2	HF	5-fluorotetralin,	30	183
				6-fluorotetralin	70	
9,10-Dihydro-anthracene	25	CH_2Cl_2	HF	1-fluoro-9,10-dihydroanthracene,	9	184
				3-fluoro-9,10-dihydroanthracene	21	
Acenaphthene	25	CH_2Cl_2	HF	3-fluoroacenaphthene,	50	184
				5-fluoroacenaphthene	20	
Trypticene	25	CH_2Cl_2	HF	1-fluorotrypticene,	12	184
				2-fluorotrypticene	23	
Naphthalene	−78 – 20 [a]	CH_2Cl_2		1-fluoronaphthalene,	50	185
				2-fluoronaphthalene	11	
		CH_2Cl_2		mixture of 1-fluoro, 2-fluoro- and 1,4-difluoronaphthalenes	75	186
Anthracene	−12 – 12 [a]	CH_2Cl_2		9-fluoroanthracene,	26	185
				1-fluoroanthracene,	45	
				2-fluoroanthracene	9	
Phenanthrene	−78 – 20 [b]	CH_2Cl_2		9-fluorophenanthrene	33 – 40	185, 187
	25	CH_2Cl_2	HF	mixture of mono-, di-, tri- and tetrafluoro-phenanthrenes	79	188
Pyrene	−125 to −78 [b]	CH_2Cl_2		mixture of monofluoropyrenes	52	189
Benzo[*a*]pyrene	−78 to −45	CH_2Cl_2		6-fluorobenzo[*a*]pyrene	26	190
Perylene	25	C_6F_{12}		difluoroperylene,	10	191
				3-fluoroperylene	30	
1-XC_6F_5 (X = F, H, Cl, Br, C_6F_5)	20	CH_2Cl_2	BF_3	1-X-heptafluorocyclohexa-1,4-dienes	> 80	192
C_6F_5Cl	25	CH_2Cl_2	BF_3	1-chloroheptafluorocyclohexa-1,4-diene	83	193
C_6F_5Br	25	CH_2Cl_2	BF_3	1-bromoheptafluorocyclohexa-1,4-diene	81	193
Decafluorobiphenyl	25	CH_2Cl_2	BF_3	1-(pentafluorophenyl)heptafluorocyclohexa-1,4-diene	73	193
C_6F_5H	25	CH_2Cl_2	BF_3	1,2,3,3,4,6,6-heptafluorocyclohexa-1,4-diene	75	193
C_6F_6	25	CH_2Cl_2	BF_3	octafluorocyclohexa-1,4-diene	74	193
	20	CH_2Cl_2	HF	the same	40	194
Octafluoro-naphthalene	20	CH_2Cl_2	HF	perfluoro-1,4-dihydronaphthalene,	42	194 – 196
				perfluoro-1,2-dihydronaphthalene	4	
2-Methoxyhepta-fluoronaphthalene	25	CH_2Cl_2	BF_3	2-methoxynonafluoro-1,4-dihydronaphthalene	35	197
2-Ethoxyheptafluoro-naphthalene	25	CH_2Cl_2	BF_3	2-ethoxynonafluoro-1,4-dihydronaphthalene	40	197

[a] At 10^{-6} mm Hg; [b] at 10^{-5} mm Hg.

Aromatic aldehydes react with XeF_2 in CH_2Cl_2 in the presence of HF to give the ethers **62** in 67% – 86% yields, the maximum yields being achieved with 4 – 5 equiv. of HF.[208, 209]

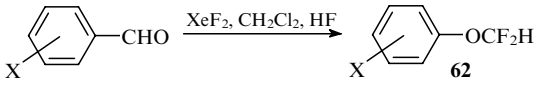

62

X = H, 4-Me, 4-Cl, 4-OMe, 4-OC_5H_{11}, 4-CO_2H, 4-CO_2Me, 2-NO_2, 3-NO_2, 4-NO_2, Ts.

The difluoromethoxylation of aromatic aldehydes carrying electron-donor substituents, such as acetamido- and methoxy groups, is accompanied by fluorination of the aromatic ring.[208]

The difluoromethyl ethers **62** are formed as a result of rearrangement which probably occurs *via* the intermediates **63** in the reaction of the fluorohydrins **64** with XeF_2.[208]

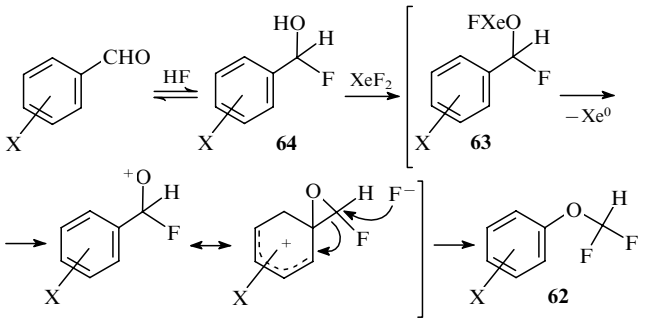

The aryl ketones **65** and **66a–c** react with XeF_2 in a similar way to give the fluorinated phenol ethers **67** and **68a–c** in low yields with considerable recovery of the starting compounds.[141,210,211]

$$\underset{\mathbf{65}}{ArCOCH_2X} \xrightarrow[24\ h,\ 25\ ^\circ C]{1\ equiv.\ XeF_2,\ HF,\ CH_2Cl_2} \underset{\mathbf{67}}{ArOCF_2CH_2X}$$

Ar = Ph, C_6F_5, 2-$NO_2C_6H_4$; X = H, F.

$$\underset{\mathbf{66a-c}}{Ar^1COAr^2} \xrightarrow[24\ h,\ 25\ ^\circ C]{1\ equiv.\ XeF_2,\ HF,\ CH_2Cl_2} \underset{\mathbf{68a-c}}{Ar^1OCF_2Ar^2}$$

$Ar^1 = Ar^2$ = Ph (**a**); Ar^1 = Ph, Ar^2 = 4-$NO_2C_6H_4$ (**b**);
$Ar^1 = Ar^2 = C_6F_5$ (**c**).

2-Fluoroindan-1-one (**69**) reacts with 1 equiv. of XeF_2 in HF–Py to give 2,2,3-trifluoro-3,4-dihydro-2*H*-benzo[*b*]pyran (**70**) and 2,2,3,6-tetrafluoro-3,4-dihydro-2*H*-benzo[*b*]pyran (**71**) as the main products.[210] 2,2-Difluoroindanedione **72** yields tetrafluorobenzopyrone **73** with XeF_2 in the presence of HF.

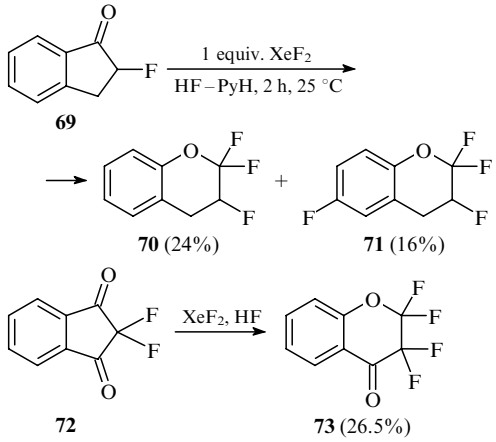

The reactions of the benzyl alcohols **74** with XeF_2 afforded the aryl fluoromethyl ethers **75** in high yields.[212] The yield of the main product increases in the presence of electron-withdrawing substituents, *e.g.*, for R = 3-NO_2, it reaches 85%. Fluorinated ethers are not formed if benzyl alcohols contain hydroxy-, alkoxy- or alkylamino groups.[212]

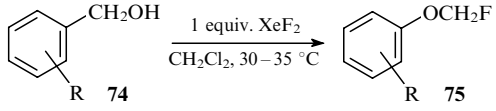

R = H, 2-NO_2, 3-NO_2, 4-NO_2, 4-Me, 3-F.

Presumably, this reaction occurs *via* the intermediate **76** and according to the same mechanism as does the synthesis of the difluoromethyl ethers **62** from aldehydes. The reaction is probably catalysed by HF; therefore, on the whole, it represents an autocatalytic process.[212]

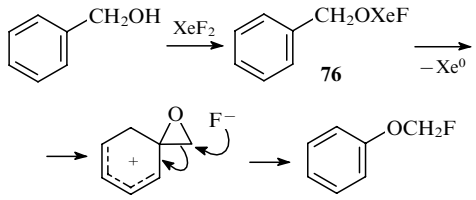

The reaction of indan-1-one with XeF_2 is accompanied by ring expansion resulting in the difluoro-substituted dihydrobenzopyran **77**. The α-fluoroketones **79** and **80a–c** are formed in the reaction of indan-2-one and the enol acetates **78a–c** with XeF_2. The fluorination products of the aromatic ring have not been found in either case.[211]

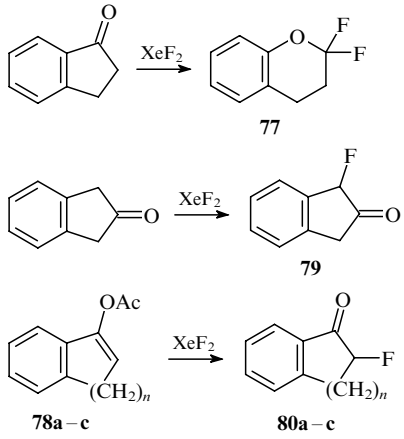

n = 1 (**a**), 2 (**b**), 3 (**c**).

The [2.2]metaparacyclophane system contains two types of aromatic rings, *viz.*, *para*- and *meta*-substituted ones. Reutov *et al.*[213] proposed a method for selective introduction of functional groups into this compound based on the use of XeF_2. It was shown that two cyclophane derivatives (**82** and **83**) containing a fluorine atom in the *para*- and *meta*-substituted benzene rings are formed from non-substituted [2.2]paracyclophane (**81**) after addition of an equimolar amount of XeF_2. Mixing of the reaction components in a Teflon vessel with CH_2Cl_2 did not result in any reaction between them, at least within one hour. The reaction could be initiated only after addition of an equimolar amount of CF_3CO_2H.

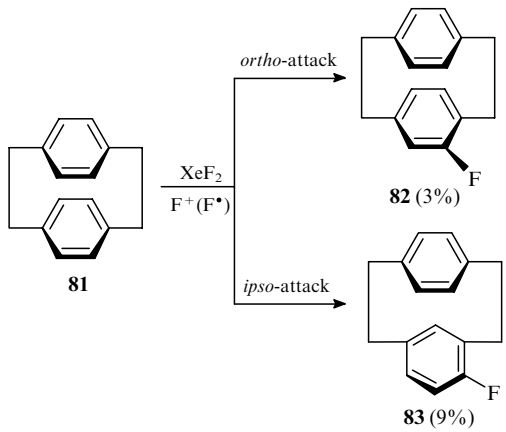

As mentioned above, the reaction of phenol with XeF_2 is nonselective.[198] 4-Fluorophenol was obtained from 2,6-di-*tert*-butylphenol in high yield using a two-step synthesis, *viz.*, fluorination by XeF_2 at low temperatures and subsequent treatment of the monofluoride **84** with $AlCl_3$ resulting in the elimination of

isobutylene and the formation of *p*-fluorophenol.[214] It is of note that fluorination of phenols can also be achieved through the use of *N*-fluoropyridinium triflate.[215, 216]

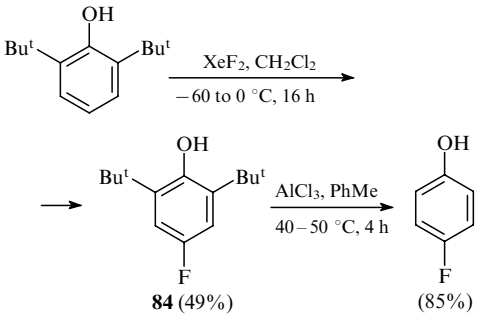

It is known [217] that XeO_3 and XeF_2 decompose in the presence of water to form a vast array of products, *e.g.*, HO$^{\bullet}$ radicals, hydrogen peroxide, molecular oxygen, XeO and the superoxide ion. It can be assumed that these products will effectively hydroxylate arenes. Indeed, heating or irradiation of a XeO_3 solution with a high-pressure mercury lamp at 20 °C in aqueous acetonitrile in the presence of benzene results in hydroxylation of the latter. The induction period of this reaction can be significantly reduced by addition of a catalytic amount of CrO_3.[218, 219] Xenon difluoride in aqueous acetonitrile is a more efficient hydroxylating reagent. In this case, the induction period is small, the initial rate of the reaction and the yield of phenol being strongly dependent on the concentration of water in the solution. HOXeF is a likely intermediate.[219]

Ethylbenzene is slowly oxidised by XeO_3 to acetophenone in the presence of the tetraphenylporphyrin manganese complex (TPP)MnOAc (TPP is tetraphenylporphyrin) in aqueous acetone. In this case, XeO_3 acts as an oxygen donor and is transferred by the metal-porphyrin catalyst to the substrate containing C–H bonds.[218]

A method for iodination of aromatic compounds by a mixture of XeF_2 with iodine or *N*-iodosuccinimide has recently been described.[172, 220] It is noteworthy that the same mixture was used for iodofluorination of alkenes. The IF generated from xenon difluoride is less reactive than that synthesised from I_2 and F_2. Presumably, in this case we deal with the reaction of an IF–XeF_2 complex with alkenes and aromatic compounds.[206]

The reaction of fluorene (**85a**) or dibenzofuran (**85b**) with XeF_2 in the presence of $BF_3 \cdot OEt_2$ gives a mixture of the monofluorides **86a**,**b**–**88a**,**b**.[221]

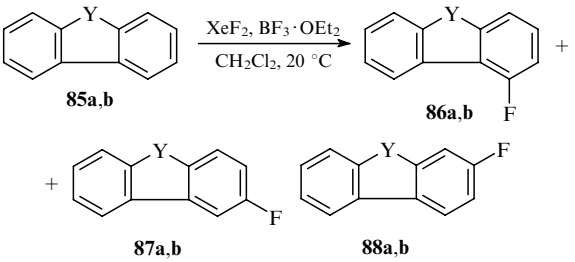

Y = CH_2 (**a**), O (**b**).

The reaction of XeF_2 with 1-R-2,3,4,5-tetrafluorobenzene (R = H, F, Br, NO_2) or 1-R-2,3,4,6-tetrafluorobenzene (R = H, CF_3) in HF or CH_2Cl_2–$BF_3 \cdot OEt_2$ results in the substitution of F for the hydrogen atom in the aromatic ring.[222] Only the addition reaction occurs in 1-R-2,3,5,6- (R = H, Br, CF_3) or 1-bromo-2,3,4,6-tetrafluorobenzenes under these conditions. The role of radical cations as intermediate compounds has been discussed.[222]

V. Reactions of xenon difluoride with organic acids and their derivatives

Earlier, it was shown (see Section II) that the reaction of XeF_2 with protic oxygen-containing acids gives unstable compounds of the FXeOR and $Xe(OR)_2$ types, which manifest strong electrophilic properties with respect to unsaturated and aromatic compounds. The reaction of benzoic acid with XeF_2 in an excess of benzene which gives phenyl benzoate in up to 70% yield is an example.[223, 224]

$$PhCO_2H + PhH + XeF_2 \longrightarrow PhCO_2Ph + 2\,HF + Xe$$

Biphenyl (1%–5%) is formed along with phenyl benzoate. Kinetic studies have shown that this reaction occurs *via* the formation of $PhCO_2XeF$ or $(PhCO_2)_2Xe$ with their subsequent reactions with benzene.[224]

For different benzoic acid derivatives, the yields of phenyl esters depend essentially on the structure of the original acid.[225] In the case of *p*-fluorobenzoic acid, the yield of the corresponding phenyl ester reached 68%, whereas for *o*-toluic acid it was as small as 3%, which can be due to steric hindrances preventing the formation of the intermediate compound.

$$RC_6H_4CO_2H + XeF_2 \longrightarrow RC_6H_4CO_2XeF + HF$$

$$RC_6H_4CO_2XeF + PhH \longrightarrow RC_6H_4CO_2Ph + HF + Xe$$

R = H, 2-NO_2, 3-NO_2, 4-NO_2, 2-Me, 3-Me, 4-Me, 4-Br, 4-F, 4-Cl.

The possibility of incorporation of benzoyloxy groups into toluene, fluoro-, chloro-, bromo- and nitrobenzene using the XeF_2–$PhCO_2H$ system has been studied.[226] The kinetic data and the isomeric composition of the reaction products suggest that the benzoyloxy group is introduced into *o*- and *p*-positions of toluene, chloro- and bromobenzene. The nitro group deactivates the nucleus so that no esters are formed. The relative rates of acyloxylation of benzene derivatives in the presence of XeF_2 decrease in the following order: $MeC_6H_5 > ClC_6H_5 > BrC_6H_5 > NO_2C_6H_5$. The experimental data suggest the electrophilic type of this reaction. The electrophilic reagent PhCOOXeF is deficient of electrons on the xenon atom and therefore attacks the positions with increased electron density in substituted benzenes.[226] Kinetic studies of the reaction of benzene with Ph[^{14}C]OOH revealed that benzoic acid is involved in the formation of phenyl benzoate and is not decarboxylated with the liberation of radiolabelled carbon dioxide.[227]

Aromatic dicarboxylic acids can be dehydrated by XeF_2 or undergo more profound conversions. The reaction of phthalic acid with XeF_2 (1 : 2) results in phthalic anhydride in 26% yield. Under the same conditions, 2,2′-diphenic acid (**89**) generates 3,4-benzocoumarin (**90**) in 30% yield along with a small amount of the anhydride.[228] The formation of compound **90** is due to partial decarboxylation of the intermediate with subsequent intramolecular acyloxylation.

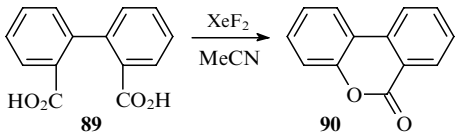

The reaction of fluoroxenon trifluoroacetate (**5d**) with aromatic derivatives has also been studied. It was shown in particular that hexamethylbenzene reacts with the *in situ* generated compound **5d** to give pentamethylbenzyl trifluoroacetate (**91**) in good yield, while the reaction with XeF_2 in the presence of HF in CH_2Cl_2 gives pentamethylbenzyl fluoride (**92**) in 72% yield.[182]

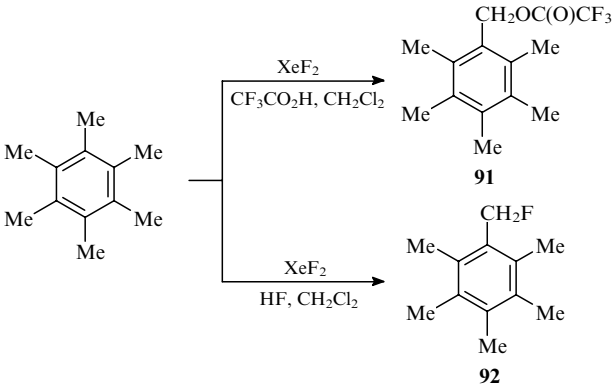

91 **92**

Acids react with one equivalent of XeF_2 in dichloromethane or chloroform to give alkyl fluorides in 20% to 95% yields.[229, 230] This reaction, like other reactions occurring in the presence of XeF_2, is catalysed by HF and thus represents an autocatalytic process. This conversion is a method for carbon chain shortening by one atom as a result of the halodecarboxylation reaction.

$$RCO_2H + XeF_2 \xrightarrow{25\ ^\circ C,\ 8-16\ h} RF + Xe + HF + CO_2$$

R = $PhCH_2$ (76%), $Ph(CH_2)_2$ (76%), $Ph(CH_2)_3$ (60%), $Me(CH_2)_8$ (54%), Ph_2CHCH_2 (63%), $Me(CH_2)_{14}$ (62%), $MeC(O)CH_2CH_2$ (82%), 2-norbornyl (74%), 1-adamantyl (82%), $PhOCH_2$ (64%), 2,4-$Cl_2C_6H_3OCH_2$ (84%), Ph_3C (65%), $PhC(OMe)CF_3$ (95%), $PhCH_2$ (76%), $PhCH(CH_2CO_2H)CH_2$ (60%), $PhCH_2CHCO_2H$ (68%), Ph (20%), $Br(CH_2)_3$ (91%).

Alkanoic and arylalkanoic acids containing primary radicals, aryloxyacetic and dicarboxylic acids are highly susceptible to fluorodecarboxylation. Carboxylic acids containing secondary radicals form fluoro derivatives in low yields, whereas carboxylic acids with tertiary radicals react as smoothly as the acids with primary radicals. Those acids which contain other protic functional groups, *e.g.*, amino acids, cholic acid, *etc.*, as well as cinnamic acid do not enter into this reaction. Benzoic acid yields benzoyl fluoride in a low yield.

The proposed mechanism [230] of fluorodecarboxylation entails the intermediate formation of xenon carboxylates.[91, 116, 182, 226]

$$RCO_2H \xrightarrow[-HF]{XeF_2} [RCO_2XeF] \xrightarrow[F^-]{a} RF + Xe + HF + CO_2$$

$$[RCO_2XeF] \xrightarrow{b} RCO_2^{\bullet} + Xe + F^{\bullet}$$

$$RCO_2^{\bullet} \xrightarrow[-CO_2]{} R^{\bullet} \xrightarrow[-Xe,\ -F^-]{XeF^{\bullet}} R^+ \xrightarrow{F^-} RF$$

According to Patrick *et al.*,[230] the reaction follows both ionic (route *a*) and radical mechanisms (route *b*). Acids containing primary and secondary radicals react by route *a*, whereas acids containing tertiary radicals and arylalkanoic acids react by route *b*. Route *a* is realised when the reaction is carried out in the presence of $[Bu_4^nN]^+[^{18}F]^-$. This made it possible to obtain 2-phenyl-1-[^{18}F]fluoroethane and 3-bromo-1-[^{18}F] fluoropropane in high radiochemical yields [230, 231] and opened a possibility of replacing the carboxy group by substituents other than the fluorine atom.[230]

$$PhCH_2CH_2CO_2H + XeF_2 + [^{18}F]^- \longrightarrow PhCH_2CH_2[^{18}F]\ (40\%)$$

$$Br(CH_2)_3CO_2H + XeF_2 + [^{18}F]^- \longrightarrow Br(CH_2)_3[^{18}F]\ (78\%)$$

The reaction with 3-phenylpropionic acid affords no elimination side products or those involving the aromatic ring. 4-Phenylbutyric acid also reacts smoothly with XeF_2 and undergoes no intramolecular rearrangements characteristic of radical processes,[230] which makes it different from the reaction with $Pb(OAc)_4$, which results in cyclisation.[232]

It could be expected that 1,2-diphenylethane would be the main reaction product of XeF_2 with 3,3-diphenylpropionic acid, since such rearrangement is well known for phenylethyl radicals.[233] However, 2,2-diphenyl-1-fluoroethane is formed instead. Presumably, this reaction is in some respect analogous to the Borodin – Hunsdiecker reaction [234, 235] where the rearrangement products are not detected either, which makes it different from the Kochi reaction.[236, 237]

Racemic 1-methoxy-1-phenyl-1,2,2,2-trifluoroethane (**94**) was obtained in 95% yield by fluorodecarboxylation of the optically active (+)-α-methoxy-α-trifluoromethylphenylacetic acid (**93**). In the presence of $[Bu_4^nN]^+[^{18}F]^-$, this reaction gave compound **94**-[^{18}F] in 65% radiochemical yield.[230]

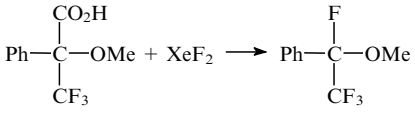

93 **94**

Pyridylacetic acid reacts with XeF_2 in the presence of HF in dichloromethane to give products the compositions of which are typical of a radical reaction.[238]

$$PyCH_2COOH \xrightarrow[CH_2Cl_2]{XeF_2,\ HF} PyCH_2CH_2Py + PyMe + PyCH_2F + PyCHCl_2 + PyCH_2Cl$$

(58%) (10%) (<1%) (17%) (11%)

The reaction of hept-6-enoic acid (**95**) with XeF_2 gives 6-fluorohex-1-ene (**96**) and fluoromethylcyclopentane (**97**).[238, 239] Fluorocyclohexane was not detected. In this case, the feasibility of a radical mechanism was unambiguously confirmed by direct EPR identification of the alkyl radicals **98** and **99** (trapped by α-phenyl-*N*-*tert*-butylnitrone). Additional experiments demonstrated the impossibility of interconversion of the fluorides **96** and **97**. The rate constant for the second-order reaction ($k = 1.1 \times 10^6$ litre mol^{-1} s^{-1}) was determined at 25 °C.[239]

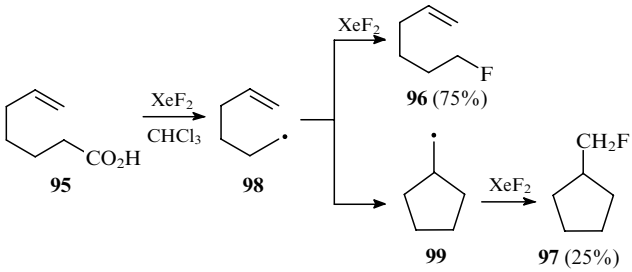

95 **98** **96** (75%) **99** **97** (25%)

endo-Norbornane 2-carboxylic acid (**100**) does not afford fluoro derivatives in the reaction with XeF_2, but rather gives 2-*exo*-norbornyl *endo*-norbornane-2-carboxylate (**101**) in 72% yield. The *exo*-position of the alcoholic function is explained by the generation of the 2-norbornyl cation, which reacts with nucleophiles to give exclusively products with an *exo*-configuration of the substituents.[238]

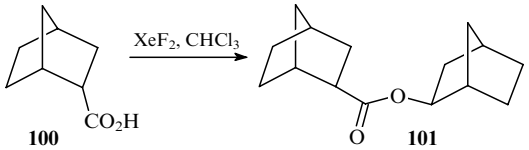

100 **101**

The reaction of the L-tartaric acid derivatives **102** with XeF_2 is non-stereospecific. The *meso*-difluoro derivative **103** (yield 36%) was isolated as the main product.[238]

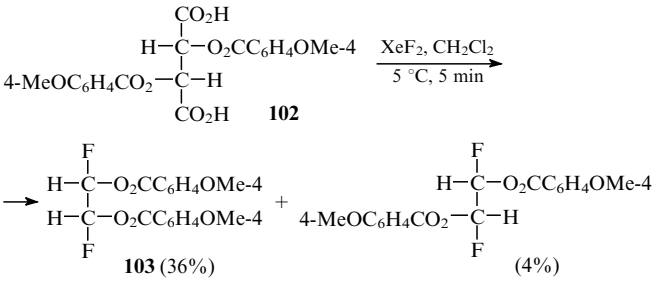

Patrick *et al.*[230] suggested that the reaction of 3-phenylbicyclo[1.1.1]pentane-1-carboxylic acid (**104a**) with XeF_2 generates a dimer; however, later it was shown [238] that this reaction yields the hydrocarbon **105a**. 3-Methoxycarbonylbicyclo[1.1.1]pentane-1-carboxylic acid (**104b**) and (−)-camphanic acid **106** are also decarboxylated by XeF_2 to give compounds **105b** and **107** in 80% and 85% yields, respectively.[239]

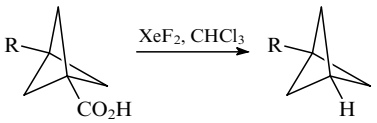

104a,**b** **105a**,**b**

R = Ph (**a**), CO_2Me (**b**).

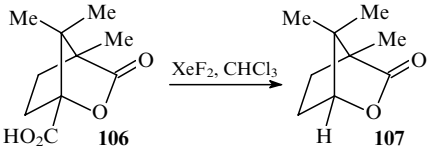

The reaction of XeF_2 with the carboxylic acids **108a**,**b** containing a thiol group gives the disulfides **109a**,**b** in a quantitative yield,[238] which is consistent with the data described in Section VIII.2.

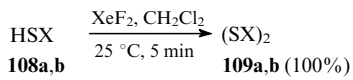

X = CH_2CO_2H (**a**), $CH_2CH_2CO_2H$ (**b**).

Fluorodecarboxylation with 1.5 equiv. of XeF_2 in dichloromethane was successfully employed for the synthesis of bridged cage fluorides.[238, 240]

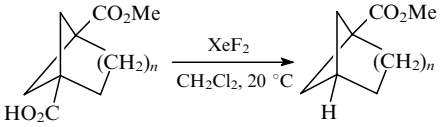

n = 0 (**104b**, **105b**); 1 (**110**, **111**).

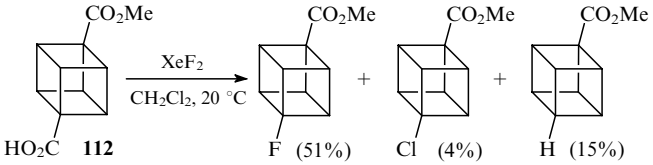

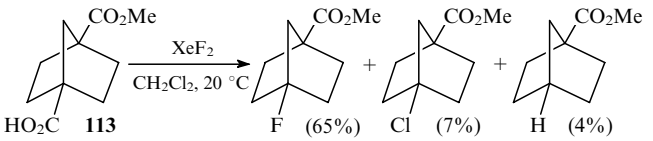

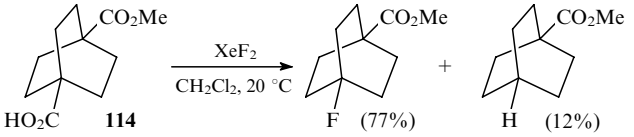

The yields and the compositions of the reaction products depend on the cage compound used. For example, 3-methoxycarbonylbicyclo[1.1.1]pentane-1-carboxylic (**104b**) and 3-methoxycarbonylbicyclo[2.1.1]hexane-1-carboxylic (**110**) acids yield exclusively the reduced decarboxylation products **105b** and **111**, whereas the monoester of a dicarboxylic acid of the cubane series (**112**) and 4-methoxycarbonylbicyclo[2.2.1]heptane-1-carboxylic acid (**113**) afford a mixture of fluorides, chlorides and reduction products. 4-Methoxycarbonylbicyclo[2.2.2]octane-1-carboxylic acid **114** forms no chlorination products under these conditions.[240]

Decarboxylation of some carboxylic acids by XeF_2 is accompanied by the formation of free radicals and can be used for their generation. Halogenocarboxylic acids, particularly trifluoroacetic acid, are especially prone to such reactions. The reaction of trifluoroacetic acid with the corresponding substrate in the presence of XeF_2 was used by Tanabe *et al.*[241] for the incorporation of the trifluoromethyl radical into aromatic and heterocyclic compounds. The reaction with benzene gives trifluoromethylbenzene in 33%–38% yield. An analogous reaction takes place in the case of other perfluorocarboxylic acids.[241]

Ar = Ph, 1,4-$Cl_2C_6H_4$, 4-$ClC_6H_4CO_2Me$, 4-ClC_6H_4NHAc, 3,5-$Cl_2C_6H_3NHAc$, 2,5-$F_2C_6H_3NHAc$.

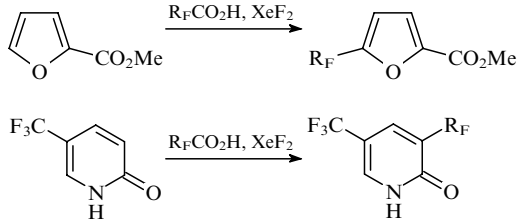

R_F = CF_3, C_2F_5, C_3F_7.

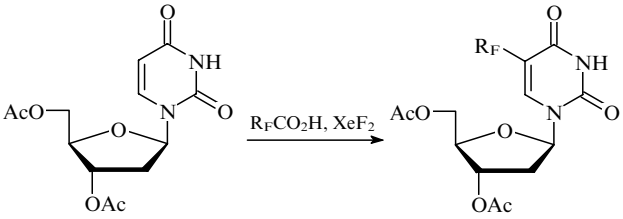

R_F = CF_3, C_2F_5.

If a heterocyclic compound contains a thiol group, perfluoroalkylation occurs exclusively at the sulfur atom.[242] In this case, disulfides are formed as side products in the same manner as in the case of acids containing a thiol group.[238]

The trifluoromethylation [243] was extended to trimethylsilyl derivatives of arenes.[241] Thus the reaction of compounds **115a**,**b** with trimethylsilyl trifluoroacetate yields a mixture of the regioisomers **116a**,**b** and **117a**,**b**. The products of *ipso*-substitution of the trimethylsilyl group were not detected.[241]

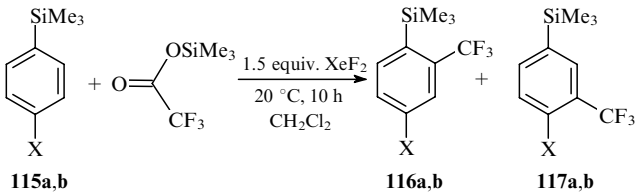

115a,**b** **116a**,**b** **117a**,**b**

Compound	X	Yield (%)	
		116	**117**
115a	Cl	9	34
115b	NHAc	8	29

Perfluorodicarboxylic acids can generate biradicals in the reaction with XeF_2. Thus the reaction of perfluoroglutaric acid (**118**) with XeF_2 in benzene results in 1,3-diphenylhexafluoropropane (**119a**) (yield 47%). 1,3-Bis(*p*-tolyl)- (**119b**) and 1,3-bis-(4-fluorophenyl)hexafluoropropane (**119c**) are formed in toluene or fluorobenzene in 62% and 65% yields, respectively.[244] The reaction of the dicarboxylic acid **118** with XeF_2 in the presence of elementary chlorine or bromine was used to prepare 1,3-dichloro- or 1,3-dibromohexafluoropropanes.

$$HO_2C(CF_2)_3CO_2H + XeF_2 \longrightarrow$$

118

ArH, 15–20 °C → $Ar(CF_2)_3Ar + HF + CO_2 + Xe$ (**119a–c**); Ar = Ph (**a**), MeC_6H_4 (**b**), FC_6H_4 (**c**)

Cl_2 or Br_2, 0–5 °C → $X(CF_2)_3X + HF + CO_2 + Xe$; X = Cl (54%), Br (71%)

The reaction of XeF_2 with the corresponding aromatic substrate in the presence of carboxylic acids containing different functional groups allows the introduction of polyfunctional substituents into the molecule of an aromatic compound. The high value of this reaction was demonstrated using chlorofluoro- or difluoronitroacetic acid as examples.[245]

$$O_2NCF(R^1)CO_2H + 1/2\ XeF_2 + PhR^2 \longrightarrow$$

120

R^1 = Cl → $O_2NCFClC_6H_4R^2$ (**121a–c**)

R^1 = F → $O_2NCF_2C_6H_4R^2$ (**121d–f**) + $O_2NCF_2CO_2C_6H_4R^2$ (**122d–f**)

R^1 = Cl: R^2 = H (**a**), Me (**b**), F (**c**); R^1 = F: R^2 = Me (**d**), F (**e**), H (**f**).

It was found that the structures of the reaction products depend on the substituent R^1 in the original acid **120**. Thus for R^1 = Cl, the reaction gives the alkylation products **121a–c**, whereas for R^1 = F, aryl difluoronitroacetates **122d–f** are formed in addition to compounds **121d–f**, which is probably due to the higher stability of the intermediate difluoronitroacyl radical.[245]

In contrast with non-substituted carboxylic acid, the reactions of the halogeno nitro carboxylic acids **123a,b** with XeF_2 yield halogenodinitromethanes.[246]

$$O_2NCFXCO_2H \xrightarrow{XeF_2}$$

123a,b

X = F → $CF_2(NO_2)_2 + CF_4 + CO_2 + Xe + HF$

X = Cl → $CFCl(NO_2)_2 + CFCl_2NO_2 + CF_4 + CO_2 + Xe + HF$

X = F (**a**), Cl (**b**).

If this reaction is carried out in the presence of chlorine, bromine or nitrogen oxides, the carboxy group in fluorochloro- (**123a**) or difluoronitroacetic acids (**123b**) can be replaced by the corresponding functional groups; compounds **124** are formed in satisfactory yields.[247] If the reaction is carried out in aromatic solvents, they undergo alkylation.[245, 248]

$$O_2NCF(X)CO_2H + XeF_2 \xrightarrow{Y_2} O_2NCFXY + CO_2 + Xe + HF$$

123a,b → **124a–f**

$Y_2 = Cl_2, Br_2, N_2O_4$; X = F, Y = Br (**a**); X = Cl, Y = Br (**b**); X = F, Y = NO_2 (**c**); X = Cl, Y = NO_2 (**d**); X = F, Y = Cl (**e**); X = Y = Cl (**f**).

Xenon difluoride reacts with carboxylic acid imides. Thus the reaction of perfluorosuccinimide (**125a**) and -glutarimide (**125b**) with XeF_2 gives *N*-fluoroimides (**126a,b**).[249]

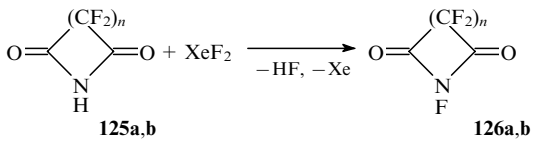

125a,b → **126a,b**

n = 2 (**a**), 3 (**b**).

The reactions of phthalimide (**127**) and saccharin (**128**) or their potassium salts with XeF_2 in dry benzene result in the *N*-phenyl derivatives of the corresponding imides **129** and **130** in 14% – 22% yields. In addition to *N*-phenyl derivatives, biphenyl is formed as a side product; its yield is lower in the reactions of potassium salts.[250]

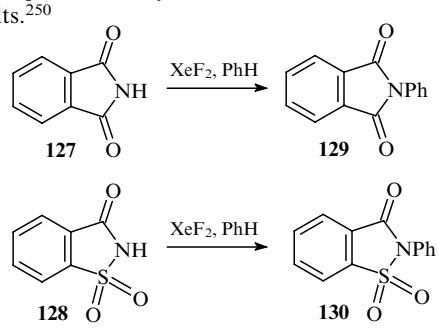

127 → **129**; **128** → **130**

The reaction of trimethylsilyl arenecarboxylates **131** with XeF_2 in dichloromethane or hexaflurobenzene results in the aryloxycarbonyl fluorides **132**. Arenes or aryl fluorides generated from the corresponding aryl radicals are the main reaction products in acetonitrile.[251]

$$ArCO_2SiMe_3 \xrightarrow{XeF_2} \begin{cases} \xrightarrow{C_6F_6 \text{ or } CH_2Cl_2} FCO_2Ar + Xe + Me_3SiF \\ \xrightarrow{MeCN} ArF + Xe + Me_3SiF + CO_2 \end{cases}$$

131 → **132**

Ar = 4-$Bu^tC_6H_4$, 4-MeC_6H_4, 3-ClC_6H_4, 4-$MeOC_6H_4$, 4-$CF_3C_6H_4$.

The transformation of compounds **131** into compounds **132** is the first example of the $R^1CO_2R^2 \rightarrow R^2CO_2R^1$ rearrangement. A mechanism for this reaction has been proposed, which includes one-electron oxidation and the formation of a radical cation and a radical anion.[251]

$$(ArCO_2SiMe_3)^{+\bullet} + (XeF_2)^{-\bullet} \longrightarrow$$

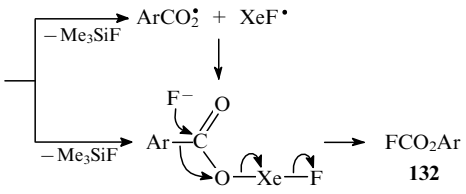

132

Using this approach, the electron-enriched centre, *i.e.*, the oxygen atom of the carbonyl group, can be converted into an electron-deficient centre using a temporary group. This is an example of so-called Umpolung.[251]

VI. Organic xenon(II) compounds containing the C–Xe bond

The chemistry of organoxenon compounds has been developing intensively in the past two decades. This trend was initiated by the appearance of a report [13] on the synthesis of $Xe(CF_3)_2$ (**133**). This compound is sublimed in *vacuo*, is stable at low temperatures and can be stored for two weeks at liquid nitrogen temperature. Upon decomposition, it gives XeF_2 and a mixture of fluorocarbons.

$$C_2F_6 \xrightarrow{\Delta} 2\dot{C}F_3 \xrightarrow[-F_2]{XeF_2} Xe(CF_3)_2$$

133

This experiment and the results of ion cyclotron resonance studies of the reaction mixture containing H_2, Xe and MeF [253,254] which were aimed at the determination [252] of the strength of the Xe–C bond (43±8 kcal mol^{-1}) gave impetus to further investigations into the synthesis of new compounds containing Xe–C bonds. Thus the formation of the methylxenon(II) cation was established in an equilibrium reaction which included a transfer of methyl cation from Me_2F^+ to Xe. The physicochemical characteristics of the equilibrium ($K = 0.16\pm0.05$, $\Delta G^\circ = 1.1\pm0.2$ kcal mol^{-1}, $\Delta S^\circ = 9.6\pm1.0$ kcal mol^{-1} K^{-1}, $S^\circ(MeXe^+) = 60.5$ cal mol^{-1} K^{-1}, $\Delta H^\circ = 4.0\pm0.5$ kcal mol^{-1}) confirmed [255] the earlier obtained [252] data on the strength of the Xe–C bond in $MeXe^+$ (55.2±2.5 kcal mol^{-1}).

Compound **133** had long been the only genuine organic xenon derivative. Further developments in the chemistry of organoxenon compounds confronted the task of creating stable xenon derivatives by a correct choice of ligands linked to xenon atoms. For xenon compounds, as for any other hypervalent compounds,[153,154,256] fluorine-containing ligands are the most suitable ones. However, despite the presence of fluorine-containing ligands in compound **133**, its stability was insufficient even for conducting routine spectral analyses.[257–259] It was suggested [260–262] that perfluorinated compounds containing a Xe–C bond have been formed as intermediates. These conclusions were inferred from the structures of the reaction products assuming that they might be formed exclusively as a result of incorporation of xenon into the C–E bond (E is an element). These investigations provided a basis for the development of a methodology of synthesis of stable organic xenon derivatives.

This approach was realised almost simultaneously by Naumann and Tyrra,[263] and Frohn and Jacobs and coworkers.[257,264,265] A procedure for the preparation of stable organic compounds with a covalent Xe–C bond, *e.g.,* of the $[Xe(C_6F_5)]^+X^-$ type, was proposed based on the cleavage of the C–B bond. Thus the low-temperature reaction of tris(pentafluorophenyl)boron with XeF_2 in CH_2Cl_2 gives the pentafluorophenylxenon salt **134a** (yields 40% [257] and 92% [266]) which separates from the reaction mixture as a colourless precipitate and could be recrystallised from acetonitrile. This compound is stable in the crystalline state for a long time at −60 °C; its solutions in acetonitrile are unstable at room temperature. A similar reaction in acetonitrile gives the pentafluorophenylxenon salt **134b**.[263]

$$B(C_6F_5)_3 + XeF_2 \xrightarrow[-30\ ^\circ C]{CH_2Cl_2} \underset{\mathbf{134a}}{[C_6F_5Xe]^+[C_6F_5BF_3]^-}$$

$$B(C_6F_5)_3 + XeF_2 \xrightarrow[0\ ^\circ C]{MeCN} \underset{\mathbf{134b}}{[C_6F_5Xe]^+[(C_6F_5)_3BF]^-}$$

Presumably, the boron compounds $B(C_6F_5)_3$, $[B(C_6F_5)_3F]^-$, $BF_3\cdot MeCN$ and BF_4^- identified by ^{11}B NMR spectroscopy could be formed by dismutation of a putative intermediate **135**.[263]

$$\underset{\mathbf{135}}{B(C_6F_5)_{3-x}} + XeF_2 \longrightarrow (3-x)\,B(C_6F_5)_3 + x\,BF_3$$

$x = 1, 2.$

It should be noted that the dismutation results also in the formation of a weak BF_3–XeF_2 complex [267] which readily reacts with pentafluorobenzene derivatives to give 1-R-heptafluorocyclohexa-1,4-dienes (R = H, F, Cl, Br, C_6F_5).[193] Heptafluorocyclohexa-1,4-diene and octafluorocyclohexa-1,4-diene were identified as the side products [263] using ^{19}F NMR.

The structures of compounds **134a**,**b** were established from NMR [268–270] and X-ray diffraction data.[263,271]

Some chemical properties of compounds **134** have been studied. Thus the reaction of the salts **134a**,**b** with water or D_2O is accompanied by the formation of C_6F_5H or C_6F_5D.[257,263] The salt **134a** reacts with halide ions in acetonitrile with the liberation of xenon and the formation of halopentafluorobenzene;[257,263] the salts **134a**,**b** form the corresponding adducts **136**–**139** with halopentafluorobenzenes,[257,263] tellurium-[263] or phosphorus-containing compounds.[257]

$$\underset{\mathbf{134b}}{[C_6F_5Xe]^+[(C_6F_5)_3BF]^-} \xrightarrow{KF} C_6F_6 + Xe + K[(C_6F_5)_3BF]$$

$$\xrightarrow{Te(C_6F_5)_2} \underset{\mathbf{136}}{[(C_6F_5)_3Te]^+[(C_6F_5)_3BF]^-} + Xe$$

$$\xrightarrow{C_6F_5I} \underset{\mathbf{137}}{[(C_6F_5)_2I]^+[(C_6F_5)_3BF]^-} + Xe$$

$$\underset{\mathbf{134a}}{[C_6F_5Xe]^+[C_6F_5BF_3]^-} \longrightarrow$$

$$\xrightarrow[Hal = I, Br]{[R_4N]^+Hal^-} C_6F_5Hal + Xe + R_4N^+[C_6F_5BF_3]^-$$

$$\xrightarrow{(4\text{-}CF_3C_6H_4)_3P} \underset{\mathbf{138}}{[C_6F_5(p\text{-}CF_3C_6H_4)_3P]^+[C_6F_5BF_3]^-} + Xe$$

$$\xrightarrow{C_6F_5Hal} \underset{\mathbf{139}}{[(C_6F_5)_2Hal]^+[C_6F_5BF_3]^-} + Xe$$

The pentafluorophenylxenon cation in compound **134a** reacts with benzylcyanide and triphenylmethane containing activated C–H bonds to give the nitriles **140** and **141** in the former case and tetraarylmethane **142** and the biphenyl derivative **143** in the latter case.[264,265]

$$\mathbf{134a} \xrightarrow[-Xe,\ -HF]{PhCH_2CN} \underset{\mathbf{140}}{Ph(C_6F_5)CHCN} + \underset{\mathbf{141}}{Ph(C_6F_5)_2CCN} + (C_6F_5)_2BF$$

$$\mathbf{134a} \xrightarrow[-Xe,\ -HF]{Ph_3CH} \underset{\mathbf{142}}{Ph_3CC_6F_5} + \underset{\mathbf{143}}{C_6F_5C_6H_4(Ph_2)CC_6F_5} + (C_6F_5)_2BF$$

The reaction of compound **134a** with bis(pentafluorophenyl)-cadmium results in perfluorobiphenyl (**144**) and pentafluorobenzene (**145**). The same products are formed in the reaction of XeF_2 with one equivalent of $Cd(C_6F_5)_2$.[266] Both reactions seem to occur *via* the intermediate **146**, which eliminates xenon to generate the radical $^\bullet C_6F_5$.

$$\underset{\mathbf{134a}}{[C_6F_5Xe]^+[(C_6F_5)_2BF_2]^-} + Cd(C_6F_5)_2 \longrightarrow \underset{\mathbf{146}}{[C_6F_5XeC_6F_5]} \xrightarrow{-Xe} \cdots$$

$$XeF_2 + Cd(C_6F_5)_2 \xrightarrow{-CdA_2}$$

$$\cdots \longrightarrow {}^\bullet C_6F_5 \longrightarrow \underset{\mathbf{144}}{C_6F_5C_6F_5}$$

$$\xrightarrow[-Solv^\bullet]{SolvH} \underset{\mathbf{145}}{C_6F_5H}$$

A = F or $[(C_6F_5)_2BF_2]^-$; SolvH is solvent.

The anion in compound **134b** can be replaced by using AsF_5.[258,272]

$$\underset{\mathbf{134b}}{C_6F_5Xe^+[(C_6F_5)_3BF]^-} + AsF_5 \xrightarrow[-20\ ^\circ C]{MeCN} \underset{\mathbf{134c}}{C_6F_5Xe^+AsF_6^-} + B(C_6F_5)_3$$

The salt **134c** formed is stable at temperatures up to 125 °C. Its chemical properties have been investigated.[272,273] The reaction with halide anions in acetonitrile yields different products depending on the nature of the anion. Thus the reaction with the fluoride anion which is a hard nucleophile yields a C_6F_5H–$C_6F_5C_6F_5$ mixture, whereas the reactions with I^-, Br^- and Cl^- anions give C_6F_5X (X = I, Br, Cl). The reactions with compounds containing the HF_2^- anion gives a mixture of C_6F_6, C_6F_5X and $C_6F_5C_6F_5$.[273] The salt **134c** was further used for the synthesis of the organoxenon compound **147** by anionic exchange with an aqueous solution of cesium pentafluorobenzoate. Compound **147** is thermally stable up to 85±3 °C ($T_{1/2} \approx 3$ h at 35 °C).[272,274,275]

$$C_6F_5Xe^+AsF_6^- + C_6F_5CO_2Cs \xrightarrow{D_2O} C_6F_5XeOCOC_6F_5$$
134c **147**

The structure of compound **147** was established by X-ray diffraction analysis.[275] The length of the C–Xe bond (2.122 Å) is larger than that in the cation $[MeCN\cdots XeC_6F_5]^+$ (2.092 Å), whereas the Xe–O bond (2.367 Å) is much longer than those in other known xenon derivatives (2.12–2.21 Å).[87,89,276–279] It should be noted that the Xe–O bond in compound **147** cannot be regarded as a purely ionic bond because of the essential differences in the lengths of the C–O bonds (1.171 and 1.220 Å) in the C_6F_5COO group,[275] which is inconsistent with an ionic carboxylate (1.26 Å).[280]

The reaction of XeF_2 with arylboranes gave the arylxenonium salts **134d**,**e**.[257,263,271,281–284]

$$(3\text{-}CF_3C_6H_4)_2BF + XeF_2 \longrightarrow [3\text{-}CF_3C_6H_4Xe]^+[3\text{-}CF_3C_6H_4BF_3]^-$$
134d

$$(4\text{-}FC_6H_4)_3B + XeF_2 \longrightarrow [4\text{-}FC_6H_4Xe]^+[(4\text{-}FC_6H_4)_2BF_2]^-$$
134e

The synthesis of organoxenon compounds from arylboranes can be carried out in the presence of boron trifluoride.[257,266,271,281,285,286] The resulting salts **134f**,**g** are obtained in good yields.

$$BAr_3 + 3\,XeF_2 + 2\,BF_3 \longrightarrow 3\,ArXe^+BF_4^-$$
134f,**g**

Ar = C_6F_5 (**f**), 2,4,6-$F_3C_6H_2$ (**g**).

The structure of compound **134g** was established by ^{129}Xe, ^{19}F, ^{13}C and ^1H NMR spectroscopy. The absolute value of $^1J(^{129}Xe-{}^{13}C)$, equal to 103.6 Hz (see Ref. 271), is much smaller than that in the cation $C_6F_5Xe^+$ [$^1J(^{129}Xe-{}^{13}C)$ = 119 Hz],[257,263] which suggests the existence of short and, as a consequence, strong bonds and the relative stability of compound **134g**. Some reactions of compounds **134f**,**g** have been studied.[271]

134f,**g** → ($Te(C_6F_5)_2$, 20 °C) $[Te(C_6F_5)_2Ar]^+BF_4^- + Xe$

134f,**g** → (KCl) $ArCl + Xe + KBF_4$

134f,**g** → (IC_6F_5, 60 °C) $Xe + [C_6F_5IAr]^+BF_4^-$

Compounds **134f**,**g** are inert with respect to atmospheric oxygen and water and can be stored in dry air for 21 days without any visible alterations, while their hydrolysis in aqueous acetonitrile is completed within 7 days.

Cyclic voltammograms of compounds of the X^+Y^- type, where X = C_6F_5Xe, $C_6F_5N_2$, C_6F_5Br, C_6F_5I and $(C_6F_5)_4P$, were obtained in 0.1 M solution of Bu_4NBF_4 in MeCN.[287] The minimum and maximum values of electroreduction potentials were obtained for $C_6F_5Xe^+$ and $(C_6F_5)_4P^+$ cations, respectively. The attachment of the first electron to the cations $C_6F_5Xe^+$ and $C_6F_5N_2^+$ is accompanied by the evolution of Xe or N_2 and the generation of the $^{\bullet}C_6F_5$ radical, which either undergoes dimerisation or abstracts hydrogen from MeCN. The first step in the electroreduction of other cations is followed by the liberation of pentafluorophenyl derivatives, *e.g.*, C_6F_5Br, C_6F_5I or $(C_6F_5)_3P$, which undergo further reduction.[287]

XeF_2 was used in the synthesis of new organoxenon compounds.[288,289] The reaction of stoichiometric amounts of XeF_2 and trifluoroacetic acid in CCl_3F at −20 °C gives xenon bis(trifluoroacetate) **6d**,[89–91] which further reacts with trifluoromethanesulfonic acid at −40 °C. This can be accompanied by the formation of the intermediate **148**; indirect evidence can be derived from the appearance of a singlet in the ^{129}Xe NMR spectrum at δ = 400 and the generation of signals at δ = −69.1 ($OCOCF_3$) and −75.6 (OSO_2CF_3) in the ^{19}F NMR spectrum. Compound **148** reacts with fluorine-containing arenes to give the arylxenon triflates **134h**–**k**.[288]

$$XeF_2 + 2\,CF_3CO_2H \xrightarrow[-40\ ^\circ C]{CCl_3F} Xe(OCOCF_3)_2 \xrightarrow{TfOH}$$
6d

$$\longrightarrow [Xe(OCOCF_3)OTf] \xrightarrow{ArH} ArXeOTf$$
148 **134h**–**k**

Ar = 2,4,6-$F_3C_6H_2$ (**h**), 3,5-$(CF_3)_2C_6H_3$ (**i**), 1-F-3-$(CF_3)C_6H_3$ (**j**), 2-F-5-$NO_2C_6H_3$ (**k**).

It is noteworthy that this reaction does not occur if FXeOTf (**5b**) is used as a starting material, while the reaction of 1,3-$F_2C_6H_4$ with the intermediate **148** gives a mixture of Xe(2,4-$F_2C_6H_3$)(OTf) and Xe(3,5-$F_2C_6H_3$)(OTf) (10 : 1) (^{129}Xe NMR data) and several side products. The reaction of 1-F-3-$(CF_3)C_6H_4$ with the intermediate **148** gives compound **134j** and some non-identified products, whereas 1,3,5-$(CF_3)_3C_6H_3$ does not react at all. The addition of arenes devoid of a fluorine, chlorine or trifluoromethyl substituent to the reaction mixture results in immediate decomposition.[288]

A method for the synthesis of cycloalkenylxenon(II) salts by the reaction of (pentafluorophenyl)xenon(II) hexafluoroarsenate **134c** with XeF_2 in HF has been developed.[273,274,290–295] Thus the reaction of the salt **134c** with XeF_2 results in the addition of two or four fluorine atoms to the aromatic ring to afford the salts **149** or **150**.[290]

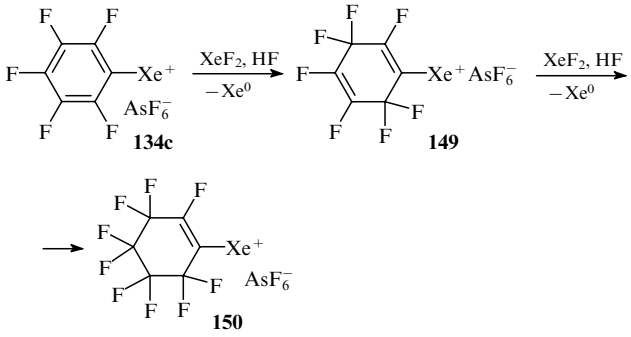

Compounds **149** and **150** are white crystalline substances stable at room temperature and soluble in MeCN. Their structures were established on the basis of ^{19}F, ^{13}C and ^{129}Xe NMR spectral data and chemical transformations.

The salts **149** and **150** react with the bromide anion or benzene in acetonitrile to give products with composition 1-R-1,4-C_6F_7 or 1-R-C_6F_9 (R = Br, Ph), respectively.[296,297] The reaction of the salt **149** with sodium fluoride in acetonitrile results in a ring contraction and the formation of perfluoro-3-methylenecyclopentene (**151**).

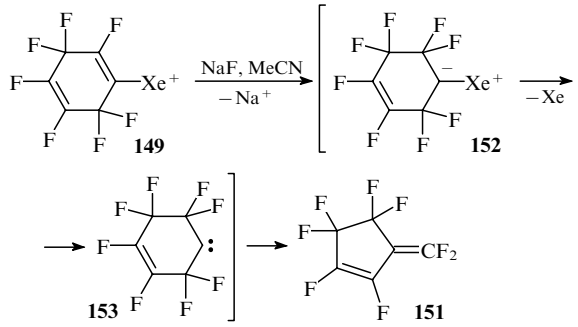

The diene **151** was the main product in the reaction mixture and was unambiguously identified on the basis of ^{19}F NMR spectra (see Ref. 291). Its formation can be interpreted in terms of the HSAB concept. Being a hard base, the nucleophilic fluoride

anion predominantly attacks the hard electrophilic centre of C(2) rather than the soft electrophilic centre of xenon(II). Elimination of xenon from the intermediate **152** results apparently in the carbene **153**, which is further transformed into the reaction product **151**.[291]

The relative reactivities of alkenyl- and arylxenon(II) derivatives were studied in a competitive reaction with tetramethylammonium chloride in acetonitrile. The conversion of the salt **149** was 67% and that of the salt **134c** was 19%. These results and the compositions of the reaction products demonstrate the high electrophilicity of the xenon atom linked to the perfluorocyclohexen-1-yl group.[295]

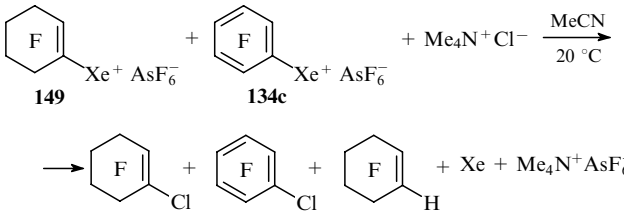

A method for the synthesis of trifluorovinylxenon(II) tetrafluoroborate (**152**) by the reaction of trifluorovinylboron difluoride with XeF_2 in CH_2Cl_2 at −40 °C has been developed recently. The salt **152** is a white solid, which decomposes at temperatures above 0 °C. Its solution in anhydrous HF is stable at 20 °C for several hours but rapidly decomposes in MeCN.[298]

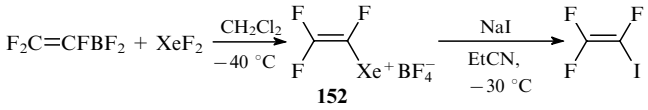

The reaction of the salt **152** with an excess of sodium iodide in EtCN at −30 °C results in trifluoroiodoethylene, which is an indirect proof of the structure of compound **152**.[298]

The alkynylxenon fluoroborate **153** was synthesised using a similar approach.[299] The borofluoride complex **154** generated from lithium *tert*-butylacetylide and BF_3 reacts with XeF_2 in CH_2Cl_2 at −40 °C to give the salt **153** the structure of which was established by NMR and IR spectroscopy. Compound **153** is relatively stable in chloroform at −30 °C, but slowly decomposes at room temperature.[299]

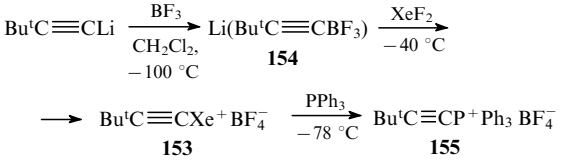

The salt **153** reacts with nucleophiles, *e.g.*, triphenylphosphine, at −78 °C to give the stable phosphonium salt **155**,[299] which confirms its structure.

The attempts to prepare xenon-containing salts from other alkynes were unsuccessful. However, some organoxenon tetrafluoroborates could be detected by ^{129}Xe NMR (see Ref. 299).

VII. Reactions of xenon difluoride with nitrogen-containing compounds

Considerable experience has been gained in the study of reactions of xenon derivatives with nitrogen-containing compounds.

Earlier it was shown[300] that aniline and benzylamine are fluorinated with XeF_2 in the absence of a catalyst without involving the NH-bonds. Unlike benzene derivatives, pyridine easily reacts with XeF_2 in the absence of a catalyst to give 2-fluoro- (35%), 3-fluoro (20%) and 2,6-difluoropyridines (11%).[300] 8-Hydroxyquinoline is converted into 5-fluoro-8-hydroxyquinoline (35%) under the action of XeF_2.[300] On the other hand, imidazo[1,2-*b*]pyridazine is not fluorinated by XeF_2.[301] The reaction of XeF_2 with tetrabutylammonium salts of arenesulfamides **156a–c** in benzene yielded *N*-sulfoazepines **157a–c** presumably formed as a result of generation and subsequent incorporation of nitrene into the benzene ring.[302,303] The yields of the azepines **157a–c** increase as the temperature increases.

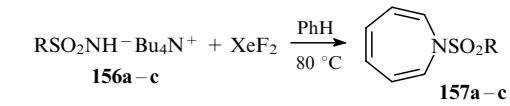

Compound **157**	R	Yield (%)
a	Ph	47
b	Me	41
c	4-MeC_6H_4	42

The reaction of uracil with XeF_2 in hydrofluoric acid or anhydrous hydrogen fluoride results in 5-fluorouracil (**158**) in small yield.[304]

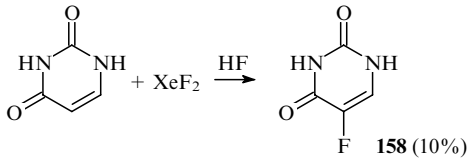

The reaction of the substituted pyrrole **159** with XeF_2 in acetonitrile at 20 °C results in the fluoride **160** and the imide **161**.[305] If the reaction was carried out in dichloromethane, 3-methoxycarbonylmethyl-4-methoxycarbonylethyl-2-formyl-5-chloropyrrole was isolated in 24% yield; its formation is explained by the involvement of the solvent in the reaction.

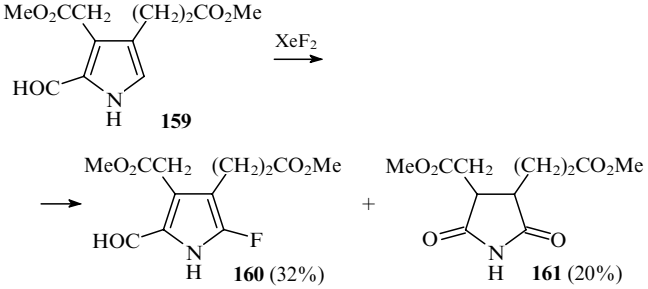

It should be noted that XeF_2 was found to be a most suitable reagent for the fluorination of pyrroles containing electron-withdrawing groups.[305]

The nitrone **162** reacts with XeF_2 to generate a stable nitroxyl radical **163**,[306] which can be converted into an ammonium salt by a reaction with ammonia.

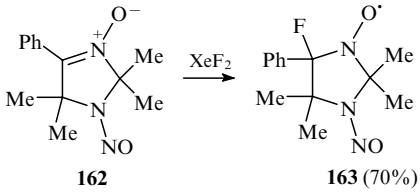

The reaction of aliphatic nitro compounds with xenon difluoride has been studied in detail.[307–313] Thus it was shown that the potassium salt of 1,1-dinitroethane (**164**) reacts with XeF_2 in CH_2Cl_2 to give a mixture of compounds.[307]

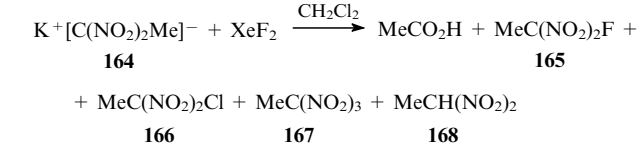

When this reaction was carried out in dry dichloromethane, 1,1-dinitro-1-fluoroethane (**165**) was the main product, whereas the chlorodinitro derivative **166** was predominantly formed in

CH_2Cl_2 saturated with water. The addition of nitrogen oxides to the reaction mixture increases the yield of 1,1,1-trinitroethane (**167**) to 22%. When this reaction is carried out in dry CH_2Cl_2, the addition of KCl and Na_2CO_3 does not influence the ratios of the reaction products. However, the yield of compound **166** in aqueous CH_2Cl_2 increases after addition of KCl, whereas 1,1-dinitroethane (**168**) is not formed in the presence of sodium carbonate. Compound **168** does not react with XeF_2 in CH_2Cl_2 at room temperature. As the reaction mixture contains simultaneously 1,1-dinitroethane and its salt, one can anticipate the formation of a self-condensation product of compound **168**, *viz*., 2,5,5-trinitro-3-aza-4-oxa-hex-2-ene, which was in due course detected. The data obtained suggest[307] that this reaction occurs by a radical or a radical-ion mechanism.

The reaction of dinitromethane, trinitromethane and phenyldinitromethane salts with XeF_2 in different solvents (CH_2Cl_2, MeCN, CCl_4) have also been studied.[308, 309] In this case, the formation of fluorination products, *e.g*., fluorodinitromethyl compounds, was accompanied by the formation of reaction products involving solvent molecules, *viz*., dinitromethyl compounds in CH_2Cl_2 (CH-form) and chlorodinitromethyl compounds (in CH_2Cl_2 and CCl_4) Acetonitrile was found to be resistant to XeF_2 and intermediate radical species. The fluorination of 1,1-dinitroethane and phenyldinitromethane in acetonitrile occurs with high selectivity.[308]

The reaction of the potassium salt of nitroform with XeF_2 in acetonitrile containing 50 vol.% of benzene or THF is accompanied by the formation of a complex mixture of products.[309]

$$^{-}C(NO_2)_3 + XeF_2 \xrightarrow[MeCN]{PhH} FC(NO_2)_3 + HC(NO_2)_3 + PhNO_2 + PhC(NO_2)_3 + PhF + PhPh + FCH(NO_2)_2 + PhC(NO_2)_2F$$

$$^{-}C(NO_2)_3 + XeF_2 \xrightarrow[MeCN]{THF} FC(NO_2)_3 + HC(NO_2)_3 + FCH(NO_2)_2 + \text{(O)}C(NO_2)_3 + \text{(O)}CF(NO_2)_2$$

It is of note that the side fluorination products of anions of dinitromethyl compounds with XeF_2 in various solvents are similar to the reaction products of dinitromethyl radicals, generated by electrochemical oxidation of polynitroalkane anions, with solvents. This similarity can be explained by the identity of the intermediate species.[309]

Xenon difluoride can play the role of a single-electron oxidant with respect to both 1,1-dinitrocarbanions and the difficultly oxidisable nitroazole anions.[310] Thus the reaction of the potassium salt of 3-nitro-1,2,4-triazole (**169**) with XeF_2 in acetonitrile results in the non-ionised 3-nitro-1,2,4-triazole (**170**) (yield 70%–80%). A 3:2 mixture of 3-nitro- (**170**) and 1-phenyl-3-nitro-1,2,4-triazoles (**171**) is formed in the MeCN–PhH system.

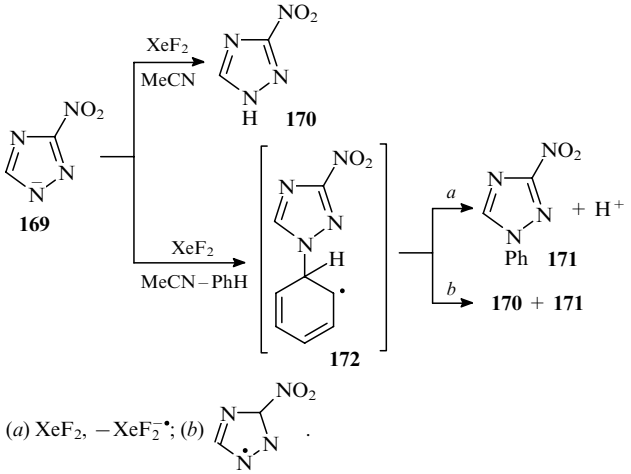

(*a*) XeF_2, $-XeF_2^{-\bullet}$; (*b*)

Presumably, compound **171** is formed as a result of generation of the radical **172**. The latter can be rearomatised by two equally probable routes, *viz*., by single-electron oxidation and deprotonation (route *a*) and by abstraction of the hydrogen atom by the 3-nitro-1,2,4-triazole radical (route *b*).[310] However, the latter route is less probable, since benzene has a much higher oxidation potential ($E_{1/2}$ = 2.02 V[314]) than the triazole anion [$E_{1/2}$ = 1.77 V (see Ref. 315)].

The reactions of potassium salts of 1,1-dinitrobut-2-enonitrile (**173a**) and the respective amide (**173b**) with XeF_2 were studied in order to compare the reactivities of the dinitromethyl group and the double bond. These reactions give the fluorination products **174a**,**b** in high yields.[311]

$$[RCH{=}CHC(NO_2)_2]^{-}K^{+} + XeF_2 \xrightarrow{MeCN} RCH{=}CHCF(NO_2)_2 + KF + Xe$$

173a,**b** **174a**,**b**

R = CN (**a**), $CONH_2$ (**b**).

Selective fluorination of the dinitromethyl anion without affecting the double bond can be explained by the absence of a catalyst (HF), since the reaction was carried out in a vessel made of ordinary silicate glass which is known to be an effective chemical acceptor of HF. According to ^{1}H NMR and GLC data, this reaction gives < 5% admixtures. When the fluorination was performed in a reactor made of a fluoropolymer resistant to HF, this resulted in a mixture of products, which can be assigned to the occurrence of HF-catalysed side reactions, *e.g*., the fluorination of the double bond.[311]

The kinetics of fluorination of salts of dinitromethyl compounds by XeF_2 has been studied.[312, 313] The kinetics is described by second-order equations, first-order with respect to each reagent. The nature of the cation in the salt does not influence the value of the fluorination rate constant in the concentration range from 10^{-3} to 10^{-5} mol litre^{-1}. The thermodynamic activation parameters ($\Delta H_{298}^{\neq}$ = 30–60 kJ mol^{-1}, $\Delta S_{298}^{\neq}$ = -60 to -130 J mol^{-1} K^{-1}) lie in the range characteristic of an S_N2 reaction.

A mechanism of the reaction of dinitro compounds with XeF_2 has been proposed.[307, 309, 310, 313] Its first step probably includes single-electron oxidation of the dinitro compound anion by XeF_2. The reaction products result from the reaction of the solvent molecules with the radical species formed in the first step. The CH_2Cl_2 molecules serve as the source of chlorine and hydrogen atoms, whereas the radical of the original dinitro compound serves as the source of NO_2.

$$R\dot{C}(NO_2)_2 + F^{-} \longrightarrow [RC(NO_2)_2F]^{-\bullet} \xrightarrow{XeF_2\,(\dot{X}eF)} RC(NO_2)_2F$$

$$[RC(NO_2)_2]^{-} + \dot{N}O_2 \longrightarrow [RC(NO_2)_3]^{-\bullet} \xrightarrow{XeF_2\,(\dot{X}eF)} RC(NO_2)_3$$

The rates of the reaction of XeF_2 with salts of *ortho*-, *meta*- and *para*-substituted aryldinitromethanes in MeCN were measured by spectrophotometric methods.[313] The relationship between the structures of the substrates and their reactivities with respect to XeF_2 is described by linear free energy equations using inductive, resonance and steric constants of the substituents. For the overwhelming majority of dinitromethyl compounds, it was found that the rate of fluorination of the corresponding dinitrocarbanion decreases with the increase in the CH-acidity.

Xenon difluoride acting as a single-electron oxidant converts the nitroxyl radicals **175** into the oxoammonium fluorides **176**, nitroso compounds **177** and **178** and the products of more profound oxidation.[316]

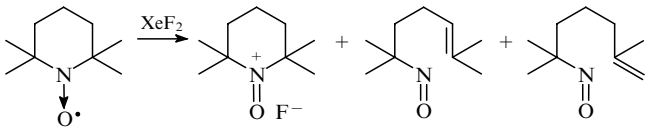

175 **176** **177** **178**

The general stoichiometric equation for the oxidation was derived from the kinetic data.[316]

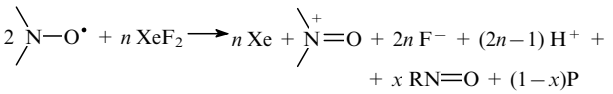

P are reaction products.

A convenient procedure for the synthesis of fluorocarbonyl-substituted hydrazines **179** and **180** in the reaction of XeF_2 with isocyanates has been developed.[317] The reaction of XeF_2 with perfluoroazapropene yields tetrakis(trifluoromethyl)hydrazine **181**.[317]

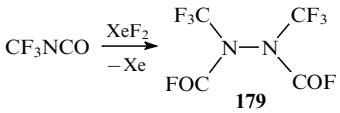

179

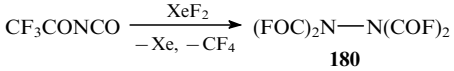

180

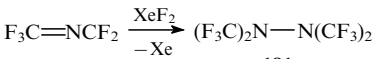

181

A compound containing the Xe–N bond was first synthesised by the reaction of XeF_2 with di(fluorosulfuryl)imide (**181**).[318–320]

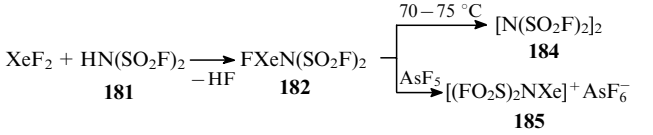

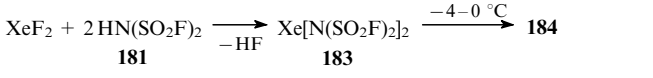

Mono- (**182**) or bis[*N*,*N*-di(fluorosulfuryl)imido]xenon fluorides **183** can be obtained depending on the reagent ratio. The structures of compounds **182** and **183** were confirmed by X-ray diffraction analysis.[321–323] The magnitude of the angle C–Xe–N (174.5°) corresponds to the structure of a distorted trigonal bipyramid with the substituents in the axial positions. The length of the Xe–C bond (2.092 Å) is comparable with that of the C–I bond.[153] The coordinate bond Xe–N (2.681 Å) in compounds **134a**,**b** is much longer than the covalent bond Xe–N.[323, 324] The decomposition of compounds **182** and **183** is accompanied by the formation of the dimer **184**. The intermediate radical $^{\bullet}N(SO_2F)_2$ was detected by EPR. The reaction of compound **182** with AsF_5 gives the salt **185**.[319, 322, 324]

N-Trimethylsilyl(trifluoromethylsulfonyl)amine (**186**) was used as the starting material for the preparation of bis[bis(trifluoromethylsulfonyl)imido]xenon (**187**), which is a stable compound and decomposes only at 72 °C to generate the radical $^{\bullet}N(SO_2CF_3)_2$.[325]

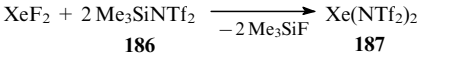

186 **187**

The attempt to prepare compounds containing a Xe–C bond by the reaction of HCN with XeF_2 was unsuccessful. However, the fact that xenon-containing cations manifest the properties of Lewis acids[326] made it possible to synthesise xenon derivatives containing the Xe–N bond from HCN.[327–330] The first adiabatic ionisation potential of HCN (13.80 eV) was determined from photoionisation data.[331] The electron affinity of the XeF^+ cation is 10.9 eV. It may therefore be assumed that HCN will be resistant to the oxidative attack of XeF^+, and $HC{\equiv}NXeF^+$ should manifest satisfactory thermal stability. Indeed, compounds **188a–g** containing covalent Xe–N bonds were synthesised by the reaction of $XeF^+AsF_6^-$ or $Xe_2F_3^+AsF_6^-$ with HCN or nitriles.[327–330]

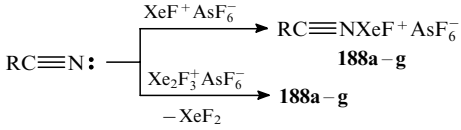

R = H (**a**), Me (**b**), CH_2F (**c**), Et (**d**), C_2F_5 (**e**), C_3F_7 (**f**), C_6F_5 (**g**).

Compounds **188a–g** were characterised by spectral methods.[328] The reaction product with hydrogen cyanide (**188a**) is a white crystalline substance stable below −60 °C. The derivatives **188e–g** containing perfluoroalkyl radicals are even less stable; they were characterised by spectral methods without being isolated from the reaction mixtures. The nature of the bond in the cation $HC{\equiv}NXeF^+$ has been discussed.[328] It is of note that the corresponding fluorokrypton salts were synthesised by an analogous scheme in the reaction of the cation KrF^+ with nitriles (the electron affinity of the cation KrF^+ is 13.2 eV).[330, 332]

Equimolar amounts of $XeF^+AsF_6^-$ and perfluoropyridine (I_p = 10.08 eV) react in anhydrous HF at −20 to −30 °C to give the salts **189a**,**b** containing the Xe–N bond. Removal of the solvent (HF) at −50 °C leads to the formation of a white solid substance which represents a mixture of XeF_2 with the salts **190a**,**b** and **191a**,**b** containing no xenon (data from the Raman spectra). BrF_5 appeared to be a more suitable solvent than HF in the formation of the salts **189a**,**b**.[329]

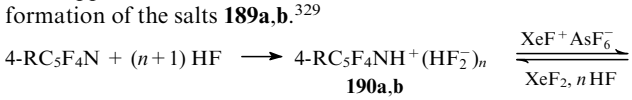

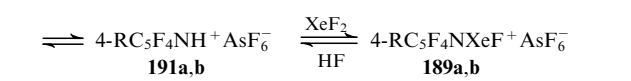

R = F (**a**), CF_3 (**b**).

The reaction of trifluoro-*s*-triazine (I_p = 11.50 eV) with $XeF^+AsF_6^-$ (1 : 1) for 4 h at room temperature gives the crystalline compound **192** which is stable at room temperature; this compound was characterised by spectral methods.[330]

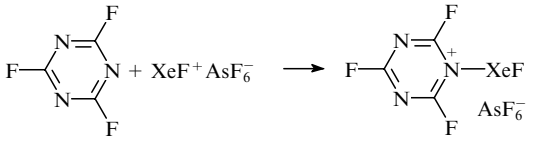

192

The reaction of the salt **193**, prepared by the reaction of trifluoroacetamide (I_p = 10.77 eV) with AsF_5, with xenon difluoride resulted in the organoxenon compound **194**.[333] The salt **193** was isolated in the crystalline state. At 0 °C, it rapidly decomposes to give gaseous products.

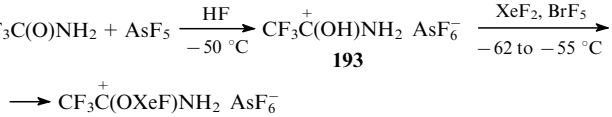

193 **194**

Rapid removal of HF from a solution containing $XeF^+AsF_6^-$ and $CF_3C(O)NH_2$ at −50 °C affords a white precipitate of composition identical to that of compound **195**; the salt **194** was not detected.[333]

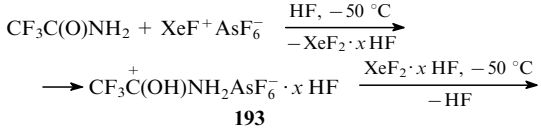

193

$$\longrightarrow CF_3\overset{+}{C}(OH)NH_2AsF_6^- \cdot XeF_2 \cdot x\,HF$$
195

A detailed study of the reaction of xenon difluoride with HN_3, NaN_3 and NaOCN in H_2O, anhydrous HF and SO_2ClF has been published.[334] An analysis of reaction products made it possible to suggest the formation of $FXeN_3$ (**196**) and FXeNCO (**197**) as intermediates, which react according to the following schemes:

$$[FXeN_3] \xrightarrow[-HF,\ -Xe]{H_2O} [HON_3] \xrightarrow{-N_2} [HON] \xrightarrow{-N_2}$$
196

$$\longrightarrow HON{=}NOH \xrightarrow[-H_2O]{} N_2O,$$

$$[FXeNCO] \xrightarrow[-HF,\ -Xe]{H_2O} [HONCO] \xrightarrow{2\,H_2O} HONH_2 + H_2O + CO_2.$$
197

Ab initio quantum-chemical calculations of the structural parameters of both intermediates have been made.[334] The data obtained suggest that the Xe–F bond in the intermediates **196** and **197** (2.051 and 2.024 Å, respectively) is longer than that in bis[(difluorosulfuryl)imido]fluoroxenon **182** (1.97 Å) and in XeF_2 (1.977 Å).[318, 320, 322–325, 328] The calculated length of the Xe–N bond (2.21 Å) in compound **197** is comparable with the experimentally determined value (the length of the corresponding bond in compound **182** is 2.20 Å). The Xe–N distance (2.32 Å) in compound **196** is much longer (2.318 Å).[328] The thermodynamic possibility of formation of the intermediates **196** and **197** was demonstrated using an energy cycle for gas-phase reactions. The enthalpies of the reactions were calculated on the basis of the literature data.[334]

$$XeF_2\,(gas) + NH_3\,(gas) \longrightarrow$$
$$\longrightarrow FXeN_3\,(gas) + HF\,(gas)\ (\Delta H^\circ < -12.1\ kcal\ mol^{-1}).$$

$$XeF_2\,(gas) + HNCO\,(gas) \longrightarrow$$
$$\longrightarrow FXeNCO\,(gas) + HF\,(gas)\ (\Delta H^\circ < -12.1\ kcal\ mol^{-1}).$$

The synthesis of $NO^+XeF_5^-$ and $NMe_4^+XeF_5^-$ in the reaction of XeF_4 with NOF or $Me_4N^+F^-$ (see Ref. 335) and the synthesis of $NF_4^+XeF_7^-$ from XeF_6 and $NF_4^+HF_2^-$ were documented.[336]

VIII. Oxidative fluorination of organoelement compounds by xenon difluoride and its derivatives

Oxidative fluorination of organoelement compounds by xenon difluoride and its derivatives presents theoretical and practical interest. The first reports on the feasibility of oxidative fluorination of iodine to IF_5 (see Ref. 29) and of SO_2 to SO_2F_2 (see Refs. 29 and 337) appeared in the late 1960's to early 1970's. Later, the reactions of other elements, their oxides, halides and carbonyls with XeF_2 were also studied, which demonstrated convincingly the high potentials of the oxidative fluorination.[338]

The transformations of organoelement compounds under the action of XeF_2 are extremely diverse and depend on the structures of the radicals linked to the heteroatom, the degree of oxidation of the heteroatom, the reaction conditions, the nature of the solvent, *etc*. The examples of the application of XeF_2 for fluorination of the majority of classes of organoelement compounds are now available.

1. Reactions of XeF_2 with Group VII organoelement compounds

a. Reactions of organoiodine compounds with XeF_2

Organoiodine compounds are among the first to have been subjected to oxidative fluorination by XeF_2. These studies were aimed at a search for convenient methods for the preparation of difluoro-λ^3-iodanylalkenes (arenes) used for fluorination of unsaturated compounds.[339–342] The first report on the oxidative fluorination of methyl iodide by XeF_2 was published in the early 1970's. The difluoro-λ^3-iodanylalkene synthesised (**198a**)[339] was rather unstable and could only be characterised by spectral methods. However, despite its low stability this compound was used for iodofluorination of alkenes.[343–346]

Later, this method of the synthesis of difluoro-λ^3-iodanylalkanes (arenes) was extended to a vast variety of alkyl- and aryl iodides. Iodobenzene,[347] substituted aryl iodides[348] as well as perfluoroalkyl- and perfluoroaryl iodides[349] are easily fluorinated by XeF_2. In the case of 1-iodo-3,5-dichlorobenzene and iodopentafluorobenzene, the excess of XeF_2 converts difluoro-λ^3-iodanylarenes into tetrafluoro-λ^5-iodanylarenes in quantitative yields,[349] while the reaction of difluoro-λ^3-iodanylbenzene (**198b**) with XeF_2 results in the fluorination of the aromatic nucleus and the formation of tetrafluoro-λ^5-iodanylbenzene.[349, 350]

$$RI + XeF_2 \xrightarrow{20\ ^\circ C} RIF_2 + Xe$$
198a–k

R = Me (**a**), Ph (**b**), CF_3CH_2 (**c**), C_6F_5 (**d**), 3,5-$Cl_2C_6H_3$ (**e**), 2-$CF_3C_6H_4$ (**f**), 3-$MeOC_6H_4$ (**g**), 4-$MeOC_6H_4$ (**h**), 3-ClC_6H_4 (**i**), 4-ClC_6H_4 (**j**), 3-$NO_2C_6H_4$ (**k**).

Difluoro-λ^5-iodanylbenzene (**198l**) immobilised on a polymeric support was synthesised using XeF_2 as a soft fluorinating reagent.[351, 352] The polymeric reagent was used for the fluorination of alkenes.[353, 354]

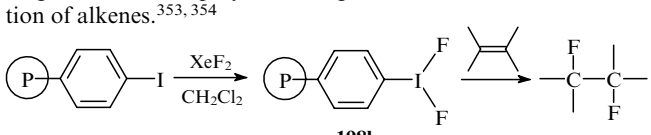

198l

(P) is polymeric support.

In the majority of cases, (difluoro-λ^3-iodanyl)alkanes are unstable.[339] However, treatment of a solution of 4-iodotricyclene in tetrachloromethane with a sixfold excess of XeF_2 and subsequent removal of the solvent and the excess of XeF_2 yield a light-yellow solid stable product **198m**.[355]

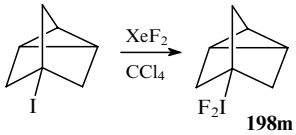

198m

In some cases, the reaction of iodoalkanes with XeF_2 results in the substitution of fluorine for iodine instead of oxidation. This takes place in the reaction of XeF_2 with polycyclic bridged iodides. Fluorinated bicycloalkanes and polycycloalkanes are formed in high yields.[240, 356]

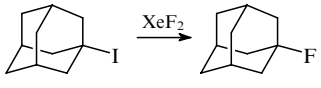

(85%)

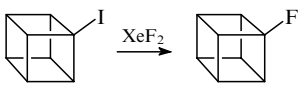

(80%)

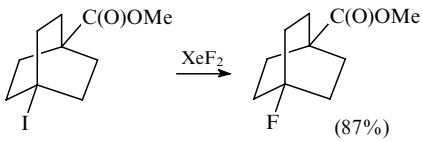

(87%)

It is assumed that this reaction occurs by a carbocationic mechanism. Initially, the difluoro-λ^3-iodanylalkanes generated undergo heterolytic cleavage of the C–I bond to give IF_2^- and the carbocations containing a cationic centre at the head of the bridge.[343] The carbocation can further react either with the fluoride anion to give a fluoride or with CH_2Cl_2 to give a chloride.

Stable cations usually generate fluorides, whereas highly reactive cations, such as cubyl or norbornyl cations, react nonselectively to give chlorides. Their content in the reaction mixture correlates with the calculated values of the carbocation energies.[356]

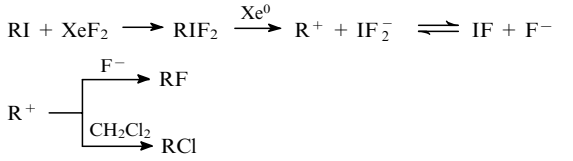

Recently, divalent xenon derivatives other than XeF_2, *e.g.*, xenon bis(trifluoroacetate) (**6d**),[89–91] xenon fluoro(triflate) (**5b**)[89] and xenon fluoro(mesylate) (**5c**),[89] came into use. Thus the reagent (**6d**) obtained *in situ* from XeF_2 and trifluoroacetic acid in the presence of trifluoroacetanhydride reacts with aryl iodides to give bis(trifluoroacetoxy)-λ^3-iodanylarenes **199**–**201**.[357] In the absence of trifluoroacetanhydride, this reaction affords μ-oxobis-[trifluoroacetato(aryl)] iodides (**202**) the structure of which was established by X-ray diffraction analysis.[357, 358]

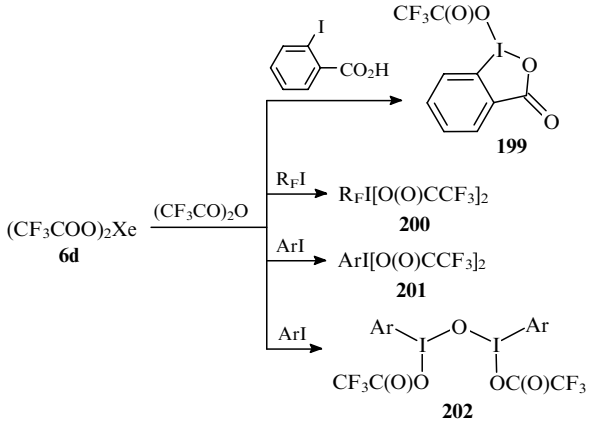

Ar = Ph, 4-MeC_6H_4, 2-MeC_6H_4, 4-PhC_6H_4, 4-[$MeC(O)O]C_6H_4$, 4-$NO_2C_6H_4$, 3-$NO_2C_6H_4$, 2-Me-4-$NO_2C_6H_3$; R_F = C_3F_7, C_4F_9.

A one-step procedure for the generation of iodanylarenes directly from aryl iodides[359–367] is based on their oxidation by xenon fluorosulfonate which gives salts of the type **203**.

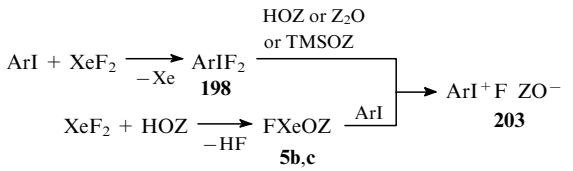

Z = Tf (**b**), Ms = SO_2Me (**c**); TMS = Me_3Si.

The interest in the sulfonates **203** is due to the fact that they can react with aromatic compounds and terminal alkynes to give the corresponding diaryliodonium (**204**, **205**) and alkenyl(aryl)-iodonium salts **206**.[359, 363, 365]

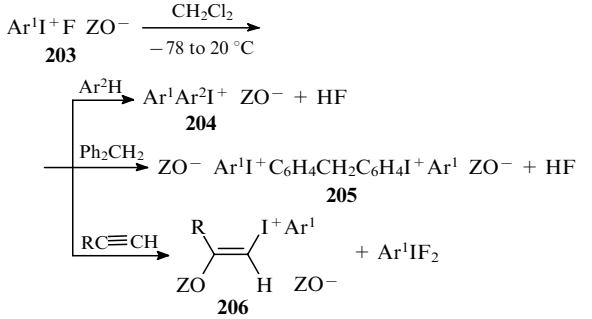

Z = Tf, Ms; Ar^1, Ar^2 = Ph, 4-MeC_6H_4, 2-MeC_6H_4, 4-$NO_2C_6H_4$;
R = H, Pr^n, Bu^n, n-C_8H_{17}, CH_2OH, CH_2OMe, CH_2Cl, $(CH_2)_2OH$.

It is noteworthy that in earlier studies the alkenyl(aryl)iodonium sulfonates **206** were obtained by electrophilic addition of [PhIO–HOTf] to alkynes.[368–373] The use of xenon derivatives **5b**,**c** for the synthesis of the salts **203** allows one-pot synthesis of β-functionalised vinyliodonium salts from iodobenzene and terminal acetylenes.

The reagent **5b** oxidises 1,4-diiodobenzene resulting in the bistriflate **207** which reacts with terminal alkynes to yield (*p*-phenylene)alkenyliodonium salts **208**.[364, 365]

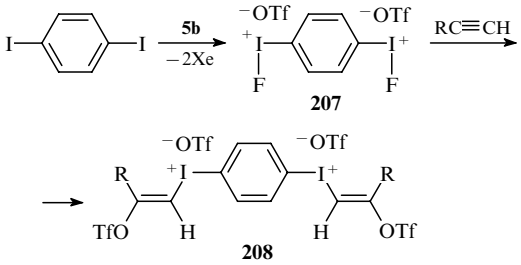

R = H, Me, Et, Ph, Pr^n, n-C_8H_{17}, CH_2Cl.

The oxidation of iodoarenes by bis(nitrodifluoroacetoxy)xenon (**6k**) yields the iodonium salts **209** in 65%–80% yields.[374, 375]

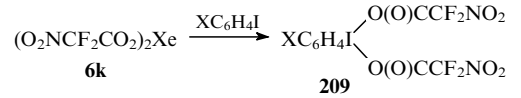

X = H, 4-Me, 4-F, 4-MeO, 3-CF_3, 4-NO_2, 4-Cl.

The reaction of $XeF^+AsF_6^-$ with HI in solution has been studied.[376]

According to *ab initio* calculations, the enthalpy of the reaction of XeF_2 with HI is equal to -63.4 kcal mol^{-1} (see Ref. 376).

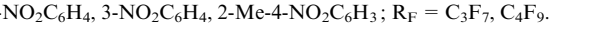

b. Reactions of organobromine compounds with XeF_2

Nesmeyanov *et al.*[377] have demonstrated that bromine can in principle be oxidised in mononuclear bromoarenes. However, this is possible only with XeF_2. The difluorides **210** formed react with different arenes in the presence of boron trifluoride etherate to give the diarylbromonium salts **211**, their structures were confirmed by independent syntheses, *viz.*, by decomposition of arenediazonium tetrafluoroborates in the presence of the corresponding bromoarenes. In some cases, the formation of bromonium salts could be detected using ^{19}F NMR spectra. The yields of the salts **211** do not exceed 5%. Fluorination and oxidation of aromatic nuclei is the main route of this reaction even at -70 °C.

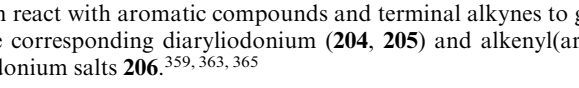

Ar^1 = 4-FC_6H_4, 4-ClC_6H_4, 4-MeC_6H_4, 2-$MeO_2CC_6H_4$;
Ar^2 = Ph, 4-FC_6H_4, 4-ClC_6H_4, 4-MeC_6H_4.

2. Reactions with Group VI organoelement compounds

a. Reactions of organosulfur compounds with XeF_2

Owing to the high oxidation potential of XeF_2, its reaction with sulfur-containing compounds occurs vigorously at low temperatures. Oxidative fluorination of sulfur-containing compounds, *viz.*, methyl phenyl sulfide, tetrahydrothiopyrones and thiochromanone, by XeF_2 was carried out for the first time in 1976 by Zupan.[378] The reaction of XeF_2 with diaryl or alkyl aryl sulfides results in the formation of sulfur(IV) and sulfur(VI) compounds;

the structures of the original sulfides influence the direction of the reaction. The nature of substituents at the α-carbon atom is the most important factor. The sulfides containing no α-hydrogen atoms are smoothly converted into difluorosulfuranes.[379] The presence of Me, CH_2 and CH fragments vicinal to the sulfur atom results in the formation of α-fluoro sulfides. For example, methyl phenyl sulfide is oxidised to fluoromethyl- (**212**) or difluoromethyl phenyl sulfide (**213**) depending on the amount of XeF_2 used.[378, 379]

$$PhSMe + XeF_2 \xrightarrow[25\ ^\circ C]{HF,\ CH_2Cl_2} \underset{\mathbf{212}\ (67\%)}{PhSCH_2F} \xrightarrow[25\ ^\circ C]{XeF_2\cdot HF,\ CH_2Cl_2} \underset{\mathbf{213}\ (58\%)}{PhSCHF_2}$$

Sometimes, the reaction of alkyl aryl sulfides with XeF_2 gives unsaturated sulfides. This is due to the low stability of α-fluoroalkyl sulfides and their proneness to eliminate HF. Thus the reaction of isopropyl phenyl sulfide with XeF_2 at −10 °C gave the fluorination product **214**, whereas isopropenyl phenyl sulfide (**215**) was obtained at 0 °C.[379]

$$PhSCHMe_2 \xrightarrow{XeF_2} \begin{cases} \xrightarrow[-10\ ^\circ C,\ 30\ min]{MeCN} \underset{\mathbf{214}\ (>90\%)}{PhSCFMe_2} \\ \xrightarrow[0\ ^\circ C,\ 2\ min]{MeCN} \underset{\mathbf{215}\ (>90\%)}{PhSC(Me)=CH_2} \end{cases}$$

The reaction of XeF_2 with diphenyl sulfide and subsequent hydrolysis of the reaction products afford diphenyl sulfoxide or sulfone. Presumably, diphenyldifluoro- (**216**), diphenyldifluorooxo-λ⁴-sulfanes (**217**) and diphenyltetrafluoro-λ⁴-sulfane (**218**) are formed as the intermediate products.[380]

$$Ph_2S \xrightarrow[HF]{XeF_2} \underset{\mathbf{216}}{[Ph_2SF_2]} \begin{cases} \xrightarrow{OH^-} Ph_2SO \xrightarrow[HF]{XeF_2} \underset{\mathbf{217}}{Ph_2S(O)F_2} \xrightarrow{OH^-} Ph_2SO_2 \\ \xrightarrow[HF]{XeF_2} \underset{\mathbf{218}}{Ph_2SF_4} \xrightarrow{OH^-} Ph_2SO_2 \end{cases}$$

The fluorination of thiochroman-4-one (**219a**) or its 3-bromo derivative (**219b**) results in thiochromen-4-ones (**220a**,**b**), whereas the reaction of 3,3-dibromothiochroman-4-one (**219c**) gives 3,3-dibromo-2-fluorothiochroman-4-one (**220c**).[378, 380]

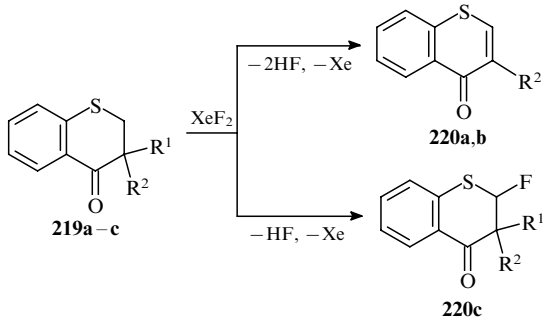

219a–c **220a**,**b** **220c**

R^1, R^2 = H (**a**); R^1 = H, R^2 = Br (**b**); R^1 = R^2 = Br (**c**).

The reaction of thio-4-pyrone with XeF_2 gives dihydro-2,6-diphenylthio-4-pyrone (**221**) which is dehydrogenated by XeF_2.[378]

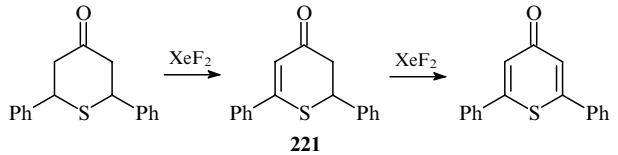

221

The reaction of dimethyl sulfide with XeF_2 has been studied in detail. In the absence of a solvent, this reaction is explosive. Dilution of the reaction mixture with trichlorofluoromethane results in FCH_2SMe which further reacts with the excess of dimethyl sulfide to give the salt **222**.[381] It is of note that the reaction of dimethyl sulfide with XeF_2 in the presence of BF_3 or AsF_5 is not accompanied by fluorination of the methyl group but the salts **223** are formed instead.

$$Me_2S \xrightarrow{XeF_2} MeSCH_2F \xrightarrow[HF]{Me_2S} \underset{\mathbf{222}}{[Me_2SCH_2SMe]^+[F(HF)_n]^-}$$

$$Me_2S \xrightarrow[A]{XeF_2} \underset{\mathbf{223}}{[Me_2SF]^+[AF]^-}$$

A = BF_3, AsF_3.

The intermediate formation of the salts **223** in this reaction was confirmed by ^{19}F NMR spectral data and independent synthesis. The cation $[Me_2SCH_2SMe]^+$ is generated only in the presence of a protic acid. It is suggested[381] that $R_2S^+X^-$ or $R_2S^+XeFX^-$ are formed as intermediates. The latter are used[382] for the fluorination of carbanions.

The reactions of sodium derivatives of diethyl malonate or of substituted malonates with XeF_2 in CH_2Cl_2 result in the dimers **224**. The fluorination products **225** were isolated in the presence of $BF_3\cdot Et_2O$. The methylthio derivatives of the malonates **226** are formed along with the fluorination products **225** after addition of dimethyl sulfide to the reaction mixture.[382] It is interesting to note that the reaction of diethyl nitromalonate with XeF_2 gives only a dimer of the type **224**.

$$RC^-(CO_2Et)_2Na^+ \xrightarrow{XeF_2} \underset{\mathbf{224}}{\left[(EtO_2C)_2C(R)\right]_2} \quad (CH_2Cl_2)$$

$$RC^-(CO_2Et)_2Na^+ \xrightarrow[CH_2Cl_2,\ BF_3\cdot Et_2O]{XeF_2} \underset{\mathbf{225}}{RC(F)(CO_2Et)_2}$$

$$RC^-(CO_2Et)_2Na^+ \xrightarrow[BF_3\cdot Et_2O,\ Me_2S]{XeF_2,\ CH_2Cl_2,} \mathbf{225} + \underset{\mathbf{226}}{RC(SMe)(CO_2Et)_2}$$

R = H, Me, Et, C_5H_{11}, Bn, NO_2.

The highest yields of the reaction products are obtained for equimolar ratios of the reagents and at low temperatures (−78 °C).[382]

The reaction of XeF_2 with fluorinated sulfides generated easily hydrolysable aryl trifluoromethyl difluorosulfuranes **227**.[383]

$$4\text{-}RC_6H_4SCF_3 + XeF_2 \xrightarrow{HF} \underset{\mathbf{227}}{4\text{-}RC_6H_4SF_2CF_3} + Xe$$

R = H, Cl, NO_2.

Thus, the reaction of sulfides with XeF_2 affords three main types of reaction products, *viz*., α-fluoroalkyl sulfides, dehydrofluorination products and sulfoxides or sulfones. A mechanism of this reaction has been proposed.[384]

The reaction of Ph_2SO with XeF_2 in the presence of ~1% solution of Et_4NCl in CH_2Cl_2 at 20 °C results in the difluoride **217** in quantitative yield.[385]

$$Ph_2SO + XeF_2 \xrightarrow[CH_2Cl_2]{Et_4NCl} \underset{\mathbf{217}}{Ph_2S(O)F_2} + Xe$$

In the absence of Cl^-, the reaction is sluggish (2–6 days). Apparently, the chloride anion promotes the generation of the fluoride anion, which behaves as a strong base in CH_2Cl_2 in the absence of HF.[386, 387] The reaction mechanism proposed by Ou and Janzen[385] which includes the formation of the anion **228** and its oxidation to the radicals **229**–**231** is corroborated experimentally by the identification of the radical XeF• (spectroscopic data).[388]

$$2Cl^- + XeF_2 \longrightarrow 2F^- + Cl_2 + Xe$$

$$Ph_2SO \underset{}{\overset{F^-}{\rightleftharpoons}} \underset{\mathbf{228}}{Ph_2S(O)F^-} \overset{e^-}{\rightleftharpoons} \underset{\mathbf{229}}{Ph_2S(O)F^\bullet} \overset{XeF_2}{\rightleftharpoons}$$

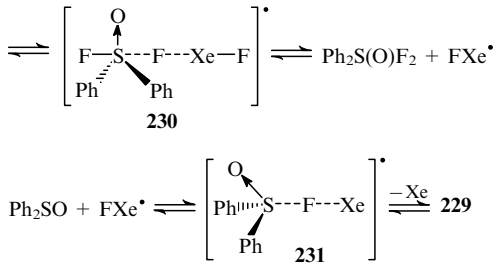

Compounds **232a–c** (*cis*- and *trans*-isomers) were synthesised in the reaction of XeF_2 with ArSSAr or $ArSF_3$ in the presence of a chloride anion source, *viz*., Et_4NCl.[389] Individual isomers can be obtained by varying the reaction conditions and the ratios of the reagents. The maximum yield of the *trans*-**232a** (89%) is achieved for the $Ph_2S_2 : Et_4NCl : XeF_2$ ratio of 1 : 2 : 8, that of the *cis*-**232c** (83%), for the $(4\text{-}O_2NC_6H_4)_2S_2 : Et_4NCl : XeF_2$ ratio of 1 : 2 : 6. In each case, the formation of side products ($ArSF_5$ and $ArSOF_3$) and fluorination of the solvent took place.

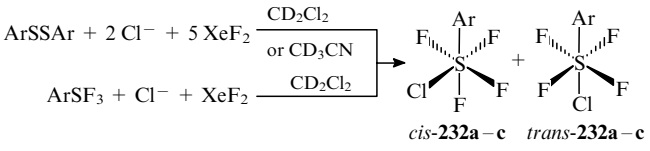

Ar = Ph (**a**), 4-MeC_6H_4 (**b**), 4-$O_2NC_6H_4$ (**c**).

A scheme with the nomenclature N-X-L (where X is the central atom, N is the number of valent electrons and L is the number of ligands)[390] illustrates the mechanism of this reaction which includes the formation of the anion **233**, its oxidation to the radical **234**[391] and subsequent recombination.[389] With a decrease in the content of the radical Cl•, the concentration of $ArSF_5$ should increase, which was confirmed experimentally.[389]

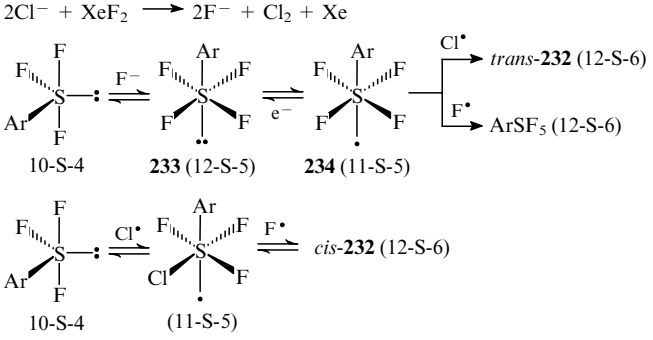

The highly selective oxidative fluorination of sulfides by XeF_2 was used for incorporating one or two fluorine atoms into the carbon chains of biologically active substances. For example, the fluorination of the methionine derivatives **235a–d** by XeF_2 (−20 to 20 °C) occurs regiospecifically and involves the MeS group.[392, 393]

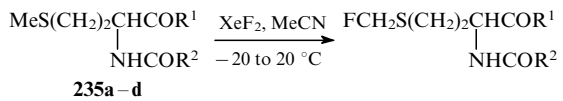

235a–d

R^1 = OMe, R^2 = CF_3 (**a**); R^1 = $OC_6H_4NO_2$-4, R^2 = OBu^t (**b**);
R^1 = $OC_6H_4NO_2$-4, R^2 = CF_3 (**c**); R^1 = $NHCH_2C(O)OEt$,
R^2 = OCH_2Ph (**d**).

The reaction of XeF_2 with methyl ester of β-biotin (**236**) results in the diastereomers of 6-fluorobiotin methyl ester **237a**,**b**.[394]

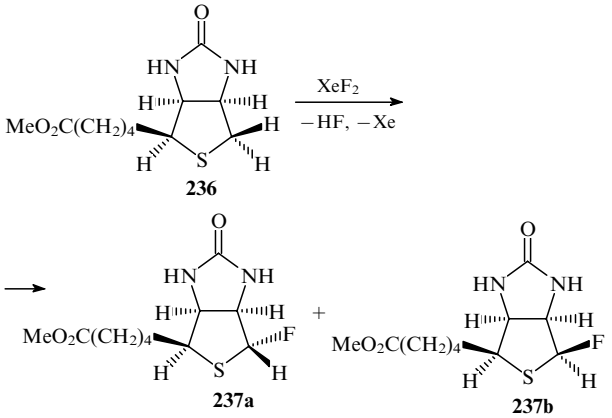

The reaction of 2′,3′-di-*O*-acetyl-5′-*S*-(4-methoxyphenyl)-5′-thiouridine (**237**) with XeF_2 yields a mixture of diastereomeric 2′,3′-di-*O*-acetyl-5′-fluoro-5′-*S*-(4-methoxyphenyl)-5′-thiouridines (**238**).[395]

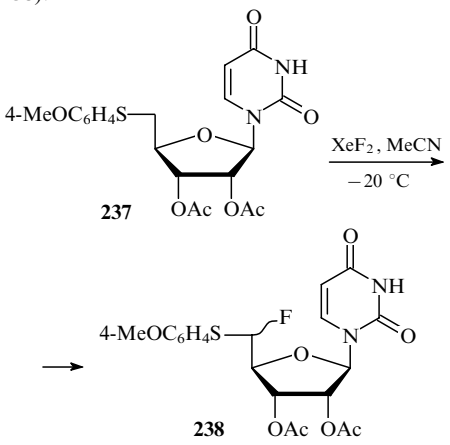

Xenon difluoride was also used for the fluorination of 3′,5′-di-*O*-acetyl-2′-*S*-alkyl(aryl)-2′-thiouridines. Thus the reaction of compound **239** with XeF_2 affords a mixture of diastereoisomeric 3′,5′-di-*O*-acetyl-2′-*S*-alkyl(aryl)-2′-fluoro-2′-thiouridines **240** in 22% yield.[396] This reaction is accompanied by partial oxidation of the sulfur atom in the initial sulfides **239** and the formation of the sulfoxides **241**.

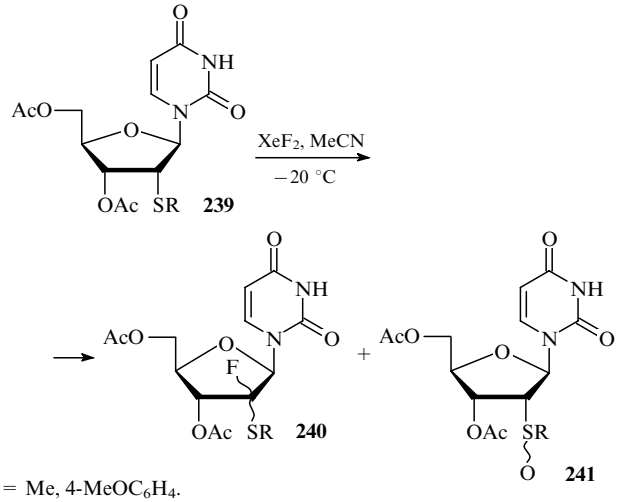

R = Me, 4-$MeOC_6H_4$.

A convenient method for the synthesis of 5′-(fluoromethylthio)adenosine derivatives (**242**) (yield 70%) by regioselective fluorination of 5-methylthioadenosine derivatives **243** by XeF_2 has been proposed.[397] In this case, as in the fluorination of the

5′-arylthioadenosine,[398] methionine [392] and biotin derivatives,[394] the reaction occurs at the least substituted carbon atom.

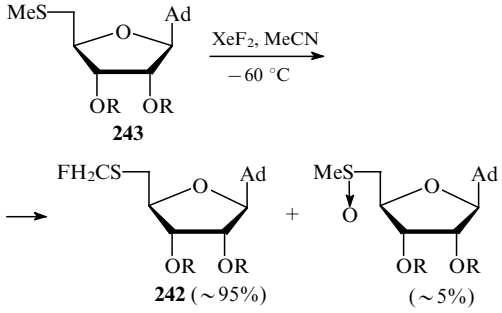

R = Bz, Ac; Ad is 9-adenine.

In contrast to sulfides, thiols and thiophenols are not fluorinated by XeF_2, but are usually oxidised to disulfides in quantitative yields. The structure of the radical at the sulfur atom and the thiol : XeF_2 ratio do not influence the direction of this reaction.[379]

$$2\,RSH + XeF_2 \longrightarrow RSSR + 2\,HF + Xe$$

R = Me, Pr^i, Bu^t, Ph.

Under drastic conditions, disulfides also react with XeF_2. Thus, fusion of bis(pentafluorophenyl) disulfide with XeF_2 at 85 °C in a sealed tube for 3 h yields a mixture of $C_6F_5SF_3$ and C_6F_5SOF which are identified by their ^{19}F NMR spectra (see Ref. 20).

$$C_6F_5SSC_6F_5 + XeF_2 \xrightarrow[-Xe]{} C_6F_5SF_3 \xrightarrow{H_2O} C_6F_5S(O)F$$

The use of XeF_2 in reactions with polychloropyridinethiols allowed one to develop new methods for perfluoroalkylation and oxyfluorination of thiol groups as well as for the oxidation of polychloropyridines to *N*-oxides. Thus the reaction of 2,3,5,6-tetrachloropyridine-4-thiol with XeF_2 in HF gave 4-fluorosulfonyl-2,3,5,6-tetrachloropyridine (**244**) and 4-fluorosulfonyl-2,3,5,6-tetrachloropyridine *N*-oxide (**245**).[399,400] This reaction is accompanied by oxidation of the original thiol into bis(2,3,5,6-tetrachloro-4-pyridyl) disulfide.

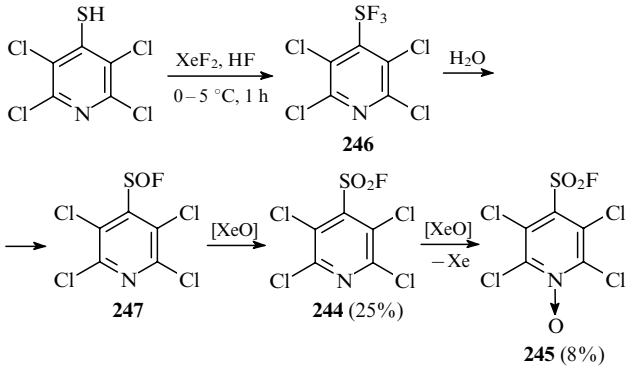

A reaction scheme which allows one to get insight into the mechanism of formation of the fluorosulfonyl fragment has been suggested.[400] Initially, the thiol group is fluorinated by XeF_2 in the presence of HF to the derivative **246** which is easily hydrolysed to the sulfoxide **247** and the sulfonylfluoride **244**. The latter can be converted into compound **245** by oxidation with [XeO] species formed in the hydrolysis of XeF_2 (the bonding energy of Xe—O is 7 kcal mol^{-1} which corresponds to the weakly bound atomic oxygen).[62–64]

A new method for perfluorination of polychloropyridinethiols which is based on the thermolysis of the xenon bisperfluorocarboxylates **6d**,**l**,**m** in the presence of thiols has been described.[242, 399–404]

Table 2. Perfluoroalkylation of pyridinethiols.

Reagent (method of generation)	Compound **248**	R	R_F	Yield (%)	Ref.
6d (A)	**a**	Cl	CF_3	66	242
6d (B)	**a**	Cl	CF_3	36.5	242, 399
6d (A)	**b**	CCl_3	CF_3	45	242
6d (A)	**c**	CN	CF_3	50	242
6l (B)	**d**	Cl	C_3F_7	85	242, 399
6m (B)	**e**	Cl	C_2F_5	85	404

Thermolysis is carried out either using the preformed reagents **6d**,**l**,**m** (method A) or with the simultaneous *in situ* generation of the xenonates **6d**,**l**,**m** (method B).

This reaction yields the polychloroperfluoroalkylthiopyridines **248**; their yields depend on the mode of generation of the xenonates **6d**,**l**,**m** (Table 2). It was found that the reactivity of the thiol group decreases with an enhancement of the acceptor properties of the substituent R.[242, 399–404]

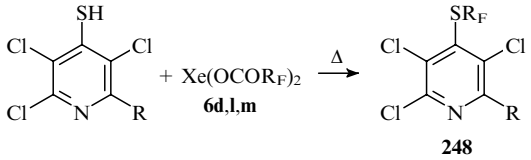

R_F = CF_3 (**d**), C_2F_5 (**l**), C_3F_7 (**m**).

This method allows direct perfluoroalkylation of thiols including those containing substitution-sensitive groups.[405]

4-Trifluoromethyl-2,3,5,6-tetrafluorothiopyridine (**249**) is formed upon the *in situ* generation of the xenonate **6d** in the presence of di(1,3,5,6-tetrafluoro-4-pyridyl) disulfide with simultaneous thermolysis at 50–60 °C (yield 41%).[242, 406]

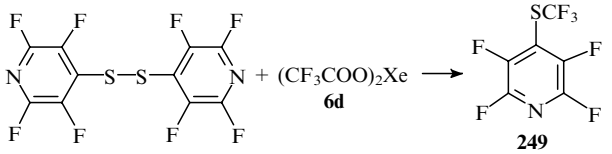

Xenon difluoride selectively oxidises the sulfur atom in compounds containing the S—N bond and the S—N bond is retained. Thus the S(IV) derivatives **252** and **253** containing the imidosulfenyl group are formed from compounds **250** and **251** in the absence of a catalyst, whereas compound **252** is further oxidised into S(VI) compound **254,** when BF_3 is used as a catalyst.[407]

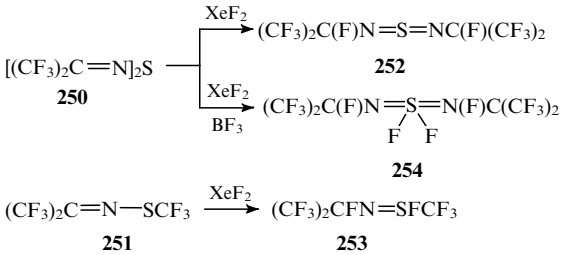

The pseudo-triene system of the isocyanate **255** undergoes 1,3- and 1,5-difluorination by XeF_2 in the absence of a catalyst resulting in compounds **256** and **257**. The N^1-(heptafluoroisopropyl)-N^2-(fluorocarbonyl)-*S*,*S*-difluorosulfodiimide (**258**) is formed in the presence of BF_3.[408]

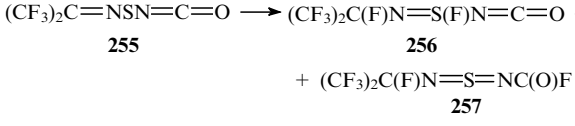

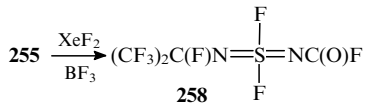

255 $\xrightarrow[BF_3]{XeF_2}$ $(CF_3)_2C(F)N{=}S(F){=}NC(O)F$ **258**

The oligomeric di-λ^4-thiatriazine **259** is easily fluorinated by XeF_2 with the preservation of the ring and the formation of the *cis*-difluoride **260**.[409,410]

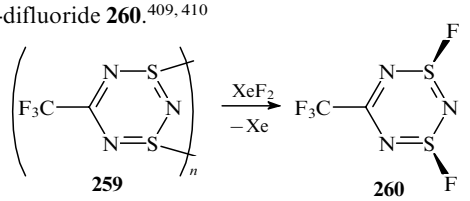

259 $\xrightarrow[-Xe]{XeF_2}$ **260**

N-Sulfinylperfluoroalkylamines **261** are converted into *N*-perfluoroalkyl-*S*,*S*-difluorosulfoximides **262** by XeF_2 in perfluorodecalin.[411]

$$R_FNSO + XeF_2 \xrightarrow[-Xe]{20\ ^\circ C} R_FNSOF_2$$

261 **262**

R_F = CF_3 (54%), C_2F_5 (50%).

The synthesis of sulfonyl fluorides from sulfonyl chlorides is effected by direct substitution of fluorine for chlorine. For example, the reaction of XeF_2 with methane-, benzene-, *p*-toluene- and pentafluorobenzenesulfonyl chlorides affords the corresponding sulfonyl fluorides as the main products upon heating for 4–10 h (yields 20%–80%). This reaction is carried out in acetonitrile or without the solvent. In some cases, fluorination of the aromatic nucleus takes place.[412]

$$RSO_2Cl \xrightarrow{XeF_2} RSO_2F$$

R = Me, Ph, C_6F_5, *p*-MeC_6H_4.

Recent reports suggest the use of $XeF^+MF_6^-$ salts (M = As, Sb) as the oxidants. It was shown in particular that $XeF^+MF_6^-$ reacts with the sulfides R^1SR^2 ($R^1 = R^2 = C_6F_5$;[413] $R^1 = CF_3$, $R^2 = Me$;[414,415] $R^1 = R^2 = Me$[381,414,415]) and thiols RSH [R = Me, CF_3 (see Ref. 416)] to give the fluorosulfonium cations of the type $R^1R^2S^+(F)MF_6^-$ and with disulfides R^1SSR^2 [$R^1 = R^2 = CF_3$; $R^1 = Me$, $R^2 = CF_3$; $R^1 = R^2 = Me$;[417] $R^1 = R^2 = Cl$ (see Ref. 418)] to give the sulfonium salts $[R^1SS(F)R^2]^+MF_6^-$. The reaction of the λ^4-sulfanes **263** with $XeF^+MF_6^-$ (M = As, Sb) gives the corresponding fluorosulfonium salts **264** and XeF_2[418] which cannot convert S(IV) into S(VI) due to its lower oxidation capacity in comparison with the cation XeF^+ (see Ref. 326).

$$R_nSF_{4-n} + XeF^+MF_6^- \longrightarrow R_nS^+F_{3-n}MF_6^- + XeF_2$$

263 **264**

R = CF_3; *n* = 0, 1, 2; M = As, Sb.

It should be noted that in the case of the λ^4-sulfanes **263**, $XeF^+MF_6^-$ salts behave as Lewis acids rather than oxidants. Their oxidative properties are manifested in the reaction with trifluoromethane sulfinyl fluoride. The S–F bond in $CF_3S(O)F$ is relatively strong as can be judged from its length (1.591 Å).[419] Depending on the nature of the element, this reaction affords either (trifluoromethyl)difluorosulfinyl hexafluoroantimonate (**265**) or the adduct **266**.[419] The reaction with dimethyl sulfoxide gives similar adducts.[419]

$$XeF^+MF_6^- \xrightarrow{CF_3S(O)F} \begin{cases} M = Sb: & Xe + [CF_3S(O)F_2]^+SbF_6^- \ (\mathbf{265}) \\ M = As: & CF_3S(O)F\cdot AsF_5 + XeF_2 \ (\mathbf{266}) \\ Me_2SO: & Me_2S(O)F\cdot MF_5 + XeF_2 \end{cases}$$

M = As, Sb.

The reaction of bis(trifluoromethyl) sulfoxide with $XeF^+SbF_6^-$ yields the salt **267** which was identified by spectral methods.[419,420] It is assumed that its first step involves a cationic attack of the sulfoxide oxygen atom by XeF^+, whereas the second step consists in the intramolecular migration of the fluoride anion to the sulfur atom. The second step seems to be hindered by steric shielding of the reaction centre by two CF_3 groups.[327]

$$(CF_3)_2SO + XeF^+SbF_6^- \longrightarrow [(CF_3)_2SOXeF]^+SbF_6^-$$

267

The reaction of thionyl chloride with $XeF^+MF_6^-$ is accompanied by the elimination of Xe and the formation of the salt **268**.[419]

$$2OSCl_2 + 3XeF^+MF_6^- \longrightarrow 2[OSClF_2]^+MF_6^- + Cl_2 + MF_5 + 3Xe$$

268

M = As, Sb.

The reaction of bis(2,2′-biphenylyl)-λ^4-sulfane **269** with 1 equiv. of XeF_2 in the presence of $BF_3\cdot OEt_2$ gives the bis(tetrafluoroborate) **270** which reacts with excess water or a dilute solution of an alkali to give cyclic sulfoxide **271** in a quantitative yield.[421]

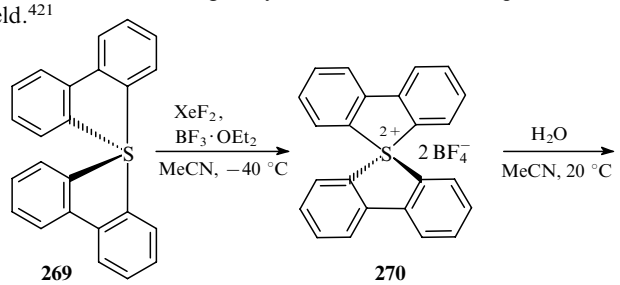

269 **270**

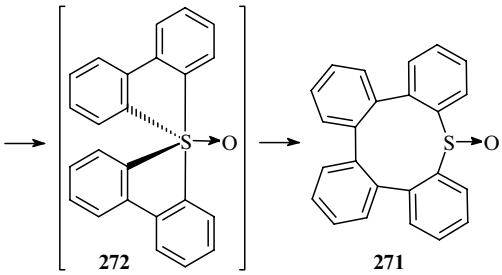

272 **271**

The formation of the sulfoxide **271** is associated with the C–C ligand coupling in the oxide **272**.[422]

The first compound containing the Xe–S bond, *viz*., HXeSH, was studied by spectral methods.[423,424] It was generated by photolysis of H_2S in a xenon matrix at 7.5 K and represents a particular case of a compound with the general formula HXY, where X = Xe, Kr, and Y is the fragment with a higher electron affinity (H, Cl, Br, I, CN, NC).[425–428]

b. Reactions of organoselenium compounds with XeF_2

For selenium, the transition into a four-coordinated state occurs much easier than for sulfur. Aryl trifluoromethyl selenides form more stable fluorides with XeF_2 than the corresponding sulfides. Thus compounds **273** react with XeF_2 in the presence of HF to give aryl trifluoromethyl difluoro-λ^4-selanes **274** in quantitative yields.[429] Bis(pentafluorophenyl) diselenide forms the pentafluorophenyl trifluoro-λ^4-selane (**275**) with XeF_2.

$$4\text{-}RC_6H_4SeCF_3 \xrightarrow[HF]{XeF_2} 4\text{-}RC_6H_4SeF_2CF_3$$

273 **274**

R = H, Cl, NO_2.

$$C_6F_5SeSeC_6F_5 \xrightarrow[HF]{XeF_2} C_6F_5SeF_3$$

275

An efficient procedure for vicinal fluoroselenenation of alkynes by addition of synthetic equivalents of the selanyl fluoride

RSeF generated *in situ* from XeF_2, diaryl, dibenzyl or dialkyl diselenides has been developed.[430] The direction of this reaction depends on the structures of the alkyne and the diselenide. Thus symmetric dialkylacetylenes react smoothly with XeF_2 and diphenyl diselenide to give the vicinal (fluoroalkenyl)phenyl selenides **276** in high yields.[430]

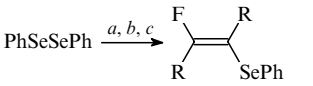

276 (72% – 87%)

R = Me, Et, Pr, Bu; (*a*) XeF_2, CH_2Cl_2, −20 °C, 15 min;
(*b*) RC≡CR, −20 °C, 0.5 h, (*c*) 20 °C, 1 h.

Terminal alkynes do not react with PhSeBr and AgF (sonication);[431] phenylacetylene forms the adduct **277a** with XeF_2 and diphenyl diselenide in 27% yield. Under these conditions, hex-1-yne affords a mixture of *E*-isomers of the adducts **277b** and **278b** in a 3 : 1 ratio (total yield 31%).[430]

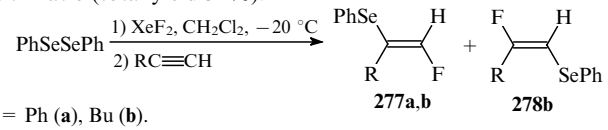

277a,**b** **278b**

R = Ph (**a**), Bu (**b**).

The reaction of asymmetrical inner alkynes with XeF_2 and $(PhSe)_2$ also results in the vicinal fluoroselenenation products **279a**–**e** and **280a**–**e** (total yield 26% – 83%).[430]

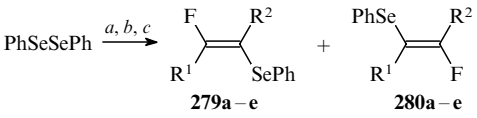

279a–**e** **280a**–**e**

R^1 = Ph, R^2 = Me (**a**); R^1 = Bu, R^2 = Me (**b**); R^1 = Bu, R^2 = Et (**c**);
R^1 = Bu, R^2 = Pr^i (**d**); R^1 = Bu, R^2 = Bu^t (**e**);
(*a*) XeF_2, CH_2Cl_2, −20 °C, 15 min;
(*b*) $R^1C{\equiv}CR^2$, −20 °C, 0.5 – 2 h; (*c*) 20 °C, 1 – 2.5 h.

Compounds **279** or a mixture of the selenides **279** and **280** are exclusively formed depending on the nature of the substituent in the alkyne. Thus 1-phenylpropyne and the sterically hindered 2,2-dimethyloct-3-yne react with XeF_2 and $(PhSe)_2$ to give exclusively the isomers **279a**,**e**, while hept-2-yne and oct-3-yne give a mixture of the isomeric selenides **279b**,**c** and **280b**,**c** in a *ca.* 1 : 1 ratio. The proportion of the isomer **279d** increases significantly in the case of 2-methyloct-3-yne.[430]

It can be expected that cycloalkynes will behave similarly in reactions with XeF_2 and $(PhSe)_2$. However, it was found that only cycloundecyne and cyclododecyne react selectively to give the adducts **281a**,**b** (yields 68% and 80%, respectively), whereas cyclooctyne and cyclodecyne yield a mixture of non-identified products.[430]

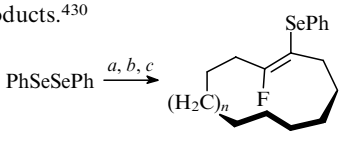

281a,**b**

n = 1 (**a**), 2 (**b**); (*a*) XeF_2, CH_2Cl_2, −20 °C, 15 min; (*b*) 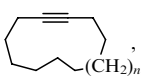 , −20 °C, 1 h; (*c*) 20 °C, 1 h.

The reactions of other diselenides with XeF_2 and alkynes including functionally substituted ones have been studied.[432] These reactions resulted in the adducts **282**.[430, 432]

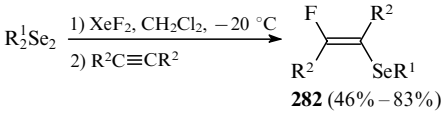

282 (46% – 83%)

R^1 = Me, Et, Pr^i, Bn, Bu^t, 2-$NO_2C_6H_4$, $CH_2CH(OMe)_2$, $(CH_2)_3CO_2Et$, $(CH_2)_3CO_2H$, $(CH_2)_2NMe_2$, CH_2SiMe_3; R^2 = Me, Et, Pr, Bu.

Trimethylphenylselanylsilane and *tert*-butyldimethylphenylselanylsilane react with oct-4-yne under analogous conditions to give the adducts **283** (yields 73% and 82%, respectively). Contrary to expectations, alkynes do not react with the PhSeNCO – XeF_2 system.[430]

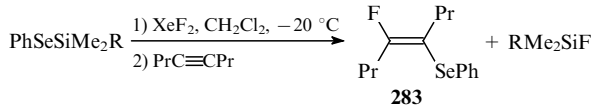

283

R = Me, Bu^t.

The fluorophenylselenenation of various phosphaalkynes resulting in the adducts **284** has been studied.[433]

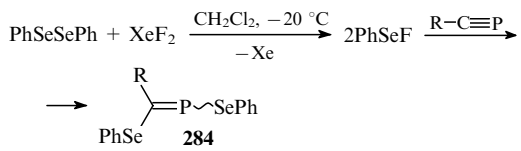

284

R = Bu^t, adamantyl.

Alkenes also react with XeF_2 and $(PhSe)_2$ in CH_2Cl_2 to give readily hydrolysable vicinal phenylselanylfluoroalkanes. The yields of the products depend on the reaction conditions and decrease dramatically with an increase in temperature.[434]

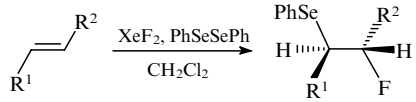

R^1 = H, Me, Bu, CH_2CN; R^2 = H, CH_2CN, CO_2Me, SO_2Ph.

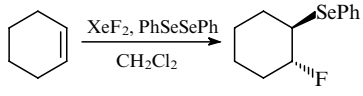

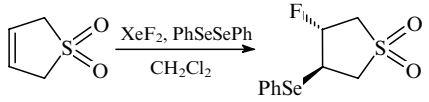

The *in situ* generated PhSeF is more reactive than PhSeCl or PhSeBr; it reacts even with electron-deficient alkenes and 2,5-dihydrothiophene 1,1-dioxide. Since the Se – F bond is more polar than the Se – Cl and Se – Br bonds, the PhSe fragment in PhSeF bears a higher positive charge than that in PhSeBr and PhSeCl and is therefore more electrophilic. Indirect evidence in favour of this assumption was obtained from spectral data.[434]

Bis(2,2′-biphenylene)-λ^4-selane (**285**) reacts with XeF_2 in acetonitrile at −40 °C to give the bis(2,2′-biphenylene)difluoro-λ^6-selane (**286**) in 54% yield.[435]

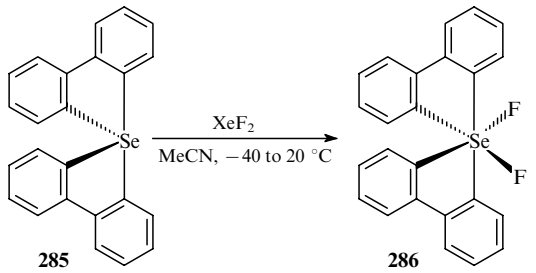

285 **286**

c. Reactions of organotellurium compounds with XeF_2

Organotellurium compounds react smoothly with XeF_2 to give derivatives of Te(IV) and Te(VI). XeF_2 was successfully used for the synthesis of a vast variety of aryltellurium(VI) fluorides from diaryl tellurides or Te(IV) derivatives.[389, 436]

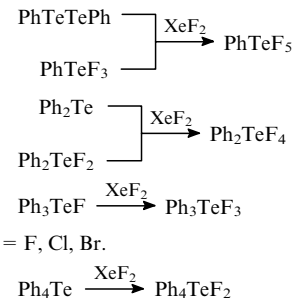

X = F, Cl, Br.

Bis(trifluoromethyl)tellurium difluoride **287** was synthesised by fluorination of bis(trifluoromethyl) telluride by XeF_2 in an acetonitrile–Freon-11 mixture.[437] Bis(pentafluorophenyl) ditelluride reacts with XeF_2 to give the pentafluorophenyltellurium trifluoride (**288**) with the cleavage of the Te–Te bond and the oxidation of Te(II) to Te(IV).[429]

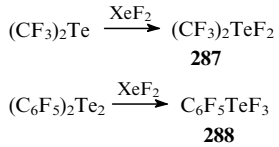

The oxidative fluorination of 2,5-dihydrotellurophene by xenon difluoride results in 2,5-dihydrotellurophene 1,1-difluoride (**289**).[438]

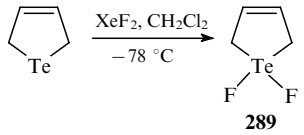

Special mention should be made of an unsuccessful attempt at the fluorotellurination of oct-4-yne by the Ph_2Te_2–XeF_2 or $PhTeSiMe_3$–XeF_2 systems.[430]

3. Reactions of XeF_2 with Group V organoelement compounds

a. Reactions of organophosphorus compounds with XeF_2

Xenon difluoride smoothly oxidises phosphorus(III) to phosphorus(V) in various phosphorus derivatives. Under these conditions, other functional groups present in the molecule are not involved as a rule. Thus the oxidation of (1-hydroxyhexafluoroisopropyl)diphenylphosphine (**290**) yields the pentavalent phosphorus derivative **291**.[439]

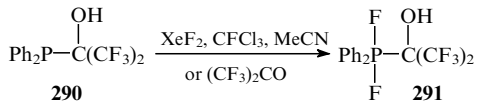

High selectivity is also observed in the oxidation of compounds containing a P–H bond. Thus the reaction of primary and secondary phosphines with XeF_2 gives the corresponding difluorides **292** and **293** in high yields.[347,440]

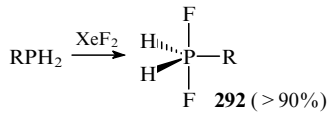

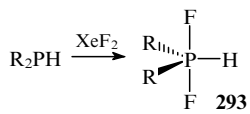

R = Ph, CH_2CH_2CN.

Oxidative fluorination also takes place in reactions with arylchlorophosphines **294** where it occurs simultaneously with the substitution of fluorine for chlorine. Triphenylphosphine (**294d**) is quantitatively converted into triphenyldifluorophosphorane **295d**,[347] whereas the chlorine-containing phosphines **294a–c** react with XeF_2 to give the fluoro-substituted phosphoranes **295a–c** in quantitative yields. No intermediate formation of chlorofluorophosphoranes was detected.[353]

n = 0 (**a**), 1 (**b**), 2 (**c**), 3 (**d**).

The fluorination of four-coordinated phosphorus derivatives containing P–H bonds results in fluorides.[441]

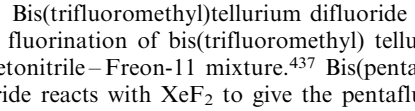

The oxidation of organic derivatives of phosphorus(III) containing P–N, P–S or P–O bonds is complicated due to easy elimination of PF_5 which is accompanied by the formation of compounds containing a P = X fragment (X = N, O, S). For example, the fluorination of bis(difluorophosphino)methylamine (**296**) by XeF_2 gives difluorophosphino(tetrafluorophosphoranyl)methylamine (**297**), which undergoes dimerisation to give compound **298**.[442]

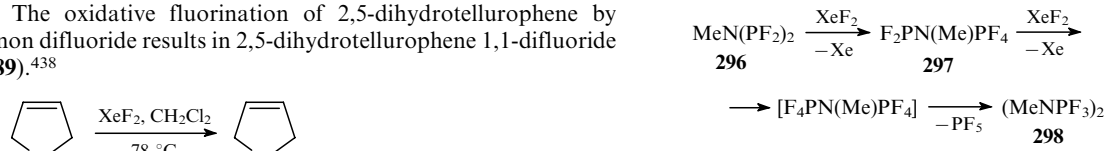

The oxidation of organic derivatives of phosphorus(III) containing P–N, P–S or P–O bonds is complicated due to easy elimination of PF_5 which is accompanied by the formation of compounds containing a P = X fragment (X = N, O, S). For example, the fluorination of bis(difluorophosphino)methylamine (**296**) by XeF_2 gives difluorophosphino(tetrafluorophosphoranyl)methylamine (**297**), which undergoes dimerisation to give compound **298**.[442]

Silyl esters and silyl-substituted amides of trivalent phosphorus acids are oxidised by XeF_2 to dialkylphosphofluoridates or dialkyl fluorophosphazenes, respectively.[441]

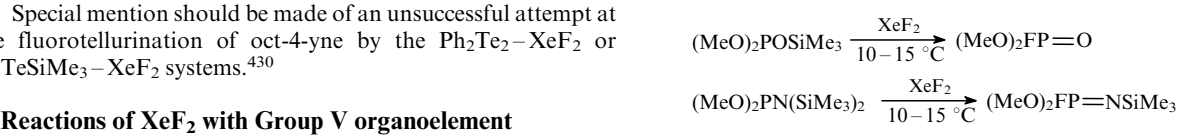

An unusual reaction takes place on the interaction of isobutyl phosphodifluoridite with catalytic amounts of XeF_2. In this case, the *tert*-butylphosphonic difluoride was isolated as the main product in 50% yield.[441,443]

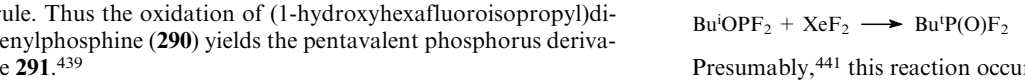

Presumably,[441] this reaction occurs through the formation of alkoxytetraphenylphosphorane, which disproportionates with the formation of the isobutyl cation.[443] The latter undergoes isomerisation and reacts with the original phosphite to afford the final product.

b. Reactions of organoarsenic derivatives with XeF_2

The reactions of XeF_2 with organoarsenic derivatives were studied in the single example.[351]

It is quite probable that in other cases the behaviour of As(III) compounds in the reaction with XeF_2 will also not be different from that of P(III) derivatives.

c. Reactions of organoantimony compounds with XeF_2

To date, reactions of XeF_2 with antimony derivatives have been studied relatively little.

Xenon difluoride fluorinates aromatic derivatives of trivalent antimony in quantitative yields under mild conditions. Trifluorodiphenylantimony and difluorotriphenylantimony were prepared from fluorodiphenylstibine (or trifluorodiphenylacetoxystibine) and triphenylstibine, respectively.[444] Tris(pentafluoro-

phenyl)stibine yields difluoro tris(pentafluorophenyl)antimony in its reaction with XeF_2.[262]

$$Sb(C_6F_5)_3 \xrightarrow{XeF_2} Sb(C_6F_5)_3F_2 + Xe$$

d. Reactions of organobismuth compounds with XeF_2

Oxidative fluorination of triphenylbismuth with XeF_2 is the most convenient and available method for the preparation of trisubstituted bismuth difluoride[445] which is interesting as a fluorinating reagent.[446, 447]

$$Ar_3Bi + XeF_2 \longrightarrow Ar_3BiF_2 + Xe$$

Ar = Ph, C_6F_5.

However, tris(trifluoromethyl)bismuth yields the bismuth trifluoride, CF_4 and Xe even at -60 °C. Their formation is attributed either to the trifluoromethylation of the XeF^+ intermediate or the degradation of the pentavalent bismuth derivative.[445]

$$Bi(CF_3)_3 + 3\,XeF_2 \longrightarrow BiF_3 + 3\,CF_4 + 3\,Xe$$

The reactions of XeF_2 or $XeF^+MF_6^-$ (M = As, Sb, Ta) with tris(pentafluorophenyl)bismuth have been studied.[448] In both cases, $(C_6F_5)_3BiF_2$ was isolated from the reaction mixture with trace amounts of pentafluorobenzene which provides indirect support for the formation of xenon compounds, such as C_6F_5XeF or $C_6F_5Xe^+MF_6^-$.[262]

4. Reactions of XeF_2 with Group IV organoelement compounds

a. Reactions of organosilicon compounds with XeF_2

Reactions of organosilicon compounds with XeF_2 were studied for compounds containing Si–Cl, Si–H, Si–C, Si–O, Si–S and Si–N bonds.

The reactions of XeF_2 with chlorosilanes are completed within several minutes. However, the yields of fluorosilanes depend on the number of chlorine atoms to be substituted in the original molecule. Mono- and dichlorosilanes are easily fluorinated to give fluoro- and difluorosilanes.[440]

$$2R_3SiCl + XeF_2 \xrightarrow{MeCN} 2R_3SiF + Xe + Cl_2$$

$$Me_2SiCl_2 + XeF_2 \xrightarrow{MeCN} Me_2SiF_2 + Xe + Cl_2$$

R = Me, Et, Ph.

If the molecule contains a hydrogen atom, difluorosilanes are formed in satisfactory yields. A stepwise mechanism of this reaction which includes initial fluorination of the Si–H bond has been proposed.[440]

$$R_2SiHCl \xrightarrow{XeF_2} R_2SiHF \xrightarrow{Cl_2} R_2SiClF \xrightarrow{XeF_2} R_2SiF_2$$

R = Ph, Me.

Triarylchlorosilanes yield products of more profound conversions.[440]

The reaction of allylchlorodimethylsilane with XeF_2 is accompanied by the cleavage of the Si–C bond to afford difluorodimethylsilane in a quantitative yield.[440]

Compounds containing alkoxy groups at the silicon atom react with XeF_2 at a very slow rate (within 4–5 days).[399] On the other hand, the reaction of XeF_2 with *tert*-butylthiotrimethylsilane in acetonitrile occurs easily and affords di-*tert*-butyl disulfide and flurotrimethylsilane in high yields.[347]

$$Me_3SiSBu^t + XeF_2 \xrightarrow{MeCN} Bu^tSSBu^t + Me_3SiF + Xe$$

Bu^tSSSBu^t and Bu^tSH are formed as side products. In the absence of a solvent, this reaction yields a mixture of products.[347]

The reaction of XeF_2 with nitrogen-containing silanes is accompanied by the cleavage of Si–N bonds resulting in the formation of fluorotrimethylsilane in > 90% yield. Presumably, this reaction occurs by a radical mechanism. The formation of $FXeNR_2$ (see Ref. 423) and FXeSR (see Refs. 318–321) as intermediate products was proposed.

$$Me_3SiNR_2 + XeF_2 \xrightarrow{MeCN} Me_3SiF + Xe + R_2\dot{N}$$

$$R_2\dot{N} \xrightarrow{R = Me} MeN{=}CH_2 \longrightarrow \text{polymer}$$

$$R_2\dot{N} \xrightarrow{MeCN} R_2NH$$

The ability of XeF_2 to cleave smoothly the Si–N bonds in polyfunctional compounds was used in the synthesis of the hexamethyltriamido-*N*-fluorophosphazene (**299**) from hexamethyltriamido-*N*-trimethylsilylphosphazene (**300**).[449]

$$\underset{\mathbf{300}}{(Me_2N)_3P{=}NSiMe_3} + XeF_2 \xrightarrow[-15\ ^\circ C]{MeCN} \underset{\mathbf{299}}{(Me_2N)_3P{=}NF} + Me_3SiF + Xe$$

An attempt to synthesise a compound containing the Xe–N bond by the reaction of XeF_2 with $Me_3SiN{=}C(CF_3)_2$ was unsuccessful. This reaction gave Xe, Me_3SiF and $(CF_3)_2C{=}NH$.[347]

It was found that trimethylpentafluorophenylsilane (**301a**) does not react with XeF_2 in acetonitrile at 20 °C. However, the addition of a catalytic amount of anhydrous CsF to the reaction mixture results in the formation of pentafluorobenzene and decafluorobiphenyl in 58% and 11% yields, respectively. In acetonitrile, this reaction is completed within 15–20 min, but in $CFCl_3$ or SO_2FCl trimethylpentafluorophenylsilane (**301a**) does not react with XeF_2 even in the presence of CsF, apparently due to the low solubility of the latter.[450–452]

$$\underset{\mathbf{301a-d}}{ArSiMe_3} + XeF_2 \xrightarrow[10-20\ ^\circ C]{CsF,\ MeCN} ArH + ArAr + Xe + Me_3SiF$$

Ar = C_6F_5 (**a**), 4-$CF_3C_6F_4$ (**b**), 4-C_5F_4N (**c**), 4-$CF_3C_6H_4$ (**d**).

Arylsilanes **301a**,**b** react similarly with XeF_2 in the presence of anhydrous KF and RbF.[450]

Trimethyl-4-tetrafluoropyridylsilane (**301c**) reacts with XeF_2 very slowly in the absence of a catalyst and within several minutes in the presence of CsF.[450]

In contrast to fluorinated arylsilanes, their hydrocarbon analogues (phenyl-, 4-tolyltrimethylsilane, tetraphenylsilane) do not enter into the reaction with XeF_2 and CsF even on heating at 40–60 °C for several hours.[451] The presence of the electron-withdrawing CF_3 group in (4-trifluoromethylphenyl)trimethylsilane (**301d**) increases its reactivity in comparison with trimethylphenylsilane. It reacts with XeF_2 to give benzotrifluoride and 4,4′-bis(trifluoromethyl)biphenyl, although the conversion is low.[450]

^{19}F CIDNP was used to establish a radical mechanism of the Si–C bond cleavage.[450] This reaction seems to be convenient for generating polyfluoroaryl and polyfluorohetaryl radicals under mild conditions. Chemical reactions occurring in the arylsilane–XeF_2–CsF system and the CIDNP data offer the most probable mechanism for this reaction.

$$C_6F_5SiMe_3 \overset{F^-}{\rightleftharpoons} \left[C_6F_5SiFMe_3\right]^- \xrightarrow[-XeF^{\bullet}, -F^{\bullet}]{XeF_2} \left[C_6F_5SiFMe_3\right]^{\bullet} \xrightarrow[-Me_3SiF]{} [C_6F_5]^{\bullet} \longrightarrow C_6F_5H + C_{12}F_{10}$$

A radical mechanism has also been proposed for the reaction of aryltrimethylsilanes **302a**–**d**.[453] It was shown that compounds **302a**–**d** react with two equivalents of XeF_2 to give the *para*-fluoro derivatives **303**. Moreover, this reaction gives the isomeric monofluoroarylsilanes **304**, the difluorides **305** and 1,4-difluorobenzene (**306**) as is the case with the reaction involving acetyl hypofluorite, the well-known radical fluorinating agent.[453]

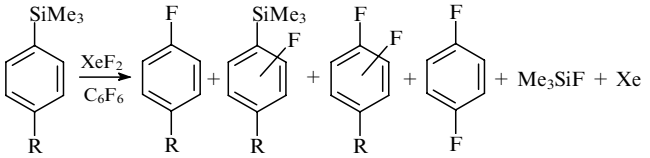

302a–d **303a–d** **304a–d** **305a–d** **306**

Compounds **302**	R	Yield (%)			
		303	**304**	**305**	**306**
a	H	65	0	0	35
b	Bu^t	86	8	6	0
c	OMe	61	39	0	0
d	Cl	82	12	6	0

This reaction occurs through the formation of the cationoid intermediate **307**, which is stabilised not only due to the β-effect of the silyl substituent but also due to the interaction of the cationic centre with the non-bonding molecular orbital of the hypervalent xenon.[453]

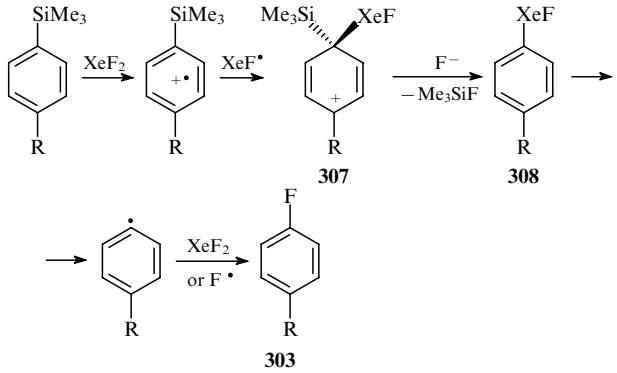

The subsequent reaction with the fluoride anion results in the intermediate **308** (see Section VI) which further yields the aryl fluorides **303a–d**.

Xenon difluoride is a convenient reagent for converting vinyl silanes into vinyl halides. This reaction was used in particular in the synthesis of 5-(2-halovinyl) derivatives of the pyrimidine nucleosides **309**.[454]

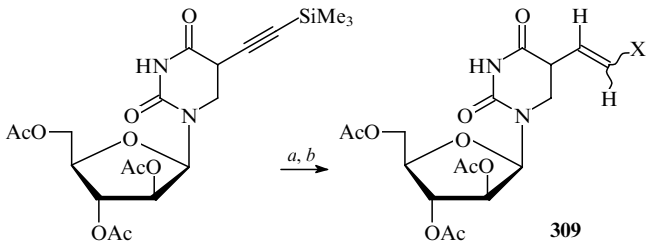

X = $SiMe_3$, I, Br, Cl;

(*a*) $Pd/CaCO_3$, , AcOEt; (*b*) XeF_2, MX (MX = LiCl, LiBr, NaI), PhH.

b. Reactions of organotin compounds with XeF_2

Aryltrimethylstannanes react with XeF_2 with cleavage of the C–Sn bond and can be used for the generation of aryl radicals. Thus trimethyl(phenyl)stannane reacts with XeF_2 rather slowly, *viz*., the conversion of the original compound reaches 80% after 12 h. In the presence of $BF_3 \cdot Et_2O$ as the catalyst, this reaction is strongly accelerated but yields a complex mixture of products.[455]

XeF_2 reacts with aryltrimethylstannanes more selectively in the presence of catalytic amounts of a palladium benzonitrile complex. Thus biaryls are formed in good yields from the aryltrimethylstannanes **310**; the yields of side products (benzene, chlorobenzene) do not exceed 1%–2%.[455]

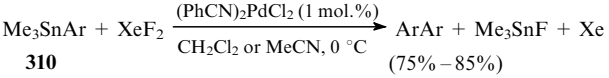

Ar = Ph, 1-naphthyl.

If a molecule contains a functional group which can react with the radical, cascade reactions may be triggered. Thus the reaction of 2-trimethylstannyl(but-3-enyl)benzene (**311**) with XeF_2 in the presence of a Pd complex results in 1-methylindan (**312**) in a satisfactory yield. In this case, no homocoupling reaction occurs.[455]

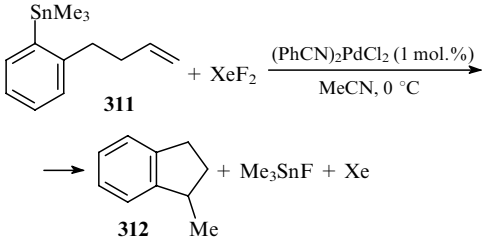

Organotin compounds can be used for the synthesis of organofluorine derivatives.[456–462] Thus the reaction of the vinylstannanes **313** and **314** with XeF_2 in the presence of silver triflate (~1:1.5) and a catalytic amount of 2,6-di-*tert*-butyl-4-methylpyridine in dichloromethane results in the vinyl fluorides **315** and **316**.

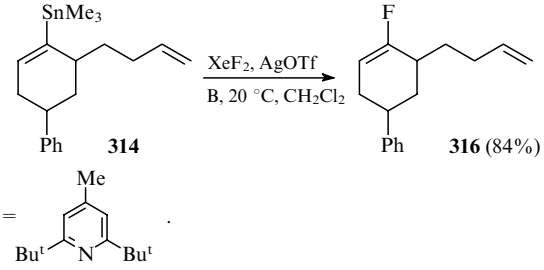

It should be noted that in contrast to compound **311**, the stannane **314** does not undergo cyclisation.[463]

Diverse functional groups in the vinylstannane molecule do not inferfere with this reaction. Thus this approach was used for the synthesis of the vinyl fluorides **317–320**.[460–462]

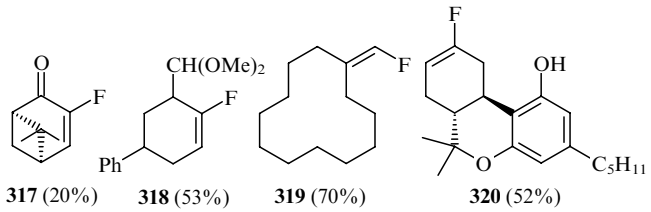

317 (20%) **318** (53%) **319** (70%) **320** (52%)

5. Reactions of XeF_2 with organoaluminium compounds

The oxidation of organoaluminium compounds (OAC) by XeF_2 is an exothermic reaction. Any contact of even small amounts of the reagents in the absence of a solvent brings about an explosion. Oxidation in solutions (toluene appeared to be the most suitable one) is associated with chemiluminescence,[261] which is similar to that observed on oxidation of OAC by oxygen.[464] It was found that this reaction involves exclusively the C–Al or the H–Al bond. The reactions of Et_3Al, $(EtO)_2AlEt$, Et_2AlCl and Bu^i_2AlH with XeF_2 gave Et_2AlF, $(EtO)_2AlF$, EtAlClF and Bu^i_2AlF (yields 95%, 97%, 80% and 79%, respectively). In addition to the above-mentioned products, Xe and C_2H_6 are formed as the main products, while C_2H_4 and C_4H_{10} are formed as admixtures. The AOC : XeF_2 ratio of 2:1 ensures the reaction of XeF_2 with the

most reactive substituent (H, Alk, Cl) bound to Al. The reactivities of the substituents decrease in the following order: H > Alk > Cl.[465]

The mechanism of the reaction of OAC with XeF_2 in toluene was studied in the example of a model compound $(EtO)_2AlEt$ containing only one non-oxidised Al–C bond.[465,466] The redox reaction begins with the formation of the intermediate complex **321** in which the electron is transferred from the OAC to the electrophilic XeF_2.[467] The reactive intermediates, *viz*., $^{\bullet}C_2H_5$ radicals, are converted through three main routes, *viz*., they react with each other to give ethane, ethylene and butane; they attack toluene at the side chain to give bibenzyl or at the aromatic ring to give ethyl-, diethyltoluenes and bitolyls. Chemiluminescence is evoked as a result of excitation and generation of the $^{\bullet}XeF$ radicals formed in the reaction of polarised ethyl radicals with XeF_2.[466,467]

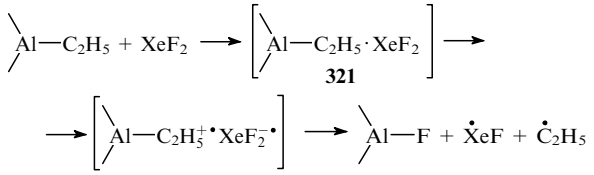

The effects of luminescence activators, *viz*., 9,10-dibromoanthracene, pyrene, *p*-terphenyl and the $[Ru(bipy)_3Cl_2\cdot(OAC)_n]$ complex (bipy is 2,2′-bipyridyl) on the chemiluminescence of the reaction of $(EtO)_2AlEt$ with XeF_2 in solution have been studied.[468] It was shown that enhanced luminescence is a result of involvement of the activator in the oxidation–reduction process.[468]

6. Reactions of XeF_2 with Group II organoelement compounds

a. Reactions of organomagnesium compounds with XeF_2

The direction of the reactions of the Grignard reagents **322a–c** with XeF_2 in diethyl ether at 20 °C depends on the structure of the substrate. Thus decylmagnesium bromide reacts with XeF_2 to give 2-ethoxydecane (**323a**), decane (**324a**) and eicosane (**325a**) in a total yield 98%. In the case of benzylmagnesium bromide, the total yield of the three main reaction products **323b–325b** is 80%; benzyl bromide was detected among side products. The composition of the reaction mixture is even more complicated in the reaction of phenylmagnesium bromide with XeF_2. In this case, the main products **323c–325c** are formed in a total yield 70% (the side products include bromobenzene, bromophenyl, mono- and dibromoacetophenone, *etc*.).[469]

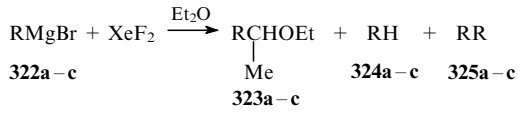

R = n-$C_{10}H_{21}$ (**a**), Bn (**b**), Ph (**c**).

A method for incorporating a trifluoromethyl group into the molecules of aromatic compounds has been proposed[470,471] which includes the conversion of aryl halides (more preferably, bromides) into the corresponding Grignard reagents and their subsequent reaction with carbon disulfide and XeF_2.

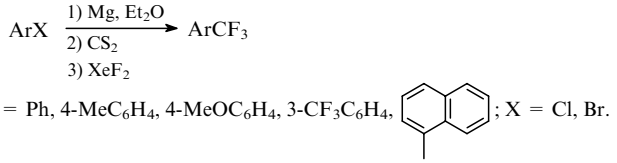

b. Reactions of organomercury compounds with XeF_2

The C–Hg bond in the reaction of XeF_2 with the mercury derivatives R_2Hg is cleaved to yield a mixture of products, such as RHgF (or RHgF + HgF_2), RF, RR, *etc*.[260,472]

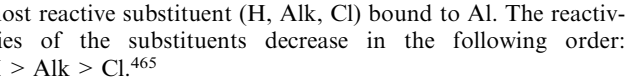

R = 4-$MeOC_6H_4$, 4-$Me_2NC_6H_4$, Bn, 4-$EtO_2CC_6H_4$, PhC≡C.

This reaction is carried out in an argon atmosphere to avoid the formation of oxygen-containing products. In the case of di(phenylethynyl)mercury, PhC≡CF is unstable and could not therefore be detected in the reaction mixture. However, indirect evidence for the formation of this compound was obtained upon treatment of the reaction mixture with tetraethylammonium bromide after complete liberation of xenon eventually resulting in PhC≡CBr in 43% yield.[472]

The efficiency of this reaction is judged by the temperature at which the liberation of xenon occurs. The reactivities of R_2Hg were found to decrease in the following order depending on R: $PhCH_2$ > *p*-$Me_2NC_6H_4$ > PhC≡C > *p*-$MeOC_6H_4$ > *p*-EtO_2C–C_6H_4. Hence, XeF_2 acts as an electron acceptor, while R_2Hg acts as an electron donor. Presumably, this reaction is a radical process involving an initial transfer of an electron from R_2Hg to XeF_2. The absence of R_2Hg fluorination products in the reaction mixture suggests that the C–Hg bond is cleaved by XeF_2 more easily than the C–H or C–C bond.[260,472]

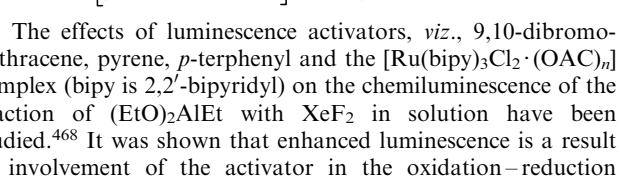

It should be noted that XeF_2 also reacts readily with mercury dihalides to give mercury difluoride in a quantitative yield. This reaction occurs especially easily with HgI_2.[472]

7. Reactions of other organometallic compounds with XeF_2

Many metals, *e.g*., iridium, react with XeF_2 to yield metal fluorides.[473] The high oxidation potential of XeF_2 allows the oxidation of carbonyl complexes of some metals. Thus the cationic complex tricarbonylbis(triethylphosphine)iridium(I) **326** reacts with XeF_2 to give the complex **327**.[474]

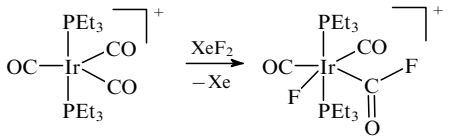

This approach can be used for preparing fluorinecarbonyl complexes of other metals.

The reactions of $[M_2(CO)_{10}]$ (M = Mn, Re) with $Xe(OTeF_5)_2$ at −78 °C in CH_2Cl_2,[475] and the reactions of $[Os_3(CO)_{12}]$,[476] $[Ir_4(CO)_{12}]$[421,477,478] and $[Ru_3(CO)_{12}]$[479] with XeF_2 in the presence of HF have been studied.

IX. Miscellaneous reactions

It was shown that the fluorination of polyethylene with XeF_2 in liquid media follows a radical mechanism.[480] The oxidation of methane by XeF_2 in aqueous media at 10–25 °C gives a mixture of MeOH (8%), MeF (2%) and CO_2 (50%).[481] The reaction of $CF_3COOXeF$ and $(CF_3COO)_2Xe$ with adamantane and its 1-halogeno (Cl, Br) derivatives results in a mixture of isomeric trifluoroacetoxyadamantanes.[482] The use of a new reagent, *viz*., I_2–XeF_2, has been documented recently.[483] Its application allows one to convert terminal alkenes into geminal difluorides.[484–486] The hypothetical mechanism of this reaction is discussed.[486]

A new line of research in the chemistry of fullerenes associated with their fluorination has evolved and is developing actively.[487] It was found that noble gas fluorides, particularly xenon difluoride, can be successfully used for the fluorination of fullerenes.[487–489]

* * *

The data discussed in the review provide convincing evidence that xenon chemistry is developing successfully and XeF_2 is applicable to miscellaneous synthetic tasks. The reagents based on the xenon derivatives considered in the review surpass well-known classical reagents and can often replace them.

References

1. N Bartlett *Proc. Chem. Soc.* 218 (1962)
2. V Zemva, R Hagiwara, W J Casteel, K Lutar, A Jesih, N Bartlett *J. Am. Chem. Soc.* **112** 4846 (1990)
3. D Schröder, J N Harvey, M Arschi, H Schwarz *J. Phys. Chem.* **108** 8446 (1998)
4. D R Brown, M J Clegg, A J Downs, R C Fowler, A R Minihan, J R Norris, L Stein *Inorg. Chem.* **31** 5041 (1992)
5. L Stein, W W Henderson *J. Am. Chem. Soc.* **102** 2856 (1980)
6. R Cipollini, F Grandinetti *J. Chem. Soc., Chem. Commun.* 773 (1995)
7. M Attina, F Bernardi, F Cacace, I Rossi *Chem. Eur. J.* **5** 1186 (1999)
8. R Hoppe, W Dähne, H Mattauch, K-M Rödder *Angew. Chem., Int. Ed. Engl.* **1** 599 (1962)
9. H H Claassen, H Selig, J G Malm, *J. Am. Chem. Soc.* **84** 3593 (1962)
10. K Lutar, A Smalc, B Zemva, S A Kinkead *Inorg. Synth.* **29** 4 (1992)
11. R D LeBlond, D D DesMarteau *J. Chem. Soc., Chem. Commun.* 555 (1974)
12. C T Goetschel, K R Loos *J. Am. Chem. Soc.* **94** 3018 (1972)
13. L J Turbini, R E Aikman, R J Lagow *J. Am. Chem. Soc.* **101** 5833 (1979)
14. A V Eletskii, S N Spirin, E V Stepanov, B B Chaivanov *Eksperimental'noe i Teoreticheskoe Issledovanie Protsessov Vzaimodeistviya Atomarnogo Ftora s Kristallicheskim Ksenonom* (Experimental and Theoretical Investigations of Processes of Interaction of Atomic Fluorine with Crystalline Xenon) Preprint of Institute of Nuclear Energy, No. 3836/13, Moscow, 1983
15. J H Holloway *J. Fluorine Chem.* **33** 149 (1986)
16. J H Holloway *Chem. Br.* **23** 658 (1987)
17. N Bartlett *The Chemistry of the Noble Gases* (Amsterdam: Elsevier, 1971)
18. D T Hawkins, W E Falconer, N Bartlett *Noble Gas Compounds. A Bibliography: 1962–1976* (New York: Plenum, 1978)
19. P Laszlo, G J Schrobilgen *Angew. Chem.* **100** 495 (1988)
20. V V Bardin, Yu L Yagupol'skii, in *Ftoriruyushchie Reagenty v Organicheskom Sinteze* (Fluorinating Agents in Organic Synthesis) (Ed L S German, S M Zemskov) (Novosibirsk: Nauka, 1987) p. 63
21. J H Holloway *Noble Gas Chemistry* (London: Methuen, 1968)
22. A B Neiding, V B Sokolov *Usp. Khim.* **43** 2146 (1974) [*Russ. Chem. Rev.* **43** 1043 (1974)]
23. R E banks (Ed.) *Fluorine Chemistry at the Millennium: Fascinated by Fluorine* (Amsterdam: Elsevier, 2000)
24. O Bostrup *Dan. Kemi* **76** 35 (1995)
25. M R C Gerstenberger, A Haas *Angew. Chem., Int. Ed. Engl.* **20** 647 (1981)
26. G Resnati *Tetrahedron* **49** 9385 (1993)
27. G A Olah, R D Chambers, G K Surya Prakash (Eds) *Synthetic Fluorine Chemistry* (New York: Wiley, 1992)
28. M Hudlicky, A E Pavlath (Eds) *Chemistry of Organic Fluorine Compounds (ACS Monograph. Ser.)* Vol. 187 (Washington, DC: American Chemical Society, 1995)
29. V A Legasov, V N Prusakov, B B Chaivanov *Reaktsii Okislitel'nogo Ftorirovaniya Diftorida Ksenona* (Reactions of Oxidative Fluorination of Xenon Difluoride) Preprint of Institute of Nuclear Energy, No. 2185, Moscow, 1972
30. R Filler *Isr. J. Chem.* **17** 71 (1978)
31. M Zupan, in *The Chemistry of Functional Groups, Supplement D: The Chemistry of Halides, Pseudo-Halides, and Azides* Parts 1, 2 (Eds S Patai, Z Rappoport) (Chichester: Wiley, 1983) p. 657
32. J A Wilkinson *Chem. Rev.* **92** 505 (1992)
33. M A Tius *Tetrahedron* **51** 6605 (1995)
34. V V Zhdankin *Izv. Akad. Nauk, Ser. Khim.* 1849 (1993) [a]
35. V K Brel, N S Zefirov, in *Chemistry of Hypervalent Compounds* (Ed. Kin-ya Akiba) (New York: Wiley-VCH, 1999) p. 389
36. F Sladky *Allg. Prakt. Chem.* **22** 213 (1971)
37. T Cleveland, C R Landis *J. Am. Chem. Soc.* **118** 6020 (1996)
38. V A Legasov, A S Marinin *Zh. Neorg. Khim.* **27** 2408 (1972) [b]
39. W W Dukat, J H Holloway, E G Hope, P J Townson, R L Powell. *J. Fluorine Chem.* **62** 293 (1993)
40. C L Chernick, J G Malm *Inorg. Synth.* **8** 258 (1966)
41. W E Falconer, W A Sunder *J. Inorg. Nucl. Chem.* **29** 1380 (1967)
42. J G Malm, E H Appelman *At. Energy Rev.* **7** 3 (1969)
43. F Schreiner, G N McDonald, C L Chernick *J. Phys. Chem.* **72** 1162 (1968)
44. J L Weeks, C L Chernick, M S Matheson *J. Am. Chem. Soc.* **84** 4612 (1962)
45. L V Streng, A G Streng *Inorg. Chem.* **4** 1370 (1965)
46. S M Williamson *Inorg. Synth.* **11** 147 (1968)
47. J H Holloway *J. Chem. Sos., Chem. Commun.* 22 (1966)
48. M-Sh Liao, Q-E Zhang *J. Phys. Chem. A* **102** 10 647 (1998)
49. V N Mit'kin, S V Zemskov *Izv. Akad. Nauk SSSR, Ser. Neorg. Mater.* **17** 1897 (1981) [c]
50. J B Nielsen, S A Kinkead, J D Purson, P G Eller *Inorg. Chem.* **29** 1779 (1990)
51. H Dang, L Huag, Q Xu, R Yang, B Zhang, D Wang, Z Lu *Wuji Huaxue Xuebao* **12** 18 (1996); *Chem. Abstr.* **125** 24 976 (1996)
52. A V Eletskii, V A Legasov, S N Spirin, E V Stepanov, B B Chaivanov *Dokl. Akad. Nauk SSSR* **280** 909 (1985) [d]
53. D R MacKenzie, R H Wiswall, in *Noble Gas Compounds* (Chicago; London: University of Chicago Press, 1963) p. 81.
54. A D Kirshenbaum, L V Streng, A G Sreng, A V Grosse *J. Am. Chem. Soc.* **85** 360 (1963)
55. J H Holloway *Educ. Chem.* **10** 140 (1973)
56. C R Bieler, K C Janda *J. Am. Chem. Soc.* **112** 2033 (1990)
57. K Seppelt *Angew. Chem.* **91** 199 (1979)
58. A Filippi, A Troiani, M Speranza *J. Phys. Chem. A* **101** 9344 (1997)
59. E H Appelman *J. Am. Chem. Soc.* **90** 1900 (1968)
60. A Schneer-Ergey, K Kozmutza *Magy. Kem. Foly.* **78** 486 (1972)
61. I Feher, M Semptey *Magy. Kem. Foly.* **76** 141 (1970)
62. A A Goncharov, Yu N Kozlov, A P Purmal' *Zh. Fiz. Khim.* **52** 2870 (1978) [e]
63. A A Goncharov, Yu N Kozlov *Zh. Fiz. Khim.* **52** 945 (1978) [e]
64. A A Goncharov, Yu N Kozlov, A P Purmal' *Zh. Fiz. Khim.* **55** 1633 (1981) [e]
65. D F Smith *Science* **140** 899 (1963)
66. K O Christe, W W Wilson *Inorg. Chem.* **27** 2714 (1988)
67. C L Chernick, H H Claassen, J G Malm, P L Plurien, in *Noble Gas Compounds* (Chicago; London: University of Chicago Press, 1963) p. 287
68. K Seppelt, H H Rupp *Z. Anorg. Allg. Chem.* **409** 331 (1974)
69. W W Wilson, K O Christe *Inorg. Chem.* **26** 916 (1987)
70. K O Christe, W W Wilson *Inorg. Chem.* **27** 1296 (1988)
71. K O Christe, W W Wilson *Inorg. Chem.* **27** 3763 (1988)
72. H P A Mercier, G J Schrobilgen *Inorg. Chem.* **32** 145 (1993)
73. J B Nielsen, S A Kinkead, P G Eller *Inorg. Chem.* **29** 3621 (1990)
74. H Selig *Inorg. Chem.* **5** 183 (1966)
75. G J Moody, H Selig *Inorg. Nucl. Chem. Lett.* **2** 319 (1966)
76. G J Schrobilgen, D Martin-Rovet, P Charpin, M Lance *J. Chem. Soc., Chem. Commun.* 894 (1980)
77. J H Holloway, V Kaučič, D Martin-Rovet, D R Russell, G J Schrobilgen, H Selig *Inorg. Chem.* **24** 678 (1985)
78. K O Christe, D A Dixon, J C P Sanders, G J Schrobilgen, S Tsai, W W Wilson *Inorg. Chem.* **34** 1868 (1995)
79. K O Christe, E C Curtis, D A Dixon, H P Mercier, J C P Sanders, G J Schrobilgen *J. Am. Chem. Soc.* **113** 3351 (1991)
80. A Ellern, K Seppelt *Angew. Chem., Int. Ed. Engl.* **34** 1586 (1995)
81. J Foropoulos Jr, D D DesMarteau *Inorg. Chem.* **21** 2503 (1982)
82. L D Shustov, N S Tolmacheva, Sh Sh Nabiev, E K Il'in, V D Klimov, V P Ushakov *Zh. Neorg. Khim.* **34** 1673 (1989) [b]
83. V K Isupov, A V Oleinik, N N Aleinikov *Zh. Neorg. Khim.* **34** 2080 (1989) [b]
84. N N Aleinikov, S A Kashtanov, I A Pomytkin, A M Sipyagin *Izv. Akad. Nauk, Ser. Khim.* 184 (1995) [a]
85. Yu M Kiselev, N E Fadeeva, A I Popov, M V Korobov, V V Nikulin, V I Spitsyn *Dokl. Akad. Nauk SSSR* **295** 378 (1987) [d]
86. V A Legasov *Vestn. Akad. Nauk SSSR* (12) 3 (1976) [f]
87. N Bartlett, M Wechsberg, F O Sladky, P A Bulliner, G R Jones, R D Burbank *J. Chem. Soc., Chem. Commun.* 703 (1969)
88. M Eisenberg, D D DesMarteau *Inorg. Nucl. Chem. Lett.* **6** 29 (1970)

89. M Wechsberg, P A Bulliner, F O Sladky, R Mews, N Bartlett *Inorg. Chem.* **11** 3063 (1972)
90. F O Sladky *Monatsh. Chem.* **101** 1571 (1970)
91. J I Musher *J. Am. Chem. Soc.* **90** 7371 (1968)
92. M Eisenberg, D D DesMarteau *Inorg. Chem.* **11** 1901 (1972)
93. R G Syvret, G J Schrobilgen *J. Chem. Soc., Chem. Commun.* 1529 (1985)
94. R G Syvret, G J Schrobilgen *Inorg. Chem.* **28** 1564 (1989)
95. K Seppelt *Angew. Chem., Int. Ed. Engl.* **11** 723 (1972)
96. K Seppelt, D Lentz, G Kloeter *Inorg. Synth.* **24** 27 (1986)
97. F O Sladky *Monatsh. Chem.* **101** 1559 (1970)
98. H P A Mercier, J C P Sanders, G J Schrobilgen *J. Am. Chem. Soc.* **116** 2921 (1994)
99. F O Sladky *Inorg. Synth.* **24** 33 (1986)
100. V K Brel, A S Koz'min, V I Uvarov, N S Zefirov, V V Zhdankin, P J Stang *Tetrahedron Lett.* 5225 (1990)
101. B Cremer-Lober, H Butler, D Naumann, W Tyrra *Z. Anorg. Allg. Chem.* **607** 34 (1992)
102. K Seppelt, D Lentz, in *Progress in Inorganic Chemistry* Vol. 29 (New York: Wiley, 1982) p. 167
103. T Birchall, R D Myers, H DeWaard, G J Schrobilgen *Inorg. Chem.* **21** 1068 (1982)
104. L Turowsky, K Seppelt *Inorg. Chem.* **29** 3226 (1990)
105. R G Syvret, K M Mitchell, J C P Sanders, G J Schrobilgen *Inorg. Chem.* **31** 3381 (1992)
106. D Lentz, K Seppelt *Angew. Chem., Int. Ed. Engl.* **17** 356 (1978)
107. E Jacob, D Lentz, K Seppelt, A Simon *Z. Anorg. Allg. Chem.* **472** 7 (1981)
108. L Turowsky, K Seppelt *Z. Anorg. Allg. Chem.* **609** 153 (1992)
109. D Lentz, K Seppelt *Angew. Chem., Int. Ed. Engl.* **18** 66 (1979)
110. G A Schumacher, G J Schrobilgen *Inorg. Chem.* **23** 2923 (1984)
111. T-C Shieh, N C Yang, C L Chernick *J. Am. Chem. Soc.* **86** 5021 (1964)
112. T C Shieh, E D Feit, C L Chernick, N C Yang *J. Org. Chem.* **35** 4020 (1970)
113. S A Shakelford, R R McGuire, J L Pflug *Tetrahedron Lett.* 363 (1977)
114. M Zupan, A Pollak *J. Chem. Soc., Chem. Commun.* 845 (1973)
115. M Zupan, A Pollak *Tetrahedron* **33** 1017 (1977)
116. A Gregorčič, M Zupan *J. Org. Chem.* **44** 4120 (1979)
117. A Gregorčič, M Zupan *J. Org. Chem.* **44** 1255 (1979)
118. M Zupan, A Pollak *J. Org. Chem.* **41** 4002 (1976)
119. S Stavber, M Zupan *J. Fluorine Chem.* **10** 271 (1977)
120. D F Shellhamer, M L Ragains, B T Gipe, V L Heasley, G E Heasley *J. Fluorine Chem.* **20** 13 (1980)
121. M Zupan, B Šket *J. Org. Chem.* **43** 696 (1978)
122. A Gregorčič, M Zupan *J. Org. Chem.* **49** 333 (1984)
123. M Zupan, A Pollak *J. Org. Chem.* **42** 1559 (1977)
124. B Šket, M Zupan *J. Chem. Soc. Perkin Trans. 1* 2169 (1977)
125. M Zupan, A Gregorčič, A Pollak *J. Org. Chem.* **42** 1562 (1977)
126. S A Shakelford *Tetrahedron Lett.* 4265 (1977)
127. S A Shakelford *J. Org. Chem.* **44** 3485 (1979)
128. A Gregorčič, M Zupan *Bull. Chem. Soc. Jpn.* **53** 1085 (1980)
129. A Gregorčič, M Zupan *J. Fluorine Chem.* **24** 291 (1984)
130. R A Hildreth, M L Druelinger, S A Shakelford *Tetrahedron Lett.* **23** 1059 (1982)
131. A Gregorčič, M Zupan *Tetrahedron* **33** 3243 (1977)
132. D F Shellhamer, R J Conner, R E Richardson, V L Heasley, G E Heasley *J. Org. Chem.* **49** 5015 (1984)
133. S Rozen, R Filler *Tetrahedron* **41** 1111 (1985)
134. T B Patrick, R Mortezania *J. Org. Chem.* **53** 5153 (1988)
135. G S Garrett, T J Emge, S C Lee, E M Fischer, K Dyehouse, J M McIver *J. Org. Chem.* **56** 4823 (1991)
136. B Zajc, M Zupan *J. Chem. Soc., Chem. Commun.* 759 (1980)
137. G L Cantrell, R Filler *J. Fluorine Chem.* **27** 35 (1985)
138. B Zajc, M Zupan *J. Org. Chem.* **47** 573 (1982)
139. T Tsushima, K Kawada, T Tsuji *Tetrahedron Lett.* **23** 1165 (1982)
140. E Differding, G M Ruegg *Tetrahedron Lett.* **32** 3815 (1991)
141. M Zupan, A Pollak *J. Org. Chem.* **39** 2646 (1974)
142. W Korytnyk, S Valentekovic-Horvath, C R Petrie III *Tetrahedron* **38** 2547 (1982)
143. W Korytnyk, S Valentekovic-Horvath *Tetrahedron Lett.* **21** 1493 (1980)
144. C C Geilen, N Loch, W Reutter, K Seppelt, F Oberdorfer *Tetrahedron Lett.* **33** 2435 (1992)
145. N N Aleinikov, I A Pomytkin, S A Kashtanov, O N Efimov, A F Zueva *Izv. Akad. Nauk SSSR, Ser. Khim.* 2850 (1988) [a]
146. F O Sladky, P A Bulliner, N Bartlett *J. Chem. Soc., A* 2179 (1969)
147. N S Zefirov, V V Zhdankin, A A Gakh, P J Stang *Izv. Akad. Nauk SSSR, Ser. Khim.* 1196 (1990) [a]
148. N S Zefirov, A A Gakh, V V Zhdankin, P J Stang *J. Org. Chem.* **56** 1416 (1991)
149. V K Brel, V I Uvarov, N S Zefirov *J. Fluorine Chem.* **54** 34 (1991)
150. V K Brel, A A Gakh, V V Zhdankin, N S Zefirov, A S Koz'min, A A Korkin, T G Kutateladze, R Caple, S A Lermontov, I G Plokhikh, S O Safronov, P J Stang, N G Chovnikova *Dokl. Akad. Nauk SSSR* **313** 1131 (1990) [d]
151. V I Uvarov, V K Brel *Izv. Akad. Nauk, Ser. Khim.* 764 (1994) [a]
152. A L Henne, E C Ladd *J. Am. Chem. Soc.* **58** 402 (1936)
153. A Varvoglis *Hypervalent Iodine in Organic Synthesis* (London: Academic Press, 1997)
154. P J Stang, V V Zhdankin *Chem. Rev.* **96** 1123 (1996)
155. N Sh Pirkuliev, V K Brel, N S Zefirov *Usp. Khim.* **69** 118 (2000) [*Russ. Chem. Rev.* **69** 105 (2000)]
156. V V Zhdankin, R Tykwinski, B Berglund, M Mullikin, R Caple, N S Zefirov, A S Koz'min *J. Org. Chem.* **54** 2609 (1989)
157. V V Zhdankin, M Mullikin, R Tykwinski, B Berglund, R Caple, N S Zefirov, A S Koz'min *J. Org. Chem.* **54** 2605 (1989)
158. N S Zefirov, T M Kasumov, A S Koz'min, V D Sorokin, V R Polishchuk *Zh. Org. Khim.* **30** 321 (1994) [g]
159. N S Zefirov, V V Zhdankin, Yu V Dan'kov, V D Sorokin, V N Semerikov, A S Koz'min, R Caple, B A Berglund *Tetrahedron Lett.* **27** 3971 (1986)
160. N S Zefirov, N Sh Samsoniya, T G Kutateladze, V V Zhdankin *Zh. Org. Khim.* **27** 220 (1991) [g]
161. N S Zefirov, V V Zhdankin, Yu V Dan'kov, V V Samoshin, A S Koz'min *Zh. Org. Khim.* **20** 444 (1984) [g]
162. V V Zhdankin, P J Stang *Tetrahedron* **54** 10927 (1998)
163. N S Zefirov, V V Zhdankin, A S Koz'min *Tetrahedron Lett.* **27** 1845 (1986)
164. D F Shellhamer, C M Curtis, D R Hollingsworth, M L Ragains, R E Richardson, V L Heasley, G E Heasley *Tetrahedron Lett.* **23** 2157 (1982)
165. D F Shellhamer, C M Curtis, R H Dunham, D R Hollingsworth, M L Ragains, R E Richardson, V L Heasley, S A Shackelford, G E Heasley *J. Org. Chem.* **50** 2751 (1985)
166. D F Shellhamer, S L Carter, R H Dunham, S N Graham, M P Spitsbergen, V L Heasley, R D Chapman, M L Druelinger *J. Chem. Soc., Perkin Trans. 2* 159 (1989)
167. D F Shellhamer, S L Carter, M C Chiaco, T E Harris, R D Henderson, W S C Low, B T Metcalf, M C Willis, V L Heasley, R D Chapman *J. Chem. Soc. Perkin Trans. 2* 401 (1991)
168. M L Druelinger, D F Shellhamer, R D Chapman, S A Shackelford, M E Riner, S L Carter, R P Callahan, C R Youngstrom *J. Chem. Soc. Perkin Trans. 2* 787 (1997)
169. M Zupan, M Metelko, S Stavber *J. Chem. Soc. Perkin Trans. 1* 2851 (1993)
170. S Rozen, E Mishani, M Kol *J. Am. Chem. Soc.* **114** 7643 (1992)
171. D F Shellhamer, M J Horney, A L Toth, V L Heasley *Tetrahedron Lett.* **33** 6903 (1992)
172. D F Shellhamer, M J Horney, B J Pettus, T L Pettus, J M Stringer, V L Heasley *J. Org. Chem.* **64** 1094 (1999)
173. S Stavber, T Sotler, M Zupan, R G Syvret, J M Dobrolsky Jr, A Popovič *J. Org. Chem.* **59** 5891 (1994)
174. Ch A Ramsden, R G Smith *J. Am. Chem. Soc.* **120** 6842 (1998)
175. D R MacKenzie, J Fajer *J. Am. Chem. Soc.* **92** 4994 (1970)
176. M J Shaw, H H Hyman, R Filler *J. Am. Chem. Soc.* **91** 1563 (1969)
177. M J Shaw, H H Hyman, R Filler *J. Am. Chem. Soc.* **92** 6498 (1970)
178. M Ya Turkina, I P Gragerov *Zh. Org. Khim.* **11** 340 (1975) [g]
179. US P. 3 833 581; *Ref. Zh. Khim.* 12 N 136P (1975)
180. M J Shaw, H H Hyman, R Filler *J. Org. Chem.* **36** 2917 (1971)
181. S Stavber, M Zupan *J. Org. Chem.* **48** 2223 (1983)
182. M Zupan *Chimia* **30** 305 (1976)
183. B Šket, M Zupan *J. Org. Chem.* **43** 835 (1978)
184. B Šket, M Zupan *Bull. Chem. Soc. Jpn.* **54** 279 (1981)
185. S P Anand, L A Quarterman, P A Christian, H H Hyman, R Filler *J. Org. Chem.* **40** 3796 (1975)

186. M Rabinovitz, I Agranat, H Selig, C-H Lin *J. Fluorine Chem.* **10** 159 (1977)
187. I Agranat, M Rabinovitz, H Selig, C-H Lin *Chem. Lett.* **32** 1271 (1975)
188. M Zupan, A Pollak *J. Org. Chem.* **40** 3794 (1975)
189. E D Bergmann, H Selig, C-H Lin, M Rabinovitz, I Agranat *J. Org. Chem.* **40** 3793 (1975)
190. I Agranat, M Rabinovitz, H Selig, C-H Lin *Experientia* **32** 417 (1976)
191. M T Stephenson, H J Shine *J. Org. Chem.* **46** 3139 (1981)
192. S Stavber, M Zupan *J. Chem. Soc., Chem. Commun.* 969 (1978)
193. S Stavber, M Zupan *J. Org. Chem.* **46** 300 (1981)
194. V V Bardin, G G Furin, G G Jakobson *Zh. Org. Khim.* **18** 604 (1982) [g]
195. V V Bardin, G G Furin, G G Jakobson, in *Tez. Dokl. Vsesoyuz. Konf. Pamyati A E Favorskogo, Leningrad, 1980* (Abstracts of Reports of the All-Union Conference on A E Favorskii Memory, Leningrad, 1980) p. 110
196. G G Jakobson, V V Bardin, G G Furin, in *The IIIrd Regular Meeting of Soviet-Japanese Fluorine Chemists, Tokyo, 1983* p. 14.1
197. B Zajc, M Zupan *Bull. Chem. Soc. Jpn.* **55** 1617 (1982)
198. S P Anand, L A Quarterman, H H Hyman, K G Migliorese, R Filler *J. Org. Chem.* **40** 807 (1975)
199. A A Goncharov, Yu N Kozlov, A P Purmal' *Zh. Fiz. Khim.* **51** 2839 (1977) [e]
200. H Koudstaal, C Olieman *Recl. Trav. Chim. Pays-Bas* **100** 246 (1981)
201. M Zupan, A Pollak *J. Fluorine Chem.* **7** 443 (1976)
202. L N Nikolenko, T I Yurasova, A A Man'ko *Zh. Obshch. Khim.* **40** 938 (1970) [h]
203. A A Avramenko, V V Bardin, A I Karelin, V A Krasil'nikov, P P Tushin, G G Furin, G G Jakobson *Zh. Org. Khim.* **21** 822 (1985) [g]
204. V V Bardin, I V Stennikova, G G Furin, G G Jakobson, in *Stroenie i Reaktsionnaya Sposobnost' Kremniiorganicheskikh Soedinenii (Tez. Dokl. 3-go Vsesoyuz. Simpoziuma), Irkutsk, 1985* [Structure and Reactivity of Organosilicon Compounds (Abstracts of Reports of the 3rd All-Union Symposium), Irkutsk, 1985] p. 133
205. V V Bardin, I V Stennikova, G G Furin, G G Jakobson *Zh. Org. Khim.* **21** 458 (1985) [g]
206. G Firnau, R Chirakal, S Sood, S Garnett *Can. J. Chem.* **58** 1449 (1980)
207. G Firnau, R Chirakal, S Sood, S Garnett *J. Labelled Compd. Radiopharm.* **18** 7 (1981)
208. Z Planinsek, S Stavber, M Zupan *J. Fluorine Chem.* **45** 141 (1989)
209. S Stavber, Z Koren, M Zupan *Synlett* 265 (1994)
210. B Zajc, M Zupan *J. Org. Chem.* **55** 1099 (1990)
211. S Stavber, B Šket, B Zajc, M Zupan *Tetrahedron* **45** 6003 (1989)
212. S Stavber, M Zupan *Tetrahedron Lett.* **34** 4355 (1993)
213. V A Nikanorov, V I Rozenberg, V G Kharitonov, D Yu Antonov, V A Mikul'shina, M V Galakhov, D P Krut'ko, N S Kopelev, V N Guryshev, V P Yur'ev, O A Reutov *Dokl. Akad. Nauk SSSR* **315** 1388 (1990) [d]
214. I Takemoto, K Yamasaki *Biosci. Biotechnol. Biochem.* **58** 594 (1994)
215. T Umemoto, S Fukami, G Tomizawa, K Harasawa, K Kawada, K Tomita *J. Am. Chem. Soc.* **112** 8563 (1990)
216. G G Furin, A A Fainzilberg *Usp. Khim.* **68** 725 (1999) [*Russ. Chem. Rev.* **68** 653 (1999)]
217. S A Kashtanov, N N Aleinikov, F I Dubovitskii *Izv. Akad. Nauk SSSR, Ser. Khim.* 2678 (1987) [a]
218. G B Shul'pin, M M Kats, Yu N Kozlov *Izv. Akad. Nauk SSSR, Ser. Khim.* 2654 (1988) [a]
219. M M Kats, Yu N Kozlov, G B Shul'pin *Zh. Obshch. Khim.* **61** 1835 (1991) [h]
220. D F Shellhamer, B C Jones, B J Pettus, T L Pettus, J M Stringer, V L Heasley *J. Fluorine Chem.* **88** 37 (1998)
221. M Zupan, J Iskra, S Stavber *J. Org. Chem.* **63** 878 (1998)
222. V V Bardin, L N Shchegoleva, H J Frohn *J. Fluorine Chem.* **77** 153 (1996)
223. L N Nikolenko, L D Shustov, T N Bocharova, T N Yurasova, V A Legasov *Dokl. Akad. Nauk SSSR* **204** 1369 (1972) [d]
224. L D Shustov, T N Bocharova, T I Yurasova, N G Marchenkova, V A Legasov, L N Nikolenko *Zh. Obshch. Khim.* **43** 841 (1973) [h]
225. T N Bocharova, N G Marchenkova, L D Shustov, T Yu Prokof'eva, L N Nikolenko *Zh. Obshch. Khim.* **43** 1325 (1973) [h]
226. L D Shustov, T D Tel'kovskaya, L N Nikolenko *Zh. Org. Khim.* **11** 2137 (1975) [g]
227. L D Shustov, T D Tel'kovskaya, L N Nikolenko *Zh. Obshch. Khim.* **44** 2564 (1974) [h]
228. L D Shustov, M N Semenova, L N Nikolenko *Zh. Obshch. Khim.* **48** 1903 (1978) [h]
229. T B Patrick, K K Johri, D H White *J. Org. Chem.* **48** 4158 (1983)
230. T B Patrick, K K Johri, D H White, W S Bertrand, R Mokhtar, M R Kilbourn, M J Welch *Can. J. Chem.* **64** 138 (1986)
231. G J Schrobilgen, G Firnau, R Chirakal *J. Chem. Soc., Chem. Commun.* 198 (1981)
232. D I Davies, C Waring *J. Chem. Soc., C* 1865 (1968)
233. J W Wilt, in *Free Radicals* Vol. 1 (Ed. J K Kochi) (New York: Wiley, 1973) p. 333
234. C V Wilson *Org. React.* **9** 332 (1957)
235. L Kaplan, in *Free Radicals* Vol. 2 (Ed. J K Kochi) (New York: Wiley, 1973) p. 372
236. J K Kochi *J. Am. Chem. Soc.* **87** 2500 (1965)
237. R A Sheldon, J K Kochi *Org. React.* **19** 179 (1972)
238. T B Patrick, S Khazaeli, S Nadji, K Hering-Smith, D Reif *J. Org. Chem.* **58** 705 (1993)
239. D P Curran, E Bosch, J Kaplan, M Newcomb *J. Org. Chem.* **54** 1826 (1989)
240. E W Della, N J Head *J. Org. Chem.* **57** 2850 (1992)
241. Y Tanabe, N Matsuo, N Ohno *J. Org. Chem.* **53** 4582 (1988)
242. A M Sipyagin, I A Pomytkin, S V Pal'tsun, N N Aleinikov, V G Kartsev *Dokl. Akad. Nauk SSSR* **311** 1137 (1990) [d]
243. G G Furin *Usp. Khim.* **69** 538 (2000) [*Russ. Chem. Rev.* **69** 491 (2000)]
244. V K Brel, V I Uvarov, N S Zefirov, P J Stang, R Caple *J. Org. Chem.* **58** 6922 (1993)
245. V I Uvarov, V K Brel, I V Martynov, N N Aleinikov, S A Kashtanov *Izv. Akad. Nauk SSSR, Ser. Khim.* 2650 (1988) [a]
246. I V Martynov, V K Brel, V I Uvarov, I A Pomytkin, N N Aleinikov, S A Kashtanov *Izv. Akad. Nauk SSSR, Ser. Khim.* 466 (1988) [a]
247. I V Martynov, V K Brel, V I Uvarov, N N Aleinikov, S A Kashtanov *Izv. Akad. Nauk SSSR, Ser. Khim.* 2639 (1988) [a]
248. V K Brel, A S Koz'min, I V Martynov, V I Uvarov, N S Zefirov, V V Zhdankin, P J Stang *Tetrahedron Lett.* **31** 4799 (1990)
249. Yu L Yagupol'skii, T I Savina *Zh. Org. Khim.* **17** 1330 (1981) [g]
250. L D Shustov, L N Nikolenko *Zh. Obshch. Khim.* **53** 2408 (1983) [h]
251. P Nongkunsarn, Ch A Ramsden *J. Chem. Soc., Perkin Trans. 1* 121 (1996)
252. D Holtz, J L Beauchamp *Science* **173** 1237 (1971)
253. H S Johnston, R Woolfolk *J. Chem. Phys.* **41** 269 (1964)
254. J Berkowitz, W A Chupka, P M Guyon, J H Holloway, R Spohr *J. Phys. Chem.* **75** 1461 (1971)
255. J K Hovey, T B McMahon *J. Am. Chem. Soc.* **108** 528 (1986)
256. T Umemoto *Chem. Rev.* **96** 1757 (1996)
257. H J Frohn, S Jacobs *J. Chem. Soc., Chem. Commun.* 625 (1989)
258. H J Frohn, S Jacobs, G Henkel *Angew. Chem., Int. Ed. Engl.* **28** 1506 (1989)
259. R J Lagow, L J Turbini, R E Aikman, M M Brezinski *J. Fluorine Chem.* **45** 12 (1989)
260. K P Butin, Ya M Kiselev, T V Magdesieva, O A Reutov *Izv. Akad. Nauk SSSR, Ser. Khim.* 716 (1982) [a]
261. R G Bulgakov, G Ya Mastrenko, G A Tolstikov, B N Yakovlev, V P Kazakov *Izv. Akad. Nauk SSSR, Ser. Khim.* 2644 (1984) [a]
262. W Tyrra, D Naumann *Can. J. Chem.* **67** 1949 (1989)
263. D Naumann, W Tyrra *J. Chem. Soc., Chem. Commun.* 47 (1989)
264. W Breuer, H J Frohn, M Giesen, S Jacobs, in *Chemiedozenten–Tagung 1989 (Abstracts of Reports), Bielefeld, 1989* p. 108
265. W Breuer, H J Frohn, M Giesen, S Jacobs, in *The 12th International Symposium on Fluorine Chemistry, 1988* p. 213
266. H J Frohn, S Jakobs, C Rossbach *Eur. J. Solid State Inorg. Chem.* **29** 729 (1992)
267. H Meinert, S Rudiger *Z. Chem.* **9** 35 (1969)
268. C J Jameson, in *Multinuclear NMR* (Ed. J Mason) (New York; London: Plenum, 1987)

269. S Tanaka, M Sugimoto, H Takashima, M Hada, H Nakatsuji *Bull. Chem. Soc. Jpn.* **69** 953 (1996)
270. C I Ratcliffe *Annu. Rep. NMR Spectrosc.* **36** 123 (1998)
271. H Butler, D Naumann, W Tyrra *Eur. J. Solid State Inorg. Chem.* **29** 739 (1992)
272. H J Frohn, A Klose, G Henkel *GIT Fachz. Lab.* **37** 752 (1993)
273. H J Frohn, A Klose, V V Bardin, A J Kruppa, T V Leshina *J. Fluorine Chem.* **70** 147 (1995)
274. H J Frohn, A Klose, V V Bardin *J. Fluorine Chem.* **64** 201 (1993)
275. H J Frohn, A Klose, G Henkel *Angew. Chem., Int. Ed. Engl.* **32** 99 (1993)
276. V M McRae, R D Peacock, D R Russell *J. Chem. Soc., Chem. Commun.* 62 (1969)
277. N Bartlett, M Wechsberg, G R Jones, R D Burbank *Inorg. Chem.* **11** 1124 (1972)
278. L K Templeton, D H Templeton, K Seppelt, N Bartlett *Inorg. Chem.* **15** 2718 (1976)
279. R J Gillepsie, G J Schrobilgen, D R Slim *J. Chem. Soc., Dalton Trans.* 1003 (1977)
280. A F Wells *Structural Inorganic Chemistry* (Oxford: Clarendon Press, 1984) p. 920
281. H J Frohn, C Rossbach *Z. Anorg. Allg. Chem.* **619** 1672 (1993)
282. H J Frohn, S Jakobs, C Rossbach, in *The 13th International Symposium on Fluorine Chemistry, Bochum, 1991* A 8
283. H J Frohn, S Jakobs, C Rossbach *J. Fluorine Chem.* **54** 8 (1991)
284. V V Bardin, H J Frohn *J. Fluorine Chem.* **60** 141 (1993)
285. D Naumann, H Butler, R Gnann, W Tyrra *Inorg. Chem.* **32** 861 (1993)
286. D Naumann, H Butler, R Gnann *Z. Anorg. Allg. Chem.* **618** 74 (1992)
287. S Datsenko, N Ignat'ev, P Barthen, H J Frohn, T Scholten, T Schroer, D Welting *Z. Anorg. Allg. Chem.* **624** 1669 (1998)
288. D Naumann, W Tyrra, R Gnann, D Pfolk *J. Chem. Soc., Chem. Commun.* 2651 (1994)
289. D Naumann, W Tyrra, R Gnann, D Pfolk, T Gilles, K F Teble *Z. Anorg. Allg. Chem.* **623** 1821 (1997)
290. H J Frohn, V V Bardin *J. Chem. Soc., Chem. Commun.* 1072 (1993)
291. H J Frohn, V V Bardin *Mendeleev Commun.* 114 (1995)
292. H J Frohn, V V Bardin *Z. Naturforsch., B Chem. Sci.* **51** 1011 (1996)
293. H J Frohn, V V Bardin *Z. Naturforsch., B Chem. Sci.* **53** 562 (1998)
294. H J Frohn, A Klose, T Schroer, G Henkel, V Buss, D Opitz, R Vahrenhorst *Inorg. Chem.* **37** 4884 (1998)
295. H J Frohn, V V Bardin *Z. Anorg. Allg. Chem.* **622** 2031 (1996)
296. V V Bardin *J. Fluorine Chem.* **89** 195 (1998)
297. A A Avramenko, V V Bardin, G G Furin, A I Karelin, V A Krasil'nikov, P P Tushin *Zh. Org. Khim.* **24** 1443 (1988) [g]
298. H J Frohn, V V Bardin *J. Chem. Soc., Chem. Commun.* 919 (1999)
299. V V Zhdankin, P J Stang, N S Zefirov *J. Chem. Soc., Chem. Commun.* 578 (1992)
300. S P Anand, R Filler *J. Fluorine Chem.* **7** 179 (1976)
301. M Zupan, A Pollak *J. Fluorine Chem.* **8** 275 (1976)
302. S V Kovalenko, V K Brel, N S Zefirov *Izv. Akad. Nauk, Ser. Khim.* 1841 (1994) [a]
303. S V Kovalenko, V K Brel, N S Zefirov, P J Stang *Mendeleev Commun.* 68 (1998)
304. T I Yurasova *Zh. Obshch. Khim.* **44** 956 (1974) [h]
305. J Wang, A I Scott *Tetrahedron* **50** 6181 (1994)
306. I A Grigor'ev, L B Volodarsky, V F Strichenko, I A Kirilyuk *Tetrahedron Lett.* **30** 751 (1989)
307. I V Tselinskii, A A Mel'nikov, L G Varyagina, A E Trubitsin *Zh. Org. Khim.* **21** 2490 (1985) [g]
308. I V Tselinskii, A A Mel'nikov, A E Trubitsin *Zh. Org. Khim.* **23** 1657 (1987) [g]
309. I V Tselinskii, A A Mel'nikov, A E Trubitsin *Zh. Org. Khim.* **24** 688 (1988) [g]
310. A E Trubitsin, A A Mel'nikov, M S Pevzner, I V Tselinskii, M E Niyazymbetov, V A Petrosyan *Izv. Akad. Nauk SSSR, Ser. Khim.* 736 (1989) [a]
311. I V Tselinskii, A A Mel'nikov, A E Trubitsin, G M Frolova *Zh. Org. Khim.* **26** 69 (1990) [g]
312. I V Tselinskii, A A Mel'nikov, A E Trubitsin *Zh. Org. Khim.* **26** 272 (1990) [g]
313. A E Trubitsin, A A Mel'nikov, I V Tselinskii, A M Popov *Zh. Org. Khim.* **26** 2007 (1990) [g]
314. V A Petrosyan, M E Niyazymbetov *Izv. Akad. Nauk SSSR, Ser. Khim.* 368 (1988) [a]
315. M E Niyazymbetov, V A Petrosyan, A A Gakh, A A Fainzil'berg *Izv. Akad. Nauk SSSR, Ser. Khim.* 2390 (1987) [a]
316. V A Golubev, N N Salmina, B L Korsunskii, N N Aleinikov, F N Dubovitskii *Izv. Akad. Nauk, Ser. Khim.* 778 (1978) [a]
317. W Sundermeyer, M Witz *J. Fluorine Chem.* **34** 251 (1986)
318. G J Schrobilgen, J H Holloway, P Granger, C Brevard *Inorg. Chem.* **17** 980 (1978)
319. D D DesMarteau *J. Am. Chem. Soc.* **100** 6270 (1978)
320. D D DesMarteau, R D LeBlond, S F Hossain, D Nothe *J. Am. Chem. Soc.* **103** 7734 (1981)
321. J F Sawyer, G J Schrobilgen, S J Sutherland *J. Chem. Soc., Chem. Commun.* 210 (1982)
322. R Faggiani, D K Kennepohl, C J L Lock, G J Schrobilgen *Inorg. Chem.* **25** 563 (1986)
323. J F Sawyer, G J Schrobilgen, S J Sutherland *Inorg. Chem.* **21** 4064 (1982)
324. G A Schumacher, G J Schrobilgen *Inorg. Chem.* **22** 2178 (1983)
325. J Foropoulos Jr, D D DesMarteau *J. Am. Chem. Soc.* **104** 4260 (1982)
326. H Selig, J H Holloway *Top. Curr. Chem., Inorg. Chem.* **124** 33 (1984)
327. A A A Emara, G J Schrobilgen *J. Chem. Soc., Chem. Commun.* 1644 (1987)
328. A A A Emara, G J Schrobilgen *Inorg. Chem.* **31** 1323 (1992)
329. A A A Emara, G J Schrobilgen *J. Chem. Soc., Chem. Commun.* 257 (1988)
330. G J Schrobilgen *J. Chem. Soc., Chem. Commun.* 1506 (1988)
331. V H Dibeler, S K Liston *J. Chem. Phys.* **48** 4765 (1968)
332. G J Schrobilgen *J. Chem. Soc., Chem. Commun.* 863 (1988)
333. G J Schrobilgen, J M Whalen *Inorg. Chem.* **33** 5207 (1994)
334. A Schulz, T M Klapötke *Inorg. Chem.* **36** 1929 (1997)
335. K O Christe, E C Curtis, D A Dixon, H P Mercier, J C P Sanders, G J Schrobilgen *J. Am. Chem. Soc.* **113** 3351 (1991)
336. K O Christe, W W Wilson *Inorg. Chem.* **21** 4113 (1982)
337. N Bartlett, F O Sladky *J. Chem. Soc., D* 1046 (1968)
338. Yu M Kiselev *Koord. Khim.* **23** 83 (1997) [i]
339. J A Gibson, A F Janzen *J. Chem. Soc., Chem. Commun.* 739 (1973)
340. J Bornstein, M R Borden, F Nunes, H I Tarlin *J. Am. Chem. Soc.* **85** 1609 (1963)
341. W Carpenter *J. Org. Chem.* **31** 2688 (1966)
342. J J Edmans, W B Motherwell *J. Chem. Soc., Chem. Commun.* 881 (1989)
343. M Zupan, A Pollak *J. Org. Chem.* **41** 2179 (1976)
344. S Stavber, M Zupan *J. Fluorine Chem.* **12** 307 (1978)
345. M Zupan *Synthesis* 473 (1976)
346. M Zupan, A Pollak *J. Chem. Soc., Perkin Trans. 1* 1745 (1976)
347. J A Gibson, R K Marat, A F Janzen *Can. J. Chem.* **53** 3044 (1975)
348. M Zupan, A Pollak *J. Fluorine. Chem.* **7** 445 (1976)
349. I I Maletina, V V Orda, N N Aleinikov, B L Korsunskii, L M Yagupol'skii *Zh. Org. Khim.* **12** 1371 (1976) [g]
350. H J Frohn, V V Bardin *Z. Naturforsch., B Chem. Sci.* **51** 1015 (1996)
351. M Zupan, A Pollak *J. Chem. Soc., Chem. Commun.* 715 (1975)
352. M Zupan *Collect. Czech. Chem. Commun.* **42** 266 (1977)
353. K Alam, A F Janzen *J. Fluorine Chem.* **36** 179 (1987)
354. A Gregorčič, M Zupan *Bull. Chem. Soc. Jpn.* **50** 517 (1976)
355. G W Bradley, J H Holloway, H J Koh, D G Morris, P G Watson *J. Chem. Soc., Perkin Trans. 1* 3001 (1992)
356. E W Della, N J Head, W K Janowski, C H Schiesser *J. Org. Chem.* **58** 7876 (1993)
357. A N Chekhlov, T M Kasumov, V K Brel, N S Zefirov *Zh. Strukt. Khim.* **37** 940 (1996) [j]
358. T M Kasumov, V K Brel, Yu K Grishin, N S Zefirov, P J Stang *Tetrahedron* **53** 1145 (1997)
359. T M Kasumov, N Sh Pirguliyev, V K Brel, Yu K Grishin, N S Zefirov, P J Stang *Tetrahedron* **53** 13139 (1997)
360. T M Kasumov, V K Brel, K A Potekhin, E V Balashova, N S Zefirov *Dokl. Akad. Nauk* **351** 644 (1996) [d]
361. T M Kasumov, V K Brel, K A Potekhin, A S Koz'min, E V Balashova, Yu S Struchkov, N S Zefirov *Dokl. Akad. Nauk* **349** 634 (1996) [d]

362. T M Kasumov, V K Brel, K A Potekhin, E V Balashova, N S Zefirov, P J Stang *Dokl. Akad. Nauk* **353** 770 (1997) [d]
363. N Sh Pirkuliev, V K Brel, T M Kasumov, N G Akhmedov, N S Zefirov *Zh. Org. Khim.* **35** 1633 (1999) [g]
364. N Sh Pirguliyev, V K Brel, T M Kasumov, N S Zefirov, P J Stang *Synthesis* 1297 (1999)
365. N Sh Pirkuliev, Candidate Thesis in Chemical Sciences, Moscow State University, Moscow, 1999
366. T M Kasumov, V K Brel, A S Koz'min, N S Zefirov, K A Potekhin, P J Stang *New J. Chem.* **21** 1347 (1997)
367. N Sh Pirguliyev, V K Brel, N S Zefirov, P J Stang *Mendeleev Commun.* 189 (1999)
368. T Kitamura, R Furuki, K Nagata, H Taniguchi, P J Stang *J. Org. Chem.* **57** 6810 (1992)
369. T Kitamura, R Furuki, H Taniguchi, P J Stang *Tetrahedron Lett.* **31** 703 (1990)
370. T Kitamura, R Furuki, H Taniguchi, P J Stang *Tetrahedron* **48** 7149 (1992)
371. P J Stang, V V Zhdankin, N S Zefirov *Mendeleev Commun.* 159 (1992)
372. T Kitamura, R Furuki, H Taniguchi, P J Stang *Mendeleev Commun.* 148 (1991)
373. T Kitamura, R Furuki, K Nagata, L Zheng, H Taniguchi *Synlett* 193 (1993)
374. V I Uvarov, V K Brel *Izv. Akad. Nauk, Ser. Khim.* 1629 (1994) [a]
375. V I Uvarov, V K Brel *Zh. Obshch. Khim.* **64** 2060 (1994) [h]
376. T M Klapötke *Heteroatom. Chem.* **8** 473 (1997)
377. A N Nesmeyanov, I N Lisichkina, A S Kulikov, A N Vanchikov, T P Tolstaya, V A Chertkov *Dokl. Akad. Nauk SSSR* **243** 1463 (1978) [d]
378. M Zupan *J. Fluorine Chem.* **8** 305 (1976)
379. R K Marat, A F Janzen *Can. J. Chem.* **55** 3031 (1977)
380. M Zupan, B Zajc *J. Chem. Soc., Perkin Trans. 1* **9** 965 (1978)
381. A M Forster, A J Downs *J. Chem. Soc., Dalton Trans.* 2827 (1984)
382. T B Patrick, S Nadji *J. Fluorine Chem.* **39** 415 (1988)
383. Yu L Yagupol'skii, T I Savina *Zh. Org. Khim.* **15** 438 (1979) [g]
384. A Gregorčič, B Zajc, M Zupan *Phosphorus Sulfur* **6** 107 (1979)
385. X Ou, A F Janzen *Can. J. Chem.* **74** 2002 (1996)
386. K O Christe, W W Wilson *J. Fluorine Chem.* **47** 117 (1990)
387. J E Gordon *The Organic Chemistry of Electrolyte Solutions* (New York: Wiley, 1975)
388. G Zerza, G Sliwinski, N Schwentner, G J Hoffman, D G Imre, V A Apkarian *J. Chem. Phys.* **99** 8414 (1993)
389. X Ou, G M Bernard, A F Janzen *Can. J. Chem.* **75** 1878 (1997)
390. C W Perkins, J C Martin, A J Arduengo, W Lau, A Alegria, J K Kochi *J. Am. Chem. Soc.* **102** 7753 (1980)
391. X Ou, A F Janzen *Inorg. Chem.* **36** 392 (1997)
392. A F Janzen, P M C Wang, A E Lemire *J. Fluorine Chem.* **22** 557 (1983)
393. K Hatano *Chem. Pharm. Bull.* **46** 1337 (1998)
394. X Huang, B J Blackburn, A F Janzen *J. Fluorine Chem.* **47** 145 (1990)
395. M J Robins, S F Wnuk, K B Mullah, N K Dalley *J. Org. Chem.* **56** 6878 (1991)
396. M J Robins, K B Mullah, S F Wnuk, N K Dalley *J. Org. Chem.* **57** 2357 (1992)
397. G Guillerm, M Gatel *J. Chem. Soc., Perkin Trans. 1* 153 (1994)
398. M J Robins, S F Wnuk, K B Mullah, N K Dalley, C-S Yuan, Y Lee, R T Borchardt *J. Org. Chem.* **59** 544 (1994)
399. A M Sipyagin, I A Pomytkin, N N Aleinikov, S V Pal'tsun, V G Kartsev, in *Tez. Dokl. VI Vsesoyuz. Konf. po Khimii Ftororganicheskikh Soedinenii, Novosibirsk, 1990* (Abstracts of Reports of the VIth All-Union Conference on the Chemistry of Organofluorine Compounds, Novosibirsk, 1990)
400. A M Sipyagin, I A Pomytkin, S V Pal'tsun, N N Aleinikov *Khim. Geterotsikl. Soedin.* 58 (1994) [k]
401. A M Sipyagin, I V Efremov, I A Pomytkin, S A Kashtanov, N N Aleinikov *Khim. Geterotsikl. Soedin.* 1291 (1994) [k]
402. A M Sipyagin, Z G Aliev *Khim. Geterotsikl. Soedin.* 1278 (1994) [k]
403. A M Sipyagin, Z G Aliev *Khim. Geterotsikl. Soedin.* 1495 (1993) [k]
404. A M Sipyagin, I A Pomytkin, S V Pal'tsun, N N Aleinikov *Chem. Heterocycl. Compd.* **30** 52 (1994)
405. V N Boiko, G M Shchupak, N V Ignat'ev, L M Yagupol'skii *Zh. Org. Khim.* **15** 1245 (1979) [g]
406. V S Ershov, S A Kashtanov, I V Efremov, I A Pomytkin, A M Sipyagin, N N Aleinikov *Khim. Geterotsikl. Soedin.* 1703 (1995) [k]
407. J Varwing, R Mews *J. Chem. Res. (S)* 245 (1977)
408. H Steinbeisser, R Mews *J. Fluorine Chem.* **17** 505 (1981)
409. R Maggiulli, R Mews, H Oberhammer, W-D Stohrer *J. Fluorine Chem.* **45** 77 (1989)
410. E Jaudas-Presel, R Maggiulli, R Mews, H Oberhammer, T Paust, W-D Stohrer *Chem. Ber.* **123** 2123 (1990)
411. W Leidinger, W Sundermeyer *Chem. Ber.* **115** 2892 (1982)
412. S A Volkova, Z M Sinyutina, L N Nikolenko *Zh. Obshch. Khim.* **44** 2592 (1974) [h]
413. R Minkwitz, G Nowicki, H Preut *Z. Anorg. Allg. Chem.* **573** 185 (1989)
414. R Minkwitz, A Werner *Z. Naturforsch., B Chem. Sci.* **43** 403 (1988)
415. R Minkwitz, G Nowicki *Z. Naturforsch., B Chem. Sci.* **44** 1343 (1989)
416. R Minkwitz, G Nowicki *Inorg. Chem.* **31** 225 (1992)
417. R Minkwitz, G Nowicki *Inorg. Chem.* **30** 4426 (1991)
418. R Minkwitz, W Molsbeck *Z. Anorg. Allg. Chem.* **612** 35 (1992)
419. A J Downs, G S McGrady, E A Barnfield, D W H Rankin, H E Robertson, J E Boggs, K D Dobbs *Inorg. Chem.* **28** 3286 (1989)
420. R Minkwitz, U Lohmann, H Bormann *Z. Anorg. Allg. Chem.* **622** 889 (1996)
421. S Sato, H Ameta, E Horn, O Takahashi, N Furukawa *J. Am. Chem. Soc.* **119** 12374 (1997)
422. T Kawashima, F Ohno, R Okazaki, H Ikeda, S Inagaki *J. Am. Chem. Soc.* **118** 12455 (1996)
423. M Pettersson, J Lundell, L Khriachtchev, E Isoniemi, M Räsänen *J. Am. Chem. Soc.* **120** 7979 (1998)
424. M Yamanishi, K Hirao, K Yamashita *J. Chem. Phys.* **108** 1514 (1998)
425. M Pettersson, J Lundell, M Räsänen *J. Chem. Phys.* **102** 6423 (1995)
426. M Pettersson, J Lundell, M Räsänen *J. Chem. Phys.* **103** 205 (1995)
427. M Pettersson, J Nieminen, L Khriachtchev, M Räsänen *J. Chem. Phys.* **107** 8423 (1997)
428. M Pettersson, J Lundell, L Khriachtchev, M Räsänen *J. Chem. Phys.* **109** 618 (1998)
429. R Kasemann, D Naumann *J. Fluorine Chem.* **41** 321 (1988)
430. H Poleschner, M Heydenreich, K Spindler, G Haufe *Synthesis* 1043 (1994)
431. Y Usuki, M Iwaoka, S Tomoda *Chem. Lett.* 1507 (1992)
432. H Poleschner, M Heydenreich, U Schilde *Liebigs Ann. Chem.* 1187 (1996)
433. K K Laali, W Fiedler, M Regitz *J. Chem. Soc., Chem. Commun.* 1641 (1997)
434. K Uneyama, M Kanai *Tetrahedron Lett.* **31** 3583 (1990)
435. S Sato, H Arakawa, E Horn, N Furukawa *Chem. Lett.* 213 (1998)
436. K Alam, A F Janzen *J. Fluorine Chem.* **27** 467 (1985)
437. D Naumann, S Herberg *J. Fluorine Chem.* **19** 205 (1982)
438. J Bergman, L Engman *J. Am. Chem. Soc.* **103** 2715 (1981)
439. A F Janzen, O C Vaidya *Can. J. Chem.* **51** 1136 (1973)
440. J A Gibson, A F Janzen *Can. J. Chem.* **49** 2168 (1971)
441. S A Lermontov, A V Popov, S I Zavorin, I I Sukhojenko, N V Kuryleva, I V Martynov, N S Zefirov, P J Stang *J. Fluorine Chem.* **66** 233 (1994)
442. A H Cowley, R C-Y Lee *Inorg. Chem.* **18** 60 (1979)
443. S A Lermontov, A V Popov, V O Zavel'skii, I I Sukhozhenko, N V Kirilova, I V Martynov. *Izv. Akad. Nauk SSSR, Ser. Khim.* 682 (1990) [a]
444. L M Yagupol'skii, V I Popov, N V Kondratenko, B L Korsunskii, N N Aleinikov *Zh. Org. Khim.* **11** 459 (1975) [g]
445. D Naumann, W Tyrra *J. Organomet. Chem.* **334** 323 (1987)
446. I G Rakov, Candidate Thesis in Chemical Sciences, Institute of Physiologically Active Compounds, Russian Academy of Sciences, Chernogolovka, 1997
447. S A Lermontov, D M Rakov, N S Zefirov, P J Stang *Phosphorus Sulfur Silicon Relat. Elem.* **92** 225 (1994)
448. R Minkwitz, B Baeck *ACS Symp. Ser.* **555** 90 (1994)
449. I V Martynov, R G Gafurov, A K Ustinov, N N Aleinikov, S A Kashtanov. *Izv. Akad. Nauk SSSR, Ser. Khim.* 1437 (1987) [a]
450. V V Bardin, I V Stennikova, G G Furin, T V Leshina, G G Jakobson *Zh. Obshch. Khim.* **58** 2580 (1988) [h]

451. V V Bardin, H J Frohn *J. Fluorine Chem.* **90** 93 (1998)
452. A P Lothian, C A Ramsden *Synlett* 753 (1993)
453. G W M Visser, R E Herder, F J J de Kanter, J D M Herscheid *J. Chem. Soc., Perkin Trans. 1* 1203 (1988)
454. M J Robins, S Manfredini *Tetrahedron Lett.* **31** 5633 (1990)
455. S A Klyuchinskii, M-A M Abid-Albaki, V S Zavgorodnii *Zh. Obshch. Khim.* **64** 161 (1994) [h]
456. M A Tius, J K Kawakami *Synth. Commun.* **22** 1461 (1992)
457. M A Tius, J K Kawakami *Synlett* 207 (1993)
458. D P Matthews, S C Miller, E T Jarvi, J S Sarbol, J R McCarthy *Tetrahedron Lett.* **34** 3057 (1993)
459. H F Hodson, D J Madge, D A Widdowson *Synlett* 831 (1992)
460. M A Tius, J K Kawakami *Tetrahedron* **51** 3997 (1995)
461. M A Tius, G S K Kannangara *Tetrahedron* **48** 9173 (1992)
462. M A Tius, G S K Kannangara, M A Kerr, K J S Grace *Tetrahedron* **49** 3291 (1993)
463. A L J Beckwith, D M O'Shea *Tetrahedron Lett.* **27** 4525 (1986)
464. G A Tolstikov, S K Minsker, Z G Bulgakov, G Ya Maistrenko, A V Kuchin, U M Dzhemilev, V P Kazakov *Izv. Akad. Nauk SSSR, Ser. Khim.* 2631 (1979) [a]
465. R G Bulgakov, V N Yakovlev, G Ya Maistrenko, G A Tolstikov, V P Kazakov *Izv. Akad. Nauk SSSR, Ser. Khim.* 490 (1986) [a]
466. R G Bulgakov, V N Yakovlev, R A Sadykov, G Ya Maistrenko, V P Kazakov, G A Tolstikov *Metalloorg. Khim.* **2** 339 (1989) [l]
467. G A Tolstikov, R G Bulgakov, S K Minsker, G Ya Maistrenko, A V Kuchin, U M Dzhemilev, V P Kazakov *Khim. Vys. Energ.* **15** 248 (1981) [m]
468. V P Kazakov, V N Yakovlev, G Ya Maistrenko *Khim. Vys. Energ.* **31** 133 (1997) [m]
469. Z Bregar, S Stavber, M Zupan *J. Fluorine Chem.* **44** 187 (1989)
470. Z Bregar, M Zupan, in *The 8th International Conference on Organic Synthesis (IUPAC), Helsinski, 1990* p. 123
471. M Zupan, Z Bregar *Tetrahedron Lett.* **31** 3357 (1990)
472. K P Butin, Yu M Kiselev, T V Magdesieva, O A Reutov *J. Organomet. Chem.* **235** 127 (1982)
473. R C Burns, I D MacLeod, T A O'Donnell, T E Peel, K A Phillips, A W Waugh *J. Inorg. Nucl. Chem.* **39** 1737 (1977)
474. A J Blake, R W Cockman, E A V Ebsworth, J H Holloway *J. Chem. Soc., Chem. Commun.* 529 (1988)
475. M C Crossman, E G Hope, L J Wootton *J. Chem. Soc., Dalton Trans.* 1813 (1998)
476. S A Brewer, J H Holloway, E G Hope *J. Chem. Soc., Dalton Trans.* 1067 (1994)
477. S A Brewer, A K Brisdon, J H Holloway, E G Hope, L A Reck, P G Watson *J. Chem. Soc., Dalton Trans.* 2945 (1995)
478. S A Brewer, J H Holloway, E G Hope, P G Watson *J. Chem. Soc. Dalton Trans.* 1577 (1992)
479. K S Coleman, J H Holloway, E G Hope *J. Chem. Soc., Dalton Trans.* 11713 (1997)
480. V P Zubov, S D Stavrova, I P Chikhacheva, O A Prudnikova, G A Fedorova, G B Barsamyan, V B Sokolov *Zh. Prikl. Khim.* **71** 848 (1998) [n]
481. Yu N Kozlov, A P Moravskii, A M Uskov, A E Shilov *Kinet. Katal.* **31** 251 (1990) [o]
482. A I Yurtanov, V A Piven', S K Baidildaeva, A V Sliz'kii, V K Brel *Zh. Org. Khim.* **32** 848 (1996) [g]
483. D L Shellhamer, B C Jones, B J Pettus, T L Pettus, J M Stringer, V L Heasley *J. Fluorine Chem.* **88** 37 (1998)
484. T B Patrick, L Zhang *Tetrahedron Lett.* **38** 8925 (1997)
485. T B Patrick, L Zhang, Q Li *J. Fluorine Chem.* **102** 11 (2000)
486. T B Patrick, S Qian *Org. Lett.* **2** 3359 (2000)
487. R Taylor *Izv. Akad. Nauk, Ser. Khim.* 852 (1998) [a]
488. O V Boltalina, A K Abdul-Sada, R Taylor *J. Chem. Soc., Perkin Trans. 2* 981 (1995)
489. L G Bulusheva, A V Okotrub *Rev. Inorg. Chem.* **19** 79 (1999)

[a] — *Russ. Chem. Bull. (Engl. Transl.)*
[b] — *Russ. J. Inorg. Chem. (Engl. Transl.)*
[c] — *Inorg. Mater. (Engl. Transl.)*
[d] — *Dokl. Chem. Technol., Dokl. Chem. (Engl. Transl.)*
[e] — *Russ. J. Phys. Chem. (Engl. Transl.)*
[f] — *Herald Russ. Acad. Sci. (Engl. Transl.)*
[g] — *Russ. J. Org. Chem. (Engl. Transl.)*
[h] — *Russ. J. Gen. Chem. (Engl. Transl.)*
[i] — *Russ. J. Coord. Chem. (Engl. Transl.)*
[j] — *J. Struct. Chem. (Engl. Transl.)*
[k] — *Chem. Heterocycl. Compd. (Engl. Transl.)*
[l] — *Organomet. Chem. (Engl. Transl.)*
[m] — *High Energy Chem. (Engl. Transl.)*
[n] — *Russ. J. Appl. Chem. (Engl. Transl.)*
[o] — *Kinet. Catal. (Engl. Transl.)*

Russian Chemical Reviews **70** (4) 265 – 284 (2001) © 2001 Russian Academy of Sciences and Turpion Ltd

DOI 10.1070/RC2001v070n04ABEH000638

Size effects in chemistry of heterogeneous systems

N F Uvarov, V V Boldyrev

Contents

I.	Introduction	265
II.	Size effects in single-component systems	266
III.	Heterogeneous multicomponent solid-phase systems (composites)	271
IV.	Mechanochemical synthesis of nanocomposites and nanoparticles	278
V.	Chemical properties of nanoscale systems	280
VI.	Conclusion	282

Abstract. Size effects in single-component and multicomponent solid-phase systems are discussed. Peculiarities of the size effects in microcrystalline and nanoscale systems are analysed. Methods for mechanochemical synthesis of nanoparticles are considered. Chemical properties of nanoscale systems are analysed. Particular attention is paid to the results of studies of the properties of nanocomposites and nanoparticles. Problems concerning their stability and the possibility of mechanochemical synthesis of these systems are discussed. The bibliography includes 175 references.

I. Introduction

The understanding of basic principles and the development of new methods for the synthesis of functional materials with unusual and valuable properties is a key problem of solid state chemistry. Currently, 'dry' (*i.e.*, partially or completely solvent-free) technologies are known to be the most efficient and ecologically safe way to carry out chemical reactions.[1]

Mechanochemical processes meet this requirement. A mechanochemical reaction is a multistage process proceeding by a complex mechanism, which requires that many factors be taken into account when optimising the conditions for mechanical activation of reactants. The mechanism of a mechanochemical reaction involves the following main stages: initial deformation of the crystal structures of reactants; formation and accumulation of both point and linear defects and interaction between them; dispersion of the reactants into blocks; formation of intermediate metastable states in the regions of phase contacts and, finally, chemical homogenisation of the reaction product followed by its relaxation to reach a thermodynamically equilibrium state.

These processes have been best studied for metals where mechanochemical reactions proceed with relative ease. However, the results of recent investigations showed that ionic and molecular crystals are also promising objects for studying mechanochemical processes. In ionic crystals, the charge and potential of the double electrical layers on the phase boundaries have a pronounced effect on the interphase interaction. In molecular crystals, there is a broad spectrum of chemical bonds differing in nature, direction and energy and each type of these bonds is characterised by a specific response to mechanical treatment. By varying the type and positions of functional groups in the molecules of the crystal one can control the mechanism of mechanochemical reactions, which is of great importance for the synthesis of advanced materials.

Mechanical activation of heterogeneous mixtures allows preparation of nanocomposites with unusual properties, including supramolecular systems. Supramolecular nanoscale systems comprise chemically active components (substrates) bound to particular atoms or molecular groups of the carrier matrices (receptors) by non-covalent interactions. Such systems have been poorly studied as yet; however, a novel class of materials based on them has been designed. Unique properties of these materials are due to both specific types of intramolecular and intermolecular interactions in the bulk of the substrate and the character of the receptor – substrate interactions. Here, the role of receptor can be played by either the molecular fragments or by a particular sublattice in the crystal structure of the reactant (intercalated compounds or 'guest – host' inclusion compounds), or by active groups on the surface of heterogeneous inclusions, which favour the formation of, *e.g.*, Langmuir films or other surface layers.

A salient feature of supramolecular heterogeneous systems is the strong interface interaction, which depends on many interrelated factors including chemical, structural, morphological and thermodynamic ones. This interaction is responsible for the structural rearrangement in the substrate and for the changes in its thermodynamic, transport and chemical properties. In certain systems, the cationic or protonic conductivity of an ionic salt (substrate) can increase by several orders of magnitude and unusual phases can be stabilised in the receptor – substrate contact region. For instance, composites of the ionic salt – oxide type are candidates for the synthesis of supramolecular solid electrolytes based on them. Of considerable interest are also heterogeneous systems of the molecular crystal – oxide type.

Theoretical analysis of the mechanism of the surface interaction between different phases is a complicated problem. Currently, the properties of intergrain and phase boundaries in metals have been fairly well investigated. However, the ionic crystal – oxide or molecular crystal – oxide interfaces are still inadequately explored both experimentally and theoretically. Experimental studies are hampered by the problems of controlling the morphol-

N F Uvarov Institute of Solid State Chemistry and Mechanochemistry, Siberian Branch of the Russian Academy of Sciences, ul. Kutateladze 18, 630128 Novosibirsk, Russian Federation. Fax (7-383) 232 28 47. Tel. (7-383) 232 56 45. E-mail: uvarov@solid.nsk.su
V V Boldyrev Novosibirsk State University, ul. Pirogova 2, 630090 Novosibirsk, Russian Federation. Fax (7-383) 239 71 01. Tel. (7-383) 232 15 50

Received 20 November 2000
Uspekhi Khimii **70** (4) 307 – 329 (2001); translated by A M Raevsky

ogy of the composite, which leads to irreproducibility of the results obtained. Modern calculations require the inclusion of the contributions of not only covalent, hydrogen and van der Waals interactions but also long-range Coulomb and dipole–dipole interactions, which makes them rather difficult. Moreover, consideration of characteristic features of real interface structures is also of great importance. Nevertheless, one can carry out trial calculations of the energetically favourable surface configurations for systems of the molecular crystal (substrate)–oxide (receptor) type using the known model interaction potentials. Such estimates would be useful for targeted search of a substrate for a particular receptor.

Since the action range of surface forces is confined to a thin near-surface layer, one can expect that nanocomposites will hold the greatest promise for the synthesis of supramolecular systems. Nanocomposites are heterophasic systems, which represent dense aggregates of nanoparticles of both phases, which are uniformly distributed in the bulk. The particle size of a nanocomposite does not exceed 10 nm. In nanocomposites, virtually the whole bulk of the substrate is in the interface region, which allows experimental investigations of its physicochemical properties at the nanoscale level. To date, the properties of nanocomposites have been poorly studied, since the preparation of these systems by conventional methods is an extremely complicated task. Mechanical activation facilitates considerably the grinding of the active component and its spreading over the oxide (receptor) surface, thus favouring strong adhesive interaction.

It is known that the physical and chemical properties of solids change as the particle size decreases. These types of phenomena are usually called size effects. Numerous papers dealing with theoretical and experimental studies of size effects have appeared (see, *e.g.*, reviews [2–13]). Currently, it has been reliably shown that size effects are inherent in all solids; some phenomenological models have been proposed for qualitative or semiquantitative description of these effects.

Size effects have been best studied for metals and to a lesser degree for ionic crystals. For many materials, size effects are observed at relatively large grain size. For instance, the diffusion coefficient, conductivity and mechanical properties of a material become dependent on the average grain size (L) for $L \sim 10^3 - 10^4$ nm; as L reduces to $10 - 10^2$ nm, the melting temperature decreases and a change in the crystal lattice parameter of the material is observed. Size effect is most pronounced in nanoscale dispersed systems with a characteristic particle size in the range from 1 to 10 nm. In this case, the properties of the material can change basically, *e.g.*, it can undergo a transformation into a high-temperature phase or another high-energy state, which cannot be realised under standard conditions.

In heterogeneous systems, size effects depend on some additional factors such as the chemical nature of the components of the heterogeneous mixture, the particle morphology (spatial distribution of the components in the bulk of the composite) and the interface interaction. Consideration of these factors is a complicated problem and no satisfactory theoretical model for the description of size effects in composites has been proposed so far. The most pronounced changes in the properties are observed in both pure substances (undoped homogeneous individual compounds) and nanocomposites if the average particle size in these systems is less than 10 nm.

Recently, the interest increased in the studies of unusual effects observed in nanoscale systems. This is not surprising since the processes proceeding in such systems serve as the basis for future solid-state nanotechnologies. However, chemical reactions in solid-phase mixtures are still the least investigated aspect of solid state chemistry. This is to a great extent due to the necessity of taking into account specific features of small particles involved or formed in the reactions. For instance, the reaction system can become a nanocomposite where the properties of reactants differ substantially from those at equilibrium in the stage of nucleation of the reaction product phase. In this review, we tried to describe the most plausible mechanisms of the influence of size effects on the course of physicochemical (including mechanochemical) processes in heterogeneous solid-phase systems. In presenting the material, we pass from simple systems to more complex ones. First, size effects in isolated particles of simple substances are considered. Then, we discuss size effects in ensembles of small particles, in heterogeneous systems of different morphologies and in the nanoparticles formed in the initial stages of heterogeneous chemical reactions and prepared by mechanical activation.

II. Size effects in single-component systems

Size effects can be arbitrarily divided into two types. Weak effects where insignificant changes in the physicochemical properties of a substance are observed with an increase in the specific surface area (*i.e.*, with reduction of the particle size) belong to the first type of size effects. Here, all the changes observed can be explained by surface effects. As a rule, these effects are usually observed in crystals with a characteristic size exceeding 10 nm. These systems will be referred to as microcrystalline ones.

Strong effects where dramatic changes in the properties of a substance cannot be interpreted in terms of conventional surface phenomena belong to the second type of size effects. Most often, they are observed for very fine particles with a characteristic size of less than 10 nm. These systems will be referred to as nanoscale ones.

In this review, we will compare these two types of size effects and follow a gradual transformation of microcrystalline systems into nanoscale ones.

1. Microcrystalline systems

It has been experimentally shown that physicochemical properties of substances change noticeably as the particle size changes in the range from 10 to 100 nm. As mentioned above, the effects observed in this case are explained by the influence of the surface on the properties of crystals. As L decreases, the fraction of surface atoms increases. A 10 nm isotropic crystal of a simple substance has $\sim 1\% - 5\%$ of the atoms on the surface. The classical Gibbs thermodynamics treats all the excess thermodynamic characteristics of such fine particles, which differ from the corresponding bulk values, as being due to surface effects.

Let us consider a small particle of a substance. Ignoring adsorption, the excess Gibbs free energy, ΔG, per unit area of the tension surface is the surface tension γ of the substance. For an isotropic medium (*e.g.*, a liquid), γ equals the surface energy of the substance, σ. If the particle size (here, the diameter of a drop of the liquid) is much larger than the characteristic molecular size, the tension surface virtually matches the geometric surface of the particle. For a spherical particle, the excess energy is

$$G_s = \gamma A = \sigma A = \sigma \frac{6V}{L}, \tag{1}$$

where A, V and L are the surface area, volume and diameter of the particle, respectively. Generally, the surface tension, $\hat{\gamma}$, of a phase in an anisotropic medium is a tensor quantity. For a slightly curved surface, it is defined as the difference between the proper local value of the stress tensor, $\hat{E}$, and its bulk value, $\hat{E}_\alpha$, extrapolated to the same point and is found by integration

$$\hat{\gamma} = \int_{-\infty}^{\infty} (\hat{E} - \hat{E}_\alpha) \mathrm{d}z, \tag{2}$$

where z is the coordinate normal to the surface of the layer. The absolute value of γ is defined as half the spur (trace) of the surface tension tensor

$$\gamma = \frac{1}{2} \mathrm{Tr} \langle \hat{\gamma} \rangle = \frac{1}{2} (\gamma_{11} + \gamma_{22}). \tag{3}$$

For a liquid or an isotropic medium, $\gamma = \gamma_{11} = \gamma_{22}$ and expression (1) holds. In the crystalline phase, the surface area

can be increased in two independent ways, *viz*., by increasing the number of surface atoms and by elastic deformation of a crystal. A specific feature of a solid is the presence of an immobile structural component, the chemical potential of which is considered to be a tensor quantity.[14,15] Nonuniformity of the chemical potential distribution over the surface layer of the crystal can lead to substantial difference between the surface tension at and surface energy of different surface areas. Owing to anisotropy of the crystal lattice, each face of the crystal is characterised by its own values of the surface tension and surface energy. In addition to the crystal faces, some contribution to the excess energy of the crystal also comes from the excess energy due to the presence of edges and vertices. Assuming an ideally smooth surface, the surface tension of *i*th crystal face is related to the surface energy by the following relationship

$$\gamma_i = \sigma_i + A_i \frac{\mathrm{d}\sigma_i}{\mathrm{d}A_i}. \tag{4}$$

The effective surface energy of a crystal with N faces, M edges and Z vertices equals [16]

$$\sigma = \left(\sum_i^N \sigma_i A_i + \sum_j^M k_j l_j + \sum_k^Z \varepsilon_k \right) A^{-1}, \tag{5}$$

where k_j is the energy of formation of the jth edge, l_j is the length of the jth edge, ε_k is the energy of formation of the kth vertex (these parameters depend on the crystal shape) and $A = \sum A_i$ is the total tension surface area. The terms in formula (5) describe the contributions of crystal faces, edges and vertices to the excess energy of the crystal ignoring surface stress. For a crystal with an equilibrium shape,

$$\sigma \approx \frac{3V}{A} \frac{\sigma_i}{h_i},$$

where h_i is the distance from the Wulf point to the ith crystal face. It is appropriate to choose the parameter [16]

$$L = \frac{6V}{A} \tag{6}$$

as the characteristic crystal size.

If the parameters σ and L of a crystal are defined by formulae (5) and (6), an additional term can be entered into Eqn (1) and it can be rewritten in the form

$$G_\mathrm{s} = \gamma A = \sigma A + \Delta G_\mathrm{e} = \sigma \frac{6V}{L} + \Delta G_\mathrm{e}, \tag{7}$$

where ΔG_e is the elastic strain energy

$$\Delta G_\mathrm{e} \approx \sum A_i \frac{\mathrm{d}\sigma_i}{\mathrm{d}A_i}.$$

In real microcrystals, the ΔG_e value depends on many factors such as the crystal shape, the tension surface area A, the type of lattice symmetry, presence of defects in the crystal, *etc*. Estimation of the elastic strain energy in real crystals is a complicated problem. Expression (7) holds for both the liquid and crystalline phases (note that the contribution of elastic strain energy is nonzero only in crystals, since for liquid $\Delta G_\mathrm{e} = 0$).

As follows from the general thermodynamic expression for the Gibbs free energy,

$$G(P,T,A) = U + PV - TS + \sigma A + \Delta G_\mathrm{e}(A), \tag{8}$$

where U, V, S are the internal energy, volume and entropy of a crystal at a pressure P and temperature T, the surface area of the crystal plays the role of an additional external parameter that defines the thermodynamic properties of the material.

If the substance is highly dispersed, the contributions of the surface-dependent terms become noticeable. This leads to specific size effects such as changes in the crystal lattice parameters, low-temperature (at temperatures close to 0 K) heat capacity, the Debye temperature, phase transition temperatures and stabilisation of unusual phases. The electronic structure of the substance also changes, which is responsible for unusual optical, electrical and magnetic properties.

Among all the size effects, the effect of a decrease in the phase transition (*e.g*., melting) temperature, T_t, of small particles has been studied in most detail. Transition temperatures are determined assuming that the corresponding phases have equal Gibbs energies. In the framework of the classical Thomson model for an isolated particle, the relative change of T_t is a linear function of $1/L$ (see Refs 17–19).

$$\frac{T_\mathrm{t}}{T_\mathrm{t}^0} = 1 - \frac{6(\gamma_\alpha V_\alpha - \gamma_\beta V_\beta)}{H_\mathrm{t}} \frac{1}{L}, \tag{9}$$

where T_t^0 and H_t are the temperature and enthalpy of the phase transition from the high-temperature α-phase to the low-temperature β-phase, respectively; γ_α and γ_β are the surface tensions of the α- and β-phases at temperature T_t, respectively; and V_α and V_β are the molar volumes of the α- and β-phases, respectively. Deviation of the experimental dependences of $T_\mathrm{t}/T_\mathrm{t}^0$ on $1/L$ from linear ones can be explained by the formation of a thin film of the liquid phase on the surface of a crystal owing to melting of small particles,[20] by the dependence of γ_α and γ_β on the particle size [21] or by the contribution of elastic strain energy $\Delta G_\mathrm{e}(A)$.[11] In the last-mentioned case, Eqn (9) can be represented in the form

$$\frac{T_\mathrm{t}}{T_\mathrm{t}^0} = 1 - \frac{6(\sigma_\alpha V_\alpha - \sigma_\beta V_\beta)L^{-1} + \Delta G_\mathrm{e}(L)}{H_\mathrm{t}}, \tag{10}$$

where σ_α and σ_β are the specific surface energies of the α- and β-phases, respectively. From Eqn (10) it follows that the transition temperature depends not only on the particle size and specific surface energy, but also on the change in the molar volume, the elastic strain energy difference between two phases, $\Delta G_\mathrm{e}(L)$, and the enthalpy of the phase transition. In the case of melting, the term $\Delta G_\mathrm{e}(L)$ includes the contribution of elastic strain energy of the crystalline phase at the melting temperature.

Neglecting the ΔG_e contribution allows construction of the phase diagrams of a substance in the T–$(1/L)$ coordinates. They can be used not only for the estimation of changes in the transition temperatures, but also for the prediction of the phase size effect with a decrease in the crystal size below a certain critical value.[6,7,13] This effect manifests itself in, *e.g*., stabilisation of new phases which are atypical of the macrocrystal. Currently, numerous experimental studies have confirmed the existence of phase size effects in both films [6,7] and polycrystalline samples.[11,13] For instance, the equilibrium crystal structure of Al_2O_3 was found to be dependent on particle size. If the radius of alumina particles does not exceed 35 nm, the γ-phase is stable; if the particle size increases, γ-Al_2O_3 undergoes transformations into β-, ε-, θ- and α-Al_2O_3.[8] The formation of amorphous phases in a number of systems can also be due to size effects.[7,22,23]

In the early studies on size effects, changes in the crystal structure of small particles were explained by the effect of excess pressure,

$$\Delta p = \frac{4\gamma}{L},$$

produced owing to surface tension.[2,4] Indeed, isolated particles of many metals, alkali metal halides, oxides and nitrides exhibit a monotonic decrease in the lattice parameter with a decrease in L, which corresponds to positive Δp values. However, the unit cell parameters of nanocrystals (*e.g*., Si, Se, Cr and Pd) increase as the particle size decreases.[3] Most often, a decrease in L leads to stabilisation of high-temperature modifications rather than high-pressure phases. An explanation [24] of this fact involves the assumption of the effective negative pressure in small particles, so that the classical concept of the Laplacian pressure cannot be generally used to describe their properties.

Recently, intensive research has been carried aimed at the synthesis of highly dispersed materials such as metals, oxides, ceramics and high-melting compounds. Currently, substances with the characteristic particle size of less than 100 nm are usually classified as nanocrystalline materials.[25,26] Most of the systems studied to date are characterised by a grain size, L, ranging from 10 to 100 nm and their properties differ insignificantly from those of large crystallites. Hence, they should be considered as microcrystalline rather than nanoscale systems. As will be shown below, the systems with a particle size smaller than 10 nm can be classified as nanoscale ones. Diverse morphologies of, *e.g.*, the particles of ceramic materials complicate the problem of description of their physical properties using a unified approach. Particular effects, such as the appearance of additional contribution to the heat capacity, a decrease in the Debye temperature, an increase in the coefficients of thermal expansion and enhanced diffusion depend on the state of intergrain boundaries and can be described in the framework of an additive model which takes into account the contributions of the bulk and the surface to the physical properties of a material. In this case, the intergrain boundaries and pores in the material can be considered as specific metastable phases, the concentrations of which increase as L decreases. On the other hand, such characteristics as the magnitude of microstresses or elastic properties of the materials under study are strongly dependent on the prehistory of a sample (*viz.*, on the procedure for its preparation and heat or mechanical pretreatment). For samples with relatively large grain size, these properties can be satisfactorily described using the Hall–Petch model. As the grain size becomes less than 10 nm, the response of the dislocation structure, formed owing to the presence of intergrain boundaries, to mechanical action becomes hardly predictable;[8,12,27] however, this can also be due to inadequate experimental procedures employed in studies of these materials.

2. Nanoscale systems

Numerous experimental studies have shown that if the particle size is less than the critical size $L_c \sim 10$ nm, the bulk properties of materials change noticeably. A particle of size $L \approx 10$ nm contains 10^4-10^5 atoms, of which 1%–5% are on the surface of the particle and contribute largely to the physicochemical properties. Ensembles of such particles form nanoscale (nanocrystalline) systems in which the following characteristic effects are observed.

1. Structural changes. If $L < L_c$, the average interatomic distance in the crystal changes dramatically and the crystal lattice parameter a becomes dependent on L. In the near-surface layer, the interplanar spacings along the normal to the surface are smaller than in the bulk of the crystal,[3,4] which is due to the nonsymmetrical action of interatomic forces on the near-surface atoms. High-resolution electron microscopy (HREM) studies have shown that the region of noticeable changes in the lattice parameter is confined to five or six atomic planes and has a characteristic size $\lambda_s \sim 1-3$ nm. The same values have been obtained in calculations on alkali halide crystals.[28,29] The λ_s value can be considered as the action range of surface forces or the effective thickness of the crystal surface. The entire near-surface region of thickness λ_s is in the state that is characteristic of the surface and the crystal structure of this region depends on particular characteristics of the surface. In this connection, mention may be made that the structure of, *e.g.*, nanoscale particles of metal glasses, which is experimentally determined from the radial distribution functions, differs from the structure of the same glasses in bulk specimens.[10]

2. Changes in thermodynamic properties. In nanocrystalline systems, the Debye temperature decreases and an additional contribution to the low-temperature heat capacity of the material appears, which increases as the particle size decreases.[2,11,12,30] These effects can be explained by changes in the vibrational states of the nanocrystal,[3,4,12] namely, by 'softening' of the spectrum (an increase in the number of low-frequency modes owing to a decrease in the number of high-frequency modes) with a decrease in L. Qualitatively, 'softening' of spectra can be explained by the action of the pure surface effects: the atoms on the surface of a bulk crystal are characterised by increased amplitudes and lower vibration frequencies. However, analysis of the behaviour of the atomic Debye–Waller factors using the data of X-ray diffraction study has shown[3] that changes in the Debye temperature in nanocrystals cannot be explained only by the contribution of the vibrations of the surface atoms since a decrease in L causes a stronger lattice 'softening' than it could be expected. This means that not only the vibrational frequencies of the surface atoms, but also those of the atoms in the bulk of the nanocrystal are lowered. Yet another interesting feature of nanocrystals is that both the entropy of melting and the melting temperature decrease as L decreases.[11] Since changes in the vibrational entropy makes the major contribution to the entropy of melting, this effect is also explained by the 'softening' of the lattice of the nanocrystal with the decrease in its size.

3. Phase size effect. This is an example of a specific type of manifestation of structural and thermodynamic changes in materials. Phase size effect is most pronounced in nanoscale systems. A decrease in L down to 10–100 nm leads to stabilisation of high-temperature phases in both nanocrystals and microcrystals. In some instances, phases that are not characteristic of a given substance (including the amorphous phase) can be formed.[2,6,7,8] Structural data for even smaller particles are lacking; however, numerous theoretical studies suggest that simple substances (metals, inert gases) occur in the form of polyatomic clusters as the particle size reduces to several nanometres.[3,4,31,32]

4. Changes in the electronic properties of materials. Among the effects experimentally observed in nanoscale systems, the quantum size effect[4,7,33,34] seems to be the most interesting for chemistry. If the size of a crystal is comparable with the de Broglie wavelength of elementary excitations, the quantisation conditions of electron energy are changed and the energy bands split into a system of energy levels (Fig. 1). In semimetals, this effect leads to the appearance of low-temperature oscillations of the kinetic coefficients and optical absorption with a decrease in the thickness of specimens (films).[7] In wide-band semiconductor crystals, electronic excitation results in the formation of loosely bound electron–hole pairs. In this case, the quantum size effect manifests itself markedly as changes in the optical spectra, namely, reduction of L leads to an increase in both the energy at the maximum of the absorption band and the exciton peak intensity and to a shift of the luminescence spectrum towards the short-wavelength region. The pattern of the absorption spectrum becomes similar to that of the spectra of individual macromolecules. Semiconductor nanocrystals possessing these properties are called 'quantum dots'; they can be used in optoelectronics and are currently

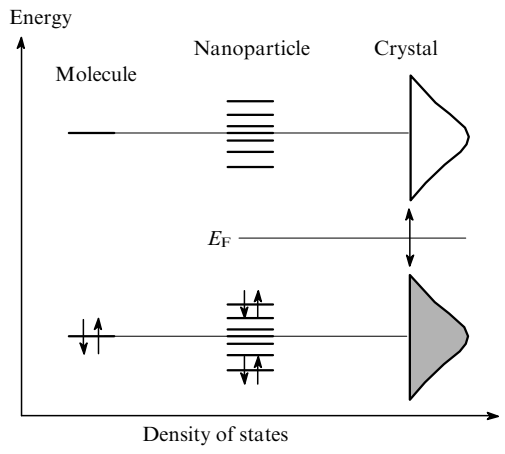

Figure 1. Electronic spectra of an isolated molecule, a nanoparticle and a semiconductor crystal. E_F is the Fermi level.

intensively studied.[33,34] As the size of ferromagnetic crystals reduces to $\sim 10-100$ nm, the coercive force increases and a decrease in the Curie temperature is observed. However, further decrease in the particle size causes a decrease in the coercive force and disappearance of ferromagnetic properties owing to the effect of superparamagnetism.[4] Ferromagnetic clusters with sizes of the order of several nanometres or layered structures with the layer thicknesses of the same order of magnitude possess abnormally high magnetoresistance coefficients.[35–37]

The above-mentioned effects can hardly be explained in the framework of the commonly accepted theory of surface phenomena. A correct mention has been made [3] that the concept of surface tension loses its meaning in the case of nanocrystals since all atoms can be treated as surface ones. Changes in the interatomic distances in small particles are mainly due to the decrease in the number of atoms in the particle,[3] which means that the size effect is a collective property of all the atoms constituting the particle. Therefore, it is helpful to follow the changes in the properties of materials on going from molecules to clusters, then to nanocrystals and, finally, to conventional bulk crystals in order to gain a deeper insight into the phenomena observed.

Let us consider pure substances with a Lennard-Jones potential of the interatomic interaction. If the number of atoms in a particle, N, is small ($N \leqslant 7$), regular polyhedral clusters are formed. If $7 < N < 13$, a large number of isomeric forms of the clusters exists, the energies of the isomers being only slightly different. If $N = 13$, a relatively stable icosahedral cluster is formed. Using this cluster as a 'seed', one can obtain larger icosahedral clusters with $N = 55$, 147, 309, 561, *etc*., by building up the atomic layers on the cluster faces.[3,4,31,32] Seldom, can large crystals of the icosahedral phase (quasicrystals) be obtained.[38,39] In addition to icosahedral clusters, pentagondodecahedral ones are also relatively stable. Owing to the presence of the five-fold symmetry axes, an increase in the cluster size should inevitably result in the development of elastic strain. According to theoretical estimates, the icosahedral and dodecahedral structures become unstable for $N \approx 500$, which corresponds to the particle size $L > \sim 2$ nm. In this case, the particle is broken into tetrahedral blocks with a close-packed, face-centred cubic (fcc) structure separated by defect domains such as systems of twin boundaries, dislocations and disclinations.[4,40] These defects provide the thermodynamic stability of the particle; in other words, small crystalline particles with imperfect structure are in the thermodynamically equilibrium state. Further increase in N leads to stabilsation of the defect-free Wulf polyhedra, the shape of which is determined from the minimum condition for the surface energy of the crystal.

Thus, each substance is characterised by two 'threshold' lengths denoted as L_1 and L_2. If the particle size of a substance is less than L_1, the particle spontaneously breaks down into nanocrystalline blocks. If $L < L_2$, a phase transition into an X-ray amorphous phase (ensemble of clusters) occurs in the particle. It should be mentioned that for small particles there is a great number of different atomic configurations with close energies.[41] This makes the concept of the equilibrium state of a particle ambiguous and is responsible for a gradual, diffuse character of phase transitions in the nanoscale systems. In particular, melting of clusters is considered as a dynamic equilibrium between the 'solidlike' and 'liquidlike' clusters that coexist at any temperature.[41,42]

On going from individual clusters to ensemble of nanoparticles, the effect of intergrain boundaries on the physicochemical properties of the ensemble becomes noticeable. Since the number of surface atoms in a nanoparticle is comparable with that in the bulk, in the case of random packing of particles the structure of each crystallite is 'tuned' to correspond to the local environment, which leads to effective broadening of the intergrain boundaries. Information on the structure of intergrain boundaries in nanoscale materials is contradictory. Both strongly disordered boundaries with a loose amorphous structure [9,10] and the boundaries with relatively high concentration of atoms (typical of bulk polycrystals) are observed.[12] In a 10 nm nanocrystal with an intergrain boundary width of 0.5–1 nm, the fraction of the atoms situated on these boundaries reaches 15%–30% of the total number of atoms.[10,12] Depending on the conditions for the preparation and annealing of ceramic nanoparticles, the structures of the intergrain boundaries can be different. Freshly prepared specimens have more disordered structures compared to either sintered or simply stored specimens in which the boundary atoms are ordered to form conventional intergrain boundaries. This is accompanied by the growth of crystallites owing to a decrease in the concentration of disordered boundary atoms. According to molecular dynamics calculations of model ensembles using the Coulomb or Lennard-Jones interatomic potentials,[43,44] these relaxation processes should be observed after intense mechanical deformation of nanoscale systems.

3. Transport properties of microcrystals and nanocrystals

Polycrystalline materials are characterised by increased mobility of atoms. This has been confirmed in studies on the kinetics of sintering and recrystallisation,[45] diffusion of radioactive isotopes [46] and ionic conductivity.[47,48] In bulk crystals, diffusion and mass transfer occur by migration of point defects which has an activation character. Earlier, enhanced diffusion in fine crystallites was thought to be due to changes in the concentration of vacancies caused by curvature of the crystallite surface. In fact, the expression for the excess concentration of point defects in a metal near the curved surface, $[V_M]$, obtained using the Thomson–Kelvin equation for the equilibrium of vacancies in crystal, has the form [45]

$$[V_M] = [V_M]_\infty \exp\left(-\frac{2\gamma\upsilon}{RkT}\right) = [V_M]_\infty \exp\left(-\frac{Q}{kT}\right), \qquad (11)$$

where $[V_M]_\infty$ is the concentration of defects in the bulk and R is the radius of curvature. If $\gamma = 100$ erg cm^{-2} and $\upsilon = 10$ cm^3 mol^{-1}, the curvature of the surface makes an additional contribution, Q, of 0.003 eV ($R = 10$ nm) and 0.03 eV ($R = 1$ nm) to the energy of formation of defects. This effect can lead to a noticeable increase in the concentration of defects only in very fine particles with the size of about 1 nm.

Currently, it is accepted that the activation energy of grain boundary diffusion in metals is lower than that of bulk diffusion; this is explained by the relatively loose local grain boundary structure and by high concentration of boundary defects.[10,46] The formation of a defect in the bulk of a metal involves two stages,[49] namely, the formation of a pair comprising an excess atom above the surface and a vacancy in the surface layer and detachment of the vacancy from the surface followed by its diffusion into the interior of the metal. This is illustrated in Fig. 2 in which the plots of changes in the free energy of the crystal upon the formation of a surface vacancy and its diffusion into the bulk of the metal are also presented. In the first stage, surface disordering occurs: the metal atom M goes out of the surface layer on the outer surface of the crystal, which leads to the formation of a pair of defects, *viz*., the adatom, M_s, and a vacancy in the surface layer, V_{Ms}. The concentration of defects on the surface, $[V_{Ms}]$, and in the bulk, $[V_M]_\infty$, are determined by the corresponding energies of formation (g_s and g_0, respectively)

$$[V_{Ms}] = [M_s] = \exp\left(-\frac{g_s}{2kT}\right), \qquad (12)$$

$$[V_M]_\infty = \exp\left(-\frac{g_0}{kT}\right). \qquad (13)$$

Surface diffusion can occur owing to both migration of atoms over the outer surface and migration of vacancies within the surface layer. In polycrystals, the role of the outer surface is played

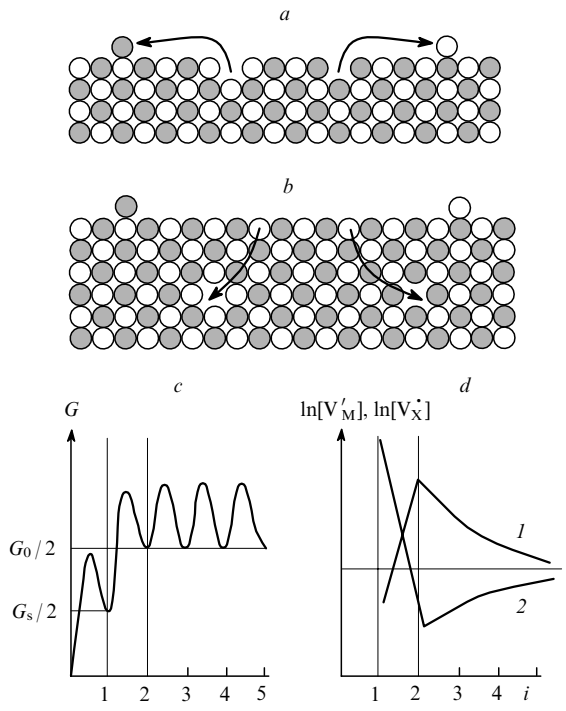

Figure 2. Schematic representation of the elementary act of surface disordering (*a*) and the formation of a Schottky defect in the bulk of a crystal (*b*) as well as change in the Gibbs free energy of the crystal upon the formation of a defect (*c*) and the spatial distribution of defects in the near-surface layer of the ionic crystal of the MX type (*d*).
$[V'_M]$ is the concentration of cationic vacancies (*1*), $[V^{\bullet}_X]$ is the concentration of anionic vacancies (*2*); *i* is the order number of the near-surface layer along the normal to the surface directed into the interior of the crystal ($i = 1$ corresponds to the outer surface of the crystal).

by the intergrain boundaries; in this case, $[M_s] \approx 1$ and surface disordering is described by the equation

$$[V_{Ms}] = \exp\left(-\frac{g_s}{kT}\right). \tag{14}$$

The energy of formation of a defect and, hence, the concentration of defects in the bulk of the crystal are determined by the fundamental properties of matter rather than surface disordering. On the contrary, the g_s value can vary between 0 and g_0 depending of many factors such as orientation of the surface, the type of intergrain boundary, adsorption of impurities on the surface, *etc*.[50] Hence, the activation energy of surface diffusion should depend on the procedure for the preparation of a given material.

In ionic crystals of the MX type, surface disordering is accompanied by the formation of the electrical double layer since both cationic (V'_{Ms}) and anionic ($V^{\bullet}_{Xs}$) vacancies within the surface layer can be formed independently in accordance with the equations of quasichemical reactions

$$0 \rightleftarrows V'_{Ms} + M^{\bullet}_s, \tag{15}$$

$$0 \rightleftarrows V^{\bullet}_{Xs} + X'_s \tag{16}$$

(here, zero corresponds to a perfect crystal).

As in the case of metals, the concentration of uncharged surface defects should be completely determined by the energy of formation of these defects

$$g_s = (g_{V_M})_s + (g_{V_X})_s.$$

However,

$$(g_{V_M})_s \neq (g_{V_X})_s,$$

hence, an excess surface charge and the corresponding surface potential φ_s appear. The magnitude of φ_s depends on the energy difference between the quasichemical surface disordering reactions:[50]

$$\varphi_s = \frac{(g_{V_X})_s - (g_{V_M})_s}{2e}. \tag{17}$$

The concentration of the Schottky defects in the bulk of a crystal is determined by the equilibrium constant of a quasichemical reaction involving the formation energy of bulk defects of g_0,

$$0 \rightleftarrows V'_{M\infty} + V^{\bullet}_{X\infty}. \tag{18}$$

The concentrations of defects on the surface,

$$[V'_{Ms}] = [V'_{M\infty}] \exp\left(\frac{g_0 - g_s}{2kT} + \frac{e\varphi_s}{kT}\right), \tag{19}$$

$$[V^{\bullet}_{Xs}] = [V^{\bullet}_{X\infty}] \exp\left(\frac{g_0 - g_s}{2kT} - \frac{e\varphi_s}{kT}\right) \tag{20}$$

depend on both the surface potential (17) and the additional contribution of the surface disordering. In the absence of the latter, (*i.e*., in a particular case $g_0 = g_s$), Eqns (19) and (20) coincide with the expressions obtained in the framework of Frenkel's model.[51, 52] Analogous expressions can also be obtained for crystals with Frenkel defects.

The parameter φ_s can be considered as the potential jump at the crystal – vacuum interface; this takes into account the properties of the surface, in particular, specific adsorption of charged particles (vacancies) on the surface. The defects localised on the surface can form a dense diffusion layer. At low concentrations of defects, the properties of this layer (or the space charge region) are described in the framework of the Gouy – Chapman model. The concentration of defects in the diffusion layer is calculated using the Poisson – Boltzmann equation which relates the space charge to the potential. The simplified expression for the ionic conductivity due to the electrical double layer has the form [53]

$$\varkappa = \frac{B}{L} T^{-1/2} \exp\left[\left(-\frac{h_0}{4} + \frac{e\varphi_s}{2} - E_m\right)(kT)^{-1}\right], \tag{21}$$

where B is the constant which includes all temperature-independent terms, h_0 is the enthalpy of formation of the defect, E_m is the migration energy of the defects that form the electrical double layer; for simplicity, the entropy contribution to φ_s is taken as zero. The expression for the conductivity of the diffusion layer written in the coordinates of the Arrhenius equation has the form:

$$\log(\varkappa T^{1/2}) = \log\frac{B}{L} - \frac{E_a}{kT},$$

where the activation energy of conductivity is

$$E_a = \frac{h_0}{4} - \frac{e\varphi_s}{2} + E_m.$$

Two regions corresponding to the high-temperature and low-temperature conductivities can be seen on the plot of experimental temperature dependence of the conductivity of a polycrystalline ionic salt. The former corresponds to the intrinsic conductivity, while the latter is due to the contribution of surface defects and is described by Eqn (21).

The mobility and transport properties of atoms in small crystals or in clusters have not been studied so far. Nevertheless, computer simulation predicts high mobilities of the atoms and points out that a distinctive feature of the mechanism of migration is its collective character.[3, 54] This has been confirmed by the results of experimental studies of nanocrystalline powders of pure substances.[55–57] For instance, the coefficient of self-diffusion in

copper nanocrystals at 271 K is 14 to 20 orders of magnitude greater than in conventional bulk copper.[55] An analogous effect was also found in studies of bulk diffusion in nickel nanocrystals.[56]

However, one should treat the interpretation of the results obtained in studies of self-diffusion with caution. A critical analysis [58] of the experimental results obtained in a study of diffusion in Cu, TiO_2 and Pd nanocrystals [57] has shown that correct consideration of the diffusion 'suction' into the bulk of the crystal makes the coefficient of surface diffusion in Cu nanocrystals typical of polycrystalline copper rather than abnormally high. It has also been mentioned [58] that the coefficients of oxygen diffusion in TiO_2 nanocrystals are 5–6 orders of magnitude greater than in bulk crystals and that the coefficients of diffusion of the dissolved hydrogen in palladium nanocrystals are greater than in the bulk specimen.

III. Heterogeneous multicomponent solid-phase systems (composites)

Generally, a solid-phase composite is a complex, heterogeneous multicomponent system which comprises several real solid phases considered as components. By a real solid phase is meant a totality of single crystals of different sizes, which contain impurities, point lattice defects, dislocations and pores as well as free surfaces (*e.g.*, cracks, intergrain and outer boundaries). Many properties of composites depend on their morphologies, namely, the particle size distribution of each phase and mutual spatial arrangement of monophasic domains. From the standpoint of connectivity of their components, composites can be divided into (i) three-dimensional random mixtures of different phases, (ii) layered and (iii) columnar structures.[59,60] Film and porous structures can also be considered as composites. Real heterogeneous systems are usually characterised by mixed morphologies.

When studying composites, one should take into account both the properties of each individual phase and those of interphase boundaries. If different phases interact with one another, the interfaces can exhibit specific properties that are characteristic of neither of the individual phases. It is appropriate to use the thermodynamic approach to describe the properties of heterogeneous systems and find the conditions for their stability. We will restrict ourselves to consideration of two possible types of the surface interaction (a weak interaction and a strong one) between components of a simple system taking a two-phase composite as an example.

1. Interface interaction and sintering of composite

For a two-phase composite composed of macrocrystalline phases (phase 1 and phase 2) with weak interaction between them, the Gibbs energy, G, can be thought to be approximately equal to the sum of the Gibbs energies of the pure components:

$$G = G_1 + G_2 .$$

In real polycrystalline specimens, the energies G_1 and G_2 depend not only on the bulk parameters but also on a number of additional factors such as the presence of (i) dislocations and corresponding elastic strain, (ii) point defects, (iii) interfaces and outer surfaces, *etc*. Assuming that the largest contribution to the total excess Gibbs energy of the real pure components comes from their surface energies, one can write:

$$G = G_1 + G_2 + G_s = (G_1^\circ + G_2^\circ) + (G_{s1} + G_{s2}). \qquad (22)$$

Here, G_1° and G_2° are the standard Gibbs energies and G_{s1} and G_{s2} are the surface energies of the components, which are defined for each component by expression (7).

Long-term heat treatment of such a composite leads to conventional sintering accompanied by growth of crystallites of both phases and annealing of dislocations.[45] After sintering, the Gibbs energy of each phase becomes close to its bulk value, G_1° and G_2°, and the system reaches a thermodynamic equilibrium. If the mixture was mechanically treated in such a manner that the particle sizes of one or both components decreased substantially, a post-annealing phase separation will occur in the composite to give a mixture of the initial macrocrystalline phases (Fig. 3 *a*).

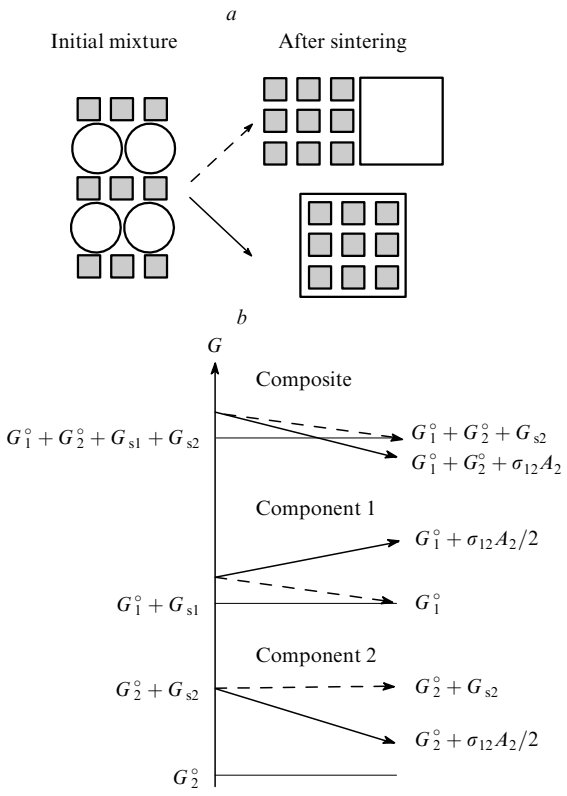

Figure 3. Schemes of sintering (*a*) and changes in the Gibbs energy of a composite (*b*) in the absence of adhesion between the components (dashed arrows) and in the case of strong adhesion (solid arrows).

Let us consider the case where the rates of recrystallisation and annealing of the component 1 are much higher than those of the component 2. The expression for the Gibbs energy of the composite annealed at the sintering temperature of the component 1 can be written in the form

$$G = G_1^\circ + G_2^\circ + \sigma_2 A_2 + \Delta G_{e2} . \qquad (23)$$

After sintering, the component 1 reaches an equilibrium state ($G_1 = G_1^\circ$), though the entire system remains thermodynamically nonequilibrium since the component 2 remains dispersed. Changes in the Gibbs energy of the composite are schematically shown in Fig. 3 *b*.

If surface interaction occurs between the constituent phases of the composite, an additional term, G_{s12}, appears in the expression for the Gibbs energy; this term represents the total change in the Gibbs energy of a heterogeneous system owing to the appearance of interphase contacts

$$G = G_1 + G_2 + G_{s12}. \qquad (24)$$

The G_{s12} is calculated as follows

$$G_{s12} = \sigma_{12} A_{12} ,$$

where σ_{12} is the specific surface energy of the interface and A_{12} is the interface area between the components 1 and 2. The contribution of the elastic strain energy should be taken into account by introducing additional terms, ΔG_{e1} and ΔG_{e2}. The total Gibbs energy of the composite with inclusion of surface interaction is

$$G = (G_1^\circ + \sigma_1 A_1 + \Delta G_{e1}) + (G_2^\circ + \sigma_2 A_2 + \Delta G_{e2}) + \sigma_{12} A_{12} . \qquad (25)$$

The expression for the Gibbs energy of the component 2 of the composite can be obtained from Eqn (25)

$$G_2 = G_2^\circ + \sigma_2 A_2 + \sigma_{12}\frac{A_{12}}{2} + \Delta G_{e2}, \quad (26)$$

assuming that the interface energy is evenly distributed between the components 1 and 2. The contribution of the elastic strain energy, ΔG_{e2}, to the total energy of the phase 2 is mainly determined by the elastic strain energy due to the crystal lattice misfit at the phase 1 – phase 2 interface and by the energy of misfit dislocations formed in the near-interface regions.[6–8] Calculations of G_e values are very complicated even for simple thin film morphology, which make estimation of this contribution in composites difficult. Nevertheless, irrespective of the character of elastic strain (a dilation or compression strain), the contribution ΔG_{e2} is always positive and should increase with an increase in A_{12}. Thus, the third and fourth terms in expression (26), which determine the energy of the phase 2, depend on the interface area in the composite.

Sintering of a mixture of a low-melting component 1 with the greater self-diffusion coefficient with nanoparticles of a high-melting compound 2 can lead to both a decrease and an increase in the interface area A_{12}. In the former case, sintering results in conventional recrystallisation of the phases. In the latter case, which is of particular interest for solid state chemistry, the formation of the interface is thermodynamically favourable if

$$\frac{dG}{dA_{12}} < 0.$$

Sintering is accompanied by an increase in the interface area A_{12}. Neglecting the dependences of the specific surface energies and elastic strain energy on the surface area (or particle size) and expressing σ_{12} in terms of the free energy of adhesion (σ_a),

$$\sigma_{12} = \sigma_1 + \sigma_2 - \sigma_a,$$

one can write

$$\frac{dG}{dA_{12}} = \sigma_1\frac{dA_1}{dA_{12}} + \sigma_2\frac{dA_2}{dA_{12}} + \sigma_1 + \sigma_2 - \sigma_a. \quad (27)$$

The formation and growth of the interface (the so-called 'sticking') have been considered in detail.[45, 61, 62] The mechanism and kinetics of 'sticking' are different in two cases defined by the conditions

$$\sigma_a < 2\sigma_1, \quad (28)$$

$$\sigma_a > 2\sigma_1. \quad (29)$$

If condition (28) is met, a 'neck' is formed between two particles of the composite. The shape and size of the 'neck' depend on the shapes and sizes of the particles and on σ_1, σ_2 and σ_a. Inequality (29) is known as the Gibbs – Smith condition for ideal wetting of films. If this condition is met, phase 1 completely covers the particle of the phase 2 after sintering.

Inequalities (28) and (29) also determine the growth mechanism of the films of the phase 1 on a support formed by the phase 2. Growth of island films according to the Volmer – Weber mechanism is observed in the former case while a steady layer-by-layer growth of films according to the Franck – van der Merve mechanism is observed in the latter case.[6, 63] The inequality (29) follows from expression (27) if

$$\frac{dG}{dA_{12}} < 0, \quad \frac{dA_1}{dA_{12}} \approx 1, \quad \frac{dA_2}{dA_{12}} = -1,$$

i.e. if a decrease in the free surface area of the component 2 (the support) leads to the formation of an equivalent free surface area of the component 1 (the film). Considering the general case of an arbitrary morphology of the initial mixture of the components 1 and 2, one can see that the newly formed free surfaces of the component 1 can overlap if the distance between the surfaces of the phase 2 is sufficiently short (see Fig. 3 *b*). Complete overlap of these free surfaces makes the derivative dA_1/dA_{12} close to zero and, assuming that the following conditions are met,

$$\frac{dG}{dA_{12}} < 0, \quad \frac{dA_1}{dA_{12}} = 0, \quad \frac{dA_2}{dA_{12}} \approx -1$$

from Eqn (27) it follows that

$$\sigma_a > \sigma_1. \quad (30)$$

This inequality determines the condition for spreading of the component 1 over the surfaces of the phase 2 in the composite. Comparison of inequalities (30) and (29) (the condition for ideal wetting or epitaxy in films) shows that the surface interaction in composites must be much stronger and requires a lower adhesion energy than in conventional film structures. It is known that roughness of a surface improves its wetting and that the roughness factor can vary between 0 and 1. Inequality (30) corresponds to the limiting case where the coefficient of roughness of the surface of the phase 2 is equal to unity.

If condition (29) or (30) is met, a spontaneous increase in the interface area or 'wetting' of the well-developed surface of the component 2 with the component 1 occurs in the system. If compound 2 is in the nanocrystalline state, the effective particle size of the phase 1 can be substantially reduced. In other words, an unusual effect, *viz.*, self-dispersion of the component 1 to give a two-phase nanocomposite, will be observed. Self-dispersion is an indicator of a strong interface interaction in the system. This interaction will occur during the long-term sintering of the composite until the entire surface of the component 2 will be covered with the component 1. In this limiting case, $A_{12} \approx A_2$ and the system reaches the state of metastable equilibrium, where

$$G = (G_1^\circ + G_2^\circ) + \sigma_{12} A_2 + (\Delta G_{e1} + \Delta G_{e2}), \quad (31)$$

$$G_1 = G_1^\circ + \sigma_{12}\frac{A_2}{2} + \Delta G_{e1}(A_2). \quad (32)$$

The effect of self-dispersion was experimentally observed in, *e.g.*, solid-phase sintering of composites $AgCl - Al_2O_3$ (see Ref. 64), $AgI - Al_2O_3$ (see Ref. 65) and $Li_2SO_4 - Al_2O_3$ (see Ref. 66). An analogous effect was detected in the heterogeneous systems based on alkali nitrates and halides such as $LiNO_3 - Al_2O_3$ and $NaNO_3 - Al_2O_3$ (see Ref. 67), $RbNO_3 - Al_2O_3$ and $CsNO_3 - Al_2O_3$ (see Ref. 68), $NaCl - Al_2O_3$, $KCl - Al_2O_3$ and $RbCl - Al_2O_3$ (see Ref. 53). This is indicative of strong adhesion of ionic salts to the alumina surface.

Analysis of expression (32) shows that the properties of an ionic salt depend not only on the standard thermodynamic parameters of the material, but also on the contribution of the energy of interface interaction, which increases as the oxide surface area increases. If the components are taken in a 50 : 50 (vol.%) ratio and mixed uniformly and an ideal wetting of the entire surface of the oxide with the MX component is achieved, the effective MX grain size is nearly equal to half the particle size of the oxide. In the composites with nanoscale oxide particles ($\sim$10 nm), the size of the MX particles becomes sufficiently small to provide noticeable size effects.

2. Adhesion energy and formation of point defects at the interface

Stable interphase contacts require that the energy of adhesion be sufficiently high. Generally, the mechanism of adhesion depends on the character and strength of the interaction between the atoms arranged on the contacting surfaces. The authors of classical monographs on adhesion [69–71] have studied the systems in which the major contribution to the surface interaction comes from the dispersion forces. In this case, the energy of adhesion can be calculated using the Hamaker – de Buhr theory

$$\sigma_a = 2(\sigma_{d1}\sigma_{d2})^{1/2} + \sigma'_{12}, \quad (33)$$

where σ_{d1} and σ_{d2} are the contributions of the dispersion forces to the surface energies of the components 1 and 2, respectively, and the last term includes the contributions of the non-dispersion interactions, *viz*., the ion–ion, donor–acceptor, dipole–dipole interaction, *etc*. In composites of the ionic salt–oxide type, it is the last term of expression (33) that makes the largest contribution to the energy of adhesion. In the absence of the electrical double layers, the σ_a value can be approximately estimated using the model of 'weak boundary layers',[72] according to which the work of adhesion is equal to the geometric mean of the works of cohesion of the components

$$\sigma_a \approx (W_1 W_2)^{1/2} = 2(\sigma_1 \sigma_2)^{1/2}. \quad (34)$$

From relationships (34), (29) and (30) it follows that self-dispersion should occur if $\sigma_2 > \sigma_1$ and be enhanced with a decrease in σ_1. Among alkali halides, lithium salts are characterised by the highest specific surface energies σ, while cesium salts are characterised by the lowest ones, the σ values being monotonically decreased on going from fluorides to iodides.[29] Therefore, self-dispersion should proceed most easily in the composites based on cesium iodide and have the lowest rate in the systems based on lithium fluoride. However, it was noted [70] that the model of 'weak boundary layers' [72] does not take into consideration specific characteristics of the interface in composites (its morphology and the presence of surface-active centres), which prevents a correct separation of the contributions of different types of interactions to the surface energies of the components, and does not assume the formation of the double surface layers.[72] Therefore, this model allows only qualitative estimation. To carry out more reliable calculations, one should take into account the structure of the contact surface and the potentials of the ion–ion interactions at the ionic crystal–oxide interface, which represents an extremely complicated problem that has not been solved so far. Approximate estimates of the surface energy using the Harkins 'broken bond' method have shown [13, 69, 73] that σ increases in proportion to the crystal lattice energy for isostructural compounds, the coefficient of proportionality being dependent on the type of the corresponding crystallographic plane. Comparison of the σ values for alkali halides [29] with the corresponding values for oxides Al_2O_3, FeO, MgO and SiO_2 (100–300 and 600–1200 erg cm^{-2}, respectively) [13, 69] shows that the wetting condition (30) should be met for the composites based on ionic halides and high-melting oxides including alumina.

Physically, a tendency of the components of composites of the ionic salt–oxide type to decrease the surface energy owing to the ion–ion interaction at the interface is the reason for rerrangement of surface layers. To a first approximation, the MX–A interface energy (MX is the ionic salt and A = Al_2O_3)

$$G^s_{MX-A} = \sigma_{MX-A} A_{MX-A} \approx \approx E_{M-Al} + E_{Al-X} + E_{M-O} + E_{X-O} \quad (35)$$

is determined by the sum of the energies of the cation–cation ($M^+ - Al^{3+}$), cation–anion ($Al^{3+} - X^-$ and $M^+ - O^{2-}$) and anion–anion ($X^- - O^{2-}$) interactions. For the sake of simplicity, let us assume that strong interfacial interaction provides a structural correspondence between the crystal lattices of the MX and A phases. Since the energies E_{M-Al}, E_{X-Al}, E_{M-O} and E_{X-O} differ from one another, an ideal structure of the boundary layer of each phase will be distorted to provide an additional gain in the surface energy owing to the mutual approach (or removal) of different surface ions. The magnitudes of the displacements of the ions from ideal positions are determined by the balance of energies E_i. Since the sizes of the anions of alumina and most of MX salts are larger than those of the cations, one can expect that, provided that both contacting phases are close-packed, the cations at the interface are displaced to longer distances than anions. As a result, an intermediate, positively charged layer enriched with cations is formed between the surface layers of the components (Fig. 4) and

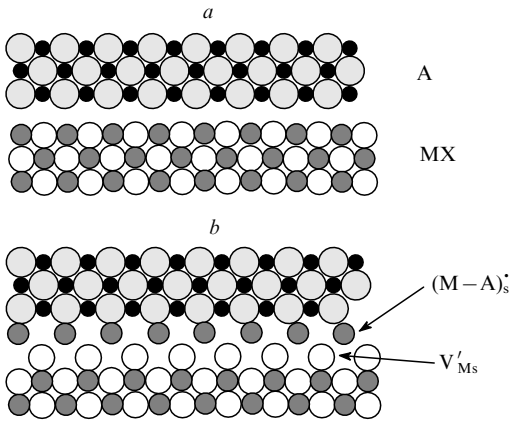

Figure 4. A scheme for the formation of defects at the interface between two binary ionic compounds.
Initial surfaces (*a*) and interface (*b*).

a layer of cationic vacancies (V'_{Ms}). Such a structural relaxation can be represented as the following quasichemical reactions:

$$0 \rightleftarrows V'_{Ms} + (M-A)_s^{\bullet}, \quad (36)$$

$$0 \rightleftarrows V'''_{Al} + (Al-MX)_s^{\bullet\bullet\bullet}, \quad (37)$$

which describe the surface disordering in MX (36) and Al_2O_3 (37) at the MX–A interface. In addition to reaction (36), interstitial cations also can be transferred into the space charge layer [48, 74]

$$M_i^{\bullet} \rightleftarrows (M-A)_s^{\bullet}. \quad (38)$$

The formation of surface defects at the MX–A interface can also proceed by other mechanisms. If the energy of the interaction between aluminum cations and X anions is sufficiently high, the following reactions can proceed at the interface:[75]

$$0 \rightleftarrows V_X^{\bullet} + (X-A)'_s, \quad (39)$$

$$0 \rightleftarrows M_i^{\bullet} + (X-A)'_s. \quad (40)$$

Reaction (39) is analogous to reaction (36) except that the role of cations is played by the anions; this can occur in composites based on fluorides, *e.g*., PbF_2–A (A = CeO_2, ZrO_2, SiO_2, Al_2O_3).[75] Reaction (40) can be observed in $AgF-Al_2O_3$ composites. Since the binding energy of Al–X dramatically decreases on going from fluoride anions to other halide anions, the reactions (39) and (40) in $MX-Al_2O_3$ systems are unlikely. More probable is the reaction

$$0 \rightleftarrows X'_i + (M-A)_s^{\bullet}, \quad (41)$$

which can occur in the salt-based MF_2-SrCl_2 composites with the anti-Frenkel defects.

Shukla *et al*.[75] proposed to use the pE value of the isoelectric point of an oxide as an indicator of the surface activity of the oxide. Indeed, equations analogous to Eqns (36) and (39) can also be written for the surface interaction of an oxide with water

$$H_2O \rightleftarrows OH' + (H-A)_s^{\bullet}, \quad (42)$$

$$2H_2O \rightleftarrows H_3O^{\bullet} + (OH-A)'_s, \quad (43)$$

The former reaction dominates for oxides with p$E > 7$ (*e.g*., Al_2O_3, CeO_2) and the latter is predominant for oxides with p$E < 7$ (ZrO_2, SiO_2). By analogy with aqueous solutions one can expect that the surface reactions (36), (38) and (41) are typical of composites with basic oxides (p$E > 7$), while reactions (39) and (40) are typical of acid oxides (p$E < 7$). Currently, the lack of experimental data makes it impossible to assess the transferability of the model of acid-base equilibria in aqueous solutions to

composites. Nevertheless, the competition between the processes (36) and (42)

$$V'_M + (M-A)^{\bullet}_s + H_2O \rightleftarrows OH' + (H-A)^{\bullet}_s + M^*_M , \qquad (44)$$

where M^*_M is a cation with a zero effective charge, can be responsible for deterioration of the ionic conductivity of the composites $AgCl-Al_2O_3$ (see Ref. 64) and $AgI-Al_2O_3$ (see Ref. 65) and for the appearance of protonic conductivity in the composites $Li_2SO_4-Al_2O_3$ (see Ref. 76) and $M(NO_3)_n-Al_2O_3$ (see Refs 77 and 78) in a humid atmosphere.

3. Ionic conductivity of composites

In essence, reactions (36)–(41) represent the formation of an electrical double layer at the $MX-Al_2O_3$ interface. The formation of this layer affects the properties of the oxide; *e.g.*, a decrease in the Néel temperature of iron(III) oxide was observed in $AgI-Fe_2O_3$ composites.[79] The effect of the electrical double layer on the properties of the ionic salt is even more pronounced. A change in the energy upon the displacement of the ion from its normal (equilibrium) position characteristic of isolated MX crystal to the space charge layer (Δg_{i-A}) can be considered as the work of charging of the surface; therefore, Δg_{i-A} is related to the surface potential at the MX–A interface

$$\varphi_{As} \sim \frac{\Delta g_{i-A}}{q_i} , \qquad (45)$$

where q_i is the charge of the displaced ion. The exact φ_{As} value is determined not only by the Δg_{i-A} value, but also by the contribution of the spatial relaxation of the oxide ions; therefore, relationship (45) should be considered only as a correlation between Δg_{i-A} and φ_{As}. If adhesive binding is strong, the Δg_{i-A} value is always negative; hence

$$\varphi_{As} > 0 \text{ for } q_i < 0$$

and

$$\varphi_{As} < 0 \text{ for } q_i > 0.$$

For $T = 0$, there is a dense layer on the surface of the MX particle contacting the oxide. This layer is analogous to the Helmholtz layer. An increase in temperature leads to the formation of a diffusion space charge layer built of cationic vacancies, which is responsible for enhanced conductivity of the composite since the ion mobility in the dense layer is low. The mobilities of defects in the diffusion layer are taken to be equal to their mobilities in the bulk of the crystal[48,74] since the concentration of defects in this layer is low and the crystal structure remains unchanged (no deformations, surface phase transitions, *etc.*). In this case, the conductivity of the composite is given by expression (21) with φ_{As} introduced instead of φ_s and the migration energy E_m corresponding to those defects which form the diffusion layer; for the sake of simplicity, the entropy contribution to φ_{As} is taken as zero. For low potential φ_{As}, which corresponds to a relatively weak surface interaction, the conductivity is low and the activation energy of conductivity is

$$E_a = \frac{h_0}{4} - \frac{e\varphi_{As}}{2} + E_m .$$

Here, E_a ranges from $h_0/4 + E_m - e\varphi_{As}/2$ to $h_0/4 + E_m$ and depends on the state of the MX–A interface (on the presence of structural defects, adsorbed impurities, *etc.*). Therefore, the conductivity parameters measured in the experiments are poorly reproducible, which is sometimes observed in poorly sintered composites.

If the surface potential φ_{As} is high, the energy of adhesion is rather high, which favours the formation of a dense interphase contact and a substantial increase in the charge density in the diffusion layer. As φ_{As} increases, the concentration of surface defects increases and at a surface potential equal to

$$\varphi_{As} = \frac{h_0}{2e} , \qquad (46)$$

a full coverage of the surface with the similarly charged ions or defects is attained. If $e\varphi_{As} > h_0/2$, several layers of similarly charged ions should be on the surface, which is unlikely. Thus, the condition (46) determines the maximum value of the surface potential $e\varphi_{As}$ in a composite.[53] In composites with high surface potential, the concentration of surface defects is close to the limiting value. In this case, the conductivity and activation energy of conductivity are given by the relationships

$$\varkappa = \frac{A}{L} T^{-1/2} \exp\left(-\frac{E_m}{kT}\right),$$
$$E_a = E_m . \qquad (47)$$

The results obtained using these expressions are in good agreement with the experimental data for composite systems $AgCl-Al_2O_3$, $AgBr-Al_2O_3$, $TlCl-Al_2O_3$ and $LiI-Al_2O_3$.[48]

Certain new factors affecting the transport properties of ionic salts appear on going to nanoscale systems. The assumption of constant mobilities of defects within the diffusion layer and in the bulk of the crystal is acceptable if the thickness of the space charge region, $2\lambda_D$, does not exceed the size of the MX crystal. It is reasonable to assume that the mobilities of defects within the diffusion layer of the crystal depend on the position of the defect owing to the drag effect of the ion 'atmosphere'. Near the MX–A interface, the defect mobility is low; it gradually increases with distance from the surface and reaches a maximum deep in the interior of the crystal. Size reduction of the MX crystal (this can be achieved by increasing the concentration of A) leads to a decrease in the defect mobilities and to an increase in the activation energy of conductivity, which is equal to the migration energy of the defect. This effect is noticeable if the crystal size L is less than $2\lambda_D$. In fact, the activation energy of conductivity in $AgI-Al_2O_3$ nanocomposites monotonically increases as the oxide concentration increases.[65]

If $L < \lambda_D$, the total concentration of defects in the bulk of the crystal becomes high. The defect–defect interactions in crystals can lead to phase transitions into the superionic state.[80–82] It cannot be ruled out that the superionic phases can be formed in the near-surface region of the crystal. The formation of the superionic phase on the surface of the pure ionic crystal has been reported;[83] in composites, this seems to be even more probable.

If the concentration of defects, n, is temperature-independent, the expression for conductivity has the form

$$\varkappa = n\left(\frac{e^2 a^2 v_0}{6kT}\right)\exp\left(\frac{S_m}{k}\right)\exp\left(-\frac{E_m}{kT}\right), \qquad (48)$$

where a is the jump length of the defect, v_0 is the vibrational frequency of the mobile ion and S_m is the entropy of migration, which can be calculated using the formula for the compensation effect

$$S_m = \frac{E_m}{T^*} ,$$

observed in alkali halide crystals. In this case, $T^* = 2.1 \times 10^3$ K.[84] The formula given below[85] relates the conductivity of the composite at 25 °C to the activation energy of conductivity and to the concentration of defects in the MX particles; it includes the compensation effect and uses two empirical parameters, $a = 0.3$ nm and $v_0 = 3 \times 10^{-12}$ s^{-1}, typical of ionic crystals,

$$\log \varkappa_{25}\,(\text{S cm}^{-1}) = \log n\,(\text{cm}^{-3}) - 14.5\,E_a\,(\text{eV}) - 20.55. \qquad (49)$$

Figure 5 presents the experimental data for different composites. The straight lines were plotted using Eqn (49) with different defect concentrations. The experimental data for a number of superionic conductors are also shown in Fig. 5. As can be seen, the

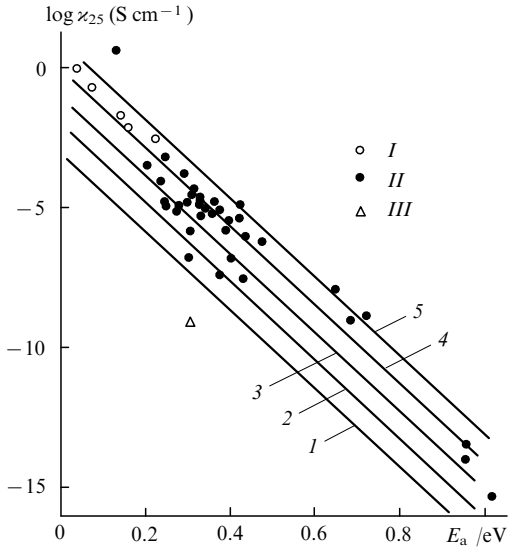

Figure 5. Theoretical (straight lines) and experimental (points) dependences of the conductivity of superionic conductors (*I*), composites (*II*) and AgCl single crystal (*III*) at 25 °C on the activation energy for conductivity at different concentrations of defects: 10^{17} (*1*), 10^{18} (*2*), 10^{19} (*3*), 10^{21} (*4*) and 10^{22} cm^{-3} (*5*).[85]

concentration of defects in the composites with the highest conductivity is also high and close to the corresponding values for superionic conductors. This indicates the possibility of stabilisation of disordered phases in composites.

4. Size effects in heterophasic systems

In studies of thin films it has been shown that the structures of solids in the near-interface regions depend strongly on peculiarities of the morphology and energetics of the contacting planes. As a rule, the epitaxial interphase contact is the most energetically favourable. In the case of strong adhesive binding, building up the layer of phase 2 on a support proceeds by the van der Merve mechanism. Owing to the crystal lattice misfit between the adjacent phases, elastic strain is accumulated in the bulk of the component 2 (the elastic strain energy increases as the thickness of the layer of phase 2 increases).[6, 86, 87] According to calculations,[88] the continuous layer is destroyed after reaching a certain critical thickness h_c and a network of misfit dislocations is formed at the interface. If the lattice misfit parameter lies between 0.1% and 1%, the calculated thickness of the epitaxial layer, h_c, is $\sim$5–25 nm (see Ref. 88), which is consistent with the experimental data. If the rate of film precipitation is high, thin films with an amorphous structure are deposited on the support instead of the epitaxial layer. As the temperature or the thickness of the layer increases, the amorphous phase undergoes transformation into a crystalline film.[7] The formation of thin epitaxial or amorphous films can be considered as manifestation of the phase size effect in heterogeneous systems, *viz*., the reduction of the characteristic size (film thickness) leads to the formation of new surface phases.

In composites, the role of the thickness of the epitaxial layer is played by the average distance between the grains of the inert component 2 (r_{22}). At low concentrations of the phase 2, the distance between the grains of this phase exceeds h_c and the properties of the phase 1 are similar to those of the island thick films oriented parallel to the faces that confine the intergrain space. On the contrary, at high concentrations of the component 2, the phase 1 is distributed in the micropores of the phase 2 after sintering. In this case, if the grain size of the phase 2 is sufficiently small (less than 10 nm), one gets $r_{22} < h_c$ and the phase 1 occurs in the form of a thin layer or a surface phase. Since the properties of substances in the surface phase differ substantially from the bulk properties of the same substance, two phases can coexist in composites, *viz*, the surface phase with anomalous properties and a conventional bulk polycrystalline phase with a high concentration of dislocations.

Thermodynamic properties of substances coated on solid supports in the form of adsorbed layers or thin films differ from their bulk properties.[2–7, 18, 19, 89] Noticeable distinctions between the thermodynamic properties appear at a characteristic crystal size of $\sim$10 nm.[2–7] Changes in the temperatures of phase transitions that occur in the bulk of the component 1 can be estimated using the formula

$$\frac{T_t}{T_t^0} = 1 - \left(\sigma_{\alpha 1}A_{\alpha 1} + \sigma_{\beta 1}A_{\beta 1} + \frac{\sigma_{\alpha 12}A_{\alpha 12} - \sigma_{\beta 12}A_{\beta 12}}{2} + \Delta G_e\right)H_t^{-1}, \quad (50)$$

where the subscripts α and β correspond to the α- and β-phases at temperature T_t, respectively, and ΔG_e is the excess elastic strain energy difference between these phases. If the changes in the volume and ΔG_e upon the phase transition are small ($A_{\alpha 1} \approx A_{\beta 1} \sim L^{-1}$; $A_{\alpha 12} \sim A_{\beta 12} \sim L^{-1}$; $\Delta G_e \approx 0$), the temperature of the phase transition into the α-phase decreases, which is usually observed in thin films. Some examples of the phase diagrams constructed in the coordinates T_t–(T, L^{-1}) for different supported metal films are available in the literature (see Refs 6–8, 18, 19). According to these phase diagrams, transition temperatures can decrease by hundreds of degrees upon reduction of L to 10 nm.[6, 7] Generally, the temperatures of phase transitions in composites can either decrease or increase depending on the particular form of the functions $G^\circ = f(T)$, $\sigma = f(T)$ and $\Delta G_e = f(T)$ for a given component in different phases.

The results of studies on the physicochemical properties of composites $AgI-Al_2O_3$ (see Refs 65, 90–94), $Li_2SO_4-Al_2O_3$ (see Ref. 66), $LiNO_3-Al_2O_3$, $NaNO_3-Al_2O_3$, $KNO_3-Al_2O_3$ (see Ref. 67), $RbNO_3-Al_2O_3$ (see Refs 68 and 95), $CsNO_3-Al_2O_3$ (see Ref. 68), $CsHSO_4-SiO_2$ (see Refs 96 and 97), $CsCl-Al_2O_3$ (see Ref. 98) with the specific surface area of Al_2O_3 particles, s, of 270 m^2 g^{-1} show that nanocomposites prepared by self-dispersion technique exhibit unusual structural, thermodynamic and transport properties. Thermodynamic calculations for all the above-mentioned systems showed that bulk chemical interaction at the temperatures of synthesis of nanocomposites is thermodynamically unfavourable. This is also confirmed by the results of special experiments on the sintering of the initial mixtures under 'severe' conditions (high temperatures and long-term heat treatment).

Thermodynamic properties of silver iodide in $(1-x)AgI-xAl_2O_3$ nanocomposites differ substantially from those of pure AgI. This can be illustrated by nearly complete absence of the thermal effect at 147 °C upon the phase transition into the α-phase of AgI in the nanocomposite with high Al_2O_3 concentrations ($x > 0.8$). Presumably, the superionic α-phase is stabilised in the composite; however, the absence of AgI reflections in the X-ray diffraction patterns (including those typical of the α-phase) suggests that silver iodide is in the amorphous state. This is also confirmed by the absence of a thermal effect at the melting transition in AgI (see Ref. 93) and by the unusual luminescence spectra observed upon UV irradiation of the nanocomposite.[94] More detailed studies have shown that an increase in the Al_2O_3 content in the composite leads to a gradual change in the properties of silver iodide. Namely, two phase transitions are observed instead of one $\alpha \rightarrow \beta$ transition, which gradually disappear as x increases. Both transitions are characterised by distinct hysteresis loops on the plots of the temperature dependences of conductivity and heat capacity, the temperature of the high-temperature phase transition depends slightly on x, while the temperature of the low-temperature phase transition decreases appreciably as the mole fraction of Al_2O_3 increases (see Refs 92 and 93).

This suggests that silver iodide can occur in two crystalline states during sintering of the composites under study. These are

the bulk state with the properties of pure AgI and the surface state localised at the $AgI-Al_2O_3$ interface. The properties of the latter are affected by the interfacial interaction. Like the bulk state, the surface crystalline state can be in the high-temperature and low-temperature disordered phases. As the Al_2O_3 content increases, the effective intercrystallite distance in the oxide (and the effective particle size of AgI) decreases and the conductivities of both phases approach each other, thus indicating a gradual levelling of distinctions between the phases.

In addition to this effect, the increase in the concentration of Al_2O_3 leads to a dramatic decrease in the enthalpies of melting and $\beta \rightarrow \alpha$ phase transition in AgI, which points to the appearance of the interface amorphous AgI phase in the composites (Fig. 6). At sufficiently high concentration of alumina, nearly all the silver iodide can be stabilised in the interface amorphous state.[91,93,94] It was shown that doping of AgI with Al_2O_3 leads to a decrease in the temperature and enthalpy of the phase transition in AgI.[99,100] This is in excellent agreement with the results of our investigations of composites with low Al_2O_3 content. However, the authors of the papers cited (*cf.* Refs 99 and 100) have observed only minor changes in the transition temperature and enthalpy, since the heterogeneous additive used in their experiments was a relatively coarse-grained (0.06 μm) Al_2O_3. The use of alumina with a grain size of 0.01 μm allowed us to observe much more pronounced effects.

Composites $MNO_3-Al_2O_3$ (M is an alkali metal) (see Refs 67, 68, 95) and the $CsHSO_4-SiO_2$ system[96,97] behave analogously. DTA studies of composites $(1-x)RbNO_3-xAl_2O_3$ have shown[95] that all the phase transition temperatures of $RbNO_3$ including the melting temperature remain virtually unchanged upon sintering, whereas the enthalpies of the phase transitions decrease dramatically. For $x \geqslant 0.7$, the DTA curves exhibit no peaks indicating the presence of crystalline $RbNO_3$ in the composite (Fig. 7). Instead, a weak broad peak appears near 250 °C with the maximum intensity for $0.4 < x < 0.6$.

These effects are not observed in the composites containing coarse-grained Al_2O_3 (with grain sizes of several micrometres),

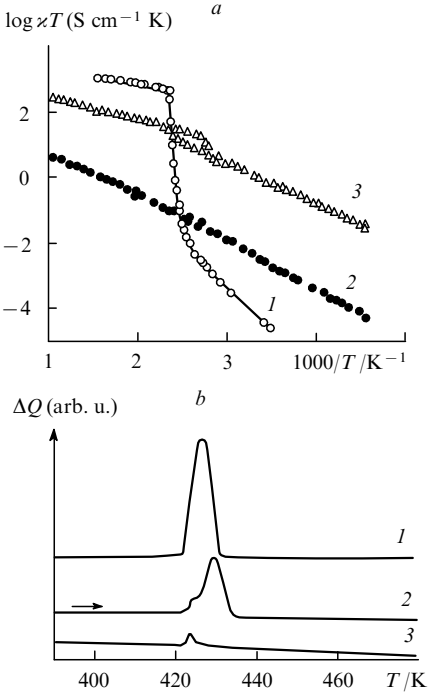

Figure 6. Temperature dependences of conductivity (*a*) and DTA curves (*b*) for pure AgI and the $(1-x)AgI-xAl_2O_3$ composites.[93]
AgI (*1*), $x = 0.6$ (*2*), $x = 0.8$ (*3*).

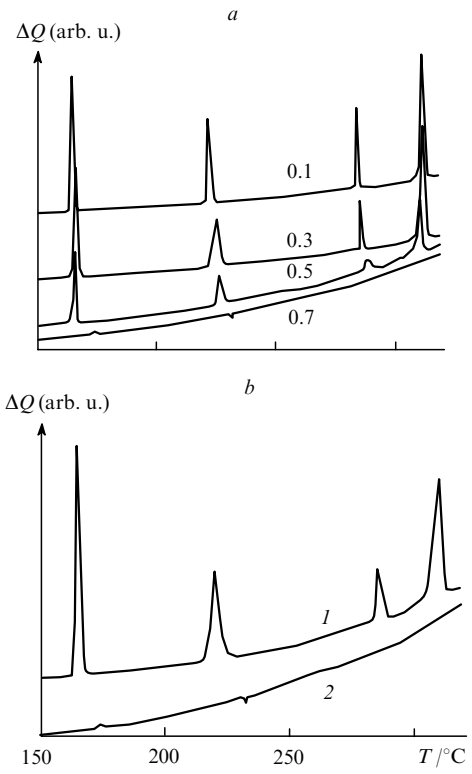

Figure 7. DTA curves for the $(1-x)RbNO_3-xAl_2O_3$ composites with a specific surface area of 270 $m^2\ g^{-1}$ (*a*) and for the $0.7\ RbNO_3-0.3\ Al_2O_3$ composites (*b*) with a specific surface area of 10 (*1*) and 270 $m^2\ g^{-1}$ (*2*). Figures near the curves shown in Fig. 7 *a* represent *x* values.[95]

which means that they are due to the influence of the oxide grain surface. Electron diffraction studies and conductivity measurements revealed the formation of an amorphous phase of $RbNO_3$ in the $RbNO_3-Al_2O_3$ composites. The thermal effect at 250 °C is due to the glass transition in the amorphous phase and the transition temperature is much higher than the calculated value (−55 °C).[101] However, it should be taken into account that in this case the amorphous $RbNO_3$ phase is formed at the $RbNO_3-Al_2O_3$ interface and its properties can be very different from those of pure amorphous rubidium nitrate. The results of thermodynamic studies of $RbNO_3-Al_2O_3$ composites are consistent with those obtained by the ionic conductivity measurements, Raman spectroscopy and X-ray diffraction analysis.[95]

The concentration and thickness of the interface phase in composites can be estimated using a simple brick-wall model for cubic particles.[85,93,95] The model is based on the assumption that the brick size is equal to the particle size of the dispersed additive (L_A) and uses the following formulae for the calculation of the volume fraction, f_s, or the mole fraction, x_s, of the interface phase

$$f_s = \beta \frac{2\lambda}{L_A} f(1-f), \tag{51}$$

$$x_s = \beta \frac{2\lambda}{L_A} \frac{\gamma x(1-x)}{1+x(\gamma-1)}, \tag{52}$$

where β is the geometric factor, λ is the thickness of the surface layer, f and x are the volume fraction and molar concentration of the dispersed phase 2 (the oxide A), respectively, and the coefficient γ depends on the densities (d) and molecular masses (μ) of the components and is defined as follows

$$\gamma = \frac{\mu_A d_1}{\mu_1 d_A}.$$

The fraction of the ionic salt (f_1 or x_1) that remained in the bulk phase can be calculated using the expressions

$$f_1 = 1 - f - f_s = \left(1 - f\beta\frac{2\lambda}{L_A}\right)(1-f), \quad (53)$$

$$x_1 = 1 - x - x_s = 1 - x - \beta\frac{2\lambda}{L_A}\frac{\gamma x(1-x)}{1+x(\gamma-1)}. \quad (54)$$

These formulae are convenient for estimating the thickness of the interface phase provided that the particle size of the dispersed component, L_A, is known. The ratio λ/L_A and the thickness of the interface phase, λ, can be estimated from the concentration dependence of any extensive characteristic of the phase 1 in the composite using expressions (53) or (54) (Fig. 8). According to calculations, the amorphous layer in $AgI-Al_2O_3$ and $RbNO_3-Al_2O_3$ composites is respectively 3 [93] and 4 nm [95] thick.

Studies of the conductivity of the nitrate-based composites revealed a substantial increase in the low-temperature conductivities and disappearance of the conductivity jumps observed upon phase transitions. Note that the Arrhenius plots of the temperature dependences of conductivity are nonlinear (Fig. 9). Among the composites based on alkali nitrates, the greatest increase in conductivity is observed for the $LiNO_3$-based ones. At 100 °C, the conductivity of the composite $0.5\,LiNO_3-0.5\,Al_2O_3$ is 7 orders of magnitude higher than that of pure lithium nitrate.[67] The smallest increase in conductivity is observed for the $CsNO_3-Al_2O_3$ system.[68] Similar effects were also found in $CsHSO_4-SiO_2$ composites.[96,97] Here, the physicochemical characteristics of cesium hydrosulfate depend on the pore size of silica gel used as a dispersed additive, that is, there is an optimum pore size ($\sim$2 nm) at which the thermodynamic, structural and transport properties of $CsHSO_4$ change to the greatest extent.[97]

Physicochemical properties of lithium sulfate change substantially on going from the bulk crystal to $(1-x)Li_2SO_4-xAl_2O_3$ nanocomposites.[66,85] The low-temperature ionic conductivity of the composite substantially increases while the well-defined (for pure Li_2SO_4) phase transition becomes diffuse in the composite (Fig. 10). The results of DTA studies of these composites showed that lithium sulfate occurs in two states at low oxide concentrations. One state exhibits the properties of the initial Li_2SO_4 while the other state possesses the properties of the phase localised near the $Li_2SO_4-\gamma$-Al_2O_3 interface. If the content of Al_2O_3 additive, x, exceeds 0.5, virtually the whole lithium sulfate is stabilised in the interface phase after sintering. In composites with the oxide particle size of the order of several nanometres the concentration of the interface phase is very low and no additional thermal effect is observed. Compared to the pure substance, the phase transition in the interface phase of Li_2SO_4 occurs at a much lower temperature (470 °C).

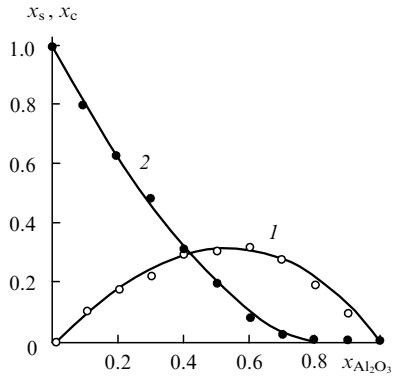

Figure 8. Dependences of the mole fraction of the interface amorphous phase (x_s) (curve *1*) and crystalline phase (x_c) (curve *2*) of AgI on the Al_2O_3 content in the $AgI-Al_2O_3$ composites according to DSC measurements of the enthalpy of the $\alpha-\beta$ phase transition in AgI. Solid lines represent the results of calculations with $\lambda \approx 4$ nm and $L_A \approx 10$ nm.[93]

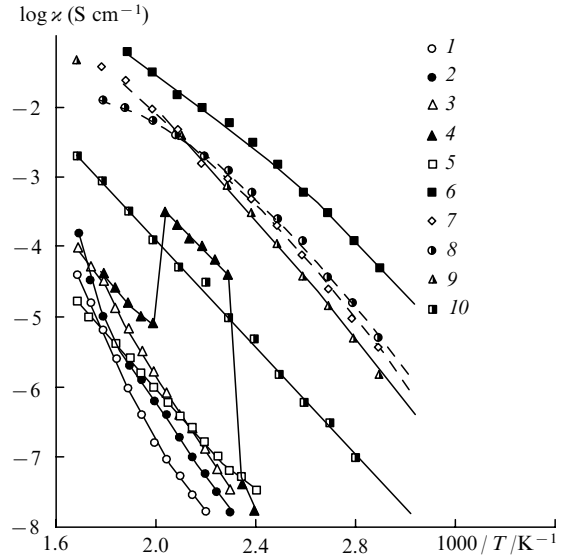

Figure 9. Temperature dependences of conductivities of nitrates MNO_3 (*1–5*) and composites $0.5MNO_3-0.5Al_2O_3$ (*6–10*); M = Li (*1*, *6*), Na (*2*, *7*), K (*3*, *8*), Rb (*4*, *9*) and Cs (*5*, *10*).[67,68]

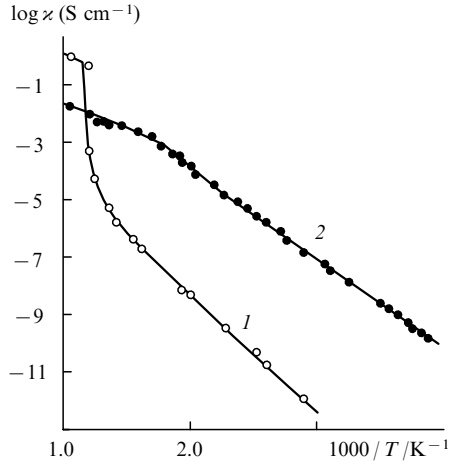

Figure 10. Temperature dependences of the ionic conductivities of pure Li_2SO_4 (*1*) and the $(1-x)Li_2SO_4-xAl_2O_3$ nanocomposite (*2*).[66]

In this case, the mechanism of adhesion involves a stage of surface chemical reaction between Li_2SO_4 and Al_2O_3 resulting in the formation of a thin interface lithium aluminate layer. The thickness of this layer was estimated at 1–2 monolayers on the surface of the Al_2O_3 grains. Analysis of the X-ray and electron diffraction patterns of the nanocomposite points to epitaxial character of the lithium sulfate layers, which is due to the close (111) interplanar spacing in Li_2SO_4 and Al_2O_3 and to strong adhesion of Li_2SO_4 to the alumina surface. Lithium aluminate forms an intermediate layer and represents a specific 'glue', which provides a denser epitaxial contact between the Li_2SO_4 and Al_2O_3 nanocrystals.

The nanocomposite $0.33\,Li_2SO_4-0.67\,Al_2O_3$ can be prepared in two ways, *viz.*, by sintering of the starting materials and by decomposition of the precursor, $Li_2SO_4 \cdot 4\,Al(OH)_3 \cdot mH_2O$.[85] The second method allows one to synthesise a nanocomposite with uniform distribution of the components and an average particle size of less than 10 nm for both Li_2SO_4 and Al_2O_3 (Fig. 11). If the alumina particles are uniform in size, both synthetic procedures

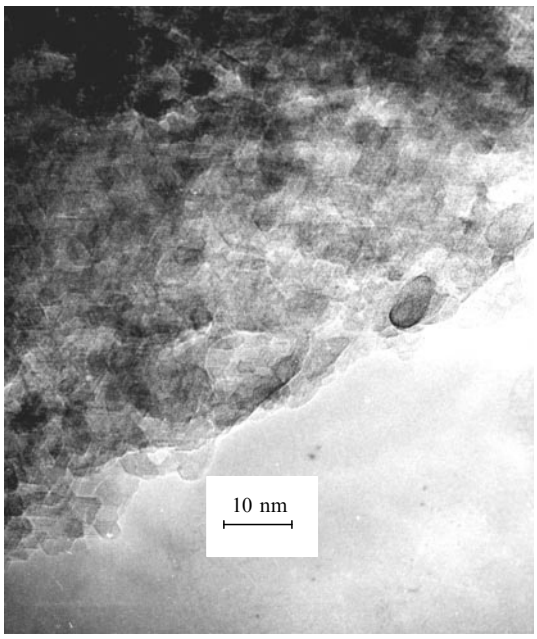

Figure 11. Morphology of the $Li_2SO_4-Al_2O_3$ nanocomposite obtained by thermal decomposition of its precursor, $Li_2SO_4 \cdot 2Al(OH)_3 \cdot mH_2O$.[66]

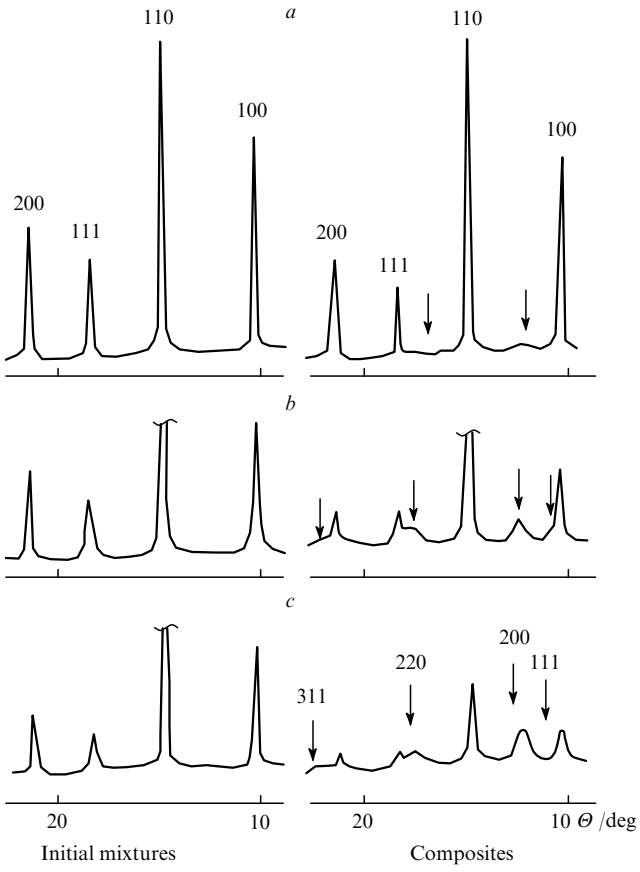

Figure 12. X-Ray diffraction patterns of the initial mixtures and $(1-x)CsCl-xAl_2O_3$ composites after long-term sintering at 600 °C. Arrows denote the reflections corresponding to the fcc phase of CsCl, figures denote the crystallographic plane indices.
$x = 0.3$ (*a*), 0.6 (*b*), 0.8 (*c*).

result in the formation of nanocomposites with identical structural, transport and thermodynamic characteristics after sufficiently long-term heat treatment of the mixtures. This indicates that the composites reached metastable thermodynamic equilibrium. Decomposition of precursors, $Li_nX \cdot 2nAl(OH)_3 \cdot mH_2O$, allows the preparation of nanocomposites with different lithium salts Li_nX (X = F, Cl, Br, I, SO_4, PO_4); these systems exhibit high ionic conductivities.[85]

X-Ray diffraction and DTA studies of $(1-x)CsCl-xAl_2O_3$ composites (with Al_2O_3 with a specific surface area, σ, of 270 $m^2\ g^{-1}$) showed that long-term sintering leads to stabilisation of a high-temperature CsCl phase localised at the interface (Fig. 12).[53,98] No changes are observed in the X-ray diffraction patterns as the particle size of Al_2O_3 increased up to ~ 1 μm; this is in agreement with the known results.[102] The size effect, *i.e.*, stabilisation of the high-temperature CsCl phase, seems to be due to the interface interaction, which is most pronounced in the composites with nanocrystalline additives.

In the ionic salt – Al_2O_3 systems, lithium salts form nanocomposites somewhat more easily than rubidium and cesium salts and iodides form nanocomposites more easily than chlorides or fluorides. This points to important role of the polarising power of the cation and the polarisability of the anion in the mechanism of surface interaction.

IV. Mechanochemical synthesis of nanocomposites and nanoparticles

Mechanochemical processes proceed at low temperatures where the formation of a perfect crystal structure is difficult. Therefore, the use of mechanochemistry for the synthesis of metastable products, in particular, nanoparticles and nanocomposites, is of considerable interest.[103–109] Mechanochemical methods for the preparation of nanocrystalline materials have been intensively developed recently [105–108] and investigations into the fundamental problems associated with the formation, relaxation and stabilisation of metastable states during mechanical activation seem to be of great importance.

1. Mechanical action on a solid and the formation of nanoscale systems

Mechanical action leads to the development of elastic stress in the crystal. For different reasons (crystal lattice anisotropy, specific features of electronic and ionic properties, different energies of chemical bonds), elastic stress relaxation can follow different mechanisms such as vibrational and electronic excitations, ionisation of chemical bonds, bond cleavage, rearrangements of atoms and migration of atoms and ions.[109] By varying the intensity and character of mechanical action one can control the properties of materials obtained by mechanical activation.[104]

One of the most often encountered effects accompanying mechanical activation is failure which leads to grinding of the particles of a substance. Failure is preceded by accumulation, interaction and concentration of defects as well as by crack formation and propagation into the interior of the crystal. However, direct mechanical grinding of a solid usually does not allow preparation of nanoparticles since mechanical activation leads to acceleration of mass transfer owing to the formation of metastable defects. In addition, the stored elastic strain energy is partly transformed into thermal energy and the temperature in the impact zone can be significantly increased, thus favouring both recrystallisation of the substance and 'healing' of defects that prevent grinding.[106]

Mechanical activation of heterogeneous mixtures seems to be more promising for the preparation of nanoparticles. Initially, the harder component acts as a crusher, thus favouring finer grinding of the softer component. Dispersion in deeper activation stages is due to the interfacial interaction between the components; here, the soft component plays the role of surfactant and facilitates the grinding of the harder component owing to the Rehbinder effect.

Mechanochemical reactions in heterogeneous mixtures represent the most efficient method for the preparation of nanocomposites.[106–108] In this case, nanoparticles of a new phase are

formed at the interface or as a result of decomposition of metastable states stabilised upon mechanical activation of the mixture. A unique feature of mechanochemical processes is the possibility of 'deformation mixing' (mechanical alloying) of the components of a mixture, *i.e.*, mixing of the starting components at the atomic level.[105–109] Mechanical alloying occurs at low temperatures whereupon diffusion is retarded. This allows stabilisation of various metastable intermediates including nanoparticles.

2. Methods for mechanochemical synthesis of nanocomposites and nanoparticles

Mechanochemical synthesis of nanocomposites in metal systems is fairly well studied. The main classes of mechanochemical reactions used for the preparation of metal nanocomposites are as follows.[110]

1. Conventional mechanical treatment of a composite resulting in transformation of one of the components into the nanocrystalline state.

This is the simplest and most widely used procedure for the preparation of nanocomposites by exposing mixtures of solids to high-power mechanical impulses. If one component of a mixture is hard while the other is soft, mechanical treatment will lead to comminution of the former and deformation of particles of the latter. This can result in the formation of a composite comprising plate-like particles of the soft component with a thickness of several nanometres separated by large nanoparticles of the hard component.

This type of nanocomposites has been obtained in, *e.g.*, bimetallic systems Cr–Fe,[111] Ni–Ti[112] and Ce–Yb[113] (for a detailed list of systems, see the review by Matteazzi *et al.*[114]). Mechanically alloyed $Cu_{30}Cr_{170}$ has been obtained by treatment of a Cu–Cr mixture[115] and studied by EXAFS, DSC and anomalous scattering of synchrotron radiation. It was shown that the alloy represents a nanocomposite rather than a solid solution of copper in chromium and that the Cu nanoparticles occur in the metastable phase. Mechanical treatment of a Cu–Co mixture, 80 : 20 (at.%), allowed the preparation of a nanocomposite containing nanoscale cobalt particles.[116] Thorough field-ion microscopy studies of the structure of the nanocomposite showed that the material contains both individual 15-nm Co nanoparticles and 1–3-nm cluster inclusions of Co atoms in the copper matrix.[117] The presence of small Co clusters is responsible for anomalous magnetoresistance of the nanocomposite. Layered Co–Cu structures obtained by vapour deposition or using pulse electrochemical deposition also possess analogous properties.[118]

2. Transformation of an amorphous phase into a nanocrystal owing to the elastic strain energy stored during mechanical treatment, *e.g.*, preparation of nanocomposites from amorphous alloys based on iron and aluminium:[119]

$$A_aB_b \text{ (amorphous solid)} \longrightarrow A_aB_b \text{ (nanocrystal)}.$$

Yet another example is the transformation of amorphous Fe–Si–B alloys into nanocrystals upon mechanical treatment. The process can be either accelerated by addition of cobalt or slowed down by addition of niobium (this can inhibit crystallisation and retain the amorphous alloy). The reasons for the transformation of the amorphous phase into a crystalline one upon mechanical treatment have been discussed.[120–122] If mechanical treatment is carried out in air, the formation of nanocomposite is often favoured by the formation of an oxide film on the metal surface.[119]

3. Decomposition of an amorphous phase (usually, an intermetallide) to give one of the components in the form of nanoparticles:

$$A_aB_b \text{ (amorphous solid)} \longrightarrow$$
$$\longrightarrow c\,A \text{ (nanocrystal)} + A_{a-c}B_b \text{ (amorphous solid)}.$$

4. More complex mechanochemical reactions:

$$a\,A + b\,B \longrightarrow A_aB_b \text{ (nanocrystals)},$$

$$A_aB_b + C \longrightarrow A_aB_bC \text{ (nanocrystals)},$$

$$A_aB_b + C_cD_d \longrightarrow A_aB_bC_cD_d \text{ (nanocrystals)}.$$

Mechanical alloying of the mixtures of different metals with graphite, silicon or tin is used for the preparation of carbide,[114,123] silicide and stannide nanoparticles.[124] Nanocomposites can also be obtained by mechanochemical solid-phase displacement and exchange reactions, *e.g.*, by the interaction of iron nitride with aluminium or silicon or by the reaction of iron carbide with chromium[125]:

$$Fe_{2.5}N + Al \longrightarrow AlN \text{ (nanocrystals)} + 2.5\,Fe,$$

$$4\,Fe_{2.5}N + 3\,Si \longrightarrow Si_3N_4 \text{ (nanocrystals)} + 10\,Fe,$$

$$Fe_3C + 3\,Cr \longrightarrow (Fe,Cr)_3C \text{ (nanocrystals)}.$$

Hydrogenation of an intermetallide $Pr(Co_{1-x}Cu_x)_5$ results in the formation of copper and cobalt nanoparticles with sizes 10–20 nm incorporated into the matrix of hydrogenation products $Pr(Co_{1-y}Cu_y)_5H_x$ and PrH_2 (see Ref. 126).

Specific methods are used if one needs to obtain nanoparticles of a single component of a nanocomposite rather than the nanocomposite itself. For instance, nickel–zinc ferrite nanoparticles with sizes 8–50 nm were obtained by long-term (200 h) heat treatment of a mixture of the ferrite and quartz.[127] To separate the metals from quartz and other components, the mixture was treated with 2 M $HClO_4$ for 1 h. This kind of treatment makes the particles on the ferrite surface charged, whereas other particles remain uncharged; this phenomenon is used for the separation of the mixture. Ferrite particles form a sol that can be destroyed by controlled change in the pH.

An efficient method for preparation and isolation of nanoparticles from mechanically alloyed composites has been proposed recently.[128–130] Nanoparticles were formed by solid-phase exchange reactions chosen in such a way that the by-products be readily soluble while the desired product, *i.e.*, nanoparticles, be insoluble in conventional solvents. For instance, ZnS nanoparticles were prepared by the solid-phase mechanochemical reaction

$$ZnCl_2 + CaS \longrightarrow ZnS + CaCl_2.$$

The newly formed zinc sulfide particles with an average size of 500 nm were found to represent aggregates comprised of smaller particles with characteristic sizes of 10–12 nm. The formation of aggregates can be prevented by adding calcium chloride to the initial mixture; in this case, the desired product is obtained as separated ZnS particles of size 7–9 nm. Calcium chloride is removed from the mixture of reaction products by selective dissolution in methanol followed by centrifugation. A similar procedure is used for the synthesis of CdS nanoparticles following the reaction

$$CdCl_2 + Na_2S \longrightarrow CdS + 2\,NaCl.$$

The starting mixture was additionally diluted with NaCl. After mechanical treatment for 1 h the mixture was washed with water to remove NaCl. The sizes of the CdS particles formed were from 4 to 8 nm (*i.e.*, less than the Bohr radius of an exciton), which allowed the mechanochemical synthesis of 'quantum dots'.

Mechanochemical reduction of oxides is also known. The use of a peroxide instead of oxide allows transformation of this reaction into self-propagating high-temperature synthesis.[131] By performing the reaction in the 'smouldering' (incomplete combustion) rather than conventional combustion regime (this can be achieved by changing the heat treatment regime of the mixture or by diluting it with an inert compound), one can obtain the reaction product in the form of nanoparticles with sizes 40–50 nm. Using this regime in the reactions of BaO_2 with metals, mixed titanium-molybdenum oxide, barium aluminate and barium stannate nanoparticles were obtained.[131]

Preparation of zinc ferrite nanoparticles by mechanical treatment of a mixture of zinc and iron oxides represents yet another example of mechanochemical synthesis of nanoparticles of complex oxides from simple ones. However, in this case heating leads to rapid growth of stable large ferrite crystals.[132] Mechanical treatment of the preliminarily prepared zinc ferrite, α-Fe_2O_3 and γ-Al_2O_3 nanoparticles also leads to their growth.[133] Therefore, optimisation of reaction conditions (in particular, mechanical treatment) should receive due attention when performing mechanochemical synthesis of nanoscale materials.

A specific case of mechanical activation of a topochemical reaction has been studied.[134] Intercalation of γ-$Al(OH)_3$ (gibbsite) with lithium salts from solution was shown to result in the development of wedging stress in the gibbsite lattice. This leads to an increase in the interlayer distances in the gibbsite structure, thus improving the intercalation conditions. Relaxation of mechanical stress can lead to the appearance of lattice defects. This will also favour an enhancement of the reactivity of gibbsite and can be used for carrying out various chemical reactions in the interlayer space of gibbsite.[135–138]

A salient feature of this type of reactions is the possibility of crystallographic control of mutual orientation of the reactants, intermolecular distances and their mobilities. Nanoparticles can be prepared by intercalating the reactants into the interlayer space. They can be formed either if both reactants are present within the interlayer space or if the second reactant (*e.g.*, oxygen) is supplied from the outside to oxidise the first reactant in the interlayer space. Nanoparticles thus formed can sometimes be retained within the interlayer space, as is the case of $[MnO_x(OH)_4]^{4-2x-y}$ nanoparticles formed by the reaction of the intercalated permanganate ions and unsaturated organic acids.[139] In other cases, the products can form a separate phase and break down the layered matrix structure, as in the thermal decomposition of complexes intercalated into the structure of hydrargillite (monoclinic gibbsite).[140]

V. Chemical properties of nanoscale systems

In studies of nanoparticles and heterogeneous nanoscale systems it is of great importance to take into account a 'feedback' between the reactivities of solid reactants and the character of the reaction between them.[1]

There are different forms of such a 'feedback'. Sometimes, it can arise owing to the development of mechanical stress due to the absence of structural correspondence between the starting substances and the reaction product (the so-called misfit).[141,142] In other cases, the reaction product can affect the electron–hole equilibrium or the concentration of ionic defects in the region adjacent to the starting point of the reaction. Finally, the 'feedback' can manifest itself in transformation of a kinetically controlled reaction into a diffusion-controlled one if the molecular volume of the product is larger than the molecular volumes of the starting materials. It should also be kept in mind that the 'feedback' can depend on the particle size of the solid reactants and products.

1. Properties of particles formed in the initial stages of heterogeneous chemical reactions

Let us consider the oxidation of lower iron and manganese oxides as an example. Here, the size effect can manifest itself in the dependence of the composition of the reaction products on the sizes of their particles. In some instances, the mechanism of a solid-phase reaction can change upon change in the particle sizes of the reactants. This is thought to be due to transformation of a homogeneous system into a heterogeneous one, as is the case of, *e.g.*, oxidation of Fe_3O_4 into Fe_2O_3.[143,144] Oxidation of fine Fe_3O_4 particles with a size less than 300 nm is a homogeneous process which involves the formation of a solid solution of oxygen in the magnetite lattice accompanied by gradual transformation of the Fe_3O_4 crystal lattice into the γ-Fe_2O_3 lattice. Oxidation of larger Fe_3O_4 particles is a heterogeneous process since the Fe ions have no time to diffuse through the whole bulk of the particle, so it is only the surface layer that is oxidised. The appearance of the oxide concentration gradients and the development of stress in the surface layer of the particles facilitate the nucleation of rhombohedral Fe_2O_3. Analogously, fine Mn_3O_4 particles are oxidised into Mn_5O_8, whereas oxidation of large particles gives α-Mn_2O_3.[145] Similar effects seem to be expected for other systems.

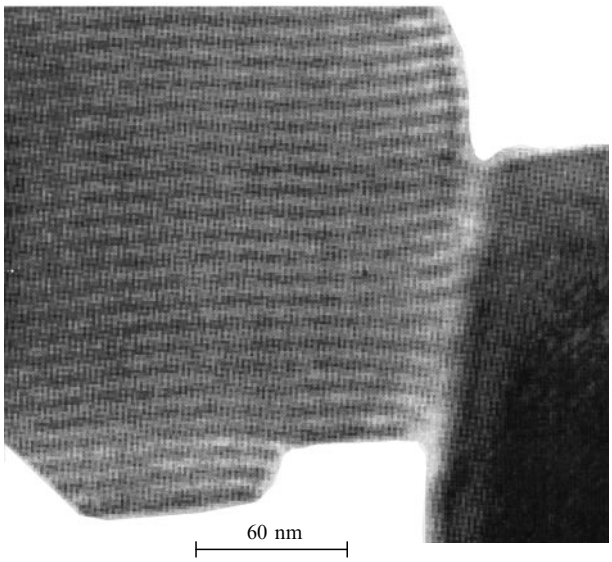

Figure 13. A HREM image of the AgBr–silver stearate interface.[153]

Size effect manifests itself in a somewhat different manner in the chemical and physical development of the latent photographic image, which begins as the Ag particle size exceeds a certain minimum value.[146–148] The usual chemical development involves treatment of silver bromide with a solution of a reducing agent and is due to the catalytic activity of Ag clusters formed upon aggregation of the surface silver atoms and comprising at least five atoms.[149,150] Physical development, or the appearance of an image owing to the deposition of the metal atoms from a solution on the potential crystallisation centres, occurs as the Ag crystallites become larger than the critical size of $\sim$4 nm.

Palladium-free metallisation of dielectrics is similar to physical development and proceeds analogously.[151,152] The process involves deposition of particles on a copper catalyst (obtained by thermal decomposition of copper hypophosphite) from a solution containing the copper salt and a reducing agent. The best results are obtained when the particle size of the copper catalyst is $\sim$25 nm. An increase in the particle size up to 80 nm leads to substantial reduction of the catalytic activity.

Treatment of silver stearate with bromides results in the formation of nanoscale AgBr particles which serve as sensitisers for silver carboxylates; the latter are candidates for modern photographic processes.[153] The case in point is as follows. Treatment of silver carboxylate with a KBr solution results in the formation of an AgBr particle and leads to the carboxylate lattice distortion at the AgBr–silver carboxylate interface owing to misfit. A HREM image of the AgBr–silver stearate interface is presented in Fig. 13. If the electron beam is oriented parallel to the basal plane of silver stearate, the layers of silver ions form rows of dark bands. As can be seen, these layers are disordered in the interface region and form an interfacial defect zone several nanometres wide. This zone seems to play a significant role in the sensitisation of silver stearate contacting the AgBr particles.

2. Catalytic properties

As mentioned above, the chemical properties of a substance including catalytic ones change on going from a bulk specimen

to a nanocrystal.[34, 154] For instance, the shifts of the energies of the conduction and valence bands in opposite directions cause changes in the photocatalytic properties of semiconductor particles. Khairutdinov[34] has reported numerous examples of the effect of particle sizes on the optical and redox properties as well as on the kinetics of photochemical processes in various oxide and sulfide systems. In particular, it has been shown that the specific photocatalytic activity of TiO_2 depends on its particle size. Unusual chemical properties of α-$Fe_2O_3-SnO_2$ nanocomposites have also been reported.[155] A salient feature of this system obtained by mechanical alloying of a mixture of oxides in high-energy mechanical activators is the high sensitivity and selectivity towards ethanol vapours and a moderate sensitivity to the accompanying gases, CO and CH_4. This is mainly due to the very large area of the contact surface between the two oxides and to the presence of tin ions on the surface of α-Fe_2O_3 particles. As a result, the oxide α-Fe_2O_3, initially assumed to be insensitive to ethanol vapours, acquires sensitivity and a gas sensor based on it allows detection of 1000 ppm of ethanol vapour in air.

A correlation was found between the particle size of a platinum catalyst and its catalytic activity in the reaction of hydrogenation of *p*-chloronitrobenzene, which is often used as a test for catalytic activity in hydrogenation reactions.[156] Using commercial catalysts, the process can proceed up to the stage of formation of chloroaniline. The use of nanoscale platinum particles with sizes 3–4 nm allows the hydrogenation to reach deeper stages with the formation of aniline and cylohexylamine. Nanocrystalline platinum catalyst also appeared to be suitable for further hydrogenation of cylohexylamine to give dicylohexylamine as the end product.

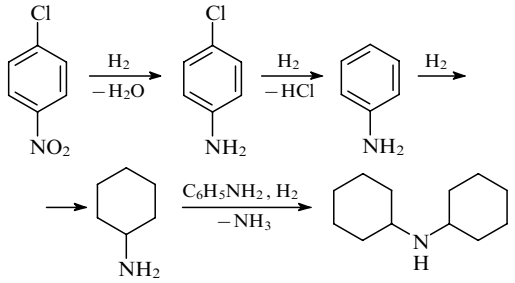

Finally, zinc ferrite nanoparticles were found to exhibit better sorption properties toward H_2S as compared to conventional pure ferrite.[125]

3. Hydrogenation of metal systems

Hydrogenation and dehydrogenation of magnesium have been studied.[157] The use of nanocomposites formed upon mechanical treatment of mixtures of magnesium with nickel and other metals leads to an increase in the rate of hydrogenation and in the yields of the end products. The rate of hydrogen absorption and the hydrogen capacity of the mechanically alloyed composite with stoichiometry Mg_2Ni also increased. Taking $LaNi_5$ as an example, it was shown that the addition of a hydrogenation catalyst (*e.g.*, palladium) to the system together with mechanically treated absorbent leads to even greater increase in the rate of hydrogen intake. Nanocomposites obtained by mechanical treatment of $Fe_{40}Ti_{60}$, $Fe_{50}Ti_{50}$ and $Fe_{67}Ti_{33}$ alloys and by direct mechanochemical alloying of elemental Fe and Ti were found to have a high hydrogen capacity. Compared to the starting alloys, these nanocomposites absorb hydrogen at lower pressures and are stable towards the phase transition of the materials into the γ-phase. Unusual properties of the alloys were explained by the presence of mechanical stress in the crystallites constituting the nanocomposites.

4. Electrochemical and anti-corrosion properties

Electrodes made of mechanically alloyed Ti_2Ni nanocomposite were found to be more efficient in the electrochemical production of hydrogen gas than those produced by conventional procedures.[158]

A distinguishing feature of mechanically alloyed nanomaterials is improved corrosion resistance.[159] Nanostructured material with stoichiometry $Fe_{32}Ni_{36}Cr_{14}P_{12}B_6$ obtained by crystallisation of an amorphous alloy exhibits a higher corrosion resistance than the initial alloy.[160] This was explained by the possibility of fast diffusion of Cr atoms towards the surface along numerous block boundaries in the composite followed by the formation of a protective layer. A similar effect has also been observed.[161] However, it does not always happen that the corrosion resistance increases. In studies of the behaviour of electrochemically deposited Ni–P alloys in 0.1 M H_2SO_4 (see Ref. 162) it was shown that nanocomposites exhibited a reduced corrosion resistance compared to bulk nickel owing to enhanced activities at block boundaries and the possibility of accelerated propagation of the reaction along these boundaries. Nanocomposites with stoichiometry $FeAl_8$ also exhibit a reduced corrosion resistance towards H_2SO_4 and Na_2SO_4 solutions.[163]

Overvoltage (up to 900 mV) on steel cathodes is one of the main sources of energy loss in the electrochemical production of chlorates. It was proposed to use nanocrystalline cathodes prepared by mechanochemical activation of a $RuO_2-Fe-Ti$ mixture.[164] The mechanically alloyed nanocomposite appeared to be an excellent material for cathode production. At a current density of 250 mA cm^{-2} and 70 °C, the overvoltage on the nanocomposite cathodes decreases by 300 mV, which allows a 15% reduction of the expenditure of electrical energy in the production of chlorates. A nanostructured material obtained by mechanical alloying of Ti and TiO in an Ar atmosphere exhibits similar properties.[165] The nanocomposite with oxygen content between 18.5 at.% and 33 at.% can be used as a cathode material in electrochemical production of sodium chlorate. At the operating current density of 250 mA cm^{-2} and solution temperature of 70 °C, the overvoltage on this cathode is 600 mV, which is nearly half as large as the overvoltage on the cathode made of metallic titanium (1107 mV).

5. Size effects in the chemistry of solid organic compounds

Back in the late 1930s, it was found that stearic acid, which usually crystallises in stable β-form, undergoes transformation into the α-form as the crystal size reduces.[166] As the size of molecular crystals decreases, the temperature of the $\alpha-\beta$-transition and the heat of melting also decrease. A change in the ratio between the surface area and volume of molecular crystals leads to changes in both dissolution rate and solubility. Reduction of the size of molecular crystals of chemical compounds used as medicinal drugs to submicron level enhances their biological assimilation and therapeutic efficiency.

Since microscopic and nanoscale molecular crystals are prone to aggregation, it is desirable to place nanoparticles obtained by certain procedures on a support or to prepare nanocomposites of the molecular crystal–support type. One of the well-known and popular methods for the preparation of this sort of nanocomposites involves treatment of the molecular crystal–support mixture in a mechanical activator. This procedure can be conveniently used to prevent transformations of highly active, metastable polymorphous crystalline modifications formed during mechanochemical activation into stable, low activity ones.[167, 168] Here, it is appropriate to refer to a number of studies on the preparation of highly active, readily soluble forms of aspirin, sulfathiazole and other medicinal drugs in order to eliminate their major drawback of low solubility.[169–173]

6. Specific chemical properties of nanocrystals of ionic compounds

Incomplete compensation of the anion and cation charges in ionic compounds leads to the appearance of charged nanoparticles; this is a reason for changes in their chemical properties on going from bulk crystals to nanocrystals.[174] This can be followed taking alkali

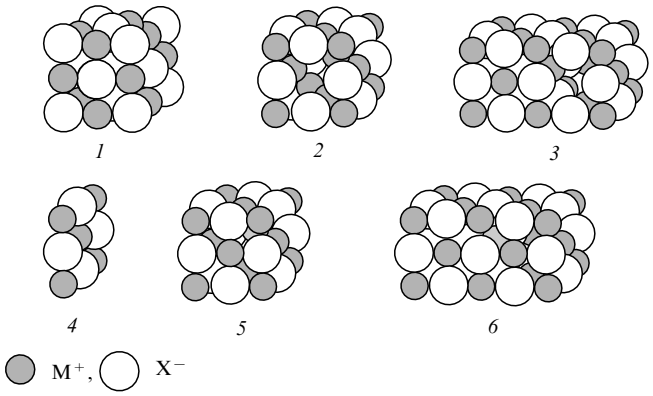

Figure 14. Structures of a (3, 3, 3) nanocrystal of an ionic salt MX (*1*) and clusters that are reactive (*2*, *3*) and passive (*4*–*6*) towards chemisorption of NH_3.
$[M_{14}X_{13}]^+$ (*1*), $[Na_{13}F_{12}]^+$ (*2*), $[Na_{22}F_{21}]^+$ (*3*), $[M_5X_4]^+$ (*4*), $[M_{14}F_{13}]^+$ (*5*) and $[M_{23}X_{22}]^+$ (*6*).[174]

halides as an example. It is known that alkali halide vapours contain charged clusters comprised of, in particular, a small odd number of ions.[175] In larger particles, electroneutrality can also be violated. Figure 14 presents the structure of a cubic nanocrystal of the (3, 3, 3) type (figures denote the number of ions along three edges). As compared to the ideal cubic lattice of ionic salt MX, the nanocrystal lattice is built in such a way that the X^- anions protrude out while the metal cations are recessed.

Charged nanocrystals possess some characteristic properties. For instance, adsorption of polar molecules such as NH_3 and H_2O occurs in different manner depending on the number of lattice sites on the crystal edges. Perfect crystals of the (3, 3, 3) or (3, 3, 5) types do not adsorb polar molecules at room temperature. The loss of two ions (M^+ and X^-, or a single MX unit) leads to the appearance of pits on the surface and to enhancement of the reactivity of crystals. In Fig. 14, the structures of clusters $[M_nX_{n-1}]^+$ (M = Na, X = F) with such pits are shown. These clusters are highly reactive towards NH_3. The structures of $[M_nX_{n-1}]^+$ clusters that are passive towards ammonia are also shown in Fig. 14. It should be mentioned that the cluster structure remains unchanged after the adsorption of a polar molecule.

The reaction of $[Na_{53}F_{52}]^+$ nanoparticles with the surface of silicon occurring in their collisions is yet another example of the reactions of ionic nanoscale clusters. Upon collision, a single fluorine atom is transferred to the silicon surface to form a F–Si bond. The reaction occurs only if the silicon surface is pure. If the silicon surface is preliminarily passivated with hydrogen, the collision event will only result in the cleavage of the nanoparticle.

Condensation of metal atoms on the surface of a nanoparticle leads to the formation of the structures similar to F-centres, where an electron is mainly localised at the anionic vacancy site. These centres are characterised by very low ionisation potentials, *e.g.*, 3 eV for $(Na^+)_n(F^-)_{n-1}e^-$ and 5 eV for $(Cs^+)_{13}(I^-)_{11}e^-$. As the temperature increases, the electron can wander onto the metal cation. A neutral metal atom thus formed leaves the surface. In the case of a perfect nanocrystal without anionic vacancies, an electron that is loosely bound to the surface forms a surface centre, which is a strong electron donor. Photolysis of nanocrystals leads to transfer of the electron from the anion to the cation followed by desorption of a halogen atom from the surface. The transfer energy lies between the energies of analogous transfer in diatomic molecules MX and in bulk $(MX)_\infty$ crystals.

By and large, studies of alkali halide nanocrystals showed that they are more passive towards many reagents as compared to bulk crystals. On the other hand, nanocrystals are prone to self-aggregation; therefore, the search for protective coatings for stabilisation of nanocrystals is topical.

VI. Conclusion

Size effects play an important role in chemical processes including mechanochemical reactions. One should distinguish two groups of size effects. Some of them, inherent in microcrystalline systems, are due to the purely surface phenomena. Stronger phase size effects manifest themselves if the particle size is less than 10 nm. In the former case, the properties of a substance can be interpreted in terms of the classical thermodynamic approach, which includes standard models for taking into account the contribution of surface effects. A basically new situation appears on going to nanoparticles since virtually the whole bulk of the sample under study falls within the action range of surface forces and classification of the atoms into the surface atoms and bulk ones becomes unjustified. In this case, a nanoparticle should be considered to be a cluster or a macromolecule, the structural, thermodynamic and transport properties of which are strongly different from those of the macrocrystal.

Various size effects are observed in heterogeneous systems represented by microcrystalline and nanoscale composites, the properties of which are affected by the interface interaction. Particularly strong are the interface effects typical of heterogeneous systems with the ionic type of bonding. Here, the interface interaction involves the stage of formation of surface defects, which leads to abrupt increase in the ionic conductivity. Similarly to isolated nanoparticles, the material nanocomposites are made of occurs in unusual states and its properties (like those of the adsorption layers) are to a great extent determined by the characteristics of the interface, *i.e.*, by the interatomic interactions within the adjacent phases in the near-surface region.

Practically, nanocomposites represent a promising class of advanced materials with unique electronic properties and high molecular, atomic and ionic mobilities. Mechanochemical processes in heterogeneous mixtures are strongly influenced by size effects, which is of great importance for solving practical tasks associated with controlling the process intensity and obtaining the desired reaction products. Problems which have arisen in this case are directly related to studies of the effect of particle size on the catalytic, electrochemical and specific chemical properties of materials. Therefore, further investigations of size effects in heterogeneous systems are of great theoretical and practical importance.

This review has been written with the financial support of the Programme 'Fundamental Problems of Modern Chemistry. Chemical Transformations Involving Nanoscale and Supramolecular Systems' of the Russian Federation Ministry of Industry, Science and Technology (Grant No. 3) and the US Civilian Research and Development Foundation (Grant REC-008).

References

1. V Boldyrev, M Boulens, B Delmon *The Control of Reactivity of Solids* (Amsterdam: Elsevier, 1979)
2. I D Morokhov, L I Trusov, S P Chizhik *Ul'tradispersnye Metallicheskie Sredy* (Ultradispersed Metallic Media) (Moscow: Atomizdat, 1977)
3. Yu I Petrov *Klastery i Malye Chastitsy* (Clusters and Small Particles) (Moscow: Nauka, 1986)
4. S A Nepiiko *Fizicheskie Svoistva Malykh Metallicheskikh Chastits* (Physical Properties of Small Metallic Particles) (Kiev: Naukova Dumka, 1985)
5. Yu I Vesnin *Vtorichnaya Struktura i Svoistva Kristallov* (Secondary Structure and Properties of Crystals) (Novosibirsk: Institute of Organic and Inorganic Chemistry, Siberian Branch, Russian Academy of Sciences, 1997)
6. L S Palatnik, I I Papirov *Epitaksial'nye Plenki* (Epitaxial Films) (Moscow: Nauka, 1971)
7. Yu F Komnik *Fizika Metallicheskikh Plenok. Razmernye i Strukturnye Effekty* (The Physics of Metallic Films. Size and Structural Effects) (Moscow: Atomizdat, 1979)

8. V G Gryaznov, L I Trusov *Prog. Mater. Sci.* **37** 289 (1993)
9. H Gleiter *Prog. Mater. Sci.* **33** 223 (1989)
10. H Gleiter *J. Appl. Cryst.* **24** 79 (1991)
11. R A Andrievskii, A M Glezer *Fiz. Met. and Metalloved.* **88** 50 (1999) [a]
12. A I Gusev *Usp. Fiz. Nauk* **168** 55 (1988) [b]
13. V L Tauson, M G Abramovich *Fiziko-Khimicheskie Prevrashcheniya Real'nykh Kristallov v Mineral'nykh Sistemakh* (Physicochemical Transformations of Real Crystals in Mineral Systems) (Novosibirsk: Nauka, 1988)
14. A I Rusanov *Solid State Ion.* **75** 275 (1995)
15. A I Rusanov *Zh. Obshch. Khim.* **70** 353 (2000) [c]
16. A I Rusanov *Fazovye Ravnovesiya i Poverkhnostnye Yavleniya* (Phase Equilibria and Surface Effects) (Leningrad: Khimiya, 1967)
17. P Pawlow *Z. Phys. Chem.* **65** 545 (1909)
18. A I Bublik, B Ya Pines *Dokl. Akad. Nauk SSSR* **87** 215 (1952) [d]
19. B Ya Pines *Ocherki o Metallofizike* (Essays on Metallophysics) (Khar'kov: Khar'kov University, 1961)
20. C R M Wronski *Br. J. Appl. Phys., J. Phys. D* **18** 1731 (1967)
21. M Hasegawa, K Hoshino, M Watabe *J. Phys. F., Met. Phys.* **10** 619 (1980)
22. V A Pavlov *Fiz. Met. Metalloved.* **59** 629 (1985) [a]
23. Yu G Sidorov, E M Trukhanov *Poverkhnost'* (6) 106 (1992)
24. I D Morokhov, S P Chizhik, N T Gladkikh, L K Grigor'eva, S V Stepanova *Dokl. Akad. Nauk SSSR* **248** 603 (1979) [d]
25. H Gleiter *Nanostruct. Mater.* **1** 1 (1992)
26. R W Siegel *Phys. New Mater.* **27** 65 (1994)
27. D G Morris *Mechanical Behaviour of Nanostructured Materials* Vol. 2 (Eds M Magini, F H Wohlbier) (Materials Science Foundations Trans. Technology Publications, Zuerich: 1998)
28. G C Benson, T A Claxton *J. Chem. Phys.* **48** 1356 (1968)
29. P W Tasker *Philos. Mag. A Phys. Condens. Matter Defects Mech. Prop.* **39** 119 (1979)
30. N X Sun, K Lu *Phys. Rev. B, Condens. Matter* **54** 6058 (1997)
31. J Friedel *Ann. Phys.* **1** 257 (1976)
32. M R Hoare, P Pal *Adv. Phys.* **20** 161 (1971)
33. A P Alivisatos *Science* **271** 933 (1996)
34. R F Khairutdinov *Usp. Khim.* **67** 125 (1998) [*Russ. Chem. Rev.* **67** 109 (1998)]
35. C L Chien, J Q Xiao, J S Jiang *J. Appl. Phys.* **73** 5309 (1993)
36. D S Lashmore, M P Dariel *J. Electrochem. Soc.* **135** 1221 (1988)
37. S S Parkin, Z C Li, D J Smith *Appl. Phys. Lett.* **58** 2710 (1991)
38. E Yu Ivanov, I G Konstanchuk, B B Bokhonov, V V Boldyrev *React. Solids* **7** 167 (1989)
39. J Eckert, L Schultz, E Hellstern *Appl. Phys. Lett.* **55** 117 (1989)
40. S Ino *J. Phys. Soc. Jpn.* **27** 941 (1969)
41. D J Wales *Science* **271** 925 (1996)
42. T L Hill *Thermodynamics of Small Systems* Part I (New York: Benjamin, 1963)
43. I I Gainutdinov, Yu T Pavlyukhin, V V Boldyrev *Dokl. Akad. Nauk* **344** 189 (1995) [d]
44. I I Gainutdinov, Yu T Pavlyukhin *Dokl. Akad. Nauk* **350** 206 (1996) [d]
45. Ya E Geguzin *Fizika Spekaniya* (The Physics of Caking) (Moscow: Nauka, 1984)
46. B S Bokshtein, Ch V Kopetskii, L S Shvindlerman *Termodinamika i Kinetika Granits Zeren v Metallakh* (Thermodynamics and Kinetics of Grain Boundaries in Metals) (Moscow: Metallurgiya, 1986)
47. J Maier *Ber. Bunsenges. Phys. Chem.* **90** 26 (1986)
48. J Maier *Prog. Solid State Chem.* **23** 171 (1995)
49. V N Chebotin *Fizicheskaya Khimiya Tverdogo Tela* (Physical Chemistry of Solids) (Moscow: Khimiya, 1982)
50. I M Lifshits, A M Kosevich, Ya E Geguzin, in *Poverkhnostnaya Diffuziya i Rastekanie* (Surface Diffusion and Spreading) (Ed. Ya E Geguzin) (Moscow: Nauka, 1969) p. 243
51. Ya I Frenkel' *Kineticheskaya Teoriya Zhidkostei* (Kinetic Theory of Liquids) (Moscow: Academy of Sciences of the USSR, 1945)
52. K L Kliewer, K S Koehler *Phys. Rev. A., At. Mol. Opt. Phys.* **140** 1226 (1965)
53. N F Uvarov, Doctoral Thesis in Chemical Sciences, Institute of Solid State Chemistry and Mechanochemistry, Siberian Branch, Russian Academy of Sciences, Novosibirsk, 1998
54. J Horvath, U Landman *Phys. Rev. Lett.* **82** 3835 (1999)
55. J Horvath, R Birringer, H Gleiter *Solid State Commun.* **62** 319 (1987)
56. B S Bokshtein, G D Breze, P V Kurkin *Izv. Vyssh. Uchebn. Zaved., Chernaya Metallurgiya* **1** 49 (1994)
57. H J Hoffler, R S Averback, H Hahn, H Gleiter *J. Appl. Phys.* **74** 3832 (1993)
58. S M Klotsman *Fiz. Met. Metalloved.* **75** 5 (1993) [a]
59. R E Newnham, D P Skinner, L E Cross *Mater. Res. Bull.* **13** 525 (1978)
60. U Stuhr, H Wipf, T J Udovic, J Weissmueller, H Gleiter *Nanostruct. Mater.* **6** 555 (1995)
61. B Ya Pines, N I Sukhinin *Zh. Tekhn. Fiz.* **26** 2100 (1956) [e]
62. A A Chernov, E I Givargizov, Kh S Bagdasarov, L N Dem'yanets, V A Kuznetsov, A N Lobachev (Eds) *Sovremennaya Kristallografiya* (Modern Crystallography) (Moscow: Nauka, 1980) Vol. 3
63. N F Uvarov, J Maier *Solid State Ion.* **61** 251 (1993)
64. N F Uvarov, V G Ponomareva *Dokl. Aksd. Nauk* **351** 358 (1996) [d]
65. N F Uvarov, E F Hairetdinov, B B Bokhonov, N B Bratel *Solid State Ion.* **86**–**88** (Pt I) 573 (1996)
66. N F Uvarov, B B Bokhonov, V P Isupov, E F Hairetdinov *Solid State Ion.* **74** 15 (1994)
67. N F Uvarov, E F Hairetdinov, I V Skobelev *Solid State Ion.* **86**–**88** 577 (1996)
68. N F Uvarov, I V Skobelev, B B Bokhonov, E F Hairetdinov *J. Mater. Synth. Proc.* **4** 391 (1996)
69. A Adamson *Physical Chemistry of Surfaces* (New York: Wiley, 1974)
70. A D Zimon *Adgeziya Plenok i Pokrytii* (Adhesion of Films and Coatings) (Moscow: Khimiya, 1977)
71. M J Jaycock, G D Parfitt *Chemistry of Interfaces* (New York: Ellis Horwood, 1981)
72. Ya O Bikerman *Usp. Khim.* **41** 1431 (1972) [*Russ. Chem. Rev.* **41** 651 (1972)]
73. A I Rusanov *Dokl. Akad. Nauk SSSR* **261** 700 (1981) [d]
74. J Maier *J. Phys. Chem. Solids* **46** 309 (1985)
75. A K Shukla, R Manoharan, J B Goodenough *Solid State Ion.* **26** 5 (1988)
76. B Zhu, B-E Mellander *Solid State Ion.* **77** 244 (1995)
77. B Zhu *Solid State Ion.* **125** 397 (1999)
78. B Zhu, B-E Mellander *Solid State Ion.* **70** (Pt 1) 285 (1994)
79. Z-Y Zhao, C-Y Wang, S-Y Dai, L-Q Chen *Solid State Ion.* **9**/**10** 1175 (1983)
80. Yu Ya Gurevich *Dokl. Akad. Nauk SSSR* **222** 143 (1975) [d]
81. J B Boyce, B A Huberman *Phys. Rep.* **51** 190 (1979)
82. N G Hainovsky, J Maier *Phys. Rev. B, Condens. Matter* **51** 15789 (1995)
83. V N Bondarev, A B Kuklov *Elektrokhimiya* **26** 1397 (1990) [f]
84. N F Uvarov, E F Hairetdinov *J. Solid State Chem.* **62** 3 (1985)
85. N F Uvarov, V P Isupov, V Sharma, A K Shukla *Solid State Ion.* **51** 41 (1992)
86. V M Kosevich, V M Ievlev, L S Palatnik, A I Fedorenko *Struktura Mezhkristallitnykh i Mezhfaznykh Granits* (Structure of Crystallite and Phase Boundaries) (Moscow: Metallurgiya, 1980)
87. L S Palatnik, M Ya Fuks, V M Kosevich *Mekhanizm Obrazovaniya i Substruktura Kondensirovannykh Plenok* (The Mechanism of Formation and Substructure of Condensed Films) (Moscow: Nauka, 1972)
88. W A Jesser, D Kulmann-Wilsdorf *Phys. Status Solidi B* **19** 95 (1967)
89. V A Gusev, V A Gagarina, E M Moroz, E A Levitskii *Kinet. Katal.* **17** 500 (1976) [g]
90. N F Uvarov, M C R Shastry, K J Rao *Rev. Solid State Sci.* **4** 61 (1990)
91. E F Hairetdinov, N F Uvarov *Mater. Sci. Forum* **88**–**90** 723 (1992)
92. N F Uvarov, E F Khairetdinov, N B Bratel' *Elektrokhimiya* **29** 1406 (1993) [f]
93. N F Uvarov, P Vanek, M Savinov, V Zelezny, J Studnicka, J Petzelt *Solid State Ion.* **127** 253 (2000)
94. N F Uvarov, A A Politov, in *Abstracts of Reports of the 12th International Conference on Solid State Ionics, Thessaloniki, 1999* M-06-P
95. N F Uvarov, P Vanek, Yu I Yuzyuk, V Zelezny, J Studnicka, B B Bokhonov, V E Dulepov, J Petzelt *Solid State Ion.* **90** 201 (1996)
96. V G Ponomareva, N F Uvarov, G V Lavrova, E F Hairetdinov *Solid State Ion.* **90** 161 (1996)
97. V G Ponomareva, G V Lavrova, L G Simonova *Solid State Ion.* **118** 317 (1999)
98. N F Uvarov, L I Brezhneva, E F Hairetdinov *Solid State Ion.* **136**–**138** 1273 (2000)

99. P Chowdary, V B Tare, J B Wagner *J. Electrochem. Soc.* **132** 123 (1985)
100. A C Khandkhar, J B Wagner *Solid State Ion.* **20** 267 (1986)
101. C A Angell, D B Helphrey *J. Phys. Chem.* **75** 2306 (1971)
102. A Kumar, K Shahi *Solid State Ion.* **68** 71 (1994)
103. G Heinike *Tribochemistry* (Berlin: Akademie-Verlag, 1984)
104. V V Boldyrev *Eksperimental'nye Metody v Mekhanokhimii Tverdykh Neorganicheskikh Veshchestv* (Experimental Methods in Mechanochemistry of Solid Inorganic Substances) (Novosibirsk: Nauka, 1983)
105. C C Koch *Annu. Rev. Mater. Sci.* **19** 121 (1989)
106. E G Avvakumov *Mekhanicheskie Metody Aktivatsii Khimicheskikh Protsessov* (Mechanical Methods of Activation of Chemical Processes) (Novosibirsk: Nauka, 1986)
107. *Mekhanokhimicheskii Sintez v Neorganicheskoi Khimii* (Mechanochemical Synthesis in Inorganic Chemistry) (Novosibirsk: Nauka, 1991)
108. *Proceedings of the 1st International Symposium on Mechanical Alloying, Kyoto, 1991*
109. P Yu Butyagin *Usp. Khim.* **63** 1031 (1994) [*Russ. Chem. Rev.* **63** 965 (1994)]
110. E Gaffet, M Abdellaoui, N N Malhourux-Gaffet *Mater. Trans. JIM* **36** 198 (1995)
111. M Dadras, D S Morris *Scr. Metall. Mater.* **28** 1245 (1993)
112. T Itsukaichi, M Umemoto, J G Cabanas-Moreno *Scr. Metall. Mater.* **29** 583 (1993)
113. E Ivanov, K Sumiyamann, H Yamauchi, K Jamai, K Suzuki *J. Alloys Compd.* **198** 195 (1993)
114. P Matteazzi, G Le Caer, A Mocellin *Ceram. Int.* **23** 39 (1997)
115. K B Gerasimov, S V Pavlov, S V Mytnichenko, V A Chernov, S G Nikitenko *J. Alloys Compd.* **252** 179 (1997)
116. M A Uimin, A Ye Yermakov, V V Serikov, A Yu Korobeinikov, A K Shtolz *Phys. Status Solidi A* **165** 337 (1998)
117. V A Ivchenko, M A Uimin, A Ye Yermakov, A Yu Korobeinikov *Surf. Sci.* **440** 420 (1999)
118. A V Demenko, A I Maslii, V V Boldyrev *J. Mater. Synth. Proc.* **3** 303 (1995)
119. A R Yavary, O Dabrohlav *Mater. Sci. Forum* **225–227** 295 (1996)
120. M L Trudeau, R Schulz, D Dussault, A Van Neste *Phys. Rev. Lett.* **64** 99 (1990)
121. R Schulz, M Simoneau, J Lantegne *Physica C* **233** 113 (1994)
122. R Schulz, M L Trudeau, D Dussault, A Van Neste, L Dignard-Bailey *Mater. Sci. Eng. A, Struct. Mater.* **179** 516 (1994)
123. P Matteazzi, G LeCaer *J. Am. Ceram. Soc.* **74** 1382 (1991)
124. P Matteazzi, G LeCaer *Proc. Adv. Mater. 1* **135** 20 (1991)
125. P Matteazzi, G LeCaer *J. Alloys Compd.* **187** 305 (1992)
126. A Ye Yermakov, N V Mushnikov, M A Uimin, N K Zajkov, A Yu Korobeinikov, A K Shtolz, V V Serikov *Mater. Sci. Forum* **269–272** 907 (1998)
127. G Nicoara, D Fratiloiu, M Nogues, J L Dormann, F Vasiliu *Mater. Sci. Forum* **235–238** 145 (1997)
128. P G McCormick, in *Handbook on the Physics and Chemistry of Rare Earth* Vol. 24 (Amsterdam: Elsevier, 1997) p. 47
129. T Tsuzuki, W T A Harrison, P G McCormick *J. Alloys Compd.* **281** 146 (1998)
130. T Tsuzuki, J Ding, P G MacCormick *Physika B* **239** 378 (1997)
131. T F Grigorjeva, A P Barinova, G N Kryukova, V V Boldyrev, in *Proceedings of the 5th European Conference on Advanced Materials, Processes and Applications, Dodrecht, 1997* Vol. 2, p. 333
132. V Sepelak, A Yu Rogachev, U Steinike, D-Chr Uecker, F Krumeich, S Wissman, K D Becker *Mater. Sci. Forum* **235–238** 139 (1997)
133. B B Bokhonov, I G Konstanchuk, V V Boldyrev *Mater. Res. Bull.* **30** 1277 (1995)
134. A P Nemudry *React. Solids* **3** 317 (1987)
135. A V Besserguenev, A M Fogg, R J Francis, S J Price, D O'Hare, V P Isupov, B P Tolochko *Chem. Mater.* **9** 241 (1997)
136. V P Isupov, Doctoral Thesis in Chemical Sciences, Institute of Solid State Chemistry and Mechanochemistry, Siberian Branch, Russian Academy of Sciences, Novosibirsk, 1998
137. V Rives, M A Ulibarri *Coord. Chem. Rev.* **181** 61 (1999)
138. V P Isupov, L E Chupakhina, R P Mitrofanova, K A Tarasov *Zh. Strukt. Khim.* **39** 453 (1998) [h]
139. E I Bakchinova, V P Isupov, V A Poluboyarov, V V Boldyrev *Dokl. Akad. Nauk* **324** 592 (1992) [d]
140. V P Isupov, K A Tarasov, L E Chupakhina *Dokl. Akad. Nauk* **324** 1217 (1992) [d]
141. V V Boldyrev, E V Boldyreva *Mater. Sci. Forum* **88–90** 711 (1992)
142. E V Boldyreva *J. Therm. Anal.* **38** 89 (1992)
143. W Feitknecht *Pure Appl. Chem.* **9** 423 (1964)
144. B Gillot, A Rousset, G Dupre *J. Solid State Chem.* **25** 263 (1978)
145. B Gillot, J Tyranowic, A Rousset *Mater. Res. Bull.* **10** 775 (1975)
146. H Reinder, L Hamburger *Recl. Trav. Chim. Pays-Bas* **50** 475 (1931)
147. E A Galashin *Dokl. Akad. Nauk SSSR* **184** 639 (1969) [d]
148. C E Mees, T H James *The Theory of Photographic Process* (New York: Macmillan, 1966)
149. J F Hamilton, P C Logel *Photogr. Sci. Eng.* **18** 507 (1974)
150. J W Mitchell *J. Imaging Sci. Technol.* **38** 193 (1995)
151. O I Lomovskii, Doctoral Thesis in Chemical Sciences, Institute of Solid State Chemistry and Mechanochemistry, Siberian Branch, Academy of Sciences of the USSR, Novosibirsk, 1990
152. A Ya Lushnikov, O I Lomovskii *Izv. Sib. Otd. Akad. Nauk SSSR, Ser. Khim. Nauk* (2) 18 (1989)
153. B B Bokhonov, L P Burleva, W C Frank, J R Miller, M R V Sahyun, D R Whitcomb, J M Winslow, C Zou *J. Imaging Sci. Technol.* **40** 85 (1996)
154. J F Hamilton *J. Vac. Sci. Technol.* **13** 319 (1976)
155. J Z Jiang, R Lin, W Lin, K Nielsen, S Morup, K Dam-Johansen, R Clasen *J. Phys. D Appl. Phys.* **30** 1459 (1997)
156. G Vitulli, E Pitzalis, A Verrazani, P Pertici, P Salvadori, G Marta *Mater. Sci. Forum* **235–238** 929 (1997)
157. I G Konstanchuk, E Yu Ivanov, V V Boldyrev *Usp. Khim.* **67** 75 (1998) [*Russ. Chem. Rev.* **67** 69 (1998)]
158. T Benameur, B Rezgui, A R Yavary, R Durand *Mater. Sci. Forum* **235–238** 917 (1997)
159. E M Gutman *Mekhanokhimiya i Zashchita Metallov ot Korrozii* (Mechanochemistry and Protection of Metals from Corrosion) (Moscow: Metallurgizdat, 1981)
160. S J Trope, B Ramaswami, K T Aust *J. Electrochem. Soc.* **135** 2162 (1988)
161. O El Kedim, M Tachikart, E Gaffet *Mater. Sci. Forum* **225–227** 825 (1996)
162. R Rofagha, R Langer, A M El-Sherik, U Erb, G Palumbo, K T Aust *Scr. Metall. Mater.* **25** 2867 (1991)
163. M Schneider, W Zeiger, D Scharnweber, H Worch *Mater. Sci. Forum* **225–227** 819 (1996)
164. A Van Neste, S H Yip, S Jin, S Boily, E Ghali, D Guay, R Schulz *Mater. Sci. Forum* **225–227** 795 (1996)
165. E Tremblay, O Savadogo, S Boily, A Van Neste, R Schulz *Mater. Sci. Forum* **225–227** 813 (1996)
166. P A Thiessen *Angew. Chem.* **51** 318 (1938)
167. A Ikekawa, S Hoyakawa *Bull. Chem. Soc. Jpn.* **54** 2587 (1981)
168. A M Dubinskaya *Khim.-Farm. Zh.* **23** 755 (1989)
169. T Shakhtshneider, V V Boldyrev, in *Reactivity of Molecular Solids* (Eds E Boldyreva, V V Boldyrev) (Chichester: Wiley, 1999) p. 271
170. A V Dushkin, Z U Rykova, T P Shakhtshneider, V V Boldyrev *Int. J. Mechanochem. Mech. Alloying* **1** 48 (1994)
171. A Yu Yagodin, A V Dushkin, V V Boldyrev *Pharmazie* **3** 69 (1991)
172. V V Boldyrev, T P Shahtshneider, L P Burleva, V A Severzev *Drug Develop. Industr. Pharm.* **20** 1103 (1994)
173. T P Shakhtshneider, M A Vasilchenko, A A Politov, V V Boldyrev *Int. J. Pharm.* **130** 25 (1996)
174. R L Whetten *Acc. Chem. Res.* **26** 49 (1993)
175. P Davidovits, D L McFadden (Eds) *Alkali Halide Vapours* (New York: Academic Press, 1979)

[a] — *Phys. Met. Metallogr. (Engl. Transl.)*
[b] — *Physics-Uspekhi (Engl. Transl.)*
[c] — *Russ. J. Gen. Chem. (Engl. Transl.)*
[d] — *Dokl. Chem. Technol., Dokl. Chem. (Engl. Transl.)*
[e] — *Tech. Phys. (Engl. Transl.)*
[f] — *Russ. J. Electrochem. (Engl. Transl.)*
[g] — *Kinet. Catal. (Engl. Transl.)*
[h] — *Russ. J. Struct. Chem. (Engl. Transl.)*
[i] — *Chem. Pharm. J. (Engl. Transl.)*

Russian Chemical Reviews **70** (4) 285 – 298 (2001) © 2001 Russian Academy of Sciences and Turpion Ltd

DOI 10.1070/RC2001v070n04ABEH000639

Size effects in electrochemistry

O A Petrii, G A Tsirlina

Contents

I.	Introduction	285
II.	Size effects in diffusion kinetics. Microelectrodes and microcells.	286
III.	Electrical double layer as a nanostructure	288
IV.	Size effects in electrocatalysis	289
V.	Size effects in the elementary act of charge transfer	291
VI.	Size effects in processes of new phase formation in electrochemical systems	292
VII.	Electrochemical nanotechnologies	293
VIII.	Conclusion	295

Abstract. General characteristics of size-dependent phenomena in electrochemical systems are given. Primary attention is paid to methodical achievements of nanoelectrochemistry, which is a line of research created over the last 15 years. The development of the main concepts of electrochemistry initiated by the stream of nanoscopic information is considered. The prospects for local studies of processes on charged interfaces, elementary steps of these processes and application of nanoelectrodes and related systems in interdisciplinary fields are discussed. The bibliography includes 198 references.

I. Introduction

Electrochemistry studies homogeneous condensed ionic systems (solutions, melts, solid electrolytes) and heterogeneous systems which include electrified interfaces. The spatial scales of heterogeneous electrochemical systems vary over a wide range (Table 1). Correspondingly, the size effects observed in them are numerous and diversified, and quite a number of them are analogous to those in homogeneous electrochemical systems. However, the latter are beyond the scope of this review.

Characteristic dimensions of conventional components of electrochemical systems (electrodes, electrolytes and membranes) cover 5 – 10 orders of magnitude. The lower boundaries of the corresponding intervals approach typical sizes of specific space regions (layers) that arise only at the electrode – electrolyte, electrode – membrane and electrolyte – membrane junctions. In electrochemical systems, the concentration distribution of components near the electrode differs from that in the bulk. As the distance from the interface increases, this distribution changes, *i.e.*, the system contains nonuniform regions. The structure of such a region is considered in detail in Refs 1 – 3. Below, we only briefly comment on the concepts employed in this article.

O A Petrii, G A Tsirlina Department of Chemistry, M V Lomonosov Moscow State University, Leninskie Gory, Moscow 119899, Russian Federation. Fax (7-095) 939 01 71. Tel. (7-095) 939 55 01.
E-mail: petrii@elch.chem.msu.ru (O A Petrii)
Tel. (7-095) 939 13 21 (G A Tsirlina)

Received 21 November 2000
Uspekhi Khimii **70** (4) 330 – 344 (2001); translated by T Ya Safonova

Table 1. Characteristic scales of elements of electrochemical systems and devices.

Elements	Size intervals /m	Components
Electrodes for practical applications	0.1 – 10	metals, semiconductors, composition materials
for research	10^{-3} – 10^{-2}	
microelectrodes	10^{-5} – 10^{-4}	
ultramicroelectrodes	10^{-8} – 10^{-6}	
thin-film electrodes	$< 10^{-8}$	
Electrolyte layers		solutions, melts, solid electrolytes
electrolysers	0.1 – 10	
research cells	10^{-3} – 0.1	
thin-layer cells	10^{-6} – 10^{-5}	
microcells	10^{-7} – 10^{-6}	
Membranes	10^{-7} – 10^{-2}	polymers, porous inorganic materials
Diffusion layers	10^{-6} – 10^{-4}	all electrolyte components
Chemisorption layers	10^{-10} – 10^{-9}	the same
'Electronic tails' and near-surface layers in semiconductors	$< 10^{-11}$	electrons and other charge carriers

When an electrode process occurs on an interface, the boundary layer is depleted of the corresponding reactant and(or) enriched with the products formed. Insofar as diffusion rates are finite, a region always exists in which the concentration of one or several components depends on the distance. We call this region the diffusion layer and usually consider it as an electrolyte component.

A uniform distribution of components can also be disturbed under equilibrium conditions. Boundary regions that arise in the process are called the 'electrical double layer' (EDL).† Charged species are distributed in the EDL under the effect of different electrostatic interactions, the concentration of ions either decreasing or increasing with an increase in the distance from the

† This name is associated with the concept of metallic and ionic plates of a hypothetical capacitor commonly used as the interface model.

boundary. If the interaction of an ion with a charged electrode is much stronger than its interaction with induced charges, then the concentration distribution much resembles the diffuse distribution of charges in an ionic atmosphere and is described by a parameter having the meaning of the Debye screening length and equivalent to the effective thickness of the diffuse part of EDL, namely, the ionic diffuse layer.

If certain components of a system specifically interact with the electrode material, then a chemisorption layer (the dense part of EDL) is formed between the surface and the diffuse layer. For the vast majority of electrode–solution systems, dense layers are formed involving solution molecules and often exclusively by such molecules.

According to modern notions of the interface structure, the adsorbate layers and the 'edges' of surface atoms on metal electrodes are spatially separated with a gap in between attributed to the emerging electronic gas ('electronic tail'). In electrochemical systems, the properties of this gap depend on the electrode potential (charge). For semiconducting electrodes, the spatial dispersion of charge carriers is also characteristic of near-to-surface solid-phase layers.

We can assess the properties of electrochemical systems from electrochemical responses, *viz*., different dependences of electrical signals (current, potential, voltage) on time and also on polarisation conditions (for instance, modulation frequency and amplitude during ac polarisation). Size effects arise when the system's parameters are commensurate with the characteristic quantities that determine a particular response.

We can distinguish several basic groups of size effects caused either by the scale commensurability of two and more subsystems, or 'intrinsic' size-dependent properties of individual subsystems. Each of these groups merits special consideration (*e.g*., see Refs 4–30). In this review, we consider the general features of size effects in electrochemical systems and give them a sort of classification. The prospects of using size effects for intensifying electrode processes and also for technological (including nanotechnological) applications are discussed. The presented list of references does not exhaust all the literature (otherwise, it would be extremely large) and contains, apart from reviews, only representative papers of recent years.

Size-dependent thermodynamic properties of electrochemical systems related to equilibria involving two-dimensional adsorption layers and nanocrystals are the subject of an interdisciplinary research field that shares its frontiers with colloid chemistry, surface science and solid-state physical chemistry. Studies of other electrochemical size effects also show a trend for integration and are combined by a recently formed separate research field, *viz*., nanoelectrochemistry. Along with inherent electrochemical techniques, this actively developing new scientific discipline extensively uses probe techniques for local surface studies,[14,16,17,20,21,31–34] diffraction[35] techniques, and also optical[36,37] and small-angle X-ray methods[38] (including those *in situ*[39]).

Originally, nanoelectrochemistry was developed on the basis of studying classical size effects (for instance, the dependences of surface conductivity on film thickness[8]). However, during the past decade, it has begun to encroach more actively on the province of quantum size-dependent phenomena. The development of nanoelectrochemistry is also stimulated by the progress in electronics; the latter branch, in turn, diversifies its elemental basis due, in particular, to the introduction of micro- and nanoelectrochemical technologies. The reason for such a 'feedback' resides in the fact that by extending the scope of electrochemical systems to the nanoscale, one substantially strengthens the material basis of electrochemistry and sharply enhances its experimental potentialities.

The possibilities of experimental studies of micro- and nanoelectrochemical systems are largely determined by the facilities for measuring small currents and charges. The characteristic settling times usually lie within hundreds of milliseconds, and, even if we pass to the femtoampere range, the lower limit of measured charge will fall within 10^{-16} and 10^{-15} C. These values exceed the charges consumed in electrochemical reactions of single ions and molecules approximately by three orders of magnitude. At present, the unique measurements with nanosecond resolution have severe restrictions on the lower limit of the measured current. The crucial obstacle that prevents lowering of the limit mentioned results from the fact that characteristic polarisation capacities of micro- and nanoelectrochemical systems are commensurable with the inherent capacities of the measuring devices.

II. Size effects in diffusion kinetics. Microelectrodes and microcells.

The uppermost limit on the scale of size-dependent properties of electrochemical systems is occupied by those manifesting themselves in electrochemical processes with diffusion-controlled rates. Such properties are studied in detail for the systems in which the dimensions of either electrodes or layers of electrolyte solutions are commensurable with the diffusion layer thickness (micrometer range that may be upscaled, for instance, due to gravitation effects). That is why, when separating microelectrodes and microcells into a special class of electrochemical systems, the upper limits of sizes (volumes) cannot always be determined unambiguously, being dependent on the configuration and convection conditions.

For the majority of microelectrodes, such a limit is ~ 10 μm. For disk, spherical, semispherical, conical and microdrop liquid electrodes exact relationships for the dependences of the limiting diffusion current I_d on the characteristic size r were obtained.[40–42] Similar size limits for microcells are determined by a condition of the overlapping of diffusion layers for two electrodes between which the current flows.[43] The corresponding quantitative expressions are very complicated; hence, the applications of microcells are largely related to *in situ* surface spectroscopy (the so-called thin-layer cells for minimising absorption in the solution bulk) and microtechnologies. In those cases, the cell volume contains actually no regions with constant concentrations of reactants, and different non-steady-state size-dependent distributions of solution components can arise.

The most important basic application of microelectrodes deals with the determination of kinetic parameters of electrode processes and is limited by the ratio between the corresponding rate constants and the limiting currents of reactant delivery.

As an example, we consider the limiting diffusion current density i_d, which corresponds to the rate of an electrode process at a slow delivery of a reactant. For an electrode of a common (macroscopic) size r exceeding substantially the diffusion layer thickness, i_d is independent of the electrode configuration and determined only by the diffusion coefficient of the reactant D and its concentration c. Correspondingly, for an electrode of a geometric surface area S, the diffusion current

$$I_d = i_d S = \text{const}\ cD^m r^2, \tag{1}$$

where the power index $m < 1$.

The values of the constant and m are determined by the parameters that characterise the convection conditions (rotation velocity of a solid electrode, streaming velocity of a liquid metal from a capillary, *etc*.) and by the electrode shape and described by the rigorous relationships deduced within the framework of the planar diffusion model. Inasmuch as i_d and the rate of electron transfer stage are proportional to c, it is difficult to overcome the diffusion limitations and determine the rate constant for the electron transfer on common-size electrodes for quick processes.

When the diffusion layer thickness is commensurable with electrode dimensions, the planar diffusion model does not operate due to a significant role of edge effects. For example, for a disk microelectrode,

$$i_d = \text{const}'\ c\sqrt{D}r^{-1}. \tag{2}$$

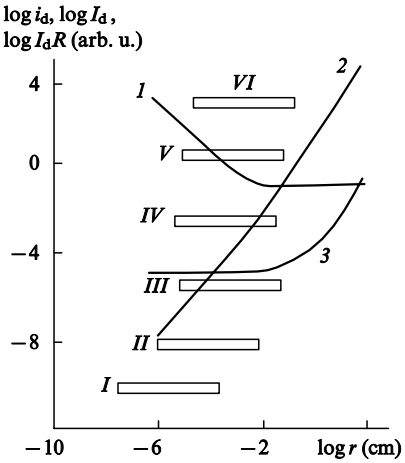

Figure 1. Size dependences of electrochemical responses (*1–3*) and typical scales of various nanotechnological processes (*I–VI*); (*1*) i_d, (*2*) I_d, (*3*) I_dR; (*I*) nanostructurisation in STM configuration, (*II*) electron-beam technologies, (*III*) ion-beam technologies, (*IV*) holographic lithography, (*V*) X-ray lithography, (*VI*) photolithography. Plotted on the basis of the results taken from Refs 19, 24.

Correspondingly, I_d turns out to be proportional to r rather than to r^2, which affects the dependence of the ohmic potential drop I_dR on r (where R is the resistance of the solution layer between the working electrode and a point in which the potential is measured by a reference electrode). Figure 1 illustrates how the most important characteristics of electrochemical systems tend to vary.

In the case of fast delivery of a reactant, regardless of the electrode size, the rate of an electrode process is proportional to the surface area (in the absence of other types of size effects, see Sections IV and V). Hence, with a decrease in r, it becomes possible to overcome the diffusion limitations for still faster reactions. Microelectrodes allow quantitative measurement of the rate constants of an order of magnitude of centimetres per second, whereas the limits of conventional rotating and dropping electrodes do not exceed 10^{-2} cm s^{-1}.

To determine the rate constants of fast reactions, the arrays of microelectrodes which include flow-through channel systems with ensembles of microband electrodes are also widely used.[44] A rotating ring-disk electrode can be considered as the first array electrode which allowed measurement of the kinetics of separate steps of electrode processes, owing to its optimum hydrodynamics.[45] The electrochemical responses of electrode arrays are characterised by special types of size dependences determined by the relative positions of their fragments (for instance, by the spaces between them).

Microelectrodes are widely used in electroanalysis,[46,47] especially for solving environmental and biological problems (for example, in electrochemical measurements *in vivo* in the monitoring of the composition of biological media, diffusion of drugs and poisons, accumulation of glucose, *etc.*). These applications stimulated further miniaturisation of electrodes. As a result, a large class of the so-called ultramicroelectrodes with surface areas of less than 1 μm^2 was developed.[48,49]

Modern methods of insulation of the surfaces of metal wires and other items provide electrodes of characteristic sizes of $\sim$ 10 nm (sometimes named nanodes). Standardisation of the geometry (shape) of nanodes presents a particular problem which can be solved by using nanosize materials of known structures, for example, carbon nanotubes as the electrodes.[50]

The term 'nanoelectrodes' is sometimes used in a different context when considering the phenomena in solutions of monodispersed colloidal metals. Thus when stabilising colloidal gold particles in dichloroethane by ferrocene-containing organic molecules, the responses of redox transformations of the latter could be detected in the single contacts of particles (nanoelectrodes) with the polarising macroelectrodes.[51] In this case, an analogy can be traced with well known suspension electrodes in which macroelectrodes play the role of current collectors.[52]

A new impact for the development of microelectrode technology was made in the end of the 1980s when Bard *et al.*[15] proposed a basically new method for carrying out local studies of surface processes and phenomena, namely, the technique of scanning electrochemical microscopy (SECM). This technique is based on the possibility of measuring the current on a probe microelectrode as a function of the distance h between the probe and the surface of an electrode under study of arbitrary dimensions dipped into a solution containing a redox system with a high electron-transfer rate constant and known diffusion coefficients of redox forms. When the diffusion layers of the probe and the electrode under study overlap (which occurs if h is commensurable or less than r), the processes on both electrodes can either be accelerated or decelerated, depending on the potentials of the probe and the electrode. The corresponding relationships for steady-state and non-steady-state currents in SECM configuration were derived as two-dimensional integral equations (for example, see Ref. 26) for systems with different geometry of probes and surfaces under study as applied to both heterogeneous and homogeneous processes.

Inasmuch as the diffusion layer boundary repeats to a certain extent the surface relief, the SECM technique allows one to visualise the latter with submicron resolution. Scanning tunnelling microscopy (STM) in air may be considered as a version of SECM, because the surface under study always bears an ultrathin film of condensed moisture playing the role of a liquid electrolyte.[53] The resolution that can be achieved depends largely on the curvature radius of the probe tip (even for tips of uncertain general geometry). Moreover, the size of the tip exerts the most critical effect on distortions of the images of surface fragments with small curvature radii. The corresponding size effects can be simulated numerically,[54] and there is a prospect of using advanced models for different convolution procedures (*e.g.*, for recovery of real images of the surface studied and for the determination of the tip geometry from the distortions of standard surface images). The development of the STM method provided special procedures for the pretreatment of well characterised tips, which are common for all probe techniques including SECM.[55,56]

The resolution in the SECM technique is enhanced if a non-uniform surface contains areas of different nature where the rates of local processes differ. Various specialised versions of SECM are developed, for instance, those for the studies of enzymic processes,[57] combined technique (SECM – probe microscopy[43]) and related techniques for investigations on the boundaries of two immiscible liquids.

A unique result achieved in SECM configuration is the measurement of responses of an electrochemical transformation of a single molecule.[58–60] This became possible owing to the accumulation of the signals from multiple successive reversible transformations of a reactant and its product in a limited solution volume between a deepened probe ultramicroelectrode ($r \approx 10$ nm) and a planar surface (Fig. 2). It is the localisation of small solution portions in micro- and nanocells the volumes of which can be reduced down to 10 nl and realisation of systems with two ultramicroelectrodes arranged along a common axis at a small distance from one another that will determine further progress in this field.[61]

Certain basic problems of microelectrochemistry formulated only recently[24,26,48] still remain unsolved. They pertain to the analysis of the potential distribution for overlapped diffusion and diffuse layers (including the case of diffuse layers of two closely spaced electrodes). This is observed, for example, in the configuration of electrochemical tunnelling microscopes (*in situ* STM). Under these conditions, certain anomalies are observed which have not yet found unambiguous explanations.[62] Thus the cathodic deposition of a metal phase can occur at electrode potentials

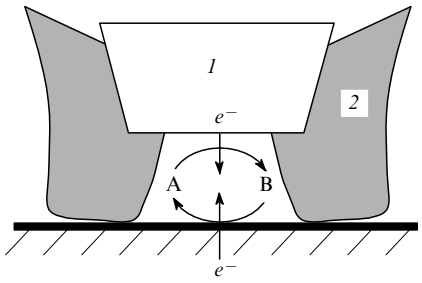

Figure 2. A scheme of a microcell for measuring electrochemical transformations of single molecules.[15]
(*1*) Ultramicroelectrode, (*2*) insulation; A and B are oxidised and reduced reactant forms, respectively.

banned by formal thermodynamics. Hence, one cannot rule out the possibility that distortions in the surface equipotentiality can occur in the vicinity of the tunnelling gap. It is still more probable that the configurations used do not provide correct measurement of the potential drop between the working and reference electrodes.

III. Electrical double layer as a nanostructure

As noted above, an electrochemical interface demonstrates a sufficiently complicated space distribution of components, due to chemisorption and electrostatic factors.[23, 63, 64]

Being the most important EDL characteristic, the zero-charge potential is directly related to the physical properties of electrodes (for example, the electronic work function).[63] Its value depends on both the electrode material nature and the crystallographic orientation of the surface. For a thin-film (especially, semiconducting) electrode, such a thickness can be reached that permits the work function to manifest size-dependent effects;[65] correspondingly, variations of film thickness can cause changes in the electrode charge *vs*. potential dependence.[7]

The models of EDL structure deal with space distributions of the potential in the dense and diffuse parts. For electrodes with pronounced heterogeneous structures and compositions, the potential can vary not only along a normal to the surface but also in parallel to it, both in the dense and diffuse parts. Comprehensive phenomenological models are developed for size-dependent parameters of EDL on polycrystalline surfaces constructed from different lattice faces with different values of zero-charge potential.[66] For small heterogeneities, EDL structure is well approximated by a model with a uniform diffuse layer. With an increase in the heterogeneity size, transition layers appear between neighbouring regions of diffuse layers of different structures. Probe techniques make it possible to study the heterogeneities of the potential distribution near the surface and describe quantitatively the interaction between the diffuse layers of the electrode and the probe.[62] This may be considered as further development of the approaches dealing with interaction of crossed filament electrodes.[63]

In the general case, the EDL is a multicomponent system in which not only concentrations but also the states of species may differ from those in the bulk. For example, the lateral Coulomb repulsion of ions adsorbed with charge transfer [67] weakens so that their surface coverage can reach a complete layer. The phenomenon of the formation of adatomic submonolayers stabilised by the interaction with the support is called *underpotential deposition* (UPD), because it provides deposition before the redox system involved reaches its equilibrium potential (for example, the deposition of adatoms M at potentials more positive than the equilibrium potential of an M/M^{n+} system). The different rates of formation and dissolution of adatomic monolayers compared with metal phases also point to the differences between these systems. Apparently, the properties of a layer start to approach those of a phase only after the deposition of the third or fourth monolayer.

Like adatoms, the molecules of organic adsorbates form structurally non-uniform adsorption layers. In the case of strong lateral interactions, different domains appear on a supporting surface, their structures being dependent on the surface geometry and charge as well as on the presence of other adsorbates. Two-dimensional condensation [68] typical of adamantane and camphor derivatives and of certain amino acids is a spectacular manifestation of lateral interactions. For adsorption with partial charge transfer (or without it at all), the co-adsorption of anions and cations can be responsible for the formation of closely packed monolayers. For example, the adsorption of multicharged polyoxometalate anions is accompanied by the formation of the so-called salt-like layers.[69–71]

Many adsorbates were reliably shown to preferentially adsorb on defective surface sites and behave specifically with respect to surface areas of different coordination.[72, 73] Figure 3 shows, as an example, the results on CO adsorption on high-index faces of a platinum single crystal. A size effect manifests itself in an increase in the surface coverage by CO molecules on areas with a high density of steps (*i.e*., with a decrease in the terrace length). For well characterised systems, the general thermodynamic approach was applied for the analysis of the contributions made by terraces and steps into reversible adsorption processes and, in particular, for the elucidation of the effects of surface crystallography on the observed zero total charge potential value.[72] Moreover, we can assume that the electronic work function is different in different surface points and, apparently, it makes sense to invoke the concept of the local work function (and, correspondingly, the local zero free charge potential [74]). An argument for such an assumption may be the difference in adsorbabilities of the surfaces of terraces and steps.

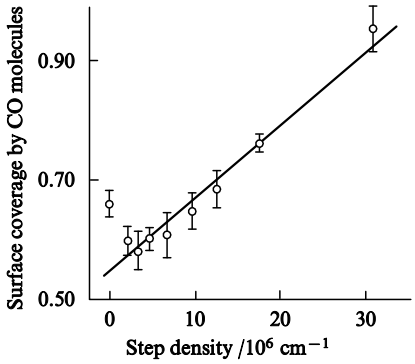

Figure 3. Surface coverage by adsorbed CO species determined from the coulometric data in 100 mM $HClO_4$ as a function of atomic step density on Pt[n(111) × (111)] single-crystal faces.[72]

It should be noted that, along with equilibrium properties of adlayers, the characteristic sizes of areas of given configurations also strongly affect the dynamic characteristics of adsorption processes. For instance, STM data at high time resolution showed that during the formation of the second layer of silver adatoms on a gold electrode surface diffusion on terraces proceeds more quickly than that on sites near the steps.[75] As a result, the adatoms are stabilised near the steps, which is beneficial for the smoothing of the relief in the early deposition stages (Fig. 4). The dynamics of adatomic-layer fragments can be followed in STM experiments with high time resolution.[24]

Unusual nanosize structures with barrier properties are formed by alkanethiol molecules adsorbed on metal atoms

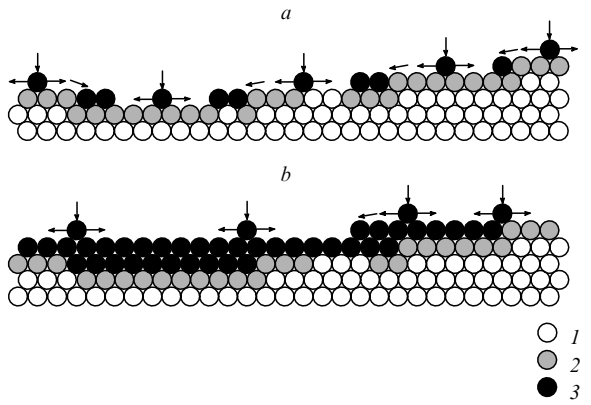

Figure 4. Schematic representation of a mechanism of silver deposition on an Au(100) surface.[75]
(*a*) Initial stages, (*b*) formation of multilayer deposit; (*1*) gold atoms, (*2*) silver atoms in equilibrium states, (*3*) mobile adatoms (marked by arrows) and silver adatoms incorporated into the lattice.

owing to chemical (virtually irreversible) interaction of terminal thiol groups with metals.[76–78] For example,

$$RSH + Hg - e^- \longrightarrow Hg(SR) + H^+.$$

By changing the alkyl chain length, one can obtain, with high precision, a sufficiently closely packed interlayer of molecules arranged in parallel (the area occupied by a thiol centre is ~ 20 Å^2) with a thickness invariant over the surface. The capacitances of alkanethiol-modified electrodes do not exceed several microfarads per square centimetre and decrease for longer alkyl chains.[79] This suggests that the solvent is practically completely forced out from the EDL dense part, and a uniform dielectric interlayer is formed on the interface. Alkyl chains are shown not to be arranged along a normal to the surface but to be bent at a substantial angle (up to 40°). Peculiarities of the formation and properties of alkanethiol layers are sensitive to surface defects,[77] which offers a unique possibility of diagnosing the latter, for example, by following different manifestations of the barrier properties of alkanethiol layers during charge-transfer processes. These systems can also be applied for studying the discrete charging of double layers formed on small particles that operate as nanoelectrodes.[80]

Considerable progress in studies of nanosize structures became evident with the possibility of visualisation of adsorbates *in situ* by probe techniques.[17, 76, 81, 82] Special attention should be drawn to the potentialities of these techniques for studying adsorption-induced phenomena, such as the appearance of surface stresses and the surface reconstruction.[83, 84] Thus the latter can be simulated on the atomic level according to the results for faces of single crystals of gold and platinum (Fig 5).

However, the problem of interpretation of STM data still remains sufficiently complicated, because the electrical double layers of a probe electrode and a scanned surface tend to overlap and interact with one another.[62]

Studies of the EDL structure on an atomic level is important for quantitative description of the interaction of reactants with electrified interfaces, *i.e.*, for the solution of problems of electrochemical kinetics. These studies can also shed light on the microscopic origin of discreteness-of-charge effects arising in the specific adsorption of ions, the effects exerted by metal hydrophilicity on the dense-layer capacitance, *etc.*, which were considered so far within the framework of phenomenological approaches. Modern approaches to building physical models of charged interfaces are surveyed in Ref. 23.

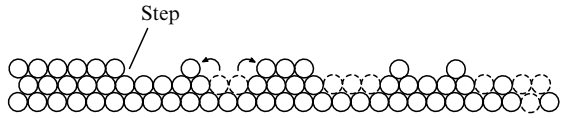

Figure 5. A scheme of island formation on a Pt(111) surface induced by potential cycling in a region that includes oxygen adsorption.[84]

IV. Size effects in electrocatalysis

Size-dependent electrochemical phenomena occur in chemisorptive and electrocatalytic processes that take place on highly dispersed, small (for instance, ultrathin) and surface-heterogeneous electrodes. In such processes, the heterogeneities of characteristic sizes commensurable with either the thicknesses or lateral periods of adsorption layers (nanosize range) play a significant role.

Many active electrocatalysts represent the so-called nanostructurised materials that exhibit periodic inhomogeinities not only on the surface but also in the bulk.[22, 85] Nanostructures are at equilibrium only in rare cases, most commonly they are metastable, but long-lived.

Nanosize materials were introduced into the practice of electrochemical studies long before the methods of their structural, morphological and electronic characterisation became available. First of all, these were the electrodes with well developed surfaces (the ratio of the real surface area S_{real} to the geometric area S being equal to 1000 and higher) of platinum-group metals consisting of nanocrystals.[4, 6, 7] For them, the experimentally determined rates of electrocatalytic processes, the surface coverages by adsorbates and the polarisation capacitances were referred not to the individual characteristics of small particles but to the values of S_{real}.[86, 87] It is the dependence of the specific (calculated per S_{real}) activity on the fabrication method that was the subject of numerous studies aimed at intensification of practically important processes applied mainly in fuel cells.

The concepts of the related structural (size) effects in heterogeneous catalysis[88] as applied to dispersed electrodes have also generated certain simplified notions based on the analysis of 'electronic' and 'structural' factors. For example, the latter factor was considered in the mitohedral approach,[89] which was developed further in the 1980s–1990s. During this period, well characterised electrode materials of similar compositions but substantially differing in surface coordination became available, *viz.*, faces of single crystals and polycrystalline materials with pronounced preferential crystallographic orientations.[10] Numerous attempts were undertaken (for example, see Refs 4, 12) to describe the activities of small metal particles in terms of an additive approach to the contributions of low-index faces. Usually, the ratio of faces on the surface was calculated for ideal equilibrium crystals (in the nanosize range, it strongly depends on the grain size).

Although a number of activity–surface coordination relationships have been revealed, the attempts to substantiate the decisive role of crystallographic orientation in electrocatalysis by dispersed materials have failed for virtually all actively studied processes of oxidation of organic compounds and hydrogen, as well as of oxygen reduction. Undeniably, the main reason for the deviations between experimental and model dependences lies in the non-equilibrium nature of small particles of real catalysts. It is also significant that the particle sizes used in the calculations were not necessarily determined by direct methods.

The technique of high-resolution electron microscopy[90–92] made it possible to refine the data on the real geometry of nanosize particles for a number of materials. However, the potentialities of this technique for the analysis of multilayer deposits and dispersed electrodes are limited. Reliable results are obtained mainly for smooth carbon supports with low surface coverages by catalysts. It should be noted that the interactions of small particles with the support substantially complicate the behaviour of these systems;[6, 7] no adequate models exist for the description of these

interactions. The activity – particle size relationships for different electrocatalytic processes are analysed in several papers (*cf.* Refs 92–98). However, these relationships pertain to relatively narrow intervals of particle sizes. Moreover, the technological methods of fabricating catalysts with different particle sizes do not provide permanence of several important structural characteristics. In different studies, the specific activity was shown either to increase or to decrease with an increase in the particle size not only in the nanometre range but also in submicron range for which one can hardy expect any manifestations of equilibrium 'structural' (and, all the more, 'electronic') size effects.

To date, different dispersed materials based on platinum and palladium have been examined by means of the STM technique with a nanometre resolution.[99–101] A comparative analysis of the data on the real surface area, porosity [102] and characteristic sizes of surface fragments (independently determined by different techniques) allows highly reliable conclusions to be drawn on the real structures of nanosize electrocatalysts: the latter include globules constituted by quasispherical particles. Sufficiently wide size distributions of particles and globules are revealed for electrodeposited dispersed catalysts. This result requires that a great number of property – size relationships be reconsidered for those cases where the sizes were estimated from S_{real}: the particle size thus determined certainly exceeds that corresponding to the distribution maximum. At a high degree of screening (or coalescence) of particles in the globules, the aforementioned differences can reach an order of magnitude, as in the case of certain materials based on electrodeposited palladium.[101]

At present, the controversial views on the structure of different boundary regions in nanosize electrocatalysts, first of all, of intergrain boundaries in globules of metal crystals pose a problem which is extremely difficult to solve experimentally. Probably, as in the case of other nanostructurised materials,[22,85] it is these highly defective regions that play a significant role in adsorption and electrocatalytic phenomena. For a number of cases, a phenomenological analysis [103,104] based on an assumption of high surface defectiveness of these electrocatalysts makes it possible to find a self-consistent set of experimental results. However, it fails to rationalise the nature of defective surface regions.

Yet another aspect of size-dependent electrocatalytic effects that manifest themselves on the scale of molecular sizes is associated with the structure of chemisorption layers. The mechanisms of the vast majority of electrocatalytic processes involve strongly bound adsorbates for which co-adsorption and competitive adsorption play important roles.[9]

A rather universal type of size effect occurs within the framework of the mechanism known as bifunctional catalysis.[9] This mechanism is realised on bi- and milticomponent surfaces where the process is controlled by the chemical reaction of two different adsorbates. Electrocatalytic hydrogenation of organic substances involving hydrogen atoms and their oxidation involving adsorbed hydroxyl radicals may serve as examples of these processes. The activity of a catalyst proves to be highest where its surface contains simultaneously two components which selectively chemisorb the species involved in the slow stage of the reaction. In this case, both the mutual arrangement of components and the ratio of their surface concentrations are of importance. Particularly, there exists an optimum (depending on the reactant structures) size of surface areas with one or another composition which provides the greatest number of reaction sites. Such an area is always commensurable with the size of the adsorbate species. Homogeneous alloys which exhibit no pronounced segregation and adatomic submonolayers are typical bifunctional catalysts. Figure 6 shows the rate of electrocatalytic oxidation of ethylene glycol on platinum covered by different amounts of tin adatoms as a function of the electrode potential.[105] Tin adatoms are the adsorption centres for active oxygen species and exhibit the maximum activity at medium surface coverages.

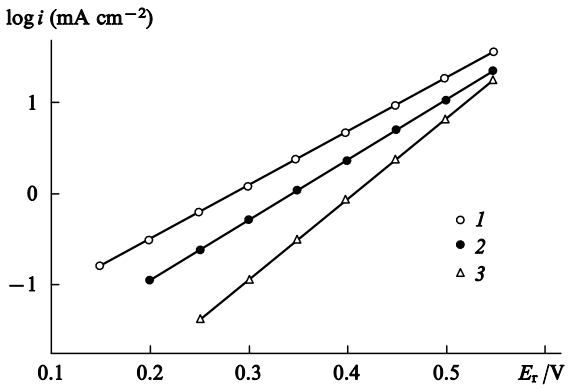

Figure 6. Steady-state polarisation curves of ethylene glycol oxidation (0.5 M, in the presence of 1 M NaOH) on platinised platinum modified by tin adatoms.[105]
Surface coverage by adatoms: (*1*) 0, (*2*) 0.76, (*3*) 0.48; E_r is the potential referred to the reversible hydrogen electrode.

If a process is controlled by the recombination of atoms, then, conversely, optimisation of the electrocatalyst requires an increase in the number of neighbouring active adsorption centres of the same nature. For this mechanism, the dependence of the process rate on the geometry and sizes of reaction sites can be well simulated by hydrogen evolution on platinum-group metals modified by different adatoms. Depending on their sizes, adatoms can occupy one, two or three neighbouring positions otherwise available for adsorbed hydrogen. In real systems, we cannot always provide a uniform distribution of a modifying additive over the surface; therefore, the observed effects of recombination inhibition appear to be smaller than is expected. This situation can be used for solving the inverse problem, *viz.*, studying the geometry of island structures.

Yet another typical mechanism of electrocatalysis (first of all, for processes involving organic substances on platinum-group metals, Fig. 7) occurs for two and more parallel processes of

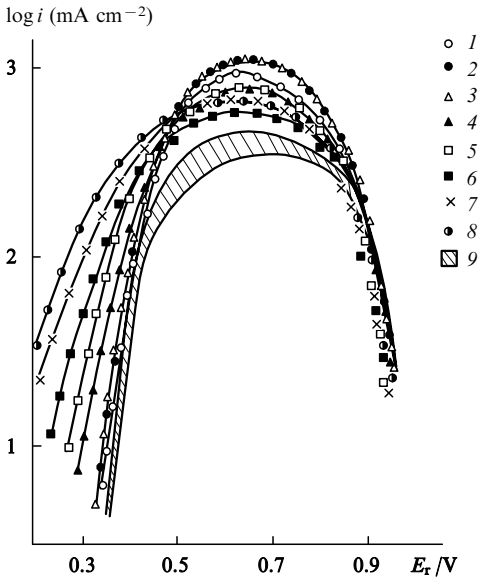

Figure 7. Steady-state polarisation curves of formic acid oxidation (1 M, in the presence of 0.5 M H_2SO_4) on platinised platinum modified by thallium adatoms.[106]
Concentration of added Tl^+ /mM: (*1*) 0.01 (*2*) 0.033, (*3*) 0.1, (*4*) 0.33, (*5*) 0.48, (*6*) 0.96, (*7*) 1.9, (*8*) 4.8, (*9*) 0. In the vicinity of the maximum, current fluctuations occur with the amplitude shown by the dashed area.

reactant chemisorption, one of which produces non-reactive strongly bound adsorbates that partly block the surface. For such self-inhibited catalytic processes, the selective suppression of the inhibitor adsorption is an important size-dependent factor. In systems with organic reactants, the blocking adsorbate occupies usually several neighbouring surface sites; hence, its formation is hindered by foreign adatoms that modify the surface (the so-called 'third-body effect'[9]). This is exemplified in Fig. 7 by the data on the acceleration of formic acid oxidation on platinum modified by thallium adatoms each blocking three neighbouring adsorption centres, according to estimates. The 'third-body' effect is manifested only in the ascending branch of the curve in the potential region where the process is inhibited by strongly adsorbed CO-like species.

Blocking adsorbates of this and nearby components are formed in both the destructive adsorption of various organic molecules and immediately in the adsorption of CO molecules. Thus the problem of designing systems with a pronounced 'third-body effect' is of prime significance for the solution of an urgent applied problem, *viz.,* preparation of CO-tolerant catalysts.

In principle, macrokinetic effects in systems with porous catalysts can be also assigned to size effects. These are discussed in detail by Chizmadzhev *et al.*[107]

V. Size effects in the elementary act of charge transfer

At present, subnanometre-scale size effects are actively studied on the molecular level within the framework of theoretical descriptions of electrochemical interfaces and attendant processes of the transfer of charged species (for example, see Refs 108–112). In such a consideration, both the sizes of molecular subsystems (reactant and product species involved in the charge transfer, solvent molecules adsorbed on electrodes) and the characteristic scales of electron density distribution are of substantial importance. Charge transfer processes cannot be studied without invoking quantum-mechanical approaches, which in turn requires a changeover from spatial scales to spatial–temporal scales.

The probability of electron transfer in an electrode–reactant system is determined by a number of factors that depend on the characteristic sizes of reaction layers.[108] The most 'large-scale' and complex factor is the distance of the closest approach of a reactant to the surface $z_{\lim}$, which is determined by steric restrictions and by chemisorptive and electrostatic interactions.

For ionic and molecular reactants, such distances do not usually exceed fractions of several tenths a nanometre. If $z_{\lim} > 1$ nm, we speak of the 'long-range' electron transfer. The limiting value $z_{\lim}$ is arbitrary and is determined by a substantial attenuation of the electron overlap, which exponentially depends on the electrode–reactant distance. By introducing the transmission coefficient K, one may represent this dependence as follows:[108]

$$K = \text{const}'' \exp\left(-\frac{z}{b}\right), \tag{3}$$

where the parameter b depends on the degree of electron delocalisation and is of an order of magnitude of a hundredth part of a nanometre. Usually, the delocalisation of reactant electrons plays the decisive role, in particular, the greatest b values (< 0.1 nm) are known for transition-metal complexes in which the charge transfer proceeds to orbitals of a mixed nature.

In principle, all reactant species located at any distance from the surface contribute to the observed rate; however, the contributions of species located in a thin near-surface layer not exceeding $z_{\lim}$ prevail. In place of the parameter $z_{\lim}$, another parameter of the same order of magnitude δz known as the reaction layer volume is used, for example, in the expression for the current density (rate of the process)

$$i = \text{const}''' (z_{\lim})\, \delta z \exp\left(-\frac{E_a}{RT}\right), \tag{4}$$

where E_a is the activation energy, R is the universal gas constant, T is the temperature. In modelling the electron transfer, δz is determined by integrating the expression (3) within the limits from $z_{\lim}$ to the infinity.

The 'long-range' transfer can be observed in systems with barrier layers on the electrode surfaces[79, 113, 114] and is studied most comprehensively for thiol systems. In particular, unambiguous dependences of the transfer rate on the barrier layer thickness are established. Thiol layers with redox-active terminal substituents that provide rigid localisation of the reactant are widely used.[115] The introduction of two redox centres, with a variable distance between them, into a thiol molecule is an interesting extension of this approach (Fig. 8).

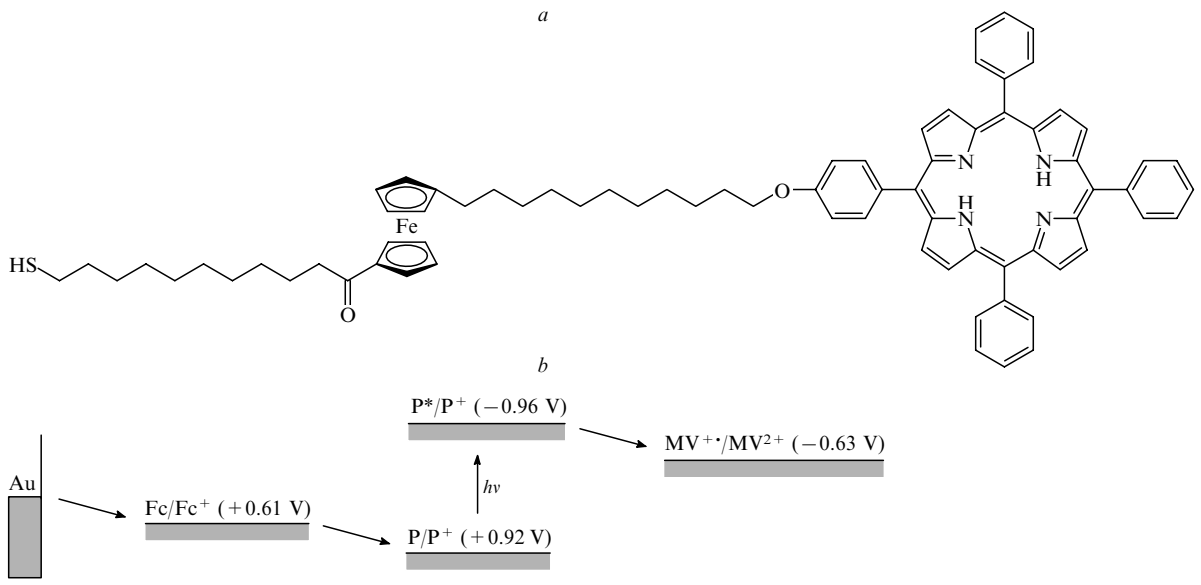

Figure 8. A scheme of a model system with two fixed redox centres, *viz*., those based on ferrocene (Fc/Fc^+) and porphyrin (P/P^+) (*a*) and the sequence of charge transfer steps to different redox centres (*b*).[116] A self-assembled layer of substituted thiols is immobilised on the surface of an illuminated gold electrode in a solution of methyl viologen (redox pair $MV^{+\bullet}/MV^{2+}$); the equilibrium potentials of the corresponding systems are shown in parentheses.

'Long-range' charge transfer is also observed for reactant species of considerable intrinsic sizes and with a pronounced degree of localisation of the transfer site (metalloproteins,[112] polynuclear complexes [71]). It should be noted that the characteristic length of the 'electronic tail' (and, correspondingly, electron overlap) depends on the electrode charge; however, the theoretical analysis of these dependences is possible so far only in terms of simplified models.[109]

The quantity z_{lim} affects not only the ovelap, which determines the prexponential factor in the equation for the rate constant of electrode reactions, but also different components of E_a: the work terms of reactants and products (if we deal with charged species, the Coulomb interactions weaken with the distance from the interface as the potential changes) and the solvent reorganisation energy. A detailed theoretical consideration of this problem is given in Refs 117, 118.

Pronounced size effects can be observed in photoelectrochemical processes involving semiconducting particles separated from the metal surface by barrier layers. The size effects are caused by a shift of absorption edge when the diameter of particles ranges from 10 to 20 nm.[119, 120] Substantial acceleration of photoelectrochemical processes occurs on passing from massive to nanosize semiconductors. This phenomenon has already found a practical application, *viz*., in photoelectrolysis of water.[121] Similar 'intrinsic' size effects of metal particles should be weaker and manifest themselves for particles with sizes below 5–7 nm. However, in principle, there exist no methodical obstacles from discovering them in the nearest future.

Prediction of the kinetics of electron transfer by taking into account all size-dependent factors becomes possible only when adequate ion–molecular models of reaction layers are built. For a number of systems, this problem can successfully be solved by invoking quantum-chemical methods [122] based on the quantum-mechanical theory of the charge-transfer elementary act.[123] Along with the classical effects of the cation size which manifest themselves in the reduction of anions on a negatively charged surface,[124] we must especially mention the inhibition of electron transfer with increase in the ligand size for a number of transition-metal complexes.[125] For non-symmetrical reactants, this dependence gives rise to various orientation effects in reaction layers.[126]

The independent (additional) possibilities of experimental simulation of the size effects of a quantum origin are provided by carrying out electron transfer processes in the STM configuration at fixed tunnelling voltages, which govern the location of energy levels of transferred electrons in the metal.[110, 127] Interesting similarities between STM and electrochemical responses can be traced for polyatomic reactants with dense outer barrier layers and for gold clusters, particularly those stabilised by alkanethiols.[128] In both cases, the current responses reveal the appearance of Coulomb blocking (up to six steps separated by potential intervals of ~ 0.3 V). The latter system, which allows one to trace the dependence of electrochemical responses on the cluster size, is considered in the literature as 'transition': for a small number of atoms in a cluster, the differences between the electrochemical charging of the gold cluster ('nanoelectrode') and an electrode process involving this cluster as a reactant in solution actually vanish.[129]

VI. Size effects in processes of new phase formation in electrochemical systems

A complex combination of size effects of different origins is realised in electrochemical processes with the formation of new phases, for instance, in electrocrystallisation processes.[25]

In the nucleation on electrode surfaces (as in the formation of a new phase in a homogeneous medium), the key role is played by supersaturation determined by the electrode potential deviation from the equilibrium value for a given redox system (overpotential η). A redox-system component formed as a result of a transfer of n electrons takes part in the nucleation process. A thermodynamic description of this phenomenon relies on the analysis of the probabilities of formation and dissolution of new-phase nuclei [5] and gives the following expression for the critical nucleus radius r_c (the minimum size, for which the probability of dissolution of a nucleus formed does not exceed the probability of its further growth):

$$r_c = \frac{\gamma A}{nF\eta} \quad \text{or} \quad r_c = \frac{2\sigma\upsilon}{nF\eta},$$

where γ is the surface tension of a two-dimensional nucleus, A is the area occupied by a mole of the substance in a monoatomic layer, F is the Faraday number, σ is the surface tension of a three-dimensional nucleus, and υ is the molar volume. When estimating the size of an extremely small critical nucleus, one cannot use the value σ characteristic of macroscopic fragments of the same solid, because, in principle, this parameter is size-dependent.

For the analysis to be correct, the EDL structure and involvement of chemisorbed solvent molecules and other solution components, as well as adatoms should also be taken into account. All these factors affect the surface energy of a nucleus and, hence, its critical size. Along with thermodynamic models, non-thermodynamic models of nucleation on the electrode surface have also been developed.[25] The latter are based on either a statistical dynamic approach or on quantum-chemical studies of different-size clusters.

The mentioned factors also play an important role in the description of steady-state and non-steady-state kinetics of nucleation and growth of new-phase particles on electrodes: in many cases, these factors can change the rate and the limiting stage of a process. Largely pertaining to potentiostatic models, the expressions for the non-steady-state current of nucleation–growth of a unit nucleus and nuclei ensembles are described in detail in numerous reviews (for example, see Refs 5, 14, 130). The time-dependent nucleus size plays a key role in deriving such expressions. The other important parameters include the number of active nucleation centres, the nucleation rate constant and a parameter characterising the kinetics of the limiting stage (the diffusion coefficient or the rate constant for electron transfer). Moreover, even the simplest approximations (for example, for the formation of spherical or semispherical nuclei on a uniform plane) allow the criteria for diagnosing the nucleation type: two-dimensional or three-dimensional growth, diffusion or kinetic control, the ratios of nucleation and growth rates, to be found. The nucleation type is elucidated from experimental current transients (for instance, power dependences at small times) by analysing the maximum current corresponding to the hindrance of growth due to the coalescence of neighbouring nuclei.

From electrochemical data, by using the corresponding algorithms, one can indirectly characterise the morphology of a system at any moment of deposition (even for a crystal size commensurable with the atomic size). However, the differences between the properties of real and model systems cause substantial deviations of the calculated values from the experimental results. For example, the calculated concentrations of active centres are often several orders of magnitude lower than those found from electron microscopy data (direct visualisation of grown crystals).

Model systems for which the active centres represent certain surface areas (for example, dislocations) and the growth rate of a new phase is limited by a process localised immediately on the surface, *viz*., the surface diffusion, are of special interest [25, 130] In this case, the key size-dependent factor is the distance between the growth steps which incorporate the adatoms slowly diffusing over the surface. However, it is difficult to fabricate such systems, especially when using real polycrystalline materials the active centres (and point defects) of which may be represented by any surface areas with small radii of curvature. The exchange of adatoms on the growth steps can be observed by means of STM.[24]

The methods of independent determination of the number and sizes of nuclei at different moments are of prime interest, especially

those that do not require the electrode to be withdrawn from solution. These requirements are fulfilled by the STM technique realised with an atomic resolution *in situ* in electrolyte solutions.[16, 17, 20, 73, 131–133] However, at present, local changes in the deposition conditions that occur near the probe, especially, for nucleation under diffusion control cannot be reliably eliminated. It was also reported that nanosize crystals are unstable in the electric field around the probe if adhesion is low (for example, this concerns the important group of model processes of metal deposition on highly oriented pyrographite). An efficient approach to the determination of the number and sizes of nuclei consists in substitution of the background solution for the deposition solution without opening the circuit.[73] The probe is brought to the surface after all the deposition stages studied are completed. This, however, dramatically reduces the time resolution.

The techniques of atomic-force microscopy in a noncontact mode progressively gain importance.[32, 134] The advantage of such methods is the possibility of studying objects of low conductivities, for example, in electroplating on wide-band semiconductors,[31, 32] in structural transformations of polymer deposits during dedoping [135] and in the course of formation of nanosize barrier oxide layers.[136] Combined photo-assisted probe techniques are being actively developed.[21, 33] It should be noted that quantitative probe-microscopic data on nanosize particles of electrodeposits (*i.e.*, where the radius of curvature of a probe is commensurable with that of the particles) can be obtained only when special convolution procedures are used, the algorithms of which are being extensively developed.[54, 137, 138]

A quantitative description of electrochemical responses in the formation of a new phase is complicated by the appearance of the so-called screening zones caused by the overlap of either the neighbouring nuclei or the corresponding diffusion layers. Certain effects of this sort can be simulated, which however always increases the number of fitting parameters, thus reducing the diagnostic possibilities of the model. Experimentally, the overlap can be avoided if the distances between the active centres are of an order of a micrometre: in this case a single nucleus can be grown on an ultramicroelectrode.[139, 140] In fact, such experiments allow one to observe the elementary events that constitute the nucleation process and then to use the obtained information for the analysis of the growth of ensembles.

Screening under diffusion control can also be used for obtaining the so-called fractal deposits (for example, see Ref. 141). Such deposits are formed in thin-layer cells, which includes the boundaries of two immiscible liquids and the solution–air interfaces. The main contribution to the growth of a new phase is made by the secondary nucleation processes which can be intensified by pulsed deposition modes (Fig. 9). Simulation of secondary nucleation which plays a significant role in many systems is a very complicated task, which defies analytical solution unless being considerably simplified. In this case, numerical techniques should be invoked.[143]

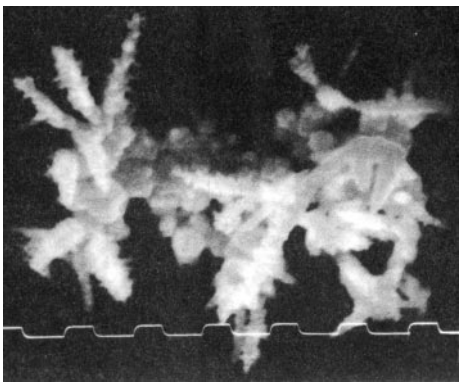

Figure 9. SEM image of platinum deposit on a carbon surface electroplated from a solution of 40 mM H_2PtCl_6 by square-wave pulses.[142] The horizontal measuring interval is 1 μm.

The technological possibilities of electrocrystallisation are extremely high and today are only partly used. The systems in which the crystals are formed on the surface of preliminarily developed adatomic submonolayers allow variation of the geometry of deposits on a nanolevel. In these layers, various two-dimensional phase transitions occur, and three-dimensional growth of nuclei is initiated by different mechanisms on domains of different structures.[144]

Tuning the fine structures by using the accompanying adsorption phenomena is also possible in the dissolution of metals: the processes of this group can be generally considered as electrocrystallisation with the formation and growth of cavity-type nuclei.

For the studies on the nanoscale level, a more precise control over the processes of new phase growth in the presence of organic additives traditionally used in industrial electroplating as the brighteners is possible by varying the ratio of the rates of nanocrystal growth in different directions.[145] Deposition of unusually long-lived metastable highly defective solids deserves mention as a promising approach.[146–148] The deposition becomes possible due to the formation of crystals on electrodes under substantially non-equilibrium conditions. A related direction is associated with the controlled variation of the stoichiometry of multicomponent phases that are deposited.[149–151]

In connection with the development of nanotechnology (see the next Section), it seems reasonable to outline the range of materials which can be deposited or formed by electrochemical mechanisms. On inert supports, one can carry out cathodic deposition of metals, alloys and certain semiconducting materials based on sulfur, selenium and tellurium and of solid complex compounds (for example, Prussian Blue and its analogues). The latter are of interest for electrochromic and sensor devices. Using anodic deposition on inert supports, one can obtain oxides and hydroxides,[152] different polymers [153, 154] and salt phases with variable electrophysical properties.[155] Anodising of metals in specially chosen media results in the formation of nanosize layers of passivating oxides many of which exhibit high photochemical activities.[156]

The formation of intercalates is an extremely important group of electrocrystallisation processes. Crystallisation of a new phase proceeds in the electrode bulk and, as a rule, is controlled by solid-state diffusion. Strains caused by intercalation can be observed by probe techniques.[157] Rapid intercalation processes are typical of a number of oxohydroxide phases and are accompanied by changes in the oxygen stoichiometry, which often proceed simultaneously with the proton transfer. High intercalation rates can be reached, for example, in materials based on oxides of ruthenium [158] and tin [159] for lattices of certain oxygen deficiencies. In such materials, as in metal hydrides, intercalation seems to be accompanied by the formation of nanosize regions with different compositions. The structure of intergrain boundaries is of principal significance for the reversibility and rate of intercalation, in particular for prevention of cracking by changing the local composition of grains.[22]

VII. Electrochemical nanotechnologies

Electrochemical fabrication of small-size articles occupies an important place in the system of chemical materials science and design of new materials having special properties. The mechanisms of formation or removal of individual small portions of solids play a decisive role in the field of electrochemical nanotechnology. These mechanisms are not quite clear which prevents the use of the most important advantage of electrochemical methods of fabricating nanoobjects, *viz.*, their controllability and the possibility of on-line quantitative monitoring. The controllability is provided by carrying out a process at a fixed potential (similar modes of deviation from equilibrium are practi-

cally unrealisable in beam and in CVD and PVD technologies). In the general case, monitoring is provided by measuring current and charge. The sensitivity to the rate of product accumulation is determined by the aforementioned limits of measuring these parameters. Additional possibilities of monitoring will arise with the use of a quartz-crystal microbalance technique, which can easily be realised in electrochemical systems, but have not yet found any practical application.

The existing nanotechnologies can be classified as local [31] and non-local.[19, 160] Most often, the latter represent different versions of lithographic techniques, *i.e.*, multistage combined technologies using photoinduced processes.

Non-local nanotechnologies based on different self-organisation processes in electrochemical systems represent an alternative to lithography. A typical example is the anodic electrosynthesis of alumina in which the ordered cylindrical pores with diameters of several tens nanometres are characterised by an extremely narrow size distribution.[145, 161] Being of interest for catalysis, this nanotube material [162] is widely used in combined technologies as a nanosize matrix. Metals [163, 164] and carbon materials [165] can be deposited into the pores of such an alumina matrix, and then alumina is removed at room temperature by dissolving it in alkali or HF. Similar processes can be realised for certain polymeric matrices (Fig. 10).

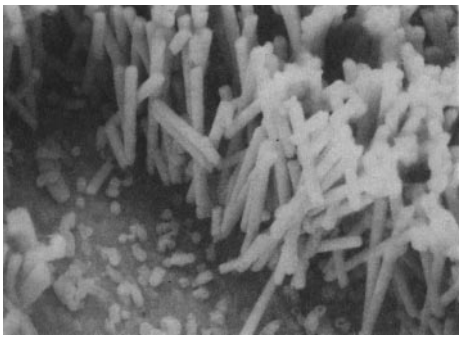

Figure 10. SEM image of an array of gold nanowires fabricated by electroplating into a polycarbonate matrix (after removal of the matrix).[166]

Electrodeposition of a metal into a porous matrix (templating) and co-deposition of a metal and a matrix (quasitemplating) form the basis of technologies for production of metallised conducting polymers.[167, 168]

Under certain conditions, the phenomenon of the formation of ordered new-phase nuclei in the absence of a matrix can also be used in nanotechnologies, for instance, in the preparation of catalytically active materials with particles of fixed sizes and also in combined low-temperature technologies for the preparation of semiconducting particles.[169–172]

Electrodeposition of lamellar bimetallic structures which is carried out either by different step-wise modes from a complex electrolyte or by consecutive deposition from different solutions constitute a separate group of processes. Continuous alternating 2-nm layers can be reproducibly obtained in systems characterised by two-dimensional growth. Layer-by-layer deposition finds wide application in the technologies of preparation of magnetic bimetallic materials.[173–176] Layer-by-layer deposition of single layers of semiconducting oxide phases [177] and of special polymeric compositions [178] is promising for the preparation of semiconducting superlattices.

Cathodic deposition of Cu/Cu_2O structures in the presence of organic complexones in a weakly alkaline medium, which is carried out in a simplest galvanostatic mode, is an example of a nanoelectrochemical technology for fabricating lamellar compositions.[179–181] Deposition of alternating layers of nanosize thicknesses is accomplished owing to a spontaneous initiation of potential oscillations caused by periodic changes in the pH and copper ion concentration in the near-electrode layer. In future, this method can be extended to other oscillating electrode processes.

The methods of dispersing metals by anodic dissolution are also worth being mentioned. Bach and coworkers [182–185] appear to be the first to apply this approach for the preparation of platinum colloids in aqueous media in the electric arc. In less severe conditions, a similar method is possible for palladium in non-aqueous solvents.[186] However, the problem of stabilisation of colloids is demanding, which requires introduction of organic additives in most cases.

We also assign the methods of immobilisation of molecular ensembles, clusters and metal particles on electrode surfaces to electrochemical nanotechnologies. The particles are bound with the surface by adsorption induced by the potential (charge) of an electrode. In a number of cases, this process occurs under electrophoretic supply and often involves surfaces preliminarily functionalised, for example, by alkanethiols. The best developed methods are those of colloid immobilisation [54, 187–189] which provide virtually monodispersed coatings. When using weak stabilisers, for example, citrates, it is possible to simultaneously provide a narrow size distribution of particles and their high adsorbabilities (Fig. 11).

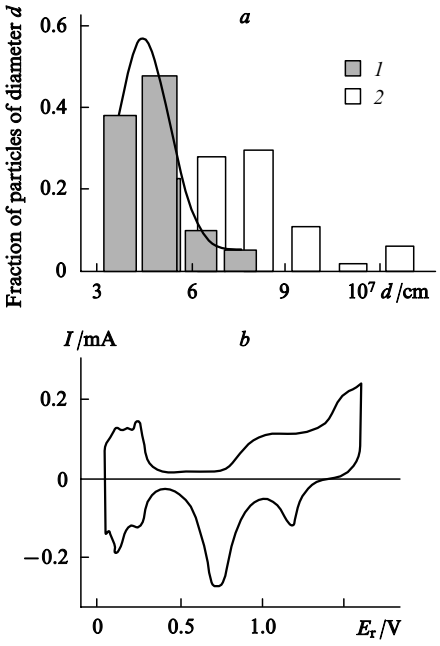

Figure 11. Size distribution of particles of immobilised platinum citrate colloid on polycrystalline gold (*a*) and potentiodynamic curve of the immobilised colloid (*b*). The distribution is plotted from STM data (*1*); for comparison, a wider distribution (*2*) corresponding to platinum electrodeposition is shown.[54]

Various local nanotechnologies can be realised in the configuration of probe microscopes [18] based on diverse processes. Thus one can locally deposit polymers and metals either by supplying reagents from the solution bulk [190] or by generating them on the probe tip.[191] It is also possible to modify a surface by transferring metal to it from the probe during short mechanical contact.[192] In this process, no electrochemical reaction occurs, and adsorption phenomena on the charged surface appear to play a significant role in the stabilisation of clusters formed. Figure 12 shows a scheme of this procedure. The methods of local etching near the tip, which are realised in STM configuration (both *in situ* [193] and *ex situ* [194]) where the role of an electrolyte is played by the moisture concentrated from air, are also gaining acceptance.

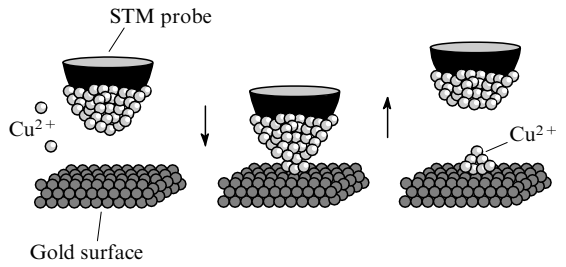

Figure 12. A procedure for local modification of a gold surface by copper clusters in an STM configuration.[20]

The adsorption and related combined nanotechnologies based on self-organisation in two-dimensional layers and spontaneous chemical deposition employ efficiently electrochemical methods to govern the process.[195]

Local modification of a surface in a scanning mode with the formation of sufficiently stable cluster ensembles is sometimes called electrochemical nanolithography.[192–193] The response time of probe microscopes leaves only few chances for nanolithography in fabricating items on the nanosize scale. However, with the progress in nanoelectronics, the scale of these electrochemical technologies will clearly increase. We can offer quite a number of examples where island, lamellar and other nanostructures formed by applying electrochemical methods are successfully used as quantum wells, superlattices, tunnelling diodes, *etc*.

Apparently, one of the main directions is associated with the achievement of quantum-size and resonance effects on the tips of STM probes modified electrochemically or by adsorption.[196, 197] In particular, this involves the quest for systems with a negative differential resistance. Figure 13 shows an example of such a response for a local quasi-one-dimensional nanostructure.

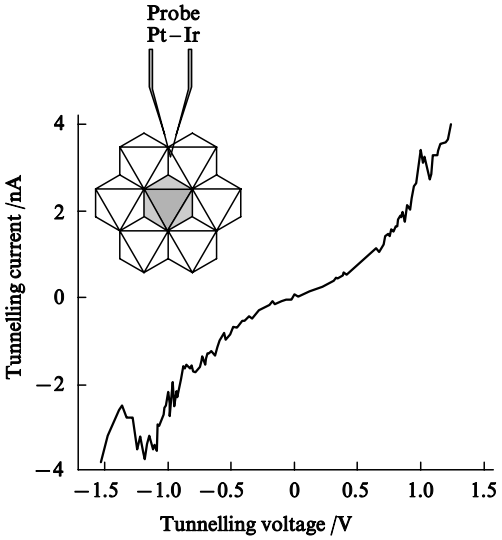

Figure 13. Tunnelling current *vs*. voltage characteristic demonstrating the negative differential resistance effect using a probe modified by heteropoly molybdate.[197]

VIII. Conclusion

The material reported in this review does not exhaust all the approaches to the research and application of size effects in electrochemistry. At present, prospects for the development of nanoelectrochemistry appear to be somewhat remarkable. This is associated with the fact that, in principle, possibilities of governing the operations on an atomic level have already been demonstrated. However, such achievements are realisable only at the lower limits of the possibilities of the available equipment.

An on-line observation of elementary steps of electrochemical charge transfer, even if for relatively slow reactions, seems to be most impressive.[24] However, this will require a substantial decrease in the operation time of probe techniques (to date, scanning of 50 images per second with an atomic resolution is apparently a record, however, not as yet for liquid phases). Conceptually, electrochemistry arrives at quite a novel stage of development when we must reconsider many common concepts and relationships. This reconsideration concerns now, particularly, the modification of the traditional Nernst equation of the equilibrium potential when applied to nanosize materials and the relationships of the classical theory of electrocrystallisation. Which of the predicted issues will remain in the status of science fiction and which will enter common research and technological practice and when this will occur, depends on many factors. However, the fast progress of nanochemistry in the recent years lends optimism.

Great expectations are associated with the integrating trends of different branches of physics and chemistry. Carrying out their experiments, modern scientists actually deal not only with elementary events that accompany transformations of single atoms and molecules, but also with transition states.[198] In the near future it may become possible to transform the experimental basis of these studies so as to adapt it to electrochemical systems.

This work was supported by the Ministry of Industry, Science and Technologies of the Russian Federation and the Foundation 'Integration' (United Educational and Research Centre A0114). We are grateful to the Corresponding member of the RAS Professor Yu M Polukarov for discussing the topical problems of nanochemistry.

References

1. J Goodisman *Electrochemistry: Theoretical Foundation* (Chichester: Wiley, 1987)
2. W Schmickler *Interfacial Electrochemistry* (Oxford: Oxford University Press, 1995)
3. B B Damaskin, O A Petrii *Vvedenie v Elektrokhimicheskuyu Kinetiku* (Introduction to Electrochemical Kinetics) (Moscow: Vysshaya Shkola, 1983)
4. K Kinoshita, P Stonehart, in *Modern Aspects of Electrochemistry* Vol. 12 (Eds J O'M Bockris, B E Conway) (New York: Plenum, 1979)
5. A I Danilov, Yu M Polukarov *Usp. Khim.* **56** 1082 (1987) [*Russ. Chem. Rev.* **56** 619 (1987)]
6. V S Bagotsky, A M Skundin *Electrochim. Acta* **29** 757 (1984)
7. V S Bagotsky, A M Skundin *Electrochim. Acta* **29** 951 (1984)
8. G N Mansurov, O A Petrii, V P Nedoshivin, A S Bluvshtein, in *Elektrokhimiya (Itogi Nauki i Tekhniki)* [Electrochemistry (Advances in Sciences and Engineering Series)] (Moscow: Izd. VINITI, 1988) Vol. 27, p. 62
9. O A Petrii, G A Tsirlina, in *Elektrokhimiya (Itogi Nauki i Tekhniki)* [Electrochemistry (Advances in Sciences and Engineering Series)] (Moscow: Izd. VINITI, 1988) Vol. 27, p. 3
10. O A Petrii, G A Tsirlina, in *Elektrokhimiya (Itogi Nauki i Tekhniki)* [Electrochemistry (Advances in Sciences and Engineering Series)] (Moscow: Izd. VINITI, 1991) Vol. 34, p. 3
11. S Makerjee *J. Appl. Electrochem.* **20** 537 (1990)
12. R R Adzis, in *Advances in Electrochemistry and Electrochemical Engineering* Vol. 13 (Ed. H Gerischer) (New York: Wiley-Interscience, 1984) p. 159
13. A Hamelin, in *Modern Aspects of Electrochemistry* Vol. 16 (Eds J O'M Bockris, B E Conway) (New York: Plenum, 1985) p. 1
14. A I Danilov *Usp. Khim.* **64** 818 (1995) [*Russ. Chem. Rev.* **64** 767 (1995)]
15. A J Bard, D E Cliffel, C Demaille, F F Fan, M Tsionsky *Ann. Chim.* **87** 15 (1997)
16. E T Yu *Chem. Rev.* **97** 1017 (1997)

17. A A Gewirth, B K Niece *Chem. Rev.* **97** 1129 (1997)
18. R M Nyffenegger, R M Penner *Chem. Rev.* **97** 1195 (1997)
19. J W Schultze, V Tsakova *Electrochim. Acta* **44** 3605 (1999)
20. D M Kolb, M A Schneeweiss *Interface* (1) 26 (1999)
21. L F Garfias-Mesias, W H Smyrl *Electrochim. Acta* **44** 3651 (1999)
22. H Gleiter *Acta Mater.* **48** 1 (2000)
23. R Guidelli, W Schmickler *Electrochim. Acta* **45** 2317 (2000)
24. D M Kolb *Electrochim. Acta* **45** 2387 (2000)
25. E Budevski, G Staikov, W J Lorenz *Electrochim. Acta* **45** 2559 (2000)
26. M V Mirkin, B R Horrocks *Anal. Chim. Acta* **406** 119 (2000)
27. A Kaifer, M Gomez-Kaifer *Supramolecular Electrochemistry* (Weinheim: Wiley-VCH, 1999)
28. W J Lorenz, W Plieth (Eds) *Electrochemical Nanotechnology. In situ Local Probe Techniques at Electrochemical Interfaces* (Weinheim: Wiley-VCH, 1998)
29. R Schuster, V Kirchner, P Allongue, G Ertl *Science* **289** 98 (2000)
30. K Krischer, in *Modern Aspects of Electrochemistry* Vol. 32 (Eds B E Conway, J O'M Bockris, R E White) (New York: Kluwer Academic Plenum, 1999) p. 1
31. M Cerisier, C Van Haesendonck, J-P Celis *J. Electrochem. Soc.* **146** 1829 (1999)
32. J V Zoval, R M Stiger, P R Biernacki, R M Penner *J. Phys. Chem.* **100** 837 (1996)
33. T Miki, H Yanagi *Langmuir* **14** 3405 (1998)
34. J Li, E Wang *Electroanalysis* **8** 107 (1996)
35. G Lehmpfuhl, Y Uchida, M S Zei, D M Kolb, in *Imaging of Surfaces and Interfaces. Frontiers in Electrochemistry* Vol. 5 (Eds J Lipkowski, P N Ross) (New York: Wiley-VCH, 1999) p. 57
36. M A Lovell, M J Walters, D Roy *Phys. Chem. Chem. Phys.* **1** 1985 (1999)
37. P Christensen, A Hamnett *Electrochim. Acta* **45** 2443 (2000)
38. D I Kochubei *EXAFS-Spektroskopiya Katalizatorov* (EXAFS Spectroscopy of Catalysts) (Novosibirsk: Nauka, 1992)
39. M Fleischmann, B W Mao *J. Electroanal. Chem.* **229** 125 (1987)
40. Q Fulian, A C Fisher, G Denuault *J. Phys. Chem. B* **103** 4387 (1999)
41. R D Martin, P R Unwin *J. Electroanal. Chem.* **439** 123 (1997)
42. L Koene, M Sluyters-Rehbach, J H Sluyters *J. Electroanal. Chem.* **402** 57 (1996)
43. C E Jones, J V Macpherson, Z H Barber, R E Somekh, P R Unwin *Electrochem. Commun.* **1** 55 (1999)
44. P B Mills, W J Aixill, F Prieto, J A Alden, R G Compton, M Rueda *J. Phys. Chem. B* **102** 6573 (1998)
45. A N Frumkin, L N Nekrasov *Dokl. Akad. Nauk SSSR* **126** 115 (1959) [a]
46. M Koudelka-Hep, P D van der Wal *Electrochim. Acta* **45** 2437 (2000)
47. M J Schöning, P Schroth, S Schütz *Electroanalysis* **12** 645 (2000)
48. C Amatore *C.R. Acad. Sci.* **323** 757 (1996)
49. M Fleischmann, B S Pons, D R Rolison, P P Schmidt *Ultramicroelectrodes* (Morganton, NC: Datatech. Systems, 1987)
50. J K Campbell, L Sun, R M Crooks *J. Am. Chem. Soc.* **121** 3779 (1999)
51. S J Green, J J Stokes, M J Hostetler, J Pietron, R W Murray *J. Phys. Chem. B* **101** 2663 (1997)
52. O A Petrii, A V Losev, in *Elektrokhimiya (Itogi Nauki i Tekhniki)* [Electrochemistry (Advances in Sciences and Engineering Series)] (Moscow: Izd. VINITI, 1979) Vol. 14, p. 120
53. S Yu Vassiliev, A V Denisov *Zh. Tekhn. Fiz.* **70** 100 (2000) [b]
54. S Yu Vassiliev, S N Pron'kin, G A Tsirlina, O A Petrii *Elektrokhimiya* **37** 523 (2001) [c]
55. A J Nam, A Teraen, T A Lusby, A J Melmed *J. Vac. Sci. Technol. B* **13** 1556 (1995)
56. B Zhang, E Wang *Electrochim. Acta* **39** 103 (1994)
57. C Kranz, G Wittstock, H Wohlschlager, W Schuhmann *Electrochim. Acta* **42** 3105 (1997)
58. F F Fan, A J Bard *Science* **267** 871 (1995)
59. A J Bard, F-R F Fan *Acc. Chem. Res.* **29** 572 (1996)
60. F-R F Fan, A J Bard *Science* **277** 1791 (1997)
61. R Schuster, V Kirchner, X H Xia, A M Bittner, G Ertl *Phys. Rev. Lett.* **80** 5599 (1998)
62. Z-X Xie, D M Kolb *J. Electroanal. Chem.* **481** 177 (2000)
63. A N Frumkin *Potentsialy Nulevogo Zaryada* (Zero-Charge Potentials) (Moscow: Nauka, 1982)
64. M A Vorotyntsev, A A Kornyshev *Elektrostatika Sred s Prostranstvennoi Dispersiei* (Electrostatics of Media with Space Dispersion) (Moscow: Nauka, 1993)
65. E L Nagaev *Phys. Rep.* **222** 199 (1992)
66. M D Levi, B B Damaskin, I A Bagotskaya, in *Elektrokhimiya (Itogi Nauki i Tekhniki)* [Electrochemistry (Advances in Sciences and Engineering Series)] (Moscow: Izd. VINITI, 1983) Vol. 19, p. 3
67. O A Petrii, A S Lapa, in *Elektrokhimiya (Itogi Nauki i Tekhniki)* [Electrochemistry (Advances in Sciences and Engineering Series)] (Moscow: Izd. VINITI, 1987) Vol. 24, p. 3
68. A N Frumkin, N V Fedorovich, E V Stenina, in *Elektrokhimiya (Itogi Nauki i Tekhniki)* [Electrochemistry (Advances in Sciences and Engineering Series)] (Moscow: Izd. VINITI, 1978) Vol. 13, p. 5
69. H Matsumoto, I Oda, J Inukai, M Ito *J. Electroanal. Chem.* **356** 275 (1993)
70. Y-G Kim, S-L Yau, K Itaya *J. Am. Chem. Soc.* **118** 393 (1996)
71. M I Borzenko, G A Tsirlina, O A Petrii *Elektrokhimiya* **36** 509 (2000)
72. V Climent, R Gomez, J M Feliu *Electrochim. Acta* **45** 629 (1999)
73. S Strobac, O M Magnussen, R J Behm *Phys. Rev. Lett.* **83** 3246 (1999)
74. P N Ross *J. Chim. Phys.* **88** 1353 (1991)
75. N Ikemiya, K Yamada, S Hara *Surf. Sci.* **348** 253 (1996)
76. G E Poirier *Chem. Rev.* **97** 1117 (1997)
77. R Yamada, K Uosaki *Langmuir* **14** 855 (1998)
78. D Hobara, K Miyake, S Imabayashi, K Niki, T Kakiuchi *Langmuir* **14** 3590 (1998)
79. K Slowinski, R V Chamberlain, C J Miller, M Majda *J. Am. Chem. Soc.* **119** 11 910 (1997)
80. S Chen, R W Murray, S W Feldberg *J. Phys. Chem. B* **102** 9898 (1998)
81. P Sautet *Chem. Rev.* **97** 1097 (1997)
82. T C Ta, V Konda, M T McDermott *J. Phys. Chem. B* **103** 1295 (1999)
83. W Haiss, J K Sass *J. Electroanal. Chem.* **386** 267 (1995)
84. P Christensen *Chem. Rev.* **92** 197 (1992)
85. H Gleiter *Nanostruct. Mater.* **6** 3 (1995)
86. S Trasatti, O A Petrii *J. Electroanal. Chem.* **327** 353 (1992)
87. T D Gladysheva, B I Podlovchenko *Vest. Mosk. Univ., Ser. 2, Khim.* **38** 3 (1997) [d]
88. S Z Roginskii *Geterogennyi Kataliz. Nekotorye Voprosy Teorii* (Heterogeneous Catalysis. Some Theoretical Problems) (Moscow: Nauka, 1979)
89. O M Poltorak, V S Boronin *Zh. Fiz. Khim.* **40** 153 (1969) [e]
90. K Shimazu, K Uosaki, H Kita, Yo Nodosaka *J. Electroanal. Chem.* **256** 481 (1988)
91. K Shimazu, D Weishaar, T Kuwana *J. Electroanal. Chem.* **233** 223 (1987)
92. Y Takasu, N Ohashi, X-G Chang, Y Murakami, H Minagawa, S Sato, K Yahikozawa *Electrochim. Acta* **41** 2595 (1996)
93. K Yahikozawa, Y Yamashita, Y Matsuda, Y Takasu *Chem. Express* **7** 597 (1992)
94. T Frelink, W Visscher, J A R van Veen *J. Electroanal. Chem.* **382** 65 (1995)
95. A Kabbadi, F Gloaguen, F Andolfatto, R Durand *J. Electroanal. Chem.* **373** 251 (1994)
96. I G Gasella, E Desmondi *Electroanalysis* **8** 447 (1996)
97. M Watanabe, I Salyusa, P Stonehart *J. Electroanal. Chem.* **271** 213 (1989)
98. G Kokkinidis, A Papoutsis, D Stoychev, A Milchev *J. Electroanal. Chem.* **486** 48 (2000)
99. M E Martins, C F Zinola, G Andreasen, R C Salvarezza, A J Arvia *J. Electroanal. Chem.* **445** 135 (1998)
100. O A Petrii, G A Tsirlina, S N Pron'kin, F M Spiridonov, M L Khrushcheva *Elektrokhimiya* **35** 12 (1999) [c]
101. M Yu Rusanova, G A Tsirlina, O A Petrii, T Ya Safonova, S Yu Vassiliev *Elektrokhimiya* **36** 517 (2000) [c]
102. T D Gladysheva, E I Shkol'nikov, Yu M Vol'fkovich, B I Podlovchenko *Elektrokhimiya* **18** 435 (1982) [c]
103. M L Khrushcheva, G A Tsirlina, O A Petrii *Elektrokhimiya* **30** 755 (1994) [c]
104. S N Pron'kin, O A Petrii, G A Tsirlina, D J Schiffrin *J. Electroanal. Chem.* **480** 112 (2000)
105. N V Smirnova, O A Petrii *Elektrokhimiya* **24** 522 (1988) [c]

106. G A Tsirlina, V N Andreev, Yu B Vassiliev, V E Kazarinov *Elektrokhimiya* **23** 556 (1987) [c]
107. Yu A Chizmadzhev, V S Markin, M R Tarasevich, Yu G Chirkov *Makrokinetika Protsessov v Poristykh Sredakh* (Macrokinetics of Processes in Porous Media) (Moscow: Nauka, 1971)
108. A M Kuznetsov *Charge Transfer in Physics, Chemistry and Biology, Mechanisms of Elementary Processes and Introduction to the Theory* (Berkshire: Gordon and Breach, 1995)
109. A A Kornyshev, A M Kuznetsov, J Ulstrup *J. Phys. Chem.* **98** 3832 (1994)
110. J E T Andersen, A A Kornyshev, A M Kuznetsov, L L Madsen, P Muller, J Ulstrup *Electrochim. Acta* **42** 819 (1997)
111. A M Kuznetsov, J Ulstrup *J. Inclusion Phenom. Macrocycl. Chem.* **35** 45 (1999)
112. Q Chi, J Zhang, E P Friis, J E T Andersen, J Ulstrup *Electrochem. Commun.* **1** 91 (1999)
113. K Slowinski, K U Slowinska, M Majda *J. Phys. Chem. B* **103** 8544 (1999)
114. K Slowinski, H K Y Fong, M Majda *J. Am. Chem. Soc.* **121** 7257 (1999)
115. V Chechik, C J M Stirling *Langmuir* **14** 99 (1998)
116. K Uosaki, T Kondo, T Kanai, K Iso-o *Z. Phys. Chem.* **212** 23 (1999)
117. Yu I Kharkats *Elektrokhimiya* **9** 881 (1973) [c]
118. A M Kuznetsov, E D German *Elektrokhimiya* **26** 931(1990) [c]
119. M Miyake, T Torimoto, T Sakata, H Mori, H Yoneyama *Langmuir* **15** 1503 (1999)
120. S Drouard, S G Hickey, D J Riley *Chem. Commun.* 67 (1999)
121. D A Tryk, A Fujishima, K Honda *Electrochim. Acta* **45** 2363 (2000)
122. R R Nazmutdinov, G A Tsirlina, O A Petrii, Yu I Kharkats, A M Kuznetsov *Electrochim. Acta* **45** 3521 (2000)
123. A M Kuznetsov, J Ulstrup *Electrochim. Acta* **45** 2339 (2000)
124. W R Fawcett, in *Electrocatalysis* (Eds J Lipkowski, P N Ross) (New York: Wiley-VCH, 1998) p. 323
125. V Yu Kotov, G A Tsirlina, O A Petrii *Elektrokhimiya* **34** 365 (1998) [c]
126. G A Tsirlina, Yu I Kharkats, R R Nazmutdinov, O A Petrii *Elektrokhimiya* **35** 19 (1999) [c]
127. C Im, K M Engenhardt, S Gregory *Phys. Rev. B* **59** 3153 (1999)
128. R C Ingram, M J Hostetler, R W Murray, T G Schaaff, J Khoury, R L Whetten, T P Bigioni, D K Guthrie, P N First *J. Am. Chem. Soc.* **119** 9279 (1997)
129. J J Pietron, J F Hicks, R W Murray *J. Am. Chem. Soc.* **121** 5565 (1999)
130. J A Harrison, H R Thirsk, in *Electroanalytical Chemistry* Vol. 5 (Ed. A J Bard) (New York: Marcel Decker, 1971) p. 67
131. R Q Hwang, M C Bartelt *Chem. Rev.* **97** 1063 (1997)
132. J V Zoval, J Lee, S Gorer, R M Penner *J. Phys. Chem. B* **102** 1166 (1998)
133. F Gloaguen, J M Leger, C Lamy, A Marmann, U Stimming, R Vogel *Electrochim. Acta* **44** 1805 (1999)
134. Q Wu, D Barkey *J. Electrochem. Soc.* **144** L261 (1997)
135. Y Kurima, J Walton, G E Thompson, R C Newman, G C Wood, K Shimizu *Phylos. Mag. B, Phys. Condens. Matter Electron. Opt. Magn. Prop.* **70** 1 (1994)
136. M Costa, F Chao, E Museux, C Tian *J. Chim. Phys.* **92** 939 (1995)
137. P M Williams, K M Shakesheff, M C Davies, D E Jackson, C J Roberts, S J B Tendler *J. Vac. Sci. Technol. B* **14** 1557 (1996)
138. J S Villarubia *J. Res. Natl. Inst. Stand. Technol.* **102** 425 (1997)
139. A Milchev, E Michailova, R Lacmann, B Muller-Zulow *Electrochim. Acta* **38** 535 (1993)
140. J P Sousa, S Pons, M Fleischmann *J. Chem. Soc., Faraday Trans.* **90** 1923 (1994)
141. L Zeiri, O Younes, S Efrima, M Deutsch *J. Phys. Chem. B* **101** 9299 (1997)
142. J L Zubimendi, G Andreasen, W E Triaca *Electrochim. Acta* **40** 1305 (1995)
143. J Strutwolf, M Wünsche, H Meyer, R Schumacher *Z. Phys. Chem.* **208** 239 (1999)
144. T A Sorenson, D W Suggs, I Nandhakumar, J L Stickney *J. Electroanal. Chem.* **467** 270 (1999)
145. H Natter, R Hempelmann *J. Phys. Chem. B* **100** 19525 (1996)
146. J V Zoval, P R Biernacki, R M Penner *Anal. Chem.* **68** 1585 (1996)
147. M Yu Rusanova, M Grden, A Czerwinski, G A Tsirlina, O A Petrii, T Ya Safonova *J. Solid State Electrochem.* **5** (3) (2001)
148. O A Petrii, T Ya Safonova, G A Tsirlina, M Yu Rusanova *Electrochim. Acta* **45** 4117 (2000)
149. Y Mastai, G Hodes *J. Phys. Chem. B* **101** 2685 (1997)
150. G A Tsirlina, O A Petrii, S Yu Vassiliev *J. Electroanal. Chem.* **414** 41 (1996)
151. G A Tsirlina, O A Petrii *J. Electroanal. Chem.* **404** 33 (1996)
152. O A Petrii, G A Tsirlina, in *Advances in Electrochemistry Sciences Electrochemical Engineering* Vol. 5 (New York: Wiley-VCH, 1998) p. 61
153. M E G Lyons (Ed.) *Electroactive Polymer Electrochemistry* Pt 1 (New York: Plenum, 1994)
154. M E G Lyons (Ed.) *Electroactive Polymer Electrochemistry* Pt 2 (New York: Plenum, 1996)
155. P Batail, K Boubekeur, M Fourmigue, J-C P Gabriel *Chem. Mater.* **10** 3005 (1998)
156. J W Schultze, M M Lohrengel *Electrochim. Acta* **45** 2499 (2000)
157. D Alliata, P Häring, O Haas, R Kötz, H Siegenthaler *Electrochem. Commun.* **1** 5 (1999)
158. J M Miller, B Dunn *Langmuir* **15** 799 (1999)
159. G A Tsirlina, Yu E Roginskaya, G G Postovalova, S Yu Vassiliev *Elektrokhimiya* **35** 1385 (2000) [c]
160. M Datta, D Landolt *Electrochim. Acta* **45** 2535 (2000)
161. A I Vorobyova, V A Sokol, E A Outkina *Appl. Phys. A, Solids Surf.* **67** 487 (1998)
162. G Patermarakis, K Moussoutzanis, J Chandrinos *Appl. Catal. A* **180** 345 (1999)
163. M L Sandrock, C D Pibel, F M Geiger, C A Foss *J. Phys. Chem. B* **103** 2668 (1999)
164. H Matsuda, H Tanaka, N Baba *Chem. Lett.* 621 (1990)
165. T Kyotani, B K Pradhan, A Tomita *Bull. Chem. Soc. Jpn.* **72** 1957 (1999)
166. W Kautek, S Reetz, S Pentzien *Electrochim. Acta* **40** 1461 (1995)
167. Yu M Maksimov, B I Podlovchenko, T L Azarchenko *Electrochim. Acta* **43** 1053 (1998)
168. C-H Yang, T-C Wen *Electrochim. Acta* **43** 207 (1998)
169. G S Hsiao, M G Anderson, S Gorer, D Harris, R M Penner *J. Am. Chem. Soc.* **119** 1439 (1997)
170. M A Anderson, S Gorer, R M Penner *J. Phys. Chem. B* **101** 5895 (1997)
171. S Gorer, G S Hsiao, M G Anderson, R M Stiger, J Lee, R M Penner *Electrochim. Acta* **43** 2799 (1998)
172. S Gorer, J A Ganske, J C Hemminger, R M Penner *J. Am. Chem. Soc.* **120** 9584 (1998)
173. T Szczurek, T Rausch, M Schlesinger, D D Snyder, C H Olk *J. Electrochem. Soc.* **146** 1777 (1999)
174. Y Jyoko, S Kashiwabara, Y Hayashi, W Schwarzacher *Electrochem. Solid-State Lett.* **2** 67 (1999)
175. G Wouters, M Bratoeva, J-P Celis, J R Roos *J. Electrochem. Soc.* **141** 397 (1994)
176. A Cziraki, I Gerocs, B Fogarassy, B Arnold, M Reibold, K Wetzig, E Toth-Kadar, I Bakonyi *Z. Met.kd.* **88** 781 (1997)
177. J R Switzer, M Shane, R Phillips *Science* **247** 444 (1990)
178. G Inzelt, M Pineri, J W Schultze, M A Vorotyntsev *Electrochim. Acta* **45** 2403 (2000)
179. A Bonnefont, R Kostecki, F McLarnon, J C Arrayet, L Servant, F Argoul *J. Electrochem. Soc.* **146** 4101 (1999)
180. E W Bohannan, L-Y Huang, F S Miller, M G Shumsky, J A Switzer *Langmuir* **15** 813 (1999)
181. J A Switzer, B M Maune, E R Raub, E W Bohannan *J. Phys. Chem. B* **103** 395 (1999)
182. N A Bach, N A Balashova *Zh. Fiz. Khim.* **6** 43 (1936) [e]
183. N A Bach, A A Rakov *Zh. Fiz. Khim.* **10** 18 (1937) [e]
184. N A Balashova, N A Bakh *Zh. Fiz. Khim.* **10** 575 (1937) [e]
185. N A Bach, A V Zimin *Zh. Fiz. Khim.* **13** 1064 (1939) [e]
186. M J Reetz, W Helbig *J. Am. Chem. Soc.* **116** 7401 (1994)
187. R S Ingram, R W Murray *Langmuir* **14** 4115 (1998)
188. M Giersig, P Mulvaney *Langmuir* **9** 3408 (1993)
189. Sh K Shaikhutdinov, F A Muller, G Meste, R J Behm *J. Catal.* **163** 492 (1996)
190. R M Nyffenegger, R M Penner *J. Phys. Chem. B* **100** 17041 (1996)
191. W Li, G S Hsiao, D Harris, R M Nyffenegger, J A Virtanen, R M Penner *J. Phys. Chem. B* **100** 20103 (1996)

192. D M Kolb, J C Ziegler, G E Engelmann *Z. Phys. Chem.* **208** 151 (1999)
193. H Sugimura, N Nakagiri *J. Vac. Sci. Technol. A, Vac. Surf. Films* **14** 1223 (1996)
194. F P Zamborini, R M Crooks *J. Am. Chem. Soc.* **120** 9700 (1998)
195. K Seshadri, A M Wilson, A Guiseppi-Elie, D L Allara *Langmuir* **15** 742 (1999)
196. G A Tsirlina, O A Petrii, S Yu Vassiliev *Electrochim. Acta* **41** 1887 (1996)
197. A M Dykhne, S Yu Vassiliev, O A Petrii, A G Rudavets, G A Tsirlina *Dokl. Akad. Nauk* **368** 467 (1999) [a]
198. A L Buchachenko *Vest. Akad. Nauk* **69** 833 (1999) [f]

[a] — *Dokl. Chem. Technol., Dokl. Chem. (Engl. Transl.)*
[b] — *Tech. Fiz. (Engl. Transl.)*
[c] — *Russ. J. Electrochem. (Engl. Transl.)*
[d] — *Moscow Univ. Bull. (Engl. Transl.)*
[e] — *Russ. J. Phys. Chem. (Engl. Transl.)*
[f] — *Herald Russ. Acad. Sci. (Engl. Transl.)*

Russian Chemical Reviews **70** (4) 299 – 320 (2001) © 2001 Russian Academy of Sciences and Turpion Ltd

DOI 10.1070/RC2001v070n04ABEH000617

Pyridopyridines

V P Litvinov, S V Roman, V D Dyachenko

Contents

I.	Introduction	299
II.	1,5-Naphthyridines	299
III.	1,6-Naphthyridines	302
IV.	1,7-Naphthyridines	311
V.	2,6-Naphthyridines	313
VI.	2,7-Naphthyridines	314

Abstract. Studies on the development of procedures for the synthesis of five isomeric pyridopyridines, *viz*., 1,5-, 1,6-, 1,7-, 2,6- and 2,7-naphthyridines, their chemical properties and biological activities performed over the last 15 years are surveyed and systematised. The bibliography includes 223 references.

I. Introduction

Pyridopyridines (diazanaphthalenes, napthyridines) are fused heterocyclic systems containing two nitrogen atoms in the adjacent rings. Naphthyridine derivatives attract interest because of the broad spectrum of their biological activities. These compounds are used in diagnostics and treatment of different human diseases (including HIV infection), agriculture, animal husbandry for external- and internal-parasite control, in industry as preservatives and components of lubricating coolants for metal processing, in analytical chemistry as ligands, *etc*.

Previously, we have considered general methods for the synthesis of naphthyridines, their structures and properties.[1] In the present review, we survey procedures for the synthesis of five isomeric pyridopyridines, *viz*., 1,5-, 1,6-, 1,7-, 2,6- and 2,7-naphthyridines, their chemical properties and biological activities. For convenience, the data are systematised according to the types of isomeric naphthyridines.

II. 1,5-Naphthyridines

The major synthetic approach to the construction of the 1,5-naphthyridine system involves condensation of 3-aminopyridine derivatives with dicarbonyl compounds followed by the intramolecular reaction of the pyridine ring with the terminal carbonyl group under the action of acid catalysts to form a C–C bond. This approach serves as the basis for well-known syntheses according to Skraup, Friedländer, Knorr, *etc*.[1] Amino derivatives of pyridine,[2] indole,[3–6] and quinuclidine,[7] oximes of the isoquinoline series[8–10] and substituted anilines[11] were successfully used as substrates in these reactions.

Unlike the above-listed reactions, condensation of cycloalkanone diethyl acetals **1** with 3-amino-2-chloropyridine (**2**) afforded azomethines **3** whose successive treatment with lithium diisopropylamide (LDA) and thioesters **4** gave rise to aryl(hetaryl)cyclo(penta – octa)[*b*][1,5]naphthyridines **5**.[2]

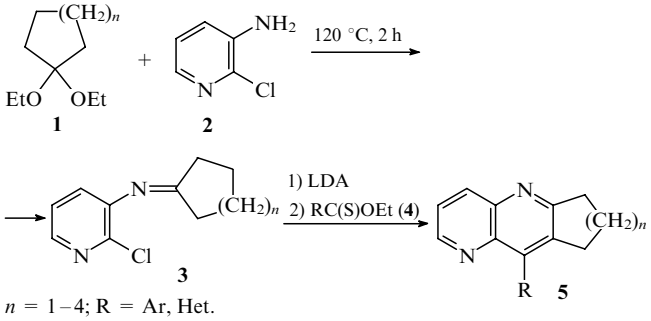

n = 1–4; R = Ar, Het.

Tryptamine, tryptophan and their derivatives are widely used in the synthesis of indolo[3,2,1-*de*][1,5]naphthyridine derivatives. Thus refluxing of tryptamine (**6**) with 2-formylbenzoic acid (**7**) in alcohol followed by the addition of concentrated hydrochloric acid afforded hexahydrobenzo[*h*]indolo[3,2,1-*de*][1,5]naphthyridine hydrochloride (**8**) used as the starting compound in the synthesis of compounds **9** and **10**. The latter have an application in the treatment of oxygen deficiency.[3]

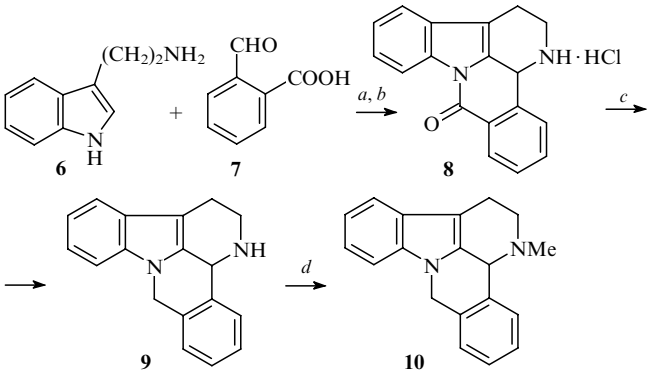

(*a*) EtOH, Δ, 2.5 h; (*b*) HCl; (*c*) $LiAlH_4$, $AlCl_3$;
(*d*) 37% CH_2O, $NaBH_3CN$, AcOH, MeCN, 20 °C, 2 h.

V P Litvinov N D Zelinsky Institute of Organic Chemistry, Russian Academy of Sciences, Leninsky prosp. 47, 119991 Moscow, Russian Federation. Fax (7-095) 135 53 28. Tel. (7-095) 135 88 37
S V Roman, V D Dyachenko T G Shevchenko Lugansk State Pedagogical Institute, ul. Oboronnaya 2, 348011 Lugansk, Ukraine.
Fax (38-064) 255 31 27. Tel. (38-064) 253 83 94

Received 27 July 2000
Uspekhi Khimii **70** (4) 343 – 367 (2001); translated by T N Safonova

1,5-Naphthyridine derivatives **11** and **12** prepared from α,α-dimethyltryptamine (**13**) and ethyl 3-chlorocarbonylpropionate are also used in the case of cerebral-vascular insufficiency and oxygen deficiency. Cyclisation of the intermediate **14** was carried out under the action of $POCl_3$ and KBH_4.[4]

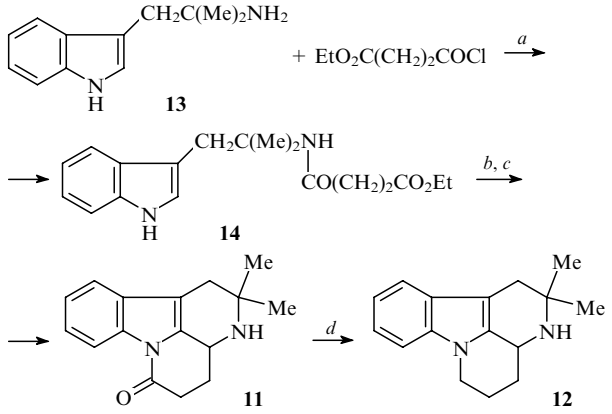

(*a*) Py, 20 °C, 1 h; (*b*) $POCl_3$; (*c*) KBH_4, EtOH – AcOH (5 : 1); (*d*) $LiAlH_4$, $AlCl_3$.

Indolonaphthyridine **15** was prepared by cyclocondensation of tryptophan (**16**) with 2-oxoglutaric acid (**17**) upon refluxing in methanol in the presence of HCl.[10]

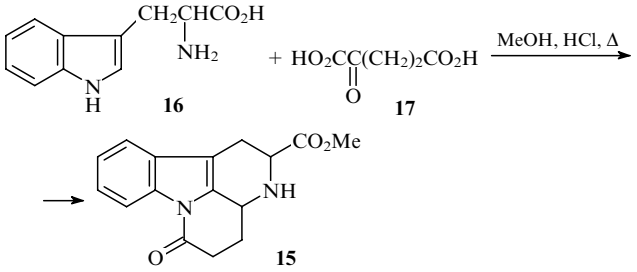

The chemical properties of 1,5-naphthyridines and the possibilities of their use for the preparation of biologically active compounds have been studied extensively. In particular, bromination of three isomeric thieno[*c*][1,5]naphthyridines **18a** – **c** and their *N*-oxides with tetrabutylammonium perbromide or bromine in the presence of $SOCl_2$ was investigated.[12] The reactions involving *N*-oxides proceed with higher regioselectivity. Thus bromination of thienonaphthyridine **18b** with tetrabutylammonium perbromide afforded a mixture of halogeno derivatives **19a** – **c**, whereas bromination of its *N*-oxide **20** under the same conditions gave rise to bromide **21** in 55% yield (23% of the initial compound remained unconsumed).[12]

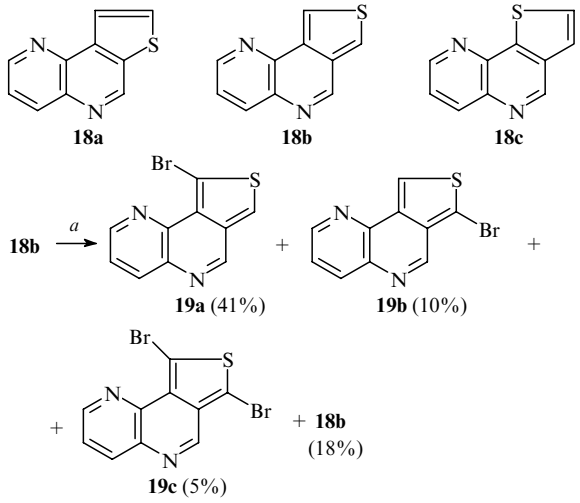

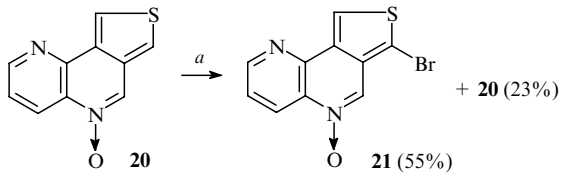

(*a*) 1.2 equiv. $Bu_4N^+Br_3^-$, $NaHCO_3$, CH_2Cl_2, 20 °C.

One of the recent major procedures used in the synthesis of biologically active 1,5-naphthyridines is based on the replacement of the halogen atom at position 4 of the naphthyridine ring.[13–23] Thus substituted 1,5-naphthyridin-4-ylamines **22** were prepared by the reactions of 4-chloro-1,5-naphthyridines **23** with aminophenols **24** – **26**[13–15] or by the Mannich reaction of 8-(4-hydroxyphenylamino)naphthyridines **27**.[16, 17]

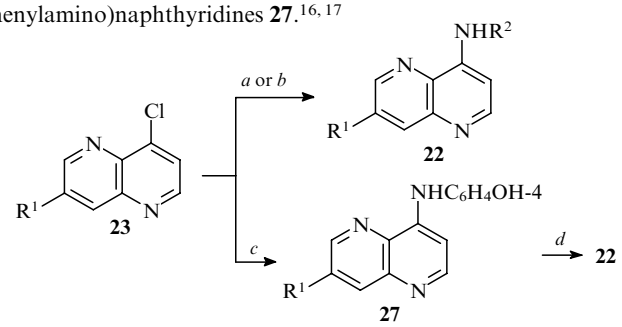

R^1 = H, Me, Cl, Br, CF_3;

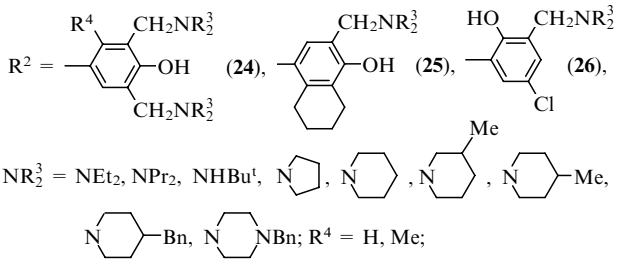

(*a*) H_2NR^2, MeOH (EtOH), HCl, Δ; (*b*) $AcNHR^2$, MeOH (EtOH), HCl, Δ; (*c*) $4\text{-}HOC_6H_4NH_2 \cdot HCl$, MeOH, Δ; (*d*) CH_2O, HNR^3_2, EtOH, Δ.

The compounds **22** exhibit antimalarial activity both *in vitro* and *in vivo*. This activity is less pronounced in the case of R^1 = Br or CF_3 and R^2 = Me or Et.[14, 15]

(7-Bromo-1,5-naphthyridin-4-yl)(piperidin-2′-yl)methanol, which is a potential antimalarial drug of a new type, was synthesised in four steps starting from 4,7-dibromo-1,5-naphthyridine.[22]

The reaction of 4-chloro-1,5-naphthyridine with 4-fluorophenol (**28**) afforded 4-(4-fluorophenoxy)-1,5-naphthyridine (**29**) exhibiting fungicidal and insecticidal activities.[23]

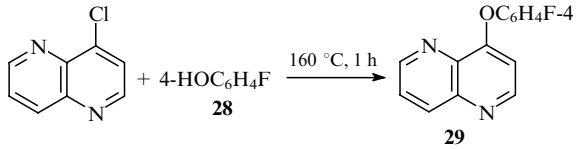

Cross-coupling of 1,5-naphthyridines **30** containing the bromine or iodine atom at position 4 with organotin, -silicon or -boron compounds **31** in the presence of $Pd(PPh_3)_4$ gave rise to aryl-substituted 1,5-naphthyridines **32** covered by a patent as herbicides.[24]

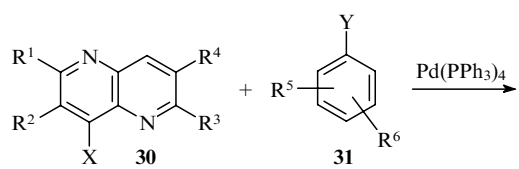

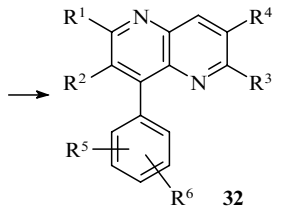

32

R^1 = Alk(C_1–C_4), OAlk, SAlk; R^2 = H, Me, F, Cl;
R^3–R^6 = H, Alk(C_1–C_4), OAlk, CN, Hal; X = Br, I;
Y = $SnMe_3$, $SiMe_3$, $B(OH)_2$.

The chlorine atom in 2- or 4-chloronaphthyridines was replaced by the iodine atom under the action of NaI in the presence of hydroiodic acid yielding 2- or 4-iodo-1,5-naphthyridines, respectively.[25] It was noted[25] that treatment of 2-iodo-1,5-naphthyridine with $NaNO_2$ in DMF gave rise to 2,2′-bis(1,5-naphthyridyl) ether (**33**) in 44% yield, whereas an analogous reaction with 4-iodo-1,5-naphthyridine did not proceed.

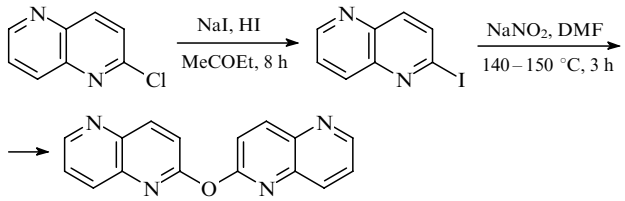

33

In 6-chloronaphtho[1′,2′:4,5]thieno[2,3-c][1,5]naphthyridine (**34**), the chlorine atom is readily replaced by the amino or hydrazinoamino group and also is reduced to yield the corresponding 1,5-naphthyridine derivatives **35**–**37**. Under the action of ethyl orthoformate, the hydrazine **37** underwent cyclisation to give triazole **38**[26] (Scheme 1).

Reductive cyclisation of esters **39** afforded 1,5-naphthyridine derivatives **40**, which were dimerised under the action of acids.[27]

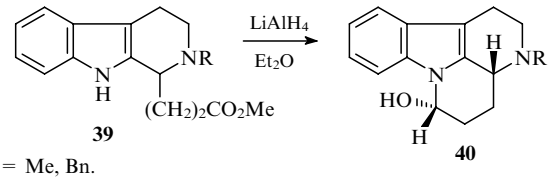

39 **40**

R = Me, Bn.

Methyl (±)-3-ethyl-2,3,3*a*,4-tetrahydro-1*H*-indolo[3,2,1-*de*]-[1,5]naphthyridine-6-carboxylate (**41**) possessing psychostimulating activity was prepared by alkylation of ester **42** with iodoethane in DMSO or by dehydration of hydroxy derivative **43**.[28]

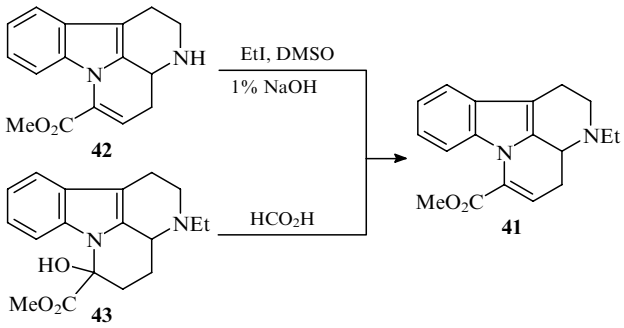

42 **43** **41**

1,5-Naphthyridine derivatives, like other isomeric pyridopyridines, were found in many natural substances and were used for the construction of a series of efficient medicines.

Recently, the previously unknown dimeric indole alkaloid cimiciduphytine (**44**) containing the 1,5-naphthyridine fragment[29] and derivatives of eburnane alkaloids **45** exhibiting hypotensive and pain-relieving activities have been isolated from naturally occurring sources. These compounds are suitable for the treatment of cerebral circulation disturbance.[30–35]

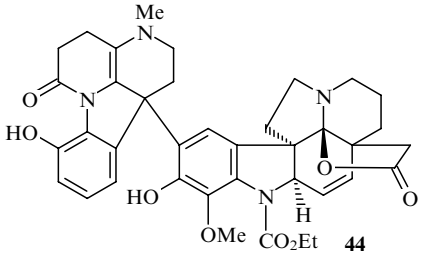

44

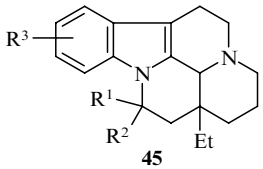

45

R^1 = H: R^2 = H, CO_2Me, CO_2Et, CH_2OH; R^1–R^2 = O;
R^3 = H, Cl, NO_2.

A derivative of penicillanic acid **46** was covered by a patent as an antibiotic.[36] Derivatives of hydroxy acid **47** were covered by a patent as anthelmintics.[37]

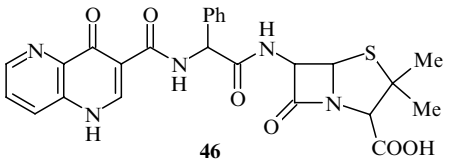

46

Scheme 1

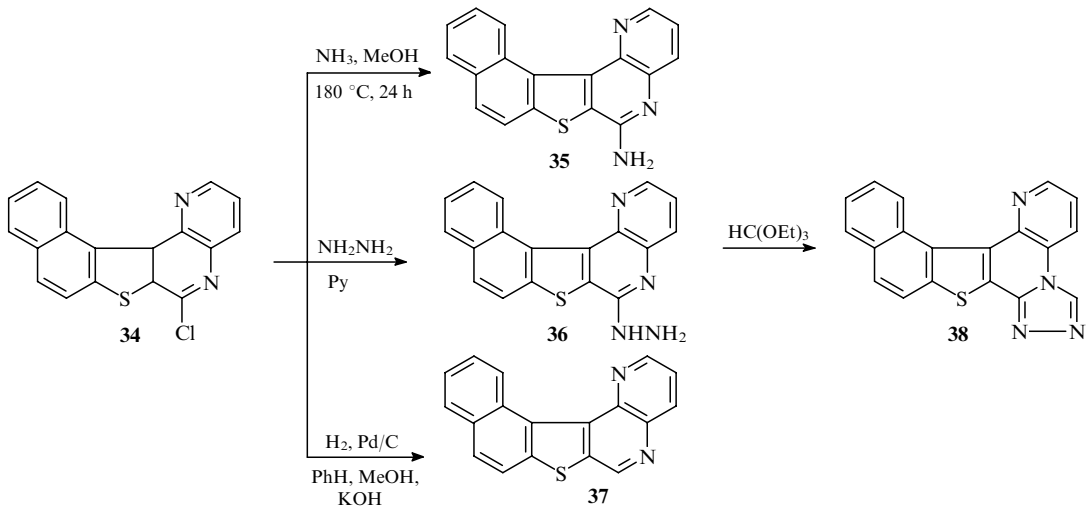

34 **35** **36** **37** **38**

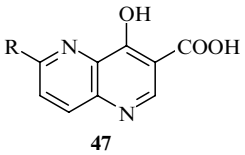

47

R = OEt, OPr, 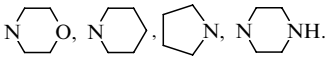

Derivatives of annelated benzoindolo-1,5-naphthyridines suitable for improvement of memory attenuated by drugs were described.[3,5] These are benzo[*b*][1,5]naphthyridines, which are analogues of inhibitors of neurokinin NK_1-receptors. Various 1,5-naphthyridine derivatives, in particular, 2-naphthyridinecarboxamide, possessing antiviral activity were also reported.[38].

Complexes **48** of Group IB or VIII metals with 1,5-naphthyridine derivatives **49** were synthesised.[39] The compounds **48** are used for the preparation of singlet oxygen. These compounds serve as sensitisers in photoinitiation of polymerases and electrophotography and as redox catalysts in organic reactions.[39]

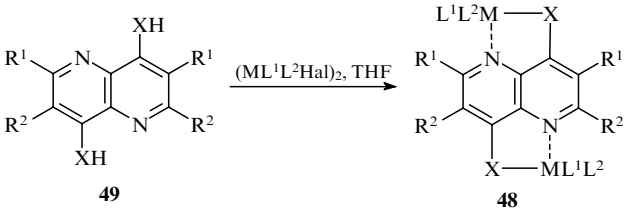

49 **48**

R^1, R^2 = H, Me, Et, cyclo-Alk(C_3–C_7); R^1–R^2 = $(CH_2)_n$, n = 3–6; X = O or S, M is Group IB or VIII metal; L^1, L^2 = Hal, NO, PPh_3, CN, CO.

The electronic structures and the UV spectral parameters of six isomeric formyl-substituted 4,6-benzo-1,5- and -1,6-naphthyridines were calculated.[40]

III. 1,6-Naphthyridines

Chemistry and biological activities of 1,6-naphthyridine derivatives were studied in much more detail than those of 1,5-, 1,7- and 2,7-naphthyridine derivatives. A wide variety of approaches to their syntheses are available.

One of the promising procedures for the synthesis of 1,6-naphthyridine derivatives involves functionally substituted pyridones as the starting compounds. Thus enamines **50** prepared from 6-formylpyrid-2-ones underwent cyclisation upon refluxing with ammonium acetate in DMF to give 1,6-naphthyridin-2-ones **51** in good yields.[41–47] *N*-Oxides **52** were prepared by cyclisation of the enamines **50** under the action of hydroxylamine hydrochloride.[42,45] The reactions of the compounds **50** with amines in methanol or DMF afforded 6-substituted 1,2,5,6-tetrahydro-1,6-naphthyridin-2-ones **53**.[48]

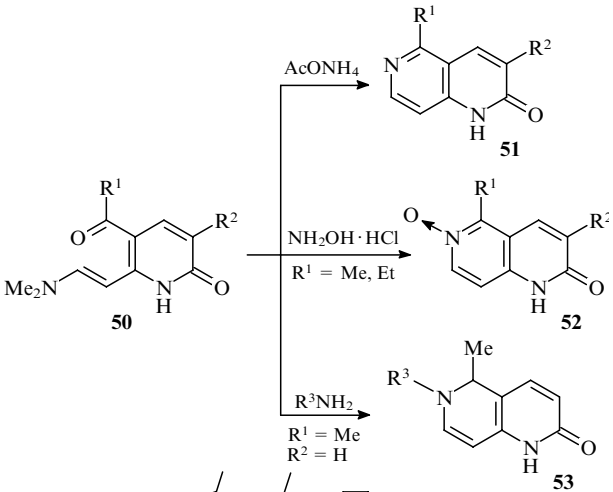

50 **51** **52** **53**

R^1 = Me, Et, Pr, Bu, Ph, 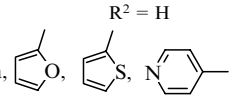 ;

R^2 = H, Br, CN; R^3 = 4-$MeOC_6H_4$, NH_2, NMe_2.

Treatment of enamine **54** derived from 5-cyano-6-formyl-2-pyridone with gaseous HBr in AcOH gave rise to 5-bromo-1,6-naphthyridin-2-one (**55**). The bromine atom in the compound **55** is readily replaced by nitrogen nucleophiles. This fact was used in the synthesis of 1,6-naphthyridine derivatives **56**–**58**.[49–52] The compounds **51**, **52** and **55**–**58** exhibit cardiotonic activity.[41–52]

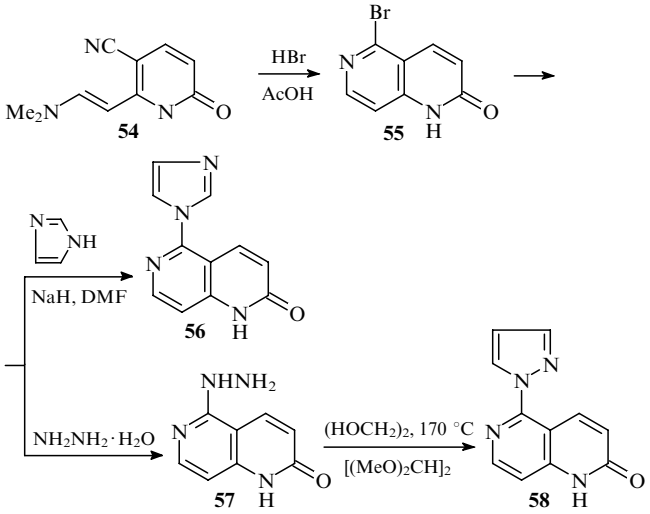

54 **55** **56** **57** **58**

1,6-Naphthyridin-5(6*H*)-ones **59a**–**g** were prepared by the reactions of pyridines **60a**–**g** with 1,3,5-triazine upon refluxing in ethanol in the presence of sodium ethoxide. The reaction of the compound **60a** with dimethylformamide diethyl acetal gave rise to enamine **61**. The reactions of the latter with amines upon refluxing in ethanol, DMF, *m*-xylene or pyridine afforded 6-substituted naphthyridinone derivatives **62**.[53,54] Refluxing of vicinal diamines **63** with enamine **61** yielded naphthyridinones **64**, which were converted into tetracyclic derivatives **65** under the action of $POCl_3$.[55]

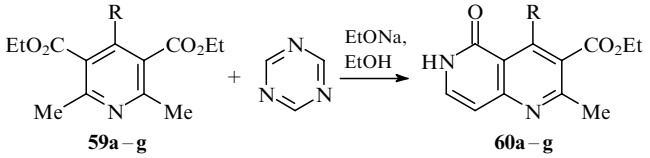

59a–**g** **60a**–**g**

R = H (**a**), Ph (**b**), 4-ClC_6H_4 (**c**), 3,4-$(MeO)_2C_6H_3$ (**d**), 2-$NO_2C_6H_4$ (**e**), 4-$NO_2C_6H_4$ (**f**), 3-pyridyl (**g**).

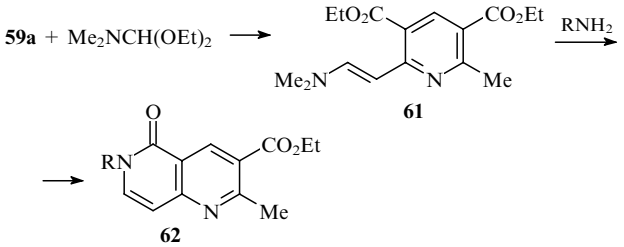

61 **62**

R = H, Ph, 2-FC_6H_4, 4-FC_6H_4, 3-$F_3CC_6H_4$, 2-$NH_2C_6H_4$.

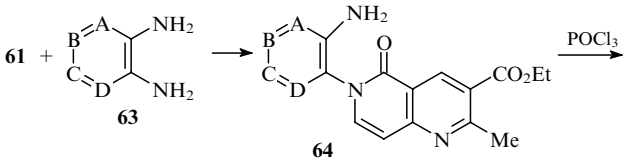

63 **64**

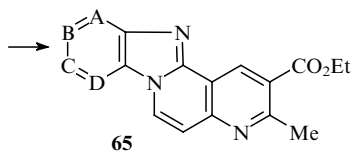

65

A = B = C = D = CH; A = B = C = CH, D = N; A = N, B = C = D = CH; A = C = D = CH, B = N; A = C = N, B = D = CH; A = C = CH, B = D = N.

The reactions of 1,4-dihydropyridines with 1,3,5-triazine in the presence of a base afforded 1,4-dihydro-1,6-naphthyridines **66a**–**h**. These compounds can also be prepared in two stages by the reactions of 1,4-dihydropyridines with dimethylformamide diethyl acetal followed by treatment of aminovinyl intermediates **67** with ammonia.[56] The compounds **66a**–**h** were covered by patents as agents promising in the treatment of cardiovascular diseases.[57–61]

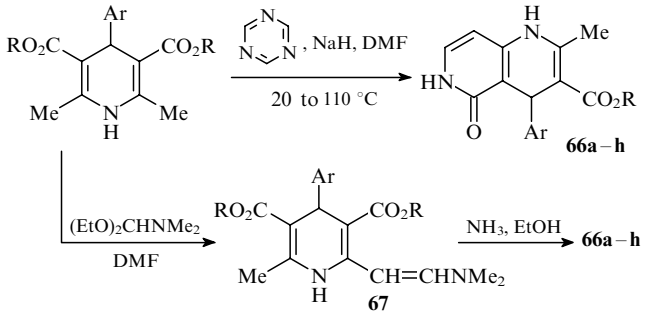

Ar = Ph (**a**), 4-ClC_6H_4 (**b**), 2-$NO_2C_6H_4$ (**c**), 2-pyridyl (**d**), 2-thienyl (**e**), 2-FC_6H_4 (**f**), 2-$CF_3C_6H_4$ (**g**), 2-F-3-ClC_6H_3 (**h**);
R = Me, Et, Bu^t.

Substituted pyridones are widely used as the starting compounds in the synthesis of substituted 1,6-naphthyridines. Thus the reactions of 1,3,5-triazine with pyridones **68a**,**b** yielded annelated 1,6-naphthyridines **69a**,**b**. The tricyclic compounds **69** containing the cyclopropyl substituent were covered by patents as efficient antibiotics.[62] Pyrido[2,3-*b*][1,6]naphthyridine **70** prepared from 1,4-dihydropyridine **71** possesses spasmolytic activity and is used in the treatment of cerebral, cardiac and peripheral artery diseases.[63]

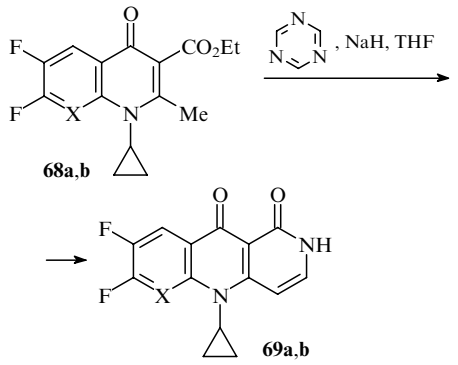

X = N (**a**), CF (**b**).

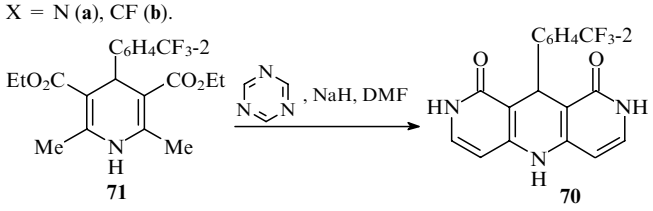

The reactions of 5-alkanoyl(aroyl)-6-methylpyridin-2(1*H*)-ones with *N*-bromosuccinimide in CCl_4 afforded bromides **72**. Successive treatment of the latter with $(Me_2N)_2CHOBu^t$ (Bredereck's reagent) and ammonium acetate gave rise to 5-alkyl(aryl)-3-bromo-1,6-naphthyridin-2(1*H*)-ones **73** in high yields.[64] The compounds **73** were converted under the successive action of $POCl_3$ and ammonia into 5-alkyl(aryl)-2-amino-3-bromo-1,6-naphthyridines **74**, which are promising starting compounds for the preparation of new biologically active compounds.

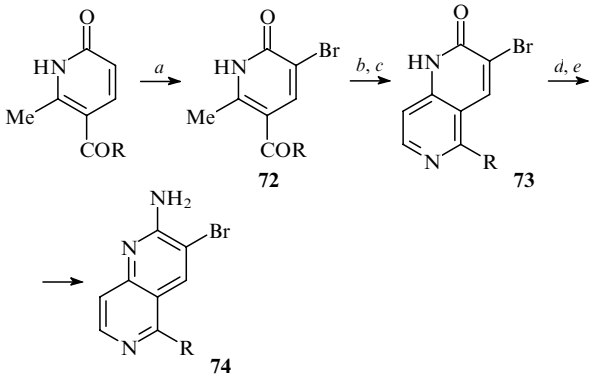

R = Me, Et, Pr^n, Bu^i, Ph, 4-$NO_2C_6H_4$;
(*a*) NBS (*N*-bromosuccinimide), CCl_4; (*b*) $(Me_2N)_2CHOBu^t$, dioxane; (*c*) NH_4OAc, DMF; (*d*) $POCl_3$; (*e*) NH_3, EtOH.

The Knoevenagel reaction of substituted 4-amino-3-formylpyridin-2-ones with CH-acids in the presence of piperidine was used in the synthesis of 2-imino-1,6-naphthyridin-5(6*H*)-ones (**75**) possessing antitubercular activity.[65]

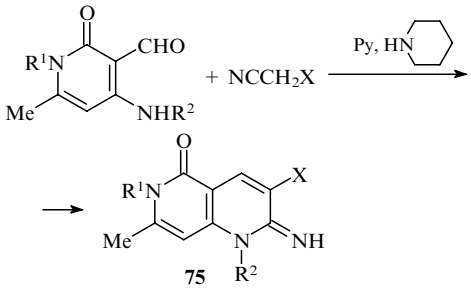

R^1, R^2 = $PhCH_2$, $Ph(CH_2)_2$; X = CN, CO_2H, CO_2Me, CO_2Et, 4-$NO_2C_6H_4$.

When heated with $POCl_3$, substituted pyridone **76** underwent cyclisation with simultaneous replacement of the 2-oxo group by the chlorine atom to give 3-chloro-4-cyanobenzo[*b*][1,6]naphthyridine **77**.[66,67]

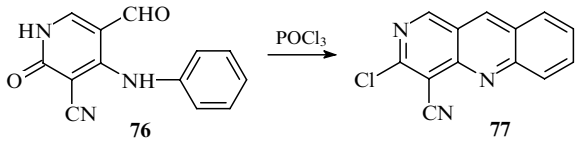

The reaction of pyridone **78** with carbon disulfide and sodium hydride in benzene followed by methylation with iodomethane produced the 5,7-bis(methylthio)-1,6-naphthyridinone derivative **79**.[68]

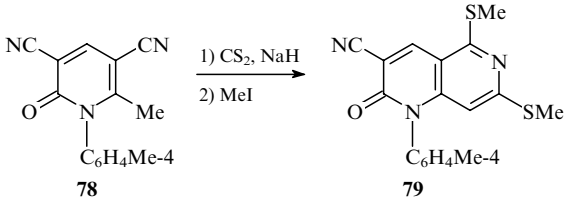

5,6,7,8-Tetrahydro-1,6-naphthyridin-5-ones **80** were synthesised by the reactions of 4-amino-5,6-dihydropyridin-2(1*H*)-one with amino ketone hydrochlorides.[69]

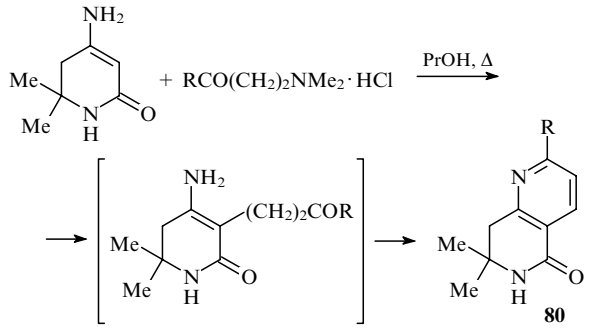

R = Ph, 4-$MeOC_6H_4$, 4-ClC_6H_4.

Piperidones are used as starting compounds in the synthesis of 1,6-naphthyridines. Thus the reactions of *N*-substituted piperidones **81a**,**b** with 2-amino-4-chlorobenzoic acid afforded 2-aryl(heteryl)tetrahydrobenzo[*b*][1,6]naphthyridines **82a**,**b**, which serve as inhibitors of interleukin 1 and were covered by patents as antiinflammatory agents.[70–72]

The reaction of the compound **82a** with phenylhydrazine in the presence of concentrated hydrochloric acid gave rise to pyrazolo[4,3-*c*]quinoline (**83**) exhibiting antiinflammatory activity.[70,72]

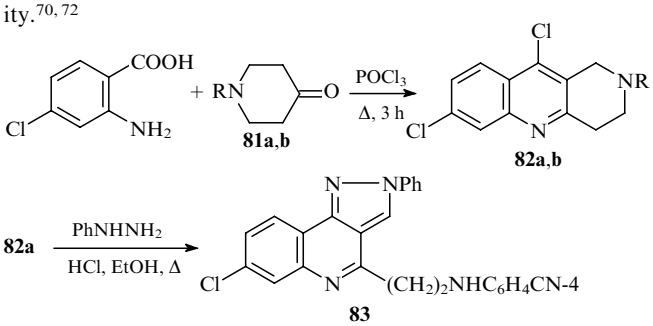

R = 4-NCC_6H_4 (**a**), pyrimidin-2-yl (**b**).

The reactions of *N*-benzylpiperidin-4-one (**84**) with 3-aminoacrolein and its homologues were used for the preparation of 5,6,7,8-tetrahydro-1,6-naphthyridines **85a**–**c**.[73]

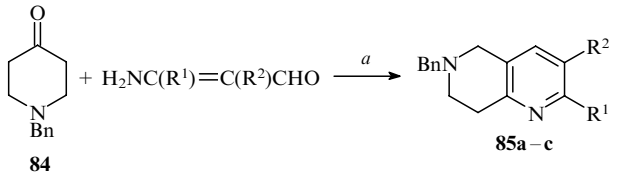

$R^1 = R^2 = H$ (**a**); R^1 = Me, R^2 = H (**b**); R^1 = H, R^2 = Me (**c**);
(*a*) NH_2 AcO^-, Et_3N, 120 °C, 24 h.

Partially hydrogenated 1,6-naphthyridines **86** were synthesised by the Hunch condensation of aromatic aldehydes with 2,4-dioxopiperidine (**87**) and derivatives of 3-aminocrotonic acid.[74] The compounds **86** were covered by a patent as drugs for the treatment of cardiovascular diseases.[75]

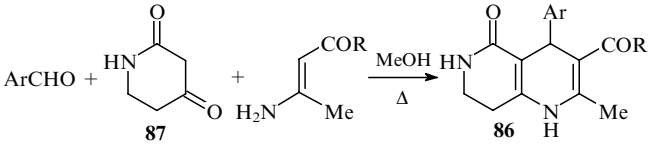

R = MeO, EtO, MeNH, Et_2N, $NH(CH_2)_2OH$.

The reactions of 6-amino-5-methylisoquinolin-1(2*H*)-one (**88**) with 4-chloronicotinic acid (**89a**) or ethyl 4-chloro-2,6-dimethylnicotinate (**89b**) afforded amino-substituted 6-aminoisoquinolines **90a**,**b**, which underwent cyclisation to form 5*H*-isoquinolino[6,7-*b*][1,6]naphthyridin-12-ones **91a**,**b**, respectively.[76] The latter were used in the synthesis of 10-substituted 1,6-naphthyridine derivatives **92a**,**b** and **93a**,**b**, which are analogues of 9-azaellipticine possessing antitumour activity. However, it appeared that the replacement of the pyrrole fragment in 9-azaellipticine by the 4-pyridone fragment led to a loss of biological activity.[76]

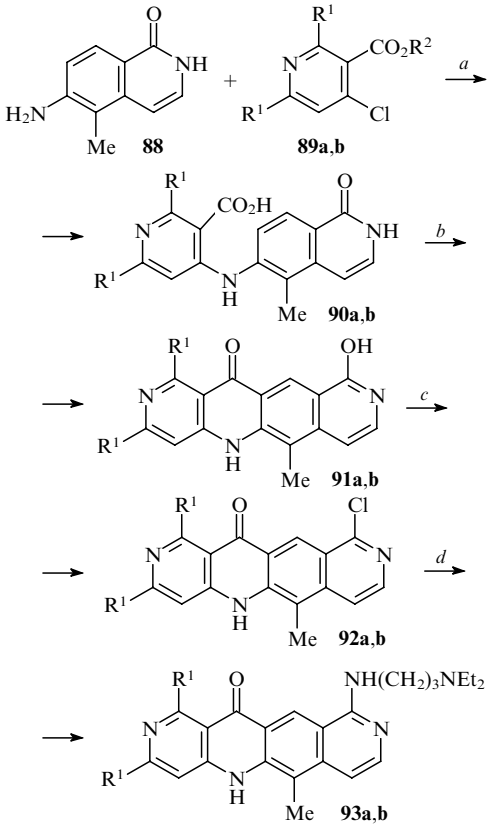

$R^1 = R^2 = H$ (**a**), R^1 = Me, R^2 = Et (**b**); (*a*) H_2SO_4, CF_3CO_2H; (*b*) H_2SO_4 or CF_3SO_3H; (*c*) $POCl_3$, PCl_5; (*d*) $NH_2(CH_2)_3NEt_2$.

Pyridinecarboxylamides are widely used in the synthesis of 1,6-naphthyridines. Thus heating of a mixture of 2-methylnicotinamide with *N*,*N*-dimethylacetamide dimethyl acetal in the presence of NaH gave rise to 7-methyl-1,6-naphthyridin-5(6*H*)-one (**94**), which is used for eliminating harmful effects caused by ionising radiation or chemotherapeutic agents during tumour treatment.[77]

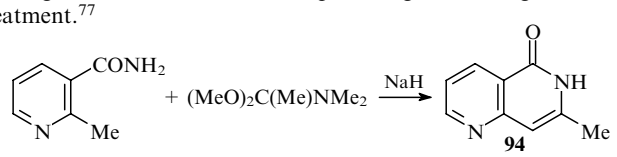

When heated in polyphosphoric acid (PPA), 6-phenyl-2-styrylnicotinamides (**95**) underwent cyclisation to form substituted 5-oxo-5,6,7,8-tetrahydro-1,6-naphthyridines **96**.[78] Analogously, benzo[*b*][1,6]naphthyridines **98** were prepared from amides of the quinoline series **97**.[78–80] Naphthyridine **98** ($R^1 = R^2 = H$) was also synthesised by cyclisation of 3-cyano-2-styrylquinoline **99** under the action of a mixture of polyphosphoric and sulfuric acids.[80]

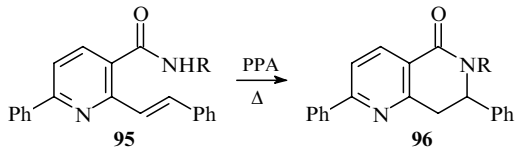

R = $CH_2=CHCH_2$, iso-C_5H_{11}, Ph, 3-MeC_6H_4.

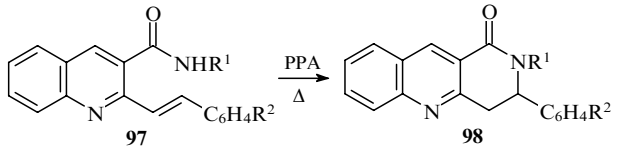

R^1 = H, Ph, Bn; R^2 = H, 4-MeO, 3-Br.

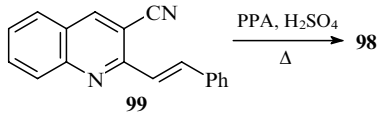

The reactions of *N*-substituted 2-chloro- or 4-chloronicotinamides with nitriles containing the active methylene group in the presence of bases were used for the preparation of amino derivatives of 1,6-naphthyridin-5(6*H*)-one or 2,7-naphthyridin-1(2*H*)-one, respectively.[81,82]

A procedure was developed for the synthesis of dodecahydroisoquinolino[2,1-*g*][1,6]naphthyridines **100** based on diethyl-2-methylnicotinamide (**101**) and 3,4-dihydroisoquinolines **102a**,**b**. The compounds **100** are highly efficient α_2-adrenoreceptor antagonists[83,84] and were covered by patents as drugs for the treatment of hypertonia, depression and diabetes, for inhibition of thrombocyte aggregation and for weight reduction.[85–90]

It should be noted that the structural analogue of α-yohimbine, *viz*., 6-methoxy-*N*-methylsulfonyl-6*H*-isoquinolino[2,1-*g*][1,6]naphthyridine (**100**, R^1 = MeO, R^2 = $MeSO_2$, the preparation RS-15385),[91] proved to be a very efficient drug in the treatment of impotence. A laboratory procedure for its preparation on a kilogram scale was developed.[92,93]

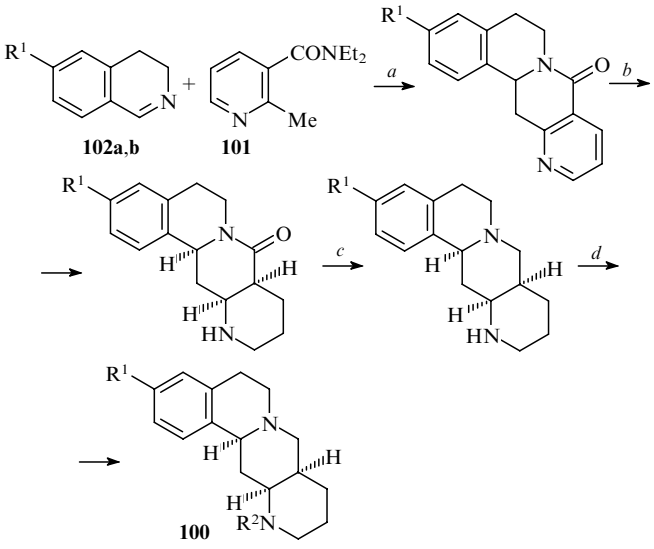

R^1 = H (**102a**), MeO (**102b**); R^2 = $MeSO_2$, $MeO(CH_2)_2SO_2$, $HO(CH_2)_2SO_2$, Bu^tNHSO_2, H_2NSO_2, Me_2NCO, $Cl(CH_2)_3SO_2$;
(*a*) Pr^i_2NLi, THF, −40 °C; (*b*) H_2, Rh/Al_2O_3, AcOH; (*c*) $LiAlH_4$, THF, Δ; (*d*) R^2X (X = Cl, Br), CH_2Cl_2, Et_3N.

Reductive cyclisation of substituted isoquinoline **103**, which was prepared from 6,7-dimethoxy-1-methylisoquinoline (**104**) in four steps, was successfully used in the synthesis of 8,9-dimethoxy-1*H*-benzo[*d*,*e*][1,6]naphthyridine (aaptamine) (**105**). The latter compound was isolated from sea sponge *Aaptos aaptos* and exhibits sympatholytic and hypotensive activities.[94,95]

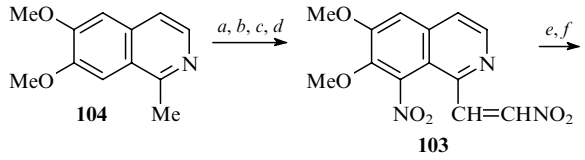

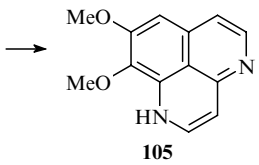

(*a*) HNO_3, −40 °C; (*b*) SeO_2, dioxane; (*c*) $MeNO_2$, Al_2O_3; (*d*) Al_2O_3, PhH, Δ; (*e*) Fe, AcOH, 20 °C, 2 h; (*f*) 90 °C, 45 min.

Pyranopyridines are convenient starting compounds in the synthesis of 1,6-naphthyridine derivatives. Thus, the reaction of 7-phenylpyrano[4,3-*b*]pyridin-5-one (**106**) with gaseous ammonia in ethanol was accompanied by the replacement of the oxygen atom of the pyran ring by the nitrogen atom to form hydroxynaphthyridine **107**. The latter was dehydrated with an alcoholic solution of HCl to give 7-phenyl-1,6-naphthyridin-5(6*H*)-one (**108a**). Treatment of pyranopyridine with propylamine led to the pyran ring opening to form 2-phenacyl-*N*-propylpyridine-3-carboxamide (**109**), which underwent cyclisation under the action of a 5% HCl solution giving rise to *N*-propyl-substituted naphthyridinone **108b**.[96]

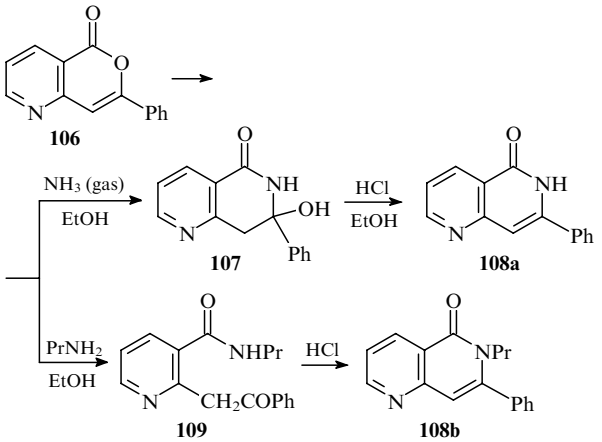

Analogous reactions of 7-methylpyrano[4,3-*b*]pyridines **110** with ammonia or aliphatic primary amines afforded 1,6-naphthyridinones **111**.[97]

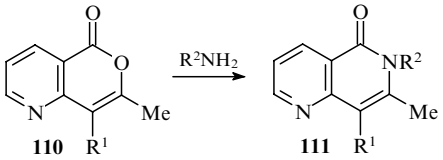

R^1 = Ac, CO_2Et; R^2 = H, Me, Bu, $(CH_2)_2NH_2$, $(CH_2)_2OH$, CH_2=$CHCH_2$.

1,6-Naphthyridin-2(1*H*)-ones **113** were prepared from pyrano[4,3-*b*]pyridine-2,7-diones **112** by successive treatment with NH_3, HBr and Zn in acetic acid.[98] It was believed that the attack of the ammonia molecule on the C(5) atom led to the pyran ring opening. Subsequent decarboxylation afforded a tautomeric mixture of substituted tetrahydropyridines **114a**,**b**. Dinitrile **115** generated by elimination of the ammonia molecule underwent cyclisation under the action of HBr to form 1,6-naphthyridine derivative **116**. Dehydrobromination with Zn in acetic acid gave rise to the final products **113**.

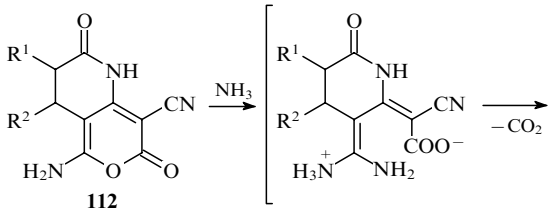

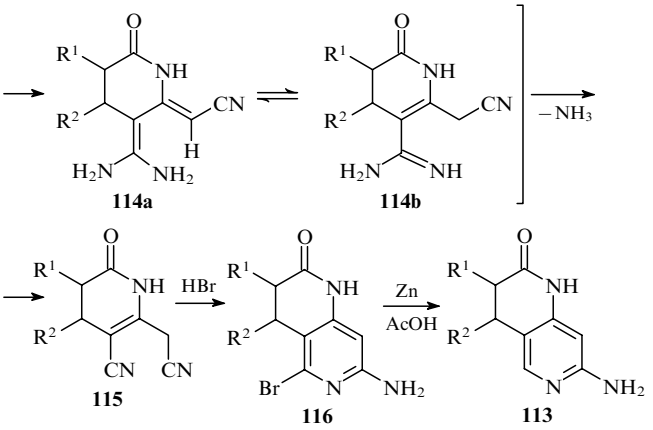

R^1, R^2 = H, Me, Ph.

Successive treatment of *N*-substituted 4-aminopyridines **117** with *tert*-butyllithium and 1,3-chloroiodopropane yielded tetrahydro-1,6-naphthyridines **118**.[99]

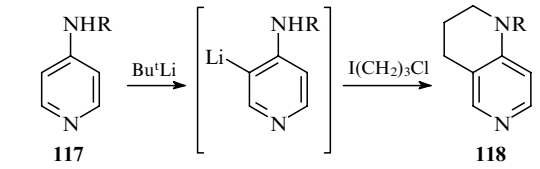

R = $COBu^t$, CO_2Bu^t.

The reaction of chlorocarbonic ester with the lithium derivative of enamine **119**, which was prepared by the reaction of 2,4,6-trimethylpyridine with benzonitrile and phenyllithium, afforded a mixture of 1,6-naphthyridin-5(6*H*)-ones **120** and **121**.[100]

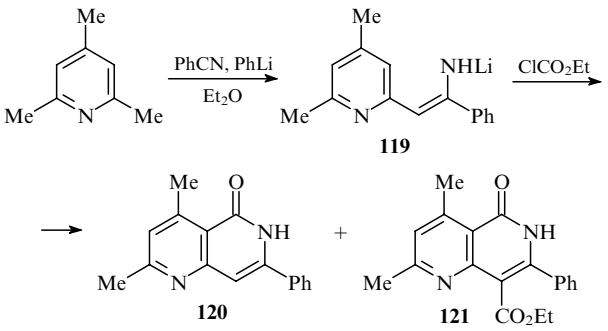

A convenient procedure was developed [101, 102] for the synthesis of 1,6-naphthyridine derivatives **122** containing the alkylselanyl substituent at position 7. Thus multicomponent condensation of cyanoselenoacetamide (**123**), 2-furfurylideneacetoacetic ester (**124**) and alkyl halides was carried out under the action of a twofold excess of *N*-methylmorpholine. The reaction involves the Thorpe dimerisation of the amide **123** yielding compound **125**, its reaction with a molecule of furfurylideneacetoacetic ester (**124**) to form adduct **126**, regioselective cyclocondensation of the adduct **126** producing substituted 1,4-dihydro-1,6-naphthyridine-7-selenolate (**127**) and alkylation of the selenolate **127** with alkyl halides giving rise to naphthyridines **122**.

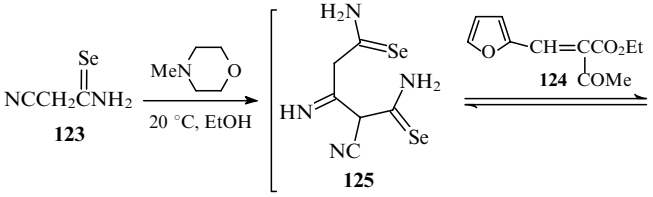

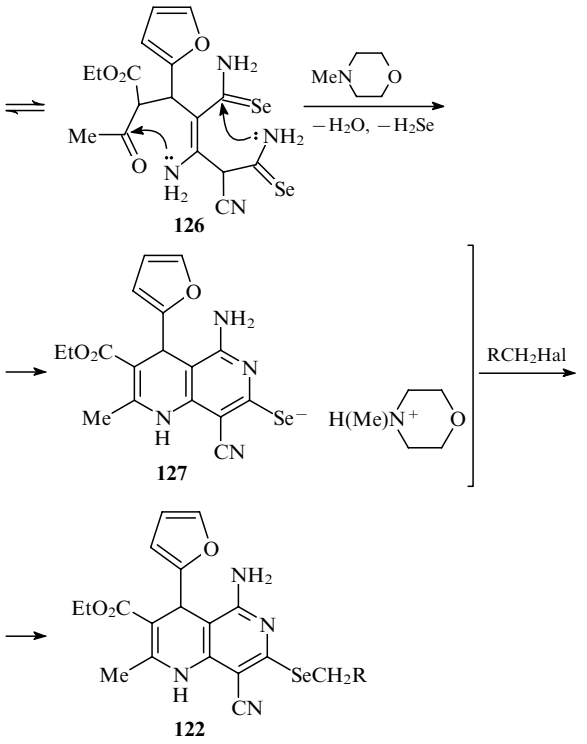

R = H, Me, Et, Pr, C_5H_{11}, CH_2Br, $(CH_2)_3Br$, $C(Me)=CH_2$, $HC=CH_2$, CO_2Et; Hal = I, Br, Cl.

This procedure also allows one to construct the naphthyridine system from other α,β-unsaturated carbonyl compounds under mild conditions.[103]

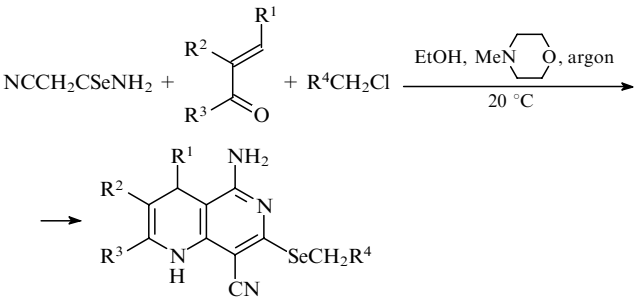

R^1–R^3 = H, Alk, Ar, Het, CN, COOH, COOAlk, COAr, COHet, $CONH_2$, CONHAr; R^4 = Alk.

Multicomponent heterocyclisation of benzaldehyde with malononitrile and its dimer **128** in the presence of piperidine or morpholine was used for the construction of the 1,6-naphthyridine system **129**. Heterocyclisation was accompanied by the insertion of the cyclic-amine fragment into the molecule to form the compounds **129**.[104]

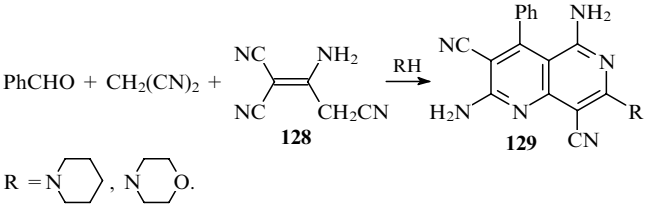

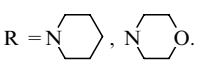

An ingenious method for the construction of the 1,6-naphthyridine system with the use of the 'chelate' methodology was developed.[105] Thus the reaction of 3-acetyl-4-amino-5,5,5-trifluoro-3-penten-2-one (**130**) with Ph_2BOBu afforded chelate complex **131** in which the oxygen atom was replaced by the nitrogen atom upon heating with primary amines. The resulting complexes

132 reacted with two equivalents of dimethylformamide dimethyl acetal to give 5-trifluoromethyl-1,6-naphthyridin-4(1*H*)-ones **133** in 77%–87% yields. It was believed [105] that the complexes **132** reacted with dimethylformamide dimethyl acetal to give condensation products at the methyl groups (**134**), which underwent deborylation with simultaneous cyclisation of intermediates **135** under the action of the methanol eliminated.

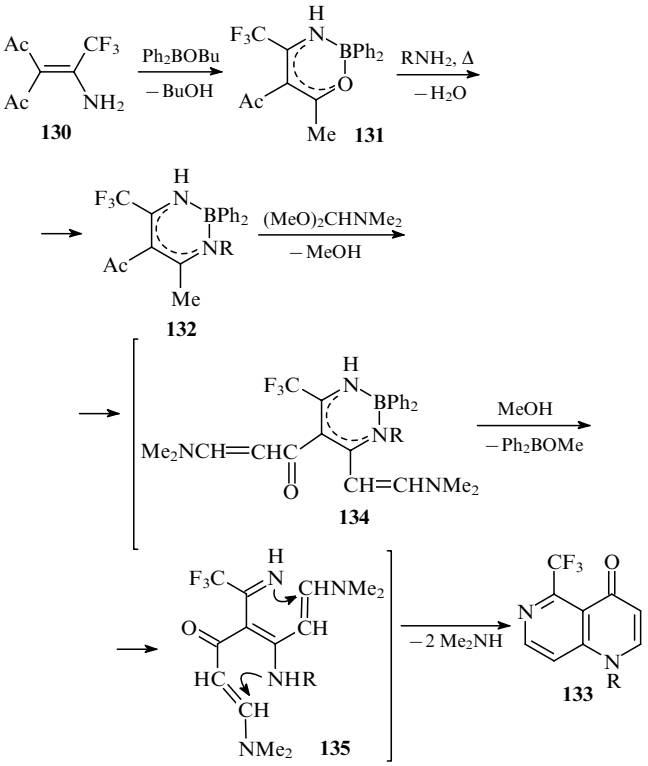

R = Bu, Bn.

Ethyl (4,6-diamino-3,5-dicyano-2-pyridyl)acetate **136** or (4,6-diamino-3,5-dicyano-2-pyridyl)acetanilide **137** were converted into 1,6-naphthyridine-5,7(6*H*,8*H*)-dione **138** upon refluxing in acetic acid in the presence of HCl. Treatment of the ester **136** with trichloroacetonitrile in the presence of triethylamine afforded naphthyridine **139**.[106]

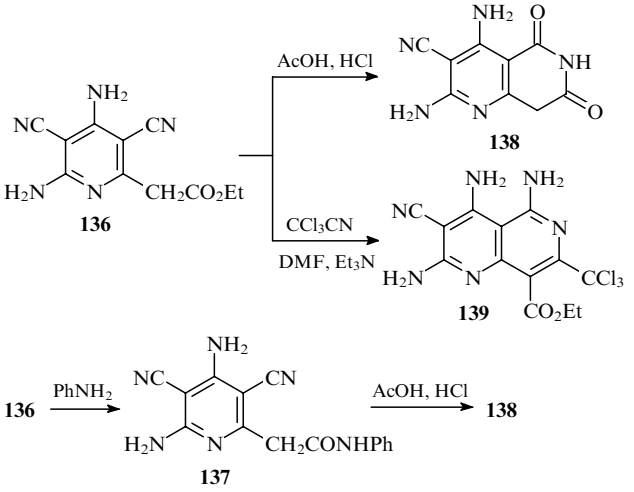

6-Methyl-2,4-diphenyl-5,6,7,8-tetrahydro-1,6-naphthyridine (**140**) was synthesised by cyclocondensation of benzylideneacetophenone (**141**) with enamino nitrile **142** in the presence of sodium ethoxide.[107]

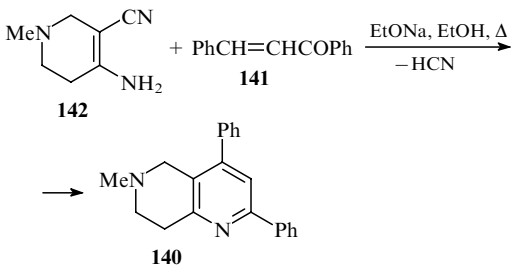

Of other procedures for the synthesis of 1,6-naphthyridines, noteworthy is three-component cyclisation of 2,3-dioxobutanal phenylhydrazone (**143**) with diethyl 3-amino-2-cyanopent-2-enedioate (**144**) and ammonium acetate to form substituted 1,6-naphthyridine-5,7(3*H*,6*H*)-dione **145**. Polyfunctionalised pyridine derivative **146** was obtained as the intermediate in this reaction.[108]

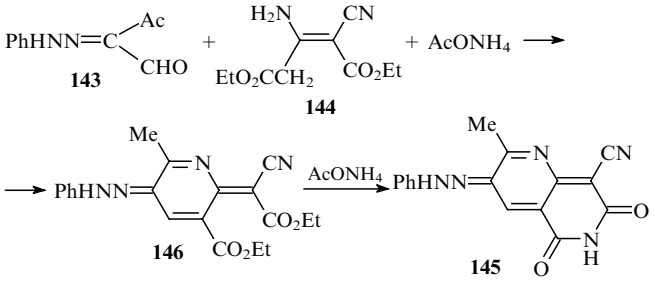

The synthesis of partially hydrogenated *N*-substituted tetrahydro-3-nitro-1,6-naphthyridines **147** involved diene condensation with the inversion of electrophilicity. 5-Nitropyrimidine reacted as the diene component with enamines **148**. Elimination of HCN from adducts **149** followed by elimination of pyrrolidine from intermediates **150** afforded the products **147**.[109]

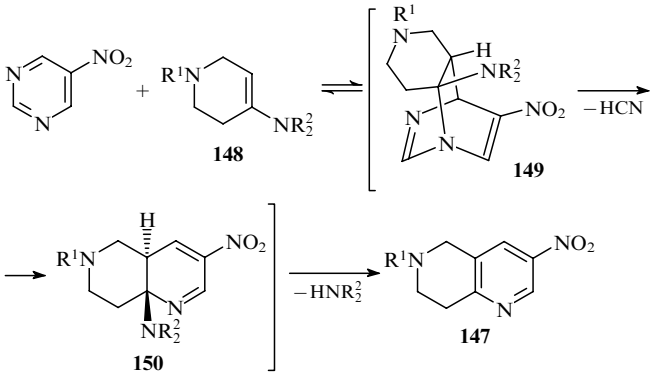

R^1 = Me, Ac; NR_2^2 = .

A handy procedure for the one-pot synthesis of the previously unknown 1-substituted 1,2,3,4,5,6,7,8-octahydro-1,6-naphthyridines **151**, which are convenient building blocks and precursors of

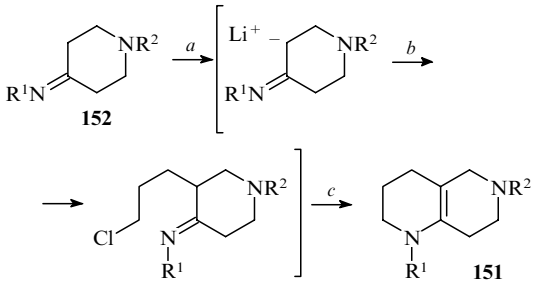

R^1 = Ph, CH_2Ph, (dl)-CH(Me)Ph, (*S*)-CH(Me)Ph; R^2 = Me, Bn, COPh; (*a*) LDA or Et_2NLi, THF, −30 °C, 30 min; (*b*) $Cl(CH_2)_3Br$, −78 °C; (*c*) Δ, 4 h.

biologically active compounds, was developed. The procedure involves metallation of imines **152** with lithium diisopropylamide or diethylamide followed by alkylation of the lithium derivatives with 1,3-bromochloropropane and intramolecular cyclisation of the resulting chloroalkylamines.[110]

2-Benzyl-1,6-dimethyl-3,10-di(methoxycarbonyl)-8-phenyldecahydro-1,6-naphthyridin-4-one was synthesised and its structure was confirmed by X-ray diffraction analysis.[111]

At the end of the section dealing with the synthesis of 1,6-naphthyridines, let us consider special procedures for the preparation of their annelated analogues. Thus a general procedure involves cyclisation of carbonyl derivatives of 4-chloropyridine with aromatic and heterocyclic amines under the action of acids. The reactions of 3-benzoyl-4-chloropyridine with substituted anilines afforded amine **153**, which underwent cyclisation under the action of polyphosphoric acid to form 1,6-naphthyridine derivatives **154** [112] (see also the synthesis of the compounds **91a**,**b** [76]).

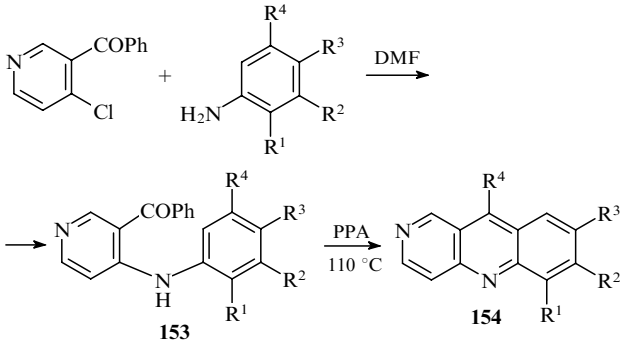

R^1, R^2 = H, OH, OMe, Cl; R^1–R^2 = CH=CH–CH=CH;
R^3 = H, OMe, NO_2; R^4 = H, OMe.

2-Chloronicotinoyl chloride (**155**) was used as the starting compound in the synthesis of heteryl-annelated 1,6-naphthyridines. Its reactions with 4,5-dihydro-1*H*-imidazolines (**156a**) or tetrahydropyrimidines (**156b**) gave rise to the corresponding *N*-acyl derivatives **157a**,**b**, which underwent cyclisation under the action of potassium *tert*-butoxide to yield imidazo- (**158a**) or pyrimido[1,2-*g*][1,6]naphthyridinones (**158b**), respectively. The compounds **158a**,**b** exhibit antiallergic and antiinflammatory activities.[113, 114]

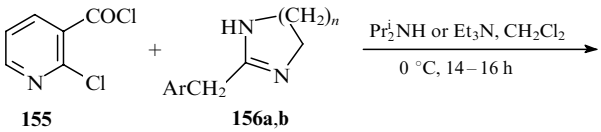

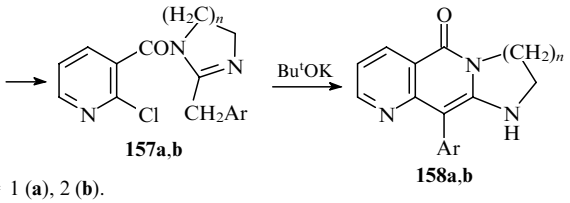

n = 1 (**a**), 2 (**b**).

The reactions of 3-aminocoumarins **159** with 2-chloronicotinoyl chloride (**155**) or 2-chloro-3-formylquinoline (**160**) afforded *N*-acyl derivatives **161** or Schiff bases **162**, which were dehydrochlorinated under the action of bases with simultaneous cyclisation to give benzopyrano[3,4-*h*][1,6]naphthyridines **163** or **164**, respectively (Scheme 2).[115, 116]

Flash pyrolysis of aminopyridine derivatives **165a**–**c** gave rise to intermediates **166a**–**c** containing the heterodiene system. Intramolecular cyclisation of the latter involving the substituent R produced annelated naphthyridines **167**–**169**.[117]

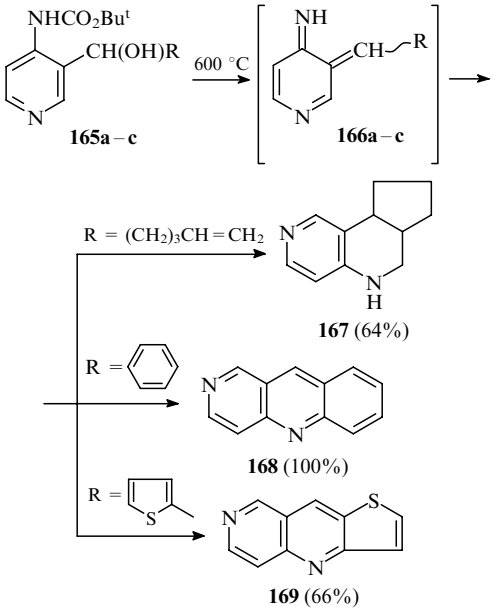

R = $(CH_2)_3CH=CH_2$ (**a**), Ph (**b**), 2-thienyl (**c**).

Dihydrobenzo[*h*][1,6]naphthyridines **170** and **171** were synthesised by Eu(fod)$_3$-catalysed intramolecular Diels–Alder cyclisation of the diene system of oxazoles **172** and **173**, respectively, with the double bond of the side-chain substituent.[118]

Scheme 2

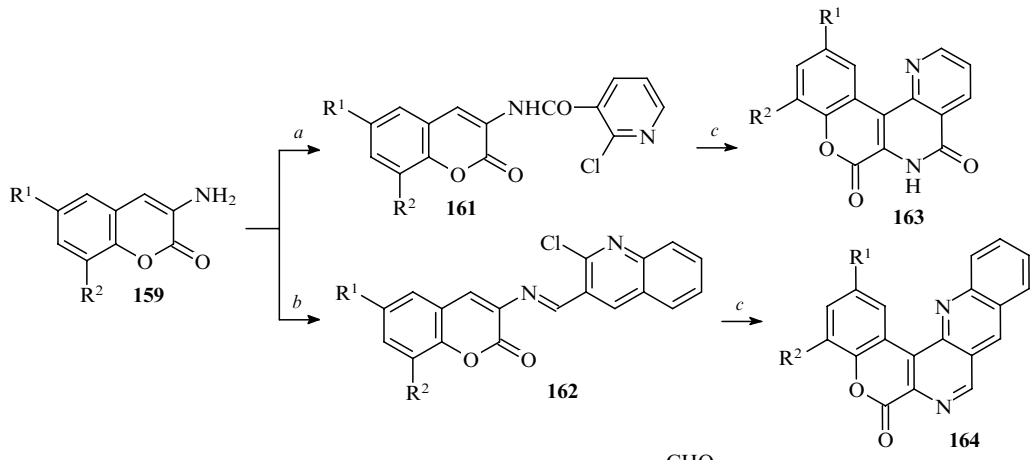

R^1 = H, Br, Cl; R^2 = H, OMe, Br; (*a*) **155**, Et_3N, PhH, Δ, 8 h; (*b*) 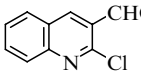 (**160**), AcOH; (*c*) Py or Et_3N–$PdCl_2$.

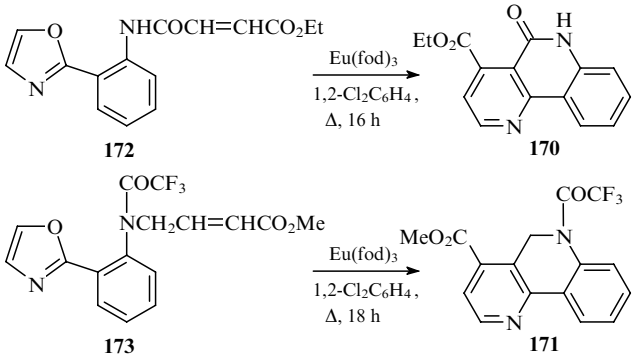

Eu(fod)$_3$ = Eu[Bu^{t}C(O)CH$_2$C(O)(CF$_2$)$_2$CF$_3$]$_3$.

1,3-Dipolar cycloaddition of 3-phenylpropynal (**174a**) or phenyl phenylethynyl ketone (**174b**) to the *N*-aminopyridinium salt **175** afforded a mixture of isomeric pyrazolo[1,5-*a*]pyridines **176a**,**b** and **177a**,**b**. Debenzylation of the compounds **176a**,**b** followed by successive treatment with formaldehyde and sodium cyanoborohydride gave rise to naphthyridines **178a**,**b**. Oxidation of the latter with *m*-chloroperbenzoic acid yielded *N*-oxides **179a**,**b**.[119]

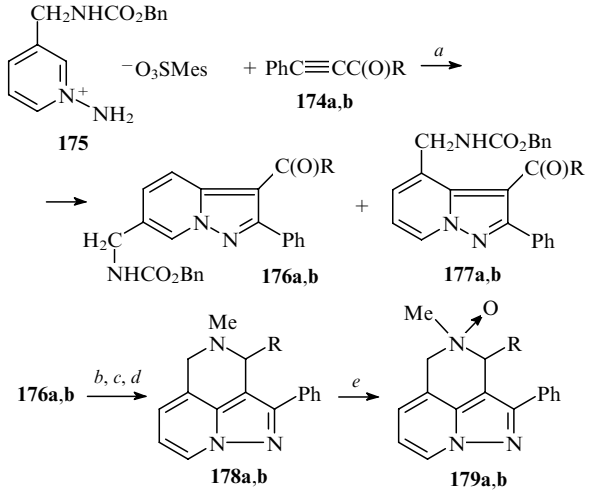

R = H (**a**), Ph (**b**); Mes = 2,4,6-Me$_3$C$_6$H$_2$; (*a*) K$_2$CO$_3$, MeCN; (*b*) 30% HBr, AcOH; (*c*) HCHO; (*d*) NaBH$_3$CN; (*e*) 3-ClC$_6$H$_4$CO$_2$H.

Dihydrobenzo[*h*][1,6]naphthyridines **180** and **181** can be prepared from 4,6-dimethyl-2-(2-nitrophenyl)-1,2-dihydropyridine-3,5-dicarboxylic esters (**182**) according to two procedures,

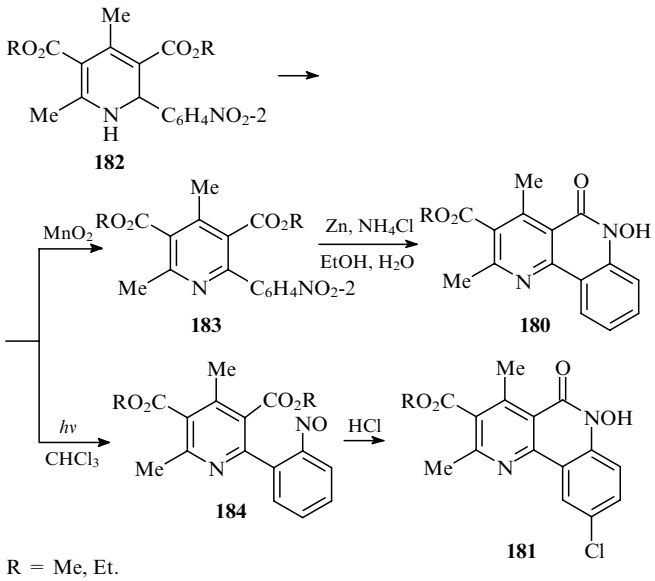

R = Me, Et.

viz., by oxidation of the dihydro derivative **182** to form pyridinedicarboxylic ester **183** followed by reduction of the nitro group with simultaneous cyclisation or by storage of a solution of the compound **182** in chloroform in sunlight to give nitroso compound **184**, which undergoes cyclisation under the action of concentrated HCl.[120]

Treatment of a solution of pyrido[1,2,3-*de*][1,4]benzooxazine **185** with a 60% NaOH solution in DMF followed by the addition of methyl isocyanate afforded the tetracyclic 1,6-naphthyridine derivative **186**. The reactions of the latter with substituted pyrrolidines or piperazines gave rise to amino derivatives **187**. The compounds **186** and **187** and their salts possess bactericidal properties.[121]

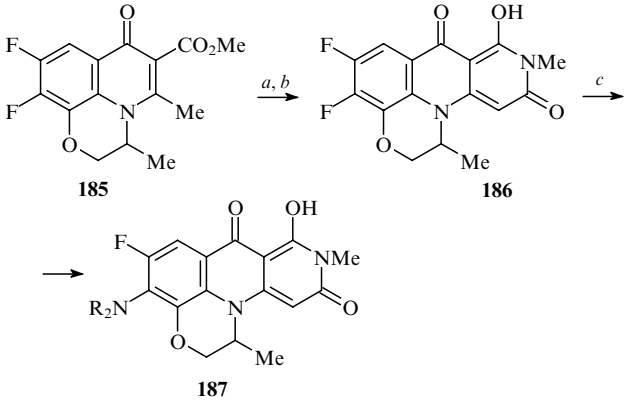

NR$_2$ are substituted pyrrolidinyls or piperazinyls;
(*a*) 60% NaOH, DMF; (*b*) MeNCO; (*c*) R$_2$NH, DMSO.

Amido and thioamido derivatives of α,β-unsaturated nitriles were used in the synthesis of annelated 1,6-naphthyridines. Thus substituted benzothiazolo[3,2-*g*][1,6]naphthyridin-5-ones (**188** and **189**) were prepared by refluxing 3-hydroxy-1*H*-pyrido-[2,1-*b*]benzothiazol-1-one (**190**) with arylmethylidenecyano(thio)-acetamides **191** and **192**, respectively, in ethanol in the presence of triethylamine.[122]

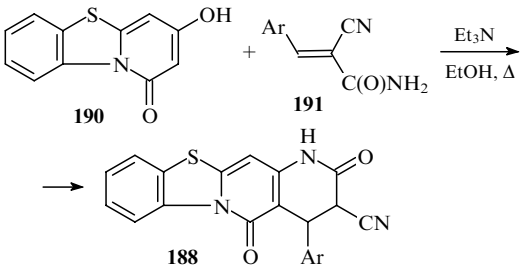

Ar = 4-MeOC$_6$H$_4$, 4-ClC$_6$H$_4$.

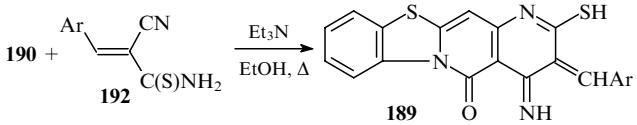

Ar = Ph, 4-MeOC$_6$H$_4$.

Thermal isomerisation of 3-(2,2-dicyanovinyl)-4-aminopyridines **193** in DMSO afforded a mixture of annelated 1,6-naphthyridines **194** and azepines **195**.[123]

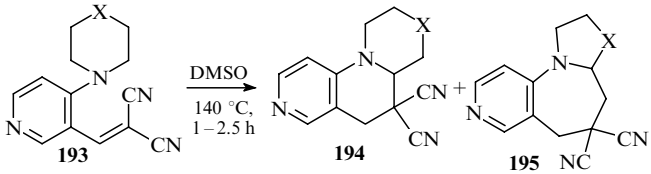

X = CH$_2$, NPh, O, S.

Of other procedures for the synthesis of annelated 1,6-naphthyridines, noteworthy is three-component condensation of the malononitrile dimer, salicylaldehyde and acetone giving rise to 1,6-naphthyridines **196**.[124]

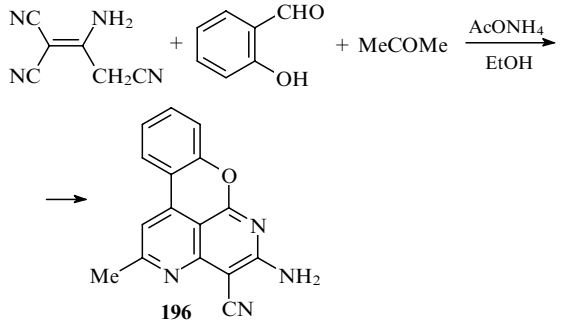

Considerable recent attention has been focused on procedures for modifications of 1,6-naphthyridine derivatives with the aim of searching for new biologically active compounds. Thus condensation of 2-amino-3-bromo-1,6-naphthyridines **74** with potassium *O*-ethyl xanthate in *N*-methylpyrrolidone afforded thiazolo[4,5-*b*][1,6]naphthyridine-2(3*H*)-thiones **197** whose subsequent methylation and hydrolysis of the methyl group in the presence of sodium methoxide afforded thiazolonaphthyridones **198** inhibiting adenosine-3′,5′-cyclophosphate phosphodiesterase (cAMP PDE III).[64]

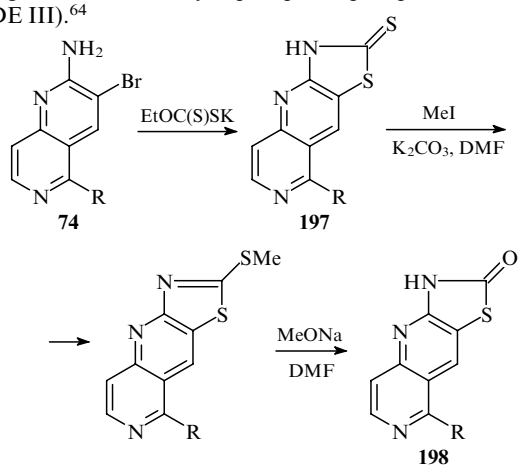

R = Me, Et, Pr^n, Bu^i, Ph, 4-$NO_2C_6H_4$.

The structural fragment of hydrogenated pyrido[3,2-*ij*]-1,6-naphthyridin-6-one **199** is present in the alkaloid matrine (sophocarpidine) found in dried roots of several plants belonging to the genus *Sophora*.

The compound **199** was synthesised from 1,6-naphthyridin-5(6*H*)-one (**200**) in six steps.[125] The key stage of the scheme consists in the Heck reaction of 8-iodo-5-methoxy-1,6-naphthyridine (**201**) with ethyl acrylate. Reduction of the double bond in the resulting derivative **202** and cyclisation of compound **203** under the action of sodium methoxide complete the synthesis.

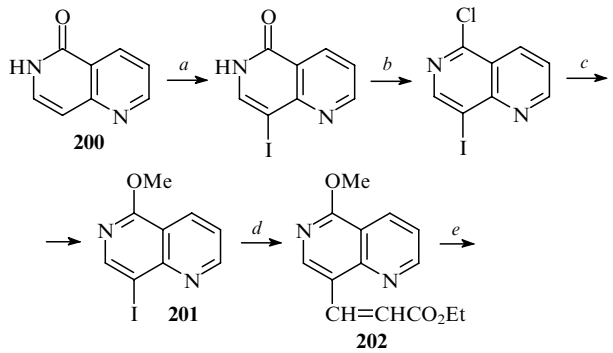

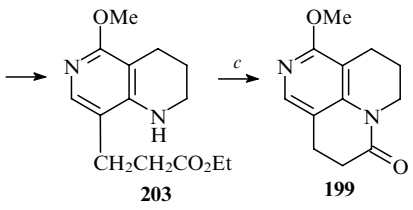

(*a*) I_2, 4M NaOH, 80 °C, 4 h; (*b*) $POCl_3$; (*c*) MeONa, MeOH; (*d*) $CH_2=CHCO_2Et$, $Pd(OAc)_2$, Et_3N, MeCN; (*e*) H_2, PtO_2, MeOH.

Condensation of 7-amino-8-cyano-1,2,3,4-tetrahydro-1,6-naphthyridine (**204**) with dimethylformamide diethyl acetal afforded azomethine **205**. Its treatment with ammonia gave rise to 1-amino-7,8,9,10-tetrahydropyrimido[4,5-*h*][1,6]naphthyridine (**206**).[126]

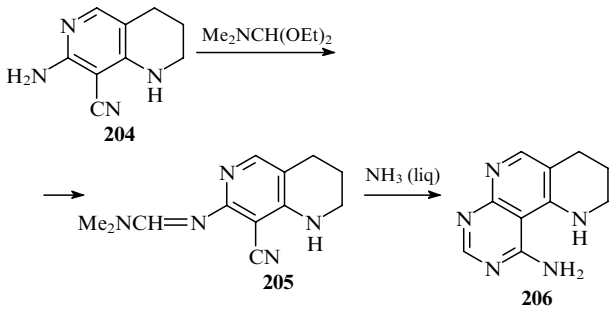

Diazotisation of the amine of the naphthyridine series **207** with a solution of sodium nitrite in 10% H_2SO_4 afforded naphthyridinone **208**, which was used as the starting compound in the synthesis of the antagonist of benzodiazepine receptors **209**.[127–129]

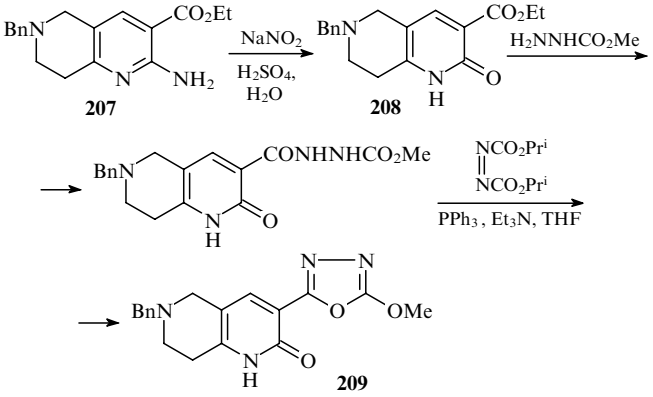

The compounds **210**, including 1,6-naphthyridine derivatives, as well as octahydronaphthyridines **211** are of interest from the pharmacological standpoint.[130–134] Thus the compounds **210** possess low toxicity and are used as components of drugs for prophylaxis and treatment of infectious diseases caused by various pathogenic bacteria.[130–133] Octahydronaphthyridines **211** are used in the treatment of depression or in cases of abstinence.[134]

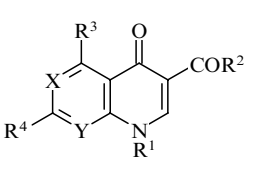

R^1 = H, Et, $(CH_2)_2OH$, $(CH_2)_2Cl$, $CH_2=CH$, cyclo-Alk; R^2 = OH, OAlk; R^3 = H, Hal, NH_2; R^4 = H, Alk, Hal; X, Y = N, CH

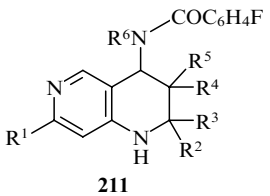

R^1 = H, Alk(C_1–C_6), CF_3, CN, NO_2; R^2, R^3 = H, Alk(C_1–C_4); R^2–R^3 = $(CH_2)_n$, n = 2–4; R^4 = H, Me, Et; R^5 = OPh, OBn, NO_2; R^6 = H, Alk(C_1–C_6)

The 1,6-naphthyridine fragment is present in the cephem molecule (**212**), which is active with respect to both gram-positive and gram-negative bacteria.[135]

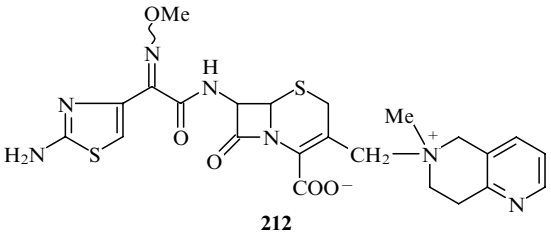

212

Recently, 1,4-dihydro-4-oxo-1,6-naphthyridine derivatives have also been covered by patents as antibacterial agents.[136] 1,4-Dihydro-5-isopropoxy-2-methyl-4-(2-trifluoromethylphenyl)-1,6-naphthyridine-3-carboxylic esters are efficient components of cytokinin inhibitors.[137] 1,6-Naphthyridine-2-carboxylamides were covered by patents as drugs used in the therapy and prophylaxis of cytomegalovirus infection.[138] 1,2,3,4,5,6,7,8-Octahydro-1,6-naphthyridine derivatives were covered by patents as anticonvulsive agents[139] and tachykinin NR_3-receptor antagonists.[140] Oxadiazolyl-substituted 1,6-naphthyridin-2-ones were covered by patents as benzodiazepine receptor antagonists.[141]

IV. 1,7-Naphthyridines

Among procedures for the synthesis of 1,7-naphthyridines, four-component condensation of 1-benzyl-3-hydroxy-5-piperidone (**213**) with 2,3-dichloro-6-fluorobenzaldehyde, acetoacetic esters and ammonium acetate giving rise to 1,4,5,6,7,8-hexahydro-1,7-naphthyridin-5-one-3-carboxylic esters **214** attracts attention due to its simplicity. The compounds **214** and their *N*-debenzylation products **215** exhibit hypotensive activity.[142, 143]

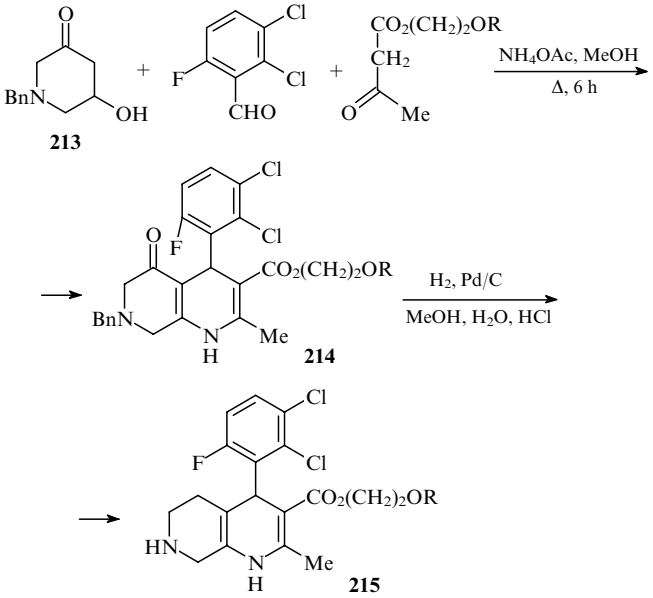

213 **214** **215**

R = Ph, 2,3-$Cl_2C_6H_3$.

3-Aroylpyridine-2-carboxylic acids **216** were used as the starting compounds for the preparation of 7-methyl-1,7-naphthyridin-8(7*H*)-one derivatives **217**, which are new strong neurokinin NK_1-receptor antagonists.[144]

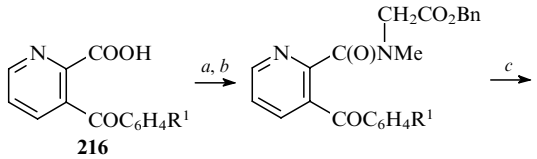

216

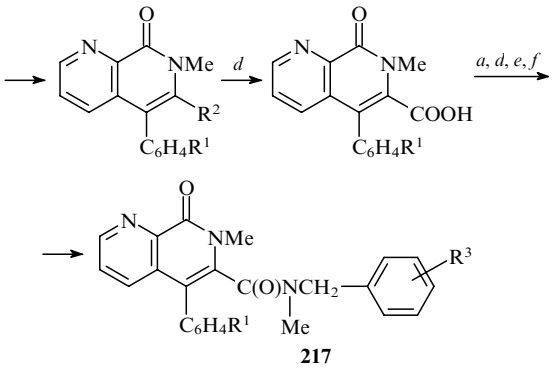

217

R^1 = H, 4-Me, 4-F; R^2 = CO_2CH_2Ph, CN, CHO, $CONH_2$;

R^3 = 3,5-$(CF_3)_2$, 2-MeO, 2-Cl, 2,5-Cl_2;

(*a*) $SOCl_2$, DMF, THF; (*b*) $BnCO_2CH_2NHMe \cdot HCl$, Et_3N, CH_2Cl_2;

(*c*) 1,8-diazabicyclo[5.4.0]undec-7-ene, PhMe; (*d*) H_2, Pd/C, MeOH;

(*e*) $R^3C_6H_4CH_2NH_2$, Et_3N, CH_2Cl_2; (*f*) MeI, NaH, DMF.

The reactions of *N*-substituted pyridine-2,3-dicarboxylimides **218** with sodium alkoxides afforded a mixture of 5-hydroxy-1,7-naphthyridin-8(7*H*)-ones **219** and 8-hydroxy-1,6-naphthyridin-5(6*H*)-ones **220**.[145]

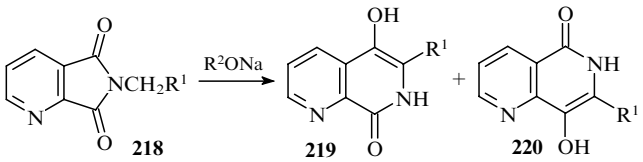

218 **219** **220**

R^1 = CO_2Me, CO_2Et, CO_2Pr^i, COPh; R^2 = Me, Et.

Treatment of 1,8-bis(bromomethyl)isoquinolinium bromide (**221**) prepared from 1,8-dimethylisoquinoline with secondary amines yielded *N*,*N*-dialkylbenzo[*de*][1,7]naphthyridinium bromides **222**.[146]

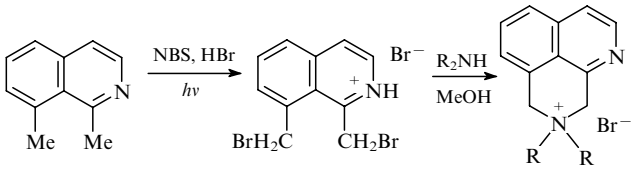

221 **222**

R = Me, Et, Pr^n, Pr^i.

Condensation of the lithium salt, which was prepared by metallation of Schiff bases **223** with lithium diisopropylamide, with ethyl 3-acetyl-2-halogenonicotinates, 3-cyano-2-halogenopyridines or 3-acetyl-2-halogenopyridines **224** gave rise to 6,8-diaryl-1,7-naphthyridines **225**.[147]

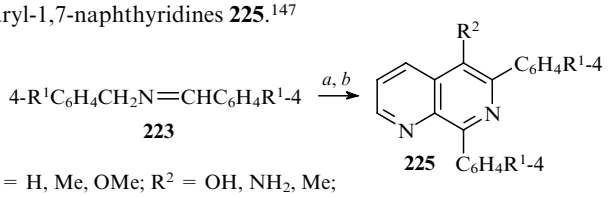

223 **225**

R^1 = H, Me, OMe; R^2 = OH, NH_2, Me;

(*a*) Pr^i_2NLi; (*b*) 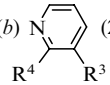 (**224**), R^3 = CO_2Et, CN, COMe; R^4 = Cl, Br.

The imino derivative of tetrahydro-1,7-naphthyridinedione **226** was synthesised by the reaction of acid chloride **227** with aniline in ether.[148]

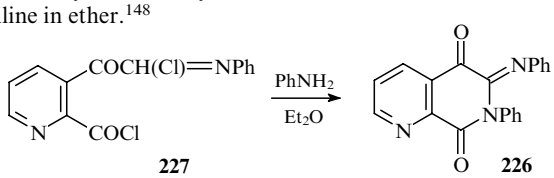

227 **226**

With the aim of searching for new antimalarial drugs among annelated 1,7-naphthyridines, compounds **228** were synthesised. Cyclisation of amino acid **229**, which was prepared from 2-iodonicotinic acid, under the action of $POCl_3$ in polyphosphoric acid afforded 10-hydroxy-2-methoxybenzo[*b*][1,7]naphthyridine **230**. The subsequent reactions with $POCl_3$ and then with aminophenols complete the synthesis. The preliminary assay of the biological activities of the compounds **228** demonstrated that these compounds are inferior to the well-known antimalarial agent pyronaridine.[149]

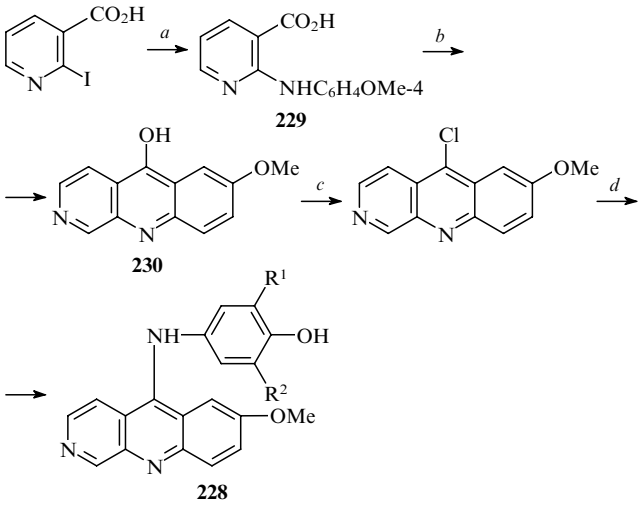

229 **230** **228**

R^1, R^2 = H, CH_2NEt_2;

(*a*) H_2N–C$_6$H$_4$–OMe; (*b*) $POCl_3$, PPA; (*c*) $POCl_3$;

(*d*) H_2N–C$_6$H$_3$(R^1)(R^2)–OH.

Treatment of (*S*)-*N*-[*N*-(4-methylpent-3-enyl)pyrrolin-2-ylmethylidene]-*o*-toluidine (**231**) with Lewis acids ($FeCl_3$, $SnCl_4$, $AlCl_3$, $MeAlCl_2$, Me_2AlCl, $EtAlCl_2$, Et_2AlCl or $BF_3 \cdot OEt_2$) or Brønsted acids (CF_3COOH or TsOH) led to formal Diels–Alder heterocyclisation giving rise to 1,7-naphthyridines **232a**,**b** in yields of > 80%. The isomer ratio depends substantially on the nature of the catalyst used. In the case of monodentate Lewis acids of the $MeAlCl_2$ or $EtAlCl_2$ type, the *cis*-isomer **232a** was obtained as the major product (99%), whereas the reactions involving bidentate Lewis acids of the $SnCl_4$ type or Brønsted acids afforded predominantly the *trans*-isomer **232b** (87%–99%).[150]

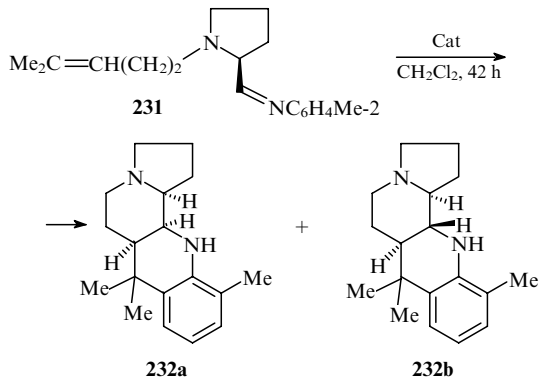

231 **232a** **232b**

1,2,3-Triazolo[1,5-*a*][1,7]naphthyridines **235a**,**b** were synthesised by the reactions of diethyl acetone-1,3-dicarboxylate (**233**) with *ortho*-substituted azides of the pyridine series **234a**,**b**.[151]

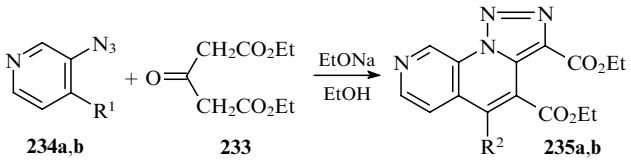

234a,**b** **233** **235a**,**b**

R^1 = CN (**234a**), CO_2Et (**234b**); R^2 = NH_2 (**235a**), OH (**235b**).

Reduction of 7-nitrobenzo[*f*][1,7]naphthyridine **236** with iron in 80% acetic acid gave rise to amine **237**, whose condensation with aromatic aldehydes afforded benzoimidazo[4,3-*fg*][1,7]-naphthyridines (**238**) exhibiting antibacterial and antifungal activities.[152, 153]

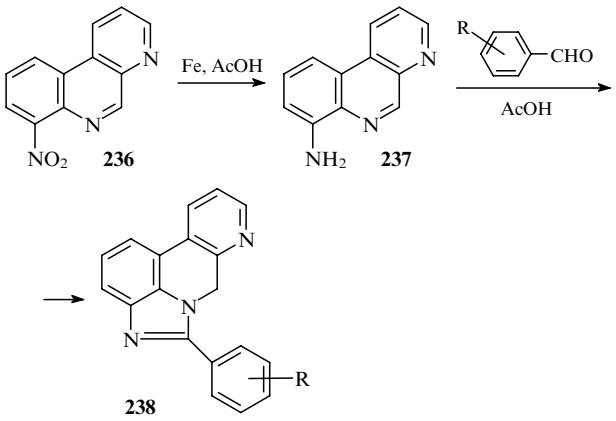

236 **237** **238**

R = H, Me, NO_2, Cl.

The rearrangement of amine of the 1,2-dihydrofuro[3,2-*f*]-[1,7]naphthyridine series produced naphthyridine derivative **239** containing the spirocyclopropane fragment.[154] The reactions of analogous 1,2-dihydrofuro[2,3-*h*][1,7]naphthyridine derivatives containing the hydroxyalkylamino group with $POCl_3$ afforded imidazo[2,1-*f*]- (**240a**) or pyrimidino[2,1-*f*][1,7]naphthyridinones (**240b**) bearing the spirocyclopropane fragment.[155]

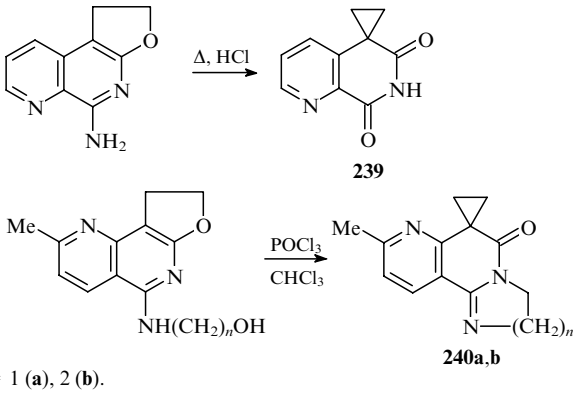

239 **240a**,**b**

n = 1 (**a**), 2 (**b**).

The reactions of 5,8-dihalogeno-1,7-naphthyridines with potassium amide in liquid ammonia were demonstrated to give mixtures of aminohalogeno, monohalogeno and monoamino derivatives of 1,7-naphthyridines.[156]

The reactivity of 4,6-benzo[*h*][1,7]naphthyridine in the Diels–Alder reactions with maleic acid and dimethyl acetylenedicarboxylate was examined. In the former case, the corresponding quaternary salt was obtained, whereas the latter reaction afforded adduct **241**.[157] 6-Ethoxycarbonyl- (**242a**) and phenacylmethylides (**242b**) were used as 1,3-dipolar reagents in the reactions with methacrylic acid, methyl methacrylate, butyl vinyl ether, methyl vinyl ketone, maleic anhydride and dimethyl acetylenedicarboxylate.[157, 158]

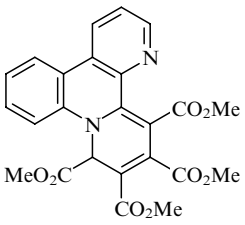

241

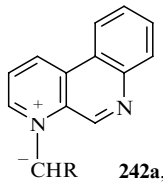

R = CO_2Et (**a**), PhCO (**b**). **242a,b**

The reactions of 6-acetamido-8-bromo-1,7-naphthyridine (**243**) with substituted piperazines in the presence of NaH afforded 6-acetamido-8-(4-R-piperazin-1-yl)-1,7-naphthyridines **244** possessing antiinflammatory, antiarrhythmic, cardiotonic, vasodilator, broncholytic, diuretic and antichlolinergic activities.[159–162]

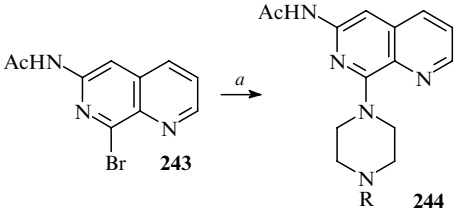

243 **244**

R = H, $(CH_2)_2OH$, CHO, Ar; (*a*) NR, $EtO(CH_2)_2OH$, NaH.

Hydrochloride of the derivative of 1,7-naphthyridine-3-carboxylic acid **245**, which lowers high blood pressure, was prepared from compound **246** and oxirane **247** upon refluxing in MeOH followed by saturation of the reaction mixture with HCl.[163]

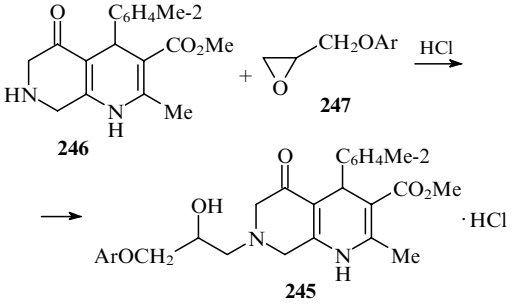

246 **247** **245**

1,7-Naphthyridone derivatives **248** were covered by patents as antibacterial agents.[164–166] Naphthyridinium derivatives **249** were covered by a patent as antidiabetic drugs.[167]

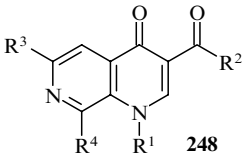

248

R^1 = H, Et, Bn; R^2 = OH, OAlk; R^3, R^4 = Hal, Me_2N, OAlk.

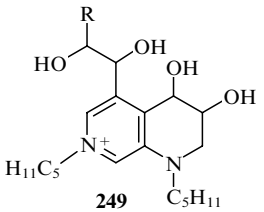

249

R = H, $HOCH_2CH(OH)$.

The data on different biological activities exhibited by a series of other 1,7-naphthyridine derivatives have also been reported in recent years.[157, 168–172]

V. 2,6-Naphthyridines

Judging from the number of papers published over the last 15 years, the chemistry of 2,6-naphthyridines attracted much less attention than that of 1,5-, 1,6- or 1,7-naphthyridines. Of the synthetic procedures developed over this period, noteworthy is oxidative cyclisation of 4-carbamoyl-3-(2-hydroxyethyl)quinolines **250a–c** under the action of CrO_3 in glacial AcOH giving rise to benzo[*c*][2,6]naphthyridines **251a–c**. The latter were used in the synthesis of 2,6-naphthyridine derivatives **252–254**.[173]

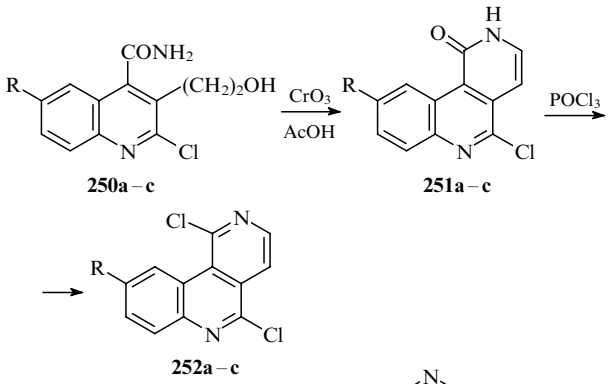

250a–c **251a–c**

252a–c

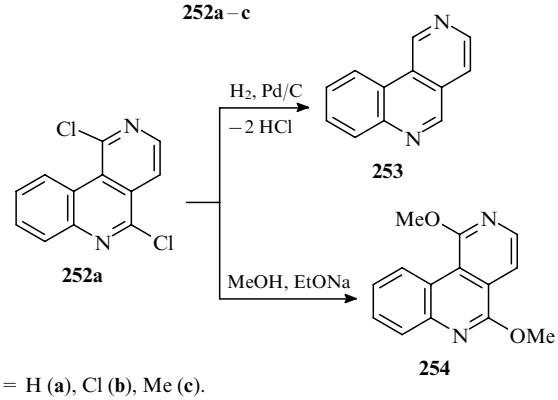

252a **253** **254**

R = H (**a**), Cl (**b**), Me (**c**).

Treatment of toluidides of halogen-substituted acetoacetic acids with sodium hydride in dioxane led to intermolecular cyclisation to form completely hydrogenated 2,6-naphthyridinetetrone **255**.[174]

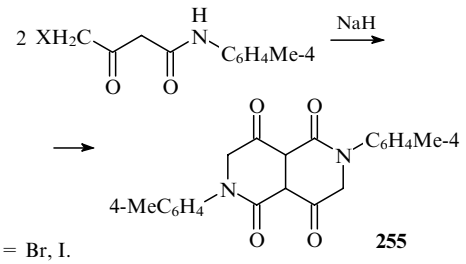

X = Br, I. **255**

Indolo[1,7-*bc*][2,6]naphthyridine **256** is a strong and selective antagonist of serotonin receptors of the 5-$HT_{2C/2B}$ subtypes possessing relatively weak affinity for 5-HT_{2A} subtype receptors.[175–177] The compound **256** was synthesised starting from indoline (**257**) and isonicotinoyl chloride.[175] Oxidation of the compound **256** with MnO_2 afforded indolonaphthyridine **258**. Yet another approach to the compound **256** involves oxidation of the double bond in compound **259** with ozone or osmium tetroxide followed by treatment with methylamine.[178] The indolonaphthyridines **256** and **258** were covered by patents as drugs for the treatment of appetite disturbance, obsessive states (phobia and depressions) and other diseases.[177, 178]

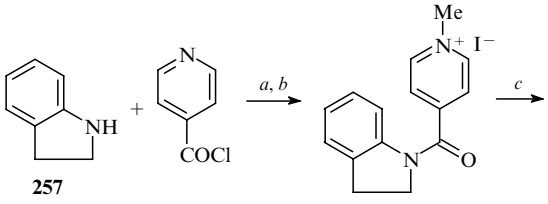

257

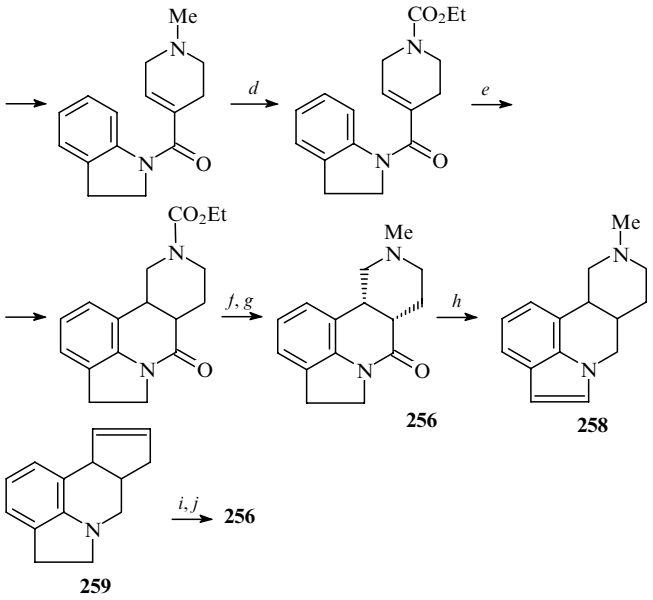

(*a*) Et_3N; (*b*) MeI; (*c*) $NaBH_4$; (*d*) $ClCO_2Et$; (*e*) *hv*; (*f*) AlH_3, THF; (*g*) (−)-di-*p*-tolyltartaric acid; (*h*) MnO_2; (*i*) O_3 (OsO_4); (*j*) $MeNH_2$.

The reactions of 1,6-dialkyl-1,6-diazacyclodeca-3,8-diynes **260** with different organic solvents (cyclohexa-1,4-diene, 9,10-dihydroanthracene or cyclooctane) as scavengers or with such reagents as HCl or MeOH proceed with high regioselectivity according to the Ad_E2 mechanism to give 1,2,3,5,6,7-hexahydro-2,6-naphthyridines **261** in quantitative yields. The reaction of the diyne **260** with H_2O in the presence of H_2SO_4 afforded naphthyridone **262** in 15% yield.[179, 180]

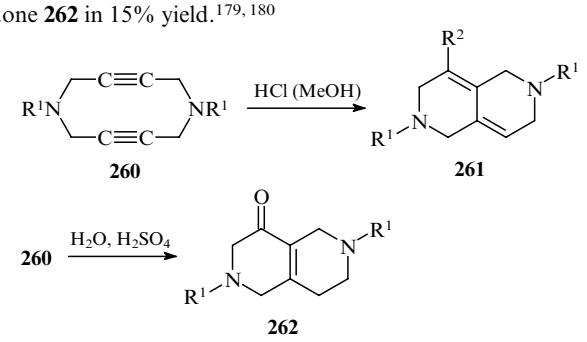

R^1 = Me, Et, Pr^i; R^2 = Cl, OMe.

Cyclisation of anilide of 3-(2-hydroxyethyl)pyridine-2-carboxylic acid occurred under the action of diethyl azodicarboxylate and Ph_3P. Subsequent treatment of the resulting 2,6-naphthyridine **263** with phenacyl bromide and then with sodium borohydride afforded octahydro-2,6-naphthyridine **264** covered by a patent as a medicine for prophylaxis and treatment of schizophrenia and depressions.[181]

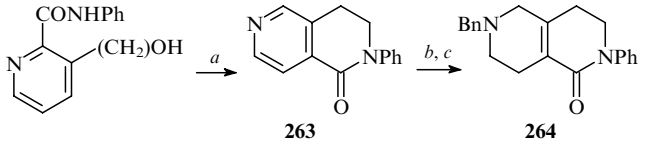

(*a*) $EtO_2CN{=}NCO_2Et$, Ph_3P, THF; (*b*) BnBr, PhMe; (*c*) $NaBH_4$, MeOH.

It was reported that 2-methoxy-12-methoxycarbonyl-2,6,8,9-tetrahydro-1*H*-indolo[7*a*,1*a*][2,6]naphthyridine isolated from seeds of *Erythrina melanacantha* Yarms can be used in the treatment of different forms of hypertonia and as an inhibitor of thrombocyte agglutination.[182]

VI. 2,7-Naphthyridines

Various approaches to the synthesis of 2,7-naphthyridines are available. Thus dianilide of 3-oxoglutaric acid **265** reacted with malononitrile in the presence of sodium acetate to give pyridone derivative **266**, whereas the reaction of the compound **265** with ethyl cyanoacetate in pyridine afforded tetrahydropyridinedione derivative **267**. The compounds **266** and **267** underwent cylcisation upon heating with triethylamine in DMF to form substituted 2,7-naphthyridine-3,6-diones **268** and **269**, respectively.[183]

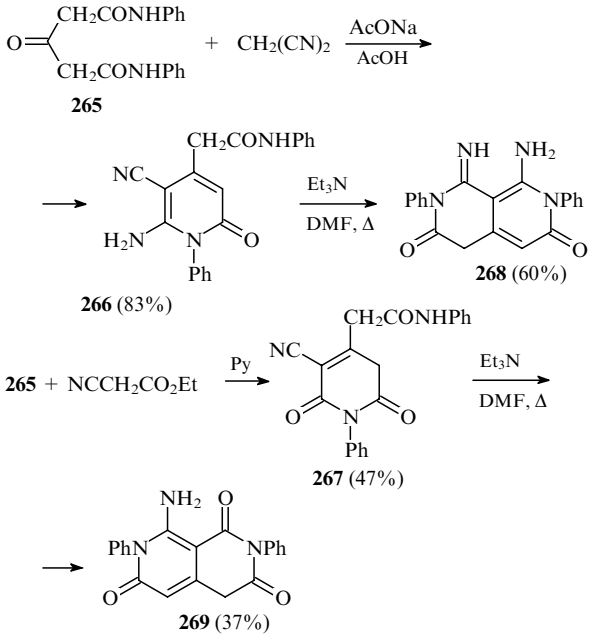

Dieckmann cyclisation of bis(2-methoxycarbonylethyl)alkylamines under the action of sodium methoxide gave rise to sodium salts of 4-hydroxy-3-methoxycarbonyltetrahydropyridines **270**. Condensation of the latter with cyanoacetamide afforded 4-cyano-1-hydroxy-5,6,7,8-tetrahydro-3-oxo-2,7-naphthyridines whose hydrolysis gave rise to 4-carbamoyl derivatives **271** exhibiting antiarrhytmic activity.[184]

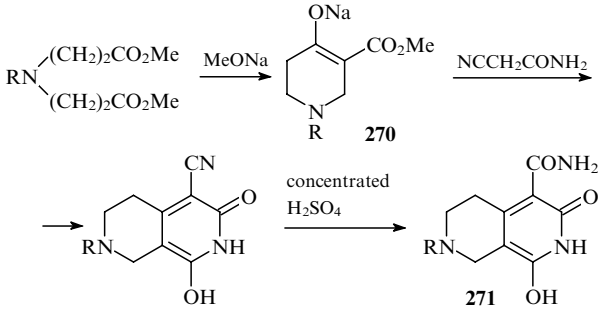

R = Et, Bn.

One of procedures for the preparation of alkyl-substituted 2,7-naphthyridines involves acylation of alcohols, ketones or alkenes in the presence of $AlCl_3$ followed by treatment of the reaction mixture with ammonia. However, these reactions are not necessarily regioselective. Thus, the reactions of acetyl chloride with *tert*-butyl alcohol or isobutylene in the presence of $AlCl_3$ followed by treatment with NH_4OH gave rise to 1,3,6,8-tetramethyl-2,7-naphthyridine along with other reaction products.[185, 186]

1-Alkyl-3,6,8-trimethyl-2,7-naphthyridines **273** were regioselectively prepared by the reactions of pyran **272** with an excess of fatty acid chlorides in the presence of $AlCl_3$ followed by treatment with liquid ammonia.[187]

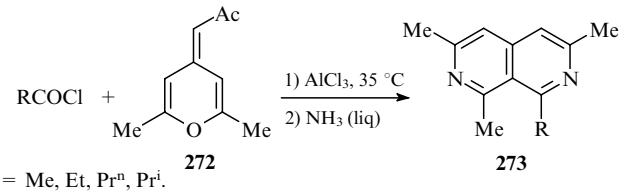

272 **273**

R = Me, Et, Pr^n, Pr^i.

Acylation of ketones **274** or enones **275** in the presence of $AlCl_3$ proceeded nonselectively. Subsequent treatment with liquid ammonia afforded a mixture of 1,3,6,8-tetraalkyl-2,7-naphthyridines **276** and **277** along with symmetrically substituted naphthyridines **278** and picolines.[188]

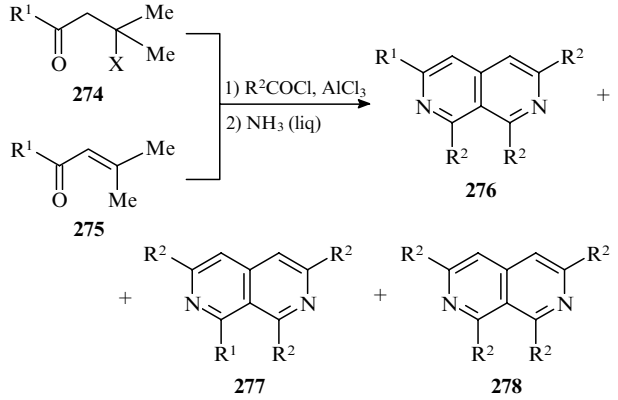

274 **276** **275** **277** **278**

R^1, R^2 = Me, Et, Pr^i; X = OH, OMe.

Yet another reaction used in the synthesis of 2,7-naphthyridine derivatives involves intramolecular cyclisation of enamino nitriles under the action of acid catalysts. Thus compound **279** underwent cyclisation to form 1-hydroxy-2,7-naphthyridine (**280**), which was used in the synthesis of sedative agent **281**.[189]

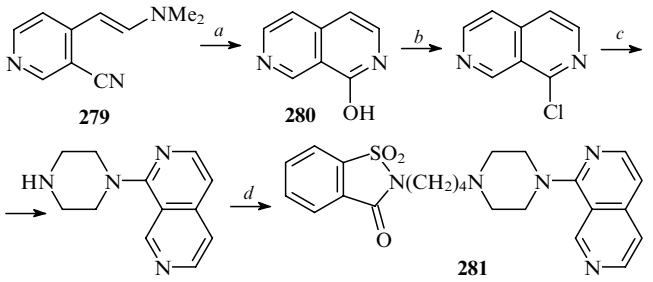

279 **280** **281**

(*a*) 30% HBr, AcOH; (*b*) $POCl_3$; (*c*) HN NH, Bu^tOK, Bu^tOH;

(*d*) 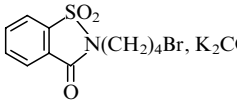

Analogous cyclisation of enamino nitrile **282** in polyphosphoric acid afforded benzo[*c*][2,7]naphthyridine **283**, which was converted into perlolinium chloride (**284**) [herbaceous alkaloid perloline (**285**)].[190] The mass spectra of the compound **285** were measured.[191]

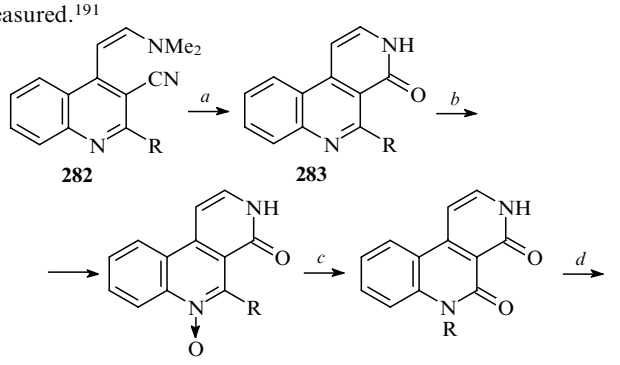

282 **283**

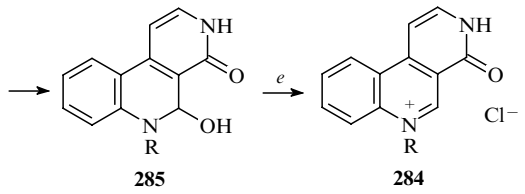

285 **284**

R = 3,4-$(MeO)_2C_6H_3$; (*a*) PPA; (*b*) 3-$ClC_6H_4CO_3H$; (*c*) *hv*, MeOH; (*d*) $[MeO(CH_2)_2O]_2AlH_2Na$; (*e*) HCl.

Yet another approach to the synthesis of 2,7-naphthyridines involves recyclisation of pyridinothiopyranothiones and pyridinopyranones. Thus recyclisation of thiopyranothiones **286** upon heating with morpholine, piperidine or piperazine in anhydrous ethanol proceeded through the nucleophilic attack of the amine on the thiocarbonyl group, the cleavage of the C(1)–S bond of the thiopyran ring and the rearrangement to form finally 2,7-naphthyridine-3(2*H*)-thiones **287**. It was demonstrated that the compounds **287** in the crystalline state exist in the equilibrium with the thiol form **288**. Their methylation with Me_2SO_4 or MeI in aqueous or ethanolic solutions of KOH produced thiomethyl derivatives **289** exhibiting antibacterial activity.[192]

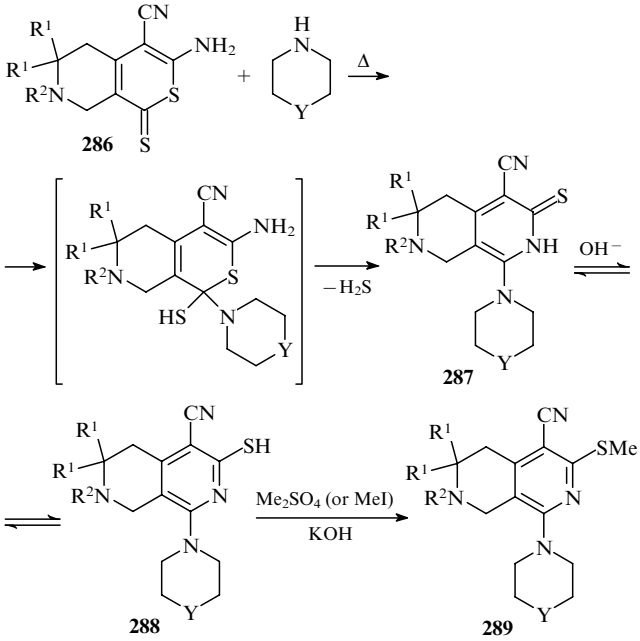

286 **287** **288** **289**

R^1 = H, Me; R^2 = Me, $CH_2CH=CH_2$; Y = O, CH_2, NH.

Condensation of substituted pyrano[4,3-*b*]pyridin-5-one **290** with dimethylformamide dimethyl acetal in xylene yielded enamine **291**, which underwent recyclisation to 2-alkyl-5-cyano-8-phenacyl-2,7-naphthyridin-1(2*H*)-ones **292** upon treatment with primary amines.[193] It was demonstrated that the change in the sequence of the addition of the reagents to the pyranone **292** (first, treatment with benzylamine and then condensation with dimethylformamide dimethyl acetal) resulted in 8-benzoyl-6-benzyl-3-cyano-4-(2-dimethylaminovinyl)-2-phenyl-1,6-naphthyridin-5(6*H*)-one (**293**).

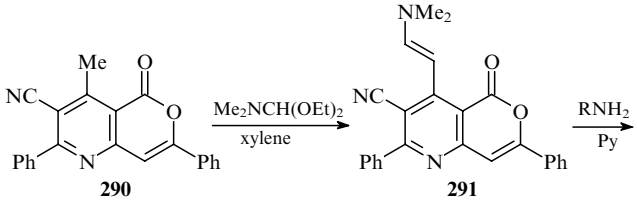

290 **291**

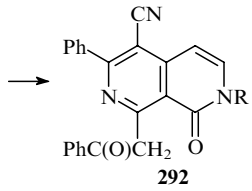

292

R = Pr, Bn.

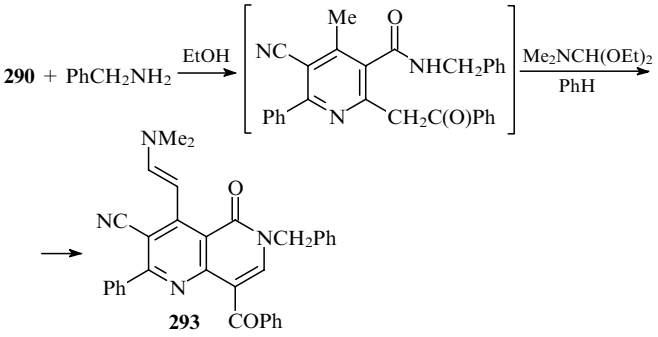

293

The reactions of 3-(phenylcarbamoyl)coumarin (**294**) with ketones in the presence of ammonium acetate in ethanol at 20 °C or in the absence of a solvent at 170 °C yielded benzo[*c*][2,7]-naphthyridines **295**.[194]

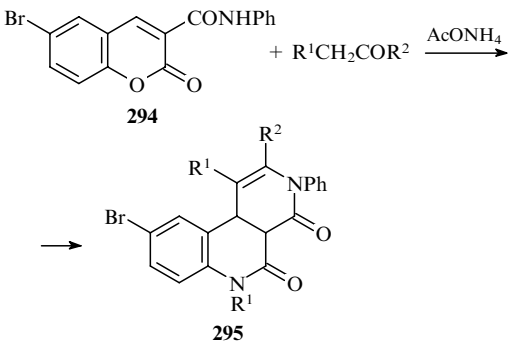

294

295

R^1 = H, Me; R^2 = Me, Et; R^1–R^2 = $(CH_2)_4$.

Fused tetrahydro-2,7-naphthyridine-1,6-diones (**296**–**298**) were also synthesised by reductive cyclisation of difuropyridine **299** and furopyridine **300**.[195]

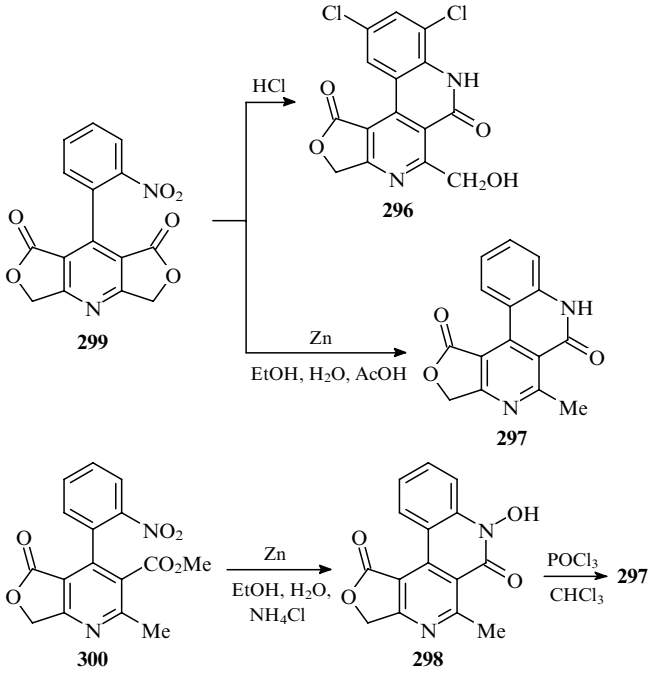

296

299

297

300

298

Annelated 2,7-naphthyridines were prepared according to a number of other approaches. Thus the reaction of hexahydro-3-oxoisoquinoline-4-carboxamide (**301**) with dimethylformamide diethyl acetal afforded a mixture of 4,5-trimethyl-1,2,7,8-tetrahydro-2,7-naphthyridine-1,8-dione (**302**) with another O-alkylation product **303**.[196]

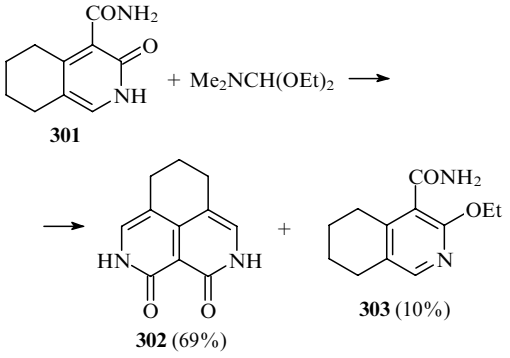

301

302 (69%)

303 (10%)

3-(2,3-Dihydrothiazol-2-ylidene)tetrahydropyridinedinone (**304**) underwent cyclocondensation upon treatment with benzaldehyde to form thiazolo[2,3-*a*][2,7]naphthyridine (**305**).[197]

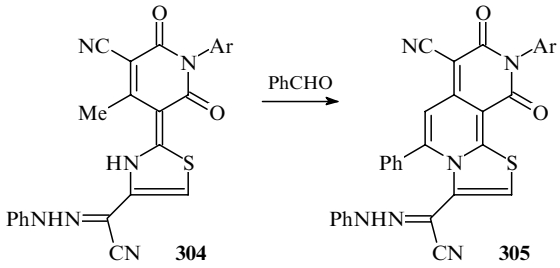

304

305

Enamine **330** underwent cyclisation to give 2,7-naphthyridine **307** under the action of ammonium chloride. The compound **307** was converted into benzo[*f*]pyrido[2′,3′:3,4]pyrrolo[2,1-*a*]-[2,7]naphthyridine **308** on treatment with H_2SO_4.[198]

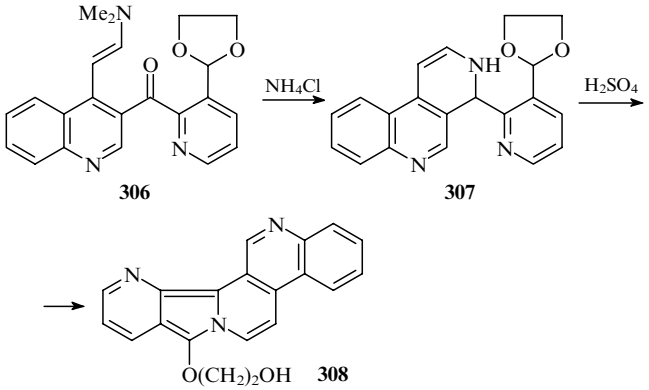

306

307

308

Photocyclisation (irradiation with a low-pressure mercury lamp, the power was 10 W, MeOH, N_2 atmosphere, 5 h) of 4-methylidene-3-nicotinoyltetrahydro-1,3-benzothiazine **309** gave rise to a mixture of isomeric 6*H*,8*H*-naphthyridino-1,3-benzothiazin-8-ones **310** and **311**.[187]

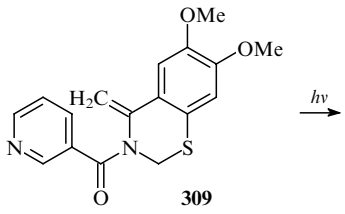

309

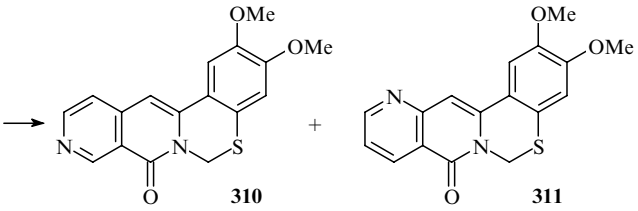

Intramolecular cyclodehydrobromination of substituted *N*-[(4-bromo-3-pyridyl)methyl]anilines **312** followed by dehydrogenation of intermediates **313** afforded benzonaphthyridines **314**.[199]

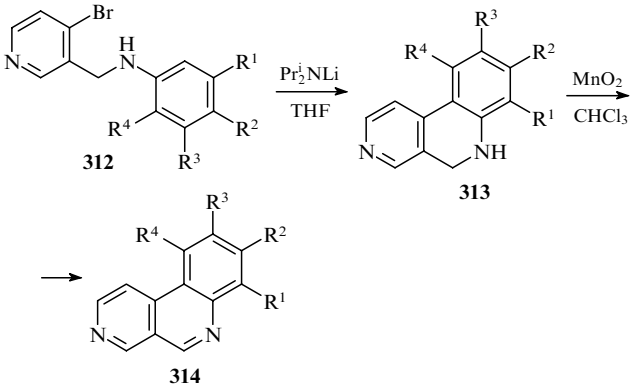

R^1, R^2, R^3, R^4 = H, Me, OMe.

Treatment of isoquinoline derivative **315** with ethyl 4-chloromethylnicotinate **316** in the presence of Bu^tOK gave rise to isoquinoline derivative **317**, which underwent cyclisation to form isoquinolino[2,1-*b*][2,7]naphthyridin-8-one (**318**).[200] The latter was not reduced with $NaBH_4$ or $NaBH_3CN$ in AcOH or Ac_2O, though this compound in AcOH was converted into derivatives **319** upon hydrogenation with hydrogen over Pt.

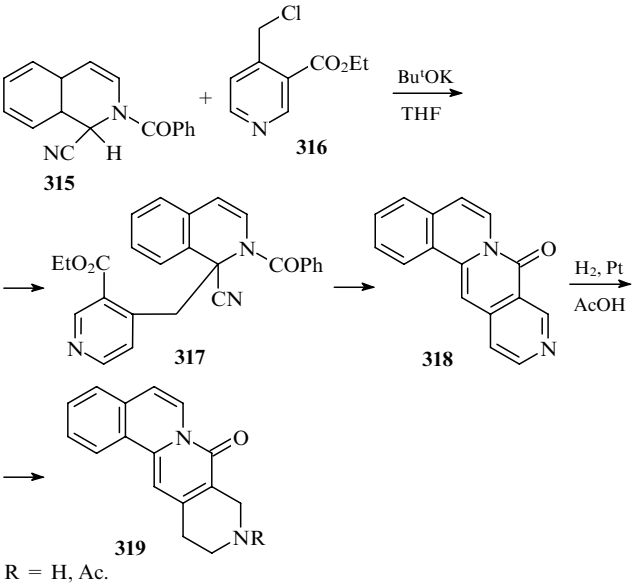

R = H, Ac.

Refluxing of substituted heterylamines **320** with a threefold excess of ethyl isocyanate in pyridine gave rise to partially hydrogenated fused 2,7-naphthyridines **321**.[201]

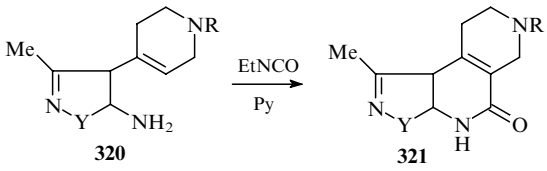

R = Me, Ac; Y = O, NMe.

An ingenious method for the preparation of annelated tetramethylthio-substituted 2,7-naphthyridine **322** is based on cyclisation of 2,6-bis[bis(methylthio)methylidene]cyclohexylidenemalononitrile (**323**) under the action of gaseous HBr.[202]

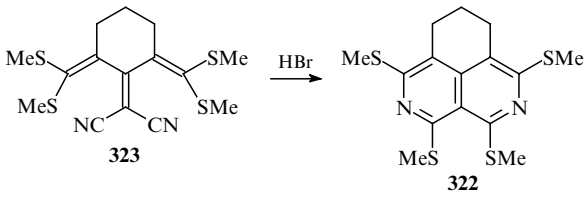

Dehydrogenation of 5,6-dihydro derivatives of 2,7-naphthyridines **324**, which were prepared by the addition of organolithium compounds to 4-substituted benzo[*c*][2,7]naphthyridines (**325**), afforded naphthyridines **326**.[203]

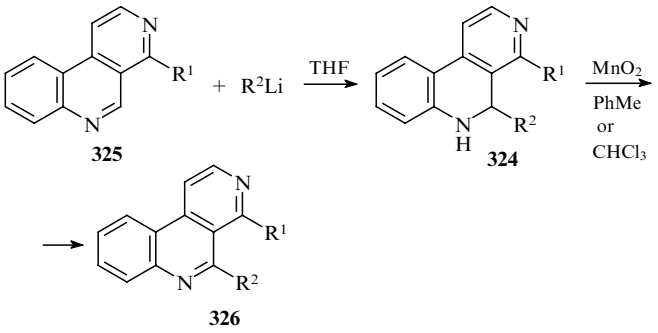

R^1 = F, Cl, $CONPr^i_2$; R^2 = Bu, Ar, Het.

Substituted tetrahydrothieno[2,3-*c*][2,7]naphthyridines **327** were prepared by the reaction of naphthyridinethione **328** with derivatives of chloroacetic acid in ethanol in the presence of sodium ethoxide (the Thorpe–Ziegler reaction).Their neurotrophic properties were investigated.[204]

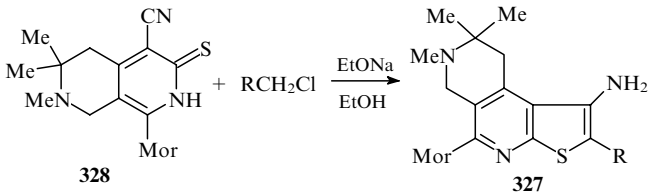

Mor = ; R = CN, $CONH_2$.

UV irradiation of *N*-aroyleneamide **329** in methanol or aqueous acetonitrile afforded a mixture of regioisomeric spirocycloadducts **330** and **331**. The solvent was not involved in the reaction performed in cyclohexane, and R = H in the compounds **330** and **331**.[205]

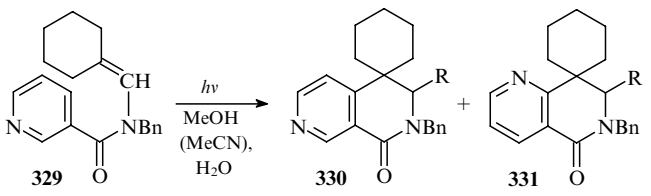

R = OMe, OH.

In a number of studies, the structural 2,7-naphthyridine fragment was found to be a component of alkaloids alangimaridine (**332**),[206] isoalamarine (**333**),[207] alamaridine (**334**) and *epi*-alamaridine,[208] nauclefine (**335**),[209,210] naulafine (**336**),[211] normalindine (**337**),[212] eudistones **338**,[213] cystodytins **339**–**341**,[214] kuanoniamines **342**,[215] meridine (**343**) possessing fungistatic activity,[216] alkaloids **344** and **345** exhibiting high antifungal and anticancer activities [217] and other biological compounds, such as sampangine (**346**) possessing antibacterial activity,[218,219] the biosynthetic precursor of camptothecin **347** exhibiting anticancer activity,[220] an analogue of olivecin **348** [221] and benzo derivatives **349** suitable for the treatment of asthma and lowering of blood pressure.[222] The data on antispasmodic activity of 2,7-naphthyridine derivatives were also reported.[223]

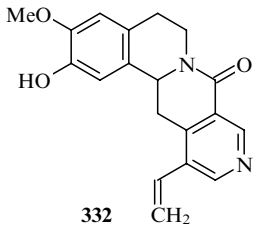

332

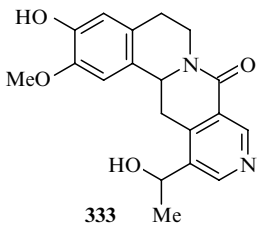

333

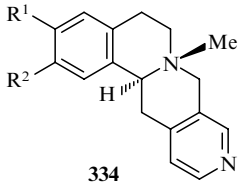

334

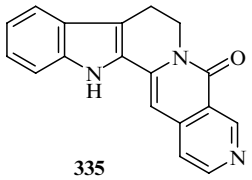

335

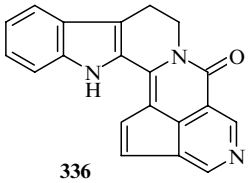

336

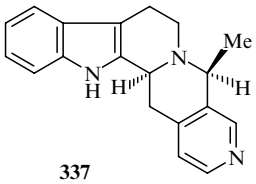

337

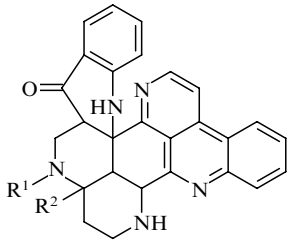

338

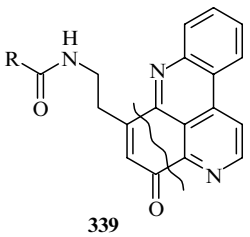

339

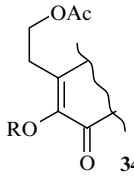

340

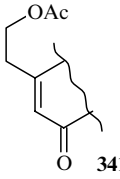

341

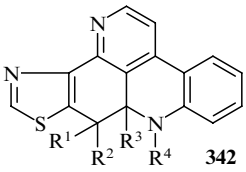

342

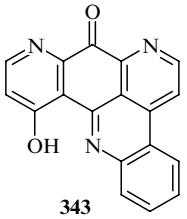

343

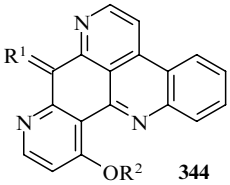

344

R^1 = O, S, NOAlk(Ar), R^2 = Alk

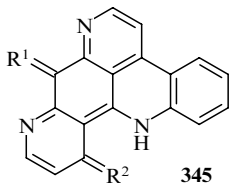

345

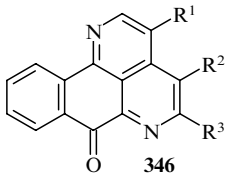

346

R^1, R^2 = O, S, NOAlk(Ar).

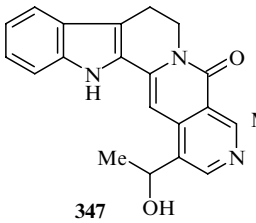

347

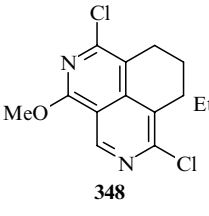

348

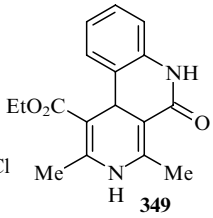

349

* * *

Analysis of the data on the synthesis, properties and biological activities of five isomeric pyridopyridines (1,5-, 1,6-, 1,7-, 2,6- and 2,7-naphthyridines) published over the last 15 years is indicative of a lively interest in different aspects of the chemistry of these heterocyclic systems. This interest is generally associated with the practical utility of their derivatives possessing a very broad spectrum of biological activities.

This review has been written with the financial support of the Russian Foundation for Basic Research (Project No. 99-03-32965).

References

1. V P Litvinov, S V Roman, V D Dyachenko *Usp. Khim.* **69** 218 (2000) [*Russ. Chem. Rev.* **69** 201 (2000)]
2. A Couture, E Deniau, P Grandclaudon, C Simion *Synthesis* 1227 (1993)
3. Fr. Appl. 2 548 667; *Chem. Abstr.* **103** 71 302 (1985)
4. Eur. P. 130 878; *Chem. Abstr.* **102** 220 856 (1985)
5. H Irikawa, Y Okumara *Bull. Chem. Soc. Jpn.* **60** 3797 (1987)
6. Eur. P. 327 426; *Chem. Abstr.* **114** 23 970 (1991)
7. G Viti, D Giannotti, R Nannicini, G Balacco, V Pestellini *Tetrahedron Lett.* **35** 5939 (1994)
8. US P. 4 652 567 (1987)
9. US P. 4 742 061 (1988)
10. US P. 4 7421 71 (1986)
11. WO PCT 9 818 795; *Chem. Abstr.* **128** 321 632 (1998)
12. J Malm, A B Hörfeldt, S Gronowitz *Heterocycles* **37** 331 (1994)
13. G B Barlin, S J Ireland *Aust. J. Chem.* **41** 1727 (1988)
14. G B Barlin, C Jiravinyu *Aust. J. Chem.* **43** 1175 (1990)
15. G B Barlin, C Jiravinyu *Aust. J. Chem.* **44** 151 (1991)
16. G B Barlin, W-L Tan *Aust. J. Chem.* **38** 905 (1985)
17. G B Barlin, W-L Tan *Aust. J. Chem.* **39** 51 (1986)
18. G B Barlin, S J Ireland, T M T Nguyen, B Kotecka, K H Rieckmann *Aust. J. Chem.* **47** 1143 (1994)
19. G B Barlin, S J Ireland, Ch Jiravinyu, Yan Jing-He *Aust. J. Chem.* **44** 677 (1991)
20. G B Barlin, W-L Tan *Aust. J. Chem.* **38** 459 (1985)
21. G B Barlin, W-L Tan *Aust. J. Chem.* **37** 2469 (1984)
22. G B Barlin, S J Ireland, C Jiravinyu, T M T Nguyen, B Kotecka, K H Rieckmann *Aust. J. Chem.* **46** 1695 (1993)
23. US P. 5 240 916; *Ref. Zh. Khim.* 13 O 85P (1995)
24. US P. 5 110 347; *Ref. Zh. Khim.* 3 O 274P (1994)
25. M Wozniak, M Tomula *Liebigs Ann. Chem.* 471 (1993)
26. R N Castle, S Pakray, G E Martin *J. Heterocycl. Chem.* **28** 1997 (1991)
27. A Achenbach, B Düthorn, R Waibel *Liebigs Ann. Chem.* 1159 (1992)
28. FR. P. 2 590 990; *Ref. Zh. Khim.* 15 O 118P (1988)
29. A A Adesomoju, M V Lakshmikantham, M P Cava *Heterocycles* **32** 1461 (1991)
30. Czech P. 216 622; *Ref. Zh. Khim.* 8 O 156P (1985)
31. Swiss P. 646 166; *Ref. Zh. Khim.* 14 O 167P (1985)
32. Fr. P. 2 562 894; *Ref. Zh. Khim.* 15 O 146P (1986)
33. BRD P. 3 409 185; *Ref. Zh. Khim.* 19 O 102P (1986)
34. Jpn. P. 60-248 688; *Ref. Zh. Khim.* 23 O 166P (1986)
35. L Czibula, A Nemes, G Visky, M Farkas, Z Szombathelyi, E Karpati, P Sohar, M Kessel, J Kreidl *Liebigs Ann. Chem.* 221 (1993)

36. BRD P. 279 887; *Ref. Zh. Khim.* 8 O 135P (1991)
37. Jpn. P. 59-93 080; *Ref. Zh. Khim.* 8 O 136P (1985)
38. WO PCT 99 29318; *Chem. Abstr.* **131** 44 810 (1999)
39. BRD P. 4 105 386; *Chem. Abstr.* **118** 82 835 (1993)
40. W Sliwa, B Minanowska *Pr. Nauk.-Wyzsza Szk. Pedagog. Czestochowa, Chem.* **1** 177 (1997); *Chem. Abstr.* **129** 175 215 (1998)
41. US P. 4 517 190 (1983)
42. US P. 4 532 247 (1983)
43. US P. 4 567 186 (1985)
44. US P. 4 559 347 (1984)
45. US P. 4 604 399 (1984)
46. US P. 4 650 806 (1985)
47. B Singh, G Y Lesher *J. Heterocycl. Chem.* **27** 2085 (1990)
48. B Singh *Synthesis* 279 (1992)
49. US P. 4 634 772 (1986)
50. US P. 4 657 915 (1986)
51. US P. 4 697 021 (1986)
52. US P. 4 716 170 (1986)
53. M Balogh, I Hermecz, G Naray-Szabo, K Simon, Z Meszaros *J. Chem. Soc., Perkin Trans. 1* 753 (1986)
54. M Balogh, I Hermecz, K Simon, L Pusztay *J. Heterocycl. Chem.* **26** 1755 (1989)
55. G Toth, A Kovacs, M Balogh, I Hermecz *J. Heterocycl. Chem.* **28** 497 (1991)
56. J Kleinschroth, K Mannhardt, J Hartenstein, G Satzinger *Synthesis* 859 (1986)
57. BRD P. 3 327 650; *Chem. Abstr.* 21 O 167P (1985)
58. BRD P. 3 431 303; *Ref. Zh. Khim.* 23 O 131P (1986)
59. BRD P. 3 502 790; *Ref. Zh. Khim.* 7 O 112P (1987)
60. BRD P. 3 605 743; *Ref. Zh. Khim.* 6 O 93P (1988)
61. BRD P. 3 602 655; *Ref. Zh. Khim.* 10 O 97P (1988)
62. Jpn. P. 477 488; *Ref. Zh. Khim.* 19 O 40P (1995)
63. BRD P. 3 609 785; *Ref. Zh. Khim.* 23 O 60P (1988)
64. B Singh, E R Bakon, G Y Lesher, Sh Robinson, P O Pennock, D C Bode, E D Pagani, R G Bentley, M J Connel, L T Hamel, P J Silver *J. Med. Chem.* **38** 2546 (1995)
65. I C Ivanov, E V Stoyanov, P S Denkova, V S Dimitrov *Liebigs Ann. Chem.* 1777 (1997)
66. N Z Tugusheva, L V Ershov, V G Granik, G Ya Shvarts, R D Syubaev, M D Mashkovskii *Khim.-Farm. Zh.* **20** 830 (1986) [a]
67. N Z Yalysheva, N P Solov'eva, V V Chistyakov, Yu N Sheinker, V G Granik *Khim. Geterotsikl. Soedin.* 1118 (1986) [b]
68. A W Erian, S M Sherif, A-Z A Alassar, Y M Elkholy *Tetrahedron* **50** 1877 (1994)
69. K-H Nietsch, R Troschütz, H J Roth *Arch. Pharm.* **318** 175 (1985)
70. US P. 4 748 246 SShA; *Chem. Abstr.* **109** 110 425 (1988)
71. US P. 4 751 305 (1987)
72. US P. 4 808 612; *Chem. Abstr.* **110** 231 609 (1989)
73. A Shiozawa, Y-i Ichikawa, C Komuro, S Kurashige, H Miyazaki, H Yamanaka, T Sakamoto *Chem. Pharm. Bull.* **32** 2522 (1984)
74. J B Sainani, A C Shah, V P Arya *Indian J. Chem.* **B34** 17 (1995)
75. BRD P. 3 502 831; *Ref. Zh. Khim.* 7 O 113P (1987)
76. C Rivalle, C Huel, E Bisagni *J. Heterocycl. Chem.* **26** 577 (1989)
77. US P. 5 391 554 (1992)
78. V I Sigova, M E Konshin *Zh. Obshch. Khim.* **54** 2083 (1984) [c]
79. S V Ukhov, M E Konshin *Khim. Geterotsikl. Soedin.* 238 (1989) [b]
80. S V Ukhov, M E Konshin *Khim. Geterotsikl. Soedin.* 92 (1992) [b]
81. A Nemazany, N Haider *J. Heterocycl. Chem.* **34** 397 (1997)
82. A Nemazany, N Haider *Electron. Conf. Heterocycl. Chem.* 1996; *Chem. Abstr.* **127** 205 495 (1997)
83. R D Clark, D B Repke, A T Kilpatrick, C M Brown, A C MacKinnon, R U Clauge, M Spedding *J. Med. Chem.* **32** 2034 (1989)
84. R D Clark, D B Repke, J Berger, J T Nelson, A T Klipatrick, C M Brown, A C MacKinnon, R U Clauge, M Spedding *J. Med. Chem.* **34** 705 (1991)
85. US P. 4 791 108 (1987)
86. Eur. P. 288 196; *Chem. Abstr.* **110** 173 210 (1989)
87. US P. 4 956 365 (1988)
88. US P. 4 960 891 (1989)
89. US P. 5 229 387 (1991)
90. US P. 5 231 181 (1991)
91. J C Rohloff, N H Dyson, J O Gardner, T V Alfredson, M L Sparacino, J Robinson III *J. Org. Chem.* **58** 1935 (1993)
92. I Hutton (Ed.) *Pharmacoproject* Vol. 13 (Richmond: PJB Publications, 1992) p. 648a
93. R D Clark, A D Michel, R L Whiting, in *Progress in Medical Chemistry* Vol. 23 (Eds G P Ellis, G B West) (Amsterdam: Elsevier, 1986) p. 1
94. P Balczewski, M K J Mallon, J D Street, J A Joule *J. Chem. Soc., Perkin Trans. 1* 3193 (1990)
95. Jpn. P. 59-48 482; *Ref. Zh. Khim.* 1 O 207P (1986)
96. N Nishiwaki, M Komatsu, Y Ohshiro *Synthesis* 41 (1991)
97. V K Jahalani, L P Ghalsasi, S P Acharya, R N Usgaonkar *Indian J. Chem.* **B28** 173 (1989)
98. P J Victory, J Teixido, J I Borrell, N Busquests *Heterocycles* **36** 1 (1993)
99. J N Reed, J Rotchford, D Strickland *Tetrahedron Lett.* **29** 5725 (1988)
100. P-L Compagnon, F Gasquez, T Kimny *Bull. Soc. Chim. Belg.* **95** 49 (1986)
101. V N Nesterov, V D Dyachenko, Yu A Sharanin, Yu T Struchkov *Izv. Akad. Nauk, Ser. Khim.* 437 (1996) [d]
102. V D Dyachenko, S V Roman, V P Litvinov *Izv. Akad. Nauk, Ser. Khim.* 121 (2000) [d]
103. S V Roman, V D Dyachenko, V P Litvinov, in *Organicheskii Sintez i Kombinatornaya Khimiya (Tez. Dokl. Mezhdunar. Konf.), Zvenigorod, 1999* [Organic Synthesis and Combinatorial Chemistry (Abstracts of Reports of the International Conference), Zvenigorod, 1999] P-58
104. S V Roman, V D Dyachenko, V P Litvinov *Khim. Geterotsikl. Soedin.* 1435 (1999) [b]
105. L S Vasil'ev, F E Surzhikov, O G Azarevich, V S Bogdanov, V A Dorokhov *Izv. Akad. Nauk, Ser. Khim.* 1510 (1994) [d]
106. R M Mohareb, S M Fahmy *Z. Naturforsch., B Chem. Sci.* **40** 1537 (1985)
107. J M Robinson, L W Brent, C Chau, K A Floyd, S L Gilham, T L McMahan, D J Magda, T J Motycka, M J Pack, A L Roberts, L A Seally, S L Simpson, R R Smith, K N Zalesny *J. Org. Chem.* **57** 7352 (1992)
108. I A El-Saaka *J. Chem. Res. (S)* 434 (1996)
109. A T M Marcelis, H C van der Plas *Tetrahedron* **45** 2693 (1989)
110. E L Gaidarova, A A Borisenko, T I Chumakov, A V Mel'nikov, I S Orlov, G V Grishina *Tetrahedron Lett.* **39** 7767 (1998)
111. T Siener, U Mueller, M Jansen, U Holzgrabe *Pharmazie* **53** 442 (1998)
112. R N Radinov, S D Simova, M A Haimova *Izv. Khim. Bulg. Akad. Nauk* **22** 144 (1989); *Ref. Zh. Khim.* 24 Zh 432 (1989)
113. R Friary, J H Schwerdt, V Seidl, F J Villani *J. Heterocycl. Chem.* **27** 189 (1990)
114. US P. 5 070 086 (1990)
115. K R Prasad, M Darbarwar *Synth. Commun.* **22** 2479 (1992)
116. K R Prasad, M Darbarwar *Org. Prep. Proced. Int.* **27** 547 (1995)
117. C W G Fishwick, R C Storr, P W Manley *J. Chem. Soc., Chem. Commun.* 1304 (1984)
118. J I Levin *Tetrahedron Lett.* **30** 2355 (1989)
119. Y Miki, O Tomii, M Utsunomiya, S Takemura, M Ikeda *Chem. Pharm. Bull.* **34** 3588 (1986)
120. K Görlitzer, C Heinrici *Arch. Pharm.* **321** 477 (1988)
121. Jpn. P. 491 090; *Ref. Zh. Khim.* 2 O 91P (1995)
122. S M Hussain, A M El-Reedy, T M Abdin *Gazz. Chim. Ital.* **118** 623 (1988)
123. V Ojea, I Muinelo, M C Figueroa, M Ruiz, J M Quintela *Synlett* 622 (1995)
124. J Svetlik, F Turecek, V Hanus *J. Chem. Soc., Perkin Trans. 1* 2053 (1988)
125. T Sakamoto, N Miura, Y Kondo, H Yamanaka *Chem. Pharm. Bull.* **34** 2018 (1986)
126. N I Smetskaya, A M Zhidkova, N A Mukhina, V G Granik *Khim. Geterotsikl. Soedin.* 1287 (1984) [b]
127. US P. 5 367 078 (1993)
128. US P. 5 424 433 (1994)
129. US P. 5 424 434 (1994)
130. Jpn. P. 58-7626; *Ref. Zh. Khim.* 2 O 123P (1985)
131. S Mishio, T Hirose, A Minamida, J-i Matsumoto, S Minami *Chem. Pharm. Bull.* **33** 4402 (1985)
132. US P. 5 180 719 (1991)
133. US P. 5 281 703 (1993)

134. WO PCT 94-12173; *Ref. Zh. Khim.* 3 O 76P (1996)
135. Jpn. P. 59-219 292; *Ref. Zh. Khim.* 1 O 184P (1986)
136. A Belicova, M Seman, V Milata, D I Ilavsky, L Ebringer *Folia Microbiol.* (*Prague*) **42** 193 (1997); *Chem. Abstr.* **127** 63 024 (1997)
137. Jpn. P. 10 182 462; *Chem. Abstr.* **129** 153 228 (1998)
138. WO PCT 97-34 894; *Chem. Abstr.* **127** 318 884 (1997)
139. WO PCT 98-54 184; *Chem. Abstr.* **130** 38 370 (1999)
140. WO PCT 99-00 388; *Chem. Abstr.* **130** 110 251 (1999)
141. WO PCT 99-03 857; *Chem. Abstr.* **130** 125 079 (1999)
142. US P. 4 596 873 (1985)
143. US P. 4 618 678 (1985)
144. H Natsugari, Y Ikeura, Y Kiyota, Y Ishichi, T Ishimaru, O Saga, H Shirafuji, T Tanaka, I Kamo, T Doi, M Otsuka *J. Med. Chem.* **38** 3106 (1995)
145. M Blanco, M G Lorenzo, I Perillo, C B Schapira *J. Heterocycl. Chem.* **33** 361 (1996)
146. A Niimi, Y Nagao, Y Abe, T Misono *Chem. Express* **6** 45 (1991)
147. A Couture, P Grandclaudon, C Simion, P Woisel *J. Chem. Soc., Perkin Trans. 1* 2643 (1995)
148. L Capuano, W Hell, C Wamprecht *Liebigs Ann. Chem.* 132 (1986)
149. P-E Zhu, Ch Chen *Pharm. Ind.* **19** 55 (1989); *Ref. Zh. Khim.* 5 O 120 (1990)
150. F Linkert, S Laschat, M Knickmeier *Liebigs Ann. Chem.* 985 (1995)
151. R K Smalley, M Teguiche *Synthesis* 654 (1990)
152. M Paluszewski, W Sliwa *Aust. J. Chem.* **46** 1115 (1993)
153. Pol. P. 167 956; *Ref. Zh. Khim.* 20 O 46P (1996)
154. T Hirota, T Matsushita, K Sasaki, S Kashino *Heterocycles* **41** 2565 (1995)
155. K Sasaki, A S S Rouf, T Hirota *J. Heterocycl. Chem.* **33** 49 (1996)
156. M Wozniak *Pol. J. Chem.* **62** 305 (1988)
157. B Bachowska, T Zujewska *Pol. J. Chem.* **70** 1324 (1996)
158. G Matusiak *Aust. J. Chem.* **52** 149 (1999)
159. Jpn. P. 62-30 780; *Ref. Zh. Khim.* 2 O 83P (1988)
160. US P. 4 690 924 (1986)
161. Jpn. P. 63-48 277; *Ref. Zh. Khim.* 15 O 88P (1989)
162. US P. 4 866 176; *Ref. Zh. Khim.* 17 O 69P (1990)
163. US P. 4 551 534 (1984)
164. S Radl, P Hradil *Collect. Czech. Chem. Commun.* **56** 2420 (1991)
165. P Hradil *Cesk. Farm.* **41** 55 (1992)
166. P Hradil *Cesk. Farm.* **41** 194 (1992)
167. Eur. P. 563 797; *Chem. Abstr.* **120** 106 978 (1994)
168. WO PCT 97-03 074; *Chem. Abstr.* **126** 199 561 (1997)
169. WO PCT 97-48 368; *Chem. Abstr.* **128** 88 786 (1998)
170. WO PCT 98-18 796; *Chem. Abstr.* **128** 321 633 (1998)
171. Jpn. P. 10 109 989; *Chem. Abstr.* **129** 16 149 (1998)
172. Y Ikeura, T Ishimaru, T Doi, M Kawada, A Fujishima, H Natsugari *Chem. Commun.* 2141 (1998)
173. P Rajamanickam, P Shanmugam *Synthesis* 541 (1985)
174. N S Ibrahim, K U Sadek, S I Aziz, M H Elnagdi *Z. Naturforsch., B Chem. Sci.* **40** 129 (1985)
175. J Nozulak, H O Kalkam, P Floersheim, D Hoyer, P Scoeffter, H R Buerki *J. Med. Chem.* **38** 28 (1995)
176. H Mühle, J Nozulak, J Cercus, E Küsters, U Buetler, G Penn, W Zaugg *Chimia* **50** 209 (1996)
177. BRD P. 473 550; *Chem. Abstr.* **117** 111 583 (1992)
178. BRD P. 4 027 018; *Ref. Zh. Khim.* 2 O 76P (1993)
179. R Gleiter, J Ritter *Angew. Chem., Int. Ed. Engl.* **33** 2470 (1994)
180. J Ritter, R Gleiter *Liebigs Ann. Chem.* 1179 (1997)
181. Br. P. 2 299 582; *Ref. Zh. Khim.* 12 O 64P (1997)
182. BRD P. 3 336 194; *Ref. Zh. Khim.* 10 O 13P (1986)
183. A M El-Reedy, M K A Ibrahim, S M Hussain, H H Moharram *J. Prakt. Chem.* **331** 745 (1989)
184. E G Paronikyan, S N Sirakanyan, A S Noravyan, T O Asatryan, K Zh Markaryan, R A Aleksanyan *Khim.-Farm. Zh.* **30** (6) 13 (1996) [a]
185. C H Erre, C M A Roussel *Bull. Soc. Chim. Fr., Pt. 2* 449 (1984)
186. F A Selimov, O G Rutman, U M Dzhemilev *Izv. Akad. Nauk SSSR, Ser. Khim.* 688 (1986) [d]
187. C Roussel, A Merier, M Gartier *J. Org. Chem.* **52** 2935 (1987)
188. C H Erre, C M A Roussel *Bull. Soc. Chim. Fr., Pt. 2* 454 (1984)
189. US P. 4 859 671 (1988)
190. A B Ridley, W C Taylor *Aust. J. Chem.* **40** 631 (1987)
191. G Dannhardt, K K Mayer, L Steindl *Chem. Ztg.* **109** 139 (1985)
192. E G Paronikyan, G V Mirzoyan, A S Noravyan, D A Avakimyan, Yu Z Ter-Zakharyan *Khim.-Farm. Zh.* **27** (11) 29 (1993) [a]
193. V A Dorokhov, A Yu Yagodkin, V S Bogdanov, S V Baranin *Izv. Akad. Nauk, Ser. Khim.* 1079 (1997) [d]
194. M Y El-Kady, G H Sayed, A M El-Gendy, M El-Sherif *Egypt. J. Chem.* **28** 63 (1985)
195. K Görlitzer, U Bartke, E Schmidt *Arch. Pharm.* **324** 105 (1991)
196. L T Guss, L V Ershov, V G Granik *Khim. Geterotsikl. Soedin.* 1696 (1987) [b]
197. R M Mohareb, H F Zohdi, S M Sherif, W W Wardkhan *Tetrahedron* **50** 5807 (1994)
198. F Bracher *J. Heterocycl. Chem.* **30** 157 (1993)
199. C F Nutailis, S R Marsh *J. Heterocycl. Chem.* **29** 971 (1992)
200. E Reimann, H Bened *Arch. Pharm.* **327** 539 (1994)
201. G Winters, A Sala, A de Paoli, V Ferri *Synthesis* 1052 (1984)
202. GDR P. 279246; *Ref. Zh. Khim.* 18 O 75P (1991)
203. C Cochennec, P Rocca, F Marsais, A Godart, G Queguiner *J. Chem. Soc., Perkin Trans. 1* 979 (1995)
204. E G Paronikyan, G V Mirzoyan, A S Noravyan, E M Arzanunts, R S Sukasyan, I S Sarkisyan, I M Nazaryan, I A Dzhagatspanyan *Khim.-Farm. Zh.* **31** (10) 34 (1997) [a]
205. J-C Gramain, Y Troin, D Vallee-Goyet *Tetrahedron* **47** 7301 (1991)
206. Jahangir, M A Brook, D B MacLean, H L Holland *Can. J. Chem.* **65** 2362 (1987)
207. U S Chowdhury *Tetrahedron* **46** 7893 (1990)
208. E Reimann, H Renz *Monatsh. Chem.* **125** 1397 (1994)
209. Jahangir, M A Brook, D B MacLean, H L Holland *Tetrahedron* **43** 5761 (1987)
210. R Vohra, D B MacLean *Heterocycles* **39** 445 (1994)
211. D B Repke Jr, M A Brook, R D Clark, J T Nelson *Heterocycles* **27** 2289 (1988)
212. A W Rey, W A Szarek, D B MacLean *Heterocycles* **32** 1143 (1991)
213. H-Y He, D J Faulkner *J. Org. Chem.* **56** 5369 (1991)
214. M A Ciufolini, N E Byrne *J. Am. Chem. Soc.* **113** 8016 (1991)
215. G P Gunawardana, F E Koehn, A Y Lee, J Clardy, H-Y He, D J Faulkner *J. Org. Chem.* **57** 1523 (1992)
216. P J McCarthy, T P Pitts, G P Gunawardana, M Kelly-Borges, S A Pomponi *J. Natur. Prod.* **55** 1664 (1992); *Ref. Zh. Khim.* 13 E 80 (1993)
217. US P. 5 182 287 (1991)
218. US P. 5 128 344 (1990)
219. US P. 5 227 383 (1991)
220. B K Carte, C DeBrosse, D Eggleston, M Hemling, M Mentzer, B Poehland, N Troupe, J W Westley, S M Hecht *Tetrahedron* **46** 2747 (1990)
221. L Mathew *J. Indian Inst. Sci.* **72** 345 (1992); *Ref. Zh. Khim.* 19 Zh 209 (1993)
222. US P. 4 478 834; *Ref. Zh. Khim.* 13 O 168P (1985)
223. E G Paronikyan, S N Sirakanyan, R G Paronikyan, A S Noravyan, in *Khimiya Fiziologicheski Aktivnykh Soedinenii (Tez. Dokl. Vsesoyuz. Konf.), Chernogolovka, 1989* [The Chemistry of Physiologically Active Compounds (Abstracts of Reports of the All-Union Conference), Chernogolovka, 1989] p. 193

[a] — *Chem. Pharm. J. (Engl. Transl.)*
[b] — *Chem. Heterocycl. Compd. (Engl. Transl.)*
[c] — *Russ. J. Gen. Chem. (Engl. Transl.)*
[d] — *Russ. Chem. Bull. (Engl. Transl.)*

Russian Chemical Reviews **70** (4) 321 – 332 (2001) © 2001 Russian Academy of Sciences and Turpion Ltd

DOI 10.1070/RC2001v070n04ABEH000603

Mechanism of thermal decomposition of silanes

A A Onischuk, V N Panfilov

Contents

I.	Introduction	321
II.	Thermal decomposition of monosilane	322
III.	Homogeneous pyrolysis of disilane	325
IV.	Heterogeneous decomposition of silanes	326
V.	Aerosol formation in the pyrolysis of silanes	327
VI.	The composition of the solid product	329
VII.	Conclusion	330

Abstract. Data on the mechanism of thermal decomposition of silanes are generalised. The main stages of the process are distinguished and characterised. Attention is concentrated on the elementary homogeneous reactions, deposition of silicon from the gas phase and formation of aerosols. Various models of formation of aerosols are considered. The results of theoretical and experimental investigations of this process are discussed. Data on the chemical composition of the solid product of silane pyrolysis (wall deposit and aerosol particles) are presented. It is noted that the hydrogen content in the solid product varies over wide limits. The bibliography includes 211 references.

I. Introduction

Thermal decomposition (pyrolysis) of silanes is used in microelectronics to obtain polycrystalline silicon and amorphous silicon layers, which explains the researchers' interest in this process. Dozens of investigations devoted to pyrolysis of silane are published annually, however, it should be emphasised that this process has been studied to a much lesser extent than pyrolysis of their closest structural analogues, *viz*. alkanes. For example, it is known that the homogeneous pyrolysis (cracking) of alkanes follows a non-branched chain mechanism. Rice's quantitative scheme suggested back in the 1930s (Ref. 1) allows one to calculate the composition of cracking products for any individual hydrocarbon. The results of the calculations obtained by this scheme fit the experimental data. The study of the influence of heterogeneous factors on the pyrolysis of hydrocarbons [2] has led to a concept of the involvement of surface in both the stages of chain initiation and termination and the stages of chain propagation.

By now, the mechanism of silane pyrolysis (unlike that of hydrocarbon pyrolysis) has not been studied adequately. Due to the lower Si—H and Si—Si bond strengths in silanes in comparison to those of the C—C and C—H bonds in hydrocarbons, pyrolysis of silanes occurs at much lower temperatures and high-molecular-mass silane derivatives are not the final products, but rather intermediates. The final products of the thermal decomposition of silanes are gaseous hydrogen and the solid phase, *viz*., silicon

$$Si_nH_{2n+2} \longrightarrow n\,Si + (n+1)\,H_2\,. \qquad (1)$$

It should be noted that the reaction generally cannot go to completion due to the experimental conditions. So the solid product is usually hydrogenated (containing chemically bound hydrogen) rather than pure silicon. The lower the reaction temperature the higher the hydrogen content in the solid product. Besides, under real conditions, stable gaseous substances (Si_2H_6, Si_3H_8, Si_4H_{10}, *etc*.) are obtained in addition to hydrogen.

Silane pyrolysis is a complex process including numerous homogeneous and heterogeneous elementary steps. At lower pressure ($P < 1$ kPa), heterogeneous stages prevail [3–7] and the solid product deposits on the reactor walls, while at high pressures homogeneous elementary reactions dominate and the solid product is obtained mainly in the form of aerosol particles.[8,9] Usually, the thermal decomposition of silanes is studied in a static reactor ($600 < T < 750$ K),[10–19] in a flow reactor ($800 < T < 1000$ K) [10,14,20–29] and in shock tubes ($900 < T < 2000$ K).[30–35] The solid product is most often amorphous hydrogenated silicon. The content of hydrogen in the solid product expressed as the [H]/[Si] ratio varies from ~ 2 (Ref. 15) 0.5 (Ref. 27) and 0.15 (Ref. 8) at low temperature and a short reaction period to < 0.01 (Ref. 36) at high temperature and a long reaction time.

Under definite conditions, the intermediate solid product (hydrogenated silicon) formed in the course of pyrolysis influences the kinetics and mechanism of this process. In particular, such influence results in acceleration of the reaction when silicon with a highly developed surface (owing to the precipitation of aerosol particles) is obtained.[37,38] As the composition of the solid product changes during the reaction, its reactivity changes, *i.e*., a solid phase of variable composition is formed, which affects the kinetics and mechanism of the process.[3] This is the key feature of the pyrolysis of silanes.

In the present review, elementary reactions, the processes of silicon precipitation on the reactor walls, the formation of aerosols and elementary reactions occurring in the solid product in the pyrolysis are considered. It should be mentioned that certain aspects of the thermal decomposition of silanes have been

A A Onischuk, V N Panfilov Institute of Chemical Kinetics and Combustion, Siberian Branch of the Russian Academy of Sciences, ul. Institutskaya 3, 630090 Novosibirsk, Russian Federation. Fax (7-383) 234 23 50. Tel. (7-383) 233 13 22.
E-mail: onischuk@ns.kinetics.nsc.ru (A A Onischuk)
Tel. (7-383) 233 23 81. E-mail: panfilov@ns.kinetics.nsc.ru (V N Panfilov)

Received 10 May 2000
Uspekhi Khimii **70** (4) 368 – 381 (2001); translated by A V Serov

discussed in detail. Thus homogeneous elementary stages of the process have been described thoroughly in a number of publications.[39–44] In the reviews,[45,46] the data on chemical vapour deposition (CVD) are systematised and some peculiarities of this process are explained. The results of studies on aerosol formation in the silane pyrolysis have been analysed.[8,9,47] In the present review, we avoid repeating the above-mentioned publications; in particular, elementary homogeneous reactions and CVD processes are not considered in detail. The attention is concentrated on those aspects which, in our opinion, either require an additional discussion (for example, the contribution of radical reactions) or provide more complete information on the pyrolysis of silanes.

II. Thermal decomposition of monosilane

1. Primary decomposition of the monosilane molecule

The reactions of the thermal decomposition of monosilane have been described most thoroughly. There are many viewpoints on whether the process of primary decomposition of SiH_4 into SiH_2 and H_2 under different conditions is homogeneous or heterogeneous. Thus according to an investigation of the silane pyrolysis in a static reactor ($P = 5-30$ kPa, $T = 650-700$ K) where the initial reaction rate did not depend on the surface to the volume ratio (S/V), the authors came to the conclusion that the primary reaction proceeds homogeneously.[15] This process was studied in static and flow reactors [10] (under lower pressure) and a conclusion as to the heterogeneity of the primary pyrolysis reaction in the whole range of pressures from 1 to 10^4 Pa was made assuming that the rate of the initial decomposition of silane at $P = 10$ Pa is proportional to the S/V ratio. This conclusion [10] was the subject of criticism. In particular, O'Neal and Ring [48] on the basis of results obtained earlier [15] reinterpreted the data given in the paper cited [10]. Taking into consideration that the heterogeneous primary decomposition prevails at pressures below 100 Pa, they proved convincingly that under high pressure (> 1 kPa) the primary decomposition proceeds as a homogeneous process. Studies on monosilane pyrolysis by laser heating (without influence of the reactor walls) confirm this conclusion. The activation energy of the laser-induced monosilane pyrolysis at 2.7 kPa (Ref. 49) was measured to be 221 ± 29 kJ mol^{-1}, which corresponds to the results obtained earlier in shock tubes [30] and in a static reactor.[15] Investigations into the silane pyrolysis under continuous wave (c.w.) CO_2 laser radiation and a total pressure of the mixture equal to 4×10^4 Pa allowed representation of the effective rate constant for the silane pyrolysis as $10^{11.5\pm0.6}\exp[-219\pm8(\text{kJ mol}^{-1})/RT]$ (Ref. 50); the value of the activation energy obtained in this study agrees with those given elsewhere.[15,30,49]

At present, it is believed that at $P > 1$ kPa the primary monosilane decomposition occurs as a homogeneous reaction and at lower pressures it is heterogeneous.[5,51]

2. The role of radical reactions in the monosilane pyrolysis

A detailed study of the mechanism of the homogeneous monosilane pyrolysis in a static reactor was first carried out by Purnell and Walsh.[15] The kinetics of the pyrolysis was characterised in the initial (conversion below 3%) and middle (conversion of 10%–20%) stages of the process. In the initial stage, the reaction had the order $\sim3/2$ with respect to monosilane, and the stoichiometry was described by the equation

$$2.39\,SiH_4 = Si_2H_6 + 0.13\,Si_3H_8 + 1.26\,H_2\,.$$

The total pressure in the reactor did not change with time and the solid product was not deposited. In the intermediate stage, the reaction was first order with respect to monosilane, the total pressure in the reactor increased and the formation of the solid product was observed.

Two alternative mechanisms were suggested which explained the experimental result, *viz*., the molecular mechanism

$$SiH_4 \longrightarrow SiH_2 + H_2\,, \tag{2}$$

$$SiH_2 + SiH_4 \longrightarrow Si_2H_6\,, \tag{3}$$

$$SiH_2 + Si_2H_6 \longrightarrow Si_3H_8 \tag{4}$$

and the radical mechanism

$$SiH_4 \longrightarrow {}^{\bullet}SiH_3 + H^{\bullet}, \tag{5}$$

$$H^{\bullet} + SiH_4 \longrightarrow H_2 + {}^{\bullet}SiH_3\,, \tag{6}$$

$${}^{\bullet}SiH_3 + SiH_4 \longrightarrow Si_2H_6 + H^{\bullet}, \tag{7}$$

$$2\,{}^{\bullet}SiH_3 \longrightarrow Si_2H_6\,. \tag{8}$$

It was noted that the reaction order 3/2 can be explained both by the radical and the molecular mechanism (it is suggested that the process in the latter proceeds in the region of the dependence of the rate constant on pressure, *viz*., in the 'fall-off' regime). Later, the calculations of the reaction constant of the unimolecular decomposition of monosilane (reaction 2) by the Rice–Ramsperger–Kassel–Marcus (RRKM) method [30] confirmed the reaction order 3/2 observed by Purnell and Walsh. Nevertheless, the discussion on the possible role of radical reactions in the thermal decomposition of monosilane continues to be topical for the last two decades.

Cleavage of the Si–H bond rupture in the SiH_4 molecule (reaction 5) is the key reaction in the radical mechanism. The Si–H bond energy was measured both by the experimental and theoretical methods. For example, interpreting the experimental data on the kinetics of the reaction between I_2 and SiH_4 in the gas phase, Doncaster and Walsh [52] estimated the H_3Si-H bond energy as 378 ± 5.1 kJ mol^{-1}. The energy of this bond found in the investigation of the reaction of SiH_3 with HI (HBr) was 384 ± 2.0 kJ mol^{-1} (298 K),[53] and in the experiments on SiH_4 photo-ionisation at 150 K it was found to be equal to 372 ± 7 kJ mol^{-1} (Ref. 54).

It should be mentioned that the values of the H_3Si-H bond energy found experimentally agree with the theoretical values. Thus Sax and Kalcher [55] have calculated the enthalpies of formation and Gibbs energies of silicon hydrides containing up to three silicon atoms. According to these calculations, the dissociation energy of the H_3Si-H bond is 383.7 kJ mol^{-1}. The H_3Si-H bond energy obtained in the determination of atomisation energies for a series of AH_n hydrides (where A is an element of the I–VII groups of the second and third periods of the Periodic Table) is 384 kJ mol^{-1}.[56] According to the calculation carried out by Ho *et al*.,[57] the value of the energy is 384 kJ mol^{-1}, later,[58] it was established as 382 kJ mol^{-1}.

The average value of the H_3Si-H bond energy obtained in the above-mentioned studies is 381 ± 13 kJ mol^{-1}. This does not agree with the experimental activation energy (233 kJ mol^{-1}) of monosilane decomposition in the initial stage of the process.[15] (Besides, for the rate of the monosilane chain decay to fit the experimentally observed rates, the chain length should exceed 10^6, but as it follows from the experimental results obtained in shock tubes,[30] the average number of collisions of the monosilane molecule with the molecules of products does not exceed 50 under these conditions.) However, the activation energy value equal to 233 kJ mol^{-1} agrees with the calculated data on the activation energy of the reaction (2).[59–64]

At present, it is acknowledged that the primary stage of the monosilane decomposition is the dissociation of the SiH_4 molecule into SiH_2 and H_2 and not H_3Si-H bond cleavage; but the significance of the contribution of the radical reactions to the next pyrolysis stages still remains an open question. Numerous publications deal with the role of SiH_3 in the process of the thermal monosilane decomposition. Thus the pyrolysis of an equimolar mixture of SiH_4 and SiD_4 was studied in flow and static reactors.[14] The formation of mixed silanes and disilanes and the differences in the results obtained in static and flow reactors could be rationalised by the mechanism implying the involvement of SiH_3.

Thermal decomposition of monosilane in the presence of acetylene in a flow reactor at 690–710 K was studied by Haas

and Ring.[24] Based on the analysis of the reaction products, it was suggested that the silyl radicals were the major products of the initial decomposition.

In an investigation into the decomposition of monosilane in a single-pulse shock tube at 1200–1300 K, it was concluded [33] that the observed decomposition rate of monosilane cannot be explained by the radical mechanism; therefore, the primary act of the monosilane decomposition is the unimolecular elimination of H_2. The rate constants for the H_2 elimination from SiH_4 were calculated by the RRKM method. Comparison of the calculated and experimental [15] values showed that they differ more than forty-fold, which led to the conclusion that the chain mechanism is predominant under the static reactor conditions.

The thermal decomposition of SiH_4 in a static reactor in the presence of ethylene was carried out in order to determine whether the primary act of the monosilane decomposition occurs according to the molecular mechanism (*i.e.*, as the result of H_2 elimination from the SiH_4 molecule).[18] The analysis of the pyrolysis products suggested that the SiH_3 radicals formed in the slow heterogeneous process of the Si—H bond cleavage participate, though to a minor extent, in the pyrolysis of silane. This suggestion was confirmed by performing a pyrolysis of a SiH_4–SiD_4 mixture and detecting a rather high content of HD in the hydrogen fraction.

The initial acceleration of the silane pyrolysis in static and flow reactors in the range of pressures from 1 to 10^4 Pa was found,[10] which could be explained by the liberation of radicals from the surface into the gas phase or by the hydrogen atom elimination into the gas phase followed by chain reaction [processes (6) and (7)].

The gas-phase pyrolysis of monosilane in the mixture of Ar and SF_6 under c.w. CO_2-laser radiation was investigated.[50] The total pressure of the mixture was 4×10^4 Pa, while the partial pressure of monosilane was 10^2–10^3 Pa. The influence of propene additives as an inhibitor of radical reactions was studied experimentally. It was established that the effective rate constant for the silane pyrolysis decreases on the addition of propene. Presumably, in the presence of an inhibitor the reaction proceeds in accordance with the molecular mechanism and is characterised by an activation energy of 281.5 kJ mol^{-1}. In the absence of an inhibitor, the radical stages become sifnificant and the effective activation energy of this process decreases to 217 kJ mol^{-1}.

A series of experiments on the monosilane decomposition in the presence of alkenes and acetylene in a static reactor was carried out in order to find out whether silyl radicals take part in the pyrolysis of monosilane.[11] The analysis of the kinetics of the pyrolysis of the silane–acetylene mixture gave additional information on the nature of the monosilane thermal decomposition. According to the first-order kinetics obtained for this mixture, it was determined that silyl radicals do not participate in the decomposition under conditions examined. A possible scheme of the radical mechanism of monosilane decomposition in the presence of alkenes, according to which lower alkanes should be formed, was suggested. The absence of lower alkanes among the experimentally detected products led to the conclusion that the silyl radicals do not contribute considerably to the reaction.

The results of the investigation on the pyrolysis of a SiH_4–SiD_4 mixture under static conditions and under reduced pressures, in particular, the kinetic curves of the H_2, HD and D_2 formation, showed [12] that HD concentration in the initial stage of the process increased more slowly than in the following stages. The analysis of the formation of isotopic hydrogen molecules shows that the molecular mechanism of the monosilane decomposition is predominant. The sequence of the formation of mixed deuteriosilanes

$$\left.\begin{array}{l} SiH_4 \longrightarrow SiH_3D \\ SiD_4 \longrightarrow SiHD_3 \end{array}\right\} \longrightarrow SiH_2D_2,$$

was determined as being due to the exchange reactions involving the SiH_3 radical, *e.g.*

$$^{\bullet}SiH_3 + SiD_4 \longrightarrow SiH_3D + {}^{\bullet}SiD_3. \quad (9)$$

The concentrations of Si_2H_6, $Si_2H_2D_4$ and Si_2D_6 in the initial stage of the pyrolysis exceed those of other deuteriodisilanes. This fact proves the predominance of the disilane formation upon the reaction SiH_2 with SiH_4. Thus, the features of formation of isotopic hydrogen molecules and deuteriodisilanes points to the significance of the contribution made by the molecular mechanism.

In studies on the heterogeneous decomposition of monosilane at 0.5–4 Pa, the liberation of hydrogen atoms and SiH_3 radicals into the gas phase was observed.[61] The heated surface was placed directly close to the ionisation source in such a way that practically all the radicals evolved from the surface into the gas phase could reach the inlet of the ionisation chamber virtually without collisions with the gas molecules. At $T > 1800$ K, almost all the hydrogen obtained upon the decomposition SiH_4 is liberated as H atoms, while a part of hydrogen is liberated as H_2 molecules at $T < 1800$ K. The elimination of hydrogen in the temperature range 1300–1800 K is characterised by the activation energy 176 kJ mol^{-1}, while at $T < 1300$ K the activation energy is 46 kJ mol^{-1}. The effectiveness of the formation of SiH_3 radicals in the heterogeneous silane decomposition is 0.014–0.05. The liberation of SiH_3 radicals from the surface takes place as the result of the exchange of the hydrogen atom between the SiH_4 molecule and the free bond localised on the surface.

Direct detection of SiH_3 radicals in the thermal decomposition of monosilane in a flow reactor was investigated by the method of laser magnetic resonance.[28] A mixture of monosilane and argon (the total pressure was 60–500 Pa, the partial pressure of monosilane was 2.3–18 Pa) was used. The concentration of SiH_3 radicals changed from 10^{10} to 10^{12} cm^{-3} as the temperature of the reactor was raised from 830 to 1250 K (10% of SiH_4 at the total pressure of 400 Pa). It was suggested that SiH_3 radicals are formed in the heterogeneous processes.

The possibility of the chemical induction of the monosilane pyrolysis was shown.[19] This was carried out in a cylindrical metal reactor. A mixture of SiH_4 and O_2 with the oxygen percentage below 2% was introduced at room temperature and the reaction was initiated by spark ignition or by chemical ignition. The degree of conversion of monosilane was up to 60%. At definite concentration ratio of SiH_4 and O_2 and pressures, the mixture can ignite spontaneously even at room temperature, which is the chemical method of ignition. If the necessary $[SiH_4]:[O_2]$ ratio is established in a small volume of a reactor, self-ignition occurs. Then the burning front spreads over the whole volume, which results in the significant burnout of monosilane. The decomposition of silane presumably has branched-chain character under these conditions. Oxygen is required only in the stage of chain initiation. The atoms and radicals formed in this stage take part in the chain reactions of the monosilane decomposition, which results in significant consumption of monosilane. The average chain length is ~ 10.

Studies of the monosilane pyrolysis under static conditions at $P = 0.2$–5 kPa show that an increase in the specific surface (S/V) at $T = 669$ K gives rise to an increase in the decomposition rate, while at $T = 779$ K it results in its reduction.[4] The dependences obtained were interpreted in the terms of the radical chain mechanism and it was suggested that the rate of the heterogeneous decomposition of monosilane increases with the increase in the ratio S/V at low temperatures, while at high temperatures the rate of the heterogeneous chain termination increases.

It was supposed that the chain process plays a considerable role in the pyrolysis of monosilane [reactions (6) and (7)].[62] The activation energies obtained by *ab initio* quantum-chemical calculations were found to be 36 and 133 kJ mol^{-1} for these reactions, respectively.

Hydrogen atom formation during the monosilane pyrolysis in a shock tube was studied.[35] The reaction was followed by monitoring light absorption by the hydrogen atoms at the wavelength $\lambda = 121.6$ nm. An Ar/SiH_4 mixture was used (the total

pressure was 1 – 1.5 atm, the relative concentration of monosilane in the mixture was $\sim 10^{-5}$). The time dependence of the hydrogen atom concentration was obtained. The features of this dependence are as follows: the change in the concentration at low temperatures is S-shaped; the maximum concentration increases as the temperature increases to $\sim$ 1600 K and decreases as the temperature increases from 1600 to 2300 K. Furthermore, at $T \geqslant 1800$ K the two-stage formation of hydrogen atoms is evident, as the characteristic time of the accumulation of hydrogen exceeds significantly the decomposition time of SiH_4. These features confirm the complex character of the processes of the hydrogen atom formation

$$Si + SiH_2 \longrightarrow {}^{\bullet}Si(H)Si + H^{\bullet}, \quad (10)$$

$$Si + H_2 \longrightarrow {}^{\bullet}SiH + H^{\bullet}, \quad (11)$$

$$Si + Si(H_2)Si \longrightarrow {}^{\bullet}Si_3H + H^{\bullet}, \quad (12)$$

$$H_2 + M \longrightarrow H^{\bullet} + H^{\bullet} + M. \quad (13)$$

Thus, the monosilane pyrolysis results in significant amount of hydrogen (5% – 10% of the initial silane concentration) even under homogeneous conditions and at high dilution. The hydrogen atoms are formed not upon the decomposition of SiH_4 or SiH_2, but rather in the secondary bimolecular reactions. It was concluded that the hydrogen might take part in the chain process which includes the reaction (6) and

$$ {}^{\bullet}SiH_3 + M \longrightarrow {}^{\bullet}SiH + H_2 + M, \quad (14)$$

$$SiH_4 + SiH \longrightarrow {}^{\bullet}Si_2H_4 + H^{\bullet}. \quad (15)$$

The rate constants for the radical reactions should be determined to evaluate the importance of these reactions in the thermal decomposition of monosilane. Unfortunately, the information on these reactions in the literature is poor. The rate constants [63] for the reactions of SiH_3 with Si_2H_6, of SiH_3 with SiD_4 and of H with SiH_4 ($T = 300$ K) are $\leqslant (7\pm4)\times10^{-15}$, $\leqslant (4\pm2)\times10^{-14}$, $\leqslant (2.5\pm0.5)\times10^{-13}$ cm^3 s^{-1}, respectively.[63] According to the calculations of the activation energy, the rate constant for the reaction (7) should be $1\times10^{-10}\exp[-56.1(\text{kJ mol}^{-1})/RT]$ cm^3 s^{-1}.[64] The calculated activation energy for the reaction (7) is 133 kJ mol^{-1}.[62] For the reaction [65]

$$ {}^{\bullet}SiH_3 + SiH_4 \longrightarrow {}^{\bullet}Si_2H_5 + H_2 \quad (16)$$

the rate constant is

$$k_{16} = 2.94\times10^{-12}\exp\left[-\frac{18.4\ (\text{kJ mol}^{-1})}{RT}\right].$$

The values of the rate constant for reaction (5) calculated based on the variation theory of the transition state for the temperature range 200 – 1000 K (Ref. 66) agree with the experimental values.

The above-mentioned data show that the role of the radical reactions in the monosilane pyrolysis is not clear. Nevertheless, the following conclusions can be made. First, under the conditions of the homogeneous pyrolysis, the primary reaction of the silane decomposition is the dissociation of SiH_4 to H_2 and SiH_2 [reaction (2)]. Second, the conditions under which radical reactions make considerable contribution exist probably even at relatively high pressures (where homogeneous reactions are predominant). In static and flow reactors, the radicals are apparently formed in heterogeneous reactions.[67]

The later statement can be confirmed by the following data. Studies of monosilane pyrolysis in a flow reactor for a mixture of 5% SiH_4 and 95% Ar (the total pressure was 6.6 kPa) gave the constants of the decomposition of monosilane at 843 and 933 K, *viz*., 0.25 and 3.6 s^{-1}, respectively. Let us estimate the possible contribution of the radical reactions to this process. The concentration of SiH_3 radicals formed in the monosilane pyrolysis in a flow reactor for a mixture of 10% SiH_4 and 90% Ar (the total pressure was 400 Pa) was measured by the method of laser magnetic resonance and was found to be 1×10^{10} and 5×10^{10} cm^{-3} at 843 and 933 K, respectively.[28] The signal for SiH_3 was proportional to the total pressure squared (the content of the silane in the initial mixture was constant) and to the partial pressure of the silane (the total pressure was fixed). Extrapolating the results obtained [28] for the mixture of 5% SiH_4 and 95% Ar (the total pressure was 6.6 kPa), we obtain $[SiH_3] \approx 1\times10^{12}$ and 5×10^{12} cm^{-3} at $T = 843$ and 933 K, respectively. The ratio of the (Ref. 65) reaction rate to $[SiH_4]$ can be calculated using the rate constant for the reaction (16). At 843 and 933 K, this ratio is 0.2 and 1.37 s^{-1}, respectively. Thus the estimated rate of the reaction (16) is close to the rate of the monosilane decomposition measured experimentally. Unfortunately, the development of the expression for the rate constant for the reaction (16) has not been described in detail.[65] Thus, the estimate given may suggest that the contribution of the radical reactions to the process of pyrolysis can be significant.

3. The mechanism of homogeneous pyrolysis of monosilane

At present, it is believed (see *e.g*. Ref. 39) that the main contribution to the process of the homogeneous monosilane pyrolysis (at least, in the early stages) is made by the following reactions

$$\begin{aligned} &SiH_4 \rightleftharpoons SiH_2 + H_2, \\ &SiH_2 + SiH_4 \rightleftharpoons Si_2H_6, \\ &SiH_2 + Si_2H_6 \rightleftharpoons Si_3H_8, \\ &SiH_2 + Si_3H_8 \rightleftharpoons Si_4H_{10}. \end{aligned} \quad (17)$$

Silylene (SiH_2) formed in the reaction of primary monosilane decomposition reacts with another molecule of monosilane to give disilane. Silylene reacts consecutively with disilane to give trisilane, with trisilane to give tetrasilane, *etc*. The formation of polysilanes is accompanied by their dissociation and the formation of substituted silylenes

$$Si_2H_6 \rightleftharpoons H_3SiSiH + H_2, \quad (18)$$

$$Si_3H_8 \rightleftharpoons SiH_3SiH_2SiH + H_2. \quad (19)$$

The reactions of substituted silylenes with monosilane result in the formation of trisilane, tetrasilane, *etc*.

$$SiH_4 + H_3SiSiH \rightleftharpoons Si_3H_8, \quad (20)$$

$$SiH_4 + SiH_3SiH_2SiH \rightleftharpoons Si_4H_{10}. \quad (21)$$

In addition, the isomerisation reactions

$$H_3SiSiH \rightleftharpoons Si_2H_4, \quad (22)$$

$$SiH_3SiH_2SiH \rightleftharpoons Si_3H_6, \quad (23)$$

unimolecular elimination of hydrogen, *e.g*.,

$$Si_2H_4 \rightleftharpoons Si_2H_2 + H_2, \quad (24)$$

$$Si_2H_2 \rightleftharpoons Si_2 + H_2, \quad (25)$$

$$Si_3H_6 \rightleftharpoons Si_3H_4 + H_2, \quad (26)$$

etc, take place.

The intermediate product Si_2H_2 is represented by two isomers, $Si(H_2)Si$ being more stable.[39,68] The Si_3H_4 species also has two isomers.[47]

Transition from the initial stage of the pyrolysis to intermediate one is accompanied by the acceleration of the process. Devyatykh and coworkers [16] were the first to investigate this phenomenon. This transition was described in more detail by Purnell and Walsh,[15] and the first mechanism of the initial acceleration was suggested in their monograph (Ref. 69). The reactions are autocatalytic processes with SiH_3SiH as an intermediate product.

$$\begin{aligned} &SiH_2 + SiH_4 \rightleftharpoons Si_2H_6 \longrightarrow SiH_3SiH + H_2, \\ &SiH_3SiH + SiH_4 \rightleftharpoons Si_3H_8 \longrightarrow SiH_2 + Si_2H_6. \end{aligned} \quad (27)$$

The results of simulation [39] have shown that the initial acceleration observed under the conditions of a static reactor [15] agree with the mechanism involving reactions (27). It should be noted that the initial acceleration in the process of the monosilane pyrolysis in a flow reactor was also described based on the mechanism of the reactions (27).[27, 67]

An alternative heterogeneous mechanism of the initial acceleration of the silane pyrolysis under the conditions of a static reactor [15] was suggested.[13, 70] Modification of the surface during the reaction was supposed to be the reason for the initial acceleration. As the result, SiH_2 is liberated from the surface into the gas phase accelerating the homogeneous process. This mechanism was criticised,[39] as the pyrolysis rate and the product ratio did not depend on the S/V ratio.[15] Furthermore, the homogeneous mechanism of the initial acceleration was supported by the results obtained in the silane pyrolysis where the influence of the reactor walls was eliminated (shock tubes [30] and laser pyrolysis [49]).

At present, the rate constants for numerous homogeneous elementary reactions occurring in the monosilane pyrolysis have been established. In particular, for the numerical simulation of the monosilane pyrolysis, one can use the parameters of the Arrhenius equation

$$k = A\exp\left(-\frac{E}{RT}\right),$$

where A is a pre-exponential factor, E is the activation energy.

The parameters A and E for the initial decomposition of the monosilane molecule [reaction (2)] in the pyrolysis of undiluted silane for the range of pressures are given in Table 1.

Table 1. Parameters of the Arrhenius equation for the reaction of primary monosilane decomposition in the range of temperatures 800 – 1500 K.[60]

P /Pa	A /s^{-1}	E /kJ mol^{-1}
0.1	1.5×10^{7}	214.4
1.3	1.5×10^{8}	214.4
13	1.5×10^{9}	214.4
1.3×10^{2}	1.5×10^{10}	214.4
1.3×10^{3}	1.5×10^{11}	214.8
1.3×10^{4}	1.8×10^{12}	218.6
1.3×10^{5}	1.7×10^{13}	223.6
∞	3.4×10^{15}	250.4

Table 2. Parameters of the Arrhenius equation (A /cm^3 s^{-1} or s^{-1}; E /kJ mol^{-1}) for the reactions occurring in the silane pyrolysis.

Reaction	A	E	Ref.
$SiH_2 + H_2 \rightarrow SiH_4$	9.8×10^{-13}	−2.3	40
$SiH_4 + SiH_2 \rightarrow Si_2H_6$	1.3×10^{-10}	−3.0	40
$Si_2H_6 \rightarrow SiH_2 + SiH_4$	1.3×10^{15}	213	43
$Si_2H_6 + SiH_2 \rightarrow Si_3H_8$	3.1×10^{-10}	−1.9	40
$Si_3H_8 \rightarrow SiH_2 + Si_2H_6$	4.9×10^{15}	222	42
$Si_3H_8 + SiH_2 \rightarrow Si_4H_{10}$	3.7×10^{-10}	−2.0	40
$Si_4H_{10} \rightarrow Si_3H_8 + SiH_2$	6.31×10^{15}	223.6	70
$Si_2H_6 \rightarrow H_3SiSiH + H_2$	7.9×10^{15}	237	70
$H_3SiSiH + H_2 \rightarrow Si_2H_6$	2.8×10^{-10}	9.2	70
$Si_3H_8 \rightarrow SiH_3SiH_2SiH + H_2$	1.8×10^{15}	229	70
$SiH_3SiH_2SiH + H_2 \rightarrow Si_3H_8$	2.83×10^{-10}	9.2	70
$SiH_4 + H_3SiSiH \rightarrow Si_3H_8$	6.6×10^{-11}	−10.9	70
$Si_3H_8 \rightarrow SiH_4 + H_3SiSiH$	9.3×10^{14}	209	42
$SiH_4 + SiH_3SiH_2SiH \rightarrow Si_4H_{10}$	6.6×10^{-11}	−10.9	70
$Si_4H_{10} \rightarrow SiH_4 + SiH_3SiH_2SiH$	4.4×10^{15}	210.3	70
$H_3SiSiH \rightarrow Si_2H_4$	6.2×10^{9}	6.5	72
$Si_2H_4 \rightarrow H_3SiSiH$	1.3×10^{10}	52.7	72
$SiH_3SiH_2SiH \rightarrow SiH_3SiHSiH_2$	6.2×10^{9}	6.5	70, 71
$SiH_3SiHSiH_2 \rightarrow SiH_3SiH_2SiH$	1.3×10^{10}	52.7	70, 71

In order to apply the data of Table 1 to the mixture of monosilane and argon, the parameters of the Arrhenius equation for several other elementary reactions of the silane pyrolysis are given in Table 2.

III. Homogeneous pyrolysis of disilane

Possible elementary reactions occurring in the thermal decomposition of disilane are described in the theoretical studies (Refs 72 – 75), while experimental investigations into the pyrolysis of disilane and higher silanes are presented in other papers (Refs 32, 42 – 44, 76, 77). Chromatographic analysis of the pyrolysis products of disilane carried out under static conditions at $P = 3\times10^3 - 10^4$ Pa and $T = 560 - 610$ K shows that the products are monosilane, trisilane, two tetrasilane isomers and hydrogen.[76] The parameters of the Arrhenius equation for the reactions of formation of monosilane, trisilane and hydrogen were determined. The mechanism of decomposition of disilane is following: the initial stage is the Si_2H_6 dissociation into SiH_2 and SiH_4, SiH_2 reacts further with Si_2H_6 to form Si_3H_8 and with Si_3H_8 to form Si_4H_{10}, *etc*. The experimental data suggest that hydrogen is a secondary reaction product.

The kinetics of the disilane decomposition was studied in a single-pulse shock tube in the temperature range 850 – 1000 K and at $P = (3.1 - 3.6)\times10^5$ Pa.[44] It was considered that two primary reactions of the disilane decomposition, *viz*., the forward reaction (18) and the reverse reaction (3) occur simultaneously. The parameters of the Arrhenius equation for these reactions were found (see Table 2).

Thermolysis of disilane under static conditions was experimentally studied by Martin, Ring and O'Neal.[43] The dependences of rate constants for this process on temperature and pressure were obtained. The calculated parameters of the Arrhenius equation differ substantially from those found by Bowrey and Purnell.[76]

The experimental investigation of the thermolysis of disilane, as well as tri- and tetrasilane under the conditions of a static reactor was continued later.[42] The parameters of the Arrhenius equation for the primary decomposition reactions of these silanes were found.

Studies of the kinetics of the disilane thermal decomposition in a shock tube at 1000 – 3100 K have shown that disilane generally decomposes into SiH_2 and SiH_4.[32]

The process of the thermolysis of disilane at $T = 300 - 1000$ K and $P = 100 - 1000$ Pa was studied by resonance enhanced multiphoton ionisation (REMPI) and multiphoton ionisation (MPI) methods.[78] The formation of silicon atoms during the pyrolysis was detected by REMPI method.

Thus, according to the above-mentioned data, the reactions

$$Si_2H_6 \longrightarrow SiH_2 + SiH_4,$$

$$Si_2H_6 + SiH_2 \longrightarrow Si_3H_8,$$

$$Si_3H_8 + SiH_2 \longrightarrow Si_4H_{10} \quad etc.$$

are predominant in the primary stage of the disilane pyrolysis.

Furthermore, the formation of silylsilylene H_3SiSiH and hydrogen as a result of dissociation of disilane, *viz*., the forward reaction (18), takes place. Silylsilylene is in equilibrium with its isomer disilene Si_2H_4 [equilibrium (22)].

Silylsilylene reacts actively with disilane (and other silanes), for example,

$$H_3SiSiH + Si_2H_6 \longrightarrow Si_4H_{10}. \qquad (28)$$

Thus, pyrolysis of disilane can proceed with an acceleration of the process due to the additional consumption of Si_2H_6 as the result of its reaction with H_3SiSiH and other substituted silylenes.

IV. Heterogeneous decomposition of silanes

Silicon deposition on the surface as the result of the heterogeneous silane decomposition has been described in detail in several reviews (see *e.g.* 45, 46). Hence, the processes of CVD are considered only in brief in the present review. The publications on the heterogeneous pyrolysis can arbitrarily be divided into two groups: the first group includes studies on the rate of formation of silicon films depending on macroscopic conditions (such as temperature, pressure and composition of a gas mixture); the second group deals with investigations into elementary heterogeneous reactions on the well-characterised ideal surface of single-crystal silicon using modern methods of analysis of the surface.

1. Growth of silicon films upon heterogeneous decomposition of silanes

Studies on the rate of formation of silicon films by the CVD method are aimed at the search for the optimum deposition conditions. Generally, this is associated with technological demands for microelectronics. Experiments were mostly carried out at reduced pressures to avoid the formation of aerosol particles, the deposition of which on the surface of growing layers impairs the product quality. In majority of investigations into CVD, silane [5, 60, 79–93] and disilane [5, 60, 80, 81, 89, 94–99] served as precursors of silicon films. The conditions of deposition in these investigations were so chosen, that the contribution of the homogeneous reactions was negligible. Thus, using the data from these publications, one can determine the reaction sticking coefficient of monosilane (ε_s) and disilane (ε_{ds}). For instance, ε_s is calculated using the equation

$$\varepsilon_s = \frac{W\rho}{Zm}, \tag{29}$$

where W is the rate of the film growth (cm s^{-1}); ρ is the density of the growing silicon film ($\rho \approx 2$ g cm^{-3}); Z is the collision frequency of the monosilane molecules with the unit surface area; m is the mass of the silicon atom. The value of ε_{ds} is calculated by the same manner.

Summing up the results given in the above-cited papers, we derived the equations for the reaction sticking coefficient of monosilane and disilane for a wide range of temperatures and partial pressures of these substances ($750 < T < 1000$ K, $2 \times 10^{-4} < p_s < 2$ kPa, $1 \times 10^{-4} < p_{ds} < 1$ kPa) [27]

$$\varepsilon_s = 10^{3.0}\exp\left[-\frac{148\ (\text{kJ mol}^{-1})}{RT}\right](p_s)^{-0.59}, \tag{30}$$

$$\varepsilon_{ds} = 10^{1.6}\exp\left[-\frac{119\ (\text{kJ mol}^{-1})}{RT}\right](p_{ds})^{-0.70}, \tag{31}$$

where p_s and p_{ds} are partial pressures of silane and disilane, respectively. The dependences of the reaction sticking coefficient of mono- and disilanes on their partial pressures are shown in Figs 1 ang 2.

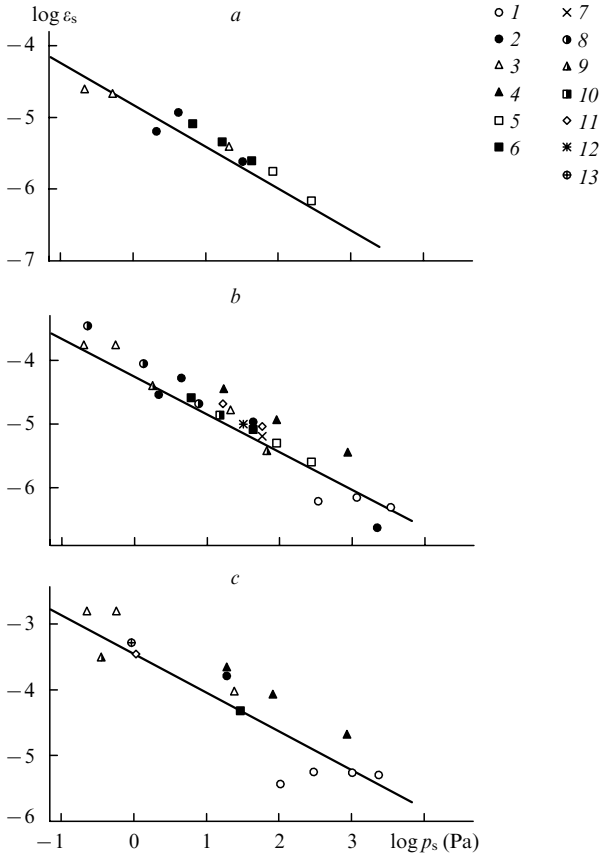

Figure 1. Dependence of the reaction sticking coefficient of monosilane on its partial pressure over the surface of the growing silicon layer at 813 (*a*), 863 (*b*) and 950 K (*c*).
Straight lines are plotted using the Eqn (30), the experimental points (*1*)–(*13*) are taken from Refs 92, 5, 81, 87, 86, 84, 88, 96, 95, 91, 85, 93 and 82, respectively.

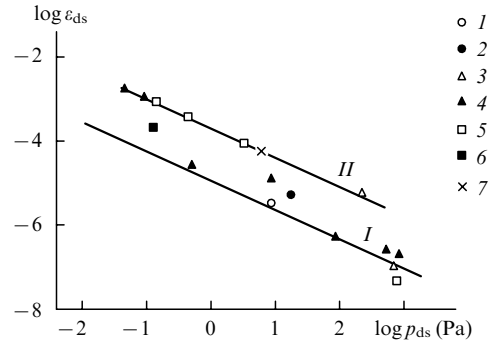

Figure 2. Dependence of the reaction sticking coefficient of disilane on its partial pressure over the surface of the growing silicon layer at 738 (*I*) and 863 K (*II*).
Straight lines are plotted using the Eqn (31), the experimental points (*1*)–(7) are taken from Refs 5, 96, 79, 99, 95, 91 and 94, respectively.

The reaction sticking coefficient of trisilane is approximately the same as those of disilane (for the same range of partial pressures).[89] It is noteworthy that the transport of the molecules from the gas phase to the reactor walls does not limit the process of film growth in the range of temperatures mentioned.[46] Using the Eqns (29)–(31), the growth rate of the silicon film in the heterogeneous decomposition of silane and disilane can be estimated for a wide range of temperatures and pressures.

2. Dissociative adsorption of silanes on the ideal surface of single-crystal silicon

Information on heterogeneous elementary reactions which occur in the pyrolysis of silane on the surface of a solid product formed, *viz.*, amorphous hydrogenated silicon is rather scarce. However, the mechanism of silicon growth on the well-characterised ideal Si(111) and Si(100) surfaces is discussed in numerous studies. Modern methods of the analysis of surface such as thermodesorption,[98] low-energy electron diffraction,[98, 100, 101] secondary-ion mass spectrometry,[102] scanning tunnelling microscopy,[103–108] reflection high-energy electron diffraction [109–111] are used in these investigations.

It was found that two neighbouring dangling bonds participate in elementary reactions of heterogeneous decomposition of mono- and disilane.[104, 107] The elementary reaction of the heterogeneous monosilane decomposition can be represented by the reaction [104, 108, 112–114]

$$SiH_4 + 2\_ \longrightarrow \underline{H} + \underline{SiH_3}. \quad (32)$$

Hereinafter, the symbol _ denotes an active centre of the surface (dangling bond), $\underline{H}$ and $\underline{SiH_3}$ mean that H and SiH_3 are bound to the surface (mono- and trihydride groups, respectively).

The elementary reaction of the heterogeneous decomposition of disilane occurs as follows [105, 115, 116]:

$$Si_2H_6 + 2\_ \longrightarrow \underline{SiH_3} + \underline{SiH_3}. \quad (33)$$

Alternatively, the following version is possible (Refs 115, 117, 118):

$$Si_2H_6 + 2\_ \longrightarrow \underline{Si_2H_5} + \underline{H}. \quad (34)$$

Trihydride groups are unstable at high temperatures and decompose in the reaction presented below [105, 113, 116, 119–121]:

$$SiH_3 + 2\_ \longrightarrow \underline{\underline{SiH_2}} + \underline{H}, \quad (35)$$

where $\underline{\underline{SiH_2}}$ is the group bound to two surface silicon atoms.

V. Aerosol formation in the pyrolysis of silanes

Three characteristic stages of aerosol formation in the pyrolysis of silanes can be distinguished: (1) nucleation, *i.e.*, the formation of nuclei which grow much faster than they decompose; (2) growth of single particles in the processes of 'condensation' and coagulation; (3) the formation of agglomerates consisting of individual primary particles. The stage of nucleation is the least studied.

1. Experimental investigation into aerosol formation

Aerosol formation can take place in the process of thermal decomposition of silane under certain conditions. The regimes of an epitaxial reactor which favour aerosol formation were studied by Eversteijn.[122] Mixtures of silane with hydrogen under atmosphere pressure were used. Aerosol formation occurred above certain critical concentration of silane, and this lower limit of silane concentration was registered at different temperatures. The critical silane concentration depended on the temperature of the reactor and changed from 0.248% to 0.002% as temperature increased from 1050 to 1410 K.

The process of aerosol formation in an epitaxial reactor was also studied by Murthy *et al.*[123] Mixtures of silane with argon under atmosphere pressure were used. If the concentration of silane at the reactor entrance exceeded 0.2%, 'smoke' was observed at the exit from the reactor at 1370 K. The onset of gas-phase nucleation was determined from 'smoke' formation. The critical concentration of silane decreased with the increase in temperature.

Investigations into aerosol formation in flow reactors were carried out.[9, 26, 124–129] Critical concentrations of silane in the decomposition of its mixtures with inert gases and hydrogen at low temperatures were determined by Slootman and Parent.[9] These experiments were carried out in a vertical flow reactor under atmosphere pressure. It was found that the critical concentration of silane for all carrier gases is inversely proportional to temperature. Homogeneous nucleation in inert gases began at relatively low temperatures. In the experiments with mixtures of silane with hydrogen, aerosol formation was observed at much higher temperatures. It is necessary to consider chemical reactions inhibiting the formation of aerosol particles to rationalise the increase in temperatures. It was suggested that the large excess of hydrogen influences kinetics of gas-phase processes, *viz.*, favours reverse reactions with silylene, which results in the decrease in the concentration of aerosol particle precursors.

Qian *et al.*[124] carried out experiments in a low-pressure flow reactor using pure silane. The residence time of silane in a hot zone was ~ 1 s. The beginning of the homogeneous nucleation was established by appearance of a weak smoke-forming flash. The critical concentration of silane (above which the nucleation was observed) increased ~ 1.26-fold on the increase in temperature from 970 to 1020 K.

The mechanism of deposition of polycrystalline silicon from silane was studied in a low-pressure flow reactor.[125] Mixtures of silane with nitrogen were used. The formation of aerosol particles was determined from laser light scattering. If the pressure of the silane exceeded the critical value (the initial content of silane in the mixture being the same), the intensity of the scattered light increased sharply. Thus for the initial mole fraction of silane equal to 0.3, the flow rate 400 $cm^3\ min^{-1}$ and temperature 1000 K, an abrupt increase in the intensity of the scattered light was observed at ~ 85 Pa. Electron microscopic studies of particles formed at 130 Pa suggest that these particles are single crystals with characteristic sizes from 5 to 10 nm.

Studies of the growth of silicon particles formed upon pyrolysis of silane in a multistage flow reactor followed by condensation, showed that the formation of the primary silicon particles as the result of homogeneous nucleation took place in the first stage.[126, 127] In the second stage, the primary particles served as the 'condensation nuclei' for the products of heterogeneous decomposition of silane and the intermediate products formed in the homogeneous pyrolysis. It was noted that the regime of spontaneous homogeneous nucleation can be realised provided such parameters as flow rate, silane concentration and temperature profile are properly selected. The morphology of the particles and their crystal structure were studied by electron microscopy. It was found that the particles are non-agglomerated spheres with the size of ~ 0.1 μm. The major part of the particles has crystal structures.

A method of synthesis of spherical particles homogeneous in size in a reactor with five heating zones was described.[128] The particle morphology was determined by electron transmission microscopy method and their crystal structures were determined by X-ray and electron diffraction.

Particles obtained in a flow reactor were shown to be clusters resulting from the homogeneous decomposition of silane, nucleation and coagulation.[26] The sizes of the clusters varied from 1 to 10 μm. X-Ray diffraction analysis revealed that the particles have crystalline structures.

The results of an experimental study of aerosol formation under static conditions were given in Refs 4 and 17. The formation of aerosols upon thermal decomposition of silane under pressure of 0.3–4.5 Pa and 750–830 K was investigated.[4] The aerosol particle formation was followed by monitoring changes in optical transmission at wavelengths of 515 and 755 nm. It was suggested that the precursors of aerosol are silicon atoms.

The critical character of the dependence of aerosol formation on the silane pressure was rationalised as being due to competition of the homogeneous nucleation and silicon deposition on the reactor walls.[17]

The investigation of aerosol formation in the pyrolysis of mono- and disilane diluted with argon was carried out in a shock tube.[8] The aerosol particle formation was followed by monitoring the absorption of laser radiation at two different wavelengths. Information on the sizes, compositions and the number concentrations of particles was obtained. The investigation of the particles by such methods as electron diffraction, electron transmission microscopy and secondary-ion mass spectroscopy shows that the particles are spherical with their diameters ranging from 10 to 40 nm. These particles are weakly agglomerated and contain 15 at.% of hydrogen.

A number of investigations [130–135] was devoted to the study of aerosol formation upon heating of silane by laser radiation. The formation of particles in mixtures of silane with argon under the action of a CO_2-laser was investigated by Flint and coworkers.[130, 131] The sizes and number concentrations of the particles were determined from the results of the measurement of

scattered and passed radiation. It was concluded that silicon particles are formed as amorphous silicon with subsequent crystallisation on passing into hotter reaction zones.

The silicon powder obtained upon laser heating of silane was analysed.[133, 134] Physicochemical parameters of the powder were determined, using a number of methods: the sizes of the particles and crystallites were determined by electron transmission microscopy and scanning electron microscopy, while the density was determined by the method of helium pycnometry. The crystal structures and sizes of the crystallites were determined by X-ray diffraction (considering the width of X-ray diffraction lines using the Debye–Sherrer formula), electron diffraction and dark-field electron microscopy. It was found that both separate spherical silicon particles and chain agglomerates are formed in the laser pyrolysis. The sizes of the primary particles incorporated in these agglomerates are in the range 10–100 nm. The particles are built of separate crystallites with the size ~ 15 nm.

The morphology of aerosol silicon particles formed upon decomposition of silane is of particular interest. Coagulation of these particles results in agglomerates of irregular structures.[128, 136] Analogous agglomerates of Ag,[137, 138] TiO_2,[136, 139–144] SiO_2[141, 144–147] and soot[148–150] are formed in natural and industrial processes.[151] These structures can be characterised by the fractal dimension $D_f < 3$, which is the exponent in the ratio

$$M \propto \left(\frac{R}{a}\right)^{D_f}, \tag{36}$$

which relates the mass of the agglomerate M to its radius R, a is the average radius of the primary particles. The silicon agglomerates formed upon pyrolysis of monosilane at temperatures 800–1720 K had the fractal dimension $D_f = 1.5–1.7$ (Refs 29, 136).

2. The mechanism of aerosol formation

Much attention has been paid to the mechanism of aerosol formation in the thermal decomposition of silanes. A mechanism of the formation of particles from silicon atoms was suggested based on investigation of aerosol formation upon thermal decomposition of monosilane under static conditions in the range of temperatures 723–1070 K and pressures 66–1335 kPa.[17] Studies of thermal decomposition of silane at 770–1070 K have led to a conclusion that the particles could be formed from Si and Si_2 atoms.[21, 22] A model of homogeneous polymerisation in the gas phase for the conditions of low-pressure reactors was suggested.[125] According to this model, the particles are formed from SiH_2. A model of particle formation from disilane was considered by White *et al.*[13] and Ring and O'Neal.[70] An assumption was made that trisilane could be a precursor of the solid product in the processes of the deposition on the reactor walls and homogeneous polymerisation.[39] Decomposition of pentasilane was considered to be the initial stage of aerosol formation.[152] A model of aerosol formation in low-pressure reactors which allows identification of the conditions of homogeneous nucleation and those under which heterogeneous reactions predominate was suggested by Sladek.[153] This model is based on the competition of nucleation processes and diffusion of aerosol precursors to the reactor walls.

A model of aerosol formation upon silane pyrolysis was given.[154] The calculations for the temperature range 900–2400 K were made based on the classical nucleation theory and assumption that aerosols are formed from silicon atoms. The critical nucleus contained several silicon atoms at 900–2000 K. Yet another theoretical investigation of silicon nucleation in silane decomposition was made based on the classical nucleation theory.[155]

Simulation of the aerosol formation process in the silicon layer deposition from mono- and disilane at atmospheric pressure showed that the basis of the mechanism is the growth of aerosol particles as the result of the consecutive addition of silylenes.[77]

A kinetic model of aerosol formation in thermal decomposition of silane was described.[156] The essence of this model is that a nucleus of an $(SiH_m)_n$ particle is formed in the initial stage as the result of homogeneous reactions; its further growth occurs due to its reaction with silane.

A mechanism of the formation of silicon hydride clusters in the silane pyrolysis was discussed.[47] This model contains detailed chemical information on the relative stabilities and reactivities of different possible silicon hydride clusters. The model allows one to calculate the rate of the particle nucleation. Thermodynamic properties of the silicon hydride clusters were estimated. The mechanism includes reversible and irreversible formation of silicon hydrides: the former reactions involve particles containing up to 10 Si atoms, while the latter reactions involve particles containing 11–20 Si atoms. The key intermediates and reactions leading to the formation of the particles were determined, the dependence of their formation on the conditions of the reaction was studied.

A detailed kinetic model describing pyrolysis of the initial molecules and the homogeneous nucleation of the silicon particles under shock tube conditions was considered.[8] The kinetic scheme contains 117 elementary reactions and includes 42 types of molecules (from fully hydrogenated Si_nH_{2n+2} to unsaturated Si_nH_{2n}, Si_2H_2 and non-hydrogenated silicon Si_n clusters). The model describes the process of coagulation of aerosol particles and their growth due to the CVD process.

Numerical solutions of discrete-sectional equations of the aerosol dynamics, which take account of the interaction of separate clusters for various reactor types were described.[128, 157] Simplified equations of reaction and coagulation which permit one to predict rapidly the aerosol evolution were derived. The influence of the initial vapour concentration, reaction time, seeds and temperature profile on the properties of the highly dispersed particles formed in silane pyrolysis was estimated.

Numerical stimulation of aerosol formation under the heterogeneous-homogeneous thermal decomposition of silane was made.[67] The model allows one to calculate the following time-dependent parameters: the degree of silane decomposition, di- and trisilane concentration, the concentration and dispersity of aerosol particles formed, the hydrogen content and the concentration of active centers (in the form of dangling bonds) in particles. These data agree reasonably with the experimental results.

The results of the above-mentioned studies show that the modern concepts on the process of aerosol formation are contradictory and its mechanism is not sufficiently studied. A reason for the disagreement as to the mechanism of aerosol formation is the insufficiency of experimental data. As a rule, the experiment gives only some parameters of the process such as the sizes of the particles,[8, 128] or temperature and the concentration of silane required for the onset of homogeneous nucleation.[4, 9, 17, 122–126] Nevertheless, based on the available literature data general features of aerosol formation in the silane pyrolysis can be formulated. The initial stage of this process is the formation of Si_mH_n clusters. The thermochemical calculations[47] show that for small sizes of clusters ($m \leqslant 10$) the rate of their decomposition is relatively high, which leads to a decrease in the number of silicon atoms in the clusters

$$Si_{m+l}H_{2(n+k)} \longrightarrow Si_mH_{2n} + Si_lH_{2k}. \tag{37}$$

In other words, the concentration of this kind of clusters depends on a quasi-equilibrium between the formation reactions of these clusters due to the agglomeration of smaller clusters

$$Si_mH_{2n} + Si_lH_{2k} \longrightarrow Si_{m+l}H_{2(n+k)}, \tag{38}$$

and the decay of lager clusters [see reaction (37)], on one side, and involvement of these clusters in analogous reactions of agglomeration and decay, on the other side. The rate of cluster decomposition is relatively small for larger cluster sizes ($m > 10$); since the dissociation of a large cluster requires that larger numbers of the Si–Si bonds were cleaved than in the dissociation of a smaller

cluster. Thus, the clusters with $m > 10$ may be regarded as particles and the rate of the formation of clusters with $m > 10$, as the rate of nucleation.[47] Further, the rate of the particle growth is determined largely by coagulation.[67]

VI. The composition of the solid product

The detailed investigations on the chemical composition of aerosol particles formed in thermal decomposition of silane are virtually not documented and the data on the solid product of the reaction which deposits on the reactor walls during the silane pyrolysis are very scarce. Therefore, the experimental data concerning this aspect should be analysed in more detail than in the previous sections.

The solid product (a deposit on the reactor walls and aerosol particles) of thermal decomposition of silane represents polycrystalline silicon [8] (high temperatures and/or long reaction time) or amorphous hydrogenated silicon [3] (mild temperatures and/or short reaction periods). The content of hydrogen in the solid pyrolysis product vary over a wide range (see Section I).

The bound hydrogen present in amorphous hydrogenated silicon has been actively studied over the last three decades. Detailed information on the vibration modes of mono- (SiH) and polyhydride [SiH_2, $(SiH_2)_n$, SiH_3] groups present in amorphous hydrogenated silicon was obtained (see, *e.g.*, Refs 158–162). IR spectra contain three characteristic absorption bands in the range of frequencies 550–750, 800–950 and 1900–2300 cm^{-1} (Ref. 158). Two peaks at ~ 2000 and 2100 cm^{-1} can be found in the range of frequencies 1900–2300 cm^{-1}. A doublet with maxima at 845 and 880 cm^{-1} or a single peak with maximum at 880 cm^{-1} is most often observed in the range 800–950 cm^{-1}. The data allow one to compare different vibration modes with absorption bands observed in the IR spectra of silanes (Table 3).

Table 3. Vibration frequencies of the Si—H bond observed in the IR-spectra of silanes.

Group	Vibration type	Frequencies /cm^{-1}
SiH	stretching	2000
	bending	630
SiH_2	stretching	2090
	scissors	880
	oscillation	630
SiH_3	stretching	2120
	deformation	905, 860
$(SiH_2)_n$	stretching	2090–2140
	scissors	890
	oscillation	845
	the same	630

The absorption peak at ~ 2100 cm^{-1} has to be discussed separately. It was supposed earlier [163, 164] that the stretching vibrations of the monohydride groups manifest themselves only at ~ 2000 cm^{-1}. However, it is well known that the stretching vibrations of the monohydride groups localised on the surface of single-crystal (Refs 116, 165 and references cited therein) and amorphous silicon [166, 167] have the frequencies at ~ 2100 cm^{-1}. Furthermore, lines at 2140,[168] 2100,[169] 2085,[170, 171] 2068 cm^{-1} (Ref. 172) were found in the IR spectra of the amorphous hydrogenated silicon, while absorption at 800–950 cm^{-1} (corresponding to the polyhydride groups, see Table 3) was absent. Heating of amorphous hydrogenated silicon resulted in an increase in the absorption intensity at 2100 cm^{-1} without any absorption at 800–950 cm^{-1}.[173, 174] These results suggest that two types of monohydride groups, which have absorption lines at 2000 and 2100 cm^{-1}, are possible in amorphous hydrogenated silicon. Using aerosol particles of amorphous hydrogenated silicon as an example, it was shown that the SiH groups with the vibration frequency ~ 2000 cm^{-1} do not interact with atmospheric oxygen, unlike the groups with the frequency ~ 2100 cm^{-1} (Refs 3, 175). The interaction of the latter is characterised by a decrease in the line intensity at 2100 cm^{-1} and appearance of absorption in the region 2170–2300 cm^{-1}. The absorption in this region is generally ascribed to monohydride groups where the hydrogen and oxygen atoms are bound to the same silicon atom (Si—O—Si—H).[176–182]

The hydrogen evolution method is a most informative method used for the investigation of amorphous hydrogenated silicon.[183–194] This method allows one to obtain quantitative information on the content of hydrogen in groups of different structures. The essence of this method can be described in the following way. A sample of amorphous hydrogenated silicon is heated at a constant rate (20–40 K min^{-1}), which results in the evolution of hydrogen. The amount of the hydrogen evolved is determined by the increasing pressure or by mass spectroscopy. The sample is heated to the $T \sim 920$–950 K, where crystallisation takes place and all the hydrogen releases to the gas phase. The results of the hydrogen evolution are usually represented as the dependence of the rate of evolution on temperature. Two temperature regions, *viz.*, 570–770 and 770–920 K can be distinguished. In the former region one [185–191, 193, 194] or two [183, 186, 188, 189, 191] peaks are observed. The hydrogen evolution in this temperature region is described by the first-order process and is not diffusion-limited.[185, 190] It is supposed that the low-temperature peak in this region is associated with elimination of hydrogen from the polyhydride groups,[183, 187–189, 194] while the high-temperature peak is determined by elimination of hydrogen from the monohydride groups.[183, 188] In the region 770–920 K, a peak the location of which depends on the rate of heating is observed. Hydrogen evolution in this case is described by the kinetics with an order exceeding the first order.[185–187, 189, 192] This peak is associated with the elimination of hydrogen from the monohydride groups.[183, 185–189] In relation to the interpretation of the peaks in the evolution spectra of hydrogen, it is worthwhile to note the investigations into the thermal desorption of hydrogen from the (111) and (100) faces of silicon single crystal [113, 195–202] and from the surface of porous crystalline sample.[202] It was found [198, 202] that the desorption of hydrogen from di- and trihydride groups occurs at 640–715 K, while from monohydride groups, at 720–820 K.

Detailed comparison of the IR spectra and the hydrogen evolution spectra for the aerosol particles of amorphous hydrogenated silicon formed upon thermal decomposition of monosilane in a flow reactor was described.[36, 175] The evolution spectra of the samples of aerosol particles withdrawn from the flow contain two relatively sharp peaks with the maxima at 670 and 760 K and a broad peak with the maximum at 780 K. It was found that the sharp peaks are determined by the evolution of hydrogen from poly- and monohydride groups with the frequency of stretching vibrations 2000 cm^{-1}, while the broad peak is determined by the evolution of hydrogen from monohydride groups with the frequency of stretching vibrations ~ 2100 cm^{-1}.

The investigations into amorphous hydrogenated silicon by the proton magnetic resonance method (Refs 203–205) show that the spectra represent superposition of two lines, *viz.*, a broad (20–30 kHz) one and a narrow (3–4 kHz) one. The hydrogen giving the broad line is called the 'clustered' phase and hydrogen giving the narrow line is called the 'dilute' phase. Hydrogen atoms of the both phases are bound to silicon atoms by covalent bonds. The difference between these two phases is that hydrogen atoms of the 'clustered' phase are located close to each other, while the hydrogen atoms of the 'dilute' phase are isolated.

For the aerosol particles of the amorphous hydrogenated silicon obtained upon thermal decomposition of monosilane, the data of IR spectroscopy were compared to those of the hydrogen evolution, on one hand, and the data from NMR spectroscopy, on the other hand.[3] It was concluded that the hydrogen of the

'clustered' phase is a constituent of mono- (vibration frequency is 2000 cm^{-1}) and polyhydride groups. The hydrogen of the 'dilute' phase is a constituent of monohydride groups with the vibration frequency 2100 m^{-1}. Experimental results suggest that the SiH groups of the 'clustered' phase are localised inside the amorphous silicon network [206] as 'hydrogen complexes', *viz*., extended defects stabilised by hydrogen.[207–211] The monohydride groups of the 'dilute' phase are localised on the surfaces of interconnected microvoids and microchannels.

VII. Conclusion

Thermal decomposition of silanes is a complex process including different stages. Arbitrarily, the main components of the mechanism of this process are as follows:

1. Homogeneous elementary reactions.

2. Heterogeneous reactions occuring on the surface of the silicon deposited on the reactor walls.

3. The formation of precursors of aerosol particles (molecular clusters Si_mH_n, $m = 10-20$) which exist in the equilibrium with gaseous intermediate products.

4. Homogeneous nucleation, *i.e*., the formation of the smallest aerosol particles, the rates of forward growth reactions for which exceed substantially those of the reverse reactions.

5. Heterogeneous deposition of molecules and smaller clusters on the surface ('condensation').

6. Coagulation and coalescence of particles. In the initial stages where the rate of coalescence exceeds that of the coagulation, more or less spherical particles are formed. In the following stages where the coagulation becomes predominant, particle agglomerates (the so-called primary particles) are formed.

7. Agglomeration of primary particles, *i.e*., the transformation of several neighbouring particles into one primary particle.

8. Chemical and structural changes in aerosol particles.

To explain the pyrolysis mechanism in general each of the above-mentioned stages has to be investigated in detail because of their close relations and mutual influence on each other. Only thorough study with the help of modern physicochemical methods can give the detailed representation of this process.

References

1. F O Rice *J. Am. Chem. Soc*. **55** 3035 (1933)
2. N A Vasil'eva, R A Buyanov, K I Zamaraev *Khim. Fiz*. **3** 688 (1984) [a]
3. A A Onischuk, V P Strunin, R I Samoilova, A V Nosov, M A Ushakova, V N Panfilov *J. Aerosol Sci*. **28** 1425 (1997)
4. R G Aivazyan, V V Azatyan, L F Satunkina *Kinet. Katal*. **37** 492 (1996) [b]
5. B A Scott, R D Estes, J M Jasinski *J. Chem. Phys*. **89** 2544 (1988)
6. A G Gasparyan, G B Rostomyan, R A Badalyan, G A Arutyunyan *Kinet. Katal*. **29** 935 (1988) [b]
7. M S Sukhov *Izv. Akad. Nauk, Neorg. Mater*. **18** 1077 (1982) [c]
8. M Frenklach, L Ting, H Wang, J M Rabinowitz *Isr. J. Chem*. **36** 293 (1996)
9. F Slootman, J-C Parent *J. Aerosol Sci*. **25** 15 (1994)
10. R Robertson, D Hils, A Gallagher *Chem. Phys. Lett*. **103** 397 (1984)
11. J W Erwin, M A Ring, H E O'Neal *Int. J. Chem. Kinet*. **17** 1067 (1985)
12. N K Serdyuk, V P Strunin, E N Chesnokov, V N Panfilov *Kinet. Katal*. **26** 790 (1985) [b]
13. R T White, R L Espino-Rios, D S Rogers, M A Ring, H E O'Neal *Int. J. Chem. Kinet*. **17** 1029 (1985)
14. M A Ring, M J Puentes, H E O'Neal *J. Am. Chem. Soc*. **92** 4845 (1970)
15. J H Purnell, R Walsh *Proc. R. Soc. London, A Math. Phys. Sci*. **293** 543 (1966)
16. G G Devyatykh, V M Kedyarkin, A D Zorin *Zh. Neorg. Khim*. **10** 1528 (1965) [d]
17. S V Maklakov, R G Aivazyan, V V Azatyan, P V Zhirkov, L F Satunkina *Mendeleev Commun*. 120 (1995)
18. P Neudorfl, A Jodhan, O P Strausz *J. Phys. Chem*. **84** 338 (1980)
19. R G Aivazyan, V V Azatyan, V I Kalachev, V I Rubtsov *Fiz. Goreniya Vzryva* **30** 85(1994)
20. G Cochet, H Mellottee, R Delbourgo *J. Chim. Phys*. **71** 1363 (1974)
21. W G Breiland, M E Coltrin, P Ho *J. Appl. Phys*. **59** 3267 (1986)
22. W G Breiland, P Ho, M E Coltrin *J. Appl. Phys*. **60** 1505 (1986)
23. S K Iya, R N Flagella, F S DiPaolo *J. Electrochem. Soc*. **129** 1531 (1982)
24. C H Haas, M A Ring *Inorg. Chem*. **14** 2253 (1975)
25. B A Scott, R D Estes *Appl. Phys. Lett*. **55** 1005 (1989)
26. G Hsu, R Hogle, N Rohatgi, A Morrison *J. Electrochem. Soc*. **131** 660 (1984)
27. A A Onischuk, V P Strunin, M A Ushakova, V N Panfilov *Int. J. Chem. Kinet*. **30** 99 (1998)
28. L N Krasnoperov, V V Nosov, A V Baklanov, V N Panfilov *Khim. Fiz*. **7** 528 (1988) [a]
29. A A Onischuk, A I Levykin, V P Strunin, K K Sabelfeld, V N Panfilov *J. Aerosol Sci*. **31** 1263 (2000)
30. C G Newman, H E O'Neal, M A Ring, F Leska, N Shipley *Int. J. Chem. Kinet*. **11** 1167 (1979)
31. V N Votintsev, I S Zaslonko, V S Mikheev, V N Smirnov *Kinet. Katal*. **27** 972 (1986) [a]
32. H-J Mick, M W Markus, P Roth, V N Smirnov *Ber. Bunsenges. Phys. Chem*. **99** 880 (1995)
33. C G Newman, M A Ring, H E O'Neal *J. Am. Chem. Soc*. **100** 5945 (1978)
34. M Koshi, S Kato, H Matsui *J. Phys. Chem*. **95** 1223 (1991)
35. H-J Mick, P Roth, V N Smirnov, I S Zaslonko *Kinet. Katal*. **35** 485 (1994) [a]
36. A A Onischuk, V P Strunin, M A Ushakova, V N Panfilov *Phys. Status Solidi B* **186** 43 (1994)
37. A A Onischuk, V P Strunin, M A Ushakova, V N Panfilov *Khim. Fiz*. **11** 1136 (1992) [a]
38. A A Onischuk, V P Strunin, M A Ushakova, V N Panfilov *Khim. Fiz*. **13** (5) 129 (1994) [a]
39. R Becerra, R Walsh *J. Phys. Chem*. **96** 10856 (1992)
40. J M Jasinski, R Becerra, R Walsh *Chem. Rev*. **95** 1203 (1995)
41. I Safarik, V Sandhu, E M Lown, O P Starausz, T N Bell *Res. Chem. Intermed*. **14** 105 (1990)
42. J G Martin, H E O'Neal, M A Ring *Int. J. Chem. Kinet*. **22** 613 (1990)
43. J G Martin, M A Ring, H E O'Neal *Int. J. Chem. Kinet*. **19** 715 (1987)
44. J Dzarnoski, S F Rickborn, H E O'Neal, M A Ring *Organometallics* **1** 1217 (1982)
45. J M Jasinski, S M Gates *Acc. Chem. Res*. **24** 9 (1991)
46. J M Jasinski, B S Meyerson, B A Scott *Ann. Rev. Chem*. **38** 109 (1987)
47. M T Swihart, S L Girshick *J. Phys. Chem., B* **103** 64 (1999)
48. H E O'Neal, M A Ring *Chem. Phys. Lett*. **107** 442 (1984)
49. J M Jasinski, R D Estes *Chem. Phys. Lett*. **117** 495 (1985)
50. V V Nosov, S M Repinskii, F N Dul'tsev *Kinet. Katal*. **25** 530 (1984) [a]
51. R Robertson, A Gallagher *J. Chem. Phys*. **85** 3623 (1986)
52. A Doncaster, R Walsh *Int. J. Chem. Kinet*. **13** 503 (1981)
53. J A Seetula, Y Feng, D Gutman, P W Seakins, M J Pilling *J. Phys. Chem*. **95** 1658 (1991)
54. J Berkowitz, J P Greene, H Cho, B Ruščić *J. Chem. Phys*. **86** 1235 (1987)
55. A F Sax, J Kalcher *J. Phys. Chem*. **95** 1768 (1991)
56. J A Pople, B T Luke, M J Frisch, J S Binkley *J. Phys. Chem*. **89** 2198 (1985)
57. P Ho, M E Coltrin, J S Binkley, C F Melius *J. Phys. Chem*. **89** 4647 (1985)
58. P Ho, C F Melius *J. Phys. Chem*. **94** 5120 (1990)
59. M S Gordon, T N Truong, E K Bonderson *J. Am. Chem. Soc*. **108** 1421 (1986)
60. B S Meyerson, J M Jasinski *J. Appl. Phys*. **61** 785 (1987)
61. J Doyle, R Robertson, G H Lin, M Z He, A Gallagher *J. Appl. Phys*. **64** 3215 (1988)
62. A Tachibana, K Yamaguchi, S Kawauchi, Y Kurosaki, T Yamabe *J. Am. Chem. Soc*. **114** 7504 (1992)
63. S K Loh, J M Jasinski *J. Chem. Phys*. **95** 4914 (1991)

64. M S Gordon, D R Gano, J S Binkley, M J Frish *J. Am. Chem. Soc.* **108** 2191 (1986)
65. M E Coltrin, R J Kee, J A Miller *J. Electrochem. Soc.* **133** 1206 (1986)
66. J Espinosa-Garsta, J Sanson, J C Corchado *J. Chem. Phys.* **109** 466 (1998)
67. A A Onischuk, A I Levykin, V P Strunin, M A Ushakova, R I Samoilova, K K Sabelfeld, V N Panfilov *J. Aerosol Sci.* **31** 879 (2000)
68. G Raabe, J Michl *Chem. Rev.* **85** 419 (1985)
69. J H Purnell, R Walsh *Chem. Phys. Lett.* **110** 330 (1984)
70. M A Ring, H E O'Neal *J. Phys. Chem.* **96** 10848 (1992)
71. M E Coltrin, R J Kee, G H Evans *J. Electrochem. Soc.* **136** 819 (1989)
72. P Ho, M E Coltrin, J S Binkley, C F Melius *J. Phys. Chem.* **90** 3399 (1986)
73. P M Agrawal, D L Thompson, L M Raff *J. Chem. Phys.* **92** 1069 (1990)
74. H K Moffat, K F Jensen, R W Carr *J. Phys. Chem.* **96** 7695 (1992)
75. H K Moffat, K F Jensen, R W Carr *J. Phys. Chem.* **96** 7683 (1992)
76. M Bowrey, J H Purnell *Proc. R. Soc. Lond. A, Math Phys. Sci.* **321** 341 (1971)
77. C J Giunta, R J McCurdy, J D Chapple-Sokol, R G Gordon *J. Appl. Phys.* **67** 1062 (1990)
78. J E Johannes, J G Ekerdt *J. Electrochem. Soc.* **141** 2135 (1994)
79. R J Bogaert, B N Baron, M T Klein, T W F Russell, R E Rocheleau *J. Electrochem. Soc.* **136** 2960 (1989)
80. P A Breddels, H Kanoh, O Sugiura, M Matsumura *Jpn. J. Appl. Phys.* **29** L1750 (1990)
81. W A P Claassen, J Bloem, W G J N Valkenburg, C H J van den Brekel *J. Cryst. Growth* **57** 259 (1982)
82. J H Comfort, R Reif *J. Electrochem. Soc.* **136** 2386 (1989)
83. T J Donahue, R Reif *J. Electrochem. Soc.* **133** 1691 (1986)
84. D W Foster, A J Learn, T I Kamins *J. Vac. Sci. Technol. B* **4** 1182 (1986)
85. G Harbeke, L Krausbauer, E F Steigmeier, A E Widmer, H F Kappert, G Neugebauer *J. Electrochem. Soc.* **131** 675 (1984)
86. M K Hatalis, D W Greve *J. Appl. Phys.* **63** 2260 (1988)
87. F Hottier, R Cadoret *J. Cryst. Growth* **52** 199 (1981)
88. T I Kamins, M M Mandurah, K C Saraswat *J. Electrochem. Soc.* **125** 927 (1978)
89. H Kanoh, O Sugiura, M Matsumura *Jpn. J. Appl. Phys.* **32** 2613 (1993)
90. H Kanoh, O Sugiura, P A Breddels, M Matsumura *IEEE Electron Device Lett.* **11** 258 (1990)
91. B S Meyerson, B A Scott, R Tsui *Chemtronics* **1** 150 (1986)
92. A M Beers, J Bloem *Appl. Phys. Lett.* **41** 153 (1982)
93. W L M Weerts, M H J M de Croon, G B Marin *J. Electrochem. Soc.* **145** 1318 (1998)
94. Y Mishima, M Hirose, Y Osaka, K Nagamine, Y Ashida, N Kitagawa, K Isogaya *Jpn. J. Appl. Phys.* **22** L46 (1983)
95. R J Buss, P Ho, W G Breiland, M E Coltrin *J. Appl. Phys.* **63** 2808 (1988)
96. D Meakin, K Papadopoulou, S Friligkos, J Stoemenos, P Migliorato, N A Economou *J. Vac. Sci. Technol. B* **5** 1547 (1987)
97. R S Rosler *Solid State Technol.* **20** (4) 63 (1977)
98. Y M Wu, R M Nix *Surf. Sci.* **306** 59 (1994)
99. M Sadamoto, J H Comfort, R Reif *J. Electron. Mater.* **19** 1395 (1990)
100. C C Cheng, J T Yates Jr *Phys. Rev. B, Condens. Matter* **43** 4041 (1991)
101. R Jones *Physica B* **170** 181 (1991)
102. S M Gates, C M Chiang *Chem. Phys. Lett.* **184** 448 (1991)
103. J J Boland *Phys. Rev. B, Condens. Matter* **44** 1383 (1991)
104. U Memmert, A Berko, R J Behm *Surf. Sci.* **323** L441 (1995)
105. Y Wang, M J Bronikowski, R J Hamers *Surf. Sci.* **311** 64 (1994)
106. D-S Lin, E S Hirschorn, T-C Chiang, R Tsu, D Lubben, J E Greene *Phys. Rev. B, Condens. Matter* **45** 3494 (1992)
107. D Albertini, F Thibaudau, L Masson, F Salvan *Surf. Sci.* **350** L216 (1996)
108. M Fehrenbacher, J Spitzmuller, M Pitter, H Rauscher, R J Behm *Jpn. J. Appl. Phys.* **36** 3804 (1997)
109. M Suemitsu, H Nakazava, N Miyamoto *Surf. Sci.* **357**–**358** 555 (1996)
110. H Hirayama, T Tatsumi, N Aizaki *Appl. Phys. Lett.* **52** 1484 (1988)
111. K Werner, S Butzke, S Radelaar, P Balk *J. Cryst. Growth* **136** 338 (1994)
112. M Suemitsu, K-J Kim, H Nakazawa, N Miyamoto *Appl. Surf. Sci.* **107** 81 (1996)
113. S M Gates, C M Greenlief, D B Beach, P A Holbert *J. Chem. Phys.* **92** 3144 (1990)
114. Z Jing, J L Whitten *Phys. Rev. B, Condens. Matter* **44** 1741 (1991)
115. L-Q Xia, M E Jones, N Maity, J R Engstrom *J. Chem. Phys.* **103** 1691 (1995)
116. K J Uram, U J Jansson *Surf. Sci.* **249** 105 (1991)
117. M Suemitsu, H Nakazawa, T Morita, N Miyamoto *Jpn. J. Appl. Phys.* **36** L625 (1997)
118. J Braun, H Rauscher, R J Behm *Surf. Sci.* **416** 226 (1998)
119. Y Suda, D Lubben, T Motooka, J E Greene *J. Vac. Sci. Technol. A, Vac. Surf. Films* **8** 61 (1990)
120. S M Gates, S K Kulkarni *Appl. Phys. Lett.* **58** 2963 (1991)
121. D Lubben, R Tsu, T R Bramblett, J E Greene *J. Vac. Sci. Technol. A, Vac. Surf. Films* **9** 3003 (1991)
122. F C Eversteijn *Philos. Res. Rep.* **26** 134 (1971)
123. J U M S Murthy, N Miyamoto, M Shimbo, J Nishizava *J. Cryst. Growth* **33** 1 (1976)
124. Z M Qian, H Michiel, A van Ammel, J Nijs, R Mertens *J. Electrochem. Soc.* **135** 2378 (1988)
125. C H J van den Brekel, L J M Bollen *J. Cryst. Growth* **54** 310 (1981)
126. J J Wu, R Flagan *J. Appl. Phys.* **61** 1365 (1987)
127. M K Alam, R C Flagan *Aerosol Sci. Technol.* **5** 237 (1986)
128. J J Wu, H V Nguyen, R C Flagan *Langmuir* **3** 266 (1987)
129. T Kojima, K Usui, T Furusawa *J. Chem. Eng. Jpn.* **22** 683 (1989)
130. J H Flint, R A Marra, J S Haggerty *Aerosol Sci. Technol.* **5** 249 (1986)
131. J H Flint, J S Haggerty *Aerosol Sci. Technol.* **13** 72 (1990)
132. M Ehbrecht, F Huisken *Phys. Rev. B, Condens. Matter* **59** 2975 (1999)
133. W R Cannon, S C Danforth, J S Haggerty, R A Marra *J. Am. Ceram. Soc.* **65** 330 (1982)
134. J S Haggerty, W R Cannon, in *Laser-Induced Chemical Processes* (Ed. J I Steinfeld) (New York; London: Plenum, 1981) p. 183
135. R Fantoni, E Borsella, S Piccirillo, C A Nannetti, R Ceccato, S Enzo *Appl. Surf. Sci.* **43** 308 (1989)
136. S N Rogak, R C Flagan, H V Nguyen *Aerosol Sci. Technol.* **18** 25 (1993)
137. A Schmidt-Ott *J. Aerosol Sci.* **19** 553 (1988)
138. A P Weber, U Baltensperger, H W Gäggeler, A Schmidt-Ott *J. Aerosol Sci.* **27** 915 (1996)
139. H D Jang, S K Friedlander *Aerosol Sci. Technol.* **29** 81 (1998)
140. S Morooka, T Yasutake, A Kobata, K Ikemizu, Y Kato *Int. Chem. Eng.* **29** 119 (1989)
141. S H Ehrmann, S K Friedlander, M Zachariah *J. Aerosol Sci.* **29** 687 (1998)
142. S N Rogak, U Baltensperger, R C Flagan *Aerosol Sci. Technol.* **14** 447 (1991)
143. A Kobata, K Kusakabe, S Morooka *Am. Inst. Chem. Eng. J.* **37** 347 (1991)
144. K Okuyama, Y Kousaka, N Tohge, S Yamamoto, J J Wu, R C Flagan, J H Seinfeld *Am. Inst. Chem. Eng. J.* **32** 2010 (1986)
145. A J Hurd, W L Flower *J. Colloid Interface Sci.* **122** 178 (1988)
146. J E Martin, D W Schaefer, A J Hurd *Phys. Rev. A, Gen. Phys.* **33** 3540 (1986)
147. G D Ulrich, J W Riehl *J. Colloid Interface Sci.* **87** 257 (1982)
148. R J Samson, G W Mulholland, J W Gentry *Langmuir* **3** 272 (1987)
149. S di Stasio *J. Aerosol Sci.* **30** 325 (1999)
150. H X Zhang, C M Sorensen, E R Ramer, B J Olivier, J F Merklin *Langmuir* **4** 867 (1988)
151. A A Onischuk, V P Strunin, M A Ushakova, V N Panfilov *J. Aerosol Sci.* **28** 207 (1997)
152. A Yuuki, Y Matsui, K Tachibana *Jpn. J. Appl. Phys.* **26** 747 (1987)
153. K J Sladek *J. Electrochem. Soc.* **118** 654 (1971)
154. C S Herrick, D W Woodruff *J. Electrochem. Soc.* **131** 2417 (1984)
155. F E Kruis, J Schoonman, B Scarlett, *J. Aerosol Sci.* **25** 1291 (1994)
156. V P Pimenov, V I Chernyak, A I Gorbunov *Khim. Fiz.* **7** 1520 (1988) [a]
157. J J Wu, H V Nguyen, R C Flagan, K Okuyama, Y Kousaka *Am. Inst. Chem. Eng. J.* **34** 1249 (1988)

158. G Lucovsky, W B Pollard, in *The Physics of Hydrogenated Amorphous Silicon (II)* (Eds J D Joannopoulous, G Lucovsky) (Berlin; Heidelberg; New York; Tokio: Springer, 1984) p. 86
159. M Cardona *Phys. Status Solidi B* **118** 463 (1983)
160. G Lucovsky *J. Non-Cryst. Solids* **76** 173 (1985)
161. G Lucovsky *J. Non-Cryst. Solids* **141** 241 (1992)
162. W B Pollard, G Lucovsky *Phys. Rev. B, Condens. Matter* **26** 3172 (1982)
163. M H Brodsky, M Cardona, J J Cuomo *Phys. Rev. B, Condens. Matter* **16** 3556 (1977)
164. G Lucovsky, R J Nemanich, J C Knights *Phys. Rev. B, Condens. Matter* **19** 2064 (1979)
165. U Jansson, K J Uram *J. Chem. Phys.* **91** 7978 (1989)
166. Y Toyoshima, K Arai, A Matsuda, K Tanaka *J. Non-Cryst. Solids* **137**/**138** 765 (1991)
167. N Maley, I Szafranek, L Mandrell, M Katiyar, J R Abelson, J A Thornton *J. Non-Cryst. Solids* **114** 163 (1989)
168. E C Freeman, W Paul *Phys. Rev. B, Condens. Matter* **18** 4288 (1978)
169. D Masson, L Paquin, S Poulin-Dandurand, E Sacher, A Yelon *J. Non-Cryst. Solids* **66** 93 (1984)
170. A T M Wilbers, G J Meeusen, M Haverlag, G M W Kroesen, D C Schram, H Kersten *Thin Solid Films* **204** 59 (1991)
171. D Dellafera, R Labusch, H H Roscher *Philos. Mag. B, Phys. Condens. Matter. Electron. Opt. Magn. Prop.* **45** 607 (1982)
172. M J van den Boogaard, B G C van den Ree, H Meiling, R E I Schropp, W F van der Veg *Physica B* **170** 281 (1991)
173. H Shanks, C J Fang, L Ley, M Cardona, F J Demond, S Kalbitzer *Phys. Status Solidi B* **100** 43 (1980)
174. C J Fang, K J Gruntz, L Ley, M Cardona, F J Demond, G Muller, S Kalbitzer *J. Non-Cryst. Solids* **35**/**36** 255 (1980)
175. A A Onischuk, V P Strunin, M A Ushakova, R I Samoilova, V N Panfilov *Phys. Status Solidi B* **193** 25 (1996)
176. G Lucovsky, J Yang, S S Chao, J E Tyler, W Czubatyj *Phys. Rev. B, Condens. Matter* **28** 3225 (1983)
177. G Lucovsky, J Yang, S S Chao, J E Tyler, W Czubatyj *J. Non-Cryst. Solids* **59**/**60** 609 (1983)
178. G Lucovsky, S S Chao, J Yang, J E Tyler, W Czubatyj *J. Vac. Sci. Technol. A, Vac. Surf. Films* **2** 353 (1984)
179. J S Knights, R A Street, G Lucovsky *J. Non-Cryst. Solids* **35**/**36** 279 (1980)
180. P John, I M Odeh, M J K Thomas, M J Tricker, J I B Wilson, *Phys. Status Solidi B* **105** 499 (1981)
181. G Lucovsky, W B Pollard *J. Vac. Sci. Technol. A, Vac. Surf. Films* **1** 313 (1983)
182. G Lucovsky *Solid State Commun.* **29** 517 (1979)
183. M Pinarbasi, N Maley, A Myers, J R Abelson *Thin Solid Films* **171** 217 (1989)
184. S Furukawa, N Matsumoto, T Toriyama, N Yabumoto *J. Appl. Phys.* **58** 4658 (1985)
185. W Beyer, H Wagner *J. Non-Cryst. Solids* **59**/**60** 161 (1983)
186. S R Das, S Charbonneau, D F Williame, J B Webb, J R MacDonald, D R Polk, S Zukotynski, J Perz *Can. J. Phys.* **63** 852 (1985)
187. J A McMillan, E M Peterson *J. Appl. Phys.* **50** 5238 (1979)
188. D K Biegelsen, R A Street, C C Tsai, J C Knights *Phys. Rev. B, Condens. Matter* **20** 4839 (1979)
189. M H Brodsky *Thin Solid Films* **50** 57 (1978)
190. S Oguz, M A Paesler *Phys. Rev. B, Condens. Matter* **22** 6213 (1980)
191. F Kozlowski, V Petrova-Koch, A Kux, W Stadler, A Fleischmann, H Sigmund *J. Non-Cryst. Solids* **137**/**138** 91 (1991)
192. W Beyer, H Wagner *J. Appl. Phys.* **53** 8745 (1982)
193. H Fritzsche, M Tanielian, C C Tsai, J Gaszi *J. Appl. Phys.* **50** 3366 (1979)
194. P John, I M Odeh, M J K Thomas, M J Tricker, F Riddoch, J I B Wilson *Philos. Mag. B, Phys. Condens. Matter. Electron. Opt. Magn. Prop.* **42** 671 (1980)
195. K Sinniah, M G Sherman, L B Lewis, W H Weinberg, J T Yates Jr, K C Janda *J. Chem. Phys.* **92** 5700 (1990)
196. S M Gates *Surf. Sci.* **195** 307 (1988)
197. S M Gates, C M Greenlief, D B Beach *J. Chem. Phys.* **93** 7493 (1990)
198. C M Greenlief, S M Gates, P A Holbert *Chem. Phys. Lett.* **159** 202 (1989)
199. S M Gates, R R Kunz, C M Greenlief *Surf. Sci.* **207** 364 (1989)
200. B G Koehler, C H Mak, D A Arthur, P A Coon, S M George *J. Chem. Phys.* **89** 1709 (1988)
201. M L Wise, B G Koehler, P Gupta, P A Coon, S M George *Surf. Sci.* **258** 166 (1991)
202. P Gupta, V L Colvin, S M George *Phys. Rev. B, Condens. Matter* **37** 8234 (1988)
203. M A Petrich *Magn. Reson. Rev.* **16** 183 (1993)
204. J B Boyce, S E Ready *Physica B* **170** 305 (1991)
205. H Eckert *Progr. Nucl. Magn. Reson. Spectrosc.* **24** 159 (1992)
206. A A Onischuk, R I Samoilova, V P Strunin, E N Chesnokov, R N Musin, V S Bashurova, A G Maryasov, V N Panfilov *Appl. Magn. Reson.* **15** 59 (1998)
207. W B Jackson, S B Zhang *Physica B* **170** 197 (1991)
208. N M Johnson *J. Non-Cryst. Solids* **137**/**138** 11 (1991)
209. F Buda, G L Chiarotti, R Car, M Parinello *Physica B* **170** 98 (1991)
210. A H Mahan, D L Williamson, B P Nelson, R S Crandall *Phys. Rev. B, Condens. Matter* **40** 12024 (1989).
211. M A Robertson, S K Estreicher *Phys. Rev. B, Condens. Matter* **49** 17040 (1994)

[a] — *Chem. Phys. Rep. (Engl. Transl.)*
[b] — *Kinet. Catal. (Engl. Transl.)*
[c] — *Inorg. Mater. (Engl. Transl.)*
[d] — *Russ. J. Inorg. Chem. (Engl. Transl.)*

Russian Chemical Reviews **70** (4) 333 – 355 (2001) © 2001 Russian Academy of Sciences and Turpion Ltd

DOI 10.1070/RC2001v070n04ABEH000654

Physiologically active compounds interacting with serotonin (5-hydroxytryptamine) receptors

O N Zefirova, N S Zefirov

Contents

I.	Introduction	333
II.	Classification of serotonin receptors	333
III.	Ligands of serotonin 5-HT_{1A} subtype receptors	334
IV.	Ligands of serotonin 5-HT_{1B} and 5-HT_{1D} subtype receptors	338
V.	Ligands of serotonin receptors of other 5-HT_1 subtypes	341
VI.	Ligands of serotonin 5-HT_2 subtype receptors	342
VII.	Ligands of serotonin 5-HT_3 subtype receptors	346
VIII.	Ligands of serotonin 5-HT_4 subtype receptors	349
IX.	Ligands of serotonin receptors of other subtypes	350

Abstract. The data on the structures of organic compounds active with respect to serotonin (5-hydroxytryptamine) receptors are systematised. Various aspects of their design are considered. The bibliography includes 296 references.

I. Introduction

The problems connected with the design of physiologically active compounds are discussed in the literature in terms of medicinal chemistry;† therefore, they are usually not very well known to a broad circle of organic chemists. The present review is aimed at the systematisation of the published data on the design of physiologically active compounds interacting with serotonin receptors and the analysis of effects of their chemical structures on their activities.

It is known that the physiological role of serotonin (5-hydroxytryptamine) (**1**, 5-HT) in the human brain consists in the regulation of various psychoemotional reactions. In addition, serotonin controls thermal regulation, sensory perception (particularly, pain sensitivity), *etc*. Recent studies have shown that disturbances in serotonin metabolism and/or functional activities of serotonin regulators are related to the pathogenesis of schizophrenia, depressive and anxiety states, alcoholism, drug abuse, *etc*.

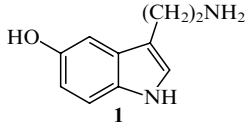

1

These findings have stimulated the interest that emerged over the past decade in the design of chemical compounds involved in the neurotransmission mediated by serotonin.

O N Zefirova, N S Zefirov Department of Chemistry, M V Lomonosov Moscow State University, Leninskie Gory, 119899 Moscow, Russian Federation. Fax (7-095) 939 30 26. Tel. (7-095) 939 48 78.
E-mail: olgaz@org.chem.msu.ru (O N Zefirova)
Tel. (7-095) 939 16 20. E-mail: zefirov@org.chem.msu.ru, zefirov@org.chem.msu.su (N S Zefirov)

Received 22 January 2001
Uspekhi Khimii **70** (4) 382 – 407 (2001); translated by R L Birnova

We hope that this review, which generalises structural approaches to the design of compounds interacting with serotonin receptors, will inspire synthetic chemists to make a radically new contribution to this branch of medicinal chemistry.

II. Classification of serotonin receptors

Serotonin (**1**) is a biogenic amine which manifests an extremely broad range of biological activities with respect to the central nervous system and other body organs and tissues. In the human central nervous system, it acts as a neurotransmitter, *i.e*., a chemical compound which transmits information from one nerve cell to another.[3] In the course of transmission, neurotransmitter molecules are released into the space separating membranes of the interacting cells where they bind to the corresponding receptors on the surfaces of target cells. It is this event that represents perception of information. The specificity of neurotransmitter – receptor interactions is determined by the structures of both the receptor and the neurotransmitter.

Serotonin receptors represent proteins incorporated into cell plasmatic membranes, which transform molecular signals from serotonin and its analogues into specific cell responses. The capability of chemical compounds of binding to their specific receptors underlies their effects on serotoninergic transmission. The effects of the majority of compounds presently used for the treatment of mental disorders, anxiety, schizophrenia, obesity, migraine, *etc*., are thought to be based on their involvement in serotoninergic transmission. These compounds act as agonists (activators) or antagonists (blockers) of the corresponding receptors. It should be noted that the interactions of chemical compounds with receptors are considered from the standpoint of both affinity (*i.e*., binding ability) and intrinsic activity (*i.e*., the ability to produce a biological response by means of structural or conformational changes in the receptor). (Affinity is numerically expressed by the reverse value of the equilibrium dissociation constant of the ligand – receptor complex. Apparently, antagonists possess no intrinsic activities.) The existence of partial

† The subject of medicinal chemistry is the search for, and the structural design [1,2] of, physiologically active compounds (drugs), the elucidation of chemical structure – activity relationships and, finally, the solution of the opposite structure – activity problem, *viz*., the design of compounds with predetermined properties.

agonists, *i.e.*, those which cannot produce maximum activation of their specific receptors and, as a consequence, maximum biological effect irrespective of their concentrations, is also possible.

The discovery of an immense variety of serotonin receptors of different subtypes in the past decade has brought about significant changes in their classification and nomenclature. Here, we shall adhere to the classification proposed by a special IUPAC commission according to which the 14 presently known subtypes of serotonin receptors are further divided into seven groups ($5HT_1 - 5HT_7$) depending on their amino acid sequences and the similarity of their signal transmission mechanisms.[4–6] Activation of serotonin receptors triggers the mechanism which involves a cascade of membrane proteins interacting sequentially with one another. In a definite step, signal transmission involves secondary messengers, *i.e.*, molecules or ions endowed with the ability of inducing conformational changes in the proteins involved in specific cellular processes. $5HT_3$ receptors which form ionic channels and transmit signals directly from nervous cells by ionic currents are the only exception.

The discovery of various subtypes of serotonin receptors led to the conclusion that the majority of presently known drugs, influencing serotoninergic transmission, act simultaneously on several subtypes of 5-HT receptors. Therefore, the design of selective ligands aimed at more efficient treatment with minimum side effects has been and still remains the problem of paramount importance, to say nothing of the fact that the design of selective ligands may culminate in the elaboration of radically new treatment schedules.

III. Ligands of serotonin 5-HT_{1A} subtype receptors

High concentrations of 5-HT_{1A} subtype serotonin receptors were found in the brain cortex where they are thought to play a crucial role in the processes associated with emotions. It has presently been demonstrated that these receptors are involved in the pathogenesis of various mental diseases, whereas ligands (especially agonists) interacting with these receptors were recommended as candidates for the treatment of various anxiety states, phobias, depressions, Alzheimer's disease (senile dementia), as analgesics, *etc.*[7–9] It is of note that 5-HT_{1A} receptors display a high degree of similarity to other receptor systems of the organism, such as adrenergic and dopaminergic systems, which significantly complicates the search for their selective ligands.

The simplest structural modifications of the serotonin molecule, *viz.*, the introduction of substituents into the benzene ring or restriction of the conformational mobility of the side chain, afforded several high-affinity 5-HT_{1A} agonists, *e.g.*, amines **2** and **3**. However, like serotonin itself, these compounds are not selective and interact with different subtypes of serotonin receptors (predominantly, with 5-HT_{1B}, 5-HT_{1D} and 5-HT_{2C}).[10,11]

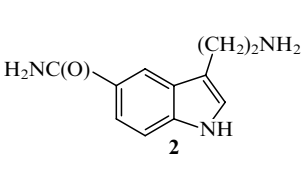

2

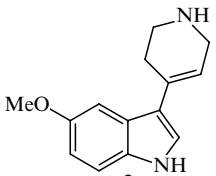

3

8-Hydroxy-2-dipropylaminotetralin (**4a**) was among the first most active and selective agonists of 5-HT_{1A} receptors,[12,13] the (+)-(*R*)-enantiomer being fully agonist and manifesting the highest affinity. The main structure–activity regularities for compounds of the type **4** are as follows. The presence of the hydroxy group in position 8 is essential for the binding and provides 500-fold higher selectivity with respect to serotonin receptors in comparison with dopamine receptors (the shift of the OH group into positions 5 or 7 sharply decreases the selectivity), while the hydroxy group in position 8 may be replaced by OMe, Ac or other groups (but not the carboxy group) without any loss in the affinity and selectivity, although the agonistic activity sometimes decreases noticeably, as in substitution by Ac.[14] The presence of two propyl substituents at the nitrogen atom is an optimum for affinity, selectivity and agonistic activity, although some variations in substituents, *e.g.*, replacement of one Pr^n group by $CH_2CH=CHI$ (compound **4b**),[15] enhance significantly the binding of the ligand to the receptor.

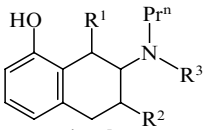

4a–d

$R^1 = R^2 = H$: $R^3 = Pr^n$ (**a**),
$CH_2CH=CHI$ (**b**);
$R^1 = Me$, $R^2 = H$, $R^3 = Pr^n$ (**c**);
$R^1 = H$, $R^2 = Me$, $R^3 = Pr^n$ (**d**).

The introduction of small substituents (*e.g.*, Me) into positions 1 (compound **4c**)[16] or 3 (compound **4d**)[17] of the alicyclic fragment of the molecule results in compounds manifesting different activities. The tetralin (1*S*,2*R*)-isomer **4c** displays nearly the same affinity as compound **4a**, but is much inferior to the latter with regard to intrinsic activity and is a weak partial agonist. The derivatives containing a methyl group in position 3 bind less effectively to 5-HT_{1A} receptors, although some of them, *e.g.*, the (2*S*,3*S*)-isomer of the tetralin **4d**, manifest high intrinsic activities.[18]

The transition to tricyclic structures afforded several potent 5-HT_{1A} agonists (*e.g.*, the *trans*-isomer **5**),[19] whereas the synthesis of rigid octahydrobenzo[*g*]quinolines yielded weak 5-HT_{1A} agonists, among which the amine **6** was the most active compound.[17] Notice that these cyclic analogues were used for the preparation of pharmacophore models of compounds interacting with 5-HT_{1A} receptors.‡

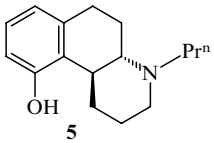

5

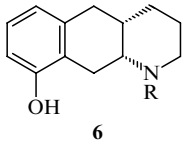

6

And, finally, it should be noted that the introduction of a fluorine atom into position 5 of compound **4a**, which gives compound **7**, changes quite unexpectedly the binding pattern. Thus the (*R*)-isomer of the tetralin **7**, is a full agonist and is somewhat less active than compound **4a**, while the (*S*)-isomer of compound **7** is a strong antagonist of 5-HT_{1A} receptors and its affinity is nearly an order of magnitude lower than that of the (*R*)-enantiomer.[20–22]

The amine **4a** was used as a prototype for the design of yet another structural class of 5-HT_{1A} agonists, *viz., trans*-(arylcyclopropyl)amines **8**.[16,23] The analysis of the structure–activity relationships in this series of compounds revealed that the introduction of electron-withdrawing substituents into the phenyl ring decreases the affinity for 5-HT_{1A} receptors, whereas electron donor or aromatic substituents (with the exception of bulky ones), *e.g.*, 2- or 3-thienyl substituents, enhance the affinity. Unlike the aminotetralin **4a**, compounds of this series are highly stereoselective, only (1*R*,2*S*)-isomers manifesting high activities.

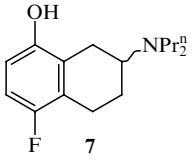

7

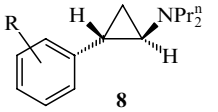

8

Yet another class of 5-HT_{1A} agonists, *viz.*, (*R*)-apomorphine analogues structurally close to aminotetralins **4** are known.

‡ The pharmacophore entails specific spatial arrangement of the binding groups essential for the optimum interaction with the receptor and causing (or blocking) a specific biological reaction. It is a purely structural concept which is neither a genuine molecule nor a genuine association of functional groups.

(*R*)-Apomorphine is a non-selective agonist of dopamine receptors. Structure–activity studies of its derivatives resulted in compounds which do not interact with dopamine receptors but are selective towards serotonin receptors. 11-Hydroxy-10-methylaporphine (**9**) with a methyl group in position 10 (instead of the hydroxy group in aporphine) is the most potent and selective compound. It is of note that only the (*R*)-enantiomer manifests agonistic activity, whereas the variations of substituents in positions 10, 11 and at the nitrogen atom reduce this activity in comparison with the amine **9**. These findings suggest that a hydrogen bond is formed between the hydroxy group in position 11 and serine-168 in the receptor protein and that a 'pocket' for the methyl group in position 10 exists in the binding site of the 5-HT_{1A} receptor.[24,25]

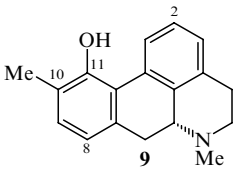

9

Compounds **10**–**12** provide other examples of cyclic systems that interact with 5-HT_{1A} receptors. Although these compounds are not selective, being active with respect to other receptors, they have been used for the construction of computer models of the ligand-binding site of 5-HT_{1A} receptors.[26–28]

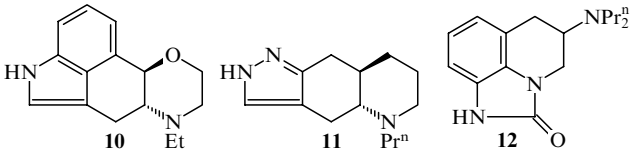

10 **11** **12**

Other structural variations in compound **4a** included the introduction of heteroatoms into the bicyclic fragment. For example, the 5-methoxy derivative **13** manifests the same high reactivity as aminotetralin (**4a**) and, which is more important, is more selective towards the 5-HT_{1A} receptor.[29] The main structure–affinity relationships for this class of compounds can be summarised as follows. Tertiary amines manifest higher affinity for the receptor than secondary and primary amines; substituents at the nitrogen atom can be rather bulky and the presence of MeO, CO_2Me and $CONH_2$ groups in position 5 provides both tight binding and the selectivity towards 5-HT_{1A} receptors.[30]

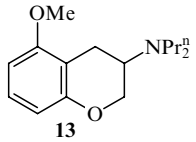

13

Buspirone derivatives constitute a large and very important structural class of 5-HT_{1A} receptor ligands.[31–33] Buspirone (**14a**) manifests high affinity for 5-HT_{1A} receptors and is endowed with agonistic activity. This is the only known compound specific for this subtype of receptor that has been recommended for clinical application as an antidepressant drug. Structural modifications of the imide and piperazine fragments and variations in the lengths of the alkyl chains were carried out aimed at a search for more active and selective buspirone analogues. These studies showed that the imide fragment of compound **14a** can be replaced by bioisosteric groups,§ *e.g.*, like those in gepirone (**14b**), ipsapirone (**14c**), tandospirone (**14d**), *etc.*[34–36] These groups should be lipophilic,[37–39] although the role of steric effects may also be significant.[40] Interestingly, some compounds, *e.g.*, substituted piperazine (**15**),[41] devoid of the cyclic amine fragment in the side chain, also manifest agonistic activities towards 5-HT_{1A} receptors. Heterocyclic substituents at the second nitrogen atom of the piperazine rings of buspirone and its analogues can be replaced by the phenyl substituent either non-substituted or containing an electron-withdrawing substituent in the *o*- or *m*-position to ensure higher affinity, *e.g.*, compound **16**.[42,43]

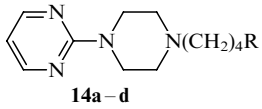

14a–d

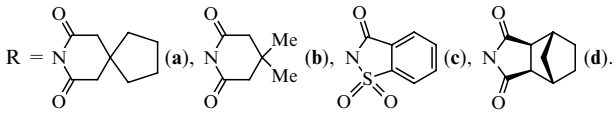

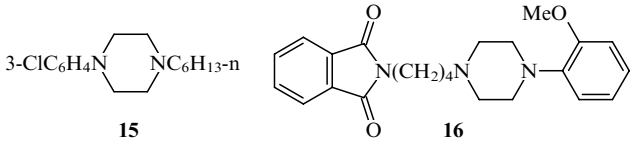

15 **16**

The optimum number of methylene groups in the linker needed for manifestation of maximum affinities of buspirone analogues for 5-HT_{1A} receptors is four, although some compounds with three and even two (less frequently) methylene groups also manifest noticeable affinities, *e.g.*, compound **17**.[44–46] Moreover, high affinity can persist upon substitution of heteroatoms for some methylene groups in the chain as is the case with ether **18**[47,48] or amide **19**.[49] Variations in the chain length and structure strongly affect its selectivity towards serotonin receptors in comparison with adrenoceptors and dopaminergic receptors.[50,51] Thus the selectivities of the bicyclohydantoin derivatives **20a**,**b** for 5-HT_{1A} can be improved by reducing the length of the intermediate alkyl chain to one methylene group ($n = 1$), although such modification causes a significant decrease in their affinities.[52]

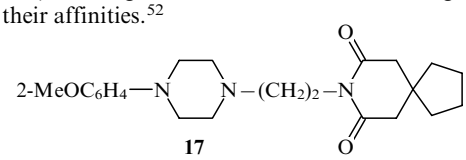

17

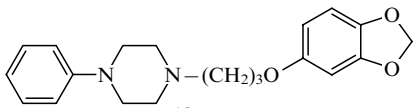

18

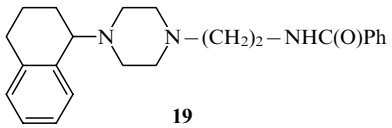

19

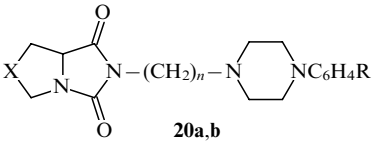

20a,**b**

$n = 1–4$; X = CH_2 (**a**), $(CH_2)_2$ (**b**).

Computer simulation studies aimed at rationalisation of such an increase in the selectivities of the bicyclohydantoin derivatives **20a**,**b** revealed[53] that compounds with $n = 1$ and $n = 4$ bind differently to the receptor. The fact that the derivatives with $n = 1$ manifest agonistic activities towards 5-HT_{1A} receptors (albeit rather weakly) suggests[53] that the protein molecule has a 'non-pharmacophoric' pocket (*i.e.*, the site docking 'non-essential' fragments of the ligand molecule rather than the pharmacophore group), which docks the imide group of the ligand

§ A bioisoster is a compound prepared by the replacement of an atom or a group of atoms (*e.g.*, a functional group) by other structural fragments with 'preserved' biological activity. The bioisosteric equivalence rules were established experimentally and are widely used in medicinal chemistry.

containing one methylene bridge. Its selectivity is attributed to the fact that adrenoceptors have no such pocket.

It is noteworthy that the majority of buspirone analogues mentioned above and buspirone itself, despite their high affinities for 5-HT_{1A} receptors, do not manifest any high intrinsic activities and are thus partial agonists. Moreover, some of them, *e.g.*, compounds **17** and **18** or the succinimide analogue **21** [54, 55] are sometimes classified as antagonists due to their very low intrinsic activities.

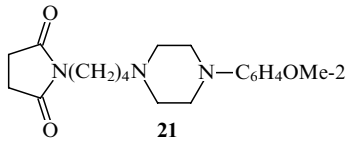

21

Studies aimed at the design of 5-HT_{1A} agonists containing simultaneously the groups constituting the essential fragments of the two main classes of 5-HT_{1A} ligands, *viz.*, aminotetralin (**4a**) and buspirone (**14a**) analogues, have become very popular in the past decade. An imide or a bioisosteric group, such as substituents R in buspirone (**14a**), gepirone (**14b**), ipsapirone (**14c**), *etc.*, were attached to the amino group of the benzopyran fragment of compound **13** through an alkyl chain, resulting in compounds **22**. Studies of structure–affinity relationships of these compounds revealed that compounds **22a–c** containing imide or sulfanylamide substituents manifested the highest activities and selectivities, whereas the preferred length of their side chains was four methylene groups, although sulfonylamide derivatives are also active even if their chains contain two methylene groups.[56]

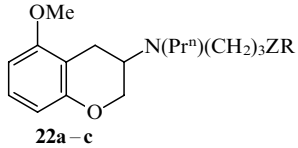

22a–c

Z = CH_2: R = 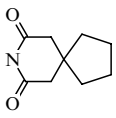 (**a**), 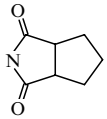 (**b**);

Z = CH_2NHSO_2, R = C_6H_4Me-4 (**c**).

High activities and selectivities of analogues of compounds **22** with limited mobilities of their side chains due to incorporation of the alkylamino groups into ring structures were predicted using the pharmacophore model of 5-HT_{1A} receptor agonists [17] and QSAR.¶ It should be noted that in many cases the restriction of conformational mobilities of functional groups is a classical approach in medicinal chemistry, since this allows stabilisation of the conformation which is the most suitable for the interaction with the receptors. The spiropyrrolidine- and spiropiperidinebenzopyrans **23** and **24** synthesised manifest high agonistic activities and selectivities with respect to 5-HT_{1A} receptors, though not exceeding those of compounds **22a–c**. In our opinion, it is expedient to carry out a detailed analysis of other types of restriction of conformational mobility in the side chains of such compounds. It is also noteworthy that compounds **23** and **24** are partial agonists of 5-HT_{1A} receptors and manifested the properties of antidepressant and anxiolytic drugs *in vivo*.[60]

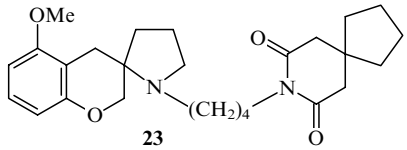

23

¶ QSAR is the abbreviation for 'quantitative structure–activity relationships'. This branch of medicinal chemistry is aimed at establishing the relationships between the properties (activities) and structural parameters of compounds (see, *e.g.*, Refs 2, 57–59).

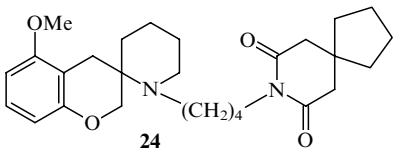

24

Benzodioxane derivatives which constitute another structural class of effective 5-HT_{1A} receptor ligands are being studied intensively. Compound **25** is one of the most potent and selective partial agonists.[61–63]

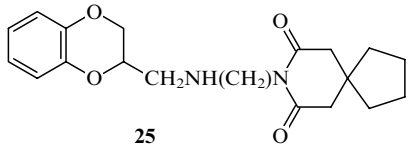

25

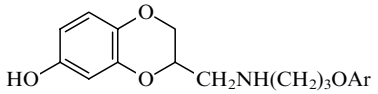

26

Ar = C_6H_4R, Het.

In such structures, as in any other buspirone (**14a**) analogues, the bridging chain may be elongated and modified, as in the case of the high-affinity partial agonists **26**, although such modification sometimes causes significant reduction in their selectivities.[64] Therefore, the search for structural modifications of benzodioxanes which might afford compounds endowed with the ability to distinguish among the binding sites of adrenoceptors and dopaminergic 5-HT_{1A} receptors was continued. It was found [65] that benzopyran (**27**), the unsaturated analogue of benzodioxanes, manifests high affinity for 5-HT_{1A} receptors and partial agonistic activity; the presence of a double bond in its ring and the absence of the oxygen atom in position 1 strongly depress its binding to adrenoceptors, which makes this compound more selective with respect to serotonin receptors. The acyclic benzodioxane analogue (compound **28**) is, contrariwise, less selective towards 5-HT_{1A} receptors than compounds **26**, although they retain their high affinities for these receptors.

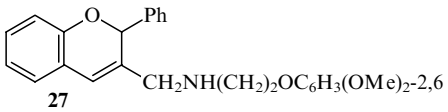

27

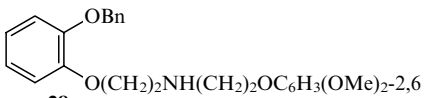

28

Benzodioxane derivatives with substituents in the benzene rings, *e.g.*, flesinoxan (**29**), also manifest high selectivities and agonistic activities.[66] Studies of structure–affinity relationships revealed that the main contribution to the binding of compound **29** to the receptor is made by the lipophilic substituent at the N(4) atom (the 4-fluorophenyl fragment may be replaced by the phenyl, thiophene or cyclohexane fragment without any loss in activity, but not by polar five- or six-membered heterocyclic substituents). Also, the amide group hardly takes part in the binding to the receptor but, rather, acts as a bridge and may therefore be replaced by other fragments. Structural modifications may also involve the

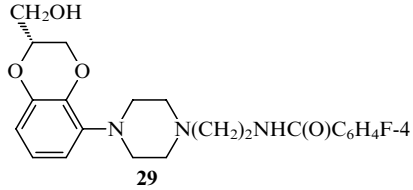

29

aryl substituent at N(1); these affect not only the affinities of the analogues but also their selectivities in comparison with dopamine receptors.[66]

An intensive search for 5-HT_{1A} receptor ligands characterised by high intrinsic activities is now in progress, since the majority of the known ligands are partial agonists. Full 5-HT_{1A} agonists were found in a new class of compounds, *viz*., 6-substituted pyridylmethylamine derivatives **30**. These ligands were selected using a special model of 5-HT_{1A} receptor activation according to which the intrinsic activities of 5-HT_{1A} ligands depend on their abilities to stabilise the positive charge generated on the receptor protein upon its binding to the agonist. The pyridine ring was chosen as a group endowed with this ability. Therefore, the pyridine derivatives of the type **30** were constructed in order to obtain full agonists of 5-HT_{1A} receptors.

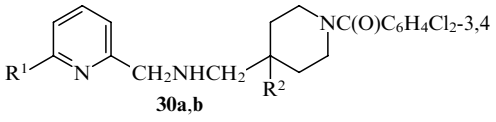

30a,**b**

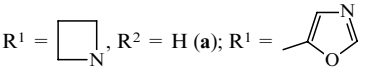

The results of QSAR studies suggest that the abilities of compounds to activate the corresponding receptors strongly depend on the nature and position of substituents in the pyridine ring. Thus a substituent (preferrably an electron-donor substituent) should be present in position 6. Compounds **30a**,**b** were finally found to be full agonists of 5-HT_{1A} receptors and possess the highest affinities and selectivities.[67] Moreover, the agonistic activities and selectivities of these compounds and some of their pharmacological characteristics can be improved by introducing the fluorine atom (R^2 = F).[68]

As shown above, structure–activity studies of 5-HT_{1A} receptor ligands are mainly directed at the search for selective compounds. However, special mention should be made of other relevant tasks, such as the search for compounds acting simultaneously as dopaminergic receptor antagonists and serotonin 5-HT_{1A} agonists. These compounds hold much promise in the therapy of schizophrenia and other mental disorders; some of them, *e.g*., the piperazine derivative **31**, are undergoing clinical trial.[69] Certain structurally related compounds, *e.g*., ziprasidone (**32**), manifest antagonistic activities towards 5-HT_2 receptors.[70]

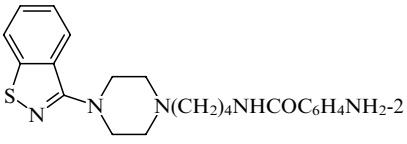

31

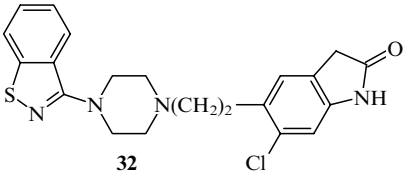

32

Since this review is aimed at the structural analysis of serotonin receptor ligands, their affinities, intrinsic activities and selectivities, we shall not dwell on the search for ligands for the related types of receptors, although in these studies 5-HT-selective ligands can also be found. Thus the search for ligands of dopaminergic receptors revealed that compound **33** possessed affinity and selectivity exclusively with respect to 5-HT_{1A} receptors.[71]

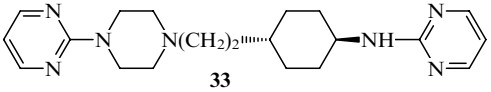

33

To complete the consideration of problems related to the design of 5-HT_{1A} agonists, it should be noted that although such ligands are rather numerous, all of them belong to a limited set of structural classes of compounds. Moreover, only some of these ligands interact with 5-HT_{1A} receptors in a selective manner and very few of them are full agonists. In this context, a search for agonists among novel classes of compounds is a very important task, since it helps elucidation of the structure–activity relationships for ligands and sheds more light on the structural peculiarities and functional roles of the corresponding receptors.

Antagonists of 5-HT_{1A} receptors have been studied in lesser detail, although they could in principle be used for the treatment of various diseases of the central nervous system. Some presently known β-adrenoceptor blockers, *e.g*., pindolol (**34**),[72,73] cyanopindolol (**35**),[74,75] *etc*., manifest antagonistic activities towards 5-HT_{1A} receptors, the (−)-(*S*)-enantiomers being more active. These compounds are also active with respect to other subtypes of serotonin receptors.

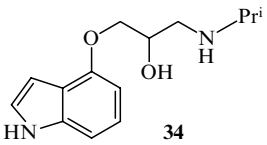

34

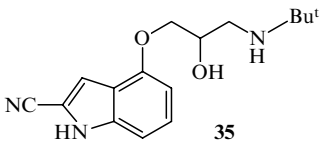

35

Numerous studies aimed at a search for selective antagonists of 5-HT_{1A} receptors have led to compounds **7** and **36**.[76,77] It was also found that many compounds previously assigned to 5-HT_{1A} antagonists, *e.g*., the piperazine derivative **37**,[78] spiroxatrine **38**,[79,80] *etc*., are in fact not genuine antagonists but manifest partial agonistic and low intrinsic activities.† It should be noted that the main approach to the design of compounds **36**–**38** consists in the introduction of bulky lipophilic substituents into the structures of 5-HT_{1A} receptor agonists. This approach is widely used in medicinal chemistry for the construction of antagonists, since the presence of additional hydrophobic interactions between the ligand and the receptor in the vicinity of the binding site increases the strength of binding to such an extent that the receptor appears to be completely blocked by the compound.

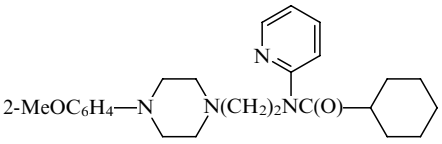

36

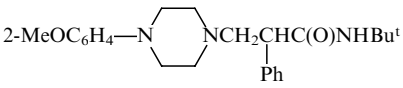

37

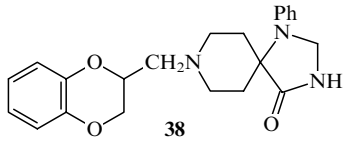

38

Until recently, there was no evidence in the literature concerning the differences in the structural requirements for agonists or antagonists of 5-HT_{1A} receptors.[18] Special mention should be made of investigations into effects of substituents on the intrinsic activities of chromanes of the type **39** which, like benzodioxanes **26**, represent high-affinity 5-HT_{1A} ligands.[81,82] Modifications of the benzene ring in their side chains revealed that the *p*-methoxy group plays a crucial role in both affinity and antagonistic activity of compound **39a**, whereas other substituents diminish both the

† The term 'silent antagonist' was specially introduced to distinguish among genuine antagonists, *i.e*., those devoid of agonistic activity, and partial agonists.

binding and the blocking properties. Modifications of the chromane ring showed that the introduction of F, Cl and OMe (but not OH and Me) into position 6 results in strong antagonists (compounds **39b**,**c**,**d**), whereas the introduction of analogous substituents into positions 5 and 7 yields partial agonists. The differences in the antagonistic activities of this series of compounds cannot be explained by different distribution of their electron densities, since the introduction of both electron-donor (*e.g.*, OMe) and electron-withdrawing groups (*e.g.*, Cl) affords full antagonists, whereas compound **39e** containing the hydroxy group manifests the properties of a partial agonist.

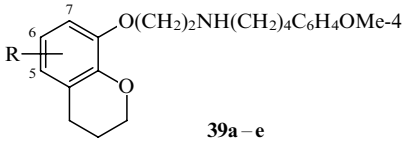

39a–e

R = H (**a**), 6-F (**b**), 6-Cl (**c**), 6-OMe (**d**), 6-OH (**e**).

In all probability, the antagonistic properties of the majority of structural classes of 5-HT_{1A} ligands depend on many factors and not necessarily depend on those factors which determine the strength of binding of the ligand to the receptor, *i.e.*, affinity. This circumstance and the fact that even minor structural modifications of 5-HT_{1A} receptor antagonists often cause significant reduction in their affinities, selectivities and antagonistic activities call for further investigations using computer simulation of the receptor structure and ligand docking (in this context, docking is a molecular simulation technique aimed at a search for the optimum matching of the ligand to the binding site).[83] On the whole, the search for selective antagonists of 5-HT_{1A} receptors is a complicated but very urgent task, since no preparations of this class have been recommended for the clinical use thus far.

IV. Ligands of serotonin 5-HT_{1B} and 5-HT_{1D} subtype receptors

Serotonin 5-HT_{1B} and 5-HT_{1D} subtype receptors are rather densely localised in the human brain. They contain extremely similar amino acid sequences despite being encoded by two different genes. These two subtypes can pharmacologically be separated using several non-selective 5-HT_2 antagonists (*e.g.*, ketanserin, see below);[53,84–86] however, their functional roles in the organism have not been established yet because only a very small number of selective ligands to these receptors are known. It is known that blocking of 5-HT_{1B} receptors results in coronary vasodilation,[87] therefore, their selective antagonists can be used for the treatment of various cardiovascular disorders. They are also recommended for use as effective fast-acting antidepressant drugs.[88,89] Agonists of 5-HT_{1D} receptors are putative antimigraine drugs, since their activation causes the brain vasodilation, diminishes pulsation, *etc*. In recent years, 5-HT_{1B} and 5-HT_{1D} subtype ligands have attracted considerable attention in connection with the design of an efficient antimigraine drug sumatriptan (**40**), which appeared to be a 5-$HT_{1B/1D}$ receptor agonist.[90–93] Sumatriptan has very few side effects, but causes coronary vasodilation, which is controlled by 5-HT_{1B} receptors (see above). This, too, calls for the design of selective agonists of 5-HT_{1B} and 5-HT_{1D} receptors.

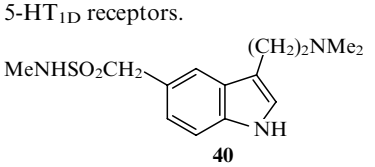

40

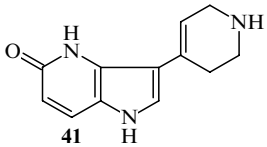

41

A fairly large group of 5-HT_{1B} and 5-HT_{1D} receptor agonists includes serotonin or tryptamine derivatives, such as amines **2** and **3**, which represent non-selective agonists of 5-$HT_{1B/1D}$ and 5-HT_{1A} receptors. Interestingly, the amine **41**,[94–96] which is a close analogue of compound **3**, is much more active and selective towards the 5-HT_{1B} receptor. Close serotonin analogues include sumatriptan (**40**) itself and its numerous derivatives, such as naratriptan (**42**),[97,98] rizatriptan (**43**),[97,99,100] zolmitriptan (**44**),[101,102] eletriptan,[103] avitriptan,[104] almotriptan[97,105] and frovotriptan (**45**).[85,106] The majority of these compounds are candidates for antimigraine drugs and have passed clinical trials or are in the final stages. Their structures vary largely by changing substituents in the indole fragment or by restricting conformational mobility of the side chain containing an amino group.

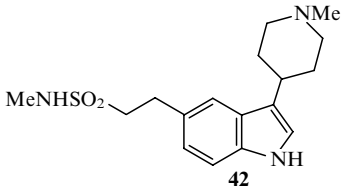

42

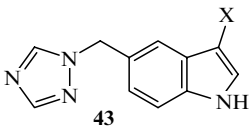

43

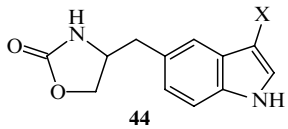

44

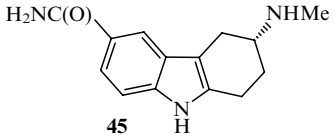

45

X = $(CH_2)_2NMe_2$.

Compounds **42**–**45** possess high affinities for 5-HT_{1D} receptors. However, they are non-selective and only 1.5–3-fold less active with respect to 5-HT_{1B} receptors. Comparison of the structures obtained suggest that the basic amine, the indole fragment and the substituent in position 5 involved in the formation of a hydrogen bond as an acceptor or a donor are the key groups needed for their efficient binding to the receptor. QSAR studies aimed at improving the activities and selectivities of serotonin and tryptamine derivatives towards 5-HT_{1D} receptors included variations of substituents at the C(5) atom.

It was found[43] that in the case of alkoxy substituents the optimum length of the alkyl chain needed for the binding to 5-$HT_{1B/1D}$ receptors is 8 or 9 carbon atoms; with shorter chains, the selectivity is lost, while with longer chains, the affinity is decreased. Thus 5-nonyloxytryptamine (**46**) represents a high-affinity agonist, which is more selective towards 5-HT_{1B} than towards 5-HT_{1D} receptors and is practically inactive towards 5-HT_{1A} receptors. It should be noted, however, that no compounds capable of distinguishing 5-HT_{1B} and 5-HT_{1D} receptors with a high degree of selectivity could thus far be obtained by changing the lengths and degree of ramification of the alkoxy substituents.[43]

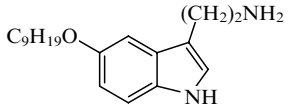

46

The variations in the substituents in position 5 revealed that the latter can be rather bulky as in the case of compounds **47**,[88,107] **48**[108–110] and **49**,[111–112] which are more selective towards 5-HT_{1D} than towards 5-HT_{1B} receptors. This is suggests the existence of a deep pocket in the binding site of 5-$HT_{1D/1B}$ receptor proteins adjacent to C(5) of the serotonin molecule. According to some data, it is in the size of this domain that 5-$HT_{1D/1B}$ receptors differ from the 5-HT_{1A} receptor,[113] although some of compounds mentioned, as expected, manifest low affinities for the latter.

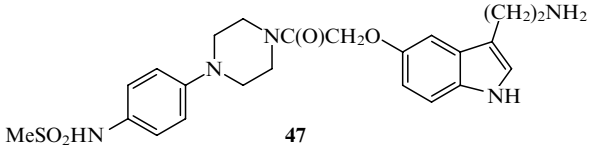

47

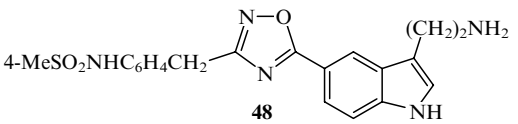

48

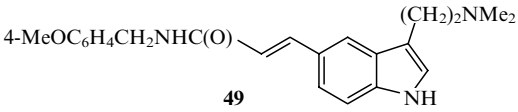

49

It is noteworthy that the introduction of a triflate group (compounds **50**), which is bioisosteric to the carboxy or the methoxy group,[114] increases the selectivity towards 5-HT_{1D} receptors 10 – 15-fold in comparison with 5-HT_{1B} receptors.[115]

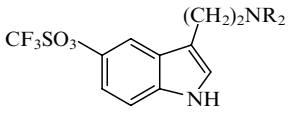

50

R = Me, Et.

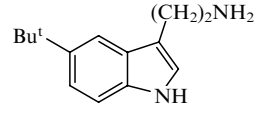

51

It is of note that until recently the ability of the substituent in position 5 to be involved in the formation of a hydrogen bond was thought to be a necessary prerequisite for high affinity, since virtually all presently known 5-HT_{1D} receptor agonists have at least one heteroatom (N, O or S) in this position. However, the recently discovered 5-alkyltryptamine analogues devoid of heteroatoms in position 5 possess high affinities for 5-HT_{1D} receptors. This affinity increases as the size of the lipophilic group increases, reaching a maximum in the *tert*-butyl derivative **51**.[85] The resulting compounds are not highly selective, *viz*., their maximum selectivities towards 5-HT_{1D} receptors are only four times greater than towards 5-HT_{1B} receptors. The fact that the formation of a hydrogen bond involving the substituent at the C(5) atom of serotonin is not critical for the manifestation of its high affinity for 5-HT_{1D} receptors points to the hydrophobicity of the spacious pocket in the vicinity of C(5). This finding allows one to expand significantly the range of possible substituents at this atom.

The variations in substituents in position 3 are much less documented. However, there are recent data to show that the selectivity towards 5-HT_{1B} and 5-HT_{1D} receptors can be enhanced by introduction of structurally more complex substituents in this position. Thus it was shown that the tryptamine analogue **52a** containing the pyrrolidine ring possesses an order of magnitude higher affinity for 5-HT_{1D} receptors than for 5-HT_{1B} receptors. On the other hand, the analogous *N*,*N*-dimethylamino derivative **52b** is non-selective.[116, 117]

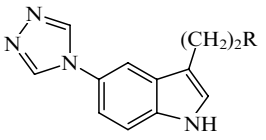

52a,**b**

R = (**a**), NMe_2 (**b**).

It is thought that the region in the receptor which binds the fragment at the C(3) atom contains an aspartic acid residue.[117] The steric requirements for the binding to this domain in both types of receptors can be determined by modifying this fragment.[117] Studies of series of compounds **53** and **54** revealed that 5-HT_{1D} receptors can bind bulky groups. It was therefore assumed that this domain contains a spacious binding pocket. At the same time, compounds containing smaller substituents bind more effectively to 5-HT_{1B} receptors. For example, compounds **53** or **54** which are full agonists of 5-HT_{1D} receptors manifest 100- and 140-fold higher selectivities towards them. Hence, the selectivity towards each of these two receptor subtypes can be provided by a correct choice of a substituent in the structural domain responsible for the binding to the aspartate residue. It is of note that the presence of a bulky substituent at C(3) can in principle increase the affinities for 5-HT_{1A} receptors (see above). However, the above-mentioned series includes compounds (*e.g*., **54**, $R^1 = CH_2Ph$, $R^2 = H$) which are selective with respect to both 5-HT_{1B} and 5-HT_{1A} receptors.[117]

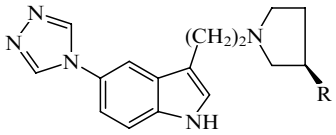

53

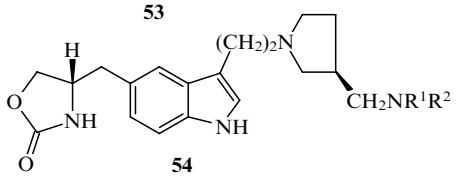

54

Many (3-piperazinopropyl)indoles, *e.g*., compound **55a**, also manifest high (up to 200-fold) selectivities towards 5-HT_{1D} *vs*. 5-HT_{1B} receptors.[118] The selectivity increases 300- to 500-fold upon introduction of the hydroxy group or the fluorine atom into the propyl chain (compound **55b**).[119] The distal nitrogen atom of piperazine does not seem to be essential for the binding to this receptor, since the corresponding piperidine analogues, *e.g*., compound **55c**, also manifest high affinities.[120] The distal nitrogen atom can also be displaced into the exocyclic position without any loss of its affinity,[120] as in the case of the 4-aminopiperidine derivative **55d**.[116] The selectivities of the ligands **55a** – **d** towards 5-HT_{1D} receptors suggest that these are less sensitive to changes in the position of the nitrogen atom than 5-HT_{1B} receptors despite close homology of these two proteins. This circumstance can further be used in the structural design.

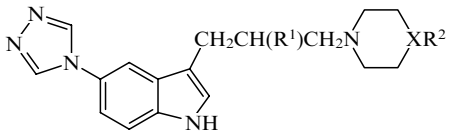

55a – **d**

R^1 = H, X = N, R^2 = $(CH_2)_2C_6H_4F$-3 (**a**); R^1 = OH, F; X = N, R^2 = Ph, C_6H_4F-3 (**b**); R^1 = H, X = CH, R^2 = Bn (**c**); R^1 = H, X = CH, R^2 = N(Me)Bn (**d**).

Among other full and partial agonists of 5-HT_{1B} and 5-HT_{1D} receptors structurally different from tryptamine, special mention should be made of arylpiperazines, *e.g*., compounds **56** [121, 122] and **57**,[121, 123] which display very low selectivities towards 5-HT_{1B} subtype receptors. As expected, these compounds possess high

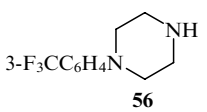

56

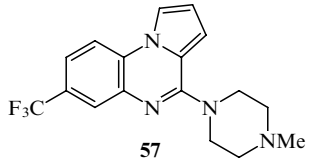

57

affinities with respect to the 5-HT_{1A} receptor. More recently synthesised compounds of this series include alniditane (**58**) [124] as well as compounds **59** [125] and **60**.[126]

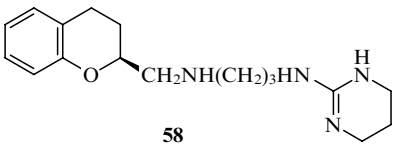

58

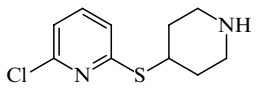

59

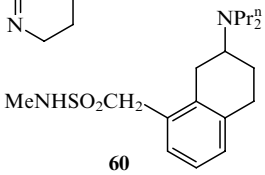

60

The adrenoceptor agonist oxymethazoline (**61**) manifests agonistic activity towards both 5-HT_{1B} and 5-HT_{1D} receptors

and is among the most promising lead compounds ‡ for the design of 5-$HT_{1D/1B}$ agonists.[127]

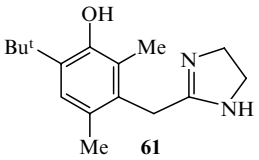

61

However, an analysis of structural requirements for the binding of benzylimidazolines of the general formula **62** to these receptors revealed that far from all substituents in the aromatic ring of compound **61** are necessary for the manifestation of high affinity. Thus the hydroxy group in position 3 of compounds **62** can be removed without any noticeable decrease in their affinities for 5-HT_{1D} subtype receptors. However, such modification decreases 50-fold the affinity for 5-HT_{1B} subtype receptors. Moreover, the contribution of the bulky substituent at the C(4) atom to the binding to 5-HT_{1D} receptors is greater. Therefore, some structural modifications of compounds **62** (*cf.*, *e.g.*, compounds **62a**,**b**) lead to a 100-fold increase in the selectivities towards 5-HT_{1D} receptors. Compounds **62a**,**b** are agonists, their affinities for adrenergic receptors are lower than that of compound **61**. It should be noted that the transition to amidines **63** decreases both their affinities and selectivities towards 5-HT_{1D} subtype receptors.[113]

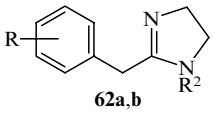

62a,**b**

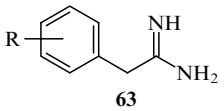

63

R^1 = 4-Bu^t (**a**), 6-Me (**b**).

Thus, the overwhelming majority of agonists of 5-HT_{1B} and 5-HT_{1D} receptors represent tryptophan analogues; therefore, these types of new lead compounds could be useful in the search for the next generation of agonists able to distinguish between these two subtypes of receptors.

The main efforts of chemists engaged in the search for antagonists are directed at the synthesis of compounds more selective towards 5-$HT_{1B/1D}$ subtype receptors in comparison with other serotonin receptors. As mentioned above, some aryloxyalkylamines, such as the well-known β-adrenoceptor antagonist propranolol (**64**), are characterised also by low affinities for 5-HT_{1A} and 5-HT_{1B} receptors and usually represent antagonists or very weak partial agonists of these receptors.

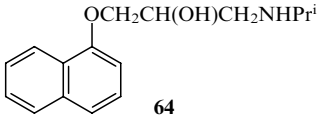

64

Studies of binding of their analogues to 5-$HT_{1D/1B}$ receptors [128] revealed that the presence of the hydroxy group in the side chain is not necessary, whereas the substitution of the CH_2 group for the oxygen atom in the ether group results in the loss of affinity. The affinity for 5-HT_{1B} subtype receptors can be increased by reducing the length of the side chain to two CH_2 groups or by using a primary or a secondary amine with smaller alkyl groups, *e.g.*, compound **65**. Replacement of the naphthalene fragment by a substituted phenyl ring is also possible, but in this case the affinity will decrease by an order of magnitude as in compounds **66** and **67**.[129] In our opinion, the structures of these lead compounds are not very suitable for the design of antagonists, since the compounds obtained interact with adrenoceptors, but are virtually non-selective towards 5-HT_{1B} subtype receptors in comparison with 5-HT_{1D} subtype receptors. Moreover, some high-affinity compounds, *e.g.*, compound **65**, lose their antagonistic properties and behave as agonists towards the corresponding receptors.

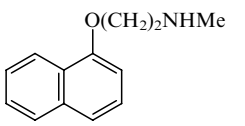

65

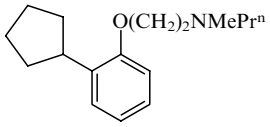

66

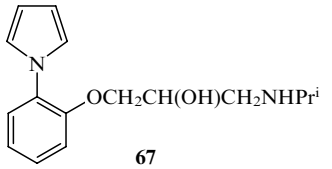

67

It is of note that until recently virtually no selective 5-$HT_{1B/1D}$ antagonists existed and studies into receptor binding were carried out with other compounds, *e.g.*, methiothepin (**68**), which interacts with other serotonin, dopaminergic and adrenergic receptors.

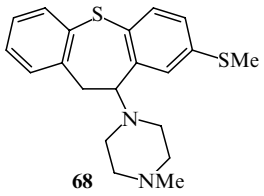

68

Benzanilide (**69**) is the first example of a selective 5-$HT_{1D/1B}$ antagonist, although it does not discriminate between the subtypes. This finding has played a crucial role in the characterisation of 5-$HT_{1D/1B}$ receptors. However, subsequent studies using cloned human receptors revealed that compound **69** is not a full antagonist, it rather acts as a partial agonist.[130,131] Therefore, the construction of selective antagonists required further investigations.

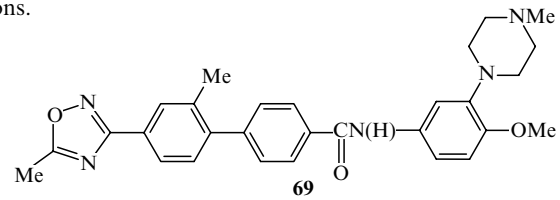

69

Sumatriptan (**40**), zolmitriptan (**44**) and other tryptamine analogues were used for the design of 5-$HT_{1B/1D}$ antagonists based on the corresponding selective agonists. QSAR studies of the factors affecting both the activity and selectivity as well as simulation using pharmacophore models of 5-$HT_{1D/1B}$ receptors [132] revealed that certain geometrical and conformational restrictions can result in the displacement of the indole nucleus from the site (which is arbitrarily termed as the aromatic binding site) specific, *e.g.*, for zolmitriptan (**44**). It was demonstrated that the retention of high affinity can be accompanied by a significant decrease in intrinsic activity. Later, it was shown that the antagonistic effect is manifested if only the pyrrole moiety of tryptamine (rather than the whole indole nucleus) is displaced. In other words, it was necessary to modify the structure of the agonist in such a fashion that the interaction of the pyrrole double bond with the π-electrons of the receptor in their specific domain would be blocked and the agonistic response would correspondingly be prevented. To achieve this, it was proposed to design an electron-deficient aromatic system by introducing electron-withdrawing substituents into position 2 of zolmitriptan (**44**). The presence of a substituent in position 2 not only makes the indole system electron-deficient, but also restricts the conformational mobility of the side chain. The alkyl chain in position 5 was also varied in order to confer greater mobility on this substituent.[132]

‡ The 'lead compound' is one of the basic concepts in medicinal chemistry which denotes a structural prototype for the future drug. The lead compound manifests definite physiological activity and its structure serves as the basis for the design of a new drug.[2]

This approach was successful, *viz*., the resulting tryptamine derivatives of the type **70** contain heterocyclic substituents comprising the carbonyl group R^2 (this group is critical for selectivity as compared with that of 5-HT_{2A} receptors)[133] and represent highly active full antagonists of 5-HT_{1B} receptors. These are also selective towards other serotonin receptors including sometimes compounds **70a**,**b** 5-HT_{1D} subtype receptors. Substitution of the amide group for the ester group in position 2 afforded less active and less selective antagonists; high affinities and selectivities were restored only after the introduction of bulky substituents to the nitrogen atom, *e.g*., compound **71**. It is believed[134] that this substituent can occupy the aromatic binding site in the receptor by pushing the indole nucleus out from this site.

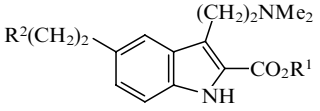

70a,**b**

R^1 = Et: R^2 = 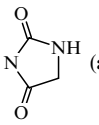 (**a**), 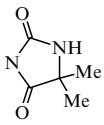 (**b**).

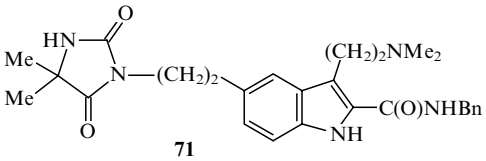

71

Yet another example is the design of 5-$HT_{1D/1B}$ receptor antagonists from the corresponding agonists.[88] Assuming that the tryptamine fragment in compound **47** is responsible for the intrinsic activity (by analogy with serotonin), while the arylpiperazine moiety is mainly responsible for the binding to the receptor, it was suggested to replace the tryptamine fragment in compound **47** by a non-selective ligand manifesting antagonistic activity towards 5-$HT_{1D/1B}$ receptors (in this particular case, the 1-naphthylpiperazine fragment) which would result in their selective antagonists. This was the case, *e.g*., for compounds **72**. Studies of these compounds showed that they are indeed selective towards 5-$HT_{1D/1B}$ receptors and many of them are full antagonists. However, the antagonistic activity depends on the aryl substituent of the arylpiperazine side chain and is maximum for Ar = 2-MeC_6H_4 or 2,3-$Me_2C_6H_3$. This suggests that the binding of this fragment also contributes to the intrinsic activity of the ligand.[88]

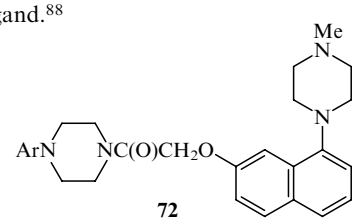

72

Recently, a series of antagonists based on the above-mentioned partial agonist **69**, which was successfully used as the lead compound in the design of compounds selectively blocking 5-HT_{1D} and 5-HT_{1B} subtype receptors, have been synthesised. These include primarily benzamide (**73**),[112,135] the structural analogue of compound **69**, which is a strong antagonist much more selective towards 5-HT_{1B} subtype receptors. Variations in the substituent R of its methylated analogues **74a**–**d** revealed that all these compounds bind to the receptor to approximately the same degree and in the same manner (like compound **73**) and manifest low affinities for 5-HT_{1A} and 5-HT_{1D} subtype receptors; their agonistic activities depend critically on the conformation of their side chains. Compound **74a** and the (*Z*)-alkenyl derivative **74b** act as strong antagonists resembling compound **73**, whereas the alkynyl derivative **74d** and the (*E*)-alkenyl derivative **74c** manifest pronounced agonistic activities.[89]

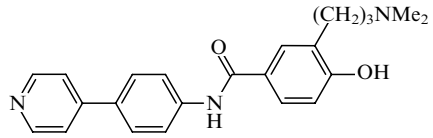

73

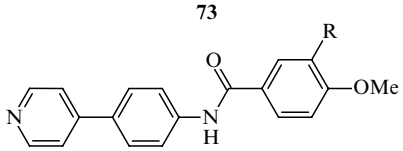

74a–**d**

R = $(CH_2)_3NMe_2$ (**a**), (*Z*)-CH=$CHCH_2NMe_2$ (**b**), (*E*)-CH=$CHCH_2NMe_2$ (**c**), C≡CCH_2NMe_2 (**d**).

It should be noted that substitution of the flexible aminoalkyl side chain for the piperazine ring in compound **69** (compounds **75a**,**b**) decreases their intrinsic activities with respect to 5-HT_{1B} receptors.[89,136] These data demonstrate the significant role of the spatial orientation of the aminoalkyl fragment in the design of 5-HT_{1B} antagonists, although it is still impossible to describe this notion in terms of conformation, since some conformationally rigid analogues of compounds **69** can also act as full antagonists. Thus compound **76** is a selective 5-HT_{1B} antagonist; its design was based on the use of a computer model of 5-HT_{1B}, 5-HT_{1D}, 5-HT_{1E}, 5-HT_{2A} and 5-HT_{2C} receptors.[86,137]

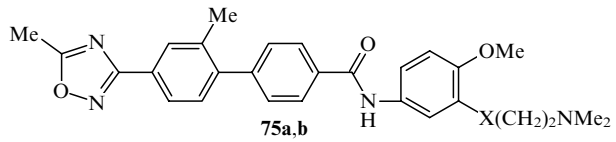

75a,**b**

X = O (**a**), CH_2 (**b**).

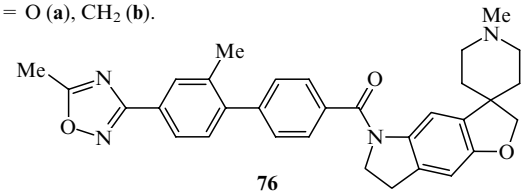

76

In conclusion, we shall refer to the structure of compound **77**, the recently discovered selective antagonist of 5-HT_{1D} receptors.[138] This compound possesses 60-fold higher affinity with respect to 5-HT_{1D} subtype receptors than to 5-HT_{1B} subtype receptors and is virtually inactive with respect to other serotonin receptors.

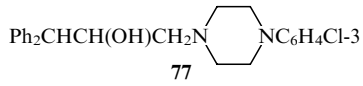

77

It is necessary to stress again that only a few compounds are known which interact with each of the above-mentioned subtypes with high selectivities, which is due to the structural similarity of 5-HT_{1B} and 5-HT_{1D} receptors. However, the present-day structural requirements for the design of such ligands are becoming more and more understandable and their number will be increasing.

V. Ligands of serotonin receptors of other 5-HT_1 subtypes

The 5-HT_{1E} and 5-HT_{1F} subtype receptors have been studied to a much lesser degree than those of other 5-HT_1 subtypes. It is known that they are present in large concentrations in brain and display high structural similarity as regards their amino acid sequences. The non-selective 5-HT_1 agonist, *viz*., the amine **2**, manifests *ca*. 1000-fold lower affinity for 5-HT_{1E} subtype recep-

tors than for the 5-HT_{1B} subtype receptors.[139,140] This is explained by the presence of the lysine–glutamic acid pair in the binding site of the 5-HT_{1E} receptor protein instead of the less polar isoleucine–serine (5-HT_{1B}) pair or the valine–serine pair (5-HT_{1D}). Presumably, this results in the formation of a salt bridge between lysine and the aspartate residue which plays the key role in the ligand binding. Compound **78a** is the agonist of 5-$HT_{1E/1F}$ receptors but does not discriminate between them and possesses low affinity. No selective or highly active ligands of 5-HT_{1E} receptors have been identified so far and the function of these receptors still remains to be established.

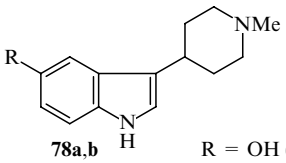

78a,**b** R = OH (**a**), 4-$FC_6H_4CONH_2$ (**b**).

Recently, studies of the functions and ligands for 5-HT_{1F} receptors have attracted the attention of many research groups due to the detection of high affinity of sumatriptan (**40**) for 5-HT_{1F} receptors (which was about an order of magnitude lower than for 5-HT_{1D} receptors). It was assumed that some (probably all) effects of sumatriptan in the alleviation of migraine symptoms are due to its binding to these receptors. The recently discovered indole derivative **78b** is their first and the only selective agonist;[141–143] no antagonists of 5-HT_{1F} receptors have been identified yet.

VI. Ligands of serotonin 5-HT_2 subtype receptors

The family of serotonin 5-HT_2 receptors is classified into three subtypes, *viz*., 5-HT_{2A}, 5-HT_{2B} and 5-HT_{2C}. The first two subtypes occur widely in peripheral tissues where they regulate muscle contraction; therefore, their ligands are used in the therapy of cardiovascular diseases. As for 5-HT_{2C} subtype receptors, they are localised exclusively in the central nervous system; their ligands produce psychotropic effects, *e.g*., their antagonists are used as anxiolytic and sedative drugs.

A series of 5-HT_2 receptor agonists were obtained by the simplest modifications of the serotonin structure. Thus α-methyl-5-hydroxytryptamine (**79**)[48,144,145] is a full high-affinity agonist of 5-HT_{2B} subtype receptors which manifests 10- and 100-fold lower affinities for 5-HT_{2C} and 5-HT_{2A} receptors, respectively. Similar selectivity profiles hold following the introduction of the thienylmethoxy substituent into position 5 (compound **80**).[146–148]

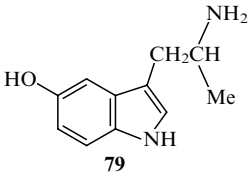

79

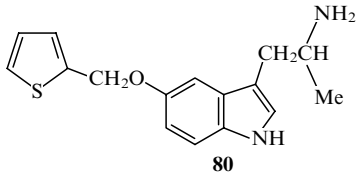

80

5-Methoxytryptamine also manifests higher affinity for 5-HT_{2B} receptors than for 5-HT_{2A} and 5-HT_{2C} receptors (25- and 400-fold, respectively), although it is non-selective towards other serotonin receptors. The introduction of a bulky bromobenzyl substituent into the amino group of 5-methoxytryptamine results in the ligand **81** which possesses high affinity and selectivity with respect to 5-HT_{2A} receptors,[149] but manifests the properties of a partial agonist.

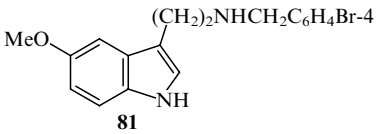

81

Bioisosteric substitution of thienepyrrole fragments for the tryptamine indole nucleus was undertaken in an attempt to design 5-HT_2 agonists. However, the resulting compounds **82** and **83** displayed somewhat lower activities towards 5-HT_2 receptors than the corresponding indole analogues (compound **82** is nearly 4 times more selective with respect to 5-HT_{2C} receptors than to 5-HT_{2A} and 5-HT_{2B} receptors). Moreover, this transformation increased significantly the affinity for 5-HT_{1A} receptors.[150] On the whole, these data corroborate the fact that different subtypes of serotonin receptors are highly sensitive to minor changes in the electronic characteristics of the aromatic systems.

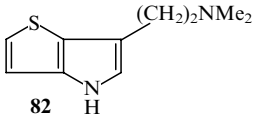

82

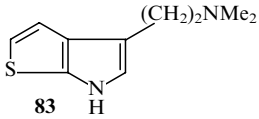

83

Studies of restriction of conformational mobility in the aminoethyl side chain of serotonin have led to the *N*-methylpyrrolidine derivative **84** (R = 5-OMe) and its analogues which manifested very high agonistic activities, being more selective towards 5-HT_{2A} subtype receptors. The activities of these compounds strongly depend on their stereochemistry, *viz*., (*R*)-enantiomers manifest *ca*. 30-fold higher affinities than (*S*)-enantiomers.[151,152]

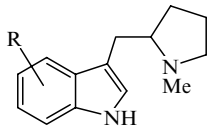

84

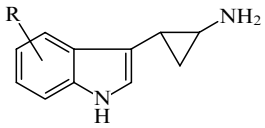

85

It is of note that conformationally rigid serotonin analogues containing cyclopropane fragments (**85**) in their side chains are somewhat more selective towards 5-HT_{2C} receptors, the fluoro derivative (**85**, R = 5-F) being the most active compound.[153,154] Noteworthy, the electron-withdrawing fluorine atom in the benzene ring not only decreases the affinity of this compound for 5-HT_{1A} receptors (see above) but also seems to be responsible for higher selectivity towards 5-HT_{2C} receptors in comparison with 5-HT_{2A} receptors. A similar dependence was demonstrated for other fluorotryptamines.[155]

The agonists manifesting higher selectivities towards 5-HT_{2C} subtype receptors were identified among halogeno derivatives of other structural classes, *e.g*., of piperazine. The diamine **86**, a partial agonist of 5-HT_{2C} receptors, which possesses 10-fold lesser affinity for 5-HT_{2A} receptors, is the most popular among them.[48,156–159] Structural variations in its molecule revealed that substitution of the pyrazine ring for the benzene ring increased significantly its selectivity and intrinsic activity; thus, the affinity of compound **87**,[160,161] a full agonist of 5-HT_{2C} subtype receptors, is 25 times higher than for 5-HT_{2A} subtype receptors.

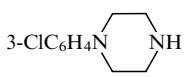

86

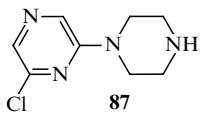

87

Agonists of 5-HT_{2C} receptors have recently been identified among indole derivatives manifesting high selectivities towards 5-HT_{2A} subtype receptors. Earlier, it was found[162] that isotryptamines (**88**) with the 2-aminopropyl side chain attached to the nitrogen atom are bioisosteric to the corresponding tryptamines as regards their binding to serotonin receptors. Affinity studies of a series of isotryptamines **88** and their analogues, *viz*., indenopyrroles **89**, revealed[155] that many of them, *e.g*., compounds **88a**,**b** and **89a**,**b**, are high-affinity full agonists of 5-HT_{2C} receptors which are 20- to 100-fold more selective towards 5-HT_{2A} receptors. It is noteworthy that the selectivities of *S*-isomers are higher than those of the corresponding *R*-isomers.[155] It should be noted that tryptamine structural isomers of some of these derivatives manifest nearly identical affinities but much lower selectivities with respect to 5-HT_{2C} receptors.

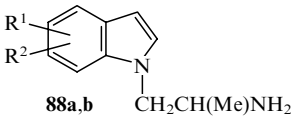

88a,**b**

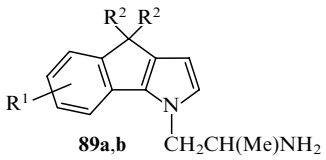

89a,**b**

R^1 = 5-F: R^2 = H (**a**), 6-Cl (**b**). R^1 = 7-OMe: R^2 = H (**a**), Me (**b**).

Phenylisopropylamines **90a** and phenylethylamines **90b** [163–165] which constitute a large group of high-affinity 5-$HT_{2A/2C}$ receptors have been the subjects of in-depth studies into the structure–activity relationships aimed at establishing the topologies of the binding sites of this particular subtype of serotonin receptors (see, *e.g.*, Refs 166–169). These studies demonstrated that high affinities for 5-$HT_{2A/2C}$ receptors require that certain structural requirements are fulfilled, such as the presence of a two-carbon chain between the amino group and the phenyl ring, the presence of methoxy groups in positions 2 and 5 of the aromatic ring and the presence of the hydrophobic substituent X in position 4. Assuming that the methoxy groups in compounds **90a**,**b** bind to two serine residues in the receptor protein, Nichols *et al.*[166,170] synthesised the cyclic derivatives **91**–**94** in order to study the geometry of this binding. It was found that compound **91** having a '*syn*-conformation' of the tetrahydrofuran ring relative to the aminoalkyl chain is practically inactive towards 5-$HT_{2A/2C}$ receptors, whereas the activity of the analogous compound **92** with the '*anti*-orientation' of these fragments is as active as that of the acyclic analogue **90a**.

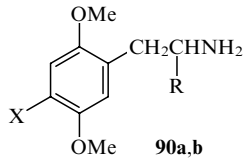

90a,**b**

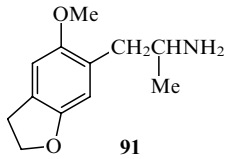

91

R = Me (**a**), H (**b**);
X = Alk, Hal, AlkS, F_3C *etc*.

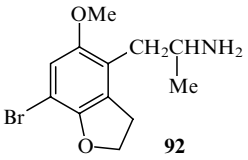

92

Substitution of the oxygen-containing heterocycle for the methoxy group in position 2 produces an opposite effect, *viz*., the '*anti*-analogues' of the type **93** compounds are inactive, whereas compound **94** is a potent agonist. As expected, structurally rigid compounds, *e.g*., compound **95** with two dihydrofuran fragments mimicking effectively active binding conformations of the methoxy groups in compounds **90a**,**b**, appeared to be high-affinity agonists of 5-$HT_{2A/2C}$ receptors. In this case, benzodihydrofuran-containing compounds represent effective conformationally restricted bioisosteres of aromatic methoxy groups.[169]

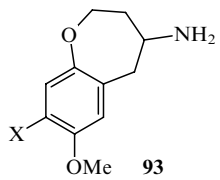

93

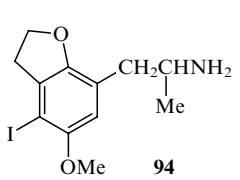

94

Substitution of furan fragments (see, *e.g*., compound **96**) [169] for dihydrofuran fragments made it possible to enhance also the agonistic activity with respect to 5-$HT_{2A/2C}$ receptors by an order of magnitude. Compounds of the type **96** manifest the highest affinities among other known ligands. Unfortunately, none of these compounds discriminate between 5-HT_{2A} and 5-HT_{2C} subtype receptors; the affinities of these compounds for 5-HT_{2B} receptors are severalfold lower because of similarities of the binding domains of the corresponding receptors.

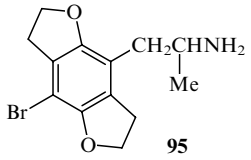

95

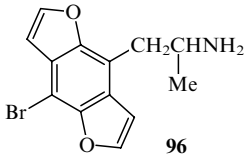

96

The attempts to lock the geometry of the aminopropyl side chain in compounds **90a**,**b** showed that its incorporation into the aminotetralin or the aminoindan rings results in the loss of activity towards 5-$HT_{2A/2C}$ receptors, whereas its introduction into the side chain of the cyclopropane ring, as in *trans*-2,5-dimethoxy-4-methylphenylcyclopropylamine, enhances the activity.[154,171]

As can be seen from the above survey, the structural classes of 5-HT_2 agonists are not very diverse and their design is poorly documented in the literature. This can probably be attributed to the strong hallucinogenic effect of these agonists,[172] which makes them unsuitable as therapeutics. Antagonists of 5-HT_2 subtype receptors can be used as drugs in treatment of ischemia and other vascular disorders.[173]

So far, several structural classes of 5-HT_2 antagonists have been identified. The most prominent position is occupied by ergolines and related compounds which manifest the properties of partial agonists or antagonists with respect to the corresponding receptors [174] [the former include the classical hallucinogenic agent, *viz*., lysergic acid diethylamide (LSD, **97**)].[174–176] Numerous antagonists of 5-HT_2 receptors have been synthesised based on ergolines and related compounds; the main strategy consisted in the introduction of various substituents [most frequently, at C(8)] assuming that this might enhance the antagonistic activity due to their additional binding to the receptor. This resulted in potent 5-HT_2 antagonists, such as compounds **98**,[177,178] **99a**–**c**, *etc*.[176,179–182]

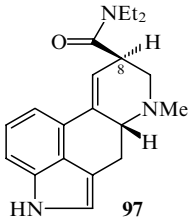

97

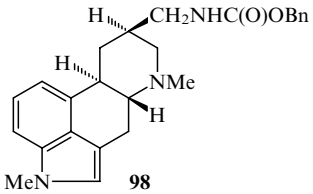

98

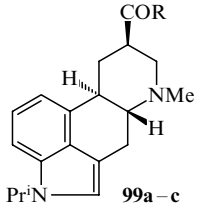

99a–**c**

R = O–⟨⟩–OMe (**a**), HN–⟨⟩ (**b**), HO–⟨⟩–HN (**c**).

Subsequent computer simulation of the binding of ergolines to 5-HT_2 receptors [174] showed that the presence of an aromatic ring in the vicinity of phenylalanine-340 of the receptor is an essential structural feature which ensures high-affinity binding owing to π- or hydrophobic interactions. This prompted synthesis of a series of ergolines and related compounds of the type **100a**,**b** devoid of the acyl fragment at C(8). Indeed, the resulting compounds manifested high affinities for 5-HT_2 antagonists and high selectivities as regards other subtypes of serotonin receptors. Thus, the ergoline structure of 5-HT_2 antagonists can in principle be reduced to a simple tetracyclic indoloquinoline system without any detriment to the affinity and antagonistic activity.[182]

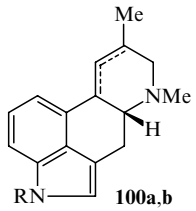

100a,b

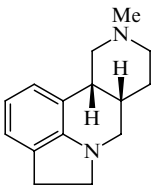

101

R = H (**a**), Pr^i (**b**).

Other structural modifications of ergoline analogues included variations of substituents at the nitrogen atom of the indole moiety. It was shown that the introduction of small alkyl substituents, including branched ones, into this position is possible.§ In some cases, the antagonistic activity is enhanced due to the presence of a double bond in positions 9 and 10 present also in lysergic acid.[182] The literature data on the role of substituents in position 4 of the cyclohexane ring are controversial: in some cases, the methoxy group at C(4) of the cyclohexane ring significantly enhances the antagonistic activity,[187] but has no effect in other cases.[182]

The majority of ergoline derivatives are active with respect to serotonin 5-HT_1, adrenergic and other receptors, but are non-selective towards 5-HT_2 subtype receptors. However, recent systematic screening of ergoline-related compounds disclosed the naphthyridine (**101**),[188–190] a highly selective antagonist of 5-$HT_{2B/2C}$ receptors which does not interact with 5-HT_1 receptors. This compound will probably serve as a prototype for the design of novel selective ligands.

Distant analogues of the long-known non-selective ligand **102**,[191,192] such as ketanserin (**103**)[193,194] and its derivatives which manifest certain selectivities towards 5-HT_{2A} receptors, constitute another large structural class of 5-HT_2 antagonists.[191,192] Ketanserin (**103**) is used in the clinical practice as an antihypertensive drug.

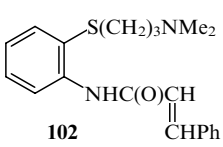

102

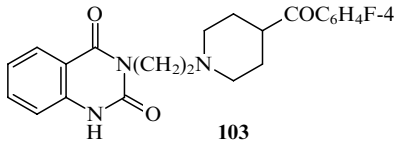

103

Studies of the structure–activity relationships in ketanserin derivatives have revealed the following features. The carbonyl group in position 2 of quinazoline can be replaced by the thiocarbonyl group, and a phenolic hydroxy group can be introduced into position 6. The two-carbon side chain can be replaced by the $(CH_2)_4$, but not by the $(CH_2)_3$ chain, which decreases the activity 100-fold.[195] Piperidine ring-opening also decreases the affinity. Although the 4-fluorobenzoyl group is present in the majority of ketanserin analogues, it can be replaced by the benzylidene [as in the case of ritanserin (**104**)] or a similar group. However, the benzylic carbon atom should be sp^2-hybridised [*cf.* the carbonyl group in ketanserin (**103**) or the double bond in ritanserin (**104**) and risperidone (**105**)]. Although a certain role in the affinity for 5-HT_{2A} receptors is played by the quinazoline-2,4-dione fragment,[195] this may be replaced by the pyridopyrimidine or thiazolopyrimidine fragment[196] or structurally simplified, as in compound **106**.[197] The latter modification is more appropriate because it affords 120-fold enhancement of selectivity towards 5-HT_{1C} receptors for which ketanserin manifests high affinity. It is of note that some ketone **106** analogues having a shortened bridging chain, *e.g.*, compound **107**,[198] are also potent selective antagonists of 5-HT_2 receptors. However, none of the above-mentioned compounds distinguish among different subtypes of 5-HT_2 receptors.

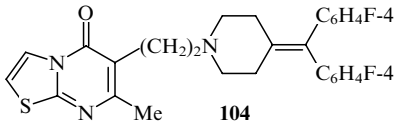

104

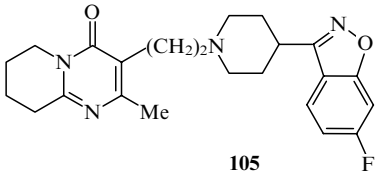

105

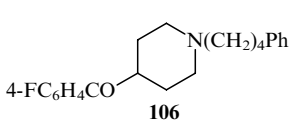

106

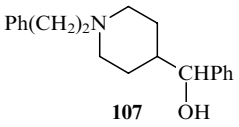

107

Variations in the quinazolidinedione fragment of ketanserin analogues have led to a large family of 5-HT_2 antagonists, *viz.*, triazaspirodecanones; their classical representative is spiperone (**108**).[197,199] This compound manifests rather high affinity for dopaminergic and 5-HT_{1A} receptors, and is also one of the few ligands binding more selectively (*ca.* 1000-fold) to 5-HT_{2A} subtype receptors than to 5-HT_{2C} subtype receptors.

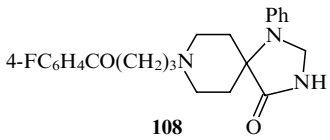

108

Molecular 'dissection' of this compound into its two basic fragments revealed that 1,3,8-triazaspirodecanone (**109**) is absolutely inactive towards 5-HT_1 and 5-HT_2 receptors, while the piperidine derivative **110** (R = H) manifests moderate affinity for 5-HT_{2A} receptors, which is 150-fold lower than that of spiperone (**108**), but is inactive towards 5-HT_1 and 5-HT_{2C} receptors. The introduction of the anilino group into position 4 of piperidine (**110**, R = NHPh) increases its affinity for 5-HT_{2A} receptors; however, the resulting compound manifests 150-fold lower selectivity towards 5-HT_{2C} receptors than spiperone (**108**).[200] These findings are suggestive of the important role of the imidazolidinone fragment in the reactivity and selectivity of spiperone (**108**). This conclusion is corroborated by the fact that the spiperone derivatives **111** containing geminal amino groups and an amide group instead of an imidazolidine ring are less selective towards 5-HT_{2A} receptors. Moreover, the affinities of some spiperone analogues decrease dramatically after the removal of the lactam carbonyl group, which points to its significance for the binding to the receptor.

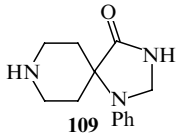

109

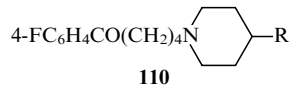

110

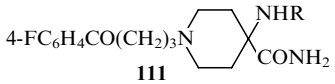

111

Other modifications of the spiperone (**108**) structure showed that substitution of the cyclohexyl fragment for the phenyl substituent at the N(1) atom increases its affinity twofold, whereas the substitution of alkyl groups decreases it. However, the

§ It should be noted that ergolines non-substituted at N(1) manifest higher affinities for human 5-HT_2 receptors than for the corresponding rat receptors,[183,184] although the only structural difference between these receptors is associated with the amino acid 242 residue (serine in humans and alanine in rats).[185,186] Presumably, serine and the NH group of indole in non-substituted ergolines form a hydrogen bond, whereas hydrophobic interactions occur between alanine and the alkyl group of the substituted ergolines.

selectivity towards 5-HT_{2A} subtype receptors increases in comparison with 5-HT_{2C}, 5-HT_{1A} and dopaminergic receptors.[201] Contrariwise, analogous substituents at the N(3) atom significantly decrease the selectivity.[201,202] It was shown also that the carbonyl group in the spiperone (**108**) molecule may be replaced by the ether group (compound **112**) with the preservation of activity and a small increase in the selectivity towards 5-HT_{2A} receptors in comparison with 5-HT_{2C} receptors. Such analogues can further be used as new structural prototypes in the search for affinity ligands to 5-HT_{2A} receptors.[200,201]

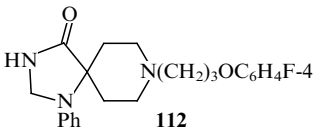

112

The sulfonylamide derivative **113** assayed recently among spiperone analogues (**108**) is attractive, because unlike compound **108** it manifested antagonistic activity and 100-fold higher selectivity towards 5-HT_{2C} receptors in comparison with 5-HT_{2A} and 5-HT_{2B} receptors. Moreover, this compound virtually did not bind to other serotonin receptors.[203,204]

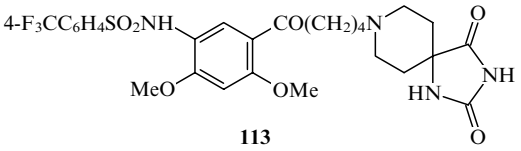

113

Progress has also been achieved in the design of selective antagonists of 5-HT_{2B} receptors. It was found that the indole derivative **114** manifests 150-fold higher affinity for 5-HT_{2B} receptors than for 5-HT_{2A} receptors, but is non- selective with respect to 5-HT_{2C} receptors.[205] The selectivity to the latter was virtually unenhanced upon partial restriction of conformational mobility of the linking chain (compound **115**); however, this approach makes it possible to increase the affinity for 5-HT_{2B} receptors and to decrease the affinity for 5-HT_{2A} receptors. A highly selective antagonist of 5-HT_{2B} receptors was obtained by substitution of the methylisothiazole fragment for the pyrimidine fragment (**114** → **116**), but the activity of the resulting compound is not very high.[206,207]

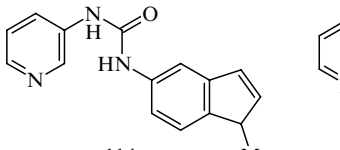

114

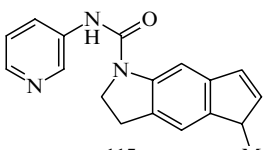

115

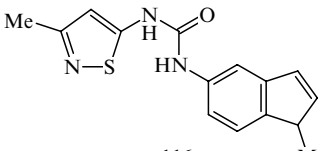

116

More active and selective (with respect to 5-HT_{2B} receptors) compounds were prepared based on the alkaloid yohimbine (**117**), which exhibits low affinity for this type of receptor itself. Elucidation of the key elements essential for the antagonistic activity of this alkaloid towards 5-HT_{2B} receptors was carried out by sequential simplification of its structure, resulting in high-affinity derivatives **118** and **119**. The affinities of these compounds and some of their analogues for 5-HT_{2B} receptors were 100–200-fold higher than for 5-HT_{2A} and 5-HT_{2C} receptors; these were practically inactive with respect to adrenergic receptors (in contrast to the original alkaloid **117**).[173] Structure–activity studies revealed an unusual and interesting fact, namely, it was found that the introduction of the methoxy substituent into position C(6) of compound **118** [which corresponds to position C(5) of the serotonin molecule] decreases the affinity, whereas the introduction of two methyl substituents into positions C(7) and C(8) increases it to a unique extent.[173] This suggests that the direct structural analogies of serotonin and the corresponding fragments of compounds **118** and **119** do not reflect their actual orientation during their binding to the receptor and demands further investigation.

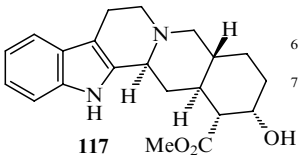

117

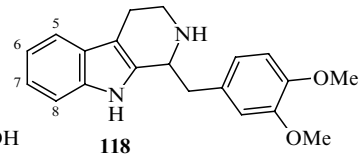

118

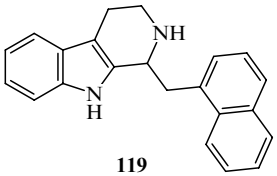

119

A new structural class of 5-HT_2 antagonists based on 5-HT_{2A} agonists of the type **90a** has recently been found. Compound **90a** (X = $CH_2CH_2CH_2Ph$) containing a phenylpropyl substituent in position 4 has become the first representative of this class. Structure–activity studies of some of its analogues established a surprising fact, *viz*., that the presence of methoxy groups in the ring is not a necessary prerequisite for their high affinities. However, this feature holds only for antagonists (for agonists, see above). This indicates that the phenylpropyl substituent can change the binding profile to the receptor.[165,208] Further developments in this field can be expected in the nearest future.

And finally, there exists a vast class of compounds manifesting nearly identical antagonistic activities towards serotonin 5-HT_2 and dopamine receptors which can be used as efficient antischizophrenic drugs. The neuroleptic drug clozapine (**120a**) is a classical representative of these compounds.[165,209,210] This possesses somewhat higher selectivity towards serotonin receptors of the 5-HT_{2A} subtype, whereas its desmethyl derivative **120b** manifests higher affinity for 5-HT_{2C} receptors.[211,212] A large number of their presently known analogues comprise a lipophilic tricyclic system,[213] which may contain additional heteroatoms (*e.g*., compound **121**) or be devoid of them (*e.g*., compound **122**).[214,215] Tetracyclic analogues such as mianserin (**123**) are also known.[216,217] A detailed survey of the work devoted to the design of compounds similar to compounds **120**–**123** or mixed-type antipsychotic drugs belonging to other structural classes is beyond the scope of the present review, which considers only compounds selective towards serotonin receptors.

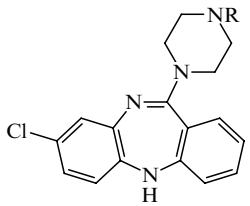

120a,**b**

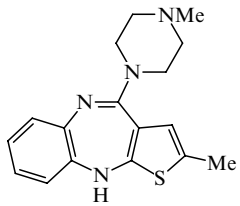

121

R = Me (**a**), H (**b**).

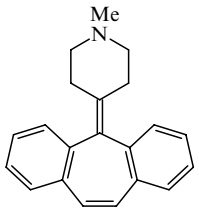

122

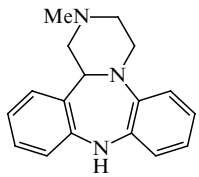

123

It should be stressed that the selectivities of antagonists towards serotonin 5-HT_2 receptors as opposed to dopaminergic (D_2) receptors are difficult to achieve. This problem was the central issue in special studies aimed at comparative structural analysis of binding sites of both types of receptors (see, *e.g.*, Ref. 218). Although the structural requirements for the affinities of both receptors are very close, they have certain steric differences, which makes it possible to predict the selectivities of various compounds to 5-HT_2 receptors.

To conclude this chapter, it should be emphasised that the search for 5-HT_2 ligands employed mainly simple screening procedures, without recourse to computer simulation or pharmacophore hypotheses. Nevertheless, the design of such ligands entails efficient structural approaches. Moreover, the use of pharmacophore and receptor models developed in the last few years and modern QSAR methods [174, 218, 219] leaves hope that progress in this area will finally be achieved.

VII. Ligands of serotonin 5-HT_3 subtype receptors

Receptors of the 5-HT_3 subtype are the only serotonin receptors that form ion channels penetrable for monovalent cations and calcium ions. The ligands interacting with this type of receptor have been in the focus of attention in the past decade, primarily in connection with the design of antagonists, some of which proved to be efficient antiemetic drugs. Antagonists of 5-HT_3 receptors can also be used for the treatment of schizophrenia and other mental disorders. The putative therapeutic role of 5-HT_3 agonists is based on their ability to control the release of the neuromediator acetylcholine in the brain, which makes these compounds promising for the treatment of neurodegenerative diseases associated with cholinergic transmission disturbances. In addition, 5-HT_3 agonists can be used as antidepressant and analgesic drugs.

Since the mechanism of signal transmission by 5-HT_3 receptors is different from those of other serotonin receptors, its ligands often possess unique structures and manifest high selectivity. Thus quaternary amines of the type *N*,*N*,*N*-trimethyl-5-hydroxytryptamine do not bind to any other subtypes of serotonin receptors.

Agonists of 5-HT_3 receptors have been studied less thoroughly than their antagonists and are less numerous. The most well-known of them is 5-hydroxy-2-methyltryptamine (**124**) which possesses lower affinity than serotonin but much higher selectivity towards 5-HT_3 subtype receptors and preserves simultaneously agonistic activity.[145, 220, 221]

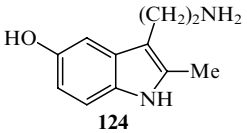

124

The other two structural groups of 5-HT_3 subtype agonists include arylpiperazines and arylbiguanides; their classical representatives are quipazine (**125a**) [222, 223] and 1-phenylbiguanide (**126**, R = H).[224] These compounds had been neglected for a long time, apparently because of the high selectivity but low affinity of phenylbiguanide for 5-HT_3 receptors. At the same time, arylpiperazines of the general formula **127** display higher affinities for 5-HT_2 receptors but are less selective and are active with respect to a vast variety of other serotonin receptors (see above). The number of publications devoted to the design of arylpiperazine and arylbiguanide analogues has increased markedly over the past decade; studies in this field were designed to increase the affinities of arylbiguanides and the selectivities of arylpiperazines.

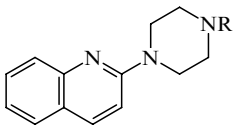

125a,**b**

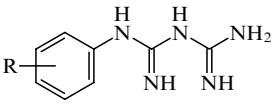

126

R = H (**a**), Me (**b**).

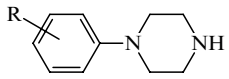

127

For the first trend, the key hypothesis was that both classes of compounds occupy the same aromatic binding site on 5-HT_3 receptors; therefore, the structure–activity dependences for arylpiperazines **127** can be extrapolated to arylbiguanides. The main structure–activity regularity for arylpiperazines **127** is that the chlorine atom in the *m*-position of the benzene ring is the only substituent (R) studied which produces a significant increase in affinity. This cannot be replaced by any other electron-withdrawing substituent (*e.g.*, CF_3). Substitution of the naphthyl substituent (compound **128a**) for the phenyl substituent, the introduction of the nitrogen atom into the benzene or the naphthalene fragment (compound **128b**) and the conversion of the NH group of piperazine into an exocyclic amino group (compound **129**) also affords high-affinity compounds.[225–227] It should be noted that the majority of these compounds manifest pronounced antagonistic activities and behave as partial agonists.¶

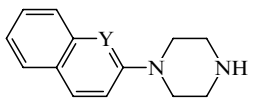

128a,**b**

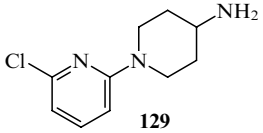

129

Y = CH (**a**), N (**b**).

In contrast, all the arylbiguanide derivatives under study are full agonists of 5-HT_3 receptors and manifest high selectivities towards them. As in the case of piperazine compounds, the introduction of the chlorine atom into the *m*-position affords the high-affinity compound **126** (R = 3-Cl), and 2-naphthylbiguanide binds 100 times more effectively than 1-phenylbiguanide.[229–233] These data unambiguously demonstrate the validity of the hypothesis about the similarity of binding profiles (or binding sites) of arylpiperazines **127** and arylbiguanides **126**. It is of note that the affinities of 3-chlorophenyl- (**130**) and 2-naphthylguanides (**131**) which also act as 5-HT_3 receptor agonists manifest the highest (by one or two orders of magnitude) affinities among other structurally related arylguanides [233] and can thus be regarded as representatives of a new structural class of serotonin receptor agonists.

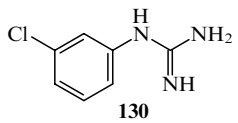

130

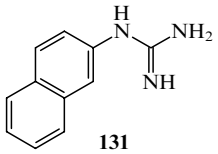

131

Investigations into the increase in the selectivities of arylpiperazines towards 5-HT_3 receptors have led to the synthesis of a vast variety of effective ligands endowed with a broad range of intrinsic activities, *viz.*, from full agonists to full antagonists. In the majority of studies, quipazine (**125a**) was used as the structural lead; its simplest modifications showed that the *N*-methyl analogue **125b** [225] manifests nearly identical affinity for 5-HT_3 recep-

¶ Some arylpiperazine derivatives manifest complex activity profiles with respect to 5-HT_3 subtype receptors. Thus the intrinsic activity of quipazine (**125a**) depends on the type of the cells comprising these receptors. It was shown that quipazine behaves as an agonist for some of these receptors and an antagonist for other receptors.[228]

tors but does not bind to 5-HT_{1B} receptors (according to more recent data, the *N*-methyl substituent is the most suitable substituent for many quipazine analogues [234]).

Earlier, it was shown that the 5-HT_{1B} receptor ligand **57** which contains a pyrrole ring and is inactive towards 5-HT_3 receptors acquires high affinity for these receptors upon removal of the trifluoromethyl group. Therefore, a vast majority of studies aimed at modification of the quipazine structure include the introduction of a condensed pyrrole ring into the quinoline system.[234–236] Among compounds of the general formula **132**, the derivatives manifesting the highest affinities for 5-HT_3 receptors possess the properties of partial (R^1 = H, 6-, 7- or 9-F; R^2 = H, Alk, CH_2 = $CHCH_2$) and full (R^1 = 9-Me, R^2 = Me; R^1 = 7-OH, R^2 = Me) agonists, the latter being the strongest 5-HT_3 agonists presently known.[237]

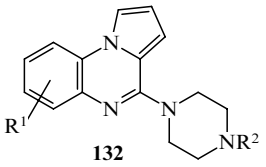

132

The introduction of lipophilic groups into the quipazine molecule yields the derivatives **133**–**135**, which behave as antagonists of the corresponding receptors or partial agonists endowed with low intrinsic activities, *e.g.*, compound **136**.[228]

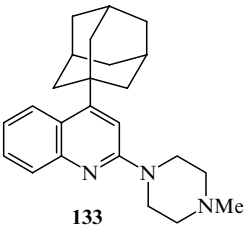

133

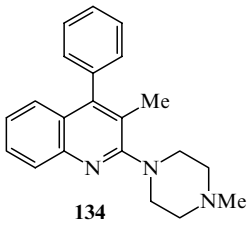

134

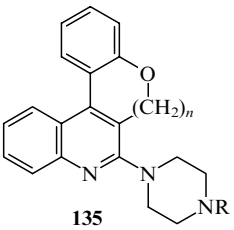

135

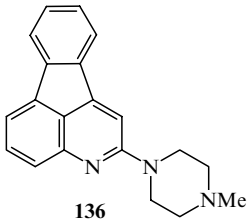

136

n = 0–2, R = H, Alk.

QSAR studies of quipazine derivatives containing various heteroaromatic fragments revealed several compounds (*e.g.*, compounds **137**–**139**) manifesting high activities, high selectivities and different intrinsic activities with respect to 5-HT_3 receptors. Thus compound **137** is the partial agonist, compound **138** is the antagonist, while compound **139** is the agonist of the corresponding receptors.[238]

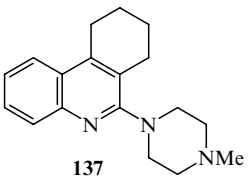

137

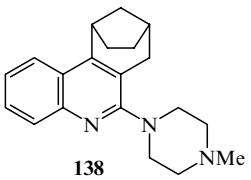

138

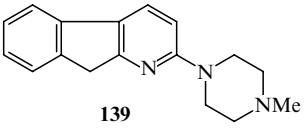

139

This finding was used in the design of a binding model of quipazine derivatives (both agonists and antagonists) to 5-HT_3 receptors.[238, 239] According to this model, the high-affinity interaction with the receptor involves the formation of a hydrogen bond between the protonated terminal nitrogen atom of piperazine and the carboxylate anion of the amino acid residue in 5-HT_3 receptors (there is conformational restriction for the bulk of the substituent at this nitrogen atom), the formation of a hydrogen bond between the nitrogen atom in the heterocycle and the corresponding hydrogen bond donor in the receptor and, finally, the specific interaction between the aromatic ring and the corresponding amino acid residue of the receptor (there is a size restriction of substituents in the region of aromatic ring fusion). Presumably, the first two interactions make a weighty contribution to affinity.[240] Moreover, favourable van der Waals interactions which are supposed [238] to be critical for the modulation of intrinsic activities with respect to 5-HT_3 receptors (*cf.* structures **137**–**139**) can be triggered in that domain of the receptor molecule which corresponds to the quinoline fragment. However, the structural determinants responsible for the intrinsic activities of quipazine derivatives are in fact more complicated, since the changes in their activities can be provoked even by any apparently insignificant changes in the heterocyclic backbone of quipazine. Thus compounds **140a**,**b** which contain neither bulky, nor lipophilic substituents in their nuclei behave nevertheless as 5-HT_3 antagonists.[240, 241]

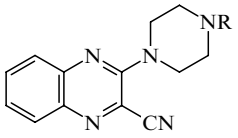

140a,**b** R = H (**a**), CH_2 = $CHCH_2$ (**b**).

QSAR studies aimed at the search for effective 5-HT_3 agonists and antagonists based on quipazine give an insight into the molecular fragments essential for the strong binding of the ligands to the receptors and allow the prediction of novel high-affinity compounds. However, elaboration of structural requirements for their agonistic and antagonistic activities is hardly possible without detailed computer simulation studies.

As indicated above, the main progress in the design of 5-HT_3 ligands is associated with the synthesis of its selective antagonists some of which have already found application in clinical practice. The majority of 5-HT_3 antagonists represent aryl- or hetarylamide derivatives. We shall briefly summarise the main concepts and results of structure–activity studies of 5-HT_3 antagonists with special emphasis on the latest data.

The first potent and selective 5-HT_3 antagonists prepared were based on the non-selective dopamine receptor ligand metoclopramide (**141**), which had long been used as an antiemetic drug. Studies from the early 1980's showed that metoclopramide and some cocaine (**142**) analogues manifest relatively weak antagonistic activities towards one of the serotonin subtype receptors [242] further identified as 5-HT_3.[243] This activity is responsible for the antiemetic effect of metoclopramide. Further modifications of metoclopramide structure as well as of the structures of analoguous and lead compounds consisted in conformational restriction of the side chain, modification of the amide fragment and substitution of an oxygen-containing ring for the *o*-alkoxy group.

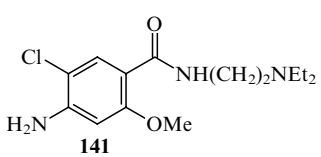

141

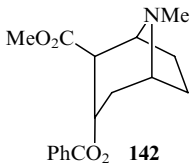

142

The introduction of the quinuclidine residue into the side chain of metoclopramide (**141**) afforded zacopride (**143**), which is a potent selective antagonist of 5-HT_3 receptors.[244, 245] Modifications including the introduction of a tropane fragment and variations of substituents in the ring give compound **144a** which is also a potent selective antagonist of this subtype of receptors.[246] Its analogue **144b** containing two methyl groups possesses virtually the same activity. It should be noted that side chain

modifications included the variations in its 'mobile' fragment. Thus phenylurea derivatives containing an alkoxy group in the *o*-position (*e.g.*, compound **145**) manifested high antagonistic activities.[247]

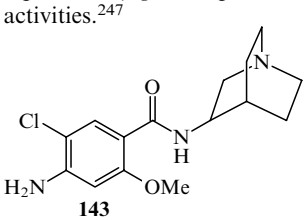

143

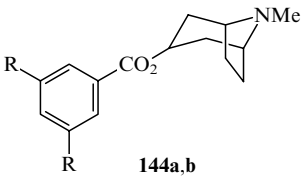

144a,b

R = Cl (**a**), Me (**b**).

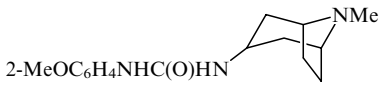

145

The benzene ring of these compounds was subjected to structural modification. Thus substitution of the indole ring for the disubstituted benzene ring in compounds **144a,b** which affords tropisetron (**146**) [144] significantly increases the affinity. A similar effect is observed upon the replacement of the aryl substituent in the urea derivative **145** by hetaryl substituents (compounds **147** and **148**).[248, 249]

Tropisetron (**146**) is a selective 5-HT_3 ligand used in clinical practice as an antiemetic drug, like its more active structural analogue granisetron (**149**) containing a 9-azabicyclo[3.3.1]nonane residue in the side chain.[250]

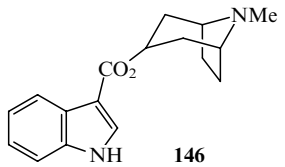

146

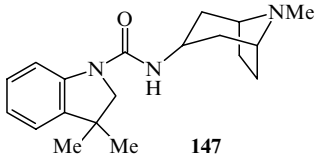

147

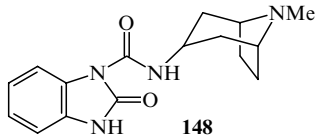

148

Modification of the 'mobile' fragment of the side chain resulted in the ketoamide (**150**), a high-affinity and selective 5-HT_3 ligand although manifesting the properties of a partial agonist.[251]

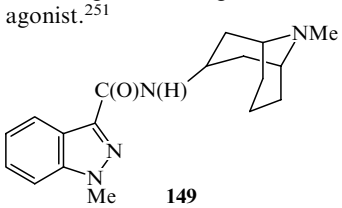

149

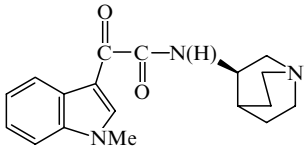

150

It is of note that these modifications were carried out together with the search for effective 5-HT_3 ligands among indole derivatives. Thus compounds **151** and **152** containing an imidazole fragment in their side chains were synthesised [252] and ondansetron (**153**),[253] the conformationally rigid analogue of compound **152**, a potent selective antagonist of 5-HT_3 receptors. Ondansetron (**153**) is the most well-known 5-HT_3 antagonist widely used as an antiemetic drug in combined therapy of tumour diseases.[254]

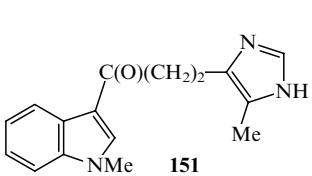

151

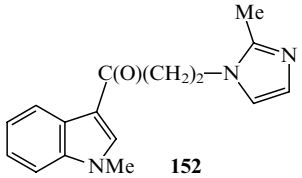

152

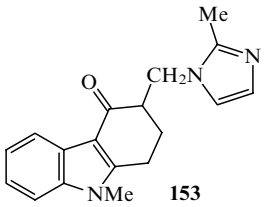

153

A modification of the amide group of metoclopramide (**141**) included the formation of the benzotriazine fragment (compound **154**). Since this modification increases the activity in comparison with the 'open' analogues of the type **155**, it is assumed that the active conformation of benzamides in the 5-HT_3 receptor should involve a planar arrangement of the carbonyl group.[255] Similar results were obtained for a series of ondansetron analogues (**153**) in which ketones fused to the indole fragment were 4 times as active as the non-cyclic analogue **152**.[255]

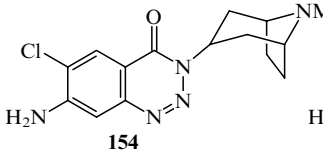

154

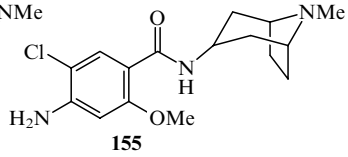

155

Yet another version of cyclisation is the incorporation of an amide group into a new ring in the side chain. The idea of this transformation stems from bioisosterism of benzamide and phenylimidazolidin-2-one fragments. Comparison of the structures of metoclopramide (**141**) and the dopamine receptor antagonist zetidoline (**156**) prompted an idea about the introduction of azabicyclic or other equivalent structural fragments of 5-HT_3 antagonists into the phenylimidazolidinonalkyl group. Indeed, several high-affinity antagonists of the 5-HT_3 receptor were identified among a series of compounds of the general formula **157**, and a compound with $R^1 = R^3 = R^6 = R^7 = H$, $R^2 = R^4 = Cl$, $R^8 = Me$ is characterised by unusually high affinity.[256] It should be noted also that the indole derivative **158** containing an oxadiazole residue mimicking the amide group instead of the bicyclic substituent is a specific antagonist of 5-HT_3 receptors.[257]

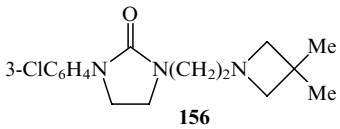

156

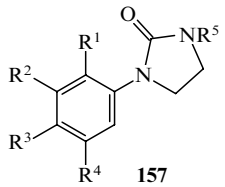

157

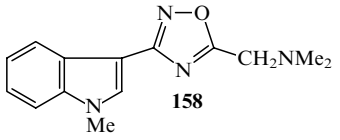

158

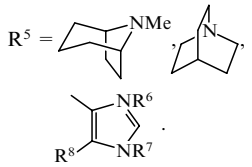

Substitution of a fused oxygen heterocycle for the *o*-alkoxy group is also a modification of the metoclopramide (**141**) structure. This modification resulted in several high-affinity selective 5-HT_3 antagonists, *e.g.*, the quinuclidine derivative **159** [258, 259] and zatosetron **160**.[260] In all these cases, the presence of the chlorine atom is a necessary prerequisite for the high activities of these compounds.

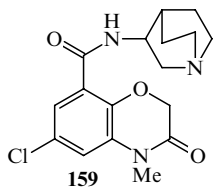

159

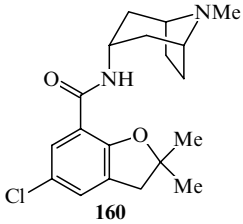

160

Many pharmacophore models have been suggested for 5-HT_3 antagonists. The differences between them originate from different models and different 5-HT_3 ligands used in their development. Critical analysis of five pharmacophore models [247, 248, 251, 261–263] disclosed the following essential components required for manifestation of high affinity, *vis*., the presence of an aromatic ring, the carbonyl group directly attached to the aromatic ring and a basic amine. The aromatic ring can represent a structural element of benzoate, benzamide, indole or imidazole fragments. As mentioned above, the carbonyl group can be replaced by an equivalent bioisosteric group, *e.g*., the 1,2,4-oxadiazole or the imidazolidin-2-one fragment. The presence and accessibility of the amine nitrogen plays a significant role in certain models,[261–263] although the details of this binding are still unknown.[264] It should be stressed, however, that some antagonists (*e.g*., compound **157**) do not fit into these structural models. The lack of correlation brought forth the necessity for modification of the binding profile of the receptor, *viz*., two additional hydrophobic binding sites were identified in the domain surrounding the aromatic ring.[257, 265] Pharmacophore models have proved to be a useful tool for the rational design of 5-HT_3 antagonists. Thus these models were used to predict high affinities of 3-aminopyridazines **161** and **162** containing a piperazine fragment for 5-HT_3 receptors.[265]

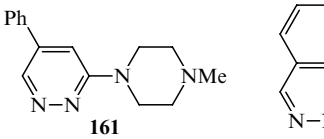

161

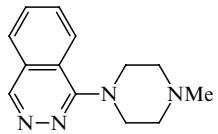

162

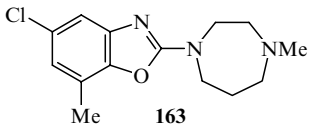

163

It should finally be noted that the number of publications devoted to the design of 5-HT_3 antagonists has presently lessened, presumably due to progress already achieved in this area. Nevertheless, the search for novel structural classes of 5-HT_3 antagonists is a vital problem in the endeavour to go far beyond the scope of tryptamine, metoclopramide and arylpiperazine derivatives. In novel compounds, such as compound **163** containing a seven-membered ring, modifications involve the same fragments. Compound **163** is a high-affinity partial agonist of 5-HT_3 receptors with low intrinsic activity.[266, 267]

VIII. Ligands of serotonin 5-HT_4 subtype receptors

Serotonin 5-HT_4 subtype receptors were discovered in the late 1980's and cloned in 1995;[268] their molecular structures and some functional characteristics have not been described until very recently.[269] Various therapeutic applications for their agonists and antagonists, *e.g*., in the treatment of intestinal disorders, arrhythmias and diseases associated with the loss of the cognitive ability, are based on the localisation of this receptor in gastrointestinal tract, atrium and urinary bladder tissues as well as in the central nervous system.

Some non-selective antagonists of serotonin receptors, mostly of 5-HT_3 receptors, *e.g*., metoclopramide (**141**), possess partial agonistic activities towards 5-HT_4 receptors. Therefore, metoclopramide (**141**) and its ester analogue **164**[270] manifesting the properties of a weak antagonist and 30-fold selectivity towards 5-HT_4 receptors than to 5-HT_3 receptors were used as the lead compounds in the design of more selective 5-HT_4 ligands.

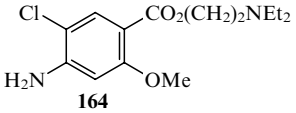

164

The general scheme of the design of these ligands resembles in many features that for 5-HT_3 antagonists and includes, in the first place, different versions of restriction of conformational mobility and modification of the amine side chain. The agonist **165**[271] and the antagonist **166** (a quaternised butyl analogue of renzapride (which is a partial agonist of the 5-HT_3 receptor) were among the first compounds manifesting somewhat higher selectivity towards 5-HT_4 receptors in comparison with 5-HT_3 receptors. This modification is based on a significant decrease in the activities of quaternary salts of 5-HT_3 antagonists with substituents bulkier than the methyl group at the nitrogen atom.[272, 273] Special mention should also be made of the original macrocyclic benzamide (**167**) which represents a partial agonist twice as selective towards 5-HT_4 receptors as towards 5-HT_3 receptors, which does not interact with other receptors.[274]

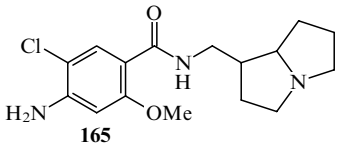

165

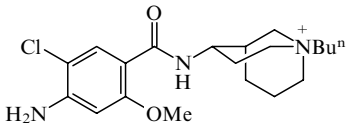

166

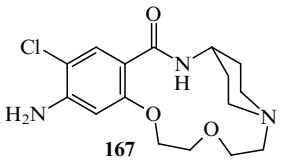

167

The close structural analogues of compound **164**, *viz*., the piperidine derivatives **168** and **169a**,**b**, are potent selective partial agonists of 5-HT_4 receptors (their intrinsic activities are 50% – 60%).[275–277] The classical approach to decrease the intrinsic activity of compound **169b** by introducing bulky lipophilic substituents proved to be successful. Thus the derivative **169c**[275, 278] manifests high antagonistic activity and 100-fold higher selectivity towards 5-HT_4 receptors than towards other serotonin receptors. It is of note that the changes in the structural activity of compound **168** from the agonistic to the antagonistic one is achieved by less significant structural modification, *viz*., through the introduction of two methyl groups into positions 3 and 5 of the piperidine ring. For the derivative **169a**, the decrease in the intrinsic activity is achieved through structural simplification, whereas the analogue **170** containing an additional carbon atom in the side chain but devoid of the lipophilic butyl substituent is a full 5-HT_4 antagonist manifesting high affinity and noticeable selectivity.[279, 280]

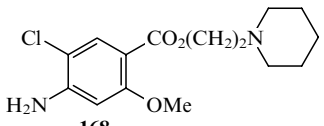

168

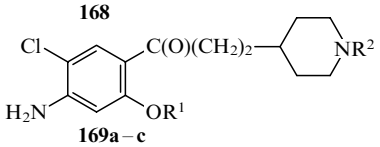

169a–c

R^1 = Me: R^2 = Bu (**a**), $(CH_2)_2NHSO_2Me$ (**b**); R^1 = $CH_2C_6H_3(OMe)_2$-3,5, R^2 = $(CH_2)_2NHSO_2Me$ (**c**).

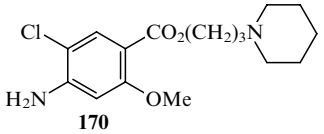

170

These and some other examples of this kind, *e.g*., the fact that metoclopramide (**141**) is a partial agonist of 5-HT_4 receptors and its ester analogue **164** is a 5-HT_4 antagonist, suggest that even minor structural changes may provoke dramatic changes in the intrinsic activities of 5-HT_4 ligands. A hypothesis of the existence of two binding sites in the 5-HT_4 receptor was developed to rationalise this fact.[277]

Substitution of an oxygen-containing ring for the *o*-alkoxy group in the piperidine-substituted metoclopramide derivatives (**141**) was efficient in the design of both 5-HT_3 and 5-HT_4 antagonists. Thus chlorine-substituted benzodioxanes **171a**,**b**[281] and the iodo derivative **171c**[282,283] proved to be selective 5-HT_4 antagonists with affinities exceeding that of compound **164** 1000-fold and even more.

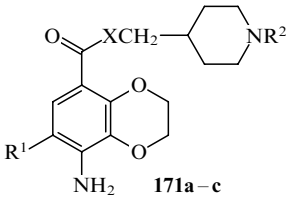

171a–c

R^1 = Cl, R^2 = Bu^n, X = O (**a**); R^1 = Cl, R^2 = $(CH_2)_3C_6H_3(OMe)_2$-3,4, X = CH_2 (**b**); R^1 = I, R^2 = Bu^n, X = O (**c**).

Substitution of the indole fragment for the benzene rings in many metoclopramide derivatives mentioned above was also effective. Compounds **172** and **173**[284,285] and their tricyclic analogue **174**[285] proved to be high-affinity selective 5-HT_4 antagonists. The attempts to modify the indole fragment revealed that benzoimidazoles **175** containing the piperazine fragment in their side chains manifest high affinities for 5-HT_4 receptors. Interestingly, compound **175** (where R = cyclo-C_3H_5) behaved as a potent antagonist, whereas that with R = Pr^i was a partial agonist manifesting very high intrinsic activity.[286] This is yet another example of reversal of the pharmacological profile of structurally related compounds, which provides additional evidence in favour of the hypothesis postulating the existence of two binding sites in the 5-HT_4 receptor.

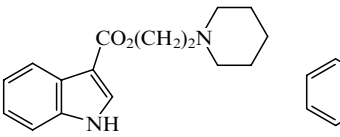

172

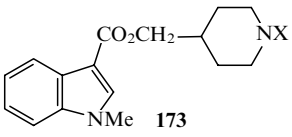

173

X = $(CH_2)_2NHSO_2Me$.

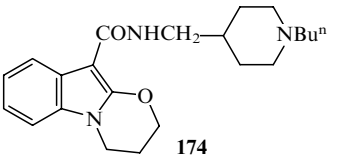

174

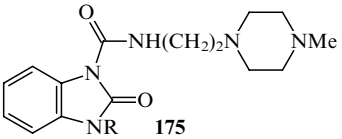

175

Conformational analysis of serotonin and zacopride (**143**) which also manifests agonistic activity towards its receptor disclosed very potent and selective 5-HT_4 agonists among indole derivatives close to serotonin and made it possible to propose a model of a binding site for 5-HT_4 agonists corresponding to the serotonin analogue **176a**. The latter appeared to be a high-affinity full agonist of 5-HT_4 receptors towards which it was more selective than to other serotonin and dopaminergic receptors.[287,288] The affinity of this compound can be increased through the introduction of lipophilic substituents into the side chain. Thus the derivatives **176b**,**c** are full agonists with the affinities exceeding that of serotonin severalfold. Compound **176d** binds to the receptor 300 times more effectively than serotonin but manifests the properties of a partial agonist. These compounds are among the most potent and selective 5-HT_4 agonists presently available.[287,288]

Some 5-HT_4 ligands were found among the derivatives of quipazine (**125a**), which also represents a 5-HT_3 ligand. The majority of compounds of this kind, *e.g.*, compound **177**, manifest partial agonistic activity towards 5-HT_4 receptors and simultaneously act as 5-HT_3 antagonists[289] which makes them promising candidates for gastrokinetic agents.

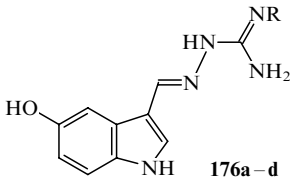

176a–d

R = H (**a**), C_5H_{11} (**b**), $(CH_2)_2Ph$ (**c**), $(CH_2)_2C_6H_3Cl_2$-3,4 (**d**).

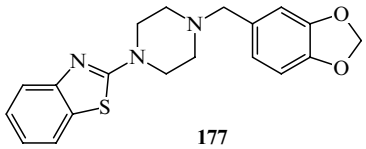

177

It should be stressed in conclusion that despite the construction of a fairly large number of potent and sufficiently selective 5-HT_4 ligands, they manifest predominantly antagonistic activities. Full selective agonists are fewer in number, but are therapeutically more valuable. Moreover, very many 5-HT_4 ligands do not possess high pharmacodynamic characteristics needed for their clinical application. It is for this reason that the main attention has presently been focussed on those modifications of the ligand structure which might improve their pharmacodynamic characteristics. To this end, amide, carbamate or ketone groups are introduced into the side chains of compounds **170** instead of ester groups.[290,291] Among compounds with improved pharmacodynamic characteristics, compounds **171b** and **174** and the recently prepared compound **178**,[290,292] a long-acting, potent and selective 5-HT_4 antagonist, deserve special mentioning.

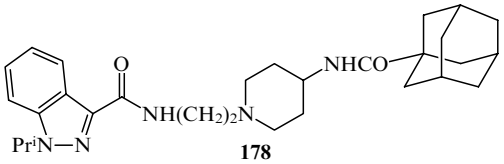

178

IX. Ligands of serotonin receptors of other subtypes

Among other subtypes of serotonin receptors, 5-HT_5 (further classified into 5-HT_{5A} and 5-HT_{5B}), 5-HT_6 and 5-HT_7 receptors are the least known. Highly selective ligands to 5-HT_5 and 5-HT_6 receptors have not been identified yet; therefore, their functional and, perhaps, therapeutic values have been studied relatively little. It is suggested that 5-HT_7 receptors play a role in the pathophysiology of certain sleep disturbances, depressive states and schizophrenia; also their stimulation causes vasodilation.

Studies of the effects of many classical ligands of serotonin receptors on these subtypes revealed that 5-carboxamidotryptamine (**2**) and LSD (**97**) manifested high, whereas compound **4a** manifested moderate, affinities for 5-HT_{5A} and 5-HT_7 receptors.[293] Many non-selective 5-HT_2 antagonists, such as methiothepin (**68**), methergoline (**98**), ritanserin (**104**), *etc.*, bind to 5-HT_6 and 5-HT_7 receptors manifesting high or moderate affinities. Very strong binding is observed in the interaction of some mixed-action antipsychotic drugs, *e.g.*, clozapine (**120a**) and pimozide (**179**), with these receptors.[294]

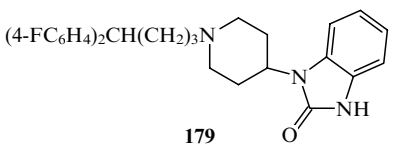

179

It is not until very recently that a series of studies devoted to the design of selective ligands of some of the above-mentioned receptor groups have been published.[295,296] Thus it was found that 5-HT_6 receptors match small alkyl substituents in position 2 of the indole ring of serotonin. The ethyl derivative **180** which represents

a full 5-HT_6 agonist manifests the highest affinity and binds to the receptor 5 times more strongly than serotonin. Compound **180** manifests only moderate affinity for some other types of serotonin receptors, being the most selective 5-HT_6 agonist known so far. Substitution of the phenyl group for the ethyl substituent does not influence the affinity but decreases dramatically the intrinsic activity. These data suggest that 2-substituted tryptamines can be used in the design of both selective agonists and antagonists of 5-HT_6 receptors.[296]

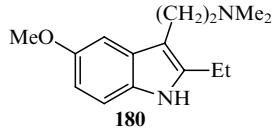

180

A selective ligand of 5-HT_7 receptors was prepared based on sulfamide **181**, which has been found as a result of wide screening and manifesting moderate affinity and weak selectivity towards 5-HT_7 receptors; its *R*,*R*-configuration was found to be important for binding. Modifications of compound **181** revealed that the methyl group in the piperidine ring may be shifted to position 4, whereas the naphthalene ring may be replaced by other aromatic substituents. Thus sulfamide **182** appeared to be two orders of magnitude more selective towards 5-HT_7 receptors than to other serotonin receptors. Compound **182** is the first example of an effective selective ligand endowed with 5-HT_7 antagonistic activity, although its affinity for these receptors is not very high.[295]

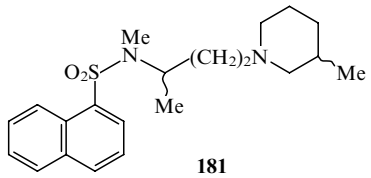

181

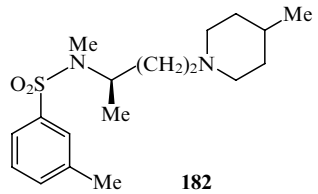

182

* * *

A vast variety of compounds interacting with serotonin receptors with high affinity have been prepared by the methods employed in medicinal chemistry. Selectivity is the major problem in the design of new ligands, since the family of serotonin receptors is characterised by a large set of structurally similar subclasses. Although this problem can successfully be overcome for some of 5-HT subtypes, for other 5-HT receptors, particularly for 5-HT_{1E}, 5-HT_{1F}, 5-HT_{5A}, 5-HT_{5B}, 5HT_6 and 5-HT_7, the design of selective ligands presents a challenge. Its successful solution will help better understanding of the functional roles of receptors in the organism. Obviously, progress in the search for ligands to serotonin receptors will depend on further advances in X-ray diffraction analysis, which will provide a basis for refining of computer models and docking studies of ligands pertaining to different structural classes.

References

1. O N Zefirova, N S Zefirov *Vestn. Mosk. Univ., Ser. 2, Khim.* **41** 43 (2000) [a]
2. O N Zefirova, N S Zefirov *Vestn. Mosk. Univ., Ser. 2, Khim.* **41** 103 (2000) [a]
3. O N Zefirova, N S Zefirov *Zh. Org. Khim.* **36** 1273 (2000) [b]
4. D Hoyer, G R Martin *Behav. Brain Res.* **73** 263 (1996)
5. D Hoyer, G Martin *Neuropharmacology* **36** 419 (1997)
6. L Uphouse *Neurosci. Biobehav. Rev.* **21** 679 (1997)
7. P Blier, C de Montigny *Trends Pharmacol. Sci.* **15** 220 (1994)
8. A Fletcher, I A Cliffe, C T Dourish *Trends Pharmacol. Sci.* **14** 41 (1993)
9. M Hamon *Trends Pharmacol. Sci.* **15** 36 (1994)
10. M S Beer, J A Stanton, Y Bevan, N S Chauhan, D N Middlemiss *Eur. J. Pharmacol.* **213** 193 (1992)
11. E Zifa, G Fillion *Pharmacol. Rev.* **44** 401 (1992)
12. D N Middlemiss, J R Fozard *Eur. J. Pharmacol.* **90** 151 (1983)
13. D R Helton, W E Colbert *J. Pharm. Pharmacol.* **46** 902 (1994)
14. H Yu, Y Liu, U Hacksell, T Lewander *Eur. J. Pharmacol.* **231** 69 (1993)
15. Z-P Zhuang, M-P Kung, H F Kung *J. Med. Chem.* **36** 3161 (1993)
16. L-E Arvidsson, A M Johansson, U Hacksell, J L Nilsson, K Svensson, S Hjorth, T Magnusson, A Carlsson, B Andersson, H Wikström *J. Med. Chem.* **30** 2105 (1987)
17. C Mellin, J Vallgarda, D L Nelson, L Björk, H Yu, N-E Anden, I Csöregh, L-E Arvidsson, U Hacksell *J. Med. Chem.* **34** 497 (1991)
18. L J Cornfield, G Lambert, L E Arvidsson, C Mellin, J Vallgarda, U Hacksell, D L Nelson *Mol. Pharmacol.* **39** 780 (1991)
19. H Wikström, B Andersson, T Elebring, J Jacyno, N L Allinger, K Svensson, A Carlsson, S Sundell *J. Med. Chem.* **30** 1567 (1987)
20. B B Höök, L Cortizo, A M Johansson, A Westlind-Danielsson, N Mohell, U Hacksell *J. Med. Chem.* **39** 4036 (1996)
21. L Björk, L J Cornfield, D L Nelson, S E Hillver, N E Anden, T Lewander, U Hacksell *J. Pharmacol. Exp. Ther.* **258** 58 (1991)
22. S-E Hillver, L Björk, Y-L Li, B Svensson, S Ross, N-E Anden, U Hacksell *J. Med. Chem.* **33** 1541 (1990)
23. J Vallgarda, U Appelberg, L E Arvidsson, S Hjorth, B E Svensson, U Hacksell *J. Med. Chem.* **39** 1485 (1996)
24. M H Hedberg, T Linnanen, J M Jansen, G Nordvall, S Hjorth, L Unelius, A M Johansson *J. Med. Chem.* **39** 3503 (1996)
25. M H Hedberg, J M Jansen, G Nordvall, S Hjorth, L Unelius, A M Johansson *J. Med. Chem.* **39** 3491 (1996)
26. G S Baxter, D A Craig, D E Clarke *Naunyn Schmiedebergs Arch. Pharmacol.* **343** 439 (1991)
27. R D Titus, E C Kornfeld, N D Jones, J A Clemens, E B Smalstig, R W Fuller, R A Hahn, M D Hynes, N R Mason, D T Wong, M M Foreman *J. Med. Chem.* **26** 1112 (1983)
28. R F Heier, L A Dolak, J N Duncan, D K Hyslop, M F Lipton, I J Martin, M A Mauragis, M F Piercey, N F Nichols, P J K D Schreur, M W Smith, M W Moon *J. Med. Chem.* **40** 639 (1997)
29. J M Cossery, H Gozlan, U Spampinato, C Perdicakis, G Guillaumet, L Pichat, M Hamon *Eur. J. Pharmacol.* **140** 143 (1987)
30. E Hammarberg, G Nordvall, R Leideborg, M Nylof, S Hanson, L Johansson, S-O Thorberg, B R Tolf, E Jerning, G T Svantesson, N Mohell, C Ahlgren, A Westlind-Danielsson, I Csöregh, R Johansson *J. Med. Chem.* **43** 2837 (2000)
31. K L Goa, A Ward *Drugs* **32** 114 (1986)
32. A Gobert, J-M Rivet, L Cistarelli, C Melon, M J Millan *Neuroscience* **93** 1251 (1999)
33. B J Cao, R J Rodgers *Psychopharmacology (Berlin)* **139** 185 (1998)
34. D P Taylor, S L Moon *Neuropeptides* **19** (Suppl.) 15 (1991)
35. K Ishizumi, A Kojima, F Antoku *Chem. Pharm. Bull.* **39** 2288 (1991)
36. I van Wijngaarden, M T M Tulp, W Soudijn *Eur. J. Pharmacol.* **188** 301 (1990)
37. M Abou-Gharbia, U R Patel, M B Webb, J A Moyer, T H Andree, E A Muth *J. Med. Chem.* **31** 1382 (1988)
38. R K Raghupathi, L Rydelek-Fitzgerald, M Teitler, R A Glennon *J. Med. Chem.* **34** 2633 (1991)
39. B J van Steen, I van Wijngaarden, M T M Tulp, W Soudijn *J. Med. Chem.* **36** 2751 (1993)
40. B J van Steen, I van Wijngaarden, M T M Tulp, W Soudijn *J. Med. Chem.* **37** 2761 (1994)
41. J L Mokrosz, M Pietrasiewicz, B Duszynska, M T Cegla *J. Med. Chem.* **35** 2369 (1992)
42. R A Glennon, S -S Hong, M Dukat, M Teitler, K Davis *J. Med. Chem.* **37** 2828 (1994)
43. R A Glennon, S S Hong, M Bondarev, H Law, M Dukat, S Rakhit, P Power, E Fan, D Kinneau, R Kamboj, M Teitler, K Herrick-Davis, C Smith *J. Med. Chem.* **39** 314 (1996)

44. J M Greuel, T Glaser *Eur. J. Pharmacol.* **211** 211 (1992)
45. T Sharp, L I Backus, S Hjorth, S R Bramwell, D G Grahame-Smith *Eur. J. Pharmacol.* **176** 331 (1990)
46. H T Yang, M Endoh *Br. J. Pharmacol.* **122** 1541 (1997)
47. T Matsuda, Y H Seong, H Aono, T Kanda, A Baba, K Saito, A Tobe, H Iwata *Eur. J. Pharmacol.* **170** 75 (1989)
48. G Baxter, G Kennett, F Blaney, T Blackburn *Trends Pharmacol. Sci.* **16** 105 (1995)
49. Y El Ahmad, E Laurent, P Maillet, A Talab, J F Teste, R Dokhan, G Tran, R Ollivier *J. Med. Chem.* **40** 952 (1997)
50. A Orjales, L Alonso-Cires, L Labeaga, R Corcostegui *J. Med. Chem.* **38** 1273 (1995)
51. J-L Peglion, H Canton, K Bervoets, V Audinot, M Brocco, A Gobert, S Le Marouille-Girardon, M J Millan *J. Med. Chem.* **38** 4044 (1995)
52. M L Lopez-Rodriguez, M L Rosado, B Benhamu, M J Morcillo, A M Sanz, L Orensanz, M E Beneitez, J A Fuentes, J Manzanares *J. Med. Chem.* **39** 4439 (1996)
53. M L Lopez-Rodriguez, M J Morcillo, T K Rovat, E Fernandez, B Vicente, A M Sanz, M Hernandez, L Orensanz *J. Med. Chem.* **42** 36 (1999)
54. G Griebel, R J Rodgers, G Perrault, D J Sanger *Psychopharmacology (Berlin)* **144** 121 (1999)
55. G Griebel, R J Rodgers, G Perrault, D J Sanger *Neuropharmacology* **39** 1848 (2000)
56. T Podona, B Guardiola-Lemaitre, D -H Caignard, G Adam, B Pfeiffer, P Renard, G Guillaumet *J. Med. Chem.* **37** 1779 (1994)
57. R T Kroemer, E Koutsilieri, P Hecht, K R Liedl, P Riederer, J Kornhuber *J. Med. Chem.* **41** 393 (1998)
58. H Kubinyi *QSAR: Hansch Analysis and Related Approaches.* (Eds R Mannhold, P Krogsgaard-Larsen, H Timmerman) (Weinheim: VCH, 1993)
59. H Kubinyi, in *The Quantitative Analysis of Structure-Activity Relationships* Vol. 1 (Ed. M E Wolff) (New York: Wiley, 1995) p. 497
60. C Comoy, C Marot, T Podona, M-L Baudin, L Morin-Allory, G Guillaumet, B Pfeiffer, D-H Caignard, P Renard, M -C Rettori, G Adam, B Guardiola-Lemaitre *J. Med. Chem.* **39** 4285 (1996)
61. S Buisson-Defferier, M van den Buuse *Eur. J. Pharmacol.* **223** 133 (1992)
62. S E Gartside, P J Cowen, S Hjorth *Eur. J. Pharmacol.* **191** 391 (1990)
63. P van den Hooff , M Galvan *Eur. J. Pharmacol.* **196** 291 (1991)
64. R E Mewshaw, J Kavanagh, G Stack, K L Marquis, X Shi, M Z Kagan, M B Webb, A H Katz, A Park, Y H Kang, M Abou-Gharbia, R Scerni, T Wasik, L Cortes-Burgos, T Spangler, J A Brennan, M Piesla, H Mazandarani, M I Cockett, R Ochalski, J Coupet, T H Andree *J. Med. Chem.* **40** 4235 (1997)
65. W Quaglia, M Pigini, A Piergentili, M Giannella, G Marucci, E Poggesi, A Leonardi, C Melchiorre *J. Med. Chem.* **42** 2961 (1999)
66. W Kuipers, C G Kruse, I van Wijngaarden, P J Standaar, M T M Tulp, N Veldman, A L Spek, A P Ijzerman *J. Med. Chem.* **40** 300 (1997)
67. B Vacher, B Bonnaud, P Funes, N Jubault, W Koek, M-B Assie, C Cosi *J. Med. Chem.* **41** 5070 (1998)
68. B Vacher, B Bonnaud, P Funes, N Jubault, W Koek, M-B Assie, C Cosi, M Kleven *J. Med. Chem.* **42** 1648 (1999)
69. A M Birch, P A Bradley, J C Gill, F Kerrigan, P L Needham *J. Med. Chem.* **42** 3342 (1999)
70. H R Howard, J A Lowe III, T F Seeger, P A Seymour, S H Zorn, P R Maloney, F E Ewing, M E Newman, A W Schmidt, J S Furman, G L Robinson, E Jackson, C Johnson, J Morrone *J. Med. Chem.* **39** 143 (1996)
71. D Wustrow, T Belliotti, S Glase, S R Kesten, D Johnson, N Colbry, R Rubin, A Blackburn, H Akunne, A Corbin, M D Davis, L Georgic, S Whetzel, K Zoski, T Heffner, T Pugsley, L Wise *J. Med. Chem.* **41** 760 (1998)
72. E M Clifford, S E Gartside, V Umbers, P J Cowen, M Hajos, T Sharp *Br. J. Pharmacol.* **124** 206 (1998)
73. R Corradetti, N Laaris, N Hanoun, A M Laporte, E Le Poul, M Hamon, L Lanfumey *Br. J. Pharmacol.* **123** 449 (1998)
74. H Giles, S J Lansdell, M L Bolofo, H L Wilson, G R Martin *Br. J. Pharmacol.* **117** 1119 (1996)
75. A Hoey, C Jackson, G Pegg, M Sillence *Br. J. Pharmacol.* **117** 712 (1996)
76. A Fletcher, E A Forster, D J Bill, G Brown, I A Cliffe, J E Hartley, D E Jones, A McLenachan, K J Stanhope, D J Critchley, K J Childs, V C Middlefell, L Lanfumey, R Corradetti, A M Laporte, H Gozlan, M Hamon, C T Dourish *Behav. Brain Res.* **73** 337 (1996)
77. E A Forster, I A Cliffe, D J Bill, G M Dover, D Jones, Y Reilly, A Fletcher *Eur. J. Pharmacol.* **281** 81 (1995)
78. I A Cliffe, C I Brightwell, A Fletcher, E A Forster, H L Mansell, Y Reilly, C Routledge, A C White *J. Med. Chem.* **36** 1509 (1993)
79. D B Bylund, H S Blaxall, L J Iversen, M G Caron, R J Lefkowitz, J W Lomasney *Mol. Pharmacol.* **42** 1 (1992)
80. D L Nelson, E W Taylor *Eur. J. Pharmacol.* **124** 207 (1986)
81. T Yasunaga, R Naito, T Kontani, S Tsukamoto, T Nomura, T Yamaguchi, T Mase *J. Med. Chem.* **40** 1252 (1997)
82. T Yasunaga, T Kimura, R Naito, T Kontani, F Wanibuchi, H Yamashita, T Nomura, S Tsukamoto, T Yamaguchi, T Mase *J. Med. Chem.* **41** 2765 (1998)
83. M J Mokrosz, B Duszynska, A J Bojarski, J L Mokrosz *Bioorg. Med. Chem.* **3** 533 (1995)
84. J M Zgombick, L E Schechter, S A Kucharewicz, R L Weinshank, T A Branchek *Eur. J. Pharmacol.* **291** 9 (1995)
85. Y-C Xu, J M Schaus, C Walker, J Krushinski, N Adham, J M Zgombick, S X Liang, D T Kohlman, J E Audia *J. Med. Chem.* **42** 526 (1999)
86. L M Gaster, F E Blaney, S Davies, D M Duckworth, P Ham, S Jenkins, A J Jennings, G F Joiner, F D King, K R Mulholland, P A Wyman, J J Hagan, J Hatcher, B J Jones, D N Middlemiss, G W Price, G Riley, C Roberts, C Routledge, J Selkirk, P D Slade *J. Med. Chem.* **41** 1218 (1998)
87. J Longmore, C M Boulanger, B Desta, R G Hill, W N Schofield, A A Taylor *Br. J. Clin. Pharmacol.* **42** 431 (1996)
88. C Jorand-Lebrun, P J Pauwels, C Palmier, C Moret, P Chopin, M Perez, M Marien, S Halazy *J. Med. Chem.* **40** 3974 (1997)
89. M Lamothe, P J Pauwels, K Belliard, P Schambel, S Halazy *J. Med. Chem.* **40** 3542 (1997)
90. M D Ferrari, P R Saxena *Trends Pharmacol. Sci.* **14** 129 (1993)
91. K L Dechant, S P Clissold *Drugs* **43** 776 (1992)
92. C M Perry, A Markham *Drugs* **55** 889 (1998)
93. K W Weitzel, M L Thomas, R E Small, J V Goode *Pharmacotherapy* **19** 957 (1999)
94. R N Iyer, C W Bradberry *J. Pharmacol. Exp. Ther.* **277** 40 (1996)
95. M D Lee, V J Aloyo, S J Fluharty, K J Simansky *Psychopharmacology (Berlin)* **136** 304 (1998)
96. A C Trillat, I Malagie, K Scearce, D Pons, M C Anmella, C Jacquot, R Hen, A M Gardier *J. Neurochem.* **69** 2019 (1997)
97. M J Gawel *Can. J. Clin. Pharmacol.* **6** 20A (1999)
98. R Salonen *Int. J. Clin. Pract.* **53** 552 (1999)
99. L J Street, R Baker, W B Davey, A R Guiblin, R A Jelley, A J Reeve, H Routledge, F Sternfeld, A P Watt, M S Beer, D N Middlemiss, A J Noble, J A Stantor, K Scholey, R J Hargreaves, B Sohal, M I Graham, V G Matassa *J. Med. Chem.* **38** 1799 (1995)
100. D Deleu, Y Hanssens *J. Clin. Pharmacol.* **40** 687 (2000)
101. C M Spencer, N S Gunasekara, C Hills *Drugs* **58** 347 (1999)
102. R M Gallagher, G Dennish, E L Spierings, R Chitra *Headache* **40** 119 (2000)
103. A Al Shekhlee, R Reed *Neurology* **55** 735 (2000)
104. P R Saxena, P De Vries, W Wang, J P Heiligers, v A Maassen, W A Bax, F D Yocca *Naunyn Schmiedebergs Arch. Pharmacol.* **355** 295 (1997)
105. H C Diener, H Kaube, V Limmroth *J. Neurol.* **246** 515 (1999)
106. A A Parsons, R Valocik, P Koster, P Raval, R Gagnon, N Tilford, G Feuerstein *J. Cardiovasc. Pharmacol.* **32** 995 (1998)
107. M Perez, C Fourrier, I Sigogneau, P J Pauwels, C Palmier, G W John, J-P Valentin, S Halazy *J. Med. Chem.* **38** 3602 (1995)
108. M S Beer, J A Stanton, Y Bevan, A Heald, A J Reeve, L J Street, V G Matassa, R J Hargreaves, D N Middlemiss *Br. J. Pharmacol.* **110** 1196 (1993)
109. A Heald, J A Stanton, S A Osborne, D N Middlemiss, M S Beer *Eur. J. Pharmacol.* **264** 213 (1994)
110. L J Street, R Baker, J L Castro, M S Chambers, A R Guiblin, S C Hobbs, V G Matassa, A J Reeve, M S Beer, D N Middlemiss, A J Noble, J A Stanton, K Scholey, R J Hargreaves *J. Med. Chem.* **36** 1529 (1993)

111. S J Starkey, M Skingle *Neuropharmacology* **33** 393 (1994)
112. J W Clitherow, D I Scopes, M Skingle, C C Jordan, W Feniuk, I B Campbell, M C Carter, E W Collington, H E Connor, G A Higgins, D Beattie, H A Kelly, W C Mitchell, A W Oxford, A H Wadsworth, M B Tyers *J. Med. Chem.* **37** 2253 (1994)
113. H Law, M Dukat, M Teitler, D K H Lee, L Mazzocco, R Kamboj, V Rampersad, T Prisinzano, R A Glennon *J. Med. Chem.* **41** 2243 (1998)
114. C Sonesson, T Barf, J Nilsson, D Dijkstra, A Carlsson, K Svensson, M W Smith, I J Martin, J N Duncan, L J King, H Wikström *J. Med. Chem.* **38** 1319 (1995)
115. T A Barf, P de Boer, H Wikström, S J Peroutka, K Svensson, M D Ennis, N B Ghazal, J C McGuire, M W Smith *J. Med. Chem.* **39** 4717 (1996)
116. J L Castro, L J Street, A R Guiblin, R A Jelley, M G Russell, F Sternfeld, M S Beer, J A Stanton, V G Matassa *J. Med. Chem.* **40** 3497 (1997)
117. F Sternfeld, A R Guiblin, R A Jelley, V G Matassa, A J Reeve, P A Hunt, M S Beer, A Heald, J A Stanton, B Sohal, A P Watt, L J Street *J. Med. Chem.* **42** 677 (1999)
118. M S Chambers, L J Street, S Goodacre, S C Hobbs, P Hunt, R A Jelley, V G Matassa, A J Reeve, F Sternfeld, M S Beer, J A Stanton, D Rathbone, A P Watt, A M MacLeod *J. Med. Chem.* **42** 691 (1999)
119. M B van Niel, I Collins, M S Beer, H B Broughton, S K F Cheng, S C Goodacre, A Heald, K L Locker, A M MacLeod, D Morrison, C R Moyes, D O'Connor, A Pike, M Rowley, M G N Russell, B Sohal, J A Stanton, S Thomas, H Verrier, A P Watt, J L Castro *J. Med. Chem.* **42** 2087 (1999)
120. J L Castro, I Collins, M G N Russell, A P Watt, B Sohal, D Rathbone, M S Beer, J A Stanton *J. Med. Chem.* **41** 2667 (1998)
121. P Schoeffter, D Hoyer *Naunyn Schmiedebergs Arch. Pharmacol.* **339** 675 (1989)
122. F Chaouloff, S Aguerre, P Mormede *Neuropharmacology* **37** 1159 (1998)
123. R F Neale, S L Fallon, W C Boyar, J W Wasley, L L Martin, G A Stone, B S Glaeser, C M Sinton, M Williams *Eur. J. Pharmacol.* **136** 1 (1987)
124. J E Leysen, W Gommeren, L Heylen, W H Luyten, I van de Weyer, P Vanhoenacker, G Haegeman, A Schotte, P van Gompel, R Wouters, A S Lesage *Mol. Pharmacol.* **50** 1567 (1996)
125. E Schlicker, U Werner, M Hamon, H Gozlan, B Nickel, I Szelenyi, M Gothert *Br. J. Pharmacol.* **105** 732 (1992)
126. M A Petty, J Elands, M P Johnson, M D Linnik, E Hamel, M A Moskowitz, W S Lee, D R McCarty, M Hibert, B M Baron *Eur. J. Pharmacol.* **336** 127 (1997)
127. P Schoeffter, D Hoyer *Eur. J. Pharmacol.* **196** 213 (1991)
128. A M Ismaiel, M Dukat, H Law, R Kamboj, E Fan, D K H Lee, L Mazzocco, D Buekschkens, M Teitler, M E Pierson, R A Glennon *J. Med. Chem.* **40** 4415 (1997)
129. P C Waldmeier, M Williams, P A Baumann, S Bischoff, M A Sills, R F Neale *Naunyn Schmiedebergs Arch. Pharmacol.* **337** 609 (1988)
130. P J Pauwels, F C Colpaert *Neuropharmacology* **34** 235 (1995)
131. J M Watson, M J Burton, G W Price, B J Jones, D N Middlemiss *Eur. J. Pharmacol.* **314** 365 (1996)
132. R C Glen, G R Martin, A P Hill, R M Hyde, P M Woollard, J A Salmon, J Buckingham, A D Robertson *J. Med. Chem.* **38** 3566 (1995)
133. G P Moloney, A D Robertson, G R Martin, S MacLennan, N Mathews, S Dodsworth, P Y Sang, C Knight, R Glen *J. Med. Chem.* **40** 2347 (1997)
134. G P Moloney, G R Martin, N Mathews, A Milne, H Hobbs, S Dodsworth, P Y Sang, C Knight, M Williams, M Maxwell, R C Glen *J. Med. Chem.* **42** 2504 (1999)
135. M R MacLean, R A Clayton, A G Templeton, I Morecroft *Br. J. Pharmacol.* **119** 277 (1996)
136. C Roberts, G W Price, L Gaster, B J Jones, D N Middlemiss, C Routledge *Neuropharmacology* **36** 549 (1997)
137. I T Forbes, S Dabbs, D M Duckworth, P Ham, G E Jones, F D King, D V Saunders, F E Blaney, C B Naylor, G S Baxter, T P Blackburn, G A Kennett, M D Wood *J. Med. Chem.* **39** 4966 (1996)
138. E Schlicker, K Fink, G J Molderings, G W Price, M Duckworth, L Gaster, D N Middlemiss, J Zentner, J Likungu, M Gothert *Naunyn Schmiedebergs Arch. Pharmacol.* **356** 321 (1997)
139. S Leonhardt, K Herrick-Davis, M Titeler *J. Neurochem.* **53** 465 (1989)
140. E M Parker, D G Izzarelli, L Lewis-Higgins, D Palmer, R A Shapiro *J. Neurochem.* **67** 2096 (1996)
141. S Shepheard, L Edvinsson, M Cumberbatch, D Williamson, G Mason, J Webb, S Boyce, R Hill, R Hargreaves *Cephalalgia* **19** 851 (1999)
142. D S Dupuis, F C Colpaert, P J Pauwels *Br. J. Pharmacol.* **124** 283 (1998)
143. K W Johnson, J M Schaus, M M Durkin, J E Audia, S W Kaldor, M E Flaugh, N Adham, J M Zgombick, M L Cohen, T A Branchek, L A Phebus *Neuroreport* **8** 2237 (1997)
144. B P Richardson, G Engel, P Donatsch, P A Stadler *Nature (London)* **316** 126 (1985)
145. H Wilson, W J Coffman, M L Cohen *J. Pharmacol. Exp. Ther.* **252** 683 (1990)
146. M S Duxon, G A Kennett, S Lightowler, T P Blackburn, K C Fone *Neuropharmacology* **36** 601 (1997)
147. G A Kennett, K Ainsworth, B Trail, T P Blackburn *Neuropharmacology* **36** 233 (1997)
148. G A Kennett, B Trail, F Bright *Neuropharmacology* **37** 1603 (1998)
149. R A Glennon, M Dukat, M El-Bermawy, H Law, J De los Angeles, M Teitler, A King, K Herrick-Davis *J. Med. Chem.* **37** 1929 (1994)
150. J B Blair, D Marona-Lewicka, A Kanthasamy, V L Lucaites, D L Nelson, D E Nichols *J. Med. Chem.* **42** 1106 (1999)
151. M Gerasimov, D Marona-Lewicka, D M Kurrasch-Orbaugh, A M Qandil, D E Nichols *J. Med. Chem.* **42** 4257 (1999)
152. J E Macor, J Blake, C B Fox, C Johnson, B K Koe, L A Lebel, J M Morrone, K Ryan, A W Schmidt, D W Schulz, S H Zorn *J. Med. Chem.* **35** 4503 (1992)
153. S Vangveravong, D E Nichols *J. Org. Chem.* **60** 3409 (1994)
154. S Vangveravong, A Kanthasamy, V L Lucaites, D L Nelson, D E Nichols *J. Med. Chem.* **41** 4995 (1998)
155. M Bös, F Jenck, J R Martin, J L Moreau, A J Sleight, J Wichmann, U Widmer *J. Med. Chem.* **40** 2762 (1997)
156. G Curzon, G A Kennett *Trends Pharmacol. Sci.* **11** 181 (1990)
157. K C Fone, R H Austin, I A Topham, G A Kennett, T Punhani *Br. J. Pharmacol.* **123** 1707 (1998)
158. I Lucki, H R Ward, A Frazer *J. Pharmacol. Exp. Ther.* **249** 155 (1989)
159. Y Sugimoto, J Yamada, T Yoshikawa, K Horisaka *Eur. J. Pharmacol.* **307** 75 (1996)
160. P J Conn, E Sanders-Bush *J. Pharmacol. Exp. Ther.* **242** 552 (1987)
161. S K Hemrick-Luecke, R W Fuller *Eur. J. Pharmacol.* **311** 207 (1996)
162. R A Glennon, J M Jacyno, R Young, J D McKenney, D Nelson *J. Med. Chem.* **27** 41 (1984)
163. R A Glennon, R Raghupathi, P Bartyzel, M Teitler, S Leonhardt *J. Med. Chem.* **35** 734 (1992)
164. D E Nichols, S Frescas, D Marona-Lewicka, X Huang, B L Roth, G A Gudelsky, J F Nash *J. Med. Chem.* **37** 4346 (1994)
165. M R Seggel, M Y Yousif, R A Lyon, M Titeler, B L Roth, E A Suba, R A Glennon *J. Med. Chem.* **33** 1032 (1990)
166. A P Monte, D Marona-Lewicka, M A Parker, D B Wainscott, D L Nelson, D E Nichols *J. Med. Chem.* **39** 2953 (1996)
167. A P Monte, S R Waldman, D Marona-Lewicka, D B Wainscott, D L Nelson, E Sanders-Bush, D E Nichols *J. Med. Chem.* **40** 2997 (1997)
168. A P Monte, D Marona-Lewicka, M M Lewis, R B Mailman, D B Wainscott, D L Nelson, D E Nichols *J. Med. Chem.* **41** 2134 (1998)
169. M A Parker, D Marona-Lewicka, V L Lucaites, D L Nelson, D E Nichols *J. Med. Chem.* **41** 5148 (1998)
170. D E Nichols, S E Snyder, R Oberlender, M P Johnson, X Huang *J. Med. Chem.* **34** 276 (1991)
171. M P Johnson, C A Mathis, A T Shulgin, A J Hoffman, D E Nichols *Pharmacol. Biochem. Behav.* **35** 211 (1990)
172. R A Glennon, M Titeler, J D McKenney *Life Sci.* **35** 2505 (1984)
173. J E Audia, D A Evrard, G R Murdoch, J J Droste, J S Nissen, K W Schenck, P Fludzinski, V L Lucaites, D L Nelson, M L Cohen *J. Med. Chem.* **39** 2773 (1996)

174. M S Choudhary, N Sachs, A Uluer, R A Glennon, R B Westkaemper, B L Roth *Mol. Pharmacol.* **47** 450 (1995)
175. R A Glennon *Neuropsychopharmacology* **3** 509 (1990)
176. M L Cohen, C J Parli, R W Fuller *J. Pharmacol. Exp. Ther.* **251** 1006 (1989)
177. C S Aulakh, J L Hill, D L Murphy *J. Pharmacol. Exp. Ther.* **263** 588 (1992)
178. G Bagdy, A F Sved, D L Murphy, K Szemeredi *Eur. J. Pharmacol.* **210** 285 (1992)
179. M L Cohen, R W Fuller, K D Kurz, C J Parli, N R Mason, D B Meyers, J K Smallwood, R E Toomey *J. Pharmacol. Exp. Ther.* **244** 106 (1988)
180. M L Cohen, D W Robertson, W E Bloomquist, H C Wilson *J. Pharmacol. Exp. Ther.* **261** 202 (1992)
181. J W Misner, W L Garbrecht, G Marzoni, K R Whitten, M L Cohen *J. Med. Chem.* **33** 652 (1990)
182. H H Pertz, H -C Milhahn, E Eich *J. Med. Chem.* **42** 659 (1999)
183. M P Johnson, J E Audia, J S Nissen, D L Nelson *Eur. J. Pharmacol.* **239** 111 (1993)
184. D L Nelson, V L Lucaites, J E Audia, J S Nissen, D B Wainscott *J. Pharmacol. Exp. Ther.* **265** 1272 (1993)
185. M P Johnson, R J Loncharich, M Baez, D L Nelson *Mol. Pharmacol.* **45** 277 (1994)
186. H T Kao, N Adham, M A Olsen, R L Weinshank, T A Branchek, P R Hartig *FEBS Lett.* **307** 324 (1992)
187. W L Garbrecht, G Marzoni, K R Whitten, M L Cohen *J. Med. Chem.* **31** 444 (1988)
188. H O Kalkman, V Neumann, J Nozulak, M D Tricklebank *Eur. J. Pharmacol.* **343** 201 (1998)
189. P O Mora, C F Netto, F G Graeff *Pharmacol. Biochem. Behav.* **58** 1051 (1997)
190. J Nozulak, H O Kalkman, P Floersheim, D Hoyer, P Schoeffter, H R Buerki *J. Med. Chem.* **38** 28 (1995)
191. J E Leysen, F Awouters, L Kennis, P M Laduron, J Vandenberk, P A Janssen *Life Sci.* **28** 1015 (1981)
192. P A Pierce, J Y Kim, S J Peroutka *Naunyn Schmiedebergs Arch. Pharmacol.* **346** 4 (1992)
193. Z Razzaque, J Longmore, R G Hill *Eur. J. Pharmacol.* **283** 199 (1995)
194. J M Van Nueten, P A Janssen, J Van Beek, R Xhonneux, T J Verbeuren, P M Vanhoutte *J. Pharmacol. Exp. Ther.* **218** 217 (1981)
195. Y Watanabe, H Usui, S Kobayashi, H Yoshiwara, T Shibano, T Tanaka, Y Morishima, M Yasuoka, M Kanao *J. Med. Chem.* **35** 189 (1992)
196. F Darchen, D Scherman, P M Laduron, J P Henry *Mol. Pharmacol.* **33** 672 (1988)
197. J L Herndon, A Ismaiel, S P Ingher, M Teitler, R A Glennon *J. Med. Chem.* **35** 4903 (1992)
198. C J Schmidt, V L Taylor, G M Abbate, T R Nieduzak *J. Pharmacol. Exp. Ther.* **256** 230 (1991)
199. P Seeman, H H van Tol *Trends Pharmacol. Sci.* **15** 264 (1994)
200. A M Ismaiel, J De los Angeles, M Teitler, S Ingher, R A Glennon *J. Med. Chem.* **36** 2519 (1993)
201. K A Metwally, M Dukat, C T Egan, C Smith, A DuPre, C B Gauthier, K Herrick-Davis, M Teitler, R A Glennon *J. Med. Chem.* **41** 5084 (1998)
202. R H Mach, J R Jackson, R R Luedtke, K J Ivins, P B Molinoff, R L Ehrenkaufer *J. Med. Chem.* **35** 423 (1992)
203. D W Bonhaus, K K Weinhardt, M Taylor, A DeSouza, P M McNeeley, K Szczepanski, D J Fontana, J Trinh, C L Rocha, M W Dawson, L A Flippin, R M Eglen *Neuropharmacology* **36** 621 (1997)
204. D W Bonhaus, C L Rocha, M W Dawson, R M Eglen *Ann. N.Y. Acad. Sci.* **861** 269 (1998)
205. I T Forbes, G A Kennett, A Gadre, P Ham, C J Hayward, R T Martin, M Thompson, M D Wood, G S Baxter, A Glen, O E Murphy, B A Stewart, T P Blackburn *J. Med. Chem.* **36** 1104 (1993)
206. I T Forbes, P Ham, D H Booth, R T Martin, M Thompson, G S Baxter, T P Blackburn, A Glen, G A Kennett, M D Wood *J. Med. Chem.* **38** 2524 (1995)
207. I T Forbes, G E Jones, O E Murphy, V Holland, G S Baxter *J. Med. Chem.* **38** 855 (1995)
208. C S Dowd, K Herrick-Davis, C Egan, A DuPre, C Smith, M Teitler, R A Glennon *J. Med. Chem.* **43** 3074 (2000)
209. A Y Deutch, B Moghaddam, R B Innis, J H Krystal, G K Aghajanian, B S Bunney, D S Charney *Schizophr. Res.* **4** 121 (1991)
210. H Y Meltzer *Psychopharmacology (Berlin)* **99** (Suppl.) S18 (1989)
211. S Fox, J Brotchie *Eur. J. Pharmacol.* **301** 27 (1996)
212. M Kuoppamaki, E Syvalahti, J Hietala *Eur. J. Pharmacol.* **245** 179 (1993)
213. G Campiani, V Nacci, S Bechelli, S M Ciani, A Garofalo, I Fiorini, H Wikstrlm, P de Boer, Y Liao, P G Tepper, A Cagnotto, T Mennini *J. Med. Chem.* **41** 3763 (1998)
214. D Hoyer, D E Clarke, J R Fozard, P R Hartig, G R Martin, E J Mylecharane, P R Saxena, P P Humphrey *Pharmacol. Rev.* **46** 157 (1994)
215. A Moran, C Velasco, T Salvador, M L Martin, L San Roman *Br. J. Pharmacol.* **113** 1358 (1994)
216. B E Leonard *Adv. Biochem. Psychopharmacol.* **31** 301 (1982)
217. R A Newton, J M Elliott *J. Neurochem.* **69** 1031 (1997)
218. K Andersen, T Liljefors, K Gundertofte, J Perregaard, K P Bögesö *J. Med. Chem.* **37** 950 (1994)
219. T Borowski, M Krol, E Broclawik, T C Baranowski, L Strekowski, M J Mokrosz *J. Med. Chem.* **43** 1901 (2000)
220. A M Ismaiel, M Titeler, K J Miller, T S Smith, R A Glennon *J. Med. Chem.* **33** 755 (1990)
221. D A Craig, R M Eglen, L K Walsh, L A Perkins, R L Whiting, D E Clarke *Naunyn Schmiedebergs Arch. Pharmacol.* **342** 9 (1990)
222. S J Peroutka, A Hamik *Eur. J. Pharmacol.* **148** 297 (1988)
223. N A Sharif, E H Wong, D N Loury, E Stefanich, A D Michel, R M Eglen, R L Whiting *Br. J. Pharmacol.* **102** 919 (1991)
224. S J Ireland, M B Tyers *Br. J. Pharmacol.* **90** 229 (1987)
225. R A Glennon, A M Ismaiel, B G McCarthy, S J Peroutka *Eur. J. Pharmacol.* **168** 387 (1989)
226. A Bachy, M Heaulme, A Giudice, J C Michaud, I A Lefevre, J Souilhac, L Manara, M B Emerit, H Gozlan, M Hamon *Eur. J. Pharmacol.* **237** 299 (1993)
227. E Edwards, E Hampton, C R Ashby, J Zhang, R Y Wang *Brain Res.* **733** 21 (1996)
228. M Anzini, A Cappelli, S Vomero, G Giorgi, T Langer, M Hamon, N Merahi, B M Emerit, A Cagnotto, M Skorupska, T Mennini, J C Pinto *J. Med. Chem.* **38** 2692 (1995)
229. G J Kilpatrick, A Butler, J Burridge, A W Oxford *Eur. J. Pharmacol.* **182** 193 (1990)
230. M I Sepulveda, S C Lummis, I L Martin *Br. J. Pharmacol.* **104** 536 (1991)
231. F G Boess, M I Sepulveda, S C Lummis, I L Martin *Neuropharmacology* **31** 561 (1992)
232. M I Niemeyer, S C Lummis *Br. J. Pharmacol.* **123** 661 (1998)
233. M Dukat, A A Abdel-Rahman, A M Ismaiel, S Ingher, M Teitler, L Gyermek, R A Glennon *J. Med. Chem.* **39** 4017 (1996)
234. G Campiani, A Cappelli, V Nacci, M Anzini, S Vomero, M Hamon, A Cagnotto, C Fracasso, C Uboldi, S Caccia, S Consolo, T Mennini *J. Med. Chem.* **40** 3670 (1997)
235. H Prunier, S Rault, J-C Lancelot, M Robba, P Renard, P Delagrange, B Pfeiffer, D-H Caignard, R Misslin, B Guardiola-Lemaitre, M Hamon *J. Med. Chem.* **40** 1808 (1997)
236. S Rault, J-C Lancelot, H Prunier, M Robba, P Renard, P Delagrange, B Pfeiffer, D-H Caignard, B Guardiola-Lemaitre, M Hamon *J. Med. Chem.* **39** 2068 (1996)
237. G Campiani, E Morelli, S Gemma, V Nacci, S Butini, M Hamon, E Novellino, G Greco, A Cagnotto, M Goegan, L Cervo, F D Valle, C Fracasso, S Caccia, T Mennini *J. Med. Chem.* **42** 4362 (1999)
238. A Cappelli, M Anzini, S Vomero, L Mennuni, F Makovec, E Doucet, M Hamon, G Bruni, M R Romeo, M C Menziani, P G de Benedetti, T Langer *J. Med. Chem.* **41** 728 (1998)
239. A Cappelli, A Donati, M Anzini, S Vomero, P G de Benedetti, M C Menziani, T Langer *Bioorg. Med. Chem.* **4** 1255 (1996)
240. A Cappelli, M Anzini, S Vomero, L Canullo, L Mennuni, F Makovec, E Doucet, M Hamon, M C Menziani, P G de Benedetti, G Bruni, M R Romeo, G Giorgi, A Donati *J. Med. Chem.* **42** 1556 (1999)
241. A Monge, J A Palop, J C Del Castillo, J M Caldero, J Roca, G Romero, J Del Rio, B Lasheras *J. Med. Chem.* **36** 2745 (1993)

242. J R Fozard, A T Mobarok Ali *Eur. J. Pharmacol.* **49** 109 (1978)
243. V Derkach, A Surprenant, R A North *Nature (London)* **339** 706 (1989)
244. W L Smith, R S Alphin, C B Jackson, L F Sancilio *J. Pharm. Pharmacol.* **41** 101 (1989)
245. W W Smith, L F Sancilio, J B Owera-Atepo, R J Naylor, L Lambert *J. Pharm. Pharmacol.* **40** 301 (1988)
246. J R Fozard *Naunyn Schmiedebergs Arch. Pharmacol.* **326** 36 (1984)
247. J Bermudez, S Dabbs, F D King *J. Med. Chem.* **33** 1932 (1990)
248. J Bermudez, S Dabbs, K A Joiner, F D King *J. Med. Chem.* **33** 1929 (1990)
249. M Turconi, M Nicola, M G Quintero, L Maiocchi, R Micheletti, E Giraldo, A Donetti *J. Med. Chem.* **33** 2101 (1990)
250. J Bermudez, C S Fake, G F Joiner, K A Joiner, F D King, W D Miner, G J Sanger *J. Med. Chem.* **33** 1924 (1990)
251. R D Clark, J M Muchowski, K K Weinhardt, M P Dillon, C-H Lee, K R Bley, D W Bonhaus, E H F Wong, R M Eglen *Bioorg. Med. Chem. Lett.* **5** 1853 (1995)
252. G J Kilpatrick, K T Bunce, M B Tyers *Med. Res. Rev.* **10** 441 (1990)
253. A Butler, J M Hill, S J Ireland, C C Jordan, M B Tyers *Br. J. Pharmacol.* **94** 397 (1988)
254. M A Liberman, S Howe, M Lane *Am. J. Surg.* **179** 60 (2000)
255. F D King (Ed.) *Medicinal Chemistry: Principles and Practice* (Cambridge: Royal Society of Chemistry, 1994)
256. F Heidempergher, A Pillan, V Pinciroli, F Vaghi, C Arrigoni, G Bolis, C Caccia, L Dho, R McArthur, M Varasi *J. Med. Chem.* **40** 3369 (1997)
257. C J Swain, R Baker, C Kneen, J Moseley, J Saunders, E M Seward, G Stevenson, M Beer, J Stanton, K Watling *J. Med. Chem.* **34** 140 (1991)
258. T Fukuda, M Setoguchi, K Inaba, H Shoji, T Tahara *Eur. J. Pharmacol.* **196** 299 (1991)
259. K Haga, K Inaba, H Shoji, Y Morimoto, T Fukuda, M Setoguchi *Jpn. J. Pharmacol.* **63** 377 (1993)
260. D W Robertson, W B Lacefield, W Bloomquist, W Pfeifer, R L Simon, M L Cohen *J. Med. Chem.* **35** 310 (1992)
261. T Rosen, A A Nagel, J P Rizzi, J L Ives, J B Daffeh, A H Ganong, K Guarino, J Heym, S McLean, J T Nowakowski, A W Schmidt, T F Seeger, C J Sick, L A Vincent *J. Med. Chem.* **33** 2715 (1990)
262. A W Schmidt, S J Peroutka *Mol. Pharmacol.* **36** 505 (1989)
263. C J Swain, R Baker, C Kneen, R Herbert, J Moseley, J Saunders, E M Seward, G I Stevenson, M Beer, J Stanton, K Watling, R G Ball *J. Med. Chem.* **35** 1019 (1992)
264. R D Clark, A B Miller, J Berger, D B Repke, K K Weinhardt, B A Kowalczyk, R M Eglen, D W Bonhaus, C H Lee, A D Michel *J. Med. Chem.* **36** 2645 (1993)
265. Y Rival, R Hoffmann, B Didier, V Rybaltchenko, J -J Bourguignon, C G Wermuth *J. Med. Chem.* **41** 311 (1998)
266. Y Sato, M Yamada, S Yoshida, T Soneda, M Ishikawa, T Nizato, K Suzuki, F Konno *J. Med. Chem.* **41** 3015 (1998)
267. M Yamada, Y Sato, K Kobayashi, F Konno, T Soneda, T Watanabe *Chem. Pharm. Bull.* **46** 445 (1998)
268. C Gerald, N Adham, H T Kao, M A Olsen, T M Laz, L E Schechter, J A Bard, P J Vaysse, P R Hartig, T A Branchek *EMBO J.* **14** 2806 (1995)
269. O Blondel, M Gastineau, Y Dahmoune, M Langlois, R Fischmeister *J. Neurochem.* **70** 2252 (1998)
270. K H Buchheit, R Gamse, H J Pfannkuche *Naunyn Schmiedebergs Arch. Pharmacol.* **345** 387 (1992)
271. D L Flynn, D L Zabrowski, D P Becker, R Nosal, C I Villamil, G W Gullikson, C Moummi, D-C Yang *J. Med. Chem.* **35** 1486 (1992)
272. T P Blackburn, G S Baxter, G A Kennet, F D King, D C Piper, G I Sanger, D R Thomas, N Upton, M D Wood *Psychopharmacology* **110** 357 (1993)
273. F D King, M S Hadley, K T Joiner, R T Martin, G J Sanger, D M Smith, G E Smith, P Smith, D H Turner, E A Watts *J. Med. Chem.* **36** 683 (1993)
274. M Langlois, D Yang, B Bremont, S Shen *Bioorg. Med. Chem. Lett.* **5** 795 (1995)
275. R M Eglen, D W Bonhaus, L G Johnson, E Leung, R D Clark *Br. J. Pharmacol.* **115** 1387 (1995)
276. S Elz, A Keller *Arch. Pharm. (Weinheim)* **328** 585 (1995)
277. D Yang, J-L Soulier, S Sicsic, M Mathe-Allainmat, B Bremont, T Croci, R Cardamone, G Aureggi, M Langlois *J. Med. Chem.* **40** 608 (1997)
278. S S Hegde, D W Bonhaus, L G Johnson, E Leung, R D Clark, R M Eglen *Br. J. Pharmacol.* **115** 1087 (1995)
279. R M Eglen, E H Wong, A Dumuis, J Bockaert *Trends Pharmacol. Sci.* **16** 391 (1995)
280. R M Eglen, K Bley, D W Bonhaus, R D Clark, S S Hegde, L G Johnson, E Leung, E H F Wong *Br. J. Pharmacol.* **110** 119 (1993)
281. R D Clark, A Jahangir, L A Flippin, J A Langston, E Leung, D W Bonhaus, E H Wong, L G Jonhnson, R M Eglen *Bioorg. Med. Chem. Lett.* **5** 2119 (1995)
282. A J Kaumann, L M Gaster, F D King, A M Brown *Naunyn Schmiedebergs Arch. Pharmacol.* **349** 546 (1994)
283. L M Gaster, A J Jennings, G F Joiner, F D King, K R Mulholland, S K Rahman, S Starr, P A Wyman, K A Wardle, E S Ellis, K J Sanger *J. Med. Chem.* **36** 4121 (1993)
284. J D Gale, C J Grossman, J W Whitehead, A W Oxford, K T Bunce, P P Humphrey *Br. J. Pharmacol.* **111** 332 (1994)
285. L M Gaster, G F Joiner, F D King, P A Wyman, J M Sutton, S Bingham, E S Ellis, G J Sanger, K A Wardle *J. Med. Chem.* **38** 4760 (1995)
286. I Tapia, L Alonso-Cires, P L Lopez-Tudanca, R Mosquera, L Labeaga, A Innerarity, A Orjales *J. Med. Chem.* **42** 2870 (1999)
287. K-H Buchheit, R Gamse, R Giger, D Hoyer, F Klein, E Kllppner, H-J Pfannkuche, H Mattes *J. Med. Chem.* **38** 2326 (1995)
288. K-H Buchheit, R Gamse, R Giger, D Hoyer, F Klein, E Klöppner, H-J Pfannkuche, H Mattes *J. Med. Chem.* **38** 2331 (1995)
289. A Monge, M del Carmen Pena, J A Palop, J M Caldero, J Roca, E Garcia, G Romero, J del Rio, B Lasheras *J. Med. Chem.* **37** 1320 (1994)
290. J M Schaus, D C Thompson, W E Bloomquist, A D Susemichel, D O Calligaro, M L Cohen *J. Med. Chem.* **41** 1943 (1998)
291. J-L Soulier, D Yang, B Bremont, T Croci, U Guzzi, M Langlois *J. Med. Chem.* **40** 1755 (1997)
292. M-L Cohen, W Bloomquist, J M Schaus, D C Thompson, A D Susemichel, D O Calligaro, I Cohen *J. Pharmacol. Exp. Ther.* **277** 97 (1996)
293. M Wood, M Chaubey, P Atkinson, D R Thomas *Eur. J. Pharmacol.* **396** 1 (2000)
294. B L Roth, S C Craigo, M S Choudhary, A Uluer, F J Monsma Jr, Y Shen, H Y Meltzer, D R Sibley *J. Pharmacol. Exp. Ther.* **268** 1403 (1994)
295. I T Forbes, S Dabbs, D M Duckworth, A J Jennings, F D King, P J Lovell, A M Brown, L Collin, J J Hagan, D N Middlemiss, G J Riley, D R Thomas, N Upton *J. Med. Chem.* **41** 655 (1998)
296. R A Glennon, M Lee, J B Rangisetty, M Dukat, B L Roth, J E Savage, A McBride, L Rauser, S Hufeisen, D K H Lee *J. Med. Chem.* **43** 1011 (2000)

[a] — *Moscow Univ. Bull. (Engl. Transl.)*
[b] — *Russ. J. Org. Chem. (Engl. Transl.)*

Russian Chemical Reviews **70** (5) 357 – 372 (2001) © 2001 Russian Academy of Sciences and Turpion Ltd

DOI 10.1070/RC2001v070n05ABEH000636

Chemical chromaticity: potential of the method, application areas and future prospects

V M Ivanov, O V Kuznetsova

Contents

I.	Introduction	357
II.	The main chromaticity characteristics and relationships between them	358
III.	The theoretical aspects of the chemical chromaticity method	360
IV.	Practical applications of the chromaticity method	366
V.	Conclusion	370

Abstract. Data on the application of the chromaticity method in chemical analysis and in various branches of industry are surveyed. The potential of the method is demonstrated and the prospects of its further development are discussed. The bibliography includes 196 references.

I. Introduction

Chromaticity is a science that deals with methods for colour measurement and its quantitative characterisation. The chromaticity method involving calculation of colour characteristics from the available spectral parameters of a test sample makes it possible to both differentiate between spectrally similar compounds and obtain additional information about them. In view of this, researchers are interested in the informative potential of the method, its field of application and limitations.

A great number of studies on the elaboration of visual detection systems and image processing have been published to date; most of these are comprehensive specialised monographs that mostly deal with the traditional methods for colour measurement and data processing.[1–5] However, so far this perfect mathematical apparatus has been little employed in analytical chemistry, although there are a number of computerised spectroscopic analytical procedures that use colour measuring systems.[4]

The appearance of a characteristic colour upon a chemical reaction is normally used in qualitative analysis for the detection of elements. It is well known that our vision is very sensitive to small absolute light intensity and distinguishes hues rather well. Not only can an eye compare two radiations but it can also determine which one is more (or less) intense. Colorimetric systems are designed and perfected for the quantitative evaluation of radiation. For some time, their practical use was hindered by the complexity of the hardware required. The need for determination of the compositions of complex dye mixtures used in the textile industry has served as an impetus for the development of the chromaticity method. The solution of this problem has made it possible not only to develop compact light-measuring instruments but also to create a mathematical apparatus for the calculation of concentration dependences from the colour changes in the test samples.

There are two basic methods for colour measurement which differ in the calculation procedure: one is based on the spectral composition of radiation and the other is based on the number of individual colours in a mixture resulting in the colour to be determined. According to this classification, all colorimetric instruments and procedures for the calculation of chromaticity coordinates can arbitrarily be divided into two types, depending on the quantity to be measured:

1. The chromaticity coordinates are calculated from the known spectral composition of radiation from a test compound (absorption and reflectance spectra, *etc*.). This method is believed to be the most accurate.[6]

2. The measured general function of colour addition (which in many cases corresponds to the sensitivities of photocells) is used to determine directly the chromaticity coordinates of the required component. The development of this method is hampered due to the difficulty of manufacturing photocells with the required spectral sensitivities.

The measurement inaccuracy of a colorimetric instrument is predicted as a function of the principle of its operation.[7–10]

Chromaticity measurements are successfully used in spectrophotometric titration,[11–13] as well as for characterisation of the forms in which indicators exist.[14–17] Chromaticity measurements are even more promising in chemical analysis in the absence or with minor use of instrumentation. Owing to the development of visual-detection express methods, the problem arises of determination of the content of a compound from the overall change in the colour of a test sample (the so-called test-methods); this problem can only be solved by chromaticity measurement methods which approximate most exactly the characteristics of human vision.

The methods of objective colour measurement with computer data processing are popular in many branches of industry, *e.g*., in the printing and paint industries,[18,19] textile industry,[20–22] glass industry[23,24] and pharmaceutical industry.[25,26] In addition, colour is an important parameter of the quality of food.[27,28] There are so many application fields of chromaticity measurement methods that they cannot all be listed.

To our knowledge, only one review on the application of the chromaticity method has appeared over the last ten years.[14] However, more than 200 publications on various aspects of the method have been published over the same period. These vast literature data are scattered, which hampers the studies, especially for those scientists who just start working in this field. In view of this, the purpose of our review is to discuss the analytical

V M Ivanov, O V Kuznetsova Department of Chemistry, M V Lomonosov Moscow State University, Leninskie Gory, 119899 Moscow, Russian Federation. Fax (7-095) 932 88 46. Tel. (7-095) 939 22 77

Received 16 November 2000
Uspekhi Khimii **70** (5) 411 – 428 (2001); translated by S S Veselyi

capabilities and practical applications of the chromaticity method and to estimate the major trends and prospects in this field.

II. The main chromaticity characteristics and relationships between them

In essence, spectroscopic methods of analysis involve the detection of optical radiation parameters of a test sample. As a rule, these are the space–time distributions of radiation, its amplitude, frequency, phase, polarisation and coherence ratio. Measurement of the analytical signal is based on changes in these parameters due to interaction of the optical radiation with the object that is analysed (light absorption, reflection, dispersion) and on changes in the characteristics of the object itself upon exposure to light due to photochromism, electrooptical effects, luminescence and other phenomena.[6] The main informative parameters of optical monitoring in analytical chemistry include amplitude-related parameters, such as optical density (A), diffuse reflection coefficient (R), luminescence intensity (I_{lum}), *etc*. Integral characteristics (the total colour differences measured photometrically) are almost never used for this purpose.

According to Grassman's laws,[1] colour determination requires that three parameters be measured independently; two of them characterise the colour and the third one, the intensity. However, these parameters are used extremely seldom in analytical chemistry because of certain specific features of quantitative measurements.

Spectroscopic analysis does not allow direct determination of the chemical composition of a compound. It gives indirect information in the form of a suitable measurable physical quantity, such as optical density, diffuse reflectance, *etc*. An additional independent parameter, such as wavelength or frequency, is introduced in order to describe the spectrum. Chemical analytical techniques are mostly based on the amplitude-related characteristics and the values of these independently measured parameters. A similar approach is used for measurement of chromaticity characteristics.[29]

The mathematical description of colour in colorimetry is based on the experimental fact that each colour can be represented as a mixture (sum) of certain amounts of three linearly independent colours.[2] The basic colours include red (R), green (G) and blue (B), *i.e*., three monochromatic radiations with wavelengths (λ) of 700, 546.1 and 435.8 nm, respectively.[30]

The colour gamut diagram in this system is shown in Fig. 1. The point S_1 corresponds to a colour within the colour gamut, while S_2 corresponds to a colour outside the gamut. It is most convenient to illustrate this representation geometrically. The three basic colours serve as axes in the orthogonal coordinate system, while any colour determined by three chromaticity coordinates is reflected by a vector **S** (see Fig. 1)

$$\mathbf{S} = R\mathbf{R} + G\mathbf{G} + B\mathbf{B}, \qquad (1)$$

where R, G and B are the red, green and blue chromaticity coordinates, respectively; **R**, **G** and **B** are the unit vectors of these colours that are mixed. Connection of the unit basic colour points ($R = 1$, $G = 1$, $B = 1$) with each other gives a triangle located in the unit plane. A remarkable feature of this plane is that the colour vectors having different lengths but the same direction cross it in the same point S, which characterises the colour saturation. In order to establish the position of the point S on the unit plane, the chromaticity coordinates r, g, b are introduced; these are related to the chromaticity coordinates R, G, B as follows:

$$r = \frac{R}{R+G+B}; \quad g = \frac{G}{R+G+B}; \quad b = \frac{B}{R+G+B}. \qquad (2)$$

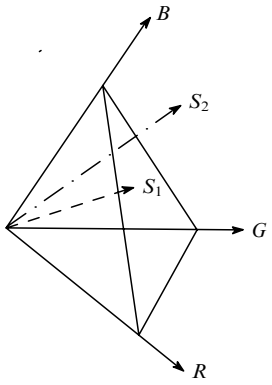

Figure 1. The RGB three-coordinate colour space.[30]

It follows from relationships (2) that $r + g + b = 1$, *i.e*., two chromaticity coordinates are sufficient to determine unambiguously the position of a point on the unit plane.

The colour perception by humans is taken into account based on experiments with colour mixing. In these experiments, one has to equalise visually pure spectral colours of equal intensity (which correspond to monochromatic lights with various wavelengths) with mixtures of the three basic colours produced by an analytical instrument. To make the comparison, pure spectral light and a mixture of the three basic colours are arranged alongside on two halves of the photometric comparison field. Upon equalisation, the amounts of the three basic colours are measured and their ratios to the unit amounts of these colours are determined. The values obtained are the chromaticity coordinates of the colour that is equalised in the selected chromaticity coordinate system. This procedure does not allow equalisation of the majority of pure spectral colours with mixtures of the three basic colours provided by the instrument. In such cases, a certain amount of one of the basic colours is added to the colour to be equalised, *i.e*., the chromaticity coordinate is allowed to be negative. Based on the estimates given by several observers, one calculates the averaged amounts of the three basic colours (specific chromaticity coordinates) which produce a mixture visually indistinguishable from the pure spectral colour. The graphic plots of the basic colour amounts on the wavelength represent the so-called colour addition curves. Based on these curves, one can calculate the fractions of the basic colours required to obtain a mixture visually indistinguishable from a colour with a complex spectral composition. For this purpose, the colour of a complex radiation is represented as a sum of pure spectral colours corresponding to its monochromatic components (with account of their intensities). The possibility of such representation is based on one of Grassman's laws, according to which the chromaticity coordinates of the colour of a mixture are equal to the sums of the corresponding coordinates of all of the colours mixed.

The addition functions are positive for the colours included in the RGB colour gamut. However, if a colour is outside the gamut, the addition functions become negative, which is inconvenient for calculations. In order to overcome this drawback, the International Commission on Illumination (CIE) summarised the known colour properties and formulas for colour variation calculations. As a result, a non-orthogonal three-colour system (XYZ) was created, which describes the spectral properties of a test object as three-dimensional vector coordinates.[2] The integral separation of the light radiation intensity into three components is convenient for correlation with human vision (due to the existence of red-, green- and blue-sensitive fibres in the eye retina).

The XYZ coordinate system is based on the following assumptions:

— the XYZ chromaticity coordinates are always positive for all real colours;

— the Y coordinate defines the colour brightness;

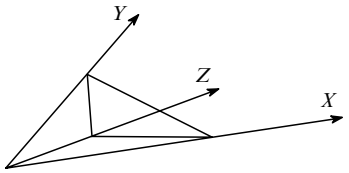

Figure 2. The XYZ three-coordinate colour space.[2]

— the chromaticity coordinates of white equal-energy radiation correspond to the centre of gravity of a triangle located in the unit plane (Fig. 2).

The following relationships are used for conversion from the RGB system of basic colours to the XYZ system:

$$\mathbf{X} = X_R\mathbf{R} + X_G\mathbf{G} + X_B\mathbf{B}, \tag{3}$$

$$\mathbf{Y} = Y_R\mathbf{R} + Y_G\mathbf{G} + Y_B\mathbf{B}, \tag{4}$$

$$\mathbf{Z} = Z_R\mathbf{R} + Z_G\mathbf{G} + Z_B\mathbf{B}, \tag{5}$$

where X_R, X_G, X_B, Y_R, Y_G, Y_B, Z_R, Z_G and Z_B are coordinates of the basic colours in the three-coordinate RGB space. It should be noted that these values have also been standardised. The chromaticity coordinates in the new colour space will have the form

$$x = \frac{X}{X+Y+Z}, \quad y = \frac{Y}{X+Y+Z}, \quad z = \frac{Z}{X+Y+Z}, \quad x+y+z = 1. \tag{6}$$

A unit plane is a right-angled triangle called the chromaticity plot; its vertices are located in the intersection points with the vectors of the basic colours. The vectors of spectral colours cross the unit plane along the pure spectral colour line (Fig. 3), which limits the region of existence of the real colours.

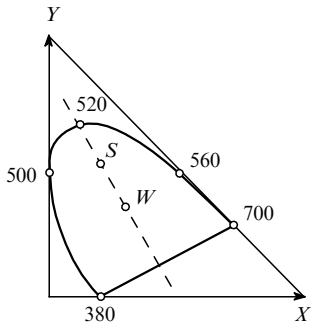

Figure 3. A unit plane in the XYZ system and the line of pure spectral colours (the solid curve).[2]
The S and W points correspond to the chromaticity coordinates of a given colour and white colour. The numbers indicate the irradiation wavelengths (λ /nm).

In addition to the X, Y, Z coordinates, there are other characteristics such as hue [$T(\lambda)$] and colour purity (P), which define unambiguously the radiation chromaticity. Obviously, any real colour can be obtained by additive mixing of white radiation with the appropriate monochromatic radiation. The hue is determined by the intersection point of the straight line which passes through the chromaticity coordinates of a given colour and the white colour (see points S and W in Fig. 3) with the pure spectral colour line (Fig. 4). The colour purity shows the ratio in which the monochromatic and white colours are mixed; the purity of monochromatic radiation is equal to unity and that of white radiation is equal to zero.

It should be noted that the use of the colour plot in the XYZ system (CIE, 1931) meets certain difficulties. For example, some

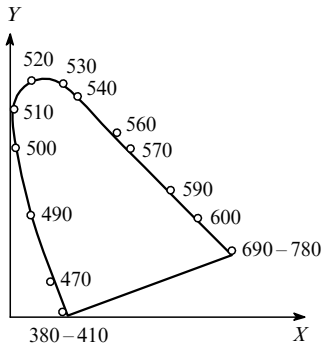

Figure 4. A colour diagram in the XYZ system.[2]
The numbers indicate the irradiation wavelengths (λ /nm).

distances between pairs of points in the plot (see Fig. 4) do not correlate with the visual perception of humans, since the scale of the plot is non-uniform. In addition, it does not give information regarding the colour lightness. The systems considered above provide only a quantitative estimate of the colour, but one cannot estimate visually the difference between two colours using these systems, since the distances between points in the colour space do not correspond to a difference reliably visible by eye. Several attempts have been undertaken to create such an equicontrast space where the distance between two points would correlate with visible colour variation. However, none of these attempts have been successful to date. The International Commission on Illumination has proposed several quasi-equal contrast systems of this kind; *CIELAB* (1976) is most popular of these systems. The L, A, B coordinates in this system are related to the X, Y, Z coordinates by the following relationships:

$$L = 116\,(Y/Y_W)^{1/3} - 16, \tag{7}$$

$$A = 500\,(X/X_W)^{1/3} - (Y/Y_W)^{1/3}, \tag{8}$$

$$B = 200\,(Y/Y_W)^{1/3} - (Z/Z_W)^{1/3}, \tag{9}$$

where L is lightness; A and B are the chromaticity coordinates (A is used for the red-green axis; B, for the yellow-blue axis); X_W, Y_W, Z_W are the coordinates of the white colour in the XYZ system; the axes A and B lie in a plane perpendicular to the L axis (Fig. 5).

The distance between two points in the three-coordinate LAB colour space characterises the total colour difference (ΔE) calculated using the formula

$$\Delta E = \sqrt{(\Delta L)^2 + (\Delta A)^2 + (\Delta B)^2}. \tag{10}$$

The hue (T) and saturation (S) are determined by the following relationships:

$$S^2 = A^2 + B^2, \qquad T = \operatorname{arctg}(B/A). \tag{11}$$

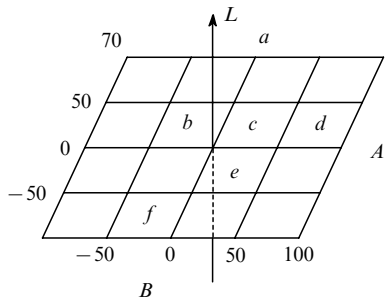

Figure 5. The LAB three-coordinate colour space. The white (a), green (b), grey (c), yellow (d), purple (e) and blue (f) regions.[30]

The yellowness (G) and whiteness (W) are expressed by the equations

$$G = \frac{100(1.28X - 1.06Z)}{Y}, \quad W = 100 - \Delta E. \tag{12}$$

The *CIELAB* colour space is most suitable for calculations, since equal distances between the points corresponding to different colours in any part of this coordinate system correlate with visual perception, enabling one to introduce a convenient measure for the quantitative determination of colour differences. In practice, the chromaticity coordinates in the *XYZ* and *CIELAB* systems and the colour characteristics of the objects of interest are obtained, *e.g.*, from the diffusion reflectance spectrum, as follows:

$$X = k \sum_{\lambda} S(\lambda)\bar{x}(\lambda)R(\lambda)\Delta\lambda, \tag{13}$$

$$Y = k \sum_{\lambda} S(\lambda)\bar{y}(\lambda)R(\lambda)\Delta\lambda, \tag{14}$$

$$Z = k \sum_{\lambda} S(\lambda)\bar{z}(\lambda)R(\lambda)\Delta\lambda, \tag{15}$$

where k is the normalising coefficient; $S(\lambda)$ is the radiation spectral density from one of the standard light sources A, C or D_{65} in relative units; $\bar{x}$, $\bar{y}$ and $\bar{z}$ are the colour addition functions; $R(\lambda)$ is the measured diffuse reflection coefficient. For self-luminous objects:

$$k = \frac{100}{\sum_{\lambda} S(\lambda)\bar{y}(\lambda)\Delta\lambda}.$$

Upon introduction of the factor k, the chromaticity coordinates for non-self-luminous objects are expressed in the scale where $Y = 100$.

Thus, chromaticity characteristics are more informative than the spectral ones, although they cannot be used without analysis of diffuse reflection spectra. The use of chromaticity characteristics in analytical chemistry expands the possibilities of studying processes that occur in test samples. The colorimetric instruments and calculation methods created for this purpose make it possible to detect colour changes and to use colour measurements for the analysis of objects.[31–33]

III. The theoretical aspects of the chemical chromaticity method

The most common task in the broad range of analyses carried out with the use of chromaticity involves the determination of metal ions. It is easy to understand that the essence of the method requires that the metals be transformed into coloured compounds, in most cases into complexes with organic ligands. These compounds can be analysed both in solution and in solid state (in the form of sorbates); in the latter case, the detection limit can be lowered by pre-concentration. Metals are mostly transformed into coloured compounds using the classical organic reagents employed in conventional spectrophotometry. Chromaticity studies on the properties of these organic reagents (optical and chromaticity parameters, *etc.*) is an important but insufficiently studied stage in the development of analytical procedures.

1. Studies of the state of organic reagents in solution and in the sorbent phase

Studies of the properties of organic reagents are important for expanding the analytical capabilities of chromaticity.[34] In view of this, the optical and chromaticity characteristics of Arsenazo III in solution and in the adsorbed state on an AV-17 anion-exchange resin have been studied. The chromaticity functions (CF) of Arsenazo III, namely the chromaticity coordinates x, y, z in the *XYZ* system, lightness (L), chromaticity coordinates A, B in the *CIELAB* system, colour saturation (S), yellowness (G), hue (T), as well as colour differences with respect to saturation (ΔS), lightness (ΔL) and tint (ΔT), were measured relative to a white colour standard with a diffuse reflection coefficient R equal to 0.98. It is assumed for an absolutely white body that $R = 1$, $W = 100$, and both ΔE and G equal zero. The functions R, W, L, X, Y, Z should be lower and ΔE should be higher for coloured compounds that absorb and reflect light simultaneously; these differences are the more significant the more intense the coloration of compounds. In agreement with this, the values of the functions R, W, L, X, Y, Z for sorbates, the coloration of which is more intense than that of solutions due to concentration, are lower, namely, they vary from 20 to 40 (for R in the range 0.2–0.4), whereas for solutions they vary from 80 to 70 (for R in the range 0.8–0.7). Of the CF, the yellowness provides the most abundant colour information. For an absolutely white body, $G = 0$; for yellow and red bodies, $G > 0$, while for green and blue ones, $G < 0$. The inflexion points in the plots (Fig. 6) correspond to regions of transition between the forms. Changes in the magnitude and sign of G in the inflexion points can indicate the state of the organic reagent in the test medium. In Arsenazo III solutions at pH < 5, the yellowness becomes positive as they contain H_8R molecules and ions such as H_7R^- (pH < 2), H_6R^{2-}, H_4R^{4-} (pH ≈ 4.6), which are red. At pH > 9.6, the yellowness is negative (−10), since the blue ions (HR^{7-} and R^{8-}) dominate in the solution. On the contrary, the G values are positive and rather high (from 40 to 120) for all sorbates and reach a maximum (120) at pH 12. It was inferred from these data that only the red ions, most likely the single-charged H_7R^- ions, are sorbed on the anion-exchange resin. Sorption of two- and multicharged ions is hampered or impossible due to steric hindrance. Ivanov *et al.*[34] suggested the use of molar CF coefficients (the ratio of the signal of a given CF to the concentration of the complexing agent expressed in mol litre^{-1}) which increase in the series: $R < G < B < L$, $X < S$, $A < W < \Delta E < Z < Y$. It was also found that the molar CF coefficients are 1.5–2.5 orders higher than the molar absorption coefficients (ε). This suggests that the

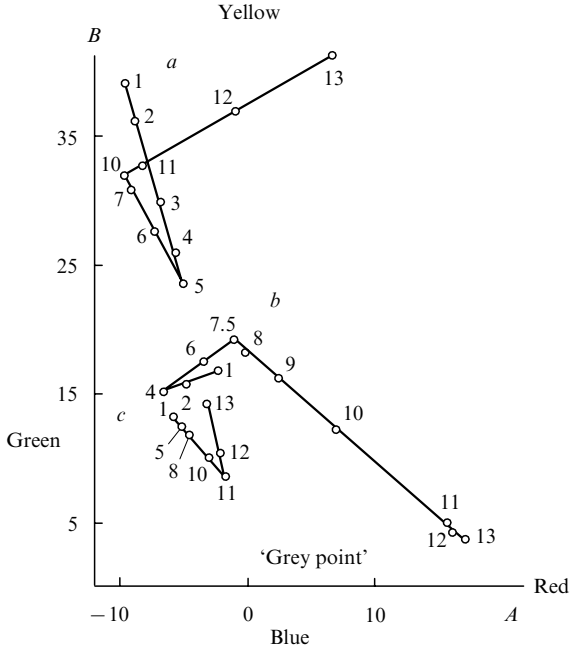

Figure 6. Changes in the A and B chromaticity coordinates (*CIELAB*) of 4-(2-pyridylazo)resorcinol (PAR) (*a*), 4-(2-thiazolylazo)resorcinol (TAR) (*b*) and 1-(2-pyridylazo)-2-naphthol (PAN) (*c*) solutions as functions of the medium acidity.[41]
Solution concentrations ($10^5 c$ /mol litre^{-1}): (*a*) 5, (*b*) 1.5, (*c*) 2.5. Acetone concentration (vol.%): (*a*) 0, (*b*) 10, (*c*) 20; the ionic strength (I) equals 0.1. The numbers indicate the pH of the solutions.

use of CF is promising for an increase in the sensitivity of determinations.

2. Studies of acid – base properties of reagents

In the majority of studies, spectrophotometric methods are used to determine the dissociation constants of organic reagents. In these methods, dependences of optical density on the solution pH are obtained and then processed graphically or by semi- or bilogarithmic computational methods. A correct choice of wavelengths is very important when measuring the optical density. They normally correspond to the maxima of light absorption by various ionic and molecular forms of the reagents. The situation becomes more complicated if the positions of the maxima differ insignificantly and especially if tautomeric equilibria exist and are imposed on the dissociation equilibria.

Changes in the properties of the equilibrium states of a reagent can be recorded using the chromaticity coordinates of the *CIELAB* equicontrast chromaticity system.[30] These values provide data on the integral distribution of light absorption in an equilibrium system tested in a broad range of wavelengths (380 – 720 nm). This allows one to avoid inaccuracies associated with a wrong choice of the range of the reagent absorption spectrum where the measurements are carried out. Thus, the reliability of the results obtained increases considerably.

Two methods exist for the determination of the equilibrium constants (pK_a).

1. Colour saturation (S) is plotted *versus* the solution pH at various reagent concentrations, then pK_a is determined graphically or calculated using the equation

$$pK_a = pH_1 + \frac{(pH_2 - pH_1)(\Delta S_1' - \Delta S_1)}{(\Delta S_2 - \Delta S_2') + (\Delta S_1' - \Delta S_1)}, \qquad (16)$$

where pH_1 and pH_2 are pH values around the assumed pK value; ΔS_1, ΔS_2, $\Delta S_1'$ and $\Delta S_2'$ are the changes in saturation depending on whether the equilibrium is shifted from alkaline to acid or from acid to alkaline medium, respectively.[35]

2. Differential plots of the reagent colour on the medium acidity are used:

$$SCD = \frac{\Delta S}{\Delta pH},$$

where the *SCD* (specific colour discrimination) parameter characterises the change in the colour saturation upon a change in pH.

The latter method is more accurate and has proved itself well in titrimetric methods.[36–39] Its application in complexonometric titration is discussed in detail elsewhere.[30,40] Of considerable interest was the use of the differential method for the determination of dissociation constants in spectroscopic analytical methods (diffuse reflection spectroscopy, solid-phase spectrophotometry). Heterocyclic azo compounds, namely, PAN, PAR and TAR, have been chosen,[41] since these are well studied as metallochromic indicators.

a. Determination of dissociation constants in solutions

It is known that PAR, TAR and PAN can exist in three main forms, *viz*., protonated at the nitrogen atom, neutral (molecular) and anionic (formed due to dissociation of the hydroxy groups) depending on the medium acidity.[42]

The variations of the chromaticity coordinates A and B (*CIELAB*) of model solutions of PAR, TAR and PAN at various pH values are shown in Fig. 6. It follows from the general character of these dependences that there are discrete pH values where the colour changes proportionally to the content of the form in which the reagent exists in the solution, and the differential plots of the colour of PAR, TAR and PAN *versus* the medium acidity should contain maxima corresponding to the pK values of the reagents. Differential curves of this type are usually analysed using the *SCD* parameter.[43,44] Morozko *et al*.[41] made calculations based on the numerical values of colour saturation. The dissociation constants found by the graphical method were found to be close to those obtained by the method of isosbestic points (Table 1).

Table 1. Dissociation constants of PAR, TAR and PAN in water – acetone solutions determined by chromaticity method and the method of isosbestic points ($I = 0.1$).

Reagent	Acetone concentration (vol.%)	Constant	pK_i obtained by	
			chromaticity method [a]	method of isosbestic points
PAR	0 [b]	pK_{NH}	2.7 ± 0.1	2.55 ± 0.15 (see [42])
	0 [b]	p$K_{p\text{-OH}}$	5.3 ± 0.2	5.47 ± 0.09 (see [45])
	0 [b]	p$K_{o\text{-OH}}$	11.5 ± 0.2	11.36 ± 0.08 (see [46])
TAR	10	pK_{NH}	1.0 ± 0.2	–
	10	p$K_{p\text{-OH}}$	5.8 ± 0.2	5.9 (see [47])
	10	p$K_{o\text{-OH}}$	9.5 ± 0.2	9.4 (see [48])
	20	pK_{NH}	1.0 ± 0.1	–
	20	p$K_{p\text{-OH}}$	6.3 ± 0.1	6.15 ± 0.22 (see [49])
	20	p$K_{o\text{-OH}}$	9.8 ± 0.2	9.68 ± 0.19 (see [49])
	40	pK_{NH}	0.8 ± 0.2	–
	40	p$K_{p\text{-OH}}$	7.1 ± 0.2	7.33 ± 0.17 (see [45])
	40	p$K_{o\text{-OH}}$	12.1 ± 0.2	12.32 ± 0.18 (see [45])
PAN	10	pK_{NH}	2.1 ± 0.2	2.32 ± 0.04 (see [50])
	10	pK_{OH}	11.9 ± 0.2	12.0 ± 0.03 (see [50])
	20	pK_{NH}	1.9 ± 0.2	1.90 ± 0.03 (see [51])
	20	pK_{OH}	12.0 ± 0.2	12.22 ± 0.05 (see [51])
	40	pK_{NH}	1.7 ± 0.2	2.09 ± 0.08 (see [52])
	40	pK_{OH}	12.2 ± 0.2	12.63 ± 0.06 (see [52])

[a] Reported data;[41] [b] measurements in water.

In a number of studies on acid – base equilibria in solutions of heterocyclic azo compounds,[53,54] it was noted that the region of existence of the reactive molecular form of an organic reagent expands with a decrease in the dielectric constant (ε) of the medium. This statement has been checked by the chromaticity method for model water – acetone solutions of PAN, PAR and TAR.[41] Figure 7 shows these dependences for TAR. The character of changes in the pK_{NH} and pK_{OH} constants makes it possible to conclude that as the content of the organic solvent increases, the reaction occurs in a more acidic medium (pK_{NH} decreases with a decrease in ε), whereas the stability of the complex increases (pK_{OH} increases with a decrease in ε).

The effect of the solvent on the pK_{NH} and pK_{OH} values for TAR was demonstrated by measuring the half-widths of *SCD* peaks (Table 2). The narrower the peak the closer the pK value

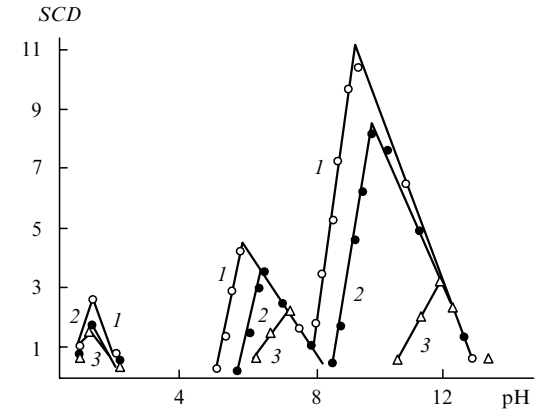

Figure 7. Variation of *SCD* of a TAR solution ($c = 10^{-5}$ mol litre^{-1}) as a function of acetone concentration and pH.[41] Acetone concentration (vol.%): (*1*) 10, (*2*) 20, (*3*) 40.

Table 2. Peak half-widths *SCD* ($\Delta p_{0.5}H_i$) as a function of acetone concentration.[41]

Parameter	$\Delta p_{0.5}H_i$ at acetone concentrations (vol.%)		
	10	20	40
$\Delta p_{0.5}H_{NH}$	0.4 ± 0.1	1.2 ± 0.2	0.3 ± 0.1
$\Delta p_{0.5}H_{p\text{-OH}}$	1.0 ± 0.2	1.2 ± 0.2	0.5 ± 0.2
$\Delta p_{0.5}H_{o\text{-OH}}$	1.2 ± 0.2	1.3 ± 0.2	0.6 ± 0.2

found graphically to that found by calculation. The results obtained suggest a sharper colour change of the reagent forms existing in solution upon both the variation of the medium acidity and the increase in the content of the polar solvent.

b. Determination of dissociation constants in the sorbent phase

The chromaticity approach to the determination of the state of organic reagents has been well proved for solutions.[55, 56] On the other hand, studies of protolytic reactions of these organic compounds on sorbent surfaces are no less important for investigation of the properties of the modified sorbents. First, protolytic equilibria characterise the reactivities of compounds, because this type of reaction is restricted to a larger extent than, *e.g.*, complexation processes. Hence, the data obtained allow one to estimate rather reliably the reactivities of different functional groups of the sorbent and of the organic compound immobilised thereon. In addition, the knowledge of the acid–base properties of reagents is necessary for the quantitative description of the stability of complexes on sorbent surfaces.

The state of TAR in the phases of silica (Silochrom C-120) and an anion-exchange resin with styrene–divinylbenzene matrix (AV-17 × 8) was studied[41] by diffuse reflectance spectroscopy (DRS) and by solid-phase spectrophotometry (SPS). The TAR dissociation constants have been found using the graphical and chromaticity calculation methods based on Fig. 8: the values of pK_{NH}, $pK_{p\text{-OH}}$ and $pK_{o\text{-OH}}$ were 1.5 ± 0.2, 6.6 ± 0.2 and 10.8 ± 0.2 for Silochrom C-120 and 1.0 ± 0.2, 5.7 ± 0.2 and 9.4 ± 0.2 for the anion-exchange resin AV-17 × 8, respectively.

Let us note that the above values of the TAR dissociation constants on AV-17 × 8 are close to those obtained for solutions. For TAR sorbed on silica, the dissociation equilibrium is shifted to the more alkaline region in comparison with solutions. This can probably be explained by specific interactions in the sorbate–sorbent system and by destruction of the silica skeleton (at pH > 10)[57] and possible dissociation of silicic acid ($pK_1 = 9.9$, $pK_2 = 11.8$, $pK_3 = 13.7$).[58]

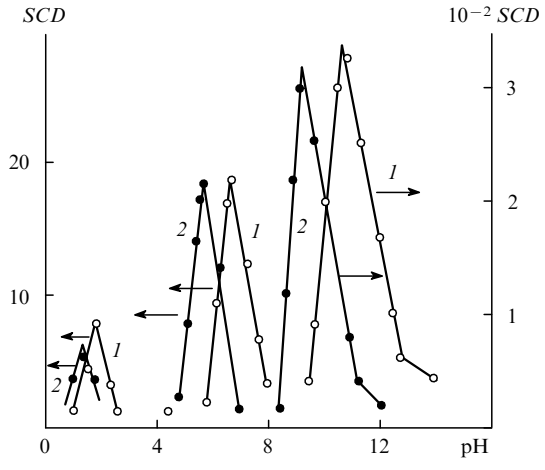

Figure 8. Variation of *SCD* of modified sorbents as a function of medium acidity.[41]
Systems: (*1*) SG–TAR, $c = 20$ μmol g^{-1} (DRS method); (*2*) AV-17 × 8–TAR, $c = 10$ μmol g^{-1} (SPS method). Sorbent fractions 200–350 μm.

It can be concluded that the quantitative description of equilibrium in the sorbent phase is a much more complicated task which usually involves a number of simplifications and assumptions that cannot be verified strictly. In spite of this, studies of equilibria on solid phase surfaces by the chromaticity method not only facilitate experimental procedures but are also of undoubted interest for researchers, as complex-forming sorbents are widely used in analytical chemistry.

3. Increasing the sensitivity of determination of metal ions

It is important to know the chromaticity parameters of complexes in order to expand the determination capabilities of chromaticity methods for elements. The use of chromaticity coordinates can increase both the determination selectivity and its sensitivity, as CF vary over broader limits than optical density or the diffuse reflectance coefficient.

Complexation of a series of transition metals, *viz.*, Cu^{II}, Zn^{II}, Ni^{II}, Mn^{II}, Fe^{III}, Cr^{III}, Co^{II}, Co^{III}, with PAN immobilised on silica gel (SG–PAN) was studied.[59, 60] It was found that the chromaticity coordinates of the SG–PAN surface in the air-dry state are strictly constant, *viz.*, $A = 77.0 \pm 0.5$ and $B = 34.0 \pm 0.5$. Basically, the chromaticity coordinates should remain constant. However, since various masking substances (for example, sodium thiosulfate for masking copper and sodium fluoride for masking iron) were added and the medium acidity was changed during the experiments, the initial chromaticity coordinates of SG–PAN changed also. These changes were particularly pronounced in the case of Mn^{II} and Cr^{III}, because the determination was carried out at pH 10.0, *i.e.*, near the critical acidity of the sorbent (pH 11.0) where it undergoes decomposition (depolymerisation). Owing to cleavage of hydrogen bonds and desorption of PAN, the chromaticity coordinates in the reference experiment are close to the 'grey point'. An increase in the absolute content of a metal ion in the solution changes the chromaticity coordinates of the complex proportionally and linearly; the saturation point of SG–PAN remains virtually constant. This means that the saturation point can serve as an individual characteristic for the detection of elements in solution. This point is usually determined using such parameters as the hue and saturation. In this case, the hue allows one to judge to which primary colour the given colour corresponds. For example, the hue of zinc is 625 nm, *i.e.*, a red colour. Saturation shows to what degree the hue is expressed in the given colour. The higher the saturation the brighter the colour of a complex adsorbed by SG–PAN.

The optimum conditions for the complexation of rare-earth metal (REM) ions, *viz.*, La, Nd, Sm, Tb, Dy, Ho, Er, Yb, with PAR were determined.[61] For all of the complexes, correlation equations for the dependence of CF on the REM concentration in the range of 0.4–2.0 μg ml^{-1} were obtained. As an example, Fig. 9 presents such dependences for erbium pyridylazoresorcinate; for the other REM studied, similar dependences were observed. It was shown that of all CF studied, the chromaticity coordinate A, the yellowness (G) and the hue (T) have the maximum magnitudes; the use of these quantities allows one to increase the determination sensitivity 35–50-fold in comparison with the sensitivity that can be achieved by spectrophotometry. Unfortunately, no correlations between the optical (such as molar absorption coefficients) or chromaticity characteristics and the properties of metal ions (for example, ionic radii) could be found.[61]

Later,[62] the features of complexation of some REM with organic reagents of various classes were studied. In particular, the complexation of lanthanum, terbium and erbium with 2-(5-bromo-2-pyridylazo)-5-diethylaminophenol (5-Br-PAAP) was studied with and without cationic (dodecyltrimethylammonium bromide), anionic (sodium dodecylsulfate) and non-ionic (OP-7) surfactants at various concentrations of organic solvents. The majority of CF depend linearly on the element concentration in

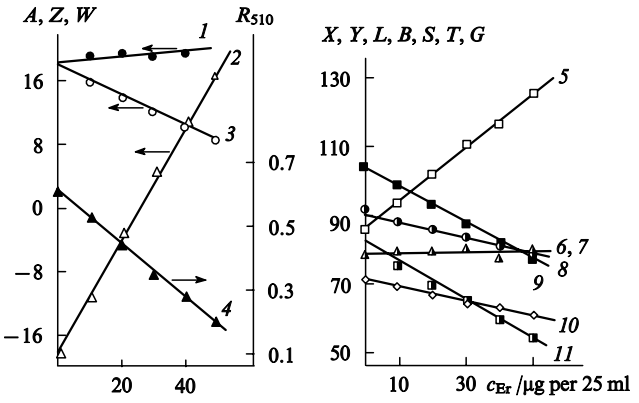

Figure 9. Dependence of the colour functions of erbium 4-(2-pyridylazo)resorcinate on the erbium concentration:[61]
(*1*) whiteness (*W*), (*2*) the chromaticity coordinate *A* in the *CIELAB* system, (*3*) the chromaticity coordinate *X* in the *XYZ* system, (*4*) diffuse reflectance coefficient at $\lambda = 510$ nm (R_{510}), (*5*) yellowness (*G*) (*6*) the chromaticity coordinate *B* in the *CIELAB* system, (*7*) saturation (*S*), (*8*) the *L* coordinate in the *CIELAB* system, (*9*) hue (*T*), (*10*) the *X* coordinate and (*11*) the *Y* coordinate in the *XYZ* system.

solution. However, for some functions, *e.g.*, for *T*, *Z*, *A* and *W*, this proportionality is violated, though the reasons for these anomalies are as yet unclear. The molar absorption coefficients were compared to the molar CF coefficients of the complexes under optimal complexation conditions. The *G*, *S* and *B* values were found to be the most sensitive characteristics. For complexes of lanthanum, erbium and terbium, the molar CF coefficients decrease in the series $G > S > B > W > Y > X > Z > L$, $B > G > S > Y > A > W > X > L$ and $B > S > W > Y > A > X > L$, respectively.

It was also shown that the use of CF provides an essential increase in the sensitivity of REM determination, *viz.*, by a factor of 25 – 100 in comparison with photometric methods (*cf.* Ref. 61).

Similar studies were carried out for complexes of erbium with Arsenazo I, Arsenazo III and Chlorophosphonazo III.[63] The molar CF coefficients for these complexes decrease in the series $G > B > Y > X > Z > L > W > A$ for Arsenazo I, $T > A > S > G > W > X > B > Y > L$ for Arsenazo III and $T > G > S > A > W > B > Y > X$ for Chlorophosphonazo III.

A study on the dependence of colour functions on the optical path length showed that all of them, except hue, change proportionally with the increase in the optical path, but the proportionality coefficient does not correlate with the molar coefficients of these functions. In addition, the sign of the change in a CF does not always coincide with the sign of its molar coefficient. These anomalies are explained [63] by the existence of complex non-linear relationships between the CF. Thus, the CF should be measured at the same layer thicknesses rather than be referred to 1 cm, as is common in photometry according to the Bouguer – Lambert – Beer law.[64] The main chemical-analytical characteristics of complexes in solutions used for the determination of metals by the chromaticity method are listed in Table 3.

A study of indium complexation with PAR,[66] PAN [67] and 5-Br-PAAP [68,69] showed that the CF depend linearly on the In content in the same concentration range (0.07 – 0.53 μg ml^{-1}) as in a study by the DRS method.

Eriochrome cyanine R (ECR) was used for the determination of trace amounts of aluminium [70–72] and beryllium [73,74] by DRS and chromaticity methods. Study on the effect of the sorbent nature on the sorption of complexes showed that the sorption ability of aluminium complexes increases in the following series of sorbents: AV-17 × 8 < silica gel < Chromaton-N-Super < cellulose. The sensitivity and reproducibility are better for colour functions than for the diffuse reflectance coefficient. The sensitivity of functions in the aluminium determination decreases in the series $G > Y > L > B > W > S > A > R$ for Chromaton-N-Super and $G > Y > B > L > S > W > A > R$ for cellulose.

Table 3. Chemical and analytical parameters of complexes in solutions in metal determination by chromaticity ($c_{min} = 0.1$ mg litre^{-1}).

Reagent	Element	pH	CP [a] range /mg litre^{-1}	Ref.
PAR	La	8.1 – 8.9	0.4 – 2.0	61
	Nd	8.0 – 9.0	0.4 – 2.0	61
	Sm	8.3 – 9.1	0.4 – 2.0	61
	Tb	8.0 – 8.6	0.4 – 2.0	61
	Dy	8.0 – 9.0	0.4 – 2.0	61
	Ho	8.5 – 9.1	0.4 – 2.0	61
	Er	8.0 – 9.5	0.4 – 2.0	61
	Yb	7.0 – 8.0	0.4 – 2.0	61
Arsenazo I	Er	6.0 – 8.5	0.4 – 2.4	63
Arsenazo III	Er	2.5 – 4.5	0.4 – 1.6	63
Chlorophosphonazo III	Er [b]	2.0 – 5.0	0.025 – 0.800	63
Lumogallion	Mo^{VI}	2.0 – 3.5	0.23 – 0.90	65
Magnezone	Mo	2.0 – 4.9	0.23 – 0.90	65

[a] CP is the linear region of the calibrating plot; [b] $c_{min} = 0.01$ mg litre^{-1}.

Beryllium interferes in the determination of aluminium; however, the beryllium – ECR complex is not sorbed by cellulose, which allows selective determination of aluminium in the presence of beryllium. The detection limit for aluminium with cellulose as the sorbent was found to be 0.004 mg litre^{-1}. The procedures developed were used for the determination of aluminium in natural water and in sodium acetate.

The complexation of nickel with dimethylglyoxime (DMG) and benzyldioxime (BD) was studied.[75] The complexes obtained were sorbed on silica gel. It was found that the optical and chromaticity characteristics form the following series in terms of determination sensitivity for nickel: $R < S < A < L < Y$ for SG – BD – Ni and $R < L \approx S < A < Y \approx T$ for SG – DMG – Ni.

Thus, the diffuse reflectance coefficient is the least sensitive colour function of coloured immobilised nickel complexes. The highest error of nickel determination is observed if the chromaticity coordinate *A* and saturation are used. The sorption of nickel complexes with DMG and BD on microcrystalline cellulose (MCC) was also studied.[76] It was found that the sensitivity of the CF increased as follows: $R < B < G < L < S < T < A < W = \Delta E < Y$ for MCC – DMG – Ni and $R < B < S < L < T < A < W = \Delta E < G < Y$ for MCC – BD – Ni.

One can see that if MCC is used, a greater number of the CF depend linearly on the nickel concentration and the order in the sensitivity series changes. Simultaneously, the detection limit becomes lower.

The CF of molybdenum(VI) complexes with *o*,*o*′-dihydroxyazo compounds [lumogallion (LG) and IREA Magnezon (MG)] and with heterocyclic azo compounds (PAR, 5-Br-PAAP) in the presence or in the absence of a third component (hydroxylamine) were determined.[65] In all cases, the three-component systems are not inferior, and in most cases superior, to two-component systems with respect to optical characteristics.

Microquantities of Co^{II}, Ni^{II}, Fe^{II} and Fe^{III} in the form of complexes with nitroso-R-salt (NRS) were determined by measurement of chromaticity coordinates of a membrane filter after concentration of metal complexes on it; the detection limits were 0.1 – 0.4 μg.[77] This reagent was also used to find conditions for the separate determination of Fe^{II} and Fe^{III} ions (see Ref. 78). The chemical and analytical characteristics of adsorbed metal complexes determined by the chromaticity method are listed in Table 4.

Three-coordinate chromaticity was used in a study of the behaviour of the $Fe(bipy)_2(CN)_2$ complex (where bipy indicates bipyridyl) in 17 different organic solvents.[81] The chromaticity

Table 4. Conditions for the determination of metal ions in a sorbent phase by chromaticity.

Reagent	Reagent structure	Element	Sorbent	pH	c_{min} /mg litre^{-1}	CP range /mg litre^{-1}	Ref.
PAN	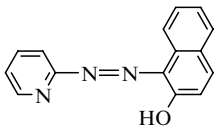	Co^{II}	SG-120	3.0 – 5.0	0.04	0.5 – 5.0	59
		Co^{III}	"	3.0 – 5.0	0.01	0.03 – 0.30	79
		Cu^{II}	"	5.0 – 8.0	1.0	0.5 – 5.0	60
		Cr^{VI}	"	2.5 – 4.5	0.1	5.0 – 50.0	60
		Fe^{III}	"	5.0 – 6.5	0.3	10.0 – 100.0	60
		In^{III}	"	4.5 – 4.8	0.04	0.2 – 0.6	67
		Mn^{II}	"	5.0 – 7.5	0.05	5.0 – 50.0	60
		Ni^{II}	"	6.0 – 9.0	0.03	0.5 – 5.0	60
		Pd^{II}	"	3.0 – 4.5	0.02	0.06 – 1.60	79
		Zn^{II}	"	7.5 – 10.0	0.03	5.0 – 50.0	60
PAR	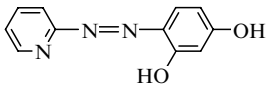	Co^{III}	"	0.5 – 1.0	0.02	0.06 – 1.00	79
		In^{III}	"	4.8 – 5.2	0.01	0.04 – 0.30	66
		Mo^{VI}	"	4.7 – 5.8	0.03	0.1 – 0.9	65
		Mo^{VI}	AV-17	4.6 – 6.1	0.3	0.95 – 3.80	65
		Pd^{II}	SG-120	0.5 – 3.0	0.1	0.3 – 2.0	79
5-Br-PAAP	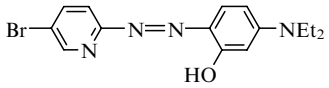	In^{III} (see [a])	"	3.8 – 5.2	0.0003	0.008 – 0.600	68
		In^{III}	"	3.5 – 5.0	0.002	0.008 – 0.640	69
		Mo^{VI}	"	5.0 – 6.0	0.04	0.05 – 0.19	65
TAN [b]	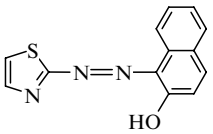	Co^{III}	"	4.0 – 6.0	0.02	0.06 – 1.00	79
		Pd^{II}	"	3.0 – 4.5	0.1	0.3 – 2.0	79
TAR	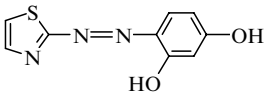	Co^{II}	"	4.0 – 8.0	0.005	0.05 – 1.00	80
		Co^{III}	"	0.6 – 1.5	0.006	0.05 – 1.00	79
		Cu^{II}	"	6.5 – 8.5	0.005	0.05 – 1.00	80
		Ni^{II}	"	5.2 – 6.8	0.005	0.05 – 1.00	80
		Pd^{II}	"	0.5 – 2.0	0.04	0.13 – 1.60	79
		Zn^{II}	"	5.6 – 7.4	0.01	0.15 – 5.00	80
LG	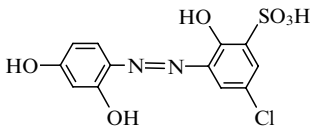	Mo^{VI}	AV-17	2.0 – 3.5	0.1	0.23 – 0.90	65
MG	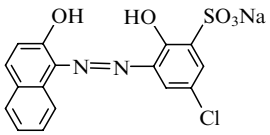	Mo^{VI}	"	2.0 – 4.9	0.1	0.23 – 0.90	65
DMG	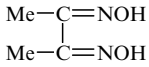	Ni^{II}	MCC	9.5 – 10.5	0.2	0.7 – 2.5	76
		Ni^{II}	SG-120	9.5 – 10.5	0.6	0.6 – 3.3	75
BD	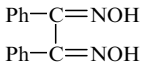	Ni^{II} (see [c])	"	7.8 – 8.8	0.3	0.3 – 1.3	75
		Ni^{II}	MCC	8.5 – 10.0	0.1	0.3 – 1.3	76
NRS	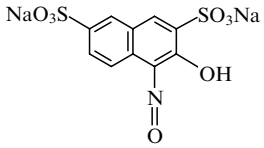	Co^{II}	membrane	–	0.1	0.3 – 3.0	77
		Fe^{II}	"	–	0.3	1.0 – 10.0	77
		Fe^{III}	"	–	0.4	1.5 – 20.0	77
		Ni^{II}	"	–	0.2	0.5 – 5.0	77
ECR	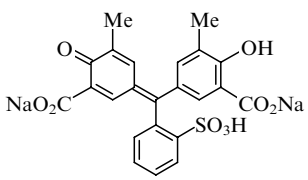	Al^{III} (see [c])	MCC	5.9 – 6.2	0.004	0.004 – 0.040	76

[a] Indium oxide was used as the subject of the study; [b] 1-(2-thiazolylazo)-2-naphtol; [c] natural water was used as the subject of the study.

coordinates allow one to compare all spectral changes occurring in a system on going from one solvent to another. In particular, the hue was used as the basic characteristic. Equations relating the T values with the acceptor numbers of the solvents (AN), the Dimroth–Reichardt parameter (Et) and the Kosover parameter (z) were found:

$$AN = (-29.15 \pm 3.68) + (0.20 \pm 0.01)T, \quad (17)$$

$$T = (151.66 \pm 8.79) + (4.71 \pm 0.30)\,AN, \quad (18)$$

$$T = (73.29 \pm 58.24) + (75.55 \pm 1.22)Et, \quad (19)$$

$$T = (167.02 \pm 55.89) + (6.15 \pm 0.77)\,z. \quad (20)$$

The results obtained make it possible to predict the acid–base properties of solvents based on the hue.

Thus, the chromaticity method provides a considerable increase in the determination sensitivity of microquantities of metals, especially if pre-concentration is used. In view of this, it would be of interest to survey the chromaticity characteristics of complexes used in analytical chemistry, first of all, in photometry. Based on this systematisation, one could try to find regularities of the effect of the reagent structure on chromaticity functions (as has already been made in photometry [42]) in order to select the most valuable organic reagents and hence to develop new determination procedures. In our opinion, this task is made much easier owing to the fact that, with rare exceptions, the optimum complexation conditions found by optical methods (including DRS) coincide with the optimum conditions for chromaticity analysis.

4. Increasing the determination selectivity of metal ions

Photometric methods are promising for the determination of mixtures of elements which form complexes with the same reagent either under different conditions (pH, temperature) or with different positions of their light absorption maxima. In the latter case, derivative spectrometry or two-wave spectrometry is used. Sometimes, this lowers the detection limit;[82] the latter can also be lowered by pre-concentration of complexes, including coloured compounds, on various sorbents or by changing the method for signal recording (for example, DRS). The greatest effect is usually achieved by a combination of analytical procedures with selection of the method for signal recording. However, selective signal recording is still an issue of topical interest.

On the other hand, the chromaticity method makes it possible to increase the determination selectivity of metal ions. For example, the chromaticity method enables separate determination of microquantities of copper and zinc in water after concentration by sorption on SG–PAN.[83] The equations for the calculation of the content of metal ions are derived using vector addition of the analytical signals

$$\Delta A_\Sigma = \sqrt{\sum_i \Delta A_i^2}\,, \quad (21)$$

where ΔA_i is the colour difference with respect to lightness (ΔL), saturation (ΔS) or shading (ΔE). This set of fourth-order equations is solved by the decahotomy method using the SVI.LAB program created by Morozko and Ivanov,[83] which allows determination of no more than two metals based on the total change in the chromaticity coordinates of a sample. Quite satisfactory results were obtained; however, determination of copper and zinc should be carried out in separate aliquots of the test solution.

In a development of this approach, the possibility of separate determination of cobalt and palladium in mixtures after concentration by chromaticity analysis with subsequent calculation of the amounts of these metals using the equations by Ivanov *et al.*[79] was studied. Cobalt and palladium were chosen due to the anomaly of the colours of their complexes with PAN (green to bluish-green) in comparison with complexes of other elements (reddish-violet) rather than by the similarity of their chemical and analytical properties, and also because they can be used to demonstrate the advantages of chromaticity as an analytical method.

Due to the closeness of the absorption (reflection) maxima of both complexes, cobalt and palladium cannot be determined separately by the DRS method because of overlap of the signals. Therefore, the effect of the sorption conditions on their chromaticity characteristics was studied.

Heterocyclic azo compounds immobilised on silica form green complexes with cobalt and palladium which differ in hue (yellowish-green and bluish-green, respectively). Recording of the colour change *versus* the content of metal ions in a solution with the use of the chromaticity coordinates A and B provides the possibility of using these differences for the separate determination of the ions in a mixture by measuring the signal at one wavelength. For example, Fig. 10 shows such dependences for complexes adsorbed on SG–PAN. If the absolute content of a metal ion in the solution (and, hence, in the sorbate) increases, the chromaticity coordinates of the sorbate surface change proportionally; the saturation point of the sorbate with respect to each metal does not change upon further increase in concentration of the corresponding ion in the solution.

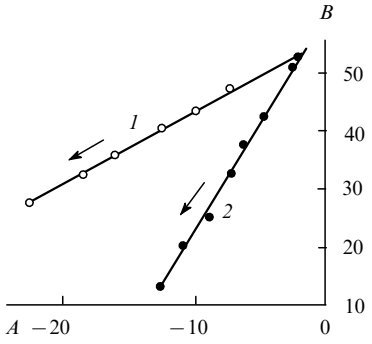

Figure 10. Effect of cobalt (*1*) and palladium (*2*) concentration on the chromaticity coordinates A and B of sorbates on SG–PAN at pH 3.[79] The arrows show the increasing metal concentration.

The equations derived for the change in the chromaticity coordinates of the sample (Table 5) are used to find conditions for separate determination of metal ions in solutions. It was suggested to use the signal separation factor (α) as a measure of completeness of separation; it is calculated using the following equations:

$$\begin{aligned} &\alpha = |\operatorname{arctg} K_{M_1} - \operatorname{arctg} K_{M_2}|, \\ &\text{if } |\operatorname{arctg} K_{M_1} - \operatorname{arctg} K_{M_2}| < 90^\circ; \\ &\alpha = 180^\circ - |\operatorname{arctg} K_{M_1} - \operatorname{arctg} K_{M_2}|, \\ &\text{if } |\operatorname{arctg} K_{M_1} - \operatorname{arctg} K_{M_2}| \geqslant 90^\circ, \end{aligned} \quad (22)$$

where K_{M_1} and K_{M_2} are the slopes of plots of the chromaticity coordinates A and B of the sorbent on the concentration of metal ions M_1 and M_2, respectively.

The magnitude of α is affected by the error of determination of the analytical signal (chromaticity coordinates). It was found experimentally for the Spectroton colorimeter that separate determination of two metals is satisfactory for $\alpha \geqslant 25^\circ$.

For all of the sorbents studied, dependences of the chromaticity coordinates A and B on the content of cobalt and palladium in solution were obtained and the following signal separation factors were found:

Sorbent	SG–PAN	SG–PAR	SG–TAN	SG–TAR
α	27°	21°	20°	15°

Table 5. Chromaticity coordinates of cobalt(III) and palladium(II) complexes on the sorbent surface.

Ion	Reagent	Equation of the sorbent colour change	Range of the sorbent colour change,[a] $(A_i, B_i)-(A_j, B_j)$	Saturation point /μg of ion
Co^{III}	TAR	$B = (28 \pm 0.1)A + (28.3 \pm 0.7)$	(7.0, 48.0)–(−7.5, 8.0)	10.97
	TAN	$B = (1.8 \pm 0.05)A + (29.5 \pm 0.4)$	(−0.5, 28.5)–(−14.0, 4.0)	18.00
	PAR	$B = (4.7 \pm 0.1)A + (19.6 \pm 0.3)$	(1.3, 25.5)–(−2.5, 8.0)	8.40
	PAN	$B = (3.9 \pm 0.05)A + (62.3 \pm 0.2)$	(−2.5, 52.5)–(−12.5, 13.0)	18.00
Pd^{II}	TAR	$B = (1.15 \pm 0.05)A + (38.5 \pm 0.5)$	(7.0, 48.0)–(−18.0, 11.0)	21.10
	TAN	$B = (1.1 \pm 0.1)A + (30.1 \pm 0.6)$	(−0.5, 28.5)–(−19.0, 9.0)	21.00
	PAR	$B = (1.5 \pm 0.1)A + (23.7 \pm 0.1)$	(1.3, 25.5)–(−10.0, 8.5)	13.10
	PAN	$B = (1.2 \pm 0.05)A + (55.6 \pm 0.2)$	(−2.5, 52.5)–(−14.0, 4.0)	35.60

[a] Saturation was used as the reference experiment.

It was concluded on the basis of the data obtained that the separation factor increases on going from thiazole azo compounds to pyridine ones and from resorcinol to naphthol. Only SG–PAN complies with the criterion of satisfactory separation ($\alpha \geqslant 25^\circ$). So this sorbent was chosen for the concentration of cobalt and palladium followed by their determination by the chromaticity method.

The concentrations were calculated using the following set of equations:

$$\Delta L_\Sigma^2 = (a_{11} + b_{11}x_1)^2 + (a_{12} + b_{12}x_2)^2,$$
$$\Delta S_\Sigma^2 = (a_{21} + b_{21}x_1)^2 + (a_{22} + b_{22}x_2)^2, \quad (23)$$

where ΔL_Σ and ΔS_Σ are the lightness and saturation, respectively, for the sum of the two metals; a_{ij} and b_{ij} $(i, j = 1, 2)$ are the factors of the calibration plot for the dependence of the chromaticity coordinates A and B on the metal ion concentrations (see Table 5); x_1 and x_2 are the unknown concentrations of the cobalt and palladium ions, respectively.

This fourth-order set of equations has four different parameters (four x_1 and x_2 pairs) which, in the general, case satisfy the solution. The sets of equations were solved on a personal computer using the Newton method. The amounts of cobalt and palladium (in 20 ml of solution) were varied from 0.5 to 5.0 μg and from 2.0 to 20.0 μg, respectively. Satisfactory results of separate determination of these metals in model mixtures were obtained; they were close to the data of analysis by the DRS method on the SG–TAR sorbent.

Of the greatest interest is the possibility of increasing the selectivity in the determination of metal ions which form reddish-violet complexes, since it is impossible to determine individual metals in a mixture in this spectral region by other methods (DRS, SPS) without masking or separation. TAR was selected as the reagent.[80] The possibility of separate determination was studied for copper, nickel and zinc in the presence of iron and cobalt. The optimum conditions for the sorption of these metals are indicated in Table 4.

The detectability of colour changes depending on the content of metal ions in solution with the use of chromaticity coordinates A and B implies that it is possible to carry out separate determination of ions in two- and three-component mixtures. Figure 11 shows such dependences for sorbates of complexes on SG–TAR. The data obtained were processed by the least-squares method.

Based on the calibration plots for the dependences of the chromaticity coordinates A and B on the content of copper, nickel, zinc and cobalt, the following signal separation factors were found:

M_1-M_2	Cu–Zn	Cu–Ni	Zn–Ni
α	23°	13°	37°

One can see that the nickel–zinc pair satisfies the criterion of separate determination. It should be noted that copper interferes in the simultaneous separate determination of nickel and zinc,

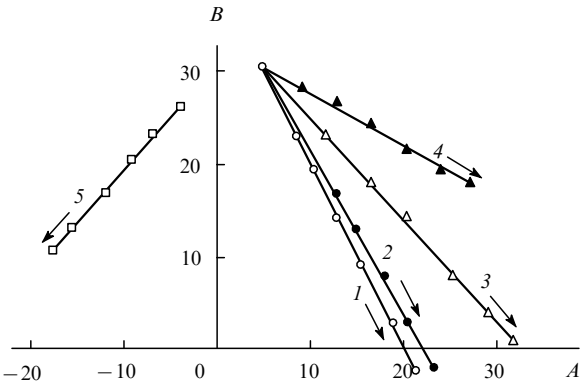

Figure 11. Dependence of the chromaticity coordinates A and B of sorbates on SG–TAR on the content of cobalt(II) (*1*), nickel (*2*), copper (*3*), zinc (*4*) at pH 7.0 and cobalt(III) (*5*) at pH 2.0.[80]
The arrows show the increasing metal concentration.

therefore it is masked with sodium thiosulfate. The ΔL and ΔS values obtained were used to calculate nickel and zinc concentrations using the set of Eqns (23).

Separate determinations of nickel and zinc in the presence of copper and cobalt were carried out similarly, except that the concentrations were calculated using a modified set of equations:

$$\Delta L_\Sigma^2 = (a_{11} + b_{11}x_1)^2 + (a_{12} + b_{12}x_2)^2 + d_1,$$
$$\Delta S_\Sigma^2 = (a_{21} + b_{21}x_1)^2 + (a_{22} + b_{22}x_2)^2 + d_2, \quad (24)$$

where x_1 and x_2 are the unknown concentrations of nickel and zinc ions, respectively; d_1 and d_2 are constants describing the contribution of cobalt to the set of equations.

The contribution of cobalt was estimated by determining its content at $\lambda = 610$ nm. The procedures described above were used to determine nickel, zinc and cobalt in a standard soil sample SP-3.

The above version of chromaticity analysis allows separate determination of 0.03–0.30 μg ml^{-1} cobalt and 0.013–0.130 μg ml^{-1} palladium, as well as 0.05–1.00 μg ml^{-1} nickel and 0.15–5.00 μg ml^{-1} zinc. The advantages of chromaticity for increasing the selectivity of determination of metal ions in two-, three- and four-component mixtures have been shown.

IV. Practical applications of the chromaticity method

1. Application of the chromaticity method in chemical analysis

Let us dwell on the most interesting practical applications of chromaticity. At present, the test procedures are becoming more and more popular. A test metal ion is usually identified by the colour of a complex it forms with a test reagent.[84] In the case of

acid – base indicators, the colour change upon decrease or increase in the medium pH is recorded. General-purpose test paper (pH 1 – 10) or reactive test papers used for qualitative and semi-quantitative analysis can serve as obvious examples.[84, 85] A colour change of the paper (sorbent) after a reaction indicates the presence of the ion in question in the test solution. Only the colour change is usually observed while the laws of this process are not recorded.

Construction of calibration test scales for the visual determination using the known dependence of the total colour difference (ΔE) on the content of the test element allows minimisation of inaccuracy of a test technique and quantitative description of not only the intensity but also of the colour change. Since one colour discrimination threshold corresponds to one ΔE unit in the equicontrast colorimetric system (*CIELAB*), the concentrations of the test element are chosen in accordance with a certain ΔE step to be determined most precisely by a human eye.

Even before the equicontrast *CIELAB* system had been developed, it was noticed that the difference in intensity of luminous fluxes is felt reliably if they differ by approximately 10% (see Ref. 6). The total colour difference is measured in the range of 0 – 100 arbitrary units, hence 10% corresponds to a step of $\Delta E = 10$. If colour is to be recognised from the surface of a reactive paper (sorbent) by a human, it is recommended to create test scales with $\Delta E \geqslant 10$ (see Ref. 86).

If a test sample loses its own colour or discolours due to the analytical reaction and the colour of the test sample support is close to white (for example, in the case of silica), the test scale should better be constructed using the inverse quantity, *viz*., the whiteness of the test sample, $W = 100 - \Delta E$ (see Ref. 68).

The dependence of the variation of the W and ΔE parameters of a test sample on the content of the test microelement has the shape of a logarithmic curve.[59] Thus, for a constant step $\Delta E = 10$ the concentration of a given microelement in a test sample changes in a geometrical progression, which is often suggested for the construction of a visual test scale.[87] In this case, the total colour difference of 10 arbitrary units between the original test sample (E_0) and a test sample following reaction of the microelement to be tested (E) is considered as the lowest determination threshold: $E - E_0 = 10$ (or $W - W_0 = 10$).

It was shown convincingly that the use of heterocyclic azo compounds immobilised on various sorbents makes it possible to achieve low detection limits in sorption-spectroscopic analyses in combination with high sensitivity and good reproducibility of results. In some cases, selective express techniques for the determination of microelements can be created using such reagents.

According to the general ideology of test methods for the environmental control, three basic rules were used as a guide in the development of sorption-spectroscopic procedures.[86]

1. The identification and determination of microelements in the environmental objects should be carried out quickly. This is achieved by comparing the indicator test sample with a standard scale.

2. It is necessary to provide the documentation of the test or the possibility of performing post-instrumental chemical analysis, which is realistic only for stable test samples.

3. The reactions should be contrasting.

The chromaticity method allows one to create an equicontrast chromaticity test scale well discernible by the human's eye. Based on the functional relationship between ΔE and the content of a test element in an object with a colour difference threshold $\Delta E \geqslant 10$, it is possible to construct a calibration test scale with a minimum error. Therefore, the descriptions of sorption-spectroscopic determination procedures involve the $\ln(\Delta E) = f(c)$ dependences in a mathematically processed form.

The non-selective colour difference parameter based on lightness (ΔL) is applicable for the post-instrumental determination of the content of a microelement in a test sample, provided that the chemical reactions which can be used for the sorption-spectroscopic analysis occur selectively and the reaction products are extracted quantitatively. The latter can be predicted to a certain extent based on the regularities of the sorption extraction of reagents by sorbent surfaces that we have studied.

The potential of the chromaticity method with the use of chromaticity coordinates is demonstrated in this study (Ref. 86) for the development of selective sorption-spectroscopic procedures for the separate simultaneous determination of cobalt(III) and palladium(II), copper(II) and zinc(II) using TAR immobilised on silica gel (SG – TAR). The capacity of the sorbent with respect to the reagent determined from saturation curves for metals was 20 μmol g^{-1} (see Refs 79, 80).

An advantage of the sorption version of testing is that it allows one to change the sensitivity of determination of a microelement by varying the sample volume, which is impossible if reagent test papers are used.

When a coloured compound formed and the sorbent sedimented, its colour was compared with the standard calibration colour scale for microelement determination, using the step $\Delta E = 10$ for making the test scale. The sorbates for the test scale were placed in test tubes with a diameter of 4 mm. The test scale obtained in this way is stable for at least five years.

2. Application of the chromaticity method in other fields of science and industry

a. Food chemistry

The greatest number of studies deal with the use of the chromaticity method for monitoring the production of foodstuffs, quality of cultures grown and in wine-making.

The effect of the growth conditions (greenhouse or open air) of hot pepper on its chromaticity characteristics[88] showed that the amount of pigments in pepper grown in a greenhouse can be predicted using the chromaticity coordinates A and B and the ratio A/B. For pepper grown in the open air, a similar correlation is observed for the values L and A/L.

The *CIELAB* system was used to estimate the quality of tomatoes,[89] tinned mushrooms[90] and potato chips.[91] It was found that the angle between the coordinates A and B depends on the colour of vegetables. A similar correlation with the L coordinate is not always observed. In particular, a study on the darkening of cut-off lettuce *versus* time[92] did not show such a dependence.

The *XYZ* chromaticity system can be used to classify honeys[93] and to estimate the natural sweetener from the cactus tree.[94] In this case, some other characteristics (viscosity, glucose content, *etc*.) were used along with the chromaticity coordinates. The chromaticity coordinates were also used to monitor production of sausages,[95, 96] in particular, to study the effect of the content of soybean proteins on the colour characteristics of the product.[95]

The three-coordinate colour system was used to study the first phase of milk turning[97, 98] and to estimate the colour of milk prepared from powder.[99] A theory allowing the preparation of emulsions with certain colour characteristics has been developed.[100] In this case, the chromaticity coordinates are calculated from the diffuse reflectance coefficient (R). The theoretical calculations are in good correlation with the experimental results. The variations of the chromaticity characteristics of soybean milk during the grinding of soy beans have also been studied.[101]

The chromaticity systems *CIEXYZ*, *CIELUV* and *CIELAB* were successfully employed for the characterisation of anthocyans isolated from red grapes,[28, 102] raspberry[103] and strawberry.[104] The effect of an atmosphere enriched with carbon dioxide on the decomposition of strawberry after harvesting was studied.[104]

Two hundred and twenty four model solutions of cyanine copigmented with rutin were studied. The procedure is based on measurements of the total colour difference and the copigment : pigment ratio. The strongest effect is reached at pH 3 – 5 and low copigment : pigment ratio (1 : 1).[105] The chromaticity system *CIELAB* is the best to describe the colour changes observable by a human eye.

The kinetics of colour changes in apples, bananas, beets and potatoes in the course of drying (convective and vacuum drying at 50, 70 and 90 °C) was studied.[106]

The effect of pasteurisation on the chromaticity characteristics of grapefruit juice [107] and pear juice [108] was studied. It was shown that the strongest changes are observed for the saturation and the chromaticity coordinate *B*, in particular, this allows one to monitor the decrease in the content of vitamin C and the discoloration of orange juice during storage at 4–24 °C (Ref. 109).

Two reviews are devoted to the spectrophotometry of wines.[110, 111] It was noted that the *CIELAB* chromaticity system is most promising as it allows one to create any colour scales, quickly compare the results of different operators in various flow points and is advantageous as it requires simple equipment. For port as an example, the effects of temperature, pH, sugar content and time on the colour characteristics of wines was studied.[111, 112] A simpler method for the calculation of the chromaticity coordinates of white, red and pink wines and brandy [27, 33] based on the measurement of the reflectance signal at three fixed wavelengths (440, 540 and 610 nm) was suggested. The method was tested for 690 wine samples.

The effect of pH and content of anthocyans on the chromaticity characteristics of a number of wines was studied.[113–117] Satisfactory correlations were found between the degree of ionisation of anthocyans and the wavelength of absorption maximum (λ_{max}) and between the degree of ionisation of anthocyans and the colour intensity.[114] It was noted that a decrease in the medium acidity increases the colour intensity and the degree of ionisation of anthocyans.[113]

The effect of pretreatment of red table wine with sulfur dioxide on their colour, phenolic composition and quality was studied.[118] It was shown that wines untreated with SO_2 darken faster than the treated wines.

b. Textile industry

The chromaticity method is used for the selection of colours in the dyeing of natural and synthetic fibres, for the control of fading of coloured cloths and fibres and for monitoring the formation of brown spots on paper-based materials.

The observed colours are produced by subtractive and additive methods. In subtractive synthesis, colour appears due to selective absorption of a portion of radiation from a light beam falling on an object. This occurs upon successive passage of a light beam through a series of differently coloured media (for example, colour films) or upon passage of light through a solution containing several dyes. Subtractive synthesis is the basis of the modern methods of colour photography, cinematography and three-colour printing. Required colours of materials formed by several dyes are obtained using this method.

The subtractive synthesis method makes it possible to blend various colours by using triads of dyes whose colours correspond to three linearly independent colours in various ratios. The painting compounds most suitable for these purposes have yellow, light-blue and purple colours. A particularly wide scale is obtained in the case where these are 'ideal' colours. A characteristic feature of the spectra of such dyes is that radiation of each of the three spectral zones is either absorbed completely or transmitted completely. The dyes that have such spectra are ideal for various processes of colour reproduction and allow one to blend virtually any colour.

If real dyestuffs are used, their transmission spectra are characterised by the absence of complete transmission in any of the zones, and the palette of the colours obtained becomes narrower and reproduction of high-purity colour is impossible. Therefore, a number of studies was devoted to the development of dyes the properties of which approached those of ideal dyes.

Several regression models for the optimal selection of dyes for various fibres have been developed.[20, 22, 119, 120]

Three 9-phenylxanthene derivatives were synthesised and used for dyeing polyacrylonitrile and polyamide cloths. All of the products were subjected to chromaticity characterisation.[121] Aqueous extracts of black tea were used for dyeing cotton and jute fibres.[21] The fibre colours were monitored using the *CIELAB* system.

The effect of the solvent system $CCl_3COOH-CH_2Cl_2$ on the ability of cotton yarn to undergo dyeing was studied. The chromaticity characteristics of dyes were studied by varying the concentration and duration of treatment of yarn with the solvent.[122]

A number of natural dyes were used for the colouring of synthetic fibres (polyester, nylon, acrylic and acetate fibre).[123] It was noted that the fibre colour saturation increased with the increase in the treatment temperature and this effect is especially strong in the case of nylon fibres.

The dependence of the chromaticity characteristics of nylon fibres on the conditions of its heating was studied.[124] The temperature was varied from 150 to 180 °C; the time was varied from 2 to 10 h.

The resistance of 15 dyes for cotton fibres and their mixtures to fading was studied.[125] The samples were irradiated with a xenon arc lamp. It was shown that the fibres dyed with a combination of dyes always faded less than the samples dyed with just one dye.

The effect of pH of the starting cochineal solution on the chromaticity characteristics of fibres was studied.[126] The pH values were set using solutions of hydrochloric, sulfuric, nitric and phosphoric acids. It was found that the chromaticity coordinate *B* decreases with the increase in pH of the starting solution; in addition, the coordinates *L*, *A*, *B* decrease regularly on storing the solutions from 1 to 21 days. This effect was most pronounced if phosphoric acid was used for setting the pH.

New synthetic polyoxyalkylene–polyurethane water-repellent fibres were obtained.[127] Polarising fibres from poly(vinyl alcohol) which possess constant light absorption in the visible region were described.[128] Such fibres can be used for making liquid-crystal displays and polarising screens.

The so-called fluorescent (or optical) whiteners are known, *i.e.*, compounds that absorb radiation with wavelengths of 340–400 nm and transform it into radiation with wavelengths of 415–466 nm (in the visible region of the spectrum). Depending on the wavelength of the absorbed light, fluorescence of different colours is observed, *viz.*, violet (the fluorescence maximum is observed at 415–429 nm), dark blue (at 430–440 nm) and light-blue (at 466 nm). The most popular optical whiteners have light-blue fluorescence (radiation with wavelengths of 400–500 nm). Unlike optical whiteners, fluorescent dyes absorb light in the visible spectrum region, like ordinary dyes. As a consequence of fluorescence of dyes, their brightness increases. Optical whiteners are used like ordinary dyes and are often referred to as white dyes.

White paper, cellulose and other cloths and fibres partially absorb light in the shortwave part of the spectrum and thus become yellowish. If optical whiteners are applied on such yellowed objects, the former radiate light with wavelengths of 400–500 nm and hence compensate for the absorbed part of visible light and complement the spectrum of the reflected light. As a result, the degree of whiteness of the objects increases, *i.e.*, an optical (fluorescent) whitening effect is observed. Optical whiteners are widely used for whitening natural and synthetic materials (cotton, wool, viscose, hair, silk, cellulose acetates, polyamides, polyurethanes, polyacrylonitrile, polypropylene, polyester), paper, plastics, for improvement of colour of dyed cloths, *etc.* The *CIELAB* system was used to study the reasons for the appearance of brown spots on materials based on paper (ancient books, paintings).

Optical whiteners are added to washing powders and compositions for dry cleaning. They should have good light resistance, resistance against acids and bases, oxidants and reducing agents and should not form complexes with metals. Bleaching with such substances is similar to dyeing with direct and acid dyes: cellulose fibres are treated with suitable optical whiteners in neutral or weakly alkaline media, while polyamide fibre, silk and wool are

treated in weakly acidic media. Dispersion whiteners are used for polyester and acetate fibres, and cationic whiteners, for polyacrylonitrile fibres.

The synthesis and properties of some unsubstituted triazinylstilbenes as fluorescent whitening agents were described.[129] The spectral and thermal characteristics, the whitening effect for cotton and the chromaticity coordinates were determined. Fluorescent dyes based on naphthalene-1,8-dicarboxylic anhydride suitable for the dyeing of polyamide fibres and epoxy resins were synthesised. The relationship between the dye structure and the colour characteristics was discussed.[130]

The effect of fluorescent additives on the colour saturation of fibres was studied.[131] For this purpose, a cotton fibre was dyed using eight dye types with five various saturation levels. The fibres obtained were treated with two types of fluorescent additives. It was shown that the addition of fluorescent compounds increased the saturation of red and dark blue hued fibres and decreased that of yellow hued fibres.

The total colour difference was used to characterise a coated antibacterial polyester fibre.[132]

A new composition based on esters was suggested for dry cleaning of cotton cloths.[133] The efficiency of laundry disks in the removal of spots from cotton and polyester fibres with the use of detergents in the absence of water was studied.[134] It was shown using chromaticity characteristics that these detergents are not superior to the compounds used for 'wet cleaning'.

c. Geochemistry and mineralogy

The *CIELAB* system allows one to distinguish the hues of precious stones (the alexandrite effect).[135] Depending on the hue, precious stones can be grouped as follows: type 1 — alexandrite, fluorite, spinel, tourmaline; type 2 — glass; type 3 — sapphire; type 4 — garnet. Such functions as lightness and saturation can be used for documentary characterisation of the differences observed.

The microscopy and photometry of ores over the period of 1890–1998 was reviewed.[136] In particular, it was emphasised that identification of ore materials includes plotting of chromaticity diagrams as an obligatory stage.

The chromaticity characteristics of a rare sulfide deposit with the composition Cu_5FeS_6 were obtained.[137]

The chromaticity coordinates ware applied to determine the nature of the colour of the Mozambiquean beryls. It was found that the green colour appears due to the presence of chromium ions in the aluminium crystal lattice, while the purple colour is due to the presence of manganese ions.[138]

A method for non-destructive determination of metal corrosion products with the use of the chromaticity characteristics of the *CIELAB* system was suggested.[139] Studies of alloys based on copper, zinc and aluminium showed that an increase in the content of zinc and aluminium first increases the lightness and yellowness to a certain value and then decreases these values.[140, 141] The results obtained have enabled the creation of differently coloured alloys, *viz*., copperish-red, goldish-yellow, brown, purple and, finally, silverish-grey.

The colour characteristics have been utilised for the description of protective and decorative coatings from chromium and titanium[142–144] and for painted steel panels.[145]

d. Production of glasses and ceramics

The chromaticity characteristics were used to control the colour range of glasses[146–149] and ceramics.[150–152] Twenty five antique glass samples were studied. It was shown that the three fragment types, *i.e*., bluish-green, light-blue and yellowish-green, result from the combinations $Fe^{II}-Fe^{III}$, $Fe^{II}-Co^{II}$ and $Fe^{II}-FeS$, respectively.[148] It was suggested to make grey and bronze glasses[149] by using combinations of such additives as Co_3O_4, Nd_2O_3 and V_2O_5, MnO_2, Er_2O_3. The resulting glass colour was monitored using chromaticity characteristics.

A series of studies was devoted to the effect of temperature–time modes on the synthesis of pigments.[23, 150–153] It was found that the heat treatment temperature is the most important factor determining the colour of the pigments obtained. An optimal temperature should hinder the formation of colourless or weakly coloured compounds. The formation of significant amount of a glassy phase resulting in dissolution of coloured crystal phases is also undesirable.[23, 150–152]

A procedure for the preparation of ceramics by coprecipitation of hydroxides was suggested. The particle sizes of the resulting polymeric hydroxides are comparable to those of colloid species. Such compounds can be transformed into ceramics of a certain colour at lower temperatures compared to those employed in the oxide technology.[152]

A study on the effect of temperature on the colour stability of series of differently coloured ceramic samples showed that the yellowish-brown ceramics are most unstable.[24]

e. Pharmacology and fabrication of cosmetics

In the pharmaceutical industry, chromaticity is used as a reliable method to control the production of dental compositions, to check the uniformity of coatings on pills, *etc*. For example, the hue of silver-containing alloys was made similar to the colour of human tooth enamel by adding cerium dioxide, which discolours silver, to the alloys. The addition of 0.1% CeO_2 causes an essential (threefold) discoloration of the alloys without any loss of strength.[25]

The relationship between the colour of dental cement and paste was studied using chromaticity characteristics.[154] Metal ceramics for tooth crowns were created and characterised by chromaticity.[155, 156]

The value of total colour difference was utilised to control the uniformity of coatings on pills.[157]

The absorption and diffuse reflection spectra of structural isomers of riboflavin tetrabutyrates were obtained.[26] The specific feature of these compounds is that their colour characteristics in the solid state differ depending on the type of the structural isomer, whereas in solution, all of the spectra are identical. This is explained by intramolecular reactions occurring in the solid phase, which result in hydrogen bond formation. The chromaticity method allows one to distinguish one isomer from another.

Tinted powders for correction of face colour were created; they consist of micas covered with granular metal oxides (titanium, iron and their mixtures) and have definite values of the chromaticity coordinates.[158] Studies of the reaction of Methylene Blue with natural white mica and with synthetic sodium-type mica[159] showed that Methylene Blue reacts with both types of mica on heating in the absence of a solvent; as a result, the chromaticity coordinates change strongly (the purple colour changes to light-blue). The resulting compounds are water-insoluble due to immobilisation of Methylene Blue on mica.

Chromaticity characteristics were used to compare a number of sunscreens.[160]

f. Electronic industry, preparation of colour coatings, radio-engineering and photo-engineering

A series of studies dealt with the development of light-emitting diodes.[161–168] It was found that green sources provide a long life of electron-beam tubes and improve the radiating characteristics.[163] A chromaticity-based method for the correction of the electron-beam tube characteristics was developed.[164]

It was suggested to use bathocuproin[161] and triphenyl amine derivatives[169] as blocking layers for organic light-emitting diodes. The diodes were characterised by the chromaticity coordinates X and Y; it was proven on this basis that the source has pure red, dark blue or green radiation.[170–172]

New sources for three-coordinate chromaticity[173] containing red and green reverse lenses were created. Sources based on polymers and oligomers[174] cover a broad spectral range, *viz*., from dark blue through white to green. A series of powder radiation sources were synthesised.[175–178] The effect of the content of Sm^{III} (see Ref. 179), Zn^{II} (see Ref. 180) and Tm^{III} (see

Ref. 181) added to fluorescent powders on the chromaticity characteristics of irradiation was studied.

Resins based on an aromatic polyester with improved colour characteristics were created;[182, 183] the advantages of copolymers of *N*-vinylcarbazole and *N*-phenyl-2-(2-thienyl-5-vinyl)-5-(2′-thienyl)pyrrole were shown.[184]

The synthesis of new copolymers containing electron- and hole-conducting elements (oxadiazole and carbazole, respectively) and an irradiator (naphthalimide) was reported.[185] Their luminescence spectra were studied and the chromaticity coordinates were calculated.

A new process for obtaining a photographic image consisting of an absorbing dye and a sensitive dye was created; the dyes were selected in such a manner that their λ_{max} values were equal. This made it possible to improve the image characteristics in the red spectral region.[186] A uniform image in the blue spectral region was obtained using silver halide grains (95 mol.% AgCl).[187] A material containing photosensitive microcapsules that included fuchsine was used to form the purple layer of the photographic image.[188]

Coatings for steel sheets resistant against changes in weather conditions were developed;[189] they can be suitable for roofs, cars, doors and mechanisms. A mixture of yellow pigments for traffic signs with good reflection properties has been developed.[190] The theory and practice of colour measurement for powder coatings were covered in a review [18] which provided recommendations on controlling the colour of these coatings. A method for the creation of coloured powders by mixing dry powders was suggested.[191] Blending the required powder colour is simplified by plotting the colour diagrams.[192]

A computer-aided method for blending the colour of paints was reported.[193] The panels are coated with various mixtures of a colour and white paints; the reflection signal is measured, and the chromaticity coordinates are calculated. The values obtained are compared with those in a standard database. Such a technique simplifies the colour blending and increases its accuracy.

The optical properties of paint coatings formed on a surface depend on the nature of the pigment and the film-forming agent, on the volume concentration of the pigment and on the surface geometry.[19] The changes in the spectral composition of the light reflected by samples upon increase in their brightness due to application of a polymeric layer were estimated by changes in the optical characteristics in the *CIELAB* system (L, S, T, ΔE). Upon application of the first layer 10–20 μm thick, a sharp decrease in reflection coefficients and increase in lightness are observed; further increase in the layer thickness affects these characteristics only slightly. For light-blue and light-green coatings, the hue decreases continuously with the increase in the layer thickness: the colour vector turns clockwise. The hue of orange samples remains unchanged. This results from the fact that light dispersion is stronger in the short-wave spectral region.

V. Conclusion

Over many years, the progress in colour-measuring systems was restrained by the low technological level. Therefore, simultaneously with development of the equicontrast colorimetric system (*CIELAB*) by the International Commission on Illumination, colorimetric instruments and calculation methods were created which made it possible to record colour and use colour measurements in the analysis. Today, the chromaticity method, especially combined with computer programs for processing spectral data, has become widely popular in polygraphy and in the paint, textile, glass, pharmaceutical and food industries and in a number of other branches of industry.

One can hope that the chromaticity method will be used more widely in analytical chemistry, especially in the cases where the analytical signal is directly related to the colour of the compound to be determined, for example, in the approximate evaluation of the content of a compound from the colour intensity. Test methods, which basically do not require complicated instruments, are promising for fast batch analysis. The use of chromaticity systems which approach as much as possible the colour characteristics of human vision should favour the development of express analysis methods.

In our opinion, chromaticity will also be used more widely in spectroscopic analysis, since the use of optical radiation as the information carrier seems to be undoubtedly promising.

Along with broadening of the scope of the method, one should note two important directions of its development. First, these are studies devoted to the methodology and metrology of the chromaticity processing of spectra, as well as development of the theoretical basis. Publications on this topic have already appeared.[194–196] Second, broadening of the scope of chromaticity can serve as an impetus for improvement of the available instruments and development of new ones and for the creation of databases and software.

References

1. E A Kirillov *Tsvetovedenie* (Colour Science) (Leningrad: Legprombytizdat, 1987)
2. B Judd *Opt. Soc. Am.* **23** 359 (1993)
3. R M Evans *An Introduction to Color* (New York: Wiley, 1959)
4. P Hawker *Int. Broadcast Eng.* **17** 13 (1986)
5. M Minnaert *Licht en Kleur in het Landschap* (Zutphen: Thieme, 1949)
6. Z Marczenko *Kolorymetrijczne Oznaczanie Pierwiastkow* (Warszawa: Wydawnictwo Naukowo-Techniczne, 1968)
7. V I Lagutin *Izmer. Tekhn.* (2) 27 (1987)
8. V I Lagutin *Izmer. Tekhn.* (5) 40 (1982)
9. A V Balashov, V P Kargin, N A Kuz'micheva, V I Lagutin *Izmer. Tekhn.* (7) 27 (1989)
10. V I Lagutin *Metrologiya* (8) 58 (1981)
11. K M M K Prasad, S Rahem *Analusis* **20** 401 (1992)
12. S Kortly, K Vytras *Sb. Ved. Praci Vysoka Skola Chem. Technol. Pardubice* **19** 21 (1969)
13. J Cacho, A Garnica, C Nerin *Anal. Chim. Acta* **162** 113 (1984)
14. K M M K Prasad, S Raheem, P Vijayaleksmi, C K Sastri *Talanta* **43** 1187 (1996)
15. V A Jadhav *J. Indian Chem. Soc.* **74** 697 (1997)
16. J M Calatayud, M M C Pascual, F P Campins *Anal. Chem.* **58** 200 (1986)
17. M Roses *Anal. Chim. Acta* **204** 311 (1988)
18. L Liang, Y Cui *Tiliao Gongye* **28** 35 (1998); *Chem. Abstr.* **130** 126 293 (1999)
19. I Yu Zvonkina, E A Indeikin *Lakokrasoch. Mater. Prim.* (2–3) 25 (1999)
20. Y S W Li, C W M Yeun, K W Yeung, K M Sin *J. Soc. Dyers Colour.* **115** 95 (1999)
21. H T Deo, B K Desai *J. Soc. Dyers Colour.* **115** 224 (1999)
22. A Gillchrist, J Nobbs *J. Soc. Dyers Colour.* **115** 4 (1999)
23. P Mirti *Archaeometry* **40** 45 (1998)
24. X Wu, H Xu, S Song *Zhonghua Kouqiang Yuxue Zazhi* **32** 350 (1997); *Chem. Abstr.* **130** 129 886 (1999)
25. W J O'Brien, K M Boenke, J B Jackson, C L Groh *Dent. Mater. Volume Date* **14** 365 (1999)
26. R Tawa, S Okumura, K Taguchi, K Fujiwara *Yakuzaigaku* **58** 179 (1998); *Chem. Abstr.* **130** 301 761 (1999)
27. F Ayala, J F Echavarri, A I Negueruela *Am. J. Enol. Vitic.* **48** 364 (1997)
28. F J Heredia, E M Francia-Aricha, J C Rivas-Gonzalo, I M Vicario, C Santos-Buelga *Food Chem.* **63** 491 (1998)
29. Yu A Zolotov *Vestn. Akad. Nauk SSSR* (11) 63 (1991) [a]
30. *J. Opt. Soc. Am.* **64** 896 (1974)
31. N Knesaurek *Croat. Chem. Acta* **70** 955 (1997)
32. T Nakatsuka *DIC Tech. Rev.* **5** 9 (1999); *Chem. Abstr.* **131** 206 188 (1999)
33. F Ayala, J F Echavarri, A I Negueruela *Am. J. Enol. Vitic.* **48** 357 (1997)
34. V M Ivanov, N I Ershova, V N Figurovskaya *Zh. Anal. Khim.* **54** 1153 (1999) [b]

35. D Escolar, M R Haro, A Saucedo, J Ayuso, A Jimenez, J A Alvarez *Appl. Spectrosc.* **50** 1290 (1996)
36. J M Calatayud, M M C Pascual, S S Vines *Quim. Anal. (Barselona)* **5** 83 (1986)
37. K Vytras, J Vytrasova, S Kortly *Talanta* **22** 529 (1975)
38. J M Calatayud, M M C Pascual, S S Vines *Analusis* **13** 87 (1985)
39. K M M K Prasad, S Raheem *Talanta* **38** 793 (1991)
40. J M Calatayud, M M C Pascual, R M Marin Saez *Analusis* **14** 508 (1986)
41. S A Morozko, O V Kuznetsova, V M Ivanov *Zh. Anal. Khim.* **52** 1146 (1997) [b]
42. V M Ivanov *Geterotsiklicheskie Azotsoderzhashchie Azosoedineniya* (Heterocyclic Nitrogen-Containing Azo Compounds) (Moscow: Nauka, 1982)
43. V M Bhuchar, V P Kukreja, S R Das *Anal. Chem.* **43** 1847 (1971)
44. E Bosch, E Casassas, A Izquiedro, M Roses *Anal. Chem.* **56** 1422 (1984)
45. V M Ivanov, A I Busev, V N Figurovskaya, T F Rudometkina *Zh. Anal. Khim.* **29** 988 (1974) [b]
46. A I Busev, V M Ivanov *Zh. Anal. Khim.* **22** 382 (1967) [b]
47. N Kaneniva, F Yoshizawa, Y Homma *Kanazawa Daigaku Yakugakubu Kenkyu Nempo* **10** 42 (1960); *Ref. Zh. Khim.* 24 V 108 (1961)
48. T F Rudometkina, V M Ivanov, A I Busev *Zh. Anal. Khim.* **32** 1674 (1977) [b]
49. A I Busev, V M Ivanov, L S Krysina *Vestn. Mosk. Univ., Ser. 2, Khim.* (3) 80 (1968) [c]
50. V M Ivanov *Usp. Khim.* **45** 456 (1976) [*Russ. Chem. Rev.* **45** 213 (1976)]
51. N S Ershova, V M Ivanov, A I Busev *Zh. Anal. Khim.* **28** 2220 (1973) [b]
52. V M Ivanov, A I Busev, N S Ershova *Zh. Anal. Khim.* **28** 214 (1973) [b]
53. T Saito *Talanta* **41** 811 (1994)
54. M C Valencia, S Boundra, J H Bosque-Sandra *Analyst* **118** 1333 (1993)
55. J Cacho, C Nerin, L Ruberte, E Rivas *Anal. Chem.* **54** 1446 (1982)
56. M Miroslaw-Boruch *Ann. Univ. Mariae Curie-Sclodowska Sect. A: Chem. Volume Date* **46–47** 101 (1995)
57. G V Lisichkin (Ed.) *Modifitsirovannye Kremnezemy v Sorbtsii, Katalize i Khromatografii* (Modified Silica in Sorption, Catalysis and Chromatography) (Moscow: Khimiya, 1986)
58. Yu Yu Lur'e *Spravochnik po Analiticheskoi Khimii* (Handbook on Analytical Chemistry) (Moscow: Khimiya, 1989)
59. V M Ivanov, S A Morozko, S V Kachin *Zh. Anal. Khim.* **49** 857 (1994) [b]
60. S A Morozko, V M Ivanov *Zh. Anal. Khim.* **50** 629 (1995) [b]
61. V M Ivanov, B Dashdendev, V N Figurovskaya *Zh. Anal. Khim.* **54** 1259 (1999) [b]
62. V M Ivanov, B Dashdendev, V N Figurovskaya *Zh. Anal. Khim.* **56** 23 (2001) [n]
63. V M Ivanov, N V Ermakova *Vestn. Mosk. Univ., Ser. 2, Khim.* 41 174 (2000) [c]
64. V M Ivanov, N V Ermakova *Zh. Anal. Khim.* **56** 586 (2001) [b]
65. G A Kochelaeva, V M Ivanov, G V Prokhorova *Zh. Anal. Khim.* **55** 18 (2000) [b]
66. V M Ivanov, N I Ershova *Vestn. Mosk. Univ., Ser. 2, Khim.* 39 101 (1998) [c]
67. V M Ivanov, N I Ershova *Vestn. Mosk. Univ., Ser. 2, Khim.* 38 396 (1997) [c]
68. N I Ershova, V M Ivanov *Anal. Chim. Acta* **368** 235 (1998)
69. V M Ivanov, N I Ershova *Vestn. Mosk. Univ., Ser. 2, Khim.* 39 170 (1998) [c]
70. N I Ershova, V M Ivanov *Anal. Chim. Acta* **408** 145 (2000)
71. N I Ershova, V M Ivanov, in *Tez. Dokl. IV Vseros. Konf. 'Analiz Ob'ektov Okruzhayushchei Sredy', Krasnodar, 2000* (Abstracts of Reports of the IVth All-Union Conference 'Analysis of Environmental Objects, Krasnodar, 2000] p. 295
72. N I Ershova, V M Ivanov, in *Pittsburgh Conference on Analytical Chemistry and Applied Spectroscopy (Abstracts of Reports), Orlando, 1999* p. 2101
73. V M Ivanov, N I Ershova, in *The 10th Russian–Japan Joint Symposium on Analytical Chemistry (Abstracts of Reports), Moscow, 2000* p. 131
74. N I Ershova, V M Ivanov, in *Tez. Dokl. IV Vseros. Konf. 'Analiz Ob'ektov Okruzhayushchei Sredy', Krasnodar, 2000* (Abstracts of Reports of the IVth All-Union Conference 'Analysis of Environmental Object, Krasnodar, 2000] p. 296
75. V M Ivanov, N I Ershova *Vestn. Mosk. Univ., Ser. 2, Khim.* 40 22 (1999) [c]
76. N I Ershova, V M Ivanov *Fr. J. Anal. Chem.* **363** 641 (1999)
77. F Yokota, M Endo, S Abe *Bunseki Kagaku* **48** 1135 (1999); *Chem. Abstr.* **132** 131 394 (1999)
78. F Yokota, S Abe *Anal. Commun.* **34** 111 (1997)
79. V M Ivanov, O V Kuznetsova, O V Grineva *Zh. Anal. Khim.* **54** 263 (1999) [b]
80. V M Ivanov, O V Kuznetsova *Zh. Anal. Khim.* **55** 998 (2000) [b]
81. T Tlaczala *Pol. J. Chem.* **71** 823 (1997)
82. S B Savvin, L M Trutneva, O P Shvoeva, V K Belyaeva, I N Marov *Zh. Neorg. Khim.* **36** 393 (1991) [d]
83. S A Morozko, V M Ivanov *Zh. Anal. Khim.* **52** 858 (1997) [b]
84. L V Boeva, V A Kimstach, T F Lifintseva *Gidrokhim. Mater.* (110) 152 (1991)
85. V M Ostrovskaya *Zh. Anal. Khim.* **32** 1820 (1977) [b]
86. O V Kuznetsova, Candidate Thesis in Chemical Sciences, Moscow State University, Moscow, 2000
87. M I Krivosheev, A K Kustarev *Tsvetovye Izmereniya* (Colour Measurements) (Moscow: Energoizdat, 1990)
88. R Gómez, J E Pardo, F Navarro, R Varón *J. Sci. Food Agric.* **77** 268 (1998)
89. J E Pardo, J Tardaguila, R Varón, F Navarro, R Gómez *Riv. Sci. Aliment.* **26** 387 (1996); *Chem. Abstr.* **126** 185 238 (1997)
90. M Rodrigo, C Calvo, T Sanchez, C Rodrigo, A Martinez *Int. J. Food Sci. Technol.* **34** 161 (1999)
91. S Segnini, P Dejmek, R Öste *Lebensm.-Wiss. Technol.* **32** 216 (1999)
92. G Peiser, G López-Gálvez, M Cantwell, M E Saltveit *Postharvest Biol. Technol.* **14** 171 (1998)
93. R Mateo, F Bosch-Reig *J. Agric. Food Chem.* **46** 393 (1998)
94. C Saenz, P Mecklenburg, A M Estevez, E Sepulveda *Acta Hortic.* **438** 135 (1997); *Chem. Abstr.* **131** 115 551 (1999)
95. B Baco, P Pipek, W Dolata, T Radomyski *Pol. J. Food Nutr. Sci.* **6** 51 (1997)
96. J Chasco, G Lizaso, M J Beriain *Meat Sci.* **44** 203 (1996)
97. T M P Cattaneo, R Lizzano, R Giangiacomo *Ind. Aliment.* **38** 233 (1999)
98. R Giangiacomo, R Lizzano, S Barzaghi, T M P Cattaneo, A S Barros *J. Near Infrared Spectrosc.* **6** 205 (1998)
99. F J Morales, M A J S Van Boekel *Int. Dairy J., Volume Date* **8** 907 (1999); *Chem. Abstr.* **131** 115 507 (1999)
100. D J McClements, W Chantrapornchai, F Clydesdale *J. Food Sci.* **63** 935 (1998)
101. A Obata, M Matsuura *Nippon Shokuhin Kagaku Kogaku Kaishi* **44** 768 (1997); *Chem. Abstr.* **128** 12 749 (1998)
102. J A Fernandez-Lopez, L Almela, J A Munoz, V Hidalgo, J Carreno *Food Res. Int. Volume Date* **31** 667 (1999)
103. B De Ancos, E Gonzalez, M P Cano *Z. Lebensm.-Unters. Forsch. A* **208** 33 (1999)
104. M I Gil, D M Holcroft, A A Kader *J. Agric. Food Chem.* **45** 1662 (1997)
105. J-F Gonnet *Food Chem.* **66** 387 (1999)
106. M K Krokida, E Tsami, Z B Maroulisz *Drying Technol.* **16** 667 (1998)
107. H S Lee, G A Coates *J. Food Sci.* **64** 663 (1999)
108. A Ibarz, S Garza, J Pagan *Alimentaria (Madrid)* **298** 87 (1998)
109. H S Lee, C S Chen *J. Agric. Food Chem.* **46** 4723 (1998)
110. O D D Soares, P Barros *Bull. O.I.V.* **72** 192 (1999); *Chem. Abstr.* **131** 242 314 (1999)
111. O D D Soares, P Barros *Proc. SPIE–Int. Soc. Opt. Eng.* **3991** 799 (1998); *Chem. Abstr.* **131** 4383 (1999)
112. M E Melendez, M C Ortiz, M S Sanchez, L A Sarabia, M Iniguez *Quim. Anal. (Barselona)* **18** 119 (1999)
113. E La Notte, V A Luizzi, M Esti, T Rinaldi *Vignevini* **22** 29 (1995)
114. F J Heredia, M Guzman-Chozas *Sci. Aliments Volume Date* **15** 551 (1995)
115. L Gao, B Girard, G Mazza, A G Reynolds *J. Agric. Food Chem.* **45** 2003 (1997)

116. J A Larrauri, C Sánchez-Moreno, P Rupérez, F Saura-Calixto *J. Agric. Food Chem.* **47** 1603 (1999)
117. R Gil-Munoz, E Gomez-Plaza, A Martinez, J M Lopez-Roca *Food Res. Int. Volume Date* **30** 699 (1998)
118. J Bakker, P Bridle, S J Bellworthy, C Garcia-Viguera, H P Reader, S J Watkins *J. Sci. Food Agric.* **78** 297 (1998)
119. J Rieker, K Wobser, W Ruettiger *Textilveredlung* **32** 261 (1997)
120. Y S W Li, C W M Yuen, K W Yeung, K M Sin *J. Soc. Dyers Colour.* **115** 22 (1999)
121. T Konstantinova, G Kirkova, R Betcheva *Dyes Pigm.* **38** 11 (1998)
122. S Rajendran, S S Ramasamy, S P Mishra *Am. Dyest. Rep.* **88** 16 (1999)
123. M Komori *Sensoku Kogyo* **47** 68 (1999); *Chem. Abstr.* **131** 6473 (1999)
124. A A Hamsa, I M Fouda, M A Kabeel, M El-Shrif, I M El-Sharkawy *Polym. Polym. Compos.* **7** 53 (1999)
125. D Nandy *Text. Res. J.* **69** 16 (1999)
126. E Kashino, K Kanbe *Kyoritsu Joshi Tanki Daigaku Seitkatsu Kagakuka Kiyo* **41** 1 (1998); *Chem. Abstr.* **130** 67 705 (1999)
127. Jpn. Appl. 91 212; *Chem. Abstr.* **131** 244 553 (1999)
128. Jpn. P. 288 396; *Chem. Abstr.* **130** 326 249 (1999)
129. T N Konstantinova, Hr I Konstantinov, R I Betcheva *Dyes Pigm.* **43** 197 (1999)
130. T Philipova *Rev. Roum. Chim.* **41** 591 (1996)
131. Y Yamaguchi, M Nagayama *Kyoritsu Joshi Tanki Daigaku Seitkatsu Kagakuka Kiyo* **38** 15 (1995)
132. Jpn. P. 324 145; *Chem. Abstr.* **131** 20 188 (1999)
133. US P. 375 812; *Chem. Abstr.* **131** 259 224 (1999)
134. A C Lumley, B M Gatewood *Book Pap. — Int. Conf. Exhib. AATCC* 38 (1998); *Chem. Abstr.* **130** 298 329 (1999)
135. Y Liu, J E Shigley, E Fritsch, S Hemphill *J. Gemmol.* **26** 371 (1999)
136. A J Criddle *Miner. Assoc. Can. (Short Course Ser.)* **27** 1 (1998); *Chem. Abstr.* **130** 141 721 (1999)
137. M M Boldyreva, O A Yakovleva, I G Manilov *Vestn. St. Petersb. Univ., Ser. 7, Geolog., Geograf.* (3) 97 (1996)
138. V P Sontsev, G V Bukin *Geolog. Geofiz.* **38** 1625 (1997)
139. Jpn. P. 304 392; *Chem. Abstr.* **127** 124 619 (1997)
140. B M Li, X Zhang *Gov. Rep. Announce* **95** (20) 122 (1995)
141. M Z B Hussein, Z Zainal, S Nadarajah *Sci. Int. (Lahore)* **10** 223 (1998)
142. T D Radjabov, A I Kamardin, Sh U Pulatov *Vide: Sci., Tech.* Appl. 279 Suppl. 158 (1996)
143. C Mitterer, P H Mayrhofer, W Waldhauser, E Kelesoglu, P Losbichler *Surf. Coat. Technol.* **108–109** 230 (1998)
144. M Nose, T Nagae, M Yokota, S Saji, M Nakada *Nippon Kinzoku Gakkaishi* **63** 944 (1999); *Chem. Abstr.* **131** 340 230 (1999)
145. O Moerk, A S Jotun, E Reck *Faerg Larck Scand.* **44** 4 (1998)
146. US P. 97-53 822; *Chem. Abstr.* **130** 128 786 (1999)
147. US P. 97-925 393; *Chem. Abstr.* **131** 326 196 (1999)
148. S Dubernet, M Scvoerer *Verre (Versailles)* **2** 26 (1996)
149. Br. P. 97-11 736; *Chem. Abstr.* **130** 186 006 (1999)
150. I A Levitskii, T V Biryuk *Steklo Keram.* (4) 3 (1995)
151. Eur. P. 99-101 891; *Chem. Abstr.* **131** 148 033 (1999)
152. M N Kopylovich, A K Baev, A A Chernic, in *Proceedings of International Symposium on Process of Handl. Powders Dusts, Minsk, 1997* p. 69; *Chem. Abstr.* **127** 98 744 (1997)
153. R D Sytnik, I G Kiiula, O A Ignatyuk *Steklo Keram.* (3) 12 (1995)
154. X Wang, J M Powers *Zhonghua Kouqiang Yuxue Zazhi* **34** 58 (1999); *Chem. Abstr.* **131** 78 338 (1999)
155. Y-H Koh, B-S Han, J-H Lee *Yoop Hakhoechi* **32** 1203 (1995); *Chem. Abstr.* **124** 97 662 (1996)
156. M Nakayama, N Ando *Shigaku* **86** 768 (1999); *Chem. Abstr.* **131** 106 770 (1999)
157. T Noguchi, H Takahashi, H Abe, T Takeuchi *Yakuzaigaku* **59** 43 (1999); *Chem. Abstr.* **131** 134 503 (1999)
158. Jpn. P. 97-310 337; *Chem. Abstr.* **131** 49 203 (1999)
159. Y Watanabe, N Tanigawa, Y Murata, C Kimura, Y Kanzaki, T Tanaka, M Matsumoto *Nippon Koshohin Kagakkaishi* **19** 164 (1995); *Chem. Abstr.* **124** 298 385 (1996)
160. B S Rosenstein, M A Weinstock, R Harib *Photodermatol. Photoimmunol. Photomed.* **15** 75 (1999)
161. Y Kijia, N Asai, S-I Tamura *Jpn. J. Appl. Phys. Part 1* **38** (9A) 5274 (1999); *Chem. Abstr.* **131** 304 758 (1999)
162. Jpn. P. 97-233 613; *Chem. Abstr.* **130** 259 310 (1999)
163. Jpn. P. 94-33 592; *Chem. Abstr.* **124** 18 010 (1996)
164. Jpn. P. 97-342 865; *Chem. Abstr.* **129** 168 173 (1998)
165. R S Deshpande, V Bulović, S R Forrest *Appl. Phys. Lett.* **75** 888 (1999)
166. US P. 97-48 449; *Chem. Abstr.* **130** 58 898 (1999)
167. Y Nakanishi, M Takahashi, Y Hatanaka *Shizuoka Daigaku Denshi Kogaku Kenkyusho Kenkyu Hokoku* **30** 47 (1995); *Chem. Abstr.* **124** 40 751 (1996)
168. Y B Xin, W Tong, C J Summers *Appl. Phys. Lett.* **74** 1567 (1999)
169. Z Xie, Y Li, J Huang, Y Wang, C Li, S Liu, J Shen *Synth. Met.* **106** 71 (1999)
170. G Bogner, A Debray, G Heidel, K Hoehn, U Mueller, P Schlotter *Proc. SPIE — Int. Soc. Opt. Eng.* **3621** 143 (1999)
171. S Tokito, T Tsutsui, Y Taga *J. Appl. Phys.* **86** 2407 (1999)
172. Y Hamada, H Kanno, T Tsujioka, H Takahashi, T Usuki *Appl. Phys. Lett.* **75** 1682 (1999)
173. US P. 98-144 876; *Chem. Abstr.* **131** 108 749 (1999)
174. Y Z Wang, R G Sun, F Medhdadi, G Leising, T M Swager, A J Epstain *Synth. Met.* **102** 889 (1999)
175. Y Li, D Dai, S Cai *Zhongguo Xitu Xuebao* **14** 16 (1996); *Chem. Abstr.* **125** 233 383 (1996)
176. B M Sinel'nikov, T V Ishchenko, L N Krivosheeva, A V Sautiev, A A Mikhalev, V M Ishchenko *Neorg. Mater.* **32** 947 (1996) [e]
177. S-S Sun *Displays* **19** 145 (1999)
178. W Tong, Y B Xin, W Park, C J Summers *Appl. Phys. Lett.* **74** 1379 (1999)
179. U Rambabu, P K Khanna, S Buddhudu *Mater. Lett.* **38** 121 (1999)
180. U Rambabu, S R Sainkar, N S Hussain, S Buddhudu *Solid State Commun.* **110** 685 (1999)
181. S Buddhudu, U Rambabu, T Balaji, K Annapurna *Mater. Chem. Phys.* **43** 195 (1996)
182. Eur. P. 96-111 746; *Chem. Abstr.* **126** 238 840 (1997)
183. M Brehmer, J Lub, P Van Dewitte *Mol. Cryst. Liq. Cryst. Sci. Technol. Sect. A* **331** 2193 (1999)
184. D S K Mudigonda, D L Meeker, D C Loveday, J M Osborn, J P Ferraris *Polymer* **40** 3407 (1999)
185. W Zhu, H Tian, A Elschner *Chem. Lett.* 501 (1999)
186. US P. 97-943 346; *Chem. Abstr.* **131** 51 985 (1999)
187. Jpn. P. 97-117 577; *Chem. Abstr.* **130** 31 120 (1999)
188. Jpn. P. 97-308 480; *Chem. Abstr.* **131** 11 536 (1999)
189. Jpn. P. 98-93 553; *Chem. Abstr.* **131** 300 627 (1999)
190. Jpn. P. 97-53 002; *Chem. Abstr.* **130** 169 603 (1999)
191. Jpn. P. 98-88 465; *Chem. Abstr.* **131** 300 662 (1999)
192. Jpn. P. 98-84 216; *Chem. Abstr.* **131** 287 764 (1999)
193. Jpn. P. 98-48 610; *Chem. Abstr.* **131** 171 585 (1999)
194. D L MacAdam *Color Measurement* (Berlin; Heidelberg; New York: Springer, 1981)
195. A D Sule *Colourage* **40** (12) 31 (1993)
196. Yu V Kostina, V K Runov, A G Borzenko, in *The 10th Russian–Japan Joint Symposium on Analytical Chemistry (Abstracts of Reports), Moscow, 2000* p. 96

[a] — *Herald Russ. Acad. Sci. (Engl. Transl.)*
[b] — *J. Anal. Chem. (Engl. Transl.)*
[c] — *Moscow Univ. Bull. (Engl. Transl.)*
[d] — *Russ. J. Inorg. Chem. (Engl. Transl.)*
[e] — *Inorg. Mater. (Engl. Transl.)*

Russian Chemical Reviews **70** (5) 373 – 403 (2001) © 2001 Russian Academy of Sciences and Turpion Ltd

DOI 10.1070/RC2001v070n05ABEH000656

X-Ray synchrotron radiation in physicochemical studies

Ya V Zubavichus, Yu L Slovokhotov

Contents

I.	Introduction	373
II.	Design of a storage ring and parameters of synchrotron radiation	374
III.	Interaction of X-rays with matter	378
IV.	X-Ray methods of physicochemical analysis	380
V.	The main trends of applied studies using synchrotron radiation	393
VI.	Conclusion	396

Abstract. Modern modifications of the conventional X-ray methods of physicochemical analysis (X-ray and electron spectroscopy, diffraction methods, *etc*.) and new combined techniques using X-ray synchrotron radiation are considered. Unique characteristics of synchrotron radiation are noted, namely, continuous spectrum, exceptionally high intensity, polarisation, coherence, pulse nature, *etc*. The key trends in the use of combined methods in chemistry and materials science including studies of substances under extreme conditions, the study of rapid processes, studies with high spatial resolution are discussed. The achievements in the applications of synchrotron radiation are illustrated by examples from various fields of chemistry and related sciences. The bibliography includes 405 references..

I. Introduction

Development of modern science relies to a great extent upon the set of available investigation tools. Many methods of physicochemical analysis commonly applied in chemistry are based on interaction of a substance under study with electromagnetic radiation of various spectral ranges. Several independent groups of methods can be distinguished based on the spectral range used, *e.g*., infrared, visible, ultraviolet and X-ray radiation. Radiation in the required spectral range is usually generated using special sources (such as gas discharge tubes, lamps, lasers, X-ray tubes) characteristic of classical versions of each method. Each source type requires its own experimental methodology, which takes into account the specific features of the interaction of this radiation with matter.

Integration of natural sciences over the last decade of the XXth century affected the techniques of physicochemical analysis stimulating their convergence. A unified approach to the generation of electromagnetic radiation of different spectral ranges is based upon a fundamental principle of electrodynamics: the electromagnetic radiation is generated by a charged particle moving with an acceleration. In particular, electrons or positrons, which move along a curved trajectory in a magnetic field with a velocity close to the velocity of light, generate a flux of photons in a broad spectral range, *i.e*., synchrotron radiation (SR) (Fig. 1).

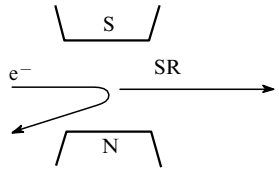

Figure 1. Generation of synchrotron radiation upon movement of an electron in a magnetic field.

Accelerators of charged elementary particles (typically, electrons or positrons) operating in a stationary regime of a storage ring can conveniently serve as powerful SR sources. In such large-scale facilities, ultrarelativistic electrons,† moving along a closed-loop orbit in an evacuated chamber of a storage ring with curvature radius of a few tens of meters, emit extremely intense electromagnetic radiation with a continuous spectrum ranging from far infrared to hard X-ray (Fig. 2). The energies of electrons in storage rings of different constructional designs can vary from hundreds of eV up to several GeV. Upon an incremental increase in the electron energy, the spectral maximum of the SR generated shifts from ultraviolet through hard ultraviolet (vacuum ultraviolet, VUV) and soft X-ray up to hard X-ray, respectively.[1–8]

Modern SR sources gradually become collective use research centres. Such centres accommodate up to a few tens of experimental stations, which function in the 24×7 mode shift by shift servicing specialists from various institutions and fields of science — from nuclear physics to molecular biology and materials science. Along with synchrotron modifications of established and widely accepted methods using traditional X-ray sources, unique purely synchrotron-based specialised techniques are rapidly developing. Applications of SR in industry are also expand-

Ya V Zubavichus, Yu L Slovokhotov A N Nesmeyanov Institute of Organoelement Compounds, Russian Academy of Sciences, ul. Vavilova 28, 117813 Moscow, Russian Federation. Fax (7-095) 135 50 85. Tel. (7-095) 135 93 04. E-mail: yan@xafs.ineos.ac.ru (Ya V Zubavichus) E-mail: slov@xafs.ineos.ac.ru (Yu L Slovokhotov)

Received 1 February 2001
Uspekhi Khimii **70** (5) 429 – 463 (2001); translated by Ya V Zubavichus

† The term ultrarelativistic particles is commonly referred to those, the kinetic energy of which $E \gg m_0c^2$, where m_0 is the rest mass of the particle and c is the velocity of light. Velocities of such species are virtually constant and very close to the velocity of light; thus any increase in their kinetic energies leads to the increase in their relativistic masses.

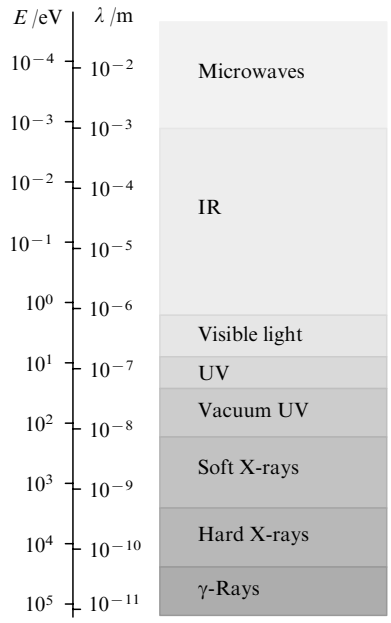

Figure 2. Spectral ranges of electromagnetic radiation, which can be generated by modern synchrotron radiation sources.

ing, in particular, in the manufacture of microelectronics (microchips, printed circuit boards, *etc*.) and micromechanics (micromotors, micropumps) devices. In this connection, applied industrial methods, such as deep X-ray lithography and LIGA technology (German acronym for a 3-stage technological process of microfabrication including lithography, electrodeposition and moulding), have made tremendous progress.[9] Medical applications utilising SR are evolving as well, especially ones aimed at early diagnostics and radiotherapy of various diseases, including cancer and at imaging of human internal organs and tissues with high contrast and spatial resolution (mammography, angiography, radiography).[10] Synchrotron techniques are successfully used in environmental studies, *e.g*., for detection of trace amounts of heavy metal pollutants in industrial wastes, aerosols, soils and in biological objects — plants, living tissues, *etc*.[11]

Currently, there are about 40 operating SR sources worldwide and more than 10 new sources are under construction. In Russia, starting from the late 70's, the Siberian Synchrotron Radiation Centre (SSRC) continuously functions on the basis of the VEPP-3 ‡ storage ring (2 GeV) at the G I Budker Institute of Nuclear Physics of the Siberian Branch of the Russian Academy of Sciences in Novosibirsk.[12] Recently, a new upgraded VEPP-4 storage ring (6 GeV) has been put into operation in the SSRC. Construction of a dedicated storage ring 'Sibir'-2' (2.5 GeV) has been finished at the Kurchatov Synchrotron Radiation Source (KSRS) in the Russian Research Centre 'Kurchatov Institute' in Moscow;[13] two new synchrotron centres in Dubna and Zelenograd are in the construction phase.

An important benefit of storage rings is their environmental safety,§ which distinguishes such facilities advantageously from, for example, neutron sources, *viz*., nuclear reactors. Even a major accident on an electron storage ring cannot result in any radiation pollution of the environment. Work at a synchrotron radiation centre does also not imply any health risk for researchers provided that they obey elementary safety rules and regulations.

All of the main methods utilising electromagnetic radiation are represented at the modern synchrotron radiation centres. A substantial organisational advantage of the SR sources is that all the state-of-the-art techniques and advanced instrumentation are concentrated in one centre and even in one building. This makes it possible to conduct comprehensive studies with the use of a broad range of complementary experimental techniques as well as stimulates mutual influence and integration of different experimental approaches and ideas.

This review is devoted to applications of SR in chemistry and related disciplines, *viz*., chemical materials science, biochemistry and molecular biology. Since it is virtually impossible to cover all modern trends in the SR applications, we have confined ourselves to discussion of only instrumental techniques based on X-ray part of the synchrotron radiation spectrum. For the same reason, we did not consider such technological applications of SR as X-ray lithography and the methods in which synchrotron radiation is used for triggering physicochemical processes, *e.g*., photochemical reactions and radiation-induced degradation (to get familiar with this field one may see, for example, Ref. 14, where synthesis of amino acids from a gaseous mixture of nitrogen, water and carbon dioxide at atmospheric pressure under irradiation by intense photon beams is described). For a detailed review of modern technological applications of SR see Ref. 15. Among non-X-ray synchrotron methods we should mention various types of UV spectroscopy [5] and synchrotron IR spectroscopy, which have been actively developed over the last years, especially its varieties with high spatial (microspectroscopy) [16] and time resolution.[17]

X-Ray-based instrumental techniques, which are most important for chemistry, include X-ray diffraction methods (in particular, single-crystal X-ray crystallography), X-ray and electron spectroscopy. In 'classical' laboratory versions of these methods, allowing detailed exploration of atomic and electronic structures of substances, traditional X-ray sources, *viz*., X-ray tubes, are used. However, synchrotron radiation sources have several significant advantages. Synchrotron X-ray beams are more intense than radiation of the high-energy X-ray tubes with rotating anodes by several orders of magnitude. Such a gain in intensity allows one to shorten the data acquisition time and investigate fine effects which would require very lengthy experiments with traditional sources. A considerable portion of energy emitted by an X-ray tube lies in a narrow spectral range (anode characteristic radiation), whereas the high intensity of synchrotron radiation is uniformly distributed over the entire X-ray spectral range. With 'white' synchrotron radiation, it is possible to select the wavelength most appropriate in each particular case or scan over a certain wavelength range during the experiment, which extends significantly the potential of traditional X-ray techniques. Yet another advantage of SR is relatively small cross-section and low divergence of X-ray beams, which can further be focused and collimated using X-ray optics. This approach is successfully applied in X-ray microprobe methods and in studies of substances under extreme ¶ conditions (it has to be mentioned, however, that focusing X-ray optics is now frequently used in laboratory devices as well). Pulse structure, polarisation and coherence of synchrotron radiation are other factors, which are of great interest and potential for applications.

II. Design of a storage ring and parameters of synchrotron radiation

1. Building blocks of a storage ring

A storage ring is an accelerator of charged light particles (electron or positrons) in which ultrarelativistic particles move along a closed-loop trajectory with velocity close to the velocity of light emitting an intense photon flux. The energy lost by electrons during each revolution as emitted radiation is compensated in a special electromagnetic acceleration system, *viz*., radiofrequency

‡ Russian acronym for electron-positron colliding beams.

§ In this respect, it is indicative that several storage rings are constructed in residential areas of large cities, *e.g*., BESSY (Berlin) and KSRS (Moscow).

¶ The term extreme condition refers here to the limiting achievable (high and low) temperatures and superhigh pressures, which are created using specialised instruments to apply to substances under study.

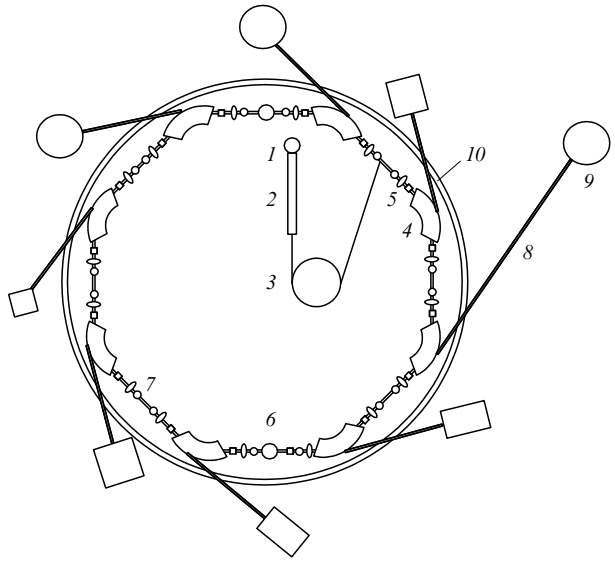

Figure 3. Design of a storage ring, the SR source: (*1*) is an electron gun, (*2*) is a linear preaccelerator (linac), (*3*) is a ring preaccelerator (booster), (*4*) is a bending magnet, (*5*) is a system of 'magnetic lenses', (*6*) is a radiofrequency resonator, (*7*) is a straight section suitable for accommodation of specialised insertion devices, (*8*) is a channel, (*9*) is an experimental station, (*10*) is a biological protection concrete wall.

resonator. The storage ring is designed to maintain a stationary regime of particles' movement rather than to generate a single pulse of particles with the maximum energy (as in the case of elementary particle accelerators in nuclear physics).

A storage ring includes the following indispensable components (Fig. 3):

— an electron source (*1*), which is, as a rule, a standard high-power electron gun based on the thermoelectric emission;

— a system for preacceleration and injection of electrons: linear (linac) (*2*) or ring (booster) (*3*) preaccelerators;

— a hollow torroidal chamber of the accelerator where the beam of ultrarelativistic electrons moves. High vacuum has to be maintained in this chamber (10^{-9}–10^{-10} Torr) in order to reduce energy losses of the electrons due to collisions with background molecules;

— a system of bending magnets (magnetic dipoles) (*4*), which define closed-loop trajectory of the electrons' movement. Between the bending magnets the particles move linearly. It is in the bending magnets that the synchrotron radiation directed tangentially to the beam trajectory is generated (see Fig. 1);

— a system of magnetic lenses (*5*), *viz*., magnetic quadrupoles and higher-order magnets, which is used for the electron beam focusing;

— an electromagnetic system (*6*) is used for the acceleration of electrons up to ultrarelativistic velocities as well as for compensation of energy losses due to emitted radiation (radiofrequency resonator);

— specialised magnetic devices (insertion devices) (*7*), *viz*., undulators and wigglers, are inserted in straight sections between the bending magnets. These devices are used for the generation of SR with enhanced characteristics compared to the bending magnet radiation. Though these are optional components of a storage ring, they are installed in the majority of modern storage rings;

— a biological protection concrete wall (*10*) adsorbs background radiation of the storage ring. Photon beams are guided by evacuated channels (*8*) through the biological protection wall to the experimental station (*9*), where experimental stations and all devices for investigations and other works based on SR utilisation are situated.

2. Design parameters of a storage ring and characteristics of synchrotron radiation

The main parameters of a storage ring as an SR source are as follows: the orbit radius R, along which the electrons move (in modern facilities, it is typically 10–30 m), electron energy E (1–6 GeV), magnetic field (B) in bending magnets (1–2 T) and their number and electron current I, which is an integral measure of the total number of electrons in the storage ring chamber (50–500 mA). These parameters are interlinked by the following relations:[4–7]

$$R = \frac{E}{eB}\,, \tag{1}$$

where e is the electron charge;

$$I = \frac{2\pi e N_e R}{c}\,, \tag{2}$$

where c is the velocity of light and N_e is the total number of electrons in the chamber.

The stability of an electron (or positron)† beam is characterised by a beam lifetime, which is the time required for the electron current to decrease by a factor of $\sim$2.7 (it corresponds to a decrease in $\ln I$ by unity). Beam lifetime depends primarily upon the vacuum quality in the chamber and can range from a few to a few tens hours. This governs the frequency of electron re-injections to the storage ring chamber required in order to maintain the intensity of SR at the appropriate level.

Design parameters of a storage ring determine the characteristics of SR it generates. Spectral distribution of the SR is commonly characterised by a critical wavelength λ_c or critical energy

$$E_c = \frac{hc}{\lambda_c}\,,$$

(h is the Plank constant); λ_c is chosen so that the total energy emitted by the source at the wavelengths longer than λ_c was equal to the total energy emitted at shorter wavelengths.

Size of a synchrotron radiation source is defined by the emittance ε; this quantity is the product of a linear size of the emitting area of the electron beam by the divergence angle of the photon beam. Typical values of the vertical and horizontal emittances of modern SR sources lie in the range of 10^{-10}–10^{-8} and 10^{-8}–10^{-6} m rad, respectively.

The intensity of SR is characterised by its brilliance, which is determined as number of photons emitted in 1 s from the emitting surface unity into the solid angle unity within the certain photon energy bandwidth (BW). Usually, the bandwidth is chosen to be equal to 0.1% of E_p (E_p is the photon energy), the so-called 0.1% BW. Thus, the unit of measure of the brilliance is photon s^{-1} mm^{-2} rad^{-2} (0.1% BW)$^{-1}$. Other intensity characteristics include spectral flux, which is obtained by multiplication of the brilliance by horizontal and vertical emittances, and total flux, which is obtained by integration of the spectral flux over the entire range of the wavelengths emitted.

Total power W emitted by the electron beam per revolution and the critical wavelength depend on the electron energy in the beam, electron current and the orbit radius:

$$W \sim \frac{I\gamma^4}{R}\,, \tag{3}$$

where $\gamma = E/m_0c_2$ is the relativistic (Lorentz) factor of an electron (m_0 is the rest mass of the electron) and

† Positron beams are used, for example, in the DCI storage ring (Orsay, France). The design of all storage rings in the SSRC (VEPP series) allows physical experiments using colliding electron–positron beams (which are accelerated in opposite directions within the same chamber). Similar principles are implied in the German PETRA accelerator (Hamburg, Germany): its name stands for Positron-Electron Tandem Ring Accelerator.

$$\lambda_c = \frac{4\pi eR}{3\gamma^3}. \quad (4)$$

Most widespread types of insertion devices are undulators and wigglers. These are multipole magnetic systems with an intense magnetic field B (0.1 – 10 T depending on the device type) and alternating polarity. The trajectory of electrons becomes strongly curved in the magnetic field of insertion devices, thus the synchrotron radiation with specially selected characteristics can be generated (Fig. 4). Spectral distribution of synchrotron radiation emitted by a bending magnet, wiggler and undulator is shown in Fig. 5; the spectrum from a 'classical' X-ray tube is also given for comparison. Yet another type of specialised magnetic insertion devices is long undulators or free-electron lasers (FEL), which act as sources of coherent monochromatic SR. Currently, more than 100 insertion devices are in operation in the synchrotron radiation centres world-wide.

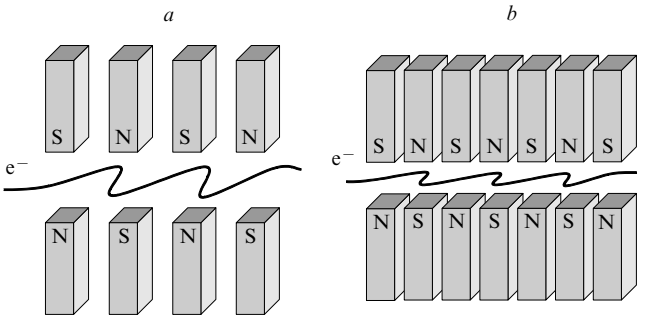

Figure 4. Specialised insertion devices: wiggler (*a*) and undulator (*b*)

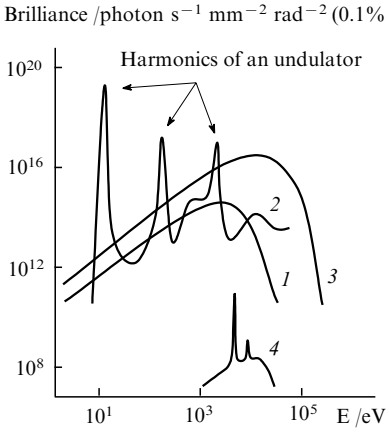

Figure 5. Spectral distribution of SR generated by bending magnet (*1*), undulator (*2*) and wiggler (*3*). For comparison, emission spectrum of an X-ray tube is also shown (*4*).

Adjacent curved sections of the electrons' trajectory within an N-pole wiggler emit independently, which leads to an increase in the intensity of SR by a factor of N compared to radiation of a bending magnet. Yet another advantage of wigglers is that they allow for creation of magnetic fields much stronger (5 – 10 T) than in a bending magnet since in the latter the value of B is linked to the orbit radius [see Eqn (1)], which results in a shift of the critical wavelength to higher energy. This is achieved by using superconducting magnets, which induce transverse 'beats' of the electrons' trajectory with amplitude of a few tenths mm. One wiggler may contain from several up to several tens of magnetic poles.

Compared to wiggler, an undulator is characterised by a larger number of magnetic poles, smaller separation between them and a weaker magnetic field ($\sim$1 T). The operation parameters of an undulator are chosen so as to achieve interference of the emission by adjacent curved trajectory sections. As a result of this interference, spectral distribution of the SR generated exhibits intensity maxima, *i.e.*, the so-called undulator harmonics. The intensity of the harmonics, which is proportional to N^2 is much higher than that generated by both bending magnets and wigglers. Furthermore, the radiation emitted by an undulator is more directed, *i.e.*, its emittance is diminished.[18] Due to differences in physical background and underlying mathematical formalism, synchrotron and undulator radiation are considered separately in the high-energy physics.

An important parameter of the SR is its polarisation, *i.e.*, the existence of preferred directions of the electric field vector. There are two types of the 'pure' polarisation, *viz.*, linear polarisation (the electric field vector oscillates in a certain plane) and circular one (the electric field vector precesses clockwise or counter-clockwise in the plane perpendicular to the direction of the wave propagation). In contrast to X-rays generated by X-ray tubes, synchrotron radiation is always completely polarised. The bending magnet radiation is linearly polarised in the plane of electrons' movement. Upon deviations from this plane up or down, the radiation becomes partially circularly polarised (elliptic polarisation). The synchrotron radiation generated in insertion devices (wigglers or undulators) also exhibits linear or circular polarisation depending on the design of the corresponding device (for example, for generation of circularly polarised SR, helical undulators or elliptic multipole wigglers can be used).

Yet another important characteristic of SR is its coherence, *i.e.*, correlation in oscillations of the electromagnetic field at different space points and at different time moments. The coherence determines the ability of radiation to produce an interference pattern; the planned fourth-generation SR sources approach lasers in this respect. There are two types of coherence, *viz.*, temporal (longitudinal) coherence, which depends mostly on monochromaticity of the SR beam and is characterised by the longitudinal coherence length, and spatial (transverse) coherence, which is, first of all, determined by the emittance of the source.

Synchrotron radiation has a pulse structure. Due to relativistic effects, the electron beam in the storage ring is split into separate moving clusters (bunches), each bunch is of a few cm in length. Therefore, electron current through a bending magnet is not continuous and the SR generated contains periodic pulses with duration of a few tens ps with nanosecond intervals between them. Under certain injection conditions, it is possible to achieve the state where only one bunch of electrons moves in the storage ring (single-bunch mode). In this case, both pulse durations and intervals between them are highly regular, which can be of great importance for time-resolved studies of fast processes.

The key parameter of a SR source is its emittance. It is the emittance, which depends upon perfection of the magnetic system of the source, that reflects most clearly the level of industrial technology involved in the construction of the storage ring. As a rule, the emittance is correlated with the brilliance: the smaller the emittance the higher the brilliance. In addition brilliance depends on the electron current. According to the value of emittance, all the operating synchrotron centres (Table 1) can be conventionally subdivided into generations. First-generation storage rings built in the 60's have the emittance of 100 – 500 nm rad. They were designed and constructed within the scopes of nuclear physics research programmes and thus were not optimised for applications based on utilisation of the synchrotron radiation and such applications took only small portion of the all available beamtime. SR studies on the first-generation storage rings were often conducted in parallel to the main studies on high-energy physics of the electron, positron, or electron – positron colliding beams (in the so-called 'parasitic' mode). In the 80's, the second-generation storage rings with emittance of the order of 50 – 150 nm rad appeared. These accelerators were specialised for SR applications, so they are often referred to as dedicated sources. Most of storage rings which are in operation nowadays belong to the second

Table 1. Characteristics of several storage rings.

Storage ring name (city, country)	Circumference /m	Energy /GeV	Maximum current /mA	Emittance /nm rad	Number of stations	Startup year [a]
DORIS III (Hamburg, Germany)	289.2	4.5	120 (e^+)	404	42	1974 (1995)
VEPP-3 (Novosibirsk, Russia)	74.4	2.0	250 (e^-)	270	9	1975
SRS (Daresbury, UK)	96	2.0	250 (e^-)	104	39	1980
DCI (Orsay, France)	94.6	1.85	300 (e^+)	1600	21	1980
Photon Factory (Tsukuba, Japan)	187	2.5	770 (e^-)	36	21	1982 (1997)
NSLS (Stoney Brook, USA)	170.1	2.6	300 (e^-)	100	70	1982
VEPP-4 (Novosibirsk, Russia)	366	6.0	80 (e^+, e^-)	1200	7	1979 (1992)
BEPC (Bejing, PRC)	65	2.2	100 (e^+, e^-)	76	7	1988
ALS (Berkeley, USA)	196.8	1.9	400 (e^-)	6	19	1993
PLS (Pohang, South Korea)	280.6	2.0	100 (e^-)	12	7	1994
MAX II (Lund, Sweden)	90	1.5	200 (e^-)	8.8	7	1994
SRRC (Hsinchu, Taiwan)	120	1.5	240 (e^-)	19	8	1994
ESRF (Grenoble, France)	844	6.0	200 (e^-)	4	50	1994
ELETTRA (Trieste, Italy)	259.2	2.0	300 (e^-)	7	9	1995
APS (Chicago, USA)	1104	7.0	300 (e^-)	8.2	68	1996
LNLS (Campinas, Brazil)	93.2	1.37	160 (e^-)	100	9	1996
SPRing-8 (Harima, Japan)	1436	8.0	100 (e^-)	5.6	61	1997
Sibir'-2 (Moscow, Russia)	124.1	2.5	300 (e^-)	76	4	1999

[a] In parentheses, the year of last large update of the storage ring is specified.

generation. Several most modern storage rings built in the 90's are classified as third-generation storage rings. They are characterised by emittance of the order of 1 – 10 nm rad and, as a constructive design feature, contain many straight sections in their vacuum chamber between bending magnets for installation of insertion devices. Brilliance of SR sources increases by 2 – 3 orders of magnitude with each new generation.[19] For example, brilliance [photon s^{-1} mm^{-2} rad^{-2} $(0.1\%\ BW)^{-1}$] of first-generation SR sources is $10^9 - 10^{12}$, of second-generation SR sources, it is $10^{12} - 10^{15}$, of third-generation SR sources, it is $10^{18} - 10^{23}$ and $> 10^{24}$ as expected for X-ray free-electron lasers. For comparison, brilliance of standard X-ray tubes and X-ray tubes with rotating anode is only $10^6 - 10^7$.

The modern SR sources generate radiation, which is more intense than that of X-ray tubes by a factor of $10^8 - 10^{14}$. Further modernisation of third-generation storage rings will soon lead to a 'diffraction limit' of a single electron emittance (ε_0)

$$\varepsilon_0 = \frac{\lambda}{2\pi}$$

(where λ is the wavelength of emitted photons), which is equal to 16 pm at $\lambda = 1$ Å ($E = 12$ keV). Thus the currently exploited SR sources are close to the physical limit of brilliance 10^{24} photon s^{-1} mm^{-2} rad^{-2} $(0.1\%\ BW)^{-1}$. The advent of fourth-generation sources with emittance of the order of 0.01 nm rad is related to new technological schemes, such as utilisation of linear accelerators or multi-ring recuperator accelerators and FELs.[12]

3. Components of experimental stations

Special channels guide synchrotron radiation generated in bending magnets, wigglers or undulators to experimental stations (see. Fig. 3). High vacuum should be maintained in these channels, as in the main chamber, in order to minimise losses and radiation background due to absorption of photons by molecules of gases within the channel. Though exact instrumentation of each station largely depends on the specificity of the method used, several main components are common for most stations. These are X-ray optics elements, X-ray monochromators and X-ray detectors.[20]

Virtually in all the cases, optical transformation of the primary SR beam is necessary for experiments, *viz*., collimation (transformation of a divergent beam into a parallel one) and focusing (transformation of a divergent or parallel beam into a convergent one). X-Ray beams with small linear sizes are widely used in X-ray microprobe techniques, X-ray microscopy and microspectroscopy. X-Ray monochromators, which allow one to extract a narrow spectral band with certain (and variable in most cases) wavelength from 'white' synchrotron radiation, are also often considered as X-ray optical elements.

The main tasks of the X-ray optics development include the increase in the energy and spatial resolution and the decrease in the intensity losses associated with the interaction of the respective elements with SR beams. Optical schemes for focusing and monochromatisation of visible light beams (and also, to a great extent, in IR and soft UV spectral ranges), *viz*., lenses, prisms, *etc*., are based on the dispersion phenomenon, *i.e*., the dependence of the refraction coefficient on the wavelength. However, the refraction coefficient for X-rays in most of materials is very close to unity and virtually independent of the wavelength (see below). Besides, soft X-rays are strongly absorbed by virtually all materials (including air). Thus alternative basic principles are used in X-ray optics, such as total external reflection at incidence angles less than 0.1° (grazing incidence), Fresnel scattering and Bragg diffraction.

Most typical optical elements aimed at collimating and focusing the synchrotron X-ray beams include: grazing incidence concave mirrors (toroidal, spherical, cylindrical, *etc*.), curved single crystals, Fresnel zone plates (FZP), Bragg Fresnel lenses (Bragg Fresnel optics, BFO) and tapered capillaries (Fig. 6). Minimal linear size of an X-ray beam achieved in modern SR centres using microcapillary techniques is 20 – 50 nm. The disadvantage of tapered capillaries is strong divergence of the focused beam after the focal point, so they should be mounted very closely to the sample under investigation. FZP and BFO allow one to produce virtually parallel X-ray beams with linear sizes of the order of 1 μm. In applications which do not require very high spatial resolution, concave X-ray mirrors are most commonly used. Generally, an X-ray mirror represents a glass or silicon support coated with a fine and extremely smooth layer of non-oxidisable noble metals (Rh, Pt or Au). A focusing mirror allows amplification of SR beam intensity by 1 – 2 orders of magnitude at the costs of decrease in its linear size.

Some of the aforementioned optical elements (curved crystals, FZP, BFO) can also play a role of a monochromator. In addition, multilayer periodical structures and coatings as well as gratings are often used as monochromators for soft X-rays. Multilayer X-ray mirrors produce sufficiently high intensity of the reflected

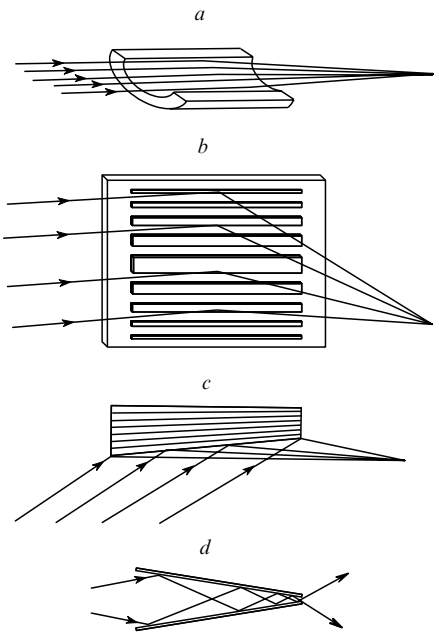

Figure 6. Main types of optical elements for collimating and focusing X-ray SR:
(*a*) X-ray mirror, (*b*) Bragg trensel lens, (*c*) focusing multilayer mirror, (*d*) tappered capillary.

beam even at usual incidence angles (up to a few degrees) and simultaneously focus and monochromatise the primary beam.

In the hard X-ray range, single crystals oriented in a diffracting position by one of its crystallographic planes are most typical monochromators. Among such monocromators, flat single-crystal plates, channel-cut monochromators and more advanced double crystal monochromators with two independent drives are well known. Upon variation of an incident radiation wavelength, the exit-axis of a channel-cut monochromator can drift by a few millimeters, whilst the independent drives of two single crystals make it possible to fix the spatial direction of the monochromatised beam.

The most important characteristic of a monochromator is its energy (or wavelength) resolution $\Delta E/E$ (or $\Delta\lambda/\lambda$). For example, energy resolution of a monochromator based on a flat mosaic graphite crystal with the diffracting plane [002] is $\sim 10^{-2}$; for double crystal monochromator with Si [111] crystals, this value is $\sim 10^{-4}$. Higher resolution can be achieved by utilising low-intensity reflections from higher-order crystallographic planes along directions almost perpendicular to the crystal surface (back reflections). For instance, monochromators with Si [13 13 13] crystals in the back reflection geometry allow one to reach a $\Delta\lambda/\lambda$ resolution of $\approx 10^{-8}$. For experiments requiring very high energy resolution, systems of nested double crystal monochromators are often applied (Fig. 7). A very promising direction in the field of X-ray monochromatisation is the utilisation of the resonance nuclear diffraction phenomenon, which allows one to reach resolutions down to 10^{-10}. It has to be noted that monochromatisation of a 'white' SR beam (extraction of a narrow spectral band) is always accompanied by great losses in intensity.

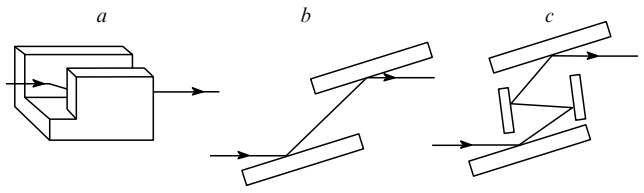

Figure 7. Examples of X-ray monochromators: (*a*) channel-cut monochromator, (*b*) double-crystal monochromator with independent drives for both crystals, (*c*) a system of two nested double-crystal monochromators.

An X-ray beam monochromatised using Bragg diffraction from a single crystal is always contaminated with higher harmonics, *i.e.*, radiation components with an energy multiple of the main component. In order to reject these harmonics, grazing incidence mirrors are often used with parameters adjusted so that the total reflection condition holds for the main component only; higher harmonics in this case pass without changing direction. In double-crystal monochromators, the harmonic rejection can be achieved by slight detuning of the two diffracting crystalline planes (this is however accompanied by noticeable losses in the main component intensity).

In some methods, (*e.g.*, in the energy-dispersive modification of XAFS spectroscopy, see below), similar X-ray optical elements based on Bragg diffraction (in particular, curved single crystals) are used not for monochromatisation but for decomposition of the 'white' beam into spectral components and defining certain spatial directions for photons with different energies (crystal-polychromators).

For control and modification of SR polarisation properties, a specialised polarised optics is used: crystal-polarisers, X-ray quarter-wave plates, phase retarders, *etc*. The state-of-the-art of modern X-ray optics is discussed in detail in a number of reviews (see, for example, Refs 1–4, 20–22).

Virtually any experiment utilising X-ray radiation requires measurement of beam intensities (primary, transmitted through a sample, fluorescent, *etc*.). For this purpose, X-ray detectors are used. Basic characteristics of an X-ray detector are sensitivity, linearity range, maximum load, counting rate, energy and spatial resolution. The following types of detectors are most often used in modern synchrotron radiation centres: photographic films and plates, ionisation chambers, proportional counters, scintillation detectors, solid state semiconducting detectors and charge-coupled devices (CCD).

Depending on spatial resolution, all detectors can be subdivided into point and position-sensitive detectors (PSD). In turn, the latter can be linear (1*D*) or two-dimensional (2*D*). PSDs allow registration of X-ray intensity distribution over a certain spatial area. Of them, multichannel (multiwire) proportional counters, detectors of the type Image Plates (which transform X-rays into visible light in recurring cycles 'energy storage as crystalline lattice defects – stimulated emission in the visible spectral range upon laser irradiation') and CCDs are most popular.

Scintillation counters and ionisation chambers are 'classical' X-ray detectors. They possess extremely high sensitivity (down to registration of single photons). Ionisation chambers are often used as primary beam monitors due to their wide linearity range and ability to operate under conditions of very intense X-ray beams. For some specific tasks (such as imaging, small angle scattering, sample adjustment in a beam), photofilm and photosensitive paper are still in use.

Solid-state semiconducting detectors exhibit high energy resolution. They are applied in cases where a spectral distribution analysis of the detected X-ray radiation is required. Avalanche photodiodes (APD), where each photon coming into the semiconducting diode generates an 'avalanche' of electron – hole pairs are the fastest of the modern X-ray detectors. Such detectors allow intensity measurements for very short pulses of SR (~ 0.1 ns), so they are widely adopted in time-resolved studies of fast processes.

III. Interaction of X-rays with matter

Upon interaction with the matter, X-ray radiation can be scattered or absorbed. These processes as well as combined phenomena of inelastic and anomalous scattering form the basis of X-ray methods of physicochemical analysis.

When a photon is scattered on a particle of a medium and changes its directions, its energy can either be conserved (elastic scattering) or partially transferred to the matter (inelastic scattering). Inelastic scattering can be due to various channels of energy transfer including excitation of collective vibrations of atomic nuclei in a crystalline lattice (phonons) or charge carriers, *viz*., electrons and holes in a conduction zone (plasmons); excitation of electrons from valence zone to vacant energy levels with creation of electron – hole pairs; ionisation of core level electrons of light elements (the so-called X-ray Raman scattering).

For standard energy of a primary beam of ~ 10 keV, inelastic losses due to phonon excitations have the order of a few meV, plasmon losses and losses due to electron – hole pairs creation lie in the range of 0.5 – 10 eV, ionisation of core electron levels may lead to losses of several tens or hundred eV (depending on the binding energy of the excited level). In the case of very hard X-ray radiation, the energy of which is much larger than the binding energies of electrons in atoms, the dominant channel of inelastic scattering is the Compton scattering of X-ray photons on quasi-free electrons (without quantum restrictions on the momentum and energy transfer). Harder γ-radiation with energy starting from several MeV (which usually is not produced by standard SR sources and thus is not considered in detail in this review ‡) interacts with the matter through the mechanisms of elementary particles' transformation, for example, by generation of electron – positron pairs.

Elastic (coherent) scattering of X-ray photons depends primarily on their interaction with electron shells of atoms (Thomson scattering). Since the energies (*i.e*., the wavelengths) of all the scattered photons are the same, elastic scattering can lead to diffraction, *i.e*., a spatial redistribution of the scattered beam intensity as a result of interference of waves coming from different atoms. When atomic arrangement has a translational symmetry (as in crystals), diffraction reflections, *i.e*., narrow maxima of the scattered wave intensity arise at certain directions. Furthermore, a persistence of a mean local atomic order even in amorphous substances gives rise to sinusoidal oscillations of the smooth (without sharp maxima) elastically scattered background as a function of the scattering angle. Diffraction phenomena form the basis of a number of experimental techniques which allow studies of fine details in the structure of the matter, including local atomic environment, supramolecular arrangement and periodicity elements (types of partial ordering).[23, 24]

Absorption of X-ray photons leading to attenuation of the photon beam as it propagates in a medium is primarily related to the photoelectric effect, *i.e*., photoionisation of inner electronic shells of atoms. In this case, a vacancy (hole) in the respective core electron level and a free electron are generated. All the methods of X-ray absorption spectroscopy are based on the analysis of X-ray absorption coefficient as a function of the energy of incident photons. Energy and spatial distribution of the photoelectrons generated in this process are the main subject of X-ray photoelectron spectroscopy techniques.[25]

The excited state with a vacancy in the core level (X-ray term), to which an atom transfers upon absorption of an X-ray photon, is metastable with a lifetime not longer than 10^{-15} – 10^{-16} s. The photoionised atom tends to diminish its energy by filling the core level hole with an electron from higher-lying levels. This can be achieved either through emission of an X-ray photon of lower energy (X-ray fluorescence) or through a radiationless two-electron process involving a transition of one electron from a higher electronic level to the core level vacancy with simultaneous detachment of a second electron (the Auger process). X-Ray fluorescence is the dominant direction of decay of an X-ray term with a *K*-shell hole (*K*-term) for atoms with atomic numbers $Z > 20$ and with $Z > 90$ for an *L*-term (Fig. 8).

‡ Recently, generation of hard γ-rays using Compton back scattering of a laser light on ultrarelativistic electrons has been developed in several synchrotron radiation centres (see, for example, Ref. 12).

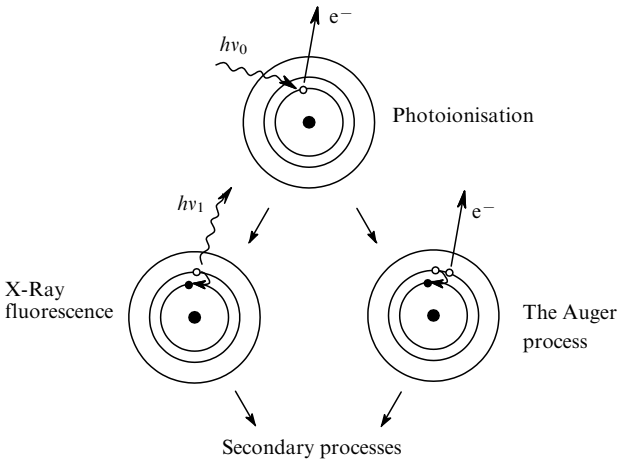

Figure 8. The main processes occurring in matter upon absorption of an X-ray photon.

X-Ray fluorescence and the Auger process result in new holes and thus evoke a cascade of secondary processes, such as emission of secondary electrons, fluorescence in the longer wavelength region, *etc*. In particular, secondary processes can lead to the appearance of luminescence in the visible light range. This phenomenon forms the physical background of the XEOL (X-ray excited optical luminescence) method. Energy transferred to the system from the absorbed X-ray photon can result in cleavage of chemical bonds and detachment of molecular fragments (photostimulated ion desorption, PSID). X-Ray absorption by semiconducting materials is accompanied by an increase in concentration of charge carriers in the conduction zone and thus by an increase in their conductivities. Secondary processes initiated by absorption of X-ray photons are widely utilised in various techniques like X-ray fluorescence spectroscopy, Auger electron spectroscopy, secondary electron spectroscopy, *etc*.

Absorption of X-ray photons in matter can also occur due to nuclear excitations. In particular, the Mössbauer spectroscopy is based on this phenomenon. Generally, this technique is not considered as a sort of X-ray spectroscopy but rather referred to as a distinct field, *viz*., γ-spectroscopy. However such a discrimination is arbitrary: the energy of the nuclear transition in the ^{57}Fe isotope, most often exploited in the Mössbauer spectroscopy (14.4 keV) is close and even slightly less than the energy of characteristic radiation produced by an Mo K_α X-ray tube, which is most popular in X-ray diffraction experiments (17.4 keV). The energy of nuclear excitations for many other isotopes commonly studied by Mössbauer spectroscopy lies also in the range of 10 – 100 keV attainable with modern SR sources. As in the case of electron excitations, excited nuclear states are metastable (however their lifetimes are substantially longer than that of electronic states, *viz*., $\sim 10^{-7}$ s) and the excited nucleus reverts back to its ground state with emission of an X-ray photon of the corresponding energy. The energy of emitted photon may be equal to (elastic or coherent nuclear scattering), or slightly less (inelastic scattering) than, that of the initial radiation. Due to longer lifetime of excited nuclear states, absorption and emission bands associated with nuclear transitions are exceptionally narrow.[26]

When X-ray beam strikes an interface, X-ray reflection occurs with the reflection angle equal to the incidence angle. However, in contrast to, for example, visible light, the probability of the X-ray reflection decreases rapidly with an increase in the incidence angle and for large incidence angle common for visible light optics, the X-ray beam simply crosses the interface not changing its direction. Noticeable X-ray reflection can be observed only at very small grazing incidence angles ($\sim 0.1\,^\circ$) under conditions of the so-called total external reflection. Under this condition, the penetration

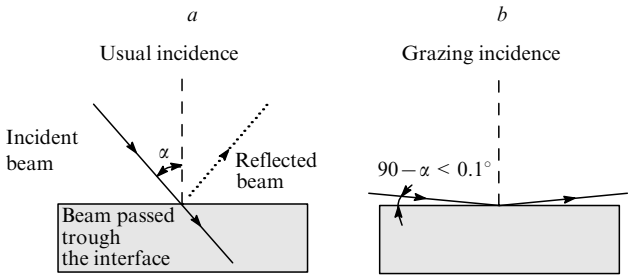

Figure 9. Reflection of an X-ray beam from a surface under conditions of usual (*a*) and grazing (*b*) incidence.

depth of X-ray radiation into the matter is only of a few atomic layers (Fig. 9). This phenomenon has to be taken into consideration in design of X-ray mirrors and focusing microcapillaries; moreover, it is the basis of a number of surface investigation techniques.

IV. X-Ray methods of physicochemical analysis

All X-ray-based research methods can be classified based on the processes which accompany interaction of X-rays with the matter. According to this principle, the following groups of methods can be formulated: X-ray spectroscopy, X-ray electron spectroscopy, X-ray diffraction and X-ray inelastic scattering. Additional independent groups include methods utilising effect of the resonance nuclear scattering (Mössbauer spectroscopy) and imaging techniques.

1. X-Ray spectroscopy

a. X-Ray absorption spectroscopy

The subject of X-ray absorption spectroscopy is the analysis of the X-ray absorption coefficient (μ) as a function of the incident photons energy $\mu = \mu(E)$. In the most common transmission mode, the linear absorption coefficient is determined by the formula

$$\mu = \ln\frac{I_0}{I_t}, \qquad (5)$$

where I_0 and I_t are intensities of the incident X-ray beam and the beam transmitted through the sample. This formula coincides with the respective relations for linear absorption coefficients in other spectral ranges (UV, visible, IR), since X-ray absorption also obeys the Bouguer – Lambert – Beer law, which links attenuation and optical path of radiation propagating in a medium. The major part of modern X-ray absorption spectroscopy studies is performed using SR, since they require scanning the incident beam energy over a broad spectral range.

The X-ray absorption coefficient increases sharply for certain values of incident radiation energy superimposed on a smooth $\mu(E)$ curve monotonically decreasing with an increase in the energy. This resonance absorption induced by photoionisation of atoms of a certain element (see above) define 'triangular' shape of X-ray absorption bands (Fig. 10 *a*). Near the absorption edge, the $\mu(E)$ manifests a fine structure. The fine structure is subdivided into two types, *viz*., X-ray absorption near-edge structure XANES (Fig. 10,*b*) and extended X-ray absorption fine structure expressed as $\psi(k)$ EXAFS (Fig. 10 *c*). XANES covers the energy range from ~50 eV before the absorption edge up to 100 – 150 eV after it. This fine structure is composed of relatively narrow resonance bands generated by electron transitions from the core level to vacant energy levels up to complete ionisation (*i.e*., photoionisation) along with broader bands associated with electron transitions to quasi-bound states (multiple scattering). The oscillatory structure EXAFS, which appears as a result of a free photoelectron scattering on the local atomic environment, is observed in the energy range of 100 – 1000 eV above the absorption edge.

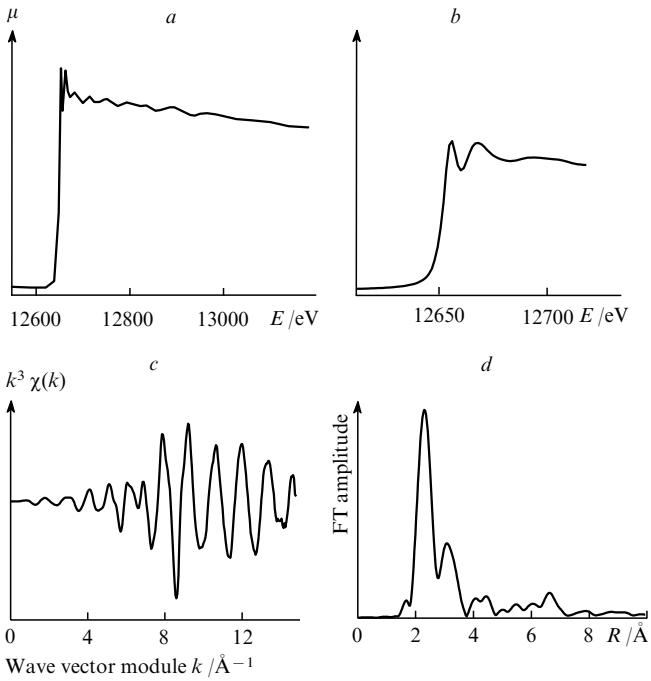

Figure 10. Steps of an EXAFS data processing:
(*a*) an experimental X-ray absorption spectrum; (*b*) the amplified XANES region; (*c*) the normalised EXAFS curve, *i.e*., the oscillating part of the X-ray absorption coefficient; (*d*) the Fourier transform (FT) of the normalised EXAFS curve, the maxima of the Fourier transform correspond to the coordination spheres around the central atom.

XANES spectroscopy is used in studies of electronic structure of substances, including determination of the energy and symmetry of vacant orbitals in molecules or unoccupied zones above the Fermi level in solids. In particular, using this method, information on the oxidation state and coordination symmetry of the central atom can be obtained.[27,28] Analysis of EXAFS gives additional structural information on the local order around the absorbing atom, including the type and the number of closest neighbours as well as interatomic distances within a sphere with the radius of 5 – 6 Å (see Fig. 10 *d*).[29,30] In addition to the interatomic distances, bond angles can be found using such modern approaches as the assessment of multiple photoelectron scattering or simultaneous fitting of spectra measured at the absorption edges of several elements in the sample. In modern X-ray absorption spectroscopy, a common term XAFS (or XAS), which covers both EXAFS and XANES, is often used.

Since the intensities of all the secondary processes are determined by the number of X-ray photons absorbed (*i.e*., by the number of holes generated in the core level), the quantum yields of these processes are proportional to the X-ray absorption coefficient and their energy dependencies exhibit XAFS-like fine structures. For example, such a fine structure is manifested in the dependence of the X-ray fluorescence intensity I_f on the energy of incident photons. Due to substantially higher signal-to-background ratio, the fluorescence yield defined as the ratio of I_f to the intensity of the excitation radiation I_0

$$\mu(E) = \frac{I_f}{I_0},$$

is 10 to 100-fold more sensitive to the oxidation state and local atomic environment of the photoionised atom than the X-ray absorption coefficient measured in the transmission mode.

XAFS in the fluorescence yield mode can be used for the analysis of the oxidation state and coordination of admixture atoms (in concentrations down to 0.1% – 0.2%).[31] Registration of the total or the Auger electron yield

$$\mu(E) = \frac{i_e}{I_0},$$

(where i_e is the electron current) as a function of incident photon energy leads to enhancement of EXAFS sensitivity to surface layers of the sample since the escape depth of electrons does not exceed 50–100 Å.[32] The optical luminescence yield in XEOL [33] or the ion yield in PSID [34] can be used in a similar way.

XAFS allows investigations of substances in any aggregate state. Therefore, it is applicable to the solution of a broad range of structural chemical problems related to the electronic state and local atomic surroundings of a certain element. Methods of X-ray absorption spectroscopy proved to be efficient in structural investigations of semiconductors,[35] superconductors,[36] amorphous glasses and alloys,[37] polymeric electrolytes,[38] ceramics,[39] metallocentres in biomolecules,[40–42] supported catalysts,[43–45] metallic nanoclusters,[46–48] *etc*. XAFS studies of solutions reveal information on structural rearrangements of molecules,[49] solvation mechanisms and structures of solvate shells of ions.[50,51] This method can be used for structural monitoring of reactions in solutions (*e.g*., electrochemical processes).[52] Structural studies of melts give important information on the nature of the interatomic interactions.[53]

In the soft X-ray range at the absorption edges of light elements, such as B, C, N, O and F (the excitation energies from 100 to 1000 eV), the X-ray absorption fine structure is usually referred to as NEXAFS (near-edge X-ray absorption fine structure).[54] Soft X-rays are strongly absorbed in matter (photon free path is only a few tens of nm), therefore NEXAFS is a surface-sensitive technique. The corresponding spectra are generally recorded in vacuum or in a helium atmosphere in the total electron yield mode. The NEXAFS spectroscopy is widely applied for characterisation of polymers,[55] chemisorbed molecules,[56] adsorbed monolayers,[57] Langmuir–Blodgett films, *etc*. For example, thin films of higher fullerenes, which are available only in minute quantities, have been characterised using this method.[58] Though extended oscillating structure is not very prominent in NEXAFS spectra, they are sensitive to the long-range atomic ordering,[57,58] which allows identification of, for example, conformations of long-chain hydrocarbon fragments or individual atomic clusters C_n with $n \leqslant 96$ (Fig. 11).[58]

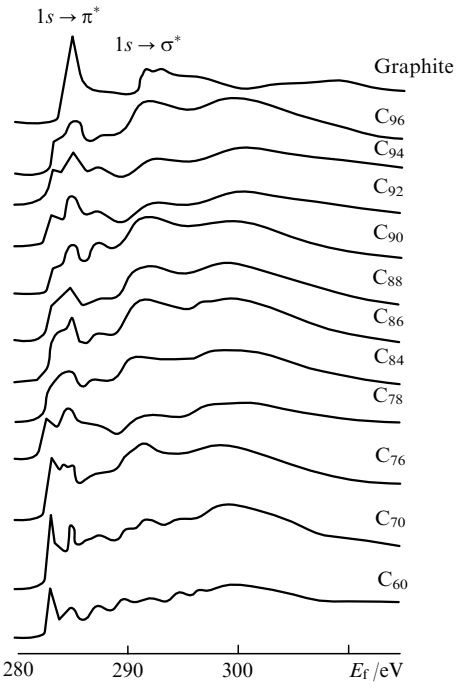

Figure 11. Carbon *K*-edge NEXAFS spectra for a series of fullerenes C_n ($n = 60–96$). Electronic transitions making principal contributions into the respective absorption bands are shown.[58]

Recently, significant attention has been drawn to XAFS spectroscopy in the energy range of 1.5–3 keV, which is intermediate between hard (> 5 keV) and soft (< 1 keV) X-rays.[59] Such techniques require expensive ultrahigh vacuum equipment, which is generally utilised in the soft X-ray region, but methodological approaches developed for hard X-ray studies can be applied to them. As an example, SOEXAFS (soft EXAFS) may be mentioned. The aforementioned energy range covers *K* absorption edges of such key elements as magnesium (~1.30 keV), aluminium (~1.56 keV) and silicon (~1.84 keV), which form the base for many building materials and composites, natural minerals, supports for catalysts, organometallic reagents, *etc*.[60–62] Furthermore, *K*-edges of phosphorus (2.14 keV) and sulfur (2.47 keV), which are constituent of many organic molecules, also belong to this region.[63]

b. X-Ray fluorescence spectroscopy

Methods of X-ray fluorescence (emission) spectroscopy (XRF) are based on detection and spectral analysis of the secondary radiation emitted by a substance following absorption of monochromatic or 'white' synchrotron radiation. They are in active use for elemental analysis of specimens of various origin.[64] An X-ray emission spectrum in XRF analysis measured usually in a broad energy range (typically up to a few tens keV) presents a set of characteristic emission lines corresponding to electron transitions from occupied levels to core holes. Modern synchrotron radiation-based X-ray fluorescence analysis is one of the most sensitive and accurate non-destructive methods for the determination of trace element concentration. In routine multi-element analysis, the lowest detection limit for a broad range of elements from calcium to actinides reaches the level of 0.1 ppm (*i.e*., 10^{-7} g g^{-1});[65] ~0.1 mg of a sample is required to carry out the measurement and the measurement itself takes a few minutes. This enables compositional analysis of samples available only in very small amounts, such as in the case of microelement distribution in lunar rock probes (Fig. 12).[66] In dedicated studies optimised for quantitative analysis of a single element or a limited range of elements, the sensitivity as high as ~1 ppb (*i.e*., 10^{-9} g g^{-1}) and even several ppt (*i.e*., 10^{-12} g g^{-1}) in the analysis of aerosols pumped through a filter, can be achieved.[67]

High-resolution X-ray fluorescence spectroscopy is an established technique for characterisation of the electronic structure of matter, *viz*., for the determination of energy distribution of occupied electronic states below the Fermi level. Information on the electronic structure collected by this method is complementary

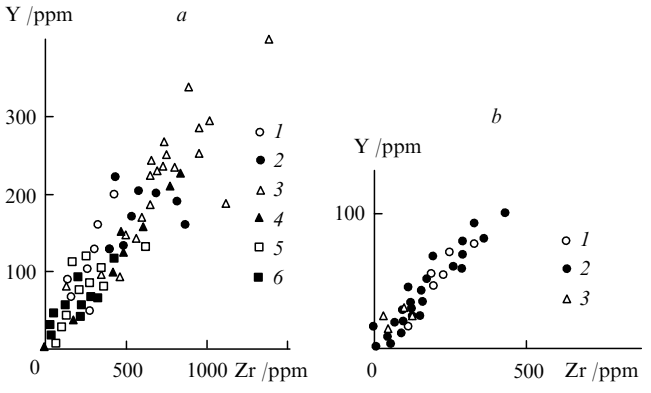

Figure 12. Zirconium *vs*. yttrium concentration correlations in samples of lunar rocks collected in 'Apollo' (*a*) and 'Luna' (*b*) space missions as determined using synchrotron X-ray fluorescence analysis.[66]
(*a*): (*1*) Apollo-11, (*2*) Apollo-12, (*3*) Apollo-14, (*4*) Apollo-15, (*5*) Apollo-16, (*6*) Apollo-17; (*b*): (*1*) Luna-16, (*2*) Luna-20, (*3*) Luna-24.

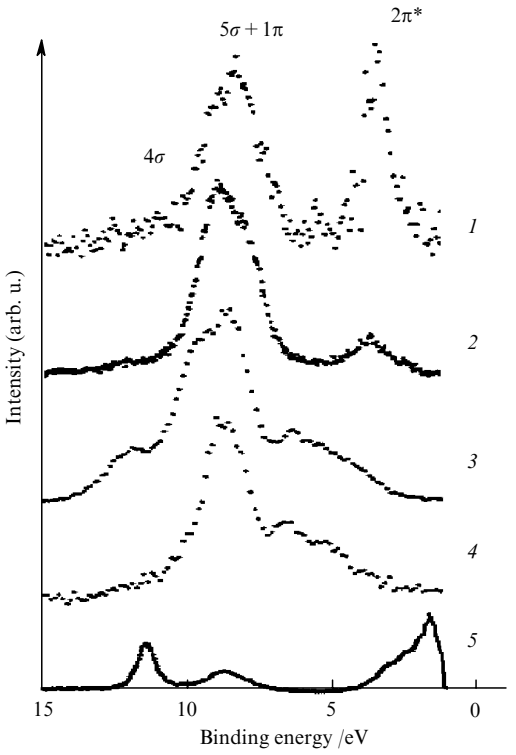

Figure 13. High-resolution soft X-ray fluorescence (C K_α and O K_α) of CO adsorbed on the (100) face of Ni single crystal.[70]
X-ray C K_α fluorescence: (*1*) perpendicular to the surface of Ni(100) face (π-components make major contribution); (*2*) parallel to the adsorbed layer. X-ray O K_α fluorescence: (*3*) parallel to the adsorbed layer; (*4*) perpendicular to the adsorbed layer; (*5*) usual XPS spectrum.

to that obtained using X-ray absorption spectroscopy. Exact positions of X-ray fluorescence lines recorded with high precision depend upon the oxidation state and coordination environment of the element under study.[68] High-resolution XRF spectroscopy can thus be considered as an analogue of the X-ray photoelectron spectroscopy (see next section), which does not require recourse to ultrahigh vacuum equipment. X-Ray fluorescence spectroscopy in the soft X-ray region is particularly informative in studies of organic molecules.[69–71] Resonant photoionisation of atoms of a certain element achieved using monochromatic radiation with the specially adjusted energy (resonant X-ray emission) enhances selectively the intensities of transitions to the vacant level generated in this process and of all the transitions in the cascade of associated secondary processes. This leads to a substantial increase in the sensitivity.[72] For instance, in a study of CO chemisorbed on metallic Ni, this approach allowed one to demonstrate experimentally donation of electrons from the Ni atoms to the $2\pi^*$ molecular orbital of CO (Fig. 13 and Scheme 1).

Scheme 1

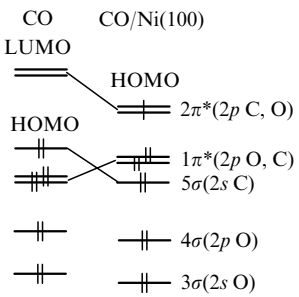

(LUMO is the lowest unoccupied molecular orbital; HOMO is the highest occupied molecular orbital).

Recent achievements in the field of applications and instrumentation of synchrotron X-ray fluorescence spectroscopy are discussed in reviews.[64, 73, 74]

c. X-Ray electron spectroscopy

In traditional methods of X-ray electron spectroscopy, the energy distribution of electrons knocked out of the sample by an X-ray beam is analysed. There are several types of X-ray electron spectroscopy, such as X-ray photoelectron spectroscopy (XPS, sometimes also referred to as ESCA, *i.e.*, electron spectroscopy for chemical analysis), Auger electron spectroscopy (AES), secondary electron spectroscopy (SES), *etc.* All the electron spectroscopy techniques are used for surface studies since the electron escape depth in the energy range typical of these methods does not exceed 50 – 100 Å.

XPS and AES are common methods for quantitative analysis of the surface chemical composition. Positions of lines in the XPS spectra correspond to binding energies of the corresponding electron levels, *i.e.*, they give information on the electronic state of atoms at the surface (chemical shift of core levels) and energy structure of the valence zone. Several other effects are manifested in XPS and give additional information, *viz.*, spin-orbit splitting of lines into multiplets, two-electron excitation processes (low energy shake-up and shake-off satellites), inelastic energy losses of photoelectrons (characteristic bulk and surface plasmons). The use of SR increases the sensitivity and energy resolution of the method noticeably due to high intensity of SR and availability of strictly monochromatic X-ray beams, respectively.[75] Variation of the excitation energy, for example, allows one to distinguish photoelectron and the Auger lines in complex spectra (the positions of the Auger lines, in contrast to photoelectron ones, do not depend on the excitation energy).[25, 76]

As in the case of XRF, additional information can be obtained from XPS spectra provided that the excitation energy is chosen close to one of the edges of resonance absorption (resonant photoemission). This method, in particular, can be used for the determination of contributions of certain atomic orbitals to molecular orbitals, which is important for chemical bonding description, for example, in transition metal complexes with π-ligands (Fig. 14).[77, 78] By varying energy of the incident beam, incidence angle or electron escape angle, one may reconstruct concentration *vs.* depth profiles of the elements under study.

A new promising branch of photoelectron spectroscopy, *viz.*, angular-resolved X-ray photoelectron spectroscopy (ARXPS),[79]

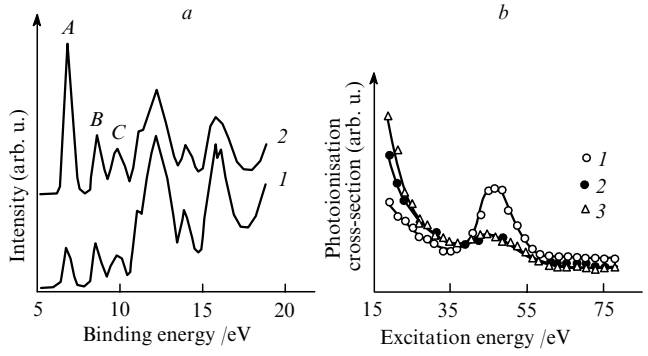

Figure 14. Valence zone photoelectron spectra of the π-complex $Ti(\eta^7\text{-}C_7H_7)(\eta^5\text{-}C_5H_5)$ for two different excitation energies (*a*) and dependence of relative photoionisation cross-sections for bands *A*, *B* and *C* upon the excitation energy (*b*).
(*a*) Excitation energy /eV: (*1*) 33, (*2*) 48; (*b*) band: (*1*) *A*, (*2*) *B*, (*3*) *C*. Sharp increase in the band *A* intensity for the excitation energy of ~48 eV due to approach of the excitation energy to the $M_{II,III}$ absorption edge of Ti ($3p \rightarrow 3d$ resonance) indicates that this band is mostly composed of Ti $3d$ atomic orbital; bands *B* and *C* correspond to molecular orbitals with significant contribution of the ligand orbitals.[77]

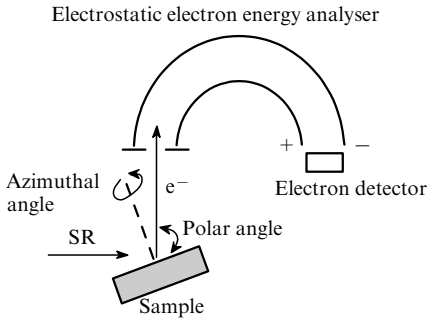

Figure 15. A scheme of a photoelectron spectrometer for recording angular-resolved spectra.

is actively developing in modern SR centres over the last years. This method is based on registration of a spatial distribution of photoelectrons with certain kinetic energies (Fig. 15). Analysis of this distribution allows one to extract the contribution of photoelectron scattering on local atoms surrounding the photoionised atom, *i.e.*, the effect of the photoelectron diffraction. In contrast to other techniques utilising electron diffraction, such as low-energy electron diffraction (LEED) or reflected high-energy electron diffraction (RHEED), the photoelectron diffraction is observed in systems both with and without long-range atomic ordering of a surface. ARXPS, like XAFS, allows studies of local atomic environment of photoionised atoms in samples with disordered or partially ordered surface structure. In particular, this method proved its effectiveness in studies of sorption–desorption processes. This allows one to reveal positions and orientations of diatomic or more complex molecules adsorbed on crystallographic faces of metal single crystals and to estimate adlayer–support distances as a function of adsorbate concentration. Photoelectron diffraction can be applied to structural characterisation of various surface systems, *viz.*, thin films, epitaxial deposits, surface alloys, metal–semiconductor interfaces, oxide layers, supported metal nanoclusters, products of ion-implantation, as well as processes like growth of interfaces and surface phase transitions including melting.[80–82]

Further development of the theory and instrumentation of ARXPS has lead to appearance of a new method for surface structural studies, *viz.*, photoelectron holography. Photoelectron holography is based on mathematical processing of large body of data on the intensities of photoelectron lines obtained by varying the sample orientation relative to the incident beam and detector (both azimuthal and polar scans) and excitation X-ray radiation energy. Holographic processing of ARXPS data allows complete reconstruction of spatial arrangement of atoms within the sphere with a radius of 5–20 Å around the photoionised atom with an accuracy in atomic positions of 0.02–0.05 Å.[83] Similar approaches are being developed in Auger electron spectroscopy and X-ray fluorescence spectroscopy.[84]

2. X-Ray diffraction methods

a. Single crystal X-ray diffraction

X-Ray diffractometry is a most important experimental method of modern structural chemistry. This allows one to determine the atomic structure of a single crystal (including unit cell parameters, space group, coordinates and types of atoms within the unit cell and parameters of their thermal vibrations). Based on atomic coordinates, any structural characteristics like interatomic distances, bond and torsion angles, *etc.*, can easily be calculated. In contrast to the majority of structural methods, X-ray diffractometry allows complete objective determination of a crystal structure without prior knowledge of any of its structural characteristics and even chemical composition.

The set of experimental data measured by X-ray diffractometry includes angle coordinates and intensities of reflections generated by diffraction of X-rays on a single crystal. The scattering of X-rays occurs primarily on electron shells; thus, mathematical processing of the experimental data (Eulerian angles and intensities of reflections) allows reconstruction of the electron density distribution $\rho(r)$ in the unit cell. In routine diffraction experiments, distinct maxima of the $\rho(r)$ function corresponding to the centres of atoms, are revealed with the accuracy of 0.01–0.02 Å. Based on high-precision data, fine features of the electron density distribution functions, such as valence electrons redistribution due to formation of chemical bonds, as well as other physicochemical characteristics of a crystal related to $\rho(r)$ can be analysed. Qualitatively, the redistribution of electron density can be visualised in deformational electron density maps $\Delta\rho(r)$ obtained by subtraction of the promolecule's electron density [composed of spherically symmetric non-interacting atoms whose positions are determined from the 'high-angle' refinement of the structure versus reflections with high $(\sin\theta)/\lambda$ ratio, where θ is the diffraction angle and λ is the wavelength] from the total experimental $\rho(r)$ function.

Currently, the most popular technique in chemical X-ray crystallography is the conventional single crystal diffractometry based on diffraction of monochromatic X-ray beam on a single crystal. X-Ray tubes are most often used as an X-ray source. A serious disadvantage of this method is very strict requirements to the quality of a sample under study. It has to be a well-formed single crystal with linear dimensions of approximately 0.1–1 mm and a sufficient diffraction power at a fixed wavelength (typically, characteristic Mo K_α $\lambda = 0.71$ Å or Cu K_α $\lambda = 1.54$ Å radiation). If a crystal is smaller than the dimensions mentioned or it is of poor quality (due to domain misorientation, static or dynamic disorder of molecules or molecular fragments in the unit cell, *etc.*), the routine structure solution becomes very complicated or even impossible. Such accompanying phenomena as X-ray absorption, anomalous dispersion, multiple diffraction and extinction (deviations of X-ray reflection intensities from the values predicted by the kinematic X-ray scattering theory) further decrease accuracy of the X-ray diffraction results.[23,24]

The use of SR in X-ray crystallography eliminates many restrictions of this method. Due to high intensity of SR beams with a capability of their further focusing and collimation by X-ray optics, it is possible to collect reflection sets of satisfactory quality for weakly diffracting and very small crystals. Low divergence of SR beams leads to improvement of angle resolution in high-precision diffraction experiments.[85–88]

Routine synchrotron X-ray crystallographic studies of low-molecular-weight compounds are now developing in two principal directions, *viz.*, investigations of samples not applicable to laboratory diffractometry (*e.g.*, due to a weak diffraction power)[89,90] and experimental investigations of electron density distribution in crystals.[91] Nowadays, crystals with linear dimensions down to several micrometers can be characterised by X-ray diffraction in synchrotron centres.[92,93] Such crystals are commonly formed in a chemical synthesis[94] and they are particularly typical in geology and mineralogy.[95,96] For mounting of such small crystals onto a diffractometer, special methods and devices (for example, on the stage of an electron microscope) are required.[97,98]

In the 90's, systematic studies of electron density distribution in crystals based on high-precision diffraction experiments were started in synchrotron radiation centres. Data acquisition time required for these studies shortened down to 15–20 hours from 10–15 days needed with laboratory equipment. Furthermore, requirements for the quality of single crystals for the studies also became not so strict as, for example, in high-precision studies (Fig. 16).[99–102] Application of hard X-ray radiation reduces absorption and extinction and increases the resulting accuracy due to larger number of observed reflections with high $(\sin\theta)/\lambda$ ratio. In high-precision laboratory experiments, Ag K_α line of X-ray tubes ($\lambda = 0.56$ Å) is used whereas several studies with synchrotron radiation wavelengths as short as 0.3–0.1 Å have been reported.[103–105]

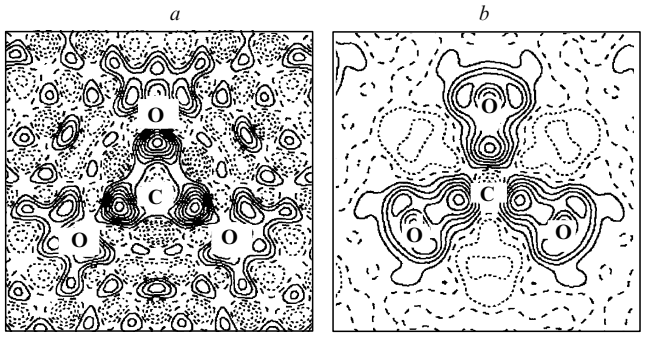

Figure 16. Static deformational electron density maps $\Delta\rho(r)$ reconstructed in high-precision X-ray diffraction studies of $MnCO_3$ single crystal (section in the plane of the carbonate group, solid lines correspond to positive and dashed lines to negative deformational electron density; contours are drawn with a step of 0.1 e $Å^{-3}$): (*a*) data collected on a laboratory diffractometer, (*b*) SR data (Photon Factory, Tsukuba, Japan).[100]

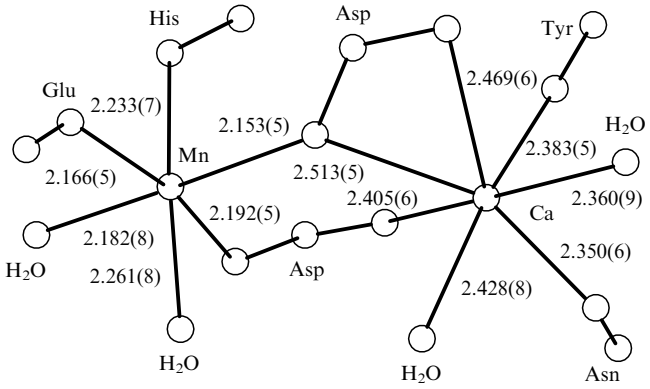

Figure 17. Geometry of the metallocentre in the protein concanavalin A determined using synchrotron X-ray single-crystal diffraction with accuracy typical of low molecular-weight compounds (the synchrotron centre CHESS, Ithaca, USA, $\lambda = 0.92$ Å). Only the atoms of amino acid fragments coordinated to the metal atoms are shown. The crystallographic parameters are as follows: orthorhombic, $a = 89.55(2)$ Å, $b = 86.46(2)$ Å, $c = 62.11(1)$ Å, space group $I222$, 116923 observed reflections, 19158 least-squares parameters refined for 2134 independent non-hydrogen atoms, $R_F = 12.2\%$.

In processing of high-precision synchrotron X-ray diffraction data, the most advanced computational techniques are applied, *viz*., multipole refinement and topological analysis of the $\rho(r)$ function.[99,106] Comparison of SR-based and laboratory approaches shows that the accuracy of synchrotron diffraction experiments is at least not lower than that obtained using laboratory diffractometers and is noticeably higher in many cases (see Fig. 14).[100,107,108] For example, one of the most accurate structures ever solved from single crystal X-ray diffraction data is racemic DL-serine: data collected at HASYLAB (Hamburg, Germany) at the wavelength of 0.45 Å.[99]

Currently, X-ray crystallography is widely applied in studies of biological macromolecules (proteins, nucleic acids, polysaccharides, viruses, *etc*.).[109] Single crystals of biopolymers possess large unit cells with parameters of 50 – 500 Å containing up to several hundred thousand independent atoms. For this reason, measurement and structure solution techniques applied in this field have to be noticeably altered. The 'classical' X-ray diffraction study allows one to reconstruct the electron density map of the crystal of a biopolymer with a relatively low resolution (3 – 5 Å), in which typical functional groups or fragments rather than single atoms can be seen on a partially resolved background of hydration water molecules (which can occupy 15% – 20% of the crystal volume). Furthermore, large and well formed single crystals of biopolymers are extremely difficult to grow and they easily decompose under X-ray irradiation, since the standard data acquisition can take several weeks on a laboratory diffractometer.

Distinct advantages of synchrotron radiation-based techniques caused a very fast growth of their application to crystallographic studies of proteins and other biopolymers.[100–113] According to Biosync (an international organisation of SR users in the field of structural biology), the fraction of SR in all diffraction studies of new crystal structures of biological macromolecules has grown from 18% in 1990 to 44% in 1996.[114] Presently, almost a half of all studies in protein crystallography is performed using SR sources. In a number of cases, the use of SR allowed one to achieve the resolution comparable to the standard resolution in small-molecule X-ray crystallography. Thus in an X-ray diffraction study of the protein concanavalin A (molecular weight 25 000), the resolution of 0.93 Å has been reached, which made it possible to reveal and refine the positions of all 2134 non-hydrogen atoms within the unit cell in the anisotropic approximation.[115] Since the ratio of the number of independent reflections *vs*. refined parameters was relatively high, accuracy comparable to that of small-molecule crystallography has been obtained (Fig. 17). Even higher resolution of 0.54 Å has been achieved in the diffraction study of the oligopeptide cramine and the deformation electron density map has been analysed for the first time for a protein molecule (data collected at HASYLAB).[116]

As a recognition of great importance of structural biology for the modern science, the 1997 Nobel prize in chemistry was awarded to the international team including J E Walker (UK), P D Boyer (USA) and J C Skou (Dennmark) for the determination of the enzymatic mechanism of the intercellular synthesis of adenosine triphosphate (ATP). The key stage of the investigation was the single crystal structure study of the enzyme complex F1-ATPase using SR diffraction data collected in Daresbury Laboratory (UK).

This enzyme is a constituent of the ATP-synthase complex, which catalyses the last stage of the intercellular ATP synthesis by oxidative phosporylation of adenosine diphosphate. The solution of the structure of F1-ATPase (molecular weight 371 000, orthorhombic, unit cell parameters $285 \times 108 \times 140$ Å, space group $P2_12_12_1$) took 12 years. To date, it is the largest non-centrosymmetric crystal structure solved from X-ray diffraction data.[117]

In addition to conventional diffractometry, the Laue diffraction method is widely applied in synchrotron crystallographic studies of proteins. In this method, the diffraction pattern is obtained by 'white' X-ray beam scattering on a rotationally fixed single crystal. Combined utilisation of intense synchrotron radiation and area detectors allows investigations of extremely small single crystals (with a volume of ~ 0.1 μm^3) with a very short data acquisition time (several ns). The unprecedented volume for a single crystal of gold studied by this method[118] is $\sim 10^{-3}$ μm^3. During recent years, special techniques for data recording and processing have been developed in this field, which allow at present the *ab initio* (*i.e*., without any *a priori* structural models) solution of relatively simple structures solely from Laue diffraction data[119,120] and refinement of structures of any complexities.[121]

Yet another direction in the development of synchrotron X-ray crystallography is magnetic scattering. The incorporation of relativistic effects gives corrections of the X-ray scattering amplitude due to interaction of X-ray photons with magnetic moments of electrons. In a classical X-ray diffraction studies, scattering of photons on magnetic moments is several orders of magnitude weaker than that on charge density. However, the magnetic component increases in the case of very hard X-rays (80 – 100 keV). Furthermore, the magnetic scattering intensity can be substantially enhanced (by 3 – 4 orders of magnitude) when the scattered wavelength approaches an absorption edge of an element with unpaired electrons in the sample (the so-called X-ray

resonance exchange scattering). In this case, the intensity of magnetic scattering of photons achieves the intensity of scattering on electron charge density.[122]

Magnetic X-ray scattering leads to the appearance of forbidden diffraction maxima (extinction condition violations) and superstructure reflections corresponding to the sublattice of magnetic atoms. With synchrotron X-ray sources of high intensities it is possible to record magnetic reflections both in the resonance region and far from the absorption edges.[123,124] It allows investigations of magnetic structures of paramagnetic crystals. In this respect, magnetic scattering of SR turns into an important alternative for the traditional technique in this field, *viz*., magnetic scattering of polarised neutrons. Magnetic X-ray scattering is widely used for studies of magnetic ordering in compounds of *f*-elements (lanthanides and actinides).[125] One of the first demonstrations of research capabilities of the technique has been the confirmation of helical magnetic structure (*i.e*., heliomagnetism, a particular case of antiferromagnetic ordering) in a number of rare-earth metals, in particular, in holmium.[126]

Yet another emerging trend of synchrotron X-ray crystallography is the so-called perturbation crystallography, covering structural investigations of crystals in an external perturbing field, such as mechanical deformation, electrostatic or magnetic field and crystals of substances in excited states.[127] For instance, an X-ray diffraction study has been performed for a single crystal of 2-methyl-4-nitroaniline (exhibiting non-linear optical and piezoelectric properties) in an external electric field (NSLS, Stony Brook, USA). Changes in unit cell parameters and intensities of selected reflections for the crystal placed into the electrostatic field of 3.9×10^6 V m^{-1} have been explained by rotation of the molecules tending to align their dipole moments with the direction of the external field.[128] Changes in unit cell parameters and electron charge density redistribution have been observed in a crystal of deuterated potassium dihydrophosphate KD_2PO_4 (manifesting segnetoelectric and piezoelectric properties) in the electrostatic field of 1.3×10^6 V m^{-1}. Upon application of the external field, a phase transition with alteration of space group and syngony ($I42d \rightarrow Fdd2$) has been detected.[129]

A combined study using IR and X-ray diffraction data for a single crystal of the $Na_2[Ru(NO_2)_4(NO)OH] \cdot 2H_2O$ photochromic complex with excitation by a laser pulse has been carried out in ESRF (Grenoble, France).[130] An excited state of the molecule (with relative population of 0.2–0.3) has been detected and structurally characterised. The excitation is accompanied by elongation of the N–O bond by 0.19(5) Å and decrease in the Ru–N–O bond angle by 6(2)°. Earlier, a non-zero population of an excited state with changed geometry of the MNO fragment has been observed for (η^5-C_5H_5)NiNO by XAFS spectroscopy.[131]

b. X-Ray powder diffraction

Techniques of X-ray powder diffraction (XRD) or X-ray phase analysis are the main fast methods for structural characterisation of polycrystalline samples. In XRD, the dependence of scattering intensity as a function of a single scattering angle 2θ, is measured. Compared to single crystal X-ray diffractometry, X-ray powder diffraction methods are much more versatile allowing studies of a broader range of samples including compact workpieces, partially ordered multiphase systems, polymers, thin films, layered nanocomposites, minerals and so on. XRD is applicable to solution of such problems as qualitative identification and semi-quantitative analysis of crystalline phases in mixtures, estimation of degree of crystallinity and sizes of crystallites in polymers, analysis of preferred orientation and textures in materials, investigations of phase transitions and equilibria in solids, determination of unit cell parameters as a function of the phase chemical composition or external conditions (pressure, temperature), structural monitoring of solid-phase reactions, *etc*.

XRD is routinely used in laboratories with X-ray tubes as the X-ray source. However, during the last decade measurement of XRD patterns in synchrotron centres (especially for samples with low diffracting power and substances available in small amounts) become more and more common (Fig. 18). Most important areas of the SR X-ray powder diffraction are high-precision and high-resolution diffractometry, which allows *ab initio* structure solution in combination with the structure refinement using the full-profile analysis (Rietveld method) solely from powder diffraction data; diffraction investigations of partially ordered and amorphous samples; time-resolved studies of processes in solids.[12,20,132] As in synchrotron X-ray crystallography, position-sensitive detectors are widely utilised in SR-based XRD (typically, curved linear 1*D* PSDs capable of simultaneous full pattern registration in the 2θ range from 0° up to 165–170°).

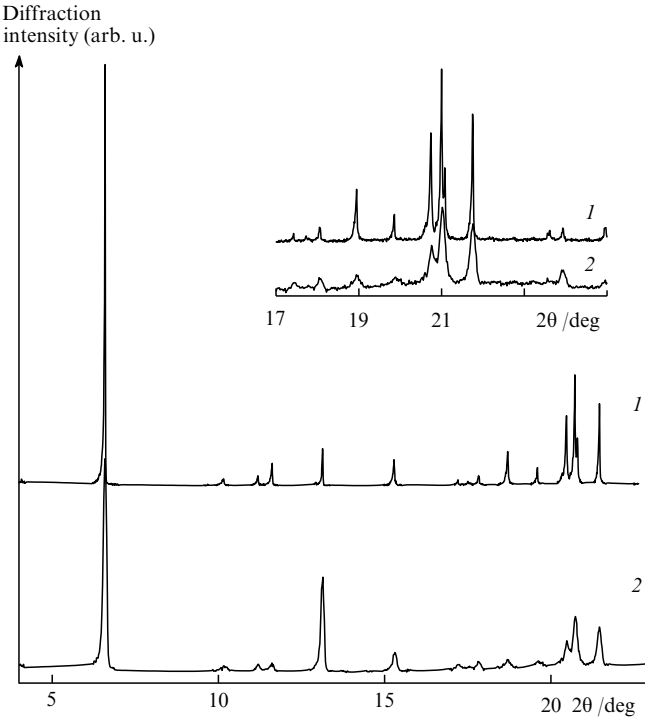

Figure 18. X-Ray powder diffraction patterns for radical-ion salt $BEDTTTF^+ \cdot C_{60} \cdot I_3^-$ (BEDTTTF stands for bis-ethylenedithiotetrathiafulvalene).
(*1*) – SR pattern (VEPP-3 storage ring, Novosibirsk, λ = 1.5402 Å, angle step 0.01°, exposure time 1 h); (*2*) – laboratory pattern (DRON-3 diffractometer, X-ray tube Cu K_α, $\lambda \approx$ 1.5418 Å, 45 kV × 20 mA, angle step 0.02°, exposure time 20 h).

Depending on the instrumental setup, two methods of XRD can be distinguished: conventional angle-dispersive diffraction (when a fixed-wavelength monochromatic X-ray beam is used) and energy-dispersive diffraction (when the scattering intensity is measured at the constant scattering angle and the wavelength of the incident beam is varied).[133] Energy-dispersive X-ray powder diffraction can be accomplished only on SR sources; this modification of XRD is very useful in structural investigations of matter under extreme conditions. In the case of angle-resolved diffractometry, due to high collimation and degree of monochromaticity of X-ray beams, resolution of weak reflections is substantially better than that obtained using laboratory diffractometers; the profiles of reflections are narrower and more regular. Using SR, it becomes possible to achieve good signal-to-noise statistics for very short time intervals (down to ms); thus it allows registration of minor crystalline phases present in the sample in very low concentration ($\sim$0.1%).[134] All these factors substantially facilitate data processing including full-profile analysis of powder patterns by the Rietveld method. The latter is used to refine positions of atoms within the unit cells by fitting the calculated intensity profile $I(2\theta)$ to the experimental curve; the

accuracy of this procedure may approach that of single crystal X-ray crystallography.[135]

The main unsolved problem in the powder crystallography is the selection of the initial approximation, *i.e.*, structure solution. In synchrotron XRD patterns, up to a few hundred individual reflections can be revealed. Thus it turns possible to solve *ab initio*, in a routine mode, relatively complex structures with up to several tens of independent atoms in the unit cell. For structure solution, both algorithms widely adopted in crystallography of small-molecular-weight compounds (direct methods, the Patterson method) and *ad hoc* techniques (maximum entropy, maximum likelihood and Monte Carlo methods, trial-and-error search among sterically allowed orientations of a fragment with known geometry in the unit cell with variation of selected structural parameters such as torsion angles, *etc.*) are used. The reliability of the Rietveld refinement results can be enhanced by fitting the structural model *versus* several independent experimental data sets (for example, *vs.* synchrotron diffraction patterns measured at different wavelengths). Recently, the Rietveld refinement combined with trial-and-error search for most probable atomic configurations proved to be very efficient in structure solution from powder diffraction data.[136–139]

The number of various structures of organic,[140–142] inorganic,[143–146] and organometallic[147,148] compounds solved *ab initio* based on synchrotron XRD data has now reached several hundreds. Synchrotron XRD is actively employed in structural studies of fullerene derivatives,[149] such as endohedral metallofullerenes $Sc@C_{82}$,[150] $Y@C_{82}$, $Sc_2@C_{84}$ (which are available only in a few mg),[151] dimeric azafullerene $(C_{59}N)_2$,[152] low-temperature modification of fullerene bromide $C_{60}Br_{24}\cdot 2Br_2$ (see Ref. 153), *etc*. In certain cases, this method allows one to solve independently several components of a multiphase system without their separation. For example, it was possible to determine crystal structures of two polymorph modification of cyclopentadienyl rubidium from synchrotron powder diffraction pattern of their mixture (Fig. 19).[154] The electron density distribution revealing features at the subatomic level for a series of simple inorganic solids, *viz.*, BN, Mg, Be, was successfully reconstructed based on synchrotron X-ray powder diffraction and using the maximum entropy method (MEM).[155–157]

Structural investigations of textured samples, which can be considered as an intermediate step between a single crystal and a polycrystalline powder with random orientation of crystallites, can also be facilitated if SR is used up to the possibility of routine structure solutions by direct methods.[158] In this case, a typical routine includes measurement of an XRD pattern at different orientations of the sample in the X-ray beam. In contrast to synchrotron experiments, such a procedure with the laboratory diffractometers usually leads to a substantial line broadening due to high divergence of the incident beam produced by an X-ray tube.

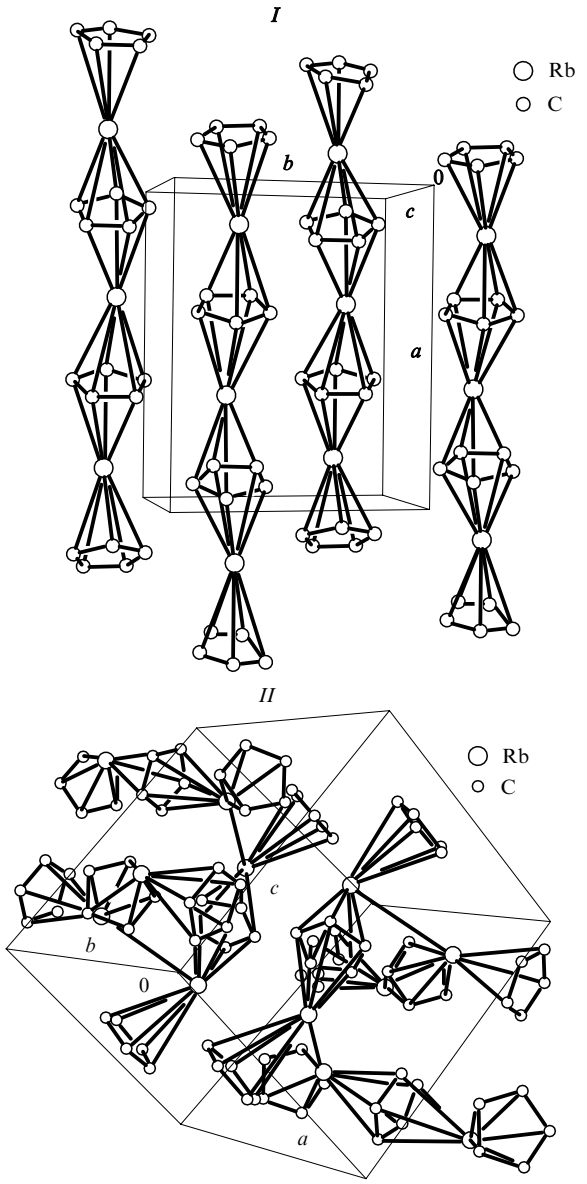

Figure 19. Crystal structures of two polymorphic modifications of $Rb(C_5H_5)$ differing from each other in spatial arrangement of infinite Cp – Rb – Cp chains. The structures have been solved *ab initio* based on the synchrotron powder diffraction pattern for their mixture.[154]
(*I*) Space group *Pnma*, a = 10.799 Å, b = 8.962 Å, c = 5.706 Å (chains are arranged along the a axis); (*II*) space group *Pbcm*, a = 9.340 Å, b = 10.967 Å, c = 10.549 Å (chains are arranged along both the b and c axes).

c. X-Ray scattering by amorphous and partially ordered samples

When X-ray radiation is scattered by a completely amorphous solid or by a liquid, the dependence of intensity on the scattering angle exhibits no sharp diffraction maxima. The Fourier transformation of smooth oscillations observed in this dependence gives rise to a radial distribution function (RDF). The maxima in this curve correspond to interatomic distances. A classical version of this method § has a limited applicability, since the interpretation of results for systems more complex than monocomponent or binary is often ambiguous. For example, noncrystalline scattering of synchrotron X-rays with the energy of 101.2 keV (HASYLAB centre) has been utilised for the analysis of RDF in normal and heavy water. In this study, small systematic differences in interatomic distances between oxygen atoms forming H-bonds with different hydrogen isotopes (the Ubbelohde effect) have been revealed.[159]

Noncrystalline scattering of hard X-rays is a promising technique for structural characterisation of glasses and other inorganic materials with disordered structures, since in this case, the amplitudes of scattering on light atoms become negligible and thus only interatomic distances related to heavy atoms are seen in RDF, which facilitates substantially their interpretation. Analysis of oscillations in the noncrystalline X-ray scattering curves up to high values of the diffraction vector

$$Q = \frac{4\pi \sin\theta}{\lambda}$$

allows determination of interatomic distances with the accuracy of *ca.* 0.01 Å.[160,161] For instance, in a study of a short-range order around barium atoms in $BaSi_2O_5$ using non-crystalline scattering

§ This method is also often referred to as the method of radial electron density (RED), wide-angle X-ray scattering (WAXS), or partial distribution functions (PDF).

of synchrotron X-rays with the energy of 150 keV over the Q range of 0.8 – 38.7 Å^{-1}, long Ba – Ba distances at 4.5 – 4.8 Å have been revealed.[162] For measurements of this kind, intense SR beams produced by insertion devices (wigglers and undulators) in third-generation storage rings are most suitable.

In substances with partially ordered structures (defect-rich, disordered and dynamic phases, liquid crystals, thin films, intercalation compounds, polymers, *etc.*) as well as in phases with non-crystallographic ordering (modulated and incommensurate phases, quasi-crystals), the types of spatial symmetry can be different for different directions and/or components of the sample. Intercalation compounds of layered matrices (such as transition metal dichalcogenides, graphite, *etc.*) may be mentioned as examples of partially ordered systems. They often exhibit a strictly parallel stacking of alternating 'guest/host' layers, long-range order within host layers combined with the possibilities of phase transitions in two-dimensional guest layers and orientational disorder of adjacent layers. Powder diffraction patterns for such systems often contain relatively narrow reflections together with wide diffuse features. Important structural information can be extracted in this case from the analysis of shapes and widths of diffraction lines [133, 135] and diffuse scattering.[163, 164]

A variety of partial ordering is particularly typical of biopolymers and other biological systems.¶ In SR-based studies of such systems, two-coordinate detectors are conveniently used. The measured patterns are usually adjusted to fit some *a priori* model, which corresponds to a structure of a segment of polymer chain, conformation of the chain, fibre orientation, *etc.*[165, 166]

d. Small-angle X-ray scattering

Small-angle X-ray scattering (SAXS) is based on the scattering of X-rays on optical inhomogeneities of the sample (atomic aggregates, cavities) with the size of the order of several tens of nm. Experimentally, scattering intensity is registered as a function of scattering angle in the region of small angles from several angular minutes up to a few degrees, *i.e.*, for diffraction vector moduli $0 < Q \leqslant 0.2$ (see Refs 167 – 169). In such small angle diffraction patterns, usual diffraction maxima corresponding to reflections from long-periodicity atomic planes with interplanar distances 10 – 50 nm (100 – 500 Å) can be observed. A periodic structure can also be formed by packing of supramolecular objects (polymer globules, nanoparticles, *etc.*). By analysing the scattering intensity decrease function for a sample with completely irregular structure, one may retrieve information on the mean particle size (or inhomogeneity regions) in the sample as well as estimate the shape and size distribution of such particles (Fig. 20).

SAXS plays a very important role in characterisation of polymer morphology (including biopolymers), conformations of macromolecules in solutions,[170, 171] colloid systems,[172] submicro- and nanoparticles as well as in studies of such processes as phase segregation in amorphous glasses, gelation, nucleation, crystal growth, amorphisation, *etc.*[173 – 175] Small divergence of synchrotron X-ray beams extends the capabilities of the technique enabling collection of scattering data at very small angles corresponding to interplanar distances up to ~1000 nm [ultra-small angle X-ray scattering (USAXS)].[176 – 178]

¶ Studies of biological objects using X-ray crystallography, non-crystalline diffraction, small angle scattering (see below) and XAFS are often merged under the common term 'structural biology'.

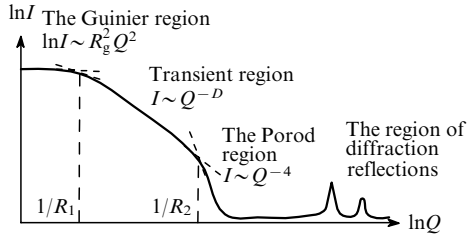

Figure 20. General view of a small angle X-ray scattering curve on an inhomogeneous sample.
R_1 is radius of aggregates; R_2 is radius of particles composing fractal aggregates; R_g is gyration radius of aggregates; D is fractal dimensionality.

3. Inelastic X-ray scattering

Analysis of energy distribution of scattered X-rays forms the basis of a number of methods.[179 – 181] As has been mentioned above (see Section III), inelastic losses accompanying X-ray scattering are due to several distinct physical processes (Fig. 21). Processing of phonon and plasmon loss spectra allows one to reconstruct dynamic structural factors (which describe the collective dynamics of a multiparticle system) for nuclei and electrons, respectively. The dynamic factor of nuclei is linked with many important characteristics of materials, such as strength, compressibility, sound velocity, *etc.*

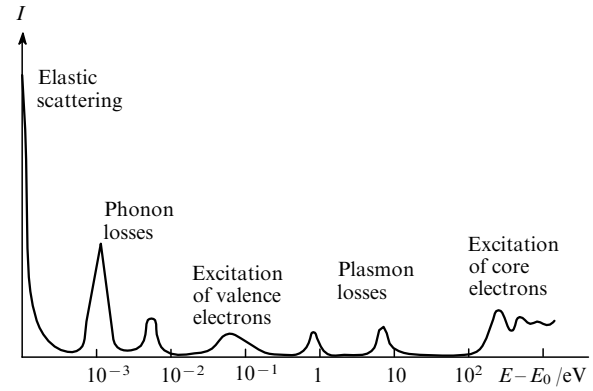

Figure 21. Characteristic energy losses in inelastic X-ray scattering spectra.

Phonon spectra of solids are close analogues of vibrational molecular IR spectra. For studies of phonon structure of crystals, inelastic neutron scattering is traditionally used. However, application of synchrotron X-rays has a number of advantages, in particular, for small crystals as well as for amorphous or liquid samples.[182, 183] In order to study atomic vibrations using inelastic X-ray scattering, a very high degree of the incident beam monochromaticity is required, so development of this method has become possible after the appearance of third-generation SR sources, systems of nested monochromators and monochromatisation techniques based on resonance nuclear diffraction (see Section IV.4).

Spectra of plasmon vibrations of electrons in the conduction zone for such solids as metals, semi- and superconductors contain important information on microscopic mechanisms of conductivity and other electrophysical properties. Spectra of energy losses corresponding to electron excitations allow determination of electron transitions, *i.e.*, studies of energy band structure of solids (similarly to the analysis of electronic states of molecules by UV spectroscopy).[184, 185] The Compton scattering profiles can be transformed into the Fermi surface maps, which reveal the distribution of electron moments in the conduction zone.[186] Many electrophysical characteristics of metals and semiconductors can be calculated based on this distribution.

X-Ray Raman scattering becomes increasingly important in chemical studies.[187, 188] Similarly to conventional Raman scattering employed in Raman spectroscopy, X-ray Raman satellites are produced by a quantified transfer of energy from photons to the sample under study. However, it is phonon loss spectra that are the closest analogues of molecular Raman spectra, whereas X-ray Raman scattering has several special features. First of all, the energy lost by an X-ray photon is consumed to induce photo-

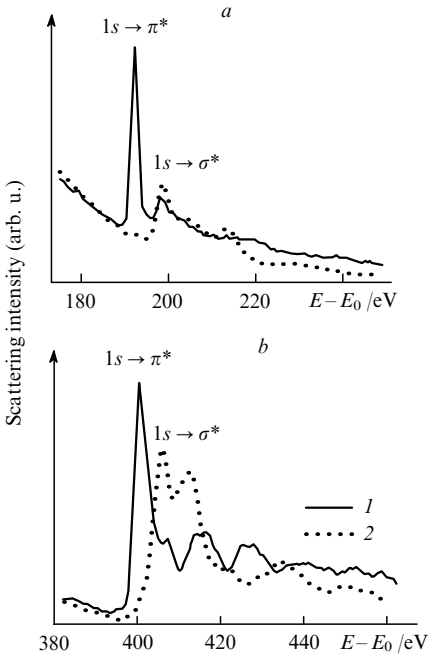

Figure 22. Boron (*a*) and nitrogen (*b*) *K*-edge X-ray absorption fine structures according to X-ray Raman scattering on a boron nitride single crystal in transmission (*1*) and reflection (*2*) modes.[180]
(*1*) The scattering vector is parallel to the *c*-axis of the crystal; (*2*) scattering vector is perpendicular to the *c*-axis of the crystal; excitation energy ~7 keV.

ionisation of light elements rather than excitation of vibrational modes and thus the respective amount of energy transfer exceeds the energy of vibrations by 5–6 orders of magnitude. Second, only low-energy satellites are observed in X-ray Raman scattering which represent triangular-shaped extended bands with an edge rather than narrow resonance maxima (Fig. 22).

Low-energy Raman satellites observed in inelastic scattering of a hard monochromatic X-ray beam (~10 keV) due to photoionisation of 1*s* shells manifest XAFS-like fine structure. Thus, X-ray Raman scattering allows one to measure XAFS spectra for the elements, the absorption edges of which lie in the soft X-ray region (50–500 eV), if one operates with ordinary hard X-ray radiation in air. This technique allows one to obtain the same information on the electronic state and local atomic environment of light elements as is given by NEXAFS or electron energy loss spectroscopy (EELS) under ultrahigh vacuum conditions. This technique is particularly promising for investigations of substances under extreme conditions, since such experiments usually require sample environment non-transparent for soft X-rays. X-Ray Raman scattering has been applied to study electronic structure of light elements, such as Li, Be, C, *e.g.*, in graphite intercalation compounds with alkaline metals (carbon 1*s*-edge) as well as in LiC_6 intercalate (lithium 1*s*-edge).[189–191]

When the energy of inelastically scattered X-ray radiation is close to resonance absorption of one of elements in the sample, the so-called resonant inelastic X-ray scattering (RIXS) is observed. The physical background of RIXS is very similar to that of resonant X-ray emission (see above). The difference in these two processes is reflected in their quantum description: the RIXS is a one-stage process; meanwhile in the resonant X-ray emission, two stages can be distinguished, *viz.*, absorption and re-emission (during lifetime of the excited state, part of the information on absorbed photon, such as its initial moment, can be lost due to internal conversion processes). The RIXS method can be efficiently used to explore fine features of electronic structures of solids: many electron transitions (excitation channels) non-detectable in absorption or non-resonant inelastic scattering spectra clearly manifest themselves in RIXS.[192, 193]

4. Synchrotron radiation Mössbauer spectroscopy

Transitions of atomic nuclei to low-lying quantum excited states for many elements lie in the hard X-ray region of the energy range 10–100 keV. When the energy of the incident X-ray radiation coincides with the energy of a nuclear transition, resonance nuclear absorption occurs, also known as nuclear γ-resonance or the Mössbauer effect. Each Mössbauer isotope (possessing low-lying excited states) is characterised with its own distinct set of nuclear transitions. Nuclear absorption bands are very narrow, their widths are usually 10^{-8}–10^{-10} eV ($\Delta E/E \approx 10^{-14}$). For comparison, the width of absorption bands associated with valence electron transitions is $\sim 10^{-7}$ eV ($\Delta E/E \approx 10^{-8}$) and that with core electron transitions is 1–10 eV ($\Delta E/E \approx 10^{-3}$). In this connection, measurements of resonance nuclear absorption are possible only with X-ray beams of the extremely high degree of monochromaticity. In the conventional laboratory modification of Mössbauer spectroscopy, excited nuclei of the isotope under study produced upon a radioactive decay are normally used as an excitation energy source; for example:

$$^{57}Co \rightarrow {}^{57}Fe^{*} \rightarrow {}^{57}Fe + \gamma. \qquad (6)$$

Other techniques of strictly monochromatic γ-rays generation, such as target activation with a neutron beam or collision of atoms with high-kinetic-energy ions (Coulomb nuclei activation) are available in nuclear research centres.†

Isotopic (or chemical) shift of the nuclear excited level energy and quadrupole splitting of the level are the parameters that are measured in Mössbauer spectra. Furthermore, hyperfine magnetic splitting of spectral lines is observed for magnetically ordered systems. These parameters represent fingerprints for each individual compound; so these allow rather straightforward and unambiguous determination of the oxidation states of an element, symmetry of coordination environment and degree of its distortion.

A major disadvantage of the conventional Mössbauer spectroscopy is a limited number of monochromatic γ-sources available. The predominant part of all Mössbauer studies is performed for a few elements which have convenient γ-active isotopes, such as ^{57}Fe, ^{119}Sn, ^{121}Sb, ^{151}Eu. In principle, utilisation of SR eliminates this restriction since X-ray radiation with continuous energy distribution up to 100 keV and higher is made available (this is particularly true for the third-generation SR sources and insertion devices). The Mössbauer effect on synchrotron radiation was first observed in the mid 80's.[194] Now, experimental stations for the experiments in this field are installed in several SR centres, such as HASYLAB, ESRF, APS, SPring-8.[195, 196]

Single crystal X-ray monochromators do not provide the degree of monochromaticity required for the convenient modification of Mössbauer absorption spectroscopy. In this relation, the so-called nuclear forward scattering (NFS) technique is under active development in the field of synchrotron Mössbauer spectroscopy. In this method, a sample is irradiated by a very fast pulse of monochromatised SR with energy close to the energy of resonance nuclear absorption and photons scattered in the direction of the primary beam (forward scattering) are registered.[197]

Under such experimental conditions, a fast-decaying background signal of X-rays elastically scattered by electrons is observed immediately after the excitation pulse followed by a coherent nuclear scattering (nuclear fluorescence) with a delay of the order of 100 ns, corresponding to the lifetime of a nuclear

† In the classical version of Mössbauer spectroscopy, the energy difference between the incident radiation emitted by nuclei of a source and resonance absorption of target nuclei is compensated by movement of a sample due to the Doppler effect; thus shifts of Mössbauer spectral lines are usually measured in velocity units (mm s^{-1}).[26]

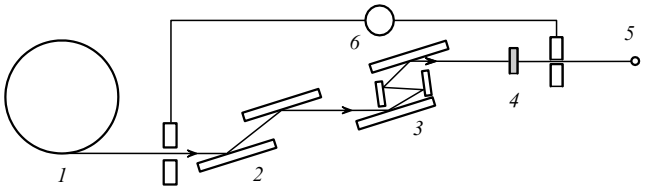

Figure 23. A scheme of a device for measurement of Mössbauer spectra in the NFS mode with utilisation of pulsed synchrotron radiation.
(*1*) Pulsed SR source, (*2*) pre-monochromator ($\Delta E/E \simeq 10^{-4}$), (*3*) high-resolution monochromator ($\Delta E/E \simeq 10^{-7}$), (*4*) sample, (*5*) APD, (*6*) delay circuit (~ 100 ns).

excited state (Fig. 23). In this signal extracted with a specialised delay circuit and measured with a fast-counting detector, such as an avalanche photodiode (APD), decaying oscillations of the scattered beam intensity (quantum beats) are observed. Quantitative parameters of these oscillations can be transformed into normal Mössbauer characteristics [197] implying that the information similar to that of conventional Mössbauer spectra can be obtained (sometimes with higher accuracy).

Up to now, first experiments have been conducted on 'exotic' Mössbauer nuclei, which however are potentially important for chemistry, such as ^{67}Zn, ^{61}Ni, ^{40}K, ^{73}Ge and a number of lanthanides and actinides. Synchrotron Mössbauer spectroscopy is a promising research tool in bioinorganic chemistry [196, 197] and structural materials science (materials under high pressures,[198–200] time-resolved studies of fast processes, magnetic properties [201, 202]).

Coherence of nuclear scattering can be violated as a result of various dynamic processes involving excited nuclei.[203] For instance, diffusion of excited nuclei leads to a faster decay of quantum beats. This phenomenon (quasi-elastic nuclear scattering [204–206]) is used in NFS studies of single crystals for determination of length and direction of elementary diffusion jumps. Energy distribution of nuclear fluorescence at non-zero scattering angles relative to the excitation beam (inelastic nuclear scattering [207]) gives information on phonon structure of a crystal lattice, *i.e.*, on collective dynamics of nuclei in the time scale comparable to the lifetime of excited states.[208]

Yet another important trend in development of synchrotron Mössbauer spectroscopy is the so-called resonance nuclear diffraction.[209] When a single crystal containing a Mössbauer isotope (for example, yttrium iron garnet enriched with ^{57}Fe isotope) is irradiated by a synchrotron X-rays with the energy close to resonance excitation of the nucleus (under Bragg's conditions), all the inelastic nuclear scattering processes are suppressed and the beam reflected becomes highly monochromatic. X-Ray monochromators based on the resonance nuclear diffraction provide the highest energy resolution available to date allowing one to extract exceptionally narrow spectral lines corresponding to energies of Mössbauer nuclei resonance absorption from incident beams of a medium degree of monochromaticity. Such high-resolution monochromators are used in Mössbauer studies and in phonon structure studies of solids by means of inelastic X-ray scattering.[210]

5. Imaging techniques

Synchrotron X-ray radiation (as well as electromagnetic radiation of other spectral regions) can be used for production of magnified images of various objects. SR-based imaging techniques include X-ray microscopy, X-ray diffraction topography, computed tomography along with methods widely adopted in medical applications, such as radiography, subtraction angiography, mammography, *etc*.

With respect to spatial resolution, X-ray microscopy occupies an intermediate position between optical and electron microscopy. Synchrotron radiation-based X-ray microscopy benefits from the possibility of varying such characteristics of the incident X-ray beam as energy and polarisation. Besides, utilisation of hard X-rays (7–30 keV) does not require an ultrahigh vacuum analytical chamber (in contrast to all modifications of electron microscopy). This enables *in vivo* studies of biological systems and strongly facilitates investigations of large objects. Standard spatial resolution of hard X-ray microscopy is ~ 0.25 μm. Utilisation of soft X-rays (0.2–1.2 keV) in combination with advanced X-ray optics, such as FZP and BFO, makes spatial resolution of 30–50 nm attainable. Penetration depth of soft X-rays into a condensed matter is higher than that of electrons, thus, the samples which are opaque for transmission electron microscope can be studied by X-ray microscopy. Furthermore, the use of electron beams induces greater radiation damage of the sample compared to synchrotron X-rays.

Yet another advantage of X-ray microscopy is the possibility to achieve element and even valence contrast by varying the incident radiation wavelength and using absorption edges. Studies of biological objects are usually performed in the energy range referred to as the 'water window', *viz*., 280–550 eV. In this range, absorption by oxygen atoms (and thus by water molecules always abundantly present in biological samples) is relatively weak. By varying the beam energy within the 'water window' it becomes possible to achieve contrast in visualisation of, for example, carbon and nitrogen atoms and thus independently estimate the spatial distribution of proteins and nucleic acids in the sample. X-Ray microscopy can be subdivided into contact, projection and scanning modifications depending on mutual orientation of SR source, sample and detector.[211–214] Recent achievements in the field of synchrotron X-ray microscopy are considered in detail in the monograph.[215]

X-Ray diffraction topography is a method of defect imaging in crystals. It is based on the analysis of intensity distribution of scattered radiation within the diffraction spot.[216] Using X-ray topography it is possible to visualise point defects and dislocations with spatial resolution of 2–3 μm, to analyse their dynamics upon application of a mechanical stress (for example, in piezoelectric crystals), as well as to study local distortions, deformations, inhomogeneities and microcracks in nearly perfect crystals.[217] Diffraction topography is sensitive to gradients of unit cell parameter deformations $\Delta a/a$ of the order of $\sim 10^{-7}$. This method can be used efficiently in studies of large single crystals which are opaque for visible light. The principal field of application of this technique is technological control of perfect crystals, for example, in manufacturing semiconductors. Utilisation of SR in this field leads to increase in the spatial resolution and decrease in exposure times (and therefore radiation damage to the sample).[216–219] X-Ray topography can be utilised as a fast preliminary test of single crystal quality. This can be particularly important in protein crystallography where diffraction experiments are very expensive and time-consuming.

X-Ray computed tomography allows visualisation of internal structure of samples in different cross-sections. The image is reconstructed by mathematical processing of transmitted intensity profiles for various mutual orientations of the sample and radiation source.[220, 221] This method is used for characterisation of such objects as technological workpieces, biological and geological samples (*e.g.*, microcavities and micropores in minerals). For image reconstruction, parallel or divergent, 'white' or monochromatic synchrotron X-ray beams can be used. The spatial resolution of X-ray tomography is a few micrometers.[222] As in the case of X-ray microscopy, the contrast of reconstructed images can be noticeably enhanced if incident radiation wavelength is chosen close to the absorption edges of certain elements in the sample. For instance, distribution of light and heavy elements throughout the sample may be independently reconstructed from X-ray tomography data collected at two strongly different wavelengths [dual photon absorptiometry–computed tomography (DPA-CT)].

In modern imaging techniques, utilisation of the coherent properties of SR acquires increasing importance. In this connection, coherent synchrotron X-ray radiation of third-generation SR sources allows one to achieve phase contrast besides standard absorption contrast in images. Absorption contrast is obtained as a result of differences in X-ray absorption coefficients of different points in the sample, whereas phase contrast is due to phase shifts of scattered coherent radiation, which gives rise to an interference pattern superimposed on the sample image. This interference pattern depends upon sample-to-detector distance and therefore very high contrast images may be obtained by adjusting this distance.[223–225]

Coherent properties are also utilised in a new SR-based visualisation technique, *viz*., X-ray photon correlation spectroscopy (XPCS) or intensity fluctuation spectroscopy. This method is an X-ray analogue of visible light dynamic scattering, which is widely used in studies of colloid systems. The X-ray photon correlation spectroscopy is based on observation of a real-time evolution of the speckle interference pattern produced by scattering of coherent X-ray radiation on disordered samples. Using this method, it is possible to study low-frequency dynamic processes (10^{-3}–10^{6} Hz) in the sample and visualise short-range density fluctuations within the distances range of the order of 1 nm.[226] This method has been successfully applied to study Brownian motion of metal nanoparticles[227] and copolymer micelles in solutions,[228] dynamics of charge density waves, critical fluctuations near the point of order–disorder phase transitions in amorphous alloys,[229] conformational dynamics of polymers upon glassification,[230] *etc*.

6. Other methods

a. Utilisation of anomalous scattering

In the theoretical description of X-ray scattering on atoms, the atomic scattering factor f_0 (sometimes also referred to as atomic form factor) is of key importance. The atomic scattering factor is a smooth function of scattering angle θ, monotonically decreasing with an increase in θ from 0° to 180°. Atomic scattering factors for adjacent elements in the D I Mendeleev Periodic Table are close. Over a wide range of wavelengths, f_0 is virtually independent of incident radiation energy.

However, if incident radiation energy approaches an X-ray absorption edge of an element in the sample, a wavelength-dependent correction to f_0 has to be introduced into the scattering formalism. This correction term is commonly referred to as anomalous dispersion (Fig. 24). In the energy range of X-ray resonance absorption, scattering is accompanied by intensity attenuation. In this case, the total atomic scattering factor $f(\theta,\lambda)$ formally acquires a complex value

$$f(\theta,\lambda) = f_0(\theta) + f'(\theta,\lambda) + if''(\theta,\lambda), \tag{7}$$

where f_0 is the wavelength-independent part of atomic scattering factor (rapidly decreasing with an increase in scattering angle);

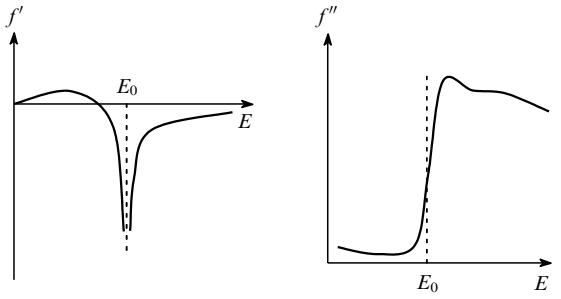

Figure 24. Real (f') and imaginary (f'') parts of anomalous dispersion correction to the atomic scattering factor as functions of the radiation energy.

f' and f'' are real and imaginary parts of the anomalous dispersion, respectively. The imaginary part of the anomalous dispersion is directly proportional to the X-ray absorption cross-section, *i.e*., to X-ray absorption coefficient μ, and its real part is linked with the imaginary part by the Kramers–Kronig dispersion relation

$$f'(\omega) = \frac{2}{\pi}\int_0^\infty \frac{\omega' f''(\omega')}{\omega^2 - (\omega')^2}\,\mathrm{d}\omega', \tag{8}$$

where ω is the radiation frequency.

An anomalous dispersion contribution may substantially distort scattering intensities compared to values calculated on the base of f_0 only. In contrast to f_0, the f' and f'' terms only weakly depend on the scattering angle, so the relative contribution of anomalous dispersion is higher for large scattering angles. As a rule, the energies of X-ray absorption edges for adjacent elements in the D I Mendeleev Periodic Table differ from each other by a few hundreds of eV, consequently, account for anomalous dispersion leads to substantial differences in atomic scattering factors (and thus to different X-ray scattering patterns) for such elements when the scattered radiation wavelength is close to an X-ray absorption edge of one of these two elements. Moreover, due to different chemical shifts of X-ray absorption edges in different compounds of one element, atomic scattering factors can become noticeably different even for atoms of one element in different chemical environment or charge state (valence contrast). Advanced techniques based on application of anomalous scattering and respective experimental diffraction results are thoroughly discussed in a number of recent publications.[231–233]

The anomalous scattering combines X-ray absorption and scattering phenomena. In order to utilise it in diffraction experiments, it is necessary to collect diffraction data with incident radiation of continuously variable wavelength (which is possible only with synchrotron sources) or to carry out a series of diffraction experiments at several wavelengths, at least one of which being close to an X-ray absorption edge of an element in the sample. In the latter case, the difference between two diffraction patterns in the proximity of the edge and apart from it will be primarily caused by scattering on the absorbing atoms.

Anomalous scattering of synchrotron radiation is widely used in powder X-ray diffraction. Using this approach, atoms of certain elements can be precisely located in the unit cell, which substantially facilitates structure solution. This technique is often referred to as resonance X-ray diffraction. In studies of amorphous samples using anomalous wide-angle X-ray scattering (AWAXS), partial radial distribution functions may be determined separately for each heavy element.[232] This makes interpretation of experimental results much more reliable and unambiguous. A similar approach is adopted in anomalous small-angle X-ray scattering (ASAXS), for example, for determination of mean size and size distribution of particles in supported metal catalysts and nanoparticles stabilised in polymer matrices or for analysis of metal distribution in bimetallic nanoclusters.[234–236]

In conventional single crystal X-ray crystallography, account for anomalous dispersion can be used in determination of the absolute configuration of a non-centrosymmetrical (chiral) crystal and its constituent molecules. When SR is used, data collection at the wavelength of resonance absorption allows unambiguous establishment of the chemical nature of anomalously scattering atoms as well as charge states for crystallographically non-equivalent atoms of one element in mixed-valence complexes, the so-called valence contrast X-ray crystallography. Capabilities of this technique has been demonstrated for a series of inorganic substances in which atoms of one element in different oxidation states occupy crystallographically non-equivalent positions, *e.g*., Fe_3O_4,[237] $GaCl_2$,[238] $NbSe_3$,[239] as well as for a number of mixed-valence polynuclear complexes.[240, 241]

Utilisation of anomalous dispersion in X-ray crystallography is most logically implemented in the multi-wavelength anomalous diffraction (MAD) method, which becomes increasingly popular in protein crystallography.[242–245] For a single crystal containing atoms of heavy elements, it is possible to estimate experimentally the phase of any reflection based on its intensity at three different wavelengths before, directly at and above the X-ray absorption edge of the corresponding element. Thus, MAD helps to overcome the key problem of single crystal X-ray crystallography, the so-called problem of initial phases: in order to transform the set of diffraction data into the target electron density distribution map, it is necessary to assign certain phases (which cannot be directly determined from standard diffraction experiment) to experimentally measured intensities of reflections. In small-molecule crystallography, reliable direct methods of statistical estimation of the initial phases have been developed, whereas in protein crystallography, the search for initial phases remains very complicated and not always solvable problem.

Determination of reflection phases using MAD is a much more laborious procedure than common diffraction measurements, however the information obtained is often worth the time spent. The MAD method gradually displaces multiple isomorphous replacement (MIR) method in protein crystallography. This formerly popular but much less versatile method is based on comparison of diffraction data sets for crystallographically isomorphous derivatives of a protein with different heavy substituents. Many biological macromolecules in their native form contain heavy elements (iron, molybdenum, zinc, copper, manganese, *etc.*) and thus the MAD-phasing procedure is directly applicable to them. Recently, first experiments have been undertaken, which demonstrated in principle the possibility of MAD application in the soft X-ray region at the absorption edges of sulfur and phosphorus. However technical problems arose related to rapid radiation-induced decomposition of the sample due to strong X-ray absorption.[246, 247]

Heavy anomalously scattering atoms can be introduced into samples under study by chemical methods. For instance, calcium or magnesium ions in biological molecules can be replaced by heavier lanthanide ions; zinc ions, by mercury, *etc.* In this case, the substituted derivative does not have to be crystallographically isomorphous to the native protein (which is a prerequisite for MIR), it is sufficient that the primary amino acid sequence and the main conformation of the protein molecule are conserved. Heavy elements can be introduced into biological molecules as labelling fragments, which are chemical analogues of their native building blocks. Among such labels, selenomethionine for proteins (MAD at the Se *K*-edge) and brominated uracil for nucleic acids (MAD at the Br *K*-edge) are most often used. Yet another route for incorporating heavy elements into crystals is to perform a diffraction experiment under pressure of Xe. In this case, Xe atoms replace water molecules in cavities of the crystal lattice without disturbing the general structure of the biopolymer, and MAD-phasing at Xe *K*-edge is then applied.[248]

Anomalous dispersion can be efficiently used to enhance research capabilities of X-ray absorption spectroscopy.[249] In this connection, the diffraction anomalous fine structure (DAFS) method, which can be considered as a diffraction modification of XAFS, is actively developing. In the DAFS method, the intensity of a selected diffraction reflection is measured while varying the incident radiation energy so as to pass across an X-ray absorption edge of a certain element. Since imaginary part of the anomalous dispersion is directly proportional to the X-ray absorption coefficient μ, the dependence of reflection intensity upon the incident radiation energy manifests XAFS-like fine structure.

The DAFS method can be applied to studies of both single crystals and polycrystalline powders. In particular, it is useful for investigations of mixtures of polycrystalline powders since it allows registration of XAFS spectra at the edge for a certain element separately for each phase. Furthermore, since crystallographically non-equivalent atoms of one element make different contributions to the intensity of different reflections, DAFS data measured for several diffraction reflections allow one to extract contributions into XAFS spectrum from each crystallographically independent group of atoms of a certain element. Capabilities of DAFS have been demonstrated on such classes of substances as spinels, complex oxides, superconductors, *etc.*[250–252]

b. X-Ray standing waves

In addition to anomalous dispersion, X-ray absorption and diffraction phenomena are manifested simultaneously in the method of X-ray standing waves (XSW).[253] Under conditions of a specular reflection or Bragg's diffraction in a nearly perfect single crystal, the intensity of the electromagnetic wave is redistributed so as to form a standing wave. Differences in local intensities of the electromagnetic field in points of nodes and antinodes of the standing wave lead to different absorption and thus to different yield of all secondary processes, such as X-ray florescence, photo- and Auger electron emission, *etc.* in the corresponding atomic layers.[254, 255] Experimentally, it is manifested in a strong dependence of intensity of respective secondary processes on the incidence angle of the X-rays on the crystal or on the wavelength of the X-rays at constant incidence angle. In the latter case, the geometry of normal incidence of radiation to the surface of the crystal is often selected; this technique is referred to as normal incidence X-ray standing waves (NIXSW).[256]

The XSW method, among very few other instrumental techniques, allows structural investigations of amorphous near-surface layers of crystals with thicknesses from several nm to several μm. It is also used for precise measurement of layer thickness in multilayer periodic structures as well as for localisation of impurity atoms in crystal lattices, *e.g.*, dopant atoms in semiconducting single crystals, implanted ions, guest metal ions in biomembranes, *etc.*[257–259] For example, XSW has been applied to study gallium arsenide single crystals with a surface doped with silicon using various techniques. As has been shown in the case of molecular beam epitaxy, all silicon atoms occupy the gallium positions of the crystal lattice. In contrast, in the case of ion implantation followed by annealing (or thermally activated diffusion), only 30% of Si atoms regularly occupy the gallium positions, the rest of Si atoms occupy random positions and of them $\sim$6% occupy the As positions.[260] Modern theoretical concepts underlying the XSW method, its instrumentation and applications are discussed in recent reviews.[256, 261]

c. Surface study methods in the geometry of grazing incidence

X-Ray reflectometry method is based on the analysis of X-ray reflectivity coefficient as a function of the X-ray incidence angle. In a number of cases, this method gives important information on the atomic structure of near-surface layers.[262] As has been mentioned above (see Section III), under conditions of total external reflection, the ratio of reflected radiation approaches unity and the incident radiation does not penetrate deep into the sample interacting only with the thin near-surface layer ($\sim$10 nm). This effect can be used in order to increase surface sensitivity of 'classical' bulk X-ray methods (such as X-ray spectroscopy and diffraction). In particular, total reflection X-ray fluorescence (TRXRF) is used for quantitative analysis of trace atoms (including light elements starting from boron) in near-surface regions of semiconductors, materials modified by ion implantation, *etc.*[263–265] Due to small penetration depth of X-rays into the sample under total reflection conditions, the method is extremely sensitive: the lowest detection limit expressed as absolute mass of an admixture is of the order of femtograms (10^{-15} g).[266] This method is used for admixture level control in such very pure objects as semiconducting single crystals.[267]

Grazing-incidence X-ray diffraction (GI-XRD) is used in studies of single crystal surfaces and other materials with atomically ordered surfaces, in particular, those with specific two-dimensional ordering. Recently, this method has been applied to such objects as self-assembled monomolecular layers, Langmuir–

Blodgett, epitaxial, atomic deposition and CVD films, as well as two-dimensional crystals of lipophilic systems (fatty acids and their salts, ω-amino acids, phospholipids) at the water–air interface.[268–275]

Grazing incidence small-angle X-ray scattering is used for characterisation of thin films and supported catalysts.[276] Measurement of X-ray reflectivity coefficient as a function of incident radiation energy at the incidence angle close to the angle of total external reflection allows registration of XAFS spectra for near-surface layers: X-ray reflectivity coefficient is correlated with complex refraction coefficient, imaginary part of which is directly proportional to the absorption coefficient $\mu(E)$ [see Eqn (7)]. This technique is commonly referred to as Refl-EXAFS. The term SEXAFS (surface EXAFS) is also sometimes used but it combines an entire set of surface-sensitive techniques for EXAFS registration including, in addition Refl-EXAFS, total electron yield, yield of photon stimulated ion desorption and so on.[277–279]

d. The use of polarisation of synchrotron radiation

The use of polarisation of electromagnetic radiation in physicochemical analysis of substances with anisotropic atomic structures is based on dichroism, *i.e.*, the dependence of optical properties of substances on the direction of the electric vector in the electromagnetic wave propagating through the substance. For instance, plane-of-polarisation rotation angle per optical path unit is a key characteristic of substances with asymmetric (chiral) atomic structures; meanwhile, circular dichroism (CD) spectra give important information on mutual orientation of chromophore groups in molecules.

In contrast to X-ray radiation produced by traditional sources, *viz.*, X-ray tubes, synchrotron radiation is always completely polarised. Similarly to visible light optics, two types of dichroism, *viz.*, linear and circular, can be distinguished in the X-ray region. Polarisation of SR is most widely used in X-ray spectroscopy, since it primarily affects the probability of electron transitions. In the case of molecule excitation by a linearly polarised SR, the probability of an electronic transition of a certain symmetry depends on the mutual orientation of the electronic transition dipole moment (difference between dipole moments of the molecule in the ground and excited states) and polarisation direction of the excitation radiation. Upon resonant photoionisation of an atom by linearly polarised X-rays, the photoelectron wave generated does not possess spherical symmetry: the probability of the photoelectron propagation is the maximum in the plane of polarisation and is equal to zero in the perpendicular plane. In EXAFS, in particular, this results in the situation where atoms from the local environment lying exactly in this plane dominate in the Fourier transforms.[280]

A prerequisite for manifestation of linear X-ray dichroism is ordering and strict orientation of the sample under study relative to the incident SR beam. For example, adsorbed monolayers, which exhibit strong anisotropy of properties in the directions parallel to the layer (interaction within the layer) and perpendicular to the layer (adsorbate–support interactions), can be efficiently studied using polarisation-dependent NEXAFS spectroscopy. This anisotropy causes a distinct dependence of X-ray absorption spectra on the incidence angle of the polarised SR beam or on the polarisation direction at the constant incidence angle. In particular, in the case of grazing-incidence, σ and π polarisations of the incident beam are often used, which probe interactions parallel and perpendicular to the sample surface, respectively.[281] Utilisation of linear polarisation of SR in X-ray microscopy with element contrast allows one to determine real-space orientation of atomic fragments in polymeric fibres, since the shape of the absorption edge (NEXAFS spectrum) becomes sensitive to the orientation of certain chemical bonds, such as C=C and C=O, which have a pronounced π*-resonance.[54, 212, 282]

Intercalation compounds into layered matrices (such as graphite and its chemical derivatives, transition metal dichalcogenides, phosphates, *etc.*) constitute another group of objects for which the application of X-ray spectroscopy with linearly polarised SR is particularly informative. These systems in many cases manifest virtually ideal texture with the layers of matrix strictly parallel to the surface of the sample. Thus, using polarisation-dependent XAFS it is possible to determine, for instance, orientation of molecules within the intercalated layers.[283, 284]

Analysis of polarisation-dependent EXAFS spectra for potassium niobate (perovskite type) made it possible to determine crystallographic directions of niobium atom shifts out of centres of octahedra formed by oxygen atoms in the phase transition.[285] Studies of distortions in planar square CuO_4 fragments in single crystals of high-temperature superconducting phases gave additional information on the mechanism of superconductivity.[286, 287]

In quantum mechanical description of polarised light properties, the term photon spin is often used. A photon, being a boson, possesses spin quantum number $S = 1$ and two allowed spin moment projections $m_S = \pm 1$ (the projection $m_S = 0$ is prohibited for a photon due to its zero rest mass). A beam of photons with $m_S = 1$ corresponds to the right and with $m_S = -1$ to the left circular polarisation. The electrons with a defined spin direction (coinciding with the photon spin) are excited upon absorption of circularly polarised photons (spin polarisation). If in the substance under study, all atomic magnetic moments are co-aligned (this is the case for a one-domain ferromagnetic or for a paramagnetic placed in a magnetic field), a distinct dependence of X-ray absorption coefficient on mutual orientation of the sample macroscopic magnetic moment and circular polarisation direction of the synchrotron radiation is manifested in XANES spectra (Fig. 25). This phenomenon first observed in 1987[288] was called X-ray magnetic circular dichroism (XMCD). Over recent years, the field of XMCD experienced rapid development since using this technique it is possible to analyse magnetic properties of materials at the atomic level, *viz.*, with element specificity determine magnetic moments of atoms and identify spin and orbital contributions.[289, 290]

XMCD (its realisation is possible only in synchrotron radiation centres) has already become an established technique for characterisation of magnetic materials: thin films of 3*d*-metals

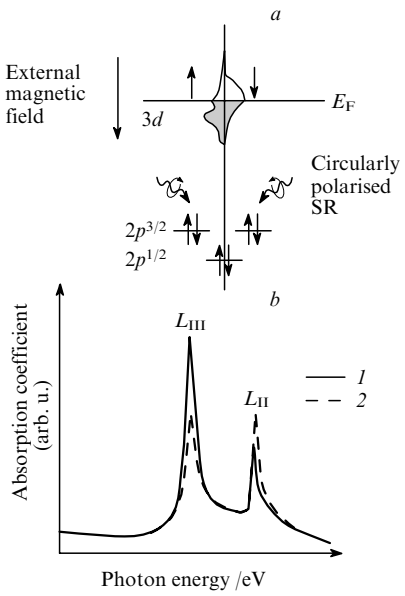

Figure 25. Scheme of the origin of circular dichroism in X-ray absorption spectra (*a*) and typical XMCD spectrum at $L_{II,III}$-edges of 3*d*- and 4*d*-metals (*b*).
Circular polarisation of the incident beam is chosen so as to excite electrons with spins parallel (*1*) and antiparallel (*2*) to the external magnetic field.

(Fe, Co, Ni), lanthanide and actinide derivatives, materials with giant magnetoresistance (strong dependence of conductivity on the applied magnetic field), *etc*. Giant magnetoresistance is typical, for instance, of multilayers with alternating ferro- and diamagnetic layers. Such materials are promising in information storage technology.[291–294]

In 1995, X-ray natural circular dichroism XNCD (*i.e*., X-ray circular dichroism, which is manifested without application of external magnetic field) was observed in some chemical systems, *e.g*., in chiral paramagnetic crystals.[295–297] Soft X-ray circular dichroism spectroscopy is widely used for characterisation of helical protein structures.[298]

The EXAFS spectra measured with circularly polarised SR produce RDF curves where atoms with non-zero magnetic moments dominate (spin-polarised or 'magnetic' EXAFS) (Fig. 26).[299, 300] The X-ray circular dichroism is actively employed in modern versions of spin-resolved photoelectron spectroscopy.[301, 302]

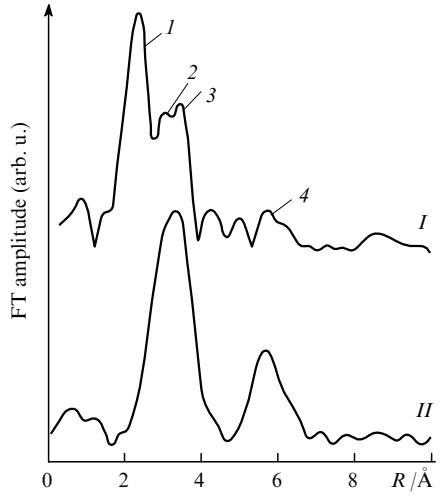

Figure 26. Normal (*1*) and magnetic (*2*) EXAFS spectra taken at Ho L_{II}-edge for $Ho_3Fe_5O_{12}$.
(*1*) Ho–O 2.3–2.4 Å; (*2*) Ho–Fe 3.0–3.7 Å; (*3*) Ho–Ho 3.7 Å; (*4*) Ho–Ho 5.6 Å.[299]

In contrast to X-ray spectroscopy, polarisation properties of SR have not found broad applications in X-ray diffraction techniques, though many phenomena accompanying diffraction exhibit polarisation dependence, which can be used for extraction of additional information. Besides, polarisation has to be taken into consideration in development and optimisation of X-ray optical elements designed for experiments with SR. Thus when linearly polarised X-rays with energy close to an X-ray absorption edge of an element in the sample is scattered by a low-symmetry single crystal, the dependence of atomic scattering factor on the scattering angle becomes anisotropic. This anisotropy is due to the fact that the absorption coefficient for the crystal (and thus corrections to the atomic scattering factor owing to the anomalous dispersion) will be different for non-equivalent crystallographic directions. In particular, this leads to the appearance of diffraction reflections forbidden by extinction conditions. This phenomenon is called anisotropic anomalous scattering (AAS) or forbidden reflection near-edge diffraction (FRNED). It can be used for determination of positions of anomalously scattering atoms within the unit cell.[303–305] For such forbidden reflections, the polarisation type and direction of the scattered wave can be different from those of the incident SR, this change being dependent on the specific crystal structure.[306] Utilisation of circularly polarised SR in X-ray crystallography makes determination of absolute configurations of chiral molecules in single crystals more reliable. X-Ray topography with circularly polarised SR is used for visualisation of magnetic domains.[307] Polarisation dependence of reflection intensities in magnetic scattering allows separation of total magnetic moment density into spin and orbital contributions.[308]

V. The main trends of applied studies using synchrotron radiation

1. Combined X-ray techniques

In majority of cases, application of only one, even quite powerful instrumental method, appears insufficient to get insight into the atomic and electronic structure of real objects (a probable exception is X-ray crystallography of small molecules). Therefore, complex SR-based studies with involvement of a number of complementary X-ray techniques are more desirable. The organisational structure of synchrotron centres itself (concentration of highly skilled staff and advanced instrumentation in one building) promotes such a convergence stimulating interchange of ideas between different experimental techniques. Moreover, a limited number of experimental stations installed at modern international synchrotron radiation centres is used by numerous research groups with diverse scientific interests. Under such operational conditions, each experimental station has to be sufficiently flexible and versatile and allow solution of a wide range of research problems with minimum hardware modifications.[309–312]

Among many advanced combined techniques routinely applied in SR centres to the studies of short- and long-range atomic order in various materials, the following combinations are most popular: XRD/XAFS (simultaneous registration of powder diffraction pattern and EXAFS spectrum) and XRD/DAFS (simultaneous registration of powder diffraction pattern and diffraction anomalous fine structure spectrum).[313–315] Specialised software has been developed for simultaneous refinement of crystal structure parameters from the experimental data of both methods.[316] For structural characterisation of semi-crystalline and amorphous polymers, SAXS/XRD or SAXS/WAXS combinations are used.[317] Protein crystallography is often supplemented with EXAFS data in order to determine exact geometry of metal centres.[318] Besides, in experiments based on the MAD method, measurement of X-ray absorption spectrum from the very same crystal as used in the diffraction experiment is required for the calculation of f' and f'' anomalous dispersion terms [see Eqn (8)] used in the phasing procedure. An ultrahigh vacuum chamber is the most expensive part of any device designed for surface studies. In order to use it with maximum efficiency, the respective device should be equipped with a broad range of functionality, for example, for utilisation of angular resolved photoelectron spectroscopy, X-ray standing waves, SEXAFS, *etc*.[319] A similar consideration is applicable to techniques based on utilisation of circularly polarised SR, where combination of magnetic scattering, XMCD, spin-polarised EXAFS, spin-resolved X-ray photoelectron spectroscopy, *etc*., in one device could be required.

Synchrotron radiation-based methods are often combined with traditional laboratory analytical methods, for example, XRD can be combined with differential scanning calorimetry for studies of phase transitions,[317, 320] the combination 'Quick-EXAFS/IR' can be used for the characterisation of matrix synthesis products.[321] Laboratories for chemical, biological and materials science studies in modern SR centres are equipped with the modern instruments for realisation of traditional analytical techniques. The availability of traditional facilities (chromatographs, lasers, presses, scanning tunnelling and transmission electron microscopes, *etc*.) is particularly important for investigations of such complex objects as surfaces, advanced materials, biological systems, *etc*.

The trend to combine several different techniques in one device is realised in a new SR-based method, *viz*., event correlation or coincidence spectroscopy. In this method, several types of secondary emissions (fluorescent photons, photoelectrons, Auger

electrons, secondary ions) initiated by resonance absorption of X-ray photons are simultaneously detected using specialised electronic circuits. As an example of this approach, mention can be made of photoelectron-photoion coincidence (PEPICO) spectroscopy, which implies simultaneous registration of photoelectrons and ions (with a time-of-flight mass spectrometer) produced by photoionisation of a free molecule by an X-ray photon. Other event correlation methods, such as Auger-photoelectron coincidence, photoelectron-fluorescent photon coincidence, *etc*., are also developing. These methods are used in investigations of photochemical reactions, determination of electronic structure and lifetime of excited states, studies of dynamics of photoionisation and photodissociation of chemical bonds in free molecules or ions in the gas phase.[322–327]

2. Studies of substances under extreme conditions

Studies of matter under extreme conditions are of great importance for many fields of modern materials science, condensed state physics, geochemistry, mineralogy and geology. A key component of devices for high-pressure researches is a diamond anvil cell (DAC), which allows production of pressures up to a few hundreds GPa at areas of several square micrometers (Fig. 27). The choice of diamond as the material for such a high-pressure cell is dictated by its unique properties, such as extremely high mechanical strength combined with transparency for hard X-rays. A disadvantage in this case is unavoidable presence of glitches due to Bragg's reflections from walls of the cell. For local heating of the sample, a laser beam can be used and for cooling, a flow of liquid helium. The temperature and pressure inside the DAC can be monitored using structural (unit cell parameters, bond lengths) or spectral characteristics of an internal standard. A ruby crystal is often used as an internal standard with the shift of optical luminescence line as a parameter enabling monitoring. Experimental stations capable to achieve conditions ($T \approx 6000$ K, $P \approx 200$ GPa) close to that in the Earth's core ($T \approx 5000$ K, $P \approx 300$ GPa) are in routine operation for several years in a number of synchrotron radiation centres.[328–333]

Along with static studies, dynamic investigations of substances and materials under microsecond impacts or in propagating blast waves are of significant practical importance. The usefulness of synchrotron radiation in studies of this kind relates primarily to its high intensity (which allows beam penetration through the sample environment) and to the temporal beam modulation in the single-bunch mode of the storage ring operation.

XRD (especially its energy-dispersive modification), X-ray crystallography, EXAFS and X-ray topography are most commonly applied for characterisation of substances under high pressures. High-pressure studies using synchrotron Mössbauer spectroscopy are also under rapid development over recent years.[199, 200] It has to be stressed that on most of specialised devices for high-pressure studies, several physical techniques are

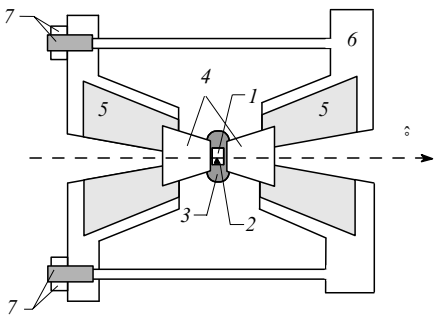

Figure 27. General view of a high-pressure cell.
(*1*) A sample under study, (*2*) a ruby crystal (internal standard used for pressure monitoring), (*3*) gasket, (*4*) tapered diamond anvils, (*5*) diamond anvil holder made of hard alloy, (*6*) steel housing, (*7*) pressure regulation mechanism (mechanic, pneumatic, hydraulic, *etc*.).

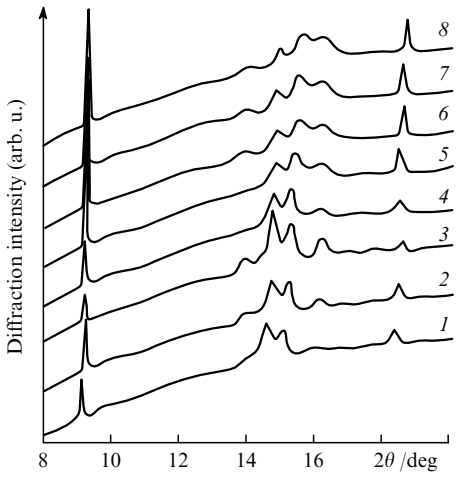

Figure 28. X-Ray powder diffraction patterns of solid oxygen at room temperature in the pressure range of 77–116 GPa (ESRF, Grenoble, France).[341]
P /GPa: (*1*) 77, (*2*) 85, (*3*) 88, (*4*) 96, (*5*) 101, (*6*) 105, (*7*) 110, (*8*) 116. At $P \sim 96$ GPa, a structural phase transition associated with oxygen metallisation occurs.

realised.[333, 334] Recently, equations of state for such substances as molecular hydrogen, helium, oxygen, carbon and water have been determined up to pressures > 100 GPa (Fig. 28) based on results obtained using SR. Phase diagrams of compounds which form the Earth's mantle and thus are very important in order to achieve understanding of geochemical processes (metallic iron, silicon, quartz, silicates and aluminosilicates) have been studied in a broad range of temperatures and pressures.[335–337] Results on structural monitoring of catalytic graphite–diamond transformation in the presence of magnesium carbonates and metallic nickel[338] and structural transition of carbon dioxide into polymeric quartz-like structure and further to metallic state have been reported.[339] In the last years, metallic states of substances and their mixtures which are gaseous under normal conditions (H_2, NH_3, CH_4, *etc*.), have become attainable, which allows simulation of the state of the matter in cores of distant planets of the Solar system: Saturn, Uranus and Neptune.[340–342]

A large part of all experiments with substances under extreme conditions is devoted to detection of unusual chemical properties and to studies of structure and properties of compounds not existing under normal temperatures and pressures. In particular, single crystals of molecular complexes formed in the hydrogen–methane system under high pressures, *viz*., $(CH_4)_2H_2$ and $(CH_4)(H_2)_2$, have been studied by synchrotron X-ray crystallography.[342] In another study, structural behaviour of potassium under high pressures has been investigated.[343] It has been shown that K forms intermetallides with 3*d*-metals, which implies that its chemical properties approach those of transition metals. Pressure-induced phase transitions in semiconducting, superconducting and magnetic materials often become subjects of SR-based studies.[344–347] Such transitions are sometimes accompanied by a change of coordination type or charge state of one of elements in the sample with preservation of overall stoichiometry.[348, 349] Structures and transformations of substances in supercritical media are widely studied. In particular, in a series of studies,[350–352] structural changes of hydration shells of such ions as Rb^+, Sr^{2+} and Br^- upon transition of water into a supercritical state have been monitored and a decrease of mean coordination number in the first coordination sphere has been revealed as a common effect.

3. Studies with high spatial resolution

Modern X-ray optics is capable of producing soft X-ray beams with linear size of several tens nm and hard X-ray beams of

submicron size. Technical progress in this field stimulates development of X-ray microprobe techniques: spatial resolution of such techniques has approached that of classical microprobe techniques utilising beams of charged particles, *viz*., electrons, protons or ions.[353–355] At the same time, synchrotron radiation gives access to a broader range of experimental techniques due to the possibility of detecting secondary radiation of various types, varying excitation energy, using polarisation and so on.‡

Microdiffraction (especially in the Laue modification) is used in studies of single grains and intergrain regions in compact polycrystalline materials (metals, composites, ceramics, semi- and superconductors),[362, 363] in analysis of local ordering areas in liquids or systems with a heavy disorder, in X-ray crystallographic investigations of submicron single crystals (clays, micas, zeolites)[364] and in structural characterisation of microscopic mineral inclusions in biological tissues.[365] Single fibre molecules are studied with synchrotron X-ray microdiffraction.[366] Spatially resolved X-ray fluorescence spectroscopy allows one to map the distribution of elements in a sample with resolution of the order of micrometers. Microprobe modifications of X-ray absorption spectroscopy (EXAFS, XANES, NEXAFS) give additional information on the chemical state and local environment of atoms in the sample under study (Fig. 29).[212, 367] Microprobe modification of XPS (sometimes referred to as 'Super-ESCA') is actively used for characterisation of minute amounts of hardly accessible or hazardous substances. For instance, an XPS study of curium oxide available in the amount of ~ 1 μg has been performed at the ALS synchrotron radiation centre (Berkley, USA).[368] The average beam size in this experiment was ~ 50 μm and the mass of the sample actually irradiated and contributing to the spectrum is estimated by the authors as only 4 ng. Spatially resolved information on supramolecular organisation of various objects can be obtained using microprobe modification of SAXS.[369, 370]

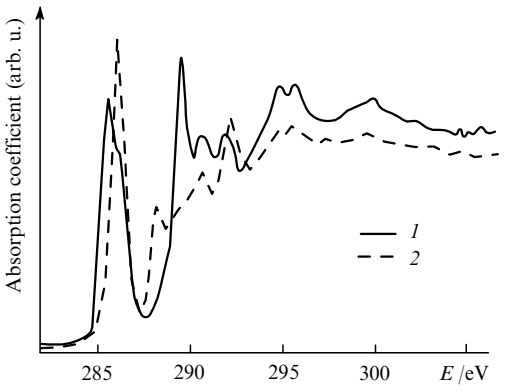

Figure 29. Micro-NEXAFS spectra (carbon *K*-edge) for thin polymeric films with area of 0.1 μm^2 on a scanning X-ray microscope (NSLS, Stony Brook, USA).[212]
(*1*) Polyethylene terephthalate; (*2*) polycarbonate.

Synchrotron X-ray microprobe techniques are routinely used for characterisation of spatially inhomogeneous objects including biological systems (cells, living tissues, bones), natural samples (microinclusions in minerals, coals, soils), advanced materials (ceramics, nanocomposites) as well as for environmental control of industrial wastes. Recently, the use of X-ray microdiffraction has been suggested as an express diagnostic tool for multilayer optoelectronics devices.[371] A set of synchrotron microprobe techniques (X-ray fluorescence, diffraction, XANES) with spatial resolution of 3×20 μm^2 has been used for determination of chemical composition, crystal structure and charge states of atoms in thin phosphor films of $MAlO_3$ (M is a rare-earth metal) grown by combinatorial synthesis.[372] Convergence of SR-based microprobe spectroscopic techniques and X-ray microscopy (see Section IV) during the last decade has lead to emergence of a new research area, *viz*., spectromicroscopy.[356]

‡ Instrumental realisation of X-ray microprobe techniques in modern synchrotron radiation centres and results of recent applications of these techniques are thoroughly discussed in a special issue of *Journal of Electron Spectroscopy and Related Phenomena*,[356] as well as in a number of books and reviews (see, for example, Refs 215, 357–361).

4. Time-resolved studies of processes

Evolution of SR sources and instrumentation, *viz*., gain in brightness, focusing optics optimisation, design of fast and sensitive detectors, development of specialised techniques for data collection and processing, has lead to a substantial decrease in the time required for conduction of an X-ray experiment with SR. Collection of XRF, EXAFS or SAXS data on facilities of modern SR centres may take only a few milliseconds. This approach is of great interest for chemistry, since it makes real-time studies of reaction dynamics possible. SR intensity is sufficiently high to obtain reliable results when the beam passes through walls of a chemical reactor (reaction chamber) or sample environment of another type. That is why most of synchrotron radiation-based methods can be realised *in situ* (see, for example, a special issue of *MRS Bulletin* dedicated to *in situ* studies of materials using synchrotron techniques[373]).

Real-time diffraction (the term 'diffraction cinema' is sometimes used) allows one to investigate dynamics of solid-state reactions, to detect formation of crystalline intermediates and, in the case of heterogeneous reactions, to follow the movement of the reaction front (interface).[20] Hydrothermal synthesis is one of the most promising fields in modern inorganic chemistry. This allows simulation of geochemical processes of natural mineral synthesis and preparation of new micro- and mesoporous materials, which can be applied as molecular sieves, ion-exchange resins, adsorbents, *etc*. The applicability of synchrotron real-time X-ray powder diffraction to studies of hydrothermal synthesis reactions is discussed in Refs 374, 375.

Changes in local environment of a reacting centre in the course of a chemical reaction can be analysed by means of Quick-EXAFS. In particular, such an approach has been utilised for detection of changes in local atomic order in active centres of catalysts.[376, 377] Time-resolved EXAFS can be used as well for structural monitoring of chemical transformations in solutions.[378, 379] Under the term Quick-EXAFS, the techniques with a rapid rotation of a standard crystal monochromator or so-called energy-dispersive EXAFS with a fixed crystal polychromator and a linear detector, are usually meant.[380–382]

Recently,[383] a new method aimed at a decrease in the XAFS data acquisition time has been proposed. It is based on a variation of the electron beam trajectory within insertion devices by adjusting operational parameters of the electromagnetic focusing system (Fig. 30) In this case, the crystal monochromator remains immobile and the beam intensity can be measured with a 'point' detector, *i.e*., ionisation chamber, which has better characteristics (such as counting rate, accuracy and sensitivity) compared to modern linear detectors. As an alternative of the aforementioned instrumental techniques of Quick-EXAFS, a stop-flow method can be used. This implies withdrawal of samples from a reaction mixture at required time intervals followed by their instant freezing and investigation using standard techniques.[384]

Time-resolved X-ray photoelectron spectroscopy enables investigations of chemical reactions at surfaces. For instance, this technique has been applied in studies of kinetics of NO reduction by molecular hydrogen on a single crystal face (553) of rhodium.[385] Data collected at the Super-ESCA station of the ELETTRA synchrotron centre allowed authors to detect intermediate unstable species (atomic nitrogen, atomic hydrogen, NH_x) and suggest a mechanism explaining the oscillatory dynamics of this reaction.

Time-resolved studies of biological processes give insights into mechanisms of key biochemical processes. For example, over the

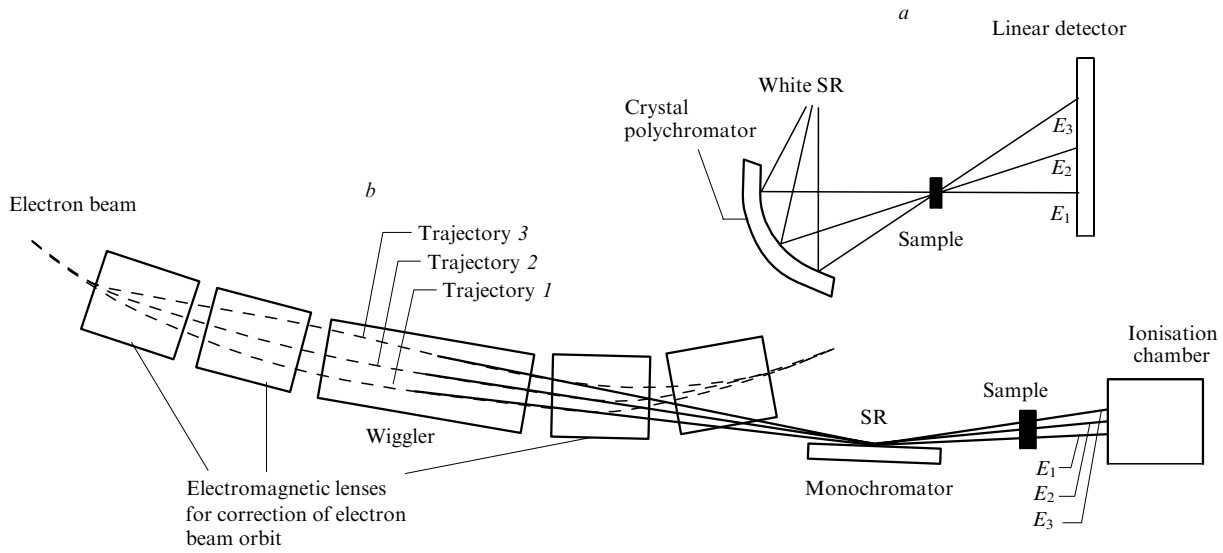

Figure 30. Experimental schemes for Quick-XAFS registration.[383]
(*a*) Energy-dispersive XAFS, (*b*) fast registration of XAFS by varying the electron trajectory within the channel of a storage ring.

last years, a substantial progress has been reached in understanding molecular mechanisms of muscle functioning thanks to SR-based studies of conformational transitions and supramolecular organisation changes of muscles under contraction and relaxation. Systematic real-time diffraction and SAXS studies of muscles are carried out in several international SR centres.[386, 387]

A combination of powerful third-generation SR sources and fast-counting 2*D* position-sensitive detectors opens new avenues in dynamic structural studies by means of Laue diffraction. Within this approach, a method of single crystal X-ray crystallography with time resolution down to tens of picoseconds is realised for biological macromolecules.[388, 389] In this modification of the 'diffraction cinema', a series of Laue patterns is registered during successive pulses of SR with a storage ring operating in the single-bunch mode. This approach is of great potential importance for investigations of enzymatic reactions. As one of the first applications of this technique, structural changes occurring in a single crystal of carboxy-myoglobin upon visible light-induced decarbonylation (Fig. 31) have been investigated.[390–392]

Capabilities offered by storage rings operating in the single-bunch mode are far from full realisation. A traditional method in this field is optical luminescence excited by X-ray pulse: its spectrum and decay dynamics are the key parameters in characterisation of new semiconducting and scintillating materials.[393] With a high level of confidence, we may suggest that in the immediate future, the interest of researchers in temporally modulated SR will increase, since this can supplement research capabilities of many of the aforementioned techniques with time resolution.

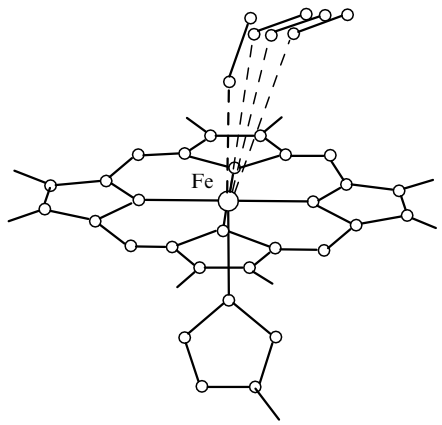

Figure 31. Migration of CO (dashed lines) in the initial stages of carboxy-myoglobin decarbonylation initiated by a visible light flash (ESRF). Atomic positions are determined by refinement of a common initial structural model *versus* a series of successive Laue-diffractograms measured for a single crystal of the substance with time resolution of ~ 10 ps.[392]

VI. Conclusion

Research capabilities of SR in chemistry and related sciences are wide and yet not fully realised. Over the last 30 years, introduction of synchrotron radiation into physicochemical analysis has resulted in substantial improvement of the accuracy and sensitivity of a few tens of physical methods. New synchrotron radiation centres are being constructed and the user community of the existing ones expands rapidly. The number of research papers reporting results obtained with the use of SR is thousands per year.

Starting from 1994, the International Union of Crystallography publishes a dedicated *Journal of Synchrotron Radiation*, in which over 1000 papers on various synchrotron radiation-related topics have already been published.

Key international and Russian national conferences with a dominant or major portion of synchrotron studies in their scope that took place over the period of 1994–2000, are listed in Table 2.

In certain fields of modern science (such as protein crystallography or XAFS), the synchrotron techniques has taken a leading position. And in such directions as development of MAD applications in crystallographic studies of biological polymers or time-resolved structural studies using Laue-diffraction, the last few years can be considered as a real breakthrough. Investigations of magnetic properties of materials using circularly polarised X-ray SR play an important role in modern technology.

Instrumentation of SR studies is under constant upgrade and sophistication. SR sources are evolving leading to even higher brilliance and stability and lower divergence of SR beams. According to predictions of machine R&D groups from several synchrotron centres [SSRL (Stanford, USA), ESRF, NSLS], fourth-generation SR sources may come into reality in the immediate future. In parallel, new ideas in the field of X-ray optics are emerging, which allows production of highly intense narrow-focus beams. Progress in this field is based to a great

Table 2. Large conferences held in 1994 – 2000 with a substantial portion of synchrotron topics in their scopes.

Year	Conference name	City	Country	Ref.[a]
1994	The Fifth International Conference on Synchrotron Radiation Instrumentation (SRI'94)	New York	USA	394
1994	The Tenth All-Russian Conference on Synchrotron Radiation (SR-94)	Novosibirsk	Russia	395
1994	The Eighth International Conference on X-ray Absorption Fine Structure (XAFS-8)	Berlin	Germany	396
1995	The 16th European Crystallography Meeting (ECM-16)	Lund	Sweden	–
1996	The First International Conference on Application of SR in Materials Science (SRMS-1)	Chicago	USA	–
1996	XAFS-9	Grenoble	France	397
1996	SR-96	Novosibirsk	Russia	398
1996	The 17th Symposium of the International Union of Crystallography (IUCr-17)	Seattle	USA	
1997	SRI'97	Himeji	Japan	399
1997	European Conference 'SR and Surface'	Castelvecco Pascoli	Italy	
1997	International Conference Frontiers in Synchrotron Radiation Spectroscopy' (FSRS'97)	Tokyo	Japan	400
1997	The First All-Russian Conference on the Application of X-rays, Synchrotron Radiation, Neutrons and Electrons to Studies of Materials (XRSNE-97)	Dubna	Russia	–
1997	ECM-17	Lisbon	Portugal	–
1998	SRMS-2	Kobe	Japan	–
1998	The Sixth International Conference on Applications of SR in Biophysics	Chicago	USA	–
1998	The Fourth European Conference on High-Resolution X-ray Diffraction and Topography (XTOP98)	Durham	England	–
1998	International School-Symposium 'SR in Natural Sciences'	Ustron-Jazovec	Poland	401
1998	XAFS-10	Chicago	USA	402
1998	ECM-18	Prague	Chech Republic	
1998	SR-98	Novosibirsk	Russia	403
1999	IUCr-18	Glasgow	Scotland	–
1999	XRSNE-99	Moscow	Russia	–
2000	SRI'2000	Berlin	Germany	–
2000	XAFS-11	Ako City	Japan	404
2000	ECM-19	Nancy	France	–
2000	SR-2000	Novosibirsk	Russia	–

[a] References to conference proceedings published in refereed journals.

extent on the latest achievements of X-ray lithography applications, which is also under active development in synchrotron centres. New fast, precise and sensitive X-ray detectors as well as X-ray monochromators with higher energy resolution appear. With improvement of coherent properties of SR, essentially new directions, such as X-ray holography, become possible. A breakthrough in imaging techniques can be expected with development of X-ray free-electron lasers.

Therefore, we may conclude that synchrotron radiation is one of the most promising points of growth for modern science. Starting from the 90's, the main SR centres turned into a new type of economic enterprises aimed at production of complex physical data. The overwhelming part of studies in modern centres have applied character and are tightly linked to technology. Despite the essentially profitless nature of 'photon factories' (for instance, costs of 1 h of beamtime on an EXAFS station, which is one of the 'cheapest' synchrotron techniques, is US \$200 – 400), contribution of synchrotron studies into modern competitive production is substantial. It explains, why the bulk of synchrotron studies in developed countries steadily increases and why many commercial companies tend to construct own stations at third-generation SR sources (for example, see review [405] on the use of synchrotron methods for characterisation of microelectronics materials prepared by the IBM R&D division on the basis of experimental results obtained at the NSLS).

Up to the 80's, the Soviet Union has been one of the world leaders in the field of synchrotron radiation theory and instrumentation. Many important steps in maturation of synchrotron radiation as a research tool have been made in the USSR. One of the first synchrotrons was constructed in 1964, experimental observation of synchrotron radiation dates back to 1971, undulators were designed in 1977, superconducting multipole wigglers in 1979 and helical undulators — sources of circularly polarised quasi-monochromatic radiation in 1983. Presently, G I Budker Institute of Nuclear Physics, where Siberian Synchrotron Radiation Centre (SSRC) operates, maintains a leading position in this field. Insertion devices, position-sensitive detectors and other high-tech devices designed and produced in BINP are used in many SR centres over the world: CAMD (Baton Rouge, USA), HASYLAB (Hamburg, Germany), Photon Factory (Tsukuba, Japan), PLS (Pohang, South Korea).

Meanwhile, the level and the volume of the applied synchrotron studies in Russia is noticeably lower than those in the largest world centres in USA, Japan and Western Europe. To the date of publication of this review, there is only one routinely operating national SR centre, Siberian synchrotron radiation centre (SSRC) in Novosibirsk, with a first-generation storage ring VEPP-3. Kurchatov synchrotron radiation source with the dedicated 'Sibir'-2' storage ring is on the stage of startup already for several years. Neither of the advanced complex techniques discussed above is involved in routine studies, which directly determine the level of modern science instrumentation. The authors hope that this review will draw attention of Russian researchers to this hot area of modern science.

This review has been written with the financial support of the Russian Foundation for Basic Research (Project No. 99-03-

32810), International Center for Diffraction Data (ICDD) and INTAS (Y V Z Grant YSF00-4095). We would like to thank our colleagues A A Ulyanov (Department of Geology, Moscow State University) and V A Strel'tsov (University of West Australia), who have kindly provided the results of their studies used as illustrations in this review, and O A Belyakova who provided us with materials of School on Synchrotron Radiation (Trieste, Italy, December 1997). The authors also express deep gratitude to D I Kochubey, B P Tolochko and specialists of SSRC for help in collaboration for many years.

References

1. E-E Koch (Ed.) *Handbook of Synchrotron Radiation* Vol. 1 (Amsterdam: North-Holland, 1983)
2. G V Marr (Ed.) *Handbook of Synchrotron Radiation* Vol. 2 (Amsterdam: North-Holland, 1987)
3. G B Brown, D E Moncton (Eds) *Handbook of Synchrotron Radiation* Vol. 3 (Amsterdam: North-Holland, 1991)
4. S Ebashi, M Koch, E Rubenstein (Eds) *Handbook of Synchrotron Radiation* Vol. 4 (Amsterdam: North-Holland, 1991)
5. I M Ternov, V V Mikhailin *Sinkhrotronnoe Izluchenie. Teoriya i Eksperiment* (Synchrotron Radiation. Theory and Experimnt) (Moscow: Energoatomizdat, 1986)
6. G N Kulipanov, A N Skrinskii, in *Rentgenospektral'nyi Metod Izucheniya Struktury Amorfnykh Tel. EXAFS-Spektroskopiya* (X-Ray Spectral Method for Investigation of the Structure of Amorphous Solids. EXAFS Spectroscopy) (Ed. G M Zhidomirov) (Novosibirsk: Nauka, 1988) p. 94
7. I M Ternov *Usp. Fiz. Nauk* **165** 429 (1995) [a]
8. H Winick *J. Synchr. Radiat.* **5** 168 (1998)
9. M Madou *Fundamentals of Microfabrication* (Boca Raton, FL; New York: CRC Press, 1997)
10. M Ando, C Uyano (Eds) *Medical Application of Synchrotron Radiation* (Berlin: Springer, 1998)
11. D G Schulze, P M Bertch *Adv. Agronomy* **55** 1 (1995)
12. *Otchet Sibirskogo Tsentra Sinkhrotronnogo Izlucheniya za 1998 g.* (Report of the Siberian Centre of Synchrotron Radiation for 1998) (Novosibirsk: Institute of Nuclear Physics, Siberian Branch of Russian Academy of Sciences, 2000)
13. *Kurchatov Synchrotron Radiation Source, 1993-1994. Activity Report, Moscow, 1995*
14. Y Utsumi, J Takahashi *Jpn. J. Appl. Phys. 2, Lett,* **37** L1268 (1998)
15. R K Kupka, F Bouamrane, C Cremers, S Megtert *Appl. Surf. Sci.* **164** 97 (2000)
16. P Dumas, G L Carr, G P Williams *Analysis* **28** 68 (2000)
17. R A Palmer, G D Smith, P Chen *Vib. Spectrosc.* **19** 131 (1999)
18. B Diviacco, R P Walker *Nucl. Instrum. Methods Phys. Res. A* **368** 522 (1996)
19. J L Laclare *J. Phys. IV, Colloq. (France)* **7** C2-39 (1997)
20. G N Kulipanov (Ed.) *Difraktometriya s Ispol'zovaniem Sinkhrotronnogo Izlucheniya* (Difractometry with the Use of Synchrotron Radiation) (Novosibirsk: Nauka, 1989)
21. V V Aristov, A I Erko, B Vidal *Diffraction X-Ray Optics* (London: IOP Publ., 1995)
22. A G Michette *Optical Systems for Soft X-Rays* (New York: Plenum, 1986)
23. B K Vainshtein *Sovremennaya Kristallografiya* (Modern Crystallography) (Moscow: Nauka, 1979) Vol. 1
24. L A Aslanov *Instrumental'nye Metody Rentgenostrukturnogo Analiza* (Instrumental Methods of X-Ray Diffraction Analysis) (Moscow: Moscow State University, 1982)
25. D Briggs, M P Seach (Eds) *Practical Surface Analysis by Auger and X-ray Photoelectron Spectroscopy* (New York: Wiley, 1983)
26. F F Fujita *Contemp. Phys.* **40** 323 (1999)
27. D C Koningsberger, R Prins (Eds) *Principles, Applications, Technique of EXAFS, SEXAFS and XANES* (New York: Wiley, 1988)
28. S S Husnain (Ed.) *X-Ray Absorption Fine Structure* (New York: Ellis Horwood, 1991)
29. G M Zhidomirov (Ed.) *Rentgenospektral'nyi Metod Izucheniya Struktury Amorfnykh Tel. EXAFS-Spektroskopiya* (X-Ray Spectral Method for Investigation of the Structure of Amorphous Solids. EXAFS Spectroscopy) (Novosibirsk: Nauka, 1988)
30. B K Teo *EXAFS: Basic Principles and Data Analysis* (Berlin: Springer, 1986)
31. G A Waychunas, G E Brown Jr *Adv. X-Ray Anal.* **37** 607 (1994)
32. H Ebel, R Svagera, M F Ebel *Microchim. Acta* **125** 165 (1997)
33. A Rogalev, J Goulon *J. Phys. IV, Colloq. (France)* **7** C2-565 (1997)
34. G Thornton, D R Warburton, I W Owen, C H Richardson, R Mcgrath, I T Mcgovern, D Norman *J. Phys. (France)* **47** NC-8-179 (1987)
35. B A Bunker, Z Wang, Q Islam *Ferroelectrics* **120** 23 (1991)
36. A Di Cicco, M Berrettoni *Phys. Lett. A* **176** 375 (1993)
37. A Di Cicco, M Minicucci *J. Synchr. Radiat.* **6** 255 (1999)
38. R G Linford *Chem. Soc. Rev.* **24** 267 (1995)
39. M Gautier-Soyer *J. Eur. Ceram. Soc.* **18** 2253 (1998)
40. C D Garner *Adv. Inorg. Chem.* **36** 303 (1991)
41. V K Yachandra *Methods Enzymol.* **246** 638 (1995)
42. P J Riggs-Gelasco, T L Stemmler, J E Penner-Hahn *Coord. Chem. Rev.* **144** 245 (1995)
43. P Johnston, P B Wells *Radiat. Phys. Chem.* **45** 393 (1995)
44. Y Iwasawa (Ed.) *X-Ray Absorption Fine Structure for Catalyst and Surfaces* (Singapore: World Sci., 1996)
45. J Evans *Chem. Soc. Rev.* **26** 11 (1997)
46. K Asakura, W-J Chun, M Shirai, K Tomishige, Y Iwasawa *J. Phys. Chem. B* **101** 5549 (1997)
47. N Toshima, T Yonezawa *New J. Chem.* **22** 1179 (1998)
48. I I Moiseev, M N Vargaftik, in *Catalysis by Di- and Polynuclear Metal Cluster Complexes* (Eds R D Adams, F A Cotton) (New York: Wiley-VCH, 1998) p. 395
49. H Huang, C H Liang, J E Penner-Hahn *Angew. Chem., Int. Ed. Engl.* **37** 1564 (1998)
50. H Tanida, H Sakane, I Watanabe *J. Chem. Soc., Dalton Trans.* **15** 2321 (1994)
51. Y Inada, K Sugimoto, K Ozutsumi, S Funahashi *Inorg. Chem.* **33** 1875 (1994)
52. L R Sharpe, W R Heineman, R C Elder *Chem. Rev.* **90** 705 (1990)
53. A Di Cicco, M Minicucci, A Filipponi *Phys. Rev. Lett.* **78** 460 (1997)
54. J Stöhr *NEXAFS Spectroscopy* (Berlin: Springer, 1992)
55. J Kukuma, B P Tommer *J. Electron Spectrosc. Relat. Phenom.* **82** 53 (1996)
56. J Taborski, P Vaterlein, H Dietz, U Zimmermann, E Umbach *J. Electron Spectrosc. Relat. Phenom.* **75** 129 (1995)
57. G Hühner, M Kinzler, Ch Wlll, M Grunze *Phys. Rev. Lett.* **67** 851 (1991)
58. R Mitsumoto, H Oji, I Mori, Y Yamamoto, K Osato, Y Ouchi, H Shinohara, K Seki, K Umishita, S Hino, S Nagase, K Kikushi, Y Achiba *J. Phys. IV, Colloq. (France)* **7** C2-525 (1997)
59. J Wong, Z U Rek, M Rowen, T Tanaka, F Schafers, B Muller, G N George, I J Pickering, G Via, B Devries, G E Brown, M Froba *Physica B* **208**–**209** 220 (1995)
60. P Ildefonse, G Cals, A M Flank, P Lagarde *Nucl. Instrum. Methods Phys. Res. B* **97** 172 (1995)
61. D C Koningsberger, J T Miller *Catal. Lett.* **29** 77 (1994)
62. M Kamijo, N Umesaki, K Fukui, C Guy, K Tadanada, M Tasumisago, T Minami *J. Non-Cryst. Solids* **177** 187 (1994)
63. S Paste, V Gotte, C Goulon-Ginet, A Rogalev, J Goulon, P Georget, J Marcilloux *J. Phys. IV, Colloq. (France)* **7** C2-665 (1997)
64. P J Potts, A T Ellis, P Kregsamer, C Streli, M West, P Wobrauschek *Annu. Rep. Anal. At. Spectrom.* **14** 1773 (1999)
65. V A Trounova, K Z Zolotarev, V B Baryshev, M A Phedorin *Nucl. Instrum. Methods Phys. Res. A* **405** 532 (1998)
66. L N Tarasov, A F Kudryashova, A A Ulyanov, V B Baryshev, K V Zolotarev *Nucl. Instrum. Methods Phys. Res. A* **405** 590 (1998)
67. E J Nordgren *J. Electron Spectrosc. Relat. Phenom.* **78** 25 (1996)
68. A N Artemiev, M M Vsevolodov, D P Grechukhin, A V Zabelin, V N Kosyakov, S V Romanov, A A Soldatov *Nucl. Instrum. Methods Phys. Res., A* **359** 266 (1995)
69. J Nordgren, J Guo *J. Electron Spectrosc. Relat. Phenom.* **110**–**111** 1 (2000)
70. E J Nordgren *J. Phys. IV, Colloq. (France)* **7** C2-9 (1997)
71. J Guo, J Nordgren *J. Electron Spectrocs. Relat. Phenom.* **110**–**111** 105 (2000)

72. F M F De Groot *J. Electron Spectrosc. Relat. Phenom.* **92** 207 (1998)
73. G M Bancroft, Y-F Hu *Inorg. Electron Struct. Spectrosc.* **1** 443 (1999)
74. M Taniguchi *J. Alloys Compd.* **286** 114 (1999)
75. A Nillson, in *Application of Synchrotron Radiation* (Berlin: Springer, 1995) p. 65
76. C Laubschat *J. Electron Spectrosc. Relat. Phenom.* **96** 127 (1998)
77. J C Green, N Kaltsoyanis, K H Sze, M MacDonald *J. Am. Chem. Soc.* 116 (1994)
78. X Li, G M Bancroft, R J Puddephatt, Y-F Hu, K H Tan *Organometallics* **15** 2890 (1996)
79. A M Bradshaw, C S Fadley, N Mertensson (Eds) *Future Perspectives of X-Ray Photoelectron Spectroscopy with Synchrotron Radiation. J. Electron Spectrosc. Relat. Phenom.* **75** (0) (Special Issue) (1995)
80. A M Bradshaw, D P Woodruff, in *Application of Synchrotron Radiation. Springer Ser. Surface Science* Vol. 35 (Ed. W Ebernardt) (Berlin, Heidelberg: Springer, 1995) p. 127
81. C S Fadley, A P Kaduwela, M A Vannove, Z Hussain *J. Electron Spectrosc. Relat. Phenom.* **75** 273 (1995)
82. C S Fadley *Prog. Surf. Sci.* **54** 341 (1997)
83. L J Terminello, B L Petersen, J J Barton *J. Electron Spectrosc. Relat. Phenom.* **75** 299 (1995)
84. C S Fadley, in *Synchrotron Radiation Research: Advances in Surface and Interface Science. Techniques* Vol. 1 (Ed. R Z Bachrach) (New York: Plenum, 1992) p. 421
85. M M Harding *Acta Crystallogr., Sect. B* **51** 432 (1995)
86. J R Helliwell *Acta Crystallogr., Sect. A* **54** 738 (1998)
87. P Coppens *Synchrotron Radiation Crystallography* (London: Academic Press, 1992)
88. P Coppens *J. Appl. Crystallogr.* **26** 499 (1993)
89. M M Harding *Mater. Sci. Forum* **228** 3 (1996)
90. P Coppens, R Bolotovsky, V Kezerashvili, A Darovsky, Y Gao *Trans. Am. Crystallogr. Assoc.* **31** 11 (1997)
91. P Coppens, G Wu, A Volkov, Y Abramov, Y Zhang, W K Fullagar, L Ribaud *Trans. Am. Crystallogr. Assoc.* **34** 51 (2000)
92. W Rieck, H Euler, H Schulz *Acta Crystallogr., Sect. A* **44** 1099 (1988)
93. R W Broach, R L Bedard, S G Song, J J Pluth, A Bram, C Riekel, H-P Weber *Chem. Mater.* **11** 2076 (1999)
94. E F Skelton, J D Ayers, S B Qudri, N E Moulton, K P Cooper, L W Finger, H K Mao, Z Hu *Science* **253** 1123 (1991)
95. K D Eichnorn *Eur. J. Mineral.* **9** 673 (1997)
96. R B Neder, M Bourghammer, Th Grasl, H Schulz *Z. Kristallogr.* **211** 763 (1996)
97. K Oshumi, K Hagiya, M Okhmasa *J. Appl. Crystallogr.* **24** 340 (1991)
98. R B Neder, M Burghammer, T Crasl, H Schulz *Z. Kristallogr.* **211** 365 (1996)
99. R Flaig, T Koritzansky, J Janczak, H-G Krane, W Morgenroth, P Luger *Angew. Chem., Int. Ed. Engl.* **38** 1397 (1999)
100. E N Maslen, V A Streltsov, N R Streltsova, N Ishizawa *Acta Crystallogr., Sect. B* **51** 929 (1995)
101. K Eichhorn, A Kirfel *Acta Crystallogr., Sect. B* **47** 843 (1991)
102. B B Iversen, F K Larsen, A A Pinkerton, A Martin, A Darovsky, P A Reynolds *Inorg. Chem.* **37** 4559 (1998)
103. H Graafsma, M Souhassou, A Puig-Molina, S Harkema, E Kvick, C Lecomte *Acta Crystallogr., Sect. B* **54** 193 (1998)
104. F Frolow, L Chernyak, D Cahen *Tern. Mult. Compd.* **152** 67 (1998)
105. F S Nielsen, P Lee, P Coppens *Acta Crystallogr., Sect. B* **42** 359 (1986)
106. T Koritsanszky, R Flaig, D Zobel, H G Krane, W Morgenroth, P Luger *Science* **279** 356 (1998)
107. T Koritzanszky, in *International Union Crystallography XVIIIth Congress and General Assembly (Collected Abstracts), Glasgow, 1999* M09.OD.002
108. B B Iversen, in *International Union Crystallography XVIIIth Congress and General Assembly (Collected Abstracts), Glasgow, 1999* M09.OD.003
109. B K Vainshtein, V M Fridkin, V L Indenbom *Sovremennaya Kristallografiya* (Modern Crystallography) (Moscow: Nauka, 1979) Vol. 2, p. 193
110. P F Lindley *Radiat. Phys. Chem.* **45** 367 (1995)
111. K Moffat, Z Ren *Curr. Opin. Struct. Biol.* **7** 689 (1997)
112. J R Helliwell, S Ealick, P Doing, T Irring, M Szemenyi, *Acta Crystallogr., Sect. D* **49** 120 (1993)
113. W Minor, D R Tomchick, Z Otwinowski *Structure* (*London*) **8** R105 (2000)
114. *Structural Biology and Synchrotron Radiation: Evaluation of Resources and Needs* http://www.ornl.gov/hgmis/biosync
115. A Deacon, T Gleichmann, A J Kalb, H Price, J Raftery, G Bradbrook, J Yariv, J R Helliwell *J. Chem. Soc., Dalton Trans.* **93** 4305 (1997)
116. C Jelsch, M M Teeter, V Pickon-Pesme, R H Blessing, C Lecomte, in *International Union Crystallography XVIIIth Congress and General Assembly (Collected Abstracts), Glasgow, 1999* M11.BB.004
117. J P Abrahams, A G W Leslie, R Lutter, J E Walker *Nature (London)* **370** 621 (1994)
118. D H Bilderback, S A Hoffmann, D J Thiel *Science* **263** 201 (1994)
119. B M Kariuki, M M Harding *J. Synchr. Radiat.* **2** 185 (1995)
120. X J Yang, Z Ren, K Moffat *Acta Crystallogr., Sect. D* **54** 367 (1998)
121. R B G Ravelli, M L Raves, S H W Scheves, A Schouten, J Kroon, *J. Synchr. Radiat.* **6** 19 (1999)
122. T Bruckel, M Lippert, B Bouchard, T Schmidt, J R Schneider, W Jauch *Acta Crystallogr., Sect. A* **49** 679 (1993)
123. M J Cooper, W G Stirling *Radiat. Phys. Chem.* **56** 85 (1999)
124. T Bruckel *Acta Phys. Pol. A* **91** 669 (1997)
125. D Mannix, S Langridge, G H Lander, J Rebizant, M J Longfield, W G Stirling, W J Nutall, S Coburn, S Wasserman, L Soderholm *Physica B* **262** 125 (1999)
126. D Gibbs, D E Moncton, K L D'Amico, J Bohr, B H Grier *Phys. Rev. Lett.* **55** 234 (1985)
127. H Graafsma, G W J C Heunen, C Schulze *J. Appl. Crystallogr.* **31** 414 (1998)
128. H Graafsma, A Paturle, L Wu, H-S Sheu, J Majewski, G Poorthuis, P Coppens *Acta. Crystallogr., Sect. A* **48** 113 (1992)
129. S J van Reeuwijk, H Graafsma, in *International Union Crystallography XVIIIth Congress and General Assembly (Collected Abstracts), Glasgow, 1999* P05.10.005
130. A Puig-Molina, H Mueller, H Graafsma, A Kvick, in *International Union Crystallography XVIIIth Congress and General Assembly (Collected Abstracts), Glasgow, 1999* P11.19.025
131. L X Chen, M K Bowman, Zh Wang, P A Montano, J R Norris *J. Phys. Chem. B* **98** 9457 (1994)
132. H Fuess *An. Quim. Int. Ed.* **94** 388 (1998)
133. A N Fitch, in *Proceedings of the 6th Summer School on Neutron Scattering: Complementary between Neutron and Synchrotron X-Ray Scattering* (Ed. A Furrer) (New York: World Sci., 1998) p. 41
134. B A Latella, B H O'Connor *J. Am. Ceram. Soc.* **80** 2941 (1997)
135. P Norby *J. Appl. Crystallogr.* **30** 21 (1997)
136. P G Fagan, R B Hammond, K J Roberts, R Docherty, A P Chorlton, W Jones, G D Potts *Chem. Mater.* **7** 2322 (1995)
137. W I F David, K Shankland, N Shankland *Chem. Commun.* 931 (1998)
138. K D Knudsen, P Pattison, A N Fitch, R J Kernik *Angew. Chem., Int. Ed. Engl.* **37** 2340 (1997)
139. A Kern, A Coelho, in *International Union Crystallography XVIIIth Congress and General Assembly (Collected Abstracts), Glasgow, 1999* P05.OD.001
140. R J Chernik, A K Cheetham, C K Prout, D J Watkin, A P Wilkinson, B T M Willis *J. Appl. Crystallogr.* **24** 222 (1991)
141. A N Fitch, H Jobic *J. Chem. Soc., Chem. Commun.* 1516 (1993)
142. R E Dennibier, M Pink, J Sieler, P W Stephens *Inorg. Chem.* **36** 3398 (1997)
143. R E Morris, J J Owen, A K Cheetham *J. Phys. Chem. Solids* **56** 1297 (1995)
144. M A Roberts, A N Fitch, A V Chadvick *J. Phys. Chem. Solids* **56** 1353 (1995)
145. R W Broach, R M Kirchner, N K McGuire, C C Chao *J. Phys. Chem. Solids* **56** 1363 (1995)
146. T R Jensen, P Norby, A N Christensen, J C Hanson *Microp. Mesop. Mater.* **26** 77 (1998)
147. D M Poojary, A Clearfield *J. Organomet. Chem.* **512** 237 (1995)
148. R E Dennibier, U Behrens, F Olbrich *J. Am. Chem. Soc.* **120** 1430 (1998)

149. J E Fischer, G Bendele, R Dinnebier, P W Stephens, C L Lin, N Bykovets, Q Zhu *J. Phys. Chem. Solids* **56** 1445 (1995)
150. E Nishibori, M Takata, M Sakata, M Inakuma, H Shinohara *Chem. Phys. Lett.* **298** 79 (1998)
151. E Nishibori, M Takata, M Sakata, H Shinohara *J. Synchr. Radiat.* **5** 977 (1998)
152. C M Brown, L Cristofilini, K Kordatos, K Prassides, C Bellavia, R Gonzales, K M Keshavorz, F Wude, A K Cheetham, J P Zhang, W Andreoni, A Currion, A N Fitch, P Pattison *Chem. Mater.* **8** 2548 (1996)
153. R E Dinnebier, P W Stephens, J K Carter, A N Lommen, P A Heiney, A R McGhie, L Branrd, A B Smith *J. Appl. Crystallogr.* **28** 327 (1995)
154. R E Dennibier, F Olbrich, S van Smaalen, P W Stephens *Acta Crystallogr., Sect. B* **53** 153 (1997)
155. Y Kubota, M Takata, M Sakata *J. Phys., Condens. Matter* **5** 8245 (1993)
156. M Takata, Y Kubota, M Sakata *Z. Naturforsch., A Phys. Sci.* **48** 75 (1993)
157. S Yamamura, M Takata, M Sakata *J. Phys. Chem. Solids* **58** 117 (1997)
158. T Wessels, C Baerlochev, L B McCusker *Science* **284** 477 (1999)
159. C J Benmore, B L Tomberli, P A Egelstaff, in *International Union Crystallography XVIIIth Congress and General Assembly (Collected Abstracts), Glasgow, 1999* P06.OF.001
160. J Poulsen, J Neuefeind, H B Neumann, J R Schneider, M D Zeider *J. Non-Cryst. Solids* **188** 63 (1995)
161. S Mobilio, C Meneghini *J. Non-Cryst. Solids* **232**–**234** 25 (1998)
162. H Schlenz, R Grabinski, A Kirfel, in *International Union Crystallography XVIIIth Congress and General Assembly (Collected Abstracts), Glasgow, 1999* P07.10.001
163. T R Welberry, Th Proffen *Acta Crystallogr., Sect. A* **54** 661 (1998)
164. T R Welberry, in *International Union Crystallography XVIIIth Congress and General Assembly (Collected Abstracts), Glasgow, 1999* K07.03.001
165. A Mahendrasingam, V T Forsyth, R Hussain, R J Greenall, W J Pigram, W Fuller *Science* **233** 195 (1986)
166. G Büldt, K Konno, K Nakanishi, H-J Plöhn, B N Rao, N A Dencher *Photochem. Photobiol.* **54** 873 (1991)
167. W Bras, A J Ryan *Adv. Colloid Interface Sci.* **75** 1 (1998)
168. J C Dore, A N North, J C Rigden *Radiat. Phys. Chem.* **45** 413 (1995)
169. C Riekel, P Bosecke, O Diat, P Engstrom *J. Mol. Struct.* **383** 291 (1996)
170. G Panick, R Malessa, R Winter, R Gert, K J Frye, C A Royer *J. Mol. Biol.* **275** 90 (1998)
171. G Barone, Z Sayers, D Svergun, M H J Koch *J. Synchr. Radiat.* **6** 1031 (1999)
172. M Megens, C M Van Kats, P Bosecke, V L Vos *J. Appl. Crystallogr.* **30** 637 (1997)
173. A F Craevich, O L Alves, L C Barbosa *Rev. Sci. Instrum.* **66** 1338 (1995)
174. A Craevich *J. Phys. I, Gen Phys. Stat. Phys Condens. Matter Cross.-Discipl. Phys.* **2** 801 (1992)
175. M F Butler, A M Donald, A J Ryan *Polymer* **38** 5521 (1997)
176. P P E A de Moor, T P M Beelen, B U Komanchek, O Dlat, R A Santen *J. Phys. Chem. B* **101** 11077 (1997)
177. J S Rigden, A N North, A R Mackie *Prog. Colloid Polym. Sci.* **93** 63 (1993)
178. A N North, J S Rigden, A R Mackie *Rev. Sci. Instrum.* **63** 1741 (1992)
179. E D Isaacs, P M Platzman *Phys. Today* **49** 40 (1996)
180. H Hayashi, N Watanabe, Y Udagawa *J. Synchr. Radiat.* **5** 1052 (1998)
181. F Sette, G Ruocco *Eur. News* **26** 78 (1995)
182. G Ruocco, F Sette *Bull. Soc. Fr. Phys.* **115** 25 (1998)
183. E Burkel *Rep. Prog. Phys.* **63** 171 (2000)
184. N G Alexandropoulos *Nucl. Instrum. Methods Phys. Res. A* **308** 267 (1991)
185. W Schülke, U Bonse, H Nagasawa, A Kaprolat, A Berthold *Phys. Rev. B* **38** 2112 (1988)
186. C Blaas, J Redinger, S Manninen, V Honkimäki, K Hämäläinen, P Suortti *Phys. Rev. Lett.* **75** 1984 (1995)
187. K Tohji, Y Udagawa *Phys. Rev. B* **39** 7590 (1989)
188. F Gelmukhanov, H Agren *Physica B* **208**–**209** 100 (1995)
189. H Nagasawa *J. Phys., Pt 2 (Paris)* **48** (C-9) 863 (1987)
190. W Schülke, A Berthold, A Kaprolat, H-J Güntherodt *Phys. Rev. Lett.* **60** 2217 (1988)
191. W Schülke, K-J Gabriel, A Berthold, H Shulte-Schrepping *Solid State Commun.* **79** 657 (1991)
192. Y Ma, *J. Electron Spectrosc. Relat. Phenom.* **79** 131 (1996)
193. G Dräger *Surf. Invest.* **13** 447 (1998)
194. U van Bärck, R L Mössbauer, E Gerdau, R Rüffer, R Holletz, G Smirnov, P Hanson *Phys. Rev. Lett.* **59** 355 (1987)
195. H Grünsteudel, W Meyer-Klaucke, A X Trautwein, H Winkler, O Leupold, J Metge, E Gerdau, H D Rüter, A Q R Baron, A I Chumakov, H F Grünsteudel, R Rüffer, M Haas, E Realo, D Mandon, R Weiss, H Toftlund, in *Bioinorganic Chemistry: Transition Metals in Biology and Their Coordination Chemistry* (Ed. A X Trautwein) (New York: Wiley-VCH, 1997) p. 760
196. A X Trautwein, H Paulsen, E Realo, H D Rüter, H Grünsteudel, R Weiss, M Haas, H Winkler, O Leupold, D Mandon, B F Matzanke, W Meyer-Klaucke *Inorg. Chim. Acta* **275** 334 (1998)
197. V Schünemann, H Winkler *Rep. Prog. Phys.* **63** 263 (2000)
198. W Sturhahn, E E Alp, T S Toellner, P Hession, M Hu, J Sutter *Hyperfine Interact. (Netherlands)* **113** 47 (1998)
199. S Nasu *Hyperfine Interact. (Netherlands)* **113** 97 (1998)
200. M Pleines, R Lübbers, M Strecker, G Wortmann, O Leupold, Yu Shvyd'ko, E Gerdau, J Metge *Hyperfine Interact. (Netherlands)* **120** 181 (1999)
201. R Lübbers, M Pleines, H-J Hesse, G Wortmann, H F Grünsteudel, R Rüffer, O Leupold, J Zukrowski *Hyperfine Interact. (Netherlands)* **120** 49 (1999)
202. L Nielsen, A Mugarza, M F Rozu, R Coehoorn, R M Junglblut, F Rozeboom, A Q R Baron, A I Chumakov, R Rüffer *Phys. Rev. B* **58** 8590 (1998)
203. V G Kohn, G V Smirnov *Hyperfine Interact. (Netherlands)* **123**–**124** 327 (2000)
204. B Sepiol, C Czihak, A Meyer, G Vogl, J Metge, R Rüffer *Hyperfine Interact. (Netherlands)* **113** 449 (1998)
205. B Sepiol, A Meyer, G Vogl, R Rüffer, A I Chumakov, A Q R Baron *Phys. Rev. Lett.* **76** 3220 (1996)
206. B Sepiol, A Meyer, G Vogl, H Franz, R Rüffer *Phys. Rev. B* **57** 10433 (1998)
207. A Chumakov, R Rüffer *Hyperfine Interact. (Netherlands)* **113** 59 (1998)
208. A I Chumakov, A Barla, R Rüffer, J Metge, H F Grünsteudel, H Grünsteudel, J Plessel, H Winklemann, M M Abd-Elmeguid *Phys. Rev. B* **58** 254 (1998)
209. E Gerdau, U van Bürck, in *Resonant Anomalous X-Ray Scattering* (Eds G Materlik, C J Sparks, K Fischer) (Amsterdam: Elsevier, 1994) p. 589
210. R Rohlsberger *Hyperfine Interact. (Netherlands)* **123**–**124** 455 (2000)
211. J Kirz, M Howells *Q. Rev. Biophys.* **28** 33 (1995)
212. H Ade, X Zhang, S Cameron, C Costello, J Kirz, S Williams *Science* **258** 972 (1992)
213. H Ade, B Hsiao, G Mitchell, E Rightor, A P Smith, R Cieslinski *Mater. Res. Soc. Proc.* **375** 293 (1995)
214. H Ade *Trends Polym. Sci.* **5** 58 (1997)
215. J Thieme, G Schmahl, E Umbach, D Rudolf (Eds) *X-Ray Microscopy and Spectromicroscopy* (Berlin: Springer, 1998)
216. M Moore *Radiat. Phys. Chem.* **45** 427 (1995)
217. F Zontone, L Moncini, R Barrett, J Baruchel, J Hartwig, Y Epelboin *J. Synchr. Radiat.* **3** 173 (1996)
218. B K Tonner *Acta Phys. Pol.* **86** 537 (1994)
219. J Baruchel, in *X-Rays and Neutrons Dynamical Diffraction. Theory and Applications* (Ed. A Authier) (New York: Plenum, 1996) p. 199
220. P Jacobs, E Sevens, M Kunnen *Sci. Total Environ.* **167** 161 (1995)
221. U Bonse, F Busch *Prog. Biophys. Mol. Biol.* **65** 133 (1996)
222. W S Haddad, I McNulty, J E Trebes, E H Anderson *Proc. SPIE — Int. Soc. Opt. Eng.* **2516** 102 (1995)
223. A Snigirev, I Snigireva, V Kohn, S Kuznetsov, I Schelokov *Rev. Sci. Instrum.* **66** 5486 (1995)
224. A Snigirev, I Snigireva, A Suvorov, M Kocsis, V Kohn *ESRF Newslett.* **24** 23 (1995)
225. A A Snigirev, C Raven *Bull. Soc. Fr. Phys.* **110** 10 (1997)

226. G Grmbel, D Abernathy, T Thurn-Albrecht, W Steffen, A Patkowski, G Meier, E W Fischer *ESRF Newslett*. **26** 10 (1996)
227. S B Dieker, R Pindak, R M Fleming, I K Robinson, L Berman *Phys. Rev. Lett*. **75** 449 (1995)
228. S G J Mochrie, A M Mayes, A R Sandy, M Sutton, S Brauer, G B Stephenson, D L Albernathy, G Grmbel *Phys. Rev. Lett*. **78** 1275 (1997)
229. S Brauer, G B Stephenson, M Sutton, R Brmning, E Dufresne, S G J Mochrie, G Grübel, J Als-Nielsen, D Abernathy *Phys. Rev. Lett*. **74** 2010 (1995)
230. Z H Kai, B Lai, W B Yun, I McNulty, K G Huang, T P Russel *Phys. Rev. Lett*. **73** 82 (1994)
231. K Burger, D Cox, R Papoular, W Prandl *J. Appl. Crystallogr*. **31** 789 (1998)
232. K Burger, W Prandl, S Doyle *Z. Kristallogr*. **212** 493 (1997)
233. D M Proserpio, G Artioli, S Mulley, G Chacon, C Zheng *Chem. Mater*. **9** 1463 (1997)
234. A Noudon *NATO Adv. Stady Inst. Ser. C, Math. Phys. Sci*. **452** 203 (1995)
235. H G Haubold, X H Wang, H Jungbluth, G Goerigk, W Schilling *J. Mol. Struct*. **383** 283 (1996)
236. B Bouchetfabre, P Dangelo, N V Pvel *Nucl. Instrum. Methods Phys. Res. B* **97** 539 (1995)
237. S Sasaki, T Toyoda, K Yamanaki, K Okhubo *J. Synchr. Radiat*. **5** 920 (1998)
238. A P Wilkinson, A K Cheetham, D E Cox *Acta Crystallogr., Sect. B* **47** 155 (1991)
239. Y Gao, M R Pressprich, P Coppens *Acta Crystallogr., Sect. A* **49** 21 (1993)
240. Y Gao, A Frast-Jensen, M R Pressprich, P Coppens *J. Am. Chem. Soc*. **114** 9214 (1992)
241. G Wu, Y Zhang, L Ribaud, P Coppens, C Wilson, B B Iversen, F K Larsen *Inorg. Chem*. **37** 6078 (1998)
242. W A Hendrickson *Science* **254** 54 (1991)
243. W A Hendrickson, C M Ogata *Methods Enzymol*. **276** 494 (1997)
244. W A Hendrickson *J. Synchr. Radiat*. **6** 845 (1999)
245. A Cassetta, A M Deacon, S E Ealick, J R Helliwell, A W Thompson *J. Synchr. Radiat*. **6** 822 (1999)
246. S Stuhrmann, K S Bartels, W Brannwarth, R Doose, F Dauvergne, A Gabriel, A Knochel, M Marmotti, H B Stuhrmann *J. Synchr. Rad*iat. **4** 298 (1997)
247. S Sturmann, K Bartels, M Hütch, M Marmottti, Z Zaiers, J Tomas, K Trams, H B Sturmann, in *Problemy Sovremennoi Kristallografii. Strukturnye Issledovaniya Kristallov* (Problems in Modern Crystallography. Structural Investigation of Crystals) (Moscow: Nauka, 1996) p. 276
248. M Schiltz, A Kvick, O S Svensson, W Shepard, E dela Fortelle, T Pranfe, R Kahn, G Brigogne, R Fourme *J. Synchr. Radiat*. **4** 287 (1997)
249. I J Pickering, M Sansone, J Marsch, G N George *J. Am. Chem. Soc*. **115** 6302 (1993)
250. J Vacinova, J L Hadeau, P Wolfers, J P Lauriat, E Elkain *J. Synchr. Radiat*. **2** 236 (1995)
251. J P Attfield *Mater. Sci. Forum* **228** 201 (1996)
252. G Materlik, C J Sparks, K Fischer (Eds) *Resonant Anomalous X-Ray Scattering. Theory and Applications* (Amsterdam: Elsevier, North-Holland, 1994)
253. R M Imamov, E Kh Mukhamedzhanov, in *Problemy Sovremennoi Kristallografii. Strukturnye Issledovaniya Kristallov* (Problems in Modern Crystallography. Structural Investigation of Crystals) (Moscow: Nauka, 1996) p. 132
254. J B Peclka, A Cedola, S Lagomarsino, S di Fonzo, W Jark, G Soullie *J. Alloys Compd*. **286** 313 (1999)
255. S-H Yang, B S Mun, A W Kay, S-H Kim, J B Kortright, J H Underwood, Z Hussain, C S Fadley *Surf. Sci*. **461** L557 (2000)
256. D P Woodruff *Prog. Surf. Sci*. **57** 1 (1998)
257. A Lessmann, S Brennan, B Materlik, M Schuster, H Riechert *Rev. Sci. Instrum*. **66** 1428 (1995)
258. Y Qian, N C Sturchio, R P Chiarello, P F Lyman, T-L Lee, M J Bedzyk *Science* **265** 1555 (1994)
259. M Sugiyama, S Maeyama, M Oshima *Rev. Sci. Instrum*. **67** 3182 (1996)
260. A Shi, P L Cowan, S Southworth, L Fotiadis, C Hor, B Harlin, F Moore, E Dobisz, H Dietrich *J. Appl. Phys*. **73** 8161 (1993)
261. M V Kovalchuk, A Y Kazimirov, S I Zheludeva *Nucl. Instrum. Methods Phys. Res. B* **101** 435 (1995)
262. J Als-Nielsen, in *Handbook of Synchrotron Radiation* (Eds G B Brown, D E Moncton) (Amsterdam: North-Holland, 1991) Vol. 3, p. 471
263. H Aiginger, P Wobrauschek, C Streli *Anal. Sci*. **11** 471 (1995)
264. R S Hockett *Mater. Res. Soc. Symp. Proc*. **354** 377 (1995)
265. C Streli *J. Trace Microprobe Techn*. **13** 109 (1995)
266. P Wobrauschek *J. Anal. At. Spectrom*. **5** 333 (1998)
267. R S Hockett *Adv. X-Ray Anal*. **37** 565 (1994)
268. Z H Ming, Y L Soo, S W Huang, Y H Kao, K Stair, G Devane, C Choi-Feng, T Chang, L P Fu, G D Gilliland, J Klem, M Hafich *Mater. Res. Soc. Symp. Proc*. **417** 325 (1996)
269. F D'Acapito, F Zontone *J. Appl. Crystallogr*. **32** 234 (1999)
270. G Capiccio, M Leoni, P Scardi, V Sessa, M L Terranova *Adv. Cryst. Growth* **203** 285 (1996)
271. J Reiche, D Janietz, T Baberka, D Hofmann, L Brehmer *Nucl. Instrum. Methods Phys. Res. B* **97** 416 (1995)
272. D Jacqemain, S G Wolf, F Leveiller, M Deutsch, K Kjaer, J Als-Nielsen, M Lanav, L Leiserowitz *Angew. Chem., Int. Ed. Engl*. **31** 130 (1992)
273. J F Legrand, A Renault, O Konovalov, E Chevigny, J Als-Nielsen, G Grübel, B Berge *Thin Solid Films* **248** 95 (1994)
274. C Bohm, F Leveiller, D Jacquemain, H Mohwald, K Kjaer, J Als-Nielsen, I Weissbuch, L Leiserowitz *Langmuir* **10** 830 (1994)
275. I Weissbuch, I Kuzmenko, M Berfeld, L Leiserowitz, M Lahav *J. Phys. Org. Chem*. **13** 426 (2000)
276. A Naudon, D Thiaudiere *J. Appl. Crystallogr*. **30** 822 (1997)
277. P Borthen, H H Strehblow *J. Phys. IV, Colloq. (France)* **7** C2-187 (1997)
278. K Tani, T Nanjyo, S Masui, H Saisho *J. Synchr. Radiat*. **5** 1141 (1998)
279. J Kowai, S Hayakawa, Y Kitajima, Y Gohshi *Anal. Sci*. **11** 519 (1995)
280. E Dartyge, A Fontaine, F Baudelet, C Giorgetti, S Pizzini, H Tolentiono *J. Phys. I (France)* **2** 1233 (1992)
281. G P Hastie, J Johnstone, K J Roberts, D Fisches *J. Cryst. Growth* **166** 67 (1996)
282. H Ade, B Hsiao *Science* **262** 1427 (1993)
283. N V Bausk, S B Erenburg, N F Yudanov, L N Mazalov *J. Phys. IV, Colloq. (France)* **7** C2-1167 (1997)
284. N V Bausk, S B Erenburg, N F Yudanov, L N Mazalov *Zh. Strukt. Khim*. **36** 932 (1995) [b]
285. V A Shuvaeva, K Yanagi, K Sakaue, H Terauchi *J. Synchr. Radiat*. **6** 367 (1999)
286. N V Bausk, L N Mazalov, A I Rykov, V F Vratskikh, V P Predtechenskii, Yu S Varlamov *Bull. Mater. Sci*. **14** 865 (1991)
287. N V Bausk, L N Mazalov, A I Rykov, V F Vratskikh, M R Predtechenskii, Yu D Varlamov *Zh. Strukt. Khim*. **33** 88 (1992) [b]
288. G Schütz, W Wagner, W Wilhelm, P Kienele, R Zeller, R Frahm, G Materlik *Phys. Rev. Lett*. **58** 737 (1987)
289. S G Ovchinnikov *Usp. Fiz. Nauk* **42** 869 (1999) [a]
290. J B Kortright, D D Awschalom, J Stohr, S D Bader, Y U Idzerda, S S Parkin, I K Schuller, H-C Siegmann *J. Magn. Magn. Mater*. **207** 7 (1999)
291. J Stöhr *J. Electron Spectrosc. Relat. Phenom*. **75** 253 (1995)
292. J Stlhr, R Nakajima *J. Phys. IV, Colloq. (France)* **7** C2-47 (1997)
293. E Dartyge, F Baudelet, C Giorgetti, S Odin *J. Alloys Compd*. **277** 526 (1998)
294. G A Sawatzky, F M F De Groot, S Altieri, N B Brookes, S L Hulbert, J B Goedkoop, B Sinkovic, E Shekel, L H Tjeng, R Hesper, E Pellegrin *J. Electron Spectrosc. Relat. Phenom*. **92** 11 (1998)
295. L Alagna, T Prosperi, S Turchini, J Goulon, A Rogalev, C Goulon-Ginet, C R Natoli, R D Peacock, B Stewart *Phys. Rev. Lett*. **80** 4799 (1998)
296. J Goulon, C Goulon-Ginet, A Rogalev, V Gotte, C Malgrange, C Brouder, C R Natoli *J. Chem. Phys*. **108** 6394 (1998)
297. B Stewart *J. Phys. IV, Colloq. (France)* **4** C9-179 (1994)
298. J C Sutherland, in *Circular Dichroism: Conformational Analysis of Biomolecules* (Ed. G D Fasman) (New York: Plenum, 1996) p. 599
299. G Schütz, D Ahlers *J. Phys. IV, Colloq. (France)* **7** C2-59 (1997)

300. G Schümtz, P Fischer, K Attenkofer, M Knulle, D Ahlers, S Stahler, C Detlefs, H Ebert, F M F De Groot *J. Appl. Phys.* **76** 6453 (1994)
301. S Imada, S Suda *J. Electron Spectrosc. Relat. Phenom.* **92** 1 (1998)
302. G Schonhense *J. Phys., Condens. Matter* **11** 9517 (1999)
303. V A Belyakov, V E Dmitrienko *Usp. Fiz. Nauk* **158** 679 (1989) [a]
304. V E Dmitrienko, in *Problemy Sovremennoi Kristallografii. Strukturnye Issledovaniya Kristallov* (Problems in Modern Crystallography. Structural Investigation of Crystals) (Moscow: Nauka, 1996) p. 84
305. A Kirfel, A Petcov *Acta Crystallogr., Sect. A* **48** 247 (1992)
306. A Kirfel, W Morgenroth *Acta Crystallogr., Sect. A* **49** 35 (1993)
307. J Baruchel, M Shlenker, in *X-Rays and Neutrons Dynamical Diffraction. Theory and Applications* (Ed. A Authier) (New York: Plenum, 1996) p. 187
308. M Sacchi *Surf. Rev. Lett.* **7** 175 (2000)
309. J Als-Nielsen, G Materlik *Phys. Today* **48** 34 (1995)
310. J V Smith *Analyst* **120** 1231 (1995)
311. A R Gerson, P J Halfpenny, S Pizzini, R Ristic, K J Roberts, D B Sheen, J N Sherwood *X-Ray Charact. Mater.* 105 (1999)
312. S K Sinha *Jpn. J. Appl. Phys., Part 1* **38** 1 (1999)
313. B S Clausen *Catal. Today* **39** 293 (1998)
314. J M Thomas, G N Greaves *Catal. Lett.* **20** 337 (1993)
315. B S Clausen, H Topsoe, R Frahm *Adv. Catal.* **42** 315 (1998)
316. N Binsted, M J Pack, M G Weller, J Evans *J. Am. Chem. Soc.* **118** 10200 (1996)
317. W Bras, G R Mant, G E Derbyshire, D Bouch, J Sheldon, J Dingis, J Ryan *Rev. Sci. Instrum.* **66** 1314 (1995)
318. S Husnain, K O Hodgson *J. Synchr. Radiat.* **6** 852 (1999)
319. H Oyanagi, I Owen, M Grimshaw, P Head, M Martini, M Saito *Rev. Sci. Instrum.* **66** 5477 (1995)
320. I Haita, H Takahashi, S Matuoka, Y Amemiya *Thermochim. Acta* **253** 149 (1995)
321. O M Wilkin, N A Young *J. Synchr. Radiat.* **6** 204 (1999)
322. M Richter *J. Electron Spectrosc. Relat. Phenom.* **76** 21 (1995)
323. J-E Rubensson, J Lüning, M Neeb, B Kuepper, S Eisebitt, W Eberhardt *Phys. Rev. Lett.* **76** 3919 (1996)
324. R A Bartynski, E Jensen, S L Hulbert, C-C Kao *Prog. Surf. Sci.* **53** 155 (1996)
325. S Vinton, S P Harte, G Charlton, V R Dhanak, G Thornton, W B Westerveld, J van Eck, J van de Weg, H G M Heideman, J B West *Chem. Phys. Lett.* **252** 107 (1996)
326. H Biehl, K J Boyle, D M Smith, R P Tuckett *Chem. Phys.* **214** 357 (1997)
327. U Becker *J. Electron Spectrosc. Relat. Phenom.* **112** 47 (2000)
328. A R Ravishankara, S Solomon, A A Turnipseed, R F Warren *Science* **259** 194 (1993)
329. R J Nelmes, M I McMahon *J. Synchr. Radiat.* **1** 69 (1994)
330. H K Mao, R J Hemley *High Press. Res.* **14** 257 (1996)
331. M I McMahon *Mater. Sci. Forum* **278** 1 (1998)
332. K Brister *Rev. Sci. Instrum.* **68** 1629 (1997)
333. J P Itié, A Polian, D Martinez, V Briois, A Di Cicco, A Filipponi, A San Miguel *J. Phys. IV, Colloq. (France)* **7** C2-31 (1997)
334. A San Miguel, J P Itié, A Polian *Physica B* **208 – 209** 506 (1995)
335. S K Saxena, L S Dubovinsky, P Haggvist, Y Cerenius, G Shen, H K Mao *Science* **269** 1703 (1995)
336. M Hanfland, U Schwarz, K Syassen, K Takemura *Phys. Rev. Lett.* **82** 1197 (1999)
337. K J Kingma, H K Mao, R J Hemley *High Press. Res.* **14** 363 (1996)
338. W Utsumi, T Muzutani, O Shimomura, T Taniguchi, S Nakano, N Nishiyama, K Funakoshi, in *International Union Crystallography XVIIIth Congress and General Assembly (Collected Abstracts), Glasgow, 1999* P08.CC.007
339. Ch-S Yoo, in *International Union Crystallography XVIII Congress and General Assembly. (Collected Abstracts)* Glasgow 1999. M08.OC.004
340. P Loubeyre, R Le Toullec, D Häusermann, M Hanfland, R J Hemley, H K Mao, L W Finger *Nature (London)* **383** 702 (1996)
341. D Hüusermann *Phys. Scr.* **66** 102 (1996)
342. Somoyazulu, L W Finger, R J Hemley, H K Mao *Science* **271** 1400 (1996)
343. L J Parker, T Aton, J B Badding *Science,* **273** 95 (1996)
344. S H Tolbert, A P Alivisatos *Ann. Rev. Phys. Chem.* **46** 595 (1995)
345. R J Nelmes, M I McMahon, in *Semiconductors and Semimetals* (Eds T Suski, W Paul) (New York: Academic Press, 1998) . 34
346. H Wilhelm, C Cros, E Reny, G Demazlau, M Hanfland *J. Mater. Chem.* **8** 2729 (1998)
347. Y Soldo, J L Hazemann, D Aberdam, M Inui, K Tamura, D Raoux, E Pernot, J F Jal, J Dupuy-Philon *Phys. Rev. B* **57** 258 (1998)
348. D Andrault, J Peryronnean, F Farges, J P Itié *Physica B* **208 – 209** 327 (1995)
349. C Roux, D M Adams, J P Itié, A Polian, D N Hendrickson, M Verdaguer *Inorg. Chem.* **35** 2846 (1996)
350. D M Pfund, J C Darab, J L Fulton, Y Ma *J. Phys. Chem. B* **98** 13 102 (1994)
351. J L Fulton, D M Pfund, S L Wallen, M Newville, E A Stern, Y J Ma *J. Chem. Phys.* **105** 2161 (1996)
352. S L Wallen, B J Palmer, D M Pfund, J L Fulton, M Newville, Y J Ma, E A Stern *J. Phys. Chem. A* **101** 9632 (1997)
353. K Jannsen, F C Adams, M L Rivers, K W Jones *Scanning Microsc. Suppl.* **7** 191 (1997)
354. G E Ice *X-Ray Spectrom.* **26** 315 (1997)
355. A Iida *X-Ray Spectrom.* **26** 359 (1997)
356. *J. Electron Spectrosc. Relat. Phenom.* **84** (1 – 3) (Special Issue) (1997)
357. C Riekel *Rep. Prog. Phys.* **63** 233 (2000)
358. P Chevallier, P Populus, A Firsov *X-Ray Spectrom.* **28** 348 (1999)
359. G Margaritondo *Jpn. J. Appl. Phys., Part 1* **38** 8 (1999)
360. M Kiskinova, M Marsi, E Di Fabrizio, M Gentili *Surf. Rev. Lett.* **6** 265 (1999)
361. N Fukumoto, Y Kobayashi, M Kurahashi, I Kojima *Spectrochim. Acta, B* **54** 91 (1999)
362. T Ungar, J I Langford, R J Cernik, G Voros, R Pflaumer, G Oszlanyi, I Kovacs *Mater. Sci. Eng., A* **247** 81 (1998)
363. A A MacDowell, C H Chang, H Padmore, J R Patel, A C Thompson *Mater. Res. Soc.* **524** 55 (1998)
364. A Snigirev, I Snigireva, C Riekel, A Miller, L Wess *J. Phys. IV, Colloq. (France)* **3** 443 (1993)
365. A Rindby, P Voglis, P Engström *Biomaterials* **19** 2083 (1998)
366. C Riekel, A Cedola, F Heidelbach, K Wagner *Macromolecules* **30** 1033 (1997)
367. S M Kuznetsov, I I Snigireva, A A Snigirev, P Engström, C Riekel *Appl. Phys. Lett.* **65** 1 (1994)
368. J D Denlinger, E Rotenberg, T Warwick, G Visser, J Nordgren, J-H Guo, P Skytt, S D Kevan, K S McCutcheon, D Shuh, J Bucher, N Edelstein, J G Tobin, B P Tonner *Rev. Sci. Instrum.* **66** 1342 (1995)
369. C Riekel, P Engström, C Martin *J. Macromol. Sci. Phys.* **37** 587 (1998)
370. M Müller, C Czihak, G Vogl, P Fratzl, H Schober, C Riekel *Macromolecules* **31** 3953 (1998)
371. Z H Cai, W Rodrigues, P Ilinsky, D Legnini, B Lai, W Yun, E D Isaacs, K E Lutterford, J Grenko, R Glew, S Stutz, J Vandenberg, R People, M A Alam, M Hybertsen, L J P Ketelsen *Appl. Phys. Lett.* **75** 100 (1999)
372. E D Isaacs, M Marcus, G Aeppli, X D Xiang, X D Sun, P Schultz, H K Kao, G S Kargile, R Haushalter *Appl. Phys. Lett.* **73** 1820 (1998)
373. P A Montano, H Oyanagi (Eds) *In Situ Synchrotron Radiation Research in Material Science*; *MRS Bull.* **24** (1) (Special Issue) (1999)
374. P Norby *Mater. Sci. Forum* **228** 147 (1996)
375. D O'Hare, J S O Evans, R J Francis, P S Halasyamoni, P Norby, J Hanson *Microp. Mesopor. Mater.* **21** 253 (1998)
376. T Shido, R Prins *Curr. Opin. Solid State Mater. Sci.* **3** 330 (1998)
377. J M Corker, F Levebrre, C Lecuyer, V Dufaud, F Quignard, A Choplin, J Evans, J-M Bisset *Science* **271** 966 (1996)
378. G Sankar, J M Thomas, D Waller *J. Phys. Chem.* **96** 7485 (1992)
379. N Yoshida, T Matsushita, S Soigo, H Oyanagi, H Hashimoto, M Fujimoto *J. Chem. Soc., Chem. Commun.* 354 (1990)
380. L M Murphy, B R Dobson, M Neu, C A Ramsdale, R W Strange, S S Hasnain *J. Synchr. Radiat.* **2** 64 (1995)
381. A Dent, J Evans, M Newton, J Corke, J A Russell, M B Abdul-Rahman, S Fiddy, R Mathew, R Farrow, G Salvini, P Atkinson *J. Synchr. Radiat.* **6** 381 (1999)
382. M Hagelstein, A Fontaine, J Goulon *Jpn. J. Appl. Phys., Part 1* **32** 240 (1993)

383. S G Nikitenko, B P Tolochko, A N Aleshaev, G N Kulipanov, S I Mishnev *J. Phys. IV, Colloq. (France)* **7** C2-549 (1997)
384. Y Inada, H Hayashi, S Funahashi, M Nomura *Rev. Sci. Instrum.* **68** 2973 (1997)
385. P D Cobden, B E Nieuwenhuys, F Esch, A Baraldi, G Vomelli, S Lizzit, M Kiskinova *Surf. Sci.* **416** 264 (1998)
386. J Harford, J Squire *Rep. Prog. Phys.* **60** 1723 (1997)
387. A A Vazina, P M Sergienko, A M Gadzhiyev, V M Aulchenko, Yu V Usov, M V Yasenev *Nucl. Instrum. Methods Phys. Res. A* **359** 220 (1995)
388. K Moffat *Acta Crystallogr., Sect. A* **54** 833 (1998)
389. K Moffat *Trans. Am. Crystallogr. Assoc.* **34** 39 (2000)
390. V Srajer, T-Y Teng, T Ursby, C Pradervand, Z Ren, S Adachi, W Schieldkamp, D Bourgeois, M Wulff, K Moffat *Science* **274** 1726 (1996)
391. M Wulff, F Schotte, G Naylor, D Bourgeois, K Moffat, G A Mourou *Nucl. Instrum. Methods Phys. Res. A* **398** 69 (1997)
392. T-Y Teng, V Črajer, K Moffat *Biochemistry* **36** 12087 (1997)
393. V V Mikhailin *Nucl. Instrum. Methods Phys. Res. A* **448** 461 (2000)
394. J B Hasting, S L Hulbert, G P Williams (Eds) *Proceedings of the 5th International Conference on Synchrotron Radiation Instrumentation*; *Rev. Sci. Instrum.* **66** (2) (1995)
395. G N Kulipanov, V F Pindyurin (Eds) *Proceedings of the 10th National Synchrotron Radiation Conference* (*SR-94*); *Nucl. Instrum. Methods Phys. Res. A* **359** (1 – 2) (1995)
396. K Baberschke, D Arvanitis (Eds) *Proceedings of the 8th International Conference on X-Ray Absorption Fine Structure*; *Physica B* **208** – **209** (1995)
397. *Proceedings of the 9th International Conference on X-Ray Absorption Fine Structure*. (Eds. J.Goulon C.Goulon-Ginet N.B.Brookes). *J. Phys. IV Colloq. (France)* **7** (C2) 1997
398. *Proceedings of the 11th National Synchrotron Radiation Conference (SR-96). (Ed. G.N.Kulipanov). Nucl. Instrum. Methods Phys. Res., A* **405** (23) 1998
399. S S Hasnain, R Helliwell, H Kamitsubo (Eds) *Proceedings of the 6th International Conference on Synchrotron Radiation Instrumentation*; *J. Synchr. Radiat.* **5** (3) (1998)
400. A Kakizaki, A Kotani (Eds) *Proceedings of the 6th International Symposium 'Frontiers in Synchrotron Radiation Spectroscopy'*; *J. Electron. Spectrosc. Relat. Phenom.* **92** (1 – 3) (1998)
401. W Pazkowicz, E Sobczak (Eds) *Proceeding of the 4th Inthernational School and Symposium on Synchrotron Radiation in Natural Science; J. Alloys Compd.* **286** (1998)
402. S S Hasnain, R Helliwell, H Kamitsubo (Eds) *Proceedings of the 10th International Conference on X-ray Absorption Fine Structure*; *J. Synchr. Radiat.* **6** (3) (1999)
403. G N Kulipanov (Ed.) *Proceedings of the 12th National Synchrotron Radiation Conference* (*SR-98*); *Nucl. Instrum. Methods Phys. Res. A* **448** (1 – 2) (2000)
404. S S Hasnain, H Kamitsubo, D M Mills (Eds) *Proceedings of the 11th International Conference on X-Ray Absorption Fine Structure*; *J. Synchr. Radiat.* **8** (2) (2001)
405. J L Jordan-Sweet *IBM J. Res. Dev.* **44** 457 (2000)

[a] — *Physics-Uspekhi (Engl. Transl.)*
[b] —*J. Struct. Chem. (Engl. Transl.)*

Russian Chemical Reviews **70** (5) 405 – 424 (2001) © 2001 Russian Academy of Sciences and Turpion Ltd

DOI 10.1070/RC2001v070n05ABEH000644

Regio- and stereochemistry of 1,3-dipolar cycloaddition of nitrile oxides to alkenes

R P Litvinovskaya, V A Khripach

Contents

I.	Introduction	405
II.	Cycloaddition of nitrile oxides to allylic and homoallylic alcohols and their derivatives	406
III.	Cycloaddition of nitrile oxides to unsaturated amines, amides and related compounds	407
IV.	Cycloaddition of nitrile oxides to acrylates, crotonates and acrylamides	409
V.	Cycloaddition of nitrile oxides to alkenes in the presence of Lewis acids	412
VI.	Cycloaddition of nitrile oxides to unsaturated aldehyde derivatives	414
VII.	Alkenylboronates in cycloaddition reactions with nitrile oxides	415
VIII.	Vinyl- and allylphosphine oxides in cycloaddition reactions with nitrile oxides	416
IX.	The nitrile oxide method in carbohydrate chemistry	416
X.	Steroid alkenes as dipolarophiles in cycloaddition reactions with nitrile oxides	417
XI.	Other examples of cycloaddition of nitrile oxides to acyclic alkenes	420

Abstract. The published data on the chemistry of intermolecular 1,3-dipolar cycloaddition of nitrile oxides to different types of alkene derivatives are systematised. Various aspects of stereo- and regiochemistry of this reaction are considered. The bibliography includes 182 references.

I. Introduction

1,3-Dipolar cycloaddition of nitrile oxides to unsaturated systems is commonly used in the synthesis of heterocyclic compounds.[1–5] This is due to at least two reasons. First, nitrile oxides react with a great diversity of dipolarophiles by virtue of their high reactivities [1] and, second, the reaction products, *viz*., isoxazoles and 4,5-dihydroisoxazoles, can be used as starting compounds for various synthetic transformations including synthesis of natural compounds and their analogues.[2,3]

This review summarises the published data on 1,3-dipolar cycloaddition of nitrile oxides to alkenes. Problems of regio- and stereochemistry of intermolecular cycloaddition (as a rule, to non-cyclic dipolarophiles) are considered in more detail.

Nitrile oxides are usually generated by treating hydroximoyl chlorides with triethylamine, by dehydrating primary nitro derivatives with isocyanates or by oxidising aldoximes with *N*-chlorosuccinimide.[6–8] New effective approaches to the generation of nitrile oxides have been developed in recent years, *e.g*., from aldoximes under the action of sodium hypochlorite,[9] from hydroximoyl chlorides in the presence of silver(I) acetate [10] or from conjugated nitroalkenes under the action of titanium(IV) chloride.[11] The latter approach allows preparation of α-functionalised nitrile oxides.

R P Litvinovskaya, V A Khripach Institute of Bioorganic Chemistry, National Academy of Sciences of Belarus, ul. Akad. Kuprevicha 5/2, 220141 Minsk, Belarus. Fax (37-517) 264 86 47. Tel. (37-517) 263 76 15. E-mail: litvin@ns.iboch.ac.by (R P Litvinovskaya)
Tel. (37-517) 264 76 48. E-mail: khripach@ns.iboch.ac.by (V A Khripach)

Received 7 December 2000
Uspekhi Khimii **70** (5) 464 – 485 (2001); translated by R L Birnova

Usually, it is only regiochemistry that is the matter of discussion in the cycloaddition of nitrile oxides to terminal alkenes, *viz*., the formation of a single regioisomer, *i.e*., 3,5-disubstituted ($R^1 = H$) or 3,5,5-trisubstituted (R^1 = Alk, Ar, *etc*.) 4,5-dihydroisoxazole.[12–17]

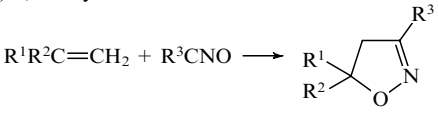

The analysis of stereochemical aspects of these reactions points to their low stereoselectivities [18,19] unless carried out under special conditions (see below).

Non-symmetrical 1,2-disubstituted alkenes usually give two regioisomers.[20–24] However, reactions of certain compounds manifest high regioselectivities with nitrile oxides. Thus the addition of acetonitrile oxide to the coumarin derivative **1** gave the regioisomeric dihydroisoxazoles **2a** and **3a** in a 75 : 3 ratio, whereas 4-methoxybenzonitrile oxide afforded exclusively the regioisomer **3b**.[25]

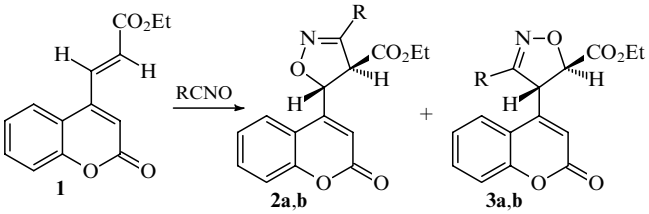

R = Me (**a**), 4-$MeOC_6H_4$ (**b**).

Attempts at performing asymmetric 1,3-dipolar cycloaddition using chiral alkenes or nitrile oxides have been undertaken, however, stereoselective introduction of a new asymmetric centre using chiral nitrile oxides was only partly successful.[26–29] Thus the reaction of the optically active nitrile oxide **4** with the alkene **5** afforded a mixture of diastereomers **6** in a 2.5 : 1 ratio.[30] Reactions with other nitrile oxides yield nearly equimolar mixtures of diastereomers.

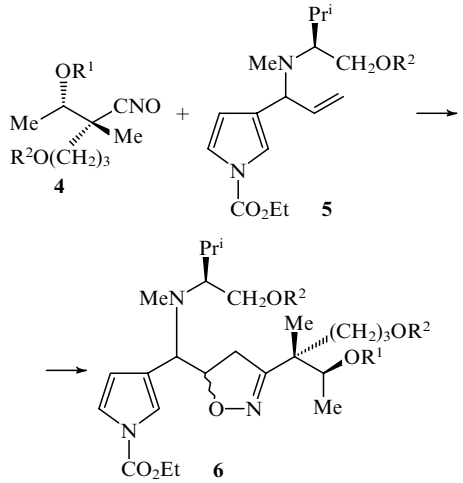

$R^1 = CH_2OMe$; $R^2 = Bu^tMe_2Si$.

II. Cycloaddition of nitrile oxides to allylic and homoallylic alcohols and their derivatives

Allylic alcohols and their esters with a chiral centre in the α-position are often used as dipolarophiles; however, the diastereoselectivity of these reactions is not always high. As a rule, reactions of nitrile oxides with allylic alcohols give predominantly *syn*-isomers.[31,32] Cycloaddition of alkenes containing protected hydroxy groups in the α-position to the double bond increases the stereoselectivity.[33–36] The reaction of the nitrile oxide **7a** with (*S*)-(+)-*O*-isopropylidenebut-3-ene-1,2-diol (**8**) is among the first examples of regioselective cycloaddition of nitrile oxides to allylic alcohols; this resulted in the *anti*-adduct **9a** (**9a** : **10a** = 4 : 1) as the main product.[35] In this case, the stereochemistry of the cycloaddition reaction is governed by the oxygen-containing substituent in the allylic position.

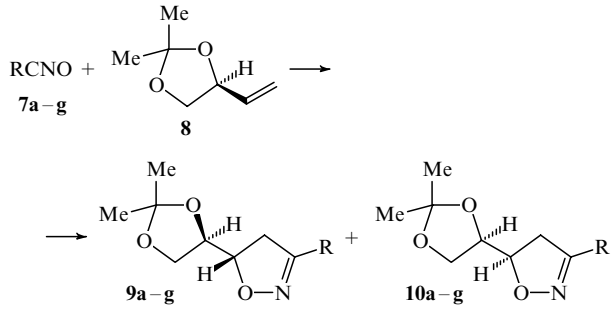

R = EtO_2C (**a**), Me (**b**), $THPOCH_2$ (**c**) (THP =), Ph (**d**),

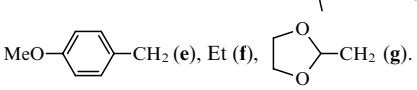

Nitrile oxides **7b–g** also react with compound **8** with high diastereoselectivities with the predominant formation of *anti*-addition products (80%–94%); the selectivity of this reaction is only weakly dependent on the structure of the nitrile oxide.[34] But-3-ene-1,2-diol containing unprotected hydroxy groups manifests low diastereoselectivity in reactions with nitrile oxides, this is somewhat higher with dioxolanes analogous to compound **8**.[33] The highest diastereoselectivity is achieved with spiroketals of vicinal diols.[36] It is assumed[34] that the cycloaddition proceeds predominantly *via* the transition state corresponding to the conformer **A** (the Kozikovsky model). Nitrile oxide attacks the C=C bond on the side opposite to the C–O bond (indicated by an arrow). Thus, the allylic oxygen atom displays an *anti*-directing (the so-called antiperiplanar) effect. According to the calculations made by Houk *et al.*,[37] this is due to minimisation of secondary interactions of the non-bonding orbitals.

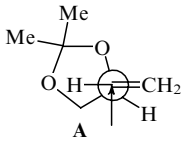

The cycloadditions of pivalo- and benzonitrile oxides to α-hydroxyallylsilane (**11a**) and its *O*-derivatives **11b–g** have been studied.[31,38] Compound **11a** yields a mixture of *syn*- and *anti*-adducts with a small excess of the *syn*-isomer **13a**; with different acylated derivatives, the stereoselectivity of this reaction is weakly affected, whereas silyl ether **11b** gives predominantly the *anti*-addition products **12b** (yield 94%).

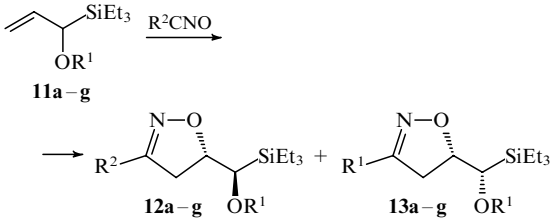

R^1 = H (**a**), $SiMe_2Bu^t$ (**b**), COMe (**c**), CO_2Me (**d**), 4-$MeOC_6H_4CO$ (**e**), COPh (**f**), 4-$NO_2C_6H_4CO$ (**g**); R^2 = Bu^t, Ph.

It was shown[31] that the *syn*-selectivity of cycloaddition of nitrile oxides, which is characteristic of the majority of allylic alcohols studied so far, decreases with the increase in the proton-accepting capacity of the solvent used.

The stereochemistry of cycloaddition of benzonitrile oxides to allylic alcohols and their ethers, allylic chlorides and 3,3-diphenylprop-1-ene has been studied in detail.[39,40]

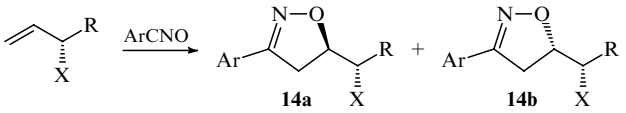

R = Me, Ph, Et, Bu^t; X = OH, OMe, OBn, OTHP, $OSiMe_2Bu^t$, Cl, Ph, Me; Ar = Ph, 4-$NO_2C_6H_4$.

In this case, too, allylic ethers react with nitrile oxides in a stereoselective manner to give the *anti*-addition products **14a** (up to 95% for X = OMe, $OSiMe_2Bu^t$); the selectivity of this reaction increases with the increase in the size of the substituent R. Alcohols yield predominantly the *syn*-addition products **14b**, albeit with low selectivity. The replacement of the ether allylic substituent by Cl, Ph or Me results in a complete or partial loss of stereoselectivity. It is of note that the ratio of the diastereomers strongly depends on the nature of the substituent in the nitrile oxide. Such a behaviour of allylic halides has been described by other authors.[41,42]

Based on the experimental data[37,43,44] and the calculations of transition state models of 1,3-dipolar cycloaddition of nitrile oxides to alkenes, it was suggested that the majority of transition states are structurally close to that shown in Fig. 1*a*. In this case, the substituents in the allyl position can be localised outside, inside or in the *anti*-position with respect to the C–O bond formed.

The main product is formed from the transition state **A** where the largest substituent (L) is in the *anti*-position, whereas the medium substituent (M) is located inside (Fig. 1*b*). The transition state **B** (Fig. 1*c*) yields the minor isomer. The outside position is more sensitive to steric factors due to the interaction of nitrile oxide with the oxygen atom. The electronic characteristics of substituents play a prominent role. Since cycloaddition of nitrile oxides is related to weakly electrophilic reactions, the donor substituent in the allylic position of the transition state is preferably in the *anti*-position, while the acceptor substituents are

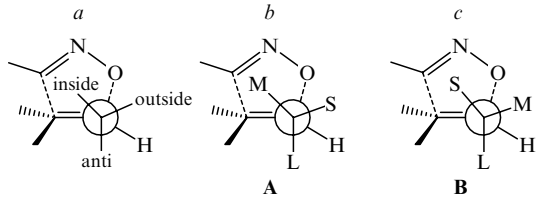

Figure 1. The transition state models in the reaction of 1,3-dipolar addition of nitrile oxides to alkenes.[43,44]
Designations for substituents: L is large, M is medium, S is small.

localised either inside or outside (in order to minimise electronic interactions).[39]

This transition state model commonly referred to as the Houk model provides a rationale for the effects of substituents on the stereochemistry of 1,3-dipolar cycloaddition.

The formation of a hydrogen bond between the oxygen atom of the nitrile oxide and the hydroxy groups of cyclic allylic alcohols results in stabilisation of the *threo*-transition state **A** (Fig. 1*b*). The relatively low stereoselectivities in the case of acyclic allylic alcohols can be assigned to the fact that conformations **A** and **B** compete with one another in the transition state.[43,44]

It is of note that the increase in stereoselectivity with the increase in the size of the substituent R in the allylic alcohol fits well the Houk model, but cannot be explained in terms of the Kozikovsky transition state model.[34]

Thus the cycloaddition of nitrile oxides to terminal alkenes with different sizes of substituents in the allylic positions gives predominantly the diastereomers **15**. The stereoselectivity depends on the relative sizes of the medium (M) and large (L) groups and varies from very low (M = Me, L = Et, **15**:**16** = 1:1) to moderate (M = Me, L = Bu^t, **15**:**16** = 4:1). The same tendency is observed where M = AlkO group, although the stereoselectivity is somewhat higher in this case. The *anti*-diastereomer **17** usually predominates over the *syn*-diastereomer **18** (~3:1). For R^2 = Bu^i, it is the *anti*-isomer that is predominantly formed. The ratios of *syn*- to *anti*-products in these reactions change little with the change in steric and electronic factors in both the nitrile oxide substituent R^3 and the oxygen atom substituent R^1.[39]

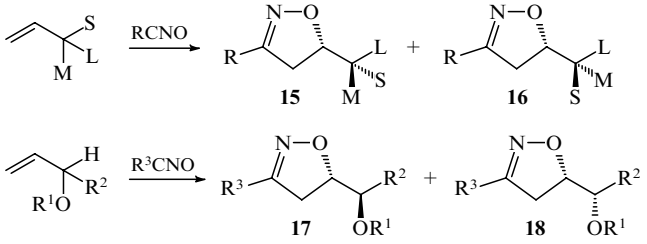

Assuming that the steric and electronic effects of the trimethylsilyl group[43] in the allylic position favour the formation of *anti*-cycloadducts, the behaviour of silanes of the type **19** has been studied in the reaction with nitrile oxides.[45]

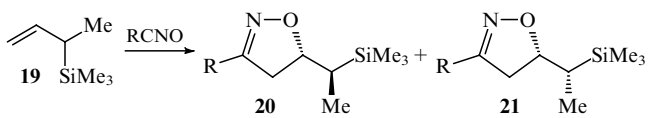

R = Ph, Bu^t.

However, the diastereoselectivity of this reaction was low, although the main product **20** (60% – 65%) was formed in accord with the Houk model. Thus, high diastereoselectivity is difficult to achieve in the absence of an oxygen-containing substituent in the allylic position,.

Recent studies have shown[46] that the ratio of 5- and 4-silyl-substituted adducts **22a** and **22b** obtained by cycloaddition of nitrile oxides to trialkoxy(vinyl)silanes depends on the nature of substituents at the silicon atom and the method used to generate nitrile oxides. This reaction is especially selective for R^1 = Me$_3$SiO and R^2 = Me (**22a**:**22b** = 10:1).

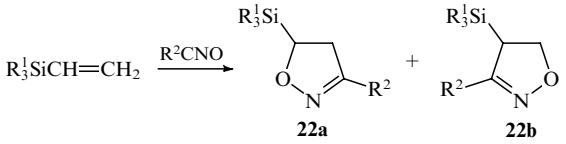

R^1 = MeO, EtO, Me$_3$SiO, $\overline{\text{NCH}_2\text{CH}_2\text{O}}$; R^2 = Me, Et, Ph.

It was shown[47] that cycloaddition of nitrile oxides to 1,1-disubstituted alkenes **23** containing a hydroxy- or an alkoxy group in the allylic position (the so-called Baylis – Hillman adducts) gives predominantly the *syn*-isomers **24**, the stereoselectivity of the reaction being dependent on the substituent R.

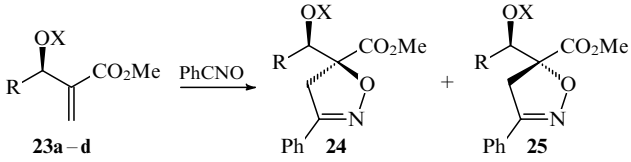

Compound **23**	R	X	Ratio **24**:**25**	Compound **23**	R	X	Ratio **24**:**25**
a	Me	H	3:1	**c**	Pr^i	H	32:1
		Bu^{t}Me$_2$Si	6:1			Bu^{t}Me$_2$Si	7:1
		Ac	1:1			Ac	9:1
b	Pr^n	H	12:1	**d**	Ph	H	2:1
		Bu^{t}Me$_2$Si	7:1			Bu^{t}Me$_2$Si	4:1
		Ac	3:1			Ac	1:1

III. Cycloaddition of nitrile oxides to unsaturated amines, amides and related compounds

The directing effect of the nitrogen atom in the allylic position has been studied in less detail than that of the oxygen atom. Cycloadditions of nitrile oxides to vinylglycine and 2-aminobut-3-en-1-ol have been described;[48–50] the selectivities of these reactions were low. Reactions of nitrile oxides with (*R*,*S*)-4-vinyl-2-phenyl-4,5-dihydrooxazole (**26a**), *N*-benzyloxycarbonyl-(4*R*)-vinyl-2,2-dimethyloxazolidine (**26b**) and (2*R*)-(*N*-benzyloxycarbonyl)but-3-enol (**26c**) have been studied.[51] It was found that the selectivities of the reactions of the cyclic compounds **26a**,**b** are higher than that of the acyclic analogue **26c**; the *erythro*-isomers of the 4,5-dihydroisoxazoles **27** are the main products. The reaction of alkene **26a** with EtO$_2$CCNO oxide occurs with the highest selectivity (the **27**:**28** ratio is 82:18).

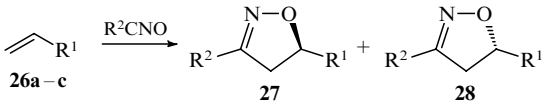

R^1 = 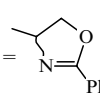 (**a**), 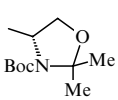 (**b**), 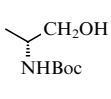 (**c**);

R^2 = Ph, EtO$_2$C, Br.

The effect of introduction of an asymmetric centre into the nitrile oxide component has been studied.[52] Cycloaddition of, *e.g.*, 4,5-dihydrooxazole-4-carbonitrile oxide **29**, to styrene yields a 1:1 mixture of 5-phenyl-4,5-dihydroisoxazoles **30** and **31**. This phenomenon is attributed to the large distance between the asymmetric centre of the molecule and the newly formed centre.

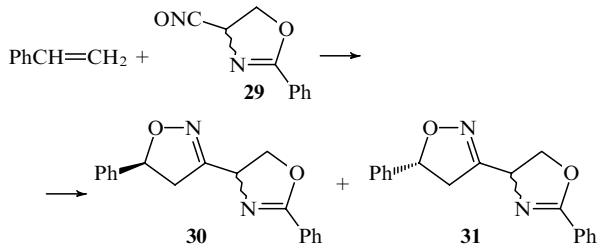

A series of 3-substituted cyclopentenes **32a–p** including amides **32f–p** have been studied as dipolarophiles;[53] variation of the amide acyl group made it possible to change the acidity of the proton in the amide substituent

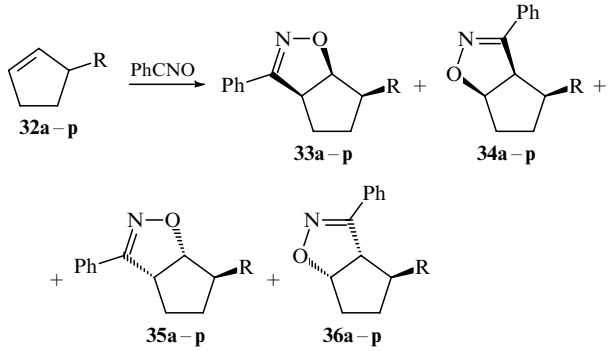

R = Me (**a**), NMe_2 (**b**), OMe (**c**), OAc (**d**), OH (**e**), NHCOPh (**f**), NMeCOPh (**g**), NHCOMe (**h**), $NHCOCF_3$ (**i**), $NHCOC_4F_9$ (**j**), NHCSMe (**k**), $NHCOC_6H_4OMe$-4 (**l**), $NHCOC_6H_4CF_3$-3 (**m**), $NHCOC_6H_4NO_2$-4 (**n**), $NHSO_2Me$ (**o**), $NHSO_2CF_3$ (**p**).

The content of cycloadducts formed as a result of the nitrile oxide attack on the alkene on the *anti*-side with respect to the substituent *R* exceeded 92% for compounds containing a methyl (**32a**), a dimethylamino (**32b**), a methoxy (**32c**) or an acetoxy (**32d**) group in the allylic position. The reaction of compound **32e** containing an allylic hydroxy group in diethyl ether afforded the adduct **33e** in 30% yield. This adduct was formed due to the formation of a hydrogen bond in the transition state of the reaction. If the reaction is carried out in benzene, which binds a proton more weakly than ether, the yield of the product **33e** increases to 50%. It is assumed that the hydroxy derivative **32e** forms a hydrogen bond with the solvent in ether and with nitrile oxide in benzene. The cycloaddition of the allylic benzamide **32f** yielded the adducts **33f** and **36f** (9 : 1), which can also be ascribed to the formation of a hydrogen bond in the transition state **C** of the cycloaddition.

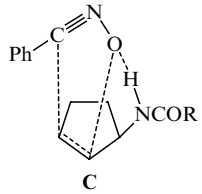

C

The model proposed sheds more light on the effects of solvents and amide substituents on the reaction rate. The product **33f** is predominantly formed in accordance with the model **C**, since the energy of its transition state decreases due to the formation of a hydrogen bond, while the energies of the transition states leading to the other three products are not changed. Therefore, the alkene **32f** should be more reactive than compounds unable to form hydrogen bonds with the nitrile oxide. Indeed, experiments on competitive reactions of compounds **32f**,**g** with pivalonitrile oxide yielded three products all of which were formed by cycloaddition of nitrile oxide to the alkene **32f** and the yield of the adduct of the type **33** reached 85%.

Competitive cycloadditions in benzene, 1,2-dimethoxyethane, dimethylformamide and hexamethylphosphoramide (HMPA) have been studied in order to establish the role of the solvent in this reaction.[54] It was found that the tertiary amide **32g** is much less reactive than the amide **32f**. In the case of the amide **32g**, the nature of the solvent influences neither the degree of conversion of the starting compounds, nor the ratios of the reaction products. Contrariwise, in the case of the amide **32f** the concentration of the reaction product **33f** increases significantly with the increase in the proton-donor capacity of the solvent; while the degree of conversion of the starting compounds changes only slightly. When the reaction was carried out in HMPA, the distribution of the reaction products was similar for both amides, which can be explained within the framework of the model **C**. Substitution of nitrile oxide for the solvent as a hydrogen-bonding acceptor decreases the rate of formation of the adduct **33f**, but the rates of formation of other reaction products change little, as a result of which the total degree of conversion decreases.

The model **C** suggests also that the yields of cycloadducts of the type **33** depend on the ability of the amide to form a hydrogen bond. Thus studies of amides **32h–p** revealed a marked tendency of an increase in the reaction selectivity with increase in the acidity of the amide proton. It is of interest that the sulfonamide group for which the acidity of the proton is the highest in this series, does not manifest high selectivity. In all probability, the bulky sulfonyl group prevents the formation of the transition state **C**. The effects of other factors should not be ruled out either.

These data show that the introduction of a disubstituted amide substituent into the allyl position of alkenes can change both the regio- and stereoselectivity of cycloaddition of nitrile oxides. The formation of hydrogen bonds in the transition state also plays a significant role in this effect.

It is of note that the selectivities of cycloaddition reactions with acyclic allylic amides studied earlier [55–58] are low. However, it was shown [59] that amide substituents influence the selectivity of cycloaddition stronger than the allylic hydroxy groups, this effect being especially well-pronounced in the case of cyclic amides.

The stereoselectivity of cycloaddition of the homoallylic amides **37a–d** to nitrile oxides is low in all cases, being comparable to that of the homoallylic alcohol **37e** and amine **37f**.

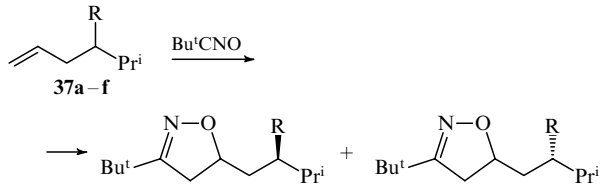

R = NHCOMe (**a**), $NHCOCF_3$ (**b**), $NHSO_2Me$ (**c**), $NHSO_2CF_3$ (**d**), OH (**e**), NH_2 (**f**).

The regioselectivity of cycloaddition of pivalonitrile oxide to allylic and homoallylic acyclic amides containing a disubstituted double bond is also low, *e.g.*, the regioisomers **38a** and **38b** are formed in a ~2 : 1 ratio.[59]

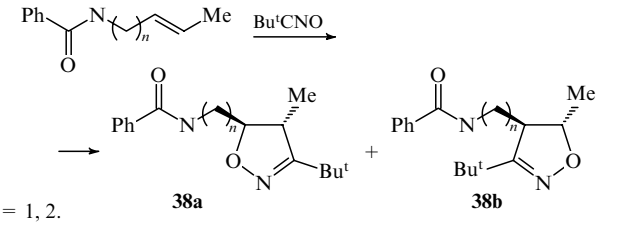

n = 1, 2.

At 20 °C, the cycloaddition occurs slowly; after 5 days, 70% of the original alkene remains unconsumed. At 80 °C, the yield is higher, but the regioselectivity is still very low. It was concluded [59] that the formation of a hydrogen bond in the transition state of acyclic systems is not critical, otherwise the amount of the regioisomer **38a** would have been much higher.

The hydroxy group plays the role of a proton donor when hydroxamic acid **39** is used as a dipolarophile. This reaction gave three isomers (**40** : **41** : **42** = 11 : 2 : 4). This suggests that the hydroxy group of hydroxamic acid is a better directing group than the hydroxy groups of alcohols and produces an effect comparable to that of the NH groups.[59]

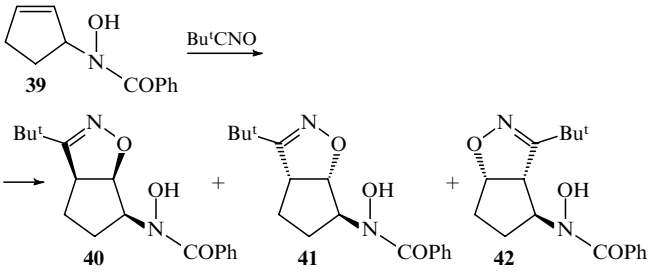

IV. Cycloaddition of nitrile oxides to acrylates, crotonates and acrylamides

An efficient approach to optically active dihydroisoxazoles might become both an alternative to the well-known aldol-type reactions and a new method for the synthesis of enantiomerically pure primary amines. Two approaches to asymmetric induction in the cycloaddition of nitrile oxides were used, *viz*., the introduction of an allylic asymmetric centre into a dipolarophile [34, 35] or the use of a chiral nitrile oxide.[27] The attempts at developing efficient procedures for diastereoselective 1,3-dipolar cycloaddition of nitrile oxides using menthyl ethers of allylic alcohols [60] were unsuccessful.

Thus 1,3-dipolar cycloaddition of 4-nitrobenzonitrile oxide with optically active acrylate **43a** and allylic ether **43b** yielded a mixture of the diastereomers **44** and **45**, the diastereomeric excess in favour of the latter was only 4%. The selectivity of the reaction of 4-nitrobenzonitrile oxide with the bornyl ester **43c** was somewhat higher. Pronounced stereoselectivity was observed only in the reaction of the sulfonamide derivatives **43d**,**e** with isobutyronitrile oxide and cyclohexanonitrile oxide. The diastereomers **44** having *S*-configurations of the newly formed chiral centres were the main isomers in these reactions.[61]

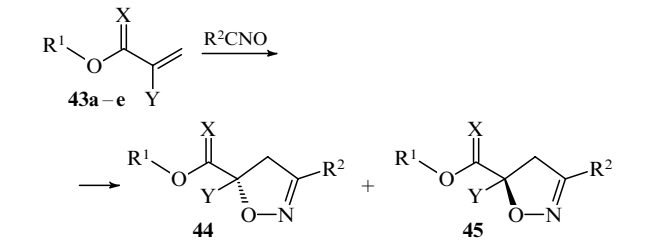

R^1	X	Y	Compound **43**	R^2	Ratio **44** : **45**
	O	H	**a**	4-$NO_2C_6H_4$	1 : 1
	CH_2	H	**b**	4-$NO_2C_6H_4$	1 : 1
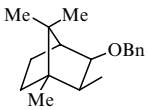	O	H	**c**	4-$NO_2C_6H_4$	1 : 1
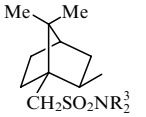	O	H	**d**	Bu^t	1 : 3
	O	H	**d**	Ph	1 : 4
	O	Me	**e**	4-$NO_2C_6H_4$	1 : 2
	O	Me	**e**	Bu^t	1 : 1
	O	Me	**e**	Ph	1 : 1

R^3 = Pr^i, C_6H_{11}

It is assumed [61] that the major diastereomers **44** result from the cycloaddition of the nitrile oxide to *s-cis*-confomers **A** of acrylates **43d**,**e**, whereas minor diastereomers are formed by addition to the *s-trans*-conformers **B**.

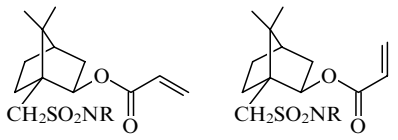

Later it was demonstrated [5] that the acrylates **43d**,**e** containing sulfonamide groups enter into other cycloaddition reactions predominantly in the *s-cis*-conformations.

Optically active 4,5-dihydroisoxazoles were synthesised by Akiyama *et al*.[62, 63] who added nitrile oxides to chiral acrylates where cyclitols played the role of auxiliary chiral substituents. The acrylates **46a**–**d** gave mixtures of dihydroisoxazoles **47** and **48** in the reactions with benzonitrile oxide (R^2 = Ph). The diastereoselectivities in the case of esters containing methoxymethyl (**46a**) and benzyl (**46b**) substituents were low, whereas the presence of bulky *tert*-butyldimethyl- and *tert*-butyldiphenylsilyl substituents in esters **46c**,**d** provided high π-facial selectivity. This stereochemical result is due to the fact that the major isomer **47** is formed from the *s-cis*-conformer of the acrylate. The bulky *tert*-butyldiphenylsilyl group effectively blocks the attack from the opposite side of the double bond. The maximum diastereoselectivity was achieved when the reaction was carried out in benzene.

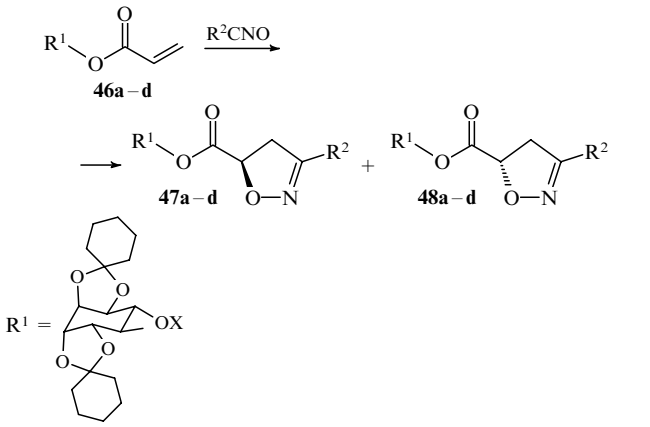

Compound **46**	X	R^2	Ratio **47** : **48**	Compound **46**	X	R^2	Ratio **47** : **48**
a	CH_2OMe	Ph	1 : 2	**d**	Bu^tPh_2Si	Me	10 : 1
b	Bn	Ph	1 : 1	**d**	Bu^tPh_2Si	Et	9 : 1
c	Bu^tMe_2Si	Ph	5 : 1	**d**	Bu^tPh_2Si	$n\text{-}C_5H_{11}$	9 : 1
d	Bu^tPh_2Si	Ph	19 : 1	**d**	Bu^tPh_2Si	Bu^t	10 : 1
				d	Bu^tPh_2Si	4-ClC_6H_4	9 : 1

The cycloaddition of 4-cyanobenzonitrile oxide to isobutyl vinylacetate affords a racemic mixture of dihydroisoxazoles.[64] It was found that the hydrolysis of this mixture using the lipase PS30 gave optically pure [4,5-dihydro-3-(4-cyanophenyl)isoxazol-5-yl]acetic acid with the *R*-configuration of the chiral centre.

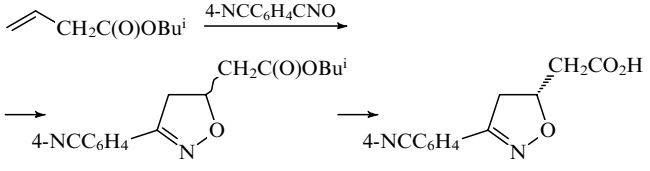

The addition of nitrile oxides to bornyl crotonates **49** (R^2 = Me) gave two regioisomeric cycloadducts **50** and **51**, each representing a mixture of diastereomers.[65]

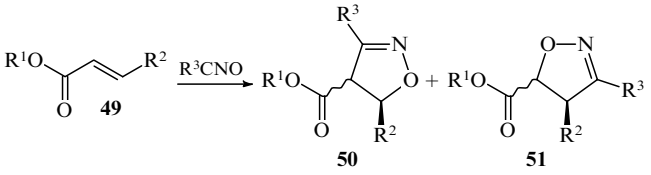

R^1	R^2	R^3	Yield of adducts (%)	
			50	**51**
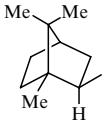	Me	Ph	65	22
	Me	Me	75	25
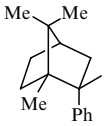	Me	Ph	56	26
	Me	Me	46	25
	H	Me	–	79
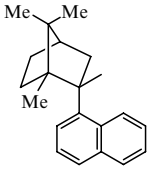	Me	Ph	63	28
	Me	Me	76	24
	H	Me	–	94

The diastereoselectivity of this reaction is > 80%. The diastereomers were separated and enantiomerically pure 4,5-dihydroisoxazoles were obtained after the cleavage of the ester bond. The regioselectivity of this reaction does not depend on either the substituent in the bornyl residue or the nature of nitrile oxide.

The addition of nitrile oxides to acrylates **49** (R^2 = H) results in an almost overriding formation of the sterically preferrable products **51**. The diastereoselectivity of this reaction is comparable to that of crotonates, which points to the similarity of the transition states generated by the attack of the dipole at the least shielded side of the alkene having an *s-cis*-conformation.[66]

The reaction of methyl cinnamate **52a** with nitrile oxides affords a mixture of regioisomeric dihydroisoxazoles **53a** and **54a** (4 : 1).[67] Quite unexpectedly, the use of other cinnamic acid derivatives, *e.g.*, the tertiary amides **52b–f**, changed the regioselectivity of this reaction, whereas in the case of primary and secondary amines the regioselectivity was the same as with esters. It is also surprising that the substituent at the nitrogen atom virtually did not affect the regiochemistry of the reaction. Hence, its regioselectivity can be varied using different cinnamic acid derivatives and different nitrile oxides.

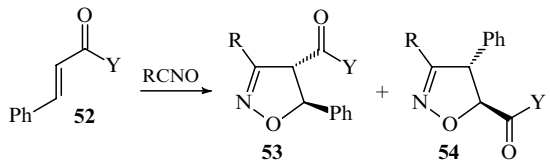

Compound **52**	Y	Ratio **53** : **54**
a	OMe	4 : 1
b	NEt_2	1 : 3
c	$N(Me)CH_2CO_2Me$	1 : 2
d	$N(Ph)CH_2CO_2Me$	1 : 2
e	L-proline methyl ester	see [a]
f	$N(CH_2CO_2Et)_2$	1 : 3

[a] Compound **54** is the main reaction product.

The use of chiral acrylamides as dipolarophiles has been reported;[68–73] acrylamides can have two low-energy rotamers due to rotation around the C–N bond. Cycloaddition of nitrile oxides to the optically active acryloylsultam **55** gives a mixture of diastereomers **56** and **57**; however, the diastereoselectivity of this reaction is rather high, especially in non-polar solvents.[68]

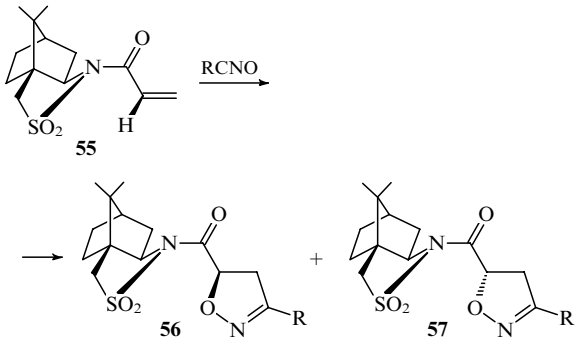

R	Solvent	Ratio **56** : **57**
Bu^t	C_6H_{14}	19 : 1
Bu^t	PhMe	9 : 1
Bu^t	CH_2Cl_2	4 : 1
Ph	C_6H_{14}	19 : 1
Me	C_6H_{14}	9 : 1
Et	C_6H_{14}	9 : 1
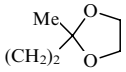	PhH	7 : 1

These results prompted a transition state model the existence of which was confirmed by X-ray diffraction analysis of compound **55**.[68]

According to calculations,[74] the dipole–dipole interaction of the C=O and S=O groups and, as a consequence, steric destabilisation, are absent only in the *s-trans*-conformer. However, this model cannot be applied to reactions promoted by Lewis acids, since the predominant conformation changes upon chelation.[74]

The results of quantum-mechanical calculations of the energy and geometrical parameters of various transition states suggest [75] that Coulomb interactions are the main factor which determines diastereofacial differentiation. The Coulomb interactions of the oxygen atom of the nitrile oxide with the sultam oxygen *endo*-atom and, to a lesser degree, with the sulfur atom determine the energy predominance of the transition states during the approach of nitrile oxide to the double bond above the sultam ring which affords compounds of the type **56** (although the approach of the nitrile oxide to the double bond under the sultam ring is sterically more favourable and results in the formation of isomers **57**).

It was shown [21,76] that methacryloylsultam **58a** is inactive in the reaction with nitrile oxides and provides low asymmetric induction, whereas this reaction is completely regiospecific (the ratio of diastereomers **59a** is ~2 : 1; the stereochemistry of the major reaction product was not determined).

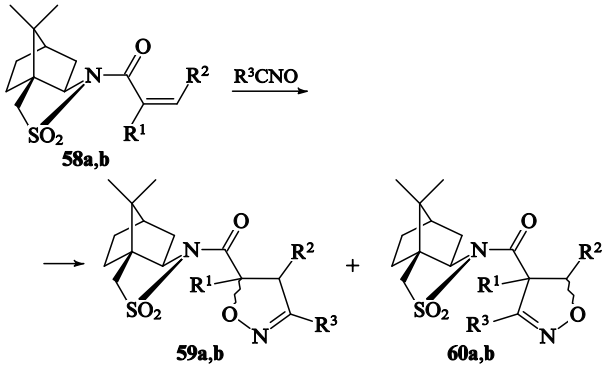

R^1 = Me, R^2 = H (a); R^1 = H, R^2 = Me (b); R^3 = Et, Bu^t, Ph.

Crotonoylsultam **58b** ensures high diastereoselectivity (the diastereomer ratio is 9 : 1); however, the regioselectivity of this reaction is rather low and four products are formed. The regioisomers **59b** and **60b** are formed in nearly equal amounts.

High selectivity is also reached with the Rebek benzooxazolimides **61**,[77] which manifest a unique ability to control the selectivity of the reaction owing to the U-shape of the molecule. The ratio of the regioisomers **62** : **63** reaches 99 : 1.

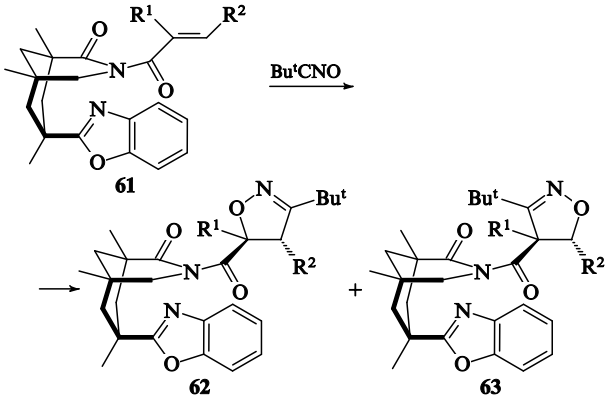

R^1 = H, Me; R^2 = H, Me, Ph, CO_2Et.

The addition of nitrile oxides to acrylamides[69] and α,β-unsaturated esters[78] containing a symmetrical chiral imidazolidine substituent in the β-position is characterised by extremely high diastereoselectivity. However, the former are difficult to obtain, while the latter manifest low regioselectivities. The reactions of 2,2-dimethyl-(4*S*,5*S*)-diphenyl-*N*,*N*′-diacryloylimidazolidine (**64**) and 2,2-dimethyl (4*R*)-phenyl-*N*-acryloylisoxazolidine (**65**) with benzonitrile oxide are highly diastereoselective.[79] Compound **64** yielded a mixture of the diastereomeric cycloadducts **66a** and **66b** in a ~ 5 : 1 ratio, whereas the reaction with compound **65** afforded a mixture of dihydroisoxazoles **67a** and **67b** (~ 4.5 : 1).

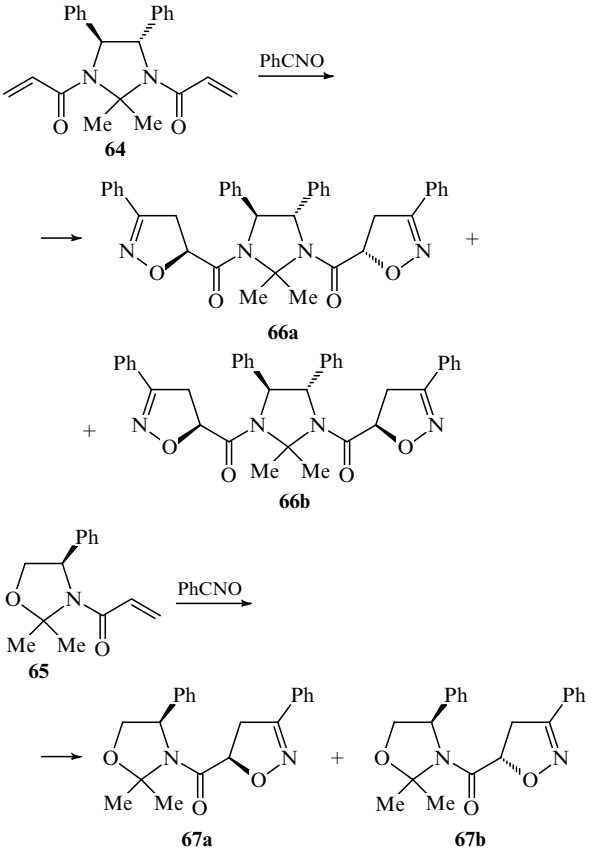

In both cases, hydrolysis of the reaction products leads to the corresponding dihydroisoxazoles possessing high optical purity. Based on the structure of the products **66a**,**b** and **67a**,**b**, it may be concluded that acrylamides **64** and **65** have an *s-cis*-conformation in the transition state, and benzonitrile oxide attacks the double bond from the side opposite to the phenyl substituent.

Studies of reactions of unsaturated compounds with benzonitrile oxide by the method of competing reactions[21] made it possible to construct an approximate scale of alkene reactivities, *viz*., activated monosubstituted > activated 1,1-disubstituted > non-activated 1,1-disubstituted = activated *trans*-1,2-disubstituted.

A high level of diastereoselectivity was achieved using compounds **68** which represent Kemp's triacid derivatives with chiral centres at one of the nitrogen atoms as dipolarophiles.[69,76] The adducts **69** with the *R*-configuration of the newly formed chiral centre are formed in more than 98% diastereomeric excess. It was noted that the pseudoenantiomeric alkene gives a C(5′)-isomeric dihydroisoxazole.

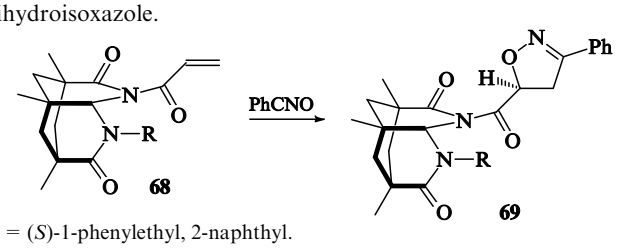

R = (*S*)-1-phenylethyl, 2-naphthyl.

1,3-Dipolar cycloaddition of nitrile oxides to the chiral acrylamides **70a**–**d** derived from (*S*)-proline and (*S*)-indoline-2-carboxylic acid yields chiral 4,5-dihydroisoxazoles **71** and **72**.[80] The stereoselectivity of this reaction is largely determined by the structure of the dipolarophile and is practically independent of the solvent used but varies depending on the nitrile oxide structure. The dipolarophiles **70a**–**d** differ in their steric characteristics. The largest steric factor is inherent in compound **70c** due to the presence of two phenyl rings, whereas the steric factor in the rigid molecule of alkene **70d** is determined by the effect of the cyclohexane ring. In the latter case, the stereoselectivity is the highest (up to 95% of the isomer **71d** is formed).

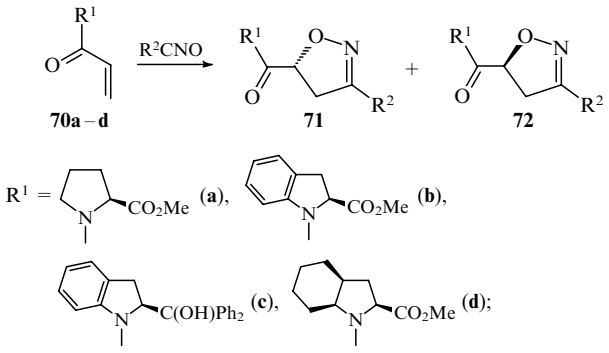

R^2 = Me, Et, Ph, 3,5-$Cl_2C_6H_3$, 4-MeC_6H_4.

The asymmetric cycloaddition to α,β-unsaturated esters **73a**–**c** containing chiral imidazolidine substituents in the β-position has been studied.[78] With methyl acrylate **73a**, the regio- and stereoselectivity of the reaction is low, *viz*., the *trans*-isomers **74** are formed in small excess. The addition of the unsaturated esters **73b**,**c** containing a symmetrically substituted imidazolidine unit was regio- or diastereoselective depending on the nature of the substituent at the nitrogen atom of the heterocycle. Thus the reaction of the acrylate **73b** was regiospecific and afforded different regioisomers depending on the nature of the nitrile oxide. However, in all cases studied the products represented mixtures of diastereomers [~(3–2) : 1]. With compound **73c**, this reaction occurred with low regioselectivity [the ratio of the regioisomers

74 : 75 was (3 – 2) : 1]; however, each regioisomer in this mixture represented an individual (4*S*,5*S*)-diastereomer.

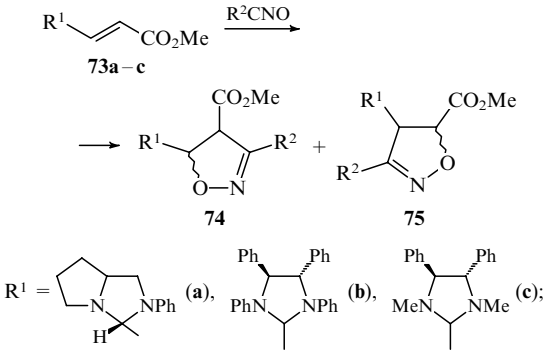

R^2 = Ph, 4-MeOC$_6$H$_4$.

The reactions of acrylates **76** with a (4*R*,7*S*)-7-isopropyl-4-methyl-4,5,6,7-tetrahydro-2*H*-indazol-3-yl fragment as an auxiliary chiral substituent have been studied.[81] Mixtures of two regioisomers **77** and **78** were obtained, the regioselectivity decreased if the reaction was carried out in more polar solvents. The nature of the substituent R^2 in the dipolarophile weakly affected the yield and the regioselectivity.[82] The acrylate **76** (R^2 = H) gives predominantly the cycloadduct **77** with benzonitrile oxide, whereas the corresponding cinnamate (**76**, R^2 = Ph) yields a mixture of the regioisomers **77** and **78**.

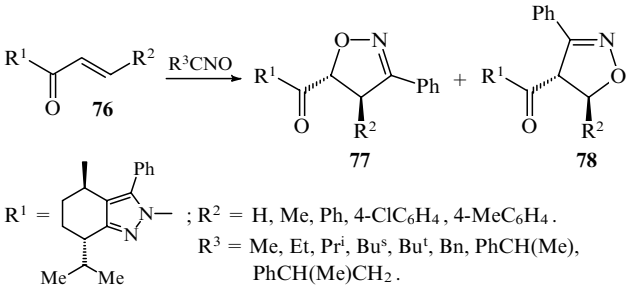

R^1 = ; R^2 = H, Me, Ph, 4-ClC$_6$H$_4$, 4-MeC$_6$H$_4$.
R^3 = Me, Et, Pr^i, Bu^s, Bu^t, Bn, PhCH(Me), PhCH(Me)CH$_2$.

Reactions of nitrile oxides prepared from oximes **79** or **80** with *N*-acryloyl-(2*R*)- or -(2*S*)-bornane-10,2-sultams **81a**,**b** have been successfully used in the synthesis of pseudodipeptides.[83] (5*R*)-Diastereomers of dihydroisoxazoles **82** or **83** containing a chiral fragment XCO in position 5 were formed predominantly from 89% to 100%.

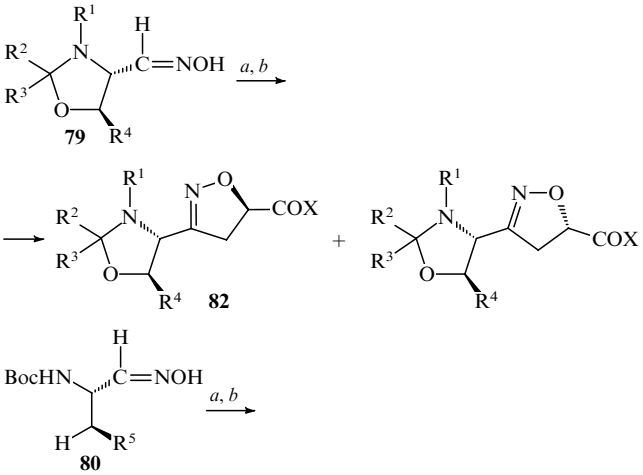

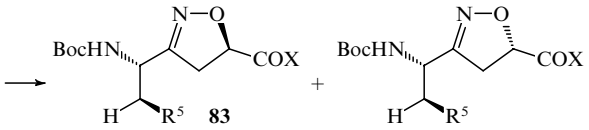

R^1 = Boc, OCOBn; R^2 = H, R^3 = Bu^t; R^2 = R^3 = Me; R^4 = H, Me; R^5 = OSiBu^{t}Me$_2$, CHMe$_2$, Ph;

(*a*) *N*-bromosuccinimide;

(*b*) XCOCH=CH$_2$ (**81a**,**b**), where X = 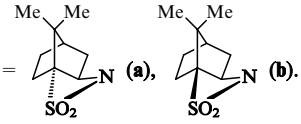

As can be seen from the data presented, in the majority of cases the addition of nitrile oxides to substituted alkenes results in the adducts containing substituents in position 5. However, there are exceptions to this rule. Thus 1,3-dipolar cycloaddition of 4-*tert*-butylbenzonitrile oxide to 6^A-acrylamido-6^A-deoxy-β-cyclodextrin gives predominantly 4-substituted dihydroisoxazole[84] (the regioisomeric ratio is 4 : 1). This effect is due to the formation of an intermediate 'host – guest' complex between the cyclodextrin fragment and nitrile oxide.

An efficient method for regio- and stereocontrol over the addition of nitrile oxides to the double bond of α,β-unsaturated diketones which makes use of chiral *S*-oxides of their cyclic dithioketals, *viz*., the diastereomeric 2-R-2-crotonoyl-1,3-dithiane *s*-oxides **84**, has been proposed.[85] The reaction with nitrile oxides is regioselective for both *syn*-**84** and *anti*-**84**; the former reacts with benzonitrile oxide to give products **85a** and **85b** in a 5 : 1 ratio, whereas for the latter the ratio is 1 : 3.

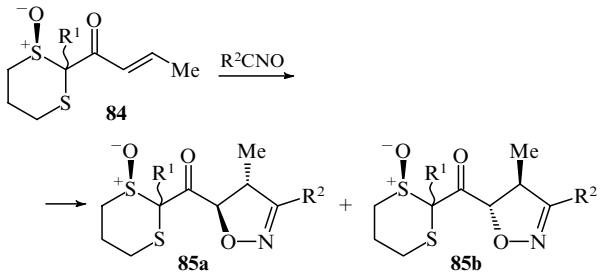

R^1 = Me, Et; R^2 = Me, Bu^i, Ph, Mes.

V. Cycloaddition of nitrile oxides to alkenes in the presence of Lewis acids

Lewis acids catalyse cycloaddition reactions of nitrile oxides to alkenes.[86–89] Thus the reaction of hydroximoyl chlorides with Grignard reagents yields the nitrile oxide complexes **86**. The first step includes *O*-metallation to give the intermediate **87** which undergoes 1,3-elimination of metal halide to give the nitrile oxide which further reacts with metal halide to give the complex **86**.

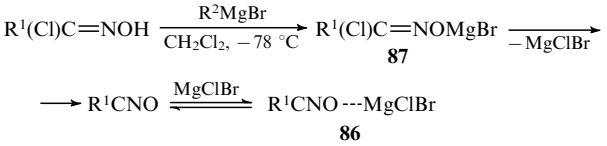

In the presence of ethylmagnesium bromide[86] the reaction rate of hydroximoyl chlorides with allylic alcohols **88** increases; no side products, *e.g*., nitrile oxide dimers, are hereby formed. Cycloaddition occurs in a *syn*-selective manner (up to 95%). Free nitrile oxides generated under the action of triethylamine manifested only weak *syn*-selectivities.

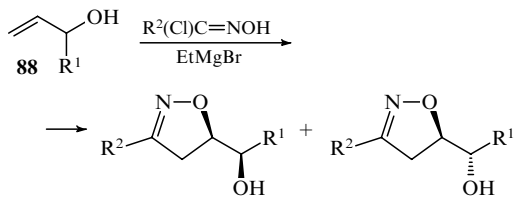

R^1 = Me, Et; R^2 = Ph, 4-$MeOC_6H_4$.

The nitrile oxide complexes of the type **86** can be generated under the action of other organometallic compounds (*e.g.*, Bu^nLi, Et_2Zn, Et_3Al); however, stereoselectivities of reactions are much lower in these cases. The complexes formed in the reaction with Et_2AlCl and $EtAlCl_2$ did not react with allylic alcohols **88** at all.[86]

The cycloaddition of nitrile oxides coordinated to Lewis acids to 1,1-disubstituted alkenes **89a–e** has been studied.[89] The formation of 4,5-dihydroisoxazoles always proceeds with high yields. The cycloaddition of acrylates **89a–d** with hydroxy groups in their chiral centres to free nitrile oxides is accompanied by the formation of a mixture of the diastereomers **90a–d** and **91a–d**, the *anti*-addition products **91a–d** being the main isomers. The proportion of the *anti*-adducts **91** decreases if nitrile oxides are used as complexes with LiCl, whereas magnesium and zinc complexes yield predominantly the cycloadducts **90a–d**. The highest *syn*-selectivity (98%) is observed in the presence of a twofold excess of magnesium alkoxide.

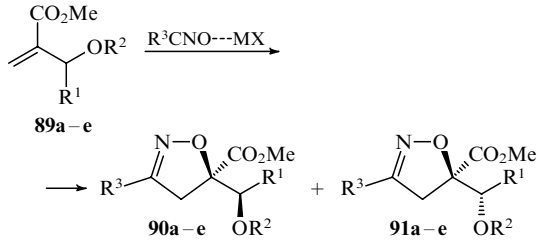

MX = $MgBr_2$, $ZnEt_2$, LiCl, $Mg(OAlk)_2$.

Compound **89**	R^1	R^2	R^3
a	Me	H	Ph
b	Me	H	4-$MeOC_6H_4$
c	Me	H	Bu^t
d	Et	H	Ph
e	Me	$SiMe_3$	Ph

A transition state model which accounts for the formation of *syn*- and *anti*-cyloaddition products has been proposed (Fig. 2).[89]

According to this model, the metal atom in the nitrile oxide–Lewis acid complex is coordinated to the hydroxy group of the dipolarophile. The transition state represents a system of condensed five-membered rings bent along the C(2)–O bond. Localisation of the substituent R^1 at the chiral centre inside the bent condensed system (Fig. 2 *a*) produces significant steric hindrances. Therefore, this reaction occurs *via* a sterically less hindered *syn*-transition state (Fig. 2 *b*). This model explains the effect of the coordinative capacity of the metal atom on the stereoselectivity of this reaction. Lithium and zinc form no stable complexes. In the presence of magnesium salts, dipolarophiles undergo ionisation to produce stronger complexes with metals, as a result of which their *syn*-selectivities increase.

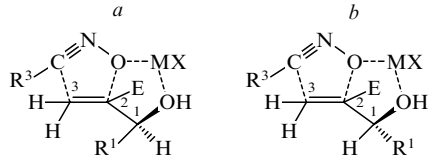

E = CO_2Me.

Figure 2. The transition states of the reaction of cycloaddition of nitrile oxides to chiral homoallylic alcohols **89a–d**.[89]
(*a*) *anti*-transition state, (*b*) *syn*-transition state; E = CO_2Me.

If the hydroxy group is protected by a bulky trimethylsilyl substituent (compound **89e**), the formation of a chelate complex in the transition state is less favourable; therefore, the alkene **89e** yields the *anti*-isomers **91** with moderate stereoselectivities (73%–79%) irrespective of the method used for the generation of nitrile oxides.

An alternative approach to increase in the stereoselectivity of nitrile oxide addition to alkenes is the use of magnesium alkoxides obtained by the reaction of allylic alcohols [86] or α,β-unsaturated ketones [90] with organomagnesium compounds. This reaction occurs in a *syn*-stereoselective manner. The maximum selectivity is reached with 2 equivalents of the alkoxide and decreases when the reaction is carried out in THF.

In the case of magnesium alkoxides **92** prepared from the corresponding allylic alcohols, the cycloaddition is regioselective and affords the cycloadducts **93** and **94**; with 2 equivalents of alkoxides **92** the *syn*-addition products **93** are predominantly formed.[86]

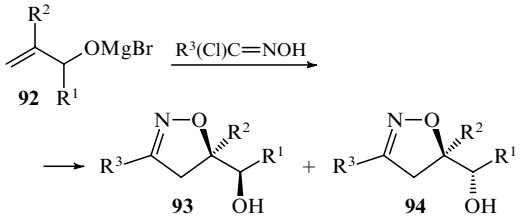

R^1	R^2	R^3	Ratio **93** : **94**
Me	H	Ph	96 : 4
Et	H	Ph	99 : 1
Et	H	4-$MeOC_6H_4$	89 : 11
Pr^i	H	Ph	97 : 3
Bu^n	Me	Ph	96 : 4

The application of this methodology to alkoxides of homoallylic alcohols resulted in the exclusive formation of the regioisomers **96** and **97** from terminal alkenes with no or very small diastereoselectivity.[86]

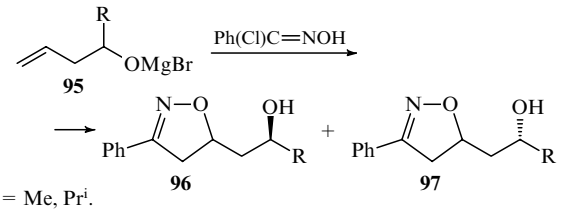

R = Me, Pr^i.

It should be noted that the control over the selectivity of 1,3-dipolar cycloaddition by coordination to metals proved to be efficient in those cases where internal alkenes were used as dipolarophiles. The cycloaddition of nitrile oxides to allylic alcohols **98** in the presence of ethylmagnesium bromide is regiospecific with the predominant formation of the *syn*-adduct **99** (94%), whereas the nitrile oxide generated under the action of triethylamine gave a mixture of compounds **99** and **100** in a 55 : 12 ratio and up to 18% of diastereomers of 4,5-dihydroisoxazole **101**, the total yield of the reaction products being much lower.

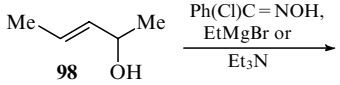

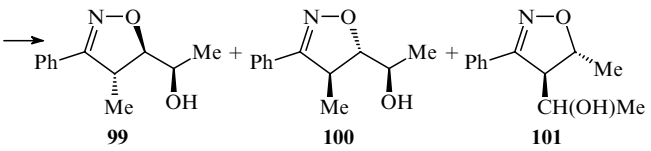

99 **100** **101**

The cycloaddition of nitrile oxides to dienes which contain a hydroxy group in both the allylic and homoallylic positions has been studied.[91] Thus the reaction of hexa-1,5-dien-3-ol (**102a**) with benzonitrile oxide generated under the action of Et_3N gives a mixture of the cycloadducts **103a** and **104a** (the diastereomeric ratios were 2 : 1 and 3 : 2, respectively), *i.e.*, under these conditions, the double bond of the allylic fragment was only a little more reactive than that of the homoallylic fragment.

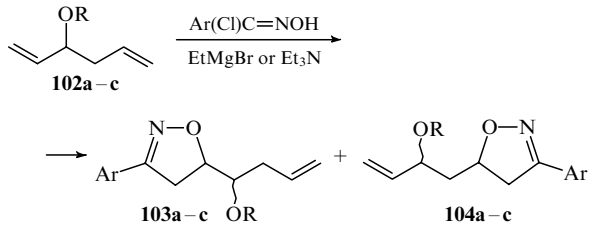

102a–c **103a–c** **104a–c**

R = H (**a**), Ac (**b**), $SiMe_2Bu^t$ (**c**); Ar = Ph, 2,6-$Cl_2C_6H_3$.

When EtMgBr is used to generate nitrile oxide, the reaction is chemoselective with respect to the allylic fragment, the *syn* : *anti*-diastereomeric ratio in compound **103** being 99 : 1. Thus the magnesium alkoxide methodology proved to be more efficient for allylic alcohols than for homoallylic alcohols.

The influence of hydrogen bond formation on the cycloaddition of 2,6-dichlorobenzonitrile oxide to compounds **102a–c** has been studied.

In weakly polar solvents, such as benzene or dichloromethane, nitrile oxide forms a hydrogen bond with the hydroxy group of the alcohol **102a** and coordinates to the double bond of the allylic fragment (the transition state **A** is more favourable than **B**), compound **103a** being the main product. The use of polar solvents, *e.g.*, DMF, prevents the formation of the hydrogen bond, and thus the product **104a** becomes predominant.

In the case of a protected hydroxy group (compounds **102b**,**c**), no hydrogen bond can be formed; therefore, acetate **102b** gives predominantly the adduct **104b** irrespective of the polarity of the solvent used. In addition, the homoallylic double bond in the acetoxy derivative **102b** becomes more reactive as a dipolarophile due to steric repulsion between the acetoxy group and nitrile oxide. For compound **102c**, the yield of dihydroisoxazole **104c** increases even more due to significant steric hindrances.

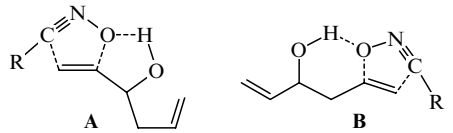

A **B**

High *syn*-selectivity in the addition to the double bond of the allylic fragment of magnesium alkoxide prepared from the alcohol **102a** can be explained in terms of the reaction mechanism. Magnesium alkoxide forms five-membered intermediates **C** or **D**, the latter being much less stable due to steric hindrances created by the propenyl substituent.

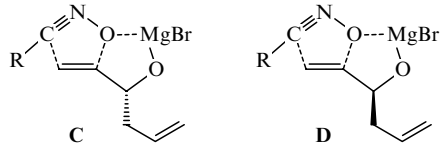

C **D**

Thus the allylic double bond is relatively more reactive in the reaction of 1,3-dipolar cycloaddition of nitrile oxides to hexa-1,5-dien-3-ols than the homoallylic bond due to the formation of a hydrogen bond. In acetyl or silyl derivatives of the alcohol **102a**, it is the isolated homoallylic bond that is more reactive. Chelation with magnesium derivatives results in high regio- and diastereoselectivity. It should be noted that the products of simultaneous addition at two bonds were also isolated.

Reactions of 1,3-dipolar cycloaddition of benzonitrile oxide with 3,3-disubstituted allylic alcohols **105** proceed with very low regioselectivity; the nature of the substituent practically does not influence the ratio of the cycloadducts **106** and **107**.[92] In the case of magnesium alkoxides (X = MgBr), the reaction rate increases considerably and so does the regioselectivity,[93,94] this effect being observed exclusively with more than 1 equivalent of magnesium alkoxide. Similar results were obtained for mesitylenecarbonitrile oxide.[94]

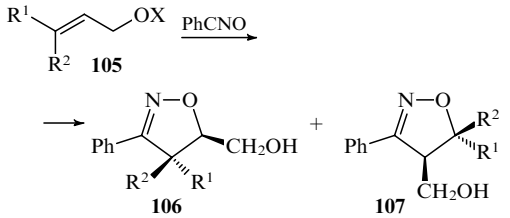

105 **106** **107**

R^1 = H, Me, Pr^i, Ph; R^2 = H, Me, Pr^n; X = H, MgBr.

The cycloaddition of 2,6-dichlorobenzonitrile oxide to magnesium alkoxides **108** obtained by treatment of α,β-unsaturated aldehydes and ketones with Grignard reagents has been studied.[90] This reaction is regio- and diastereoselective and results in the *syn*-adducts **109**.

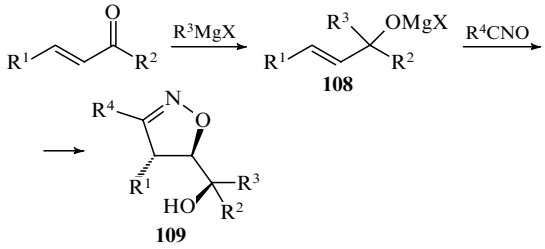

108 **109**

R^1 = H, Me; R^2 = H, R^1-R^2 = CH_2CH_2; R^3 = Me, Et; R^4 = 2,6-$Cl_2C_6H_3$.

Encouraging results were also obtained with cyclopentenone; however, the attempts to carry out an analogous reaction with cyclohexenone were without success.

VI. Cycloaddition of nitrile oxides to unsaturated aldehyde derivatives

Cycloaddition to cinnamaldehyde is one of few examples of cycloaddition of aceto- and benzonitrile oxides to α,β-unsaturated aldehydes.[95] In addition to the expected products, *e.g.*, 4-formyl-5-phenyl-3-R-4,5-dihydrooxazoles, bis-adducts were isolated due to the cycloaddition of nitrile oxide to the carbonyl group of the primary cycloadducts. Therefore, in subsequent experiments the carbonyl groups of α,β-unsaturated aldehydes were protected prior to their cycloaddition to nitrile oxides.

The reactions of cyclic acetals **110** with nitrile oxides[96] gave predominantly the adducts **111**. The desired regioselectivity can be attained by varying the nitrile oxide structure. For example, for R^1 = CO_2Et and R^2 = Ph the **111** : **112** ratio is 99 : 1.

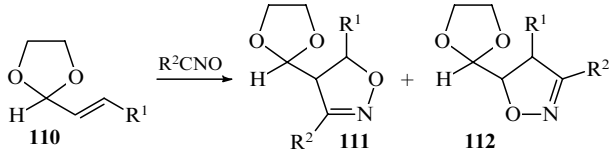

110 **111** **112**

R^1 = Ph, CO_2Et, Et; R^2 = Ph, Me, Pr^i.

The compositions of cycloaddition products in the case of β-substituted α,β-unsaturated aldehyde derivatives depend on the nature of the protective groups.[97] The cycloaddition to cyclic acetals **113a**,**b** yields predominantly the regioisomers with an acetal substituent in position 4, whereas for dithioacetals **113c**,**d** the regioselectivity is opposite. Calculations led to a conclusion that the orientation in this case of the dithioacetal group is determined by the steric factor, whereas that in the case of the acetal group is determined by the interaction of the frontal orbitals.

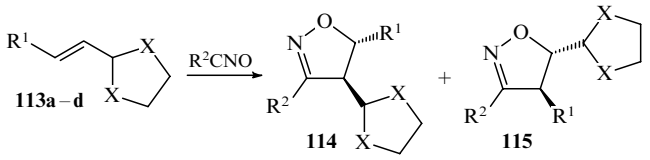

113a–d **114** **115**

Compound **113**	R^1	X	R^2	Ratio **114** : **115**
a	Ph	O	Ph	91 : 9
	Ph	O	4-$MeOC_6H_4$	17 : 1
b	Me	O	$PhCH_2$	9 : 1
c	Ph	S	Ph	17 : 83
	Ph	S	4-$MeOC_6H_4$	27 : 73
d	Me	S	$PhCH_2$	3 : 7

Thus, by varying the protecting group in the α,β-unsaturated aldehyde, one can change the regioselectivity of the reaction resulting in substituted 4,5-dihydroisoxazoles with the formyl substituent in different positions.

High stereoselectivity is achieved in the addition of nitrile oxides to 2-hydroxybut-3-enal dithioacetal derivatives.[98] Thus the diastereoselectivity of the cycloaddition of nitrile oxides to 2-silyloxybut-3-enal dithioacetals **116** virtually does not depend on either the size of the protective group at the oxygen or the sulfur atoms or the nature of the substituent. The *anti*-isomers **117** are formed as the main products and the maximum diastereoselectivity (96%) is achieved with the bulky dithioacetal group ($R^2 = Bu^t$). However, the yield of this reaction depends, to some extent, on the nature of the nitrile oxide; the total yield of the cycloadducts **117** and **118** is low (25%–26%) with $R^1 = SiMe_2Bu^t$, $R^2 = Bu^t$ and $R^3 = CO_2Et$ or CH_2OBn.

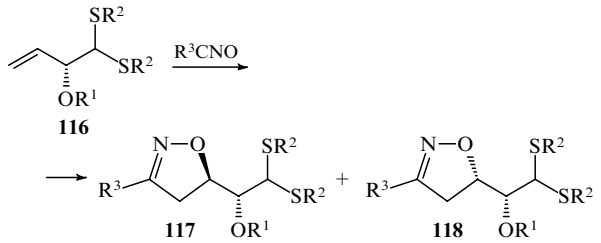

116 **117** **118**

R^1 = Bn, $SiMe_2Bu^t$; R^2 = Ph, $(CH_2)_3$, Bu^t; R^3 = Me, Ph, 4-$MeOC_6H_4$,

, CO_2Et, CH_2OBn.

Deprotection of the aldehyde group occurs with high yields and without epimerisation of the chiral centres, which apparently makes this method especially attractive from the synthetic point of view.[98]

VII. Alkenylboronates in cycloaddition reactions with nitrile oxides

Organoboron derivatives, particularly alkenylboronate derivatives are readily available and are often used in synthetic practice as convenient building blocks.[99] The possibility of the use of alkenylboronates as dipolarophiles in cycloaddition with nitrile oxides has been studied.[100–102] It is of note that an attempt at enhancing the reactivity of the double bond in alkenylboranes by introducing stronger electron-withdrawing groups, such as borabicyclononyl, catecholboryl or $BHal_2$ groups, has not led to the desired effect.[103]

It was found that the vinylboronates **119a–g** react with nitrile oxides in a regiospecific manner to give 4,5-dihydroisoxazoles **120a–g**, their yields being only little dependent on the changes in the nitrile oxide structure. α-Substituted alkenylboronates **119h**,**i** gave also 4,5-dihydroisoxazoles **120h**,**i** containing a boronate residue in position 5 as the reaction products, while the trisubstituted compound **119j** gave no cycloadducts. β-Substituted alkenylboronates **119k–m** do not afford products similar to compounds **120**; this reaction gave 4,5-dihydroisoxazoles **121k**,**l** or isoxazole **122** containing no boronate substituent.

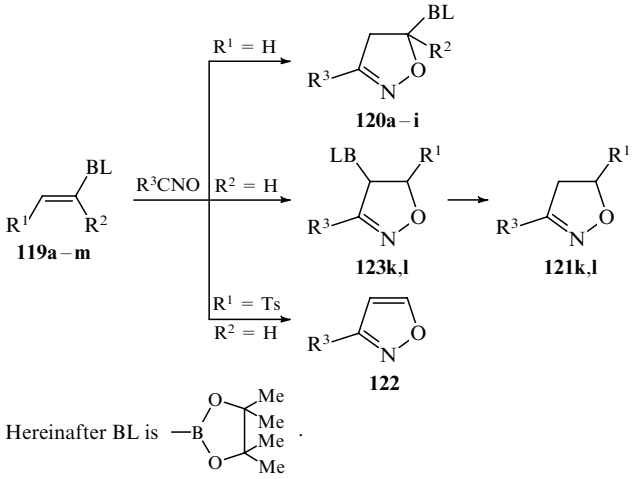

119a–m **120a–i** **123k**,**l** **121k**,**l** **122**

Hereinafter BL is .

Substrate **119**	R^1	R^2	R^3	Reaction product
a	H	H	4-ClC_6H_4	**120a**
b	H	H	Me	**120b**
c	H	H	Bu^t	**120c**
d	H	H	CO_2Et	**120d**
e	H	H	COMe	**120e**
f	H	H	$(CH_2)_3CO_2Me$	**120f**
g	H	H	$CH_2CH(OMe)_2$	**120g**
h	H	Me	4-ClC_6H_4	**120h**
i	H	Ph	4-ClC_6H_4	**120i**
j	$(CH_2)_4$		4-ClC_6H_4	–
k	Bu	H	4-ClC_6H_4	**121k**
l	MeOCO	H	4-ClC_6H_4	**121l**
m	Ts	H	4-ClC_6H_4	**122**

A mechanism of cycloaddition has been proposed [101] based on the results of the reaction of vinylboronates with diazo compounds.[104] According to this mechanism, nitrile oxide is added regioselectively to *cis*-alkenylboronates **119k–l** to give 4,5-dihydroisoxazoles **123** with a boronate residue in position 4. Similar compounds were isolated and characterised in previous studies.[105] Spontaneous 1,3-migration of the boronate residue and subsequent hydrolysis give 4,5-dihydroisoxazoles **121**. Elimination of TsOH in the case where R^1 = Ts results in isoxazole **122** (R^3 = 4-ClC_6H_4).[106]

An effective procedure for the synthesis of 4-hydroxy-4,5-dihydroisoxazoles using vinylboronates has been proposed.[105] Thus 1,3-dipolar cycloaddition of nitrile oxides to 2-substituted *trans*-alkenylboronates **124** gives 4,5-dihydroisoxazoles **125** with a boronate substituent in position 4 as the main regioisomers. Treatment of the reaction mixture with Bu^tO_2H gives *trans*-hydroxy-4,5-dihydro-4-isoxazoles **126** in high yields (75%–88%).

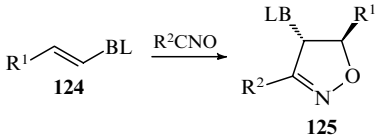

124 **125**

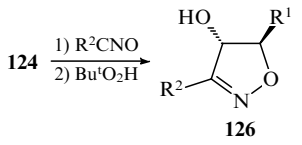

R^1 = Pr^n, CH_2OAc, Ph, Bu^n, CO_2Me, $(CH_2)_3Cl$; R^2 = Ph, 4-$MeOC_6H_4$.

The cycloaddition of nitrile oxides to allylboranes **127** has been studied.[101] As in the case of alkenylboranes, one regioisomer **128** is formed. Allylboranes containing a chiral centre in the α-position yield a nearly equimolar mixture of diastereomers with nitrile oxides; their stereochemistry has not been established.

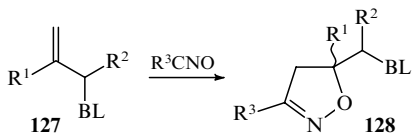

R^1 = H, Me; R^2 = H, Cl, C_6H_{13}, C_5H_9; R^3 = Bu^t, 4-ClC_6H_4.

Thus, 1,3-dipolar cycloaddition of nitrile oxides to alkenyl- or allylboronates and subsequent oxidative deborylation of the adducts formed is a direct route to 4-hydroxy- or 5-hydroxyalkyl-4,5-dihydroisoxazoles.

The reaction of [3-R-4,5-dihydroisoxazol-2-yl]boranes **120a**–**h** with diiodomethane in the presence of MeLi yields their homologues.[107]

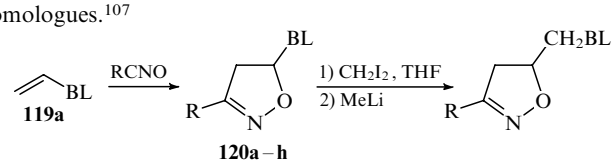

R = 4-ClC_6H_4 (**a**), Me (**b**), Bu^t (**c**), CO_2Et (**d**), COMe (**e**), Ph (**f**), $(CH_2)_2CO_2Me$ (**g**), CMe_2OSiMe_3 (**h**).

Cycloaddition of nitrile oxides to the optically active alkenylboronate **129** gives four products; the total yield of 4,5-dihydroisoxazoles **130a**,**b** is ~50%, whereas that of (4*S*,5*S*)- and (4*R*,5*R*)-4-hydroxy-4,5-dihydroisoxazoles **130c**,**d** is ~45%, *erythro*-isomers being predominant in both cases.[108] Thus, this reaction occurs in a regiospecific manner but with moderate stereoselectivity. Compounds **130a**,**b** are formed as a result of deborylation of the primary 4,5-dihydroisoxazoles which contain a boronate substituent in position 4 (like compounds **123a**,**b**).

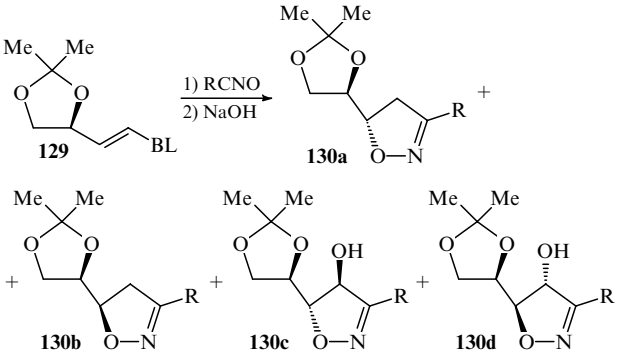

R = Ph, 4-ClC_6H_4.

Compounds **130c**,**d** were the only reaction products (**130c** : **130d** ≈ 4 : 1) when *tert*-butyl peroxide was used for the generation of nitrile oxide.

VIII. Vinyl- and allylphosphine oxides in cycloaddition reactions with nitrile oxides

1,3-Dipolar cycloaddition of nitrile oxides to racemic methylphenylvinylphosphine oxide results in phosphorus-containing 4,5-dihydroisoxazoles **131a**,**b** and **132a**,**b** in good yields.[109] The isomers **131a**,**b** with a phosphine oxide substituent in position 5 either predominate or are the only reaction products. The cycloaddition occurs with a significant (~40%) diastereofacial selectivity. According to X-ray diffraction data, compound **131a**, which exists in an *erythro*-configuration, has a conformation in which the C–O and P=O bonds are in the *anti*-position.

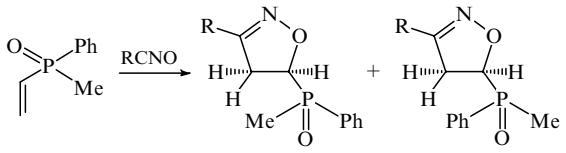

R = Ph, Me.

1-R-Propenyldiphenylphosphine oxides **133** were studied in the reaction of 1,3-dipolar cycloaddition.[110]

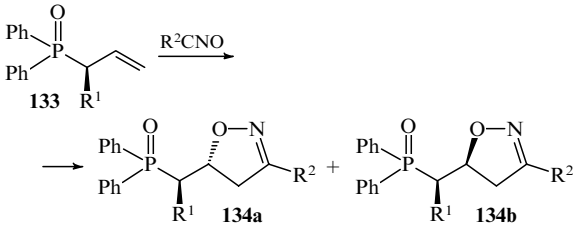

R^1 = Me, Et, Pr, C_6H_{11}, $C_{11}H_{23}$, CO_2Et, $(CH_2)_nCO_2Me$;
R^2 = H, Me, Et, Pr, Bu^i.

Cycloadducts are not formed, if nitrile oxides contain a bulky substituent R^2. In other cases, the reaction proceeds at a very slow rate. The *anti*-addition products **134a** are predominant in all cases. This is one of the few examples of cycloaddition reactions where the substituent in the nitrile oxide has a stronger influence than the substituent R^1 in the allylic position. It was suggested [110] that the extremely bulky phosphorus-containing substituent in the Houk transition state occupies a position opposite to that of the ring which is formed, whereas the R^1 group and the allylic hydrogen atom are localised inside and outside, respectively. Branched substituents R^2, *e.g.*, Pr^i, are too bulky for these positions; therefore, alkenes **133** do not form cycloadducts with such nitrile oxides.

IX. The nitrile oxide method in carbohydrate chemistry

Cycloaddition of nitrile oxides to alkenes is used in the synthesis of various sugar derivatives. The nitrile oxide method proved to be a convenient procedure for the elongation of a carbon chain in the synthesis of higher sugars. The 1,3-dipolar cycloaddition of the simplest nitrile oxides to the double bonds of the sugar derivatives **135a**–**d** has been studied.[111–116] The reaction of compounds **135a**,**b**,**d** with nitrile oxides is regioselective and gives 4,5-dihydroisoxazoles **136** and **137** which contain the sugar moiety in position 5 (74 : 26 and 97 : 3, respectively). The major diastereomers of the adducts **136** have the *R*-configurations of the newly formed chiral centres. Quite a different result is obtained for the corresponding D-ribose derivative **135c**,[113,115] which represents an epimer of compound **135a** as regards the homoallylic C(3) atom. In this case, the *syn*- and *anti*-adducts **136** and **137** are formed in approximately equal amounts. This reaction is the first

example of the dependence of the composition of nitrile oxide cycloaddition products on the configuration of the chiral centre in the homoallylic position.

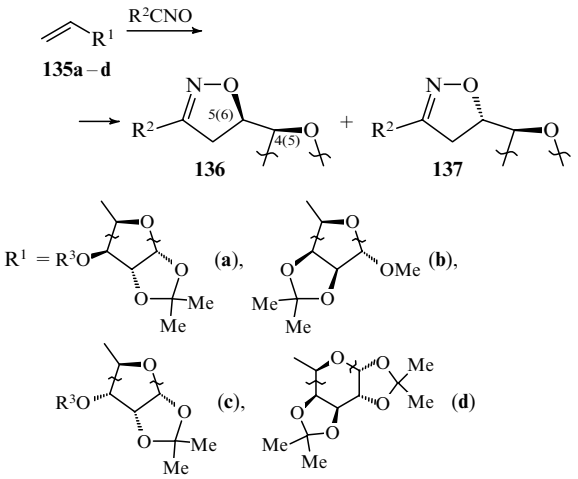

R^2 = Ph, CO_2Et; R^3 = H, OH, OMe, OBn, Ac, Ar.

The 1,3-dipolar addition of ω-unsaturated heptoses and hexoses **138a**,**b** to the nitrile oxide **139** was used in the synthesis of 7-deoxytrideca- and 6-deoxydodecadialdoses.[117] It should be noted that this reaction is one of the few examples of asymmetric induction by a chiral nitrile oxide. Both alkenes react regiospecifically and with high diastereoselectivity to give predominantly the *anti*-adducts **141a**,**b** (**141** : **140** = 4 : 1 and 14 : 3, respectively).

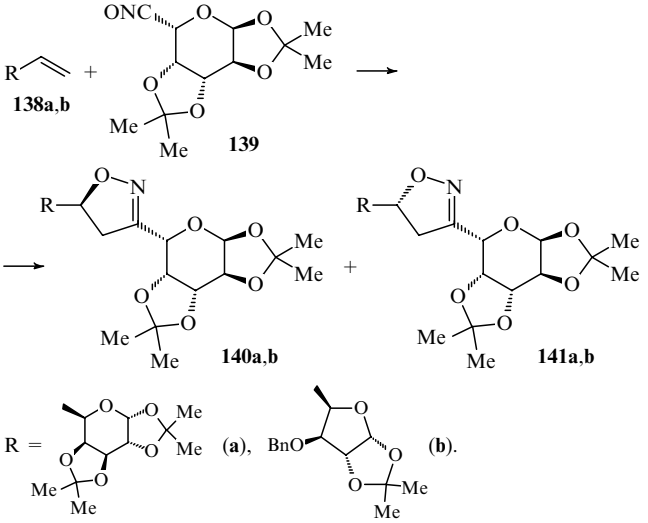

The stereo-controlled cycloaddition of the alkene **138b** to nitrile oxides derived from D-xylose (**142a**) or D-arabinose (**142b**) has been carried out. In both cases, the reaction is regiospecific and diastereoselective with the predominance (up to 80%) of the diastereomers **143** having *R*-configurations of the newly formed chiral centres.[118]

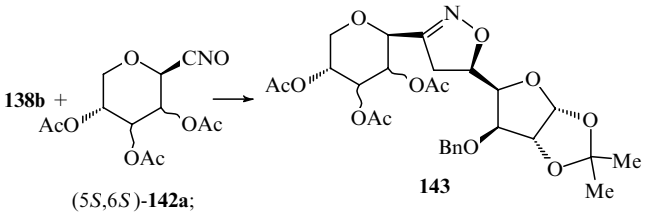

(5*S*,6*S*)-**142a**;
(5*R*,6*R*)-**142b**.

Similar results were obtained with L- or D-arabinonitrile (**145**),[119] oxide derivatives **144** and glyceronitrile oxide (**146**).[115]

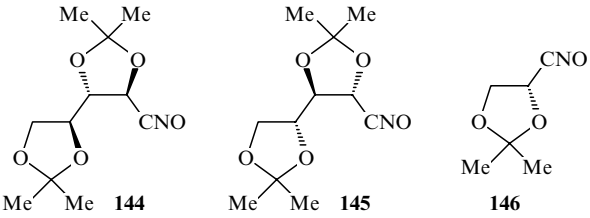

The 1,3-dipolar cycloaddition of nitrile oxides to nitroalkenes and α,β-unsaturated carbonyl compounds **147a**–**d** containing a sugar moiety has been studied. For alkenes **147b**–**d**, this reaction is regio- and stereoselective and yields exclusively the diastereomers **148** with the *trans*-configuration of substituents at the C(4) and C(5) atoms.[120]

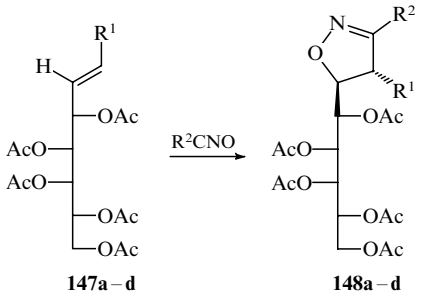

R^1 = NO_2 (**a**), Ac (**b**), CO_2Me (**c**), CO_2Et (**d**); R^2 = Me, Ph, Mes, Br.

Based on molecular-mechanical models and the structure of the reaction products, it was suggested [120] that in this case it is the stable transition state **A** that is realised. This conclusion is in good agreement with the anti-periplanar effect of the acetoxy group in the allylic position.

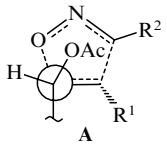

The regioselective cycloaddition of tetrahydropyranyloxyacetonitrile oxide to the nitrogen bases **149** containing vinyl groups results in the nucleoside aza analogues **150** possessing antiviral activities.[121, 122]

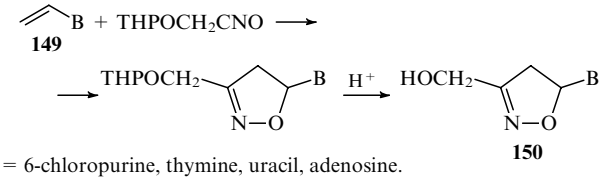

B = 6-chloropurine, thymine, uracil, adenosine.

X. Steroid alkenes as dipolarophiles in cycloaddition reactions with nitrile oxides

1,3-Dipolar cycloaddition of nitrile oxides to steroid alkenes has been studied using compounds with a double bond in both the cyclic part of the molecule (*e.g.*, $\Delta^{5(6),16(17)}$-steroids) and the side chain.

The addition of nitrile oxides to the disubstituted double bond of the steroids **151a**–**d** occurs at a slow rate and sometimes requires a large excess of nitrile oxide; its result does not change upon modification of the steroid skeleton but strongly depends on the nature of the substituent R^2 of the nitrile oxide.[123] No cycloaddition products were found for R^2 = Pr^i.

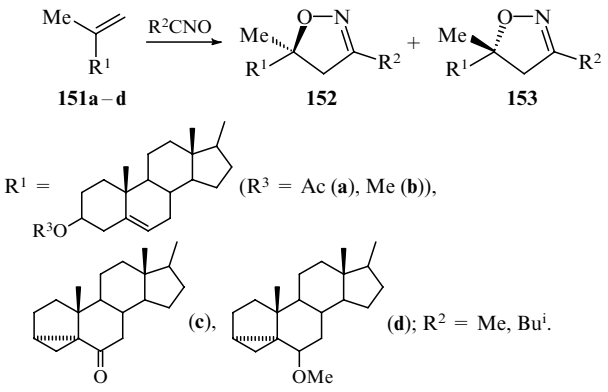

This addition is regiospecific leading exclusively to the formation of 4,5-dihydroisoxazol-5-yl derivatives and stereoselective (**152** : **153** = 3 : 1). The main epimer is formed as a result of an attack of the nitrile oxide at the double bond from the sterically less hindered side (the α-region of the steroid).

1,3-Dipolar cycloaddition of nitrile oxides to the 17β-hydroxy-17α-vinyl estrone derivative **154a** proceeds in a regiospecific and stereoselective manner [**155** : **156** = (10 – 15) : 1]. The stereoselectivity of the reaction decreases on going to the steroids of the androstane series **154b,c** (**155:156** = 1:1) for R^2 = Me and 3 : 1 for R^2 = Pr^i.[124, 125]

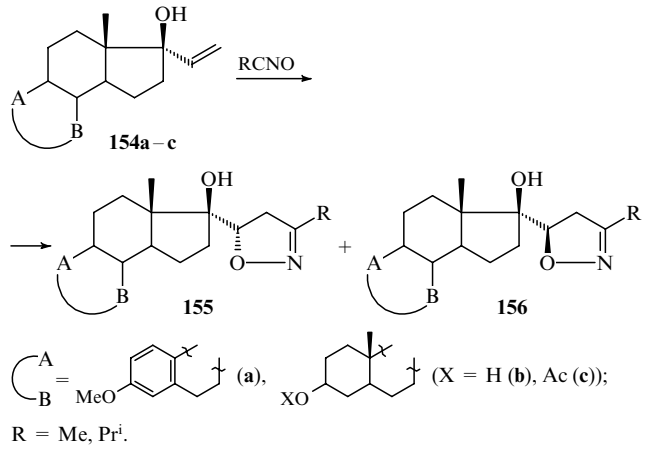

The steroid derivatives **157a** – **i** containing a but-2-enyl substituent in the ring *D* have been studied in the reaction of 1,3-dipolar cycloaddition to nitrile oxides.[126 – 132] In all cases, this

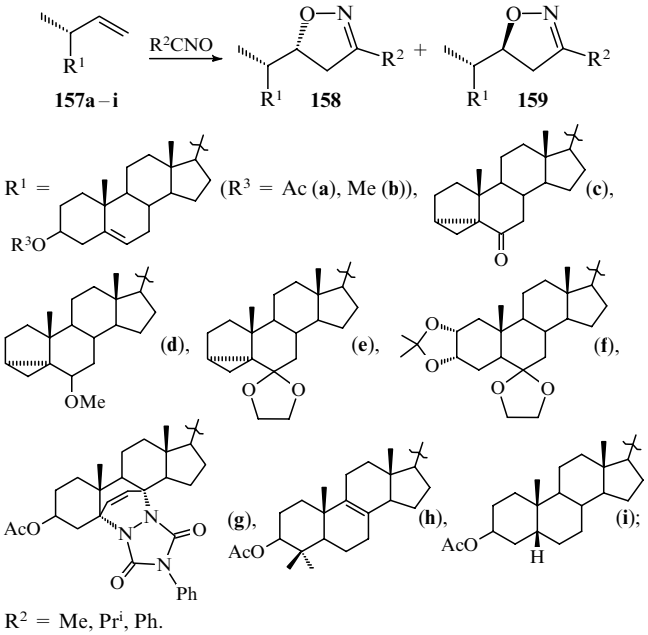

reaction gave a mixture of the 5′-epimeric 4,5-dihydroisoxazol-5-yl steroids **158** and **159**. The ratio of the epimers (5′*R*)-**158** and (5′*S*)-**158** depends on the structures of both the nitrile oxide and the steroid. In some cases, the reaction possessed pronounced stereoselectivity, *e.g.*, the **158** : **159** ratio in the reaction of compound **157h** with benzonitrile oxide is 4.5 : 1, whereas the reaction of the alkene **157f** with isobutyronitrile oxide is not selective. The reaction of compound **157g** with nitrile oxides is a special case, for it gives only one reaction product **158** (R^2 = Me, Pr^i).

1,3-Dipolar cycloaddition of nitrile oxides to steroidal allylic alcohols **160a** – **c** [126, 132, 133] affords the adducts **161** and **162**; the *threo*-isomers **161** are formed with high stereoselectivities. The cycloaddition of EtO_2CCNO to compound **160b** gave only one diasteromer, *viz.*, 4,5-dihydroisoxazole **161b** (R^2 = CO_2Et), albeit in a low yield.

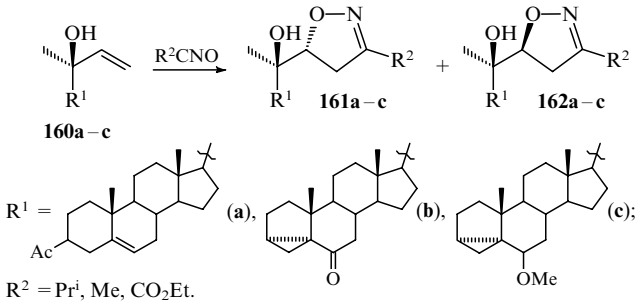

The stereochemistry and the ratio of the reaction products in the cycloaddition of nitrile oxides to the Δ^{23}-steroids **163** is determined by the nature of the oxygen-containing substituents in the α- and β-positions to the double bond and the configuration of the C(20) and C(22) centres in the starting dipolarophile (Table 1).[134 – 138]

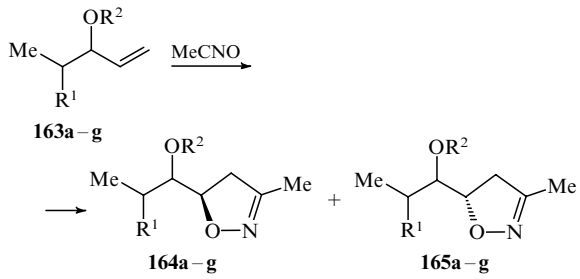

The cycloaddition of acetonitrile oxide to the steroid **163a** containing a (22*S*)-hydroxy group occurs in a regio- and stereoselective manner with the predominant formation of the *threo*-isomers **164a**. The ratio of the epimers formed in the reaction with (22*S*)-acetoxy derivative **163b** was 1 : 1 (with a concomitant decrease in the degree of conversion). The use of the (20*S*,22*R*)-hydroxy derivative **163c** also resulted in the predominant formation of the *threo*-isomer **165c**, whereas in the case of the (22*R*)-acetoxy derivative **165d** the epimers were formed in a 1 : 1 ratio and the degree of conversion was also decreased. This reaction becomes stereospecific upon protection of the hydroxy group by a bulky *tert*-butyldimethylsilyl substituent (compound **163e**), however, the (22*R*,5′*S*)-diastereomer **165e** is formed in a low yield. The (22*S*,5′*S*)-diastereomer **165f** was predominant upon cycloaddition of the (20*R*,22*R*)-22-hydroxy derivative **163f**, but the stereoselectivity of this reaction was not very high. When the (20*R*,22*R*)-22-acetoxy derivative **163g** is used as a dipolarophile, the *syn*-cycloaddition product **165g** is formed in a large excess which is in contrast to the reactions with the acetoxy derivatives **163b** and **163d**.

These reaction patterns differ basically from those for non-steroid compounds and suggest the possible formation of a transition state (an intermediate complex) including nitrile oxide and the allylic hydroxy group of the steroid molecule.[2] The structure of the transition state depends on the nature of the

Table 1. The stereochemistry and ratios of reaction products in the reaction of acetonitrile oxide with the steroids **163**.

R^1	R^2	Compound **163**	Configuration of the C(20) and C(22) centres	Total yield	Ratio of adducts **164** and **165**
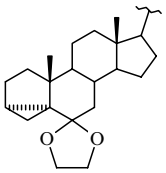	H	**a**	(20*S*,22*S*)	88	4 : 1
	Ac	**b**	(20*S*,22*S*)	81 [a]	1 : 1
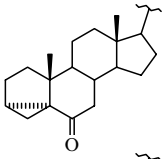	H	**c**	(20*S*,22*R*)	88	1 : 4
	Ac	**d**	(20*S*,22*R*)	90 [b]	1 : 1
	$SiMe_2Bu^t$	**e**	(20*S*,22*S*)	16 [c] 25 [e]	see [d]
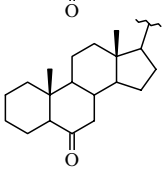	H	**f**	(20*R*,22*R*)	70	1 : 2
	Ac	**g**	(20*R*,22*S*)	78 [f]	1 : 4

[a] The conversion is 41%. [b] The conversion is 38%. [c] 20 °C. [d] Only the adduct **165** is formed. [e] 60 °C. [f] The conversion is 40%.

steroid fragment and the configuration of the allylic and homoallylic centres.

The reaction of acetonitrile oxide with the 20-hydroxy-20-propenyl steroids **166b**,**d** containing the homoallylic hydroxy groups occurs without any noticeable stereoselectivity to afford approximately equal amounts of the epimeric 4,5-dihydroisoxazoles **167b**,**d** and **168b**,**d**.[139]

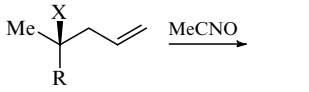

166a–d

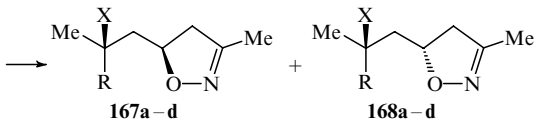

167a–d **168a–d**

R = 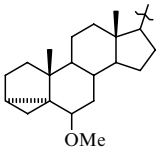 : X = H (**a**), OH (**b**);

R = 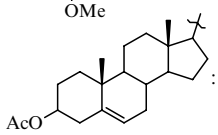 : X = H (**c**), OH (**d**).

This reaction is also non-stereoselective with the steroid alkenes **166a**,**c** devoid of hydroxy groups.[140]

The first attempts to use steroidal nitrile oxides **169a**,**b** and **170a–d** [141–144] as dipoles in reactions with alkenes revealed that the cycloaddition which occurs in a regioselective manner yields one regioisomer in the form of epimeric pairs of 4,5-dihydroisoxazol-3-yl steroids. However, this reaction is non-stereoselective for both C(22)- (**169a**,**b**) and C(23)-nitrile oxides (**170a–d**).

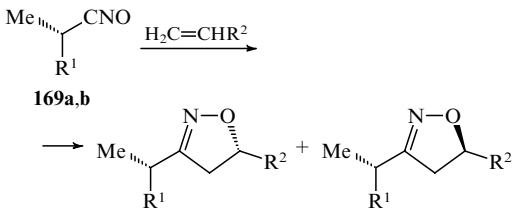

169a,**b**

R^1 = 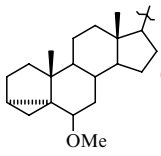 (**a**), 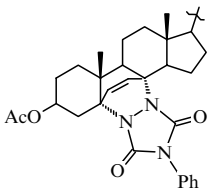 (**b**);

R^2 = CH_2OH, CH_2OAc, CMe_2OH, Ac, CH_2Br, Pr^i.

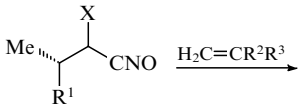

170a–d

R^1 = 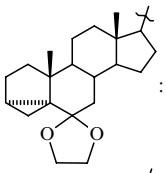 : X = H (**a**), OAc (**b**);

R^1 = 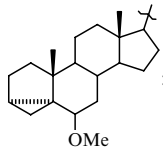 : X = H (**c**), OAc (**d**);

R^2 = H, R^3 = Me; R^2 = Me, R^3 = Pr^i.

The reactions of 3-methylidene-17-acetoxyandrostane (**171**) with aceto- and benzonitrile oxides gave mixtures of 3α- and 3β-isomers of the spiro derivatives **172** and **173** with the predominance of the former isomers (2.5–3) : 1.[145,146] The reactions of the steroid **171** with nitrile oxides RCNO, where R = $EtCO_2$, 2,4,6-$Me_3C_6H_2$, always give the only cycloaddition products, *viz*., the 3α-isomers **172** (yields 60% and 25%, respectively). The addition of triphenylacetonitrile oxide to alkene **171** yields a 1 : 1 mixture of two epimeric 4,5-dihydroisoxazoles in a total yield of 87%.[147]

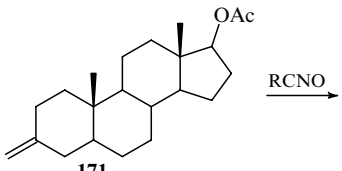

171

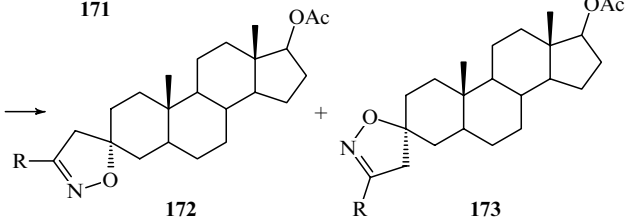

172 **173**

R = Me, Ph, Mes, CO_2Et, Ph_3C.

It was reported [145] that 1,3-dipolar cycloaddition of nitrile oxides to 17-methylidene steroids gives regioisomeric 4,5-dihydroisoxazoles *spiro*-conjugated to the steroid fragment in position 17. However, the configuration of the C(17) centre of the steroid has not been established (yield 60% – 70%).[145]

The stereochemistry of 1,3-dipolar cycloaddition of nitrile oxides to steroidal compounds with an endocyclic double bond is usually determined by the attack of the nitrile oxide from the less protected α-region of the steroid. Thus cycloaddition of arenecarbonitrile oxides to the spirost-5-ene derivatives [148] is regio- and stereoselective and results in 3′-substituted [5α,6α-*d*]-4,5-dihydroisoxazoles.

The published data concerning the addition of nitrile oxides to the Δ^{16}-bond of steroids are controversial.[149–155] In some cases, only [17α,16α-*d*]-4,5-dihydroisoxazoles or [16α,17α-*d*]-4,5-dihydroisoxazoles are exclusively formed, but the formation of two regioisomers was also reported. The composition of reaction products depends on the structure of the 1,3-dipole and the method used for its generation. It is of note that sometimes the Δ^5-bond and the cross-conjugated (3-oxo-1,4-diene) system are not involved in this reaction.

XI. Other examples of cycloaddition of nitrile oxides to acyclic alkenes

It was noted [105, 156, 157] that 1,3-dipolar cycloaddition of some achiral vinyl sulfones to nitrile oxides studied previously proceeds without any noticeable regioselectivity.

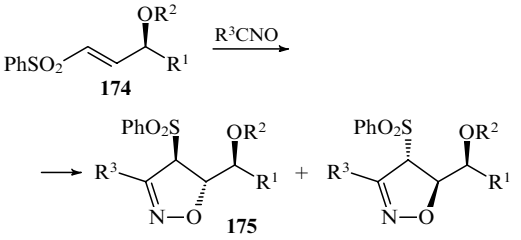

174 **175**

R^1 = Et, Pr^i; R^2 = Ac, MOM, Bu^tMe_2Si; R^3 = Me, Ph.

The reaction of the chiral vinyl sulfones **174** with nitrile oxides does not go to completion even in the presence of a large excess of the 1,3-dipole (the conversion is 36% – 68%).[158] In this case, only the regioisomers with the phenylsulfonyl group at C(4) are formed. The stereoselectivity of this reaction depends on the nature of substituents in both the alkene and nitrile oxide, however, the *anti*-adducts **175** are always predominant and in the case of the bulky substituents R^1 and R^2 they are virtually the only isolated products,[158] which is in agreement with the Houk model.

The first attempts at cycloaddition of nitrile oxides to the homochiral vinyl ethers **176a–f** [159] resulted in reaction products in low yields and with low diastereoselectivities.[160]

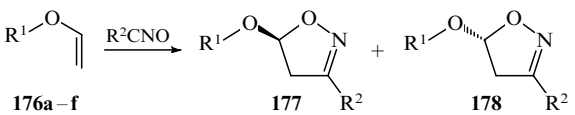

176a–f **177** **178**

R^1 = (–)-menthyl (**a**), 8-phenylmenthyl (**b**), (1*S*)-*endo*-bornyl (**c**), (*R*)-PhCH(CO_2Me) (**d**), (*S*)-1-(2-naphthyl)ethyl (**e**), (*S*)-1-phenylbutyl (**f**);
R^2 = Me, Et, Pr^n, Bu^t, Ph, $Ph(CH_2)_2$, 4-$NO_2C_6H_4$.

The best results were obtained for the vinyl ether **176e**,[161] *viz*., the ratio of the isomers **177** : **178** is (3–4) : 1 in reactions with almost all nitrile oxides. X-Ray diffraction data suggest that compounds **177** with the *R*-configurations of the newly formed chiral centres at the C(5) atoms are the predominant isomers.

1,3-Dipolar cycloaddition of nitrile oxides to allenes yields several reaction products.[162] The reaction of *N*,*N*-diarylamino allenes **179** with 1 equiv. of 3,5-dichloro-2,4,6-trimethylbenzonitrile oxide gives the adduct **180** with the involvement of the α,β-double bond and a small amount of the spirobisadduct **181**.[163]

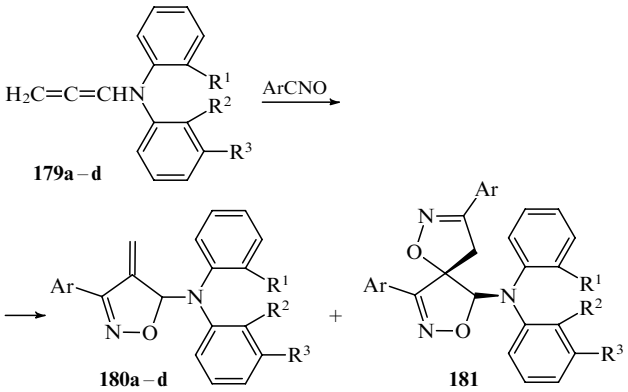

179a–d **180a–d** **181**

R^1 = R^2 = R^3 = H (**a**); R^1 – R^2 = $(CH_2)_2$, R^3 = H (**b**);
R^1 – R^2 = CH = CH, R^3 = H (**c**); R^1 = R^2 = H, R^3 = Me (**d**);
Ar = 3,5-Cl_2-2,4,6-Me_3C_6.

The reaction of the allenes **179** with 2 equivs. of the nitrile oxide gives only spiro compounds **181**. The α,β-double bond in the allenes **179** is more reactive due to the activating and polarisation effects of the nitrogen-containing substituent, which also controls the regio- and stereoselectivity of this reaction.

It was shown [164] that the fragment of proline benzyl ester plays the role of an effective chiral auxiliary group in the asymmetric addition of nitrile oxides to the alkenes **182**. This gives a mixture of the isomers **183** and **184** with the predominance of the former isomer. The regioselectivity does not depend on the reaction temperature and the nature of the substituent R^1. The reaction of the alkene **185** with benzo- and pivalonitrile oxides yields the adducts **186** and **187** in 10 : 1 and 9 : 1 ratios, respectively.[164]

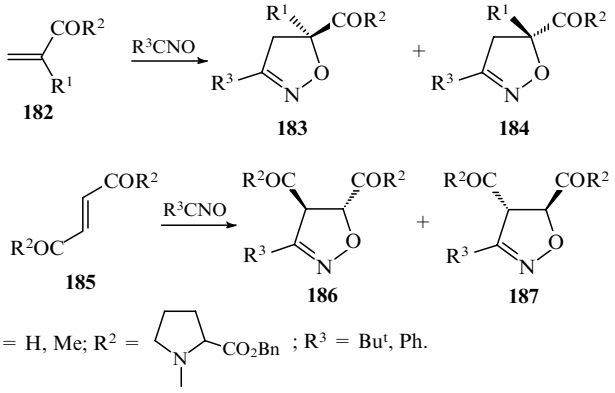

182 **183** **184**

185 **186** **187**

R^1 = H, Me; R^2 = ; R^3 = Bu^t, Ph.

3-Vinylcephalosporins **188** were used in the synthesis of novel 3-substituted cephalosporins **189**.[165] It was found that compounds **188** do not react with nitrile oxides generated from nitroalkanes under the action of phenyl isocyanate in the presence of triethylamine or *N*,*N*,*N*′,*N*′-tetramethylurea.

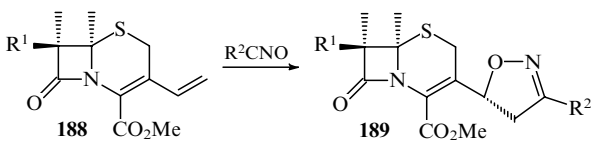

188 **189**

R^1 = BnCONH, $PhOCH_2CONH$; R^2 = Me, Et.

4,5-Dihydroxyisoxazoles **189** could be synthesised by the reaction of alkenes **188** with silyl nitronates as synthetic equivalents of nitrile oxides. These reactions result in *N*-silyloxyisoxazolidines which undergo spontaneous elimination of the trimethylsilanol group to yield 4,5-dihydroisoxazoles **189**; this reaction is regio- and stereoselective.

The simultaneous presence of C=C and C=N bonds in the molecule poses the problem of chemoselectivity.[166] Thus benzonitrile oxide and pivalonitrile oxide react with the heterodienes **190a**,**b** containing a terminal C=C bond to give the substituted 4,5-dihydroisoxazoles **191** in good yields. The cycloaddition of benzonitrile oxide to the β-substituted substrates **190c**–**e** involves exclusively the C = N bond resulting in 4,5-dihydro-1,2,4-oxadiazoles **192**. In this case, *E*-isomers react faster than *Z*-isomers. Compounds **190c**–**f** do not react with pivalonitrile oxide, apparently due to steric hindrance.[167]

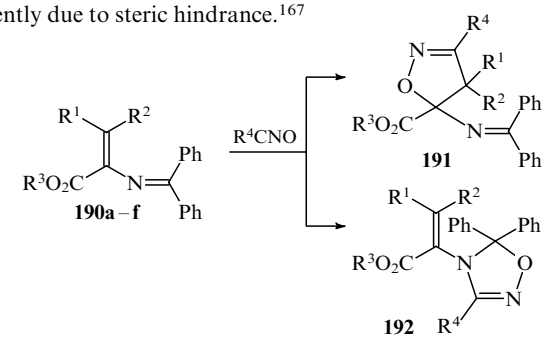

$R^1 = R^2 = H$: R^3 = Me (**a**), Et (**b**); R^1 = Me, $R^2 = H$, R^3 = Me (**c**); $R^1 = H$, $R^2 = R^3$ = Me (**d**); R^1 = Ph, $R^2 = H$, R^3 = Me (**e**); $R^1 = H$, R^2 = Ph, R^3 = Me (**f**); R^4 = Ph, Bu^t.

The irontricarbonyl complexes **193a**–**d** can be used to prepare 4,5-dihydroisoxazoles with a high degree of stereoselectivity.[168] This reaction results in the predominant formation of the epimers **194** [**194** : **195** = (7–9) : 1]. It is noteworthy that the formation of the isomers **195** is explained [168] by the presence of *cis*-rotamers in the original complexes **193**.

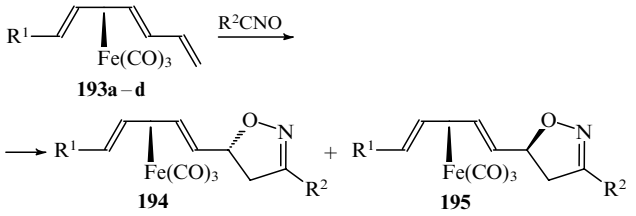

R^1 = Me (**a**), Et (**b**), Bu^t (**c**), Ph (**d**); R^2 = Me, CO_2Me, $CH_2OSiPh_2Bu^t$.

The chiral synthesis of (+)-(*S*)-[6]-gingerol was performed using the complex **193a**.[169]

It was shown that the use of the chromiumtricarbonyl complexes of the styrene derivatives **196** in the reaction with 3,5-dichloro-2,4,6-trimethyl-benzonitrile oxide results in the stereoselective synthesis of the adducts **197** with the *S*-configurations of the newly formed chiral centres at the C(5) atoms.[170] It is of note that the reaction of nitrile oxides with styrene proceeds in a non-stereoselective manner.

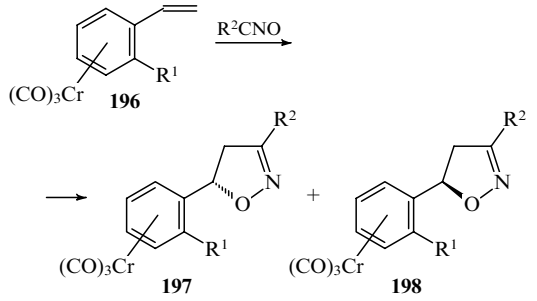

R^1 = OMe, Me, Cl; R^2 = 3,5-Cl_2-2,4,6-Me_3C_6.

R^1	Ratio **197** : **198**
OMe	80 : 20
Me	98 : 2
Cl	96 : 4

The cycloaddition of nitrile oxides to the η^1-allyliron complexes **199** [171] yields mixtures of 4,5-dihydroisoxazoles **200**. In the case of the chiral complexes **199b**,**c**, mixtures of diastereomeric 4,5-dihydroisoxazoles **200b**,**c**,**e**,**f** are formed in (59–93) : (41–7) ratios.

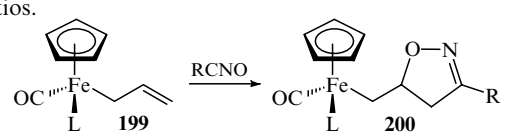

R = Ph: L = CO (**a**), (**b**), PPh_3 (**c**); R = Mes: L = CO (**d**); 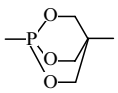 (**e**), PPh_3 (**f**).

The 1,3-dipolar addition of arenecarbonitrile oxides to the chiral vinyl sulfoxides **201** occurs with high regio- and stereoselectivity and results in (4*S*,5*R*,R_S)-4,5-dihydroisoxazoles **202**.[172, 173]

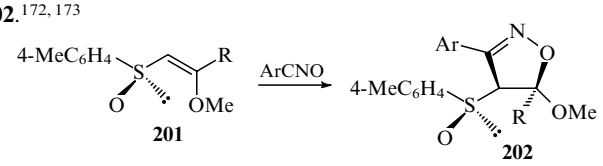

R = CH_2F, CHF_2, CF_3, C_2F_5;
Ar = Ph, 2,6-$Cl_2C_6H_3$, 3,5-Cl_2-2,4,6-Me_3C_6.

The effect of the sulfinyl group is much less pronounced if the latter is in the β-position relative to the double bond.[174] This reaction is characterised by full regioselectivity but moderate stereoselectivity and results in the formation of chiral 4,5-dihydroisoxazoles. Thus, the addition of 3,5-dichloro-2,4,6-trimethylbenzonitrile oxide to the allylic sulfoxide **203** results in the diastereomers **204** and **205** in a 1.4 : 1 ratio.[174]

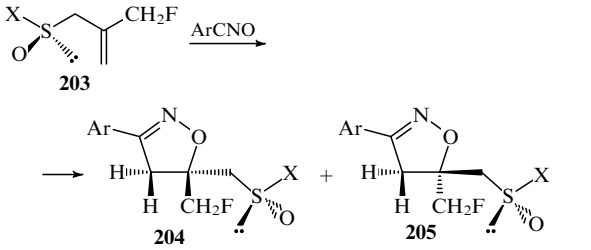

X = 4-MeC_6H_4; Ar = 3,5-Cl_2-2,4,6-Me_3C_6.

A mixture of the diastereomers **207** and **208** (2 : 1) is formed in the reaction of (*Z*)-allylic sulfoxide **206** with 3,5-dichloro-2,4,6-dimethylbenzonitrile oxide.

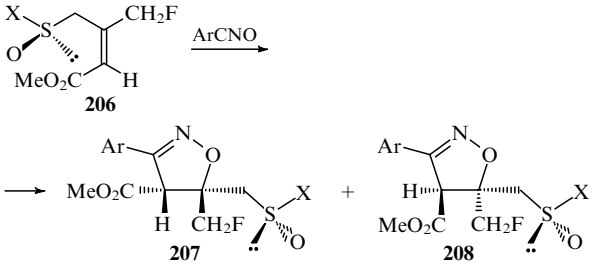

X = 4-MeC_6H_4; Ar = 3,5-Cl_2-2,4,6-Me_3C_6.

The dipolarophiles **209** have two chiral centres, *viz*., the sulfinyl group and the oxygen-containing substituent in the allylic position. Both functional groups influence the stereochemistry of the 1,3-dipolar cycloaddition.[175] The reactions of compounds (3*S*,R_S)-**209** with arenecarbonitrile oxides give mixtures of 4,5-dihydroisoxazoles **210** and **211**. In all cases studied, the epimers **210** were predominant (up to 67%).

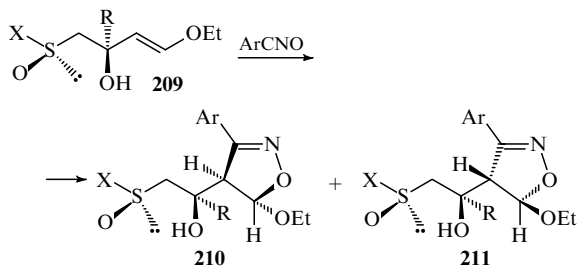

X = 4-MeC$_6$H$_4$; R = CF_3, CF_2Cl;
Ar = 3,5-Cl$_2$-2,4,6-Me$_3$C$_6$, 2,6-Cl$_2$C$_6$H$_3$.

It was found [176, 177] that baker's yeast *Saccharomyces cerevisiae* are effective chiral catalysts in reactions of asymmetric cycloaddition of nitrile oxides. Thus the addition of nitrile oxides to alkenes **212a–c** in the presence of baker's yeast and cyclodextrin gives 4,5-dihydroisoxazoles **213a–c** with high stereoselectivity.

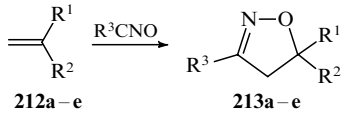

212a–e **213a–e**

R^1 = H: R^2 = 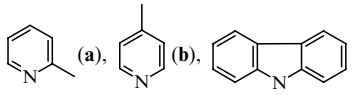 (**a**), (**b**), (**c**);

R^1 = Me: R^2 = CN (**d**), CO_2Me (**e**);

R^3 = Mes, 2,6-Cl$_2$C$_6$H$_3$, 2,4,6-(MeO)$_3$C$_6$H$_2$;

The electron-deficient dipolarophiles **212d,e** also gave optically active 4,5-dihydroisoxazoles **213d,e**.[178]

However, some authors [179] argue against this conclusion assuming that the isolation of only one enantiomer is due to the loss of the second enantiomer in the recrystallisation.

It was noted that cycloaddition of nitrile oxides to captodative alkenes **214** occurs in a regioselective manner and results in the isoxazoles **215**.[180] Here, alkenes **214** behave as acetylene equivalents.

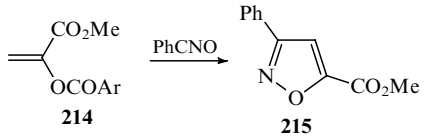

214 **215**

* * *

Thus, 1,3-dipolar cycloaddition of nitrile oxides to the double bond can be applied to various classes of compounds. In the majority of cases, this occurs with good yields and high regio- and, sometimes, stereoselectivity which allows its use for the solution of complex problems of organic synthesis. The reaction products, *viz*., 4,5-dihydroisoxazoles, present interest from the standpoint of their biological activities.[181, 182] In our opinion, further investigations into the cycloaddition of nitrile oxides to alkenes will be associated with the search for novel catalysts and chiral substituents for regio- and stereo-controlled addition.

References

1. C Grundmann, P Grunanger *The Nitrile Oxides* (New York: Springer, 1971)
2. A P Kozikowski *Acc. Chem. Res.* **17** 410 (1984)
3. P G Baraldi, A Barco, S Benetti, G P Pollini, D Simoni *Synthesis* 857 (1987)
4. F A Lakhvich, E V Koroleva, A A Akhrem *Khim. Geterotsikl. Soedin.* 435 (1989) [a]
5. D P Curran *Adv. Cycloadd.* **1** 129 (1988)
6. A A Akhrem, V A Khripach, F A Lakhvich, M I Zavadskaya, O A Drachenova, I A Zorinayu *Zh. Org. Khim.* **25** 2120 (1989) [b]
7. T Mukaijama, T Hoshino *J. Am. Chem. Soc.* **82** 5339 (1960)
8. K E Larsen, K B G Torssell *Tetrahedron* **40** 2985 (1984)
9. E Malamidou-Xenikaki, X N Stampelos, E Coutouli-Argyropoulou *J. Heterocycl. Chem.* **33** 563 (1996)
10. Yu Tokunaga, M Ihara, K Fukumoto *Heterocycles* **43** 1771 (1996)
11. G Kumaran, G H Kulkarni *J. Org. Chem.* **62** 1516 (1997)
12. O Moriya, H Takenaka, Y Urata, T Endo *J. Chem. Soc., Chem. Commun.* 1671 (1991)
13. A Baranski, E Cholewka *Pol. J. Chem.* **65** 319 (1991)
14. M H D Postema *Tetrahedron* **48** 8545 (1992)
15. J I Levin, P S Chan, J Couplet, T K Bailey, G Vice, L Thibauet, F Lai, A M Venkatesan, A Cobuzzi *Bioorg. Med. Chem. Lett.* **4** 1703 (1994)
16. C W Holzapfel, K Bischofberger, J Olivier *Synth. Commun.* **24** 3197 (1994)
17. A Studer, D P Curran *Tetrahedron* **53** 6681 (1997)
18. K Halling, K B G Torssell, R G Hazell *Acta Chem. Scand.* **45** 736 (1991)
19. G Burton, G J Clarke, J D Douglas, A J Eglington, C H Frydrych, J D Hinks, N W Hird, E Hunt, S F Moss, A Naylor, N H Nicholson, M J Pearson *J. Antibiot.* **49** 1266 (1996)
20. R Alguacil, F Farina, M V Martin *Tetrahedron* **52** 3457 (1996)
21. D P Curran, T A Heffner *J. Org. Chem.* **55** 4585 (1990)
22. K Bast, M Christl, R Huisgen, W Mack, R Sustman *Chem. Ber.* **106** 3258 (1973)
23. K Bast, M Christl, R Huisgen, W Mack *Chem. Ber.* **106** 3312 (1973)
24. J Mann, B Pietrzak *Tetrahedron* **45** 1549 (1989)
25. D N Nicolaides, K C Fylaktakidou, K E Litinas *J. Heterocycl. Chem.* **33** 967 (1996)
26. T-J Lu, L-J Sheu *J. Chin. Chem. Soc. (Taipei)* **42** 877 (1995)
27. A P Kozikowski, Y Kitagawa, J P Springer *J. Chem. Soc., Chem. Commun.* 1460 (1983)
28. R H Jones, G C Robinson, E J Thomas *Tetrahedron* **40** 177 (1984)
29. D A Barr, M J Dorrity, R Grigg, J F Malone, J Montgomeri, S Rajviroonigit, P Stevenson *Tetrahedron Lett.* **31** 6569 (1990)
30. A P Kozikowski, A P Cheng *Tetrahedron Lett.* **28** 3189 (1987)
31. D P Curran, S A Gothe *Tetrahedron* **44** 3945 (1988)
32. V Jiger, I Muller, R Schohe, M Frey, R Ehrler, B Hafele, D Schroter *Lect. Heterocycl. Chem.* **8** 79 (1985)
33. V Jiger, R Schohe, E F Paulus *Tetrahedron Lett.* **24** 5501 (1983)
34. A P Kozikowski, A K Ghosh *J. Org. Chem.* **49** 2762 (1984)
35. A P Kozikowski, A K Ghosh *J. Am. Chem. Soc.* **104** 5788 (1982)
36. M B Gravestock, R M Paton, C J Todd *Tetrahedron Asymmetry* **6** 2723 (1995)
37. P Caramella, N G Rondan, M N Paddon-Row, K N Houk *J. Am. Chem. Soc.* **103** 2438 (1981)
38. A Kamimura *J. Synth. Org. Chem. Jpn.* **50** 808 (1992)
39. K N Houk, S R Moses, Y-D Wu, N G Rondan, V Jiger, R Schohe, R Fronczek *J. Am. Chem. Soc.* **106** 3880 (1984)
40. K N Houk, H-Y Duh, Y-D Wu, S R Moses *J. Am. Chem. Soc.* **108** 2754 (1986)
41. J Chanet-Ray, M O Charmier-Januario, S Chou, R Vessiere *J. Chem. Res. (S)* 382 (1994)
42. V Jäger, R Müller, T Leibold, M Hein, M Schwarz, M Fengler, L Jaroskova, M Paetzel, P LeRoy *Bull. Soc. Chim. Belg.* **103** 491 (1994)
43. N G Rondan, M N Paddon-Row, P Caramella, J Mareda, P H Muller, K N Houk *J. Am. Chem. Soc.* **104** 4974 (1982)
44. R Annunziata, M Benaglia, M Cinquini, L Raimondi *Tetrahedron* **49** 8629 (1993)
45. D P Curran, B H Kim *Synthesis* 312 (1986)
46. E Lukevics, V Dirnens, A Kemme, J Popelis *J. Organomet. Chem.* **521** 235 (1996)
47. R Annunziata, M Benaglia, M Cinquini, F Cozzi, L Raimondi *J. Org. Chem.* **60** 4697 (1995)
48. G Keum, Y J Chung, B H Kim *Bull. Korean Chem. Soc.* **13** 343 (1992)
49. T Moriwake, S Hamano, S Saito, S Torii *Chem. Lett.* 2085 (1987)
50. S Fushiya, H Chiba, A Otsubo, S Nozoe *Chem. Lett.* 2229 (1987)
51. E C Boyd, R M Paton *Tetrahedron Lett.* **34** 3169 (1993)

52. A J Blake, E C Boyd, R O Gould, R M Paton *J. Chem. Soc., Perkin Trans. 1* 2841 (1994)
53. D P Curran, S-M Choi, S A Gothe, F-t Lin *J. Org. Chem.* **55** 3710 (1990)
54. T Nishi, Y Morisawa *Heterocycles* **29** 1835 (1989)
55. A A Hagedorn III, B J Miller, J O Nagy *Tetrahedron Lett.* **21** 229 (1980)
56. P A Wade, S M Singh, M K Pillay *Tetrahedron* **40** 601 (1984)
57. A P Kozikowski, X M Cheng *Tetrahedron Lett.* **26** 4047 (1985)
58. D M Vyas, Y Chiang, T W Doyle *Tetrahedron Lett.* **25** 487 (1984)
59. D P Curran, S A Gothe, S M Choi *Heterocycles* **35** 1371 (1993)
60. W Oppolzer, G Poli, C Starkemann, G Bernardinelli *Tetrahedron Lett.* **29** 3559 (1988)
61. D P Surran, B H Kim, H P Piyasena, R J Loncharich, K N Houk *J. Org. Chem.* **52** 2137 (1987)
62. T Akiyama, H Nishimoto, K Ishikawa, S Ozaki *Chem. Lett.* 447 (1992)
63. T Akiyama, K Okada, S Ozaki *Tetrahedron Lett.* **33** 5763 (1992)
64. L Zhang, J C Chung, T D Costello, I Valvis, P Ma, S Kauffman, R Ward *J. Org. Chem.* **62** 2466 (1997)
65. T Olsson, K Stern, G Westman, S Sundell *Tetrahedron* **46** 2473 (1990)
66. T Olsson, K Stern, S Sundell *J. Org. Chem.* **53** 2468 (1988)
67. M A Weidner-Wells, S A Fraga, J P Demers *Tetrahedron Lett.* **35** 6473 (1994)
68. D P Surran, B H Kim, J Daugherty, T A Heffner *Tetrahedron Lett.* **29** 3555 (1988)
69. D P Curran, K Jeong, T A Heffner, J Rebek *J. Am. Chem. Soc.* **111** 9238 (1989)
70. S Kanemasa, K Onimura *Tetrahedron* **48** 8645 (1992)
71. B H Kim, J Y Lee *Tetrahedron Asymmetry* **2** 1359 (1991)
72. B H Kim, D P Curran *Tetrahedron* **49** 293 (1993)
73. S Kanemasa, K Onimura *Tetrahedron* **48** 8631 (1992)
74. W Oppolzer *Tetrahedron* **43** 1969 (1987)
75. K S Kim, B H Kim, W M Park, S J Cho, B J Mhin *J. Am. Chem. Soc.* **115** 7472 (1993)
76. J A Stack, T A Heffner, S J Geib, D P Curran *Tetrahedron* **49** 995 (1993)
77. D P Curran, M-H Yoon *Tetrahedron* **53** 1971 (1997)
78. S Kanemasa, T Hayashi, H Yamamoto, E Wada, T Sakurai *Bull. Chem. Soc. Jpn.* **64** 3274 (1991)
79. S Kanemasa, K Onimura, E Wada, J Tanaka *Tetrahedron Asymmetry* **2** 1185 (1991)
80. Y H Kim, S H Kim, D H Park *Tetrahedron Lett.* **34** 6063 (1993)
81. C Kashima, I Fukuchi, K Takahashi, A Hosomi *Tetrahedron Lett.* **34** 8305 (1993)
82. C Kashima, K Takahashi, I Fukuchi, K Fukusaka *Heterocycles* **44** 289 (1997)
83. B H Kim, Y J Chung, G Keum, J Kim, K Kim *Tetrahedron Lett.* **33** 6811 (1992)
84. A G Meyer, C J Easton, S F Lincoln, G W Simpson *Chem. Commun.* 1517 (1997)
85. P C B Page, M Purdie, D Lathbury *Tetrahedron* **53** 1061 (1997)
86. S Kanemasa, M Nishiuchi, A Kamimura, K Hori *J. Am. Chem. Soc.* **116** 2324 (1994)
87. S Kanemasa, S Kabayashi, M Nishiuchi, H Yamamoto, E Wada *Tetrahedron Lett.* **32** 6367 (1991)
88. S Kanemasa, M Nishiuchi *Tetrahedron Lett.* **34** 4011 (1993)
89. S Kanemasa, S Kobayashi *Bull. Chem. Soc. Jpn.* **66** 2685 (1993)
90. H R Kim, J H Song, S Y Rhie, E K Ryu *Synth. Commun.* **25** 1801 (1995)
91. J N Kim, H R Kim, E K Ryu *Synth. Commun.* **23** 1673 (1993)
92. G Bianchi, C De Micheli, R Gandolfi, P Grunanger, P V Finzi, O V de Pava *J. Chem. Soc., Perkin Trans. 1* 1148 (1973)
93. S Kanemasa, M Nichiuchi, E Wada *Tetrahedron Lett.* **33** 1357 (1992)
94. S Kanemasa, K Okuda, H Yamamoto, S Kaga *Tetrahedron Lett.* **38** 4095 (1997)
95. F De Sarlo, A Guarna, A J Brandi *J. Heterocycl. Chem.* **20** 1505 (1983)
96. T-Y Lu, J-F Yang, L-J Sheu *J. Org. Chem.* **60** 7701 (1995)
97. A Kamimura, K Hori *Tetrahedron* **50** 7969 (1994)
98. R Annunziata, M Cinquini, F Cozzi, L Raimondi *Tetrahedron* **44** 4645 (1988)
99. A Pelter, K Smith, H C Brown *Borane Reagents* (London: Academic Press, 1988)
100. M Jazouli, B Carboni, R Carrie, M Soufiaoui, L Toupet *J. Heteroatom. Chem.* **5** 513 (1994)
101. M Jazouli, S Baba, B Carboni, R Carrie, M Soufiaoui *J. Organomet. Chem.* **498** 229 (1995)
102. J D Bonk, M D Avery *Tetrahedron Asymmetry* **8** 1149 (1997)
103. D A Singleton, J P Martinez, G M Ndip *J. Org. Chem.* **57** 5768 (1992)
104. D S Matteson *J. Org. Chem.* **27** 4293 (1962)
105. R H Wallace, J Liu *Tetrahedron Lett.* **35** 7493 (1994)
106. M Barzaghi, P L Beltrame, P D Croce, P D Buttero, E Licandro, S Maiorana, G Zecchi *J. Org. Chem.* **48** 3807 (1983)
107. R H Wallace, K K Zong *Tetrahedron Lett.* **33** 6941 (1992)
108. A Zhang, Y Kan, G Zhao, B Jiang *Tetrahedron* **56** 965 (2000)
109. A Brandi, P Cannavo, K M Pietrusiewicz, M Zablocka, M Wieczorek *J. Org. Chem.* **54** 3073 (1989)
110. S K Armstrong, E W Collington, J G Kight, A Naylor *J. Chem. Soc., Perkin Trans. 1* 1433 (1993)
111. R M Paton, A A Young *J. Chem. Soc., Chem. Commun.* 132 (1991)
112. R M Paton, A A Young *J. Chem. Soc., Perkin Trans. 1* 629 (1997)
113. A J Blake, R O Gould, K E McGhie, R M Paton, D Reed, I H Sadler, A A Young *Carbohydr. Res.* **216** 461 (1991)
114. M De Amici, C De Micheli, A Ortisi, G Gatti, R Gandolfi, L Toma *J. Org. Chem.* **54** 793 (1989)
115. A J Blake, G Kirkpatrick, K E McGhie, R M Paton, K J Penman *J. Carbohydr. Chem.* **13** 409 (1994)
116. A J Blake, R O Gould, R M Paton, A A Young *J. Chem. Res. (S)* 482 (1993)
117. R M Paton, A A Young *J. Chem. Soc., Chem.Commun.* 993 (1994)
118. R M Paton, K J Penman *Tetrahedron Lett.* **35** 3163 (1994)
119. K E McGhie, R M Paton *Tetrahedron Lett.* **34** 2831 (1993)
120. M Mancera, I Roffe, J A Galbis *Tetrahedron* **51** 6349 (1995)
121. H -J Gi, Y Xiang, K Zhao *J. Org. Chem.* **62** 88 (1997)
122. Y Xiang, J Chen, R F Schinazi, K Zhao *Bioorg. Med. Chem. Lett.* **6** 1051 (1996)
123. A V Baranovskii, R P Litvinovskaya, V A Khripach *Zh. Org. Khim.* **26** 1274 (1990) [b]
124. R P Litvinovskaya, S V Drach, Yu I Lapchinskaya, V A Khripach *Zh. Org. Khim.* **37** 57 (2001) [b]
125. R P Litvinovskaya, A S Lyakhov, S V Drach, V A Khripach, A A Govorova *Zh. Obshch. Khim.* **70** 1571 (2000) [c]
126. H G Cutler, T Yokota, G Adam (Eds) *Brassinosteroids: Chemistry, Bioactivity and Applications* (Washington, DC: American Chemical Society 1991)
127. R K Tkhaper, I G Reshetova, A V Kamernitskii, R P Litvinovskaya *Izv. Akad. Nauk SSSR, Ser. Khim.* 969 (1991) [d]
128. USSR P. 1 747 455; *Byull. Izobret.* (26) 80 (1992)
129. Russ. P. 1 786 807; *Byull. Izobret.* (3) 321 (1996)
130. V A Khripach, R P Litvinovskaya, S V Drach *Zh. Org. Khim.* **29** 717 (1993) [b]
131. R P Litvinovskaya, N V Koval', V A Khripach *Khim. Geterotsikl. Soedin.* 267 (1998) [a]
132. A I Verenich, A A Govorova, N M Galitskii, A V Baranovskii, R P Litvinovskaya, V A Khripach *Zh. Strukt. Khim.* 552 (1992) [e]
133. A A Akhrem, V A Khripach, R P Litvinovskaya, A V Baranovskii, M I Zavadskaya, A N Kharitonovich, E V Borisov, F A Lakhvich *Zh. Org. Khim.* **25** 1901 (1989) [b]
134. R P Litvinovskaya, S V Drach, V A Khripach *Mendeleev Commun.* 215 (1995)
135. R P Litvinovskaya, V A Tereshko, S V Drach, V A Khripach *Zh. Obshch. Khim.* **66** 859 (1996) [c]
136. R P Litvinovskaya, A S Lyakhov, A A Govorova, S V Drach, V A Khripach *Bioorg. Khim.* **23** 147 (1997) [f]
137. R P Litvinovskaya, S V Drach, V A Khripach *Zh. Org. Khim.* **35** 1653 (1999) [b]
138. R P Litvinovskaya, S V Drach, V A Khripach *Zh. Org. Khim.* **36** 1838 (2000) [b]
139. R P Litvinovskaya, S V Drach, E A Ermolenko, V A Khripach *Zh. Org. Khim.* **34** 1037 (1998) [b]
140. V A Khripach, V N Zhabinskii, N D Pavlovskii *Zh. Org. Khim.* **35** 390 (1999) [b]
141. V A Khripach, V N Zhabinskii, A I Kotyatkina *Zh. Org. Khim.* **29**1569 (1993) [b]

142. R P Litvinovskaya, Doctoral Thesis in Chemical Sciences, Institute of Bioorganic Chemistry, National Academy of Sciences of Belarus, Minsk, 1998
143. R P Litvinovskaya, S V Drach, V A Khripach *Zh. Org. Khim.* **33** 201 (1997) [b]
144. V A Khripach, V N Zhabinskii, N D Pavlovskii *Zh. Org. Khim.* **34** 59 (1998) [b]
145. C Parini, S Colombi, A Ius, R Longhi, G Vecchio *Gazz. Chim. Ital.* **107** 559 (1977)
146. J Kalvoda, H Kaufmann *J. Chem. Soc., Chem. Commun.* 209 (1976)
147. H Kaufmann, J Kalvoda *J. Chem. Soc., Chem. Commun.* 210 (1976)
148. A U Siddiqui, A H Siddiqui, T S Ramaiah *J. Indian Chem. Soc.* **69** 282 (1992)
149. W Fritsch, G Seidl, H Ruschig *Liebigs Ann. Chem.* **677** 139 (1964)
150. U Stache, W Fritsch, H Ruschig *Liebigs Ann. Chem.* **685** 228 (1965)
151. G W Moersch, E L Wittle, W A Neuklis *J. Org. Chem.* **43** 1272 (1965)
152. T Kwon, A S Heiman, E T Oriaku, K Yoon, H J Lee *J. Med. Chem.* **38** 1048 (1995)
153. M Khalil, M F Maponya, D H Ko, Z You, E I Oriaku, H J Lee *Med. Chem. Res.* 52 (1996)
154. A Ius, C Parini, G Sportoletti, G Vecchio, G Ferrara *J. Org. Chem.* **36** 3470 (1971)
155. T Kametani, H Furuyuma, T Honda *Heterocycles* **19** 357 (1982)
156. P Saramella, E Albini, T Bandiera, A C Coda, P Grunanger, F M Albini *Tetrahedron* **39** 689 (1983)
157. A Bened, R Durand, D Pioch, P Geneste *J. Org. Chem.* **47** 2461 (1982)
158. J De Blas, J C Carretero, E Dominguez *Tetrahedron Asymmetry* **6** 1035 (1995)
159. T V Rajan Babu, G S Reddy *J. Org. Chem.* **51** 5458 (1986)
160. A N Boa, S E Booth, D A Dawkins, P R Jenkins, J Fawcett, D R Russell *J. Chem. Soc., Perkin Trans. 1* 1277 (1993)
161. A N Boa, D A Dawkins, A R Hergueta, P R Jenkins *J. Chem. Soc., Perkin Trans. 1* 953 (1994)
162. G Broggini, G Zecchi *Gazz. Chim. Ital.* **126** 479 (1996)
163. G Broggini, G Molteni, G Zecchi *J. Chem. Res. (S)* 203 (1993)
164. H Waldmann *Liebigs Ann. Chem.* 1013 (1990)
165. J Pitlik *Synth. Commun.* **24** 243 (1994)
166. C Balzamini, G Spadoni, A Bedini, M Lanfranchi, M Pellinghelli *J. Heterocycl. Chem.* **29** 1593 (1992)
167. G Spadoni, C Balsamini, A Bedini, E Duranti, Tontini *J. Heterocycl. Chem.* **29** 305 (1992)
168. T LeGall, J-P Lellouche, L Toupet, J-P Beaucourt *Tetrahedron Lett.* **30** 6517 (1989)
169. T LeGall, J-P Lellouche, J-P Beaucourt *Tetrahedron Lett.* **30** 6521 (1989)
170. C Baldoli, P Buttero, S Maiorana, G Zecchi *Tetrahedron Lett.* **34** 2529 (1993)
171. W Malisch, J Zöller, M Schwarz, V Jäger, A M Arif *Chem. Ber.* **127** 1243 (1994)
172. P Bravo, L Bruche, A Merli, G Fronza *Gazz. Chim. Ital.* **124** 275 (1994)
173. P Bravo, L Bruche, M Crucianelli, A Farina, S V Meille, A Merli, P Seresini *J. Chem. Res. (S)* 348 (1996)
174. P Bravo, L Bruche, P Seresini, M Zanda, A Arnone *J. Heterocycl. Chem.* **34** 489 (1997)
175. A Arnone, P Bravo, L Bruche, P Seresini *J. Chem. Res. (S)* 198 (1996)
176. K R Rao, N Bhanumathi, P B Sattur *Tetrahedron Lett.* **31** 3201 (1990)
177. K R Rao, Y V D Nageswar, H M Sampathkumar *J. Chem. Soc., Perkin Trans. 1* 3199 (1990)
178. R K Rao, Y V D Nageswar, N Bhanumathi, T N Srinivasan *Indian J. Chem.* **B33** 171 (1994)
179. C J Easton, C M Hughes, E R Tiekink *Tetrahedron Lett.* **36** 629 (1995)
180. R Jimenez, L Perez, J Tamariz, H Salgado *Heterocycles* **35** 591 (1993)
181. Ch Samoutsis, S Nikolaropoulos *J. Heterocycl. Chem.* **35** 731 (1998)
182. S V Drach, R P Litvinovskaya, V A Khripach *Khim. Geterotsikl. Soedin.* 291 (2000) [a]

[a] — *Chem. Heterocycl. Compd. (Engl. Transl.)*
[b] — *Russ. J. Org. Chem. (Engl. Transl.)*
[c] — *Russ. J. Gen. Chem. (Engl. Transl.)*
[d] — *Russ. Chem. Bull. (Engl. Transl.)*
[e] — *J. Struct. Chem. (Engl. Transl.)*
[f] — *Russ. J. Bioorg. Chem. (Engl. Transl.)*

Russian Chemical Reviews **70** (5) 425 – 447 (2001) © 2001 Russian Academy of Sciences and Turpion Ltd

DOI 10.1070/RC2001v070n05ABEH000635

Problems of control of the reactivity of macroradicals and the growth of polymer chains

D F Grishin, L L Semyonycheva

Contents

I. Introduction 425
II. Coordination interactions of organic compounds of Group II and III elements with macroradicals and their influence on chain propagation 425
III. Growth of the polymer chain in the presence of stable radicals and iniferters 435
IV. Characteristic features of homo- and co-polymerisation of vinyl monomers in the presence of organoelement compounds derived from Group V elements 441
V. Conclusion 443

Abstract. Data on the influence of stable radicals, iniferters, organoelement compounds and other active additives on the reactivity of macroradicals and the elementary steps of the (co)polymerisation of acrylic and some other monomers are generalised. New approaches to the control of the lifetime of the polymer chain and of the chain propagation stage are analysed. The problems of synthesis of compositionally homogeneous homo- and copolymers by radical polymerisation are considered. The bibliography includes 247 references.

I. Introduction

Polymerisation involving radical species has long been and still remains the key method for the synthesis of polymers. Obvious advantages of radical polymerisation are the methodical and technical simplicity of its implementation and good reproducibility of the results. A significant drawback of the method which somewhat delays its practical use is the difficulty of controlling the kinetics of polymerisation and compositional homogeneneity of the products, caused by the fact that the reactivity of free radicals participating in the polymerisation barely depends on the medium composition or other conditions.[1–4]

In this connection, development of effective methods for controlling the growth and the lifetime of a polymer chain is a topical task. This problem could be solved if it were possible to change the reactivity of the chain-propagating radicals in the required manner.

In recent years, several new approaches for controlling the growth of a polymer chain under the conditions of radical polymerisation have been proposed. These approaches include reversible inhibition by stable radicals, the use of iniferters as controlling initiators of a new type and the use of catalytic amounts of stable radicals or coordinatively unsaturated organoelement compounds (OEC) as reactive additives, *etc*. These methods have been used to develop effective methods for the synthesis of compositionally uniform polymeric materials with a specified set of properties. This review is devoted to the analysis of these methods.

D F Grishin, L L Semyonycheva Research Institute of Chemistry, N I Lobachevsky Nizhnii Novgorod State University, prosp. Gagarina 23/5, 603600 Nizhnii Novgorod, Russian Federation.
Fax (7-831) 235 64 80. Tel. (7-831) 265 81 62.
E-mail: grishin@ichem.unn.runnet.ru (D F Grishin)
Tel. (7-831) 265 74 51 (L L Semyonycheva)

Received 13 November 2000
Uspekhi Khimii **70** (5) 486 – 510 (2001); translated by Z P Bobkova

II. Coordination interactions of organic compounds of Group II and III elements with macroradicals and their influence on chain propagation

The search for the ways of target-directed change in the reactivity of monomers and chain-propagating radicals directly during polymerisation is one of the most important aspects in the studies on the methods of synthesis of polymeric materials of a particular structure with specified properties.

In the 1970 – 1980s, the vigorous studies concerning the use of protic and aprotic Lewis acids (halides of Group II and III elements and some transition metals) for controlling the reactivity of vinyl and, especially, acrylic monomers carried out in a number of leading scientific schools of the world gave rise to a new line of research in the synthetic chemistry of polymers, namely, coordinated radical polymerisation.[5–7]

It was found that Lewis acids, which are strong electron acceptors, can substantially influence the electron density distribution over the monomer π-bond and functional group and are thus able to change the kinetic parameters of homo- and copolymerisation and the relative activities of monomers. On the basis of this approach, original methods for the synthesis of alternating and compositionally homogeneous copolymers, physiologically active high-molecular-mass compounds, graft and block copolymers, and a number of promising composite materials have been developed.

The main drawback of this method for modification of polymeric materials is that the controlling additive is introduced, as a rule, in a substantial excess with respect to the initiator (1% – 5% relative to the monomer). This leads to contamination of the resulting polymer. The cost of its purification is high; therefore, this method for the control of the composition and structure of polymers does not have prospects in industry.

The use of OEC as initiators has laid the foundations of a new stage in the development of the synthetic chemistry of polymers.

The Ziegler – Natta catalysts proposed for the synthesis of homo- and copolymers of alkenes and dienes are of limited utility for (co)polymerisation of vinyl monomers, especially acrylates,

because these monomers are highly reactive towards the components of these organometallic catalysts.[8]

Conversely, initiating systems based on alkyl derivatives of non-transition elements and oxidants including organic and organoelement peroxides (OEP) not only initiate efficiently radical homo- and copolymerisation of a broad range of monomers but also control the composition of copolymers and the kinetics of processes; they also change noticeably the properties of polymers. Based on the analysis of the characteristic features of polymerisation kinetics and unusual properties of macromolecules synthesised in the presence of organoelement initiators, it was initially suggested and later convincingly proved that the features mentioned above are related to the coordination interaction of the OEC with the growing radical. This interaction promotes an increase in the electron-withdrawing properties (electrophilicity) of the macroradical.[9–11]

1. The effect of coordinatively unsaturated organoelement compounds on the polymerisation kinetics of vinyl monomers and on the molecular-mass characteristics of polymers

Among organoelement initiators of the redox type, it is necessary first of all to distinguish compositions based on alkyl derivatives of boron and aluminium, which possess a number of advantages over the conventional radical initiators.[11–20] In particular, boron and aluminium alkyl derivatives in combination with organic and organoelement peroxides permit one to carry out polymerisation of vinyl monomers, which occurs at a high initial rate over a broad temperature range,† from 0 to 50 °C,[13–15] and copolymerisation of vinyl monomers with alkenes and allylic monomers.[23–25] Polymers and copolymers prepared in the presence of these organoelement initiators have unusual properties such as stability against thermal treatment and unusual molecular-mass characteristics; copolymers possess a number of unique mechanical properties.[13–29]

In view of the fact that the rates of chain propagation during the synthesis are high and based on the studies of some physicochemical properties of the prepared polymers, it has been suggested [14,27–29] that components of an organoelement initiator not only participate in the stage of generation of chain-propagating radicals but also influence the chain propagation and termination stages.

It is known that unsaturated compounds including monomers are able to be coordinated to OEP.[30–32] In these compounds, monomers act as electron density donors. On the one hand, complex formation increases the rate of peroxide decomposition and, hence, increases the initiation rate, while, on the other hand, it favours redistribution of electron density on the monomer π-bond and thus changes the reactivity of the monomer including that with respect to radicals. Similar complexes of vinyl monomers with Lewis acids (metal halides) have long been known and studied in detail.[5] It was shown reliably by IR [33–36] and NMR [37] spectroscopy that metal halides are coordinated to the carbonyl group of the monomer. The constants of complex formation of organic compounds of Group III elements with methyl methacrylate (MMA) and acrylonitrile (AN) were estimated taking organoaluminium compounds as examples.[38]

If the concentration of the OEC used as the initiator amounts to 0.01 mol.% – 0.05 mol.%, the formation of OEC complexes with radicals,[39–41] including polymeric radicals, appears more likely.[28,33] Upon the OEC – radical coordination interaction, the electron-withdrawing properties of the growing macroradical are enhanced and its reactivity with respect to the multiple bonds in monomers increases. This interaction results in a higher rate constant for chain propagation. In addition, due to steric factors and the enhanced electrophilicity of the species, the rate constant for chain termination decreases.

† For vinyl chloride (VC), this range is −60 to 50 °C.[15,19,21,22]

In a series of studies,[17–19,40,41] it was demonstrated that the addition of catalytic amounts of OEC derived from Group II and III elements in a polymerising mixture which contains peroxide and azo initiators entails an increase in the rate of polymerisation of (meth)acrylic and some vinyl monomers and markedly influences the properties of the resulting polymers (Table 1).

Table 1. Influence of triisobutylborane (TIBB) on the rate of polymerisation (V) of vinyl monomers and the molecular mass (MM) of polymers (T = 313 K).

Monomer	Initiator (0.1 mol.%)	TIBB (mol.%)	$10^4 V$ /mol litre^{-1} s^{-1}	10^{-3} MM
VA	AIBN	0.0	0.3	737
		0.2	1.7	614
		0.3	6.0	503
BA	DCHPD	0.0	0.3	2680
		0.2	19.9	610
		0.4		440
		0.6		380
		0.8		200
AN	AIBN	0.0	21.0	–
		0.5	159.2	–
		1.0	295.1	–
		1.5	237.3	–
MMA	DCHPD	0.0	0.7	610
		0.2	1.1	586
		0.4	1.5	560
			1.8	
AA	DCHPD	0.0	0.09	9.4
(in THF)		0.015	0.22	–
		0.045	0.56	–
		0.060	1.12	7.7
St	DCHPD	0.0	3.4	1800
		0.2	3.6	1780
		0.3	3.7	1660

Note. The following designations are used: VA is vinyl acetate, AIBN is azobisisobutyronitrile; BA is butyl acrylate, DCHPD is dicyclohexyl peroxydicarbonate, AA is acrylamide, St is styrene.

Thus the rate of polymerisation of AN and butyl acrylate (BA) increases by almost two orders of magnitude upon introduction of trialkylborane in the system. Meanwhile, although organoboron compounds are capable of initiating homolytic decomposition of hydroperoxides,[42,43] they do not exert catalytic action on the decomposition of acyl peroxides [in particular, benzoyl peroxide (BP)[44] or dicyclohexyl peroxydicarbonate (DCHPD)],[18] or other compounds,[45] used in the studies cited as initiators. The researchers concluded that the accelerating influence of trialkylboranes on the polymerisation of polar vinyl monomers can be due exclusively to the coordination interaction of the growing macroradicals with the boron atom in the OEC. This interaction occurs either directly at the reaction centre (with participation of the unpaired electron), or at the functional group

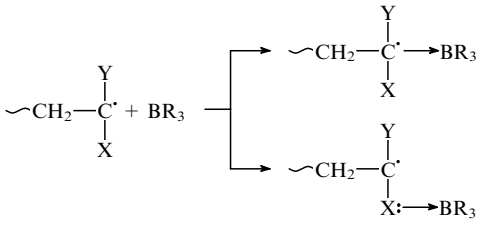

(1)

(where X is a functional group, Y is the hydrogen atom or a methyl group), or simultaneously at both sites with delocalisation of the unpaired electron

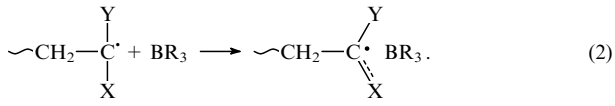

(2)

On the basis of studies of copolymerisation of MMA with electron-donating monomers involving binary trialkylborane–OEP initiators,[11,14] it was suggested that the Lewis acid might be involved in the coordination interaction with the poly(methyl methacrylate) (PMMA) radical; this hypotheisis was proved by EPR spectroscopy[28,46] and confirmed by quantum-chemical calculations.[47] In addition, it was shown by quantum-chemical calculations[48] that in the case of radicals containing a C=O group in the α-position to the reaction centre, the reaction centre is delocalised over three atoms.

Unlike metal halides (Lewis acids), organometallic additives introduced in the system in amounts comparable with the initiator concentration (0.1 mol.% – 0.5 mol.% with respect to the monomer), influence appreciably the growth of the polymer chain. This fact indicates unambiguously that an increase in the polymerisation rate in the presence of these compounds is due to complex formation of the OEC exactly with the macroradical rather than with the monomer.

It has been suggested[49] that one OEC molecule can participate consecutively in several chain propagation steps, while retaining the growing macroradical in its coordination sphere. In this case, chain propagation occurs in a cyclic reaction complex which incorporates the growing macroradical, the monomer, and the complex-forming agent.

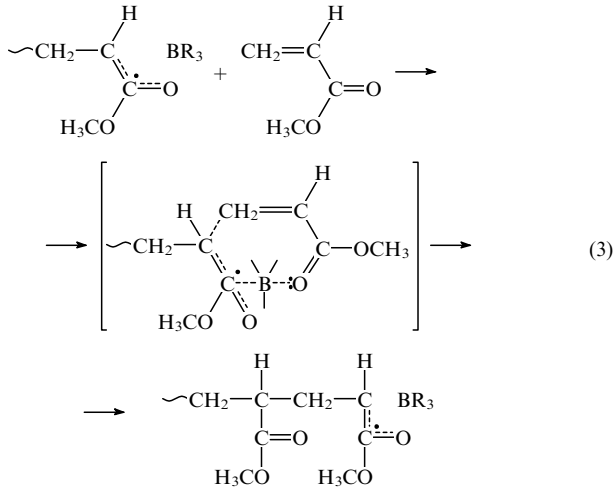

(3)

A similar mechanism involving an eight-membered reaction complex has been proposed by Kabanov[50] to interpret the increase in the propagation rate constant in the polymerisation of MMA in the presence of metal halides and by Smirnova and coworkers,[51,52] who studied copolymerisation of acrylic acid with VA (vinyl acetate) in the presence of germanium salts. In our opinion, the above-presented reaction complex [see Eqn (3)], which includes the allylic delocalised macroradical is thermodynamically and geometrically more stable.

It was found[53] that the addition of trialkylborane accelerates processes with monomers containing a polar substituent. In the case of styrene, organoelement additives have little influence on the polymerisation. Apparently, this is due to the fact that the St macroradical contains no functional groups capable of being coordinated to trialkylborane; therefore, the additive almost does not change the electrophilicity of the growing macroradical. The coordination directly to the reaction centre, namely, to the carbon atom carrying the unpaired electron is relatively unlikely. Moreover, this interaction can create steric hindrance to chain propagation. It is not by chance that the St polymerisation rate is lower in the presence of some organic compounds of Group III elements than without any complex-forming additives.[49]

The features of electronic and spatial structures of the growing macroradical play a crucial role in the chain propagation stage of coordinated radical polymerisation. On the one hand, coordination of an OEC molecule to a macroradical increases the electrophilicity of the latter and thus enhances its reactivity with respect to the monomer π-bond. It is evident that this effect is more pronounced in the case of polymerisation of sterically nonhindered monomers such as BA, AN and VA. On the other hand, upon the coordination interaction of the radical with OEC, the size of the reaction centre increases and additional steric hindrance to the chain propagation can arise. In the case of bulky radicals, for example, those of PPMA or polystyrene (PS), steric factors are, naturally, more significant in the chain propagation step than in the case of the BA or VA macroradicals. This is why the activating effect of Group III element alkyl derivatives is manifested most clearly in the polymerisation of esters and other functional derivatives of acrylic acid (amides, nitriles). The effect involved in the polymerisation of methacrylates, for example, MMA and butyl methacrylate (BMA) is much less pronounced.

The structure of OEC also influences the reactivity of the chain-propagating radicals and, hence, the kinetic parameters of polymerisation of acrylic monomers. For example, replacement of the alkyl radical in the trialkylborane molecule by a halogen atom [dibutylboron bromide (DBBB)] deteriorates the coordination capacity of boron due to the partial blocking of its vacant *p* orbital ($p_\pi - p_\pi$ conjugation). As a consequence, DBBB is less active as a controller of acrylate polymerisation than TIBB (triisobutylborane).[49]

Similar regularities can be observed in the case of phenyl derivatives of boron. Triphenylborane and dibutylphenylborane[53] were found to accelerate polymerisation of acrylic monomers to a smaller extent than TIBB.

This can be due both to the steric restrictions involved in the coordination of triphenylborane to the growing polymer radical and to the conjugation of one phenyl group of the substituent with the vacant *p* orbital of boron. Consequently, as in the case of DBBB, the electron-withdrawing capacity of the central atom in the OEC decreases. These results do not contradict the published data on the relationship of the reactivities of alkyl and phenyl derivatives of boron.[54]

The alkyl derivatives of boron analogues — aluminium, gallium and indium — also increase somewhat the rate of polymerisation of acrylic monomers and VA;[49] however, as in the case of DBBB, their influence on the chain propagation stage is less pronounced than that of TIBB. The difference between the effects of organoboron compounds, on the one hand, and organoaluminium, -gallium and -indium compounds, on the other hand, is, apparently, due to different coordination capacities of the central atoms in the OEC and, as a consequence, their dissimilar influence on the reactivity of the macroradical. A similar consideration can be used to interpret the lower efficiency, compared to that of trialkylboranes,[53] of zinc and cadmium alkyl derivatives as controllers of the polymer chain growth in the polymerisation of acrylic monomers.

Thus, alkyl derivatives of boron exert a greater influence on chain propagation in the radical polymerisation of vinyl monomers than other coordinatively unsaturated OEC derived from Group II and III elements.[54]

The participation of OEC in the elementary steps of polymerisation (chain propagation, transfer, termination) opens broad opportunities for controlling the MM of the resulting polymers. The introduction in the polymerisate of boron alkyl derivatives in amounts commensurable with the concentration of the initiator decreases substantially the MM. The calculated constants for the chain transfer to TIBB are 1×10^{-2} for MMA and 2.2×10^{-2} for VA.[53] The addition of TIBB also influences markedly the MM of poly(butyl acrylate) when polymerisation is carried out in an ethyl acetate solution.[49] The molecular mass of the polymer decreases with an increase in the OEC concentration; upon the introduction of 0.8 mol % of trialkylborane, it decreases by more than an order

of magnitude. The calculated constant for chain transfer to the organoboron compound is 7.4×10^{-2}; this is somewhat higher than the constant for chain transfer to TIBB during MMA polymerisation and appreciably higher than the chain transfer constant to BA (0.3×10^{-4}).[55]

The high constants of chain transfer to trialkylboranes can be due to two processes involving the macroradical and the OEC. One process is free-radical substitution of the growing polymer radical for the alkyl radical in OEC

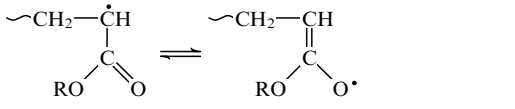
(4)

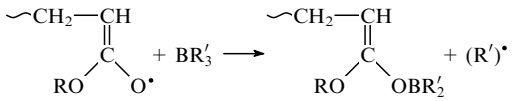
(5)

R, R′ is alkyl (isobutyl, ethyl, n-butyl).

Using EPR spectroscopy and quantum-chemical calculations, it has been shown [48] that (meth)acrylate macroradicals are prone to exist in a state typical of alkyl radicals, *i.e.*, the reaction centre is delocalised to give both carbon- and oxygen-centred radicals [Eqn (4)]. However, the rate constant for the replacement of alkyl radicals in trialkylborane by oxygen-centred radicals [Eqn (5)] is rather high, $\sim 10^5$ litre mol^{-1} s^{-1}.[56]

The second process which is also favourable for the control of the polymer MM is the abstraction of a hydrogen atom from the α-methylene unit of an alkyl group in OEC by the growing macroradical.

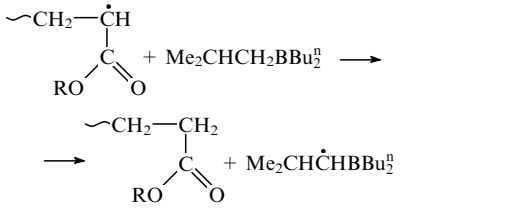
(6)

The occurrence of this reaction was proved unambiguously by EPR using the spin trap technique in a study of the influence of small additives of methyl acrylate (MA) and other acrylic monomers on the polymerisation of MMA with organoelement initiators.[57] The rate constant for this reaction in the case of triethylborane is $\sim 10^4$ litre mol^{-1} s^{-1}.[56]

In the polymerisation of styrene (St), the MM of the product barely changes, which is consistent with the results of kinetic measurements and indicates that OEC does not interact with the growing macroradical of PS.[49, 53]

The influence of added OEC on the molecular-mass distribution (MMD) of polymers has been studied by gel permeation chromatography (GPC).[58] In the presence of AIBN as the initiator, a unimodal MMD curve is observed; however, when TIBB is added to the system, the curve becomes clearly bimodal. As a consequence, the polydispersity of samples increases somewhat. Evidently, in the presence of TIBB, the growth of the polymer chain occurs in parallel by two mechanisms, namely, coordinated radical and radical mechanisms.

On the one hand, OEC is coordinated to the growing macroradical, thus increasing its electrophilicity and, hence, its reactivity with respect to the monomer. As noted above, chain propagation takes place in a cyclic reaction complex [see, for example, Eqn (2)]. This interaction changes the chain propagation and termination rate constants and decreases the MM of the polymer. On the other hand, growth of the polymer chain occurs simultaneously by the classical radical mechanism

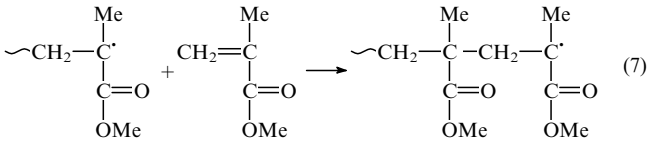
(7)

A bimodal MMD curve is also observed when polymerisation of MMA is carried out with a binary initiator, TIBB–di-*tert*-butylperoxytriphenylantimony (DPA), which is an efficient low-temperature initiator controlling polymerisation of vinyl monomers.[13, 15, 19, 22, 32, 44]

The conclusions drawn confirm indirectly the results of studies of the MMD of PS samples synthesised in the presence of various OEC derived from Group II and III elements.[52] The introduction of these compounds barely influences both the general pattern of the MMD curve and the degree of polydispersity of samples. It has been noted above that OEC do not react with the growing polystyrene radical due to electronic and steric factors.[49, 58] Therefore, in the polymerisation of St, chain propagation follows only the traditional radical mechanism without participation of the complex-forming agent.

Thus, the data outlined above indicate that organic compounds of Group III elements provide effective control of the molecular-mass characteristics of polyacrylates. This way of controlling polymerisation of acrylic monomers opens up new opportunities for the synthesis of polymers with novel physicochemical and practical properties. A certain drawback of the proposed method is the higher polydispersity of the resulting polymers, caused by the fact that polymerisation in the presence of organoelement additives follows two parallel mechanisms.

2. Specific influence of phenolic inhibitors on homo- and copolymerisation of vinyl monomers in the presence of organic compounds of Group III elements

Hydroquinone, ionol, diphenylolpropane and some other phenols are known inhibitors of radical polymerisation; they are traditionally used as stabilisers for the storage of vinyl monomers. The inhibiting efficiency substantially increases in the presence of oxygen; this may be due to oxidation of phenols to quinones, which retard chain propagation more appreciably.[59]

According to the most popular viewpoint,[59, 60] the inhibitory influence of hydroquinone is due to the easy abstraction of the active hydrogen atom from the phenol molecule giving rise to a phenoxyl radical.

$$R^{\bullet} + ArOH \longrightarrow R-H + ArO^{\bullet}. \qquad (8)$$

The phenoxyl radical, which exhibits a low reactivity towards the monomer multiple bond, is unable to initiate a radical process (polymerisation).

Back in the 1960s, it was found [61–64] that the addition of some OEC derived from Group III elements makes it possible to carry out polymerisation of MMA in the presence of BP or AIBN to a high degree of conversion, despite the presence of comparable amounts of hydroquinone. Apparently,[56] in the presence of OEC, the phenoxyl radicals undergo a fast S_R2 substitution reaction.

$$ArO^{\bullet} + MR_3 \longrightarrow R^{\bullet} + ArOMR_2 \qquad (9)$$

M is a Group II or III metal.

The alkyl radicals formed in this reaction can subsequently initiate polymerisation. It is in these processes that organoboron compounds can act as chain transfer agents in the polymerisation of acrylates. As noted above, the rate constants for the chain transfer in peroxide-initiated polymerisation of MMA are equal to 0.015 for tri-n-butylborane and 0.01 for TIBB.[20]

A somewhat different interpretation of the absence of inhibitory influence of phenols on polymerisation in the presence of OEC was proposed by Arimoto,[62] who suggested that trialkylborane is coordinated to the growing macroradical through the unpaired electron of the latter.

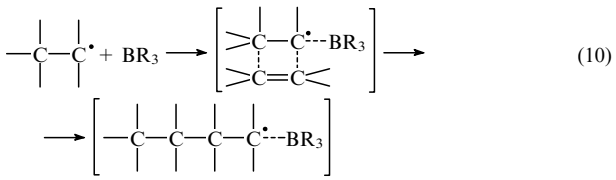

(10)

As a consequence, the reaction centre of the radical becomes blocked and the interaction with phenol is made impossible. It should be noted that Grotewold *et al.*[61] cast doubt on the experimental results obtained by Arimoto.

In some studies published in the 1990s,[16–18, 65] it was shown that diphenylolpropane and hydroquinone are not merely inactive as inhibitors of radical polymerisation of acrylates in the presence of trialkylboranes but, conversely, accelerate it. Indeed, the rates of MMA and AN polymerisation markedly increase in the presence of organic compounds of Group III elements, the effect becoming more pronounced with an increase in the contents of OEC and the above-mentioned diphenols. Similar data have also been obtained for reactions carried out in the presence of alkylalkoxy boron derivatives.[44]

This unusual accelerating effect can be due to some extent to the occurrence of chain transfer to the OEC [Eqn (9)]. However, this fact alone cannot account for the absence of the inhibiting effect in the polymerisation of MMA, AN, and MA in the presence of substantial concentrations of hydroquinone and diphenylolpropane (an order of magnitude higher than the initiator concentration) or for the absence of inhibiting effect after the introduction of Lewis acids in the system which undergoes polymerisation.[66–68] The unusual behaviour of phenols can be explained in terms of the coordinated radical mechanism of (co)polymerisation of acrylic monomers on organoelement initiators. In the presence of electron acceptors such as Lewis acids, the macroradical and the monomer are coordinated to components of the initiator. The complex formation of OEC with the monomer activates the monomer;[58] this enables initiation of the polymerisation by phenoxyl radicals.

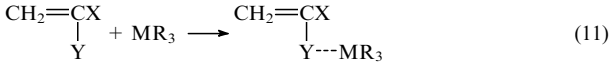

(11)

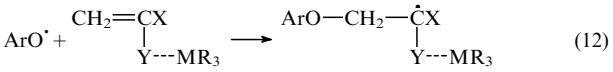

(12)

M is a Group III metal.

The coordinated macroradical, unlike the non-coordinated one, exhibits enhanced electrophilicity with respect to the monomer π-bond, which results in a higher propagation rate constant.[5, 11, 18]

The occurrence of reaction (12) is also confirmed by the fact that IR- and UV-spectroscopic studies show the presence of phenoxy groups in the MMA polymer. This view on the kinetics of polymerisation of acrylates in the presence of OEC and inhibitors is indirectly supported by the absence or attenuation of the inhibiting effect in MMA polymerisation in the presence of Group III metal halides.[66–68] In this case, S_R2 reactions [Eqn (9)] are impossible in principle; therefore, the effect observed can be interpreted in terms of either the Arimoto scheme, or reactions (11) and (12), or the cyclic mechanism of chain propagation [see Eqn (3)].[7, 20, 49] The same trialkylborane molecule can be involved in several consecutive chain propagation events, while retaining the growing macroradical in the coordination sphere of the boron atom and 'receiving' (coordinating) new monomer molecules. Chain propagation in the cyclic reaction complex hampers the interaction of the growing macroradical with the inhibitor.

It is the processes considered above that account for the increase in the rate of MMA, AN and MA polymerisation in the presence of organic compounds of Group III elements and phenols such as hydroquinone and diphenylolpropane. However, in the case of ionol, which is a sterically hindered phenol, polymerisation rate somewhat decreases.[7, 16] This appears to be due to the fact that reactions (9) and (12) are much less efficient for ionol than for hydroquinone or diphenylolpropane.

In view of the foregoing, it can be assumed that the vacant orbitals of TIBB accept electron density through coordination to the macroradical. This increases the electrophilicity of the coordinated poly(methyl methacrylate) radicals; therefore, they become relatively 'inert' with respect to the abstraction of a hydrogen atom from phenol. In addition, chain propagation takes place in the cyclic reaction complex, which also hampers the reaction of the macroradical with the active hydrogen atom of the phenol hydroxy group. As a consequence, polymerisation of MMA proceeds up to a high degree of conversion in the presence of a 10-fold excess of the inhibitor with respect to OEC.

Phenolic inhibitors have also a certain influence on the polymer MM.[7, 16, 49, 65] In particular, the molecular mass of PMMA decreases upon the introduction of phenols. However, this influence is not so pronounced (as could be expected) as that observed in the absence of OEC or in the presence of conventional chain transfer agents.

Oxygen plays an important role in the mechanism of inhibition of radical polymerisation by various phenols. According to one view,[59] the influence of oxygen reduces to the oxidation of phenol to the corresponding stable radical or quinone. In the presence of organic compounds of boron or aluminium or of benzoquinone, polymerisation of MMA proceeds without an induction effect.[40, 61–64] The inhibitory effect of benzoquinone after the addition of TIBB depends on the [TIBB] : [benzoquinone] molar ratio. If the amount of benzoquinone is smaller than that of TIBB, the inhibitory action has virtually no effect on the polymerisation kinetics. The process occurs up to a high degree of conversion and the molecular mass of PMMA changes insignificantly. In the absence of OEC, benzoquinone efficiently inhibits polymerisation of acrylates: the rate of polymerisation in the initial stages is close to zero, the limiting degree of conversion is less than 0.5%.[49, 58]

As the benzoquinone concentration increases, the rate of polymerisation decreases. However, even with a twofold excess of benzoquinone with respect to alkylborane, it is markedly higher than that in the absence of OEC. Analysis of the publications cited and data on the reactivity of organoboron compounds and quinones point to efficient consumption of trialkylborane and quinone.[69–74]

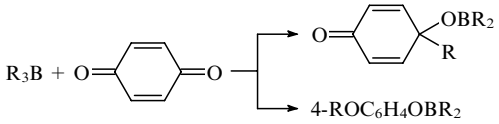

(13)

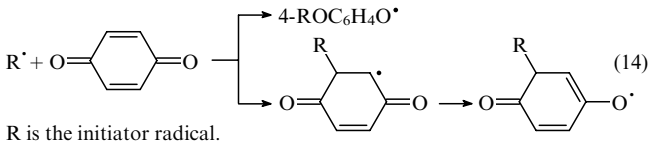

(14)

R is the initiator radical.

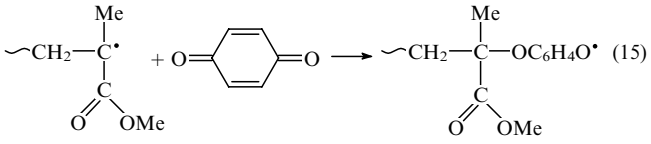

(15)

Reaction (14) and the regularities of inhibition of alternating copolymerisation by quinones have been studied comprehensively by EPR spectroscopy by Golubev,[70] who used the reactions of benzoquinone, naphthoquinone, and fluoranil with organic radicals of different electrophilicity as examples to demonstrate that the abnormally slight influence of quinoid-type radical inhibitors on the alternating copolymerisation is related to substantial polar effects involved in this reaction. In accordance with this concept, the increase in the electrophilicity of macroradicals upon the coordination to OEC should substantially influence the reactivity

of the macroradical with respect to the quinone [chain termination, Eqns (13)–(15)].

It is beyond doubt that in the presence of OEC in a polymerising system, the factor of polarity would play a vital part in the attenuation of the inhibiting effect of quinones. In particular, the phenoxyl radicals generated in processes (13)–(15) enter into S_R2 substitution to give alkyl radicals able to initiate polymerisation once again [see Eqn (9)]. Judging from the average chain length, two chain transfers to the trialkylborane molecule take place.[63]

The influence of organoaluminium compounds on the polymerisation of acrylates in the presence of benzoquinone is equally efficient.[58] The rate of polymerisation increases with an increase in the [triethylaluminium]:[benzoquinone] ratio, passes through a maximum, and then decreases. This was attributed[64] to the occurrence of two mechanisms of initiation; one of them is related to the decomposition of the initiator into radicals and the other, to the generation of radical centres upon decomposition of the triethylaluminium complex with quinone. In view of the analysis of products of the reaction of organoaluminum compounds with quinones, the latter mechanism seems quite debatable.

Apparently, in this case, as for trialkylborane, both the heterolytic reaction [Eqns (13)–(15)] and the homolytic transfer of the reaction centre to the metal atom in OEC [see Eqn (9)] take place. In addition, whereas in the case of TIBB, the reaction can involve two alkyl groups, in the case of triethylaluminium, only one group is involved[64] (the rate constant for chain transfer is equal to 89 litre $mol^{-1} s^{-1}$; for comparison, the rate constant for chain propagation is 576 mol $litre^{-1} s^{-1}$.[75]).

Organoelement compounds formed by Group III elements and the inhibitors chosen accelerate not only homo- but also copolymerisation of MMA with a number of vinyl monomers, including St, VA, and methacrylic acid (MAA).[7] Similar features have also been found for the MAA–VA pair of monomers. It was shown in relation to the copolymerisation of these monomers in the presence of hydroquinone and OEC that the inhibitor participates in the chain propagation and termination stages and influences the dependence of the copolymer composition on the composition of the monomer mixture.[17] For MAA contents in the monomer mixture ranging from 20 mol.% to 80 mol %, the addition of hydroquinone virtually does not change the composition of the MAA–VA copolymer, which does not depend on the composition of the monomer mixture. In the Kelen–Tudoc calculation of the copolymerisation constants, the intermediate calculated parameters (η and ψ) are found to deviate from the linear dependence; this is evidence supporting the coordinated radical mechanism of copolymerisation.

3. The coordinated radical copolymerisation of vinyl and some other monomers in the presence of organoelement initiators

At present, copolymerisation is an important method for the preparation of polymers with a specified set of chemical and physical properties because it is difficult in most cases to control the properties of homopolymers. Meanwhile the need to control these properties is a topical task in preparing materials for various purposes.[4, 76]

Copolymerisation normally affords random copolymers, the composition and properties of which are determined by the composition of the monomer mixture and the reactivity of monomers and chain-propagating radicals. However, there exist monomer pairs copolymerisation of which gives polymers with regular alternation of the units. As a rule, strict alternation of monomer units is observed if one monomer is a clear-cut donor of electron density, and the other one is an acceptor. Since the number of monomers with clearly defined electron-withdrawing properties is small [maleic anhydride and its derivatives, sulfur(IV) dioxide], the number of monomer pairs that can form alternating copolymers is also few.

The main method for controlling the composition of copolymers is introduction of special additives, usually, protic and aprotic acids, into the system. The latter are coordinated to the monomers or to the chain-propagating radicals and thus enhance their electron-withdrawing properties and provide the possibility of preparing alternating copolymers.[5, 77, 78] The main drawback of this method of modification of polymer materials is that the controlling additive is introduced in a large excess with respect to the initiator (1–3 orders of magnitude), which results in contamination of the polymer formed. The cost of polymer purification is high; therefore, the use of this method to control the polymer composition on an industrial scale is non-expedient.

The use of organoelement initiators based on Group III element organic compound and peroxides eliminates this drawback because the controlling influence of these additives on chain propagation manifests itself, as noted above, when catalytic amounts of the initiator are used (0.01 mol %–1.00 mol %).

The complex formation effects in the radical copolymerisation in the presence of Lewis acids are largely determined by the electronic structure of the monomer.[6, 79] In the possible limiting cases, either one monomer or both monomers react with the complex-forming agent. Both situations are analysed below.

It has been shown in relation to a number of monomer pairs that an organoelement initiator influences directly the variation of the copolymer composition and the copolymerisation rate *vs.* the composition of the monomer mixture. The controlling influence of OEC is most pronounced in the copolymerisation of (meth)acrylates with electron-donating monomers.[7, 58] For instance, in the copolymerisation of MMA with allyl chloride (AC) with a classical radical initiator AIBN, the copolymer is enriched in the more active monomer, MMA, in each section of the composition curve (the relative activities of the monomers are $r_{MMA} = 3.05$; $r_{AC} = 0.05$).[23, 77] The rate of copolymerisation decreases with an increase in the content of AC in the monomer mixture. When a binary initiator, TIBB–DPA, is used,[80] the composition curve is S-shaped. A section in which the copolymer composition does not depend on the composition of the monomer mixture can be clearly seen in the curve; in this case, the trend for the alternation of monomer units is close to its limiting value.

The relative activities of both monomers become much less different and smaller than unity (Table 2); the product $r_1 r_2 \rightarrow 0$, pointing to a coordinated radical mechanism of (co)polymerisation.[5, 6] This is also indicated by the deviation from linearity of the calculated parameters in the determination of the copolymerisation constants by the Kelen–Tudoc method.

Organoelement initiators, even present in low concentrations (0.01 mol %–0.10 mol %), have a noticeable controlling influence on the composition and structure of the MMA–AC copolymer. This is due to the coordination of the growing macroradical to the components of the initial system. Studies of the separate effects of the initiator components on the dependence of the copolymer composition on the composition of the monomer mixture indicate that TIBB, which contains a boron atom with a vacant *p* orbital, plays the most active role in the complex formation with the macroradical.[80] Its coordination to the growing poly(methyl methacrylate) radical induces electron density redistribution in the radical, increases the radical electrophilicity, and enhances its reactivity towards the π-bond of the electron-donating monomer AC.

The variation of the rate of copolymerisation of AC with MMA as a function of the initial composition of the monomer mixture has a clear-cut maximum at a monomer ratio close to the equimolar ratio. This is evidence in favour of the coordinated radical mechanism of copolymerisation and also provides grounds for believing that the monomers and macroradicals form a cyclic reaction complex in the chain propagation stage.

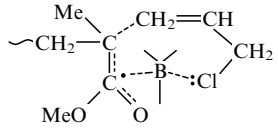

Table 2. Effective values for the relative activity of monomers.

Monomers		r_1	r_2	Initiator	Monomers		r_1	r_2	Initiator
1	2				1	2			
AN	VA	4.05	0.06	AIBN	MMA	VDC	2.50	0.50	AIBN
		0.97	0.20	TIBB – TBP			1.04	0.06	TIBB – DPA
		0.90	0.04	TIBB – TBPT	MMA	VC	15.0	0.02	AIBN
		0.85	0.05	TIBB – TBPG			6.7	0.02	TIBB – TBPA
		0.40	0.03	TIBB – TBPA	MMA	AA	1.03	0.03	TIBB – TBPS
		0.35	0.42	TIBB – DPA	VA	VDC	0.03	3.60	AIBN
AN	AC	3.05	0.05	AIBN			0.12	0.20	TIBB – DPA
		3.78	0.15	TIBB – DPA	VA	VC	0.23	1.68	AIBN
AN	MMA	0.15	1.35	PB			0.58	0.97	TIBB – DPA
		0.15	1.10	TIBB – oxygen	VA	VPD	0.20	3.02	AIBN
		0.04	1.53	TIBB – TPB			0.32	0.19	TIBB – TBP
		0.15	0.75	TIBB – TBPT			0.17	0.15	TIBB – TBPG
		0.26	0.67	TIBB – TBPG			0.30	0.28	TIBB – DPA
		0.10	0.64	TIBB – DPA	VPD	St	0.05	5.20	DCHPD
AN	VC	2.80	0.04	AIBN			0.05	0.96	TIBB – DPA
		2.20	0.05	TIBB – oxygen			0.29	0.94	TIBB – TBPG
		0.86	0.05	TIBB – DPA	St	AA	0.15	0.25	BP
		0.74	0.05	TIBB – TBPA			0.87	0.04	TIBB – TBPA
AN	VDC	0.91	0.37	AIBN	St	MAA	0.15	0.70	BP
		0.12	0.14	TIBB – DPA			0.27	0.03	TIBB – TBPA
AN	MAA	0.15	5.50	AIBN	Ethylene	VA	1.00	1.30	AIBN
		0.15	0.43	TIBB – DPA			0.80	1.20	TIBB – DPA
AN	St	0.04	0.40	AIBN			0.95	1.10	TIBB – TBPS
		0.19	0.45	TBPS	Ethylene	VC	0.24	3.60	AIBN
		0.14	0.26	TBPT			0.22	0.50	TIBB – DPA
		0.04	0.27	TIBB – DPA			0.20	2.0	Ziegler – Natta
MMA	MAA	0.58	1.40	BP	MMA	St	0.32	0.33	DCHPD – DPA
		0.95	0.99	AIBN – TIBB			0.50	0.60	TIBB – oxygen
		1.07	0.62	AIBN – DPA					
		1.10	0.85	AIBN – TBPS	Propene	VC	0.28	0.39	TIBB – DPA
		0.45	0.28	TIBB – DPA	Hex-1-ene	VC	0.05	0.65	TIBB – DPA
MMA	AC	48.10	0.03	AIBN			0.06	0.88	TIBB – TBPA
		0.57	0.03	TIBB – DPA			0.13	0.94	TIBB – TBPS
MMA	St	0.46	0.52	DCHPD	Hex-1-ene	AN	0.0	12.2	AIBN
		0.37	0.57	TIBB – DPA			0.10	4.60	TIBB – DPA

Note. The following designations are used: VDC is vinylidene chloride, AA is acrylic acid, VPD is vinylpyrrolidone, TBP is *tert*-butyl peroxide; TBPT is *tert*-butylperoxytriethyltin; TBPG is *tert*-butylperoxytriethylgermane; TBPS is *tert*-butylperoxytriphenylantimony; TBPS is *tert*-butylperoxytrimethylsilane.

The cyclic mechanism of propagation prevents the destructive chain transfer to the allylic monomer; this accounts for the high degree of conversion in the copolymerisation of AC with acrylates.

The presence of fragments with double bonds in the MMA – AC copolymer ($\sim$4% – 5%) can be explained by assuming that allyl-type radicals formed upon abstraction of a hydrogen atom from AC can again initiate polymerisation in the presence of OEC by the following scheme:

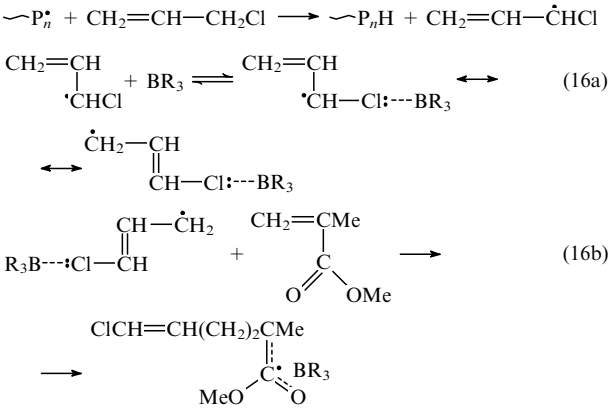

(16a)

(16b)

Coordination of OEC to an allyl type radical increases the radical electrophilicity and reactivity with respect to the π-bond of the monomer. The coordinated allylic radical, unlike a non-coordinated one, is able to re-initiate polymerisation [Eqn (16b)].

The possibility of initiating polymerisation by an allylic macroradical in the presence of Lewis acids (metal halides) was also mentioned in other publications. [5, 81, 82]

The NMR spectra of MMA – AC copolymers and syndiotactic PMMA coincide,[80] which confirms the radical mechanism of the copolymerisation of MMA with AC.

A thermomechanical study of MMA – AC copolymers showed [80] a sharp decrease in the glass transition temperature and a decrease in the ultimate strength and in the modulus of elasticity of copolymers with respect to the corresponding characteristics of the MMA homopolymer prepared both with the DPA – TIBB initiating system [83] and with a classical radical initiator.[84] Hence, the presence of AC (10 mol % – 15 mol %) in the copolymer has a substantial influence on its properties.

The decrease in the glass transition temperature of the MMA – AC copolymer noted above extends the temperature range of the highly elastic state of the copolymer and thus increases its frost resistance, which is significant for practical purposes.

Copolymerisation of AC with the electron-donating VA monomer in the presence of organoelement initiators proceeds to a lower degree of conversion (less than 10% over a period of 7 days)[85,86] than copolymerisation of AC with acrylates. This copolymer was also found to contain fragments with double bonds, which can serve as evidence for initiation of the polymerisation by allyl-type radicals in the presence of OEC [see Eqns (16a,b)].

In the copolymerisation of AN and AC, the formation of a cyclic reaction complex is impossible for steric reasons;[87] therefore, the influence of an organoelement initiator on the dependences of the copolymer composition and copolymerisation rate on the composition of the monomer mixture is less pronounced.[80] In all sections of the composition curve, the copolymer is enriched in AN, which is more reactive ($r_1 > 1$, $r_2 < 1$), although the relative activities of the monomers found in AIBN- and OEP-initiated reactions differ somewhat from each other.

Conversely, copolymerisation of MMA with an electron-donating monomer (St) is subject to regularities[27,88] similar to those observed in the copolymerisation of the MMA – AC pair, namely, the variation of copolymerisation rate as a function of the initial composition of the monomer mixture passes through an extremum (this may also imply the formation of a reaction complex in the chain propagation stage) and the relative activities of both monomers are much smaller than unity.

According to NMR study of the MMA – St copolymers synthesised using DCHPD and organoelement initiators, the microstructures of the specimens obtained are markedly different.[88] The copolymer synthesised in the presence of DCHPD shows a good agreement of the calculated content of triads with that found experimentally. However, in the case of the copolymer prepared in the presence of an organoelement initiator, the discrepancy between the experimental and theoretical values is substantial, indicating that the Mayo – Lewis scheme is inapplicable under these conditions. The ratio of triads calculated from the relative activities in accordance with the pre-terminal unit model showed that the Mertz – Alfrey – Goldfinger equation describes the polymerisation process much more adequately. It can be seen from the data presented that the effect of the pre-terminal unit is not the only factor able to change the copolymer composition. This indicates once again that complex formation between the monomer and the initiator and especially, between the initiator and the macroradical contributes significantly to the change in the monomer relative activities.

Analysis of the dependences of the instantaneous and gross compositions of MMA – St copolymers on the degree of conversion shows that the product of copolymerisation in the presence of DCHPD is enriched in MMA at high degrees of conversion. Initiation by the TIBB – OEP system gives rise to a copolymer with a narrower composition distribution of fractions.[88]

Hirai *et al.*,[89,90] who studied the controlling influence of boron compounds on the composition of the MMA – St copolymer, demonstrated that photoinitiation in the presence of 1 mol % of boron trichloride or ethylboron dichloride gives rise to an alternating St – MMA copolymer. On the basis of kinetic measurements and study of the microtacticity of copolymers, it was concluded that copolymerisation involves the ternary complex 'MMA – St – organoboron compound'. It was noted that diethylboron chloride and triethylborane have a weaker effect on the composition of the MMA – St copolymer than trialkylboranes. In the presence of boron trifluoride, homopolymerisation of styrene takes place.

It has been proposed[91] to use a mixture of alkylboron halides for the synthesis of alternating copolymers of acrylates with alkenes over a broad temperature range (−150 to 100 °C) and at a relatively low pressure (< 100 atm). The degree of conversion reaches 70% over 5 – 6 h. However, the controlling effect of the organoelement additive shows itself only when the amount of the additive is comparable with the monomer concentration. In this case, the influence of OEC on the copolymer composition is likely to be due to the coordination interaction of the OEC with the monomer rather than with the macroradical.

Blends based on organoelement derivatives of Group II elements in combination with Group IV element halides influence the composition of copolymers in a similar way.[92]

An efficient controlling influence of the binary initiator trialkylborane – OEP can be traced in the copolymerisation of AN with VA.[14,93,94] In the case of the classical radical initiator AIBN, the AN – VA copolymer is enriched in AN, which is the more reactive monomer ($r_{AN} = 4.05$, $r_{VA} = 0.06$) at any composition of the monomer mixture. When the organoelement initiator TIBB – OEP is employed, the composition curve is S-shaped. A section in which the copolymer composition barely depends on the composition of the monomer mixture can be clearly distinguished on the curve; this suggests the trend for alternation of the monomer units in the copolymer and points to the coordinated radical mechanism of copolymerisation. The same is indicated by equalisation of the relative activities of the monomers: $r_{AN} = 0.35$; $r_{VA} = 0.42$ (for comparison, r_1 and r_2 found in terms of the $Q-e$ scheme are 4.27 and 0.06, respectively) and by the deviation from linear dependence of the calculated parameters in the Kelen – Tudoc determination of the copolymerisation constants.

In our opinion, the very pronounced influence of low concentrations of the initiator (0.1 mol % – 1.0 mol %) is due to the coordination interaction of the growing macroradical with the components of the initiating system. Important roles should be played by both trialkylborane, which has a vacant orbital at the boron atom, and the organoelement peroxide. This interaction results in electron density redistribution and contributes to the stabilisation of the species

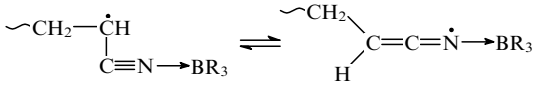

The decrease in the relative activity of AN, found as the ratio of the rate constant for the reaction of the radical with the like monomer (K_{11}) to the rate constant for its reaction with the foreign monomer (K_{12})

$$r_{AN} = \frac{K_{11}}{K_{12}},$$

in the presence of OEC can be related to either a decrease in K_{11}, or an increase K_{12}, or a simultaneous change of both rate constants in the above-indicated directions. These changes can be brought about by an increase in the electron-withdrawing properties of the polyacrylonitrile radical coordinated to the OEC. It is evident that an increase in the electrophilicity decreases the reactivity of the macroradical towards the π-bond of AN (the monomer with a strong electron-withdrawing group) and increases the reactivity towards VA (the electron-donating monomer).

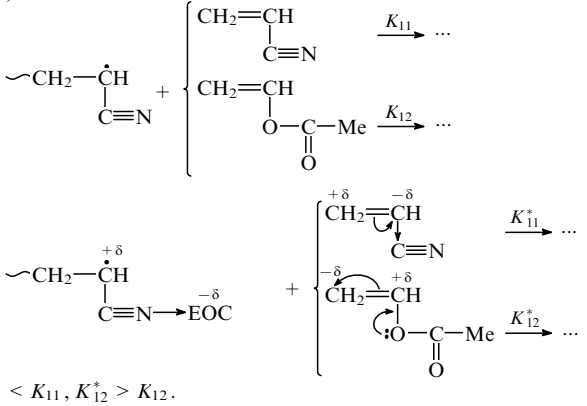

$K^*_{11} < K_{11}$, $K^*_{12} > K_{12}$.

These changes result in a substantial decrease in the relative activity of acrylonitrile ($r^*_{AN} < r_{AN}$).

The rate constant for the addition to VA of the poly(vinyl acetate) radical coordinated to the OEC increases, while that for the addition to AN decreases. As a consequence, the relative activities of the monomers which undergo copolymerisation (AN and VA) become nearly equal and smaller than unity (see Table 2), which generates the trend for alternation of the monomer units. The relative activity of AN changes more sharply than the copolymerisation constant of VA; this indicates that complex formation of OEC with the polyacrylonitrile radical is the governing factor in this system.

The dependence of the rate of copolymerisation of AN with VA in the presence of organoelement initiator on the composition of the monomer mixture has a clear-cut maximum, as in the case of the MMA – AC monomer pair.[14] This points to a coordinated radical character of the process. Similar features have been found for the copolymerisation of AN with MAA, acrylic acid and MMA.[7] As for the AN – VA pair of monomers, the composition curve has a section in which the copolymer composition virtually does not depend on the composition of the monomer mixture. It can be seen from the data of Table 2 that the relative activities of the monomers in the presence of organelement initiators differ markedly from the values calculated using the $Q-e$ scheme or published data. The observed levelling of the relative activities of monomers entails the compositional uniformity of the resulting polymer.

The influence of the components of organelement initiators on the dependence of the copolymer composition on the composition of the monomer mixture in the case of MMA – MAA monomer pair is equally significant.[95] When copolymerisation of these monomers is carried out without OEC additives (AIBN initiation, see Table 2), the copolymer is enriched in the more active monomer, MAA, at any composition of the monomer mixture. In the case of a binary organoelement initiator, TIBB – DPA, the composition curve follows an S-shaped pattern, and the relative activities of both monomers are substantially smaller than unity. The product of the copolymerisation constants tends to zero, pointing to the alternation of monomer units in the copolymer.

Studies of the separate influence of components of the binary organoelement initiator on the chain propagation[27] demonstrated that the addition of 0.2 mol % of TIBB (the concentration of the AIBN initiator is 0.1 mol %) results in substantial levelling of the relative activities of the monomers (see Table 2). The addition of an organosilicon peroxide to AIBN also influences appreciably the reactivities of the monomers and the chain-propagating radicals — the copolymer is enriched in MMA in each section of the curve. The effective values of the relative activities of MMA and MAA are also subject to the controlling influence of DPA, which is an efficient co-initiator for trialkylboranes.[13–15] Thus, both components of the organoelement initiator (alkylborane and OEP) have a controlling influence on the copolymerisation of acrylic monomers.

Copolymerisation of MMA with an electron-donating monomer (St) is influenced by components of an organoelement initiator in a different way.[88] For the polymerisation of these monomers initiated by organoelement initiators, the composition curve is also S-shaped. The relative activities of both monomers are smaller than unity, their numerical values being slightly dependent on the initiator. However, for the MMA – St monomer pair with the use of organoelement initiators, the dependence of the copolymerisation rate on the composition of the monomer mixture has a clear-cut maximum at a nearly equimolar monomer ratio, which is indicative of a coordinated radical copolymerisation mechanism and of the participation of the initiator components in the propagation stage.

The different effects of OEC as weak Lewis acids on the copolymerisation of MMA with MAA and with St are due to the fact that in the former case, the two monomers (MMA and MAA) are similar in structure and electron-withdrawing properties and thus both can react with the complex-forming agent, whereas in the latter case (MMA and St), only one monomer, namely, MMA, reacts with the Lewis acid.

These conclusions are in good agreement with the results of kinetic studies of the copolymerisation of AN with VA and with (meth)acrylates.[7,93–95]

The effect of the heteroatom of the organoelement peroxide on the copolymer composition and the copolymerisation rate was also found for the AN – St pair of monomers at 343 – 353 K,[96] although it is less pronounced than in the case of a binary organoelement initiator.

A quantitative estimate of the change in the reactivity (including electrophilicity) of macroradicals and monomers induced by coordination to the components of an organoelement initiator is provided by the $Q-e$ parameters of the Alfrey – Price equation.[97,98] These parameters are known to have a clear physical meaning and to correlate with the energy of localisation, the order and the π-electron density of the monomer double bond. Comparative analysis of the published Q and e values for various vinyl monomers and the values of these parameters calculated using the relative activities of monomers for the case of organoelement initiators shows that the introduction of organoelement additives changes these values appreciably. Indeed, judging by the Q and e parameters, in the presence of the binary TIBB – OEP initiator, *N*-vinylpyrrolidone acts as an electron density acceptor ($e = 0.94$) rather than an electron density donor ($e = -1.0$), as usual.[97]

Similar regularities have been observed for other vinyl monomers (Table 3): the parameter e, which characterises the electronic structure of the monomer, substantially increases.

Table 3. The parameters Q and e for several vinyl monomers.

Monomer	Q	e	Monomer	Q	e
St	1.0	0.8	MA	0.74	0.40
	1.0	0.8		0.76	0.45
AN	0.60	1.20	VC	0.04	0.20
	0.90	1.33		0.94	0.97
VPD	0.20	−1.00	VDC	0.22	0.36
	1.31 [a]	1.89 [a]		0.29	1.07
AA	1.15	0.77		0.33	0.94
	0.34	1.03		0.50 [d]	0.34 [d]
MAA	1.50	0.68		0.50 [e]	1.50 [e]
	0.86	1.39	VA	0.03	−0.22
	0.74 [b]	0.40 [b]		0.85	−0.06
	1.15 [c]	0.53 [c]			

Note. The values obtained in the absence of initiators are given above the stroke; those in the presence of the organoelement initiator TIBB – DPA are below the stroke.

Additives: [a] tin tetrachloride, [b] dimethylformamide, [c] Lewis base, [d] TBPG – TIBB, [e] acetic acid.

An increase in the numerical value of e in (meth)acrylates attests to an increase in the energy of conjugation and a decrease in the electrophilicity of the double bond. This means an increase in the reactivity of the monomer π-bond towards elctrophilic radicals.

It has been found within the empirical Alfrey – Price scheme that an increase in the parameter e, which is related to the polarity of the monomer double bond, entails an increase in the rate constant for propagation and, hence, in the rate of homo- and copolymerisation.[97,98] As noted above, this is actually observed in the study of the kinetics of homo- and copolymerisation of (meth)acrylates in the presence of catalytic amounts of organoelement compounds.

The efficient controlling influence of organoelement initiators based on trialkylboranes and Group IV – V element peroxides is also manifested in those cases where both monomers involved in copolymerisation are electron donors but contain functional

groups able to be coordinated to Lewis acids. These monomers can be represented, for example, by VPD and VA.[99] The results of studies of the kinetic dependences for the composition and structure of copolymers point unambiguously to a coordinated radical mechanism of copolymerisation. The monomers form a reaction complex with the components of the initiator during the chain propagation stage: the dependence of the copolymerisation rate on the composition of the monomer mixture has an extremum in the region of equimolar amounts of monomers in the initial mixture.

An organoelement initiator has a substantial influence on the copolymerisation of VPD with VDC, which are 'naturally alternating' comonomers.[99,100] The composition curve is S-shaped when DCHPD is used as an initiator. When copolymerisation of this pair is carried out with a binary initiator, TIBB–OEP, the resulting copolymer is enriched in VDC.

Organosilicon peroxides have a controlling influence on the copolymerisation of acrylates in the presence of sulfuryl chloride and phosphorus trichloride;[101,102] however, for the monomer pairs considered in the studies cited, this influence is less pronounced than that in the case of Group III element OEC; this is undoubtedly due to the difference between the electron-withdrawing properties of the modifiers.

Thus, catalytic amounts of coordinatively unsaturated OEC not only effectively initiate low-temperature polymerisation of vinyl monomers but also have a controlling effect on the kinetic parameters of copolymerisation of a broad range of monomers and the composition of copolymers.

The compositional uniformities of macromolecules for one– and two-centre copolymerisation are substantially different.[103] Therefore, important information on the chain propagation mechanism can be gained by performing copolymerisation of a broad range of monomers.

It was found in relation to copolymerisation of MMA with MAA that the integral curves for the distribution over composition for MMA–MAA copolymers synthesised in the presence of a conventional organic (DCHPD)[104] and organoelement (TIBB–DPA)[105] initiators are different. The curve for DCHPD is unimodal,[104] while that obtained with organoelement initiators is bimodal.[105]

When acrylates are made to copolymerise with alkenes, the controlling effect of OEC is not so pronounced as in the copolymerisation of vinyl monomers with each other. The rates of copolymerisation of AN with cyclohexene and hex-1-ene, MMA with ethylene, and VA with ethylene [106] decrease linearly with an increase in the alkene content in the monomer mixture. The degree of conversion does not exceed 30%. The relative activities still differ somewhat from those found for classical radical initiators but this difference is less significant than in the case of copolymerisation of two vinyl monomers.[7] Apparently, this is due to the fact that alkenes and, especially, chain-propagating radicals derived from them, are less prone to form complexes than monomers containing functional groups or atoms with lone electron pairs.

In should be noted that low-pressure radical copolymerisation of ethylene and α-olefins with polar vinyl monomers is quite a topical problem in polymer chemistry. This is especially true for the synthesis of VC copolymers with α-olefins.

Vinyl chloride and α-olefins are known to undergo efficient polymerisation at low pressure according to different mechanisms, namely, polymerisation of VC follows a radical mechanism, while ethylene and its homologues polymerise by a coordination mechanism in the presence of Ziegler–Natta catalysts.[107,108] It is impossible to synthesise VC–olefin copolymers with a high degree of conversion under technologically beneficial conditions in the presence of conventional initiators. The highest degree of conversion on the Ziegler–Natta catalysts does not exceed 24% (in the presence of electron-donor additives, 30%),[109] that in the presence of AIBN is 17%.[110]

It should be noted that physicochemical properties of VC copolymers with ethylene or α-olefins, *e.g.*, good processability, great elongation at rupture, enhanced specific impact strength, *etc.*, make them promising as plastics. In addition, the introduction of even 5%–10% of ethylene units in poly(vinyl chloride) markedly decreases the cost of manufacture of the polymer. The absence of efficient initiators holds up large-scale production of these copolymers.

As shown above, the coordination-radical initiators based on OEC with Group III elements and OEP with Group IV elements, due to the specific features of their structure, occupy an intermediate position between the traditional radical initiators and Ziegler–Natta catalysts. With these initiators, copolymerisation of VC with ethylene and with α-olefins can be carried out at high rates and high degrees of conversion with minimum energy expenditure.[106,111,112]

The degree of conversion in the homopolymerisation of alkenes initiated by these compounds does not exceed 3%–5%, which may be due to the specific features of radical formation in the TIBB–OEP systems.[57,113] However, copolymerisation of ethylene and other alkenes with vinyl monomers can be performed in the presence of the TIBB–OEP systems over a broad range of compositions and with high yields.

Using the vinyl acetate–ethylene and AN–hex-1-ene monomer pairs as examples, the activation energies for copolymerisation on the TIBB–*tert*-butylperoxytetraphenylantimony binary initiator were estimated to be 25.8 and 36.4 kJ mol^{-1}, respectively.[29,106] These values are much lower than the activation energies found for the use of diazo compounds and acyl peroxides as initiators and are close to the data for homopolymerisation of vinyl monomers with organoelement initiators.

The rate of copolymerisation of alkenes with vinyl monomers and the degree of conversion depend substantially on the composition of the monomer mixture and the number of carbon atoms in the alkene molecule. Thus in the case of the VC–ethylene pair, the yield of the copolymer reaches 90% over a period of 5–6 h.[112]

As the alkyl chain length in the alkene increases, the rate of polymerisation and the degree of conversion decrease; in the case of oct-1-ene, the yield of the copolymer does not exceed 20%. Additional introduction of an initiator results in only a slight increase in the yield. The reason for the decrease in the degree of conversion on passing from ethylene to α-olefins is probably related to the chain termination involving the active hydrogen atoms in the α-position relative to the alkene double bond.

In the case where traditional radical initiators or Ziegler–Natta catalysts are used in the VC copolymerisation with alkenes, the possibility of varying the copolymer composition is quite limited. The course of the composition curves and the relative activities of the monomers indicate that the copolymer is enriched in one monomer at any composition of the initial mixture. This is due to the considerable difference between the reactivities of VC and alkenes. The use of the trialkylborane–OEP systems results in substantial equalisation of the copolymerisation constants. Thus the composition curve for VC copolymerisation with ethylene or other alkenes follows an S-shaped pattern; for alkene contents in the monomer mixture ranging from 30 mol.% to 70 mol.%, the copolymer composition is virtually constant and does not depend on the composition of the mixture.[112]

The introduction of alkene units in vinyl polymers influences the physicochemical properties of the product in a definite manner. In particular, in the case of the ethylene–VA pair of monomers, the intrinsic viscosity of the copolymer increases with an increase in the alkene fraction. Conversely, the intrinsic viscosity (and MM) of the ethylene–VC copolymer decreases with an increase in the ethylene mole fraction. We calculated the Fickentcher constant (K_F), characterising the MM of poly(vinyl chloride) for a number of VC–alkene copolymer specimens.[114] The constant proved to be much lower (K_F = 40–70) than in the case of poly(vinyl chloride) synthesised with these initiators.[22] A decrease in the Fickentcher constant is known to facilitate

processing and to enhance the plasticity of the polymeric product.[14] It is worthy of note that an increase in the concentration of the initiator for an invariant ratio of the monomers in the mixture decreases the viscosity of the copolymers and slightly (by 5% – 6%) increases the degree of conversion.[106]

Thus, the use of coordinatively unsaturated OEC able to change the reactivity of macroradicals in a desired manner is an efficient technique for controlling the growth of the polymer chain under conditions of radical polymerisation. One more way of controlling the lifetime of a polymer chain aimed at synthesising compositionally uniform polymers is the use of stable radicals.

III. Growth of the polymer chain in the presence of stable radicals and iniferters

In recent years, a new concept of controlled processes called 'pseudo-living'-chain ‡ (or 'living'-chain) radical polymerisation has been vigorously developing. This polymerisation is of considerable interest as a simple and reliable method for the synthesis of polymers with a definite structure and specified properties.

The essence of the 'pseudo-living' polymerisation is as follows.[76, 117 – 120] The polymerisate contains catalytic amounts of active additives of a specific type (for example, stable radicals or their sources, complex ions of variable-valence metals, and other chain propagation controllers), able to undergo a reversible reaction with chain-propagating active radicals ($R^{\bullet}$) to give a labile adduct [R–X], which decomposes under certain conditions to recover the same chain-propagating macroradical.

$$R^{\bullet} + {}^{\bullet}X \rightleftharpoons RX. \qquad (17)$$

An important feature of 'pseudo-living' radical processes is alternation of the periods of chain propagation, termination and re-initiation. An obvious advantage of this approach is that the polymer chain grows step-by-step, *i.e.*, it becomes possible to control the lifetime of the growing radical. This brings about the following specific features of both the polymerisation kinetics and the properties of the resulting polymer:

— the number of polymer chains and active centres remains constant at any degree of conversion;

— starting from a low degree of conversion, the polymer MM continuously increases, the number-average MM value (M_n) increasing linearly with the degree of conversion;

— a narrow polydispersity (M_w/M_n, where M_w is the weight-average MM) of the polymer is observed at any degree of conversion;

— the isolated products of polymerisation can also act as macroinitiators; the addition of a new portion of the monomer results in further polymerisation and an increase in the polymer MM;

— when two or more monomers are added successively, block copolymers are formed.

Although the 'pseudo-living' radical polymerisation is a relatively new line in the research dealing with controlled radical processes, quite a few organic and organoelement compounds which permit radical polymerisation to be carried out in the 'living' regime have been proposed to date. Currently, more than a hundred publications devoted to this topic appear annually, and this flow does not decrease.§

‡ The process has been called 'pseudo-living' radical polymerisation because it has some features peculiar to the ionic 'living' polymerisation in which no chain termination takes place and chain propagation is continued until the monomer is exhausted.[115, 116]

§ Suffice it to say that in the section 'Radical Polymerisation' of the World Congress 'IUPAC MACRO-2000,' the problems of 'pseudo-living' polymerisation were the most vigorously discussed topic: of 36 oral reports and 51 posters, 17 reports and 20 posters were related to 'pseudo-living' polymerisation; and 18 posters were presented at the separate poster session on 'pseudo-living' polymerisation.[121]

Depending on the active additives (chain propagation controllers) used, the processes carried out in the 'living'-chain regime can be classified into the following types:

— polymerisation involving stable carbon-centred radicals and nitroxides, first of all, 2,2,4,4-tetramethyl-1-piperidinoxyl (TEMPO) and its analogues;

— polymerisation in the presence of spin traps and other potential sources of stable radicals;

— polymerisation using iniferters, controlling initiators of a new type;

— polymerisation in the presence of OEC, mainly, transition metal halides (atom transfer radical polymerisation — ATRP).

1. 'Pseudo-living'-chain polymerisation with participation of carbon-centred radicals and nitroxides

Examples of using stable radicals for controlling the kinetic parameters of radical polymerisation are well known and have been described fairly comprehensively not only in original publications but in relevant monographs.[76] Stable radicals, for example, galvinoxyl, phenoxyl and nitroxide spin adducts are active acceptors of free radicals, including polymeric radicals, over a broad temperature range. In recent years, in relation to the development of the reversible inhibition concept,[122 – 124] the interest in these compounds, especially nitroxides, has substantially increased as they can be used to control the chain propagation.

An important feature of some nitroxides is reversible interaction with a number of growing polymeric radicals at temperatures above 100 °C. This opens up some prospects for controlling the growth and, mainly, the lifetime of the polymeric chain. Over a fairly short period, the studies on the influence of nitroxides [76, 118 – 120, 125 – 136] and alkoxyamines [76, 118 – 120, 137 – 139] have occupied a prominent place in the research on 'pseudo-living' polymerisation.

The compounds used most often to control the lifetime of the growing chain include TEMPO [125 – 133] and its substituted analogues such as 4-methoxy-2,2,6,6-tetramethyl-1-piperidinoxyl,[137] 4-hydroxy-2,2,6,6-tetramethyl-1-piperidinoxyl,[135] *etc.* These nitroxides are used both as such (in the case of thermally initiated polymerisation) and in combination with traditional radical initiators (BP, AIBN, *etc.*).[125 – 136, 140] 'Pseudo-living' polymerisation in the presence of nitroxides based on TEMPO is normally carried out at temperatures of 95 – 130 °C; it is most typical of St and its derivatives (4-bromostyrene,[137] 3- and 4-chloromethylstyrenes,[140] *etc.*), as well as some acrylic monomers.[127, 135] However, it should be noted that in the case of acrylates, nitroxide spin adducts are much less efficient. In all probability, this is due to the fact that the bond (C – O – N) formed according to reaction (17) between the growing macroradical and the nitroxide is stronger, and hence, less labile in the case of polyacrylate radicals than in the case of styrene. Thus, dissociation of this bond requires more energy and, correspondingly, a higher temperature. However, raising the temperature of the synthesis can result in irreversible transformation of the terminal fragment into hydroxylamine.[120, 141] This may account for the fact that in the case of acrylates and other vinyl monomers, 'pseudo-living' mechanism could not be induced by increasing polymerisation temperature to 150 °C.[130, 135, 142, 143] Nevertheless, poly(butyl acrylate) with M_n = 10 500 – 27 000 and M_w/M_n = 1.53 has been prepared in the presence of 2,2,6,6-tetramethyl-4-hydroxy-1-piperidinoxyl at 150 °C.[135] Copolymerisation of St with BA in the presence of TEMPO using an azeotropic monomer mixture (St : BA = 7 : 3) at 120 °C also proceeds by a 'pseudo-living' mechanism.[144]

Kuchanov [124] has studied the effect of nitroxides on block polymerisation of St carried out at 120 °C, with different initial concentrations of TEMPO and without initiators.[124] In the presence of an initiator, polymerisation follows a 'pseudo-living' mechanism,[129, 144, 145] as indicated by the absence of a gel effect and low polydispersity coefficients of the resulting polymer as well

as by the increase in MM following an increase in the degree of conversion. 'Pseudo-living' copolymerisation of St with BA was carried out under similar conditions.[144]

In the presence of TEMPO, block copolymers of St with MMA and with butyl methacrylate have been synthesised.[128,146] It was shown that PS macromolecules are capable of re-initiating polymerisation. Yoshida and Sugita[147] combined cationic and radical polymerisation to prepare a biterminal polymer, poly-(styrene-β-tetrahydrofuran), with two terminal TEMPO radicals, which subsequently undergoes copolymerisation with St to give triblock copolymer.

A detailed and thoroughly justified description of the kinetic features of the 'living'-chain polymerisation in the presence of nitroxides has been reported.[120]

In addition to nitroxides, stable radicals of other classes have also found use in 'pseudo-living' radical polymerisation processes. In particular, the influence of the triphenylmethyl (trityl) radical, formed upon homolytic decomposition of hexaphenylethane (HPE)

$$Ph_3C-CPh_3 \longrightarrow 2\,Ph_3C^{\bullet}, \quad (18)$$

on the polymerisation of acrylic monomers has been studied. It was shown[148,149] in relation to the AIBN-initiated polymerisation of MMA at 80 °C that in the presence of excess HPE ([HPE] : [AIBN] > 5), the process switches to the 'pseudo-living' regime, which is characterised by successive increase in the polymer MM and suppression of the gel effect at high degrees of conversion. However, unlike nitroxides (TEMPO and its analogues), which do not react with the monomer double bond, the triphenylmethyl radical can itself initiate polymerisation.[148,150] Therefore, radical polymerisation of MMA in the presence of HPE has a number of specific features.

It was shown[148,150] that polymerisation of MMA at 80 °C with the addition of HPE and in the absence of AIBN proceeds very slowly (polymerisation time up to a high degree of conversion at [HPE] = 0.1 mol % is ~50 h; for the same AIBN concentration, it is 2–3 h) and exhibits features of a 'pseudo-living' process. In particular, gel effect is scarcely observed, the MM of the polymer linearly increases with an increase in the degree of conversion, and the polydispersity decreases with an increase in the degree of conversion of the monomer. The researchers cited[150] convincingly demonstrated that in this case, polymerisation of MMA follows a two-stage 'pseudo-living' mechanism.

The first stage is due to fast consumption of the trityl radicals in chain initiation and termination. At this stage, a reactive PMMA oligomer containing trityl groups at both ends of the chain is formed and rapidly accumulated

$$Ph_3C^{\bullet} + MMA \longrightarrow Ph_3C-MMA^{\bullet}, \quad (19)$$

$$Ph_3C-MMA^{\bullet} + {}^{\bullet}CPh_3 \longrightarrow Ph_3C-MMA-CPh_3\,. \quad (20)$$

The terminal bond in this oligomer remains labile. The PMMA oligomer re-initiates polymerisation at the second stage of the process, giving rise to a polymeric product in the system. During polymerisation at the second stage, the average MM continuously increases due to the formation of the polymer with a higher molecular mass and gradual consumption of the oligomer.

By analysis of the molecular-mass characteristics of the synthesised PMMA, interesting features of this process were identified.[148,150] The products formed at the first stage show a bimodal MMD. The position of the low-molecular-mass mode corresponding to oligomers virtually does not change during the process; however, its area gradually decreases. The high-molecular-mass mode shifts to higher MM with an increase in the degree of conversion, and its area increases. At high degrees of conversion, the oligomer mode virtually disappears, and the chromatogram becomes unimodal. Similar changes in the MMD of the final product — PMMA — were also observed when MMA polymerisation was carried out in the presence of specially synthesised and isolated oligomer.

Taking into account the experimental data considered above on the polymerisation of MMA in the presence of HPE, the following mechanism of the AIBN-initiated formation of PMMA was proposed.[148,150] Hexaphenylethane dissociates at 80 °C to afford trityl radicals, which initiate polymerisation; the rate constant for this reaction is 1×10^{-3} litre mol^{-1} s^{-1} (the rate of initiation at [HPE] = 5.0×10^{-3} mol litre^{-1} is 5×10^{-5} mol litre^{-1} s^{-1}). In parallel with this process, initiation at a rate of 5×10^{-8} mol litre^{-1} s^{-1} due to the thermal decomposition of AIBN takes place. It is clear that initiation caused by decomposition of AIBN at the beginning of the process can be neglected. The resulting oligomers re-initiate polymerisation; the parallel polymerisation due to initiation by AIBN also continues. The ratio of the rates of these processes is determined by the ratio of the initial concentrations of HPE and AIBN (the rate constants of these reactions are close[1]). If excess HPE is used (for example, [HPE] : [AIBN] > 50), the mechanism of this process is close to the 'pseudo-living' polymerisation mechanism.

In the opinion of the researchers cited,[148–150] HPE can be regarded as an iniferter because in the absence of a reactive competing agent, initiator (in this case, AIBN), the relatively inert trityl radical has time to attack the monomer and participates in the step of initiation of polymerisation; however, the rate of polymerisation with HPE is much lower than the rate of the AIBN-initiated process.

The diphenylmethyl and (trimethylsilyloxy)diphenylmethyl radicals, formed upon decomposition of tetraphenylethane[117,151–154] and bis(trimethylsilyloxy)tetraphenylethane,[117,155] respectively, behave similarly to the trityl radical in the 'pseudo-living' thermal polymerisation. In the first stage consisting of initiation and termination of the growing chains, the radicals formed upon thermal decomposition are rapidly consumed, and the reactive oligomeric product is accumulated. This product re-initiates polymerisation in the second stage of the process, which gives rise to the polymeric product. The polymers formed in the first stage are characterised by a bimodal MMD. The position of the low-molecular-mass mode, corresponding to oligomers, barely changes during the process; however, its area gradually decreases.

Study of copolymerisation of vinyl monomers in the presence of stable carbon-centred radicals is of obvious interest. The first data on the mechanism of copolymerisation involving carbon-centred radicals were obtained back in 1985.[156,157]

The use of *O*,*O*′-diisopropyl xanthogen sulfide (DXS) as a controlling additive made it possible to perform 'pseudo-living' copolymerisation of St with MA at 120–140 °C.[158,159] A specific feature of this process is a substantial decrease in the copolymerisation rate. Apparently, this is due to the fact that the rate of re-initiation in this system is lower than the rate of initiation;[159] this is obviously due to the difference between the energies of the S–S bond in the dissociating DXS and the C–S bond in the terminal group of the copolymer

$$Pr^iO-\underset{\underset{S}{\|}}{C}-S-S-\underset{\underset{S}{\|}}{C}-OPr^i \longrightarrow 2\,{}^{\bullet}S-\underset{\underset{S}{\|}}{C}-OPr^i \quad (21)$$

$$\sim CH_2\underset{\underset{R}{|}}{CH}-S-\underset{\underset{S}{\|}}{C}-OPr^i \longrightarrow \sim CH_2\underset{\underset{R}{|}}{CH}^{\bullet} + {}^{\bullet}S-\underset{\underset{S}{\|}}{C}-OPr^i \quad (22)$$

It can be seen from Eqn (22) that under these conditions, the stable S-centred radical formed acts as both an initiator and a chain propagation controller, similarly to carbon-centred radicals such as the trityl[148–150] or diphenylmethyl radical.[151–155] The copolymers considered are gradient polymers the properties of which differ from the properties of random polymers.[159]

2. Controlled radical polymerisation in the presence of spin traps and other sources of stable radicals

As noted above, a substantial drawback of the control of chain propagation by stable radicals is that the use of these species allows one to perform 'pseudo-living' radical polymerisation only at relatively high temperatures, above 100 °C. It is clear that development of effective methods for conducting polymerisation in the 'living'-chain regime at lower temperatures, normal for radical polymerisation of vinyl monomers under industrial conditions (50–80 °C), is a topical problem of synthetic polymer chemistry.

In this respect, the use of peroxides and azo compounds (typical radical initiators) in combination with active additives able to generate stable radicals, chain propagation controllers, directly in the polymerisation system (*in situ*) appears to be promising for performing controlled polymerisation. Nitroso compounds, nitrones, and other acceptors of free radicals used as spin traps in the studies of homolytic processes in organic and polymer chemistry can be used for this purpose.[160] For example, the use of *C*-phenyl-*N*-*tert*-butylnitrone (PBN) and 2-methyl-2-nitrosopropane (MNP) as effective controllers of the lifetime of a polymer chain for a number of vinyl monomers of various structures has been proposed.[161–169] These compounds exert an effective controlling influence on the polymerisation of various monomers in the temperature range of 50–80 °C.

On the basis of analysis of experimental data on the reactivity of nitrones and nitroso compounds, the following scheme of chain propagation in the presence of these additives was proposed.[161–163]

At the first stage, MNP (or PBN) react with the growing macroradical ($\sim P_n^{\bullet}$) to give a stable nitroxide.

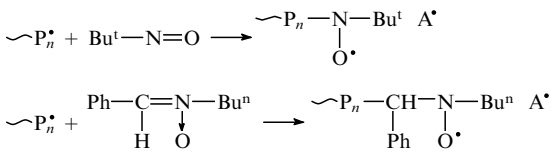

(23)

The nitroxide spin adduct $A^{\bullet}$ further reacts with the chain-propagating radical $\sim P_n^{\bullet}$ to give a labile bond

$$\sim P_n^{\bullet} + {}^{\bullet}A \rightleftharpoons [\sim P_n\text{---}A]. \quad (24)$$

The reversible reaction (24) results in alternation of the 'sleeping' and 'living' periods of the polymeric radical: the monomer (M) molecules add successively to the macroradical; thus, the polymer chain grows.

$$[\sim P_n\text{---}A] + M \longrightarrow [\sim P_{n+1}\text{---}A]. \quad (25)$$

The lability (relative instability) of the resulting $[\sim P_{n+1}\text{---}A]$ bond under conditions of polymerisation of vinyl monomers (50–80 °C) is due to both high stability of the nitroxide spin adduct ($A^{\bullet}$) and specific features of the structure of the polymeric radical ($\sim P_n^{\bullet}$). In particular, the energy of the R^1-O bond in the R^1-O-N bridge of the $R^1-O-N(R^3)R^2$ type nitroxide adducts formed according to Eqn (23) depends appreciably on the nature of radicals surrounding the N–O group, especially on their spatial structure. Thus in the case of TEMPO, a known controller of chain propagation, or the methyl radical, the bond energy is ~30 kcal mol^{-1}. Apparently, this is why TEMPO and its analogues are able to control efficiently the radical polymerisation of St and some acrylic monomers only at relatively high temperatures (100–130 °C). For a more bulky ethyl radical, the energy of this bond is ~25 kcal mol^{-1}, and in the case of sterically hindered *tert*-butyl or polyacrylate radicals, it is even lower (~20 kcal mol^{-1}).

When vinyl monomers are made to polymerise in the presence of PBN (or MNP), the nitrogen atom in the $R^1-O-N(R^3)R^2$ nitroxide adduct is linked to even more bulky and sterically hindered radicals. For example, in the case of MMA and MNP, it is linked to a *tert*-butyl radical (from MNP) and two polyacrylate radicals, having a high-molecular-mass 'tail'.

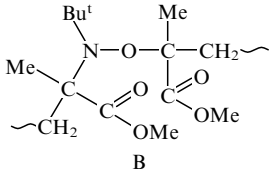

B

The strength of this bond is much lower than that in the case of TEMPO; naturally, it will dissociate rather easily at lower temperatures to give the initial radicals.

Moreover, since the nitroxide adduct B is formed initially upon the interaction of two bulky radicals directly during the synthesis of the polymer at a temperature of 50–80 °C, it cannot be ruled out that the chemical bond between the chain-propagating radical ($\sim P_n^{\bullet}$) and the nitroxide spin adduct ($A^{\bullet}$) is a vibrationally excited molecule (an analogue of a radical pair in the $[\sim P_n\text{---}A]$ solid matrix) even at the instant of formation.

To date, 'pseudo-living' polymerisation in the presence of PBN has been accomplished for a number of vinyl monomers, namely, MMA,[161–164, 166–168] butyl methacrylate, BA, St, and VC.[165–167] The main process parameters and the properties of polymers prepared in the presence of PBN are listed in Table 4. Some common features of the mechanism of the 'pseudo-living' radical polymerisation in the presence of PBN can be distinguished.

In particular, the introduction of a controlling additive results in an appreciable decrease, down to complete suppression, of the gel effect and allows conduction of the polymerisation to high degrees of conversion (80%–90%). It is very important for practical purposes that the time of polymerisation increases insignificantly (with respect to that for the process without an additive), as a rule, not more than twofold (see Table 4). The duration of polymerisation of St and MMA by the 'pseudo-living'

Table 4. Some kinetic parameters for the polymerisation of vinyl monomers in the presence of PBN and molecular-mass characteristics of polymers (initiator AIBN, 0.1 mol.%).

Monomer	[PBN] (mol.%)	T /°C	$10^4 V$ /mol litre^{-1} s^{-1}	Time /h	Degree of monomer conversion (%)	$10^6 M_\eta$	M_w/M_n	Ref.
MMA	–	50	1.2	8	91	4.3	>2.0	161, 162
	0.80	50	0.8	17	75	1.2	1.7	
BA	–	65	2.1	2	98	–	>2.0	169
	0.02	65	0.1 [a]	7	65	0.7 [b]	1.7	
BMA	–	50	1.1	12	99	10.7	–	169
	0.2	50	0.8 [a]	24	78	6.5	–	
VC	–	50	9.1	3	92	70 [c]	2.5	165
	0.01	50	0.6	5	89	66 [c]	1.7	

[a] The rates are given for [PBN] = 0.1 mol.%. [b] The M_n value. [c] The Fickentcher constants are given.

radical mechanism is known to increase severalfold in the presence of TEMPO,[125–136] triphenylmethyl radicals[148–150] or other radicals. The PBN concentration at which the gel effect is suppressed depends on the structures of the monomer and, especially, the growing macroradical; in any case, this concentration is commensurable with the content of the initiator (0.01 mol.%–0.80 mol.%).[161, 162, 164, 169]

The number-average and viscosity-average (M_η) molecular masses of the polymer prepared in the presence of PBN follow a linear dependence on the degree of conversion, which is typical of polymerisation by the 'pseudo-living' mechanism. The shift of the low-molecular-mass shoulder and the whole mode to higher molecular masses with an increase in the degree of conversion of the monomer can be clearly seen in the MMD curves.[161, 162, 169]

An important feature of the proposed controller is the fact that stable radicals able to control chain propagation are formed directly during polymerisation as a result of interaction of the macroradicals with an additive introduced to the system, which effectively controls the synthesis of macromolecules even at 50–80 °C.

A shortcoming of this method for controlling the growth of a polymer chain is that the MMD of the resulting polymer is broader than, for example, in the case of ATRP.[76, 119, 120] In our opinion, this is due to the inhomogeneity of high-molecular-mass nitroxides formed by reaction (23) as chain propagation controllers.

It should be noted that the structures of the macroradical and the monomer have a substantial influence on the polymerisation kinetics and the polymer MM under the conditions of reversible inhibition in the presence of PBN. Thus comparison of acrylic monomers, namely, MMA, butyl methacrylate and BA, shows that the process involving BA occurs at higher temperature (> 65 °C) and at much lower concentrations of the active additive and has a longer induction period than the processes with MMA or butyl methacrylate.[166–169]

The differences in the regularities of polymerisation of MMA and butyl methacrylate, on the one hand, and BA, on the other hand, are undoubtedly due to specific features of the structure of growing macroradicals and the reactivity of the macroradicals towards nitroxide spin adducts. Thus, from a thermodynamic standpoint, sterically hindered PMMA and poly(butyl methacrylate) macroradicals (tertiary radicals) form a weaker and, hence, a more labile bond with the nitroxide used as a chain propagation controller [reaction (23)]. In the case of polymerisation of BA, the bond between the nitroxide spin adduct and the growing macroradical of poly(butyl acrylate) (secondary radical) is stronger and more stable against dissociation. As a consequence, in the case of polymerisation of BA, the 'living'-chain mechanism can be accomplished at a higher temperature. In addition, the rate constant for the acceptance of secondary and tertiary radicals by a spin trap (PBN) are known to differ by almost an order of magnitude. In our opinion, this can account for the long induction period in BA polymerisation and for the possibility of using lower concentrations of nitrone as a controller of the chain propagation than those required in the polymerisation of MMA and butyl methacrylate.[166–169]

The foregoing is confirmed by the data on the polymerisation of VC[165, 166, 168] and St[166, 168] in the presence of PBN: the growing polymer radicals derived from these monomers are secondary radicals; hence, as in the case of BA, the controlled process takes place at a lower PBN concentration.

It was shown in relation to the polymerisation of MMA that the use of MNP as a controlling additive entails effects similar to those observed with PBN; in the latter case, the control of the polymer chain propagation requires lower concentrations of the additive (0.005 mol.% – 0.01 mol.%). Apparently, this is due to higher constants for the acceptance of macroradicals by nitroso compounds than by nitrones.[163, 166–169]

3. Iniferters as controlling initiators of polymerisation of a new type

Yet another elegant method for performing controlled radical polymerisation proposed in recent years is based on the use of a special class of initiators called iniferters.¶ These compounds decompose rather readily to give free radicals ($A^\bullet$) and ($B^\bullet$)

$$A-B \rightleftharpoons A^\bullet + B^\bullet. \quad (26)$$

One radical is reactive ($A^\bullet$), it can react with the monomer and thus initiate the chain propagation. The second radical ($B^\bullet$) is reactive only with respect to the growing macroradical and can react with it according to the reversible inhibition pattern

$$A^\bullet + M \longrightarrow A-M^\bullet, \quad (27)$$

$$A-M^\bullet + {}^\bullet B \rightleftharpoons A-M-B. \quad (28)$$

Chain termination *via* recombination of the growing macroradical with the primary radical of the iniferter [reaction (28)] occurs much faster than chain termination *via* recombination or disproportionation of the growing radicals. In addition, iniferter participates in chain transfer reactions.

In terms of their chemical nature, the iniferters known to date can be conventionally divided into three groups.

In the iniferters of the first group, homolytic decomposition of both the initial and the resulting macromolecular initiator involves a labile bond of the same chemical nature. Examples of these iniferters are alkoxyamines[76, 118–120, 137–142] and alkylthiocarbamates.[170–174]

In the case of second-group iniferters, the steps of decomposition of the initial and macromolecular initiators involve bonds of different chemical natures. This group of iniferters includes, for example, phenylazotriphenylmethane[117, 148, 175, 176] and some thio iniferters.[117]

Binary redox systems based on organic and organoelement compounds and the corresponding oxidants (sterically hindered quinones, oxytriazenes, *etc*.) can be classified as the third type of iniferters.[177–182]

Alkoxyamines, which are used most often as iniferters, are compounds of the $R-M_n-X$ type, where R is the radical formed upon decomposition of a conventional initiator of radical polymerisation (BP, AIBN, DCHPD[135, 183–189]), M is the monomer (most often, St), X is a nitroxide (as a rule, TEMPO or its analogue).

It has been noted above that the parameters of polymerisation in the presence of TEMPO are close to the parameters of 'living' ionic processes; this is due to the high re-initiation constant by reaction (17). In this connection, vigorous studies into the use of alkoxyamines as iniferters are being carried out.

Numerous publications have been devoted to the synthesis of new alkoxyamines[189–195] and their application in the polymerisation processes. The results of these studies can be used to select the compounds $R-M_n-X$ the half-life of which is shorter than the period of complete polymerisation transformation by factors of tens or even hundreds;[120] this, in turn, can increase the efficiency of a nitroxide as a 'pseudo-living' polymerisation agent. An important indication of a 'living' process is polydispersity. If ordinary quadratic termination does not take place, the polydispersity of the polymer should be equal to unity. Polystyrene samples with polydispersity values close to unity have been obtained with a number of alkoxyamines.[120]

The results of kinetic studies of the mechanism of 'living' radical polymerisation of St in the presence of alkoxyamines and of analytical calculation studies were considered in detail in a review.[120] Polymerisation in the presence of alkoxyamines occurs by the following scheme:

¶ The term iniferter is composed of the names of elementary steps of radical polymerisation: ini (initiation), fer (transfer), ter (termination).[117, 124]

$$\begin{aligned} &R-R \longrightarrow 2\,R^{\bullet}\ \text{(initiation)},\\ &R-X \longrightarrow R^{\bullet} + X^{\bullet},\\ &R^{\bullet} + X^{\bullet} \longrightarrow R-X,\\ &R^{\bullet} + M \longrightarrow R-M^{\bullet},\\ &R^{\bullet} + R^{\bullet} \longrightarrow R-R. \end{aligned} \qquad (29)$$

The process kinetics has the following specific features: the rate of polymerisation is proportional to the monomer concentration and does not depend on the alkoxyamine concentration; the polymer MM increases linearly with an increase in the degree of polymerisation (this regularity holds, at least, up to $M_n = 20\,000 - 30\,000$); the polydispersity of the polymer normally first decreases with an increase in the degree of conversion and then increases; the polydispersity coefficient fluctuates depending on the process conditions but, as a rule, it remains less than 1.3; the concentration of the stable nitroxide (EPR detection) is equal to 0.1% – 1.0% relative to the initial concentration of the alkoxyamine throughout the whole process.[196]

Computer analysis of the kinetic data and the molecular-mass characteristics[197–199] made it possible to establish correlations between reaction parameters (temperature, concentration of the reactants) and the properties of 'living' polymerisation agents [the rate constants for the forward and back reactions (28)]. These results can be used to choose the optimum conditions for performing polymerisation of St with a particular iniferter.

However, it should be noted that, similarly to the polymerisation in the presence of TEMPO (and, evidently, for the same reasons), these compounds can be used at temperatures above 100 °C and only for polymerisation of St and its analogues[137,140,198,200,201] and copolymerisation or preparation of block copolymers of St with other monomers, most commonly, acrylates.[202–204]

Dissociation of alkoxyamines at high temperatures (above 135 °C) has been studied in detail in relation to 1-methylbenzyloxy-2,2,6,6-tetramethyl-1-piperidine[205] and its derivatives resulting from decomposition of BP in St.[141] The process follows two pathways, one to give a reactive hydrocarbon radical and a stable nitroxide (it is this reaction that is responsible for the 'living' polymerisation mechanism) and the other, giving rise to an unsaturated hydrocarbon and hydroxylamine (hydride transfer).

Alkoxyamines based on TEMPO have been used[206–209] to synthesise densely cross-linked glassy polymers by 'pseudo-living' radical three-dimensional polymerisation; copolymerisation of St with MA was taken as an example. Due to the 'pseudo-living' polymerisation mechanism, the point at which a continuous network was formed was shifted appreciably towards higher degrees of conversion (> 17% – 35%) compared to that observed for conventional three-dimensional radical polymerisation.

Block copolymerisation of St and its analogues with acrylates has proved to be a more efficient method for the extension of the scope of application of alkoxyamines. Block copolymers based on PS or on St copolymers with acrylates with high St contents prepared in the presence of alkoxyamines have been considered in detail in reviews[120,210] and monographs.[76,119]

The use of derivatives of thiocarbamates as photoiniferters has been studied extensively.[124,170–174] Unlike the iniferters which decompose at high temperatures, thiocarbamates tend to decompose on exposure to UV radiation at much lower temperatures than alkoxyamines. The polymerisation of St in the presence of these reagents has all the main features of 'pseudo-living' polymerisation.[173,174]

An EPR study of the photo decomposition of *S*-benzyl *N*,*N*-diethyldithiocabamate and PS containing a terminal dithiocarbamate group induced by UV radiation (λ = 365 nm, 25 °C) has shown[120,211] that decomposition follows the same mechanism with rupture of the C – S bond to give reactive benzyl (or polystyrene) and stable *N*,*N*-diethyldithiyl radicals.

$$\mathrm{BnSC(S)NEt_2} \xrightarrow{h\nu} \mathrm{Bn^{\bullet}} + {}^{\bullet}\mathrm{SC(S)NEt_2} \qquad (30)$$

$$\sim\!\mathrm{CH_2CH(Ph)SC(S)NEt_2} \longrightarrow \sim\!\mathrm{CH_2CH^{\bullet}(Ph)} + {}^{\bullet}\mathrm{SC(S)NEt_2} \qquad (31)$$

By assuming that decomposition of these compounds occurs by the same mechanism, one can explain the fact that the regularities of polymerisation in the presence of low- and high-molecular-mass iniferters — *S*-benzyl *N*,*N*-diethyldithiocabamate and the PS containing a terminal dithiocabamate group — prove to be qualitatively the same.

Research into the photo and thermal decomposition of thio iniferters showed[212–215] that decomposition of symmetric molecules involves either the S – S bond

$$\mathrm{RSSR} \xrightarrow{h\nu} 2\,\mathrm{RS^{\bullet}} \qquad (32)$$

R = Ph, $\mathrm{C(S)NAlk_2}$,

or both the S – S and C – S bonds

$$\begin{aligned} &\mathrm{RSSR} \xrightarrow{h\nu} 2\,\mathrm{RS^{\bullet}},\\ &\mathrm{RSSR} \xrightarrow{h\nu} \mathrm{R^{\bullet}} + {}^{\bullet}\mathrm{SSR} \end{aligned} \qquad (33)$$

R = C(O)Ph.

In the case of nonsymmetric dithiocarbamates and dithiocarbonates $\mathrm{R(CH_2)_nSC(S)NAlk_2}$ and $\mathrm{R(CH_2)_nSC(S)OAlk}$ (R = Ph, R′CO), the formation of dithiyl (stable) radicals needed to induce 'pseudo-living' polymerisation takes place only for the compounds $\mathrm{BnSC(S)NAlk_2}$, BnSC(S)OAlk and AlkCOO. $\mathrm{.CH_2SC(S)NAlk_2}$.[216–218]

Other compounds that can be attributed to the class of iniferters in question include HPE,[148–150] tetraphenylethane[117,151–154] and bis(trimethylsilyloxy)tetraphenylethane,[117,155] which do decompose under polymerisation conditions to yield symmetric inert radicals but only in the case where they are added without an initiator. In the absence of an active competing agent, initiator, the low-reactivity radical has time to attack the monomer and participates in the initiation of polymerisation. However, the rate of polymerisation in the presence of HPE or related tetraphenylethane or bis(trimethylsilyloxy)tetraphenylethane is much lower than that of the process initiated by AIBN or an organic peroxide.

Another type of iniferters includes phenyl azotriphenylmethane (PAT); the use of this compound as the initiator of 'pseudo-living' polymerisation of MMA was first described by Otsu and Matsumoto.[117]

The thermal decomposition of PAT occurs at a high rate with rupture of the C – N bond; it is accompanied by evolution of nitrogen and gives rise to phenyl and triphenylmethyl radicals according to the following scheme

$$\mathrm{Ph-N=N-CPh_3} \longrightarrow \mathrm{Ph^{\bullet}} + \mathrm{N_2} + {}^{\bullet}\mathrm{CPh_3}.$$

The reactive phenyl radicals initiate polymerisation, while the relatively stable triphenylmethyl radicals participate only in the chain termination by macroradicals to give a terminal bond. As has already been noted, the terminal bonds are fairly labile thermally and their homolytic cleavage results in re-initiation of polymerisation. It was found that up to a degree of conversion of ~2%, the polymerisation rate of MMA[148,175] and MA[176] increases (as in the presence of HPE); subsequently, in the transient region up to degrees of conversion of 5% – 15%, the rate markedly decreases; finally, gradual self-acceleration of the reaction starts. The dependence of the MM on the degree of conversion for polymer samples is linear up to 50% degree of conversion.

The MMD follows a specific pattern of variation during polymerisation, namely, the products formed at degrees of con-

version ranging from 1% to 7% exhibit a unimodal MMD and are oligomeric products. As the degree of conversion increases, the MMD curves become bimodal: a second mode arises, which shifts to higher MM as polymerisation advances, and its area continuously increases. The position of the oligomeric mode does not change; however, its area gradually decreases. When the degree of conversion is high (nearly limiting), the oligomeric mode completely disappears, and the MMD of the resulting PMMA and poly(methyl acrylate) becomes again unimodal. A similar pattern of variation of the MMD is observed for 'pseudo-living' polymerisation of MMA involving trityl radicals.[148–150] Evidently, the mechanism of formation of PMMA in the presence of PAT is underlain by the same processes as in the initiation by AIBN with HPE [148–150] (see the previous Section).

An interesting feature of MMA polymerisation in the presence of PAT has been identified.[148,175] Starting with some degree of conversion (40% – 50%), the MMD mode stops moving to higher molecular masses, *i.e.*, the contribution of the 'pseudo-living' polymerisation to the formation of the polymer markedly decreases. In the opinion of the researchers cited, this may be due to the fact that the trityl radical is capable of initiating polymerisation of the acrylate, giving rise to a conventional 'dead' polymer, this process being more active at high degrees of conversion. In addition, accumulation of the 'dead' polymer in the system can be due to side reactions, resulting in deactivation of the labile bond in the macroiniferter, namely, isomerisation of the triphenylmethyl radical followed by its addition to the macroradical, which occurs in parallel with the formation of the labile bond [219]

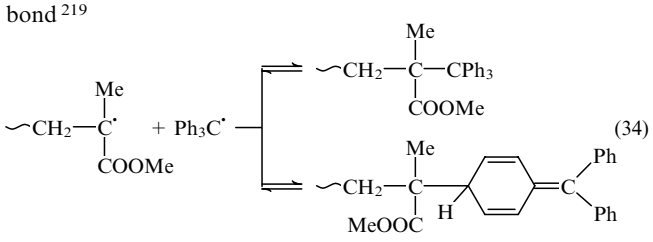

(34)

and disproportionation of these radicals [219]

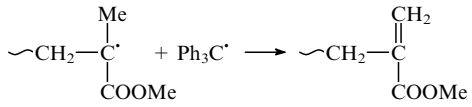

(35)

As noted above, decomposition of the symmetric molecules of thio iniferters involves either the S – S bond or both the S – S and C – S bonds [see reactions (32) and (33)]. The former route yields symmetric S-centred radicals, which can initiate polymerisation without AIBN or peroxide. We have already discussed data on the use of DXS as a controlling additive in the copolymerisation of vinyl monomers.[158,159] The stable S-centred radical arising according to reactions (32) and (33) under the indicated conditions acts as both an initiator and a chain propagation controller and can be attributed to the class of iniferters under consideration because the labile bond in the terminal group of the copolymer is the C – S bond.

Original binary initiators and chain propagation controllers based on oxytriazenes and oxidants (metal oxides, organic and inorganic peroxides and hydroperoxides) have been proposed.[179–182] It was found by EPR spectroscopy that, owing to the simultaneous generation of reactive phenyl radicals (chain propagation initiators) and nitroso compounds, which can react with chain-propagating radicals to give nitroxides (which control the chain propagation), these systems are able, on the one hand, to initiate radical polymerisation, and, on the other hand, to act as process controllers.

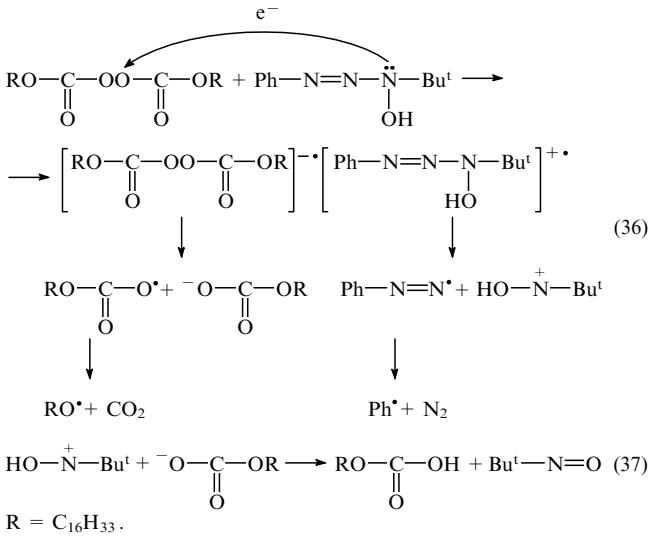

(36) (37)

The possibility of realisation of a similar single-electron transfer mechanism in the reaction of acyl peroxides with substituted amines has been demonstrated previously.[220]

In addition, it cannot be ruled out that secondary reactions take place between triazene and the alkoxide radicals derived from the peroxide, which results in triazene decomposition.

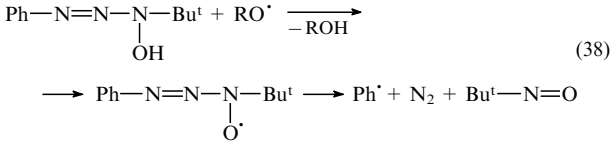

(38)

The presence of nitroxides in the polymerisate was detected by EPR using the spin trap technique [a triplet with the splitting constant at nitrogen a_N = 15.6 Oe corresponding to the adduct of the nitroso compound with the poly(methyl methacrylate) radical].

Polymerisation of MMA in the presence of oxytriazene, like that in the presence of MNP,[163,166–168] proceeds under relatively mild temperature conditions (50 – 60 °C) and exhibits features peculiar to 'pseudo-living' polymerisation, namely, the absence of gel effect in the polymerisation up to high degrees of conversion, linear increase in the MM following an increase in the degree of conversion, relatively low polydispersity, *etc.*[179–182] Thus, these systems can be regarded as a sort of binary iniferter.

Yet another example of unusual initiators and controllers of polymer chain propagation is provided by compositions based on sterically hindered quinones and OEC. Thus it has been found [177,178] that 3,5-di-*tert*-butylquinone, used traditionally as the inhibitor of radical processes, when combined with trialkylborane, is able not only to initiate effectively radical polymerisation of various monomers but also to control the propagation of the polymeric chain according to the 'pseudo-living' mechanism. It was found by EPR spectroscopy and by kinetic measurements that the rate of MMA polymerisation is comparable in this case with the rate of polymerisation of acrylic monomers in the presence of traditional radical initiators, AIBN and acyl peroxides, and in some cases, even exceeds it.

Analysis of the data obtained shows that several processes occur in the system. One process is the reaction of quinone, for example, with TIBB, which gives rise to radicals carrying the polymerisation.

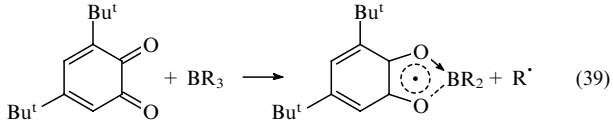

(39)

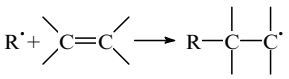

(40)

The occurrence of reaction (39) has also been assumed in other studies [221, 222] (this assumption was made taking account of the results of EPR investigations of the reaction of quinones with alkyl derivatives of Group III elements, in particular, gallium). In addition, the chain-propagating radicals can react with quinones to give oxygen-centred radicals of the phenoxyl type, which react with TIBB to generate new alkyl radicals,[223] able to initiate polymerisation.

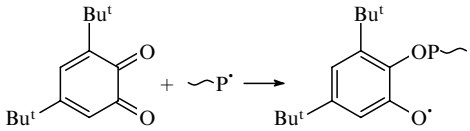

(41)

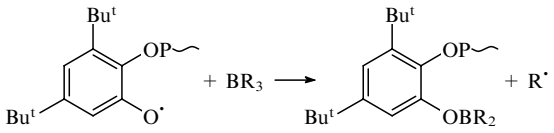

(42)

P is the chain-propagating (polymeric) radical.

The dependence of MM of poly(methyl methacrylate) synthesised in the presence of the 3,5-di-*tert*-butylquinone – TIBB system on the degree of conversion is linear over a broad range of MM values, from 17 000 to 200 000. As the degree of conversion increases, the polymer MMD mode moves continuously to higher molecular masses. This type of dependence of the polymer MM on the degree of conversion is characteristic of 'pseudo-living' chain propagation, including that in the presence of iniferters. It can be seen from Eqn (39) that the reaction of the components of the 3,5-di-*tert*-butylquinone – TIBB binary initiator furnishes the reactive alkyl radical R$^{\bullet}$, capable of initiating polymerisation, and a stable radical (A$^{\bullet}$), which can be coordinated to the chain-propagating radical to afford a labile bond.

$$\sim P^{\bullet} + {}^{\bullet}A \rightleftharpoons [\sim P^{\bullet}\text{---}{}^{\bullet}A]. \quad (43)$$

The polymer chain grows according to a stepwise pattern as a result of consecutive steps of cleavage of the terminal labile bond [$\sim$P---A] and consecutive addition of some number of monomer units to give a new labile bond according to the scheme

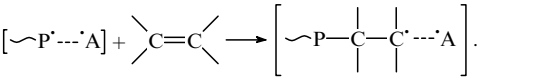

(44)

Thus, quinones combined with OEC act as a sort of low-temperature binary iniferters. In this case, the reactive radical (R$^{\bullet}$) which initiates polymerisation and the stable radical (A$^{\bullet}$) which controls the chain propagation are generated directly in the reaction system upon the reaction of the components of a binary initiator with each other [see Eqns (39) – (43)].

Similar regularities are also characteristic of some other quinones and OEC derived from Group III — V elements.[224]

Original initiators-chain propagation controllers based on sterically hindered trialkylboranes and oxidants have been proposed by Chung *et al.*[225] These investigators were the first to use stable boron-containing radicals produced upon oxidation of 1-octyl-9-borabicyclononane to control the chain propagation in the polymerisation of MMA. The use of this additive brings about the features typical of 'pseudo-living' radical polymerisation. It is of fundamental importance that, unlike most known systems, with this system the process occurs at room temperature which allows one to eliminate the undesirable thermal constituent of the process, which markedly deteriorates the MMD of the polymer.

4. Radical polymerisation in the 'living' chain regime in the presence of organoelement compounds

The use of OEC as chain propagation controllers in the 'pseudo-living' radical polymerisation of vinyl monomers opens up prospects for modelling 'pseudo-living' processes using individual features of the metal or non-metal atom in OEC.

Processes in which organic compounds of transition metal halides are used to control the growth of a polymer chain have been studied to date.[76, 119, 226 – 228]

It is known [229] that transition metal halides with the formula $X^n - Y_m - L_x$ (X is a transition metal, n is the valence of the metal, Y is chloride or bromide, L is an organic ligand, most often, a Lewis base) containing metal in a lower oxidation state react with alkyl halides (RX) at $\sim$100 °C to give the alkyl radicals R$^{\bullet}$ capable of initiating polymerisation. Simultaneously, oxidation of the transition metal takes place according to the reversible Kharasch reaction.[229]

$$R - X + X^n - Y_m - L_x \rightleftharpoons R^{\bullet} + X^{n+1} - Y_m - L_x, \quad (45)$$

$$R^{\bullet} + xM \longrightarrow R - M_x^{\bullet}, \quad (46)$$

M is monomer.

When this reaction was induced in the medium of a vinyl monomer, stepwise growth of the polymer chain was observed, *i.e.*, a 'pseudo-living' chain process took place.

Currently, a broad range of OEC (copper, iron, palladium and other compounds) are used as controlling additives; the organic ligands most often contained in these systems are 2,2′-bipyridine,[230, 231] 4,4′-di(non-5-yl)-2,2′-bipyridine,[232 – 236] triphenylphosphine,[226 – 228, 237] *etc*. The alkyl halides normally used for this purpose include alkyl(or aryl) bromides and dialkyl(or diaryl)- alkylaryl bromides.[226, 230, 232, 233, 235, 236]

For a series of vinyl monomers, namely, St,[226, 228, 232 – 235] MA,[233, 234] MMA,[226, 232, 234, 237 – 239] AN [230] and so on, the ATRP process has been accomplished [see redox reaction (45)]. The rate of this process is rather high; therefore, all the polymer chains are initiated almost simultaneously; this allows the manufacture of polymers with a polydispersity close to unity (1.05 – 1.30).[227, 228, 230, 232 – 239] Unlike the controlling additives on the basis of stable radicals considered above, the ATRP agents are not incorporated in the polymer chain and, hence, they can be regarded as analogues of catalysts.

In addition to transition metal compounds (for example, as in ATRP), other OEC are also employed to induce 'pseudo-living' radical polymerisation. As early as in the 1970s, Academician G A Razuvaev and co-workers [240, 241] synthesised block copolymers of MMA with AN using radical initiation by organo-mercury and -tin compounds. It was established by emission spectroscopy that PMMA contained mercury in the terminal groups, and subsequently these macromolecules can act as peculiar macroinitiators. The molecular mass of the secondary polymer is twice as high as the MM of the initial one, which confirms indirectly the possibility of a 'pseudo-living' chain mechanism.

IV. Characteristic features of homo- and co-polymerisation of vinyl monomers in the presence of organoelement compounds derived from Group V elements

The coordinatively unsaturated OEC containing Group II and, especially, Group III elements participate directly in the chain propagation step. The addition of compounds derived from Group IV and V elements also influences the elementary steps in polymerisation. These compounds have vacant *d* orbitals, which stipulates their electron density acceptor properties.

Tin and germanium tetrachlorides can influence significantly co-polymerisation of MAA esters with MMA.[51, 52] The introduction of 1 mol.% of these compounds to a polymerisate gives rise to alternating copolymers. Conversely, the addition of tetrabutyltin

barely influences either polymerisation rate or the MM of polymers. Apparently, this is due to the fact that vacant *d* orbitals of the tin atom are removed from the nucleus and, therefore, the electron-acceptor capacity of these orbitals is too low to activate the chain-propagating radical. Electron-donating alkyl radicals do not promote the coordinating capacity of OEC either. Data on the copolymerisation of MMA with MAA in the presence of tetrabutyltin additives confirm the conclusion that the activities of monomers and growing macroradicals virtually do not change.

Meanwhile, the controlling effect of Group IV element halides on the copolymerisation of acrylates, described by Smirnova and coworkers,[51, 52] can be explained by the fact that inorganic Lewis acids are more prone to form intermolecular complexes than organic compounds of the same elements.

A specific position is occupied by OEC containing Group V elements because they contain both a lone electron pair in the *p* orbital suitable for a nucleophilic attack and vacant *d* orbitals, which can give rise to electron-withdrawing properties.

It has been shown [242, 243] that the addition of alkyl derivatives of bismuth and antimony influences directly the kinetic parameters of polymerisation of vinyl monomers. Thus the rate of BA and VA polymerisation increases by more than an order of magnitude in the presence of catalytic amounts of triisobutylbismuth. The addition of triethylantimony markedly accelerates not only bulk polymerisation of acrylates but also solution polymerisation in ethyl acetate, which is a polar solvent and can be regarded as a hydrogenated analogue of MMA in terms of its electronic structure; like the monomer, it contains an ester group able to be coordinated to electron density acceptors. Organic compounds of bismuth and antimony, like those of Group III elements, do not exert any substantial catalytic effect on the decomposition of an initiator such as AIBN either in inert hydrocarbons or in the presence of vinyl monomers.[53]

Thus, the data presented above indicate unambiguously that acceleration of polymerisation of acrylic monomers in the presence of OEC containing Group V elements is due to the direct participation of these additives in the chain propagation stage.

It should be noted that catalytic amounts of OEC accelerate chain propagation in the polymerisation of VA and BA much more efficiently than in the polymerisation of MMA, which is in good agreement with the results of investigations into the influence of Group III element compounds on the polymerisation of acrylates.

The phenyl derivatives of Group V elements stable against oxidation by atmospheric oxygen also activate somewhat the process of MMA polymerisation. The accelerating effect of these derivatives decreases in the series $Ph_3Bi > Ph_3Sb > Ph_3As$, which is in line with the variation of nucleophilic properties of these compounds.

It is clear that the influence of organic derivatives of Group V elements on the polymerisation of acrylic monomers is directly related to the presence of the lone electron pair in the *p* orbital. This conclusion is supported by the fact that introduction of pentaphenylantimony in the polymerisate barely changes the polymerisation rate and the polymer MM.[242, 243]

Apparently, during its growth, a macroradical reacts with the metal atom in the OEC to give a four-coordinate radical complex

$$\sim P^{\bullet} + \ddot{E}R_3 \longrightarrow [\sim P^{\bullet}\text{---}\dot{E}R_3], \qquad (47)$$

where $\sim P^{\bullet}$ is the growing macroradical; E is a Group V element (antimony, bismuth); R = Et, Ph, Bu^i.

It is known [56] that, owing to the lone electron pair in the *p* orbital and free *d* orbitals, Group V elements are capable of expanding their electron shells. It has been shown by EPR [56] that compounds of trivalent Group V elements can react with free oxygen- and carbon-centred radicals; as this takes place, the coordination number increases to four and the corresponding intermediates are formed [reaction (47)].

The $[\sim P\text{---}ER_3]$ bond thus formed between the growing macroradical and a Group V element is labile and can be cleaved either yielding the initial compounds (OEC and the chain-propagating radical, which can continue polymerisation) or with the 'ejection' of a radical from the organoelement compound (S_R2 substitution).

$$\left[\sim P^{\bullet}\text{---}\dot{E}R_3\right] \longrightarrow \sim P^{\bullet} + \ddot{E}R_3 \quad \text{or} \quad \sim P\ddot{E}R_2 + R^{\bullet} \qquad (48)$$

Thus, one of the variants for the participation of OEC in the chain transfer stage and in the control of MM is realised.

It cannot be ruled out that in the presence of coordinatively unsaturated OEC, chain propagation takes place *via* insertion of the monomer at the labile $[\sim P^{\bullet}\text{---}\dot{E}R_3]$ bond to give a new coordinated macroradical.

$$\left[\sim P^{\bullet}\text{---}\dot{E}R_3\right] + CH_2{=}\underset{\displaystyle X}{\underset{|}{CH}} \longrightarrow \left[\sim P^{\bullet}\text{----}\dot{E}R_3 \;\; CH_2{=}\underset{\displaystyle X}{\underset{|}{CH}}\right] \longrightarrow \left[\sim P{-}CH_2{-}\underset{\displaystyle X}{\underset{|}{\dot{C}H}}\text{---}\dot{E}R_3\right] \qquad (49)$$

Thus, OEC is coordinated to the growing macroradical and thus participates directly in chain propagation and prevents bimolecular chain termination upon recombination of growing macroradicals. This type of process can be considered as a variant of 'pseudo-living' polymerisation.

It has been noted above that an increase in the rate of complex-radical polymerisation in the presence of metal halides can be explained by assuming the cyclic mechanism of chain propagation.[5] Similarly to OEC containing Group III elements, the alkyl derivatives of antimony and bismuth have a more pronounced influence on the chain propagation in the polymerisation of VA and BA than in the polymerisation of MMA.[242, 243] Since the distributions of electron density in the molecules of alkyl acrylates and methacrylates (for example, in MMA and BA) differ insignificantly,[79] it can be suggested that steric factors make the crucial contribution to the change in the kinetic parameters of polymerisation (in particular, the rate constants for chain propagation). The absence of substituents at the central carbon atom in the butyl acrylate radical makes the reaction centre more readily accessible for the coordination to OEC and subsequent chain propagation than in the case of MMA (tertiary radical).

The mechanism of chain propagation proposed above is also supported by the absence of inhibitory effect upon joint introduction of hydroquinone and triethylantimony in the polymerisate.[53] The organoelement additive enters into the coordination interaction with the growing macroradical and thus 'blocks' the reaction centre and prevents its interaction with the inhibitor. Consequently, the rate of polymerisation and the MM of polymers virtually do not change in the presence of hydroquinone and triethylantimony.

The character of influence of benzoquinone (a more effective inhibitor of radical polymerisation) on the kinetics of the processes studied is determined by the quinone concentration in the monomer mixture.[53] When the ratio [benzoquinone] : [triethylantimony] < 1, the rate of polymerisation virtually does not change. Conversely, with an excess of the quinone, polymerisation is retarded.

This pattern of variation indicates, apparently, that at least two independent processes take place. One process is fast reaction of triethylantimony with benzoquinone in which quinone is reduced to hydroquinone.[244, 245] As noted above, hydroquinone influences only slightly the kinetics of polymerisation of acrylic monomers in the presence of organic compounds of Group V elements. In addition, when [benzoquinone] : [triethylantimony] > 1, the excess benzoquinone reacts with the growing macroradical to give stable phenoxyl radicals; as a consequence, polymerisation also slows down. The substantial decrease in the molecular mass of PMMA upon introduction of the quinone

confirms the assumption that it participates in the chain termination step.[243]

Organoelement compounds containing Group V elements not only influence the rate of polymerisation of vinyl monomers but also control the MM of polymers, the effect being more pronounced than that induced by the addition of trialkylboranes.[53]

The addition of triethylantimony in amounts comparable with the concentration of the initiator markedly decreases the MM of poly(butyl acrylate) both for bulk polymerisation and for solution polymerisation in ethyl acetate.[243] The molecular mass of the polymer decreases with an increase in the OEC concentration: on introduction of 0.8 mol.% of triethylantimony, it decreases by more than an order of magnitude. The rate constant for the chain transfer to triethylantimony amounts to 0.118, which markedly exceeds the corresponding value for the chain transfer to the monomer (0.003).

The rate constants for the chain transfer to triisobutylbismuth in the polymerisation of MMA and VA calculated from experimental data are equal to 0.011 and 0.71, respectively.[242, 243] The values for the chain transfer to antimony and bismuth alkyl derivatives considerably exceed the corresponding parameters for TIBB (1×10^{-2} and 2.2×10^{-2} for MMA and VA, respectively).[20, 53] The very high rate constants for chain transfer in the polymerisation of BA and VA can be due to the occurrence of two processes involving the macroradical and OEC. One process, namely, free-radical substitution of the growing polymeric radical for the alkyl radical in organo-antimony and -bismuth compounds, occurs by a scheme similar to that presented above for trialkylboranes [see reactions (4) and (5)]. The rate constant for the substitution of oxygen-centred radicals for the alkyl radicals in triethylantimony is $\sim 10^5$ litre mol^{-1} s^{-1} (see Refs 246 and 247).

The second process, which also contributes to the control of the polymer MM, is abstraction of a hydrogen atom from the alkyl group of the OEC by the growing macroradical [similarly to Eqn (6)]. The occurrence of this reaction was proved unambiguously by EPR using the spin trap technique in a study of the influence of minor additives of methyl acrylate and other acrylic monomers on the control of the PMMA molecular mass during polymerisation involving organoelement initiators.[113]

It was found that, like trialkylboranes, organic compounds of antimony and bismuth also influence the composition of copolymers. Thus in the case of the MMA – MAA pair of monomers, the addition of triethylantimony in amounts commensurable with the concentration of the initiator induces transition from the copolymer enriched in one component ($r_{MAA} = 1.40$, $r_{MMA} = 0.08$) to strict alternation of units in the copolymer.[243] The appearance of alternation of units can be explained by an increase in the rate of cross propagation as a result of the formation of a cyclic reaction complex involving the monomer, the growing macroradical and the OEC. It is noteworthy that, as in the case of TIBB, the flat section in the composition curve corresponds to an MAA content in the copolymer, equal to 0.66 mol.%. This indicates that MAA is involved in the chain propagation step as a dimer.[243] Triethylantimony also influences somewhat the regularities of copolymerisation of MAA with the electron-donor St monomer:[53] the introduction of triethylantimony substantially increases the rate of copolymerisation; however, neither the composition of the copolymers, nor the relative activities of the monomers change noticeably.

The difference from the copolymerisation of the MAA – MMA pair of monomers is caused by the different in kind structures of MMA (electron density acceptor) and St (electron density donor), and the corresponding macroradicals.

Thus, OEC containing Group V elements participate directly in the elementary steps of polymerisation of vinyl monomers and control efficiently polymerisation kinetics and the MM and composition of copolymers prepared both in the bulk and in solution.

V. Conclusion

The effective methods for controlling the reactivity of macroradicals developed to date permit the preparation of homo- and copolymers uniform in composition and molecular mass. The control is attained *via* active influence on the elementary processes of polymerisation including the chain propagation step. The introduction of very small amounts of active additives makes it possible to achieve substantial and, what is more important, targeted change in the reactivity of the macroradicals and to control systematically the polymer chain propagation. It is of prime importance that some OEC, spin traps, iniferters and other controllers of chain propagation considered above are active when present in amounts comparable with the concentration of the initiator. Hence, in the future, they could be used in the industrial synthesis of polymers.

The analysis of published data given above demonstrates, in our opinion, considerable achievements in the development of controlled radical polymerisation — a new and promising line of research in the synthetic chemistry of polymers.

The review was supported by the Russian Foundation for Basic Research (Project No. 99-03-33346).

References

1. Kh S Bagdasar'yan *Teoriya Radikal'noi Polimerizatsii* (Theory of Radical Polymerisation) (Moscow: Nauka, 1966)
2. G Odian *Principles of Polymerization* New York: McGraw-Hill, 1974)
3. S S Ivanchev *Radikal'naya Polimerizatsiya* (Radical Polymerisation) (Leningrad: Khimiya, 1985)
4. G Moad, D H Solomon *The Chemistry of Free Radical Polymerization* (London: Pergamon Press, 1995)
5. V A Kabanov, V P Zubov, Yu D Semchikov *Kompleksno-Radikal'naya Polimerizatsiya* (Complex-Radical Polymerisation) (Moscow: Khimiya, 1987)
6. J M G Gowie (Ed.) *Alternating Polymerization* (New York; London: Plenum, 1985)
7. D F Grishin *Vysokomol. Soedin., Ser. B* **36** 1574 (1994) [a]
8. B A Dolgoplosk, E I Tinyakova *Reaktsii Metalloorganicheskikh Soedinenii kak Redoks-Protsessy* (Reactions of Organometallic Compounds as Redox Processes (Moscow: Nauka, 1981)
9. N V Yablokova, Yu A Aleksandrov *Usp. Khim.* **58** 908 (1989) [*Russ. Chem. Rev.* **58** 534 (1989)]
10. M I Kabachnik (Ed.) *Metalloorganicheskie Soedineniya i Radikaly* (Organometallic Compounds and Radicals) (Moscow: Nauka, 1985)
11. D F Grishin *Khim. Khim. Tekhnol.* **36** (1) 3 (1993)
12. E B Milovskaya *Usp. Khim.* **42** 881 (1973) [*Russ. Chem. Rev.* **42** 384 (1973)]
13. G A Razuvaev, V A Dodonov, Yu A Ivanova *Dokl. Akad. Nauk SSSR* **250** 119 (1980) [b]
14. D F Grishin, V A Dodonov, O V Zolotova *Dokl. Akad. Nauk SSSR* **319** 395 (1991) [b]
15. V A Dodonov, Yu A Ivanova, D F Grishin, L L Semyonycheva, in *Novye Initsiiruyushchie Sistemy na Osnove Boralkilov i Elementoorganicheskikh Mono- i Diperoksidov pri Polimerizatsii Vinilkhlorida* (Modern Initiation Systems Based on Boron Alkyls and Organoelement Mono- and Diperoxides for Polymerisation of Vinyl Chloride) (Dzerzhinsk: Research Institute of Polymers, 1981) p. 52
16. V A Dodonov, D F Grishin *Vysokomol. Soedin., Ser. B* **35** 47 (1993) [a]
17. D F Grishin, S V Vashurina *Vysokomol. Soedin., Ser. A* **35** 1236 (1993) [a]
18. V A Dodonov, D F Grishin, I N Aksenova *Vysokomol. Soedin., Ser. B* **35** 2070 (1993) [a]
19. V A Dodonov, L L Semyonycheva, M B Gorshkova *Vysokomol. Soedin., Ser. B* **26** 101 (1984) [a]
20. G A Razuvaev, V A Dodonov, I N Aksenova *Vysokomol. Soedin., Ser. B* **28** 66 (1986) [a]
21. V A Dodonov, L L Semyonycheva, E V Sazonova, Yu A Ivanova *Vysokomol. Soedin., Ser. B* **25** 235 (1983) [a]
22. L L Semyonycheva, Candidate Thesis in Chemical Sciences, Gor'kii State University, Gor'kii, 1989
23. D F Grishin, A B Radbil' *Vysokomol. Soedin., Ser. A* **35** 1421 (1993) [a]

24. D F Grishin, V A Dodonov *Plastmassy* (2) 5 (1992)
25. D F Grishin, V A Dodonov, M Yu Maleeva *Zh. Prikl. Khim.* **65** 1902 (1992) [c]
26. L L Semyonycheva, D N Bort, V A Dodono, in *Fiziko-Khimicheskie Osnovy Sinteza i Pererabotki Polimerov (Mezhvuzovskii Sbornik)* [Physicochemical Foundations of Synthesis and Processing of Polymers (Intercollegiate Collection)] (Gor'kii: Gor'kii State University, 1983) p. 36
27. D F Grishin, O Yu Chinyaeva *Vysokomol. Soedin., Ser. B* **35** 156 (1993) [a]
28. V A Dodonov, L L Semyonycheva, Yu V Ovchinnikov, V A Titova *Khim. Khim. Tekhnol.* **36** (3) 90 (1993)
29. D F Grishin, P S Razmaev *Khim. Khim. Tekhnol.* **34** (8) 47 (1991)
30. V V Gorbatov Yu A Kurskii, Yu A Aleksandrov, N V Yablokova *Zh. Obshch. Khim.* **49** 365 (1979) [d]
31. Yu A Aleksandrov, V V Gorbatov, V G Tsvetkov, N V Yablokova *Zh. Obshch. Khim.* **49** 933 (1979) [d]
32. D F Grishin, Candidate Thesis in Chemical Sciences, Gor'kii Polytechnical Institute, Gor'kii, 1981
33. V B Golubev, V P Zubov, L I Valuev, G S Naumov, V A Kabanov, V A Kargin *Vysokomol. Soedin., Ser. A* **11** 2689 (1969) [a]
34. Yu D Semchikov, A N Egorochkin, A V Ryabov *Vysokomol. Soedin., Ser. B* **15** 893 (1973) [a]
35. S Taruke, S Okamura *J. Polym. Sci., Polym. Chem. Ed.* **5** 1083 (1967)
36. Z A Tikhonova, Yu D Semchikov, A V Ryabov, T I Liogon'kaya, in *Tr. po Khimii i Khimicheskoi Tekhnologii (Mezhvuzovskii Sbornik)* [Proceedings on the Chemistry and Chemical Technology (Intercollegiate Collection)] (Gor'kii: Gor'kii State University, 1975) No. 3, p. 21
37. T Ikegami, J Hirai *J. Polym. Sci., Polym. Chem. Ed.* **8** 463 (1970)
38. L M Dubinina, V V Amerik, B A Krentsel', E F Petrov, A F Kozhevnik *Izv. Akad. Nauk SSSR, Ser. Khim.* 2667 (1979) [e]
39. G A Abakumov *Zh. Vses. Khim. O-va im D I Mendeleeva* **24** 156 (1979) [f]
40. V A Dodonov, D F Grishin *Vysokomol. Soedin., Ser. B* **35** 137 (1993) [a]
41. D F Grishin, A A Moikin, L L Semyonycheva, E V Kolyakina *Polimery* **35** 860 (2000)
42. S S Ivanchev, L B Shumnyi, V V Konovalenko *Vysokomol. Soedin., Ser. A* **22** 2735 (1980) [a]
43. L V Shumnyi, T A Kuznetsov, V V Konovalenko, S S Ivanchev *Vysokomol. Soedin., Ser. B* **25** 759 (1983) [a]
44. I N Aksenova, Candidate Thesis in Chemical Sciences, Gor'kii State University, Gor'kii, 1987
45. A G Davies, B P Roberts, J S Scaiano *J. Chem. Soc., Perkin Trans. 2* 803 (1972)
46. D F Grishin, A A Moykin, in *Proceedings of Free Radical Polymerization, Genua, 1996* p. 47
47. S K Ignatov, A G Razuvaev, D F Grishin, M V Kuznetsov *Vysokomol. Soedin., Ser. A* **41** 1587 (1999) [a]
48. E B Milovskaya, T G Zhuravleva, P I Dolgopol'skaya, L I Veselova *Vysokomol. Soedin., Ser. A* **6** 412 (1964) [a]
49. D F Grishin, A A Moikin *Vysokomol. Soedin., Ser. B* **38** 1909 (1996) [a]
50. V A Kabanov, in *Proceedings of International Symposium of Macromolecular Chemistry, IUPAC, Budapest, 1969* p. 435
51. L A Smirnova, T E Knyazeva, Yu D Semchikov, Sh I Modeva, A N Egorochkin, G S Kalinina, E G Lyutin *Vysokomol. Soedin., Ser. A* **22** 2137 (1980) [a]
52. S A Bulgakova, L A Smirnova, Yu D Semchikov, T E Knyazeva, Sh I Modeva *Vysokomol. Soedin., Ser. B* **23** 691 (1981) [a]
53. A A Moikin, Candidate Thesis in Chemical Sciences, Nizhnii Novgorod State University, Nizhnii Novgorod, 1998
54. A N Nesmeyanov, R A Sokolik *Metody Elementoorganicheskoi Khimii (Bor, Alyuminii, Gallii, Indii, Tallii)* [Methods of Organoelement Chemistry (Boron, Aluminium, Gallium, Indium, Thallium)] (Moscow: Khimiya, 1964)
55. A D Jenkins, A Ledwith *Reactivity, Mechanism and Structure in Polymer Chemistry* (London: Wiley-Interscience, 1971)
56. K U Ingold, B P Roberts *Free-Radical Substitution Reactions* (New York: Wiley-Interscience, 1974)
57. V A Dodonov, D F Grishin, V K Cherkasov, G A Razuvaev *Vysokomol. Soedin., Ser. A* **24** 451 (1982) [a]
58. D F Grishin, Doctoral Thesis in Chemical Sciences, Nizhnii Novgorod State University, Nizhnii Novgorod, 1994
59. B A Dolgoplosk, E I Tinyakova *Metalloorganicheskii Kataliz v Protsessakh Polimerizatsii* (Organometallic Catalysis in Processes of Polymerisation) (Moscow: Nauka, 1985)
60. B A Dolgoplosk, E I Tinyakova *Generirovanie Svobodnykh Radikalov i Ikh Reaktsii* (Generation of Free Radicals and Their Reactions) (Moscow: Nauka, 1982)
61. J Grotewold, E A Lissi, A E Villa *J. Polym. Sci., Part A* **6** 3121 (1968)
62. F S Arimoto *J. Polym. Sci., Part A* **4** 275 (1966)
63. E Arancibia, J Grotewold, E Lissi, A Villa *J. Polym. Sci., Part A* **7** 3430 (1969)
64. J Grotewold, M Hirschler *J. Polym. Sci., Polym. Chem. Ed.* **15** 393 (1977)
65. V A Dodonov, I N Aksenova, S N Zaburdyaeva *Vysokomol. Soedin., Ser. B* **34** 34 (8) (1992) [a]
66. F G Sattor, R D Lundberg *J. Polym. Sci., Part B, Polym. Lett.* **10** 583 (1972)
67. M Hirooka *J. Polym. Sci., Part B, Polym. Lett.* **10** 171 (1972)
68. J Furukawa, S Tsuruta, J Kiji *J. Polym. Sci., Part A* **11** 1819 (1973)
69. D F Grishin *Usp. Khim.* **62** 1007 (1993) [*Russ. Chem. Rev.* **62** 951 (1993)]
70. V B Golubev, Doctoral Thesis in Chemical Sciences, Moscow State University, Moscow 1987
71. B M Mikhailov, Yu N Bubnov *Bororganicheskie Soedineniya v Organicheskom Sinteze* (Organoboron Compounds in Organic Synthesis) (Moscow: Nauka, 1977)
72. V A Kondin, V N Alyasov, V K Cherkasov, V P Maslennikov, G A Abakumov *Zh. Obshch. Khim.* **58** 583 (1988) [d]
73. Y Florenscy, M Kuran, A Pasynkewich, K Kwes *J. Organomet. Chem.* **112** 21 (1976)
74. G A Tolstikov, V P Yur'ev *Alyuminiiorganicheskii Sintez* (Organoaluminium Synthesis) (Moscow: Nauka, 1976)
75. J Grotewold, M Hirchier *J. Polym. Sci., Polym. Chem. Ed.* **15** 383 (1977)
76. K Matyjaszewski *Controlled Radical Polymerisation* (Oxford: Oxford University Press, 1998)
77. B A Krentsel' (Ed.) *Novoe v Chereduyushcheisya Sopolimerizatsii* (New in Alternating Copolymerisation) (Moscow: Institute of Petrochemical Synthesis, Academy of Sciences of the USSR, 1983)
78. J Furukava *Vysokomol. Soedin., Ser. A* **21A** 2591 (1979) [a]
79. Yu A Eizner, B L Erusalimskii *Elektronnyi Aspekt Reaktsii Polimerizatsii* (The Electronic Aspect of Polymerisation) (Leningrad: Khimiya, 1976)
80. D F Grishin, A B Radbil', T I Radbil' *Vysokomol. Soedin., Ser. A* **36** 1256 (1994) [a]
81. V F Kulikova, I V Savinova, V P Zubov, V A Kabanov, P S Pulak, V A Kargin *Vysokomol. Soedin., Ser. A* **9** 299 (1967) [a]
82. V P Zubov, Author's Abstract of the Doctoral Thesis in Chemical Sciences, Moscow State University, Moscow, 1970
83. Z V Orlova, Candidate Thesis in Chemical Sciences, Research Institute of Polymers, Dzerzhinsk, 1983
84. M M Gudimov, B V Perov *Organicheskoe Steklo* (Organic Glass) (Moscow: Khimiya, 1983)
85. V A Dodonov, A E Tsvetkov, L V Adaevskaya, in *Fiziko-Khimicheskie Osnovy Sinteza i Pererabotki Polimerov* (Physicochemical Foundations of Synthesis and Processing of Polymers) (Gor'kii: Gor'kii State University, 1985) p. 28
86. V A Dodonov, A E Tsvetkov, S S Dolinin, in *Fiziko-Khimicheskie Osnovy Sinteza i Pererabotki Polimerov* (Physicochemical Foundations of Synthesis and Processing of Polymers) (Gor'kii: Gor'kii State University, 1985) p. 16
87. Yu D Semchikov, Author's Abstract of the Doctoral Thesis in Chemical Sciences, Gor'kii State University, Gor'kii, 1974
88. V A Dodonov, O Yu Chinyaeva, D F Grishin *Vysokomol. Soedin., Ser. B* **33** 470 (1991) [a]
89. H Hirai, K Takenchi *Macromol. Chem., Rapid. Commun.* **1** 541 (1980)
90. H Hirai, K Takenchi, M Kamiyama *J. Polym. Sci., Polym. Chem. Ed.* **19** 2581 (1981)
91. US P. 4 121 032; *Ref. Zh. Khim.* 11 S 225P (1979)
92. Jpn P. 52-205 12; *Ref. Zh. Khim.* 4 S 224P (1978)
93. D F Grishin, V A Dodonov, O Yu Zolotova *Vysokomol. Soedin., Ser. B* **33** 643 (1991) [a]
94. D F Grishin, V A Dodonov *Khim. Khim. Tekhnol.* **35** (9) 107 (1992)
95. D F Grishin, V A Dodonov, O Yu Zolotova, V K Cherkasov *Vysokomol. Soedin., Ser. A* **34** (7) 33 (1992) [a]

96. L N Nistratova, E R Nikiforova, Yu D Semchikov, in *Fiziko-Khimicheskie Osnovy Sinteza i Pererabotki Polimerov* (Physico-chemical Foundations of Synthesis and Processing of Polymers) (Gor'kii: Gor'kii State University, 1985) p. 96
97. L J Young *J. Polym. Sci.* **54** 411 (1961)
98. Yu D Semchikov *Vysokomol. Soedin., Ser. A* **32** 243 (1990) [a]
99. D F Grishin, T V Zakharova *Vysokomol. Soedin., Ser. B* **34** (7) 18 (1992) [a]
100. D F Grishin, V A Dodonov, E V Bobina *Vysokomol. Soedinen., Ser. B* **34** (4) 41 (1992) [a]
101. N A Kopylova, E G Kabanova, N V Yablokova, Yu D Semchikov, V A Puzankova *Vysokomol. Soedin., Ser. A* **31** 301 (1989) [a]
102. N A Kopylova, N V Yablokova, T M Pisareva, E G Kabanova, Yu D Semchikov, Yu A Aleksandrov *Vysokomol. Soedin., Ser. B* **29** 506 (1987) [a]
103. V A Myagchenkov, S Ya Frenkel' *Kompozitsionnaya Neodnorodnost' Sopolimerov* (Composition Heterogeneity of Copolymers) (Leningrad: Khimiya, 1988)
104. V A Myagchenkov, E V Kuznetsov, O A Iskhakov, V M Luchkina *Vysokomol. Soedin.* **5** 724 (1963) [a]
105. D F Grishin *Khim. Khim. Tekhnol.* **41** (11) 69 (1998)
106. D F Grishin, V B Zhislina *Khim. Khim. Tekhnol.* **35** (7) 47 (1992)
107. R A Terteryan, in *Khimiya i Tekhnologiya Vysokomolekulyarnykh Soedinenii (Itogi nauki i Tekhniki)* [The Chemistry and Technology of Polymers (Advances in Science and Engineering Series)] (Moscow: Izd. VINITI, 1986) Vol. 21, p. 96
108. G P Belov *Plastmassy* (11) 29 (1980)
109. A Misono, Y Uchida, K Yamada *J. Polym. Sci.* **5** 401 (1967)
110. A Misono, Y Uchida, K Yamada *Bull. Chem. Soc. Jpn.* **40** 2366 (1967)
111. USSR P. 17 000 109; *Byull. Izobret.* (47) 97 (1991)
112. D F Grishin, V A Dodonov *Plastmassy* (2) 5 (1992)
113. G A Razuvaev, V A Dodonov, D F Grishin, V K Cherkasov *Dokl. Akad. Nauk SSSR* **253** 113 (1980) [b]
114. E N Zil'berman *Poluchenie i Svoistva Polivinilkhlorida* (Synthesis and Properties of Polyvinyl Chloride) (Moscow: Khimiya, 1968)
115. M Szwarc *Nature(London)* **178** 1168 (1956)
116. M Szwarc, V Levy, R Mikovich *J. Am. Chem. Soc.* **78** 2656 (1956)
117. T Otsu, A Matsumoto *Adv. Polym. Sci.* **136** 75 (1998)
118. S M Mel'nikov, E N Yudakov, in *Khimiya* (The Chemistry) (Moscow: Moscow State University, 1994) p. 147
119. K Matyjaszewski *Controlled/Living Radical Polymerisation* (Oxford: Oxford University Press, 2000)
120. G V Korolev, A P Marchenko *Usp. Khim.* **69** 447 (2000) [*Russ. Chem. Rev.* **69** 409 (2000)]
121. *Proceedings of the 38th Macromolecular IUPAC Symposium. World Polymer Congress IUPAC MACRO 2000, Warsaw, 2000* Vol. 1
122. B R Smirnov *Vysokomol. Soedin., Ser. A* **32** 583 (1990) [a]
123. V M Lagunov, I V Golikov, B R Smirnov, G V Korolev *Vysokomol. Soedin., Ser. B* **29** 1442 (1987) [a]
124. S I Kuchanov *Usp. Khim.* **60** 1346 (1991) [*Russ. Chem. Rev.* **60** 689 (1991)]
125. P Bertin, B Boutevin, P Gramain, in *Proceedings of Symposium on Free Radical Polymerization: Kinetics and Mechanisms, Geneva, 1996* P. 122
126. F Takeshi, T Tomoya, in *Proceedings of Symposium on Free Radical Polymerization: Kinetics and Mechanisms, Geneva, 1996* p. 63
127. A A Il'in, B R Smirnov, N V Ribin, I V Golikov, M M Mogilevich, in *Proceedings of Symposium on Free Radical Polymerization: Kinetics and Mechanisms, Geneva, 1996* p. 206
128. W Devonport, L Michalak, E Malmstrom, M Mate, K Bulent, C J Hawker, G G Barclay, R Sinta *Macromolecules* **30** 1929 (1997)
129. M Yu Zaremskii, Yu I Stoyachenko, A V Plutalova, M B Lachinov, V B Golubev *Vysokomol. Soedin., Ser.* **41A** 389 (1999)
130. K Matyjaszewski, S G Gaynor, D Greszta, D Mardare, T Shigemoto *J. Phys. Org. Chem.* **8** 306 (1995)
131. K Matyjaszewski, S G Gaynor, D Greszta, D Mardare, T Shigemoto *Macromol. Symp.* **98** 73 (1995)
132. D Mardare, T Shigemoto, K.Matyjaszewski. *Polym. Prepr. (Am. Chem. Soc. Div. Polym. Chem.)* **35** 557 (1994)
133. K Matyjaszewski, S G Gaynor, D Greszta, D Mardare, T Shigemoto, J-S Wang *Macromol. Symp.* **95** 217 (1995)
134. T Fukuda, A Goto, K Ohno *Macromol. Rapid Commun.* **21** 151 (2000)
135. N A Listigovers, M K Georges, P G Odell, B Keoshkerian *Macromolecules* **29** 8992 (1996)
136. D Mardare, T Shigemoto, K.Matyjaszewski. *Polym. Prepr. (Am. Chem. Soc. Div. Polym. Chem.)* **35** 778 (1994)
137. E Yoshida. *J. Polym. Sci., Polym. Chem. Ed.* **34** 2937 (1996)
138. W Devonport, L Michalak, E Malmström, M Mate, B Kurdi, C J Hawker, G G Barclay, R Sinta *Macromolecules* **30** 1929 (1997)
139. B Keoshkerian, M K Georges, D Boils-Boissier *Macromolecules* **28** 6381 (1995)
140. P M Kazmaier, K Daimon, M K Georges, G K Hamer, R P N Veregin *Macromolecules* **30** 2228 (1997)
141. K Ohno, Y Tsujii, T Fukuda *Macromolecules* **30** 2503 (1997)
142. D Benoit, S Grimaldi, J Finet, P Tordo, M Fontanille, Y Gnanou *Polym. Prepr. (Am. Chem. Soc., Div. Polym. Chem.)* **38** (1) 729 (1997)
143. M Georges, M Quinlan, B Keoshkerian, P Odell *Polym. Prepr. (Am. Chem. Soc., Div. Polym.Chem.)* **37** (2) 507 (1996)
144. A V Plutalova, M Yu Zaremskii, M G Pavlov, E S Garina M B Lachinov, V B Golubev *Vysokomol. Soedin., Ser. B* **41** 552 (1999) [a]
145. M Yu Zaremskii, Yu I Stoyachenko, A V Plutalova, E S Garina, M B Lachinov, V B Golubev, in *Proceedings of the 36th IUPAC Symposium on Macromolecules, Seoul, 1996* p. 723
146. V A Khrenov, M Yu Zaremskii, V B Golubev *Vest. Mosk. Univ., Ser 2, Khim.* 9 (1997) [g]
147. E Yoshida, A Sugita *Macromolecules* **29** 6422 (1996)
148. E V Chernikova, Author's Abstracts of Candidate Thesis in Chemical Sciences, Moscow State University, Moscow, 1997
149. E V Chernikova, Z A Pokataeva, E S Garina, M B Lachinov, V B Golubev *Vysokomol. Soedin., Ser. A* **40** 221 (1998) [a]
150. E V Chernikova, Z A Pokataeva, E S Garina, M B Lachinov, V B Golubev *Vysokomol. Soedin., Ser. B* **40**1205 (1998) [a]
151. A Bledzki, D Braun *Makromol. Chem.* **182** 1047 (1981)
152. T Otsu, A Matsumoto, T Tazaki *Polym. Bull.* **17** 323 (1987)
153. R Guerrero, P Chaumont, J E Herz, G Beinert *Eur. Polym. J.* **30** 851 (1994)
154. L Hajji, R Guerrero, G Beinert, J E Herz, A Bieber, J J Andre *Macromol. Theory Simul.* 1105 (1995)
155. M E Leon-Saenz, G Morales-Balado, R Guerrero-Santos, in *Proceedings of Symposium on Free Radical Polymerization: Kinetics and Mechanisms, Geneva, 1996* p. 181
156. T Otsu, A Kuriyama *Polym. J.* **17** 97 (1985)
157. T Otsu, T Tazaki *Polym. Bull.* **16** 277 (1986)
158. M Yu Zaremskii, A A Lyakhov, E S Garina, M V Lachinov *Dokl. Akad. Nauk* **347** 766 (1996) [b]
159. M Yu Zaremskii, A A Luzin, E S Garina, V B Golubev, M B Lachinov *Vysokomol. Soedin., Ser. A* **39** 1286 (1997) [a]
160. V E Zubarev *Metod Spinovykh Lovushek* (The Method of Spin Traps) (Moscow: Moscow State University, 1984)
161. D F Grishin, L L Semyonycheva, E V Kolyakina *Dokl. Akad. Nauk* **362** 634 (1998) [b]
162. D F Grishin, L L Semyonycheva, E V Kolyakina *Vysokomol. Soedin., Ser. A* **41** 609 (1999) [a]
163. D F Grishin, L L Semyonycheva, E V Kolyakina *Mendeleev Commun.* 250 (1999)
164. D F Grishin, L L Semyonycheva, E V Kolyakina *Vest. Nizhegorodsk. Univ., Ser. Khim.* 156 (1999)
165. D F Grishin, L L Semyonycheva, K V Sokolov, E V Kolyakina *Vysokomol. Soedinen., Ser. B* **42** 1263 (2000) [a]
166. E V Kolyakina, D F Grishin, L L Semyonycheva, K V Sokolov, in *Vtoroi Vserossiiskii Karginskii Simpozium 'Khimiya i Fizika Polimerov v Nachale XXI Veka' (Tez. Dokl.), Chernogolovka, 2000* [The Second All-Russian Kargin Symposium 'The Chemistry and Physics of Polymers in the Beginning of the XXIst Century' (Abstracts of Reports), Chernogolovka, 2000] Vol. 1, p. 2
167. D F Grishin, in *Proceedings of the 38th Macromolecular IUPAC Symposium. World Polymer Congress IUPAC MACRO 2000, Warsaw, 2000* Vol. 1, p. 172
168. E V Kolyakina, D F Grishin, L L Semyonycheva, in *Proceedings of the 38th Macromolecular IUPAC Symposium. World Polymer Congress IUPAC MACRO 2000, Warsaw, 2000* Vol. 1, p. 227
169. E V Kolyakina, L L Semyonycheva, D F Grishin *Zh. Prikl. Khim.* **94** 483 (2001) [c]
170. T Otsu, M Yoshida *Macromol. Chem., Rapid Commun.* **3**127 (1982)

171. P Lambrinos, M Tardi, A Polton, P Sigwalt *Eur. Polym. J.* **26** 1125 (1990)
172. S R Turner, R W Blewins *Macromolecules* **23** 1856 (1990)
173. S I Kuchanov, M Yu Zaremskii, A V Olenin, E S Garina, V B Golubev *Dokl. Akad. Nauk SSSR* **303** 371 (1989) [b]
174. M Yu Zaremskii, A V Olenin, E S Garina, S I Kuchanov, V B Golubev, V A Kabanov *Vysokomol. Soedin., Ser. A* **33** 2167 (1991) [a]
175. E V Chernikova, E S Garina, M Yu Zaremskii, M B Lachinov, A V Olenin, V B Golubev *Vysokomol. Soedin., Ser. A* **37** 1638 (1995) [a]
176. E V Chernikova, Z A Pokataeva, E S Garina *Vysokomol. Soedin., Ser. B* **42** 1530 (2000) [a]
177. D F Grishin, A A Moikin, V K Cherkasov *Vysokomol. Soedin., Ser. A* **41** 595 (1999) [a]
178. A A Moikin, E P Smirnova, D F Grishin, in *Vserossiiskaya Konferentsiya 'Metalloorganicheskaya Khimiya na Rubezhe XXI Veka' (Tez. Dokl.), Moskva, 1999* [All-Russian Conference 'Organometallic Chemistry on the Boundary of the XXIst Century' (Abstracts of Reports), Moscow, 1999] Vol. 3, p. 1
179. D F Grishin, A A Moykin, E P Smirnova, M V Pavlovskaya, L L Semyonycheva *Mendeleev Commun.* 152 (2000)
180. M V Pavlovskaya, D F Grishin, L L Semyonycheva, A A Moikin, E P Smirnova, in *Vtoroi Vserossiiskii Karginskii Simpozium 'Khimiya i Fizika Polimerov v Nachale XXI Veka' (Tez. Dokl.), Chernogolovka, 2000* [The Second All-Russian Kargin Symposium 'The Chemistry and Physics of Polymers in the Beginning of the XXIst Century' (Abstracts of Reports), Chernogolovka, 2000] Vol. 2, p. 3
181. D F Grishin, in *Mezhdunarodnaya Konferentsiya 'Metalloorganicheskie soedineniya — Materialy Budushchego Tysyacheletiya' (Tez. Dokl.), Nizhnii Novgorod, 2000* [International Conference 'Organometallic Compounds — Materials of the Future Millennium' (Abstracts of Reports), Nizhnii Novgorod, 2000] p. 58
182. M V Pavlovskaya, D F Grishin, L L Semyonycheva, in *Mezhdunarodnaya Konferentsiya 'Metalloorganicheskie soedineniya — Materialy Budushchego Tysyacheletiya' (Tez. Dokl.), Nizhnii Novgorod, 2000* [International Conference 'Organometallic Compounds — Materials of the Future Millennium' (Abstracts of Reports), Nizhnii Novgorod, 2000] p. 113
183. US P. 4 581 429; *Chem. Abstr.* **102** 221 335 (1986)
184. C J Hawker *J. Am. Chem. Soc.* **116** 1185 (1994)
185. J M Catala, F Bubel, S O Hammouch *Macromolecules* **28** 8441 (1995)
186. R D Puts, D Y Sogah *Macromolecules* **29** 3323 (1996)
187. C J Hawker *Angew. Chem., Int. Ed. Eng.* **34** 1456 (1995)
188. C J Hawker, J L Hedrick *Macromolecules* **28** 2993 (1995)
189. M-O Zink, A Kramer, P Neswadba *Macromolecules* **33** 8106 (2000)
190. G Ananchenko, H Fischer, in *Proceedings of the the 38th Macromolecular IUPAC Symposium. World Polymer Congress IUPAC MACRO 2000, Warsaw, 2000* Vol. 1, p. 217
191. L Longo, R Fusco, P Accomazzi, L Bonoldi, R Po, G Schimperna, N Cardi, in *Proceedings of the 38th Macromolecular IUPAC Symposium. World Polymer Congress IUPAC MACRO 2000, Warsaw, 2000* Vol. 1, p. 223
192. N Cardi, M Caldararo, M Cardaci, R Po, G Schimperna, in *Proceedings of the 38th Macromolecular IUPAC Symposium. World Polymer Congress IUPAC MACRO 2000, Warsaw, 2000* Vol. 1, p. 224
193. A Kramer, P Nesvadba, W Wunderlich, M-O Zink, in *Proceedings of the 38th Macromolecular IUPAC Symposium. World Polymer Congress IUPAC MACRO 2000, Warsaw, 2000* Vol. 1, p. 226
194. M-O Zink, P Nesvadba, A Kramer, in *Proceedings of the 38th Macromolecular IUPAC Symposium. World Polymer Congress IUPAC MACRO 2000, Warsaw, 2000* Vol. 1, p. 228
195. P Nesvadba, A Kramer, W Wunderlich, M-O Zink, in *Proceedings of the 38th Macromolecular IUPAC Symposium. World Polymer Congress IUPAC MACRO 2000, Warsaw, 2000* Vol. 1, p. 229
196. T Fukuda, T Terauchi *Chem. Lett.* 293 (1996)
197. H Fischer *Macromolecules* **30** 5666 (1997)
198. D Greszta, K Matyjaszewski *Macromolecules* **29** 7661 (1996)
199. J He, H Zhang, J Chen, Y Yang *Macromolecules* **30** 8010 (1997)
200. G G Barclay, C J Hawker, H Ito, A Orellana, P R L Malenfant, R F Sinta *Macromolecules* **31** 1024 (1998)
201. N Ide, T Fukuda *Macromolecules* **30** 4268 (1997)
202. M Yu Zaremskii, Yu I Stoyachenko, V A Hrenov, O A Kononenko, N V Alexeev, E S Garina, V B Golubev, in *Proceedings of New Approaches Polymer Synthesis Macromolecular Formation, St. Petersburg, 1997* p. 010
203. T Fukuda, T Terauchi, A Goto, Y Tsujii, T Miyamoto, Y Shimizu *Macromolecules* **29** 3050 (1996)
204. C Marestin, C Noel, A Gyuot, J Claverie *Macromolecules* **31** 4041 (1998)
205. I Li, B A Howell, K Matyjaszewski, T Shigemoto, P B Smith, D B Priddy *Macromolecules* **28** 6692 (1995)
206. A Goto, T Terauchi, T Fukuda, T Miyamoto *Polym. Prepr. Jpn.* **45** 1261 (1996)
207. G V Korolev, M P Berezin, G M Bakova, I S Kochneva *Vysokomol. Soedin., Ser. B* **42** 2190 (2000) [a]
208. I S Kochneva, G V Korolev, M P Berezin, G M Bakova, in *Vtoroi Vserossiiskii Karginskii Simpozium 'Khimiya i Fizika Polimerov v Nachale XXI Veka' (Tez. Dokl.), Chernogolovka, 2000* [The Second All-Russian Kargin Symposium 'The Chemistry and Physics of Polymers at the Beginning of the XXIst Century' (Abstracts of Reports), Chernogolovka, 2000] Vol. 1, p. 2
209. G V Korolev, L S Kochneva, G M Bakova, M P Berezin, in *Proceedings of the 38th Macromolecular IUPAC Symposium. World Polymer Congress IUPAC MACRO 2000, Warsaw, 2000* Vol. 1, p. 221
210. B Amedure, B Boutevin, P Gramain *Adv. Polym. Sci.* **127** 87 (1997)
211. V B Golubev, M Yu Zaremskii, S M Mel'nikov, A V Olenin, V A Kabanov *Vysokomol. Soedin., Ser. A* **36** 320 (1994) [a]
212. A F Barton, J C Bevington *Trans. Faraday Soc.* **62** 433 (1966)
213. M M Zigmunt, B I Shapiro, A S Kuz'minskii *Vysokomol. Soedin., Ser. A* **15** 2361 (1973) [a]
214. T Sato, M Abe, T Otsu *Makromol. Chem.* **180** 1165 (1979)
215. T Sato, M Abe, T Otsu *Makromol. Chem.* **178** 1951 (1977)
216. M Okawara, T Nakai, T Morishita, E Imoto *Kogyo Kagaku Zasshi* **67** 2108 (1964); *Ref. Zh. Khim.* 17 S 93 (1965)
217. M Okawara, T Nakai, E Imoto *Kogyo Kagaku Zasshi* **69** 973 (1966); *Ref. Zh. Khim.* 12 S 108 (1967)
218. M Niwa, N Nigashi, M Shimizu, A Matsumoto *Makromol. Chem.* **189** 2187 (1988)
219. J R Ebdon, T N Huckerby, B J Hunt, S Rimmer, M J Shepherd, M Teodorescu *Polymer* **39** 4943 (1998)
220. E G E Hawkins *Organic Peroxides* (London: F F Spon, 1961)
221. A V Kondin, V N Alyasov, V K Cherkasov, V P Maslennikov, G A Abakumov *Zh. Obshch. Khim.* **58** 583 (1988) [d]
222. G A Razuvaev, G A Abakumov, E S Klimov, E N Gladyshev, P Ya Bayushkin *Izv. Akad. Nauk SSSR, Ser. Khim.* 1128 (1977) [e]
223. D F Grishin, A A Moykin *Mendeleev Commun.* 34 (1998)
224. D F Grishin, A A Moikin, in *Metallokompleksnyi Kataliz Polimerizatsionnykh Protsessov, Chernogolovka, 1998* (Metallocomplex Catalysis of Polymerisation Processes, Chernogolovka, 1998) p. 22
225. T C Chung, W Janvicul, H L Lu. *J. Am. Chem. Soc.* **118** 705 (1996)
226. Ph Lecomte, I Drapier, Ph Dubois, Ph Teyssie, R Jerome *Macromolecules* **30** 7631 (1997)
227. H Uegaki, Y Kotani, M Kamigaito, M Sawamoto *Macromolecules* **30** 2249 (1997)
228. Y Kotani, M Kamigaito, M Sawamoto *Macromolecules* **32** 2420 (1999)
229. W Urry, M Kharasch *J. Am. Chem. Soc.* **66** 1438 (1944)
230. K Matyjaszewski, S M Jo, H Van der Park, S G Gaynor *Macromolecules* **30** 6398 (1997)
231. T Grimaud, K Matyjaszewski *Macromolecules* **30** 2216 (1997)
232. K Matyjaszewski, M Wei, J Xia, N E McDermott *Macromolecules* **30** 8161 (1997)
233. T E Patten, J Xia, T Abernalthy, K Matyjaszewski *Science* **272** 866 (1996)
234. J Xia, K Matyjaszewski *Macromolecules* **30** 7692 (1997)
235. K Matyjaszewski, S Coca, S G Gaynor, M Wei, B E Woodworth *Macromolecules* **30** 7348 (1997)
236. J-S Wang, K Matyjaszewski *Macromolecules* **28** 7572 (1995)
237. Y Kotani, M Kato, M Kamigaito, M Sawamoto *Macromolecules* **29** 6979 (1996)
238. T Ando, M Kamigaito, M Sawamoto *Macromolecules* **30** 4507 (1997)
239. V Percec, H J Kim, B Barboiu *Macromolecules* **30** 8526 (1997)

240. G A Razuvaev, Yu D Semchikov, S F Zhil'tsov, V A Sokolova, L M Mazanova *Dokl. Akad. Nauk SSSR* **231** 353 (1976) [b]
241. G A Razuvaev, S F Zhil'tsov, L I Lyadkova, V N Kashaeva, V A Sokolova, L M Mazanova *Vysokomol. Soedin., Ser. A* **23** 575 (1981) [a]
242. D F Grishin, A A Moikin *Dokl. Akad. Nauk* **356** 766 (1997) [b]
243. D F Grishin, A A Moikin *Vysokomol. Soedin., Ser. A* **40** 1266 (1998) [a]
244. E Furimsny, J A Howard, J R Morton *J. Am. Chem. Soc.* **95** 6574 (1973)
245. H Yao-Zang, C Chen, Z Fanghea, L Yi *J. Organomet. Chem.* **378** 147 (1989)
246. J K Kochi, P J Krusic *J. Am. Chem. Soc.* **91** 3942 (1969)
247. A G Davies, B P Roberts *J. Organomet. Chem.* **19** 17 (1969)

[a] — *Polym. Sci. (Engl. Transl.)*
[b] — *Dokl. Chem. Technol., Dokl. Chem. (Engl. Transl.)*
[c] — *Russ. J. Appl. Chem. (Engl. Transl.)*
[d] — *Russ. J. Gen. Chem. (Engl. Transl.)*
[e] — *Russ. Chem. Bull. (Engl. Transl.)*
[f] — *Mendeleev Chem. J. (Engl. Transl.)*
[h] — *Moscow Univ. Bull. (Engl. Transl.)*

Russian Chemical Reviews **70** (6) 449 – 469 (2001) © 2001 Russian Academy of Sciences and Turpion Ltd

DOI 10.1070/RC2001v070n06ABEH000664

Femtochemistry

O M Sarkisov, S Ya Umanskii

Contents

I.	Introduction	449
II.	Characteristic features of femtosecond pulses	449
III.	The main objectives of femtochemistry	451
IV.	Experimental methods of femtochemistry	451
V.	Dynamics of intramolecular processes and of transition states in a chemical transformation	452
VI.	The kinetics of ultrafast chemical reactions	457
VII.	Control of intramolecular dynamics and an elementary chemical event	462
VIII.	The prospects of femtochemistry	466

Abstract. The review is devoted to a new field of chemistry — femtochemistry. New, in principle, possibilities of investigation and control of chemical reactions by means of ultrashort coherent light pulses are considered. The general concepts are illustrated by numerous examples of femtochemical studies of the dynamics and kinetics of elementary chemical reactions in the gas and condensed phases. The prospects of femtochemistry are discussed.
The bibliography includes 172 references.

I. Introduction

How does an elementary chemical reaction occur? What are intermediate configurations of a reacting system? How can the route and the rate of a chemical reaction be controlled? Chemists have asked themselves these questions throughout the history of the development of chemistry. However, the profundity of both the questions and the answers depends on the level of understanding of elementary processes and on the experimental capabilities.

Until quite recently, in all experiments dealing with elementary reactions the time evolution of either reactants or reaction products has been recorded. However, on the path from reactants to products, the molecular system passes through various structures (states) which can no longer be considered as reactants but cannot yet be regarded as products. From the experimenter's viewpoint, the range of interatomic distances corresponding to these structures is a 'black box' because the experiment does not provide any information about these structures or their change. Chemists call this range of interatomic distances the transition state,[1] and the time evolution of atom configurations in this 'black box' is called transition state dynamics. The passage of a reacting molecular system through the transition state represents an elementary step of a chemical reaction. The reaction path is usually characterised by the dependence of the potential energy on interatomic distances.

Theorists try to reconstruct the transition state dynamics from the results of investigations of the kinetics of reactants and products. However, it turned out that this often cannot be done unambiguously; experimental data are needed. The problem lies in the fact that the residence time of a molecular system in the 'black box' is very short, ~ 100 fs (1 fs = 10^{-15} s). Therefore, special laser equipment is required to detect the events taking place over this 100-fs period.

The appearance of a new tool — light pulses with durations of 10 – 100 fs — provided the possibility of detecting tiny changes, about 0.1 Å, in the distances between atoms in a molecular system; this triggered a new line of research in chemical physics, namely, femtochemistry. This field of investigations makes it possible to answer the questions posed above at a new, in principle, level; to verify some fundamental assumptions which we use; to distinguish the regions where they are no longer valid; and to discover new ways of controlling a chemical transformation. In 1999, an American scientist A Zewail was awarded the Nobel Prize for studies in the field of femtochemistry. Although femtochemistry is 'young' (its age can be estimated as 12 years), several reviews have been published (see, for example, publications [2–6]). In this review, we attempt to examine, from different standpoints, the rapidly developing approaches and concepts as well as new problems arising in this field.

II. Characteristic features of femtosecond pulses

Before discussing the problems of femtochemistry, let us consider characteristic features of ultrashort light pulses and new experimental capacities brought about by these features.

In a system of coordinates the z axis of which coincides with the direction of propagation of a laser pulse, the components of the electric field strength $E(t) = [E_x(t),E_y(t),E_z(t)]$ of a femtosecond light pulse for a specified point in space can be written in the form

$$\begin{aligned} E_x(t) &= E_{x0}\mathrm{f}(t)\cos[\omega_0 t + \delta_x + \alpha(t)], \\ E_y(t) &= E_{y0}\mathrm{f}(t)\cos[\omega_0 t + \delta_y + \alpha(t)], \\ E_z(t) &= 0. \end{aligned} \qquad (1)$$

In these equations, E_{x0} and E_{y0} are the maximum values of the x and y components of the field strength, respectively, f(t) is the

O M Sarkisov, S Ya Umanskii N N Semenov Institute of Chemical Physics, Russian Academy of Sciences, ul. Kosygina 4, 117334 Moscow, Russian Federation. Fax (7-095) 938 24 84. Tel. (7-095) 939 74 97.
E-mail: sarkisov@femto.chph.ras.ru (O M Sarkisov)
Tel. (7-095) 939 74 36. E-mail: unan@center.chph.ras.ru
(S Ya Umanskii)

Received 27 February 2001
Uspekhi Khimii **70** (6) 515 – 538 (2001); translated by Z P Bobkova

time dependence of the envelope of the pulse, t is the current time, ω_0 is the carrier light frequency related to the carrier wavelength λ_0 in the following way:

$$\lambda_0 = \frac{2\pi c}{\omega_0},$$

δ_x and δ_y are the phase constants and $\alpha(t)$ is the function describing the frequency modulation over the pulse duration. The polarisation of light in the pulse is characterised by the ratio E_{x0}/E_{y0} and by the δ_x and δ_y values. The pulse envelope $f(t) \propto \sqrt{I(t)}$, where $I(t)$ is the time dependence of light intensity in the pulse, can have different forms. However, irrespective of this, it is determined by pulse duration (τ).

Most often, Gaussian pulses with the envelope

$$f(t) = \exp\left(-\frac{t^2 2\ln 2}{\tau^2}\right), \tag{2}$$

and the frequency modulation

$$\alpha(t) = \frac{1}{2}\gamma t^2, \tag{3}$$

where γ is the temporal chirp (the parameter determining the rate of phase modulation) are considered. When $t = \pm\tau/2$, the light intensity in the pulse is equal to half its maximum.

Thus, parameters characterising a femtosecond pulse include pulse duration τ, field amplitude, carrier frequency and the function $\alpha(t)$ (expressed in most cases in terms of the temporal chirp γ).

It is known that a field can also be specified by spectral characteristics

$$\mathscr{E}_j(\omega) = \int_{-\infty}^{+\infty} E_j(t)\exp(i\omega t)\mathrm{d}t, \tag{4}$$

where $j = x, y$. Usually, the functions $f(t)$ and $\exp[i\alpha(t)]$ vary much more slowly than $\exp(i\omega_0 t)$; therefore, it can be written that

$$\mathscr{E}_j(\omega) = \frac{1}{2}\exp(-i\delta_j)F_j(\omega-\omega_0), \tag{5}$$

where

$$F_j(\omega-\omega_0) = E_{j0}\int_{-\infty}^{+\infty} f(t)\exp\{i[(\omega-\omega_0)t-\alpha(t)]\}\mathrm{d}t. \tag{6}$$

The function $F_j(\omega-\omega_0)$ is complex-valued and can be represented in the form

$$F_j(\omega-\omega_0) = |F_j(\omega-\omega_0)|\exp[i\varphi(\omega-\omega_0)], \tag{7}$$

where

$$|F_j(\omega-\omega_0)| \propto \sqrt{S(\omega)},$$

$S(\omega)$ is the the pulse power spectrum measured experimentally. The spectral phase $\varphi(\omega-\omega_0)$ is related to the functions $f(t)$ and $\alpha(t)$ in a complex manner. For Gaussian pulses, these functions are determined by relations (2) and (3), respectively. Therefore,

$$\varphi(\omega-\omega_0) = \frac{1}{2}\beta(\omega-\omega_0)^2,$$
$$\beta = \frac{4\gamma\tau^4}{16(\ln 2)^2 + \gamma^2\tau^4}. \tag{8}$$

The β parameter is called spectral chirp.

An important spectral characteristic of a femtosecond pulse is the width of its spectrum at the half-height of the amplitude ($\Delta\omega$). The spectral width is determined by the uncertainty relation

$$\tau\Delta\omega = \text{const}. \tag{9}$$

The value of const depends on the shape of the pulse and the chirp envelope. For a Gaussian pulse with $\gamma = 0$ (this pulse is usually referred to as transform-limited), const = 2.773. In the case of chirped pulses (*i.e.*, those with $\gamma \neq 0$), the constant can acquire arbitrarily large values depending on the chirp value.

Now we shall list the main experimental capacities resulting from the properties of femtosecond pulses.

First, due to the short pulse duration, evolution of processes can be studied with a temporal resolution even higher than the duration of the pulse itself. When the velocity of an atom is 10^5 cm s^{-1} and $\tau = 10^{-14}$ s, changes in the internuclear distances of about 0.1 Å can be detected. This means that not only the formation of products but also the time evolution of the nuclear configuration can be monitored with high accuracy in real time within the time scale of vibrational motion.

Second, since the spectral width of femtosecond pulses is rather large, several quantum states with different energies can be excited simultaneously. For example, a transform-limited pulse with $\tau = 10^{-14}$ s has the spectral width $\Delta\omega = 1100$ cm^{-1}. This light pulse can excite simultaneously several vibrational quantum states.

Third, a coherent light pulse can be obtained. In combination with the aforesaid, this means that coherent excitation of several vibrational or rotational states is possible. This new type of an excited state is called a non-stationary quantum state or a coherent nuclear wave packet.†

A specific feature of these states is that several eigen energy states with definite relative phases of atomic motion in a molecule can be subjected simultaneously to coherent excitation. The scheme of non-stationary and stationary quantum states of a molecule is shown in Fig. 1.

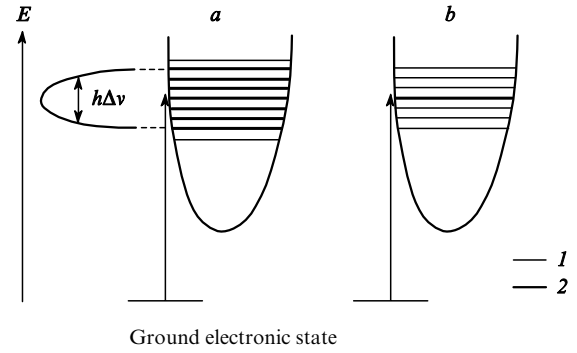

Figure 1. Non-stationary (*a*) and stationary (*b*) vibrational quantum states of a molecule. The horizontal lines mark unoccupied (*1*) and occupied (*2*) stationary vibrational states.

Fourth, due to high intensity (peak power) of femtosecond pulses with the pulse energy being relatively low, multiphoton absorption processes giving rise to highly excited molecular systems can be easily accomplished and numerous methods of non-linear spectroscopy can be used without heating the sample. Under the action of such pulses on a gas or a solid, light pulses with a broad spectral range (supercontinuum) and X-ray and electron pulses are generated. It should also be noted that light field intensities (10^{10} V cm^{-1}) exceeding even the intensities of intramolecular fields can be attained rather easily.

Thus, the use of femtosecond light pulses makes it possible to attain high temporal resolution, to create coherent non-stationary quantum states, to produce highly excited molecules, to act upon the potential energy surface (PES) and to generate ultrashort light, electron and X-ray pulses.

† The notion of wave packet was introduced in 1926 by E Schrödinger; however, it has virtually not been used in chemistry.

III. The main objectives of femtochemistry

How does the study of reactions within the femtosecond time scale pertain to practical chemistry? Indeed, the duration of an elementary reaction in practical chemistry is much longer than 100 fs. This is due to the fact that an elementary reaction includes both a fast chemical event and the preceding slower intra- and intermolecular energy exchange processes.

For an unimolecular chemical event to occur, the following processes should take place:

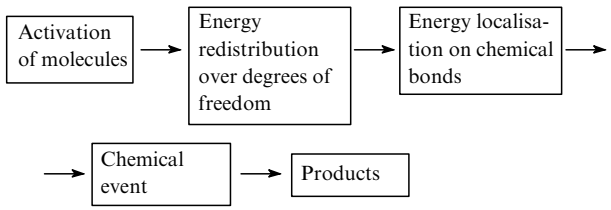

Activated molecules should possess a sufficiently high energy, which can be acquired either upon collisions, or due to a chemical reaction, or upon absorption of photons. Usually, this energy is redistributed very rapidly (in about 0.1 – 1 ps) over different vibrational degrees of freedom of the molecule. Then a fluctuation should occur, after which a certain energy is concentrated in the required site of the molecule, for example, in the form of vibrations of atoms of the bond to be cleaved. Only after this, does the chemical event take place. The time scale of the chemical event itself is 10 – 100 fs.

The specific features of new instrumentation noted above determine the following lines of research in femtochemistry: study of the dynamics of intramolecular processes and the transition state in a chemical transformation; study of the kinetics of ultrafast chemical reactions; control of the intramolecular dynamics and of the path of an elementary chemical reaction.

Now we shall briefly explain what is the purpose of each of these lines of investigation.

The goal of the first line is to obtain more detailed and substantiated views on the nuclear dynamics in a molecular system (either reacting or not). This refers both to the dynamics of intramolecular processes (coherent motion of nuclei, energy redistribution or localisation, *etc*.) and time evolution of the configurations of the molecular system on passing from reactants to products. In this connection, the possibility of creating a coherent wave packet (rotational, vibrational or electronic) in the molecular system is of fundamental importance. The most significant for chemistry is the vibrational wave packet in which several vibrational states undergo simultaneously coherent excitation. In this case, it can be said that intramolecular dynamics of nuclei is the time evolution of the vibration-rotational wave packets. A significant feature of this description is that phase characteristics of the nuclear motion are taken into account. However, it is known that after some time, dephasing takes place; as a consequence, the nuclear dynamics becomes incoherent and the regular nuclear motion switches to stochastic motion.

The purpose of the second line is to gain information on the kinetics of ultrafast reactions. Within the framework of this line of research, investigators are interested in the time evolution of the reactant or product concentration rather than in the phase characteristics of the nuclear motion. The features of femtosecond pulses most significant for this line of research include short duration, which allows implementation of techniques with high temporal resolution (using these techniques, one can study ultrafast reactions), and high intensity (this allows excitation of molecules with visible light to high energies).

The third line of research in femtochemistry is the most 'ambitious'. In this case, all the above-mentioned features of femtosecond pulses are significant. The possibility of creating femtosecond pulses opens new, in principle, opportunities for controlling intramolecular processes and the path of elementary chemical reactions. The idea of this control is based on the fact that, by using femtosecond pulses, one can switch the reacting system to a transition state with a definite initial wave function and then control the time evolution of this state. Due to the coherence of the light pulse, the initial state of the system can be created as a well-defined coherent wave packet. By changing the carrier frequency and the amplitude and phase characteristics of a femtosecond light pulse, it is possible to create in the initial (zero) instant of time different nuclear wave packets, the dynamics of which can be substantially different. The high temporal resolution allows researchers to 'monitor' the evolution of the transition state in order to act upon the system PES by one more femtosecond light pulse at the required point in time.

IV. Experimental methods of femtochemistry

Typical experimental methods of femtochemistry are based on the use of two femtosecond pulses according to the 'pump – probe' pattern (Fig. 2). The first pulse (λ_1) creates a wave packet in the electronically excited state. After some period of time, a second pulse (λ_2) probes the changes that have taken place. After the probe pulse, the molecular system passes into a different electronic state [either upper (Fig. 2 *a*) or lower (Fig. 2 *b*) in energy] and, owing to this transition, the response of the system to the action of the pump and probe pulses as a function of the time delay between them is recorded. The 'pump – probe' pattern makes it possible to detect both the dynamics of the motion of atoms (wavelength λ_2) and the kinetics of product formation (wavelength λ_2').

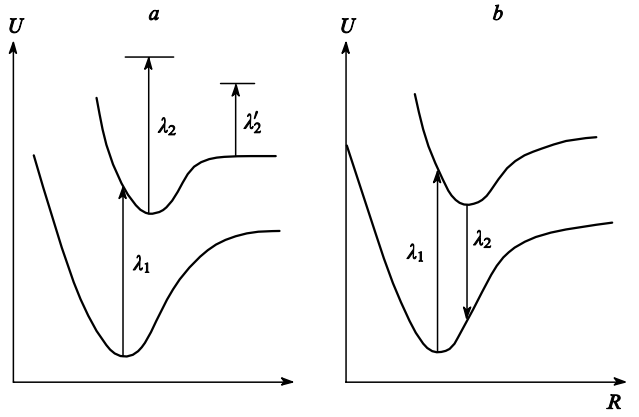

Figure 2. Simplest patterns of the 'pump – probe' technique. U is potential energy, R is the distance between the nuclei, λ_1 is the wavelength at the centre of the pump pulse spectrum, λ_2 is the wavelength at the centre of the spectrum of the pulse probing the transition state dynamics; λ_2' is the wavelength at the centre of the spectrum of the pulse probing the reaction products.

A typical scheme of the setup is shown in Fig. 3. A laser (as a rule, a dye or titanium-sapphire laser) usually pumped by a continuous-wave argon or solid-state laser generates consecutive femtosecond light pulses. The energy of these pulses is increased in a laser amplifier. The amplified pulse passes through a compensator of the envelope velocity dispersion (not shown in the Figure) and is then split into two components. One component is used as the pump pulse and the other, as the probe pulse. Both pulses pass through facilities which allow one to change the pulse parameters (carrier frequency, chirp, duration). The variable time delay between the pump and probe pulses is ensured by an optical delay line in which the optical path length of one of the pulses can vary. The pump and probe pulses are focussed on the specimen. The response to the two pulses as a function of the delay between them is recorded using a detector. The characteristics recorded as the response can include photoinduced absorption,[7–9] fluorescence,[10–12] stimulated radaiation,[13] miltiphoton ionisation[14]

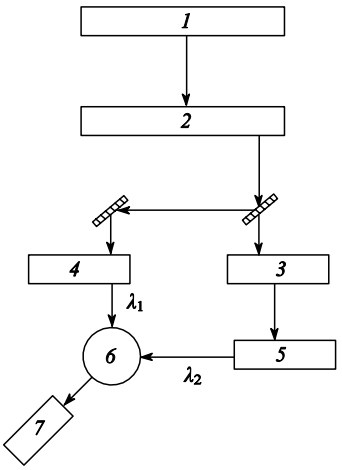

Figure 3. Experimental setup used for the 'pump – probe' experiments. (*1*) generator of femtosecond pulses; (*2*) optical amplifier of the pulse energy; (*3*, *4*) devices for changing the parameters of femtosecond light pulses, (*5*) optical line of the time delay between the pump and probe pulses; (*6*) reaction zone, (*7*) device for recording the response of the molecular system to the action of two pulses.

(often recorded using time-of-flight mass spectrometry techniques [15, 16]), rotation of the polarisation plane, [17] *etc*.

It is worth noting that the high intensity of femtosecond pulses permits utilisation of any non-linear spectroscopy technique developed to date in which several pulses are used.[18, 19] A special group of methods includes those in which the second pulse is focussed onto a target in order to generate ultrashort supercontinuum,[20, 21] electron [22–25] or X-ray [26, 27] pulses, which then serve as the probe pulses.

Supercontinuum pulses are used most effectively to study solutions. Primary processes in solutions result in broad absorption spectra of reactants, intermediate states and products. These spectra overlap, which markedly hampers interpretation of experimental data obtained at a particular wavelength. Regarding the time evolution of the intermediate states, more information is provided by an approach according to which time evolution of a broad spectrum of photoinduced absorption is recorded. This requires an ultrashort pulse which emits light over a broad spectral range. A supercontinuum the spectrum of which covers the whole visible region can serve as the source of such a pulse in femtochemistry. The methods that make use of this approach are documented.[20, 21]

Ultrashort pulses of electrons and X-rays are also used as probe pulses. In this case, diffraction of electrons or X-rays after reflection from the specimen under study is detected. By recording the diffraction pattern of electrons or X-rays at various points in time after the action of the pump light pulse, one can gain information on the structure of intermediates and the dynamics of structural changes. The methods based on electron diffraction are applicable only to gas media, while those based on X-ray diffraction are suitable also for condensed media. For example, electron diffraction has been used to determine the structure of an intermediate species.[22] The diffraction of X-rays has been used as yet only to detect the dynamics of structural changes in the absence of a chemical reaction. Thus time evolution of the arrangement of cadmium atoms in films of organic compounds heated by femtosecond light pulses has been studied.[26] There are publications in which absorption of the probe X-ray pulse is used to investigate photochemical reactions. For example, a study by Raksi *et al*.[27] deals with photodissociation of SF_6 molecules.

V. Dynamics of intramolecular processes and of transition states in a chemical transformation

It has been noted above that, due to the great spectral width, a coherent femtosecond light pulse excites a non-stationary quantum state, *viz*., a coherent wave packet (rotational, vibrational or electronic). The dynamics of nuclear motion shows itself in the time evolution of this packet. High temporal resolution permits real-time detection of the dynamics of wave packets.

A great number of theoretical studies devoted to the dynamics of coherent nuclear wave packets both in di- and polyatomic systems have been published.[28–36] Let us consider some properties of vibrational wave packets in relation to diatomic molecules in the absence of a chemical transformation.

Usually wave packets of this type are formed in some electronically excited state $|1\rangle$, to which dipole radiation transitions from the ground electronic state $|0\rangle$ are allowed. For simplicity, we assume that the pump pulse has a Gaussian shape, carrier frequency ω_0, duration τ and temporal chirp γ. Let us also assume that the crucial contribution to the wave packet is made by the ground vibrational state (the state with the vibrational quantum number $\upsilon = 0$) of the ground electronic state. Then at the instant of termination of the action of the light pulse ($\tau_f \approx \tau$), the vibrational wave packet $\Psi_1(R, \tau_f)$ (R is the distance between the nuclei) in the electronically excited state $|1\rangle$ has the form

$$\Psi_1(R, \tau_f) = \sum_{\upsilon} \varphi_{1\upsilon}(R) C_\upsilon(\tau_f, \tau, \gamma). \tag{10}$$

Here $\varphi_{1u}(R)$ are the vibrational wave functions of the molecule in the electronic state $|1\rangle$ corresponding to the vibrational quantum number υ and the vibration energy $\varepsilon_{1\upsilon}$ measured in relation to the minimum of the electronic potential curve of the state $|1\rangle$, while the complex coefficients are

$$C_\upsilon(\tau_f, \tau, \gamma) \approx S_{00,1\upsilon} \exp\left\{-i\frac{\varepsilon_{1\upsilon}\tau_f}{\hbar} - i\frac{\beta(\tau,\gamma)[\varepsilon_{1\upsilon} - (\omega_0 - T_{e1})]^2}{2\hbar^2}\right\} \times \times \exp\left[-\frac{\varepsilon_{1\upsilon} - (\omega_0 - T_{e1})^2}{2\Gamma^2(\tau,\gamma)}\right], \tag{11}$$

where $S_{00,1u}$ are the overlap integrals of the wave function of the ground vibrational state of the $|0\rangle$ electronic term and the wave functions $\varphi_{1\upsilon}(R)$, T_{e1} is the distance between the bottom of the ground state and the first excited state, the spectral chirp $\beta(\tau, \gamma)$ is defined by the formula (8), and

$$\Gamma^2(\tau,\gamma) = \gamma^2\frac{\tau^2}{4\ln 2} + \frac{4\ln 2}{\tau^2}. \tag{12}$$

The evolution of the wave packet $\Psi_1(R, \tau_f)$ that has formed by the instant τ_f at $t > \tau_f$ obeys the temporal Schrödinger equation for a free molecule and, hence, the corresponding non-stationary wave function has the form

$$\Psi_1(R, t) = \sum_{\upsilon} \varphi_{1\upsilon}(R) C_\upsilon(\tau_f, \tau, \gamma) \exp\left[-i\frac{(t-\tau_f)\varepsilon_{1\upsilon}}{\hbar}\right]. \tag{13}$$

The probability of obtaining in measurements the value ε_υ for the vibrational energy of the molecule the state of which is described by the non-stationary wave function $\Psi_1(R, t)$ is equal to $|C_\upsilon(\tau_f, \tau, \gamma)|^2$ and does not depend on time t. A significant feature of the wave packet is the fact that the probability density for finding a molecule with the distance R between the nuclei

$$|\Psi_1(R,t)|^2 = \sum_{\upsilon}|C_\upsilon|^2\varphi_{1\upsilon}^2(R) + \sum_{\upsilon>\upsilon'} 2|C_\upsilon| \times \tag{14}$$

$$\times \left\{\cos\left[\frac{(t-\tau_f)(\varepsilon_{1\upsilon} - \varepsilon_{1\upsilon'})}{\hbar} + \mathrm{Arg}(C_{\upsilon'}) - \mathrm{Arg}(C_\upsilon)\right]\right\} \times$$

$$\times \varphi_{1\upsilon}(R)\varphi_{1\upsilon'}(R)$$

(unlike the stationary states) depends on time t. This can be interpreted as movement of the wave packet along the PES.

The dynamics of wave packets in model anharmonic oscillators has been studied theoretically in detail.[28–36] It was found that it consists of two stages. The first stage is spreading of the packet with splitting into several sub-packets. Subsequently these sub-packets can be completely restored, owing to interference, to give the initial wave packet within time T/x, where T is the period of classical vibrations and x is the anharmonicity parameter. Similar results are obtained in numerical calculations for real systems, for example, for the I_2 molecule. Figure 4 shows the $|\Psi(R,t)^2|$ functions for the I_2 molecule in the electronically excited state $B0_u^+$ for three delay times calculated in relation to experimental data obtained by Sarkisov *et al.*[12] It can be seen that in the initial time instant, the vibrational wave packet is localised in space; then motion of the centre of gravity and spreading of the packet take place. The spreading is due to the fact that the phases of the Fourier components of the packet become less correlated with one another.

A vivid description of wave packet dynamics can be obtained by using representation of the quantum state of the system in terms of the Wigner distribution function in the phase space (see, for example, Ref. 37). The Wigner function for an anharmonic molecular oscillator is written as

$$W(R,P,t)=\frac{1}{\pi\hbar}\int_{-\infty}^{+\infty}\exp\left(i\frac{Px}{\hbar}\right)\rho_1^{(\mathrm{vib})}(R+x,R-x,t)\mathrm{d}x, \quad (15)$$

where P is the momentum conjugate to the coordinate R, $\rho_1^{(\mathrm{vib})}(R+x,R-x,t)$ is the density matrix for the molecular oscillator in a coordinate representation (the definition for the notion of a density matrix can be found, for example, in Ref. 31); in particular, if the state of the molecular oscillator is described by the wave function $\Psi_1(R,t)$, then

$$\rho_1^{(\mathrm{vib})}(R+x,R-x,t)=\Psi_1(R+x,t)\Psi_1^*(R-x,t). \quad (16)$$

The Wigner distribution function is an analogue of the classical distribution function in the phase space. However, this analogy should not be understood literally because, due to quantum fluctuations, $W(R,P,t)$ is not a positively defined function. To get rid of the 'non-classical' behaviour of the Wigner distribution function for quasi-classical quantum states (for example, vibrational wave packets of diatomic molecules in typical femtosecond experiments), it is averaged over regions of the phase space (about $2\pi\hbar$). The function used most often is the following 'coarse-grained' distribution function (it is called sometimes the Husimi function):

$$W_{\mathrm{H}}(\bar{R},\bar{P},\sigma,t)=\frac{1}{\pi}\int_{-\infty}^{+\infty}\mathrm{d}R\int_{-\infty}^{+\infty}W(R,P,t)\times \quad (17)$$

$$\times\exp\left[-\frac{(\bar{R}-R)^2}{\sigma^2}-\frac{(\bar{P}-P)^2\sigma^2}{\hbar^2}\right]\mathrm{d}P,$$

where σ is a parameter expressed in units of length. The variables $\bar{R}$ and $\bar{P}$ can be regarded as the classical coordinate and the momentum of the molecular oscillator, respectively.

Lozovoy *et al.*[37] calculated, in relation to experiments described in other publications,[12,38] the Husimi distribution functions for the vibrational wave packets formed by the pump pulse in the $B0_u^+$ electronic state of the I_2 molecule. The results of calculations for two delay times show that at $\Delta t = 149$ fs, the packet is still localised, while at $\Delta t = 4944$ fs, it has split into four sub-packets. At longer times, interference takes place, resulting in the restoration of the initial wave packet. The physical pattern of the dynamics of the vibrational wave packet in a diatomic molecule in the absence of bond rupture can be described as follows. The packet is first spread, which is due to the 'disturbance' of the relative phases of various Fourier components of the wave packet. Then it is divided into sub-packets, the Fourier components of which have similar phases. These packets interfere either constructively or destructively; this may result in more localised wave packets. Thus, for diatomic molecules, the intramolecular dynamics can be represented as splitting and restoration of wave packets.

The dynamics of vibrational wave packets in the absence of chemical transformations of the diatomic iodine molecule in the electronically excited state $B0_u^+$ is manifested as time oscillation of the response in the 'pump–probe' experiment. This response is a dependence of the signal intensity (I) on the delay between the pump and probe pulses (Δt). Figure 5 shows the experimental data and the results of calculations of the response function in accordance with the theory developed by Sarkisov and co-workers.[39] This theory allows one to derive the response function of the 'pump–probe' experiment for diatomic molecules at various parameters of the pump and probe light pulses. The

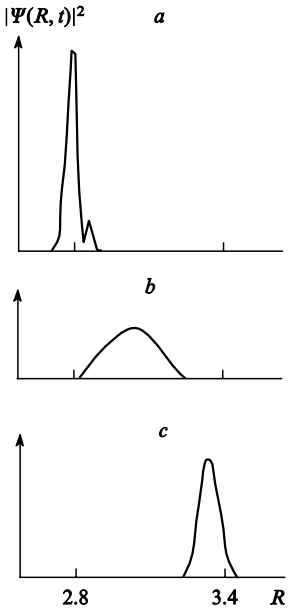

Figure 4. Dynamics of the vibrational wave packets in the bound electronic state $B0_u^+$ of the iodine molecule: distribution of the probability density $|\Psi(R,\mathrm{t})|^2$ of the occurrence of nuclei at distances R for time delays $\Delta t = 0$ (*a*), 30 (*b*), 60 fs (*c*).

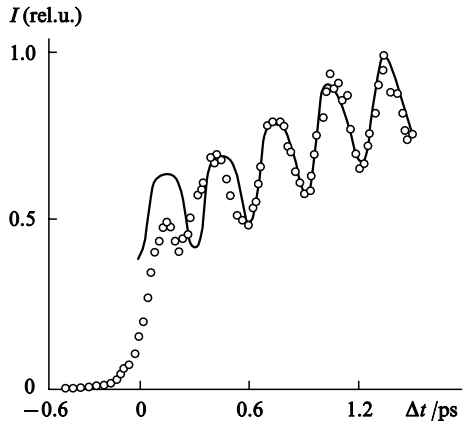

Figure 5. Superimposed oscillation signals in 'pump–probe' experiments for an iodine molecule in an electronically excited state.[12]
The dots show experimental data and the curve corresponds to calculations.

calculated response function for the detection of fluorescence is in good agreement with the experimental data without adjustable parameters. The deviation of the theoretical curve from the experimental points at short Δt values is due to overlap of these pulses (the theory used [39] does not imply this overlap.)

In terms of the classical theory, the vibrations of atoms in a diatomic molecule are represented as vibrations of two masses connected by a spring. Within the framework of the theory of stationary quantum states, the vibrations of nuclei are not considered at all. Only introduction of the notion of wave packets does provide a view on the vibrations from the quantum standpoint.

What are the dynamics of wave packets for polyatomic molecules? To answer this question, the dynamics of nuclear wave packets in a triatomic molecule (NO_2) has been studied.[40] In experimental studies, the author utilised the resonance variant of the stimulated scattering. The pump pulse had a circular polarisation; this made it possible to eliminate the influence of molecular rotation on the detected response. First, a coherent vibrational wave packet in an adiabatic electronically excited state was formed. The lifetime of this packet is determined by the interaction of the electronically excited and ground states. As a result of this interaction, the intramolecular non-adiabatic electron-vibrational dynamics switches from a regular to a stochastic mode. The experiments showed (and calculations confirmed) that this transition takes place over a period of 500 fs.

In the NO_2 molecule, the terms of the electronically excited and ground states undergo strong interaction; this provides grounds for regarding it as a model of a complex molecule. Therefore, it can be assumed that for polyatomic molecules, transition from a regular dynamic mode to the stochastic mode will take place in approximately the same time period (500 fs – 2 ps). Indeed, the wave packet dynamics manifested in the oscillations of the recorded signals has been observed for many complex molecules (see, for example, a number of studies [41–44]); in all cases, the time of oscillations did not exceed several picoseconds. As an example, we shall consider the results of a study [42] devoted to intramolecular vibrational dynamics of the azulene molecule during the internal conversion from the electronic state S_1 to the ground electronic state. In the experiments, both probe and pump pulses were shorter than 20 fs. Damped oscillations of the signal upon excitation of the molecule to the S_1 state with an excess of vibrational energy of >1300 cm^{-1} were observed. The damping time was 0.7 ps. Analysis showed that the main contribution to oscillations is made by only two (the corresponding frequencies are 160 and 200 cm^{-1}) of the 48 vibration modes. Thus, for large molecules, femtosecond pump pulses can generate vibrational wave packets consisting of a limited number of vibration modes. This example shows that the coherence of the atomic motion in a molecular system can also be retained on a picosecond scale.

Experimental methods have now been developed which provide the generation of rotational wave packets and recording of their dynamics not only in the excited but also in the ground electronic state.[17,45] The dynamics of the rotational wave packets observed experimentally for the NO_2 molecule in the ground electronic state is illustrated by Fig. 6. It can be seen that the signal reflecting the evolution of the rotational wave packet has the form of beats. Experiments were carried out using the method of non-resonance stimulated Raman light scattering. The pump and probe pulses are linearly polarised at an angle of 45° with respect to each other. The variation of the rotation angle of the plane of polarisation of the probe pulse as a function of Δt was detected. The rotational constants determined from this dependence coincide with the rotational constants determined by conventional microwave spectroscopy techniques.

Currently, approaches are being formed aimed at the formation and detection of vibrational wave packets in the ground electronic state. For example, as applied to diatomic molecules, methods for four-wave mixing of three pulses with a femtosecond

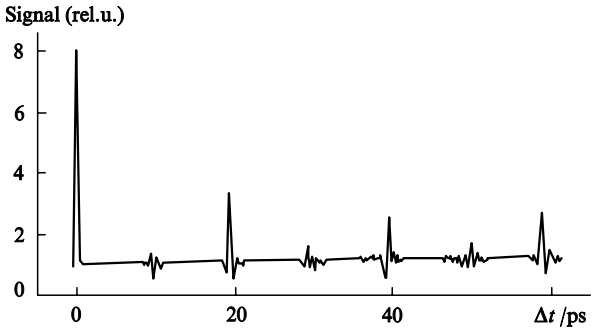

Figure 6. Experimentally observed dynamics of rotational wave packets for the NO_2 molecule in its ground electronic state.[17]

temporal resolution are being developed.[46–48] Methods for generation of vibrational wave packets in polyatomic molecules in the ground electronic state with excitation energies of either higher or lower than the dissociation threshold of these molecules have been proposed.[49,50]

Now we shall consider the intramolecular dynamics in the presence of a chemical transformation beginning also with a diatomic molecule. The most interesting example is pre-dissociation of the NaI molecule (Fig. 7). This system is characterised by avoided crossing of the covalent and ionic potential curves (Fig. 7 *a*). Both the dynamics of the transition state $[Na\cdots I]^{\#}$ and

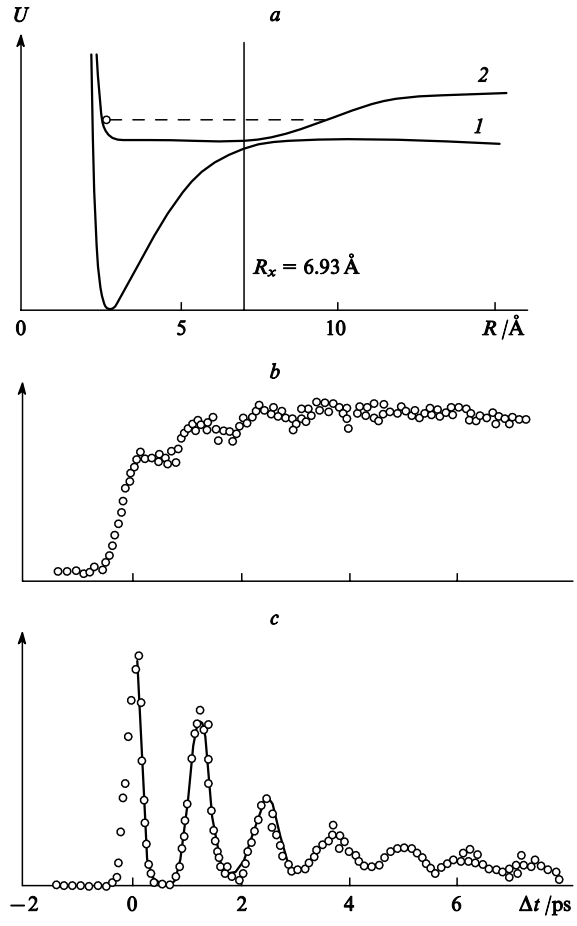

Figure 7. Dynamics of NaI dissociation.[51]
(*a*) potential energy curves for the ground (*1*) and excited (*2*) electronic states; (*b*) kinetics of accumulation of free Na atoms; (*c*) experimental monitoring of the $[Na\cdots I]^{\#}$ transition state.

the coherent kinetics of the formation of the pre-dissociation product, a sodium atom, were measured. The transition state dynamics gives an oscillating response with a decreasing amplitude. The decrease in the amplitude is related to 'skipping' of a part of the wave packet to a different electronic potential curve. Apparently, this is the first example of experimental real-time monitoring of the dynamics of intramolecular motion accompanied by non-adiabatic electron transitions. The product (sodium atom) is formed when the wave packet approaches the avoided crossing point. If we dealt with stationary states, the kinetics would be exponential with a rate constant equal to the vibration frequency multiplied by the probability of the non-adiabatic transition. However, in this case, the situation is different. When the wave packet is far from the avoided crossing region, the product yield does not increase. This type of kinetics is due to coherence; therefore, we call it coherent kinetics. By averaging the kinetics over all phases of wave packets, we shall obtain exponential kinetics.

It should be noted than the vibrationally coherent reactions induced by femtosecond pulses can take place in complex systems in various media. When these reactions occur, coherent wave packets can in some cases be observed experimentally in the products. Three reactions can be considered as examples, namely, decomposition of CH_2I_2 upon multiphoton absorption,[52] proton transfer in the 2-(2′-hydroxyphenyl)benzothiazole molecule [42] and the reaction responsible for the primary stage of vision.[53]

In the first reaction, the CH_2I_2 molecules were excited due to two-photon absorption on exposure to a femtosecond pulse with a carrier wavelength of 308 nm. Over a period of less than 100 fs, the carbene CH_2 and the iodine molecule in a non-stationary vibrationally excited state of the electronic state D' are formed.

In the case of proton transfer in the 2-(2′-hydroxyphenyl)benzothiazole molecule,[42] clear-cut damped oscillations of stimulated fluorescence were observed 60 fs after excitation with the probe pulse. The authors consider that the observed oscillations occur after the proton transfer has taken place. Analysis showed that only four of the 69 vibration modes (118, 254, 289 and 529 cm^{-1}) are involved in the formation of the vibrational wave packet, the predominant contribution to oscillations being made by only two vibration modes (118 and 254 cm^{-1}). The damping time for the contribution of the mode with a frequency of 118 cm^{-1} is 0.3 ps; that for each of other modes is $\sim$1 ps.

The third reaction is photoinduced isomerisation of the retinal chromophore in rhodopsin; more precisely, isomerisation of the excited 11-*cis*-retinal in the ground electronic state.[53] The 11-*cis*-retinal molecule was excited by a femtosecond pulse and the oscillating time dependence of the absorption of the product with a period of 550 fs was recorded. Two important experimental facts are worth mentioning: (i) the reaction occurs over a period of 200 fs; (ii) the reaction product was formed in a non-stationary vibrationally excited state of the ground electronic state. The researchers cited [53] give the affirmative answer to the question 'Does the vibrational coherence play an important role in the primary stage of vision?' They consider that avoided crossing of PES takes place and the wave packet can 'skip' from one PES to another and attribute the effective quantum yield of the reaction (0.67) to the reaction time (200 fs). The probability of this skip depends on the wave packet velocity in the avoided crossing region. If the velocity of the wave packet motion is decreased, the quantum yield of photoisomerisation should diminish. To confirm this hypothesis, femtosecond experiments on photoisomerisation of isorhodopsin were carried out. It was found that isorhodopsin isomerisation affords the same product, bathorhodopsin. It was suggested that the initial velocity of wave packet motion after excitation is lower in the case of isorhodopsin than in the case of rhodopsin. This was confirmed in experiments: the reaction proceeds more slowly (over 600 fs) and has a lower quantum yield (0.22). Therefore, the investigators concluded that the quantum yield is determined by the reaction dynamics rather than by the vibrational relaxation processes, as had been considered previously.

There are several publications in which the coherent wave packets have been observed when investigating elementary reactions within the femtosecond and sub-picosecond time scales. For example, vibrational coherence was observed in the photodissociation of OCS in the gas phase,[54] photodissociation of $Mn_2(CO)_9$ [55] and $Cr(CO)_6$,[41] intramolecular proton transfer,[56] femtosecond processes in proteins [57] and electron transfer.[58–62] For example, in a study of the hexamethylbenzene complex with tetracyanoethylene (TCE), oscillations were detected both in absorption and in fluorescence.[59, 60, 62] In a study of donor–acceptor interactions, Rubtsov and Yoschihara [61] have used various electron donors (carbazole, 1-chloronaphthalene, *N*-methylaniline) and acceptors (TCE, chloranil, fluoranil). It was shown that for each particular acceptor, irrespective of the nature of the donor, the same oscillation frequency in the fluorescence signal is observed: 155 cm^{-1} for TCE (oscillation period 215 fs), 178 cm^{-1} for chloranil (oscillation period 187 fs) and 212 cm^{-1} for fluoranil (oscillation period 157 fs). Hence, the oscillations are due to the formation of the vibrational wave packet associated with the excitation of a particular electron acceptor in the donor–acceptor complex.

It should be noted that the use of laser spectroscopy with ultrahigh temporal resolution often makes it possible to gain information on not only the product formation and the reactant decay but also on the transition state dynamics without observing the vibrational coherence. These studies also made a substantial contribution to the development of the views on the transition state dynamics. First of all, this refers to the study of electron transfer processes in molecular systems with intervalent transitions in organometallic compounds,[63, 64] charge recombination in photoexcited donor–acceptor complexes without covalent bonds,[59–70] charge separation and recombination in donor–acceptor supramolecules with covalent bonds.[70–75]

Studies of electron transfer in non-covalent donor–acceptor complexes and intervalent transitions in metal complexes provided important information on the dynamics of relaxation of their dipole environment.[61–68] These studies showed that, in addition to orientational relaxation, an important role is played by the libration motion of the medium dipoles.[60, 63, 64] In the same publications, it is noted that the single-mode approximation (when one average frequency of intramolecular vibrations is taken) is insufficient for describing the internal re-organisation of the system.

A situation typical of covalently bonded supramolecules is that an optical transition from the ground state gives rise to a locally excited state, which passes subsequently into a charge transfer state. The covalently bonded donor–acceptor supramolecules 'mimic' the charge separation process in a photosynthetic centre.[71, 72] Charge separation can take place both on the pico- and on the femtosecond time scale. This has been demonstrated [75] in relation to charge separation in the tetra-*meso*-substituted ferrocenylporphyrin molecules. The researchers studied the relaxation dynamics in various tetra-*meso*-substituted ferrocenylporphyrins, Fc_4PH_2, $ZnFc_4P$, $Fc_4PH_4^{2+}$ and $TCE:Fc_4PH_2$ (Fc is ferrocene, P is porphyrin), by the 'pump–probe' method. A supercontinuum was used as the probe pulse. The differential absorption in the 380–600 nm spectral range was recorded. Under the action of a femtosecond pulse with a wavelength of 610 nm, the $Q^1(\pi^*-\pi)$ state of the electron acceptor (porphyrin molecule) was excited, the ferrocene molecule serving as the electron donor. The formation of the charge transfer state $P^- - Fc^+$ from the locally excited $Q(\pi^*-\pi)$ state takes place over a period of $\sim$200–210 fs in the case of Fc_4PH_2 and $ZnFc_4P$. However, in the case of $Fc_4PH_4^{2+}$ and $TCE:Fc_4PH_2$, transition to the charge transfer state requires at least 10 ps. The different time scales of transition are, apparently, due to different conformation flexibilities of the porphyrin ring. Note that the transition to the charge transfer state occurs faster than the relaxation of solvent

molecules. A higher rate of electron transfer compared to the rate of relaxation of solvent molecules is also observed for complexes containing no covalent bonds.[62, 65] To interpret these facts, it is necessary to use new approaches to the standard views on electron transfer.

Other examples of investigation into transition state dynamics without observing the coherent wave packets can be found in a number of publications devoted to elucidation of the problem whether a reaction follows a stepwise or a concerted mechanism. Stepwise reactions differ from concerted ones in that the potential curves along the reaction coordinate have an intermediate minimum between the minima corresponding to reactants and products. In some cases, the reaction mechanism can be established rather easily. For example, photodecomposition reactions of acetone,[76] fluoroethane [77] and cyclic ketones [78] occur by stepwise mechanisms. This is proved (by experiment) by the fact that the primary and secondary bond ruptures occur at different time instants. The decomposition of CH_2I_2 upon multiphoton excitation [52] follows a concerted mechanism, which is confirmed by the short reaction time (< 50 fs) and by the product being formed in a non-stationary coherent state. However, it is often difficult to elucidate the reaction mechanism; this requires methods with a very high temporal resolution. Examples of reactions that follow stepwise and concerted mechanisms are listed in Table 1.

Table 1. Examples of reactions occurring by stepwise and concerted mechanisms.

Reaction	λ_1 /nm	Mechanism	t /fs	Ref.
$Fe(CO)_5 + 2\,h\nu \rightarrow$ $\rightarrow FeCO + 4\,CO$	400	concerted	~ 100	79
$Fe(CO)_5 + h\nu \rightarrow$ $\rightarrow Fe(CO)_4^* + CO$, $Fe(CO)_4 \rightarrow Fe(CO)_3 + CO$	267	stepwise	~ 100 ~ 3000	80
cyclo-$C_4H_8 \rightarrow 2\,C_2H_4$ (in the ground electronic state)	–	the same	~ 700	81
Cyclohexene $\rightarrow$ $\rightarrow$ ethylene + butadiene (in the ground electronic state)	–	concerted, stepwise	~ 200	82
Two-proton transfer in 2,2′-bipyridine-3,3′-diol	300 – 400	the same	~ 50 $\sim 10\,000$	83, 84

The first example is related to the photochemistry of metal carbonyls, which are widely used as photocatalysts and for the production of high-purity metallic films on various surfaces. Photodecomposition of these compounds has been studied using femtosecond spectroscopy techniques. For example, the ultrafast dynamics of photofragmentation of $Mn_2(CO)_{10}$, namely, rupture of the metal – metal and metal – ligand bonds occurring over hundreds of femtoseconds, has been studied.[85] The dynamics of $M(CO)_6$ dissociation (M = Cr, W, Mo) in solutions has been investigated [86] using femtosecond IR spectroscopy. It was found that the primary reaction in the UV photolysis is ejection of one CO group, which takes place over a period of less than 240 fs. Let us analyse decomposition of $Fe(CO)_5$ in the gas phase in more detail. Two groups of researchers [79, 80] have considered an important point, namely, whether the molecule loses one or several CO ligands after photoexcitation. The viewpoints of the researchers cited are appreciably different.

In experiments described in one of these publications,[79] the 'pump – probe' procedure was used. The pump pulse had a carrier wavelength of 400 nm. Upon the absorption of two photons, a transition state with an excitation energy of 50 000 cm^{-1} was formed. The probe pulse had a carrier wavelength of 800 or 400 nm. Using a time-of-flight mass spectrometer, the ions of both the starting compound and all the fragments of $Fe(CO)_n^+$ decomposition ($n = 0 - 5$) were detected. The experiments showed that the decay times of all the $Fe(CO)_n^+$ cations ($n = 2 - 4$) were nearly equal and amounted to ~ 100 fs. (Time characteristics of the growth of signals of the cations were not detected.) The maxima of signals of these cations are shifted in time relative to the maximum of the $Fe(CO)_5^+$ signal by 20 ± 5 fs for $Fe(CO)_4$, by 30 ± 5 fs for $Fe(CO)_3$ and by 60 ± 15 fs for $Fe(CO)_2$. Only for FeCO and Fe, were the kinetic characteristics of the growth of signals observed, the formation kinetics of iron atoms being correlated with the kinetics of the decay of FeCO. This means that dissociation of FeCO is a subsequent reaction which occurs with a characteristic time of 230 fs. The following model was proposed to interpret the experimental data. The excitation is followed by structural rearrangement of the transition state during the first 20 ± 5 fs; consequently, the distance between the centers of gravity of $Fe(CO)_4$ and CO increases relative to the equilibrium distance. With this transition state geometry, after absorption of the photons from the probe pulse, the parent molecule is converted into the corresponding ion, which decomposes to give the detectable $Fe(CO)_4^+$ ion and CO. Within 30 ± 5 fs after the pump pulse, a new configuration of the transition state appears (apparently, two CO ligands are separated from the Fe atom by distances greater than the equilibrium distance). The probe pulse induces the transformation of the parent molecule into the corresponding ion, which decomposes to give the detectable $Fe(CO)_3^+$ ion and two CO molecules. The origin of the detectable $Fe(CO)_2^+$ and $FeCO^+$ cations is explained in approximately the same way. Within the framework of this model, the observable ions are 'fingerprints' of the time evolution of the transition state. Thus, upon absorption of two photons with a wavelength of 400 nm, the reagent loses four CO ligands in ~ 100 fs. Since this value corresponds to the time scale of the period of the Fe – CO bond vibrations (the typical range is 80 – 100 fs), the researchers concluded that the reaction

$$Fe(CO)_5 + 2\,h\nu \longrightarrow FeCO + 4\,CO$$

occurs by a concerted mechanism.

The same reaction was studied by similar methods in another study.[80] Five consecutive processes with time constants of 21, 15, 30, 47 and 3300 fs were detected after the pump pulse. However, the four faster processes were attributed to intermediate intramolecular processes taking place in the excited $Fe(CO)_5$ molecule and in the primary product $Fe(CO)_4$ formed in an electronically excited state. In the opinion of the researchers cited, the second step of CO elimination, *i.e.*, transition of $Fe(CO)_4$ to $Fe(CO)_3$, occurs in the ground electronic state over a longer period (3.3 ps). They discussed the possibility of a concerted reaction mechanism and concluded that it does not take place.

The conclusions made in the two studies discussed above are contradictory. However, it should be noted that Trushin *et al.*[80] performed excitation of the $Fe(CO)_5$ molecule by one-photon absorption at a wavelength of ~ 267 nm, while in the study by Banares *et al.*,[79] this was done by two-photon excitation at ~ 400 nm. Therefore, in the latter case, the $Fe(CO)_5$ molecule could have a much greater excitation energy and, perhaps, different parameters of the initial vibrational wave packet. In addition, both groups of scientists did not control the structure of the pump pulse, although it is known, for example, that the chirp of the pump pulse can result in an increase in the product yield in the channel corresponding to the concerted mechanism. Thus, the question of the mechanism of this reaction remains open.

The second example is opening of the cyclobutane ring giving rise to two ethylene molecules.[81] Two mechanisms of this reaction are discussed in the literature — concerted (described by the Woodward – Hoffman rule) and stepwise (a biradical two-step mechanism). By investigating the kinetics of the decay of biradicals, the authors [81] arrived at the conclusion that the reaction follows the stepwise biradical mechanism. They believe that a

small potential well (4 kcal mol^{-1}) corresponding to the intermediate species, biradicals, is present near the top of the barrier.

The third example is represented by decomposition of cyclohexene and other cyclic compounds.[82] Experimental data and trajectory calculations showed that the reactions follow two mechanisms, a concerted and a stepwise biradical mechanism. In the researchers' opinion, the contributions of the two types of mechanisms to the overall reaction rate are dictated by the asymmetry of the molecular structure, localisation of the activated complex and the height of the potential barrier.

The problem of the search for an experimental criterion which would be indicative of a concerted reaction mechanism has been discussed.[82,87] It is generally accepted that several bonds are modified simultaneously in a concerted reaction — some of them are cleaved and some new bonds are formed. However, the notion of simultaneity for the experimenter has not been defined. The authors of the publications considered believe that a well-posed criterion should be related to the time scale of the movement along the reaction coordinate. This means that only the real-time dynamics of intermediate structures can substantiate the concept of concertness. It should be emphasised that the notion of concerted reactions has usually been related only to the structure of PES. In femtochemistry, realisation of either concerted or stepwise mechanism can also depend on the way of production of the wave packet, in particular, on the degree of its coherence.

The last-mentioned example refers to the studies of intramolecular two-proton transitions in electronically excited states. Two-proton transfer in the 2,2′-bipyridine-3,3′-diol molecule has been studied.[83,84] It was found that this transfer can follow two mechanisms, namely, a one-step concerted mechanism and a two-step mechanism comprising two successive steps of one-proton transfer.

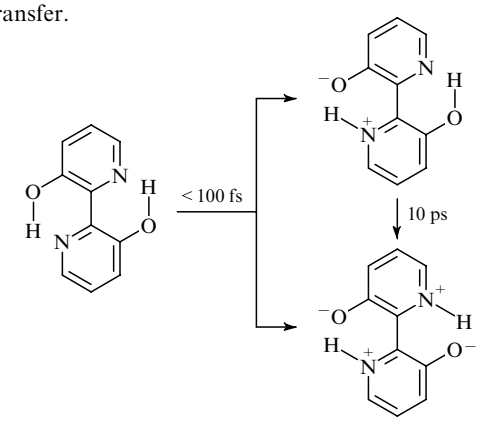

The concerted reaction and the first step in the stepwise process occur in less than 100 fs, while the last step requires ~10 ps.

One of the studies cited [84] is devoted to the dependence on the excitation energy of the ratio of the reaction yields obtained from the different channels. It was shown that an increase in the vibrational energy in the electronically excited state S_1 results in a higher ratio of the yields of mono- and diketo tautomeric products. The predominance of the concerted mechanism at low excitation energies was attributed to the fact that there exists a potential barrier for the first step, which affords the monoketo tautomer. Due to presence of an electrophilic substituent in these molecules, the one-proton transfer takes place.[88] This was demonstrated using tautomerisation of 6-methoxycarbonyl-2,2′-bipyridine-3,3′-diol as an example. The one-proton transfer in this molecule takes < 150 fs.

Yet another example is provided by the proton transfer processes in 7-azaindole dimers. They can be regarded as model processes mimicking tautomerisation in DNA pairs. Time evolution during the intramolecular tautomerisation of 7-azaindole dimers containing two N—H bonds has been investigated.[89] The molecular structures in which the transfer of one or two protons takes place are shown below

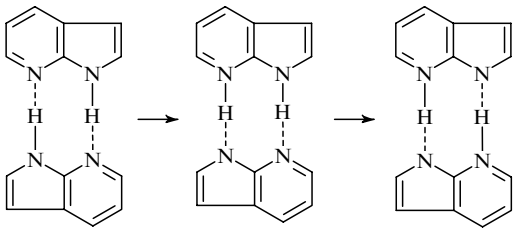

On exposure to a femtosecond pulse at 305–310 nm, the dimers formed in a molecular beam passed to an electronically excited state. Ionisation of various structures under the action of the probe pulse (wavelength 605 nm) took place at different points in time after the pump pulse. The result of ionisation was recorded by a time-of-flight mass spectrometer. The femtosecond temporal resolution made it possible to follow the motion of protons in each intermediate and to determine the characteristic times of this motion in the absence of a solvent. It was found that the first step of proton transfer occurs in several hundreds of femtoseconds, while the second step, which yields tautomer, is much slower, it proceeds over a period of several picosends. When the hydrogen atoms are replaced by deuterium atoms, the time scales of tautomerisation reactions change substantially. The mechanism of these processes has been discussed,[89] in particular, the role of quantum tunnelling in it. Nevertheless, the question of whether the two-proton transfer follows a concerted or a stepwise mechanism has been brought up in subsequent studies.[90–92] In these publications, the possibility of existence of active and inactive dimers with respect to tautomerisaton reactions and the role of solvation effects are discussed. It was shown [91] that clustering of water does not induce the formation of reaction-inactive dimers; the researchers concluded that the two-proton transfer follows a stepwise mechanism. However, Catalan *et al.*[92] believe that this transfer in 7-azaindole dimers occurs by a concerted mechanism. The conclusions made in this study provoked scientific discussion. Remarks concerning the publication cited [92] can be found in a study by Folmer *et al.*[93] The authors investigated this reaction using the 'Coulomb explosion' technique and concluded that it follows a stepwise mechanism.

VI. The kinetics of ultrafast chemical reactions

Study of the kinetics of a process includes monitoring of the time evolution of the concentration of a reactant or a product. This means that the populations of quantum levels rather than the dynamics of wave packets should be detected (we are not interested in the phase caracteristics of the nuclear motion). The features of femtosecond pulses significant for this line of femtochemistry include high temporal resolution and high intensity. Using these pulses with multiphoton absorption, it is possible to produce and to study molecules in high electronic states the lifetimes of which are very short.

Currently, vigorous studies dealing with the chemistry of highly excited molecules are being carried out. It is obvious that the rates and the ratios of channels of these reactions depend substantially on intramolecular processes such as conversion from highly excited electronic states, S_n, energy redistribution over vibrational modes and vibrational relaxation caused by intermolecular energy transfer to the solvent.

In a study of electron relaxation, it has been shown [94,95] that excitation of high electronic states in, for example, coumarin 481, oxazine 1 and sulforhodamine, is accompanied by internal conversion processes ($S_n \rightarrow S_1$), which occur in 180–280 fs. This conclusion is based [94] on the results of the following experiments. Coumarin 481 molecules in cyclohexane were excited by a pulse (duration 100 fs, wavelength 267 nm) to some electronic state S_n, the energy level of which is 12 000 cm^{-1} higher than the energy level S_1. From measurement of the kinetics of fluorescence (the up-conversion) related to the $S_1 \rightarrow S_0$ transition, the researchers reached a conclusion about the time characteristics of the $S_n \rightarrow S_1$

internal conversion. By investigating intramolecular processes for various porphyrins, it was found that the lifetime of the porphyrin molecule as the free base (H_2P) in the S_3 state is shorter than 40 fs, while that in the S_2 state is 90 fs. These and other data attest that the time scale of these processes is < 300 fs.

In some publications (see, for example, Refs 96–100), it is concluded that intramolecular energy redistribution occurs much faster, namely, in tens of femtoseconds. A somewhat different opinion was expressed by Hasche *et al.*,[100] who consider that redistribution of vibrational energy is faster (30–200 fs) for approximately iso-energetic vibrational levels and slower (200–1000 fs) for vibrational levels with appreciably different frequencies. Much longer times are required for relaxation of vibrational energy, *i.e.*, for the transfer of vibrational energy to the molecules of the environment. The time scale of these processes is about tens of picoseconds.[94, 101]

Let us consider examples of kinetic measurements for reactions of the following classes: bond rupture in electronically excited molecules, elimination of electronically excited molecules, decomposition of vibrationally excited molecules in the ground electronic state, photoisomerisation, bimolecular reactions in van der Waals complexes, bimolecular association reactions (*i.e.,* reactions in which the reactants are free and no chemical transformations take place upon collision; however, for definite distances between the reactants, photon absorption can take place; this induces the formation of a bond).

Examples of unimolecular reactions proceeding within femto- and sub-picosecond time scales are presented in Table 2. Below we discuss these reactions in more detail.

Table 2. Characteristic times (τ) of some ultrafast unimolecular reactions.

Reaction number	Reaction	t /fs	Ref.
Bond rupture in electronically excited molecules			
1	$(ICN)^e \rightarrow I + CN$	200	102
2	$(CH_3I)^e \rightarrow CH_3 + I$ (see [a])	100–200	103
3	$(CD_3I)^e \rightarrow CD_3 + I$ (see [a])		
4	$(C_2F_4I_2)^e \rightarrow (C_2F_4I)^* + I^*$ (see [b])	200	77
5	$(C_2F_4I_2)^e \rightarrow (C_2F_4I)^* + I$		
Elimination from electronically excited molecules			
6	$(CH_2I_2)^e \rightarrow CH_2 + I_2(D')$ (see [a])	< 100	52
7	$(NH_3)^e \rightarrow NH(c^1) + H_2$ (see [c])	< 50	104
Isomerisation of electronically excited molecules			
8	Isomerisation of spironaphthooxazine, multistep process	3000	21, 105, 106
Tautomerisation of electronically excited molecules			
9	$A^e \rightarrow T^e$	60	107
10	$T^e \rightarrow$ decay (A^e is the ketone form of methyl salicylate, T^e is the enol form of methyl salicylate)	> 1000	107
Decomposition of vibrationally excited radicals in the ground electronic state			
11	$(C_2F_4I)^* \rightarrow C_2F_4 + I$ (see [c])	25 000	77
12	$(CH_3CO)^* \rightarrow CH_3 + CO$	500	76
13	$[CH_2(CH_2)_{n-2}C{=}O]^* \rightarrow CH_2(CH_2)_{n-2} + CO$ (n = 4, 5, 6, 10)	100	78

Note. The superscript '*e*' designates electronically excited species, and '*' marks vibrationally excited species. Excitation energy/eV: [a] 8; [b] 4.7; [c] 10.

Dissociation of ICN from an electronically excited state (see Table 2, reaction *1*) takes place on the repulsive term. The kinetics of formation of the CN product has been measured experimentally.[102] The time of bond rupture was determined by comparing experimental data (obtained with ultrahigh temporal resolution) with the results of calculations in terms of the diatomic approximation.

After decomposition of the $(CH_3I)^e$ and $(CD_3I)^e$ molecules (see Table 2, reactions *2* and *3*) (each molecule gained an excitation energy of 8 eV due to two-photon absorption) from Rydberg states, the time evolution of processes was recorded for 100–200 fs.[103] An appreciable isotope effect was observed.

The electronically excited $(C_2F_4I_2)^e$ molecule is formed after exposure of $C_2F_4I_2$ to a femtosecond light pulse with a wavelength of 277 nm. Decomposition of the electronically excited molecule takes place along two channels over a period of 200 fs giving rise to the vibrationally excited $(C_2F_4I)^*$ radical in the ground electronic state and a iodine atom. One channel provides an electronically excited iodine atom, and the other channel, a non-excited iodine atom (see Table 2, reactions *4* and *5*, respectively).

Both mechanisms of decomposition of $(C_2F_4I_2)^e$ and the mechanism of decomposition of the $(C_2F_4I)^*$ radicals formed in the ground electronic state have been studied.[77] The results of this study are discussed in more detail below, when considering the processes with participation of vibrationally excited radicals in the ground electronic state.

Elimination reactions of highly excited molecules occur due to multiphoton absorption. Femtosecond pulses have a high on-peak power; therefore, multiphoton processes readily take place. An example is reaction *6* (see Table 2), namely, gas-phase decomposition of a CH_2I_2 molecule excited by multiphoton absorption, induced by absorption of two photons with a wavelength of 310 nm (excitation energy 8 eV).[52] One product of this reaction is molecular iodine, which exists in a non-stationary quantum state; reaction time < 100 fs. Note that for low excitation energies, rupture of the C–I bond to give an iodine atom is the main reaction channel.

Yet another example is decomposition of ammonia induced by five-photon absorption ($\lambda = 615$ nm).[104] If the excitation energy of the ammonia molecule is 10 eV, decomposition by reaction *7* takes place (see Table 2); if it amounts to ~ 8 eV, the following reaction proceeds:

$$NH_3 \longrightarrow NH_2 + H.$$

These examples illustrate the potential of methods with the use of femtosecond pulses for the development of the chemistry of electronically excited molecules.

A large number of publications are devoted to photoisomerisation induced by femtosecond pulses (see, for example, papers [9, 21, 105–117]). In particular, many studies deal with isomerisation of electronically excited molecules of various photochromic compounds in solutions. On exposure to light, photochromic compounds can undergo reversible intramolecular transformations accompanied by a change in the absorption spectrum. This property of photochromic compounds can be used for generation of various optico-electronic devices. In particular, the possibility of using them for three-dimensional optical memory is discussed.[115, 116] Let us consider photoisomerisation of unsubstituted indoline spiro compounds, namely, spironaphthopyran (SNP), spironaphthooxazine (SNPO) and spirophenanthrooxazine (SPO).

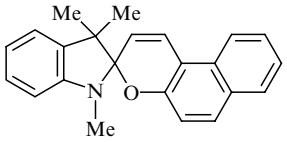

SNP

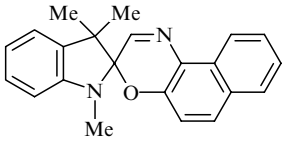

SNPO

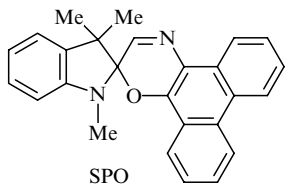

SPO

Photoisomerisation is transition of form A into form B, which has a planar structure similar to the structure of merocyanine dyes. For example,

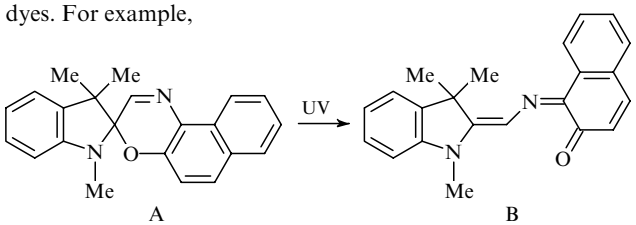

A B

Femtosecond pulses with durations of 170–400 fs have been used.[112–114] It was found that isomerisation proceeds *via* singlet states and is completed within a picosecond time scale.

The mechanism of these reactions has been studied in more detail in several publications.[21, 105, 106] The pump pulse centred at a wavelength of 308 nm had a duration of 70 fs. Probing was performed using a supercontinuum in the spectral range of 420–590 nm. For each of the three compounds, the dynamics of the photoinduced absorption spectra was recorded with a high temporal resolution for different time intervals after the action of the pump pulse. Figure 8 illustrates the dynamics of the photoinduced absorption spectra recorded experimentally for spirophenanthrooxazine. It was found that the reaction mechanism does not change when the position of the aromatic rings changes. On the basis of experimental data and quantum-chemical calculations, a photoisomerisation mechanism including the following processes was proposed:

(0) $A(S_0) + h\nu \longrightarrow A(S_2)$,

(1) $A(S_2) \longrightarrow A(S_1)$,

(2) $A(S_1) \longrightarrow X^*$,

(3) $X^* \longrightarrow B$.

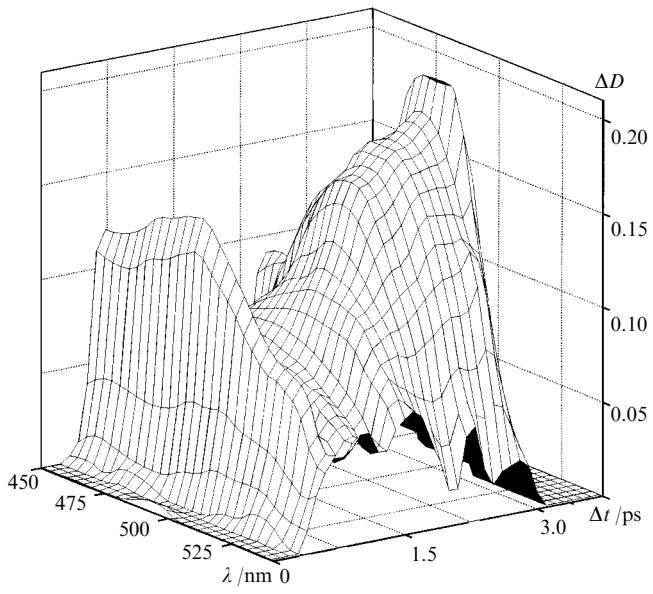

Figure 8. Dynamics of the photoinduced absorption spectra for SPO.[106] ΔD is the optical density change.

Here $A(S_i)$ ($i = 1, 2$) is molecule A in the singlet electronic state S_i; X is an intermediate species, which is characterised by rupture of the bond between spiro carbon and oxygen. It is worth noting that the experimental approach developed in a series of publications[21, 104] made it possible to observe the time evolution of the $S_2 \rightarrow S_1$ transition, vibrational relaxation in the S_1 electronic state, the formation of the intermediate species X*, which is the *cis*-cisoid isomer in the electronically excited state, and the formation of X and of the reaction products — forms B of the corresponding spiro compounds. The last-mentioned reaction includes the following steps: non-adiabatic $X^* \rightarrow X$ transition and the transition of X into species B. However, it was impossible to separate these steps in time, due to the superposition of the absorption spectra for species X and B. Therefore, both steps are written as a single reaction, which appears to be limited by the rotation of the molecule about bonds of the opened ring. The results of experimental studies for SNPO are shown in Fig. 9. Absorption of a light quantum brings the molecule to the S_2 excited state. This is followed by transition to the vibrational levels of the S_1 electronic state. This transition shows itself as accumulation of molecules $A(S_1)$; this is detected by a change in the absorption spectra observed for delays of up to 110 fs (Fig. 9 *a*). The next stage is transition of molecule $A(S_1)$ into the state X* (this intermediate state was observed by low-temperature phosphorescence[109]), which is characterised by rupture of the bond between the spiro carbon atom and the oxygen atom. The species X* is detected on the basis of absorption spectra in the spectral range of 420–450 nm; the variation of the concentration of X* is illustrated by Fig. 9 *b*. The next step is non-adiabatic transition of the system from the excited state X* to the ground electronic state X. The molecule acquires the possibility of rotating around the

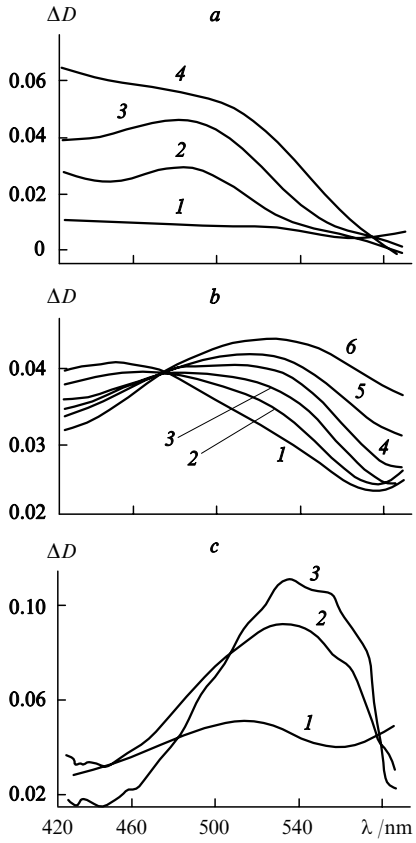

Figure 9. Photoinduced absorption spectra of SNPO for various time delays between the pump and probe pulses.
Δt /fs: (*a*) −110 (*1*), 0 (*2*), 73 (*3*), 185 (*4*); (*b*) 665 (*1*), 739 (*2*), 812 (*3*), 886 (*4*), 960 (*5*), 1034 (*6*); (*c*) 960 (*1*), 3600 (*2*), stationary absorption spectrum of the reaction product (*3*).

bonds of the opened ring. Figure 9 *c* shows the variation of the absorption spectra associated with this process. The absorption spectrum for a delay of 3.6 ps shown in the same figure is similar to the known steady-state absorption spectrum of form B.

The calculation of the dynamics of this reaction is as yet too complicated; therefore, the experimental data were processed within the framework of the kinetic scheme presented above. This processing made it possible to describe quantitatively the three-step mechanism of photoisomerisation of the compounds under consideration in terms of the rate constants k_i (i = 1, 2, 3). The following values were obtained (fs):

Compound	k_1^{-1}	k_2^{-1}	k_3^{-1}
SNP	100	250	1800
SNPO	80	230	1000
SPO	100	300	2000

It can be seen that the rate constants found for the three compounds are virtually equal. Only the k_3 value, which, as noted above, is determined by the rate of rotation around the C–C and C–N bonds, does differ substantially in the case of SNPO. This is apparently due to the fact that rotation around the C–C bonds occurs more easily than rotation around the C–N bonds.[118]

Of substantial interest for researchers are tautomerisation reactions in which intramolecular proton transfer takes place. These reactions are involved in many chemical and biological systems; in some systems, these processes are photochromic, although no pronounced structural changes take place.

Tautomerisation has been studied in the vapour phase,[119] in supersonic molecular beams [89] and in solutions.[83, 84, 90–92, 120, 121] Herek *et al.*[119] investigated the methyl salicylate system in which a proton migrates from one oxygen atom to the other. This process is accompanied by the change of the structure from the ketone form (before the transfer) to the enol form (after the transfer). The authors consider that the proton transfer takes place over a period of 60 fs. At longer times (picosecond time scale), non-radiative decay of the resulting structure takes place, caused by intramolecular energy relaxation or dissociation. In the studies mentioned above [83, 84, 89, 90–92] dealing with one- and two-proton transfer reactions in bipyridinediols and 7-azaindole dimers, it was found that the transfer of two protons can occur both as a synchronous process and as two consecutive steps. Each step includes the transfer of one proton, the first proton migrating much faster than the second one. Neuwahl *et al.*[120] studied the same processes but employed other experimental methods. This work confirmed the results of a previous study;[83] according to these estimates, primary processes of one- and two-proton transfer in bipyridinediols occur over periods of < 50 fs.

The researchers cited above consider that the proton transfer takes place in electronically excited states. A different point of view is expressed by Takeda *et al.*,[121] who studied intramolecular proton transfer in 2-(2′,4′-dinitrophenyl)pyridine; they assumed that no intermediate or final products in excited states are formed. Only three different intermediate photoinduced absorption spectra were observed in the experiments. To interpret experimental data, they proposed a model which is often used to describe photochromic reactions. Under the action of excitation, the molecule passes into the singlet excited state S_1 (the $S_1 \rightarrow S_n$ transition was observed experimentally); relaxation of the excited state gives rise to an intermediate product in its ground electronic state, and subsequently, the final product is formed. According to author's estimate, the intramolecular proton transfer requires 320–500 fs. This is several times longer than the duration of proton transfer in other systems.[122, 123] In our opinion, the absence of excited intermediate species is unlikely. The assumption of the researchers cited [121] is based on the fact that they did not observe any luminescence. However, we have considered above a model of photoisomerisation of spiro compounds in which photoinduced absorption by the intermediate electronically excited product without luminescence was recorded.

Most of unimolecular reactions with photoactivation proceed in accordance with statistical laws. This is due to the fact that intramolecular redistribution of energy occurs in 0.1–1 ps, *i.e.*, over a period much shorter than the characteristic time of decomposition of the molecule. For a reaction not to obey the statistical laws, decomposition must be faster than the intramolecular redistribution of the vibrational energy. This requires a very fast excitation of the molecule to high energies. This process has been realised.[68] The molecule passed into an electronically excited state upon the action of a femtosecond pulse. Fast decomposition of the electronically excited molecule gave rise to vibrationally excited radicals in the ground electronic state. The degree to which the vibrational excitation surpasses the potential barrier to radical decomposition in the ground electronic state depends on the height of the barrier and on the wavelength of the pump light pulse. By adjusting the wavelength of the pump light pulse and by choosing an appropriate molecular system, one can obtain radicals with either slight or substantial vibrational excitation exceeding the potential barrier. The above-mentioned decomposition of vibrationally excited $(C_2F_4I)^*$ radicals generated in reactions *4* and *5* can be considered as an example of the former situation. The vibrationally excited radical decomposes along two pathways to give C_2F_4 together with excited or non-excited iodine atoms

$$(C_2F_4I)^* \longrightarrow C_2F_4 + I, \qquad \text{(reaction } 14\text{)}$$

$$(C_2F_4I)^* \longrightarrow C_2F_4 + I^*. \qquad \text{(reaction } 15\text{)}$$

The reaction was studied in a supersonic molecular beam using a time-of-flight mass spectrometer (multiphoton ionisation was induced by a second femtosecond pulse with a wavelength of 304 nm). The kinetics of product formation, the velocity distribution of I and I* atoms and the anisotropy of product dispersion in reactions *4*, *5* (see Table 2) and *14*, *15* were measured. The yields of I and I* atoms were 0.7 and 0.3, respectively. The average proportion of the translational energy was 59% for reaction *4* and 67% for reaction *5*. With allowance for the energy conservation law, the distribution of internal energy in the intermediate $(C_2F_4I)^*$ radical was determined. This distribution proved to be broad and to have two maxima located at 12 and 17 kcal mol^{-1}.

The vibrationally excited radical decomposes over a period of 25 ps. The measurements showed that only 30% of the excited radicals formed in reaction *4* decompose by channels *14* and *15*. On the basis of this result and of the distribution of internal energy in the radical, the potential barrier to reaction *14* was estimated to be $\sim$15 kcal mol^{-1}. Preliminary calculations resorting to the statistical theory indicate that decomposition by pathway *14* takes place within a picosecond time scale, which is in line with experimental results (although analysis of the velocity distribution of I and I* atoms showed that some molecules decompose faster than it follows from calculations).

Yet another example is decomposition of highly vibrationally excited $(RCO)^*$ radicals in the ground electronic state.[76] On exposure to a femtosecond pulse, electronically excited acetone molecules R^1COR^2 (R^1 = Me, R^2 = Et) are formed. Decomposition of electronically excited molecules (excitation energy 186 kcal mol^{-1}) takes place over a period of $\sim$100 fs. This affords vibrationally excited $(R^1CO)^*$ and $(R^2CO)^*$ radicals in the ground electronic state. Decomposition of the acetyl radical requires 500 fs (that of the propionyl radical lasts 750 fs) for an excitation energy of $\sim$65 kcal mol^{-1}. This time of decomposition is much shorter than the time calculated in terms of the Rice–Ramsperger–Kassel–Marcus (RRKM) statistical theory. This low rate of radical decomposition has been attributed [76] to the fact that upon photoexcitation, only a minor part of vibrational energy (less than the equilibrium energy) is evolved on the reaction coordinate, namely, the C–C bond.

The next example refers to the research into highly vibrationally excited radicals of the $[CH_2(CH_2)_{n-2}C=O]^*$ type in their ground electronic state.[78] The number of carbon atoms n in these

radicals was 4, 5, 6 and 10. These radicals were formed upon photodissociation (which took 100 fs) of the corresponding cyclic ketones. Decomposition of the vibrationally excited radicals does not obey statistical laws. This is proved by two facts. First, the reactions occur over a period of ~ 100 fs, which is several orders of magnitude shorter than the values calculated in terms of the statistical theory. Second, the reaction time barely depends on the number of carbon atoms in the radical and hence, on the number of vibrational degrees of freedom.

Thus, using femtosecond procedures, it is possible to generate vibrationally excited radicals with various, including non-statistical, distributions of intramolecular energy and to study decomposition of these radicals. An approach to the investigation of intramolecular processes at high vibrational energies and new ways of conducting reactions to circumvent the statistical laws have been considered.[76]

A complicated experimental problem of femtochemistry is fixing the zero point of time. Therefore, the question of the possibility of investigation of bimolecular reactions in van der Waals complexes has long remained open. The following approach has been proposed.[85] A weakly bonded van der Waals complex (VDWC) incorporating a molecule of one reactant is assembled in a supersonic molecular beam. Under the action of a femtosecond pulse, the second reactant is formed in the VDWC. In this case, the instant of action of the light pulse which generates the reacting system can be taken to be zero. Some examples of bimolecular reactions studied by femtosecond spectroscopy techniques are listed in Table 3.

Table 3. Examples of bimolecular reactions in VDWC.

Reaction number	Reaction	VDWC	t /fs	Ref.
Exchange reaction				
16	$H + CO_2 \rightarrow OH + CO$	$IH\cdots CO_2$	1000	124
Reactions with electron transfer				
17	$PhH + I_2 \rightarrow PhHI + I$	$PhH\cdots I_2$	1000	125
18	$PhH + I_2 \rightarrow PhHI + I^*$	$PhH\cdots I_2$	200	
Photoassociation reaction				
19	$Hg + Hg + h\nu \rightarrow Hg_2$	–	–	126

The first example is bimolecular reaction *16* in the $IH\cdots CO_2$ VDWC. On exposure to the light pulse, the I–H bond is cleaved. This point in time is taken to be zero. The hydrogen atom starts to move and then reacts with CO_2 to give the OH radical. If the structure of the complex is known, it becomes possible to study the bimolecular reaction that takes place with a specified rate and a specified impact parameter. In this particular case, it was shown [124] that reaction *16* proceeds *via* the step of formation of a long-lived complex over several picoseconds. A similar technique has been utilised to study [127] the bimolecular reaction

$$Br + I_2 \longrightarrow BrI + I.$$

The second example includes charge transfer reactions *17* and *18*. These reactions have been studied using various electron donors (D), for example, $D = C_6H_6$,[125] C_2H_5S.[128] A common feature of these reactions is a correlation between the ionic and covalent terms. In these reactions, the weakly bonded D···I complex consists of electron-donor molecules D and iodine. The complex was irradiated by a femtosecond pulse; as a consequence, the molecular system passed to a transition state in the ionic part of the potential curve (Fig. 10). This means that an electron has passed from the donor to the acceptor. The system moves along the term, enters the area of Coulomb attraction and approaches the avoided crossing point at which two channels of product

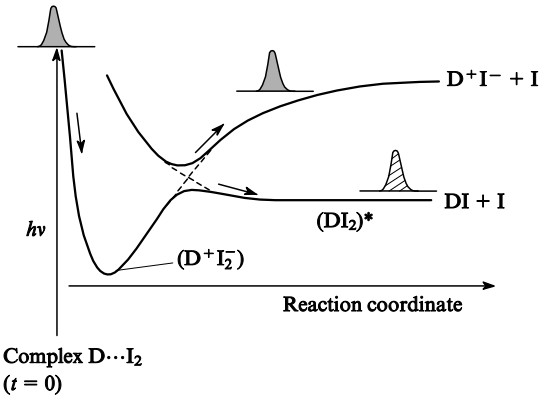

Figure 10. Chart of the potential energy change along the coordinate of the reaction $D\cdots I_2 \rightarrow DI + I$ (or $D^+I^- + I$).
After absorption of light by a weakly bound complex, the nuclei start to move towards the pseudo-crossing point of the ionic and covalent terms; after the pseudo-crossing point has been passed, two reaction channels appear.

formation appear. In the studies under consideration, the iodine atom was detected and its velocity was measured by time-of-flight mass spectrometry. As a rule, the formation of iodine atoms with two different velocities corresponding to the two channels was observed (for example, if benzene is used as the electron donor, these velocities are 400 and 1000 m s^{-1}). The channel yielding the excited iodine atom (the faster iodine atoms) is implemented over a period of 200 fs, while the channel giving rise to the non-excited iodine atom is performed in 1000 fs.

The third example is bimolecular photoassociation *19* in which an excited Hg_2 molecule is produced from two mercury atoms under the action of a femtosecond pulse. The potential curve for the Hg_2 molecule is repulsive. The femtosecond pulse allows the system to switch from the repulsive state to the binding state. The resonance character of this transition is determined by the pulse wavelength and the distance (the impact parameter) separating the mercury atoms in the ground electronic state. Thus, by varying the pulse wavelength, the mercury atoms participating in the reaction can be selected according to their impact parameters. The dynamics of the excited molecules thus formed can be studied by time-resolved fluorescence methods.

In the examples discussed above, the molecular systems were considered to be isolated. However, if the chemical reaction occurs in solution, the solvent has a substantial influence on it. After excitation of the molecular system by a femtosecond pulse, two types of fast dynamic processes can take place, namely, intramolecular processes (redistribution of electronic and vibrational energy) and intermolecular processes (vibrational relaxation and solvation of excited molecules). Information concerning these processes is gained most often from the shifts of time-resolved absorption, fluorescence and stimulated emission spectra for times of less than several picoseconds.[129–131] It was found that in many cases, the dynamics of solvation includes two steps, a faster step with a duration of < 200 fs and a slower step occurring within the picosecond time scale. The fast step is often attributed to intramolecular processes, while the slow step is ascribed to intermolecular relaxation, the formation and destruction of hydrogen bonds, *etc*.

The interaction of the solvent with the dissolved substance has a substantial influence on not only intermolecular but also intramolecular processes in the latter. Thus in a study of the dynamics of formation and rupture of a hydrogen bond and its influence on the rate of relaxation of the *trans*-retinal molecule in the S_3 and S_2 electronic states in a butan-1-ol–cyclohexane mixture,[132] it was found that the lifetime of the molecule in the S_3 state in pure cyclohexane is 30 fs, while that in the S_2 state is 0.7 ps; upon the

addition of butanol, these periods increase by factors of ~ 7 and ~ 2.5, respectively. The increase in the lifetime of the molecule in the S_2 state resulted in higher quantum yields of fluorescence and isomerisation. In another publication,[131] bithiophene, tertiophene and quaterthiophene oligomers have been studied in solution and photoinduced absorption and fluorescence spectra have been detected. For time periods of < 1 ps after excitation, spectral shifts were observed; they were interpreted as relaxation processes, resulting in an equilibrium between the excited oligomers and their solvation shells.

Femtosecond vibrational spectroscopy can serve as an efficient tool for the study of solvation mechanisms. For example, coumarin 102 has been studied (using C_2Cl_4 and $CHCl_3$ as solvents).[133] The carbonyl group of coumarin dyes was found to be linked to a solvent molecule by a hydrogen bond; the researchers showed how the presence of this bond is manifested in the dynamics. In the experiment, coumarin 102 was transferred to the electronically excited S_1 state by the action of a 100-fs light pulse with a frequency of 1500 to 1750 cm^{-1}, and the evolution of the absorption vibrational spectrum in the ground and in excited states and in polar ($CHCl_3$) and non-polar (C_2Cl_4) solvents was detected with a temporal resolution of 200 fs. In the spectrum of a coumarin solution in a non-polar solvent, the absorption band of the C=O bond was located at 1735 cm^{-1}, which is a characteristic frequency for a free carbonyl group. For the electronically excited state, a decrease in the dipole moment of the transition was observed; however, no significant shift of the C=O vibration band was found. In the case of a coumarin solution in a polar solvent, the absorption frequency of the C=O vibrations is markedly displaced, namely, to 1700 cm^{-1} for the coumarin molecule in its ground electronic state. This shift is attributed to the presence of a hydrogen bond between the $CHCl_3$ molecule and the C=O group of coumarin in its ground electronic state. For the electronically excited state, the frequency of the C=O mode shifts to 1740 cm^{-1}, *i.e.*, it is close to that in a non-polar solvent. This points to the absence of a hydrogen bond in the electronically excited state.

In the examples considered above, we virtually did not mention studies dealing with femtosecond processes in proteins. Detailed information concerning these processes has been reported.[53, 57, 134–138]

VII. Control of intramolecular dynamics and an elementary chemical event

Chemical reactions are controlled at the macroscopic level by changing reaction conditions — pressure, temperature and other parameters. Attempts at controlling an elementary reaction by changing the character of the interaction of light with reactants have been undertaken long ago.[139]

The development of femtosecond pulses, which permit one to change the transition state dynamics, opens new, in principle, opportunities of controlling an elementary chemical reaction and, hence, the product yield. Let us consider various approaches which can be helpful in developing this line of research.

1. Non-statistical unimolecular reactions. The approach using non-statistical unimolecular reactions is based on the generation of vibrationally excited molecules with such an intramolecular distribution of vibrational energy that the unimolecular reaction proceeds to give desired products. The attempts to perform selective reactions in this way have been made for one-photon[140] and infrared multiphoton excitation.[141] However, it was found that unimolecular reactions induced by photoactivation took place in line with statistical laws, according to which the rate constants for these reactions do not depend on intramolecular energy distribution but are dictated by the total vibrational energy. This was due to the fact that intramolecular energy redistribution occurs faster (within 0.1–1 ps) than decomposition of the molecule. In order to control the decomposition route and to obtain desired products, it is necessary to localise the excitation energy in a particular fragment of the molecule; this should be done during the reaction.

This method of control can be realised using femtosecond pulses. Under the action of these pulses, the molecules are excited very rapidly; due to multiphoton absorption, the excitation energy can be so high that decomposition occurs faster than the intramolecular energy redistribution; the initial intramolecular distribution of the excitation energy can be changed by varying the amplitude and phase characteristics of the femtosecond light pulse.

The reactions considered above can serve as examples of processes in which femtosecond pulses are used to study non-statistical decomposition of vibrationally excited radicals. The first example is decomposition of the highly vibrationally excited $(R^1CO)^*$ and $(R^2CO)^*$ radicals (R^1 = Me, R^1 = Et) in their ground electronic state.[76] These radicals are formed upon decomposition of ketone molecules R^1COR^2 induced by a femtosecond pulse and taking 50–100 fs. When the vibrational excitation energy is ~ 65 kcal·mol^{-1}, rupture of the C–C bond in the acetyl radical takes place in 500 fs. This decomposition period is ten times as long as that calculated in terms of the RRKM statistical theory. According to the researchers' viewpoint, upon decomposition of the parent ketone molecule, the vibrational energy in the resulting $(R^1CO)^*$ and $(R^2CO)^*$ radicals is distributed non-uniformly; more precisely, only a minor portion of this energy has evolved onto the reaction coordinate along the C–C bond. During 500 fs, the vibrational energy does not have time to be redistributed; therefore, this coordinate receives less vibrational energy than expected in accordance with the statistical law.

The second example is stepwise decomposition of cyclic ketones with various numbers of carbon atoms (n = 4, 5, 6 and 10). After excitation of the molecules of cyclic ketones by a femtosecond pulse, the first C–C bond is cleaved to give radicals of the $[CH_2(CH_2)_{n-2}C=O]^*$ type in their ground electronic state. This cleavage requires ~ 50 fs. The species thus formed contains a store of non-statistically distributed vibrational energy, which is much greater than the energy needed to split off the carbon oxide. It was shows[78] that the rates of decomposition calculated by the statistical theory are two to four orders of magnitude lower than the measured rates. It was also noted that the measured decomposition rates virtually do not depend on the number of atoms in the decomposing species, whereas calculations in terms of statistical theory predict a decrease in the rate of decomposition by orders of magnitude following the change in the number of carbon atoms from 4 to 10. These results can be interpreted only by assuming that biradicals formed in the ground electronic state have a substantial energy of vibrational excitation in the reaction coordinate sufficient for their subsequent decomposition. Since decomposition proceeds faster than the energy redistribution over various vibrational modes, initially, there is much more energy in the reaction coordinate than would be there after statistical redistribution of the vibrational energy.

Hence, if decomposition can follow two channels, then, using femtosecond pulses, it is possible to create molecules in which the vibrational energy located on the reaction coordinate of one channel exceeds the threshold value, while that on the reaction coordinate of the other channel is lower than the threshold value. Thus, by varying the fraction of the vibrational energy on one or another reaction coordinate, one can direct the reaction along one channel.

2. Dynamics of wave packets. The known methods for laser separation of isotopes proposed by Letokhov[141] are based on small isotope shifts in the spectra of atoms and molecules. To implement these methods, monochromatic laser sources with tuned wavelength are required. An experiment dealing with the laser separation of bromine isotopes using femtosecond pulses has been described.[142]

The new approach to the separation of isotopes makes use of specific features of the wave packet dynamics. If wave packets for the isotopes of bromine molecules ($^{79}Br_2$ and $^{81}Br_2$) are created,

the wave packet dynamics in the two isotopic molecules will be different. During short periods of time, the differences related to the dissimilar vibration frequencies are insignificant. However, the time evolution of wave packets goes through periodic destructions and revivals.[37] Therefore, the deviations of the wave packet dynamics are accumulated in the isotopic molecules, and at times of the order of tens of nanoseconds, they would be sufficient for choosing the instant for acting upon the molecule of only one isotope by another femtosecond pulse. Averbukh *et al.*[142] employed a 100-fs pulse tunable in the region of 550 – 590 nm for the formation of wave packets. The second femtosecond pulse having the same duration and a wavelength of 340 nm was used for ionisation. The delay between the pulses was varied up to 50 ps. Ionised molecules were detected using a time-of-flight mass spectrometer. An isotope ratio of ~250% was attained.

3. Action on the PES. Femtosecond pulses can be used to control the dynamics of the transition state by changing the PES at the required time instant. Let us consider a simple example. Suppose that there are two crossing terms with different types of symmetry; a wave packet moves along one of the terms, without 'feeling' the other term, and forms products C and D. At the instant the wave packet approaches the crossing point of the terms, a femtosecond pulse acts upon the PES. The pulse would induce splitting of the terms. As a consequence, the wave packet continues moving but along the other potential term; this may give products A and B. This approach to the control of the reaction has been proposed and implemented in experiments on photodissociation of OClO.[143] The reaction proceeds by two channels

$$\mathrm{OClO} + h\nu \begin{cases} \rightarrow \mathrm{O} + \mathrm{ClO} \\ \rightarrow \mathrm{Cl} + \mathrm{O_2} \end{cases}$$

For low intensities of the pump pulse, both products are formed in a ratio corresponding to known published data. However, as the intensity of the pump pulse increases, the rate along the channel resulting in molecular oxygen starts to increase non-linearly, while the rate along the channel yielding ClO decreases. The time delay between the pump and probe pulses in these experiments was 40 ps. In the authors' opinion, these changes are due to distortions of the potential energy surface. The following model is possible: the pulse induces the formation of the electronically excited state $^2A_2$ ($^2A_2 \leftarrow X\,^2B_1$). This is followed by internal conversion to the $^2A_1$ electronic state, from which dissociation of OClO takes place to give ClO. Transition to the $^2B_2$ state is hindered; therefore, the amount of molecular oxygen formed is small. Upon an increase in the intensity of the pump pulse, the PES is distorted and transition to the $^2B_2$ state occurs much more easily; therefore, the fraction of the molecular oxygen increases. The yield of molecular oxygen increases following an increase in the pump pulse intensity (I) in proportion to I^4. In the study cited, the $\mathrm{ClO} : \mathrm{O_2}$ ratio varied by a factor of 12 and the intensity of the excitation field reached a value of 1.5×10^{12} W cm^{-2}.

It should be noted that intensities of 10^{18} W cm^{-2} can be attained in a field of focussed femtosecond pulses; therefore, the light field strength can reach 10^{10} V cm^{-1}. Thus, we can deal with fields exceeding the intraatomic fields (10^9 V cm^{-1} for the hydrogen atom). Under the action of so strong fields, distortion of PES can take place for a short period. The use of strong fields for the target-directed distortion of PES would apparently be an object of the future studies.

4. Dynamics of non-adiabatic transitions. A scheme for controlling the molecular evolution with the use of non-adiabatic transitions up and down in energy was first proposed by Tanor and Rice.[144] The scheme assumes the possibility of acting at a required instant upon the wave packet, generated by a pump pulse, by another pulse in order to bring the system to a different state. This approach is illustrated by Fig. 11, which shows the variation of the potential energy along the reaction coordinate for two electronic terms. Let us consider the molecule ABC. If there is

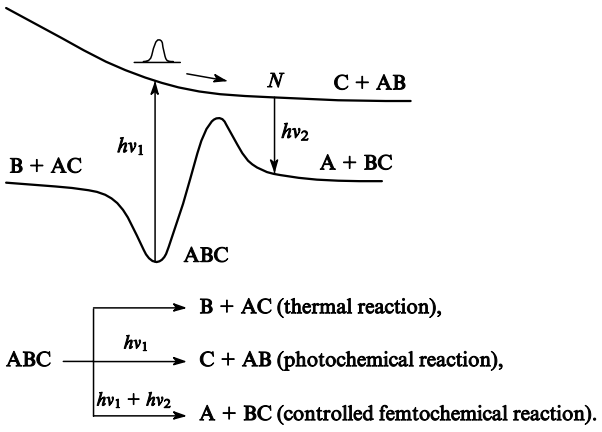

Figure 11. Scheme for the control of the reaction using non-adiabatic transitions performed at definite time instants.

a high potential barrier on the right, only B and AC can be formed as the reaction products in the case of thermal activation. Upon photoactivation by stationary light, the reaction yields C and AB. Irradiation with a femtosecond pulse gives a wave packet, which moves along the direction marked by the arrow. In femtochemistry, the wave packet dynamics is controlled in the real-time mode. By acting on the molecular system by a femtosecond pulse at the instant the wave packet reaches point N (to shift it down in energy to the right slope of the potential barrier), the reaction can be directed at the selective formation of only products A and BC. It should be emphasised that in terms of the model considered, these products cannot be obtained using other activation methods. The formation of iodine molecules in different electronically excited states[145] and the formation of Na^+ or Na^{2+} ions induced by a pair of femtosecond pulses with different time delays between the pulses[146] can be regarded as experimental illustrations of this approach. However, no convincing examples of the experimental use of this type of control can be found in the literature yet.

5. Orientation dynamics — control of the geometry of reactant approach. The efficiency of a reaction both in the gas and in the condensed phases is known to depend substantially on the mutual orientation of the colliding partners. In the gas phase, a specified orientation of one reactant with respect to the other is usually attained in crossed molecular beams on application of uniform or non-uniform electric fields. In recent years, attempts to use electromagnetic field pulses for creation of molecules with a predominant direction of the dipole moment have been made more and more often. Femtosecond pulses are used for the formation of coherent rotational wave packets in the ground electronic state.[17, 147, 148] In this case, the orientation varies with time while repeating the previous orientations rather than remaining static, as in the case where conventional techniques are used. The control of the geometry of reactant approach can be clearly demonstrated in relation to bimolecular reactions in VDWC. An example is provided by bimolecular reaction *16* in the $\mathrm{IH}\cdots\mathrm{CO_2}$ van der Waals complex (see Table 3) considered above. Under the action of the first femtosecond pulse, the I—H bond is cleaved, and the hydrogen atom starts moving towards CO_2. At a certain instant, the second femtosecond pulse creates a coherent rotational packet in the CO_2 molecule. By changing the time delay between the first and second pulses, one can control flying of the hydrogen atom towards CO_2 molecules having different orientations, *i.e.*, study the dependence of the product yield on the geometry of reactant approach. Naturally, there can be any other molecule in place of CO_2.

6. Coherent dynamics. The approaches being developed most successfully are those in which phase characteristics of the laser pulses are used. Several theoretical approaches have been elaborated; they envisage the use of phase characteristics of the exciting

light for controlling the yield of products in an elementary reaction. Shapiro and Brumer [149] proposed a scheme similar to the scheme of the interference of light which had passed along two channels and had arrived at the initial point with different phases. Similarly, two wave packets characterised by the wave functions ψ_1 and ψ_2 can follow different paths. If they come to the same final state, the probability of occurrence in this state is proportional to the total wave function squared. Hence, the amplitudes of the two wave functions should be summed up before squaring. The probability of the occurrence of the system in a particular state depends on the cross term which includes the phases of different wave functions. This approach has been implemented experimentally, for example, by Zhu *et al.*[150] A beam of DI molecules was excited by two laser beams, by one photon ($\lambda = 118$ nm) from the first beam and three photons ($\lambda = 354$ nm) from the second beam. The phase correlation between these beams was varied by passage of both light beams through a transparent gas medium: the refractive indices at different wavelengths are different; therefore, by varying the pressure inside the gas cell, one can control the phase. The excited DI molecules decay along two channels, $DI^+ + e^-$ and $D + I(^2P_{1/2})$. As expected, the relative yield is a sinusoidal function of the difference between the phases.

For creating a nuclear wave packet with definite phase and amplitude characteristics, the use of chirped femtosecond pulses has been proposed;[151] this would markedly simplify the control schemes for elementary chemical processes. First, under the influence of these pulses, multiphoton processes of light absorption occur more easily. Second, a femtosecond pulse is spectrally broad and it becomes possible to generate vibrational and rotational wave packets with different initial phases of the Fourier components by changing the phase characteristics of the pulse. Third, two wave packets with the wave functions ψ_1 and ψ_2 can be produced. The probability that the system occurs in a particular state depends on the cross term, which includes phases of different wave functions.

The influence of the chirp on the intramolecular dynamics and on photophysical and photochemical processes involving diatomic molecules is illustrated by examples presented in Table 4. It can be seen that the quantum yields in the processes considered above depend on the chirp of the pump pulse. When the pump pulse intensity is high (strong fields), the quantum yield of fluorescence of dyes in solution depends on the sign of the chirp (see the last example in Table 4).

Let us illustrate the variation in the vibrational dynamics for the iodine molecule in the electronically excited state as a function of the chirp sign.[37] For this purpose, we shall consider the results of calculations of the wave packet dynamics in the Wigner representation of the quantum state of the system, *via* the 'coarse-grained' Wigner distribution function in the phase space using relation (15). These calculations utilised the results of experiments performed under conditions where all the parameters including the magnitude of β remained invariant, only the sign of the chirp being changed. The dependence of the Husimi function W_H on the classical coordinate and the momentum (characterised by the change in the degree of blackening) for different times elapsed after absorption of the pump pulse is illustrated in Fig. 12. The density maps corresponding to wave packets formed by the pump pulse with $\beta = -2000$ fs^2 are shown at the left; those for the pulse with $\beta = 2000$ fs^2 are on the right. It can be seen that the wave packets formed by the pulse with a negative chirp retain localisation for much longer periods. This means that the intramolecular dynamics of atoms can be influenced by controlling phase characteristics of the pulses. By changing synchronisation of the atomic motion in the transition state and by varying phase characteristics of the pump pulse, one can control the transition state dynamics, *i.e.*, the product yields in an elementary chemical reaction.

Table 4. Examples of influence of the chirp on some physicochemical processes.

Process	Result	Ref.
$Na_2 + n\,h\nu \rightarrow Na^+ + e$ $Na_2 + n\,h\nu \rightarrow Na_2^+ + e$	the quantum yield of the ions depends on the chirp	152
$NaI + h\nu_1 \rightarrow NaI$ $(NaI)^* \rightarrow Na + I$ $(NaI)^* + h\nu_2 \rightarrow Na^* + I$	the Na*/Na ratio depends on the chirp	153
The vibrational dynamics of I_2 in the electronically excited state	the vibrational dynamics depends on the chirp	37, 154
The rotational dynamics of D_2 and N_2 in the ground electronic state	the rotational dynamics depends on the chirp	17, 147
Fluorescence of LD690 dye molecules	the fluorescence quantum yield depends on the chirp	155

In recent years, experimental works have been published, which demonstrated that the phase characteristics of the pulse can influence appreciably the channels of product yields in photodissociation of polyatomic molecules.

Multiphoton photodissociation of CH_2I_2 has been studied.[156] The normal channel for the photodissociation of this molecule is the formation of iodine atoms in the electronically excited and ground states and the CH_2I radical. However, it is known that in the case of one-photon absorption in the vacuum ultraviolet region (> 9 eV), one more channel exists ($\sim$1%), which affords molecular iodine in the $D'^3\Pi_g$ state and, to a small extent, in the electronically excited *f* states. In the study cited, the dependence of the multiphoton photodissociation of CH_2I_2 on the sign and the magnitude of the linear chirp was measured. Pulses with a carrier wavelength of 624 nm and with a duration of 47 fs were used in the experiments. Excitation was performed both by pulses centred at 624 nm and by pulses obtained by doubling the frequency, *i.e.*, centred at 312 nm. The value of the spectral chirp β was varied from -2000 to 2400 fs^2. The well-known fluorescence of the molecular iodine at 342 nm is a consequence of multiphoton absorption of light with a wavelength of 624 nm. The maximum yield of molecular iodine in the electronically excited state D' was observed at $\beta = -500$ fs^2, while the minimum yield was found at $\beta = -2400$ fs^2. The yield of molecular iodine varied by a factor of 2.9. The dependence of the product yield on the chirp value was also observed when the CH_2I_2 molecule was excited by pulses with a wavelength of 312 nm. However, the variation of the yield of molecular iodine in the excited state followed the opposite pattern: the highest yield was observed at $\beta = -2400$, whereas the lowest yield was observed at $\beta = -500$ fs^2. The chirp follows a quadratic dependence on the pulse duration. The absence of symmetry in the dependence of the product yields on the chirp relative to the zero chirp indicates that the observed variations of the yields are related to the phase characteristics of the pump pulse rather than to the pulse duration.

The second example is multiphoton photodissociation of ammonia. One-photon excitation with an energy higher than $\sim$6 eV is known to induce decomposition of ammonia to give the NH_2 radical in the ground state X^2B_1 and the hydrogen atom (the first channel).

Excitation of an ammonia molecule to 9.4 eV gives rise to the second channel, reaction *7* (see Table 2).[157]

Multiphoton photodissociation of ammonia under the action of femtosecond pulses centred at 615 nm (2 eV) has been studied.[104] The duration of the transform-limited pulse was 50 fs. To have an energy of excitation of the molecule higher than 9.4 eV, five photons should be absorbed. Since the excitation energy equal to 10 eV is still insufficient for ionisation, the molecule decomposes according to the two above-noted channels. The NH radical formed in photodissociation *7* occurs in the

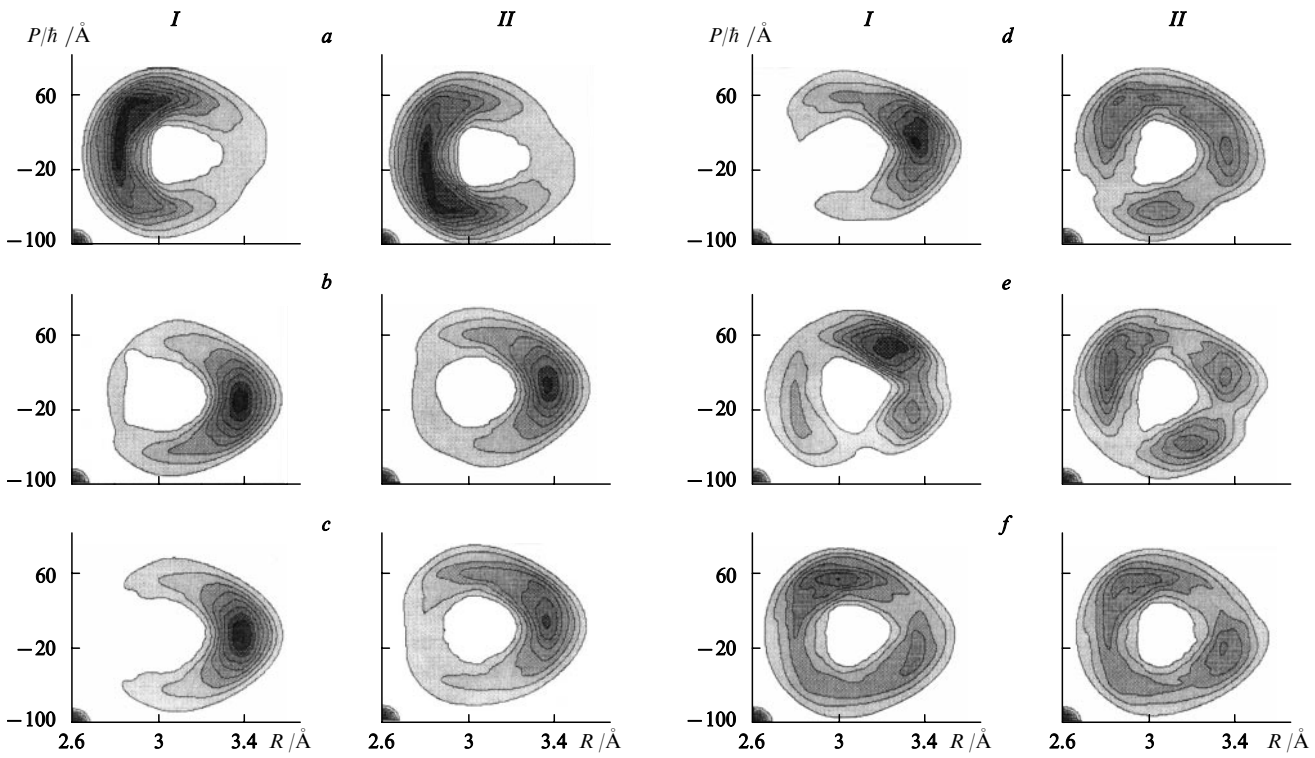

Figure 12. Dependence of the Husimi function on the classical coordinate (abscissa) and the momentum (ordinate) at different times (t) after absorption of the pump pulse for $\beta = -2000$ fs^2 (I), 2000 fs^2 (II).[37]
t /fs: (*a*) 0, (*b*) 150, (*c*) 750, (*d*) 1950, (*e*) 3150, (*f*) 4960.

electronically excited state $c^1\Pi$, from which fluorescence related to the $c^1\Pi \rightarrow a^1\Delta$ transition is observed at 324 nm.[157] Thus, the quantum yield of the ammonia decomposition according to the second channel can be judged by fluorescence intensity, which is proportional to the concentration of the NH($c^1\Pi$) radical. In the study cited, the variation of the integral fluorescence (F) in the spectral region of 300–340 nm was recorded as a function of the intensity of pump pulses (I). It was shown that experimental data are described adequately by the equation

$$F = A(\beta)(I)^5,$$

where $A(\beta)$ is the coefficient depending on the spectral chirp. This relation was used to determine the coefficient $A(\beta)$, expressed in relative units and reflecting the influence of the chirp on the photodissociation of ammonia by the second channel. Figure 13 presents the $A(\beta)$ dependences normalised to the $A(\beta = 0)$ values. The fluorescence intensity is proportional to the number of NH($c^1\Pi$) radicals formed; therefore, the plot in Fig. 13 reflects the dependence of the quantum yield of these radicals in relative units on the value of the spectral chirp. The ratio of the maximum quantum yield to the minimum quantum yield equals 12. It should also be noted that the variation of the quantum yield is non-symmetric with respect to the zero chirp; this implies that the observed changes are mainly related to the phase characteristics of the femtosecond pulse rather than to the pulse duration.

Taking these two reactions as examples, it was demonstrated that the product yields can be controlled using phase characteristics of the pump pulses. However, it has already been noted that the characteristic times of coherence of nuclear wave packets are normally 100–1000 fs. Hence, the reactions of excited molecules should occur over even shorter periods of time; this requires relatively high excitation energies (in the examples considered above, the excitation energies were 10–12 eV). The PES parameters for these energies are unknown; therefore, there arises the problem of determining and analysing these parameters for complex molecular systems for which quantum-chemical calcu-

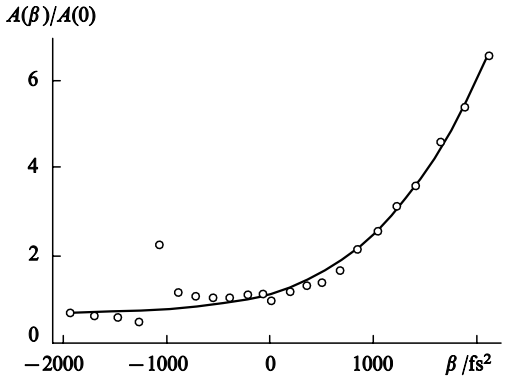

Figure 13. Yield of the product NH($c^1\Pi$) *vs.* the value of the spectral chirp.

lations are difficult to perform. In this connection, some researchers are developing a different approach. Thus it has been found [158] that a scheme with the use of a feedback with the product yields can be implemented within the framework of optimal control theory; this method permits determination of pulse shape and spectral content. This scheme maximises the yield of a definite product. Experiments of this type have been carried out;[159] the researchers performed automated optimisation of the control of the reaction channels using photodissociation of the $LFe(CO)_2Cl$ molecule (L is cyclopentane) as an example. This molecule contains different bonds between the metal and the ligands (Fe–CO, Fe–Cl and Fe–L). On exposure to femtosecond pulses, products are formed *via* two channels; one channel implies rupture of only one Fe–CO bond, while according to the other channel, all the ligands, except Cl, are detached. Both products are detected by means of a mass spectrometer. The measured ratio of the product weights is fed to a computer and is processed in terms of a definite

algorithm. An instruction is devised according to which the phase characteristics of a femtosecond pulse change in such a way as to ensure a higher ratio of product weights. The minimum ratio is 1.2, and the maximum ratio is 4.9. In the opinion of the authors, the global minimum has not yet been found. Therefore, it is expected that this range of ratios can be markedly extended.

The effects caused by the chirp are related to the characteristics of the PES and to the wave packet dynamics. The change in the chirp of the pump pulse results in different distributions of the initial phases of the steady states (the superposition of which makes the wave packet); this influences the dynamics of the atomic motion in the transition state. The qualitative scheme for the control of the product yields by phase characteristics of the femtosecond pulse is shown below in relation to a planar tetraatomic molecule CA_3:

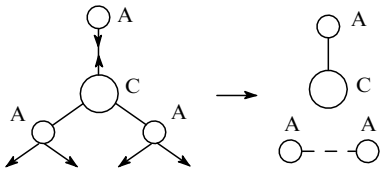

The standard photodissociation channel for molecules of this type involves rupture of the C–A bond where the vibrational energy is evolved on the stretching vibration, which determines the reaction coordinate. Let as assume that the wave packet consists of antisymmetric and bending vibrations, which determine the reaction coordinate by a concerted mechanism. If the motion of A atoms is so synchronised that two bonds are synchronously stretched and their bending vibrations, occurring in parallel with stretching, participate in the formation of the new A–A bond, the concerted mechanism would be realised more efficiently. It appears that synchronisation of the motion of atoms can be used to make a fairly large class of reactions follow a concerted mechanism.

Examples of control of reactions proceeding in condensed media upon one-photon absorption have been considered above. Studies [83, 84] of one- and two-proton transfer in the 2,2′-bipyridine-3,3′-diol molecule induced by femtosecond pulses in solutions was considered in Section V. Since these processes take place over periods of $< 50-100$ fs, it is reasonable to assume that the two-proton transfer follows a concerted mechanism. Then, by changing the chirp of the pump pulse, one can change the ratio of the channels of one- and two-proton transfer. Petrukhin and coworkers [160, 161] studied one- and two-proton transfer in 2,2′-bipyridine-3,3′-diol induced by femtosecond pulses in a hexane solution. The pumping was performed by pulses centred at a wavelength of 308 nm, while probing was accomplished by a supercontinuum pulse in the spectral range of 400–620 nm. The time evolutions of the photoinduced absorption spectra in the 400–470 nm range and of the photoinduced 'brightening' in the 470–620 nm range were monitored in experiments. It was found that photoinduced 'brightening' at a wavelength of 500 nm was due to stimulated emission from the excited diketo tautomer under the action of the probe pulse, while the photoinduced absorption at $\sim$450 nm is due to the $S_n \rightarrow S_1$ transitions in both the monoketo and diketo tautomers. It was found that the time evolution of brightening and absorption depends on the chirp of the pump pulse. In the opinion of the researchers, this is indicative of the fact that the ratio of the channels of one- and two-proton transfer is determined by both the sign and the magnitude of the chirp of the pump pulse. Hence, the reaction can also be controlled in the condensed phase.

VIII. The prospects of femtochemistry

In our opinion, the research in femtochemistry will develop vigorously in the near future according to four main lines.

The first line is the control of chemical reactions. We believe that the control of chemical reactions and physical processes aimed at obtaining desired products will be among the most promising fields of development of femtochemistry. In the majority of studies which have been considered in this review, pulses with durations of several tens of femtoseconds have been employed. Only a few studies operating with femtosecond pulses shorter than 10 fs are available. Obviously, chemical laboratories would be gradually equipped with lasers able to generate pulses with ever decreasing durations. This means that the coherent chemistry will cover more and more objects; it will become possible to use coherent wave packets even for those systems in which stochastisation occurs very rapidly. First, due to the shortening of a pulse, its spectral width increases; hence, the number of steady states included in the nuclear wave packet formed and the set of the initial phase distributions will increase. This markedly extends the range of variation of the amplitude and phase characteristics of the femtosecond pulse and thus enhances the capacity of controlling the dynamics of the molecular system in the transition state. Second, for very short pulse durations, localisation of the nuclear wave packet can reach even 0.005 Å. This makes it possible to increase the accuracy of controlling the orientation dynamics and non-adiabatic transitions. In other words, shortening of femtosecond pulses would provide the possibility of extending the number of molecular systems suitable for realisation of coherent reactions and of increasing substantially the selectivity. It is by virtue of femtosecond pulses that new schemes of controlling the processes such as photoionisation, fluorescence and light absorption would be implemented experimentally and substantiated theoretically in the near future. It appears that these schemes would include several femtosecond pulses (with different chirps) and time delays between them. Schemes of this type have already been proposed (see, for example, studies [162, 163]). We expect that the development of the above-considered approaches to the control of chemical reactions would result in the near future in the development of selective environmentally clean chemical technologies. Apparently, these technologies would be economically rational only for the preparation of expensive materials in small quantities. The approaches in question will become especially promising for the control of functional properties of nanostructures.

The shortening of the duration of pump pulses down to values at which the 'energy span' (ΔE) will be comparable with the bond energy (for a pulse duration of 1 fs, the ΔE value is $\sim$40 kcal mol^{-1}) will result in the development of new schemes for the control of chemical reactions. With sufficiently short pulses, it will be possible to generate electron wave packets in which several electronic quantum states are excited simultaneously. One can hope that schemes for controlling the electron motion in these packets would be designed.

The second line is the wave packet dynamics in the ground electronic state. Most of the examples considered in this review, especially for coherent chemistry, referred to reactions in which the reactant was in the electronically excited state. This is due to the fact that it is much more difficult to form vibrational packets in the ground electronic state than in an electronically excited state. As noted above, experimental methods are being currently developed [46–50] for the formation of coherent vibrational wave packets with excitation energies both higher and lower than the dissociation threshold. In this connection, two factors are significant: the decrease in the duration of femtosecond pulses and development of multi-pulse methods. The setting of shorter pulses in the practice of chemical experiment would substantially improve the possibilities of formation of coherent vibrational wave packets in the ground electronic state. Indeed, in this case, it is easier to use several femtosecond pulses to generate the required wave packets due to downward non-adiabatic transitions. The possibility of creating vibrational wave packets in the ground electronic state would appear as a result of multiphoton absorption of infrared femtosecond pulses. The increase in the probability of this

absorption is due to the fact that it would be possible to form a wave packet on the basis of high-frequency symmetrical vibration modes; consequently, the multiquantum factor for absorption would markedly decrease. We believe that the number of investigations into the coherent dynamics of the transition state for reactions in the ground electronic state will essentially increase in the near future.

The third line is the time evolution of the structural changes with femtosecond temporal resolution. Femtosecond pulses with a duration of 10^{-14} s allow the detection of shifts equal to 0.1 Å; however, conversion of the response function into the distance between the atoms is rather easy for diatomic molecular systems but very difficult for polyatomic molecular systems. In other words, the values measured in spectroscopic experiments cannot be transformed in the general case into the coordinates of moving atoms. An alternative variant is to develop methods that allow determination of the structures of intermediate species with a femtosecond temporal resolution.

By irradiating a target with a powerful femtosecond pulse, one can generate electron or X-ray pulses; measurement of electron or X-ray diffraction provides information on the time evolution of the positions of nuclei. Electron diffraction occurs only in the gas phase; X-ray diffraction can also be studied in condensed media. At present, these approaches are used in procedures with picosecond and sub-picosecond temporal resolution.

Time-resolved ultrafast electron diffraction has been used to study photodissociation of CF_2I_2 on irradiation with light pulses ($\lambda = 307$ nm).[22] It was found that abstraction of two iodine atoms is completed within ~ 4 ps; the structure of the resulting CF_2 radical was determined. The radical is formed in the ground electronic state with the following interatomic distances: C–F 1.30 (±0.02) Å, F···F 2.06 (±0.06) Å.

No convincing examples of using time-resolved X-ray diffraction have been reported yet. Therefore, study of the dynamics of positions of the cadmium atoms in a film containing 83 layers of cadmium atoms after heating the film by a femtosecond light pulse[26] can be referred to as an example. In this study, the dependence of the intensity of the diffraction signal on the delay between the heating light pulse and the probe X-ray pulse was measured. The experimental results obtained bear information on the time evolution of the shift of cadmium atoms from the corresponding layers with a sub-picosecond temporal resolution.

Evidently, spectroscopic measurements in dynamic investigations would be gradually replaced by measurements of this type.

The fourth line of research is femtochemistry with spatial resolution. Femtosecond spectroscopy has provided methods that allow investigations to be performed with high temporal resolution. Using scanning tunnelling microscopy, surface images (including those containing single adsorbed species) with angstrom spatial resolution were obtained for the first time; the energy distribution of surface electrons and the migrations of surface atoms have been measured; new nano-scale surface structures have been assembled. New spectroscopic techniques were developed which allow measurement of the vibrational spectra of single adsorbed species using a scanning tunnelling microscope, detection of single paramagnetic centres on the surface of oxidised metals, study of photoisomerisation of individual molecules, *etc.*[164–166] However, the number of problems the solution of which requires methods with high temporal and spatial resolution constantly increases. In recent years, several approaches to the development of these methods have been used.

The first approach is aimed at creating the possibility of performing detection by light pulses with high spatial resolution. However, the light pulses in the conventional optics are subject to a diffraction limit, which makes impossible a spatial resolution of less than $\sim\lambda/2$. In several recent years, so-called 'near-field optics' which permits a substantial improvement of the spatial resolution has been developed. The simplest implementation of the near-field optics is to replace the set of lenses by pointed optical light guide with the hole diameter d at the tip smaller than the wavelength. The near field decays rapidly with an increase in the distance from the light guide. Therefore, the specimen is mounted at distances less than d. Within the framework of this approach, it is possible to perform femtochemical investigations with a spatial resolution of tens of nanometers. The schemes used for the excitation of molecules have been reported.[167, 168]

Another approach is based on combination of femtosecond pulses with photoelectron spectroscopy. Light pulses generate electrons, which can be detected with high spatial resolution. This approach has been realised by Secatskii *et al.*[169] The researchers used very sharp silicone pins at the end of which femtosecond pulses were focused. These pulses induced two-photon emission of electrons, which was detected by a microscope. It was demonstrated that femtosecond two-photon laser photoelectron microscopy can ensure a spatial resolution of up to 3 nm.

An approach representing an attempt to combine femtosecond pulses with scanning tunnelling microscopy has been reported.[170, 171] Illumination of the tunnel gap with femtosecond pulses was combined with detection of components of the tunnelling current, which follow a non-linear dependence on the intensity of light pulses. In the opinion of the authors, this route could provide both high spatial and high temporal resolutions.

It has been noted[172] that modern chemistry cannot be conceived without coherence and high spatial and temporal resolutions. It is these points that appear to become important factors in the development of chemistry.

This work was supported by the Russian Foundation for Basic Research (Project Nos. 99-03-33500 and 00-03-40118).

References

1. J C Polanyi, A H Zewail *Acc. Chem. Res.* **28** 119 (1995)
2. A H Zewail *Femtochemistry: Ultrafast Dynamics of the Chemical Bond* (Singapore: World Sci., 1994)
3. J Manz, L Wöste (Eds) *Femtosecond Chemistry* (Weinheim: VCH, 1995)
4. V Sundstrom (Ed.) *Femtochemistry and Femtobiology: Ultrafast Reaction Dynamics at Atomic Scale Resolution* (London: Imperial College Press, 1997)
5. A H Zewail *J. Phys. Chem. A* **104** 5660 (2000)
6. O M Sarkisov *Zh. Vses. Khim. O-va im. D I Mendeleeva* **35** 669 (1990) [a]
7. T Kuhne, P Vohringer *J. Chem. Phys.* **105** 10 788 (1996)
8. F Laermer, T Elsaesser, W Kaiser *Chem. Phys. Lett.* **156** 381 (1989)
9. D V Malakhov, F E Gostev, N I Koroteev, V V Lozovoi, S A Magnitskii, O M Sarkisov, D G Tovbin, A A Titov *Khim. Fiz.* **18** (7) 18 (1999) [b]
10. M J Rosker, M Dantus, A H Zewail *J. Chem. Phys.* **89** 6113 (1988)
11. L E Berg, M Beutter, T Hansson *Chem. Phys. Lett.* **253** 327 (1996)
12. O M Sarkisov, F E Gostev, V V Lozovoi, E A Sviredenkov, A A Titov, V G Tovbin, S Ya Umanskii *Izv. Akad. Nauk, Ser. Khim.* 594 (1996) [c]
13. Y Chen, L Hunziker, P Ludowise, M Morgen *J. Chem. Phys.* **97** 2149 (1992)
14. S Rutz, K Kobe, H Kulling, E Schreiber, L Woste *Z. Phys. D* **26** 276 (1993)
15. D Zhong, A H Zewail *J. Phys. Chem. A* **102** 4031 (1998)
16. L Wang, H Konguchi, T Suzuki *Faraday Discuss.* **11** 37 (1999)
17. D G Tovbin, V V Lozovoy, F E Gostev, A A Titov, S A Antipin, S Ya Umanskiy, O M Sarkisov *Chem. Phys. Lett.* **303** 458 (1999)
18. N Brabec, F Krausz *Rev. Mod. Phys.* **72** 545 (2000)
19. M Schmitt, G Knopp, A Materny, W Kiefer *Chem. Phys. Lett.* **270** 9 (1997)
20. S A Kovalenko, N P Ernsting, J Ruthmann *Chem. Phys. Lett.* **258** 445 (1996)
21. A N Petrukhin, S A Antipin, F E Gostev, V S Marevtsev, O M Sarkisov, A A Titov, D G Tovbin, V A Barachevskii, Yu V Strokach *Khim. Fiz.* **19** (2) 90 (2000) [c]
22. J Cao, H Ihee, A H Zewail *Chem. Phys. Lett.* **290** 1 (1998)
23. H Ihee, J Cao, A H Zewail *Chem. Phys. Lett.* **281** 10 (1997)

24. M Ya Schelev, in *Proceedings of the 20th International Congress of High-Speed Photography and Photonics, Moscow, 1998* Vol. 3516, p. 923
25. M Ya Shelev, G I Bryukhnevich, V I Lozovoi, M A Monastyrski, A M Prokhorov, A V Smirnov, N S Vorobiev *Opt. Eng.* **37** 2249 (1998)
26. Ch Rishel, A Rousse, I Uschmannt, P-A Albouy, J-P Geindre, P Audebert, J C Gauthier, E Forster, J-L Martin, A Antonetti *Nature (London)* **390** 490 (1997)
27. F Raksi, K R Wilson, Zh Jiang, A Ikhlef, Ch Y Cote, J-C Kiefer *J. Chem. Phys.* **104** 6066 (1996)
28. D J Tannor, R Kosloff, S A Rice *J. Chem. Phys.* **85** 5805 (1986)
29. R D Coalson, M Karplus *J. Chem. Phys.* **93** 3919 (1990)
30. H Metiu, V Engel *J. Chem. Phys.* **93** 5693 (1990)
31. M Gruebele, A H Zewail *J. Chem. Phys.* **98** 883 (1993)
32. B Reischl *Chem. Phys. Lett.* **239** 173 (1995)
33. V A Kovarskii *Zh. Eksp. Teor. Fiz.* **110** 1216 (1996)
34. J S Cao, K R Wilson *J. Chem. Phys.* **107** 1441 (1997)
35. I M Umanskii, V V Eremin, N E Kuz'menko *Zh. Fiz. Khim.* **72** 899 (1998) [d]
36. K Mishima, K Yamashita *J. Mol. Struct.* **462** 483 (1999)
37. V V Lozovoy, O M Sarkisov, A S Vetchinkin, S Ya Umanskii *Chem. Phys.* **243** 97 (1999)
38. V V Lozovoy, S A Antipin, F E Gostev, A A Titov, D G Tovbin, O M Sarkisov, A S Vetchinkin, S Ya Umanskii *Chem. Phys. Lett.* **284** 221 (1998)
39. V V Lozovoy, O M Sarkisov, S Ya Umanskii *Khim. Fiz.* **14** (8) 83 (1995) [b]
40. D G Tovbin, Candidate Thesis in Chemical Sciences, Institute of Chemical Physics of the Russian Academy of Sciences, Moscow, 1999
41. S A Trushin, W Fuss, W E Schmid, K L Kompa *J. Phys. Chem. A* **102** 4129 (1998)
42. A J Wurzer, S Lochbruner, E Riedle *Appl. Phys. B* **71** 405 (2000)
43. B J Homoelle, M D Edington, W M Diffey, W F Beck *J. Phys. Chem. B* **102** 3044 (1998)
44. S Savikhin, W Struve *Biophys. J.* **67** 2002 (1994)
45. V E Subotin, D G Tovbin, S Ya Umanskii, O M Sarkisov *Khim. Fiz.* **19** (11) 3 (2000) [b]
46. M Schmitt, G Knopp, A Materny, W Kiefer *J. Phys. Chem. A* **102** 4059 (1998)
47. I Pastirk, V V Lozovoy, B I Grimberg, E J Brown, M Dantus *J. Phys. Chem. A* **103** 10226 (1999)
48. I Pastirk, V V Lozovoy, B I Grimderg, E J Brown, M Dantus *Faraday Discuss.* **113** 401 (1999)
49. R Pausch, M Heid, T Chen, W Kiefer, H Schworer *J. Chem. Phys.* **110** 9560 (1999)
50. J Manz, M Oppel, G K Paramonov *J. Phys. Chem. A* **102** 4271 (1998)
51. T S Rose, M J Rosker, A H Zewail *J. Chem. Phys.* **88** 6672 (1988)
52. U Marvet, M Dantus *Chem. Phys. Lett.* **256** 57 (1996)
53. Q Wang, R W Schoenltin, L A Peteanu, R A Mathies, Ch V Shank *Science* **266** 422 (1994)
54. A Hishikawa, K Ohde, R Itakura, S Liu, K Yamanouchi, K Yamashita *J. Phys. Chem. A* **101** 694 (1997)
55. A Waldman, S Ruhman, S Shaik, G N Sastry *Chem. Phys. Lett.* **230** 110 (1994)
56. C Chudoba, E Riedle, M Pfeiffer, T Elsaesser *Chem. Phys. Lett.* **263** 622 (1996)
57. M H Vos, J-L Martin *Biochim. Biophis. Acta* **1411** 1 (1999)
58. D C Arnett, P Vohringer, N F Scherer *J. Am. Chem. Soc.* **117** 12262 (1995)
59. I Rubtsov, K Yoschihara *J. Phys. Chem. A* **101** 6138 (1997)
60. M Hayaschi, T-S Yang, J Yu, A Mebel, R Chang, S Lin, I Rubtsov, K Yoschihara *J. Phys. Chem. A* **102** 4797 (1998)
61. I Rubtsov, K Yoschihara *J. Phys. Chem. A* **103** 10 202 (1999)
62. K Wynne, C Galli, R Hochstrasser *J. Chem. Phys.* **100** 4156 (1994)
63. K Tominaga, D Kliner, A Johnson, N Levinger, P Barbara *J. Chem. Phys.* **98** 1228 (1993)
64. G C Walker, P F Barbara, S K Doorn, Y Dong, J T Hupp *J. Phys. Chem.* **95** 5712 (1991)
65. T Asahi, N Mataga *J. Phys. Chem.* **95** 1956 (1991)
66. V A Nadtochenko, N N Denisov, I V Rubtsov, A P Moravskii *Izv. Akad. Nauk, Ser. Khim.* 1151 (1996) [c]
67. V A Nadtochenko, N N Denisov, P P Levin *Izv. Akad. Nauk, Ser. Khim.* 1078 (1995) [c]
68. V A Nadtochenko, N N Denisov, I V Rubtsov, A S Lobach, P P Levin, in *Recent Advances in the Chemistry and Physics of Fullerenes and Related Materials* (Eds K Kadish, R Ruoff) (Pennington: The Electrochemical Society, 1994) p. 1645
69. P Y Cheng, D Zhong, A H Zewail *J. Chem. Phys.* **103** 5153 (1995)
70. P Y Cheng, D Zhong, A H Zewail *Chem. Phys. Lett.* **242** 368 (1995)
71. T Haberle, J Hirsch, H Pollinger, H Heitele, M E Michel-Byerle, C Anders, A Dohling, C Krieger, A Ruckemann, H A Staab *J. Phys. Chem.* **100** 18269 (1996)
72. H Pollinger, H Heitele, M E Michel-Byerle, M Tercel, H A Staab *Chem. Phys. Lett.* **209** 251 (1993)
73. T Asahi, M Ohkohchi, R Matsusaka, N Mataga, R P Zhang, A Osuka, K Maryama *J. Am. Chem. Soc.* **115** 5665 (1993)
74. H Heitele, F Pollinger, T Haberle, M E Michel-Byerle, H A Staab *J. Phys. Chem.* **98** 7402 (1994)
75. V A Nadtochenko, D V Khudyakov, O M Sarkisov, N M Loim, in *Abstracts of 18th Conference of the Condensed Matter Division of the European Physical Society, Motreuaux, Switzerland, 2000* p. 317
76. S K Kim, J Guo, J S Baskin, A H Zewail *J. Phys. Chem.* **100** 9202 (1996)
77. D Zhong, S Ahmad, A H Zewail *J. Chem. Soc.* **119** 5978 (1997)
78. E W-G Diau, J L Herek, Z H Kim, A H Zewail *Science* **279** 847 (1998)
79. L Banares, T Baumert, M Bergt, B Kiefer, G Gerber *J. Chem. Phys.* **108** 5799 (1998)
80. S A Trushin, W Fuss, K L Kompa, W E Schmid *J. Phys. Chem. A* **104** 1997 (2000)
81. S Pedersen, J L Herek, A H Zewail *Science* **266** 1359 (1994)
82. E W-G Diau, S De Feyter, A H Zewail *Chem. Phys. Lett.* **304** 134 (1999)
83. H Zhang, P van der Meulen, M Glasbeek *Chem. Phys. Lett.* **253** 97 (1996)
84. D Marks, P Prosposito, H Zhang, M Glasbeek *Chem. Phys. Lett.* **289** 535 (1998)
85. S K Kim, S Pedersen, A H Zewail *Chem. Phys. Lett.* **233** 500 (1995)
86. T Lian, S E Bromberg, V C Asplund, H Yang, C B Harris *J. Phys. Chem.* **100** 11994 (1996)
87. S De Feyter, E W-G Diau, A A Scala, A H Zewail *Chem. Phys. Lett.* **303** 249 (1999)
88. D Marks, H Zhang, P Borowicz, A Grabowska, M Glasbeek *Chem. Phys. Lett.* **309** 19 (1999)
89. A Douhal, S K Kim, A H Zewail *Nature (London)* **378** 260 (1995)
90. A Nakajima, M Hirano, R Hasumi, K Kaya, H Watanabe, C C Carter, J M Williamson, T Miller *J. Phys. Chem. A* **101** 392 (1997)
91. D E Folmer, E S Wisniewski, S M Hurley, A W Castleman Jr *Proc. Natl. Acad. Sci. USA* **96** 12 980 (1999)
92. J Catalan, J C Valle, M Kasha *Proc. Natl. Acad. Sci. USA* **96** 8338 (1999)
93. D E Folmer, E S Wisniewski, A W Castleman *Chem. Phys. Lett.* **318** 637 (2000)
94. K Ohta, T J Kang, K Tominaga, K Yoschihara *Chem. Phys.* **242** 103 (1999)
95. F Laermer, W Israel, T Elsaesser *J. Opt. Soc. Am. B* **7** 1604 (1990)
96. S Arimoto, T Yamazaki, T Okada, S Tagkagi, T Arai, K Tokumary *Chem. Phys. Lett.* **242** 644 (1995)
97. S H Ashworth, T Hasche, M Woerner, E Riedle, T Elsaesser *J. Chem. Phys.* **104** 5761 (1996)
98. M L Horng, J A Gardecki, A Papazyan, M Maroncelli *J. Phys. Chem.* **99** 17311 (1995)
99. S A Kovalenko, J Ruthmann, N P Ernsting *J. Chem. Phys.* **109** 1894 (1998)
100. T Hasche, S H Ashworth, E Riedle, W Woerner, T Elsaesser *Chem. Phys.* **104** 5761 (1996)
101. T Elsaesser, W Kaiser *Annu. Rev. Phys. Chem.* **42** 83 (1991)
102. M Dantus, M Rosker, A H Zewail *J. Chem. Phys.* **89** 10 6128 (1987)
103. M H M Janssen, M Dantuc, H Guo, A H Zewail *Chem. Phys. Lett.* **214** (3/4) 281 (1993)
104. F E Gostev, A E Dzhailaubekov, A N Petrukhin, A A Titov, S Ya Umanskii, O M Sarkisov *Khim. Fiz.* **19** (12) 11 (2000) [b]

105. S A Antipin, A N Petrukhin, F E Gostev, V S Marevtsev, A A Titov, D G Tovbin, A I Shienok, V A Barachevskii, Yu P Strokach, O M Sarkisov *Khim. Fiz.* **19** (4) 3 (2000) [b]
106. S A Antipin, A N Petrukhin, F E Gostev, V S Marevtsev, A A Titov, V A Barachevsky, Yu P Strocach, O M Sarkisov *Chem. Phys. Lett.* **331** (5/6) 378 (2000)
107. N Tamai, T Saika, T Shimidzu, M Irie *J. Phys. Chem.* **100** 4689 (1996)
108. R J Sension, S T Repinec, A Z Szarka, R M Hochstrasser *J. Chem. Phys.* **98** 6291 (1993)
109. W Fus, W E Schmid, S A Trushin *J. Chem. Phys.* **112** 8347 (2000)
110. J S Baskin, L Banares, S Pedersen, A H Zewail *J. Phys. Chem.* **100** 11 920 (1996)
111. M V Alfimov, F V Balakin, S P Gromov, Yu V Zaushitsyn, O A Fedorova, N I Koroteev, A V Pakulev, A Yu Resnyanskii, A P Shkurinov *Zh. Fiz. Khim.* **73** 1871 (1999) [d]
112. N Ernstng *Chem. Phys. Lett.* **159** 526 (1989)
113. N Ernsting, T Arthetengeland *J. Phys. Chem.* **95** 5502 (1991)
114. N Tamai, H Masuhara *Chem. Phys. Lett.* **191** 189 (1992)
115. D A Partnenopoulos, P M Rentzepis *Science* **245** 843 (1989)
116. N I Koroteev, S A Krikunov, S A Magnitskii, D V Malakhov, V V Shubin *Jpn. J. Appl. Phys.* **37** 2279 (1998)
117. W A Noyes Jr, G S Hammond, J N Pits (Eds) *Advances in Photochemistry* (New York: Interscience, 1968) Vol. 5, p. 329
118. V S Marevtsev, N L Zaichenrj *J. Photochem. Photobiol. A, Chem.* **102** 197 (1997)
119. J L Herek, S Pedersen, L Banares, A H Zewail *J. Chem. Phys.* **97** 9046 (1992)
120. F V R Neuwahl, P Foggi, R G Brown *Chem. Phys. Lett.* **319** 157 (2000)
121. J Takeda, D D Chung, J Zhou, K A Nelson *Chem. Phys. Lett.* **290** 341 (1998)
122. M Wiechmann, H Port, F Laermerr, W Frey, T Elsaesser *Chem. Phys. Lett.* **165** 28 (1990)
123. B J Schwartz, L A Peteanu, C B Harris *J. Phys. Chem.* **96** 3591 (1992)
124. N F Scherer, C Sipes, R B Bernstein, A H Zewail *J. Chem. Phys.* **92** 5239 (1990)
125. P Y Cheng, D Zhong, A H Zewail *J. Chem. Phys.* **105** 6216 (1996)
126. U Marvet, Q Zhang, M Dantus *J. Phys. Chem. A* **102** 4111 (1998)
127. M Gruebele, I R Sims, E D Potter, A H Zewail *J. Chem. Phys.* **95** 7763 (1991)
128. D Zhong, A H Zewail *Proc. Natl. Acad. Sci. USA* **96** 2602 (1999)
129. J Ruthmann, S A Kovalenko, N P Ernsting, D Ouw *J. Chem. Phys.* **109** 5466 (1998)
130. E T J Nibbering, F Tschirschwitz, C Chudoba, T Elsaesser *J. Phys. Chem. A* **104** 4236 (2000)
131. D V Lap, D Grebner, S Rentsch, H Naarmann *Chem. Phys. Lett.* **211** 135 (1993)
132. Sh Yamaguchi, H Hamaguchi *J. Phys. Chem. A* **104** 4272 (2000)
133. S Chudoba, E T J Nibbering, T Elsaesser, in *Xth International Conference on Ultrafast Phenomena, Garmish-Partenkirchen, Germany, 1998* p. 134
134. A R Holzwarth, M G Muller *Biochemistry* **35** 11820 (1996)
135. O Kuhn, V Sundstrom *J. Chem. Phys.* **107** 4154 (1997)
136. R Kumble, S Palese, R W Visschers, P L Dutton, R M Hochstrasser *Chem. Phys. Lett.* **261** 396 (1996)
137. S L Logunov, T M Masciangioli, V F Kamalov, M A El-Sayed *J. Phys. Chem. B* **102** 2303 (1998)
138. Ch Wan, T Fiebig, Sh O Kelley, Ch R Treadway, J K Barton, A H Zewail *Proc. Natl. Acad. Sci. USA* **96** 6014 (1999)
139. R N Zare *Science* **279** 1875 (1998)
140. M N Ashfold, J E Baggott *Molecular Photodissociation Dynamics* (London: Royal Society of Chemistry, 1987)
141. V N Bagratashvili, V S Letokhov, A A Makarov, E A Reabov *Multiple Photon Infrared Laser Photophysics and Photochemistry* (Harwood: Academic Publishers, 1984)
142. I Sh Averbukh, M J J Vraking, D M Villeneuve, A Stoloq *Phys. Rev. Lett.* **77** 3518 (1996)
143. P Ludowise, M Blackwell, Y Chen *Chem. Phys. Lett.* **258** 530 (1996)
144. D J Tanor, S A Rice *J. Chem. Phys.* **83** 5013 (1985)
145. R M Bowmann, M Dantus, A H Zewail *Chem. Phys. Lett.* **174** 546 (1990)
146. T Baumert, G Gerber *Isr. J. Chem.* **34** 103 (1994)
147. R Uberna, M Khalil, R M Williams, J M Papanicolas, S R Leone *J. Chem. Phys.* **108** 9259 (1998)
148. E Hertz, O Faucher, B Lavorel, F D Via, R Chaux *Phys. Rev. A* **61** 3816 (2000)
149. M Shapiro, P Brumer *J. Chem. Phys.* **84** 4103 (1986)
150. L Zhu, K Suto, J A Fiss, R Wada, T Seideman, R J Gordon *Phys. Rev. Lett.* **79** 4108 (1997)
151. S Ruhman, R Kosloff *J. Opt. Soc. Am. B* **7** 1748 (1990)
152. A Assion, T Baumert, J Helbing, V Seyfried, G Gerber *Chem. Phys. Lett.* **259** 488 (1996)
153. V A Arkarian, C J Bardeen, J Che, P Cong, B Kohler, J L Krause, C C Martens, M Messina, V V Yacovlev, K R Wilson, R Zadoyan, in *Ultrafast Phenomena* (Berlin: Springer, 1996) p. 112
154. B Kohler, V V Yacovlev, J Che, J L Krause, M Messina, K R Wilson *Phys. Rev. Lett.* **74** 3360 (1995)
155. G Gerullo, C J Bardeen, Q Wang, C V Shank *Chem. Phys. Lett.* **262** 362 (1996)
156. I Pastric, E J Brown, Q Zhang, M Dantus *J. Chem. Phys.* **108** 4375 (1998)
157. N Washida, G Inoe, M Suzuki *Chem. Phys. Lett.* **114** 274 (1985)
158. R S Judson, H Rabitz *Phys. Rev. Lett.* **68** 1500 (1992)
159. A Assion, T Baumert, M Bergt, T Brixner, B Kiefer, V Seyfried, M Strehle, G Gerber *Science* **282** 919 (1998)
160. V A Senekerimyan, A N Petrukhin, S A Antipin, F E Gostev, in *XLIII Nauchnaya Konferentsiya MFTI 'Sovremennye Problemy Fundamental'nykh i Prikladnykh Nauk', Dolgoprudnyi, 2000* (The XLIIIth Scientific Conference of Moscow Physical Engineering Institute 'Current Problems of Fundamental and Applied Sciences, Dolgoprudnyi, 2000) p. 49
161. F.V.R.Neuwahl, P.Foggi, R.G.Brown *Chem. Phys. Lett.* **319** 157 (2000)
162. A M Zheltikov, A N Naumov *Kvantovaya Elektron.* **30** 6 (2000) [e]
163. T Hornung, R Meier, M Motzkus *Chem. Phys. Lett.* **326** 445 (2000)
164. S A Kovalevskii, F I Dalidchik, M V Grishin, N N Kolchenko, B R Shub *Appl. Phys. A* **66** 125 (1998)
165. M V Grishin, F I Dalidchik, S A Kovalevskii, N N Kolchenko *Ultramicroscopy* **79** 203 (1999)
166. N S Maslova, A I Oreshkin, V I Panov, S A Magnitskii *Solid State Commun.* **117** 41 (2001)
167. A Lewis, U Ben-Ami, N Kuck, G Fish, D Diamant, L Lubovsky, K Lieberman, Sh Katz, A Saar, M Roth *Scanning* **17** 3 (1995)
168. A A Ezhov, S A Magnitskii, D A Muzychenko, V I Panov, in *Zondovaya Mikroskopiya-99. Materialy Vserossiiskogo Soveshchaniya, Nizhnii Novgorod, 1999* (Probe Microscopy-99. Materials of All-Russian Meeting, Nizhnii Novgorod, 1999) p. 125
169. S K Secatskii, S V Checalin, A L Ivanov, Yu A Matveets, A G Stepanov, V S Letokhov *J. Phys. Chem. A* **102** 4148 (1998)
170. W Pfeiffer, F Sattler, S Volger, G Gerber, J Y Grand, R Moller *Appl. Phys. B* **64** 265 (1997)
171. V Gerstner, A Knoll, W Pfeiffer, F Thon, G Gerber *J. Appl. Phys.* **88** 4851 (2000)
172. A L Buchachenko *Usp. Khim.* **68** 99 (1999) [*Russ. Chem. Rev.* **68** 85 (1999)]

[a] — *Mendeleev Chem. J. (Engl. Transl.)*
[b] — *Chem. Phys. Rep. (Engl. Transl.)*
[c] — *Russ. Chem. Bull. (Engl. Transl.)*
[d] — *Russ. J. Phys. Chem. (Engl. Transl.)*
[e] — *Quantum. Electron. (Engl. Transl.)*

Russian Chemical Reviews **70** (6) 471 – 490 (2001) © 2001 Russian Academy of Sciences and Turpion Ltd

DOI 10.1070/RC2001v070n06ABEH000657

Ultrafast nonradiative transitions between higher excited states in organic molecules

V L Ermolaev

Contents

I.	Introduction	471
II.	Single-photon excited fluorescence from higher excited S_n levels to the ground-state level	473
III.	Fluorescence due to transitions from higher excited S_n levels under conditions of stepwise excitation of molecules	476
IV.	Lifetimes of higher excited S_n states estimated from fluorescence quantum yields and absorption integrals	481
V.	Delayed fluorescence from higher excited S_n states due to triplet – triplet annihilation	481
VI.	Lifetimes of higher excited S_n states of molecules estimated from homogeneous broadening of absorption spectra	484
VII.	Lifetimes of higher excited S_n states estimated from picosecond and femtosecond spectroscopy data	486
VIII.	Ultrafast nonradiative transitions involving triplet states	487
IX.	Conclusion	488

Abstract. Ultrafast nonradiative transitions between electronic levels of aromatic and dye molecules, competing with fast photochemical reactions (*e.g.*, electron or proton transfer, photoisomerisation, *etc.*), are considered. The results of determination of the rate constants for nonradiative transitions between higher excited singlet and triplet states using different methods are summarised. The experimental data are interpreted in terms of the exchange-resonance theory of nonradiative transitions. The bibliography includes 189 references.

I. Introduction

In his lecture at the XIX Mendeleev Congress academician A L Buchachenko noted that the development of experimental techniques that use short laser pulses has widened the horizons of chemistry. Fresh ideas thus introduced into chemistry have been embodied into femtochemistry.[1] The subject of femtochemical studies is ultrafast reactions, such as proton or electron transfer in acid – base (donor – acceptor) pairs, *cis* – *trans*-isomerisation with detection of the *twist*-conformation, photogeneration and relaxation of electron-hole pairs in semiconductors, elementary stages in photosynthesis, molecular decomposition, *etc.*[2, 3] Topicality of research into ultrafast processes is emphasised by the fact that the 1999 Nobel Prize in chemistry was awarded to A H Zewail, one of the originators of femtochemistry.

Single-photon excitation of a complex organic molecule to a higher excited singlet state (HESS) S_n ($n > 1$) is followed by transient relaxation processes. These processes, as well as transformations of excess electronic energy thus supplied to the molecule, are of considerable interest in studying the mechanisms of photochemical reactions in the vapour phase and in solutions. Most of the photochemical reactions of organic compounds in solutions are known to proceed involving the first excited singlet (S_1) and triplet (T_1) states. Both of them usually have rather long, on the molecular scale, lifetimes (from several nanoseconds for the S_1 states to hundreds of microseconds in liquids and tens of seconds in solid solutions for the T_1 states). However, the characteristic times of many fast photochemical reactions (electron and proton transfer, isomerisation, *etc.*) are much shorter. This suggests the involvement of other, upper excited states of the molecules (whose lifetimes are much shorter compared to those of the S_1 and T_1 states) in these reactions. Some of the fast reactions are considered in this review as examples. It should be noted that the possibility of estimating the HESS lifetimes has appeared only in the last decades. Nevertheless, a large body of experimental data obtained by direct and indirect methods has been accumulated to date. Therefore, it is of interest to analyse them, to assess their reliability and to consider possible mechanisms of excitation relaxation.

S I Vavilov was the first to obtain experimental data which allowed estimation of the rates of nonradiative transitions between the HESS of complex organic molecules (dyes) in solutions. He had shown experimentally[4, 5] that the quantum yields of dye fluorescence in solutions are independent of the wavelength of exciting radiation. In other words, light emission (fluorescence) always occurs from the first excited (fluorescent) S_1 level irrespective of the level to which the molecule was excited after absorption of a light quantum (the Vavilov law).

Attempts to observe emission from the HESS of complex molecules under standard conditions have failed for long. This means that emission from these levels (with rate constants of the order of $10^7 - 10^8$ s^{-1}) is accompanied by a competing fast nonradiative process (with a rate constant of at least 10^{12} s^{-1}). This interpretation is also supported by the fact that the fluorescence spectrum of a complex molecule in solution is independent of the wavelength of exciting light.

After establishment of the triplet nature of the metastable phosphorescent state of aromatic molecules[6, 7] the Vavilov law was supplemented by Kasha's rule,[8] according to which emission of light from complex molecules always occurs from the lowest excited level of a given spin multiplicity. The Vavilov law and Kasha's rule can be illustrated by a diagram of singlet (S_n) and triplet (T_n) vibronic energy levels of complex organic molecules (Fig. 1). Fulfilment of the Vavilov law and Kasha's rule means that the rate constants for nonradiative transitions (k_{nr}) from the S_n and T_n ($n \geqslant 2$) levels to the S_1 and T_1 levels, respectively, are

V L Ermolaev The State Unitary Enterprise 'All-Russian Scientific Centre, S I Vavilov State Optical Institute', Birzhevaya Liniya 12, 199034 St. Petersburg, Russian Federation. Fax (7-812) 328 37 20. Tel. (7-812) 328 46 08 (ext. 426). E-mail: ermol@soi.spb.su

Received 2 February 2001
Uspekhi Khimii **70** (6) 539 – 561 (2001); translated by A M Raevsky

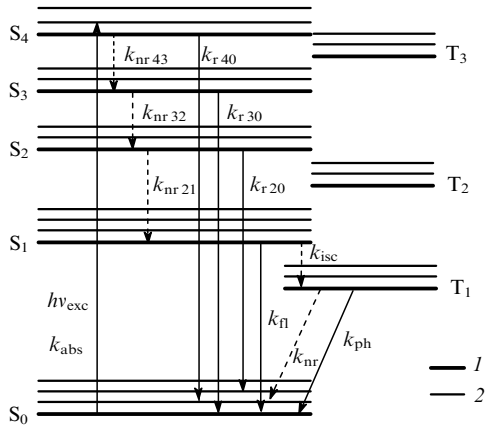

Figure 1. An energy level diagram illustrating transitions between vibronic levels of organic molecules.
Here and in Figs 2, 5–7 and 9 thick (*1*) and thin (*2*) lines denote electronic and vibronic energy levels, respectively. Notations of singlet energy levels: S_0 is the ground-state level and S_1, S_2, S_3 and S_4 are the first (fluorescent), second, third and fourth excited energy levels, respectively. Notations of triplet energy levels: T_1, T_2 and T_3 are the lowest (phosphorescent), second and third excited levels, respectively. Solid and dashed vertical lines respectively denote radiative and nonradiative transitions. Notations of rate constants: k_{r30} is the rate constant for the $S_3 \rightarrow S_0$ radiative transition (the radiative rate constant), $k_{r10} \equiv k_{fl}$ is the usual fluorescence rate constant, k_{nr32} is the rate constant for the $S_3 \rightarrow S_2$ nonradiative transition (internal conversion), k_{isc} is the rate constant for intersystem crossing (spin-forbidden $S_1 \rightarrow T_1$ nonradiative transition), k_{ph} is the phosphorescence rate constant, k_{nr} is the rate constant for nonradiative transition from the lowest triplet to the ground singlet state and k_{abs} is the absorption rate constant.

three for more orders of magnitude higher than the corresponding rate constants for radiative transitions (radiative rate constants, k_r) and intersystem crossing rate constants. However, this estimate says nothing about the rate constants for particular nonradiative transitions, *e.g.*, $S_n \rightarrow S_{n-1}$, $S_{n-1} \rightarrow S_{n-2}$, *etc*. However, knowledge of these rate constants is of interest for both research into fundamental problems of luminescence, photochemistry and photobiology and estimation of limiting energy characteristics of, *e.g.*, dye lasers and Q switches.

Recently, some experimental methods have been developed that allowed the obtaining of quantitative information on the rates of nonradiative transitions between higher excited energy levels of molecules. These are as follows:

1. Measurements of fluorescence spectra and yields from upper excited levels by direct single-quantum excitation of corresponding energy levels.

2. Measurements of $S_n \rightarrow S_0$ luminescence spectra and yields using a stepwise two-photon excitation technique, $S_0 + hv_1 \rightarrow S_1 + hv_2 \rightarrow S_n$ ($n > 1$).

3. Measurements of the fluorescence spectra from higher excited singlet levels populated *via* triplet–triplet annihilation.

4. HESS lifetime estimation from the results of (i) experiments on 'hole burning' in absorption spectra at low temperatures, (ii) linewidth measurements in fluorescence excitation spectra in supersonic jets or (iii) bandwidth measurements in structured emission spectra from higher excited levels.

5. Direct HESS lifetime measurements using picosecond or femtosecond spectroscopy.

6. Estimation of the rates of ultrafast nonradiative transitions involving triplet states.

Before presenting the results of particular experimental studies on the rates of nonradiative transitions we will briefly outline elements of modern quantum-mechanical theories of nonradiative transitions in complex organic molecules. According to formal theory of nonradiative transitions,[9–11] excitation of a molecule leads to its transition to a non-stationary excited state. Owing to short duration of the excitation pulse and high density of final vibronic states inherent in polyatomic molecules, nonradiative deactivation of the initial non-stationary state occurs exponentially. The rate constant for such a process, k_{nr}, is calculated using first-order, time-dependent perturbation theory. This process corresponds to the 'statistical limit' case.[12]

If the adiabatic approximation holds, the wave function of the system, $\Psi_{ma}(\mathbf{r}, \mathbf{Q})$, can be written as the product of electron wave function, $\varphi_{ma}(\mathbf{r}, \mathbf{Q})$, and vibrational wave function, $\chi_a(\mathbf{Q})$,

$$\Psi_{ma}(\mathbf{r}, \mathbf{Q}) = \varphi_m(\mathbf{r}, \mathbf{Q})\chi_a(\mathbf{Q}),$$

where $\mathbf{r}(r_1, r_2, r_3,...)$ are the electron coordinates, $\mathbf{Q}(Q_1, Q_2, Q_3,...)$ are the coordinates of atomic nuclei and the indices m and a denote the energy level and vibrational state, respectively.

Usually, the operator of nonadiabaticity, $V_{ma,nb}$ (m and n denote the energy levels and a and b denote the corresponding vibrational states), is considered as a perturbation inducing the nonradiative transition. Approximate expression for the matrix element of transition between the excited electronic state n and the state m with a lower energy has the form:

$$V_{ma,nb} \approx$$
$$\approx -\sum_i \frac{h^2}{M_i} \int \chi_{ma}(\mathbf{Q}) \left\langle \varphi_m(\mathbf{r}, \mathbf{Q}) \left| \frac{\partial}{\partial Q_1} \right| \varphi_n(\mathbf{r}, \mathbf{Q}) \right\rangle \frac{\partial}{\partial Q_1} \chi_{nb}(\mathbf{Q}) \mathrm{d}\mathbf{Q} +$$
$$+ \frac{1}{2} \sum_i \frac{h^2}{M_i} \int \chi_{ma}(\mathbf{Q}) \left\langle \varphi_m(\mathbf{r}, \mathbf{Q}) \left| \frac{\partial^2}{\partial Q_1^2} \right| \varphi_n(\mathbf{r}, \mathbf{Q}) \right\rangle \chi_{nb}(\mathbf{Q}) \mathrm{d}\mathbf{Q},$$

where M_i is the mass of the nucleus of ith atom. Neglecting the term containing the second derivatives of electron wave functions and simplifying this expression,[13] we get

$$V_{ma,nb} \approx \left\langle \varphi_m(\mathbf{r}, \mathbf{Q}) \left| \frac{\partial}{\partial Q_i} \right| \varphi_n(\mathbf{r}, \mathbf{Q}) \right\rangle = \frac{\langle \varphi_m(\mathbf{r}, \mathbf{Q}) | \partial U / \partial Q_i | \varphi_n(\mathbf{r}, \mathbf{Q}) \rangle}{E_m(\mathbf{r}, \mathbf{Q}) - E_n(\mathbf{r}, \mathbf{Q})},$$

where $U(\mathbf{r},\mathbf{Q})$ is the Coulomb energy of the interaction between electrons and nuclei and $E(\mathbf{r},\mathbf{Q})$ is the adiabatic potential for the excited state.

The total rate of a nonradiative transition between the states n and m can be written as the sum of partial transition probabilities

$$k_{r\,nm} = \frac{2\pi}{h} \sum_{a,b} |V_{ma,nb}|^2 p(nb) \delta(E_{ma} - E_{nb}).$$

Here, $p(nb)$ is the population of the initial vibronic state, δ is the Dirac delta function and E_{ma} and E_{nb} are the energies of the vibronic states ma and nb, respectively.

The aforesaid represents a framework of the general theory of nonradiative transitions. In the text below, we will consider the exchange-resonance theory of nonradiative transitions in ions and complex molecules developed by Sveshnikova, the author of this review and Bodunov.[14–16] According to this theory, all vibrations of a molecule under study are divided into two types, namely, promoting-accepting vibrations and accepting ones.

The first type of vibrations comprises high-frequency, strongly anharmonic vibrations responsible for the vibrational absorption spectrum of the molecule in both fundamental and overtone regions. These vibrations are usually almost inactive in vibronic molecular spectra since corresponding Franck–Condon integrals are close to zero.

The second type of vibrations comprises those responsible for the vibronic spectrum of the molecule due to nonzero Franck–Condon integrals. Often, these vibrations appear to be totally symmetric and are therefore inactive in the vibrational absorption spectrum of the molecule. For instance, the totally symmetric vibrations of aromatic molecules associated with changes in the C–C distances belong to accepting vibrations.

Bodunov[15] used the operator of nonadiabaticity as a perturbation inducing the nonradiative transition. He divided molecular

vibrations into two above-mentioned types and showed that the expression for the rate constant for the nonradiative transition between two electronic levels, k_{nr}, can be written using the overlap integral of the normalised vibronic emission spectrum of a molecule due to transition between the corresponding levels, $f(E)$, and the vibrational absorption spectrum of the same molecule, $\sigma(E)$

$$k_{nr} \approx \left|\overline{\langle\varphi_m|\frac{\partial U}{\partial Q_k}|\varphi_n\rangle}\right|^2 \int f(E)\sigma(E)E^{-(s+1)}\mathrm{d}E.$$

Here, the horizontal line denotes averaging over the first type of vibrations; $s = 3$ for dipole and $s = 5$ for quadrupole radiation. This formula is similar to the Förster–Dexter formulae for the nonradiative energy transfer between energy donor and acceptor, except that the transfer occurs intramolecularly to decrease the electron energy and to increase the vibrational energy. Validity of the exchange-resonance theory of nonradiative transitions was experimentally proved taking lanthanide ions in solutions,[14,17] transition-metal complexes[17,18] and (with some limitations) complex aromatic molecules[17–19] as examples. It should be noted that this theory was developed assuming a weak coupling between the energy levels involved in the transition, though this is not necessarily true in the case of HESS.

In this review, we will analyse the results of experimental studies from the standpoint of the exchange-resonance theory of nonradiative transitions, since this theory predicts that k_{nr} is proportional to k_r. Unfortunately, the rate constants for radiative transitions between higher excited singlet states are unknown for most of the molecules studied; nevertheless, in some instances such correlations can be found.

Recently, a number of reviews concerning fast photophysical and photochemical processes in complex organic molecules have been published (see, *e.g.*, excellent reviews[20,21]). However, the authors of these studies placed the emphasis on the vibrational energy redistribution after excitation of the molecules, whereas the problem of electronic relaxation was only briefly outlined. On the other hand, a large body of information on electronic relaxation reported in numerous studies allows some generalisation of the results obtained.

II. Single-photon excited fluorescence from higher excited S_n levels to the ground-state level

Beer and Longuet-Higgins[22] were the first who reported a strongly supported example of violation of the Vaviov law and Kasha's rule. They studied fluorescence of an azulene solution under conditions of single-quantum excitation and provided convincing proofs of the fact that the fluorescence observed after excitation of the solution into the second or shorter-wavelength absorption bands is due to transition from the second excited to the ground-state level ($S_2 \rightarrow S_0$). Azulene fluorescence was observed in the near UV spectral region (at about 28 000 cm^{-1}), though the long-wavelength absorption band of this compound lies near 14 000 cm^{-1}. These experimental observations were confirmed in more recent studies of azulene and a large number of its derivatives.[23–25] The quantum yields of $S_2 \rightarrow S_0$ fluorescence of a number of azulene derivatives were found to be as high as several percent while the S_2 state lifetimes were as long as 1.4 ns. The results obtained in these studies were briefly outlined in a monograph.[26]

Much weaker was the $S_2 \rightarrow S_1$ fluorescence of azulene observed in the region from 14 000 to 9500 cm^{-1} (710–1050 nm).[27–30] Thorough measurements allowed[31] the determination of the quantum yield ratio of the $S_2 \rightarrow S_0$ and $S_2 \rightarrow S_1$ fluorescence ($q_{fl\,20}$ and $q_{fl\,21}$, respectively)

$$\frac{q_{fl\,20}}{q_{fl\,21}} = 450 \pm 100.$$

This value characterises the ratio of the rate constants for radiative transitions from the S_2 level to the ground-state and first excited levels. From the standpoint of the exchange-resonance theory of nonradiative transitions[14] the low probability of $S_2 \rightarrow S_1$ internal conversion is due to not only the wide energy gap between these levels and minor changes in the molecular configuration in the S_1 state compared to those for the molecular configuration in the S_2 state, but also forbiddenness of the radiative transition between these levels.

Hirata and Lim[32] studied fluorescence of azulene and perdeuterated azulene vapours and, in particular, its dependence on the excess vibrational energy in the S_2 state. They suggested that a direct internal conversion from the second excited singlet state to the ground state can occur in the azulene molecule bypassing the S_1 state. Unfortunately, this assumption was not strengthened by convincing proofs, so that the arguments adduced by the authors had little force.

$S_2 \leftarrow S_0$-Fluorescence excitation spectra of azulene cooled in a supersonic jet have been studied.[33] It was found that the fluorescence excitation spectrum of the $S_2 \leftarrow S_0$ transition exhibits a fine vibrational structure. The fluorescence excitation spectra for transitions from the ground-state level to the S_3 and S_4 levels were found to be substantially broadened due to fast conversion from these levels to the S_2 state.

Direct measurements of fluorescence decay times from the S_2 state of 2-haloazulene and 1,3-dihaloazulene molecules in solution have been carried out.[34] It was shown that intersystem crossing to the triplet manifold with the rate constant $k_{isc}(S_2 \rightsquigarrow T_n)$ can occur in the molecules of compounds studied in addition to the $S_2 \rightsquigarrow S_1$ internal conversion and $S_2 \rightarrow S_0$ and $S_2 \rightarrow S_1$ transitions.

Table 1 lists the fluorescence quantum yields, energy level positions [$E(S_2)$], energy gaps (ΔE), rate constants for radiative and nonradiative transitions between different energy levels as well as the second excited singlet state lifetimes, $\tau(S_2)$, for azulene and a number of its derivatives.[31–51] For comparison, mention may be made that the $S_1 \rightarrow S_0$ fluorescence of azulene in solution ($\sim$14 000 cm^{-1}) is characterised by very low quantum yield ($\sim 10^{-4}$–10^{-6}) (see Refs 24 and 35) and a decay time, $\tau(S_1)$, estimated at 1.9 (see Ref. 36) or 1 ps (see Ref. 37).

The dynamics of isolated azulene molecules in the S_1 state has been studied in detail by femtosecond-resolved mass spectrometry in molecular beams.[38] The dephasing time of azulene was found to be shorter than 100 fs. With an excess vibrational energy of $\sim$2000 cm^{-1}, the $S_1 \rightarrow S_0$ internal conversion time in azulene vapours was estimated at 900±100 fs. It was concluded that, despite the wide energy gap ($\sim$14 000 cm^{-1}), such a high internal conversion rate can be rationalised by considering the conical intersection of the potential energy surfaces (PES) of the S_1 and S_0 states near the PES minimum of the S_1 state, as was suggested earlier.[22,39]

Luminescence studies[40] of azulene derivatives allowed the determination of the order in which light emission appears. At low temperatures, an increase in the energy of the S_1 level and narrowing of the $\Delta E(S_2-S_1)$ gap lead to the appearance of the $S_1 \rightarrow S_0$ fluorescence. At room temperature, the $S_2 \rightarrow S_0$ fluorescence remains the dominant process. At higher temperatures, the usual $S_1 \rightarrow S_0$ fluorescence prevails. A feature of azulene derivatives is the low-temperature $T_1 \rightarrow S_0$ phosphorescence.

Interesting results were obtained in studies of the fluorescence of 1,3,5,7-tetra-*tert*-butylindacene (TTBI), a representative of nonalternant antiaromatic hydrocarbons.[41] Similarly to azulene, TTBI has a low intensity transition in the near IR region [$E(S_1)$ = 9300 cm^{-1}] and has an intense, allowed transition in the visible spectral region [$E(S_2)$ = 18 300 cm^{-1}]. The authors of this study[41] succeeded in observing the $S_2 \rightarrow S_0$ fluorescence of a TTBI solution in cyclohexane (see Table 1). A salient feature of this compound is violation of the cascade character of internal conversion, so that the $S_2 \rightsquigarrow S_0$ nonradiative transition appears to be more probable than the $S_2 \rightsquigarrow S_1$ transition. In accordance with the proposed exchange-resonance mechanism of nonradiative transitions,[15] this violation can be suggested to be due to substantial increase in the probability of the $S_2 \rightarrow S_0$ radiative

Table 1. Characteristics of transitions from the second singlet level for a number of organic molecules.

Compound	Solvent	$E(S_2)$ /cm^{-1}	$\Delta E(S_2-S_1)$ /cm^{-1}	$q_{fl\,20}$	$k_{r\,20}$ /s^{-1}	$\tau(S_2)$ /ps	$10^{-8}\,k_{nr\,21}$ /s^{-1}	Ref.
Azulene	cyclohexane	28 300	14 000	3.1×10^{-2}	2.2×10^{7}	1400	6.9	35
	isopentane (at 190 K)	28 300	14 000	6.8×10^{-5} (see [a])	4.0×10^{4} (see [b])	1400	5.9	31
1,3-Dichloroazulene	cyclohexane	27 000	14 300	5.8×10^{-2}	3.6×10^{7}	830	6.934	34
1,3-Dibromoazulene	ethanol	–	12 400	4.4×10^{-2}	5.5×10^{7}	310	–	34
1,3,5,7-Tetra-*tert*-butylindacene	cyclohexane	18 300	9100	9×10^{-5}	10^{8}	2.5	4×10^{3} (see [c])	41
Xanthione	fluorinated hydrocarbons	24 000	7970	1.4×10^{-3}	8×10^{6}	175	5.7×10	51
	trimethylpentane	23 400	7500	5×10^{-4}	1×10^{7}	45	2.1×10^{5}	49
2,2,3,3-Tetramethyl-indanethione	fluorinated hydrocarbons	26 800	11 000	1.4×10^{-1}	1.6×10^{8}	880	9.7	51

Note. Measurements were mostly carried out by direct single-quantum excitation at room temperature.
[a] The $q_{fl\,21}$ value, [b] the $k_{r\,21}$ value, [c] the $k_{nr\,20}$ value.

transition compared to that of the $S_2 \rightarrow S_1$ transition and to the larger value of the Franck–Condon factor for the former transition. According to quantum-mechanical calculations,[41] the geometric parameters of the TTBI molecule in the S_2 and S_1 states are close, but they differ appreciably from those for the S_0 state.

Fluorescent properties of solutions of another representative of antiaromatic compounds, 1,3,5-tri-*tert*-butylpentalene, have been studied theoretically and experimentally.[42] Emission observed in the region near 27 000 cm^{-1} with a quantum yield of 2×10^{-3} after excitation by light with $\lambda = 313$ nm was assigned to the $S_3 \rightarrow S_0$ transition. The interpretation of the results obtained in this study appeared to be the subject of a discussion.[4,44] The role of conical intersection of the PES of the S_1 and S_0 states in quenching of usual fluorescence was pointed out.[44]

A study of fluorescence from the second excited singlet level of [18]-annulene (18A), a representative of alternant hydrocarbons, and its monofluoro derivative (F18A) in 3-methylpentane matrix at 4 K has been reported.[45] Symmetric (D_{6h}) molecular skeleton of 18A comprises 18 carbon atoms while the S_1 and S_2 states of the molecule are in the regions of 12 500 and 21 400 cm^{-1}, respectively. Both 18A and F18A were found to be $S_2 \rightarrow S_0$ fluorescent with rather high yields, the latter being also $S_1 \rightarrow S_0$ fluorescent (in this case, the fluorescence yield was 100 times lower). Nickel and Hertzberg[46] studied fluorescence of biphenylene (an antiaromatic hydrocarbon) in 3-methylpentane solution at 130 K. They found that the fluorescence yield from the second excited level is more than two orders of magnitude lower than that of the $S_1 \rightarrow S_0$ fluorescence, namely, $q_{fl}(S_1 \rightarrow S_0) = 2.3\times10^{-4}$.

Thioketones represent another class of compounds characterised by rather high fluorescence yields for transitions of their molecules from the second excited singlet state.[47–50] Huber and Mahaney were the first who reported the emission from the S_2 level of aromatic thioketone molecules taking xanthione as an example.[47] Shortly, their paper was followed by a series of related studies carried out using a large number of alkyarylthioketones.[48–50] For thioketone molecules, the orbital forbidden $S_1(n,\pi^*) \leftarrow S_0$ transition is near 15 000 cm^{-1} (the molar extinction coefficient at the absorption band maximum, ε_{max}, is 20 mol^{-1} litre cm^{-1}), while the allowed $S_2(\pi,\pi^*) \leftarrow S_0$ transition is near 23 500 cm^{-1} ($\varepsilon_{max} = 16\,000$ mol^{-1} litre cm^{-1}).[49,51]

The $S_2 \rightarrow S_0$ fluorescence bands are observed in the violet spectral region ($\sim$22 500 cm^{-1}) while those of the long-wavelength $S_1 \leftarrow S_0$ transition are observed in the near IR spectral region ($\sim$15 000 cm^{-1}). It should also be noted that no $S_1 \rightarrow S_0$ fluorescence was found. On the other hand, $T_1 \rightarrow S_0$ phosphorescence is observed even at room temperature, with a quantum yield (in frozen solution) can be as high as 10%.

Fluorescence from the second excited state of xanthione and related molecules is strongly quenched upon addition of saturated and aromatic hydrocarbons, which is indicative of a photochemical reaction between the thioketones and hydrocarbons.[50–54] The highest $S_2 \rightarrow S_0$ fluorescence yields were obtained in solutions of perfluoroalkanes (*e.g.*, $q_{fl\,20} = 0.014$ for xanthione at room temperature, see Table 1). The dipole $S_2 \rightarrow S_1$ radiative transition in the xanthione molecule is forbidden.[49] This substantially decreases the probabilities of nonradiative transitions in accordance with the proposed exchange-resonance mechanism of these transitions.[15]

A solution of 4-*H*-1-benzopyran-4-thione (BPT) in perfluoro-1,3-dimethylcyclohexane has been studied in detail.[55–57] It was shown that the phosphorescence quantum yield is independent of the frequency of exciting light up to 36 300 cm^{-1} (the $S_0 \rightarrow S_4$ transition). This fact contradicts the conclusion drawn previously[58,59] that the phosphorescence yield decreases by 30% upon excitation into the $S_0 \rightarrow S_1$ band as compared to direct excitation to the T_1 state. On the other hand, a 25% decrease in the $S_2 \rightarrow S_0$ fluorescence yield under excitation into the $S_0 \rightarrow S_4$ band was found. This was associated with changes in the rate of internal conversion from the S_2 state;[57] is it also implied that excitation to upper states leads to an increase in the vibrational energy of the molecule. Intersystem crossing from the HESS to the triplet manifold (namely, to higher excited triplet levels) due to the strong spin-orbit coupling, followed by fast internal conversion to the T_1 state also seems not to be improbable in thioketones.

Maciejewski *et al.*[60] proposed a method for determination of quantum yields of intramolecular nonradiative transitions, $q_{nr}(S_m \rightarrow S_{m-i})$ ($i = 1, 2, \ldots, m$), between different energy levels of complex organic molecules. The method was evaluated taking three aromatic thioketones dissolved in a perfluorinated hydrocarbon and directly excited to the S_3 state as examples. To determine the $q_{nr}(S_m \rightarrow S_{m-i})$ values, the relative fluorescence quantum yields $q_r(S_{m-1})$, $q_r(S_{m-2})$, ... $q_r(S_1)$ from all lower lying energy levels should be known. The authors of this study used the phosphorescence yield of thioketones, $q_r(T_1)$, instead of the usual fluorescence yield, $q_r(S_1)$, assuming that the T_1 state is populated exclusively *via* the S_1 state and thioketones exhibit no S_1 fluorescence. (The latter statement is incorrect since it is known[55,57] that for BPT the S_1 fluorescence intensity is $\sim$0.01 of the phosphorescence intensity at room temperature.) The relative quantum yields of nonradiative transitions between different excited singlet levels can also be estimated by comparing the absorption and fluorescence excitation spectra from different lower-lying energy levels. The internal conversion and emission quantum yields (q_{nr} and q_r, respectively) for the three thioketones are listed in Table 2.

The starting point of the study[60] was to rationalise marked violations of the cascade mechanism of internal conversion observed even for molecules with rather wide energy gaps (this

Table 2. Characteristics of nonradiative and radiative transitions in thioketones dissolved in perfluoro-1,3-dimethylcyclohexane, obtained at room temperature.[60]

Transition characteristics	Xanthione-1,3,4,5,6,8-d_6	Xanthione-h_8	4*H*-1-Benzopyran-4-thione
$q_{nr}(S_4 \rightsquigarrow S_2)$	–	–	(0.74)
$q_{nr}(S_3 \rightsquigarrow S_2)$	0.90	0.72	0.74 (0.82)
$q_{nr}(S_3 \rightsquigarrow S_1)$	0.0	0.04 (?)	0.11 ($\sim$0.0)
$q_{nr}(S_3 \rightsquigarrow S_0)$	0.10 (?)	0.24 (?)	0.15 ($\sim$0.0)
$q_{nr}(S_2 \rightsquigarrow S_1)$	0.96	0.85	0.88 (1.0)
$q_{nr}(S_2 \rightsquigarrow S_0)$	0.0	0.14 (?)	0.10 ($\sim$0.0)
$q_r(S_2 \rightsquigarrow S_0)$	0.042	0.014	0.023
$q_r(T_1 \rightsquigarrow S_0)$	0.078	0.038	0.076
$q_r(S_1 \rightsquigarrow S_0)$	0.0	0.0	0.0 (0.01)
$\tau(S_2)$ /ps	606	178	210
$E(S_1)$ /cm^{-1}	16 000	16 000	16 800
$\Delta E(S_2-S_1)$ /cm^{-1}	8000	7900	8600
$\Delta E(S_3-S_2)$ /cm^{-1}	4900	5000	4800
$\Delta E(S_3-S_1)$ /cm^{-1}	12 900	12 900	13 400

Note. The data taken from Ref. 57 are given in parentheses.

particularly refers to quantum yields of the $S_3 \rightsquigarrow S_0$ and $S_2 \rightsquigarrow S_0$ nonradiative transitions, see Table 2). The authors cited suggested that these violations can be accounted for either by large differences between the electronic matrix elements appearing in the expression for the rate constant of nonradiative transition or by conical intersection of the PES when moving over the hypersurface of the S_3 state towards a distorted local minimum. In interpretation proposed in the study,[16] the above-mentioned matrix elements represent the rate constants for radiative transitions between corresponding energy levels. Conical intersection of the PES provides a direct transition to the ground state.

Difficulties in measuring q_{nr} should be pointed out. First, this is a strong overlap of the bands corresponding to population of different HESS in the absorption spectrum, especially if the intensities of neighbouring bands differ substantially, as is the case of the $S_3 \rightsquigarrow S_0$ and $S_2 \rightsquigarrow S_0$ transitions in thioketones. Because of this, information on violation of cascade mechanism of nonradiative transitions between excited levels in particular molecules including thioketones should be considered very carefully. For instance, Nickel[61] thoroughly studied nonradiative transitions in BPT and came to conclusion that there is no good reason to assume direct internal conversion from the S_2 and S_3 states of thioketone molecules to the ground state.† Fast appearance of an impurity (a photochemical reaction product) in the thioketone solution has also been reported.[56]

The method proposed by Maciejewski *et al.*[60] allows the obtaining of complete information on the nonradiative transitions between all energy levels only if direct single-quantum excitation of a HESS will give rise to fluorescence from all lower-lying levels. However, this is possible (and only for the S_2 state!) for a limited number of molecules (thioketones, several porphyrins, *etc.*). If direct single-quantum excitation gives rise only to S_1 fluorescence, one can only point to deviations from the Vavilov law and Kasha's rule which were repeatedly checked using many molecules.

Bright $S_2(\pi,\pi^*) \rightarrow S_0$ fluorescence of 1,8-(1′,8′)-naphthalylnaphthalene solutions, characterised by $q_{fl} = 0.18$ and $t = 3$ ns was observed,[62] despite the narrow gap between S_2 and S_1 levels [$\Delta E(S_2-S_1) = 5000$ cm^{-1}]. However, such a high quantum yield of fluorescence due to transition from the S_2 level in combination with the narrow energy gap seems to be unrealistic. Presumably, in this case there was a contribution of impurity or product of a photochemical reaction. Similarly to thioketones and azulene, no $S_1(n,\pi^*) \rightarrow S_0$ usual fluorescence was observed, only phosphorescence was found in this case.

† Private communication.

Direct single-quantum excitation of porphin derivatives also gives rise to the $S_2 \rightarrow S_0$ (or $S_3 \rightarrow S_0$) fluorescence. This fluorescence ($\sim$23 000 cm^{-1}) was first studied by Gouterman *et al.*[63] The fluorescence spectrum was found to be a mirror image of intense Soret absorption band. More detailed studies of this fluorescence have shown[64,65] that the highest quantum yield ($q_{fl\,20} = 1.2 \times 10^{-3}$) is observed for Zn-tetrabenzoporphyrin solutions. For metal-free tetrabenzoporphyrin, the absolute quantum yield of 'blue' fluorescence is nearly an order of magnitude lower (1.8×10^{-4}). It was also found that tetrabenzoporphyrin complexes with metals with partly filled *d*-shell exhibit no 'blue' fluorescence detectable under conditions of single-quantum excitation.

In a study[66] of Co(II) and Ni(II) complexes with crown ethers and phthalocyanine derivatives it was shown that the $S_2 \rightarrow S_1$ internal conversion time is shorter than 500 fs. Effect of complexation of *meso*-tetraphenylporphyrins (TPP) with trivalent Y, Lu and Th on the 'blue' fluorescence has been studied.[67] All the complexes under study, *viz.*, YTPP(acac), LuTPP(acac) and ThTPP(acac), exhibit fluorescence from the S_2 level with nearly equal quantum yields (0.001). In contrast to this, the quantum yield of usual fluorescence of these complexes decreases substantially in the above-mentioned order, which indicates that intersystem crossing has no effect on quenching of the S_2 level of porphyrins. No fluorescence from the second singlet level was found for free base TPP.[67,68] In spite of nearly equal energy gaps $\Delta E(S_2-S_1)$ for metal complexes with octaethylporphyrins (OEP) and TPP, such OEP as H_2OEP, AlClOEP and ZnOEP exhibit no $S_2 \rightarrow S_0$ fluorescence.[68] $S_2 \rightarrow S_0$-Fluorescence of tetra-*para*-tolylporphyrin complexes with Sm(III), Eu(III), Gd(III), Tb(III), Yb(III) and Lu(III) in ethanol has been studied.[69] Weak quenching (by factors of $\sim$1.5 to 3.0) of fluorescence of paramagnetic complexes with Gd(III), Sm(III) and Tb(III) as well as strong quenching of fluorescence for the complexes with Eu(III) and Yb(III) was explained by the appearance of charge-transfer states lying between the S_1 and S_2 levels on the energy scale. [Among lanthanide ions, Eu(III) and Yb(III) are known to possess the highest electron affinities.]

Due to the short lifetime of the S_2 state, 'blue' fluorescence of porphyrins is strongly polarised even in solutions of low viscosity (in contrast to usual $S_1 \rightarrow S_0$ fluorescence of organic compounds).[60] This feature was used[70] to separate out the $S_2 \rightarrow S_0$ fluorescence. Frequency modulation was performed using polarisers while signal measurements were carried out with an amplifier with synchronous detection. This experimental procedure allows one to separate out the desired fluorescence against the background of the impurity usual fluorescence, since the impurities emit natural light and their signal is not modulated. The quantum yield of S_2 fluorescence of Zn-ethioporphyrin under conditions of single-quantum excitation was 7.5×10^{-5}. An up-conversion study of the S_2 fluorescence decay and S_1 fluorescence rise of Zn(TPP) complexes in ethanol has been reported.[71] It was shown that the decay of the S_2 fluorescence at 430 nm and the rise of the S_1 fluorescence near 600 nm are characterised by the same time constant of 2.3 ps. A more complex picture is observed for the spectral region between these bands, which indicates a contribution of 'hot' luminescence.

$S_2 \rightarrow S_0$-Fluorescence studies of dye molecules under conditions of single-quantum excitation have been carried out taking Brilliant Green[72] and Malachite Green[73,74] dyes as examples.

Lipsky *et al.*[75–77] studied single-quantum induced fluorescence of aromatic molecules from the second and upper levels. Alkylbenzenes were excited with a Hg resonance line at $\lambda = 184.9$ nm (the vacuum UV spectral region). Very weak $S_2 \rightarrow S_0$ (or $S_3 \rightarrow S_0$) fluorescence bands appeared on the short-wavelength wing of the usual fluorescence spectra. To single them out, quenchers of usual fluorescence (CCl_4, CCl_3H, cyclo-C_7F_{14}) were added to the solutions. In contrast to usual fluorescence,

Table 3. Characteristics of nonradiative transitions from the second (or upper) singlet levels in a number of organic molecules.

Compound	Solvent	$E(S_2)$ /cm^{-1}	$\Delta E(S_2-S_1)$ /cm^{-1}	$q_{fl\,20}$	$k_{r\,20}$ /s^{-1}	$\tau(S_2)$ /ps	$k_{nr\,21}$ /s^{-1}	Ref.
Zn-Tetrabenzoporphyrin	–	23 300	7400	1.2×10^{-3}	5.2×10^{8}	3	3.3×10^{11}	65
		–	–	(1.6×10^{-3})	–	–	–	63
Zn-Ethioporphyrin	DMF	24 450	7200	7.5×10^{-5}	–	–	–	70
Tetrabenzoporphyrin	"	–	–	1.8×10^{-4}	–	0.4	2.5×10^{12}	70
Brilliant Green	ethanol, 77 K	21 800	6300	1.0×10^{-4}	5×10^{7}	2	5×10^{11}	72
p-Xylene	isooctane	41 000	6600	2.9×10^{-5}	2.9×10^{8}	0.1	1.0×10^{13}	75
	"	–	(34 400)	(1.3×10^{-5})	–	–	(1.5×10^{14})	77
	"	48 800 (see [a])	7800 (see [b])	1.2×10^{-5}	3.0×10^{9} (see [c])	0.004	2.5×10^{14}	75
		–	–	(5×10^{-6})	–	–	–	77
Naphthalene	"	44 050 (see [a])	–	2.2×10^{-5}	–	–	(8×10^{13})	76
	"	–	–	(2×10^{-5})	–	–	–	77
Pyrene	"	36 000 (see [a])	7000	5×10^{-6}	–	–	–	76

Note. Measurements were carried out using direct single-quantum excitation technique at room temperature. The values obtained from measurements in the vapour phase are given in parentheses. [a] The $E(S_3)$ value, [b] the $E(S_3-S_2)$ value, [c] the $k_{r\,30}$ value.

almost no quenching of the S_2 and S_3 fluorescence occurs due to the short lifetimes of these states. Presumably, impurity emission that precludes the observation of fluorescence from HESS of the molecules under study is also quenched simultaneously. Selected characteristics of nonradiative transitions in these molecules are listed in Table 3. High rates of internal conversion and small differences between them in solutions and as vapours, indicative of intramolecular process, are noteworthy.

Carotenoids play an important role in many processes occurring in living organisms. In particular, they serve as pigment protectors in cells of green plants and purple bacteria against their destruction by singlet oxygen. A systematic study of fluorescence of β-carotenes and their analogues, linear polyenes, has been carried out.[78] It was found that the energy gap $\Delta E(S_1-S_0)$ becomes narrower and the yield of usual fluorescence decreases as the polyene chain length increases. The fluorescence yield decreases from 7×10^{-3} for the polyene with five conjugated bonds down to 4×10^{-6} for β-carotene (solutions in hexane at room temperature). Among the compounds under study, the longest molecular chains were those of decapreno-β-carotene and dodecapreno-β-carotene with 15 and 19 double bonds, respectively. These compounds exhibited only S_2 fluorescence with the quantum yield $q_{fl\,20}\approx5\times10^{-5}$. The S_2 state lifetime, $\tau(S_2)$, estimated from q_{fl20} was ~100 fs. Therefore, despite the decrease in the usual fluorescence yield with lengthening of the molecular chain, fluorescence from the second excited level of these molecules remains nearly constant.

Weak $S_2\rightarrow S_0$ fluorescence was observed in an anthracene crystal directly excited by a resonance Hg line at $\lambda=254$ nm.[79] The ratio of fluorescence yields from the S_2 and S_1 states was estimated at $\sim5\times10^{-6}$ and $\tau(S_2)$ was roughly estimated at $\approx10^{-13}$ s.

However, measurements of fluorescence spectra and quantum yields of fluorescence due to transitions from the second and upper excited singlet states under conditions of direct single-quantum excitation are impossible for most of fluorescent complex organic compounds. This is due to the low fluorescence quantum yields, superimposition of impurity luminescence in solvents and in insufficiently purified substances under study and to the Rayleigh and Raman scattering.

In conclusion, mention may be made of an interesting example of fluorescence from a triplet rather than singlet higher excited state.[80] Irradiation of 9,10-dibromoanthracene and 9-bromoanthracene solutions in undegassed hexane by a high-power Xe lamp resulted in weak fluorescence near 840 nm for the former and near 865 nm for the latter compound. This phenomenon was suggested to be due to the $T_2\rightarrow T_1$ radiative transition. Fluorescence was excited in the regions of conventional absorption spectra of these compounds. The T_2 levels were populated *via* $S_1\rightarrow T_2$ intersystem crossing. The T_2 levels of the molecules under study are near the corresponding S_1 levels on the energy scale and the energy gaps, $\Delta(T_2-T_1)$, are $\simeq12\,000$ cm^{-1}. The $T_2\rightarrow T_1$ fluorescence quantum yield was estimated at 8×10^{-7} and the T_2 state lifetime, $\tau(T_2)$, was estimated at $\simeq10^{-11}$ s.[80]

III. Fluorescence due to transitions from higher excited S_n levels under conditions of stepwise excitation of molecules

The appearance of pulsed laser excitation sources allowed studies of ultrafast relaxation processes from HESS using the stepwise excitation technique. Essentially, the method is as follows. Excitation of a molecule by the first quantum leads to population of the first (fluorescent) excited singlet state S_1. Being in the thermalised S_1 state, the molecule absorbs the second quantum, thus populating an upper excited singlet state (Fig. 2)

$$S_0+h\nu_1\rightarrow S_1+h\nu_2\rightarrow S_n\ (n\geqslant2).$$

This excitation technique allows easy observation of fluorescence spectra corresponding to $S_n\rightarrow S_0$ transitions ($n\geqslant2$) with quantum yields of the order of $10^{-6}-10^{-7}$. It appears to be

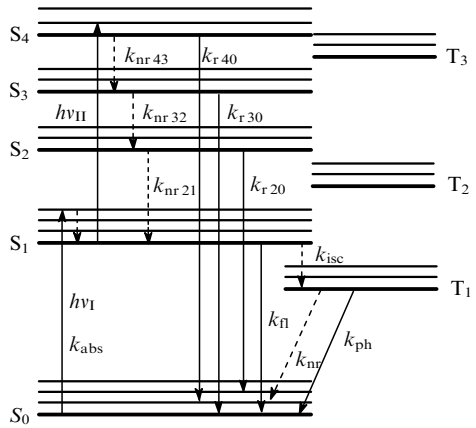

Figure 2. An energy level diagram illustrating nonradiative transitions between higher excited singlet states under conditions of two-quantum stepwise excitation and fluorescence due to transitions from the HESS to the ground state of the molecule;
$h\nu_I$ and $h\nu_{II}$ are the first and second excitation quanta, respectively.

particularly convenient when using tunable lasers generating nanosecond pulses and operating at repetition rates from 5 to 50 Hz. The method has the advantage that stepwise excitation has no effect on the fluorescent impurity molecules in the compound under study and in the solvent, whose absorption spectra are observed in the region of $S_n \leftarrow S_0$ ($n \geqslant 2$) transitions. In addition, the spectrum under study is not overlapped with the Raman spectrum since the latter is shifted up to 3000 cm^{-1} with respect to the former. To simplify the interpretation of the results obtained, nanosecond pulses were used with moderate radiation flux levels. (In this case, the use of picosecond and femtosecond laser pulses is less appropriate since it is accompanied by an increase in the contribution of two-photon excitation which affects also the impurity molecules). The best combination of molecular properties for performing stepwise excitation studies includes sufficiently high fluorescence yields, S_1 state lifetimes of the order of several nanoseconds and rather large absorption cross-sections for the $S_n \leftarrow S_1$ transitions.[81]

The first studies on fluorescence spectra corresponding to transitions from higher excited states to the ground state obtained by stepwise excitation technique date back to the late 1960s and early 1970s.[82–86] In particular, Terenin *et al.*[82] observed blue fluorescence of a chlorophyll solution excited by a high power ruby laser. Violet fluorescence of an aluminum phthalocyanine chloride solution was studied under similar conditions.[83] It was also found that the action of high-power radiation of a ruby laser on a solution of cyanine dye in methanol leads to the appearance of blue fluorescence with its intensity proportional to the squared exciting radiation intensity.[84] These results were subjected to criticism.[87,88] Blue fluorescence was suggested to be due to photochemical decomposition products of the dye. However, blue fluorescence was also observed in a CW excitation study of cryptocyanine.[89] The authors of this study found that the blue and red fluorescence excitation spectra match each other and the UV absorption spectrum in the UV spectral region. The quantum yield of the blue fluorescence was 10^{-4}.[89]

The potentialities of the stepwise excitation technique for studying fluorescence from higher excited states of complex molecules have been demonstrated in a series of studies by Lin, Topp *et al.*[90–95] They used a dye laser with an output of 0.1 to 0.5 mJ per ~ 5 ns pulse, pumped by a nitrogen laser operated at a repetition rate of up to 50 Hz. Fluorescence due to transitions from higher excited singlet states was detected using a monochromator and a photomultiplier with synchronous detection (the signal was averaged over 100–300 pulses). To eliminate scattered visible fluorescence, a light filter was placed in front of the monochromator. The advantages of consecutive stepwise excitation over simultaneous excitation by picosecond pulses with the same energy at the same wavelength were demonstrated taking rubrene as an example.

Stepwise excitation experiments can be performed even using a high-power CW laser. For instance, the $S_3 \rightarrow S_0$ fluorescence spectrum of tetracene (a solution in methylcyclohexane) was measured using an Ar laser with an output of 0.8 W at 233 K by focusing the laser light on a flow-through cell.[96] This is the first observation of fluorescence accompanying the transition from HESS of aromatic hydrocarbon molecules under conditions of stepwise excitation.

In studies of $S_n \rightarrow S_0$ fluorescence spectra of rhodamine B and rhodamine 6G (solutions in ethanol) at 300 K Lin and Topp[91] observed three prominent bands in the region 250–400 nm for each compound, at 275, 320 and 382 nm for rhodamine B and at 270, 310 and 377 nm for rhodamine 6G. The shapes of these band systems were found to be nearly mirror images of the three-band systems corresponding to electronic transitions in the absorption spectra of the dyes. The fluorescence band of rhodamine 6G at 377 nm matches that measured in the earlier[85,86] and more recent[97] studies. Polarisation spectrum measurements confirmed the presence of three electronic transitions in the observed fluorescence spectrum. It should be noted that positions of the fluorescence bands of the rhodamines at 382 and 377 nm remain virtually unchanged upon variation of the second quantum frequency from 22 000 to 18 000 cm^{-1}.

Stepwise excitation technique was used to study a large number of aromatic hydrocarbon molecules characterised by several electronic transitions in this spectral region.[92–95] It was shown that electronic relaxation of higher excited singlet states of organic molecules occurs until vibrational equilibration is established after the excitation event. Studies of $S_n \rightarrow S_0$ transitions in the 3,4,9,10-dibenzopyrene molecule revealed the appearance of a fine vibrational structure in the spectral region adjacent to the effective excitation frequency [$\nu_{ef} = \nu_{0-0}(S_1) + \nu_2$] after excitation by the second quantum (540–610 nm). It was found that this fine structure depends on the frequency of the second excitation quantum. The spacing between the observed bands (1460 ± 60 cm^{-1}) is close to that of the principal progression in the $S_1 \rightarrow S_0$ fluorescence spectrum (1440 ± 50 cm^{-1}). Topp and Lin[93] suggested that the observed vibrational structure of the spectrum is caused by the anti-Stokes Raman scattering; however, they did not rule out that a phenomenon similar to the Personov effect[98,99] is observed in this case.

Distinctions between the structures of the spectra measured near the excitation level have been found for centrosymmetric molecules and those without a centre of symmetry.[94] Under conditions of two-step excitation, selection rules forbid transitions of centrosymmetric molecules in those states from which radiative transitions to the S_0 ground state are allowed. Indeed, judging from the sum of the $S_1 \leftarrow S_0$ transition frequency and the second absorbed quantum frequency, in this case the fluorescence spectrum begins 'some distance' from its conventional position.

Stepwise excitation studies of a large number of fluorescent dyes and aromatic molecules in solutions at room temperature and at 77 K have been carried out.[100–106] It was found that intramolecular nonradiative transitions from higher excited singlet levels in dyes and most complex aromatic compounds in solutions occur in a cascade manner, *i.e.*, consecutively involving all the lower-lying electronic levels. This conclusion was drawn based on comparison of the shape of fluorescence spectra of organic molecules excited by the second quantum with varied frequency in states with different energies. The $S_n \rightarrow S_0$ ($n \geqslant 2$) fluorescence spectra of Magdale Red dye (a solution in ethanol) at 77 K are shown in Fig. 3 while those of 1,2-benzanthracene (a solution in ethanol) at 293 K are presented in Fig. 4. The spectra shown in Figs 3 and 4 exhibit prominent bands that are mirror images of corresponding $S_n \leftarrow S_0$ absorption bands. In addition, the intensity ratio of the $S_n \rightarrow S_0$ and $S_{n-k} \rightarrow S_0$ bands ($k < n$) remains constant as the energy of the second quantum varies.

The ratio of the areas under the bands corresponding to different $S_n \rightarrow S_0$ transitions characterises the relative quantum yield of a given fluorescence transition. Given the absolute quantum yield of a particular intramolecular transition, it is possible to determine the absolute quantum yields for other transitions. The corresponding radiative rate constant can be found from the area under that absorption band which is the mirror image of the fluorescence band of the given transition. Then, one can estimate the S_n state lifetimes

$$\tau(S_n) = \tau_r(S_n \leftarrow S_0)\, q_{fl}(S_n \rightarrow S_0).$$

Here, $\tau_r(S_n \leftarrow S_0)$ is the inverse of the rate constant for the $S_n \rightarrow S_0$ radiative transition and $q_{fl}(S_n \rightarrow S_0)$ is the fluorescence quantum yield. The fluorescence quantum yields and decay times thus obtained are listed in Table 4.

The results of analysis of the spectra presented in Figs 3 and 4 and those reported elsewhere[97,100–106] are sufficient to allow the following conclusions.

First, stepwise excitation of a molecule to an S_n ($n \geqslant 2$) state leads to the appearance of the spectral bands corresponding to the $S_n \rightarrow S_0$, $S_{n-1} \rightarrow S_0$, $S_{n-2} \rightarrow S_0$, *etc.* transitions in the fluorescence spectrum of the molecule.

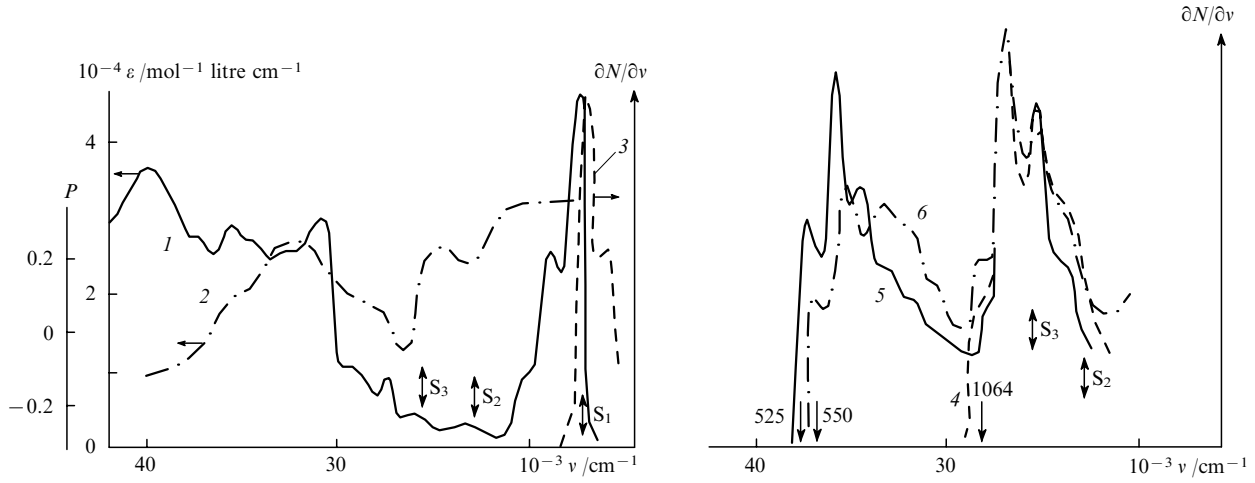

Figure 3. Magdale Red spectra (a solution in ethanol).
The $S_n \leftarrow S_0$ absorption spectrum at 77 K (*1*); polarisation spectrum of $S_1 \rightarrow S_0$ fluorescence excitation as function of excitation frequency at 293 K (a solution in glycerol) (*2*), see also a separate *P* scale; $S_1 \rightarrow S_0$ fluorescence spectrum at 77 K (*3*) and $S_n \rightarrow S_0$ ($n \geqslant 2$) fluorescence spectra (*4–6*) obtained under conditions of stepwise excitation from the S_1 state at λ_{exc} = 1064, 550 and 525 nm, respectively. Double vertical arrows denote the energy levels of S_n electronic states on the frequency scale. Single arrows denote the energy levels achieved under conditions of stepwise excitation. *N* is the number of absorbed quanta.

Second, for most of molecules (except for those characterised by strongly different equilibrium nuclear configurations in the S_1 and S_0 states) each band in the $S_n \leftarrow S_0$ absorption spectrum has a nearly mirror image in the $S_n \rightarrow S_0$ fluorescence spectrum.

Third, if excitation of a molecule by the second quantum leads to population of an upper S_k ($k > n$) state and if the S_n levels are populated by $S_k \rightsquigarrow S_{k-1} \rightsquigarrow S_n$ electronic relaxation, the shape of fluorescence spectra and, in particular, the shape of particular bands corresponding to $S_n \rightarrow S_0$ transitions and the band intensity ratios are in most cases independent of the energy of the second quantum.

Fourth, distortion of the fluorescence spectra from higher excited states is observed only if the total energy of the $S_1 \rightarrow S_0$ transition and the second excitation quantum is larger than the ionization energy of the molecule under study in solution (see Figs 3 and 4).

To obtain additional experimental verification of the assumption of cascade character of intramolecular electronic relaxation, the absolute quantum yields ($q_{fl\,n0}$) of $S_n \rightarrow S_0$ fluorescence were measured at different energies of the second excitation quantum. By the quantum yield of fluorescence due to intramolecular transitions from higher excited electronic states under conditions of stepwise excitation is meant the ratio of the number of the quanta emitted in the form of $S_n \rightarrow S_0$ fluorescence to the number of molecules excited to the S_n state. Determination of $q_{fl\,n0}$ requires knowledge of the number of absorbed (the $S_n \leftarrow S_1$ transition) and emitted ($S_n \rightarrow S_0$ transition) quanta. The former parameter is complicated to calculate. Previously,[97, 100–106] it was estimated

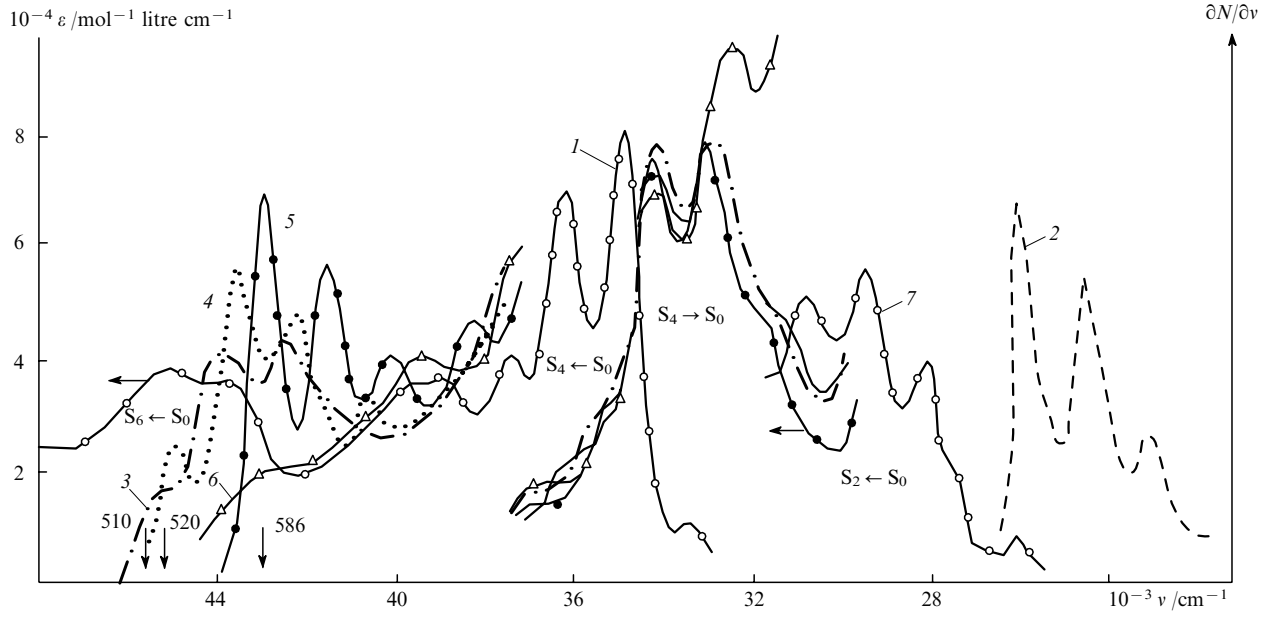

Figure 4. Spectra of 1,2-benzanthracene (a solution in ethanol) at 293 K.[72]
The $S_n \leftarrow S_0$ absorption (*1*) and $S_1 \rightarrow S_0$ fluorescence (*2*) spectra. The $S_n \rightarrow S_0$ ($n \geqslant 2$) fluorescence spectra obtained under conditions of stepwise excitation from the S_1 state at λ_{exc} = 510, 520, 586 and 340 nm, respectively (*3–6*); enlarged representation of the $S_n \leftarrow S_0$ absorption spectrum (*7*) (8 times along the ordinate axis). The spectral width of the instrumental response function was 200 cm^{-1}.

Table 4. Characteristics of transitions from the HESS of organic molecules (fluorescence spectra and yields were measured using stepwise excitation technique).

Compound	n	ΔE_{n0} /cm^{-1}	$\Delta E_{n,n-1}$ /cm^{-1}	$q_{\mathrm{fl}\,n0}$	$k_{\mathrm{r}\,n0}$ /s^{-1}	$k_{\mathrm{nr}}(S_n \rightarrow S_{n-1})$ /s^{-1}	τ_n /ps	Ref.
Solvent — ethanol, 77 K								
Brilliant Green	2	21 800	6300	1×10^{-4}	5×10^{7}	5×10^{11}	2	97
	4	30 600	4500	2×10^{-6}	8.3×10^{7}	4.2×10^{13}	0.024	
Rhodamine B	2	22 800	5100	3×10^{-6}	1×10^{7}	3.3×10^{12}	0.3	97
	3	24 600	1800	4×10^{-6}	1.4×10^{7}	3.6×10^{12}	0.28	
	4	27 700	3100	1×10^{-5}	4×10^{7}	4.0×10^{12}	0.25	
	5	31 800	4100	4×10^{-6}	1.4×10^{8}	3.3×10^{13}	0.03	
Magdale Red	2	23 300	6000	1.5×10^{-6}	8.3×10^{6}	5.6×10^{12}	0.18	97
	3	25 500	2200	4.5×10^{-6}	1.3×10^{7}	3.0×10^{12}	0.33	
Solvent — ethanol, 293 K								
Rhodamine 6G	2	24 300	5600	2×10^{-6}	1×10^{7}	5.0×10^{12}	0.2	97
	3	25 650	–	–	–	–	–	
	4	28 400	2750	1×10^{-5}	5×10^{7}	5.0×10^{12}	0.2	
Pyrene	4	36 300	6000	7×10^{-6}	4×10^{8}	5.0×10^{13}	0.02	97
	5	41 000	4700	1.8×10^{-5}	5×10^{8}	2.9×10^{13}	0.035	
	6	~44 500	~3500	$\sim6\times10^{-6}$	$\sim3\times10^{8}$	$\sim4.5\times10^{13}$	~0.022	
1,2-Benzanthracene	4	34 500	1100	4×10^{-5}	6.7×10^{8}	1.7×10^{13}	0.06	97
	5	38 500	4000	1.3×10^{-5}	5×10^{8}	3.8×10^{13}	0.026	
	6	43 000	4500	1.3×10^{-5}	7×10^{8}	5.6×10^{13}	0.018	
9,10-Di-*n*-propylanthracene	2	37 700	< 3000	3×10^{-5}	1.4×10^{8}	4.3×10^{13}	0.023	107
α-Naphthylphenyloxazole	2	35 300	7800	4×10^{-6}	(1.6×10^{8})	–	(0.024)	104
	3	41 000	5700	5.6×10^{-6}	(6.7×10^{8})	–	(0.010)	
3,4.9,10-Dibenzopyrene	2	25 500	2300	–	–	–	0.2	95
	3	30 100	4600	–	–	–	> 0.1	
	4	34 100	4000	–	–	–	0.08	
	5	37 600	3500	–	–	–	–	
	6	41 500	3900	5×10^{-5}	2.2×10^{9}	–	0.04	

Note. The values estimated from the linewidths in structured fluorescence spectra and unreliable results due to difficulties of the determination of the emission rate constant owing to changes in the molecular configuration in the excited state are given in parentheses.

from changes in the intensity of transmitted laser radiation with the frequency ν_2 upon turning on a laser with the frequency ν_1 and from the amplitude of additional opto-acoustical signal which appeared upon simultaneous illumination of the object under study by two laser pulses.[107]

The fluorescence quantum yield was also estimated [108] from the following relationship

$$q_{\mathrm{fl}\,n0} = \frac{I_{\mathrm{fl}\,n0}}{I_{\mathrm{fl}\,10}\sigma_{1n}I_{\mathrm{ex}\,2}\tau_{\mathrm{r}1}},$$

where $I_{\mathrm{fl}\,n0}$ and $I_{\mathrm{fl}\,10}$ are the integrated intensities of the S_n and S_1 fluorescence, respectively; σ_{1n} is the absorption cross-section for the $S_n \leftarrow S_1$ transition, $I_{\mathrm{ex}\,2}$ is the power density of exciting radiation with the frequency ν_2 and $\tau_{\mathrm{r}1}$ is the radiative lifetime of the S_1 state.

Table 5 lists the results obtained for α-naphthylphenyloxazole, pyrene and 1,2-benzanthracene. As can be seen, the $q_{\mathrm{fl}\,n0}$ values are independent of energy of the second quantum within the experimental error. This is a strong argument in favour of the cascade mechanism of electronic relaxation of HESS.

Let us analyse the spectra of fluorescence accompanying transitions from the HESS of most of the molecules studied, obtained under conditions of stepwise excitation. The following picture is observed in the region adjacent to the frequency corresponding to the sum of the energies of the S_1 state and the second excitation quantum. The $S_n \rightarrow S_0$ fluorescence spectra (S_n is the state directly populated by absorption of the second quantum) exhibit a more pronounced vibrational structure compared to the $S_n \leftarrow S_0$ absorption spectra of the same molecules obtained under the same conditions and to the fluorescence

Table 5. Absolute $S_n \rightarrow S_0$ fluorescence quantum yields ($q_{\mathrm{fl}\,n0}$) measured using stepwise excitation technique.[97, 104]

Compound	ν_1 /cm^{-1}	ν_2 /cm^{-1}	Energy level to be excited	$10^6 q_{\mathrm{fl}\,n0}$ (see [a])	$10^6 q_{\mathrm{fl}\,n0}$ (see [b])
α-Naphthyl-phenyl-oxazole	27500	16 950	S_3	4.0 ± 0.8	5.6 ± 1.5
		18 200	S_3	3.5 ± 0.8	4.9 ± 1.5
		19 250	S_4	4.2 ± 0.8	5.8 ± 1.5
Pyrene	26000	16 950	S_4	3.0 ± 1.0	3.5 ± 1.0
		18 200	S_5	4.0 ± 1.5	4.5 ± 1.5
		19 250	S_6	5.0 ± 2.0	6.0 ± 2.0
1,2-Benz-anthracene	25900	16 950	S_5	35 ± 8	–
		18 200	S_6	35 ± 8	–
		19 250	S_6	35 ± 8	–

Note. Measurements were carried out in ethanol solutions at 293 K.
[a] Given are the $q_{\mathrm{fl}\,20}\times10^6$ values ($\nu_{\max} \approx 33\,200$ cm^{-1}) for α-naphthyloxazole and $q_{\mathrm{fl}\,40}\times10^6$ values ($\nu_{\max} \approx 34\,500$ cm^{-1}) for pyrene and 1,2-benzanthracene; [b] given are the $q_{\mathrm{fl}\,30}\times10^6$ values ($\nu_{\max} \approx 39\,300$ cm^{-1}) for α-naphthyloxazole and $q_{\mathrm{fl}\,50}\times10^6$ values ($\nu_{\max} \approx 41\,500$ cm^{-1}) for pyrene.

spectra from the HESS populated *via* relaxation from higher excited levels (see Figs 3 and 4).

Positions of all the fluorescence bands observed depend on the frequency of the second quantum. On the other hand, neither the structure nor the relative intensities of the fluorescence bands corresponding to transitions from the lower-lying HESS populated *via* relaxation remain unchanged (see curves *4–6* in Fig. 3 and curves *4* and *5* in Fig. 4).

If the frequency of the second excitation quantum varies within $\Delta\nu_2 < 1500$ cm^{-1}, the entire spectral region in question (it will be remembered that this is a region of the fluorescence spectrum) is shifted simultaneously with the position of the level to be populated. An increase in $\Delta\nu_2$ leads to substantial redistribution of vibronic band intensities. Further increase in the frequency ν_2 (by several thousands of cm^{-1}) causes the appearance of spectral bands corresponding to emission of nearly the same intensity; however, the new bands exhibit no pronounced vibrational structure.

The appearance of structured $S_n \rightarrow S_0$ fluorescence spectra can probably be rationalised by the effect of selective excitation of molecules with a particular configuration into a broad $S_n \leftarrow S_0$ absorption band by spectrally narrow (~ 0.5 cm^{-1}) radiation with the frequency ν_2. Due to ultrashort lifetimes of the S_n states (10 – 100 fs) of those molecules which exhibit structured spectra, inhomogeneous line broadening in the $S_n \leftarrow S_1$ absorption spectrum can be considered as manifestation of specific molecular conformations due to low-frequency, out-of-plane vibrations of the aromatic rings.

This explanation is also supported by the fact that Brilliant Green and Zn-tetrabenzoporphyrin exhibit no structured spectra upon excitation of the relatively long-lived ($\sim 1-3$ ps) S_2 state. On the other hand, stepwise excitation of Brilliant Green by the second quantum ($\lambda_2 = 500-620$ nm) and population of the S_5 level ($\tau_5 \leqslant 24$ fs) leads to the appearance of a structured spectrum. This is consistent with the assumption that the structured spectra are observed upon transitions from electronically and vibrationally unrelaxed states, while the excited states with the picosecond lifetimes undergo at least partial vibrational relaxation.

It was assumed [97, 103] that the effect in question (the appearance of structured spectra) is to some extent similar to the Personov effect, *i.e.*, the appearance of the $S_1 \rightarrow S_0$ fluorescence spectra with well-resolved fine structure under the action of selective laser excitation of organic molecules in solid solutions at 4 K (see Refs 98 and 109).

There are some distinctions between these effects. First, a structured spectrum appears in the case where one electronic transition ($S_n \leftarrow S_1$) is selectively excited while another transition ($S_n \rightarrow S_0$) is used for the detection of structured emission. Conventional Personov effect is not observed in this situation since the two transitions are uncorrelated. Second, structured spectra are observed in liquid solutions without cooling them down to the liquid helium temperature (though liquid solutions can be considered as solid ones during a time of the order of tens of femtoseconds). Third, corresponding vibronic levels are noticeably broadened (up to hundreds of cm^{-1}) due to the short lifetimes of the excited states, whereas in the case of the Personov effect the linewidths are equal to hundredth and thousandth fractions of cm^{-1}. Finally, structured spectra appeared under conditions of stepwise excitation are observed only for those molecules for which the 0 – 0 band of the $S_1 \rightarrow S_0$ transition is only slightly inhomogeneously broadened.

The appearance of a structured fluorescence spectrum under conditions of stepwise excitation was explained in another manner.[110] The authors of this study assumed that the observed fluorescence is due to anti-Stokes resonant vibronic Raman scattering (ARVRS). An energy level diagram illustrating the proposed [110] formation mechanism of structured emission spectrum is shown in Fig. 5. ARVRS occurs if excitation of a molecule to the S_1 state after absorption of the first quantum is followed by absorption of the second excitation quantum with the frequency ν_2. As a result, transition of the molecule to a vibrational electronic ground-state level is accompanied by scattering of a quantum corresponding to the frequency $\nu_2 + \nu_{0-0}(S_1-S_0) - \Sigma n_i \nu_i$. Later, the authors of other studies [108, 111, 112] supported this explanation and pointed to the similarity of the observed spectrum and the usual fluorescence spectrum shifted towards the high-frequency region.

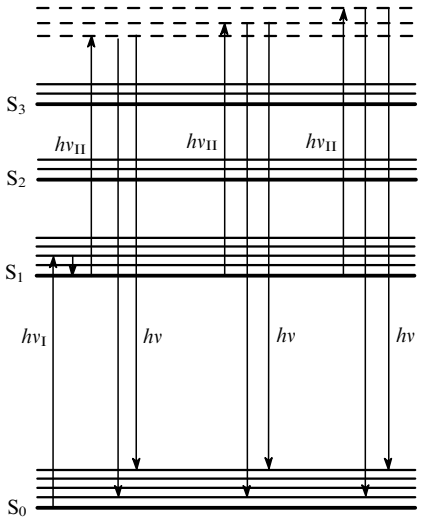

Figure 5. An energy level diagram illustrating the ARVRS mechanism. Dashed lines denote virtual energy levels involved in the Raman scattering. Vertical lines corresponding to ARVRS are denoted as $h\nu$.

Nevertheless, we dissent from the proposed [110] explanation for the experimental observations. Let us adduce some arguments in favour of the interpretation of structured emission appearing under conditions of stepwise excitation of organic molecules as fluorescence.

If an excited level is populated *via* relaxation from upper levels rather than by direct excitation, the integrated intensity of the structured spectrum is nearly the same as the emission intensity in the same spectral region.[97]

The bands in the structured spectrum are much broader than those in the $S_1 \rightarrow S_0$ fluorescence spectrum. On the other hand, the ARVRS mechanism requires that the width of the short-wavelength band in the structured spectrum obtained under conditions of stepwise excitation and the width of the 0 – 0 band in the $S_1 \rightarrow S_0$ fluorescence spectrum be equal.

If a molecule in the S_1 state is excited by a second quantum and if the energy of this quantum is sufficiently high for the molecule to undergo photoionisation, the fluorescence yield from higher excited states should decrease dramatically. It is just the situation that is observed in the experiments. For instance, in the case of rhodamine B the fluorescence yield from HESS decreases by more than an order of magnitude as the frequency ν_2 is varied from 19 000 cm^{-1} to $\nu_2 > 32\,000$ cm^{-1}. Assuming that structured emission is due to ARVRS, there is no grounds for such a large decrease in the emission intensity, since the process involves only virtual high-lying states.

Nonradiative energy transfer from a higher excited state of 1,2-benzanthracene, which was stepwise excited to the region of structured spectrum, to benzene and xylene molecules has been observed.[112] This transition was interpreted as ARVRS. However, the authors of this study noted that nonradiative energy transfer from the virtual levels involved in ARVRS is rather strange.

The problem of 'hot' fluorescence bands in emission spectra due to transitions from HESS has been considered.[113] If a molecule excited to an upper singlet state by the second quantum relaxes to a lower-lying HESS, a substantial excess vibrational energy is stored in the latter state. Hence, it is logical to expect the appearance of 'hot' fluorescence bands in the emission spectrum from this state. If the HESS lifetimes are shorter than the time of vibrational energy redistribution within a complex molecule, the intensities of 'hot' fluorescence bands are determined by the population probability of the states in question *via* internal conversion from upper electronic states and by the rate of the initial stage of energy exchange between the optically active and inactive vibrations. At first glance, the intensities of 'hot' bands in

the emission spectrum must be strongly dependent on the excess vibrational energy in the emitting S_n ($n > 1$) state and, hence, on the energy of the second quantum. However, as can be seen in Fig. 4, the $S_4 \rightarrow S_0$ fluorescence bandshape of 1,2-benzanthracene depends only slightly on the second-quantum energy when it is varied from 17 100 to 28 200 cm^{-1} (for the S_4 state, this corresponds to an excess vibrational energy lying between 8400 and 19 500 cm^{-1}). Considering a 'hot' fluorescence band lying 1400 cm^{-1} above the 0–0 band of the $S_4 \rightarrow S_0$ transition, Lyubimtsev [113] has come to the conclusion that cascade relaxation passes through an optically active vibrational state (1400 cm^{-1}) with a unit probability.

IV. Lifetimes of higher excited S_n states estimated from fluorescence quantum yields and absorption integrals

Determination of a HESS lifetime requires knowledge of the ratio of absolute quantum yield of $S_n \rightarrow S_0$ fluorescence to the number of absorbed second quanta and the radiative rate constant for the same transition. The latter parameter can be estimated using the absorption integral for the band corresponding to the $S_n \leftarrow S_0$ transition.[114, 115]

$$\tau_n = \frac{q_{\mathrm{fl}\,n0}}{k_{\mathrm{r}\,n0}}.$$

A number of studies concerning this subject have been reported.[97, 100, 106] It was found that the HESS lifetimes of organic molecules in solutions vary from several picoseconds for the S_2 states of certain molecules to 10–20 fs for the S_n states, $n = 3–6$. The τ_n values of the order of tens of femtoseconds mean that the electronic relaxation rates of these states are higher than the intramolecular vibrational relaxation rates which were estimated at hundreds of femtoseconds.[19, 116, 117] Elsaesser and Kaiser [20] proposed to distinguish between two types of vibrational excitation relaxation, *viz*., fast relaxation for the energy redistribution between isoenergetic vibrational states and slow relaxation corresponding to the relaxation to lower-lying energy levels. Transfer of excess vibrational energy from the molecule under study to the environment (solvent molecules) proceeds at lower rates and is characterised by the times of the order of several tens of picoseconds.[19, 116] Therefore, the cascade relaxation of the HESS of organic molecules (except for the S_2 state of a certain molecules) can be considered as occurring with conservation of the energy supplied to the molecules. Variation of the excess vibrational energy was found to have a slight effect on the band position and shape in the $S_n \rightarrow S_0$ fluorescence spectra, though in some cases this energy was varied by 10 000 cm^{-1} and more.

Electronic relaxation times of the HESS of aromatic and dye molecules are nearly equal to the period of optically active vibrations ($\nu = 1200–1600$ cm^{-1}) or even shorter.

To verify such interesting results, attempts have been undertaken at estimating the HESS lifetimes using other methods. For instance, the τ_v values were found from the line broadening in the structured spectra appearing upon selective excitation by the second quantum of the HESS lying near the initially excited state.[97, 104] The spectral widths of vibronic bands (the first vibronic band) in such spectra were compared with the spectral width of the 0–0 band in the usual fluorescence spectrum. In those cases where the 0–0 bands were only slightly inhomogeneously broadened (pyrene, 1,2-benzanthracene, phenanthrene, $T = 77$ K), the structured spectra were additionally broadened. Assuming that the broadening of the upper (S_n) and lower (S_1, S_0) levels is uncorrelated, the broadening $\Delta\nu'_{n0}$ due to the short lifetime of the S_n state (*i.e*., the homogeneous width) was estimated using the formula

$$\Delta\nu'_{n0} = \sqrt{[\Delta\nu_{n0}(S_n - S_0)]^2 - [\Delta\nu_{10}(S_1 - S_0)]^2},$$

where $\Delta\nu_{v0}$ and $\Delta\nu_{10}$ are the halfwidths of the corresponding bands.

The broadening calculated using this formula (300 cm^{-1} for the S_6 states of pyrene and 1,2-benzanthracene) corresponds to the lifetime of these states, $\tau_6 = 18$ fs.

These τ_6 values are in reasonable agreement with the estimates obtained for pyrene ($\tau_6 = 15–30$ fs) and 1,2-benzanthracene ($\tau_6 = 18$ fs) from the absolute quantum yields of fluorescence.

The rate constants for nonradiative transitions between the HESS are calculated using the absolute quantum yields of the $S_n \rightarrow S_0$ fluorescence and the radiative rate constants estimated from the band integral in the $S_n \leftarrow S_0$ absorption spectrum. It should be noted that the results of calculations of the absorption band integral refer to the molecule which is in the S_0 state and has its equilibrium configuration. However, the molecule excited from the S_1 state to a HESS after absorption of the second quantum retains the configuration of the former state. If the equilibrium molecular configurations in the S_1 and S_0 states differ only slightly, these estimates of τ_v are justified. However, in some cases (*e.g*., *p*-terphenyl or 2,5-diphenyloxazole) the molecular configuration in the excited (S_1) state is substantially different from the ground-state (S_0) configuration. This manifests itself in different patterns of their absorption and usual fluorescence spectra. According to X-ray diffraction data, the ground-state structure of the *p*-terphenyl molecule is nonplanar.[118] On the other hand, quantum-chemical calculations [119] showed that in the case of fluorescence emission this molecule has a nearly planar configuration. Clearly, the oscillator strengths of electronic transitions and the corresponding energy levels can vary over a wide range upon changes in the molecule geometry (Fig. 6).

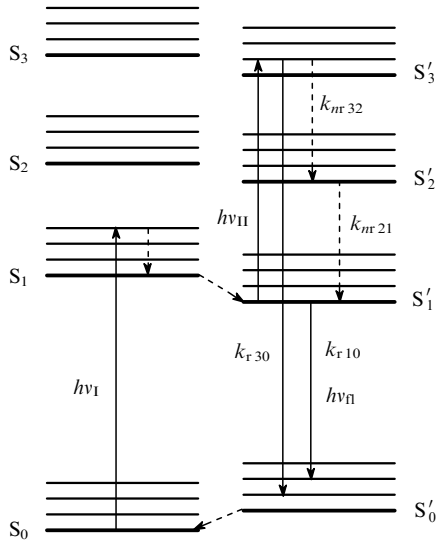

Figure 6. An energy level diagram illustrating two-quantum stepwise excitation of a molecule in the case of variations of the molecular configuration or solvate environment during the lifetime of the fluorescent (S_1) state. The energy levels belonging to the triplet manifold are not shown.

V. Delayed fluorescence from higher excited S_n states due to triplet–triplet annihilation

As has been shown experimentally,[120] annihilation of two molecules being in the lowest triplet state (the so-called triplet–triplet annihilation) can lead to generation of both the first and upper excited singlet (and triplet) states of the molecules:

$$T_1 + T_1 \rightarrow S_n + S_0, \; n \geqslant 1.$$

This process leads to the appearance of not only the usual $S_1 \rightarrow S_0$ fluorescence, but also the $S_n \rightarrow S_0$ ($n > 2$) delayed fluorescence due to triplet–triplet annihilation. This feature was used to detect the phenomenon in question. The first successful experiments were carried out taking 1,2-benzanthracene and fluoranthene dissolved in paraffin oil as examples. A schematical energy level diagram of the interacting molecules is shown in Fig. 7.

Triplet–triplet annihilation studies of a number of aromatic compounds, *e.g.*, naphthalene (S_2), phenanthrene (S_3), triphenylene (S_3), 1,2-benzanthracene (S_3), pyrene (S_2), chrysene (S_3), fluoranthene (S_4) and *N*-methylcarbazole (S_4, S_2?), anthraquinone (S_3, S_4), xanthone (S_3) have been carried out.[121–124] (The singlet state generated after triplet–triplet annihilation is given in parentheses.)

Triplet–triplet annihilation induced fluorescence from the HESS is observed using a phosphoroscope. This allows effective suppression of the stray exciting light, though the usual fluorescence light [it is nearly four orders of magnitude more intense than the $S_n \rightarrow S_0$ ($n \geqslant 1$) fluorescence] remains. In contrast to the stepwise excitation method, triplet–triplet annihilation technique does not allow variation of the energy of the second quantum over a wide range. However, in the former case it is difficult to observe the region near the short-wavelength limit of the usual fluorescence in the fluorescence spectra from HESS, since this spectral region is, as a rule, used for excitation of the molecule under study to the S_1 state by the first quantum. As a result, the stray light precludes measurements of the weak $S_n \rightarrow S_0$ ($n \geqslant 1$) fluorescence spectrum. Triplet–triplet annihilation techniques provides much better conditions for the observation of this spectral region (Fig. 8).

Delayed fluorescence spectra of 1,2-benzanthracene, fluoranthene, pyrene and chrysene solutions in methylcyclohexane at 193 K were obtained by triplet–triplet annihilation technique and corrected for the quantum spectral sensitivity of the experimental setup.[121] All the above-mentioned compounds exhibit clearly seen

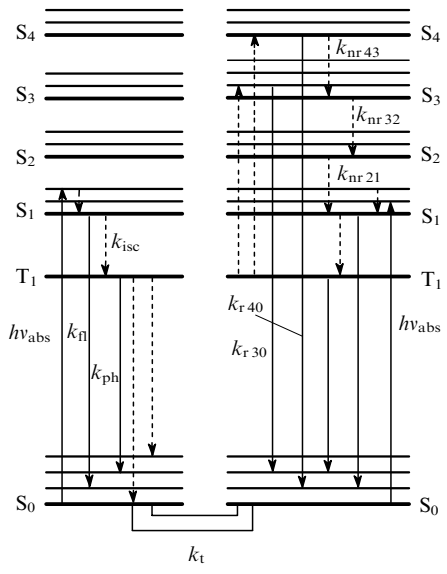

Figure 7. Schematic representation of energy level diagram for nonradiative transitions between higher excited singlet states of a molecule (fluorescence corresponding to transitions from the HESS to the ground state due to triplet–triplet annihilation). Vertical solid and dashed lines denote radiative and intramolecular nonradiative transitions, respectively. The system of dashed lines linked by upward-looking brackets (see the bottom of the diagram) corresponds to the interaction between two triplet molecules accompanied by energy transfer from one to the other molecule and excitation of the latter to a higher excited singlet state (k_t). The energy level diagram for the system of higher excited triplet states of the molecules and the scheme illustrating their triplet–triplet annihilation induced excitation are not shown.

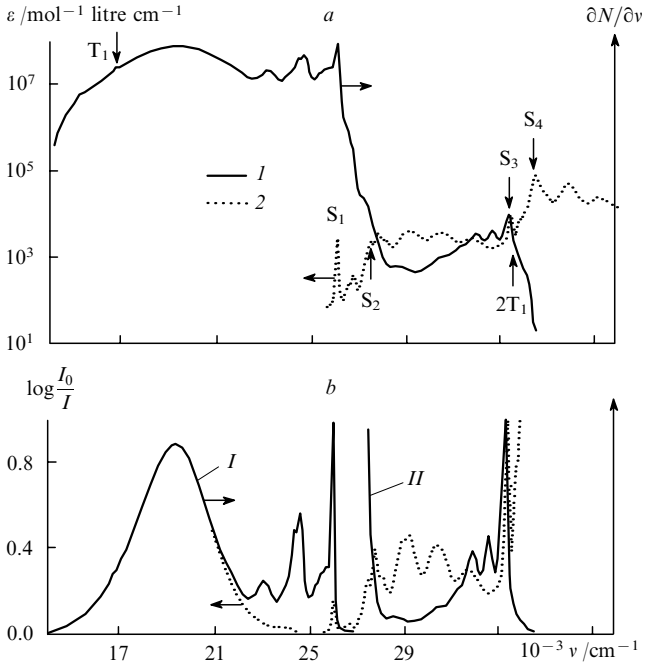

Figure 8. Spectrum of delayed fluorescence due to triplet–triplet annihilation (*1*) and absorption (*2*) spectrum of 1,2-benzanthracene (a 5×10^{-5} mol litre^{-1} solution in methylcyclohexane) measured at $\lambda_{exc} = 365–366$ nm ($T = 193$ K) (I_0 is the initial intensity).
The 'as-measured' (*I*) and expanded (9150 times along the ordinate axis, *II*) representation of the spectra.[121]

$S_n \rightarrow S_0$ fluorescence spectra. In some instances, the $S_n \rightarrow S_0$ fluorescence band appears to be a mirror image of the $S_n \leftarrow S_0$ absorption band, as in the stepwise excitation studies.

$S_n \rightarrow S_0$-Fluorescence spectra of *N*-methylcarbazole (NMC) dissolved in heptane and toluene (Tol) have been studied.[123] Triplet–triplet annihilation was found to induce both fluorescence from HESS of the NMC molecules and sensitised fluorescence of toluene, which is due to the nonradiative energy transfer from the HESS of *N*-methylcarbazole to the toluene molecule. This process can be schematically described as follows:

$$T_1(\text{NMC}) + T_1(\text{NMC}) \rightarrow S_n(\text{NMC}) + S_0(\text{NMC}),$$

$$S_n(\text{NMC}) \rightarrow S_0(\text{NMC}) + h\nu_{fl},$$

$$S_n(\text{NMC}) + S_0(\text{Tol}) \rightarrow S_0(\text{NMC}) + S_1(\text{Tol}),$$

$$S_1(\text{Tol}) \rightarrow S_0(\text{Tol}) + h\nu_{sens\ fl}.$$

Triplet–triplet annihilation of Cd-tetrabenzoporphyrin molecules also induces delayed fluorescence from the S_2 state.[125] In this case, the triplet state was sensitised by triplet–triplet energy transfer from Pd-tetraphenylporphyrin molecules which exhibit only weak S_2 fluorescence [$q_{fl}(S_2 \rightarrow S_0) < 10^{-5}$].

Hetero-triplet–triplet annihilation of azulene and fluoranthene solution in isopentane leads to the appearance of fluorescence from the second excited singlet level of azulene.[126, 127] These studies allowed the determination of the lifetime of the lowest triplet state for azulene (48 μs) and the quantum yields of intersystem crossing for this molecule, $q(S_1 \rightarrow T_1) = 4 \times 10^{-6}$ and $q(S_2 \rightarrow T_1) = 4 \times 10^{-2}$. The rate constants for intersystem crossing, corrected for the lifetimes of azulene molecule in the S_1 and S_2 states (see Table 1), were found to be $k(S_1 \rightsquigarrow T_1) = 2 \times 10^6$ s^{-1} and $k(S_2 \rightsquigarrow T_1) = 2.8 \times 10^7$ s^{-1}. Delayed $S_2 \rightarrow S_0$ fluorescence of 4,6,8-trimethylazulene due to homo-triplet–triplet annihilation was observed[128] at 27 680 cm^{-1} using sensitisation of triplet states by adding phenazine to the solution (the T_1 energy is 15 630 cm^{-1}). Hetero-triplet–triplet annihilation of anthracene and xanthone molecules was used[129] to study fluorescence from the S_6 ($^1B_{3u}^+$) level of anthracene, perdeuterated anthracene and

9,10-dimethylanthracene in their solutions in 1,1,2-trichlorotrifluoroethane. The intensity ratio of the $S_6 \rightarrow S_0$ fluorescence to the $S_1 \rightarrow S_0$ usual fluorescence was found to be $\sim 10^{-6}$. Triplet–triplet annihilation of biphenylene (an antiaromatic compound) sensitised with *N*-methylcarbazole in an isopentane–cyclopentane mixture at 178 K allowed the detection [130] of very weak $S_2 \rightarrow S_0$ fluorescence of this compound, which was not previously observed using direct excitation techniques (see Section II). This indicates a rather high sensitivity of the triplet–triplet annihilation method.

A method was proposed for increasing the intensity ratio of the fluorescence from the HESS and usual fluorescence.[123] It involves the addition of quenchers of the S_1 state to the solution under study. The potentialities of this method were demonstrated taking delayed fluorescence due to triplet–triplet annihilation of pyrene in the presence of efficient quenchers (diethylaniline and triethylamine) as an example. (The additives should be efficient quenchers of the lowest excited singlet state rather than the triplet state and be transparent to delayed $S_n \rightarrow S_0$ fluorescence due to triplet–triplet annihilation. They should also not enter into photochemical reactions with the compound under study.) This experimental technique was used in precise measurements of the $S_2 \rightarrow S_0$ fluorescence spectrum of pyrene.[123]

Interesting results were obtained [56] in studies of annihilation delayed fluorescence of 4*H*-1-benzopyran-4-thione (BPT) in perfluoro-1,3-dimethylcyclohexane. The experimentally determined probability of generation of the S_2 state by triplet–triplet annihilation was found to be 0.03. This is much lower than the statistical coefficient for the creation of a singlet state by triplet–triplet annihilation (0.25), obtained assuming that the quintet state is inaccessible from 'energy' considerations. The authors of this study mentioned that the probability obtained (0.03) is of the same order of magnitude as the known parameters for anthracene (0.08) and phenanthrene (0.02). The observed generation of the S_2 state of BPT by triplet–triplet annihilation was interpreted [56] as a special case of Förster's (exchange-resonance) energy transfer mechanism.‡ However, the lack of data on the $T_1 \rightarrow S_n$ absorption spectra of BPT precludes calculations of S_2 generation. Note that exchange-resonance mechanism of energy transfer between T_1 states should be common to processes of generation of both S_n and T_n states and that in the case of similar intensities of the spin-allowed and spin-forbidden transitions in the BPT molecule the $T_1 \rightarrow S_n$ spectra are indistinguishable from the $T_1 \rightarrow T_n$ ones.

The HESS lifetimes were estimated from the broadening of the 0–0 vibronic bands in the absorption spectra compared to the 0–0 band of the long-wavelength transition. Another method used for estimating the τ_v values involved the determination of (i) the quantum yield ratios of $S_n \rightarrow S_0$ fluorescence and delayed $S_1 \rightarrow S_0$ fluorescence under the same conditions and (ii) the rate constants for radiative $S_n \rightarrow S_0$ transitions from the absorption integrals for the corresponding $S_n \leftarrow S_0$ transitions. The estimates obtained are listed in Table 6.

Triplet–triplet annihilation technique has a drawback consisting in uncertainty in the identification of the annihilation-generated HESS, since the excitation probability distribution of these states is determined by the overlap integral of the $T_1 \rightarrow S_0$ emission and $S_n \leftarrow T_1$ absorption spectra normalised to a unit band area. Unfortunately, if the phosphorescence spectra are, as a rule, known, almost no information on the $S_n \leftarrow T_1$ absorption spectra is available. In the case of triplet–triplet annihilation, intersystem crossing becomes allowed in the $S_n \leftarrow T_1$ transitions; however, the effect of the Franck–Condon factors persists.[131]

Katoh and Kotani [132] studied fluorescence from the HESS of an anthracene crystal upon fusion of two singlet (S_1) excitons. They also investigated [133] $S_n \rightarrow S_0$ fluorescence of an anthracene crystal using a two-step laser excitation technique.

‡ Eisenberger *et al.*[56] pointed out that triplet–triplet annihilation of aromatic hydrocarbon molecules follows the exchange-resonance energy transfer mechanism. They used a much higher rate constant for the $T_1 \rightarrow S_0$ transition in BPT.

Table 6. Characteristics of transitions from the HESS of organic molecules.

Compound	n	ΔE_{n0} /cm^{-1}	$\Delta E_{n,n-1}$ /cm^{-1}	$q_{\mathrm{fl}\,n0}$	$k_{\mathrm{r}\,n0}$ /s^{-1}	k_{nr} ($S_n \rightarrow S_{n-1}$) /s^{-1}	τ_n /ps	Ref.
Solvent — isopentane–methylpentane mixture, T = 4 K								
Phenanthrene	2	33 900	5000	–	–	1.3×10^{13}	(0.08)[a]	144
	2	–	–	–	–	–	(0.5)[b]	146
Solvent — methylcyclohexane, T = 190 K								
Pyrene	2	29 600	2600	3.5×10^{-5}	3.8×10^{8}	1.1×10^{13}	0.09	123
	2	–	–	–	–	2.5×10^{13}	($\geqslant$0.04)	123
	4	36 300	6000	7×10^{-6}	4×10^{8}	5.0×10^{13}	0.02	123
Solvent — methylcyclohexane, T = 193 K								
1,2-Benzanthracene	3	33 400	5580	5.5×10^{-6}	4.2×10^{7}	7.7×10^{12}	0.13	121
Fluoranthene	4	34 700	3700	1.1×10^{-5}	4×10^{8}	3.8×10^{13}	0.026	121
	4	–	–	–	–	$\sim 2.0 \times 10^{13}$	($\sim$0.05)	121
Chrysene	3	36 800	6000	1.9×10^{-5}	10^{9}	5.3×10^{13}	0.019	121
	3	–	–	–	–	$\sim 5.9 \times 10^{13}$	($\sim$0.017)	121
Solvent — 1,1,2-trichloro-1,2,2-trifluoroethane, T = 243 K								
Anthraquinone	3	36 500	7000	10^{-5} (see [c])	–	–	–	124
	4	40 000	3500	–	–	–	–	124
Xanthone	3	35 000	5700	10^{-6} (see [c])	–	–	–	124

Notes. Decay times and rate constants of nonradiative transitions were obtained by triplet–triplet annihilation technique. The values estimated from the linewidths in structured spectra are given in parentheses.
[a] At 4 K, [b] in a supersonic jet, [c] experimental conditions: $c = 10^{-5}$ mol litre^{-1}, deoxygenated.

VI. Lifetimes of higher excited S_n states of molecules estimated from homogeneous broadening of absorption spectra

The method of estimation of the HESS lifetimes from the data on homogeneous line broadening in absorption spectra is based on the uncertainty relation, which relates the lifetime of an excited electronic or vibronic state of a molecule under study to the homogeneous broadening of the corresponding energy level

$$\tau_n = \frac{1}{2\pi c \Delta\nu_{1/2}},$$

where, τ_n is the lifetime of the energy level (in seconds), c is the velocity of light (in cm s^{-1}) and $\Delta\nu_{1/2}$ is the halfwidth of the energy level (in cm^{-1}). At first glance, τ_n values can be simply determined using this formula after measuring any absorption or emission line corresponding to the transition between the ground and excited states. Indeed, since the ground-state lifetime is infinitely long, this state contributes negligibly to the homogeneous broadening of the spectrum. However, there is also inhomogeneous broadening, which much exceeds the homogeneous broadening in the case of solutions, and the broadening due to phase relaxation.[134]

Subsequently several experimental methods for elimination or strong suppression of inhomogeneous broadening were developed.[135–142] These are as follows:

— low-temperature measurements of absorption and luminescence spectra of crystals;

— measurements of impurity spectra from crystals in those cases where the impurity molecule under study can be easily incorporated into the unit cell of the matrix crystal (*e.g.*, a naphthalene molecule in durene crystal);

— spectral line narrowing in Shpolskii matrices;

— obtaining of narrow fluorescence spectra using the Personov effect upon excitation to the region of the 0–0 electronic transition by monochromatic radiation;

— 'hole burning' in absorption spectra using photochemical reactions or another mode-selective technique for removal of 'inhomogeneously broadened' molecules with specified electronic energy;

— obtaining of extremely narrow absorption or fluorescence spectra in free supersonic jets.

Narrowing of spectral lines broadened due to phase relaxation is achieved by cooling the samples under study. Therefore, the above-mentioned experimental methods are, as a rule, applicable at temperatures close to the liquid helium temperature. Ignoring phase relaxation requires preliminary measurements and analysis of the temperature dependence of linewidths.

Hochstrasser and Marzzacco[134] studied the $T_n \leftarrow S_0$ and $S_n \leftarrow S_0$ absorption spectra of a number of aromatic compounds in the crystalline phase at 4.2 K. Presumably, they were the first who considered substantial broadening of vibronic bands in the absorption spectra upon excitation to the second and upper electronic states. For instance, marked broadening of vibronic lines was found in the spectra of pyrazine and its derivatives, phenazine, 9,10-diazaphenanthrene, naphthalene and its halogen derivatives in the region of the $T_2 \leftarrow S_0$ transition. According to Kasha's rule, excitation of a molecule to the second triplet state should be followed by fast internal conversion to the lowest triplet state. A similar broadening was observed in the singlet–singlet absorption spectra of naphthalene and quinoxaline molecules incorporated into durene crystals, of naphthalene and quinoxaline vapours and of naphthaldehyde. These spectra exhibited narrow $S_1 \leftarrow S_0$ absorption lines which were substantially broadened on approaching the lines corresponding to the $S_2 \leftarrow S_0$ transition.

Studies of vibronic absorption linewidths of different singlet–singlet transitions of anthracene, coronene and 1,2-benzperylene in Shpolskii matrices revealed[135] noticeable narrowing of the $S_n \leftarrow S_0$ ($n \geqslant 1$) lines with a decrease in the temperature from 300 to 77 K. Further reduction of temperature down to 4.2 K was found to have little effect on the linewidths. Narrowing of the $S_1 \leftarrow S_0$ line was followed down to 4.2 K. The linewidths for a number of compounds are listed in Table 7. However, the $S_1 \leftarrow S_0$ linewidths were found to be strongly overestimated since the S_1 state lifetimes of the molecules under study estimated from these linewidths are nearly three orders of magnitude shorter than the

Table 7. HESS lifetimes of organic molecules estimated from vibronic bandwidths.

Compound	Matrix	T/K	$S_n \leftarrow S_0$	ν/cm^{-1}	Homogeneous linewidth/cm^{-1}	τ_n/ps	Method	Ref.
Anthracene	n-hexane	4.2	$S_1 \leftarrow S_0$	26 234	6.2	0.08	Shpolskii effect	135
	"	77	$S_2 \leftarrow S_0$	39 140	280	0.019	the same	135
	"	77	$S_3 \leftarrow S_0$	45 080	400	0.013	"	135
Coronene	n-heptane	4.2	$S_1 \leftarrow S_0$	23 450	2.1	2.6	"	135
	"	4.2	$S_2 \leftarrow S_0$	28 440	4.1	1.3	"	135
	"	77	$S_3 \leftarrow S_0$	32 870	300	0.018	"	135
	"	77	$S_5 \leftarrow S_0$	46 600	350	0.015	"	135
1,12-Benzoperylene	n-hexane	4.2	$S_1 \leftarrow S_0$	24 636	2.4	2.2	"	135
	"	77	$S_2 \leftarrow S_0$	25 800	420	0.013	"	135
	"	77	$S_5 \leftarrow S_0$	44 580	1400	0.004	"	135
	"	77	$S_6 \leftarrow S_0$	47 100	800	0.007	"	135
Zn-Tetraphenyl-porphyrin	poly(methyl methacrylate)	4	$S_2 \leftarrow S_0$	23 600	7.8	1.4[a]	hole burning technique	141
	poly(vinyl butyral)	4	$S_2 \leftarrow S_0$	23 480	6.5	1.6	the same	141
	see[b]		$S_2 \leftarrow S_0$	25 120	4.0	1.3	supersonic jet	142
Zn-Tetratolyl-tetrabenzo-porphyrin	"	20	$S_2 \leftarrow S_0$	?	6.1	1.7	the same	141
Tetrabenzopor-phyrin derivative	THF–Et_2O (1 : 1) mixture	4.2	$S_2 \leftarrow S_0$	16 500	25	0.2	hole burning technique	140
		4.2	$S_3 \leftarrow S_0$	23 040	11	0.48	the same	140
Free porphyrin base	see[b]	–	$S_2 \leftarrow S_0$	19 884	11	0.48	supersonic jet	142

[a] From fluorescence yields, [b] vapour in a supersonic jet.

measured lifetimes. Analysis of the results obtained in the above-mentioned studies [136–139] shows that these linewidths much exceed the natural linewidths even in the Shpolskii matrices; determination of the natural linewidths requires the Personov holes [98, 99] to be 'burnt' in the absorption lines.

The linewidths of transitions to upper excited singlet states also seem to be overestimated.

A series of studies on free porphyrin base dissolved in the Shpolskii matrices has been reported.[136–139] The homogeneous linewidths were determined using a photochemical hole burning technique based on the tautomeric transformations involving inner hydrogen atoms of the porphyrin molecule.[64, 136] Samples were irradiated by a tunable single-mode laser with a frequency jitter of $\sim$10 MHz. The contribution of phase relaxation was determined from the temperature dependences of the 0–0 linewidths in the range from 1.5 to 4.2 K. The homogeneous width of the 0–0 line for the $S_1 \leftarrow S_0$ transition was found to be $\sim$9 MHz (0.0003 cm^{-1}) at 1.5 K,[137] which corresponded to the experimentally observed $S_1 \leftarrow S_0$ fluorescence decay time of free porphyrin base in n-octane at 4.2 K (17 ns). This indicates that the hole burning technique does allow measurements of homogeneous line broadening, thus providing a means for determination of the lifetimes of the excited states of organic molecules.

The lifetimes of vibronic levels for the S_1 state of free porphyrin base in n-octane at 4.2 K (Table 8) were determined using the same procedure.[139] The homogeneous holewidth of the 0–0 band was found to be $\sim$9 MHz, whereas those of the vibronic bands for the same transition were varied from 5 to 150 GHz (0.1–7 cm^{-1}). Both hole burning and measurements of vibronic bandwidths in the spectra corresponding to transitions to upper electronic excited levels were performed using a tunable pulsed laser with a bandwidth of $\sim$1 cm^{-1}.

The lifetimes of several vibrational levels of the S_1 state of free porphyrin base at 4.2 K vary from 1 to 30 ps (Table 8). Totally symmetrical modes in the frequency range from 150 to 1160 cm^{-1} are characterised by substantial variations of the lifetimes. For the modes with frequencies lying between 1340 and $\sim$1580 cm^{-1}, the lifetimes of vibrational levels were estimated at 1.0 to 1.6 ps irrespective of the vibrational mode symmetry. This is in reasonable agreement with the results of measurements of the lifetimes of vibrational levels of organic molecules obtained by other experimental methods.[116, 117] Note that the rates of vibrational relaxation of most of higher excited states are much lower than those of electronic relaxation (see Tables 2–5).

The S_3 state lifetimes of a tetrabenzoporphyrin derivative [a solution in THF–Et_2O (1 : 1) mixture] determined from hole burning experiments at 4.2 K and estimated from the $S_3 \rightarrow S_0$ fluorescence quantum yield have been compared.[140] As in the preceding case, holes were burnt using photochemically induced tautomeric transformation involving inner hydrogen atoms of porphyrin molecule. The hole halfwidth was found to be 10 cm^{-1} for the $S_3 \leftarrow S_0$ transition (λ_{max} = 434 nm), which corresponded to the S_3 level lifetime, τ_3, of 0.53 ps. The lifetime of the same state estimated from the $S_3 \rightarrow S_0$ fluorescence quantum yield and the ratio of the radiative rate constants for the $S_3 \rightarrow S_0$ and $S_1 \rightarrow S_0$ transitions (these were determined from the absorption spectrum) was 1.2 ps. The discrepancy between the two τ_3 values is not too large; however, it seems to be greater than the experimental error. Position of the S_2 level of the tetrabenzoporphyrin derivative has also been determined.[140] The corresponding band in the absorption spectrum is overlapped with vibronic bands of the $S_1 \leftarrow S_0$ transition. However, hole burning measurements allowed the observation of the 0–0 band of the $S_2 \leftarrow S_0$ transition at 606 nm and estimation of the S_2 state lifetime at 0.38 ps. The lifetime of the vibronic sublevel of the S_1 state with an energy of 1108 cm^{-1} was also determined: the hole halfwidth was found to be 0.18 nm, which corresponded to a vibronic level lifetime of 1.1 ps.

Hole burning technique was used for studying internal conversion in Zn-tetraphenylporphyrin molecules incorporated into polymeric matrices at 4 K.[141] The homogeneous broadening in the Soret band was close to that found in the preceding case [140] (see Table 7). Supersonic jet measurements have led to similar results.[142, 143]

The HESS lifetimes were estimated by the photophysical (optical) hole burning method.[144] Previously,[145] this experimental technique was used in a study on the temperature dependence of phase relaxation of the S_1 state of Zn-porphyrin molecule. To burn holes in the $S_2 \leftarrow S_0$ absorption band of phenanthrene (a solution in isopentene–2-methylpentane mixture at 4.2 K), molecules were excited to a triplet state by irradiating samples by the light of a pulsed dye laser with frequency doubling. Absorption was measured using a high-resolution double monochromator. A phosphoroscope was constructed to provide alternate illumination of a sample placed in a cryostat by the laser light and by the transmitted light of a Xe lamp. The homogeneous halfwidth of hole burnt was found to be 67 cm^{-1}, which corresponded to the $S_2(0)$ state lifetime of phenanthrene, τ_2, of 0.079 ps. The lifetime of the S_2 vibronic state (400 cm^{-1}), also determined by both resonance and off-resonance hole burning techniques, was found to be nearly the same. On the other hand, homogeneous linewidth measurements of isolated phenanthrene molecules in a supersonic jet have led to a value of 0.5 ps for $\tau_2(0)$.[146] The reason for such a large difference between the estimates of the lifetimes of the second excited state of phenanthrene molecules is still to be clarified. Indeed, since fast internal conversion occurs intramolecularly, one would expect similar rates of internal conversion for the molecule in the condensed phase and in the vapour phase. Unfortunately, comparable information on the rate constants for internal conversion from higher excited states in the condensed phase and in supersonic jets for the same molecules is scarce.

Nickel and Wick [147] studied the vibrational structure of the S_0-S_2 absorption band of coronene in poly(methyl methacrylate) at 1.8 K by the photophysical hole burning technique. The lifetime of the vibronic S_2 states, estimated from the homogeneous width of resonance transitions, was found to be somewhat shorter than 2 ps. This is in reasonable agreement with the results obtained by different authors [148, 149] who observed fluorescence from the S_2 state of coronene under conditions of direct single-quantum excitation and with the results of measurements of the homogeneous width of fluorescence excitation lines in the Shpolskii matrices and in a supersonic jet. Such a relatively long lifetime of the S_2 state [with the energy gap $\Delta E(S_2-S_1) \simeq 5000$ cm^{-1}] seems to be due to high molecular symmetry and forbiddenness of the $S_2(^1B_{1u}) \rightarrow S_1(^1B_{2u})$ radiative transitions. Unlike phenanthrene, the homogeneous linewidth of coronene is nearly the same both in a supersonic jet and in the low-temperature matrix.

A large body of information on the linewidths in the molecular spectra (including those of porphyrins) obtained in supersonic jet studies has been reported.[142, 143, 146]

Table 8. Lifetimes of vibrational levels of the S_1 state of free base porphyrin molecules (a solution in n-octane) at 4.2 K.[139]

ν /cm^{-1}	Mode symmetry	Homogeneous width /GHz	τ /ps
0 [a]	A_g	0.017	9.4×10^3
155	A_g	82	1.9
307	A_g	50	3.2
710	A_g	5	32
783	B_{1g}	44	3.6
943	A_g	96	1.7
970	B_{1g}	103	1.5
1161	A_g	5.4	30
1340	A_g	150	1.0
1355	B_{1g}	120	1.3
1583	A_g	100	1.6

[a] The 0–0 transition.

VII. Lifetimes of higher excited S_n states estimated from picosecond and femtosecond spectroscopy data

In the last decade, direct measurements of the HESS lifetimes of organic molecules were reported. To measure the decay of very weak emission from these states with femtosecond resolution is a complicated problem. Conventional experimental techniques involve consecutive stepwise excitation by two picosecond or femtosecond light pulses with a small pulse delay. The second pulse is used for measuring the kinetics of either the induced absorption spectrum or the absorption spectrum reconstruction for the lower-lying state (laser photolysis with picosecond or femtosecond resolution). Excitation by the second pulse also allows photoionisation of a molecule followed by mass-spectrometric or another type of detection of the cation formed or electron detached. Recently, a large number of studies concerning measurements of ultrafast luminescence decay kinetics by luminescence up-conversion, *i.e.*, 'mixing' of weak luminescence with an optically delayed femtosecond pulse in a nonlinear crystal, were reported.

When comparing different methods for studying the dynamics of internal conversion from HESS, preference should be given to those which allow the observation of fluorescence kinetics due to transition from these states. Studies of molecular absorption spectra induced by laser pulses are complicated by three factors, *viz.*, transition-state absorption, ground-state 'bleaching' and stimulated emission from the excited state. The results of second-pulse induced photoionisation studies are also ambiguous.

A stepwise photoionisation study of the lifetime of the S_2 state (35 900 cm^{-1}) of naphthalene in a supersonic jet has been reported.[150] However, only the upper bound of the lifetime of this state (10^{-11} s) was estimated due to instrumental limitations on the pulse duration (6 ps). Quenching of the S_2 fluorescence of Zn(TPP) in acetonitrile due to the addition of dichloromethane has been studied by an up-conversion technique.[151] The lifetime $\tau(S_2)$ of ZnTPP was found to be 3.5 (in acetonitrile) and 0.75 ps (in dichloromethane). Since the S_2 state lifetime is very short, the concentration dependence of fluorescence quenching can be described using the Perrin model:

$$\ln\frac{I_0}{I} = VN_A[CH_2Cl_2],$$

where I_0 is the radiation intensity without a quencher, I is the radiation intensity, $V = (4/3)\pi R^3$ is the action range of the quencher ($R = 15$ Å) and N_A is the Avogadro constant. It was found [151] that quenching of fluorescence from the S_1 state of Zn(TPP) with dichloromethane is inefficient. The authors suggested that quenching of the S_2 fluorescence is due to electron transfer.

Internal conversion in complexes of Zn-porphyrin (ZnP) derivatives and free porphyrin base (H_2P) dissolved in benzene has been studied by femtosecond fluorescence spectroscopy.[152] For ZnP, two fast components of the $S_2(B) \rightarrow S_0$ fluorescence decay were associated with the $S_2 \rightarrow S_1$ internal conversion with a time constant of 150 fs (spectral changes in the region of the $S_2 \rightarrow S_0$ transition) and with vibrational relaxation to the $S_1(Q)$ state with a time constant of 600 fs (spectral changes in the region of the $S_1 \rightarrow S_0$ transition). Free porphyrin base exhibits ultrafast relaxation of the $S_3(B)$ state ($\tau < 40$ fs), fast relaxation of the $S_2(Q_y)$ state with a time constant of 90 fs and a slower vibrational relaxation of the $S_1(Q_x)$ state. A fluorescence up-conversion study of fluorescence decay from the $S_3(^1B_b)$ state of tetracene in solution using 280 fs pulses was carried out.[153] The decay time, τ, of the ($S_3 \rightarrow S_0$) fluorescence of tetracene in the UV region was estimated to be $\sim$120 fs. Usual fluorescence from the $S_1(^1L_a)$ level was found to arise with the same rate constant.

Decay kinetics of the S_2 and S_1 states of Malachite Green dye in different solvents (methanol, water, ethylene glycol and water–glycerol mixture) has been studied by femtosecond fluorescence up-conversion spectroscopy (pulse separation $\Delta t = 90$ fs).[154] The decay times in an aqueous solution were estimated at 0.27 ps for $\tau(S_2)$ and at 0.54 ps for $\tau(S_1)$. If the molecule is excited to the second singlet state, the rise of the S_1 fluorescence and the decay of the S_2 fluorescence occur with the same rate constant.

Femtosecond time-resolved photoelectron spectroscopy ($\Delta t < 200$ fs, $\lambda = 252$ nm) was used for studying ultrafast internal conversion in 1,3,5-hexatriene, which is one of the simplest representatives of polyenes.[155] The S_1 state lifetimes were estimated at 730 and 270 fs for *cis*- and *trans*-hexatriene, respectively. The authors of this study suggested that relaxation process occurs as a cascade, *viz.*, $S_2 \rightsquigarrow S_1 \rightsquigarrow S_0$. The estimate of the S_2 state lifetime, $\tau(S_2) \leqslant 50$ fs, is consistent with that obtained earlier [156] from the homogeneous width of the $S_2 \leftarrow S_0$ absorption line at 250 nm in supersonic jets. The S_2 state decay times were estimated at 50 fs for *trans*-hexatriene and at 20 fs for *cis*-hexatriene. This is close to the S_2 state lifetime of *trans*-hexatriene vapours (40 fs) obtained from the data on resonant Raman scattering.[157]

Femtosecond up-conversion studies of the effect of molecular structure and solvent on the S_2 state lifetimes of carotenoids have been reported.[158, 159] They revealed violation of Kasha's rule [8] and Ermolaev–Sveshnikova's rule [160, 161] (the sum of the fluorescence and triplet-state generation quantum yields equals unity for solutions of fluorescent compounds) in the case of linear polyenes including carotenoids. It was pointed also out that the main emission of molecules with C_{2h} symmetry originates from the S_2 level (the $S_2 \rightarrow S_1$ radiative transition is forbidden). If the molecular symmetry is broken, the S_1 emission becomes stronger. The τ_2 values for the three compounds studied lie between 100 and 200 fs. More recently, in studies of neurosporene (a linear carotenoid) it has been shown [162] that excitation to the S_2 state with an excess vibrational energy of $\sim$3000 cm^{-1} leads to the appearance of a time-dependent $S_2 \rightarrow S_0$ fluorescence spectrum. This was explained by the vibrational energy redistribution in the S_2 state from the Franck–Condon active modes to other (dark) modes with a time constant of 35–40 fs, followed by the $S_2 \rightarrow S_1$ internal conversion occurring in 250 fs.

The effect of hydrogen bond formation/dissociation on the relaxation rate of the S_3 and S_2 states of *trans*-retinal molecules (a solution in butan-1-ol–cyclohexane mixture) on the subpicosecond time scale has been first studied recently.[163] The $S_3[B_u^+(\pi,\pi^*)]$ and $S_2[A_g^-(\pi,\pi^*]$ state lifetimes of the molecules under study in neat butan-1-ol (200 fs and 1.8 ps, respectively) were found to be much longer than the corresponding lifetimes in neat cyclohexane (30 fs and 0.7 ps, respectively). In the S_2 state, all the *trans*-retinal molecules are hydrogen-bonded. The increase in the fluorescence and the isomerisation quantum yields and the decrease in the triplet quantum yield upon hydrogen bond formation were explained by the prolonged lifetime of the S_2 state of *trans*-retinal. The authors cited were the first to study the formation and cleavage of a hydrogen bond in a subpicosecond time.

Hirata *et al.*[164, 165] studied the dependence of the rate constant for the $S_2 \rightarrow S_1$ internal conversion on the energy gap width in the molecules of (i) diphenylacetylene and its derivatives and (ii) *trans*-α,ω-diphenylpolyenes with different chain length (solutions in n-hexane and THF were used in both cases). The S_2 state lifetimes of diphenylpolyenes with the molecular chains of length from 3 to 8 monomer units and the energy gaps of width from 1600 to 4800 cm^{-1} varied insignificantly (500 ± 100 fs) and increased only slightly with the decrease in the temperature. The rate constant for the $S_1 \rightarrow S_0$ nonradiative transition increased by three orders of magnitude for the same diphenylpolyenes.

A femtosecond laser flash photolysis study on fast photo-induced reactions of *trans*-azobenzene excited to the S_2 state (in solutions at 303 K, $\sim$200 fs resolution) has been reported.[166] Analysis of the induced absorption decay curve measured in the region 370–450 nm revealed its two-exponential structure and

allowed determination of the time constants which appeared to be different for different solvents. The time constant for the fast exponent, τ_1, was found to be 0.9 ps for hexane, cyclohexane and hexadecane and 1.2 ps for acetonitrile. That for the slow exponent, τ_2, was found to be 13 ps for the hydrocarbons and 16 ps for acetonitrile. The authors suggested that the decay of the fast exponent is due to deactivation of the $S_2(\pi,\pi^*)$ state. The appearance of the slow exponent was explained by the presence of an intermediate excited singlet state lying between the S_2 and S_1 states on the energy scale, corresponding to the *twist*-conformer of the excited *trans*-azobenzene molecule. The dynamics of the S_2 and S_1 states of *trans*-4-n-butyl-4′-methoxyazabenzene in hexane has been studied [167] by a similar experimental technique with the same resolution. The time constants were estimated at $\approx$250 fs for $\tau(S_2)$ and at 2.3 ps for $\tau(S_1)$.

Femtosecond time-resolved photoelectron spectroscopy was used for measuring the S_n state lifetimes of pyrazine molecules in a supersonic jet.[168] In particular, the lifetime of the S_2 state, $\tau(S_2)$, was estimated at 20 fs. A supersonic jet study of the S_2 state of benzene – ammonia complexes has been reported.[169] The S_2 state lifetime was estimated at $\sim$100 fs.

Fluorescence of coumarin 481 in cyclohexane at 293 K, which appeared after excitation by 100 fs pulses at λ = 267 nm has been studied in detail.[170] The molecules were excited to an S_n state lying 12 000 cm^{-1} higher than the S_1 state and then the dynamics of the rise of the $S_1 \rightarrow S_0$ fluorescence was observed using up-conversion technique. The time constant of the rise of the fluorescence in the region 419 – 475 nm was found to be 280 to 220 fs. This time was interpreted as that required for completion of the $S_n \rightarrow S_1$ internal conversion. It was also suggested that intramolecular redistribution of vibrational energy in the S_1 and S_0 states occurs with strongly different rates.[170]

However, there is also another concept of the redistribution of excess vibrational energy in the ground and first excited states after optical excitation.[20] The authors came to conclusion that vibrational excitation is redistributed in the S_0 and S_1 states of dye molecules with the same rate constant. Based on analysis of their original studies and published data, they also suggested that in most cases redistribution of excess vibrational energy involves two stages. The first stage is fast, with a time constant τ_1 estimated at 30 to 200 fs, while the second stage is slow, with a time constant τ_2 estimated at 200 to 1000 fs. It was assumed that the fast stage is due to the interaction of isoenergetic vibrational levels, whereas the slow stage is due to coupling of levels with different energies. Yet another assumption is that the time required to 'cool' a vibrationally 'overheated' molecule *via* transfer of excess energy to the environment (solvent molecules) should be much longer (from 15 to 40 ps for different solvents).

The dynamics of IR 125 dye in ethylene glycol solution was studied by pump-probe experiments.[171, 172] The pump pulse duration was 30 fs (λ = 425 nm) while the probe pulse width was 20 fs (λ = 850 nm). It was found that a dye molecule excited to an S_n ($n > 1$) state by a pulse at λ = 425 nm arrives at the S_1 state within 50 fs; however, the time constant of S_1 population (accumulation of molecules at the minimum of the PES of this state) is much larger ($\sim$1 ps).

A number of papers concerning nonradiative transitions between higher excited electronic levels of the molecules comprised of ten or smaller number of atoms was reported. In particular, the S_2 state lifetimes of acetone and its deuterated analogue in the vapour phase were studied using femtosecond photoionisation (λ_{exc} = 194 nm, λ_{ion} = 295 nm).[173] It was found that $\tau(S_2)$ = 13.5 ps for acetone-d_6 and 4.7 ps for acetone-h_6. In this case, the S_1 state lifetimes of both molecules ($<$ 150 fs) are shorter than the corresponding S_2 state lifetimes. This is similar to azulene and β-carotenes.

VIII. Ultrafast nonradiative transitions involving triplet states

A salient feature of aromatic and dye molecules is the possibility of ultrafast nonradiative transitions involving triplet states. Naturally, the question arises of the rates of such transitions.

Liu and Edman [174] studied photoisomerisation reactions of various alkenes sensitised by anthracene and its derivatives. All the reaction pathways were known to pass through triplet states. The authors assumed that the photoreactions can proceed only *via* excited molecules of anthracene and its derivatives. Since the lowest triplet levels of anthracenes lie much below those of alkenes, it was suggested that the reactions under study proceed due to energy transfer from the second triplet level (T_2) of the anthracenes and that the T_2 level is populated *via* intersystem crossing from the S_1 state. [The T_2 level of the sensitiser molecules lies somewhat lower than their first excited singlet level, $E(T_2)$ = 25 000 – 26 000 cm^{-1}]. Among all the alkene reactions studied, the highest quantum yield (0.042) was found for *cis – trans* isomerisation of piperylene in benzene (0.2 M) at 293 K sensitised by 9,10-dibromoanthracene. Assuming that the rate constant for triplet – triplet energy transfer from the T_2 level is equal to the diffusion rate constant, the T_2 state lifetime of 9,10-dibromoanthracene was estimated at 1.3×10^{-10} s.[175]

An alternative explanation for the results obtained by Liu and Gale [175] has been put forward in a paper [176] concerning fluorescence quenching of haloanthracenes by naphthalene and phenanthrene. Taking into account a correlation between the rate constants for quenching and the spin-orbit coupling constants of anthracene derivatives, the authors concluded that a spin-forbidden, singlet – triplet energy transfer occurs in this case. Similarly to the earlier results,[175] the most pronounced effect was observed for 9,10-dibromoanthracene. It was also assumed [176] that this process should also lead to population of triplet states of the energy acceptor and can induce alkene isomerisation.

Only a few observations of the fluorescence due to triplet – triplet transitions have been reported. For instance, $T_2 - T_1$ fluorescence was detected upon excitation of certain anthracene derivatives dissolved in methylcyclohexane to the S_1 state.[80, 177] Fluorescence spectra were measured in air at room temperature. The 0 – 0 bands in the $T_2 - T_1$ fluorescence spectra of these compounds lie in the region from 840 to 960 nm (12 000 – 10 400 cm^{-1}) and are nearly mirror images of the long-wavelength $T_n \leftarrow T_1$ absorption bands. The $T_2 \rightarrow T_1$ fluorescence quantum yields were estimated at 10^{-6} for 9,10-dibromoanthracene [$\tau(T_2) = 2 \times 10^{-12}$ s] and at 5×10^{-8} for the unsubstituted anthracene [$\tau(T_2) = 10^{-13}$ s]. These values are in poor agreement with indirect estimates of the T_2 state lifetime of anthracene, obtained from the results of photochemical sensitisation studies.[178]

Keller [179] was the first to report on the reverse intersystem crossing from higher excited triplet states of aromatic molecules to the excited singlet levels. At 77 K, aromatic molecules in a glassy matrix were excited by UV irradiation to populate the lowest triplet state. Then the molecules were excited by visible light into the $T_n \leftarrow T_1$ absorption bands and their UV fluorescence accompanying the $S_1 \rightarrow S_0$ transition (Fig. 9) was observed. The fluorescence intensity was proportional to the intensity of visible light and the fluorescence lifetime was identical to the lifetime of the lowest triplet T_1 state. The quantum yield of the triplet – singlet intersystem crossing process (the ratio of the number of $T_n \rightarrow S_1$ transitions to the number of photons absorbed by the T_1 state) is small, namely, 5×10^{-7} for naphthalene, 2×10^{-6} for quinoline and 10^{-6} for fluorene. Kobayashi *et al.*[180] also observed the $S_1 \rightarrow S_0$ fluorescence of anthracene and its 9-methyl and 9-phenyl derivatives due to reverse intersystem crossing. The quantum yield of the $T_n \rightarrow S_1$ intersystem crossing was estimated at 5×10^{-6} for anthracene and at 8×10^{-5} for 9-phenylanthracene. More recently [181] some arguments were adduced in favour of assumption that the S_1 state of 9,10-dibromoanthracene molecule is

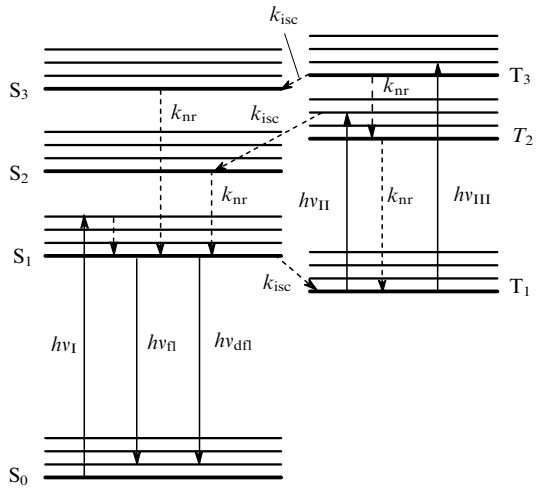

Figure 9. An energy level diagram illustrating the appearance of delayed fluorescence (ν_{dfl}) after excitation of a molecule to a higher excited triplet state and intersystem crossing from this state to the singlet manifold.

populated *via* absorption of a light quantum by the T_1 state and is also due to the $S_m \leftarrow T_1$ transition. Population of the fluorescent state of perylene vapours *via* excitation of the lowest triplet state by consecutive irradiation by two laser pulses has been reported.[182]

A version of Keller's technique [179] which uses stepwise excitation by nanosecond laser pulses has been proposed in studies of xanthene dyes (eosin, erythrosin and Rose Bengal) in polymeric matrices.[183, 184] The authors simultaneously observed both the delayed fluorescence induced by the second delayed pulse and the decrease in the optical density of the triplet–triplet absorption, which was rationalised by the occurrence of the $T_n \rightarrow S_m$ reverse intersystem crossing. Thus, a competition of nonradiative intersystem crossing with internal conversion over the triplet manifold is implied. This is quite probable since the molecules studied contain heavy Br or I atoms. However, too high quantum yields of the process [183, 184] are suspicious because the spin-forbidden transition competes with the spin-allowed process of internal conversion over the triplet manifold.

Similar approach was used in studies of the $S_1 \rightarrow S_0$ fluorescence of Rose Bengal in aqueous solutions (a phosphate buffer, pH 7.0).[185] Fluorescence appeared after stepwise excitation of the dye molecules from the lowest triplet state to excited triplet states, followed by reverse intersystem crossing to the singlet manifold and emission. An intense absorption band at $\lambda_{max} = 1063$ nm was detected by near-infrared laser flash photolysis measurements and assigned to the $T_2 \leftarrow T_1$ transition.[185] It was found that excitation of the dye by the second harmonic of a Nd laser ($\lambda = 532$ nm, $t_{pulse} = 134$ ps) to the S_1 state leads to population of the T_1 triplet state with a probability of 0.98 and to fluorescence emission with a quantum yield of 0.02. The second pulse of the fundamental frequency of the Nd laser excited the solution with a delay of 34 ns to populate the T_2 state since the fundamental frequency of neodymium penetrates the long-wavelength triplet–triplet absorption band.

Population of the T_3 state was achieved by irradiating the solution by the second pulse ($\lambda = 632$ nm) with the same delay. Then, the dependence of the intensity of two-step, laser-induced delayed fluorescence on the intensity of laser pulses was measured and analysis using a simplified kinetic scheme was performed. As a result, the quantum yield of the $T_2 \rightarrow S_1$ reverse intersystem crossing, $q(T_2,S_1)$, was estimated at 0.014 and the T_2 state lifetime, $\tau(T_2)$, was found to be 5.8 ps.[185] No $S_1 \rightarrow S_0$ fluorescence was observed upon two-step laser-induced excitation at $\lambda_2 = 632$ nm *via* the T_1 state. Therefore, only the upper bound of the reverse intersystem crossing yield from the T_3 state, $q(T_3 \rightarrow S_n)$, was estimated at 0.06. These results strongly disagree with those obtained in earlier studies,[183, 184], according to which $q(T_3 \rightarrow S_n) = 0.74$. Previously,[183] this value was estimated from the decrease in the T_1 state population of the dye after irradiation by the second pulse at $\lambda_2 = 632$ nm.

Table 9. Quantum yields of reverse intersystem crossing for excited triplet levels of Rose Bengal dye molecule.[185]

Energy level	E /cm^{-1}	$\Delta E(T_n \rightarrow S_n)$ /cm^{-1}	$\Delta E(T_n \rightarrow T_{n-1})$ /cm^{-1}	$q(T_n \rightarrow S_n)$
T_2	23 550	4030	9435	0.014
T_3	31 130	2820	7580	< 0.06
T_4	32 500	640	1370	0.8

Previously (see, *e.g.*, Refs 186 and 187), it was assumed that the reverse intersystem crossing occurs mainly from the T_2 level. However, the results of measurements of the quantum yield $q(T_n \rightarrow S_n)$ for Rose Bengal rule out this assumption. Table 9 lists the quantum yields of reverse intersystem crossing, positions of triplet levels and the energy gaps between them and the nearest lower-energy triplet and singlet levels of the Rose Bengal molecule. As can be seen, the quantum yields of reverse intersystem crossing are satisfactorily described by the 'energy gap law'; however, it should be remembered that internal conversion over the triplet manifold leads to the energy gap narrowing with increase in the level number. This casts some doubts on the too high yield of reverse intersystem crossing from the T_4 level, though the strength of the spin-orbit coupling between particular triplet and singlet states plays a significant role in this case.[185]

It was found that the addition of LiBr in combination with stepwise excitation to HESS leads to an increase in the quantum yield of triplet rhodamine generation in solution.[188]

IX. Conclusion

The results obtained using different methods of determination of the rate constants for ultrafast nonradiative transitions, considered in this review are, with rare exception, in reasonable agreement with one another. Those obtained by recently developed but rather widely used direct picosecond and femtosecond methods for measuring the fluorescence decay have for the most part confirmed indirect estimates based on the fluorescence yields from HESS under conditions of single-quantum or two-quantum excitation to corresponding levels and found from the homogeneous absorption linewidths. It was established that in most cases the HESS lifetimes of organic and dye molecules are of the order of tens of femtoseconds. The only exception is the second excited singlet state (S_2), the lifetime of which for a number of molecules is much longer, so that it can be considered as a specific state similar to the fluorescent state (S_1). More complex is the problem of theoretical interpretation of experimental results. Correspondence between the observed rate constants and predictions of modern theories of nonradiative transitions is fragmentary. In some instances even the 'physical' or 'chemical' mechanism responsible for the nonradiative transition remains unclear. Undoubtedly, the development of femtosecond measuring devices will provide the possibility of obtaining new information on transitions between HESS. For instance, only in the very recent past has it been possible to observe non-exponential fluorescence decay due to transitions from the HESS, which is interpreted as superimposed 'hot' fluorescence.

'Physical' ultrafast nonradiative transitions can occur by tunneling and as conical intersections of the PES of excited states. Comprehensive theory of nonradiative transitions, based on calculations of possible fast processes due to such conical intersections in complex molecules is now at an early stage. The state-of-the-art in multidimensional theory of nonadiabatic transitions

in the case of conical intersections of the PES has been recently considered in a special issue of the *Chemical Physics* journal.[189]

The author expresses his gratitude to Dr. B Nickel for submitting materials and valuable discussions and to Prof. V A Benderskii for valuable critical comments. This review has been written with the financial support of the Russian Foundation for Basic Research (Project No. 00-03-32208) and the Ministry of Industry, Science and Technology of the Russian Federation.

References

1. A L Buchachenko *Usp. Khim.* **68** 99 (1999) [*Russ. Chem. Rev.* **68** 85 (1999)]
2. A H Zewail *Femtochemistry: Ultrafast Dynamics of the Chemical Bond* (Singapore: World Sci., 1994)
3. V Sundstrom (Ed.) *Femtochemistry and Femtobiology* (Singapore: World Sci., 1998)
4. S I Vavilov*Philos. Mag.* **43** 307 (1922)
5. S I Wawilow *Z. Phys.* **42** 311 (1927)
6. A N Terenin *Acta Phys. Chim. USSR* **18** 210 (1943)
7. G Lewis, M Kasha *J. Am. Chem. Soc.* **66** 2100 (1944)
8. M Kasha *Discuss. Faraday Soc.* **9** 14 (1950)
9. R Englman *Nonradiactive Decay of Ions and Molecules in Solids* (Amsterdam: North-Holland, 1979)
10. E S Medvedev, V I Osherov *Teoriya Bezyzluchatel'nykh Perekhodov v Mnogoatomnykh Molekulakh* (The Theory of Nonradiate Transitions in Polyatomic Molecules) (Moscow: Nauka, 1983)
11. E S Medvedev, V I Osherov *Radiationless Transition in Polyatomic Molecules (Ser. Chemical Physics)* Vol. 57 (Berlin: Springer, 1995)
12. A Nitzan, J Jortner, P M Rentzepis *Proc. R. Soc. London, A Math. Phys. Sci.* **327** 367 (1972)
13. J Jortner, S A Rice, R M Hochstrasser, in *Advances in Photochemistry* (Eds J N Pitts Jr, G S Hammond, W A Noyes Jr) (New York; London: Wiley, 1969) Vol. 7, p. 149
14. E B Sveshnikova, V L Ermolaev *Opt. Spektrosk.* **30** 379 (1971) [a]
15. E N Bodunov *Opt. Spektrosk.* **40** 942 (1976) [a]
16. V L Ermolaev, E B Sveshnikova, E N Bodunov *Usp. Fiz. Nauk* **166** 279 (1996) [b]
17. V L Ermolaev, E N Bodunov, E B Sveshnikova, T A Shakhverdov *Bezyzluchatel'nyi Perenos Energii Elektronnogo Vozbuzhdeniya* (Nonradiate Transfer of Electronic Excitation Energy) (Leningrad: Nauka, 1977)
18. V L Ermolaev, E B Sveshnikova *Chem. Phys. Lett.* **23** 349 (1973)
19. V L Ermolaev, E B Sveshnikova *Acta Phys. Pol. A* **95** 299 (1999)
20. T Elsaesser, W Kaiser *Annu. Rev. Phys. Chem.* **42** 83 (1991)
21. G B Tolstorozhev, S A Tikhomirov *Zh. Prikl. Spektrosk.* **65** 635 (1998)
22. M Beer, H C Longuet-Higgins *J. Chem. Phys.* **23** 1390 (1955)
23. G Viswanath, M Kasha *J. Chem. Phys.* **24** 574 (1956)
24. B D Wagner, D Tittelbach-Helmrich, R P Steer *J. Phys. Chem.* **96** 7904 (1992)
25. D Huppert, J Jortner, P M Rentzepis *J. Chem. Phys.* **56** 4826 (1972)
26. J B Birks *Photophysics of Aromatic Molecules* (London; New York; Sydney; Toronto: Wiley-Interscience, 1969)
27. P M Rentzepis, J Jortner, R P Jones *Chem. Phys. Lett.* **4** 599 (1970)
28. D Huppert, J Jortner, P M Rentzepis *Chem. Phys. Lett.* **13** 225 (1972)
29. G D Gillispie, E C Lim *J. Chem. Phys.* **65** 4314 (1976)
30. G D Gillispie, E C Lim *J. Chem. Phys.* **68** 4578 (1977)
31. D Klemp, B Nickel *Chem. Phys. Lett.* **130** 493 (1986)
32. Y Hirata, E C Lim *J. Chem. Phys.* **69** 3292 (1978)
33. M Fujii, T Ebata, N Mikami, M Ito *Chem. Phys.* **77** 191 (1983)
34. G Eber, S Schneider, F Dorr *Chem. Phys. Lett.* **52** 59 (1977)
35. S Murata, C Iwanaga, T Toda, H Kokubun *Ber. Bunsenges. Phys. Chem.* **76** 1176 (1972)
36. E P Ippen, C V Shank, R L Woerner *Chem. Phys. Lett.* **46** 20 (1977)
37. C V Shenk, E P Ippen, O Teschke, R L Fork *Chem. Phys. Lett.* **57** 433 (1978)
38. E W-G Diau, S De Feyter, A H Zeweil *J. Chem. Phys.* **110** 9785 (1999)
39. M J Bearpark, F Bernardi, S Clifford, M Olivucci, M A Robb, B R Smith, T Vreven *J. Am. Chem. Soc.* **118** 169 (1996)
40. G Eber, F Gruneis, S Schneider, F Dorr *Chem. Phys. Lett.* **29** 397 (1974)
41. R Klann, R J Bauerle, F Laermer, T Elsaesser, M Niemeyer, W Luttke *Chem. Phys. Lett.* **169** 172 (1990)
42. A Falchi, C Gellini, P R Salvi, K Hafner *J. Phys. Chem. A* **102** 5006 (1998)
43. A Falchi, C Gellini, P R Salvi, K Hafner *J. Phys. Chem. A* **104** 1078 (2000)
44. M J Bearpark, M A Robb *J. Phys. Chem. A* **104** 1075 (2000)
45. U P Wild, H J Griesser, V D Tuan, J F M Oth *Chem. Phys. Lett.* **41** 450 (1976)
46. B Nickel, J Hertzberg *Chem. Phys.* **132** 219 (1989)
47. J R Huber, M Mahaney *Chem. Phys. Lett.* **30** 410 (1975)
48. M H Hui, P de Mayo, R Suan, W R Ware *Chem. Phys. Lett.* **31** 257 (1975)
49. M Mahaney, J R Huber *Chem. Phys.* **9** 371 (1975)
50. A Maciejewski, R P Steer *J. Am. Chem. Soc.* **105** 6738 (1983)
51. A Maciejewski, R P Steer *Chem. Rev.* **93** 67 (1993)
52. A Maciejewski, R P Steer *J. Phys. Chem.* **92** 6939 (1988)
53. M Szymanski, R P Steer *J. Phys. Chem.* **96** 8719 (1992)
54. M Szymanski, A Maciejewski, J Kozlowski, J Koput *J. Phys. Chem. A* **102** 677 (1998)
55. H Eisenberger, B Nickel *J. Chem. Soc., Faraday Trans.* **92** 733 (1996)
56. H Eisenberger, B Nickel, A A Ruth, R P Steer *J. Chem. Soc., Faraday Trans.* **92** 741 (1996)
57. B Nickel, H Eisenberger, M T Wick, R P Steer *J. Chem. Soc., Faraday Trans.* **92** 1101 (1996)
58. M Szimanski, A Maciejewski, R P Steer *J. Phys. Chem.* **92** 2485 (1988)
59. M Szimanski, A Maciejewski, R P Steer *J. Photochem. Photobiol. A* **57** 405 (1991)
60. A Maciejewski, M Milewski, M Szimanski *J. Chem. Phys.* **111** 8462 (1999)
61. B Nickel *J. Lumin.* **44** 1 (1989)
62. J Cai, E C Lim *J. Chem. Phys.* **95** 3014 (1991)
63. L Bajema, M Gouterman, C B Rose *J. Mol. Spectrosc.* **39** 421 (1971)
64. I E Zalesskii, V N Kotlo, A N Sevchenko, K N Solov'ev, S F Shkirman *Dokl. Akad. Nauk SSSR* **210** 312 (1973) [c]
65. V N Kotlo, K N Solov'ev, S F Shkirman *Izv. Akad. Nauk SSSR, Ser. Fiz.* **39** 1972 (1975)
66. A V Nikolaitchik, M A J Rodgers *J. Phys. Chem. A* **103** 7597 (1999)
67. L A Martarano, Ch-P Wong, W DeW Horrocks Jr, A M Goncalves *J. Phys. Chem.* **80** 2389 (1976)
68. Y Kurabayashi, K Kikuchi, H Kokubun, Y Kaizu, H Kobayashi *J. Phys. Chem.* **88** 1308 (1984)
69. M P Tsvirko, G F Stelmakh, V E Pyatosin, K N Solovyov, T F Kachura *Chem. Phys. Lett.* **73** 80 (1980)
70. V L Ermolaev, I P Kotlyar, V A Lyubimtsev, V G Maslov *Opt. Spektrosk.* **52** 3 (1982) [a]
71. N Mataga, Y Shibata, H Chosrowjan, N Yoshida, A Osuka *J. Phys. Chem. B* **104** 4001 (2000)
72. V L Ermolaev, V A Lyubimtsev *Tr. Gos. Opt. Inst. im. S I Vavilova* **65** (199) 20 (1987)
73. A Janovski, J Rzeszotarska *J. Lumin.* **21** 409 (1980)
74. M Yoshizawa, K Suzuki, A Kubo, S Saikan *Chem. Phys. Lett.* **290** 43 (1998)
75. T A Gregory, S Lipsky *J. Chem. Phys.* **65** 296 (1976)
76. F Hirayma, T A Gregory, S Lipsky *J. Chem. Phys.* **58** 4696 (1973)
77. T A Gregory, F Hirayma, S Lipsky *J. Chem. Phys.* **58** 4697 (1973)
78. P O Andersson, S M Bachilo, R-L Chen, T Gillbro *J. Phys. Chem.* **99** 16199 (1995)
79. R Katoh, S Fujiyoshi, M Kotani *Chem. Phys. Lett.* **292** 621 (1998)
80. G D Gillispie, E C Lim *J. Chem. Phys.* **65** 2022 (1976)
81. L A Hallidy, M R Topp *Chem. Phys. Lett.* **46** 8 (1977)
82. A Terenin, G Kobyshev, G Lialin *Photochem. Photobiol.* **5** 689 (1966)
83. W E Gibbs *Appl. Phys. Lett.* **11** 113 (1967)
84. A Muller, E Pfluger *Chem. Phys. Lett.* **2** 155 (1968)
85. M D Galanin, Z A Chizhikova *Kratkie Soobshch. po Fizike* (4) 35 (1971)
86. M D Galanin, Z A Chizhikova *Izv. Akad. Nauk SSSR, Ser. Fiz.* **36** 941 (1972)
87. E N Kaliteevskaya, T K Razumova *Opt. Spektrosk.* **36** 1118 (1974) [a]
88. D Leupold, R Konig, B Voigt *J. Lumin.* **9** 113 (1974)
89. V Rehak, A Novak, M Titz *Chem. Phys. Lett.* **52** 39 (1974)
90. G C Orner, M R Topp *Chem. Phys. Lett.* **36** 295 (1975)
91. H-B Lin, M R Topp *Chem. Phys. Lett.* **47** 442 (1977)
92. H-B Lin, M R Topp *Chem. Phys. Lett.* **48** 251 (1977)

93. M R Topp, H-B Lin *Chem. Phys. Lett.* **50** 412 (1977)
94. H-B Lin, M R Topp *Chem. Phys. Lett.* **67** 273 (1979)
95. M R Topp, H-B Lin, K-J Choi *Chem. Phys.* **60** 47 (1981)
96. B Nickel, G Roden *Ber. Bunsenges. Phys. Chem.* **81** 281 (1977)
97. V A Lyubimtsev, Candidate Thesis in Physicomathematical Sciences, Leningrad State University, Leningrad, 1989
98. R I Personov, E I Al'shits, L A Bykovskaya *Opt. Commun.* **6** 169 (1972)
99. B M Kharlamov, R I Personov, L A Bykovskaya *Opt. Commun.* **12** 191 (1974)
100. V L Ermolaev, V A Lyubimtsev *Izv. Akad. Nauk SSSR, Ser. Fiz.* **47** 1405 (1983)
101. V L Ermolaev, V A Lyubimtsev *Opt. Spektrosk.* **56** 1026 (1984) [a]
102. V L Ermolaev, V A Lyubimtsev *Opt. Spektrosk.* **60** 74 (1986) [a]
103. V L Ermolaev, V A Lyubimtsev *Opt. Spektrosk.* **60** 970 (1986) [a]
104. V A Lyubimtsev, V L Ermolaev *Opt. Spektrosk.* **61** 511 (1986) [a]
105. V A Lyubimtsev, V L Ermolaev *Opt. Spektrosk.* **61** 766 (1986) [a]
106. V L Ermolaev, V A Lubimtsev *Acta Phys. Pol. A* **71** 731 (1987)
107. A A Krasheninnikov, A V Shablya *Opt. Spektrosk.* **60** 70 (1986) [a]
108. V P Klochkov, V L Bogdanov *Zh. Prikl. Spektrosk.* **43** 5 (1985)
109. R I Personov, E I Al'shits, L A Bykovskaya *Pis'ma Zh. Eksp. Teor. Fiz.* **15** 609 (1972)
110. A P Veduta, M D Galanin, B P Kirsanov, Z A Chizhikova *Pis'ma Zh. Eksp. Teor. Fiz.* **11** 157 (1970)
111. V L Bogdanov, in *Topics in Fluorescence Spectroscopy. Nonlinear and Two-Photon-Induced Fluorescence* (Ed. J R Lakowicz) (New York; London: Plenum, 1997) Vol. 5, p. 211
112. V L Bogdanov, V P Klochkov *Opt. Spektrosk.* **48** 34 (1980) [a]
113. V A Lyubimtsev *Izv. Akad. Nauk SSSR, Ser. Fiz.* **54** 391 (1990)
114. T P Kravets *Izv. Mosk. Inzh. Uchil., Ser. 2* (6) (1912)
115. S J Strickler, R A Berg *J. Am. Chem. Soc.* **37** 814 (1962)
116. N M Cottfried, A Seilmeier, W Kaiser *Chem. Phys. Lett.* **111** 326 (1984)
117. J Scherer, A Seilmeier, W Kaiser *J. Chem. Phys.* **83** 3948 (1985)
118. J L Baudour, H Caillean, W B Yelon *Acta Crystallogr., Sect. B, Struct. Crystallogr.* **33** 1773 (1977)
119. G V Maier, V P Shcherbina *Opt. Spektrosk.* **52** 1063 (1982) [a]
120. B Nickel *Chem. Phys. Lett.* **27** 84 (1974)
121. B Nickel *Helv. Chim. Acta* **61** 198 (1978)
122. B Nickel *Chem. Phys. Lett.* **71** 238 (1980)
123. B Nickel, G Roden *Chem. Phys.* **53** 243 (1980)
124. B Nickel, G Roden *Chem. Phys. Lett.* **74** 368 (1980)
125. G F Stel'makh, M P Tsvirko *Opt. Spektrosk.* **50** 998 (1981)
126. B Nickel *Chem. Phys. Lett.* **68** 17 (1979)
127. Y J Kray, B Nickel *Chem. Phys.* **53** 235 (1980)
128. D Klemp, B Nickel *Chem. Phys. Lett.* **97** 66 (1983)
129. B Nickel, G Roden *Chem. Phys.* **66** 365 (1982)
130. J Hertzberg, B Nickel *Chem. Phys.* **132** 235 (1989)
131. D L Dexter *J. Chem. Phys.* **21** 836 (1953)
132. R Katoh, M Kotani *Chem. Phys. Lett.* **201** 141 (1993)
133. R Katoh, M Kotani *Chem. Phys. Lett.* **300** 734 (1999)
134. R M Hochstrasser, C Marzzacco *J. Chem. Phys.* **49** 971 (1968)
135. J L Richards, S A Rice *Chem. Phys. Lett.* **9** 444 (1971)
136. S Voelker, J H van der Waals *Mol. Phys.* **32** 1703 (1976)
137. S Voelker, R M Macfarlane, A Z Genack, H P Trommsdorff, J H van der Waals *J. Chem. Phys.* **67** 1759 (1977)
138. S Voelker, R M Macfarlane, J H van der Waals *Chem. Phys. Lett.* **53** 8 (1978)
139. S Voelker, R M Macfarlane *Chem. Phys. Lett.* **61** 421 (1979)
140. V G Maslov *Opt. Spektrosk.* **50** 1091 (1981) [a]
141. M Vacha, Sh Machida, K Horie *J. Phys. Chem.* **99** 13163 (1995)
142. U Even, J Jortner, J Friedman *J. Phys. Chem.* **86** 2273 (1982)
143. U Even, J Magen, J Jortner *J. Chem. Phys.* **77** 4384 (1982)
144. B Dick, B Nickel *Chem. Phys.* **110** 131 (1986)
145. R M Shelby, R M Macfarlane *Chem. Phys. Lett.* **64** 545 (1979)
146. A Amirav, M Sonnenschein, J Jortner *J. Phys. Chem.* **88** 5593 (1984)
147. B Nickel, M T Wick *Chem. Phys.* **168** 111 (1992)
148. C-J Ho, J Babbitt, M R Topp *J. Phys. Chem.* **91** 5599 (1987)
149. R Jefferson, J Babbitt, C-J Ho, M R Topp *J. Phys. Chem.* **92** 2422 (1988)
150. A Hiraya, Y Achiba, N Mikami, K Kimura *J. Chem. Phys.* **82** 1810 (1985)
151. H Chosrowjan, S Tanigichi, T Okada, S Takagi, T Arai, K Tokumaru *Chem. Phys. Lett.* **242** 644 (1995)
152. S Akimoto, T Yamazaki, I Yamazaki, A Osuka *Chem. Phys. Lett.* **309** 177 (1999)
153. N Sarkar, S Takeuchi, T Tahara *J. Phys. Chem. A* **103** 4808 (1999)
154. C C Hayden, D W Chandler *J. Phys. Chem.* **99** 7897 (1995)
155. D R Cyr, C C Hayden *J. Chem. Phys.* **104** 771 (1996)
156. D G Leopold, R D Pandley, J L Roebber, R J Hemley, V Vaida *J. Chem. Phys.* **81** 4218 (1984)
157. A B Myers, K S Pranata *J. Phys. Chem.* **93** 5079 (1989)
158. M Mimuro, U Nagashima, S Nagaoka, S Takaichi, I Yamazaki, Y Nishimura, T Katoh *Chem. Phys. Lett.* **204** 101 (1993)
159. M Mimuro, S Akimoto, S Takaichi, I Yamazaki *J. Am. Chem. Soc.* **119** 1452 (1997)
160. V L Ermolaev *Usp. Fiz. Nauk* **80** 3 (1963) [b]
161. V L Ermolaev, E B Sveshnikova *Acta Phys. Pol.* **34** 771 (1968)
162. S Akimoto, I Yamazaki, S Takaichi, M Mimuro *Chem. Phys. Lett.* **313** 63 (1999)
163. Sh Yamaguchi, H Hamaguchi *J. Phys. Chem. A* **104** 4272 (2000)
164. Y Hirata, T Okada, N Mataga, T Nomoto *J. Phys. Chem.* **96** 6559 (1992)
165. Y Hirata, K Mashima, H Fukumoto, K Tani, T Okada *Chem. Phys. Lett.* **308** 176 (1999)
166. I K Lednev, N-Q Ye, R E Hester, J N Moore *J. Phys. Chem.* **100** 13338 (1996)
167. J Azuma, N Tamai, A Shishido, T Ikeda *Chem. Phys. Lett.* **288** 77 (1998)
168. V Stern, P Farmanara, W Radloff *J. Chem. Phys.* **112** 4460 (2000)
169. W Radloff, Th Freudenberg, H-H Ritze, V Stern, K Weyers, F Noack *Chem. Phys. Lett.* **245** 400 (1995)
170. K Ohta, T J Kang, K Tominaga, K Yoshihara *Chem. Phys.* **242** 103 (1999)
171. T Hasche, S H Ashworth, E Riedle, M Woerner, T Elsaesser *Chem. Phys. Lett.* **244** 164 (1995)
172. S H Ashworth, T Hasche, M Woerner, E Riedle, T Elsaesser *J. Chem. Phys.* **104** 5761 (1996)
173. J C Owrutsky, A P Baronawski *J. Chem. Phys.* **110** 11206 (1999)
174. R S H Liu, J R Edman *J. Am. Chem. Soc.* **90** 213 (1968)
175. R S H Liu, D M Gale *J. Am. Chem. Soc.* **90** 1897 (1968)
176. V L Ermolaev, E B Sveshnikova *Opt. Spektrosk.* **28** 601 (1970) [a]
177. G D Gillispie, E C Lim *Chem. Phys. Lett.* **63** 355 (1979)
178. R O Campbell, R S H Liu *J. Am. Chem. Soc.* **95** 6560 (1973)
179. R A Keller *Chem. Phys. Lett.* **3** 27 (1969)
180. Sh Kobayashi, K Kikuchi, H Kokubun *Chem. Phys. Lett.* **42** 494 (1976)
181. K Kikuchi, H Fukumura, H Kokubun *Chem. Phys. Lett.* **123** 226 (1986)
182. N A Borisevich, L M Bolot'ko, A V Doronin, A A Sukhodola *Opt. Spektrosk.* **63** 1036 (1987) [a]
183. G A Ketsle, L V Levshin, S N Letuta *Opt. Spektrosk.* **68** 344 (1990) [a]
184. G A Ketsle, L V Levshin, Yu N Lantukh, S N Letuta *Izv. Akad. Nauk SSSR, Ser. Fiz.* **54** 473 (1990)
185. J M Larkin, W R Donaldson, T H Foster, R S Knox *Chem. Phys.* **244** 319 (1999)
186. S Reindl, A Penzkofer *Chem. Phys.* **211** 431 (1996)
187. P C C Lee, M A J Rodgers *Photochem. Photobiol.* **45** 79 (1987)
188. V V Ryl'kov, E A Cheshev *Opt. Spektrosk.* **63** 1030 (1987) [a]
189. Y Yaas, M Klissinger, S Zilberg (Eds) *Conical Intersection in Photochemistry, Spectroscopy and Chemical Dynamics*; *Chem. Phys.* **259** (2 – 3) (Spec. Issue) (2000)

[a] — *Opt. Spectrosc. (Engl. Transl.)*
[b] — *Physics-Uspekhi (Engl. Transl.)*
[c] — *Dokl. Chem. Technol., Dokl. Chem. (Engl. Transl.)*

Russian Chemical Reviews **70** (6) 491 – 508 (2001) © 2001 Russian Academy of Sciences and Turpion Ltd

DOI 10.1070/RC2001v070n06ABEH000610

Design of site-specific RNA-cleaving reagents

V N Silnikov, V V Vlassov

Contents

I.	Introduction	491
II.	General problems of the design of site-specific RNA-cleaving reagents	491
III.	Catalysts of RNA cleavage	492
IV.	Site-specific RNA-cleaving reagents	499

Abstract. Data on chemical compounds capable of cleaving ribonucleic acids under physiological conditions are systematised and generalised. The possibilities of the design of site-specific RNA-cleaving reagents are considered. The bibliography includes 245 references.

I. Introduction

Reagents capable of performing efficient and specific cleavage of nucleic acids (NA) are required in molecular-biological investigations, used for the development of genetic-engineering techniques and employed in genetic engineering and gene therapy. Selective NA-specific cleaving reagents can be used for the preparation of biologically active gene-targeting compounds capable of suppressing or modulating expression of particular genetic programs. The design of such compounds offers possibilities of influencing the origin of pathological states.[1–4] This line of investigation can revolutionise the strategy of treatment of virtually all diseases.

The construction of NA-cleaving reagents for all the above-mentioned applications is a complicated problem because cleavage should proceed under nearly physiological conditions. Preparations used as therapeutic drugs should act strictly selectively on particular sequences in the compositions of certain types of nucleic acids. Side processes must be excluded, and the efficiency of the reaction with the target nucleic acid should be high to suppress functioning of the latter as completely as possible.

Since the design of gene-targeting chemical reagents is a topical problem, this line of investigation has been developed intensively in recent years. Presently, the following types of compounds are primarily used for DNA cleavage.

1. Compounds containing variable-valence metal complexes as reactive groups. The latter catalyse oxidation processes resulting in nucleoside degradation.[5–7]

2. Enediynes capable, under certain conditions, of generating biradical species, which react with both DNA chains and cause their cleavage.[8]

3. Alkylating reagents whose reactions weaken the glycoside bond in modified nucleosides resulting in their degradation.[9,10]

Recently, reagents cleaving DNA according to a photooxidation mechanism[11,12] as well as reagents based on natural and synthetic metal-independent antibiotics (varacin, lissoclinotoxin, *etc*.) generating hydroxyl radicals[13] have gained wide acceptance. Mechanisms of DNA hydrolysis, which occurs through interactions of radicals with various nucleic-acid elements, were considered in detail in reviews.[5,14,15]

Unlike DNA, RNA are substantially more stable to oxidative cleavage[16] (in particular, under the action of metal-dependent antibiotics, such as bleomycin,[17,18] and enediyne antibiotics, such as neocarzinostatin, esperamycin, *etc*.[19]) due to higher stability of the glycoside bond in ribonucleotides compared to that in deoxyribonucleotides. At the same time, hydrolytic cleavage of RNA proceeds much more readily.

Recently, considerable study has been given to the mechanisms of RNA cleavage with various compounds and to the design of catalysts for directed RNA cleavage. Data accumulated in this field and the construction of the first chemical RNA-cleaving agents exhibiting higher specificity compared to that of natural enzymes call for generalisation and analysis of the results of the investigations.

A very interesting line of investigation aimed at designing RNA-targeting agents involves the construction of ribozymes, *viz*., catalysts based on RNA or DNA. Different classes of ribosimes, procedures for their construction and the mechanisms of RNA cleavage under the action of these catalysts were considered in detail in reviews.[20–24]

The results of studies in the field of construction of artificial catalysts whose active groups catalysing hydrolysis of phosphodiester bonds are involved in conjugates with oligonucleotides, peptides and intercalates have not been systematised. The present review is intended to close this gap and is devoted to the main classes of compounds capable of catalysing RNA depolymerisation under physiological conditions and to their use in the preparation of 'synthetic ribonucleases' for directed cleavage of particular sequences of ribonucleic acids.

II. General problems of the design of site-specific RNA-cleaving reagents

Compounds capable of performing selective site-specific RNA cleavage must, like enzymes, contain two domains, *viz*., an RNA-binding domain, which can form a specific complex with particular RNA regions (target regions), and an RNA-hydrolysing domain performing hydrolysis of phosphodiester bonds adjacent to the binding sites or located in their vicinity (Fig. 1). Some

V N Silnikov, V V Vlassov Novosibirsk Institute of Bioorganic Chemistry, Siberian Branch of the Russian Academy of Sciences, prosp. Akad. Lavrent'eva 8, 630090 Novosibirsk, Russian Federation.
Fax (7-383) 233 36 77. Tel. (7-383) 233 37 62.
E-mail: Silnik@niboch.nsc.su (V N Silnikov)
Tel. (7-383) 233 33 28 (V V Vlassov)

Received 11 July 2000
Uspekhi Khimii **70** (6) 562 – 580 (2001); translated by T N Safonova

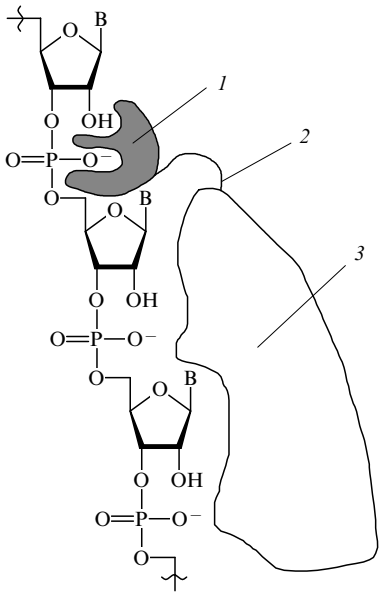

B, heterocyclic base residue.

Figure 1. Overall structure of synthetic ribonucleases;
(*1*) an RNA-hydrolysing fragment or a reactive group, (*2*) a linker, (*3*) an RNA-binding fragment.

peptides forming complexes with particular nucleotide sequences or elements of the three-dimensional RNA structure as well as low-molecular-weight organic compounds, such as intercalators,[25] polycations [26] and aminoglycosides,[27] can provide selectivity of RNA binding. Selected aspects of interactions of low-molecular-weight ligands with nucleic acids have been considered previously.[28–30] Oligonucleotides and their analogues are the most promising affine structures for directed action on RNA. A complementary oligonucleotide can be directed at any nucleotide sequence of interest. An additional advantage of these reagents is the fact that all these compounds can be synthesised with the use of a universal technology. Nucleotide sequences consisting of 15–20 units are unique even in genomes with complex organisation, this length of complementary oligonucleotides being sufficient to provide recognition and efficient binding with an RNA target under physiological conditions. Recently, a series of oligonucleotide analogues, which are resistant to cell enzymes and can form more stable complexes with nucleic acids than those of natural oligonucleotides, have been designed.[31–36]

Natural RNA-hydrolysing compounds, *viz*., enzymes and antibiotics, can be used as RNA-cleaving groups. Thus compounds, which can perform selective RNA cleavage in the vicinity of sequences involved in binding of conjugates, were synthesised based on oligodeoxyribonucleotides and natural enzymes, *viz*., ribonucleases A, S [37,38] and H.[39,40] However, enzymes contain their own RNA(DNA)-binding affine structures along with catalytic centres, which is necessarily reflected in the specificity of such conjugates and in the effects caused by these conjugates in biological systems. Due to this fact as well as to the complexity of the synthesis of these conjugates, enzymes and natural antibiotics show little promise as reactive groups.

RNA-hydrolysing fragments or reactive groups whose properties have little effect on the recognition of nucleic acid by a conjugate are agents of choice.

III. Catalysts of RNA cleavage

The presence of 2′-hydroxyl groups in RNA makes possible hydrolytic cleavage of these biopolymers according to the mechanism of intramolecular transesterification. RNA cleavage by this mechanism is widespread in nature, for example, in reactions catalysed by ribonucleases and ribozymes. It is reasonable to employ processes occurring in active centres of ribonucleases and ribozymes in the construction of RNA-cleaving chemical reagents.

It should be taken into account that high efficiency of natural enzymes results from functioning of complex active centres that arise in the course of evolution, while reactive groups forming a catalytic centre taken alone are generally weak catalysts of the corresponding processes. In the construction of artificial catalysts for the action on biopolymers, it is very important to provide the necessary spatial arrangement of all participants of the catalytic process by using the corresponding linkers.

1. Mechanism of hydrolytic cleavage of ribonucleic acids

Many enzymes and ribozymes cleave ribonucleic acids according to the mechanism of intramolecular transesterification through the nucleophilic attack of the oxygen atom of the 2′-hydroxyl group at the phosphorus atom. This reaction can proceed by two stereochemical mechanisms. One mechanism is realised when the angle α (Fig. 2) is close to 180° and the distance d between the

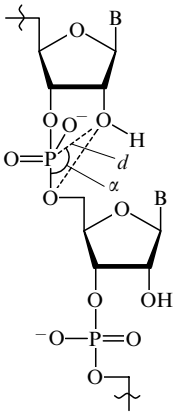

B, heterocyclic base residue.

Figure 2. Principal parameters responsible for the reactivity of phosphodiester bonds in RNA;
d is the 2′-O–P distance (Å) and α is the 5′-O–P–3′-O angle.

reacting groups < 3 Å (the linear mechanism), whereas another mechanism takes place when the angle α is close to 90° (the related mechanism). In the former case, the AE mechanism (an analogue of the S_N2 mechanism) is realised. The latter mechansim requires an additional stage, *viz*., migration of the leaving group from the equatorial to apical position (pseudorotation).[41] Pseudorotation was postulated for hydrolysis of a number of model compounds.[42–44] It was assumed that 3′→ 2′-isomerization in ribonucleotides also involves pseudorotation.[45] However, hydrolysis proceeded according to the linear mechanism in all cases for which the mechanism of catalytic RNA cleavage under the action of ribozymes or enzymes was established. Possible mechanisms of hydrolytic RNA cleavage under various conditions were considered in detail in a number of reviews and original studies.[45–47] The structural parameters of the regions of some RNA in which spontaneous hydrolysis is highly probable were analysed.[48] The dimensionless parameter F varying from 0 to 1 (for notations of α and d, see Fig. 2) was used as an integral value characterising stability of phosphodiester bonds in RNA sequences.

$$F = \frac{\alpha - 45}{180 - 45} \cdot \frac{(3\text{Å})^3}{d^3}.$$

It appeared that the parameter F characterising the mutual spatial arrangement of the oxygen atom of the 2′-hydroxyl group, the phosphorus atom and the oxygen atom at the 5′-terminus of

the leaving nucleoside correlates well with stability of the internucleotide bonds. The structural elements with $F = 0.5-0.8$ correspond to sites of spontaneous hydrolysis, whereas stable regions are characterised by the parameter F of 0.1–0.15. Hydrolytically labile sites with low values of the parameter F are rare exceptions. Generally, heterocyclic bases in these sites form either noncanonical GA pairs or CpA(UpA) sequences in single-stranded regions in which short-lived structures (which are able to undergo cleavage according to the linear mechanism, but which are not detected by NMR spectroscopy and X-ray diffraction analysis) can, apparently, arise.

Low values of the parameter F are also typical of double-stranded RNA regions in which the phosphodiester bonds are characterised by high stability.

It should be noted that experimental data on the high hydrolytic lability of some sequences in RNA are available. However, no explanation for these data was offered. Thus, cleavage of the phosphodiester bonds in the CpA(UpA) sequences in single-stranded RNA occurs most readily, which is not clearly understood.[49] These sequences in short single-stranded oligoribonucleotides undergo cleavage in the presence of various proteins (T7 RNA polymerase, T4 polynucleotide kinase, lysozyme or trypsin) and some polymers, such as polyethylene glycol, dextran or polyvinyl pyrrolidone.[50–52] The efficiency of cleavage depends on the length of the oligonucleotide and on the nature of the flanking nucleotides. Thus, the ratio between the rates of hydrolysis of the bonds in the UA sequence for GUAC, GUAU and CGUA is 1 : 6 : 16, whereas the corresponding ratio for GUAA, CGUAA and UCGUAA is 1 : 4 : 6. The change of the nucleotide residue X at the 3′-terminus in the XUAA tetranucleotide has virtually no effect on the rate of hydrolysis, whereas the efficiency of GUAX cleavage decreases in the series X = G > A > U > C by a factor of three.[53]

It was also demonstrated that the UpA and CpA sequences in the loop regions of RNA are cleaved in the presence of nonionic [Triton X-100 (**1**) or Genapol X-100 (**2**)] or zwitterionic [zwittergent 3–10 (**3**) or an amide derivative of cholic acid (**4**)] detergents at concentrations corresponding to the critical concentrations of micelle formation.[54] Efficiency of hydrolysis is independent of the micelle size. The maximum rate of hydrolysis is achieved in the case of the loop consisting of five nucleotide units.[50] Anionic detergents, such as sodium dodecyl sulfate or deoxycholic acid, suppress cleavage.

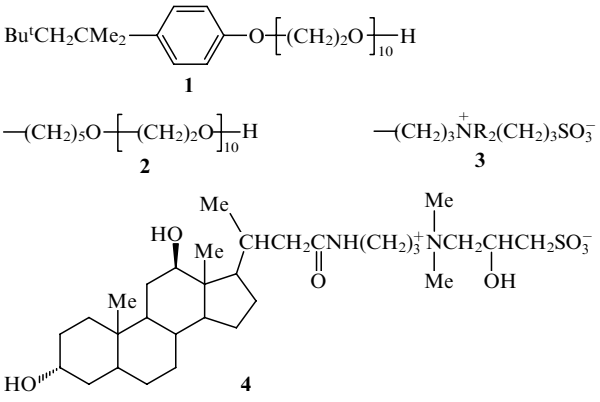

It can be suggested that the compounds **1**–**4** influence RNA in such a way that in some of its regions, *viz*., in the pyrimidine–purine sequences, the oxygen atom of the 2′-hydroxyl group of ribose and the internucleotide phosphate are brought into proximity and the angle α is increased, the resulting geometry being most favourable for spontaneous cleavage of the phosphodiester bonds. However, the mechanism of this reaction as well as the reasons for high lability of the CpA and UpA fragments still remain to be elucidated.

2. Hydrolysis of ribonucleic acids involving metal ions and metal complexes

Presently, abundant data on hydrolysis of ribonucleic acids involving various metal ions are available. Destruction of ribonucleic acids under the action of the Zn^{2+}, Ni^{2+}, Ca^{2+}, Co^{2+}, Cu^{2+}, Mg^{2+}, Mn^{2+}, Pb^{2+}, Al^{3+} and Ln^{3+} ions and ions of other lanthanides has received the most study. Some of these ions can cause RNA cleavage under physiological conditions.

Metal ions are involved in active centres of many enzymes hydrolysing phosphodiester bonds, such as phosphomono-,[55] phosphodi-[56,57] and phosphotriesterases.[58] In some cases, these ions serve as cofactors necessary for functioning of ribozymes taking part in chemical catalysis of cleavage of phosphodiester bonds.[59] Below are considered the schemes of cleavage of phosphodiester bonds in RNA with the participation of metal ions. Metal ions can be involved in catalytic processes as Lewis acids by reacting directly with the oxygen atom of the phosphate group (**A**),[60] with a nucleophile (for example, with the hydroxide anion) (**B**)[61] or with the oxygen atom of the leaving group (**C**). In addition, metal ions can be indirectly involved in catalysis. Thus, these ions can either coordinate a water molecule and act as intramolecular general acid catalysts (**D**) or coordinate the hydroxide anion and act as intramolecular general base catalysts (**E** or **F**).[62,63]

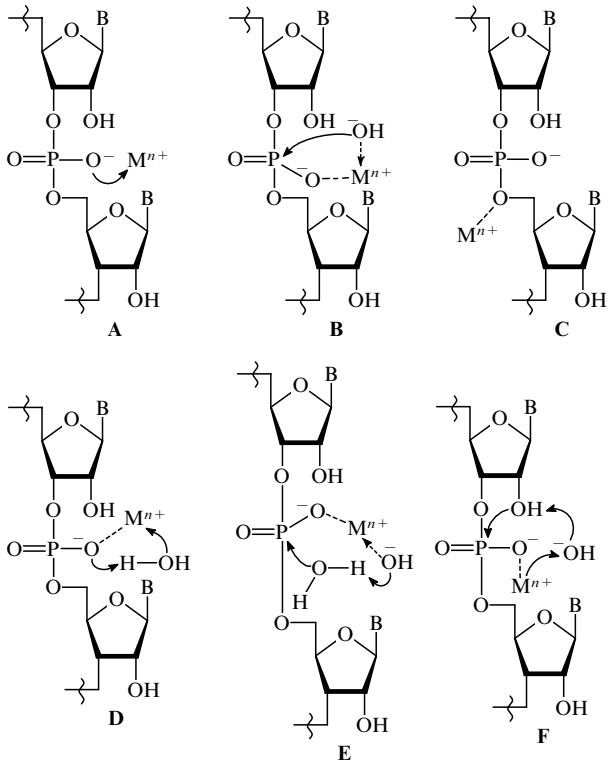

Apparently, hydrolytic RNA cleavage with different metal ions can proceed by one or another mechanism or according to a combination of them. Two main models of the participation of metal ions in hydrolysis of phosphodiester bonds were proposed. According to the model **G**, the metal ion and the hydroxide anion coordinated to this ion are involved in the catalytic reaction.[64–68] The model **H** is based on the mechanism accepted for such natural enzymes as alkaline phosphatase and DNA polymerase I[57,69] and assumes the participation of two metal ions one of which coordinates the hydroxyl group and the second ion activates the oxygen atom of the leaving group. Most of the results obtained in studies of RNA hydrolysis catalysed by metal ions can be interpreted based on both the models **G** and **H**.[70] X-Ray diffraction data for some ribozymes provide evidence in favour of the reaction mechanism involving one metal ion.[64,71] However, information on substantial acceleration of RNA hydrolysis

under the action of the $Mg^{2+}-Pb^{2+}$ (see Ref. 72), $Nd^{3+}-Pb^{2+}$ (see Refs 73 and 74), $La^{3+}-Fe^{3+}$ and $La^{3+}-Sn^{4+}$ pairs [75] can be interpreted only within the framework of the model **H**.

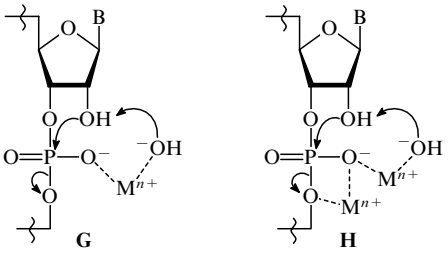

G **H**

Using the ApA dinucleotide as an example, it was demonstrated that the phosphodiester bond can be hydrolysed under the action of both the hydroxy complex of La^{3+} (see Ref. 76) and the binuclear hydroxy complex $[La_2(OH)]_5^{+}$.[77] The rate of hydrolysis was increased by four orders of magnitude on going from the mono- to the binuclear complex.[78] It can be suggested that hydrolysis can proceed involving either one or two metal ions depending on the reaction conditions. Within the frameworks of all mechanisms proposed, metal ions, which are stronger Lewis acids and have a larger coordination sphere, should be more efficient catalysts of hydrolytic cleavage. In this connection, considerable study should be given to cleavage of phosphodiester bonds under the action of the Ce^{4+} (see Ref. 79) and Zr^{4+} ions.[80, 81]

The rate of hydrolysis of phosphodiester bonds in RNA catalysed by metal ions depends on the nature of the flanking nucleosides. Thus, hydrolysis of the phosphodiester bond in ApA in a solution of the Tm^{3+} salt (0.01 mol litre^{-1}) proceeded 4.8–5.1 times faster than that in UpU.[82] In studies of hydrolysis of six different nucleotide pairs (UpG, CpC, GpA, ApU, UpA and ApA) in solutions of the Lu^{3+} salt (0.01 mol litre^{-1}), the reaction rate for the UpG dinucleotide, which underwent hydrolysis most rapidly, was found to be 2.2 times higher than that for ApA, which is the most stable under these conditions.[82] The presence of the 3′-terminal phosphate group leads to substantial acceleration of hydrolysis of the internucleotide phosphate bond in dinucleotides due, apparently, to more efficient cation binding. Thus, hydrolysis of the phosphodiester bond in ApAp in the presence of Zn^{2+} ions proceeded more rapidly than that in ApA. At the same time, the presence of the 2′-terminal phosphate group or the 2′,3′-cyclophosphate group exerts only a slight effect on the rate of hydrolysis.[83] Analogous results were obtained in other studies as well.[84, 85] It was shown that the 3′-terminal phosphate group in oligodeoxynucleotides containing a ribonucleotide unit, *viz.*, Up(Tp)$_n$Tp or Up(Tp)$_n$T ($n = 0-4$ or 7), at the 5′-terminus accelerates hydrolysis even if it is spaced at seven nucleotide units.[86] Apparently, the observed 5–20-fold acceleration of hydrolysis of poly(U) compared to UpU under the action of the Mg^{2+}, Co^{2+}, Ni^{2+}, Cd^{2+} or Zn^{2+} ions is attributable to the polyelectrolyte effect of the total negative charge of poly(U).[87]

The ability of metal ions to catalyse hydrolysis varies over a wide range depending on the nature of the substrate. Thus, the activity of metal ions in the hydrolysis of ApA decreases in the series Tm = Lu > Y > Nd = Eu = Sm > Ce = Sc = Gd = Tb > Pr = Dy > Ho = Er > Yb > La.[76] At the same time, the activity of metal ions in hydrolysis of 3′,5′-cycloadenosinemonophosphate (which is one of the intermediate hydrolysis products of ApA) under analogous conditions decreases in the series Ce $\gg$ Pr > Nd = La > Y = Sm = Dy > other lanthanides.[88]

Evidently, the differences in the rate of hydrolysis in the dunucleotide pairs as well as in more complex substantces arise from the different complex-forming ability of various fragments of nucleic acids. Problems of complex formation of metal ions with nucleic acids were considered in detail in a review. [89]

Hydrolysis of RNA in the presence of various metal ions is widely used for revealing the cation-binding sites in nucleic acids.[90–94] The magnesium, lead and lanthanide ions can catalyse selective cleavage of phosphodiester bonds in the regions of some specific elements of the three-dimensional RNA structure.[95–99] The sensitivity of these reactions to the orientation of the ligands was used in studies of the RNA structure in solution and for comparison of the three-dimensional structures of mutant tRNA and 5SRNA.[100, 101] It was demonstrated [102] that sequences of ribonucleic acids in complexes with oligodeoxynucleotides do not undergo hydrolysis in the presence of Eu^{3+} or La^{3+} complexes, apparently, because the conformational flexibility of RNA, which is necessary for efficient ion binding and for transesterification, is limited upon formation of the duplex. In imperfect complexes, loop single-stranded regions are cleaved more rapidly.[103] The effects of the nucleotide sequence and the size of the loop region on the efficiency of RNA hydrolysis in the presence of the Pb^{2+} and Zn^{2+} ions as well as in the presence of their complexes were examined in detail.[104] The efficiency of hydrolytic cleavage was demonstrated to be increased as the size of the loop increases and as the hydrolysed phosphodiester bond moves away from the stalk fragment. The results obtained confirmed once again the necessity of conformational flexibility of the ribosephosphate fragment subjected to hydrolysis.

Due to the ability of complexes of lanthanides,[105, 106] copper,[107] zinc and some other metals [108] to catalyse hydrolysis of phosphodiester bonds, they can be considered as potential hydrolytically active groups in the synthesis of conjugates with organic compounds and oligonucleotides. The lanthanide ions, which are strong Lewis acids [109] and have a flexible coordination sphere,[110] are believed to be the most promising catalysts. The construction of highly stable metal complexes, which are simultaneously characterised by the high acidity of the central atom, presents a contradictory problem. However, a number of metal complexes (for example, compounds **5**–**8**) possessing high stability with retention of high activity in hydrolysis were prepared.[85, 106, 111, 112] It was demonstrated that catalytic RNA cleavage can proceed in the presence of zinc(II) [85] and lanthanum(III) [106] complexes. The rate of RNA hydrolysis in the presence of different metal complexes depends on pH. This suggests that, as in the case of free metal ions, hydrolysis of phosphodiester bonds occurs, apparently, with the participation of two molecules of the metal complex. In this case, one molecule acts as a Lewis acid, whereas the second molecule coordinates the hydroxide anion and acts as a base.[113, 114]

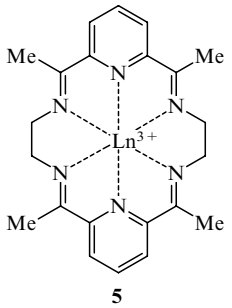

5

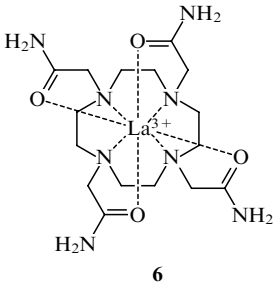

6

Ln = La, Eu, Tb, Lu.

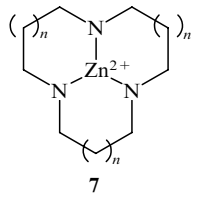

7

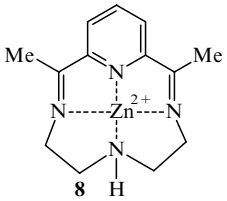

8

$n = 2, 3$.

3. Reagents modelling active centres of metal-dependent enzymes catalysing phosphoester-bond cleavage

Hydrolytic centres of metal-dependent enzymes, which are involved in hydrolysis of phosphoester bonds in various sub-

strates, often contain two complex-forming domains consisting of the amino acid residues His, Asp(Asn), Glu, Arg and Lys (in different combinations) and one of hydroxyl-containing amino acids, *viz*., Ser or Tyr. The distances between the metal ions (Ca^{2+}, Zn^{2+}, Mn^{2+}, Mg^{2+} and Fe^{3+}) in the active centres are in the range of 3–5 Å. In addition, the hydrolytic centres may contain one or several such amino acids as Glu, Arg, Lys, His or Ser. The functional groups of these amino acids are not directly bound to the metal ions and act as additional base, acid or nucleophilic catalysts (see reviews [115–118]). Active centres of some enzymes contain one (staphylococcus nuclease [119] and nuclease Sm from *Serratia marcescens* [120]) or more than two metal ions (nuclease P1).[121] Below are considered the principal structural elements of the active centres of natural metal-dependent enzymes, which hydrolyse phosphoester bonds in various substrates and contain from one to three metal ions, *viz*., staphylococcus nuclease (**9**), phosphorylase C from *Bacillus cereus* (**10**) and purpuric acid phosphatase (**11**).

Owing to success achieved in the synthesis of stable metal complexes and progress made in the determination of the structures of active centres and elucidation of the mechanisms of action of enzymes, which hydrolyse phosphoester bonds in various substrates, a broad range of synthetic catalysts, which serve as functional and structural models of natural enzymes, have been synthesised in recent years.[122–124]

Binuclear metal complexes based on the Zn^{2+} (see Refs 125–127), Cu^{2+} (see Refs 128–130), Co^{3+} (see Refs 131 and 132) and La^{3+} ions [133, 134] were prepared. The efficiency of hydrolysis in the presence of binuclear metal complexes appeared to be much higher than that in the case of their mononuclear analogues. This is particularly essential for the Zn ions, which are weak Lewis acids and whose mononuclear complexes do not catalyse hydrolysis.[129, 135] Compounds **12**–**16** proved to be the most efficient catalysts among all polynuclear metal complexes modelling active centres of natural enzymes. In particular, hydrolysis of the phosphoester bond in the model substrate in the presence of the complex **12**, which is a structural and functional model of D-fructose 1,6-bis(phosphate-1) phosphatase, proceeded 10^3 times more rapidly than that in the presence of similar cobalt complexes.[132] Analogous results were obtained for the copper complex **13**. In the presence of the latter the rates of hydrolysis of phosphoester bonds in various compounds are increased by a factor of $(1-2.7) \times 10^4$.[129] It should be noted that in the case of hydrolysis of natural substrates in the presence of polynuclear metal complexes, metal ions can interact not only with phosphate residues, but also with heterocyclic bases as a result of which these compounds acquire particular substrate specificity. Thus, the relative rates of cleavage upon hydrolysis of ribonucleoside-2′,3′-cyclophosphates of adenosine, guanine, uridine and cytosine in the presence of the binuclear copper complex **15** are 1.5, 8.5, 4.3 and 1, respectively, whereas the relative rates in the presence of the complex **16** are 31.1, 1, 2.9 and 5.1, respectively.[130] The ratio between the rates of hydrolytic cleavage of the GpG dinucleotide, which is most readily hydrolysed, and the most stable ApA dinucleotide in the presence of the trinuclear zinc complex **14** was 163 : 1.[136]

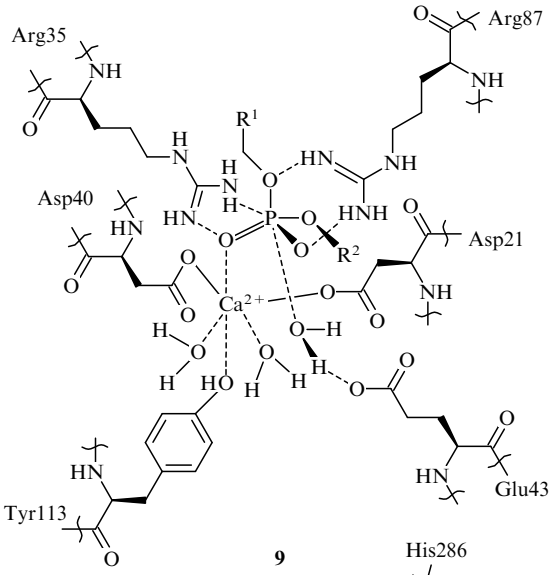

9

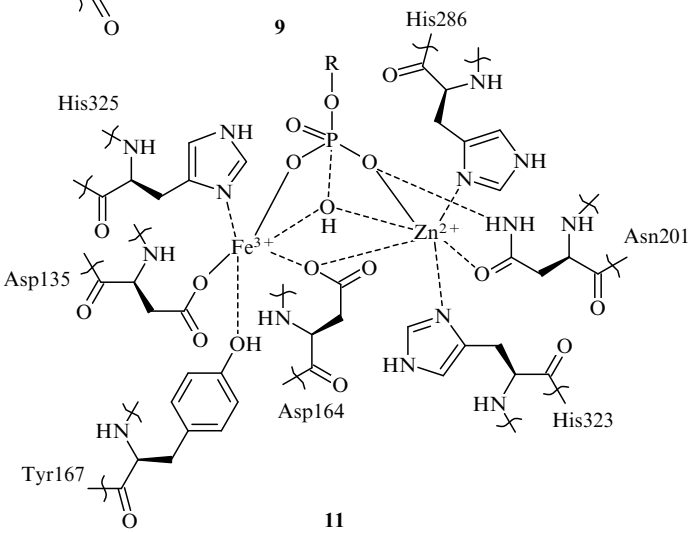

11

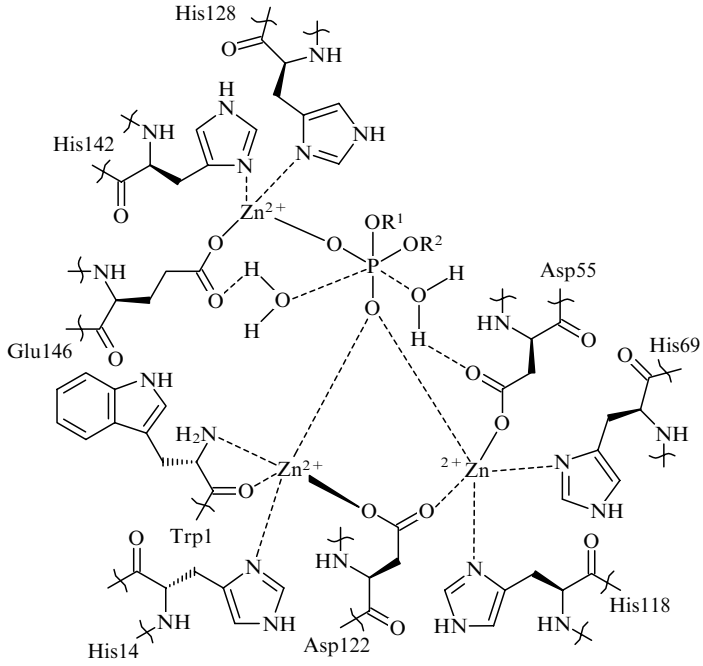

10

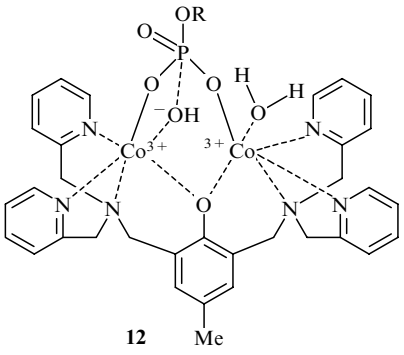

12

R = 4-$NO_2C_6H_4$.

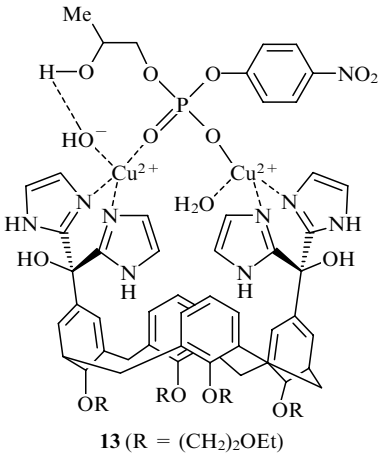

13 (R = $(CH_2)_2OEt$)

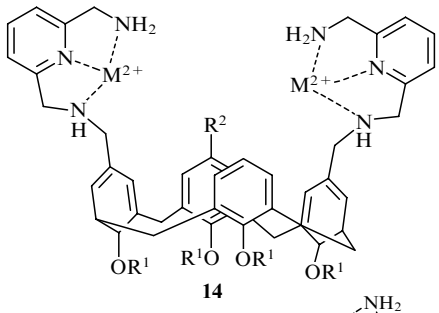

14

R^1 = $(CH_2)_2OEt$; R^2 = H, M = Zn, Cu.

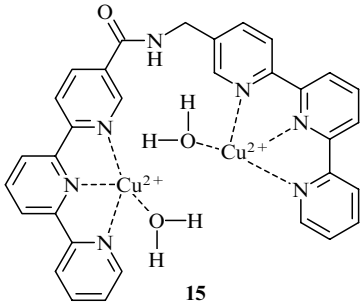

15

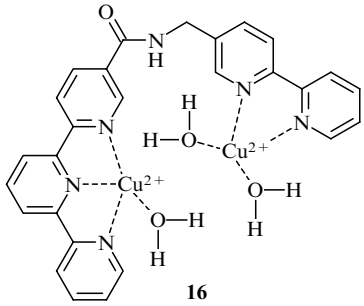

16

Below are listed compounds **17**–**22** modelling hydrolytic centres of enzymes, which act as acid catalysts (**20**–**22**), base catalysts (**17**, **18** and **22**) or nucleophilic catalysts (**19**) and whose active centres contain functional groups that are not bound to metal ions.[137–140]

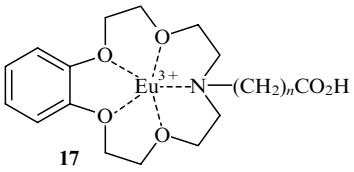

17

n = 1–3.

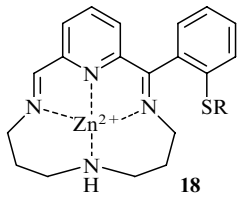

18

R = H, .

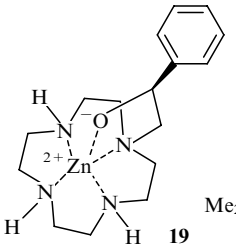

19

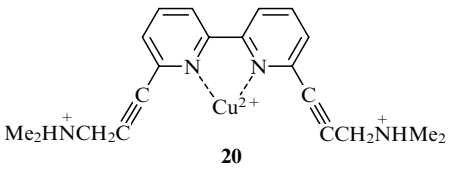

20

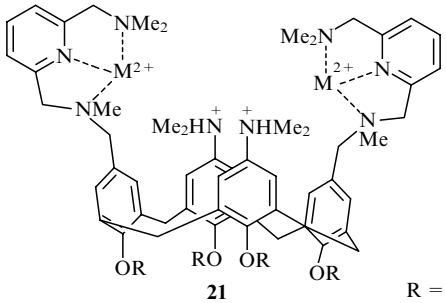

21

R = $(CH_2)_2OEt$

Modelling of the active centres of such enzymes requires a more rigid mutual spatial arrangement of the reactive groups compared to that in compounds containing only metal ions with flexible and bulky coordination spheres. In most cases, the compounds **17**–**22** proved to be only insignificantly more efficient than the basis metal complexes.

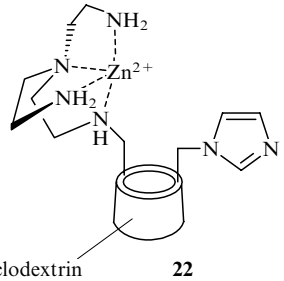

Cyclodextrin **22**

Probably, this is attributable to the unfavourable spatial arrangement of the reactive centres. The efficiency of cleavage is increased by a factor of 10^3–10^4 when the mutual arrangement of all participants of the catalytic process is optimum.[141, 142] Models of the active centres of natural enzymes based on metal complexes containing additional functional groups, which are not involved in complex formation, were discussed in detail in a review.[143]

4. Hydrolysis of ribonucleic acids with amino compounds and cationic peptides

Hydrolysis of RNA is catalysed by various amino compounds.[144] In the studies of hydrolysis of bis(4-nitrophenyl) and bis(2,4-dinitrophenyl) phosphates with diamines of the general formula $Me_2N(CH_2)_nNMe_2$ (**23a**–**c**) [n = 1 (**a**), 2 (**b**) or 3 (**c**)], two possible mechanisms of cleavage of the phosphodiester bonds were proposed. One of these mechanisms (**A**) is realised in the case of hydrolysis involving diamines as the corresponding monocations. The second mechanism (**B**) assumes the participation of neutral diamines. Thus hydrolysis in the presence of the diamines **23a**–**c** as monocations was accelerated by a factor of 870, 74 and 190, respectively, compared to hydrolysis in the presence of trimethylamine. In addition, the isotope effect, which was expected for

general acid catalysis, was observed when H_2O was replaced by D_2O ($k_H : k_D = 1.6$ for the diamine **23a**). The diamines **23a–c** in the neutral form exhibit substantially higher catalytic activity (1400–2040 times higher than that of trimethylamine), the isotope effect being absent. Apparently, in the latter case, the positive charge that arises in the course of the nucleophilic attack at the phosphorus atom (the transition state **B**) is electrostatically stabilised by the free electron pair of the second nitrogen atom.[145]

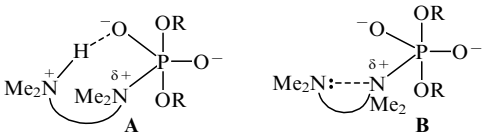

A **B**

R = 4-$NO_2C_6H_4$, 2,4-$(NO_2)_2C_6H_3$.

Hydrolysis of poly(A), poly(C) and poly(U) in solutions of polyamines (1–2 mol litre^{-1}), such as ethylenediamine, triethylenetetramine, *etc.*, was investigated.[146] It appeared that ethylenediamine possesses the highest catalytic activity, the efficiency of hydrolysis (50 °C, 2 days) in a solution of ethylenediamine (1 mol litre^{-1}) being decreased in the series poly(A) > poly(U) > poly(C) (33%, 28% and 16%, respectively). Under these conditions, poly(G) was not hydrolysed.[147]

Apparently, the weak hydrolytic activity of bleomycin (metal-dependent antibiotic) in the absence of metal ions is explained by the presence of aliphatic amino groups.[148] Regular peptides containing arginine and(or) lysine can accelerate hydrolysis of the phosphodiester bonds in ApAp and poly(A).[149–151] The regular peptides poly(Leu-Lys-Lys-Leu) and poly(Leu-Lys) capable of forming α-helices and β-folds, respectively, exhibit the highest activity in hydrolysis. In their complexes with RNA, the ratio $Lys^+ : PO_4^- = 2 : 1$ was achieved. Distortion of the polypeptide structure by introducing proline (Pro-Leu-Lys-Leu-Lys) or with the use of the D,L-isomers (D,L-Leu-D,L-Lys) leads to a sharp decrease in the catalytic activity of peptides. It should be noted that hydrolysis is not accelerated in the presence of poly(His), poly(Arg-Glu-Glu) and a number of other regular peptides containing various functional groups. No activity was also observed for the Ac-Leu-Lys-NHEt dipeptides. Apparently, the fact that the distances between the phosphate residues in the ribonucleotide (6.2 Å) coincide with the distances between the positive charges in poly(Leu-Lys-Lys-Leu) (6 Å) and poly(Leu-Lys) (6.9 Å) plays a decisive role in the manifestation of the catalytic activity exhibited by the above-mentioned peptides in RNA hydrolysis (Fig. 3).[152, 153]

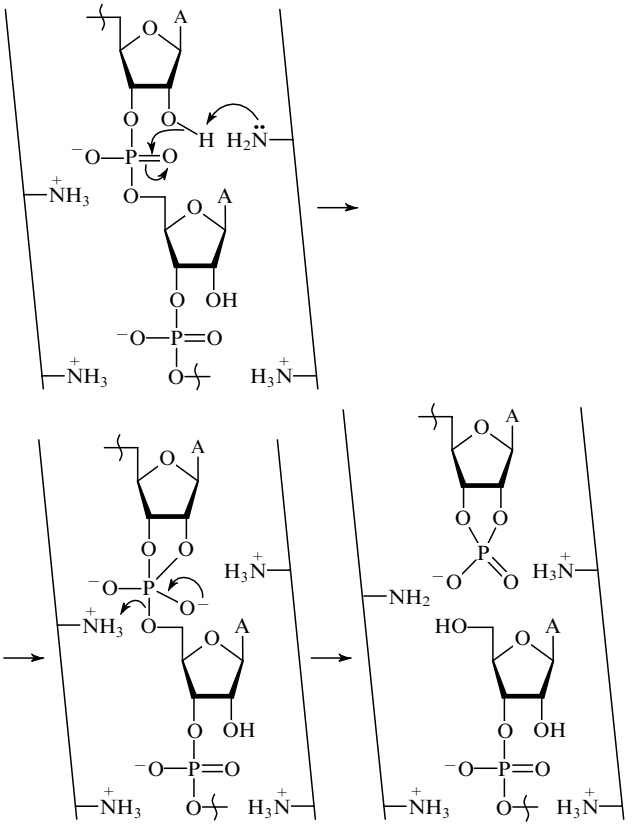

A, heterocyclic base residue.

Figure 3. The assumed mechanism of hydrolytic RNA cleavage under the action of polycharged peptides.

On the whole, both polyamines and regular peptides ehxibit low hydrolytic activity. Thus, the degree of depolymerisation of ApAp under the action of the most active regular peptide, *viz.*, poly(Leu-Lys), at 50 °C (pH 8.0) was 85% after 7 days.[150] After 2 days, the degree of depolymerisation of poly(A), poly(U) and poly(C) under the action of the most active polyamines at 50 °C (pH 8.0) varied from 16% to 69%.[147]

5. Reagents modelling active centres of metal-independent ribonucleases

Of metal-independent ribonucleases, ribonucleases A and T1 have received the most study. Both enzymes were found to cleave phosphodiester bonds in RNA according to the mechanism of intramolecular transesterification under conditions of acid–base catalysis. The scheme of the 'classical' two-step mechanism of acid–base catalytic hydrolysis of phosphodiester bonds in ribonucleic acids under the action of RNase A involves transesterification to form cyclic phosphodiester **24** followed by its hydrolysis. The abstraction of the proton from the 2′-hydroxyl group of the ribose residue under the action of the base **25** and the transfer of the proton from the fragment **26** to the oxygen atom of the leaving group are the key stages of this mechanism (Scheme 1).[154, 155] The details of interactions of the amino acid residues in the active centre both with each other and with the substrate have consistently been refined.[156–159]

Breslow and coworkers[160] proved that the active centres of ribonulceases can, in principle, be modelled by small molecules. The authors found that RNA hydrolysis was catalysed by a neutral concentrated (1–2 mol litre^{-1}) imidazole buffer and then synthesised a conjugate of cyclodextrin with molecules containing imidazole fragments. This conjugate catalysed hydrolysis of a model substrate, *viz.*, *tert*-butylcatechol 1,2-cyclophosphate.[161]

Hydrolysis of RNA with imidazole conjugates or an imidazole buffer proceeded most efficiently at pH 7, which corresponds, as in the case of ribonuclease A, to the mechanism of general acid–base catalysis, *i.e.*, one protonated and one nonprotonated imidazole fragment were involved in hydrolysis. Breslow examined three possible bisimidazole conjugates of cyclodextrin and found that only one of them, which is characterised by the spatial arrangement of the imidazole rings most favourable for the cleavage of the phosphodiester bond, exhibited catalytic activity in hydrolysis of the model phosphodiester.[162] Some conjugates of cyclodextrin containing various combinations of the imidazole and amino groups, cyclic and acyclic ethers and metal complexes also possess phosphoesterase activity with respect to model substrates.[163–166] Prakash *et al.*[167] proposed a structure modelling ribonuclease A in which the same imidazole fragment acts as a base and a proton donor. The model proved to be suitable in the presence of zinc ions, which stabilise the transition state and cause an increase in the electrophilicity of the phosphorus atom (structure **27**, Scheme 2). The authors believed[167] that hydrolytic cleavage of the phosphodiester bond in the diribonucleotide proceeds according to the related transfer mechanism (Section III.1). It was assumed that the leaving group in the structure **27** is located rather close to the 2′-hydroxyl group. The proton transfer from the 2′-hydroxyl group of the substrate to the

Scheme 1

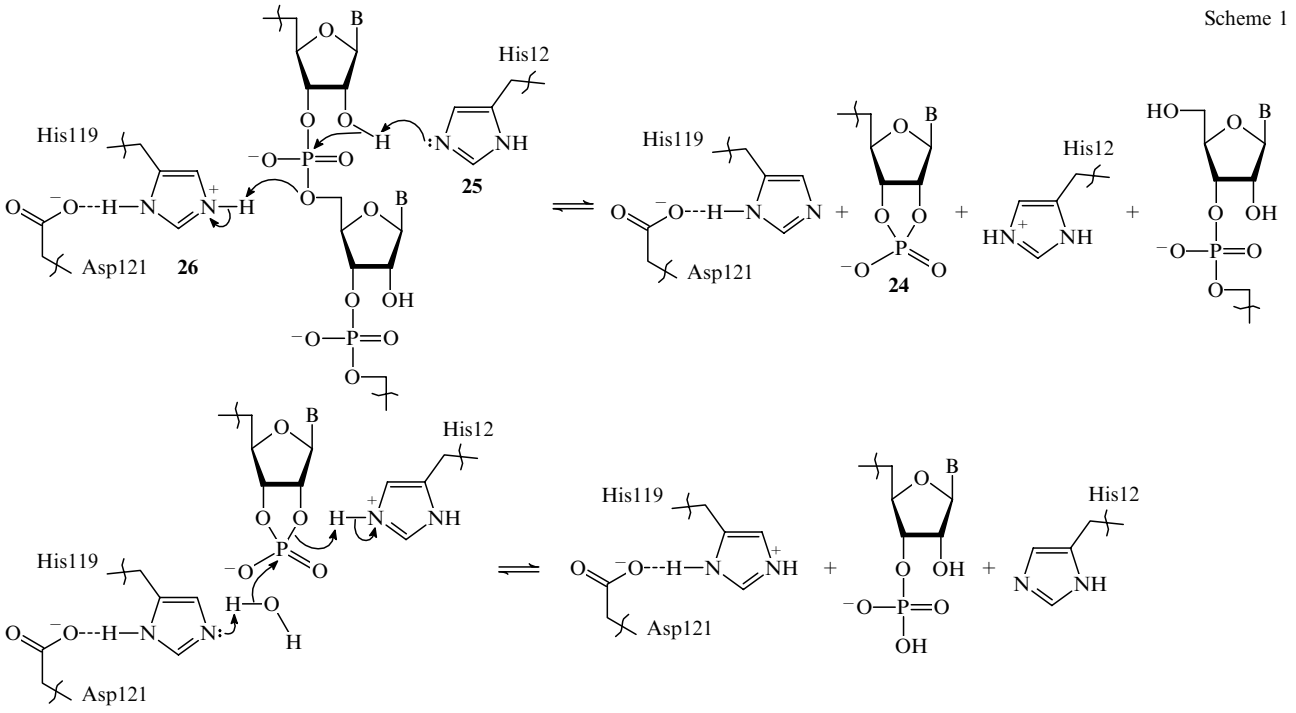

B, heterocyclic base residue.

Scheme 2

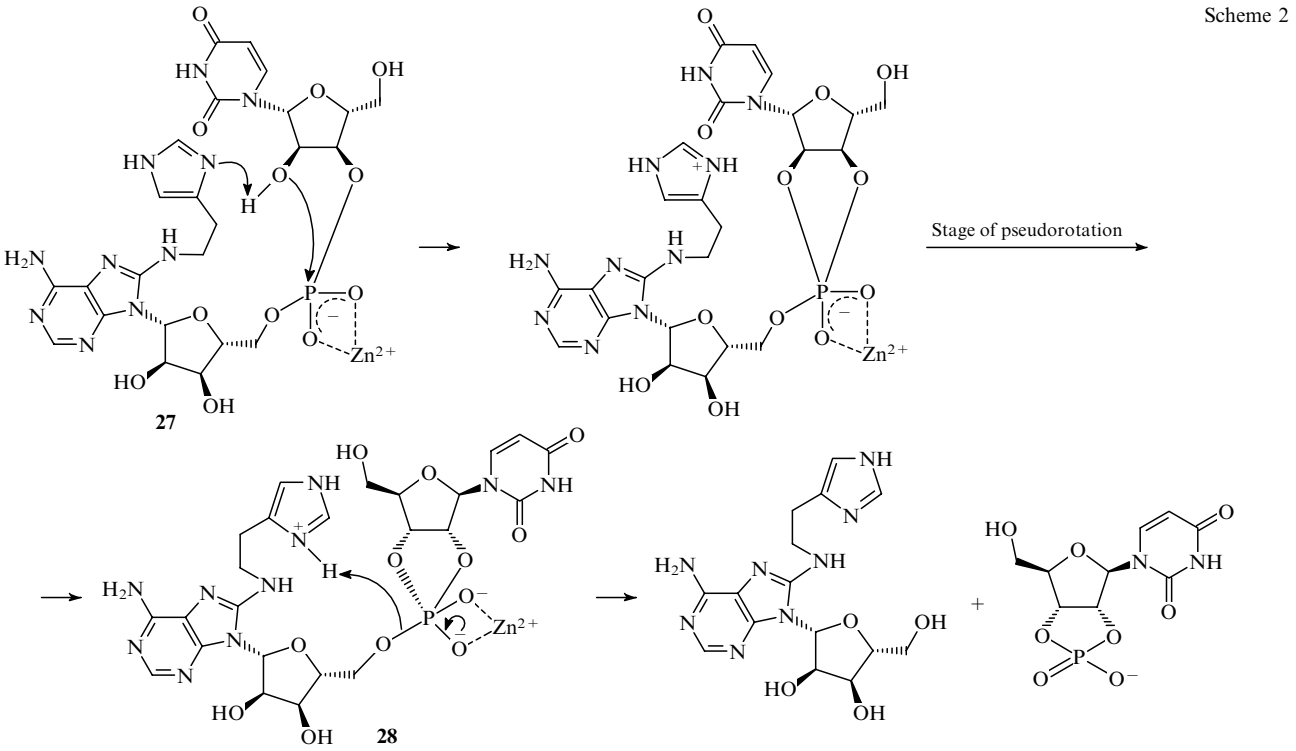

imidazole fragment and the stage of pseudorotation are followed by the cleavage of the phosphodiester bond involving a proton of the same imidazole fragment (intermediate **28**). This mechanism requires an additional stage of pseudorotation; however, the process can involve the same histamine fragment as proton donor and proton acceptor.

More recently, hydrolytic RNA cleavage under the action of imidazole and its conjugates with cationic and intercalating compounds has been studied in detail.[168, 169] It was demonstrated that these compounds can be used as structural probes in studies of the secondary structures of RNA and RNA–deoxyoligonucleotide complexes in solutions.[168, 169]

Hydrolysis with both an imidazole buffer and imidazole conjugates proceeds predominantly in single-stranded regions of RNA. Apparently, this is associated with the lower conformational flexibility of nucleotides in double-stranded regions and the less favourable spatial arrangement of the 2′-hydroxyl group with respect to the phosphorus atom of the internucleotide phosphate group. It should be noted that the rate of hydrolysis with an imidazole buffer is independent of the nucleotide sequence in the region subjected to cleavage (Fig. 4), whereas imidazole conjugates have a pronounced tendency for cleavage at the pyrimidine – purine regions.[168]

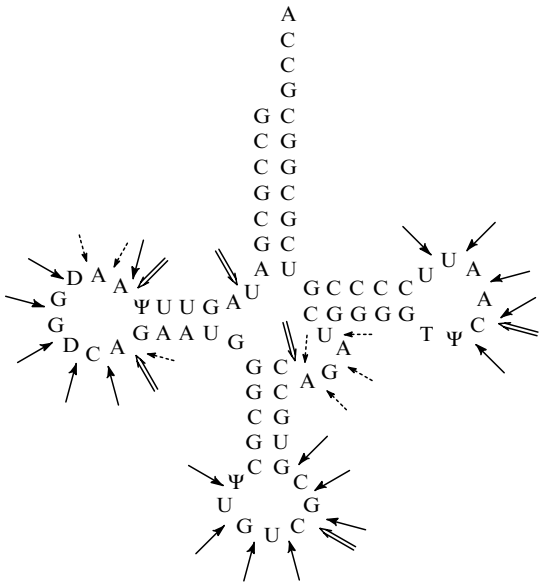

Figure 4. Structure and major cleavage sites of $tRNA^{Asp}$.
The most probable and less probable sites of cleavage under the action of an imidazole buffer are indicated by single and dashed arrows; the sites of cleavage under the action of imidazole conjugates are indicated by doubled arrows.

Modelling of the active centre of staphylococcus nuclease (nuclease S) is also of interest. The structure and the mechanism of action of nuclease S were established based on X-ray diffraction data, results of kinetic studies and data on substitutions of amino acids in the active centre of the enzyme.[170–172]

It is assumed that due to coordination by the guanidinium groups, the phosphate ion adopts the conformation favourable for hydrolysis with nuclease S. Simultaneously, the five-coordinate intermediate state of the phosphorus atom is stabilised. Although being a metal-dependent enzyme, nuclease S, like other compounds containing guanidinium groups, can be bound to the phosphate anions[173,174] and accelerate hydrolysis of the phosphodiester bonds in the absence of metal ions.[175] Hydrolysis of phosphodiester bonds under the action of compounds containing the guanidinium fragments is accelerated in the presence of external or internal nucleophiles.[176,177] Yet another type of hydrolytic centre combining elements of the active centre of RNase A (general base catalysis with imidazole) and nuclease S (coordination of the phosphate anion and stabilisation of the five-coordinate state of the phosphorus atom) was proposed by Oost and Kalesse.[178] The compounds synthesised contained the imidazole fragment and one or two guanidinium groups bound to a steroid core through spacers of different lengths. Most of the compounds synthesised exhibited low hydrolytic activity with respect to the model substrate, *viz*., 2′-hydroxypropyl 4-nitrophenyl phosphate. The efficiency of hydrolysis depended on both the number of guanidinium groups (two groups were better than one group) and their positions with respect to the steroid rings as well as on the length of the linker. The most efficient construction, *viz*., **29**, also exhibited a low hydrolytic activity with respect to UpU ($k = 2.4 \times 10^{-4}$ h^{-1}, 60 °C, pH 7.5). At the same time, simpler compounds containing only guanidinium groups [1,3-bis(guanidinium)propane] or simultaneously guanidinium and imidazole fragments {1,3-bis(guanidinium)-2[2-(1*H*-imidazol-4-yl)ethylamino]propane} appeared to be hydrolytically inactive.

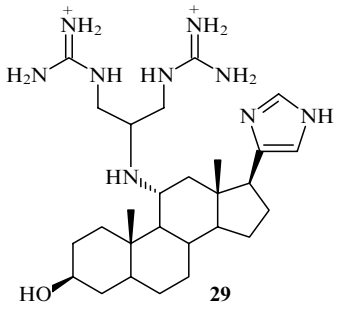

29

Therefore, functional models of the active centres of natural ribonucleases can be, apparently, obtained by constructing molecules which contain basic and acidic catalytic centres adopting particular orientations.

Most often, synthetic ribonucleases contain imidazole residues (an analogue of His12 in RNase A) or the carboxylate anion (an analogue of Glu58 in RNase T1) as a base and the protonated imidazole fragment as a proton donor (analogously to His119 and His92, respectively). Apparently, efficiency of catalysis can be improved by introducing positively charged groups (amino or guanidinium) into the catalytic centre to achieve a particular orientation of the phosphate ion with respect to the catalytic centres and to stabilise the five-coordinate intermediate state of the phosphorus atom. Probably, the introduction of the nucleophilic group (for example, the hydroxyl group simulating the 2′-hydroxyl group of ribose) into the reactive centre will allow one to construct catalysts hydrolysing phosphodiester bonds in DNA.[179]

IV. Site-specific RNA-cleaving reagents

Site-specific RNA cleavage can be performed with the use of reagents containing groups which form complexes with particular nucleotide sequences or elements of the three-dimensional RNA structure. The most evident method for solving this problem is the use of oligonucleotides complementary to the predetermined primary sequences of the RNA target. In addition, a number of low-molecular-weight ligands possessing affinity for particular spatial structural elements of RNA are available.

1. Conjugates based on polycyclic compounds

Catalytically active groups can be added to polyaromatic compounds capable of intercalating into double-stranded regions of nucleic acids *via* flexible linkers. Synthetic constructions containing polycyclic intercalating compounds and metal complexes are widely used for DNA cleavage.[180,181] Efforts were made to prepare compounds which can hydrolyse RNA, by adding various combinations of guanidinium, amino and carboxyl groups to intercalating compounds. Some most active representatives of such conjugates were synthesised based on acridine (**30** and **31**),[182–184] phenazine (**32**),[185] isoalloxazine (**33**)[186] and anthraquinone (**34a**,**b**).[187]

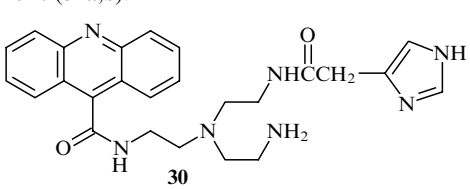

30

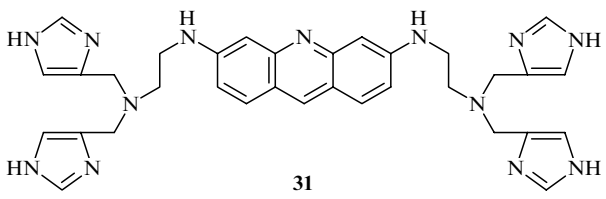

31

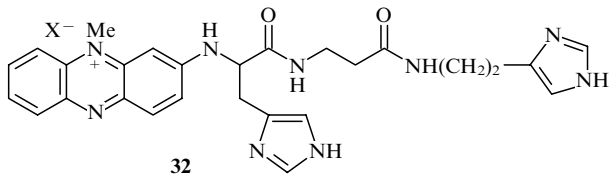

32

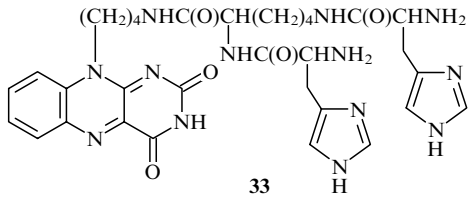

33

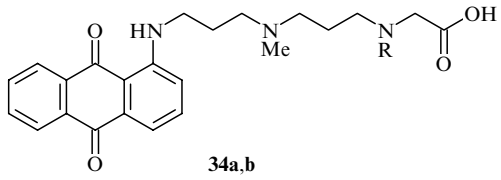

34a,**b**

R = H (**a**), CH_2CO_2H (**b**).

The substrates (tRNA, mRNA and synthetic oligonucleotides) employed did not enable one to perform a reliable comparison of the catalytic activity of the conjugates **30**–**34**. Generally, the catalytic activity is determined based on the disappearance of the initial nucleotide-containing substance without analysis of the hydrolysis products. This procedure does not allow one to reveal relationships between the structures of synthetic ribonucleases and their catalytic activity. We synthesised a series of compounds, which differ by both the structure of the linkers and the combination of reactive groups in the catalytic centre.[186] The phenazine conjugates whose RNA-hydrolysing centres contained two imidazole fragments, which were separated from the intercalator by the linker consisting of 8–14 C—C or C—N bonds, possessed the highest activity. The compounds containing the imidazolyl fragment and the carboxyl group exhibited somewhat lower activity.

The conjugates **30**–**32** and **34a** exhibited pronounced specificity with respect to cleavage of the CpA and UpA sequences in single-stranded RNA regions.[185,186] The exceptions are the isoalloxazine conjugate **33** (see Ref. 186) and the anthraquinone conjugate **34b** (see Ref. 187) containing two carboxyl groups. Hydrolysis of $tRNA^{Phe}$ in the presence of the anthraquinone derivative **34a** containing one carboxyl group proceeded predominantly at the CpA regions. However, when one more carboxyl group was introduced into the RNA-hydrolysing centre (the compound **34b**), the phosphodiester bonds in the GpA and GpG sequences were predominantly subjected to hydrolysis, and GpC was hydrolyzed to a lesser degree.

The low activity of most of the conjugates based on polycyclic compounds is attributable to the fact that these conjugates are inserted between RNA turns thus stabilising its double-stranded structure. In this case, the catalytic groups are located in the RNA region most resistant to hydrolysis. The use of long linkers makes possible localisation of the catalytic groups in the region of more labile single-stranded RNA fragments, which, in turn, provides higher efficiency of hydrolysis.[187]

2. Conjugates based on polycations

Unlike conjugates based on polycyclic compounds, which tend to be bound to double-stranded fragments of nucleic acids, conjugates based on cationic compounds are bound to RNA through Coulomb interactions, thus providing their homogeneous distribution over all sterically accessible phosphodiester bonds of the RNA target. Conjugates **35**–**39** based on synthetic and natural polyamines containing the imidazole and 1,4-diaminobutane fragments as the RNA-hydrolysing groups were described.[188–192]

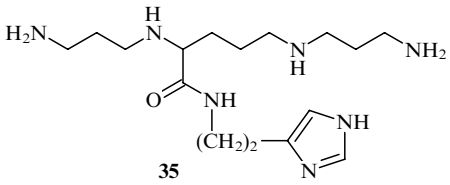

35

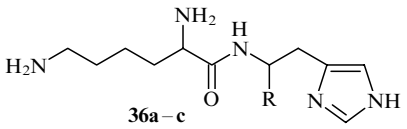

36a–**c**

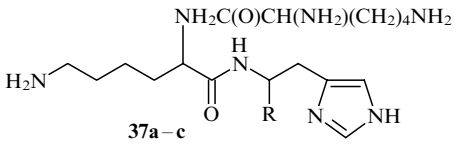

37a–**c**

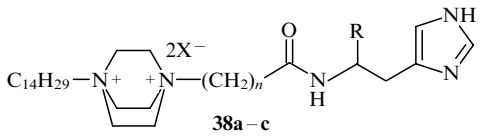

38a–**c**

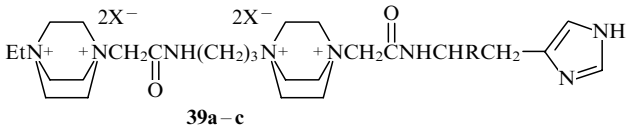

39a–**c**

35–**39**: R = H (**a**), CO_2H (**b**), CO_2Me (**c**).

As mentioned above, 1,4-diaminobutane and imidazole at concentrations of 1–2 mol litre^{-1} promote RNA hydrolysis. Synthetic ribonucleases **35**–**39** based on conjugates of imidazole with polyamines efficiently catalyse hydrolysis at substantially lower concentrations (10^{-3}–10^{-5} mol litre^{-1}), which is indicative of the synergistic action of the individual elements of these constructions. A sharp decreases in the efficiency of catalysis on going from imidazole conjugates to *N*-methylimidazole conjugates [188] and the manifestation of an isotope effect ($k_H/k_D = 2.28$) upon hydrolysis of dinucleosidemonophosphate CpA in water and D_2O (see Ref. 169) indicate that acid–base catalysis occurs at the limiting reaction stage. The catalytic activity of the compounds **35**–**39** was investigated in experiments with synthetic oligonucleotides, various tRNA and fragments of virus RNA. The conjugates **35**–**39** were demonstrated to provide high rates of cleavage of the phosphodiester bonds in the 5′-Py-A motifs in single-stranded RNA regions.[188–190] It should be noted that no preferential binding of the conjugates to phosphates of the above-mentioned motifs compared to other internucleotide phosphates was assumed. The conjugates studied contained different RNA-binding fragments, while the RNA targets had different structures. Hence, high instability of pyrimidine–purine sequences in RNA can be explained only by their characteristic features. The conjugates **35**–**39**, which are able to perform efficient and specific depolymerisation of RNA under mild conditions, can be considered as an alternative for RNase A in studies of the secondary structure of RNA.[168,188]

Menger and coworkers [193,194] proposed to carry out hydrolytic cleavage of phosphodiester bonds in RNA with the use of compounds **40b** and **41b**, which, unlike the conjugates **35**–**39**, are nucleophilic catalysts. Due to the electronegative substituent in the β position, the aldehyde groups in the compounds **40a** and **41a** are hydrogenated in weakly alkaline and neutral solutions to give the highly nucleophilic catalysts **40b** and **41b**. Owing to the

positive charge of the nitrogen-containing fragment, the nucleophilic group is localised in the vicinity of the phosphodiester bond. The authors believed that the presence of the alkyl substituent leads to the enhancement of the efficiency of hydrolysis due to micellar catalysis (by analogy with the micellar analogues of serine proteases proposed previously [195]). The catalysts **40** and **41** accelerated hydrolysis of the model compound, *viz*., of bis-(4-nitrophenyl) phosphate, by a factor of 1800 and 750, respectively, compared to the rate of hydrolysis in the absence of catalysts. It should be noted that micellar catalysis led to acceleration by only a factor of 210.[193, 194] Since examples of cleavage of natural RNA substrates in the presence of catalysts of this type are lacking in the literature, the efficiency of these catalysts cannot be compared with that of compounds functioning based on the general acid – base catalysis.

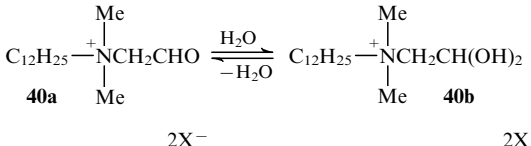

40a **40b**

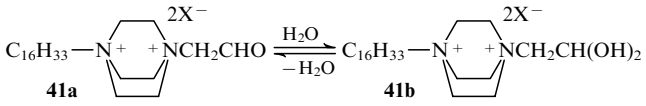

41a **41b**

Catalysts for cleavage of phosphodiester bonds based on polyamines were constructed using methods of combinatorial chemistry.[196] A mixture of several carboxylic acids was activated by water-soluble carbodiimide in the presence of polyallylamine with a molecular weight of 30 000 – 40 000. The ratio between the components was chosen so that the total degree of acylation of the amino groups of the polymer was 5% – 45%. A large library of water-soluble polymers with a statistical arrangement of functional groups was obtained by varying both the ratio between the carboxylic acids in the reaction mixture and the degree of modification of the initial polyamine.

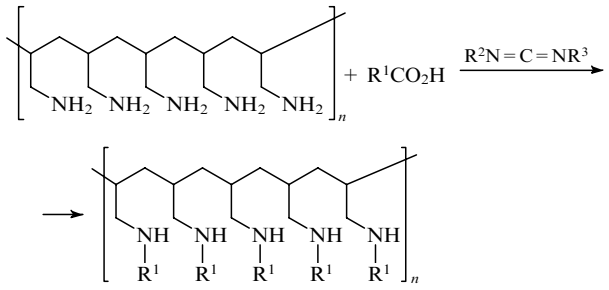

R^1 = HO_2C, 4-HOC_6H_4, 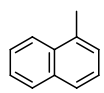 , 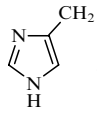 , $(CH_2)_2NHCNH_2$,

$HOCH_2$, $HS(CH_2)_2$, C_7H_{15}; R^2 = Et, R^3 = $(CH_2)_3NMe_2$.

The catalytic activity of the compounds synthesised was determined from the degree of hydrolysis of bis(4-nitrophenyl) phosphate in the presence of metal ions (Mg^{2+}, Zn^{2+} or Fe^{3+}). This approach made it possible to reveal a series of polymers accelerating hydrolysis by a factor of 20 000 – 30 000. Polyamine containing 7.5% of caprylic-acid residues, 15% of imidazolylacetic-acid residues and 10% of 4-hydroxybenzoic-acid residues in the presence of iron ions proved to be most active (k_{cat}/k = 31 400).[197] The drawback of this approach is the lack of information on the structures of catalytically active sites. At the same time, methods of combinatorial chemistry make possible the rapid determination of functional groups necessary for particular catalytic processes to proceed efficiently.

Synthetic constructions based on macrocyclic polyamines are of particular interest. In these compounds, the catalytic and affine centres merge together. The efficiency of binding of macrocycles with RNA can be additionally enhanced by addition of the former to polyaromatic compounds.[198] The cleavage of the phosphodiester bond in adenosine-5′-triphosphate catalysed by macrocyclic polyamine **42** is presented in Scheme 3. Compounds of the type **42** did not exhibit hydrolytic activity with respect to nucleic

Scheme 3

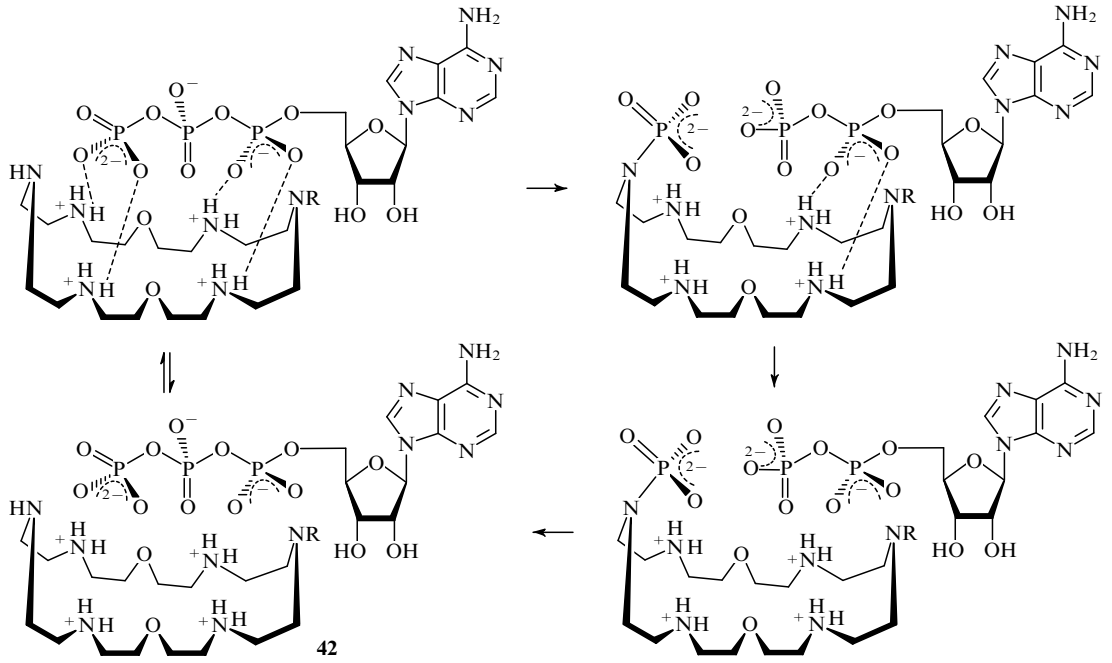

42

R = 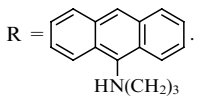 .

acids.[199] However, the construction of synthetic catalysts based on molecules whose functional groups have a limited degree of freedom shows considerable promise.

3. Conjugates based on oligonucleotides

In the construction of oligonucleotide conjugates, virtually all types of the above-described catalytic groups were used (see reviews [200–204]). These groups were introduced into the midpoint of the oligonucleotide address (Fig. 5 *a*) or were added to the terminal fragments of the nucleotides (Fig. 5 *b*). The first mode of construction of conjugates seems to be attractive because subsequent RNA cleavage under the action of these conjugates leads to a substantial decrease in stability of the complexes of the conjugate with the substrate, which should be favourable for hydrolysis under the catalytic conditions. At the same time, the catalytic group in the complex of RNA with such a conjugate is located in the region of the duplex structure characterised by high stability.[102] When located at the terminus of the oligonucleotide, the catalytic group in the resulting complex is oriented toward the more labile single-stranded structure. However, the stability of the complex after RNA cleavage remains virtually unchanged. Therefore, exchange of the conjugate between depolymerised RNA and intact RNA is hindered, which should retard efficient functioning of the catalysts.

Conjugates containing catalytic groups attached to the 5′-terminal phosphate group differ substantially in efficiency of RNA depolymerisation. For the Lu^{3+} complex, which was prepared *in situ* based on oligo-DNA containing the iminodiacetic-acid residue (**43**) at the 5′-terminus, the degree of polymerisation was 17%

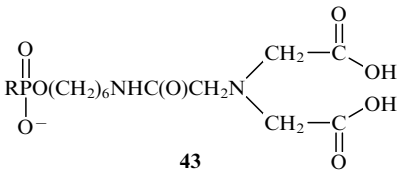

43

R, oligonucleotide residue.

(37 °C, 8 h). In the case of conjugates based on macrocyclic Eu^{3+} complexes **44a**,**b**, the degree of depolymerisation was 30% (37 °C, 18 h) and 80% – 90% (37 °C, 16 h), respectively.[206] The introduction of the same metal complexes at position 5 of thymidine located at the midpoint of the oligonucleotide address gave rise to inactive [205] or weakly active [206] conjugates. The catalytic activity of oligonucleotide conjugates **45** containing copper complexes at position 5 of thymidine also appeared to be low. Thus the degree of cleavage upon incubation of RNA with such conjugates at 45 °C for 72 h was at most 18% – 25%.[207]

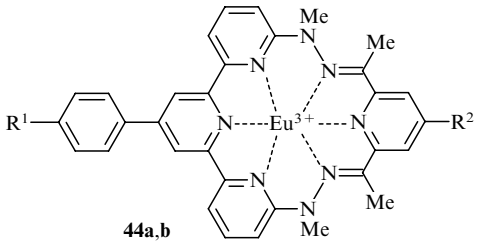

44a,**b**

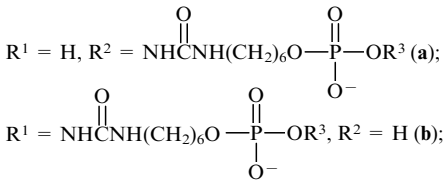

R^3, oligonucleotide residue.

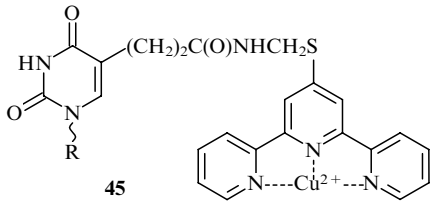

45

R, oligonucleotide residue.

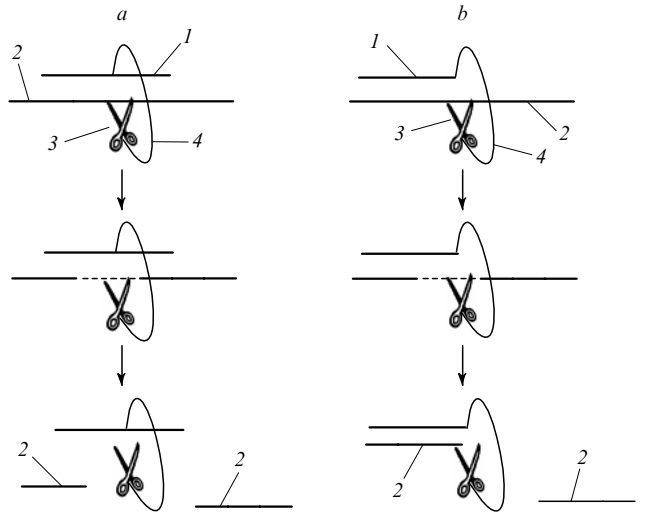

Figure 5. Main approaches to the construction of superspecific synthetic ribonucleases based on oligonucleotide conjugates;
(*a*) introduction of catalytic groups at the midpoint of the oligonucleotide address, (*b*) the addition to the terminal fragment; (*1*) is an oligonucleotide, (*2*) is an RNA target, (*3*) is a catalytic group, (*4*) is a linker.

High efficiency of cleavage is achieved when hydrolytic groups are located in the region of loop structures of the RNA target (Fig. 6 *a*). As mentioned above, phosphodiester bonds in loop regions of nucleic acids are characterised by high sensitivity with respect to cleavage under the action of reagents of different nature.[72, 103, 104, 208, 209] The efficiency of RNA cleavage with conjugates forming loop structures with RNA was as high as 92%, whereas that in analogous reactions involving conjugates forming perfect complexes was at most 7%.[205]

In the case of addition of a metal complex at the 5′-terminal phosphate group of the oligonucleotide address, hydrolysis of phosphodiester bonds occurs at a distance from one to seven nucleotide units depending on the type of the linker.[204, 210] In the case of formation of an artificial loop in the vicinity of the 5′-terminus, the cleavage is virtually quantitatively reoriented from the single-stranded region to the loop, the total degree of hydrolysis being increased.[205] It was demonstrated that synthetic ribonucleases based on 12-unit 2′-modified oligoribonucleotides, which were constructed on the above-described principle, can execute up to 40 events of RNA cleavage in the course of incubation at 37 °C during 64 h (at a reagent concentration of 1×10^{-3} mol litre^{-1}) in the presence of a 50-fold excess of RNA.[211]

Yet another way of increasing the flexibility of the sugar-phosphate core in the target RNA region is based on the replacement of one nucleotide unit in the oligonucleotide address by a non-nucleotide insertion.[212]

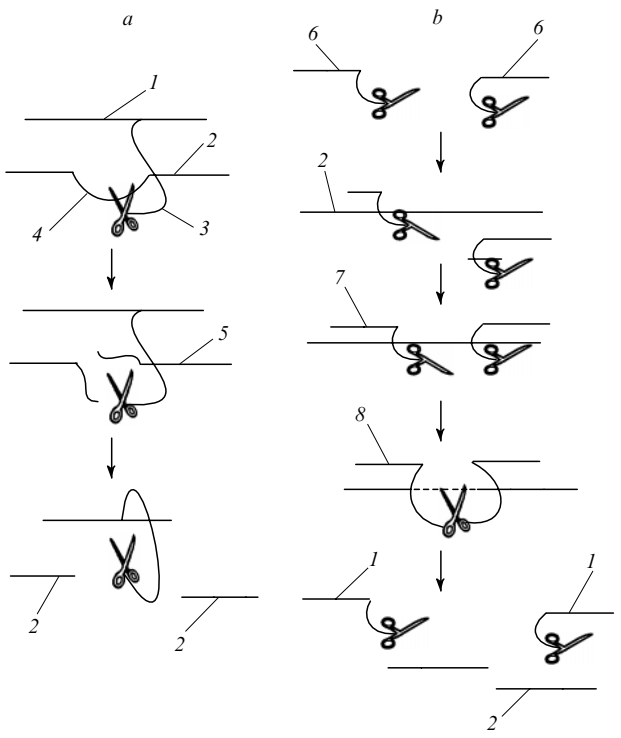

Figure 6. Principles of construction of synthetic ribonucleases based on conjugates containing noncomplementary regions (*a*) and based on module conjugates (*b*);
(*1*) is oligonucleotide, (*2*) is an RNA target, (*3*) is a linker, (*4*) is a noncomplementary region, (*5*) RNA cleavage, (*6*) are oligonucleotides containing components of the catalytic centre, (*7*), formation of the catalytic centre at the RNA target, (*8*) RNA cleavage.

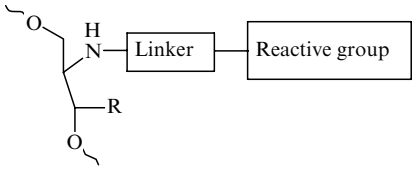

R = H, Me.

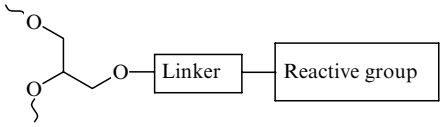

The ability of these oligonucleotide conjugates to cleave RNA under catalytic conditions was exemplified by conjugates **46a** containing macrocyclic Dy^{3+} complexes.[213]

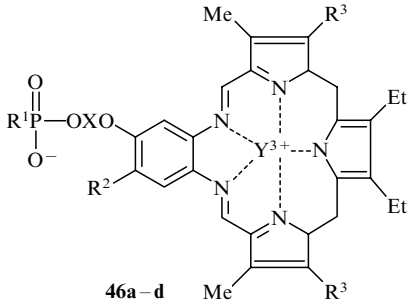

R^1 is the oligonucleotide residue; R^2 = H, OMe; R^3 = $(CH_2)_3OH$, Et; X = $(CH_2)_3$, $(CH_2)_6$, $(CH_2)_6NHCOCH_2$; Y = Dy (**a**), La (**b**), Lu (**c**), Eu (**d**).

A promising approach to the construction of RNA-cleaving oligonucleotide conjugates involves the design of module (binary) reagents (see Fig. 6 *b*). The approach is based on separation of the catalytic centre into two fragments and the synthesis of conjugates of these fragments with oligonucleotides complementary to the adjacent regions of the RNA target. The catalytic centre arises only in the case of formation of a proper ternary complex in which two inactive structures are recombined to form a catalytically active centre. This centre can be formed either by individual reactive groups involved in natural ribonucleases (for example, two imidazole fragments) or by poorly reactive metal complexes forming more reactive binuclear catalytic centres. Undoubtedly, this approach imposes much more rigid limitations on both the structural parameters of the fragments of the reactive centre and the geometry of the conjugates as a whole. However, this approach has a number of important advantages, *viz*., it makes possible the improvement in specificity of the reaction with the target sequence and allows one to exclude side reactions of the conjugates with non-target biopolymers.

The most efficient conjugates of **46a–d** contain complexes of rare-earth metals (La^{3+}, Lu^{3+}, Eu^{3+} or Dy^{3+}) as catalytic groups. Dissociation of these ions from the metal complexes can lead to nonspecific cleavage of other biopolymers resulting in their high toxicity in biological systems. Recently, binuclear zinc complexes have been proposed for solution of this problem. Under physiological conditions, zinc ions by themselves cannot efficiently catalyse depolymerisation of biopolymers, whereas the efficiency of their binuclear complexes is rather high.[214]

Reagents based on oligonucleotide conjugates with catalytic groups, which do not contain metal ions, seem to be more promising because they allow one to exclude completely any cofactors. In combination with high specificity of the oligonucleotide address, the above fact may enable one to prepare compounds capable of performing efficient cleavage of the target RNA sequences leaving other biopolymers intact. However, some groups (amino and carboxyl groups, heterocyclic fragments) exhibit substantially lower catalytic activity than metal ions and metal complexes. High efficiency of hydrolysis in the presence of organic compounds is achieved only in the case of the optimum spatial arrangement of all groups involved in the catalytic process. Oligonucleotide derivatives containing ethylene-[215] or propylenediamine[216] at the 5′-terminus are the simplest RNA-cleaving conjugates, which do not contain metal ions. Cleavage of $tRNA^{Phe}$ under the action of a 19-unit oligonucleotide conjugate containing the diamine residue was reported.[217] The efficiency of this reaction was 10% after incubation at 50 °C for 4 h. Similar efficiency was observed upon cleavage of a 30-unit model oligoribonulceotide under the action of an analogous conjugate.[218] In both cases, the 5′-CpA sequences in the region of the reagent localisation were subjected to hydrolysis. The introduction of oligoamines through a non-nucleotide insertion at the midpoint of the conjugate leads to a decrease in efficiency of hydrolysis under analogous conditions to 3%.[219] At the same time, the degree of hydrolysis performed at 40 °C for 4 h with the use of a 10-unit oligopeptidylnucleotide containing diethylenetriamine at the 5′-terminus instead of the 19-unit oligodeoxyribonucleotide was 30%, and hydrolysis was quantitative after 24 h.[220] The target used in the latter study differed from that employed in the study [217] by the single substitution G → C as a result of which the CpApCpA fragment was present in the region of location of the hydrolytic group. Both bonds in CpA were subjected to hydrolysis, but to a different degree.

In the absence of metal ions, conjugates containing fragments, which bear the 1,4-diaminobutyl, *N*-propylimidazolium or histamine residues at the 3′-terminal phosphates of oligonucleotides, do not exhibit catalytic activity in hydrolysis of the model oligoribonucleotide. The histamine-containing compound exhibited weak activity upon introduction of zinc ions into the reaction mixture.[221] In a latter study, the polyuridyl sequence was used as the target.

The synthesis of oligonucleotide conjugates containing the $(Leu\text{-}Arg)_nGlyNH_2$ oligopeptides (n = 2–4) at the 5′-terminal

phosphate was reported.[222, 223] Incubation of a model 14-unit oligoribonucleotide with the complementary six-unit oligodeoxyribonucleotide whose oligopeptide fragment consists of alternating Leu-Arg pairs led to cleavage of the RNA target. In the case of the conjugate containing three Leu-Arg pairs, prolonged incubation (48 h, 37 °C) resulted in insignificant cleavage (~5%) of the target at the CpU site in the vicinity of the localisation site of the oligopeptide. In experiments with conjugates bearing two or four Leu-Arg pairs, the efficiency of cleavage under these conditions reached 30% and 70%, respectively. In the latter case, two GpA sequences and, to a lesser extent, UpU located in the double-stranded region of the complex were the major cleavage sites. In the case of incubation of *E. coli* $tRNA^{Phe}$ with conjugates based on the pTCAATC oligonucleotide, which is complementary to two sequences in the anticodon and TΨC loops, the phosphodiester bonds in the region of the D loop, in the TΨC loop and, to a lesser extent, in the anticodon region of this tRNA were cleaved. Cleavage of the phosphodiester bonds in the non-target region of the D loop was related to the possible spatial proximity to the TΨC loop possessing the partial binding site of the reagent.[222, 223] Unlike the model 14-unit oligoribonucleotide, the site of tRNA subjected to hydrolysis under the action of the reagent ($n = 3$ or 4) was independent of the length of the peptide residue, although the degree of hydrolysis of the target was also substantially decreased on going from $n = 4$ to $n = 3$. The maximum efficiency of hydrolysis was 80% ($n = 4$, 48 h, 20 °C).

We prepared oligonucleotide conjugates containing the bisimidazolium fragments at the 5′- or 3′-terminal phosphate.[224] The activity of the conjugates was tested using yeast phenylalanine tRNA as well as pre- and mini-exons of mRNA from *Leishmania amazonensis*. In the case of $tRNA^{Phe}$, the C(61)A(62) and C(63)A(64) sequences located in the vicinity of the hydrolytically active groups were subjected to cleavage, in all cases the highest efficiency of cleavage being observed at the CpA bond separated from the binding site of the reagent by three nucleotide units. The reagent containing the catalytic group at the 3′-terminal phosphate appeared to be somewhat more active than its 5′-analogue. After incubation at 37 °C for 8 h, the total efficiency of tRNA cleavage at three sites reached 60%.[225] In the case of the mini-exon of mRNA from *Leishmania amazonensis*, the efficiency of hydrolysis for the 17-unit oligonucleotide containing the bisimidazolium fragment at the 3′-terminus was 100% after 5 h. Cleavage proceeded primarily at the CpA sequences (80%) in the region of the expected localisation of the reactive groups. Similar results were obtained for oligonucleotide conjugates whose 5′-terminal phosphates bear synthetic fragments containing the imidazole fragment and the aliphatic amino group.[226] An increase in the length of the spacer, which links the bisimidazole fragments with the oligonucleotide address, as well as the introduction of reactive groups through a non-complementary nucleotide residue led to substantial enhancement of the efficiency of hydrolysis. Incubation of $tRNA^{Phe}$ with such conjugates at 37 °C for 3–5 h resulted in quantitative RNA cleavage (Fig. 7). Hydrolysis was completely inhibited in the presence of an oligonucleotide complementary to the cleavage sites (indicated by arrows, the oligonucleotide A, see Fig. 7).[227] Dendrimeric oligonucleotide conjugates containing from 2 to 24 imidazole residues were proposed.[228] This approach seems to be attractive for the synthesis of libraries of oligonucleotide conjugates containing not only imidazole fragments, but also other functional groups typical of the active centres of natural enzymes.

Methods of combinatorial chemistry can be used not only for the construction of reactive groups, but also for the choice of the RNA region most favourable for hydrolysis. The synthesis of a library of 8-unit 2′-*O*-modified oligoribonucleotides with random sequences was reported.[229] Each oligonucleotide contains the Eu^{3+} complex **44** at the 5′-terminus. Four hydrolysis sites were found after incubation of this library with 39-unit RNA (1 mmol litre^{-1} of the conjugates, 50 nmol litre^{-1} of RNA, 37 °C) for even 2 h. This result was unexpected because the

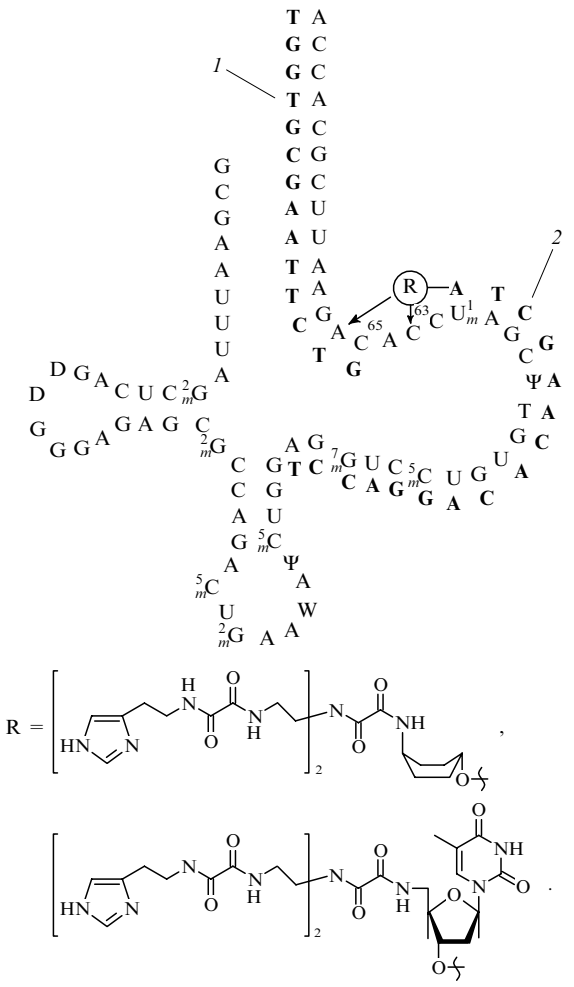

Figure 7. Metal-independent catalytic groups R used in the construction of synthetic ribonucleases based on oligonucleotide conjugates.
Sites of $tRNA^{Phe}$ cleavage with bisimidazole oligonucleotide conjugates are indicated by arrows; (*1*) oligonucleotide A, (*2*) oligonucleotide B.

concentration of each particular conjugate in the reaction mixture was no higher than 15 pmol litre^{-1}.

Two radically different approaches to the synthesis of oligonucleotide conjugates with various ligands, *viz*., the introduction of ligands in one of the stages of the oligonucleotide synthesis and the post-synthetic modification of the oligonucleotide, are of considerable current use.[230] Several alternative procedures for performing both strategies are available. The first approach most often involves the automated synthesis of oligonucleotides based on amidophosphites of protected nucleosides and ligands. Monomeric blocks containing fragments of various metal complexes[231–235] and imidazole-containing constructions[236–240] were proposed for the preparation of synthetic ribonucleases based on oligonucleotide conjugates. The successive synthesis of the oligonucleotide and catalytic fragments of the conjugate at the same solid-phase carrier is a promising variation of this approach.[221, 241] However, this approach is unavailable for the majority of potential consumers of these conjugates because of the necessity of synthesising unique amidophosphites in each particular case and the problems associated with the choice of protective groups and procedures for their removal in the case of the successive synthesis of oligonucleotide conjugates. On the contrary, the synthesis of oligonucleotides containing functional groups along with 5′- or 3′-terminal phosphates and amino, hydroxyl and carboxyl groups was well developed by many biochemical companies due to which the post-synthetic modification of oligonucleotides shows considerable promise. Variations

Scheme 4

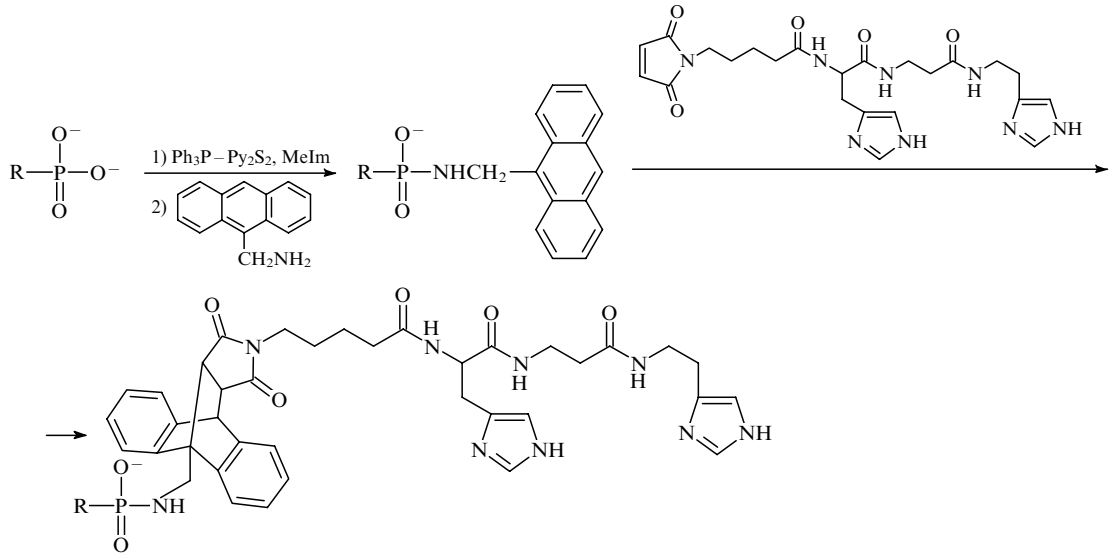

R is deoxyoligonucleotide; MeIm is methylimidazole.

of the functionalisation of the above-mentioned groups were considered in the studies.[230, 242] The latter approach was widely used in the synthesis of ribonucleases containing metal complexes,[103, 205, 210, 211, 229] polyamines[215, 219] or imidazole derivatives.[226] The soft procedure for activation of the terminal phosphate group[243] makes possible the preparation of oligonucleotide conjugates with molecules bearing aliphatic amino groups without protection of the imidazole[224, 225, 244] or guanidinium[222, 223] fragments. Beloglazova *et al.*[245] proposed an ingenious approach to the preparation of oligonucleotide conjugates with molecules containing virtually any functional groups necessary for the design of highly efficient catalytic centres. The authors attached the catalytic centre to the terminal phosphate group of deoxyoligonucleotide by a Diels–Alder reaction between the anthracene fragment and the double bond of a maleimide group (Scheme 4).

* * *

Intensive studies on the construction of synthetic catalysts for the specific cleavage of ribonucleic acids have resulted in the preparation of promising compounds belonging to a new family of structural probes for investigation of RNA conformations and for the design of conjugates of antisense oligonucleotides. Low-molecular-weight synthetic catalysts capable of cleaving RNA with an efficiency and selectivity close to those typical of natural ribonulceases are as yet unavailable. However in many cases, this efficiency is not necessary. In particular, in spite of low efficiency, synthetic ribonucleases as structural probes have advantages over natural enzymes. For example, when binding with RNA, ribonuclease A, which is an enzyme catalysing hydrolysis predominantly of pyrimidine–purine sites in single-stranded regions, changes the RNA structure and even leads to untwisting of double-stranded regions, which limits the possibilities of its use in structural studies. Small synthetic molecules do not destroy the structures of nucleic acids and cleave the latter only within single-stranded regions existing in the native molecule, which allows one to obtain information on the biologically active RNA structure.

Studies both aimed at examining processes occurring in the active centres of enzymes and directed towards modelling of these processes in small chemical nucleases are being continued. It is hoped that synthetic nucleases, which may be highly competitive with natural biocatalysts and even outperform them in efficiency, will be prepared in the coming years. Such compounds can help in designing a new generation of highly efficient antiviral and anticancer drugs.

References

1. D G Knorre, V V Vlassov, V F Zarytova, A V Lebedev, O S Fedorova *Design and Targeted Reactions of Oligonucleotide Derivatives* (Raton, FL: Boca Press, 1994)
2. D S Sigman, A Mazumder, D M Perrin *Chem. Rev.* **93** 2295 (1993)
3. P D Cook, in *Antisense Research and Applications* (Eds S T Crooke, B Lebleu) (Raton, FL: Boca Press, 1993)
4. C Helene, J-J Tulme, in *Oligodeoxynucleotides. Antisense Inhibitors of Gene Expression* (Ed. J S Cohen) (London: Macmillan, 1989)
5. D G Knorre, O S Fedorova, E I Frolova *Usp. Khim.* **62** 70 (1993) [*Russ. Chem. Rev.* **62** 65 (1993)]
6. W K Pogozelski, T D Tullius *Chem. Rev.* **98** 1089 (1998)
7. C J Burrows, J G Muller *Chem. Rev.* **98** 1109 (1998)
8. J L Hue, Y C Xue, M Y Xie, R Zhang, T Otani, Y Minami, Y Yamada, M Casaazza *Proc. Natl. Acad. Sci. USA* **90** 2822 (1993)
9. D G Knorre, V V Vlassov *Prog. Nucl. Acids Res. Mol. Biol.* **32** 291 (1985)
10. K Kido, H Inoue, E Ohtsuka *Nucl. Acids Res.* **20** 1339 (1992)
11. B Armitage *Chem. Rev.* **98** 1171 (1998)
12. B Armitage, T Koch, H Frydenlund, H Örum, H-G Batz, G B Schuster *Nucl. Acids Res.* **25** 4674 (1997)
13. T Chatterji, K S Gates *Bioorg. Med. Chem. Lett.* **8** 535 (1998)
14. G Pratviel, J Bernadou, B Meunier *Angew. Chem., Int. Ed. Engl.* **34** 746 (1995)
15. J Bernadou, G Pratviel, B Meunier, in *DNA and RNA Cleavers and Chemotherapy of Cancer and Viral Diseases* (Ed. B Meunier) (Dordrecht: Kluwer Academic, 1995) p. 211
16. H H Thorp *Chem. Biol.* **7** 33 (2000)
17. J Stubbe, J W Kozarich *Chem. Rev.* **87** 1107 (1987)
18. R M Burger *Chem. Rev.* **98** 1153 (1998)
19. J-M A Battigello, M Cui, S Roshong, B J Carter *Bioorg. Med. Chem.* **3** 839 (1995)
20. T Tuschl, J B Thomson, F Eckstein *Curr. Opin. Struct. Biol.* **5** 296 (1995)
21. L Jaeger *Curr. Opin. Struct. Biol.* **7** 324 (1997)
22. N G Walter, J M Burke *Curr. Opin. Chem. Biol.* **2** 24 (1998)
23. W G Scott *Curr. Opin. Struct. Biol.* **8** 720 (1998)
24. D Sen, C R Geyer *Curr. Opin. Chem. Biol.* **2** 680 (1998)
25. W D Wilson, L Ratmeyer, M Zhao, L Strekowski, D Boykin *Biochemistry* **32** 4098 (1993)
26. L Frydman, P C Rossomando, V Frydman, C O Fernandez, B Frydman, K Samejima *Proc. Natl. Acad. Sci. USA* **89** 9186 (1992)
27. K Michael, Y Tor *Chem. Eur. J.* **4** 2091 (1998)
28. C S Chow, F M Bogdan *Chem. Rev.* **97** 1489 (1997)
29. M G Wallis, R Schroeder *Prog. Biophys. Mol. Biol.* **67** 141 (1997)
30. F Leclerc, R Cedergren *J. Med. Chem.* **41** 175 (1998)
31. M Egli *Angew. Chem., Int. Ed. Engl.* **35** 1894 (1996)
32. M J Soth, J S Nowick *Curr. Opin. Chem. Biol.* **1** 120 (1997)

33. C Apple, C Leumann *Chem. Biol.* **5** 209 (1998)
34. A M Kawasaki, T P Prakash, A S Fraser, M Prhave, G B Inamati *Nucleosides Nucleotides* **18** 1737 (1999)
35. T P Prakash, A M Kawasaki, G Vasquez, A S Fraser, M D Casper, P D Cook, M Manoharan *Nucleosides Nucleotides* **18** 1381 (1999)
36. S K Singh, P Nielsen, A A Koshkin, J Wengel *Chem. Commun.* 455 (1998)
37. R N Zuckermann, P G Schultz *J. Am. Chem. Soc.* **110** 6592 (1988)
38. R N Zuckermann, D R Corey, P G Schultz *J. Am. Chem. Soc.* **110** 1614 (1988)
39. Y Uchiyama, H Inoue, E Ohtsuka, C Nakai, S Kanaya, Y Ueno, M Ikehara *Bioconjugate Chem.* **5** 327 (1994)
40. C Nakai, A Konishi, Y Komatsu, H Inoue, E Ohtsuka, S Kanaya *FEBS Lett.* **339** 67 (1994)
41. D Barton, W D Ollis (Eds) *Comprehensive Organic Chemistry* Vol. 2 (Oxford: Pergamon Press, 1979)
42. F H Westheimer *Acc. Chem. Res.* **1** 70 (1968)
43. D-M Zhou, K Taira *Chem. Rev.* **98** 991 (1998)
44. T Uchimaru, S Kawahara, S Tsuzuki, K Matsumura, K Taira *J. Mol. Struct.* **469** 215 (1999)
45. M Oivanen, S Kuusela, H Lönnberg *Chem. Rev.* **98** 961 (1998)
46. S Mikkola, E Stenman, K Nurmi, E Yousefi-Salakdeh, R Strömberg, H Lönnberg *J. Chem. Soc., Perkin Trans. 2* 1619 (1999)
47. E Mäki, M Oivanen, P Poijirvi, H Lönnberg *J. Chem. Soc., Perkin Trans. 2* 2493 (1999)
48. G A Soukup, R R Breaker *RNA* **5** 1308 (1999)
49. A Bibillo, K Ziomek, M Figlerowicz, R Kierzek *Acta Biochim. Pol.* **46** 145 (1999)
50. H Hosaka, I Sakabe, K Sakamoto, S Yokoyama, H Takaku *J. Biol. Chem.* **269** 20 090 (1994)
51. R Kierzek *Collect. Czech. Chem. Commun. (Spec. Issue)* **61** 161 (1996)
52. R Kierzek *Nucl. Acids Res.* **20** 5079 (1992)
53. R Kierzek *Nucl. Acids Res.* **20** 5073 (1992)
54. A Riepe, H Beier, H J Gross *FEBS Lett.* **457** 193 (1999)
55. D Gani, J Wilkie *Chem. Soc. Rev.* **24** 55 (1995)
56. A Lahm, S Volbeda, D J Suck *J. Mol. Biol.* **215** 207 (1990)
57. L S Beese, T A Steitz *EMBO J.* **10** 25 (1991)
58. M M Benning, J M Kuo, F M Raushel, H M Holden *Biochemistry* **34** 7973 (1995)
59. W G Scott *Curr. Opin. Chem. Biol.* **3** 705 (1999)
60. D R Jones, L F Lindoy, A M Sargeson *J. Am. Chem. Soc.* **105** 7327 (1983)
61. P Hendry, A M Sargeson *Prog. Inorg. Chem.* **38** 201 (1990)
62. T C Bruice, A Tsubouchi, R O Dempsy, L P Olson *J. Am. Chem. Soc.* **118** 9867 (1996)
63. J K Bashkin, L A Jenkins *J. Chem. Soc., Dalton Trans.* 3631 (1994)
64. W G Scott, J T Finch, A Klug *Cell* **81** 991 (1995)
65. S C Dahm, W B Derrick, O C Uhlenbeck *Biochemistry* **32** 13040 (1993)
66. S Kuusela, H Lönnberg *J. Phys. Org. Chem.* **5** 803 (1992)
67. S Kuusela, H Lönnberg *J. Phys. Org. Chem.* **6** 347 (1993)
68. R S Brown, J C Dewan, A Klug *Biochemistry* **30** 4785 (1991)
69. P S Freemont, J M Friedman, L S Beese, M R Sanderson, T A Steitz *Proc. Natl. Acad. Sci. USA* **85** 8924 (1988)
70. B W Pontius, W B Lott, P H von Hippel *Proc. Natl. Acad. Sci. USA* **94** 2290 (1997)
71. W G Scott, A Klug *Trends Biochem. Sci.* **21** 220 (1996)
72. T Pan, O C Uhlenbeck *Nature (London)* **358** 560 (1992)
73. N Sugimoto, T Ohmichi *FEBS Lett.* **393** 97 (1996)
74. T Ohmichi, N Sugimoto *Biochemistry* **36** 3514 (1997)
75. M Irisawa, M Komiyama *J. Biochem.* **117** 465 (1995)
76. M Komiyama, K Matsumura, Y Matsumoto *J. Chem. Soc., Chem. Commun.* 640 (1992)
77. K Matsumura, M Komiyama *J. Biochem.* **122** 387 (1997)
78. P Hurst, B K Takasaki, J Chin *J. Am. Chem. Soc.* **118** 9982 (1996)
79. S J Frandkin *Curr. Opin. Chem. Biol.* **5** 201 (2001)
80. J Visscher, A W Schwartz *Nucl. Acids Res.* **20** 5749 (1992)
81. R Ott, R Krämer *Angew. Chem., Int. Ed. Engl.* **37** 1957 (1998)
82. K Matsumura, Y Matsumoto, M Komiyama *Nucl. Acids Symp. Ser.* **27** 11 (1992)
83. J J Butzow, G L Eichhorn *Biochemistry* **10** 2019 (1971)
84. A George, P Draganac, W R Farkas *Inorg. Chem.* **24** 3627 (1985)
85. V M Shelton, J R Morrow *Inorg. Chem.* **30** 4295 (1991)
86. S Kuusela, M Rantanen, H Lönnberg *J. Chem. Soc., Perkin Trans. 2* 2269 (1995)
87. S Kuusela, H Lönnberg *J. Chem. Soc., Perkin Trans. 2* 2301 (1994)
88. J Sumaoka, M Yashiro, M Komiyama *Nucl. Acids Symp. Ser.* **27** 37 (1992)
89. S A Kazakov, in *Bioorganic Chemistry* (Ed. S M Hecht) (New York: Oxford University Press, 1996) p. 224
90. L S Behlen, J R Sampson, A B DiRenzo, O C Uhlenbeck *Biochemistry* **29** 2515 (1990)
91. J Wrzesinski, D Michalowski, J Ciesiolka, W J Krzyzosiak *FEBS Lett.* **374** 62 (1995)
92. N A Kolchanov, I I Titov, I E Vlassova, V V Vlassov *Prog. Nucl. Acids Res. Mol. Biol.* **53** 131 (1996)
93. J Ciesiolka, M Yarus *RNA* **2** 785 (1996)
94. I Majerfeld, M Yarus *RNA* **4** 471 (1998)
95. R S Brown, B E Hingerty, J C Dewan, A Klug *Nature (London)* **303** 543 (1983)
96. R S Brown, J C Dewan, A Klug *Biochemistry* **24** 4785 (1985)
97. D Michalowski, J Wrzesinski, W Krzyzosiak *Biochemistry* **35** 10 727 (1996)
98. J Ciesiolka, J Gorski, M Yarus *RNA* **1** 7538 (1995)
99. M Wech, I Majerfeld, M Yarus *Biochemistry* **36** 6614 (1997)
100. B Dichtl, T Pan, A B DiRenzo, O C Uhlenbeck *Nucl. Acids Res.* **21** 351 (1993)
101. J Ciesiolka, S Lorenz, V A Erdmann *Eur. J. Biochem.* **204** 575 (1992)
102. K A Kolasa, J R Morrow, A P Sharma *Inorg. Chem.* **32** 3983 (1997)
103. D Huesken, G Goodall, M J J Blommers, W Jahnke, J Hall, R Haener, H E Moser *Biochemistry* **35** 16591 (1996)
104. I Zagorowska, S Kuusela, H Lönnberg *Nucl. Acids Res.* **26** 3392 (1998)
105. M Yashiro, A Ishikubo, M Komiyama *J. Biochem.* **120** 1067 (1996)
106. J R Morrow, L A Buttrey, V M Shelton, K A Berback. *J. Am. Chem. Soc.* **114** 1903 (1992)
107. L A Jenkins, J K Bashkin, M E Autry *J. Am. Chem. Soc.* **118** 6822 (1996)
108. D P Weiner, T Wiemann, M M Wolfe, P Wentworth Jr, K D Janda *J. Am. Chem. Soc.* **119** 4088 (1997)
109. S J Oh, K H Song, J W Park *J. Chem. Soc., Chem. Commun.* 575 (1995)
110. J Sumaoka, S Miyama, M Komiyama *J. Chem. Soc., Chem. Commun.* 1755 (1994)
111. U Baykal, E U Akkaya *Tetrahedron Lett.* **39** 5861 (1998)
112. R Breslow, D Berger, D-L Huang *J. Am. Chem. Soc.* **112** 3686 (1990)
113. P R Norman, R D Cornelius *J. Am. Chem. Soc.* **104** 2356 (1982)
114. M K Stern, J K Bashkin, E D Sall *J. Am. Chem. Soc.* **112** 5357 (1990)
115. N Sträter, W N Lipscomb, T Klabunnde, B Krebs *Angew. Chem., Int. Ed. Engl.* **35** 2024 (1996)
116. D E Wilcox *Chem. Rev.* **96** 2435 (1996)
117. J A Cowan *Chem. Rev.* **98** 1067 (1998)
118. R A Kovall, B W Matthews *Curr. Opin. Chem. Biol.* **3** 578 (1999)
119. D J Weber, A K Meeker, A S Mildvan *Biochemistry* **30** 6103 (1991)
120. S V Shlyapnikov, E V Blaganov, V M Levdikov, V Yu Lunin, V V Lunin, A M Mikhailov, Kh Betzel', K R Raiyashankar, M Perbandt *Mol. Biol.* **33** 454 (1999) [a]
121. A Volbeda, A Lahm, F Sakiyama, D Suck *EMBO J.* **10** 1607 (1991)
122. J K Bashkin *Curr. Opin. Chem. Biol.* **3** 752 (1999)
123. E K van den Beuken, B L Feringa *Tetrahedron* **54** 12985 (1998)
124. E Rizzarelli, G Vecchio *Coord. Chem. Rev.* **188** 343 (1999)
125. R Breslow, S Singh *Bioorg. Chem.* **16** 408 (1998)
126. W H Chapman Jr, R Breslow *J. Am. Chem. Soc.* **117** 5462 (1995)
127. S Matsuda, A Ishikubo, A Kuzuya, M Yashiro, M Komiyama *Angew. Chem., Int. Ed. Engl.* **37** 3284 (1998)
128. M Wall, R C Hynes, J Chin *Angew. Chem., Int. Ed. Engl.* **32** 1633 (1993)
129. P Molenveld, J F J Engbersen, H Kooijman, A L Spek, D N Reinhoudt *J. Am. Chem. Soc.* **120** 6726 (1998)
130. S Liu, Z Luo, A D Hamilton *Angew. Chem., Int. Ed. Engl.* **36** 2678 (1997)

131. Y Chung, E U Akkaya, T K Venkatachalam, A W Czarnik *Tetrahedron Lett*. **31** 5413 (1990)
132. J S Seo, N-D Sung, R C Hynes, J Chin *Inog. Chem*. **35** 7472 (1996)
133. A Tsubouchi, T C Bruice *J. Am. Chem. Soc*. **116** 11 614 (1994)
134. K G Rogunathan, H-J Schneider *Angew. Chem., Int. Ed. Engl*. **35** 1219 (1996)
135. M Yashiro, A Ishikubo, M Komiyama *J. Chem. Soc., Chem. Commun*. 1793 (1995)
136. P Molenveld, J F J Engbersen, D N Reinhoudt *Angew. Chem., Int. Ed. Engl*. **38** 3189 (1999)
137. A Roigk, O V Yescheulova, Yu V Fedorov, O A Fedorova, S P Gromov, H-J Schneider *Org. Lett*. **1** 833 (1999)
138. S D Dong, R Breslow *Tetrahedron Lett*. **39** 9343 (1998)
139. E Kövári, R Krämer *J. Am. Chem. Soc*. **118** 12704 (1996)
140. P Molenveld, J F J Engbersen, D N Reinhoudt *Eur. J. Org. Chem*. 3269 (1999)
141. E Kimura, Y Kodama, T Koike, M Shiro *J. Am. Chem. Soc*. **117** 8304 (1995)
142. R Krämer *Coord. Chem. Rev*. **182** 243 (1999)
143. J Costamagna, G Ferraudi, B Matsuhiro, M Campos-Vallette, J Canales, M Villagrán, J Vargas, M J Aguirre *Coord. Chem. Rev*. **196** 125 (2000)
144. M Komiyama, K Yoshinari *J. Org. Chem*. **62** 2155 (1997)
145. M Komiyama, K Yoshinari *J. Chem. Soc., Chem. Commun*. 1880 (1989)
146. K Yoshinari, M Komiyama *Nucl. Acids Symp. Ser*. **26** 23 (1991)
147. K Yoshinari, K Yamazaki, M Komiyama *J. Am. Chem. Soc*. **113** 5899 (1991)
148. M V Keck, S M Hecht *Biochemistry* **34** 12029 (1995)
149. B Barbier, A Brack *Orig. Life Evol. Biosph*. **17** 381 (1987)
150. B Barbier, A Brack *J. Am. Chem. Soc*. **110** 6880 (1988)
151. B Barbier, A Brack *Orig. Life Evol. Biosph*. **20** 139 (1990)
152. M Perello, B Barbier, A Brack *Int. J. Protein Res*. **38** 154 (1991)
153. B Barbier, A Brack *J. Am. Chem. Soc*. **114** 3511 (1992)
154. H Shindo, M B Hayes, J S Cohen *J. Biol. Chem*. **251** 2644 (1976)
155. C N Pace, U Heinemann, U Hahn, W Saenger *Angew. Chem., Int. Ed. Engl*. **30** 343 (1991)
156. G A Sowa, A C Hengge, W W Cleland *J. Am. Chem. Soc*. **119** 2319 (1997)
157. B D Wladkowski, L A Svensson, L Sjolin, J E Landner, G L Gilliland *J. Am. Chem. Soc*. **120** 5488 (1998)
158. L W Schultz, D J Quirk, R T Raines *Biochemistry* **37** 8886 (1998)
159. D M Perreault, E V Anslyn *Angew. Chem., Int. Ed. Engl*. **36** 432 (1997)
160. R Breslow, M Labelle *J. Am. Chem. Soc*. **108** 2655 (1986)
161. R Breslow, J B Doherty, G Guillot, C Lipsey *J. Am. Chem. Soc*. **100** 3227 (1978)
162. E Anslyn, R Breslow *J. Am. Chem. Soc*. **111** 5972 (1989)
163. C G Ferguson, G R J Thatcher *Org. Lett*. **1** 829 (1999)
164. J Yu, Y Zhao, M J Holterman, D L Venton *Bioorg. Med. Chem. Lett*. **9** 2705 (1999)
165. M J Han, K S Yoo, J Y Chang, T-K Ha *Angew. Chem., Int. Ed. Engl*. **39** 347 (2000)
166. J Yan, R Breslow *Tetrahedron Lett*. **41** 2059 (2000)
167. T P Prakash, S S Kunta, K N Ganesh *Tetrahedron* **50** 11699 (1994)
168. R Giege, B Felden, V N Silnikov, M A Zenkova, V V Vlassov *Meth. Enzymol*. **318** 147 (2000)
169. M A Zenkova, N L Chumakova, A V Vlassov, N I Komarova, A G Ven'yaminova, V V Vlassov, V N Silnikov *Mol. Biol* **34** 456 (2000) [a]
170. D W Hibler, N J Stolowich, M A Reynolds, J A Gerlt, J A Wilde, P H Bolton *Biochemistry* **26** 6278 (1987)
171. E H Serpersu, J McCracken, J Peisach, A S Mildvan *Biochemistry* **25** 68 (1986)
172. E H Serpersu, J McCracken, J Peisach, A S Mildvan *Biochemistry* **27** 8034 (1988)
173. R P Dixon, S J Geib, A D Hamilton *J. Am. Chem. Soc*. **114** 365 (1992)
174. F Chu, L S Flatt, E V Anslyn *J. Am. Chem. Soc*. **116** 4194 (1994)
175. D M Perreault, L A Cabell, E V Anslyn *Bioorg. Med. Chem*. **5** 1209 (1997)
176. M W Göbel, J W Bats, G Dürner *Angew. Chem*. **104** 217 (1992)
177. V Jubian, A Veronese, R P Dixon, A D Hamilton *Angew. Chem., Int. Ed. Engl*. **34** 1237 (1995)
178. T Oost, M Kalesse *Tetrahedron* **53** 8421 (1997)
179. M-S Muche, M W Göbel *Angew. Chem., Int. Ed. Engl*. **35** 2126 (1996)
180. S A Ross, M Pitié, B Meunier *Eur. J. Inorg. Chem*. 557 (1999)
181. V Steullet, D W Dixon *Bioorg. Med. Chem. Lett*. **9** 2935 (1999)
182. J Smith, K Ariga, E V Anslyn *J. Am. Chem. Soc*. **115** 362 (1993)
183. A Lorente, J F Espinosa, M Fernández-Saiz, J - M Lehn, W D Wilson, Y Z Yi *Tetrahedron Lett*. **37** 4417 (1996)
184. C-H Tung, Z Wei, M J Leibowitz, S Stein *Proc. Natl. Acad. Sci. USA* **89** 7114 (1992)
185. M A Podyminogin, V V Vlassov, R Giege *Nucl. Acids Res*. **21** 5950 (1993)
186. V N Silnikov, N P Luk'yanchuk, G V Shishkin, R Zhizhe, V V Vlassov *Dokl. Akad. Nauk* **364** 690 (1999) [b]
187. M Endo, K Hirata, T Ihara, S Sueda, M Takagi, M Komiyama *J. Am. Chem. Soc*. **118** 5478 (1996)
188. V V Vlassov, G Zuber, B Felden, J-P Behr, R Giege *Nucl. Acids Res*. **23** 3161 (1995)
189. D A Konevets, M A Zenkova, V N Silnikov, V V Vlassov *Dokl. Akad. Nauk* **360** 554 (1998) [b]
190. D A Konevetz, I E Beck, N G Beloglazova, I V Sulomenko, V N Silnikov, M A Zenkova, G V Shishkin, V V Vlassov *Tetrahedron* **55** 503 (1999)
191. X H Li, R Wan, Q Zhang, Y F Zhao *Chin. Chem. Lett*. **9** 333 (1998)
192. N S Zhdan, I L Kuznetsova, A V Vlassov, V N Silnikov, M A Zenkova, V V Vlassov *Bioorg. Khim*. **25** 723 (1999) [c]
193. F M Menger, L G Whitesell *J. Am. Chem. Soc*. **107** 707 (1985)
194. F M Menger, R A Persichetti *J. Org. Chem*. **52** 3451 (1987)
195. M L Bender, M Komiyama, in *Bioorganic Chemistry* (Ed. E E van Tamelen) (New York: Academic Press, 1977) p. 19
196. F M Menger, Z X Fei *Angew. Chem., Int. Ed. Engl*. **33** 346 (1994)
197. F M Menger, A V Eliseev, V A Migulin *J. Org. Chem*. **60** 6666 (1995)
198. M P Mertes, K B Mertes *Acc. Chem. Res*. **23** 413 (1990)
199. M W Hosseini, A J Blacker, J-M Lehn *J. Am. Chem. Soc*. **112** 3896 (1990)
200. M Komiyama *J. Biochem*. **118** 665 (1995)
201. R Hiner, J Hall *Antisense Nucl. Acids Drug Dev*. **7** 423 (1997)
202. B N Trawick, A T Daniher, J K Bashkin *Chem. Rev*. **98** 939 (1998)
203. V V Vlassov, V N Silnikov, M A Zenkova *Mol. Biol*. **32** 62 (1998) [a]
204. M Komiyama, J Sumaoka *Curr. Opin. Chem. Biol*. **2** 751 (1998)
205. D Magda, R A Miller, J L Sessler, B L Iverson *J. Am. Chem. Soc*. **116** 7439 (1994)
206. J Hall, D Husken, R Häner *Nucl. Acids Res*. **24** 3522 (1996)
207. J K Bashkin, E I Frolova, U Sampath *J. Am. Chem. Soc*. **116** 5981 (1994)
208. T Pan, B Dichtl, O C Uhlenbeck *Biochemistry* **33** 9561 (1994)
209. I J Brittain, X Huang, E C Long *Biochemistry* **37** 12 113 (1998)
210. J Hall, D Husken, U Pieles, H E Moser, R Hiner *Chem. Biol*. **1** 185 (1994)
211. R Hiner, J Hall, A Pfützer, D Hmsken *Pure Appl. Chem*. **70** 111 (1998)
212. M A Reynolds, T A Beck, P B Say, D A Schwartz, B P Dwyer, W J Daily, M M Vaghefi, M D Metzler, R E Klem, L J Arnold *Nucl. Acids Res*. **24** 760 (1996)
213. D Magda, M Wright, S Crofts, A Lin, J L Sessler *J. Am. Chem. Soc*. **119** 6947 (1997)
214. S Matsuda, A Ishikubo, A Kuzuya, M Yashiro, M Komiyama *Angew. Chem., Int. Ed. Engl*. **37** 3284 (1998)
215. M Komiyama, T Inokawa, T Shiiba, N Takeda, K Yoshinari, M Yashiro *Nucl. Acids Symp. Ser*. **29** 197 (1993)
216. A Kuzuya, Y Azuma, T Inokava, K Yoshinari, M Komiyama *Nucl. Acids Symp. Ser*. **37** 209 (1997)
217. M Komiyama, T Inokava *J. Biochem*. **116** 719 (1994)
218. M Komiyama, T Inokawa, K Yoshinari *J. Chem. Soc., Chem. Commun*. 77 (1995)
219. M Endo, Y Azuma, Y Saga, A Kuzuya, G Kawai, M Komiyama *J. Org. Chem*. **62** 846 (1997)
220. J C Verheijen, B A L M Deiman, E Yeheskiely, G A van der Marel, J H van Boom *Angew. Chem., Int. Ed. Engl*. **39** 369 (2000)
221. J Hovinen, A Guzaev, E Azhayeva, A Azhayev, H Lönnberg *J. Org. Chem*. **60** 2205 (1995)

222. D V Pyshnyi, M N Repkova, S G Lokhov, E M Ivanova, A G Ven'yaminova, V F Zarytova *Bioorg. Khim.* **23** 497 (1997) [c]
223. D Pyshnyi, M Repkova, S Lokhov, E Ivanova, A Venyaminova, V Zarytova *Nucleosides Nucleotides* **16** 1571 (1997)
224. V Silnikov, G Zuber, J-P Behr, R Gige, V Vlassov *Phosphorus Sulfur Silicon Relat. Elem.* **109–110** 277 (1996)
225. V Vlassov, T Abramova, T Godovikova, R Gige, V Silnikov *Antisense Res. Dev.* **7** 39 (1997)
226. K Ushijima, H Gouzu, K Hosono, M Shirakawa, K Kogosima, K Takai, H Takaku *Biochem. Biophys. Acta* **1379** 217 (1998)
227. N G Beloglazova, N N Polushin, V N Silnikov, M A Zenkova, V V Vlassov *Dokl. Akad. Nauk* **369** 827 (1999) [b]
228. N N Polushin *Collect. Czech. Chem. Commun., Coll. Symp. Ser.* **2** 145 (1999)
229. D Hüken, A Deichert, J Hall, R Häner *Nucleosides Nucleotides* **18** 1507 (1999)
230. A S Butorin, G N Grimm, K Elen *Mol. Biol.* **34** 946 (2000) [a]
231. A S Modak, J K Gard, M C Merriman, K A Winkeler, J K Bashkin, M K Stern *J. Am. Chem. Soc.* **113** 283 (1991)
232. J K Bashkin, J Xie, A T Daniher, U Sampath, J L-F Kao *J. Org. Chem.* **61** 2314 (1996)
233. G Wang, D E Bergstom *Tetrahedron Lett.* **34** 6721 (1993)
234. J Hovinen *Bioconjugate Chem.* **9** 132 (1998)
235. H Inoue, M Shimizu, T Furukawa, T Tamura, M Matsui, E Ohtsuka *Nucleosides Nucleotides* **18** 1503 (1999)
236. J K Bashkin, J K Gard, A S Modak *J. Org. Chem.* **55** 5125 (1990)
237. J K Bashkin, S M Sondhi, U Sampath, A d'Avignon *New J. Chem.* **18** 4604 (1994)
238. N N Polushin, B-ch Chen, L W Anderson, J S Cohen *J. Org. Chem.* **58** 4606 (1993)
239. G Wang, D E Bergstom *Tetrahedron Lett.* **34** 6725 (1993)
240. T H Smith, J V LaTour, D Bochkariov, G Chaga, P S Nelson *Bioconjugate Chem.* **10** 647 (1999)
241. A Yu Karyagin, T V Abramova, V N Silnikov, G V Shishkin *Izv. Akad. Nauk, Ser. Khim.* 536 (2000) [d]
242. G N Grimm, A S Boutorine, C Helene *Nucleosides Nucleotides* **19** 1943 (2000)
243. D G Knorre, P V Alekseev, Y V Gerassimova, V N Silnikov, G A Maksakova, T S Godovikova *Nucleosides Nucleotides* **17** 397 (1998)
244. L Yurchenko, V Silnikov, T Godovikova, G Shishkin, J-J Toulme, V Vlassov *Nucleosides Nucleotides* **16** 1721 (1997)
245. N G Beloglazova, V N Silnikov, M A Zenkova, V V Vlassov *FEBS Lett.* **481** 277 (2000)

[a] — *Mol. Biol. (Engl. Transl.)*
[b] — *Dokl. Chem. Technol., Dokl. Chem. (Engl. Transl.)*
[c] — *Russ. J. Bioorg. Chem. (Engl. Transl.)*
[d] — *Russ. Chem. Bull. (Engl. Transl.)*

Russian Chemical Reviews **70** (6) 509 – 533 (2001) © 2001 Russian Academy of Sciences and Turpion Ltd

DOI 10.1070/RC2001v070n06ABEH000640

Affinity sorbents containing nucleic acids and their fragments

I G Shishkina, A S Levina, V F Zarytova

Contents

I.	Introduction	509
II.	Solid supports and linkers	509
III.	Chemical methods for the immobilisation of nucleic acids	513
IV.	Immobilisation of nucleic acids in the course of solid-phase synthesis	524
V.	Miscellaneous methods of immobilisation of nucleic acids	524
VI.	Immobilisation of nucleic acids using enzymes and avidin – biotin interactions	524
VII.	The use of matrices containing nucleic acids	525
VIII.	Conclusion	528

Abstract. The published data on the main methods for the preparation of polymeric supports containing nucleic acids (NA) or their fragments (oligonucleotides) are reviewed with special emphasis on chemical immobilisation. Some physical and physicochemical immobilisation techniques, including those based on the use of enzymes and avidin – biotin interactions and preparation of NA-containing supports by direct oligonucleotide synthesis on these supports are considered. A special section is devoted to the application of NA-containing sorbents for the isolation of individual NA and proteins as well as in hybridisation analysis including those utilising DNA chips and DNA biosensors. The bibliography includes 391 references.

I. Introduction

Polymeric supports containing nucleic acids (NA) and their fragments have long attracted the attention of specialists in different fields of biochemistry, gene engineering and molecular biology. In the past decade, such supports have successfully been used in hybridisation analysis for research purposes as well as in medicine for the diagnostics of infectious, cancer, genetic and other diseases. NA-Containing matrices are efficient tools for isolation of individual NA and NA-dependent enzymes. The synthesis of affinity sorbents is based on the following principle: the ligands (in our case, NA, oligonucleotides or polynucleotides) are immobilised on a polymeric support (a matrix) through a linker or a spacer, or without them. With the advent of automated synthetic techniques, oligonucleotides have become commercially readily available, which makes them especially attractive as ligands. Native NA are also immobilised as ligands for the solution of some practical tasks.

I G Shishkina, A S Levina, V F Zarytova Novosibirsk Institute of Bioorganic Chemistry, Siberian Branch of the Russian Academy of Sciences, prosp. Acad. Lavrent'eva 8, 630090 Novosibirsk, Russian Federation. Fax (7-383) 233 36 77. Tel. (7-383) 239 62 75.
E-mail: igshishkina@hotmail.com (I G Shishkina)
Levina@niboch.nsc.ru (A S Levina)
Tel. (7-383) 239 62 24. E-mail: Zarytova@niboch.nsc.ru (V F Zarytova)

Received 15 March 2001
Uspekhi Khimii **70** (6) 581 – 608 (2001); translated by R L Birnova

All presently known methods for immobilisation of oligonucleotides and NA can be conventionally divided into chemical methods, which involve covalent binding of NA to the support, and other methods, which include all the procedures demanding special equipment or technology (*e.g.*, synthesisers, irradiation, *etc.*) in addition to the support, NA and chemicals.

This review is devoted to the description of the main methods for the preparation of NA-containing sorbents, their properties and applications. It should be noted that these methods can be used for immobilisation of not only oligo(poly)nucleotides, but also their analogues and peptide-nucleic acids (PNA) in which the sugar-phosphate backbone is replaced by the peptide chain. A separate section is devoted to the use of NA-containing matrices for the isolation of individual NA and proteins as well as in hybridisation analysis (including DNA chips and DNA biosensors).

II. Solid supports and linkers

1. Supports

Before we pass to the consideration of various procedures for immobilisation of NA, we shall dwell briefly on the requirements placed upon polymeric supports to be used in the design of 'ideal' affinity matrices. These include:

(1) insolubility (to avoid the loss of the ligand attached and contamination of the isolated compound with the dissolved support);

(2) accessibility of the immobilised ligand for the formation of complexes with specific biomolecules;

(3) zero adsorption capacity (to prevent non-specific interactions);

(4) high reactivity essential for chemical modification of the support surface;

(5) chemical stability under conditions employed for the attachment of ligands as well as sorption and desorption of the products and regeneration of the matrix;

(6) high resistance to microbes and enzymes;

(7) hydrophilicity (to reduce non-specific sorption due to hydrophobic interactions);

(8) commercial availability.

The requirements for the nature, shape, composition and mechanical strength of the solid support vary depending on the experimental task. The most popular supports can be divided into two groups, *viz.*, natural and synthetic ones (Table 1). High-

Table 1. Commercially available carriers.

Carrier	Commercial name	Manufacturer
Natural supports		
Agarose	Sepharose, Superose	Pharmacia, LKB
	Bio-Gel A	Bio-Rad
	Ultrogel	IBF
Cellulose	Cellulose	Whatman
Dextran	Sephadex	Pharmacia
Synthetic supports		
Polyacrylamide supports	Bio-GelP	Bio-Rad
	Trisacryl GF-2000, Sephacryl	IBF Biotechnics
	Ultrogel	Pharmacia
	Azlactone beads	IBF
	3M Emphaze biosupport	3M Corporation
		Pierce Chemical
Polymethacrylate supports	TSK-Gel Toyopearl HW	Tosoh Corporation
	Fractogel TSK	EM Science, Merck
	HEMA	TESSEK Ltd.
	Separon, Spheron	Alltech Associates
	Eupergit	Rohm Pharma
Polystyrene supports	Porous supports	PerSeptive Biosystem
	Polystyrene balls	Pierce Chemical
	Dyno particles	Trondheim
	TentaGel	Rapp Polymers
	MerckoGel	Merck
Glass supports		
	CPG glass	Pierce Chemical
	Glass beads	Jenco, Supelco
	Microscope glass slides	Fisher Scientific
		Menzel-Glaser

pressure affinity chromatography demands hard materials, whereas in column chromatography performed at normal pressure hardness is not a critical factor. The relatively small specific surface area in non-porous supports can largely be compensated by the reduced size (down to the micron level) of the support particles with the preservation of their satisfactory hydrodynamic characteristics. Porous supports are suited to affinity chromatography where the size of the analysed molecules is much smaller than that of the matrix pores. In the majority of cases, sorbents represent spherical granules with the size of 40 to 150 μm, whereas silica gel-based sorbents for high-performance affinity chromatography have a particle size of about 10 μm.

Modern studies often utilise membranes as supports. They are usually manufactured from various polymeric materials, such as cellulose, polyamide (nylon), polyacrylonitrile, polysulfone, polypropylene, polyesters, polyethylene, *etc*. Cellulose, nylon and poly(ethylene terephthalate) are the most popular supports, since they allow easy incorporation of various functional groups. Cover glasses and polystyrene immunological assay plates are widely used in hybridisation analysis.

Some supports incorporating various functional groups (Table 2) accessible for immobilisation of ligands are commercially available; however, they demand additional modification prior to application because they partly lose their activities upon storage. Therefore, we shall consider some synthetic procedures leading to such sorbents along with the principal known methods for the preparation of affinity sorbents containing NA or their fragments.

2. Linkers and spacers

Oligonucleotides and NA can be immobilised directly on the surface of the solid support; however, this can result in steric hindrance to subsequent reactions with biomolecules, especially in the case of planar supports, such as membranes and slides. To prevent this, immobilisation is carried out with the use of linkers or spacers which hold the ligand at some distance away from the surface and thus make it more accessible for further interactions.

In the absence of linkers, immobilisation can be carried out by virtually all physical methods (*e.g.*, UV irradiation, sorption on the surface by drying) or by direct synthesis of oligonucleotides on glass [1] or on aminated polypropylene.[2] However, immobilisation is usually performed after incorporation of spacers into the oligonucleotide and/or on the surface of the support.[3–40] The larger is the distance between the immobilised ligands and the surface, the more accessible they are for the reaction with the dissolved molecules. Most often, the role of linkers is played by linear aliphatic chains containing different numbers of hexamethylenediamine, 6-aminocaproic acid or ethylene glycol units. In addition to the length, an important role is played by the nature of the linker, which may govern the extent of non-specific sorption. This can be overcome through the use of linker chains consisting of hydrophilic molecules, *e.g.*, 1,3-diaminopropan-2-ol or amino acid residues. Hydrophilic linkers of any length can be designed from phosphoroamidites of various diols [8] or by stepwise addition of 1,3-diaminopropan-2-ol and bromoacetic acid.[9,10] The linkers are usually attached to the support by the same methods as ligands. Silica gel and glass are premodified by (3-aminopropyl)-triethoxysilane (**1**),[11–13] (3-glycidyloxypropyl)trimethoxysilane (**2**),[3,4,13–15] [*N*-(2-aminoethyl)-3-aminopropyl]trimethoxysilane (**3**), (diethylenetriaminopropyl)trimethoxysilane (**4**)[16] or other trialkoxysilanes.[17–21] The number of immobilisation sites can be increased by an order of magnitude using branched linkers, such as dendrimers (**5**).[22]

Oligonucleotides with linkers (3–11 units) attached to their 5′- (see Refs 7, 23–28) or 3′-terminal [15,29] phosphates, to the apurinisation sites,[30] to the amino group of 5-methyldeoxycytidine,[31,32] to C(5) of deoxyuridine [33–36] or to C(8) of deoxyadeno-

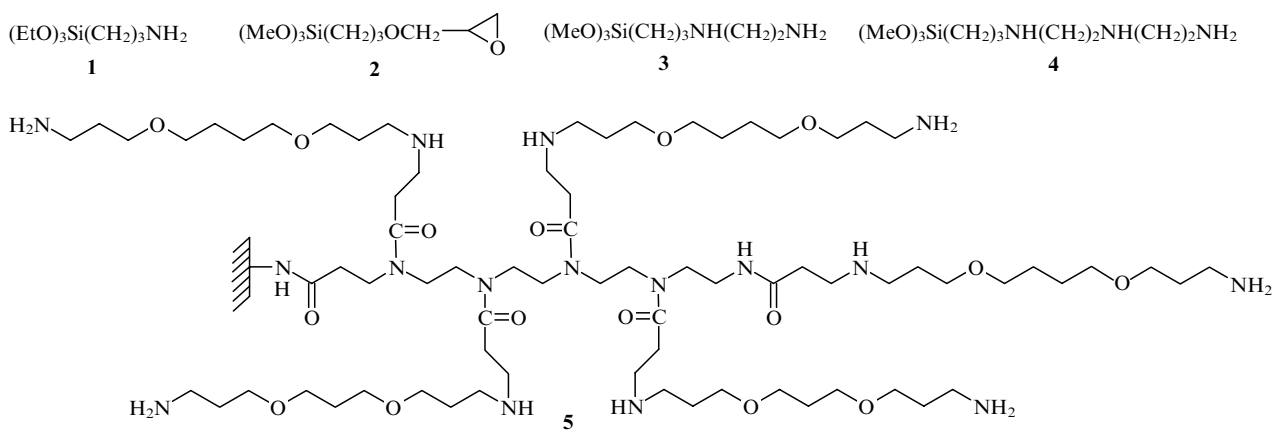

Table 2. Supports for the immobilisation of ligands.

Functional groups of supports	Ligand	Groups of supports formed after immobilisation of the ligand	Commercial name of the support	Manufacturer
—$CONHNH_2$	LCHO	—C(O)NHN=CHL	Affi-Gel Hz gel, Affi-Prep Hz support	Bio-Rad
			Agarose adipic acid hydrazide	Pharmacia
			Carboxymethylcellulose hydrazide	Sigma, Supelco
			3M Emphaze hydrazide biosupport	Pierce
			Hydrazide beads	Pierce, Sigma, Supelco
			Polyacrylamide hydrazide	Sigma, Supelco
			Polyacrylhydrazidoagarose	Pierce
—$OC(O)NH(CH_2)_2NHCO$—C$_6$H$_4$—$HgCl$	LSH	—$OC(O)NH(CH_2)_2NHCO$—C$_6$H$_4$—$HgSL$	Immobilized *p*-chloromercuribenzoate gel	Pierce
			Affi-Gel 501gel	Bio-Rad
—$OCH_2CH(OH)CH_2SS$—C$_5$H$_4$N	LSH	—$OCH_2CH(OH)CH_2SSL$	Thiopropyl-activated	
			Agarose	Sigma, Supelco
			Sepharose 6B	Pharmacia, Sigma, Supelco
			Thiolagarose	ICN
—O—C(=NCH(CO_2H)CONHCH(C(O)$NHCH_2CO_2H$)SS—C$_5$H$_4$N)—O—	LSH	—O—C(=NCH(CO_2H)CONHCH(C(O)$NHCH_2CO_2H$)SSL)—O—	Activated thiolsepharose 4B	Pharmacia, Supelco
—$NH(CH_2)_3NHC(=NH)(CH_2)_3SS$—C$_6H_3$($CO_2H$)($NO_2$)	LSH	—$NH(CH_2)_3NHC(=NH)(CH_2)_3SSL$	Immobilized TNB-thiol	Pierce
—$CH_2NHCOCH_2I(Br)$	LSH	—$CH_2NHCOCH_2SL$	Ultralink iodoacetyl	Pierce
			Bromoacetylagarose	ICN, Calbiochem
			Bromoacetylcellulose	Sigma
—O—C(=NH)—O—	LNH_2	—O—C(=NL)—O—	Cyanogen bromide-activated	
			Agarose, Sepharose 6M B	Sigma, Supelco
			Agarose CL-4B	Fluka
			Sepharose 4B	Fluka, Sigma, Supelco, Pharmacia
—$OCH_2CH(O)CH_2$	LOH LNH_2	—$OCH_2CH(OH)CH_2XL$ X = O, NH	Epoxy-activated	
			Agarose	Pierce, Sigma, Supelco
			Sepharose 6B	Pharmacia, Sigma, Supelco
			Eupergit C	Rohm Pharma, Supelco
			Oxirane acrylic beads	Sigma
			Polymercarrier VA-epoxy	Riedel-de Haen
			POROS 20 EP	PerSeptive Biosystem
			Supelcosil epoxy 540	Supelco
			Toyopearl AF-epoxy-650M	Supelco, Tosoh Co.

Table 2 (continued).

Functional groups of supports	Ligand	Groups of supports formed after immobilisation of the ligand	Commercial name of the support	Manufacturer
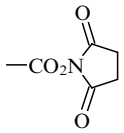	LNH_2	—OC(O)NHL	*N*-Hydroxysuccinimide-activated	
			Agarose	Sigma, Supelco
			CH-Sepharose	Fluka, Sigma, Supelco
			Sepharose, Superose	Pharmacia
			Affi-Gel, Affi-Prep support	Bio-Rad
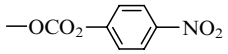	LNH_2	—OC(O)NHL	Nitrophenyl-activated Agarose	Sigma, Supelco
	LNH_2	—OC(O)NHL	Carbonyldiimidazole(CDI)-activated	
			Agarose	Sigma, Supelco
			Trisacryl GF-200, TSK HW-65F	IBF Biotechnics
			Reacti-Gel (6X, GF-2000, HW-65F) Supports	Pierce
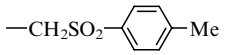	LSH LNH_2	—CH_2XL X = NH, S	Tosyl-activated	
			Agarose	Pierce, Sigma, Supelco
			Dynabeads M280	Dynal Inc.
—$CH_2OSO_2CH_2CF_3$	LSH LNH_2	—CH_2XL X = NH, S	Tresyl-activated Agarose	Pierce, Schleicher & Schuell, Sigma, Supelco
			Toyopearl AF-tresyl-650M	Supelco, Tosoh Co.
—OCH_2CHO	LNH_2	—OCH_2CH_2NHL	Toyopearl AF-formyl-650M	Tosoh Co.
			Aldehydeagarose	Sigma

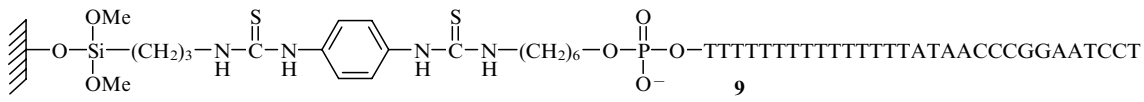

9

sine [37] are immobilised on commercially available supports (see Table 2) bearing relatively short linkers (2–11 units).

There is no general agreement as regards the dependence of hybridisation properties of immobilised oligonucleotides on the linker's length. It was noted [6, 16] that the hybridisation abilities of immobilised oligonucleotides are enhanced with increase in the linker's length. It is also suggested [8, 38, 39] that efficient hybridisation requires the optimum length of the spacer to be selected. The use of linkers (**6**–**8**) containing different numbers of repeating units has also been documented.[8]

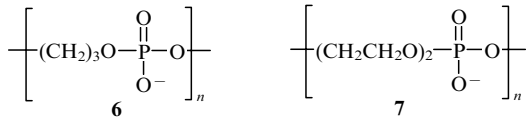

6 **7**

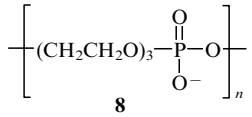

8

The maximum efficiency of hybridisation is achieved for $n = 8-10$ with all three types of units. This suggests that the yields of hybridisation products depend not only on the length of the linker, but also on its structure (in this case, probably, on the number of negative charges). The maximum increase in the yields of hybridisation products (150-fold in comparison with the yields in the absence of the spacer) was observed with the linkers **7** and **8** for $n = 8$. With a further increase in the number of units, the hybridisation ability diminishes, and for $n = 25-30$ the yields of the hybridisation products are virtually the same as in the absence of the linker.

However, it was shown [40] that the length of the linker between the polyacrylamide support and an oligonucleotide does not influence the stability of a duplex formed. This is consistent with the results of the above-cited studies and those devoted to the sequencing of DNA by hybridisation on oligonucleotide microchips.[41–47] Presumably, the optimum length of the linker depends on many factors, such as the nature of the support, the ligand and the linker itself, and should be chosen experimentally for each particular task. It is noteworthy that immobilisation on granulated supports can be made using short linkers or no linkers at all, whereas films and slides demand longer linkers.

In order to increase the distance between the surface and an oligonucleotide to be immobilised, the latter sometimes is elongated by introducing additional chains consisting of thymidine units [*e.g.*, oligo$(dT)_{1-400}$][17, 19, 48, 49] or non-essential oligonucleotide sequences (*cf.* **9**).[7, 18]

III. Chemical methods for the immobilisation of nucleic acids

Immobilisation of NA by covalent binding to polymeric supports is achieved by the reaction of available or incorporated functional groups of the oligonucleotide with reactive groups of the support. In this review, the chemical methods used for the formation of a covalent bond between the ligand and the polymer are divided into two large groups, *viz.*,

(1) immobilisation of functionalised and/or activated NA on nucleophilic supports, and

(2) immobilisation of NA on supports containing electrophilic groups.

It should be noted that the functional groups of the natural nucleic acids (hydroxy groups of ribose, phosphoric acid residues and heterocyclic bases [50]) possess nucleophilic properties and react with the electrophilic groups of the polymer. These reactions usually yield numerous binding sites of the ligands to the supports, which results in the loss of the full-value interactions of immobilised NA with biomolecules. To prevent this, NA are modified by introduction of additional functional groups which are more reactive than the corresponding functional groups of the natural NA.

1. Immobilisation of functionalised and activated nucleic acids on nucleophilic supports

Immobilisation of NA and their fragments on solid supports containing surface nucleophilic groups (*e.g.*, hydroxy, thiol or amino groups) can be achieved by preliminary activation of the functional groups of the ligand (Fig. 1).

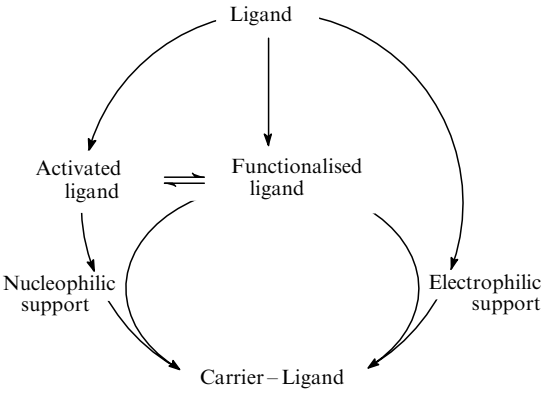

Figure 1. Chemical methods for the immobilisation of ligands.

The introduction of functional groups into poly- and oligonucleotides has been the subject of several reviews.[51–53] Most often, the post-synthetic introduction of additional functional groups involves terminal phosphate groups using reagents which affect other functional groups of NA to a much lesser extent. Carbodiimides, arenesulfonyl chlorides, 2,4,6-trimethylbenzoyl chloride, *etc.*, are commonly used for this purpose.[54–58] The reactive oligonucleotide derivatives formed are unstable and used for the introduction of additional functional groups into oligonucleotides or for direct immobilisation on solid supports immediately following preparation.

a. Activation of nucleic acids by carbodiimides

The addition of NA using carbodiimides **10a**–**c** has been one of the earliest approaches to the preparation of affinity sorbents and has continued to be a very popular procedure.[50–64] This method is based on the ability of carbodiimides to activate either the carboxy groups of polymers or the terminal phosphate group of NA. Carbodiimide-activated oligonucleotides react readily with amino or thiol groups of solid supports. Reactions with hydroxyl-containing supports proceed less effectively.

The carbodiimide method is used for the immobilisation of mono-, oligo-, polydeoxyribonucleotides and DNA in both organic solvents using dicyclohexylcarbodiimide (**10a**)[50–62] and aqueous media using water-soluble carbodiimides, *e.g.*, 1-(3-dimethylaminopropyl)-3-ethylcarbodiimide (**10b**)[13, 18, 24, 25, 65, 66] or 1-cyclohexyl-3-(2-morpholinoethyl)carbodiimide metho-*p*-toluenesulfonate (**10c**).[25, 67]

$R^1N{=}C{=}NR^2$

10a–c

$R^1 = R^2$ = cyclo-C_6H_{11} (**a**); R^1 = Et, $R^2 = Me_2N(CH_2)_3$ (**b**);

R^1 = cyclo-C_6H_{11}, R^2 = 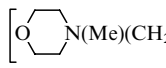 $[SO_3C_6H_4Me\text{-}4]^-$ (**c**).

The mechanism of activation of phosphate groups of oligonucleotides by carbodiimides has been studied in detail and some side reactions have been revealed.[68–73] Protonation of carbodiimides and the formation of intermediate unstable reactive *O*-phosphorylisourea derivatives **11** is the limiting step of this reaction.[74] This stage is also inhibited by strongly basic nucleophilic groups of the support. Besides, protonated nucleophilic groups do not react with compounds **11**. As a consequence, the yield of the final product **12** decreases if polymers with strongly basic groups are used. The substituted *O*-phosphorylisoureas **11** can also be transformed into side products, *e.g.*, be hydrolysed with the liberation of the original phosphate group and urea or undergo consecutive conversions leading to pyrophosphates, polyphosphates and *O*-phosphorylisourea derivatives.[75] The latter, in turn, produce non-reactive *N*-pyrophosphorylurea derivatives **13**[75,76] or *N*-phosphorylurea derivatives **14**.[66,77–79]

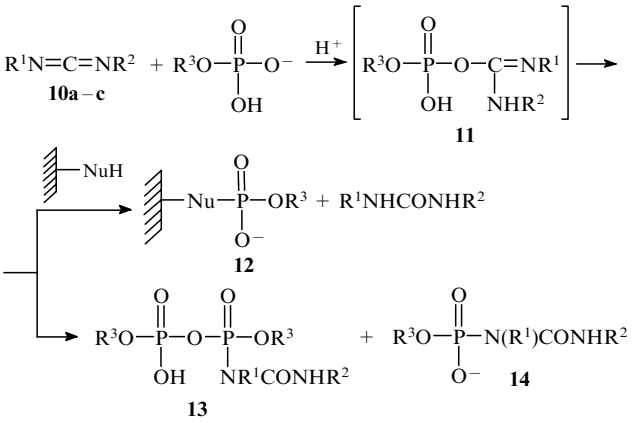

R^3, oligonucleotide residue; NuH = NH, SH, OH.

In the activation of oligonucleotides by carbodiimides resulting in compounds **11**–**14**, modification of internucleotide phosphate groups[76,79] and heterocyclic bases[69,80] is observed. In the case of oligodeoxyribonucleotides, the reaction with the internucleotide phosphate groups results in the urea derivatives **15**,[76] whereas the reaction with oligoribonucleotides leads to the isomerisation and cleavage of the internucleotide bonds.[51,81]

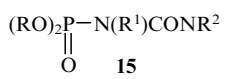

The activation of the terminal phosphate group of the nucleotide by carbodiimide in alkaline media (pH $\geqslant$ 8) can be accompanied by nucleophilic addition of the anion formed from the heterocyclic base to the double bond of the carbodiimide. This reaction affects the bases containing a CONH group, *i.e.*, the N(3) atom in the uracil and thymine residues and the N(1) atom in the guanine residues.[69]

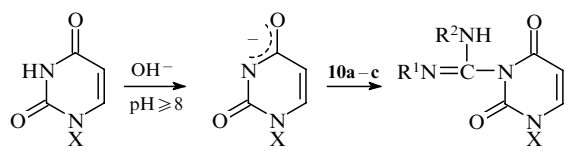

X, oligonucleotide residue.

The rate of the limiting stage can be accelerated, the yield of the target product **12** in the immobilisation of the oligonucleotide derivatives **11** can be increased and the modification of the internucleotide phosphodiester groups and heterocyclic bases by carbodiimides can be overcome if the reaction is carried out in weakly acidic media (pH 4.25–5.0).[80] In this case, the carbodiimide-activated terminal phosphate group of an oligonucleotide reacts predominantly with the amino, thiol or hydroxy groups on the surface of the support.

The selectivity and efficiency of oligonucleotide immobilisation increases slightly after functionalisation of their 5′-phosphate groups by linkers containing a terminal carboxy group,[18,82] which reacts with the amino groups of the support after its activation by carbodiimide.

An alternative approach consists in the activation of the carboxy groups of the polymer by carbodiimides (see Section III.2). In this case, immobilisation of nucleotides and oligonucleotides on supports involves the amino groups of the heterocyclic bases or linkers attached to the 3′- (see Refs 66, 83) or 5′- (see Refs 25, 84) terminal phosphates of the oligonucleotides.

Immobilisation of NA and oligonucleotides by the carbodiimide method is carried out on virtually all available solid supports, *e.g.*, cellulose, Sepharose,[59–63,72,85] Sephacryl,[23,65,67] Sephadex,[23,73,85] SiO_2-based supports[12,18,64,65,86,87] and various membranes.[66,82,83,88] In addition to conventional supports, magnetic carriers (*e.g.*, polystyrene-coated magnetite particles)[25] and latex microspheres (polystyrene beads able to form colloidal suspensions)[24] are used. The resulting matrices are used in hybridisation analysis[12,13,18,23,25,66,67] and in affinity chromatography.[63,89]

The efficiency of immobilisation of oligonucleotides on polymeric supports can be increased by performing activation by carbodiimides in the presence of nucleophilic catalysts, *e.g.*, imidazole, triazole or tetrazole, which generate the corresponding phosphoramidates;[24,25,65,73,88] the latter manifest high reactivities towards nucleophiles after protonation of the azole units. Phosphorimidazolidates **16** are commonly used.[88,90,91]

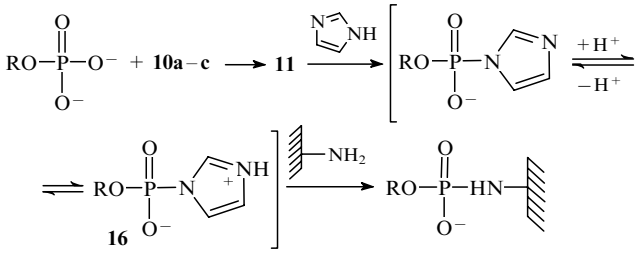

R, oligonucleotide residue.

The addition of compounds containing hydroxy groups with higher acidities, *e.g.*, *N*-hydroxysuccinimide or *N*-hydroxybenzotriazole, to the reaction mixture instead of nucleophilic catalysts results in the formation of the activated NA esters **17**.[73,92]

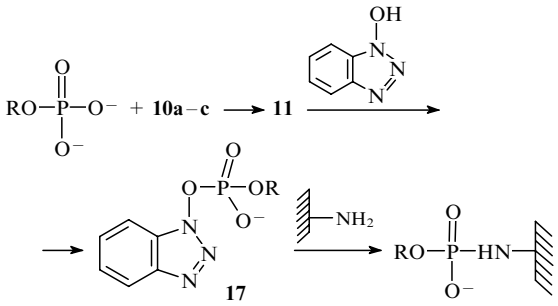

R, oligonucleotide residue.

The main advantage of the last two approaches is the lack of side reactions, since the derivatives **16** and **17** are more stable than the *O*-phosphorylisoureas **11**. The compounds **16** and **17** react with the amino groups of the support more efficiently, which increases the yield on immobilisation.

b. Activation of nucleic acids by 2,4,6-trimethylbenzoyl chloride

High reactivity of the title reagent with respect to the terminal and internucleotide phosphate groups ensures rapid formation of the corresponding mixed anhydrides. In aqueous media, only the mixed anhydride **18** formed upon reaction with the terminal phosphate persists.[93,94] This is used for the immobilisation of deoxyribonucleic acids on polymers containing nucleophilic amino groups. In aqueous media, immobilisation is due to the formation of a phosphoramide bond between the terminal 5′-phosphate group of the oligonucleotide and the primary amino group of the polymer (the product **19**).[57,95]

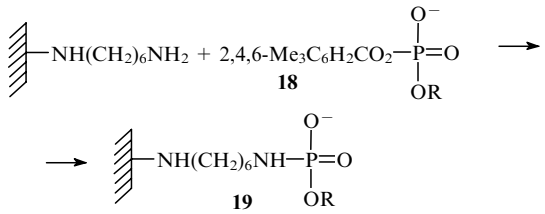

R, oligonucleotide residue.

In the study by Shumyantseva and Khomutov,[96] the activated oligonucleotide **18** was immobilised on aminooxybutylcellulose **20**. The resulting affinity sorbent **21** is stable only at pH 7.0 due to the high lability of the alkoxyamide bond. In addition, binding of oligonucleotides to the polymer **20** occurred involving the amino groups of cytidine to give the product **22**, most probably due to transamination in aqueous media.[56,94]

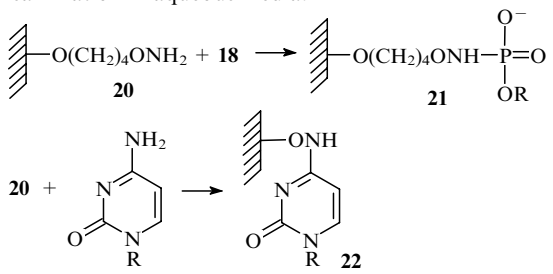

R, oligonucleotide residue.

This method has not gained wide acceptance despite the fact that TMP, AMP, CMP, d(pT)$_3$, d(pA)$_3$ and other oligonucleotides[57,95,96] were immobilised on polysaccharide supports in fairly good yields (0.05–0.15 mmol of the nucleotide per 1 g of the support). The significant disadvantages of this method are the lengthy immobilisation step (> 3 days) and side reactions (*e.g.*, the formation of pyrophosphates of oligonucleotides, reactions involving internucleotide phosphates and the heterocyclic bases of oligonucleotides). This method is inappropriate for the immobilisation of ribooligonucleotides and RNA, since mixed anhydrides favour the formation of cyclophosphates in the activation step, subsequent isomerisation and cleavage of the internucleotide bonds.[93]

c. Activation of the terminal phosphates of oligonucleotides by the triphenylphosphine–dipyridyl disulfide redox couple

The triphenylphosphine–dipyridyl disulfide redox couple ($Ph_3P-Py_2S_2$) was first recommended for use as a condensation reagent for peptide and oligonucleotide syntheses by Mukaiyama *et al.*[97,98] The following reaction scheme was proposed:[98]

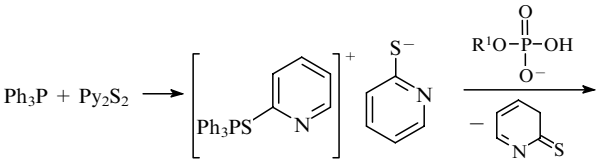

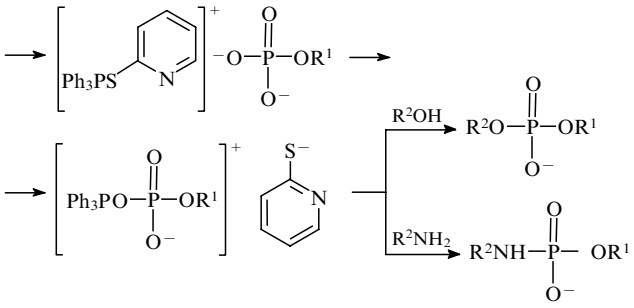

R^1, nucleotide or oligonucleotide residue; R^2 = Alk, Ar.

However, the reaction of an oligonucleotide with highly basic amino groups in the presence of the Ph_3P-PyS_2 couple occurs at a slow rate and with low yields, which places certain restrictions on its practical application. A detailed study of this system by Zarytova *et al.*[99–102] revealed that the $Ph_3P-Py_2S_2$ couple selectively activates the terminal phosphate group of an oligonucleotide in the presence of nucleophilic catalysts with the formation of the zwitterionic oligonucleotide derivatives **23**.

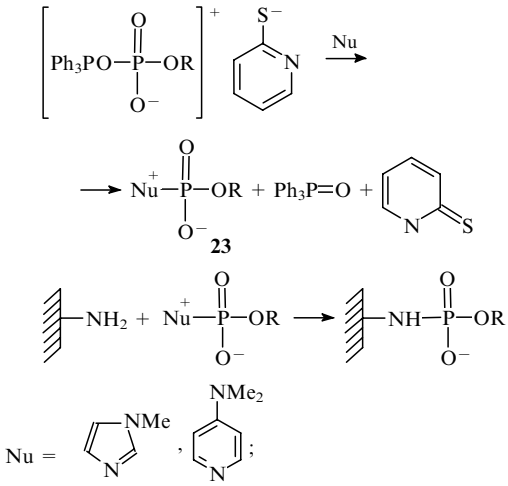

R, nucleotide or oligonucleotide residue.

It should be emphasised that heterocyclic bases and internucleotide phosphate groups are not involved in the activation, which precludes the formation of side products. Therefore, this approach can be used for the activation of both deoxyoligonucleotides and their analogues and, which is especially important, of ribooligonucleotides without migration of the C(3)–C(5′) internucleotide bond.

The activated derivatives **23** react rapidly and virtually quantitatively with primary amines to yield oligonucleotide phosphoramides.[100] The activated oligonucleotide **23** can easily be immobilised provided the primary amino group is localised on its surface.[101,102] The immobilisation is completed within 2 h in aqueous alkaline media or in organic solvents. Up to 97% of the starting oligonucleotide material binds to the support, which enables one to control and vary the capacities of affinity sorbents. Any material can be used as a support, but silica gel[103–105] and polymethacrylate gels[101,106] are especially widely used. The matrices with immobilised oligonucleotides were used for affinity chromatography of NA-dependent proteins,[101,106] nucleic acids and their analogues.[102–105] The $Ph_3P-Py_2S_2$ couple can be recommended for the immobilisation of ribooligonucleotides and RNA, since in contrast with the known condensation reagents (*e.g.*, carbodiimides, arenesulfonyl chlorides, azoles, 2,4,6-trimethylbenzoyl chloride), it does not react with internucleotide phosphates and nucleophilic centres of heterocycles and no corresponding side products are formed.

d. Activation of nucleic acids by bifunctional reagents

Activation and subsequent immobilisation of NA and their fragments can be achieved through the use of bifunctional reagents. The reactions with bisoxiranes, disuccinimidyl carbonate, carbonyldiimidazole and glutaraldehyde will be considered in detail in Section III.2.

The bifunctional reagents also include 2,4,6-trichloro-1,3,5-triazine (**24**), which reacts with the primary amino group of a spacer introduced into the oligonucleotide in the course of its synthesis.[27]

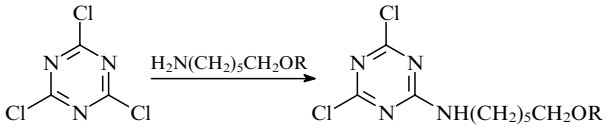

24 **25**

R, oligonucleotide residue

The triazine derivatives of oligonucleotides **25** are stable for at least one week at 4 °C and can be immobilised on any supports containing amino (see Refs 6, 27) or thiol groups.[6] The resulting sorbents are characterised by low non-specific sorption of proteins and NA and are stable under hybridisation conditions.[27, 107]

e. Reductive amination with nucleic acids and oligonucleotides containing aldehyde groups

Reductive amination is based on the well-known reaction of aldehydes and ketones with primary amines resulting in the formation of Schiff's bases. The reduction of Schiff's bases by sodium borohydride affords stable secondary amines.

$$R^1NH_2 + O{=}CHR^2 \rightleftharpoons R^1N{=}CHR^2 \xrightarrow{NaBH_4} R^1NHCH_2R^2$$

Immobilisation based on this method requires that NA or oligonucleotides contained aldehyde groups. This requirement is easy to meet in the case of ribooligonucleotides, RNA and deoxyoligonucleotides carrying a 3′-terminal ribose moiety. The *cis*-diol group of the terminal ribose is selectively oxidised by sodium periodate. The aldehyde groups formed (compound **26**) react with supports containing surface amino [108–111] and hydrazide [112–114] groups.

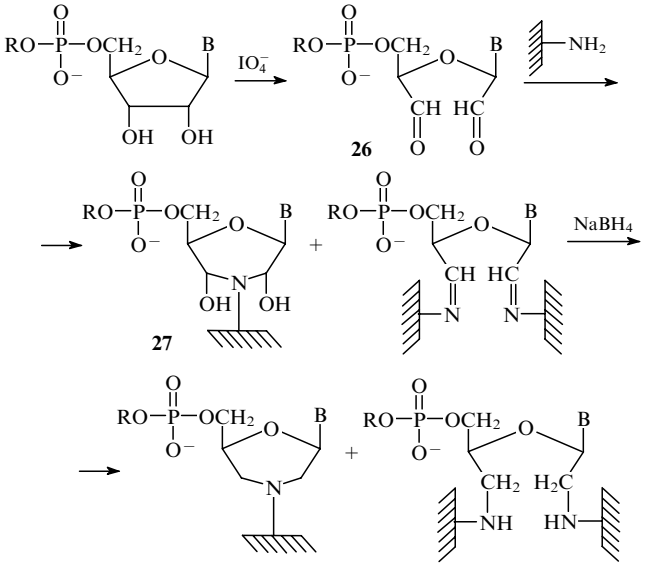

R, ribooligonucleotide, RNA or deoxyoligonucleotide;
B, heterocyclic base.

In this reaction, the dialdehyde can react both with one amino group of the support (to give the morpholine derivative **27** [50, 52]) and with two amino groups leading to bisadducts. Since the derivatives of the type **27** are stable only at pH > 9 and phosphate undergoes β-elimination at pH < 8, they should be reduced with sodium borohydride or cyanoborohydride immediately after preparation.

A decrease in the yield of the immobilisation products can also be due to the cleavage of the 5′-C—O bond in the periodate oxidation product **26** in alkaline media (β-elimination) resulting in the splitting of the modified nucleoside from the 3′-end of RNA.[50]

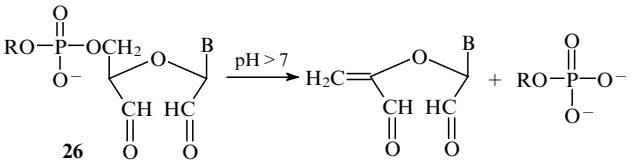

26

Immobilisation on supports containing hydrazide groups occurs with higher yields, since hydrazones do not require treatment with reductants, being more stable than azomethines.[29] It should be noted, however, that the binding of an oligonucleotide to the support through the aliphatic amino group formed upon reduction is stronger [29] than that formed through the hydrazone group.

Reductive amination was used for efficient immobilisation of all ribonucleoside mono-, di- and triphosphates [114–118] on cellulose and agarose (Sepharose) modified by amino or hydrazide groups. The sorbents formed were used in affinity chromatography of proteins, such as myosins [118] and the elongation factors Tu and Ts.[110] Reductive amination is the main technique in immobilisation of ribonucleotides. Polyribonucleotides [poly(A) and poly(U)] following oxidation of the *cis*-glycol groups were attached to polysaccharide supports.[111, 115, 119] Among numerous studies aimed at immobilisation of RNA by this method,[112, 116, 119–121] special mention should be made of those studies [115, 117, 122, 123] in which ribosomal RNA were covalently attached to hydrazide-agarose and used for the isolation and purification of ribosomal proteins. tRNAs immobilised on polysaccharide templates [111, 115, 124] were used for the purification of aminoacyl-tRNA synthases.[125–128]

Recent developments in oligonucleotide synthesis have stimulated studies aimed at the synthesis of oligodeoxyribonucleotides containing a terminal ribonucleoside unit. Its 3′-*cis*-glycol group is oxidised and used for immobilisation of oligodeoxynucleotides on solid supports.[29, 64, 129, 130] The affinity matrices thus prepared are widely used in hybridisation analysis and sequencing of DNA.[42, 43, 45, 131–133]

Immobilisation of NA and their fragments by reductive amination can also be achieved by the introduction of the aldehyde groups into the supports. One can synthesise polymers of virtually any type containing reactive aldehyde groups. The methods of their synthesis will be discussed in Section III.2.i.

f. Immobilisation of nucleic acids containing thiol groups

The introduction of chemically reactive thiol groups into NA and their fragments [53] allows specific immobilisation of such ligands by conventional methods, *e.g.*, on supports containing epoxy groups (Section III.2.b) or active halogen atoms (Section III.2.e).[134] Special procedures can also be used for this purpose. Thiol groups can be introduced in the last step of the phosphoramidite oligonucleotide synthesis, *e.g.*, using commercial phosphorylating reagents, such as phosphoramidites of *S*-protected thio alcohols.[49, 134, 135]

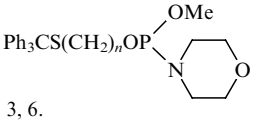

n = 3, 6.

The removal of all protective groups (including the trityl group) by silver nitrate leads to an oligonucleotide containing a

5′-terminal thiol group.[49, 135] Thiol groups can either be introduced into the 3′-end of an oligonucleotide in the initial stage of the synthesis,[16, 136] or incorporated into the isolated oligonucleotide by an enzymic reaction, *viz*., using ATP containing a γ-thiol group.[137]

An alternative approach consists in preliminary incorporation of an easily modifiable aliphatic amino group into the terminal 5′-phosphate group of an oligonucleotide.[90] The reaction of the spacer amino group of the deblocked oligonucleotide with 3,3′-dithiobis-*N*-(propionyloxy)succinimide in the presence of a disulfide bond reductant, *e.g*., dithioerythritol (DTE), dithiothreitol (DTT), cysteine or mercaptoethanol, affords an oligonucleotide containing a thiol group.

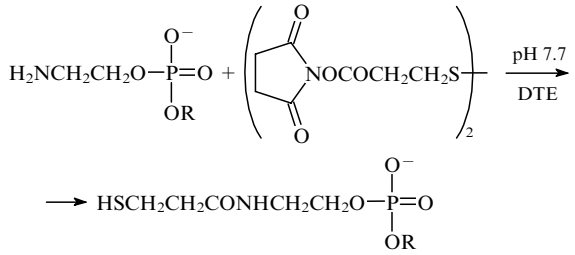

R, oligonucleotide residue; DTE, dithioerythritol.

Oligonucleotides containing thiol groups (SH-oligonucleotides) can be selectively immobilised on solid supports containing thiol groups, *i.e*., through the formation of a disulfide bond. Prior to immobilisation, the thiol groups of oligonucleotides can be activated by 2,2′-dipyridyl disulfide.[6]

If the supports and oligonucleotides contain non-activated thiol groups, the formation of the disulfide bond between NA and the matrix occurs under the action of oxidants (I_2 or H_2O_2).[49] Polysaccharides, glass (CPG),[90] magnetite particles coated with a silicon-containing polymer (Biomag),[49] polyacrylamide (Trisacryl, Sephacryl)[28] and polymethacrylate[6] are widely used as supports. Owing to the ease of the formation and the cleavage of the disulfide bonds by oxidising and reducing agents, thiol matrices are often used for reversible immobilisation of oligonucleotides containing thiol groups.

Immobilisation of purified SH-oligonucleotides proceeds rapidly and specifically. The resulting matrices manifest high stability and purity in hybridisation analysis[28, 49, 90] and in the purification of DNA-dependent proteins.[137] It should be noted, however, that the susceptibility of the thiol groups to oxidation creates storage problems. In the course of time, intermolecular disulfide bonds and side products can be formed. Immobilisation of SH-oligonucleotides on activated or functionalised supports will be considered below (Section III.2.f).

2. Immobilisation of nucleic acids on electrophilic supports

Native non-modified NA and their fragments are immobilised on functionalised and activated supports. Such supports can also be used for immobilisation of NA containing primary aliphatic amino or thiol groups introduced either in the course of or following the synthesis. The methods for the incorporation of the functional groups on the surface of supports able to react with the corresponding groups of the ligand will be discussed below.

a. Activation of supports by cyanogen bromide

A method of the activation of supports containing hydroxy groups by cyanogen halides was first proposed in 1967 for immobilisation of proteins and peptides.[138] The activation is usually carried out by cyanogen bromide at pH 10–11.[139–141] The reactive cyanate **28** formed upon activation reacts with the free hydroxy group of the support to give the reactive cyclic imidocarbonate **29** and the inactive carbamate **30**.[142, 143] A significant contribution to the development of this method was made by Cuatrecasas[144] who has selected the conditions for the immobilisation of various ligands including NA.[145]

In the early 1970's, this method became a routine procedure for the immobilisation of NA.[84, 139, 140, 146–150] The attachment of NA occurs at the amino groups of heterocyclic bases of a polynucleotide. In this way, polyuridylic[147, 149] and polyadenylic[139] acids and RNA[84, 141, 150] have been immobilised. After immobilisation of NA, the remaining reactive groups of the support are blocked by treatment with 1 M 2-aminoethanol.

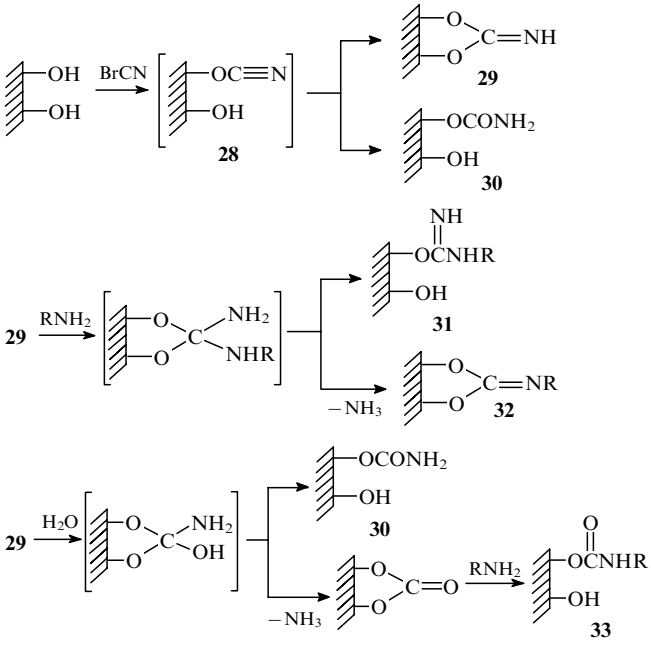

It was shown that the isourea derivatives **31** were the main products formed in the immobilisation of a single-stranded DNA (0.2 mol litre^{-1} of 2-morpholinoethanesulfonic acid, pH 8.0) in formamide[139, 145]; the *N*-substituted imidocarbonates **32** and carbamates **33** are formed in lesser amounts.

This method is most commonly used for the immobilisation of single-stranded DNA[139, 140, 146, 151, 152] and RNA.[84, 139, 141, 150] It was possible to prepare polymeric supports of high capacity and specificity despite possible reaction of the amino groups of heterocycles with activated supports. However, the affinity properties of the sorbents containing short oligonucleotides are weak, since the NH_2 groups of the heterocyclic bases involved in the covalent binding to the polymer cannot take part in the complex formation.

Immobilisation of poly- and oligonucleotides on cyanogen bromide-activated supports is much more selective when the linkers containing aliphatic primary amino groups are attached to either the 5′- or the 3′-end of the oligonucleotide chain[54–58, 153] or the internucleotide phosphate group.[154] However, in this case, too, partial immobilisation of the ligand occurs through heterocyclic bases.[155]

Nucleoside mono-, di- and triphosphates, such as AMP,[156, 157] ADP,[158, 159] ATP,[160] UMP,[58, 161] GTP[58] and dCp_4 (see Ref. 162), were immobilised on cyanogen bromide-activated Sepharose (all the nucleotides contained linkers with primary aliphatic amino groups incorporated into the phosphate groups or the heterocyclic bases). These sorbents were used for the purification of ribonucleotide reductase of phage T4,[160] the cap-binding protein[163] and deoxynucleotide kinase of *Lactobacillus*.[162]

The disadvantages of this method are as follows. First, immobilisation of the ligand must be carried out immediately after the activation of the support because of the low stability of the reactive groups formed upon treatment with cyanogen bromide. Second, cyanogen bromide is a toxic substance. Third, the basic isourea groups of the support **31** (pK_a = 9.5) formed by the reaction with the primary amine appear to be positively charged at physiological pH values, which confers undesirable anion-exchanging properties on such affinity sorbents. Moreover, this reaction yields numerous side products, while the binding sites of

nucleotides cannot be determined with certainty. On storage, the ligand is gradually split off from the polymeric support.[113, 146, 164] It was shown [153] that affinity matrices prepared by immobilisation of oligothymidylates containing 5′-terminal amino groups on cyanogen bromide-activated cellulose retain their stabilities in aqueous media during one week at 22 °C and for only 24 h at 42 °C. Most probably, this is due to the instability of the *N*-substituted isourea derivatives **31**.[143]

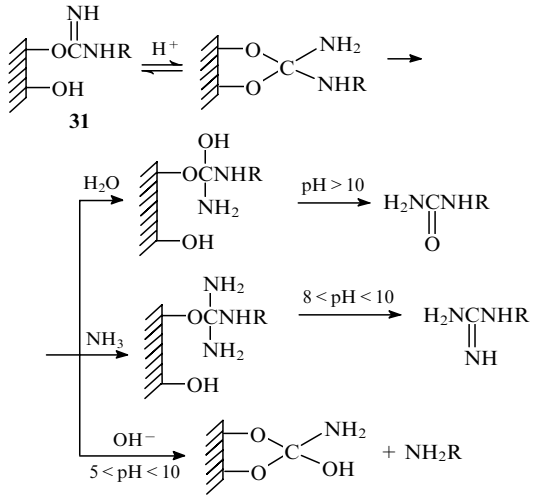

However, despite these drawbacks this method is widely employed for the immobilisation of DNA, RNA and synthetic oligonucleotides [165–170] aiming at the preparation of affinity matrices which are further used for the isolation and purification of DNA-dependent proteins.

b. Activation of supports by oxiranes

Bifunctional oxiranes were first recommended for the incorporation of reactive groups into polymeric supports and the stabilisation of gels by cross-linking.[171] The hydroxy groups of supports are usually activated by the diglycidyl ether of 1,4-butanediol at pH > 7.0.[37, 172, 173] This treatment affords a polymer containing reactive epoxy groups, which react with the nucleophilic groups of the ligands.

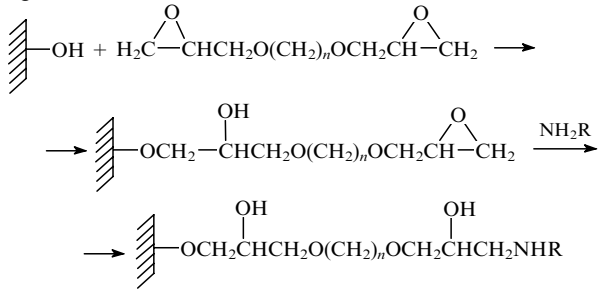

Epichlorohydrin is also used for the preparation of supports containing epoxy groups.[78, 107, 114] At present, epoxy groups are often incorporated on silica gel [3, 174] and glass [15, 175] using trimethoxysilanes **2** rather than polysaccharides.

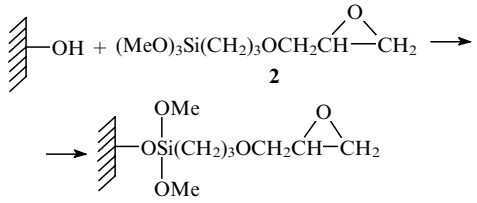

As a rule, immobilisation of ligands containing amino, hydroxy or other nucleophilic groups on the supports containing epoxy groups occurs smoothly at pH 9–13 (8–20 h, 20–25 °C). The unconsumed epoxy groups are blocked by treatment with 2-aminoethanolamine (1 mol litre^{-1}). This method was used for the covalent binding of polynucleotides and some DNAs.[37, 172, 173, 176] The efficiency of binding of polynucleotides changed in the series: poly(dT) > poly(dC) = poly(dA) > poly(dG).[172] As nucleotides usually contain many functional groups, the exact binding site for polynucleotides is difficult to establish and therefore this is not always specified.[172, 173] For example, it is believed [37] that the immobilisation of the C(8)-hydroxyethylthio derivative of cyclo-AMP on a polymeric support containing epoxy groups is achieved by its binding through the terminal hydroxy group of the linker.

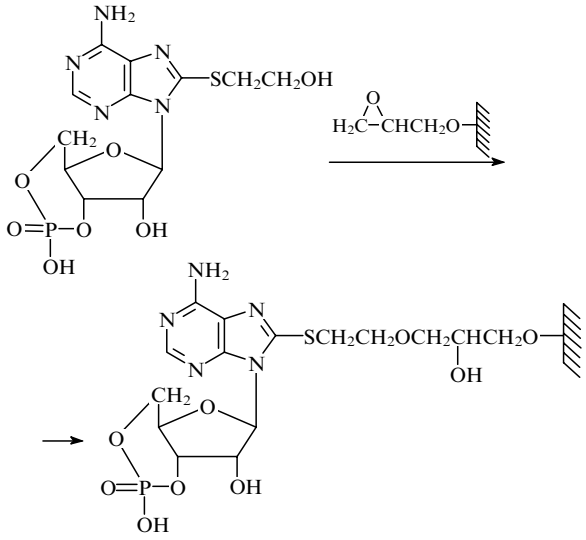

It was shown that the immobilisation of oligodeoxyribonucleotides in concentrated (2.7 mol litre^{-1}) potassium phosphate occurs predominantly through purine bases.[177] Despite its obvious advantages over other methods, this method has only one disadvantage, *viz*., the uncertainty of the binding site of nucleic acids. The use of an extended bisoxirane reagent ensures the introduction of a long uncharged hydrophilic arm between the ligand and the polymer surface, which is especially convenient for chromatography of large biomolecules. The affinity sorbents prepared on such supports are rather stable, since the ligand is attached through an ether bond, and the immobilisation is not accompanied by non-specific sorption of biopolymers.[15, 171] Immobilisation of biologically active ligands on mechanically stable silica gels containing epoxy groups allows preparation of matrices for high-performance affinity chromatography. It should be remembered, however, that some supports are unstable in alkaline media where such immobilisation takes place.

c. Supports containing *N*-hydroxysuccinimide groups

The idea to use *N*-hydroxysuccinimide esters as reactive groups for the formation of amide bonds with the primary amino groups of ligands was first formulated and realised in studies devoted to peptide synthesis.[178, 179] High solubility of *N*-hydroxysuccinimide in water and organic solvents makes it a convenient reagent for the activation of various polymeric surfaces.

The supports containing esterified *N*-hydroxysuccinimide **34** are obtained by treating the polymers containing terminal carboxy groups with *N*-hydroxysuccinimide in the presence of dicyclohexylcarbodiimide (DCC) in dry solvents.[26, 180]

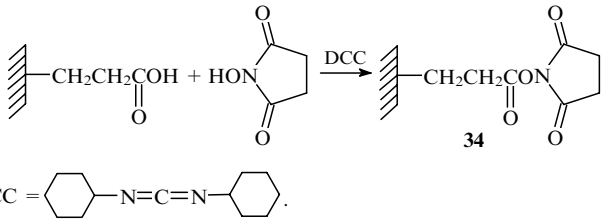

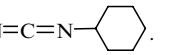

Bifunctional reagents, *e.g*., *N*,*N*′-disuccinimidyl carbonate (**35a**) or *N*-succinimidyloxycarbonyl chloride (**35b**), are used for

the activation of supports containing hydroxy or amino groups.[22, 181]

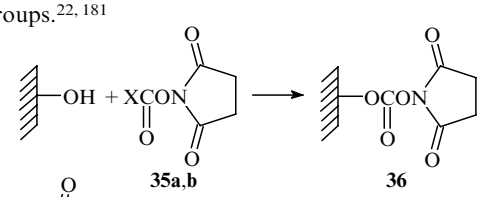

35a,**b** **36**

X = 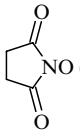 NO (**a**), Cl (**b**).

The *N*-hydroxysuccinimide esters **34** and **36** react rapidly with oligonucleotides containing aminoalkyl groups at the 5′-terminal phosphate (**37a**–**d**) or in the heterocyclic bases in buffer solutions (pH 7.5–9.0) resulting in the formation of stable amide bonds.

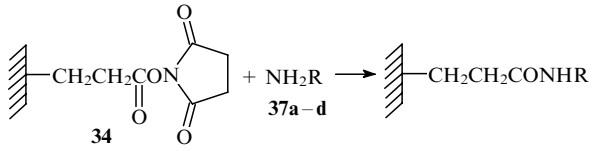

34 **37a**–**d**

R = $(CH_2)_6NH(pT)_{29}$ (**a**), $(CH_2)_2SS(CH_2)_2NH(pN)_{29}$ (**b**), $(CH_2)_{12}O(pCTT)_7$ (**c**), $(CH_2)_2O(pT)_{18}$ (**d**).

It was shown [65] that immobilisation of a 29-membered oligonucleotide occurs predominantly through the amino group of 6-aminohexyl linker attached as 5′-phosphoramidates (**37a**). Immobilisation through the cystaminyl linker (**37b**) is less efficient, while binding through the amino group of the heterocyclic bases proceeds to a smaller degree. Unfortunately, the capacity of the affinity sorbents thus obtained does not exceed 1 nmol g^{-1} at best, apparently, due to rapid hydrolysis of the activated ester **34**. The efficiency of immobilisation is higher in non-aqueous media where competitive hydrolysis is reduced to a minimum.

Hydrolysis of the reactive surface groups of the support **34** yields carboxy groups which confer ion-exchange properties on the affinity sorbent, while unconsumed groups of the activated support **36** are gradually hydrolysed to regenerate the starting groups.

An interesting approach to the immobilisation of double-stranded fragments of DNA on *N*-hydroxysuccinimide-activated Sepharose has been proposed.[31, 182] A 39-membered oligonucleotide was synthesised with a hairpin and a 1,6-diaminohexane unit was introduced into a heterocyclic base of the hairpin loop. The incorporated amino group was used for the attachment of the oligonucleotide to the polymer. Any double-stranded DNA fragments containing the corresponding sticky ends can be bound then to the immobilised oligonucleotide using DNA-ligase.

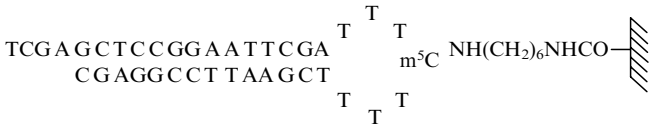

Supports with immobilised poly- and oligonucleotides were used in hybridisation analysis [21, 22, 183] and affinity chromatography.[7, 26] Thus the amino-containing oligonucleotide $(CTT)_7$ **37c** was immobilised on Sepharose and this sorbent was used for the isolation of plasmid pXL2563 containing GAA sites due to triplex formation.[7] Column chromatography on silica gel containing immobilised 5′-aminoethyloctadecathymidylate (**37d**) was successfully used for the separation of a mixture of adenylates A_{12}–A_{18}.[26]

d. Diazotised supports

The azo coupling reaction has long attracted the attention of investigators engaged in immobilisation of nucleotides, since the introduction of aromatic amino groups into the support can be performed under mild conditions. Different approaches to the synthesis of polymers containing aromatic amino groups are shown in Scheme 1.[144, 184–186] Such supports are usually prepared by the reduction of the corresponding aromatic nitro compounds.[187] Diazotisation of aromatic amino groups is carried out with sodium nitrite in acidic media.

Immobilisation of native nucleic acids on diazotised supports, such as compounds **38a**–**d** (see Scheme 1), involves exclusively heterocyclic bases.[25, 67, 184] The introduction of spacer groups into oligonucleotides, *e.g.*, the introduction of phenol residues into 5′-phosphate groups, results in the predominant (up to 87%) immobilisation at this particular group.[188]

Scheme 1

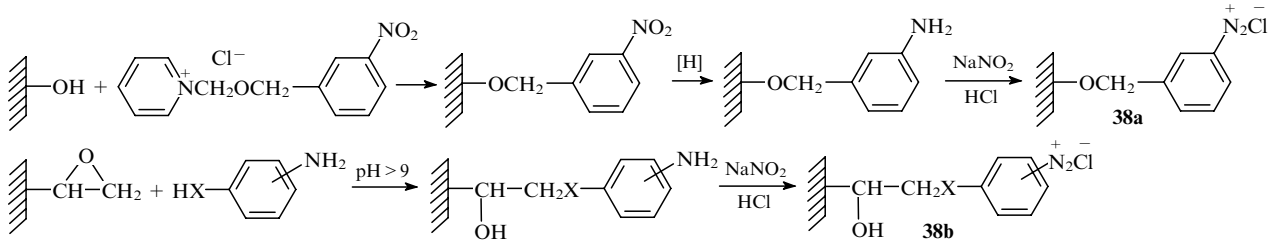

X = NH, S.

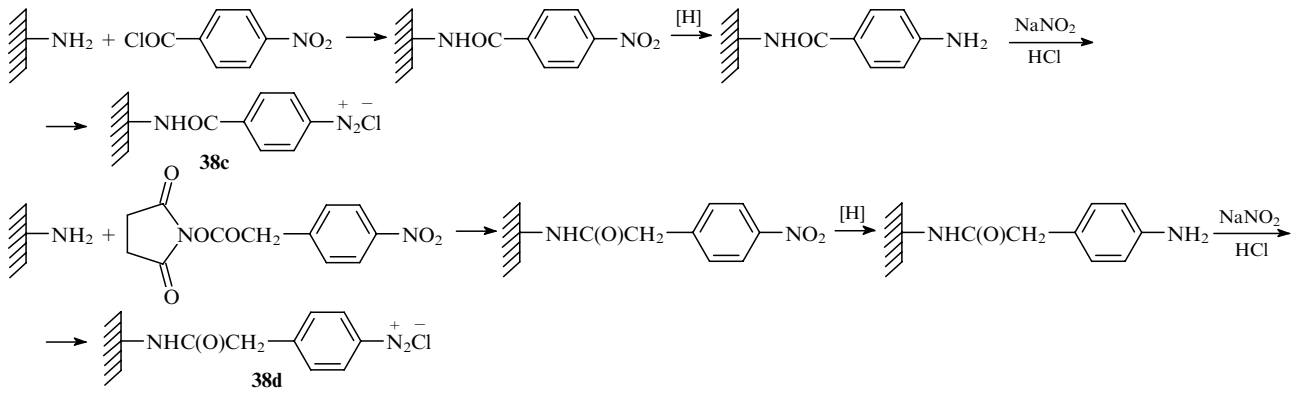

The azo coupling reaction consists in electrophilic substitution where the diazonium ion plays the role of an attacking agent. This reaction can be visually monitored by following colouration of the support. Immobilisation of 5′-AMP (**39**) at the C(8) atom of the heterocyclic base on agarose containing diazo groups is an example.[189]

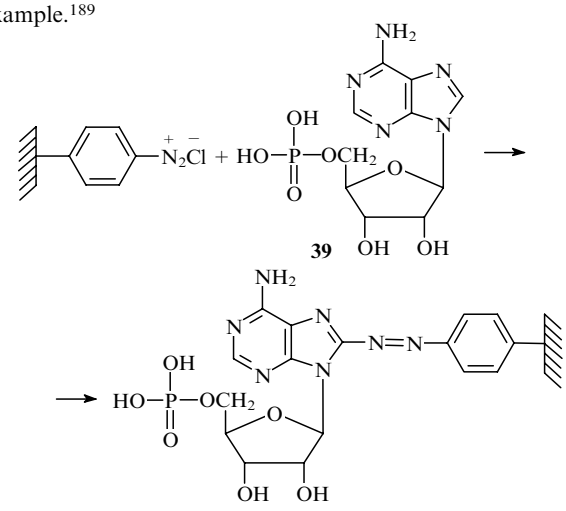

Azo coupling can be accompanied by the reaction of diazonium salts with the amino groups of heterocyclic bases, which affords a diazoamino compound.[190]

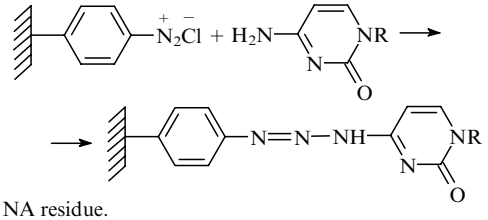

R, NA residue.

In addition to reactions of diazonium salts with heterocyclic bases of nucleic acids, side reactions with water (to give phenols) and aromatic amino groups which are always present on the surface of such supports can also take place. If azo couping occurs at a slow rate, the formation of phenol and the cross-linking of the polymeric support can predominate.[185]

Aromatic diazo compounds are rather unstable, they decompose at elevated temperatures and upon illumination. Therefore, diazotised supports are used immediately after their synthesis. They can also be treated with $NaBF_4$ or $NaPF_6$ to give more stable tetrafluoroborates or hexafluorophosphates.[185]

Denatured DNA and RNA immobilised by this method were used mostly in hybridisation analysis.[184, 185, 191] Good results were obtained with the use of supports **38b** (see Scheme 1) containing diazophenylsulfide groups.[140] Immobilised cyclic DNA was used as a template in an asymmetric polymerase reaction.[192]

The efficiency of immobilisation on diazotised supports is differently estimated by different authors, *viz*., from 795 μg of the nucleotide per 1 g of the support [146] to trace amounts.[25] Affinity sorbents prepared by azo coupling are usually unstable. Up to 50% of immobilised DNA is lost within the first 2–3 days at 45 °C irrespective of the nature of the matrix.[146] Low non-specific sorption of biopolymers on diazotised supports is their main advantage.

Cellulose or paper filters containing diazo groups are most commonly used for immobilisation of DNA; however, Sephacryl proved to be the best polymer for such immobilisation.[67] Magnetic particles were also tested, however, with little effect.[25]

e. Supports containing active halogen atoms

Activation of oligonucleotides by 2,4,6-trichloro-1,3,5-triazine (**24**) was considered in Section III.1.d. In this section, we shall consider the preparation of supports activated by 2,4,6-trichloro-1,3,5-triazine and their use for the immobilisation of ligands. The reactions of polynucleotides and NA with non-modified polysaccharides (cellulose and dextran) in the presence of 2,4,6-trichloro-1,3,5-triazine (**24**) [107] which permit consecutive substitution of chlorine atoms will also be discussed.

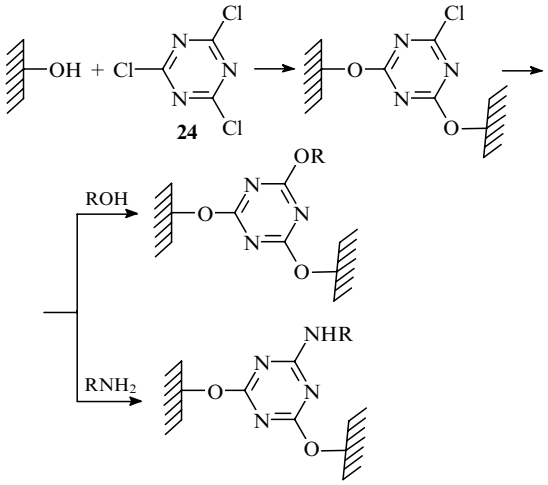

R, NA or oligonucleotide residue.

When the activation is carried out in an alkaline medium, two chlorine atoms react with the hydroxy groups of the supports resulting in the binding of triazine to the polymers. The third chlorine atom remains intact and can be substituted by the amino or hydroxy groups of the ligand to be attached.[193, 194] It was shown that immobilisation of DNA using 2,4,6-trichloro-1,3,5-triazine involves predominantly the amino groups of the heterocyclic bases.[107] As a result, the multipoint binding of DNA and oligonucleotides to the polymer makes the ligand less accessible for the interaction with the complementary polynucleotides in solution. Immobilisation of oligonucleotides bearing an amino group-containing linker at the 5′-end occurs selectively through the introduced amino group.[107, 194] However, even in this case the yields of the addition products are rather low due to the low accessibility of the chlorine atom in the triazine-containing support.

In order to increase the efficiency and selectivity of the method, it was suggested to activate the supports by 2-amino-4,6-dichloro-1,3,5-triazine (**40**).[142, 193]

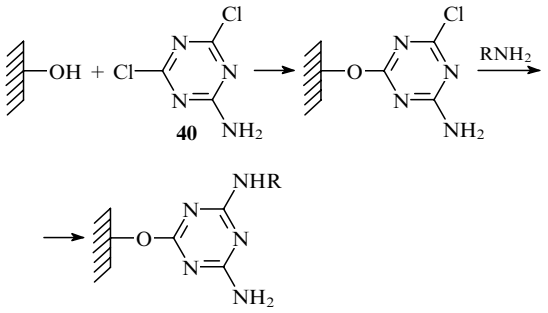

R, oligonucleotide residue.

The presence of an amino group in the triazine **40** decreases the reactivity of one of the chlorine atoms with respect to nucleophilic attack and thus prevents cross-linking of the polymer. The remaining chlorine atom reacts exclusively with strong nucleophiles, *e.g*., with the aliphatic amino group of the spacer introduced into an oligonucleotide.[193]

Triazine-activated polymers are fairly stable at elevated temperatures and can be stored for several weeks at 4 °C. The use of matrices with immobilised DNA or poly(U) made it possible to isolate both proteins and the complementary chains of NA.[193] However, application of this method is restricted by the high toxicity of trichlorotriazine.

The carboxy groups of polyethylene terephthalate films can easily be converted into acid halide groups upon treatment with PCl_3, PCl_5, $POCl_3$, $SOCl_2$ or $(COCl)_2$ in the presence of DMF.

The polymers **41** containing acid halide groups react with the nucleophilic groups of the ligands. Immobilisation carried out under anhydrous conditions involves predominantly primary amino groups of the spacer incorporated into the 5′-terminal phosphate groups of oligonucleotides.[195] The stability of the sorbents **42** is provided by the stability of the amide bond formed. The films containing immobilised oligonucleotides obtained by this method were successfully used in hybridisation analysis.[196]

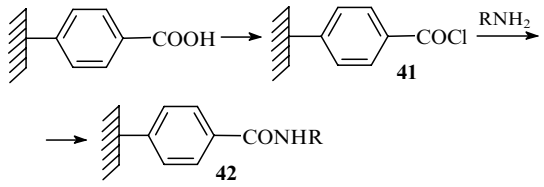

R, NA or oligonucleotide residue.

A chloromethylated styrene–divinylbenzene copolymer can also be used for the immobilisation of ligands. This approach was used for the attachment of 5′-ATP through the triphosphate residue.[197]

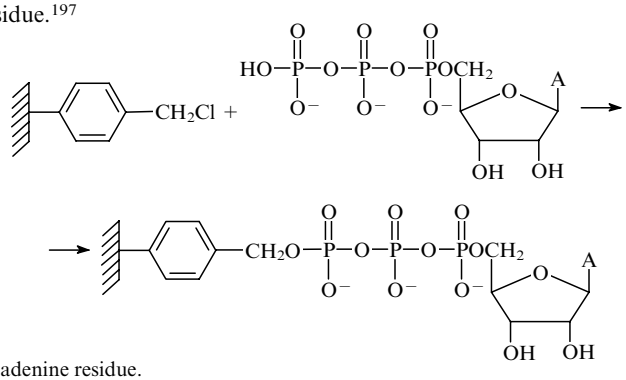

A, adenine residue.

Halogenoacetyl agarose has become especially popular among commercially available supports containing active halogen atoms (see Table 2). This sorbent is resistant to hydrolysis; therefore, the immobilisation procedure can be carried out in aqueous buffers. The best results were obtained in the case of immobilisation of oligonucleotides containing thiol groups. To prevent attachment at heterocyclic bases, the SH-containing oligonucleotide obtained with the use of T4 kinase and γ-thiol-ATP was hybridised with the complementary chain.[137] The duplex formed was attached to bromoacetyl agarose. The immobilisation occurred exclusively at the 5′-terminal thiolphosphate group of the oligonucleotide. If required, the complementary chain could be removed.

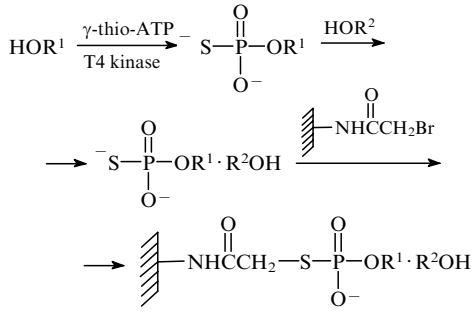

R^1,R^2, complementary oligonucleotide residues.

f. Activated supports for the immobilisation of SH-containing oligonucleotides

Immobilisation of NA and their fragments containing thiol groups on supports containing epoxy groups or active halogen atoms[134] has been described in Sections III.2.b and III.2.e, respectively. SH-containing ligands can also be immobilised using other methods.

Oligonucleotides containing thiol groups can selectively be immobilised on solid supports containing thiol groups owing to the formation of disulfide bonds. The supports are pretreated with *p*-chloromercuribenzoate, di(3-ethoxycarbonyl-4-nitrophenyl) disulfide, 2,2′-dipyridyl disulfide or 2,2′-dithiobis(5-nitropyridine).[90, 144]

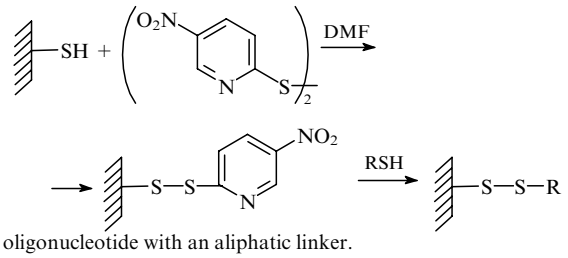

R, oligonucleotide with an aliphatic linker.

High thiophilicity of mercury ions allows the attachment of SH-containing oligonucleotides to modified polymers (*e.g.*, to agarose) containing HgCl groups.[90]

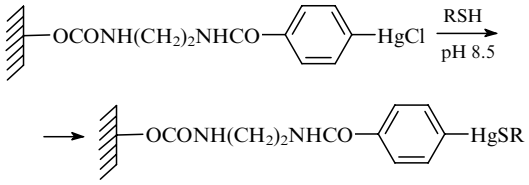

R, oligonucleotide with an aliphatic linker.

The reaction of the thiol groups with the maleimide residues present on the polymer surface is yet another approach to the immobilisation of SH-containing oligonucleotides. Maleimide can be incorporated into virtually all materials containing primary amino groups using succinimidyl 4-(maleimidophenyl)butyrate (**43**) or maleic anhydride.[11, 16, 136]

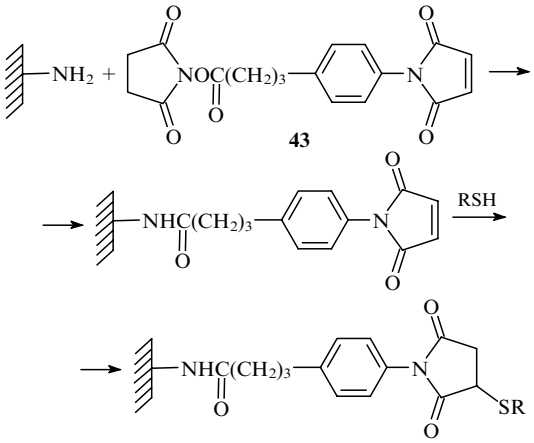

The nucleophilic addition of SH-containing oligonucleotides to the double bonds of the support **44** in a buffer solution occurs rapidly (2 h at 4 °C) resulting in the formation of a stable bond between the support and an oligonucleotide.

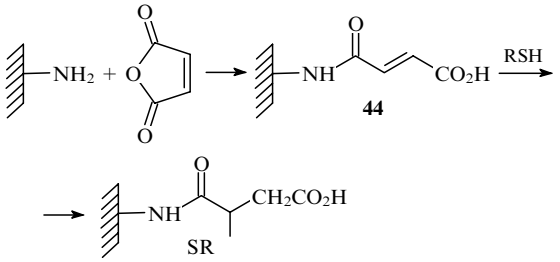

R, oligonucleotide residue.

g. Activation of supports by carbonyldiimidazole

Hydroxy and carboxy groups of supports can easily be activated by *N*,*N*′-carbonyldiimidazole (**45**). This reagent earlier proposed for peptide synthesis [198] is now successfully used for the immobilisation of ligands containing primary amino groups.[199, 200]

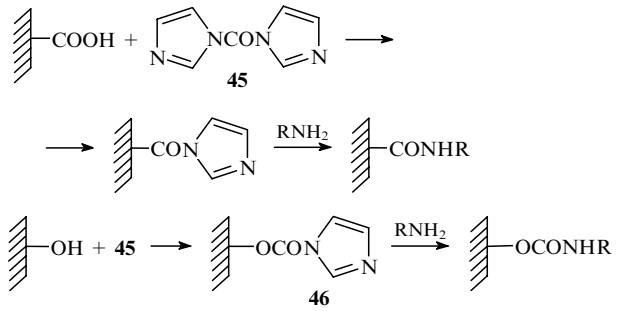

R, oligonucleotide residue.

The activation of polymers is performed in non-aqueous media; the optimum conditions for the immobilisation of ligands must be selected for each particular case. The high efficiency of the ligand attachment in dry solvents is due to the lack of competitive hydrolysis. Affinity matrices prepared by this method are rather stable, since the amide bond formed between the support and the ligand is very strong. The support **46** is stable in dry solvents for several years. The half-life time of the hydrolysis of imidazolyl carbamate **46** is several hours. Thus activated agarose loses completely its activity in aqueous buffers only after 30 h at pH 8.5–9.0.[200] Following elimination of CO_2 and imidazole, the support **46** is converted into the original hydroxyl-containing carrier devoid of charged groups, which excludes the manifestation of ion-exchange properties of the support and non-specific sorption of biomolecules. It is noteworthy that the half-lifetime of the hydrolysis of cyanogen bromide- or hydroxysuccinimide-activated supports is several minutes.

However, despite the advantages of the above-described imidazole-containing supports the immobilisation of, *e.g.*, 6-aminohexylphosphoryl-dCTP and 5′-aminoalkyloligonucleotides, occurs with low yields.[3, 201] This method has not found wide application for the immobilisation of NA and its fragments.

h. Activation of supports by sulfonyl chlorides

Organic sulfonyl chlorides, such as *p*-toluenesulfonyl chloride (TsCl), 2,2,2-trifluoroethanesulfonyl chloride (TrsCl) and methanesulfonyl chloride (MsCl), are potent acylating agents, which convert hydroxy groups of a carrier into reactive sulfonates to afford the supports **47**–**49**.[202–204]

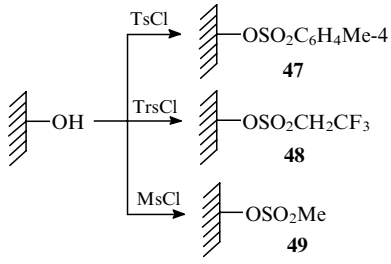

TsCl = $ClSO_2C_6H_4Me$-4, TrsCl = $ClSO_2CH_2CF_3$, MsCl = $ClSO_2Me$.

Immobilisation of oligonucleotides on the supports **48** [205] and **49** [29] occurs exclusively through the amino group of a spacer attached to the 5′- or 3′-end of the oligonucleotide. In the absence of aminospacers, immobilisation through heterocyclic bases and terminal phosphate groups of oligonucleotides proceeds with lower yields. Immobilisation on the support **49** occurs with low yields,[29] whereas polymers **48** are used for the preparation of affinity sorbents with high capacities; these are used for purification of DNA-dependent proteins.[205] The sulfonate residues are good leaving groups and the reactivities of the activated supports depend on the nature of the sulfonate and decrease in the following order: Trs > Ts > Ms. Thus, the support **49** is the most stable and the least reactive. The supports **47**–**49** are stable in non-aqueous media and can be stored for several weeks at 4 °C in aqueous HCl (1 mmol litre^{-1}) without any loss in their activities. Immobilisation of NA containing thiol or primary amino groups on sulfonyl chloride-activated supports occurs as the nucleophilic substitution of the sulfonate residue with the formation of a stable bond between the nucleophile and the carbon atom of the original support. The attachment of the ligand can be carried out in both aqueous and organic media. Immobilisation on the more reactive polymers **48** is more efficient at neutral pH values at 4 °C, whereas that on the carriers **47** is better performed at pH 9–11.[204]

i. Supports containing aldehyde groups (reductive amination)

Immobilisation of NA and their fragments by reductive amination can be carried out using two approaches. The first of them consists in the introduction of the aldehyde groups into NA and their subsequent immobilisation on supports containing hydrazide or primary aliphatic amino groups (see Section III.1.e). The second approach includes the incorporation of aldehyde groups into supports and their subsequent application for the immobilisation of NA through the amino groups of heterocyclic bases or through introduced spacer groups. The latter version is considered in this section.

Aldehyde groups can be introduced into supports by different methods. Polysaccharide supports containing diol groups are oxidised by sodium periodate to give the modified polymer **50** with high content of the aldehyde groups. The supports devoid of hydroxy groups are modified by glutaraldehyde (**51**), glycidol (**52**), an oligomer containing aldehyde groups (**53**) or compounds which are further oxidised by periodate. Some examples of preparation of polymers of virtually any type containing aldehyde groups are shown in Scheme 2.

The aldehyde groups of the polymer react readily with ligands containing primary amino groups to give Schiff's bases. The latter are further reduced by $NaBH_4$, $NaBH_3CN$ or the pyridine–borane complex ($Py \cdot BH_3$). Unlike sodium borohydride, the last two reagents rapidly reduce the Schiff's bases, but not the aldehyde groups.[29, 206] It should also be noted that $NaBH_4$ is decomposed in acidic media, whereas $NaBH_3CN$ functions effectively at pH 4–10. It was recommended to replace highly toxic $NaBH_3CN$ by the $Py \cdot BH_3$ complex.[29]

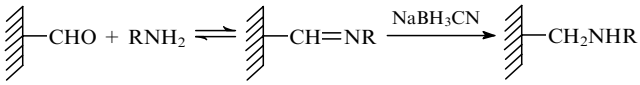

Oligonucleotides with incorporated aminospacers are immobilised in good yields on supports containing aldehyde groups to form strong bonds.[11, 12, 29, 30] However, this is accompanied by the addition of oligonucleotides through the amino groups of the heterocyclic bases. Especially strong non-specific immobilisation was observed in the case of supports activated by glutaraldehyde (**51**).[29]

The glutaraldehyde **51** is used to prepare affinity sorbents with a high content of NA. This reagent brings about cross-linking of the polysaccharides with nucleotides and NA (DNA, RNA [207], NAD [208]) through primary amino groups of the modified carriers (aminoethylcellulose,[207] aminohexylsepharose [208]) and the heterocyclic bases. High concentrations of the ligand on the carrier results from additional intramolecular cross-linking of the ligand, which is often a drawback, especially in affinity chromatography.

Scheme 2

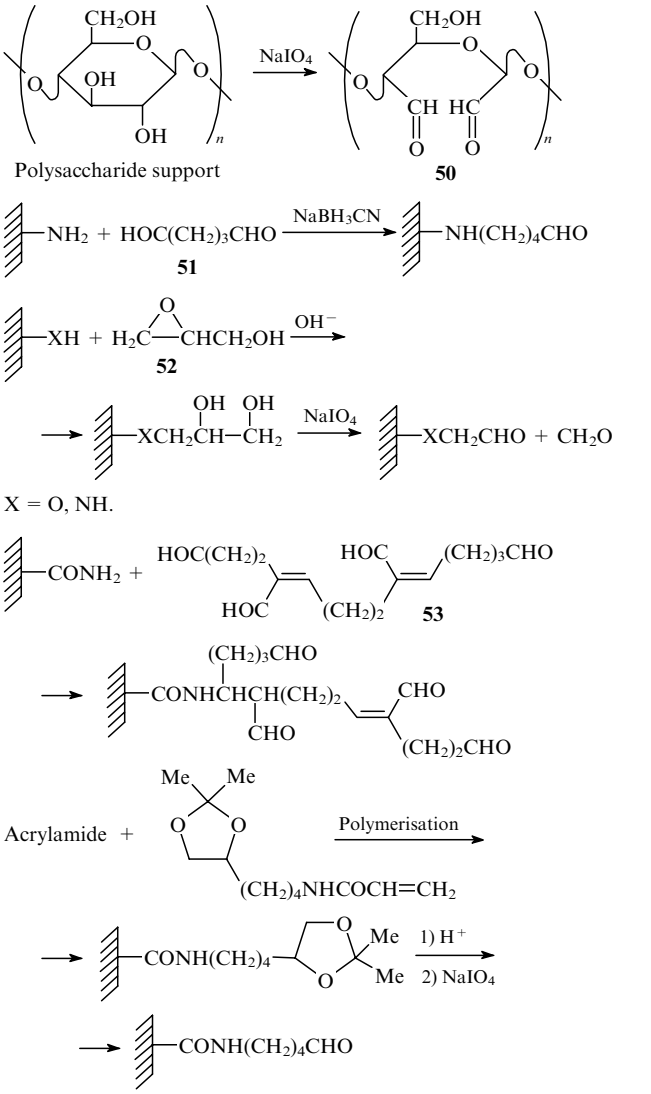

j. Supports bearing isothiocyanate groups

The isothiocyanate group is yet another functional group which rapidly reacts with aliphatic primary amino groups to give stable thiourea derivatives. 1,4-Phenylene diisocyanate can be used for the activation of virtually all polymers containing primary amino groups.[17, 19, 22] Immobilisation of oligonucleotides on isothiocyanate-containing supports occurs with good yields[17, 19] and is not accompanied by immobilisation of non-modified oligonucleotides.[19, 22] The remaining isothiocyanate groups of the activated carrier undergo gradual hydrolysis to amino groups, which imparts ion-exchange properties to the affinity matrices.

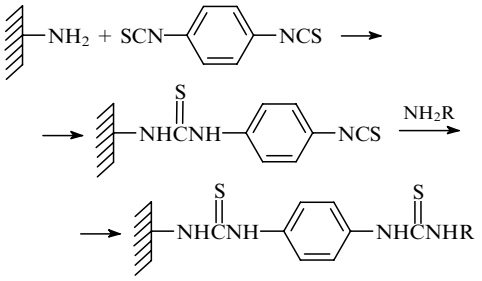

3-Isothiocyanatopropyltriethoxysilane [209] or 1-(3-trimethoxysilylpropyl)-3-(4-isothiocyanatophenyl)thiourea [19] can be used for the modification of glass surfaces. This one-step procedure is used for the preparation of glasses bearing reactive isothiocyanate groups.

k. The four-component condensation

The Ugi reaction is a multicomponent condensation leading to *N*-alkylamides under mild conditions [171, 210–212] and involves α-addition of electrophilic compounds containing C=N bonds to isocyanides **54**. The immonium salt **55** formed in the reaction of a carboxylic acid with an amine and an aldehyde or a ketone is added to isocyanide. Intramolecular acylation affords the final product **56**.

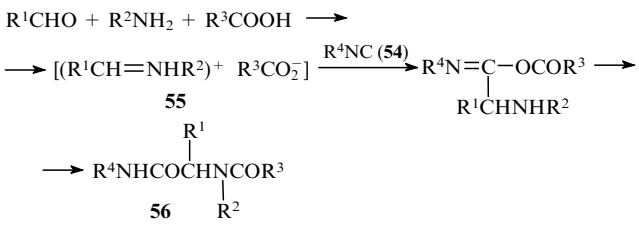

The three soluble reactants may be varied depending on the nature of the functional groups (isocyanide,[201] carboxy, aldehyde or amino groups [212]) present on the support surface.

The reaction of 5′-AMP with Sepharose modified by 4,4′-diaminodiphenylmethane in the presence of cyclohexyl isocyanide and acetaldehyde is an example of the Ugi reaction employed for the preparation of modified supports.[171, 212, 213] In this case, the role of an anion of the immonium salt **55** is played by the phosphoric acid residue of 5′-AMP and not by the carboxy group (Scheme 3).

The best results (39 mg g^{-1}) were obtained in the immobilisation of RNA on Sepharose containing amino groups.[212] However, this method has not found wide application due to the side reactions between the functional groups of the nucleotides and the components of this complex system.

Scheme 3

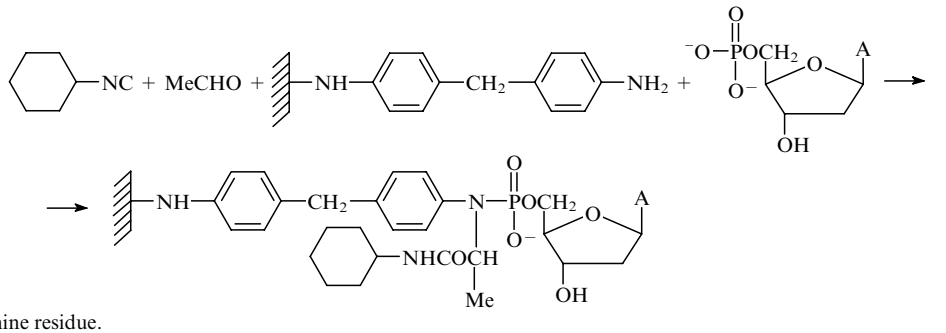

A, adenine residue.

IV. Immobilisation of nucleic acids in the course of solid-phase synthesis

The development of automated methods for oligonucleotide synthesis offered new opportunities for the preparation of affinity matrices bearing covalently bound oligonucleotides. The carriers on which oligonucleotides are synthesised can be used as affinity sorbents. This obviates the necessity of removal of the nucleotide material from the carrier and its further immobilisation on the support. However, one essential step, *viz*., purification of the newly synthesised oligonucleotide and the estimation of the quality of the immobilised material, is lost.

The last step in any solid-phase oligonucleotide synthesis includes the removal of protective groups from the heterocyclic bases and splitting of the nucleotide material from the support by treatment with concentrated ammonia. Elimination of the nucleotide material under deblocking conditions can be excluded if oligodeoxythymidylates [214] devoid of protective groups are synthesised or if supports are used containing primary aliphatic amino [8, 22, 215] or hydroxy [1, 216–218] anchor groups or the hydroxy groups of preliminarily attached nucleosides.[31, 219] Oligonucleotide synthesis on such supports results in the formation of an ether bond resistant to ammonia. Monomers containing non-conventional protective groups of heterocyclic bases are also used in the synthesis of affinity sorbents; their removal requires milder conditions,[220] which do not cause the destruction of the ester bond between the support and the nucleotide residue.

In addition to macroporous glass [8, 31, 214, 216, 217, 220] and glass slides,[22] polyacrylmorpholide,[31] polypropylene,[215] silica gel [31] and Teflon copolymers [216] are used as supports for oligonucleotide synthesis. The affinity matrices based on them manifest good hybridisation properties [8, 215, 217] and can be used for the isolation of mRNA [214] and DNA-specific proteins.[216]

The advantages and disadvantages of different supports in the synthesis of oligonucleotide libraries (combinatorial synthesis) have been reviewed in detail.[218] TentaGel (polyoxyethylene-coated polystyrene beads, Rapp Polymere GmbH) and Merck-Gel [partially hydrolysed poly(vinyl acetate), Merck KgaA] were recognised as the best granulated carriers. Their capacities with respect to the first fragment (nucleoside) are 120 and 700 μmol g^{-1}, respectively (*cf.* 30–50 μmol g^{-1} for conventional supports); the elongation of the oligonucleotide chain occurs also with high yields.

At present, new procedures and equipment for oligonucleotide synthesis on films and glass slides used as DNA chips and DNA sensors are being developed (see Section VII.2.b).

V. Miscellaneous methods of immobilisation of nucleic acids

Physical and physicochemical methods have been used for the immobilisation of NA earlier than other methods. Adsorption, UV irradiation and mechanical incorporation into different gels are especially popular nowadays.

Adsorption of DNA on cellulose is a very simple and rather widespread procedure which consists in freeze-drying [221–223] or conventional drying [222, 224] of cellulose impregnated with solutions of NA. The DNA-cellulose thus prepared is successfully used for purification of DNA-dependent proteins. However, such DNA-cellulose is not always suitable for hybridisation of NA because of instability of the nucleotide material at elevated temperatures and its easy desorption in buffers of low ionic strength. Nevertheless, non-covalent sorption of DNA fragments on nitrocellulose filters is a very popular procedure for the preparation of samples for hybridisation analysis [225] despite its obvious disadvantages, such as the loss of the nucleotide material during multistage hybridisation assays, fragility of cellulose after vacuum treatment, *etc*.

The development of polymerase chain reaction (PCR) and the advent of new methods of hybridisation assay brought forth the need for rapid immobilisation of NA fragments on the surface of microplates. Adsorption of oligonucleotides on such surfaces is carried out in the presence of high salt concentrations (NaCl, tetramethylammonium chloride) and/or cationic detergents (cetyltrimethylammonium bromide, dimethyloctylamine hydrochloride).[88, 226–229] Presumably, in this case immobilisation occurs exclusively by virtue of hydrophobic interactions between the oligonucleotides and the support surface.[88] It was noted [22] that adsorption is selective as regards surfaces which possess hydrophilic properties.[226] Although the mechanism of such immobilisation is not completely understood, the samples prepared by this method are widely used in hybridisation assays.[88, 227, 228]

Yet another procedure consists in the application of polyelectrolyte films onto glass surfaces and the sorption of DNA or polynucleotides occurs owing to ion-exchange interactions.[230, 231]

Nucleic acids and their fragments can be immobilised on different supports upon irradiation with UV light.[155, 222, 223, 232–235] Side reactions occurring in the ligands are not significant and do not prevent the application of these systems in affinity chromatography of proteins and enzymes.[222, 232, 234] The use of specially prepared photosensitive supports, *e.g*., cellulose [236] or microporous Nylon 6 [237] containing aryl azide residues, increases significantly the maximum capacity and efficiency of photoimmobilisation of NA. The sensitivity of hybridisation assays with these matrices is 2- to 4-fold higher than that obtained with matrices prepared by conventional sorption on nitrocellulose. This may be ascribed to mild immobilisation conditions which do not affect the structure of NA.

Nucleic acids or their fragments can be immobilised on polyacrylamide,[238, 239] agar [240] or on glass slides bearing the acrylamide groups,[20, 241] which allows the preparation of sorbents with high content of the nucleotide material. The advantage of this method is that the immobilisation can be carried out on virtually any surface.[241, 242]

To ensure higher selectivity of immobilisation, copolymerisation is carried out with oligonucleotides functionalised with groups containing multiple bonds (*e.g*., pyrrolyl,[242] allyl [20] or acrylamide [241]).

$$NH_2C(O)CH{=}CH_2 + CH_2{=}CHC(O)NH(CH_2)_nR \xrightarrow{\text{Polymerisation}}$$

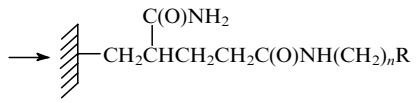

R, oligonucleotide residue.

VI. Immobilisation of nucleic acids using enzymes and avidin–biotin interactions

Recently, streptavidin- or avidin-containing sorbents have gained wide acceptance for the attachment of biotin-modified DNA or oligonucleotides. In these matrices, immobilisation of oligonucleotides is achieved due to the formation of a stable avidin–biotin complex ($K_d \approx 10^{-15}$ mol litre^{-1}) rather than a covalent bond. Such sorbents are easily and rapidly prepared by mechanical mixing of a streptavidin carrier and a biotin-modified oligonucleotide and used for the isolation of proteins and enzymes,[35, 36, 243–246] DNA sequencing [34, 247] and hybridisation assays.[248, 249] However, these sorbents possess a number of disadvantages, such as non-specific sorption of proteins which is more pronounced in the case of avidin-containing matrices,[250, 251] than in the case of streptavidin supports.[252] The remaining avidin residues are blocked by bovine serum albumin or methyl mannoside;[253] buffers of high ionic strength are used for chromatography.

Short and homogeneous oligonucleotides are more accessible and can be immobilised more easily than long NA fragments. The sorbents containing oligo(dT) [especially oligo$(dT)_{25}$-Dynabeads] and oligo(dA) have now become especially popular.[254–256] Immo-

bilisation of large fragments of NA on these or any other supports containing short oligonucleotides (10–20 nucleotide residues) can be carried out enzymically using ligase, by attaching specially synthesised or isolated long fragments of NA,[24, 257] or using DNA-polymerase, by completing the mRNA [258, 259] or the DNA template [260] which forms complexes with the short oligonucleotide on the polymer.

VII. The use of matrices containing nucleic acids

1. Affinity chromatography

The solution of the key problems of molecular biology and biochemistry related to the structure and interactions between biopolymers demands the use of special techniques allowing the isolation of individual biopolymers from complex multicomponent mixtures. Thus proteins, enzymes, NA, oligonucleotides and their analogues are necessary in a pure state for the studies of their structures as well as for protein-NA, DNA-DNA and RNA-DNA recognitions. These biomolecules can be isolated by affinity chromatography on sorbents containing immobilised NA or oligonucleotides. This method is based on the ability of ligands immobilised on insoluble supports to form highly specific complexes with macromolecules, which dissociate under definite conditions (*e.g.*, either upon change in the ionic strength or pH of the eluent or upon increase in temperature).

a. Isolation of individual nucleic acids and their fragments

The principle of affinity chromatography of NA was first applied to the isolation of oligo- and polynucleotides having homogeneous sequences. The possibility of fractionation of oligonucleotides on supports containing immobilised polynucleotides has been noted in the early papers.[60, 61, 261] A series of papers devoted to affinity chromatography of poly(A)-mRNA,[214, 254, 262, 263] NA or oligonucleotides containing homogeneous sequences were published in the late 1980's–early 1990's owing to the development of methods of synthesis of oligonucleotides and the accessibility of novel carriers.[26, 264] However, this method was not successful for the isolation of individual oligonucleotides or longer sequences devoid of homogeneous inserts. Present-day studies widely employ commercial supports carrying immobilised homogeneous oligonucleotides, most commonly, oligo(T) supports. The use of durable materials, such as silica gel, glass and some methacrylate-based copolymers as supports allows high-performance affinity chromatography and complete separation of oligonucleotides differing in length by one base.[105]

Affinity chromatography of heterogeneous oligonucleotides and NA has become possible following development of efficient methods for immobilisation of heterogeneous oligonucleotides on insoluble supports. Matrices containing relatively short (10–15-mers) immobilised oligonucleotide fragments complementary to a region of an oligonucleotide to be purified have been used for the isolation of extended (more than 30-mers) synthetic oligonucleotides which can hardly be purified by conventional chromatographic methods.[102, 104] This approach was applied for the isolation of a synthetic 34-membered oligonucleotide representing a deoxy copy of an RNA fragment of the Russian tick-borne encephalitis virus on LiChrosorb-NH_2 bearing an immobilised 17-membered oligonucleotide complementary to the 5′-end of the 34-membered fragment (Fig. 2).[102]

Apart from synthetic oligonucleotides, individual NA and DNA fragments obtained upon scission of DNA with restriction enzymes can be isolated by affinity chromatography from complex mixtures (see Fig. 2).[102, 104] This approach was used to obtain highly enriched $tRNA^{Phe}$ from human placenta [103] utilising two successive affinity chromatography steps on matrices containing immobilised oligonucleotides complementary to the CCA-end of tRNA (the first step) and to a site in the anti-codon loop of $tRNA^{Phe}$ (the second step).

Both single- and double-stranded NA can be isolated from cell extracts on sorbents carrying immobilised specific oligonucleotides. In the latter case, oligonucleotides should be able to form triplexes with definite regions of NA, as can be exemplified by purification of the DNA plasmids pTS2 (Ref. 265) and pXL2563 (Ref. 7) from cell extracts.

b. Separation of diastereomeric mixtures of non-ionic oligonucleotide analogues

Considerable interest in oligonucleotide analogues containing modified internucleotide phosphate groups, *viz.*, methylphosphonates and phosphotriesters, can be explained by their physicochemical and biological properties, *e.g.*, resistance to nucleases, sorption on cell membranes, penetration inside the cell and ability to form complexes with the complementary regions of NA. Since these analogues contain an asymmetric internucleotide phosphorus atom, they represent mixtures consisting of a large number of diastereomers which differ in the stabilities of the complementary complexes formed. Individual diastereomers are necessary for detailed investigations of physicochemical properties and biological behaviour of oligonucleotide analogues in cellular systems.

For the first time, chromatographic separation of diastereomers of nonathymidilyluridine octaethyl ester into fractions was carried out on a column with poly(A) cyanogen bromide-activated Sepharose.[266] However, individual diastereomers of non-ionic analogues of oligonucleotides could be obtained only by high-performance affinity chromatography.

The silica gel-based sorbent LiChrosorb bearing the octanucleotide pTGTTTGGC immobilised through the 5′-terminal phosphate group was used for the isolation of individual diastereomers of the heterogeneous octanucleotide GCCAAACA ethyl esters at a constant column temperature.[105] This allowed separa-

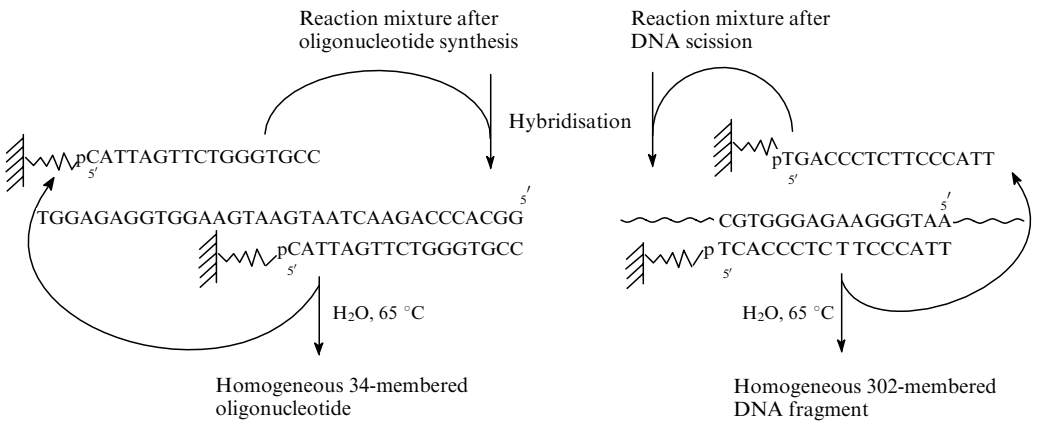

Figure 2. Affinity chromatography.

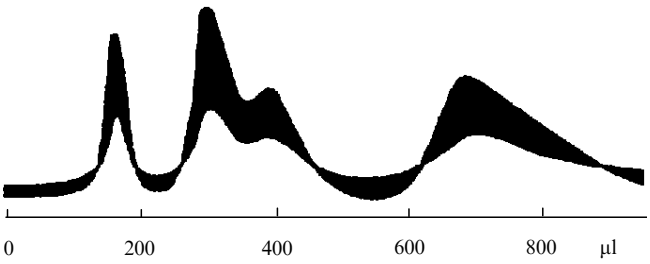

Figure 3. A chromatographic separation profile of a mixture of four diastereomers of the octanucleotide GpCpCpAp_{OEt}Ap_{OEt}ApCpA ethyl esters on an affinity sorbent (LiChrosorb) containing pTGTTTGGC immobilised through the 5′-terminal phosphate group.[105]

tion of stereoisomers of the octanucleotide GCCAAACA containing one, two or three phosphotriester groups (Fig. 3). The same affinity sorbent was successfully used to obtain individual diastereomers of the heptanucleoside methylphosphonate $Cp_{Me}Cp_{Me}Ap_{Me}$ $Ap_{Me}Ap_{Me}Cp_{Me}A$; the absolute configurations of these diastereomers have been established.[267]

c. Isolation of NA-dependent enzymes

At present, affinity chromatography on cellulose and Sepharose containing calf thymus DNA has become a routine procedure for obtaining pure preparations of NA-dependent proteins which are non-specific as regards the nucleotide sequence. Purification of site-specific proteins is carried out on sorbents with immobilised oligonucleotides having the corresponding recognition sites. Most of the proteins isolated represent transcription and replication protein factors (for a comprehensive description, see the reviews [181, 268, 269]). The list given in these reference can be supplemented by several other papers [36, 137, 270, 271] describing the methods for the preparation of affinity sorbents used for the purification of these proteins. Affinity chromatography was also used for the isolation of some receptors.[62, 168, 252]

Isolation of site-specific restrictases is of the greatest interest, since affinity matrices in this particular case should be resistant to enzymes to be isolated. The restriction endonucleases *Eco*RI [272] and *Sph*I [273] hydrolyse DNA only in the presence of Mg^{2+} ions, whereas in the absence of Mg^{2+} ions they bind to the site-bearing DNA. This property is used for their isolation. For the isolation of IIS-type restrictases (*Fok*I, *Hga*I, *Sfa*NI), which hydrolyse DNA at a site other than the recognition site, a duplex which incorporates the recognition sites for these enzymes but contains no sites necessary for DNA hydrolysis has been synthesised.[101] The structure of the duplex is given below (the corresponding recognition sites are enclosed in boxes). One of the oligonucleotides of the duplex was covalently linked to the methacrylate-based polymeric support.

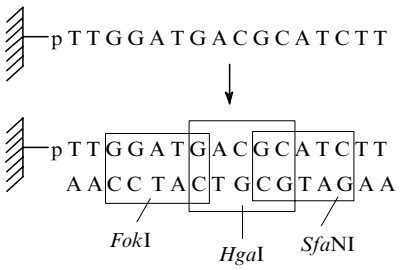

Sorbents containing immobilised oligonucleotide duplexes, which, in turn, contain non-canonical base pairs, are used for the isolation of DNA repair enzymes responsible for mismatch correction. Thus thymine-DNA glycosylase [274, 275] was isolated on an affinity DNA sorbent containing a dG : U mismatch, however, in only trace amounts. Highly purified biologically active mismatch-specific DNA glycosylases (MutM and MutY) responsible for the removal of the oxidised form of guanine from DNA as well as for mismatch correction were isolated by affinity chromatography.[106] This study utilised a support (Toyopearl-AF) carrying an immobilised oligonucleotide duplex containing the non-canonical pairs $N8^{oxo}$-dC or rA-dG (where $N8^{oxo}$ is 8-oxonebularine, an analogue of the oxidised form of guanine).

Affinity chromatography on oligonucleotide-containing sorbents allows both the isolation of NA-dependent proteins and studies of their interactions with immobilised NA fragments.[106, 276]

2. Hybridisation assay

Molecular hybridisation of NA is based on the fundamental property of complementary chains of NA to form stable duplexes. This method allows rapid testing of mutated viral NA and viroids and is distinguished by high specificity, sensitivity and reproducibility. The main stages of the hybridisation analysis have been described in detail.[277–282]

The sensitivity of this method is determined by the choice of procedures for the detection of oligonucleotide probes carrying radioactive ([^{32}P]), fluorescent and other labels.

The selection of a support and the procedure for the immobilisation of NA or oligonucleotides is the key problem in any solid-phase hybridisation assay, which is determined by a specific goal in each particular case.

Dot-blot hybridisation includes immobilisation of a denatured portion of total NA to be tested on nitrocellulose.[283–289] Polystyrene immunological microwell plates are employed for the automation of serial tests of clinical samples.[290, 291] Immobilisation of NA targets or specific cloned fragments is carried out by physicochemical methods, *e.g.*, by sintering at 80 °C or by UV irradiation.

Blot-hybridisation in which a NA preparation is hydrolysed by restriction enzymes subjected to fractionation (*e.g.,* separation according to the molecular mass) by gel electrophoresis and further transferred to a support from the gel is a more efficient method of analysis. After immobilisation on the support, NA are hybridised with labelled probes (the so-called Southern blot DNA assay) [225] and Northern blot (RNA assay).[292] Currently, the Southern blot is used for the detection of PCR products and determination of the reaction specificity.[293–295] Nitrocellulose filters [225, 292, 296, 297] and nylon membranes [298, 299] (less frequently, *p*-azidobenzoylcellulose [236]) or dried gels following fractionation of NA fragments [300] are commonly used for the fixation of the nucleotide material. Sandwich blot is a promising approach to the analysis of NA in non-purified specimens containing proteins, polysaccharides and other components.[301] This method is based on the use of two different oligo- or polynucleotide fragments complementary to different sites of the NA to be assayed. One of these fragments is immobilised on a support, whereas the other is soluble and carries a reporter group (*e.g.*, a radiolabel, a biotin residue, *etc.*). After hybridisation and removal of admixtures and the excess of the second (labelled) probe, the NA that has formed a complementary complex with the nucleotide immobilised on the support is detected by the label bound. A vast number of solid supports and immobilisation procedures have been used for sandwich blot. Initially, nitrocellulose filters have been used,[302, 303] which were replaced by mechanically stronger nylon membranes [304] and more handy polypropylene and polystyrene immunological microwell plates.[32, 305–307] Hybridisation of NA with oligonucleotide probes immobilised on the surface of microgranulated supports is a way of acceleration of the hybridisation. Different versions of this approach using Sephacryl,[67] polyacrylamide,[28] nylon [27] and polystyrene beads [304, 308, 309] and magnetic microparticles [25, 219, 304, 310] have been described. The use of magnetic microparticles has an additional advantage, since they can easily be concentrated from suspensions, which significantly simplifies manipulations with samples.

'Reverse dot blot' [48] implies the introduction of a label into the NA or its fragment obtained by PCR. After hybridisation of a labelled NA with an oligonucleotide immobilised on a solid

support, the complementary hybrid formed is detected by virtue of the label bound to the support. Nylon [48, 66, 83, 311] and poly(ethylene terephthalate) [195, 312, 313] membranes, immunological microwell plates [314, 315] and glass [17, 316] have been used as supports for the reverse dot blot. The use of cover glasses in hybridisation assays is especially convenient, since glass is readily available, inexpensive and has a well-studied surface which is easy to modify and is suitable for fluorescent detection. Immobilisation of oligonucleotides is usually carried out by photochemical or various chemical methods.

3. DNA chips and DNA sensors

The development of effective methods for the immobilisation of oligonucleotides as well as array-based mapping methods have led to the design of microchips with immobilised oligonucleotide sets (arrays). Such DNA chips which represent slides (usually, glass slides) containing an immense variety of immobilised oligonucleotides (tens of thousands of DNA fragments) find ever growing application in molecular biology, medicine, biotechnology, *etc.*

Initially, microchips were proposed for the sequencing of nucleic acids (the so-called SBH method, sequencing by hybridisation).[132, 317–319] It was assumed that the use of arrays with a complete set of immobilised octanucleotides ($65536 = 4^8$) would make it possible to determine the unknown sequences of nucleic acids by hybridisation assays. However, it was found that serious problems are inherent in the SBH method and not much success in this area has been achieved yet. These studies have shown, however, that microchips can find wide application in the analysis of gene expression and mutations as well as in the diagnostics of genetic, infectious and cancer diseases.[320–334]

There are two main approaches to the preparation of DNA microchips, *viz.*, the synthesis of oligonucleotides directly on surfaces [4, 5, 8, 175, 215, 217, 218, 321, 333–341] and immobilisation of presynthesised oligonucleotides on slides of glass or other materials.[17, 19, 22, 30, 131, 133, 248, 322, 323, 330–332, 342–344]

The former approach has been realised in such methods as combinatorial photolithography on glass slides or other supports using photoreactive protective groups.[321, 337–341] Irradiation of slides through a cover mask results in the removal of photoreactive protective groups from the oligonucleotide chains at the predetermined sites so that the next monomeric unit is coupled to the deblocked oligonucleotide chain. By shifting the mask and by iterating the irradiation and coupling procedures, one can obtain ultimately surfaces containing a large number of oligonucleotides of predetermined sequences at specified points. Despite its obvious economic expediency, direct synthesis of oligonucleotides on surfaces suffers from one serious disadvantage, since it does not provide 100% yields in coupling steps, which can result in errors in further analysis.

The latter approach to the manufacture of DNA microchips entails the use of isolated and purified oligonucleotides.

Thorough pre-washing and etching prior to immobilisation is a very important stage. These are necessary for the removal of admixtures (grease, dirt, dust, *etc.*) and for the generation of surface hydroxy groups.[345, 346] The washing procedure makes use of organic solvents (most commonly, methanol) or potent oxidants (*e.g.*, hydrogen peroxide). The activation of the glass surface is achieved by inorganic acids or alkalis (HF, HCl, HNO_3, H_2SO_4 or NaOH). This is followed by the introduction of functional groups on the slide surface for subsequent reactions using silanes of the general formula $(R^1O)_3Si(CH_2)_nR$,[2] where R^1 = Me or Et and R^2 is a functional group (see compounds **1**–**4** in Section III.2). The reactions considered in the foregoing sections are used for covalent attachment of oligonucleotides onto the surface of glass slides. Here we shall cite a paper [344] which describes a novel approach. Oligonucleotides or cDNA with linkers containing 5′-terminal SH or $CH_2=CH$ groups were preincubated with the corresponding trimethoxysilanes, after which the conjugates obtained were immobilised on non-modified glasses.

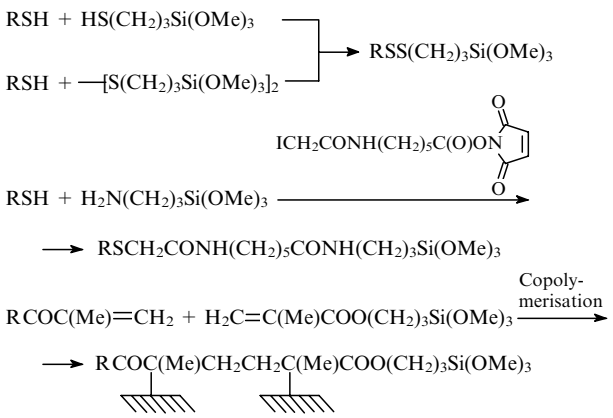

R, oligonucleotide or cDNA.

The nature and the lengths of the linkers binding the oligonucleotide to the surface are important characteristics for effective hybridisation. Steric accessibility of oligonucleotides for complementary interaction can be achieved through the use of long-chain linkers. The efficiency of hybridisation increases severalfold through the use of spacers of appropriate lengths [8, 38, 320, 331–333] (see Section III.2). The amount of the immobilised oligonucleotide referred to the unit of surface area (the surface capacity) is yet another important characteristic of DNA chips; this should not exceed a certain optimum value in order to avoid steric hindrances during subsequent hybridisation. The capacity is not very high (0.01–1.00 pmol mm^{-2}) [8, 15–17, 19, 20, 242, 333] but sufficient for successful assays. The optimum capacity of 0.25–0.35 pmol mm^{-2} for the immobilisation of polynucleotides (150–350 b.p.) has been recommended.[17]

Obviously, the sensitivity of a hybridisation assay increases with an increase in capacity. This is achieved using several approaches, *viz.*, by attachment of oligonucleotides to branched linkers (dendrimers) [22] and by formation of acrylamide,[20, 29, 30, 45, 347–349] agarose [183] or gelatine [350] layers on glass surfaces, which ensures 'three-dimensional' attachment of oligonucleotides. In this case, the capacities of oligonucleotides referred to the unit of surface area is much higher than in two-dimensional immobilisation and can amount to 30 pmol mm^{-2},[45] while steric accessibility of oligomers for subsequent hybridisation is preserved.

In early studies, radiolabelled probes were used for the detection of signals in hybridisation assays. However, other labels incorporated into oligonucleotide probes, such as biotin, digoxigenin, chemiluminophores, fluorescent and enzymic labels, also gained wide acceptance.[302, 308, 351]

Physical methods of detection have come into use owing to the recent progress in DNA chip technology. The DNA sensors (biosensors), like other biosensors, provide rapid and direct detection both with labels and without them. The use of biosensors allows kinetic studies of hybridisation processes. The topology of immobilised oligonucleotides in films applied onto the surfaces of slides and fine details of molecular interactions at the film-solution interface are also investigated.[337–341, 352–356] Thus the effects of the shape, length and composition of the double helix formed on the efficiency of hybridisation have been studied.[4, 357, 358]

DNA sensors can utilise piezoelectric technologies for measuring the changes in the oscillation frequencies of crystals bearing immobilised oligonucleotides during the sorption of the complementary DNA chain,[359–362] surface plasmon resonance technology (in this case, the refractive index of the metal surface changes upon binding of the soluble ligand to the ligand immobilised on the metal film),[363–366] scanning microscopy [352, 367] and X-ray photoelectron spectroscopy (XPS).[353] Electrochemical detection makes use of electrodes bearing immobilised oligonucleotides which change their electrical characteristics in the course of hybridisation.[365, 368–370] Optical sensors able to detect changes

in the optical properties (*e.g.*, refractive index, interference, *etc.*) of films are also widely used for the detection of hybridisation of DNA chains on the surfaces containing immobilised oligonucleotides.[230, 371 – 373]

These methods ensure high sensitivity, *i.e.*, the detection of nano- and picogram quantities of compounds.

The design of DNA chips and DNA sensors is an explosively developing field of science and biotechnology. Advances in this area will be a breakthrough in the diagnostics of genetic, cancer and infectious diseases as well as in medicine and pharmacology.

4. Enzymic synthesis on NA templates

Immobilised synthetic oligonucleotides and NA as templates or primers for enzymic synthesis of oligo- and polynucleotides can repeatedly be used for the synthesis of complementary oligonucleotide chains, which simplifies the separation of the final product from the templates. The latter circumstance is especially important, since along with the template or the primer the reaction mixture contains the enzyme and a large excess of nucleoside triphosphates (NTP) used as substrates for NA biosynthesis.

DNA polymerases of bacteriophage T7,[34, 374] polymerase I of *E.coli*, the Klenow fragment [85, 257, 260, 375, 376] and Taq polymerase [377 – 380] are used in solid-phase enzymic synthesis of DNA or DNA fragments. cDNAs synthesised on oligo(dT)-bearing supports (*e.g.*, cellulose,[258, 259, 381] latex [382 – 384] or magnetic particles [374]) by transcription of the corresponding poly(A) – mRNAs in the presence of RNA-dependent DNA polymerase (reverse transcriptase) are most often used as templates. Some authors recommend to immobilise plasmids [34] or bacteriophages [192, 376] containing incorporated exogeneous DNAs (including cDNAs) [192] and utilise them as templates for subsequent enzymic synthesis on supports. Using primers complementary to the 3′-terminal region of the immobilised template, one can obtain full complementary DNA.[85, 192, 257, 380] Enzymic template synthesis permits one to introduce various functional groups and labels into DNAs and their fragments [257, 375] using primers, dNTP or terminating dideoxyribonucleoside triphosphates (ddNTP) carrying the corresponding functional groups. The addition of one or all the four ddNTP with different labels to the reaction mixture along with four dNTP makes it possible to obtain series of labelled products and to determine the oligonucleotide sequence of the immobilised DNA.[34, 378, 379]

The chemical synthesis of oligoribonucleotides and RNA is more complicated than that of oligodeoxyribonucleotides, hence, the interest in enzymic methods is obvious. Biosynthesis of RNA is carried out using DNA-dependent RNA polymerases, *e.g.*, RNA polymerases of T7 [129, 385, 386] and *E.coli*.[381, 387, 388] Immobilised oligodeoxyribonucleotides [129, 385, 386, 388] and cDNA are used as templates for oligoribonucleotide and mRNA syntheses, respectively.[381, 387] The amount of the final products can be increased by means of PCR technology, while modern magnetic particles (Dynabeads) ensure easier separation of the products synthesised.

Enzymic synthesis on immobilised NA templates is used for the replication, transcription and sequencing of nucleic acids as well as for the introduction of functional groups and labels and the construction of genomic and cDNA libraries.

VIII. Conclusion

The work considered in this review demonstrates the immense diversity of methods for immobilisation of NA on solid supports. Immobilisation of NA on activated supports are especially widely used. In this case, native NA is immobilised non-specifically through many points. However, this results in the preparation of affinity matrices with higher capacities. The attachment of nucleotides and oligonucleotides containing additional reactive groups occurs much more selectively, *i.e.*, without affecting the heterocyclic bases and with the preservation of their abilities for affinity interactions.

Physical immobilisation methods are irreproducible and non-specific. The advantage of chemical approaches is the possibility to use the immobilisation methods corresponding to a specified experimental task. The stability of affinity sorbents under various conditions and the procedure used for the removal of the ligand from the support can be determined in advance provided that the nature of the bond between the ligand and the support is known.

Reactions of ligands containing amino or thiol groups with the reactive groups of the support have become especially widespread among other methods of immobilisation of NA and their fragments. The attachment of oligonucleotides containing amino groups to supports containing aldehyde groups is a common procedure. The method utilising the $Ph_3P-Py_2S_2$ couple as an activating reagent has proved to be efficient in the binding of oligonucleotides with terminal phosphate groups to granulated polymers. In the case of planar supports, *e.g.*, films and glasses, it is more expedient to use methods implying the activation of the functional groups of the support or utilise bifunctional cross-linking reagents, *e.g.*, 1,4-phenylene diisocyanate. It should be noted, however, that no universal immobilisation procedure exists and both the support and the immobilisation procedure should be chosen for each particular case.

NA-containing carriers have found wide acceptance for both research and applied purposes. A number of reviews devoted to this topic has been published in recent years.[326, 328, 347, 389 – 391] The supports with immobilised oligonucleotides are used as sorbents in affinity chromatography in order to obtain highly purified individual NA or their fragments. Affinity chromatography seems to be the only efficient procedure for the separation of diastereomeric mixtures of non-ionic oligonucleotide analogues. Affinity oligonucleotide-containing matrices have proved to be highly efficient for the isolation of nucleotide-dependent enzymes. Such supports are also used in solid-phase enzymic synthesis of DNA, RNA and their fragments.

Special mention should be made of NA-containing carriers for hybridisation assays, which underlie the diagnostics of many diseases. It is used for detecting mutations, viral and bacterial NA, *etc.* This method is gaining increasing popularity for genetic expertise in medical and forensic practice.

The trend which includes the design and application of DNA microchips is developing explosively in recent years. These tools have proved to be useful in various fields of biology and medicine. Their unique properties are based on the fact that a small area of glass slides contains a large amount of immobilised oligonucleotides, which allows a great number of assays to be conducted simultaneously.

The use of immobilised oligonucleotides as biosensors adds novel unique capabilities to the arsenal of modern analytic techniques. They permit one to obtain information more rapidly, simply and less expensively than in conventional hybridisation techniques. The novel devices, *viz.*, DNA biosensors, hold tremendous potential in many areas, *e.g.*, clinical analyses for forensic expertise, monitoring of the environment, food quality, *etc.*

References

1. G Cohen, J Deutsch, J Fineberg, A Levine *Nucl. Acids Res.* **25** 911 (1997)
2. R S Matson, J B Rampal, P J Coassin *Anal. Biochem.* **217** 306 (1994)
3. K Ernst-Cabrera, M Wilchek *Anal. Biochem.* **159** 267 (1986)
4. U Maskos, E M Southern *Nucl. Acids Res.* **20** 1679 (1992)
5. E M Southern, S C Case-Green, J K Elder, M Johnson, K U Mir, L Wang, J C Williams *Nucl. Acids Res.* **22** 1368 (1994)
6. H Hakala, H Lönnberg *Bioconjugate Chem.* **8** 232 (1997)
7. P Wils, V Escriou, A Warnery, F Lacroix, D Lagneaux, M Ollivier, J Crouzet, J-F Mayaux, D Scherman *Gene Ther.* **4** 323 (1997)
8. M S Shchepinov, S C Case-Green, E M Southern *Nucl. Acids Res.* **25** 1155 (1997)

9. J Turkova *Affinity Chromatography* (Amsterdam: Elsevier, 1978)
10. V Jirku, J Turkova *Methods Enzymol.* **135** 341 (1987)
11. M Yang, R Y C Kong, N Kazmi, A K C Leung *Chem. Lett.* 257 (1998)
12. M Zammatteo, L Jeanmart, S Hamels, S Courtois, P Louette, L Hevesi, J Remacle *Anal. Biochem.* **280** 143 (2000)
13. L Henke, P A E Piunno, A C McClure, U J Krull *Anal. Chim. Acta* **344** 210 (1997)
14. B S Sproat, D M Brown *Nucl. Acids Res.* **13** 2979 (1985)
15. J B Lamture, K L Beattie, B E Burke, M D Eggers, D J Ehrlich, R Fowler, M A Hollis, B B Kosicki, R K Reich, S R Smith, R S Varma, M E Hogan *Nucl. Acids Res.* **22** 2121 (1994)
16. L A Chrisey, G U Lee, C E O'Ferrall *Nucl. Acids Res.* **24** 3031 (1996)
17. Z Guo, R A Guilfoyle, A J Thiel, R Wang, L M Smith *Nucl. Acids Res.* **22** 5456 (1994)
18. B Joos, H Kuster, R Cone *Anal. Biochem.* **247** 96 (1997)
19. D Chen, Z Yan, D L Cole, G S Srivatsa *Nucl. Acids Res.* **27** 389 (1999)
20. A V Vasiliskov, E N Timofeev, S A Surzhikov, A L Drobyshev, V V Shick, A D Mirzabekov *Biotechniques* **27** 592 (1999)
21. N P Gerry, N E Witowski, J Day, R P Hammer, G Barany, F Barany *J. Mol. Biol.* **292** 251 (1999)
22. M Beier, J D Hoheisel *Nucl. Acids Res.* **27** 1970 (1999)
23. T R Gingeras, D Y Kwoh, G R Davis *Nucl. Acids Res.* **15** 5373 (1987)
24. J N Kremsky, J L Wooters, J P Dougherty, R E Meyers, M Collins, E L Brown *Nucl. Acids Res.* **15** 2891 (1987)
25. V Lund, R Schmid, D Rickwood, E Hornes *Nucl. Acids Res.* **16** 10861 (1988)
26. T A Goss, M Bard, H W Jarrett *J. Chromatogr.* **508** 279 (1990)
27. J Van Ness, S Kalbfleisch, C R Petrie, M W Reed, J C Tabone, N M J Vermeulen *Nucl. Acids Res.* **19** 3345 (1991)
28. E Fahy, G R Davis, L J DiMichele, S S Ghosh *Nucl. Acids Res.* **21** 1819 (1993)
29. E N Timofeev, S V Kochetkova, A D Mirzabekov, V L Florentiev *Nucl. Acids Res.* **24** 3142 (1996)
30. D Proudnikov, E Timofeev, A Mirzabekov *Anal. Biochem.* **259** 34 (1998)
31. S Pochet, T Huynh-Dinh, J Igolen *Tetrahedron* **43** 3481 (1987)
32. J A Running, M S Urdea *Biotechniques* **8** 276 (1990)
33. M Shimkus, J Levy, T Herman *Proc. Natl. Acad. Sci. USA* **82** 2593 (1985)
34. T Hultman, S Stahl, E Hornes, M Uhlen *Nucl. Acids Res.* **17** 4937 (1989)
35. M Leblond-Francillard, M Dreyfus, F Rougeon *Eur. J. Biochem.* **166** 351 (1987)
36. O S Gabrielsen, E Hornes, L Korsnes, A Ruet, T B Øyen *Nucl. Acids Res.* **17** 6253 (1989)
37. W Weber, C-W Vogel, H Hilz *FEBS Lett.* **99** 62 (1979)
38. Y Zhang, M Y Coyne, S G Will, C H Levenson, E S Kawasaki *Nucl. Acids Res.* **19** 3929 (1991)
39. P A E Piunno, U J Krull, R H E Hudson, M J Damha, H Cohen *Anal. Chim. Acta* **288** 205 (1994)
40. A V Fotin, A L Drobyshev, D Y Proudnikov, A N Perov, A D Mirzabekov *Nucl. Acids Res.* **26** 1515 (1998)
41. Yu P Lysov, A A Chernyi, A A Balaev, F N Gnuchev, K L Bitti, A D Mirzabekov *Mol. Biol.* **29** 104 (1995) [a]
42. M A Livshits, V L Florentiev, A D Mirzabekov *J. Biomol. Struct. Dyn.* **11** 783 (1994)
43. D Guschin, G Yershov, A Zaslavsky, A Gemmell, V Shick, D Proudnikov, P Arenkov, A Mirzabekov *Anal. Biochem.* **250** 203 (1997)
44. A Kunitsyn, S Kochetkova, E Timofeev, V Florentiev *J. Biomol. Struct. Dyn.* **14** 239 (1996)
45. S Parinov, V Barsky, G Yershov, E Kirillov, E Timofeev, A Belgovskiy, A Mirzabekov *Nucl. Acids Res.* **24** 2998 (1996)
46. S Dubiley, E Kirillov, Y Lysov, A Mirzabekov *Nucl. Acids Res.* **25** 2259 (1997)
47. I B Ivanov, G M Ershov, V E Barskii, A I Bel'govskii, E V Kirillov, E Ya Kreindlin, S V Parinov, N V Mologina, A D Mirzabekov *Mol. Biol.* **31** 159 (1997) [a]
48. R K Saiki, P S Walsh, C H Levenson, H A Erlich *Proc. Natl. Acad. Sci. USA* **86** 6230 (1989)
49. Ph J R Day, P S Flora, J E Fox, M R Walker *Biochem. J.* **278** 735 (1991)
50. N K Kochetkov, E I Budovskii, E D Sverdlov, N A Simukova, M F Turchinskii, V N Shibaev, in *Organicheskaya Khimiya Nukleinovykh Kislot* (Organic Chemistry of Nucleic Acids) (Moscow: Khimiya, 1970)
51. D G Knorre, V F Zarytova, A G Badashkeeva, O S Fedorova *Biotekhnologiya (Itogi Nauki i Tekhniki)* [Biotechnology (Advances in Science and Engineering Series)] (Moscow: Izd. VINITI, 1991) Vol. 37
52. S Agrawal *Methods Mol. Biol.* **26** 93 (1994)
53. J A Fidanza, H Ozaki, L W McLaughlin *Methods Mol. Biol.* **26** 121 (1994)
54. B Chu, L E Orgel *Methods Mol. Biol.* **26** 145 (1994)
55. D G Knorre, V V Vlassov, V F Zarytova, A V Lebedev, O S Fedorova, in *Design and Targeted Reactions of Oligonucleotide Derivatives* (Boca Raton, FL: CRC Press, 1994) p. 101
56. V V Shumyantseva, R M Khomutov *Bioorg. Khim.* **3** 1471 (1977) [b]
57. V V Shumyantzeva, N I Sokolova, Z A Shabarova *Nucl. Acids Res.* **3** 903 (1976)
58. V N Shibaev, Yu Yu Kusov, N A Kalinchuk, N K Kochetkov *Bioorg. Khim.* **3** 120 (1977) [b]
59. E K F Bautz, B D Hall *Proc. Natl. Acad. Sci. USA* **48** 400 (1962)
60. P T Gilham *J. Am. Chem. Soc.* **84** 1311 (1962)
61. P T Gilham *J. Am. Chem. Soc.* **86** 4982 (1964)
62. S C Gross, S A Kumar, H W Dickerman *J. Biol. Chem.* **257** 4738 (1982)
63. T Y Shih, M A Martin *Biochemistry* **13** 3411 (1974)
64. WO PCT 9 009 393; *Chem. Abstr.* **149** 247 682 (1990)
65. S S Ghosh, G F Musso *Nucl. Acids Res.* **15** 5353 (1987)
66. M G Ivanovskaya, I A Kozlov, N A Naryshkin, Z A Shabarova *Bioorg. Khim.* **21** 535 (1995) [b]
67. J A Langdale, A D Malcolm *Gene* **36** 201 (1985)
68. H G Khorana *Some Recent Developments in the Chemistry of Phosphate Esters of Biological Interest* (New York: Wiley, 1961)
69. Z A Shabarova, A A Bogdanov *Khimiya Nukleinovykh Kislot i Ikh Komponentov* (The Chemistry of Nucleic Acids and Their Components) (Moscow: Khimiya, 1978)
70. J P Riehm, H A Scheraga *Biochemistry,* **5** 99 (1966)
71. A Williams, I T Ibrahim *Chem. Rev.* **81** 589 (1981)
72. P T Gilham *Biochemistry* **7** 2809 (1968)
73. D Rickwood *Biochim. Biophys. Acta* **269** 47 (1972)
74. G T Babkina, D G Knorre, L G Olenchich *Izv. Sib. Otd. Akad. Nauk SSSR, Ser. Khim. Nauk* (1) 120 (1972)
75. V F Zarytova, E M Ivanova, A V Lebedev *Bioorg. Khim.* **2** 189 (1976) [b]
76. D G Knorre, V F Zarytova *Nucl. Acids Res.* **3** 2709 (1976)
77. M G Ivanovskaya, N A Naryshkin, Z A Shabarova *Bioorg. Khim.* **21** 454 (1995) [b]
78. D G Knorre, T N Shubina *Kinet. Katal.* **5** 637 (1964) [c]
79. V F Zarytova, E M Ivanova, A V Lebedev *Bioorg. Khim.* **2** 1196 (1976) [b]
80. M G Ivanovskaya, M B Gottikh, Z A Shabarova *Nucleosides Nucleotides* **6** 913 (1987)
81. V F Zarytova, V K Rait, T S Chernikova *Bioorg. Khim.* **3** 1626 (1977) [b]
82. M G Ivanovskaya, I A Kozlov, I V Lebedeva, Z A Shabarova *Mol. Biol.* **28** 1176 (1994) [a]
83. Y Zhang, M Y Coyne, S G Will, C H Levenson, E S Kawasaki *Nucl. Acids Res.* **19** 3929 (1991)
84. M V Berridge, A I Aronson *Anal. Biochem.* **53** 603 (1973)
85. A Panet, H G Khorana *J. Biol. Chem.* **249** 5213 (1974)
86. W H Scouten, in *Affinity Chromatography. Bioselective Adsorption on Inert Matrices* (New York: Wiley, 1981) Vol. 59, p. 349
87. V I Latich, V P Varlamov, N N Semenova, S V Rogozhin *Biokhimiya* **45** 1597 (1980) [d]
88. T T Nikiforov, Y H Rogers *Anal. Biochem.* **227** 201 (1995)
89. V G Allfrey, A Inoue *Methods Cell Biol.* **17** 253 (1978)
90. R Bischoff, J M Coull, F E Regnier *Anal. Biochem.* **164** 336 (1987)
91. B C F Chu, G M Wahl, L E Orgel *Nucl. Acids Res.* **11** 6513 (1983)
92. M B Gottikh, M G Ivanovskaya, E A Skripkin, Z A Shabarova *Bioorg. Khim.* **16** 514 (1990) [b]
93. V L Drutsa, V F Zarytova, D G Knorre, A V Lebedev, N I Sokolova, Z A Shabarova *Nucl. Acids Res.* **5** 185 (1978)

94. V L Drutsa, V F Zarytova, D G Knorre, A V Lebedev, N I Sokolova, Z A Shabarova *Dokl. Akad. Nauk SSSR* **233** 595 (1977) [e]
95. V V Nosova, I S Vel'moga, N I Sokolova, Z A Shabarova, M A Prokof'ev *Dokl. Akad. Nauk SSSR* **219** 1134 (1974) [e]
96. V V Shumyantseva, R M Khomutov *Bioorg. Khim.* **4** 1477 (1978) [b]
97. T Mukaiyama, R Matsueda, M Suzuki *Tetrahedron Lett.* 1901 (1970)
98. T Mukaiyama, M Hashimoto *J. Am. Chem. Soc.* **94** 8528 (1972)
99. V F Zarytova, T S Godovikova, I V Kutyavin, L M Khalimskaya, in *Reactive Oligonucleotide Derivatives as Affinity Reagents and Probes in Molecular Biology* (Eds K S Bruzik, W J Stec) (Amsterdam: Elsevier, 1987) p. 149
100. T S Godovikova, V F Zarytova, L M Khalimskaya *Bioorg. Khim.* **12** 475 (1986) [b]
101. S Kh Degtyarev, P A Belavin, I G Shishkina, V F Zarytova, L P Gavryuchenkova, S N Morozov *Bioorg. Khim.* **15** 358 (1989) [b]
102. V F Zarytova, I G Shishkina *Anal. Biochem.* **188** 214 (1990)
103. V F Zarytova, G G Karpova, D A Mundus, I G Shishkina *Bioorg. Khim.* **16** 1069 (1990) [b]
104. T V Abramova, N V Amirkhanov, V V Gorn, V F Zarytova, E I Frolova, I G Shishkina *Bioorg. Khim.* **17** 232 (1991) [b]
105. I A Vtorushina, Yu A Gorbunov, V F Zarytova, N I Komarova, A V Lebedev, S G Lokhov, A V Manaenko, A N Sinyakov, I G Shishkina *Bioorg. Khim.* **18** 92 (1992) [b]
106. I G Shishkina, N V Bulychev, A P Grollman, F Johnson *Int. J. Bio-Chromatogr.* **3** 329 (1997)
107. B M Kurinenko, F F Shagi-Mukhamedova, A M Nuzhina *Bioorg. Khim.* **1** 1624 (1975) [b]
108. P T Gilham *Adv. Exp. Med. Biol.* **42** 173 (1974)
109. P T Gilham *Methods Enzymol.* **21** 191 (1971)
110. G R Jacobson, J P Rosenbusch *FEBS Lett.* **79** 8 (1977)
111. A A Nedospasov, R M Khomutov *Bioorg. Khim.* **4** 645 (1978) [b]
112. D L Robberson, N Davidson *Biochemistry* **11** 533 (1972)
113. A Weissbach, M Poonian *Methods Enzymol.* **34** 463 (1974)
114. M Wilchek, R Lamed *Methods Enzymol.* **34** 475 (1974)
115. M B Ustav, Ya L Remme, A Ya Lind, R L-E Villems *Bioorg. Khim.* **5** 365 (1979) [b]
116. N Ulbrich, I G Wool, E Ackerman, P B Sigler *J. Biol. Chem.* **255** 7010 (1980)
117. H R Burrell, J Horowitz *FEBS Lett.* **49** 306 (1975)
118. A Oplatka, O Muhlrad, R Lamed *J. Biol. Chem.* **251** 3972 (1976)
119. A S Butorin, S K Vasilenko *Izv. Sib. Otd. Akad. Nauk SSSR, Ser. Khim. Nauk* (9) 143 (1976)
120. E Junowicz, S E Charm *Biochim. Biophys. Acta* **428** 157 (1976)
121. N V Belitsina, S M Elizarov, M A Glukhova, A S Spirin, A S Butorin, S K Vasilenko *FEBS Lett.* **57** 262 (1975)
122. M Ustav, R Villems, A Lind *FEBS Lett.* **82** 259 (1977)
123. J O Langland, S M Pettiford, B L Jacobs *Protein Exp. Purif.* **6** 25 (1995)
124. D G Knorre, S D Myzina, L S Sandakhchiev *Izv. Sib. Otd. Akad. Nauk SSSR, Ser. Khim. Nauk* (3) 135 (1964)
125. C M Joyce, J R Knowles *Biochem. Biophys. Res. Commun.* **60** 1278 (1974)
126. P Remy, C Birmele, J P Ebel *FEBS Lett.* **27** 134 (1972)
127. S Bartkowiak, J Pawelkiewicz *Biochim. Biophys. Acta* **272** 137 (1972)
128. J J Befort, N Befort, G Petrissant, P Remy, J-P Ebel *Biochimie* **56** 625 (1974)
129. A A Ëlov, E M Volkov, T G Reintamm, T S Oretskaya, Z A Shabarova *Bioorg. Khim.* **15** 159 (1989) [b]
130. S Agrawal, C Christodoulou, M J Gait *Nucl. Acids Res.* **14** 6227 (1986)
131. Yu P Lysov, V P Florent'ev, A A Khorlin, K R Khrapko, V V Shik, A D Mirzabekov *Dokl. Akad. Nauk SSSR* **303** 1508 (1988) [e]
132. K R Khrapko, Y P Lysov, A A Khorlin, V V Shik, V L Florentiev, A D Mirzabekov *FEBS Lett.* **256** 118 (1989)
133. K R Khrapko, Y P Lysov, A A Khorlin, I B Ivanov, G M Ershov, S K Vasilenko, V L Florent'ev, A D Mirzabekov *DNA Sequence* **1** 375 (1991)
134. R Blanks, L W McLaughlin *Nucl. Acids Res.* **16** 10283 (1988)
135. B A Connolly, P Rider *Nucl. Acids Res.* **13** 4485 (1985)
136. L A Chrisey, C E O'Ferrall, B J Spargo, C S Dulcey, J M Calvert *Nucl. Acids Res.* **24** 3040 (1996)
137. S-H Kang, X Xu, O Heidenreich, S Gryaznov, M Nerenberg *Nucl. Acids Res.* **23** 2344 (1995)
138. R Axen, J Porath, S Ernback *Nature (London)* **214** 1302 (1967)
139. M S Poonian, A J Schlabach, A Weissbach *Biochemistry* **10** 424 (1971)
140. D J Arndt-Jovin, T M Jovin, W Bihr, A-M Frischauf, M Marquardt *Eur. J. Biochem.* **54** 411 (1975)
141. A F Wagner, R L Bugianesi, T Y Shen *Biochem. Biophys. Res. Commun.* **45** 184 (1971)
142. B A Klyashchitskii, V S Shapot *Usp. Biol. Khim.* **17** 234 (1976)
143. J Kohn, M Wilchek *Biochem. Biophys. Res. Commun.* **107** 878 (1982)
144. P Cuatrecasas *J. Biol. Chem.* **245** 3059 (1970)
145. S C March, I Parikh, P Cuatrecasas *Anal. Biochem.* **60** 149 (1974)
146. H Bmnemann, P Westhoff, R G Herrmann *Nucl. Acids Res.* **10** 7163 (1982)
147. U Lindberg, T Persson *Eur. J. Biochem.* **31** 246 (1972)
148. G Vassart, H Brocas, P Nokin, J E Dumont *Biochim. Biophys. Acta* **324** 575 (1973)
149. J N Ihle, K-L Lee, F T Kenney *J. Biol. Chem.* **249** 38 (1974)
150. J Kempf, N Pfleder, J M Egly *J. Chromatogr.* **147** 195 (1978)
151. S G Siddell *Eur. J. Biochem.* **92** 621 (1978)
152. J C Schabort *J. Chromatogr.* **73** 253 (1972)
153. L Clerici, F Campagnari, J F M de Rooij, J H van Boom *Nucl. Acids Res.* **6** 247 (1979)
154. N I Sokolova, I V Ponomarenko, Z A Shabarova, M A Prokof'ev *Dokl. Akad. Nauk SSSR* **253** 1395 (1980) [e]
155. C R Lowe, P D G Dean, in *Affinity Chromatography* (London: Wiley, 1974) p. 200
156. P D G Dean, D B Craven, M J Harvey, C R Lowe *Adv. Exp. Med. Biol.* **42** 99 (1974)
157. H Guilford, P-O Larsson, K Mosbach *Chem. Scr.* **2** 165 (1972)
158. P Brodelius, P-O Larsson, K Mosbach *Eur. J. Biochem.* **47** 81 (1974)
159. I P Trayer, H R Trayer, D A P Small, R C Bottomley *Biochem. J.* **139** 609 (1974)
160. O Berglund, F Ecstein *Eur. J. Biochem.* **28** 492 (1972)
161. R Barker, K W Olsen, J H Shaper, R L Hill *J. Biol. Chem.* **247** 7135 (1972)
162. S Ikeda, R P Swenson, D H Ives *Biochemistry* **27** 8648 (1988)
163. N R Webb, R V J Chari, G DePillis, J W Kozarich, R E Rhoads *Biochemistry* **23** 177 (1984)
164. G I Tesser, H-U Fisch, R Schwyzer *Helv. Chim. Acta* **57** 1718 (1974)
165. J T Kadonaga, R Tjian *Proc. Natl. Acad. Sci. USA* **83** 5889 (1986)
166. Z Hostomsky, J Smrt, L Arnold, Z Tocik, V Paces *Nucl. Acids Res.* **15** 4849 (1987)
167. D Staiger, F Becker, J Schell, C Koncz, K Palme *Eur. J. Biochem.* **199** 519 (1991)
168. G G F Mason, A-M Witte, M L Whitelaw, C Antonsson, J McGuire, A Wilhelmsson, L Poellinger, J A Gustafsson *J. Biol. Chem.* **269** 4438 (1994)
169. A Denizli, E Pikin *J. Chromatogr. B., Biomed. Sci. Appl.* **666** 215 (1995)
170. G S Cox, D W Gutkin, M J Haas, D E Cosgrove *Biochim. Biophys. Acta* **1396** 67 (1998)
171. J Porath *Biochimie* **55** 943 (1973)
172. L G Moss, J P Moore, L Chan *J. Biol. Chem.* **256** 12655 (1981)
173. P A Lazo *Biochem. J.* **217** 331 (1984)
174. P O Larsson, M Glad, L Hansson, M-O Mansson, S Ohlson, K Mosbach *Adv. Chromatogr.* **21** 41 (1983)
175. E M Southern, U Maskos, J K Elder *Genomics* **13** 1008 (1992)
176. H Potuzak, P D G Dean *Nucl. Acids Res.* **5** 297 (1978)
177. J B Wheatley, M H Lyttle, M D Hocker, D E Schmidt Jr *J. Chromatogr. A* **726** 77 (1996)
178. G W Anderson, J E Zimmerman, F M Callahan *J. Am. Chem. Soc.* **86** 1839 (1964)
179. S Sakakibara, N Inukai *Bull. Chem. Soc. Jpn.* **38** 1979 (1965)
180. M Wilchek, K L Knudsen, T Miron *Bioconjugate Chem.* **5** 491 (1994)
181. M Wilchek, T Miron, J Kohl *Methods Enzymol.* **104** 3 (1984)

182. S Pochet, B Arcangioli, T Huynh-Dinh *Nucl. Acids Res.* **16** 1619 (1988)
183. V Afanassiev, V Hanemann, S Wölfl *Nucl. Acids Res.* **28** e66 (2000)
184. B E Noyes, G R Stark *Cell* **5** 301 (1975)
185. B Seed *Nucl. Acids Res.* **10** 1799 (1982)
186. J K Inman, H M Dintzis *Biochemistry* **8** 4074 (1969)
187. D Barton, W D Ollis (Eds) *Comprehensive Organic Chemistry* Vol. 2 (Oxford: Pergamon Press, 1979)
188. M Fontanel, H Bazin, R Tzhoule *Bioconjugate Chem.* **4** 380 (1993)
189. V V Korshak, M I Shtil'man, in *Polimery v Protsessakh Immobilizatsii i Modifikatsii Prirodnykh Soedinenii* (Polymers in Processes of Immobilisation and Modification of Natural Compounds) (Moscow: Nauka, 1984)
190. E N Moudrianakis, M Beer *Proc. Natl. Acad. Sci. USA* **53** 564 (1965)
191. J C Alwine, D J Kemp, G R Stark *Proc. Natl. Acad. Sci. USA* **74** 5350 (1977)
192. P L Ashley, R J MacDonald *Anal. Biochem.* **140** 95 (1984)
193. J F M De Rooij, G Wille-Hazeleger, A B J Vink, J H van Boom *Tetrahedron* **35** 2913 (1979)
194. J H van Boom, J F M de Rooij, L Clerici, F Campagnari *Nucl. Acids Res. (Spec. Publ.)* **4** 85 (1978)
195. T S Godovikova, T N Orlova, E Yu Dobrikova, V A Shamanin, V F Zarytova, N V Vorob'eva, N A Serdyukova, N Yu Shamanina, I O Petruseva, N D Pitsenko *Bioorg. Khim.* **20** 1196 (1994) [b]
196. Russ. P. 1 808 014; *Byull. Izobret.* (13) 227 (1993)
197. M A Harpold, M Calvin *Nature (London)* **219** 486 (1968)
198. R Paul, G W Anderson *J. Org. Chem.* **27** 2094 (1962)
199. G J Bartling, H D Brown, S K Chattopadhyay *Nature (London)* **243** 342 (1973)
200. M T W Hearn *Methods Enzymol.* **135** 102 (1987)
201. G S Bethell, J S Ayers, W S Hancock , M T W Hearn *J. Biol. Chem.* **254** 2572 (1979)
202. K Nilsson, K Mosbach *Eur. J. Biochem.* **112** 397 (1980)
203. K Nilsson, K Mosbach *Biochem. Biophys. Res. Commun.* **102** 449 (1981)
204. K Nilsson, K Mosbach *Methods Enzymol.* **135** 65 (1987)
205. H-C Kirch, H Krüger, H S Holthausen *Nucl. Acids Res.* **19** 3156 (1991)
206. R F Borch, M D Bernstein, H D Durst *J. Am. Chem. Soc.* **93** 2897 (1971)
207. V V Romanov, V K Starostina *Biotekhnologiya* **7** 618 (1987)
208. H Ukeda, K Ono, M Imabayashi, P Matsumoto, Y Osajima *Agric. Biol. Chem.* **53** 235 (1989)
209. F B Anspach, H-J Wirth , K K Unger, P Stanton, J R Davies, M T W Hearn *Anal. Biochem.* **179** 171 (1989)
210. A Freeman, M Sokolovsky, L Goldstein *Biochim. Biophys. Acta* **571** 127 (1979)
211. I Ugi *Angew. Chem.* **74** 9 (1962)
212. P Vretblad, R Axen *Acta Chem. Scand.* **27** 2769 (1973)
213. R Axen, P Vretblad, J Porath *Acta Chem. Scand.* **25** 1129 (1971)
214. T Chow, C Juby, L Yuen *Anal. Biochem.* **175** 63 (1988)
215. R S Matson, J Rampal, S L Pentoney Jr, P D Anderson, P Coassin *Anal. Biochem.* **224** 110 (1995)
216. C H Duncan, S L Cavalier *Anal. Biochem.* **169** 104 (1988)
217. U Maskos, E M Southern *Nucl. Acids Res.* **20** 1675 (1992)
218. H Seliger, R Bader, M Hinz, B Rotte, F Eisenbeiss, S Gura, B Nitzan, S Margel *React. Funct. Polym.* **43** 325 (2000)
219. C Albretsen, K-H Kalland, B-I Haukanes, L-S Havarstein, K Kleppe. *Anal. Biochem.* **189** 40 (1990)
220. Y Hayakawa, S Wakabayashi, H Kato, R Noyori *J. Am. Chem. Soc.* **112** 1691 (1990)
221. B M Alberts, F J Amodio, M Jenkins, E D Gutmann, F J Ferris *Cold Spring Harbor Symp. Quant. Biol.* **33** 289 (1968)
222. H Potuzak, U Wintersberger *FEBS Lett.* **63** 167 (1976)
223. R M Litman *J. Biol. Chem.* **243** 6222 (1968)
224. R F Baker *Anal. Biochem.* **78** 569 (1977)
225. E M Southern *J. Mol. Biol.* **98** 503 (1975)
226. T T Nikiforov, R B Rendle, P Goelet, Y-H Rogers, M L Kotewicz, S Anderson, G L Trainor, M R Knapp *Nucl. Acids Res.* **22** 4167 (1994)
227. P Cros, R Kurfmrst, P Allibert, N Battail, N Piga, V Roig, N T Thuong, B Mandrand, C Hzhlzhne *Nucl. Acids Res.* **22** 2951 (1994)
228. M M DeAngelis, D G Wang, T L Hawkins *Nucl. Acids Res.* **23** 4742 (1995)
229. V Balladur, A Theretz, B Mandrand *J. Colloid Interface Sci.* **194** 408 (1997)
230. J Piehler, A Brecht, G Gauglitz, M Zerlin, C Maul, R Thiericke, S Grabley *Anal. Biochem.* **249** 94 (1997)
231. B I Sukhorukov, G B Sukhorukov, L I Shabarchina, M M Montrel' *Biofizika* **45** 40 (2000) [f]
232. R J Britten *Science* **142** 963 (1963)
233. S Fukui, K Sonomoto, N Itoh, A Tanaka *Biochimie* **62** 381 (1980)
234. E W Khandjian *Mol. Biol. Rep.* **11** 107 (1986)
235. S M Kalachikov, V A Adarichev, G M Dymshits *Bioorg. Khim.* **18** 52 (1992) [b]
236. L A Frumgarts, S M Kalachikov, G M Dymshits, M I Dobrikov, G V Shishkin *Izv. Sib. Otd. Akad. Nauk SSSR, Ser. Khim. Nauk* (1) 81 (1988)
237. M I Dobrikov, T A Prikhod'ko, I V Safronov, G V Shishkin *Sib. Khim. Zh.* **2** 18 (1992)
238. A Wada, A Kishizaki *Biochim. Biophys. Acta* **166** 29 (1968)
239. L I Gus'kova, V P Demushkin *Usp. Khim.* **43** 1241 (1974) [*Russ. Chem. Rev.* **43** 574 (1974)]
240. E T Bolton, B J McCarthy *Proc. Natl. Acad. Sci. USA* **48** 1390 (1962)
241. F N Rehman, M Audeh, E S Abrams, P W Hammond, M Kenney, T C Boles *Nucl. Acids Res.* **27** 649 (1999)
242. T Livache, A Roget, E Dejean, C Barthet, G Bidan, R Tzhoule *Nucl. Acids Res.* **22** 2915 (1994)
243. J G Morgan, G M Dolganov, S E Robbins, L M Hinton, M Lovett *Nucl. Acids Res.* **20** 5173 (1992)
244. H Ji, L M Smith *Anal. Chem.* **65** 1323 (1993)
245. J Ostrowski, K Bomsztyk *Nucl. Acids Res.* **21** 1045 (1993)
246. G Gadaleta, D D'Elia, L Capaccio, C Saccone, G Pepe *J. Biol. Chem.* **271** 13537 (1996)
247. T Hultman, S Stahl, T Moks, M Uhlen *Nucleosides Nucleotides* **7** 629 (1988)
248. D O'Meara, P Nilsson, P-Å Nygren, M Uhlén, J Lundeberg *Anal. Biochem.* **255** 195 (1998)
249. S W Lucas, M M Harding *Anal. Biochem.* **282** 70 (2000)
250. R C Duhamel, J S Whitehead *Methods Enzymol.* **184** 201 (1990)
251. G S Wood, R Warnke *J. Histochem. Cytochem.* **29** 1196 (1981)
252. R Alon, E A Bayer, M Wilchek *Biochem. Biophys. Res. Commun.* **170** 1236 (1990)
253. G Bussolati, P Gugliotta *J. Histochem. Cytochem.* **31** 1419 (1983)
254. K S Jakobsen, E Breivold, E Hornes *Nucl. Acids Res.* **18** 3669 (1990)
255. I R Rodriguez, G J Chader *Nucl. Acids Res.* **20** 3528 (1992)
256. W H Scouten, P Konecny *Anal. Biochem.* **205** 313 (1992)
257. T Goldkorn, D J Prockop *Nucl. Acids Res.* **14** 9171 (1986)
258. M P Vitek, S G Kreissman, R H Gross *Nucl. Acids Res.* **9** 1191 (1981)
259. T G Wood, J B Lingrel *J. Biol. Chem.* **252** 457 (1977)
260. L R Solomon, L R Massom, H W Jarrett *Anal. Biochem.* **203** 58 (1992)
261. P T Gilham, W E Robinson *J. Am. Chem. Soc.* **86** 4985 (1964)
262. H Tsurui, A Suyama, A Wada *Nucl. Acids Symp. Ser.* **19** 49 (1988)
263. A S Butorin, V V Vlasov, E M Ivanova, A S Rait, I G Shishkina, L V Yurchenko, L A Yakubov *Biopolim. Klet.* **5** 71 (1989)
264. U Baumann, U Lehmann, K Schwellnus, J H van Boom, H Kuhn *Eur. J. Biochem.* **170** 267 (1987)
265. T Schluep, C L Cooney *Nucl. Acids Res.* **26** 4524 (1998)
266. G G Karpova, L O Kozlova, N P Pichko *Izv. Sib. Otd. Akad. Nauk SSSR, Ser. Khim. Nauk* (7) 96 (1983)
267. E V Vyazovkina, E V Savchenko, S G Lokhov, J W Engels, E Wickstrom, A V Lebedev *Nucl. Acids Res.* **22** 2404 (1994)
268. J T Kadonaga *Methods Enzymol.* **208** 10 (1991)
269. S Eisenberg, S C Francrsconi, Ch Civalier, S S Walker *Methods Enzymol.* **182** 521 (1990)
270. H Kawaguchi, A Assai, Y Ohtsuka, H Watanabe, T Wada, H Handa *Nucl. Acids Res.* **17** 6229 (1989)
271. C DiRusso, R P Rogers, H W Jarrett *J. Chromatogr. A* **677** 45 (1994)
272. C Pozidis, G Vlatakis, V Bouriotis *J. Chromatogr.* **630** 151 (1993)
273. G Vlatakis, V Bouriotis *Anal. Biochem.* **195** 352 (1991)
274. P Neddermann, J Jiricny *J. Biol. Chem.* **268** 21218 (1993)

275. P Neddermann, J Jiricny *Proc. Natl. Acad. Sci. USA* **91** 1642 (1994)
276. G Schnapp, H P Rodi, W J Rettig, A Schnapp, K Damm *Nucl. Acids Res.* **26** 3311 (1998)
277. J Meinkoth, G Wahl *Anal. Biochem.* **138** 267 (1984)
278. H G Pereira *BioEssays* **4** 110 (1986)
279. J A Matthews, L J Kricka *Anal. Biochem.* **169** 1 (1988)
280. U Landegren, R Kaiser, C T Caskey, L Hood *Science* **242** 229 (1988)
281. G S Sayler, A C Layton *Annu. Rev. Microbiol.* **44** 625 (1990)
282. A G Badashkeeva, D G Knorre. *Mol. Biol.* **25** 309 (1991) [a]
283. A H Al-Hakim, R Hull *Biochem. J.* **251** 935 (1988)
284. J J Leary, D J Brigati, D C Ward *Proc. Natl. Acad. Sci. USA* **80** 4045 (1983)
285. H Yokota, K Yokoo, Y Nagata *Biochim. Biophys. Acta* **868** 45 (1986)
286. C R Petrie III, A D Adams, M Stamm, J van Ness, S M Watanabe, R B Meyer Jr *Bioconjugate Chem.* **2** 441 (1991)
287. A Oser, W K Roth, G Valet *Nucl. Acids Res.* **16** 1181 (1988)
288. V A Shamanin, A G Pletnev, S G Rubin, V I Zlobin *J. Gen. Virol.* **71** 1505 (1990)
289. K Yamakawa, H Oyamada, O Nakagomi *Mol. Cell Probes* **3** 397 (1989)
290. A Oser, G Valet *Nucl. Acids Res.* **16** 8178 (1988)
291. P Hurskainen, P Dahlen, J Ylikoski, M Kwiatkowski, H Siitari, T Lövgren *Nucl. Acids Res.* **19** 1057 (1991)
292. P S Thomas *Proc. Natl. Acad. Sci. USA* **77** 5201 (1980)
293. D Y Kwoh, G R Davis, K M Whitfield, H L Chappelle, L J DiMichele, T R Gingeras *Proc. Natl. Acad. Sci. USA* **86** 1173 (1989)
294. V Deubel, M Laille, J P Hugnot, E Chungue, J L Guesdon, M T Drouet, S Bassot, D Chevrier *J. Virol. Methods* **30** 41 (1990)
295. M Shibata, H Takano, T Hironaka, K Hirai *J. Virol. Methods* **46** 279 (1994)
296. P Frossard, K L Sisco, D L Rucknagel *Anal. Biochem.* **134** 265 (1983)
297. T K Christopoulos, E P Diamandis, G Wilson *Nucl. Acids Res.* **19** 6015 (1991)
298. G M Church, W Gilbert *Proc. Natl. Acad. Sci. USA* **81** 1991 (1984)
299. S Beck *Anal. Biochem.* **164** 514 (1987)
300. M Purrello, I Balazs *Anal. Biochem.* **128** 393 (1983)
301. P J Nicholls, A D Malcolm *J. Clin. Lab. Anal.* **3** 122 (1989)
302. M Ranki, A Palva, M Virtanen, M Laaksonen, H Soderlund *Gene* **21** 77 (1983)
303. A C Syvanen *Med. Biol.* **64** 313 (1986)
304. D V Morrissey, M Lombardo, J K Eldredge, K R Kearney, E P Groody, M L Collins *Anal. Biochem.* **181** 345 (1989)
305. P Dahlen, A C Syvanen, P Hurskainen, M Kwiatkowski, C Sund, J Ylikoski, H Soderlund, T Lovgren *Mol. Cell Probes* **1** 159 (1987)
306. G H Keller, D-P Huang, M M Manak *Anal. Biochem.* **177** 27 (1989)
307. H Kohsaka, A Taniguchi, D D Richman, D A Carson *Nucl. Acids Res.* **21** 3469 (1993)
308. M S Urdea, J A Running, T Horn, J Clyne, L Ku, B D Warner *Gene* **61** 253 (1987)
309. D V Morrissey, M L Collins *Mol. Cell Probes* **3** 189 (1989)
310. A Jungell-Nortamo, A C Syvanen, P Luoma, H Soderlund *Mol. Cell Probes* **2** 281 (1988)
311. Y Tsuruta, T Yoshioka, R Suzuki, T Sakata *J. Immunol. Methods* **169** 17 (1994)
312. T I Vener, M F Turchinsky, V P Zubov, T S Godovikova, T N Orlova, V A Shamanin, V F Kulikova *Nucl. Acids Symp. Ser.* **24** 267 (1991)
313. T S Godovikova, T N Orlova, V F Zarytova, V A Shamanin, N V Vorobjova, N A Serdjukova, A G Romashchenko *Nucl. Acids Symp. Ser.* **24** 284 (1991)
314. S Kawai, S Maekawajiri, A Yamane *Anal. Biochem.* **209** 63 (1993)
315. M Shindo, A M Di Bisceglie, J Silver, T Limjoco, J H Hoofnagle, S M Feinstone *J. Virol. Methods* **48** 65 (1994)
316. U Maskos, E M Southern *Nucl. Acids Res.* **21** 2267 (1993)
317. W Bains, G Smith *J. Theor. Biol.* **135** 303 (1988)
318. R Drmanac, I Labat, I Brukner, R Crkvenjakov *Genomics* **4** 114 (1989)
319. C R Cantor, A Mirzabekov, E Southern *Genomics* **13** 1378 (1992)
320. D J Duggan, M Bittner, N Chen, P Meltzer, J M Trent *Nat. Genet.* **21** 10 (1999)
321. R J Lipshutz, T Fodor, T R Gingeras, D J Lokhart *Nat. Genet.* 21 20 (1999)
322. D D L Bowtell *Nat. Genet.* **21** 25 (1999)
323. A Vente, M Korn, G Zehetner, A Poustka, H Lehrach *Nat. Genet.* **21** 22 (1999)
324. C M Niemeyer, D Blohm *Angew. Chem.* **38** 2865 (1999)
325. T Pastinen, A Kurg, A Metspalu, L Peltonen, A-C Syvanen *Genome Research* **7** 606 (1997)
326. A Metspalu, J M Shumaker, in *Microsystem Technology. A Power Tool for Biomolecular Studies* Vol. 10 (Eds J M Kohler, T Mejevaia, H P Saluz) (Basel; Boston; Berlin: Birkhauser Verlag, 1999) p. 371
327. Z Guo, Q Liu, L M Smith *Nat. Biotechnol.* **15** 331 (1997)
328. G Ramsay *Nat. Biotechnol.* **16** 40 (1998)
329. S Granjeaud, F Bertucci, B R Jordan *BioEssays* **21** 781 (1999)
330. M Schena, D Shalon, R W Davis, P O Brown *Science* **270** 467 (1995)
331. V G Cheung, M Morley, F Aguilar, A Massimi, R Kucherlapati, G Childs *Nat. Genet.* **21** 15 (1999)
332. D J Hacia *Nat. Genet.* **21** 42 (1999)
333. J S Früchtel, G Jung *Angew. Chem.* **108** 19 (1996)
334. R J Lipshutz, D Morris, M Chee, E Hubbell, M J Kozal, N Shah, N Shen, R Yang, S P A Fodor *Biotechniques* **19** 442 (1995)
335. A C Pease, D Solas, E J Sullivan, M T Crovin, C P Holmes, S P A Fodor *Proc. Natl. Acad. Sci. USA* **91** 5022 (1994)
336. G Lowe *Chem. Soc. Rev.* **24** 309 (1995)
337. G H McGall, A D Barone, M Diggelmann, S P A Fodor, E Gentalen, N Ngo *J. Am. Chem. Soc.* **119** 5081 (1997)
338. M C Pirrung, L F G MacGall *J. Org. Chem.* **63** 241 (1998)
339. S P Fodor, J L Read, M C Pirrung, L Stryer, A T Lu, D Solas *Science* **251** 767 (1991)
340. M Beier, J D Hoheisel *Nucl. Acids Res.* **28** e11 (2000)
341. E Gentalen, M Chee *Nucl. Acids Res.* **27** 1485 (1999)
342. Yu-H Rogers, P Yiang-Baucom, Z-J Huang, V Bogdanov, S Anderson, M T Boyce-Jacino *Anal. Biochem.* **266** 23 (1999)
343. T Strother, R J Hamers, L M Smith *Nucl. Acids Res.* **28** 3535 (2000)
344. A Kumar, O Larsson, D Parodi, Z Liang *Nucl. Acids. Res.* **28** e71 (2000)
345. L C Shriver-Lake, in *Immobilised Biomolecules in Analysis* (Eds T Cass, F S Liger) (Oxford: Oxford University Press, 1998) p. 1
346. J J Cras, C A Rowe-Taitt, D A Nivens, F S Ligler *Biosens. Bioelectron.* **14** 683 (1999)
347. A D Mirzabekov *Trends Biotechnol.* **12** 27 (1994)
348. G Yershov, V Barsky, A Belgovsky, E Kirillov, E Kreindlin, I Ivanov, S Parinov, D Gushin, A Drobyshev, S Dubiley, A Mirzabekov *Proc. Natl. Acad. Sci. USA* **93** 4913 (1996)
349. A L Drobyshev, A S Zasedatelev, G M Yershov, A D Mirzabekov *Nucl. Acids Res.* **27** 4100 (1999)
350. E Ermantraut, K Wohlfart, S Wölfl, T Schulz, M Kohler, in *Microreaction Technology. Proceedings of the 1st International Conference on Microreaction* (Ed. W Ehrfeld) (Berlin; Heidelberg: Springer, 1997) p. 332
351. L-J van Doorn, B Kleter, J Voermans, G Maertens, H Brouwer, R Heijtnik, W Quint *J. Med. Virol.* **42** 22 (1994)
352. L T Mazzola, S P Fodor *Biophys. J.* **68** 1653 (1995)
353. T M Herne, M J Tarlov *J. Am. Chem. Soc.* **119** 8916 (1997)
354. R Levicky, T M Herne, M J Tarlov, S Satija *J. Am. Chem. Soc.* **120** 9798 (1998)
355. A B Steel, T M Herne, M J Tarlov *Anal. Chem.* **70** 4670 (1998)
356. S O Kelley, N M Jackson, M G Hill, J K Barton *Angew. Chem.* **111** 991 (1999)
357. U Maskos, E M Southern *Nucl. Acids Res.* **21** 4663 (1993)
358. J C Williams, S C Case-Green, K U Mir, E M Southern *Nucl. Acids Res.* **22** 1365 (1994)
359. N C Fawcett, J A Evans, L C Chien, N Flowers *Anal. Lett.* **21** 1099 (1988)
360. H Su, K M R Kallury, M Thomson, A Roach *Anal. Chem.* **66** 769 (1994)
361. C Nicolini, V Erokhin, P Facci, S Guerzoni, A Ross, P Pashkevitsch *Biosens. Bioelectron.* **12** 613 (1997)

362. J Wang, P-E Nielsen, M Jiang, X Cai, J R Femandez, D H Grant, M Ozsoz, A Begleiter, M Mowat *Anal. Chem.* **69** 5200 (1997)
363. E F A de Vries, R B M Schasfort, J van der Plas, J Greve *Biosens. Bioelectron.* **9** 509 (1994)
364. A A Kruchinin, Y G Vlasov *Sensors Actuators B* **30** 77 (1996)
365. M Yang, M E McGovern, M Thomson *Anal. Chim. Acta* **346** 259 (1997)
366. S Sawata, E Kai, K Ikebukuro, T Iida, T Honda, I Karube *Biosens. Bioelectron.* **14** 397 (1999)
367. S Kossek, C Padeste, L X Tiefenauer, H Siegenthalter *Biosens. Bioelectron.* **13** 31 (1998)
368. K M Millan, A Saraullo, S R Mikelsen *Anal. Chem.* **66** 2943 (1994)
369. J Wang, G Rivas, X Cai, E Palecek, P E Nielsen, H Shiraishi, N Dontha, D Luo, C Parrado, M Chicharro, P A M Farias, F Valera, D Grant, M Ozsoz, M Flair *Anal. Chim. Acta* **347** 1 (1997)
370. G Marazza, I Chianella, M Mascini *Biosens. Bioelectron.* **14** 43 (1999)
371. G B Sukhorukov, M M Montrel, A I Petrov, L I Shabarchina, B I Sukhorukov. *Biosens. Bioelectron.* **11** 913 (1996)
372. M Sauer, A Brecht, K Charisse, M Maier, M Gerster, I Stemmler, G Gauglitz, E Bayer *Anal. Chem.* **71** 2850 (1999)
373. C Xiao, X-E Zhang, Y-Q Chai, W-P Hu, Z-P Zhang, X-M Zhang, A F G Cass *Biosens. Bioelectron.* **13** 451 (1998)
374. T M Jovin, A Kornberg *J. Biol. Chem.* **243** 250 (1968)
375. V V Didenko *Anal. Biochem.,* **213** 75 (1993)
376. C Hansen, F Libert, G Vassart, D Christophe *Anal. Biochem.* **162** 130 (1987)
377. I Raineri, C Moroni, H P Senn *Nucl. Acids Res.* **19** 4010 (1991)
378. A Rolfs, I Weber *Biotechniques* **17** 782 (1994)
379. A Rosenthal, D S C Jones *Nucl. Acids Res.* **18** 3095 (1990)
380. S Stamm, J Brosius *Nucl. Acids Res.* **19** 1350 (1991)
381. C R Thrash, R T Schimke *J. Biol. Chem.* **252** 5615 (1977)
382. K Kuribayashi-Ohta, S Tamatsukuri, M Hikata, C Miyamoto, Y Furuichi *Biochim. Biophys. Acta* **1156** 204 (1993)
383. E Hara, T Kato, S Nakada, S Sekiya, K Oda *Nucl. Acids Res.* **19** 7097 (1991)
384. K Kuribayashi, M Hikata, O Hiraoka, C Miyamoto, Y Furuichi *Nucl. Acids Symp. Ser.* **19** 61 (1988)
385. A A Ëlov, E M Volkov, Z A Shabarova *Bioorg. Khim.* **17** 789 (1991) [b]
386. H A Marble, R H Davis *Biotechnol. Prog.* **11** 393 (1995)
387. R H Davis *Curr. Opin. Biotechnol.* **6** 213 (1995)
388. L Ya Denisova, S N Zagrebel'nyi, N M Pustoshilova, A G Ven'yaminova, V V Gorn, V F Zarytova, M N Repkova, I G Shishkina *Bioorg. Khim.* **15** 562 (1989) [b]
389. H W Jarrett *J. Chromatogr.* **618** 315 (1993)
390. V Delpech *Ann. Biol. Clin.* **58** 29 (2000)
391. M J O'Donnell-Maloney, C L Smith, C R Cantor *Trends Biotechnol.* **14** 401 (1996)

[a] — *Mol. Biol. (Engl. Transl.)*
[b] — *Russ. J. Bioorg. Chem. (Engl. Transl.)*
[c] — *Kinet. Catal. (Engl. Transl.)*
[d] — *Biochemistry (Engl. Transl.)*
[e] — *Dokl. Chem. Technol., Dokl. Chem. (Engl. Transl.)*
[f] — *Biophysics (Engl. Transl.)*

Russian Chemical Reviews **70** (7) 535 – 541 (2001) © 2001 Russian Academy of Sciences and Turpion Ltd

DOI 10.1070/RC2001v070n07ABEH000652

Paramagnetic resonance and detection of a single electron spin

A L Buchachenko, F I Dalidchik, S A Kovalevskii, B R Shub

Contents

I.	Introduction	535
II.	ESR sensitivity evolution	535
III.	Optical detection and magnetic resonance of single triplet molecules	536
IV.	Single-molecule tunnelling spectroscopy	537
V.	Tunnelling spectroscopy of a single electron spin	538
VI.	Tunneling spectroscopy of spin channels	538
VII.	Single electron spin relaxation	539
VIII.	Can single-spin ESR be detected by tunnelling spectroscopy?	539
IX.	Excited states and single-molecule chemistry	540
X.	Single-molecule spin chemistry	541
XI.	Conclusion	541

Abstract. Two methods of detection of a single electron spin, namely, optical detection (1993) and tunnelling spectroscopy (1998) are described. Both methods are based on the spin chemistry laws. Physical principles and prospects of application of these methods are considered. The bibliography includes 34 references.

I. Introduction

Electron spin resonance (ESR) spectroscopy has found numerous applications in physics, chemistry, molecular biology and medicine. This method has two key functions. First, it is used as a physical tool in studies of the structure and dynamics of spin carriers (radicals, ions, complexes, high-spin molecules, *etc*.). The hyperfine (electron – nucleus) interaction constants as well as the magnitudes of dipole (electron – electron) splitting of the Zeeman energy levels and the parameters of spin – orbit interaction, which manifests itself as different values of *g*-factors, contain structural information. The width and shape of ESR spectral lines contain information on the rotational, translational and intramolecular spin carrier dynamics. This information can be extracted by means of the spin relaxation times τ_1 and τ_2 which are determined by the rate of energy relaxation of the Zeeman reservoir and the rate of phase relaxation (*i.e*., spin precession) respectively.

Second, ESR spectroscopy is an important analytical method which is used not only in fundamental areas of science (physics, chemistry and biology), but also in ecology, archaeology, medicine and history (*e.g*., in age determination using ESR[1,2]). Analytically, the key advantage of this method is its high sensitivity. The aim of this review is to analyse the evolution of this parameter and to outline some ways toward progress in reaching the limiting sensitivity, which allows detection of a single, individual paramagnetic species.

A L Buchachenko, F I Dalidchik, S A Kovalevskii, B R Shub N N Semenov Institute of Chemical Physics, Russian Academy of Sciences, ul. Kosygina 4, 119991 Moscow, Russian Federation. Fax (7-095) 938 24 84.
Tel. (7-095) 939 74 90. E-mail: spinchem@chph.ras.ru
(A L Buchachenko)
Tel. (7-095) 939 72 59 (F I Dalidchik), (7-095) 137 82 73 (B R Shub)

Received 15 January 2001
Uspekhi Khimii **70** (7) 611 – 618 (2001); translated by A M Raevsky

II. ESR sensitivity evolution

In his pioneering paper Zavoiskii reported a sensitivity of $\sim 10^{19}$ spins. In 1959, Semenov and Bubnov[3] improved the ESR sensitivity and reached a value of $\sim 10^{11}$ spins using high-frequency modulation and automatic frequency control. Since then this value appeared to be a 'nearly limiting' one for all commercial ESR spectrometers including modern instruments. Further improvement of sensitivity up to $\sim 10^7$ spins[4] appeared to be solely due to the development of high-resolution ESR spectroscopy (an 'elite' division of ESR spectroscopy) which operates with magnetic fields of ~ 50 kŒ. The sensitivity of 'routine' ESR spectroscopy is, as a rule, $\sim 10^{11}$.

Technically, this threshold is difficult to overcome since it is determined by the low sensitivity of detectors of microwave and radiofrequency radiation (it should be remembered that classical ESR spectroscopy is based on measurements of energy losses).

A great breakthrough in studies aimed at improving the ESR sensitivity is associated with the use of a combination of the microwave pumping of the spin system with optical detection of results. High photon energy allows them to be detected even in the photon-counting regime. This provides a colossal gain in sensitivity and starts the development of non-classical ESR spectroscopy, *viz*., the so-called optically detected magnetic resonance (ODMR).

The principle of ODMR is illustrated in Fig. 1. Let us assume that a triplet radical pair with the total spin $S = 1$ is generated by photolysis or radiolysis in solution or in a solid. In the magnetic field, only two spin states are mixed. These are the triplet state T_0 with the zero spin projection and the singlet state S, whereas the other two spin states (T_+ and T_-) with the spin projections $S_z = \pm 1$ are excluded from the triplet – singlet intersystem crossing of the pair. Fast intersystem crossing from the non-reactive state T_0 to the reactive state S followed by the formation of reaction products in the radical pair leads to depopulation of the levels T_0 and S. Microwave pumping at the ESR frequency ω corresponding to the difference between the Zeeman energies of

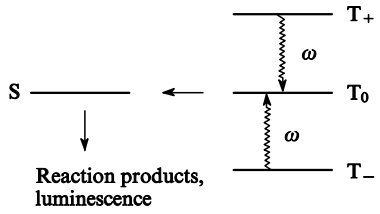

Figure 1. An energy level diagram illustrating the ODMR mechanism. Here and in Fig. 2 wavy arrows denote the microwave pumping of corresponding transitions.

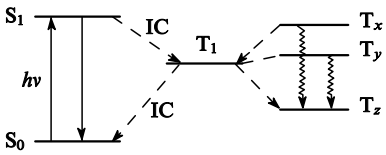

Figure 2. An energy level diagram illustrating transitions between different levels in the pentacene molecule.
Notations of energy levels: S_0 and S_1 are the ground-state singlet and excited singlet levels, respectively; T_1 is the lowest triplet state; T_x, T_y and T_z are the magnetic sublevels of the triplet state T_1. IC denotes intersystem crossing.

the states T_0-T_+ and T_0-T_- leads to an inversion drop and accumulation of electron spins on the level T_0, thus increasing the yield of reaction products. Clearly, the radical pair serves as a chemical microwave detector. If reaction products fluoresce, 'chemical reception' of microwaves can be optically detected, which is the case with ODMR. However, this is not the only reception technique since in the case of charged reaction products magnetic resonance can be detected using changes in conductivity. Generally, this technique is well known as Reaction Yield Detected Magnetic Resonance (RYDMR). Pioneering studies on RYDMR were reported by Frankevich.[5,6] Among different versions of the RYDMR method, ODMR is the most sensitive one.

The outstanding possibilities of the ODMR technique can be best illustrated by the results obtained by Molin *et al.*[7,8] taking detection of aromatic radical anions as an example. Generation of anion–cation radical pairs in the experiments on radiolysis of solutions of aromatic molecules is followed by their annihilation and creation of electronically excited luminescent molecules. The yield of such molecules is strongly dependent on the microwave pumping of ESR transitions in the radical pair. In this case the ODMR sensitivity is as high as several tens of spins. It should be noted that both pulsed and CW ODMR can be observed experimentally.

Having reached such a high sensitivity, it is logical to pose the next problem which can be formulated as detection of single-molecule ESR (or ESR of a single electron spin carrier).

III. Optical detection and magnetic resonance of single triplet molecules

Progress in photodetection technique and confocal optical microscopy has opened the possibility of visual observation and optical detection of single molecules.[9] Upon being illuminated, luminescent molecules (*e.g.*, rhodamine 6G, terrylenediimine, *etc.*) adsorbed on a surface, implanted (in low concentrations) in monomolecular layers or embedded in thin polymer films can be observed as molecular 'fireflies' using a microscope. Currently, this experimental technique has been intensely developed. It is widely used in, *e.g.*, molecular dynamics studies. Translational dynamics are studied by tracing the 'firefly' trajectory while information on rotational dynamics is obtained by measuring luminescence depolarisation. Other areas of application of the 'firefly' technique include measurements of the rates of energy transfer to neighbouring molecules, verification of the ergodic theorem, *etc.*[10,11]

Many optical chromophores used in the experiments on observation of single molecules occur in the long-lived triplet states. By placing such molecules in a permanent and a microwave magnetic field one can initiate paramagnetic resonance and detect it optically by means of observation of light emission from the molecular 'fireflies'. The possibility of using such a detection technique can be aptly illustrated taking the ODMR of single pentacene molecules in a *p*-terphenyl single crystal (the mole fraction of pentacene was $\sim 10^{-8}$) as an example. *A propos*, it is this system that was used in the first successful single-molecule ODMR experiments.[12,13]

An energy level diagram of pentacene spins, typical of almost all molecules, is shown in Fig. 2. After absorption of a quantum $h\nu$, the molecule goes from the ground state S_0 to the excited state S_1 which is then depopulated *via* fluorescence or molecular relaxation to the lowest triplet state T_1. The state T_1 is paramagnetic and triply spin degenerate. The dipole interaction between two spins leads to removal of degeneracy and the appearance of three energy levels (T_x, T_y and T_z).

The dipole electron–electron interaction is described by a tensor, the principal components of which, ε_x, ε_y and ε_z, are different with respect to different molecular axes. In ESR spectroscopy, they are usually expressed through the parameters D and E.

$$D = \frac{3}{2}\varepsilon_z,\ E = -\frac{1}{2}(\varepsilon_x - \varepsilon_y).$$

These parameters characterise the deviation of the symmetry of the dipole interaction (and, hence, spin distribution) from spherical and axial symmetry, respectively.

Dipole splitting also exists in the absence of a magnetic field. If a molecule is placed in an external magnetic field, one should take into account not only the dipole magnetic interaction, but also the Zeeman magnetic interaction, so that in the limiting case (in strong magnetic fields) the spin states T_x, T_y and T_z with the energies ε_x, ε_y and ε_z, respectively, are transformed into the corresponding canonical spin states T_+, T_0 and T_-.

Intersystem crossing from the state S_1 to the state T_1 is spin-forbidden and is thus induced by the intramolecular spin–orbit interaction, which partially removes this forbiddenness (due to exchange between the intrinsic angular momentum of an electron and its orbital angular momentum). Since the orbital angular momentum is anisotropic (*i.e.*, it takes different values with respect to different molecular axes), the spin–orbit interaction is also anisotropic. Because of this, the rate of inversion drop from the state S_1 also appears to be dependent on the symmetry of the molecule: the states T_x, T_y and T_z with the energies ε_x, ε_y and ε_z (and, correspondingly, the states T_+, T_0 and T_-) are populated at different rates.

For the same reason, the depopulation rates of these levels due to spin relaxation from the state T_1 to the ground state are also different. These differences in the population and depopulation rates of the three spin sublevels of the triplet T_1 are responsible for colossal differences in their steady-state populations. For instance, excitation of a pentacene molecule to the state S_1 followed by red $S_1 \rightarrow S_0$ fluorescence also causes population of the lowest triplet level T_1 with a probability of 0.5%. Among the triplet sublevels, the highest population rates ($1.5 \times 10^5\ s^{-1}$) are observed for the levels T_x and T_y; the depopulation rates of these levels (transition to the ground state S_0) are also high ($0.25 \times 10^5\ s^{-1}$).

For the level T_z, these rates are very low, so that in the steady-state regime only the levels T_x and T_y appear to be populated, whereas the level T_z remains nearly completely depopulated.

If microwave pumping is tuned to resonance with the energy difference between the spin levels T_x and T_z, their populations are

equalised. As a result, a proportion of pentacene molecules pass to the long-lived T_z level and are temporarily excluded from the 'community' of fluorescent molecules.

Clearly, a decrease in the fluorescence intensity of a single pentacene molecule is an indicator of magnetic resonance. Knowing the kinetic constants of photophysical and relaxation processes, one can estimate the magnitude of this effect: it reaches $\sim 20\%$ in the case of microwave pumping of the transition $T_x - T_z$.[13]

An ODMR spectrum of a single triplet pentacene molecule is shown in Fig. 3 *a*. In accord with theory, microwave pumping at the resonance frequencies of the $T_x - T_z$ and $T_y - T_z$ transitions (~ 1470 and ~ 1410 MHz, respectively) leads to noticeable (by more than 10%) decrease in the fluorescence intensity; the latter transition is less intense since the population of the level T_y is intermediate between those of the 'active' (T_x) and 'passive' (T_z) levels.

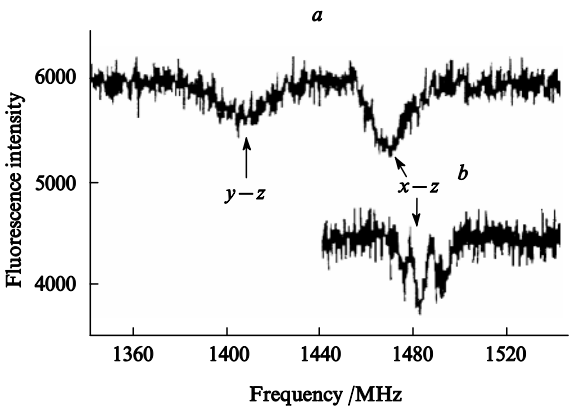

Figure 3. An ODMR spectrum of a single pentacene molecule implanted in a *p*-terphenyl crystal (*a*) and hyperfine structure of the ODMR spectrum of a pentacene molecule deuterated at all positions except for two positions at the carbon atoms lying on the central symmetry axis (*b*).

If the number of magnetic nuclei is small and the hyperfine splitting exceeds the linewidth, one can resolve the hyperfine structure in the spectrum of triplet ODMR. For instance, the ODMR spectrum of a pentacene molecule deuterated at all positions except for two protons at the carbon atoms lying on the central symmetry axis exhibits a clearly seen hyperfine structure originating from two magnetically equivalent protons (a triplet with the 1 : 2 : 1 intensity ratio) and corresponding to the $T_x \rightarrow T_z$ (Fig. 3 *b*) transition with an electron – proton interaction constant of ~ 10 MHz (~ 3.6 Gs).[13]

At first glance, observation of hyperfine structure seems to be a mysterious phenomenon. In a single-molecule experiment, nuclear configurations (a total of four for two protons of the partially deuterated pentacene) should be fixed during the time taken for one excitation – fluorescence cycle ($S_0 \rightarrow T_z \rightarrow S_0$), which is of the order of $10^{-5} - 10^{-6}$ s. The unpaired electron of the triplet molecule must experience only one nuclear configuration. However, the spectral shape suggests that it somehow 'sees' all the four pairs of spin configurations, namely, $\alpha_n\alpha_n$, $\alpha_n\beta_n$, $\beta_n\alpha_n$ and $\beta_n\beta_n$ (here, α_n and β_n denote the proton spins; the pairs $\alpha_n\beta_n$ and $\beta_n\alpha_n$ are equivalent and correspond to identical nuclear configurations).

The answer to this enigma is simple. In single-molecule ODMR experiments, the molecule experiences over 10^6 cascade excitation – fluorescence cycles during the typical measuring time (usually, about 10 min). Hence, the number of 'arrivals' at the ground state with a residence time of 100 μs during each cascade cycle is the same. Due to the dipole interaction of pentacene protons with the nuclei of neighbouring molecules and other nuclei of the indicator pentacene molecule, this time appears to be sufficient for reorientation of the spins of the pentacene protons (in spectroscopy, this is called spin diffusion or spectral diffusion). As a result, the pentacene protons have time to 'arrive' at all the four nuclear configurations during the ODMR measuring time and the final spectrum exhibits a triplet with the 1 : 2 : 1 intensity ratio (see Fig. 3 *b*).

It should be noted that reorientation of the proton spins (spectral diffusion) occurs only at those instants when the molecule is in the ground state. In the triplet state, strong electron – nuclear magnetic interaction fixes the proton spins and 'excludes' them from spectral diffusion (or, as spectroscopists say, excludes these protons from the dipole – dipole nuclear reservoir).

The hyperfine structure of the ODMR spectrum of ^{13}C nuclei of a pentacene molecule isotopically substituted at different positions is due to the same reasons.[14] However, it should be noted that all the ODMR spectra of single triplet molecules observed so far were measured for only one case, *viz*., a pentacene molecule implanted in a terphenyl crystal. Further progress of this experimental technique and extension of the areas of its application is closely related to advances of optical detection of single molecules in crystals and on the surface of solids.[15]

Magnetic resonance of single spin carriers has been intensively developed. Recently, Köhler[16] has reported an excellent review concerning the state-of-the-art and prospects of studies in the field, so that there is no need to dwell on this point.

Mention may be made of one important circumstance: it is spectral diffusion and change in the nuclear spin configurations at a single electron spin that cause a remarkable phenomenon, *viz*., a single spin Hahn echo.[17] It should be remembered that spin echo (Hahn echo) appears as a result of coherent behaviour of a spin ensemble; the observation of a single spin Hahn echo confirms the ergodic theorem, according to which averaging over the ensemble is equivalent to averaging over time.

IV. Single-molecule tunnelling spectroscopy

Recently published series of pioneering studies on tunnelling vibrational spectroscopy[18–20] has promoted the transformation of scanning tunnelling microscopy from a 'topographic' method for monitoring the atom-molecular relief of a surface into a new powerful method of chemical physics, which allows one not only to 'see' a desired single molecule, but also to identify it from 'fingerprints' (the vibronic spectrum) and even follow its chemical fate. The last-mentioned circumstance seems to be of great value owing to the possibility of observation of chemical transformations of a single molecule, which has appeared for the first time. So far classical chemistry has been concerned with molecular ensembles even in the best versions of molecular beam techniques. Modern coherent chemistry also deals with single wave packets (ensembles of coherent molecules) rather than single molecules.[21]

Physically, the idea a single-molecule, resonance tunnelling vibrational spectroscopy[18] is very simple. If a scanning tunnelling microscope operates in the field emission mode and the tip voltage exceeds the work function of electrons, the tunnelling electrons leaving the tip appear to be confined in the space between the tip and the adsorbed molecule 'sitting' on the surface under the tip. The electrons confined in this space can move between two potential barriers, *viz*., the tip and the surface. The residence time of an electron under the tip is of the order of $10^{-13} - 10^{-14}$ s (it is much longer than the mean free time), *i.e*., the space between the tip and the surface represents a specific nanoscale resonator in which standing waves (field emission resonances) appear at particular energies. Since the resonance energy depends on the tip potential, the tunnelling current as function of the bias voltage exhibits some clearly seen peaks corresponding to vibronic (resonance) energy levels of the specified adsorbed molecule which interacts with an the electron trapped in the resonator. This is a specific form of manifestation of a fundamental quantum effect called resonance bleaching of double potential barriers. Such barriers can be as 'wide and high' as it is wished, but if the

energy of the species corresponds to that of a quasi-stationary level, they appear to be penetrable.[22] The double potential barriers for which the energy of the tunnelling species can vary [23] (*e.g.*, thin layers of a dielectric containing impurity atoms or the tunnelling contacts containing adsorbed molecules) also appear to be penetrable.

In such systems, energy exchange between the tunnelling electrons and vibrational degrees of freedom of the impurity atoms or adsorbed molecules can occur, thus leading to excitation of oscillations (inelastic interaction). For those electrons whose energies correspond to those of vibronic levels of the resonator containing an adsorbed molecule, the vacuum gap between the surface and the tip becomes transparent; in this case, the tunnelling current is a maximum.

V. Tunnelling spectroscopy of a single electron spin

Tunnelling spectroscopy also allows detection of a single electron spin on the surface. This requires that the tunnelling electron be able to distinguish (discriminate) two spin states of the unpaired electron with $S_z = \pm 1/2$ (*e.g.*, the Zeeman energy levels of a paramagnetic species). There are two parameters suitable for performing such a discrimination, *viz.*, energy and spin. In typical magnetic fields $H \approx 3000$ Gs, the Zeeman energy of the unpaired electron is $\sim 10^{-5}$ eV, which is 4–5 orders of magnitude lower than the energies of the tunnelling electron and 3 orders of magnitude lower than the resolution of tunnelling spectroscopy (~ 0.01 eV). Clearly, it is impossible to use energy as a parameter for discriminating the Zeeman energy levels of the unpaired electron. This means that the other parameter, spin, should be used and that the detection principles of a single spin should be based on the spin chemistry laws.

Let us consider from this viewpoint the spin states and spin dynamics of two electron spins, the spin of a paramagnetic (probed) centre and that of a tunnelling (probing) electron. This two-spin system represents a spin analogue of the radical pair considered in the spin chemistry. It can be in two states, *viz.*, in a singlet state with the total spin $S = 0$ or in the triplet state with the total spin $S = 1$.

The energy splitting between these spin states equals the exchange energy J of two electrons in the nanoscale resonator. This means that all vibronic levels of the spin carrier situated under the tip should be split into doublets corresponding to the singlet and triplet spin states of the electron pair. The nanoscale resonator is 'transparent' to the tunnelling electrons of the electron pair irrespective of the state (singlet or triplet) of the pair at different energies (different tip potentials).

The interaction between two electrons (the tunnelling electron and the unpaired one) is identical to the interaction between radicals in a radical pair. For instance, recombination of a singlet radical pair, CH_3 and OH, involves the singlet channel only to give a singlet CH_3OH molecule, while their disproportionation involves the triplet channel (the reaction $CH_3 + OH \rightarrow {}^3CH_2 + H_2O$) to give the triplet carbene ${}^3CH_2$. Thus, formally, both channels are spin-allowed (*i.e.*, the total spins of the reagents and products in each channel conserve). However, the energy 'cost' of each channel is different, *viz.*, the former process proceeds barrierlessly (without activation energy), whereas the latter requires the overcoming of an energy barrier of ~ 6 kcal mol^{-1}.

Tunnelling spectroscopy of a single electron spin on the surface was theoretically substantiated and experimentally implemented by Dalidchik and Kovalevskii.[24] The spectrum of a O_2^- anion sitting on the TiO_2 surface (Fig. 4) exhibits a doublet splitting of each line, which is in complete agreement with theory. The splittings *1–2*, *2–3*, *1′–2′* and *2′–3′* equal 0.15 eV, which exactly corresponds to the vibrational quantum for the O–O bond in the anion (the frequency of the stretching vibrations O–O is 1180 cm^{-1}). Singlet–triplet splitting between the peaks, *i.e.*, the separations between the lines *1–1′*, *2–2′* and *3–3′*, is equal to the exchange energy of two electrons (the tunnelling

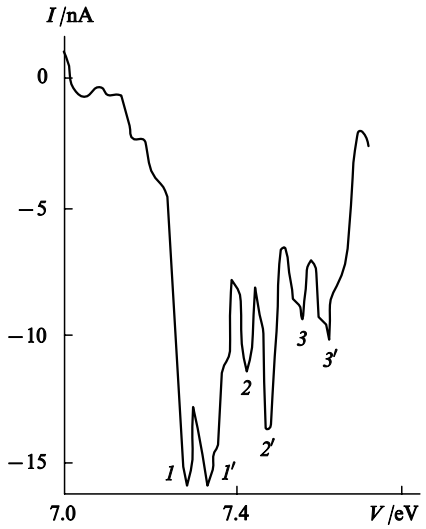

Figure 4. Tunnelling current I as function of the tip potential V (tunnelling spectrum) of a single radical anion O_2^- on the TiO_2 surface.

electron and the unpaired electron of the radical anion O_2^-) in the nanoscale resonator.

This experiment also allowed the exchange energy to be measured ($J = 0.07$ eV), which provided the possibility of estimating the size of the nanoscale resonator, R. Let us write the known relationship

$$J(R) = J_0 \exp(-\alpha R),$$

where J_0 is the exchange energy in a strongly coupled two-electron system (*e.g.*, H_2 molecule) and α is the characteristic parameter of the J decay as a function of R. Assuming that $J_0 \approx 4.5$ eV and $\alpha \approx 2$ Å^{-1}, we get $R \approx 2.1$ Å, which seems to be physically realistic for the nanoscale resonator.

VI. Tunneling spectroscopy of spin channels

As mentioned above, a single paramagnetic species can be detected using tunnelling spectroscopy due to the appearance of two resonance channels (a singlet and a triplet one) of the tunnelling current. These channels are separated by ~ 0.1 eV on the energy scale. Such a doublet splitting of vibronic levels was confirmed experimentally and discussed above (see Fig. 4). Equidistant doublet splitting of all lines in the tunnelling spectrum (on the plot of the dependence of the current I on the potential V) is an unambiguous indicator of the presence of a spin carrier (a radical or an ion) under the tip. However, direct attribution of each of the two spin channels to the singlet and triplet channel is impossible (we cannot determine to which channel the groups of lines *1*, *2* and *3* and *1′*, *2′* and *3′* in Fig. 4 belong). Based on general considerations and following Pauli, one can only suggest that the triplet level lies above the singlet one on the energy scale, *i.e.*, that the low-energy lines of the doublets correspond to the singlet channel, while their high-energy components correspond to the triplet channel. However, these considerations seem to be quite unreliable since no details of the interaction between the tunnelling electron and paramagnetic centre are currently known.

Microwave pumping is also unhelpful in distinguishing these channels since the singlet channel is ESR 'silent' while the response of the triplet channel (transitions between the states T_+, T_0 and T_-) does not produce any changes in the tunnelling current. Therefore, if microwave pumping causes no transitions between the states S and T, no transfer of the tunnelling electrons between the two channels occurs. On the other hand, yet another reason seems to be stronger: the lifetime of the electron pair in the nanoscale resonator is much shorter than the time taken for spin reorientation induced by microwave pumping. This means that

classical ESR of a single electron spin is impossible and other approaches should be used.

Imagine that the tip of a tunnelling microscope is made of a ferromagnetic material and emits spin-polarised electrons. (Such tips are widely used in topographic studies of the surface of ferromagnetic materials.[25]) If the voltage is chosen in such a way that the nanoscale resonator is 'tuned' in resonance with the singlet level, the potential barrier on the surface is transparent to the tunnelling electrons with the spins antiparallel to the spin of the paramagnetic centre. The singlet spin state of two electrons (the tunnelling electron and the unpaired one) in the nanoscale resonator is of course a combination of the spins of these electrons. Let the emitted (polarised) electrons leaving the paramagnetic tip have the spin β and the unpaired electron of the paramagnetic centre have either the spin α of β (here, the difference between the populations of the Zeeman energy levels of the electrons is neglected and the probabilities of the appearance of electrons with the spins α and β are taken to be equal). Then, the combinations αβ correspond to the singlet state of the electron pair, thus providing conditions for the tunnelling current to flow, while the combinations ββ correspond to the triplet state whose energy differs by a value of J. For the spin combinations ββ the potential barrier is impenetrable, so this contribution to the tunnelling current is locked.

Here, an important point which was first reported by Kozhushner *et al.*[26,27] should be taken into account. Due to exchange interaction between the electrons (more exactly, its nonsecular term $(1/2)J(S_+S_- + S_-S_+)$, where S_+ and S_- are the spin operators which increase and decrease the spin projection, respectively), the polarised electrons leaving the tip also polarise the spin of the unpaired electron in such a manner that its α spin it transformed into a β spin and the energy level α of the paramagnetic centre is depopulated. The system undergoes a transition from the singlet state to the triplet state and the resonance tunnelling current in the singlet channel no longer flows.

An energy level diagram illustrating the population of the Zeeman levels of both electrons in the system 'ferromagnetic tip – paramagnetic centre' is shown in Fig. 5. Initially (*a*), both energy levels corresponding to the single spin have nearly equal populations. If the tip potential differs from zero, the tunnelling current I_t proportional to $N_\beta P_\alpha$ (N_β is the population of the Zeeman energy level of the polarised tip electrons and P_α is the population of the upper Zeeman energy level α of the paramagnetic centre) flows in the system. The singlet current will flow only provided that the single spin of the paramagnetic centre will be oriented antiparallel to the spins of the tunnelling electrons, *i.e.*, in the combination βα.

It is known that

$$\frac{P_\alpha}{P_\beta} = \exp\left(-\frac{g\beta H}{kT}\right),$$

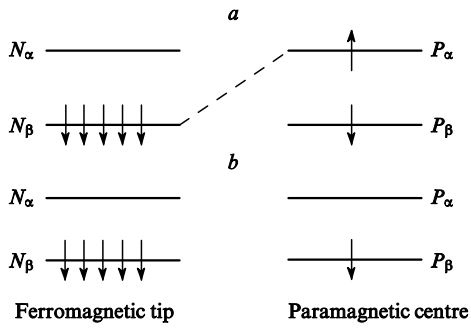

Figure 5. An energy level diagram illustrating population of the Zeeman levels in the system 'ferromagnetic tip – paramagnetic centre'. Initial state (*a*) and after passage of the tunnelling current (*b*).

where $g\beta H$ is the Zeeman splitting. Since $g\beta H \ll kT$, we get $P_\alpha \approx P_\beta$. Exchange interaction causes polarisation of the spin α of the paramagnetic centre (an analogue of the flip-flop transition in the nuclear Overhauser effect) and depopulation of the upper Zeeman energy level. As a result, only the spin combinations ββ remain in the system (Fig. 5*b*). The singlet resonance peak on the $I-V$ plot disappears and the tunnelling current (singlet channel) is locked.

The polarisation mechanism of the singlet tunnelling current lock has not been experimentally observed so far. However, should it be found, it could be possible to distinguish between the singlet and triplet channels of the resonance tunnelling current and to determine not only the magnitude, but also sign of the electron – electron exchange interaction in the nanoscale resonator. This opens new prospects for single-molecule tunnelling spectroscopy.

VII. Single electron spin relaxation

Observation of the lock effect of the singlet tunnelling channel requires that the spin of the paramagnetic species be completely polarised. This is possible only in the case of slow spin – lattice relaxation where the spin orientation of the species remains fixed between the acts of electron transport between the ferromagnetic tip and the surface. For characteristic spin relaxation times ($\tau_s \approx 10^{-8}$ s), this condition is met if the tunnelling currents are rather heavy, $I > 0.1$ nA s^{-1}. At weaker tunnelling currents, the species can have random spin orientations at the instances corresponding to the acts of interaction with the tunnelling electron; this means that both parallel and antiparallel orientations of the spins of the species and the electron are possible. During the measuring time of the tunnelling current (at specified voltage), the paramagnetic species sequentially interacts with numerous electrons leaving the tip (the number of electrons is $N = It$, where t is the measuring time). The probabilities of the singlet and triplet states of electron pairs are determined not only by the statistics of these states, but also by the kinetics of both spontaneous (relaxation) spin transitions and those induced by the polarised electron current.

In the case of ferromagnetic tip the lock rate of the singlet channel is given by the relation

$$\frac{\partial P}{\partial t} = -\left(I - \frac{1}{\tau_s}\right). \quad (1)$$

Here, P is the population of the singlet channel (*i.e.*, the population of the spin states αβ) and I is the tunnelling current of those electrons that had experienced exchange scattering by the paramagnetic centre. The first term in Eqn (1) includes the polarisation of the paramagnetic centre due to the polarised electron current (the pumping rate of the triplet channel and the depopulation rate of the singlet channel) while the second term includes the depolarisation (relaxation) rate of the triplet channel and the recovery rate of the singlet channel.

If $I > \tau_s^{-1}$ ($\partial P/\partial t < 0$), population of the triplet channel and depopulation of the singlet channel occur; the tunnelling current in the singlet channel is locked. At weak currents, where $I < \tau_s^{-1}$ ($\partial P/\partial t > 0$), the relaxation rate is higher than the population rate of the triplet channel. In this case, the weak tunnelling current cannot lock the singlet channel that remains open. In fact, the condition $I = \tau_s^{-1}$ determines the lock threshold of the tunnelling current. It allows measurements of the electron spin relaxation time of the single paramagnetic centre under conditions of tunnelling spectroscopy.

VIII. Can single-spin ESR be detected by tunnelling spectroscopy?

Novel spin spectroscopy methods, *viz.*, optical spectroscopy and tunnelling spectroscopy are based on spin combinations of two

electrons. In both cases, not only detection of single paramagnetic species, but also measurements of their spin relaxation parameters is possible. However, these methods use fundamentally different detection techniques. In the case of optical detection, the singlet channel manifests itself *via* fluorescence and, hence, some of its characteristics can be measured. The triplet channel is nondetectable; however, both the channels are strongly coupled *via* the spin–orbit and magnetic interactions, so that any changes in the triplet (nondetectable) channel affect some parameters of the singlet channel. In tunnelling spectroscopy, both these channels are detectable; however, no magnetic interaction between them occurs so that they are independent.

There is also a number of dynamic distinctions between the two above-mentioned detection techniques. In the case of optical detection, the residence time of a molecule in the triplet state is $\sim 10^{-5}$ s in each excitation–deactivation cycle. This time is much longer than that required for spin reorientation under the action of microwave pumping, $\tau_{mw} = (\gamma H)^{-1}$ (γ is the gyromagnetic ratio of an electron and H is the strength of the microwave field). Typically, $\tau_{mw} \approx 3.1 \times 10^{-7}$ s; this means that the triplet lifetime is long enough for both spin reorientation and change in the populations of the triplet levels under the action of the microwave magnetic field. In other words, the triplet state is an effective 'receiver' of external microwave radiation. In tunnelling spectroscopy, the residence time of the electron in the nanoscale resonator is very short. As mentioned above, it does not exceed 10^{-14} to 10^{-13} s. This means that the triplet states in the nanoscale resonator cannot act as effective 'receivers' of microwave radiation.

In tunnelling microscopy, single-spin magnetic resonance should be detected using non-classical approaches (*e.g.*, polarised tunnelling electrons).

In this case, the population kinetics of the spin states is similar to that considered above; however, transitions between two spin orientations of a paramagnetic species can now be stimulated not only by the tunnelling electrons, but also by microwave pumping.

This can be easily understood by considering Eqn (1) again. If resonance microwave pumping occurs (*i.e.*, the ESR conditions are met), this equation takes the form

$$\frac{\partial P}{\partial t} = -\left(I - \frac{1}{\tau_s} - \frac{1}{\tau_{mw}}\right). \qquad (2)$$

As can be seen, a new term appears, which is due to the spin relaxation induced by the microwave pumping. Spin relaxation induces additional transitions from the state ββ to the state αβ, thus additionally populating the singlet channel with a rate of τ_{mw}^{-1}. In other words, microwave pumping shifts the lock threshold of the singlet channel in such a manner that the old condition $I = \tau_{mw}^{-1}$ is replaced by a new one,

$$I = \frac{1}{\tau_s} + \frac{1}{\tau_{mw}}.$$

Since the values τ_s^{-1} and τ_{mw}^{-1} are commensurable under standard ESR conditions, the additional shift of the lock threshold of the tunnelling current in the singlet channel due to microwave pumping can be noticeable and even experimentally measurable. Moreover, experiments under conditions where $\tau_{mw}^{-1} \ll \tau_s$ can be readily set up (at $H \gg 1$ Œ). In this case, the shift of the lock threshold will be nearly completely determined by the microwave pumping. This offers considerable promise for single-spin ESR detectable from the tunnelling current. A complete theory of this phenomenon has been developed recently.[28]

IX. Excited states and single-molecule chemistry

In the aforesaid, we assumed conservation of the electron energy (it should be remembered that the Zeeman transition energies are negligible). Hence, the spin effects due to exchange interaction, relaxation and microwave pumping were associated solely with changes in the spin orientations of the paramagnetic species and tunnelling electrons. However, more complex effects can also occur, where the tunnelling electrons are responsible not only for the change in the spin orientation of the adsorbed species, but also for the excitation of internal (vibrational and/or electronic) degrees of freedom of the species. In the case of tunnelling between conductors in which all electron states below the Fermi level can be considered filled, such processes can proceed only at the voltages V exceeding the energy loss $\delta\varepsilon$ (usually, $\delta\varepsilon \gg tT$) and the dependence of I on the potential V exhibits the so-called threshold features (conductivity jumps), which appear at the voltage $eV = \delta\varepsilon$. Threshold features manifest themselves as maxima of the second derivatives of the tunnelling current with respect to the tip potential. They are observed in those cases where the tunnelling electrons excite the molecule 'sitting' under the microscope tip and induce its chemical transformations.

The possibility of observation of inelastic processes using tunnelling microscopy was predicted in 1985; however, experimental studies have been reported only recently.[29–31] For instance, it was found that molecules C_2H_2 and C_2D_2 adsorbed on the (001) surface of a copper single crystal dissociate to give C_2H and C_2D, respectively. This occurs at potentials of 2.8 V for C_2H_2 and 3.9 V for C_2D_2.[31] The C_2H and C_2D radicals thus formed undergo further dissociation to give C_2 at potentials of 2.1 and 2.7 V, respectively. In this case, large isotope effects are due to differences between the vibrational excitation cross-sections of different isotopomers rather than to isotopism of the C–H and C–D bonds. The excitation cross-section is determined by the probability of energy transfer (an inelastic process) from the 'light' tunnelling electron to the 'heavy' molecule; its magnitude is proportional to a small parameter $(a_0/R)^{2\Delta v} \leqslant 10^{-2\Delta v}$ (a_0 is the amplitude of zero-point vibrations of the molecule or constituent atoms, R is the characteristic atomic size and Δv is the change in the vibrational quantum number upon excitation). This formula readily demonstrates large isotope effect for the excitation cross-section.

Dehydrogenation was also observed for single ethylene molecules adsorbed on the Ni(110) surface (finally, ethylene loses two protons to give C_2H_2) and for benzene, pyridine and their isotopomers adsorbed on the Cu(001) surface.[31] Moreover, diffusion displacements and rotational motions of single molecules induced by the tunnelling electrons can also be observed along with their chemical transformations.

No observations of threshold features in the experiments on the excitation of adsorbed species by tunnelling electrons using a scanning tunnelling microscope (STM) have been reported so far. These features are assumed to be 'large-scale' since in this case we are concerned with electron–electron energy exchange. Of particular interest is consideration of a physically adsorbed oxygen molecule. The ground state of the molecule (a triplet $X^3\Sigma_g^-$) is separated from the nearest excited singlet state ($a^1\Delta_g$) by about 1 eV on the energy scale. The reactivity and relaxation of singlet dioxygen adsorbed on various surfaces were studied in detail by Ryskin [32] and Krylov and Shub.[33] Using different 'macroscopic', kinetic and spectroscopic methods, they first determined the relaxation times of singlet dioxygen. It was found that this parameter depends strongly on the surface characteristics and its magnitude can vary over a wide range. Optimum experimental conditions for observation of threshold features of the $X^3\Sigma_g \rightarrow a^1\Delta_g$ transitions of an oxygen molecule 'sitting' under the tip using a STM should be chosen so that the rates of stimulated and spontaneous (relaxation) transitions be comparable. This allows detection of new changes in the tunnelling current by varying the tunnelling current (*i.e.*, by changing the populations of two electronic states of the oxygen molecule). This situation is quite similar to that described above for the single spin ('self-regulation' and lock of the tunnelling current).

X. Single-molecule spin chemistry

In STM experiments, the operating current densities can be as high as 10^8 A cm^{-2}. It is for this reason that is possible to transform the equilibrium conditions into nonequilibrium ones and cause creation of nonequilibrium distributions over vibrational and electron energy levels of the single molecules 'sitting' under the tip.[34] (It should be remembered that in the case of single-molecule experiments we are dealing with ensembles of elementary events, *i.e.*, a manifold of independent interaction acts of a species with individual tunnelling electrons.) Heating leads to acceleration of chemical transformations such as desorption, dissociation, transfer of the adsorbed species from the tip to the surface, *etc*. Experiments with ferromagnetic tips allow the observation of versatile single-molecule spin chemistry effects. The simplest case is deposition of a paramagnetic species from the ferromagnetic tip on the surface containing a paramagnetic centre. It is easy to understand that at sufficiently heavy tunnelling currents (both species are polarised) recombination is forbidden. At weak currents (the spin of the species adsorbed on the surface has no definite orientation), recombination is allowed.

XI. Conclusion

Thus, classical scanning tunnelling microscopy gave impetus to the emergence and development of two new, important and promising methods, *viz*., single-molecule tunnelling spectroscopy and single-molecule chemistry.

The emergence of these methods signifies a new stage of the development of modern chemistry, which offers considerable prospects for surface sciences, catalysis, *etc*. In particular, the use of single-molecule spectroscopy and single-molecule chemistry in combination with photochemistry and femtochemistry presents new, inestimable possibilities for manipulating the molecules. In the framework of single-molecule spectroscopy and single-molecule chemistry classical spin chemistry also undergoes transformation into 'single-molecule' spin chemistry. This offers unique possibilities for spin channel detection, single electron spin manipulation and detection of ESR of a single paramagnetic centre (including triplet molecules, carbenes and ions) from the tunnelling current.

The authors express their gratitude to the Russian Foundation for Basic Research and the Federal Programme 'Integration' for financial support.

References

1. D Attanasio *EPR Newsletters* **9** 14 (1998)
2. D Attanasio, D Capitani, C Federici, A Serge *Archaeometry* **37** 377 (1995)
3. A G Semenov, N N Bubnov *Pribory Tekhnika Eksperim*. (1) 92 (1959); *Vestn. Akad. Nauk SSSR* (3) 55 (1959) [a]
4. O Ya Grinberg, A A Dubinskii, Ya S Lebedev *Usp. Khim*. **52** 1490 (1983) [*Russ. Chem. Rev*. **52** 850 (1983)]
5. E L Frankevich, A I Pristupa, V I Lesin *Chem. Phys. Lett*. **47** 304 (1978)
6. A L Buchachenko, E L Frankevich *Chemical Generation and Reception of Radio- and Microwaves* (New York: VCH, 1994)
7. V O Saik, O A Anisimov, Yu N Molin *Chem. Phys. Lett*. **116** 138 (1985)
8. O A Anisimov, V M Grigoryants, Yu N Molin *Pis'ma Zh. Eksp. Teor. Fiz*. **30** 589 (1979)
9. S Mais, J Tittel, Th Basché, C Bräuchle, W Göhde, H Fuchs, G Müllen, K Müller *J. Phys. Chem. A* **101** 8435 (1997)
10. W E Moerner, M Orrit *Science* **283** 1670 (1999)
11. F Kulzer, F Koberling, Th Crist, A Mews, Th Basché *Chem. Phys*. **247** 23 (1999)
12. J Köhler, J A J M Disselhorst, M C J M Donckers, E J J Groenen, J Schmidt, W E Moerner *Nature (London)* **363** 242 (1993)
13. J Wrachtrup, C von Borczyskowski, J Bernard, M Orrit, R Brown *Nature (London)* **363** 244 (1993)
14. J Köhler, A C J Brouwer, E J J Groenen, J Schmidt *Science* **268** 1457 (1995)
15. *Chem. Phys*. **247** (1) (Spec. Issue) (1999)
16. J Köhler *Phys. Rep*. **310** 261 (1999)
17. J Wrachtrup, C von Borczyskowski, J Bernard, R Brown, M Orrit *Chem. Phys. Lett*. **245** 262 (1995)
18. F I Dalidchik, M V Grishin, N N Kolchenko, S A Kovalevskii *Surf. Sci*. **387** 50 (1997)
19. F I Dalidchik, M V Grishin, S A Kovalevskii, N N Kolchenko *Pis'ma Zh. Eksp. Teor. Fiz*. **65** 306 (1997)
20. S A Kovalevskii, F I Dalidchik, M V Grishin, N N Kolchenko, B R Shub *Appl. Phys. A, Mater. Sci. Process*. **66** (Suppl. Pt. 1) (1998)
21. A L Buchachenko *Usp. Khim*. **68** 99 (1999) [*Russ. Chem. Rev*. **68** 85 (1999)]
22. D Bohm *Quantum Mechanics* (New York: Prentise Hall Inc., 1952)
23. F I Dalidchik *Zh. Eksp. Teor. Fiz*. **87** 1384 (1984)
24. F I Dalidchik, S A Kovalevskii *Pis'ma Zh. Eksp. Teor. Fiz*. **67** 916 (1998)
25. R Wiesendanger, in *Scanning Probe Microscopy. Analytical Methods* (Berlin: Springer, 1998)
26. M A Kozhushner, B R Shub, R R Muryasov *Pis'ma Zh. Eksp. Teor. Fiz*. **67** 484 (1998)
27. A L Buchachenko, M A Kozhushner, B R Shub *Izv. Akad. Nauk, Ser. Khim*. 1732 (1998) [b]
28. A L Buchachenko, F I Dalidchik, B R Shub *Chem. Phys. Lett*. **340** 103 (2001)
29. B C Stipe, M A Resaei, W Ho *Phys. Rev. Lett*. **81** 1263 (1998)
30. B C Stipe, M A Resaei, W Ho *Science* **279** 1907 (1998)
31. J Gaudioso, H J Lee, W Ho *J. Am. Chem. Soc*. **121** 8479 (1999)
32. M E Ryskin, Candidate Thesis in Physicomathematical Sciences, Institute of Chemical Physics, Academy of Sciences of the USSR, Moscow, 1983
33. O V Krylov, B R Shub *Neravnovesnye Protsessy v Katalize* (Non-Equilibrium Processes in Catalysis) (Moscow: Khimiya, 1990)
34. M V Grishin, F I Dalidchik, S A Kovalevskii, N N Kolchenko *Pis'ma Zh. Eksp. Teor. Fiz*. **71** 104 (2000)

[a] — *Herald Russ. Acad. Sci. (Engl. Transl.)*
[b] — *Russ. Chem. Bull. (Engl. Transl.)*

Russian Chemical Reviews **70** (7) 543 – 576 (2001) © 2001 Russian Academy of Sciences and Turpion Ltd

DOI 10.1070/RC2001v070n07ABEH000650

Electrochemical reactions of alkenes induced by anodic oxidation and their applications in organic synthesis

Yu N Ogibin, G I Nikishin

Contents

I.	Introduction	543
II.	Reactions induced by direct anodic oxidation	543
III.	Reactions induced by indirect anodic oxidation	558
IV.	Conclusion	573

Abstract. The main achievements and trends in the use of anodic oxidation and electrochemical reactions of alkenes in organic synthesis are analysed, systematised and generalised. The large potential and advantages of electrochemical methods of synthesis of organic compounds are demonstrated. These methods allow transformation of alkenes into functional derivatives the preparation of which by conventional chemical methods is either difficult or impossible. Primary attention is paid to the influence of the structures of substrates and electrolysis conditions on the regio- and stereoselectivities of the reactions. The bibliography includes 305 references.

I. Introduction

Anodic oxidation and electrochemical reactions of unsaturated organic compounds represent a vigorously developing line of research in organic electrochemistry. These reactions allow transformation of alkenes into functionally substituted compounds the synthesis of which by chemical methods is either impossible or difficult from the experimental standpoint. In many cases, electrochemical reactions are more advantageous from the environmental standpoint than chemical reactions.

This review describes systematically the published data on the reactions of alkenes taking place at the anode and in electrolyte solutions and on the use of these reactions in organic synthesis. More than 200 studies on electrooxidation of alkenes have now been published (most of them, during the last 15 years). There are several reviews [1–18] and monographs [19–23] containing data on the anodic processes involving unsaturated compounds. However, the information on electrooxidation of alkenes presented in these sources is not systematised in any way and does not reflect adequately the knowledge accumulated to date. The present review is meant to fill these gaps, to shed light upon the new trends in the development of alkene reactions induced by anodic oxidation, and to demonstrate the use of these reactions in organic synthesis taking electrooxidation of unsubstituted and functionally substituted alkenes and cycloalkenes, substituted dienes, and some other types of alkenes as examples. The review covers publications of the last two decades and also some earlier studies that have not been reflected adequately in the above-mentioned reviews and monographs.

An alkene can be directly involved in an electrochemical process upon transfer of an electron from its higher occupied molecular orbital at the anode (direct route). Alkenes can also participate in the electrochemical process *via* the reaction with electrogenerated organic or inorganic radicals ($X^{\bullet}$), ions (X^{+}), or oxidants (Ox), which can be formed from the corresponding precursors at potentials lower than the potential of alkene oxidation (indirect route).[24–26] The role of precursors can be played by the solvent, organic or inorganic anions and mediators (Scheme 1).

In accordance with the possibility of electrochemical transformations of alkenes into final products by both direct and indirect routes, the reactions considered in the review are classified into two groups.

Scheme 1

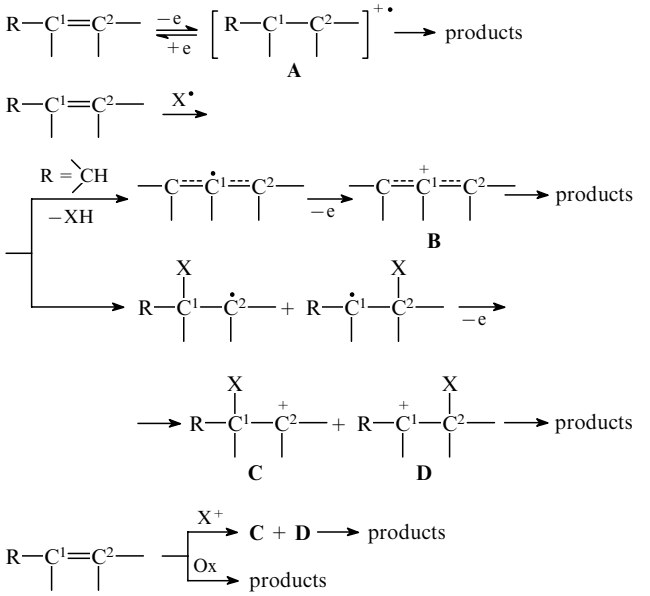

II. Reactions induced by direct anodic oxidation

The efficiency of direct anodic oxidation depends, most of all, on the rate of electron transfer from the alkenes adsorbed on the anode and is determined by their oxidation potentials. The oxidation potentials of the alkenes considered in this Section are listed in Table 1.[27–39]

Yu N Ogibin, G I Nikishin N D Zelinsky Institute of Organic Chemistry, Russian Academy of Sciences, Leninsky prosp. 47, 119991 Moscow, Russian Federation. Fax (7-095) 135 53 28. Tel. (7-095) 938 35 95 (Yu N Ogibin), (7-095) 135 53 05 (G I Nikishin)

Received 9 January 2001
Uspekhi Khimii **70** (7) 619 – 655 (2001); translated by Z P Bobkova

Table 1. Potentials of oxidation half-waves ($E_{1/2}$) for alkenes of various types.

Alkene	$E_{1/2}$ /V	Electrolyte	Solvent	Electrode	Ref.
Alkenes and cycloalkenes					
Alk-1-enes	2.7 – 2.8	Et_4NBF_4	MeCN	Pt	27 – 31
Alk-2-enes	2.2 – 2.3	Et_4NBF_4	MeCN	Pt	27 – 31
2-Methylbut-2-ene	1.65	Bu_4NClO_4	MeCN	Pt	32
2,3-Dimethylbut-2-ene	1.29	Bu_4NClO_4	MeCN	Pt	32
Cyclohexene	2.14	$LiClO_4$	MeCN	Pt	28, 32
1-Methylcyclohexene	1.70	$LiClO_4$		Pt	32
α-Pinene	1.3 – 1.4	$LiClO_4$	MeCN	Pt	30
Norbornene	2.02	$LiClO_4$	MeCN	Pt	30
Arylalkenes and arylcycloalkenes					
Styrene	1.45	$NaClO_4$	MeOH	C	33
	1.95 – 2.05	Et_4NBF_4	MeCN	Pt	33
2-Phenylpropene	1.37	$NaClO_4$	MeOH	C	33
	1.80 – 1.89	Et_4NBF_4	MeCN	Pt	27
1-Phenylpropene	1.50	$LiClO_4$	MeCN	Pt	27
1,1-Diphenylethylene	1.48 – 1.55	Bu_4NClO_4	MeCN	Pt	32, 35
1-Methoxyphenylethylene	0.90	$NaClO_4$	MeOH	C	34
4-Methylstyrene	1.38	Et_4NClO_4	MeCN	Pt	35
4-Methoxystyrene	1.15	Et_4NClO_4	MeCN	Pt	35
4-Chlorostyrene	1.76	Et_4NClO_4	MeCN	Pt	35
Allylbenzene	1.89	$LiClO_4$	MeCN	Pt	36
3-Methoxy-3-phenylprop-1-ene	1.95	$LiClO_4$	MeCN	Pt	36
1-Methoxy-3-phenylprop-1-ene	1.42	$LiClO_4$	MeCN	Pt	36
cis-Stilbene	1.38	$NaClO_4$	MeOH	C	27
trans-Stilbene	1.19	$NaClO_4$	MeOH	C	27
1-Phenylcyclohexene	1.36	$NaClO_4$	MeOH	C	32
Indene	1.25	$NaClO_4$	MeOH	C	28, 29
Acenaphthene	0.95	$NaClO_4$	MeCN	Pt	27
Acenaphthylene	1.32	Et_4NClO_4	MeCN	Pt	37
Enol ethers and esters					
1-Ethoxycycloalkenes	0.95 – 1.00	$NaClO_4$	MeOH	glass carbon	38
1-Methoxyhex-1-ene	1.04	$NaClO_4$	MeOH	glass carbon	38
1-Acetoxy-2-methylcyclopentene	1.18	$LiClO_4$	MeCN	Pt	39

Note. Hereinafter, the oxidation potentials are given in the unified scale *versus* a silver halide electrode at 25 °C; the potentials determined *versus* saturated calomel and standard hydrogen reference electrodes were decreased by 0.30 and 0.54 V, respectively.

The high oxidation potentials of alkenes with a terminal double bond hamper their direct anodic oxidation. The replacement of hydrogen atoms at double bonds by alkyl or other electron-donating groups decreases the oxidation potential and thus facilitates this process. To reach the anodic potentials at which alkenes undergo effective direct oxidation, tetrafluoroborates are used as supporting electrolytes and acetonitrile, 2,2,2-trifluoroethanol, trifluoroacetic acid or fluorosulfonic acid are used as solvents. Oxidation of activated alkenes, for example, styrenes and enol ethers (or esters), is normally carried out in methanol and ethanol, which are the best solvents for most of the electrochemical processes considered in this review. In undivided cells, these protic solvents suppress side cathodic reactions of alkenes due to easy discharge of protons. Owing to their versatile solvent capacity, they permit the use of high concentrations of the electrolyte and the organic substrate.

The transformation route of radical cations **A** (see Scheme 1) depends on their reactivity with respect to other compounds present in the reaction mixture. In most cases, radical cations behave as proton donors or electrophiles and react with nucleophiles or bases. They can also be oxidised or be involved in radical dimerisation, recombination, disproportionation and addition processes. The most typical reactions of the radical cations electrogenerated from alkenes are considered below (Sections II.1 – II.8).

1. Allylic substitution in alkenes

The allylic substitution in activated alkenes occurs *via* direct anodic oxidation, and allylic substitution in non-activated or weakly activated alkenes can occur *via* either direct or indirect anodic oxidation, or involve both types of reaction. For representing the full picture of allylic substitution, the direct and indirect routes of anodic oxidation are considered together in Section II. In both cases, cationic intermediates **B**, **C** and **D** are generated at initial stages (see Scheme 1); they enter into solvolysis (Scheme 2, pathway *a*) and deprotonation reactions (Scheme 2, pathways *b*, *c*).[30]

Scheme 2

Pathway *a*

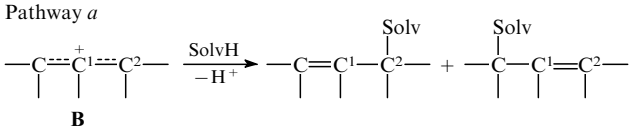

B

SolvH is protic solvent.

Pathway *b*

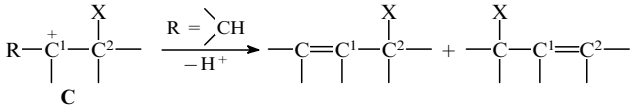

C

Pathway *c*

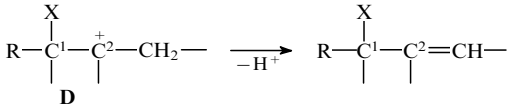

D

Allylic substitution in alkenes has been studied in relation to diisobutene,[40 – 42] cyclohexene,[30, 43 – 48] 1-, 3- and 4-methylcyclohexenes,[30] α- and β-pinenes,[30] allylbenzene,[36, 49] 4-allylanisole and some other allylarenes.[50] The efficiency and the direction of the direct anodic oxidation in undivided cells at a controlled anode potential or in the direct-current mode depends substantially on the nature of the anode material, supporting electrolyte and the solvent. This effect is attributed to different susceptibilities of electrolytes, alkenes and solvents for chemo- and electrosorption on the anode surface. Allylic substitution in non-activated alkenes — diisobutylene and cyclohexene — is most efficient in methanol with tetraalkylammonium toluene-*p*-sulfonate as the supporting electrolyte and with graphite or lead dioxide supported on graphite as the anode material. Diisobutylene is converted into a complex mixture of products mainly consisting of isomeric methoxyoctenes **1** – **6**.[41]

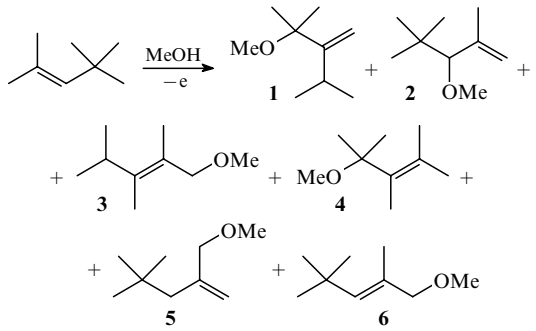

The electrolysis of cyclohexene in acetic acid gave 3-acetoxycyclohexene (**7a**) as the major product; that in methanol yielded 3-methoxycyclohexene (**7b**). In both cases, 1,2-disubstituted cyclohexanes **8a**,**b** are also formed. The composition of reaction products depends on the solvent nucleophilicity: when the electrolysis is carried out in acetic acid, radical cations **A** are converted predominantly into cations **B** and then into the product **7a**, whereas in more nucleophilic methanol, they mainly react with the solvent to give intermediates **C** and then the products **8b** and **9b**.[30] In wet acetonitrile, 3-acetamidocyclohexene (**10**) is formed.[30,43,45]

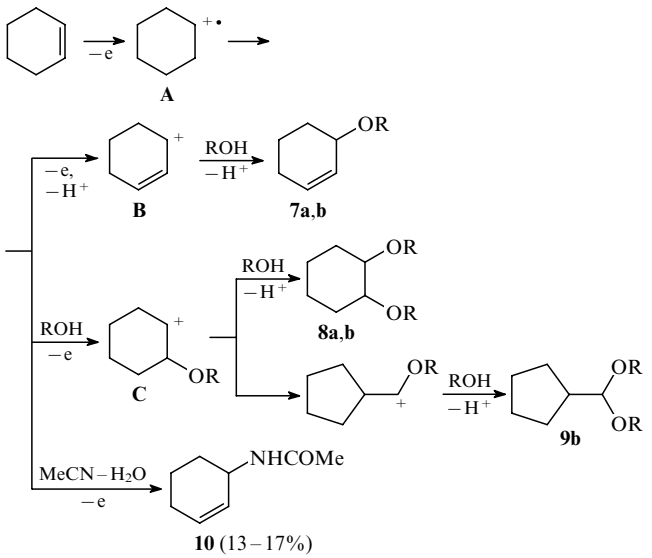

R	Yield (%)		
	7	**8**	**9**
Ac (**a**)	55	1.1	2.6
Me (**b**)	24	2.5	23

To increase the selectivity of electrochemical acetamidation of hydrocarbons, in particular, cyclohexene, the use of an ion exchange resin with sulfonate groups has been proposed.[48] In the presence of an ion exchange resin, the reactive nitrilium ions **D** formed in acetonitrile solutions are transformed into stable imidoyl sufonates **E** attached to the polymeric support. With this approach, the yield of the reaction products markedly increases and the isolation of products is substantially facilitated.

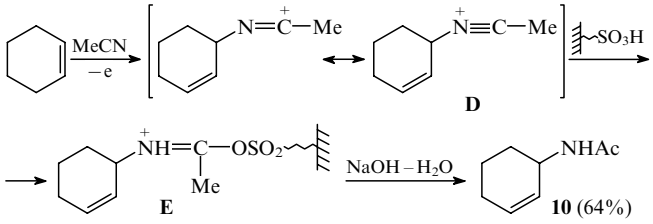

It is worth noting that acetoxylation of 1-, 3- and 4-methylcyclohexenes, oct-1-ene and oct-2-ene, gives the same products both in the electrochemical[30] and standard versions.[50–52] This is evidence in favour of participation of carbenium ions in electrochemical acetoxylation. However, the *cis*- to *trans*-isomer ratios obtained in the electrochemical and chemical acetoxylations are different; the electrochemical process yields mainly *cis*-isomers.

Electrochemical allylic acetoxylation and methoxylation of α-pinene, unlike those of methylcyclohexenes, give predominantly *trans*-isomers of substituted cyclohexenes **11a**,**b** and **12a**,**b**.[30]

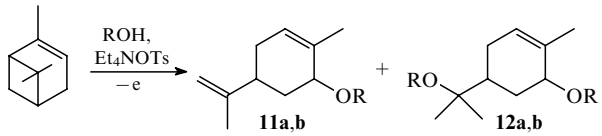

R	Yield (%) (*trans* : *cis* ratio)	
	11	**12**
Ac (**a**)	24 (2.2 : 1)	12 (2.9 : 1)
Me (**b**)	22 (6.2 : 1)	41 (2.6 : 1)

Under similar conditions, allylic methoxylation of β-pinene gives rise to a mixture of mono- and dimethoxy derivatives **13**–**16**.[30]

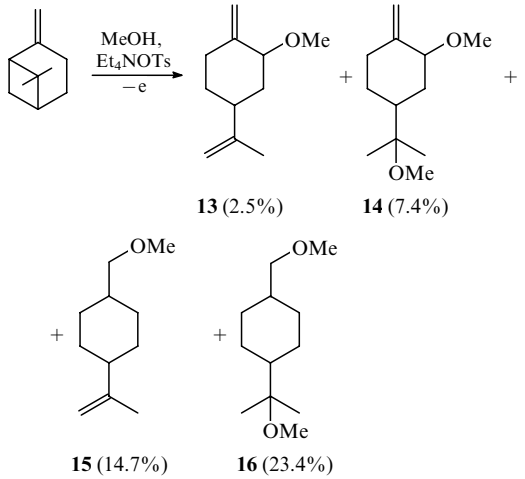

Electrooxidation of allylbenzene in methanol results initially in 3-methoxy-1-phenylprop-1-ene (**17**) and 3-methoxy-3-phenylprop-1-ene (**18**).[36]

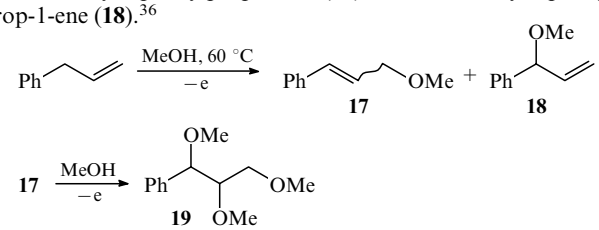

Under conditions of electrolysis, compound **17** is converted almost entirely into 1,2,3-trimethoxypropylbenzene (**19**) because of its lower oxidation potential compared to those of **18** or allylbenzene (1.42, 1.95 and 1.89 V, respectively, see Table 1). The degree of conversion and the yields of electrolysis products depend on the supporting electrolyte used (Table 2).

In the presence of acidic electrolytes (TsOH, H_2SO_4), 3-methoxy-3-phenylprop-1-ene (**18**) undergoes fast isomerisation into 3-methoxy-1-phenylprop-1-ene (**17**); as a consequence, the product of allylbenzene trimethoxylation, namely, the compound **19**, is produced predominantly. The major products formed in the presence of basic electrolytes are the allylic methoxylation products **17** and **18**. When neutral salts are used as electrolytes (Bu_4NBF, TsONa), the products of allylic methoxylation and trimethoxylation of allylbenzene are formed in comparable amounts.

Table 2. Effect of the supporting electrolyte on the degree of conversion and the yield of products of allylbenzene electrolysis.[36]

Electrolyte	Conversion (%)	Yield (%)		
		17	**18**	**19**
MeOLi	58	8	59	4
MeONa	24	4	54	9
Bu_4NBF_4	26	5	36	43
TsONa	63	4	32	25
TsOH	62	4	–	55
H_2SO_4	82	2	–	44

Note. Electrolysis under amperostatic conditions in an undivided cell (ACU), Pt anode, Cu cathode, 220 mA cm^{-2}, 6.8 F mol^{-1}, MeOH, 60 °C. Here and below, F is the quantity of electricity equal to one Faraday.

In an initial stage of electrolysis in methanol with a graphite anode and with sodium methoxide as the supporting electrolyte, 4-allylanisole is methoxylated similarly to allylbenzene at the benzylic carbon atom; however, during the subsequent, more extensive electrooxidation, it is converted into 1,1-dimethoxyallylanisole.[50]

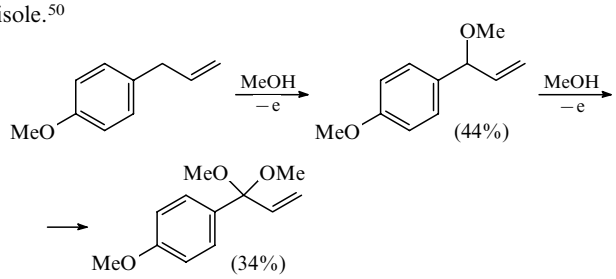

In the anodic oxidation of methyl oleate, allylic substitution also takes place. This yields predominantly unsaturated monoacetates **20** and **21** (yield of up to 60%); further electrooxidation affords unsaturated diacetates **22** and **23** (upon subsequent allylic substitution). The highest yield of the diacetates (85%) was attained when the anode current density was 8 mA cm^{-2} and the consumption of electricity was ~4 F mol^{-1} (see Ref. 53).

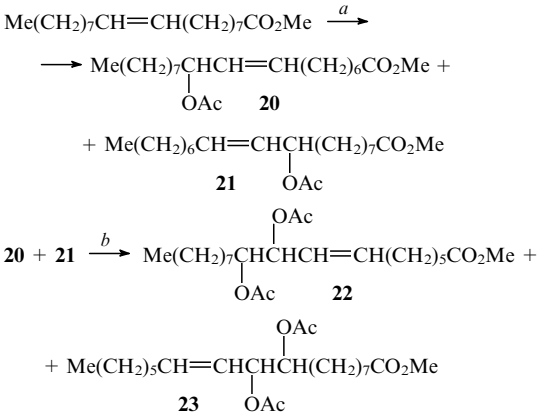

(*a*) ACU, Pt anode, 1.3 F mol^{-1}, AcOH, $LiClO_4$;
(*b*) ACU, > 1.3 F mol^{-1}.

Apart from unsaturated mono- and diacetates **20**–**23**, small amounts of the corresponding saturated mono- and diacetates are also formed.

Allylic substitution can follow an intramolecular pathway provided that the electrogenerated cation of type **B** (see Schemes 1 and 2) contains an internal nucleophile. An example of this reaction is anodic oxidation of citronellol in acetonitrile or propylene carbonate giving rise to 2-(2-methylprop-1-enyl)-4-methyltetrahydropyran (**24**), a valuable fragrance compound known as rosenoxid.[54, 55] The use of methanol instead of acetonitrile changes the electrochemical behaviour of citronellol: the yield of the product **24** decreases to 7%, while 3,7-dimethyl-6-methoxyoct-7-en-1-ol (**25**) becomes the major product of electrolysis.

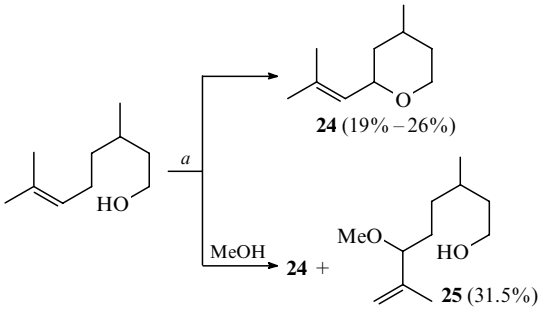

(*a*) ACU, C anode, 40 mA cm^{-2}, 2 F mol^{-1}, MeCN or propylene carbonate, Et_4NOTs.

2. Transformation of enol acetates into enols and α-acetoxy ketones

During the electrolysis of enol acetate in acetic acid, radical cations **A**, generated in the first stage, undergo electrooxidation, deprotonation, and solvolysis to give α-acetoxy-substituted allylic cations **B** and α,β-diacetoxy-substituted carbenium ions **C**. Elimination of acetyl cations from these intermediates results in enones and α-acetoxy ketones.[39, 56]

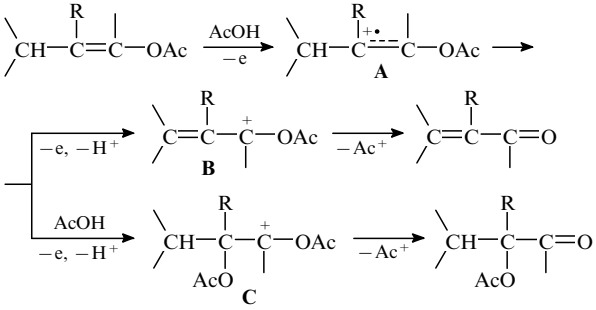

The nature of the supporting electrolyte exerts a crucial influence on the composition of the electrolysis products. Indeed, when a solution of Et_4NOTs in AcOH or in MeOH is used as the electrolyte, amperostatic electrolysis of enol acetates in a divided cell (ACD) with a carbon anode, as a rule, results predominantly (in some cases, solely) in enones;[39] when the anodic oxidation is carried out in potassium acetate or triethylamine, α-acetoxy ketones are produced (Table 3).

It is noteworthy that in an undivided cell, enol acetates are converted almost entirely into 1,6-diketones as a result of cathodic dimerisation of the enones formed. For example, enol acetates derived from cyclohexanones are transformed into bis(3,3′-dioxo)cyclohexyls.[57]

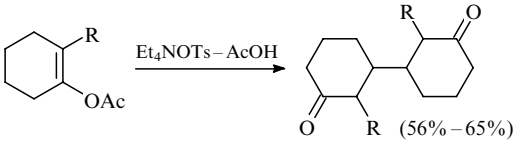

R = H, Me.

In the presence of catalytic amounts (0.4 mol % – 1.0 mol %) of metal salts (iron and copper sulfates, cobalt acetate), the cathodic dimerisation is completely suppressed and cycloalk-2-enones become the major product of electrolysis, as in a divided cell (yield 80% – 86%).[57]

Electrochemical transformation of enol acetates into enones served as the basis for the development of a general method for the synthesis of 2-mono- and 2,3-disubstituted cyclopent-2-enones.[56, 57]

Table 3. Composition of products of anodic oxidation of enol acetates in AcOH.[39, 56, 58]

Substrate	R^1	R^2	R^3	Electrolyte	Products	Yield (%)
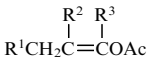	n-C_5H_{11}	H	Me	Et_4NOTs	n-$C_6H_{13}CH(OAc)COMe$ n-$C_5H_{11}CH=CHCOMe$	24 6
	Alk(C_1-C_5)	H	Me	AcOK or Et_3N	$AlkCH_2CH(OAc)COMe$	54–78
	H	H	Et	AcOK or Et_3N	AcO(Me)CHCOEt	66
	H	H, Me	Ph	AcOK or Et_3N	AcO(Me)C(R^2)COPh	47–73
	H	Me	Pr^i	AcOK or Et_3N	AcO(Me)C(Me)$COPr^i$	20
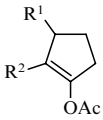	H	H		Et_4NOTs		3
					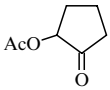	37
	H	Alk(C_1-C_9)		Et_3NOTs	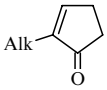	66–90
	H	Me		AcOK or Et_3N	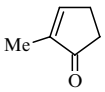	24
					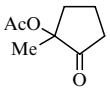	59
	H	$(CH_2)_6CO_2Me$		Et_4NOTs	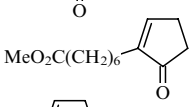	84
	H	Bn		Et_4NOTs	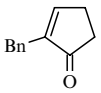	45
	n-C_5H_{11}	CH_2CO_2Me		Et_4NOTs	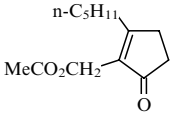	69
	H	$CH_2CH=CH_2$		AcOK or Et_3N	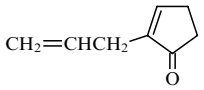	12
					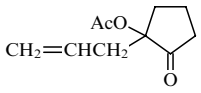	59
	H	$CH_2CH=CHMe$		AcOK or Et_3N	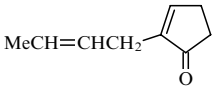	3
					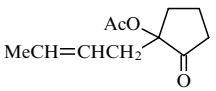	43
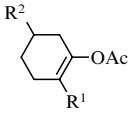	H	H		Et_4NOTs	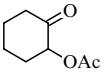	25
						9

Table 3 (continued).

Substrate	R^1	R^2	R^3	Electrolyte	Products	Yield (%)
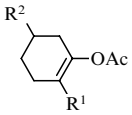	H	H		Et_4NOH	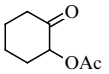	39
					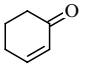	1
	H	Me		Et_4NOTs [a]	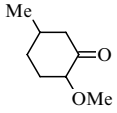	55
	Pr^i	Me		AcOK or Et_3N	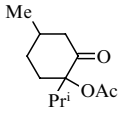	60
					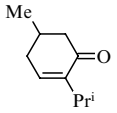	25
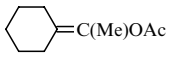				Et_4NOTs	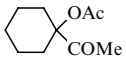	3
					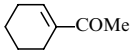	55

Note. Electrolysis under amperostatic conditions in a divided cell (ACD), carbon anode; [a] electrolysis was carried out in methanol.

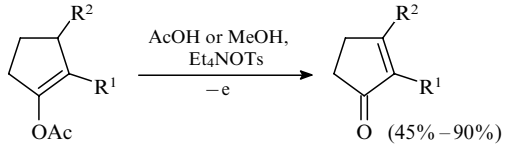

Methoxylation of enol acetates, which occurs similarly to acetoxylation, is used to accomplish 1,2-shift of the carbonyl group in ketones. An example of such transformation for substituted cyclohexanones is given below.[58]

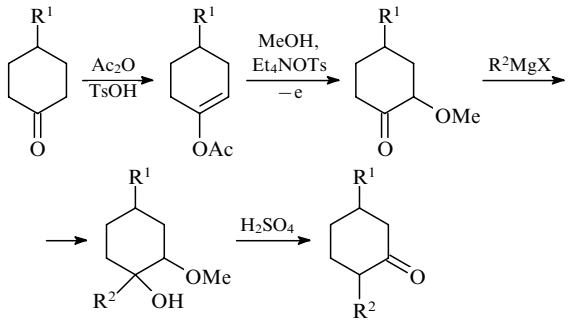

3. Reactions of enamines

Electrooxidation of enamines affords radical cations **A**, which then add a nucleophile to give radical intermediates **B**. Electrooxidation of these species followed by deprotonation of cationic intermediates **C** gives rise to enamines containing a nucleophilic substituent in the β-position. Hydrolysis of the enamines furnishes the corresponding α-substituted ketones.[59, 60]

This electrochemical process was implemented for cyclopentanone ($n = 1$) and cyclohexanone ($n = 2$) enamines. Methanol and the anions derived from acetylacetone, ethyl acetoacetate and diethyl malonate were used as nucleophiles, and a methanolic solution of sodium methoxide was used as the electrolyte.[59, 60]

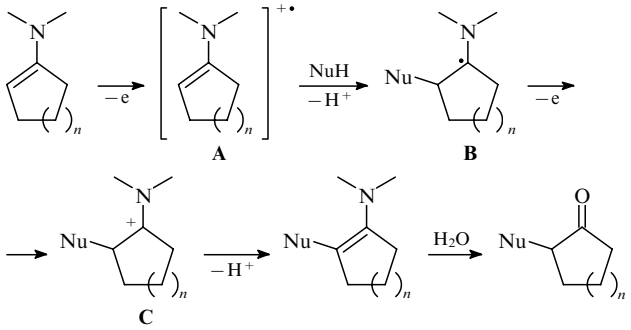

$n = 1, 2$.

N-Methoxycarbonyl-substituted enamines **26a–d** are converted into halomethoxylation products **27a–d** upon electrolysis in methanol in ammonium bromide or iodide as the supporting electrolyte.

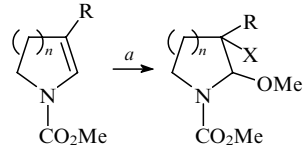

26a–d **27a–d**

Compound **26**	R	*n*	The yield of compounds **27** (%)
a	Me	1	38
b	Me	2	42
c	Et	1	66
d	Et	2	93

Compound **27d** has been used to synthesise a bicyclic derivative of α-carboxybutyrolactone **28**, which is a key intermediate in the synthesis of the alkaloid eburnamonine (**29**).[61,62]

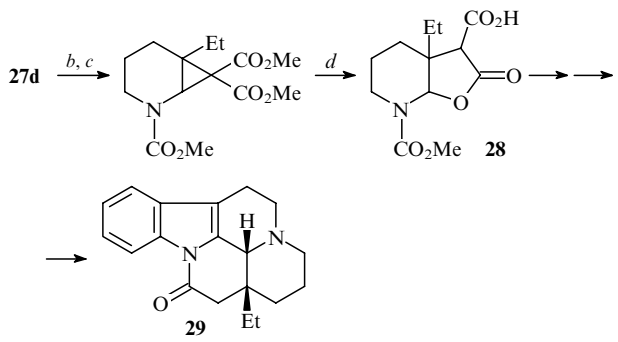

(*a*) ACU, Pt anode, 75 mA cm^{-1}, 3.5 F mol^{-1}, MeOH, NH_4X (X = Br, I); (*b*) $CH_2(CO_2Me)_2$, Et_3N, $TiCl_4$; (*c*) MeOH, 20 equiv. KOH, Δ; (*d*) DMF, Δ.

4. Dimethoxylation and diacetoxylation of alkenes

The scheme of electrochemical dimethoxylation and diacetoxylation of non-activated alkenes includes the formation of radical intermediate **A**, its electrooxidation and the reaction of the carbenium ion **B** with MeOH or AcOH.

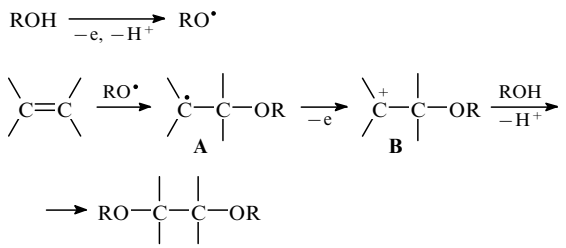

R = Me, Ac.

Electrochemical dimethoxylation of alkenes, for example, of conjugated arylalkenes and enol ethers (or esters) occurs with high selectivity and results in the formation of products in high yields. The most interesting examples are listed in Table 4.

Electrochemical dimethoxylation of weakly activated double bonds in arylalkenes (styrene, 2-phenylpropene and so on) takes place as an irreversible two-electron process (one two-electron oxidation wave is observed).[26,75] Highly activated double bonds in vinylanisole, 4-propenylanisole, α,α′-dimethoxystilbene and so on are dimethoxylated in two steps (two single-electron waves are observed), the first being reversible and the second being irreversible.[24,25,75,76]

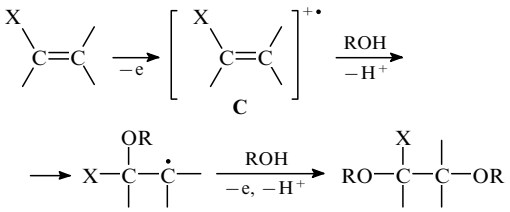

X = Ar, Bn, AlkO; R = Me, Ac.

The transfer of the first electron from the substrate molecule adsorbed on the anode, which occurs on the anode, is the rate-limiting step of this reaction. In the radical cations **C** thus formed, the highest spin density and the positive charge density are located on the β-carbon atom.[75] The process selectivity is markedly affected by the arylalkene concentration both in the solution and on the anode surface, by the current density at the anode, the anode material and the nature of the electrolyte anion.[26,40,75,77] The rate of oxidation of *trans*-alkenes is about an order of magnitude higher than that for the *cis*-isomers.[78] The yield of dimethoxylation products increases with a decrease in the substrate concentration in the solution and on the anode surface and with an increase in the current density up to values close to limiting ones; the yield sharply increases when a platinum, lead dioxide, or magnetite anode is used instead of the graphite anode[75] and sodium toluene-*p*-sulfonate is used as the electrolyte.[77] Unlike $NaClO_4$, sodium toluene-*p*-sulfonate exhibits desorption-replacing properties with respect to arylalkenes and other organic substrates; as a consequence, the substrate concentration on the anode surface during the electrolysis with TsONa is 50 times lower than that in the presence of $NaClO_4$. The same effect, although less pronounced, can be traced for tetrabutylammonium tetrafluoroborate. The highest yields (substance yield 60% – 80% and current yield 66% – 71%) of the products of dimethoxylation of arylalkenes are attained with a Pt anode, Bu_4NOTs or Bu_4NBF_4 as the supporting electrolyte and when the substrate concentration is close to 1 mol $litre^{-1}$ (see Ref. 64). Under similar conditions of electrolysis in the presence of potassium hydroxide as the electrolyte, enol ethers are converted predominantly into acetals and ketals of α-methoxy-substituted aldehydes and ketones. For example, alkyl vinyl ethers give rise to α-methoxyaldehyde acetals **30**, 1-alkoxycycloalkenes are converted into α-methoxycycloalkanone ketals **31**,[39,59,72,79] while bicyclic enol ethers yield dimethoxy-substituted oxabicycloalkanes **32**.[73,74]

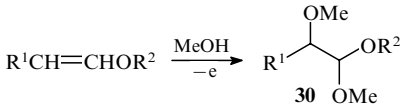

R^1	R^2	Yield of **30** (%)
H	Me	60
H	Et	68
H	Bu^n	75
n-C_6H_{13}	Me	60

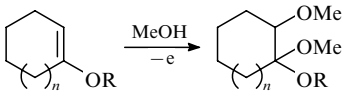

31 (45% – 60%)

n = 0, 1; R = Me, Et.

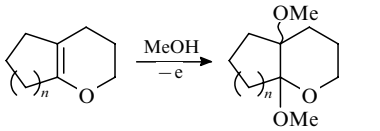

32 (64% – 68%)

n = 2, 8.

The selectivity of dimethoxylation of arylalkenes and enol ethers is substantially affected by the competing electrooxidative dimerisation and oligomerisation reactions, which will be considered in Section II.5. These side reactions are effectively suppressed by tris(4-bromophenyl)amine. In the presence of this compound, the yield of the reaction product in the dimethoxylation of propenylbenzene increases to 93%.[80]

Electrochemical diacetoxylation of alkenes at the double bond is usually accompanied by allyllic substitution; this diminishes the synthetic value of this process.

This reaction carried out in acetic acid with potassium or sodium acetate as the supporting electrolyte occurs with moderate selectivity but only for alkenes the structure of which rules out the possibility of allylic substitution, for example, stilbenes, 1,1-diphenylethylene,[81] indene and 1-alkylindenes.[82–85] In these cases, the yields of diacetoxylation products do not exceed 40%. An example is provided by 1-alkylindenes, which are converted into 1-alkyl-2,3-diacetoxyindans in 55% – 75% yields; small amounts of 2-acetoxy-1-alkyl-3-hydroxyindans (yields 6% – 20%) are formed simultaneously.[84] A mechanism for the anodic acetoxylation of indenes involving the intermediate for-

Table 4. Electrochemical dimethoxylation of arylalkenes and enol ethers under conditions of diaphragmless anodic oxidation in methanol.

Substrate	R^1	R^2	Electrolyte	Method	Product	Yield (%) [a]	Ref.
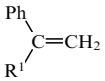	H		Bu_4NBF_4	A	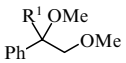	63–80	63, 64
	H		KF	A		80	64
	Me		KF	A		70	65
	Ph		Et_4NClO_4	B		69	33
	Ph		KF	A		86	65
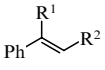	H	Me	KF	A	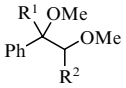	76	65
	Me	Et	KF	A		73	65
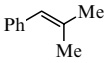			Bu_4NBF_4	A	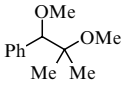	75 (63)	63
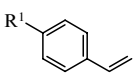	Me		KF	A	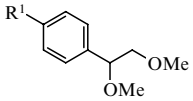	88	65
	Me		MeONa	B		36	33
	Me		Bu_4NBF_4	A		65 (52)	63
	Cl		MeONa	B		31	33
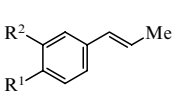	MeO	H	Bu_4NBF_4	A	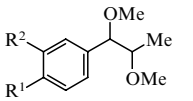	76	65
	MeO	H	KF	A		76	65
	MeO	MeO	$NaClO_4$, NaOH	B		70 (70)	66
	OCH_2O		KF	A		58	65
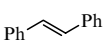			KF	A	Ph(OMe)CHCH(OMe)Ph	41	67
			MeONa	B		64	68
			Bu_4NBF_4	A	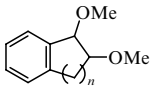	87 (72) [b]	63
			Bu_4NBF_4	C		88 [b]	69
$n = 1, 2$			Bu_4NBF_4	C		90 [c]	69
			Bu_4NBF_4	C	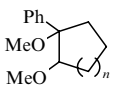	81 [b]	69
			Bu_4NBF_4	A		71 (71) [c]	63
			Bu_4NBF_4	C		76 [c]	69
$n = 1–3$			Bu_4NBF_4	C		90 [d]	69
			Bu_4NBF_4	A	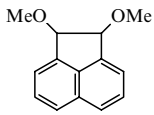	80	70
			MeONa	B, D		–	71
	Me		KOH	B	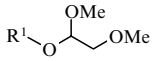	68	72
	Et		KOH	B		60	72
	Bu		KOH	B		75	72
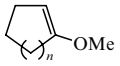			MeONa	D	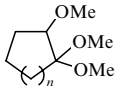	45 [b]	59
			KOH	B		60 [c]	72
$n = 1, 2$							
			KOH	B	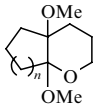	68 [b]	73, 74
			KOH	B		80 [c]	73, 74
$n = 1, 2$							
			Bu_4NBF_4	C	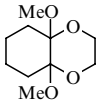	70	73, 74

Note. Method A: ACU, Pt anode, 100–220 mA cm^{-2}, 1.9–2.5 F mol^{-1}, 60 °C; method B: ACU, Pt anode, 8–80 mA cm^{-2}, 2.0–6.2 F mol^{-1}, −5–20 °C; method C: ACU, C anode, 100 mA cm^{-2}, 2.0 F mol^{-1}, 60 °C; method D: ACU, C anode, 8 mA cm^{-2}, 2.0–3.5 F mol^{-1}, ~20 °C.
[a] The substance yield (or the current yield, in parentheses) is given relative to the converted substrate; [b] $n = 1$; [c] $n = 2$; [d] $n = 3$.

mation of radical cation **33**, radical **34** and carbenium ion **35** has been proposed.[85] The side products, namely, acetoxy-3-hydroxy-derivatives **36**, are produced from cation **37**, which results from an intramolecular attack of the OAc group on the electron-deficient centre of the carbenium ion **35**.

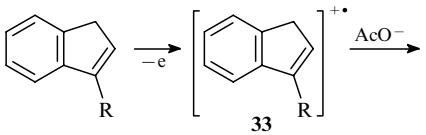

33

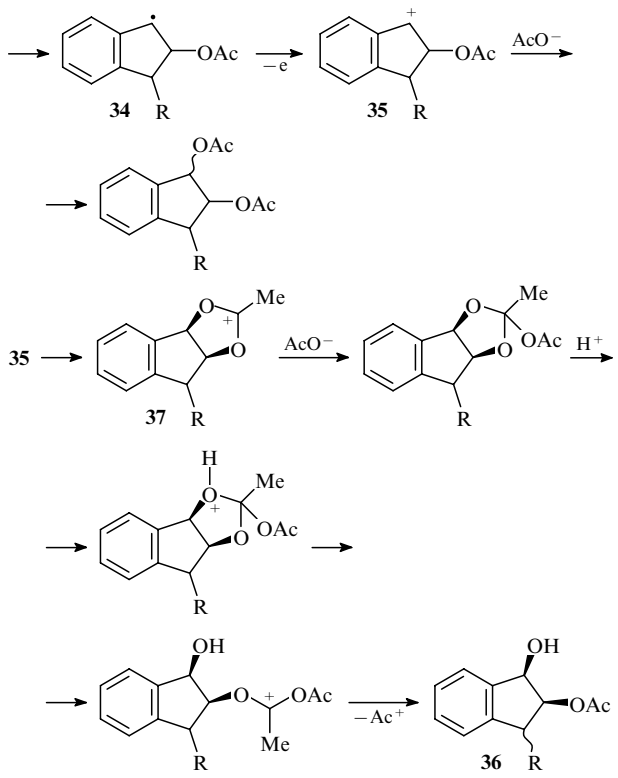

R = H, Me, Et, Pr^n, Pr^i, Bu^n, Bu^t.

5. Dimerisation of alkenes

The electrochemical transformation of alkenes into dimerised products of type **38**–**40** takes place *via* several consecutive steps. Radical cations **A** generated in the first step undergo recombination and add to the initial alkene molecules. The radical-cation and dication intermediates **B** and **C** undergo solvolysis, electrooxidation and deprotonation giving rise to unsubstituted and substituted (saturated and unsaturated) dimeric compounds.

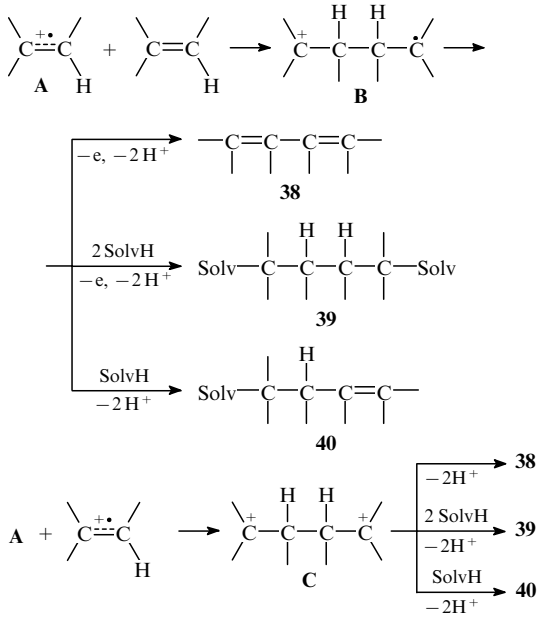

SolvH is a protic solvent.

The optimal conditions for these reactions are as follows: the initial concentration of alkene >1 mol litre^{-1}, methanol as the solvent, $NaClO_4$ as the supporting electrolyte, and a graphite anode.[33, 35, 38, 72] Under these conditions, the aliphatic and alicyclic vinyl ethers **41**, **42** are converted into ketals of 1,4-dicarbonyl compounds, which are hydrolysed to give the corresponding diketones; 5,6-dihydro-4-pyran (**43**) is converted into dimethoxy derivative **44**.[38, 72]

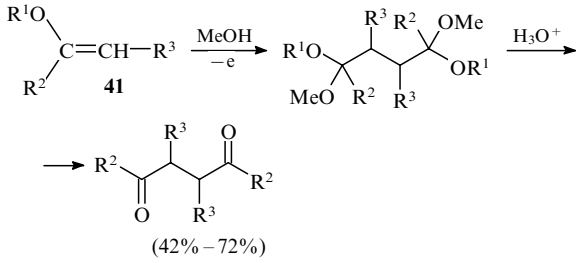

(42%–72%)

R^1 = Me, Et; R^2 = H, Et, Ph; R^3 = H, Me, Bu^n.

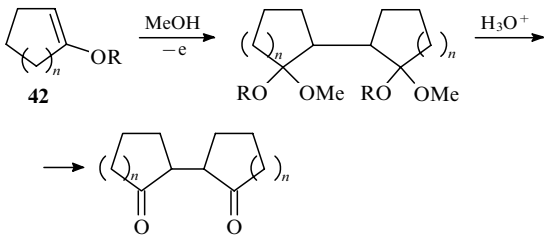

(48%–61%)

R = Me, Et; *n* = 2, 4.

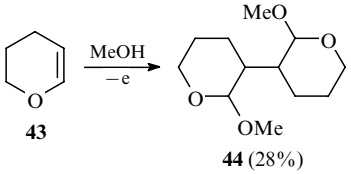

44 (28%)

Dimerisation of vinyl ethers **41**–**43** is accompanied by side addition of methanol to the double bond, which is catalysed by the protons resulting from anodic oxidation of the solvent and solvolysis of electrogenerated radical cations. To suppress this reaction, electrolysis of vinyl ethers is usually carried out in the presence of bases, for example, pyridine or 2,6-lutidine.[38]

Unlike vinyl ethers, arylalkenes are unable to add methanol under conditions of electrooxidative dimerisation; therefore, the reaction can be carried out without a base. The composition, the structure and the yield of dimerisation products of arylalkenes depend on the type of substitution at the double bond, the nature of the supporting electrolyte and the anode potential.[33, 34] Thus electrolysis of arylalkenes **45a**,**c** in the presence of sodium perchlorate yields 1,4-dimethoxy-1,4-diarylbutanes **46a**,**c** as the only or major products, while in the presence of sodium camphorsulfonate, 1,4-diaryl-1-methoxybut-1-ene **47a** and 1,4-diarylbuta-1,3-diene **48a** are formed (Table 5). Electrolysis of 2-phenylpropene (**45b**) with the $NaClO_4$ electrolyte at an anode potential of 1.6–1.7 V yields dimer **48b**; at lower potentials (1.1–1.2 V), a mixture of dimers **46b**, **47b** and **48b** in 4.2 : 2.5 : 1 ratio is formed. In the case of 4-methoxystyrene (**45c**), an increase in the potential from 0.8 to 1.2–1.3 V increases the yield of the dimer **46c** from

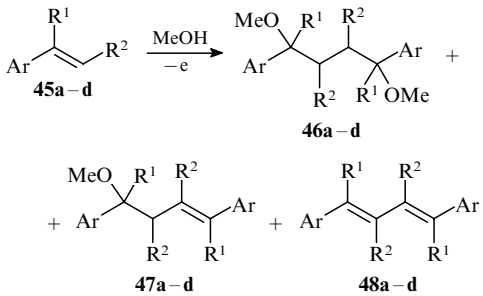

Ar = Ph, 4-$MeOC_6H_4$; R^1 = H, Me; R^2 = H; R^1–R^2 = $(CH_2)_3$.

Table 5. Electrooxidative dimerisation of arylalkenes **45** in methanol.[33, 34]

Compound **45**	Ar	R^1	R^2	Electrolyte	Potential /V	Reaction product (yield) (%)
a	Ph	H	H	$NaClO_4$–MeONa (10 : 1)	1.1	**46a** (64)
	Ph	H	H	Sodium camphorsulfonate	1.6–1.7	**47a** (28) + **48a** (36)
b	Ph	Me	H	$NaClO_4$–MeONa (10 : 1)	1.6–1.7	**48b** (67)
	Ph	Me	H	$NaClO_4$–MeONa (10 : 1)	1.1–1.2	**46b** (42) + **47b** (17) + **48b** (10)
c	4-$MeOC_6H_4$	H	H	$NaClO_4$, MeOH, CH_2Cl_2	1.2–1.3	**46c** (79)
	4-$MeOC_6H_4$	H	H	$NaClO_4$, MeOH, CH_2Cl_2	0.8	**46c** (66)
d	Ph	$(CH_2)_4$		$NaClO_4$, MeOH, CH_2Cl_2	0.9	**46d** (3.4)

Note. Electrolysis was carried out under potentiostatic conditions in an undivided cell (PCU) with a graphite anode; the current yield was determined relative to the isolated products; the initial concentration of the substrate was 5.8–6.0 mol litre^{-1}.

66% to 79%. Alkenes with a greater extent of substitution at the double bonds, for example, 1-phenylcyclohexene **45d** give the corresponding dimer **46d** in a yield of only 3.4%.

Apart from dimer **49**, the electrooxidative dimerisation of indene gives dimethoxylation product **50**.[33, 34]

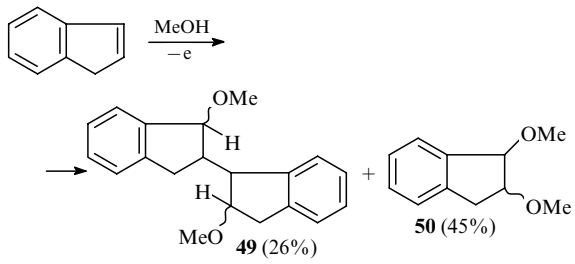

6. Intramolecular electrooxidative cyclisation

Intramolecular electrooxidative cyclisation is possible for alkenes the molecules of which contain, in addition to the C=C bond, a group capable of electrooxidative transformation into a radical-cation or a radical centre and the chain separating them consists of three to five atoms. The radical cations and radical intermediates electrogenerated from alkenes of this type, for example, from unsaturated carboxylic acids, unsaturated ethers and carbamates, activated α-stannyl or α-silyl groups, aryl(hetaryl)alkenes and non-conjugated α-alkoxy- and α-acetoxydienes, are converted into cyclic products upon intramolecular addition at the double bond followed by solvolysis or other secondary reactions. These processes are considered in more detail below, in Sections II.6.a–e.

a. Cyclisation of unsaturated carboxylic acids

In the cyclisation of unsaturated carboxylic acids, the reaction products result from intramolecular cyclisation of alkenyl radicals **51** generated by the anodic oxidation of the anions of unsaturated acids under conditions of the Kolbe reaction.

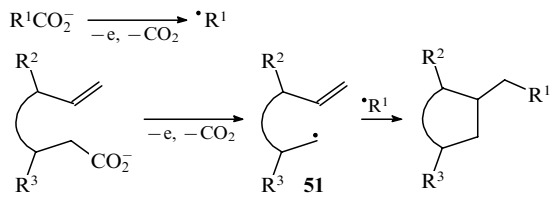

The recent comprehensive reviews devoted to this known reaction [1–4, 86] describe, along with other aspects, the results of application of anodic oxidation to the generation of radicals from carboxylic acids and investigation of the electrochemical cyclisation of unsaturated acids. Further progress along this line [87–90] resulted in the elaboration of new methods for the synthesis of natural and related cyclic products, for example, pyrrolidines **52**,[88, 89] precursors of prostaglandins **53** and **54**[90] and angular triquinanes **55**.[91]

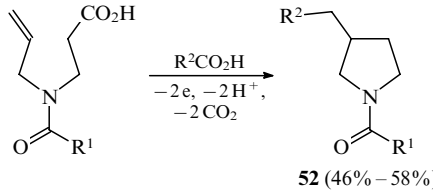

R^1 = H, Me; R^2 = Me, n-C_5H_{11}, $(CH_2)_4CO_2Me$.

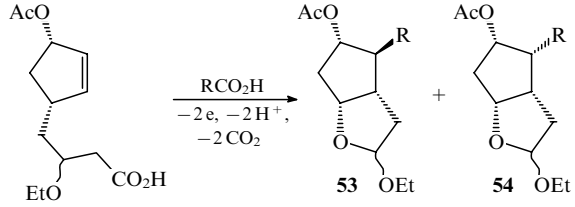

R	Yield (%)	
	53	**54**
Me	50	18
n-C_8H_{17}	40	14
$(CH_2)_2CO_2Me$	42	14
$CH_2SiMe_2CH_2$	30	8
Me_3SiCH_2	29	10
n-$C_5H_{11}COCH_2CH(SiMe_3)$	4–5	–

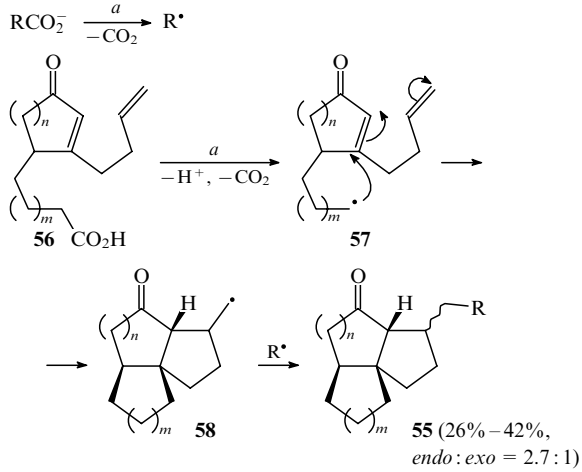

R = Me, n-C_5H_{11}, $(CH_2)_2CO_2Me$; n = 1–3, m = 1, 2; (*a*) ACU, Pt anode, steel cathode, 25 mA cm^{-2}, 1.2 F mol^{-1}, MeOH, 4 equiv. of RCO_2H neutralised by KOH to 5%, 40–45 °C.

The formation of the compounds **55** from acids **56** takes place *via* regio- and stereoselective radical tandem cyclisation initiated by anodic oxidation and giving rise to three new C–C bonds. Two

bonds are formed at the stage of cyclisation of radical **57**, and the third one, upon recombination of tricyclic radical **58** with the R$^{\bullet}$ radical generated from the saturated acid, which is used as the second reactant. This distinguishes electrochemical cyclisation from tandem cyclisations initiated by chemical methods: in this case, C–H or C–I bonds are formed at the final stage.[92–94] An advantage of the electrochemical tandem cyclisation is that it does not use organotin reagents, normally employed in the chemical version, and the combination of the initial unsaturated and saturated acids makes it possible to change the side chain of the product **55**.

b. Cyclisation of unsaturated ethers and carbamates activated by α-stannyl and α-silyl groups

Silyl, stannyl or thioaryl groups in the α-position markedly decrease the oxidative potentials of ethers or carbamates **59**; this facilitates the electrochemical transformation in oxonium (X = O) or *N*-acyliminium (X = NCO_2Me) ions.[95–101] Intramolecular cyclisation of substrates **59** yields products containing an endocyclic fluorine atom, indicating a cationic mechanism of the reaction (in the case of a radical mechanism, an exocyclic product would be formed at $n = 1$). The supporting electrolyte, namely, tetrabutylammonium tetrafluoroborate or hexafluorophosphate, serves as the source of the fluorine anion at the final stage of the process.[98]

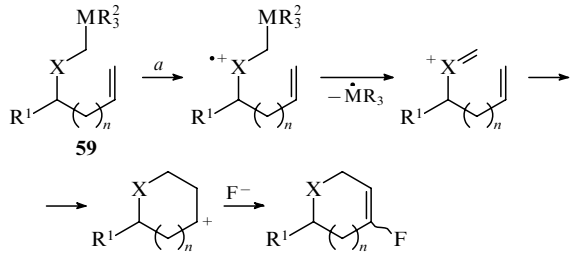

(50%–98%, *cis* : *trans* = 1.2 : 3)

M = Sn, Si; R^1 = H, Me; R^2 = Alk; X = O, NCO_2Me; n = 1, 2; (*a*) ACU, graphite anode, CH_2Cl_2, Bu_4NBF_4.

Trialkylstannyl groups exert a more pronounced activating effect than trialkylsilyl groups; as a consequence, cyclic products are formed in higher yields from stannyl derivatives.

This method has been used to convert α-stannyl-substituted arylaliphatic ethers **60a–c** into isochroman (**61a**), 6-fluoroisochroman (**61b**) and *N*-methoxycarbonyl-1,2,3,4-tetrahydroisoquinoline (**61c**). The transformation of *trans*-1-(tributylstannylmethoxy)-2-(hex-1-enyl)cyclohexane (**62**) gave rise to *trans*-3-butyl-4-bromo-1-oxadecalin (**63**).[99, 101]

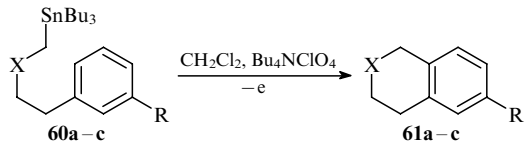

X = O: R = H (**a**, 55%), F (**b**, 80%); X = NCO_2Me, R = H (**c**, 54%).

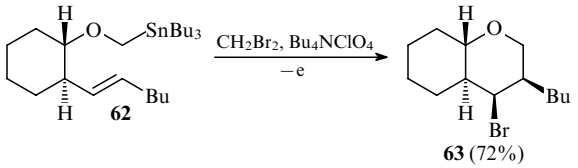

c. Cyclisation of aryl and hetarylalkenes

Intramolecular cyclisation of aryl- and hetarylalkenes is a result of transformations of radical cations **64** electrogenerated from these substrates. This cyclisation is one of the most useful reactions induced by direct anodic oxidation.[102–118]

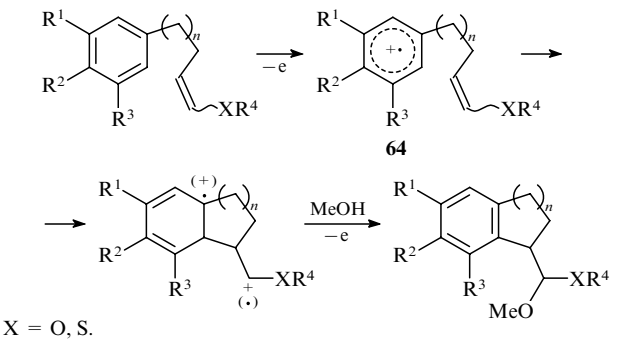

X = O, S.

The structure of the bi- and polycyclic compounds thus obtained depends on the nature and the stereochemistry of substituents at the double bond. For example, cyclisation of substrates **65–67** having related structures but differing in the nature and the positions of substituents at the double bond affords absolutely different tricyclic compounds **68–70**, precursors of natural products.[102–111]

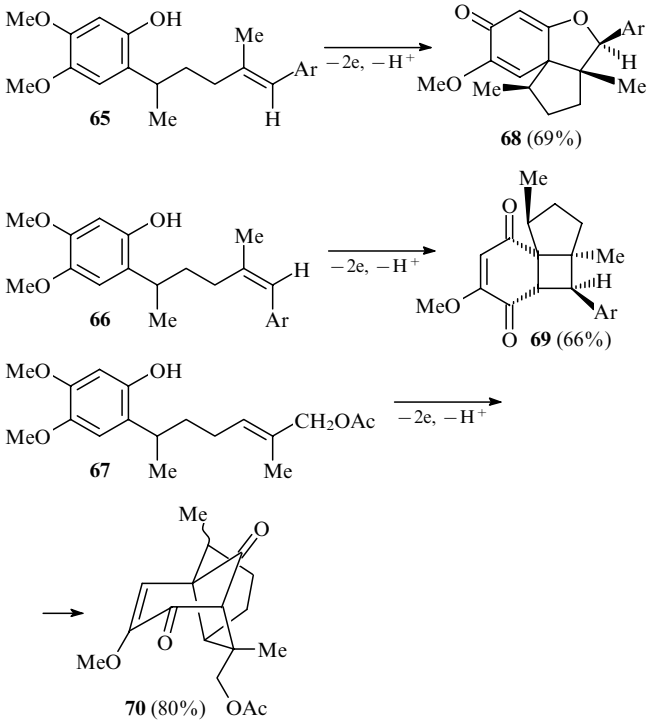

Mild experimental conditions and high product yields are important advantages of this method for the preparation of this type of polycyclic polyfunctionalised compound.

4-Hydroxy-2′-alkenylbiphenyls **71a–e** have been used as examples to study the influence of the structure of the initial substrates, electrolysis conditions and some other factors on the cyclisation. Presumably,[112, 113] the initial step represents generation of cationic intermediates **A** and **B** induced by anodic oxidation; this is followed by their cyclisation and the reaction of cations **C** with methanol giving rise to compounds **72a–e**.[112, 113]

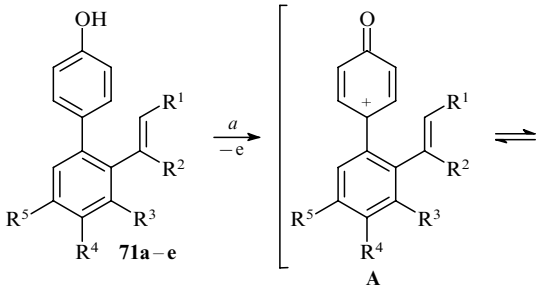

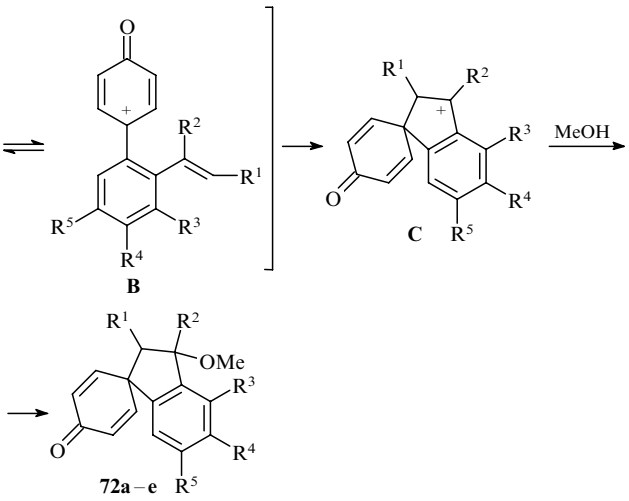

(*a*) ACD, platinum wire or glass carbon anode, 1.6–2.0 F mol^{-1}, MeOH or MeOH–AcOH (CH_2Cl_2, MeCN), $LiClO_4$, 0–20 °C.

Compound **71**	R^1	R^2	R^3	R^4	R^5	The yield of compounds **72** (%)	Ref.
a	H	H	H	H	H	16	112, 113
b	H	Me	H	H	H	85	112, 113
c	H	Ph	H	H	H	65	112, 113
d	Me	H	H	H	H	35	112, 113
e	$(CH_2)_3$		H	H	H	69	112, 113
f	H	H	Me	H	H	70	114
g	H	H	H	H	OMe	47	115
h	H	Me	H	H	OMe	84	115
i	H	Me	H	OMe	H	80	115
j	H	H	H	OMe	OMe	70	115
k	H	Me	H	OMe	OMe	92	115
l	H	Me	H	OCH_2O		70	115

The cyclisation of 4-(2′-alkenylphenyl)phenols **71b**,**c**,**e**, containing α-substituents in the alkenyl group, occurs with high yields (65%–85%). In the case of the compounds **71** in which R^2 = H the yields are much lower. The compound **71m**, containing a phenylthio group at the double bond, is converted into diketone **73**.

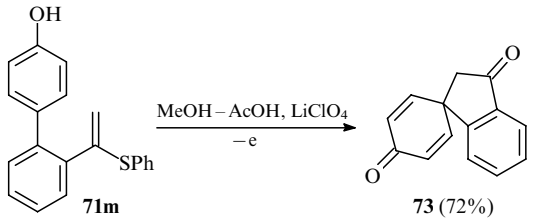

The yields of reaction products also depend on the solvent, current density, anode material and addition of mild acids, for example, acetic acid. The highest yields are attained when the reaction is carried out in a mixture of acetonitrile with methanol (4 : 1) containing 5–10 equiv. of AcOH, using lithium perchlorate as the supporting electrolyte and a current density of 0.84 mA cm^{-2} on a platinum electrode.[113]

The increase in the yields of the compounds **72** following the replacement of hydrogen at the α-carbon atom in the olefinic group by a methyl group is presumably [115] due to the fact that in this case, the cationic intermediate exists preferably in conformation **A**, in which the double bond is close to the reaction centre. For the substrates **71** in which R^2 = H, conformation **B** is preferred. A similar effect is exerted by the methyl group in the *ortho*-position to the alkenyl substituent. For example, the transformation of 4-hydroxy-2′-vinyl-3′-methylbiphenyl (**71f**) gives the cyclisation product — spirodienone **72f** — in 70% yield.[114]

Cyclisation of 4-hydroxyarylalkenes with R^2 = H containing methoxy groups in the *para*-position or both in the *para*- and *meta*-positions relative to the vinyl group (the compounds **71g**,**j**) is more efficient. Similar *meta*-methoxy-derivatives do not cyclise. Cyclisation of *para*- and *meta*-methoxy-substituted **71h**,**i**,**k**,**e** in which R^2 = Me gives products in high yields.[115]

The trimethylsilyl ethers of 4-hydroxyarylalkenes, for example, compound **74**, unlike the corresponding phenols, are converted into cyclic products in high yields even in the absence of AcOH.[114]

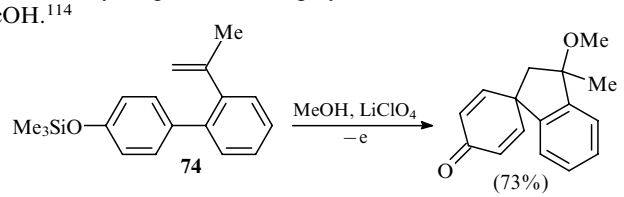

Silyl ethers can cyclise in the presence of bases. Thus, depending on the nature of the functional groups present in the substrate, this process can be carried out both in a neutral medium and in the presence of acids or bases.

Within the framework of investigation of cyclisation, anodic oxidation of aryl- and hetarylalkenes with electron-enriched double bonds has been vigorously developing in recent years.[116–118] The interest in these reactions is determined by the possibility of performing the cyclisation of arylalkenes with a regioselectivity (pathway *b*) differing from that observed in the case of the Friedel–Crafts cyclisation (pathway *a*). The cyclisation process during the anodic oxidation is based on the inversion of polarity of enol ethers. This reaction makes it possible to prepare cyclic products of various structures from the same initial substrate, depending on the method used to initiate cyclisation.

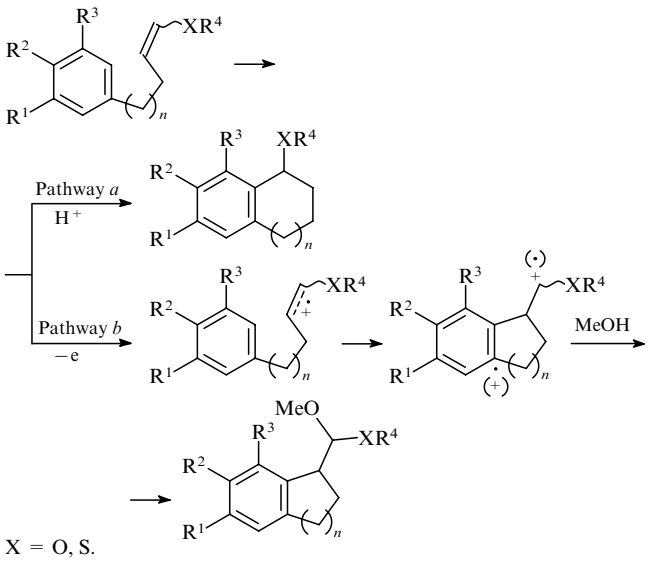

X = O, S.

Thus by anodic oxidation of enol ethers and enol thioethers **75a**–**c**, cyclisation products, namely, substituted tetralins **76a**–**c**, **77**, and **78** have been prepared in high yields. Under the same conditions, the enol ether **75d** is converted into spiro derivative **79** (Scheme 3).[116, 118]

It should be noted that cyclisation of the enol ether **75a** to give the tetralins **76a** and **77** is accompanied by the formation of 1,6- and 1,8-dimethoxytetralins, resulting from further electrooxidation. The tetralin **76b**, formed from the enol ether **75b**, is converted into 1,6,8-trimethoxytetralin **78**.[118]

Scheme 3

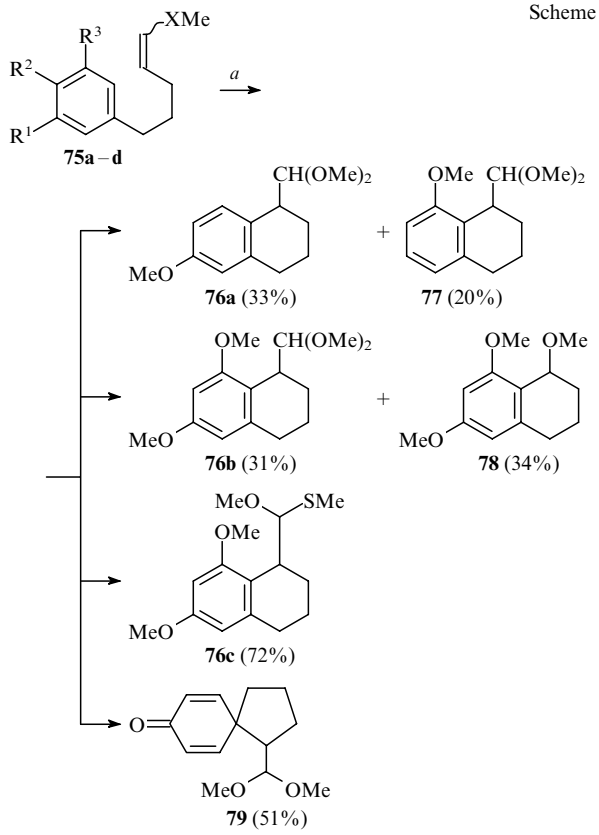

75: R^1 = OMe, R^2 = R^3 = H, X = O (**a**); R^1 = R^3 = OMe, R^2 = H, X = O (**b**), S (**c**); R^1 = R^3 = H, R^2 = OMe, X = O (**d**); (*a*) ACD, glass carbon anode, 1.6–2.0 F mol^{-1}, MeOH–CH_2Cl_2 (1 : 4), $LiClO_4$, 5 equiv. of 2,6-lutidine (2,6-Lut), ~20 °C.

These side reactions do not take place if electrolysis is carried out with a controlled potential (1.1 V). Unlike cyclisation of the enol ethers **75a**,**b**, cyclisation of the enol thioether **75c** under similar conditions occurs without further oxidation of the reaction product **76c**.

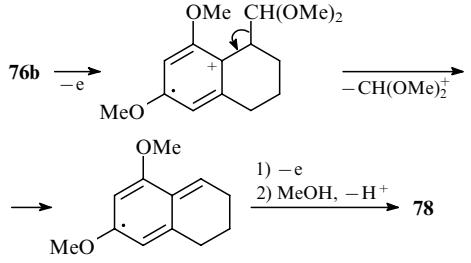

The cyclisation of furyl- (**80**) and pyrrolyl-substituted alkenes **81** containing electron-enriched double bonds induced by anodic oxidation has opened a new way for assembling bicyclic structures incorporating five-membered heterocycles.[116,117] A compound of type **82** can be used in the synthesis of furan-containing bi- and polycyclic natural products.[119–126]

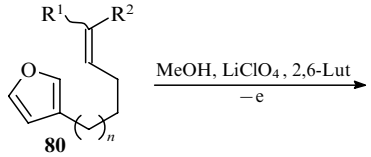

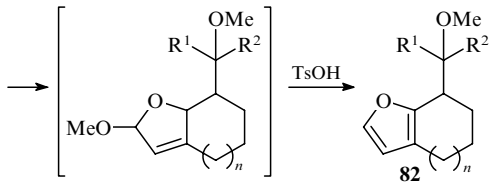

R^1 = SMe, OMe, Ph, Me, CH_2SiMe_3; R^2 = H, Me, n = 1, 2.

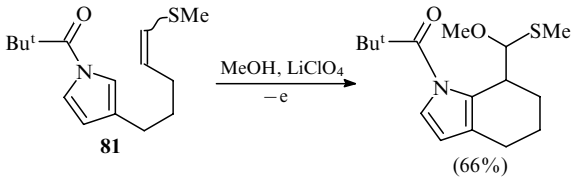

d. Cyclisation of non-conjugated 1-alkoxy-dienes

Cyclisation of non-conjugated 1-alkoxy-dienes has not yet been adequately studied. This electrochemical process, which has much in common with cyclisation of aryl- and hetarylalkenes, has found application for the synthesis of carbocyclic compounds. The value of this method is dictated by the possibility of reverting the polarity of the β-carbon atom in the initial 1-alkoxy-dienes **83a**–**m** from nucleophilic to electrophilic due to the fact that an initial stage of the process is transformation of the substrates into radical cations **84a**–**m**.[127–134] The electrolysis conditions and the yields of the reaction products **85a**–**m** are listed in Table 6.

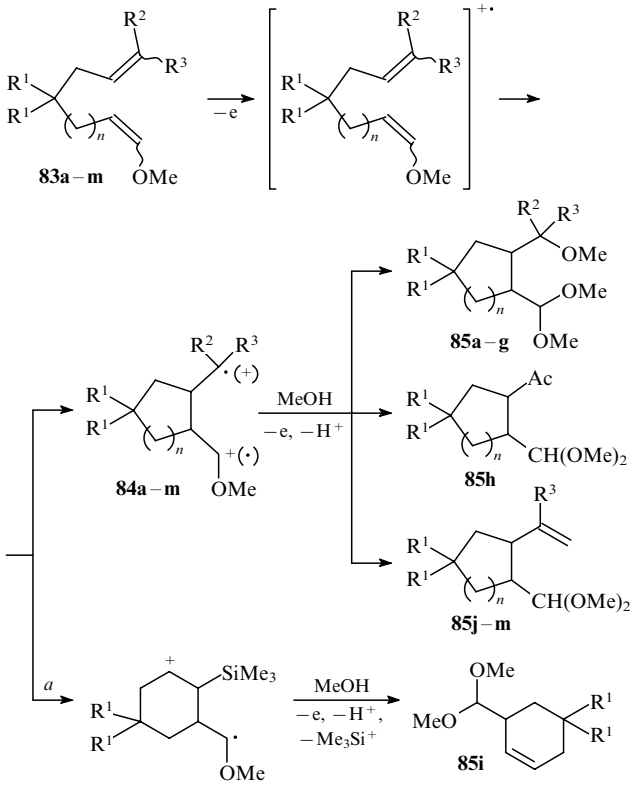

(*a*) R^1 = Me, R^2 = $SiMe_3$, R^3 = H.

The 1-methoxy-dienes **83** (n = 1–3), which contain substituents R^2 and R^3 activating the double bond, ensure the most selective formation of cyclic compounds (see Table 6).[127–134] Cyclisation of 1-methoxy-dienes **86a**,**b** does not proceed under similar conditions: these compounds are converted into unsaturated dialdehyde diacetals **87a**,**b**.

Table 6. Anodic oxidation of 1-methoxy dienes **83a**–**m**.

Compound **83**	n	R^1	R^2	R^3	Reaction product	Yield (%)	Ref.
a	1	Me	OMe	H	**85a**	68	128
b	1	H	OMe	H	**85b**	70	128
c	2	H	OMe	H	**85c**	65	128
d	3	H	OMe	H	**85d**	50	128
e	1	H	Ph	H	**85e** [a]	65–73	127, 128
f	2	H	Ph	H	**85f**	65	128
g	1	H	Me	Me	**85g**	60	128
h	1	Me	OMe	Me	**85h**	62	132
i	1	Me	$SiMe_3$	H	**85i**	29	129
j	1	Me	CH_2SiMe_3	H	**85j** [a]	84	132
k	1	Me	CH_2SiMe_3	Me	**85k**	89	128
m	2	H	CH_2SiMe_3	H	**85m**	59	128

Note. Conditions of electrolysis: ACU, Pt or wire glass carbon anode, 15 mA cm^{-2}, 2 F mol^{-1}, methanol–THF (1 : 1) or MeOH–CH_2Cl_2 (1 : 4), $LiClO_4$, 2,6-Lut. [a] A mixture of *trans*- and *cis*-isomers.

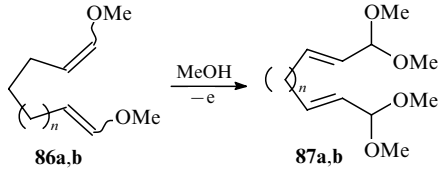

n = 4 (**a**), 12 (**b**).

The principle of electrochemical cyclisation of linear 1-methoxy-dienes has been extended successfully to compounds **88**, containing cyclopentane (m = 1) and cyclohexane (m = 2) fragments.[130, 132, 134]

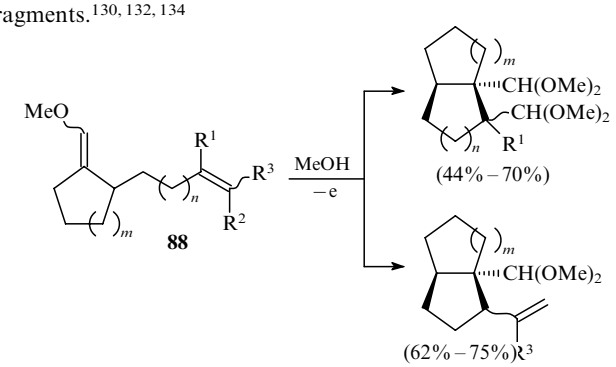

R^1, R^2 = H, Me; R^3 = OMe, $SiMe_3$; m, n = 1, 2.

e. Cyclisation of non-conjugated 1-acetoxy-dienes

Cyclisation of non-conjugated 1-acetoxy-dienes **89** has many common features with the transformation of enol acetates into enones and α-acetoxy ketones (see Section II.2). A fundamental distinction between these electrochemical processes is that radical cations **A** electrogenerated from the 1-acetoxy-dienes **89** can react with a second C=C bond acting as an internal nucleophile. The intramolecular electrophilic attack on the double bond by the cationic centre of the radical cation gives rise to cyclic radical cation **B**. The subsequent deprotonation and electrooxidation of intermediate **B** are accompanied by elimination of the acetyl cation, resulting in the formation of cyclisation product **90** and competitive formation of conjugated enones **91** or **92**.[135]

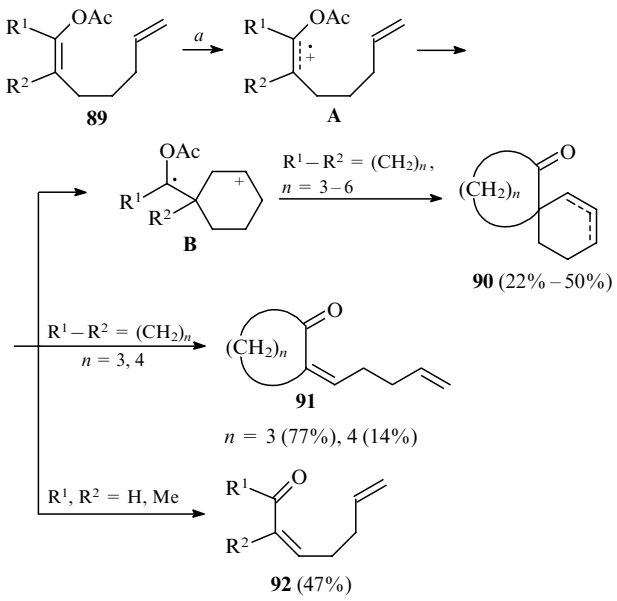

(*a*) ACU, graphite electrodes, 4–10 F mol^{-1}, AcOH, Et_4NOTs (1 mol $litre^{-1}$), ~20 °C.

Cyclisation of radical cations **A** by a radical mechanism does not occur under these conditions.

7. Transformations of alkenes with skeletal rearrangement

The transformations of alkenes with skeletal reconstruction take place as a result of rearrangement of carbenium ions, which are intermediates in the anodic oxidation of alkenes. For example, cyclohexene is converted into cyclopentanecarbaldehyde dimethyl acetal (**93**),[136] while *trans*-stilbene yields diphenylacetaldehyde dimethyl acetal (**94**).[67]

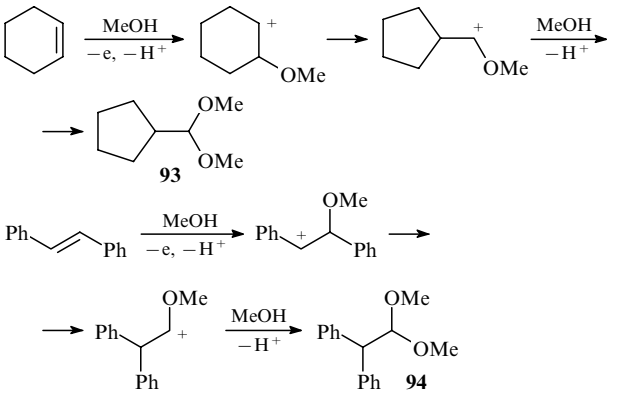

Since carbenium ions react competitively with MeOH, the dimethyl acetals **93** and **94** are formed as mixtures with 1,2-dimethoxycyclohexane and 1,2-dimethoxy-1,2-diphenylethane. When anodic oxidation of cyclohexene, *trans*-stilbene and related alkenes is carried out in trimethyl orthoformate in the presence of iodine, this side process is suppressed and acetals are produced as the only electrolysis products.[136] The promotory effect of iodine is related presumably [136] to the formation of iodonium salts, which efficiently assist the rearrangement.

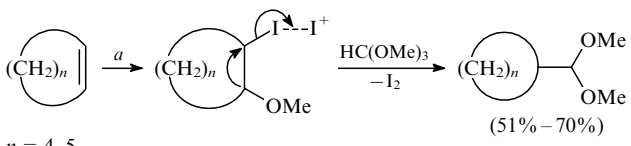

n = 4, 5.

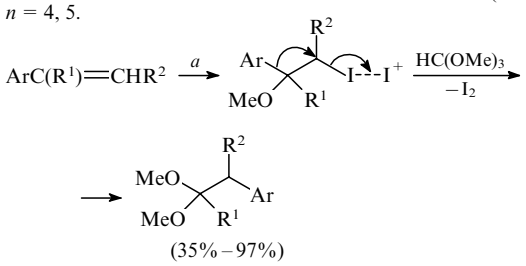

Ar = Ph, 4-MeC_6H_4, 4-$MeO_2CC_6H_4$, 4-ClC_6H_4; R^1 = H, Me; R^2 = H, Me, Ph, CH_2OMe; (*a*) ACU, graphite anode, 0.1 mA cm^{-2}, 3–17 F mol^{-1}, $HC(OMe)_3$, $LiClO_4 \cdot 3H_2O$, 0.25–1.2 equiv. I_2, 20–100 °C.

8. Cleavage of the double bond in alkenes

Electrochemical cleavage of the double bond in alkenes takes place in an aqueous or alcoholic solution. This is a two-stage process consisting of vicinal dioxygenation of the alkene double bond at the initial stage and cleavage of the C–C σ-bond in the resulting species at the subsequent stage.

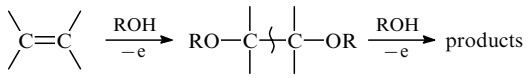

ROH is water or alcohol.

For conjugated arylalkenes, aryl(areno)cycloalkenes and enol acetates, the two stages can proceed successively as a one-pot reaction because the same electrolytes are effective for both processes. The attempts to cleave the double bond in enol ethers in the same way failed (see Section II.8.b).

a. Direct cleavage of the C=C bond in arylalkenes, aryl(areno)cycloalkenes and enol acetates

Stepwise investigation of styrene electrooxidation in methanol in an undivided cell showed that the initial and the subsequent stages of this process are affected in different ways by the nature of the electrolyte, anode material and temperature. The highest selectivity (76%–80%) of the first stage (degree of substrate conversion 90%–93%) is attained in potassium fluoride or tetrabutylammonium tetrafluoroborate as the supporting electrolyte with a platinum anode, while for the second stage a selectivity of 70%–83% (degree of conversion 85%–98%) is observed in the presence of sodium toluene-*p*-sulfonate and tetrabutylammonium tetrafluoroborate with a graphite anode.[64, 65] Operation of the overall process under conditions favourable for the second stage permits preparation of the target products in higher yields. Under these conditions, conjugated arylalkenes were converted into benzaldehyde acetals and arylketone ketals (the consumption of electricity is 4–8 F per mole of alkene).[64, 137–139]

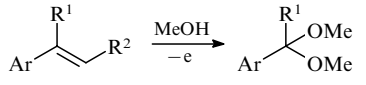

Ar = Ph, 4-MeC_6H_4, 4-$MeOC_6H_4$; R^1 = H, Me, Ph; R^2 = H, Me, Et.

1-Phenylcycloalkenes give acetal and ketal derivatives of ω-benzoylalkanals.[64, 140]

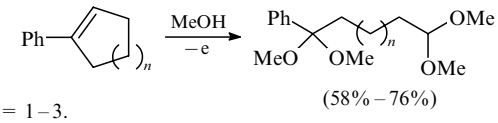

n = 1–3.

Indene (**95a**) and 1,2-dihydonaphthalene (**95b**) form the bis(acetals) **96a**,**b**.[64, 140]

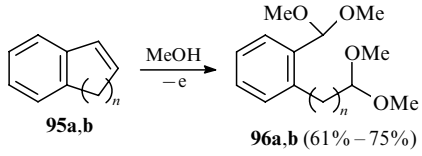

95a,**b**

96a,**b** (61%–75%)

n = 1 (**a**), 2 (**b**).

Acyclic (**97**) and cyclic (**98a**,**b**) acetals of naphthalene-1,8-dicarboxaldehyde were prepared from acenaphthene.[70] The **97** to **98a**,**b** ratio depends substantially on the electrolyte used: in the presence of potassium fluoride, these products are formed in 30% and 34% yields, respectively; in the presence of tetrabutylammonium tetrafluoroborate, the ratio is ~1 : 25 (overall yield 57%).

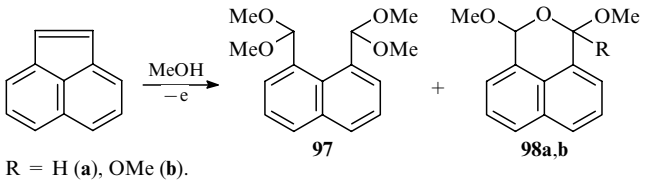

97 **98a**,**b**

R = H (**a**), OMe (**b**).

The process selectivity sharply decreases when the initial alkene concentration is higher than 1.0 mol $litre^{-1}$ because of the increase in the relative amount of the alkene involved in the side dimerisation, oligomerisation and polymerisation reactions (see Section II.5). The decrease in the alkene concentration in the reaction mixture by using its gradual addition to the electrolyte during electrolysis makes it possible to increase the product yield to 15%–20%.[65]

The predominant formation of the cyclic acetals **98** from acenaphthene is, apparently, caused by the fact that, during the electrolysis in the presence of Bu_4NBF_4, the space near the anode surface gets acidified by the electrogenerated HBF_4, which catalyses the transformation of the acetals **97** into **98a**,**b**.

The rupture of the C–C bond in glycols formed upon the electrooxidation of the double bond in conjugated arylalkenes in aqueous and water-organic media proceeds at a substantially higher rate than that in their alkyl ethers. In this case, the process cannot be stopped at the stage of formation of glycols due to the fast rupture of the C–C bond in the HO–C–C–OH fragment. Direct anodic oxidation of propenylbenzene, anethole and isosafrole has been studied in most detail.[138–142] Anisaldehyde was prepared from anethole in high substance yield (81%–85%) but a low current yield (~20%).[141, 142] The cleavage of double bond in isosafrole has not resulted in the synthesis of 3,4-methylenedioxybenzaldehyde (piperonal) in a yield higher than 34%.

Electrochemical rupture of the C=C bond in enol acetates proceeds *via* consecutive transformation into radical-cation and radical intermediates **A** and **B**, α-methoxy ketones, their semiketals, and radical cations **C** and gives rise to esters of oxoalkanoic acids.[143]

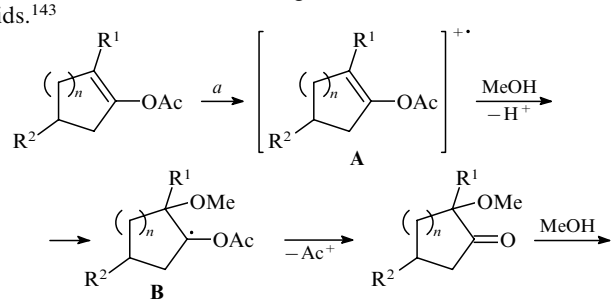

A

B

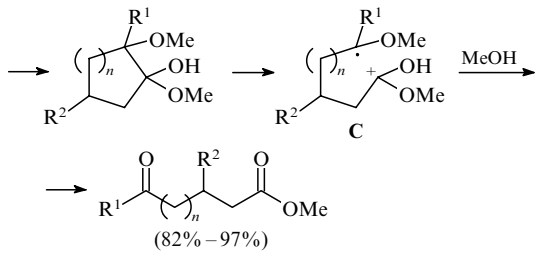

n = 1, 2; R^1, R^2 = H, Me, Pr^i; (*a*) ACU, Pt anode, 4 F mol^{-1}, MeOH – AcOH (10 : 1), $LiClO_4$, 2 – 8 °C.

Starting from (+)-menthone enol acetate, methyl (+)-3,7-dimethyl-6-oxooctanoate was prepared by this method in 74% yield.[143]

b. Direct cleavage of the double bond in cyclic enol ethers

It has been noted above that cleavage of the double bond in enol ethers cannot be carried out as a one-pot reaction with the same selectivity as for conjugated arylalkenes, aryl- and benzocycloalkenes. This is due to the fact that the electrochemical vicinal dialkoxylation of enol ethers proceeds with a satisfactory selectivity only with basic electrolytes, which are inefficient at the stage of electrooxidative cleavage of dialkoxylation products. Therefore, the process is carried out as two separate electrochemical stages with isolation of the products of dialkoxylation of enol ethers **99** – **101** after the first stage.[59, 144 – 146]

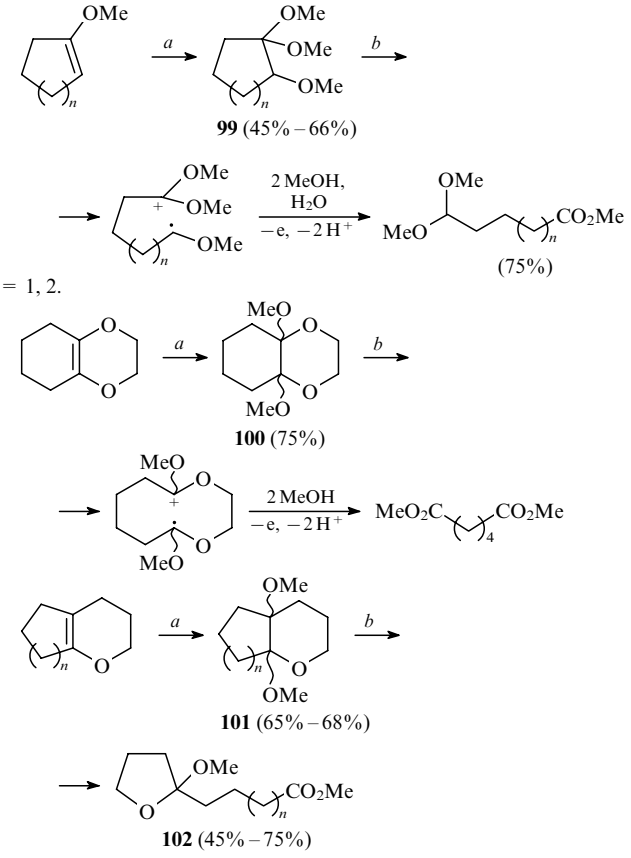

n = 2, 8; (*a*) ACU, Pt anode, 3.5 – 6.2 F mol^{-1}, MeOH, MeONa or KOH, – 5 – 20 °C; (*b*) ACU, graphite anode, 6 – 8 F mol^{-1}, MeOH, Et_4NOTs or Bu_4NBF_4, 20 °C.

The electrochemical processes at the second stage result in ring opening in the dialkoxylation products **99** – **101**. In the case of the compounds **101**, the reaction is accompanied by their electrooxidative rearrangement into methyl ω-(2-methoxytetrahydrofuryl)alkanoates **102**. The rearrangement takes place due to isomerisation of intermediates **A** into carbocations **B** *via* oxonium ions **C**. The subsequent alcoholysis of cations **B** results in the reaction product **102**.[145, 146]

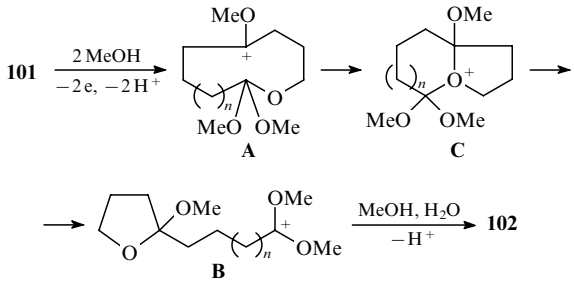

III. Reactions induced by indirect anodic oxidation

In the reactions induced by indirect anodic oxidation, unlike reactions induced by direct anodic oxidation, no direct electron transfer from the alkene molecule takes place at the anode. In this case, alkenes are involved in the electrochemical process through interaction with electrogenerated inorganic or organic radicals, ions or reagents (see Scheme 1). These intermediates arise from their precursors at potentials lower than the potentials of alkene oxidation. The process of alkene transformation into products takes place partly or entirely in the bulk solution rather than on the anode surface and is markedly facilitated and accelerated. This strategy allows one to perform electrochemical transformations of alkenes impossible in the case of direct anodic oxidation and thus extends the scope of applicability of anodic processes in organic synthesis.

The most typical precursors for the generation of oxidants and reagents in the alkene transformations induced by indirect anodic oxidation are anions of organic and inorganic acids, variable-valence metal compounds and triarylamines.

1. The reactions of alkenes with radicals electrogenerated from carboxylate anions and 1,3-dicarbonyl and related compounds

In the anodic oxidation of carboxylate, acetoacetate, malonate and cyanoacetate anions, carbon-centred radicals are generated;[1 – 4, 86] in the presence of alkenes, they add to the double bond. The resulting radical adducts **103** are converted along two routes: they either undergo pairwise or cross recombination (Scheme 4, pathways *a*, *b*) or are oxidised to give carbocations (pathway *c*). Subsequently the carbocations react with internal or external nucleophiles.[1 – 4]

Scheme 4

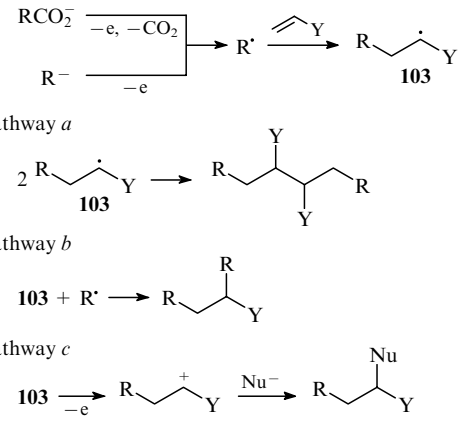

a. Reactions of alkenes with alkanoic acids

The reactions of alkenes with radicals generated from saturated acids and 1,3-dicarbonyl and related compounds have been generalised in a review,[5, 6] which covers the data published up to 1981. In this review, we consider later publications.

The main difference between alkene reactions with radicals generated by the anodic oxidation of alkanoic acids and their reactions with similar radicals generated by chemical methods is that the electrochemical method makes it possible to vary the radical concentration on the electrode surface over a broad range by varying the current density and thus to control the process. An increase in the current density favours recombination of radicals, while a decrease facilitates the oxidation of radicals. The electrochemical and chemical processes also differ in the way in which electron-withdrawing substituents Y in the alkene molecule influence the reaction route. The formyl, acetyl and alkoxycarbonyl groups direct the electrochemical reaction exceptionally to pathway *a* [147] and the chemical reaction, to pathway *a* or *b*. The alkenes $CH_2=CHY$ with electron-donating substituents Y, such as alkyl, aryl, vinyl and alkoxyl groups are converted along each of the three pathways: *a*, *b* and *c* (see Scheme 4).[5,6]

The electrochemical reactions under consideration have been studied in relation to the methylation [147] and trifluoromethylation [148–162] of acrylates,[147–159] methacrolein, vinyl ketones,[147] acrylo- and fumaronitrile,[149,160] esters of fumaric, maleic [151,152] and but-3-enoic acids,[150] alkenes,[148,149,153,154] vinyl acetate,[151,152] isopropenyl acetate, allyl chloride,[153,154] but-3-en-1-ol [161] and undec-10-enoic acid.[162] These reactions are normally carried out in an aqueous solution of a mixture of acetonitrile with partially (to 10%) neutralised acetic or trifluoroacetic acid in a cell with platinum electrodes at an anodic current density of 50–100 mA cm^{-2} and with passage of 1.1–1.5 F of electricity per mole of the acid.[147,159] Methylation and trifluoromethylation of methacrolein, vinyl ketones and acrylates results under these conditions in pairwise and cross coupling of the arising radicals to give 2:2 (**104**, **105**) and 2:1 (**106**) adducts in 40%–80% yields.[147–149,156,157] The decrease in the anodic current density to 1 mA cm^{-2} and a decrease in the temperature from 20 to 0–5 °C directs the reaction of trifluoroacetic acid with methyl methacrylate almost entirely along pathway *c* giving rise to methyl 2-acetamido-2-methyl-4,4,4-trifluorobutanoate (**107**). The compound **107** is formed upon oxidation of the initial radical adducts and the reaction of the resulting carbocations with the solvent (MeCN).[156] This change in the direction of the process is due to the fact that electrooxidation of radical adducts occurs much faster than their dimerisation.[159]

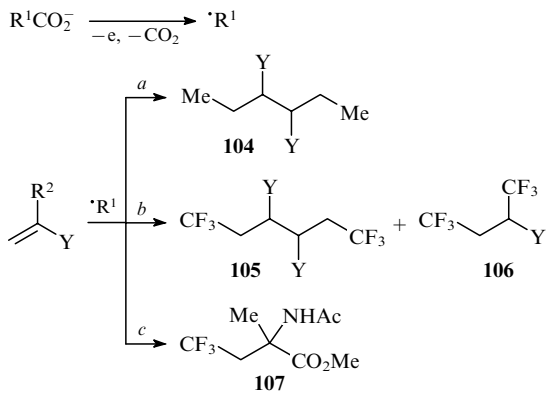

Y = CHO, Ac, CO_2H, CO_2Me, CN; (*a*) R^1 = Me, R^2 = H, 50 mA cm^{-2}; (*b*) R^1 = CF_3, R^2 = H, 50–100 üA·cü$^{-2}$; (*c*) R^1 = CF_3, R^2 = Me, Y = CO_2Me, 1 mA cm^{-2}, 0–5 °C.

b. Reactions of alkenes with 1,3-dicarbonyl and related compounds

Radical adducts formed by ethyl acetoacetate, diethyl malonate or malononitrile with vinyl ethyl ether or styrene are oxidised at the anode to cationic intermediates, which react with external or internal nucleophiles being thus converted into linear (**108**, **109**) and/or cyclic products (**110**, **111**). The adducts formed with styrene also give dimers **112**.[163]

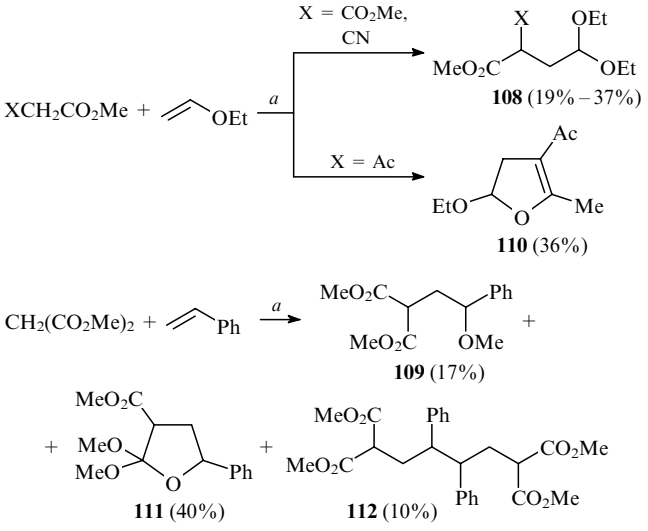

(*a*) ACU, 14 mA cm^{-2}, 1.5 F mol^{-1}, EtOH or MeOH, EtONa or MeONa.

Joint electrolysis of cycloalkane-1,3-diones **113**, **114** with alkenes affords the products of formal [3+2]-cycloaddition, dihydrofuran (**115**, **116**) and tetrahydrofuran (**117**) derivatives.[164–167]

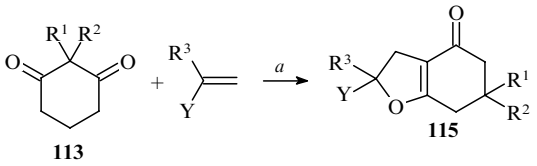

(*a*) ACU, 14 mA cm^{-2}, 1.5 F mol^{-1}, MeCN.

R^1	R^2	R^3	Y	Yield of **115** (%)
H	H	H	Ph	85
H	H	Me	$CH=CH_2$	62
H	H	H	OEt	57
Me	Me	H	Ph	97
Me	Me	H	CH_2SiMe_3	45

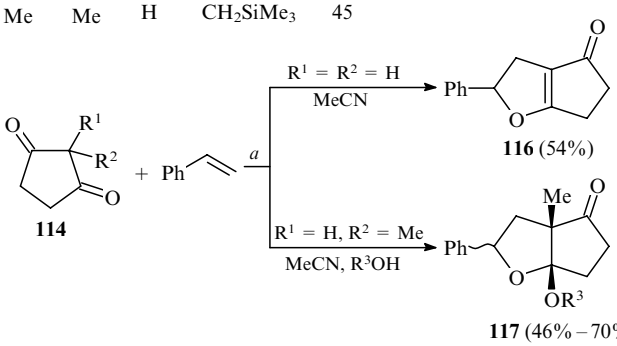

R^3 = H, Me; (*a*) ACU, 14 mA cm^{-2}, 1.5 F mol^{-1}.

2. Reactions with electrochemically generated *o*-quinonemethides

o-Quinonemethides **118** are generated upon the anodic oxidation of *o*-[1-(phenylthio)alkyl]phenols **119** in nitroethane followed by fragmentation of the radical cations **120** thus formed with elimination of the phenylthiol radicals. In the presence of alkenes, which are active acceptors of *o*-quinonemethides, cycloaddition to give chromans **121** takes place.[168,169]

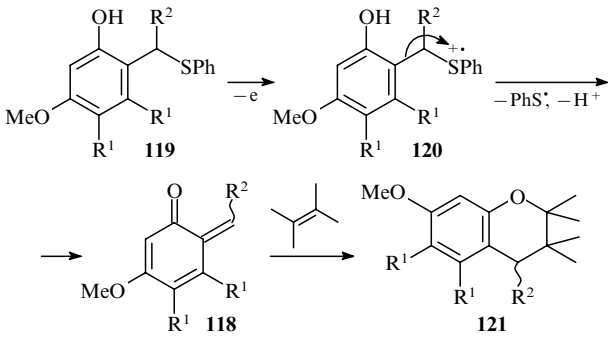

R^1 = H, OMe; R^2 = H, Alk.

3. Arylthiocarbonylation

Electrochemically initiated arylthiocarbonylation is typical of alkenyl sulfides and alkenylsilanes. In this reaction, they are converted into α-phenylthio ketones **122**.[170–172]

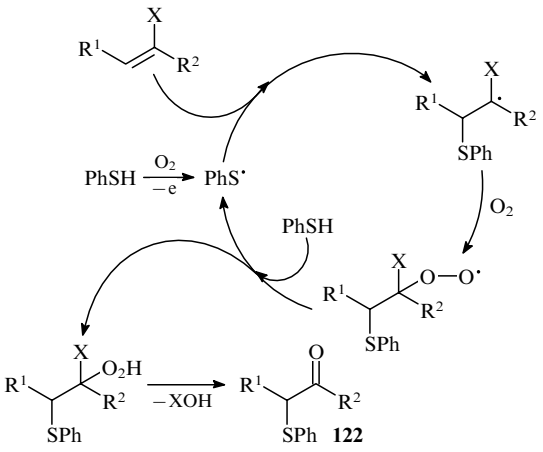

X = SPh, $SiMe_3$; R^1, R^2 = H, Alk.

The reaction is carried out in an undivided cell (at ~20 °C) in acetic acid with Et_4NOTs as the supporting electrolyte in the presence of 2–4 equiv. of benzenethiol with passage of 20 mA current for 1-min periods at 30-min intervals (0.16–1.19 F mol^{-1}) and with bubbling oxygen.

4. Halogenation, halooxygenation, haloacetamidation, epoxidation and other related reactions

Anodic oxidation initiates halogenation, halooxygenation and related reactions in aqueous MeCN or DMF or in water-alcoholic media, in the presence of chloride, bromide or iodide anions. The halide anions are readily oxidised due to the low oxidation potentials (0.8, 0.4 and 0.2 V *vs.* Ag/Ag^+, respectively), being converted into molecular chlorine, bromine and iodine; these reagents are responsible for alkene halogenation, halooxygenation and haloacetamidation [173–184] and, under certain conditions of electrolysis, epoxidation [184–193] and other related reactions (for example, azidoalkoxylation,[194] oxyselenenation, acetamidoselenenation,[195–198] acetamidosufenation,[199] intramolecular arylthio- and arylseleno-esterification and lactonisation,[200–203] and nitroacetamidation [203,204]).

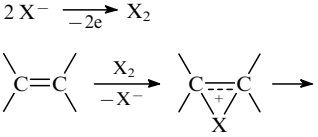

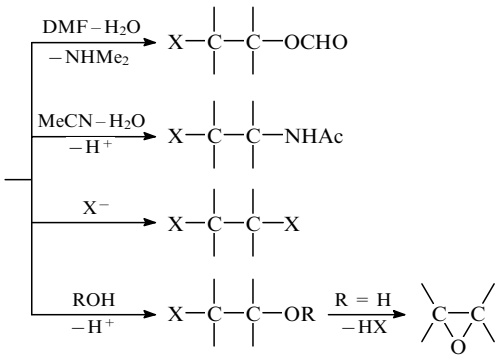

X = Cl, Br, I.

In the case of alkenes activated by electron-donating substituents, competitive formation of these products *via* radical cations is also possible.

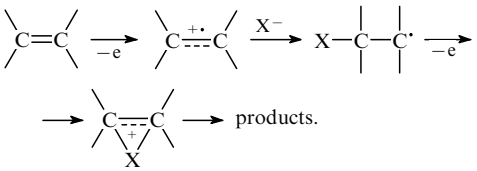

Due to the high discharge potential of fluoride anions (2.5 V), fluorination, fluorooxygenation and fluoroacetamidation of alkenes occurs exclusively with participation of radical cations.[205–207]

The composition of oxidation products in the presence of hydrogen halide salts depends considerably on the substrate type, the nature of the solvent and electrolysis conditions (Table 7, 8). A highly selective transformation of alkenes into halohydrins and epoxides takes place in water and aqueous acetonitrile or dimethylformamide with participation of bromides; sodium and tetraalkylammonium bromides as well as readily regenerable poly(4-vinylpyridine) hydrobromide are the most effective among them.[192] The selectivity of epoxidation is greatly affected by the medium pH and the anode current density. In a solution of sodium bromide in aqueous acetonitrile, the reaction medium becomes alkaline at the final stage of electrolysis in an undivided cell; this induces the transformation of the bromohydrin formed into the epoxide. Oxidation of an alkene under similar conditions with a small amount of an acid added (normally, sulfuric and hydrochloric acid) permits bromohydrin to be produced in a nearly quantitative yield. In the case of α-arylalkenes (for example, isosafrole), glycols are formed under these conditions due to hydrolysis of α-bromo-β-hydroxyalkylarenes.[184] The selectivity of transformation of alkenes into bromohydrins and epoxides sharply decreases for an anode current density of > 20 mA cm^{-2} and an anode potential of > 1.5 V. For alkenes reactive towards halogen molecules, the optimal values are 1–2 mA cm^{-2} and 0.8 V.[179,180]

Alkene bromoalkoxylation is highly selective in anhydrous alcohols at an anode current density of 100–200 mA cm^{-2} under conditions that ensure complete cathodic reduction of the dihalides formed in a competing reaction to give the initial alkene (graphite anode, nickel cathode, 30 °C, 5.6 F mol^{-1} of electricity) (see Table 8).[182]

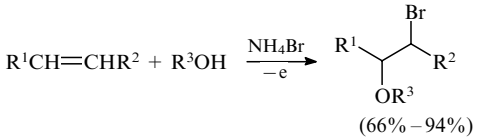

R^1 = Alk, Ar; R^2 = H, Alk; R^3 = Me, Et, Pr^i, Bu^t.

Table 7. Influence of electrolysis conditions on the composition of products of anodic oxidation of acyclic alkenes in the presence of halogen-containing mediators (20–45 °C).

Alkene	R^1	R^2	Mediator	Solvent	Method	Yield of the reaction product (%) [a]			Ref.
						mono-halide	dihalide	epoxide	
$R^1CH=CHR^2$	Alk	H	HCl	H_2O	A	(85–90)	(10)	–	173
	CH_2Cl	H	HCl	H_2O	A	(85–90)	(10)	–	173
	Alk	H	NaBr	H_2O	B	60 (90)	–	–	174
	Alk	Alk	NaX (X = Cl, Br)	H_2O	B	–	–	65–88	186–189
	Bn	Me	Et_4NBr, $NaClO_4$	MeOH	B	(50)	(35)	–	177
	Bn	Me	Et_4NI, $LiClO_4$	MeCN–H_2O	B	(51)	–	–	177
	Ph	Me	Et_4NCl, $LiClO_4$	MeCN–H_2O	C	65	–	–	178
	Ph	Me	Et_4NCl, $LiClO_4$	DMF–H_2O	C	85	–	–	178
	(*E*)-Ph	Ph	Et_4NCl, $LiClO_4$	MeCN–H_2O	C	–	65	–	178
	(*E*)-Ph	Ph	Et_4NCl, $LiClO_4$	DMF–H_2O	C	47	23	–	178
	(*E*)-Ph	Ph	$Et_4NF\cdot 3HF$	MeCN	B	34	–	–	205–207
	Ph	H	$Et_4NF\cdot 3HF$	MeCN	B	40	traces	–	206
	Ph	H	Et_4NCl, $LiClO_4$	DMF–H_2O	C	75	–	–	178
	Ph	H	NH_4Cl	MeOH–MeCN	D	95 (35)	–	–	182
	Ph	H	NH_4Br	ROH	D	65–78	–	–	182
	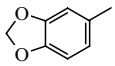	Me	NaBr	MeCN–H_2O	E	23 [c]	–	71	184
	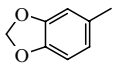	Me	NaBr, H_2SO_4	MeCN–H_2O	E	~100	–	–	184
	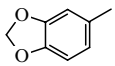	Me	NaX (X = Cl, I)	MeCN–H_2O	E	39–43 [c]	–	–	184
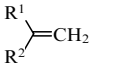	Me	Me	HCl	H_2O	A	(85–90)	10	–	173
	Alk	H	see [b]	DMF–PhH–H_2O	E	–	–	80	192
	$Cl(CH_2)_{10}$	H	see [b]	DMF–PhH–H_2O	E	–	–	62	192
	Ph	Ph	$Et_4NF\cdot 3HF$	MeCN	B	0–21	48–63	–	205–207
	Bn	H	NH_4Br	MeOH	D	93	–	–	182
	Bn	H	NH_4Br	EtOH	D	63	–	–	182
	Bn	Me	NH_4Br	MeOH	D	94	–	–	182
	H	OMe	NH_4X (X = Cl, Br)	$MeO(CH_2)_2OH$	E	87–92	–	–	180
	H	OMe	NH_4I	$MeO(CH_2)_2OH$	E	60	–	–	180
	H	OBu^n	NaN_3–NH_4OTs	MeOH	G	66–81 [d]	–	–	194
	Me	OMe	NaN_3–NH_4OTs	MeOH	G	82 [d]	–	–	194
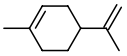			Et_4NBr, $LiClO_4$	MeOH	C	50	–	–	176
	CH_2OAc		NaCl, HCl	$Cl(CH_2)_2Cl$–H_2O (2:1)	E	85	–	–	179
	CO_2H		NaCl, HCl	CH_2Cl_2–H_2O	E	55	–	–	179
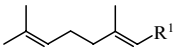	CO_2Me, CH_2OAc, CH_2SO_2Ph		MBr (Na, K, Li)	MeCN–H_2O (5:1)	E	–	–	75–91	190, 191
			Et_4NBr	MeCN–H_2O (5:1)	E	–	–	82	190, 191

Note. Method A: ACU, PbO_2 anode, 50–200 mA cm^{-2}; method B: PCU, Pt anode, 0.4–1.5 V; method C: ACU, Pt anode, 20 mA cm^{-2}, 2.0 F mol^{-1}; method D: ACU, graphite anode, 110 mA cm^{-2}, 5.6–9.5 F mol^{-1}; method E: ACU, Pt anode, 6–13 mA cm^{-2}, 4–10 F mol^{-1}; method F: ACU, Pt anode, 0.3–6.0 mA cm^{-2}, 2.1–3.5 F mol^{-1}; method G: ACD, graphite anode, 25 mA cm^{-2}, 3.0 F mol^{-1}.

[a] Substance yield (in parentheses, current yield); [b] poly(4-vinylpyridine) hydrobromide; [c] 1-[3,4-(methylenedioxy)phenyl]propane-1,2-diol; [d] α-azido ketone ketal.

When the quantity of electricity increases to 10–14 F mol^{-1} and the nickel cathode is replaced by a brass one, or by a nickel cathode coated with powdered Raney nickel, not only dibromide but also the bromo ether formed is reduced. The reaction yields ethers and thus it can formally be regarded as a very facile and effective method for the addition of alcohols to alkenes.[63, 208]

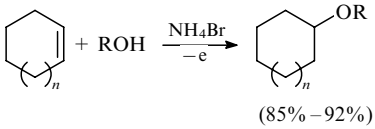

(85%–92%)

n = 1, 2, 7; R = Me, Et, CH_2CH_2OMe.

Table 8. Influence of electrolysis conditions on the composition of products of anodic oxidation of cyclic alkenes in the presence of halogen-containing mediators (20–45 °C).

Alkene	R^1	R^2	Mediator	Solvent	Method	Yield of the reaction product (%) (see [a])		Ref.
						mono-halide	dihalide	
	1	H	NH_4Br	MeOH	A	75	–	63, 182
	1	H	Et_4NBr	MeOH	B	54	14	175
	1	H	Et_4NCl	$MeCN-H_2O$	B	40	–	175
	1	H	Et_4NBr	$MeCN-H_2O$	B	–	68	175
	1	H	I_2, $LiClO_4$	$MeCN-H_2O$	C	(85)	–	177
	1	H	Et_4NCl	$DMF-H_2O$	B	58	22	175
	1	H	Et_4NBr	$DMF-H_2O$	B	16	64	175
	1	H	$Et_4NBr-(PhSe)_2$	$MeOH-H_2SO_4$	D	95–98	–	196
	1	H	$Et_4NBF_4-(PhSe)_2$	MeCN	C	77	–	197
	1, 2, 7	OMe	NH_4X (X = Cl, Br, I)	MeOH	E	85–94 [b]	–	180
	1, 2, 7	OAc	NH_4X (X = Cl, Br)	$MeCN-H_2O$	E	55–95 [c]	–	180
	1, 2, 3, 7	OAc	NaN_3-NH_4OTs	MeOH	F	67–83 [d]	–	194
	7	$OSiMe_3$	NH_4I	$MeCN-H_2O$ (3 : 1)	E	97 [c]	–	180
			MBr (M = Li, K, Na)	MeOH	E	69–74	–	180
			NH_4X (X = Br, I)	MeOH	E	93–96	–	180
			NH_4Cl	MeOH	E	60	–	180
			Et_4NBr	MeOH	E	97	–	180
			NaN_3-NH_4OTs	MeOH	F	60 [d]	–	194
			NaBr	MeOH	A	66	–	182

Note. Method A: ACU, graphite anode, 110 mA cm^{-2}, 5.6–9.5 F mol^{-1}; method B: potentiostatic conditions, a divided cell (PCD), Pt anode, 0.8–1.3 mA cm^{-2}; method C: PCU, Pt anode, 0.4–1.5 V; method D: ACU, Pt anode, 6–13 mA cm^{-2}, 4–10 F mol^{-1}; method E: ACU, Pt anode, 0.3–6.0 mA cm^{-2}, 2.1–3.5 F mol^{-1}; method F: ACD, graphite anode, 25 mA cm^{-2}, 3.0 F mol^{-1}.

[a] Substance yield (in parentheses, current yield); [b] α-halocycloalkanone dimethyl ketals. [c] α-halocycloalkanones. [d] α-azido ketone ketal.

In more profound electrooxidation of arylalkenes in the sodium bromide electrolyte, the bromo ethers formed are dehydrobrominated and the resulting enol ethers **123** are converted into α-bromoalkyl aryl ketone dimethyl ketals **124** under the action of methanol and bromine.[63, 209]

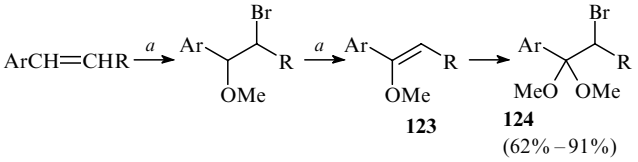

R = H, Alk; (*a*) ACU, Pt anode, brass cathode, 220 mA cm^{-2}, 9 F mol^{-1}, MeOH, NaBr, 60 °C.

Electrolysis of styrene in ethylene-, 1,3-propylene- or 1,3-butylene glycol gives rise to cyclic ketals of bromomethyl phenyl ketones **125**.[63]

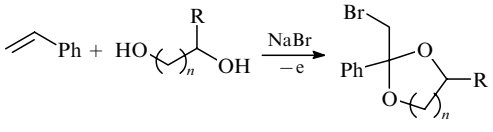

125 (66%–80%)

n = 1, 2; R = H, Me.

Anodic oxidation of enol ethers in the presence of ammonium bromide yields ketals of α-halo ketones **126**. When lithium, sodium, or potassium bromide is used, the yield of the ketals decreases by 20%–30%. α-Halo ketones **127** are formed in 55%–97% yields from enol acetates and trimethylsilyl ethers under similar conditions (see Table 8).[180]

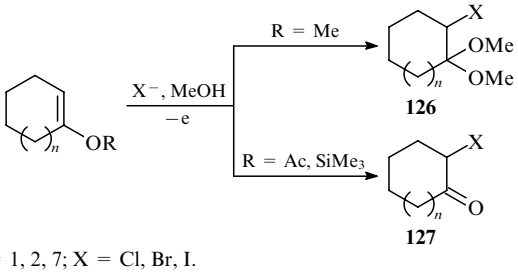

n = 1, 2, 7; X = Cl, Br, I.

Other reactions induced by anodic oxidation proceed similarly to electrochemical halooxygenation and haloacetamidation of alkenes. For example, azidomethoxylation of alkenes is documented.[194]

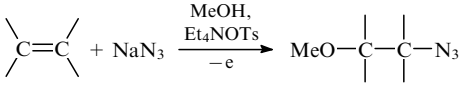

Two mechanisms have been proposed for this reaction, namely, pathway *a* for non-activated alkenes and pathway *b* for activated alkenes.[194]

Pathway *a*

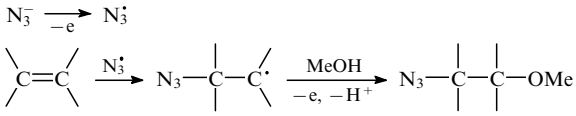

Pathway *b*

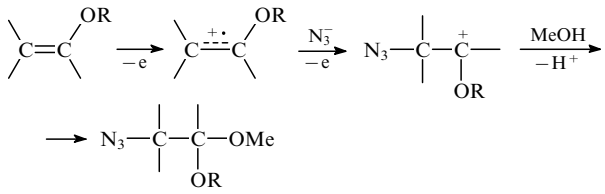

Alkene oxyselenenation – deselenenation results in allyl ethers such as **128**.[195, 196]

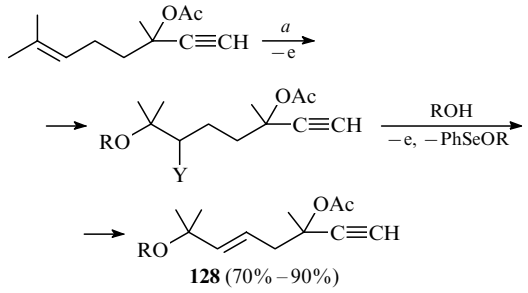

128 (70% – 90%)

R = H, Me; Y = SePh, Se(O)Ph; (*a*) ACU, Pt anode, 10 – 20 mA cm^{-2}, ROH or MeCN – H_2O, 0.1 equiv. $(PhSe)_2$, 1.5 equiv. $MgSO_4$, 60 – 70 °C.

Electrolysis of alkenes in the presence of diselenides and disulfides is accompanied by hydroxy-, alkoxy- and acetamidoselenenation [196 – 198] and acetamidosulfenation.[199]

Hydroxy-, alkoxy- and acetamidoselenenation reactions are initiated by electrogenerated halogenonium ions. Under the action of these species, diphenyl diselenide and diphenyl sulfide are converted into phenylselenenyl and phenylsulfenyl halides. These electrophilic intermediates add to alkenes, and the resulting adducts react with external or internal nucleophiles to give reaction products.

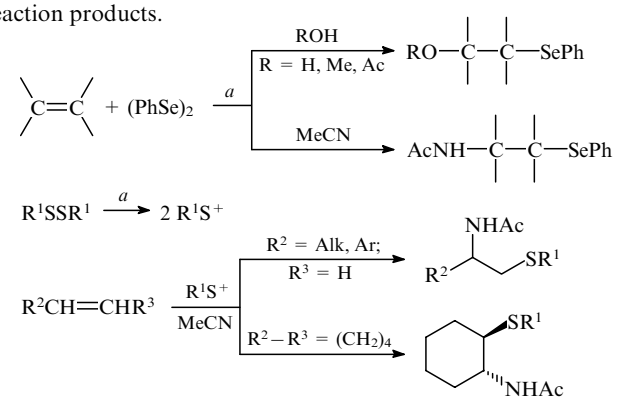

(*a*) ACU, Pt anode, 6.7 – 13 mA cm^{-2}, MeOH, AcOH, MeCN – H_2O, $Et_4NX - H_2SO_4$ (X = Cl, Br, I).

Unsaturated alcohols and acids undergo intramolecular arylthio and arylseleno esterification and lactonisation during electrolysis in the presence of disulfides and diselenides.[200 – 203] The reaction mechanism is similar to the mechanism of electrochemical alkoxyselenenation and acetamidosulfenation.

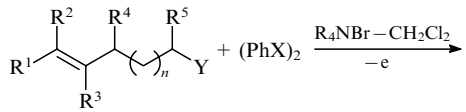

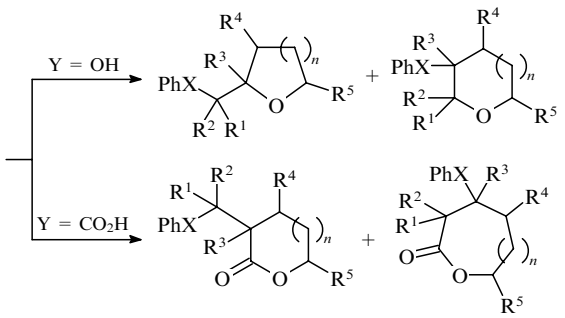

R^1, R^2, R^3, R^4, R^5 = H, Me; $R^1 - R^2$ ùöù $R^1 - R^3 = (CH_2)_m$ (m = 2, 3); n = 0, 1, 2; Y = OH, CO_2H; X = S, Se.

Electrochemical intramolecular phenylthio and phenylseleno esterification and lactonisation of unsaturated alcohols and carboxylic acids proceed with high selectivity (50% – 86%) only in the case where five- and six-membered rings are formed. If the substrate double bond is endocyclic as, for example, in cyclohexen-3-ylacetic acid, stereospecific *trans*-addition of phenylsulfenyl and phenylselenenyl halides takes place to give *cis*-fused bicyclic system **129**.[201, 202]

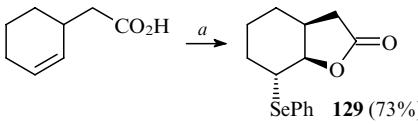

129 (73%)

(*a*) ACU, graphite anode, Cu cathode, 400 mA cm^{-2}, 6 F mol^{-1}, MeOH, 0.5 equiv. $(PhSe)_2$, NH_4Br, 15 – 20 °C.

Nitronium tetrafluoroborate resulting from anodic oxidation of N_2O_4 in MeCN adds to alkenes to give nitroacetamidation products.[203, 204]

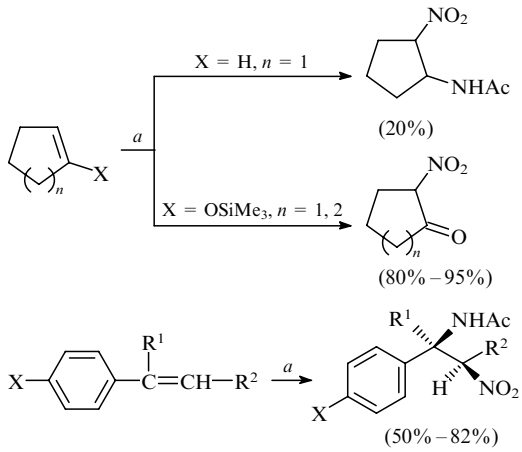

X = H, Br; R^1 = H, Me; R^2 = H, Me, Ph; (*a*) $NO_2^+ BF_4^-$ (0.25 mol litre^{-1} in MeCN), – 70 °C.

5. *o*-Nitration and diacylation

Electrochemical *o*-nitration and diacylation involve the nitrate radical NO_3 generated by the anodic oxidation of the nitrate anions.[210] In the presence of terminal alkenes and cycloalkenes, the nitrate radicals add to them, and the resulting radical adducts are converted into alkyl nitrates upon detachment of hydrogen atoms from the solvent. The resulting alkyl nitrates are transformed into the corresponding alcohols without isolation.[211]

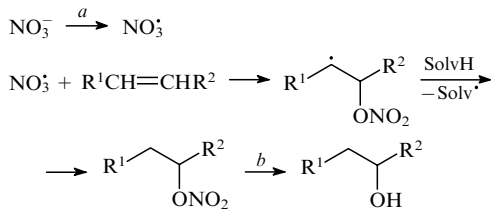

R^1 = Alk, R^2 = H; R^1-R^2 = $(CH_2)_m$ (m = 4, 6); (*a*) ACU, Pt anode, 50 mA cm^{-2}, 8 F mol^{-1}, $MeCN-H_2O-Et_2O$ (10 : 2 : 1), $LiNO_3$, 10 °C; (*b*) NaSH.

Under similar conditions of electrolysis, 1,1-di- and 1,1,2-trisubstituted alkenes furnish oxazoline derivatives.[211]

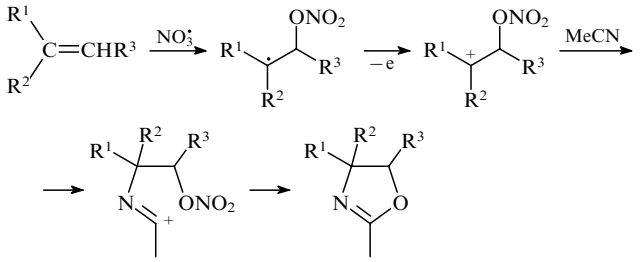

R^1 = Me, Et, n-C_9H_{19}; R^2 = Me, Et; R^3 = H, Me.

In the case where the reaction mixture contains, apart from nitrate (usually, lithium, ammonium, sodium, or potassium nitrate) and alkene, an aldehyde in a concentration sufficient for trapping nitrate radicals, diacylation of the alkene takes place.[212]

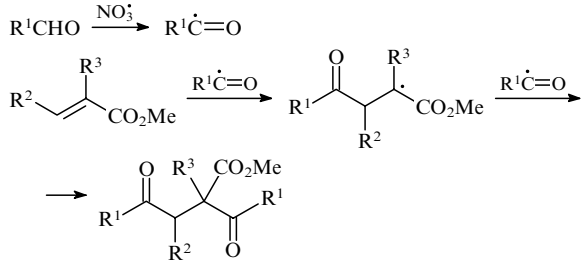

6. Hydroboration

Electrochemical hydroboration of alkenes includes two stages, namely, electrogeneration of diborane from borohydride anions and addition of the diborane formed *in situ* to alkenes to give trialkylboranes; treatment of these products with hydrogen hydroperoxide in an alkaline medium results in alkanols.[213,214]

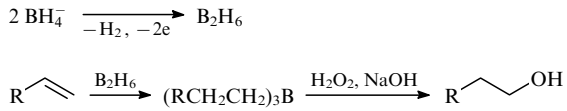

Hydroboration is carried out with the sodium iodide electrolyte under galvanostatic conditions in an undivided cell with a platinum anode and a steel cathode by passing 2 F of electricity per mole of alkene. The reaction is regio- and stereoselective and gives products in high yields. This procedure has been used to prepare primary alkanols from unsaturated and hydroxy- and acetoxy-substituted terminal alkenes (yields 64%–81%), cycloalkanols from cycloalkenes (70%–72%), (−)-*cis*-myrtanol from (−)-β-pinene (82%), *exo*-borneol from norbornene (72%), *etc*. The method is promising for organic synthesis. The electrogenerated diborane can also reduce carboxylic acids to the corresponding alcohols.[214]

7. Electrochemical cyclisation assisted by tin hydrides

The electrochemical cyclisation assisted by tin hydrides is illustrated by transformation of 2-halocyclohexyl allyl ethers into octahydro-3-methylbenzofuran **130** (yield 65%). Tin hydrides act in this reaction as precursors of tin-centred radicals and as hydrogen atom donors, while the electric current initiates this radical-chain process.[215]

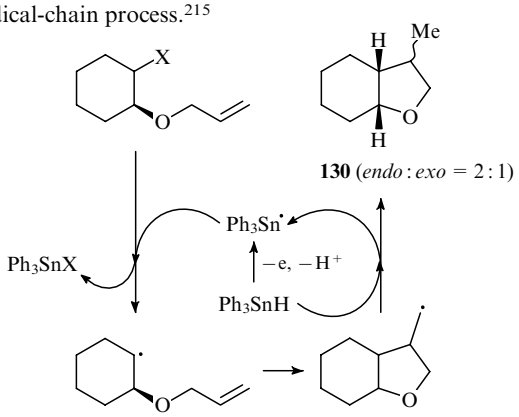

130 (*endo* : *exo* = 2 : 1)

X = Br, I; (*a*) ACD, Pt electrodes, 10 mA cm^{-2}, 0.2–0.5 F mol^{-1}, THF, Bu_4NBF_4, 1.2 equiv. Ph_3SnH, ~20 °C.

Similarly, octahydro-3-methylidenebenzofuran was prepared from 2-halocyclohexyl propargyl ethers (65%–69%), β-lactam derivative **131** was converted into dihydrocephalosporin **132**.

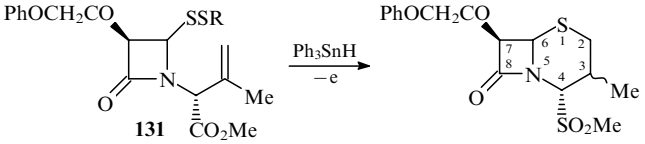

131

132 (80%, 3α : 3β = 1 : 2)

R is 2-benzothiazolyl.

These reactions can also be carried out in undivided cells. However, complete conversion of the substrate in an undivided cell required a four times greater quantity of electricity.

An advantage of the electrochemical method over the chemical methods in which azoisobutyronitrile, benzoyl peroxide, trialkylboranes, *etc*., serve as initiators[216,217] is higher stereoselectivity.

8. Phosphorylation

Indirect electrochemical phosphorylation of alkenes and cycloalkenes occurs upon the electrophilic addition of triphenylphosphinium radical cations generated by anodic oxidation of triphenylphosphine followed by electrooxidative deprotonation of the adduct thus formed. The reaction yields 1-alkenyl- and 1-cycloalkenyl-substituted triphenylphosphonium salts.[18,218–220]

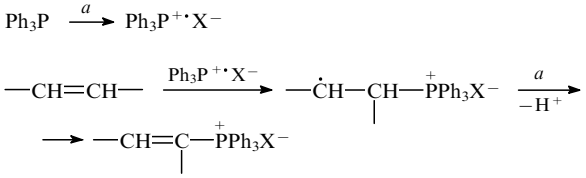

X = ClO_4, BF_4; (*a*) X^-, ACU, graphite anode, Fe cathode, 1.07 mA cm^{-2}, 2 F mol^{-1}, CH_2Cl_2, 0.2 equiv. Ph_3P, 0.5 equiv. 2,6-LutHClO$_4^-$ or 1.33 equiv. K_2CO_3, N_2 atmosphere, ~20 °C.

This reaction has been used to prepare phosphonium salts from ethylene, C_5-C_8 cycloalkenes, norbornene, substituted styrenes, vinyl and allylsilanes, α,β-unsaturated compounds, *etc*. (Table 9).[218–225] When vinyl- and allylsilanes are used, desilylation of the adducts formed initially takes place, and phosphorylated alkenes are formed as the reaction products.[220–222]

Table 9. Electrochemical triphenylphosphorylation of alkenes.

Alkene	Method	Reaction product	Yield (%)	Ref.	Alkene	Method	Reaction product	Yield (%)	Ref.
$n = 1-4$	A	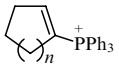	50–60	219–221	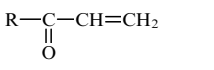 R = H, Me, Et, NH_2, OEt	B	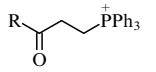	55–84	221, 224
	A	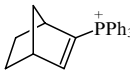	65	219–221	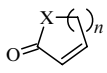 X = CH_2, n = 1, 2; X = O, n = 2	B	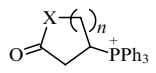	61–67	221, 224
	A	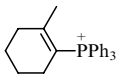	40	220, 221					
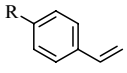 R = H, Me	A	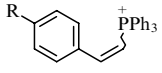	80–100	220, 221	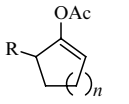 R = H, Me; n = 1–3	C	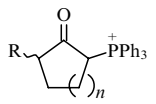	47–96	221, 225
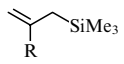 R = H, Me	B	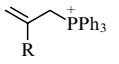	68–71	220, 221					
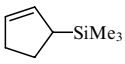	B	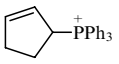	21	221–223	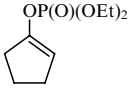	C	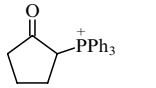	23–51	221, 224
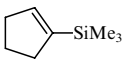	B	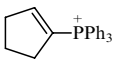	24	221–223	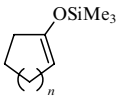 n = 1, 2	C	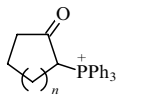	11–30	221, 224
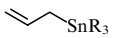	B	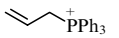	61	221–223					

Note. Method A: ACU, graphite anode, stainless-steel cathode, 1.07 mA cm^{-2}, 2 F mol^{-1}, CH_2Cl_2, 0.2–1 equiv. of Ph_3P, 0.5 equiv. of 2,6-$LutHClO_4$ or 2,6-$LutHBF_4$, ~20 °C; method B: ACU, glass carbon anode, Pb cathode, 1.1 mA cm^{-2}, 1.8 F mol^{-1}, CH_2Cl_2, 2 equiv. of Ph_3P, 0.5 equiv. of 2,6-$LutHClO_4$ or 2,6-$LutHBF_4$, K_2CO_3, ~20 °C; method C: ACU, glass carbon anode, Pb cathode, 1 mA cm^{-2}, 2 F mol^{-1}, MeCN, 1–3 equiv. of Ph_3P, 0.5 equiv. of $LiBF_4$, N_2 atmosphere, ~20 °C.

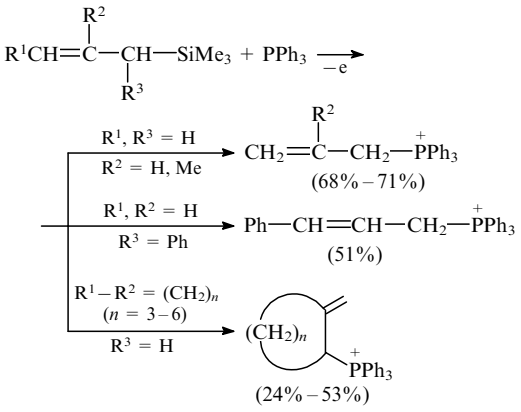

Electrochemical reactions of triphenylphosphine with vinyl ketones, acrolein, cycloalk-2-enones, ethyl acrylate, acrylamide [220, 223] and cycloalkenol ethers [220, 224] give rise to phosphorylated ketones.

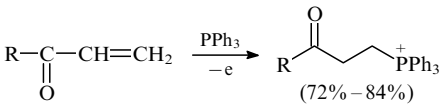

R = H, Me, Et, EtO.

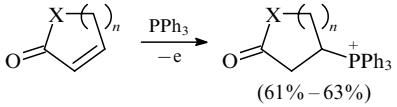

X = CH_2O, n = 1, 2.

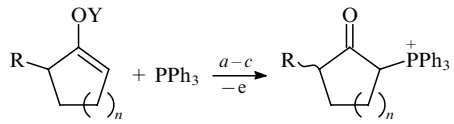

R = H, Me; n = 1–3; (*a*) Y = Ac (47%–96%); (*b*) Y = $P(O)(OEt)_2$ (23%–51%); (*c*) Y = $SiMe_3$ (11%).

Electrochemical phosphorylation of carboxy-substituted alkenes **133** by phosphines with Bu_4NBr as the supporting electrolyte results in acylphosphonium salts **134**, which are readily reduced at the cathode under the conditions of diaphragmless electrolysis to give intermediates **135**. These undergo radical cyclisation, electroreduction and protonation and are thus converted first into cyclic intermediates **136** with separated anionic, cationic and radical centres and then into cyclopentanones **137**. The reaction is carried out in an undivided cell (graphite electrodes, 2.4 mA cm^{-2}, 4 F mol^{-1}, CH_2Cl_2, 3 equiv. of X_3P (X = Ph, Bu^n), 1 equiv. of Bu^n_4NBr, 2 equiv. of $MeSO_3H$). Together with cyclopentanones **137**, aryl-substituted alkenals **138** are produced (Scheme 5).[225]

This electrochemical reaction is an example of successful use in organic synthesis of paired electrolysis in which the processes occurring at both the cathode and the anode are involved in the assembling of the final product.

By phosphorylation of alk-1-enes with the phosphines X_3P in the presence of thiols RSH (R = Pr^n, Bu^n) under conditions of electrolysis differing substantially from those used in the studies cited above,[218–225] alk-2-enylphosphonium salts **139** have been

Scheme 5

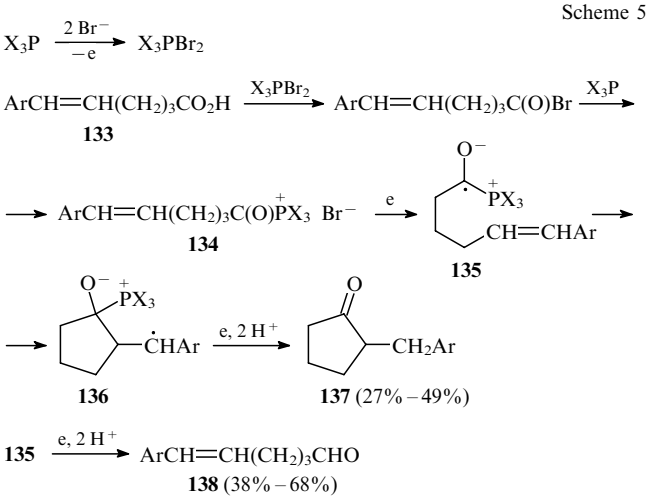

X = Ph, Bu^n; Ar = 4-YC_6H_4, Y = H, Me, MeO, Cl, Br.

prepared (yields 46%–85%). The products of alkene thioalkylation are formed as side products.[226]

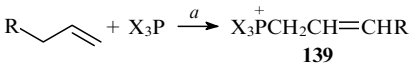

R = n-C_5H_{11}, n-C_6H_{13}; X = Mes, Bu^n; (*a*) ACD, Pt anode, Ni cathode, 4 mA cm^{-2}, 2.2–4.8 F mol^{-1}, MeCN, 0.05 equiv. X_3P, 0.75 equiv. RSH, 0.5 equiv. $NaClO_4$, 0.6 equiv. Na_3PO_4.

The processes of regiospecific phosphorylation of alkenes presented in Table 9 take place only with triphenylphosphine. If it is replaced by trialkylphosphines, trialkyl phosphites, dialkyl trimethylsilyl phosphites or phosphorous amides, the reactions yield mixtures of phosphorylation products with different positions of the C=C bond in the alkenyl or cycloalkenyl fragment. For example, electrolysis of Et_3P, Pr^n_3P or Bu^n_3P in the presence of cycloalkenes gives rise to regioisomeric cycloalkenyl phosphonium salts with the double bond in positions 1, 2 or 3.[227] This difference between the behaviours of triphenylphosphine and other phosphines in this reaction is related, in the researchers' opinion, to higher thermodynamic stability of alk-1- and cycloalk-1-enyltriphenylphosphonium salts compared to the corresponding trialkylphosphonium salts caused by the effective stabilisation of the positive charge with participation of the π-systems of the phenyl groups. Phosphorylation of hex-1-ene and cyclohexene with trialkyl and dialkyl trimethylsilyl phosphites gives rise to three types of isomeric products, while the reactions involving phosphorous mono- and diamides, yield two types of isomers.[228,229] Phosphorous amides are more basic than alkyl phosphites; thus, they can bind more efficiently the protons generated during the electrolysis, and the prototropic isomerisation of the intermediates is suppressed (Scheme 6).[229]

The yields of alk(cycloalk)-2-enylphosphonates of type **140**, **141** are 2–4 times as high as the yields of other regioisomers. In some cases, they are formed as the only products.[228,229] In the presence of diethyl phosphite or *O*,*O*-dibutyl phosphorothioite as a mediator which changes the nature of the phosphorus-containing active intermediates, the regiodirectivity of phosphorylation of alkenes by phosphorous mono- and diamides changes towards the predominant formation of alk(cycloalk)-1-enyl-substituted phosphonamidates of type **142**. For example, cyclohexenyl phosphonamidates **141** and **142** (1:2 ratio) were prepared in the presence of diethyl phosphite, together with the side product diethyl cyclohexylphosphonate (**143**).[229]

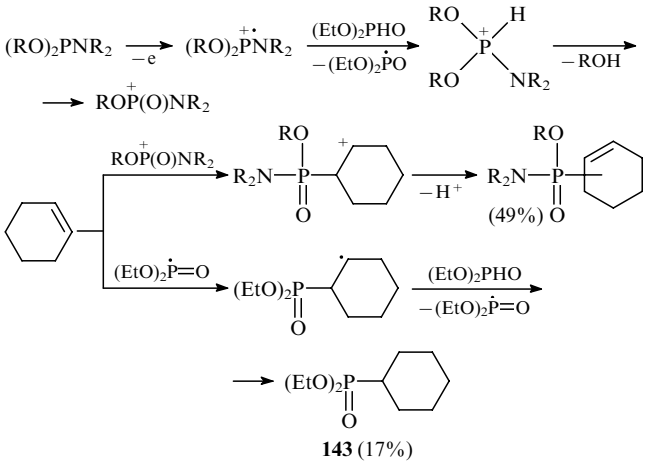

9. Hydrophosphonylation and hydrothiophosphonylation

Indirect electrochemical hydrophosphonylation of alkenes with dialkyl phosphites takes place in the presence of trialkylphosphines, trialkyl and dialkyl trimethylsilyl phosphites [Bu^n_3P, $(Pr^iO)_3P$, $(EtO)_2POSiMe_3$].[230]

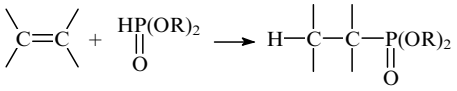

The promotory effect of these compounds is based on electric generation of the radical cations $X_3P^{+\bullet}$ at potentials at which dialkyl phosphites and alkenes are electrochemically inactive (0.8–1.6 V). The products of hydrophosphonylation are formed upon the detachment of hydrogen atoms from dialkyl phosphites by the $X_3P^{+\bullet}$ radical cations and subsequent addition of the generated $(RO)_2P(O)^{\bullet}$ radicals to alkenes. A chain transfer takes place in the reaction between the radical adducts and dialkyl phosphites.[230] The products of hydrophosphonylation of alkenes, for example, cyclohexene,[230] are formed selectively only with the assistance by trialkylphosphines.

Scheme 6

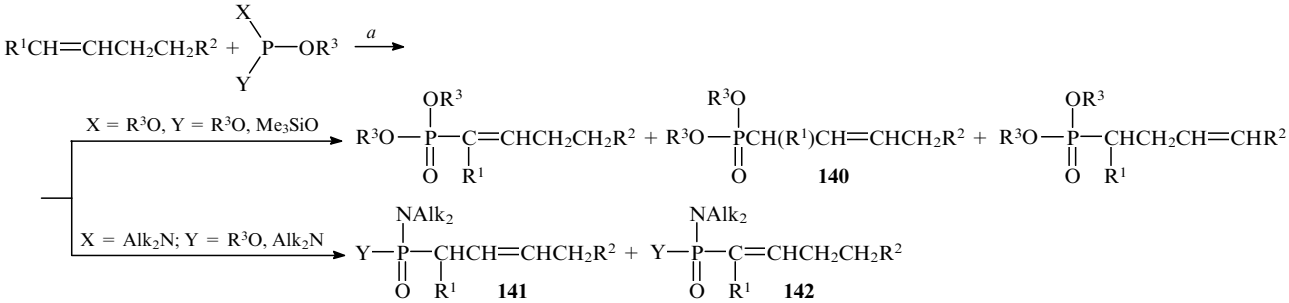

R^1, R^2 = H, Bu^n; R^1-R^2 = $(CH_2)_2$; R^3 = Alk; (*a*) ACD, Pt anode, 0.1–8 mA cm^{-2}, 1.1–1.7 F mol^{-1}, MeCN, 5–6 equiv. of alkene, 0.25 equiv. $NaClO_4$, 8 equiv. Na_3PO_4.

Trialkyl and dialkyl trimethylsilyl phosphite-initiated reactions give rise to saturated and unsaturated phosphonates derived from the mediator and the dialkyl phosphite. The triisopropyl phosphite-assisted reaction of cyclohexene with diethyl phosphite yields eight products including diethyl and diisopropyl cyclohexyl-, cyclohex-1-enyl-, cyclohex-2-enyl- and cyclohex-3-enylphosphonates. Presumably,[230] this is due to active oxidation of the intermediate radical adducts **A** by the radical cations generated from triisopropyl phosphite and to addition of the latter species to cyclohexene.

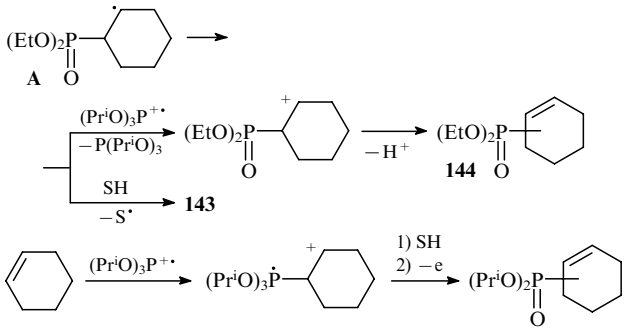

Similarly, the radical cations electrogenerated from trialkyl phosphites initiate hydrothiophosphonylation of alkenes with *O*,*O*-dialkyl phosphorothioites.[231,232]

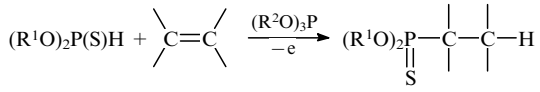

R^1 = Et, Pr^i, Bu; R^2 = Alk.

Joint electrolysis of alkenes with dialkyl phosphites or *O*,*O*-dialkyl phosphorothioites or with their sodium or lithium salts affords mixtures of alkene hydrophosphonylation (hydrothiophosphonylation) products and the products of substitution of the diethoxyphosphoryl or -thiophosphoryl group for the allylic hydrogen atom.[231–235] Thus the reaction of cyclohexene with sodium diethyl phosphite yields diethyl cyclohexyl- and cyclohexenylphosphonates **143** and **144** (overall yield 52%, 2 : 1 ratio).[232,233] A similar reaction with sodium *O*,*O*-diethyl phosphorothioite gives compounds **145** and **146** in a total yield of 87% (11 : 1 ratio).

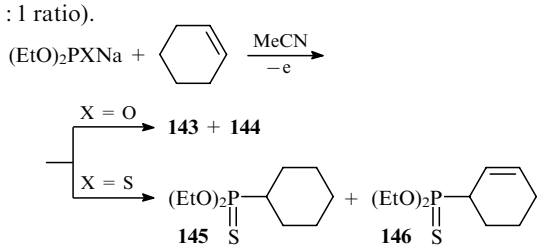

X = O, S.

In the reactions of alkenes with dialkyl phosphorothioites, the formation of phosphorylation products is completely suppressed when a 1 : 1 acetonitrile – THF mixture is used as the solvent.[232]

10. Radical-cation [4 + 2]-cycloaddition of styrenes and enamines to vinylindoles and -pyrroles induced by anodic oxidation

The radical-cation [4 + 2]-cycloaddition reactions have been vigorously studied during the last two decades. Owing to the very low activation barriers, they proceed tens or hundreds times as fast as the ordinary Diels – Alder reactions; hence, they can be performed under milder conditions. The radical-cation [2 + 4]-cycloaddition is highly regio- and chemoselective. Moreover, they can be carried out for dienophiles with electron-donating substituents at the double bond, which do not enter into conventional Diels – Alder reaction. There are strong grounds for believing that they will find extensive application in organic synthesis.[236]

The [4 + 2]-cycloaddition of enamines to 2-vinylindoles or -pyrroles acting as dienes induced by anodic oxidation[237–240] proceeds efficiently only in the case where the difference between the oxidation potentials of dienophiles and dienes does not exceed 500 mV.[241] To avoid polymerisation, there should not be hydrogen atoms at the 3-position of the pyrrole or indole ring. The radical-cation cycloaddition of enamines to 2-vinylindoles **147** includes generation of radical cations **148** at the anode, their addition to enamines **149a–d** and subsequent cyclisation, electrooxidation and deprotonation of the radical-cation cycloadducts **150a–d** to give cycloaddition products **151a–d**.[239,240] The structure and the yield of the reaction product depend most of all on the structure of the initial substrates. Electrolysis of 2-vinylindoles **147** together with methyl β-(*N*,*N*-dimethylamino)acrylate (**149a**) or substituted β-(*N*,*N*-dimethylamino)acrylonitriles **149b–d** affords compounds of the pyrido[1,2-*a*]indole series (**151a–d**), which are of interest as building blocks in the synthesis of indole alkaloids.[237,239]

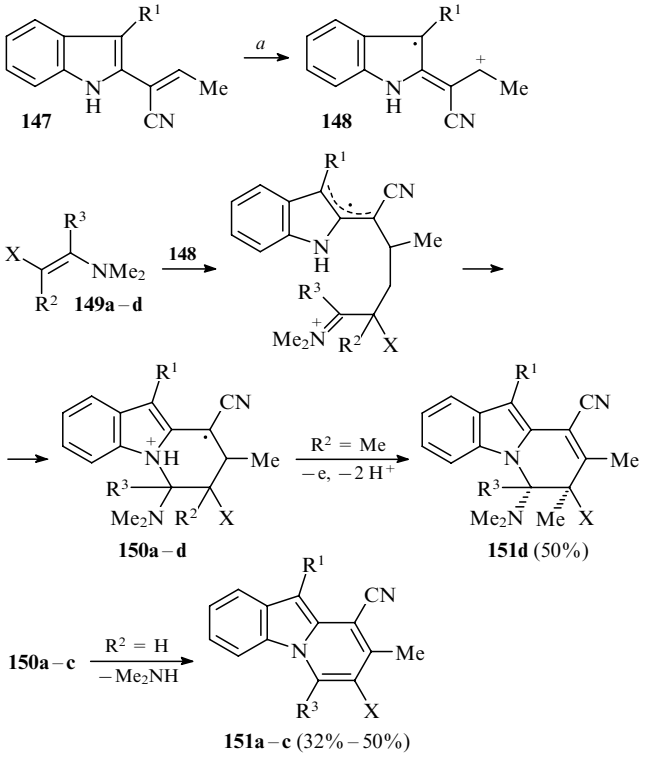

(*a*) PCU, graphite anode, 0.49 – 0.67 V, CH_2Cl_2 – MeCN (1 : 1) or MeCN, 0.1 equiv. $LiClO_4$.

Compounds **149–151**	R^1	R^2	R^3	X	Yield of **151** (%)
a	Me	H	H	CO_2Me	90–91
b	CH_2CH_2OEt	H	H	CO_2Me	62
c	Me	H	Me	CN	68
d	Me	Me	H	CN	53

Cycloaddition of the indoles **147** to 1,4,5,6-tetrahydropyridines **152a–d** or to α-(*N*,*N*-dimethylaminomethylene)butyrolactone (**153**) results in tetracyclic compounds **154a–d**, **155** of the indolo[1,2-*a*]pyridine series incorporating the skeleton of pyrrocoline alkaloids such as goniomitine.[238,239]

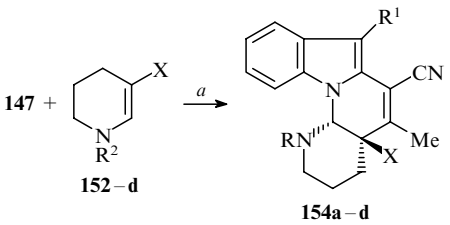

147 + **152–d** → **154a–d**

Compound **154**	R^1	R^2	X	Yield (%)
a	H	Me	CO_2Me	91
b	Me	Me	CO_2Me	62
c	H	Me	CN	68
d	H	CH_2CH_2OEt	CN	53

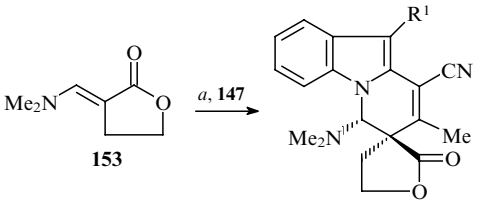

153 → **155** (52% – 53%)

(*a*) PCU, graphite anode, 0.49 – 0.67 V, CH_2Cl_2 – MeCN (1 : 1) or MeCN, 0.1 equiv. $LiClO_4$.

Polysubstituted indolizines, difficult to synthesise by other methods, have been prepared by joint electrooxidation of 2-vinylpyrroles **156** with enamines **149**.[240]

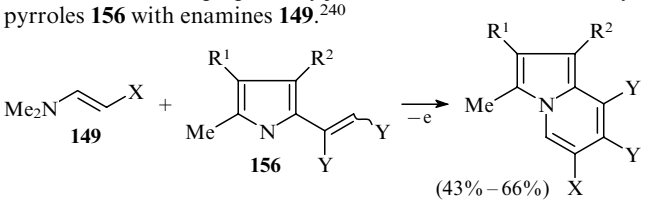

149 + **156** → (43% – 66%)

X = CO_2Me, CN, NO_2; Y = CO_2Me, CN; R^1, R^2 = Me, CO_2Me.

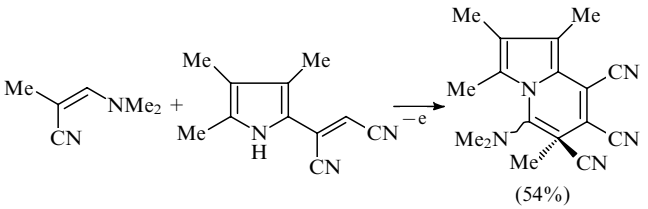

(54%)

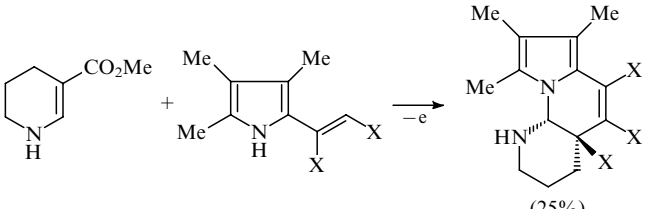

(25%)

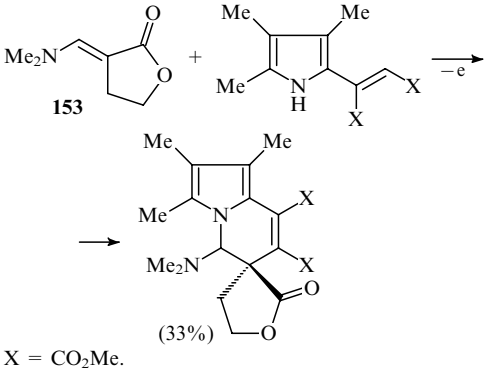

153 → (33%)

X = CO_2Me.

The tentative asynchronous mechanism of the radical-cation cycloaddition[241, 242] allows the formation of the final product as a mixture of *cis*- and *trans*-isomers because rotation around the C – C bond in the initial radical-cation adduct is possible. The formation of only *trans*-isomers indicates that cyclisation occurs much faster than the rotation around the C – C bond. Stabilisation of the radical intermediates by radical-stabilising substituents such as nitrile or alkoxycarboxyl group is favourable for the reaction.[238, 239]

11. Reactions of alkenes induced by electrooxidation of variable-valence metal compounds

Compounds of variable-valence metals (manganese, copper, palladium, ruthenium, nickel, cobalt, cerium, and thallium) act in electrochemical processes as mediators (Med) and participate in the electron transfer at the anode and in the reaction of the oxidised form of the mediator (Med_{ox}) with the substrate (RH). The reaction between RH and Med_{ox} can follow two pathways, one giving rise to a radical cation (pathway *a*) and one giving rise to a radical (pathway *b*).

Pathway *a*

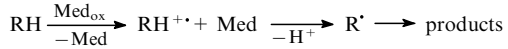

Pathway *b*

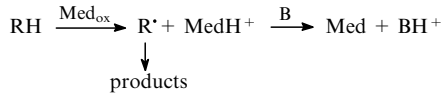

B is proton acceptor.

In many cases, compounds and complexes of variable-valence metals are used in these processes as binary mediator systems in combination with other mediators including organic compounds (CH acids, benzoquinone or triarylamines).

a. Reactions induced by electrooxidation of manganese compounds

Despite the fact that the addition of carboxylic acids, aldehydes, ketones and amines to alkenes initiated by manganese triacetate or oxidative systems based on it have been comprehensively studied,[243, 244] their extensive use is held up, most of all, by the need to introduce relatively large amounts of initiators and by problems associated with their regeneration. In the last decade, a strategy has been developed according to which this type of electrochemical reaction is carried out in the presence of a catalytic amount (0.03 – 0.2 equiv.) of $Mn(OAc)_2$, acting as a mediator and the source of electrogenerated manganese triacetate. Examples of the addition of CH acids to alkenes initiated by $Mn(OAc)_2$-based oxidative systems are listed in Table 10.

Using the $Mn(OAc)_2$–$Cu(OAc)_2$ mediator system, γ-lactones have been obtained in acceptable yields from acetic acid and styrenes,[246, 250] and alk-2-enyl- and cycloalk-2-enyl-substituted cyanoacetic esters were synthesised from ethyl cyanoacetate, alkenes and cycloalkenes.[246, 247] In these reactions the carboxymethyl and (ethoxycarbonyl)cyanomethyl radicals together with their adducts with alkenes are formed as intermediates; the former species result from single-electron oxidation of acetic acid and ethyl cyanoacetate by electrogenerated $Mn(OAc)_3$ and the latter arise upon the addition of the primary radicals to alkenes. These secondary intermediates (**A** and **B**) are further oxidised by regenerable Cu(II) ions, which react with radical adducts **A** and **B** by different mechanisms, namely, single-electron transfer for **A** and oxidative β-deprotonation for **B**.[246, 247]

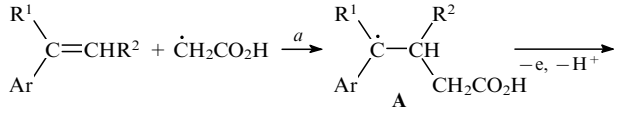

A

Table 10. Electrochemical addition of CH acids to alkenes initiated by manganese diacetate-based oxidative systems.

CH acid	Alkene	R^1	R^2	R^3	Method	Reaction product	Yield (%)	Ref.
XCH_2CO_2Et (X = CN, CO_2Et)	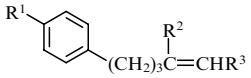	H	H	H	A	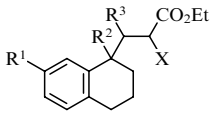	70–79	245
		Me	H	H	A		58–61	245
		F	H	H	A		53–60	245
		H	Me	H	A		60–73	245
		H	H	Me	A		37–39	245
XCH_2CO_2Et (X = CN, CO_2Et)		–	–	–	A	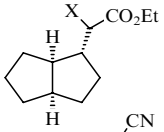	76–78	246
$NCCH_2CO_2Et$	$R^1CH=CHR^2$	Alk	H	–	A	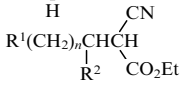 n = 2–5, 10	50–64	246, 247
$AcCH_2CO_2Et$		Alk	H, Me	–	A	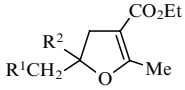	80–86	246
$PhCH_2CH(CO_2Et)_2$	$R^1CH=CHR^2$	Alk	H	–	A	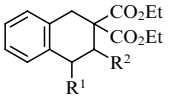	86	249
		CO_2Et	H	–	A		40	249
		Ph	Ph	–	A		75	249
		AcO	H	–	A		24	249
		see [a]	H	–	A		55	249
$PhCOCH_2NO_2$	$R^1CH=CH_2$	Bu^n	–	–	B	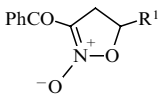	59	248
		$AcOCH_2$	–	–	B		37	248
	$Bu^nCH=CH_2$	–	–	–	B	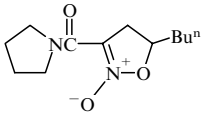	48	248
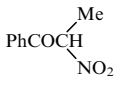	$Bu^nCH=CH_2$	–	–	–	B	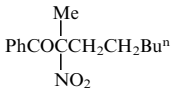	54	248

Note. Method A: ACD, graphite anode, 20–30 mA cm^{-2}, 2 F mol^{-1}, AcOH–AcOEt (13:3), 0.03–0.25 equiv. of AcONa, $Mn(OAc)_2 \cdot 4H_2O$, 60–70 °C; method B: ACD, graphite anode, 0.2–0.5 mA cm^{-2}, 2 F mol^{-1}, 0.1 equiv. of AcOH, Bu_4NBF_4, $Mn(OAc)_2 \cdot 4H_2O$, 60 °C. [a] Succinimido.

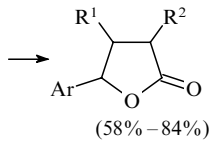

(58%–84%)

R^1 = H, Me; R^2 = H, Ph, CO_2Et, CH_2OH; Ar = Ph, 4-ClC_6H_4, 4-MeC_6H_4.

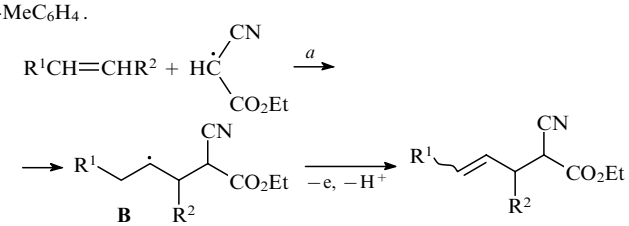

(44%–58%)

R^1 = $Me(CH_2)_n$ (n = 2, 4, 6), R^2 = H; R^1-R^2 = $(CH_2)_n$ (n = 2–5, 9); (*a*) ACD, graphite anode, 10 mA cm^{-2}, 2 F mol^{-1}, AcOH–Ac_2O (2:1), AcONa, 0.065 equiv. $Mn(OAc)_2 \cdot 4H_2O$, 0.025 equiv. $Cu(OAc)_2 \cdot H_2O$, 95–97 °C.

The binary mediator system, $Mn(OAc)_2$–$NCCH_2CO_2Et$, proved to be a good initiator of free-radical chain addition of polyhalomethanes[251] (bromomalonic esters and methyl bromoacetate) to alkenes.[251,252]

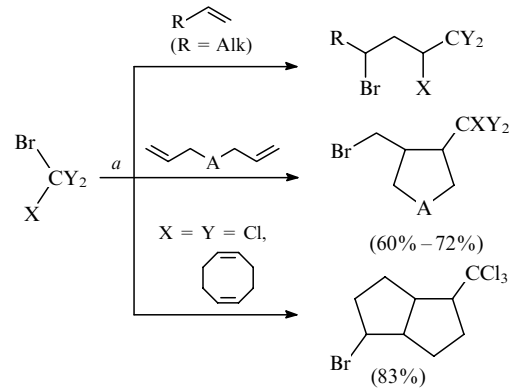

X = Y = Br, Cl; X = Br, Y = F; A = O, NAc; (*a*) ACU, graphite anode, 0.06–0.6 F mol^{-1}, AcOH, AcOK, 0.05 equiv. $Mn(OAc)_2$, 0.1 equiv. $NCCH_2CO_2Me$, 40 °C.

Certain progress has taken shape in the field of practical implementation of indirect electrooxidation with manganese diacetate as a mediator. For instance, electrosynthesis of a precursor of sorbic acid (**157**), namely, γ-vinyl-γ-butyrolactone (**158**), from butadiene and acetic acid, which allows preparation of kilograms of this compound, has been developed.[253]

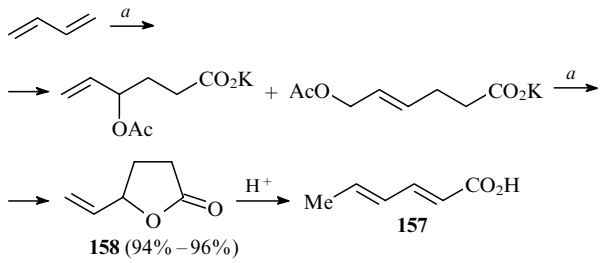

(*a*) ACU, AcOH – Ac_2O (1 : 1), AcONa, 0.1 equiv. $Mn(OAc)_2 \cdot 4H_2O$, 0.037 equiv. $Cu(OAc)_2 \cdot H_2O$, 95 – 125 °C.

b. Reactions induced by electrooxidation of palladium, ruthenium, osmium and silver compounds

The chemical prototypes of these reactions such as the Wacker process of oxidation of α-alkenes to methyl ketones,[254–256] ethylene to vinyl acetate,[257] hydroalkoxycarbonylation[258–260] and epoxidation of alkenes,[261] suffer from a number of drawbacks including the low rate of oxidation of alkenes with internal double bonds, the explosive risk from the gaseous mixtures of alkenes with oxygen, fast corrosion of the equipment induced by corrosive reaction media, *etc*. Numerous publications have been devoted to the search for new procedures for performing the above-listed reactions.[262–277] Methods of indirect anodic oxidation of alkenes using redox systems consisting of $Pd(OAc)_2$ and an organic mediator (hydroquinone, benzoquinone, their analogues or triarylamines) have been developed to date.[263–269] The mediator acts as an electrogenerated oxidant with respect to Pd(0), which results from the reaction of alkene with Pd(II).

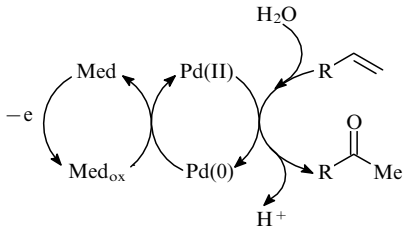

Med is hydroquinone or $(4\text{-}BrC_6H_4)_3N$; Med_{Ox} is benzoquinone or $(4\text{-}BrC_6H_4)_3N^{+\cdot}$.

This procedure has been used to perform electrooxidative transformation of alkenes into ketones[263–266] or into vinyl or allyl acetates.[267,269] Electrooxidation of alkenes in alcohols in the presence of CO yields esters of alkanoic acids (Table 11).[268]

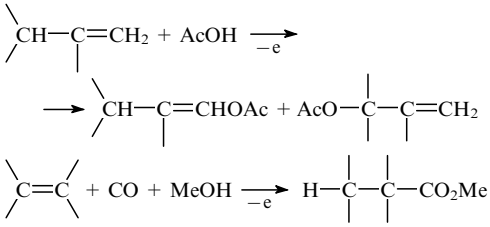

Ruthenium and silver polypyridyl complexes, the ruthenium heteropolyanion $[SiRu(H_2O)W_{11}O_{39}]^{5-}$ and potassium osmate have also shown themselves as effective mediators in indirect anodic oxidation of alkenes. Thus the complex $[Ag(bipy)_2]^+$ (bipy is 2,2′-bipyridine) catalyses epoxidation of alkenes.[270]

Table 11. Indirect anodic oxidation of alkenes with mediator systems containing catalytic amounts (0.01 – 0.1 equiv.) of $Pd(OAc)_2$ or $PdCl_2$.

Alkene	Co-mediator (equiv.)	Electrolyte	Reaction product (isomer ratio)	Yield (%)	Ref.
Dec-1-ene	BQ (0.2)	$Bu_4NBF_4 - HClO_4$	decan-2-one	92	264
	CDA (0.1)	$NaClO_4 - AcONa$	2- and 3-acetoxydec-1-enes (2 : 3)	91	269
	see [a]	LiCl	methyl undecanoates (1 : 3)[b]	73	268
(*E*)-Oct-2-ene	BQ (0.2)	$Bu_4NBF_4 - HClO_4$	octan-2,3,4-ones (6 : 3 : 1)	96	264
(*Z*)-Hept-2-ene	BQ (0.2)[a]	LiCl	methyl octanoates (1 : 3)[b]	50	268
$PhCH=CH_2$	BQ (0.2)	$Bu_4NBF_4 - HClO_4$	acetophenone	79	264
	CDA (0.1)	$NaClO_4 - AcONa$	α-acetoxystyrene	35	269
	see [a]	LiCl	methyl phenylpropionates (1 : 3)[b]	75	268
Cyclohexene	BQ (0.2)	$Bu_4NBF_4 - HClO_4$	cyclohexanone	100	264
	CDA (0.1)	$NaClO_4 - AcONa$	2- and 3-acetoxycyclohexenes (1 : 1)	29	269
	see [a]	LiCl	methyl cyclohexanecarboxylate	50	268
Cycloheptene	CDA (0.1)	$NaClO_4 - AcONa$	2- and 3-acetoxycycloheptenes (1 : 13)	72	269
Cyclohexylethylene	CDA (0.1)	$NaClO_4 - AcONa$	1-acetoxy-1-cyclohexylethylene	33	269
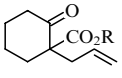 R = Me, Et	BQ (1.1)	$NaClO_4 - AcONa$	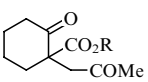	87	265
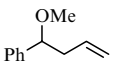	TBA (0.05)	Et_4NOTs	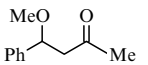	89	266
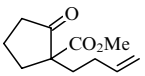	TBA (0.05)	Et_4NOTs	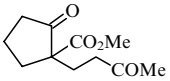	60	266
Dec-1-en-3-ol	TBA (0.05)	Et_4NOTs	3-hydroxydecan-2-one	41	266
	HQ	$LiClO_4 - AcOLi$	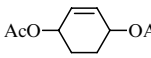	–	267

Note. PCD with alternation of electrode polarity (graphite, Pt, Ti – MnO_2), MeCN – H_2O, DMF – H_2O, MeOH or AcOH; BQ is benzoquinone, CDA is copper diacetate, TBA is tri(4-bromophenyl)amine, HQ is hydroquinone. [a] Bubbling of CO during the electrolysis; [b] ratio of esters of linear and branched acids.

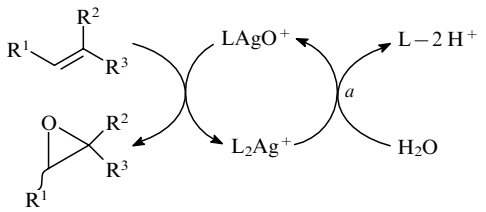

R^1	R^2	R^3	Oxirane yield (Current yield) (%)
H	H	Bu^n	– (30)
H	Me	CO_2Bu^i	87 (21)
n-C_5H_{11}	H	CO_2Me	80 (20)
MeO_2CCH_2	H	CO_2Me	90 (20)

L = bipy; (*a*) ACU, Pt or graphite anode, MeCN – H_2O (19 : 1), $LiClO_4$, 0.0125 – 0.05 equiv. AgOAc, 0.025 – 0.1 equiv. L.

Oxidation of allylic and benzylic C – H bonds and rupture of double bonds in alkenes are catalysed by the complex $[Ru(tripy)(bipy)(H_2O)]^{2+}$ (tripy is 2,2′,2″-terpyridyl).[271 – 273]

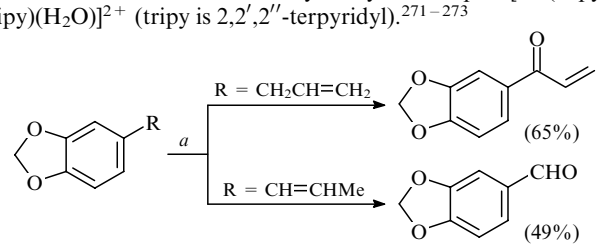

(*a*) PCD, Pt anode, 0.8 V, 3.9 F mol^{-1}, $Bu^tOH - H_2O$ (1 : 1), 0.065 equiv. $[Ru(tripy)(bipy)(H_2O)]^{2+}$, pH 6.8 (phosphate buffer), 30 °C.

Rupture of double bonds in alkenes also takes place in the presence of $SiRu(H_2O) \cdot W_{11}O_{39}^{5-} - NaIO_3$ [274] and $K_2OsO_2(OH)_4 - HIO_4$ [275] mediator systems.

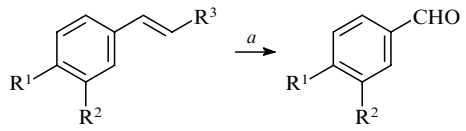

R^1	R^2	R^3	The yield of aldehyde (%)
H	H	Ph	79
MeO	H	Me	59
MeO	H	4-$MeOC_6H_4$	38
OCH_2O		Me	70

(*a*) ACD, PbO_2 anode, 8 mA cm^{-2}, 3.5 – 5.5 F mol^{-1}, $CH_2Cl_2 - H_2O$, 0.0034 – 0.006 equiv. $SiRu(H_2O)W_{11}O_{39}^{5-}$, 2 equiv. $NaIO_3$, 50 °C.

The $K_2OsO_2(OH)_4 - [K_3Fe(CN)_6]$ system catalyses alkene dihydroxylation and the subsequent cleavage of diols giving rise to ketones (total yields 62% – 91%).[276, 277]

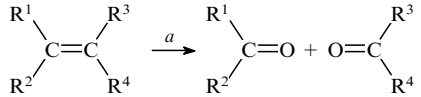

R^1, R^3 = H, Me, Ph; R^2 = H, Me; R^4 = Ph, $(CH_2)_2OCOPh$, 3,4-$(OCH_2O)C_6H_3$; (*a*) ACU, PbO_2 anode, Pt cathode, 5.6 mA cm^{-2}, 5 F mol^{-1}, MeCN – H_2O (10 : 3), Et_4NOTs, 0.04 equiv. $K_2OsO_2(OH)_4$, 0.5 equiv. HIO_4.

The electrochemical asymmetric dihydroxylation of alkenes in the presence of the $K_2OsO_2(OH)_4 - [K_3Fe(CN)_6]$ system and the Sharpless ligand is markedly superior to the corresponding chemical process in enantioselectivity and in yields of target products.[278] The main advantage of the electrochemical variant is that it implies the use of catalytic amounts of the osmate (0.002 equiv.) and the electrically regenerable oxidant, $[K_3Fe(CN)_6]$ (0.1 equiv.). In the classical version, at least a stoichiometric amount of the oxidant is required. The electrochemical dihydroxylation of styrene, 2-methyl-1-phenylpropene, *trans*-stilbene and 1,2-dihydronaphthalene results in the corresponding chiral diols; the degree of conversion is 90% – 97% and the enantiomeric yield is 90% – 100%.[276, 277]

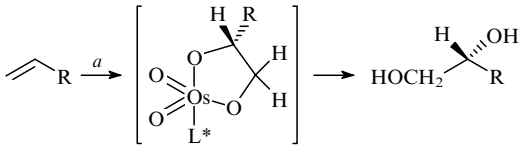

L* is the Sharpless ligand.

R	The yield of diol (%)	Configuration (*ee*)
Ph	95	*R*(–) (97.3)
Bu^n	71.2	*R*(+) (84.1)
n-C_8H_{17}	69	*R*(+) (91.8)
2-Naphthyl	87	*R*(–) (86.3)

(*a*) ACU, Pt anode, $Bu^tOH - H_2O$ (1 : 1), 0.1 equiv. $[K_3Fe(CN)_6]$, 0.002 equiv. $K_2OsO_2(OH)_4$, 0.01 equiv. L*, 0 – 20 °C.

12. Indirect electrochemical rupture of double bonds in alkenes

Indirect electrochemical rupture of double bonds in alkenes takes place with assistance of mediators and mediator systems such as manganese sulfate,[279] methanesulfonate and cerium sulfate,[280, 281] triarylamines,[80] $RuSi(H_2O)W_{11}O_{39}^{5-} - NaIO_3$,[274] $K_2OsO_2(OH)_4 - HIO_4$,[275] PhSSPh – NaBr [80] and $CuCl_2 - O_2$.[282] Two procedures have been developed: a single-stage procedure in which the electric generation of the oxidised form of the mediator (Med_{ox}) and the substrate oxidation by this species take place simultaneously in an electrolytic cell and a two-stage procedure in which the electric generation of Med_{ox} takes place in the cell, while the alkene oxidation by Med_{ox} occurs in a separate reaction vessel. These methods have been used to cleave the double bonds in 3,7-dimethyloct-6-enyl benzoate (**159**) in order to prepare 4-methyl-6-benzoyloxyhexanal (**160**);[275] and in styrenes (**161a – d**),[276, 280, 282] *trans*-stilbene (**161e**),[274, 275] anethole (**162a**)[275] and isosafrole (**162b**)[80, 271, 275, 276, 279] in order to prepare aromatic carbonyl compounds (**163a – d** and **164a,b**). The conditions of synthesis and the product yields are summarised in Table 12.

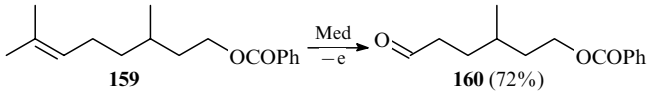

159 **160** (72%)

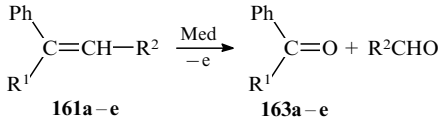

161a – e **163a – e**

$R^1 = R^2 = H$ (**a**); R^1 = Me, R^2 = H (**b**); R^1 = Ph, R^2 = H (**c**); R^1 = H, R^2 = Me (**d**); R^1 = H, R^2 = Ph (**e**).

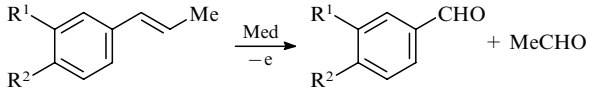

162a,b **164a,b**

R^1 = H, R^2 = MeO (**a**); $R^1 - R^2 = OCH_2O$ (**b**).

Electrooxidative cleavage of the double bonds in alkenes solves the same problems as chemical methods such as ozonolysis,[283 – 289] oxidation with chromic [290, 291] or cerium reagents,[292]

Table 12. Indirect electrooxidative cleavage of the C=C bond in alkenes.

Alkene	Mediator or mediator system (equiv.)	Method	Product	Yield (%) [a]	Ref.
159	$K_2OsO_2(OH)_4-HIO_4$ (0.04 : 0.5)	A	**160**	72 (29)	275
161b	$K_2OsO_2(OH)_4-HIO_4$ (0.04 : 0.5)	A	**163b**	71 (40)	275
161c	$K_2OsO_2(OH)_4-HIO_4$ (0.04 : 0.5)	A	**163c**	94 (42)	275
161e	$K_2OsO_2(OH)_4-HIO_4$ (0.04 : 0.5)	A	**163e**	66 (33)	275
162b	$K_2OsO_2(OH)_4-HIO_4$ (0.04 : 0.5)	A	**164b**	62 (99)	275
161a	$(MeSO_3)_2Ce(OH)_2(H_2O)$	see [b]	**163a**	89	280
161e	$SiRu(H_2O)W_{11}O_{39}^{5-}-NaIO_3$ [(0.003–0.006) : 0.5]	B	**163e**	79 (57)	274
161a	$SiRu(H_2O)W_{11}O_{39}^{5-}-NaIO_3$ [(0.003–0.006) : 0.5]	B	**164a**	59 (23)	274
162b	$SiRu(H_2O)W_{11}O_{39}^{5-}-NaIO_3$ [(0.003–0.006) : 0.5)]	B	**164b**	70 (44)	274
162b	MnO_2	see [b]	**164b**	54	279
	$Ce(SO_4)_2$	see [b]	**164b**	83	281
	$[Ru(tripy)(bipy)(H_2O)]^{2+}$ (0.065)	C	**164b**	49	271
	PhSSPh–NaBr (0.37 : 0.2)	D	**164b**	53 (70)	80
161d	$(4\text{-}BrC_6H_4)_3N$ (0.041)	E	see [c]	35	80
161a	$CuCl_2$ (0.05)–O_2	F	see [d]	(70)	282

Note. Method A: ACD, PbO_2 anode, 6.7 mA cm^{-2}, 2.5–10 F mol^{-1}, MeCN–H_2O (10 : 3), Et_4NOTs, 20 °C; method B: ACD, PbO_2 anode, 8 mA cm^{-2}, 3.5–5.5 F mol^{-1}, dichloroethane–H_2O (1 : 1), 50 °C; method C: PCD, Pt anode, 0.8 V, Bu^tOH-H_2O (4 : 1), phosphate buffer, 20 °C; method D: ACU, Pt anode, 8 mA cm^{-2}, 6.4 F mol^{-1}, MeCN–H_2O (2 : 1), ~20 °C; method E: ACU, graphite anode, 5 mA cm^{-2}, 3.5 F mol^{-1}, MeOH, $LiClO_4$, 18 °C; method F: PCD, Pt anode, 1.0 V, MeCN, $NaClO_4$, 80 °C.

[a] Substance yield (in parentheses, current yield). [b] Two-step cleavage; conditions of electric generation of Med_{ox} for $(MeSO_3)_2Ce(OH)_2(H_2O)$ and $Ce_2(CO_3)_3$: ACD, Pt anode, 200 mA cm^{-2}, 1.0 F mol^{-1}, $MeSO_3H-H_2O$, 50 °C; for MnO_2 and $MnSO_4\cdot 4H_2O$: ACD, PbO_2 anode, 200 mA cm^{-2}, 2.2 F mol^{-1}, 2 equiv. of H_2SO_4, 20 °C; for $Ce(SO_4)_2$ and $Ce_2(SO_4)_3$: ACD, Pt anode, 200 mA cm^{-2}, 1.2 F mol^{-1}, H_2SO_4, 20 °C. [c] $PhCH(OMe)_2$. [d] PhCHO.

the RuO_4–MeCHO–O_2 system,[293] *etc.*[294,295] The drawbacks peculiar to chemical methods have been largely overcome in the electrochemical method for the cleavage of double bonds in alkenes.

13. Reactions involving sacrificial metallic anodes

Electrochemical alkylation or acylation of alkenes with organic halides and acyl halides giving rise to C–C bonds is carried out using sacrificial metallic (usually, aluminium, zinc and magnesium) anodes. Their role is to suppress the formation of halogen molecules and thus to prevent halogenation of alkenes. The electrochemical formation of a C–C bond is an alternative to the reaction including deprotonation of organic CH acids induced by metals, organometallic compounds or strong bases and subsequent alkylation with the organic halide. In this case, the C–C bond formation is usually accompanied by side reactions, namely, O-alkylation, dialkylation or condensation of the substrate. In the processes with sacrificial anodes, the C–C bond is formed more selectively. For example, the reactions of activated alkenes with organic 1,1-, 1,3- and 1,4-dihalides,[296] non-activated alkenes with acylating reagents,[297,298] and cyclisation of unsaturated bromoacetals [299] afford compounds **165**–**169** in high yields.

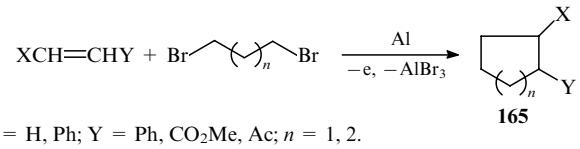

165

X = H, Ph; Y = Ph, CO_2Me, Ac; n = 1, 2.

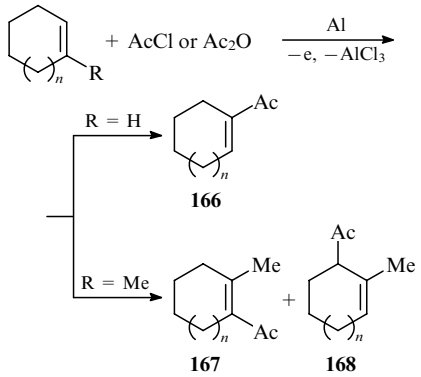

166 **167** **168**

R = H, Me; n = 1, 2.

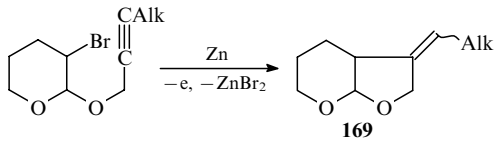

169

Besides preventing the generation of molecular bromine, a sacrificial aluminium anode participates (through Al^{3+} ions) in stabilisation of the type **A** dianions generated by cathodic reduction of the activated alkene.

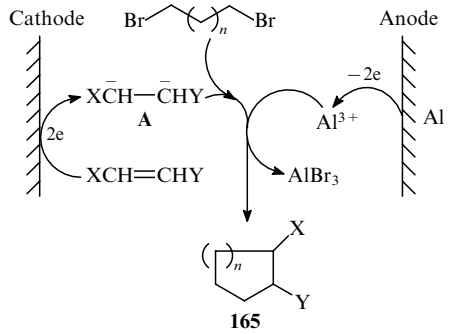

165

The substituted cycloalkanes **165** are formed in reasonable yields (30%–60%) only from activated alkenes, namely, esters of maleic, fumaric, cinnamic and acrylic acid and 4-phenylbut-3-en-2-one, upon reaction with 1,3- and 1,4-dihaloalkanes. The reaction proceeds with high stereoselectivity (isomer ratio *trans* : *cis* > 10 : 1). Cyclobutane derivatives are obtained by this method in very low yields, and only from 1,2-dichlorides. When 1,2-dibromides are used, electrochemical debromination takes place. In the reaction of dimethyl maleate with 1,3-dibromopropane, dimethyl 2-allylbutanedioate (yield 10%) and 1,2-cyclopentadicarboxylate (50%) are formed.[296]

In acylation of cycloalkenes with acetyl chloride, an aluminium anode not merely suppresses the generation of molecular chlorine but also catalyses the reaction, due to the influence of $AlCl_3$ formed during the electrochemical process. The electrochemical acylation occurs more selectively than the classical Friedel–Crafts reaction.[300–304] Joint electrolysis of equimolar amounts of acetyl chloride and cyclohexene or cycloheptene in an undivided cell at −10 to −5 °C (3 F mol^{-1}) results in complete conversion of cycloalkenes into 1-acetylcycloalkenes **166** (yields 60%–80%).[297,298] The transformation of 1-methyl-substituted cycloalkenes gives rise to two isomers, 1-acetyl-2-methylcycloalkenes **167** and 3-acetyl-2-methylcycloalkenes **168**, in a total yield of 65%–85%; the compounds **168** markedly predominate. Elec-

trochemical acetylation of acyclic alk-1-enes involves only the terminal carbon atom but the yields are relatively low (22% – 25%). The side products formed are α,β-dichlorides (1% – 10%), which become the only reaction products when a carbon or platinum anode is used.

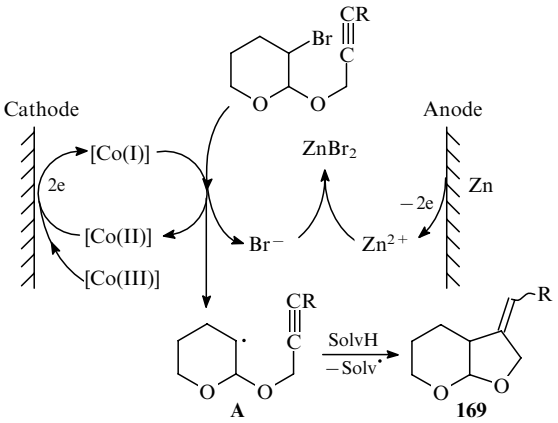

The intramolecular electrochemical cyclisation of unsaturated bromoacetals to dioxabicycloalkanes **169** is an example in which the use of sacrificial metallic anodes is combined successfully with the catalysis of the cathodic single-electron reduction of organic halides with cobaloxime. The cathodic generation of Co(I) complexes, single-electron reduction of bromoacetal to radical **A** by these complexes, cyclisation of the radical and subsequent transformation into the final product (yields 70% – 77%) are the key steps of this process.

Electrochemical reactions of alkenes with sacrificial metallic anodes provide good results in many cases where the chemical analogues either do not occur at all or are hardly suitable due to the low yields of the target products. This also eliminates the necessity of performing a labour-consuming and, in some cases, unsafe step of the synthesis of organometallic compounds. By using high current densities (up to 1 A dm^{-2}), one can produce substantial amounts of reaction products.

IV. Conclusion

Although electrochemical reactions are a powerful tool for transforming and assembling organic molecules, they are still used in most cases only by specialists and have not become a routine method of chemical synthesis. We hope that this review would be useful not only as a source of specially selected information but also as a manual for the practical use of electrochemical reactions for solving problems of organic synthesis. From this standpoint, reactions carried out in an electrolytic cell not separated into electrode compartments, which are simple in experimental implementation and require much less electricity, are more advantageous. The review demonstrates the substantial progress achieved in recent years in the investigation of alkene reactions induced by anodic oxidation and in development, on this basis, of theoretical and procedural aspects of modern organic chemistry. First of all, this refers to indirect anodic oxidation of alkenes with assistance by inorganic and organic mediators and mediator systems. Study of electrochemical processes involving these systems made it possible not only to establish the regularities and propose mechanisms of transformation of alkenes into functionally substituted products but also to elaborate simple methods which ensure high degrees of alkene conversion with minimum electricity consumption to give compounds the synthesis of which by chemical methods is either impossible or difficult from the experimental standpoint. Substantial progress has also been achieved in the study of electrochemical cyclisation, [4 + 2]-cycloaddition, phosphorylation, rupture of double bonds, and reactions involving sacrificial anodes. Methods of electrochemical transformation of alkenes and other organic compounds under conditions of diaphragmless electrolysis (in which both anodically and cathodically induced processes are involved in the assembling of the final product) have been developed. Vivid examples of this type of transformation are cyclisation of carboxy-substituted arylalkenes to give 2-benzylcyclopentanones in the presence of a tertiary phosphine (Scheme 5) [225] and indirect electrochemical reduction of carboxylic acids to the corresponding alcohols with assistance by the same reagent.[305] In our opinion, the scope of application of organic electrosynthesis should be extended. This is largely due to the fact that electric current would remain one of the most available, inexpensive and facile oxidants and reductants.

References

1. H J Schäfer *Top. Curr. Chem.* **152** 91 (1990)
2. H J Schäfer, in *Comprehensive Organic Synthesis* (Eds B M Trost, I Fleming) (Oxford: Pergamon Press, 1991) p. 633
3. H J Schäfer, in *Dachema Monographics* Vol. 112 (Weinheim: VCH, 1989) p. 399
4. E Steckhan *Angew. Chem., Int. Ed. Engl.* **25** 683 (1986)
5. H J Schäfer, E Steckhan *Angew. Chem., Int. Ed. Engl.* **8** 518 (1969)
6. H J Schäfer *Angew. Chem., Int. Ed. Engl.* **20** 911 (1981)
7. J Utley *Chim. Ind. (Milan)* **72** 324 (1990)
8. T Shono *J. Electrochem. Soc. Jpn.* **60** 964 (1992)
9. J Utley *Chem. Ind.* 215 (1994)
10. Y Matsumura *J. Electrochem. Soc. Jpn.* **62** 765 (1994)
11. T Nonaka, in *Organic Electrochemistry* (Eds H Lund, M M Baizer) (New York; Basel; Hong Kong: Marcel Dekker, 1991) p. 1131
12. M Niyazymbetov, D H Evans *Tetrahedron* **49** 9627 (1993)
13. S Torii *J. Synth. Org. Chem. Jpn.* **51** 1024 (1993)
14. J Utley *Chem. Soc. Rev.* **26** 181 (1997)
15. O N Chechina, A P Tomilov *Elektrokhimiya* **35** 149 (1999) [a]
16. K D Moeler *Top. Curr. Chem.* **185** 49 (1997)
17. B Uno, N Okumura *Recent Res. Dev. Pure Appl. Chem.* **2** (Pt. 1) 83 (1998)
18. H Maeda, H Ohmori *Acc. Chem. Res.* **32** 72 (1999)
19. S Torii *Electroorganic Synthesis. Methods and Applications* Vol. 15 (Tokyo: Monographs in Modern Chemistry, 1985) Pt. 1
20. K Yoshida *Electrooxidation in Organic Chemistry. The Role of Cation Radicals as Synthetic Intermediates* (New York, Wiley,1984)
21. M M Baizer, H Lund (Ed.) *Organic Electrochemistry* (New York: Marcel Dekker, 1988)
22. A J Fry *Synthetic Organic Electrochemistry* (New York: Wiley, 1989)
23. D Kyriacon *Modern Electroorganic Chemistry* (Berlin: Springer, 1994)
24. V D Parker, L Eberson *J. Chem. Soc., Chem. Commun.* 340 (1969)
25. L Eberson, V D Parker *Acta Chem. Scand.* **24** 3553 (1970)
26. M Katz, P Riemenschneider, H Wendt *Electrochim. Acta* **17** 1595 (1972)
27. N L Weinberg (Ed.) *Technique of Electroorganic Synthesis* Pt. II (New York; London; Sydney; Toronto: Wiley, 1975) p. 667
28. L L Miller, G D Nordblom, E A Mayeda *J. Org. Chem.* **37** 916 (1972)
29. C K Mann, K K Barnes *Electrochemical Reactions in Nonaqueous Systems* (New York: Marcel Dekker, 1970)
30. T Shono, A Ikeda *J. Am. Chem. Soc.* **94** 7892 (1972)
31. T Shono, A Ikeda, J Hayashi, S Hakozaki *J. Am. Chem. Soc.* **97** 4261 (1975)
32. R Akaba, in *Recent Advances in Electroorganic Synthesis* (Ed. S Torii) (Amsterdam: Elsevier, 1987) p. 75
33. R Engels, H J Schäfer, E Steckhan *Liebigs Ann. Chem.* 204 (1977)
34. H Baltes, E Steckhan H J Schäfer *Chem. Ber.* **111** 1294 (1978)
35. M Kojima, H Sakuragi, K Tokumaru *Chem. Lett.* 1707 (1981)
36. M N Elinson, I V Makhova, G I Nikishin *Izv. Akad. Nauk SSSR, Ser. Khim.* 1569 (1987) [b]
37. I Tanimoto, K Kushioka, T Kitagawa, K Maruyama *Bull. Chem. Soc. Jpn.* **52** 3586 (1979)
38. D Koch, H J Schäfer, E Steckhan *Chem. Ber.* **107** 3640 (1974)
39. T Shono, Y Matsumura, Y Nakagawa *J. Am. Chem. Soc.* **96** 3532 (1974)
40. R Vlădea *Rev. Roum. Chim.* **30** 151; 249 (1985)
41. R Vlădea, F Kerek *Rev. Roum. Chim.* **30** 157 (1985)

42. R Vlădea *Rev. Roum. Chim.* **31** 1691 (1986)
43. T Shono, T Kosaka *Tetrahedron Lett.* 6207 (1968)
44. A J Baggaley, R Brettle *J. Chem. Soc. C* 2055 (1968)
45. G Faita, M Flesischmann, D Pletcher *J. Electroanal. Chem.* **25** 455 (1970)
46. K Yoshida, T Kanbe, T Fueno *J. Org. Chem.* **42** 2313 (1977)
47. R Brettle, J R Sutton *J. Chem. Soc., Perkin Trans. 1* 1947 (1975)
48. A Bewick, J M Mellor, B S Pons *J. Chem. Soc., Chem. Commun.* 738 (1978)
49. G I Nikishin, M N Elinson, I V Makhova *Izv. Akad. Nauk SSSR, Ser. Khim.* 1919 (1984) [b]
50. I Barba, R Chinchila, C Gomez *J. Org. Chem.* **55** 3270 (1990)
51. G Sosnovsky, S O Lawesson *Angew. Chem.* **76** 218 (1948)
52. C Djerassi *Chem. Rev.* **43** 271 (1948)
53. C Adams, E N Frankel, J H P Utley *J. Chem. Soc., Perkin Trans. 1* 353 (1979)
54. T Shono, A Ikeda, Y Kimura *Tetrahedron Lett.* 3599 (1971)
55. L A Kheifits, V M Dashunin *Dushistye Veshchestva i Drugie Produkty dlya Parfyumerii* (Perfumes and Other Products for Perfumery) (Moscow: Khimiya, 1994) p. 172
56. T Shono, M Okawa, I Nishiguchi *J. Am. Chem. Soc.* **97** 6144 (1975)
57. H Maekawa, K Nakano, T Hirashima, I Nishiguchi *Chem. Lett.* 1661 (1991)
58. T Shono, I Nishiguchi, M Nitta *Chem. Lett.* 1319 (1976)
59. T Shono, Y Matsumura, H Hamaguchi, T Imanishi, K Yoshida *Bull. Chem. Soc. Jpn.* **51** 2179 (1978)
60. T Chiba, M Okimoto, H Nagai, Y Tanaka *J. Org. Chem.* **44** 3519 (1979)
61. T Shono, Y Matsumura, O Onomura, M Ogaki, T Kanazawa *J. Org. Chem.* **52** 536 (1987)
62. T Shono, Y Matsumura, M Ogaki, O Onomura *Chem. Lett.* 1447 (1987)
63. I V Makhova, Candidate Thesis in Chemical Sciences, Institute of Organic Chemistry, Academy of Sciences of the USSR, Moscow, 1989
64. Yu N Ogibin, A I Ilovaisky, G I Nikishin *Izv. Akad. Nauk, Ser. Khim.* 1624 (1994) [b]
65. A I Ilovaisky, Candidate Thesis in Chemical Sciences, Institute of Organic Chemistry, Russian Academy of Sciences, Moscow, 2000
66. R R Vargas, L V Pardimi, H Viertler *Tetrahedron Lett.* **30** 4037 (1989)
67. Yu N Ogibin, A I Ilovaisky, G I Nikishin *Izv. Akad. Nauk, Ser. Khim.* 2202 (1997) [b]
68. T Inoue, K Koyama, T Matsuoka, S Tsutsumi *Bull. Chem. Soc. Jpn.* **40** 162 (1967)
69. Yu N Ogibin, A I Ilovaisky, G I Nikishin *J. Org. Chem.* **61** 3256 (1996)
70. Yu N Ogibin, A I Ilovaisky, G I Nikishin *Electrochim. Acta* **42** 1933 (1997)
71. A Giirado, F Barba, J A Franco *Electrochim. Acta* **27** 1621 (1982)
72. B Belleau, Y K Au-Young *Can. J. Chem.* **47** 2117 (1969)
73. Yu N Ogibin, A O Terent'ev, A I Ilovaisky, G I Nikishin *Izv. Akad. Nauk, Ser. Khim.* 2115 (1999) [b]
74. Yu N Ogibin, A O Terent'ev, A I Ilovaisky, G I Nikishin *Elektrokhimiya* **36** 214 (2000) [a]
75. V Plazak, H Schneider, H Wendt *Ber. Bunsenges.* **78** 1373 (1974)
76. E Steckhan *J. Am. Chem. Soc.* **100** 3526 (1978)
77. M Katz, H Schneider, H Wendt *Ber. Bunsenges.* **77** 1828 (1973)
78. B D Gates, J S Swenton *Tetrahedron Lett.* **33** 2127 (1992)
79. Fr. P. 2 513 880; *Chem. Abstr.* **99** 58 750 (1983)
80. T U Bornewasser, E Steckhan, in *Electroorganic Synthesis* (Eds R D Little, N L Weinberg) (New York: Marcel Dekker, 1991) p. 205.
81. F D Mango, W A Bonner *J. Org. Chem.* **29** 1367 (1964)
82. L Cedheim, L Eberson, B Helgee, K Nyberg, R Servin, H Sternerup *Acta Chem. Scand., Ser. B* **29** 617 (1975)
83. E Bernharson, L Eberson, K Nyberg, B Rietz *Acta Chem. Scand.* **25** 1224 (1971)
84. L Cedheim, L Eberson *Acta Chem. Scand., Ser. B* **29** 904 (1975)
85. L Cedheim, L Eberson *Acta Chem. Scand., Ser. B* **29** 969 (1975)
86. V A Grinberg, Yu B Vasil'ev *Elektrokhimiya* **32** 309 (1996) [a]
87. M Huhtasaari, H J Schäfer, L Becking *Angew. Chem., Int. Ed. Engl.* **23** 980 (1984)
88. H J Schäfer, in *Recent Advances in Electroorganic Synthesis* (Ed. S Torii) (Amstardam: Elsevier, 1987) p. 3
89. L Becking, H J Schäfer *Tetrahedron Lett.* **29** 2797 (1988)
90. J Weinguny, H J Schäfer *Liebigs Ann. Chem.* 225; 235 (1994)
91. A Matzeit, H J Schäfer, C Amatore *Synthesis* 1432 (1995)
92. D P Curran, D Kim *Tetrahedron Lett.* **27** 5821 (1986)
93. D P Curran, C-T Chang *Tetrahedron Lett.* **28** 2477 (1987)
94. D P Curran, E Bosch, J Kaplan, M Newcomb *J. Org. Chem.* **54** 1826 (1989)
95. J-i Yoshida, T Maekawa, T Murata, S-i Matsunaga, S Isoe *J. Am. Chem. Soc.* **112** 1962 (1990)
96. J-i Yoshida, Y Ishichi, K Nishiwaki, S Shiozawa, S Isoe *Tetrahedron Lett.* **33** 2599 (1992)
97. J-i Yoshida, Y Morita, Y Ishichi, S Isoe *Tetrahedron Lett.* **35** 5247 (1994)
98. J-i Yoshida, Y Ishichi, S Isoe *J. Am. Chem. Soc.* **114** 7594 (1992)
99. J-i Yoshida, K Takada, Y Ishichi, S Isoe *J. Chem. Soc., Chem. Commun.* 2361 (1994)
100. J-i Yoshida, M Sugawara, N Kise *Tetrahedron Lett.* **37** 3157 (1996)
101. J-i Yoshida, K Takada, Y Ishichi, S Isoe, in *Novel Trends in Electroorganic Synthesis* (Ed. S Torii) (Tokyo: Kodansha, 1995) p. 295
102. S Yamamura, Y Shizuri, H Shigemori, Y Okuno, M Ohkubo *Tetrahedron* **47** 635 (1991)
103. S Maki, S Kosemura, S Yamamura, S Kowano, S Ohba *Chem. Lett.* 651 (1992)
104. S Maki, K Toyoda, S Kosemura, S Yamamura *Chem. Lett.* 1059 (1993)
105. S Maki, N Asaba, S Kosemura, S Yamamura *Tetrahedron Lett.* **33** 4169 (1992)
106. Y Shizuri, M Ohkuno, H Shigemori, S Yamamura *Tetrahedron Lett.* **28** 6661 (1987)
107. Y Shizuri, M Ohkuno, S Yamamura *Chem. Lett.* 113 (1989)
108. S Maki, S Kosemura, S Yamamura, S Ohba *Tetrahedron Lett.* **34** 6083 (1993)
109. Y Shizuri, S Maki, M Ohkubo, S Yamamura *Tetrahedron Lett.* **31** 7167 (1990)
110. S Maki, K Toyoda, T Mori, S Kosemura, S Yamamura *Tetrahedron Lett.* **35** 4817 (1994)
111. S Yamamura, in *Novel Trends in Electroorganic Synthesis* (Ed. S Torii) (Tokyo: Kodansha, 1995) p. 265
112. G W Morrow, J S Swenton *Tetrahedron Lett.* **28** 5445 (1987)
113. G W Morrow, Y Chen, J S Swenton *Tetrahedron* **47** 655 (1993)
114. J S Swenton, K Carpenter, Y Chen, M L Kerns, G W Morrow *J. Org. Chem.* **58** 3308 (1993)
115. J S Swenton, A Callinan, Y Chen, J J Rohde, M L Kerns, G W Morrow *J. Org. Chem.* **61** 1267 (1996)
116. K D Moeller, D G New *Tetrahedron Lett.* **35** 2857 (1994)
117. Z Tesfai, K D Moeller *J. Electrochem. Soc. Jpn.* **62** 1115 (1994); *Chem. Abstr.* **123** 169 450 (1995)
118. D G New, Z Tasfai, K D Moeller *J. Org. Chem.* **61** 1578 (1996)
119. R L Danheiser, E J Stoner, H Koyama, D S Yamashita, C A Klade *J. Am. Chem. Soc.* **111** 4407 (1989)
120. B Carte, M R Kernan, E B Barrabee, D J Faulkner *J. Org. Chem.* **51** 3528 (1986)
121. A Gopalan, P Magnus *J. Org. Chem.* **49** 2317 (1984)
122. S P Tanis, L A Dixon *Tetrahedron Lett.* **28** 2495 (1987)
123. K Hiroi, H Sato *Synthesis* 811 (1987)
124. A Padwa, M Ishida *Tetrahedron Lett.* **32** 5673 (1991)
125. F M Dean *Adv. Heterocyl. Chem.* **30** 161 (1982)
126. B H Lipshutz *Chem. Rev.* **86** 795 (1986)
127. K D Moeller, M R Marzabadi, D G New, M Y Chiang, S Keith *J. Am. Chem. Soc.* **112** 6123 (1990)
128. C M Hudson, M R Marzabadi, K D Moeller, D G New *J. Am. Chem. Soc.* **113** 7372 (1991)
129. C M Hudson, K D Moeller *J. Am. Chem. Soc.* **116** 3347 (1994)
130. K D Moeller, L V Tinao *J. Am. Chem. Soc.* **114** 1033 (1992)
131. K D Moeller, C M Hudson, L V Tinao-Wooldridge *J. Org. Chem.* **58** 3478 (1993)
132. L V Tinao-Wooldridge, K D Moeller, C M Hudson *J. Org. Chem.* **59** 2381 (1994)
133. D A Frey, S H K Reddy, K D Moeller *Electrochim. Acta* **42** 1967 (1997)
134. D A Frey, S H K Reddy, K D Moeller *J. Org. Chem.* **64** 2805 (1999)

135. T Shono, I Nishiguchi, S Kashimura, M Okawa *Bull. Chem. Soc. Jpn.* **51** 2181 (1978)
136. T Shono, Y Matsumura, S Katoh, K Ikeda, T Fujita, T Kamada *Tetrahedron Lett.* **30** 5309 (1989)
137. Yu N Ogibin, M N Elinson, A B Sokolov, G I Nikishin *Izv. Akad. Nauk SSSR, Ser. Khim.* 494 (1990) [b]
138. Yu N Ogibin, A B Sokolov, A I Ilovaisky, M N Elinson, G I Nikishin *Izv. Akad. Nauk SSSR, Ser. Khim.* 644 (1991) [b]
139. Yu N Ogibin, A I Ilovaisky, G I Nikishin *Izv. Akad. Nauk, Ser. Khim.* 2044 (1996) [b]
140. Yu N Ogibin, A I Ilovaisky, G I Nikishin *Izv. Akad. Nauk, Ser. Khim.* 2356 (1991) [b]
141. F Fichter, A Christen *Helv. Chim. Acta* **8** 332 (1925)
142. F Fichter, M Rinderspacher *Helv. Chim. Acta* **10** 102 (1927)
143. USSR P. 1 692 978; *Byull. Izobret.* (43) 95 (1991)
144. S Torii, T Inokuchi, R Oi *J. Org. Chem.* **47** 47 (1982)
145. Yu N Ogibin, A O Terent'ev, A I Ilovaisky, G I Nikishin *Mendeleev Commun.* 239 (1998)
146. Yu N Ogibin, A O Terent'ev, A I Ilovaisky, G I Nikishin *Mendeleev Commun.* 194 (1999)
147. M Chkir, D Lelandais *J. Chem. Soc., Chem. Commun.* 1369 (1971)
148. C J Brookes, P L Coe, D M Owen, A E Pedler, J C Tatlow *J. Chem. Soc., Chem. Commun.* 323 (1974)
149. C J Brookes, P L Coe, A E Pedler, J C Tatlow *J. Chem. Soc., Perkin Trans. 1* 202 (1978)
150. R N Renaud, P J Champagne *Can. J. Chem.* **53** 529 (1975); **57** 990 (1979)
151. R N Renaud, P J Champagne, M Sevard *Can. J. Chem.* **57** 2617 (1979)
152. Y Dan-oh, K Uneyama *Bull. Chem. Soc. Jpn.* **68** 2993 (1995)
153. N Muller *J. Org. Chem.* **48** 1370 (1983)
154. N Muller *J. Fluorine Chem.* **36** 163 (1987)
155. N Muller *J. Org. Chem.* **51** 263 (1986)
156. K Uneyama, H Nanbu *J. Org. Chem.* **53** 4598 (1988)
157. K Uneyama, S Makio, H Nanbu *J. Org. Chem.* **54** 872 (1989)
158. K Uneyama, O Morimoto, H Nanbu *Tetrahedron Lett.* **30** 109 (1989)
159. K Uneyama *Tetrahedron* **47** 555 (1991)
160. K Uneyama, S Watanabe *J. Org. Chem.* **55** 3909 (1990)
161. N Muller *J. Org. Chem.* **49** 4559 (1984)
162. N Muller *J. Org. Chem.* **49** 2826 (1984)
163. H J Schäfer, A Al Azrak *Chem. Ber.* **105** 2398 (1972)
164. S Torii, K Uneyama, T Onishi, Y Fujita, M Ishiguro, T Nishida *Chem. Lett.* 1603 (1980)
165. J-i Yoshida, K Sakaguchi, S Isoe *Tetrahedron Lett.* **27** 6075 (1986)
166. J-i Yoshida, K Sakaguchi, S Isoe *J. Org. Chem.* **53** 2525 (1988)
167. J-i Yoshida, K Sakaguchi, S Nakatani, S Isoe, in *Recent Advances in Electroorganic Synthesis* (Ed. S Torii) (Amsterdam: Elsevier, 1987) p. 85
168. K Chiba, M Tada *J. Chem. Soc., Chem. Commun.* 2485 (1994)
169. K Chiba, J Sonoyama, M Tada *J. Chem. Soc., Chem. Commun.* 1381 (1995)
170. J-i Yoshida, S Nakatani, S Isoe *J. Chem. Soc., Chem. Commun.* 1468 (1988)
171. J-i Yoshida, S Nakatani, S Isoe *J. Org. Chem.* **54** 5655 (1989)
172. S Nakatani, J-i Yoshida, S Isoe *Tetrahedron* **49** 2011 (1993)
173. D A Ashurov, A M Akhmedov, Zh R Alumyan *Zh. Obshch. Khim.* **44** 1842 (1974) [c]
174. V M Mel'nikov, V I Kashutin, V A Smirnov *Zh. Obshch. Khim.* **45** 2105 (1975) [c]
175. P Pouillen, R Minko, M Verniette, P Martinet *Electrochim. Acta* **24** 1189 (1979); **25** 711 (1980)
176. J A Caram, M E Martins, E G Gros, C M Marscoff *Electrochim. Acta* **35** 1163 (1990)
177. N L Weinberg, A K Hoffman *Can. J. Chem.* **49** 740 (1971)
178. M Verniette, C Daremon, J Simonet *Electrochim. Acta* **23** 929 (1978)
179. K Uneyama, N Hasegawa, H Kawafuchi, S Torii *Bull. Chem. Soc. Jpn.* **56** 1214 (1983)
180. S Torii, T Inokuchi, S Masima, T Kobayashi *J. Org. Chem.* **45** 2731 (1980)
181. S Torii, K Uneyama, H Tanaka, T Yamanaka, T Yasida, M Ono, Y Kohmoto *J. Org. Chem.* **46** 3312 (1981)
182. M N Elinson, I V Makhova, G I Nikishin *Izv. Akad. Nauk SSSR, Ser. Khim.* 829 (1988) [b]
183. M N Elinson, I V Makhova, G I Nikishin *Izv. Akad. Nauk SSSR, Ser. Khim.* 125 (1990) [b]
184. S Torii, K Uneyama, K Ueda *J. Org. Chem.* **49** 1830 (1984)
185. N Ibl, A Selvig *Chem. Ing. Tech.* **B42** 180 (1970)
186. K H Simmrock *Chem. Ing. Tech.* **48** 1085 (1976)
187. K G Ellis, R E W Jansson *Chem. Ind.* 864 (1980)
188. K G Ellis, R E W Jansson *J. Appl. Chem.* **11** 531 (1981); **13** 657 (1983)
189. C Belmont, H H Girault *Electrochim. Acta* **40** 2505 (1995)
190. S Torii, K Uneyama, M Ono, H Tazawa, S Matsunami *Tetrahedron Lett.* 4661 (1979)
191. S Torii, K Uneyama, S Matsunami *J. Org. Chem.* **45** 16 (1980)
192. J-i Yoshida, J Hashimoto, N Kawabata *J. Org. Chem.* **47** 3575 (1982)
193. N Takano, M Ogata, N Takeno *Chem. Lett.* 85 (1996)
194. K Fujimoto, Y Tokuda, Y Matsubara, H Maekawa, T Mizuno, I Nishiguchi *Tetrahedron Lett.* **36** 7483 (1995)
195. K Uneyama, M Ono, S Torii *Phosphorus Sulfur* **16** 35 (1983)
196. S Torii, K Uneyama, M Ono *Tetrahedron Lett.* **21** 2741 (1980)
197. A Bewick, D E Coe, G B Fuller, J M Mellor *Tetrahedron Lett.* **21** 3827 (1980)
198. V V Zhuikov, V Z Latynova, M Yu Postnikova, Yu M Kargin *Zh. Org. Khim.* **59** 1349 (1989) [c]
199. A Bewick, D E Coe, J M Mellor, W M Owton *J. Chem. Soc., Perkin Trans. 1* 1033 (1985)
200. N Schultz, S Töteberg-Kaulen, S Dapperheld, J Heyer, M Platen, K Schumacher, E Steckhan, in *Recent Advances in Electroorganic Synthesis* (Ed. S Torii) (Amsterdam: Elsevier, 1987) p. 127
201. S Töteberg-Kaulen, E Steckhan *Tetrahedron* **44** 4389 (1988)
202. R D Vukicevic, S Konstantinovic, M Lj Mihailovic *Tetrahedron* **47** 859 (1991)
203. A J Bloom, M Fleischmann, J M Mellor *Tetrahedron Lett.* **25** 4971 (1984)
204. A J Bloom, E H M Abd Elall, M I Al Ashmawy, J M Mellor, W M Owton, Z Abd El Samil, in *Recent Advances in Electroorganic Synthesis* (Ed. S Torii) (Amsterdam: Elsevier, 1987) p. 33
205. I N Rozhkov, I Ya Aliev, I L Knunyants *Izv. Akad. Nauk SSSR, Ser. Khim.* 1418 (1976) [b]
206. A Bensadat, G Bodennec, E Laurent, R Tardivel *Tetrahedron Lett.* 3799 (1977)
207. A Bensadat, G Bodennec, E Laurent, R Tardivel *Nouv. J. Chem.* **5** 127 (1981)
208. T Yamada, T Osa, T Matsue *Chem. Lett.* 995 (1987)
209. G I Nikishin, M N Elinson, I V Makhova *Tetrahedron Lett.* **29** 1603 (1988)
210. T Shono, S Kashimura, T Soejima, K Ohta, Y Yamaguchi, in *Recent Advances in Electroorganic Synthesis* (Ed. S Torii) (Amsterdam: Elsevier, 1987) p. 41
211. T Shono, M Chuankamnerdkarn, H Maekawa, M Ishifune, S Kashimura *Synthesis* 895 (1994)
212. T Shono, T Soejima, K Takigawa, Y Yamaguchi *Tetrahedron Lett.* **35** 4161 (1994)
213. R Shundo, Y Matsubara, I Nishiguchi, T Hirashima, H Maekawa, S Kashimura *Chem. Lett.* 2033 (1989)
214. R Shundo, Y Matsubara, I Nishiguchi, T Hiroshima *Bull. Chem. Soc. Jpn.* **65** 530 (1992)
215. H Tanaka, H Suga, H Ogawa, A K M Abdul Hai, S Torii *Tetrahedron Lett.* **33** 6495 (1992)
216. B Giese *Radicals in Organic Synthesis. Formation of Carbon–Carbon Bonds* (Press Oxford: Pergamon, 1986)
217. D P Curran *Synthesis* 417; 489 (1988)
218. H Ohmori, T Takanami, M Masui *Tetrahedron Lett.* **26** 2199 (1985)
219. H Ohmori, T Takanami, M Masui *Chem. Pharm. Bull.* **35** 4960 (1987)
220. H Ohmori, H Maeda, T Takanami, M Masui, in *Recent Advances in Electroorganic Synthesis* (Ed. S Torii) (Amsterdam: Elsevier, 1987) p. 29
221. T Takanami, K Suda, H Ohmori, M Masui *Chem. Lett.* 1335 (1987)
222. T Takanami, A Abe, K Suda, H Ohmori, M Masui *Chem. Pharm. Bull.* **38** 2698 (1990)

223. H Ohmori, T Takanami, H Shimada, M Masui *Chem. Pharm. Bull.* **35** 2558 (1987)
224. T Takanami, A Abe, K Suda, H Ohmori *J. Chem. Soc., Chem. Commun.* 1310 (1990)
225. H Maeda, T Maki, H Ohmori *Chem. Lett.* 249 (1995)
226. A S Romakhin, V A Zagumennov, E V Nikitin, Yu M Kargin *Zh. Obshch. Khim.* **65** 1321 (1995) [c]
227. V A Zagumennov, A S Romakhin, E V Nikitin *Zh. Obshch. Khim.* **69** 803 (1999) [c]
228. A S Romakhin, I P Kosachev, E V Nikitin *Zh. Obshch. Khim.* **66** 1955 (1996) [c]
229. A S Romakhin, V A Zagumennov, E V Nikitin *Zh. Obshch. Khim.* **67** 602 (1997) [c]
230. A S Romakhin, I P Kosachev, E V Nikitin, Yu A Ignat'ev, Yu M Kargin, A N Pudovik *Dokl. Akad. Nauk SSSR* **294** 1413 (1987) [d]
231. A S Romakhin, V A Zagumennov, E V Nikitin, Yu M Kargin *Zh. Obshch. Khim.* **59** 223 (1989) [c]
232. A S Romakhin, V A Zagumennov, E V Nikitin *Zh. Obshch. Khim.* **66** 256 (1996) [c]
233. A S Romakhin, I P Kosachev, V A Zagumennov, E V Nikitin *Zh. Obshch. Khim.* **67** 244 (1997) [c]
234. E V Nikitin, V A Zagumennov, A S Romakhin, I P Kosachev, Yu A Babkin *Electrochim. Acta* **42** 2205 (1997)
235. A S Romakhin, I P Kosachev, V A Zagumennov, E V Nikitin *Zh. Obshch. Khim.* **68** 159 (1998) [c]
236. J Mattay *Synthesis* 233 (1989)
237. C F Gürtler, S Blechert, E Steckhan *Synlett* 141 (1994)
238. C F Gürtler, S Blechert, E Steckhan *Angew. Chem., Int. Ed. Engl.* **34** 1900 (1995)
239. C F Gürtler, E Steckhan, S Blechert *J. Org. Chem.* **61** 4136 (1996)
240. T Peglow, S Blechert, E Steckhan *Chem. Eur. J.* **4** 107 (1998)
241. J Mlcoch, E Steckhan *Tetrahedron Lett.* **28** 1081 (1987)
242. N L Bauld *Tetrahedron* **45** 5307 (1989)
243. G I Nikishin, Yu N Ogibin *Sov. Sci. Rev., Sect. B, Chem. Rev.* **7** 99 (1985)
244. G G Melikyan, in *Organic Reactions* Vol. 49 (New York: Wiley, 1997) p. 427
245. R Shundo, I Nishiguchi, Y Matsubara, T Hiroshima *Chem. Lett.* 235 (1991)
246. R Shundo, I Nishiguchi, Y Matsubara, T Hirashima *Tetrahedron* **47** 831 (1991)
247. R Shundo, I Nishiguchi, Y Matsubara, T Hirashima *Chem. Lett.* 2285 (1990)
248. R Warsinsky, E Steckhan *J. Chem. Soc., Perkin Trans. 1* 2027 (1994)
249. F Bergamini, A Citterio, N Gatti, M Nicolini, R Sauti, R Sebastiano *J. Chem. Res. (S)* 364 (1993)
250. R Shundo, I Nishiguchi, Y Matsubara, M Toyoshima, T Hirashima *Chem. Lett.* 185 (1991)
251. J Y Nedelec, K Nohair *Synlett* 659 (1991)
252. K Nohair, I Lachaise, J-P Paugam, J-Y Nedelec *Tetrahedron Lett.* **33** 213 (1992)
253. J P Coleman, R C Hallcher, D E McMackins, T E Rogers, J H Wagenknecht *Tetrahedron* **47** 809 (1991)
254. J Tsuji *Synthesis* 369 (1984)
255. T Hosokawa, S T Murahashi *Acc. Chem. Res.* **23** 49 (1990)
256. D G Miller, D D M Wayner *J. Org. Chem.* **55** 2924 (1990)
257. S Nakamura, A Yasui *J. Catal.* **17** 366 (1970)
258. H Alper, F W Hartstock, B Despeyroux *J. Chem. Soc., Chem. Commun.* 905 (1984)
259. H Alper, F W Hartstock *J. Chem. Soc., Chem. Commun.* 1141 (1985)
260. H Alper, G Vasapollo, F W Hartstock, M Mlekuz, D J H Smith, G E Morris *Organometallics* **6** 2391 (1987)
261. R A Sheldon *Top. Curr. Chem.* **164** 23 (1993)
262. V A Shepelin *Elektrokhimiya* **11** 1767 (1975) [a]
263. J Tsuji, M Minato *Tetrahedron Lett.* **28** 3683 (1987)
264. P G Miller, D D M Wayner *Can. J. Chem.* **70** 2485 (1992)
265. H Riering, H J Schäfer *Chem. Ber.* **127** 859 (1994)
266. T Inokuchi, L Ping, F Hamaue, M Izawa, S Torii *Chem. Lett.* 121 (1994)
267. J-E Bickvall, A Gogoll *J. Chem. Soc., Chem. Commun.* 1236 (1987)
268. D M Wayner, F W Hartstock *J. Mol. Catal.* **48** 15 (1988)
269. F W Hartstock, D D M Wayner *Tetrahedron Lett.* **35** 8137 (1994)
270. C Kandzia, E Steckhan *Tetrahedron Lett.* **35** 3695 (1994)
271. M S Thompson, W F De Giovani, B A Moyer, T J Meyer *J. Org. Chem.* **49** 4972 (1984)
272. J M Madurro, G Chiericato Jr, W F De Giovani, J R Romero *Tetrahedron Lett.* **29** 765 (1988)
273. M M T Khan, A P Rao, S H Mehta *J. Mol. Catal.* **78** 263 (1993)
274. E Steckhan, C Kandzia *Synlett* 139 (1992)
275. H Tanaka, R Kikuchi, M Baba, S Torii *Bull. Chem. Soc. Jpn.* **68** 2989 (1995)
276. A P Amundsen, E N Balko *J. Appl. Electrochem.* **22** 810 (1992)
277. S Torii, P Liu, H Tanaka *Chem. Lett.* 319 (1995)
278. K B Sharpless, W Amberg, Y L Bennani, G A Crispino, J Hartung, K-S Jeong, H-L Kwong, K Morikawa, Z-M Wang, D Xu, X-L Zhang *J. Org. Chem* **57** 2768 (1992)
279. J Grimshaw, C Hua *Electrochim. Acta* **39** 497 (1994)
280. R P Kreh, R M Spotnitz, J T Lundquist *J. Org. Chem.* **54** 1526 (1989)
281. Br. P. 2 165 536; *Chem. Abstr.* **105** 153 052 (1986)
282. T Koyama, A Kitani, S Ito, K Sasaki *Chem. Lett.* 395 (1993)
283. S D Razumovskii, G E Zaikov *Ozon i Ego Reaktsii s Organicheskimi Soedineniyami* (Ozone and Its Reactions with Organic Compounds) (Moscow: Nauka, 1974)
284. *Organikum. Organisch-Chemisches Grundpraktikum* (Berlin: VEB Deutscher Verlag Wissenschaften, 1990)
285. R B Miller, J M Frincke *J. Org. Chem.* **45** 5312 (1980)
286. P J Carratt, K P C Vollhardt *Synthesis* 423 (1971)
287. M Miura, M Nojima, S Kusabayashi *J.Chem. Soc., Perkin Trans. 1* 1950 (1980)
288. O V Topalova, L A Shabrova *Zh. Org. Khim.* **11** 2444 (1975) [e]
289. L Li *Huaxue Shijie* **24** 199 (1983); *Chem. Abstr.* **100** 85 617 (1983)
290. V I Isagulyants *Sinteticheskie Dushistye Veshchestva* (Synthetic Perfumes) (Erevan: Academy of Sciences of Arm. SSR, 1946) p. 332
291. I-N Vin, A F Polyakov *Izv. Vyssh. Uchebn. Zaved., Pishch. Tekhnol.* (4) 68 (1965)
292. T-L Ho *Synthesis* 347 (1973)
293. K Kaneda, S Haruna, T Imanaka, K Kawamoto *J. Chem. Soc., Chem. Commun.* 1467 (1990)
294. H Mimoun, M M P Machirant, I S de Roch *J. Am. Chem. Soc.* **100** 5437 (1978)
295. P A Ganeshpure, S Satish *Tetrahedron Lett.* **29** 6629 (1988)
296. Y-W Lu, J-Y Nedelec, J-C Folest, J Perichon *J. Org. Chem.* **55** 2503 (1990)
297. R D Vukicevic, S Konstantinovic, Lj Joksovic, G Pouticelli, M Lj Mihailovic *Chem. Lett.* 275 (1995)
298. R D Vukicevic, Lj Joksovic, S Konstantinovic, Z Markovic, M Lj Mihailovic *Bull. Chem. Soc. Jpn.* **71** 899 (1998)
299. T Inokuchi, H Kawafuchi, K Aoki, A Yoshida, S Torii *Bull. Chem. Soc. Jpn.* **67** 595 (1994)
300. H M R Hoffmann, T Tsushima *J. Am. Chem. Soc.* **98** 6008 (1977)
301. P Beak, K R Berger *J. Am. Chem. Soc.* **102** 3848 (1980)
302. T Shono, I Nishiguchi, M Sasaki, H Ikeda, M Kurita *J. Org. Chem.* **48** 2503 (1983)
303. A Tubul, M Santelli *J. Chem. Soc., Chem. Commun.* 191 (1988)
304. F X Bates, J A Donnelly, J R Keegan *Tetrahedron* **47** 4991 (1991)
305. H Ohmori, T Maki, H Maeda, in *Novel Trends in Electroorganic Synthesis* (Ed. S Torii) (Tokyo: Kodansha, 1995) p. 34

[a] — *Russ. J. Electrochem. (Engl. Transl.)*
[b] — *Russ. Chem. Bull. (Engl. Transl.)*
[c] — *Russ. J. Gen. Chem. (Engl. Transl.)*
[d] — *Dokl. Chem. Technol., Dokl. Chem. (Engl. Transl.)*
[e] — *Russ. J. Org. Chem. (Engl. Transl.)*

Russian Chemical Reviews **70** (7) 577 – 606 (2001) © 2001 Russian Academy of Sciences and Turpion Ltd

DOI 10.1070/RC2001v070n07ABEH000661

Spectral properties of porphyrins and their precursors and derivatives

N Zh Mamardashvili, O A Golubchikov

Contents

I. Introduction 577
II. IR spectra of porphyrins and their precursors and derivatives 577
III. ^{1}H NMR spectra of porphyrins and their precursors 585
IV. Electronic absorption spectra of porphyrins and metalloporphyrins 595

Abstract. The data of IR, ^{1}H NMR and electronic absorption spectroscopy of porphyrins and their precursors and derivatives are analysed, systematised and generalised. The bibliography includes 105 references.

I. Introduction

Problems of spectroscopy of porphyrins have been considered in detail in a number of papers and monographs (see, for example, Refs 1 – 8). However, the last 10 – 15 years have been marked by impressive progress in the synthetic chemistry of porphyrins resulting in the determination of the spectral characteristics of new heterocyclic compounds (porphyrins and their intermediates) with very complex structures. It should be noted that most studies dealt with the spectra of particular porphyrins and their precursors with the aim of establishing the structures of the newly synthesised compounds. However, the results of investigations by different spectral methods, which were performed under different conditions and using a limited number of compounds, cannot necessarily be compared.

In order for the relationship between the structure and the spectral properties of complex multicontour chromophores (among which are, undoubtedly, porphyrins) to be revealed, comprehensive investigation of a diversity of compounds whose structures vary from simple to complex must be carried out. Pyrrole intermediates are of obvious interest because they can be used to follow changes in the spectral characteristics as the macrocycle undergoes chemical modifications. In the present review, we analyse, systematise and generalise the recent data of IR, ^{1}H NMR and electronic absorption spectroscopy of porphyrins and their derivatives and precursors, *viz*., of mono-, di- and tetrapyrrole compounds.

N Zh Mamardashvili Institute of Solution Chemistry, Russian Academy of Sciences, ul. Akademicheskaya 1, 153045 Ivanovo, Russian Federation. Fax (7-093) 237 85 09. Tel. (7-093) 237 85 12.
E-mail: ngm@ihnr.polytech.ivanovo.su
O A Golubchikov Ivanovo State University of Chemistry and Technology, prosp. F Engelsa 7, 153460 Ivanovo, Russian Federation.
Fax (7-093) 241 79 95. Tel. (7-093) 232 73 78

Received 29 March 2001
Uspekhi Khimii **70** (7) 656 – 686 (2001); translated by T N Safonova

II. IR spectra of porphyrins and their precursors and derivatives

IR spectroscopy enables one not only to identify compounds, but also to follow changes in various characteristics of individual chemical bonds and the molecule as a whole that occur upon chemical modifications. For example, information on the relative stabilities of corresponding chemical bonds in the molecules can be obtained by comparing the force constants of these bonds, which can be calculated from the spectral data. Since all force constants cannot necessarily be determined from the spectral data, qualitative conclusions about the relative stabilities of the bonds are often made based on the experimental vibration frequencies observed in IR spectra. These frequencies are functions of the atomic weights and the force constants of the bonds. A comparison of the frequencies of analogous vibrations for different compounds can be performed only in the case of the characteristic vibrations. The shifts of characteristic vibration frequencies are directly related to the changes in the electronic states of the bonds and the fragments within which the vibrations under consideration are localised.

Investigation of a large number of structurally similar molecules can be a help in refining the assignment of vibrations to particular fragments of the porphyrin ring.

1. Pyrroles

The assignment of virtually all bands in the IR spectrum of pyrrole (**1a**) was made[9,10] and this spectrum can be used in studies of pyrrole derivatives (Table 1). The NH stretching vibrations in the spectrum of solid pyrrole are observed in the region of $\sim$3500 cm^{-1}. In chloroform, this band is split into two components (at 3400 and 3497 cm^{-1}). The intensity of the band at 3497 cm^{-1} increases upon dilution. Therefore, the band at 3400 cm^{-1} corresponds to associated NH bonds, whereas the band at 3497 cm^{-1} is assigned to the free bonds. According to the results of calculations carried out for the isolated pyrrole molecule, the NH stretching vibration band in its spectrum is located at 3491 cm^{-1} (Table 2).

Two pronounced bands at 3100 and 3130 cm^{-1} are assigned to CH stretching vibrations of pyrrole. Calculations by the semiempirical PM3 method demonstrated[11] (see Table 2) that the more intense band (at 3100 cm^{-1}) corresponds to vibrations of the C(α)–H bonds, whereas the less intense band corresponds to vibrations of the C(β)–H bonds. The frequencies in the region of 1350 – 1600 cm^{-1} belong to skeletal vibrations of pyrrole. In the spectrum, these vibrations are observed as an intense band at 1350 cm^{-1} and a medium intensity band at 1530 cm^{-1}.

Table 1. Positions of the absorption maxima (cm^{-1}) in the IR spectra of the pyrroles **1a**–**l** (in KBr pellets).[9, 10]

Compound **1**	Pyrrole fragment			Alkyl substituent		ν(C=O)	ν(C–O)
	ν(NH)	ν(CH)	ν(C–C)	δ(CH)	γ(CH)		
a[a]	3495	3100, 3130	1350, 1530	–	–	–	–
b	3458	–	1350, 1508	1380	1004	1667	1284
c	3456	–	1348, 1510	1379	1022	1664	1290
d	3458	–	1346, 1515	1386	1018	1680	1290
e	3450	–	1360, 1530	1380	1010	1670	1280
f	3451	–	1338, 1514	1380	1015	1690	1287
g	3450	–	1328, 1517	1377	1090	1685	1273
h	3453	–	1316, 1514	1378	1065	1702	1255
i	3452	–	1320, 1517	1384	1116	1687	1268
j	3466	–	1384, 1540	1370	1088	1686	1265
k	3450	–	1357, 1578	1382	1000	1680	1295
l	3454	3108	1352, 1564	1378	994	1637	1290

[a] According to the published data.[2]

Examinations[9–12] of the spectra of substituted pyrroles **1b**–**l** demonstrated that chemical modifications of the molecule lead to essential spectral changes. Thus, the spectrum of 2-ethoxycarbonyl-3,4,5-trimethylpyrrole (**1b**) shows CH deformation vibrations of the alkyl groups.

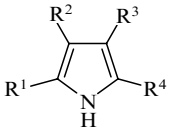

1a–**l**

Compound **1**	R^1	R^2	R^3	R^4
a	H	H	H	H
b	Me	Me	Me	CO_2Et
c	Me	Et	Me	CO_2Et
d	Me	Bu^n	Me	CO_2Et
e	Me	Bu^n	Me	CO_2Bn
f	Me	Et	Me	CO_2Bn
g	CO_2Et	Et	Me	CO_2Bn
h	CO_2Et	Et	Me	CO_2H
i	CO_2H	Et	Me	CO_2Et
j	CO_2Et	Et	Me	I
k	I	Et	Me	CO_2Et
l	H	Bu^n	Me	CO_2Et
m	H	Me	Me	H
n	Me	H	H	Me
o	Me	Me	Me	H
p	H	Me	Et	Me
q	H	Me	Et	CO_2Et
r	Me	Et	Me	CHO
s	Me	Me	Et	CHO

The skeletal vibration bands are shifted to the lower-frequency region and are more intense than the corresponding bands in the spectrum of unsubstituted pyrrole. Apparently, a rise in the intensities of these bands can be accounted for by the effect of the electron-withdrawing ester group.

This assumption is supported by the following fact. In the spectrum of 2-benzyloxycarbonyl-5-ethoxycarbonyl-4-ethyl-3-methylpyrrole (**1g**), the vibration bands of the pyrrole ring are shifted further to the low-frequency region with a simultaneous increase in their intensities. Of the molecules under consideration, the largest low-frequency shifts of skeletal vibrations are observed for the α-carboxypyrroles **1h**,**i**. Noteworthy are also the low-frequency shifts of NH vibrations of these pyrroles. The spectrum of 4-butyl-2-ethoxycarbonyl-3-methylpyrrole (**1l**) has an intense band at 3108 cm^{-1} corresponding to CH stretching vibrations of the pyrrole ring. Investigations demonstrated that this band corresponds to vibrations of the C(α)–H bond of pyrrole (the β positions are occupied by substituents). The spectral characteristics of the positional isomers **1h**,**i** and **1j**,**k** differ only slightly from each other. An increase in the size of the alkyl substituent (R) in 4-R-2-ethoxycarbonyl-3,5-dimethylpyrroles **1b**–**d** (R = Me, Et or Bu^n) is accompanied primarily by an increase in the intensity of the CH vibration bands of the alkyl groups. It should be noted that the C=O, C–O, C–OH and C–I vibrations are characteristic. The bands belonging to these vibrations are present in the spectra of all compounds of the series **1b**–**l** and allow one to

Table 2. Vibration frequencies (cm^{-1}) in the IR spectra of the pyrroles **1a**–**l** calculated by the PM3 method.[11]

Compound **1**	Pyrrole fragment			Alkyl substituent		ν(C–O)
	ν(NH)	ν(CH)	ν(C–C)	δ(CH)	γ(CH)	
a	3491	3100, 3133	1355, 1530	–	–	–
b	3453	–	1350, 1512	1384, 1390	1007	1289
c	3459	–	1356, 1516	1386, 1399	1027	1293
d	3462	–	1348, 1510	1382, 1394	1021	1296
e	3447	–	1364, 1528	1380, 1392	1012	1284
f	3453	–	1340, 1516	1380, 1391	1011	1280
g	3450	–	1325, 1515	1379, 1395	1094	1278
h	3450	–	1320, 1510	1376, 1397	1069	1252
i	3448	–	1316, 1519	1380, 1391	1119	1270
j	3466	–	1386, 1544	1373, 1389	1086	1266
k	3454	–	1350, 1576	1376, 1382	1002	1290
l	3456	3112	1354, 1564	1371, 1384	994	1284

identify the pyrrole synthesised and to establish its structure and purity.

2. Dipyrrolylmethanes

The IR spectra of dipyrrolylmethanes **2a**–**x** were measured and examined.[12–14] The structures of these compounds have been previously investigated by calculation methods (the MM + molecular mechanics method and the semiempirical PM3 method). The calculated energy parameters and geometric characteristics corresponding to the energy minima are summarised in the studies.[15,16] The energy parameters of the dipyrrolylmethane molecule are substantially affected by the substituents at positions 5 and 5′, while the effects of the alkyl substituents at positions 3, 3′, 4 and 4′ are insignificant.

As mentioned above, the NH stretching vibrations of pyrrole are observed at 3495 cm^{-1}. On going to dipyrrolylmethane (**2x**), the NH vibration band is shifted to the low-frequency region by $\sim$40 cm^{-1}. Introduction of the phenyl substituent at the *meso*-position of dipyrrolylmethane (the compound **2w**) leads to a further short-wavelength shift (by 15 cm^{-1}) of this band (Table 3). Below are given the charge distributions on the atoms of the dipyrrolylmethane molecules, which show the influence of the electronic factors upon chemical modifications of the molecule.

Thus, the presence of electron-withdrawing substituents (for example, the carboxy group) at positions 5 and 5′ of dipyrrolylmethane leads to a decrease in the electron density on the nitrogen atoms (the compound **2b**), which is accompanied by lowering of the ν(NH) frequency by $\sim$40 cm^{-1} (Tables 3 and 4). The presence of the electron-donating methoxy groups in the *meso* substituents of the carboxy derivatives **2n**,**p**,**r** causes a high-frequency shift (by $\sim$15 cm^{-1}) of the NH vibration band compared to that in the spectrum of the carboxy derivative **2b**. The larger the electron density on the nitrogen atom, the higher the vibration frequency.

Compound	Charges on atoms (arb.u.)				
	N(1)	C(2)	C(3)	C(4)	C(5)
1a	0.337	−0.315	−0.162	−0.164	−0.309
2a	0.368	−0.296	−0.159	−0.101	−0.331
2b	0.425	−0.279	−0.184	−0.068	−0.358
2f	0.339	−0.312	−0.133	−0.133	−0.312
2w	0.387	−0.305	−0.164	−0.164	−0.311

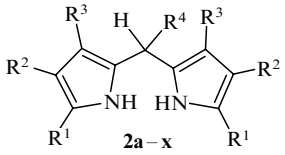

2a–**x**

Compound **2**	R^1	R^2	R^3	R^4
a	CO_2Et	Me	Me	H
b	CO_2H	Bu^n	Me	H
c	CO_2Et	Et	Me	H
d	CO_2Et	Bu^n	Me	H
e	H	Me	Me	H
f	CO_2Et	H	Me	H
g	H	Me	Bu^n	H
h	CO_2H	Me	Bu^n	Ph
i	CO_2H	Bu^n	Me	Ph
j	COH	Me	Bu^n	Ph
k	CO_2Et	Bu^n	Me	Ph
l	CO_2Et	Me	Bu^n	Ph
m	H	Me	Bu^n	4-$MeOC_6H_4$
n	CO_2H	Me	Bu^n	4-$MeOC_6H_4$
o	H	Me	Bu^n	3-$MeOC_6H_4$
p	CO_2H	Me	Bu^n	3-$MeOC_6H_4$
q	H	Me	Bu^n	2-$MeOC_6H_4$
r	CO_2H	Me	Bu^n	2-$MeOC_6H_4$
s	H	Me	Bu^n	4-$NO_2C_6H_4$
t	CO_2H	Me	Bu^n	4-$NO_2C_6H_4$
u	H	Me	Bu^n	3-$NO_2C_6H_4$
v	CO_2H	Me	Bu^n	3-$NO_2C_6H_4$
w	H	H	H	Ph
x	H	H	H	H

The intense band at 3100 cm^{-1} was assigned[12] to CH stretching vibrations of pyrrole [C(α)–H stretching vibrations]. The formation of the dipyrrole structure is accompanied by the high-frequency shift of this band by $\sim$20 cm^{-1} (see Table 3). The introduction of the aryl substituent at the *meso* position of dipyrrolylmethane has virtually no effect on CH vibrations of the pyrrole rings. The spectral characteristics of the positional isomers **2h**,**i** are very similar (see Table 4).

The intense band at 1350 cm^{-1} and the medium intensity band at 1530 cm^{-1} belong to skeletal vibrations of pyrrole. In the dipyrrolylmethane **2w**, the C–C vibration frequency of the pyrrole fragment is shifted to the low-frequency region by $\sim$5 cm^{-1}. Alkylation of the pyrrole rings and the replacement

Table 3. Positions of the absorption maxima (cm^{-1}) in the IR spectra of the pyrrole **1a** and the dipyrrolylmethanes **2c**–**g**,**m**,**o**,**q**,**s**,**u**,**w**,**x**.[12–14]

Compound	ν(NH)		ν(CH)		ν(C–C)[a]		ν(C–C)[b]	
	A	B	A	B	A	B	A	B
1a	3491	3495	3100, 3133	3100, 3130	1355, 1530	1350, 1530	–	–
2c	3448	3452	3124	3120	1335, 1517	1335, 1520	1364	1370
2d	3436	3432	3122	3125	1333, 1514	1330, 1525	1362	1370
2e	3446	3444	3123	3120	1330, 1507	1335, 1520	1364	1375
2f	3433	3430	3122	3125	1325, 1510	1330, 1520	1360	1380
2g	3434	3440	3123	3120	1325, 1512	1330, 1530	1360	1380
2m	3428	3430	3121	3120	1328, 1518	1330, 1530	1358	1360
2o	3432	3430	3121	3120	1324, 1520	1325, 1540	1358	1360
2q	3426	3421	3120	3122	1325, 1515	1330, 1525	1360	1365
2s	3448	3442	3122	3124	1326, 1521	1330, 1527	1362	1368
2u	3442	3440	3124	3128	1328, 1518	1330, 1530	1360	1360
2w	3438	3440	3124, 3166	3129, 3170	1346, 1525	1350, 1540	1362	1370
2x	3453	3455	3122, 3160	3122, 3160	1345, 1524	1330, 1530	1359	1360

Note. Here and in Tables 4 and 5, the calculated and experimental (in KBr pellets) spectra are denoted by A and B, respectively.
[a] Stretching vibrations of the pyrrole fragment; [b] stretching vibrations of the methine bridge.

Table 4. Positions of the absorption maxima (cm^{-1}) in the IR spectra of the dipyrrolylmethanes **2b**,**h**–**l**,**n**,**p**,**r**,**t**,**v**.[15, 16]

Compound **2**	ν(NH)		ν(C–C) [a]		ν(C–C) [b]		ν(C=O)
	A	B	A	B	A	B	B
b	3416	3412	1310, 1520	1315, 1520	1354	1360	1675
h	3418	3410	1318, 1512	1321, 1510	1350	1358	1670
i	3421	3427	1320, 1522	1326, 1510	1354	1357	1685
j	3438	3435	1323, 1517	1332, 1510	1350	1355	1670
k	3444	3440	1322, 1520	1330, 1510	1350	1360	1675
l	3452	3445	1326, 1525	1330, 1514	1356	1360	1680
n	3430	3427	1330, 1515	1335, 1520	1360	1366	1685
p	3432	3429	1324, 1522	1330, 1530	1362	1365	1680
r	3433	3427	1320, 1524	1324, 1520	1356	1350	1690
t	3429	3434	1324, 1618	1329, 1522	1340	1342	1675
v	3433	3438	1319, 1520	1324, 1530	1342	1340	1678

[a] Stretching vibrations of the pyrrole fragment; [b] stretching vibrations of the methine bridge.

of one of the *meso*-hydrogen atoms by the aryl group are accompanied by an increase in this shift (see Tables 3 and 4). The presence of electron-withdrawing substituents at positions 5 and 5′ of dipyrrolylmethane leads to lowering of the ν(C–C) frequency of the pyrrole fragment compared to that in the spectrum of unsubstituted dipyrrolylmethane.

Calculations of the spectra of dipyrrolylmethanes demonstrated that the intense band in the region of 1340–1365 cm^{-1} corresponds to C–C vibrations of the methane bridge. The presence of the electron-withdrawing nitro groups in the aryl *meso*-substituents leads to a substantial increase in the intensity of this band.

On going from pyrroles to dipyrrolylmethanes, the C=O, C–O and C–OH vibrations remain characteristic and allow the identification of the dipyrrolylmethane synthesised. It can be seen from the data presented in Tables 1–4 that the IR spectra of pyrroles differ substantially from those of dipyrrolylmethanes. The involvement of pyrrole in the open conjugated system of hexamethyldipyrrolylmethene as well as in the cyclic octamethylporphyrinogen system [7] is accompanied by further complications of the spectra. However, the most pronounced effect is observed when pyrrole is involved in the conjugated porphyrin macrocycle.

3. Porphyrins

The effects caused by an increase of the molecular symmetry (for example, upon formation of metal complexes) or its lowering (for example, in the case of introduction of substituents in the macrocycle) are manifested in the IR spectra of porphyrins along with the changes in stretching vibration frequencies.

When studying these effects, it is useful to consider two series of compounds: (1) porphyrins containing the hydrogen atoms at the *meso* positions of the macrocycle and substituents at the β positions of the pyrrole fragments and (2) porphyrins containing substituents at the *meso* positions and the hydrogen atoms at the β positions of the pyrrole fragments.

The IR spectra of β-alkylated porphyrins **3a**–**w** in which two and four *meso*-hydrogen atoms are successively replaced by the alkyl (CH_3–C_6H_{13} or $C_{11}H_{23}$), phenyl or aryl (C_6H_4X, X = H, 4-OMe, 3-OMe, 2-OMe, 4-NO_2 or 3-NO_2) substituents were investigated.[14, 17–21]

The geometric and energy parameters of the porphyrin molecules corresponding to the energy minima are summarised in the studies.[22, 23] The experimental vibration frequencies of the porphyrins **3a**–**w** and those calculated by the PM3 method are given in Table 5. The *meso*-alkyl substituents in the porphyrins **3a**–**g** can adopt various conformations. However, calculations by the semiempirical PM3 method demonstrated [24] that the extended zigzag chain typical of n-alkanes in the crystalline state is a preferential conformation of the alkyl substituents. The cisoid and transoid relative arrangements of the alkyl substituents at positions 5 and 15 are equally probable. The corresponding conformers shown in Fig. 1 *a*,*b* have equal energies of steric strain (365 kJ mol^{-1}). The *meso*-phenyl or *meso*-aryl substituents in the porphyrins **3h**–**s** are located perpendicular to the plane of the porphyrin macrocycle (Fig. 1 *c*,*d*).[22]

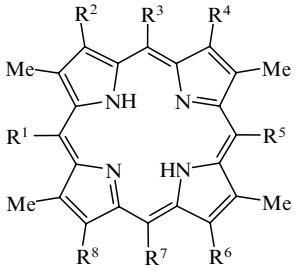

3a–**w**

Compound **3**	R^1, R^5	R^2, R^4, R^6, R^8	R^3, R^7
a	Me	Me	H
b	Et	Me	H
c	Pr^n	Me	H
d	Bu^n	Me	H
e	C_5H_{11}	Me	H
f	C_6H_{13}	Me	H
g	$C_{11}H_{23}$	Me	H
h	Ph	Bu^n	H
i	4-$OMeC_6H_4$	Bu^n	H
j	3-$OMeC_6H_4$	Bu^n	H
k	2-$OMeC_6H_4$	Bu^n	H
l	4-$NO_2C_6H_4$	Bu^n	H
m	3-$NO_2C_6H_4$	Bu^n	H
n	H	Bu^n	Ph
o	H	Bu^n	4-$OMeC_6H_4$
p	H	Bu^n	3-$OMeC_6H_4$
q	H	Bu^n	2-$OMeC_6H_4$
r	H	Bu^n	4-$NO_2C_6H_4$
s	H	Bu^n	3-$NO_2C_6H_4$
t	H	Bu^n	H
u	Et	Me	Ph
v	C_6H_{13}	Me	Ph
w	C_6H_{13}	Me	4-$OMeC_6H_4$

The out-of-plane CH deformation vibrations of porphyrins are observed in the region of 830–850 cm^{-1}. Among these are the CH vibrations of the pyrrole rings and methine bridges of the macrocycle. The γ(CH) vibration frequency of the pyrrole fragments of porphyrins increases compared to the corresponsing frequency in the spectrum of pyrrole as the interactions between

Table 5. The NH and CH vibration frequencies (cm^{-1}) of the porphyrin ring in the β-octaalkylporphyrins **3a**–**w**.[14, 17, 24]

Compound **3**	ν(NH)		δ(NH)		γ(NH)		ν(CH) [a]		δ(CH) [b]		γ(CH) [c]	
	A	B	A	B	A	B	A	B	A	B	A	B
a	3348	3346	980	960	708	695	3022	3027	1507	1502	830	832
b	3343	3342	974	963	707	695	3011	3016	1487	1497	825	832
c	3342	3340	986	964	710	700	3002	3008	1483	1491	829	834
d	3346	3345	992	970	712	700	2942	2940	1479	1484	835	836
e	3348	3346	1001	978	714	705	2926	2920	1480	1486	831	836
f	3347	3348	991	984	715	705	2907	2900	1478	1489	832	837
g	3352	3350	1003	980	721	710	2906	2880	1477	1486	833	838
h	3323	3320	992	980	720	700	2960	2960	1485	1488	840	842
i	3321	3315	1007	990	714	709	3006	3000	1484	1490	845	849
j	3323	3318	974	965	717	702	2984	2980	1478	1487	840	845
k	3332	3320	970	960	710	700	2970	2962	1481	1486	839	844
l	3325	3310	994	985	715	710	3025	3030	1494	1500	850	853
m	3332	3320	996	980	719	705	2994	2990	1479	1485	845	848
n	3327	3327	997	960	700	690	2884	2990	1490	1489	830	840
o	3318	3315	1005	986	718	706	2986	3010	1490	1500	845	850
p	3328	3320	994	978	704	690	3012	2940	1479	1485	830	840
q	3330	3324	981	970	705	690	2942	2920	1492	1500	849	852
r	3319	3310	1002	990	721	710	2931	3020	1493	1500	842	846
s	3336	3324	994	980	731	704	3014	2995	1479	1486	839	844
t	3338	3335	990	984	714	702	2994	2980	1476	1484	835	844
u	3342	3325	1010	974	728	710	3007	3060	1492	1500	–	–
v	3340	3328	1013	982	730	705	3028	3048	1484	1496	–	–
w	3347	3330	1017	990	728	700	3020	3035	1480	1492	–	–

[a] Stretching vibrations of the alkyl groups; [b] deformation vibrations of the alkyl groups; [c] out-of-plane deformation vibrations of the methine bridges.

the C(β)–C(β) bonds and the π-system of the macrocycle are weakened due to the introduction of alkyl or aryl substituents.

In the spectra of β-unsubstituted porphyrins (*meso*-tetraalkyl- and -tetraphenylporphyrins), an intense band in the region of 772–805 cm^{-1} corresponds to γ(CH) vibrations. This band is absent in the spectra of octamethyl-, octaethyl-, dodecaalkyl- and dodecaphenylporphyrins.[25–27] The γ(CH) vibration frequency depends substantially on the presence of substituents at the *meso* positions of the macrocycle. Thus, the bands at 772 and 780 cm^{-1} correspond to these vibrations in the spectra of porphyrin and *meso*-tetra(*iso*-butyl)porphyrin, respectively. This effect is more pronounced in the spectrum of tetraphenylporphyrin in which the γ(CH) vibration band is observed at 797 cm^{-1}.[25]

In the IR spectrum of 2,8,12,18-tetrabutyl-3,7,13,17-tetramethylporphyrin (**3t**), out-of-plane C(β)–H deformation vibration bands are absent, whereas an intense band at 835 cm^{-1} belongs to γ(CH) vibrations of the *meso*-hydrogen atoms (see Table 5). This band is absent in the spectra of the 5,15-dialkyl-10,20-diphenylporphyrins **3u**–**w**, whereas it is observed in the region of ~830–850 cm^{-1} in the spectra of the 5,15-dialkyl- and 5,15-diaryl-β-octaalkylporphyrins **3a**–**m**.

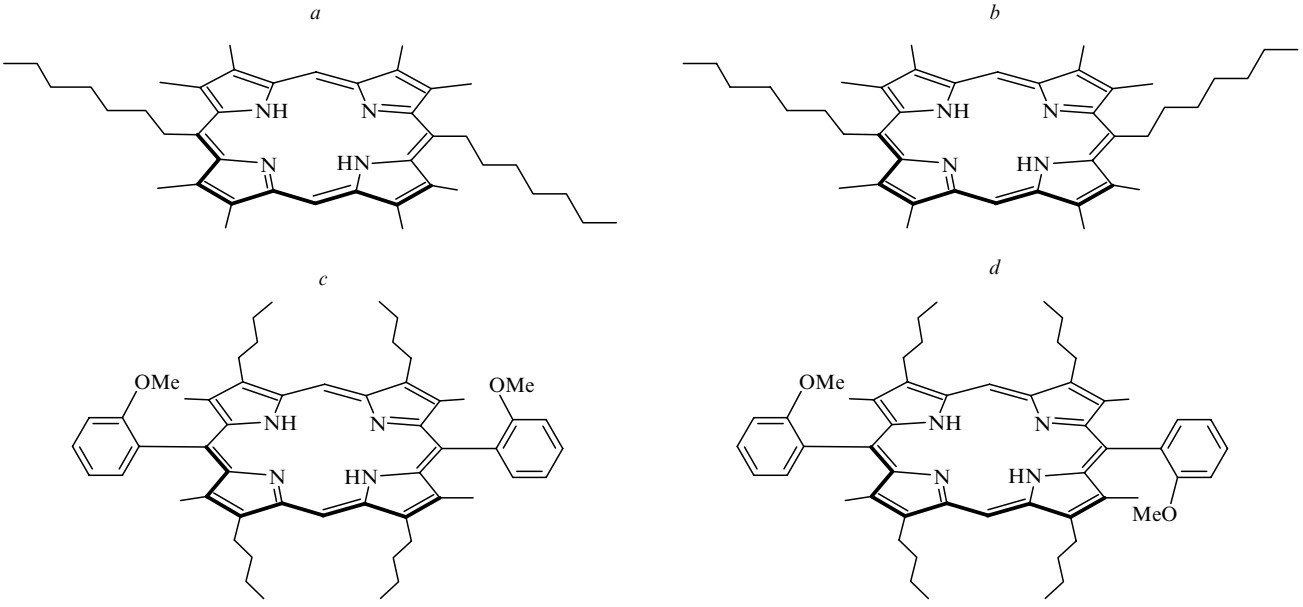

Figure 1. Cisoid (*a*) and transoid (*b*) conformers of 5,15-di-n-heptyl-2,3,7,8,12,13,17,18-octamethylporphyrin and the atropoisomers [α,α (*c*) and α,β (*d*)] of 2,8,12,18-tetrabutyl-5,15-di(2-methoxyphenyl)-3,7,13,17-tetramethylporphyrin.[22]

Table 6. The CH vibration frequencies (cm^{-1}) of the phenyl groups in the diphenyl(aryl)octaalkylporphyrins **3h**–**m**,**o**–**w** (in KBr pellets).[4, 18]

Compound **3**	γ(C(1)–H)	γ(C(2)–H)	γ(C(3)–H)	γ(C(4)–H)	γ(C(5)–H)	δ(CH)
h	–	–	–	–	745	1170, 1050
i	–	840	–	–	–	1174, 1065
j	870	–	780	–	–	1164, 1060
k	–	–	–	750	–	1179, 1050
l	–	846	–	–	–	1185, 1069
m	890	–	785	–	–	1162, 1071
o	–	844	–	–	–	1180, 1068
p	874	–	782	–	–	1170, 1067
q	–	–	–	754	–	1180, 1055
r	–	848	–	–	–	1184, 1073
s	896	–	787	–	–	1170, 1068
u	–	–	–	–	747	1172, 1060
v	–	–	–	–	750	1178, 1050
w	–	840	–	–	–	1174, 1075

Since the out-of-plane deformation vibrations of the adjacent CH bonds of the phenyl fragments, which occur in phase, strongly interact with each other, the positions of the corresponding bands in the spectra depend on the number of the above-mentioned bonds. These bands are intense and can be used for the determination of the position of the substituent in the phenyl fragment (Table 6).

The spectra of the 5,15-diphenylporphyrins **3h**,**n** have an intense band at 745 cm^{-1} due to interactions between five adjacent CH bonds (for example, in monosubstituted benzene).[25] The spectra of the di(*meta*-R-phenyl)porphyrins **3j**,**m**,**p**,**s** have bands in the regions of 780–787 cm^{-1} (three adjacent CH bonds) and 870–896 cm^{-1} (one CH bond). The spectra of the di(*ortho*-R-phenyl)porphyrins **3k**,**q** have a band at ~750 cm^{-1} (four adjacent CH bonds), whereas the spectra of the di(*para*-R-phenyl)porphyrins **3i**,**l**,**o**,**r** have a band in the region of 840–848 cm^{-1} (two adjacent CH bonds) (see Table 6).

The identification of in-plane CH deformation vibrations presents a more complicated problem. The bands in the region of 964–1060 cm^{-1} are generally assigned[28] to δ(CH) vibrations of the pyrrole fragments of porphyrins. These bands are observed as two narrow closely spaced intense bands. The spectra of β-octaalkylporphyrins have no intense bands in this region. The medium intensity bands in the region of 1484–1500 cm^{-1} belong to δ(CH) vibrations of alkyl groups. Their positions remain virtually unchanged as the length of the alkyl substituent increases (see Table 5). The in-plane CH deformation vibrations of the phenyl fragments are observed in the region of 1000–1300 cm^{-1}.[25] In the spectra of *meso*-diphenyloctaalkylporphyrins, these vibrations are observed as medium intensity bands at 1170 and 1050 cm^{-1}, which are insignificantly shifted upon introduction of electron-withdrawing or electron-donating substituents into the benzene rings (see Table 6). The spectra of the positional isomers **3h**,**n** are similar. In the spectra of tetraphenylporphyrins, the *ν*(CH) vibrations of the phenyl substituents are observed at 3100 cm^{-1}. Therefore, it is conceivable that the band at 3000 cm^{-1} has a complex nature because the CH vibrations of both the porphyrin and benzene rings are observed in this region. The spectra of the β-alkylated porphyrins **3a**–**m**,**u**–**w** have bands in the region of 2940 cm^{-1}, which, apparently, belong to CH stretching vibrations of the alkyl groups.

The skeletal vibrations of the porphyrin ring are observed in the region of 1100–1250 cm^{-1}.[24, 26] The IR spectra of the β-octaalkylporphyrin **3t** and the 5,15-dialkyl-β-octamethylporphyrins **3a**–**g** have several medium intensity bands in this region. The assignment of the skeletal vibration bands in the spectra of *meso*-phenyl-substituted porphyrins is hampered by the fact that vibrations of the porphyrin ring overlap with those of the benzene fragments. The bands in the region of 1350–1600 cm^{-1} were assigned to *ν*(C–C) vibrations of the benzene rings.[26] In the spectrum of *meso*-tetraphenylporphyrin, these vibrations are manifested as three rather weak bands (at 1489, 1570 and 1590 cm^{-1}) whose intensities become higher as the frequency increases. It is known[29] that the ratio of the intensities of these bands in the spectra of functional benzene derivatives is determined by the presence or absence of conjugation between the phenyl fragments and functional groups. In the spectrum of *meso*-tetraphenylporphyrin, alternation of the intensities of the bands is analogous to that observed in the spectrum of biphenyl.

Chemical modifications of the phenyl substituents in *meso*-phenyl-substituted porphyrins exert a substantial effect on the skeletal vibrations of the macrocycle.[25, 26] Tetra(*ortho*- and *meta*-R-phenyl)porphyrins exist as two atropoisomers due to which the band at 1200 cm^{-1} is split. The spectra of tetra(*para*-R-phenyl)-porphyrins have one intense band at about 1100 cm^{-1}, which is shifted to the low-frequency region in parallel with the increase in the mass of the substituent. The spectra of the di(*ortho*- and *meta*-R-phenyl)porphyrins **3j**,**k**,**m**,**p**,**q**,**s** have a pronounced doublet at 1200 cm^{-1}, whereas the spectra of the *para*-derivatives **3i**,**l**,**o**,**r** show an intense band at 1100 cm^{-1} (for the nitro derivatives) or at 1180 cm^{-1} (for the methoxy derivatives).

Since the nitrogen atoms in porphyrins are more electronegative than those in pyrroles, the N–H bond length (90 pm) in porphyrins is 10% smaller than that in pyrrole. Because of this, the bands at 719 and 725 cm^{-1} (which are 160 cm^{-1} higher than those in the case of pyrrole) are assigned to out-of-plane γ(NH) deformation vibrations of the porphyrin molecule, while the bands at 970 and 980 cm^{-1} (which are 160 cm^{-1} lower than those in the case of pyrrole) are assigned to in-plane δ(NH) deformation vibrations.[26, 30] The validity of this assignment is additionally confirmed by the absence of the corresponding bands in the spectra of metalloporphyrins. In the spectra of the β-octaalkylporphyrins **3a**–**w**, the γ(NH) and δ(NH) vibrations are observed in the regions of 690–710 and 960–990 cm^{-1}, respectively (see Table 5).The positions of the bands change only slightly upon *meso*-substitution. No relationship between the effects of the substituents (OMe or NO_2) in the benzene rings of the porphyrins **3i**–**m**,**o**–**s** and the NH deformation vibration frequencies was revealed.

The NH stretching vibrations of porphyrins are characteristic and their identification presents no problems. The *ν*(NH) frequency of porphyrins is ~190 cm^{-1} lower than that of pyrrole because the electron density is transferred from the pyrrole fragments to the macrocyclic aromatic π system, the lowering of the *ν*(NH) vibration frequency being accompanied by stabilisation of the porphyrin anion. Further lowering of the stretching vibration frequency (by ~15 cm^{-1}) and stabilisation of the porphyrin anion (*i.e.*, an increase of the acid ionisation constant) occur as the aromaticity increases in the porphyrin–tetraazaporphyrin–phthalocyanine series (Table 7).

Table 7. Frequencies of NH symmetrical stretching vibrations and the first-stage acid ionisation constants (K_1) for porphyrins in DMSO solutions.[7]

Porphyrin	ν(NH) /cm^{-1}	pK_1
Porphin	3305	22.35 ± 0.02
Octamethylporphyrin	3311	–
meso-Tetraphenylporphyrin	3315	21.15 ± 0.03
Tetrabenzoporphyrin	3305	18.53 ± 0.05
Tetraazaporphyrin	3300	12.36 ± 0.18
Phthalocyanine	3290	10.73 ± 0.03
Mesoporphyrin	3315	–
Deuteroporphyrin	–	25.30 ± 0.04

The ν(NH) frequency becomes higher on both deep alkylation and hydrogenation of porphyrins due to an increase of the electron density on the nitrogen atoms. The ν(NH) vibration band in the spectrum of the octaalkylporphyrin **3t** is shifted to the high-frequency region by ~ 30 cm^{-1} compared to that in the spectrum of porphyrin. This effect is further enhanced (by ~ 10 cm^{-1}) in the presence of the electron-donating alkyl substituents ($CH_3-C_6H_{13}$ or $C_{11}H_{23}$) at the *meso* positions of the macrocycle. At the same time, the introduction of aryl substituents at the *meso* positions leads to the low-frequency shift (by ~ 15 cm^{-1}) of the ν(NH) vibration bands compared to the analogous band observed in the spectrum of the porphyrin **3t** (see Table 5).

4. Metalloporphyrins

The molecular symmetry of metalloporphyrins is higher than that of porphyrins due to the replacement of two hydrogen atoms in the coordination centre of the porphyrin ligand by the metal atom and equalisation of the geometric parameters of the pyrrole fragments in metal complexes. Changes in the geometric parameters of the porphyrin molecule upon complex formation are clearly manifested in the IR spectra. Thus, the number of absorption bands decreases and their symmetry and resolution increase. These facts are associated with degeneration of the energies of particular types of vibrations as the molecular symmetry becomes higher.[2, 31–33]

In the spectra of metalloporphyrins, the following NH absorption bands disappear first: the NH stretching vibration bands in the region of 3345–3360 cm^{-1} and the NH deformation vibration bands in the regions of 720–740 and 960–980 cm^{-1}.[2, 7] In the spectra of mesoporphyrin **4a**, protoporphyrin **4b**, deuteroporphyrin **4c** and hematoporphyrin **4d**, the fingerprint region where the skeletal vibrations of the porphyrin molecule are located is most sensitive to the introduction of the metal atom.[34]

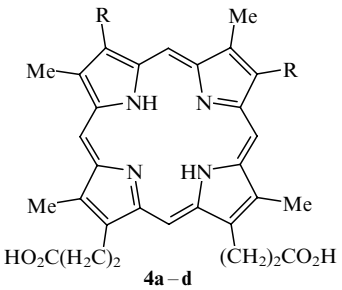

4a–d

R = Et (**a**), CH=CH$_2$ (**b**), H (**c**), CH(Me)OH (**d**).

The formation of metalloporphyrin from porphyrin leads to sharp changes in the intensities of the bands in the regions of 675–683 (I) and 705–711 cm^{-1} (II). A substantial decrease in the intensity of the band I is accompanied by an increase in the intensity of the band II. The positions of these bands depend only slightly on the nature of the metal atom. Other skeletal vibrations of the pyrrole rings of porphyrin are less sensitive to the introduction of the metal atom into the coordination centre of the molecule.

All absorption bands caused by vibrations of the peripheral substituents of porphyrin are weakly sensitive to the introduction of the metal atom. Thus, the intense band at 900 cm^{-1} observed in the spectrum of the protoporphyrin **4b** is retained on complex formation with divalent metals. On going to the porphyrin complex with Mn(III), the relative intensity of this band decreases, but its position remains unchanged. Analogous situations are observed for the complexes of the mesoporphyrin **4a** and the hematoporphyrin **4d**.[34] The presence of at least two free β positions in the pyrrole rings of porphyrin leads to substantial changes in the spectral pattern. Thus, the number of the bands in the region of 900–1000 cm^{-1} in the spectra of complexes of the deuteroporphyrin **4c** is smaller and their intensities are higher compared to those observed in the spectrum of the ligand.

The changes in the IR spectra of porphyrins on complex formation with divalent metals depend on the nature of the metal atom (Tables 8 and 9). However, the most substantial changes in the spectral characteristics of the porphyrin complexes are observed in the case of polyvalent metal ions. The formation of these complexes results in essential changes in the structure and symmetry of the metalloporphyrin molecule due to the displacement of the cation from the plane of the macrocycle.[7, 35]

In the case of *meso*-tetraphenylporphyrin complexes, the most essential changes associated with complex formation are observed in the region of the spectrum where the out-of-plane γ(CH) deformation vibrations of the pyrrole ring are manifested (~ 800 cm^{-1}).[25] The IR spectrum of *meso*-tetraphenylporphyrin has three bands in this region (at 783, 797 and 810 cm^{-1}), the intensities of the first and third bands being equal and low. The band at 797 cm^{-1} is the most intense one. In the spectrum of the corresponding metalloporphyrin, the band at 783 cm^{-1} disappears, the intensity of the band at 810 cm^{-1} decreases sharply and the latter is shifted to the high-frequency region due, apparently,

Table 8. Positions of absorption maxima (cm^{-1}) in the IR spectra of the porphyrin complexes **4a–d**.[7, 34]

Compound **4**	Complexes with				
	Zn	Cu	Co	Pd	Mn[a]
a	831	832	832	834	839
	896	897	897	898	898
	950	951	951	952	958
	982	980	985	987	989
	1193	1194	1194	1194	1195
	1435	1433	1432	1433	1434
b	835	833	834	835	838
	900	898	902	902	917
	947	948	948	950	958
	984	987	990	992	993
	1193	1196	1200	1200	1200
	1434	1433	1435	1434	1435
c	833	833	833	834	850
	898	989	898	900	920
	950	952	952	954	956
	981	984	983	984	989
	1200	1200	1200	1200	1205
	1434	1437	1437	1438	1437
d	834	832	832	834	837
	928	920	928	832	930
	952	952	954	956	955
	982	982	984	985	990
	1193	1002	1203	1208	1210
	1433	1433	1433	1432	1433

[a] Porphyrin–Mn(Cl) complexes.

Table 9. Positions of absorption maxima (cm^{-1}) in the IR spectra of *meso*-tetraaryl-substituted porphyrin complexes.[20,25]

Substituent in the benzene ring	Complexes with				
	Zn	Ni	Co	Cu	Mg
H	737	752	740	745	735
	802	809	802	797	800
	971	980	974	977	982
	1070	1079	1073	1070	1075
	1171	1166	1176	1173	1164
2-OMe	742	758	747	751	740
	805	808	803	798	801
	994	1007	996	1000	1004
	1050	1050	1051	1049	1055
	1182	1184	1181	1179	1183
3-OMe	771	785	776	781	774
	806	810	808	803	800
	847	864	852	860	855
	1005	1009	1005	1003	1002
	1076	1092	1084	1080	1079
	1172	1155	1165	1162	1166
4-OMe	794	811	800	804	792
	850	854	844	840	853
	990	1001	993	998	995
	1110	1107	1109	1107	1109
	1174	1186	1178	1174	1174
2-Me	740	752	743	747	738
	811	816	809	804	810
	993	999	995	998	990
	1055	1067	1054	1051	1056
	1182	1176	1183	1181	1188
3-Me	770	784	773	776	768
	892	899	890	885	890
	790	792	792	799	789
	1001	1005	1001	1003	1000
	1107	1107	1100	1092	1083
	1155	1186	1153	1151	1164
4-Me	787	804	792	796	789
	854	859	852	847	852
	996	1007	999	1003	1001
	992	998	996	999	990
	1110	1090	1112	1108	1109
	1188	1175	1183	1180	1174

to the fact that complex formation leads to lowering of the electron density in the macrocycle.

The high-frequency shift of the band at 797 cm^{-1} is observed in the spectra of porphyrin complexes with polyvalent metal ions. In the case of Mo(V) and W(V), this band is observed at 805 cm^{-1}.[36] Apparently, the shift of the band at 797 cm^{-1} in the spectra of complexes with polyvalent ions is associated with the geometric characteristics of these complexes in which the metal ion deviates substantially from the plane of the molecule. The noncoplanar arrangement of the metal atom reduces the possibility of transfer of the σ- and π-electron density from the nitrogen atom to the metal atom as a result of which the complexes should be destabilised.

Complex formation causes substantial changes in the frequencies and intensities of the bands in the region of 964–1030 cm^{-1} where the in-plane δ(CH) deformation vibrations of the pyrrole fragments of the porphyrin molecule are manifested. It is worthy of note that the intensity of the band at 1003 cm^{-1} in the spectrum of *meso*-tetraphenylporphyrin rises sharply upon complex formation. Koifman[34] believed that this band is associated with two types of vibrations of the pyrrole fragments, *viz*., with in-plane δ(CH) deformation vibrations and ν[C(β)–C(β)] stretching vibrations. As mentioned above, the introduction of electron-withdrawing substituents into the pyrrole ring results in a more substantial change in the dipole moment of the molecule in the course of vibration. This leads to significant changes (generally, to a rise) in the intensities of the out-of-plane and in-plane CH deformation vibration bands. By analogy, the increase in the intensity of the band at 1003 cm^{-1} in the spectrum of *meso*-tetraphenylporphyrin can be related to the electron density redistribution in the molecule upon complex formation. Apparently, the δ(CH) vibrations make the major contribution to this absorption band.

Complex formation with *meso*-tetraaryl-substituted porphyrins as well as the change of the metal atom lead to substantial changes in the region of 690–758 cm^{-1} (see Table 9) in which two out-of-plane deformation vibration bands of the aryl groups are observed. The position of one band depends on the nature of the metal atom and changes from 690 to 708 cm^{-1}.[20,25] The second band belongs to the most intense bands manifested in the IR spectra of metal complexes and is observed in the region of 732–758 cm^{-1}. The frequencies and intensities of the ν(C–C) stretching vibration bands of the benzene rings are also changed substantially upon complex formation. Thus, two intense bands appear instead of three medium intensity bands in the region of 1430–1590 cm^{-1}. It was noted[37] that the changes in the electronic structure of the *p* and *d* shells of the metal atom as well as the changes in the geometric parameters of the coordination centre caused by complex formation have no effect on the position and intensity of the ν(C–C) band (1590 cm^{-1}) in the spectrum of *meso*-tetraphenylporphyrin. Hence, there is no clear correlation between the electronic structure of the coordination centre and the ν(C–C) vibration frequency. However, it can be stated that the C–H and C–C vibrations of the benzene rings depend on the change in the symmetry of the π system of the macrocycle due to complex formation.

The spectral characteristics of the complexes of 2,8,12,18-tetrabutyl-3,7,13,17-tetramethylporphyrin (**3t**) and its *meso*-di-(**3a**–**c**,**g**–**m**) and -tetrasubstituted derivatives (**3u**,**w**) with Zn, Cu and Ni[38] are given in Table 10. Complex formation leads to the disappearance of the NH vibration bands in the IR spectra and to a decrease in the number of the bands in the regions where C–C vibrations of the pyrrole and benzene rings are manifested. In the case of both protoporphyrin and deuteroporphyrin, the spectral characteristics are less affected by the introduction of the metal ion into the coordination centre of the porphyrin molecule. However, the changes are comparable with those observed on coordination of *meso*-tetraphenylporphyrin.

The region about ~1000 cm^{-1} in which the metal-sensitive bands are most pronounced is of particular interest. The spectra of all complexes have three bands at ~980, 955 and 910 cm^{-1}, the positions of the first and third bands being dependent on the nature of metal.[27,38] The high-frequency shifts of these bands increase in the series Zn < Cu < Ni. It should be noted that the above-mentioned sequence corresponds to the hypsochromic shifts of the absorption bands in the electronic absorption spectra of the complexes of **3a**–**c**,**g**–**m**,**t**,**u**,**w** (see Table 10).[39] The bands at 955 and 910 cm^{-1} in the IR spectrum of the copper complex of octaethylporphyrin belong to deformation vibrations of the alkyl groups, which is confirmed by the absence of these bands in the spectrum of the copper complex of porphyrin.[34] The band at 980 cm^{-1} may be assigned to deformation vibrations of the porphyrin ring. An analogous assignment was made for the copper complex of octaethylporphyrin.[25]

The CH vibration frequencies of the methine bridges in the *meso*-unsubstituted (**3t**) and the *meso*-disubstituted β-octaalkylporphyrins (**3a**–**s**) depend substantially on the nature of the metal ion.[27] These frequencies at 3110, 1220 and 835 cm^{-1} belong to stretching and deformation (in-plane and out-of-plane) CH vibrations, respectively. The positions of the absorption maxima of the CH deformation vibrations of the methine bridges in porphyrins are given in Table 10. The stronger the coordination of the metal atom and the higher its electronegativity, the larger the high-frequency shift. The in-plane deformation vibrations depend on

Table 10. Positions of absorption maxima in the IR (cm^{-1}) and electronic absorption (nm) spectra of the β-octaalkylporphyrin complexes **3a–c,g–m,t,u,w**.[38,39]

Compound **3**	ν [a] for complexes with			$\lambda_{max}(\log\varepsilon)$ [b] for complexes with			Compound **3**	ν [a] for complexes with			$\lambda_{max}(\log\varepsilon)$ [b] for complexes with		
	Zn	Cu	Ni	Zn	Cu	Ni		Zn	Cu	Ni	Zn	Cu	Ni
a	834	835	836	570(3.66)	568(3.58)	556(3.42)	**k**	839	840	841	574(3.86)	570(3.90)	569(3.82)
	917	925	929	537(3.78)	534(3.74)	526(3.18)		912	920	924	540(4.29)	538(4.19)	535(4.26)
	977	982	989	409(4.63)	408(4.56)	398(4.17)		986	994	999	413(5.31)	410(5.17)	408(5.20)
	1217	1220	1226					1226	1228	1232			
b	836	837	838	570(3.65)	568(3.60)	510(3.45)	**l**	840	842	843	574(3.78)	572(3.70)	568(3.81)
	918	924	927	538(3.78)	535(3.42)	526(3.15)		907	912	921	541(4.30)	539(4.25)	536(4.20)
	982	987	992	409(4.62)	408(4.48)	398(4.20)		982	988	911	413(5.27)	410(5.20)	406(5.31)
	1231	1236	1239					1207	1214	1219			
c	835	836	837	572(3.64)	568(3.62)	558(3.38)	**m**	846	846	847	574(3.59)	570(3.59)	567(3.72)
	918	925	929	538(3.74)	536(3.42)	526(3.19)		918	924	928	540(4.17)	538(4.09)	536(4.01)
	982	988	994	410(4.61)	409(4.50)	398(4.18)		985	990	996	414(5.34)	412(5.41)	410(5.39)
	1233	1238	1242					1234	1240	1244			
g	836	836	838	572(3.60)	569(3.64)	558(3.40)	**t**	834	835	836	569(3.95)	569(3.86)	557(3.91)
	922	926	932	539(3.75)	535(3.50)	525(3.19)		911	918	922	538(3.62)	534(3.54)	526(3.60)
	984	987	995	411(4.58)	409(4.50)	397(4.19)		986	991	997	403(5.21)	399(5.17)	396(5.14)
	1234	1239	1246					1228	1231	1237			
h	836	837	838	575(3.99)	573(3.87)	570(3.79)	**u**	838	838	839	578(3.67)	576(3.60)	572(3.60)
	912	919	923	541(4.26)	539(4.31)	536(4.28)		912	917	920	544(3.82)	542(3.80)	539(3.84)
	980	985	992	412(5.01)	410(5.08)	408(5.13)		988	992	997	420(4.91)	418(4.90)	414(4.89)
	1220	1223	1229					1223	1227	1234			
i	840	842	843	573(3.96)	571(3.91)	569(3.90)	**w**	837	837	839	582(3.62)	580(3.69)	578(3.60)
	916	923	925	540(4.26)	538(4.31)	536(4.40)		915	920	924	547(3.80)	544(3.78)	542(3.81)
	980	986	992	411(5.08)	409(5.11)	406(5.21)		986	990	995	422(4.92)	420(4.94)	416(4.89)
	1222	1225	1231					1225	1228	1233			
j	838	839	840	574(3.87)	571(3.80)	5.68(3.92)							
	910	916	920	540(4.30)	537(4.38)	535(4.36)							
	988	994	998	413(5.20)	411(5.13)	409(5.27)							
	1209	1215	1220										

[a] In KBr pellets; [b] a solution in chloroform.

the nature of the metal atom more strongly than the out-of-plane vibrations. The regularity revealed for the δ(CH) and γ(CH) vibrations of the methine bridges agrees with the changes that occur at 1000 cm^{-1} in the IR spectra upon complex formation and is confirmed by the results of studies by electronic absorption spectroscopy.

Therefore, examination of the IR spectra demonstrated that the introduction of the metal ion into the porphyrin molecule affects substantially the macrocycle (particularly, its π-electron system) and causes changes in the frequencies and intensities of vibrations of most of the bonds and molecular fragments.

III. ^{1}H NMR spectra of porphyrins and their precursors

Studies performed in the last decades demonstrated that ^{1}H NMR spectra are very informative and adequately reflect the structural features of porphyrins.[40–59] The presence of the extended delocalised π-electron system of the porphyrin macrocycle gives rise to a strong ring current in the molecules placed in the magnetic field. The ring current causes anisotropic shielding of the protons located in the field of its action and (together with the diamagnetic component of paired σ-electrons) leads to a substantial shift of their signals in the ^{1}H NMR spectra. It can be stated that the ring current and aromaticity of porphyrins change in a similar way in response to the analogous changes in the molecular structure of the porphyrin and the medium, which is most clearly seen on comparison of the spectra of porphyrins and their precursors.

1. Pyrroles

The chemical shifts of protons depend on the electron density on the hydrogen atom, the ring current of the molecule, the π-electron charge on the atom bound to the proton under consideration and the steric effects resulting from interactions with the substituents or the heteroatoms involved in the ring. Generally, separation of these effects presents a considerable problem.

The introduction of substituents into the pyrrole molecule leads to essential spectral changes.[9,10,13] A comparison of the characteristics of pyrrole (**1a**) and 3,4-dimethylpyrrole (**1m**) (Table 11) demonstrated that the positions of the signals for the protons of the CH groups of the pyrrole rings remain unchanged. Apparently, the β-substitution in the pyrrole ring exerts only a slight effect on the π-electron system of the molecule. In the spectrum of 2,3,4-trimethylpyrrole (**1o**), the signals for α-H are shifted upfield by 1.06 ppm compared to those in the spectrum of unsubstituted pyrrole due, apparently, to the positive inductive effect of the methyl group. Correspondingly, the downfield shift of the signal for α-H (0.43 ppm) observed on going from 3,4-dimethylpyrrole (**1m**) to 2-ethoxycarbonyl-3-ethyl-4-methylpyrrole (**1q**) occurs due to the effect of the electron-withdrawing ester group.

The most essential changes associated with chemical modifications of the molecule are observed in the region of the signals for the protons of the β-methyl and NH groups (see Table 11). An increase in the number of methyl groups in the pyrrole ring on going from the compound **1m** to the compound **1o** causes upfield shifts of the signals for the protons of the alkyl substituents by 0.13 ppm. The introduction of the electron-withdrawing ester or formyl group into the molecule results in downfield shifts of these signals by ~0.2 ppm. Of all the structures under consideration,

Table 11. Positions and multiplicities of the signals in the ^{1}H NMR spectra of pyrrole (**1a**) and its derivatives **1b**–**s**, **5a**,**b**.[9, 10, 12]

Compound	δ(NH)	δ(β-CH_3)	δ(β-Alk)	δ(α substituent)		δ(OCH_2CH_3)	
				H	another substituent	CH_3	CH_2
1a	7.62 s (1H)	–	–	6.18 s (2H)	–	–	–
1b	9.00 s (1H)	2.08 s (3H)	1.75 s (3H)	–	2.02 s	1.30 t	4.16 q
1c	9.68 s (1H)	2.24 s (3H)	1.17 t (3H), 2.45 q (2H)	–	2.59 s	1.38 t	4.35 q
1d	8.62 s	2.20 s	0.95 t, 1.28 m, 1.82 m, 2.28 t	–	2.13 s	1.28 t	4.23 q
1e	8.84 s	2.21 s	0.84 t, 1.30 m, 1.82 m, 2.27 t	–	2.09 s	7.27 [a] m	5.22 m
1f	8.80 s	2.23 s	0.89 t, 2.41 q	–	2.01 s	7.25 [a] m	5.19 m
1g	8.75 s	2.24 s	0.84 t, 2.69 q	–	–	7.30 [a] m, 1.33 t	4.32 m
1h	9.88 s	2.54 s	0.87 t, 2.69 q	–	12.60 s	1.32 t	4.31 q
1i	10.05 s	2.53 s	0.88 t, 2.71 q	–	12.64 s	1.33 t	4.30 q
1j	8.88 s	2.20 s	0.85 t, 2.71 q	–	–	1.26 t	4.24 q
1k	9.01 s	2.18 s	0.84 t, 2.74 q	–	–	1.27 t	4.23 q
1l	9.82 s (1H)	2.22 s (3H)	0.87 t, 1.87 m, 1.29 m, 2.65 t	6.20 s (1H)	–	1.32 t	4.31 q
1m	7.17 s (1H)	2.01 s (6H)	–	6.18 s (2H)	–	–	–
1n	6.97 s (1H)	1.50 s (2H) [b]	–	–	5.11 s (6H)	–	–
1o	6.72 s (1H)	2.02 s (6H)	–	6.02 s (1H)	5.12 s (3H)	–	–
1p	6.99 s (1H)	1.86 s (3H)	1.05 t (3H), 2.37 q (2H)	5.09 s (1H)	–	–	–
1q	9.88 s (1H)	2.24 s (3H)	1.14 t (3H), 2,40 q (2H)	6.61 s (1H)	–	1.32 t	4.27 q
1r	10.87 s	2.27 s	1.05 t, 2.36 q	–	9.45 s	–	–
1s	10.09 s	2.24 s (3H)	1.21 t (3H), 2.74 q (2H)	–	6.89 s (3H), 9.58 s (1H)	–	–
5a	9.73 s	2.22 s	1.08–1.58 m, 2.18–2.44 m	–	2.14 s	1.31 t	4.25 q
5b	9.84 s	2.27 s	1.26 m, 2.27–2.48 m	–	9.54 s	–	–

Note. Hereinafter, the ^{1}H NMR spectra were measured in $CDCl_3$; the chemical shifts (δ) are given in ppm. [a] Signals for the protons of the phenyl groups; [b] signals for β-H.

this chemical shift is maximum (~0.5 ppm) in the case of the carboxy derivatives.

The chemical shifts of the signals for the protons of the NH groups are changed more substantially. Methylation of the pyrrole ring (the compounds **1a** and **1o**) is accompanied by the upfield shifts of these signals by ~0.9 ppm (see Table 11). The signals for the protons of the NH groups are shifted downfield (up to 3.3 ppm) upon introduction of electron-withdrawing groups at the α positions of pyrroles.

The spectral characteristics (the intensities and multiplicities of the signals) agree well with the structures of the pyrroles synthesised. The signals for the protons of the ester (at δ 1.2–4.5) and carboxy (at δ 9.45–12.65) groups remain very characteristic and do not overlap with the signals of other proton-containing groups.

No substantial changes in the chemical shifts of the signals for the protons of the β-alkyl substituents and functional groups are observed on going from the compounds **1c**,**q** to β-bound pyrroles **5a**,**b**.

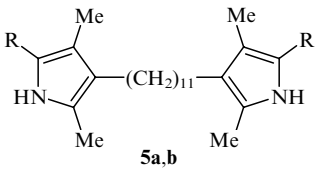

5a,**b**

R = CO_2Et (**a**), CHO (**b**).

In the ^{1}H NMR spectra of the compounds **5a**,**b**, the arrangement of the signals of the $(CH_2)_{11}$ methylene bridge linking the β positions of the pyrrole fragments is of interest.[60] The signals for the protons of two methylene groups directly bound to the pyrrole ring (see Table 11) are resolved from the signals for the protons of the remaining nine units of the bridge. The intensity distribution of the signals provides information on the relative number of equivalent protons (4 and 18, respectively). The signals for the protons of the NH groups in the spectrum of the compound **5b** are shifted upfield and are broadened compared to those observed in the spectrum of the pyrrole **1r**. Since the bispyrroles **5a**,**b** consist of two pyrrole rings separated from each other, the observed changes are, apparently, associated with the fact that solutions contain several conformers with different relative arrangements of the pyrrole nuclei. As a result, the positions of the NH groups in the bispyrrole molecule are nonequivalent (different shielding of the nuclei in different molecules or in different positions of a single molecule). On the contrary, the signals for the protons of the NH groups in the spectra of analogous dipyrrolylmethenes and biladienes are shifted downfield due to extension of the conjugated system and enhancement of the aromaticity of the pyrrole rings.[61]

2. Dipyrrolylmethanes

A comparison of the ^{1}H NMR spectra of the compounds **1b** and **2a** revealed no substantial changes in the region of the signals for the protons of the NH groups [12, 13] (Tables 11 and 12) due, apparently, to the absence of conjugation between the nearby π-electron systems of the pyrrole rings. On going from unsubstituted dipyrrolylmethane to the carboxy derivatives, the signals for the protons of the NH groups are shifted downfield (by ~0.5 ppm) due, presumably, to the electron-withdrawing effect of the carboxy groups. Methylation at the β positions of dipyrrolylmethane is accompanied by slight upfield shifts of the signals for the protons of the NH groups. The shifts successively increase on going from β-dialkyl-substituted dipyrrolylmethane to the β-tetraalkyl-substituted analogue and as the length of the alkyl substituent increases (the compounds **2a**,**c**,**d**), which is consistent with the positive inductive effect of the alkyl substituents.

The introduction of the phenyl substituent at the *meso* position of dipyrrolylmethane (the compound **2k**) leads to a slight downfield shift of the signal for the protons of the NH groups by 0.2 ppm compared to that in the spectrum of unsubstituted dipyrrolylmethane. A more substantial shift is observed in the spectrum of the structural isomer **2l**. Apparently, the above-considered changes can be attributed to the small negative inductive effect of the phenyl groups.

Chemical modifications at positions 5 and 5′ in the dipyrrolylmethane molecule (on going from the ethoxycarbonyl derivatives to the carboxy analogues) have virtually no effect on the positions of the signals for the β-alkyl protons. However, it should be noted

Table 12. Positions and multiplicities of the signals in the ^{1}H NMR spectra of dipyrrolylmethanes and their derivatives.[12–14]

Compound	δ(NH)	δ(β-CH_3)	δ(*meso*-H)	δ(Alk)	δ(Ar)
2a	9.24 s (2H)	2.92 s (6H)	3.87 s (2H)	1.87 s (6H)	–
2b	9.55 s (2H)	2.94 s (6H)	5.30 s (2H)	0.82 t (6H), 1.25 m (4H), 1.85 m (4H), 2.30 t (4H)	–
2c	9.14 s (2H)	2.97 s (6H)	3.73 s (2H)	0.98 t (6H), 2.30 q (4H)	–
2d	9.10 s (2H)	2.91 s (6H)	3.80 s (2H)	0.84 t (6H), 1.25 m (4H), 1.86 m (4H), 2.31 t (4H)	–
2f	9.20 s (2H)	2.94 s (6H)	3.78 s (2H)	6.49 s (2H)	–
2h	9.75 s (2H)	2.21 s (6H)	5.81 s (1H)	0.80 t (6H), 1.21 m (4H), 1.87 m (4H), 2.23 t (4H)	6.68 m (3H; 3,4-H), 6.90 d (2H; 2-H)
2i	9.69 s (2H)	2.22 s (6H)	5.89 s (1H)	0.79 t (6H), 1.22 m (4H), 1.90 m (4H), 2.25 t (4H)	6.61 m (3H; 3,4-H), 6.90 d (2H; 2-H)
2j	9.81 s (2H)	2.16 s (6H)	4.84 s (1H)	0.94 t (6H), 1.20 m (4H), 1.92 m (4H), 2.34 t (4H)	6.65 m (3H; 3,4-H), 6.90 d (2H; 2-H)
2k	9.32 s (2H)	2.22 s (6H)	4.01 s (1H)	0.81 t (6H), 1.19 m (4H), 1.87 t (4H), 2.28 t (4H)	6.60 m (3H; 3,4-H), 6.90 d (2H; 2-H)
2l	9.52 s (2H)	2.23 s (6H)	4.12 s (1H)	0.83 t (6H), 1.20 m (4H), 1.85 m (4H), 2.32 t (4H)	6.69 m (3H; 3,4-H), 6.90 d (2H; 2-H)
2n	9.69 s (2H)	2.20 s (6H)	5.88 s (1H)	0.81 t (6H), 1.19 m (4H), 1.89 m (4H), 2.28 t (4H)	6.70 d (2H; 3-H), 6.92 d (2H; 2-H), 3.66 s (3H; CH_3)
2p	9.48 s (2H)	2.22 s (6H)	5.31 s (1H)	0.82 t (6H), 1.21 m (4H), 1.84 m (4H), 2.34 t (4H)	6.72 m (2H; 3,4-H), 6.92 d (2H; 2-H), 3.68 s (3H; CH_3)
2r	9.52 s (2H)	2.20 s (6H)	5.89 s (1H)	0.84 t (6H), 1.20 m (4H), 1.79 m (4H), 2.34 t (4H)	6.74 m (3H; 3,4-H), 6.96 d (1H; 2-H), 3.70 s (3H; CH_3)
2t	9.54 s (2H)	2.24 s (6H)	5.83 s (1H)	0.80 t (6H), 1.24 m (4H), 1.80 m (4H), 2.36 t (4H)	6.68 d (2H; 3-H), 6.90 d (2H; 2-H)
2v	9.56 s (2H)	2.27 s (6H)	5.81 s (1H)	0.83 t (6H), 1.19 m (4H), 1.82 m (4H), 2.36 t (4H)	6.74 m (2H; 3,4-H), 6.98 d (2H; 2-H)
2x [a]	7.81 s (2H)	–	3.80 s (2H)	1.82 s (6H)	–
6a	9.07 s (4H)	2.17 s (12H)	5.44 s (2H)	0.86 t (12H), 2.29 q (8H)	6.95 t (4H; 3,4-H), 7.13 m (4H; 2-H), 4.12 m (2H; CH_2), 3.54 t (4H; CCH_2)
6b	9.62 s (4H)	2.19 s (12H)	5.36 s (2H)	0.84 t (12H), 2.31 q (8H)	7.03 m (4H; 3,4-H), 7.28 m (4H; 2-H), 4.10 m (4H; CH_2), 3.78 t (4H; CCH_2)
6c	9.20 s (4H)	2.21 s (12H)	5.28 s (2H)	0.82 t (12H), 2.30 q (8H)	7.14 m (4H; 3,4-H), 7.31 m (4H; 2-H), 4.12 m (4H; 2-CH_2), 3.84 t (4H; OCH_2)

[a] According to the published data.[30]

that the introduction of the phenyl substituent at the *meso* position of the molecule is accompanied by the upfield shifts (by ~0.7 ppm) of the signals for the protons of the methyl substituents at positions 3 and 3′ (see Table 12) due to the shielding effect of the ring current of the phenyl substituent.

In the ^{1}H NMR spectra of the 5,5′-diesters **2a**,**c**,**d**,**f**,**k**,**l**, the signals for the *meso*-protons are observed as a pronounced singlet in the region δ 3.73–4.12. As expected, the signals are shifted downfield (by ~2 ppm) on going to the 5,5′-dicarboxy derivatives **2b**,**h**,**i**,**n**,**p**,**r**, (see Table 12). The electron-withdrawing effect of the carboxy group is identical in both the *meso*-unsubstituted and *meso*-aryl-substituted dipyrrolylmethanes. The introduction of the phenyl substituent at the *meso* position of porphyrin leads to an increase in the downfield shift (by ~0.5 ppm) in the case of both the ethoxycarbonyl and carboxy derivatives. Apparently, this fact can be explained by a small negative inductive effect of the substituent. The signals for the *meso*-protons and the protons of the phenyl fragments in the structural isomers **2k**,**l** are observed at δ ~4.0 and 6.6–6.9, respectively (see Table 12). In the ^{1}H NMR spectra, the signals for the protons of the unsubstituted *meso*-phenyl groups in the compounds **2h**–**l** are observed as a doublet of the *ortho*-protons and a multiplet of the *meta*- and *para*-protons. The *para*-substitution (the compounds **2n**,**t**) results in the appearance of a doublet for the *meta*-protons along with a doublet for the *ortho*-protons. In the spectra of the *meta*-substituted dipyrrolylmethanes **2p**,**v**, the signals for the *meta*- and *para*-protons again coalesce into a multiplet.

In the spectra of the linear tetrapyrrole compounds **6a**–**c**, the signals for the *meso*-protons are shifted downfield by ~1.5 ppm, whereas the positions of the signals for the protons of the β-alkyl and NH group change only slightly compared to those in the spectra of the monomeric analogue **2c**.

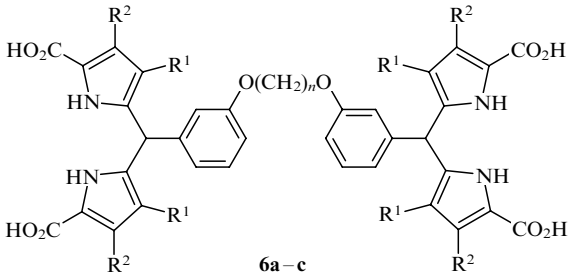

6a–**c**

R^1 = Me, R^2 = Et, n = 3 (**a**); R^1 = Et, R^2 = Me, n = 4 (**b**); R^1 = Me, R^2 = Et, n = 4 (**c**).

More substantial changes are observed in closed tetrapyrrole structures. It was found [61] that the signals for the protons of the β-alkyl and NH groups are shifted upfield by 0.65 and 0.28 ppm, respectively, on going from pyrrole to octamethylporphyrinogen due, apparently, to the positive inductive effect of the methyl groups at the β positions. The introduction of the methyl group at the α position of pyrrole also leads to the upfield shift of the signal for the β-alkyl protons.

3. Porphyrins

Conjugated macrocyclic structures are of most interest. The imposition of the external magnetic field on these molecules gives rise to ring currents, which make the major contribution to the observed chemical shifts. Theoretical analysis of the ^{1}H NMR spectra shows that the positions of the signals for the protons of porphyrins are determined primarily by the strength of ring π-electron currents (the macrocyclic current enclosing the molecule as a whole and local currents localised in the pyrrole nuclei). It should be noted that the macrocyclic current (Fig. 2) possesses the major 'bed' corresponding to the main 18-membered contour of conjugation and 'arms' formed by the semi-isolated C(β)–C(β) bonds in the pyrrolenine nuclei.

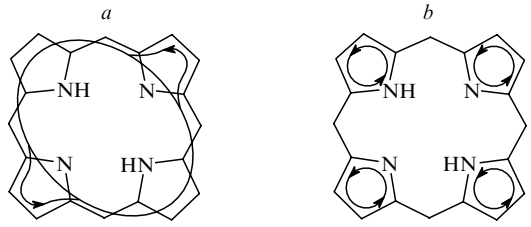

Figure 2. Schematic representation of the circuits of the ring π-electron currents in the porphyrin molecule; (*a*) the macrocyclic current, (*b*) local currents.[7, 25]

The protons at the β and *meso* positions are exocyclic with respect to the macrocyclic and local pyrrole currents and experience the deshielding influence of the latter. The signals for these protons are observed at low field (at δ from 9.7 to 11.2 for the *meso*-protons and at δ from 8.5 to 9.9 for the β-protons; see Table 13). The protons of the NH groups are exocyclic with respect to the local ring currents and endocyclic with respect to the macrocyclic current. Undoubtedly, the shielding effect of the latter prevails and the signals for the protons of the NH groups are observed at very high field (at δ from −1.4 to −4.4; see Table 13).

The β-hydrogen atoms of the pyrrole and pyrrolenine fragments are in principle nonequivalent. However, rapid (within the NMR time scale) transformations occur at room temperature and the signals for the β-protons are averaged. Two different peaks corresponding to resonance absorption of the energy by the protons of the β-CH groups of the pyrrole and pyrrolenine fragments can be observed at low temperature.[7, 62]

Table 13. Chemical shifts (ppm) of the β- and *meso*-protons and the protons of the NH groups in the ^{1}H NMR spectra of porphyrins.[7]

Porphyrin	δ(β-H)	δ(*meso*-H)	δ(NH)
Porphin	9.74	10.58	−3.76
Porphin [a]	9.92	11.22	−4.40
Octaethylporphin	–	10.18	−3.70
Ethioporphyrin-I	–	10.10	−3.67
Tetra-*iso*-butylporphyrin	9.41	–	−2.73
Tetra-n-pentylporphyrin	9.28	–	−2.75
Tetraphenylporphyrin	8.70	–	−2.81
Tetraphenylporphyrin [a]	8.45	–	−2.38
Tetra(2-methylphenyl)porphyrin	8.60	–	−2.66
Tetra(2-methoxyphenyl)porphyrin	8.65	–	−2.68
Tetra(2-bromophenyl)porphyrin	8.45	–	−2.63
Tetra(2-aminophenyl)porphyrin	8.82	–	−2.72
Tetra(3-methoxyphenyl)porphyrin	8.85	–	−2.85
Tetra(3-nitrophenyl)porphyrin	8.77	–	−2.96
Tetra(3-bromophenyl)porphyrin	8.82	–	−2.91
Tetra(3-hydroxyphenyl)porphyrin [a]	8.52	–	−2.45
Protoporphyrin	–	9.96	−4.08
Chlorin	–	9.65	−1.40
Deuteroporphyrin [a]	9.66	11.21	–

Note. In all tetrasubstituted porphyrins, the substituents are located in the *meso* positions. [a] The spectrum of a solution in CF_3CO_2H was measured.

On going from porphin to chlorin, the signals for the protons of the NH groups in the ^{1}H NMR spectra are shifted downfield, whereas the signals for the *meso*-protons are shifted upfield, *i.e.*, these signals are shifted toward each other, which is indicative of a decrease in the strength of the induced magnetic field produced by the macrocyclic ring current.[7, 62] In our opinion, two consequences of hydrogenation of one of the C(β)=C(β) bonds are responsible for these changes. First, due to hydrogenation of the C(β)=C(β) bond, the number of charge carriers providing the macrocyclic ring current is decreased by two electrons and, correspondingly, the strength of the macrocyclic ring current is diminished. Second, one of the 'arms' through which this current flows disappears, *i.e.*, the effective diameter of the ring conductor is reduced. As a result, the strength of the magnetic field induced by the macrocyclic ring current decreases.

On going from a solution of porphin (P) in deuteriochloroform to a solution in trifluoroacetic acid, the neutral form H_2P is converted into the doubly protonated form H_4P^{2+} in which the excess positive charge is located primarily on four nitrogen atoms. In this case, the electron density on the central hydrogen atoms is sharply reduced, which was confirmed by calculations for the neutral and protonated forms of porphin by the PM3 method.[63] In this connection, one would expect that the signals for the protons of the NH groups in the ^{1}H NMR spectrum will be shifted downfield upon protonation of porphin. However, the signals are shifted upfield by ~0.7 ppm (see Table 13). Simultaneously, the signals for the β- and *meso*-protons are shifted downfield. This character of the spectral changes indicates that protonation of porphin leads to a substantial increase in the strength of the magnetic field induced by the macrocyclic ring current.

Calculations [23] carried out by the PM3 method demonstrated that protonation of porphin is accompanied by a change in the geometric structure of the molecule. The C(α)–NH–C(α) fragments in the initial porphin are planar and the nitrogen atoms are sp^2-hybridised. In the protonated porphin, these fragments adopt a pyramidal structure (the nitrogen atoms have nearly sp^3 hybridisation) and the degree of involvement of the nitrogen atoms in conjugation with the α-carbon atoms is substantially reduced. This fact is confirmed by an increase in the C(α)–N bond length observed upon protonation of porphin. The above-mentioned rearrangements lead to a change in the contour of macrocyclic conjugation. In the case of protonated porphin, this conjugation is realised primarily along the outer contour of the molecule. Therefore, protonation causes an increase in the diameter of the conjugation ring resulting in upfield shifts of the signals for the internal protons and downfield shifts of the signals for the external protons.

In the case of β-alkyl substitution in porphin (on going to octaethylporphin and ethioporphyrin), the signals for the protons of the NH groups and the signals for the *meso*-protons are shifted downfield and upfield, respectively. Analogous, but more pronounced, changes are observed in the presence of a substituent in the *meso* position. It should be noted that the introduction of both electron-donating (*meso*-tetra-*iso*-butyl- and *meso*-tetra-n-pentylporphyrin) and electron-withdrawing (tetraphenylporphyrin and its derivatives) substituents gives the same results, *viz.*, the signals for β-protons and for the protons of the NH groups are shifted upfield and downfield, respectively. It seems likely that the introduction of substituents both at the β- and *meso* positions leads to reduction in the strength of the aromatic macrocyclic current regardless of the electronic nature of the substituent. The reasons for this phenomenon remain unclear.

The currents in the porphyrin molecule are substantially affected by complex formation.[7] The higher the degree of covalence of the N–H bond, the larger the decrease in the ring current due to the presence of the coordinated metal atom. Coordination to the medium-sized M^{2+} cations (M = Mg, Zn, Cd, Ni or Pd) is

accompanied by upfield shifts of the signals for the *meso*-protons (the ring current is reduced). In the spectra of the complexes in which the M^{2+} metal ion deviates from the plane due to its large radius and weak coordination interactions (M = Sn or Pb) or in the spectra of the complexes with the M^{3+} or M^{4+} ions in which the metal atom deviates from the plane of the macrocycle under the action of the extra ligands, the signals for the *meso*-protons are shifted downfield relative to those in the spectra of the porphyrin ligand. These shifts may be due to an increase in the ring current. However, this effect is insignificant and depends on the nature of the ions serving as the extra ligands.[7]

The following characteristic features should be noted in the ^{1}H NMR spectra of β-octaalkylporphyrins and their 5,15-diaryl-, 5,15-dialkyl- and 5,15-dialkyl-10,20-diaryl derivatives.[14, 19, 20, 24, 27] On going from 2,8,12,18-tetrabutyl-3,7,13,17-tetramethylporphyrin (**3t**) to 2,8,12,18-tetrabutyl-3,7,13,17-tetramethyl-5,15-diphenylporphyrin (**3h**), the most substantial changes are observed in the region of the signals for the protons of the β-methyl and NH groups (Table 14). The upfield shifts of the

Table 14. Positions and multiplicities of the signals in the ^{1}H NMR spectra of the β-octaalkylporphyrins **3a**–**f**, **h**–**w**.[14, 19, 20, 24, 27]

Compound **3**	δ(NH)	δ(β-CH_3)	δ(*meso*-H)	δ(β-Alk)	δ(*meso*-Ar)
a	−2.11 s (2H)	3.01 s (24H)	9.82 s (2H), 4.01 s (6H)	–	–
b	−2.06 s (2H)	3.09 s (24H)	9.79 s (2H), 4.08 q (4H), 2.24 t (6H)	–	–
c	−2.04 s (2H)	3.12 s (24H)	9.77 s (2H), 4.10 t (4H), 2.20 m (4H), 1.80 t (6H)	–	–
d	−2.03 s (2H)	3.11 s (24H)	9.78 s (2H), 4.14 t (4H), 2.22 m (4H), 1.92 m (4H), 1.54 t (6H)	–	–
e	−2.07 s (2H)	3.14 s (24H)	9.80 s (2H), 4.20 t (4H), 2.25 m (4H), 1.90 m (4H), 1.50 m (4H), 1.01 t (6H)	–	–
f	−2.14 s (2H)	3.18 s (24H)	9.82 s (2H), 4.32 t (4H), 2.50 m (4H), 2.16 m (4H), 1.64 m (4H), 1.09 m (4H), 0.78 t (6H)	–	–
h	−2.42 s (2H)	2.41 s (12H)	10.17 s (2H)	3.91 t (8H), 2.11 m (8H), 1.63 m (8H), 1.03 t (12H)	7.98 d (4H; *o*-H), 7.68 m (6H; *m,p*-H)
i	−2.38 s (2H)	2.42 s (12H)	10.12 s (2H)	3.85 t (8H), 2.10 m (8H), 1.67 m (8H), 1.03 t (12H)	7.82 d (4H; *o*-H), 7.14 d (4H, *m*-H), 3.98 s (6H; CH_3)
j	−2.49 s (2H)	2.50 s (12H)	10.18 s (2H)	3.93 t (8H), 2.14 m (8H), 1.67 m (8H), 1.03 t (12H)	7.61 m (4H; *o*-H), 7.55 m (4H; *m,p*-H), 3.88 s (6H; CH_3)
k [a]	−2.38 s (2H)	2.53 s (12H)	10.19 s (2H)	3.99 t (8H), 2.18 m (8H), 1.67 m (8H), 1.09 t (12H)	7.67 d (2H; *o*-H), 7.60 t (2H; *m′*-H), 7.19 t (2H; *p*-H), 7.10 d (2H; *m*-H), 3.84 s (6H; OCH_3)
k [b]	−2.37 s (2H)	2.54 s (12H)	10.17 s (2H)	3.97 t (8H), 2.17 m (8H), 1.64 m (8H), 1.02 t (12H)	7.57–7.65 m (4H; *o, m′*-H), 7.17 t (H; *p*-H), 7.10 d (2H; *m*-H), 3.78 s (6H; OCH_3)
l	−2.49 s (2H)	2.27 s (12H)	10.20 s (2H)	3.91 t (8H), 2.07 m (8H), 1.63 m (8H), 1.10 t (12H)	8.39 d (4H; *o*-H), 7.96 d (4H; *m*-H)
m	−2.47 s (2H)	2.33 s (12H)	10.17 s (2H)	3.87 t (8H), 2.03 m (8H), 1.66 m (8H), 1.02 t (12H)	8.92 s (2H; *o*-H), 8.60 d (2H; *o′*-H), 8.24 d (2H; *p*-H), 7.77 t (2H; *m*-H)
n	−2.32 s (2H)	3.41 s (12H)	10.16 s (2H)	2.91 t (8H), 1.40 m (8H), 1.36 m (8H), 1.01 t (12H)	7.99 d (4H; *o*-H), 7.72 m (6H; *m,p*-H)
o	−2.27 s (2H)	3.99 s (12H)	10.07 s (2H)	2.79 t (8H), 2.38 m (8H), 1.50 m (8H), 1.02 t (12H)	7.87 d (4H; *o*-H), 7.70 d (4H; *m*-H), 3.99 s (6H; OCH_3)
p	−2.23 s (2H)	3.92 s (12H)	10.15 s (2H)	2.92 t (8H), 2.42 m (8H), 1.56 m (8H), 1.00 t (12H)	7.84 m (4H; *o*-H), 7.64 m (4H; *m,p*-H), 3.90 s (6H; OCH_3)
q	−2.27 s (2H)	3.98 s (12H)	10.14 s (2H)	2.90 t (8H), 2.44 m (8H), 1.52 m (8H), 1.01 t (12H)	7.91 m (2H; *o*-H), 7.66 m (6H; *m,p*-H), 3.81 s (6H; OCH_3)
r	−2.20 s (2H)	3.94 s (12H)	10.16 s (2H)	2.94 t (8H), 2.46 m (8H), 1.50 m (8H), 1.01 t (12H)	8.42 d (4H; *o*-H), 7.92 d (4H; *m*-H)
s	−2.23 s (2H)	3.92 s (12H)	10.18 s (2H)	2.87 t (8H), 2.42 m (8H), 1.48 m (8H), 1.04 t (12H)	8.76 s (2H; *o*-H), 8.54 d (2H; *o′*-H), 8.20 d (2H; *p*-H), 7.72 t (2H; *m*-H)
t	−3.80 s (2H)	3.47 s (12H)	9.91 s (4H)	3.92 t (8H), 2.19 m (8H), 1.64 m (8H), 1.11 t (12H)	–
u	–	2.42 s (24H)	4.0 q (4H), 0.65 t (6H) [c]	–	7.70 m (6H; *m,p*-H), 7.96 d (4H; *o*-H)
v	–	2.44 s (24H)	4.30 t (4H), 2.54 m (4H), 2.20 m (4H), 1.64 m (4H), 1.09 m (4H), 0.62 t (6H) [c]	–	7.78 m (6H; *m,p*-H), 7.99 d (4H; *o*-H)
w	–	2.33 s (24H)	4.50 t (4H), 2.84 m (4H), 2.20 m (4H), 1.67 m (4H) 1.01 m (4H), 0.60 t (6H) [c]	–	8.42 d (4H; *o*-H), 7.94 d (4H; *m*-H), 3.92 s (6H; CH_3)

[a] α,α-Atropoisomer; [b] α,β-atropoisomer; [c] signals for the protons of the *meso*-alkyl groups.

signals for the protons of the methyl groups (by 1.06 ppm) can be attributed to the shielding effect of the ring currents of the phenyl fragments. Apparently, the signals for the protons of the NH groups are substantially shifted downfield ($\sim$1.4 ppm) due to both the negative inductive effect of the phenyl fragments and a reduction in the strength of the macrocyclic ring current. The planar porphyrin macrocycle is deformed and its aromaticity is decreased due to steric strains caused by the phenyl groups. On going from the compound **3h** to the compound **3n**, the porphyrin macrocycle undergoes further deformation due to steric interactions between the butyl and phenyl substituents resulting in the downfield shifts (by 0.1 ppm) of the signals for the protons of the NH groups. The shielding effect of the ring currents of the phenyl fragments is manifested in the upfield shifts of the signals for the protons of the butyl substituents. These shifts are maximum (1 ppm) for the CH_2 groups directly bound to the macrocycle, whereas the positions of the signals of the terminal CH_3 groups remain virtually unchanged (0.02 ppm). The introduction of the substituents into the phenyl rings of 5,15-diphenylporphyrin (*o*,*m*,*p*-OMe or *m*,*p*-NO_2) exerts only a slight effect on the positions of the signals for the *meso* protons and for the protons of the NH groups (see Table 14).

In the ^{1}H NMR spectra of the 5,15-dialkyloctamethylporphyrins **3a**–**f**, the signals for the protons of the NH groups are shifted downfield compared to those in the spectrum of the porphyrin **3t**. Apparently, this is associated with the deformation of the molecule caused by the *meso*-substitution. The magnetic field of the π-electron ring current of the porphyrin, in turn, affects the positions of the signals for the protons of the alkyl *meso*-substituents. In this case, the spectra contain individual non-overlapping signals for the protons of the methylene and methyl fragments of the alkyl substituents. Thus, the spectrum of 5,15-dihexyl-2,3,7,8,12,13,17,18-octamethylporphyrin (**3f**) has the signal for the protons of the methylene group, which is directly bound to the macrocycle, as a triplet at δ 4.32, the signal of the adjacent methylene group as a quintet at δ 2.5 and the signals for the protons of the next two CH_2 groups as quintets at δ 2.16 and 1.64.[12] The signals of the last methylene group and the terminal methyl group are observed as a sextet at δ 1.09 and a triplet at δ 0.78.

The signals of the β-methyl groups in the spectra of the compounds **3a**–**f** are shifted downfield by $\sim$0.4–0.5 ppm compared to the corresponding signals in the spectra of 5,15-diarylporphyrins, which is attributed to elimination of the shielding effect exerted by the ring currents of the *meso*-aryl substituents.

Not only the signals for the *meso*-protons, but also the signals for the protons of the NH groups disappear in the ^{1}H NMR spectra on going from the *meso*-disubstituted porphyrins to the *meso*-tetrasubstituted compounds (**3u**–**w**). The reasons for this phenomenon remain unclear. Analogous changes are observed in the spectrum of tetraphenyl-substituted β-octamethylporphyrin.[27]

The signals for the β-methyl protons of *meso*-tetrasubstituted porphyrins are observed in the region (at δ $\sim$2.4) identical to that of 5,15-diarylporphyrins (see Table 14). It should be noted that the above-mentioned region is intermediate between the regions in which these signals are observed in the spectra of the octaalkylporphyrin **3t** (at δ 3.47) and its *meso*-tetraphenyl derivative (at δ 1.76),[25] which confirms the assumption that the magnetic anisotropy of the aryl *meso*-fragments exerts an effect on the protons of the β-substituents.

The chemical shifts of the protons of the phenyl fragments are observed in the region δ $\sim$7.7–8. The signals of the unsubstituted phenyl groups of the compounds **3h**,**n**,**u**,**v** are observed as a doublet for the *ortho*-protons and a multiplet for the *meta*- and *para*-protons. The chemical shifts of the protons of the substituted phenyl fragments vary depending on the nature of the substituent. Among the spectra of the porphyrins containing the electron-donating methoxy group in the *meso*-phenyl fragment, only the spectra of the *para*-substituted compounds **3i**,**o**,**w** have pronounced individual signals, *viz*., a doublet for the *ortho*-protons and a doublet for the *meta*-protons. In the spectra of the *meta*-methoxy-substituted compounds **3j**,**p**, the corresponding signals are observed as multiplets.

In the spectra of porphyrins containing the electron-withdrawing nitro group in the *meso*-phenyl fragment (both in the *meta*- and *para*-substituted compounds), the signals are observed as pronounced multiplets. The spectra of the *para*-nitro derivatives **3l**,**r** have a doublet for the *ortho*-protons and a doublet for the *meta*-protons. The signals of the *meta*-nitro derivatives **3m**,**s** are observed as a doublet for the *para*-protons, a triplet for the *meta*-protons and a singlet and a doublet for the nonequivalent *ortho*-protons (see Table 14).

The *ortho*-methoxy-substituted porphyrin **3k** can exist as two atropoisomers (α,α and α,β), which differ by the orientation of the methoxy groups with respect to the porphyrin plane. The ^{1}H NMR spectra of these compounds are characterised by the presence of the signals for the phenyl protons as multiplets. The spectrum of the α,α-atropoisomer has two doublets for the *ortho*- and *meta*-protons and two triplets for the *meta*- and *para*-protons. The spectrum of the α,β-atropoisomer has a doublet for the *meta*-protons, a triplet for the *para*-protons and a multiplet for the *ortho*- and *meta*-protons (see Table 14).

4. Bisporphyrins

As mentioned above, the porphyrin fragments in cyclophane dimers are brought into proximity due to the bridging bonds located at the *meso* or β positions of the macrocycles. The lengths and rigidity of the bridges are responsible for the conformational flexibility of the dimer.

Interactions between the π-electron systems of the macrocycles are clearly manifested in the ^{1}H NMR spectra. The chemical shifts of the protons depend on the length of the bridge and the mutual orientation of the macrocycles.[64–86]

Dimeric porphyrins **7a**–**f** in which the porphyrin rings are linked through the β positions of the pyrrole rings by two amide bridges can exist as two isomers (*syn* and *anti*). The possibility of

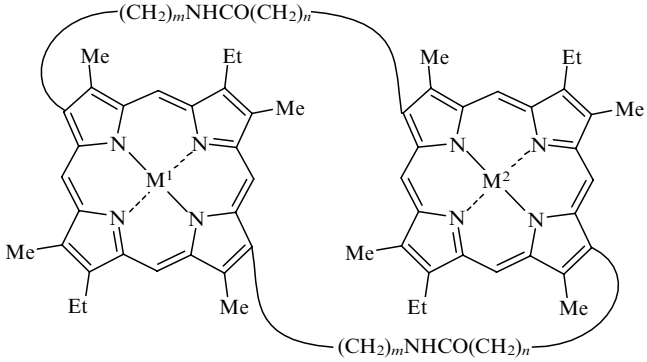

7a–**n**

Compound **7**	M^1	M^2	*n*	*m*
a	H_2	H_2	0	1
b	H_2	H_2	1	1
c	H_2	H_2	0	2
d	H_2	H_2	2	1
e	H_2	H_2	1	2
f	H_2	H_2	3	1
g	Co	H_2	1	1
h	Co	Co	1	1
i	Ag	H_2	1	1
j	Ag	Ag	1	1
k	Mn	Mn	1	1
l	Mn	Co	1	1
m	Fe	Co	1	1
n	Ag	Co	1	1

formation of a particular isomer depends on the orientation of the porphyrin fragments at the instant the second amide bond is formed.[72, 73]

Figure 3 presents the ^{1}H NMR spectrum of the *anti*-isomer of the bisporphyrin **7c**, which has signals for four *meso*-protons (at δ 9.29, 8.84 and 8.78) and signals for the protons of the alkyl substituents (at δ 3.60, 3.64, 3.68 and 3.74). The signals for the protons of the NH groups are shifted upfield (δ −7.78 and −7.81) compared to those observed in the spectra of their monomeric analogues (δ −3.75). The amide bridges in the compound **7c** contain two methylene groups each. Two of these groups bound to the NH groups give a quadruplet (δ 5.8) and a doublet (δ 4.7), whereas two other groups bound to the porphyrin fragment of the dimer give signals at δ 4.1. The signals for the methylene protons of the ethyl groups are observed in the same region. The signals for the protons of the amide groups are observed as a doublet at δ 6.97. The chemical shifts of the protons of the alkyl substituents in the compound **7c** differ only slightly from those of the analogous protons in the monomeric analogue **8** (Table 15).

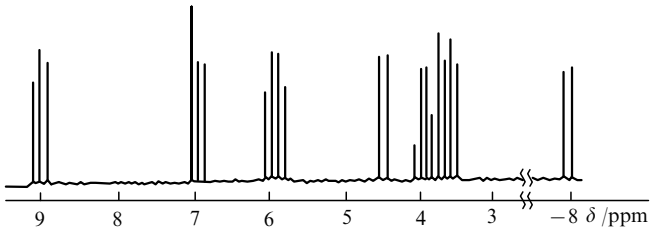

Figure 3. ^{1}H NMR spectrum of the bisporphyrin **7c** in $CDCl_3$.[73]

Three homologous dimers **9a**–**c** were investigated.[74] It was found that the porphyrin fragments approach each other by 100–120 pm as the number of the methylene groups in the bridges is decreased by one. The spectral properties are indicative of the 'face-to-face' orientation of the macrocycles.

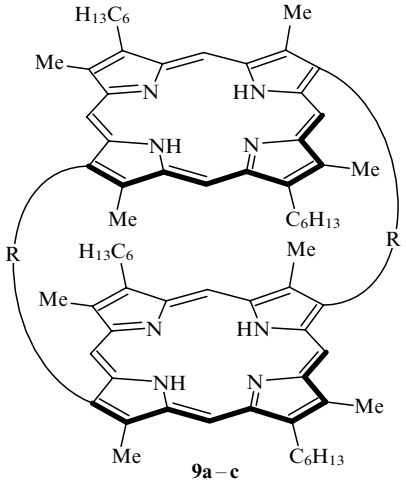

9a–**c**

R = $(CH_2)_2CO(Bu^n)(CH_2)_3$ (**a**), $CH_2CO(Bu^n)(CH_2)_3$ (**b**), $CH_2CO(Bu^n)(CH_2)_2$ (**c**).

Compound **9**	*R* /pm (see [a])	δ(NH) (see [b])	λ /nm (see [c])
a	640	−6.2	383
b	540	−6.6	540
c	420	−8.5	420

[a] The distance between the porphyrin fragments; [b] in $CDCl_3$; [c] the absorption band in the electronic absorption spectrum measured in CH_2Cl_2.

Table 15. Chemical shifts (ppm) of the protons of 4,8-di(2-ethoxycarbonylethyl)-2,6-diethyl-1,3,5,7-tetramethylporphyrin (**8**) and the dimeric porphyrins **7a**–**f**.[72]

Compound	δ($NH_{pyrrole}$)	δ(*meso*-H)	δ(CH_3)
7a	−7.81, −7.93	8.90–8.98	3.65–3.90
7b	−8.14	8.70–8.91	3.58–3.60
7c	−7.78, −7.81	8.78–9.29	3.60–3.74
7d	−8.00, −7.90	8.70–8.90	–
7e	−8.30, −8.00	8.70–8.90	–
7f	−6.2	9.00–9.40	–
8	−3.75	10.10, 10.16	3.67

^{1}H NMR spectral studies revealed the existence of two conformers of dimer **10a**. In one of them, the porphyrin rings are located parallel to each other (*anti*). In another conformer, the porphyrin rings are bent with respect to each other (*syn*, 'half-open shell').[80] The conformers occur due to rigidity of the amide bonds and their appearance depends on the relative orientation of the carbonyl groups. The spectrum of a mixture of the conformers has four signals for the protons of the NH groups (at δ −8) and twelve signals for the *meso*-protons (at δ 7–10). Four signals (at δ 9) correspond to the *meso*-protons of the *anti* conformer and eight signals belong to the *meso*-protons of the *syn* conformer. The characteristic features of the crystal structure of the compound **10a** are responsible for the rather steady existence of both conformers in equal amounts. A decrease in the intensities of the signals for the protons in the spectrum of the *anti* conformer of the zinc complex of the dimer **10b** compared to the signals for the protons of the *syn* conformer indicates that the *anti* : *syn* ratio is 1 : 9. On protonation of the porphyrin **10a**, the amount of the *anti* conformer increases and the *anti* : *syn* ratio becomes equal to 1 : 6. No hypsochromic shift of the Soret band (see Section IV) is observed in the electronic absorption spectrum of the dimer **10a** compared to the spectrum of the monomeric analogue.

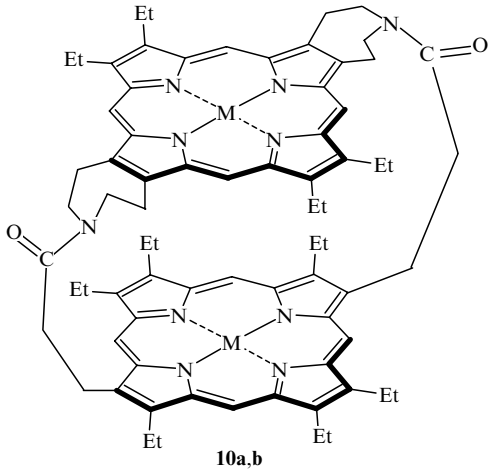

10a,**b**

M = 2H (**a**), Zn (**b**).

^{1}H NMR spectral studies established the characteristic structural features of cyclophane dimers **11a**–**d** in which the tetraphenylporphyrin fragments are linked through the *meta* or *ortho* positions of the phenyl substituents by four ether bridges.[77, 78]

The spectrum of the dimer **11a** differs from that of monomeric *meso*-tetra(3-butoxyphenyl)porphyrin in that the signals for the β-protons of the pyrrole rings are substantially split and the protons of the central CH_2 groups of the bridges give two signals. The signals for the protons of the OCH_2 and CH_2 groups are broadened. These characteristic features are retained on going from the neutral to protonated form of the dimer.

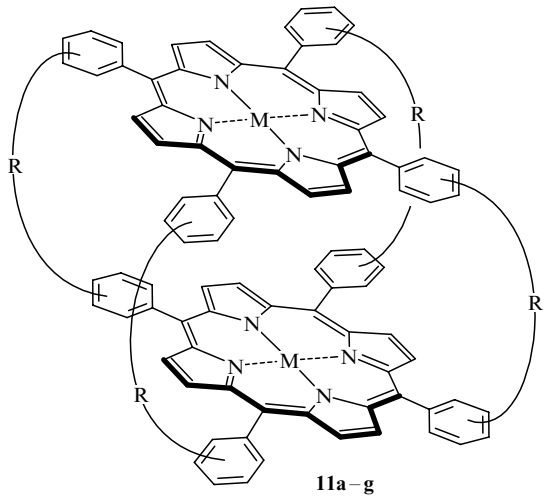

11a–g

R = *m*-O(CH$_2$)$_n$O-*m*, *n* = 4: M = H$_2$ (**a**), Zn (**b**); R = *o*-O(CH$_2$)$_n$O-*o*, *n* = 3: M = H$_2$ (**c**), Zn (**d**); R = *m*-CH$_2$NHCH$_2$-*m*, M = H$_2$ (**e**); R = *m*-CH$_2$NTsCH$_2$-*m*, M = H$_2$ (**f**); R = *m*-CH$_2$NTs-*m*, M = H$_2$ (**g**).

The cyclophane structure of the dimer imposes rigid limitations on the conformational flexibility of the O(CH$_2$)$_n$O chains. The fact that the protons of the bridging CH$_2$ groups give two signals is indicative of a skewed conformation of the ether bridges due to which the benzene rings of the adjacent macrocycles are inclined relative to each other. As a result, both fragments of tetraphenylporphyrin in the dimer adopt a nonplanar dome-shaped conformation. The resulting strain is partially relieved due to corrugation of the tetrapyrrole rings, *viz*., two opposite pyrrole fragments are bent upward, while two other fragments are bent downward. The inclination of the phenyl groups in combination with corrugation of the porphyrin macrocycle are responsible for the magnetic nonequivalence of the *ortho*-protons of the phenyl groups (external and internal) and the β-protons of the pyrrole rings. The external *ortho*-protons are located in proximity to the β-protons of the pyrrole rings directed upward, whereas the internal protons are located in proximity to the β-protons of the pyrrole rings bent downward. The distances between the pairs of the protons of the first type are smaller than those between the pairs of the protons of the second type due to which the deshielding effect of the ring currents of the macrocycle and the benzene ring in the first case is more pronounced (Table 16).

The corrugated dome-shaped conformation of the macrocycle is retained in the protonated form of the dimers. In the latter case, one pair of the protons of the NH groups is located in the centre of the macrocycle and is substantially shielded by the ring current, whereas the second pair of the protons is bent outward and the shielding effect of the ring current of the macrocycle exerted on the latter pair is weakened.

Corrugation of the porphyrin macrocycles in the protonated form of dimeric porphyrin leads to weakening of the macrocyclic ring current and strengthening of the local currents in the pyrrole fragments. For the external β-hydrogen atoms, the above-mentioned two effects compensate each other, whereas these effects with respect to the internal protons of the NH groups add up together resulting in substantial downfield shifts of the signals for these protons in the case of the dimeric porphyrin **11a** compared to its monomeric analogue (see Table 16).

The mutual effect of the macrocyclic ring currents of the adjacent porphyrin fragments leads to the nonequivalence of the protons of the NH groups in the dimer **11c**. Due to corrugation of the porphyrin rings, the distance from one pair of the protons of the NH groups to the adjacent tetrapyrrole fragment is 0.8 Å larger compared to that for the second pair.[78] This is a sufficient reason for the appearance of two signals for these protons in the ^{1}H NMR spectrum (see Table 16). The bridging groups in the dimer **11c**, unlike those in the dimer **11a**, are conformationally flexible. Judging from the fact that the positions of the signals of two OCH$_2$ groups are somewhat different (δ 4.25 and 4.11), two conformations of the bridge in solutions are rapidly (within the NMR time scale) transformed into one another. Apparently, the conformation with the unsymmetrical arrangement of the OCH$_2$ groups with respect to the tetraphenylporphyrin rings prevails.

In the ^{1}H NMR spectra of the cyclophane dimers **11e–g** in which the tetraphenylporphyrin fragments are linked through the *meta* positions of the phenyl groups by two- or three-membered bridges, the ring current exerts an even more pronounced shielding effect on the chemical shifts of the protons located below the plane of the adjacent porphyrin ring. The largest shifts are observed for the signals for the protons of the NH groups and for the *ortho*-protons of the phenyl groups because they are located between the porphyrin fragments.[79] The shifts of the signals for the β-protons of the pyrrole rings are much smaller because these protons are located at large distances from the shielding region.

Table 16. Positions and multiplicities of the signals in the ^{1}H NMR spectra of the cyclophane dimers of tetraphenylporphyrin **11a**,**c** and *meso*-tetra(3-butoxyphenyl)porphyrin.[77]

Compound	Solvent	δ(NH)	δ(β-H)	δ(H$_{bridge}$) [a]
11a	$CDCl_3$	−1.94 s	8.37 s	1.85 m (HC<u>H</u>CH$_2$O)
			9.02 s	2.27 m (<u>H</u>CHCH$_2$O)
				4.35 m (C<u>H</u>$_2$O)
	$CDCl_3$ –	−0.27 s	8.35 d	2.09 m (HC<u>H</u>CH$_2$O)
	CF_3COOH		8.51 d	2.34 m (<u>H</u>CHCH$_2$O)
				4.51 m (C<u>H</u>$_2$O)
11c	$CDCl_3$ –	−1.32 s	8.22 s	0.95 m (<u>H</u>CHCH$_2$O)
	CF_3COOH	−1.03 s	8.43 s	1.93 m (HC<u>H</u>CH$_2$O)
				4.11 t (C<u>H</u>$_2$O)
				4.25 t (C<u>H</u>$_2$O)
meso-Tetra-(3-butoxy-phenyl)por-phyrin	$CDCl_3$	−2.81 s	8.89 s	1.86 m (C<u>H</u$_2$CH$_2$O)
				4.15 t (C<u>H</u>$_2$O)

[a] The δ values are given for the underlined protons.

Compound	δ /ppm		
	NH	phenyl *o*-H	β-H
11e	−3.78	7.81	8.43, 8.46
11f	−4.42	7.14	8.17, 8.15
11g	−4.11	7.78	8.25, 8.43
Monomer [a]	−2.81	8.25	8.86

[a] 5,10,15,20-Tetra(3-bromomethylphenyl)porphyrin.

It can be seen that the mutual effect of the porphyrin fragments is strengthened as the lengths of the bridges in the compounds **11e** and **11g** decrease. Steric restrictions resulting from the presence of the bulky substituents in the bridges of the dimer **11f** lead to rotation of the macrocycles with respect to each other about the axis passing through the centres of both porphyrin rings (in the dimers **11f** and **11e**, the angle of rotation of the macrocycles with respect to each other is 26° and 13°, respectively). The molecule adopts an energetically more favourable conformation in which the porphyrin fragments, while remaining parallel to each other, are located at shorter distances and exert a more substantial shielding effect. This fact is confirmed by the ^{1}H NMR spectral data. As in the case of the dimers **11a**,**c**, the characteristic features of the cyclophane structures of the dimers **11f**,**g** are responsible for the magnetic nonequivalence of the *ortho*-protons of the benzene rings (internal and external) and the β-protons of the pyrrole rings.

In dimeric porphyrins **12a–d**, the aromatic bridge does not provide the 'face-to-face' orientation of the macrocycles.[81] This

Table 17. Positions and multiplicities of the signals in the ^{1}H NMR spectra of the dimeric porphyrins **12a**–**d** and 2,8,12,18-tetraethyl-3,7,13,17-tetramethyl-5-phenylporphyrin.[81]

Compound	δ(NH)	δ(Ar)	δ(*meso*-H)
12a	−2.27 s (4H)	7.94 s (1H), 8.32 t (1H), 8.89 d (2H)	10.15 s (4H)
12b	−1.90 s (4H)	8.00 d (2H), 8.70 d (2H)	10.34 s (4H)
12c	−3.0 s (2H), −2.1 s (2H)	7.95 s (1H), 8.29 t (1H), 8.95 d (2H)	9.83 s (1H), 10.10 s (2H), 10.15 s (2H)
12d	−3.0 s (2H), −1.95 s (2H)	8.01 d (2H), 8.74 d (2H)	9.95 s (1H), 10.26 s (2H), 10.34 s (2H)
2,8,12,18-Tetraethyl-3,7,13,17-tetramethyl-5-phenylporphyrin	−2.39 s (2H)	8.00 d (2H), 8.24 t (2H), 8.75 t (1H)	9.79 s (1H), 10.21 s (2H)

fact is clearly manifested in the ^{1}H NMR spectra of the above-mentioned compounds (Table 17). The spectra of the unsymmetrical dimers **12c**,**d** are of most interest. The signals for the protons of the NH groups in these spectra are observed as singlets at δ −2 and −3, which is indicative of the nonequivalence of the π-electron systems of the porphyrin fragments of these dimers. Neither the spectra of the unsubstituted dimers **12e**,**f** nor the spectra of the symmetrical compounds **12a**,**b** show analogous splitting of the signals for the protons of the NH groups. The spectra of the dimers **12a**,**b** have one singlet each at δ −2.27 and −1.90, respectively. The high-field signal (at δ −3.0) was assigned to the *meso*-unsubstituted porphyrin fragment in the dimers **12c**,**d**, while the low-field signal (at δ −2.1 or −1.95) was assigned to the *meso*-substituted porphyrin fragment.[81] The chemical shifts of the protons in these compounds correspond to those in the linear *meso*-bound dimers of porphyrins whose spectra have signals for the protons of the aliphatic alkyl groups at δ 1.0–4.0, signals for the *meso*-H atoms at δ 9.8–11.0 and signals for the protons of the NH groups at δ −2.0 and −3.0. The signals for the protons of the phenyl fragments are observed at δ 7.95–8.95. These chemical shifts have different values in the spectra of the dimers **12a**,**c** and **12b**,**d** (see Table 17). The multiplicities and intensities of the signals correspond to the assumed structures of the compounds.

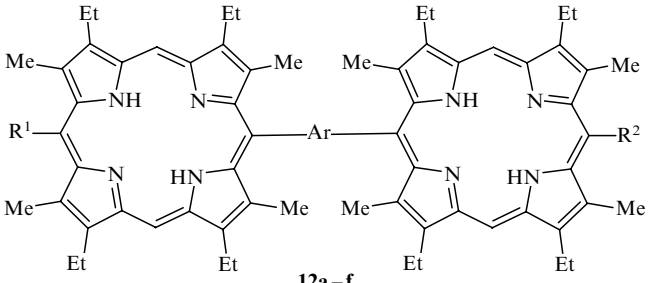

12a–**f**

$R^1 = R^2 =$ 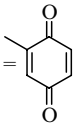 : Ar = 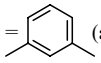 (**a**); 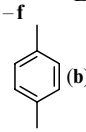 (**b**); R^1 = H, R^2 = 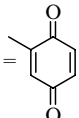 :

Ar = 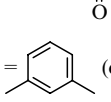 (**c**), 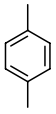 (**d**); $R^1 = R^2$ = H: Ar = 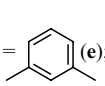 (**e**); 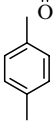 (**f**).

Dimeric *meso*-diphenyl-β-octaalkylporphyrins **13a**–**i** containing the bridging $O(CH_2)_nO$ groups at different positions of the phenyl substituent were investigated.[82–86]

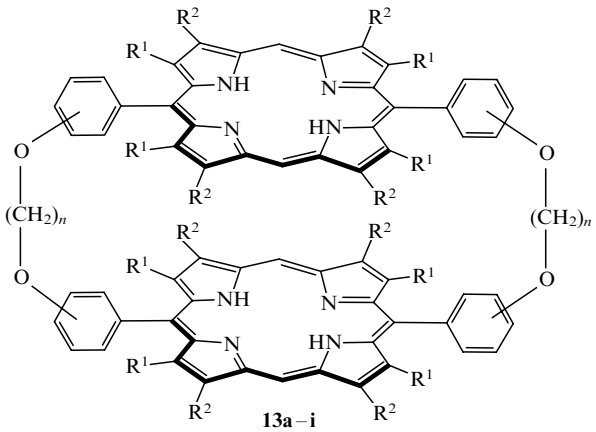

13a–**i**

R^1 = Me, R^2 = Bu: n = 2, *para* (**a**); n = 3, *para* (**b**); n = 4, *para* (**c**); R^1 = Me, R^2 = Et: n = 3, *meta* (**d**); n = 4, *meta* (**e**); R^1 = Et, R^2 = Me: n = 4, *meta* (**f**); R^1 = Me, R^2 = Bu: n = 2, *ortho* (**g**); n = 3, *ortho* (**h**); n = 4, *ortho* (**i**).

The cyclophane structures of these compounds were confirmed by the ^{1}H NMR spectral data (Table 18). The *meso*-protons and the protons of the β-CH_3 and NH groups give singlet signals. This indicates that the dimers adopt a symmetrical conformation in which the porphyrin macrocycles are located one above the other. However, it is conceivable that the singlet signals are observed due to the time-averaging of different (including unsymmetrical) conformations of the porphyrins.

In the spectra of the dimers under consideration, the signals for the protons of the NH groups are shifted upfield compared to those of the monomeric analogues **3i**–**k**, which is a manifestation of the mutual magnetic shielding of the ring currents of the aromatic macrocycles. Judging from the positions of the signals, the distance between the porphyrin fragments increases as the length of the bridging group increases (see Table 18). This distance is responsible also for the upfield shifts of the signals for the protons of the methylene groups in the spectra of the compounds **13a**,**b**,**d**,**g**,**h** (in which the number of the methylene units in the bridges n = 2 and 3) compared to the signals for the protons of the methoxy groups in the spectra of *meso*-di(methoxyphenyl)-substituted monomeric porphyrins. Starting from n = 4, these signals in the spectra of both the dimeric and monomeric compounds are observed virtually in the same region regardless of the positions of the bridging units in the benzene rings of the compounds **13c**,**e**,**i**.

The chemical shifts of the β-alkyl protons change only slightly on going from the monomers to the corresponding dimers. However, these shifts are substantially different for different structural isomers. Thus, the dimers **13e**,**f** differ by the arrangement of the methyl and ethyl groups at the β positions of the porphyrin fragments. In the porphyrin **13e**, the protons of the methyl groups experience the shielding effect of the ring currents of the phenyl substituents. In the case of the dimer **13f**, the shielding effect is exerted on the protons of the ethyl groups. The maximum shifts (1.08 ppm) are observed for the protons of the methylene groups directly bound to the macrocycle, while virtually no shifts (0.02 ppm) are observed for the signals for the protons of the CH_3 groups.

The signals for the protons of the bridging OCH_2 groups and the signals for the protons of the OCH_3 groups of the monomeric analogues are located nearly in the same region. The protons of the bridging CH_2 groups give signals at $\delta \sim 1.90$, which is characteristic of the protons of the corresponding substituents in the monomeric porphyrins.[12] Apparently, this is attributable to the fact that the peripheral substituents are not virtually enclosed by the ring current of the conformationally flexible dimers.

The signals for the protons of the phenyl groups in the spectra of the dimers **13a**–**c** are observed as a doublet for the *ortho*-

Table 18. Positions and multiplicities of the signals in the ^{1}H NMR spectra of the dimeric porphyrins **13a**–**i** and their monomeric analogues **3i**–**k**.[82–86]

Compound	δ(NH)	δ(Alk)	δ(β-CH_3)	δ(H_{phenyl})			δ(H_{bridge})		δ(*meso*-H)
				2-H, 6-H	4-H	3-H, 5-H	CH_2	OCH_2	
13a	−5.27 s (4H)	1.03 t (24H), 1.63 m (16H), 2.10 m (16H), 3.90 t (16H)	2.39 s (24H)	7.80 d (8H)	–	7.10 d (8H)	–	4.01 t (8H)	9.10 s (4H)
13b	−4.92 s (4H)	0.98 t (24H), 1.36 m (16H), 2.11 m (16H), 3.84 t (16H)	2.41 s (24H)	7.84 d (8H)	–	7.14 d (8H)	2.01 m (4H)	3.92 t (8H)	9.43 s (4H)
13c	−4.64 s (4H)	1.00 t (24H), 1.48 m (16H), 2.12 m (16H), 3.87 t (16H)	2.42 s (24H)	7.81 d (8H)	–	7.24 d (8H)	1.94 m (8H)	3.90 t (8H)	10.12 s (4H)
3i	−2.38 s (2H)	1.03 t (12H), 1.67 m (8H), 2.10 m (8H), 3.85 t (8H)	2.42 s (12H)	7.82 d (4H)	–	7.13 d (4H)	–	3.98 s (6H) [a]	10.12 s (2H)
13d	−5.82 s (4H)	0.97 t (24H), 2.97 q (16H)	3.42 s (24H)	7.69 m (8H)	7.22 m (4H)	7.22 m (4H)	1.92 m (4H)	4.25 t (8H)	9.12 s (4H)
13e	−4.32 s (4H)	1.03 t (24H), 3.91 q (16H)	2.40 s (24H)	7.71 m (8H)	7.38 m (4H)	7.38 m (4H)	1.90 m (8H)	4.02 t (8H)	10.08 s (4H)
13f	−4.28 s (4H)	1.00 t (24H), 2.99 q (16H)	3.38 s (24H)	7.80 m (8H)	7.42 m (4H)	7.42 m (4H)	1.88 m (8H)	4.02 t (8H)	10.08 s (4H)
3j	−2.49 s (2H)	1.03 t (12H), 1.67 m (8H), 2.14 m (8H), 3.93 t (8H)	2.50 s (12H)	7.61 m (4H)	7.55 m (2H)	7.55 m (2H)	–	3.88 s (6H) [a]	10.18 s (2H)
13g [b]	–	0.98 t (24H), 1.36 m (16H), 2.01 m (16H), 3.85 t (16H)	2.50 s (24H)	7.74 m (4H)	7.36 m (4H)	7.36 m (8H)	–	4.06 t (8H)	9.08 s (4H)
13h [b,c]	–	0.96 t (24H), 1.48 m (16H), 2.12 m (16H), 3.84 t (16H)	2.46 s (24H)	7.70 d (4H)	7.21 t (4H)	7.64 t (4H) 7.12 d (4H)	1.98 m (4H)	4.01 t (8H)	9.52 s (4H)
13h [b,d]	–	0.99 t (24H), 1.52 m (16H), 2.12 m (16H), 3.87 t (16H)	2.48 s (24H)	7.60 m (4H)	7.19 t (4H)	7.65 m (4H) 7.11 d (4H)	2.01 m (4H)	4.03 t (8H)	9.50 s (4H)
13h [b,e]	–	1.01 t (24H), 1.49 m (16H), 2.13 m (16H), 3.86 t (16H)	2.49 s (24H)	7.57 m (4H)	7.17 t (4H)	7.65 m (4H) 7.11 d (4H)	2.04 m (4H)	4.11 t (8H)	9.54 s (4H)
13i [b]	–	1.07 t (24H), 1.57 m (16H), 2.07 m (16H), 3.89 t (16H)	2.44 s (24H)	7.82 m (4H)	7.42 m (4H)	7.42 m (8H)	1.96 m (8H)	3.94 s (8H)	10.09 s (4H)
3k	−2.38 s (2H)	1.09 t (12H), 1.67 m (8H), 2.18 m (8H), 3.99 t (8H)	2.53 s (12H)	7.67 d (2H)	7.19 t (2H)	7.60 t (2H) 7.10 d (2H)	–	3.66 s (6H) [a]	10.19 s (2H)

[a] Signals for the protons of the methoxy group; [b] zinc complexes. Atropoisomers of the zinc complex of the dimer **13h**: [c] α,α,α,α; [d] α,β,α,α; [e] α,β,α,β.

protons (at $\delta \sim 7.8$) and a doublet for the *meta*-protons (at $\delta \sim 7.15$).

The dimers linked through the *meta* (**13d**–**f**) or *ortho* positions (**13h**,**i**) of the phenyl substituents exist as three atropoisomers, which differ by the orientations of the oxygen atoms of the ether bridges (Fig. 4). The compound **13g** containing short ether bridges ($n = 2$) does not form atropoisomers. The assignment of the signals to particular atropoisomers was made based on comparison of the chromatographic mobilities and polarities of the porphyrin molecules. From Table 19 it can be seen that the experimental data (R_f) agree with the calculated characteristics (the dipole moments of the molecules). The smaller the dipole moment of the molecule, the higher the chromatographic mobility of the atropoisomer.

The atropoisomerism of porphyrins is well studied.[89,90] For the phenyl fragments to be rotated, the macrocycle must be deformed to reduce steric interactions between the *ortho*-substituents and the protons of the NH or CH_2 groups. The addition of the side methyl groups would be expected to hinder rotation. However, the activation energy of thermal atropoisomerism is increased only slightly on going from *meso*-tetraphenylporphyrin to (*meso*-diphenyl)octamethylporphyrin. This phenomenon was

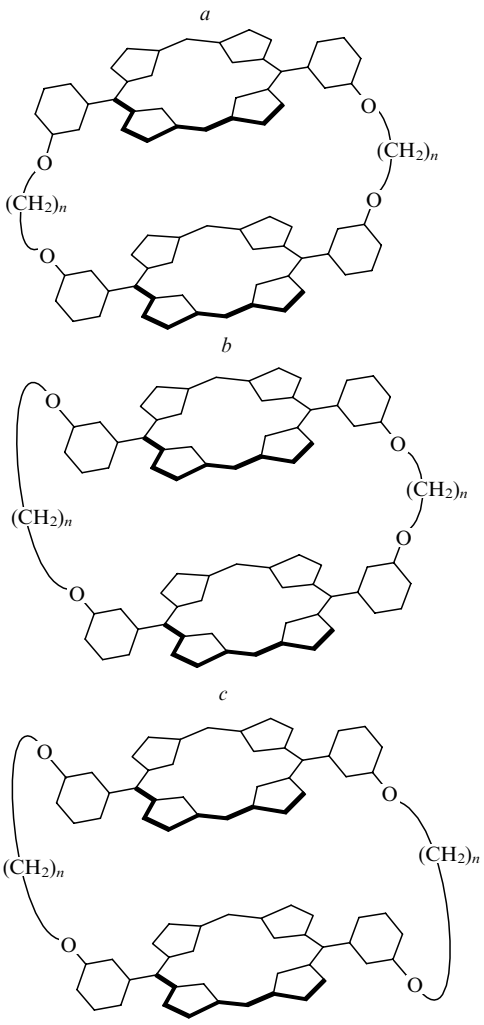

Figure 4. The α,α,α,α- (*a*), α,β,α,α- (*b*) and α,β,α,β-atropoisomers (*c*) of the dimers **12d**–**f**.[86]

accounted for by the flexibility of diphenylporphyrins.[89,90] The molecules of these compounds possess two free *meso* positions along which the ring is, apparently, folded. Therefore, steric restrictions arising from the introduction of additional β-methyl groups are compensated by flexibility of the diphenylporphyrin molecule.

Table 19. Dipole moments (μ) and chromatographic mobilities (R_f) on Silufol of the monomeric (**3h**–**m**) and dimeric (**13h**) porphyrins.[87,88]

Compound	Substituent in the benzene ring	Atropoisomer	μ /D (see [a])	R_f (see [b])
3h	H		0.107	0.60
3i	4-OMe		0.681	0.43
3j	3-OMe		0.674	0.45
3k	2-OMe	α,α	0.970	0.30
		α,β	0.100	0.65
3l	4-NO_2		0.424	0.50
3m	3-NO_2		0.026	0.75
13h	2-O$(CH_2)_4$O-2	α,α,α,α	0.075	0.61
		α,β,α,α	0.755	0.49
		α,β,α,β	1.398	0.31

[a] The dipole moments were calculated by the semiempirical CNDO and INDO methods. The conformations with the minimum energies were optimised by the block-diagonal Newton–Raphson method; [b] in the case of monomeric porphyrins, the spots were visualised with toluene; in the case of the atropoisomers of the dimeric porphyrin, the spots were visualised with a 1 : 4 pyridine–hexane mixture.

It was demonstrated [12] that, unlike the monomeric porphyrin **3k**, which readily underwent atropoisomerisation in boiling *o*-xylene (starting from one isomer, a mixture of the α,α and α,β isomers was formed in a ratio of 1 : 1), the phenyl fragments in the dimeric porphyrins cannot rotate and the atropoisomers of these compounds are stable. The ^{1}H NMR spectral data for the α,α,α,α, α,β,α,α and α,β,α,β isomers of the zinc complex of the dimer **13h** are given in Table 18. As in the case of the monomer **3k**, the spectra of the atropoisomers of the dimeric porphyrin **13h** differ only by splitting of the signals for the protons of the phenyl groups. The spectrum of the α,α,α,α atropoisomer, which is, apparently, characterised by the higher degree of equivalence of the protons, has a doublet for the *ortho*-protons and a triplet for the *para*-protons. The nonequivalent *meta*-protons give individual signals as a doublet and a triplet. The spectra of the α,β,α,α and α,β,α,β atropoisomers have a pronounced triplet for the *para*-protons and a doublet from a portion of the *meta*-protons. The signals for the other portion of the *meta*-protons and the signals for the *ortho*-protons coalesce into a multiplet.

IV. Electronic absorption spectra of porphyrins and metalloporphyrins

Electronic absorption spectra of porphyrins are very characteristic and contain four low-intensity absorption bands in the visible region and one very intense band in the violet region of the spectrum (the Soret band). The commonly accepted classification of these bands is as follows. The bands *I* and *III* in the visible region of the spectrum (Fig. 5 *a*) belong to quasi-forbidden electron transitions, whereas the bands *II* and *IV* are of electronic-vibrational origin, *i.e.*, are vibrational satellites of the bands *I* and *III*, respectively. Although possessing a number of common features, the spectra of porphyrins show substantial variations, which reflect the changes in the molecular structure and the effect of the solvent. According to the universally accepted concepts, light absorption is accompanied by excitation of the porphyrin molecule and the characteristic features of the absorption spectrum are determined by transitions of the π-electrons between two higher occupied and two lower unoccupied orbitals (the four-orbital Platt–Gouterman model [1]).

The intensity ratio of the absorption bands in the spectra of porphyrins depends on their structures in a peculiar fashion. The ethio type of the spectrum (see Fig. 5 *a*) with the intensity ratio *IV* > *III* > *II* > *I* is typical of *meso*-tetraphenylporphyrin, ethio-

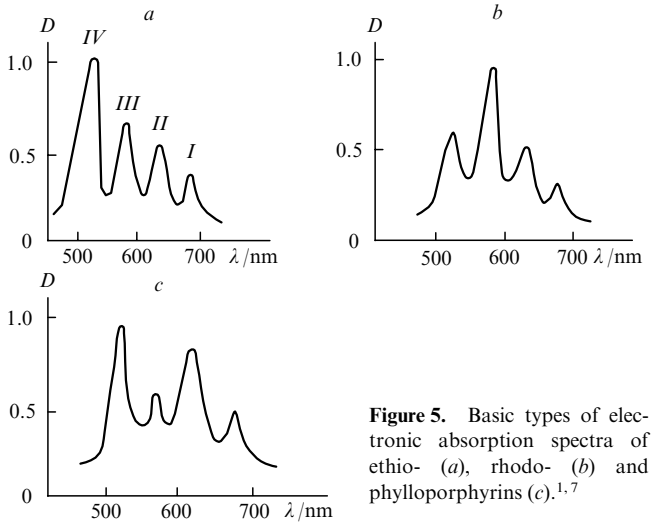

Figure 5. Basic types of electronic absorption spectra of ethio- (*a*), rhodo- (*b*) and phylloporphyrins (*c*).[1,7]

porphyrin and other symmetrically substituted porphyrins. For porphyrins characterised by the rhodo type of the spectra (Fig. 5 *b*), another sequence, *viz*., *III* > *IV* > *II* > *I*, is realised. Among the latter compounds are rhodoporphyrin and other porphyrins containing an electron-withdrawing substituent (COOH, NO_2, Cl, *etc*.) in the pyrrole fragment. Phylloporphyrin and other porphyrins containing one or two *meso*-substituents are characterised by the phyllo type of the spectrum (*IV* > *II* > *III* > *I*) (Fig. 5 *c*). Chlorin, tetrabenzoporphyrin and phthalocyanine give characteristic spectra of their own. In their spectra, the long-wavelength band *I* has the maximum intensity.

On going from porphyrin to metalloporphyrin, the symmetry of the planar macrocyclic fragment (of the π-electron cloud of the macrocycle) increases due to which the spectrum is simplified. The Soret band changes only slightly upon complex formation. The visible region of the spectra of metal complexes has two absorption bands, *viz*., the band *I* corresponding to the electron transition and the band *II* corresponding to the electronic-vibrational transition. The energy of the electron transition for the band *I* and its position in the spectrum (λ_1) can serve as reliable criteria for determining the strength and the type of the metal (M)—nitrogen chemical bond in metalloporphyrins. The band *I* is shifted hypsochromically as the strength of the M—N coordination bond in metalloporphyrins containing the planar MN_4 coordination unit increases.[91,92]

One of the most important features of metalloporphyrins is the deviation of the metal atom from the plane of the MN_4 coordination unit under the influence of the strongly coordinated molecular ligands or acido ligands. In most cases, the deviation of the metal atom from the plane is accompanied by a long-wavelength shift of the band *I*, whereas the movement of the metal atom toward the plane is accompanied by a short-wavelength shift.[7]

Therefore, electronic absorption spectroscopy is a powerful tool in studying the type and strength of the coordination bonds in metalloporphyrins, the degree of aromaticity of the macrocycle and its change upon chemical modification of the porphyrin.

1. Porphyrins

Electronic absorption spectra of porphyrins depend substantially on both the electronic and steric factors. Not only the positions and intensities of the absorption bands, but also their number can be changed. From this viewpoint, of special note is the introduction of four substituents at the *meso* positions of porphyrin. A rise in the aromaticity and an increase in the rigidity of the macrocycle lead to the complete disappearance of vibrational satellites and to a sharp increase in the intensities of the electron transition bands (Fig. 6). The band *I* in the electronic spectrum of tetraazoporphyrin is shifted to the short-wavelength region.[6]

On the whole, the introduction of substituents at the *meso* positions of the porphyrin macrocycle has a more substantial

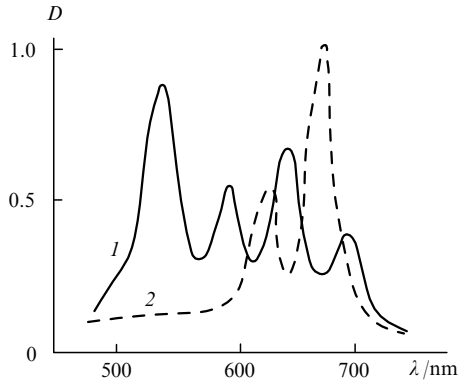

Figure 6. Electronic absorption spectra of porphyrin (*1*) and tetraazaporphyrin (*2*) in chloroform.[6,7]

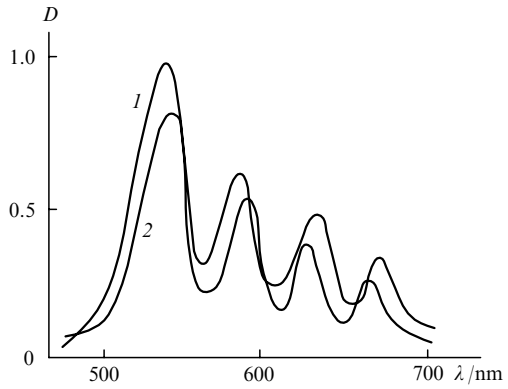

Figure 7. Electronic absorption spectra of *meso*-tetramethylporphyrin (*1*) and *meso*-tetraphenylporphyrin (*2*) in chloroform.[25]

effect on the absorption spectra than the introduction of substituents at the β positions. The *meso*-tetrasubstituted porphyrins are characterised by a distorted ethio type of spectra with rather large (25–40 nm) bathochromic shifts of the bands (Fig. 7, Table 20). It should be noted that small hypsochromic shifts of all absorption bands are observed on going from *meso*-tetramethylporphyrin to its homologues containing longer alkyl substituents.[38] Similar bathochromic shifts are observed in the electronic absorption bands on going from porphyrin to *meso*-tetraphenyl- or *meso*-tetramethylporphyrin (see Table 20). In these cases, the steric factor, apparently, prevails over the electronic effect.

The introduction of various substituents at the *para* positions of the phenyl rings of *meso*-tetraphenylporphyrin causes bathochromic shifts of the absorption bands in the visible region of the spectra. A comparison of the spectra of tetraphenylporphyrin and its *para*-substituted derivatives demonstrated that the intensities of the electron transition bands (*I* and *III*) rise as the electron-donating properties of the substituents increase. Simultaneously, the intensities of the vibrational bands (*II* and *IV*) are diminsihed.[93] The ethio type of the spectrum of tetraphenylporphyrin is distorted because the band *I* becomes more intense than the band *II*.

The presence of electron-donating substituents at the *meta* positions also leads to bathochromic shifts of the bands, the intensities of the vibrational bands being increased, while the intensities of the electron transition bands remaining virtually unchanged.[25] The spectra of *ortho*-substituted tetraphenylporphyrins are characterised by lower intensities of the electron transition bands compared to those observed in the electronic absorption spectrum of tetraphenylporphyrin. In some cases, this gives rise to the spectra of the phyllo type, for example, in the case of tetra(2-halogenophenyl)porphyrins and, particularly, in the case of tetra(2,6-dihalogenophenyl)porphyrins.

The absorption spectra are also dependent on the solvent. Thus, the bands in the electronic absorption spectra of substituted *meso*-tetraphenylporphyrins are shifted bathochromically and the intensities of the electron transition bands grow on going from nonpolar hexane to polar pyridine.[25]

It is known[39] that the introduction of methyl groups at the β positions of the porphyrin ring causes only slight bathochromic shifts of the absorption bands (5–10 nm). The effect of the *meso*-substitution on the spectral characteristics of β-alkylporphyrins and their complexes with some transition metals (Zn, Cu or Ni) was investigated.[14,17,38,39] 2,8,12,18-Tetrabutyl-3,7,13,17-tetramethylporphyrin (**3t**), which is similar in the electronic effect of the substituents to natural porphyrins, was used as the starting compound. Derivatives of the porphyrin **3t** containing aryl (**3h**–**m**) or alkyl (**3a**–**g**) substituents or aza bridges (**14m**) at positions 5 and 15 are structurally related to the most important

Table 20. Electronic absorption spectra of *meso*-tetrasubstituted porphyrins in chloroform.[25,38]

meso-Substituents	λ_{max}/nm ($\varepsilon \times 10^{-3}$/litre mol^{-1} cm^{-1})				
	I	*II*	*III*	*IV*	Soret
H	615 (1.0)	562 (3.5)	515 (2.7)	490 (9.3)	394 (174)
H [a]	620 (4.4)	568 (6.3)	535 (9.1)	500 (12.1)	400 (141)
Me	664 (3.7)	610 (2.7)	560 (5.2)	524 (6.8)	420 (112)
Ph	648 (6.4)	590 (6.1)	550 (8.6)	516 (19.4)	419 (499)
Ph [b]	694 (9.1)	602 (8.0)	shoulder	553 (9.4)	454 (164)
4-$NH_2C_6H_4$	654 (7.6)	599 (5.5)	562 (12.0)	524 (12.0)	428 (313)
4-HOC_6H_4	650 (5.2)	595 (5.07)	556 (7.9)	519 (11.4)	423 (272)
4-$MeOC_6H_4$	652 (7.4)	595 (6.1)	557 (11.9)	520 (17.7)	423 (491)
4-$MeOC_6H_4$ (see [b])	703 (3.8)	608 (4.0)	shoulder	556 (5.27)	454 (189)
4-MeC_6H_4	648 (6.8)	593 (6.2)	554 (10.3)	518 (18.8)	412 (504)
4-BrC_6H_4	650 (6.5)	592 (7.4)	551 (10.6)	516 (21.9)	412 (567)
4-$NO_2C_6H_4$	650 (3.5)	592 (5.4)	552 (7.6)	518 (15.3)	426 (228)
4-$NO_2C_6H_4$ (see [b])	697 (3.8)	600 (3.9)	shoulder	552 (4.09)	454 (246)
3-$NH_2C_6H_4$	649 (3.9)	592 (5.2)	557 (7.1)	518 (15.1)	427 (155)
3-HOC_6H_4	645 (5.1)	588 (7.5)	550 (8.4)	514 (20.2)	419 (413)
3-$MeOC_6H_4$	648 (5.2)	590 (6.7)	550 (7.8)	516 (20.6)	420 (499)
3-MeC_6H_4	648 (6.5)	592 (6.0)	551 (8.7)	517 (18.7)	420 (485)
3-BrC_6H_4	652 (6.7)	592 (6.6)	549 (8.5)	516 (20.2)	420 (456)
3-$NO_2C_6H_4$	655 (6.6)	592 (7.1)	550 (7.3)	516 (20.6)	424 (352)
2-$NH_2C_6H_4$	653 (3.1)	595 (5.2)	556 (5.8)	519 (16.2)	422 (186)
2-HOC_6H_4	652 (5.6)	590 (5.3)	548 (5.6)	515 (16.6)	419 (354)
2-$MeOC_6H_4$	646 (4.1)	590 (7.6)	547 (7.3)	514 (21.9)	419 (432)
2-MeC_6H_4	648 (4.6)	590 (6.4)	546 (6.3)	515 (20.5)	418 (477)
2-BrC_6H_4	647 (2.6)	590 (7.7)	551 (4.3)	515 (22.5)	420 (475)
2-$NO_2C_6H_4$	654 (3.0)	596 (6.7)	552 (6.8)	518 (19.4)	424 (283)
C_6F_5	657 (4.4)	583 (8.0)	538 (4.1)	507 (22.3)	414 (317)

The spectral characteristics are given: [a] for β-octamethylporphyrin; [b] for *meso*-tetraaryl-β-octamethylporphyrins.

synthetic porphyrins, *viz*., to *meso*-tetraphenylporphyrin and tetraazaporphyrin.

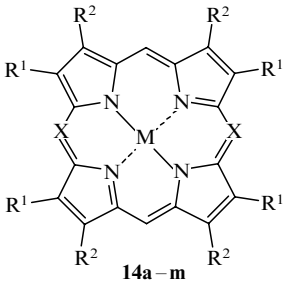

14a–m

$R^1 = R^2 = Me$, X = CMe: M = Zn (**a**), Cu (**b**), Ni (**c**); R^1 = Me, $R^2 = Bu^n$: X = CPh, M = Zn (**d**), Cu (**e**), Ni (**f**); X = CH, M = Zn (**g**), Cu (**h**), Ni (**i**); X = N, M = Zn (**j**), Cu (**k**), Ni (**l**), H_2 (**m**).

As can be seen from Fig. 8, the absorption spectra of these compounds, as well as of their zinc complexes, are similar. The spectral changes are quantitative rather than qualitative. This fact indicates that the corresponding electron transitions are of the same type and suggests that the introduction of two phenyl or alkyl substituents or the replacement of the carbon atoms at the *meso* positions by the nitrogen atoms exerts a rather small perturbing effect on the π-system of the porphyrins and their zinc complexes under study, and the π-system retains the approximate symmetry D_{2h} and D_{4h}, respectively.

It was demonstrated [17] that electron transitions in metalloporphyrins occur from the a_{1u} and a_{2u} orbitals to the e_{gx} and e_{gy} orbitals. The a_{1u} orbital has four nodal planes passing through the *meso* positions and the central nitrogen atoms. The a_{2u} orbital possesses zero electron density on the β-carbon atoms. Hence, perturbation of the π-system of metalloporphyrins at the β positions, for example, upon alkylation, destabilises the a_{1u} orbital, while the energy level of the a_{2u} orbital remains unchanged. On the contrary, perturbation at the *meso* positions and the nitrogen atoms has no effect on the a_{1u} orbital and affects the a_{2u} orbital. Two degenerate antibonding e_g orbitals differ in that one of the nodal planes of the e_{gx} orbital and one of the nodal planes of the e_{gy} orbital pass through different pairs of the nitrogen atoms (in porphyrins, NH – NH).

Figure 9 shows the changes in the energy levels of the a_{1u}, a_{2u} and e_g orbitals (taking into account their nodal properties) that occur on going from the zinc complexes of the octaalkylporphyrin **14g** to the zinc complex of the *meso*-diazaoctaalkylporphyrin **14j**. The energy levels of the higher occupied (b_1 and b_2) and lower

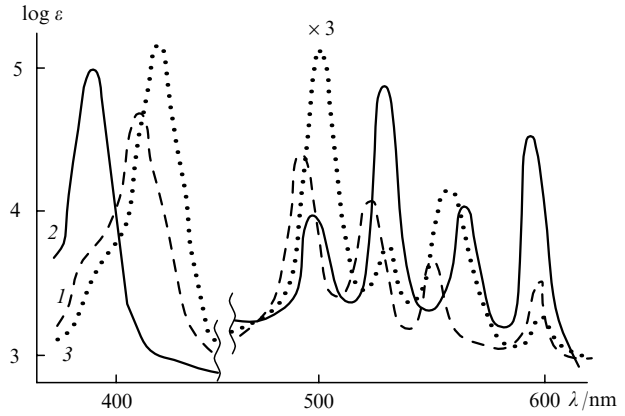

Figure 8. Electronic absorption spectra of 2,8,12,18-tetrabutyl-3,7,13,17-tetramethylporphyrin (*1*) and its 5,15-diaza- (*2*) and -diphenyl derivatives (*3*) in chloroform.[17]

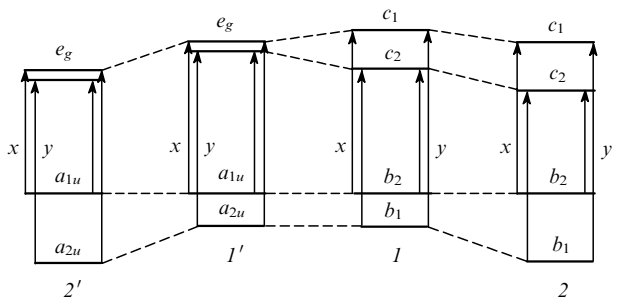

Figure 9. Scheme of the energy levels of the higher occupied and lower unoccupied orbitals of octaalkylporphyrin (*1*), its 5,15-diaza derivative (*2*) and their zinc complexes (*1′* and *2′*, respectively).[17]

unoccupied (c_1 and c_2) orbitals of free porphyrins are also presented in Fig. 9.

The replacement of the carbon atoms at the *meso* positions by the nitrogen atoms results primarily in lowering of the energy levels of the a_{2u} and e_g orbitals compared to the levels of these orbitals in the compound **14g** and, as a consequence, in weakening of the configuration interactions between the excited one-electron states $a_{1u}e_{gx}$ and $a_{2u}e_{gx}$ and between $a_{1u}e_{gy}$ and $a_{2u}e_{gy}$. Correspondingly, the intensity of the absorption band *I* in the electronic absorption spectrum of the complex **14j** is higher than that present in the spectrum of the complex **14g**. An analogous effect is observed in the case of free porphyrins. Thus, the bands *I* and *II* in the spectrum of the *meso*-diazaoctaalkylporphyrin **14m** are more intense than those in the spectrum of the octaalkylporphyrin **3t**.

Weakening of the configuration interaction would be expected to cause hypsochromic shifts of the absorption bands in the visible region of the spectra of the aza derivatives **14j**,**m** and the bathochromic shift of the Soret band. However, experimental studies demonstrated that the replacement of the carbon atoms by the nitrogen atoms has the opposite effect. Apparently, the direction of the shift of the absorption bands on going from the porphyrins **3t** and **14g** to their aza analogues **14m** and **14j** is determined by a change in the energy of the corresponding one-electron transitions, *i.e.*, by stabilisation of the a_{2u} and e_g levels in the compound **14j** and the b_1 and c_2 levels in the ligand **14m**. On going from the above-mentioned porphyrins to their aza derivatives, the intensities of the electronic-vibrational bands *II* and *IV* of the porphyrin and the band *II* of the complex are sharply diminished (see Fig. 8, Table 21). These bands borrow the intensity from the adjacent allowed Soret band.[17] The smaller the difference between the energies of the interacting transitions, the higher the efficiency of this rearrangement of the intensities. The replacement of the carbon atoms by the nitrogen atoms is accompanied by a

Table 21. Electronic absorption spectra of β-octaalkylporphyrin derivatives.[38, 39]

Compound	λ_{max} /nm (log ε)				
	I	*II*	*III*	*IV*	Soret
In chloroform					
3a	625.0 (2.98)	574.1 (3.17)	538.2 (3.21)	505.4 (3.77)	405.1 (4.61)
14a	–	570.3 (3.66)	537.1 (3.78)	–	408.6 (4.63)
14b	–	568.3 (3.58	534.1 (3.74)	–	405.7 (4.56)
14c	–	556.0 (3.42)	526.4 (3.19)	–	398.4 (4.17)
3b	626.3 (2.98)	572.4 (3.19)	539.0 (3.22)	509.4 (3.80)	405.3 (4.58)
3c	625.1 (2.93)	573.7 (3.15)	538.5 (3.20)	509.1 (3.79)	408.7 (4.60)
3d	626.3 (2.97)	572.7 (3.14)	539.7 (3.19)	509.2 (3.77)	405.1 (4.59)
3e	626.1 (2.94)	572.7 (3.13)	539.1 (3.19)	509.7 (3.76)	405.3 (4.56)
3f	626.3 (2.96)	573.0 (3.15)	539.4 (3.18)	508.4 (3.74)	407.1 (4.56)
3g	626.7 (2.91)	576.2 (3.14)	540.1 (3.17)	507.9 (3.76)	409.0 (4.62)
3h	622.0 (3.42)	574.7 (3.92)	541.1 (3.71)	508.1 (4.16)	409.8 (5.19)
14d	–	575.1 (3.99)	541.4 (4.26)	–	412.3 (5.08)
14e	–	573.2 (3.89)	539.6 (4.31)	–	410.4 (5.08)
14f	–	570.1 (3.79)	536.1 (4.28)	–	408.6 (5.14)
3i	623.6 (3.60)	572.1 (3.99)	542.4 (3.80)	508.4 (4.12)	409.4 (5.10)
3j	621.9 (3.49)	574.2 (3.71)	542.4 (3.60)	508.0 (4.01)	410.1 (5.14)
3k	622.4 (3.60)	573.8 (3.87)	541.8 (3.74)	508.2 (4.09)	409.0 (5.02)
3l	624.6 (3.41)	576.0 (3.70)	544.0 (3.52)	506.9 (4.16)	409.0 (5.17)
3m	622.5 (3.51)	576.4 (3.90)	543.0 (3.71)	507.1 (4.13)	410.4 (5.09)
14h	–	569.2 (3.86)	534.1 (3.54)	–	399.7 (5.17)
14i	–	557.1 (3.91)	526.1 (3.60)	–	396.7 (5.14)
3u	629.1 (3.48)	574.5 (3.62)	540.4 (3.68)	507.1 (4.01)	421.4 (4.89)
3v	634.5 (3.28)	576.1 (3.58)	542.1 (3.72)	508.4 (4.03)	422.1 (4.92)
14m	622.1 (4.01)	580.4 (3.64)	544.4 (4.17)	506.0 (3.69)	375.1 (5.20)
14j	–	589.3 (4.24)	548.5 (3.52)	–	378.6 (5.24)
14k	–	587.6 (4.14)	544.1 (3.41)	–	376.2 (5.14)
14l	–	576.4 (4.08)	536.4 (3.38)	–	370.1 (5.07)
In acetic acid					
3a	–	564.1 (3.89)	–	–	419.0 (5.24)
14a	–	570.3 (3.64)	537.0 (3.70)	–	405.1 (4.60)
3h	621.9 (3.78)	574.7 (4.03)	–	–	434.8 (5.21)
14d	621.9 (3.90)	574.7 (4.15)	–	–	434.0 (5.20)
3t	–	592.2 (3.49)	548.2 (3.81)	–	407.8 (5.08)
14g	–	592.4 (3.55)	548.7 (3.88)	–	407.2 (5.18)
14m	626.1 (3.81)	–	–	–	393.5 (5.10)
14j	624.6 (3.93)	–	–	–	379.9 (5.08)

hypsochromic shift of the Soret band resulting in the low intensities of the electronic-vibrational bands in the spectra of the compounds **14m** and **14j**.

A comparison of the electronic absorption spectra of the metal complexes of octaalkylporphyrin derivatives (M = Zn, Cu or Ni) demonstrated that the bands are shifted to the low-frequency region. These shifts increase in the series Zn < Cu < Ni, *i.e.*, as the strength of the metal–nitrogen coordination bond increases. An enhancement of the electronegativity of the metal atom leads to lowering of the electron density on the occupied π-orbitals of the porphyrin molecule, which is accompanied by hypsochromic shifts of the bands (particularly, of the band *I*).

An analogous regularity is also observed for the positions of the 'metal-sensitive' bands in the IR spectra of porphyrins.[11] The deformation vibration bands of the alkyl groups (at 955 and 910 cm^{-1}) and the stretching and deformation vibration bands of the *meso*-protons (at 3110, 1220 and 835 cm^{-1}) are shifted to the high-frequency region as the degree of coordination of the metal atom increases.

On going from the octaalkylporphyrin **3t** to the *meso*-diphenyloctaalkylporphyrin **3h**, the Soret band is shifted bathochromically (see Table 21). It was demonstrated [38] that the introduction of strong donor or acceptor substituents into the phenyl rings of the diphenyl-substituents porphyrins **3i**–**m** has virtually no effect on the absorption spectra. Apparently, all absorption bands are shifted bathochromically due to distortion of the planar structure of the porphyrin macrocycles due to the presence of the phenyl substituents. This suggestion is evidenced by the ^{1}H NMR spectral data.[12, 14] It is known that steric restrictions are responsible for analogous changes in the electronic absorption spectra of *ortho*-derivatives of tetraphenylporphyrin [81] and cyclophane dimeric porphyrin. [76] A comparison of the electronic absorption spectra of the structural isomers **3h** and **3n** showed that the replacement of the methyl groups at positions 3, 7, 13 and 17 of the porphyrin macrocycle by the butyl groups leads to a substantial increase in the bathochromic shift of the absorption bands resulting from additional deformation of the porphyrin molecule due to the mutual effect of the adjacent butyl and phenyl fragments.

The electronic absorption spectra of the *meso*-dialkyl-substituted octaalkylporphyrins **3a**–**g** belong to the ethio type. For the first four members of the series, the odd-even alternation of the positions of the bands *I* and *III* is observed (see Table 21).

The porphyrin rings in the *meso*-tetrasubstituted octaalkylporphyrins **3u**,**v** have distorted 'corrugated' structures giving rise to substantial bathochromic shifts and broadening of the bands in their electronic absorption spectra compared to those observed in the spectra of tetraphenylporphyrin and *meso*-disubstituted octaalkylporphyrins (see Table 21).

2. Bisporphyrins

The electronic absorption spectra of cyclophane dimeric porphyrins have the following distinguishing features as compared to the monomeric analogues:[76–86, 94–102]

(1) a relatively large hypsochromic shift and substantial broadening of the Soret band;

(2) one diffuse absorption band at the long-wavelength side of the Soret band;

(3) a small bathochromic shift in the visible region.

The shifts of the bands in the absorption spectrum are determined by two factors, *viz*., by essential interactions between two identical porphyrin fragments whose nature depends on the symmetry of the dimer (the factor of exciton interactions) and by the effect of the solvent, which reflects the different degree of solvation of the ground and excited states (the factor of solvation).

In the short-wavelength region, the effect of the first factor leads to the hypsochromic shift of the Soret band in the electronic absorption spectra of symmetrical porphyrins, while the second factor causes broadening of this band. The manifestation of the low-energy excited states is possible in the case of displacement or inclination of the porphyrin macrocycles due to which the Soret band has a shoulder at 450 nm. Small bathochromic shifts of the bands in the visible region are attributable to weakening of the effect of exciton interactions in the long-wavelength region of the spectrum.

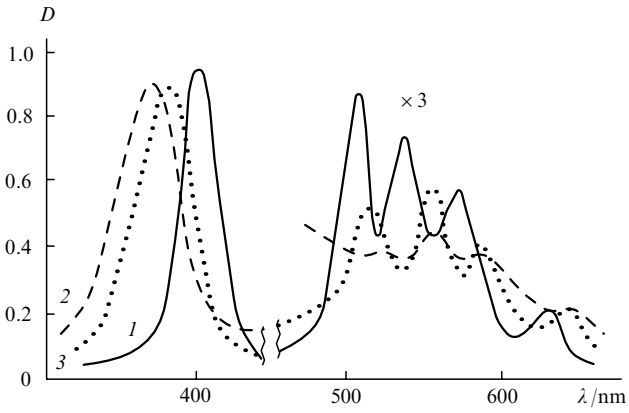

Figure 10. Electronic absorption spectra of the monomeric porphyrin **8** (*1*) and the dimeric porphyrins **7a** (*2*) and **7b** (*3*) in dichloromethane.[72]

The electronic absorption spectra of the monomeric porphyrin **8** and the β-bound dimers **7a**,**b**[72] are shown in Fig. 10.

The hypsochromic shift of the Soret band increases and the absorption bands in the visible region are shifted bathochromically and become more diffuse as the number of units in the bridge increases. The changes in the positions of the amide groups in the bridges also exert an effect on the electronic absorption spectra (Table 22).

In the electronic absorption spectra of the dimers **15a**–**d** and **16a**,**b** linked through the flexible hydrocarbon bridges and rigid aromatic fragments, respectively, the Soret band is shifted hypsochromically and the bands in the visible region are shifted bathochromically compared to those in the spectra of their monomeric analogues.[57, 70, 100] These shifts are determined by the strength of interactions between the porphyrin fragments, which depends not only on the distance between the macrocycles, but also on their mutual arrangement.

The hypsochromic shift of the Soret band in the electronic absorption spectrum of the compound **15c** containing two eight-atom bridges is 10 nm (Table 23). A decrease in the length of one bridge by two methylene units (the compound **15b**) leads to a

Table 22. Electronic absorption spectra of monomeric porphyrin (**8**) and the dimeric porphyrins **7a**–**n** in dichloromethane.[72, 73]

Compound	λ_{max} /nm				
	Soret	*IV*	*III*	*II*	*I*
7a	370	502	536	566	644
7b	376	502	544	577	626
7c	372	507	548	578	640
7d	381	–	–	–	627
7e	380	–	–	–	626
7f	384	–	–	–	624
7g	380	505	538	569	622
7h	382	–	–	554	–
7i	386	510	548	572	640
7j	392	–	526	566	–
7k	352	468	556	–	–
7l	382	473	534	560	–
7m	380	–	552	–	–
7n	384	–	520	558	–
8	400	498	536	566	620

Table 23. Electronic absorption spectra of monomeric and dimeric porphyrins in dichloromethane.[57, 70, 100]

Compound	λ_{max}/nm				
	Soret	*IV*	*III*	*II*	*I*
2,7,12,17-Tetraethyl-3,8,13,18-tetramethylporphyrin	396	496	531	566	619
15a	385	498	532	567	620
15b	390	497	531	567	620
15c	386	501	534	569	623
15d	392	502	535	570	622
16a	394	503	537	572	625
16b	378	508	542	578	630
2,8,13,17-Tetraethyl-3,7,12,18-tetramethyl-5-phenylporphyrin	402	501	537	559	626

Table 24. Characteristics of absorption and emission of the porphyrins **8** and **17**.[94, 103]

Compound	λ/nm [a]	λ_{em}/nm [b]	ϕ_{rel} [c]
8	397	621	1.0
8 [d]	402	572	1.0
8 [e]	401	596	1.0
17a	385	624	0.54
17b	388	581	0.20
17c	397	596	0.71

[a] The absorption maximum of the Soret band; the electronic absorption spectrum was measured in dichloromethane; [b] the emission spectrum was recorded in dichloromethane on irradiation in the Soret region; [c] the quantum yield of fluorescence of the dimeric complexes with respect to the corresponding monomeric complexes; [d] the Zn complex of the compound **8**; [e] the protonated form of the compound **8**.

decrease in this shift by 4 nm. Apparently, the interactions between the π-electron systems of the macrocycles are weakened and the effect of exciton interactions on the spectral properties is reduced due to inclination of the porphyrin macrocycles arising from the different length of the bridges. An analogous spectral behaviour was observed [94, 103, 104] in the case of dimers containing two flexible ester bridges.

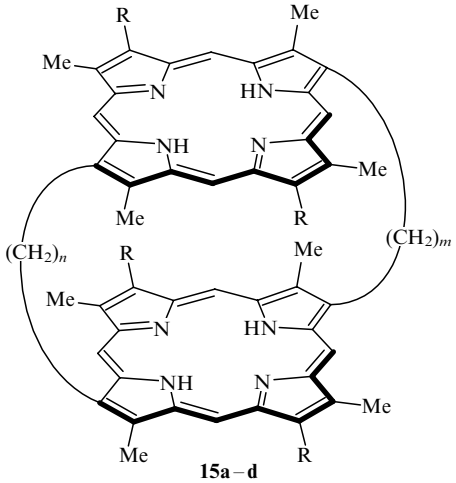

15a–d

$m = n = 5$ (**a**), $m = 8$, $n = 6$ (**b**), $m = n = 8$ (**c**), $m = n = 10$ (**d**).

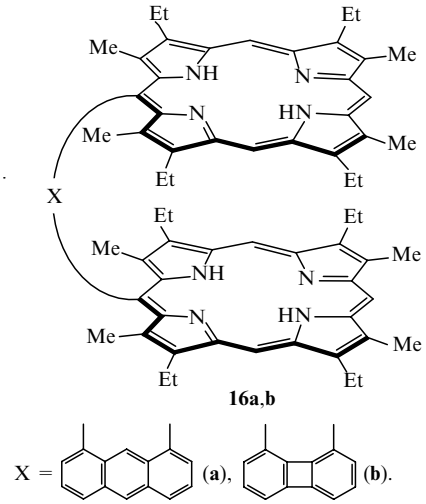

16a,b

X = (**a**), (**b**).

The Soret band in the electronic absorption spectra of the dimer **17a** and its zinc complex **17b** is broadened and is hypsochromically shifted relative to the Soret band in the spectra of the monomer **8** and its zinc complex. The distance between the macrocycles in the dimers increases and interactions between the porphyrin fragments are weakened upon protonation (Table 24).

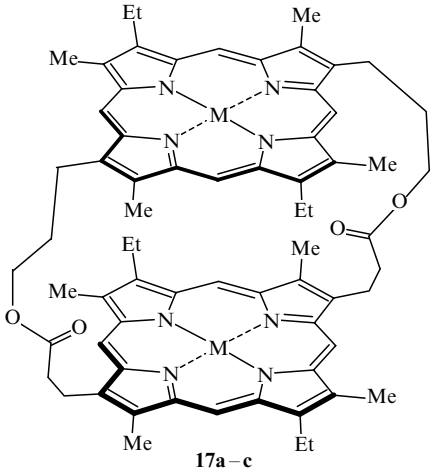

17a–c

M = H_2 (**a**), Zn (**b**), H_4 (**c**).

The dimers adopting a 'face-to-face' conformation are characterised by fluorescence quenching due to interactions between the porphyrin fragments. In the case of the dimer **17a**, this quenching was ~50% of the corresponding value for the monomeric analogue.

In the absorption spectra of the dimers containing four bridges, no hypsochromic shift is observed in the short-wavelength region (Table 25). The spectrum of the dimer **18a** containing the ester bridges is characterised (Fig. 11) by noticeable broadening and the bathochromic shift of the band in the visible region of the spectrum, while the position of the Soret band

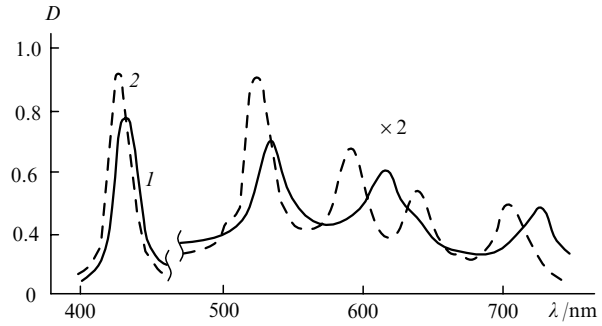

Figure 11. Electronic absorption spectra of the dimer **18a** (*1*) and tetra-*meso*-[*p*-2-(hydroxyethoxy)phenyl]porphyrin (*2*) in pyridine.[105]

Table 25. Electronic absorption spectra of monomeric and dimeric porphyrins in pyridine.[77, 104]

Compound	λ_{max} /nm				
	Soret	*IV*	*III*	*II*	*I*
11a	444	–	542	581	694
11b	446	–	–	620	666
11c	435	533	572	675	694
11e [a]	414	515	550	590	646
11f [a]	414	516	550	591	649
11g [a]	415	517	552	593	650
Tetra(*m*-butoxyphenyl)-porphyrin	420	515	550	594	651
Zn complex of tetra-(*m*-butoxyphenyl)-porphyrin	433	–	558	597	–
18a	426	523	562	584	677
18b	422	–	562	606	–

[a] The spectra were measured in chloroform.

remains unchanged.[70, 105] The absorption bands in the visible region of the spectrum of the dimer **11a** containing ether bonds are shifted bathochromically [77] by 25–40 nm and the Soret bands are shifted by 20–25 nm compared to those observed in the spectrum of the monomeric analogue (Fig. 12 *a*).

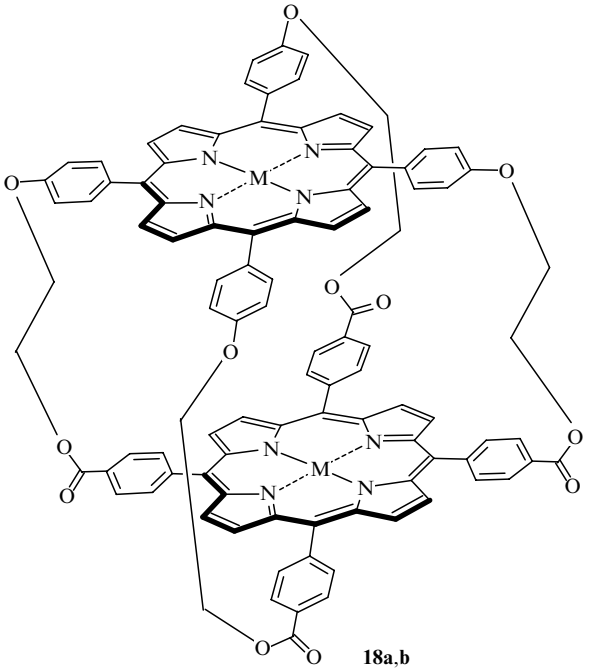

18a,**b**

M = H_2 (**a**), Zn (**b**).

This spectral behaviour of the dimer **11a** is attributed to extension of the conjugated π-electron system due to partial conjugation between the π-systems of the phenyl rings and the porphyrin macrocycles.[77] This effect is most clearly pronounced in the electronic absorption spectrum of a solution of the compound **11a** in CH_3CO_2H in which the dimer **11a** exists in the protonated form (Fig. 12 *b*).

Protonation leads to an essential increase of deformation of the macrocycle, while the dihedral angle between the mean porphyrin plane and the plane of the benzene π-systems decreases significantly. A decrease in the length of the bridge by one methylene group on going from the dimer **11a** to the dimer **11c** is accompanied by hypsochromic shifts of all bands by 7–21 nm (see Table 25). However, the bathochromic shift with respect to

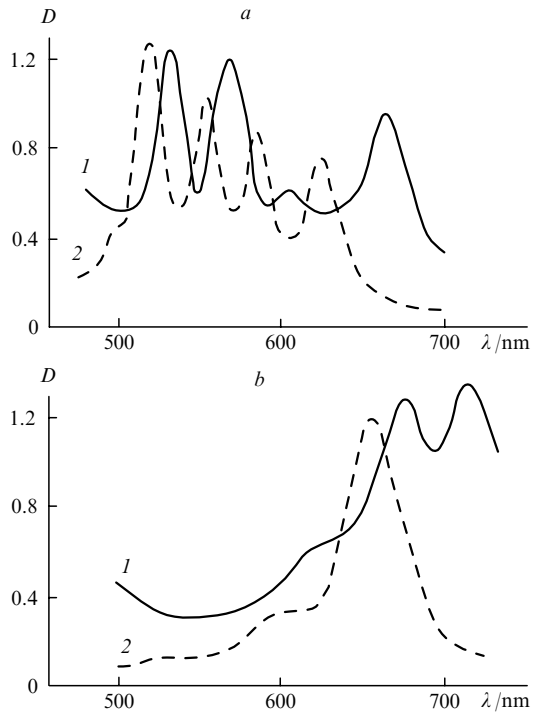

Figure 12. Electronic absorption spectra of the dimer **11a** (*1*) and tetra-*meso*-(*m*-butoxyphenyl)porphyrin (*2*) in pyridine (*a*) and acetic acid (*b*).[77]

the absorption bands in the spectrum of the monomeric analogue is retained.

In the electronic absorption spectra of the cyclophane dimers **11e**–**g**, the Soret band is shifted to the short-wavelength region by 4–5 nm and is broadened compared to the Soret band in the spectrum of the monomer (see Table 25).[79] Broadening is more pronounced in the case of the dimer **11f** in which the porphyrin fragments, while remaining parallel, are rotated with respect to each other (α_{max} = 26°). The spectral characteristics are changed due to interactions between the dipoles of the electronic transitions in two porphyrin fragments located at angles other than 0 or 180° with respect to each other. Bookser and Bruice [79] believed that the observed broadening and shifts of the bands indicate that solutions contain the dimers **11e**–**g** predominantly in a twist conformation. In this case, steric restrictions are less significant and the adjacent porphyrin rings are brought into proximity, which is also confirmed by the ^{1}H NMR spectral data.

The electronic absorption spectra (Fig. 13 *a*,*b*) of the dimeric *meso*-diphenyl-β-octaalkylporphyrins **13a**–**i** containing the $O(CH_2)_nO$ bridging groups were investigated.[82–85] The absorption bands of all dimeric porphyrins **13** are broadened and shifted hypsochromically by 5–20 nm compared to those in the spectrum of the monomeric porphyrin **3h** (Table 26). The short-wavelength shifts of the bands increase regularly as the length of the $O(CH_2)_nO$ bridge decreases and the adjacent porphyrin fragments approach each other. Considering this shift as a characteristic of the average distance between the porphyrin fragments in the dimer, it can be concluded that this distance decreases on going from the α,α,α,α to α,β,α,β atropoisomer (see Fig. 4). Calculations of the structures of the octamethyl analogues of the dimers by molecular mechanics demonstrated that the distance between the porphyrin fragments is no less than 3.6 Å.[87]

Consequently, exciton interactions between the porphyrin rings are responsible for the shifts of the absorption bands. Since the bands are shifted hypsochromically, the dimers have predominantly the 'face-to-face' orientation with the parallel arrangement of the interacting dipole moments of the electronic transitions. Each atropoisomer of the dimer exists as an equilibrium mixture of a large number of conformers. The structures of some of these

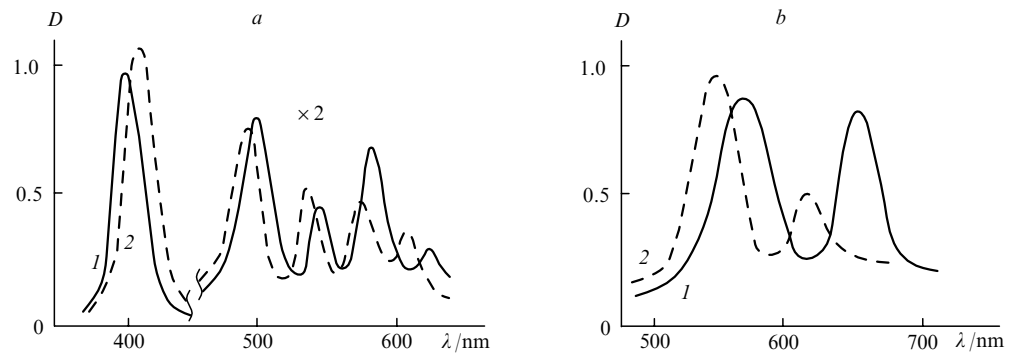

Figure 13. Electronic absorption spectra of the porphyrin **3h** (*1*) and the *meta*-bound dimer **13d** (*2*) in chloroform (*a*) and acetic acid (*b*).[82, 83]

Table 26. Electronic absorption spectra of the dimeric porphyrins **3h** and **13a**–**i**.[83, 86]

Compound	λ_{max}/nm (log ε)				
	Soret	*IV*	*III*	*II*	*I*
In chloroform					
3h	411 (5.35)	506 (4.21)	540 (3.81)	576 (3.89)	630 (3.45)
13a	405 (4.33)	503 (3.81)	538 (3.38)	573 (3.59)	626 (3.01)
13b	407 (4.91)	506 (3.99)	537 (2.45)	575 (3.63)	627 (3.19)
13c	410 (4.96)	507 (4.06)	540 (3.31)	576 (3.57)	629 (3.07)
13d [a]	393 (5.01)	497 (4.15)	531 (3.80)	565 (3.54)	621 (3.28)
13d [b]	395 (4.98)	497 (4.09)	534 (3.72)	568 (3.48)	622 (3.39)
13d [c]	394 (5.04)	496 (4.11)	530 (3.79)	566 (3.51)	621 (3.40)
13e [a]	395 (5.00)	498 (3.94)	534 (3.56)	569 (3.19)	623 (3.01)
13e [b]	396 (5.07)	500 (3.96)	537 (3.58)	571 (3.27)	623 (3.08)
13e [c]	395 (5.01)	497 (3.98)	533 (3.69)	569 (3.49)	622 (3.11)
13f [a]	397 (5.11)	501 (4.06)	541 (3.89)	573 (3.50)	624 (3.28)
13f [b]	399 (5.01)	503 (4.11)	542 (3.82)	576 (3.49)	625 (3.37)
13f [c]	397 (5.07)	500 (4.03)	539 (3.82)	576 (3.52)	623 (3.42)
13g	386 (5.10)	494 (3.96)	530 (3.60)	566 (3.27)	618 (3.08)
13h [a]	390 (4.99)	495 (3.92)	531 (3.56)	563 (3.26)	619 (3.08)
13h [b]	391 (4.92)	496 (3.89)	533 (3.42)	566 (3.36)	620 (3.13)
13h [c]	390 (4.99)	495 (3.92)	531 (3.56)	563 (3.26)	619 (3.08)
13i [a]	391 (5.08)	495 (3.90)	530 (3.57)	561 (3.28)	619 (3.07)
13i [b]	393 (5.00)	498 (3.87)	535 (3.52)	566 (3.21)	620 (3.04)
13i [c]	393 (5.01)	496 (3,94)	533 (3.60)	562 (3.20)	620 (3.00)
In acetic acid					
3h	436 (5.38)	–	572 (4.16)	–	619 (3.88)
13a	432 (4.90)	–	556 (4.51)	–	589 (3.17)
13b	435 (4.96)	–	558 (4.37)	–	593 (3.29)
13c	438 (4.93)	–	559 (4.09)	–	597 (3.11)
13d [a]	435 (4.92)	–	552 (4.42)	–	591 (3.59)
13d [b]	436 (4.87)	–	552 (4.40)	–	590 (3.50)
13d [c]	435 (4.96)	–	552 (4.42)	–	590 (3.54)
13e [a]	438 (4.91)	–	552 (4.42)	–	595 (3.51)
13e [b]	437 (4.90)	–	552 (4.48)	–	595 (3.49)
13e [c]	438 (4.94)	–	552 (4.45)	–	595 (3.54)
13f [a]	440 (4.92)	–	555 (4.43)	–	592 (3.35)
13f [b]	439 (4.81)	–	555 (4.43)	–	592 (3.29)
13f [c]	439 (4.86)	–	556 (4.45)	–	592 (3.54)
13g	427 (4.90)	–	549 (4.48)	–	583 (3.47)
13h [a]	430 (4.87)	–	550 (4.27)	–	587 (3.61)
13h [b]	431 (4.73)	–	551 (4.14)	–	588 (3.40)
13h [c]	430 (4.81)	–	550 (4.39)	–	587 (3.52)
13i [a]	433 (4.73)	–	551 (4.37)	–	591 (3.62)
13i [b]	434 (4.60)	–	552 (4.19)	–	591 (3.36)
13i [c]	434 (4.86)	–	552 (4.41)	–	592 (3.50)

Atropoisomers: [a] α,α,α,α; [b] α,β,α,α; [c] α,β,α,β.

conformers were studied by molecular mechanics (the MM+ force field). The atomic coordinates and the components of the potential energy of the optimised structures are summarised in the study.[87] From Table 27 it follows that a change from one conformer to another is generally accompanied by insignificant changes in the energy of the molecule (at most 10 kJ mol^{-1}). In spite of the fact that it is presently impossible to carry out complete analysis of the potential energy surface of such complex molecules, the existence of various conformational isomers in the gaseous phase and solutions is beyond question.

The results of geometry optimisation of dimeric porphyrins by the MM+ method (Fig. 14) demonstrated [87,88] that the aromatic tetrapyrrole macrocycle is deformed very readily. None of 15 conformers contains the planar porphyrin fragment. Conformational rearrangements of the tetrapyrrole nucleus occur through changes of the dihedral angles C–C–C–C, C–C–C–N, *etc.*, while the bond lengths and bond angles remain constant.

Each conformer of the dimeric porphyrins **13a**–**i** has its own individual absorption spectrum. It is needless to say that these spectra are qualitatively similar to the spectra of the monomeric analogues. However, in a quantitative sense these differences may be significant. One would expect that the absorption bands of the conformers with the parallel and perpendicular arrangement of the porphyrin rings will be shifted hypsochromically and bathochromically, respectively, under the influence of the exciton factor. The experimental spectra represent superpositions of the spectra of all conformers present in solution due to which the absorption bands of dimeric compounds are broadened and their intensities are lower compared to those of monomeric porphyrin. At the same time, the corresponding absorption bands in the spectra of monomeric and dimeric porphyrins do not differ in oscillator strength (f), which was calculated according to the approximate equation

$$f = (4.6 \times 10^{-9})\, \varepsilon_{max} \Delta\nu_{1/2},$$

where ε_{max} is the absorption coefficient at the absorption maximum and $\Delta\nu_{1/2}$ is the half-width of the band.

The data in Table 26 show that the absorption bands in the spectra of the *para*-bound dimers **13a**–**c** are shifted bathochromically compared to those of their *meta*- (**13d**–**f**) and *ortho*-analogues (**13g**–**i**). This phenomenon may be attributed both to an increase in the proportion of conformers of the 'half-open shell' type and to a more substantial deformation of the porphyrin macrocycle in the *para*-bound dimers.

Table 27. Strain energies of the conformers of the *ortho*-, *meta*- and *para*-bound dimers **13a**,**d**,**h** (E/kJ mol^{-1}) and their components (kJ mol^{-1}): strain energies of bonds (E_1), bond angles (E_2), torsion angles (E_3), van der Waals interactions (E_4), stretching–bending (E_5) and Coulomb interactions (E_6).[87,88]

Compound **13**	Conformer [a]	E	E_1	E_2	E_3	E_4	E_5	E_6
h	*1*	650	19	412	78	74	3	56
	2	653	20	421	86	71	1	56
	3	684	20	453	91	63	1	56
d	*4*	618	18	430	78	35	1	55
	5	599	18	423	83	20	1	54
	6	646	20	425	80	65	1	54
	7	623	20	424	85	40	1	52
	8	654	18	421	81	79	1	54
	9	591	18	419	81	14	1	58
a	*10*	669	21	431	72	90	2	53
	11	674	20	423	92	84	1	54
	12	683	21	437	99	71	2	53

[a] For notations of the conformers, see Fig. 14.

It should be noted that not only the positions of the absorption bands, but also the ratio of their intensities in the electronic absorption spectra of dimeric porphyrins are changed. In the case of *para*-bound dimers, the phyllo type of the spectrum, which is characteristic of monomeric β-octaalkyl-*meso*-diphenylporphyrins, is retained, while the spectra of the *ortho*- and *meta*-analogues belong to the ethio type (Fig. 15).

The differences in the electronic absorption spectra are reduced due to protonation of the porphyrin rings of the dimers **13a**–**i** in acetic acid and, correspondingly, to an increase of the distance between the likely charged fragments.

* * *

The data surveyed in the present review give convincing evidence that the combined use of modern spectroscopic methods enables one to obtain comprehensive information on the molecular

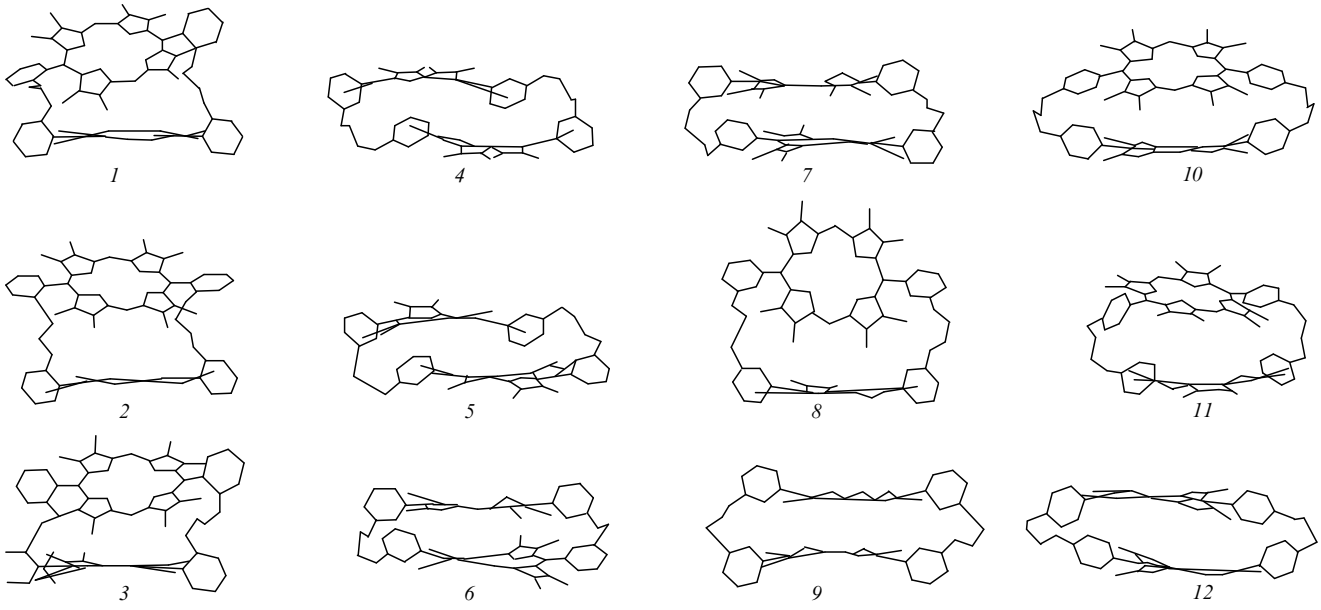

Figure 14. Conformers of the dimeric porphyrins **13h** (*1*–*3*), **13d** (*4*–*9*) and **13a** (*10*–*12*).[87,88]

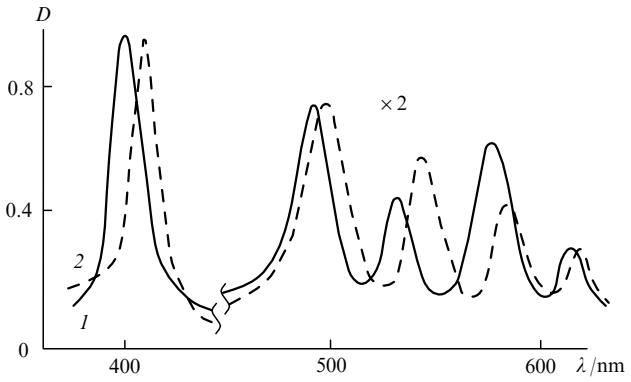

Figure 15. Electronic absorption spectra of the dimers **13a** (*1*) and **13d** (*2*) in chloroform.[83, 86]

structures of the newly synthesised compounds. The development of the spectroscopy of porphyrins provides the theoretical basis for the wider use of this unique class of tetrapyrrole macrocyclic compounds in technology, medicine and biology because the determination of the correlations between the structure and the spectral properties of the molecules can help in solving the problem of the construction of new materials with the desired properties.

This review has been written with the financial support of INTAS (Grant YSF-00-37).

References

1. G P Gurinovich, A N Sevchenko, K N Solov'ev *Spektroskopiya Khlorofilla i Rodstvennykh Soedinenii* (Spectroscopy of Chlorophyll and Related Compounds) (Minsk: Nauka i Tekhnika, 1968)
2. K N Solov'ev, L L Gladkov, A S Starukhin *Spektroskopiya Porfirinov: Kolebatel'nye Sostoyaniya* (Spectroscopy of Porphyrins: Vibrational States) (Minsk: Nauka i Tekhnika, 1985)
3. M Gouterman *J. Chem. Phys.* **30** 1139 (1959)
4. M Gouterman *J. Mol. Spectrosc.* **6** 138 (1961)
5. A H Corwin, A B Chivvis, R W Poor, D G Whitten, E W Baker *J. Am. Chem. Soc.* **90** 6577 (1968)
6. B D Berezin *Koordinatsionnye Soedineniya Porfirinov i Ftalotsianina* (Coordination Compounds of Porphyrins and Phthalocyanine) (Moscow: Nauka, 1978)
7. B D Berezin, N S Enikolopyan *Metalloporfiriny* (Metalloporphyrins) (Moscow: Nauka, 1988)
8. V A Kuz'mitskii, K N Solov'ev, M P Tsvirko, in *Porfiriny: Spektroskopiya, Elektrokhimiya, Primenenie* (Porphyrins: Spectroscopy, Electrochemistry, Applications) (Ed. N S Enikolopyan) (Moscow: Nauka, 1987) p. 7
9. N Zh Mamardashvili, O A Golubchikov *Zh. Org. Khim.* **35** 1080 (1999) [a]
10. N Zh Mamardashvili, M E Klueva, O A Golubchikov *Molecules* **5** 89 (2000)
11. N Zh Mamardashvili, S A Zdanovich, O A Golubchikov *Pirroly. Raschet Metodom Molekulyarnoi Mekhaniki* (Pyrroles. Molecular Mechanics Calculation); article deposited at the VINITI No. 3133-V97 (Moscow, 1996)
12. N Zh Mamardashvili, A S Semeikin, L V Klopova, O A Golubchikov, in *XIII Vsesoyuz. Seminar po Khimii Porfirinov i ikh Analogov (Tez. Dokl.), Samarkand, 1991* [The XIIIth All-Union Seminar on the Chemistry of Porphyrins and Their Analogues (Abstracts of Reports), Samarkand, 1991] p. 98
13. N Zh Mamardashvili, S A Zdanovich, O A Golubchikov *Zh. Org. Khim.* **34** 1234 (1998) [a]
14. N Zh Mamardashvili, A S Semeikin, O A Golubchikov *Zh. Org. Khim.* **29** 1213 (1993) [a]
15. N Zh Mamardashvili, S A Zdanovich, O A Golubchikov *Dipirrolilmetany. Raschet Metodom Molekulyarnoi Mekhaniki* (Dipyrrolylmethanes. Molecular Mechanics Calculation); article deposited at the VINITI No. 1470-V97 (Moscow, 1997)
16. N Zh Mamardashvili, S A Zdanovich, O A Golubchikov *Geometricheskie Parametry Dipirrolilmetanov. Raschet Metodom Molekulyarnoi Mekhaniki* (Geometric Parameters of Dipyrrolylmethanes. Molecular Mechanics Calculation); article deposited at the VINITI No. 1697-V97 (Moscow, 1997)
17. A S Semeikin, N Zh Mamardashvili, A V Glazunov, O A Golubchikov, B D Berezin *Izv. Vyssh. Uchebn. Zaved., Khim. Khim. Tekhnol.* **33** (9) 12 (1990)
18. N Zh Mamardashvili, A S Semeikin, O A Golubchikov, B D Berezin, in *XVII Vsesoyuz. Chugaevskoe Soveshch. po Khimii Kompleksnykh Soedinenii (Tez. Dokl.), Minsk, 1990* [The XVIth All-Union Chugaev Meeting on the Chemistry of Complex Compounds (Abstracts of Reports), Minsk, 1990] p. 120
19. N Zh Mamardashvili, S A Zdanovich, O A Golubchikov, in *Problemy Sol'vatatsii i Kompleksoobrazovaniya v Rastvorakh (Tez. Dokl. VI Mezhdunar. Konf.), Ivanovo, 1995* [The Problems of Solvation and Complex-Formation in Solutions (Abstracts of Reports of the VIth International Conference), Ivanovo, 1995] N23
20. N Zh Mamardashvili, A S Semeikin, O A Golubchikov, B D Berezin, in *III Vsesoyuz. Konf. po Khimii i Biokhimii Makrotsiklicheskikh Soedinenii (Tez. Dokl.), Ivanovo, 1988* [The Third All-Union Conference on the Chemistry and Biochemistry of Macrocyclic Compounds (Abstracts of Reports), Ivanovo, 1988] p. 318
21. N Zh Mamardashvili, O A Golubchikov *Molecules* **5** 757 (2000)
22. N Zh Mamardashvili, S A Zdanovich, O A Golubchikov *Struktura 5,15-Difenilzameshchennykh β-Oktalkilporfirinov. Raschet Metodom Molekulyarnoi Mekhaniki* (The Structure of 5,15-Diphenyl-Substituted β-Octaalkylporphyrins. Molecular Mechanics Calculation); article deposited at the VINITI No. 3703-V97 (Moscow, 1997)
23. N Zh Mamardashvili, S A Zdanovich, O A Golubchikov *Geometricheskie Parametry 5,15-Difenilzameshchennykh β-Oktalkilporfirinov. Raschet Metodom Molekulyarnoi Mekhaniki* (Geometrical Parameters of 5,15-Diphenyl-Substituted β-Octaalkylporphyrins. Molecular Mechanics Calculation); article deposited at the VINITI No. 3704-V97 (Moscow, 1997)
24. S A Zdanovich, N Zh Mamardashvili, O A Golubchikov *Zh. Org. Khim.* **32** 788 (1996) [a]
25. A S Semeikin, Doctoral Thesis in Chemical Sciences, Ivanovo Chemical Technological Institute, Ivanovo, 1995
26. S F Mason *J. Chem. Soc.* 976 (1958)
27. N Zh Mamardashvili, A M Semeikin, S A Zdanovich, O A Golubchikov, in *Pervaya Mezhdunar. Konf. po Biokoordinatsionnoi Khimii (Tez. Dokl.), Ivanovo, 1994* [The First International Conference on Biocoordination Chemistry (Abstracts of Reports), Ivanovo, 1994] p. 195
28. T A Koroleva, O I Koifman, B D Berezin *Zh. Fiz. Khim.* **55** 2007 (1981) [b]
29. R M Silverstein, G C Bussler, T C Morrill *Spectrometric Identification of Organic Compounds* (New York: Wiley, 1974)
30. S A Syrbu, A S Semeikin, B D Berezin, in *Pervaya Mezhdunar. Konf. po Biokoordinatsionnoi Khimii (Tez. Dokl.), Ivanovo, 1994* [The First International Conference on Biocoordination Chemistry (Abstracts of Reports), Ivanovo, 1994] p. 198
31. H Ogoshi, N Masai, Z-i Yoshida, J Takemoto, K Nakamoto *Bull. Chem. Soc. Jpn.* **44** 49 (1971)
32. N V Ivashin, S N Terekhov, I F Gurinovich, V V Sivchik *Zh. Prikl. Spektrosk.* **34** 124 (1981)
33. N V Ivashin, I F Gurinovich, G P Gurinovich *Zh. Prikl. Spektrosk.* **23** 1026 (1975)
34. O I Koifman, Doctoral Thesis in Chemical Sciences, Ivanovo Chemical Technological Institute, Ivanovo, 1983
35. T N Lomova, B D Berezin *Koord. Khim.* **27** 96 (2001) [c]
36. T N Lomova, N I Volkova, B D Berezin *Zh. Neorg. Khim.* **30** 626 (1985) [d]
37. B A Suleiman, G E Nikitina, A S Semeikin, N Zh Mamardashvili, O A Golubchikov, in *XX Nauch. Sessiya Rossiiskogo Seminara po Khimii Porfirinov i ikh Analogov (Tez. Dokl.), Ivanovo, 1999* [The XXth Scientific Session of Russian Seminar on the Chemistry of Porphyrins and Their Analogues (Abstracts of Reports), Ivanovo, 1999] p. 7

38. N Zh Mamardashvili, A S Semeikin, O A Golubchikov, B D Berezin, in *Problemy Sol'vatatsii i Kompleksoobrazovaniya v Nevodnykh Rastvorakh (Tez. Dokl. IV Vsesoyuz. Soveshch.), Ivanovo, 1989* [The Problems of Solvation and Complex-Formation in Non-aqueous Solutions (Abstracts of Reports of the IVIth All-Union Meeting), Ivanovo, 1989] p. 211
39. N Zh Mamardashvili, A S Semeikin, L V Klopova, O A Golubchikov *ESP β-Oktalkil-ms-difenilporfirinov v Nevodnykh Rastvoritelyakh* (EAS of β-Oktaalkyl-ms-Diphenylporphyrins in Nonaqueous Solvents); article deposited at the VINITI No. 3733-V89 (Moscow, 1989)
40. H L Anderson, J K M Sanders *J. Chem. Soc., Perkin Trans. 1* 2223 (1995)
41. H L Anderson, S Anderson, J K M Sanders *J. Chem. Soc., Perkin Trans. 1* 2231 (1995)
42. S Anderson, H L Anderson, J K M Sanders *J. Chem. Soc., Perkin Trans. 1* 2247 (1995)
43. H L Anderson, C J Walter, A Vidal-Ferran, R A Hay, P A Lowden, J K M Sanders *J. Chem. Soc., Perkin Trans. 1* 2275 (1995)
44. C C Mak, N Bampos, J K M Sanders *Angew. Chem., Int. Ed. Engl.* **37** 3020 (1998)
45. T E Clement, D J Nurco, K M Smith *Inorg. Chem.* **37** 1150 (1998)
46. R Paolesse, R K Pandey, T P Forsyth, L Jaquinod, K R Gerzevske, D J Nurco, M O Senge, S Licoccia, T Boschi, K M Smith *J. Am. Chem. Soc.* **118** 3869 (1996)
47. T Hirao, K Saito *Tetrahedron Lett.* **41** 1413 (2000)
48. H Nasri, M Debbabi *Polyhedron* **17** 3607 (1998)
49. G V Ponomarev, G V Kirillova, G B Maravin, T A Babushkina, V P Suboch *Khim. Geterotsikl. Soedin.* **6** 776 (1979) [e]
50. C-B Wang, S K Chang *Synthesis* **7** 548 (1979)
51. C K Chang *J. Am. Chem. Soc.* **99** 2819 (1977)
52. H Ogoshi, H Sugimoto, T Nishiguchi, T Watanabe, Y Matsuda, Z Yoshida *Chem. Lett.* 29 (1978)
53. H Ogoshi, H Sugimoto, Z-i Yoshida *Tetrahedron Lett.* **49** 4477 (1976)
54. M J Crossley, M M Harding, S Sternhell *J. Am. Chem. Soc.* **108** 3608 (1986)
55. G M Dubowchik, A D Hamilton *J. Chem. Soc., Chem. Commun.* 665 (1986)
56. K Maruyama, T Nagata, N Ono, A Osuka *Bull. Chem. Soc. Jpn.* **62** 3167 (1989)
57. I Abdalmuhdi, C K Chang *J. Org. Chem.* **50** 411 (1985)
58. J P Collman, J I Brauman, T J Collins, B L Iverson, G Lang, R B Pettman, J L Sessler, M A Walters *J. Am. Chem. Soc.* **105** 3038 (1983)
59. J P Collman, C E Barnes, P N Swepston, J A Ibers *J. Am. Chem. Soc.* **106** 3500 (1984)
60. B Morgan, D Dolphin *J. Org. Chem.* **52** 5364 (1987)
61. N Zh Mamardashvili, S A Zdanovich, O A Golubchikov *PMR Spektry Mono-, Di- i Tetrapirrol'nykh Soedinenii Lineinogo i Tsiklicheskogo Stroeniya* (^{1}H NMR Spectra of Mono-, Di- and Tetrapyrrole Compounds with Linear and Cyclic Structures); article deposited at the VINITI No. 1616-V95 (Moscow, 1995)
62. H Ogoshi, E-i Watanabe, N Koketsu, Z-i Yoshida *Bull. Chem. Soc. Jpn.* **49** 2529 (1976)
63. Yu B Ivanova, N Zh Mamardashvili, V B Sheinin, O A Golubchikov, in *Problemy Sol'vatatsii i Kompleksoobrazovaniya v Rastvorakh (Tez. Dokl. VII Mezhdunar. Konf.), Ivanovo, 1998* [The Problems of Solvation and Complex-Formation in Solutions (Abstracts of Reports of the VIIth International Conference), Ivanovo, 1998] p. 458
64. J Hiom, J B Paine III, U Zapf, D Dolphin *Can. J. Chem.* **61** 2220 (1983)
65. S Wolowiec *Polyhedron* **17** 1295 (1998)
66. T P Wijesekera, J B Paine III, D Dolphin *J. Am. Chem. Soc.* **105** 6747 (1983)
67. D A Ban, A F Mironov *Mendeleev Commun.* **4** 153 (1995)
68. E G Levinson, A F Mironov *Mendeleev Commun.* **3** 94 (1994)
69. A Osuka, K Maruyama, I Yamazaki, N Tamai *J. Chem. Soc., Chem. Commun.* 1243 (1988)
70. D Dolphin, J Hiom, J B Paine III *Heterocycles* **16** 417 (1981)
71. C K Chang, M-S Kuo, C-B Wang *J. Heterocycl. Chem.* **14** 943 (1977)
72. J P Collman, C S Bencosme, C E Barnes, B D Miller *J. Am. Chem. Soc.* **105** 2704 (1983)
73. J P Collman, F C Anson, C E Barnes, C S Bencosme, T Geiger, E R Evitt, R P Kreh, K Meier, R B Pettman *J. Am. Chem. Soc.* **105** 2694 (1983)
74. C K Chang *Adv. Chem. Ser.* **173** 162 (1979)
75. A Osuka, F Kobayashi, T Nagata, K Maruyama *Chem. Lett.* 287 (1990)
76. J A Anton, J Kwong, P A Loach *J. Heterocycl. Chem.* **13** 717 (1976)
77. O A Golubchikov, S G Korovina, E M Kuvshinova, A S Semeikin, A M Shul'ga, V A Perfil'ev, S A Syrbu, B D Berezin *Zh. Org. Khim.* **24** 2378 (1988) [a]
78. O A Golubchikov, in *Pervaya Mezhdunar. Konf. po Biokoordinatsionnoi Khimii (Tez. Dokl.), Ivanovo, 1994* [The First International Conference on Biocoordination Chemistry (Abstracts of Reports), Ivanovo, 1994] p. 188
79. B C Bookser, T C Bruice *J. Am. Chem. Soc.* **113** 4208 (1991)
80. G M Dubowchik, A D Hamilton *J. Chem. Soc., Chem. Commun.* 904 (1985)
81. J L Sessler, M R Johnson *Angew. Chem.* **99** 679 (1987)
82. N Zh Mamardashvili, A S Semeikin, B D Beresin, O A Golubchikov, in *Proceedings of the 3rd European Symposium on Organic Reactivity, Göteborg, 1991* p. 211
83. N Zh Mamardashvili, S A Zdanovich, O A Golubchikov *Zh. Org. Khim.* **32** 934 (1996) [a]
84. N Zh Mamardashvili, A S Semeikin, S A Zdanovich, O A Golubchikov, in *Proceedings of the Vth European Symposium on Organic Reactivity, Santiago de Compostela, 1995* p. 170
85. N Zh Mamardashvili, S A Zdanovich, O A Golubchikov, in *VII Mezhdunar. Konf. po Khimii Porfirinov i ikh Analogov (Tez. Dokl.), S.-Peterburg, 1995* [The VIIth International Conference on the Chemistry of Porphyrins and Their Analogs (Abstracts of Reports), St. Petersburg, 1995] p. 22
86. O A Golubchikov, N Zh Mamardashvili, A S Semeikin *Zh. Org. Khim.* **29** 2445 (1993) [a]
87. N Zh Mamardashvili, S A Zdanovich, O A Golubchikov *Struktura Konformerov Dimernykh Oktalkildifenilporfirinov s Mostikovymi Gruppami v o- i m-Polozheniyakh Benzol'nykh Fragmentov* (The Structure of Conformers of Dimeric β-Octaalkyldiphenylporphyrins with Bridging Groups in the *o*- and *p*-Positions of Benzene Fragments); article deposited at the VINITI No. 2941-V95 (Moscow, 1995)
88. N Zh Mamardashvili, S A Zdanovich, O A Golubchikov *Struktura Konformerov Dimernogo Oktalkilporfirina po Dannym Metoda Molekulyarnoi Mekhaniki* (The Structure of Conformers of Dimeric Octaalkylporphyrin From Molecular Mechanics Data); article deposited at the VINITI No. 2967-V95 (Moscow, 1995)
89. R Young, C K Chang *J. Am. Chem. Soc.* **107** 898 (1985)
90. A Lecas, J Levisalles, Z Renko, E Rose *Tetrahedron Lett.* **25** 1563 (1984)
91. T N Lomova, V V Morozov, E G Mozhzhukhina, B D Berezin, in *Spektroskopiya Koordinatsionnykh Soedinenii (Tez. Dokl. IV Vsesoyuz. Soveshch.), Krasnodar, 1986* [The Spectroscopy of Coordination Compounds (Abstracts of Reports of the IVth All-Union Meeting), Krasnodar, 1986] p. 264
92. T N Lomova, E G Mozhzhukhina, L P Shormanova, B D Berezin, in *V Vsesoyuz. Konf. po Koordinatsionnoi i Fizicheskoi Khimii Porfirinov (Tez. Dokl.), Ivanovo, 1988* [The Vth All-Union Conference on Coordination and Physical Chemistry of Porphyrins (Abstracts of Reports), Ivanovo, 1988] p. 64
93. N Datta-Gupta, T J Bardos *J. Heterocycl. Chem.* **3** 495 (1966)
94. C Kaldapa, J C Blais, V Carré, R Granet, V Sol, M Guilloton, M Spiro, P Krausz *Tetrahedron Lett.* **41** 331 (2000)
95. C K Chang *J. Heterocycl. Chem.* **14** 1285 (1977)
96. J A Cowan, J K M Sanders, G S Beddard, R J Harrison *J. Chem. Soc., Chem. Commun.* 55 (1987)
97. B M Trost, C R Hutchinson (Eds) *Organic Synthesis Today and Tomorrow* (Madison, WI: University of Wisconsin, 1980)
98. A Osuka, K Maruyama *J. Am. Chem. Soc.* **110** 4454 (1988)
99. C K Chang, I Abdalmuhdi *Angew. Chem.* **96** 154 (1984)
100. S S Eaton, G R Eaton, C K Chang *J. Am. Chem. Soc.* **107** 3177 (1985)
101. C K Chang, I Abdalmuhdi *J. Org. Chem.* **48** 5388 (1983)
102. J Weiser, H A Staab *Angew. Chem.* **96** 602 (1984)
103. H Ogoshi, H Sugimoto, Z-i Yoshida *Tetrahedron Lett.* 169 (1977)

104. J A Cowan, J K M Sanders *J. Chem. Soc., Chem. Commun.* 1213 (1985)
105. N E Kagan, D Mauzerall, R B Merrifield *J. Am. Chem. Soc.* **99** 5484 (1977)

[a] — *Russ. J. Org. (Engl. Transl.)*
[b] — *Russ. J. Phys. Chem. (Engl. Transl.)*
[c] — *Russ. J. Coord. Chem. (Engl. Transl.)*
[d] — *Russ. J. Inorg. Chem. (Engl. Transl.)*
[e] — *Chem. Heterocycl. Compd. (Engl. Transl.)*

Russian Chemical Reviews **70** (7) 607 – 626 (2001) © 2001 Russian Academy of Sciences and Turpion Ltd

DOI 10.1070/RC2001v070n07ABEH000665

Detonation synthesis ultradispersed diamonds: properties and applications

V Yu Dolmatov

Contents

I.	Introduction	607
II.	Synthesis and morphology	608
III.	Elemental composition and admixtures	608
IV.	Surface properties	610
V.	Phase composition, microstructure and surface texture	611
VI.	Sorption properties and exchange capacity	611
VII.	Chemical properties of ultradispersed diamonds	613
VIII.	Spectroscopy	615
IX.	Thermal analysis	616
X.	Defects of the bulk structure	616
XI.	Electrophysical properties of ultradispersed diamonds	617
XII.	Fractionation process and sedimentation stability	617
XIII.	The diamond – graphite structural phase transition	618
XIV.	A cluster model and the fractal nature of UDD aggregates	618
XV.	Comparison of properties of diamonds of different origins.	621
XVI.	Application fields of ultradispersed diamonds	621

Abstract. Published data on the properties of a novel nanomaterial *viz*., detonation synthesis ultradispersed diamonds (UDD), are summarised and systematised for the first time. Certain properties of UDD synthesised under different conditions are compared. Particular attention is drawn to substantiation of the cluster model of UDD and the fractal nature of their aggregates. The potential application fields of UDD are considered. Operating parameters of new materials are presented. The bibliography includes 110 references.

I. Introduction

Detonation synthesis ultradispersed diamonds (UDD or nanodiamonds) pertain a class of nanomaterials the fabrication, modification, and application of which attract the attention of scientists and engineers from different countries. This area of science and technology is at the boundary of solid-state physics and chemistry and thus becomes the world's most rapidly growing field as regards fundings provided for its development.

At present, a wide spectrum of nanoparticles is studied which differ in both their nature (metals, non-metals, chemical compounds) and the technologies for their production (gas-phase and plasmochemical syntheses, precipitation from colloidal solutions, thermal decomposition and reduction, mechanical synthesis, electrical-detonation and detonation syntheses) and the unique properties of particles and materials and articles manufactured on their basis. The latter aspect is of prime importance in view of the development of novel industrial technologies which include miniaturisation of facilities.

We believe that, among all types of nanomaterials, UDD represent the most interesting subject. Indeed, first of all, even a bulk diamond (*e.g*., natural diamond) exhibits a unique combination of chemical, physicochemical (particularly, thermophysical) and mechanical properties. Second, diamonds resulting from miniaturisation or, more precisely, prepared in a form of nanoparticles (mean size 4 – 6 nm) from a plasma upon detonation of powerful explosive mixtures (EM), acquire more pronounced anomalous properties.

Whereas ordinary (natural) diamonds are applied in practice, as a rule, as abrasives and cutting tools and substrates for microelectronics, the application sphere of UDD is much wider. By chemical, barochemical and thermal treatment of UDD one can impart to them different surface properties. In this connection, the attention of scientists is focused on detailed studies of characteristics and properties of diamonds and a search for new application fields.

In Russia, UDD are used as a composite material in electrochemical and chemical metal – diamond coatings, polymeric films and membranes; in different kinds of rubbers; as anti-friction and anti-wear additives to lubricants of different purposes; in finishing and super-finishing polishing compositions; in abrasives. Nanodiamonds serve in fabrication of magnetically soft and hard input media, anti-friction tribotechnological diamond-containing compositions based on thermoplastic materials (used in friction joints), abrasion-resistant structure materials based on ethylene thermoplastic co-polymers and in manufacture of radiation- and ozone-resistant rubbers. Moreover, they are most important components in the reprocessing of worn tire rubber. Studies are launched on sintering of UDD under high dynamic and static pressures (for manufacture of cutting tools, abrasives, substrates for microelectronics), on using them in medicine (as anti-cancer drugs and a component of such drugs, an effective gastroenteritis

V Yu Dolmatov Special Design Bureau (SDB) 'Tekhnolog' at the St. Petersburg State Technological Institute (Technical University), Sovetskii prosp. 33A, 193076 St. Petersburg, Russian Federation. Fax/Tel. (7-812) 100 38 98. E-mail: alsen@comset.net

Received 28 February 2001
Uspekhi Khimii **70** (7) 687 – 708 (2001); translated by T Ya Safonova

remedy, an immobiliser of biologically active substances, a super-effective sorbent for purification of blood and lymph, *etc*.).

In Russia, particularly, at SDB 'Tekhnolog' industrial technologies are developed for the detonation synthesis of UDD, which allow production of diamonds (as powders and suspensions) in amounts that run into tons.

In this review, for the first time, an attempt is undertaken to describe the properties of detonation synthesis diamonds in sufficient detail. All the available literature on UDD is analysed for the last 15 years including publications by the author.

Inasmuch as UDD are extremely complex materials and their characteristics are largely determined by the methods of preparation, chemical purification and surface modification, the properties of nanodiamonds reported in different studies can differ. The literature data reviewed do not exhaust the subject, because the approaches of different authors were different, the UDD samples used differed from one another and the studies were carried out under different conditions and often were sporadic.

II. Synthesis and morphology

Detonation-induced transformations of powerful explosives and their mixtures with the composition $C_aH_bN_cO_d$ with a negative oxygen balance (*i.e*., with the oxygen content lower than the stoichiometric value) in a non-oxidising medium yields a condensed carbon phase which involves ultradispersed diamonds.[1,2] The pressure and temperature in the detonation wave ($P-T$ parameters) correspond to the region of thermodynamic stability of diamonds ($P \geqslant 10$ GPa, $T \geqslant 3000$ K).[3,4] Such condensed carbon, which is commonly named a diamond blend (DB), can contain up to 75% UDD. Calculation and experimental methods have shown[5,6] that the primary UDD particles with diameter of $\sim$4 nm form fractal cluster structures (of 30–40-nm size) from which larger aggregates (of an order of magnitude of hundreds of nanometers) are formed. The clusters are built of a limited number of atoms (from several tens to several thousands) and, with regard to their properties, occupy an intermediate position between individual atoms and bulk solids.[7,8]

In the liquid-phase oxidation of condensed carbon, non-diamond structures gradually decompose, the most sophisticated method of chemical purification of DB being their treatment by dilute nitric acid at elevated temperature and pressure.[9,10]

According to the literature data,[11] purified UDD contain no intermediate amorphous phase. This is indicated by the shape of the (111) band in X-ray diffraction spectra and the results of electron microscopy. Depending on the conditions of the detonation synthesis, the mean size of UDD grains varies from 2 to 20 nm.

Diamond grains with sizes up to 100 nm are shown to exhibit highly defective block structures (1–3-nm blocks were observed in dark-field images).[12] With an increase in the grain size, the crystalline structure becomes more perfect. These results are confirmed in studies by high-resolution electron microscopy.[13]

It was found[14] that UDD are single-phase materials and contain no Lonsdalite, graphite and other admixtures. The size of subgrains (mosaic blocks) was found to be 4 nm by the method of diffractometry of co-ordination spheres,[15] no lattice microdistortions were revealed and the dislocation density determined from the value of subgrain size by the Williamson–Smallman relationship $N = 3/z^2$ was found to be equal to 1.8×10^{17} m^{-2}.

An X-ray diffraction pattern for UDD powders[16] also characterises UDD as a diamond phase containing no admixtures of Lonsdalite and graphite.

The coherent-scattering regions (CSR) were found to be of a mean size of 4.2 ± 0.2 nm and represent the proper UDD grains of diamond-lattice structure and an insignificant amount of aggregates of carbon atoms dispersed throughout the bulk which form no lattice and are mainly spaced at $\sim$0.15 nm from one another.[16] Along intergrain boundaries, carbon-atom aggregates are located for which the distribution in interatomic distances is close to Gaussian. The latter fact indicates that the structure of intergrain boundaries is amorphous.

Sizes of UDD crystals were estimated based on the so-called phonon confinement model.[17–19] It was shown that the nanocrystal size is 4.3 nm, which coincides with the results X-ray diffraction analysis of the same samples.[20]

In their usual state, UDD represent a powder of a specific surface area of 250–350 m^2 g^{-1} and a pore volume of 0.3–1.0 cm^3 g^{-1} (see Ref. 21). Heating of samples to 1273 K does not result in any decrease in the specific surface area. In a suspension, the size of UDD particles reaches 0.05×10^{-6} m; in a dried form, nanodiamonds represent a polydispersed powder. On heating above 873 K in an inert atmosphere, UDD particles begin to grow and acquire spherulitic shapes which measure up to $(150-200) \times 10^{-6}$ m and disintegrate at a load of 10–15 kg mm^{-2}. No polycrystals are formed in this case.

Due to the non-equilibrium conditions of their synthesis, UDD particles display a high density of defects, an active and well-developed surface (reaching 450 m^2 g^{-1}) and an excess enthalpy of formation.

III. Elemental composition and admixtures

Ultradispersed diamonds are characterised by the presence of a substantial amount of difficultly removable volatile and solid admixtures. The former include adsorbed gases (CO, CO_2, N_2), water and acids remaining after chemical purification (HNO_3, H_2SO_4). The latter group of admixtures involves non-diamond carbon, insoluble metal compounds (oxides, carbides) and salt admixtures. Powders of UDD can be considered as a certain diamond-containing composite material that consists of different carbon forms (80%–89%), nitrogen (2%–3%), hydrogen (0.5%–1.5%), oxygen (up to 10%), and an incombustible residue (0.5%–8.0%). Carbon represents a mixture of proper ultradispersed diamond (90%–97%) and non-diamond carbon (3%–10%). In detonation synthesis nanodiamonds, the impurity percentage is higher compared with other artificial diamonds (diamonds prepared by steady-state synthesis contain no less than 96% carbon); and, therefore, the effect of impurities on physical and chemical properties should be more pronounced for UDD compared with other diamonds.

Impurities present in UDD can be arbitrarily divided into the following groups:

(1) water-soluble ionised (free electrolytes);

(2) chemically bonded to the diamond surface and prone to hydrolysis and ionisation (salt forms of functional surface groups);

(3) water insoluble (mechanical impurities, non-dissociating salt and oxide forms of surface impurities);

(4) incorporated into the diamond lattice and encapsulated.

The impurities of the first and second groups are formed in the stage of chemical purification of UDD by acids.[9] Major water-soluble admixtures (first group) are removed by washing UDD with water. To make the removal more efficient, the suspensions are additionally treated by ion-exchange resins.

Surface functional groups (the second group of impurities) of the COOH, OH, SO_3H, NO_3 and NO_2 types can be considered as ionogenic with the diamond itself as the ion-exchange material.[22] In this case, treatment of UDD aqueous suspensions by ion-exchange resins, which involves demineralisation of surface groups, is also the most efficient.

Water-insoluble impurities (the third group) represent both individual microparticles of metals, oxides, carbides, salts (sulfates, silicates, carbonates) and surface compounds of salts and metal oxides incapable of dissociation. For their removal, *i.e*., transformation into soluble forms, UDD are treated by acids.

By using different methods of UDD purification, one can remove 40%–95% of the impurities of these three groups. All attempts to obtain individual UDD have failed. This is explained by the fact that the impurities of the fourth group are virtually

impossible to remove by chemical methods; moreover, the transition of third-group impurities into a soluble state is incomplete.

The main admixed elements are silicon, calcium, iron and sulfur; titanium, copper, chromium, and potassium are present virtually always in small amounts. Having an active and well-developed surface, nanodiamonds can sorb solution impurities. Hence, the presence of certain impurities, namely, silicon, potassium and, partially, iron can be attributed to the hardness of water employed in UDD purification.

Being among the major technological impurities in UDD, iron in concentrations of no less than 0.1 mass% – 0.5 mass% (which corresponds to the presence of insoluble iron compounds, preferentially on the surface) is difficult to remove.

Powders of UDD also contain substantial amounts of volatile admixtures ($\sim$10 mass%);[23] thermal treatment of UDD in vacuum (0.01 Pa) allows one to either remove the volatile impurities or substantially decrease their content. The optimum temperature of annealing is 673 K.

Ultradispersed diamonds studied in Ref. 21 were of the following composition: carbon, up to 88%; hydrogen, up to 1%; nitrogen, up to 2.5%, oxygen, up to 10%. The same ratio of elements remains after a thermal treatment up to 1273 K in either reductive (hydrogen) or neutral (argon) atmosphere. The carbon content in UDD samples passes through a maximum in a range of 973 – 1073 K, whereas hydrogen and nitrogen contents remain virtually unchanged. The maximum density of UDD was reached after heating in an argon atmosphere at 1073 K and amounted to 3.21×10^3 kg m^{-3}.

Scientists from the Russian Federation Nuclear Centre — All-Russian Research Institute of Technical Physics (RFNC-ARITP, Snezhinsk) have determined the contents of admixed elements in UDD samples manufactured at SDB 'Tekhnolog' and RFNC-ARITP (Table 1).

Table 1. Content (mass %) of admixed elements in UDD samples (AES data).

Admixture	UDD powder of UDD-STP brand [a]	Aqueous UDD suspension of UDD-TAH brand [a]	Typical UDD [b]
Fe	0.150	0.100	0.100
Cr	0.070	0.050	0.500
Si	0.300	0.100	0.150
Al	0.005	0.001	0.010
Na	0.030	0.003	0.050
K	0.002	0.002	0.002
Cu	0.005	0.002	0.003
Ca	0.002	0.002	0.010
Mg	0.005	0.003	0.005
Mn	0.001	see [c]	0.001
Ti	0.010	0.005	0.002
Pb	0.001	0.001	0.001
Total	0.580	0.270	0.840
Incombustible residue	0.950	0.400	1.400

[a] Produced at SDB 'Technolog' in accordance to specification TU 05121441-275-95. [b] Produced at RFNC-ARRITP. [c] Undetected at a sensitivity of 5×10^{-4} mass %.

Due to the fact that the time of synthesis of UDD is very short, surface carbon atoms have no time to stabilise by closure of all the bonds in the newly formed diamond lattice. They form a bond or two bonds with other elements of explosive materials, *viz*., hydrogen, nitrogen and oxygen. Hence, it is of great importance to assess the changes in the relative contents of heteroatoms that stabilise surface carbon atoms on the interface as a function of chemical treatment conditions and the degree of oxidative decomposition of DB.[24] For this purpose, an original diamond blend is treated by oxidising systems based on nitric acid and also by organic solvents, hydrocarbons and alcohols in the temperature interval of 358 – 578 K. Table 2 shows the results of the analysis as arbitrary molecular formulas calculated per 100 carbon atoms. Generally, the relative content of heteroatoms varies in a wide interval: from 5 to 35 hydrogen atoms and from 4 to 32 oxygen atoms per 100 carbon atoms. The nitrogen content varies from 2 to 4 atoms per 100 carbon atoms and is independent of the treatment conditions.

Table 2. Elemental composition of DB.[24]

Treatment conditions	Arbitrary molecular formula	Number of heteroatoms per 100 carbon atoms
DB sample		
Original, $\alpha = 0$	$C_{100}H_{5.3}N_{2.84.1}$	12.2
Treated by hydrocarbons C_nH_{2n+2}	$C_{100}H_{13.8}N_{2.94.6}$	21.3
Treated by alcohols $C_nH_{2n+1}OH$	$C_{100}H_{15.5}N_{2.68.0}$	26.1
Oxidative decomposition, $\alpha = 26.3\%$	$C_{100}H_{25.4}N_{2.922.5}$	50.8
Oxidative decomposition, $\alpha = 31.8\%$	$C_{100}H_{34.9}N_{2.923.1}$	60.9
UDD sample		
Original, $\alpha = 55.0\%$	$C_{100}H_{11.2}N_{2.29.1}$	22.5
Oxidative decomposition, $\alpha = 64.9\%$	$C_{100}H_{19.3}N_{2.123.5}$	44.9
Oxidative decomposition, $\alpha = 74.4\%$	$C_{100}H_{18.7}N_{2.022.8}$	43.5
Oxidative decomposition, $\alpha = 75.6\%$	$C_{100}H_{23.7}N_{2.422.9}$	48.8

Note: α is the degree of oxidative decomposition determined from the expression

$$\alpha = \frac{[C_{ox}] - [C_{ox}]'}{[C_{ox}]},$$

where $[C_{ox}]$ and $[C_{ox}]'$ are the mass fractions of the oxidisable carbon in original DB and UDD and in treated (oxidised) samples, respectively.

Non-oxidative treatment of DB by organic solvents (hydrocarbons C_nH_{2n+2} and alcohols $C_nH_{2n+1}OH$) does not affect the carbon skeleton of particles, but causes changes in the composition of surface functional groups. In this process, the elemental composition of DB changes regularly: relative concentrations of hydrogen and oxygen increase owing to the addition of hydrocarbon- and hydroxyl-containing fragments. The total number of heteroatoms is doubled.

In the oxidative decomposition of DB, the spectrum of carbon-to-heteroatom ratio in the products may be wider. As the action of oxidants on DB is stronger (increase in temperature, acid concentration, *etc*.), carbon gradually transforms into carbon dioxide.

First of all, the most disordered amorphous part of carbon is oxidised, next comes the turn of micrographite structures. After practically complete removal of non-diamond carbon forms from DB, the resulting UDD represent a chemically inactive material difficultly susceptible to further oxidation. Nonetheless, the author has succeeded in decomposing partially the diamond substance by long-term etching. The etching degree was 45% of UDD mass or 75.6% of the mass of original DB. The dependence of DB composition on the degree of oxidative decomposition (Fig. 1) has a complicated shape.

The minimum contents of heteroatoms correspond to both the original DB and purified UDD, the maximum values (53.5 and 44.9 heteroatoms per 100 carbon atoms) are typical of partially oxidised DB ($\alpha = 26\% - 31\%$) and etched UDD

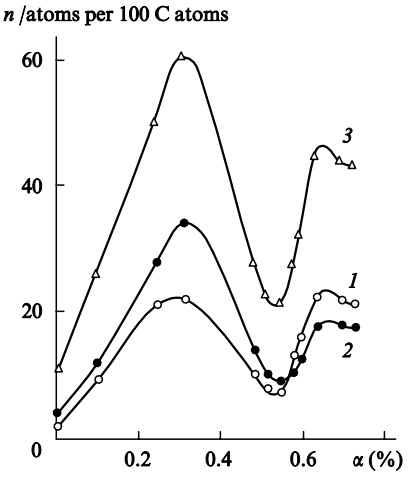

Figure 1. Elemental composition of DB as a function of the degree of oxidative decomposition (α).[24]
Relative content (n) of (*1*) oxygen, (*2*) hydrogen, (*3*) all heteroatoms.

(α = 65% – 75%), respectively. The concentrations of hydrogen and oxygen bonded to the surface vary in parallel. This makes it possible to assume that the chemical composition of surface functional groups is constantly reproduced.

For metastable structures, like partially oxidised DB and products of UDD etching, the recovery of surface-group composition results from active interactions with the reaction medium and the formation of a maximum number of heterobonds. The more stable forms, *viz*., the original DB and UDD, contain the smallest numbers of heteroatoms, which however is higher compared with that in the well-known diamond micropowders of steady-state synthesis ($C_{100}H_{1.1}O_{2.2}$) and soot ($C_{100}H_{5.1}O_{4.1}$).

From the chemical standpoint, the curves obtained allow the process of oxidative decomposition to be interpreted as two consecutive stages: (1) preferential etching of the carbon matrix at structural defects and along links between species, in the course of which the reaction surface increases and is enriched with oxidation intermediates; (2) etching of the loosened surface, gas formation and removal of surface oxidation products. A cyclic nature of these stages suggests that decomposition affects only structurally heterogeneous materials, whereas the oxidation selectively involves different structural forms.

Inasmuch as the concentrations of heteroatoms in DB and UDD are very high, a question arises of a possible location of these heteroatoms and the nature of their bonds with carbon. Calculations show that a 4-nm diamond particle consists of $\sim 12 \times 10^3$ carbon atoms, nearly 3×10^3 of which are located on the surface. For example, for UDD, we can write the following arbitrary molecular formulas: C_{75} for bulk and $C_{25}H_{11.2}N_{2.8}O_{9.1}$ for the surface atoms. Thus almost every carbon atom on the surface should be bonded to a heteroatom.

IV. Surface properties

The concentration of active hydrogen ([H_a]) on a UDD surface has been determined.[25] It is commonly agreed that a hydrogen atom bonded to an atom of any other element except carbon is active. For a carbon surface, the quantity [H_a] may serve as a measure of its enrichment by functional groups (hydroxy, carboxy, amine, sulfonic, *etc*.).

In the studies on the reaction of methylmagnesium iodide in anisole with functional surface groups of DB and UDD, three stages can arbitrarily be distinguished, *viz*., (1) the reaction with molecular impurities and the external surface (with functional groups most easily accessible), (2) the reaction with the surfaces of open pores and (3) the reaction with the surface becoming free upon mechanical destruction of UDD aggregates.

Depending on treatment conditions of DB and UDD, the density of protogenic groups in them varies from 0.34 to 2.52 μg-equiv m^{-2}, and the concentration of active hydrogen varies from 0.49 to 7.52 μg-equiv m^{-2}. The proportion of the mobile hydrogen on DB and UDD surfaces amounts to 4% – 22% of the total hydrogen content in the powders.

Surface and electrophysical properties of nanodiamonds of two different specimens (UDD-1 and UDD-2) differing in the content of incombustible residue ([I.r.]) have been studied (Table 3).[26]

Table 3. Characteristics of the nanodiamond powders studied.[26]

Parameter	UDD-1	UDD-2
[I.r.] (%)	0.75	1.16
χ /m^3 kg^{-1}	$-0.35 \cdot 10^{-8}$	0
S_{sp} /m^2 g^{-1}	167	162
C_{BET}	303	814
A /J g^{-1}	400	550
A' /J m^{-2}	2.4	3.4

Note. The parameters are specified in the text.

The amounts of incombustible residues in powders and their specific magnetic susceptibilities (χ) were measured following the procedures developed at the Bakul' Institute of Superhard Materials (Kiev, Ukraine). Adsorption and structural characteristics, *viz.,* the C_{BET} constant, the adsorption potential (A), the specific adsorption potential of UDD (A') and the specific surface area (S_{sp}) were determined by the BET method from isotherms of nitrogen low-temperature adsorption measured on an 'Akusorb-2100' instrument. For UDD samples from both specimens studied, the isotherms of the second kind are typical.

As can be seen from Table 3 the UDD-1 and UDD-2 samples have equal specific surfaces but differ somewhat in the degree of purity and especially in the adsorption potential (for UDD-2 this is 37% larger). According to the values of the C_{BET} constant found, the UDD-2 powder exhibits higher adsorption activity, which suggests that the use of the degree of purity for characterising UDD is ambiguous.

It is found[26] that the absorption band in the IR spectrum of UDD at 1640 cm^{-1} is associated with the deformation vibrations of water, both bound and free. A band at 1750 cm^{-1} corresponds to vibrations of the OH groups.

Drying of UDD powders at 393 K did not result in any noticeable qualitative changes in the spectra. This suggests that the UDD surface bears active functional groups which favour adsorption of water.

On the basis of absorption spectra of UDD powders, it was concluded that the amount of moisture in the form of bound water molecules on the surfaces of nanodiamonds is higher compared with common diamond micropowders obtained in steady-state synthesis. Carboxy and carbonyl groups were also identified. The contents of methyl and methylene groups in UDD powders were insignificant.[26]

An analysis of IR spectra revealed the presence of potassium and aluminium sulfates, chromates and their complex compounds involving silicon in incombustible residues of UDD. Most probably, all these compounds have appeared as a result of a contamination during chemical purification of UDD by chromic anhydride in sulfuric acid.[26]

The changes in the nature of a 'coat' of functional groups on the surface of nanodiamonds upon their treatment in different media, affects the susceptibility of UDD to cold pressing.[27] Table 4 shows the values of limiting pressures during the compaction and the densities of compacted UDD both non-modified and

Table 4. The effect of UDD pretreatment on the limiting compacting pressure (P_{lim}) and the density (ρ) of compacts.[27]

Parameter	Initial UDD	UDD modified by treatment with		
		H_2	CO_2	concentrated HNO_3
P_{lim} /kg cm^{-2}	800–900	300–400	1200	1200
ρ /g cm^{-3}	1.2	1.00–1.15	1.23–1.30	1.3–1.4

modified by treatment with concentrated nitric acid, hydrogen and carbon dioxide.

V. Phase composition, microstructure and surface texture

Depending on the synthesis conditions, the explosion condensed products contain either only a cubic phase of diamond or also Lonsdalite as an admixture (up to 30%).[21] The X-ray diffraction pattern of a UDD sample contains five reflections characterised by the following intensity distribution:

Reflection	(111)	(220)	(113)	(400)	(331)
Fraction (%):					
UDD sample	85.0	14.0	0.5	0.3	0.2
reference sample	44	22	18	4	12

It may be assumed that the predominance of the reflection from the (111) plane in the spectrum is associated with the spherical shapes of UDD particles.

Table 5 shows microstructure parameters of UDD specimens. Nanodiamonds formed during detonation of a trotyl–hexogen melt (60 : 40) [21] exhibit the highest microstresses of the second kind and, as a consequence, have most deformed lattices. It was found that the microstresses of UDD lattice do not change until the onset of graphitisation at 1473 K. Thus, a highly strained structure of UDD is thermally stable. Nonetheless, UDD synthesised by the aforementioned method should be expected to possess an enhanced reactivity.

Table 5. Microstructure of detonation synthesis nanodiamonds.

Coherent scattering region /nm	a/a_0 (%) [a]	Microstresses /GPa	a /nm	Ref.
4–6	1.0	10	0.3562 ± 0.0003	21
5–10	0.42–0.47	4.2–4.7	–	28
5–15	0.1	1.0	0.3572 ± 0.0004	29

Note. [a] Relative lattice distortion (a is the parameter of a real lattice, a_0 is the parameter of the diamond cubic lattice).

Peculiarities of the surface structure were studied for DB, partially oxidised DB and UDD,[30, 31] and the degree of oxidative decomposition was estimated (see footnote to Table 2).

The BET method was used for the determination of the specific surface area (S_{BET}) and the size distribution of pores from the adsorption isotherms of nitrogen. By gradually increasing the degree of oxidative decomposition (α) of DB by acids it was possible to obtain a series of specimens of partially oxidised DB containing different amounts of oxidised carbon, *viz*., from the initial DB (sample *1*) to UDD (sample *12*). Table 6 shows the texture parameters of the specimens.

The dependences of the specific surface area, the volume, and geometrical parameters of pores on the quantity α reach an extremum at $\alpha = 0.63$; at this point, S_{BET} and the volume of pores are a minimum, and C_{BET} is a maximum. At this stage of

Table 6. Parameters of DB and UDD textures.[30]

Sample	$[C_{ox}]$ (%)	α	S_{BET} /m^2 g^{-1}	V_p /cm^3 g^{-1}	C_{BET}	d_a /nm	d_d /nm
1	53.4	0	404	1.2451	108	9.1	8.8
2	44.4	0.17	409	1.0746	112	8.1	8.0
3	38.4	0.28	399	0.9931	107	7.7	7.9
4	36.3	0.32	314	0.7488	109	7.5	7.6
5	27.8	0.48	244	0.6621	133	8.6	6.8
6	27.6	0.49	209	0.5406	136	8.7	8.8
7	23.7	0.56	198	0.5236	155	9.1	9.1
8	19.5	0.63	195	0.5089	182	9.5	9.3
9	9.9	0.81	240	–	–	–	–
10	7.9	0.85	252	–	–	–	–
11	3.4	0.94	276	0.8241	135	9.8	9.6
12	1.2	0.98	290	0.8396	121	9.2	9.2

Note. Here, $[C_{ox}]$ denotes the mass fraction of oxidised carbon; V_p is the limiting volume of the sorption space at $P/P_s = 0.995$ (P is the partial pressure of nitrogen, P_s is the pressure at which the whole internal surface of pores is covered by a nitrogen monolayer); d_a is the size of an open pore; d_d is the critical neck size, *i.e*., the maximum pore size at which the atoms of an adsorbed gas can enter the adsorbent.

decomposition, a partially oxidised DB retains ~20% of non-diamond carbon. In the range of $\alpha = 0.63–0.98$, carbon particles are etched at the stressed and defective areas. Here, a new kind of surface with predominant relaxed diamond-type structures is formed. Thus, when passing from the original DB to UDD, the texture characteristics of the substances change non-monotonically. This distinguishes DB from other carbon phases (technological carbon, coals, carbon fibres) being associated, first of all, with the presence of two carbon phases, *viz*., diamond-type and non-diamond in DB, which differ in their chemical activities and oxidation mechanisms. Comparing the values of S_{BET}, C_{BET} and the volume of pores found for DB and UDD, on the one hand, and those obtained for intermediate oxidation products, on the other hand, we can conclude that the powders of detonation carbon represent organised space structures formed during multistep aggregation of original particles rather than a mechanical mixture of UDD and non-diamond carbon.

In the liquid-phase oxidation, chemical decomposition (etching) of secondary aggregates occurs, which entails regular changes in the surface area and in texture characteristics of the powders. Primary aggregates remain practically unchanged. These data taken altogether point to a structural self-organisation of detonation synthesis ultradispersed carbon.

As was discussed above, the properties of UDD surface strongly depend on the conditions of their chemical pretreatment, which in a number of cases plays a key role in the production of new composite diamond-containing materials with the required characteristics.

VI. Sorption properties and exchange capacity

The sorption properties of DB and UDD, which are extremely important characteristics for different application fields of UDD have been studied.[32]

Oxygen-containing groups present on nanodiamond surfaces [33] impart a charge to UDD aggregates in aqueous solutions; the value and sign of this charge depend on the concentration and the dissociation constant of these groups, the solution pH and the background-electrolyte concentration. Ions H^+ and OH^- are potential-determining. The dependence of the specific adsorption on the solution pH, which is observed for all powders under study, can be attributed to an increase in the degree of dissociation of surface groups with acidic properties.

In the gradual oxidation of the detonation-derived carbon, the specific adsorption changes non-monotonically and passes

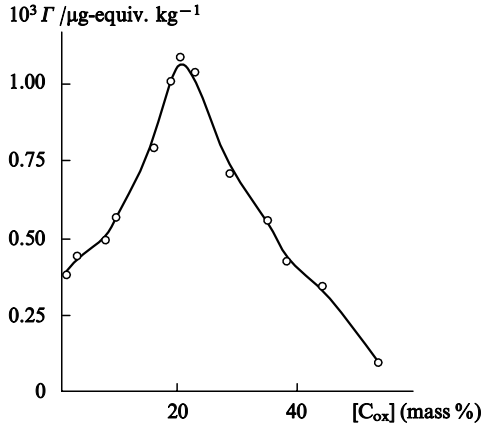

Figure 2. Specific adsorption (Γ) as a function of oxidisable carbon content in DB (pH 11).[32]

through a pronounced extremum (Fig. 2). A low specific adsorption value for the original DB is explained by the fact that this DB has been synthesised in a non-oxidative medium and thus involves a small amount of surface oxygen-containing groups.

When a DB is exposed to oxidants, two processes proceed simultaneously, *viz*., surface enrichement with oxygen-containing groups and etching of carbon. With an increase in the degree of oxidative decomposition, the surface is enriched with oxygen-containing groups, the specific adsorption would have been expected to reach a maximum and then remain constant. However, starting from 18% – 20% of residual oxidisable carbon, the specific adsorption decreases.

The presence of an extremum in the curve (see Fig. 2) reflects qualitative changes in the surface structure of DB upon treatment, namely, a transition from a graphite-like form to a diamond-like form.[31] In this transitional state, the material exhibits the best adsorption properties. The DB subjected to drastic oxidation retains only a stable diamond form. Under the conditions of mild oxidative etching, the boundary between diamond-like and non-diamond carbon shifts. The residual oxidisable carbon (the remaining 18% – 20%) actually represents a diamond-like phase, *i.e*., corresponds to the periphery of a diamond cluster.

For UDD samples listed in Table 1, the sorption capacity with respect to benzene and chloroform vapours was estimated at 292 – 294 K by a weighing method under steady-state conditions close to the isothermal ones. The results obtained are as follows.

1. The sorption capacity of a dry powder of UDD-STP (produced at SDB 'Tekhnolog') amounts to 9 mol kg^{-1} with respect to benzene vapour and 10.5 mol kg^{-1} with respect to chloroform vapour. The observation time was 15 days; 90% – 95% of adsorbate was absorbed in 2 days.

2. The sorption capacities of four fractions isolated from the suspension of UDD-TAH decrease monotonically from 8 mol kg^{-1} for the first fraction to 7 mol kg^{-1} for the fourth fraction with respect to benzene vapour and, correspondingly, from 8.5 to 7.5 mol kg^{-1} with respect to chloroform vapour. The observation time was 13.3 days; 95% – 100% of the adsorbate was adsorbed in 2 days (more quickly for chloroform).

3. For comparison, sorption capacities of certain UDD samples made at RFNC-ARITP were determined, which varied from 12 – 16 to 10 – 14 mol kg^{-1} for benzene vapour and from 14 – 19 to 12 – 17 mol kg^{-1} for chloroform vapour. A distinguishing feature of this type of UDD is that its sorption capacity gradually increases: 55% – 65% of adsorbate is adsorbed in 2 days. The adsorption capacities and rates virtually coincide for DB and diamonds isolated from it (*i.e*., the sorption capacity in fact is independent of the content of non-diamond carbon in the diamonds).

Inasmuch as the adsorption phenomenon forms the basis of many technological processes, the degrees of adsorption of heavy-metal ions on the UDD surface were estimated. For this purpose, an electrochemical technique of cathodic potentiodynamic pulses was applied.[34]

Table 7. Results on the adsorption activity studies of UDD-1 and UDD-2 powders with respect to heavy metal ions.[26]

M^{n+}	$[M^{n+}]$ in electrolyte /mol kg^{-1}	θ (%)	
		UDD-1	UDD-2
Fe^{2+}	0.1	18.0	26.5
Fe^{2+}	10	80.6	82.5
Ni^{2+}	0.1	16.0	33.0
Ni^{2+}	10	75.0	80.0
Cr^{6+}	0.1	12.0	40.0
Cr^{6+}	10	48.0	53.3

It was shown that the adsorption activities of UDD powders with respect to metal ions (iron, nickel, chromium) differ substantially (Table 7). In all experiments, the surface coverages (θ) of UDD-2 were higher. On the whole, the adsorption activity of nanodiamonds with respect to the ions under study decreases in the following order: $Fe^{2+} > Ni^{2+} > Cr^{6+}$ (Ref. 26). However, at low concentrations of metal ions (0.1 mol kg^{-1}), this sequence for UDD-2 is reversed: $Cr^{6+} > Ni^{2+} > Fe^{2+}$. With an increase in the ion concentrations from 0.1 to 10 mol kg^{-1}, the degree of surface coverage of diamond particles increases 3 – 4-fold and reaches 70% – 80%.

It was thus confirmed [26] that the adsorption activity of UDD surface depends substantially on the method of chemical purification of nanodiamonds of detonation synthesis.

Studies of surface properties of UDD isolated from DB under the action of nitric acid and atmospheric oxygen [35] and modified by different reagents [36, 37] showed UDD to possess pronounced cation-exchange properties, which manifest themselves in the exposure of nanodiamonds to aqueous solutions. It was also found that UDD represent sorbents of high activity with respect to gases.[23]

As was mentioned above, chemical purification of UDD enriches the diamond surface with oxygen-containing groups that determine its cation-exchange properties as a sorbent. The surface of UDD oxidised by atmospheric oxygen bears a greater amount of oxygen-containing groups of the acid type (*i.e*., protogenic) compared with the diamonds of liquid-phase oxidation. As a result, the former nanodiamonds possess better ion-exchange properties. Hence, UDD can serve as promising sorbents for ions of a basic nature.

On the other hand, the method for cooling of the products of detonation synthesis plays a significant role in the formation of the nanodiamond surface. Comparison [38] of nanodiamonds obtained from the same explosive compositions and with charges of the same geometry (*i.e*., fused and pressed in the same moulds) but with different cooling procedures and isolated from the synthesis products by the same methods has shown that their surfaces differ in the composition and the number of admixed functional groups including those groups that affect the ion-exchange properties. Particularly, the use of ice as a cooling agent (*i.e*., as an armour for the charge) is beneficial for the maximum protection of UDD from the subsequent graphitisation. This refers primarily to its finest crystals, which have the highest specific surface area and, hence, high sorption activity.

The sorption capacity of UDD obtained in different conditions or purified by different methods was studied with respect to cesium ions.[38] It was found that the sorption capacity of nanodiamonds synthesised under identical conditions but purified using different oxidants and different treatment conditions varied from 0.01 to 0.50 mol kg^{-1}. This suggests that this depends on the nature of the oxidant and the conditions (duration, temperature) of UDD isolation from synthesis products. Samples obtained from DB by ozone purification exhibited the highest sorption

abilities (0.4–0.5 mol kg^{-1}). The value found exceeds substantially those of known natural sorbents[39] (0.01–0.15 mol kg^{-1} with respect to cesium) and is commensurable with the sorption capacity of KU-8-2 resin (0.8 mol kg^{-1}), which is a widely used ion-exchange resin.

An analysis of IR spectra showed that the UDD samples contain different polar functional groups: OH, NH, C–O, C=O, C–H, C–N, C=N, C–O–O in different concentrations. Nanodiamonds of higher sorption capacities are characterised by higher intensities of absorption bands of oxygen-containing (C=O, in the region of 1700 cm^{-1}) and peroxide (C–O–O, 1800–1900 cm^{-1}) groups compared with other samples. Apparently, it is the presence of these groups that is responsible for the enhanced cation-exchange ability of the samples under discussion.

An IR spectrum of UDD synthesised in a gaseous cooling medium shows a wide absorption band in the region of 1600–1900 cm^{-1}, which points to a higher concentration of oxygen-containing groups which determine the cation exchange.

It was proposed to use UDD as a potential sorbent for cesium radionuclides.[38] Compared with conventional ion-exchange resins, ion-exchange materials based on nanodiamonds possess basically better new characteristics: substantially higher thermal stability (400 °C in air compared with 120–150 °C for KU-8-2 resin), resistance against aggressive media, mechanical strength, the absence of swelling and high sorbent density (3.1–3.3 g cm^{-3} against 0.7–0.8 g cm^{-3} for KU-8-2).

In the context of the commercial application of UDD for deposition of composite electroplates, it is of interest to study the behaviour of UDD hydrosols in the presence of different ions under the action of an external electrical field and without it.

Electrochemical studies of an aqueous suspension of UDD were carried out in the pH range of 3–10, at an ionic strength varying from 10^{-4} to 10^{-1} in a temperature interval from 20 to 70 °C.[40] A combination of macroelectrophoresis and potentiometric and conductometric titrations were applied. The experimental data were analysed within the framework of a model that takes into account the complex nature of UDD aggregation with the formation of primary and secondary structures.[6,41]

The dependence of the exchange capacity (G) for UDD on the pH of KCl solutions with concentrations (c) of 0.1 and 0.01 mol $litre^{-1}$ was examined by potentiometric titration. The titration curves for UDD powders and sedimentation-unstable hydrosols virtually coincide, which points to the similarity of the structures (or specific surface areas) of coagulated precipitates and dried powders. A threshold of fast coagulation of the hydrosols and loss of sedimentation stability corresponds to pH 5.5 in KCl solution with c = 0.01 mol $litre^{-1}$. With an increase in pH, the exchange capacity of UDD increases from 0.05×10^3 μg-equiv. kg^{-1} (pH 3) to $(0.4–0.6) \times 10^3$ μg-equiv. kg^{-1} (pH 10). In the pH range of 9–10, the exchange capacity of the hydrosol substantially increases, in contrast to that of the UDD powder. This reflects different dispersion of nanodiamond particles.

On the basis of the specific surface value of 322 m^2 g^{-1} found by the BET method for powder particles,[40] the surface charge density was calculated, which made it possible to roughly assess the potential of the UDD surface for both powders and hydrosols. Figure 3 shows the dependences of the surface, diffusion and electrokinetic potentials on the solution pH.

The pH-dependences of the surface (curve *1*) and diffusion (curve *2*) potentials have similar shapes. The electrokinetic potential (curve *3*) was estimated from the results of macroelectrophoresis by using a formula valid for particles with unipolar conduction.[42]

From comparison of the potentials (see Fig. 3), it follows that a substantial volume ascribed to the immobile part of the electrical double layer can be attributed not only to the presence of water layers with different structures near the nanodiamond surface, but also to the immobilisation of the dispersion medium inside the UDD aggregates. Such a conclusion is confirmed by the different

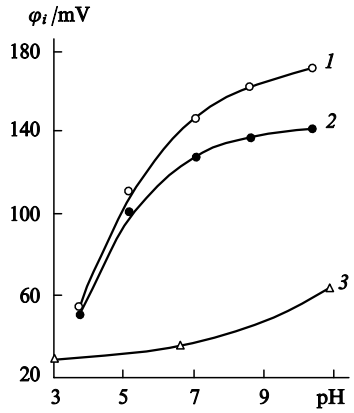

Figure 3. Dependences of (*1*) surface, (*2*) diffusion and (*3*) electrokinetic potentials (φ_i) on pH for UDD particles in a hydrosol in KCl solution (c = 0.01 mol $litre^{-1}$).[40]

shapes of the temperature dependences for electrokinetic and diffusion potentials.

At a low ionic strength (in a KCl solution with $c = 10^{-4}$ mol $litre^{-1}$), no apparent flocculation of primary aggregates occurs, and the destruction of the interfacial water layers, which proceeds at elevated temperatures, is accompanied by an increase in the electrophoretic mobility of UDD. In solutions of higher ionic strengths, the destruction of interfacial layers at elevated temperatures facilitates flocculation of primary aggregates. Water immobilised inside newly formed secondary aggregates does not necessarily take part in the motion; however, the exchanged ions retain their mobility. In this case, the electrophoretic mobility decreases and the diffusion potential remains unchanged. Indeed, the diffusion potential calculated for the isopolarisation mode from the data on the conductivity of UDD hydrosols, under an assumption of a constant size of hydrosol particles, does not decrease with an increase in the temperature (in contrast, a slight increase is observed).

Electrochemical studies of the surface allowed refinement of the structure of solid phase in UDD hysrosols. Using the values of the diffusion potentials found in potentiometric titration and the results of conductivity measurements at the isoconduction point (pH 6, KCl solution, c = 0.01 mol $litre^{-1}$), the sizes of non-conducting spherical UDD formations were determined and proved to coincide with the radii of primary aggregates (10–30 nm) estimated by electron microscopy.[6] This implies that primary aggregates are non-conducting, *i.e.*, have dense ion-impermeable structures.

Thus, UDD represent presumably a cation-exchange system with a variety of functional groups of different acidic strengths.[40] Hydrosols of UDD consist of dense primary aggregates which form ion-permeable secondary structures. Different shapes of the pH dependences for diffusion and electrokinetic potentials, as well as many other properties of UDD hydrosols as a function of pH, ionic strength and temperature are determined by the changes in their secondary structures.

VII. Chemical properties of ultradispersed diamonds

Studies of the chemical composition of DB and UDD were carried out by the methods of gas chromatography (CG), polarography, IR spectroscopy and X-ray photoelectron spectroscopy (XPS).[43] Table 8 shows the results of polarographic and GC studies of DB and UDD samples.

It follows from the data in Table 8 that the carbon of the UDD surface groups is oxidised to a higher degree and the hydrogen content is substantially lower compared with DB.

Table 8. Composition of desorbed gases and their activation energies.[43]

Sample	Composition of desorbed gases [a]		Activation energy of desorption [b] /kJ mol^{-1}
	gas	gas content /cm^3 g^{-1}	
DB [c]	CO_2	3.9	23.4
	N_2	0.7	22.5
	CH_4	4.03	47.6
	H_2	7.8	–
	CO	0.09	103.6
	NH_3	1.43	27.2
UDD [d]	CO_2	11.4	48.5
	N_2	0.83	23.0
	CH_4	1.7	28.4
	HCN	traces	–

Note. [a] Determination conditions: 673 K; desorption time, 2 h; pressure, 0.1 Pa. [b] At 573 – 773 K. [c] Elemental composition (%): C, 86.3; H, 0.4; N, 3.7; O, 9.6. [d] Elemental composition (%): C, 86.0; H, 0.1; N, 2.5; O, 11.4.

The IR spectroscopy data suggest the presence of the carbonyl, carboxy, hydroxy, methyl and nitrile groups on the surfaces of UDD and DB. Thermodesorpsion of large amounts of methane and hydrogen from a DB sample (Table 8) gives us grounds to assume that it has a different composition of surface groups. Apparently, this is associated with the following reactions involving carbon surface atoms with uncompensated bonds

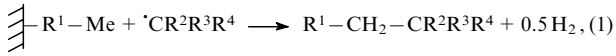

$$\equiv R^1-Me + {}^{\bullet}CR^2R^3R^4 \longrightarrow R^1-CH_2-CR^2R^3R^4 + 0.5\,H_2\,, \quad (1)$$

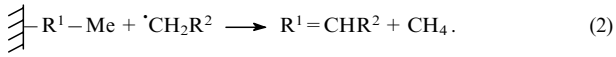

$$\equiv R^1-Me + {}^{\bullet}CH_2R^2 \longrightarrow R^1=CHR^2 + CH_4\,. \quad (2)$$

If reactions (1) and (2) do occur, then the fraction of carbon atoms with uncompensated bonds (surface atoms) amounts to no less than 1.6 %. An estimation based on these data showed that the mean particle diameter is 45 nm (no more than 300 carbon atoms).

According to XPS results [21, 43], the C_{1s} band in the spectrum of DB represents a wide asymmetric peak (half-width, $\Delta E_{1/2}$ = 4.1 eV), which narrows after bombardment with argon ($\Delta E_{1/2}$ = 2.5 eV) and takes a shape typical of graphite and fine-grain coals. In this case, the surface charging is zero, which is typical of conducting substances. These results suggest that the bulk of the sample represents the graphite phase, whereas, in the surface layer (several tens of angstrom deep), the diamond carbon phase is located.

For UDD samples (see Table 8), a symmetrical C_{1s} peak ($\Delta E_{1/2}$ = 3.3 eV) is typical, and the surface charging is + 3.3 eV. After bombardment with argon, the shape of the carbon peak remains unchanged, and the surface charging reaches + 6.2 eV, $\Delta E_{1/2}$ = 2.9 eV. It was concluded that carbon in the surface layer (no less than 10-nm deep) of a sample is represented exclusively by the diamond phase.[43] The initial sample includes nitrogen and oxygen (O : C = 0.027, N : C = 0.020) as the admixtures. After bombardment with argon, the admixture content becomes lower than the threshold sensitivity of a spectrometer.

Thus, in DB particles the diamond-like carbon phase surrounds the graphite phase or, more precisely, a non-diamond carbon form. UDD particles consist entirely of a diamond-like carbon phase. Admixtures in the form of carbon compounds with oxygen and nitrogen are accumulated preferentially in the surface layer of a particle.

In accordance with a classification of functional derivatives of diamonds, UDD pertain to a group of 'colloidal diamonds' as regards the crystal sizes and the ratio of surface carbon atoms (C_s) to the total number of carbon atoms (C_{tot}) in a diamond crystal.[44]

For nanoparticles measuring 2 – 10 nm, the number of surface C atoms with respect to their total number in the core varies from 63% to 15%, *i.e.*, from 4 to 18 internal carbon layers are present. Hence, UDD properties should largely be determined by the chemical states of their surfaces, in contrast to coarse diamond crystals with $C_s/C_{tot} \to 0$. However, to date the chemical properties of UDD remain less understood as compared with diamonds of other types.

The functional 'coat' of UDD particles, the possibilities of their chemical modification in different gaseous media, and their behaviour at elevated temperatures have been studied.[27]

The UDD samples were produced at the Research Industrial Association (RIA) 'Altai' (Biisk) and purified by using oleum – nitric acid mixtures at 523 K. The isolated UDD were dark-grey powders with microcrystals of 3 – 8 nm, which, being placed in water, formed aggregates measuring up to 2×10^{-4} m. The elemental composition of these UDD (%) is given below.

C	H	O	N	Ash content
78.6 – 78.8	0.65 – 0.70	16.5 – 17.0	1.78 – 2.16	1.34 – 2.47

The high content of oxygen in UDD agrees with the C_s/C_{tot} ratio and the amount of possible functional oxygen-containing groups on the surfaces of diamond particles of such sizes.[44]

The first step of UDD modification included drying them in air and heating the fine fraction in a flow of nitrogen at 348 K in a flow-through system. In the second stage, UDD were heated at 673 – 973 K in a flow of a gas (N_2, CO_2, CH_4, H_2, air) passed at a rate of 5.6×10^{-7} m^3 s^{-1}.

The results obtained [27] allowed the authors to assess the effect of pretreatment of UDD on the temperature of oxidation initiation. After treatment with water oxidation starts at 673 K, whereas upon exposure to a $CH_4 + CO_2$ mixture, it begins at 773 K, *i.e.*, hydroxylated surfaces are oxidised more easily.

Studies on the behaviour of UDD in oxidising gas mixtures under isothermal heating showed that the oxidants may be arranged in the following series with respect to their activities: air $\gg CO_2 > H_2O$.

It was shown that all the temperature dependences of UDD oxidation rate clearly manifest two regions. In the low-temperature region (below 673 K), the change in the UDD mass depends little on the temperature, whereas in the high-temperature region oxidation sharply accelerates with an increase in temperature.

On the basis of the results obtained, the apparent activation energies of UDD oxidation were calculated (Table 9). This table also shows the temperatures of transition to high-temperature regions for different oxidation conditions.

As is seen from the data of Table 9, the activation energies in two regions differ by a factor of 3 – 6 for the same oxidant. Probably, this is associated with the fact that, in the low-temperature region, oxidation actively involves the 'coat' of functional groups present on the surface of UDD particles and their decom-

Table 9. Apparent activation energies (E_a) of UDD oxidation in low-temperature (I) and high-temperature (II) regions.

Oxidant	Temperature of I to II transition /K	E_a /kJ mol^{-1}	
		region I	region II
$O_2 + N_2$ (20% O_2)	673	24.7 ± 1.7	96.1 ± 4.2
$O_2 + N_2$ (10% O_2)	773	24.7 ± 1.7	96.1 ± 4.2
$O_2 + N_2$ (4% O_2)	773	25.5 ± 5.9	91.1 ± 13.0
CO_2	898	36.4 ± 7.1	120.4 ± 15.0
CO_2, K_2CO_3 (see [a])	838	18.8 ± 5.0	88.6 ± 5.0
H_2O	933	22.2 ± 13.4	152.2 ± 7.1
H_2O, K_2CO_3 (see [a])	703	20.5 ± 12.1	126.7 ± 10.0

Note. [a] Successive treatment.

position products, whereas in the high-temperature region only hydroxy groups take part in the reaction. In the presence of a catalyst (K_2CO_3), the activation energies of UDD oxidation are somewhat lower than that of the noncatalysed process. On the whole, the activation energies of UDD oxidation in the high temperature region are slightly lower compared with detonation diamonds synthesised from graphite and soot [45] and twice as low as those of kimberlite diamonds.[46]

The aforementioned results confirm the presence of a 'coat' of different functional groups on the surfaces of UDD particles and suggest that this 'coat' changes as a result of chemical modification and has a pronounced effect on physical and chemical properties of UDD, particularly, the resistance of the latter against oxidising gas mixtures, their compactibility (see Table 4), *etc*.

Furthermore, the results obtained allow us to conclude that UDD represent not simply diamond-like materials (*e.g*., see Ref. 4), but typical diamonds, the surface of which, as for the other diamond types, contains different functional groups that saturate free valences of carbon surface atoms. A unique specific feature of UDD is that, with respect to the C_s/C_{tot} ratio, they occupy an intermediate position in a series of functional derivatives of diamond cores, between low-molecular forms similar to adamantane functional derivatives and the polymeric forms representing diamond macro-crystals with specific functional 'coats'. It has been shown [44] that such a mesoregion corresponds to colloidal sizes of the particles. Therefore, bearing in mind that, due to the presence of a functional 'coat', an electrical double layer can surround UDD particles in solution, it is quite reasonable to call the latter particles colloidal diamonds.

VIII. Spectroscopy

Absorption spectra of UDD powders do not reveal any specific features in the optical range. A microscopic study have shown that UDD microparticles by themselves are colourless, so that the typical colour of the powder is, most probably, caused by diffuse scattering and reflection. The microparticles demonstrated no optical anisotropy.

The refractive index of UDD estimated by the immersion technique amounted to ~ 2.55 at the wavelength of 580 nm, which is substantially higher than that of natural diamonds and artificial diamonds of steady-state synthesis.

1. Infrared spectroscopy

The diamond lattice is known to possess over 50 defect centres active in the optical spectra. Most synthetic diamonds contain nitrogen as atomic dopant of substitution. With respect to shapes of the IR spectra, diamonds are divided into two types, *viz*., (I) with one-phonon absorption and (II) without absorption in the single-phonon spectrum range. The first group includes diamonds of the Ia type the one-phonon absorption of which is caused by three independent defective centres: A (1282, 1210, 1110, 480 cm^{-1}), B1 (1332, 1175, 1000, 775, 328 cm^{-1}) and B2 (1350–1380 cm^{-1}), and the diamonds of the Ib type the one-phonon absorption of which is caused by C centres. A well developed surface of UDD (up to 4.5×10^5 m^2 kg^{-1}) and high C_s/C_{tot} ratios that determine the high concentration of surface functional groups allow the method of IR spectroscopy to be used [27] with the aim of reliable identification of the nature of these functional groups.

For insufficiently purified UDD (produced by RIA 'Altai'), the spectra measured both before and after modification revealed absorption bands of carbonyl (1730–1790 cm^{-1}) and hydroxy groups (1640, 3400 cm^{-1}). A wide band with a maximum in the range of 1100–1140 cm^{-1} is probably related to the overall absorption of a number of admixed nitrogen centres of types A (two nitrogen atoms in neighbouring substitution cites), B1 (an accumulation of vacancies 'decorated' by nitrogen), B2 (laminar formations in the cube's plane) and C (isolated nitrogen atoms substituting carbon atoms in the lattice) and the vibrations of C–O–C fragments (NO_2 groups at primary and secondary carbon atoms, SO_2OH groups, OH groups in CO_2H and at ternary carbon atoms absorb in the same range, which complicates unambiguous interpretation).

Comparison of the spectra shows that the positions and intensities of the bands of the carbonyl-group absorption vary widely depending on the UDD modification conditions. Treatment in a nitrogen atmosphere at 937 K results in elimination of carbonyl and carboxy groups, which is indicated by reduced intensities of the corresponding bands. Independently of the modifying gas used, treatment at 673 K shifts the maximum at 1730 cm^{-1} to the region of 1780–1790 cm^{-1}, which indicates the formation of $-C(O)-O-C(O)-$ structures. Insignificant changes in the spectral patterns observed after treating UDD by different kinds of gases suggest that these gases affect insignificantly the composition of surface functional groups of these UDD samples under the conditions specified.

For UDD purified by the nitric-acid procedure (SDB 'Tekhnolog'), the IR spectrum slightly differs from previous spectra and contains characteristic bands at 3500 cm^{-1} (strong, wide), 1740 and 1640 cm^{-1} (both medium), 1260 and 1170 cm^{-1} (both strong and wide) and 610 cm^{-1} (wide, of medium intensity). These bands are well reproducible irrespective of the purification procedure used and, hence, can be assumed to be caused by UDD intrinsic absorption.

A band at 1260 cm^{-1} corresponds to one-phonon absorption of the diamond lattice. Presumably the width and intensity of this band are determined by distortion of the diamond lattice,[18] diamonds of the IIa type, which contain no admixtures, do not absorb in this region. The nature of the other bands in UDD IR spectrum is unclear. Evidently, they do not coincide with any known absorption centres in diamonds. It is possible that some of these bands are caused by adsorbed nitrogen and water.

Our results allowed also us to reveal additional bands dependent on the procedure used for the isolation of UDD. For instance, the spectrum of UDD treated by nitric acid shows bands at 2940, 1390, 1505, 650 cm^{-1}, which were absent in the spectrum of UDD treated by sulfuric acid (produced at RIA 'Altai'); in turn, the latter spectrum contained bands at 2800, 2205 and 670 cm^{-1}. Apparently, the latter bands are caused by the presence on UDD surfaces of conglomerates of functional groups either chemically bound or adsorbed in the course of treatment.

In contrast, due to a substantial amount of background impurities, IR spectra of non-purified DB appear to have a substantially uniform shape with prominent regions of enhanced absorption at 3300 and 1170 cm^{-1}. The presence and width of the latter correlate with the concentration of the diamond component in DB. The spectrum of diamond-free DB reveals none of these peculiarities. It cannot be ruled out that processing of a sufficient body of experimental data will allow development of a quantitative method for the estimation of the diamond concentration in DB.

On the whole, IR spectra of UDD and DB are a good source of information on their structures.

2. NMR and ESR spectra

^{13}C NMR spectra [21] of nanodiamonds involve four signals. A signal with δ 34.5 corresponds to the diamond carbon atoms; a broad signal in the region of δ 30 is due to the fact that carbon atoms are not structurally equivalent, first of all, due to the presence of defects and the Lonsdalite phase. Weakly pronounced peaks with δ 68 and 53 can be attributed either to the effect of partially oxidised structures or the presence of nitrogen atoms in the sample.

In the ^1H NMR spectrum,[21] three overlapping peaks were observed. A signal with δ 2.2 corresponds to the isolated C–OH groups, whereas a signal with δ 3.8 corresponds to bound C–OH groups. A signal with δ 6.7 most probably belongs to S–OH groups formed on the surface of a sample during its chemical

purification (in Ref. 21, oleum–nitric acid treatment of DB was applied).

In the ESR spectra, the UDD signal at 293 K is a singlet with a g-factor of 2.003 and a half-width $\Delta H_{1/2} = 6.3-8.3$ Œ.[21] The concentration of paramagnetic particles ranges from 2.7×10^{21} to 2.0×10^{22} kg^{-1}. The parameters of this signal are most close to the ESR signal of broken bonds on the diamond surface ($g = 2.0027$, $\Delta H_{1/2} = 5.5$ Œ).[47] A similar ESR spectrum was also observed for AV detonation diamonds.[48] It is of note that, despite a high concentration of nitrogen atoms in UDD ($\sim 1.6 \times 10^{24}$ kg^{-1}) no triplet signal associated with doped nitrogen atoms that substitute carbon in the diamond lattice was observed.

3. Raman spectra

Deconvoluted profiles reveal maxima at 1580 and 1620 cm^{-1}, which coincide well with the maxima of the density-of-states function of the sp^2-bound carbon atoms. This suggests that UDD involve an amorphous graphite phase.[20] A band with a maximum at 1530 cm^{-1} can be attributed to the sp^3-bound carbon atoms of that part of the structure which is susceptible to a severe distortion. Apparently, the appearance in the spectrum of a number of specific features of the phonon density of states for the sp^3-bound carbon atoms suggests that, in addition to an amorphous graphite phase, UDD involve an amorphous diamond carbon phase.

4. X-Ray diffraction spectra

X-Ray diffraction spectra [20] of UDD samples contain wide, symmetrical diffraction maxima at $2\theta = 43.9$, 75.3 and 91.5°, which can be adequately described by Lorentz profiles and correspond to the (111), (220) and (311) reflections of the diamond-like lattice with a parameter $a_0 = 0.3565 \pm 0.0005$ nm. The average size of UDD particles determined by using the Selyakov–Scherrer relationship from the half-widths of these lines for all diffraction maxima is equal to 4.5±0.5 nm.

In the region $2\theta = 17°$, an intense localised halo is detected; further, as θ decreases, an increase in the scattered radiation is observed. An intense scattering near the incident beam is typical of diffraction on disordered amorphous structures. Apparently, the observed halo cannot be caused by diffraction on macrostructures with a long-range order and should be associated with its scattering on structural units of a middle-range order. For UDD, not only spherical particles with sizes < 4 nm, but also ordered carbon chains and packages of planes can serve as such structural units. This makes it possible to explain the high intensity of the halo compared with the intensity of the basal (111) maximum. The size of these particles roughly estimated from the halo half-width (in accordance with the Selyakov–Scherrer formula, with assumption of a spherical shape) amounts to ~1.5 nm.

Apparently, it is these small (< 4 nm) ordered particles that represent the 'amorphous' diamond and graphite phases detected in the Raman spectra.

IX. Thermal analysis

Thermal analyses of UDD were carried out either in air or in an atmosphere of an inert gas.[21] On heating in air at a rate of 10 K min^{-1}, oxidation of UDD starts at 703 K,[49] whereas oxidation of diamonds of DSD (detonation synthetic diamond), DDG (detonation diamond with graphite nuclei) and SDB 1/0 (synthetic diamond micropowder) brands begins at 863, 843 and 923 K, respectively.[50] After heating in a neutral atmosphere below 1273 K, the mass loss is 3%–4%. Heating in a CO_2 atmosphere in the temperature range from 443 to 753 K increases the sample's mass by 5%, which can be attributed to CO_2 adsorption and displacement of lighter molecules. Heating in a hydrogen atmosphere is accompanied by HCN evolution.

A complex thermal analysis of UDD carried out in our studies showed that thermograms in air manifest three characteristic regions. At 373–383 K, the mass loss is 5%–7%. This process is endothermic and reversible. An analysis of gaseous products showed that 97%–98% of the gas evolved at this temperature represents nitrogen. Hence, it can be assumed that nitrogen captured from the atmosphere desorbs.

At 523 K, the decrease in the mass of a sample is accompanied by a positive thermal effect. At 753–773 K, an extesive mass loss occurs (up to 95%), which is accompanied by a substantial thermal effect up to 1023–1053 K. Thereafter, no changes take place, and the residual mass corresponds with a 10% accuracy to the ash content of the initial sample estimated according to a standard procedure. It can be assumed that in the interval from 773 to 1023 K carbon is intensively oxidised yielding an incombustible residue. It is noteworthy that oxidation is accompanied by an intense glow.

Wet UDD lose the main mass of water in the interval from 403 to 433 K. Thereafter, the parameters vary practically in the same way as for the predried samples.

Heating in an inert gas atmosphere (helium) at 383–393 K is also accompanied by desorption of nitrogen captured from the atmosphere. In the temperature range of 673–1173 K, a sample loses up to 10% of its mass and heat is liberated. Carbon dioxide and nitrogen are evolved (the molar ratio is 4:1) and the morphology of the material changes.

At 1153–1163 K, a slight positive thermal effect is observed; however, the mass of the sample remains unchanged. The process is accompanied by changes in the morphology and colour of the material. Note that according to the literature data [21] heating in an inert atmosphere entails a practically complete removal of surface groups (adsorbed and chemically bound) from diamond crystals.

X. Defects of the bulk structure

Bulk structural defects of UDD were studied [2] by the method of electron–positron annihilation for all the modes of diamond crystallisation discussed below.

Nanodiamonds were synthesised by detonation of trotyl–hexogen welded charges with 5 mass %–70 mass % of highly dispersed hexogen in water. To estimate the effect of the hexogen concentration and the type of bulk-structure defects and the degree of dispersion of UDD on the sintering process, not only the carbon/hydrogen ratio in the explosive mixture, but also the geometry of charges affecting the time of manifestation of high pressures and temperatures and quenching conditions were varied. After chemical purification, the crystalline structures of UDD were studied by the method of electron–positron annihilation of bulk structural defects. Moreover, a technique of low-temperature adsorption of nitrogen was used for estimating the specific surface area. For studying the sintering processes, UDD of the maximum density of bulk defects (the pycnometric density of 3.05–3.10 g cm^{-3}), the mean CSR size of 1.5–2.0 nm and the maximum degree of dispersion (the specific surface area of 420 m^2 g^{-1}) were chosen. UDD powders were sintered under a pressure of 4–12 GPa. Then, the microhardnesses of sinters and the crushing strengths of the polycrystalline grinding powders obtained were determined.

It was found that with an increase in the carbon temperature and its concentration in the detonation of carbon-containing explosives the distribution curve of vacancy clusters and pores passes through a maximum, after which their concentration begins to decrease. In the region of the maximum corresponding to 3900 K, both an increase in the concentration of vacancy clusters (*i.e.*, agglomerates of vacancies) and the highest concentration of micropores of radii of 1–2 nm in UDD are reached. The aggregates, which contain several vacancies and serve as nuclei for submicropores, represent the centres that capture positrons. The presence in UDD of positronium which has never been observed in diamonds suggests that it appears on the internal surfaces of submicropores formed from vacancy agglomerates.

The absence of submicropores and a low volume density of structural defects (pycnometric density of 3.3×10^3 kg m^{-3}) in

UDD crystallised from trotyl brings these diamonds closer to SDB 1/0 diamonds. This is indicated, for instance, by identical IR spectra of their powders.

XI. Electrophysical properties of ultradispersed diamonds

Diamonds are diamagnetics with a constant magnetic susceptibility ($\chi = -0.62 \times 10^{-8}$ m^3 kg^{-1}).[51] The magnetic susceptibility of UDD substantially differs from this value (see Table 3). The specific magnetic susceptibility of any powder material characterises quantitatively the magnetic properties of the powder as a whole, being the sum of specific magnetic susceptibilities (χ_i) of all components present in the powder with account of their compositions. Table 10 shows the values of magnetic susceptibilities for UDD admixtures.[52]

Table 10. Magnetic susceptibility of admixtures in UDD powder.[52]

Component	UDD	Micropowder of steady-state synthesis	$10^8\chi_i$ /m^3 kg^{-1} (see [a])
Diamond	+	+	−(0.1 – 0.5)
Metal	traces	+	$10^3 - 10^4$
Graphite	+	+	−(0.1 – 8.2)
Carbon materials	+	−	−(0.1 – 2.0)
Gelatine	−	+	−(0.5 – 0.9)

Note. [a] Tentative value.

According to the literature data,[21] the conductivities of UDD are minimal for samples heated at 573 K (resistivity of $\sim 10^{12}$ Ω m). Subsequent heating increases the conductivity (resistivity decreases to $6.0 \times 10^{10} - 2.0 \times 10^{11}$ Ω m). If the samples are heated in a carbon-dioxide atmosphere, then, at temperatures above 1173 K, the resistivity sharply decreases to 2.3×10^4 Ω m, which apparently manifests the beginning of graphitisation.

The permittivity (ε) of different UDD samples varies in a range from 1.7 to 2.7 (Ref. 21). The dissipation factor is $0.5 \times 10^{-3} - 1.0 \times 10^{-2}$.

Thus, UDD exhibit a number of properties that distinguish them from the known types of synthetic diamonds. Despite enhanced reactivity, the diamond-like carbon phase remains stable in neutral and reductive media up to 1273 K, as regards their physicochemical characteristics.

According to our results, at ~293 K the resistivity of a pressed UDD pellet is $10^6 - 10^7$ Ω m. After moistening the pellet, the resistivity sharply increases ($< 10^3$ Ω m for a sample with 5% of water). With further moistening, the resistivity remains unchanged and appears to be determined by the amount of absorbed water. It cannot be ruled out that these data can serve as a basis for the development of a method for determining the residual moisture in UDD.

Yet another important characteristic of the diamond surface is the electrokinetic potential (ζ potential). Taking into account the fact that its value depends substantially on the state of the nanodiamond surface, ζ potential values should be expected not to differ for different fractions of the same UDD and, more so, for UDD samples obtained by different methods of purification and surface modification.

Determination of ζ potential was carried out by electrophoresis based on an electrical current-induced directed transfer of particles of the dispersed medium with respect to the liquid phase.[53] The values of ζ potential were found for three fractions, *viz*., precipitated (I), intermediate (II) and suspended (III), which were obtained from UDD manufactured at RFNC-ARITP (Table 11).

Table 11. Basic physicochemical parameters of isolated UDD fractions.[53]

Parameter	Fraction I	Fraction II	Fraction III
Appearance	light-grey readily crumbling powder	grey powder	black thread-like quasi-crystal formations
Pycnometric density ($10^{-3}\rho$) /kg m^{-3}	3.3	3.2	3.1
[I.r] (mass %)	1.6	1.3	0.9
[C_{ox}] (mass %)	1.0	1.5	1.9
Viscosity [a] of UDD aqueous suspension /MPa s			
at [UDD] = 10 kg m^{-3}	1.04	1.07	1.12
at [UDD] = 60 kg m^{-3}	1.32	1.63	5.15
Electrokinetic potential /mV	+16	+32	+39

Note. Fractions are specified in the text. [a] At 293 K.

The value of ζ potential was also determined for UDD of UDD-TAH (produced at SDB 'Tekhnolog'). The samples were preliminarily purified by ion-exchange resins. For non-fractionated UDD (UDD-TAH), the value of the ζ potential of 32 – 34 mV was found (from three experiments) at 297 – 298 K (for a comparison, ζ potential of non-fractionated and non-dried UDD produced at RFNC-ARITP and similarly pretreated was ±25 – 26 mV).

For four isolated fractions of UDD (UDD-TAH), values of +55, +76, +25 and +33 mV, respectively, were obtained. The resistances (R) of the suspensions (not exceeding 2×10^{-5} Ω) differed only insignificantly after the measurements.

XII. Fractionation process and sedimentation stability

The fractionation process has been discussed in detail.[53] It was claimed that the traditional methods of fractionation of particles with respect to composition and size based on stirring of nanodiamonds in a chosen liquid and subsequent sedimentation under the action of gravity, cannot be applied to highly dispersed colloidal systems including UDD. In the best case, fine fractions are decanted and later form aggregates during drying. The use of organic liquids cannot be accepted due to the high sorption capacity of nanodiamonds (the author of the present work thinks differently).

UDD of different purity grades are shown to include a typical set of functional groups, which remain unchanged up to the destruction of the diamond structure. These are polar OH, NH, C=O, CH and C=N functional groups. It is these groups, especially, the carbonyl and hydroxy groups that determine the trend of UDD particles to form aggregates in aqueous solutions.

Centrifugation of a sedimentation-stable suspension for different periods allowed isolation of UDD fractions (see Table 11).[53] Analysis of IR spectra of the fractions isolated showed that practically the same functional groups were present in all the fractions; however, their concentration differed for different fractions.

UDD was considered as a complex composite material, which consists of individual fractions.[53] The latter differ from one another in the nature and composition of surface groups, as well as in the sizes of aggregates.

Ultrasonication of a dry UDD powder (UDD-STP, produced by Joint Stock Company 'Diamond Centre', St. Petersburg) in water allowed preparation of a stable suspension the dispersed composition of which remained unchanged for a month and

longer.[54] The average size of formed aggregates was 300 nm. An attempt to stabilise the suspension by using different surfactants failed. The UDD particles appear to be surrounded by surfactant molecules with hydrophobic tails directed towards the aqueous medium. Thus, additional hydrophobisation of UDD particles takes place, and the stability of the latter in water decreases.

It was found [55] that, with an increase in the ability of molecules of the medium to association (acetone < benzene < propan-2-ol < water), the degree of dispersion of UDD particles in suspensions also increases. Hence, the solvation of the accessible surface of diamond clusters is favoured not only by the polarity, but also by the tendency of substances to form π-complexes.

From the practical viewpoint, the most important goal is the preparation of stable UDD suspensions in non-polar organic solvents. Nanodiamond suspensions of such a kind will allow cluster compositions based on elastomers to be developed. A real way of solving this problem is to change the nature of the surface of UDD particles from hydrophilic to hydrophobic. For this purpose, a dry nanodiamond powder was added to a benzene solution of commercial co-polydimethyl siloxane and polyisoprene.[55] The adsorption of hydrophobic polymer chains on the surface of UDD clusters was assumed to be beneficial for stabilisation of the suspension. Indeed, the authors managed to enhance the degree of dispersion of UDD in an organic solvent. A method for modifying surfaces and optimising suspensions was developed;[54, 55] for this purpose, polyisoprene proved to be most suitable. Its use for the modification of the surfaces of UDD clusters gave a suspension in which particles measuring 300 nm predominated. This suspension retained its sedimentation stability for no less than 10 days.

XIII. The diamond – graphite structural phase transition

Systematic studies of the diamond – graphite structural phase transition were carried out for UDD clusters.[20] The phase transition occurs in the course of heating in an inert atmosphere in the temperature range of 720 – 1400 K. To detect the transition, the Raman spectroscopy and X-ray diffractometry were used.

The analysis of Raman spectra and X-ray diffraction patterns makes it possible to conclude that UDD represent a cluster material of a diamond crystalline structure with nanocrystals with a characteristic size of ~4.3 nm.

A narrow range of sizes of UDD nanoclusters, *viz*., 4 – 5 nm, was often reported.[17, 56, 57] Apparently, this is explained by the fact that for nanoclusters of small sizes diamond rather than graphite constitutes the thermodynamically stable form. This assumption is confirmed by the results of calculations.[58]

The fact that the lines in the Raman spectra of nanodiamonds coincide with the maxima of the function of phonon density of states in diamond and graphite suggests that UDD involve only small amounts of amorphous diamond and graphite. Inasmuch as nanodiamond clusters, like other ultra-dispersed materials, exist only in an aggregate form,[6] the amorphous phase apparently is located inside such aggregates on the surfaces of diamond cores. The presence of the amorphous phase was also confirmed by the results of X-ray diffractometry, which made it possible to assess the characteristic sizes of particles as ~1.5 nm.

The invariant position of a maximum at 1322 cm^{-1}, which is observed in the Raman spectra with an increase in the support temperature (T_{app}) up to 1000 K, points to the absence of any substantial changes in the structure of the diamond core at such annealing temperatures. This is confirmed by the data from X-ray diffractometry, which state that the graphite phase appears only at $T_{app} > 1200$ K.

The diamond – graphite structural phase transition in the annealing in an inert atmosphere starts from the cluster surfaces. As follows from the analysis of X-ray diffraction data, the graphite phase originates as a set of equidistant graphite nanoplates with a characteristic size < 4 nm and then at $T_{app} > 1200$ K the formation of this phase predominantly involves the diamond core.

The temperature of phase transition (T_{pt}) found correlates well with the results of electron microscopy,[59] according to which the core of a nanocrystalline diamond begins to decrease only as a temperature of 1300 K is reached. This process is accompanied by the transition of carbon into an onion-like structure. A peak at 1575 cm^{-1}, which appears in the Raman spectrum and is clearly pronounced at 1400 K, was interpreted [59] as the manifestation of the carbon onion-like structure. This fact confirms the correctness of the T_{pt} value determined.

It was noted [59] that the diamond – graphite phase transition starts in UDD at substantially lower temperatures compared with diamond single crystals for which $T_{pt} > 1900$ K (see Ref. 60). Such a decrease in a phase-transition temperature, *e.g*., a melting point, was observed earlier for metal clusters.[61]

In parallel with the formation of the graphite phase on the diamond core of a cluster, ordering of sp^2-bound carbon fragments present on original UDD occurs at $T_{app} > 720$ K. Such an sp^2-coordinated crystallisation, in the course of which a disordered (amorphous) phase of carbon located between diamond cores forms continuous graphite nets (patterns), takes place beyond the crystalline diamond core and reflects the changes in the amorphous sp^2-bound carbon. This crystallisation is indicated by an increase in the band intensity at 1350 and 1600 cm^{-1} in the Raman spectra and the appearance of a fine structure in the diffraction pattern in the region of low and medium angles at $T_{app} > 1300$ K.

XIV. A cluster model and the fractal nature of UDD aggregates

Being a structure of the classical type, a UDD particle consists of a relatively dense and ordered crystal-like core and a loose chemically labile shell. The diamond core determines the basic diamond-type properties of UDD, namely, their thermal and chemical stability, heat conduction and thermal diffusivity, low electrical conductivity, the X-ray diffraction pattern quasi-abrasiveness and quasi-hardness. The cluster shell is responsible for such properties of the substance as the sign and value of the UDD surface charge, the chemical composition of surface functional groups, absorption, adsorption, chemisorption and colloidal stability of UDD particles in liquid and other media. In contrast to 'classical' metal clusters the cores and ligand shells of which are built of chemically different elements, *viz.,* metal atoms and complexing ions, in UDD clusters both the cores and the stabilising shells are largely the carbon atoms. In this case, the diamond lattice of the core can gradate to a non-diamond periphery through a system of diamond-like polyhedral polycyclic structures and net patterns. The cluster boundary is stabilised by the products of interaction of periphery carbon atoms with the environment, *viz*., gaseous detonation products, oxidising mixtures and modifying reagents. Peripheral structures play a decisive role in aggregation of diamond clusters and their interaction with matrix substances of composite materials and coatings. The presence of two carbon components in UDD particles is confirmed by a number of experimental data (*e.g*., see Refs 62 and 63).

The structure of condensed detonation products is formed during both the main process, *viz*., in the chemical-reaction zone of the detonation wave, and in the discharge stage where the explosion products are scattered and undergo the action of reflected shock waves.[1, 4, 64] In the latter case, such secondary processes as graphitisation of diamonds and amorphisation of the crystal phase are highly probable. In addition to structural and phase transformations that affect the carbon core of the particles, chemical reactions of the condensed matter with gases take place in the detonation chamber. These interactions are highly diversified due to the wide temperature range and the impact loads that operate throughout the 'life-time' of the carbon condensate in the reactor.

Taking into account the fact that condensation of the diamond substance from detonation products proceeds in fractions of several tenths of a millisecond,[1,2,4] we assumed that, first of all, in the chemical-reaction zone, the primary products of explosive decomposition of the EM are not completely homogenised [64] and, secondly, segregation of condensed and molecular components of detonation products (DP) does not manage to proceed completely. Hence, condensed DP can retain certain 'chemical markers' of the diamond formation process, namely, molecular compounds and fragments of condensed structures, the composition and structure of which can indicate the mechanism of the EM free carbon condensation and reveal the intrinsic structure of a carbon particle.

The expected chemical markers can be divided into the following four groups:

— cage, bridged, alicyclic carbon compounds, which represent the fragments of diamond and diamond-like structures characterised by sp^3-hybridisation of the carbon atoms;

— derivatives of mono- and polycyclic aromatic compounds, which represent the fragments of graphite-like structures (sp^2-hybridisation of the carbon atoms);

— aliphatic (linear and branched) compounds, which represent the fragments of the maximally amorphous carbon-cluster periphery, as well as indications of the presence of carbyne structures;

— compounds that involve C – N and C – O bonds, representing the fragments of the surface layer of particles.

To detect and analyse these 'chemical markers', we experimentally studied the products of mild thermal and organolytic decomposition of UDD and DB.

Low-temperature (cold) extraction was carried out in a Soxhlet apparatus at a solid : liquid ratio of 1 : 10 and an extraction time of 10 – 12 h. Organolytic decomposition was accomplished under the conditions of the supercritical state of the solvent where the extractive power of the liquid is a minimum. This treatment was carried out in a steel autoclave of a volume of 0.4 litre at 573 – 673 K under a pressure > 5 MPa.

The extracts obtained were studied by the methods of low-temperature luminescence and IR spectroscopies, gas-liquid chromatography, chromato-mass spectrometry and ^{1}H NMR spectroscopy.

Different types of detonation charges including a sample which contained no diamonds (the so-called 'under-developed' charge) were subjected to cold extraction. Depending on the synthesis conditions, the DB contained variable amounts of extractable substances. These are largely bi- and polycyclic aromatic hydrocarbons with a single or several substituents in the rings. Thus compounds containing sp^2- and sp^3-hybridised carbon atoms were obtained among molecular products of low-temperature extraction of DB. However, it is evident that such compounds are formed most probably from ultradispersed graphite and turbostratic carbon rather than from diamond. Under cold extraction, the solid carbon matrix is not split, but its extractant-soluble molecular components are desorbed and washed out. Hence, it can be concluded that the compounds identified are the intermediates of a transition from primary products of EM detonation to a condensed carbon phase.

The following correlation is observed between the amount of extracted polyaromatic compounds, on the one hand, and the composition and perfectness of the diamond phase in the mixture (*i.e.*, the amount of various defects on the surface and in the bulk of diamond grains, the presence of lattice distortions dependent on both the detonation conditions and the configuration of the blasting chamber), on the other hand: the maximum yield of soluble substances ($\sim$ 5%) is reached for detonation carbon that contains no diamond.

A deeper extraction in combination with partial decomposition of the solid matter was carried out at 473 – 637 K and elevated pressure, *i.e.*, under conditions of supercritical states of organic solvents used. The supercritical liquefaction of carbon proceeds most completely in pyridine, which ranks among the most active solvents.

At present, we know the composition of simplest high-temperature (hot) extracts obtained by using the following relatively mild hydrocarbon solvents (Table 12): of normal structure (heptane and decane), aromatic (benzene and toluene) and alicyclic hydrocarbons (cyclohexane) and hydronaphthalenes (tetralin and decalin). These solvents are relatively stable under experimental conditions; their extraction ability increases in the following sequence: normal < aromatic < alicyclic hydrocarbons < hydronaphthalenes.

Table 12. Aromatic heterocyclic compounds in high-temperature extracts from UDD and DB isolated using different solvents.

Compound	DB, extraction by toluene	UDD, extraction by		
		benzene	cyclo-hexane	hydro-naphthalenes
	+	–	–	–
	+	–	–	+
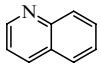	–	–	+	+
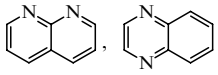	+	+	+	+
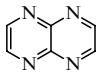	+	+	–	+
	–	–	+	+
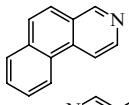	–	–	+	–
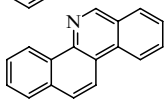	+	–	–	–

Note. Sign '+' denotes the presence of a compound in the extract.

The extracts obtained differed in colour: from light yellow (normal hydrocarbons) to dark brown (hydronaphthalenes). Upon the treatment, the ratio of diamond to non-diamond phases changed, as well as the surface properties. Supercritical liquefaction allows solubilisation of up to 10 mass % of diamond-containing phase in 30 min. In this case, relatively weak and reactive chemical bonds are cleaved including elimination of the surface groups and most disordered near-surface carbon layers of clusters. Stable macroscopic structural units are retained as a solid carbon residue, microunits survive as individual molecules which pass into solution. Among the latter, polycyclic nitrogen-containing heretocycles (Table 12) with one and two nitrogen atoms in the ring and a number of rings up to four were detected.

Taking into account the laws of organic chemistry, the formation conditions of these compounds allow us to conclude that nitrogen is incorporated into the condensed carbon (including the diamond phase) as a result of primary reactions, most probably, due to polycondensation of nitrogen-containing monomers with carbon – nitrogen bonds. At first glance, this contradicts the ESR spectra for nanodiamonds [21] which demonstrated

no characteristic triplet signal related to admixed nitrogen atoms replacing carbon in the diamond lattice. However, this a comparison rather emphasises the difference between 'common' diffusional growth of a diamond crystal and the polycondensation mechanism of the formation of UDD during the detonation process. The former involves capture of admixed nitrogen atoms into the newly formed diamond lattice and distribution of such admixed atoms throughout the crystal bulk. In contrast, the formation of UDD first involves incorporation of nitrogen (more precisely, a nitrogen–carbon pair) into an aromatic ring (with a high binding energy in the ring, which is typical of aromatic structures), and then these rings are built into a compacting prototype structure of condensed carbon. In the latter case, the paramagnetic properties of nitrogen should differ from those of admixed nitrogen atoms.

The structure of the outer shell of a diamond cluster was also assessed on the basis of the results on thermodesorption. The studies were carried out on an LKB-2091 chromato-mass spectrometer (Sweden). Thermodesorption was carried out at 573 K in a flow of helium with collection of the products in a capillary cooled by liquid nitrogen. Then, thermodesorption products were vaporised and separated by chromatography on a capillary column with a weakly polar phase (SPB-5; column length, 60 m; diameter 3.2×10^{-4} m), at a helium flow (rate of 2.5×10^{-6} m^3 s^{-1}) in a mode of programmed temperature increase from 293 to 543 K (heating rate, 4 K min^{-1}).

The mass spectra were processed and the products were identified using a built-in computer RDR-2 using a mass spectra data base. Table 13 shows the composition of substances desorbed from the surface of the diamond-containing mixture and UDD.

Table 13. Products of thermodesorption (T = 253 K) from UDD and DB surfaces.

Compound	DB	UDD	UDD-H [a]
Acetonitrile	–	++	–
Nitromethane	–	+	–
Butanal	–	+	–
Butan-2-one	–	+	+
Tetrahydrofuran	–	+	–
Ethanol	–	–	+
Acetone	–	–	+
Ethyl acetate	–	++	+++
Benzene and its homologues	++	+++	++
Alkylbenzenes:			
C_9	+	+++	–
C_{10}	+++	+	–
Alkanes:			
C_7	–	+	+++
C_8	–	+	+
C_9	–	+	–
C_{10}	+++	+++	–
C_{11}	+	+	–
Alkenes:			
C_7	–	+	–
C_8	+	+	–
C_9	–	+	–
C_{10}	–	++	–
Terpene C_{10}	+	++	–
Alkylcyclopentanes	+	–	–
Naphthalene	+	+	–

Note. Three samples of each type were analysed. The signs '+', '++' and '+++' show that the compound was detected in thermodesorption products for one, two and three samples, correspondingly. [a] After hydrogen treatment.

Only hydrocarbons are desorbed from the DB surface: saturated C_8–C_{11}, unsaturated C_8–C_9, alicyclic and aromatic. The predominance of C_{10} alkanes and, probably, n-decane ($C_{10}H_{22}$) agrees with the result that detonation products contain carbyne, the structure of which is most thermodynamically favourable in the condensation of C_{10}–C_{12} carbon chains with the formation of cumulene bonds. The proportion of aromatic hydrocarbons including C_{10} alkylbenzenes among the substances desorbed from DB is comparatively small, although the presence of polycyclic aromatic nets in DB itself is unambiguously proved.[63] Hence, the degree of sp^2-type condensation of carbon is high enough; however, the polyaromatic nets have a very disordered, predominantly aliphatic coating, *viz*., a peculiar type of hydrocarbon 'fringe'. In the desoption products from the DB surface, hydrogen is present in an inactive C–H form, which agrees with the results of determination of active hydrogen on the surface of ultradispersed carbon.[31]

The composition of the desorption products from the UDD surface is more complex and diverse. In addition to hydrocarbons, oxygen- and nitrogen-containing compounds were identified, which are formed as a result of oxidation of the carbon surface. Benzene and C_7–C_{10} homologues are abundant and are second only to C_{10}-alkanes, n-decane prevailing among the latter. Of bridged alicyclic structures, camphene and terpene $C_{10}H_{16}$ are present. Such a composition of the desorption products suggests that the appearance of the diamond structures themselves at the interface is highly improbable. Stabilisation of the diamond structure in a UDD cluster occurs *via* various transition carbon structures. An exposure of UDD to a hydrogen flow at 673 K (UDD-H in Table 13) results in irreversible desorption of most of the C_8–C_{11} hydrocarbons; however, the decomposition of surface carbon structures with the formation of C_2–C_7 hydrocarbons goes on, *i.e*., the surface metastability is reproduced.

Below, certain characteristics of UDD cluster particles are summarised together with the methods of their estimation.

Characteristic	Method
Crystalline core with 4–6-nm diameter	X-ray diffractometry
The presence of peripheral condensed structures of the following types:	
— polyaromatic nets	selective oxidation, organolysis
— aromatic heterocycles	organolysis
Stabilising system of surface compounds:	organolysis, thermodesorption, hydrogenolysis
— aliphatic units	
— bridged structures	
— aromatic rings	
Surface functional groups:	IR spectroscopy,
— carboxyl	chemical analysis,
— carbonyl	potentiometry, polarography, thermodesorption, thermovacuum desorption
— ester	
— quinone	
— nitrile	

These so very diverse and different fragments are combined into a single particle and then into an ensemble of particles in accordance with the fractal rules by a non-continuous filling of a random volume by the mass of a substance.[65] Two- and three-dimensional classical models fail to describe these particles due to their very high C_s/C_{tot} ratio. The packing and arrangement of UDD crystals also cannot be described within the frameworks of the classical theory of filling. It is assumed[6] that the aggregates formed can have a fractal structure. The practical application of UDD requires these properties to be taken into account.

An original procedure has been developed for the direct determination of the fractal dimension of UDD aggregates in hydrosols.[41] The fractal dimension (D), which varied insignificantly in the range of 2.1–2.3, was studied as a function of the

pH, ionic strength and temperature. It was found that an increase in the temperature and ionic strength and a decrease in the pH favour flocculation accompanied by a decrease in the density and fractal dimension of UDD aggregates.

A two-stage mechanism for UDD aggregation was assumed. In the first stage, relatively compact primary aggregates are formed by a particle–cluster mechanism, which takes place in the oxidation of a non-diamond component of DB during its chemical purification. The second stage of cluster–cluster aggregation with the formation of a looser secondary structure is reversible and preferentially associated with the flocculation of primary aggregates.

It is by the structural heterogeneity of the interactions of clusters both with one another and with individual carbon-containing molecules (this is associated with the fact that different particles in powder systems are surrounded by different numbers of active 'neighbours'), as well as by highly irreversible conditions of UDD formation that the fact that the experimental values of UDD fractal dimension do not correspond to any definite type of aggregation (cluster–cluster, cluster–particles) can be explained.

XV. Comparison of properties of diamonds of different origins.

Table 14 (see Ref. 66) presents comparison of the properties of finely dispersed diamond powders of different origins synthesised by three different methods.

The chemical compositions of UDD synthesised by detonation of EM with a negative oxygen balance differ in the presence of substantial amounts of oxygen. Studies of electrophoretic properties of aqueous dispersions of UDD showed that the surface of particles acquires a considerable negative charge (−78.44 mV) caused apparently by ionogenic oxygen-containing groups.

Such a powder possesses high adsorption capacity. Being a characteristic of UDD, the adsorption potential exceeds that of SDB 1/0 powder by an order of magnitude, and the specific adsorption potential exceeds the corresponding value more than twice. On the other hand, with respect to magnetic and electrophysical characteristics UDD powders differ insignificantly from commercial diamond powders SDB 1/0 synthesised under steady-state conditions. Substantial differences are also observed in the values of the degree of surface hydrophilicity and electrophoretic charge: for UDD, they are two- and ten-fold higher, respectively.

Despite their fine degrees of dispersion, UDD have the same graphitisation threshold, although the initial temperature of oxidation in air is 50 K lower for UDD as compared with SDB 1/0 diamonds synthesised under steady-state conditions.

Diamonds obtained by a detonation impact on graphite and soot in an explosive mixture consist of two phases, cubic and hexagonal (Lonsdalite). UDD powders involve only a cubic modification.

XVI. Application fields of ultradispersed diamonds

1. Electrochemical and chemical co-deposition of ultradispersed diamonds with metals

Co-deposition of UDD with metals is applied in machine-building, ship-building, aircraft, electronic, radio-engineering, medical, and jewelry industries.[71–83]

Table 14. Characteristics of diamond powders of different nature.

Characteristic	SDB 1/0 [a]	Finely dispersed diamond [b]	UDD [c]
Phase composition	diamond of a cubic symmetry (a = 0.357 nm)	diamond of a cubic (a = 0.357 nm) and hexagonal (a = 0.252 nm) symmetry or a cubic symmetry [67]	diamond of a cubic symmetry (a = 0.357 nm)
Substructure:			
CSR size /nm	undetected [d]	10–12	4 [d]
microstresses of II kind ($\Delta\alpha/\alpha$)	–	1×10^{-3}–1.9×10^{-3}	absent [d]
dislocation density /m^{-2}	–	–	1.8×10^{17} (see [d])
ρ /g cm^{-3}	3.49	3.20–3.40 (see [67])	3.30
Particle size /nm	0–2000	41–82 (see [67]), 10–50 (from graphite) 20–800 (from soot) [68]	2–50 2–20 (see [69]) 4 (see [1])
S_{sp} /m^2 g^{-1}	13.5 (see [39])	20–42 (see [67]) 20–25 (from graphite) 35 (from soot) [68]	217 150–450 (results of the author)
Elemental composition (mass %)	C — 99.0; (Ni, Mn, Cr, Fe) [e] — 0.5; Si — 0.2; B — 0.2; (O, H) [e] — 0.1	–	C — 93.2–100; O — 0–6.8; Si – traces
[I.r.] (mass %)	< 0.1	0.1 (see [67])	< 2.0
T_{ox} /K (see [f])	723	–	673
T_g /K (see [g])	1373	> 1073 (see [69])	1373–1473
R /Ω m	1×10^{11} (see [70])	–	7.7×10^{9} (see [70])
Dissipation factor at a frequency of 10^3 Hz	0.0100	–	0.0145
$10^8\chi$ /m^2 kg^{-1}	0.5 (see [70])	–	< 1.0 (see [70])
Degree of hydrophilicity /J mol^{-1} kg^{-1}	−1480 (see [70])	–	−3100 (see [70])
Electrophoretic charge of the surface /mV	−6.53	–	−78.44
Adsorption potentials:			
A /J g^{-1}	14.2 (see [70])	–	384 (see [70])
A' /J m^{-2}	1.005	–	2.16

Note. Based largely on the results given in Ref. 66; the data of other studies are specified. [a] Synthesised by a steady-state method. [b] Synthesised by detonation-impact of graphite or soot in EM. [c] Synthesised by detonation of an EM with a negative oxygen balance. [d] The results by Yu I Sozin (Bakulev Institute of Superhard Metals, Kiev). [e] Total content. [f] Initial temperature of oxidation in air. [g] Initial temperature of graphitisation in vacuum.

Metal–diamond composition coatings are characterised by the following common features: superior wear-resistance and microhardness, substantial corrosion stability, low porosity, a sharply reduced friction coefficient, substantial adhesion and cohesion, high throwing power of electrolytes.

The advantages that may be achieved by using UDD in electroplating processes are listed below.

1. The quality and competitive characteristics of manufactured articles are improved. The articles are characterised by

— better resistance to wear and high microhardness;

Coating UDD + M, where M	Resistance to wear increases by a factor of n, where n	Microhardness, $(10^3 h)$/kg mm^{-3}
Cr	2–12	1.4
Ni	5–8	0.68
Cu	9–10	0.154
Au	1.8–5.5	0.25
Ag	4–12	0.18
Sn	3	–
Al	10–13	1.5

— enhanced adhesion and a reduced friction coefficient;

— reduced porosity (the porosity decreases six- to eightfold for UDD coatings with Zn, sevenfold with Sn, sixfold with Au, eightfold with Ag, and a pore-free coating is formed with Cu);

— high insulating ability of anodic alumina films (a relative weight gain of such a film is higher by a factor of 2.0–3.5);

— corrosion stability (for UDD co-deposits with Cu, no mass loss in standard tests was observed; for co-deposits with Zn, the corrosion resistance increased two- to fourfold);

— a sharp increase in the throwing power of electrolytes (threefold for UDD with Cu, 1.5–2.0-fold for co-deposits with Zn);

— enhanced elasticity (for UDD–Cu deposits, by a factor of 2–4);

2. The service life of articles increases two- to tenfold.

3. The economy in materials, energy and labour are achieved (the coating thickness is recommended to decrease two- to threefold);

4. The effectiveness of an electroplating unit increases by 20%–50% due to a decrease in the coating thickness and (in a number of cases) an acceleration of film formation.

5. The environmental parameters of the electroplating process improve.

Addition of UDD to the electrolyte for nickel plating results in a four- to ninefold increase in the wear-resistance of nickel plates.

The UDD content in metal films varies from 0.1 mass % to 1.5 mass % for all metals and from 0.5 mass % to 40 mass % for anodic oxide films.

For a 1×10^{-6}-m thick metal layer, UDD consumption is ~ 1 carat (2×10^{-4} kg) per 1 m^2.

2. Ultradispersed diamonds in polymer compositions

Modified polymers are applied in the manufacture of aircraft, cars, tractors and ships, in medicine, chemical and petrochemical industries, production of seals, cut-off devices of various kinds, in protective and anti-friction film coatings.[79, 83–91]

a. Film coatings based on fluoroelastomers and polysiloxanes

A technology of cold vulcanisation and filling of fluoroelastomers with UDD particles allows one to obtain coatings with a number of advantages.

1. The permeability with respect to hydrocarbons and polar solvents decreases by a factor of 50, *viz*., from 1.389×10^{-7} to 0.0278×10^{-7} kg m^{-2} s^{-1}. Co-polymers with ethylene and with perfluoroalkyl vinyl ethers (protective coatings) exhibit the highest chemical resistance to acidic and alkaline salt media.

2. The coefficient of dry friction with metal decreases to 0.01.

3. The elasticity and strength parameters improve: the stretch modulus at 100% elongation and the conditional rupture strength increase more than tenfold (from 8.5 to 92 MPa and from 15.7 to 173 MPa, respectively). In this case, the elongation increases by a factor of 1.6 (from 280% to 480%), and the residual elongation decreases by a factor of 1.2 (from 108% to 81%).

4. The strength of adhesion contacts increases

(a) for active surfaces (St.3 steel, zinc, aluminium), by 200%–500% (from 1.7 to 5.1 kN m^{-1} for St.3 and from 0.5 to 3.3 kN m^{-1} for aluminium);

(b) for inactive surfaces (lead, copper), the strength of adhesion contact is 2.8–3.1 kN m^{-1};

(c) the coating developed has the following dielectric characteristics:

— at 4000 MHz, the dissipation factor is 2.58–2.71 depending on the film thickness;

— at 5000 MHz, the transmission and reflection factors may reach 15.0 and 12.4, respectively, depending on the film thickness;

— at 11 000 MHz, the transmission and reflection factors may reach 14.3 and 12.4, respectively, depending on the film thickness.

The coating retains its physical and mechanical properties and operation efficiency under a load up to 2×10^6 kg m^{-2}.

Film coatings based on UDD-modified polysiloxanes possess enhanced elasticity and strength characteristics: the modulus at 100% elongation increases by a factor of 3 (from 19 to 53 MPa); the rupture strength also triples both at 100% (from 52 to 154 MPa) and absolute (from 730% to 1970%) elongation; the tear strength increases by a factor of 1.4.

Fluorine-containing elastomers modified with UDD possess improved elasticity and strength characteristics and are resistant to thermal ageing; the modulus at 100% elongation increases by a factor of 1.6 (from 7.9 to 12.5 MPa), the resistance to rupture is 1.1-times higher (from 15.4 to 16.5 MPa), the rupture elongation increases by a factor of 1.35 (from 210% to 285%).

The resistance of UDD-modified fluoroelastomers to abrasive wear increases by a factor of 1.5–2.0, *i.e*., with respect to this parameter, they are similar to polyisoprene rubbers.

b. Rubbers

Under thermal ageing at 573 K, UDD-containing rubbers either virtually retain their physical and mechanical characteristics at a level of analogous characteristics of standard compositions (non-subjected to heating) or exceed this level. The use of UDD is beneficial for cross-linking in non-destructive changes in the course of thermal ageing.

Polyisoprene rubbers modified by UDD demonstrate enhanced elasticity and strength characteristics. Thus, for the SKI-3 isoprene rubber, the modulus at 300% elongation increases by a factor of 1.6 (from 7.7 to 12.3 MPa), the conditional tensile strength increases by a factor of 1.4 (from 20.5 to 28.2 MPa), and the tear strength increases from 139 to 148 kN m^{-1}. The maximum swelling degree of rubbers in toluene decreases by 45%. These rubbers have a higher degree of vulcanisation and increased strength characteristics (approximately 30% higher than that of standard rubbers based on SKI-3) and higher wear endurance.

The increase in elongation with an increase in the modulus observed for these rubbers contradicts the commonly accepted notions. This points to the changes in the supramolecular structure of the rubber, evidenced by a substantial cohesion increase (by a factor of 1.6: from 1.7 to 2.7 MPa).

Modification of the SKI-5 isoprene rubber by UDD particles results in a 1.6–1.8-fold increase in the controlled strength parameters (modulus at 300% elongation, rupture and tear strengths) with retention of elastic properties.

Oil-containing rubbers modified by UDD possess higher degrees of vulcanisation compared with those without UDD (the modulus at 300% elongation increases from 5.8 to 7.4 MPa, relative elongation decreases from 700% to 610%). Moreover, rubbers that contain UDD together with technological carbon have a tear strength 25%–35% higher then the reference samples.

With introduction of UDD into a standard rubber mixture SKMS-30 ARK based on a butadiene–styrene co-polymer with 30% styrene units, the cohesion strength increases by a factor of 1.5–2.0 (from 1.6 to 3.1 MPa) compared with reference samples.

Rubbers modified by UDD are distinguished by high degrees of vulcanisation, their strength characteristics being practically equal to those of reference rubber, and twice surpass them in tear strength (which increases from 71 to 135 kN m^{-1}). The modulus at 300% elongation increases by a factor of 1.44 (from 7.9 to 11.4 MPa).

Butadiene–nitrile V-14 rubbers modified by UDD exhibit improved operating characteristics: the friction coefficient decreases by a factor of 1.5, wear resistance is enhanced by a factor of 1.3, the elasticity increases by a factor of 1.7, frost resistance also improves (the glass transition temperature decreases by 8%–10%).

For RSS natural rubber (Malaysia) modified by UDD, the modulus at 300% elongation increases threefold (from 1.8 to 5.4 MPa), which is accompanied by a certain improvement in operational characteristics.

Epoxy glues based on UDD exhibit good adhesion and cohesion properties.

Nanodiamonds are applied in technologies for polymerisation from solutions and melts, chemical solidification, and in the techniques for electron-beam, flame, and electrostatic sputtering. Standard equipment is used for fabrication of UDD-containing compositions.

Polymeric compositions containing UDD display substantial advantages.

1. The quality and commercial characteristics of the production improve: the articles exhibit superior strengths, wear resistance, resistance to ageing and action of abrasives. The friction coefficient is low for polyfluoroelastomers (such as co-polymers of polyvinylidene fluoride with perfluorinated co-monomers, *e.g.*, perfluoropropene) and high for polyisoprenes (SKI-3 and SKI-5). The materials and coatings can be adapted to particular technologies and articles.

2. Cheap polymeric starting materials can be substituted for expensive ones.

3. Expensive and deficient components and materials may be saved.

Nanodiamond consumption amounts to 1–5 kg per 1000 kg rubber (polymer) and 1–5 kg per 1000 m^2 of a polymeric coating or a film.

3. Ultradispersed diamonds in lubricants, greases, and lubricating–cooling liquids.

Modified lubricant compositions are used in machinery, metal working, engine-building, ship-building, the aircraft industry and transport.[79, 83, 92–100]

Addition of nanodiamonds to oils allows one to obtain high-quality sedimentation-resistant and environmentally safe systems with superhard particles that measure $< 5 \times 10^{-7}$ m.

The merits of UDD additives to oil compositions are as follows:

1. The quality and competitive characteristics of articles improve: the service life of vehicles and equipment increases; the economy of fuel and lubricants is achieved, these additives can serve as an alternative to expensive oils and special lubricants.

2. The friction torture is reduced by 20%–40%.

3. The wear of friction surfaces decreases by 30%–40%.

4. Fast run in of friction gears is observed.

The consumption of nanodiamonds is 0.01–0.2 kg per 1000 kg of oil.

4. Ultradispersed diamonds in abrasive tools

Tools fabricated from nanodiamonds are used in abrasive, mining and metal working industries, in machinery, electronics, medicine and jewelry production.[83, 101–103]

Below, the quality indices [microhardness (h), electrical resistivity (R), heat-conductivity (γ) and permittivity (ε)] are shown for clinkers obtained from diamond powders subjected to high pressures and temperatures, both for UDD themselves and diamond-oxide compositions with vitreous oxides (diamond ceramics).

	$10^{-3}h$ /kg mm^{-2}	R /Ω m	γ /W m^{-1} K^{-1}	ε
Individual UDD	3.0–3.5	10^9–10^{12}	100–150	7–9
Diamond ceramics (UDD + MgO)	3–4	10^{10}–10^{12}	120–160	8–10

For individual UDD, the density of defect-free fragments is $(3.35–3.50) \times 10^3$ kg m^{-3}.

These clinkers (the so-called diamond glasses) can easily be cut by ultrasound and laser, ground and polished. They can be used as abrasives in the working of materials of average hardness and in electronics.

Ultradispersed diamonds metallised by transition-metal clusters possess high microhardness [$h = (6–7) \times 10^3$ kg mm^{-2}] and represent excellent tool materials.

The use of UDD (0.5%–1.5%) for enhancing the strength properties of polymeric matrices of grinding and polishing tools results in a simultaneous increase in both strength (by a factor of 1.3–1.5) and elastic (by a factor of 1.8–2.0) properties of an abrasive tool.

5. Ultradispersed diamonds in microabrasive and polishing compositions.

Polishing systems (PS) that contain UDD are used in precision finishing of materials in radio engineering, electronics, optics, medicine and machinery.[79, 104–109]

The compositions allow one to obtain perfect mirror solid surfaces of required planeness, plane-parallelism, of any geometrical shape, containing no defects and dislocations, with the contour interval $R_z = 2–8$ nm (with an average deviation from a mean hypothetical surface $\sigma = 0.5–2.0$ nm).

The advantages of UDD-containing polishing systems are as follows.

1. The minute sizes of UDD ensure the minimum surface roughness and the colloidal stability of PS.

2. The chemical stability of UDD allows one to use chemically active additives to PS and to recover PS.

3. The amount of material removed from the surface being polished is small (the material losses decrease).

4. Owing to ion-exchange and sorption properties of UDD, the removed ionic and molecular products are immobilised on the UDD surface, which provides a clean surface.

5. The fractal structure of UDD aggregates ensures a controlled structurisation in PS suspensions and the absence of stressed and disrupted surface layers on a material being polished.

6. These systems are non-toxic.

7. Polishing systems with UDD allows one to enhance the quality and competitive characteristics of polished articles and to ensure the polishing of materials technologically difficult to work.

Nanodiamond consumption is 0.001–0.01 kg per 1 m^2 of the surface worked.

6. Ultradispersed diamonds in magnetic recording systems.

Nanodiamonds are used, first of all, as anti-friction additives and physical modifiers in ferromagnetic-varnish coatings of magnetic films and disks and, secondly, as the additives to electrochemical composition films destined to improve the magnetic recording device characteristics.[77, 79, 83]

1. The addition of UDD to a ferromagnetic layer sharply reduces its domain sizes (ferromagnetic grains), *i.e.*, the density of recording increases substantially.

When introduced into a varnish to form a special film destined for cleaning of recording heads, UDD provides polishing of the latter and enhances their resistance to wear.

Magnetically soft information carriers which contain UDD display the following advantages: abrasive wear of a magnetic-carrier layer decreases, optimum conditions are provided for operation of magnetic heads and reading devices, friction of the magnetic carrier decreases and stability of its motion is provided.

The consumption of nanodiamonds is 1% – 2% of the varnish mass.

2. As compared to individual CoP coatings, magnetically soft amorphous CoP – UDD films are shown to display the following advantages: a 1.3-fold increase in microhardness, a 4.5-fold increase in the resistance to wear, a 1.4-fold decrease in friction coefficient, a 2-fold increase in the service life of magnetic-head cores without any changes in their effectiveness.

For magnetically hard polycrystalline CoP – UDD coatings compared to individual CoP coatings both electrochemically and chemically deposited, the microhardness increases by a factor of 1.2, corrosion currents decrease by a factor of 1.6, the service life of the carriers of magnetic information increases.

Magnetic characteristics of both magnetically soft amorphous films and magnetically hard coatings remain unchanged with an addition of UDD.

Nanodiamond consumption is ~ 1 carat for a layer with 1×10^{-6} m thick.

7. Biological activity of ultra-dispersed diamonds

When UDD are used as potential medical drugs, their anomalously high adsorption capacities, high specific surface areas, abundance of free electrons on the surface (a multiple radical-donor), nanoscale sizes, a great amount of oxygen-containing functional groups on crystal surfaces, chemically inert grains and surface hydrophilicity are of great importance.[79, 110]

Nanodiamonds can be applied in oncology, gastroenterology, cardiology, dermatology, for curing vessel diseases, *etc*. They display no carcinogenic and mutagenic properties and are non-toxic.

Owing to their high adsorption capacities and other specific features, nanodiamonds exhibit extremely high activities with respect to pathogenic viruses, microbes and bacteria by absorbing them intensively. Nanodiamonds are selective sorbents and supports for biologically active substances, they can significantly enhance the action of drugs. The use of UDD normalises blood pressure. Moreover, UDD are effective drugs for different gastroenteric diseases, an excellent remedy for after-effects of burns, different skin diseases and intoxication.

The use of UDD in the form of aqueous and oil suspensions is beneficial for curing cancer patients; these tend to increase the effect of drugs, relieve pains, normalise peristalsis of the bowels, improve blood characteristics and activate the immune system, remove toxins from the organism and prolonge the patient's life.

The use of UDD in chemical and radio-therapy appears to be promising in the cure of malignant tumours for prevention of the mutagenic effect of drugs. At the same time, UDD do not reduce the therapeutic effect and are capable of preventing the appearance of mutations in normal cells or generation of secondary tumours under the action of anti-tumour drugs.

A therapeutic course requires $\sim 0.02 - 0.5$ g of UDD.

* * *

Thus, this survey demonstrates that UDD microcrystals with a narrow size distribution at about 430 nm manifest extremely varied and sometimes unusual properties. Undoubtedly, physico-chemical and chemical studies of UDD will be continued. It is possible that the main application fields of nanodiamonds are still to be found, although there are good grounds to believe that UDD can be applied virtually in any field, first of all, in high technologies.

References

1. A I Lyamkin, E A Petrov, A P Ershov, G V Sakovich, A M Staver, V M Titov *Dokl. Akad. Nauk SSSR* **302** 611 (1988) [a]
2. V I Trefilov, V S Mikhalenkov, G I Savvakin, E A Tsapko, D G Savvakin *Dokl. Akad. Nauk SSSR* **305** 85 (1989) [a]
3. F P Bundy *Physica A* **156** 169 (1989)
4. A M Staver, N V Gubareva, A I Lyamkin, E A Petrov *Fiz. Goreniya Vzryva* **20** (5) 100 (1984)
5. A P Ershov, A L Kupershtokh *Fiz. Goreniya Vzryva* **27** (2) 111 (1991)
6. G V Sakovich, V D Gubarevich, F Z Badaev, P M Brylyakov, O A Besedina *Dokl. Akad. Nauk SSSR* **310** 402 (1990) [a]
7. Yu I Petrov *Klastery i Malye Chastitsy* (Clusters and Small Particles) (Moscow: Nauka, 1986)
8. H Haberland (Ed.) *Clusters of Atoms and Molecules (Springer Ser. Chem. Phys.)* Vols 52, 56, Parts I, II (Berlin: Springer, 1994)
9. V Yu Dolmatov, T M Gubarevich, R R Sataev, in *Dokl. V Vsesoyuz. Sovesh. po Detonatsii, Krasnoyarsk, 1991* (Proceedings of the Vth All-Union Meeting on Detonation, Krasnoyarsk, 1991) Vol. 1, p. 135
10. Russ. P. 2 109 683; *Byull. Izobret*. (12) 215 (1998)
11. A V Kurdyumov, N F Ostrovskaya, V B Zelyavskii, N I Borimchuk, V V Yarosh *Sverkhtv. Mater*. (4) 23 (1998)
12. G I Savvakin, V A Kotko, N F Ostrovskaya, A V Kurdyumov *Poroshk. Metall*. **10** 78 (1988)
13. T Xu, K Xu, J Zhao *Mater. Sci. Eng. B* **38** 1 (1996)
14. G P Bogatyreva, Yu I Sozin, N A Oleinik *Sverkhtv. Mater*. (4) 5 (1998)
15. Yu I Sozin *Kristallografiya* **39** 10 (1994) [b]
16. V D Andreev, Yu I Sozin *Sverkhtv. Mater*. (4) 67 (1998)
17. M Yoshikawa, Y Mori, H Obata, M Maegawa, G Katagiri, H Ishida, A Ishitani *Appl. Phys. Lett*. **67** 694 (1995)
18. A Ye Alexensky, M V Baidakova, M E Boiko, V Yu Davydov, A Ya Vul', in *Proceedings of the 3rd International Conference on the Application of Diamond Films and Related Materials, Maryland, MD, 1995* p. 75
19. E D Obraztsova, K G Korotushenko, S M Pimenov, V G Ralchenko, A A Smolin, V I Konov, E N Loubnin *Nanostruct. Mater*. **6** 827 (1995)
20. A E Aleksenskii, M V Baidakova, A Ya Vul', V Yu Davydov, Yu A Pevtsova *Fiz. Tv. Tela* **39** 1125 (1997) [c]
21. A L Vereshchagin, V F Komarov, V M Mastikhin, V V Novoselov, L A Petrova, I I Zolotukhina, N V Vychin, K S Baraboshkin, A E Petrov, in *Dokl. V Vsesoyuz. Sovesh. po Detonatsii, Krasnoyarsk, 1991* (Proceedings of the Vth All-Union Meeting on Detonation, Krasnoyarsk, 1991) Vol. 1, p. 99
22. T M Gubarevich, N M Kostyukova, R R Sataev, L V Fomina *Sverkhtv. Mater*. (5) 30 (1991)
23. A V Nozhkina, N A Kolchemanov, A A Kardanov, P Ya Detkov *Sverkhtv. Mater*. (1) 78 (2000)
24. T M Gubarevich, L S Kulagina, I S Larionova, in *Dokl. V Vsesoyuz. Sovesh. po Detonatsii, Krasnoyarsk, 1991* (Proceedings of the Vth All-Union Meeting on Detonation, Krasnoyarsk, 1991) Vol. 1, p. 130
25. T M Gubarevich, O F Turitsyna, L I Poleva, A V Tyshetskaya *Zh. Prikl. Khim*. **65** 1269 (1992) [d]
26. G P Bogatyreva, M N Voloshin, M A Marinich, V G Malogolovets, V L Gvyazdovskaya, V S Gavrilova *Sverkhtv. Mater*. (6) 42 (1999)
27. I I Kulakova, V Yu Dolmatov, T M Gubarevich, A P Rudenko *Sverkhtv. Mater*. (1) 46 (2000)
28. V I Trefilov, G I Savvakin, V V Skorokhod, Yu M Solonin, B V Fenochka *Poroshk. Metall*. **1** 32 (1979)
29. A V Anan'in, O N Breusov, V N Drobyshev, G E Ivanchikhina, A I Rogacheva, V F Tatsii, I G Shunina *Sverkhtv. Mater*. (5) 11 (1986)
30. K S Baraboshkin, T M Gubarevich, V F Komarov *Kolloid. Zh.* **54** (6) 9 (1992) [e]
31. Russ. P. 2 046 094; *Byull. Izobret*. (29) 189 (1995)
32. T M Gubarevich, N M Kostyukova, I S Larionova, L I Poleva, in *Dokl. V Vsesoyuz. Sovesh. po Detonatsii, Krasnoyarsk, 1991* (Proceedings of the Vth All-Union Meeting on Detonation, Krasnoyarsk, 1991) Vol. 1, p. 112

33. N V Novikov, V G Aleshin, A A Smekhnov, A A Shishkin, A A Shul'zhenko *Dokl. Akad. Nauk SSSR* **300** 1122 (1988) [a]
34. G P Bogatyreva, M A Marinich, V L Gvyazdovskaya, in *Proceedings of the IXth European Conference on Diamond, Diamond Like Material, Nitrides and Silicon Carbide, Crete, 1998* p. 15-4
35. G A Chiganova *Kolloid. Zh.* **56** 266 (1994) [e]
36. V I Makal'skii, V F Loktev, I V Stoyanova, in *Nauchn. Tr. ISM Akad. Nauk Ukr. SSR, Kiev, 1990* (Proceedings of the Institute of Superhard Materials, Academy of Sciences of Ukraine, Kiev, 1990) p. 48
37. T N Burushkina, V G Aleinikov, B B Donster, G I Savvakin, in *Nauchn. Tr. ISM Akad. Nauk Ukr. SSR, Kiev, 1990* (Proceedings of the Institute of Superhard Materials, Academy of Sciences of Ukraine, Kiev, 1990) p. 41
38. S I Chukhaeva, L A Cheburina *Sverkhtv. Mater.* (2) 43 (2000)
39. U G Distanov, A S Mikhailov, T P Konyukhova *Prirodnye Sorbenty SSSR* (Natural Sorbents of the USSR) (Moscow: Nedra, 1990)
40. A V Ignatchenko, A B Solokhina, M V Irdyneeva, in *Dokl. V Vsesoyuz. Sovesh. po Detonatsii, Krasnoyarsk, 1991* (Proceedings of the Vth All-Union Meeting on Detonation, Krasnoyarsk, 1991) Vol. 1, p. 166
41. A V Ignatchenko, A B Solokhina, in *Dokl. V Vsesoyuz. Sovesh. po Detonatsii, Krasnoyarsk, 1991* (Proceedings of the Vth All-Union Meeting on Detonation, Krasnoyarsk, 1991) Vol. 1, p. 164
42. S S Dukhin, V V Deryagin *Elektroforez* (Electrophoresis) (Moscow: Nauka, 1976)
43. A L Vereshchagin, L A Petrova, V V Novoselov, P M Brylyakov, V F Komarov, in *Dokl. IX Vsesoyuz. Simp. po Goreniyu i Vzryvu, Suzdal', 1989* (Proceedings of the IXth All-Union Symposium on Combustion and Explosion, Suzdal', 1989) p. 14
44. A P Rudenko, I I Kulakova, V L Skvortsova *Usp. Khim.* **62** 99 (1993) [*Russ. Chem. Rev.* **62** 87 (1993)]
45. O N Breusov, V M Volkov, N G Shunina, V F Tatsii, in *Mezhdunarodnyi Seminar 'Sverkhtverdye Materialy'* (International Seminar 'Superhard Materials') (Kiev: Naukova Dumka, 1981) p. 114
46. O Yu Zhdankina, I I Kulakova, A P Rudenko *Vestn. Mosk. Univ., Ser. 2, Khim.* **26** 497 (1985) [f]
47. N D Samsonenko, E V Sobolev *Pis'ma Zh. Eksp. Teor. Fiz.* **5** 304 (1967)
48. A V Belyankina, T A Nachal'naya, Yu I Sozin, L A Shul'man *Sintetich. Almazy* **5** 5 (1975)
49. A L Vereshchagin, G M Ul'yanova, V V Novoselov, A P Petrov, P M Brylyakov *Sverkhtv. Mater.* (5) 20 (1990)
50. O N Breusov, V M Volkov, V N Drobyshev, V F Tatsii, in *Tr. ISM Akad. Nauk Ukr. SSR, Kiev, 1990* (Proceedings of the Institute of Superhard Materials, Academy of Sciences of Ukraine, Kiev, 1984) p. 19
51. V S Veselovskii *Uglerod, Almazy, Grafit i Ugli. Metodologiya ikh Issledovaniya* (Carbon, Diamonds, Graphite and Coals. Methodology of Their Investigation) (Moscow: Section of Scientific and Technical Information, 1936) p. 176
52. G P Bogatyreva, G F Nevstruev, G D Il'nitskaya *Sverkhtv. Mater.* (1) 4 (2000)
53. S I Chukhaeva, P Ya Detkov, A P Tkachenko, A D Toropov *Sverkhtv. Mater.* (4) 29 (1998)
54. L V Agibalova, A P Voznyakovskii, V Yu Dolmatov *Sverkhtv. Mater.* (4) 87 (1998)
55. A P Voznyakovskii, V Yu Dolmatov, V V Klyubin, L V Agibalova *Sverkhtv. Mater.* (2) 64 (2000)
56. M Yoshikawa, Y Mori, M Maegawa, G Katagiri, H Ishida, A Ishitani *Appl. Phys. Lett.* **62** 3114 (1993)
57. V L Kuznetsov, M N Aleksandrov, I V Zagoruiko, A L Chivilin, E M Moroz, V N Kolomichuk, V A Likholobov, P M Brylyakov, G V Sakovitch *Carbon* **29** 665 (1991)
58. M Y Gamarnik *Phys. Rev. B* **54** 2150 (1996)
59. V L Kuznetsov, A L Chuvilin, Yu V Butenko, I Yu Mal'kov, A K Gutakovskii, S V Stankus, R Kharulin *Mater. Res. Soc. Symp. Proc.* **359** 105 (1995)
60. H Herchen, M A Cappelli *Phys. Rev. B* **43** 11740 (1991)
61. E L Nagaev *Usp. Fiz. Nauk* **162** 49 (1992) [g]
62. T M Gubarevich, Yu V Kulagina, L I Poleva *Sverkhtv. Mater.* (2) 34 (1993)
63. T M Gubarevich, Yu V Kulagina, L I Poleva, V F Pyaterikov, V Yu Dolmatov *Zh. Prikl. Khim.* **66** 1882 (1993) [d]
64. N V Kozyrev, P M Brylyakov, Sen Chel Su, M A Shtein *Dokl. Akad. Nauk SSSR* **314** 889 (1990) [a]
65. L Pietronero, E Tosatti (Eds) *Fractals in Physics: Proceedings of the Sixth Trieste International Symposium on Fractals in Physics, Trieste, 1985* (Amsterdam: North-Holland, 1986)
66. G P Bogatyreva, M N Voloshin *Sverkhtv. Mater.* (4) 82 (1998)
67. G A Adadurov, A V Baluev, O N Breusov, V N Drobyshev, A I Rogacheva, A M Sapegin, V F Tatsii *Izv. Akad. Nauk SSSR, Neorg. Mater.* **13** 649 (1977)
68. A V Kurdyumov, O N Breusov, V N Drobyshev, V A Mel'nikova, V F Tatsii *Fiz. Goreniya Vzryva* **3** 126 (1989)
69. V M Titov, V F Anisichkin, I Yu Mal'kov *Fiz. Goreniya Vzryva* **3** 117 (1989)
70. G P Bogatyreva, V V Danilenko, V L Gvyazdovskaya *J. CVD* **6** 17 (1997)
71. Russ. P. 1 694 710; *Byull. Izobret.* (44) 91 (1991)
72. Russ. P. 1 668 490; *Byull. Izobret.* (29) 123 (1991)
73. Russ. P. 1 813 812; *Byull. Izobret.* (17) 72 (1993)
74. Russ. P 2 059 022; *Byull. Izobret.* (12) 195 (1996)
75. A D Toropov, P Ya Detkov, S I Chukhaeva *Gal'vanotekh. Obrabotka Poverkhn.* **7** (3) 14 (1999)
76. S V Vashchenko, Z A Solov'eva *Gal'vanotekh. Obrabotka Poverkhn.* **1** (5–6) 45 (1992)
77. Yu V Timoshkov, T M Gubarevich, T I Orekhovskaya, I S Molchan, V I Kurmashev *Gal'vanotekh. Obrabotka Poverkhn.* **7** (2) 20 (1999)
78. A D Toropov, P Ya Detkov, S I Chukhaeva, in *Gal'vanotekhnika i Obrabotka Poverkhnosti (Tez. Dokl. Vseros. Nauchn.-Prakt. Konf. RKhTU im. D I Mendeleeva), Moskva, 1999* [Electrolytic Metallurgy and Surface Processing (Abstracts of Reports of the All-Union Scientific and Practical Conference of D I Mendeleev Russian Chemical Technological University), Moscow, 1999] p. 116
79. V Yu Dolmatov *Sverkhtv. Mater.* (4) 77 (1998)
80. V Yu Dolmatov, G K Burkat *Sverkhtv. Mater.* (1) 84 (2000)
81. G K Burkat V Yu Dolmatov, in *Gal'vanotekhnika i Obrabotka Poverkhnosti (Tez. Dokl. Vseros. Nauchn.-Prakt. Konf. RKhTU im. D I Mendeleeva), Moskva, 1999* [Electrolytic Metallurgy and Processing of Surface (Abstracts of Reports of the All-Union Scientific and Practical Conference of D I Mendeleev Russian Chemical Technological University), Moscow, 1999] p. 15
82. V Yu Dolmatov, G K Burkat, V Yu Saburbaev, M V Veretennikova, L N Sorokina, in *Materialy i Pokrytiya v Ekstremal'nykh Usloviyakh (Tez. Dokl. Mezhdunar. Konf.), Katsiveli, Ukraina, 2000* [Materials and Coatings under Extremal Conditions (Abstracts of Reports of International Conference), Katsiveli, Ukraine, 2000] p. 65
83. G V Sakovich, V F Komarov, E A Petrov, P M Brylyakov, M G Potapov, I G Idrisov, in *Dokl. V Vsesoyuz. Sovesh. po Detonatsii, Krasnoyarsk, 1991* (Proceedings of the Vth All-Union Meeting on Detonation, Krasnoyarsk, 1991) Vol. 2, p. 272
84. Russ. P. 2 100 389; *Byull. Izobret.* (36) 295 (1997)
85. A P Voznyakovskii, E A Levintova, V Yu Dolmatov, M P Greenblat, in *Proceedings of the IVth European East – West Conference and Exhibition on Materials and Processes, St. Petersburg, 1993* p. 80
86. A P Voznyakovskii, V Yu Dolmatov, E A Levintova, T M Gubarevich, in *Dokl. Mezhdunar. Konf. po Kauchuku i Rezine, Moskva, 1994* [Proceedings of International Conference on Caoutchouc and Rubber, Moscow, 1994] Vol. 2, p. 80
87. A P Voznyakovskii, L F Shelokhneva, V Yu Dolmatov, V S Bodrova *Kauchuk Rezina* **6** 27 (1996)
88. V Yu Dolmatov, V A Marchukov, V G Sushchev, M V Veretennikova, in *Materialy i Pokrytiya v Ekstremal'nykh Usloviyakh (Tez. Dokl. Mezhdunar. Konf.), Katsiveli, Ukraina, 2000* [Materials and Coatings under Extremal Conditions (Abstracts of Reports of International Conference), Katsiveli, Ukraine, 2000] p. 64
89. A P Voznyakovskii, V Yu Dolmatov, in *Materialy i Pokrytiya v Ekstremal'nykh Usloviyakh (Tez. Dokl. Mezhdunar. Konf.), Katsiveli, Ukraina, 2000* [Materials and Coatings under Extremal Conditions (Abstracts of Reports of International Conference), Katsiveli, Ukraine, 2000] p. 85

90. A P Voznyakovskii, Yu P Sokolov, V Yu Dolmatov, in *Materialy i Pokrytiya v Ekstremal'nykh Usloviyakh (Tez. Dokl. Mezhdunar. Konf.), Katsiveli, Ukraina, 2000* [Materials and Coatings under Extremal Conditions (Abstracts of Reports of International Conference), Katsiveli, Ukraine, 2000] p. 86
91. V Yu Dolmatov, A P Voznyakovski, in *Proceedings of the VIIIth European Conference of Diamond, Diamond-Like and Related Materials, Edinburgh, Scotland, 1997* p. 15.158
92. Jpn. P. 05 140 478; *Chem. Abstr.* **119** 252 218 (1993)
93. Jpn. P. 05 171 169; *Chem. Abstr.* **119** 184 591 (1993)
94. Jpn. P. 2 004 586; *Byull. Izobret.* (45–46) 102 (1993)
95. S I Shchelkanov, S V Kan, V E Red'kin, in *Dokl. V Vsesoyuz. Sovesh. po Detonatsii, Krasnoyarsk, 1991* (Proceedings of the Vth All-Union Meeting on Detonation, Krasnoyarsk, 1991) Vol. 1, p. 173
96. WO PCT 9 301 261; *Chem. Abstr.* **119** 121 057 (1993)
97. V M Sannikov, Yu M Korobeiko, in *Ul'tradispersnye Materily. Poluchenie i Svoistva (Mezhvuzovskii Sbornik), Krasnoyarsk, 1990* [Ultradispersed Materials. Production and Properties (Intercollegiate Collection), Krasnoyarsk, 1990] p. 155
98. V N Istomin, E D Rakshin, Yu D Akimov, in *Ul'tradispersnye Materily. Poluchenie i Svoistva (Mezhvuzovskii Sbornik), Krasnoyarsk, 1990* [Ultradispersed Materials. Production and Properties (Intercollegiate Collection), Krasnoyarsk, 1990] p. 161
99. A P Shingin, V E Red'kin, E D Rakshin, S V Selicheev, in *Ul'tradispersnye Materily. Poluchenie i Svoistva (Mezhvuzovskii Sbornik), Krasnoyarsk, 1990* [Ultradispersed Materials. Production and Properties (Intercollegiate Collection), Krasnoyarsk, 1990] p. 165
100. S I Shchelkanov, S V Kan, V E Red'kin, in *Ul'tradispersnye Materily. Poluchenie i Svoistva (Mezhvuzovskii Sbornik), Krasnoyarsk, 1990* [Ultradispersed Materials. Production and Properties (Intercollegiate Collection), Krasnoyarsk, 1990] p. 173
101. K S Baraboshkin, A L Vereshchagin, B F Komarov, I A Kramarenko, M G Potapov, V N Shalyuta, I I Zolotukhina, in *Dokl. V Vsesoyuz. Sovesh. po Detonatsii, Krasnoyarsk, 1991* (Proceedings of the Vth All-Union Meeting on Detonation, Krasnoyarsk, 1991) Vol. 1, p. 76
102. G I Savvakin, in *Dokl. V Vsesoyuz. Sovesh. po Detonatsii, Krasnoyarsk, 1991* (Proceedings of the Vth All-Union Meeting on Detonation, Krasnoyarsk, 1991) Vol. 2, p. 254
103. V V Sobolev, V Ya Slobodskoi, A D Sharabura, in *Dokl. V Vsesoyuz. Sovesh. po Detonatsii, Krasnoyarsk, 1991* (Proceedings of the Vth All-Union Meeting on Detonation, Krasnoyarsk, 1991) Vol. 2, p. 264
104. Russ. P. 2 082 738; *Byull. Izobret.* (18) 141 (1997)
105. A A Zakharov, V A Yuzova, N V Eristova, in *Ul'tradispersnye Materily. Poluchenie i Svoistva (Mezhvuzovskii Sbornik), Krasnoyarsk, 1990* [Ultradispersed Materials. Production and Properties (Intercollegiate Collection), Krasnoyarsk, 1990] p. 170
106. T M Gubarevich, V Yu Dolmatov *Zh. Prikl. Khim.* **66** 1878 (1993) [d]
107. T M Gubarevich, V Yu Dolmatov, in *Almaz: Fizika i Elektronika (Tr. Mosk. Seminara)* [Diamond: Physics and Electronics (Proceedings of Moscow Seminar)] (Moscow: Central Russian House of Science, 1993) No. 2, p. 81
108. Jpn. Appl. 05/156 239; *Chem. Abstr.* **119** 232 441 (1993)
109. Jpn. Appl. 04/116 198; *Chem. Abstr.* **120** 89 353 (1992)
110. V Yu Dolmatov, L N Kostrova *Sverkhtv. Mater.* (3) 82 (2000)

[a] — *Dokl. Chem. Technol., Dokl. Chem. (Engl. Transl.)*
[b] — *Crystallogr. Rep. (Engl. Transl.)*
[c] — *Phys. Solid. State (Engl. Transl.)*
[d] — *Russ. J. Appl. Chem. (Engl. Transl.)*
[e] — *Colloid J. (Engl. Transl.)*
[f] — *Moscow Univ. Bull. (Engl. Transl.)*
[g] — *Physics-Uspekhi (Engl. Transl.)*

Russian Chemical Reviews **70** (8) 627 – 639 (2001) © 2001 Russian Academy of Sciences and Turpion Ltd

DOI 10.1070/RC2001v070n08ABEH000678

Scanning tunnelling vibrational spectroscopy of single surface complexes and detection of single electron spins

F I Dalidchik, S A Kovalevskii, B R Shub

Contents

I.	Introduction	627
II.	Single molecule chemical physics of surfaces	628
III.	Threshold and resonance features of currents flowing through nanoscale tunnel junctions containing adsorbed species	628
IV.	Inelastic electron tunnelling spectroscopy with STM	630
V.	Vibrational scanning tunnelling spectroscopy using resonance features of STM currents	631
VI.	Kinetics of vibrational and spin transitions in single surface complexes	634
VII.	Scanning tunnelling spectroscopy using fluctuations of STM currents	637
VIII.	Time-resolved scanning tunnelling spectroscopy	637
IX.	Conclusion	637

Abstract. New spectroscopic techniques employing the scanning tunnelling microscope are considered. The new methods allow measurements of the vibrational spectra of single surface complexes, determination of the nonequilibrium distributions of such complexes over vibrational levels, studies on the kinetics of vibrational transitions, determination of vibrational relaxation parameters, detection of single surface electron spins and studies on the dynamics of fast surface migration of species. The physical grounds and possible applications of the methods in chemical research are also discussed. The bibliography includes 80 references.

I. Introduction

Determination of the structure and properties of surface complexes belongs to the key problems of modern chemical physics of surfaces including heterogeneous catalysis. The number of differently organised groups of adsorbed species can be rather large even in the simplest systems. For instance, the interaction of oxygen with metals can be accompanied by the formation of more than ten types of complexes, depending on the metal crystal face involved in the process, the metal oxidation state and temperature. These complexes differ not only in their adsorption sites, but also in atomic and electronic structure. Usually, such complexes coexist and interact with one another at sufficiently high coverages of the surface. In heterogeneous catalysis, the most reactive complexes play the role of active surface sites.[1, 2]

Different surface complexes can play the role of active surface sites in different stages of a catalytic reaction, *i.e.*, in the course of adsorption and surface migration and in various chemical transformations (dissociation, desorption, as well as substitution, recombination or exchange reactions). The internal structure and properties of the surface complexes have long been intensively studied by many experimental methods. However, the exact nature of the active surface sites remains a moot question as yet for the majority of systems including those studied in most detail. Determination of the exact nature faces great difficulties which are mainly associated with a large number of types of surface complexes and with low steady-state concentrations of the active sites due to their high reactivity.

Experiments with structurally and chemically homogeneous surfaces (the so-called 'ideal' surfaces) are free from these drawbacks. Carrying out high-vacuum experiments allows one to assemble macroscopic ensembles of regularly arranged surface complexes of a particular type by controlled low-temperature adsorption on microfacets of perfect single crystals.[3] The structure and properties of such systems can be studied in detail by various spectroscopic methods including optical and corpuscular ones, beam and field emission techniques, as well as steady-state and kinetic methods.[4] It should be noted that most of the widely used methods have initially been developed to study the dynamics of elementary processes in the gas phase.

Experiments with ideal surfaces have significantly extended the ideas of both the internal structure of surface structures and the dynamics of elementary acts in heterogeneous processes. In such experiments, many complexes have been found for the first time. Beam experiments provided direct evidence for the dependence of the reactivity of ideal surfaces on their atomic structure.[5] Femtosecond laser experiments allowed the characteristic times of electronic and vibrational relaxation of many surface complexes to be measured for the first time.[6] Currently, heterogeneous processes on ideal surfaces are studied with a time resolution of $\sim 10^{-13} - 10^{-14}$ s, which is sufficient for the real-time observation of the motion of individual species (molecules, ions, atoms) in elementary acts of chemical transformations.

Since 1960s, intensive studies of ideal surfaces as model systems have been carried out in many countries. The results of such studies serve as one of the main sources of information necessary for devising physical models of the interactions of atomic species with the surface and at the solid surfaces. However, the results of high-vacuum measurements bear no direct relation to the chemistry of real surfaces. Typically, the time taken to form a real surface is of the order of 10^{-7} s ($P \approx 1$ atm, $T \approx 300$ K). Such surfaces are characterised by disordered atomic structures. In real systems, the variety of types of ensembles of surface

F I Dalidchik, S A Kovalevskii, B R Shub N N Semenov Institute of Chemical Physics, Russian Academy of Sciences, ul. Kosygina 4, 119991 Moscow, Russian Federation. Fax (7-095) 137 83 18.
Tel. (7-095) 939 72 59 (F I Dalidchik), (7-095) 939 73 52 (S A Kovalevskii), (7-095) 137 82 73 (B R Shub)

Received 27 April 2001
Uspekhi Khimii **70** (8) 715 – 729 (2001); translated by A M Raevsky

complexes is much greater than in ideal systems. Often, real surfaces are covered by complexes that cannot be produced in desired amounts in high-vacuum experiments to be studied then by conventional spectroscopic methods such as IR, Auger and ESR spectroscopy, *etc*. Additionally, the dynamics of elementary acts of various heterogeneous processes in ordered and disordered ensembles of the same surface complexes can be essentially different. For chemisorbed species this is due to changes in the potential energy surfaces upon the formation of new chemical bonds, whereas in the case of physisorbed particles the distinctions can be due to multiple scattering of both products and reagents by the species surrounding the reacting complex.

Compared to modelling of gas-phase processes, the problem of devising physical models of heterogeneous surface reactions is much more complicated. The dynamics of all essential elementary gas-phase processes can be studied in detail using high-vacuum beam and optical experiments. However, the results of such experiments with ideal surfaces are insufficient to devise physical models of heterogeneous chemical reactions, especially catalytic ones, which are of prime interest in practice. Studies on the dynamics of elementary acts of gas-phase reactions can be successfully performed with femtosecond time resolution, which allows real-time monitoring of the motion of atomic species. In the case of heterogeneous chemical reactions, solving a similar problem requires not only real-time, but also real-space monitoring of the motion of atomic species and, hence, atomic-scale spatial resolution. The present state-of-the-art in chemical physics of surfaces is characterised by great demand for novel methods which would allow assembling of single complexes of adsorbed species at specified points of the surface, studies on their atomic and electronic structure, measurements of physical parameters, determination of chemical properties and studies on the dynamics of elementary acts of chemical transformations at the single-event level. Currently, the development of such methods requires the use of scanning tunnelling microscopy (STM). Hence, the new methods should be basically different from those used in studies of gas-phase processes.[7,8]

II. Single molecule chemical physics of surfaces

In experiments with STM, the atomic and electronic structure of conducting surfaces is probed with a thin metallic tip (the radius of curvature of well-fabricated tips is comparable with the characteristic atomic size) separated from the surface by a distance d of the order of 5–10 Å.[8] In this case, the overlap of the atomic orbitals of the tip and the surface is very weak and the surface–tip system represents a nanoscale tunnel junction whose conductance

$$\sigma = \frac{\partial J}{\partial V},$$

(J is the current and V is the voltage) at low voltages ($V \ll \varphi$, φ is the tip work function) is determined by the probability of electron tunnelling through the potential barrier (the barrier penetrability)

$$D(d) \propto \exp\left(-2d\sqrt{2\varphi}\right) \qquad (1)$$

and by the surface local density of electron states [$\rho(\varepsilon,\mathbf{r})$] at the position of the tip[9]

$$\sigma(V) \propto D(d)\rho[\varepsilon(V),\mathbf{R}], \qquad (2)$$
$$\varepsilon(V) = \varepsilon_F - V.$$

Here, ε and $\mathbf{r}$ are the energy and coordinate of an electron, respectively, $\mathbf{R}$ is the tip coordinate and ε_F is the Fermi level. (In the text below, we will use the system of atomic units, except otherwise specified; the tip polarity is assumed to be negative.)

According to relationship (2), displacements of the tip across the surface (at specified V and d) produce changes in the current flowing through the tunnel junction, which are proportional to the changes in the electron density $\rho[\varepsilon(V),\mathbf{R}]$, which are determined by the relief of the surface. For 'single-atom' tips, where the tunnelling current is determined by the overlap of the surface orbital with the orbital of the atom nearest to the surface, one gets $\delta J/\delta R \approx 0.1$ nA Å^{-1}. This is sufficient for 'current' imaging of a surface area with Ångström spatial resolution by simply scanning it. Spectroscopic measurements, *i.e*., measurements of the $\sigma - V$ dependences allow reconstruction of the energy distributions of electrons at specified points of the surface. [Note that relationships (1) and (2) include only the contribution of elastic tunnelling characterised by conservation of the energies of the tunnelling electrons. Usually, this is the most probable case.]

The invention of the STM[7] opened a new, amazing world of single-molecule phenomena. The STM is capable of imaging surfaces with Ångström spatial resolution and provides the possibility of seeing individual adsorbed atoms, molecules and adsorbate clusters in the real space, as well as of directly monitoring reconstruction† of ideal surfaces,[10,11] elementary acts of slow surface migration,[12] dissociation[13] and desorption.[14,15] Numerous examples of manipulating individual adsorbed species with the STM tip by their targeted desorption, adsorption, dissociation and transfer between the surface and the tip have been reported. In modern experiments with STM, the atomic and electronic structure of surfaces covered by adsorbed species are studied at the single complex level while the dynamics of heterogeneous processes is in increasing frequency studied at the single-event level. Chemical physics of surface becomes a 'single molecule' science.[16]

The opportunities of 'single molecule' chemical physics of surface seem to be almost boundless, especially taking into account continuous evolution of spectroscopic methods which make it possible to obtain information on the structure of single surface complexes and the dynamics of individual acts of elementary chemical transformations. Experiments with STM allow one not only to see individual adsorbed species and complexes and to reconstruct the corresponding electron energy distributions, but also to measure their vibrational spectra,[17,18] create and measure different types of nonequilibrium vibrational distributions[19] and reconstruct parameters of heterogeneous vibrational[20,21] and electronic[22,23] relaxation. It is also possible to study the kinetics of spontaneous and current-induced vibrational transitions in single surface complexes. (It is this kinetics that often determines the probabilities of elementary acts of chemical transformations of the complexes located under the tip of an STM.[21]) Recently, methods for detection of single surface paramagnetic centres have been proposed and evaluated.[24] Some new experimental schemes have been considered, which would initiate studies on the kinetics of spin transitions in single paramagnetic centres, measurements of spin–lattice relaxation times and relaxation times of individual electronically excited physisorbed molecules[22,23] and research in the field of detection of single molecule magnetic resonance effects.[25–27] New methods for STM studies on the dynamics of fast migration of those adsorbed atomic species whose stable images cannot be obtained have been proposed and theoretically substantiated.[28,29] The main goal of this review is to describe and analyse recent advances in single molecule heterogeneous chemistry.

III. Threshold and resonance features of currents flowing through nanoscale tunnel junctions containing adsorbed species

Most of new spectroscopic methods exploiting STMs also employ the effects of spin-dependent and inelastic electron tunnelling. The former effect is associated with the dependence of tunnelling probability on the electron spin orientation while the latter is due

† Before the invention of the STM, reconstruction of ideal surfaces was studied only by diffraction methods which allow one to obtain raw experimental information about the surface structure in the reciprocal lattice space rather than conventional coordinate space.

to processes in which energy exchange occurs between the tunnelling electrons and electronic and vibrational degrees of freedom of the adsorbed species. In experiments with STM, inelastic electron tunnelling including spin-dependent electron tunnelling can manifest themselves as two kinds of characteristic features on the $J-V$ curves, *viz*., threshold [17] and resonance features.[18]

Threshold features are observed at voltages corresponding to the opening of inelastic electron tunnelling channels. (Below the threshold voltage inelastic tunnelling of an electron is impossible since in this case the electron energy after excitation of a species located under the tip of an STM should be lower than that of the Fermi level corresponding to the highest occupied electron state.) An energy level diagram illustrating both elastic and inelastic electron tunnelling is presented in Fig. 1.

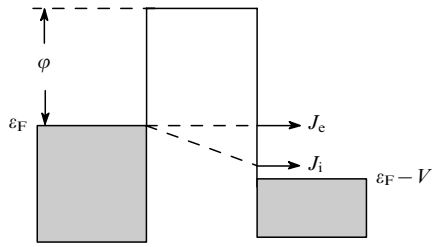

Figure 1. An energy level diagram illustrating electron tunnelling through a nanoscale tunnel junction at voltages $V \ll \varphi$; J_e and J_i are the elastic and inelastic electron tunnelling currents, respectively.

At threshold voltages $V_\omega = \omega$ (ω is the excitation energy of a species located under the STM tip) the conductance of a tunnel junction changes jumpwise

$$\sigma(V) \propto \eta(V - V_\omega), \tag{3}$$

where $\eta(x)$ is the Heaviside function

$$\eta(x) = \begin{cases} 0, & x \leqslant 0 \\ 1, & x > 0 \end{cases}$$

Experiments with STM are usually carried out at $\omega \gg kT$ (k is the Boltzmann constant and T is the temperature of the surface).

The conductance jump magnitude, $\delta\sigma(V_\omega)$, is proportional to the excitation probability of a surface complex, w_ω

$$\delta\sigma(V_\omega) \propto w_\omega \sigma^-(V_\omega), \tag{4}$$
$$\delta\sigma(V_\omega) = \sigma^+(V_\omega) - \sigma^-(V_\omega),$$
$$\sigma^\pm(x) = \sigma(x \pm 0).$$

Resonance features of the STM currents manifest themselves at voltages corresponding to 'bloomed' tunnel junctions (Fig. 2). The effect of resonance blooming of double potential barriers separated by a well with appropriate quasi-stationary electron energy level ε_0 is well known in quantum mechanics.[30] Resonance tunnelling of species involves three stages. A species tunnelling from the left half-space is captured by the well, spends some time in the quasi-stationary state and then tunnels through the second potential barrier to appear in the right half-space. Clearly, the tunnelling probability, $D(\varepsilon)$, is determined by three terms, *viz*., the resonance capture probability, Γ_1, the decay probability of the quasi-stationary state with retention of the initial tunnelling direction, Γ_2/Γ ($\Gamma = \Gamma_1 + \Gamma_2$, where Γ_2 is the probability of tunnelling through the second potential barrier) and the density of electronic states, $\rho_0(\varepsilon)$, near the quasi-stationary energy level ε_0.

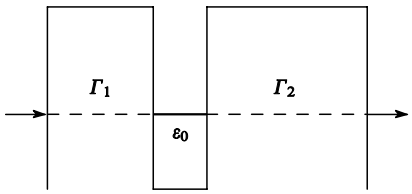

Figure 2. A scheme of tunnelling through the double potential barrier (resonance tunnelling mechanism).

$$D(\varepsilon) \approx \frac{\Gamma_1\Gamma_2}{\Gamma}\rho_0(\varepsilon), \tag{5}$$
$$\rho_0(\varepsilon) = \frac{1}{\pi}\frac{\Gamma}{(\varepsilon - \varepsilon_0)^2 + \Gamma^2}.$$

At $\varepsilon = \varepsilon_0$, the probability of tunnelling through the double potential barrier is equal to the ratio rather than product of the exponentially low probabilities of tunnelling through the single potential barriers

$$D(\varepsilon_0) \approx \frac{\Gamma_{\min}}{\Gamma_{\max}}, \tag{6}$$

where $\Gamma_{\min} = \min(\Gamma_1, \Gamma_2)$, $\Gamma_{\max} = \max(\Gamma_1, \Gamma_2)$. If $\Gamma_1 = \Gamma_2$, one gets $D(\varepsilon_0) = 1$, which means that the 'as-wide-and-high-as-it-wished' double potential barrier appears to be absolutely penetrable. This also holds for those potential barriers which contain electron traps with vibrational degrees of freedom. It has been shown that 'instantaneous' formation and decay of the quasi-stationary electron state can strongly 'shake' the slow vibrational subsystem ($\varepsilon_0 \gg \omega$, ω is the vibrational quantum), thus exciting not only single-quantum, but also multi-quantum vibrational transitions.[31]

The probability of inelastic resonance electron tunnelling, $D_{\upsilon\upsilon'}(\varepsilon)$ (υ and υ' are the vibrational quantum numbers before and after tunnelling), has the form

$$D_{\upsilon\upsilon'}(\varepsilon) = \frac{4\Gamma_1(\upsilon,\bar{\upsilon})\Gamma_2(\bar{\upsilon},\upsilon')}{[\varepsilon - \varepsilon_0(\bar{\upsilon}) + \omega\upsilon]^2 + \Gamma^2}, \tag{7}$$
$$\Gamma_{1(2)}(\upsilon,\bar{\upsilon}) = \Gamma_{1(2)}\langle\upsilon|\bar{\upsilon}\rangle^2,$$
$$\Gamma = \Gamma_1 + \Gamma_2. \tag{8}$$

Here, Γ_1 is the probability of resonance electron capture by the well in the quasi-stationary state (the probability of tunnelling through the first potential barrier), $\varepsilon_0(\bar{\upsilon}) = \varepsilon_0 + \bar{\omega}(\bar{\upsilon} + 1/2)$ is the energy of the vibronic level of the quasi-stationary state, $\bar{\upsilon}$ is the vibrational quantum number of the quasi-stationary state, $\langle\upsilon\bar{\upsilon}\rangle$ are the Franck–Condon factors and Γ_2 is the decay probability of the quasi-stationary state, followed by escape of the electron with retention of the initial tunnelling direction.

It is easily seen that if the potential barriers are characterised by equal Γ_1 and Γ_2 values and the electron energy ε takes its resonance value $\varepsilon = \varepsilon_0(\upsilon,\bar{\upsilon})$, the expression for inelastic tunnelling probability, $D_{\upsilon\upsilon'}(\varepsilon)$, does not contain exponentially small terms and, hence, double potential barriers can also be absolutely penetrable

$$D_{\upsilon\upsilon'}[\varepsilon = \varepsilon_0(\upsilon,\bar{\upsilon})] \propto \langle\upsilon|\bar{\upsilon}\rangle^2\langle\bar{\upsilon}|\upsilon'\rangle^2, \tag{9}$$
$$\varepsilon_0(\upsilon,\bar{\upsilon}) = \varepsilon_0 + \bar{\omega}\left(\bar{\upsilon} + \frac{1}{2}\right) - \omega\left(\upsilon + \frac{1}{2}\right),$$
$$\Gamma_1 = \Gamma_2.$$

It should be noted here that, strictly speaking, simple formula (7) for calculating the probabilities of elastic ($\upsilon = \upsilon'$) and inelastic ($\upsilon \neq \upsilon'$) resonance tunnelling is valid only for long-lived intermediate states ($\Gamma < \bar{\omega}$). On the other hand, the expression for the total tunnelling probability

$$D_\upsilon = \sum_{\upsilon'} D_{\upsilon\upsilon'}, \tag{10}$$

which determines the experimentally measured tunnelling current, is not subject to this limitation [see Ref. 31 which concerns the development of a general theory of inelastic resonance tunnelling and derivation of formulae that are valid at arbitrary ratios between the oscillation period, the lifetime of the quasi-stationary electron state and the times of electron tunnelling through single potential barriers $\tau_{1,2} = (\partial \ln \Gamma_{1,2}/\partial\varepsilon)^{-1}$].

Inelastic resonance tunnelling is a purely quantum-mechanical effect which can be observed in any nanoscale junctions including those formed by the tip of an STM and the surface. In this case, the role of electron traps can be played by adatoms having appropriate energy levels. However, this is a rare case which is of secondary importance. For the species which are of prime interest for practice, such as adsorbed O_2, H_2O, CO molecules, *etc*., the resonance electron energy levels lie below ε_F. The simplest (artificial) way of creating a near-surface electron trap consists of applying a voltage exceeding the tip work function for electrons to the junction.[32, 33] Figure 3 presents an energy level diagram illustrating the mechanism of electron tunnelling from the tip to a sample at such voltages, when the STM operates in the field emission mode.[34, 35] It is easily seen that in this case the tunnelling path has a segment of classically allowed motion of length l

$$l \approx \frac{V-\varphi}{V} d \approx 5-7\ \text{Å}.$$

At particular energies $\varepsilon_n(V,d)$, standing electron waves (field emission resonances, n is the resonance number) originate in this segment. In other words, a nanoscale resonator is formed near the surface, in which the tunnelling electrons are trapped to spend times

$$t_n \approx \Gamma_n^{-1} \approx \left(\frac{\partial \varepsilon_n}{\partial n}\right)^{-1} (1-\beta)^{-1}. \qquad (11)$$

Here, β is the surface reflection coefficient of an electron with energy ε_n. For pure metals, $\beta \approx 0.1-0.3$ [34, 35] and Γ_n values are sufficiently large ($\hbar\Gamma_n \approx 1$ eV, $t_n \approx 4\times10^{-15}$ s), so that the resonance maxima corresponding to different vibrational levels are overlapped. In this case, vibrational transitions of adsorbed species can manifest themselves as small-scale oscillations on the wings of broad field emission resonances.[33] For oxides and metal surfaces coated with thin oxide films, Γ_n values are much smaller [$\hbar\Gamma_n \approx 0.1$ eV, $t_n \approx 4\times10^{-14}$ s (see Refs 18, 19, 24)] and the resonance maxima corresponding to different vibrational transitions can be well resolved. Longer residence times of electrons near such surfaces can be due to the formation of space charge under the tip of the STM injecting electrons into the oxide (the current density $j \approx 10^6-10^8$ A cm^{-2}.)

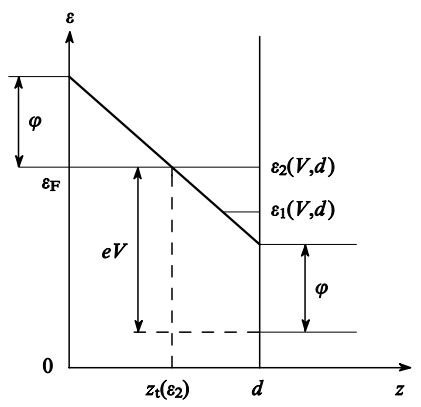

Figure 3. A scheme illustrating electron tunnelling in an STM operating in the field emission mode ($V > \varphi$);
$\varepsilon_{1(2)}(V,d)$ are the electron energy levels of field emission resonances, d is the surface – tip separation and z_t is the classical turning point.

Depending on the atomic and electronic structure of the tip, resonance features on the current – voltage characteristics of the STM can manifest themselves either as conductivity maxima [if $\rho_t(\varepsilon) \approx$ const, where $\rho_t(\varepsilon)$ is the local density of electron states at the position of the tip] or total current maxima [if $\rho_t(\varepsilon)$ exhibits a narrow peak, which is characteristic of 'single-atom' tips and tips containing adsorbed species [36, 37]]. In experimental studies of molecular adsorption on the metal and oxide surfaces by vibrational scanning tunnelling spectroscopy using resonance features of STM currents such maxima have been observed in the $J-V$ curves.[18–21, 24, 38–43]

IV. Inelastic electron tunnelling spectroscopy with STM

1. Single-quantum vibrational transitions of single adsorbed molecules

Threshold features of tunnelling currents in metal – dielectric – metal (M – D – M) junctions containing adsorbed species were predicted and experimentally found in 1966.[44] Threshold features of currents in tunnel $n-p$-junctions (tunnel diodes [45]) due to phonon excitation have been observed by Holonyak and Lesk.[46]

Since energy exchange between an electron and slow vibrational degrees of freedom of the surface is adiabatically forbidden, the probabilities of inelastic tunnelling are usually very low. According to recent estimates,[33] the probabilities of vibrational transitions can be described by a relationship

$$w_{\upsilon,\upsilon'} \propto \left(\frac{a_0}{R_0}\right)^{2|\upsilon-\upsilon'|}, \qquad (12)$$

where a_0 is the zero-point vibrational amplitude and R_0 is the equilibrium position of the oscillator simulating the vibrational subsystem. For single-quantum transitions ($|\upsilon-\upsilon'| = 1$), $w_\omega \approx 0.01-0.05$. Threshold features on the $J-V$ curves of M – D – M tunnel junctions are virtually unobservable. To distinguish them against the background noise, the dependences of $\partial\sigma/\partial V$ on V are usually measured. In this case, threshold features manifest themselves as peaks, the positions of which allow determination of the vibrational quantum energy ω.

Inelastic electron tunnelling spectroscopy of M – D – M tunnel junctions was widely used in 1970 – 1980s for measuring vibrational spectra of species adsorbed at the metal – dielectric interface (see publications on tunnelling vibrational spectroscopy, *e.g*., review [47]). These measurements were performed with macroscopic ensembles of adsorbed species. As a consequence, all the spectra measured by tunnelling vibrational spectroscopy were inhomogeneously broadened. Spectroscopy of threshold features of the STM currents is free from this drawback.

The possibility of observation of threshold features associated with single-quantum vibrational transitions in adsorbed species in experiments with STM seems to be apparent since the energy level diagrams used for illustration of elastic and inelastic tunnelling through M – D – M junctions and nanoscale tunnel junctions are the same (see Fig. 1). In essence, the problem of observation of small-scale threshold features in the experiments with STM is reduced to the problem of capabilities of the instrument the experimentalist has in hand.

As should be expected, single-quantum transition probabilities obtained in theoretical studies of the extent of threshold features of STM currents were estimated at $\sim 0.01-0.05$.[48, 49] Search for threshold features due to single-quantum vibrational transitions was carried out in many research laboratories over more than a decade. These studies were stimulated, in particular, by the necessity of solving one of the central problems of STM physics, *viz*., the problem of chemical identification of single adsorbed species, whose topographic images are strongly dependent on the scanning mode (*i.e*., on the specified V and d values).

The first example of a threshold feature associated with single-quantum excitations of stretching vibrations of the C – H bond has been reported only recently by Ho *et al*.[17] who studied

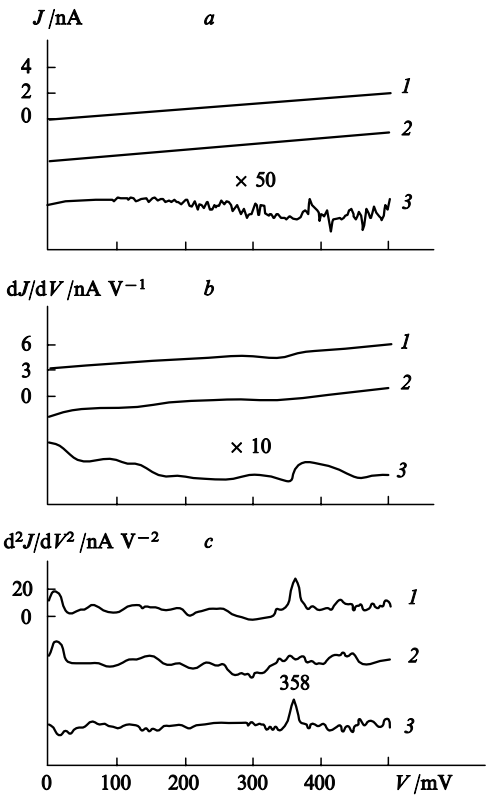

Figure 4. Threshold features of the STM current J (*a*), $\partial J/\partial V$ (*b*) and $\partial^2 I/\partial V^2$(*c*) recorded for a single acetylene molecule adsorbed on the Cu(100) surface.[17]
The curves were recorded with the STM tip positioned over the center of acetylene molecule (*1*) and over the clean surface area (*2*). Curves *3* represent the corresponding difference curves (*1*–*2*). Curves *2* and *3* are shifted along the ordinate axis.

adsorption of a single C_2H_2 molecule on the Cu(100) surface. The design of the new low-temperature STM specially developed to extend the capabilities of inelastic electron tunnelling spectroscopy to a single molecule level has been described elsewhere.[50] Some of the results obtained by Ho *et al.*[17] and presented in Fig. 4 can serve as an illustration of the difficulties associated with extraction of weak threshold signals from the intense background noise of the total current. (Recently,[51] it has been reported that Ho's continuous measurements of the spectra required signal accumulation during many hours.[17]) The isotope effect observed for deutero-substituted acetylene molecules has proven correctness of the assignment of the threshold feature shown in Fig. 4 to single-quantum vibrational transitions of the C–H bond. Later, inelastic electron tunnelling spectroscopy was used to observe elementary acts of dehydrogenation of single ethylene, benzene and pyridine molecules.[52] The topographic images obtained at different time instances allowed observation of displacements and rotations of single molecules, which would be induced by the STM current. Detection of a threshold feature due to the single-quantum vibrational excitations of CO molecules adsorbed on the Cu(001) and Cu(110) surfaces was reported.[53] However, multi-quantum (or combination) vibrational transitions, the probabilities of which do not exceed 0.001 [see expression (12)], have not been observed so far using inelastic electron tunnelling spectroscopy.

2. Electronic transitions in single adsorbed molecules

Conductance jumps of tunnelling gaps, due to vibrational transitions in adsorbed molecules represent an important but not the only example of manifestation of inelastic tunnelling in the experiments with STM. Other interesting examples are associated with electronic excitation of surface complexes. Since in this case there is no small characteristic parameter (energy exchange between two electrons having comparable energies occurs effectively), one should expect that the extent of the threshold features of STM currents associated with electronic transitions in the adsorbed species will be much greater than that observed in the case of vibrational transitions. This problem has been studied recently[22,23] taking a threshold feature associated with the $X^3\sum_g^- - a^1\Delta_g$-transition in physisorbed oxygen molecules as an example. In this case, the threshold feature should be observed at $V \approx 1$ V. Rather high probability of the excitation of oxygen molecules to the singlet state by the tunnelling electrons (the probabilities of such transitions in the gas phase can reach 10% to 15%, see Ref. 54) allows one to predict a new effect, namely, the dependence of the magnitude of the threshold jump on the tunnelling current. At currents $J \approx (w_{TS}\,\tau_{ST})^{-1}$, where w_{TS} is the excitation probability of oxygen molecules from the triplet to the singlet state by inelastically tunnelling electrons and τ_{ST} is the singlet–triplet relaxation time of oxygen, the time intervals between individual electronic transitions between the tip and the surface are insufficient for complete relaxation of the singlet oxygen molecule. Hence, the tunnelling current measured over a time interval $t \gg \tau_{ST}$ ($t \approx 10^{-3}$ s, $\tau_{ST} \approx 10^{-8}$ s) consists of two components,

$$J = J_T n_T + J_S n_S, \qquad (13)$$
$$J_{T(S)} = J_{eT(S)} + J_{iT(S)}.$$

The currents $J_{T(S)}$ are due to the tunnelling electrons which interact with the molecule that was initially in the triplet (singlet) state. In both cases, elastic and inelastic electron tunnelling is possible [the corresponding currents are $J_{eT(S)}$ and $J_{iT(S)}$]. The latter process, which is responsible for the formation of singlet oxygen, has a threshold

$$J_{iT} \propto \eta(eV - \hbar\omega_S),$$

where $\hbar\omega_S$ is the excitation energy of singlet oxygen ($\hbar\omega_S \approx 1$ eV).[1] The probabilities of different events (different types of tunnelling) are proportional to the time-average populations of the triplet and singlet states (n_T and n_S, respectively), which are determined by the kinetics of spontaneous (relaxation) and current-induced transitions. By varying the STM current (this can be done by simply changing the distance between the surface and the STM tip), *i.e.*, by changing the ratio of the excitation and relaxation rates one can achieve targeted variation of the parameters $J_{T(S)}\tau_{ST}$, which will affect the populations and, hence, the magnitude of the threshold feature of the STM current. The minimum tunnelling currents (J_{min}) at which the dependence of the conductance jump on J is observed will determine the singlet–triplet relaxation time of a single singlet oxygen molecule ($\tau_{ST} \approx J_{min}^{-1}$).

V. Vibrational scanning tunnelling spectroscopy using resonance features of STM currents

1. Multi-quantum and combination vibrational transitions in single molecules adsorbed on the oxide and metal surfaces

Measurements of vibrational spectra of surface complexes are widely used in studies of chemical processes on the surfaces of solids. Absorption IR spectroscopy,[55] electron energy loss spectroscopy,[56] tunnelling vibrational spectroscopy[47] and other versions of vibrational spectroscopy allow identification of main types of surface complexes and determination of their structure. However, these methods provide only averaged information about macroscopic ensembles of species (see above) and single-quantum vibrational transitions in them. Recently,[18–20,38,40] the method of vibrational scanning tunnelling spectroscopy (VSTS) has been developed. This technique, which uses an STM operating in the field emission mode, allowed the vibrational spectra of adsorbed species to be measured for the first time in experiments

with STM. As a rule, the bands observed in such spectra correspond to not only single-quantum, but also multi-quantum vibrational transitions including combination ones. These spectra allow virtually unambiguous chemical identification of the species located under the STM tip.

Vibrational series of field emission resonances, which allowed the first observation of the effects of inelastic resonance electron tunnelling in experiments with STM, were predicted and detected in 1997.[18] The first experiments with a commercial STM Omicron (Germany) were carried out on naturally oxidised titanium samples in air. The current–voltage characteristics obtained exhibited clearly defined groups of equidistant maxima. The current *vs.* voltage ($J-V$) dependences were measured at different points of the surface at constant separation d of the order of 5 Å, which was adjusted and maintained by choosing an appropriate current at $V_{max} = 10$ V. The currents J varied from 4 to 20 nA. The $J-V$ dependences were measured with variable V increments ranging from 0.01 to 0.05 V. To exclude small-scale fluctuations of the measured currents, the results obtained with the 0.01 V increment were averaged over two (four) close V values. It was found that at weak currents $J(V_{max})$ resonance lines appear on the $J-V$ curves only at $V > 8$ V. At $J(V_{max}) > 7$ nA, resonance features were clearly seen in the whole range of changes in V, that is, from 5 to 10 V ($\varphi \approx 5$ eV). An example of the vibrational spectra measured in the study cited [18] is shown in Fig. 5. Comparison of the measured vibrational quanta (0.1 eV) with those known for TiO_2 ($\hbar\omega \approx 0.09$ eV) allowed one to assign these lines to the vibrational transitions of the Ti–O bond. Simultaneously, spectra with $\hbar\omega \approx 0.27$ and 0.45 eV were also observed.[18] These quanta were associated with vibrational transitions in the adsorbed CO molecules and OH radicals. Further experiments were carried out in ultrahigh vacuum ($P < 10^{-9}$ Torr) with dosed adsorption of the gases under study.

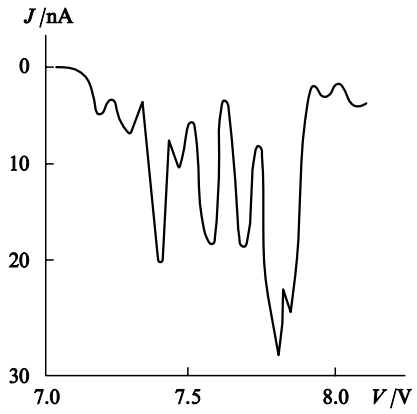

Figure 5. Vibrational spectrum of oxidised titanium ($\hbar\omega = 0.1$ eV).[18]

2. Adsorption of water on oxidised titanium. Isotope effect

Oxides are widely used as supports for many types of catalysts.[1,2] Adsorption of water on oxide surfaces has been repeatedly studied by different methods (see, *e.g.*, Ref. 57); nevertheless, one of the key issues, *viz.*, that of the forms of adsorption, remained open until the performance of the VSTS experiments.

The first measurements of the vibrational spectra of water adsorbed on the titanium surface oxidised in air using high-vacuum experiments with STM have been reported recently.[40] (This 'in-air' method was also used for measuring the vibrational spectra of water adsorbed in the nanoscale junction formed by the Ir–Pt tip and niobium.[58]) Measurements of the $J-V$ curves were preceded by a special procedure for the preparation of the surfaces under study, which included heating of samples to 550 K followed by long-term storage in high vacuum and exposure of the samples

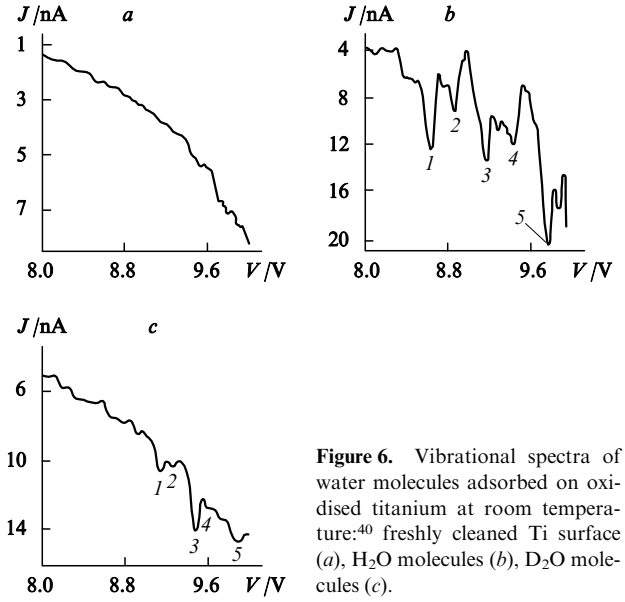

Figure 6. Vibrational spectra of water molecules adsorbed on oxidised titanium at room temperature:[40] freshly cleaned Ti surface (*a*), H_2O molecules (*b*), D_2O molecules (*c*).

to water vapour at a pressure of $\sim 10^{-6}$ Torr. After heating of the samples for ~ 2 h and subsequent storage in high vacuum the current–voltage characteristics measured at the majority of the surface points exhibited faintly visible series of field emission resonances corresponding to the vibrational frequencies of titanium oxide (see Fig. 6 *a*). Further exposure of the sample to water vapour (~ 300 K) was accompanied by significant changes in the spectral pattern; in particular, measurements at many surface points gave the spectra similar to that shown in Fig. 6 *b*. This spectrum exhibits clearly defined resonance lines corresponding to the single-quantum [$\hbar\omega_1 \approx e(V_3 - V_1) \approx 0.5$ eV, $\hbar\omega_2 \approx e(V_2 - V_1) \approx 0.2$ eV], two-quantum [$\hbar\omega_3 \approx e(V_5 - V_1) \approx 2\hbar\omega_1$] and combination [$\hbar\omega_4 \approx e(V_4 - V_1) \approx \hbar\omega_1 + \hbar\omega_2$] vibrational transitions in water molecule (the subscript at the quantities ω and V denotes the number of the resonance line in the spectrum). Small-scale maxima between the first and second (and between the third and fourth) resonances in Fig. 6 *b* correspond to the vibrations of the Ti–O bond ($\hbar\omega \approx 0.1$ eV). The magnitudes of the quanta $\hbar\omega_1$ and $\hbar\omega_2$ were found to be close to the known IR spectroscopy data on the stretching [$\hbar\omega_1(\mathrm{IR}) = 0.46$ eV] and bending [$\hbar\omega_2(\mathrm{IR}) = 0.20$ eV] vibrational quanta of H_2O molecules adsorbed on the oxidised titanium surface. It was found that the surface areas characterised by the spectra similar to that shown in Fig. 6 *b* have an island structure with the island size from 10 to 50 nm (this is typical of water adsorption on the surface of polycrystals). Blank runs with heavy water (D_2O) also gave similar spectra (see Fig. 6 *c*) with field emission resonances with the energies $\hbar\omega_1(D_2O) \approx 0.35$ eV and $\hbar\omega_2(D_2O) \approx 0.15$ eV. With an accuracy of $\sim 10\%$, this corresponded to the expected isotope effect

$$\frac{\hbar\omega(H_2O)}{\hbar\omega(D_2O)} \approx \sqrt{2}.$$

The shift of vibrational spectra towards smaller $\hbar\omega$ values represents the main, but not the only manifestation of the isotope effect. Replacement of hydrogen by deuterium leads to simultaneous change in frequency and the vibronic coupling parameter α

$$\frac{\alpha_D}{\alpha_H} \approx \sqrt{2}.$$

Correspondingly, the Franck–Condon factors determining the extent of the resonance maxima also change. For instance, for the transitions ($0 \rightarrow 1$) one gets

$$\frac{\langle 0|1\rangle_{\rm H}}{\langle 0|1\rangle_{\rm D}} = \frac{\alpha_{\rm H}}{\alpha_{\rm D}} \exp[-(\alpha_{\rm H} - \alpha_{\rm D})].$$

These relationships allow estimation of the parameter $\alpha_{\rm H}$. Using experimental data

$$\frac{J^{\rm r}_{\rm H}(\upsilon = 1)}{J^{\rm r}_{\rm D}(\upsilon = 1)} \approx 1.25,$$

where $J^{\rm r}_{\rm H,D}$ are the resonance components of the current (*i.e.*, the heights of the resonance maxima, calculated relative to the background curve), we get $\alpha_{\rm H} \approx 1.4$.

The observation of the isotope effect in the spectra of resonance features on the $J-V$ curves of the STM is unambiguous evidence for correspondence between the observed series of resonance maxima (see Fig. 6 *b*,*c*, peaks *1*–*5*) and vibrational transitions in the adsorbed water molecules. The absence of lines at $\hbar\omega \approx 0.2$ eV in particular spectra (see, *e.g.*, Fig. 7) suggests that the surface complex represents an OH radical (the value $\hbar\omega \approx 0.5$ eV corresponds to the stretching vibrational quantum of the OH radical). Hence, both types of adsorption (*viz.*, molecular and dissociative ones) on the TiO_2 surface are possible at room temperature, as was suggested recently.[57]

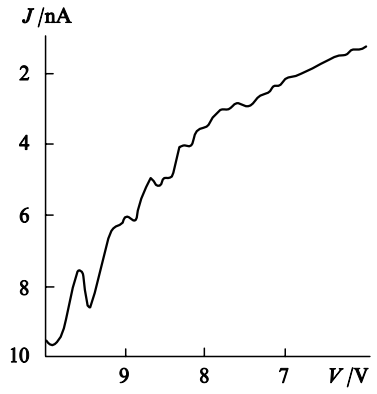

Figure 7. Vibrational spectrum of hydroxyl group adsorbed on oxidised titanium at room temperature.[41]

Vibrational scanning tunnelling spectroscopy (or spectroscopy of resonance features of STM currents) opens considerable opportunities for studies on the adsorption of various gases on the surface of oxides and metals coated with thin oxide films. The method allows one for the first time to obtain reliable chemical identification of the adsorbed species and to measure the spectra of not only single-quantum, but also multi-quantum vibrational transitions including combination ones in the adsorbed molecules and clusters. This has been exemplified by oxygen clusters adsorbed on the Al(100) surface at room temperature.[20, 39, 42]

3. Multi-quantum vibrational transitions in oxygen clusters adsorbed on aluminium

Initial stages of aluminium oxidation have been intensively studied by many experimental methods including scanning tunnelling microscopy,[59] high-resolution electron energy loss spectroscopy,[60, 61] IR spectroscopy, *etc*. Currently, it is known that at room temperature and low surface coverages the adsorbed oxygen forms small clusters with characteristic vibrational quanta $\hbar\omega_1 = 0.11-0.12$, $\hbar\omega_2 = 0.07-0.08$ and $\hbar\omega_3 = 0.036-0.040$ eV.[59–61] Low-energy electron diffraction studies[60, 61] showed that the intensities of the electron energy loss peaks depend on the oxygen dose to which the sample was exposed. At small doses [$< 10-20$ Langmuir (L), 1 L = 1 Torr s], the losses were found to be ~ 0.08 and 0.12 eV. Exposure to greater doses ($\gtrsim 100$ L) corresponding to the formation of nanoscale islands on

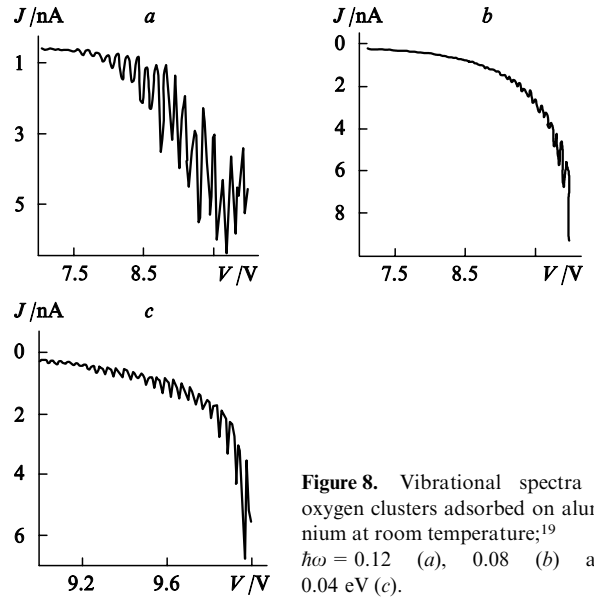

Figure 8. Vibrational spectra of oxygen clusters adsorbed on aluminium at room temperature;[19] $\hbar\omega = 0.12$ (*a*), 0.08 (*b*) and 0.04 eV (*c*).

the surface of the oxide phase resulted in the losses $\hbar\omega = 0.04$ eV. The same $\hbar\omega$ values were obtained [19] in the VSTS measurements of vibrational spectra of oxygen adsorbed on the Al(100) surface (Figs 8–10).

Experiments with the Al(100) and oxidised titanium surfaces were carried out using the same procedures for both the preparation of the surfaces and measurements of vibrational spectra with the STM. The $J-V$ curves measured for clean Al(100) surface with an increment $\Delta V = 0.01$ V exhibited no resonance features and were well described by the Fowler–Nordheim formula

$$J(V) = \exp\left(-\frac{C}{V}\right) \qquad (14)$$

($C = 10-100$ V), which corresponds to electron tunnelling from the tip of an STM operating in the field emission mode.

Measurements at different points of the surface carried out at $\sim 10-20$ L doses showed that nearly 10% of the $J-V$ curves exhibited vibrational series with $\hbar\omega_1 \approx 0.12$ eV. (The spectra with $\hbar\omega_2 \approx 0.08$ eV were observed more rarely.) This allows the determination of the sticking coefficient of oxygen to the clean Al(100) surface, $\theta \approx 0.005-0.01$. The same values were obtained in a STM study of the initial stages of Al(100) oxidation.[59]

Exposure to greater doses was accompanied by significant changes in the pattern of vibrational spectra. For instance, spectra with $\hbar\omega_3 = 0.04$ eV appeared at different points of the surface at

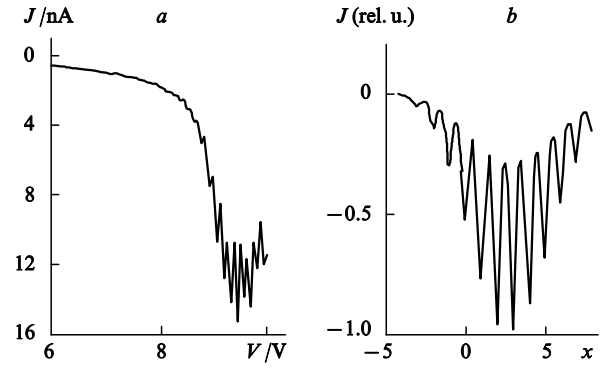

Figure 9. Vibrational spectrum of oxygen cluster adsorbed on aluminium ($\hbar\omega = 0.12$ eV, dose 20 L);[19] bell-shaped envelope (*a*) and theoretical curve calculated using formula (6) for the Boltzmann distribution over vibrational levels, $x = V/\omega$ (*b*).

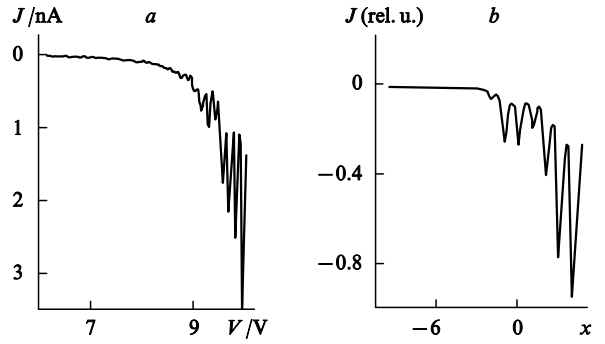

Figure 10. Vibrational spectrum of oxygen cluster adsorbed on an aluminium surface ($\hbar\omega = 0.12$ eV, dose 20 L);[19]
oscillating envelope (*a*) and theoretical curve calculated using formula (6) for the inverse distribution over vibrational levels (*b*).

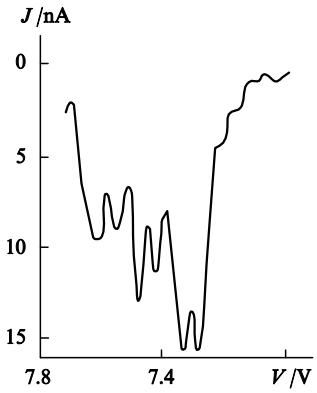

Figure 11. Doubled vibrational series of field emission resonances for paramagnetic radical ion O_2^- adsorbed on oxidised titanium (the effect of exchange splitting of resonance lines).[24]

50 L doses. Further increase in exposure doses led to a decrease in the number of spectra with the lines with larger $\hbar\omega$ (0.12 and 0.08 eV) and to rapid increase in the number of spectra with the vibrational quantum $\hbar\omega_3 = 0.04$ eV corresponding to the oxide phase. After exposure to $\sim$1000 L doses the $J-V$ curves measured at almost all points of the surface under study exhibited long series of resonance maxima corresponding to the oxide. Simultaneously, adsorption of CO molecules on the oxidised aluminium surface was observed. Such complexes can be readily identified using their spectra that exhibit lines corresponding to combination vibrational transitions

$$eV_{\upsilon_1\upsilon_2} = eV_0 + \hbar\omega_0\upsilon_1 + \hbar\omega_3\upsilon_2, \quad \upsilon_{1,2} = 0, 1, 2, \ldots, \tag{15}$$

where the largest vibrational quantum [$\hbar\omega_0 = 0.24$ eV (see Ref. 61)] equals the well-known value characteristic of the CO molecules.

4. Detection of single surface paramagnetic centres

The surfaces of oxides and oxidised metals are always covered by small amounts of paramagnetic centres [$< 1\%$ (see Ref. 2)] which are usually studied by ESR on polycrystals.[62] Attempts at detecting ESR signals from individual paramagnetic centres (PC) with the STM have been undertaken.[63, 64] Weak changes in the tunnelling currents were detected in experiments with oxidised silicon. Signals were observed at room temperature at distances $\sim$3 to 6 Å from the single point defects tentatively identified as PC. Such a dependence of the ESR signal on the tip position seems to be abnormal. The origination mechanism of 'single-atom' ESR in the case of equally populated Zeeman levels is currently unknown. The problem of integration of the ESR and STM methods needs further consideration.

Possible variants of such an integration have been considered.[25, 26] It was shown that using ferromagnetic tips (here, the tunnelling electrons are polarised) allows detection of ESR signals in the experiments with STM even at room temperature when $kT > \hbar\omega_L$ (ω_L is the Larmor frequency) and the Zeeman levels have equal equilibrium populations. This can be done with the operating currents $J > \tau_\sigma^{-1}$ (τ_σ is the characteristic spin–lattice relaxation time) at which the polarised tunnelling electrons create nonequilibrium distributions over the Zeeman levels. Practical implementation of this technique would make it possible to reveal the arrangement of paramagnetic centres on the surface using the capabilities of the STM; however, these experiments preclude measurements of *g*-factors since local magnetic fields under the ferromagnetic tip of the STM are currently unknown.

Another solution to the problem of detection with STM of a single PC has been suggested and evaluated.[24, 65] It was found that for metal oxides and metals coated with thin oxide films, the exchange splitting of the field emission resonances ($\delta_{j,n}$) can be larger than or comparable with the width of the energy level: $\delta_{j,n} \approx 0.1-0.2$ eV, $\Gamma_{j,n} \leqslant 0.1-0.04$ eV. Hence it follows that the vibrational spectra of the PC should have the form of two series of equidistant maxima on the $J-V$ curves, shifted with respect to each other by the exchange splitting $\delta V \approx 0.1-0.2$ V.

Such a spectrum has first been observed for oxidised titanium (Fig. 11). Based on the exchange splitting and the vibrational quantum magnitude ($\hbar\omega = 0.15$ eV), this PC can be unambiguously identified as a single surface paramagnetic radical ion O_2^-. [The vibrational frequency of dioxygen ion adsorbed on oxide surfaces is well known from the IR spectroscopy data:[2] $\hbar\omega(O_2^-) = 1180\ \text{cm}^{-1} = 0.15$ eV.] The characteristic spectral pattern corresponding to the adsorbed radical ion O_2^- represents a complete spin-vibrational 'portrait' of this species, which can also be used in studies of single O_2^- ions adsorbed on other surfaces. This can be exemplified by the spin-vibrational spectrum of a single O_2^- ion detected on the oxidised Al(100) surface (Fig. 12).

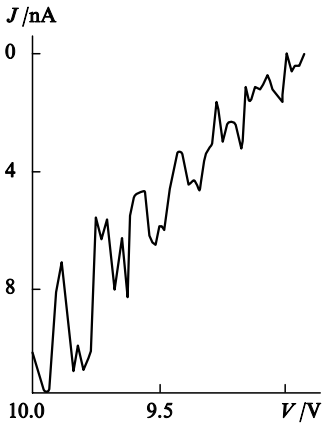

Figure 12. Spin-vibrational series for paramagnetic radical ion O_2^- adsorbed on oxidised aluminium surface.

VI. Kinetics of vibrational and spin transitions in single surface complexes

The development of new methods for detection with STM of single paramagnetic centres and measurements of multi-quantum vibrational spectra of single surface complexes creates prerequisites for the invention of 'kinetic' modifications of the scanning tunnelling spectroscopy of vibrational and spin transitions. This is of crucial importance.

According to the ergodic hypothesis, the kinetics of quantum transitions can be studied by two equivalent approaches. One of

them implies experiments with ensembles of identical subsystems while the other involves experiments with the same subsystem and multiple repetition of the transitions under study. Until recently, all kinetic modifications of spectroscopic methods were based on the first approach. However, spectroscopic measurements with ensembles can appear to be insufficiently informative in the case of inhomogeneous systems such as surfaces covered with adsorbed species. Scanning tunnelling spectroscopy of vibrational and spin transitions allows the second approach to be implemented for the first time. (In this case, the kinetics of quantum transitions in ensembles of elementary events occurring in the same surface complex rather than in ensembles of adsorbed species is studied.) These surface chemistry studies were impossible[‡] until recent publications.[18, 19, 22]

The idea of kinetic scanning tunnelling spectroscopy is very simple. In experiments with STM, the current densities can be as high as 10^{10} to 10^{11} A cm^{-2}. Thus, the time intervals between individual acts of tunnelling can be shorter (or at least comparable with the characteristic relaxation times of internal degrees of freedom of the surface complexes.) At such electron current densities, the distributions of the species located under the STM tip over vibrational states appear to be essentially nonequilibrium. If ferromagnetic tips are used, spin distributions of the species also appear to be nonequilibrium.[25, 26] Under these conditions, the average current J measured during the time of the order of 10^{-3} s includes contributions of a large number of transitions,

$$J(V) = \sum_{\upsilon,S,S_z} n(\upsilon, S, S_z) J_{\upsilon,S,S_z}(V). \tag{16}$$

Here, $n(\upsilon,S,S_z)$ is the current-dependent population of the state $|\upsilon,S,S_z\rangle$ of the surface complex 'sitting' under the STM tip, J_{υ,S,S_z} is the tunnelling current due to the electrons interacting with the species which initially was in the state $|\upsilon,S,S_z\rangle$ and S and S_z are the spin of the species and its projection, respectively.

Since individual acts of electron tunnelling are uncorrelated (the relaxation times of electronic subsystems for the surface and tip are much shorter than all other characteristic times), the kinetics of vibrational and spin transitions in the surface complex can be described by a system of balance equations

$$\frac{\partial n(v)}{\partial t} = \sum_{vv'} \left[n(v') w_{v'v} - n(v) w_{vv'} \right] = 0, \tag{17}$$

where v denotes the totality of vibrational and spin quantum numbers and $w_{v'v}$ are the probabilities of quantum transitions $v' \to v$, which, generally, can be both current induced and spontaneous (relaxation)

$$w_{v'v} = J_{v'v} + w_{\mathrm{r}\, v'v}\,. \tag{18}$$

Here, $J_{v'v}$ are the tunnelling currents corresponding to the electronic transitions for particular fixed initial (v') and final (v) values of the vibrational and spin quantum numbers of the complex and $w_{\mathrm{r}\, v'v}$ are the probabilities of spontaneous transitions.[§] Taken together, the system of equations (17) and expressions (16) and (18) make it possible to obtain a self-consistent description of the formation of resonance features on the $J-V$ curves of the STM. Resonance currents $J_{v'v}$ can be calculated using formula (7). According to expression (16), the series of field emission resonances on the $J-V$ curves depend on the distributions $n(v,S,S_z)$, which allows their reconstruction from experimental data.[19, 20, 25] From Eqns (17) and expression (18) it follows that the dependence of the distributions $n(v,S,S_z)$ on $w_{\mathrm{r}\, v'v}$ can be used for reconstructing the kinetics of spin and vibrational transitions.

Some examples of nonequilibrium spin effects, potentially observable in systems with ferromagnetic tips, have been considered recently.[25] Therefore, below we will restrict ourselves to the description of nonequilibrium effects which can be observed in the vibrational spectra of adsorbates.[19, 20]

1. Reconstruction of nonequilibrium distributions over vibrational states

The relation between the shape of the envelopes of vibrational spectra of adsorbed species and the distributions $n(\upsilon)$ can be easily understood by analysing a diagram of vertical vibrational transitions occurring in the case of capture of a tunnelling electron by a trap (resonator). Such a diagram illustrating the main model of multi-quantum vibrational transitions (the model of shifted harmonic oscillators[67]) is shown in Fig. 13. (Recent estimates[24] have shown that the vibrational frequencies of adatoms change by no more than 10% to 15% upon capture of an electron by the resonator.) It is easily seen that for the equilibrium vibrational distributions corresponding to rather weak tunnelling currents insufficient for strong heating of the vibrational subsystem

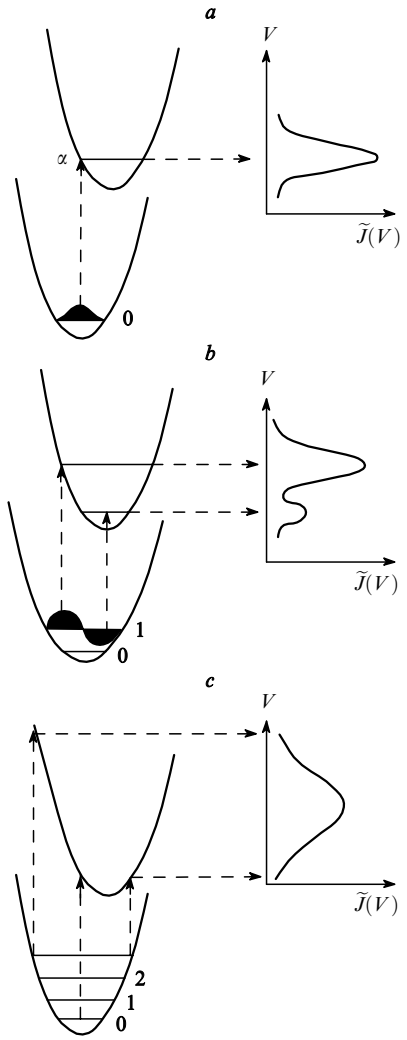

Figure 13. A scheme illustrating the formation of different types of envelopes for the vibrational spectra of adsorbates and the relation between the shape of the envelope and $\tilde{J}(V)$ and distributions over vibrational states.

[‡] It should be mentioned that single molecule spectroscopy by laser induced fluorescence also provides a means for studying the structure of and quantum transitions in single adsorbed species. However, spatially resolved experiments as well as studies on multi-quantum vibrational transitions and those involving highly excited states cannot be performed using this technique. The potentialities of this method have been considered in detail in a special issue of the *Chemical Physics* journal.[66]

[§] It will be recalled that we use the system of atomic units in which the electron charge $e = 1$.

$$n(\upsilon) = \begin{cases} 1, & \upsilon = 0 \\ 0, & \upsilon \neq 0 \end{cases}.$$

It will be recalled that usually the condition $kT \ll \omega$ is fulfilled. In this case, all the tunnelling electrons interact with the nonexcited surface complex and the envelopes of the resonance series are determined only by the Franck–Condon factors $\langle 0|\bar{\upsilon}\rangle^2$

$$\langle 0|\bar{\upsilon}\rangle^2 = \frac{\alpha^{\bar{\upsilon}} \exp(-\alpha)}{\bar{\upsilon}!}.$$

Here, α is the vibronic coupling parameter equal to the number of the energy level in which the species goes from the ground vibrational state (see Fig. 13 *a*). At $\alpha \approx 1$, the envelopes have a shape of sufficiently narrow bell-shaped curves.¶

For nonequilibrium distributions, the envelopes have a different shape. For Boltzmann-type distributions,

$$n(\upsilon) \approx \exp\left(-\frac{\upsilon}{\langle\upsilon\rangle}\right),$$

the envelopes are also bell-shaped, but have larger halfwidths which depend on $\langle\upsilon\rangle = \sum_{\upsilon} \upsilon n(\upsilon)$ (see Fig. 13 *c*). For inverse distributions, the envelopes exhibit oscillations, *i.e.*, the spectra are formed by groups of resonance maxima on the $J-V$ curves (see Fig. 13 *b*). The number of such groups, N, correlates with the number (υ_m) of the energy level with the highest population

$$N = \upsilon_m + 1.$$

Figures 8–10 present some examples of the vibrational spectra with bell-shaped and oscillating envelopes, obtained in our studies on the initial stages of the oxidation of aluminium at room temperature. The results of calculations of the $J-V$ curves using relationships (17) and (18) show the possibility of reconstructing the nonequilibrium distributions over vibrational states for the surface complexes located under the STM tip and 'heated' by the current of elastically and inelastically tunnelling electrons.

2. Kinetics of multi-quantum vibrational transitions

Combining the solution of equations (17) and calculations of vibrational series of the current–voltage characteristics of the STM using expression (16) allows the kinetics of vibrational transitions in single complexes located under the STM tip to be reconstructed from the experimental $J-V$ curves. Clearly, this also includes the reconstruction of the parameters determining the rate of vibrational relaxation of the surface complex to which the spectrum under study corresponds.

The dependences of the distributions $n(\upsilon)$ and corresponding $J-V$ curves on the excitation and de-excitation rates of vibrational degrees of freedom of surface complexes can be readily illustrated by the results of calculations presented in Figs 14–16. [Full information on the kinetics of vibrational transitions is contained in the shape of the envelopes, therefore the results of calculations of the $J(V)$ dependences are given in relative units.] The histograms of corresponding vibrational distributions calculated using formulae (7), (17) and (18) for both resonance and off-resonance V values are also shown in Figs 14–16.

In accordance with formula (7), the partial tunnelling currents ($J_{\upsilon\upsilon'}$) were approximated by resonance-type terms in which the probabilities of tunnelling from the tip to the trap, Γ_1, and from the trap to the sample, Γ_2, had the form

$$\Gamma_1 = C_1 \exp\left(-\frac{C}{V}\right), \quad \Gamma_2 = \text{const},$$

where C_1 and C are constants.

¶ Mention may be made of an analogy between inelastic resonance tunnelling and resonance absorption of light by molecules [67] and impurity centres in crystals.[68]

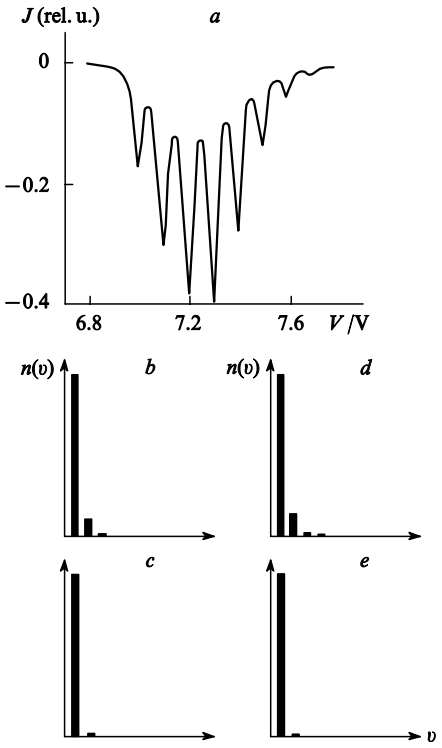

Figure 14. Vibrational spectrum with bell-shaped envelope (*a*) and distributions over vibrational levels (*b*–*e*).
Calculated using formulae (6), (16) and (17) for $w_{r\upsilon} > J_\upsilon$;
V/V: 7 (*b*), 7.05 (*c*), 7.4 (*d*) and 7.45 (*e*).

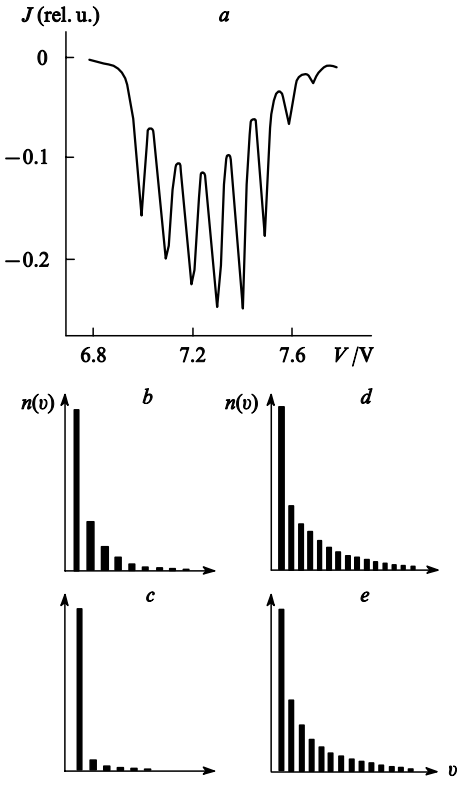

Figure 15. Vibrational spectrum with bell-shaped envelope (*a*) and distributions over vibrational levels (*b*–*e*). Calculated using formulae (6), (16) and (17) for $w_{r\upsilon} < J_\upsilon$; (*b*–*e*) see Fig. 14.

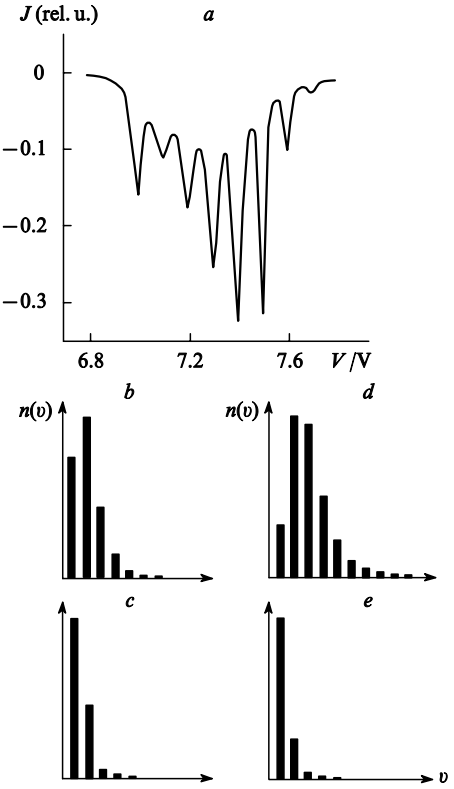

Figure 16. Vibrational spectrum with bell-shaped envelope (*a*) and distributions over vibrational levels (*b*–*e*). Calculated using formulae (6), (16) and (17) for $w_{r\upsilon} < J_\upsilon$, $w_{r\upsilon} \approx \upsilon^3$; (*b*–*e*) see Fig. 14.

Different conditions for the excitation of the vibrational subsystem by the currents $J_{\upsilon\upsilon'}$ and for current-induced and spontaneous (with the rate approximated by the dependence $w_{r\upsilon} = c_r\upsilon^n$) vibrational relaxation were simulated. This was achieved by varying the parameters Γ_1, C_1, C, Γ_2, c_r and n in such a manner that the distributions over vibrational levels corresponded to the histograms presented in Figs 14–16.

The calculated spectrum shown in Fig. 14 *a* corresponds to weak heating of the vibrational subsystem (*cf*. Fig. 13 *a*). Changes in the bell-shaped spectrum upon an increase in the temperature of the vibrational subsystem are presented in Fig. 15 *a* and the relation between the spectra with oscillating envelopes and inverse distributions $n(\upsilon)$ is illustrated by the plot shown in Fig. 16 *a*. (This type of distributions is formed if the currents are rather heavy while the vibrational relaxation is slow and its rate is a nonlinear function of the excitation level.)

VII. Scanning tunnelling spectroscopy using fluctuations of STM currents

Pioneering STM studies and direct observation of slow surface migration of species with a time resolution of the order of 0.1 s have been reported more than a decade ago.[69,70] Since then, surface diffusion was repeatedly studied by scanning tunnelling microscopy (see, *e.g.*, Refs 71 and 72). By and large, such experiments are similar to those carried out earlier with a field emission[73] and ion microscope.[74] The known procedure for reconstructing the surface migration parameters from the images taken at different time instants allows one to reconstruct the surface diffusion activation energies of species with a reasonable accuracy (~5%–15%). Unfortunately, the pre-exponential factors in the expressions for the diffusion coefficients are determined with much lower (from 1.5 to 2 orders of magnitude) accuracy. This precludes studies on the surface migration dynamics. In particular, the hop lengths distributions of the migrating species remain unknown so far. These distributions determine the rates of many heterogeneous chemical reactions, but often do not necessarily correspond to the nearest adsorption site.[1]

It is believed that the problem can be solved by studying the spectral characteristics of the noise of tunnelling currents in STM due to changes in the conductance of the tunnelling gap caused by the passage of the migrating species.[28,29,75] An optimum design of experiment using 'fluctuation scanning tunnelling spectroscopy' has been proposed and substantiated.[28,29] Suppose the STM tip scans the surface area containing the migrating species using a velocity close to the migration rate of the species. In this case, the spectral density of the low-frequency noise of the STM current strongly depends not only on the pre-exponential factor in the equation for the diffusion coefficient, but also on time taken for the migrating species to hop from one adsorption site to another one. Since even commercially sold STMs allow the surface scan velocity to be varied over a wide range (from 1 to 100 nm s^{-1}), scanning tunnelling spectroscopy using fluctuations of STM currents can be used for reconstructing the surface migration dynamics of not only slow particles, but also fast ones which cannot be imaged by surface topography measurements.

VIII. Time-resolved scanning tunnelling spectroscopy

Rapid progress in femtosecond laser spectroscopy and scanning tunnelling spectroscopy allows the surface structure to be studied with atomic-scale spatial or corresponding time resolution. This makes it possible to pose a more complicated problem of integrating the capabilities of these modern, powerful experimental methods for studying the surface.

Pioneering studies aimed at integrating the probe methods of studying solid surfaces including scanning tunnelling microscopy and femtosecond laser spectroscopy date back to early 1990s.[76–79] Currently, two main research avenues have been developed, the optical and tunnelling one, each with its specific problems and solution methods. To review them goes beyond the scope of this paper, so we will only briefly outline the state-of-the-art in the field.

In optical studies, the STM tip is replaced by a thin optical fibre brought to the surface under study to a distance shorter than the light wavelength. This type of probe instruments, *viz*., near-field scanning optical microscopes, provides atomic-scale time resolution in combination with rather high spatial resolution (~30–50 nm), which is one or two orders of magnitude higher than the resolution of conventional optical microscopes.

To achieve higher spatial resolution, one needs continue in use experimental methods employing STMs. Using the STM also allows time-resolved spectroscopic measurements to be performed by varying the conductance of the tunnel junction. As follows from expression (2), this can be done by varying the tunnelling gap or by changing the surface density of electron states (*e.g.*, by illuminating the contact) or the voltage. Each of these approaches has its own limitations that are due to inertia of the tip, finite switching rate of control circuits and small magnitudes of the tunnelling currents. Currently, time resolution achieved in experiments with STMs is no better than several picoseconds,[80] though integration of STM and femtosecond laser spectroscopy has been the subject of research activity in many research centres.

IX. Conclusion

The history of development of scanning tunnelling microscopy and spectroscopy demonstrates numerous examples of successful solutions to fundamental problems of surface chemistry and physics. One cannot but be surprised at increasing number of new possibilities provided by the STM, the perfect scientific instrument. Advanced research techniques in surface chemistry and physics owe their origin to the creators of the STM. On the other hand, mention should be made of rapid increase in applied

research in which the STM and related probe instruments (see a short review [80]) are used as instruments for assembling of various nanoclusters from individual atoms on the solid surfaces. Nanoclusters exhibit unique physical and chemical properties. For instance, they can be extremely hard and possess high adsorptive and emissive capacities and reactivity. The conductivity of nanoclusters can be controlled in a targeted manner by varying their atomic structure without changing the chemical composition, by doping them with individual impurity atoms or by applying mechanical strain or a magnetic field. Of course, this gives rise to lots of ideas associated with possible use of both single 'hand-assembled' nanoclusters and multicluster nanomaterials in different areas of chemistry, in electronics, technology, ecology, medicine, *etc*. The development of nanotechnologies also implies wide use of probe instruments. Crucial importance of nanotechnologies to high-tech processes of the 21st century has now gained general acceptance in all highly developed countries. It is a wide-spread, well-substantiated opinion that many economic, military, social, political and medicinal problems can be solved using the results of nanotechnological studies. There are strong grounds to believe that the mission of being a scientific basis for nanotechnologies falls to the single molecule chemical physics of surfaces, which has been rapidly developed in a manner much like that of the chemical physics of macroscopic ensembles of atomic species.

The authors express their gratitude to Academician A L Buchachenko for incessant support of their research, frequent discussions of the results obtained, valuable comments and criticism. We are also grateful to M V Sharova for help in preparing the manuscript.

This review has been written with the financial support of the Russian Foundation for Basic Research (Project Nos 99-03-32098 and 99-03-32100).

References

1. O V Krylov, B R Shub *Neravnovesnye Protsessy v Katalize* (Non-Equilibrium Processes in Catalysis) (Moscow: Khimiya, 1990)
2. O V Krylov, V F Kiselev *Adsorbtsiya i Kataliz na Perekhodnykh Metallakh i Ikh Oksidakh* (Adsorption and Catalysis on Transition Metals and Their Oxides) (Moscow: Khimiya, 1981)
3. L A Bol'shov, A P Napartovich, A G Naumovets, A G Fedorus *Usp. Fiz. Nauk* **122** 125 (1978) [a]
4. *Handbook of Microscopy. Application in Materials Science. Solid State Physics and Chemistry* (Weinheim: VCH, 1997)
5. M W Roberts, C S McKee *Chemistry of the Metal–Gas Interface* (Oxford: Oxford University Press, 1979)
6. H L Dai, W Ho (Eds) *Laser Spectroscopy and Photochemistry on Metal Surfaces* (Singapore: World Sci., 1995)
7. G Binnig, H Rohrer, Ch Gerber, E Weibel *Phys. Rev. Lett.* **49** 57 (1982)
8. R Wiensendanger *Scanning Probe Microscopy and Spectroscopy*. (Cambridge: Cambridge University Press, 1994)
9. J Tersoff, D R Hamann *Phys. Rev. B* **31** 805 (1985)
10. H-J Gunterrodt, R Wiesendanger (Eds) *Scanning Tunnelling Microscopy III. Springer Series in Surface Science* (Berlin: Springer, 1993)
11. R Z Bakhtizin, T Hashizume, X-D Wang, T Sakurai *Usp. Fiz. Nauk* **167** 289 (1997) [a]
12. D M Eigler, E K Schweizer *Nature (London)* **344** 524 (1991)
13. B C Stipe, M A Rezaei, W Ho, S Gaom, M Persson, B I Lindqvist *Phys. Rev. Lett.* **78** 4410 (1997)
14. L J Lauhon, W Ho *Phys. Rev. Lett.* **84** 1527 (2000)
15. Ph Avouris *Acc. Chem. Res.* **28** (3) 95 (1995)
16. A L Buchachenko *Usp. Khim.* **68** 99 (1999) [*Russ. Chem. Rev.* **68** 85 (1999)]
17. B C Stipe, M A Rezaei, W Ho *Science* **280** 1732 (1998)
18. F I Dalidchik, M V Grishin, S A Kovalevskii, N N Kolchenko *Pis'ma Zh. Eksp. Teor. Fiz.* **65** 306 (1997)
19. M V Grishin, F I Dalidchik, S A Kovalevskii, N N Kolchenko *Pis'ma Zh. Eksp. Teor. Fiz.* **71** 104 (2000)
20. F I Dalidchik, M V Grishin, S A Kovalevskii, N N Kolchenko, B R Shub *Poverkhnost'* **6** 107 (2001)
21. M V Grishin, F I Dalidchik, S A Kovalevskii, N N Kolchenko, B R Shub, in *Zondovaya Mikroskopiya-2001 (Materialy Vserossiiskogo Soveshchaniya), Nizhnii Novgorod, 2001* [Probe Microscopy-2001 (Proceedings of All-Russian Meeting), Nizhnii Novgorod, 2001] p. 131
22. E M Balashov, S O Gladkov, F I Dalidchik, M A Kozhushner, B R Shub *Khim. Fiz.* **20** (5) 85 (2001) [b]
23. E Balashov, S Gladkov, F Dalidchik, M Kozhushner, B Shub *Phys. Lett. A* **282** 47 (2001)
24. F I Dalidchik, S A Kovalevskii *Pis'ma Zh. Eksp. Teor. Fiz.* **67** 916 (1998)
25. A L Buchachenko, M A Kozhushner, B R Shub *Izv. Akad. Nauk, Ser. Khim.* 1732 (1998) [c]
26. M A Kozhushner, B R Shub, R R Muryasov *Pis'ma Zh. Eksp. Teor. Fiz.* **67** 484 (1998)
27. A L Buchachenko, F I Dalidchik, S A Kovalevskii, B R Shub *Usp. Khim.* **70** 613 (2001) [*Russ. Chem. Rev.* **70** (7) (2001)]
28. A S Prostnev, V I Chernysh, B R Shub *Khim. Fiz.* **16** (6) 25 (1997) [b]
29. A Prostnev,V Chernysh, B Shub *Chem. Phys. Rep.* **18** 13 (1997)
30. D Bohm *Quantum Mechanics* (New York: Prentise Hall Inc., 1952)
31. F I Dalidchik *Zh. Eksp. Teor. Fiz.* **87** 1384 (1984)
32. F Dalidchik, M Grishin, N Kolchenco, S Kovalevskii, in *Book of Abstracts of the 43rd International Field Emission Symposium, Moscow, 1996* p. 25
33. F Dalidchik, M Grishin, N Kolchenco, S Kovalevskii *Surf. Sci.* **387** 50 (1997)
34. G Binnig, K H Frank, H Fuchs, N Garsia, B Rehl, H Rohrer, F Salvan, A R Williams *Phys. Rev. Lett.* **55** 991 (1985)
35. R S Becker, J A Golovchenko, B S Swartzentruber *Phys. Rev. Lett.* **55** 987 (1985)
36. I-W Lyo, Ph Avouris *Science* **245** 1369 (1989)
37. N D Lang *Phys. Rev. B* **55** 9364 (1997)
38. F Dalidchik, M Grishin, N Kolchenko, S Kovalevskii, B Shub *Spectrosc. Lett.* **30** 1429 (1997)
39. F Dalidchik, M Grishin, N Kolchenko, S Kovalevskii *Ultramicroscopy* **79** 203 (1999)
40. F I Dalidchik, M V Grishin, S A Kovalevskii, N N Kolchenko, B R Shub *Pis'ma Zh. Eksp. Teor. Fiz.* **66** 37 (1997)
41. S A Kovalevskii, F I Dalidchick, M V Grishin, N N Kolchenko, B R Shub *Appl. Phys. A, Mater. Sci. Process.* **66** (Suppl. Pt.1) (1988)
42. S A Kovalevskii, F I Dalidchick, M V Grishin, B R Shub, in *Preliminary Proceedings of STM'99, Seoul, Korea, 1999* p. 673
43. M Grishin, F Dalidchik, S Kovalevskii, N Kolchenko, in *Book of Abstracts of the 45th International Field Emission Symposium, Irbid, Jordan, 1998* p. 74
44. R C Jaklevic, J Lambe *Phys. Rev. Lett.* **17** 1139 (1966)
45. V I Fistul', N Z Shvarts *Usp. Fiz. Nauk* **77** 109 (1962) [a]
46. N Holonyak, I F Lesk *Phys. Rev. Lett.* **4** 3167 (1959)
47. P K Hansma *Tunnelling Spectroscopy: Capabilities, Applications and New Techniques* (New York: Plenum, 1982)
48. B N J Persson, J E Dimuth *Solid State Commun.* **57** 769 (1986)
49. B N J Persson, A Baratoff *Phys. Rev. Lett.* **59** 339 (1987)
50. B C Stipe, M A Rezaei, W Ho *Rev. Sci. Instrum.* **70** 137 (1999)
51. J K Gimzevski, Ch Joachim *Science* **283** 1683 (1999)
52. J Gaudioso, H J Lee, W Ho *J. Am. Chem. Soc.* **121** 8479 (1999)
53. L J Lauhon, W Ho *Phys. Rev. B* **60** R8525 (1999)
54. C J Noble, P G Burke *Phys. Rev. Lett.* **68** 2011 (1992)
55. A A Davydov *IK Spektroskopiya v Khimii Poverkhnosti Okislov* (IR Spectroscopy in the Chemistry of Oxides Surface) (Novosibirsk: Nauka, 1984)
56. H Ibach, in *Electron Energy Loss Spectrometers. Springer Series in Optical Sciences* (Berlin: Springer, 1990)
57. M B Hugenschmidt, L Gamble, C T Campbell *Surf. Sci.* **302** 329 (1994)
58. I V Zakurdaev, D S Firsov, in *Zondovaya Mikroskopiya-99 (Materialy Vserossiiskogo Soveshchaniya), Nizhnii Novgorod, 1999* [Probe Microscopy-99 (Proceedings of All-Russian Meeting), Nizhnii Novgorod, 1999] p. 283
59. H Brune, J Witterlin, J Trost, G Ertl, J Wiechers, R J Behm *J. Chem. Phys.* **99** 2128 (1993)
60. C Astaldi, P Geng, K Jakoby *J. Electron. Spectrosc. Relat. Phenom.* **44** 175 (1987)
61. J L Erskine, R L Strong *Phys. Rev. B* **25** 5547 (1982)
62. A B Roitsin, V M Maevskii *Usp. Fiz. Nauk* **159** 297 (1989) [a]

63. Y Manassen, R J Hamers, J E Demuth, A J Castellano Jr *Phys. Rev. Lett.* **62** 2531 (1989)
64. D Shadal, Y Manassen *Phys. Rev. B* **44** 11528 (1991)
65. M V Grishin, F I Dalidchik, S A Kovalevskii, N N Kolchenko, B R Shub, in *Zondovaya Mikroskopiya-99 (Materialy Vserossiiskogo Soveshchaniya), Nizhnii Novgorod, 1999* [Probe Microscopy-99 (Proceedings of All-Russian Meeting), Nizhnii Novgorod, 1999] p. 63
66. *Chem. Phys.* **247** (1) (Spec. Issue) (1999)
67. M D Frank-Kamenetskii, A V Lukashin *Usp. Fiz. Nauk* **116** 193 (1975) [a]
68. G Ehrlich, F Hudda *J. Chem. Phys.* **35** 1421 (1961)
69. Y-W Mo, B S Swartrantruber, M B Webb, M L Lagally *J. Vac. Sci. Technol. A* **8** 201 (1990)
70. E Ganz, K Sattler, J Clarke *Surf. Sci.* **219** 33 (1989)
71. E Ganz, S Theiss, I-S Hwang, J Golovchenko *Phys. Rev. Lett.* **68** 1567 (1992)
72. Y-W Mo *Phys. Rev. Lett.* **71** 2923 (1993)
73. R Gomer *Rep. Progr. Phys.* **53** 917 (1990)
74. E W Müller, T T Tsong *Field Ion Microscopy. Field Ionization and Evaporation)* (Oxford: Pergamon Press; Translated into Russian; Moscow: Nauka, 1980)
75. M Sumetskii, A Kornyshev *Phys. Rev. B* **48** 17493 (1993)
76. M R Freeman, G Nunes Jr *Appl. Phys. Lett.* **63** 2633 (1993)
77. S Weiss, D F Ogletree, D Botkin, M Salmeron, D S Chemla *Appl. Phys. Lett.* **63** 2567 (1993)
78. J W P Hsu, E A Fitzgerald, Y H Xie, P J Silverman *J. Appl. Phys.* **79** 7743 (1996)
79. M J Gregor, P G Blome, R G Ulbrich, Grossmann, S Grosse, J Feldmann, W Stolz, E O Göbel, D J Arent, M Bode, K A Bertness, J M Olson *Appl. Phys. Lett.* **67** 3572 (1995)
80. R Pool *Science* **247** 634 (1990)

[a] — *Physics-Uspekhi (Engl. Transl.)*
[b] — *Chem. Phys. Rep. (Engl. Transl.)*
[c] — *Russ. Chem. Bull. (Engl. Transl.)*

Russian Chemical Reviews **70** (8) 641 – 653 (2001) © 2001 Russian Academy of Sciences and Turpion Ltd

DOI 10.1070/RC2001v070n08ABEH000630

1,3-Dipolar cycloaddition reactions of nitrile oxides in the synthesis of natural compounds and their analogues

A I Kotyatkina, V N Zhabinsky, V A Khripach

Contents

I.	Introduction	641
II.	Methods for the generation of nitrile oxides	641
III.	Methods for the transformations of isoxazoles and 4,5-dihydroisoxazoles	641
IV.	Intermolecular 1,3-dipolar cycloaddition reactions of nitrile oxides	643
V.	Intramolecular 1,3-dipolar cycloaddition reactions of nitrile oxides	647
VI.	Syntheses based on enantiocontrolled 1,3-dipolar cycloaddition reactions of nitrile oxides	649

Abstract. The published data on the use of 1,3-dipolar cycloaddition reactions of nitrile oxides in the synthesis of natural compounds and their analogues are systematised and reviewed. The bibliography includes 145 references.

I. Introduction

The cycloaddition of nitrile oxides to alkynes and alkenes is the most popular approach to the synthesis of isoxazoles and 4,5-dihydroisoxazoles.[1–7] Isoxazoles and 4,5-dihydroisoxazoles are used as intermediates in total syntheses of natural compounds. The fact that these compounds represent equivalents of definite functional groups can be exploited in different steps of the synthesis. On the other hand, isoxazoles and 4,5-dihydroisoxazoles are relatively stable compounds and remain intact in the course of multistep transformations.

The present review is devoted to the synthesis of natural compounds based on reactions of nitrile oxides with dipolarophiles with subsequent transformations of the adducts formed.

II. Methods for the generation of nitrile oxides

Nitrile oxides are usually unstable and prone to dimerisation resulting in the corresponding furoxans.[8] Therefore, they are usually generated *in situ* by dehydration of primary nitro compounds by phenyl isocyanate[9] or by dehydrohalogenation of hydroximoyl chlorides or bromides by triethylamine.[10] Hydroximoyl chlorides are generated from oximes by chlorination with chlorine, *N*-chlorosuccinimide (NCS),[11] nitrosyl chloride, sodium hypochlorite[12] or *tert*-butyl hypochlorite.[13] A procedure for the synthesis of functionalised and non-functionalised hydroximoyl chlorides, which involves treatment of nitroalkanes or conjugated nitroalkenes with titanium(IV) chloride, has been developed.[14]

Several modified procedures for the generation of nitrile oxides, *e.g.*, dehydration of nitroalkanes by toluene-*p*-sulfonic acid,[15] benzenesulfonyl chloride or ethyl chloroformate in the presence of triethylamine[16] were developed in the 1980's. All these reactions are carried out at elevated temperatures. The use of di-*tert*-butyl pyrocarbonate and catalytic amounts of *N*,*N*-dimethylaminopyridine (DMAP) allows the dehydration of nitroalkanes under much milder conditions.[17]

Chloramine T is effective for the generation of nitrile oxides from oximes.[18] This reaction is usually carried out by heating an aldoxime and an alkene in ethanol in the presence of chloramine T. Its role consists in the chlorination of aldoxime to hydroximoyl chloride. Subsequent elimination of HCl by treatment with a base results in nitrile oxide. Nitrosyl chloride or aqueous sodium hypochlorite can be used instead of chloramine T.[12]

Thermolysis of furoxans, which represent cyclic dimers of nitrile oxides, occurs under drastic conditions and is therefore seldom used;[19] thermal generation of nitrile oxides from hydroximoyl chlorides by boiling in toluene is used far more often.[20] This method was used, in particular, for the synthesis of fullereno-4,5-dihydroisoxazoles.[21]

A new method for the generation of nitrile oxides by microwave irradiation of hydroximoyl chlorides in the presence of dipolarophiles has recently been proposed. This procedure includes cycloaddition of nitrile oxides to weak dipolarophiles, such as nitriles[22] and polycyclic aromatic compounds (*e.g.*, phenanthrene, anthracene, pyrene, *etc.*) in the absence of solvents.[23] The yields of cycloaddition products exceed severalfold those obtained under standard conditions, whereas the reaction time is reduced to 3 – 10 minutes against ~ 24 h under standard conditions.

Nitrile oxides are generated from *O*-trimethylsilylhydroximoyl chlorides by treatment with potassium fluoride in acetonitrile at ~ 20 °C (see Ref. 24) or from hydroximoyl chlorides using molecular sieves (3 – 5 Å) in CH_2Cl_2.[25] In the latter case, the cycloadducts are formed in high yields, while no furoxans are formed at all.

III. Methods for the transformations of isoxazoles and 4,5-dihydroisoxazoles

Methods for the transformations of isoxazoles (**1**) and 4,5-dihydroisoxazoles are based on the lability of the N – O bond and are extremely diverse. In this section, we shall consider the main classes of compounds generated from the 1,3-dipolar cycloaddition adducts of nitrile oxides and the methods for their transformation with special emphasis on novel approaches.

A I Kotyatkina, V N Zhabinsky, V A Khripach Institute of Bioorganic Chemistry, National Academy of Sciences of Belarus, ul. Acad. Kuprevicha 5/2, 220141 Minsk, Belarus. Fax (37-517) 264 86 47. Tel. (37-517) 263 76 13. E-mail: vz@ns.iboch.ac.by (A I Kotyatkina, V N Zhabinsky) Tel. (37-517) 264 86 47. E-mail: khripach@ns.iboch.ac.by (V A Khripach)
Received 19 October 2000
Uspekhi Khimii **70** (8) 730 – 743 (2001); translated by R L Birnova

The most common procedure is the reductive scission of isoxazoles by hydrogenation over Raney nickel or platinum dioxide to afford enamino ketones **2**.[26–28]

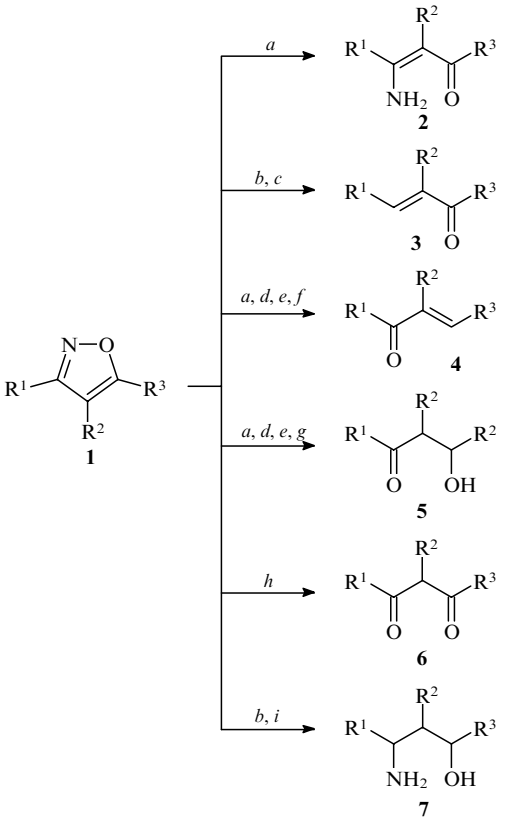

(*a*) H_2, Ni/Ra (Pt_2O), EtOH; (*b*) Na/NH_3, 3 equiv. Bu^{t}OH, THF; (*c*) *p*-TsOH, PhMe, Δ; (*d*) PhCOCl, Py; (*e*) $NaBH_4$; (*f*) H^+; (*g*) 90% AcOH; (*h*) Ni/Ra, BCl_3, MeOH–H_2O; (*i*) Ni–Al, MeOH, KOH.

Enamino ketones **2** can also be prepared by reduction of isoxazoles with sodium in liquid ammonia in the presence of 1 equiv. of Bu^{t}OH.[29] With 3 equiv. of Bu^{t}OH, this reaction yields intermediate β-amino ketones; their acid hydrolysis results in enones **3**.[29] The regioisomeric enones of the type **4** are obtained by benzoylation of enamino ketones **2** followed by reduction of the amido ketones formed and hydrolysis of the intermediate hydroxy enamides.[30] Hydrolysis of hydroxy enamides by 90% AcOH yields β-hydroxy ketones **5**.[27,31] β-Diketones **6** are prepared by catalytic hydrogenation of isoxazoles in the presence of Lewis acids.[32] Isoxazoles are reduced to amino alcohols **7** using nickel–aluminium alloys in the presence of an alkali.[33]

However, reductive scission of isoxazoles cannot be used if the substrates contain double bonds or protective groups susceptible to hydrogenolysis. In this case, cleavage of the N–O bonds is achieved by using other methods. Thus molybdenum or iron carbonyls were recommended for use in the synthesis of enamino ketones **2a–f**.[34]

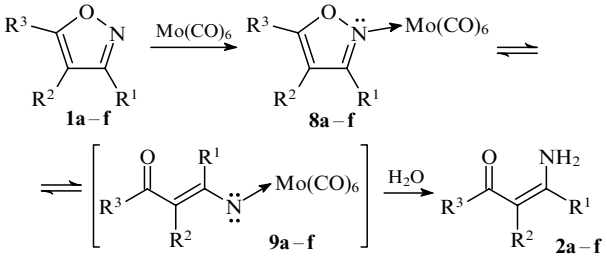

$R^1 = R^3$ = Ph, R^2 = H (**a**); R^1 = Me, R^2 = H, R^3 = Ph (**b**);
$R^1 = R^3$ = Me, R^2 = H (**c**); R^1 = Ph, $R^2 = R^3$ = H (**d**);
R^1 = Ph, $R^2 - R^3 = (CH_2)_4$ (**e**); R^1 = Ph, $R^2 - R^3 = (CH_2)_3$ (**f**).

The mechanism of this reaction includes the formation of the molybdenumhexacarbonyl complexes **8a–f** involving the nitrogen atom of the isoxazole with subsequent cleavage of the N–O bond and hydrolysis of the nitrene complexes **9a–f** to the enamino ketones **2a–f**.

The reductive opening of isoxazoles leading to enamino ketones is achieved with samarium iodide in tetrahydrofuran containing methanol as the proton source in 57% to 80% yields.[35]

Dihydrolipoamide (**10**) was used for reductive cleavage of 4,5-dihydroisoxazoles[36] [lipoamide (**11**) is a coenzyme in redox reactions occurring in living organisms]. The reductive cleavage of N–O bonds in 3,5-disubstituted isoxazoles **1b**,**c**,**g–i** under the action of compound **10** in the presence of iron(II) salts also proceeds with high yields.

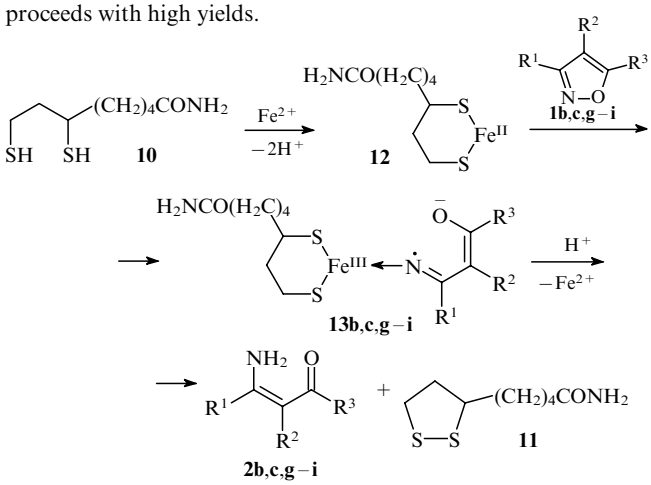

R^1 = Me, R^2 = H: R^3 = Ph (**b**), Me (**c**); $R^1 = R^2$ = H, R^3 = Me (**g**);
R^1 = Ph: R^2 = CO_2Me, R^3 = Me (**h**); R^2 = CO_2H, R^3 = Me (**i**).

It is suggested that isoxazoles **1b**,**c**,**g–i** react with the complex (**12**) to give the intermediates **13b**,**c**,**g–i** which are further hydrolysed to enamino ketones **2b**,**c**,**g–i**. Compound **10** is converted into lipoamide **11** under these conditions.

N-Methylated β-oxo amides **14a–c** are formed in high yields upon fragmentation of *N*-methylated isoxazoles **15a–c** catalysed by Et_3N.[37]

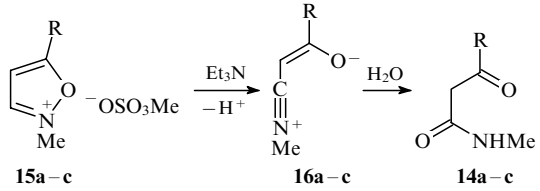

R = Me (**a**), CH=CHPh (**b**), $CH_2PO(OEt)_2$ (**c**).

The isoxazolium salts **15a–c** are deprotonated with subsequent cleavage of the N–O bond and generation of the nitrilium ions **16a–c** which are further converted into β-oxo amides **14a–c** in the presence of water.

The reductive scission of 4,5-dihydroisoxazoles **17** has long been poorly understood. A method for their reduction over Raney nickel in the presence of trifluoroacetic or hydrochloric acid, which yielded a mixture of β-hydroxy ketones **5** and their dehydration products (α,β-unsaturated ketones **4**), was developed in 1979.[38] Later,[39] it was suggested to carry out this reaction in the presence of boric acid, which afforded β-hydroxy ketones **5** in high yields. The latter can further be dehydrated into enones **4**.[40] This method for the opening of 4,5-dihydroisoxazoles is widely used in the synthesis of natural compounds.[4]

The use of rhodium on Al_2O_3 and platinum dioxide as catalysts in the hydrogenation of dihydroisoxazoles **17** has been described.[41] Amino alcohols **7** are prepared by reduction of 4,5-dihydroisoxazoles by $LiAlH_4$,[42–44] the $BH_3 \cdot Me_2S$ complex (see Ref. 45) and zinc (or sodium) borohydride in the presence of nickel chloride in methanol.[46]

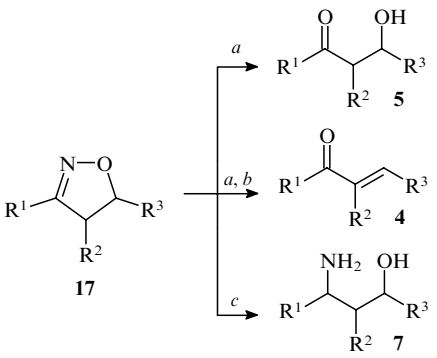

(*a*) H_2, Ni/Ra, H_3BO_3, EtOH; (*b*) p-TsOH; (*c*) $LiAlH_4$, Et_2O.

Hydroxy nitriles **18** are prepared from carboxydihydroisoxazoles.[47]

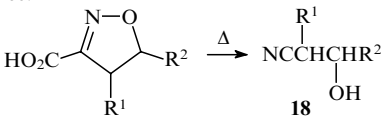

Similar to isoxazoles, 4,5-dihydroisoxazoles **17a–e** are opened under the action of molybdenum hexacarbonyl.[48] This reaction occurs *via* the complexes **19a–e** and **20a–e** which are further converted into β-hydroxy ketones **5a–e**. The complexes **19a–e** undergo retrodegradation in the absence of water.

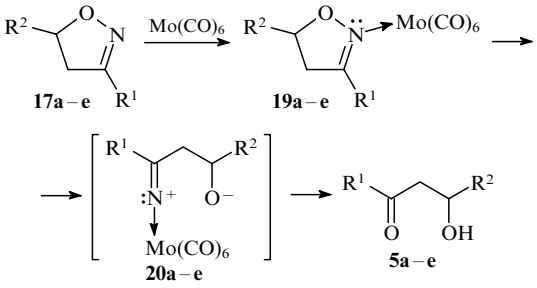

$R^1 = Me_2C(OH)$: R^2 = n-C_8H_{17} (**a**), Bn (**b**); $R^1 = MeO_2C(CH_2)_2$, R^2 = n-$C_{10}H_{21}$ (**c**); $R^1 = HO_2C(CH_2)_2$, R^2 = n-$C_{10}H_{21}$ (**d**); $R^1 = CH_3(CH_2)_5$, R^2 = (*Z*)-MeCH=CH (**e**).

The possibility of opening of dihydroisoxazoles **17f–i** by ozonolysis resulting in β-hydroxy ketones **5f–i** has been studied.[49] It is suggested that similar to oxime ozonolysis [50] this involves the electrophilic attack of ozone at the C(3) atoms of dihydroisoxazoles resulting in the formation of the intermediates **21f–i** with subsequent cleavage of C–N bonds.

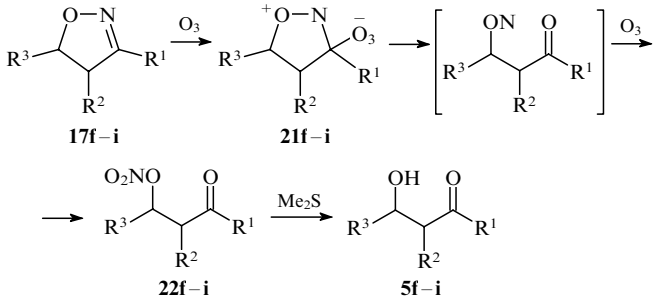

R^1 = Me, $R^2 = R^3$ = cyclo-C_5H_{11}, (**f**); R^1 = Ph, R^2 = H, R^3 = Bu^n (**g**); $R^1 = CH_2OH$, R^2 = H, R^3 = Bu^n (**h**); $R^1 = R^2 = R^3$ = Me (**i**).

Further oxidation leads to hydroxy ketone nitrates **22f–i**; their reduction by dimethyl sulfide yield β-hydroxy ketones **5f–i**. Although the yields of the final products are lower (61%–74%) than those obtained by hydrogenolysis, the ozonolysis of 4,5-dihydroisoxazoles is effective if the substrates **17** contain functional groups susceptible to hydrogenolysis.

IV. Intermolecular 1,3-dipolar cycloaddition reactions of nitrile oxides

1,3-Dipolar cycloaddition of nitrile oxides used in the synthesis of natural compounds can be effected in two ways, *viz*., as intermolecular and as intramolecular reactions. The first approach entails convergent syntheses of complex molecules from two simpler blocks. The latter approach can be used for the generation of new C–C bonds in preformed molecules and/or for the introduction of additional functional groups.

1. Synthesis of talaromycin

The structures containing spiroketal groups were discovered in insects, microorganisms, plants and fungi in the mid-1970's.[51, 52] One of the representatives of this class, *viz*., talaromycin B (**23**), was isolated from the toxic fungus *Talaromyces stipitatus*.[53] The synthesis of talaromycin involved intermolecular 1,3-dipolar cycloaddition of a nitrile oxide to the alkene.[54]

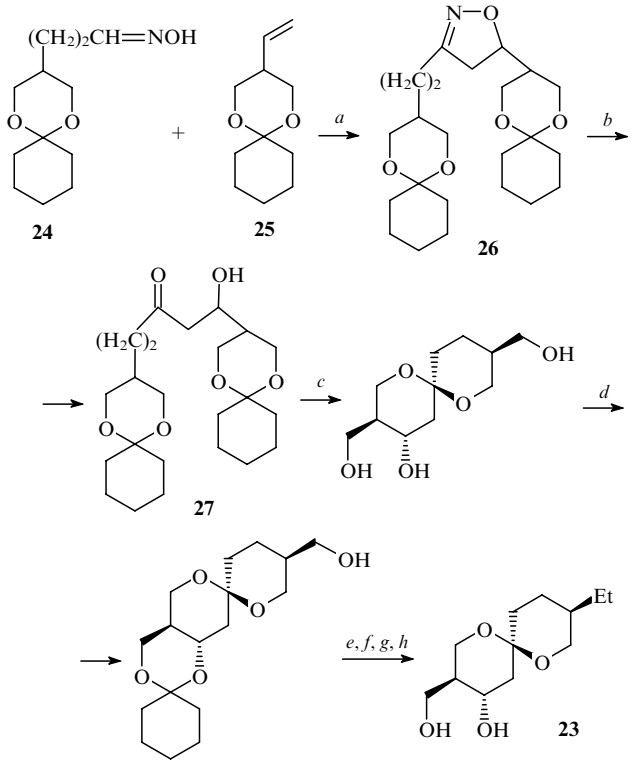

(*a*) NaOCl, Et_3N, H_2O, CH_2Cl_2 (67%); (*b*) H_2, Ni/Ra (72%); (*c*) MeOH, Amberlyst-15 (93%); (*d*) Amberlyst-15, 1-methoxycyclohexene, THF (80%); (*e*) MsCl, Et_3N, Et_2O; (*f*) NaI, Me_2CO; (*g*) Me_2CuLi, THF; (*h*) HCl, MeOH, H_2O.

The nitrile oxide generated from the oxime **24** reacted with the alkene **25** to give 4,5-dihydroisoxazole **26**. Cleavage of the N–O bond was achieved by hydrogenation over Raney nickel. Spiroketalisation of the hydroxy ketone **27** proceeded in a weakly acidic medium in the presence of Amberlyst-15 in methanol. The resulting trihydroxy derivative **28** contained the main fragments of the talaromycin (**23**) backbone. After protection of *cis*-diol groups, racemic talaromycin (**23**) was formed in a total yield of 12%.

2. Synthesis of milbemycin β_3

Intermolecular 1,3-dipolar cycloaddition of a nitrile oxide to the alkene **28** was used in the first total synthesis of yet another compound containing a spiroketal system, *viz*., milbemycin β_3 (**29**).[55] Milbemycin β_3 was isolated in 1974 [56] and is one of more than twenty compounds of the milbemycin series. The interest in these compounds is due to their high antileukemic [57] and insecticidal [58, 59] activities and low toxicities for mammals. The synthesis

of milbemycin (**29**) faced several complicated problems including stereo-controlled formation of six asymmetric centres of the molecule, *viz*., C(12), C(17), C(19), C(21), C(22) and C(23).

The first step of this synthesis included cycloaddition of the optically active 1,3-dipolarophile **28** and the nitrile oxide prepared by treatment of protected nitropropanal with methyl isocyanate. The resulting mixture of isomeric dihydroisoxazoles **30** was reduced by lithium aluminium hydride with subsequent protection of hydroxy and amino groups. The diastereomeric mixture of the ammonium salts **31** was treated with an aqueous solution of *p*-toluenesulfonic acid resulting in spiroketalisation and simultaneous deprotection of the aldehyde group. The addition of isopropenyllithium cuprate to aldehyde **32**, which was controlled by the chelate complex formed, yielded a mixture of allylic alcohols (7 : 1 in favour of the desired isomer). Compound **33** prepared by the reaction with propionyl chloride was selected for the Ireland–Claisen rearrangement. An attempt to use lithium diisopropylamide (LDA) in the synthesis of enolate was unsuccessful; the ester **33** could be deprotonated by potassium bis(trimethylsilyl)amide. Further treatment of the (*Z*)-enolate formed with trimethylchlorosilane and heating afforded the acid **34** with the required configuration of the C(12) centre. Total synthesis of the macrolide **29** required four additional steps.

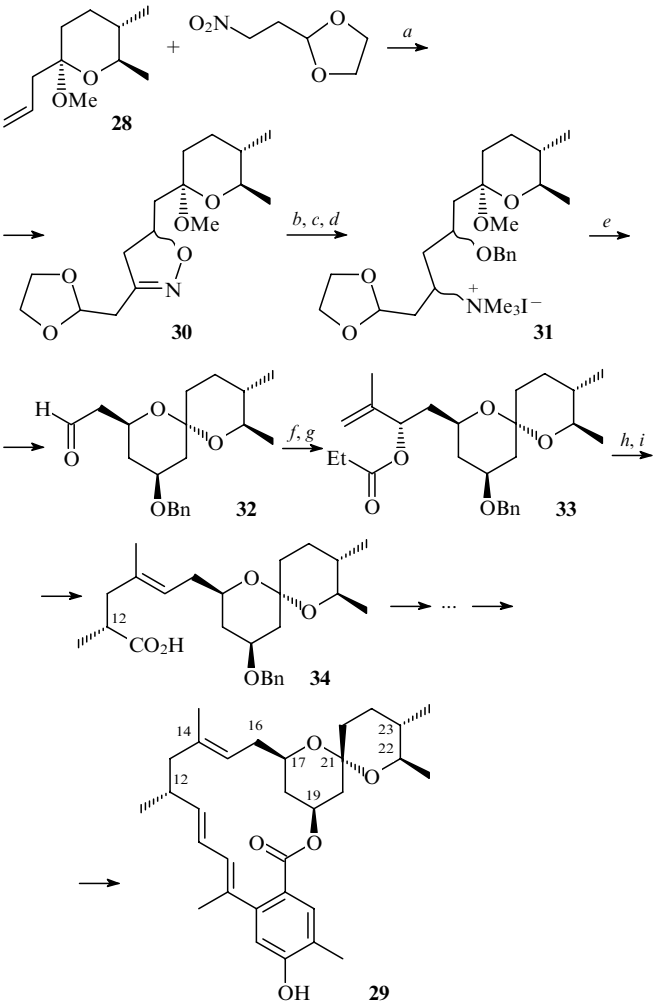

(*a*) MeNCO, Et_3N, PhH (68%); (*b*) $LiAlH_4$, Et_2O; (*c*) KH, BnI; (*d*) MeI; (*e*) TsOH, H_2O (24%–30%); (*f*) $CH_2=CH(Me)CuLi$; (*g*) EtCOCl, CH_2Cl_2, Py (63%); (*h*) $(Me_3Si)_2NK$, THF, −78 °C; (*i*) Me_3SiCl (TMSCl), 55 °C (57%).

3. Synthesis of lingbiatoxin A

The synthesis of indole **35**, the intermediate product in the synthesis of the alkaloid lingbiatoxin A (**36**), has been described.[60] It is assumed that compound **36** is a potential carcinogen and plays a key role in cell responses to some hormones and drugs. Structurally, lingbiatoxin A (**36**) represents a tricyclic compound the indole fragment in which is fused to a nine-membered ring.

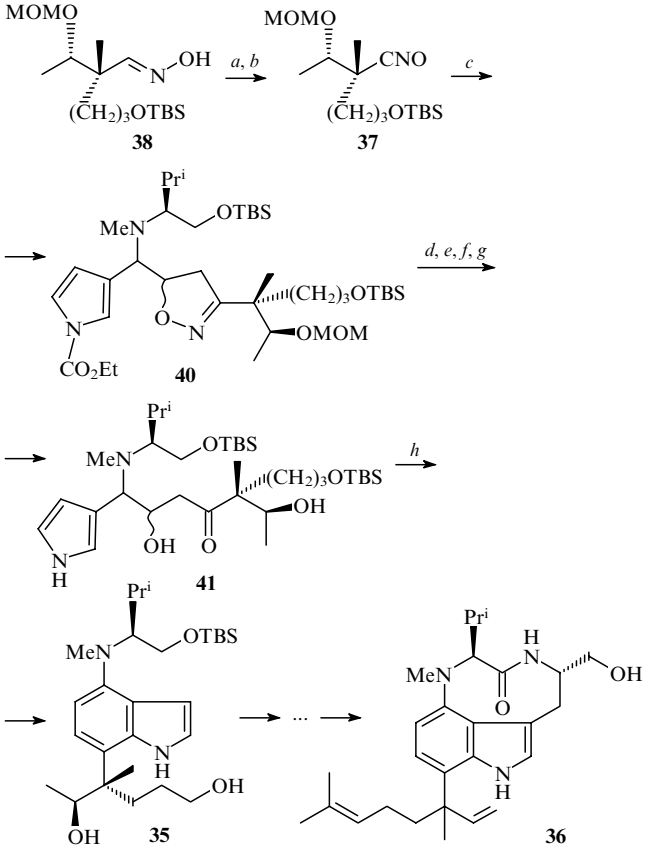

MOM — $MeOCH_2$, TBS — $SiMe_2Bu^t$; (*a*) Bu^tOCl, −78 °C; (*b*) Et_3N, 20 °C; (*c*) EtO_2CN (**39**), PhH, 80 °C, 20 h (78%); (*d*) HCl, MeOH (80 °C); (*e*) TBSCl, DMAP, THF; (*f*) 5% KOH, MeOH; (*g*) H_2, Ra/Ni, MeOH, H_2O, AcOH; (*h*) TBSOTf, CH_2Cl_2 (68%).

The strategy of this synthesis was based on the reaction of the nitrile oxide **37**, generated from the chiral oxime **38**, with the pyrrole derivative **39** as the dipolarophile. The attempts to synthesise hydroximoyl chloride (bromide) from the oxime **38** using conventional halogenating reagents (*e.g.*, *N*-chloro- or *N*-bromosuccinimide) were without success. Positive results were attained with *tert*-butyl hypochlorite in dichloromethane at −78 °C. Dehydrochlorination of hydroximoyl chloride by triethylamine at 20 °C afforded a highly stable nitrile oxide **37**, which was isolated in a pure state and characterised. The cycloaddition of the nitrile oxide **37** to the alkene **39** in benzene with heating gave 4,5-dihydroisoxazole **40**, which represented a mixture of diastereomers (2.5 : 1). The synthesis of hydroxy ketone **41** included manipulations with protective groups, elimination of the *N*-ethoxycarbonyl group and hydrogenolysis of 4,5-dihydroisoxazole under standard conditions. *tert*-Butyldimethylsilyl triflate proved to be the best catalyst in the formation of the annelated phenyl ring[61] of the indole **35**, a convenient intermediate for lingbiatoxin A (**36**).

4. Synthesis of (+)-phyllanthocin

Phyllanthocin (**42**) (Scheme 1) is an aglycone of the glycoside phyllanthoside isolated from the roots of the South American tree *Phyllanthus acuminatus* in 1977.[62] This glycoside manifests high activity against mouse leukemia P 388 and mouse melanoma B16; therefore, it was decided to carry out its clinical trials as an

Scheme 1

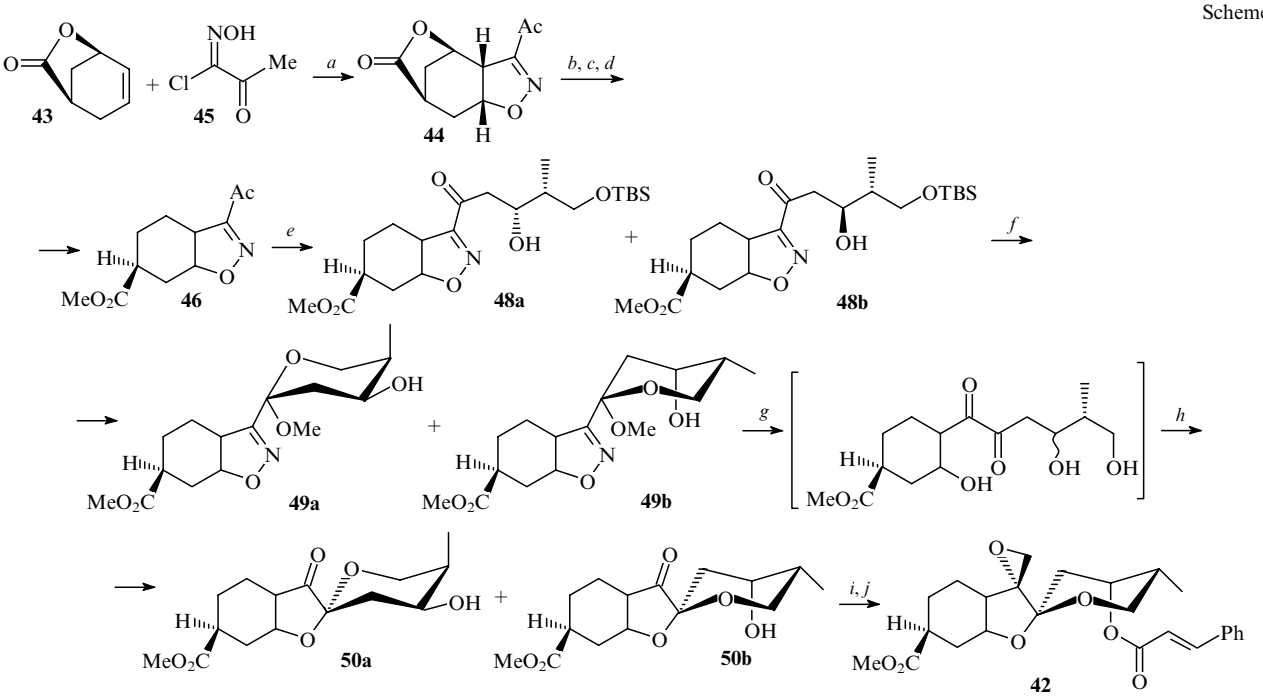

(*a*) PhMe, Δ (45%); (*b*) K_2CO_3, MeOH; (*c*) Cl(S)COPh, DMAP, CH_2Cl_2 (83%); (*d*) Bu_3SnH, azoisobutyronitrile (AIBN); (*e*) OHC 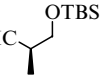 (**47**), LDA, THF (75%); (*f*) 5% HF, MeOH, 20 °C (70%); (*g*) H_2, Ni/Ra, H_3BO_3, MeOH – H_2O (89%); (*h*) CF_3SO_3H, CH_2Cl_2; (*i*) MeS(O) = CH_2, DMSO, THF, 1 h (89%); (*j*) *trans*-PhCH = CHCOCl, DMAP, CH_2Cl_2 (40%).

anticancer drug for humans.[63] Several structurally related compounds were isolated and given a common name 'phyllanthostatins'.[64] Total syntheses of (+)-phyllanthocin (**42**) have been described in a number of papers.[65–68] One of them involves 1,3-dipolar cycloaddition of a nitrile oxide to the cyclohexene derivative **43**. A detailed analysis of regio- and stereochemistry of the cycloadducts has been carried out (see Scheme 1).[69]

Lactone **43** was used as a starting compound for an increase in the stereo- and regioselectivity of the subsequent 1,3-dipolar cycloaddition reaction. The cycloadduct **44** of the required stereo- and regiochemistry was prepared by slow thermal generation of highly reactive nitrile oxide from the hydroximoyl chloride **45** in boiling toluene in the presence of the lactone **43** (yield 45%). 4,5-Dihydroisoxazole **46** was synthesised from compound **44** in three steps. Aldol condensation of the optically active aldehyde **47** with the ketone **46** gave a mixture of adducts **48a**,**b** in a 1 : 1.2 ratio.

It is of note that several attempts to open the heterocycle in compounds **48a**,**b** failed. Increased robustness of the 4,5-dihydroisoxazole ring is presumably due to its conjugation with the keto group. A mixture of isomers **48a**,**b** was converted into a mixture of methylglycosides **49a**,**b** followed by hydrogenolysis of the N – O bond in 4,5-dihydroisoxazole fragments and cyclisation of the intermediates which gave a mixture of spiroketals **50a**,**b** (1 : 18). The main isomer **50b** was converted to the target product, *viz*., (+)-phyllanthocin (**42**).

5. Synthesis of vitamin A

Vitamin A and its analogues remain in the focus of attention of synthetic chemists due to their prominent biological and pharmacological activities.[70, 71] The Grignard reaction between compounds incorporating C_6- and C_{14}-fragments of vitamin A is one of the most general approaches to the synthesis of the vitamin A backbone.[72, 73]

An alternative strategy for the construction of the basic backbone[74] consists in the simultaneous formation of the C – C bond and the introduction of functional groups in the interaction of the nitrile oxide **51** (the C_{14}-fragment) with the alkene **52** (the C_6-fragment) resulting in 3,5-disubstituted 4,5-dihydroisoxazole **53**. The cleavage of the N – O bond was achieved through the previously developed procedure using $Mo(CO)_6$.[48] The resulting β-hydroxy ketone **54** was dehydrated and enone **55** was reduced by $NaBH_4$ to the intermediate **56**, which is common in the synthesis of vitamin A. This scheme allows one to obtain large amounts of vitamin A and easy introduction of new functional groups in the synthesis of its analogues.

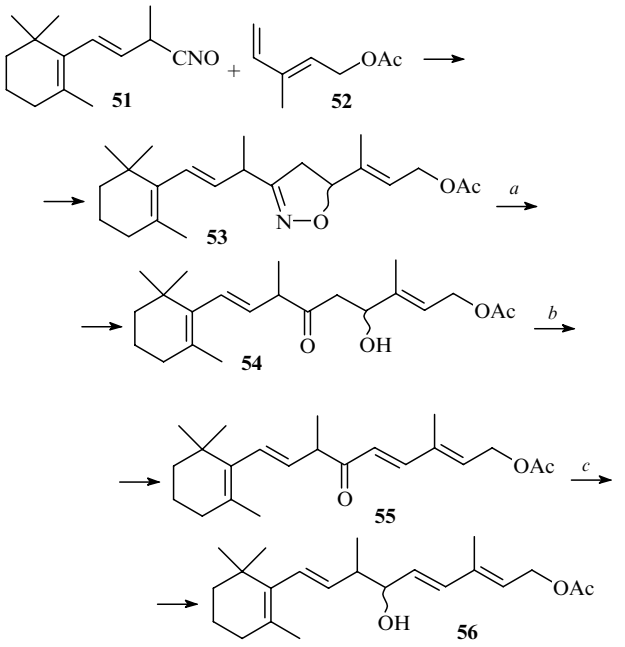

(*a*) $Mo(CO)_6$, MeCN (60%); (*b*) MsCl, Et_3N, 0 °C; (*c*) $NaBH_4$ (70%).

6. Synthesis of burseran and brassilignan

Preparations based on aloe have long been known in folk medicine.[75,76] Some aloe components are related to lignans, while certain representatives of this family possess antitumour activities and prevent metastasis.[77,78] Several approaches to the synthesis of natural lignans and their analogues manifesting biological activities have been developed.[79–82] In the majority of these syntheses, chiral compounds were used as starting materials. Achiral starting compounds were recommended for the synthesis of optically active natural lignans, *viz*., burserans **57e** and **58e** and brassilignans **57c** and **58c**, and some of their analogues.[83]

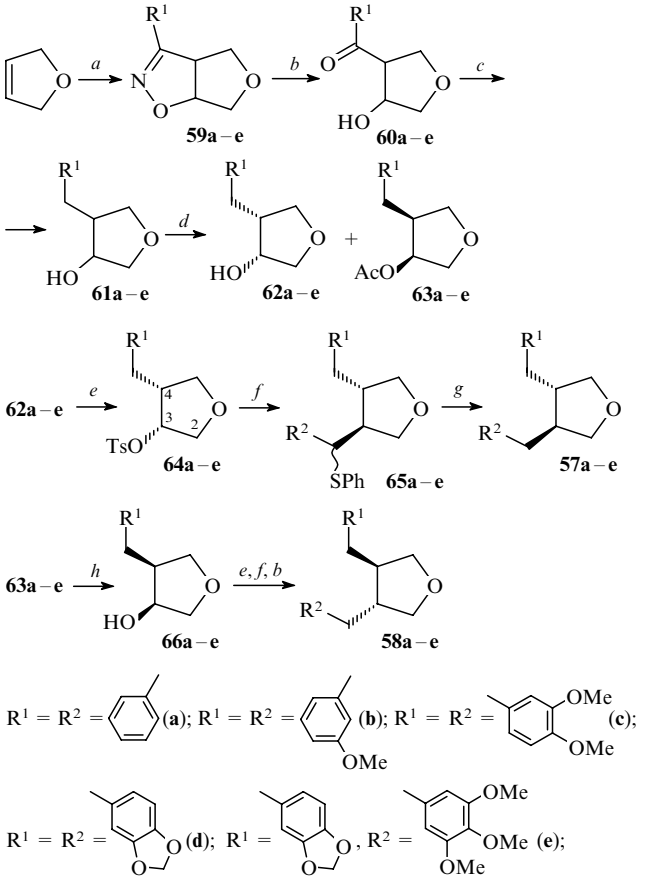

(*a*) $R^1CCl{=}NOH$, Et_3N, Et_2O, ~20 °C (58%–84%); (*b*) H_2, Ni/Ra, EtOH, H_3BO_3; (*c*) H_2, Pd/C, MeOH–H_2O; (*d*) $CH_2{=}CHOAc$, lipase PS; (*e*) MeLi, THF, −78 °C, TsCl; (*f*) R^2CH_2SPh, BuLi, THF, 0 °C; (*g*) Ni/Ra, EtOH, Δ, 20 h; (*h*) K_2CO_3, MeOH.

1,3-Dipolar cycloaddition of aromatic nitrile oxides to 2,5-dihydrofuran yielded furoisoxazoles **59a**–**e**. Hydrogenolysis of the cycloadducts **59a**–**e** over Raney nickel in the presence of a large excess of boric acid gave β-hydroxy ketones **60a**–**e** the keto group in which was reduced by hydrogen on palladium.

Lipase PS was used to separate the optical antipodes of the resulting alcohols **61a**–**e**. The absolute stereochemistry of alcohols **62a**–**e** and acetates **63a**–**e** was established later, following completion of the synthesis of the natural compounds **57e**, **58e**, **57c** and **58c**. Tosylation of compounds **62a**–**e** and **63a**–**e** (after preliminary hydrolysis) and subsequent nucleophilic substitution of the secondary tosyloxy group pursued two goals, *viz*., the introduction of the second aromatic substituent and the inversion of the C(3) centre so that the configurations of the substituents corresponded to those of the natural compounds. *p*-Toluenesulfonates **64a**–**e** gave a mixture of diastereomeric sulfides **65a**–**e**; their desulfurisation with Raney nickel in EtOH gave the target products **57a**–**e** in a total yield of 6%–16%. The same reaction sequence was applied to the isomers **66a**–**e** resulting in the preparation of optically active products **58a**–**e** (yield 6%–14%). Thus, a series of natural compounds, *viz*., burserans **57e** and **58e**, brassilignans **57c** and **58c** and artificial analogues *viz*., dehydroxycubebins **57d** and **58d**, 3,4-bis(3-methoxybenzyl)-tetrahydrofurans **57b** and **58b,** 3,4-dibenzyltetrahydrofurans **57a** and **58a**, were prepared. This method[83] gives an access to a vast variety of natural and non-natural lignans including their aza analogues owing to the high accessibility of 2,5-dihydrofuran, aromatic nitrile oxides and diverse phenyl sulfides.

7. Synthesis of higher monosaccharides

The role of monosaccharides in vital activities of animals, plants and human beings is generally acknowledged. The discovery of antibiotics[84,85] containing higher monosaccharides gave strong impetus to investigations into their synthesis.[86,87] An approach described by Poton and Young[88] is based on cycloaddition of accessible unsaturated monosaccharides to nitrile oxides with subsequent reduction of the dihydroisoxazoles formed.

Thus the reaction of the alkene **67** derived from D-glucose with the nitrile oxide **68** gave a mixture of diastereomeric 4,5-dihydroisoxazoles **69a**,**b** in a 14 : 86 ratio. Compound **69b** gave the dihydroxy ketone **70** in two steps; its reduction with sodium borohydride yielded a mixture of 6-deoxy-D- and 6-deoxy-L-*glycero*-D-*gluco*-octofuranoses **71** and **72**.

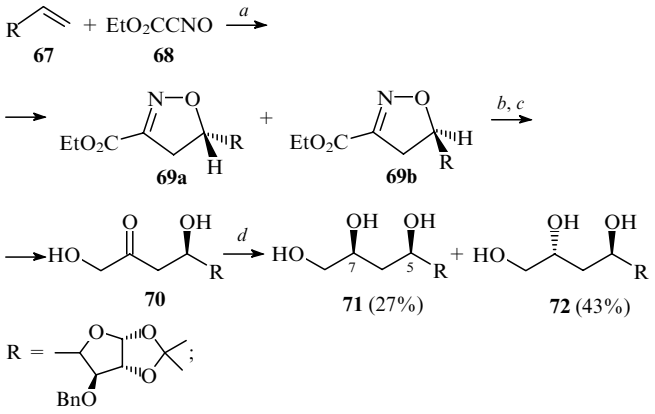

(*a*) Et_2O, Et_3N, 14 h (75%); (*b*) $NaBH_4$, THF, EtOH; (*c*) H_2, Pd/C, H_3BO_3, MeOH–H_2O, 18 h (78% **69b**); (*d*) $NaBH_4$, EtOH, H_2O.

The alkene **67** and D-glyceronitrile oxide **73** were used in the synthesis of (7*R*)- and (7*S*)-nonofuranoses **74** by the same reaction scheme.

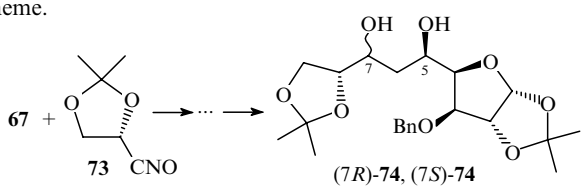

(8*S*)- And (8*R*)-7-deoxydecopyranoses **75** were prepared from the nitrile oxide **73** and the alkene **76** derived from D-galactose.

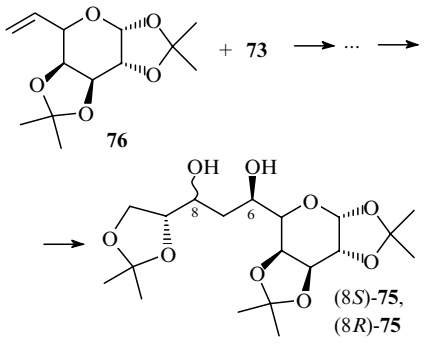

The configurations of the C(5) and C(7) centres in compounds **71**, **72** and **74** and of the C(6) and C(8) centres in compounds **75** were established on the basis of ^{1}H NMR spectroscopic data and stereochemistry of their precursors, *viz*., 4,5-dihydroisoxazoles, and confirmed by X-ray diffraction analysis. This approach enables the synthesis of diverse higher monosaccharides.

8. Synthesis of a heterocyclic analogue of daunomycin

Daunomycin is a typical representative of anthracycline antibiotics used in the chemotherapy of malignant tumours.[89,90] However, its application is restricted due to side effects including high cardiotoxicity. An attempt was made to synthesise modified anthracycline derivatives in which the benzene rings (*D*) is replaced by a heteroaromatic rings. The daunomycin analogues thus synthesised contained thiophene [91] or indole fragments [92] as rings *D* and manifested high activities comparable to that of daunomycin, but lower toxicities. The synthesis of compound **77**, an intermediate in the synthesis of the daunomycin analogue containing an isoxazole fragment as ring *D*, has been developed.[93]

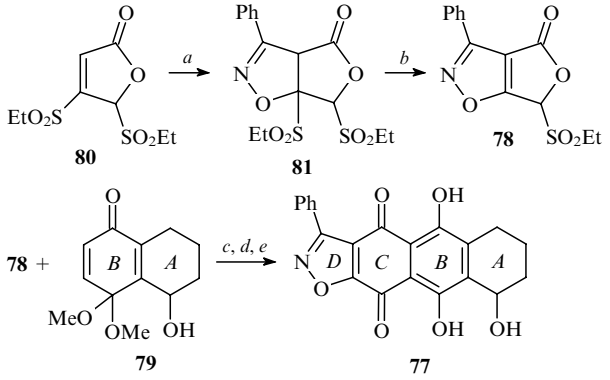

(*a*) PhCCl=NOH, molecular sieves, 20 °C, 10 h; (*b*) SiO_2 (85%); (*c*) LDA, THF, −78 °C; (*d*) −2 °C, 120 h (40%); (*e*) BCl_3, −78 °C, 45 min (50%).

The key stage in this synthesis is the annelation of furoisoxazole **78** and the bicyclic derivative **79** (the DC + BA strategy) under the action of lithium diisopropylamide. Compound **78** was synthesised by cycloaddition of benzonitrile oxide to 4,5-di(ethylsulfonyl)-2,5-dihydrofuran-2-one **80**. Numerous experiments showed [94] that this dipolarophile far exceeds other dipolarophiles as concerns reactivity. Moreover, the presence of the ethylsulfonyl group at the C(5) atom significantly affects the regio- and stereochemistry of the cycloaddition reaction, whereas the ethylsulfonyl group in position 4 enables subsequent aromatisation of compound **81** into isoxazole **78**.

V. Intramolecular 1,3-dipolar cycloaddition reactions of nitrile oxides

1. Stereoselective synthesis of ptilocaulin and its epimer

Ptilocaulin (**82**) and its epimer at the C(7) atom, *viz*., isoptilocaulin (**83**), isolated from the sea sponge *Ptilocaulis spiculfer* in 1982 [95] manifest antileukemic and antibacterial activities. These compounds have relatively simple but unusual structures in which guanidine is annelated with the hydrindan system. A seven-step stereoselective synthesis of compounds **82** and **83** has been developed,[96] which includes the formation of a six-membered carbocycle by intramolecular cycloaddition of a nitrile oxide to the double bond in the cyclopentene derivative **84**.

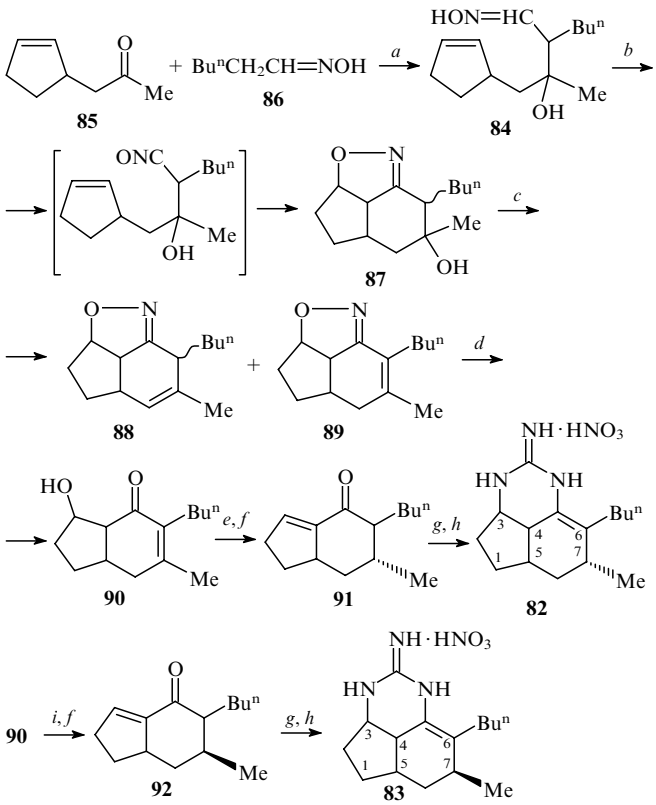

(*a*) 2 equiv. BuLi, THF, 0–20 °C, 6 h (90%); (*b*) NaOCl, CH_2Cl_2, −10 to −20 °C, 5 h (80%); (*c*) $SOCl_2$–Py, −10 °C, 40 min; (*d*) H_2, Ni/Ra, H_3BO_3, MeOH–H_2O (60%); (*e*) H_2, Pd/C (95%); (*f*) TsOH, PhH, 40 °C, 30 min; (*g*) $(H_2N)_2C$=NH, PhH, Δ, 36 h (35%); (*h*) HNO_3; (*i*) Li–$EtNH_2$, −70 °C, 30 min (85%).

Aldol condensation of the ketone **85** with the hexenal oxime (**86**) dianion yields the β-hydroxy oxime **84**. Its treatment with sodium hypochlorite gives tricyclic 4,5-dihydroisoxazole **87** as a mixture of four diastereomers. Compound **87** is dehydrated into a 1 : 1 mixture of unsaturated 4,5-dihydroisoxazoles **88** and **89** which are further subjected to reductive scission over Raney nickel. The unsaturated ketol **90** is the key intermediate in the synthesis of ptilocaulin (**83**) and its C(7) epimer (**82**).[97,98] The enone **91** prepared from the ketol **90** by hydrogenation of the double bond over palladium and subsequent dehydration reacted with guanidine to give isoptilocaulin **82**. The epimer of enone **91** with the β-configuration of the methyl group at C(7) (compound **92**) was prepared by reduction of the double bond in ketol **90** with lithium in diethylamine (in this case, the carbanion undergoes axial protonation) with subsequent dehydration. The use of lithium in liquid ammonia made it possible to achieve simultaneous reduction of the double bond and the keto group. Ptilocaulin (**83**) was prepared by heating of the enone **92** with guanidine. Compounds **82** and **83** were isolated as nitrates.

2. Synthesis of (−)-specionin

(−)-Specionin (**93**) was isolated from leaf extracts of the tree *Catalpa speciosa*.[99] This compound manifests insecticidal activity against various pests of coniferous plants which inflict severe damages to the wood-processing industry. The first synthesis of racemic specionin was carried out in 1985.[100] Synthesis of the optically active compound based on the nitrile oxide-based approach was developed by Curran *et al*.[41] The 4,5-dihydroisoxazole intermediate **94** was synthesised from the acetal **95** in eight steps.

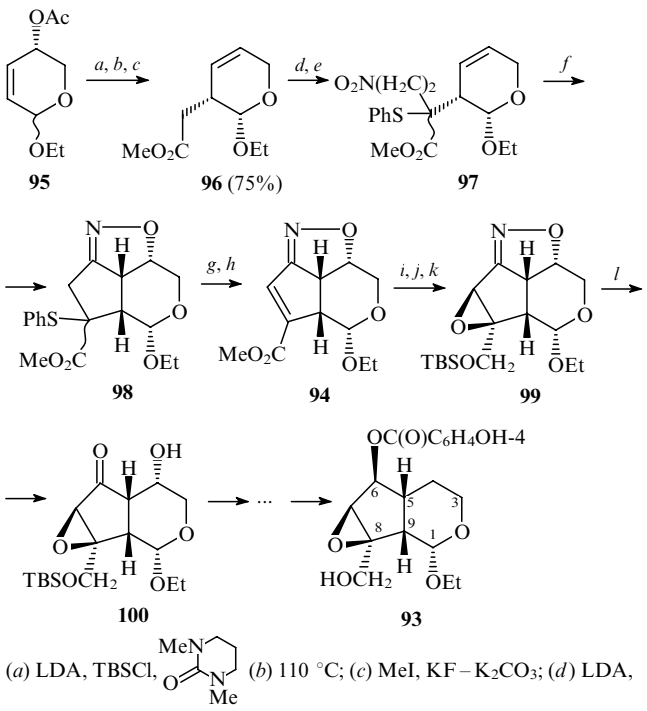

(*a*) LDA, TBSCl, (*b*) 110 °C; (*c*) MeI, KF – K_2CO_3; (*d*) LDA, PhSSPh; (*e*) LDA, $CH_2=CHNO_2$ (85%); (*f*) *p*-ClC_6H_4NCO, Et_3N, 110 °C (89%); (*g*) *m*-chloroperbenzoic acid (*m*-CPBA); (*h*) PhH, 80 °C; (*i*) $Bu^i_2Bu^nAlHLi$ (42%); (*j*) TBSCl, DMAP, Et_3N (72%); (*k*) 3,5-dinitroperbenzoic acid, Na_2HPO_4, CH_2Cl_2 (77%); (*l*) H_2, Rh/Al_2O_3 (57%).

The Ireland – Claisen rearrangement yielded compound **96**; its sulfenylation and the addition of the α-sulfite formed to nitroethylene led to the derivative **97**, which was further involved in the intramolecular cycloaddition of the nitrile oxide fragment to the double bond. The sulfide group in the tricyclic 4,5-dihydroisoxazole **98** was oxidised and the sulfoxide formed was boiled in benzene, which resulted in elimination of $PhSO_2H$ and the formation of a double bond. Selective reduction of the ester group in the derivative **94** was carried out using a complex prepared from butyllithium and diisobutylaluminium hydride; the resulting alcohol was converted into the silyl ether. Its epoxidation by 3,5-dinitroperbenzoic acid could be performed due to the resistance of the dihydroisoxazole ring to oxidants; this reaction was stereoselective and yielded a single isomer (**99**). The dihydroisoxazole ring in compound **99** was opened smoothly by hydrogenolysis in the presence of 5% rhodium on Al_2O_3 in aqueous methanol resulting in β-hydroxy ketone **100**. The use of other catalysts (*e.g.,* Ni-Ra, Pd/C, Pt_2O) in this step resulted in the destruction of the molecule. (−)-Specionin (**93**) was obtained from its precursor **100** in eight steps; the total yield was 0.5% with respect to compound **95**.

3. Synthesis of testosterone

Total synthesis of steroids, which play an extremely important role in the human organism as well as in animal and plant organisms, has been the subject of numerous investigations.[101, 102]

The use of 4,5-dihydroisoxazoles in the formation of steroid backbones was described back in the 1960-70's. In some studies, 4,5-dihydroisoxazoles were used as parts of alkylating agents bearing a masked β-diketone function [103, 104] in the synthesis of D-homotestosterone, progesterone, testosterone and 13-ethyltestosterone.

The synthesis of testosterone (**101**) made use of a new approach based on intramolecular 1,3-dipolar cycloaddition.[105] This procedure enabled the construction of the ring *B* with the β-configuration of the C(19) methyl group and simultaneous introduction of functional groups for further synthesis of ring *A*. Starting from the optically active indanone **102**, the oxime **103** was prepared in eight steps (total yield 37%). The intramolecular 1,3-dipolar cycloaddition of the nitrile oxide prepared from this oxime occurred stereospecifically and resulted in the cycloadduct **104**. Although the stereochemistry of the angular methyl group of 4,5-dihydroisoxazole formed cannot be inferred from the spectroscopic data, the structure **104** was assigned to this compound [105] on the assumption [106, 107] that the chair-like conformation is more preferable in the transition state than the boat-like conformation leading to the C(10) isomer.

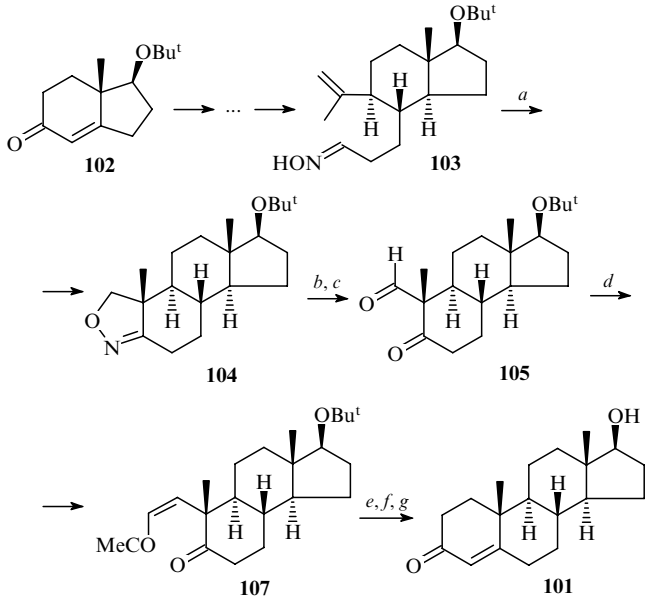

(*a*) NaClO, CH_2Cl_2 (87%); (*b*) H_2, Ni/Ra, $B(OMe)_3$, MeOH (97%); (*c*) SO_3 – Py, DMSO (97%); (*d*) $MeCOCH=PPh_3$ (**106**), $Me_2C_6H_3$ (89%); (*e*) H_2, 10% Pd/C; (*f*) KOH, MeOH; (*g*) CF_3CO_2H (76%).

The reductive opening of 4,5-dihydroisoxazole **104** over Raney nickel in the presence of trimethyl borate in aqueous methanol gave a hydroxy ketone; its oxidation yielded the aldehyde **105**. A three-carbon fragment was introduced by the Wittig reaction with 1-triphenylphosphoranylidenepropan-2-one (**106**). The resulting enone **107** was converted into testosterone *tert*-butyl ether as a result of catalytic hydrogenation and treatment with potassium hydroxide in methanol, eventually resulting in the closure of the ring *A*. Removal of the protective group from the C(17) hydroxy group completed the synthesis of testosterone **101** in a total yield of 17%. Thus, the use of intramolecular 1,3-dipolar cycloaddition of nitrile oxide enabled effective construction of testosterone rings *A* and *B*.

4. Synthesis of calicheamicin γ_1^I

Compounds related to antitumour antibiotics of the enedyine series, *e.g.,* calicheamicin γ_1^I, esperamycin A_1, dinemycin A, were isolated from cultured bacterial cells of *Micromonospora echinospora*.[108, 109] These compounds produce strong therapeutic effects by cleaving double-stranded DNA at specific sequences.[110, 111] A number of papers published soon after their discovery [112 – 116] were devoted to the synthesis of their main backbones, *e.g.*, to the racemic calicheamicin aglycone, calicheamicinone (**108**). The syntheses of oligosaccharide fragments attached to the hydroxy group at C(8) of calicheamicinone (**108**) have also been described.[117, 118]

The first enantioselective synthesis of (−)-calicheamicinone (**108**) and a total synthesis of calicheamicin γ_1^I were carried out by Nicolaou and coworkers.[119, 120] This synthesis is based on the use of the intramolecular 1,3-cycloaddition reaction of alkenyl nitrile oxide prepared from the aldoxime **109**.

This aldoxime was treated with aqueous sodium hypochlorite under standard conditions, which resulted in intramolecular cyclisation and the formation of a 4 : 1 mixture of 4,5-dihydro-

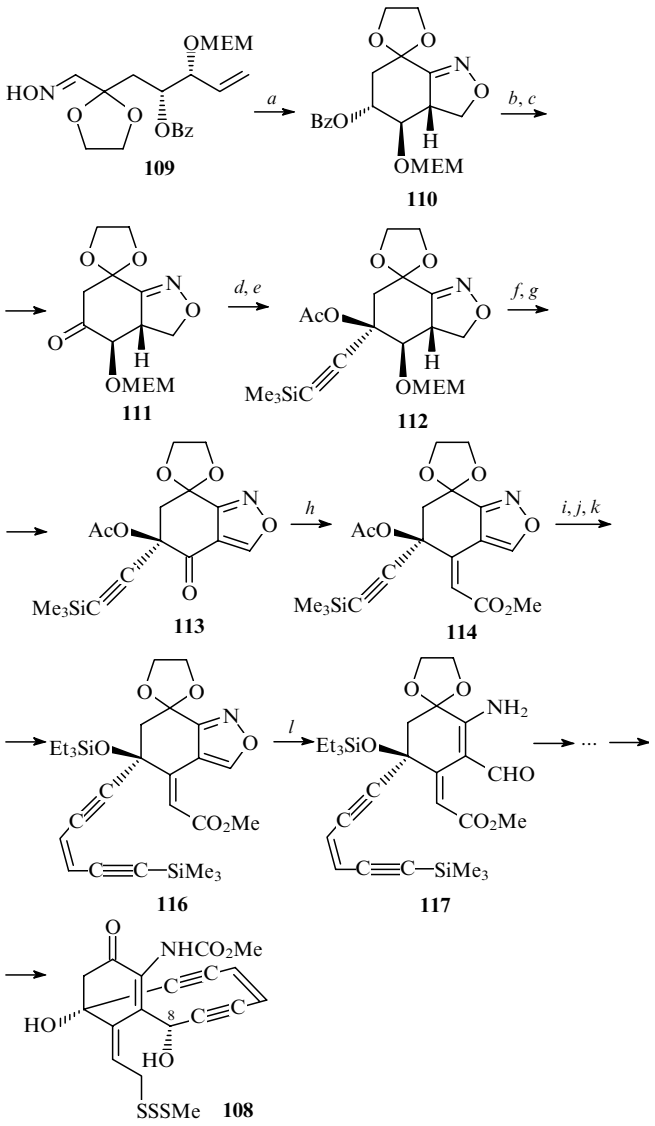

MEM is $MeO(CH_2)_2$; (*a*) NaOCl, CH_2Cl_2, 25 °C, 2 h (65%); (*b*) NaOMe MeOH, 0 °C (100%); (*c*) CrO_3, H_2SO_4, Me_2O, 0 °C (95%); (*d*) 1.5 equiv. $Me_3SiC{\equiv}CLi$, THF, −78 °C (67%); (*e*) Ac_2O, 25 °C, 3 h; (*f*) 10 equiv. $ZnBr_2$, CH_2Cl_2, 25 °C, 2 h; (*g*) $COCl_2$, DMSO (54%); (*h*) $Ph_3P{=}CHCO_2Me$, PhMe, 90 °C, 16 h (84 %); (*i*) K_2CO_3, MeOH – CH_2Cl_2, 0 °C, 6 h (90%); (*j*) Et_3SiOTf, 2,6-lutidine, CH_2Cl_2, 0 °C, 30 min (96%); (*k*) (*Z*)-$Me_3SiC{\equiv}CCH{=}CHCl$ (**115**), $Pd(PPh_3)_4$, CuI, $BuNH_2$, PhH, 0 °C, 2 h (91%); (*l*) $Mo(CO)_6$, MeCN – H_2O, 80 °C, 1.5 h (82%).

isoxazole diastereomers; the main isomer **110** was isolated in 51% yield. After removal of benzoyl protection, the secondary alcohol formed was oxidised by the Jones reagent to the ketone **111**. The nucleophilic addition of lithium (trimethylsilyl)acetylenide to the ketone **111** was fully stereoselective; the hydroxy group in the resulting acetylenic alcohol was protected by acetylation.

Removal of the methoxyethoxymethyl group in compound **112** and subsequent Swern oxidation of the alcohol formed yielded unexpectedly isoxazole **113** instead of 4,5-dihydroisoxazole. The use of other oxidants gave the same results. Therefore, the strategy of the synthesis had to be changed in favour of the Wittig reaction of the ketone **113** with methyl triphenylphosphoranylideneacetate, which resulted in selective synthesis of compound **114** having the *E*-configuration of the double bond in the enediyne fragment.

After removal of the protective trimethylsilyl group, the enyne group was introduced by high-yielding palladium-catalysed addition of (*Z*)-chloroenyne (**115**), which gave the enediyne **116**. The opening of the isoxazole ring in this molecule under the action of molybdenum hexacarbonyl in aqueous acetonitrile resulted in the enamino aldehyde **117**.

The final product of this synthesis, *i.e.*, (−)-calicheamicinone (**108**), was prepared from the aldehyde **117** in 16 steps. The total yield of compound **108** was 2.6% with respect to the starting aldoxime **109**.

5. Synthesis of zoapatanol

The intramolecular cycloaddition reaction was used to prepare compound **118**, the optically active intermediate in the synthesis of zoapatanol (**119**), one of novel diterpenoids containing an oxepane ring.[121] This is endowed with contraceptive activity [122, 123] and was isolated from the leaves of the Mexican plant *Montanoa tomentosa*.[124] Syntheses of racemic zoapatanol [125, 126] and the optically active product (Scheme 2) have been described.[127]

D-Glucose diacetonide (**120**) was used as the starting compound in the 13-step synthesis of the oxime **121**. The intramolecular nitrile oxide cycloaddition reaction was carried out under standard conditions. The resulting dihydroisoxazole **122** (a mixture of diastereomers) was reduced over Raney nickel to the hydroxy ketone **123**. Its dehydration gave α,β-unsaturated oxo ester **118** which is considered [121] to be a convenient intermediate in the synthesis of zoapatanol **119.**

VI. Syntheses based on enantiocontrolled 1,3-dipolar cycloaddition reactions of nitrile oxides

The optical purity of natural compounds is of crucial importance where they are used as medicinal drugs or plant protectors. In contrast to non-symmetrical Diels – Alder reactions, studies on enantiocontrolled cycloaddition reactions of nitrile oxides have a relatively short history.

The feasibility of stereocontrolled cycloaddition using optically active nitrile oxides or alkenes has been studied.[128, 129] Dipolarophiles containing bulky chiral auxiliaries have become especially popular. As a result, the nitrile oxide attack occurs in a strictly stereoselective manner; the chiral substituents are then removed. Chiral (−)-menthyl acrylates,[130] bornyl crotonates,[131] alkenes containing tricarboxylic Kemp's acid [132] or the Oppolzer

Scheme 2

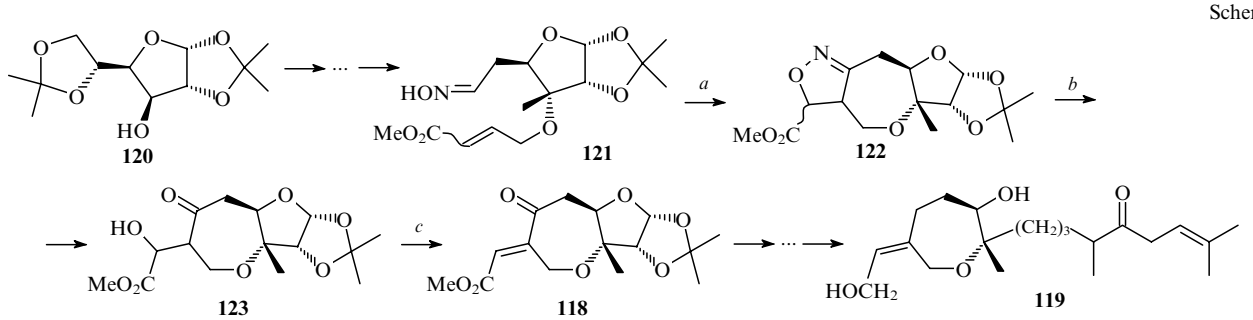

(*a*) NaOCl, CH_2Cl_2, Et_3N (61%); (*b*) Ra/Ni, H_2, MeOH – H_2O; (*c*) $MeSO_2Cl$, CH_2Cl_2, Et_3N.

sultam [133, 134] as substituents as well as alkenes coordinated to iron [135] or cobalt [136] complexes belong to such dipolarophiles.

1. Syntheses using the chiral Oppolzer reagent

The chiral Oppolzer reagent, *viz*., L-camphor sultam (**124**), was used [137] in the synthesis of several natural compounds, *e.g*., the sex pheromone of the butterfly *Hepialis californicus* [(+)-hepialone **125**)[138]], (−)-(1*R*,3*R*,5*S*)-1,3-dimethyl-2,9-dioxabicyclo[3.3.1]nonane (**126**),[139] the constituent of the Norwegian spruce bark, and (−)-(1*S*)-7,7-dimethyl-6,8-dioxabicyclo[3.2.1]octane (**127**)[140] isolated from hop oil and confering characteristic odour to beer.

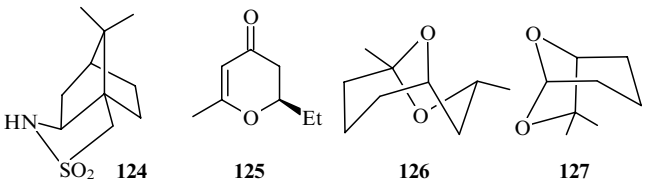

124 **125** **126** **127**

Syntheses of compounds **125**–**127** were performed according to non-sophisticated and efficient schemes the key step in which included the addition of readily accessible nitrile oxides to the amide **128** prepared by treatment of the chiral sultam **124** with acryloyl chloride in the presence of sodium hydride and CuCl. Subsequent reduction of the adducts **129** resulted in 4,5-dihydroisoxazoles **130** and regeneration of L-camphor sultam **124.**

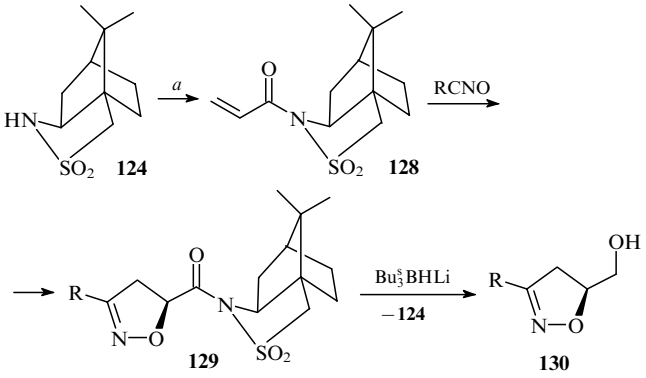

(*a*) $CH_2{=}CHCOCl$, NaH, CuCl.

(+)-Hepialone (**125**) was synthesised from the nitro ketal **131**.[137] The cycloaddition performed under standard conditions [9] yielded a mixture of epimeric 4,5-dihydroisoxazoles (88 : 12); the main diastereomer **132** was isolated by chromatography. Its reduction by L-selectride (Bu^s_3BHLi) gave the alcohol **133** with recovery of the chiral reagent **124**. Tosylation of the alcohol **133** and subsequent treatment of the *p*-toluenesulfonate with lithium

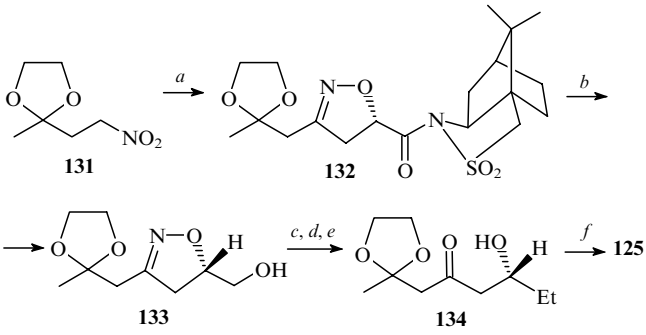

(*a*) **128**, PhNCO, Et_3N; (*b*) Bu^s_3BHLi, THF, 25 °C, 30 min (85%); (*c*) TsCl, Et_3N, DMAP, 25 °C, 26 h (100%); (*d*) Me_2CuLi, Et_2O, −5 °C, 18 h (57%); (*e*) Ni/Ra, H_2O, MeOH, H_3BO_3 (75%); (*f*) 3 M HCl, Et_2O, 25 °C, 20 h (88%).

dimethylcuprate led to the replacement of the hydroxymethyl group by the ethyl group. Reduction of 4,5-dihydroisoxazole by hydrogen over Raney nickel occurred with the retention of the original configuration of the chiral centre and yielded the β-ketol **134** . Subsequent ring closure under conditions of acid catalysis afforded the pheromone **125**.

(−)-(1*R*,3*R*,5*S*)-1,3-Dimethyl-2,9-dioxabicyclo[3.3.1]nonane (**126**) was synthesised from the oxime **135** and the amide **128**.[137] Cycloaddition gave epimeric 4,5-dihydroisoxazoles (92 : 8); the main isomer was isolated in 89% yield by column chromatography. Deoxygenation of the hydroxy group had to be carried out following removal of the chiral reagent by L-selectride.

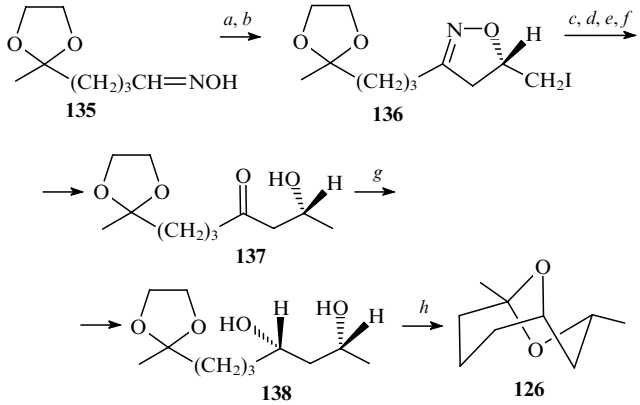

135 **136** **137** **138** **126**

(*a*) **128**, NCS, DMF; (*b*) Et_3N, Et_2O; (*c*) Bu^s_3BHLi, THF, 25 °C, 45 min (86%); (*d*) TsCl, CH_2Cl_2, Et_3N, DMAP, 9 h (83%); (*e*) NaI, $NaHCO_3$, MeCOEt, Δ (98%); (*f*) Ni/Ra, H_2, H_3BO_3, MeOH – H_2O (15 : 1), 16 h (74%); (*g*) Et_2BOMe, −70 °C, $NaBH_4$, THF – MeOH (86%); (*h*) Et_2O, 3 M HCl, 20 °C, 16 h (57%).

Initially, this was attempted by radical reduction of the iodide **136** prepared from the corresponding *p*-toluenesulfonate, which however resulted in racemisation. Numerous experiments allowed finally elaboration of the optimum conditions for such reduction [*viz*., Bu_3SnH, diazabicycloundecene (DBU), AIBN, 50 °C]. Hydrogenation of the 4,5-dihydroisoxazole **136** over Raney nickel, which was accompanied by reductive deiodination, appeared to be the shortest way to the optically pure ketol **137**. The target product **126** was obtained by treatment of the optically active 1,3-diol **138** with HCl.

(−)-(1*S*)-7,7-Dimethyl-6,8-dioxabicyclo[3.2.1]octane (**127**) was synthesised from the oxime **139**.[137] The optically pure cycloadduct **132** was isolated in 70% yield from a mixture of epimers (85 : 15). The Grignard reaction of the 4,5-dihydroisoxazole **132** with MeMgBr gave compound **140**, the chiral reagent **124** was recovered simultaneously. Reduction of the dihydroisoxazole **140** with lithium aluminium hydride occurred stereoselectively to give the optically active amino alcohol in 97% yield. The latter was deaminated with sulfamic acid and the diol **141** obtained was treated with an acid, which resulted in the target bicyclic product **127**.

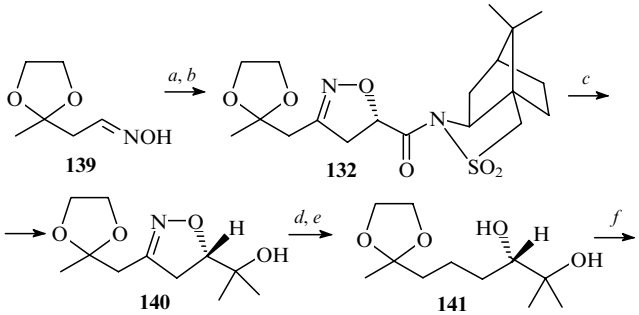

139 **132** **140** **141**

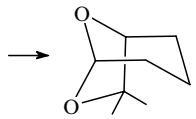

127

(*a*) **128**, NCS, CH_2Cl_2; (*b*) Et_3N, CH_2Cl_2 (70%); (*c*) MeMgBr, THF, −78 °C (72%); (*d*) $LiAlH_4$, Et_2O, −78 °C (97%); (*e*) NH_2OSO_3H, NaOH, CH_2Cl_2, 1 h, 60 °C (54%); (*f*) PhH, TsOH, 48 h, 60 °C (61%).

2. Synthesis of (+)-(*S*)-gingerol

A group of French chemists[141] studied the enantiocontrolled synthesis of dihydroisoxazoles using the chiral acyclic irontricarbonyl complex **142** as a dipolarophile. The complex **142** was prepared by olefination of optically active aldehydes coordinated to ironpentacarbonyl.[135] The method proved to be efficient in the synthesis of (+)-(*S*)-gingerol (**143**), a biologically active compound[144, 145] isolated from plants.[142–145]

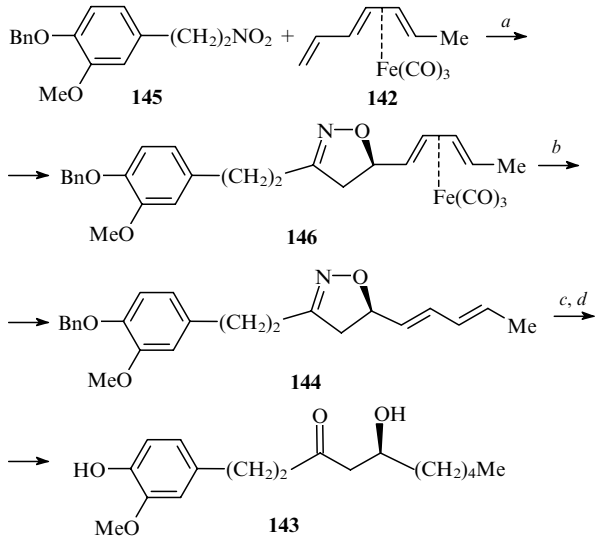

(*a*) PhNCO, Et_3N, ~20 °C, 48 h (75%); (*b*) $(NH_4)_2Ce(NO_3)_6$, MeOH, −20 °C, 25 min (62%); (*c*) H_2, Ni/Ra, H_3BO_3, MeOH – H_2O, 3.5 h (80%); (*d*) H_2, 10% Pd/C, MeOH, 20 °C, 40 min (66%).

Synthesis of compound **143** has been the subject of numerous studies; two of those employ the 1,3-dipolar cycloaddition of nitrile oxides with subsequent reductive scission of the cycloadducts formed.[31, 46] The formation of the β-hydroxycarbonyl fragment in gingerol **143** was achieved by enantioselective reduction of chiral enamido ketones[31] and transformation of chiral 3-sulfenyldihydroisoxazoles.[46]

The 4,5-dihydroisoxazole **144** was synthesised by the 1,3-dipolar cycloaddition of a nitrile oxide to the chiral acyclic irontricarbonyl complex **142**.[141] The nitrile oxide precursor, *viz*., the nitrocompound **145**, was synthesised in five steps from the readily accessible 4-benzyloxy-3-methoxybenzaldehyde (total yield 33%). The cycloaddition of triene **142** to the nitrile oxide generated from the nitro compound **145** yielded a mixture of diastereomeric 4,5-dihydroisoxazoles in a 89 : 11 ratio; the main isomer **146** was isolated in 75% yield. The irontricarbonyl complex was decomposed by oxidation with cerium ammonium nitrate in methanol. The final product, *viz*., (+)-(*S*)-gingerol (**143**), was prepared from the 4,5-dihydroisoxazole **144** in two steps. First, 4,5-dihydroisoxazole was reduced into the corresponding β-hydroxy ketone over Raney nickel under standard conditions. In this step, the diene group was partly reduced. The reduction was completed by catalytic hydrogenation over palladium.

* * *

The data presented in the rewiew illustrate the efficiency of the nitrile oxide-based approach as both an alternative to classical reactions employed in organic chemistry (*e.g.*, the aldol condensation) and an independent method aimed at the solution of complicated problems in the synthesis of pheromones, alkaloids, vitamins, monosaccharides, antibiotics, steroids and other natural compounds.

References

1. A A Akhrem, F A Lakhvich, V A Khripach *Khim. Geterotsikl. Soedin*. 1155 (1981) [a]
2. B H Lipshutz *Chem. Rev*. **86** 795 (1986)
3. S Kanemasa, O Tsuge *Heterocycles (Spec. Issue)* **30** 719 (1990)
4. A P Kozikowski *Acc. Chem. Res*. **17** 410 (1984)
5. F A Lakhvich, E V Koroleva, A A Akhrem *Khim. Geterotsikl. Soedin*. 435 (1989) [a]
6. A Annunziata, M Cinquini, F Cozzi, L Rainmondi *Gazz. Chim. Ital*. **119** 253 (1989)
7. P G Baraldi, A Barco, S Benetti, G P Pollini, D Simoni *Synthesis* 857 (1987)
8. C Grundman, P Grunangeger *The Nitrile Oxides* (Berlin: Springer, 1971)
9. T Mukaiyama, T Hoshino *J. Am. Chem. Soc*. **82** 5339 (1960)
10. C Grundmann, R Richter *J. Org. Chem*. **33** 476 (1968)
11. V Jäger, I Müller *Tetrahedron* **41** 3519 (1985)
12. P Caramella, P Grunangeger, in *1,3-Dipolar Cycloaddition Chemistry* (Ed. A Padwa) (New York: Wiley, 1984) p. 291
13. R V Stevens, N Beaulieu, W H Chan, A R Daniewski, T Takeda, A Waldner, P G Williard, U Zutter *J. Am. Chem. Soc*. **108** 1039 (1986)
14. G Kumaran, G H Kulkarni *J. Org. Chem*. **62** 1516 (1997)
15. T Shimizu, Y Hayashi, K Teramura *Bull. Chem. Soc. Jpn*. **57** 2531 (1984)
16. T Shimizu, Y Hayashi, H Shibafuchi, K Teramura *Bull. Chem. Soc. Jpn*. **59** 2827 (1986)
17. Y Basel, A Hassner *Synthesis* 309 (1997)
18. A Hassner, K M L Rai *Synthesis* 57 (1989)
19. D P Curran, C J Fenk *J. Am. Chem. Soc*. **107** 6023 (1985)
20. K B G Torssell *Nitrile Oxides, Nitrones and Nitronates in Organic Synthesis. Novel Strategies in Synthesis* (Purdue: Purdue University, 1987)
21. H Irngartinger, A Werber, T Escher *Liebigs Ann*. 1845 (1996)
22. A Diaz-Ortiz, E Diez-Darra, A De la Hoz, A Moreno, M J Gomez-Escalonilla, A Loupy *Heterocycles* **43** 1021 (1996)
23. A Corsaro, U Chiacchino, V Librando, S Fisichella, V Pistara *Heterocycles* **45** 1567 (1997)
24. R F Cunico, L Bedell *J. Org. Chem*. **48** 2780 (1983)
25. J N Kim, E K Ryu *Heterocycles* **31** 1693 (1990)
26. K H Schulte-Elte, B L Müller, G Ohloff *Helv. Chim. Acta* **56** 310 (1973)
27. P G Baraldi, A Barco, S Benetti, F Moroder, G P Pollini, D Simoni *J. Org. Chem*. **48** 1297 (1983)
28. A I Kotyatkina, V N Zhabinsky, V A Khripach, A de Groot *Collect. Czech. Chem. Commun*. **65** 1173 (2000)
29. G Buchi, J C Vederas *J. Am. Chem. Soc*. **94** 9128 (1972)
30. S Kashima, Y Yamamoto, Y Tsuda *J. Org. Chem*. **40** 526 (1975)
31. P G Baraldi, F Moroder, G P Pollini, D Simoni, A Barco, S Benetti *J. Chem. Soc., Perkin Trans. 1* 2983 (1982)
32. A P Kozikowski, S Goldstein *J. Org. Chem*. **48** 1139 (1983)
33. R Plate, P H H Hermkens, J M M Smits, R J F Nivard, H C J Ottenheijm *J. Org. Chem*. **52** 1047 (1987)
34. M Nitta, T Kobayashi *J. Chem. Soc., Perkin. Trans. 1* 1401 (1985)
35. N R Natale *Tetrahedron Lett*. **23** 5009 (1982)
36. M Kijima, Y Nambu, T Endo *J. Org. Chem*. **50** 1140 (1985)
37. P DeShong, J A Cipollina, N K Lowmaster *J. Org. Chem*. **53** 1356 (1988)
38. A A Akhrem, F A Lakhvich, V A Khripach, I B Klebanovich *Dokl. Akad. Nauk SSSR* **244** 615 (1979) [b]
39. D P Curran *J. Am. Chem. Soc*. **105** 5826 (1983)

40. A P Kozikowski, C-S Li *J. Org. Chem.* **52** 3541 (1987)
41. D P Curran, P B Jacobs, R L Elliott, B H Kim *J. Am. Chem. Soc.* **109** 5280 (1987)
42. D C Lathbury, P J Parsons *J. Chem. Soc., Chem. Commun.* 291 (1982)
43. I Müller, V Jäger *Tetrahedron Lett.* **23** 4777 (1982)
44. R Annunziata, M Cinquini, F Cozzi, A Restelli *J. Chem. Soc., Perkin Trans. 1* 2293 (1985)
45. E P Schreiner, H Gstach *Synlett* 1131 (1996)
46. R Annunziata, M Cinquini, F Cozzi, A Gilardi, A Restelli *J. Chem. Soc., Perkin Trans. 1* 2289 (1985)
47. A P Kozikowski, M Adamczyk *J. Org. Chem.* **48** 366 (1983)
48. P G Baraldi, A Barco, S Benetti, S Manfredini, D Simoni *Synthesis* 276 (1987)
49. A P Kozikowski, M Adamczyk *Tetrahedron Lett.* **23** 3123 (1982)
50. R E Erickson, P J Andrulis Jr, J C Collins, M L Lungle, G D Mercer *J. Org. Chem.* **34** 2961 (1969)
51. J W Westley *Adv. Appl. Microbiol.* **22** 177 (1977)
52. R Baker, R H Herbert, A H Parton *J. Chem. Soc., Chem. Commun.* 601 (1982)
53. D G Lynn, N J Phyllips, W C Hutton, J Shabanowitz, D I Fennell, R J Cole *J. Am. Chem. Soc.* **104** 7319 (1982)
54. A P Kozikowski, J G Scripko *J. Am. Chem. Soc.* **106** 353 (1984)
55. S R Schow, J D Bloom, A S Thompson, K N Winzenberg, A B Smith III *J. Am. Chem. Soc.* **108** 2662 (1986)
56. H Maishima, M Kurabayashi, C Tamura *Tetrahedron Lett.* 711 (1975)
57. J R Egerton, D A Ostlind, L S Blair, C H Eary, D Suhayda, S Cifelli, R F Riek, W F Campbell *Antimicrob. Agents. Chemother.* **15** 372 (1979)
58. M Ono, H Mishima, Y Takiguchi, M Terao *J. Antibiot.* **36** 509 (1983)
59. H Mishima, J Ide, S Muramatsu, H Ono *J. Antibiot.* **36** 980 (1983)
60. A P Kozikowski, X-M Cheng *Tetrahedron Lett.* **28** 3189 (1987)
61. S Nakatsuka, T Masuda, O Asano *Tetrahedron Lett.* **27** 4327 (1986)
62. S M Kupchan, E J LaVoie, A R Branfman, B Y Fei, W M Bright, R F Bryan *J. Am. Chem. Soc.* **99** 3199 (1977)
63. G R Pettit, G M Cragg, D Gust, P Brown, J M Schmidt *Can. J. Chem.* **60** 939 (1982)
64. G R Pettit, G M Cragg, M I Suffness, D Gust, F E Boettner, M Williams, J A Saenz-Renauld, P Brown, J M Schmidt, P D Ellis *J. Org. Chem.* **49** 4258 (1984)
65. P R McGuirk, D B Collum *J. Org. Chem.* **49** 843 (1984)
66. A B Smith III, M Fukui *J. Am. Chem. Soc.* **109** 1269 (1987)
67. S D Burke, J E Cobb, K Takeuchi *J. Org. Chem.* **50** 3420 (1985)
68. A B Smith III, R A Rivero *J. Am. Chem. Soc.* **109** 1272 (1987)
69. S F Martin, M S Dappen, B Dupré, C J Murthy, J A Colapret *J. Org. Chem.* **54** 2209 (1989)
70. B Blumberg *Semin. Cell Dev. Biol.* **8** 417 (1997); *Chem. Abstr.* **127** 290 808 (1997)
71. D M Kochhar *Handb. Exp. Pharmacol.* **124** 3 (1997); *Chem. Abstr.* **126** 98 741 (1997)
72. R S H Liu, A E Asato *Tetrahedron* **40** 1931 (1984)
73. J Otera, H Misawa, T Onishi, S Suzuki, Y Fujita *J. Org. Chem.* **51** 3834 (1986)
74. P G Baraldi, A Barco, S Benetti, M Guarneri, S Manfredini, G P Pollini, D Simoni *Tetrahedron Lett.* **29** 1307 (1988)
75. R S Ward *Chem. Soc. Rev.* **11** 75 (1982)
76. R S Ward *Tetrahedron* **46** 5029 (1990)
77. E Bianchi, M E Caldwell, J R Cole *J. Pharm. Sci.* **57** 195 (1968)
78. Z Getahum, L Jurd, P S Chu, C M Lin, E Hamel *J. Med. Chem.* **35** 1058 (1992)
79. T Morimoto, M Chiba, K Achiwa *Heterocycles* **33** 435 (1992)
80. N Rehnberg, G Magnusson *J. Org. Chem.* **55** 4340 (1990)
81. N Rehnberg, G Magnusson *Tetrahedron Lett.* **29** 3599 (1988)
82. M P Sibi, J A Gaboury *Synlett* 83 (1992)
83. J A Gaboury, M P Sibi *J. Org. Chem.* **58** 2173 (1993)
84. N B Perry, J W Blunt, M H G Munro, L K Pannell *J. Am. Chem. Soc.* **110** 4850 (1988)
85. X Ye, Y Quiang *Weishengwu Xuebao* **27** 156 (1987); *Chem. Abstr.* **107** 112 294 (1987)
86. S J Danishefsky, M P DeNino *Angew. Chem., Int. Ed. Engl.* **26** 15 (1987)
87. S Jeganathan, P Vogel *J. Chem. Soc., Chem. Commun.* 993 (1989)
88. R M Paton, A A Young *J. Chem. Soc., Chem. Commun.* 132 (1991)
89. K Krohn *Angew. Chem., Int. Ed. Engl.* **25** 790 (1986)
90. K Krohn *Tetrahedron* **46** 291 (1990)
91. Y Kita, M Kirihara, J Sekihachi, R Okunaka, M Sasho, S Mohri, T Honda, S Akai, Y Tamura, K Shimooka *Chem. Pharm. Bull.* **38** 1836 (1990)
92. Y Kita, M Kirihara, Y Fujii, R Okunaka, S Akai, H Maeda, Y Tamura, K Shimooka, H Ohushi, T Ishida *Chem. Pharm. Bull.* **39** 857 (1991)
93. R Alguacil, F Farina, M V Martin *Tetrahedron* **52** 3457 (1996)
94. R Alguacil, F Farina, M V Martin, M C Paredes *Tetrahedron Lett.* **36** 6773 (1995)
95. G C Harbour, A A Tymiac, K L Rinehart Jr, P D Shaw, R G Hughes, Jr, S A Mizak, J H Coats, G E Zurenko, L H Li, S L Kuentzel *J. Am. Chem. Soc.* **103** 5604 (1981)
96. A Hassner, K S K Murthy *Tetrahedron Lett.* **27** 1407 (1986)
97. B B Snider, W C Faith *J. Am. Chem. Soc.* **106** 1443 (1984)
98. A E Walts, W R Roush *Tetrahedron* **41** 3623 (1985)
99. C C Chang, K Nakanishi *J. Chem. Soc., Chem. Commun.* 605 (1983)
100. E van der Eycken, J van der Eycken, M Vandewalle *J. Chem. Soc., Chem. Commun.* 1719 (1985)
101. F J Zeelen, M B Groen *Recl. Trav. Chim. Pays-Bas* **105** 465 (1986)
102. F J Zeelen *Nat. Prod. Rep.* 607 (1994)
103. G Stork, J E McMurry *J. Am. Chem. Soc.* **89** 5464 (1967)
104. J W Scott, G Sausy *J. Org. Chem.* **37** 1652 (1972)
105. M Ihara, Y Tokunaga, K Fukumoto *J. Org. Chem.* **55** 4497 (1990)
106. K S K Murthy, A Hassner *Tetrahedron Lett.* **28** 97 (1987)
107. K Shishido, Y Tokunaga, N Omachi, K Hiroya, K Fukumoto, T Kametani *J. Chem. Soc., Chem. Commun.* 1093 (1989)
108. N Zein, A M Sinha, W J McGahren, G A Ellestad *Science* **240** 1198 (1988)
109. N Zein, M Poncin, R Nilakantan, G A Ellestad *Science* **244** 697 (1988)
110. K C Nicolaou, W-M Dai *Angew. Chem., Int. Ed. Engl.* **30** 1387 (1991)
111. W -d Ding, G A Ellestad *J. Am. Chem. Soc.* **113** 6617 (1991)
112. P Magnus, P A Carter *J. Am. Chem. Soc.* **110** 1626 (1988)
113. J N Haseltine, S J Danishefsky, G Schulte *J. Am. Chem. Soc.* **111** 7638 (1989)
114. S L Schreiber, L L Kiessling *J. Am. Chem. Soc.* **110** 631 (1988)
115. P Magnus, H Annoura, J Harling *J. Org. Chem.* **55** 1709 (1990)
116. J N Haseltine, M P Cabal, N B Mantlo, N Iwasawa, D S Yamashita, R S Coleman, S J Danishefsky, G K Schulte *J. Am. Chem. Soc.* **113** 3850 (1991)
117. K C Nicolaou, D Clark *Angew. Chem., Int. Ed. Engl.* **31** 855 (1992)
118. R L Halcomb, M D Wittman, S H Olson, S J Danishefsky, J Golik, H Wong, D Vyas *J. Am. Chem. Soc.* **113** 5080 (1991)
119. A L Smith, E N Pitsinos, C-K Hwang, Y Mizuno, H Saimoto, G R Scarlato, T Suzuki, K C Nicolaou *J. Am. Chem. Soc.* **115** 7612 (1993)
120. K C Nicolaou, C W Hummel, M Nakada, K Shibayama, E N Pitsinos, H Saimoto, Y Mizuno, K-U Baldenius, A L Smith *J. Am. Chem. Soc.* **115** 7625 (1993)
121. T K M Shing, C-H Wong, T Yip *Tetrahedron Asymmetry* **7** 1323 (1996)
122. R M Konojia, E Chin, C Smith, R Chen, D Rowand, S D Levine, M P Wachter, R E Adams, D W Hahn *J. Med. Chem.* **28** 796 (1985)
123. D W Hahn, A J Tobia, H E Rosenthale, J L McGuire *Contraception* **26** 133 (1984)
124. S D Levine, R E Adams, R Chen, M L Cotter, A F Hirsch, V V Kane, R M Kanojia, C Shaw, M P Wachter, E Chin, R Huettemann, P Ostrowski, J L Mateos, L Noriega, A Guzmán, A Mijarez, L Tovar *J. Am. Chem. Soc.* **101** 3404 (1979)
125. R C Cookson, N J Liverton *J. Chem. Soc., Perkin Trans. 1* 1589 (1985)
126. K C Nicolaou, D A Claremon, W E Barnette *J. Am. Chem. Soc.* **102** 6611 (1980)
127. B M Trost, P D Greenspan, H Geissler, J H Kim, N Greeves *Angew. Chem., Int. Ed. Engl.* **33** 2182 (1994)
128. B de Lange, B L Feringa *Tetrahedron Lett.* **29** 5317 (1988)
129. S Kanemasa, T Hayashi, H Yamamoto, E Wada, T Sakurai *Bull. Chem. Soc. Jpn.* **64** 3274 (1991)

130. D P Curran, B H Kim, H P Piyasena, R J Loncharich, K N Houk *J. Org. Chem.* **52** 2137 (1987)
131. T Olsson, K Stern *J. Org. Chem.* **53** 2468 (1988)
132. D P Curran, K-S Jeong, T A Heffner, J Rebek Jr *J. Am. Chem. Soc.* **111** 9238 (1989)
133. W Oppolzer, G Poli, C Starkemann, G Bernardinelli *Tetrahedron Lett.* **29** 3559 (1988)
134. W Oppolzer *Tetrahedron* **43** 1969 (1987)
135. T Le Gall, J-P Lellouche, L Toupet, J-P Beaucourt *Tetrahedron Lett.* **30** 6517 (1989)
136. S Dare, B Ducroix, S Bernard, K M Nicholas *Tetrahedron Lett.* **37** 4341 (1996)
137. D P Curran, T A Heffner *J. Org. Chem.* **55** 4585 (1990)
138. I Kubo, T Matsumoto, D L Wagner, J N Shoolery *Tetrahedron Lett.* **26** 563 (1985)
139. J P Vita, W Franke *Naturwissenschaften* **63** 550 (1976)
140. Y Naya, M Kotake *Tetrahedron Lett.* 2459 (1967)
141. T Le Cull, J-P Lellouche, J-P Beaucourt *Tetrahedron Lett.* **30** 6521 (1989)
142. D W Connell, M D Sutherland *Austr. J. Chem.* **22** 1033 (1969)
143. T Murata, M Shinohara, M Miyamoto *Chem. Pharm. Bull.* **20** 2291 (1972)
144. M Kobayashi, N Shoji, Y Ohizumi *Biochim. Biophys. Acta* **903** 96 (1987)
145. S Gerner, G Flanz *Deutsch. Apoth. Ztg.* **137** 4260 (1997); *Chem. Abstr.* **128** 7427 (1997)

[a] — *Chem. Heterocycl. Compd. (Engl. Transl.)*
[b] — *Dokl. Chem. Technol., Dokl. Chem. (Engl. Transl.)*

Russian Chemical Reviews **70** (8) 655 – 672 (2001) © 2001 Russian Academy of Sciences and Turpion Ltd

DOI 10.1070/RC2001v070n08ABEH000645

Sulfur ylides in the synthesis of heterocyclic and carbocyclic compounds

S N Lakeev, I O Maydanova, F Z Galin, G A Tolstikov

Contents

I.	Introduction	655
II.	Rearrangements of cyclic sulfur ylides	656
III.	Intramolecular cyclisation of sulfur ylides	665
IV.	Reactions of thiocarbonyl ylides	667
V.	Cycloaddition of ylides to alkenes	669

Abstract. Data on the use of sulfonium ylides in the synthesis of carbocyclic and heterocyclic compounds published over the last 15 years are analysed, systematised and generalised. The bibliography includes 139 references.

I. Introduction

The chemistry of ylides attracted considerable interest in the early 1950s after Wittig has discovered the reaction of phosphonium ylides with carbonyl compounds giving rise to alkenes.[1] Investigations carried out by Corey[2] and Franzen[3,4] extended the Wittig reaction to sulfur ylides and initiated extensive studies of sulfonium ylides. The further development of the chemistry of these compounds demonstrated that they could be widely used in organic synthesis.

Sulfur ylides contain a negatively charged carbon atom directly bound to a positively charged sulfur atom. In the general form, these compounds can be represented by two resonance structures, *viz*., ylide **1** and ylene **2**.[5]

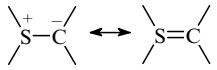

1 **2**

Sulfonium (**1**) and sulfoxonium (**3**) ylides containing two organic substituents at the sulfur atoms are most often used in organic synthesis.[6–9] Sulfinyl ylides (**4**), sulfonyl ylides (**5**), thiocarbonyl ylides (**6**) and iminosulfuranes (**7**) are also known.[8]

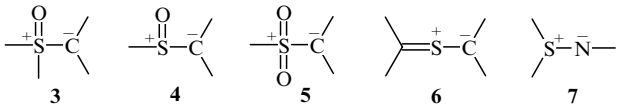

3 **4** **5** **6** **7**

Sulfur ylides act as nucleophilic reagents, their reactivities being inversely proportional to their stability. Ylides are stabilised through the electron density delocalisation under the action of electron-withdrawing substituents at the carbanionic centre. The properties of stabilised sulfur ylides are summarised and compared with the properties of non-stabilised ylides in reviews.[6,10,11]

The reactions of sulfur ylides with compounds containing C=X bonds (X = O, C or N) gained wide acceptance in organic synthesis. These reactions proceed as the nucleophilic addition followed by 1,3-elimination of a sulfur-containing group to form epoxide, cyclopropane or aziridine, respectively.[6]

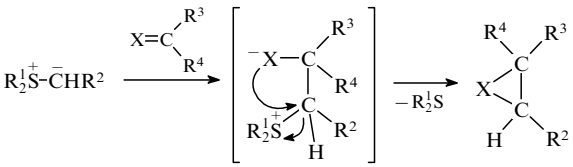

X = O, C, N.

The data on these reactions were surveyed in detail in the monograph[6] and in a series of studies.[7,12–16] Due to their zwitterionic character, sulfonium ylides are also widely used in rearrangements generating new C–C bonds (often with high stereo- and regioselectivity).[16–20] In the last decade, interest in sulfur ylides was quickened owing to their successful use in asymmetric synthesis.[16] A one-stage procedure, which has been developed recently for the synthesis of optically active epoxides and aziridines,[21,22] represents a considerable achievement in this field. Optically pure sulfur ylides, which are generated *in situ* in reactions of catalytic amounts of chiral sulfides with diazo compounds in the presence of dirhodium tetraacetate or copper acetylacetonate, react with aldehydes or imines to give epoxides or aziridines, respectively, and the sulfide is recovered and recycled to the catalytic cycle. This procedure was used for the syntheses of various substituted epoxides and aziridines in good yields and with high enantioselectivity.[16,23–25]

S N Lakeev, I O Maydanova Institute of Biology, Ufa Scientific Centre of the Russian Academy of Sciences, prosp. Oktyabrya 69, 450054 Ufa, Russian Federation. Fax (7-347) 235 26 41. Tel. (7-347) 235 53 41. E-mail: bmch@anrb.ru (S N Lakeev)
F Z Galin Institute of Organic Chemistry, Ufa Scientific Centre of the Russian Academy of Sciences, prosp. Oktyabrya 71, 450054 Ufa, Russian Federation. Fax (7-347) 235 60 66. Tel. (7-347) 235 52 88. E-mail: galin@anrb.ru
G A Tolstikov N N Vorozhtsov Novosibirsk Institute of Organic Chemistry, Siberian Branch of the Russian Academy of Sciences, prosp. Akad. Lavrent'eva 9, 630090 Novosibirsk, Russian Federation. Fax (7-383) 234 47 52. Tel. (7-383) 234 38 50. E-mail: kim@nioch.nsc.ru

Received 21 December 2000
Uspekhi Khimii **70** (8) 744 – 762 (2001); translated by T N Safonova

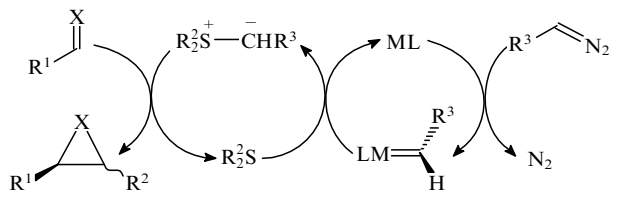

X = $Me_3Si(CH_2)_2SO_2N$, O; ML = $Rh_2(OAc)_4$, $Cu(acac)_2$.

Sulfur ylides also find wide application in the synthesis of other cyclic compounds as well as of hetero-, macro- and polycyclic structures, including natural compounds and their analogues. Special-purpose reviews devoted to this aspect are lacking. The only study dealing with this problem [13] has covered the results published up to 1986 inclusive. The present review surveys the data on the use of sulfur ylides in syntheses of complex cyclic, heterocyclic and natural compounds published over the last 15 years. Systematisation and analysis of the available data will help in evaluating the possibilities of the use of sulfur ylides in the synthesis of complex structures and give a deeper insight into prospects of the further development of this line of investigation. Reactions of ylides giving rise to three-membered carbo- and heterocycles are beyond the scope of the present review.

II. Rearrangements of cyclic sulfur ylides

Sigmatropic rearrangements of cyclic sulfur ylides were investigated in most detail. In these studies, sulfur ylides were used in the synthesis of various carbo- and heterocyclic compounds. The reactions are carried out with the use of either ylides generated *in situ* or individual compounds prepared in advance. The 1,2-Stevens rearrangements [18, 20] and 2,3-sigmatropic rearrangements of sulfur ylides find most extensive synthetic applications.[16–20, 26]

1. 1,2-Stevens rearrangements

The 1,2-Stevens rearrangements of sulfur and nitrogen ylides were discovered in 1928.[27] According to orbital symmetry rules, the concerted mechanism of this thermal rearrangement is forbidden.[28] Hence, the most probable mechanism involves the dissociation–recombination process. It was demonstrated [29, 30] that the rearrangements proceed through the formation of a radical pair, the rate of radical recombination being higher than the rate of their diffusion into a solvent.

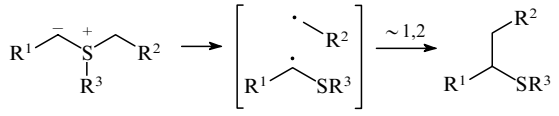

The employment of rearrangements of sulfur ylides in the synthesis of cyclic compounds appeared to be particularly promising in connection with the development of the carbene method for the generation of cyclic sulfur ylides.[20, 31–34] Ylides are formed through the electrophilic addition of a carbenoid species, which is generated from the diazo group under the action of transition metal (predominantly, Rh or Cu) compounds, to the sulfur atom.[34] These reactions are most often performed with stable diazoesters or diazoketones. Recently,[35, 36] it was demonstrated that trimethylsilyldiazomethane can also be successfully used for the generation of sulfur ylides.

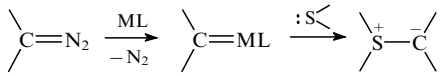

Sometimes the process is complicated by a side reaction of insertion of the carbene formed into the C–H bond. Thus intramolecular cyclisation of diazosulfide **8** afforded not only the major reaction product **9**, generated through the 1,2-rearrangement of intermediate unstable tricyclic thiophenium ylide **10**, but also a product of insertion into the C–H bond (**11**).[37]

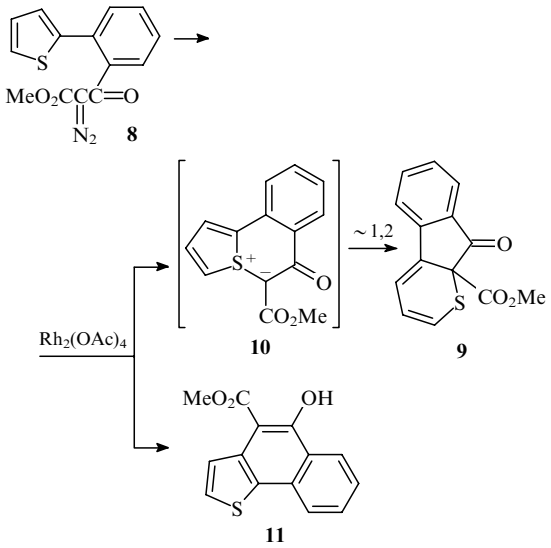

New stable four-to-seven-membered cyclic ylides were synthesised by intramolecular cyclisation of diazosulfides and their thermal rearrangements giving rise to heterocyclic compounds were carried out virtually simultaneously by two independent research groups.[38–40] It was demonstrated [38, 39] that six- and seven-membered cyclic ylides **12a**,**b** underwent the 1,2-Stevens rearrangement on heating to give the corresponding substituted cyclic thioesters **13a**,**b** in 40%–60% yields.

Decomposition of the diazoallyl sulfide **12b** catalysed by $Rh_2(OAc)_4$ afforded directly the rearranged thiepane **13b** (the yield was 59%); intermediate cyclic sulfonium ylide was not detected. The fact that the thiepane **13b** was formed through the 2,3-rearrangement rather than through the [1,2]-shift was exemplified by the reactions of diazosulfides **12c–e** containing the prenyl, cinnamyl or crotyl substituent at the sulfur atom, which were accompanied by the allylic inversion.

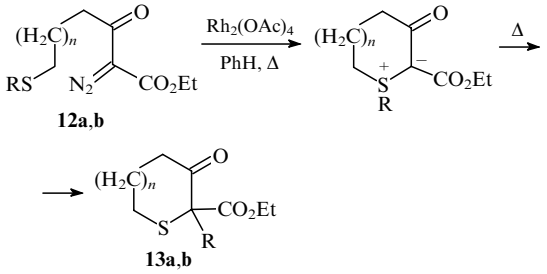

R = Bn, n = 1 (**a**); R = $H_2C{=}CHCH_2$, n = 2 (**b**).

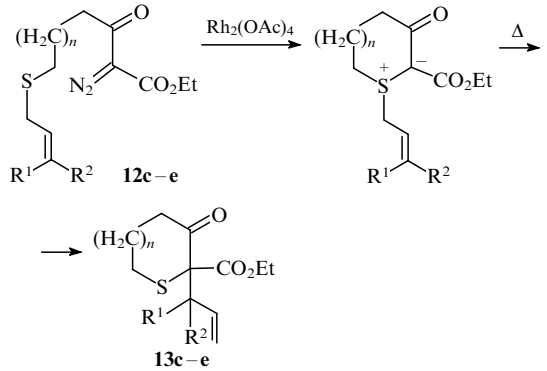

$R^1 = R^2$ = Me, n = 1 (**c**); R^1 = Ph, R^2 = H, n = 2 (**d**); R^1 = Me, R^2 = H, n = 2 (**e**).

On heating, four- (**14**) and six-membered *S*-phenyl-substituted (**15**) sulfur ylides underwent the 1,4-rearrangement to form derivatives of dihydro- (**16**) and tetrahydrofuran (**17**), respec-

tively.[40] Seven-membered and some six-membered cyclic ylides decompose giving rise to unsaturated sulfur-free compounds.[40]

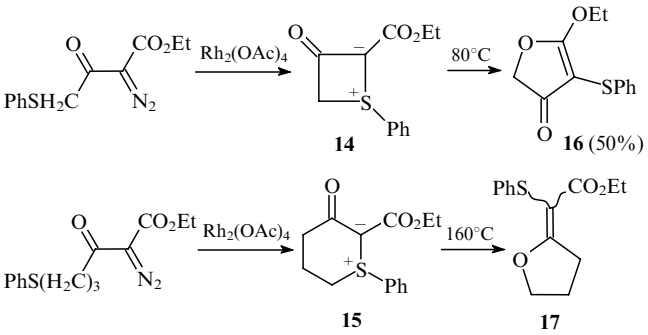

The 1,2-rearrangement of cyclic ylide **18** stabilised by two ethoxycarbonyl groups, which was formed in the reaction of 2,3-dihydroisothiazol-3-one with diazomalonic ester, was accompanied by insertion of carbene into the S–N bond to form 3,4-dihydro-1,3-thiazin-4(2*H*)-one **19**.[41]

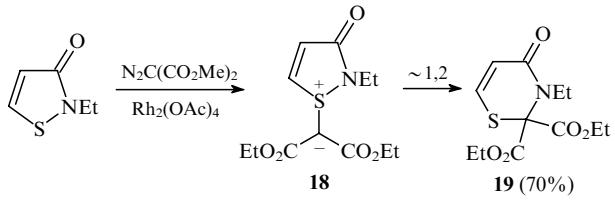

Substituted 1,3-dithianes **20** were synthesised by the 1,2-rearrangement proceeding with the cleavage of the S–S bond of intermediate 1,2-dithiolane ylides **21**.[42] The ylides **21** were generated by the reactions of cyclic disulfides with carbenes, which were prepared from diazo compounds under conditions of catalytic or photochemical reactions. If cyclic disulfides contain more than four substituents, the C–S bond in the ylides **21** can be cleaved. Subsequent desulfation of intermediates **22** afforded thietanes **23**.

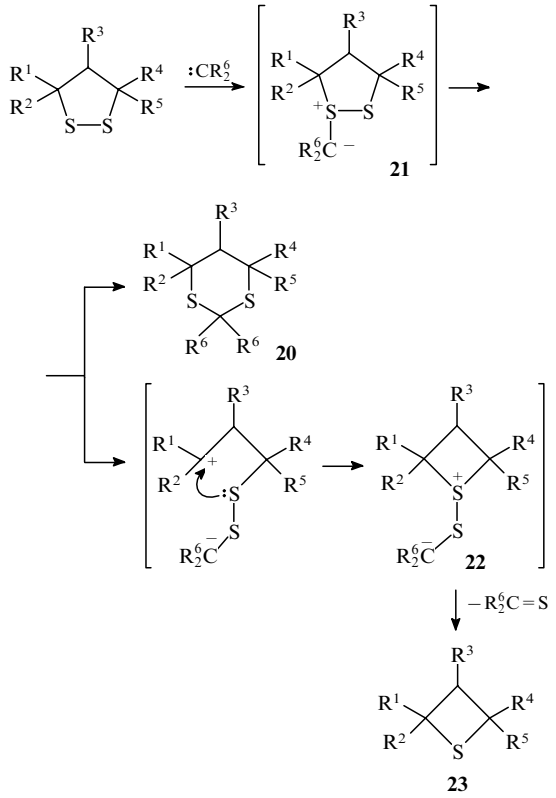

The generation of cyclic ylides by intramolecular reactions of sulfur-containing compounds with carbenes followed by their thermal rearrangements was successfully used in the synthesis of carbocyclic natural compounds. Thus the 1,2-rearrangement of ylide **24** proceeded with ring contraction to give substituted cyclopentane **25**. The latter served as the key compound in the synthesis of sesquiterpenes (±)-cuparene (**26**) and (±)-laurene (**27**).[43,44]

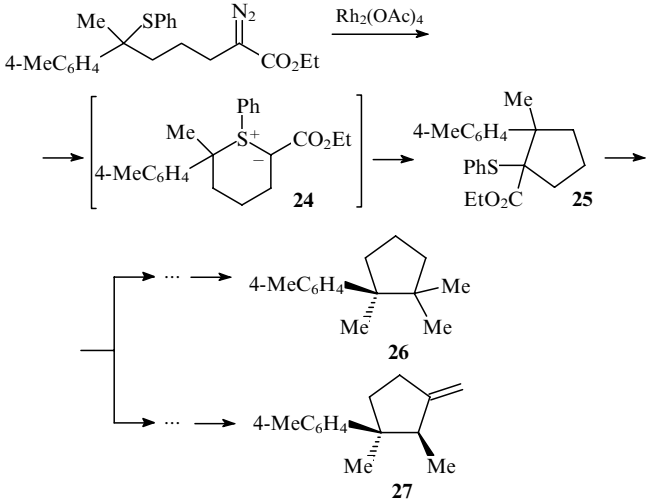

An analogous strategy was applied to the synthesis of pyrrolizidine alkaloids, *viz*., (±)-trachelanthamidine (**28a**), (±)-isoretronecanol (**28b**) and (±)-supinidine (**29**).[45,46] Diazoketone **30** was converted under the action of a rhodium catalyst into bicyclic sulfonium ylide **31** whose subsequent rearrangement afforded a compound of the pyrrolizidine series (**32**). The latter was used for the synthesis of the alkaloids **28a**,**b** and **29**.

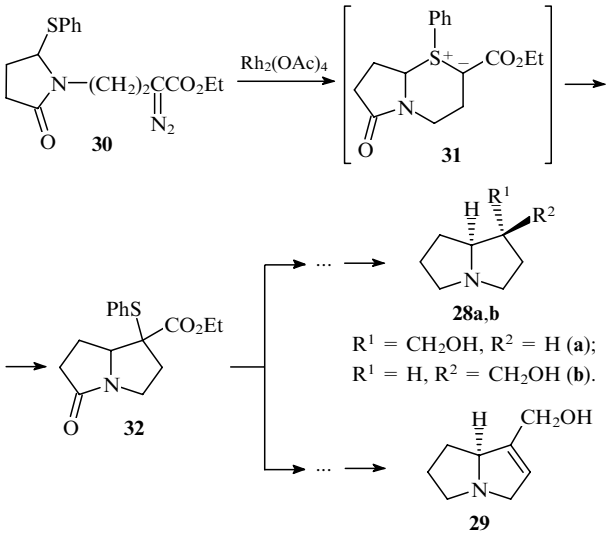

1,2-Rearrangements proceed with high stereoselectivity, particularly, at low temperature and in viscous solvents. These reactions involving chiral sulfides can be employed in asymmetric synthesis.[18] In particular, the Stevens rearrangement allows one to solve the key problem in the synthesis of natural nitrogen-containing compounds consisting in the stereoselective formation of new C–C bonds at the α position with respect to the nitrogen atom. Thus a new approach to 6-amidocarbopenicillan antibiotics was exemplified by the synthesis of bicyclic β-lactam **33**.[47] Photolysis of diazoketone **34** afforded ylide **35**, which was rearranged to give the compound **33**, the new C–C bond being formed stereoselectively.

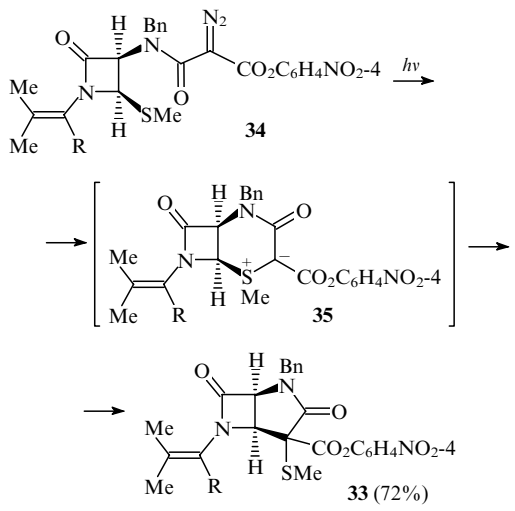

This synthetic approach was further developed in the stereoselective synthesis of alkaloids (+)-heliotridine (**36a**) and (+)-retronecine (**36b**).[48]

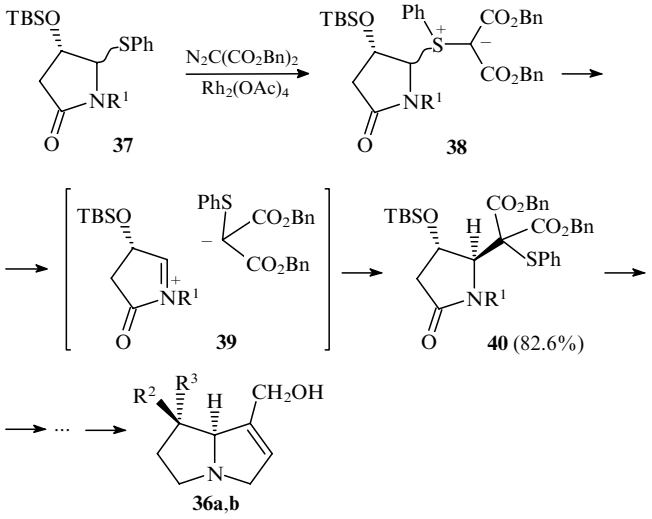

TBS is Bu^tMe_2Si;
36a: $R^1 = (CH_2)_2OC(O)Bu^t$, $R^2 = H$, $R^3 = OH$;
36b: $R^1 = (CH_2)_2OC(O)Bu^t$, $R^2 = OH$, $R^3 = H$.

The catalytic reaction of optically active sulfide **37**, which can be readily derived from (*S*)-malic acid, with dibenzyl diazomalonate afforded ylide **38** whose 1,2-rearrangement proceeded with high stereoselectivity. It is believed that the first stage of this reaction involved the cleavage of the C–S bond to produce salt **39**. The attack of the carbanion on the C=N bond proceeded predominantly from the less shielded side to form 2,3-*trans*-pyrrolidone derivative **40**, which was used as the starting compound in the synthesis of the alkaloids **36a**,**b**.

The application of the intramolecular rearrangement of cyclic sulfonium ylides allowed the development of a new method for the preparation of lactones,[49] which were used in the synthesis of C-nucleosides. Diazoacetyl thioglycoside **41** was prepared from precursor **42** according to the modified Corey method.[50] When refluxed in benzene with a catalytic amount of rhodium acetate, the compound **41** was converted into lactone **45** through sulfur ylide **43** and oxonium intermediate **44**. The lactone **45** served as the key compound in the synthesis of nucleoside antibiotic (+)-showdomycin.

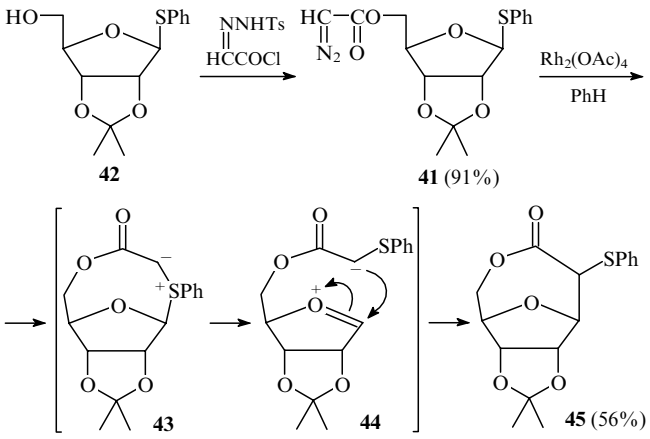

2. 2,3-Sigmatropic rearrangements

In the last two decades, the synthesis of cyclic compounds made wide use of 2,3-sigmatropic rearrangements of allylic and benzyl sulfur ylides. Baldwin was the first to carry out these studies [51–53] as early as 1968. Since then the 2,3-sigmatropic rearrangements of ylides have found many applications.

The rearrangement of allylic ylides into homoallylic sulfides can be represented in general form as follows:

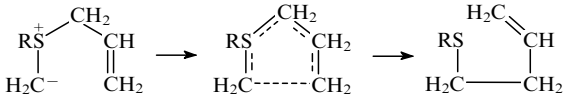

According to the orbital symmetry rules, 2,3-sigmatropic rearrangements are allowed [28] and they proceed either on heating or photolysis of ylides with complete inversion of the allylic substituent.[54,55] Since these reactions proceed by a concerted mechanism, high regio-, diastereo- and enantioselectivity are achieved, which is of particular interest from the standpoint of their application in asymmetric synthesis.

A gentle and efficient procedure for the synthesis of 3-allylisothiochroman-4-one (**46**)[56] involves the 2,3-sigmatropic rearrangement of cyclic sulfur ylide **47** formed by intramolecular cyclisation of diazosulfide **48** under the action of a rhodium catalyst.

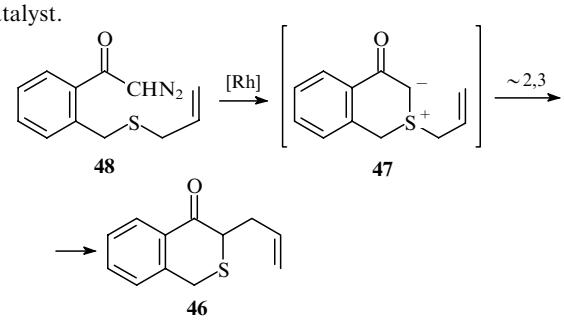

The use of chiral allylic sulfides in 2,3-sigmatropic rearrangements offers considerable possibilities for enantioselective syntheses of cyclic compounds, including analogues of natural compounds.

Thus the synthesis of optically active thioxanones **49a**–**d** was based on the 2,3-sigmatropic rearrangement of optically pure cyclic sulfur ylide **51**, which proceeded with high asymmetric induction.[57,58] Crotyl thiodiazoester **50** derived from L-valine was converted into the corresponding cyclic allylic sulfur ylide by either rhodium-catalysed intramolecular cyclisation or deprotonation of sulfonium salt **52** derived from the compound **50**. The rearrangement of the ylide **51** afforded four isomeric thioxanones **49a**–**d**. The best yield and diastereoselectivity were achieved on deprotonation of the sulfonium salt **52**.

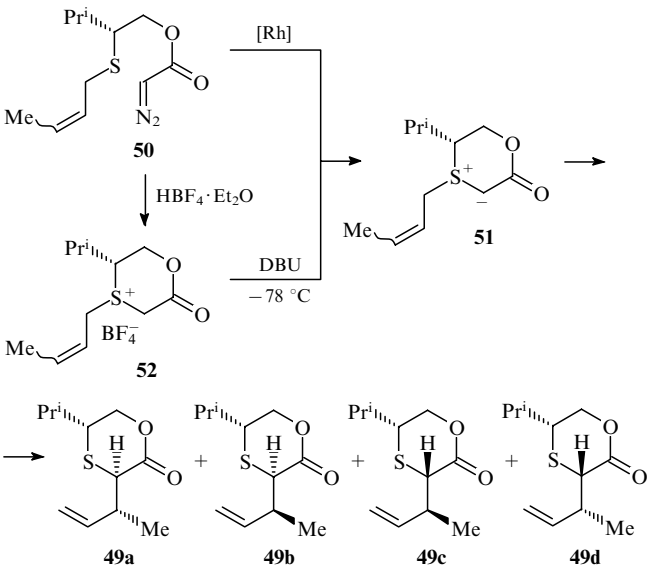

DBU is 1,8-diazabicyclo[5.4.0]undec-7-ene.

Starting compound	Reagent	Total yield (%)	Isomer ratio			
			49a	**49b**	**49c**	**49d**
(*Z*)-**50**	[Rh]	35	84	8	7	1
(*E*)-**50**	[Rh]	28	10	83	2	5
(*Z*)-**52**	DBU	66	94	4	2	traces
(*E*)-**52**	DBU	64	4	93	1	2

The reactions involving the *Z*-isomers of the compounds **50** and **52** yielded the thioxanone **49a** as the major product, whereas the reactions with the participation of the *E*-isomers gave rise to the thioxanone **49b**. This stereoselectivity was attributed [59] to the *endo* conformation of the allyl-containing five-membered ring in the prevailing transition states **A** or **B**.

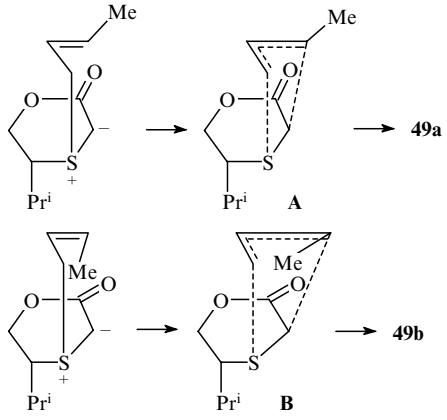

Substituted five-to-eight-membered lactones **53a**,**b** and **54a**,**b** were prepared by the 2,3-sigmatropic rearrangements of allylic sulfonium ylides **55a**,**b** and **56a**,**b** generated from the corresponding diazoesters under the action of dirhodium tetraacetate.[60–63]

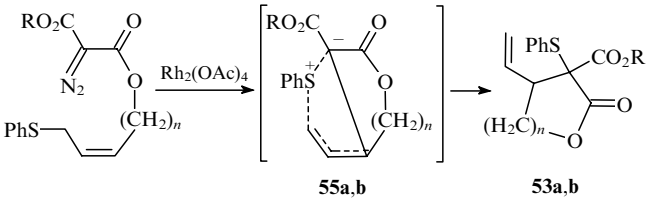

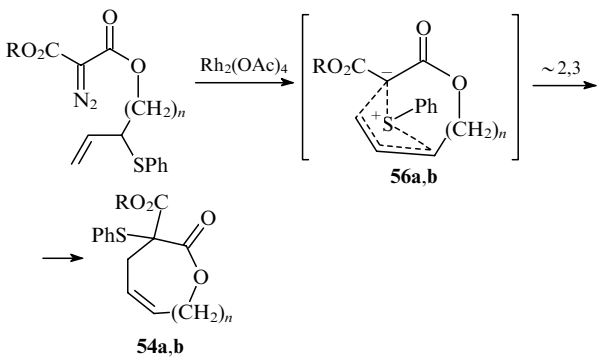

R = Me, Et; *n* = 1, 2.

Lactone **57** was prepared according to an analogous procedure and was used in the stereoselective synthesis of perhydro[2,3-*b*]furanone derivative **58**.[62]

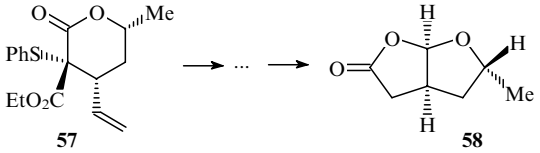

The rearrangement of sulfur ylides, which were prepared by treatment of sulfur-containing diazoketones **59** and **60** with dirhodium tetraacetate in boiling benzene, was used in a new approach to the synthesis of bridging δ-lactones **61** [64] as well as of spiro-fused five- and six-membered lactones **62a**,**b** [65] and spirocarbocyclic compounds **62c**,**d**.[66]

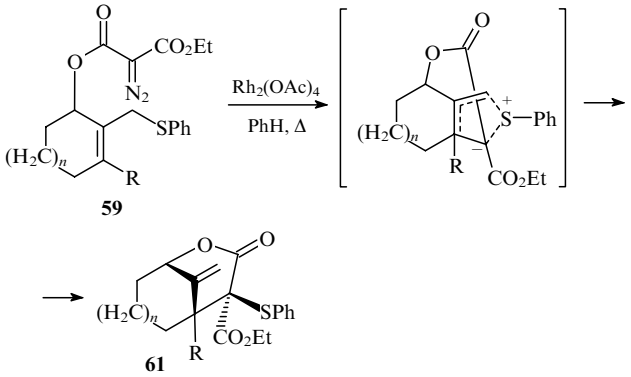

R = H, Me; *n* = 1, 2.

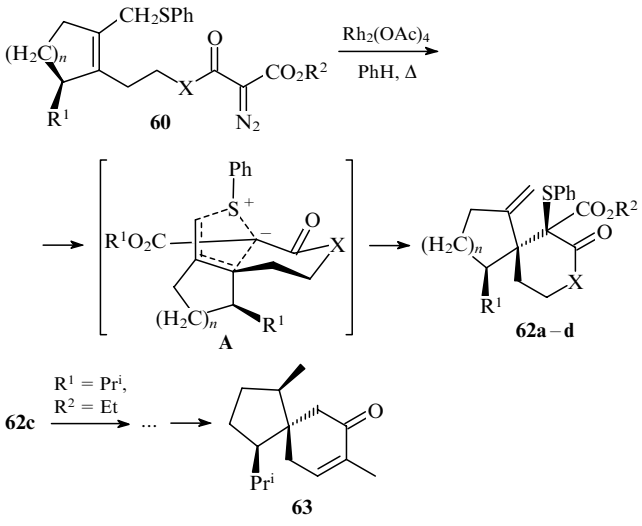

R^1, R^2 = Alk; X = O, *n* = 1 (**a**), 2 (**b**); X = CH_2, *n* = 1 (**c**), 2 (**d**).

Spiroannelation using the [2,3]-sigmatropic rearrangement *via* cyclic allylic sulfonium ylide was applied in the enantioselective synthesis of sesquiterpene (+)-acorenone B (**63**).[66] High stereoselectivity of the sigmatropic rearrangement is attributed to the fact that the less sterically hindered side opposite to the isopropyl group is favourable for the attack of the carbanion on the sulfonium reaction centre (transition state **A**).

Rhodium-catalysed stereoselective cyclisation of diazosulfide **64** followed by the 2,3-rearrangement of the resulting ylide afforded *cis*-2-oxa-9-vinyldecalin derivative **65**, which served as the starting compound in the synthesis of vernolepin (**66**).[67]

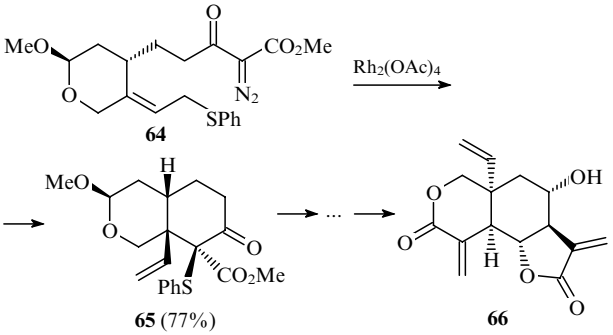

The rhodium-, copper- and palladium-catalysed stereoselective reactions of diazosulfides **67a** and **67b** were studied.[68] Depending on conditions, these reactions can afford either sulfonium ylides, which undergo the 2,3-sigmatropic rearrangement to form bicyclic compounds **68a** and **68b**, or tricyclic cyclopropane derivatives **69a** and **69b**. The latter are products of intramolecular cyclopropanation. Decomposition of the diazoamides **67a**,**b** in the presence of the rhodium complex with caprolactam gave rise predominantly to the azabicyclooctanes **68a**,**b**, whereas cyclopropane derivatives were selectively formed as the major products in the presence of catalysts containing electron-withdrawing ligands [$Rh_2(OAc)_4$, $Cu(acac)_2$, $Cu(OTf)_2$ or $Pd(OAc)_2$].

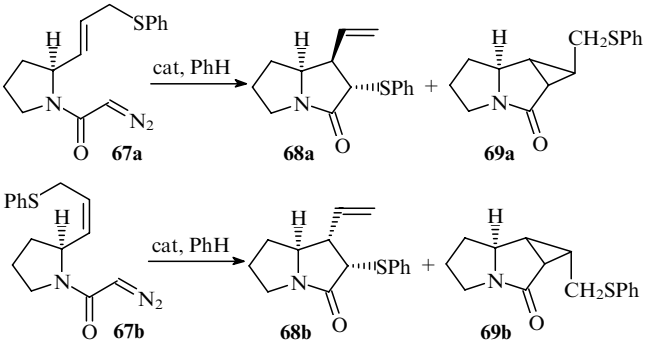

The rearrangements of diaminosulfoxonium salts of type **70** to form dihydro-2,1-benzoisothiazole derivatives **71** were described.[69] Treatment of the salts **70**, which were prepared by alkylation of sulfonimidoamides, with Bu^{t}OK resulted in the 2,3-sigmatropic rearrangement of intermediate ylides **72** to produce cyclohexadieneimine derivatives **73** in the first stage. The transfer of the hydrogen atom in the latter compounds was accompanied by rearomatisation. Cyclisation of intermediates **74** afforded the final products **71**.

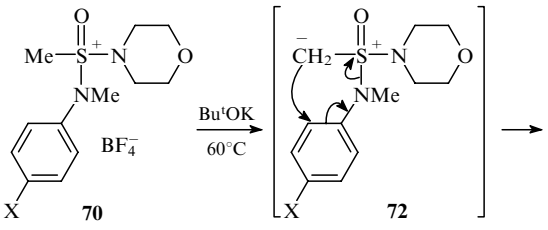

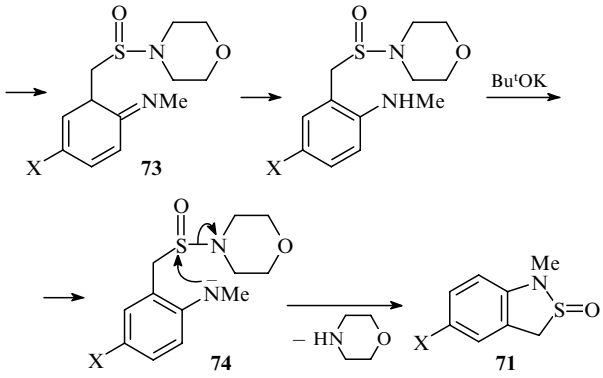

X = Me, Cl.

Yet another promising synthetic application of sulfur ylides is based on the 2,3-sigmatropic rearrangements of cyclic allylic sulfonium ylides proceeding with ring expansion.[17,70]

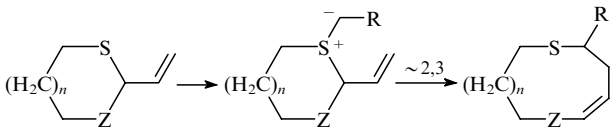

Z is the carbon atom or a heteroatom.

Ylides can be generated by reactions of cyclic α-vinyl sulfides with diazo compounds in the presence of copper [17,70] or rhodium catalysts [71] or by reactions of bases [17,70] with sulfonium salts. These procedures were used for the preparation of various macrocyclic compounds. For example, the synthesis of thiacycloundeca-4,7-diene derivative **75**, which is a precursor of aglycon of macrolide antibiotic methymycin, *viz*., methyneolide **76**, was carried out starting from tetrasubstituted thiolane **77**.[72–74] The rearrangement of ylide **78** derived from salt **79** afforded thiacyclooctene **80** from which ylide **81** was synthesised in several steps. The subsequent stereoselective 2,3-sigmatropic rearrangement of the ylide **81** gave rise to thiacycloundecadiene **75** (Scheme 1).

The 2,3-sigmatropic rearrangements of bicyclic allylic sulfonium ylides, which gave rise to compound **82** containing the thiabicyclo[6.3.1]undec-3-ene fragment, was used in the total synthesis of cytochalasines.[75,76] In this synthesis, vinyl iodide **83** served as the starting compound. The key stage of this synthesis involved the rearrangement of ylide **84** generated from sulfonium salt **85** under the action of potassium carbonate.

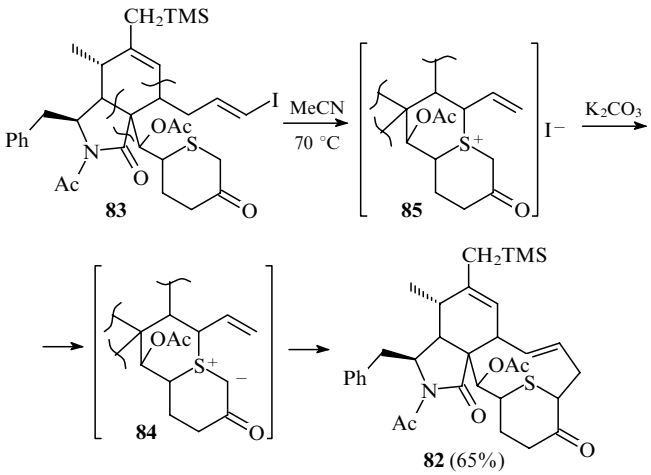

Difficultly accessible bicyclic unsaturated disulfides **86** (the so-called betweenanene structures) and **87** were synthesised.[77,78] Heating of dithioketal **88** with diazoacetate in the presence of $CuSO_4$ afforded ylide **89**, which underwent the 2,3-sigmatropic

Scheme 1

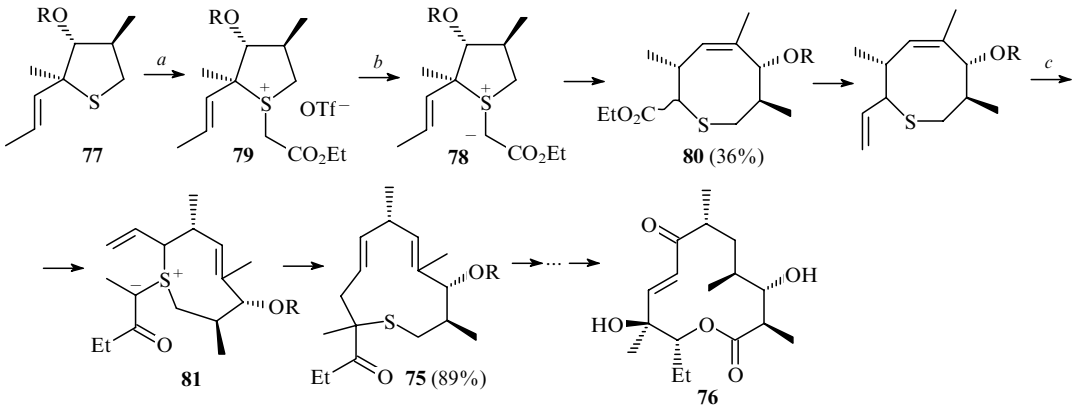

Tf = F_3CSO_2; (*a*) $TfOCH_2CO_2Et$; (*b*) K_2CO_3; (*c*) $TfOCHMeCOEt$, K_2CO_3.

rearrangement to give two geometric isomers **86** and **87** in a ratio of 4 : 1.

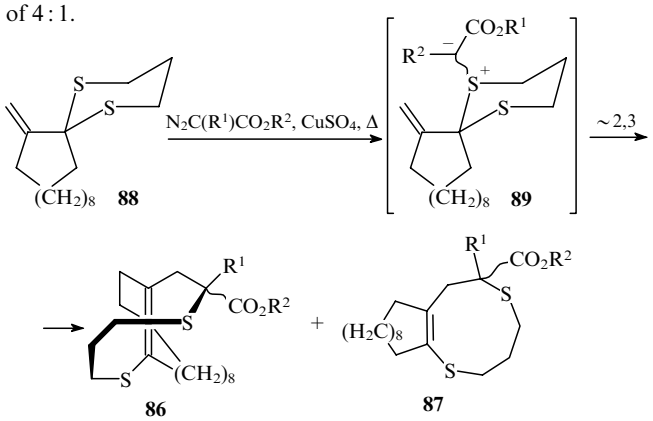

The structures of the 2,3-sigmatropic rearrangement products of acetylenic ylides **90a**–**c** derived from the corresponding sulfonium salts **91a**–**c** depend on the nature of the substituent at the triple bond. Thus the ylides containing alkyl substituents were converted into allenic sulfides **92a**,**b**, whereas the phenyl substituent promoted isomerisation into 1,3-diene **93c**.[79]

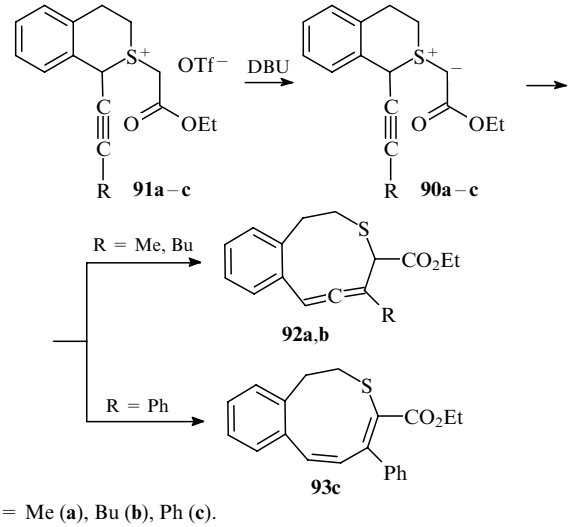

R = Me (**a**), Bu (**b**), Ph (**c**).

Aryl-substituted ylides **94** and **95**, which were formed on desilylation of salts **96** and **97**, underwent the Sommelet–Hauser rearrangement giving rise predominantly to substituted 2,5,8,9-tetrahydrodibenzo[*c*,*f*]thionines **98**[80] and 3,4,6,7-tetrahdydro-1*H*-5,2-benzooxathionines **99**, respectively.[81]

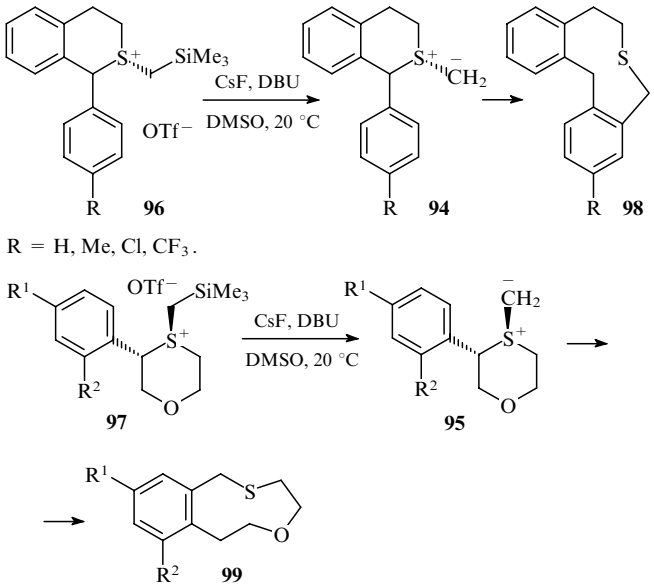

R = H, Me, Cl, CF_3.

R^1, R^2 = H, Me, OMe, CF_3.

Analogous thermal 2,3-sigmatropic rearrangements accompanied by ring expansion proceeded in the case of α-vinyl iminosulfurane ylides **100a**–**c**, which were prepared by treatment of sulfides **101a**–**c** with chloramine T in methanol at ~20 °C.[82] The rearrangements of the ylides **100a**–**c** afforded azathiacyclenes **102a**–**c**. It should be noted that treatment of 2-vinylthiepane **101c** with chloramine T gave rise to the final product **102c** even at room temperature. Attempts to isolate the intermediate ylide **100c** failed.

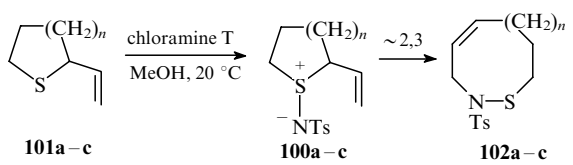

Compound **101**	*n*	Yield of **100** (%)	Temperature of the rearrangement /°C	Yield of **102** (%)
a	1	70	140	55
b	2	61	140	54
c	3	–	~20	61

Under the same conditions, benzoiminosulfuranes **103** and **104** produced 1,2- (**105**) and 3,4-benzothiazonines (**106**), respectively.[82]

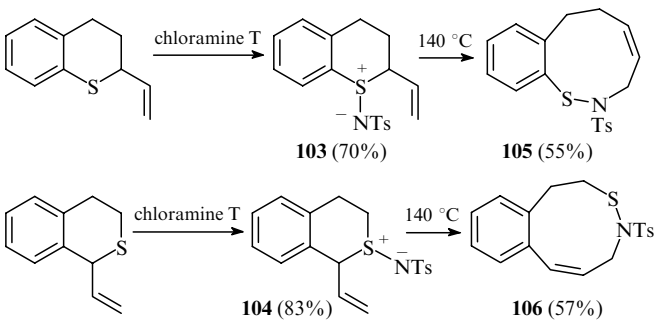

The reactions of 3,4-disubstituted 2,5-dichlorothiophenes **107** with diazoketones in the presence of rhodium catalysts afforded derivatives of a new heterocyclic system, *viz*., of 1,4-oxathiocine **108**.[83,84] The reaction scheme involves the formation of sulfur ylides **109** and their subsequent thermal 2,3-sigmatropic rearrangement proceeding through intermediates **110**. Heating of oxathiocine **111** at 110 °C gave rise to benzene derivative **112** due to elimination of the sulfur atom and 1,2-shift of the chlorine atom. It should be noted that the reactions of diazoketones with thiophenes, which do not contain chlorine atoms at positions 3 and 5, do not yield oxathiocine derivatives.

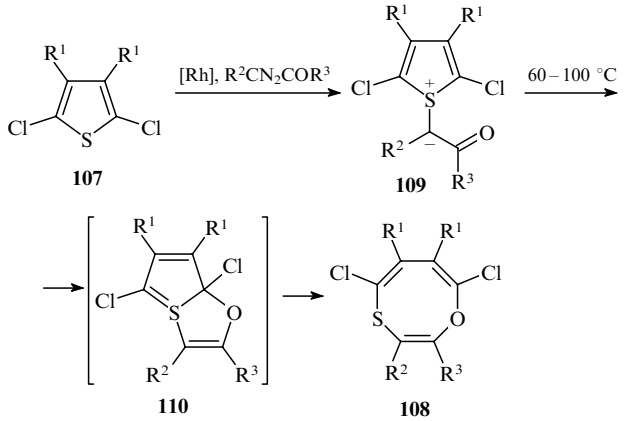

R^1 = H, Cl; R^2 = CO_2Et, CO_2Bu^t, Ts; R^3 = Me;
R^2–R^3 = $COCH_2CMe_2CH_2$.

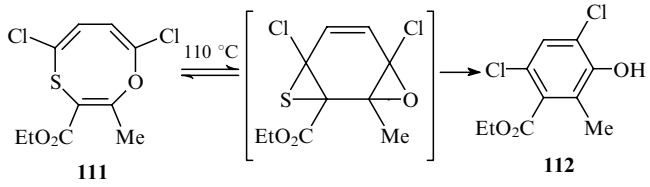

The 2,3-sigmatropic rearrangements of bi- and tricyclic sulfur ylides derived from substituted thiaphenanthrenes and isothiochromans, respectively, afforded both ring expansion products and spirane compounds.[85–88] The direction of the reaction and the structures of the final products depend essentially on the nature of the substituents at the sulfur atom and at position 1 of the initial ylide. For example, the reaction of stabilised ylide **113** with succinimide gave rise to the ring expansion product, *viz*., 2-phenyl-4,5-dihydro-3,5-benzooxathionine **114**, in high yield. The reaction mechanism involves deprotonation of intermediate **115** with the imide anion to form exocyclic methylide **116** whose 2,3-sigmatropic rearrangement yielded the target product **114**.[85] The reaction of the ylide **113** with phthalimide proceeded analogously.

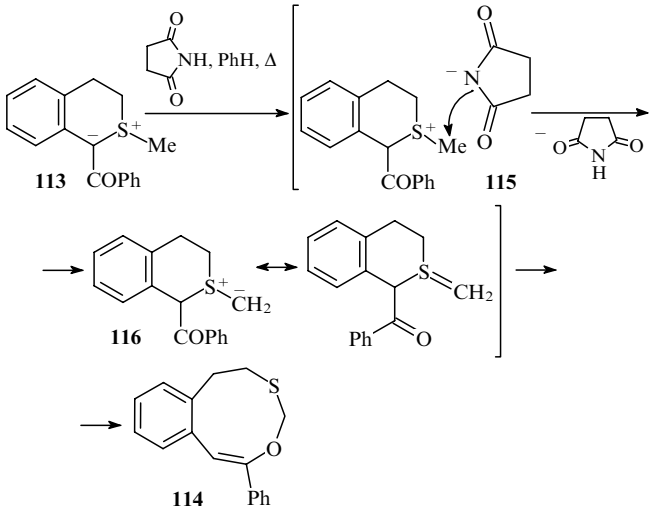

The reaction of 1-cyanoisothiochroman ylide **117a** proceeded by the same mechanism; however, due to the presence of the cyano group, the 2,3-sigmatropic rearrangement of intermediate exomethylide **118a** proceeded differently to form spirocyclic compound **119**.[86] On thermolysis, the compound **119** was isomerised to tetrahydrothiepin **120**, whereas its reactions with acetylenedicarboxylic esters afforded cycloadducts **121a**,**b**. The course of the reaction is substantially affected by the substituent at the sulfur atom. Thus the bulkier ethyl substituent in the ylide **117b** hinders the 2,3-rearrangement and the reaction gave rise to a mixture of benzothiopyran **122** and dimer **123**.

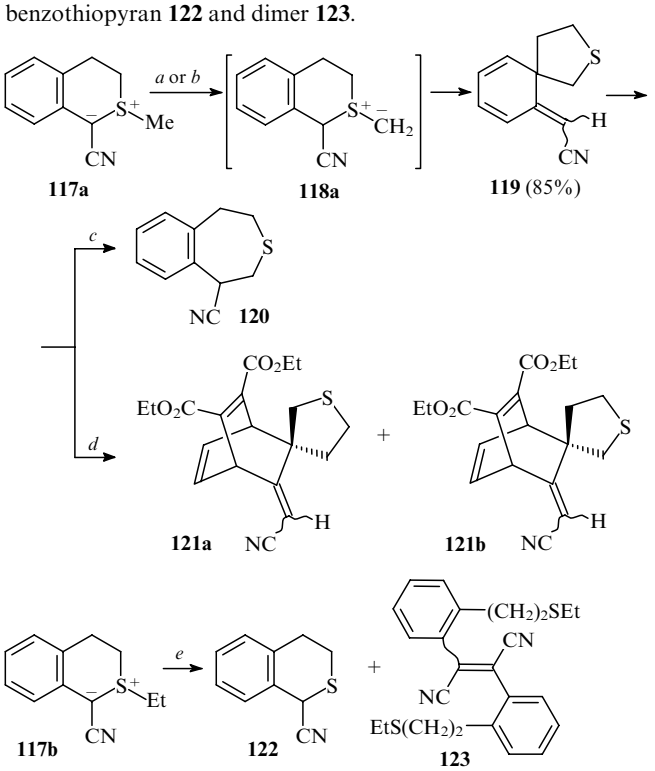

(*a*) EtOH or MeOH, Δ; (*b*) 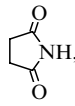 ; (*c*) 205 °C;
(*d*) $EtO_2CC{\equiv}CCO_2Et$; (*e*) EtOH, Δ.

Due to the presence of one more substituent (Cl, Br or Me) at position 1 in ylides **124**, their reactions proceeded through the 2,3-sigmatropic rearrangement involving the S–N bond. The reactions of the ylides **124** with succinimide afforded ketenimines **125**, which gave amides **126** or enol acetates **127** upon acid hydrolysis.[86]

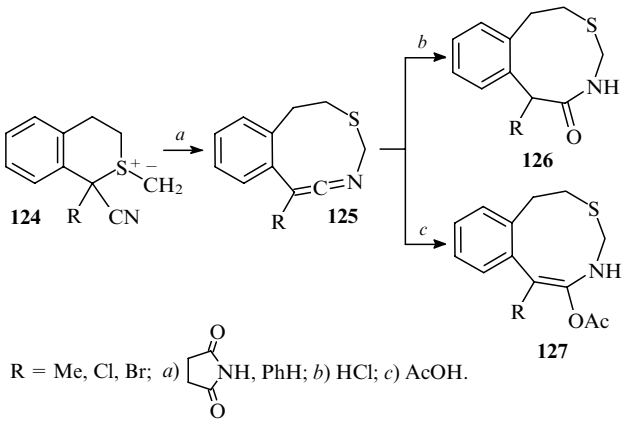

R = Me, Cl, Br; *a*) NH, PhH; *b*) HCl; *c*) AcOH.

The reactions of the 1-cyano ylides **117a**,**b** with activated acetylenes (dimethyl acetylenedicarboxylate or methyl propiolate) afforded fused compounds **128** and **129a**,**b**.[86] The methyl derivative **117a** gave a mixture of the compounds **128** and **129a** ($\sim$1 : 1) in 75% total yield. The reaction mechanism involves the intermediate formation of zwitterions **130a**,**b** whose isomerisation can take two different pathways (path *a* and path *b*). Intramolecular deprotonation of the *S*-methyl group (path *a*) gave rise to ylide **131** whose 2,3-sigmatropic rearrangement afforded the compound **128**. The nucleophilic attack of the vinyl anion on the positively charged sulfur atom produced unstable σ-sulfurane intermediate **132a**, which was converted into the ylide **129a**. The ethyl derivative **117b** gave only the doubly stabilised ylide **129b** in 31% yield.

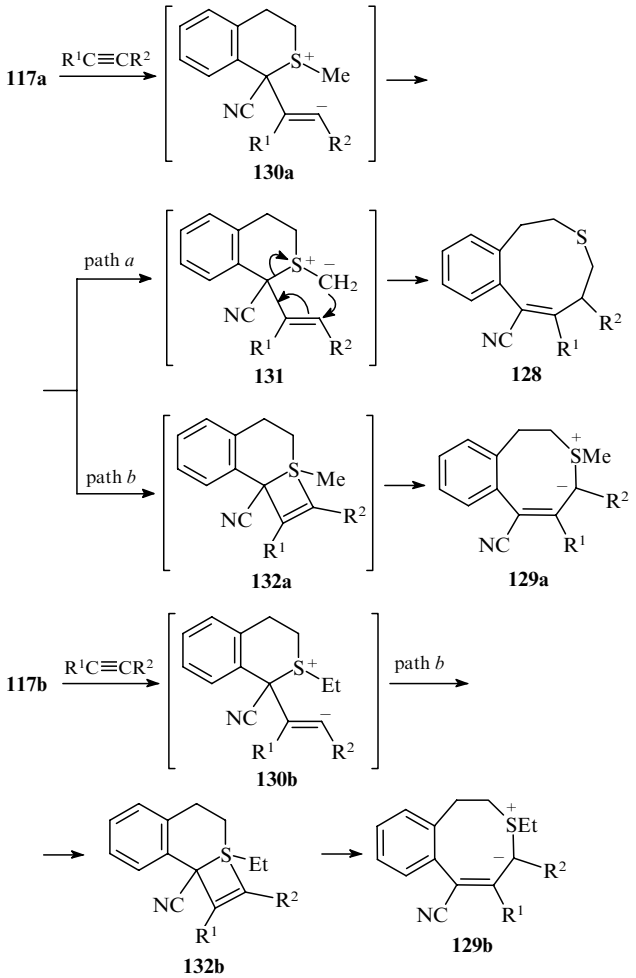

R^1 = H, R^2 = CO_2Me (**129a**); R^1 = R^2 = CO_2Me (**129b**).

The reactions of stabilised isothiochromene sulfonium ylides **133a**,**b** with acetylenic dienophiles proceeded differently.[87] These compounds reacted as heterodiene systems and the reactions proceeded as [4 + 2]-cycloaddition to yield intermediates **134a**,**b**. Depending on the solvent, subsequent conversions of these intermediates afforded either dihydrocyclopropa[*a*]naphthalene derivatives **135a**,**b** (in aprotic solvents) or naphthalene derivative **136a** (in protic solvents). It should be noted that only [2 + 1]-adduct **137** was formed in high yield in the reaction of the compound **133a** with methyl propiolate in sulfolane. This adduct was generated by the interaction of intermediate **138** with the starting ylide **133a**.

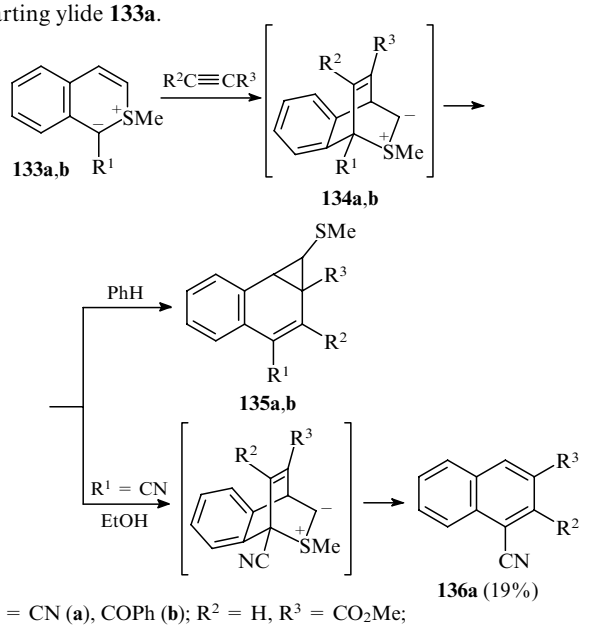

R^1 = CN (**a**), COPh (**b**); R^2 = H, R^3 = CO_2Me;
R^2 = R^3 = CO_2Me, CO_2Et.

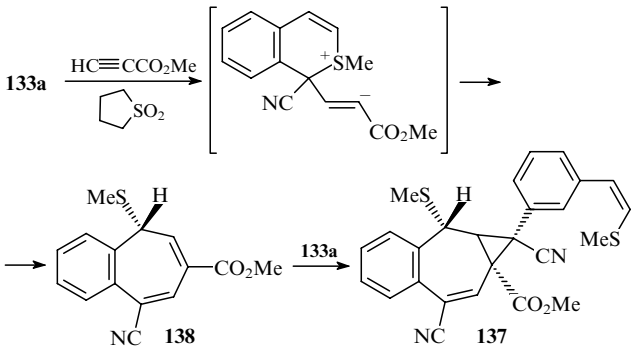

The reaction of 2-cyano-α-thiochromene ylide **139** with dimethyl acethylenedicarboxylate afforded the ring expansion product **140** in low yield.

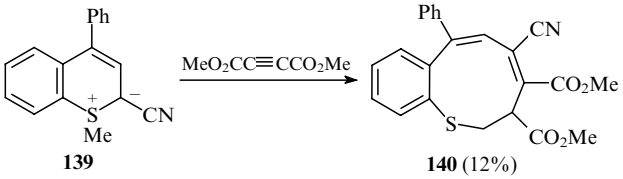

The reactions of tricyclic sulfur ylide **141a** stabilised by the adjacent cyano group (the thiaphenathrene derivative) with activated acetylenes produced spirocyclic compounds **142** (the yields were up to 31%), which underwent the 1,5-rearrangement upon heating to give dibenzothionine derivatives **143** in yields of up to 95%.[88] It is assumed that the reaction mechanism involves the formation of zwitterionic intermediates **144**, which are rearranged to exocyclic sulfonium ylides **145**. The ylides **145** can undergo the

Sommelet–Hauser rearrangement to produce the compounds **142**. In the case of the ethyl-substituted ylide **141b**, spirocyclic compounds were not formed; instead, the reaction afforded dibenzothiepin derivatives **146** as the major products (the yields were up to 38%). Since the ethyl substituent at the sulfur atom in the compound **141b** causes steric hindrances to the Sommelet–Hauser, this compound underwent the 1,2-Stevens rearrangement to form the ring expansion product **146**. The rearrangements of the zwitterions **144** afforded dibenzothiocine derivatives (in the yields of up to 22%) along with the compounds **146** (see the scheme for the formation of the compound **129a**).[86]

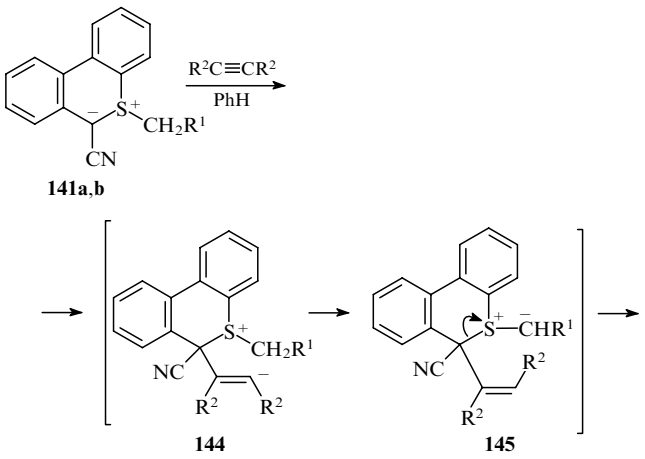

R^1 = H (**a**), Me (**b**); R^2 = CO_2Me, CO_2Et.

The reactions of sulfur ylides **147a–f**, *viz*., 9-alkyl-9-thia-10-azaphenanthrenes, with dimethyl acetylenedicarboxylate gave rise to dibenzothiazonium derivatives (compounds **148** and **149**), dibenzothiazocine derivatives (compounds **150**), 2-alkylsulfinyl-2′-vinylamionbiphenyls **151** and bis(biphenylylimino)ethane derivatives **152** (Scheme 2).[89]

The composition of the reaction products depends substantially on the substituent at the sulfur atom. Thus the compound **147a** produced predominantly dibenzothiazonine derivatives **149a** and **148a**, whereas the ylides **147b**,**c**,**d** gave predominantly dibenzothiazocine derivatives **150** and biphenyls **151**. The ylides **147e**,**f**

Scheme 2

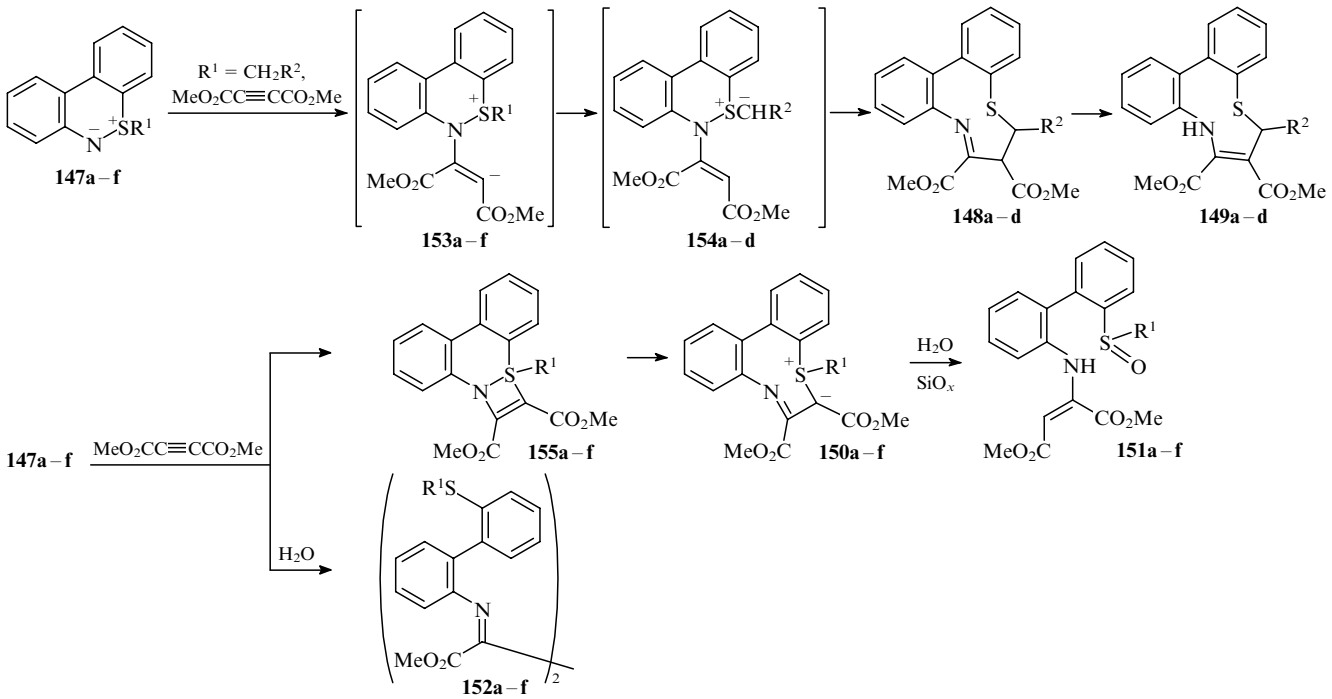

R^1 = CH_2R^2 (R^2 = H (**a**), Me (**b**), Et (**c**), C_5H_{11} (**d**)); R^1 = Ph (**e**), CH=CPh_2 (**f**).

containing the phenyl or vinyl substituent at the sulfur atom produced only dibenzothiazocine derivatives **150e**,**f**. The reaction mechanism involves the formation of zwitterions **153** and **154**. The exocyclic ylide **154** was isomerised to form the compounds **148** and **149**. The zwitterion **153** can produce intermediate **155** from which the derivatives **150** and **151** are generated or can react with water giving rise to the dimers **152**. The reactions of 9-alkylthiaazaphenanthrenes **147a – c** with methyl propiolate afforded 1 : 2 adducts, which are dibenzothiazocine derivatives **156a – c**.[89]

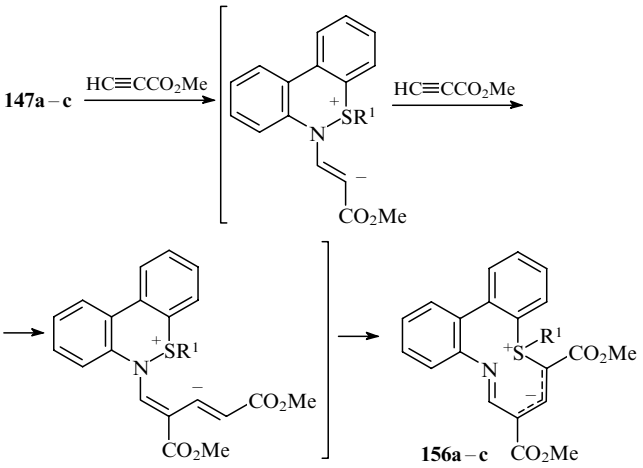

The rearrangements of tricyclic sulfonium salts **157** under the action of various bases have been studied thoroughly.[90] Thus treatment with strong bases [lithium diisopropylamide(LDA), NaH or K_2CO_3] afforded ylides **158** and **159**, which underwent the 2,3- and 1,4-sigmatropic rearrangements to form spirovinylcyclopropane derivatives **160** or tricyclic compounds **161**. The ratio of the reaction products depends on both the base used and the nature of the substituents.

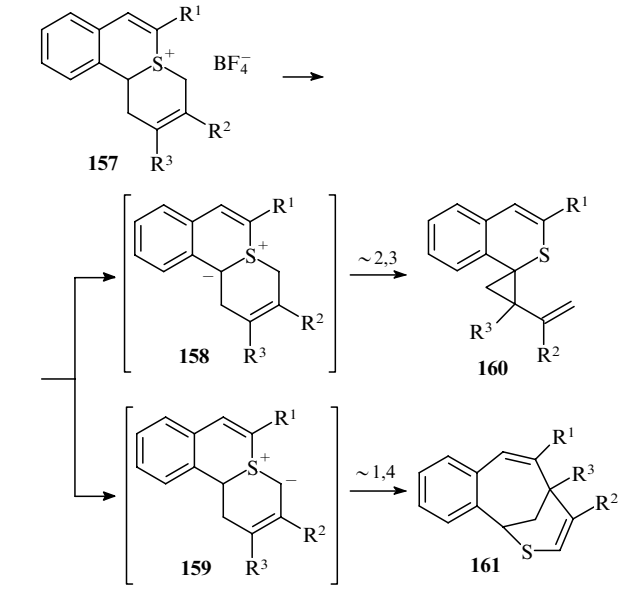

R^1	R^2	R^3	Base	Yield (%)	
				160	**161**
H	Me	Me	LDA	35	52
Bz	Me	Me	LDA	57	7
H	Me	Me	NaH	28	70
Bz	Me	Me	NaH	75	0
H	H	Me	NaH	44	45
Me	Me	Me	NaH	46	46
H	Me	Me	K_2CO_3	21	22
Bz	Me	Me	K_2CO_3	64	0

In the reactions with the salts **157**, weak bases, such as Et_3N, Et_2NH, $BuNH_2$ or AcOK, act as nucleophilic reagents and attack the CH_2 group adjacent to an electron-deficient centre to yield ring expansion products **162** in high yields.

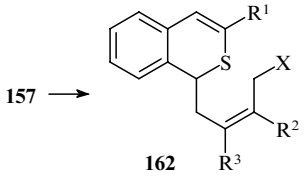

X = NEt_3BF_4, NEt_2, OAc, NHBu.

Interesting results were obtained in studies of the rearrangements of dibenzothiocine salts **163a**,**b**, which took place under the action of a KOH solution in methanol.[91] Thus the sulfoxide **163a** was converted into a mixture of enantiomers of dibenzothiepin derivative **164a**,**b** (in a ratio of ~2 : 1). Under the same conditions, the sulfide **163b** unexpectedly gave compound **165**. The assumed reaction mechanism involves the tandem of the 2,3- and 1,3-sigmatropic rearrangements with the intermediate formation of spirocyclic intermediates **166** and **167**.

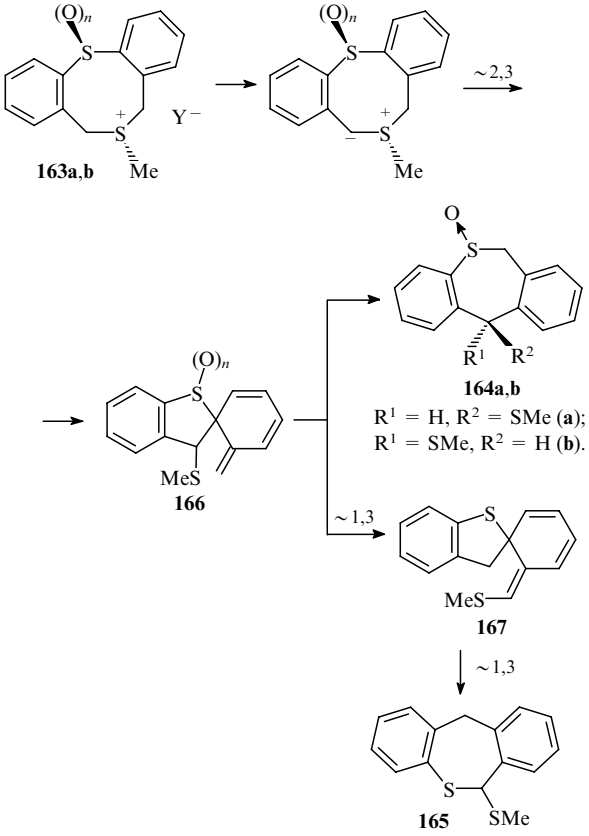

n = 1, Y = $SbCl_6$ (**a**); *n* = 0, Y = BF_4 (**b**).

III. Intramolecular cyclisation of sulfur ylides

A promising approach to the synthesis of nitrogen-containing heterocycles, including analogues of alkaloids, is based on intramolecular cyclisation of phthalimido-substituted sulfur ylides stabilised by the carbonyl group.[92–98] Under the conditions of the Arndt – Eistert reaction,[99] *N*-phthaloyl-α- (**168**) and -β-amino acids (**169**) generated bromo ketones, which were converted into the corresponding sulfonium salts. Deprotonation of these salts afforded stabilised ylides **170** and **171**, respectively, which underwent intramolecular cyclisation on heating in toluene with an equimolar amount of benzoic acid[96] to give methylthio-substituted pyrrolizidine- (**172**) and indolizidinediones **173** and **174**. It is significant that racemisation does not take place in the reactions

involving optically active ylides. Longer-chain sulfur ylides derived from γ- and δ-amino acids did not undergo cyclisation; instead, alkyl thioketones and oxobenzoates were formed as the major products.[96] The effect of the substituents in the phthalimide fragment on the regioselectivity of the reaction and the yields of the products was also studied.[97]

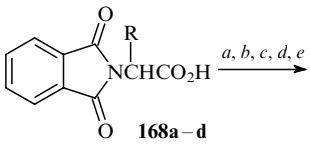

168a–d

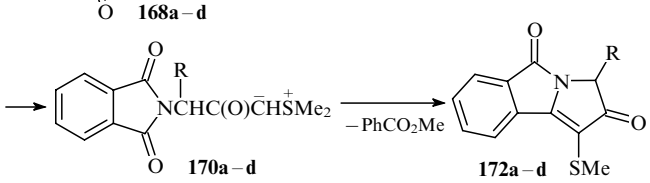

170a–d **172a–d**

Compound **172**	R	Yield (%)
a	H	86
b	Me	85
c	Pr^i	84
d	Bn	83

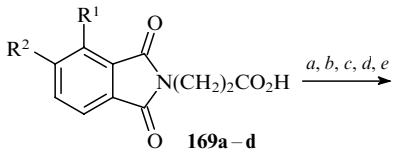

169a–d

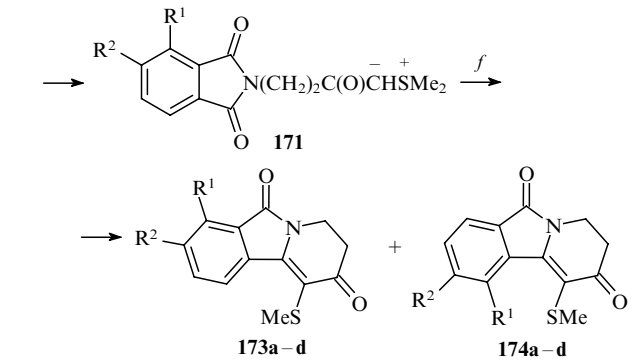

171 **173a–d** **174a–d**

Compound **169**	R^1	R^2	Yield (%)	
			173	**174**
a	H	H	86	
b	NO_2	H	52	
c	Cl	H	75	
d	H	NO_2	38	35

(*a*) $SOCl_2$; (*b*) CH_2N_2; (*c*) HBr; (*d*) Me_2S; (*e*) NaOH – K_2CO_3; (*f*) $PhCO_2H$, 110 °C.

Ylides **175** and **176** containing the tetrahydrophthalimide or succinimide fragment, respectively, instead of the phthalimide fragment did not undergo cyclisation.[97]

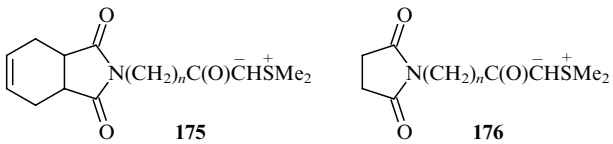

175 **176**

n = 1, 2.

Under the conditions of cyclisation, ylide **177**, which was synthesised from β-alanine and pyridine-2,3-dicarboxylic anhydride, selectively formed a tricyclic compound, *viz*., 5-methylthio-7,8-dihydro-4,8*a*-diazafluorene-6,9-dione (**178**).[98]

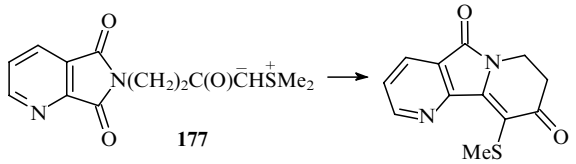

177 **178** (58%)

The assumed mechanism of a new type of intramolecular cyclisation, which is not quite typical of sulfonium ylides, involves, apparently, the attack of the anionic centre on one of the carbonyl groups of the phthalimide fragment followed by migration of the methyl group.[100, 101] The reaction ends in elimination of the methanol fragments from intermediate **179** under the action of benzoic acid to form rearrangement product **180**, methyl benzoate and water.

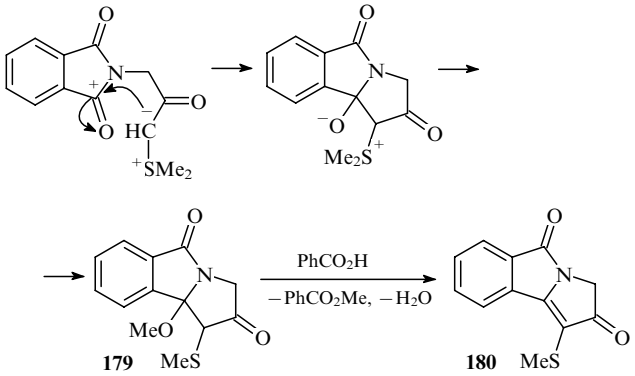

179 **180**

Intramolecular cyclisation of ylides **181** containing the sulfur atom in the ring gave rise to benzoates **182**.

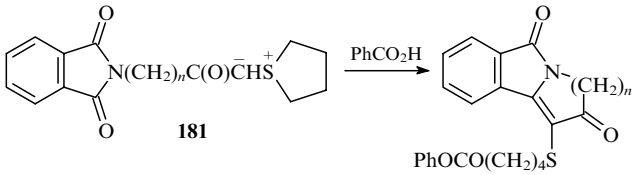

181 **182**

n = 1, 2.

Diazosulfides (*R*)- or (*S*)-**183** generated from D- or L-methionine, respectively, underwent cyclisation under the action of HBr to form optically active sulfonium salts (*R*)- or (*S*)-**185** (the yields were 54 and 62%, respectively). Subsequent treatment of these salts with potassium carbonate afforded cyclic ylides (*R*)- or (*S*)-**184** stabilised by the carbonyl group (the yields were 75% and 90%, respectively).[102]

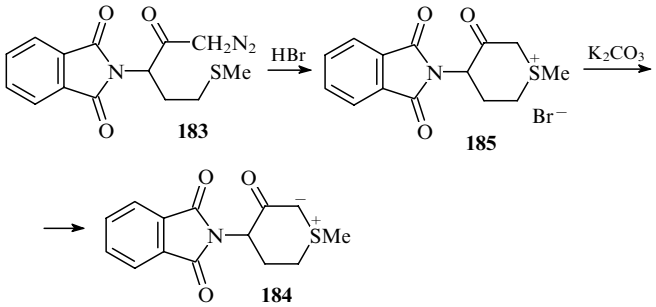

183 **185** **184**

A new approach to the stereoselective synthesis of amino acids from chiral lactams through intermediate formation of β-ketosulfoxonium ylides was developed.[103, 104] Previously,[105, 106] it was found that these ylides were converted into intermediates of the carbene type on photolysis or under the action of transition metals. The reactions of activated chiral lactams **186a**,**b** with dimethylsulfoxonium methylide were demonstrated to produce ylides **187a**,**b** in high yields.[103, 104] Under the action of rhodium

catalysts, the reactions of the ylides **187a**,**b** proceeded stereoselectively giving rise to derivatives of 4-oxopyrrolidine **188a** or 5-oxopiperidine **188b** formed as a result of cyclisation of intermediate carbenes **189a**,**b**. The compounds **188a**,**b** were used in the synthesis of optically active α-amino acids.[107]

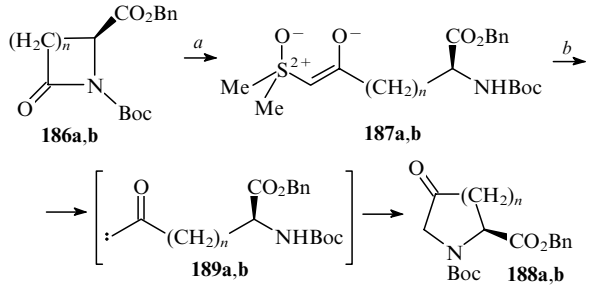

Boc = Bu^{t}OCO; n = 1 (**a**), 2 (**b**);

(*a*) $Me_2\overset{+}{S}(O)CH_2^-$, DMSO, 20 °C; (*b*) [$Rh^{2+}$].

IV. Reactions of thiocarbonyl ylides

Considerable recent attention has been given to thiocarbonyl ylides, which are readily accessible and highly reactive intermediates. Several procedures were developed for the preparation of thiocarbonyl ylides among which are the 1,3-dipolar cycloaddition of diazo compounds to thioketones to form 1,3,4-thiadiazolines followed by nitrogen elimination,[108] the addition of thioketones to oxiranes[109] or photoisomerisation of aryl vinyl sulfides.[110] Thiocarbonyl ylides readily undergo rearrangements. These compounds are involved in cycloaddition with dipolarophiles and in 1,3- and 1,5-electrocyclisations, which often proceed with high regio- and stereoselectivity. The reactions of thiocarbonyl ylides with compounds of the RXH type (X = N, O or S) giving rise to 1 : 1 adducts were also studied.[111–113] Recently, cyclisation of carbenes generated by catalytic decomposition of diazothioamides has gained wide acceptance for the preparation of thiocarbonyl ylides.[114] Thus diazothioamide **190** gave cyclic thiocarbonyl ylide **191** under the action of a rhodium catalyst. The ylide **191** was converted into enaminoketone **193** due to elimination of sulfur from intermediate episulfide **192**.[115]

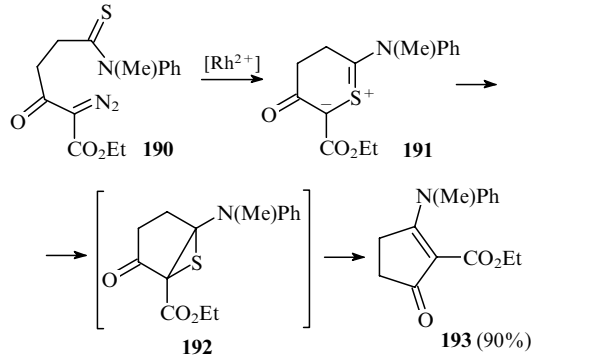

Intramolecular cyclisation of diazothioamide **194** catalysed by dirhodium tetraacetate afforded thiocarbonyl ylide **195** stabilised through the aromatic mesoionic structure. The ylide **195** reacted with *N*-phenylmaleimide according to the scheme of the diene synthesis to give adduct **196**.[115]

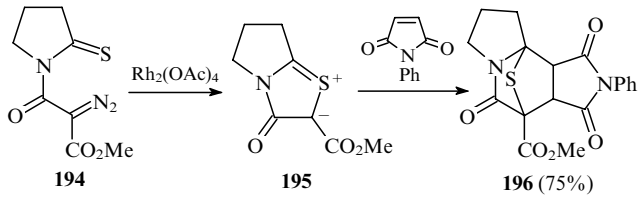

Thiocarbonyl ylides were successfully used in the synthesis of natural alkaloids.[116–120] Thus non-stabilised ylide **198** was generated from diazothioamide **197** under the action of rhodium acetate followed by the rearrangement of the latter into episulfide **199**. Isomerisation of the compound **199** afforded thioketone **200**, which underwent desulfurisation under the action of Raney nickel to yield dihydropyridone **201**.[116]

This procedure was used for the synthesis of dihydropyridone **202**, which was the key intermediate in the total synthesis of antibiotic indolisomycin **203**.[117, 118] Diazothioamide **204** was used as the starting compound.

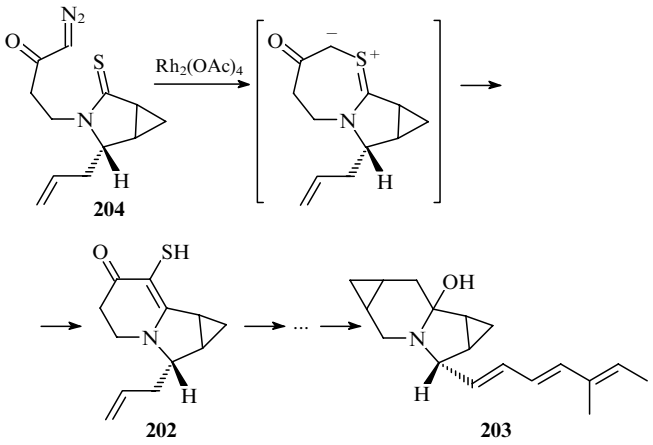

Alkaloids helenine (**205**)[119] and cephalotaxine (**206**)[120] were synthesised using compounds **207** and **208**, respectively. The latter were prepared by cyclisation of hydrazones **209** and **210**, which were synthesised from substituted benzaldehydes and *N*-amino-1,2-diphenylaziridine, in the presence of dirhodium tetraacetate. The reactions proceeded through the corresponding carbenoids and cyclic thiocarbonyl ylides (Scheme 3).

Thiocarbonyl ylide **211**, which was generated *in situ* on heating of a suspension of iodonium compound **212** in carbon disulfide in the presence of copper acetylacetonate, underwent cyclisation to yield oxathiol heterocycle **213**.[121]

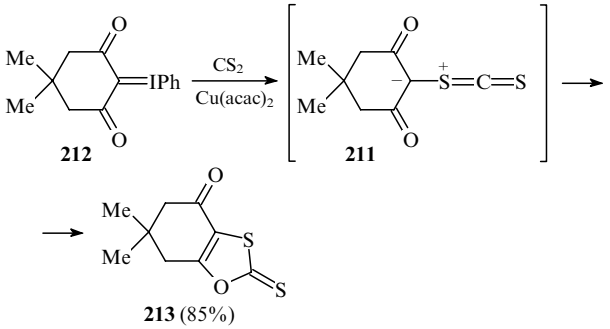

The reaction of di-*tert*-butylthioketene (**214**) with diazomalonate afforded thioketene ylide **215**, which underwent cyclisation to give 2-alkylidene-1,3-oxathiol **216**.[122]

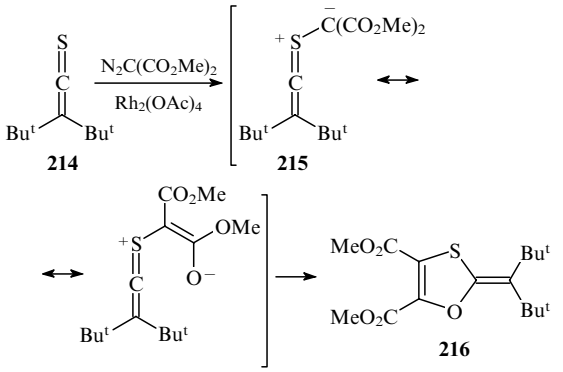

Scheme 3

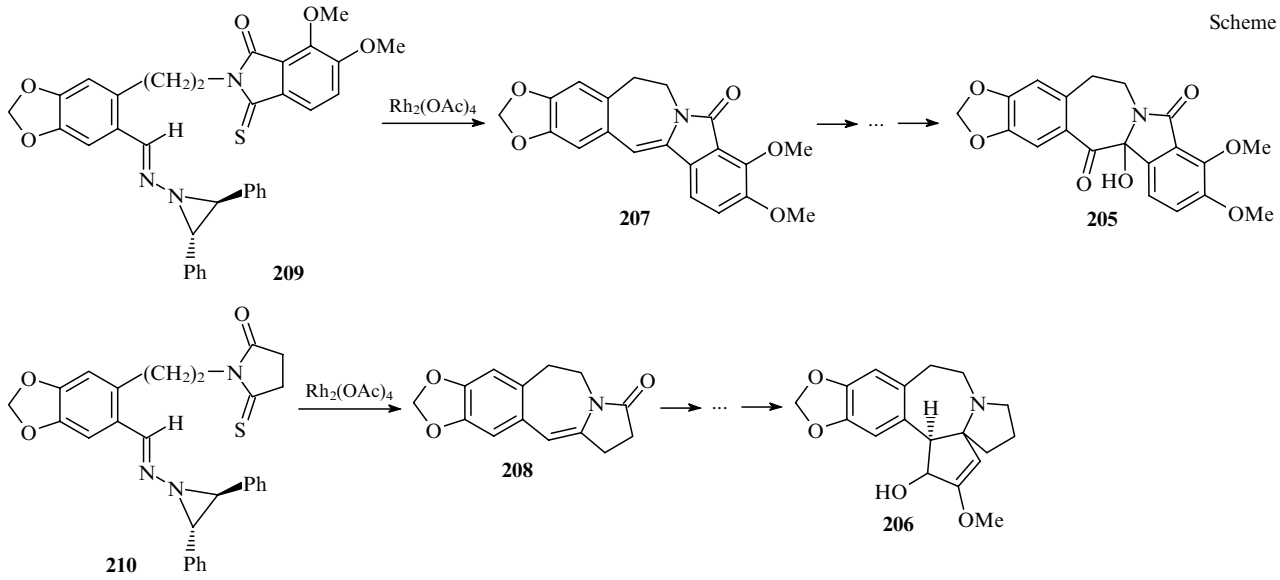

Scheme 4

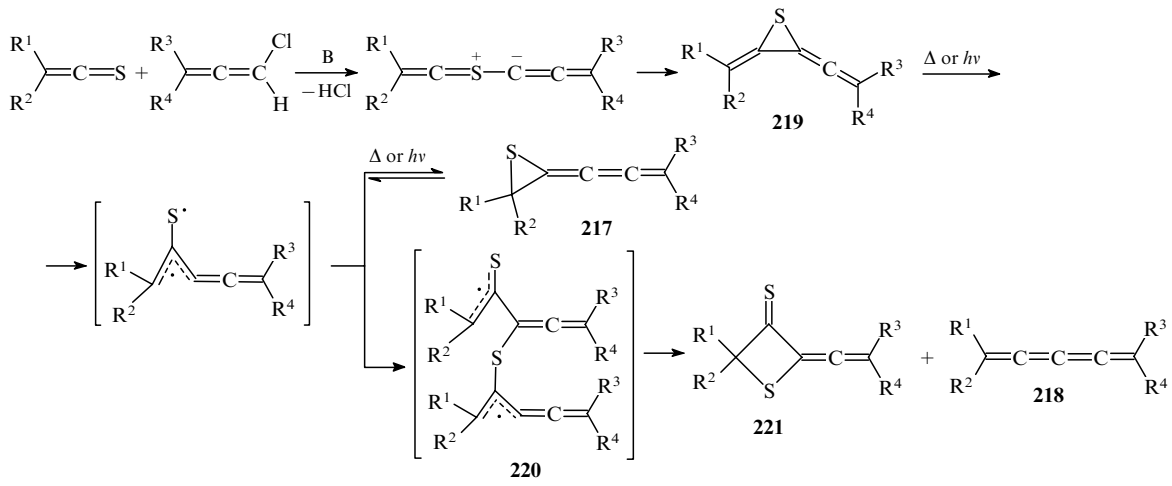

$R^1 = R^2 = R^3 = R^4 = Bu^t$; $R^1 - R^2 = CMe_2(CH_2)_3CMe_2$, $R^3 = R^4 = Bu^t$; B is a base.

Various cumulenes and cumulene episulfides were prepared by the addition of alkenylidene dicarbenes to thioketenes.[123] Episulfides **217** were isolated as stable crystal compounds, which underwent predominantly desulfurisation on heating or photolysis to give tetraenes **218** in yields from 50% to 69% and were also partially isomerised to episulfides **219**. Substituted thietanethiones **221** were obtained as by-products (9% – 20%) due to the intermolecular transfer of the sulfur atom through biradical intermediate **220** (Scheme 4).

Vinylthiocarbonyl ylides generated from vinyldiazoalkanes **222** and thiochromones **223** or **224** gave 1,3- (**225**) or 1,5-electrocyclisation (**226** or **227**) products depending on the nature of substituents in the ylide.[124] Unstable thiirane **225** (R = H) was immediately converted into diene derivative **228** with elimination of sulfur. The reactions of diazo compounds **222a**,**b** with thiochromone **224** proceeded through the formation of analogous dienes. Diazo compound **222c** containing the bulkier phenyl substituent was involved in 1,5-electrocyclisation with the thiochromones **223** and **224** to give dihydrothiophene derivatives **226** and **227**, respectively.

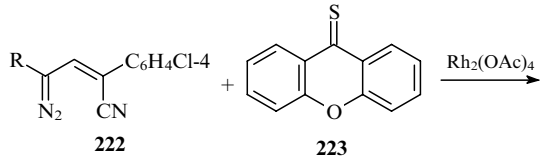

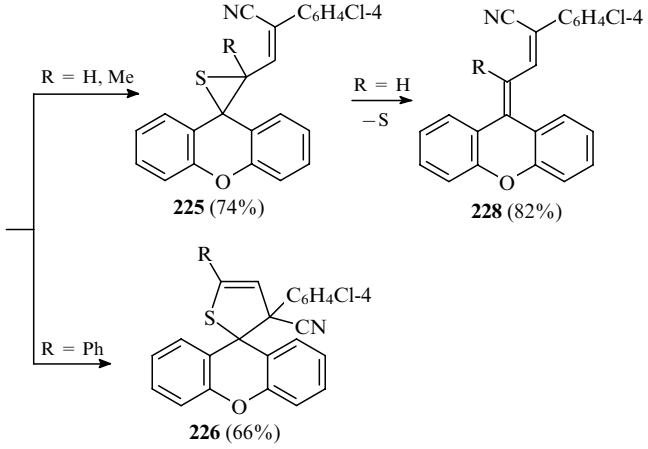

R = H (**a**), Me (**b**), Ph (**c**).

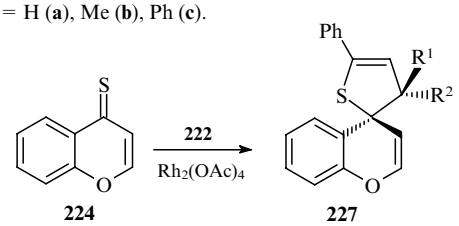

R^1 = CN, R^2 = C_6H_4Cl-4 (55%); R^1 = C_6H_4Cl-4, R^2 = CN (28%).

Amino-substituted thiocarbonyl ylide **229** underwent intramolecular condensation of a new type providing an approach to 1,6-dithia-3,9-diazaspiro[4.4]non-2-enes **230**.[125]

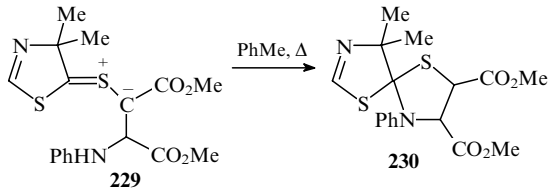

The reactions of thiocarbonyl ylide **231** with thioamides **232** were accompanied by unusual intramolecular cyclisation.[108] Adduct **233** generated initially underwent cyclisation to give 2-thia-4-azabicyclo[3.1.1]hept-2-ene derivative **234**. This is the first example of the nucleophilic addition of a cyclobutanone derivative to the carbonyl group proceeding without opening of the four-membered ring.

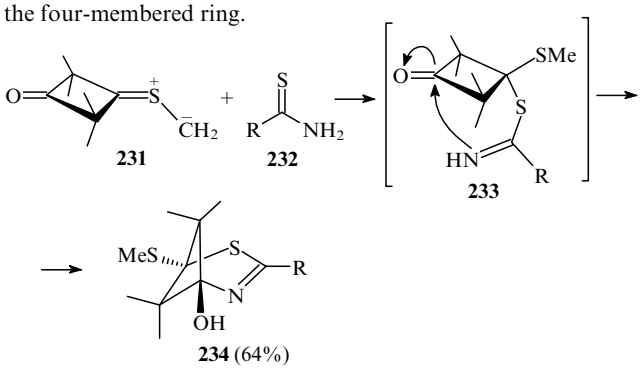

234 (64%)

R = Me, Ph.

V. Cycloaddition of ylides to alkenes

The reactions of stabilised sulfonium ylides with electron-deficient alkenes of the C=C–X=Y type generally afford cyclopropanes (the $Ad_N-E_{1,3}$ mechanism);[6] however, five-membered heterocycles can also be formed due to the involvement of the activating X=Y group, where X=Y = NO_2, N=O or N=NAr (the $Ad_N-E_{1,5}$ mechanism).[10, 13]

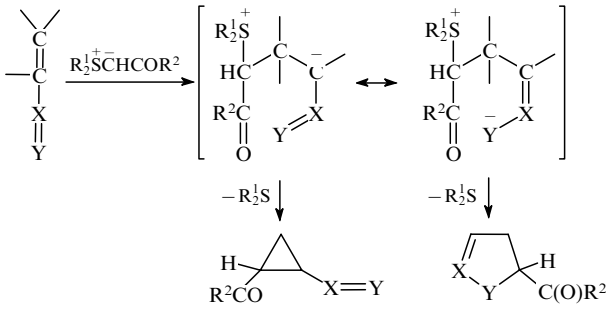

These reactions were considered in sufficient detail in the review,[13] which surveyed the data available up to 1986. Hence, we dwell only on the recent most interesting results published in the literature.

The reactions of nitroalkenes with stabilised sulfonium ylides were demonstrated [126, 127] to proceed stereoselectively to give both *trans*-4,5-dihydroisoxazole *N*-oxides **235** and substituted cyclopropanes, the ratio of the reaction products being essentially dependent on the α-alkyl substituent in nitroalkenes. In the case of bulkier substituents R, heterocyclic adducts are formed in substantially higher yields.

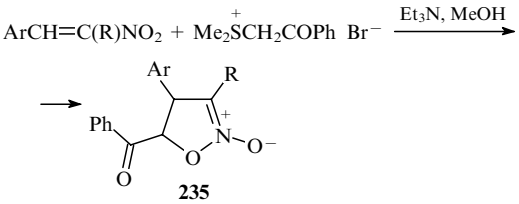

Ar = 3-$NO_2C_6H_4$, R = CO_2Et (85%); Ar = Ph, R = Me (41%).

The reactions of arylmethylenecyanothioacetamides with stabilised sulfur ylides **236** proceeded stereoselectively to give mixtures of 2-amino-4,5-dihydrothiophenes **237** and cyclopropanethiocarboxamides **238**.[128] In most cases, the dihydrothiophenes **237** were obtained as the major reaction products. For R = cyclo-C_3H_5, cyclopropane derivatives did not form at all.

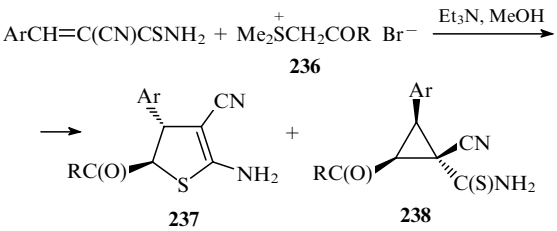

Ar = 2-MeC_6H_4, 2-$NO_2C_6H_4$, 4-$MeOC_6H_4$, 3-pyridyl, 2-thienyl;
R = Ph, 2-thienyl, cyclo-C_3H_5.

A simple and efficient procedure for the preparation of 2,5-dihydrofurans **239** containing the *N*-tosylamino substituent is based on the reaction of *N*-sulfonylimines with sulfur ylides generated from *cis*-4-hydroxybut-2-enyldimethylsulfonium salts **240**.[129] The assumed mechanism involves the formation of aziridine derivative **241**, ring opening through the attack of the internal nucleophile and subsequent cyclisation to form 2,5-dihydrofuran. The reaction involving the *trans*-isomer of the sulfonium salt **240** afforded only the aziridine derivative.

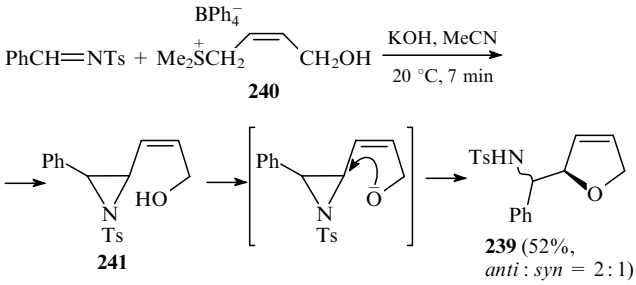

239 (52%, *anti* : *syn* = 2 : 1)

As mentioned above, thiocarbonyl ylides are readily involved in 1,3-dipolar cycloaddition to give the corresponding cycloadducts in high yields and with high regioselectively. Thus when heated, dihydrothiadiazoles **242**, which were formed in the reactions of diazomethane with derivatives of oxodithiocarboxylic acids **243**, gave intermediate **244**, which reacted with dienophiles to yield substituted thiolanes **246**–**248**.[130] In the absence of dienophile, the ylide **244** produced intramolecular cyclisation product **245**.

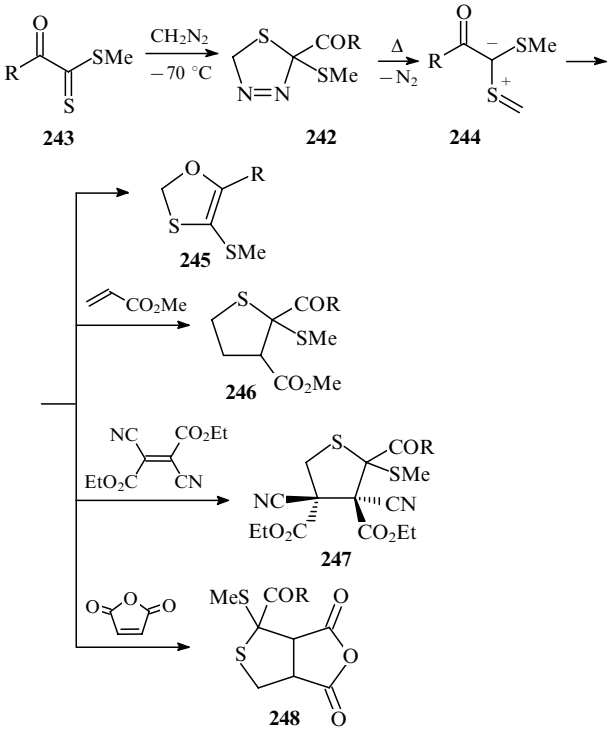

1,3-Dipolar cycloaddition of thiocarbonyl ylide **249** to sulfur dioxide gave rise to 1,2,4-oxadithiolane 2-oxide **250**.[131]

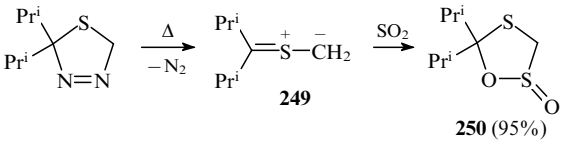

The reaction of thiocarbonyl ylide **251**, which was generated *in situ* from oxospiro[cyclobutanedihydrothiadiazole] **252**, with *trans*-1,2-bis(trifluoromethyl)-1,2-dicyanoethylene afforded thiolane **253** and stable strained cyclic ketenimine **254** in a ratio of ~1 : 4.[132]

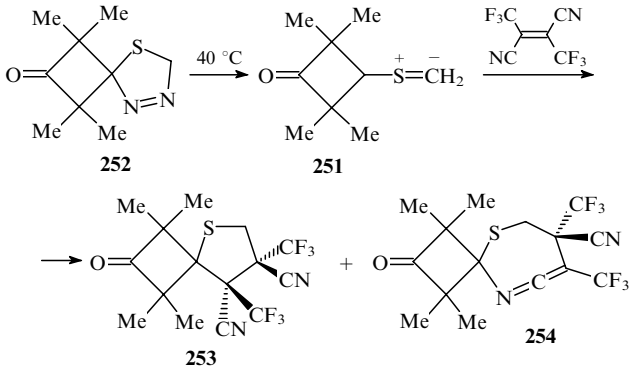

Adamantanethione-*S*-methylide (**255**) reacted with methyl acrylate to form substituted thiolane **257**, whereas its reactions with thioketones **256** gave rise to 1,3-dithiolanes **258a–c** and **259a–e**. The reactions involving thiobenzophenone (**256a**), thiofluorenone (**256b**) or thioxanthione (**256c**) produced two regioisomers.[133]

1,3-Dipolar cycloaddition of thiocarbonyl ylides **260** to thiazole-5(4*H*)-thiones **261**[134] or azodimethyl carboxylate **262**[135] proceeded with high regioselectivity to give the corresponding spirocyclic adducts **263–266** in high yields.

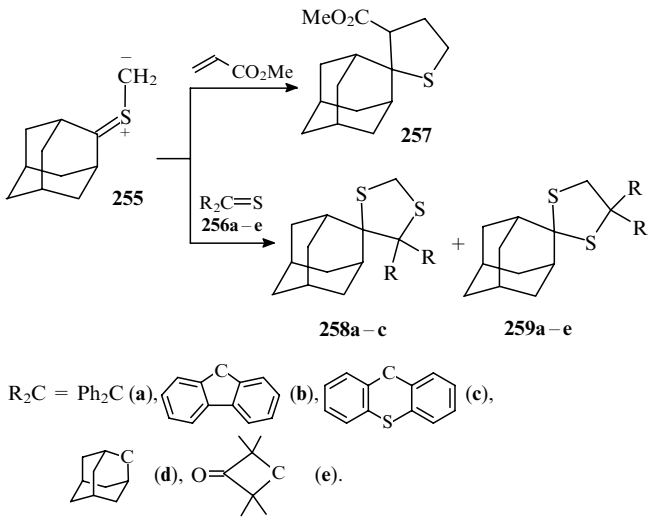

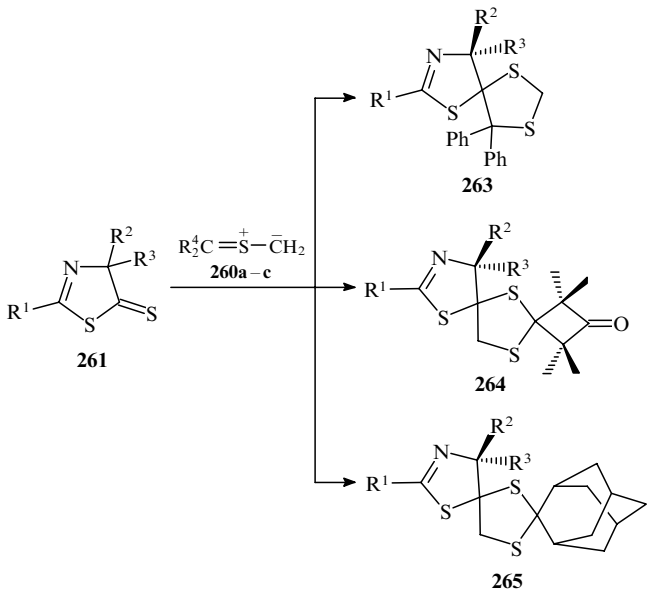

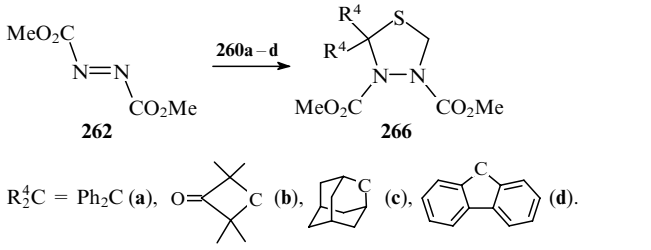

Cycloaddition of the thiocarbonyl ylides **251** and **260a** to *N*-sulfinylaniline and *N*-sulfinyltosylamide gave rise to both substituted 1,3,4-dithiazolidine 3-oxides (adducts at the N=S bond) and 1,2,4-oxadithiolane-2-tosylimides (adducts at the S=O bond).[136] The reactions of thioketones with diazoacetates performed on heating in THF[137,138] afforded acyl-substituted thiocarbonyl ylides as the initial reaction products, which either underwent 1,3- or 1,5-dipolar electrocyclisation or reacted with the second thioketone molecule to give a 1,3-dipolar cycloaddition product. The first example of 1,3-dipolar cycloaddition of thiocarbonyl ylide $CH_2=S-CH_2$ to fullerene C_{60} giving rise to a tetrahydrothiophene derivative was reported.[139] This product is a convenient starting compound for subsequent functionalisation.

* * *

As evident form the published data, the recent investigations dealt with more and more complex conversions involving sulfur ylides. We believe that the synthesis of heterocyclic compounds with unique structures and the total synthesis of natural products and biologically active synthetic analogues will be the major field of application of ylides in the coming years. The reactions of ylides producing alkaloids and alkaloid-like compounds are worthy of particular attention because they have an increasingly important place among drugs used in oncology and cardiology. There is no doubt that new biologically active compounds will be discovered among organosulfur heterocyclic compounds prepared by ylide procedures.

References

1. G Wittig, G Geissler *Justus Liebigs Ann. Chem.* **580** 44 (1953)
2. E J Corey, M Chaykovsky *J. Am. Chem. Soc.* **87** 1353 (1965)
3. V Franzen, H-J Schmidt, C Mertz *Chem. Ber.* **94** 2942 (1961)
4. V Franzen, H-E Driesen *Chem. Ber.* **96** 1881 (1963)
5. A Jonson *Ylid Chemistry* (New York: Academic Press, 1966)
6. B M Trost, L S Melvin *Sulfur Ylides, Emerging Synthetic Intermediates* (New York; San-Francisco; London: Academic Press, 1975)
7. E Block, in *The Chemistry of Sulfonium Group* (Eds C J M Stirling, S Patai) (New York: Academic Press, 1981) p. 673
8. F Bernardy, G Csizmadia, A Magini *Organic Sulfur Chemistry* (Amsterdam; Oxford; New York; Tokyo: Elsevier, 1985)
9. Yu G Gololobov, A N Nesmeyanov, V P Lysenko, I E Boldeskul *Tetrahedron* **43** 2609 (1987)
10. Yu V Belkin, N A Polezhaeva *Usp. Khim.* **50** 909 (1981) [*Russ. Chem. Rev.* **50** 481 (1981)]
11. N D Sadekov, V I Minkin, V V Semenov, S A Shevelev *Usp. Khim.* **50** 813 (1981) [*Russ. Chem. Rev.* **50** 432 (1981)]
12. C R Jonson *Acc. Chem. Res.* **6** 341 (1973)
13. N N Magdesieva, T A Sergeeva *Khim. Geterotsikl. Soedin.* 147 (1990) [a]
14. D Romo, J L Romine, W Midura, A I Meyers *Tetrahedron* **46** 4951 (1990)
15. D Romo, A I Meyers *Tetrahedron* **47** 9503 (1991)
16. A-H Li, L-X Dai, V K Aggarwal *Chem. Rev.* **97** 2341 (1997)
17. E Vedejs *Acc. Chem. Res.* **17** 358 (1984)
18. I E Marko, in *Comprehensive Organic Synthesis* (Eds B M Trost, I Fleming, G Pattenden) (Oxford: Pergamon Press, 1991) p. 913
19. O Meyer, P C Cagle, K Weickhardt, D Vichard, J A Gladysz *Pure Appl. Chem.* **68** 79 (1996)
20. T Ye, M A McKervey *Chem. Rev.* **94** 1091 (1994)
21. V K Aggarwal, H Abdel-Rahman, R V H Jones, H Y Lee, B D Reid *J. Am. Chem. Soc.* **116** 5973 (1994)
22. V K Aggarwal, A Thompson, R V H Jones, M C H Standen *J. Org. Chem.* **61** 8368 (1996)
23. V K Aggarwal, J G Ford, R V H Jones, R Fieldhouse *Tetrahedron Asymmetry* **9** 1801 (1998)
24. V K Aggarwal, J G Ford, S Fonquerna, H Adams, R V H Jones, R Fieldhouse *J. Am. Chem. Soc.* **120** 8328 (1998)
25. V K Aggarwal *Synlett* 329 (1998)
26. R Bruckner, in *Comprehensive Organic Synthesis* Vol. 3 (Eds B M Trost, I Fleming, E Winterfeldt) (Oxford: Pergamon Press, 1991) p. 873
27. T S Stevens, E M Creighton, A B Gordon, M MacNicol *J. Chem. Soc.* 3193 (1928)
28. R B Woodward, R Hoffman *The Conservation of Orbital Symmetry* (Weinheim: Verlag Chemie, 1970)
29. W D Ollis, M Rey, I O Sutherland *J. Chem. Soc., Perkin Trans. 1* 1009 (1983)
30. K Chantrapromma, W D Ollis, I O Sutherland *J. Chem. Soc., Perkin Trans. 1* 1049 (1983)
31. J Adams, D M Spero *Tetrahedron* **47** 1765 (1991)
32. A Padwa, S F Hornbuckle *Chem. Rev.* **91** 263 (1991)
33. M P Doyle, M A McKervey, T Ye *Modern Catalytic Methods for Organic Synthesis with Diazo Compounds: from Cyclopropanes to Ylides* (New York: Wiley, 1998)
34. M P Doyle, D C Forbes *Chem. Rev.* **98** 911 (1998)
35. D S Carter, D L van Vranken *Tetrahedron Lett.* **40** 1617 (1999)
36. V K Aggarwal, M Ferrara, R Hainz, S E Spey *Tetrahedron Lett.* **40** 8923 (1999)
37. H Storflor, J Skramstad, S Nordenson *J. Chem. Soc., Chem. Commun.* 208 (1984)
38. C J Moody, R J Taylor *Tetrahedron Lett.* **29** 6005 (1988)
39. C J Moody, R J Taylor *Tetrahedron* **46** 6501 (1990)
40. H M L Davies, L van T Crisco *Tetrahedron Lett.* **28** 371 (1987)
41. W D Crow, I Gosney, R A Ormiston *J. Chem. Soc., Chem. Commun.* 643 (1983)
42. W Ando, Y Kumamoto, T Takata *Tetrahedron Lett.* **26** 5187 (1985)
43. T Kametani, K Kawamura, M Tsubuki, T Honda *J. Chem. Soc., Chem. Commun.* 1324 (1985)
44. T Kametani, K Kawamura, M Tsubuki, T Honda *J. Chem. Soc., Perkin Trans. 1* 193 (1988)
45. T Kametani, H Yukawa, T Honda *J. Chem. Soc., Chem. Commun.* 651 (1986)
46. T Kametani, H Yukawa, T Honda *J. Chem. Soc., Perkin Trans. 1* 833 (1988)
47. T Kametani, A Nakayama, A Itoh, T Honda *Heterocycles* 2355 (1983)
48. T Kametani, H Yukawa, T Honda *J. Chem. Soc., Chem. Commun.* 685 (1988)
49. G Kim, S Kang, S N Kim *Tetrahedron Lett.* **34** 7627 (1993)
50. E J Corey, A G Myers *Tetrahedron Lett.* **25** 3559 (1984)
51. J E Baldwin, R E Hackler, D P Kelly *J. Am. Chem. Soc.* **90** 4758 (1968)
52. J E Baldwin, R E Hackler, D P Kelly *J. Chem. Soc., Chem. Commun.* 537; 538 (1968)
53. J E Baldwin, D P Kelly *J. Chem. Soc., Chem. Commun.* 899 (1968)
54. W Ando, S Kondo, K Nakayama, K Ichibori, H Kohoda, H Yamato, I Imai, S Nakaido, T Migita *J. Am. Chem. Soc.* **94** 3870 (1972)
55. W Ando, T Yagihara, S Kondo, K Nakayama, H Yamato, S Nakaido, T Migita *J. Org. Chem.* **36** 1732 (1971)
56. A Padwa, G E Hornbuckle, G E Fryxell, P D Stull *J. Org. Chem.* **54** 817 (1989)
57. M J Kurth, S H Tahir, M M Olmstead *J. Org. Chem.* **55** 2286 (1990)
58. S H Tahir, M M Olmstead, M J Kurth *Tetrahedron Lett.* **32** 335 (1991)
59. Y-D Wu, K N Houk *J. Org. Chem.* **56** 5657 (1991)
60. F Kido, S C Sinha, T Abiko, A Yoshikoshi *Tetrahedron Lett.* **30** 1575 (1989)
61. F Kido, S C Sinha, T Abiko, M Watanabe, A Yoshikoshi *Tetrahedron* **46** 4887 (1990)
62. F Kido, S C Sinha, T Abiko, M Watanabe, A Yoshikoshi *J. Chem. Soc., Chem. Commun.* 418 (1990)
63. F Kido, A B Kazi, A Yoshikoshi *Chem. Lett.* 613 (1990)
64. F Kido, Y Kawada, M Kato, A Yoshikoshi *Tetrahedron Lett.* **32** 6159 (1991)
65. F Kido, T Abiko, A B Kazi, M Kato, A Yoshikoshi *Heterocycles* **32** 1487 (1991)
66. F Kido, T Abiko, M Kato *J. Chem. Soc., Perkin Trans. 1* 229 (1992)
67. F Kido, T Abiko, M Kato *J. Chem. Soc., Perkin Trans. 1* 2989 (1995)
68. T A Chappie, R M Weekly, M C McMills *Tetrahedron Lett.* **37** 6523 (1996)
69. K Okuma, N Higuchi, Sh Kaji, H Takeuchi, H Ohta, H Matsuyama, N Kamigata, M Kobayashi *Bull. Chem. Soc. Jpn.* **63** 3223 (1990)
70. E Vedejs, J P Hagen *J. Am. Chem. Soc.* **97** 6878 (1975)
71. M P Doyle, J H Griffin, M S Chinn, D van Leusen *J. Org. Chem.* **49** 1917 (1984)
72. E Vedejs, R A Buchanan, P Conrad, G P Meier, M J Mullins, Y Watanabe *J. Am. Chem. Soc.* **109** 5878 (1987)
73. E Vedejs, R A Buchanan, P C Conrad, G P Meier, M J Mullins, J G Schaffhausen, C E Schwartz *J. Am. Chem. Soc.* **111** 8421 (1989)
74. E Vedejs, R A Buchanan, Y Watanabe *J. Am. Chem. Soc.* **111** 8430 (1989)
75. E Vedejs, C L Fedde, C E Schwartz *J. Org. Chem.* **52** 4269 (1987)
76. E Vedejs, J G Reid, J D Rodgers, S J Wittenberger *J. Am. Chem. Soc.* **112** 4351 (1990)
77. A Nickon, A D Rodriguez, R Ganguly, V Shirhatti *J. Org. Chem.* **50** 2767 (1985)

78. V Cere, C Paolucci, S Pollicino, E Sandri, A Fava *J. Org. Chem.* **46** 486 (1981)
79. H Sashida, T Tsuchiya *Chem. Pharm. Bull.* **34** 3644 (1986)
80. T Tanzawa, N Shirai, Y Sato, K Hatano, Y Kurono *J. Chem. Soc., Perkin Trans. 1* 2845 (1995)
81. T Kitano, N Shirai, Y Sato *J. Chem. Soc., Perkin Trans. 1* 715 (1997)
82. H Sashida, T Tsuchiya *Chem. Pharm. Bull.* **34** 3682 (1986)
83. O Meth-Cohn, E Vuorinen *J. Chem. Soc., Chem. Commun.* 138 (1988)
84. T A Modro, E Vuorinen *Phosphorus Sulfur Silicon Relat. Elem.* **74** 449 (1993)
85. T Kataoka, A Tomoto, H Shimizu, E Imai, M Hori *J. Chem. Soc., Perkin Trans. 1* 515 (1984)
86. T Kataoka, M Kataoka, M Ikemori, H Shimizu, M Hori, I Miura *J. Chem. Soc., Perkin Trans. 1* 1973 (1993)
87. M Hori, T Kataoka, H Shimizu, K-i Narita, S Ohno, H Ogura, H Takayanagi, Y Iitika, H Koyama *J. Chem. Soc., Perkin Trans. 1* 1885 (1988)
88. M Hori, T Kataoka, H Shimizu, O Komatsu, K Hamada *J. Org. Chem.* **52** 3668 (1987)
89. H Shimizu, M Ozawa, T Matsuda, K Ikedo, T Kataoka, M Hori, K Kobayashi, Y Tada *J. Chem. Soc., Perkin Trans. 1* 1709 (1994)
90. H Shimizu, S Miyazaki, T Kataoka, M Hori *J. Chem. Soc., Perkin Trans. 1* 1583 (1995)
91. K Ohkata, K Okada, K Maruyama, K Akiba *Tetrahedron Lett.* **27** 3257 (1986)
92. G A Tolstikov, F Z Galin, S N Lakeev *Izv. Akad. Nauk SSSR, Ser. Khim.* 1209 (1989) [b]
93. F Z Galin, S N Lakeev, G A Tolstikov *Khim. Geterotsikl. Soedin.* 1693 (1989) [a]
94. G A Tolstikov, F Z Galin, S N Lakeev, L M Khalilov, V S Sultanova *Izv. Akad. Nauk SSSR, Ser. Khim.* 612 (1990) [b]
95. L M Khalilov, V S Sultanova, S N Lakeev, F Z Galin, L F Chertanova, G A Tolstikov *Izv. Akad. Nauk SSSR, Ser. Khim.* 2298 (1991) [b]
96. F Z Galin, S N Lakeev, G A Tolstikov *Izv. Akad. Nauk, Ser. Khim.* 165 (1996) [b]
97. F Z Galin, S N Lakeev, G A Tolstikov *Izv. Akad. Nauk, Ser. Khim.* 2008 (1997) [b]
98. F Z Galin, S N Lakeev, L F Chertanova, G A Tolstikov *Izv. Akad. Nauk, Ser. Khim.* 2376 (1998) [b]
99. W E Bachmann, V Struve, in *Organic Reaction* (New York: Wiley, 1942)
100. S N Lakeev, Candidate Thesis in Chemical Sciences, Institute of Organic Chemistry, Ufa Research Centre of the Russian Academy of Sciences, Ufa, 1990
101. F Z Galin, Doctoral Thesis in Chemical Sciences, Institute of Organic Chemistry, Ufa Research Centre of the Russian Academy of Sciences, Ufa, 1993
102. G A Tolstikov, F Z Galin, S N Lakeev *Izv. Akad. Nauk SSSR, Ser. Khim.* 974 (1989) [b]
103. J E Baldwin, R M Adlington, C R A Godfrey, D W Gollins, M L Smith, A T Russel *Synlett* 51 (1993)
104. J E Baldwin, R M Adlington, C R A Godfrey, D W Gollins, J G Vaughan *J. Chem. Soc., Chem. Commun.* 1434 (1993)
105. E J Corey, M Chaykovsky *J. Am. Chem. Soc.* **86** 1640 (1964)
106. B Cimetiére, M Julia *Synlett,* 271 (1991)
107. K-Y Ko, K-I Lee, W-J Kim *Tetrahedron Lett.* **33** 6651 (1992)
108. J Buter, S Wassenaar, R M Kellogg *J. Org. Chem.* **37** 4045 (1973)
109. W J Middleton *J. Org. Chem.* **31** 3731 (1966)
110. W G Herkstroeter, A G Schultz *J. Am. Chem. Soc.* **106** 5553 (1984)
111. G Mloston, T Gendek, A Linden, H Heimgartner *Helv. Chim. Acta* **82** 290 (1999)
112. G Mloston, T Gendek, H Heimgartner *Pol. J. Chem.* **72** 66 (1998)
113. M Kigi, G Mloston, A Linden, H Heimgartner *Helv. Chim. Acta* **77** 1299 (1994)
114. S Takano, S Tomita, M Takahashi, K Ogasawara *Synthesis* 1116 (1987)
115. A Padwa, F R Kinder, L Zhi *Synlett* 287 (1991)
116. F G Fang, M Prato, G Kim, S J Danishefsky *Tetrahedron Lett.* **30** 3625 (1989)
117. G Kim, M Y Chu-Moyer, S J Danishefsky *J. Am. Chem. Soc.* **112** 2003 (1990)
118. G Kim, M Y Chu-Moyer, S J Danishefsky, G K Schulte *J. Am. Chem. Soc.* **115** 30 (1993)
119. F G Fang, S J Danishefsky *Tetrahedron Lett.* **30** 2747 (1989)
120. F G Fang, M E Maier, S J Danishefsky, G Schulte *J. Org. Chem.* **55** 831 (1990)
121. L P Hadjiarapoglou *Tetrahedron Lett.* **28** 4449 (1987)
122. N Tokitoh, T Suzuki, A Itami, M Goto, W Ando *Tetrahedron Lett.* **30** 1249 (1989)
123. N Tokitoh, T Suzuki, W Ando *Tetrahedron Lett.* **30** 4271 (1989)
124. M Hamaguchi, N Funakoshi, T Oshima *Tetrahedron Lett.* **40** 8117 (1999)
125. J Romanski, G Mloston, A Linden, H Heimgartner *Pol. J. Chem.* **73** 475 (1999)
126. A V Samet, A M Shestopalov, V V Semenov *Khim. Geterotsikl. Soedin.* 1136 (1996) [a]
127. G Kumaran, G H Kulkarni *Synthesis* 1545 (1995)
128. A V Samet, A M Shestopalov, V N Nesterov, V V Semenov *Izv. Akad. Nauk, Ser. Khim.* 127 (1998) [b]
129. W-P Deng, A-H Li, L-X Dai, X-L Hou *Tetrahedron* **56** 2967 (2000)
130. J R Moran, I Tapia, V Alcazar *Tetrahedron* **46** 1783 (1990)
131. G Mloston *Bull. Soc. Chim. Belg.* **99** 265 (1990)
132. R Huisgen, E Langhals, G Mloston, T Oshima *Heterocycles* **29** 2069 (1989)
133. G Mloston, R Huisgen, K Polborn *Tetrahedron* **55** 11475 (1999)
134. R Huisgen, X Li, G Mloston, R Knorr, H Huber, D S Stephensos *Tetrahedron* **55** 12783 (1999)
135. G Mloston, H Heimgartner *Helv. Chim. Acta* **74** 1386 (1991)
136. R Huisgen, G Mloston, K Polborn *Heteroat. Chem.* **10** 662 (1999)
137. M Kigi, G Mloston, H Heimgartner *Pol. J. Chem.* **72** 678 (1998)
138. M Kigi, A Linden, G Mloston, H Heimgartner *Helv. Chim. Acta* **81** 285 (1998)
139. H Ishida, M Ohno *Tetrahedron Lett.* **40** 1543 (1999)

[a] — *Chem. Heterocycl. Compd. (Engl. Transl.)*
[b] — *Russ. Chem. Bull. (Engl. Transl.)*

Russian Chemical Reviews **70** (8) 673 – 715 (2001) © 2001 Russian Academy of Sciences and Turpion Ltd

DOI 10.1070/RC2001v070n08ABEH000679

Marine polar steroids

V A Stonik

Contents

I.	Introduction	673
II.	Polyhydroxysteroids and related compounds	673
III.	Steroid sulfates	684
IV.	Steroid glycosides	692
V.	Steroidal alkaloids	703
VI.	Miscellaneous marine steroids	708
VII.	Problems of isolation and structural analysis of marine polar steroids	710
VIII.	Conclusion	711

Abstract. Structures, taxonomic distribution and biological activities of polar steroids isolated from various marine organisms over the last 8 – 10 years are considered. The peculiarities of steroid biogenesis in the marine biota and their possible biological functions are discussed. Syntheses of some highly active marine polar steroids are described. The bibliography includes 254 references.

I. Introduction

The marine biota differs essentially from the terrestrial one in taxonomic composition and extreme diversity. This includes representatives of much more numerous large animal and plant taxa (*i.e.*, animal phyla and plant divisions) in comparison with those dwelling on land. Many of these taxa contain exclusively marine organisms (*e.g.*, echinoderms, bryozoans, ascidians, nearly all divisions of algae) or comprise very small groups of terrestrial species. For example, only one sponge family inhabits freshwater reservoirs, whereas all other sponges are exclusively sea and ocean dwellers. Taxonomic peculiarities of various producers and their unusual dwelling habitat provide the rationale for the non-coincidence of structures of the absolute majority of marine secondary metabolites and natural products found in terrestrial organisms.

The uniqueness and structural diversity of natural compounds isolated from marine organisms draw the attention of chemists to this particular field. Published material devoted to this problem can now be found in virtually every issue of the majority of international chemical journals. Chemical investigations of marine organisms are making rapid strides. Of $\sim$12 000 newly discovered compounds, 1400 are marine steroids.

It is well known that steroids play an important biological role. They represent constituents of biomembranes and hormones, fulfil protective functions, stimulate plant growth, *etc.* Many representatives of this group are widely used in medicine as essentials of antiinflammatory, anabolic and contraceptive drugs. Steroids isolated from various marine organisms (marine steroids) manifest diverse biological activities. Some of them are extremely toxic against tumour cells and show antimicrobial and other effects. It is therefore not surprising that marine steroids arouse considerable interest in not only chemists, but also in pharmacologists and physicians. Besides, these compounds fall under the scope of biology and biochemistry. Studies on taxonomic distribution of marine steroids make it possible to detect compounds which can be used as chemotaxonomic markers able to resolve many moot points in systematics of marine organisms and phylogenetic relationships in the marine biota. Since marine organisms comprise a large number of the so-called living fossils, comparison of their metabolisms with those of representatives of younger taxa sheds additional light on the evolution of secondary metabolic processes.

Polar (often, water-soluble) steroids constitute an abundant group of marine steroids;† many highly active and structurally unique compounds belong to this group. Studies of marine (including polar) steroids carried out before 1987 are reviewed in a monograph.[1] Some problems related to marine polar steroids are also discussed in the reviews [2, 3] published in the early 1990's. This review is an attempt to generalise the experimental data on marine polar steroids published over the last 8 – 10 years.

II. Polyhydroxysteroids and related compounds

Marine organisms contain a great number of oxygenated sterol derivatives; the majority of these secondary metabolites are related to polyhydroxylated derivatives. These compounds were found in algae and marine invertebrates, particularly in sponges, echinoderms and octocorals (one of the orders of the Anthozoa class which in turn belongs to the phylum Coelenterata). In this section, we shall consider those oxygenated marine steroids and related compounds which have been discovered very recently, namely, after 1993 when Minale *et al.*[2] published a review devoted to polyhydroxylated marine steroids.

V A Stonik Pacific Institute of Bioorganic Chemistry, Far Eastern Branch of the Russian Academy of Sciences, prosp. 100-letiya Vladivostoka 159, 690022 Vladivostok, Russian Federation. Fax (7-423) 231 40 50. Tel. (7-423) 231 23 60, (7-423) 231 11 68. E-mail: piboc@stl.ru

Received 14 May 2001
Uspekhi Khimii **70** (8) 763 – 808 (2001); translated by R L Birnova

† Steroid compounds which contain three or more oxygen atoms as well as steroid alkaloids, sulfates, phosphates and glycosides of steroid aglycons are usually referred to as polar steroids.

1. Polyhydroxysteroids from algae

A series of steroid hydroperoxides **1a**,**b** and **2a**,**b** were isolated from the red alga *Galaxaura marginata* collected near the coasts of Taiwan.[4] These compounds manifest high cytotoxic activities against tumour cells P-388, KB, A-549, HT-29 (their semi-inhibiting concentrations, IC_{50}, lie within the range 0.2–1.0 μg ml^{-1}).

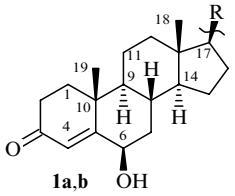

1a,**b**

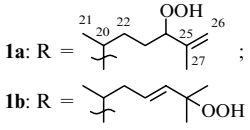

1a: R = ;

1b: R = .

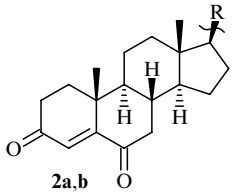

2a,**b**

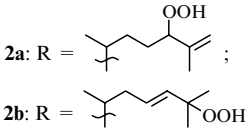

2a: R = ;

2b: R = .

The oxygenated 3,4-dinorcholestane derivative **3** was isolated from extracts of the red alga *Laurencia obtusa*.[5] The steroidal 3,6-diketone **4** oxygenated at C(16) was isolated from the alga *Jania rubens*, it exhibited high toxicity against some tumour cells ($IC_{50} \approx 0.5$ μg ml^{-1}) (see Ref. 6). The hydroperoxides **5a**,**b** isolated from the brown alga *Turbinaria conoides* also possessed cytotoxic properties.[7]

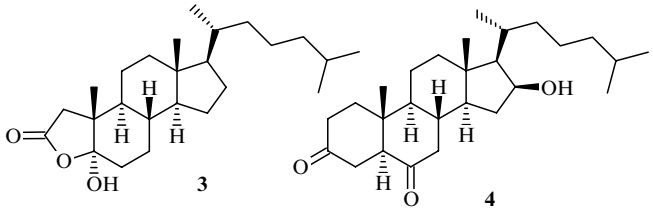

3 **4**

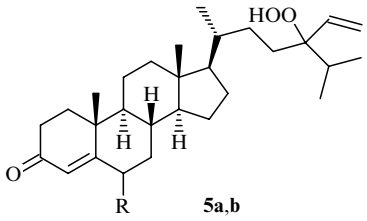

5a,**b**

5a: R = O;
5b: R = β-OH.

However, highly oxygenated sterols are not very common in algae. These metabolites are much more widely distributed in marine invertebrates.

2. Polyhydroxysteroids from sponges

The 5,6-epoxide **6** isolated from the sponge *Ircinia fasciculata* collected near the coasts of India [8] and a series of steroids isolated from the Taiwanese sponge *Xestospongia* sp., *viz*., aragusterols A–D (**7c**–**f**),[9–11] xestokerols A, B (**7a**,**b**) and aragusterols E–H (**7g**–**j**), relate to sponge polyhydroxysteroids.[12] Aragusterols and related compounds have unusual side chains, which contain cyclopropane fragments, while aragusterol C (**7e**) contains a chlorine atom in the side chain, which is a unique structural feature of natural steroids.

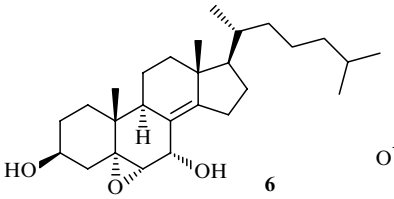

6

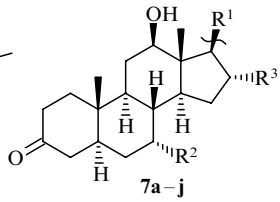

7a–**j**

Compound **7**	Name	R^1	R^2	R^3
a	xestokerol A	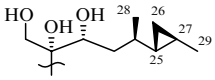	H	H
b	xestokerol B	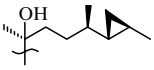	OH	H
c	aragusterol A	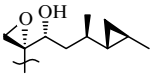	H	H
d	aragusterol B	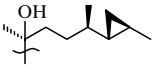	H	H
e	aragusterol C	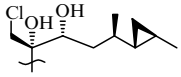	H	H
f	aragusterol D	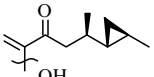	H	H
g	aragusterol E	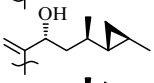	H	H
h	aragusterol F	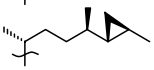	H	OH
i	aragusterol G (3α-OH)	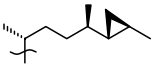	H	H
j	aragusterol H (3β-OH)	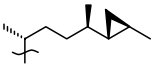	H	H

It should be noted that the presence of unusual side chains in sponge polar steroids is due to the presence in the sponges of their precursors (sterols) having identical side chains. In contrast to higher plants where sterols represent minor components, some representatives of sponges and cnidarians (coelenterates) contain unusual sterols as predominant, and sometimes single components of steroid fractions. The side chain of the steroid ketone mycalone **8** from the Australian sponge *Mycale* sp. contains a lactone fragment formed upon oxidation of the ketone precursor at C(21) and C(24).[13]

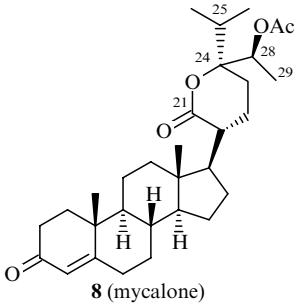

8 (mycalone)

Among the compounds mentioned above, aragusterols manifesting strong cytotoxic and antitumour activities present special interest. The IC_{50} values of aragusterols **7c** and **7d** against tumour cells (KB) are 0.042 and 0.041 μg ml^{-1}, respectively. These steroids (1.6 mg kg^{-1}) increase the lifespan of mice with leukemia L-1210 *in vivo* by 220% and 257%, respectively.

5-Epiaragusterol A synthesised from deoxycholic acid possessed cytotoxic properties comparable to those of aragusterol A (**7c**).[14] The synthesis of aragusterols from (+)-hekogenin[15] included stereoselective formation of side chains, the addition of the corresponding fragment **9** to the 20-ketosteroid **10** prepared from hekogenin and preparation of aragusterol B (**7d**) *via* the intermediate **17** with subsequent transformation of **7d** into **7c**, **7e** and **8f** (Scheme 1). The triethylsilyl (TES) derivative **10** was synthesised in six steps from the readily available hekogenin. The fragment **9**, which is structurally similar to the side chain of

Scheme 1

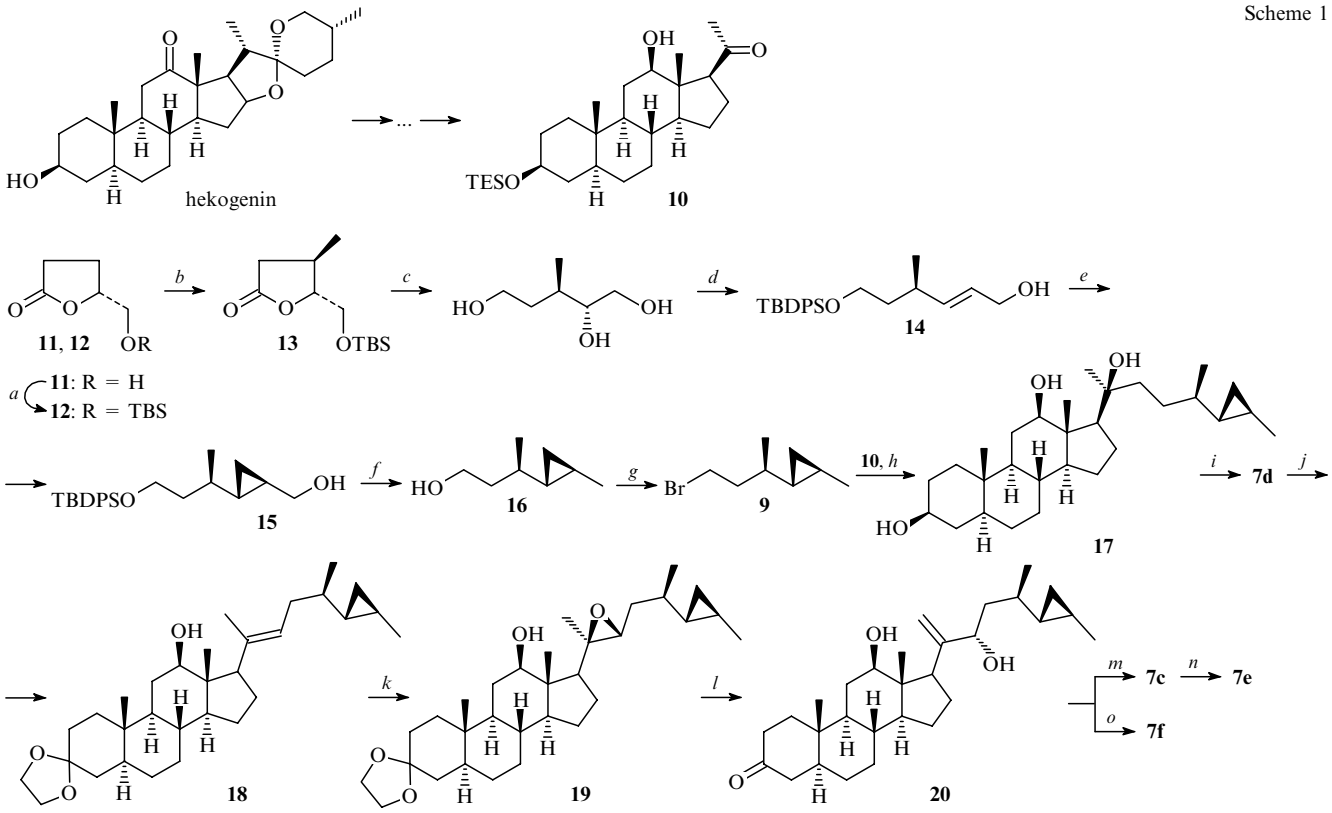

(*a*) Bu^t_3SiCl (TBSCl), imidazole, DMF (92%); (*b*) Me_2CuLi, Et_2O, −78 °C (90%); (*c*) $LiAlH_4$, THF; 80% AcOH (89%); (*d*) $Pb(OAc)_4$, K_2CO_3, benzene; $Ph_3P{=}CHCO_2Me$, benzene (67%); Bu^tPh_2SiCl (TBDPSCl), imidazole, DMF; Bu^i_2AlH (DIBAH), CH_2Cl_2, −78 °C (91%); (*e*) CH_2I_2, Et_2Zn + $BuBO_2(CH)_2(CONMe_2)_2$, CH_2Cl_2 (99%); (*f*) Ph_3P, CBr_4, CH_2Cl_2; $LiAlH_4$, THF–Et_2O; Bu^n_4NF, THF (88%); (*g*) Ph_3P, *N*-bromosuccinimide (NBS), CH_2Cl_2 (75%); (*h*) lithium naphthalenide, THF, 0 °C; Bu_4NF, THF (93%); (*i*) $Al(OBu^t)_3$, cyclohexanone, toluene (66%); (*j*) ethylene glycol, TsOH, boiling benzene (79%); (*k*) Bu^tO_2H, $VO(acac)_2$, CH_2Cl_2 (78%); (*l*) Pr^i_2NMgBr, THF (93%); 80% AcOH (98%); (*m*) *m*-CPBA, Na_2HPO_4, CH_2Cl_2, 0 °C (54%); (*n*) Li_2CuCl_4, THF (90%); (*o*) pyridinium dichromate (PDC), molecular sieves (4 Å), CH_2Cl_2 (100%).

aragusterols, was synthesised from (5*R*)-hydroxymethyl-2(5*H*)-furanone (**11**) which in its turn was prepared from L-ascorbic acid. Protection of the hydroxy group (as the tris-*tert*-butylsilyl ether) and subsequent reaction of the derivative **12** with lithium dimethylcuprate yielded the lactone **13** with high stereoselectivity. The latter was reduced, and the protective group was removed by treatment with acetic acid. The intermediate triol was converted into the allylic alcohol **14** in four steps, which included oxidation with lead tetraacetate, the Wittig reaction, protection of the hydroxy group as a silyl ether and subsequent reduction of the ester with diisobutylaluminium hydride. The key step in the synthesis of compound **9** was the conversion of the alcohol **14** into the cyclopropane derivative **15** by treatment with diiodomethane in the presence of diethylzinc and *N*,*N*,*N*′,*N*′-tetramethyl-(*S*,*S*)-tartarodiamide n-butylboronate. This reaction proceeded with high stereospecificity (yield 99%). Compound **15** was first converted into the alcohol **16** and then into the bromide **9**.

The stereoselective reaction of the 20-ketosteroid **10** with the alkyllithium derivative prepared from the bromide **9** and subsequent removal of the protective group at C(3) with tetrabutylammonium fluoride resulted in the alcohol **17** with high stereoselectivity. Its Oppenhauer oxidation gave aragusterol B (**7d**) which was further used for the synthesis of the other three aragusterols **7c**,**e**,**f** by chemical modification of the side chain *via* the intermediates **18**–**20**. The oxidation of the steroid alkene **18** to the epoxide **19** was carried out stereoselectively with *tert*-butyl hydroperoxide in the presence of vanadyl bisacetylacetonate.

The sponge *Spongia officinalis* represents the source of a series of novel 5,6-epoxysteroids **21a**–**c** and **22a**–**c** which were isolated as acetates and differed in the structures of side chains and the positions of double bonds in the steroid nuclei.[16] Compound **21a** was also isolated from *Ircinia fasciculata*.[8]

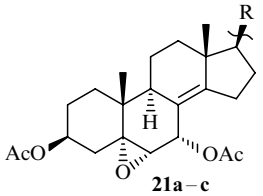

21a–**c**

21a: R = ;

21b: R = ;

21c: R = .

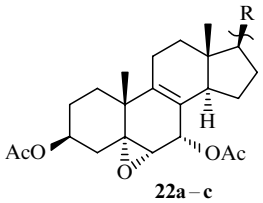

22a–**c**

22a: R = ;

22b: R = ;

22c: R = .

Steroids oxidised in positions 5 and 6 were repeatedly found in sponges where they were apparently formed from Δ^5-sterols.[17] The ketone **23** from *Spirostrella inconstans* is one of such newly discovered steroids.[18]

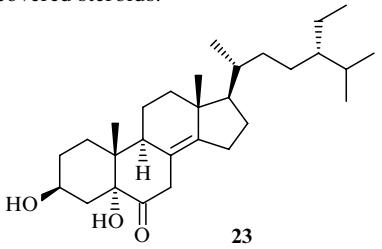

23

Incrustasterols A and B (**24a**,**b**) from the Mediterranean sponge *Dysidea incrustans* differ from other polar sponge steroids in the presence of $\Delta^{8(9)}$-7-hydroxy-9-keto- and $\Delta^{8(9)}$-7,9-diketo-fragments, which are uncommon for marine steroids.

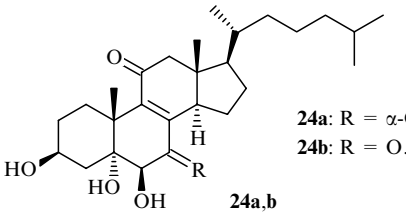

24a: R = α-OH, H;
24b: R = O.

24a,**b**

Compounds **24a**,**b** are toxic for tumour cells (lung and kidney carcinomata, melanoma).[19] These compounds were synthesised from the readily available cholest-7-enol.[20]

The so-called agosterol **25** from *Spongia* sp. abrogates drug resistance of carcinoma cells, conditioned by enhanced expression of membrane glycoproteins.[21] Xestobergsterols A–C (**26a**–**c**), which contain five carbocycles with the *cis*-fused rings *C* and *D*, were found in *Xestospongia bergquistia* and *Ircinia* sp.[22,23] Presumably, the presence of an additional ring in these steroids is due to intramolecular aldol condensation of the yet non-isolated 23-keto derivative. Compounds **26a** and **26b** manifest cytotoxic activities and inhibit the anti-IgE-induced release of histamine from mast cells when used in small doses. Thus these compounds present considerable interest as potential active substances of novel antihistamine drugs. Their activities are closely related to strong inhibition of phosphatidylinositol phospholipase C.

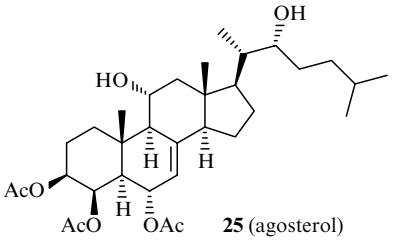

25 (agosterol)

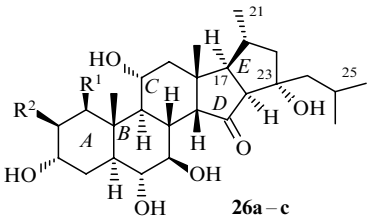

26a: $R^1 = R^2 = H$;
26b: $R^1 = H$, $R^2 = OH$;
26c: $R^1 = R^2 = OH$.

26a–**c**

Yet another polar sponge steroid with the *cis*-fused rings *C* and *D*, *viz*., contignasterol (**27**) from *Petrosia contignata*, discovered simultaneously with xestobergsterols[24] produces strong antihistamine effect. Although contignasterol is inferior to compounds **26a** and **26b** in the activity, it is far more active than antihistamine drugs routinely used in clinical practice and is the subject of intense pharmacological studies as a promising candidate for antiallergic and antiasthmatic drugs.

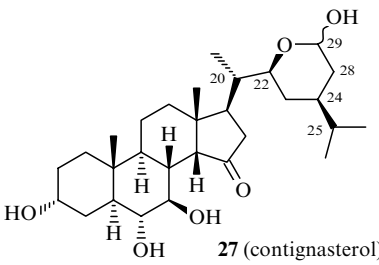

27 (contignasterol)

Geodisterol (**28**), the first marine steroid containing an aromatic ring *A*, was isolated from extracts of *Geodia* sp.[25]

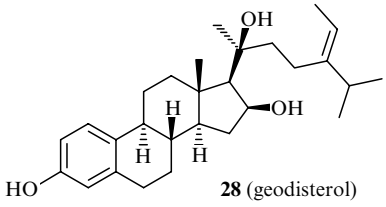

28 (geodisterol)

Previously, such compounds were referred to as hormones; however, in contrast to the latter, geodisterol (**28**) has a ten-carbon side chain characteristic of sterols. Bienmasterol (**29**) from *Bienma* sp.,[26] which is toxic against tumour cells (L-1210 and KB), contains a 22,25-diene fragment in the side chain, which is uncommon for natural steroids. An analogous fragment has been detected by us previously in baicalosterol isolated from the sponge *Baicalospongia bacilifera*.[27]

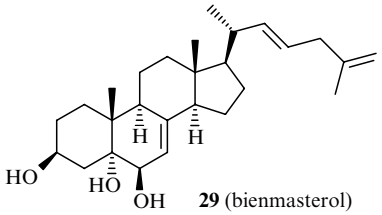

29 (bienmasterol)

Cytotoxic kicheisterones A and B (compounds **30** and **31**) with the *cis*-fused rings *A* and *B*, which contain carboxy groups in position 21 and furan fragments in the side chains, were isolated from an unidentified Hawaiian sponge of the Poecilosclerida order. These compounds are rather stable in acidic media but are easily interconverted in alkaline media to form 1 : 1 mixtures.[28]

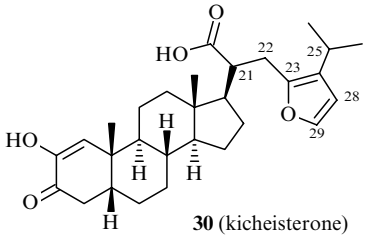

30 (kicheisterone)

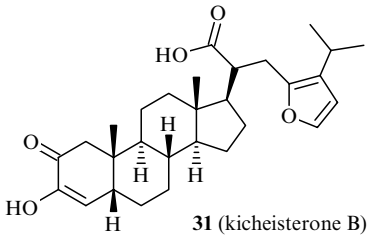

31 (kicheisterone B)

Steroids **30** and **31** were found in the sponge *Strongylacidon* sp. together with kicheisterones C–E (compounds **32a**,**b**, **33**). The latter contain chlorine atoms and belong to the group of extremely rare halogenated steroids.[29]

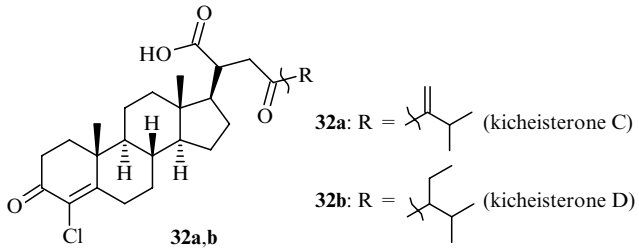

32a: R = (kicheisterone C)
32b: R = (kicheisterone D)

32a,**b**

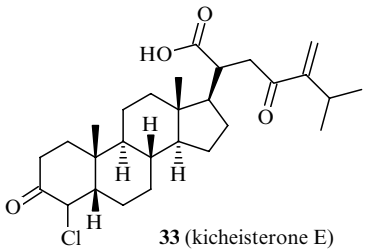

33 (kicheisterone E)

It is of note that no bromine-containing steroids have been isolated so far despite the wide occurrence of brominated metabolites in marine organisms.

Three pregnane derivatives **34a–c** from *Strongylophora* sp. were found to contain unusual (19 → 2)-lactone rings; their structures were established by X-ray diffraction analysis.[30] Hydroperoxides and related peroxides are more common for algal steroids; however, the novel biofouling inhibitor steroid **35** containing a peroxy group has recently been isolated from the sponge *Lendenfeldia chondrodes*.[31] Peroxides similar to compound **35** are readily formed by oxidation of $\Delta^{5,7}$-sterols, which are abundant in fungi, but scarce in sponges.

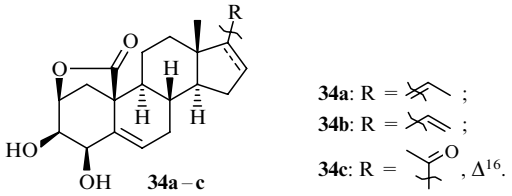

34a–c

34a: R = ;
34b: R = ;
34c: R = , Δ^{16}.

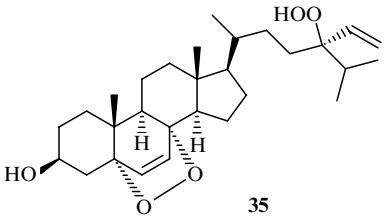

35

The novel acetylated polyhydroxysteroids **36**, **37**, **38a**,**b**[32] and related steroids[33] were detected in some sponges of the *Dysidea* genus. The steroid **37** and, to a lesser degree, steroids **38a**,**b** inhibit the binding of interleukin-8 to its specific receptor of the type A.

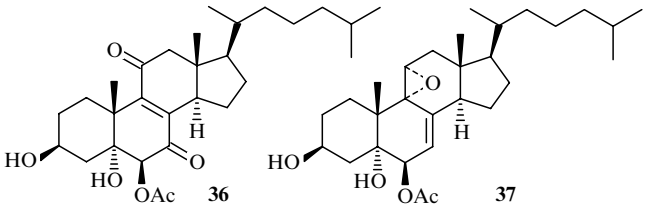

36 **37**

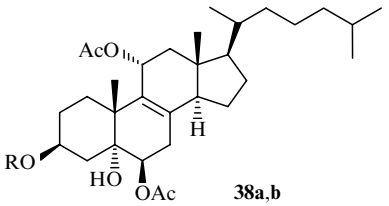

38a,**b**

38a: R = H;
38b: R = Ac.

Secosteroids occur widely in sponges. The most common of them are 9,11-secosteroids, such as blancasterol (**39**), a cytotoxic diacetate from the Northern Pacific sponge *Pleraplysilla* sp., which inhibits the growth of various tumour cells including drug-resistant cell cultures of human mammary carcinoma MCF-7.[34] Stelletasterol (**40a**), the antifungal secosteroid from *Stelletta* sp. isolated simultaneously with stelletasterone (**40b**),[35] differs from the previously known herbasterol (**40c**) from *Dysidea herbacea* only in the stereochemistry of the hydroxy group at the C(3) atom.

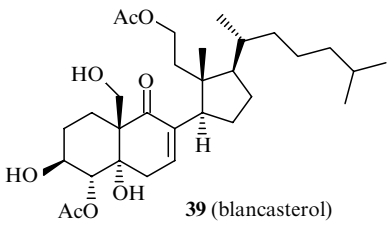

39 (blancasterol)

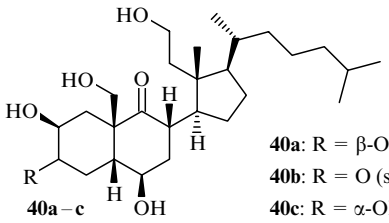

40a–c

40a: R = β-OH, H (stelletasterol);
40b: R = O (stelletasterone);
40c: R = α-OH, H (herbasterol).

Like many other marine secosteroids, luffasterols A–C (**41a–c**) from *Luffariella* sp.[36] and the related secosteroid **41d** from *Spongia matamata*[37] contain 5,6-epoxy rings. 3-Deacetylluffasterol B (**41e**) and the related compound **41f** were isolated from *Spongia agaricina*. Both compounds manifest highly toxic activities against tumour cells.[38]

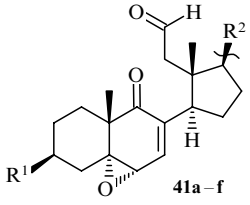

41a–f

41a: R^1 = OAc, R^2 = (luffasterol A);
41b: R^1 = OAc, R^2 = (luffasterol B);
41c: R^1 = OAc, R^2 = (luffasterol C);
41d: R^1 = OH, R^2 = ; **41e**: R^1 = OH, R^2 = ;
41f: R^1 = OH, R^2 = .

Secosteroids **42a**,**b** and **43a**,**b** along with biogenetically related oxygenated sterols **44** and **45** were found in the Mediterranean sponge *Dysidea fragilis*.[39]

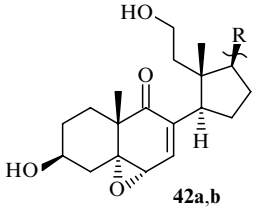

42a,**b**

42a: R = ;
42b: R = .

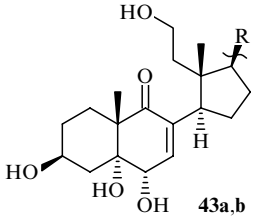

43a,**b**

43a: R = ;
43b: R = .

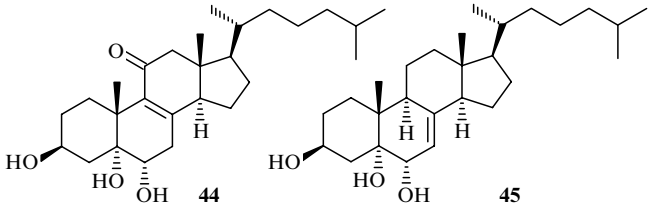

44 **45**

A series of euryspongiols **46a**–**e** and the epimeric 3α-hydroxy analogues possessing antihistamine properties were isolated from the sponge *Euryspongia* sp.[40] These compounds are the most strongly oxygenated sponge secosteroids known so far. The strong inhibiting effect of these and some other secosteroids on histamine release from mast cells during stimulation of the latter with anti-IgE suggests that marine secosteroids are promising candidates for antiallergic and antiasthmatic drugs.

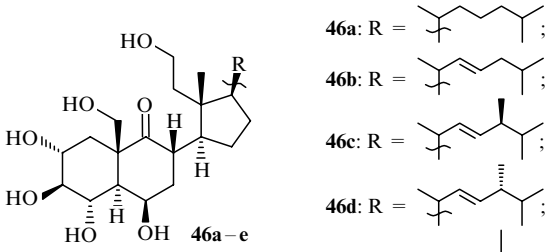

46a–**e**

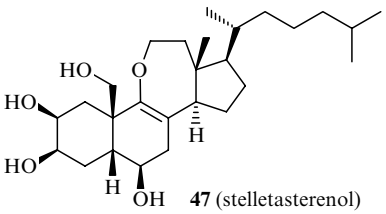

47 (stelletasterenol)

The unusual cyclic 9(11)-secosterenol, *viz*., stelletasterenol (**47**) from *Euryspongia arenaria,* contains an oxygen atom between the C(9) and C(11) atoms and manifests the properties of a PAF (platelet activation factor) agonist.[41]

In addition to 9,11-secosteroids common for marine invertebrates, sponges contain less abundant groups of compounds, which comprise 8,14- and 8,9-secosteroids. The former include jereisterol B (**48**) from *Jereicopsis graphidiophora*[42] and swinhosterols A and B (**49a**,**b**) from *Theonella swinhoe*.[43] Sponge 8,9-secosteroids are represented by unique 8α,9α-epoxy compounds, *e.g*., jereisterol A (**50a**) from *J. graphidiophora*[42] and its homologue **50b** isolated from the Senegalese sponge *Microscleroderma spirophora* together with the isomeric $\Delta^{8(14),9(11)}$ steroid **51**.[44] These compounds contain *O*-methyl groups, which occur rarely in natural steroids. Their structural analogues, *viz*., tilopiols A (**52**) and B (**53**), have recently been found in the microscopic fungus *Tilopilus plumbeoviolaceus*.[45] This finding suggests that microorganisms can be involved in the biosynthesis of sponge steroids **50a**,**b** and **51**.

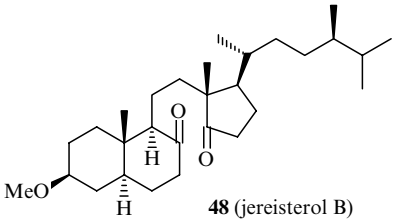

48 (jereisterol B)

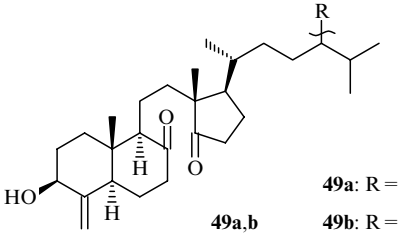

49a,**b**

49a: R = (swinhosterol A);
49b: R = (swinhosterol B).

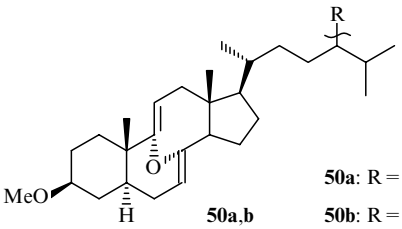

50a,**b**

50a: R = (jereisterol A);
50b: R = .

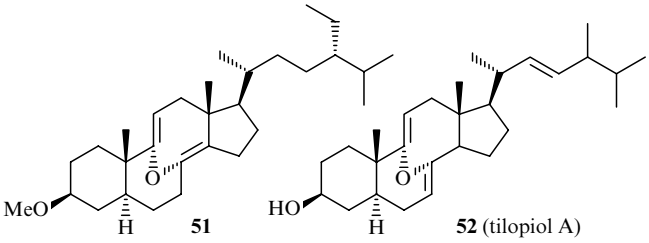

51 **52** (tilopiol A)

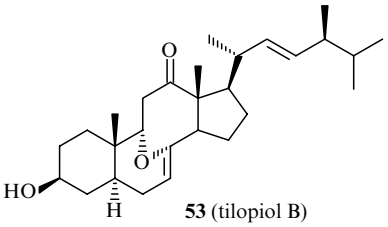

53 (tilopiol B)

It is not excluded that the great diversity of polar sponge steroids and the unique structures of many of them are due to biochemical conversions of the original sterols of both the sponge cells and microbial endosymbionts which are present in some sponges in amounts comparable to the populations of host cells. However, this hypothesis needs further verification and experiment in each particular case.

Although not a single sterol-oxidising enzyme has been isolated from sponges, symbiont bacteria, fungi or microalgae so far, such enzymes obviously differ from analogous enzymes of higher animals and terrestrial microorganisms in those sites in their sterol systems which oxidise the respective substrates. Thus some sponges were found to contain various secosteroids which are absent in terrestrial animals.

3. Polyhydroxysteroids from cnidarians

Polyhydroxysteroids are even more abundant in cnidarians (Coelenterata), particularly octocorals (soft corals) and gorgonian corals than in sponges. A great number of polyhydroxysteroids and secosteroids were detected in these marine invertebrates as long ago as 1970–1980. In the recent years, the list of these compounds was supplemented with many new names. Thus nephalsterol B (**54a**) found in *Nephthea erecta*,[46] *N. chabroli*[47] and *Litophyton arboreum*[48] [the latter contains additionally the $\Delta^{8(9)}$-triol **55** and related compounds, *e.g*., litosterol (**54b**) and nephalsterol C (**54c**)] are characteristic components of soft corals of the *Nephthea* genus. Compounds **54b**,**c** manifest strong antimicrobial activities, *viz*., they inhibit *Mycobacterium tuberculosis* by 90% and 96% when used in the doses of 3.13 and 12.5 μg ml^{-1}, respectively. The antituberculotic activity of nephalsterol B (**54a**) is less pronounced.[49]

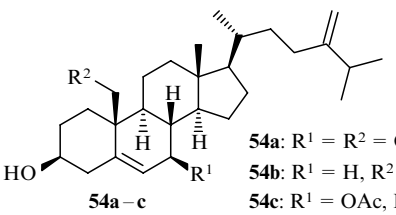

54a–**c**

54a: $R^1 = R^2 =$ OH (nephalsterol B);
54b: $R^1 =$ H, $R^2 =$ OH (litosterol);
54c: $R^1 =$ OAc, $R^2 =$ OH (nephalsterol C).

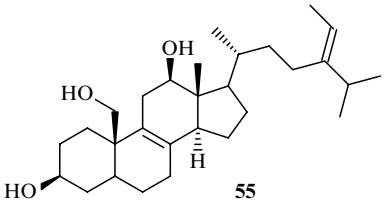

55

Some novel steroids of this series, *viz*., polyols **56a**,**b**, the triol **57** and the tetrol **58** from *Nephthea chabroli*, have recently been described.[47] Their structurally related analogues, *viz*., the triol **59** and the dihydroxy ketone **60**, were isolated from *Nephthea erecta* collected near the coasts of Taiwan.[46]

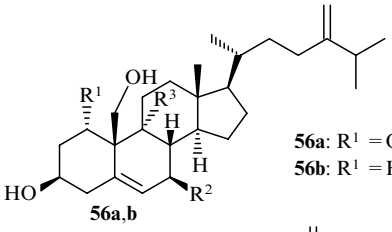

56a,**b**

56a: R^1 = OH, R^2 = R^3 = H;
56b: R^1 = H, R^2 = R^3 = OH.

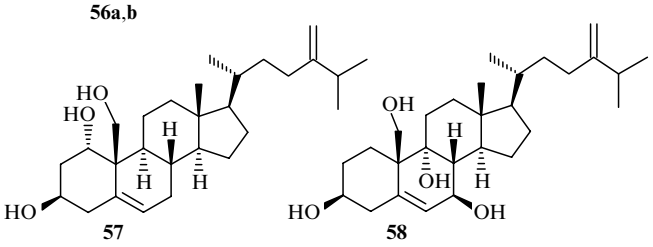

57 **58**

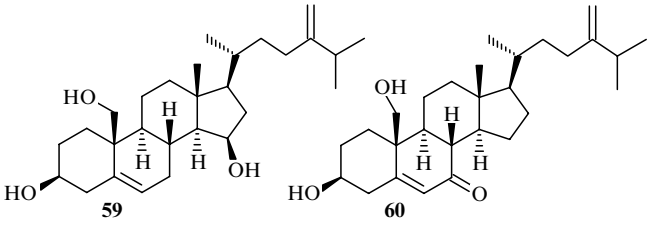

59 **60**

Triols **61a**,**c** and the tetrol **61b** from *Sinularia mayi* contain several hydroxy groups in their side chains.[50] The novel steroidal polyol **62** oxygenated at C(3), C(6), C(9) and C(11) was found in *S. hirta*.[51] The triol **63** and the corresponding glycosides were isolated from extracts of *S. gibbrosa*,[52] whereas the novel steroid pentol **64a** and its acetate **64b** were isolated from *S. dissecta*.[53] The pentol **65a** and the ketone **65b** from *Sinularia* sp.[54] and *S. microclavulata*,[55] respectively, contain oxygen atoms in the same positions, *viz*., at C(1), C(3), C(5), C(6) and C(16). The steroidal peroxide **66** from *Sinularia* sp.[56] proved to be highly toxic for tumour cells (IC_{50} = 0.4–2.7 μg ml^{-1}). This compound was isolated together with pregnenolone earlier detected in the sponge *Haliclona rubens*.[57] The stereochemistry of the C(22), C(23) and C(24) asymmetric centres of the peroxide **66** was established by comparison of its spectra with those of some synthetic model compounds.

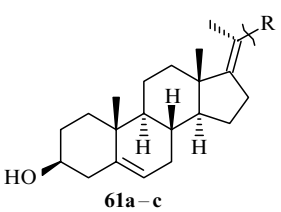

61a–**c**

61a: R = 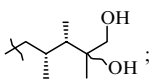 ;

61b: R = 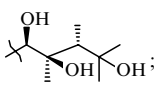 ;

61c: R = 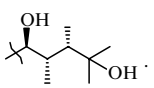 .

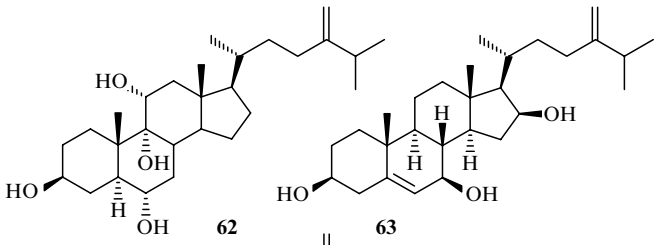

62 **63**

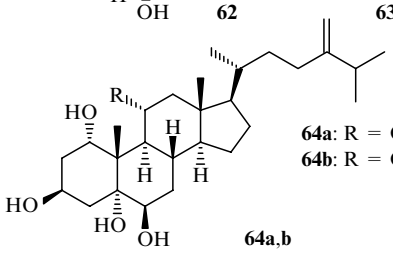

64a: R = OH;
64b: R = OAc.

64a,**b**

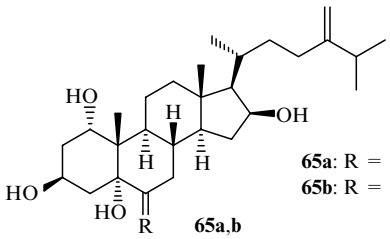

65a: R = β-OH, H;
65b: R = O.

65a,**b**

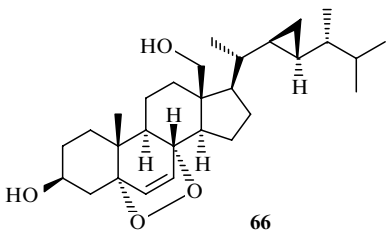

66

Several novel polar steroids were discovered in soft corals of the *Lobophyton* genus. For example, the tetrol **67** was isolated from *L. crassum*,[58] whereas two monoacetates **68a**,**b** were isolated from *L. cf. pauciflorum*.[59] These steroids contain 5α,6β-diol fragments similar to those present in oxygenated steroids isolated from soft corals of the *Sarcophyton* genus. For example, sarcoaldesterol B (**69a**) represents a deacetylated derivative of the steroid **68a**. It was isolated from the Okinawian soft coral *Sarcophyton* sp.

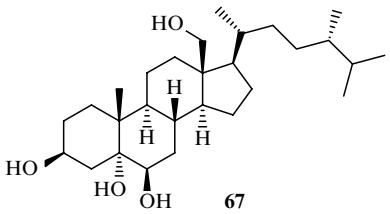

67

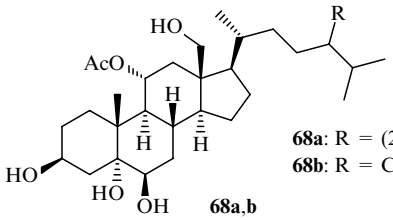

68a: R = (24*S*)-CH_3;
68b: R = CH_2=.

68a,**b**

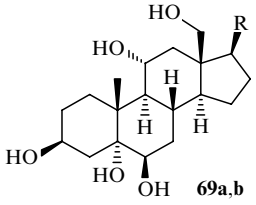

69a: R = 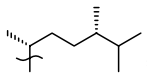 ;

69b: R = 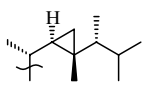 .

69a,**b**

together with sarcoaldesterol A (**69b**), which contains a side chain similar to that of gorgosterol, the well-known sterol of cnidarians.[60]

Steroids **70a**–**d** from the soft coral *S. subviride* collected near the coasts of the Andaman Islands are oxygenated to a greater degree. Some of them contain an acetate group at C(25) characteristic of polar steroids of Coelenterata.[61] Two novel polar steroids **71a**,**b** containing unique 17,20-epoxy fragments, two hippurin derivatives **72a**,**c** differing in stereochemistry at C(22) (hippurin is a well-known polar steroid of Coelenterata) and their acetates **72b**,**d**, were isolated from extracts of *S. crassocaule*.[62]

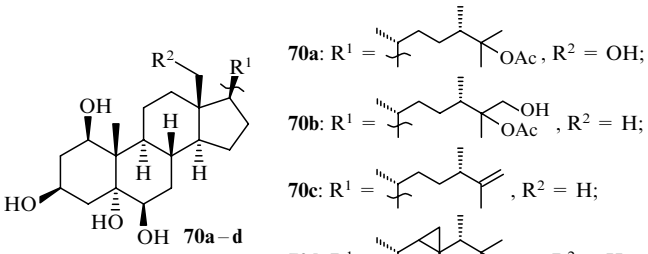

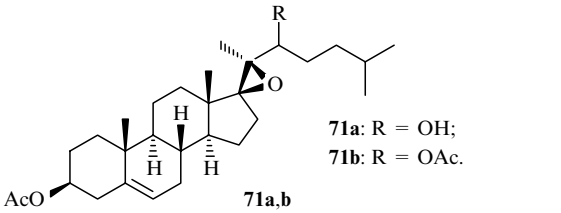

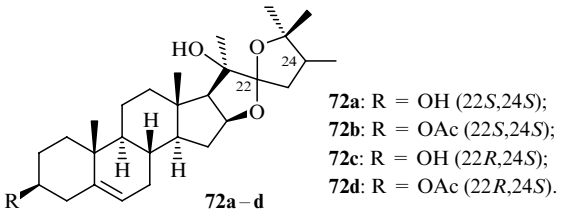

A series of polar steroids including the hippurin analogue, *viz*., compound **73**, as well as derivatives **74a**,**b**, **75** and **76** were detected in the soft coral *Alcyonium gracilum* by Shin *et al*.[63] Presumably, compound **76** is a biosynthetic precursor of all this group of secondary metabolites.

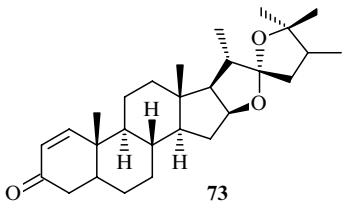

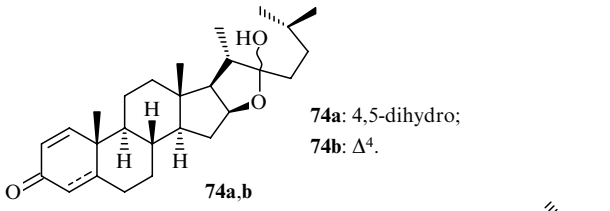

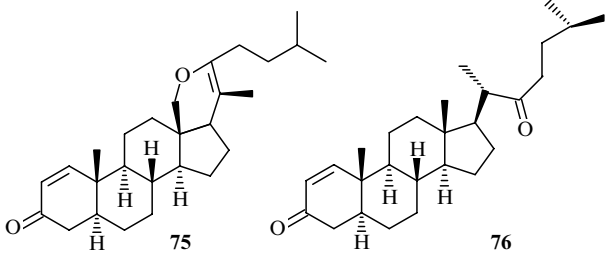

Yet another species of this genus, *viz*., *Alcyonium gracilum* (its mixture with *Dendronephthea* sp. has been studied), contains related steroids **77a**,**b**,[64] which are toxic for barnacle (*Balanus amphitrite*) larvae (LD_{100} = 100 μg ml^{-1}).

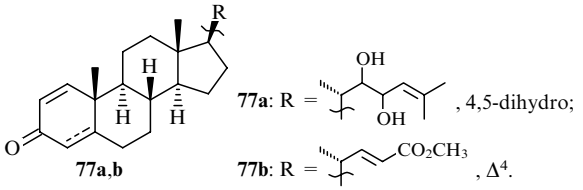

The steroidal pentol **78** was found in the soft coral *Sclerophytum* sp. together with several previously known steroids.[65] Andamansterol (**79**) [66] containing hydroxy groups in positions 9 and 11, which takes its name after the place where it was first collected (Andaman Islands), was detected in another unidentified species of the same genus. Such oxidation can precede the formation of 9,11-secosteroids widely distributed in marine invertebrates. An interesting feature of andamansterol (**79**) is the presence of a hydroxy group at C(21), which is uncommon for polar steroids of Coelenterata, but is common for steroids of some echinoderms, particularly, for ophiuroid metabolites.

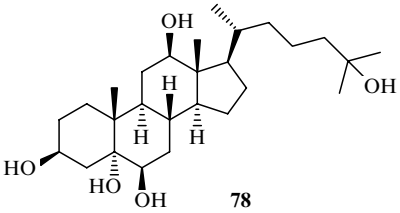

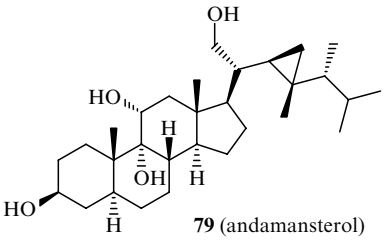

Gorgonian corals are distinguished for a great diversity of oxygenated steroids containing from 2–3 to 5–6 oxygen atoms. Thus melithasterols A–D (**80a**–**d**), each containing an 5,6-epoxy ring and an additional OH-group in position 7, were found in *Melithaea ocracea*.[67] Melithasterol A (**80a**) has recently been synthesised.[68] Steroids **81a**,**b** from *Acabaria undulata* also contain epoxide rings, however, in positions 7 and 8.[69] Anastomosacetals A–D (**82a**–**d**) from *Euplexaura anastomosans* collected near the coasts of Korea contain oxygen atoms in positions 17, 21 and 24.[70]

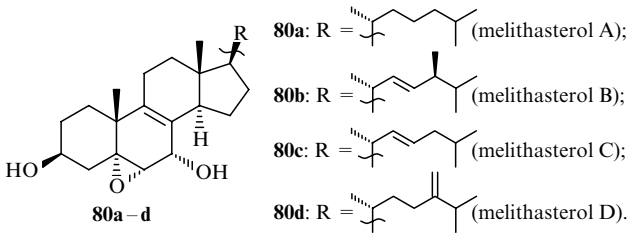

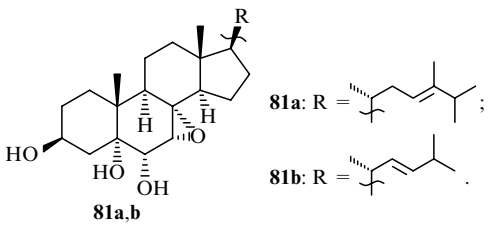

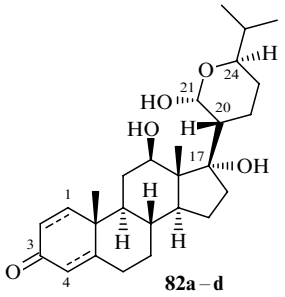

82a–**d**

82a: $\Delta^{1,4}$ (anastomosacetal A);
82b: Δ^{4} (anastomosacetal B);
82c: Δ^{1} (anastomosacetal C);
82d: 1,2,4,5-tetrahydro (anastomosacetal D).

The so-called black coral *Anthiphates subpina* related to the Antipatharia order contains steroid triols **83a**,**b** and diketone **84**, which are toxic for crustaceans.[71] The tetrol monoacetate **85a** and the corresponding tetrol **85b** were isolated from *Telesto viisei*.[72]

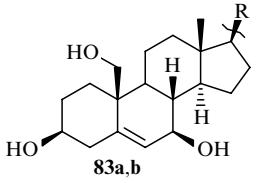

83a,**b**

83a: R = 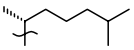 ;
83b: R = 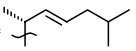 .

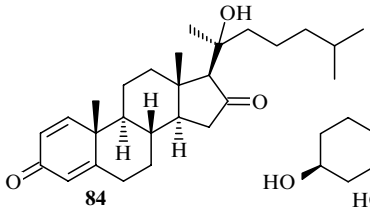

84

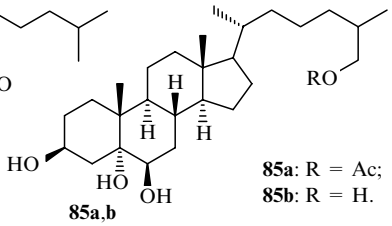

85a,**b**

85a: R = Ac;
85b: R = H.

The steroidal hemiacetal **86** possessing antimicrobial, antiviral and antitumour properties was isolated from the gorgonian coral *Ctenocella* sp.[73] Punacine (**87**) from the gorgonian coral *Lophogorgia punicea* dwelling near the coasts of Brazil contains a hydroxy group at C(17), which is uncommon for cnidarian steroids.[74]

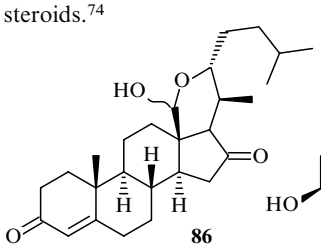

86

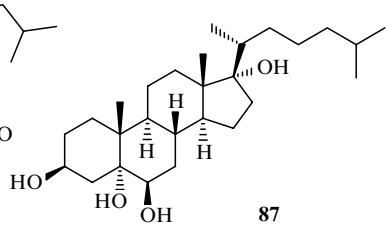

87

Polyhydroxylated steroids **88a**,**b** from the octocoral *Dendronephthea gigantea*[75] manifested moderate cytotoxic activities against tumour cells (L-1210).

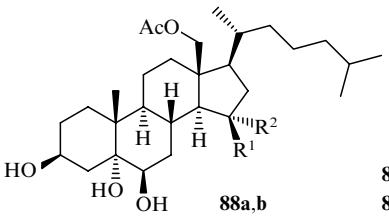

88a,**b**

88a: $R^1 = R^2 = H$;
88b: $R^1 = OH$, $R^2 = H$.

A series of steroids oxygenated in positions 1, 5, 6 and 11 (compounds **89a**,**b**, **90a**,**b**, **91a**–**d** and **92**) were isolated from the Okinawian coral *Clavularia viridis*.[76] Compounds **89a**,**b** manifest cytotoxic properties and are similar to vitanolides, the higher terrestrial plant metabolites, in the structures of their polycyclic fragments.

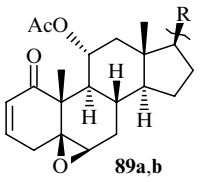

89a,**b**

89a: R = 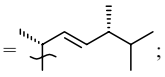 ;
89b: R = 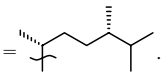 .

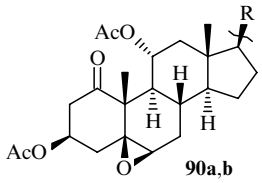

90a,**b**

90a: R = 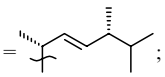 ;
90b: R = 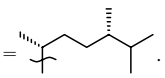 .

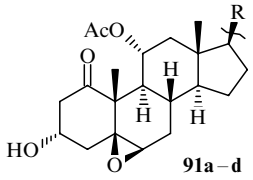

91a–**d**

91a: R = 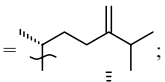 ;
91b: R = 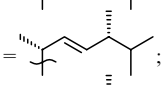 ;
91c: R = 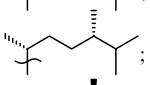 ;
91d: R = 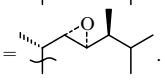 .

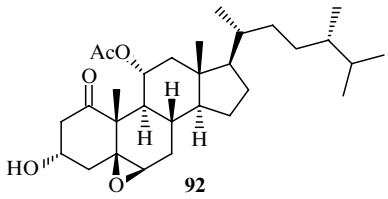

92

Secosteroids are common metabolic products of octocorals. The 9,10-secosteroids, *viz*., calicopherols A and B (**93a**,**b**), which are toxic for shrimps, were isolated from the gorgonian coral *Caligorgia* sp. collected near the coasts of Japan.[77] A series of novel calicopherols differing structurally from compounds **93a,b** have recently been isolated from the gorgonian coral *Muricella* sp. These compounds manifest high cytotoxic activities against tumour cells and inhibit phospholipase A_2.[78]

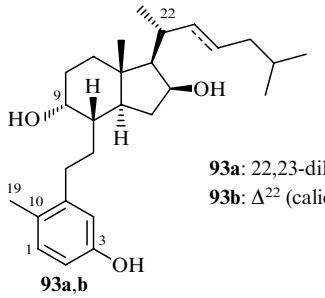

93a,**b**

93a: 22,23-dihydro (calicopherol A);
93b: Δ^{22} (calicopherol B).

9,11-Secosteroids are much more abundant in soft and gorgonian corals. Among the most recent findings, we should make reference to dioxoaldehyde **94** from *Subergorgia suberosa* collected near the coasts of India;[79] steroids **95a**–**c** from the same species collected near the coasts of the Comores Islands;[80] the epoxide **96** from the Indonesian coral *Lobophytum* sp.[81] and 4α-methylsecosteroids **97** and **98** from *Pseudopterogorgia* sp.[82] manifest moderate inhibitory activities with respect to protein kinase C and possess antiinflammatory and cytotoxic properties.

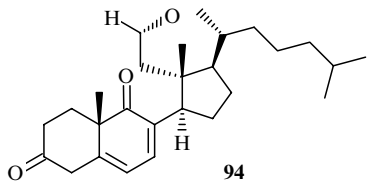

94

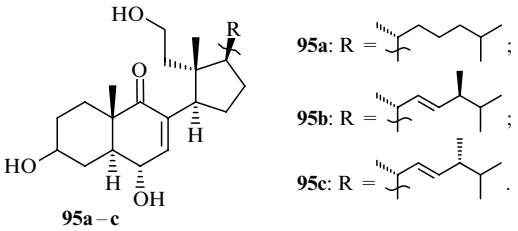

95a–c

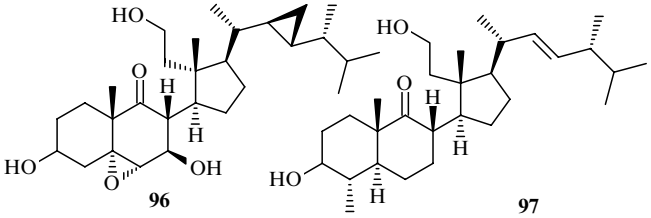

96 **97**

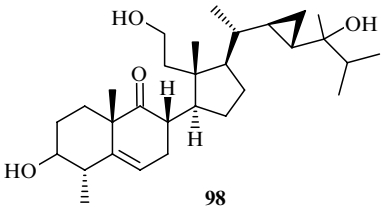

98

The unusual hemiacetal **99** (nicobarsterol) from *Sclerophytum* sp. was named after the place where it was first collected (the Nicobar Islands in the Indian Ocean).[66]

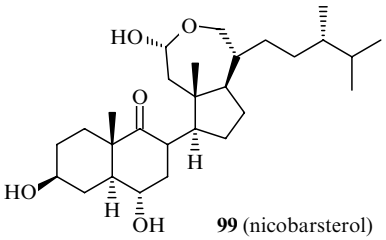

99 (nicobarsterol)

A search for novel compounds able to prevent biofouling of ship bottoms and submerged structures undertaken by the Fusetani group[93] resulted in the isolation of four novel unprecedented 13,17-secosteroids **100a**,**b** and **101a**,**b** (isogosterols A–D) from *Dendronephthea* sp. They manifested much higher antifouling activities in comparison with steroids **77a**,**b** and inhibited the settlement of barnacle (*Balanus amphitrite*) larvae when used in concentrations of ~ 2 μg ml^{-1} (see Ref. 83).

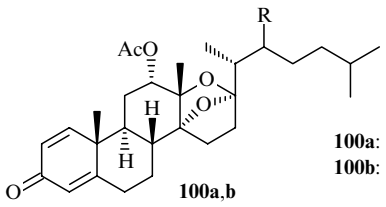

100a,**b**

100a: R = H (isogosterol A);
100b: R = OAc (isogosterol D).

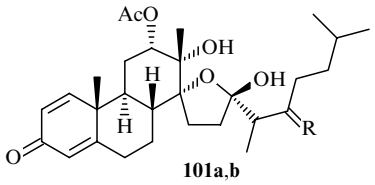

101a,**b**

101a: R = O (isogosterol B);
101b: R = OAc, H (isogosterol C).

Oxygenated steroids with the pregnane skeleton were often found in various representatives of Coelenterata; in particular, acetylated pregnanes **102a–d** and **103** have recently been found in the South African population of *Pieterfaura inilobata*.[84]

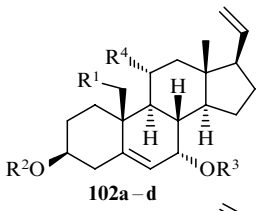

102a–d

102a: $R^1 = R^3 = H$, $R^2 = Ac$, $R^4 = OH$;
102b: $R^1 = H$, $R^2 = R^3 = Ac$, $R^4 = OH$;
102c: $R^1 = OAc$, $R^2 = Ac$, $R^3 = R^4 = H$;
102d: $R^1 = OAc$, $R^2 = R^3 = Ac$, $R^4 = OH$.

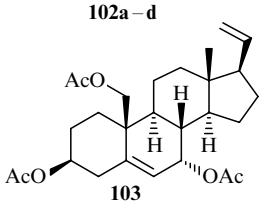

103

The detection of polar steroids in the sea pens of the Pennatulaceae order is the most uncommon case. Thus the triol **104**, the simplest oxygenated steroid formed upon oxidation of cholesterol at the 5(6)-double bond, was isolated from *Pteroides esperi*.[85]

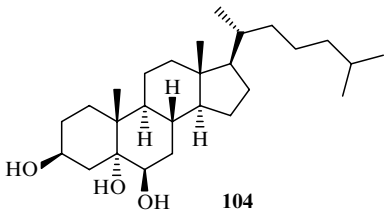

104

It should be said in conclusion that hydroxylation in Coelenterata predominantly occurs in positions 3, 5, 6, 22 and 25 and less frequently in positions 1, 2, 11, 16, *etc*. Steroids containing angular hydroxymethyl groups are widespread in these invertebrates; the oxygenation of the 19-methyl group occurs most often. In these animals, sterols can be oxidised to pregnane derivatives. 9,11-Seco compounds are as widely occurring in cnidarians as in sponges. It is noteworthy that polar steroids are seldom found in other taxa of Coelenterata, with the exception of octocorals.

4. Polyhydroxylated steroids from molluscs

Polar steroids are seldom found in molluscs, usually these are of exogenous origin, *viz*., they are consumed with food and accumulated in either an unchanged or a modified form. In most cases, the steroids accumulated in molluscs play the protective role.

For example, unusual 2α,3α-dihydroxy cross-conjugated ketones, such as diaulusterols A and B (**105a**,**b**), one of which containing a hydroxybutyrate substituent in the side chain, were detected in the nudibranch mollusc *Diaula sandiegensis*.[86] Recent *in vitro* studies of 1,2-^{13}C-acetate as a biosynthetic precursor showed that the steroid **105a** is not biosynthesised by these molluscs but is modified by addition of a substituent to the hydroxy group at C(25); this substituent is biosynthesised from acetate.[87] It is of note that nudibranch molluscs are devoid of shells and other mechanical protective means, they readily absorb toxic and deterrent metabolites from the sponges they feed on.

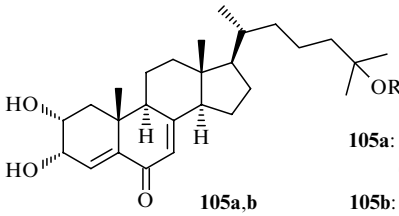

105a,**b**

105a: R = $COCH_2CH(OH)CH_3$ (diaulusterol A);
105b: R = H (diaulusterol B).

The triol **106a** and its 6-*O*-methyl derivative **106b** widely occurring in sponges were isolated from fertilised eggs of the mollusc *Aplysia juliana*.[88]

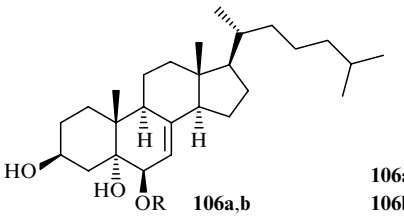

106a,**b**

106a: R = H;
106b: R = CH_3.

5. Polyhydroxysteroids of echinoderms

Echinoderms, particularly starfishes, are the source of the most oxygenated steroids. A great number of polyhydroxy derivatives have been discovered in these organisms since 1974. More than 20 novel compounds, (compounds **107**–**128**)[89–95] have been isolated recently (Table 1). The hydroxy groups in positions 3β, 6α or 6β, 8β, 15α or 15β, 16β and 26 are especially abundant in starfish steroids, while polyhydroxysteroids containing hydroxy groups in positions 4α or 4β, 7α, 14α, 24, 28 and 29 are isolated less often. Some starfish polar steroids contain eight or nine hydroxy groups,

Table 1. The structures of polyhydroxysteroids isolated from starfishes.

Compound	Unsaturation type	R^1	R^2	R^3	R^4	R^5	R^6	The side chain (R^7)	The biological source	Ref.
107	–	H	H	α-OH	H	β-OH	β-OH	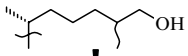	*Ceramaster patagonicus*	89
108	$\Delta^{8(14)}$	H	H	α-OH	H	β-OH	H	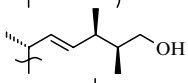	*Acodontaster conspicuus*	90
109	$\Delta^{8(14)}$	H	H	α-OH	H	β-OH	H	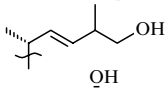	*Acodontaster conspicuus*	90
110	–	H	H	α-OH	OH	α-OH	H	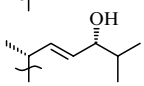	*Ceramaster patagonicus*	89
111	–	H	H	β-OH	H	α-OH	β-OH	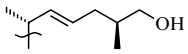	Echinasteridae gen. sp.	91
112	–	H	H	β-OH	H	α-OH	β-OH	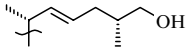	Echinasteridae gen. sp.	91
113	–	H	H	β-OH	H	α-OH	β-OH	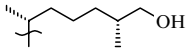	Echinasteridae gen. sp.	91
114	–	H	H	β-OH	H	α-OH	β-OH	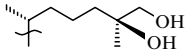	Echinasteridae gen. sp.	91
115	–	H	H	β-OH	H	α-OH	β-OH	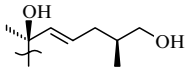	Echinasteridae gen. sp.	91
116	–	H	H	β-OH	OH	α-OH	β-OH	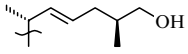	Echinasteridae gen. sp.	91
117	–	H	H	β-OH	OH	α-OH	β-OH	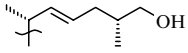	Echinasteridae gen. sp.	91
118	–	H	H	β-OH	OH	α-OH	β-OH	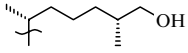	Echinasteridae gen. sp.	91
119	–	H	H	β-OH	OH	α-OH	β-OH	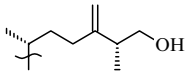	Echinasteridae gen. sp.	91
120	–	H	H	β-OH	OH	α-OH	β-OH	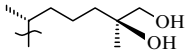	Echinasteridae gen. sp.	91
121	–	H	H	β-OH	OH	α-OH	H	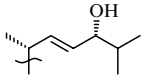	Echinasteridae gen. sp.	91
122	–	β-OH	H	α-OH	OH	β-OH	H	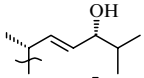	Echinasteridae gen. sp.	91
123	–	β-OH	H	α-OH	OH	β-OH	H	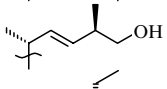	*Acodontaster conspicuus*	90
124	–	β-OH	H	α-OH	OH	β-OH	β-OH	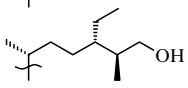	*Acodontaster conspicuus*	90
125	–	β-OH	H	β-OH	OH	β-OH	H	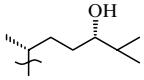	*Henricia derjugini*	93
126	–	H	α-OH	β-OH	H	α-OH	β-OH	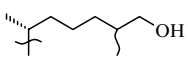	*Ctenodiscus crispatus*	94

Table 1 (continued).

Compound	Unsaturation type	R^1	R^2	R^3	R^4	R^5	R^6	The side chain (R^7)	The biological source	Ref.
127	–	H	α-OH	β-OH	H	α-OH	β-OH	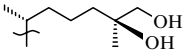	*Ctenodiscus crispatus*	94
128	–	H	α-OH	β-OH	H	α-OH	β-OH	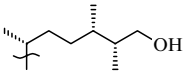	*Luidiaster dawsoni*	95

although the corresponding pentols and hexols are more common for these animals.

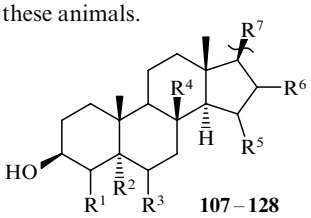

107 – 128

Sometimes starfish metabolites contain other functional groups or manifest other structural features. For example, the pentol **129** from *Luidia clathrata*[92] is a 5β-cholestane derivative in contrast to other polar steroids of this series. One of the hydroxy groups in compound **130** from Echinasteridae gen sp. is oxidised to the keto group,[91] whereas steroids **131** and **132** from *Myxoderma platyacanthus* contain carboxy groups in their side chains.[96]

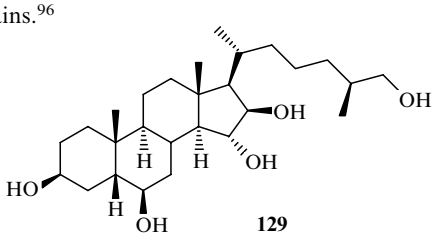

129

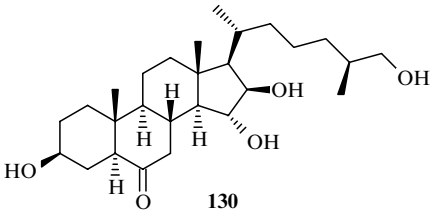

130

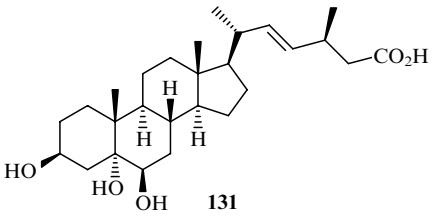

131

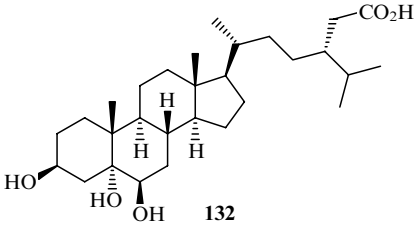

132

Recent studies on the distribution of polyhydroxy compounds in various body components and organs and structures of starfishes[97] prompted several conclusions concerning their biological roles. Since polyhydroxysteroids and related mono- and biosides were found only in digestive organs and solubilise lipid suspensions like bile acids, their role in starfishes can be similar to that of bile acids and bile alcohols in vertebrates.

Some starfish polyhydroxysteroids manifested antimicrobial activities against the gram-positive bacterium *Staphylococcus aureus* but did not inhibit the gram-negative bacterium *Escherichia coli*. A series of octols and nonols containing hydroxy groups in positions 4, 7, and 8 manifested high cytotoxic activities against human lymphoma cells JURCAT.[98]

It is interesting to note that polyhydroxysteroids are not common in other classes of echinoderms. Related sulfated polyols were found only in ophiuroids, whereas in holothurians and sea urchins polar steroids have not been identified yet. Recently, steroidal 3β,5α,6β-triols of the Δ^7-series were found in one representative of sea lilies (Crinoidea).[99]

Not all groups of marine invertebrates are rich in polyhydroxysteroids. The latter are not common for bryazoans and ascidians, but occur predominantly as ecdysteroids in crustaceans; however this group of polar steroids fall beyond the scope of the present review. In sponges, cnidarians and echinoderms, they are represented by only very few orders or classes. Notwithstanding, the immense diversity of marine polyhydroxysteroids is amazing and seems to reflect the intense evolutional search characteristic of taxa located in the basements of phylogenetic trees. Obviously, cnidarians and sponges are the most ancient animal organisms that have come down to us.

The biological roles of oxygenated sterol derivatives and related pregnane and other steroids are different in vertebrates and marine invertebrates. Whereas in the former they predominantly act as hormones and take part in digestion as bile acids, in sponges and cnidarians they usually perform protective functions, *e.g.*, they frighten away predators, inhibit the growth of pathogenic microorganisms, protect producers from fouling with algae, barnacles, molluscs, *etc.*

It is interesting to note that there are such biochemical transformations of sterols in some primitive marine invertebrates, which as happy findings of the Nature are repeated many time in other types of organisms and become to be of considerable importance in more advanced animal taxa and in higher plants. For example, as it was mentioned above, sponges and cnidarians contain pregnenolone, a biosynthetic precursor of steroid hormones of higher animals. Compounds of the spirostane series, which are analogous to aglycons of steroid saponins of higher plants, were repeatedly found in cnidarians and some other marine invertebrates. C_{28}-Steroid lactones, which are structurally similar to some witanolides (metabolites of terrestrial higher plants of the *Solanaceae* family), were found in the soft coral *Minabea* sp.[100] These biochemical parallelisms presumably testify to some degree of determinism in evolution of secondary metabolic processes occurring in living organisms.

III. Steroid sulfates

Sulfated compounds are extensively distributed in marine organisms. They were found in micro- and macroalgae, marine invertebrates (*e.g.*, sponges, echinoderms, molluscs), hemichordates and fishes. Sulfation is an essential mechanism of biosynthetic conversions occurring in the marine biota. This is not surprising, since sulfur (in the form of a sulfate ion) is the fourth most abundant

element in sea water after chlorine, sodium and magnesium. The introduction of a sulfate group increases the solubility of marine natural products and makes them biphilic, which is especially important for manifestation of their detergent and toxic activities and signal functions in various inter- and intraspecies interactions. The presence of sulfate groups ensures efficient transport of the corresponding compounds in water, while the presence of hydrophobic fragments in their molecules facilitates their binding to hydrophobic receptors of recipient organisms.

In macroalgae and some microalgae, sulfated compounds are largely represented by polysaccharides, while those in marine animals are represented by low-molecular-weight bioregulators. Over 500 sulfated secondary metabolites of different chemical groups (*e.g.*, terpenoids, carotenoids, steroids, alkaloids, aromatic metabolites, *etc.*) have been identified.[101]

Sulfated steroids constitute one of the most numerous groups of these compounds. They were mostly isolated from animals related to two large phyla of marine invertebrates, *viz.*, echinoderms (Echinodermata) and sponges (Porifera), although sulfated steroids were also found in other marine organisms. The biological functions of compounds related to this group are still poorly understood, although the facts that the least polar of them are essential components of biomembranes, while other representatives of this group are used for chemical protection against predators and pathogenic or fouling microorganisms leave no doubts.

1. Sterol sulfates

Structurally, sterol sulfates are the simplest sulfated steroids. In echinoderms, they occur as common metabolites; their concentrations in starfishes (Asteroidea), holothurians (Holothurioidea), ophiuroids (Ophiuroidea) and sea lilies (Crinoidea) amount to 4–5 mg per gram of dry tissue, those in sea urchins (Echinoidea) are somewhat lower.[1] The predominant component in the respective fractions is cholesterol sulfate **133a**. In addition, these fractions always contain sulfates of other Δ^5-sterols. Toxic representatives of holothurians and starfishes contain small amounts of sulfated stanols and sulfates of Δ^7-sterols along with sulfates of the Δ^5 series. For example, the Far Eastern holothurian *Eupentacta* (= *Cucumaria*) *fraudatrix* was found to contain polar steroids **133a**–**i**, **134a**–**k** and **135a**–**l**. Moreover, the same holothurian species contain trace amounts of sulfates of 14α-methyl-$\Delta^{9(11)}$-sterols **136a**,**b** and of triterpenoids **137** and **138**.[102] Practically all free sterols from *E. fraudatrix* are subject to sulfation, however, in different degrees. Δ^5-Sterols (in the first place, cholesterol), which are consumed with food, are sulfated in the greatest degree. In contrast with sulfates, free sterols of the Δ^5 series are present in toxic holothurians in small amounts; they can be transformed into sulfates, stanols and Δ^7-sterols. Stanols and Δ^7-sterols, contrariwise, predominate in fractions of free sterols, but are sulfated in a very low degree. These peculiarities of steroid metabolism in holothurians and starfishes are explained by the presence of toxic glycosides, which react with the membrane cholesterol and other Δ^5-sterols resulting in the formation of membrane pores. This is why cholesterol and its homologues are highly toxic for holothurian cells; their substitution by $\Delta^{9(11)}$- and Δ^7-sterols, stanols and sulfates of the type **133**, which are less capable to form membrane complexes with holothurian toxins, protects these animal cells from deleterious effects of their intrinsic glycosides.[103]

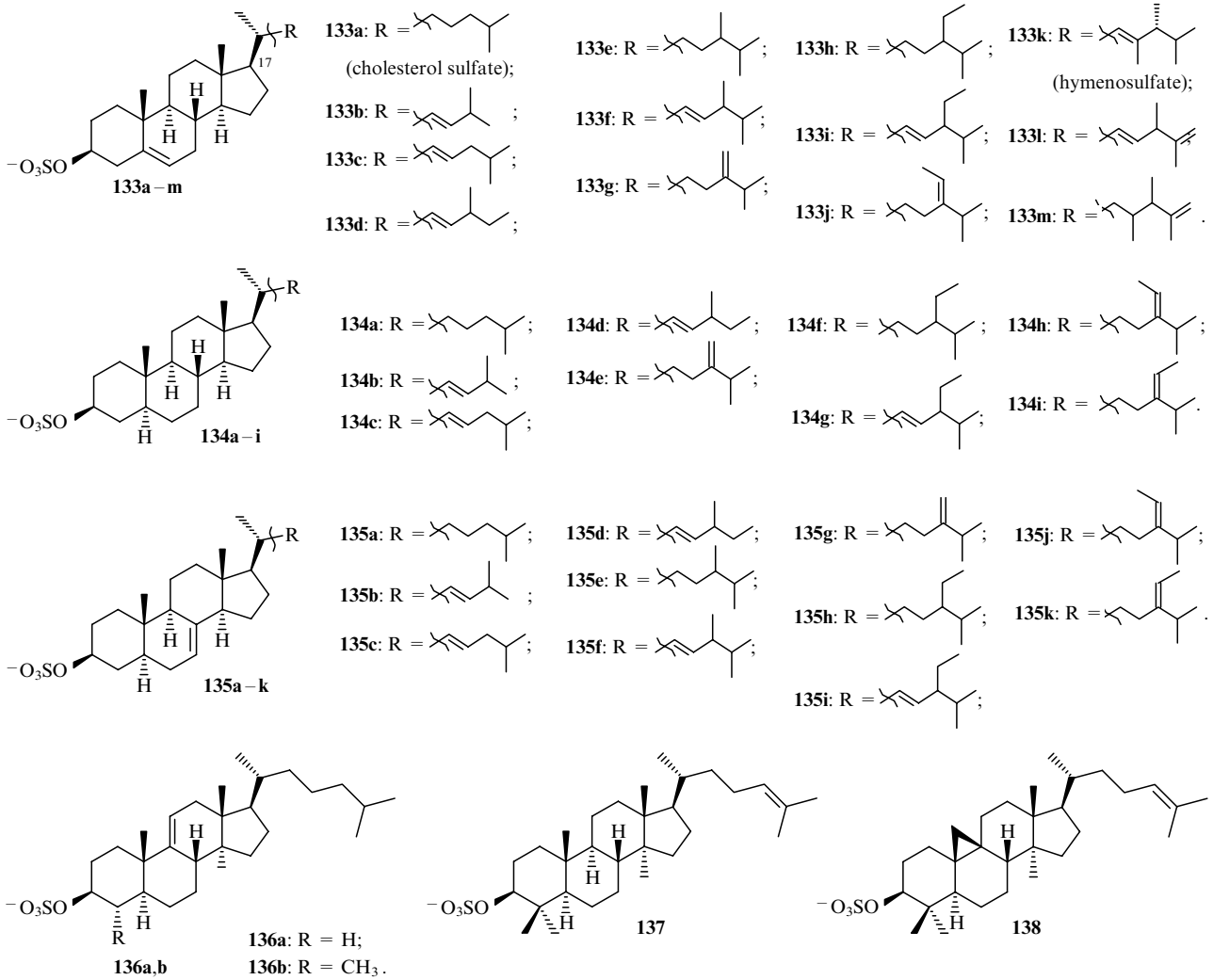

These data suggest that sulfation of free cholesterol in echinoderms is a result of their adaptation to the effects of intrinsic membranolytic toxins and that sterol sulfates fulfil a membrane-protective function by preventing the effects of these toxins on cell membranes.

Recently, Indian and Italian scientists have isolated two novel sulfated sterols **133l**,**m** from the tropical sea cucumber *Holothuria* sp.[104]

Sterol sulfates were detected not only in echinoderms but also in some other marine organisms. For example, 24-methylidene-cholesterol sulfate **133g** was detected in the diatomic microalga *Nitzchia alba* as long as 35 years ago,[105] whereas the so-called hymenosulfate **133k**, which contains an unusual side chain similar to those of some free microalgal (dynoflagellate) sterols, was found in the haptophytic microalga *Hymenomonas* sp.[106]

2. Polyhydroxysteroid monosulfates

Polyhydroxysteroid monosulfates from sponges and echinoderms contain sulfate groups in 3β- or other positions. Thus compounds **139a**–**c** containing additional hydroxy groups at C(19) were isolated from the sponge *Toxadocia zumi*.[107] A new β-1,3-glucanase inhibitor, *viz*., annasterol sulfate **140**, was isolated in our laboratory from the Pacific deep-water sponge *Poecilastra laminaris*.[108]

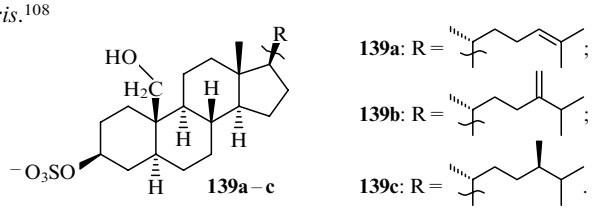

139a–**c**

139a: R = ;

139b: R = ;

139c: R = 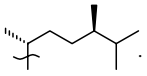 .

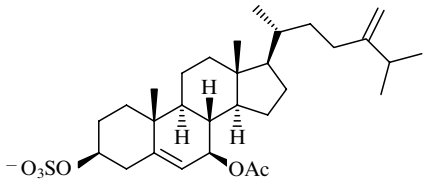

140 (annasterol sulfate)

The unusual steroid polymastiamide A (**141a**) was isolated from the sponge *Polymastia boletiformis* collected near the coasts of Norway.[109] This is the amide of a rarely occurring amino acid, *viz*., *p*-methoxyphenylglycine, and its steroidal fragment is a $\Delta^{8(14)}$-derivative methylated in position 4. Earlier, 4α-methyl-$\Delta^{8(14)}$-sterols were detected in some archaebacteria of the *Methylococcus* genus. This points to participation of symbiont bacteria in biosynthesis of compound **141a**, since archaebacteria have recently been identified as symbionts in some sponges. Polymastiamides B–F (**141b**, **142a**,**b**, **143a**,**b**) isolated from the same sponge are structurally close to polymastiamide A (**141a**). Their treatment with CH_3OH/HCl is accompanied by both migration of the double bond and aromatisation of the ring C resulting in the artificial products **144** and **145**.[110]

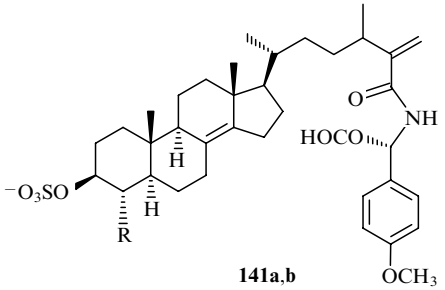

141a,**b**

141a: R = CH_3;
141b: R = H.

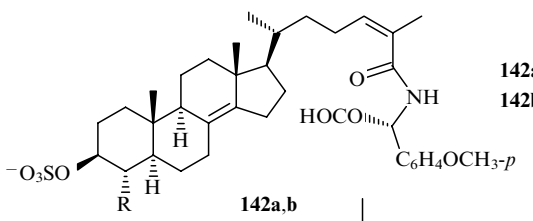

142a,**b**

142a: R = CH_3;
142b: R = H.

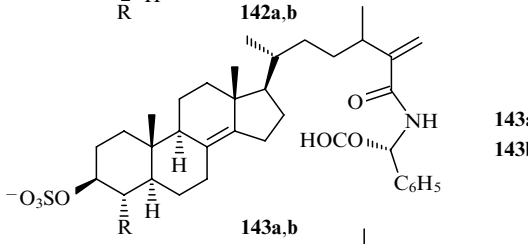

143a,**b**

143a: R = CH_3;
143b: R = H.

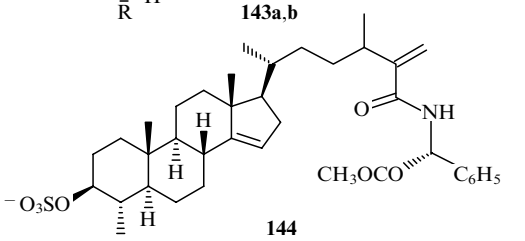

144

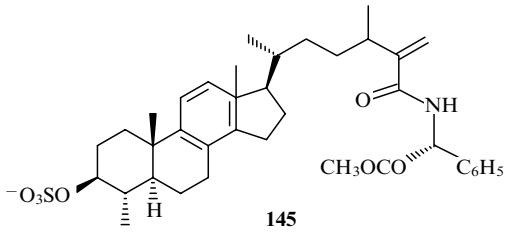

145

The steroid **146** from the sponge *Stilopus australis*[111] is unrelated to sterol derivatives, this rather resembles steroid hormones because of the presence of the pregnane skeleton.

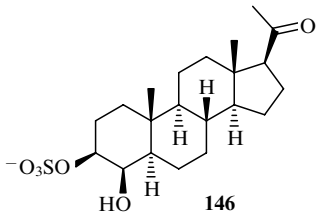

146

One of a few steroid monosulfates **147** with the sulfate group in position 2β was isolated from *Echinoclathria suhispida* collected near the coasts of Japan. Echinoclasterol sulfate **147** is a salt in which protonated tyramine is the counter-ion.[112]

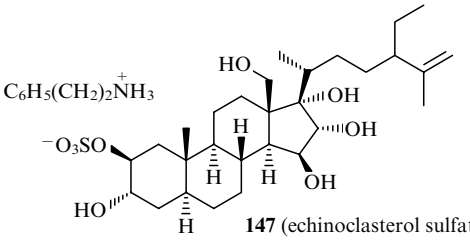

147 (echinoclasterol sulfate)

The unique cytotoxic steroid **148** containing a sulfate group in position 6α was found in the sponge *Dysidea fragilis* collected from the lagoon of Venice.[39] Haliclostanone sulfate (**149**) from the Malaysian sponge *Haliclona* still remains the only sulfated sponge steroid with an uncommon *cis*-fusion of rings *C* and *D*.[113] Sulfates of acanthosterols A–J (**150a**–**j**) from the sponge *Acanthodendrilla* sp. contain sulfate groups in position 6.[114] Thus, sponges contain various steroid metabolites, mostly those sulfated in positions 3, 2 or 6.

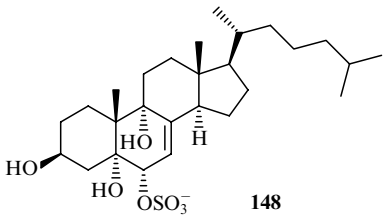

148

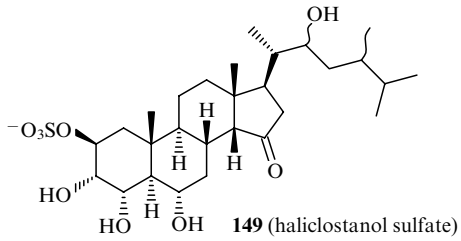

149 (haliclostanol sulfate)

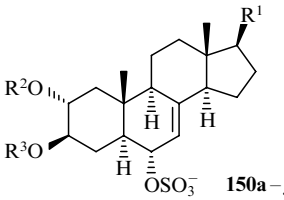

150a–**j**

Compound **150**	R^1	R^2	R^3
a	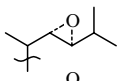	H	H
b	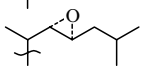	H	Ac
c	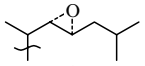	H	H
d	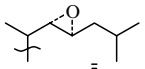	Ac	H
e	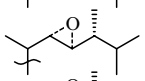	H	Ac
f	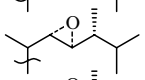	H	H
g	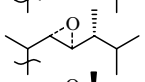	Ac	H
h	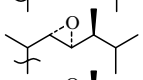	H	Ac
i	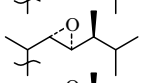	H	H
j	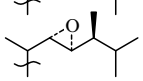	Ac	H

Non-glycosylated polyhydroxysteroid sulfates are abundant in starfishes and usually contain sulfate groups in the side chains. If sulfation takes place in the steroid nucleus, the sulfate group is bound to C(3), C(6), C(15) or C(16). Thus different starfish species contained steroids of the general formula **151**. Steroids **151a**,**c** are genuine algycons of many asterosaponins.[3, 115] Presumably, these compounds are biosynthetic precursors of asterosaponins, which are converted into them after the attachment of the carbohydrate chain. The related compound apheloketotriol (**151b**) was isolated from *Aphelasterias japonica*.[116]

The novel steroid **152** sulfated at C(6) was detected in the starfish *Oreaster reticulatus* together with 16 steroid glycosides and several polyhydroxysteroids.[117]

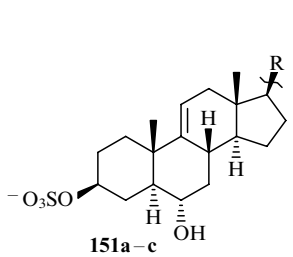

151a–**c**

151a: R = 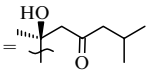 (tornasterol A sulfate);

151b: R = 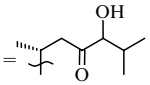 (apheloketotriol);

151c: R = (asterone sulfate).

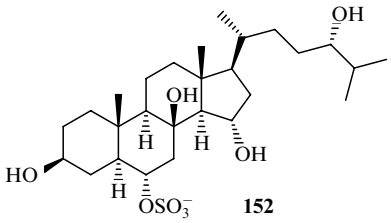

152

The monosulfates **153a**,**b** and **154** containing sulfate groups in position 15 or 16 were isolated from *Luidia clathrata*,[92] whereas the 3-monosulfate **155** was isolated from *L. quinaria*.[118]

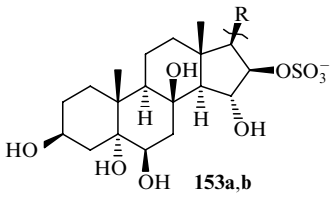

153a,**b**

153a: R = 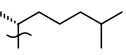 ;

153b: R = 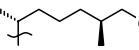 OH.

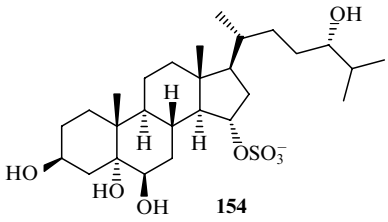

154

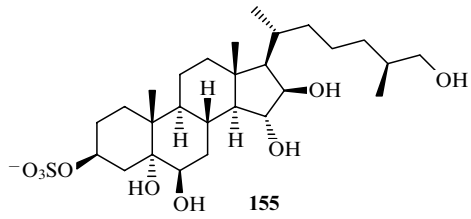

155

A large series of compounds **156b**–**e** containing sulfate groups in different positions of their side chains were found in *L. clathrata*.[92] The structurally related monosulfate **156a** was isolated from extracts of *Luidia ludwigi*.[119] The related sulfates **156f**–**i** from the starfish *Styracaster caroli*[120] collected at 2-km depth near the coasts of New Caledonia have highly oxygenated side chains. Sulfates **156j** and **156k** were isolated from the starfish *Ctenodiscus crispatus*.[94] Steroids **157a**–**c** sulfated in side chains and hydroxylated at C(16) of the side chains were found in *L. clathrata* [92] and *Styracaster caroli* (**157c**).[120]

The unusual steroidal ketones, *viz*., asterosterols B and C (**158a**,**b**) containing saturated ketone fragments in rings *B* characteristic of ecdysteroids, were isolated from antarctic starfishes belonging to the Asteriidae family.[121] These animals also contained a unique sulfate **159** with a seven-membered unsaturated lactone ring. Regioisomeric lactone rings are present in brassinosteroids, the higher-plant growth stimulants.

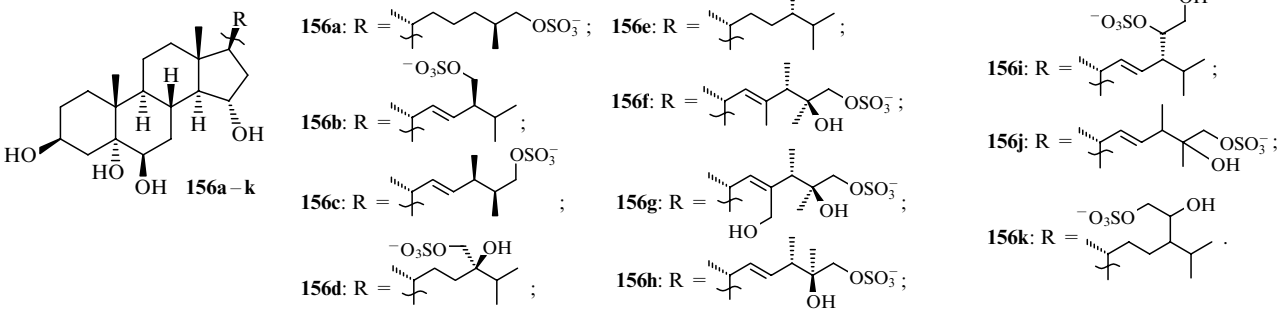

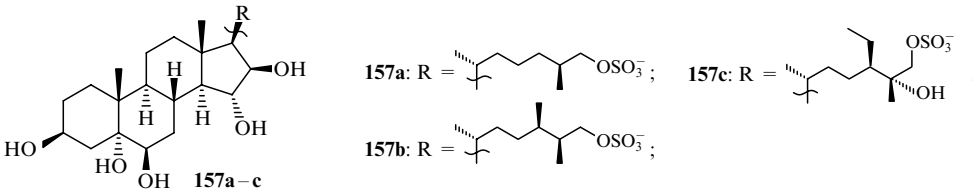

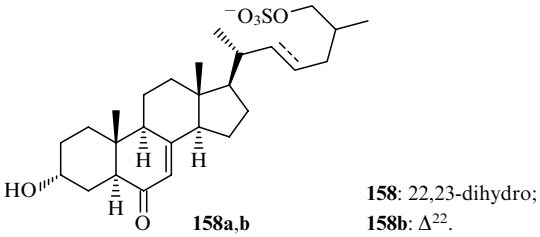

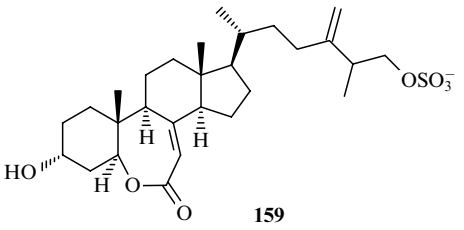

Finally, a group of steroid sulfates containing sulfate groups in the taurine fragments or in other sulfated amino alcohol fragments, which represent the corresponding amides, have been isolated recently from *Myxoderma platyacanthum* (compounds **160a**,**b**)[96] and *Styracaster caroli* (compounds **161a**–**c**).[122] In contrast to other starfish steroids, the latter are cholanic acid derivatives.

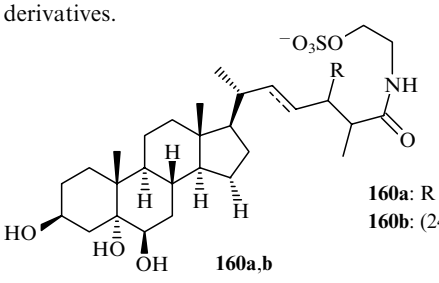

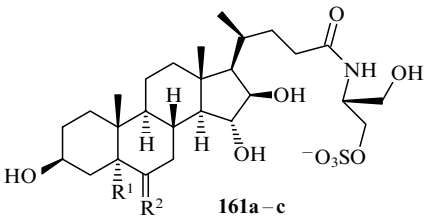

In ophiuroids (brittle stars) belonging to yet another class of echinoderms, polyhydroxysteroid sulfates are represented predominantly by 3α-derivatives. Monosulfates are less widely distributed in these animals in comparison with di- and trisulfates, although several compounds of this type have been isolated from different representatives of the class Ophiuroidea. Thus compounds **162a**,**b** were found in Far Eastern brittle stars *Ophiura leptoctenia* and *O. sarsi*.[123, 124] The monosulfated steroid **163** was isolated from *Ophiarachna incrassata* collected near the coasts of New Caledonia.[125] Later, it was found that this compound inhibits protein kinase pp $60^{v\text{-}src}$ responsible for regulation of cell growth and intercellular signalling.[126]

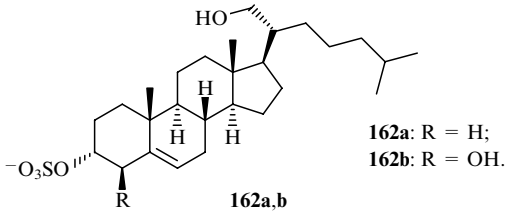

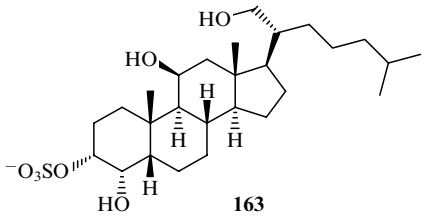

Sulfated bile alcohols from fishes (for an early review, see Ref. 1) are also related to polyhydroxysteroid monosulfates. Among those, scymnol sulfate **164a** isolated from the shark *Scymnus borealis* as long ago as in 1898 is the most widely known one. Recently, both C(24) epimers of this compound have been isolated from the shark *Lamna ditropis*.[127] The related bile alcohol, chymaerol sulfate **164b**, was found in the bile of two shark species, *viz*., *Lamna ditropis* and *Rhizoprionodon acutis*.[128] Three novel steroid sulfates **165a**,**b** and **166** were found in the bile of the sunfish *Mola mola*.[129] Compounds **165a**,**b** represent 25*R*- and 25*S*-isomers, whereas compound **166** represents a taurine conjugate of an acid, which differs from cholic acid in that one of its hydroxy groups occupies position 11 rather than 12. The novel sulfated pregnane derivative **167** was isolated from the urine of

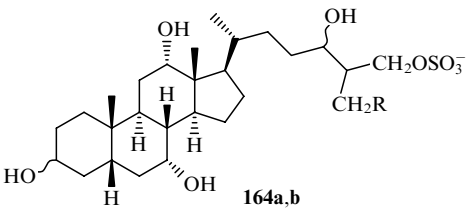

164a: R = OH, 3β-OH, 24*S* and 24*R* (scymnol sulfate);
164b: R = H, 3α-OH, 24*R* and 25*S* (chymaerol sulfate).

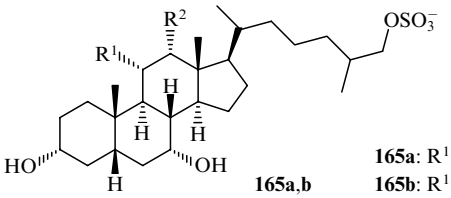

165a,**b** **165a**: R^1 = OH, R^2 = H; **165b**: R^1 = H, R^2 = OH.

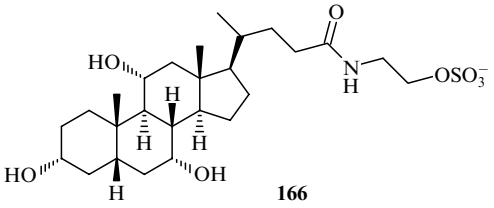

166

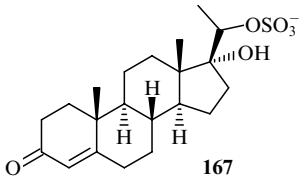

167

female salmon *Salmo solar*.[130] The most recent findings and the data obtained previously testify to the fact that sulfated steroids are extensively distributed in fishes.

3. Steroid disulfates

Some sponge steroids contain sulfate groups in positions 3α and 2β. This series of compounds includes compound **168**, a possible biogenetic precursor of halistanol sulfate,[131] which is the most widely occurring trisulfate of sponges, and weinbersterols A and B (**169a**,**b**) from the sponge *Petrosia weinbergi*. The latter have unique side chains containing cyclopropane fragments, which makes them different from other polysulfated sponge steroids. Steroids **169a**,**b** manifest antiviral activities against cat leukemia and mouse influenza viruses.[132] The absolute configurations (24*S*,28*S*) of weinbersterols A and B were established by comparing them with those of the free sterols, which represent biogenetic precursors of steroids **169a**,**b** isolated from the same sponge.[133]

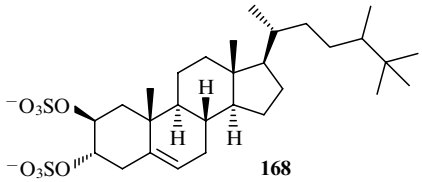

168

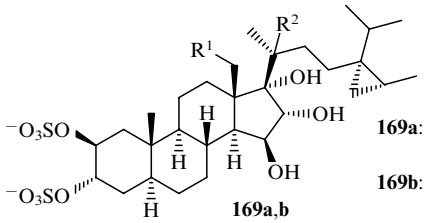

169a,**b** **169a**: R^1 = H, R^2 = OH (weinbersterol A); **169b**: R^1 = OH, R^2 = H (weinbersterol B).

Yet another group of antiviral disulfates, the so-called orthoestrols A–C from the Caribbean sponge *P. weinbergi*,[134] comprises derivatives of orthobutyric acids. The stereochemistry of orthoestrol B (**170b**) appears as 24*R*,28*S*; that of orthoestrol C (**170c**) is 24*R*.

Halistanol B disulfate (**171**) from the South African sponge *Pachastrella* sp.[135] presents interest with regard to both its structure (its side chain contains no methyl group in position 27, which makes this compound different from cholesterol) and biological activity. It inhibits the activity of the enzyme catalysing the conversion of the protein precursor of endothelin into endothelin-1 (IC_{50} = 1.3 μg ml^{-1}). Endothelin induces vascular

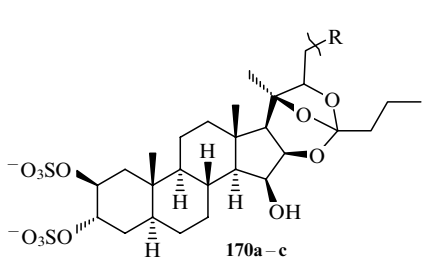

170a–**c** **170a**: R = (orthoestrol A); **170b**: R = (orthoestrol B); **170c**: R = (orthoestrol C).

spasms and is abundant in patients with hypertension and renal insufficiency. Compound **171** as an inhibitor of endothelin synthesis is a promising model substance for development of new antihypertensive drugs.

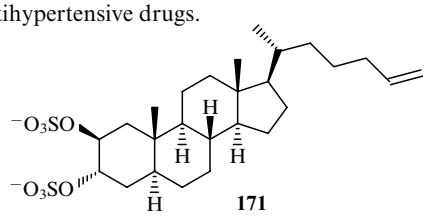

171

A series of steroid disulfates were found in starfishes and ophiuroids. Thus compounds **172a**–**d** were isolated from the starfish *Tremaster novaecaledonia*[136] and compound **172e**, from *Aphelasterias japonica*.[137]

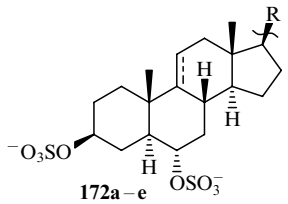

172a–**e**

172a: R = , Δ^0; **172b**: R = , Δ^0; **172c**: R = , $\Delta^{9(11)}$; **172d**: R = , $\Delta^{9(11)}$; **172e**: R = , $\Delta^{9(11)}$.

In contrast to their starfish counterparts, steroid disulfates isolated from ophiuroids have a number of specific structural features. In nearly all of them, one sulfate group is in position 3α and the second one is in the side chain at C(21). These steroids comprise stanol derivatives as well as 5(6)-unsaturated derivatives. For example, sulfated stanols of the general formulas **173** and **174** are widely distributed in various representatives of this class, *e.g.*, in more than 30 species of Ophiuroidea.[3,99] Disulfate **173a**, which was first discovered together with compound **173b**,**c** in *Ophioderma longicaudum*[138] and later in different species of Ophiuridae, Gorgonocephalidae and Asteronychnidae families,[99] is the most widespread disulfate of the general formula **173**. The steroid **173d** was isolated from the antarctic brittle star *Astrotoma agassizii*.[139]

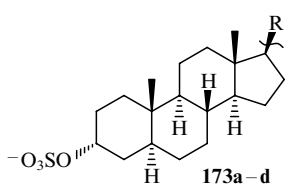

173a–**d**

173a: R = ; **173b**: R = ; **173c**: R = ; **173d**: R = , 2β-OH.

Steroid disulfates of many ophiuroids are characterised by *cis*-fusion of rings *A* and *B*. For example, compound **174a** first described by Italian scientists in 1985[140] was later discovered in various representatives of the *Ophiocoma*, *Ophioarthrum*, *Ophiolepis*, *Ophionereis* and *Ophiozona* genera.[3,99] The steroid **174b** was found in *Ophiocoma dentata*, *Ophioarthrum elegans*, *Ophiorachna incrassata*, *Ophiolepis superba* and *Ophiomastix annulosa*.[3] The steroid **174c**, which differs from the latter in the structure of its side chain, was first discovered in *Ophiocoma dentata*,[3] whereas compounds **174d**–**f** were found in *Ophiolepis superba*, which also contains additionally oxygenated derivatives **174g**,**h**,**i**.[141] The steroid **174j** containing an additional hydroxy group at C(12) was isolated from *Ophioderma longicaudum*,[138] whereas steroids **174k**,**l** were isolated from *Ophiomastix annulosa*[142] and *Ophiopholis superba*.[141] The steroid **174m** containing an unusual 5,9-epoxy fragment was found in *Ophiomastix annulosa*[142] and compound **174n** was detected in the antarctic ophiura *Astrotoma agassizi*.[139]

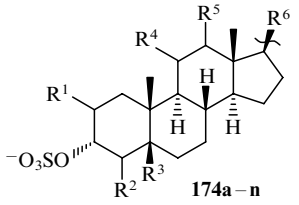

174a–**n**

Compound **174**	R^1	R^2	R^3	R^4	R^5	R^6
a	H	α-OH	H	β-OH	H	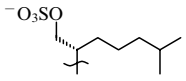
b	H	α-OH	H	H	H	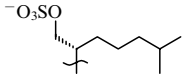
c	H	α-OH	H	H	H	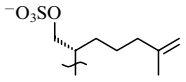
d	H	α-OH	H	H	H	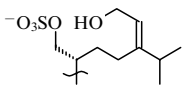
e	H	α-OH	H	H	H	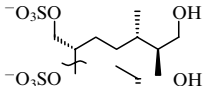
f	H	α-OH	H	H	H	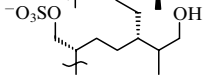
g	H	α-OH	β-OH	H	H	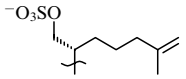
h	β-OH	α-OH	H	H	H	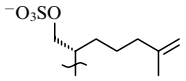
i	β-OH	α-OH	H	H	H	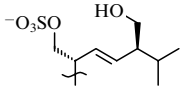
j	H	α-OH	H	β-OH	β-OH	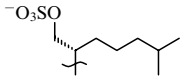
k [$\Delta^{9(11)}$]	H	α-OH	H	H	H	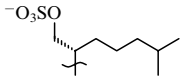
l	H	α-OH	α-OH	H	H	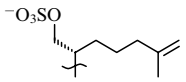
m	H	4α,9α-epoxy	H	H	H	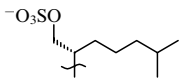
n	β-OH	H	H	H	H	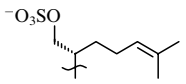

5(6)-Unsaturated steroids of the general formula **175** are often present in ophiuroids. Thus compounds **175a** and **175b** were isolated from the Far Eastern brittle star *Ophiura sarsi*[124] and steroids **175c-f** were isolated from *Ophiopholis aculeata*.[143] The steroid **175a** was also isolated from *Ophiura texturata*,[144] *Gorgonocephalus caryi*,[145] *Ophiotrix fragilis*[2] and some other species. The steroid **175g** was found in *O. texturata*,[144] the steroid **175h** was detected in *Ophiarachna incrassata*.[140] The disulfate **175i** containing three functional groups in the ring *A* was isolated from the antarctic brittle star *Ophiosparte gigas*[146] as well as from *Astroclades exiguus* and *Amphiophiura ponderosa*.[147]

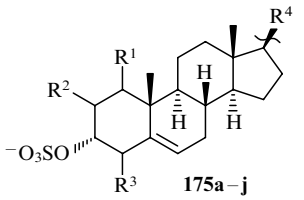

175a–**j**

Compound **175**	R^1	R^2	R^3	R^4
a	H	H	β-OH	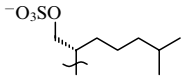
b	H	β-OH	H	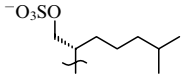
c	H	H	β-OH	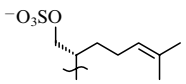
d	H	H	β-OH	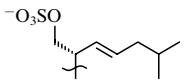
e	H	β-OH	H	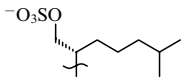
f (24*S* and 24*R*)	H	β-OH	H	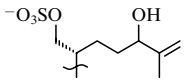
g	H	H	β-OH	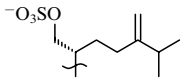
h	β-OH	H	H	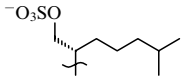
i	H	β-OH	β-OH	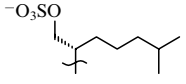
j	H	β-OH	H	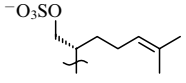

The unusual steroid disulfate **176a** was detected in the brittle star *Ophiosparte gigas*.[146] It contains a sulfate group in position 2β but not in position 3α, like other sulfates of this series. Later, this disulfate was isolated from several other representatives of this class.[99] Its 24(25)-unsaturated derivative **176b** and related ophiuroid disulfates **175j** and **174n** from *Astrotoma agassizii*[139] and their acetates manifested strong antiviral activities against the pathogenic virus HSV-2, which evokes meningitis and other severe infections in humans.[147]

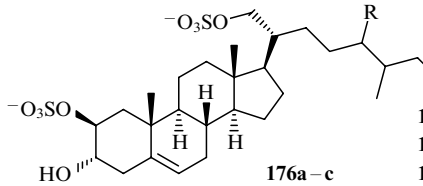

176a–**c**

176a: R = H, X = H;
176b: R = H, X = H, Δ^{24};
176c: R = H, X = OH.

The typical ophiuroid steroids **175a**,**b** and **176a** were unexpectedly found in the starfishes of the *Pteraster* genus.[148] These compounds differ from steroids of the majority of other starfish species in the stereochemistry of substituents at C(3) (3α instead of more common 3β) and oxygenation at C(21). A detailed analysis of steroids isolated from this group of starfishes led to the discovery of a compound earlier identified in ophiuroids (compound **175g**) and novel compounds **176c** and **177a**,**b** which combine structural features of steroids from brittle stars (*e.g.*, oxygenation in positions 3α and 21) and starfish (*e.g.*, oxygenation in position 26).[149] The presence of the same or structurally related secondary metabolites in brittle stars and starfishes corroborates the viewpoint of some taxonomists that these two classes of echinoderms are phylogenetically more closely related in comparison with other classes of Echinodermata.

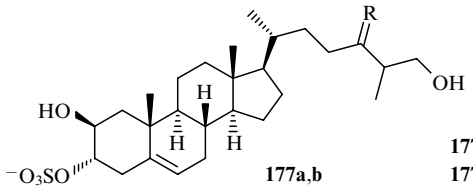

177a,**b** **177a**: R = CH_2; **177b**: R = H_2.

Disulfates from ophiuroids manifest the properties of activators of some enzymes, particularly glucanases.[150] Steroids of the Δ^5-series isolated from *Ophiopholis aculeata* activate the transport of calcium ions into different cells without disturbing the integrity of biomembranes.[151]

4. Steroid trisulfates

Trisulfated polyhydroxysteroids are typical representatives of marine metabolites. They were found in sponges and echinoderms.[1, 17, 99, 152] Halistanol sulfate (**178a**), the most widespread sponge steroid sulfate, was isolated from the sponge *Halichondria moori* in 1981 by Fusetani *et al.*[153] It contains three sulfate groups in rings *A* and *B* of the steroid tetracyclic nucleus. The structure of socotrasterol sulfate (**178b**) isolated repeatedly from different sponges was established in our laboratory.[154] Both compounds have unusual side chains, which are additionally alkylated (compared with those of terrestrial sterols). The side chain of socotrasterol sulfate is unique in that it contains two 'extra' methyl groups at C(26) and a 23(24) double bond uncommon for natural steroids. A large series of analogous natural compounds have been isolated from different sponges. These include halistanol sulfates A–D (**178c**–**f**) from *Epipolasis* sp.,[155] norsocotrasterol sulfate (**178g**) from sponges of the *Halichondridae* family,[156] dihydrosocotrasterol sulfate (ophirapstanol sulfate) **178h** from *Topsentia ophiraphidites*,[157] halistanol sulfates F–H (**178i**–**k**) from *Pseudaxinyssa digitata*,[158] compound **178l** from *Trachiopsis halichondroides*[159] and steroids **178m**–**p** from *T. halichondroides* and *Cymbastella coralliophila*.[160]

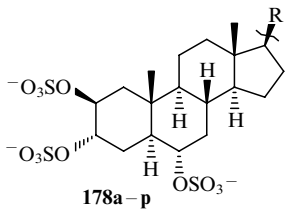

178a–**p**

Compound **178**	Name	R
a	halistanol sulfate	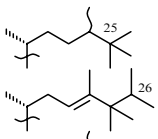
b	socotrasterol sulfate	
c	halistanol sulfate A	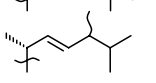
d	halistanol sulfate B	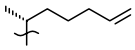
e	halistanol sulfate C	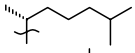
f	halistanol sulfate D	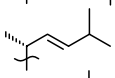
g	26-norsocotrasterol sulfate	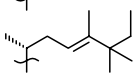
h	ophirapstanol sulfate	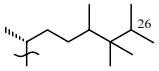
i	halistanol sulfate F	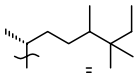
j	halistanol sulfate G	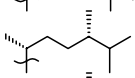
k	halistanol sulfate H	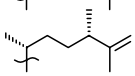
l	–	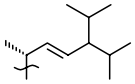
m	–	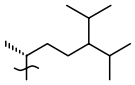
n	–	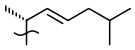
o	–	
p	–	

The sulfated steroids of this series manifest a broad range of biological activities (*e.g.*, antimicrobial, hemolytic, ichthyotoxic, *etc.*), inhibit HIV-1-induced infection,[161] suppress the activities of some enzymes including that of β-1,3-glucanase[162] and interact with the thrombin receptor.[155]

Several related trisulfates have recently been identified in sponges. These include halistanol sulfate E (**179**) from *Epipolasis* sp.,[155] which contains an additional hydroxy group at C(16), ibisterol sulfate **180a** from the sponge *Topsentia* sp., which inhibits HIV-1 and, in contrast to related steroids, possesses a 9(11)-double bond and an unusual side chain with a cyclopropane fragment.[163] Topsentiasterols **180b** and **181a**–**d** from an unidentified sponge of the *Topsentia* genus carry hydroxy groups at C(4) and in the majority of cases contain oxygenated side chains. These compounds possess antimicrobial properties.[164]

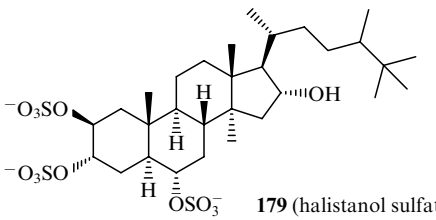

179 (halistanol sulfate E)

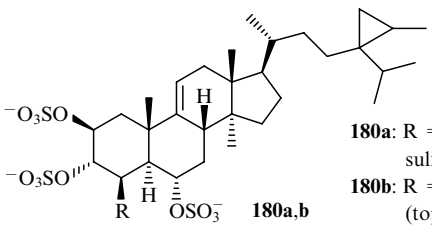

180a,**b** **180a**: R = H (ibisterol sulfate); **180b**: R = OH (topsentiasterol E).

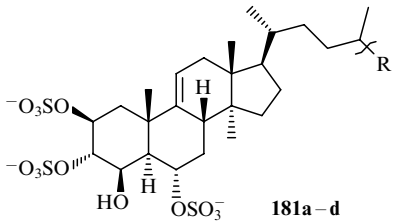

181a–d

181a: R = 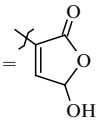 (topsentiasterol A);

181b: R = 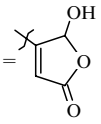 (topsentiasterol B);

181c: R = 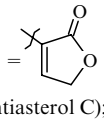 (topsentiasterol C);

181d: R = (topsentiasterol D).

Several trisulfated steroids were found in echinoderms, particularly in ophiuroids. Thus steroids **182a**,**b** were isolated from *Ophiorachna incrassata* extracts[3] and the steroid **183** was isolated from *Ophiura sarsi*.[124]

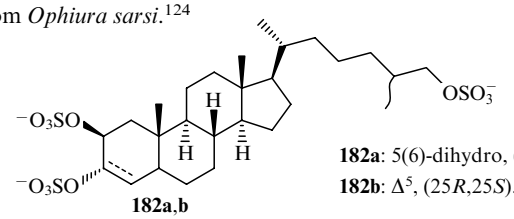

182a,**b**

182a: 5(6)-dihydro, (25*R*,25*S*);
182b: Δ^5, (25*R*,25*S*).

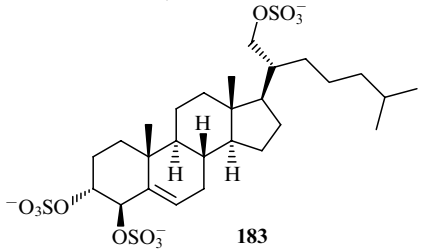

183

On the whole, sulfated steroids present substantial interest owing to their unusual chemical structures and biological activities. Some of them are attractive objects for synthetic modelling aimed at the design of novel antimicrobial, antiviral and other drugs. It is of note that sulfated steroids seem to be absent in Coelenterata. In any case, none has been isolated from these invertebrates so far.

IV. Steroid glycosides

Over a long time, steroid glycosides were considered to be typical metabolites of higher plants; however, in the last 25–30 years they were isolated from starfishes along with the corresponding polyols and sulfates.[1,3] Later, they were found in sponges, cnidarians and fishes of the *Pardachiras* genus. A small review devoted to marine steroid glycosides was published in 1996.[165] Therefore, in this section we shall consider the results of the most recent studies published 4–6 years ago and those data which have not been discussed in this review.

Marine steroid glycosides, like any other marine polar steroids, have original structures, no one of them coincides with the structures of glycosides isolated from taxonomically remote biological sources, such as terrestrial plants.

Starfish glycosides are conventionally divided into several large groups,[3] *viz*., (i) steroid glycosides, which are sulfated at C(3) [their carbohydrate chains are attached at O(6) (classical asterosaponins)]; (ii) mono- and biosides of polyhydroxylated steroid, containing as a rule carbohydrate residues in their side chains and (iii) glycosides containing carbohydrate fragments attached to C(3) and C(6) of the aglycons to form macrocycles. The structures of individual representatives of these groups are given below. Glycosides related to the first structural type, *e.g*., tornasteroside A (**184**)[166] from *Acanthaster planci* (a starfish commonly referred to as the 'crown of thorns'), differ from each other in both the structures of their carbohydrate chains which usually contain from four to six monosaccharide residues and in the structures of the aglycon side chains. Glycosides related to yet another structural type, *e.g*., nodososide (**185a**) from *Protoreaster nodosus*[167] and asterosaponin P_1 (**185b**) from *Asterina* (= *Patiria*) *pectinifera*[168]), are structurally very diverse and may contain sulfate groups.

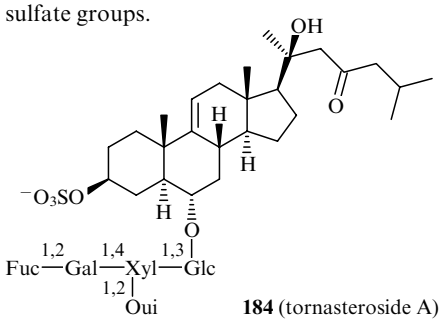

184 (tornasteroside A)

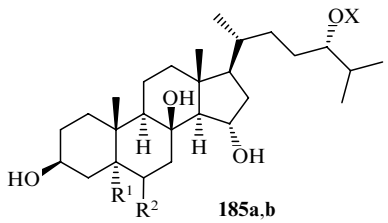

185a,**b**

185a: R^1 = OH, R^2 = β-OH, X = 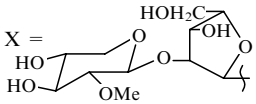 (nodososide);

185b: R^1 = H, R^2 = α-OH, X = 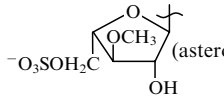 (asterosaponin P_1).

Glycosides containing carbohydrate chains involved in a macrocycle exemplified in sepositoside A (**186**)[169] were detected only in a few species of starfishes of the *Echinaster* genus.

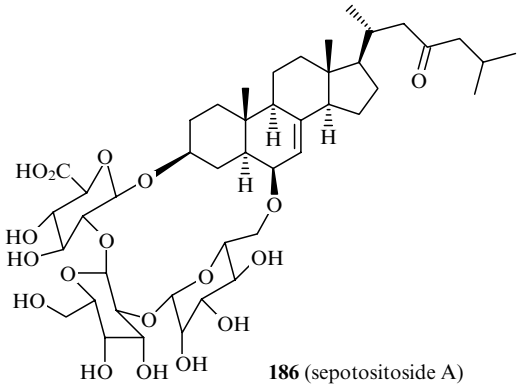

186 (sepotositoside A)

Classical asterosaponins are usually present in starfishes as complex mixtures; they are toxic to fishes, manifest cytotoxic and hemolytic activities, are predominantly accumulated in animal body walls and probably fulfil protective functions. All these compounds contain aglycons of the same structural type with a 9(11) double bond and a sulfate group at C(3), the aglycon of tornasteroside A being the most common fragment.

Tetraosides usually possess linear carbohydrate chains, whereas the carbohydrate chains of penta- and hexaosides have one or (more seldom) two branch points, predominantly at the second monosaccharide of the chain. Monosaccharides are represented mostly by pyranose forms of D-fucose, D-quinovose, D-glucose, D-galactose, D-xylose and 6-deoxy-D-*xylo*-hexos-4-

ulose (the latter contains the hydrated keto group in position 4). The glycosidic bonds have usually β-configurations.

Quite a lot of novel asterosaponin oligoglycosides have recently been isolated from starfishes (Table 2). For example, the so-called nipoglycosides A – D (**187** – **190**) were isolated from the starfish *Distolasterias nipon*[170] and brasiliensoside (**191**) was isolated from *Echinaster brasiliensis*.[171] In contrast with the glycosides from the other two species of this genus, these glycosides are devoid of carbohydrate chains incorporated in a macrocycle. Cosmasterosides A – D (**192** – **195**) containing two xylose residues each in their carbohydrate chains were isolated from the starfish *Cosmasterias lurida*.[172]

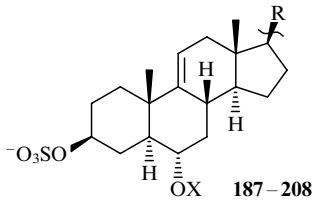

187 – **208**

In contrast to most asterosaponins containing five to six sugar residues, compounds **194** and **195** have only four monosaccharide residues. Reticulatosides A and B (**196**, **197**) and asterosaponin (**198**) containing a pregnane aglycon were found in *Oreaster reticulatus*.[117] About 20 steroid glycosides including the novel asterosaponins **199** – **203** were isolated from a non-identified starfish species belonging to the Echinasteriidae family collected near Antarctic coasts by Italian scientists,[173] whereas asteriidosides A – E (**204** – **208**) were isolated from a non-identified Antarctic species belonging to the Asteriidae family.[174]

Asterosaponin-like glycosides with 'shortened' carbohydrate chains were first isolated from *Asterias forbesi*[175, 176] and *Lethasterias nanimensis chelifera*.[115] Forbesides E, E_1, E_2 and E_3 (**209a** – **d**) and cheliferoside L_1 (**209e**) represent pregnane monoquinovosides; most of them contain additional sulfate groups in their monosaccharide residues.

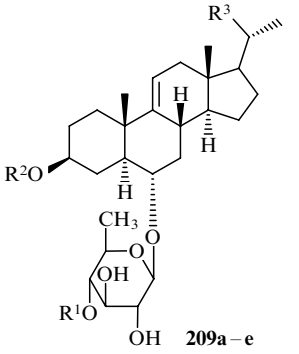

209a – **e**

Compound **209**	Name	R^1	R^2	R^3
a	forbeside E	SO_3Na	SO_3Na	OH
b	forbeside E_1	H	SO_3Na	OH
c	forbeside E_2	SO_3Na	H	OH
d	forbeside E_3	H	SO_3Na	O
e	cheliferoside L_1	SO_3Na	SO_3Na	O

Aphelasteroside C (**210a**) from *Aphelasterias japonica* differs from cheliferoside L_1 (**209e**) in its relatedness to cholestane, rather than to pregnane derivatives; its side chain contains a 23-keto-24-hydroxy fragment uncommon for asterosaponins.[116] Latespinosides A – D (**210b**,**c**, **211**, **212**) from *Asteropecten latespinus* differ from aphelasteroside C (**210a**) exclusively in the structures of their side chains, compound **212** being the first androstane steroid isolated from starfishes.[177]

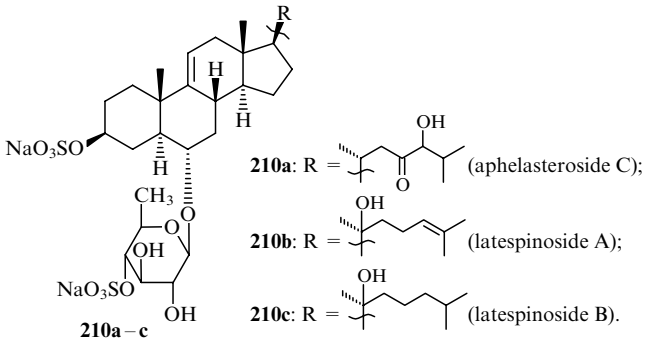

210a – **c**

210a: R = (aphelasteroside C);

210b: R = (latespinoside A);

210c: R = (latespinoside B).

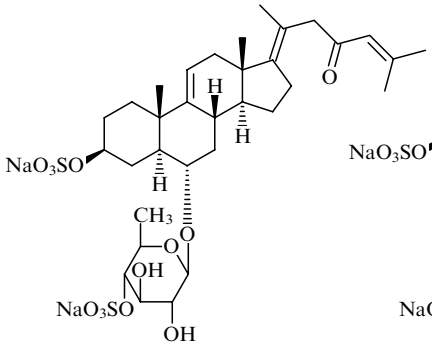

211 (latespinoside C)

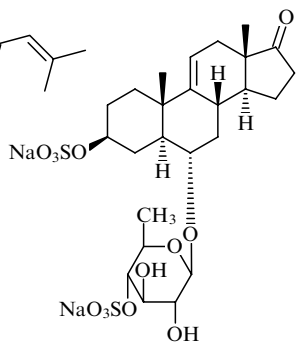

212 (latespinoside D)

Yet another recently discovered group of asterosaponins with shortened carbohydrate chains includes downeosides (**213** – **216**) from *Henricia downeyae*.[178, 179] These compounds contain one or two monosaccharide residues in their carbohydrate fragments; their high polarities are due to the presence of glucuronic acid residues, which are not common in 'classical' asterosaponins, but are present in cyclic asterosaponins. In contrast to other asterosaponins, the carbohydrate fragments in these glycosides are bound to C(3) atoms, whereas their sulfate groups are bound to C(6). Downeyosides A and B (**213a**,**b**) possess additional tetrahydrofuran rings and side chains containing three contiguous hydroxy groups at C(20), C(22) and C(23), which is uncommon for natural steroids. Downeyosides C – G and J (**214a** – **f**) resemble 'classical' asterosaponins in the structures of their side chains, whereas downeyosides K and L (**215a**,**b**) contain additional hydroxy groups at C(16). And, finally, downeyosides H and I

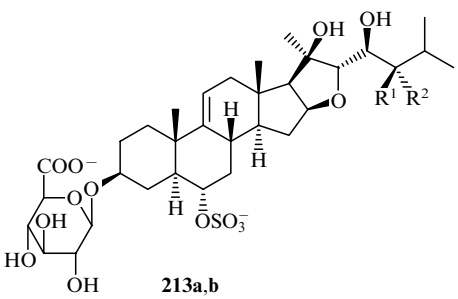

213a,**b**

213a: $R^1 = CH_3$, $R^2 = H$ (downeyoside A);
213b: $R^1 = H$, $R^2 = CH_3$ (downeyoside B).

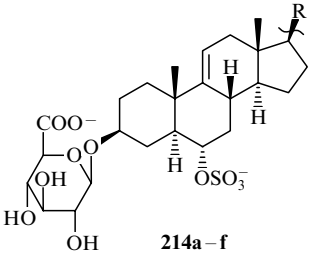

214a – **f**

214a: R = 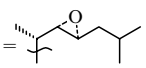 (downeyoside C);

214b: R = 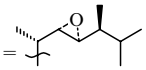 (downeyoside D);

214c: R = 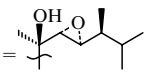 (downeyoside E);

214d: R = 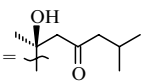 (downeyoside F);

214e: R = 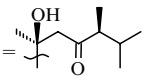 (downeyoside G);

214f: R = 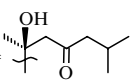 9(11)-dihydro, (downeyoside J) .

Table 2. Asterosaponins isolated from starfishes.

Compound	Name	The structure of the side chain (R)	The structure of the carbohydrate chain (X)	Ref.	Compound	Name	The structure of the side chain (R)	The structure of the carbohydrate chain (X)	Ref.
187	nipoglycoside A	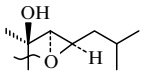	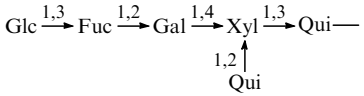	170	**198**	–		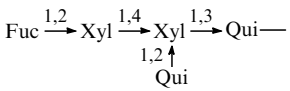	117
188	nipoglycoside B	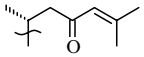	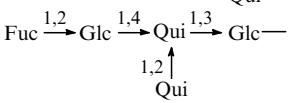	170	**199**	24-methylbrasiliensoside	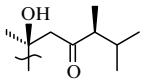	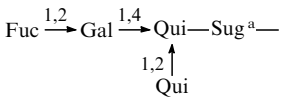	173
189	nipoglycoside C	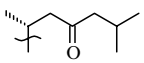	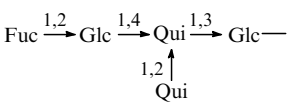	170	**200**	antarcticoside A	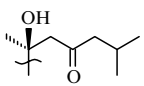	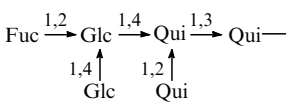	173
190	nipoglycoside D	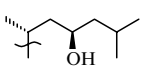	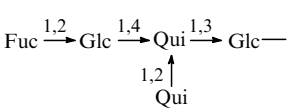	170	**201**	antarcticoside B	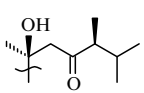	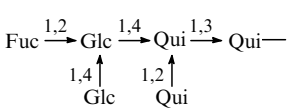	173
191	brasiliensoside	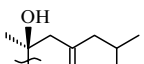	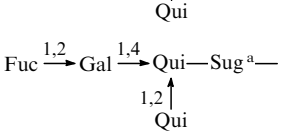	171	**202**	antarcticoside C	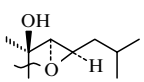	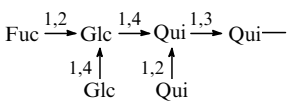	173
192	cosmasteroside A	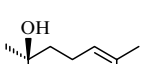	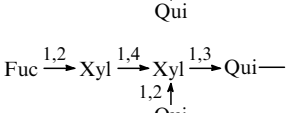	172	**203**	24-methylpectenoside A	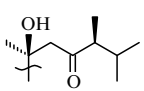	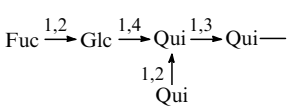	173
193	cosmasteroside B	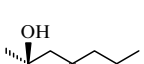	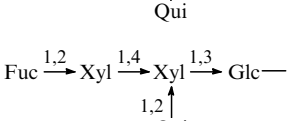	172	**204**	asteriidoside A	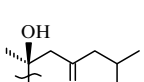	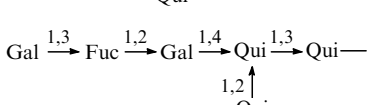	174
194	cosmasteroside C	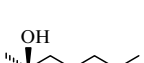	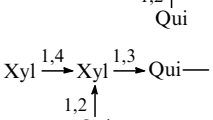	172	**205**	asteriidoside B	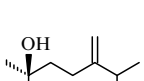	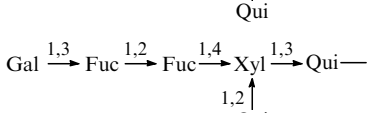	174
195	cosmasteroside D	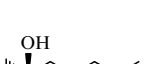	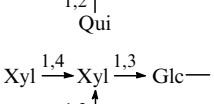	172	**206**	asteriidoside C	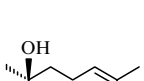	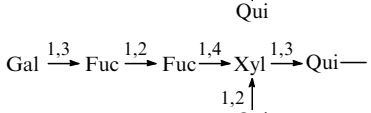	174
196	reticulatoside A	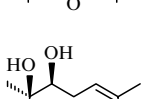	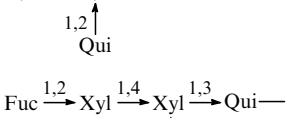	117	**207**	asteriidoside D	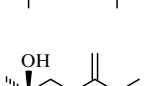	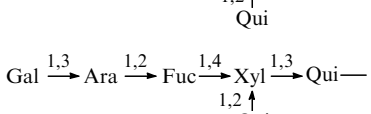	174
197	reticulatoside B	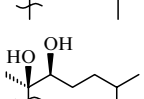	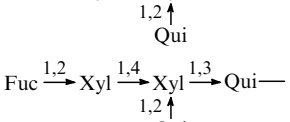	117	**208**	asteriidoside E	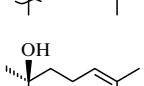	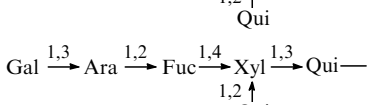	174

[a] Sug is 6-deoxy-*xylo*-hexos-4-ulose.

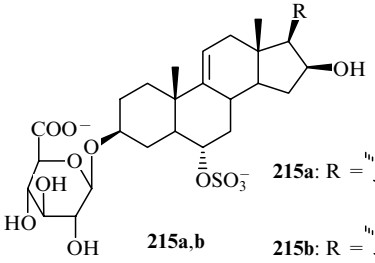

215a,**b**

215a: R = 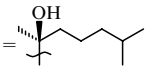 (downeyoside K);

215b: R = 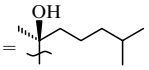 ,

9(11)-dihydro (downeyoside L).

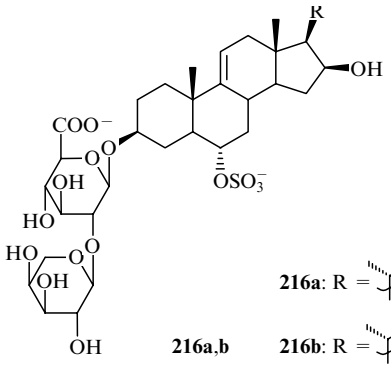

216a,**b**

216a: R = 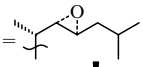 (downeyoside H);

216b: R = 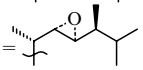 (downeyoside I).

(**216a**,**b**) are biosides, each containing an additional L-arabinose residue bound to glucuronic acid by α-glycosidic bond.

In recent years, the list of newly discovered mono- and biosides of polyhydroxysteroids has been supplemented with more than 50 new names (Table 3).

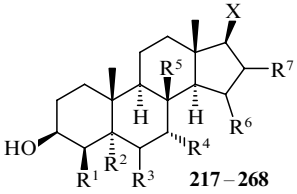

217–**268**

As a rule, the carbohydrate fragments of these compounds are bound to C(24) or C(26) (cholestane series), to C(28) or C(26) (ergostane series) and to C(29) or C(26) (stigmastane series). Xylose, its various methylated derivatives (in a pyranose form), arabinose and 3-*O*-methylarabinose (in a furanose form) are the monosaccharide components. Glucopyranose, arabinopyranose, xylofuranose, galactofuranose and fucofuranose are found less often. The glycosides of this series contain sometimes one or several sulfate groups in the carbohydrate part and the aglycons. In biosides, the monosaccharides are linked by 1,2-bonds or, less frequently, by 1,5- and 1,6-bonds (the author's data), *e.g.*, as in compounds **262**, **264**–**267**.[184–186]

Novel structural series of glycosides recently discovered in starfishes include compounds containing two monosaccharide fragments, *viz*., one at C(3) and the other in the side chain. Some representatives of this class, *viz*., distolasterosides D_1–D_3 (**269a**–**c**) were found in *Distolasterias nipon*.[187] Reinvestigations of polar steroids from the same species collected near the coasts of Japan led to the isolation of yet another steroid bisglycoside, *viz*., distolasteroside D_4 (**269d**) and distolasteroside D_5 (**270**), which contains a sulfate group instead of a monosaccharide residue at C(3).[170]

In the most recent times, this group of compounds was further expanded owing to asteriidosides F–I (**271a**,**b** and **272a**,**b**)

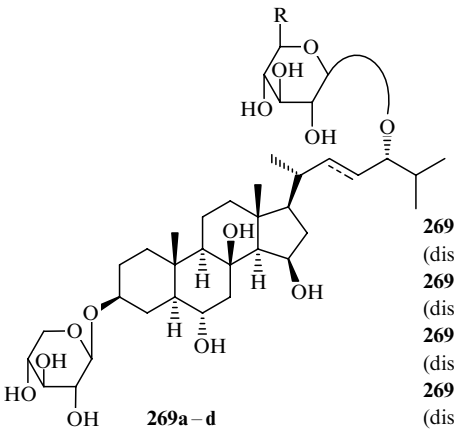

269a–**d**

269a: R = H (distolasteroside D_1);
269b: R = H, Δ^{22} (distolasteroside D_2);
269c: R = CH_2OH (distolasteroside D_3);
269d: R = $CH_2OSO_3^-$ (distolasteroside D_4).

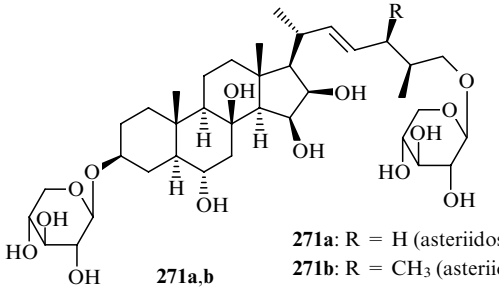

270 (distolasteroside D_5) isolated from the Antarctic starfish belonging to Asteriidae gen. sp.[174] and echinasterosides B_1 (**273**) and F (**274**) from *Echinaster sepositus*[188] and *E. brasiliensis*,[171] respectively.

271a,**b**

271a: R = H (asteriidoside F);
271b: R = CH_3 (asteriidoside G).

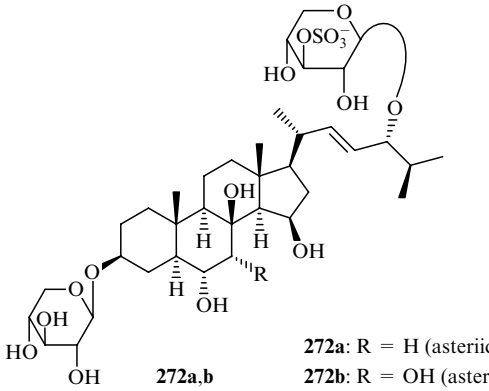

272a,**b**

272a: R = H (asteriidoside H);
272b: R = OH (asteriidoside I).

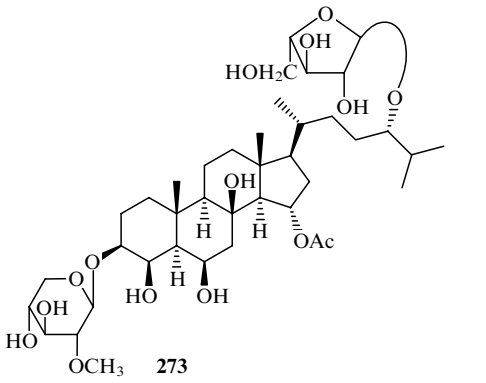

273

Table 3. Some novel polyhydroxysteroid glycosides isolated from starfishes.

Compound	Name	R^1	R^2	R^3	R^4	R^5	R^6	R^7	The side chain (X) (the double bond)	The carbohydrate fragment (Y)	The source	Ref.
217	validoside A	OH	H	6α-SO_3^-	H	OH	β-OH	H	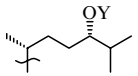	2,4-$(OCH_3)_2$-Xyl_p-(1→2)-Ara_f	*Odontaster validus*	180
218	validoside B	H	H	α-OH	H	OH	β-OH	H	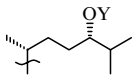	2-SO_3-3-OCH_3-Xyl_p	*Odontaster validus*	180
219	luridoside A	H	H	α-OH	H	OH	β-OH	H	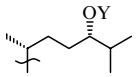	4-SO_3-Xyl_p	*Cosmasterias lurida*	181
220	luridoside B	H	H	α-OH	H	OH	β-OH	H	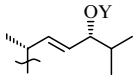	4-SO_3-Xyl_p	*Cosmasterias lurida*	181
221	helianthoside	H	H	α-OH	H	OH	α-OH	H	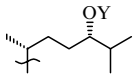	3-SO_3-Xyl_p	*Heliaster helianthus*	182
222	oreasteroside A	H	H	α-OH	H	OH	α-OH	H	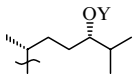	3-OCH_3-Ara_f	*Oreaster reticulatus*	117
223	oreasteroside B	H	H	α-OH	H	OH	α-OH	H	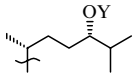	Xyl_p-(1→2)-3-OCH_3-Ara_f	*Oreaster reticulatus*	117
224	oreasteroside C	H	H	α-OH	H	OH	α-OH	H	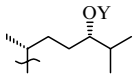	2-OCH_3-Xyl_p-(1→2)-Ara_f	*Oreaster reticulatus*	117
225	oreasteroside D	H	H	α-OH	H	OH	α-OH	H	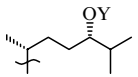	2-OCH_3-Xyl_p-(1→2)-3-OCH_3-Ara_f	*Oreaster reticulatus*	117
226	oreasteroside E	H	H	α-OH	H	OH	β-OH	H	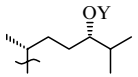	Xyl_p-(1 → 2)-3-OCH_3-Ara_f	*Oreaster reticulatus*	117
227	oreasteroside F	H	H	α-OH	H	OH	α-OH	β-OH	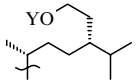	5-OCH_3-Gal_f	*Oreaster reticulatus*	117
228	oreasteroside G	H	H	6α-SO_3^-	H	OH	α-OH	β-OH	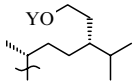	5-OCH_3-Gal_f	*Oreaster reticulatus*	117
229	oreasteroside H	H	H	6α-SO_3^-	H	OH	α-OH	H	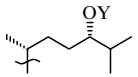	3-OCH_3-Ara_f	*Oreaster reticulatus*	117
230	oreasteroside I	H	H	6α-SO_3^-	H	OH	α-OH	H	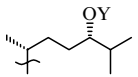	Ara_f	*Oreaster reticulatus*	117

Table 3 (continued).

Compound	Name	R^1	R^2	R^3	R^4	R^5	R^6	R^7	The side chain (X) (the double bond)	The carbohydrate fragment (Y)	The source	Ref.
231	oreasteroside J	H	H	α-OH	OH	OH	β-OH	β-OH	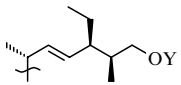	2-SO_3-3-OCH_3-Xyl_p	*Oreaster reticulatus*	117
232	oreasteroside K	H	H	α-OH	OH	OH	β-OH	β-OH	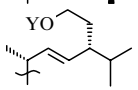	2-SO_3-3-OCH_3-Xyl_p	*Oreaster reticulatus*	117
233	antarcticoside D	OH	H	α-OH	H	OH	β-OH	H	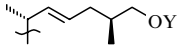	3-OCH_3-Xyl_p	Echinasteridae gen. sp.	91
234	antarcticoside E	OH	H	α-OH	H	OH	β-OH	H	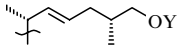	3-OCH_3-Xyl_p	Echinasteridae gen. sp.	91
235	antarcticoside F	OH	H	α-OH	H	OH	β-OH	H	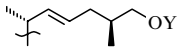	2,4-$(OCH_3)_2$-Xyl_p-(1→2)-Ara_f	Echinasteridae gen. sp.	91
236	antarcticoside G	OH	H	α-OH	H	OH	β-OH	H	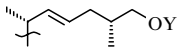	Xyl_p-(1→2)-Ara_f	Echinasteridae gen. sp.	91
237	antarcticoside H	OH	H	α-OH	H	OH	β-OH	H	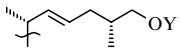	Ara_f	Echinasteridae gen. sp.	91
238	antarcticoside I	OH	H	α-OH	H	OH	β-OH	H	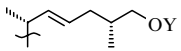	Gal_f	Echinasteridae gen. sp.	91
239	antarcticoside J	OH	H	α-OH	H	OH	β-OH	H	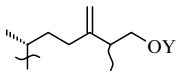	4-SO_3-3-OCH_3-Xyl_p	Echinasteridae gen. sp.	91
240	antarcticoside K	OH	H	α-OH	H	OH	β-OH	H	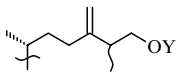	3-OCH_3-Xyl_p	Echinasteridae gen. sp.	91
241	antarcticoside L	OH	H	α-OH	H	OH	β-OH	H	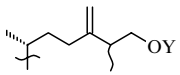	4-OCH_3-Xyl_p-(1→2)-Gal_f	Echinasteridae gen. sp.	91
242	antarcticoside M	OH	H	α-OH	H	OH	β-OH	H	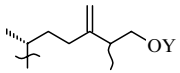	4-OCH_3-Xyl_p-(1→2)-Ara_f	Echinasteridae gen. sp.	91
243	antarcticoside N	OH	H	α-OH	H	OH	β-OH	H	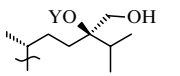	Ara_f	Echinasteridae gen. sp.	91
244	antartcicoside O	OH	H	6α-SO_3^-	H	OH	β-OH	H	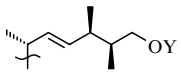	3-OCH_3-Glc_p	Echinasteridae gen. sp.	91
245	antarcticoside P	OH	H	6α-SO_3^-	H	OH	β-OH	H	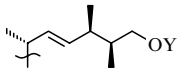	2,4-$(OCH_3)_2$-Xyl_p-(1→2)-Gal_f	Echinasteridae gen. sp.	91
246	ceramasteroside C_1	OH	H	α-OH	H	OH	β-OH	β-OH	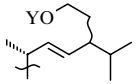	2-OCH_3-Xyl_p-(1→2)-Gal_f	*Ceramaster patagonicus*	89

Table 3 (continued).

Compound	Name	R^1	R^2	R^3	R^4	R^5	R^6	R^7	The side chain (X) (the double bond)	The carbohydrate fragment (Y)	The source	Ref.
247	ceramasteroside C_2	H	H	α-OH	H	OH	β-OH	β-OH	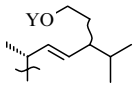	2,4-$(OCH_3)_2$-Xyl_p-(1→2)-Gal_f	*Ceramaster patagonicus*	89
248	ceramasteroside C_3	H	H	α-OH	H	OH	β-OH	β-OH	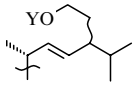	2-OCH_3-Xyl_p-(1→2)-Gal_f	*Ceramaster patagonicus*	89
249	ceramasteroside C_4	OH	H	α-OH	H	OH	β-OH	H	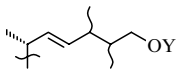	2-OCH_3-Xyl_p-(1→2)-Gal_f	*Ceramaster patagonicus*	89
250	ceramasteroside C_5	H	H	α-OH	H	OH	β-OH	H	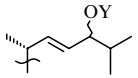	2-OCH_3-Xyl_p-(1→2)-Xyl_p	*Ceramaster patagonicus*	89
251	leptasteroside L	H	OH	β-OH	H	OH	α-OH	H	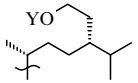	Glc_p	*Leptasterias polaris acervata*	183
252	acodontasteroside A	OH	H	6α-SO_3^-	H	OH	β-OH	H	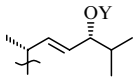	2-OCH_3-Xyl_p-(1→2)-Gal_f	*Acodontaster conspicuus*	90
253	acodontasteroside B	OH	H	6α-SO_3^-	H	OH	β-OH	H	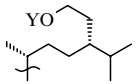	2-OCH_3-Xyl_p-(1→2)-Xyl_p	*Acodontaster conspicuus*	90
254	acodontasteroside C	OH	H	6α-SO_3^-	H	OH	β-OH	H	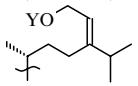	2-OCH_3-Xyl_p-(1→2)-Xyl_p	*Acodontaster conspicuus*	90
255	acodontasteroside D	OH	H	α-H	H	OH	β-OH	H	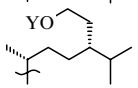	Xyl_p-(1→2)-Xyl_p	*Acodontaster conspicuus*	90
256	acodontasteroside E	OH	H	α-H	H	OH	β-OH	H	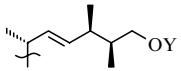	2-OCH_3-Xyl_p-(1→2)-Xyl_p	*Acodontaster conspicuus*	90
257	acodontasteroside F	OH	H	α-H	H	OH	β-OH	H	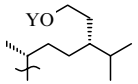	2-OCH_3-Xyl_p-(1→2)-Xyl_p	*Acodontaster conspicuus*	90
258	acodontasteroside G	OH	H	α-H	H	OH	β-OH	H	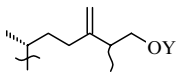	2-OCH_3-Xyl_p-(1→2)-Xyl_p	*Acodontaster conspicuus*	90
259	acodontasteroside H	H	H	α-H	H	H	β-OH	H	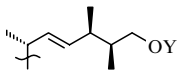 ($\Delta^{8(14)}$)	2-OCH_3-Xyl_p-(1→2)-Xyl_p	*Acodontaster conspicuus*	90

Table 3 (continued).

Compound	Name	R^1	R^2	R^3	R^4	R^5	R^6	R^7	The side chain (X) (the double bond)	The carbohydrate fragment (Y)	The source	Ref.
260	acodontasteroside I	H	H	α-H	H	H	β-OH	H	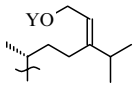 ($\Delta^{8(14)}$)	Xyl_p	*Acodontaster conspicuus*	90
261	crossasteroside P_3	H	H	α-H	H	OH	H	H	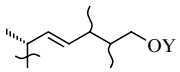 ($\Delta^{14(15)}$)	3-OCH_3-Glc_p	*Crossaster papposus*	184
262	crossasteroside P_4	OH	H	α-H	H	OH	β-OH	H	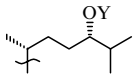	2,4-$(OCH_3)_2$-Xyl_p-(1→5)-Ara_f	*Crossaster papposus*	184
263	solasteroside S_1	H	H	β-OH	H	H	α-H	H	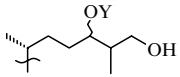	Xyl_p	*Solaster dawsoni*	185
264	solasteroside S_2	H	H	α-H	H	OH	β-OH	β-OH	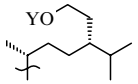	Gal_f-(1→6)-Gal_f	*Solaster dawsoni*	185
265	mediasteroside M_1	H	H	α-H	H	OH	β-OH	H	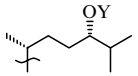	2-OCH_3-Xyl_p-(1→5)-Ara_f	*Mediaster murrayi*	186
266	mediasteroside M_2	H	H	α-H	H	OH	β-OH	H	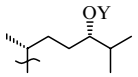	Xyl_p-(1→5)-Ara_f	*Mediaster murrayi*	186
267	mediasteroside M_3	H	H	α-H	H	OH	β-OH	H	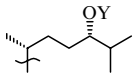	2,4-$(OCH_3)_2$-Xyl_p-(1→5)-Ara_f	*Mediaster murrayi*	186
268	mediasteroside M_4	H	H	α-H	H	OH	β-OH	H	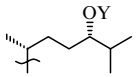	2,3-$(OCH_3)_2$-Xyl_p-(1→2)-Ara_f	*Mediaster murrayi*	186

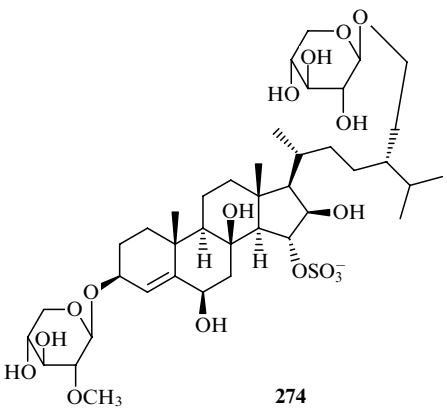

274

Yet another group of recently discovered glycosides contains only one carbohydrate fragment linked to the C(3) atom. These compounds include desulfated 26-norechinasteroside A (**275a**)

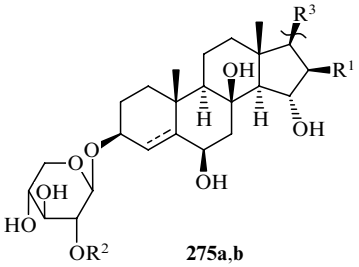

275a,**b**

Compound **275**	Name	R^1	R^2	R^3
a (Δ^4)		OH	CH_3	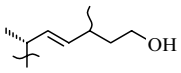
b	asteriidoside L	H	H	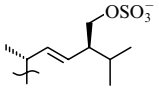

from *Henricia downeyae*,[179] compounds **276a**–**e** from *Echinaster brasiliensis*,[171] henriciosides H_2 and H_3 (**276f**,**g**) from *H. derjugini*[93] and asteriidoside L (**275b**) from Asteriidae gen sp.[174]

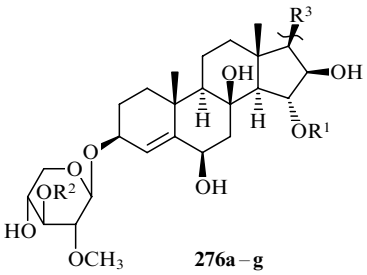

276a–**g**

Compound **276**	Name	R^1	R^2	R^3
a		SO_3^-	H	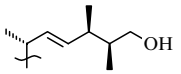
b		H	H	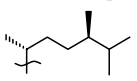
c	echinasteroside C	SO_3^-	H	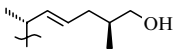
d	echinasteroside D	SO_3^-	H	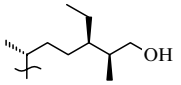
e	echinasteroside E	H	H	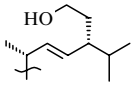
f	henricioside H_2	H	CH_3	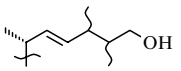
g	henricioside H_3	H	CH_3	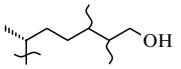

In contrast to all other polyhydroxysteroid glycosides containing one or two monosaccharide residues, cytotoxic compounds **277a**–**c** from *Fromia monilis*[189] contain three monosaccharides.

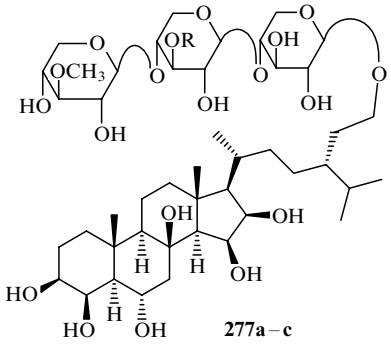

277a: R = CH_3;
277b: R = CH_3, Δ^{22};
277c: R = H.

277a–**c**

The impressive diversity of glycosides of polyhydroxysteroids and other polar steroids found in starfishes reflects the immense variety of oxidising and glycosylating enzymes present in these animals, which is comparable only to the wide occurrence of steroid-oxidising enzymes in microorganisms and glycosyl transferases in terrestrial higher plants. Several newly discovered groups of glycosides not mentioned in previous reviews[2,3] include monoquinovosides related to classical asterosaponins as well as mono- and biosides sulfated at C(6) and containing carbohydrate chains in position 3.

It should be stressed that starfish enzymes differ from known enzymes of terrestrial origin in the specificities of hydroxylation and ability to transfer mono- or oligoside residues into definite positions of sterol substrates. Sulfation of metabolites in different positions is a distinguishing feature of biogenesis of steroid glycosides in starfishes.

In other phyla of marine invertebrates, such as sponges, glycosides have been discovered much later than in starfishes. Sponge glycosides usually contain mono-, di- or trimethylsterol aglycons and carbohydrate chains linked to C(3). These metabolites were first isolated from *Asteropus sarasinosum* by Kitagawa *et al.*[190,191] Sarasinosides represent oligoglycosides of hitherto unknown dimethylsterol aglycons. They manifest high ichthyotoxic activities and moderate cytostatic activities in tests with fertilised eggs of the starfish *Asterina pectinifera*. Compounds **278a**–**c**, **279a**–**c** and **280a**–**c** were found in the starfish *A. sarasinosum* collected near the Palau Island in the Pacific Ocean,[191] whereas compounds **281**, **282a**–**b** and **283** were isolated from the same sponge species dwelling in the region of the Solomon Islands.[192] The aglycons of sarasinoside D (**281**) contain a rarely occurring 4,4,8-trimethylsterane skeleton system similar to that of scalarane sesterterpenoids, but differing from that of dammarane triterpenoids in a 1,2-shift of the methyl group from C(14) to C(13).

The so-called pachastrelloside A (**284**), which inhibits cell division in fertilised sea urchin eggs without affecting cell nuclei resulting in the formation of multinuclear unicellular embryos, was isolated from *Pachastrella* sp. Unlike other steroid glycosides, pachastrelloside A (**284**) contains monosaccharide residues in unusual positions. Thus, one of them, *viz*., galactose, is linked to C(4), whereas the other one, *viz*., xylose, is bound to C(7) of the aglycon.[193] Comparison of the aglycon structures of eryloside A (**285**) from *Erylus lendenfeldi*,[194] erylosides C and D (**286a**,**b**) from

Erylus sp.,[195] eryloside E (**287**) from *E. goffrileri*[196] and ulososides (**288**, **289**) isolated by us from *Ulosa* sp.[197,198] showed that stepwise demethylation of the lanostane or the related terpene precursor in sponges resembles the conversion of lanosterol into cholesterol in higher animals. This process consists in oxidative removal of the methyl group from position 14 and subsequent elimination of the methyl groups linked to C(4) (Table 4).

The hopaioside **290** isolated from the Micronesian sponge *Cribrochalina olemda* differs significantly from other sponge steroid glycosides.[199] This compound is related to 19-norpregnane rather than to sterol or norlanostane derivatives.

Interesting steroid glycosides were also detected in some octocorals. Most of them are monosides of the pregnane series and contain one or several acetate or propionate groups. Several novel glycosylated sterol derivatives and novel pregnane glycosides have recently been isolated from these animals. Thus α-L-fucosides containing aglycons of the 24-methylcholesterol series **291a**–**c** were found in some soft corals (*e.g.*, *Alcyonium* sp.) and some representatives of the *Sinularia* and *Lobophytum* genera.[200] The related glycosides **292a**,**b** and **293** were isolated from *Sinularia gibberosa*[52,201] and *S. grandilobata*.[202]

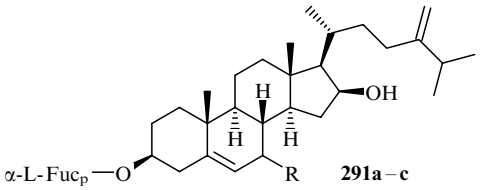

291a–**c**

291a: R = H;
291b: R = β-OH;
291c: R = α-OH.

Table 4. Sponge glycosides.

Structural formula	Compound	Structure of the carbohydrate chain (X)	Name
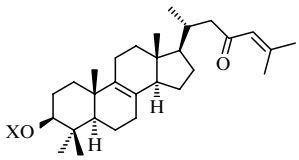	**278a**	β-1,2 β-1,6 β-1,2 Glc$_p$—Glc$_p$—NAcGlc$_p$—Xyl$_p$— β-1,4 | NAcGal$_p$	sarasinoside A_1
	278b	β-1,2 β-1,6 β-1,2 Glc$_p$—Xyl$_p$—NAcGlc$_p$—Xyl$_p$— β-1,4 | NAcGal$_p$	sarasinoside B_1
	278c	β-1,6 β-1,2 Xyl$_p$—NAcGlc$_p$—Xyl$_p$— β-1,4 | NAcGal$_p$	sarasinoside C_1
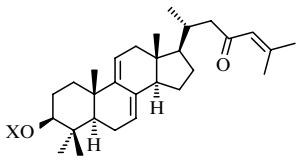	**279a**	β-1,2 β-1,6 β-1,2 Glc$_p$—Glc$_p$—NAcGlc$_p$—Xyl$_p$— β-1,4 | NAcGal$_p$	sarasinoside A_2
	279b	β-1,2 β-1,6 β-1,2 Glc$_p$—Xyl$_p$—NAcGlc$_p$—Xyl$_p$— β-1,4 | NAcGal$_p$	sarasinoside B_2
	279c	β-1,6 β-1,2 Xyl$_p$—NAcGlc$_p$—Xyl$_p$— β-1,4 | NAcGal$_p$	sarasinoside C_2
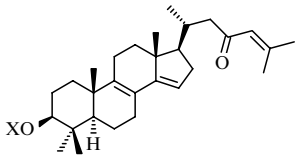	**280a**	β-1,2 β-1,6 β-1,2 Glc$_p$—Glc$_p$—NAcGlc$_p$—Xyl$_p$— β-1,4 | NAcGal$_p$	sarasinoside A_3
	280b	β-1,2 β-1,6 β-1,2 Glc$_p$—Xyl$_p$—NAcGlc$_p$—Xyl$_p$— β-1,4 | NAcGal$_p$	sarasinoside B_3
	280c	β-1,6 β-1,2 Xyl$_p$—NAcGlc$_p$—Xyl$_p$— β-1,4 | NAcGal$_p$	sarasinoside C_3
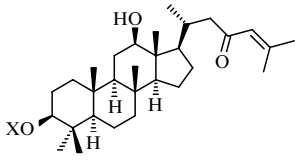	**281**	β-1,2 β-1,6 β-1,2 Glc$_p$—Xyl$_p$—NAcGlc$_p$—Xyl$_p$— β-1,4 | NAcGal$_p$	sarasinoside D
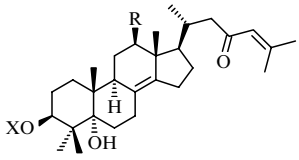	**282a** (R = H)	β-1,2 β-1,6 β-1,2 Glc$_p$—Xyl$_p$—NAcGlc$_p$—Xyl$_p$— β-1,4 | NAcGal$_p$	sarasinoside E
	282b (R = OCH_3)	β-1,2 β-1,6 β-1,2 Glc$_p$—Xyl$_p$—NAcGlc$_p$—Xyl$_p$— β-1,4 | NAcGal$_p$	sarasinoside F

Table 4 (continued).

Structural formula	Compound	Structure of the carbohydrate chain (X)	Name
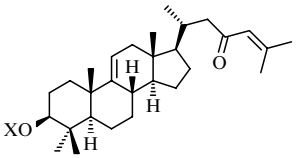	**283**	Glc_p(β-1,2)—Xyl_p(β-1,6)—NAcGlc$_p$(β-1,2)—Xyl_p— NAcGal$_p$(β-1,4)	sarasinoside G
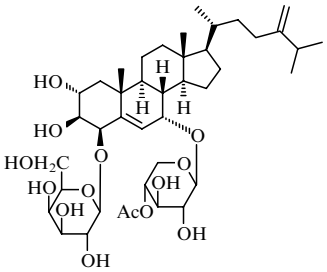	**284**	–	pachastrelloside A
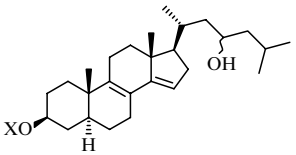	**285**	Gal_p(β-1,2)—Gal_p—	eryloside A
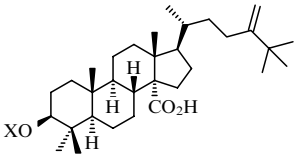	**286a**	Gal_p(1,4)—Gal_p(1,3)—Gal_p— Gal_p(1,2)	eryloside C
	286b	Gal_p(1,3)—Gal_p— Gal_p(1,2)	eryloside D
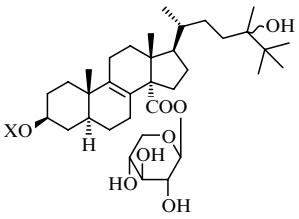	**287**	Gal_p(1,2)—NAcGlc$_p$—	eryloside E
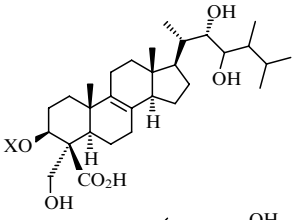	**288**	Glc_pA(β-1,6)—Glc_p—	ulososide A
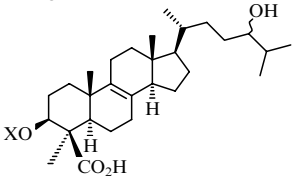	**289**	NAcGlc$_p$–	ulososide B
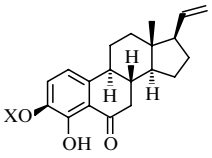	**290**	4-OAc-L-Fuc–	chopaioside

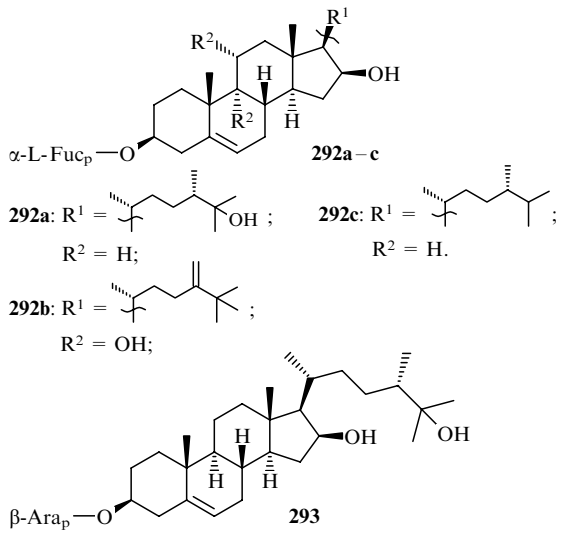

The cytotoxic pregnane glycoside verrucoside (**294**) from *Eunicella verrucosa*[203] contains L-digitalose as a carbohydrate component, enantiomeric with the corresponding 6-deoxyhexose occurring in terrestrial plants. This compound inhibits tumour cells P-388, A-549 and HT-29 (IC_{50} = 5.9, 7.2 and 6.3 μg ml^{-1}, respectively). The glycoside **295** from the gorgonian coral *Eunicea* sp. is its structural analogue.[204] Glycosides **296** and **297** from the soft corals *Scleronephthya palida*[205] and *Alcyonium* sp.[64] collected near the coasts of Thailand represent 19-norpregnane derivatives.

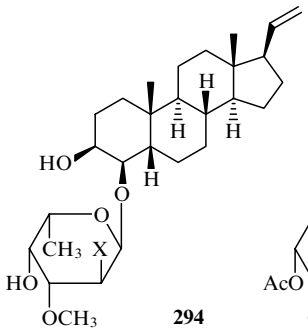

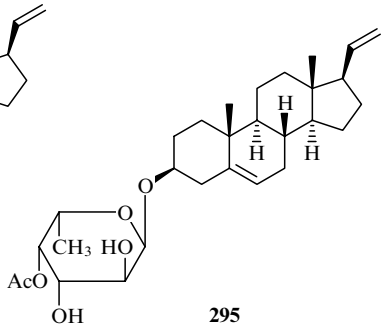

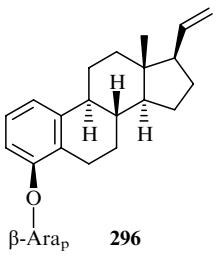

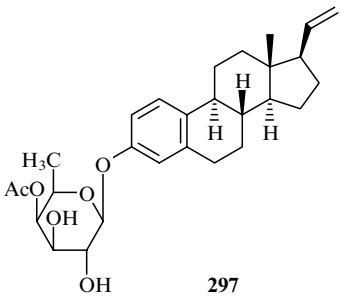

Some fish species also contain steroid glycosides. This fact is surprising in that glycosides are not common for terrestrial vertebrates. Among other known secondary marine glycoside metabolites, special mention should be made of shark reppelant compounds isolated from the corresponding glands of the sole *Pardachirus marmoratus* and the peacock fish *Pardachirus pavoninus*. Although these fishes swim extremely slowly, they successfully withstand the attacks of predatory fishes in their vehement struggle for existence under conditions of coral reefs. Both fish species belong to the same genus and secrete toxic substances at the moment of danger. These substances contain the peptides pardaxins causing paralysis of shark's gnathic muscles and two groups of toxic glycosides endowed with hemolytic activities, *viz*., pavonins **298a**,**b** and **299a**–**d** from *P. pavoninus*[206,207] and mosesines **300a**–**d** and **301** from *P. marmoratus*.[208]

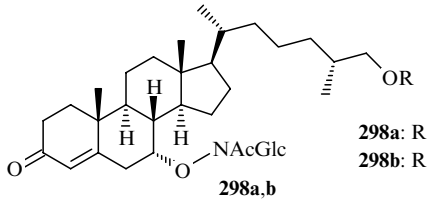

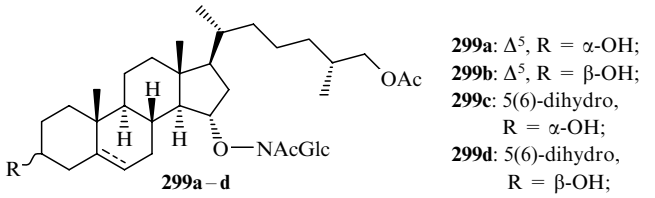

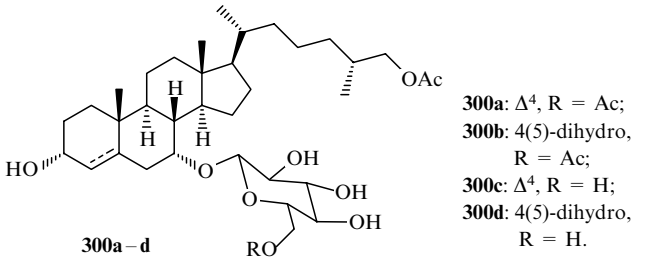

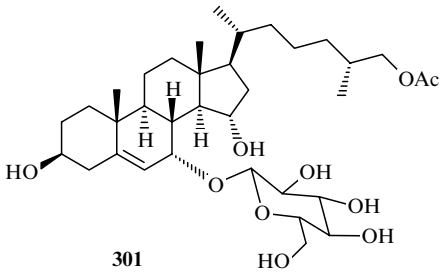

These data suggest that steroid glycosides can be synthesised by taxonomically very distant and diverse groups of marine animals (from invertebrates to fishes). As regards the diversity of their constituent biologically active steroid glycosides, starfishes resemble other well-known sources of these compounds, *viz*., higher terrestrial plants.

V. Steroidal alkaloids

Bissteroidal pyrazines constitute a special group among other natural compounds, which are supertoxic for tumour cells. The structure of cephalostatin 1 (**302a**), the first compound of this series isolated from the marine tubular worm *Cephalodiscus gilchristi* by Pettit *et al*. (USA),[209] was established by X-ray diffraction analysis. This compound in extremely low concentration was toxic for tumour cells P-388 (IC_{50} = 10^{-7}–10^{-9} μg ml^{-1}). Later, about 20 cephalostatins of this series, *e.g*., compounds **302b**–**g**, **303**, **304a**,**b**, **305**, **306a**,**b** and **307**, were isolated from this animal.[210–215]

Structurally close dimeric steroid alkaloids were unexpectedly found in the sea squirt *Ritterella tokioka* by Fusetani *et al*.[216–219] Ritterasine A (**308a**), the first compound in this series, is highly toxic for P-388 cells (IC_{50} = 3.5×10^{-3} μg ml^{-1}) (see Ref. 216). The origin of the unusual fragment containing four five-membered rings in ritterazine A and related compounds was explained by the rearrangement of the 12-hydroxy-Δ^{14}-steroid system of their precursor (Scheme 2).

Later, this group of Japanese chemists isolated more than twenty ritterazines, *e.g*., compounds **308b**, **309a**,**b**, **310**, **311**, **312a**,**b** and **313**, differing in the structures of rings *C*, *D*, *E* and *F* in one or both steroid fragments.[217–219] The majority of ritterazines appeared to be highly toxic for tumour cells; some of them manifested superhigh activities (Table 5).[218]

Scheme 2

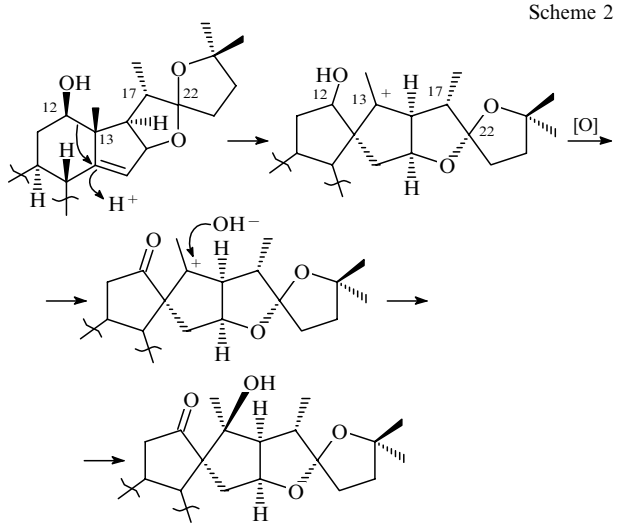

The isolation of two closely related groups of compounds from phylogenetically distant taxa, such as sea worms and ascidians, prompted a suggestion that their biosynthesis is carried out by symbiont microorganisms rather than by the host organism. Cephalostatin 7 (**305**) is the most active compound of this series. Studies carried out at the National Cancer Institute (USA) showed that its average IC_{50} for 60 strains of tumour cells was equal to 10^{-9} mol litre^{-1}. Later, this and some other dimeric steroidal alkaloids were synthesised. According to Pettit,[209] these compounds are formed by dimerisation and subsequent oxidation of steroidal α-amino ketones. Fuchs *et al.*[220] described the biomimetic synthesis of cephalostatins 7 (**305**), 12 (**307**) and ritterazin K (**311**). The starting compound in this synthesis was steroid pentacyclic aldehyde **314** prepared from readily available hekogenin acetate. This was converted *via* the intermediate ketones **315**, **316** and bromo ketones **317** and **318** into azido ketones **319** and **320** (Scheme 3). Treatment of the azido ketone mixture (1 : 1) with 6 equiv. of NaHTe in ethanol for 1 h and subsequent addition of silica gel as a mild catalyst yielded a mixture of **321** (14%), **322** (35%) and **323** (23%). Compounds

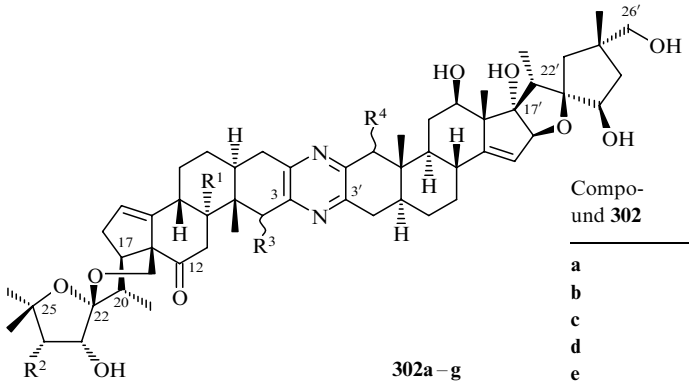

302a–**g**

Compound **302**	Name	R^1	R^2	R^3	R^4
a	cephalostatin 1	H	H	H	H
b	cephalostatin 2	OH	H	H	H
c	cephalostatin 3	OH	CH_3	H	H
d	cephalostatin 10	OH	H	H	α-OCH_3
e	cephalostatin 11	OH	H	α-OCH_3	H
f	cephalostatin 18 (22′epimer)	H	H	H	α-OCH_3
g	cephalostatin 19 (22′epimer)	H	H	α-OCH_3	H

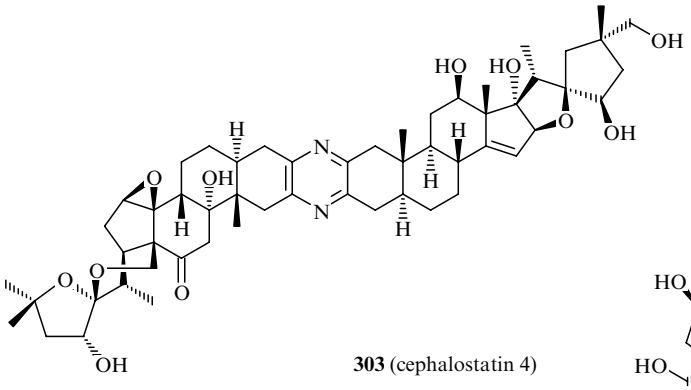

303 (cephalostatin 4)

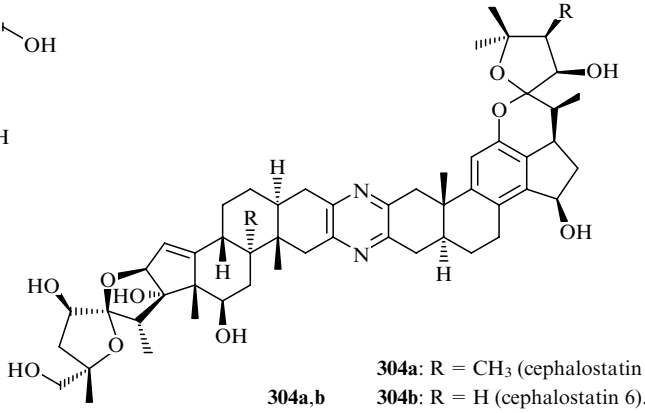

304a,**b** **304a**: R = CH_3 (cephalostatin 5); **304b**: R = H (cephalostatin 6).

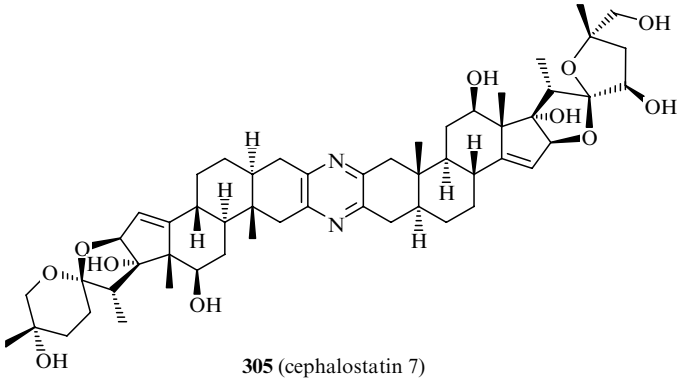

305 (cephalostatin 7)

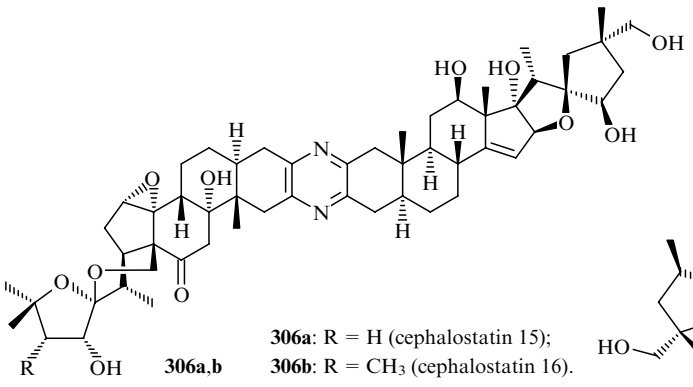

306a: R = H (cephalostatin 15);
306b: R = CH_3 (cephalostatin 16).

306a,**b**

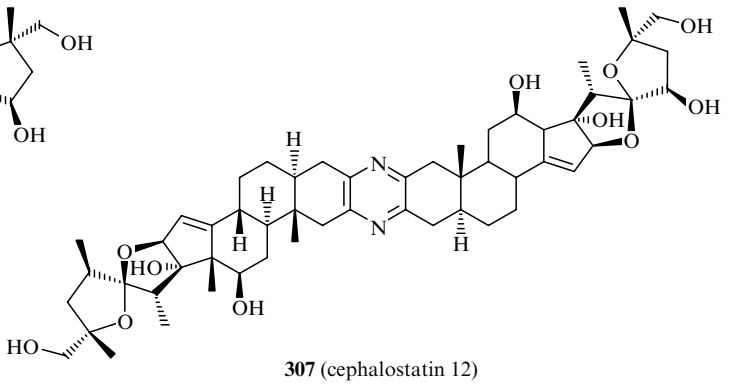

307 (cephalostatin 12)

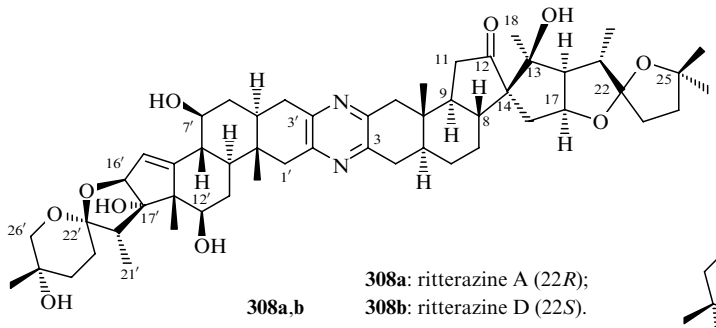

308a: ritterazine A (22*R*);
308b: ritterazine D (22*S*).

308a,**b**

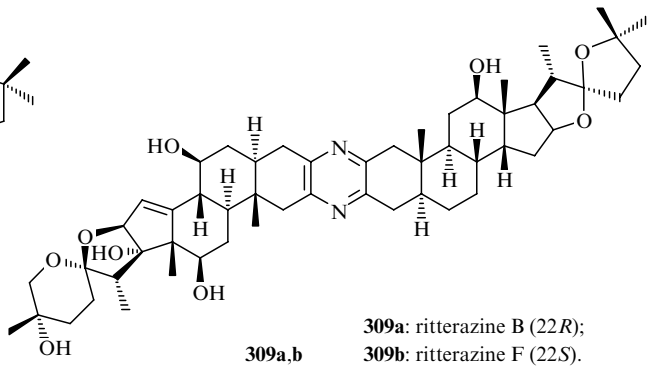

309a: ritterazine B (22*R*);
309b: ritterazine F (22*S*).

309a,**b**

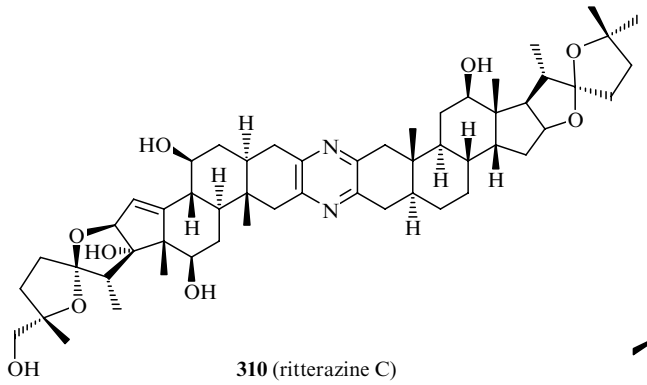

310 (ritterazine C)

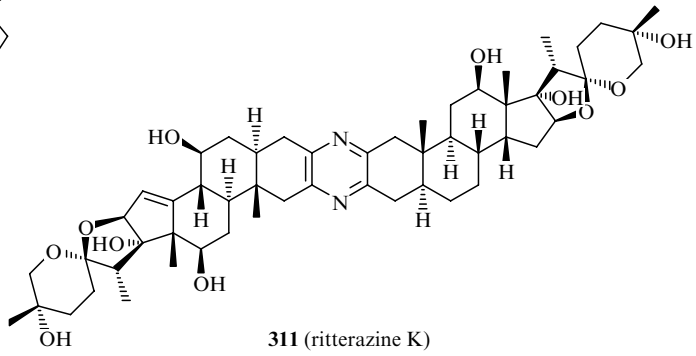

311 (ritterazine K)

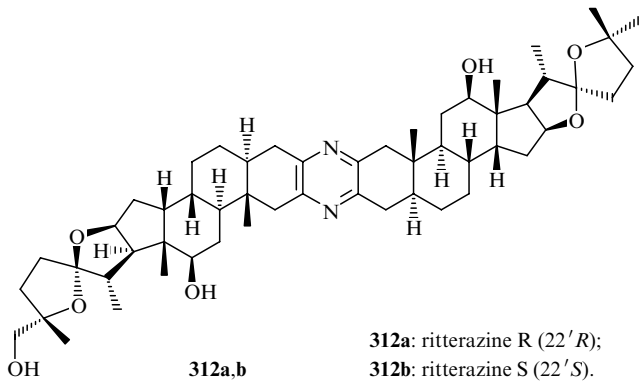

312a: ritterazine R (22′*R*);
312b: ritterazine S (22′*S*).

312a,**b**

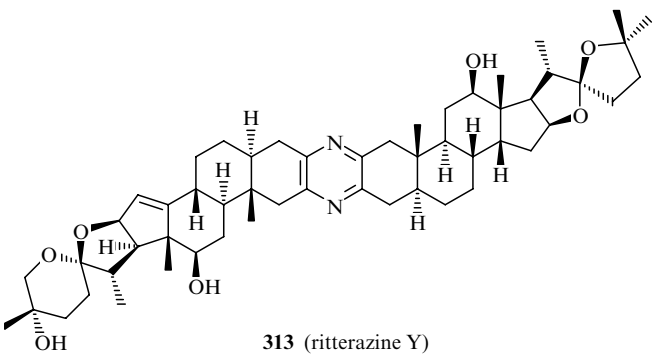

313 (ritterazine Y)

321–**323** were purified by chromatography; their subsequent deprotection gave products identical with natural cephalostatins 7 (**305**) and 12 (**307**) and ritterazine K (**311**), respectively.

Pyrazine steroidal dimeric alkaloids belong to the most toxic natural products for tumour cells presently known. The synthesis of some of them has opened new opportunities for their further pharmacological and clinical investigations.

Squalamine (**324a**), an unusual sulfated derivative of spermidine, was isolated from the shark *Squalus acanthis*.[221, 222] Its structure was determined by spectroscopic methods; the stereo-

Table 5. The cytotoxic activities of ritterazines against tumour cells P-388.[218]

Compound	IC_{50} /μg ml^{-1}	Compound	IC_{50} /μg ml^{-1}
ritterazine A	0.0035	ritterazine F	0.00073
ritterazine B	0.00015	ritterazine K	0.0095
ritterazine C	0.092	ritterazine S	0.46
ritterazine D	0.016	ritterazine Y	0.0035

Scheme 3

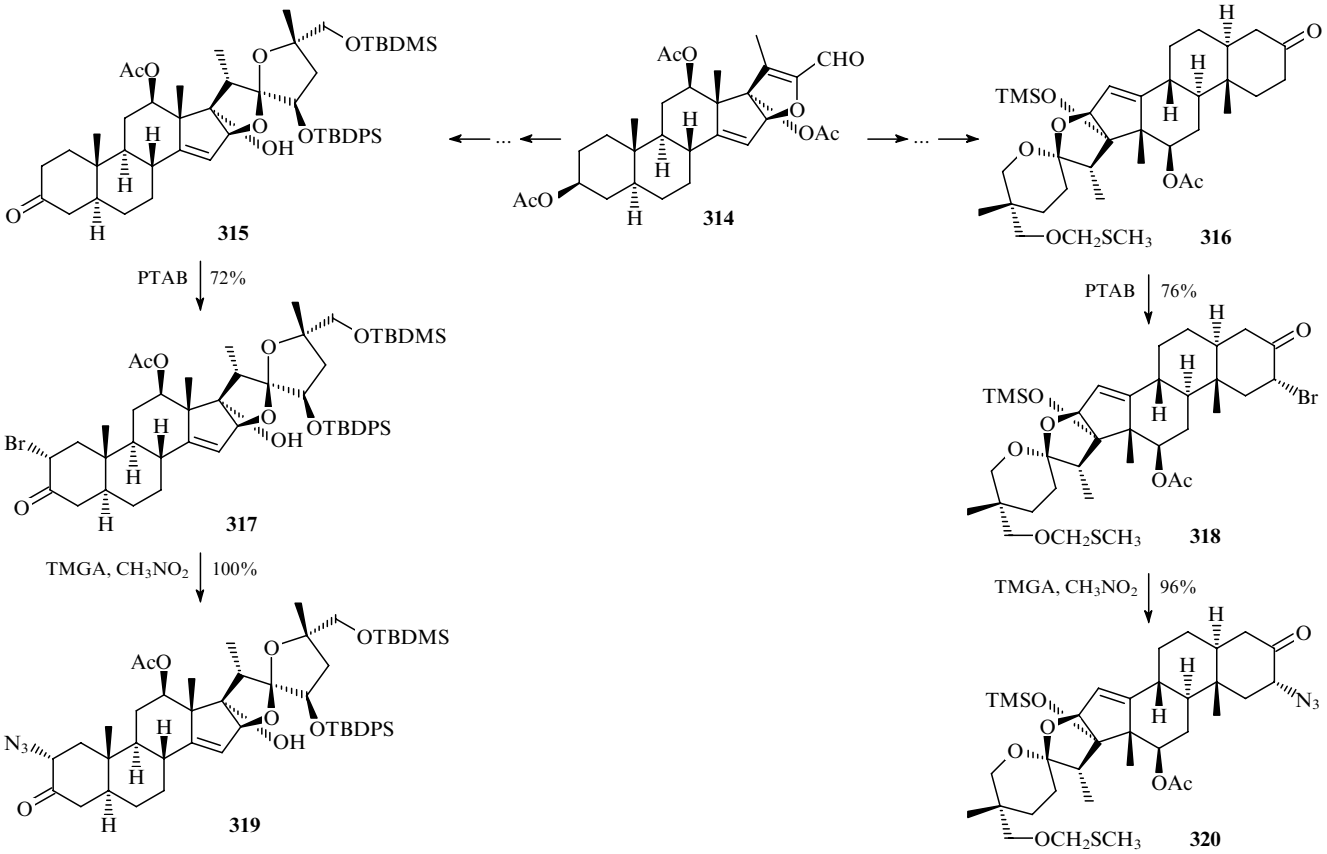

TBDMS, *tert*-butyldimethylsilyl; PTAB, phenyltrimethylammonium tribromide; TMGA, tetramethylguanidinium azide.

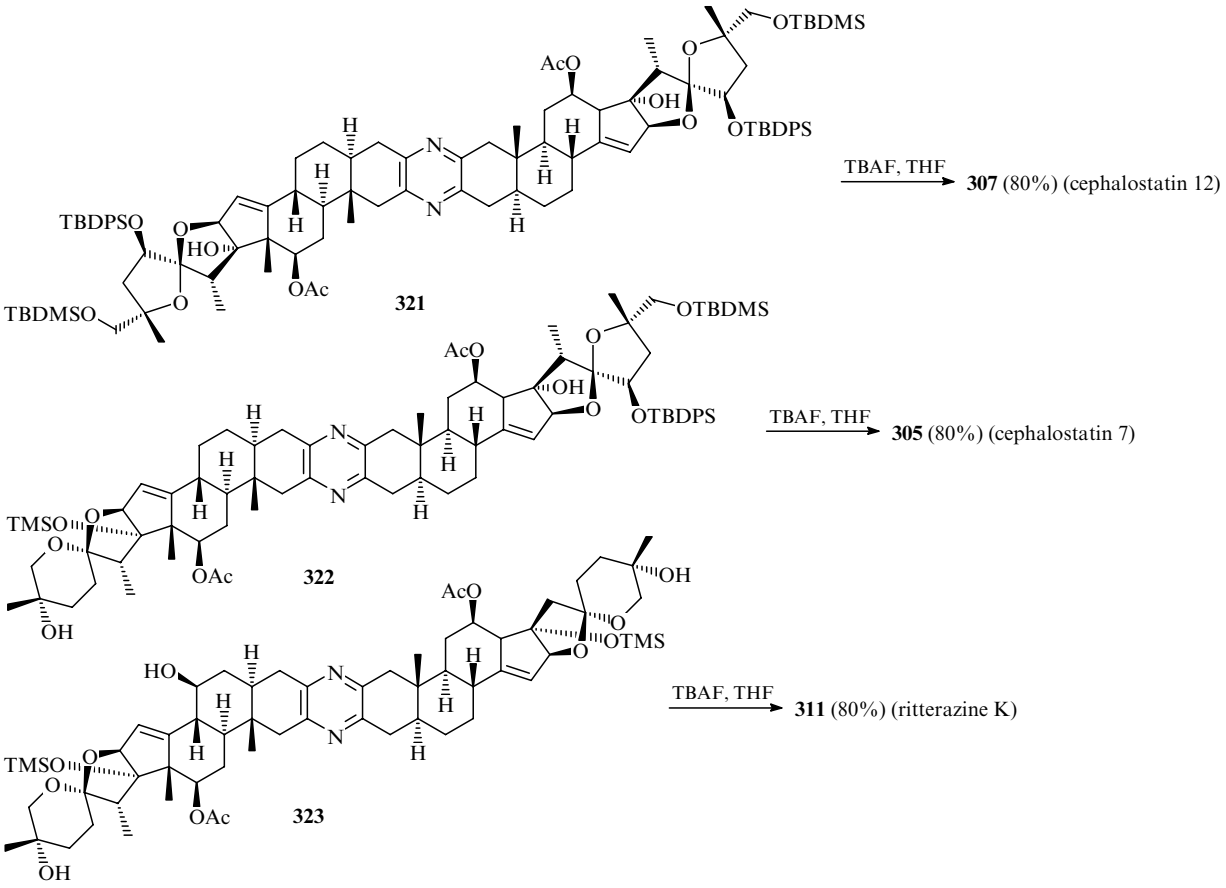

TBAF, tetrabutylammonium fluoride.

chemistry of the asymmetric centre C(24), (24*R*), was established based on the synthesis of desulfosqualamine and its (24*S*) isomer starting from stigmasterol.[223] In contrast to bile alcohols of fishes, squalamine (**324a**) is present not only in the liver and the gallbladder but also in other shark organs, *e.g.*, in the spleen and ovaries. Squalamine (**324a**) manifests interesting properties, *viz.*, its antibacterial activity is comparable to that of the broad-spectrum antibiotic ampicillin (see Table 6), but its antifungal and antiprotozoan effects are stronger.

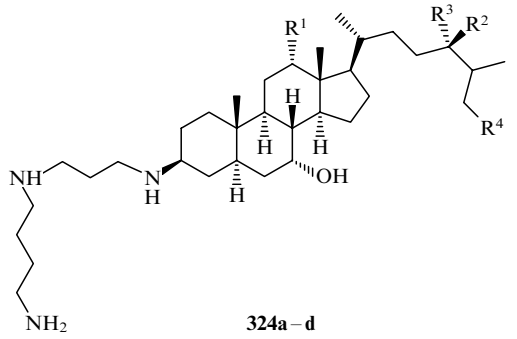

324a–d

Compound **324**	R^1	R^2	R^3	R^4
a	H	OSO_3H	H	H
b	H	OH	H	OSO_3H
c	OH	OSO_3H	H	H
d	H	OSO_3H	CH_2OH	H

Some novel alkaloids of this series, *viz.*, compounds **324b–d**, **325a**,**b**, **326** and **327**, have been isolated recently. Noteworthy, the antimicrobial activity of compound **327** is comparable to that of squalamine.[234] Compounds of this series suppress the appetite in mice and other animals, which prompted a conclusion about their role in sporadic alimentary behaviour of the shark *S. acanthis*, which eats only once in two weeks.

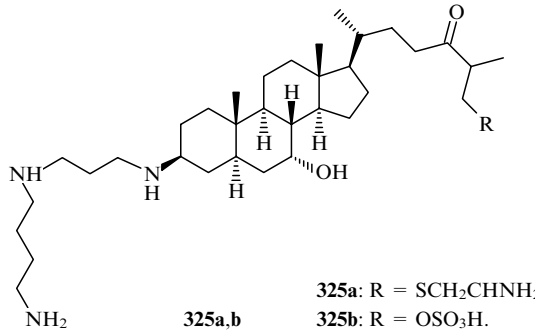

325a,**b** **325a**: R = $SCH_2CHNH_2CO_2H$; **325b**: R = OSO_3H.

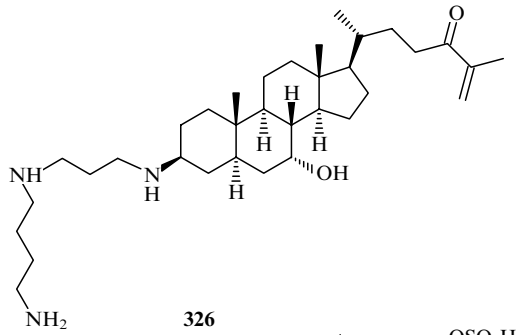

326

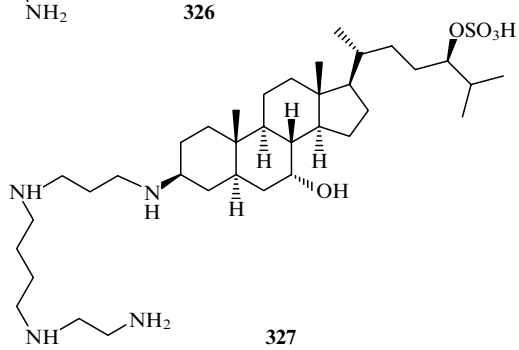

327

Table 6. Comparison of the antimicrobial activities of squalamine (minimum IC /mg ml^{-1}) and the antibiotic ampicillin.

Microorganism	Squalamine	Ampicillin
E.coli	1–2	2–4
Pseudomonas aeruginosa	4–8	62–125
Staphylococcus aureus	1–2	<1
Streptococcus faecalis	1–2	<0.25
Proteus vulgaris	4–8	8–16
Serratia marcescens	>125	4–62
Candida albicans	4–8	>125
Paramecium caudarum	4–8	>65

Two novel alkaloids **328a**,**b**[225] related to the previously known antimicrobial metabolites, plakinamides A and B (**329a**,**b**) from the sponge *Plakina* sp.,[226] were isolated from extracts of the sponge *Corticum* sp. collected near the coasts of Indonesia. Compounds **328a**,**b** are highly toxic for tumour cells and manifest moderate immunomodulating and antimicrobial activities.

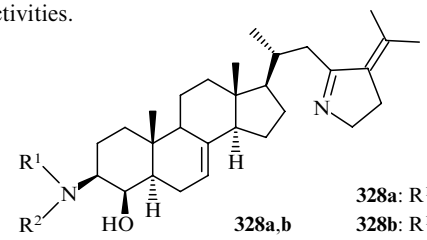

328a,**b** **328a**: $R^1 = R^2 = CH_3$; **328b**: $R^1 = COCH_3$, R^2 = H.

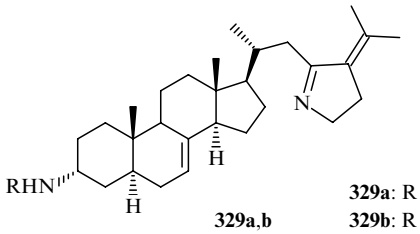

329a,**b** **329a**: R = H; **329b**: R = $COCH_3$.

The unusual steroidal alkaloids **330** and **331** with expanded ring *B* have been found recently in the Pacific sponge *Corticum* sp.[227]

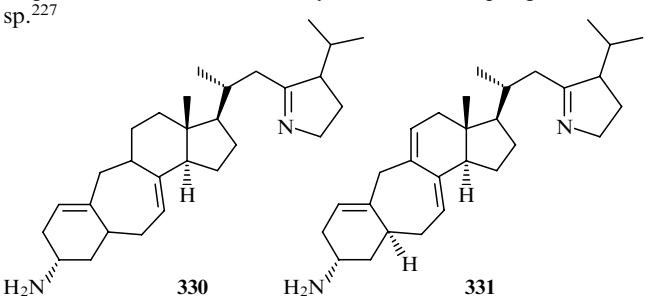

330 **331**

The steroidal oximes **332** and **333** from the sponge *Cinachyrella* sp. inhibit competitively human placental aromatase and are

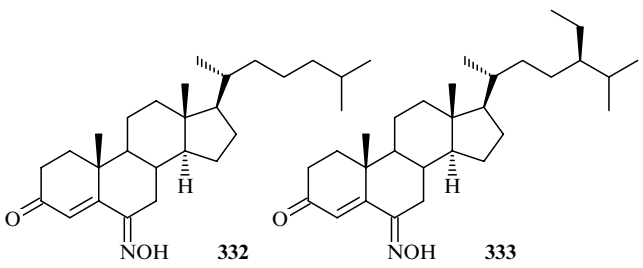

332 **333**

potential inhibitors of hormone-dependent tumours.[228] The syntheses of these compounds have been described.[229]

Although marine steroid alkaloids known thus far are not numerous, they present substantial interest with regard to their chemical structures and physiological activities.

VI. Miscellaneous marine steroids

In this section, we shall consider those marine steroids which can hardly be related to any of the above-mentioned structural groups.

Steroid phosphates were found in the starfish *Tremaster novaecaledoniae*. Tremasterols A–C (**334a–c**) related to glycosides were the first to be described.[230] The monosaccharide residues in these compounds are bound to aglycons by phosphodiester rather than glycosidic bonds. The signals for the protons at C(6) in the ^{1}H NMR spectra of tremasterols represented doublets of doublets of doublets of doublets (J = 9.5, 9.5, 7.5 and 4.5 Hz), *i.e.*, they contained an additional spin coupling constant compared with the corresponding spectra of 6α-hydroxy cholestane derivatives due to the HC–O–P coupling. Their ^{31}P NMR spectra contained triplet signals at δ 3.54, which coalesced into doublets upon irradiation of C<u>H</u>(6) or C<u>H</u>(1′), which suggests the presence of a phosphate group between C(6) and the monosaccharide residue. Chemical shifts of phosphorus atoms for phosphate and other functional groups in the ^{31}P NMR spectra are well established (see, *e.g.*, Ref. 231). Later, the steroid **335** containing sulfate and phosphate groups in positions 3 and 6, respectively, was isolated from the same starfish species.[136]

Some sponges were found to contain dimeric steroids. Thus bistheonellasterone (**336**) and bisconicasterone (**337**) were isolated from the Okinawian sponge *Theonella swinhoei* by Japanese scientists.[232,233] Compound **338** was prepared in nearly quantitative yield from theonellasterone **338** upon heating and evaporation of the latter in chloroform (50 °C, 2 h). The coupling occurred with excellent regio- and stereospecificity. It is assumed that the dimeric steroids **336** and **337** are formed as a result of the Diels–Alder cycloaddition of theonellasterone **338** to its Δ^4-isomer or, correspondingly, by cycloaddition of two molecules of conicasterone **339** to each other. Ketones **338** and **339**, the possible precursors of compounds **336** and **337**, and related compounds have been isolated from the same sponges where they occur as crystalline inclusion compounds.

Crellastatin A (**340**) was the first sulfated steroid dimer isolated from the sponge *Crella* sp.[234] The related compounds **341, 342**, *etc.*, were isolated later.[235]

Hymnosterone A (**343**), the unusual cytotoxic steroid derivative of mixed biogenesis, was isolated from the microscopic fungus *Gymnascella dankaliensis* associated with the sponge *Halichondria japonica*.[236] Hymnostatins containing a non-steroid fragment of compound **343**, *e.g.*, hymnostatin A (**344**), were detected in the same microorganism. They manifest high toxicities against tumour cells P-388.[237]

Polar steroids are seldom found in scleroactinian corals. However, steroidal acids **345a** and **346**, the carbon skeletons of which are identical with those of cholic acids, were discovered in deep-water *Deltocyanthus magnificus* by Pietra *et al.*[238]. Some of

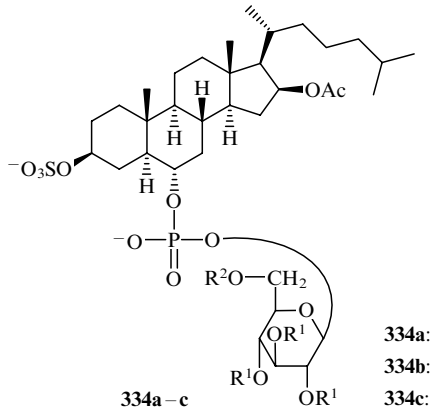

334a–c

334a: $R^1 = R^2 = H$;
334b: $R^1 = R^2 = Ac$;
334c: $R^1 = H$, $R^2 = Ac$.

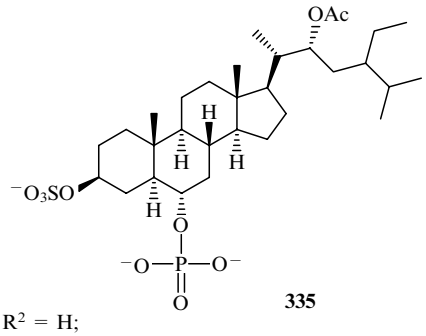

335

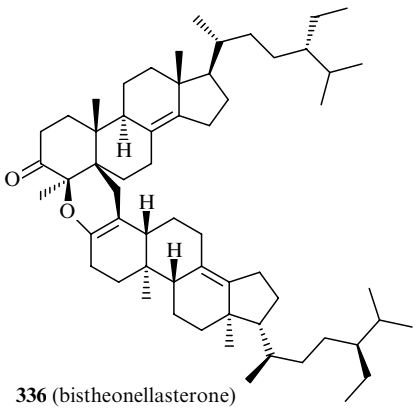

336 (bistheonellasterone)

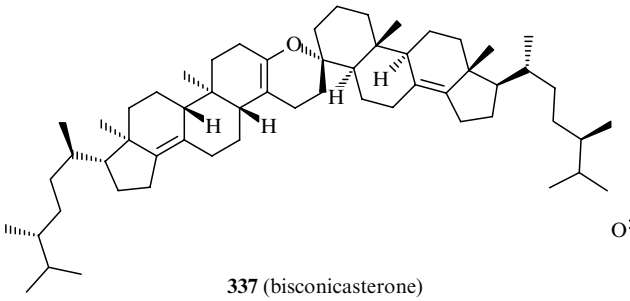

337 (bisconicasterone)

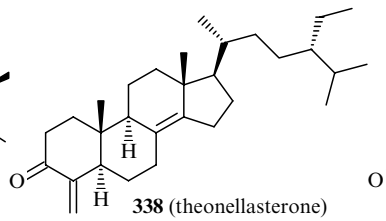

338 (theonellasterone)

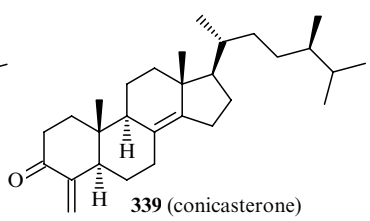

339 (conicasterone)

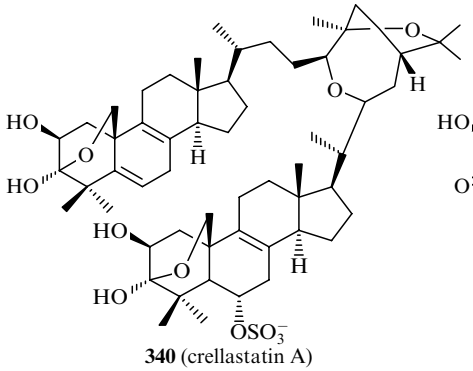

340 (crellastatin A)

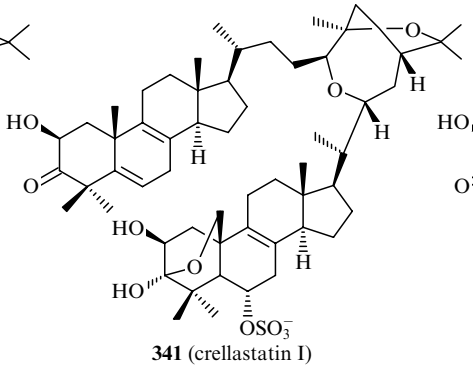

341 (crellastatin I)

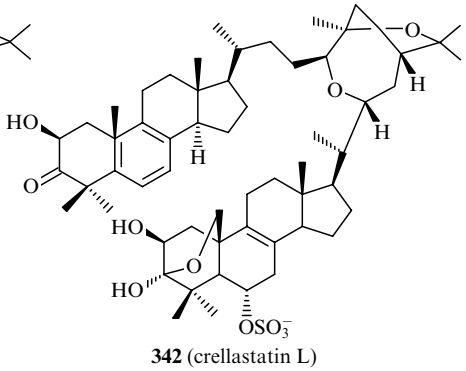

342 (crellastatin L)

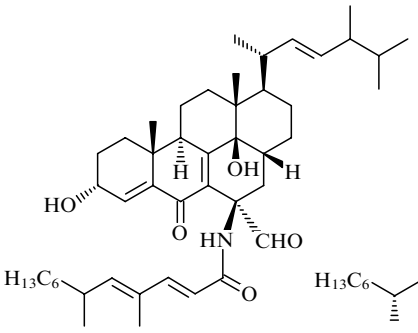

343 (hymnosterone A)

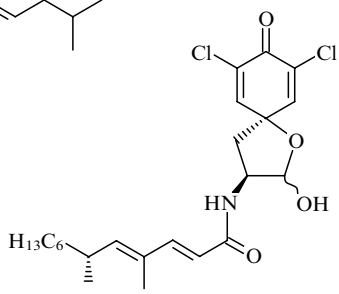

344 (hymnostatin A)

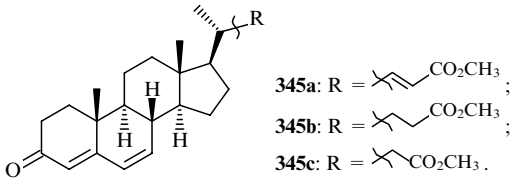

345a: R = CO_2CH_3;
345b: R = CO_2CH_3;
345c: R = CO_2CH_3.

345a – c

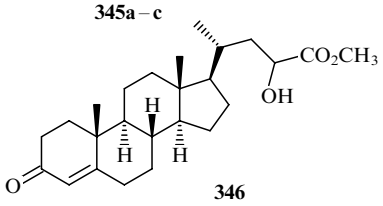

346

these compounds were isolated as methyl esters by treatment of the corresponding fractions with diazomethane.

* * *

Several interesting papers devoted to marine polar steroids were published after this review had been written. Thus Fujita *et al.*[239] reported on the isolation of two novel unusual polar steroids, *viz.*, haplosamate A (**347**) and the minor steroid **348** from the sponge *Cribrochalina* sp. dwelling near the Western coast of Japan.

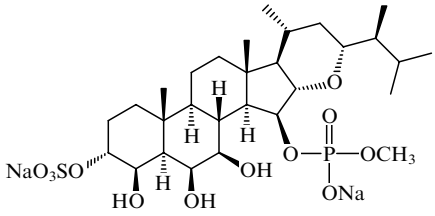

347 (haplosamate A)

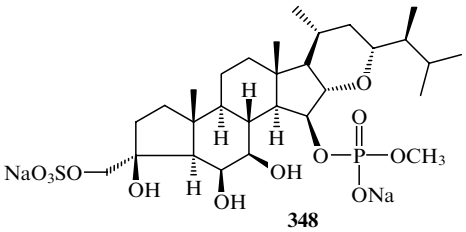

348

These compounds were discovered during the search for inhibitors of matrix metalloproteinases of the membrane type (MT-MMPs), the key enzymes in tumour metastasis. These enzymes activate progelatinase A, which causes the degradation of type IV collagen. The latter inhibits invasion of tumour cells in different body organs and tissues. It is suggested that MT-MMPs inhibitors hold considerable promise as antitumour agents. Compounds **347** and **348** inhibited MT-MMPs (IC_{50} = 150 and 160 μg ml^{-1}, respectively).

Haplosamate A was found to be identical with the inhibitor of integrase, a specific enzyme of the human immunodeficiency virus, with a tentative formula **349**, which has earlier been isolated from two Philippine sponges.[240]

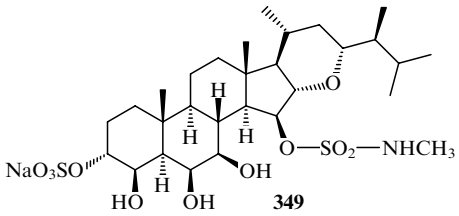

349

It was suggested that this polyhydroxylated steroid contains one sulfate group and one *N*-methylsulfamate group. However, the NMR spectra of haplosamate A displayed additional splitting of signals for certain protons, which could not be inferred from the formula **349**. Thus the proton signal corresponding to the methoxy group occurred as a doublet, which points to the presence of a phosphorus atom in this steroid. Further structural analysis corroborated the correctness of the structure **347** for haplosamate A and the compound isolated from Philippine sponges.

Haplosamate A (**347**) and the related steroid **348** are the first sponge steroids containing both sulfate and methyl phosphate groups. The absolute stereochemistry of compounds **347** and **348** was established on the basis of their chemical conversions and using a modified Mosher's method.

The structure of haplosamate B (**350**),[239] which was erroneously identified as compound **351**,[240] is even more surprising. Haplosamate B is the first polar steroid containing two phosphate and one sulfate groups; one of the phosphate groups in steroid **350** is methylated.

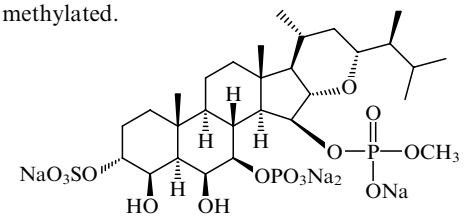

350 (haplosamate B)

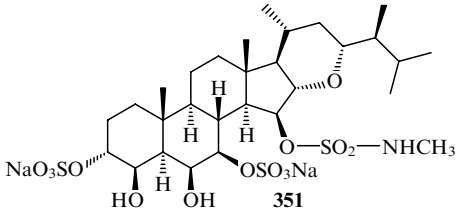

351

The number of marine steroid glycosides is rapidly increasing. A recent report is devoted to the isolation of three novel antibacterial asterosaponins, *viz.*, goniopectenosides A – C (**352a – c**), from the starfish *Goniopecten demonstrans*.[241]

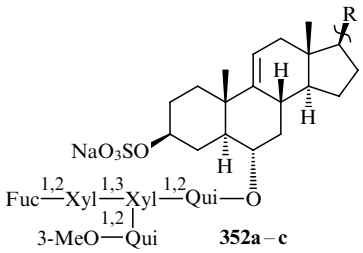

352a: R = 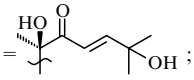 ;
352b: R = 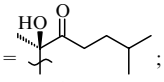 ;
352c: R = 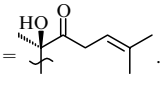 .

352a – c

The carbohydrate chains of these compounds contain a rarely occurring monosaccharide, *viz.*, 3-*O*-methylquinovose, whereas their aglycons contain a keto group in position 22 rather than in 23. The use of a new instrumental approach, *viz.*, liquid chromatography combined with NMR and mass-spectroscopic detection (LC-NMR-MS), in the analysis of the well-studied asterosaponin fraction isolated from the starfish *Asterias rubens* revealed five novel steroid glycosides named ruberosides A – D.[242]

Four novel glycosides of this series, *viz*., sarasinosides H_1, H_2, I_1 and I_2 (compounds **353a**–**d**), were isolated from the sponge *Melophlus isis* together with the previously identified sarasinosides A_1 and A_3.[243] In contrast to sarasinosides, the cytotoxic glycosides ectyoplasides A and B (**354a**,**b**) from the Caribbean sponge *Ectyoplasia ferox*,[244] represent oxygenated derivatives of 4,14-dimethylsterols and contain two galactose and one arabinose residues in their carbohydrate chains.

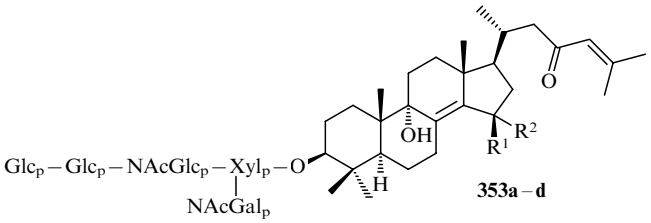

353a–**d**

353a: R^1 = OH, R^2 = H (sarasinoside H_1);
353b: R^1 = OCH_3, R^2 = H (sarasinoside H_2);
353c: R^1 = H, R^2 = OH (sarasinoside I_1);
353d: R^1 = H, R^2 = OCH_3 (sarasinoside I_2).

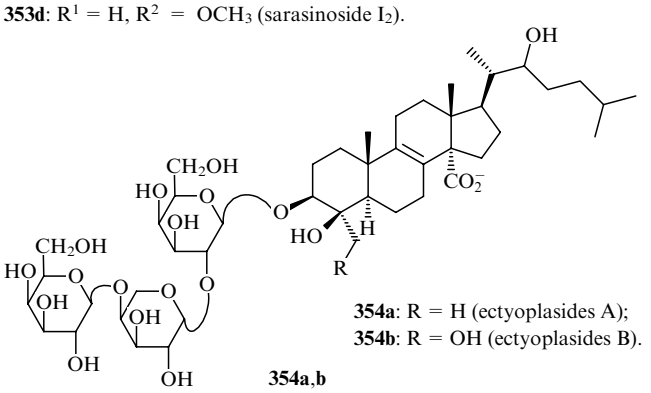

354a: R = H (ectyoplasides A);
354b: R = OH (ectyoplasides B).

354a,**b**

Yet another series of steroid glycosides, *viz*., wondosterols A–C (**355a**–**c**), were detected in a mixture of two different sponge species dwelling near the coasts of Korea.[245] These compounds contain carbohydrate chains linked to C(4) of the aglycons. Wondosterols (**355a**–**c**) belong to the same structural series as the known bioside pachastrelloside A (**284**), but differ from the majority of other sponge glycosides in that they derive from polyhydroxysterols rather than from methylsterols.

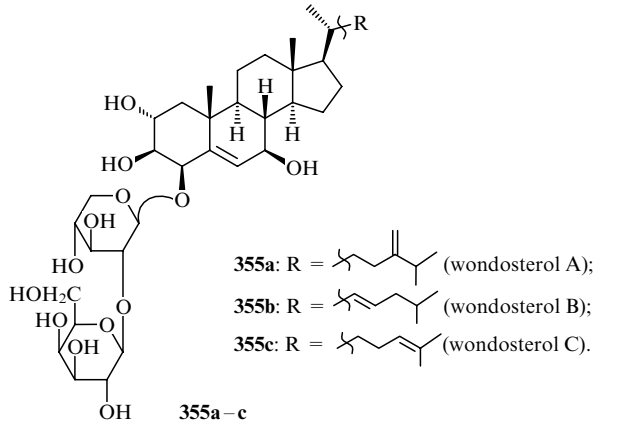

355a: R = (wondosterol A);
355b: R = (wondosterol B);
355c: R = (wondosterol C).

355a–**c**

Among novel steroids isolated from Coelenterata, special mention should be made of a series of compounds similar to witanolides isolated recently from the Okinawian soft coral *Clavularia viridis*, *viz*., the so-called jonarasterols A–C (**356a**–**c**)[246] and the steroidal pentol **357** from the soft coral *Sarcophyton trocheliophorum*,[247] which was weakly toxic against normal human leucocytes, but inhibited leukemia cells HL-60, melanoma cells M-14 and mammary carcinoma cells MCF-7 (IC_{50} = 3–5 μg ml^{-1}).

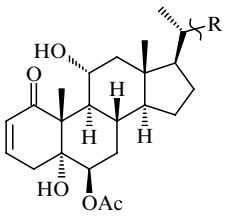

356a–**c**

356a: R = (jonarasterol A);
356b: R = (jonarasterol B);
356c: R = (jonarasterol C).

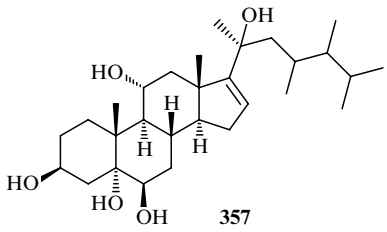

357

VII. Problems of isolation and structural analysis of marine polar steroids

Polar steroids are usually present in marine organisms as very complex mixtures of structurally related compounds, which significantly complicates their isolation and separation. These steroids may contain several functional groups or fragments. Thus trisulfated sterol derivatives are widespread in sponges, whereas steroids containing sulfate or phosphate groups in addition to monosaccharide fragments are more common for starfishes. Moreover, many highly active marine steroids are minor components of extracts where their concentrations do not exceed 0.001% of the dry weight of the corresponding organisms. Their isolation and purification present a difficult and not always solvable problem, although these procedures are usually carried out with the use of the most advanced separation techniques.

In our laboratory, we use reversed-phase column chromatography on a PTFE powder (Polychrome-1) in the first step of isolation of polar steroids. This consists in application of aqueous extracts on columns with this sorbent, elution of salts by washing the columns with water and elution of polar steroids with aqueous alcohol.[99,160]

Italian chemists perform this procedure on a column with Amberlite XAD-2.[3,165] Further separation usually requires the use of several separation techniques including gel-permeation chromatography on Sephadexes LH-20 and LH-60, adsorption chromatography on silica gel, reversed-phase HPLC as well as drop counter-current distribution. The isolation of 22 novel polar steroids from the starfish *Oreaster raticulatus*,[117] about 20 cephalostatins from *Cephalodiscus gilchristi*[211–217] and 20 ritterazines from *Ritterella tokioka*[216–219] provide illustrative examples of progress achieved.

NMR spectroscopy including the most updated techniques, *e.g*., HMBC and NOESY experiments, is the most popular structural physicochemical method. The absolute configurations of asymmetric carbon atoms of polyhydroxysteroids are often established by the Mosher's method,[248] which consists in the conversion of the corresponding hydroxy groups into ester groups by treatment with chiral *R*-(+)- and *S*-(−)-α-methoxy-α-trifluoromethylphenylacetyl chlorides (MTPA) with subsequent determination of the chemical shifts of protons at the adjacent carbon atoms of the diastereomeric esters formed. In the case of the 24*R*-configuration of the corresponding asymmetric centres in (+)- and (−)-MTPA esters, the signals corresponding to the $C(26)H_3$ and $C(27)H_3$ groups are observed at δ 0.89–0.91, whereas those for the 24*S*-isomers are found in the higher field, *viz*., at δ 0.83–0.86.

FAB-mass spectrometry is the most popular modern mass spectrometric technique for the determination of molecular masses of polar steroids and establishment of the sequences of

monosaccharide units in carbohydrate chains of steroid glycosides.

Although the chemical properties of many marine polar steroids are still poorly investigated, the use of chemical procedures for the establishment of their chemical structures sometimes demonstrates their unusual or unpredicted chemical behaviour especially in acidic media, *e.g.*, migration of the double bond in the steroid nucleus from position 8(9) to positions 8(14) and 14(15),[110, 191, 197] aromatisation of a ring in the steroid skeleton,[110] *etc*.

VIII. Conclusion

In marine organisms, steroid substrates can be oxygenated at any carbon atom without exceptions (Table 7). Even the products of steroid metabolism formed by oxidative cleavage of the bonds between the quaternary carbon atoms, *e.g.*, C(10) or C(13), and the neighbouring carbon atoms, were found in these organisms. Compounds containing hydroxy groups in methine and methylene groups instead of hydrogen atoms are even more numerous. Some representatives of starfishes, sponges and cnidarians contain steroids with three, four and even more (up to nine) hydroxy groups. Further modifications of polar steroids in marine organisms include sulfation (sponges, starfishes, ophiuroids and fishes), acylation (octocorals and some other cnidarian species and sponges), methylation (sponges), oxidation of hydroxy groups to keto and carboxy groups (sponges, cnidarians and echinoderms), phosphorylation (starfishes and sponges) and glycosylation (starfishes, sponges, fishes, cnidarians, less frequently, ophiuroids). Sometimes, biochemical conversions of polar steroids lead to the formation of nitrogen-containing derivatives, *viz*., alkaloids. All this provides evidence for the wide structural diversity of marine polar steroids.

The analysis of published data suggests that in-depth studies in this area are still in progress. In the last few years, the number of newly discovered marine steroids increases annually by 50 – 100 compounds. Many novel unexpected findings still remain to be made.

Although the biological activities and functions of marine polar steroids have not been adequately investigated yet, many of them have attracted the attention of pharmacologists and physicians. This concerns supercytotoxic antitumour compounds, efficient antimicrobial agents, inflammation inhibitors, *etc*. In-depth studies of antiinflammatory activities of contignasterol, antitumour activities of cephalostatins and specific physiological activities of other marine polar steroids are currently under way. However, the array of activities tested employed in the isolation of novel polar steroids is still rather narrow. Thus the majority of investigators have concentrated on the search for novel antitumour compounds, whereas all other types of activities of marine steroids are neglected.

The experimental data and the unusual structural peculiarities of some polar steroids attract keen attention of synthetic chemists. Recent developments in this field culminated in complete and partial syntheses of these natural compounds, their analogues and derivatives. Thus the syntheses of two novel sponge 9,10-secosteroids,[250] *viz*., calicopherol E and astrogorgiadiol (by the method of Barton [249]); of cytotoxic stolonipherones earlier isolated from the soft coral *Clavularia viridis;*[251] of incrustasterols possessing antitumour activities;[252] of xestobergsterol A obtained in 24 steps from stigmasterol [253] and of 3-epi-6,7-dideoxysestobergsterol A [254] have recently been carried out. Apparently, the synthetic trend in the study of marine polar steroids will be developed in the future.

It is obvious that the vast pool of fundamental knowledge concerning the structure, taxonomic distribution and properties of marine polar steroids created owing to joint efforts of many research groups all over the world will serve as a basis for the development of novel biotechnological approaches to their preparation in sufficiently large amounts. Close cooperation of bioorganic chemistrs and specialists in aquatic, cell and tissue cultures and gene engineering will be a valuable contribution.

In the next few years, significant progress can be anticipated in the study of biogenesis of marine steroids, particularly in isolation and investigation of enzymes responsible for their biosynthesis

Table 7. Examples of marine organisms containing oxygenation polar steroids with oxiden-containing functional groups at different positions.

Carbon atom	Marine organisms	Carbon atom	Marine organisms	Carbon atom	Marine organisms
1	sponges (*Xestospongia*), corals (*Sinularia*), *etc*.	10	gorgonian corals (*Caligorgia*), sponges (*Corticum*)	19	corals (*Nephthea*, *Antiphates*, *Litophyton*), sponges (*Toxadocia*, *Strongylophora*, *Crella*)
2	many ophiuroids, sponges (*Aplyinopsis*, *Echinoclathria*, *Halichondria*, *Topsentia*, *etc*.)	11	many sponges and corals, some ophiuroids, fishes (*Mola*)	20	many starfishes, sponges (*Petrosia*, *Geodia*), corals (*Sarcophyton*, *etc*.)
3	all marine organisms excluding bacteria	12	some fishes, sea worm (*Cephalodiscus gilchristi*), ascidia (*Ritterella tokioka*)	21	many ophiuroids, starfishes (*Pteraster*), some corals and sponges
4	many ophiuroids and starfishes, corals, sponges (*Stilopus*, *Haliclona*)	13	octocorals (*Dendronephthea*)	22	sponges (*Haliclona*, *Petrosia*, *etc*.), corals (*Alcyonium*, *etc*.)
5	many sponges, corals and starfishes, some sea lilies	14	some starfishes, sponges (*Jereicopsis*, *Theonella*)	23	many starfishes, some corals, sponges (*Xestospongia*, *Ircinia*)
6	many sponges, corals and starfishes, some sea lilies	15	many starfishes	24	many starfishes, fishes, sponges (*Crella*)
7	some starfishes and octocorals, fishes, sponges (*Poecilastra*)	16	Many starfishes, corals, sea worm (*Cephalofiscus gilchristi*)	25	some starfishes and octocorals
8	many starfishes, sponges (*Jereicopsis*, *Theonella*), fungi (*Tilopilus*)	17	sponges (*Echinoclathria*, *etc*.), corals (*Dendronephthea*), sea worm (*Cephalofiscus gilchristi*)	26	many starfishes, some fishes, sponges (*Polymastia*)
9	many sponges and corals, fungi (*Tilopilus*)	18	octocorals (*Sinularia*, *etc*.), sponges (*Echinoclathria*)	27	many starfishes, some fishes, sponges (*Polymastia*)
				28 [a]	many starfishes
				29 [b]	many starfishes, sponges (*Petrosia*)

[a] In the side chains of ergostane derivatives. [b] In the side chains of ergostane and stigmastane derivatives.

and the use of these enzymes or competent cells for targeted transformations of steroid substrates.

References

1. G B Elyakov, V A Stonik *Steroidy Morskikh Organizmov* (Steroids from Marine Organisms) (Moscow: Nauka, 1988)
2. M V D'Auria, L Minale, R Riccio *Chem. Rev.* **93** 1839 (1993)
3. L Minale, R Riccio, F Zollo, in *Progress in the Chemistry of Organic Natural Products* Vol. 62 (Eds H Herz, G W Kirby, R E Moore, W Steglich, Ch Tamm) (New York: Springer, 1993) p. 75
4. J-H Sheu, S-Y Huang, G-H Wang, C-Y Duh *J. Nat. Prod.* **60** 900 (1997)
5. M Kobayashi, O Murata, N Rao, R Chavakula, N S Sarma *Tetrahedron Lett.* **33** 519 (1992)
6. L Ktari, A Blond, M Guyot *Bioorg. Med. Chem. Lett.* **10** 2563 (2000)
7. J-H Sheu, G H Wang, P-J Sung, C-Y Duh *J. Nat. Prod.* **62** 224 (1999)
8. Y Venkateswarlu, M V R Reddy, M R Rao *J. Nat. Prod.* **59** 876 (1996)
9. K Iguchi, H Shimura, S Taira, C Yokoo, K Matsumoto, Y Yamada *J. Org. Chem.* **59** 7499 (1994)
10. K Iguchi, M Fujita, H Nagaoka, H Mitome, Y Yamada *Tetrahedron Lett.* **34** 6277 (1993)
11. H Shimura, K Iguchi, S Nakaike, T Yamagishi, K Matsumoto, C Yokoo *Experientia* **50** 134 (1994)
12. H Miyaoka, M Shinohara, M Shimomura, H Mitome, A Yano, K Iguchi, Y Yamada *Tetrahedron* **53** 5403 (1997)
13. S J Rochfort, R W Gable, R J Capon *Aust. J. Chem.* **49** 715 (1996)
14. H Mitome, H Miyaoka, H Takahashi, Y Yamada *Bioorg. Med. Chem. Lett.* **7** 691 (1997)
15. H Mitome, H Miyaoka, M Nakano, Y Yamada *Tetrahedron Lett.* **36** 8231 (1995)
16. A Migliuolo, V Piccialli, D Sica, F Giordano *Steroids* **58** 134 (1993)
17. A Aiello, E Fattorusso, M Menna *Steroids* **64** 687 (1999)
18. B Das, K V N S Srinivas *J. Nat. Prod.* **55** 1310 (1992)
19. A Casapullo, L Minale, F Zollo, C Roussakis *Tetrahedron Lett.* **36** 2669 (1995)
20. I Izzo, F De Riccardis, A Massa, G Sodano *Tetrahedron Lett.* **37** 4775 (1996)
21. S Aoki, Y Yoshioka, Y Miyamoto, K Higuchi, A Setiawan, N Murakami, Z-S Chen, T Sumizawa, S Akiyama, M Kobayashi *Tetrahedron Lett.* **39** 6303 (1998)
22. N Shoji, A Umeyama, K Shin, K Takeda, S Arihara, J Kobayashi, M Takei *J. Org. Chem.* **57** 2996 (1992)
23. J Kobayashi, H Shinonaga, H Shigemori, A Umeyama, N Shoji, S Arihara *J. Nat. Prod.* **58** 312 (1995)
24. D L Burgoyne, R J Andersen, T M Allen *J. Org. Chem.* **57** 525 (1992)
25. G-Y-S Wang, P Crews *Tetrahedron Lett.* **37** 8145 (1996)
26. C Zeng, M Ishibashi, J Kobayashi *J. Nat. Prod.* **56** 2016 (1993)
27. T N Makarieva, I A Bondarenko, A S Dmitrenok, V M Boguslavsky, V A Stonik, V I Chernih, S M Efremova *J. Nat. Prod.* **54** 953 (1991)
28. J R Carney, W Y Yoshida, P J Scheuer *J. Org. Chem.* **57** 6637 (1992)
29. J R Carney, P J Scheuer, M Kelly-Borges *J. Org. Chem.* **58** 3460 (1993)
30. J M Corgiat, P J Scheuer, J L Rios Steiner, J Clardy *Tetrahedron* **49** 1557 (1993)
31. Y Sera, K Adachi, Y Shizuri *J. Nat. Prod.* **62** 152 (1999)
32. P de Almeida Leone, J Redburn, J N A Hooper, R J Quinn *J. Nat. Prod.* **63** 694 (2000)
33. S P Gunasekera, F Schmitz *J. Org. Chem.* **48** 885 (1988)
34. J Pika, R J Andersen *Tetrahedron* **49** 8757 (1993)
35. H Li, S Matsunaga, N Fusetani *Experientia* **50** 771 (1994)
36. M V R Reddy, M K Harper, D J Faulkner *J. Nat. Prod.* **60** 41 (1997)
37. Q Lu, D J Faulkner *J. Nat. Prod.* **60** 195 (1997)
38. A Rueda, E Zubia, M J Ortega, J L Carballo, J Silvá *J. Nat. Prod.* **61** 258 (1998)
39. A Aiello, E Fattorusso, M Menna, R Carnuccio, T Iuvone *Steroids* **60** 666 (1995)
40. J Dopeso, E Quiñoá, R Riguera, C Debitus, P R Bergquist *Tetrahedron* **50** 3813 (1994)
41. I A van Altena, A J Butler, S J Dunne *J. Nat. Prod.* **62** 1154 (1999)
42. M V D'Auria, L Gomez Paloma, L Minale, R Riccio, C Debitus *Tetrahedron Lett.* **32** 2149 (1991)
43. A Umeyama, N Shoji, M Enoki, S Arihara *J. Nat. Prod.* **60** 296 (1997)
44. V Costantino, E Fattorusso, A Mangoni, M Akhin, E M Gaydou *Steroids* **59** 181 (1994)
45. S-H Wu, X-D Luo, Y B Ma, J-K Liu, D-G Wu, B Zhao, Y Lu, Q T Zheng *J. Nat. Prod.* **63** 534 (2000)
46. C-Y Duh, S-K Wang, M-J Chu, J-H Sheu *J. Nat. Prod.* **61** 1022 (1998)
47. M R Rao, U Venkatesham, Y Venkateswarlu *J. Nat. Prod.* **62** 1584 (1999)
48. R Li, S Y Wang, G L Tan, K H Long *Steroids* **59** 503 (1994)
49. K A El Sayed, P Bartyzel, X Shen, T L Perry, J K Zjawiony, M T Hamann *Tetrahedron* **56** 949 (2000)
50. M Kobayashi *J. Chem. Res. (S)* 44 (1994)
51. V Anjaneyulu, K N Rao, J S Babu, M Kobayashi *Indian J. Chem.* **33B** 144 (1994)
52. M Kobayashi, K M C A Rao, V Anjaneyulu *J. Chem. Res. (S)* 140 (1994)
53. M Kobayashi, K M C A Rao, M M Krishna, V Anjaneyulu *J. Chem. Res. (S)* 180 (1994)
54. M Kobayashi, M M Krishna, V Anjaneyulu *Chem. Pharm. Bull.* **40** 2845 (1992)
55. R S Li, K C Chang, K H Long *Steroids* **57** 3 (1992)
56. J-H Sheu, K-C Chang, C-Y Duh *J. Nat. Prod.* **63** 149 (2000)
57. J A Ballantine, K Williams *Tetrahedron Lett.* 1547 (1977)
58. Y Venkateswarlu, M Rama Rao, P Ramesh *J. Nat. Prod.* **60** 1301 (1997)
59. Q Lu, D J Faulkner *Nat. Prod. Lett.* **10** 231 (1997)
60. A Umeyama, N Shoji, M Ozeki, S Arihara *J. Nat. Prod.* **59** 894 (1996)
61. B L Raju, G V Subbarao, M C Reddy, D V Rao, C B Rao, V S Raju *J. Nat. Prod.* **55** 904 (1992)
62. A S R Anjaneyulu, M V R K Murthy, P M Gowri *J. Nat. Prod.* **63** 112 (2000)
63. Y Seo, J H Jung, J-R Rho, J Shin, J T Song *Tetrahedron* **51** 2497 (1995)
64. Y Tomono, H Hirota, Y Imahara, N Fusetani *J. Nat. Prod.* **62** 1538 (1999)
65. M Kobayashi, F Kanda, C V L Rao, S M D Kumar, G Turimurtulu, C B Rao *Chem. Pharm. Bull.* **38** 1724 (1990)
66. M Kobayashi, K Kobayashi, K V Ramana,C V L Rao, D V Rao, C B Rao *J. Chem. Soc., Perkin Trans. 1* 493 (1991)
67. M Kobayashi, F Kanda *J. Chem. Soc., Perkin Trans. 1* 1177 (1991)
68. P Ramesh, V L N Reddy, N S Reddy, Y Venkateswarlu *J. Nat. Prod.* **63** 1420 (2000)
69. J Shin, Y Seo, J-R Rho, K W Cho *J. Nat. Prod.* **59** 679 (1996)
70. Y Seo, J-R Rho, K W Cho, J Shin *J. Nat. Prod.* **59** 1196 (1996)
71. A Aiello, E Fattorusso, M Menna *J. Nat. Prod.* **55** 321 (1992)
72. G K Liyanage, F J Schmitz *J. Nat. Prod.* **59** 148 (1996)
73. X C Fretté, J F Biard, C Roussakis, J F Verbist, J Vercaute, N Pinaud, C Débitus *Tetrahedron Lett.* **37** 2959 (1996)
74. R D Epifanio, L F Maia, A C Pinto, I Hardt, W Fenical *J. Braz. Chem. Soc.* **9** 187 (1998)
75. K Yoshikawa, S Kanekuni, M Hanahusa, S Arihara, T Ohta *J. Nat. Prod.* **63** 670 (2000)
76. K Watanabe, M Iwashima, K Iguchi *Steroids* **61** 439 (1996)
77. M Ochi, K Yamada, H Kotsuki, K Shibata *Chem. Lett.* 427 (1991)
78. Y Seo, K W Cho, H Chung, H-S Lee, J Shin *J. Nat. Prod.* **61** 1441 (1998)
79. A S R Anjaneyulu, N S K Rao, G V Rao *Indian J. Chem.* **36B** 418 (1997)
80. M Aknin, V Costantino, A Mangoni, E Fattorusso, E M Gaydou *Steroids* **63** 575 (1998)
81. L A Morris, E M Christie, M Jaspars, L P van Ofwegen *J. Nat. Prod.* **61** 538 (1998)
82. H Y He, P Kulanthaivel, B J Baker, K Kalter, J Darges, D Cofield, L Wolf, L Adams *Tetrahedron* **51** 51 (1995)
83. Y Tomono, H Hirota, N Fusetani *J. Org. Chem.* **64** 2272 (1999)
84. D R Beukes, M T Davies-Coleman, D C Egglestion, R C Haltiwanger, B Tomkowiez *J. Nat. Prod.* **60** 573 (1997)
85. P K Datta, A K Ray, A K Barua, S K Showdhuri, A Patra *J. Nat. Prod.* **53** 1347 (1990)

86. D E Williams, S W Ayer, R J Andersen *Can. J. Chem.* **64** 1527 (1986)
87. J Kubanek, R J Andersen *J. Nat. Prod.* **62** 777 (1999)
88. Y Yamaguchi, Y Nakanishi, T Shimokawa, S Hashiguchi, A Hayashi *Chem. Lett.* 1713 (1992)
89. A A Kicha, A I Kalinovsky, V A Stonik *Izv. Akad. Nauk, Ser. Khim.* 190 (1997) [a]
90. S De Marino, M Iorizzi, F Zollo, L Minale, C D Amsler, B J Baker, J B McClintock *J. Nat. Prod.* **60** 959 (1997)
91. M Iorizzi, S De Marino, L Minale, F Zollo, V Le Bert, C Roussakis *Tetrahedron* **52** 10997 (1996)
92. M Iorizzi, P Bryan, J McClintock, L Minale, E Palagiano, S Maurelli, R Riccio, F Zollo *J. Nat. Prod.* **58** 653 (1995)
93. A A Kicha, A I Kalinovsky, N V Gorbach, V A Stonik *Khim. Prirod. Soedin.* 249 (1993) [b]
94. A A Kicha, A I Kalinovsky, N V Ivanchina, Yu N El'kin, V A Stonik *Izv. Akad. Nauk, Ser. Khim.* 1821 (1994) [a]
95. A A Kicha, A I Kalinovsky, N V Ivanchina, V A Stonik *Izv. Akad. Nauk, Ser. Khim.* 2088 (1998) [a]
96. E Finamore, L Minale, R Riccio, G Rinaldo, F Zollo *J. Org. Chem.* **56** 1146 (1991)
97. A A Kicha, N V Ivanchina, I A Gorshkova, L P Ponomarenko, G N Likhatskaya, V A Stonik *Comp. Biochem. Physiol.* **128B** 43 (2001)
98. L Andersson, L Bohlin, M Iorizzi, R Riccio, L Minale, W Moreno-Lopez *Toxicon* **27** 179 (1989)
99. L K Shubina, S N Fedorov, E V Levina, P V Andriyaschenko, A I Kalinovsky, V A Stonik, I S Smirnov *Comp. Biochem. Physiol.* **119B** 505 (1998)
100. M B Ksebati, F J Schmitz *J. Org. Chem.* **53** 3926 (1988)
101. J-M Kornprobst, C Sallenave, G Barnathan *Comp. Biochem. Physiol.* **119B** 1 (1998)
102. T N Makarieva, V A Stonik, I I Kapustina, V M Boguslavsky, A S Dmitrenok, V I Kalinin, M L Cordeiro, C Djerassi *Steroids* **58** 508 (1993)
103. A M Popov, N I Kalinovskaya, T A Kuznetsova, I G Agafonova, M M Anisimov *Antibiotiki* **28** 656 (1983)
104. A S R Anjaneyulu, M J R V Venugopal, L Minale, M Iorizzi, E Pelagiano *Indian J. Chem.* **37B** 262 (1998)
105. M Kates, B E Volcani *Biochem. Biophys. Acta* **116** 264 (1966)
106. M Kobayashi, M Ishibashi, H Nakamura, Y Ohizumi, Y Hirata *J. Chem. Soc., Perkin Trans. 1* 101 (1989)
107. T Nakatsu, R P Walker, J E Thompson, D J Faulkner *Experientia* **39** 759 (1983)
108. T N Makarieva, V A Stonik, O G D'yachuk, A S Dmitrenok *Tetrahedron Lett.* **36** 129 (1995)
109. F Kong, R J Andersen *J. Org. Chem.* **58** 6924 (1993)
110. F Kong, R J Andersen *J. Nat. Prod.* **59** 379 (1996)
111. M R Prinsep, J W Blunt, M H G Munro *J. Nat. Prod.* **52** 657 (1989)
112. H Y Li, S Matsunaga, N Fusetani, H Fujiki, P T Murphy, R H Willis, J T Baker *Tetrahedron Lett.* **34** 5733 (1993)
113. S Sperry, P Crews *J. Nat. Prod.* **60** 29 (1997)
114. S Tsukamoto, S Matsunaga, N Fusetani, R W M van Soest *J. Nat. Prod.* **61** 1374 (1998)
115. A A Kicha, A I Kalinovsky, V A Stonik *Khim. Prirod. Soedin.* 520 (1991) [b]
116. N V Ivanchina, A A Kicha, A I Kalinovsky, P S Dmitrenok, V A Stonik, R Riguera, C Jimenez *J. Nat. Prod.* **63** 1178 (2000)
117. M Iorizzi, G Bifulco, F De Riccardis, L Minale, R Riccio, F Zollo *J. Nat. Prod.* **58** 10 (1995)
118. P V Andriyaschenko, E V Levina, A I Kalinovsky *Izv. Akad. Nauk, Ser. Khim.* 473 (1996) [a]
119. A J Roscatagliata, M S Maier, A M Seldes *J. Nat. Prod.* **58** 1941 (1995)
120. M Iorizzi, F De Riccardis, L Minale, E Palagiano, R Riccio, C Debitus, D Duhet *J. Nat. Prod.* **57** 1361 (1994)
121. S De Marino, E Pelagiano, F Zollo, L Minale, M Iorizzi *Tetrahedron* **53** 8625 (1997)
122. F De Riccardis, L Minale, R Riccio, M Iorizzi, C Debitus, D Duhet, C Monniot *Tetrahedron Lett.* **34** 4381 (1993)
123. E V Levina, A I Kalinovsky, V A Stonik, S N Fedorov, V V Isakov *Khim. Prirod. Soedin.* 375 (1988) [b]
124. E V Levina, S N Fedorov, V A Stonik, P V Andriyaschenko, A I Kalinovsky, V V Isakov *Khim. Prirod. Soedin.* 483 (1990) [b]
125. M V D'Auria, R Riccio, L Minale, S La Barre, J Pusset *J. Org. Chem.* **52** 3947 (1987)
126. X Fu, F J Schmitz, R H Lee, J S Papkoff, D L Slate *J. Nat. Prod.* **57** 1591 (1994)
127. H Ishida, S Kinoshita, R Natsuyama, H Nukaya, K Tsuji, N Nagasawa, T Kosuge *Chem. Pharm. Bull.* **40** 864 (1992)
128. H Ishida, N Yamamoto, H Nukaya, K Tsuji, T Kosuge *Chem. Pharm. Bull.* **42** 2514 (1994)
129. H Ishida, H Nakayasu, H Miyamoto, H Nukaya, K Tsuji *Chem. Pharm. Bull.* **46** 12 (1998)
130. A Moore, A P Scott *Proc. R. Soc. London, B Biol. Sci.* **249** 205 (1992)
131. T N Makarieva, L K Shubina, A I Kalinovsky, V A Stonik *Khim. Prirod. Soedin.* 272 (1985) [b]
132. H H Sun, S S Cross, M Gunasekera, F E Koehn *Tetrahedron* **47** 1185 (1991)
133. J-L Giner, S P Gunasekera, S A Pomponi *Steroids* **64** 820 (1999)
134. F E Koehn, M Gunasekera, S S Cross *J. Org. Chem.* **56** 1322 (1991)
135. A D Patil, A J Freyer, A Breen, B Carte, R K Johnson *J. Nat. Prod.* **59** 606 (1996)
136. F De Riccardis, L Minale, R Riccio, B Giovannitti, M Iorizzi, C Debitus *Gazz. Chim. Ital.* **123** 79 (1993)
137. E Finamore, F Zollo, L Minale, T Yasumoto *J. Nat. Prod.* **55** 767 (1992)
138. I Bruno, L Minale, R Riccio, S La Barre, D Laurent *Gazz. Chim. Ital.* **120** 449 (1990)
139. A J Roccatagliata, M S Maier, A M Seldes *J. Nat. Prod.* **61** 370 (1998)
140. R Riccio, M V D'Auria, L Minale *Tetrahedron* **41** 6041 (1985)
141. M V D'Auria, R Riccio, E Uriatre, L Minale, J Tanaka, T Higa *J. Org. Chem.* **54** 234 (1989)
142. M V D'Auria, L Gomez Paloma, L Minale, R Riccio, A Zampella, J Tanaka, T Higa *Tetrahedron Lett.* **33** 4641 (1992)
143. S N Fedorov, E V Levina, A I Kalinovsky, P S Dmitrenok, V A Stonik *J. Nat. Prod.* **57** 1631 (1994)
144. M V D'Auria, L Paloma, L G Minale, R Riccio, A Zampella *J. Nat. Prod.* **58** 189 (1995)
145. I I Kapustina, T N Makarieva, V A Stonik, A I Kalinovsky *Khim. Prirod. Soedin.* 305 (1993) [b]
146. M V D'Auria, L G Paloma, L Minale, R Riccio, A Zampella *Nat. Prod. Lett.* **3** 197 (1993)
147. M J Comin, M S Maier, A J Roccatagliata, C A Pujol, E B Damonte *Steroids* **64** 335 (1999)
148. E V Levina, P V Andriyaschenko, V A Stonik, A I Kalinovsky *Comp. Biochem. Physiol.* **114B** 49 (1996)
149. E V Levina, P V Andriyaschenko, A I Kalinovsky, V A Stonik *J. Nat. Prod.* **61** 1423 (1998)
150. E V Levina, P V Andriyaschenko, S N Fedorov, L A Elyakova *Khim. Prirod. Soedin.* 647 (1994) [b]
151. D L Aminin, I G Agafonova, S N Fedorov *Comp. Biochem. Physiol.* **112C** 201 (1995)
152. R G Kerr, B J Baker *Nat. Prod. Rep.* **8** 46 (1991)
153. N Fusetani, S Matsunaga, S Konosu *Tetrahedron Lett.* **22** 1985 (1981)
154. T N Makarieva, L K Shubina, A I Kalinovsky, V A Stonik, G B Elyakov *Steroids* **42** 267 (1983)
155. S Kanazawa, N Fusetani, S Matsunaga *Tetrahedron* **48** 5467 (1992)
156. T N Makarieva, P S Dmitrenok, L K Shubina, V A Stonik *Khim. Prirod. Soedin.* 371 (1988) [b]
157. S P Gunasekera, S H Sennett, M Kelly-Borges *J. Nat. Prod.* **57** 1751 (1994)
158. G Bifulco, I Bruno, L Minale, R Riccio *J. Nat. Prod.* **57** 164 (1994)
159. T N Makarieva, L K Shubina, V A Stonik *Khim. Prirod. Soedin.* 111 (1987) [b]
160. T N Makarieva, V A Stonik, A S Dmitrenok, V B Krasokhin, V I Svetashev, M V Vysotskii *Steroids* **60** 316 (1995)
161. T C McKee, J H Cardellina II, R Raffaele, M V D'Auria, M Iorizzi, L Minale, R A Moran, R J Gulakowski, J B MaMohan, R W Buckheit, K M Snader, M R Boyd *J. Med. Chem.* **37** 793 (1994)

162. T N Zvyagintseva, T N Makarieva, V A Stonik, L A Elyakova *Khim. Prirod. Soedin.* 71 (1986) [b]
163. T C McKee, J H Cardellina II, M Tischler, K M Snader, M R Boyd *Tetrahedron Lett.* **34** 389 (1993)
164. N Fusetani, M Takahashi, S Matsunaga *Tetrahedron* **50** 7765 (1994)
165. L Minale, M Iorizzi, E Palagiano, R Riccio *Adv. Exp. Med. Biol.* **404** 335 (1996)
166. I Kitagawa, M Kobayashi *Chem. Pharm. Bull.* **26** 1864 (1978)
167. R Riccio, L Minale, C Pizza, F Zollo, J Pusset *Tetrahedron Lett.* **23** 2899 (1982)
168. A A Kicha, A I Kalinovsky, E V Levina, V A Stonik, G B Elyakov *Tetrahedron Lett.* **24** 3893 (1983)
169. F De Simone, A Dini, E Finamore, L Minale, C Pizza, R Riccio, F Zollo *J. Chem. Soc., Perkin Trans. 1* 1855 (1981)
170. M Iorizzi, L Minale, R Riccio, T Yasumoto *J. Nat. Prod.* **56** 1786 (1993)
171. M Iorizzi, F De Riccardis, L Minale, R Riccio *J. Nat. Prod.* **56** 2149 (1993)
172. A J Roccatagliata, M S Maier, A M Seldes, M Iorizzi, L Minale *J. Nat. Prod.* **57** 747 (1994)
173. S De Marino, L Minale, F Zollo, M Iorizzi, V Le Bert, C Roussakis *Gazz. Chim. Ital.* **126** 667 (1996)
174. S De Marino, M Iorizzi, E Palagiano, F Zollo, C Roussakis *J. Nat. Prod.* **61** 1319 (1998)
175. J A Findlay, Z-Q He, M Jaseja *Can. J. Chem.* **67** 2078 (1989)
176. J A Findlay, Z-Q He *J. Nat. Prod.* **53** 710 (1990)
177. R Higuchi, M Fujita, S Matsumoto, K Yamada, T Miyamoto, T Sasaki *Liebigs Ann. Chem.* 837 (1996)
178. E Palagiano, F Zollo, L Minale, L G Paloma, M Iorizzi, P Bryan, J McClintock, T Hopkins, D Riou, C Roussakis *Tetrahedron* **51** 12 293 (1995)
179. E Palagiano, F Zollo, L Minale, M Iorizzi, P Bryan, J McClintock, T Hopkins *J. Nat. Prod.* **59** 348 (1996)
180. M J Vazques, E Quinoa, R Riguera, A San Martin, J Darias *Can. J. Chem.* **71** 1147 (1993)
181. M S Maier, A Roccatagliata, A M Seldes *J. Nat. Prod.* **56** 939 (1993)
182. M J Vazques, E Quinoa, R Riguera, A San Martin, J Darias *Liebigs Ann. Chem.* 1257 (1993)
183. A A Kicha, A I Kalinovsky, V A Stonik *Izv. Akad. Nauk, Ser. Khim.* 1164 (1995) [a]
184. A A Kicha, A I Kalinovsky, V A Stonik *Khim. Prirod. Soedin.* 257 (1993) b
185. A A Kicha, A I Kalinovsky, N V Ivanchina, V A Stonik *Izv. Akad. Nauk, Ser. Khim.* 980 (1993) [a]
186. A A Kicha, A I Kalinovsky, N V Ivanchina, V A Stonik *J. Nat. Prod.* **62** 279 (1999)
187. I I Kapustina, A I Kalinovsky, S G Polonik, V A Stonik *Khim. Prirod. Soedin.* 250 (1987) [b]
188. A A Kicha, A I Kalinovsky *Khim. Prirod. Soedin.* 619 (1993) [b]
189. A Casapullo, E Finamore, L Minale, F Zollo, J B Carre, C Debitus, D Laurent, A Folgore, F Galdiero *J. Nat. Prod.* **56** 105 (1993)
190. I Kitagawa, M Kobayashi, Y Okamoto, M Yoshikawa, Y Hamamoto *Chem. Pharm. Bull.* **35** 5036 (1987)
191. M Kobayashi, Y Okamoto, I Kitagawa *Chem. Pharm. Bull.* **39** 2867 (1991)
192. A Espada, C Jiménez, J Rodriguez, P Crews, R Riguera *Tetrahedron* **48** 8685 (1992)
193. H Hirota, S Takayama, S Miyashiro, Y Ozaki, S Ikegami *Tetrahedron Lett.* **31** 3321 (1990)
194. S Carmely, M Roll, Y Loya, Y Kashman *J. Nat. Prod.* **52** 167 (1989)
195. M V D'Auria, L G Paloma, L Minale, R Riccio, C Debitus *Tetrahedron* **48** 491 (1992)
196. N K Gulavita, E W Wright, M Kelly-Borges, R E Longley, D Yardwood, M A Sills *Tetrahedron Lett.* **35** 4299 (1994)
197. A S Antonov, A I Kalinovsky, V A Stonik, E V Evtushenko, G B Elyakov *Izv. Akad. Nauk, Ser. Khim.* 1265 (1994) [a]
198. A S Antonov, A I Kalinovsky, V A Stonik *Tetrahedron Lett.* **39** 3807 (1998)
199. B K S Yeung, M T Homann, P J Scheuer, M Kelly-Borges *Tetrahedron* **50**12593 (1994)
200. M Kobayashi, F Kanda, S R Damarla, D V Rao, C B Rao *Chem. Pharm. Bull.* **38** 2400 (1990)
201. A S R Anjaneyulu, K S Sagar, C V S Prakash *Indian J. Chem.* **35B** 819 (1996)
202. V Anjaneyulu, K N Rao, P Radhika, M Kobayashi *Indian J. Chem.* **35B** 757 (1996)
203. Y Kashman, D Green, C Garcia, D Garcia Arevalos *J. Nat. Prod.* **54** 1651 (1991)
204. O M Cobar, A D Rodriguez, O L Padilla *J. Nat. Prod.* **60** 1186 (1997)
205. P Kittakoop, R Suttisri, C Chaichantipyuth, S Vethchagarun, K Suwanborirux *J. Nat. Prod.* **62** 318 (1999)
206. K Tachibana, M Sakaitani, K Nakanishi *Science* **226** 703 (1984)
207. K Tachibana, M Sakaitani, K Nakanishi *Tetrahedron* **41** 1027 (1985)
208. K Tachibana, S H Gruber *Toxicon* **26** 839 (1988)
209. G R Pettit, M Inoue, Y Kamano, D L Herald, C Arm, C Defresne, N D Christie, J M Schmidt, D L Doubek, T S Krupa *J. Am. Chem. Soc.* **110** 2006 (1988)
210. G R Pettit, M Inoue, Y Kamano, C Dufresne, N Christie, M L Niven, D L Herald *J. Chem. Soc. Chem. Commun.* 865 (1988)
211. G R Pettit, J-P Xu, Y Ichihara, M D Williams, M R Boyd *Can. J. Chem.* **72** 2260 (1994)
212. G R Pettit, Y Kamano, M Inoue, C Dufresne, M R Boyd, C L Herald, J M Schmidt, D L Doubek, N D Christie *J. Org. Chem.* **57** 429 (1992)
213. G R Pettit, Y Ichihara, J Xu, M R Boyd, M D Williams *Bioorg. Med. Chem. Lett.* **4** 1507 (1994)
214. G R Pettit, J P Xu, M D Williams, N D Christie, D L Doubek, J M Schmidt, M R Boyd *J. Nat. Prod.* **57** 52 (1994)
215. G R Pettit, R Tan, J Xu, Y Ichihara, M D Williams, M R Boyd *J. Nat. Prod.* **61** 955 (1998)
216. S Fukuzawa, S Matsunaga, N Fusetani *J. Org. Chem.* **59** 6164 (1994)
217. S Fukuzawa, S Matsunaga, N Fusetani *J. Org. Chem.* **60** 608 (1995)
218. S Fukuzawa, S Matsunaga, N Fusetani *Tetrahedron* **51** 6707 (1995)
219. S Fukuzawa, S Matsunaga, N Fusetani *J. Org. Chem.* **62** 4484 (1997)
220. T G LaCour, C Guo, S Bhandaru, M R Boyd, P L Fuchs *J. Am. Chem. Soc.* **120** 692 (1998)
221. S L Wehrli, K S Moore, H Roder, S Durell, M Zasloff *Steroids* **58** 370 (1993)
222. K S Moore, S Wehrli, H Roder, M Rogers, J N Forrest Jr, D McCrimmon, M Zasloff *Proc. Natl. Acad. Sci. USA* **90** 1354 (1993)
223. R M Moriarty, L A Enache, W A Kinney, C S Allen, J W Canary, S M Tuladhar, G Liang *Tetrahedron Lett.* **36** 5139 (1995)
224. M N Rao, A E Shinnar, L A Noecker, T L Chao, B Feibuch, B Snyder, I Sharkansky, A Sarkahian, X Zhang, S R Jones, W A Kinney, M Zasloff *J. Nat. Prod.* **63** 631 (2000)
225. J Jurek, P Scheuer, M Kellyborges *J. Nat. Prod.* **57** 1004 (1994)
226. R M Rosser, D J Faulkner *J. Org. Chem.* **49** 5157 (1984)
227. S De Marino, F Zollo, M Iorizzi, C Debitus *Tetrahedron Lett.* **39** 7611 (1998)
228. J Rodriguez, L Nuñez, S Peixinho, C Jiménez *Tetrahedron Lett.* **38** 1833 (1997)
229. H L Holland, S Kumaresan, L Tan, V C O Njar *J. Chem. Soc., Perkin Trans. 1* 585 (1992)
230. F De Riccardis, M Iorizzi, L Minale, R Riccio, C Debitus *Tetrahedron Lett.* **33** 1097 (1992)
231. D B Gerenstein *Prog. Nucl. Magn. Reson. Spectrosc.* **16** 1 (1983)
232. M Kobayashi, K Kawazoe, T Katori, I Kitagawa *Chem. Pharm. Bull.* **40** 1773 (1992)
233. Y Inouye, Y Sugo, T Kusumi, N Fusetani *Chem. Lett.* 419 (1994)
234. M V D'Auria, C Giannini, A Zampella, L Minale, C Debitus, C Roussakis *J. Org. Chem.* **63** 7382 (1998)
235. C Giannini, A Zampella, C Debitus, J-L Menou, C Roussakis, M V D'Auria *Tetrahedron* **55** 13749 (1999)
236. T Amagata, K Minoura, A Numata *Tetrahedron Lett.* **39** 3773 (1998)
237. T Amagata, M Doi, T Ohta, K Minoura, A Numata *J. Chem. Soc., Perkin Trans. 1* 3585 (1998)

238. A Guerriero, M D'Ambrosio, H Zibrowius, F Pietra *Helv. Chim. Acta* **79** 982 (1996)
239. M Fujita, Y Nakao, S Matsunaga, M Seiki, Y.Itoh, R W M van Soest, M Heubes, D J Faulkner, N Fusetani *Tetrahedron* **57** 3885 (2001)
240. A Qureshi, D J Faulkner *Tetrahedron* **55** 8323 (1999)
241. S De Marino, M Iorizzi, F Zollo, C D Amsler, S P Greer, J B McClintock *Eur. J. Org. Chem.* 4093 (2000)
242. M Sandvoss, L H Pham, K Levson, A Preiss, C Mügge, G Wünsch *Eur. J. Org. Chem.* 1253 (2000)
243. H S Lee, Y See, K W Cho, J R Rho, J Shin, V J Paul *J. Nat. Prod.* **63** 915 (2000)
244. F Cafieri, E Fattorusso, O Taglialatela-Scafati *Eur. J. Org. Chem.* 231 (1999)
245. G Ryu, B W.Choi, B H Lee, K-H Hwang, U C Lee, D S Jeong, N H Lee *Tetrahedron* **55** 13 171 (1999)
246. M Iwashima, K Nara, K Iguchi *Steroids* **65** 130 (2000)
247. H Dong, Y L Gou, R M Kini, H X Xu, S X Chen, S L M Teo, P P H But *Chem. Pharm. Bull.* **48** 1087 (2000)
248. J A Dale, H S Mosher *J. Am. Chem. Soc.* **95** 512 (1973)
249. D H R Barton, R H Hesse, M M Pechet, E J Rizzardo *J. Am. Chem. Soc.* **95** 2748 (1973)
250. G Della Sala, I Izzo, F De Riccardis, G Sodano *Tetrahedron Lett.* **39** 4741 (1998)
251. M De Filippo, I Izzo, S Raimondi, G Sodano *Tetrahedron Lett.* **42** 1575 (2001)
252. F De Riccardis, A Spinella, I Izzo, A Giordano, G Sodano *Tetrahedron Lett.* **36** 4303 (1995)
253. M E Jung, T W Johnson *Tetrahedron* **57** 1449 (2001)
254. Y Kaji, T Kaomi, A Nakamura, Y Fujimoto *Chem. Pharm. Bull.* **48** 1480 (2000)

[a] — *Russ. Chem. Bull. (Engl. Transl.)*
[b] — *Chem. Nat. Compd. (Engl. Transl.)*

Russian Chemical Reviews **70** (9) 717 – 734 (2001) © 2001 Russian Academy of Sciences and Turpion Ltd

DOI 10.1070/RC2001v070n09ABEH000675

Superconducting MgB_2 and related compounds: synthesis, properties and electronic structure

A L Ivanovskii

Contents

I.	Introduction	717
II.	Magnesium borides: a brief history of investigations (1895 – 2000)	718
III.	Magnesium diboride, a medium-T_c superconductor	720
IV.	Conclusion	730

Abstract. The discovery of superconductivity in magnesium diboride ($T_c \approx 40$ K), announced in January 2001, stimulated intensive research into the nature of superconductivity and electrophysical, magnetic and thermodynamic properties and spectroscopic characteristics of MgB_2 and related compounds. The review concerns methods for the synthesis of new MgB_2-based superconductors with more complex chemical composition. Particular emphasis is placed on the results of investigations on the electronic structure and peculiarities of chemical bonding in these compounds. Materials science aspects of practical utilisation of materials based on the new superconductor are analysed. Main results of theoretical and experimental studies in the above-mentioned fields are generalised. The bibliography includes 228 references.

I. Introduction

In his lecture at the International Symposium on Transition Metal Oxides (Sendai, South Korea, 2001) J Akimitsu announced [1] the discovery of superconductivity in MgB_2 (for more detailed information, see Ref. 2). Magnesium diboride is a relatively poorly studied representative of a broad class of metal borides.[3–14] The discovery of superconductivity in MgB_2 has immediately attracted considerable interest in this system. The transition temperature for MgB_2 ($T_c \approx 40$ K) is almost twice as high as the values of T_c for all other binary superconductors, *e.g.*, compounds and alloys with B1- (NbN, $T_c \approx 17.3$ K) or A15-type (Nb_3Ge, $T_c \approx 23$K) structures.[15,16] From the viewpoint of its properties, magnesium diboride stands apart from all known borides. For instance, the values of T_c for binary *d*-metal borides,[9,17] as well as for ternary ($LnRuB_2$, $LnRh_4B_4$) and pseudoternary $[(Ln_{1-x}Ln'_y)Rh_4B_4]$ borides [18] lie between $\leqslant 0.5$ and 8 K. The highest transition temperatures ($T_c \approx 16-23$ K) were found for intermetallic borocarbides (IBC), namely, layered quaternary compounds of the $LuNi_2B_2C$ type [19–21] belonging to 'conventional' superconductors.[22]

A distinctive feature of magnesium diboride is that the value of T_c for this compound is 'intermediate' between those of classical low-temperature (LTSC) and high-temperature superconductors (HTSC). To emphasise this feature, MgB_2 is sometimes called a medium-T_c superconductor. It is of great importance that, unlike high-temperature superconducting complex oxides, MgB_2 is a non-oxygen compound with very simple chemical composition and structure.[3–8]

The discovery of superconductivity in MgB_2 has raised a number of questions.

1. What is the nature of the superconductivity in MgB_2?
2. Is magnesium diboride a unique compound of this kind or is it the first representative of a new class of superconductors?
3. What physical and chemical properties should related superconductors possess?

Answers to these questions can predetermine a breakthrough in understanding the nature of the superconductivity in crystals and physical chemistry of inorganic compounds and in outlining possible application areas of new superconductors.

In spite of short time that has elapsed since the discovery of superconductivity in MgB_2, experimentalists and theoreticians have accumulated a great body of information about its properties.

New superconductors have been found and superconducting materials based on MgB_2 were obtained in the form of powders, single crystals, films, wires and composites. It was found that the superconductivity parameters of MgB_2 remain stable in magnetic fields and upon neutron irradiation. Magnesium diboride is characterised by high critical transport currents and, at the same time, by their low sensitivity to grain boundary contacts. These and some other properties of this novel superconductor seem to be rather attractive for its practical utilisation.

The main goal of this review is to generalise a considerable body of information about magnesium diboride, its functional properties and possible application areas accumulated to date. Taking into account a great deal of interest in MgB_2, we have briefly outlined the history of investigations of the system Mg – B and reported the available data on the properties of magnesium borides. Particular emphasis is placed on the results of recent studies on the nature of the superconductivity in and physicochemical properties of MgB_2 (including the year 2001). The review concerns the results of both theoretical modelling and experimental research into the electronic structure and the nature of chemical bonding in magnesium diboride and related compounds. Problems associated with search for new superconductors based on MgB_2 and some materials science aspects are also outlined.

A L Ivanovskii Institute of Solid State Chemistry, Urals Branch of the Russian Academy of Sciences, ul. Pervomaiskaya 91, 620219 Ekaterinburg, Russian Federation. Fax (7-343) 274 44 95. Tel. (7-343) 274 53 31. E-mail: ivanovskii@ihim.uran.ru

Received 19 April 2001
Uspekhi Khimii **70** (9) 811 – 829 (2001); translated by A M Raevsky

II. Magnesium borides: a brief history of investigations (1895–2000)

Magnesium borides were first obtained by Moissan in 1895.[23] Analysis of products of the interaction between metallic magnesium and boric anhydride revealed two magnesium borides with strongly different chemical stabilities. One of the borides was found to decompose in acids to give boranes, mostly B_4H_{10}. More recently, this boride, with the chemical composition Mg_3B_2,[24–28] was studied[24] for use as starting material in the synthesis of boranes. The assumption of the existence of the second boride, Mg_2B_4 (MgB_2), was proposed[29] based on the results of analysis of boride hydrolysis products.

Studies carried out by researchers from the USSR[3,8] and other countries[4–7] over a period of two decades, from 1950s to 1970s, serve as a basis for present-day knowledge of the system Mg–B. Magnesium borides can be obtained by (i) reduction of B_2O_3 with metallic magnesium,[23] (ii) direct interaction of elemental Mg and B, (iii) reduction of MgO with boron, (iv) reduction of Na_2BF_6 with magnesium and (v) by reactions between Mg and BCl_3 and between MgO and boron carbide.[3,8] Pioneering studies on the phase equilibria in the system Mg–B and physicochemical properties of particular magnesium borides also date back to the above-mentioned two decades.

1. Phase relations in Mg–B system

No detailed phase diagram of the system Mg–B is available. Information about stable magnesium borides is contradictory (see, *e.g.*, Refs 3–13, 30). On the one hand, the occurrence of four phases (MgB_2, MgB_4, MgB_6 and MgB_{12}) is assumed.[30] On the other hand, the assumption of the occurrence of the lowest magnesium boride, Mg_3B_2, was rejected.[31] Six magnesium boride phases (MgB_2, MgB_4, MgB_6, a variable composition phase MgB_6–MgB_{17} and two phases of unknown composition) have also been reported.[32] The following phases were found in the phase diagram of the system Mg–B reported in monograph[33]: MgB_2, MgB_4 and MgB_7 (Fig. 1). Below we will consider only those magnesium borides for which reliable structural information is available.

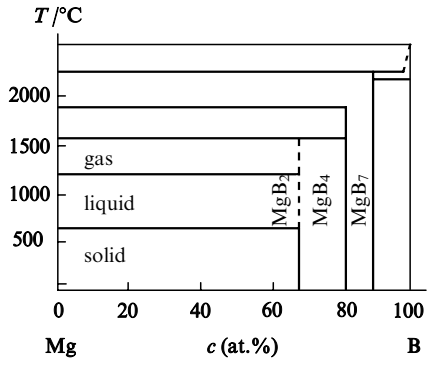

Figure 1. Phase diagram for the Mg–B system.[33]

2. Crystal chemistry of magnesium borides

Pioneering studies on the crystal structure of MgB_2 date back to the early 1950s.[34–40] Magnesium diboride has a hexagonal AlB_2-type structure. The space group is $P6/mmm$ (D^1_{6h}), the number of formula units in the unit cell $Z = 1$. Boron atoms occupy positions at the centres of trigonal prisms while magnesium atoms occupy positions at their vertices. Such prisms share all faces, thus forming a three-dimensional packing. The structure of MgB_2 can be represented as alternating planar hexagonal Mg layers and graphite-like (honeycomb) boron sheets (Fig. 2). The alternation pattern is Mg–B_2–Mg–B_2... The coordination number (CN)

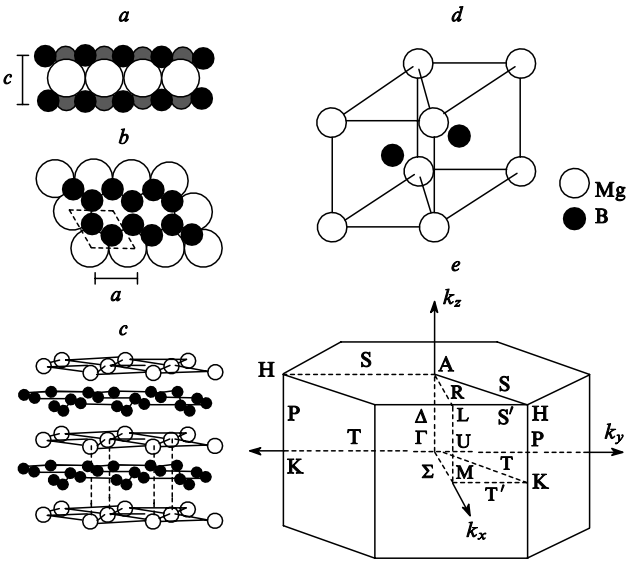

Figure 2. Structure of MgB_2.
Types of atomic packing: interlayer packing, side view (*a*); in-plane packing, top view (*b*); packing of atomic layers, side view (*c*); primitive unit cell (*d*) and the Brillouin zone (*e*).

of magnesium atoms is 20 and their coordination polyhedron (CP) is [$MgB_{12}Mg_8$]. For boron atoms, CN = 9 and the CP is [BMg_6B_3]. The atomic positions in the unit cell are as follows: Mg, 1*a* (0,0,0) and B, 2*d* (1/3, 2/3, 1/2) and (2/3, 1/3, 1/2). The lattice constants are $a = 3.0834$ and $c = 3.5213$ Å; $c/a = 1.142$. The interatomic distances are B–B ($a/\sqrt{3}$) = 1.780, B–Mg ($\sqrt{a^2/3 + c^2/4}$) = 2.503, Mg–Mg (in-plane) = 3.083 and Mg–Mg (interlayer) = 3.520 Å.[10,38–40]

Currently, more than a hundred of binary compounds with the AlB_2-type structure are known, including diborides of *p*- and *d*-elements.[3–13,38–40] Nevertheless, the problem of the existence of general physical or chemical criteria determining the conditions for the formation of structural types of various borides remains a moot question as yet. From the standpoint of crystal chemistry,[10] structural types of borides can be explained taking into account the ratio of atomic radii (r) of the components M/B (M is metal). According to the theory of symmetry of close crystal packings of spheres, an 'ideal' value of r_M/r_B for trigonal prismatic coordination is 1.89. For stable hexagonal MB_2 phases, the ratio r_M/r_B varies from 1.14 to 2.06[38] (*e.g.*, $r_M/r_B = 1.571$ for aluminium diboride and 1.758 for magnesium diboride).

Pearson[40] proposed an empirical criterion for the existence of AlB_2-type structures, namely, a correlation between structural parameters (c/a) of stable phases and the ratio r_M/r_X (here, X is an element whose atoms can form graphite-like sheets; in addition to boron, the set X can include Be, Si, Ga, Hg, Zn, Cd, Al, Cu, Ag and Au, see Refs 38–40). The ratio c/a varies from 0.59 to 1.2 (Fig. 3). As can be seen, the point corresponding to MgB_2 ($c/a = 1.142$) is located near the upper critical bound of structural stability. According to Pearson,[40] the occurrence of hexagonal CaB_2, which is the closest analogue of superconducting MgB_2 (see below), is impossible.

Magnesium tetraboride was first synthesised in 1953.[35] The crystal structure and properties of this compound have been studied in detail.[31,41–43] Crystals of MgB_4 belong to orthorhombic system (the space group $Pnam$, $Z = 4$) and are characterised by the unit call parameters $a = 5.464$, $b = 7.472$ and $c = 4.428$ Å.[42,43] The structural motif can be represented as pentagonal pyramids built of boron atoms, which form extended chains. Magnesium atoms occupy positions between boron polyhedra. The shortest distances are Mg–B = 2.392 and Mg–Mg = 3.075 Å. The atomic positions in the unit cell are as follows: Mg, 4*c*: x, y, 1/4 ($x = 0.051$, $y = 0.136$); $B_{1,2}$, 4*c*:

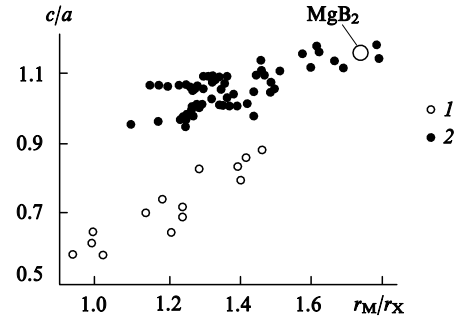

Figure 3. Dependence of the ratio of lattice parameters (c/a) on the ratio of atomic radii (r_M/r_X) for AlB_2-type binary phases MX_2;[40] c/a: <0.9 (*1*) and >0.95 (*2*).

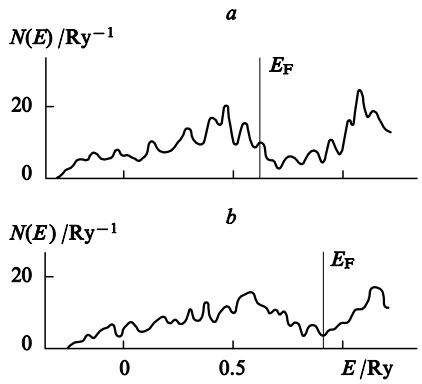

Figure 4. Total densities of states for MgB_2 (*a*) and AlB_2 (*b*) obtained from FLMTO calculations.[49]

($x_1 = 0.725$, $y_1 = 0.657$; $x_2 = 0.559$, $y_2 = 0.854$) and B_3, 8*d*: x, y, z ($x = 0.130$, $y = 0.434$, $z = 0.442$).[10] This structural type is unique in its kind since most of binary metal tetraborides [5–9, 12, 13] belong to the CrB_4 and ThB_4 structural types.

The existence of magnesium hexaboride, MgB_6, also remains a moot question as yet. It is thought that such a hexaboride represents a mixture of magnesium heptaboride MgB_7 and magnesium tetraboride MgB_4 while MgB_9 represents a mixture of MgB_7 and elemental boron.[44] The structure of magnesium heptaboride MgB_7 (Mg_2B_{14}) is characterised by a CN of 28 for the magnesium atom.[45] Similar structural elements are also inherent in $MgAlB_{14}$ ($Mg_{1-x}Al_{1+y}B_{14}$), $LiAlB_{14}$ and NaB_{15}.[10] On the other hand, MgB_7 and Mg_2B_{14} were described as individual phases with different lattice constants.[13]

3. Magnesium borides: properties, electronic structure and chemical bonding

Information about physicochemical properties of magnesium borides is scarce.[3, 8, 9, 11, 13] Only hydrolytic stability of magnesium borides and their reactions with acids have been studied in detail. It was found that boranes are formed only in the reactions with MgB_2. From the viewpoint of its reactivity and solubility in acids, this compound differs strongly from both higher magnesium borides and most of *d*-metal diborides which possess high chemical stability. Some thermochemical and thermal properties of MgB_2 (heat capacity, enthalpy, entropy and dissociation pressure, heats of formation) have been reported.[8, 9, 13]

To our knowledge, no studies on the electronic structure and the nature of chemical bonding in magnesium borides, except for MgB_2 and 'MgB_6', have been carried out so far. By analogy with other metal–boron systems, it can only be assumed that covalent B—B bonds (within boron polyhedra) should have increased importance in the overall system of interatomic interactions responsible for improvement of thermomechanical properties and chemical stability of magnesium borides on going from lower borides to higher (from MgB_2 to 'MgB_{12}').

The energy band structure of MgB_2 was studied [46–48] by the semiempirical LCAO,[47] tight binding [48] and non-self-consistent orthogonalised plane wave (OPW) methods.[46] The structures of the valence bands of MgB_2 and graphite were found to be similar.[46] The major contribution to the valence band of magnesium diboride comes from the combination of boron $p_{\sigma,\pi}$-orbitals.[47] Charge transfer occurs from Mg to B. The position of the bottom of the conduction band is determined by B boron p_π-orbitals. Comparison of the energy band structure for MgB_2 and the hypothetical crystal $\square B_2$ with 'empty' cation sublattice allowed one to draw a qualitative conclusion about the dominating role of B—B interactions in the overall system of chemical bonds.

The energy band structure as well as the chemical bonding and energy parameters of MgB_2 obtained from the first nonempirical calculations carried out by the self-consistent full-potential linear muffin-tin orbital (FLMTO) method [49] were analysed and compared with the corresponding characteristics of isostructural borides (AlB_2 and TiB_2). Among the known diborides MB_2, titanium diboride exhibits exceptionally high thermomechanical and strength properties.[7–9] The total densities of states (DOS) for MgB_2 and AlB_2 are shown in Fig. 4. The energy band structure consists of two broad bands separated by a DOS minimum (a pseudogap). A qualitative explanation for differences between the properties of MgB_2 and AlB_2 was obtained [49] in the framework of the rigid band model (RBM) [50–52] based on the structure of the valence band. According to this model, both chemical stability and thermomechanical properties of MB_2 are related to the parameter

$$V = \frac{V_b}{V_v},$$

where V_b is the width of the filled band of electron states and V_v is the total width of the valence band (up to the DOS minimum). An optimum stability corresponds to $V = 1$ (*i.e.*, all bonding bands are filled while all antibonding bands are empty). This condition holds for such *d*-metal diborides as TiB_2, ZrB_2 and HfB_2 [the valence electron concentration, VEC, is 3.33 e per atom per formula unit (see Refs 50–57)]. For MgB_2 (VEC = 2.67),[49] the calculated values are $V_v = 1.011$, $V_b = 0.912$ Ry, $V = 0.902$. For AlB_2 (VEC = 3.0 e per atom), $V_b = V_v = 1.146$ Ry, $V = 1.0$, which means that this diboride should exhibit the highest stability.

Analysis of chemical bonding in MgB_2, AlB_2 and TiB_2 using charge density maps (Fig. 5) shows that the overlap of the B—B wave functions in the plane of graphite-like sheets decreases from MgB_2 to TiB_2.[49] For TiB_2, the most pronounced is the effect of interlayer Ti—B covalent bonds, while MgB_2 is characterised by retention of spherical symmetry of the cation charge density contours. The cohesive energies (E_{coh}),† and the energies of particular (B—B, M—B and M—M) bonds were calculated (Table 1). As can be seen, the major contribution to the cohesive

† As is known, E_{coh} describes the overall effect of chemical bonding in crystals.

Table 1. Cohesive energies (E_{coh}) and energies of particular bonds (E_b) for magnesium, aluminium and titanium diboride /Ry per unit cell.[49]

Parameter	MgB_2	AlB_2	TiB_2
E_{coh}	1.26	1.42	1.58
E_b (see[a])			
M—M	0.11	0.28	0.36
B—B	0.86	0.83	0.86
M—B	0.29	0.24	0.36

[a] For calculation procedure, see Refs 53–57.

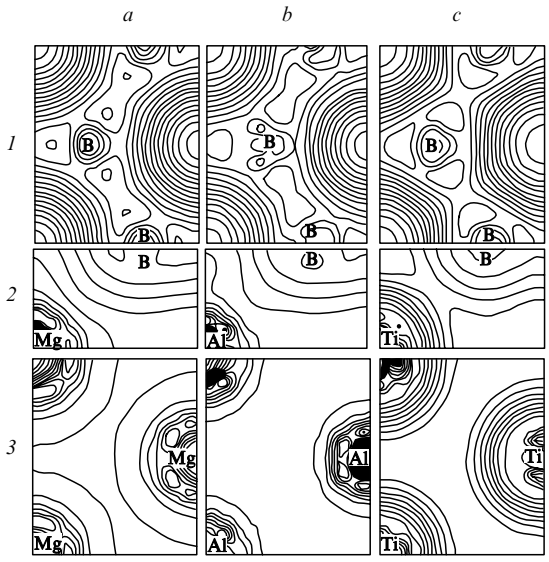

Figure 5. Charge density distributions for magnesium (*a*), aluminium (*b*) and titanium diboride (*c*): in-plane for boron sheets (*1*), in-plane for metal atom layers (*3*) and between boron sheets and metal layers (*2*).[49]

energies of MgB_2 comes from the B – B-interaction (68%). The contributions of other types of chemical bonds are much smaller (23% for B – Mg and 9% for Mg – Mg bonds). An increase in the cohesive energy on going from MgB_2 to AlB_2 is due to strengthening of the M – M bonds while the B – B and M – B binding energies vary only slightly. This is the main distinction between these compounds and *d*-metal diborides for which the value of E_{coh} depends first of all on the 'interlayer' M – B interactions.[53–57]

4. Application areas of magnesium borides

Information about application areas of magnesium borides concerns mainly MgB_2. The most attractive properties of this compound are its mechanical characteristics and high reactivity.

Magnesium diboride is used as an abrasive; polycrystalline composites based on MgB_2 and boron nitride were proposed to be used as materials for cutting devices.[13] As mentioned above, magnesium boride was used as starting material to obtain boranes following the hydrolytic decomposition reaction of the boride. Currently, the role of MgB_2 (i) as precursor in reactions of fast chemical exchange in the synthesis of refractory *d*-metal borides and ceramics based on them and (ii) in the preparation of close-packed boron nitride polymorphs has been studied intensively.

The known methods for the preparation of cubic boron nitride (c-BN), a material with record hardness, are based on heat treatment of hexagonal BN (h-BN) under pressure or precipitation from melts. Crystallisation and nucleation of c-BN are strongly affected by various catalysts, *e.g.*, C, B, Fe, Co, Ni, Cu, Al, their alloys and mixtures, as well as metal nitrides, oxides and borides.[58,59] Magnesium diboride is an efficient catalyst of spontaneous crystallisation of c-BN.[13,60–68] Studies of c-BN nucleation from melts in the system MgB_2 – BN at pressures up to 6.8 GPa and temperature up to 2000 K allowed one to determine the threshold pressure ($P \approx 4.5$ GPa) for the lower temperature bound of the c-BN phase formation ($T \approx 1630$ K).[67] The role of small additives of the third component (P, Si) on the crystallisation kinetics of c-BN in pseudoternary systems MgB_2 – BN – P (see Ref. 65) and MgB_2 – BN – Si[63,64] has been studied.

Magnesium diboride and higher magnesium borides occur among reaction products if refractory *d*-metal borides are obtained by reduction of corresponding oxides by magnesium-reduced boron

$$MO_y + B \longrightarrow MB_z + B_2O_3$$

or by magnesium reduction of such oxides

$$MO + Mg + B_2O_3 \longrightarrow MgO + MB_z.$$

At the formation temperatures of refractory borides MB_z, magnesium borides thermally decompose into boron and magnesium, the latter being removed nearly completely.[13] The procedure for preparation of dispersed ZrB_2 powders[69] is based on competitive reduction processes of ZrO_2 and boric anhydride in the system ZrO_2 – Mg – B_2O_3 (at 1100 °C) and boronation of α-Zr and Mg in the system ZrO_2 – Mg – amorphous boron (at 700 °C) followed by removal of MgO and MgB_2. A thermal reaction in the system TiO_2 – Mg – B_2O_3 in Ar atmosphere results in titanium diboride as the major product and magnesium oxide and magnesium borate ($Mg_3B_2O_6$) as side products.[70] Metal borides, solid solutions based on them and boride ceramics can also be synthesised by solid-state reactions of fast chemical exchange with participation of MgB_2.[71–73] A mechanochemical reaction in a Ti – 4% MgB_2 mixture, resulting in a nanocrystalline Ti matrix with inclusion of MgB_2 grains of size 20 to 300 nm has been studied.[74] Subsequent sintering of the reaction product at 600 °C resulted in a new compound with NiAs-type structure and unknown composition.

Along with TiB_2, B_4C, CrB_2, BN and amorphous boron, MgB_2 was announced to be an antioxidant, *i.e.*, an additive to carbon-containing refractory materials used in metallurgy to prevent them from breakdown upon oxidation of carbon in the surface layer.[75] Oxidation and phase formation in the mixture of MgB_2 synthesised in the reaction $MgB_{12} + Mg \rightarrow MgB_2$ with periclase – carbon composite have been studied as functions of temperature.[75] The process is characterised by exothermic effects, begins at ~470 °C and results in MgO, $Mg_2B_2O_5$ and boric anhydride. Similar magnesium polyborides (mixtures of amorphous boron and MgB_{12} obtained by magnesium reduction of B_2O_3) were found to behave similarly. According to DTA, the mass increased by 43%. Amorphous boron of purity 95% to 98% exhibited the best antioxidant properties; in this case, a mass increase of 124% to 147%.

The results of applied research on the use of MgB_2 as a catalyst in the synthesis of c-BN,[76] as antioxidant additive to refractory materials[77–79] and for production of dispersed alloys[80] and SiC powders (see Ref. 81) were patented.

Prospects for practical utilisation of superconducting MgB_2 will be considered below.

III. Magnesium diboride, a medium-T_c superconductor

The discovery[1,2] of superconductivity in MgB_2 and publication of pioneering studies,[82–87] in which the nature of the effect was rationalised in the framework of electron – phonon mechanism of superconductivity, has stimulated discussion about possible analogues of superconducting magnesium diboride. Both chemical composition and crystal structure aspects of the problem were considered and some other factors responsible for superconductivity were analysed. Chemical analogues of MgB_2, that is, binary and multicomponent borides, have been considered in the preceding Section of this review.

Considerable attention has been given to the role of quasi-two-dimensional (quasi-2D) structure of magnesium diboride. It has been generally thought that high lattice symmetry (preferably, cubic) is favourable for superconductivity. This can be exemplified by elemental superconductors (Nb, La under pressure and fullerite C_{60} with the transition temperatures of 9, 13 and 33 K, respectively), binary compounds (ZrN, NbN and Nb_3Ge with T_c of 10.7, 18 and 23 K, respectively) and a number of ternary compounds.[88–90]

Recently, a group of 2D-HTSC has been found. Oxides with CuO_2 layers in their structures can serve as the best known

example of these compounds. Quasi-2D β-nitrides ZrNCl (T_c = 15 K) and HfNCl (T_c = 25 K) also represent layered structures with alternating (Zr, Hf)–N and chlorine layers. Interlayer interactions in these compounds are weak and superconductivity is observed upon intercalation with alkali metal atoms.[91–93] A possible mechanism of superconductivity in anisotropic media taking into account the quasi-2D character of the energy bands has been discussed.[94]

Special attention has been given[87] to similarity in the atomic structure and electronic properties of MgB_2 and graphite. Both compounds are isoelectronic [the ionic formula of magnesium boride is $Mg^{2+}(B_2)^-$], have layered structures and exhibit a similar type of chemical bonding with strong in-plane σ-bonds and weak interlayer π-bonds. Moreover, electron-doped intercalated graphites (*e.g.*, LiC_8 and KC_8) are superconductors (up to T_c = 5 K).[95,96] There is also evidence[97] for substantial enhancement of superconductivity in specially treated fullerite C_{60} to $T_c \sim 52$ K (*cf.* $T_c \leqslant 33$ K for the known medium-T_c superconductors based on M_3C_{60}, where M is an alkali metal), which points to potentially significant role of intercalation.

The nature of these analogies can be understood by analysing the band structure and phonon spectrum of magnesium diboride. Before considering them, let us discuss methods for the synthesis of MgB_2.

1. Synthesis and properties of superconducting MgB_2

a. Synthesis of MgB_2

Currently, superconducting MgB_2 is mainly obtained as polycrystals by solid-phase synthesis from elemental B and Mg.[1,2,82–84,98–120] Synthetic procedures differ from one another in composition of starting materials, atmosphere, and heat treatment regimes. For instance, MgB_2 samples were synthesised[84] from magnesium flakes and sub-micron powder of amorphous boron which were pressed in pellets, placed on Ta foil and subsequently fired in a tube furnace under inert atmosphere (95% Ar + 5% H_2) at 600 (1 h), 800 (1 h) and 900 °C (1 h) and then lightly ground. The resulting powders were hot pressed (10 kbar, 650–800 °C) for periods between 1 and 5.5 h. The samples thus obtained were characterised by multiphase composition; however, they exhibited high critical currents.

Other sintering conditions are listed in Table 2. For instance, $Mg(^{11}B)_2$ was prepared[101] from a boron powder enriched with ^{11}B and Mg lumps placed in a BN crucible and heat-treated for 1.5 h in Ar atmosphere (P = 50 bar). No chemical composition of the sample obtained was reported. The superconductivity parameters were T_c = 39 K and the width of the transition ΔT_c = 0.4 K. Magnesium diboride samples were also synthesised[82] from a Mg : B = 2 : 1 mixture in a Ta tube placed in a quartz ampoule in Ar atmosphere. The mixture was heated to 950 °C and kept 2 h at this temperature. The procedure proposed by Gerashenko *et al.*[99] involved pressing of magnesium and amorphous boron into pellets which were placed in a Ta crucible and then subjected to two-step annealing in purified helium flow. At first, the pellets were annealed at 800 °C for 1 h. The resulting phase contained MgB_2 (78.6%), Mg (16.6%), MgO (4.7%) and BN (traces). Subsequent annealing at 875 °C (1 h) led to evaporation of the unreacted metallic magnesium. The final phase was composed of MgB_2 (89.9%), MgO (5.2%) and BN (1.7%) and characterised by T_c = 39.5 K and ΔT_c = 2.5 K. Thus, superconducting magnesium diboride powders can be obtained using rather simple synthetic procedures which do not require costly starting materials and equipment.

b. Physicochemical properties of superconducting MgB_2

The mechanism of superconductivity in MgB_2 was elucidated by measuring the isotope effect on $Mg(^{10}B)_2$ and $Mg(^{11}B)_2$ powders.[82] Replacement of ^{10}B by the heavier isotope, ^{11}B, led to a decrease in T_c from 40.2 to 39.2 K and to narrowing of the transition region by 0.1 K (Fig. 6). The isotope coefficient,

$$\alpha_B = -\frac{\Delta \ln T_c}{\Delta \ln M_B},$$

where M_B is the magnetisation of the boron sublattice, was found to be ~ 0.26. This is close to the α_B values for IBC,[105,106] the superconductivity of which is due to electron–phonon interaction (with high-frequency optical B A_{1g} modes) and is described in the framework of the Bardeen–Cooper–Schrieffer (BCS) model.[22]

Experiments with different samples[102,107,108] revealed rather high critical current densities (j_c) ($2 \times 10^4 - 10^5$ A cm^{-2}). It was found that the temperature dependences of the critical fields H_{c2} and H_{c1} near T_c have a slope of 0.012 T K^{-1} and that the magnetisation curves are reversible.[107,108] The H_{c2} anisotropy (1.73) was first measured[108] on aligned crystallite samples. The temperature dependence $H_{c1}(T)$ was reported to be linear for the whole temperature region in which superconductivity is observed.[109] At $T > T_c$, the temperature dependence of the resistivity has the form[110]

Table 2. Conditions for the synthesis of superconducting MgB_2 powders.

Atmosphere (sheath)	Sintering conditions		Phase composition	Lattice parameters /Å		T_c /K	Ref.
	T /°C	time /h		a	c		
92% Ar + 8% H_2 (Ta foil)	600 + 800 + 950, after compaction	2 + 2 + 1,	MgB_2 + MgO (impurity)	3.0815(6)	3.5191(7)	37	100
	950	2					
Inert atmosphere (a Ta tube placed in a quartz ampoule)	950	2	$Mg(^{10}B)_2$	3.1432 ± 0.03	3.5193 ± 0.03	40.2	82
Ar (Ta crucible)	850	2	$Mg(^{11}B)_2$	–	–	39.2	98
Inert atmosphere (a BN crucible on Ta foil placed in a quartz ampoule)	900, after compaction	4	single-phase $Mg(^{11}B)_2$	–	–	39	101
	1000	6					
Ar (a Ta tube in a quartz ampoule)	1200	1	–	–	3.518	–	102
MgB_2 (AA)[a]	500	72	MgB_2 + impurities (10^{-2} at.% Ni, Cu, W)	–	–	–	103
Ar (Nb tube)	900	1–3	–	–	–	–	104

[a] Commercially sold MgB_2 powder [Alfa Aesar Co, USA, assay (purity 98%)].

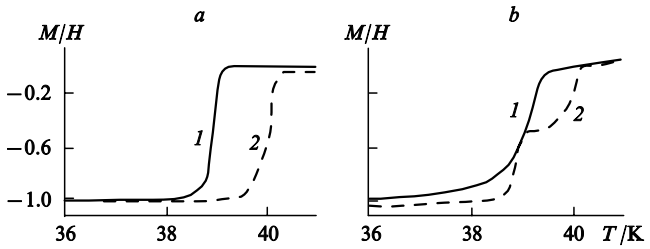

Figure 6. Isotope effect in magnesium diboride.[82]
(*a*) Magnetisation divided by magnetic field strength (M/H) as function of temperature for $Mg(^{11}B)_2$ (*1*) and $Mg(^{10}B)_2$ (*2*); (*b*) the same for $Mg(^{10}B)(^{11}B)$ (*1*) and sum of $Mg(^{11}B)_2$ and $Mg(^{10}B)_2$ data (*2*).

$$\rho(T) \approx T^2.$$

It was found that magnetic field has no effect on ρ. The Hall coefficient[111] R_H of magnesium diboride is positive (4.1×10^{-11} m^3 deg^{-1} at 100 K and a hole concentration, n, of 1.5×10^{23} cm^{-3}) and increases in the temperature range from 40 to 300 K.

An important distinction of superconducting MgB_2 from cuprate HTSC has been pointed out.[84] Due to high anisotropy, cuprate HTSC rapidly lose their performance in external fields, while the supercurrents flowing throughout even untextured, multiphase MgB_2 samples are little sensitive to weak magnetic fields. The spin–lattice relaxation rate[99,112] and the Knight shift[99] were measured by NMR spectroscopy; the behaviour of the former parameter was interpreted within the framework of *s*-wave model in the strong electron–phonon coupling limit.[112]

Magnesium diboride was also studied by the scanning tunnelling microscopy.[113–115] Particular attention was paid to the current-*vs*.-voltage characteristics used for the determination of the width of the superconducting energy gap (Δ). Large scatter of the gap widths Δ (from 5 to 7 meV, see Refs 113–115) was first of all explained by different compositions of the samples studied. The gap widths Δ were also evaluated from the tunnelling spectra of Au/MgB_2 point-contact tunnel junctions[116] (Δ = 4.3 meV) and IR reflectance spectra[117] (Δ = 4.5 meV).

The specific heat of magnesium diboride and its dependences on the magnetic field and temperature were measured,[118,119] as well as some other thermodynamic and mechanical characteristics [*e.g.*, the elasticity modulus $B_0 = 151 \pm 5$ GPa (see Ref. 120)].

The possibility of self-consistent interpretation of the results of the above-mentioned experiments in the framework of the model of electron–phonon mechanism of superconductivity in magnesium diboride[82,85–87] should be emphasised. On the other hand, Hirsch[121] proposed a 'universal' model of 'hole superconductivity' in MgB_2,[122] which implies pairing of spin carriers driven by the Coulomb interaction. However, the results obtained upon treatment of MgB_2 according to Hirsch[121] in order to increase T_c (*e.g.*, by doping with aluminium or by hydrostatic lattice compression) contradict the conclusions reported in theoretical studies based on the electron–phonon mechanism of superconductivity.

2. Electronic structure and superconductivity of MgB_2

According to McMillan,[123] the critical temperature in crystals with electron–phonon mechanism of superconductivity can be determined using the formula

$$T_c \approx \langle\omega\rangle \exp[f(\lambda)],$$

where $\langle\omega\rangle$ is the averaged phonon frequency (which is inversely proportional to the masses of the atoms), λ is the electron–phonon coupling constant [$\lambda \approx N(E_F)\langle I^2\rangle$], $N(E_F)$ is the density of states (DOS) at the Fermi level and $\langle I^2\rangle$ is the electron–ion matrix element determined by the bond ionicity. Information about the electronic structure and vibrational states of MgB_2 is of crucial importance for correct interpretation of superconductivity in and other properties of MgB_2 as well as for targeted search for new superconductors.

a. Electronic structure

The discovery of superconductivity in MgB_2 stimulated intensive theoretical[85–87,124–130] and experimental[131–133] studies of the electronic structure of magnesium diboride[85–87,124–133] and a large number of stable and metastable isostructural diborides of Li, Na,[87,125,126] Be, Ca,[124] Al,[124,126] Sc, Y, Ti, V,[124,134] Ag and Au,[127] as well as some related phases [MgB_6, CaB_6,[128] $CaSi_2$, CaSiBe,[125] $ZrBe_2$, $HfBe_2$, $CaGa_2$,[127] Mg_3BN_3 (see Ref. 129)]. Calculations were carried out using rigorous, self-consistent density functional approach.

The valence band structure of MgB_2 is determined[85–87,124–126] by the B $2p$ states which form four $\sigma(2p_{x,y})$-bands and two $\pi(2p_z)$-bands (Fig. 7). They exhibit strongly different dispersion $E(k)$. For the B $2p_{x,y}$-bands, the dispersion $E(k)$ is maximum along the $k_{x,y}$ direction (Γ–K). These bands reflect the distribution of the B states within graphite-like sheets, which have a quasi-2D type and form flat zones along the k_z direction (Γ–A). Two B $2p_{x,y}$-bands cross the Fermi level and contribute largely to the total density of states at the Fermi level [$\sim$30% (see Ref. 85)]. These bands are responsible for the metal-like properties of magnesium diboride. The Fermi level is located in the region of bonding states. Magnesium diboride exhibits hole-type conductivity, which is consistent with the results of Hall coefficient measurements.[111] Charge transfer occurs from magnesium to boron.

One of the most distinctive features[85–87,124–130] of the electronic structure of MgB_2 is the position of the B $2p_{x,y}$ energy bands. Namely, they are above the E_F at the Γ point of the

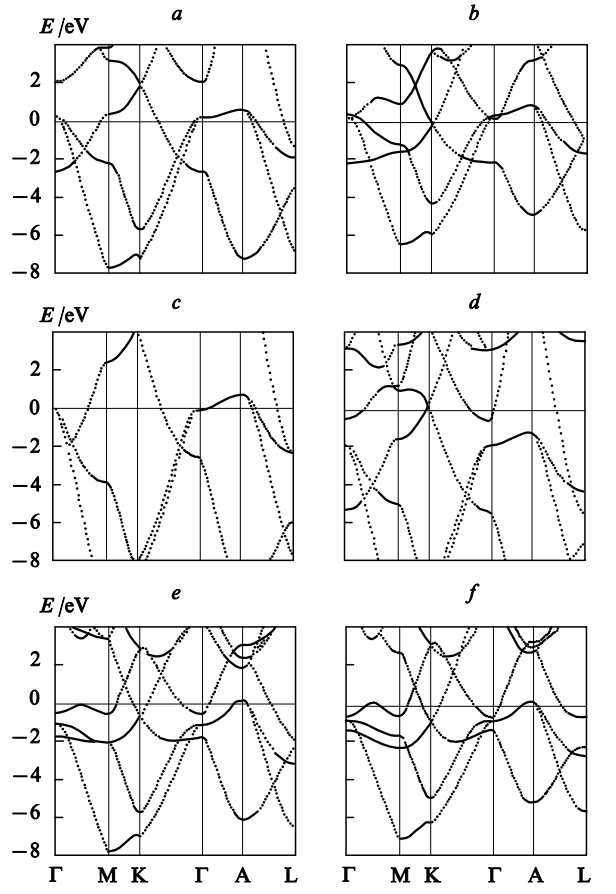

Figure 7. Energy band structures for MgB_2 (*a*), CaB_2 (*b*), BeB_2 (*c*), AlB_2 (*d*), ScB_2 (*e*) and YB_2 (*f*).[124]

Brillouin zone and form two hole-type cylinders on the Fermi surface.[85–87] The B $2p_z$-like states have a 3D-type, are oriented perpendicular to the boron sheets and are responsible for weak interlayer π bonds.[85–87, 124–126] Both π-bands cross the Fermi level and are characterised by the maximum dispersion along the k_z direction (Γ – A). The Mg *s*, *p*-states and B *s*-states are mixed with the system of B 2*p*-like bands near the valence band edge and in the conduction band. The determining role of boron in the formation of the electronic structure of MgB_2 has been particularly emphasised by Kortus *et al.*[85] who titled their communication 'Superconductivity of metallic boron in MgB_2'.

The electronic structure of magnesium diboride was studied by X-ray emission spectroscopy (XES),[131, 132] X-ray absorption spectroscopy (XAS)[131, 132] and photoemission spectroscopy (XPS).[131, 133] Comparison of the C K_α XES lines ($1s \rightarrow 2p$-transitions) for graphite and corresponding B K_α lines for MgB_2 and AlB_2 (Fig. 8) clearly demonstrates differences in positions of their emission maxima determined by the p_{xy}-states.[135] This supports the idea[85–87, 124–130] of correlation of the superconductivity in MgB_2 with the relative positions of the σ- and π-bands (the presence of hole-type σ-states). The results of XES and XAS studies[132] of the structure of B bands near the Fermi level are in excellent agreement with the results of calculations (Fig. 9). The spectra exhibit a number of resonance lines indicating the presence of a protective oxide film formed on the sample surface upon exposure to air.

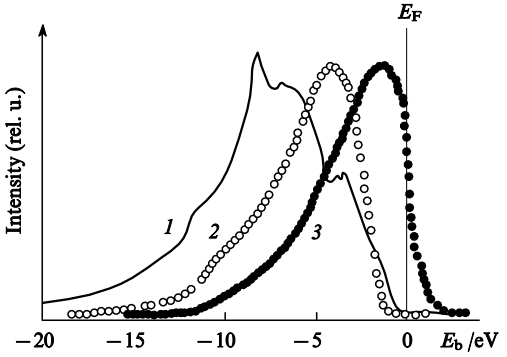

Figure 8. X-Ray emission C K_α spectra ($1s \rightarrow 2p$-transitions) for graphite (*1*) and corresponding B K_α spectra for AlB_2 (*2*) and MgB_2 (*3*).[131]

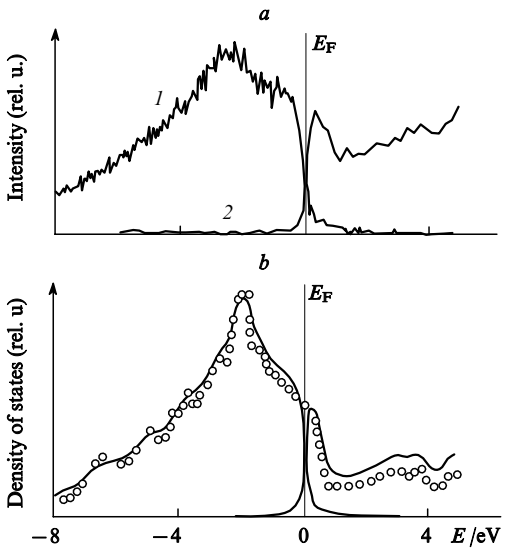

Figure 9. X-Ray emission (*1*) and absorption (*2*) spectra of boron in MgB_2 (*a*) and the DOS distribution for boron (*b*): theoretical (solid lines) and corrected for the lifetime of excited state, thermal and instrumental broadening of the experimental setup (points).[132]

High-resolution XPS studies of magnesium diboride allowed direct observation[133] of the superconducting energy gap (~4.5 meV at 15 K). This gap (~3 meV at $T = 0$ K) is of the *s*-wave character and its temperature dependence is consistent with the BCS theory.

Band structure calculations were carried out for magnesium diboride and isostructural diborides of Li, Na,[87, 126] Be, Ca,[124] Al,[124, 126] Sc, Y, Ti, V,[124, 134] Ag and Au (see Ref. 127). The band structures are compared in Figs 7 and 10. The absence of superconductivity in BeB_2 (see Ref. 136) was assumed[124] to be due to the low-energy shift of σ-bands and the absence of hole states at the Γ point, which changes the Fermi surface topology in such a manner that cylinders (along the Γ – A directions) are transformed into cones. The absence of superconductivity in AlB_2 is due to filling of σ-bands caused by the VEC increase.[83] Variations of superconducting properties for a number of *d*-metal diborides can be rationalised based on the results of calculations.[53–55, 124, 134] For ScB_2 and YB_2, the 2D-p_{xy}-bands at the A point are above the E_F (see Fig. 7), but the concentration of hole carriers is low. It is important that metal *d*-states contribute largely to $N(E_F)$. As a result, these diborides are characterised by low T_c (1.5 – 2.0 K).[9, 17] Among hexagonal transition metal diborides, the lowest T_c values should be exhibited by TiB_2, ZrB_2 and HfB_2, for which the Fermi level is located in the pseudogap.[50–55] As electron concentration increases, the *d*-band is filled and $N(E_F)$ increases[50, 52–55] (*e.g.*, for Group V and VI *d*-metal diborides). This can lead to an increase in T_c; *e.g.*, a rather high $T_c \sim 9$ K was reported for TaB_2.[137]

Analysis of the energy band structures of metastable diborides of Li, Na,[87, 126] Ca,[124] Al,[124, 126] Ag and Au (see Ref. 127) showed that the σ- and π-band configurations and band filling types

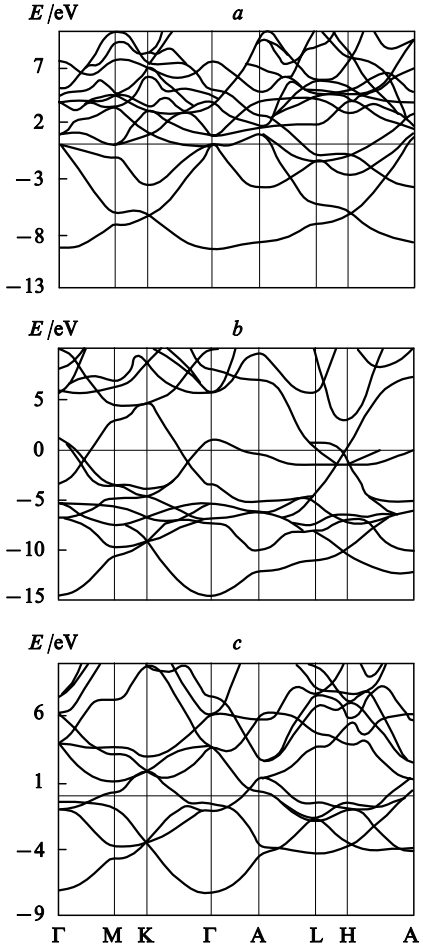

Figure 10. Energy band structures for $CaGa_2$ (*a*), AgB_2 (*b*) and $ZrBe_2$ (*c*).[127]

calculated for CaB_2 are the same as the 'optimum' parameters of superconducting MgB_2. Calcium diboride was suggested [124] to be the most probable new superconductor. Estimates [124] of the enthalpy of formation of CaB_2 (-0.12 eV per formula unit) showed the possibility of real synthesis of this compound. It is thought that calcium diboride can be stabilised by, *e.g.*, doping with isoelectronic or hole dopants (Mg, Li, Na) or by forming layered superstructures, *e.g.*, $Ca-B_2-Mg-B_2-Ca$. The electronic properties of ternary systems based on MgB_2 will be considered in the next Section of this review. Here, we will only mention that an increase in the unit cell volume will assist the formation of the electronic structure of diborides in a manner favourable for superconductivity. This can be done by, *e.g.*, isoelectronic replacement of magnesium by cations with larger atomic radii (Ca, Sr, Ba).[124]

Structural similarity between MgB_2 and hexagonal BN has been pointed out.[129] Like MgB_2, boron nitride also contains planar boron sheets while its structural stability is due to strong in-plane covalent bonds.[14, 138] The energy band structures of MgB_2 and solid solutions of composition $MgB_{2-y}N_y$, where boron was partially replaced by nitrogen, were compared.[129] Solid solutions with $y = 0.25$ and 1.00 were studied. The solution $MgB_{1.0}N_{1.0}$ (in which the composition of the non-metal sublattice formally matches the composition BN) can be considered as a model of magnesium boronitride prepared by intercalating atomic h-BN sheets with hexagonal magnesium layers. The energy band structure of the individual ternary phase Mg_3BN_3 with separated layers of different-type metalloids (B and N) was calculated.[139]

An increase in the N/B ratio in the composition of solid solutions leads to a shift of the Fermi level towards higher values, filling of antibonding states and a decrease in $N(E_F)$. The bonding B $p_{x,y}$-like bands become completely filled while the hole states are absent. According to calculations,[129] Mg_3BN_3 is a semiconductor [transition at the Γ point of the Brillouin zone, the forbidden gap (FG) width is 0.88 eV (0.065 Ry)]. The valence band structures of MgB_2 and Mg_3BN_3 are fundamentally different, *viz.*, the determining role in the mechanism of superconductivity in MgB_2 is played by the B 2*p*-bands while for Mg_3BN_3 these bands lie much below E_F and contribute negligibly to the region of the spectrum near the Fermi level.

The energy band structure of metastable cubic magnesium hexaboride (the space group *Pm*3*m*) has been studied.[140] The optimised lattice parameter corresponded to $a = 4.115$ Å. The main building blocks of the MgB_6 structure are B_6 octahedra. The energy band structure contains 10 valence bands of hybrid B 2*s*,*p*-states, which are responsible for B—B bonds both within and between B_6 octahedra. The upper filled band forms a flat zone along the $X-\Gamma$ direction and is composed of B $p_{x,y}$-orbitals involved in B—B interactions between B_6 octahedra. The first unfilled band is characterised by strong *k*-dispersion and is composed of contributions of cation states. Unlike CaB_6 (FG $\approx$ 0.0163 Ry, direct transition at the Γ point), magnesium hexaboride is a narrow-gap semiconductor with indirect transition (FG $\approx$ 0.0150 Ry, $X \rightarrow R$ transition).[10, 141–144] Despite the determining role of B—B bonds in MgB_2 and MgB_6 crystals, they possess basically different electronic properties that is, metallic for MgB_2 and semiconducting for MgB_6.

'Non-boride' AlB_2-type phases with silicon, beryllium or gallium graphite-like sheets have been reported [$CaSi_2$, CaSiBe,[125] $ZrBe_2$, $HfBe_2$, $CaGa_2$ (see Ref. 127)].

Rhombohedral $CaSi_2$ (the space group *R*3*m*) obtained under equilibrium conditions is known to be a nonsuperconducting semimetal.[145] Heat treatment of $CaSi_2$ under pressure can cause a polymorphous transformation into an AlB_2-type structure.[146] Similarity between the energy band structure of this disilicide and those of *sp*-element diborides and $CaGa_2$ (see Fig. 10)[127,146] was found.[125] The main distinctions are due to Ca *d*-orbitals which are mixed with the Si states near the bottom of the conduction band due to hybridisation. The antibonding π^*-bands are partly filled, which can be the reason for structural instability of the high-pressure phase under normal conditions. Stabilisation of hexagonal $CaSi_2$ by replacement of Si by Be was studied taking calculations of a model phase CaSiBe as an example. It was assumed [125] that (i) replacement of Si by an atom of smaller radius (*cf.* $r_{Si} = 1.34$ and $r_{Be} = 1.13$ Å) will produce 'chemical pressure', which is favourable for stabilisation of the AlB_2-type structure, and (ii) partial depletion of the π^*-band with a decrease in the electron concentration in the system will an additional stabilising factor. As was found, stabilisation of the AlB_2-type structure requires the reduction of the VEC in the system by $\sim$0.7 e.[125] The electronic properties of $HfBe_2$ and $ZrBe_2$ are fundamentally different from those of superconducting MgB_2 (see Fig. 10).

b. Electronic structure and properties of superconducting MgB_2

Some properties of MgB_2 were explained using information about its electronic structure obtained from calculations. Kortus *et al.*[85] estimated the constant λ ($\sim$1) and phonon frequencies (300–700 cm^{-1}) and calculated the T_c value within the rigid atom sphere model. Their results were found to be consistent with the experiment.[2] The *ab initio* approach was also successfully used in phonon spectrum calculations, simulation of the effect of heat treatment on superconductivity in magnesium diboride and calculations of its elasitc characteristics (see below). Calculations [134] of the electric field gradients (EFG) reflect asphericity of the electron density distribution in the vicinity of atomic nuclei and are closely related to the symmetry of their nearest environment, electronic structure and the nature of chemical bonding.

Experimental EFG values are obtained in studies of quadrupole effects in the NMR spectra of MgB_2 (see Refs 99, 112) and some other diborides.[147] Analysis of the nature and regularities of variations of the EFG depending on the energy band structure of several diborides MB_2 (M = Be, Mg, Al, Sc, Ti, V, Cr) has been reported.[134] The results are listed in Table 3. Among *sp*-metal borides, BeB_2 is characterised by the largest V_{zz} component of the EFG. For 3*d*-metal diborides, the V_{zz} component changes nonmonotonically, with a minimum for TiB_2. These changes were explained [134] based on results of band structure calculations for these phases (see Fig. 7). For boron nuclei, the EFG characterises the anisotropy of partial charge density distributions

$$V_{zz} \approx \frac{p_z - (p_x + p_y)}{2},$$

where p_z, p_x and p_y are the corresponding band populations.

Table 3. EFG components on boron nuclei in borides.

Diboride	10^{-21} V_{zz} /V m^{-2}		
	FLMTO [134]	FLAPW [148] (see [a])	experiment [147]
MgB_2	1.88	—	1.69
BeB_2	2.10	—	—
AlB_2	0.99	—	1.08
ScB_2	0.60	—	—
TiB_2	0.35	0.38	0.37
VB_2	0.38	0.39	0.43
CrB_2	0.59	0.60	0.63

[a] Full-potential linearised augmented plane wave method.

According to calculations, diborides with partially unfilled p_{xy}-bands (BeB_2, MgB_2) are characterised by the largest EFG. Additional increase in EFG for BeB_2 depends on the mutual position of the p_{xy}- and p_z-bands and is determined by an increase in the population of the latter. The increase in V_{zz} in order $TiB_2 \rightarrow VB_2 \rightarrow CrB_2$ is due to fundamentally different reasons, namely, weakening of the interlayer hybrid $p-d$ metal—boron

bonds affecting the relative position and populations of the B p_{xy}- and p_z-bands.[124] Estimation of changes in the EFG on magnesium and boron nuclei in MgB_2 with pressure (up to $P = 10$ GPa) showed that an increase in pressure has little effect on the EFG at boron nuclei, whereas the EFG at magnesium nuclei rapidly increases.[134]

c. Phonon spectrum and electron – phonon interaction

Preliminary estimation of phonon frequencies obtained from band structure calculations showed [85, 87, 149] that they were consistent with the observed T_c. The authors of pioneering studies [85, 87] reported only particular modes responsible for electron – phonon coupling. The results of phonon spectrum calculations [149–151] point to the dominating role of optical phonons in the electron – phonon interaction. Similarly to electron states of the σ-bands, these optical phonons are of quasi-2D type (along the Γ – A direction of the Brillouin zone) and correspond to the in-plane vibrational modes. An important distinction between the phonon characteristics of MgB_2 and AlB_2 (Fig. 11) consists in 'softening' of the high-frequency vibrational modes in magnesium diboride and their strong coupling ($\lambda \approx 0.75$) with electrons near the Fermi level.[150] Nonsuperconducting AlB_2 is characterised by a much smaller constant λ (0.4).[150] Inelastic neutron scattering studies [101] revealed four peaks of the generalised density of phonon states, the maximum energy of atomic oscillations was found to be higher than 90 meV. The maximum energy of acoustic phonons (36 meV) was determined from analogous experiments [98] and it was shown that optical modes are characterised by strong dispersion and form peaks at 54, 78, 89 and 97 meV. The estimate [98] of the constant λ ($\lambda \approx 0.9$) obtained using the Born – von Karman model [98] is consistent with the results of calculations by Andersen *et al.*[149]

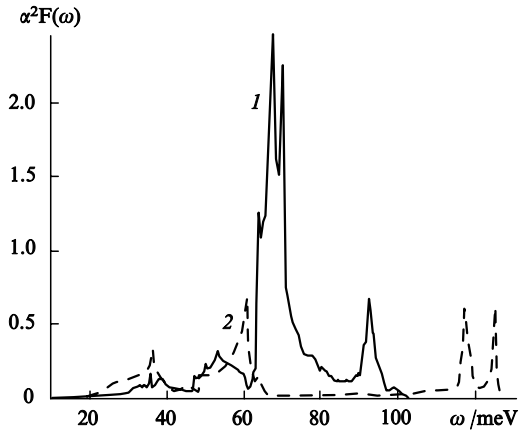

Figure 11. Eliashberg functions [$\alpha^2F(\omega)$] for MgB_2 (*1*) and AlB_2 (*2*).[150]

3. Search for new superconductors based on MgB_2 and related phases: theory and experiment

The discovery of superconductivity in MgB_2 stimulated intensive theoretical and experimental search for new related superconductors. A general trend has been to extend the variety of possible MgB_2-based superconductors by varying their chemical compositions.

a. Theoretical studies

The possibility of chemical modification of the electronic structure of 'ideal' MgB_2 by varying its chemical composition was systematically studied by the FLMTO method in the framework of supercell approach.[124, 152] The effects analysed were those produced on the band structure of MgB_2 by doping the boron sublattice with Be, C, N and O, by doping the magnesium sublattice with Be, Ca, Li, Na, Zn and Cu and by changing the diboride composition due to addition of lattice vacancies in Mg- and B-sublattices (nonstoichiometry effects). The compositions of compounds studied are listed in Table 4.

Table 4. Results of FLMTO calculations of the DOS at the Fermi level [state per (eV per formula unit)] for magnesium diboride and related binary and ternary systems.[124]

Diboride	$N(E_F)$	Diboride	$N(E_F)$
MgB_2	0.73	$Mg_{0.75}Li_{0.75}B_2$	0.73
CaB_2	0.92	$Mg_{0.50}Li_{0.50}B_2$	0.75
BeB_2	0.47	$Mg_{0.75}Na_{0.75}B_2$	0.73
$MgB_{1.75}C_{0.25}$	0.56	$Mg_{0.50}Na_{0.50}B_2$	0.76
$MgB_{1.75}$	0.61	$Mg_{0.75}Cu_{0.25}B_2$	0.89
$Mg_{0.75}B_2$	0.74	$Mg_{0.75}Be_{0.25}B_2$	0.62
		$Mg_{0.75}Zn_{0.25}B_2$	0.51

Qualitative changes in the energy band structures of solid solutions have been discussed in the framework of the RBM model.[152] It was found that dopants can act as hetero- or isoelectronic impurities which change or have no effect on the VEC in the system, respectively. According to calculations, Be impurity in the boron sublattice, Li, Na and Cu impurities in the magnesium sublattice as well as both types of lattice vacancies ('hole dopants') will, first, decrease the VEC in the system, thus leading to an increase in the concentration of hole states in the σ-band and, second, assist a shift of the E_F towards high energies with an increase in $N(E_F)$. Both these factors are favourable for superconductivity (see above). On the contrary, Al impurity in the magnesium sublattice, C, N and O impurity in the boron sublattice ('electron dopants'), will deteriorate the superconducting properties of the system due to filling of the σ-band and reduction of $N(E_F)$. In the framework of the RBM model, the role of isoelectronic replacement of Mg by Be or Ca remains unclear as yet. One can only assume that the main effects will be associated with structural factors, that is, magnesium diboride lattice distortion depending on the ratio of radii of 'host' and 'guest' elements.

Numerical calculations [124, 152] give a more complex picture (see Table 4 and Figs 12, 13). The addition of vacancies to boron sublattice ($MgB_{1.75}$) leads to a decrease in $N(E_F)$. In the series of solid solutions $MgB_{1.75}C_{0.25} < MgB_{1.75}N_{0.25} < MgB_{1.75}O_{0.25}$ the $N(E_F)$ increases nonmonotonically. This is due to the filling of antibonding states. The σ-band becomes fully occupied. It was concluded that there is no prospect for obtaining superconductivity in the system by doping the boron sublattice.[124] Based on consideration of particular binding energies (see Table 1), it was suggested that insertion of impurity into the boron sublattice is much less probable than substitution in the cation sublattice. In the latter case, the energy band structures of solid solutions $Mg_{1-x}M_xB_2$ (M = Be, Ca, Li, Na, Cu, Zn) remain essentially

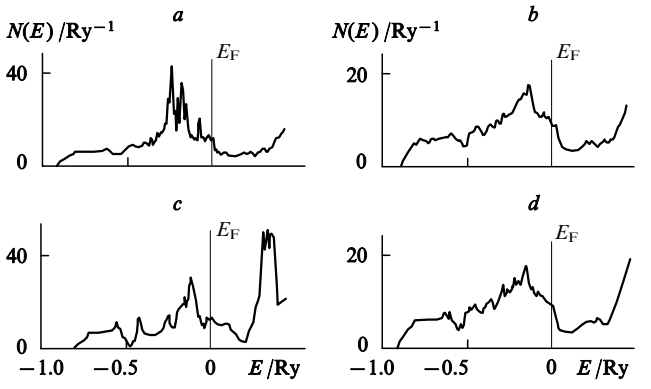

Figure 12. Total densities of states for $Mg_{0.75}Cu_{0.25}B_2$ (*a*), $Mg_{0.72}Na_{0.75}B_2$ (*b*), CaB_2 (*c*) and MgB_2 (*d*).[124]

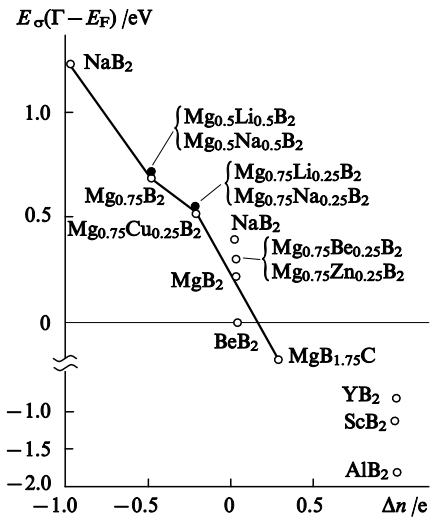

Figure 13. Dependence of the σ-band position at the Γ point of the Brillouin zone relative to the Fermi level in crystals $[E_\sigma(\Gamma - E_F)]$ on the electron concentration (relative to MgB_2, Δn) for binary diborides and ternary solid solutions based on MgB_2.[124]

similar to that of superconducting MgB_2 (see Fig. 12 and Table 4). The $N(E_F)$ value depends first of all on the impurity concentration. Hence, the main procedure for modifying the properties of magnesium diboride is to dope its cation sublattice. In addition to the VEC, electron distributions and superconductivity were also found to be dependent on the impurity concentration that affects structure peculiarities of MgB_2-based multicomponent solid solutions (first of all, the ratio between the in-plane distance and interlayer spacing).

Calculations of solid solution $Mg_{0.5}Al_{0.5}B$ [125] revealed the presence of hole states near the Z point of the Brillouin zone. It was also found that cation substitution and corresponding electron distributions cannot be completely described using the rigid band model.

Changes in the energy band structure with concentration and, in particular, the dependence of the σ-band energies on the composition of solid solutions $Mg_{1-x}Al_xB_2$ and $Mg_{1-x}Na_xB_2$ (x = 0, 1/3, 2/3, 1.0) were studied[126] using the density functional theory in the framework of supercell approach ($\sqrt{3} \times \sqrt{3}$) (Fig. 14). For $Mg_{1-x}Na_xB_2$ with any x, the top of the B p_{xy}-band at the Γ point is above E_F; in other words, the major electronic criterion for the existence of superconductivity holds. For $Mg_{1-x}Al_xB_2$, this condition is valid at $x < 0.6$. At $x > 0.6$, the hole states at the centre of the Brillouin zone disappear. The concentrations of the σ-holes (n_h /cm^{-3}) depend on the compositions of solid solutions as follows:[126]

for $Mg_{1-x}Al_xB_2$, $n_h = (0.8 + 0.8x) \times 10^{23}$,

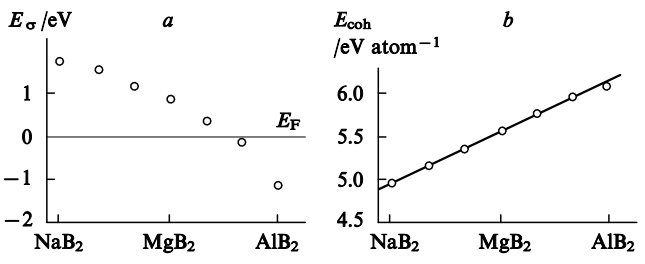

Figure 14. Changes in the σ-band position at the Γ point of the Brillouin zone (E_σ) relative to the Fermi level (*a*) and cohesive energies (*b*) in the order $NaB_2 \rightarrow Mg_{1-x}Na_xB_2 \rightarrow MgB_2 \rightarrow Mg_{1-x}Na_xB_2 \rightarrow AlB_2$.[126]

for $Mg_{1-x}Na_xB_2$, $n_h = (0.8 - 1.4x) \times 10^{23}$.

The hole concentration is a maximum ($\sim 1.6 \times 10^{22}$ cm^{-3}) for NaB_2. The cohesive energy (see Fig. 14) monotonically increases in the order $NaB_2 < Mg_{1-x}Na_xB_2 < MgB_2 < Mg_{1-x}Al_xB_2 < AlB_2$ as the corresponding bonding states in the valence band are filled.

b. Experimental studies

Theoretical studies of systems mentioned above are accompanied by experimental search [83, 136, 153–159] for new superconductors based on MgB_2 (variation of its elemental composition was mostly considered). Substitution solid solutions were synthesised using cation ($Mg_{1-x}M_xB_2$; M = Li, Be, Al, Zn, Cu) [83, 136, 153–155] and anion ($MgB_{2-y}C_y$) [156–158] sublattice substitution. Earlier,[159] only the formation of solid solutions in the MgB_2–AlB_2 system was reported.

Solid solutions were synthesised from elements in inert atmosphere, the samples obtained were analysed by elemental and structural analyses and their superconductivity parameters (T_c, ΔT_c) were measured (Table 5).

System Mg–B–Be.[155] A mixture of MgB_2 + BeB_2 phases was obtained. Beryllium diboride has a hexagonal structure (the space group $P6/mmm$, $c/a = 0.977$) and is paramagnetic at $T < 5$ K. It was found that beryllium does not replace the Mg atoms.

System Mg–B–Li.[155] The homogeneity region of solid solutions $Mg_{1-x}Li_xB_2$ was determined ($x < 0.3$). As lithium content increases, the interlayer distance remains unchanged while the in-plane B–B distance (parameter *a*) is shortened by ~0.014 Å (at $x = 0.3$). A decrease in T_c is observed beginning with $x = 0.1$ and becomes pronounced near the single-phase composition bound of the solid solution ($x = 0.3$). Loss of superconductivity occurs for the sample with $x = 0.5$.

System Mg–B–Al.[83] Two homogeneity regions of solid solutions $Mg_{1-x}Al_xB_2$ were found (see Table 5). As the Al/Mg ratio increases, anisotropic lattice compression occurs: the interlayer spacings decrease appreciably while the B–B distances do not exhibit considerable changes. This leads to structural instability of the crystal and phase transition at $x = 0.1$. A decrease in T_c in the homogeneity region of the solid solutions was explained [83] by an increase in the electron concentration and a decrease in $N(E_F)$. Analysis of the phase diagram shows that the superconducting phase is very close to the structural instability point of the system.

System Mg–B–Cu.[153, 154] Information about this system is contradictory. Abnormally high T_c = 49 K announced [153] for a sample with stoichiometric composition $Mg_{0.8}Cu_{0.2}B_2$ has not been confirmed; attempts at preparing copper-containing single-phase solid solutions failed.[154]

System Mg–B–Zn.[154] The homogeneity region for $Mg_{1-x}Zn_xB_2$ samples is up to $x = 0.1$. Analysis of the lattice parameters for a sample with $x = 0.1$ revealed their increase compared to those of MgB_2, namely, 0.17% for *a* and 0.2% for *c*. It was suggested [154] that nonmonotonic change in T_c is due to positive for the parameter *a* (in-plane B–B distances) and negative for the parameter *c* (interlayer spacings) expansion effects.

System Mg–B–C.[156–158] AlB_2-Type borocarbides $MgB_{2-x}C_x$ were synthesised from elements. Transition temperature T_c decreases in the homogeneity region ($x \leqslant 0.20$) by ~2 K (at $x = 0.20$, see Ref. 157) while the width of the transition, ΔT_c, substantially increases (by ~3–7 K as compared to 'pure' MgB_2, see Refs 156, 157). Introduction of carbon impurity leads to compression of graphite-like boron sheets: $a(MgB_2) - a(MgB_{1.8}C_{0.2}) = 0.013$ Å. The interlayer distances (the lattice parameter *c*) remain unchanged.[156] Magnesium borocarbides with much narrower homogeneity region ($x < 0.1$) were also synthesised;[158] transition temperature of these compounds decreases as the C/B ratio increases.

Table 5. Conditions for synthesis and characteristics of particular ternary systems based on MgB_2.

Starting materials [a]	Reaction conditions	Products (phase composition)	T_c /K	Lattice parameters /Å		Ref.
				a	*c*	
Mg + B + Al	95% Ar + 5% H_2, 600–900 °C	$Mg_{1-x}Al_xB_2$: solid solutions at $0 < x < 0.1$ and $0.25 < x < 0.40$ mixture of phases at $0.1 < x < 0.25$	38 ($x = 0$) 36 ($x \approx 0.1$) 0 ($x > 0.1$)	decreases as x increases		83
Mg + B + Cu	95% Ar + 5% H_2, 600–900 °C	$Mg_{0.8}Cu_{0.2}B_2$ (?) [mixture of phases $MgB_2 + Cu_2Mg + MgO$ (traces)]	49 (?)	3.068	3.505	153
	100% Ar, 600–900 °C	mixture of phases $MgB_2 + Cu_2Mg +$ + (MgO + MgB_4) (traces)	(?)	–	–	154
Mg + B + Zn	100% Ar 600–900 °C	solid solutions $Mg_{1-x}Zn_xB_2 + MgO$ (traces) + MgB_4 at $x \approx 0.1$, mixture of phases at $x > 0.1$	changes nonmonotonically	3.0841 ($x \leqslant 0.1$)	3.5250 ($x = 0.1$)	154
Mg + B + Li	100% Ar, 950 °C	$Mg_{1-x}Li_xB_2$: solid solutions at $x < 0.3$ mixture of phases at $x > 0.3$	decreases as x increases	3.070 ($x = 0.3$)	3.524 ($x = 0.3$)	155
Mg + B + Be	Ar	mixture of phases	–	–	–	136
Mg + B + C	100% Ar, 850 °C, 20 atm	$MgB_{1.8}C_{0.2}$ + MgO (traces)	$T_{c1} \approx 41$ $T_{c2} \approx 37$	3.070	3.520	156
	950 K	the same	~34	3.070	3.523	157

[a] Amorphous boron powder was used in most cases.

The synthesis of 'superstoichiometric' compositions $Mg_{1+x}B_2$ with 10 at.%, 20 at.% and 30 at.% of excess Mg added to the reaction mixture has also been reported.[157] It was found that 'superstoichiometry' has no effect on the superconductivity in magnesium diboride.

4. Materials science and some aspects of practical utilisation of MgB_2

a. Pressure dependence

Studies on the effect of pressure (as well as joint effect of pressure and temperature) on the properties of MgB_2 attract considerable attention both in solving fundamental problems of the nature of superconductivity in anisotropic media and in developing new procedures for improving the properties of superconducting MgB_2.[120, 160–166]

The structure of MgB_2 polycrystals as function of hydrostatic pressure up to 0.62 GPa was studied by neutron diffraction in the temperature range from 11 to 297 K.[163] It was found that the lattice parameters a and c change linearly with pressure, *viz*., $a = a_0 - 0.00187P$, $c = c_0 - 0.00307P$, where a_0 and c_0 are the lattice parameters under normal conditions and P is the pressure (in GPa). Essentially nonuniform lattice compression was emphasised: compression along the c axis is 64% larger than along the a axis (in the B–B plane). Similar results were obtained in synchrotron X-ray diffraction studies of isothermal compression (Fig. 15). Thermal expansion of the crystal lattice is also anisotropic and is mainly due to changes in the interlayer distances (the parameter c).[163] It was found that the effect is due to anisotropy of chemical bonding in MgB_2.[120–163]

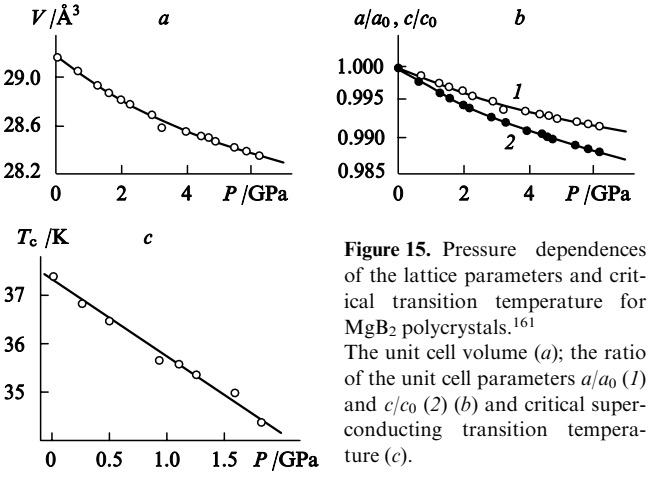

Figure 15. Pressure dependences of the lattice parameters and critical transition temperature for MgB_2 polycrystals.[161]
The unit cell volume (*a*); the ratio of the unit cell parameters a/a_0 (*1*) and c/c_0 (*2*) (*b*) and critical superconducting transition temperature (*c*).

Superconductivity parameters of MgB_2 are pressure dependent. For instance, it was found that the superconducting transition temperature decreases with a rate of -2.0 [162] and -1.6 K $(GPa)^{-1}$,[164] respectively (see Fig. 15). This is consistent with the results of calculations [165] [-1.4 K $(GPa)^{-1}$] and can be explained based on the BCS theory of the mechanism of superconductivity in magnesium diboride.[120, 165]

b. Neutron irradiation

Experiments [167] on thermal ($\Phi = 1 \times 10^{19}$ cm^{-2}) and fast ($\Phi = 1 \times 10^{18}$ cm^{-2}) neutron irradiation of MgB_2 (the total dose was greater than 10 doses per atom) were carried out with a IVV-2M nuclear reactor at $T = 350$ K. The transition temperature of irradiated samples decreased from 40 to 5 K, the residual resistance ρ_0 increased (from 0.35 to 2.0 mΩ cm) and the upper critical field exhibited minor changes ($-dH_{c2}/dT \approx 0.5$ T K^{-1}). By analogy with A15-type superconductors (Nb_3Sn, V_3Si), the results obtained were explained [167] by a decrease in $N(E_F)$. It was concluded that high radiation resistance of MgB_2 under conditions of neutron irradiation (other superconductors undergo amorphisation under such conditions) is of prime importance for practical utilisation of this compound. Irradiation of MgB_2 samples leads to anisotropic lattice expansion (mostly, to an increase in the parameter c from 3.5216 to 3.5533 Å), which is accompanied by an increase in the unit cell volume by ~1.4%.[157] The occupation number of Mg sites decreases from 0.94 to 0.89, while the occupation number of B sites remains unchanged. No antisite defects were found.

c. Grain boundary effects

Heat treatment of MgB_2 under high pressure to improve superconducting properties of highly porous (under the synthesis conditions) magnesium diboride polycrystals has been proposed.[160] At $T = 950$ °C and $P = 3$ GPa, the surface morphology of MgB_2 samples changed, their porosity decreased and the grain boundary contact area increased. High-resolution transmission electron microscopy studies of the morphology of the MgB_2 samples obtained by high-pressure sintering ($P = 3$ GPa) revealed the absence of porosity and strong connections between grains. The impurity phase (magnesium tetraboride) occurred in the form of small inclusions.[113] Specific features of some properties of

MgB_2 polycrystals, determined by the grain structure of the surface, have been discussed.[168, 169]

d. Surface and films

The development of methods for reproducible synthesis of epitaxial superconducting MgB_2 thin films for various electronic devices is one of the key problems of practical utilisation of this material. Here, the use of many conventional film growth procedures is complicated by the large differences in vapour pressure, adsorption coefficients and mobilities between boron and magnesium as well as due to a tendency of magnesium to undergo oxidation.

Currently, such films are synthesised using two, *ex situ* and *in situ*, approaches.[170–178] The former[174, 175] implies preliminary preparation of boron films which are then saturated with magnesium while the latter includes fabrication of MgB_2 films during the same run.

Currently, films with the highest current density and T_c (37–39 K) have been obtained by *ex situ* processes.[174, 175] The procedure included pulsed laser deposition (PLD) of thin boron films onto a substrate ($SrTiO_3$) followed by their reaction with magnesium vapours at 900 °C. The film surfaces were characterised[175] by well-developed grain structure. This approach has a drawback, that is, the high-temperature stage (here, temperatures are higher than the decomposition temperature of magnesium diboride). Therefore, this method is inapplicable to the growth of multilayers and heterojunctions. In addition, in the case of *ex situ* synthesis the film growth is driven by diffusion of magnesium through an already formed magnesium diboride surface layer, which makes it difficult to obtain an epitaxial relationship between the film and the substrate.[174, 175]

The *in situ* film growth involves two stages.[170–173] Initially, magnesium diboride films are prepared by PLD of various targets on different substrates, *e.g.*, Al_2O_3, $LaAlO_3$, $SrTiO_3$.[173] The targets (Fig. 16) were dispersed (< 45 μm) powders of MgB_2 synthesised from elemental boron and magnesium, commercial MgB_2 powders (AA), *etc*. Typically, the films were 100–500 nm thick. Superconductivity was observed only for films annealed in the rather narrow temperature interval (550–600 °C). Atomic force microscopy images revealed a reasonably smooth surface of these films, which is in stark contrast to the surface of the *ex situ* prepared films with well-defined grains. Films were deposited on the (100) and (111) surfaces of $SrTiO_3$ by (i) PLD of MgB_2, (ii) PLD of multilayers of MgB_2 and Mg followed by *in situ* annealing at high temperature and (iii) PLD of multilayers of Mg and B followed by *in situ* annealing at high temperature.[174] The highest superconducting transition temperature (T_c = 22 K) was observed for the films grown from magnesium diboride target. An increase in the annealing temperature deteriorates the superconductivity characteristics (for instance, T_c was no higher than 8 K after annealing at temperatures > 800 °C). This is thought to be due to layer-by-layer deviation from perfect nonstoichiometry.[174] It was emphasised that the necessary condition for growth of superconducting films consists in retaining the necessary Mg content.

Films grown *in situ* from room-temperature deposited Mg + MgB_2 powder targets and post-annealed at 600 °C were also characterised by relatively low T_c (12–22 K). It is believed that one of the key factors consists in the choice of reaction conditions to prevent oxidation of magnesium in plasma and in the film deposited. In this case, of great importance is the choice of the pressure of the inert gas in the vacuum chamber. Yet another reason for the low T_c is associated with the possibility[172] of formation of nonsuperconducting higher magnesium borides (MgB_4, MgB_7) and elemental boron, which deteriorates the superconductivity parameters of the film. The formation of magnesium borides is associated with the nature of plasma generated by the laser. In different ionisation zones, the temperature of plasma can be as high as several thousands of degrees. In this connection, of great importance are the results of thermodynamic modelling[179] of the system Mg–B using the CALPHAD technique.[180] Calculations[179] of composition–temperature, composition–pressure and pressure–temperature phase diagrams were carried out using experimental values of thermodynamic parameters of the components (MgB_2, MgB_4, MgB_7 as well as the gas, liquid and solid magnesium phases and β-boron). Magnesium diboride can be formed only at vapour pressures of magnesium falling into specific range and in particular temperature range (Fig. 17). Clearly, operation under these conditions will favour optimisation of the composition and, as a consequence, superconductivity characteristics of *in situ* grown films.

A 'mixed' film fabrication procedure has been proposed.[177] Films deposited *in situ* from MgB_2 targets in high vacuum exhibited the properties of pure metals or semiconductors; super-

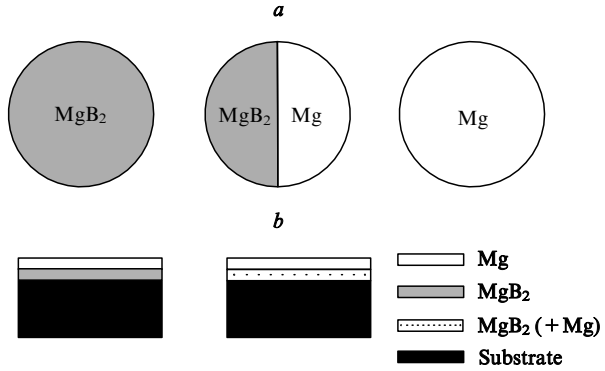

Figure 16. Schematical drawings of the targets (*a*) and chemical compositions of *in situ* prepared films (*b*).[173]

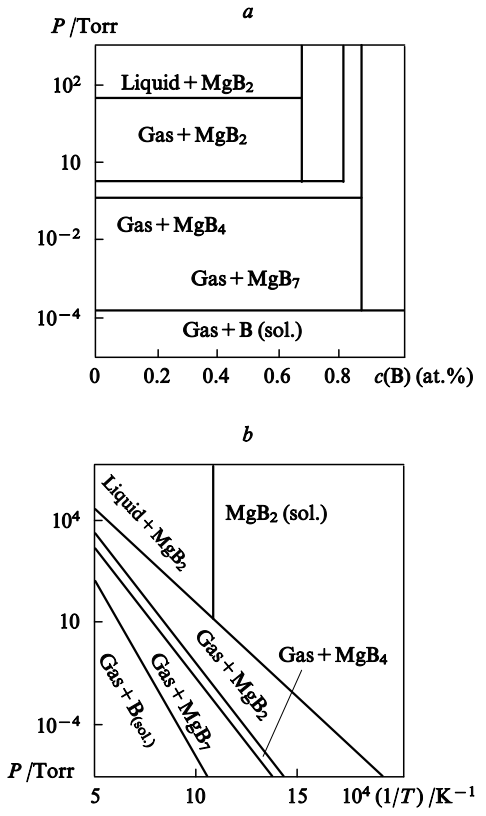

Figure 17. Calculated diagrams of the Mg–B system.
The pressure–composition diagram at T = 850 °C (*a*) and P–T-diagram for the ratio Mg : B > 1 : 2 (*b*). The 'gas + MgB_2' region corresponds to thermodynamic conditions for the preparation of MgB_2 thin films. Obtained from CALPHAD calculations.[179]

conductivity ($T_c \approx 25$ K) was observed only after additional exposure to magnesium vapours. Films with $T_c = 24$ K were obtained from stoichiometric MgB_2 targets by PLD on silicon substrates followed by heating in Ar atmosphere.[178] Uniform surface morphology and thickness of films were pointed out. Oxygen contamination of the outermost layers was assumed to be the main reason for the low T_c.

Vasquez *et al.*[181] reported a special XPS study of the elemental composition of the surface of MgB_2 polycrystals. The XPS spectrum of the surface of initial sample exhibited strong impurity signals from C and O, two signals from Mg 2*p*-state with binding energies (E_b) of 49.5 and 50.8 eV and signals from B 1*s*-states. Among the last-named group of signals, a weak peak with $E_b = 193$ eV is due to the presence of boric anhydride. The main signal of the B 1*s*-state was a doublet with the energies $E_b = 186.7$ and 187.9 eV comparable with the corresponding energies for isostructural *d*-metal diborides (187.2 – 188.5 eV, see Ref. 182).

According to Vasquez *et al.*[181] there are three main concentration zones near the MgB_2 surface. The first zone, *i.e.*, the surface of initial sample, is covered with oxide film and is substantially enriched with magnesium (the Mg : B ratio is 1 : 1.25). The oxide layer can be efficiently removed in the course of chemical purification (by, *e.g.*, 1% and 0.5% solutions of HCl and Br_2 in ethanol). The second, 'subsurface', zone under the oxide film is, on the contrary, depleted of magnesium (Mg : B = 1 : 3). In this zone, nonstoichiometry with respect to magnesium leads to a decrease in the electron density in boron sheets. The corresponding signal of B 1*s*-state is observed at higher binding energy ($E_b = 187.9$ eV). The second B 1*s*-peak ($E_b = 186.7$ eV) corresponds to the states of boron atoms in the third zone (magnesium diboride bulk with stoichiometric ratio Mg : B = 1 : 2). The energies of Mg 2*p*-level and Auger-signal are lower than that of metallic magnesium due to cationic state of Mg^{2+} in magnesium diboride.

e. New MgB_2-based superconducting materials: wires, ribbons, composites

A simple procedure for fabricating high density MgB_2 wires has been developed.[183] As mentioned above, MgB_2 polycrystals are obtained by solid-phase synthesis (a mixture of boron and magnesium powders is heat treated); mechanistically, magnesium diboride is formed *via* diffusion of Mg vapour into the boron grains. Bud'ko *et al.*[183] proposed to use this technique with boron fibres instead of powder. Boron fibres ($d \approx 100$ μm, Textron Systems, USA) and metallic magnesium taken in a stoichiometric ratio were placed in a Ta tube and heated at 950 °C for 1 h. Compared to the unreacted boron fibres, the MgB_2 wires thus obtained were brittle and somewhat deformed (see Fig. 18), but they did not break down. A tungsten core ($d \approx 15$ μm) of the starting boron fibres did not appear to be affected during the reaction, it also has no effect [183] on the superconducting characteristics of the MgB_2 wires. The diameter of the MgB_2 wires increased from 100 to 160 μm (synthesis of magnesium diboride powder is also accompanied by an increase in the particle size compared to the initial boron grains [82]). The density of wire segments was determined to be ~ 2.4 g cm^{-3} [$\sim 80\%$ of the theoretical density of MgB_2 crystal, 2.55 g cm^{-3} (see Ref. 82)]. The superconductivity parameters of the wires were $T_c = 39.4$ and $\Delta T_c = 0.9$ K. At room temperature, the wires exhibited the properties of highly conducting material (the resistivity, ρ, had a value of 9.6 μΩ cm), whereas near the critical transition temperature ($T = 40$ K) ρ decreased to 0.38 μΩ cm. Temperature dependence of the resistivity ($\rho = \rho_0 + \rho_1 T^{\alpha}$, where $\alpha \approx 2.6$) is close to that found for MgB_2 polycrystals [$\alpha \approx 2.8$, measured for $Mg(^{10}B)_2$ pellets].[82]

To choose optimum conditions for the preparation of superconducting MgB_2 wires, the mechanism of Mg diffusion into boron was systematically studied using commercialy sold boron fibres ($d = 100$ and 141 μm).[184] Boron fibres were exposed to magnesium vapours at 950 °C, the course of the reaction was monitored by the scanning electron microscopy (SEM) using the

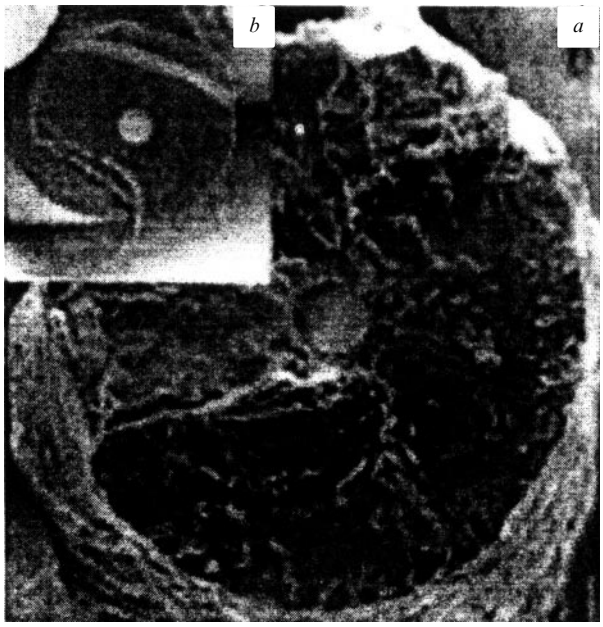

Figure 18. Electron microscope images of cross-section of a MgB_2 wire of diameter 160 μm (*a*) and unreacted boron filament with a tungsten core (*b*).[183]

SEM images of the cross-sections of the MgB_2 wires taken after time intervals. It was found that magnesium diboride begins to form after 15 min and is 50% complete after 1 h. The wire segments thus produced were of little porosity. In Fig. 19, the resistivities of MgB_2 pellets and wires are shown as functions of temperature. Different behaviour of the curves is thought to be due to larger density of wires.[184] Studies [185] on magnetotransport characteristics of dense wires revealed a very narrow resistive transition, a linear temperature dependence of H_{c2} in the range 7 K < T < 32 K and a positive curvature of this dependence near T_c. This is similar to the behaviour of layered IBC.[186–188]

Another technique for fabrication of superconducting MgB_2 wires involves placing powdered MgB_2 inside a sheath (a niobium,[189] gold, copper of nickel tube [190]). For instance, a niobium tube of diameter 6 mm was filled with MgB_2 powder and then a ribbon was prepared by cold drawing followed by rolling.[189] The ribbon with a superconducting core (a cross-section of 0.232 mm^2) had a cross-section of 2.56×0.32 mm^2.[189] At 4.2 K, the measured current density in the ribbons heated at 900 °C for 1, 2 and 3 h in an Ar atmosphere was 4.7, 7.5 and 1.1×10^4 A cm^{-2}, respectively. Experiments [190] with ribbons

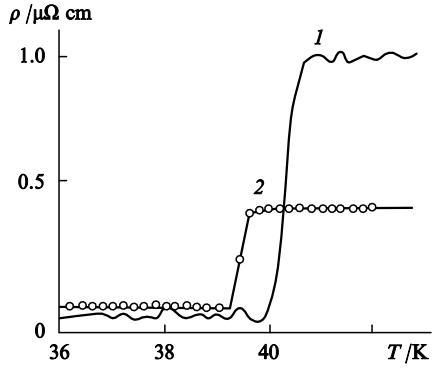

Figure 19. Resistivity of a dense MgB_2 wire (*1*) and polycrystalline MgB_2 pellet (*2*) as function of temperature.[184]

sheathed with different metals (Au, Ni, Cu) revealed the highest current density ($\sim 10^5$ A cm^{-2}) at 4.2 K for the ribbon with Ni sheath.

Magnesium diboride is highly brittle, which is typical of ceramics. Therefore, the problem of improving mechanical properties of MgB_2, *i.e.*, making the material more malleable without significant deterioration of its superconducting properties is of great importance. The most obvious way is to fabricate composites with ductile metals (or alloys) which should have low melting temperatures comparable with that of MgB_2 (1073 K) and be conductors and highly plastic substances. The formation of such composites should also not be accompanied by reactions between the ductile additive and magnesium diboride resulting in solid solutions. Recently, aluminium (T_m = 933 K) was found to be appropriate for this purpose.[191] Pellets of MgB_2–Al composite (11 vol.% Al) were prepared from MgB_2 (AA) and Al powders (the particle size of both components was 1 to 3 μm) by pressing at 500–700 K, *i.e.*, below the formation temperature of nonsuperconducting $Mg_{1-x}Al_xB_2$ solid solutions.[83] The samples were studied by scanning tunnelling microscopy and the transport and magnetic characteristics of the composites were measured. Particular attention was given to the proximity effect (the formation of a typical 'mini-gap' structure was observed, which is due to contact between magnesium diboride and aluminium, T_c^{Al} = 1.2 K) and to the effect of structural disordering on the superconducting transition temperature of the MgB_2–Al composite. The T_c value for the composite (38 K) was found to be comparable with that of pure MgB_2 (39 K).

IV. Conclusion

Information collected and systematised in this review describes the infancy of research into the properties of recently found new superconductor, MgB_2. In spite of short time that elapsed after the discovery of superconductivity in MgB_2, experimentalists and theoreticians have accumulated a great body of information about its physicochemical properties. The results obtained are of crucial importance for an understanding of the nature of superconductivity in anisotropic media. They gave a strong impetus to search for new superconductors among metal borides and related compounds and opened attractive prospects for their technological utilisation.

The state-of-the-art in this field can be outlined as follows. To date, a number of methods for the synthesis of MgB_2 have been developed. Peculiarities of the electronic structure and chemical bonding in MgB_2 as well as its electrophysical, magnetic, thermodynamic properties and spectroscopic characteristics have been studied. Based on the results of theoretical modelling and synthetic experiments, some new MgB_2-based solid solutions have been found and ways to further search for new superconductors have been directed. Materials science studies allowed the obtaining of MgB_2 powders, films, wires and composites.

On the other hand, magnesium diboride, as a medium-T_c superconductor, remains a unique compound in its kind except for a few solid solutions based on this substance. All attempts at increasing the critical transition temperature of MgB_2 or finding new superconductors with close T_c have failed so far. Many problems of the synthesis and detailed investigations of multicomponent systems with participation of magnesium diboride are still to be solved. These are, *e.g.*, studies of the phase diagrams, determination of homogeneity regions of solid solutions and criteria for optimum doping of MgB_2 as well as establishment of reasons for changes in T_c. Further search for new candidates for superconductors with graphite-like boron sheets in their structure is undoubtedly required. We believe that these problems will be the focus of research interest in the near future.

* * *

Studies on superconducting MgB_2 and related compounds have been continued in the course of preparation of the manuscript. The most interesting recent results are as follows.

Single crystals of MgB_2 have been first obtained.[192–195] A magnesium-enriched precursor sealed in a niobium ampoule was placed in a quartz tube,[192] heated to 1050 °C (1 h) and then very slowly cooled down to 700 °C (the cooling duration was 120 to 360 h). The MgB_2 single crystals were found to have various shapes (spherical, rod-like, or hexagonal-plate) depending on the cooling regime. The samples studied were characterised by excellent superconductivity parameters (T_c = 38 K and ΔT_c = 0.3 K). Experiments with MgB_2 single crystals revealed strong anisotropy of superconductivity.[192–195]

An original method for the synthesis of high density, single-phase MgB_2 ceramics with T_c = 38 K by crystallisation of magnesium diboride melt under pressure has been proposed.[196] The slope and the onset of transition to the superconducting state were found to be dependent on the grain size of the material.

Epitaxially grown, oriented MgB_2 films were prepared and their properties have been studied:[197–210] superconductivity,[197, 199–210] the Hall effect [207] and surface resistance.[206] Anisotropy of some characteristics of the oriented films (in particular, conductivity and upper critical field [198, 200]) was revealed. Degradation of superconductivity in MgB_2 films in the presence of water has been studied.[205] Preparation of nanostructured superconducting MgB_2 films has also been reported.[203] Pioneering calculations of the electronic structure of the boron- and magnesium-terminated MgB_2 (0001) surfaces have been carried out.[211, 212]

Summing up, mention may be made that there are three main lines of inverstigations in the field of search for MgB_2-related superconductors. The first research avenue is associated with extension of the class of possible MgB_2-based superconductors by varying their chemical compositions to obtain different types of solid solutions or by forming superstructures (see Section III.3). The second investigation line includes studies of a much broader spectrum of substances. Here, the search for possible superconductors has been performed among binary or multicomponent compounds which are to some extent structurally or chemically similar to MgB_2. The discovery of critical transitions in ZrB_2 (5.5 K, see Ref. 213), TaB_2 (9.5 K, see Ref. 137), Re_3B (4.7 K, see Ref. 214) and in the new phase of beryllium boride with the chemical composition $BeB_{2.75}$ and the unit cell containing 110.5 atoms (0.72 K, see Ref. 215) represent recent advances in this field.

The third line of research activity was initiated by the discovery of superconductivity at $T_c \approx 8$ K in a perovskite-like intermetallide $MgCNi_3$.[216] From the standpoint of 'renewed chemical paradigm' it was proposed [216] that the whole class of intermetallides should be considered as potential superconductors. The results obtained by Cava *et al.*[216] are of particular interest for the following reasons.

Highly symmetric structure of $MgCNi_3$ (the space group $Pm3m$) favours superconductivity. However, superconductivity in all the known isostructural compounds — oxide perovskites [*e.g.*, (Ba, K)BiO_3, see Ref. 217] — is due to electron–hole states of the oxygen atoms occupying 3*c*-type positions (0, 1/2, 1/2). Since in the $MgCNi_3$ structure these positions are occupied by Ni atoms, the mechanism of superconductivity should be of fundamentally different nature.

Most of the known 'non-oxide,' perovskite-like compounds MXM'_3 (M′ = Zn, Al, Ga, In, Sn; M = Mn, Fe; X = C, N) are ferromagnetic (and antiferromagnetic) or are characterised by more complex (mixed) types of spin ordering.[218] Hence, among structurally similar compounds, $MgCNi_3$ can be considered as an 'intermediate' between the classes of perovskite-like superconductors (oxides) and magnetics (non-oxide perovskites).

Among superconductors, nickel-containing IBC $LuNi_2B_2C$ ($T_c \approx 16$ K) and YNi_2B_2C ($T_c \approx 15.6$ K) are the closest 'chemical analogues' of $MgCNi_3$. However, unlike the last-named compound, these IBC belong to magnetic superconductors and exhibit

a distinct quasi-2D structure.[22] In addition, the Ni content in IBC is much less than in $MgCNi_3$. Taking into account clearly defined magnetic properties of nickel, the fact that superconductivity occurs in the nickel-rich compound $MgCNi_3$ is quite surprising.

Based on the results of pioneering studies on the properties of $MgCNi_3$ (the critical field, H_{c2}, the Hall coefficient, *etc*.,[219–221]) and critical transition temperatures of $MgCNi_{3-x}M_x$ (M = Mn, Co, Cu) samples doped at Ni sites, the parent compound, $MgCNi_3$, was placed into the class of 'conventional' superconductors with electron–phonon interactions.[222,223] Band structure calculations for $MgCNi_3$ (see Refs 224–227) revealed a distinctive feature, *viz*., the presence of an intense DOS peak near the Fermi level. It was found that the major contribution to $N(E_F)$ comes from the Ni 3*d*-states (~88.2%). Band structure calculations for new $MgCNi_3$-like superconductors have been carried out. The possibility of superconductivity in a nonstoichiometric (with respect to C sublattice) perovskite, in perovskite-like $ScBNi_3$ and $InBNi_3$ as well as in $MgCCo_3$ and $MgCCu_3$ (all of them are isoelectronic and isostructural to $MgCNi_3$) has been discussed.[228]

The discovery of superconductivity in intermetallic compounds MgB_2 and $MgCNi_3$ with simple and highly symmetric structures has given a creative urge to search for application areas of these promising superconductors.

The author expresses his gratitude to N I Medvedeva, V G Zubkov, V N Diev and V G Bamburov for valuable discussions.

References

1. *Perspectivnye Tekhnol*. **8** (1–2) 1 (2001)
2. J Nagamatsu, N Nakagawa, T Muranaka, Y Zenitani, J Akimitsu *Nature (London)* **410** 63 (2001)
3. G V Samsonov, L Ya Markovskii, A F Zhigach, M G Valyashko *Bor, ego Soedineniya i Splavy* (Boron, Its Compounds and Alloys) (Kiev: Academy of Sciences of Ukr. SSR, 1960)
4. B Post, F W Glaser *Refractory Binary Borides* (New York: Interscience, 1963)
5. V Aronsson, T Lundstrom, S Rundquvist *Refractory Borides, Silicides and Phosphides* (London: Methuen, 1965)
6. E L Muettertis (Ed.) *The Chemistry of Boron and its Compounds* (New York: Wiley, 1967)
7. H Goldschmidt *Interstitial Alloys* (London: Butterworths, 1967)
8. G V Samsonov, T I Serebryakova, V A Neronov *Boridy* (Borides) (Moscow: Atomizdat, 1975)
9. G V Samsonov, I M Vinitskii *Tugoplavkie Soedineniya. Spravochnik* (High-Melting Compounds. Handbook) (Moscow: Metallurgiya, 1976)
10. Yu B Kuz'ma *Kristallokhimiya Boridov* (Crystal Chemistry of Borides) (L'vov: Vishcha Shkola, 1983)
11. T Ya Kosolapov (Ed.) *Boridy i Materialy na Ikh Osnove* (Borides and Materials Based on Them) (Kiev: Institute of Problem of Materials Technology, Academy of Sciences, Ukr. SSR, 1986)
12. Yu B Kuz'ma, I F Chaban *Dvoinye i Troinye Sistemy, Soderzhashchie Bor* (Binary and Ternary Systems Containing Boron) (Moscow: Metallurgiya, 1990)
13. T I Serebryakova, V A Neronov, P D Peshev *Vysokotemperaturnye Boridy* (High-Temperature Borides) (Moscow: Metallurgiya, 1991)
14. A L Ivanovskii, G P Shveikin *Kvantovaya Khimiya v Materialovedenii. Bor, ego Splavy i Soedineniya* (Quantum Chemistry in Materials Technology. Boron, Its Alloys and Compounds) (Ekaterinburg: Izd. Ekaterinburg, 1997)
15. S V Vonsovsky, Y A Izumov, E Z Kurmaev *Superconductivity of Transition Metals, Alloys and Compounds* (Berlin: Springer, 1982)
16. L E Toth *Transition Metal Carbides and Nitrides* (New York; London: Academic Press, 1971)
17. L Leyarovska, E Leyarovski *J. Less-Common Met*. **67** 249 (1979)
18. M B Maple, O Fischer (Eds) *Superconductivity in Ternary Compounds; I. Structural, Electronic and Lattice Properties; II. Superconductivity and Magnetism* (Berlin; Heidelberg; New York: Springer, 1982)
19. R J Cava, H Takagi, B Batlogg, H W Zandbergen, J J Krajewski, W F Peck, R van Doren, R J Felder, T Siegrist, T K Mizuhashi, J O Lee, H Eisaki, S A Carter, S Uchida *Nature (London)* **367** 146 (1994)
20. R J Cava, H Takagi, H W Zandbergen, J J Krajewski, W E Peck, T Siegrist, B Batlogg, R van Doren, R J Felder, T K Mizuhashi, J O Lee, H Eisaki, S Uchida *Nature (London)* **367** 252 (1994)
21. R Nakarajan, C Mazumdar, Z Nossian, S K Dhar, K V Gopalakrishnan, L C Gupta, C Goddart, B D Padalia, R Vijayaraghavan *Phys. Rev. Lett*. **72** 274 (1994)
22. A L Ivanovskii *Usp. Khim*. **67** 403 (1998) [*Russ. Chem. Rev*. **67** 357 (1998)]
23. H Moissan *Ann. Chim. Phys*. **6** 296 (1895)
24. A Stock *Hydrides of Boron and Silicon* (Ithaca, NY: Cornell University Press, 1933)
25. N Moissan *Ann. Chim. (Paris)* **8** 87 (1906)
26. F Jones, R Taylor *J. Chem. Soc*. 1881 (1912)
27. R Ray *J. Chem. Soc*. **105** 2162 (1914)
28. M Travers, N Gupta, R Ray *Indian Inst. Sci*. **1** 1 (1914)
29. M Travers, R Ray *Proc. R. Soc. London A* **87** 153 (1913)
30. T Serebryakova *J. Less-Common Met*. **67** 499 (1979)
31. P Duhart *Ann. Chim. (Paris)* **7** 339 (1962)
32. F A Shunk *Constitution of Binary Alloys (Second Suppl)* (New York: McGraw-Hill, 1971)
33. T Massalsky (Ed.) *Binary Alloy Phase Diagrams* (New York: A S M International, 1990)
34. M Jones, R Marsh *J. Am. Chem. Soc*. **76** 1434 (1954)
35. V Russel, R Hirst, F Kanda, A J King *Acta Crystallogr*. **6** 870 (1953)
36. L Ya Markovskii, Yu D Kondrashev, G V Kapustovskaya *Zh. Obsh. Khim*. **25** 433 (1955) [a]
37. L Ya Markovskii, Yu D Kondrashev, G V Kapustovskaya *Dokl. Akad. Nauk SSSR* **100** 1095 (1955) [b]
38. P Beck (Ed.) *Electronic Structure and Alloy Chemistry of the Transition Elements* (New York; London: Wiley-Interscience, 1963)
39. K Schubert *Kristallstrukturen zweikomponentiger Phasen* (Berlin; Gottingen; Heidelberg: Springer, 1964)
40. W B Pearson *The Crystal Chemistry and Physics of Metals and Alloys* (New York; London; Sidney; Toronto: Wiley-Interscience, 1972)
41. A Guette, R Naslain, J Galy *C.R. Acad. Sci., Ser. C* **275** 41 (1972)
42. R Naslain, A Guette, M Barret *J. Solid State Chem*. **8** 68 (1973)
43. R Naslen, A Guette, J Casper, in *Bor. Poluchenie, Struktura, Svoistva* (Boron. Production, Structure, Properties) (Moscow: Nauka, 1974) p. 160
44. R Naslain, A Quette, P Hagenmuller *J. Less-Common Met*. **47** 1 (1976)
45. A Quette, M Barret, R Naslain, P Hagenmuller *J. Less-Common Met*. **82** 325 (1981)
46. I I Tupitsyn, I I Lyackovskaya, M S Nakhmanson, A A Sukhik *Sov. Phys.-Solid State* **16** 2915 (1975)
47. D Armstrong, P G Perkins *J. Chem. Soc., Faraday Trans. 2,* **75** 12 (1979)
48. J K Burdett, G J Miller *Chem. Mater*. **2** 12 (1989)
49. A L Ivanovskii, N I Medvedeva *Zh. Neorg. Khim*. **45** 1355 (2000) [c]
50. G P Shveikin, A L Ivanovskii *Usp. Khim*. **63** 751 (1994) [*Russ. Chem. Rev*. **63** 711 (1994)]
51. A F Guillermet, G Grimvall *J. Less-Common Met*. **169** 257 (1991)
52. X Wang, D Tian, L Wang *J. Phys., Condens. Matter* **6** 10185 (1994)
53. A L Ivanovskii, N I Medvedeva, Yu E Medvedeva *Mendeleev Commun*. 129 (1998)
54. A L Ivanovskii, N I Medvedeva, Yu E Medvedeva, A E Nikiforov, G P Shveikin *Metallofiz. Noveishie Tekhnol*. **20** 41 (1998)
55. A L Ivanovskii, N I Medvedeva, Yu E Medvedeva *Metallofiz. Noveishie Tekhnol*. **21** 19 (1999)
56. A L Ivanovskii, N I Medvedeva, Yu E Medvedeva, G P Shveikin *Dokl. Akad. Nauk* **361** 642 (1998) [b]
57. A L Ivanovskii, N I Medvedeva *Zh. Neorg. Khim*. **44** 1717 (1999) [c]
58. S Nakano, O Fukunaga *Diam. Relat. Mater*. **2** 1409 (1993)
59. G Bocquillon, C Loriers-Susse, J Lorieres *J. Mater. Sci*. **28** 3547 (1993)
60. T Endo, O Fukunaga, M Iwata *J. Mater. Sci*. **14** 1676 (1979)
61. T I Serebryakova, V A Ponomarenko, A I Karasev *Poroshk. Metall*. (11) 77 (1980)

62. V B Shipilo, L M Gameza, I P Guseva *Sverkhtv. Mater.* (3) 5 (1981)
63. V B Shipilo, V V Sergeev *Poroshk. Metall.* (4) 48 (1985)
64. V B Shipilo, L M Gameza *Zh. Fiz. Khim.* **63** 196 (1989) [d]
65. V B Shipilo, L M Gameza *Neorg. Mater.* **25** 51 (1989) [e]
66. V S Lysanov (Ed.) *El'bor v Mashinostroenii* (Elboron in Machine Building) (Leningrad: Mashinostroenie, 1978)
67. V L Solozhenko, V Z Turkevich, W B Holzapfel *J. Phys. Chem. B* **103** 8137 (1999)
68. T Ya Kosolapova, T V Andreeva, T V Bartnitskaya, G G Gnesin, G N Makarenko, I I Osipova, E V Prilutskii *Nemetallicheskie Tugoplavkie Soedineniya* (Nonmetallic High-Melting Compounds) (Moscow: Metallurgiya, 1985)
69. H Kobayashi, M Katoh, Y Kamiyama, T Mitamura *J. Ceram. Soc. Jpn.* **100** 172 (1992)
70. V Sundaran, K V Logan, R F Speyer *J. Mater. Res.* **12** 2657 (1997)
71. E G Gillan, R B Kaner *Chem. Mater.* **8** 333 (1996)
72. Y Guindon, L Rao, E G Gillan, R B Kaner *J. Mater. Res.* **10** 353 (1995)
73. M Gu, Z Wu, Y Jin, M Kocak *J. Mater. Sci.* **35** 2499 (2000)
74. J A Wilson, J W Steeds, D Wilkes, C M Ward-Close *J. Mater. Sci.* **36** 67 (2001)
75. V G Bamburov, O V Sivtsova, V P Semyannikov, V A Kiselev *Ogneupory Tekhn. Keram.* (2) 2 (2000)
76. Jpn. P. 62 108 710; *Chem. Abstr.* **107** 63 688 (1987)
77. Jpn. P. 5 105 532 ; *Chem. Abstr.* **119** 78 476 (1993)
78. Jpn. P. 5170 514; *Chem. Abstr.* **119** 187 176 (1993)
79. Jpn. P. 9 080 821; *Chem. Abstr.* **127** 26 010 (1997)
80. Jpn. P. 0 101 936; *Chem. Abstr.* **101** 11 276 (1984)
81. Jpn. P. 0 298 676; *Chem. Abstr.* **110** 140 420 (1989)
82. S L Bud'ko, G Lapertot, C Petrovic, C E Cunningham, N Anderson, P C Canfield *Phys. Rev. Lett.* **86** 1877 (2001)
83. J S Slusky, N Rogado, K A Regan, M A Hayward, P Khalifah, T He, K Inumaru, S M Loureiro, M K Haas, H W Zandbergen, R J Cava *Nature (London)* **410** 343 (2001)
84. D C Larbalestier, L D Cooley, M O Rikel, A A Polyanskii, J Jiang, S Patanik, X Y Cai, D M Feldman, A Gurevich, A A Squitiere, M T Naus, C B Eom, E E Hellstrom, R J Cava, K A Regan, N Rogado, M A Hayward, T He, J S Slusky, P Khalifah, K Inumaru, M Haas *Nature (London)* **410** 186 (2001)
85. J Kortus, I I Mazin, K D Belashchenko, V P Antropov, L L Boyer *Phys. Rev. Lett.* **86** 4656 (2001)
86. K D Belashchenko, M van Schlifgaarde, V P Antropov http://xxx.lanl.gov/abs/cond-mat/0102290 (2001)
87. J M An, W E Pickett *Phys. Rev. Lett.* **86** 4366 (2001)
88. J Gavaler *Appl. Phys. Lett.* **23** 480 (1973)
89. R J Cava, B Batlogg *MRS Bull.* **14** 49 (1989)
90. K Holczer, O Klein, S Huang, R B Kaner, K Fu, R L Whetten, F Diederich *Science* **252** 1154 (1991)
91. S Yamanaka, H Kawaij, K Hothehama, M Ohashi *Adv. Mater.* **8** 771 (1996)
92. H Kawaij, K Hothehama, S Yamanaka *Chem. Mater.* **9** 2127 (1997)
93. S Yamanaka, K Hotehama, H Kawaij *Nature (London)* **392** 580 (1998)
94. M Kohmoto, I Chang, J Friedel http://xxx.lanl.gov/abs/cond-mat/0103352 (2001)
95. N B Brandt, S M Chudinov, Y G Ponomarev *Modern Problems in Condensed Matter Sciences* Vol. 20 (North-Holland: Amsterdam, 1988)
96. I T Belash, A D Bronnikov, O A Zharikov, A V Palnichenko *Synth. Met.* **36** 283 (1990)
97. J H Schon, C Kloc, B Batlogg *Nature (London)* **408** 549 (2000)
98. R Osborn, E A Goremychkin, A L Kolesnikov, D G Hinks *Phys. Rev. Lett.* **87** 7005 (2001)
99. A Gerashenko, K Mikhalev, S Verkhovskii, T D'yachkova, A Tyutyunnik, V Zubkov http://xxx.lanl.gov/abs/cond-mat/0102421 (2001)
100. A G Joshi, C G Pillai, P Raj, S K Malik *Solid State Commun.* **118** 445 (2001)
101. T J Sato, K Shibata, Y Takano http://xxx.lanl.gov/abs/cond-mat/0102486 (2001)
102. O F de Lima, R A Ribeiro, M Avila, C A Cardoso, A A Coelho *Phys. Rev. Lett.* **86** 5974 (2001)
103. Ch Walti, E Felder, C Degen, G Wigger, R Monnier, B Delley, H R Ott http://xxx.lanl.gov/abs/cond-mat/0102522 (2001)
104. S X Dou, X L Wang, J Horvat, D Milliken, E W Collings, M D Sumption http://xxx.lanl.gov/abs/cond-mat/0102320 (2001)
105. D D Lawrie, J P Franck *Physica C* **245** 159 (1995)
106. K O Cheon, I R Fischer, P C Canfield *Physica C* **312** 35 (1999)
107. D K Finnemore, J E Ostenson, S L Bud'ko, G Lapertot, P C Canfield *Phys. Rev. Lett.* **86** 2420 (2001)
108. Y Takano, H Takeya, H Fujii, H Kumakura, T Hatano, K Togano, H Kito, H Ichara http://xxx.lanl.gov/abs/cond-mat/0102167 (2001)
109. S Li, H H Wen, Z W Zhao, Y Ni, Z A Ren, G C Che, H Yang, Z Y Li, Z H Zhao http://xxx.lanl.gov/abs/cond-mat/0103032 (2001)
110. C U Jung, M S Park, W N Kang, M S Kim, S Y Lee, S I Lee *Physica C* **353** 162 (2001)
111. W N Kang, C U Jung, K Kim, M S Park, S Y Lee, H Kim, E M Choi, M S Kim, S J Lee http://xxx.lanl.gov/abs/cond-mat/0102313 (2001)
112. H Kotegawa, K Ishida, Y Kitaoka, T Muranaka, J Akimitsu http://xxx.lanl.gov/abs/cond-mat/0102334 (2001)
113. G Y Sung, S H Kim, J Kim, D C Yoo, J W Lee, C U Jung, M S Park, W N Kang, D Zhonglian, S I Lee http://xxx.lanl.gov/abs/cond-mat/0102498 (2001)
114. A Sharoni, I Felner, O Millo *Phys. Rev. B* **63** 220508 (2001)
115. G Karapetrov, M Iavorone, W K Kwok, G W Gabtree, D G Hinks *Phys. Rev. Lett.* **86** 4374 (2001)
116. H Schmidt, J F Zasadzinski, K E Gray, D G Hinks *Phys. Rev. B* **63** 22 504 (2001)
117. B Gorshunov, C A Kutscher, P Haas, M Dressel, F P Mena, A B Kuz'menko, D van der Marel, T Muranaka, J Akimitsu *Eur. Phys. J. B* **21** 159 (2001)
118. R K Kremer, B J Gibson, J S Ahn http://xxx.lanl.gov/abs/cond-mat/0102432 (2001)
119. Y Wang, T Plackowski, A Junod *Physica C* **355** 179 (2001)
120. T Vogt, G Schneider, J A Hriljac, G Yang, J S Abell *Phys. Rev. B* **63** 220 505 (2001)
121. J E Hirsch *Science* **292** 1521 (2001)
122. J E Hirsch *Physica C* **341** – **348** 213 (2000)
123. W L McMillan *Phys. Rev. Ser. 2* **167** 331 (1968)
124. N I Medvedeva, A L Ivanovskii, J E Medvedeva, A J Freeman *Phys. Rev. B* **64** 220 502 (2001)
125. G Satta, G Profeta, F Bernardini, A Contonenza, S Massidda http://xxx.lanl.gov/abs/cond-mat/0102358 (2001)
126. S Suzuki, S Higai, K Nakao *J. Phys. Soc. Jpn.* **70** 1206 (2001)
127. I R Shein, N I Medvedeva, A L Ivanovskii *Fiz. Tv. Tela* (2001) (in the press) [f]
128. N I Medvedeva, Yu E Medvedeva, A L Ivanovskii http://zhurnal ape relarn ru/articles/2001/008 pdf (2000)
129. N I Medvedeva, Yu E Medvedeva, A L Ivanovskii *Dokl. Akad. Nauk* **379** (1) (2001) [b]
130. A Reyes-Serrato, D Galvan http://xxx.lanl.gov/abs/cond-mat/0103477 (2001)
131. E Z Kurmaev, I I Lyackovskaya, J Kortus, N Miyata, M Demeter, M Neumann, M Yanagihara, M Watanabe, T Muranaka, J Akimitsu http://xxx.lanl.gov/abs/cond-mat/0103487 (2001)
132. T A Callot, L Lin, G T Woods, G P Zhang, J R Thompson, M Paranthaman, D L Erderer http://xxx.lanl.gov/abs/cond-mat/0103593 (2001)
133. T Takahashi, T Sato, S Souma, T Muranaka, J Akimitsu *Phys. Rev. Lett.* **86** 4915 (2001)
134. N I Medvedeva, A L Ivanovskii, J E Medvedeva, A J Freeman, D L Novikov http://xxx.lanl.gov/abs/cond-mat/0104346 (2001)
135. C Beyreuther, R Hierl, G Wiech *Ber. Bunsenges. Phys. Chem.* **79** 1081 (1975)
136. I Felner *Physica C* **353** 11 (2001)
137. D Koczorowski, A J Zalevski, O J Zogal, J Klamut http://xxx.lanl.gov/abs/cond-mat/0103571 (2001)
138. A L Ivanovskii *Usp. Khim.* **66** 511 (1997) [*Russ. Chem. Rev.* **66** 459 (1997)]
139. N Sudo, H Hashizume, C Carvalho *J. Appl. Crystallogr.* **24** 286 (1991)

140. S V Okatov, A L Ivanovskii, N I Medvedeva, J E Medvedeva *Phys. Status Solidi A* **225** R3 (2001)
141. H Ripplinger, K Schwarz, P Blaha *J. Solid State Chem.* **133** 51 (1997)
142. S Massidda, A Continenza, T M DePascale, R Monnier *Z. Phys. B, Condens. Matter* **102** 83 (1997)
143. A L Ivanovskii, S V Okatov *Mendeleev Commun.* **11** 8 (2001)
144. S Fahy, D R Hamann *Phys. Rev. B* **41** 7587 (1990)
145. K Kusakabe, Y Tateyama, T Oguchi, S Tsuneyumi *Rev. High Pressure Sci. Technol.* **7** 193 (1998)
146. S Massidda, A Baldereschi *Solid State Commun.* **66** 855 (1985)
147. A H Silver, T Kushida *J. Chem. Phys.* **38** 865 (1963)
148. K Schwarz, H Ripplinger, P Blaha *Z. Naturforsch., A Phys. Sci.* **51** 527 (1996)
149. Y Kong, O V Dolgov, O Jepsen, O K Andersen *Phys. Rev. B* **64** 020501 (2001)
150. K Bohnen, R Heid, B Renker *Phys. Rev. Lett.* **86** 5771 (2001)
151. A Lin, I I Mazin, J Kortus http://xxx.lanl.gov/abs/cond-mat/0103570 (2001)
152. N I Mededeva, Yu E Medvedeva, A L Ivanovskii, V G Zubkov, A Friman *Pis'ma Zh. Eksp. Teor. Fiz.* **73** 378 (2001)
153. Y P Sun, W H Song, J M Dai, B Zhao, J J Du, H H Wen, Z X Zhao *Chin. Phys. Lett.* **18** 587 (2001)
154. S M Kazakov, M Angst, J Karpinski *Solid State Commun.* **119** 1 (2001)
155. Y G Zhao, X P Zhang, P T Qau, H T Zhang, S L Jia, B S Cao, M H Zhu, Z H Han, X L Wang, B L Gu http://xxx.lanl.gov/abs/cond-mat/0103077 (2001)
156. J S Ahn, E J Choi http://xxx.lanl.gov/abs/cond-mat/0103169 (2001)
157. S Zhang, J Zhang, T Zhao, C Rong, B Shen, Z Cheng *Chin. Phys.* **10** 335 (2001)
158. T Takenobu, T Ito, D H Chi, K Prassides, Y Iwasa http://xxx.lanl.gov/abs/cond-mat/0103241 (2001)
159. N V Vekshina, L Ya Markovskii, Yu D Kondrashev, T K Voevodskaya *Zh. Prikl. Khim.* **44** 958 (1971) [g]
160. C U Jung, M Park, W N Kang, K Kim, S Y Lee, S Lee *Physica C* **353** 162 (2001)
161. K Prassides, Y Iwasa, T Ito, D Chi, K Uehara, E Nushibori, M Takata, S Sakata, Y Ohishi, O Shimomura, T Muranaka, J Akimitsu *Phys. Rev. B* **64** 2509 (2001)
162. E Saito, T Taknenobu, T Ito, Y Iwasa, K Prassides, T Arima *J. Phys., Condens. Matter* **13** L267 (2001)
163. J D Jorgensen, D G Hinks, S Short *Phys. Rev. B* **63** 220508 (2001)
164. B Lorenz, R L Meng, C W Chu http://xxx.lanl.gov/abs/cond-mat/0102264 (2001)
165. I Loa, K Syassen *Solid State Commun.* **118** 279 (2001)
166. T Tomita, J J Hamlin, J S Schilling http://xxx.lanl.gov/abs/cond-mat/0103538 (2001)
167. A E Kar'kin, V V Voronin, T V D'yachkova, N I Kadyrova, A P Tyutyunnik, V G Zubkov, Yu G Zainulin, M V Sadovskii, B N Goshchitskii *JETP Lett.* **73** 570 (2001)
168. G Rubio-Bollinger, H Suderow, S Vieira *Phys. Rev. Lett.* **86** 5582 (2001)
169. A A Zhukov, K Yates, K G Perkins, Y Bugoslavsky, M Polichetti, A Berenov, J Driscoll, A D Caplin, L F Cohen *Supercond. Sci. Technol.* **14** L13 (2001)
170. W N Kang, H Kim, E Choi, C U Jung, S Lee http://xxx.lanl.gov/abs/cond-mat/0103179 (2001)
171. A Brikman, D Mijatovich, G Rijneders, V Leca, H Smodle, I Oomen, A A Golubov, F Roesthuis, S Hakema, H Hilgenkamp, D Blank, H Rogalla *Physica C* **353** 1 (2001)
172. D Blank, H Hilgenkamp, A Brikman, D Mijatovich, G Rijneders, H Rogalla *Appl. Phys. Lett.* **79** 394 (2001)
173. H M Christen, H Y Zhai, C Cantoni, M Paranthaman, B C Sales, R Rouleau, D P Norton, D K Christen, D Lowndes *Physica C* **353** 157 (2001)
174. S R Sinde, S B Ogale, R L Greene, T Venkatesan, P C Canfield, S L Bud'ko, G Lapertot, C Petrovic http://xxx.lanl.gov/abs/cond-mat/0103542 (2001)
175. C B Eom, M K Lee, J H Choi, L Belenky, X Song, L D Cooley, M T Naus, S Patanik, J Jiang, M Rickel, A Polyanskii, A Gurevich, X Y Cai, S D Bu, S E Babcock, E E Hellstrom, D C Larbalestier, N Rogano, K A Regon, M A Hayward, T He, J S Slusky, K Inumara, M K Haas, R J Cava *Nature (London)* **411** 558 (2001)
176. M Paranthaman, C Cantoni, H Y Zhai, H M Christen, T Aytug, S Sathyamuthy, E D Specht, J D Thompson, D H Lowndes, H R Kerchner, D K Christen *Appl. Phys. Lett.* **78** 3669 (2001)
177. G G Grassano, W Ramadan, V Ferrando, E Bellingeri, D Marre, C Ferdeghini, G Grasso, M Putti, A S Siri, P Manfrinetti, A Palenoza, A Chincarini http://xxx.lanl.gov/abs/cond-mat/0103572 (2001)
178. H Y Zhai, H M Chirsten, L Zhang, C Cantoni, M Paranthaman, B C Sales, D K Christen, D H Lowndes http://xxx.lanl.gov/abs/cond-mat/0103588 (2001)
179. Z K Liu, D G Schlom, Q Li, X Xi *Appl. Phys. Lett.* **78** 3678 (2001)
180. N Saunders, A P Miodownik *CALPHAD (Calculation of Phase Diagrams): a Comprehensive Guide* (Oxford: Pergamon Press, 1998)
181. R P Vasquez, C U Jung, M S Park, H-J Kim, J-Y Kim, S-I Lee *Phys. Rev. B* **64** 052510 (2001)
182. C L Perkins, R Singh, M Trenary, T Tanaka, Y Paderno *Surf. Sci.* **470** 215 (2001)
183. P C Canfield, D K Finnemore, S L Bud'ko, J E Ostenson, G Lapertot, C E Cunningham, C Petrovic *Phys. Rev. Lett.* **86** 2423 (2001)
184. S E Cunningham, C Petrovic, G Lapertot, S L Bud'ko, F Laabs, W Straszheim, D K Finnemore, P C Canfield *Physica C* **353** 5 (2001)
185. S L Bud'ko, C Petrovic, G Lapertot, C E Gunningham, P C Canfield *Phys. Rev. B* **63** 220503 (2001)
186. V Metlushko, U Welp, A Koshelev, I Aranson, G Crabtree, P C Canfield *Phys. Rev. Lett.* **79** 1738 (1998)
187. K Rathnayaka, A K Bhatnagar, A Parasiris, D Naugle, P C Canfield, B Cho *Phys. Rev. B* **55** 8506 (1997)
188. S V Shulga, S Drechsler, G Fuchs, K Muller, K Winzer, M Heinecke, K Krug *Phys. Rev. Lett.* **80** 1730 (1998)
189. M D Sumption, X Peng, E Lee, M Tomsic, E W Collings http://xxx.lanl.gov/abs/cond-mat/0102441 (2001)
190. G Grasso, A Malagoli, C Ferdeghini, S Roncallo, V Braccini, M R Cimberle, A S Siri *Appl. Phys. Lett.* **79** 230 (2001)
191. A Sharoni, O Millo, G Leitus, S Reich *J. Phys., Condens Matter* **13** L503 (2001)
192. C U Jung, J Choi, P Chowdhury, H P Kijoon, K Kim, M Park, H Kim, J Kim, Z Du, M Kim, W N Kang, S Lee, G Sung, J Y Lee http://xxx.lanl.gov/abs/cond-mat/0105330 (2001)
193. M Xu, H Kitazawa, Y Takano, J Ye, K Nishida, H Abe, A Matsushita, G Kido http://xxx.lanl.gov/abs/cond-mat/0105271 (2001)
194. J Hlinka, I Gregora, J Pokorny, A Plecenik, P Kus, L Satrapinsky, S Benacka http://xxx.lanl.gov/abs/cond-mat/0105275 (2001)
195. S Lee, H Mori, T Masui, Yu Eltsev, A Yamamoto, S Tajima http://xxx.lanl.gov/abs/cond-mat/0105545 (2001)
196. Appl. Russ. 108 865 (2001)
197. W N Kang, H Kim, E M Choi, C U Jung, S L Lee *Science* **292** 1521 (2001)
198. J H Jung, K W Kim, H J Lee, M W Kim, T W Noh, W N Kang, H Kim, E M Choi, C U Jung, S L Lee http://xxx.lanl.gov/abs/cond-mat/0105180 (2001)
199. S Patnaik, L D Cooley, A Gurevich, A A Polyanskii, J Jiang, X Y Cai, A A Squitieri, M T Naus, M K Lee, J H Choi, L Belenky, S D Bu, S D Letteri, X Song, D Schlom, S E Babcock, C B Eom, E E Hellstrom, D C Larbalestier *Supercond. Sci. Technol.* **14** 315 (2001)
200. H J Zhai, H M Christen, L Zhang, M Paranthaman, C Cantoni, B C Sales, P H Fleming, D K Christen, D H Lowndes http://xxx.lanl.gov/abs/cond-mat/0103618 (2001)
201. Z W Zhao, H H Wen, S L Li, Y M Ni, H P Yang, W N Kang, H J Kim, E M Choi, S I Lee http://xxx.lanl.gov/abs/cond-mat/0104249 (2001)
202. S F Wang, S Y Dai, Y I Zhou, Z H Chen, D F Cui, J D Yu, M He, H B Lu, G Y Yang *Chin. Phys. Lett.* **18** 967 (2001)
203. X D Zeng, A Sukiasyan, X X Xi, Y F Hu, E Wertz, Q Li, W Tian, H P Sun, X Pan, J Lettieri, D Schlom, C O Brubaker, Z Liu http://xxx.lanl.gov/abs/cond-mat/0105080 (2001)
204. A H Li, X L Wang, M Ionescu, S Soltonian, J Horvat, T Silver, H K Liu, S X Dou http://xxx.lanl.gov/abs/cond-mat/0104156 (2001)
205. H J Zhai, H M Christen, L Zhang, M Paranthaman, P H Fleming, D H Lowndes http://xxx.lanl.gov/abs/cond-mat/0104309 (2001)

206. S Y Lee, J H Lee, J S Ryu, J Lim, S H Moon, H N Lee, H G Kim, B Oh http://xxx.lanl.gov/abs/cond-mat/0105327 (2001)
207. H J Kim, W N Kang, F M Choi, M S Kim, K H P Kim, S I Lee http://xxx.lanl.gov/abs/cond-mat/0105363 (2001)
208. M H Jung, M Jaime, A H Lacerda, G S Boebinger, W N Kang, H J Kim, E M Choi, S I Lee http://xxx.lanl.gov/abs/cond-mat/0106146 (2001)
209. A Berenov, Z Lockman, X Qi, Y Bugoslavsky, L F Cohen, M H Jo, N A Stelmashenko, V N Tsaneva, M Cambara, N Hari Babu, D A Cardwell, M G Blamire, J L Mac Manus-Driscoll http://xxx.lanl.gov/abs/cond-mat/0106278 (2001)
210. C Ferdeghini, V Ferrando, G Grassano, W Ramadan, E Bellingeri, V Braccini, D Marre, P Manfrinetti, A Palenzona, F Borgatti, R Felici, T L Lee http://xxx.lanl.gov/abs/cond-mat/0107031 (2001)
211. V M Silkin, E V Chulkov, P M Echenique http://xxx.lanl.gov/abs/cond-mat/0105628 (2001)
212. Z Li, J Yang, J G Hou, Q Zhu http://xxx.lanl.gov/abs/cond-mat/0106590 (2001)
213. V A Gasparov, N I Sidorov, I I Zver'kova, M P Kulakov *JETP Lett*. **73** 532 (2001)
214. G K Strukova, V F Degtyareva, D V Shivkun, V N Zverev, V M Kiiko, A M Ionov, A N Chaika http://xxx.lanl.gov/abs/cond-mat/0105293 (2001)
215. D P Young, P W Adams, J Y Chan, F R Fronczek http://xxx.lanl.gov/abs/cond-mat/0104063 (2001)
216. T He, Q Huang, A P Ramirez, Y Wang, K A Regan, N Rogado, M A Hayward, M K Haas, J S Slusky, K Inumaru, H W Zandbergen, N P Ong, R J Cava *Nature (London)* **411** 6833 (2001)
217. A Taraphder, R Pandit, H R Krishnamurthy, T V Ramakrishnan *Int. J. Mod. Phys. B* **10** 863 (1998)
218. A L Ivanovskii *Usp. Khim*. **68** 119 (1999) [*Russ. Chem. Rev*. **68** 103 (1999)]
219. S Y Li, R Fan, X H Chen, C H Wang, W Q Mo, K Q Ruan, Y M Xiong, X G Luo, H T Zhang, L Li, Z Sun, L Z Cao http://xxx.lanl.gov/abs/cond-mat/0104554 (2001)
220. Z Q Mao, M M Rosario, R Nelson, K Wu, I G Deac, P Schiffer, Y Liu, T He, K A Regan, R J Cava http://xxx.lanl.gov/abs/cond-mat/0105280 (2001)
221. Q Huang, T He, K A Regan, N Rogado, M A Hayward, M K Haas, K Inumaru, R J Cava http://xxx.lanl.gov/abs/cond-mat/0105240 (2001)
222. M A Hayward, M K Haas, T He, K A Regan, N Rogado, K Inumaru, R J Cava http://xxx.lanl.gov/abs/cond-mat/0104541 (2001)
223. Z A Ren, G C Che, S L Jia, H Chen, Y M Ni, Z X Zhao http://xxx.lanl.gov/abs/cond-mat/0105366 (2001)
224. I R Shein, N I Medvedeva, A L Ivanovskii *JETP Lett*. **74** 122 (2001)
225. S B Dugdale, T Jarlborg http://xxx.lanl.gov/abs/cond-mat/0105349 (2001)
226. J H Shim, B I Min http://xxx.lanl.gov/abs/cond-mat/0105418 (2001)
227. D J Singh, I I Mazin http://xxx.lanl.gov/abs/cond-mat/0105577 (2001)
228. I R Shein, N I Medvedeva, A L Ivanovskii http://xxx.lanl.gov/abs/cond-mat/0107010 (2001)

[a] — *Russ. J. Gen. Chem. (Engl. Transl.)*
[b] — *Dokl. Chem. (Engl. Transl.)*
[c] — *Russ. J. Inorg. Chem. (Engl. Transl.)*
[d] — *Russ. J. Phys. Chem. (Engl. Transl.)*
[e] — *Inorg. Mater. (Engl. Transl.)*
[f] — *Phys. Solid State (Engl. Transl.)*
[g] — *Russ. J. Appl. Chem. (Engl. Transl.)*

Russian Chemical Reviews **70** (9) 735 – 776 (2001) © 2001 Russian Academy of Sciences and Turpion Ltd

DOI 10.1070/RC2001v070n09ABEH000683

Synthetic methodologies for carbo-substituted conjugated dienes

A A Vasil'ev, E P Serebryakov

Contents

I.	Introduction	735
II.	Elimination reactions	735
III.	Olefination of carbonyl compounds	742
IV.	Organometallic reactions	749
V.	The synthon approach to conjugated dienes	760
VI.	Electrocyclic reactions	763
VII.	Methods based on migration or reduction of multiple bonds	766
VIII.	Miscellaneous methods	768
IX.	Conclusion	770

Abstract. The scope of this review encompasses methods and synthetic protocols leading to conjugated dienes bearing no heteroatoms in the C=C–C=C moiety. Attention is concentrated on methodologies developed during the last decade, particularly, to the metal complex-mediated synthesis. The bibliography includes 494 references.

I. Introduction

Until about 1960, the synthetic chemistry of conjugated dienes was focused mainly on their simplest representatives. Usually, these dienes were prepared either by dehydrating diols and allylic or homoallylic alcohols or by eliminating the elements of HX (X = OAlk, OCOR, OSO_2R, Hal, *etc*.) from properly selected unsaturated substrates. However, such techniques were unsuitable for the synthesis of higher homologues, because the use of these reactions resulted in mixtures of isomers.

Then, in the mid-sixties a new period in the synthesis of conjugated dienes began, as this class of compounds became increasingly in demand. This popularity was due to the fact that dienes with fixed position of configurationally defined double bonds and with various sensitive functional groups (and their combinations) had been identified by that time as fragments of many natural products. Moreover, inter- and intramolecular Diels – Alder reactions employing conjugated dienes had become widely used tools in the synthesis of cyclic molecules.

Advances in organometallic chemistry and metal complex catalysis highlighted dienes as useful four-electron π-ligands capable of forming interesting metal complexes. These aspects of diene chemistry are considered, with due attention to details, in two recently published review collections.[1,2] Finally, stereospecific 1,4-*cis* hydrogenation of conjugated dienes using chromium carbonyl complexes proved to be an efficient, preparatively viable method for stereocontrolled synthesis of alkenes.[3,4]

Abundant literature on the synthesis of conjugated dienes has been accumulated, and systematic surveys have been periodically attempted during the last thirty years. Among early sources (up to the late 1980's), the serial edition of Houben – Weyl[5] and a few monographs and collective volumes[6–9] should be mentioned, because some chapters there are dedicated to conjugated dienes. Another good source of references (not commented on) is a compendium of reactions leading to dienes.[10] Also useful is a monograph,[11] where numerous methods for constructing conjugated dienes are cited in the context of pheromone synthesis. A review on the synthesis of conjugated polyenes, where the dienes were considered as parental polyene systems,[12] was published in 1997 in a book[1] that is nearly inaccessible in Russia. This makes the appearance of an updated review quite opportune, let alone the fact that in the last four years the chemistry of conjugated dienes has been enriched with some new and interesting synthetic methods.

This review aims at a systematic survey of selective methods for obtaining conjugated carbo-substituted dienes that were elaborated between the end of 1960 and March, 2001. Methods leading to the molecules with heteroatomic substituents on the C=C–C=C unit will be mentioned just in a few exclusive cases. The description of reactions used will be focused on their preparative aspects; the mechanisms will be mentioned only when it is necessary, since most of them have been considered in detail in original publications.

A A Vasil'ev, E P Serebryakov N D Zelinsky Institute of Organic Chemistry, Russian Academy of Sciences, Leninsky prosp. 47, 119991 Moscow, Russian Federation. Fax (7-095) 135 53 28. Tel. (7-095) 938 35 30. E-mail: vasiliev@ioc.ac.ru (A A Vasil'ev), ser@ioc.ac.ru (E P Serebryakov)

Received 1 June 2001
Uspekhi Khimii **70** (9) 830 – 873 (2001); translated by E P Serebryakov, Z P Bobkova

II. Elimination reactions

Elimination reactions leading to alkenes basically can be divided into two groups. The first group involves the ejection of a nucleofugal group and a vicinal hydrogen or metal atom. The second one involves reductive elimination of two vicinal groups. When the substrate already has a double bond adjacent to one of the groups undergoing elimination, the product of the reaction is a conjugated diene.

1. Elimination of HX

Elimination of one molecule of water from 2-methylbut-3-en-2-ol (Favorskii's method) or of two molecules of water from butane-1,3-diol (the last step in Lebedev's process) as well as catalytic

thermolysis of 4,4-dimethyl-1,3-dioxane (Farberov's method) are classical ways of obtaining dienic monomers applicable to other lower conjugated dienes. However, the conditions under which the processes are performed are too drastic to be useful for obtaining more labile, functionally substituted higher dienes.

Elimination of HX from substrates of allylic or homoallylic type proceeds regiospecifically only for molecules with specific patterns of substitution, *e.g.*, for compounds **1**[13] or **2**.[14] If the substrate contains a functional group strongly stabilising only one of the possible isomeric products, this also can favour an unambiguous course of the process (*e.g.*, in the case of reactions **3** → **4**[15] and **5** → **6**[16]).

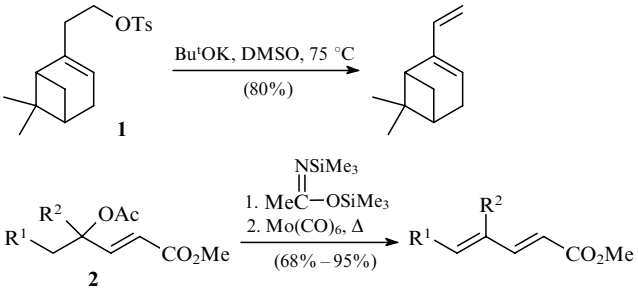

R^2 = H, CH_2R^1.

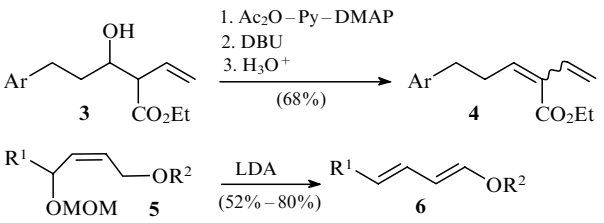

DMAP is 4-dimethyaminopyridine; DBU is 1,8-diazabicyclo-[5.4.0]undec-7-ene; MOM is methoxymethyl; LDA is lithium diisopropylamide.

Generally, elimination of HX or MX from allylic-type substrates affords isomer mixtures. However, in the presence of palladium catalysts the reaction proceeds regioselectively. In these cases substituents R^1 in starting compounds **7**–**9** can contain functional groups.[17, 18]

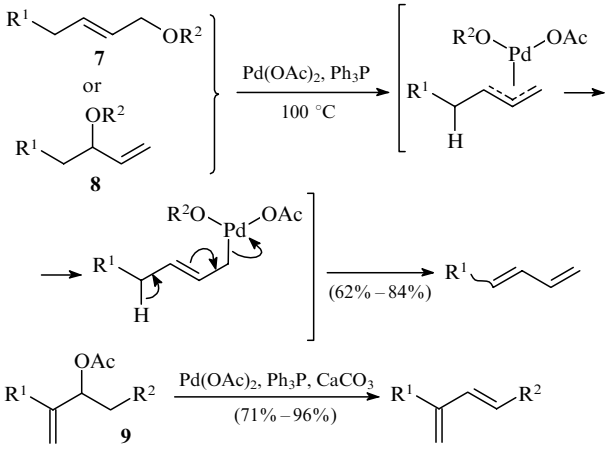

In this way neryl acetate was converted to myrcene, while geranyl acetate afforded a mixture of *cis* and *trans* isomers of β-ocymene.[19]

In the presence of palladium catalysts, the ring opening in acyclic vinylic oxiranes **10** and **11** proceeds smoothly to give α-dienols **12** and **13**.[20] The regioselectivity of these reactions depends on the position of substituents at the epoxide ring.

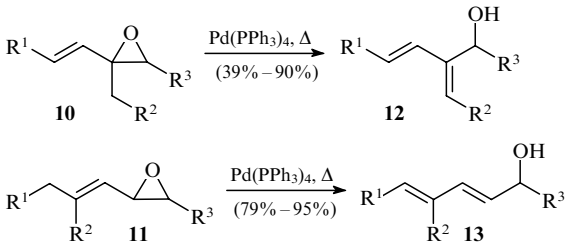

Elimination of CO_2 from alkenyl-substituted cyclic carbonates **14** takes place in the same manner, but the resulting diene **15** is obtained predominantly as the *E*,*E*-isomer whatever the configuration of the starting compound.[21]

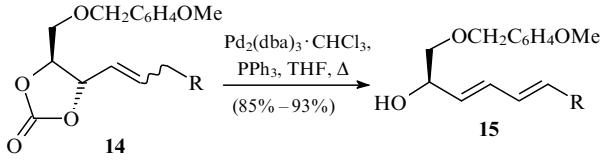

dba is dibenzylideneacetone.

Epoxides **16** (substituents R^1 and R^2 can contain ester groupings) undergo regiospecific formal dehydration mediated by organophosphorus reagents.[22, 23]

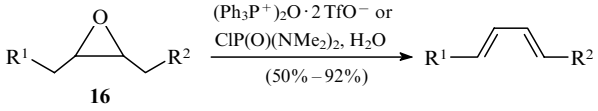

A three-step protocol of formal α,α′-elimination of water from allylic alcohols **17** is based on their chemoselective epoxidation in the presence of a silylating agent and vanadium catalysts.[24, 25] Subsequent opening of the epoxide ring in compounds **18** by mild Lewis acids proceeds regiospecifically (the ejection of proton occurs exclusively from the substituent lying in the *trans*-position relative to the silyloxy group), and affords unsaturated diols **19**. Finally, circumventional elimination of vicinal hydroxy groups from **19** gives an additional double bond. In this way nerol is readily transformed to myrcene, and geraniol to *trans*-β-ocymene.

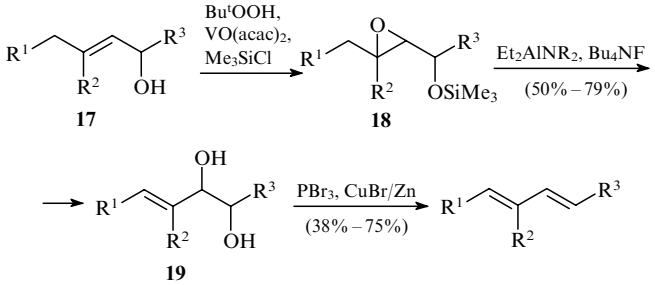

2. Deamination

An interesting method for the conversion of pyridines **20** into allylic (*Z*,*E*)-dienylamines **21** begins with quaternisation of their nitrogen atom followed by reduction, another methylation and subsequent Hofmann degradation of the resulting intermediate **A** (Scheme 1).[26, 27] Then, after yet another quaternisation, the amino group of compound **21** can be replaced by a carbonaceous substituent. The intermediate *Z*,*E*-dienes **21** can be isomerised to give the corresponding *E*,*E*-dienes **22** by treating the corresponding *N*-oxides with trifluoroacetic acid, and subsequently by reductive substitution. This protocol was employed in the synthesis of insect pheromones.[27]

3. Reductive elimination

The reduction of alk-2-ene-1,4-diols[28] **23** or of the respective ethers[29, 30] in the system $LiAlH_4 – TiCl_3$ was used in the synthesis of retinoids **24**[31, 32] and other natural products.[30, 33]

Scheme 1

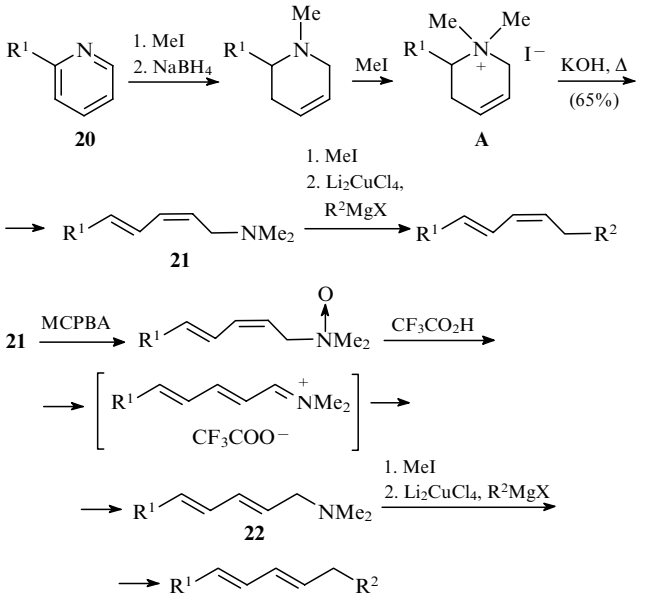

MCPBA is *m*-chloroperbenzoic acid.

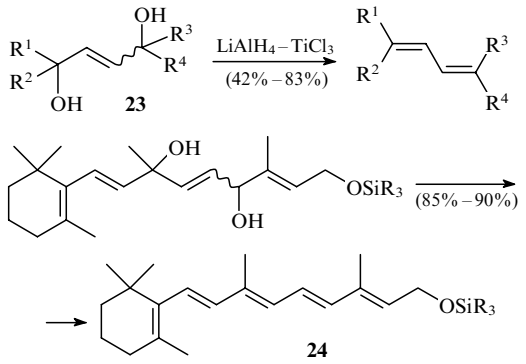

Reductive elimination of halogen atoms from 1,2,3,4-tetrahaloalkanes **25**, 1,2-dihaloalk-3-enes **26** and 1,4-dihaloalk-2-enes **27** gives 1,3-dienes in good yields. In addition to the traditional zinc,[34,35] the salts of arenetellurols were recommended.[36] In the latter case, the process can be performed readily using catalytic amount of Ar_2Te_2 that is periodically reduced by titrating the reaction mass with sodium borohydride. This method was applied to a number of linear and cyclic substrates, including those bearing additional functional groups.†

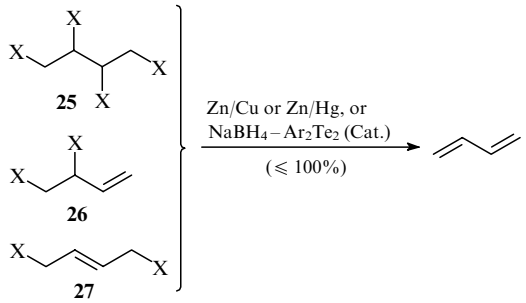

† 1,4-Dibromoalk-2-enes **27** can be prepared by treating internal[35] and, what is particularly interesting, terminal alkenes with 2 equiv. *N*-bromosuccinimide.[36] In the latter case, the bromination occurs in a stepwise mode involving allylic rearrangement. 1,2-Dibromoalk-3-enes **26** can be prepared from the corresponding diols which, in their turn, are obtainable from allylic alcohols.[25]

Reductive scission of *cis*-3-chloro-2-vinyltetrahydrofuran (**28**) with samarium iodide results in (*E*,*E*)-hexa-3,5-dien-1-ol (**29**) of > 97% geometric purity.[37] The same stereochemical result is observed in the case of 2-alkynyl-3-chlorotetrahydrofurans (**30**, $n = 1$). By contrast, their tetrahydropyran homologues (**30**, $n = 2$) in the same reaction afford the *Z*-configured enynols **31**, supposedly due to different conformational behaviour of five-membered and six-membered heterocycles.[37]

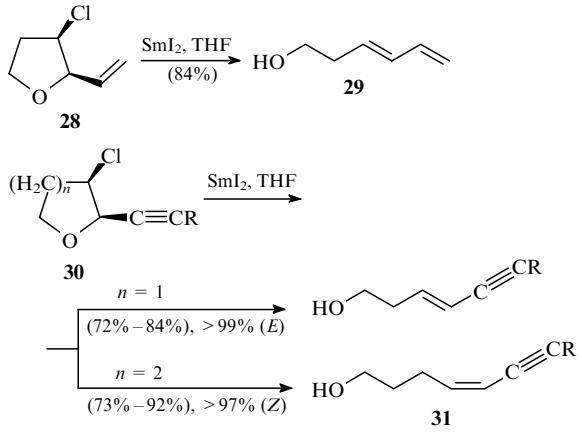

When allylic nitro compounds of the type **32** are treated with chromium(II) diacetate [$Cr(OAc)_2$ – Dipy system in dimethylformamide], their vicinal nitro- and mesyloxy (or acetoxy) groups undergo reductive elimination, which results in the formation of an additional double bond. These transformations were used to obtain conjugated dienes **33**, albeit in moderate yields.[38]

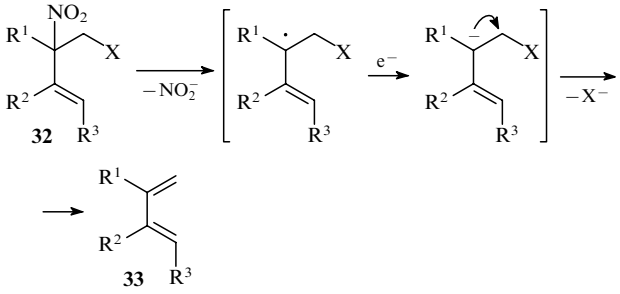

X = OMs, OAc.

4. Stereocontrolled 1,2-elimination of R_3SiX and R_3SnX

The Peterson reaction (see a review[39]) consists in simultaneous elimination of vicinal hydroxy and silyl groups and results in the formation of a double bond. This transformation can occur both in the presence of bases (*e.g.*, Bu^{t}OK, KH) and acids (AcOH, H_2SO_4). The double bond configuration in product(s) **34** depends on the reaction conditions. When the starting compound **35** is treated with a base, the primarily formed alkoxide undergoes *syn*-elimination upon which a molecule of metal silanolate is ejected. When the process is initiated with an acid, it starts with protonation of the hydroxy group, followed by *anti*-elimination of a molecule of water, together with a silyl cation.

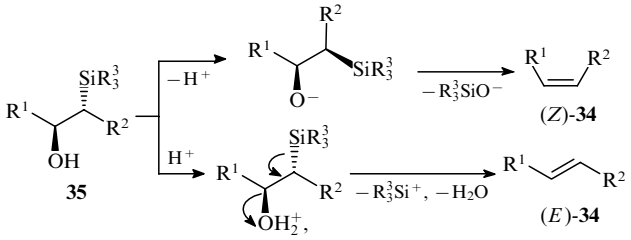

This approach can be used for the synthesis of dienes, when a double bond is already present in the starting compound. Depending on the mutual arrangement of substituents in substrates **36** and

37 and on the process conditions, one obtains diene(s) **38** in the required configuration.‡

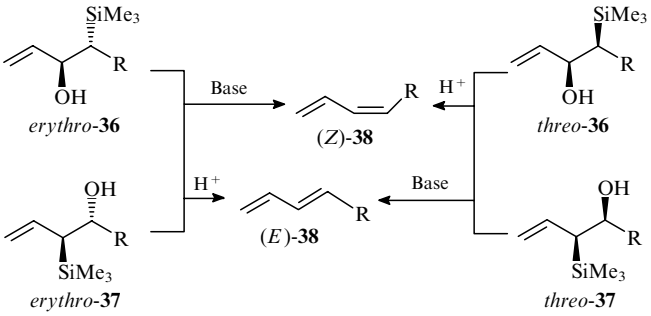

In a vinylogous version of the Peterson reaction, compounds **39** and **40** in which the allylic hydroxyl and the silyl group are located at the opposite ends of the double bond are employed as the starting substrates.[50,51] If the silyl group is attached to the terminal carbon atom (as in compounds **39** and **40**), the resulting diene **38** has always the *E*-configuration. When both the hydroxyl and the silyl group are attached to secondary carbon atoms in *erythro* relationship, the reaction affords the *E*,*E*-dienes.[52]. However, in the case of their *threo*-relationship, the resulting dienes are in the *E*,*Z*-configuration, the *Z*-bond being formed at the hydroxyl-bearing carbon atom.

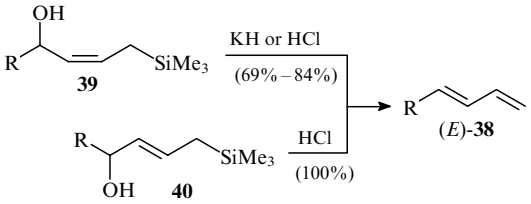

Compounds **41** containing Group IV and VI higher elements (*e.g.*, S and Sn, instead of O and Si) react similarly and spontaneously under very mild conditions; no catalyst is needed.[53]

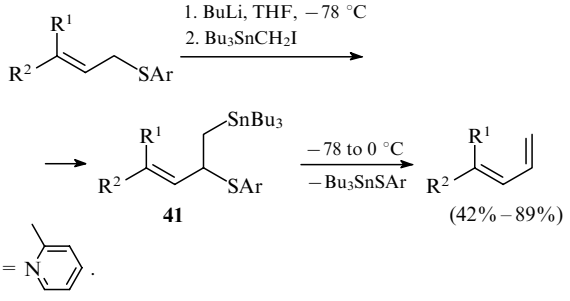

5. Oxidative 1,2-*syn*-elimination of RSeOH and RSOH

Oxidative elimination of an organoselenium fragment from aliphatic selenides is a relatively new method of alkene synthesis (see reviews [54–57]). This process involves the oxidation of a selenide to the corresponding selenoxide, which then undergoes spontaneous *syn*-elimination to give an alkene and a selenenic acid. This method has been widely used in syntheses of natural products of rather complicated structure, because there are many versatile methods for obtaining necessary organoselenium precursors (see, *inter alia*, the publications on the synthesis of α-arylseleno-γ-alkenoic acids [58–60]). Elimination of RSeOH from homoallylic selenides **42** leads to conjugated alkyl dienoates **43**.[60–65]

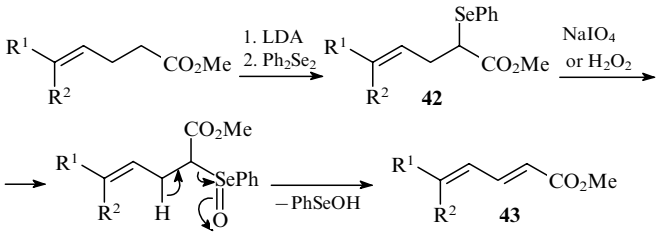

By contrast, instead of giving conjugated dienes *via* oxidative elimination, the oxidation of allylic selenides **44** mostly triggers a [2,3]-sigmatropic rearrangement that finally results in 're-arranged' allylic alcohols.[66,67]

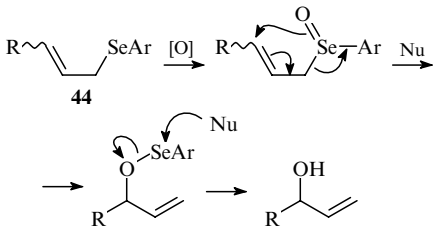

R = Alk, Ar′; Ar = *p*-$NO_2C_6H_4$.

Allylic 2,4-dinitrophenyl selenides appear to be an exclusion,[68] but even in this case, the resulting conjugated dienes are accompanied by noticeable amounts of allylic alcohols.

Due to high nucleophilicity of areneselenolates, they can open the five-membered lactone ring in compounds **45** to give selenides **46**, and subsequently conjugated dienes **47** with a functional group in the side chain.[69]

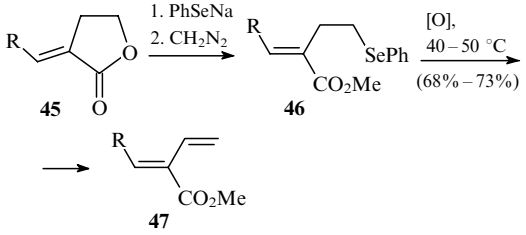

By analogy with selenoxides, aliphatic sulfoxides can undergo oxidative elimination to give alkenes, but at higher temperatures. This can be illustrated by the fragmentation of sulfoxides that were prepared by oxidising sulfides **48** and **49**.[70,71] The latter were obtained upon the addition of sulfur-containing cationoid reagents to terminal alkenes.

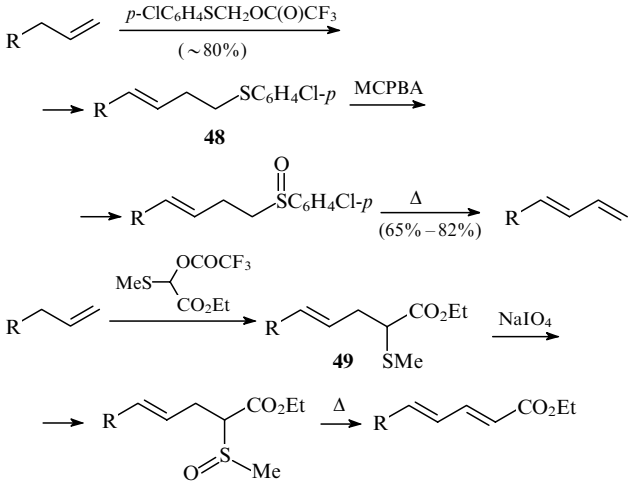

Elimination of a sulfoxide unit was used as the final stage in the synthesis of 2-hydroxymethylbuta-1,3-diene from 2-bromoethyl phenyl sulfide.[72]

‡ Various protocols for the preparation of starting β-hydroxysilanes have been elaborated.[40–49] Particularly interesting are the reagents of the type R_3SiCH_2X (X = CO_2Alk, CN, *etc.*), which are widely used in the olefination of carbonyl compounds.[46–49]

α-Sulfinyl esters **50**, immediate precursors of alkyl alka-2,4-dienoates, are stable at room temperature. They can be readily prepared from synthon **51**, which already contains a sulfoxide grouping.[73]

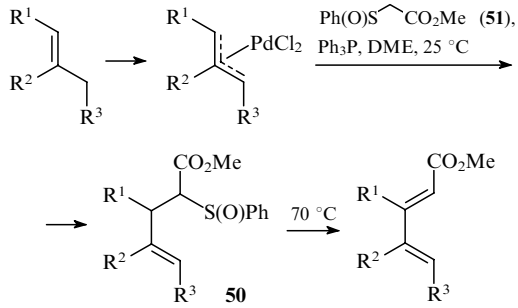

DME is 1,2-dimethoxyethane.

Unlike allylic selenoxides, allylic sulfoxides can be used for obtaining conjugated dienes.[66, 74] A convenient way of performing this process involves the esterification of allylic alcohols **52** with arenesulfenyl chlorides (the best results are obtained when Ar = 2,4-dinitrophenyl) followed by the rearrangement of intermediate sulfenates **53** into sulfoxides **54**; the latter then undergoing elimination to give dienes **55**.

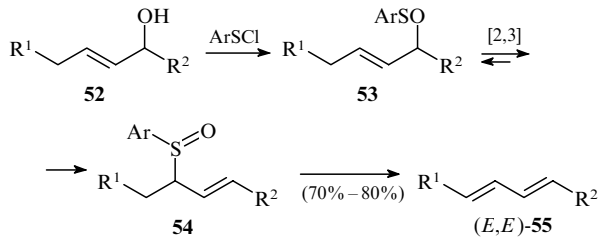

Conjugated dienes with extended carbon chains (*e.g.*, dienic alcohol **56**) can be synthesised from suitable allylic sulfides.[75]

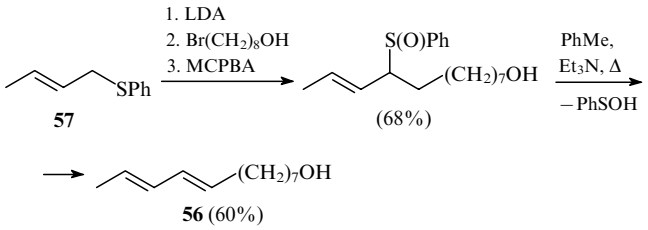

Vinyl sulfoxides of the type **58** rearrange on heating to allylic sulfoxides **59** that afford conjugated dienes upon eliminating ArSOH.[76]

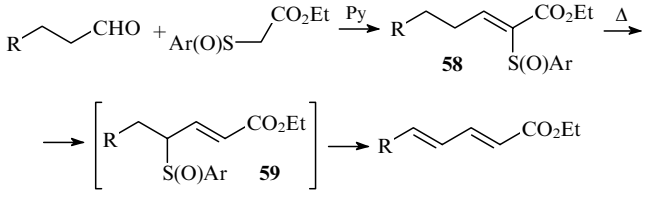

6. 1,2-Elimination of $ArSO_2H$

On treatment with bases, alkyl phenyl sulfones eject the phenylsulfinate anion to give alkenes. If the molecule of sulfone has already a double bond, this reaction leads to dienes. A synthesis of conjugated dienes from homoallylic sulfones **60** is known,[77] where the latter were obtained by sequential alkylation of bis(phenylsulfonyl)methane (**61**) first with allyl- and then with alkyl halides.

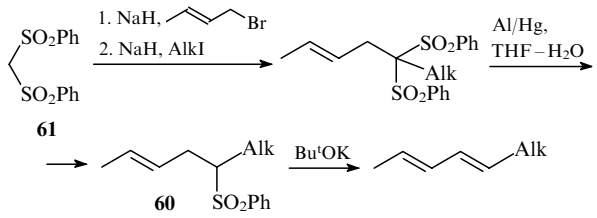

β-Acetoxysulfones **62** can be used as the precursors of alkenes **63** in the Julia method of olefination (aldol-like alkylation of an alkyl phenyl sulfone followed by acylation to give **62**, then elimination of AcOM, and reduction of the resulting vinyl sulfones **64** to give alkene **63**)[78, 79] However, when a large excess of a stronger base is used (~10 equiv.), both substituents in the acetoxy sulfone **62** undergo elimination, which gives rise to the conjugated dienes **55**.[80, 81] The dienes **55** can be obtained from the sulfones **64** either directly, or *via* intermediate allylic sulfones **65** (Scheme 2).

Scheme 2

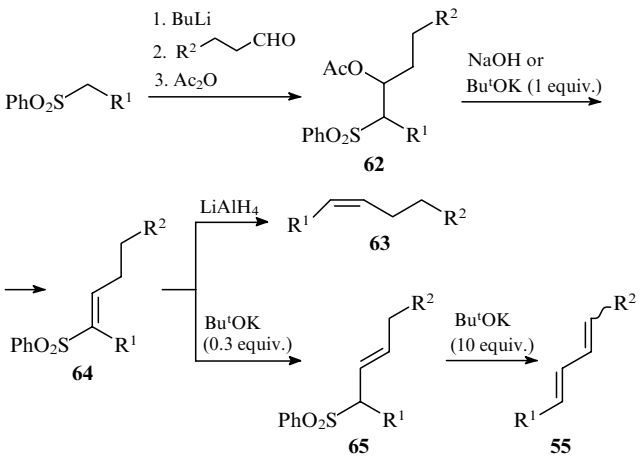

This approach is also applicable to the synthesis of amides (**66**)[82, 83] or esters (**67**)[83] of conjugated dienoic acids.

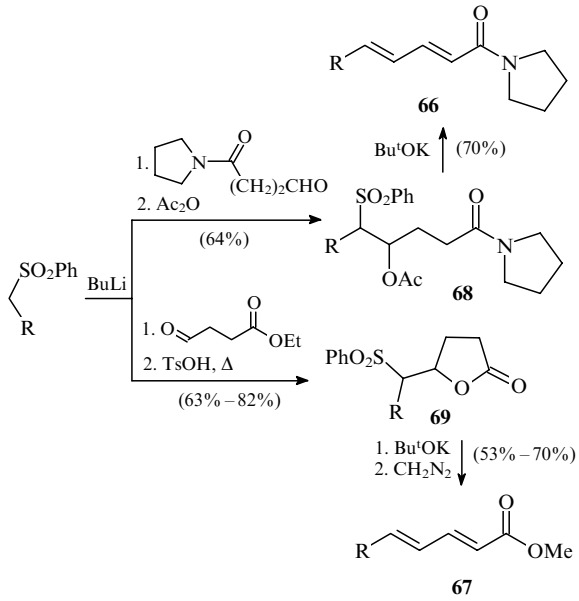

It should be noted that in the former case, there is no need to isolate the intermediate amides **68**, while in the latter case, the isolation of (1-sulfonylalkyl)butyrolactones **69** is necessary.

The terminal 1,3-dienes (*E*)-**38** are readily converted into the corresponding 2-phenylsulfonyl-1,3-dienes **70** upon treatment with $PhSO_2SePh$ (see a review[84]). The latter are strongly electrophilic, and thus are capable of adding C-nucleophiles. This is a

Scheme 3

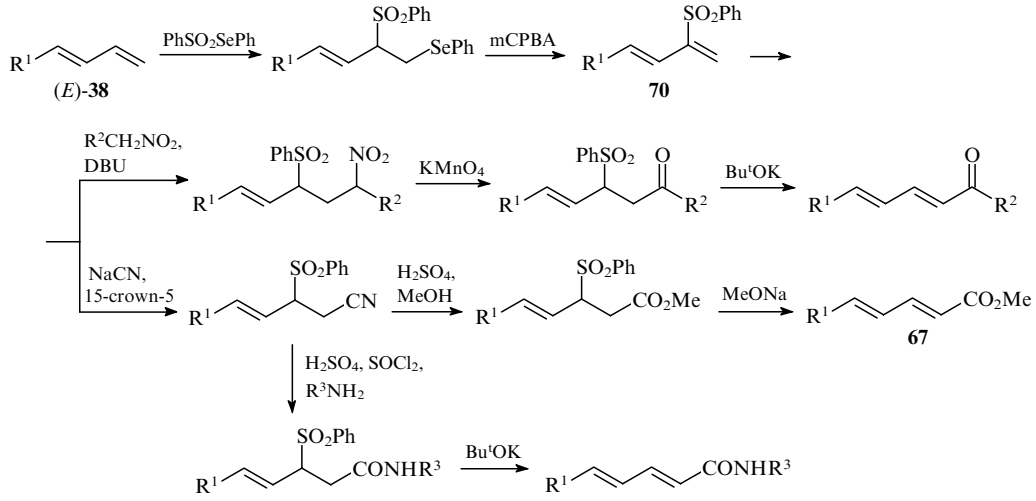

convenient method for the introduction of a functionalised alkyl substituent to the 1-position of conjugated dienes (Scheme 3).[85,86]

7. Fragmentation of α-halogen-substituted sulfones

The 'vinylogous' Ramberg–Bäcklund reaction (see a review [87]) is yet another example of obtaining 1,3-dienes from sulfones. From preparative standpoint, it is a C_1-homologation of alkenes with a view of introducing an additional double bond; bromomethylsulfonyl bromide (**71**), readily accessible upon bromination of 1,3,5-trithiane, is used here as a C_1 synthon.[88,89]

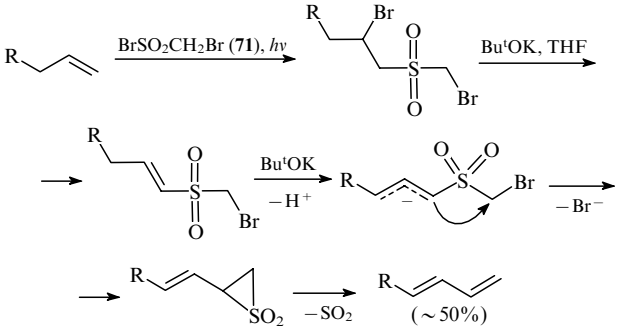

High regiospecificity of diene formation is observed when cyclic alkenes are used as the starting compounds. Thus the only products obtained from cycloalkenes are 3-methylenecycloalkenes, 1-methylcycloalkenes react to give 1,2-dimethylenecycloalkanes, and methylenecycloalkanes afford 1-vinylcycloalkenes.[90] In all cases, the yields of dienes are moderate. Functionally substituted alkenes have been rarely used in these reactions.

tert-Butyl methoxycarbonylmethyl sulfoxide (**72**) proved to be a convenient synthon for elongating the skeleton of allylic alcohols **73** by a C_2 moiety. The transformation takes place *via* intermediates **74** and **75** to afford alka-2,4-dienoic acids **76**.[91] Its final step is the Ramberg–Bäcklund reaction, the key intermediate of which is generated by deprotonating sulfone **76** and submitting the carbanion to α-chlorination with CCl_4 (not shown).

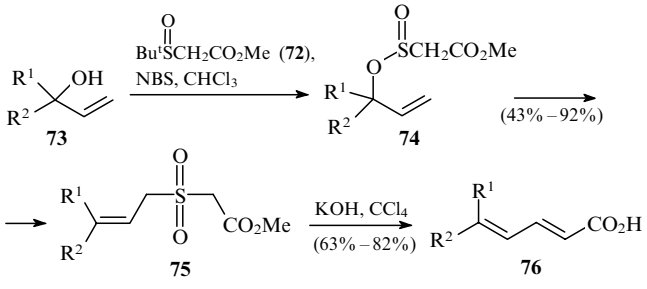

NBS is *N*-bromosuccinimide.

8. Cheletropic elimination

The ability of β-sulfolenes to undergo reversible fragmentation into 1,3-dienes and SO_2 (see a monograph [92]) underlies a versatile synthesis of dienes with somewhat sophisticated structure starting with successive α,α′-bis-alkylation of parental sulfolene **77**.[93,94] Depending on the procedure used to decompose the alkylated sulfolene **78**, one obtains either *E*,*E*- or *E*,*Z*-dienes. The parental sulfolene **77** acts in this method as a synthetic equivalent of 1,4-dianion of buta-1,3-diene. This strategy was employed in the synthesis of some pheromones of *Lepidoptera* that contain terminal or internal *E*,*E*-configured diene substructures.

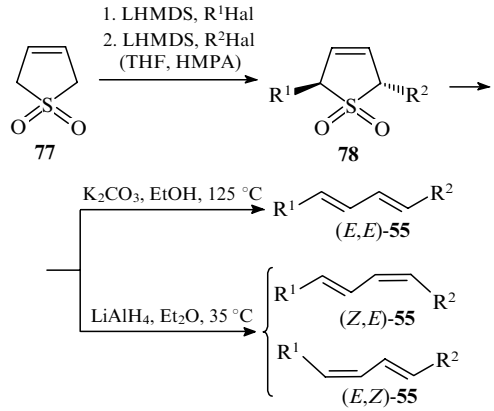

LHMDS is the lithium derivative of hexamethyldisilazane, HMPA is hexamethylphosphoramide.

For the alkylation of sulfolene-derived carbanions, it was recommended to use manganese as the counter-ion. The use of manganese counter-ion enhances the thermal stability of carbanions, so that even allylic halides with additional electrophilic groups (*e.g.*, methyl 4-bromocrotonate) [95] can be used as alkylating reagents. Another way to overcome the lability of sulfolene-derived anions is the use of its synthetic equivalent, tricyclic compound **79** (this sulfolane is prepared by cycloaddition of cyclopentadiene to 3-sulfolene). Upon vapour-phase thermolysis (650 °C), the alkylated derivatives thus formed (**80**) undergo two-step retro-fragmentation to give the *E*,*E*-configured internal dienes **55** of 91%–95% purity.[96]

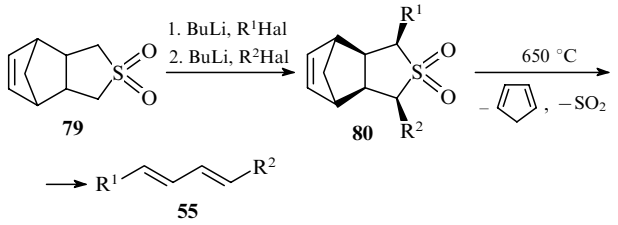

The latter approach proved useful also in the synthesis of insect pheromones.[97,98]

On treatment with NEt_3, 3-bromomethyl-3-sulfolene **81** is converted into 4-methylene-2-sulfolene **82**.[99] The latter, as well as its alkylated derivatives **83**, can readily enter into the Michael reaction with such nucleophiles as amines, thiols and nitroalkane-derived anions, which leads to modified β-sulfolenes **84** and **85** in up to 90% yields. Subsequent thermolysis of **84** or **85** gives rise to the branched 1,3-dienes with functionalised substituents.

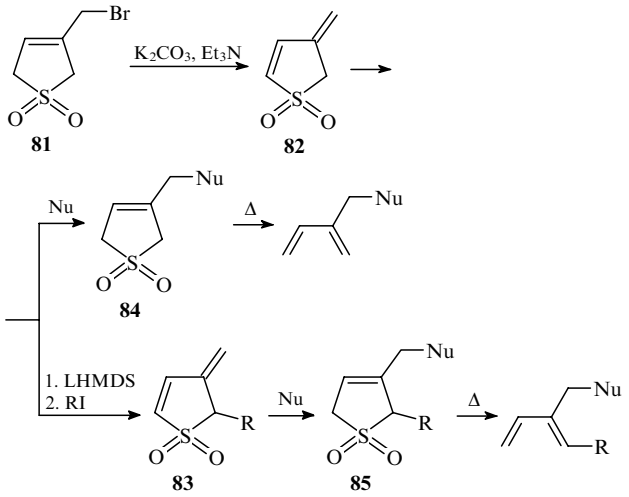

Other approaches to conjugated dienes from variously substituted and functionalised β-sulfolenes have been also reported. In one of them, readily accessible α-acylthiophenes **86** were used as the starting compounds for obtaining α-branched conjugated dienones **87** in three or four synthetic operations.[100]

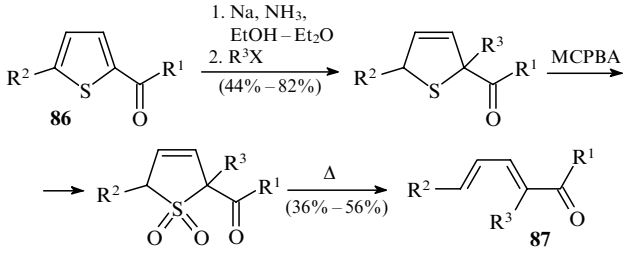

Another group of sulfolenes suitable for the synthesis of conjugated dienes can be obtained from vinylic phosphonates **88** and mercaptoacetaldehyde **89**; the synthetic protocol comprises two sequential Michael reactions followed by intramolecular Horner – Wadsworth – Emmons (HWE) reaction and oxidation.[101] It is recommendable to perform the thermolysis of sulfolenes **90** directly in the presence of electron-deficient dienophiles. This technique was employed in an elegant synthesis of compound **91**, an alkaloid of eleocanine group, from sulfolene **92**.[102]

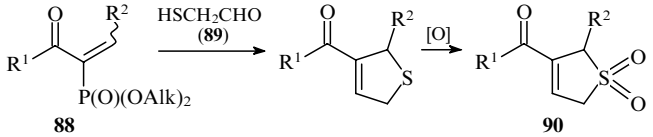

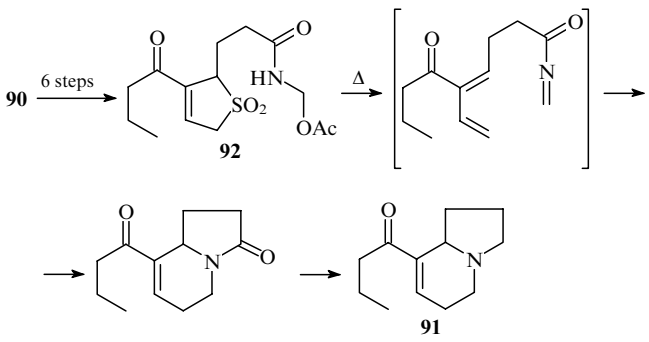

90: $R^1 = Pr^n$, $R^2 = (CH_2)_2CH=CH_2$.

β-Hydroxy acids are prone to decompose with the formation of alkenes and concomitant ejection of carboxy and hydroxy groups. If such substrates (*e.g.*, β-hydroxy acid **93**) have already a double bond, their fragmentation will give dienes. This process can be carried out by treating acids **93** either with *N*,*N*-dimethylformamide acetals [103] or with acetic anhydride.[104] Decomposition of β-acetoxy acids **94** is catalysed by palladium complexes.

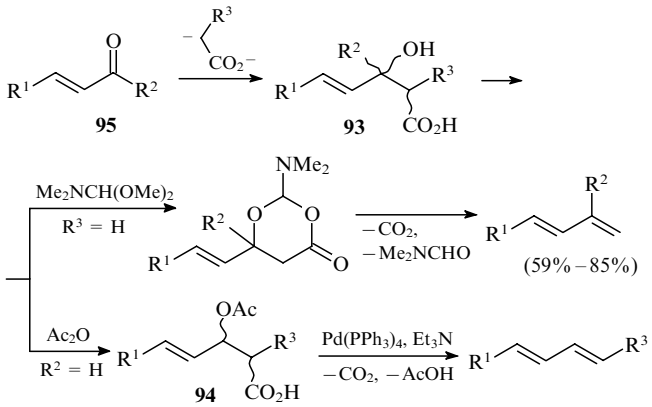

Although intermediate acetoxy acids **94** are obtained as mixtures of stereoisomers, the newly formed double bond acquires the *E*-configuration, while the double bond of the starting enal **95** ($R^2 = H$) retains its configuration in the resulting diene. These transformations were employed in stereocontrolled synthesis of the pheromones **56** and **96**.[104]

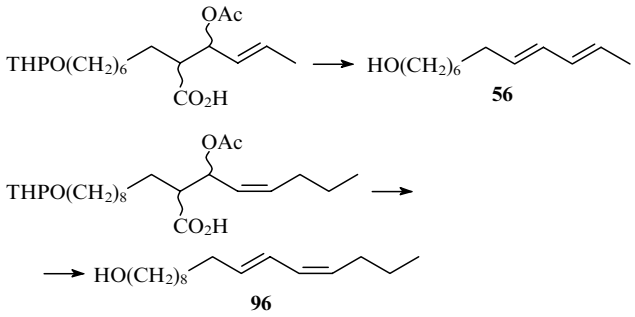

THP is tetrahydropyranyl.

Elimination of carboxy and hydroxy groups from 4-hydroxycyclohex-2-enecarboxylic acids **97** was used in the synthesis of cyclohexadienes **98**.[105]

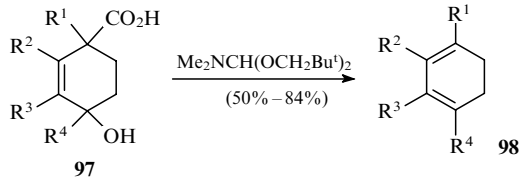

III. Olefination of carbonyl compounds

Olefination of a carbonyl compound means the replacement of its oxo group by the alkylidene grouping (Scheme 4).

Scheme 4

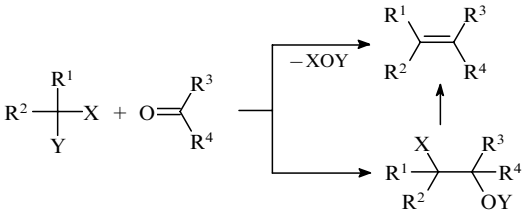

The process takes place in stepwise manner and includes the addition of olefinating agent to the C=O group followed by the elimination of an X–O–Y species from the primary adduct. In some cases elimination occurs spontaneously, in others the adduct has to be isolated first, after which the second step is carried out separately. The most widely used olefination reactions are shown in Table 1.

For the synthesis of conjugated dienes, it is necessary that one of the reactants should already possess a double bond. In general, two cases are possible: the double bond is present in the carbonyl compound (*a*), or the double bond belongs to the olefinating agent (*b*) (Scheme 5). Each of the cases displays its particular features depending on the chosen variant of olefination (see the corresponding subsections below). A detailed enough compendium on olefination of carbonyl compounds can be found in Larock's monograph,[10] but some of the methods cited there were used only to obtain monounsaturated compounds.

Scheme 5

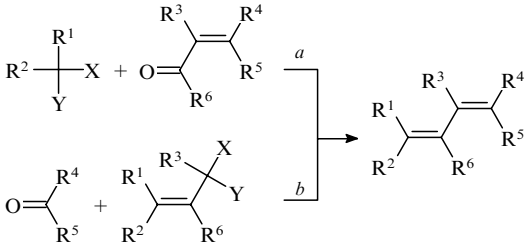

1. Condensation of CH acids with carbonyl compounds

Different variants of direct condensation of α,β-enals with active methylene compounds to give conjugated dienes are described now in all high-school textbooks. Several examples of preparation of dienoic acids are given in a review dedicated to the Knoevenagel reaction.[106] In its classical version, the highest yields (25% – 40%) are attained by heating an enal with malonic acid in pyridine [107–110] (see, *inter alia*, the preparation of octa-2,4-dienoic acid **99** from hex-2-enal **100** [109]). Instead of enal, one can use the corresponding acetal, and perform the reaction in the presence of piperidine in pyridine at 100 – 140 °C.[111] However, the yield of the dienoic acid remains about 20%.

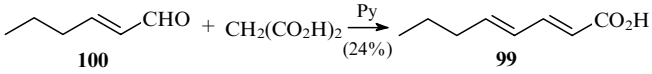

The DMAP-catalysed condensation of enals **101** with alkyl hydrogen malonates affords dienoates **103** in good yields.[112] However, noticeable amounts of deconjugated β,γ,δ,ε-dienoates are formed when β-substituted acroleins ($R^1 \neq H$) are used in the reaction.

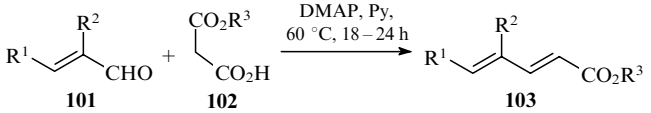

When the process is carried out at 140 °C in xylene in the presence of piperidine or its acetate, deconjugated *E* isomers of alk-3-enoic acids are formed as the main products.[113] The extension of this procedure to α,β-enals affords partly deconjugated alkyl dienoates **104**.[114] In total, the yield of isomeric dienes amounts to 60% if DMSO is used as the solvent (100 °C); however, a higher content of the 3*Z*,5*E*-isomer in total products is

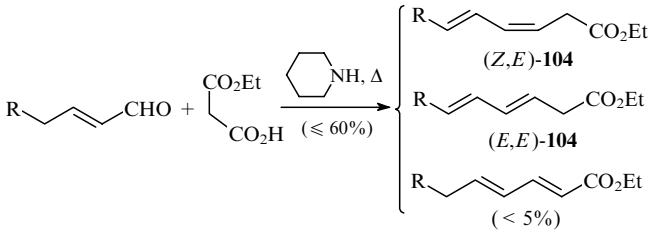

Table 1. Main types of carbonyl olefination reactions.

Olefination variant	The reagent $R^1R^2C(X)(Y)$			Comments
	X	Y	R^1 and R^2	
Aldol condensation	H	H [a]	$R^1 = CO_2R^3$, COR^3, CN	the reaction is sensitive to the nature of the carbonyl substrate
The Knoevenagel reaction	H	H [a]	$R^1 = R^2 = CO_2R^3$, CN	the reaction is characteristic of aldehydes
The Wittig reaction	$=PPh_3$		R^1 and R^2 can contain various functional groups	the reaction is sensitive to the nature of the carbonyl substrate
The Horner – Wadsworth – Emmons reaction	$P(O)(OR)_2$	H [a]	$R^1 = CO_2R^3$, COR^3, CN	the reaction is characteristic of aldehydes and less predictable with ketones
The Peterson reaction	SiR_3	H [a]	$R^1 = CO_2R^3$, CN	the reaction is applicable to nearly all types of aldehydes and ketones if they have no other reactive functional groups
The Julia – Baudin approach	SO_2Ar	H [a]	R^1 and R^2 contain no reactive functional groups	the primary adduct undergoes elimination in a separate step
The Krief reaction	SeR [b]	SeR [b]	the same	the reaction is applicable to nearly all types of aldehydes and ketones if they have no other reactive functional groups

[a] Upon activation, this hydrogen atom is replaced by a positively charged counter-ion. [b] One of these RSe groups is exchanged for lithium.

attained when xylene (140 °C) is used. The unwanted 3*E*,5*E*- and 2*E*,4*E*-isomers (the content of the latter does not exceed 5%) can be removed upon converting them into inclusion complexes with urea.

Since the esters of pentenedioic (glutaconic) acid are the vinylogues of dialkyl malonates, they readily react with unsaturated aldehydes to give substituted conjugated dienes (see a review [115]). Thus the esters of 3-methylglutaconic acid (*e.g.*, **105**) were successfully employed in the synthesis of methoprene (**106**) [R = (MeO)$Me_2C(CH_2)_3CH(Me)CH_2$] as the equivalents of isoprenoid C_5 block.[116] The primarily isolated products of condensation of aldehydes with the glutaconate **105** are configurationally pure 4-carboxy-3-methylalka-(2*Z*,4*E*)-dienoic acids, which are subsequently converted into (*E*,*E*)-3-methylalka-2,4-dienoic acids **106** in several steps.

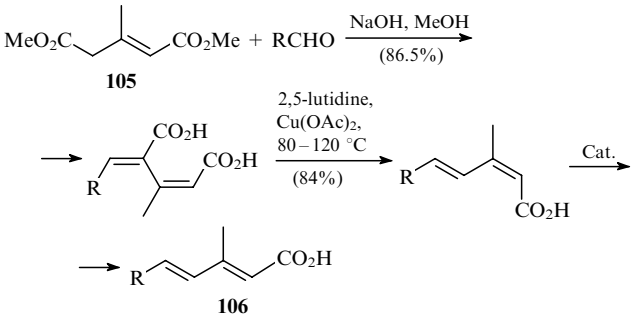

The 'classical' aldol condensation of α,β-enals with aldehydes or ketones (see a review [117]) is also used for obtaining conjugated dienes (*e.g.*, for preparing hepta-3,5-dien-2-one **107** from acetone and crotonaldehyde [118]).

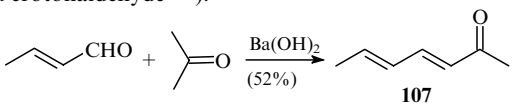

In traditional variants, hydroxides [119] or sodium sulfite [120, 121] are usually used as the bases. The yields of the products, particularly of dienals are moderate, and (quite often) even low. The yields of dienones vary over wide limits and strongly depend on the reaction conditions and on the particular nature of the reaction partners. The industrial large-scale syntheses of pseudoionone and its analogues from citral and acetone (or butan-2-one) were the objects of special research and development studies, and their conditions were duly optimised.[122]

Lately, a number of advanced procedures for directed aldol condensation have been developed. Thus high regioselectivity can be attained by using alkyl acetates or methyl ketones as the active methylene component (**108**), and lithium diisopropylamide as the base [123]. Upon treatment with LDA, ketones of the type **108** with two activated positions undergo deprotonation almost entirely at the methyl group due to the kinetic control.[124]

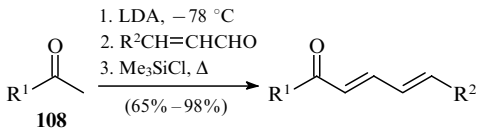

Another regioselective method of deprotonation consists in using dimethylhydrazones of asymmetric aliphatic ketones like **109**.[125]

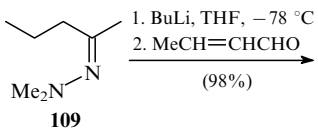

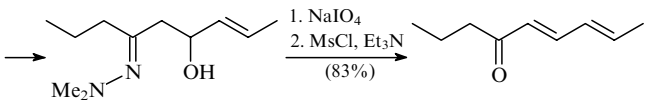

Recently [126] a conceptually new mode of aldol condensation has been developed. It consists in treating a mixture of two aldehydes, one of which is an α,β-enal, with LDA at −78 °C in the presence of aluminium tris(2,6-diphenylphenoxide) **110**. Under these conditions, α,β-enals behave exclusively as the vinylogues of the active methylene components.

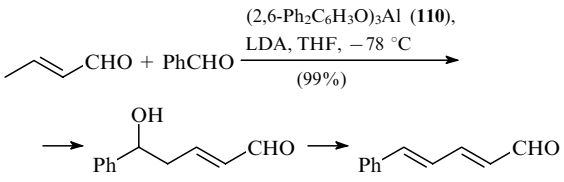

The choice of enals in this method is not confined to crotonaldehyde-like structures; higher polyenals $Me(CH=CH)_nCHO$ and conjugated enones (that react by their vinylogous anionic termini) also are suitable. Thus in 4-methylacetophenone it is the remote methyl, not the COMe group, that is activated under above conditions!

It was speculated that on mixing, the reactants form a specifically shaped conglomerate the deprotonation of which at vinylogous positions is the most favoured one. The addition of the resulting carbanion to the aldehyde component is believed to take place inside the conglomerate.

Under other conditions, the α,β-unsaturated carbonyl compounds like mesityl oxide **111** after deprotonation, add to the carbonyl substrates (electrophiles) with formation of deconjugated products, *e.g.*, **112** [127] Subsequent dehydration of the latter leads to the branched conjugated diene **113**.

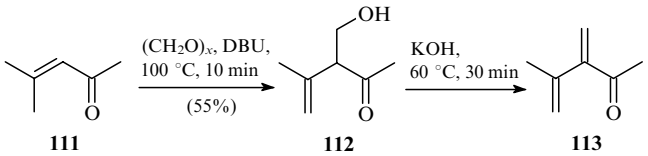

An original regio- and stereocontrolled approach to α-branched (2*Z*,4*E*)-dienoic acid relies on the use of a vinylogous synthon **114** with a methylthio group.[128]

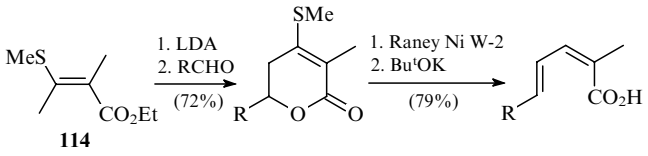

Yet another way of securing high regioselectivity in the condensation of two different carbonyl compounds is to replace conventional active methylene component by its synthetic equivalent, vinyl ether (*e.g.*, **115**). Moreover, not only aldehydes but acetals **116** can be used as carbonyl components, which operationally is more convenient. Characteristic features of this process have been thoroughly studied and discussed in a review [129] and a monograph.[130] The main shortcomings of this method are its tedious procedures and moderate yields.

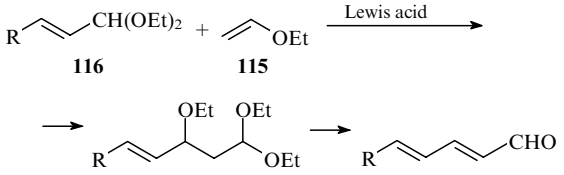

Similar results were obtained by employing ethoxyacetylene **117** instead of the active methylene component.[131–135] Using this agent, the reaction can be performed not only with aldehydes but also with ketones (**118**, $R^4 \neq H$). In this case, the overall reaction product is a mixture of stereoisomers. The process can be implemented either in the presence of $BF_3 \cdot OEt_2$, or by adding the organometallic derivative of **117** to the carbonyl component, and then by subjecting the adduct to acid hydrolysis.

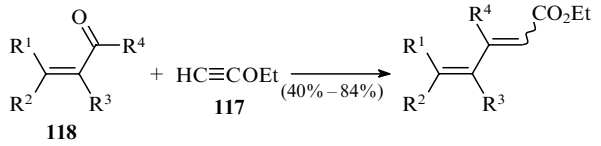

Sorbic acid (**119**, fungistatic agent for food) is manufactured industrially on a multitonne scale by a process where ketene (**120**) is used as the C_2 component.[136, 137] In the laboratory practice, it can be conveniently replaced by trimetylsilyl ketene **121**.[138]

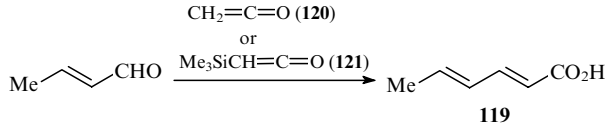

The Diels–Alder reaction of 1-alkoxybuta-1,3-dienes **122** with strongly electrophilic aldehydes leads to dihydropyran derivatives **123**, which can be subsequently transformed into dienals **124**.[139, 140] In this protocol, the compound **122** acts as a synthetic equivalent of crotonaldehyde.

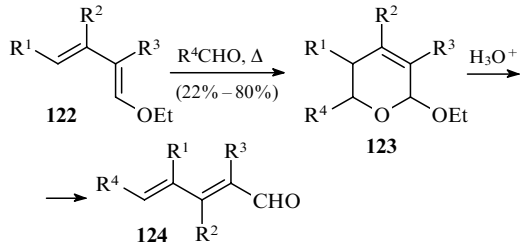

R^1, R^2, R^3 = H, Me; R^4 = H, CCl_3, CO_2Et.

2. The Wittig reaction and related processes

The Wittig reaction (in its classical or newer variants) is one of the most popular methods of olefin synthesis. Recently, its mechanistic and preparative aspects have been studied in much detail, and discussed in reviews.[141–143] In general (Scheme 6), for the construction of a conjugated diene system. it is necessary that one of the reactants, either the carbonyl compound **125** (pathway *a*) or the phosphorus-bearing compound **126** (pathway *b*) should already have a double bond in its structure.

From the standpoint of operational convenience, pathway *a* is technically simpler and thus preferable, provided that the olefinic carbonyl compound is readily accessible.

Scheme 6

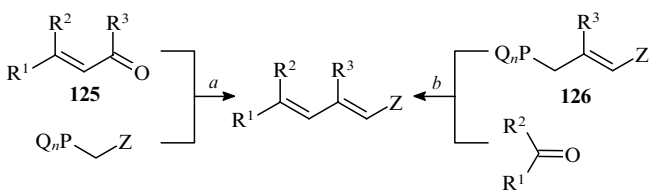

Q_nP = Ph_3P^+, $Ph_2P(O)$, $(AlkO)_2P(O)$ *etc.*; Z = Alk, Alkenyl, Ar, Het, CO_2R^4, CN, $CONR^4_2$, $C(O)R^4$ *etc.*

a. Phosphoranes

As a rule, the use of phosphoranes like $Ph_3P=CHCO_2Et$ or $Ph_3P=CHCN$ in reactions with α,β-unsaturated aldehydes is unproblematic; this is confirmed by abundant literature records. Thus a recent work describes a stereoselective *in situ* synthesis of (2*E*,4*Z*)- and (*E*,*E*)-5-bromopenta-1,3-dienoates (**127**), where the oxidation of (*Z*)- and (*E*)-3-bromoallyl alcohols was carried out in the presence of $Ph_3P=CHCO_2Et$.[144]

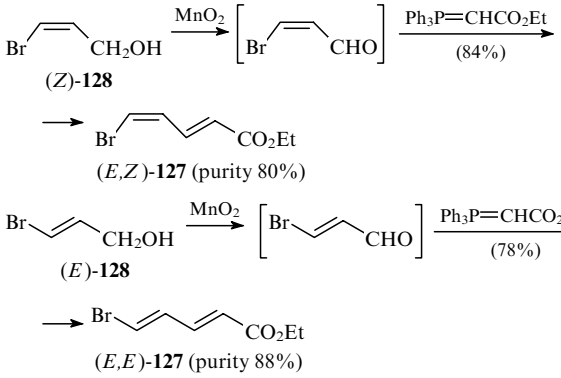

The starting α,β-enals can be obtained by elongating saturated aldehydes **129** by a C_2 fragment using 2-oxoethylidene phosphorane **130**. A stepwise process for preparing the *Z*,*E*-configured dienes **55** from alkanals **129** consisting of two sequential Wittig olefinations has been developed.[145]

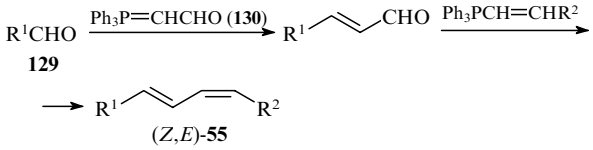

The *E*,*E*-configured 5,6-*trans*-epoxyalka-2,4-dienals **131** are obtained in moderate yields by two-step elongation of *trans*-2,3-epoxyalkanals **132** with phosporane **130** first under mild, and afterwards under somewhat more drastic conditions.[146–148] Alternatively, dienal **131** can be prepared in one step using the vinylogous phosphorane $Ph_3P=CH-CH=CHCHO$.[149]

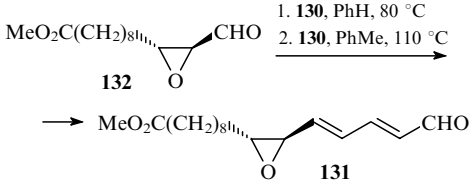

For the first stage of elongation, the phosphorane **130** can be replaced by more accessible alkoxycarbonyl-substituted phosphoranes $Ph_3P=C(CO_2Et)R$ (**133**, R = H, Alk); after that, the CO_2Et group introduced is transformed into CHO.[150] The (*E*,*E*)-dienoic acid **134** was synthesised in this way with high stereoselectivity.

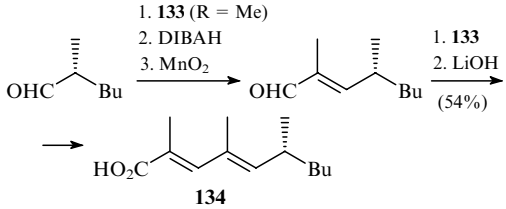

DIBAH is diisobutylaluminium hydride.

Aldol hemiacetals can be successfully used in the Wittig olefination instead of aldehydes. Thus starting from 2-deoxy-D-ribose (a naturally occuring aldol hemiacetal) or its derivatives

135, dienes **136** and **137** have been synthesised.[151, 152] Depending on the procedure employed for eliminating the 5-OH group from the intermediate dihydroxy alkenoate, the configuration of the second double bond in the target dienes can be *Z* or *E*.

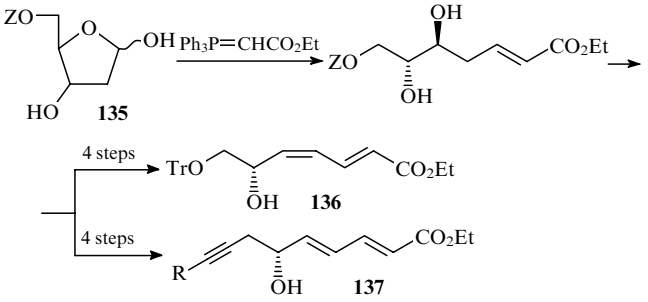

Unlike aldehydes, conjugated ketones enter reluctantly into the Wittig reactions. The α,β-enones that are not branched at the β-position sometimes enter into the Michael reaction with phosphonates of the type $(RO)_2P(O)CH_2CO_2Alk$ to give the products of 1,4-addition.[153] It is noteworthy that α-diketones **138** can react with two molecules of the above phosphonates and give conjugated dienes *via* the intermediate α,β-enone **139**.[154, 155] For the synthesis of diesters **140**, it is necessary to adopt a two-step procedure,[154] while the preparation of dinitriles **141** can be performed in one step due to the higher reactivity of the corresponding intermediate.[155]

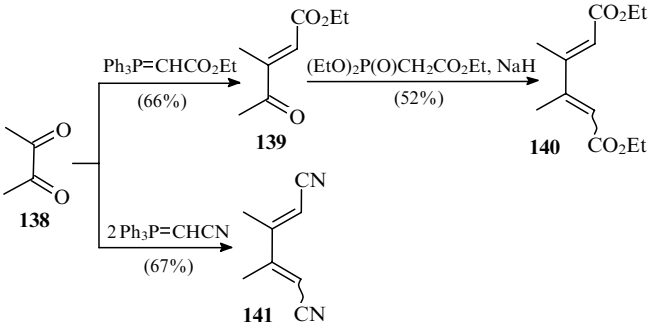

Cyclic α-diketones such as cyclobutane-1,2-dione and cyclohexane-1,2-dione also react in this way to give semicyclic dienes.

Pathway *b* of Scheme 6 looks equally attractive. The use of allylic phosphoranes **126** (Z = Alk, Ar) is justified, particularly when the precursor of the phosphonium salt, the corresponding allylic halide, is readily accessible.[156] Allylic halides of higher molecular complexity are rather difficult both to prepare and, particularly, to purify. As a consequence, roundabout approaches to allylic phosphoranes have been developed. Thus allylic phosphoranes **142** are formed *in situ* from the η^3-allylic palladium complexes **143** (prepared by heating allylic alcohols **144** or **145** in dioxane in the presence of $Pd(acac)_2$ and triphenylphosphine.[157, 158] The subsequent reaction of phosphoranes **142** with aldehydes affords conjugated dienes. This way of preparing conjugated dienes is lengthy enough and complicated by side reactions.

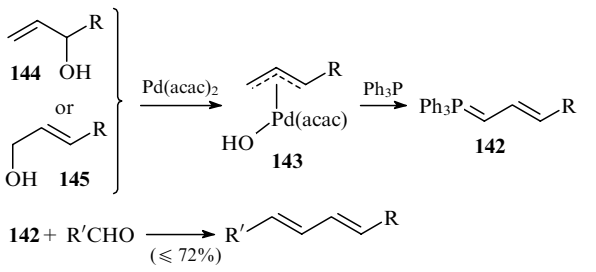

Another synthesis of conjugated dienes that involves indirect approach to allylic phosphoranes relies on the ability of (buta-1,3-dienyl)phosphonium compounds **146** to react with C-nucleophiles such as the dianions of β-dicarbonyl compounds or organocuprates.[159, 160]

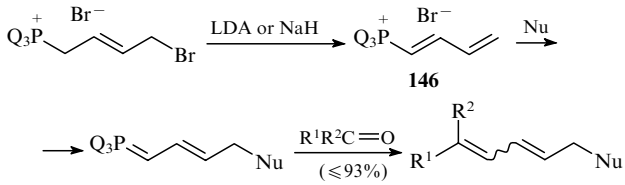

On treatment with strong bases, allyltriphenylphosphorane **147** gives metallated derivative **148**, which reacts with one molecule of a carbonyl compound as a C-nucleophile to afford the modified allylic phosphorane **149**. Then the Wittig reaction of **149** with the second molecule of aldehyde or ketone brings forth dienic alcohols **150** in moderate yields.[161]

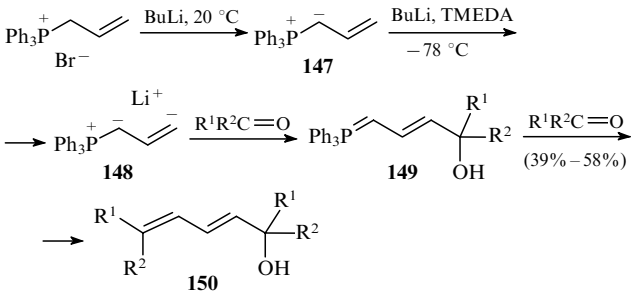

TMEDA is *N*,*N*,*N*′,*N*′-tetramethylethylenediamine.

b. Phosphonates

It is profitable to replace phosphoranes by the corresponding phosphonates of the type $(EtO)_2P(O)CH_2Z$. This variant of olefination is known as the Horner – Wadsworth – Emmons reaction. Thus the olefination of tiglic aldehyde **151** with triethyl phosphonoacetate **152** affords ethyl dienoate **153** in 90% yield.[162, 163] The newly formed double bond has almost pure *E* configuration.

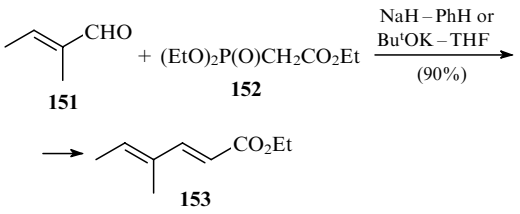

A simple procedure for implementing such a process has been proposed. It consists in mixing together and stirring an aldehyde, phosphonate **153** and concentrated aqueous K_2CO_3. The method is applicable to the synthesis of alkyl dienoates or alkadienones and provides satisfactory yields (60% – 70%).[164] Time and again, it was used in the synthesis of natural products.[4, 165, 166]

In the case of phosphonates with phenoxy groups (**154**), the stereoselectivity of olefination is reversed (with respect to the case of **152**) *i.e*, the *Z*-isomers of alk-2-enoates are produced.[167] For the reactions involving phosphonates **154**, it was recommended to use NaH, Triton B or the DBU – NaI system as the base. The reaction of hex-2-enal (**100**) with **154** afforded ethyl (2*Z*,4*E*)-octa-2,4-dienoate **155** with 97% isomeric purity.[168]

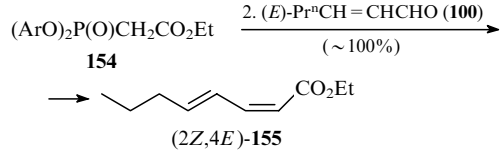

The reaction of allylic phosphonates of the type **156** with saturated aldehydes can be successfully applied to the synthesis of dienes.[169]

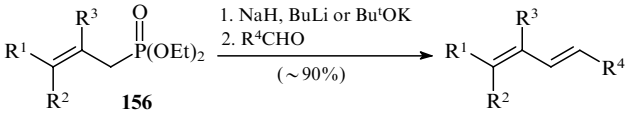

R^1, R^2, R^3 = H, Alk.

For allylic phosphonates **156** with additional functional groups (R^1 or R^2 = CO_2Alk, $CONR_2$, RCO, or CN) the HWE reaction is one of the most studied because it is widely used in the synthesis of polyenes. Such phosphonates are usually prepared by employing the Arbuzov or Michaelis–Becker reactions (see a review[142]). Recently, an interesting method for the synthesis of γ-phosphono-α,β-enones from allylic phosponates was reported.[170] Its protocol involves silylation, alkylation (if necessary) and finally acylation.

The experience accumulated since the mid-sixties suggests that the HWE reactions are sensitive to the nature of the reactants and bases used and to conditions under which they are implemented. Thus for the preparation of alkyl dienoates of the type **157**, it was recommended to use such bases as MeONa in DMF,[171] $NaNH_2$ in THF,[171] NaH in DMF,[172] and, what is particularly convenient, the systems of phase transfer catalysis: solid KOH–benzene–18-crown-6 (Cat.)[173–176] or solid KOH–benzene–$Alk_4N^+Br^-$ (Cat.).[177,178] In the latter case, 3-methylalka-2,4-dienoates **157** are formed with 90%–96% *E*,*E*-selectivity[143,178] By contrast, when the phosphonate grouping contains the 1,3,2-phospholane fragment, the reaction results in 2*Z*,4*E*-isomers (~70%–85% selectivity).[179,180]

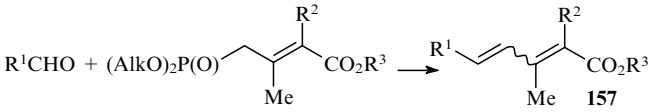

Bis(β,β,β-trifluoroethyl) esters of aliphatic phosphonic acids (Still–Gennari phosphonates) react with aldehydes to give *Z*-alkenes. The reactions of α,β-enals with bis(β,β,β-trifluoroethyl) 3-cyano-2-methylprop-2-enylphosphonate (**158**) afford the 2*Z*,4*E*-isomers of 2-methylalka-2,4-dienonitriles with high selectivity.[181] The possibility of using the phosphonate **158** for the synthesis of 1,3-dienes with *Z*-configured newly formed double bond is indicated by the reaction of (2*Z*,4*Z*)-β-ionylideneacetaldehyde (**159**) with this phosphonate.[182]

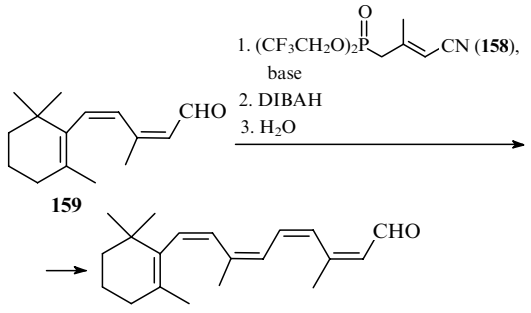

In the mixture of four stereoisomers of retinal formed in this reaction, the proportion of products with *Z*-configuration of the newly formed double bond amounts to 72%.

When non-branched phosphonocrotonates **160** are used, the yields of dienes **161** decrease (to 59% with the use of $NaNH_2$ in THF[4,166]); under conditions of phase transfer catalysis, the dienes **161** are not formed at all. However, with the use of lithium derivative of hexamethyldisalazane,[183] the dienes **161** are produced in 84% yield, whereas the use of LDA having close properties[184] provides only 27% yield. Recently, a method for the synthesis of conjugated dienes has been proposed according to which a mixture of the initial phosphonocrotonate and aldehyde is refluxed in THF in the presence of LiOH and 4 Å molecular sieves. The yield of dienes is 86%.[185] Cyclohexanones can be used successfully in place of aldehydes in this reaction.

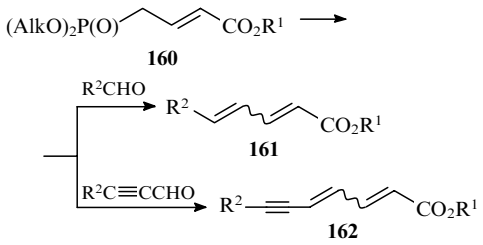

Olefination of acetylenic aldehydes by the phosphonate **160** in the presence of $NaNH_2$ in THF gives rise to the corresponding dienynoates **162** in a yield not higher than 36%.[4,186]

Apart from esters, dienals **163** have also been synthesised using this route.[187]

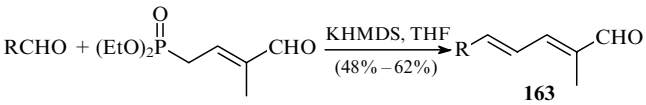

Dienic aldehydes **164** and their acetals **165** can be prepared using synthons **166** and **167** with the protected aldehyde group.[188,189]

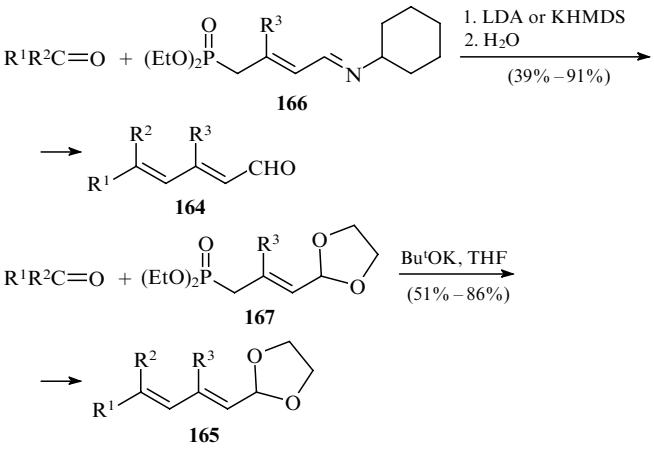

Dienyl trifluoromethyl ketones **168** are formed from dienamines **169**, tautomers of Schiff's bases **170**.[190]

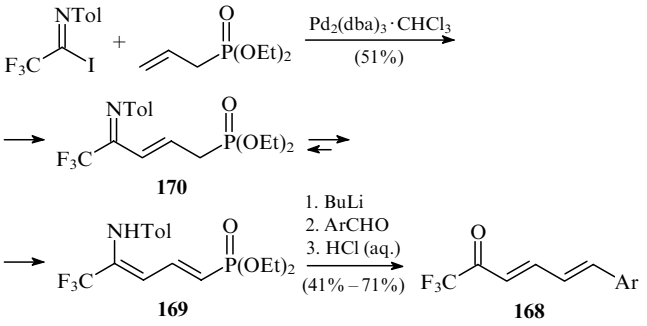

c. Allylic phosphines and phosphine oxides

Olefination of carbonyl compounds can also be performed by means of allylic phosphines **171** and allyl phosphine oxides **172**;[191] the products **38** thus formed differ in the stereochemistry of the newly formed double bond.

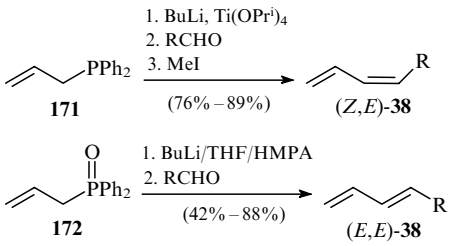

Allylic phosphine oxides with more complex structures used for the synthesis of functionally substituted conjugated dienes can be prepared from simpler phosphine oxides **173** or **174**.[192] To this end, compounds **173** and **174** are made to react with aldehydes and ketones, and the reaction products **175** and **176** are subjected to dehydration. Acidic dehydration of secondary β-hydroxyphosphine oxides **175** is accompanied by the migration of the phosphorus-containing group, while dehydration of tertiary β-hydroxyphosphine oxides **176** follows the standard pathway. In both cases, tertiary carbocation **177** is formed, which is transformed, under thermodynamic control, into thermodynamically more favourable alkene **178**. Thus the same product **179** can be prepared in different ways, which makes the phosphine-oxide route more versatile.

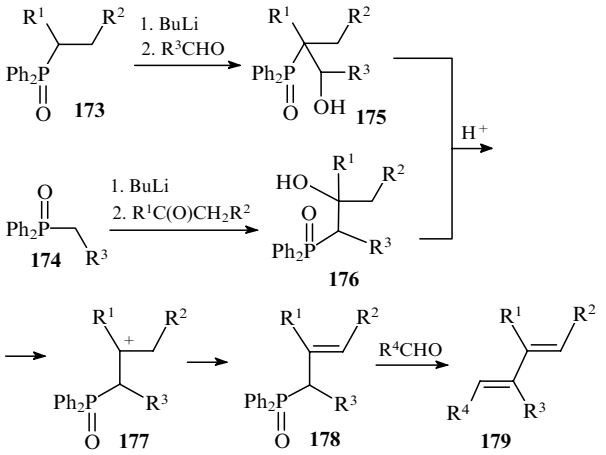

The synthesis of conjugated diene **180** containing an ethyl acetoacetate fragment as a substituent has been reported.[193] This compound was prepared using phosphine oxide **181**.

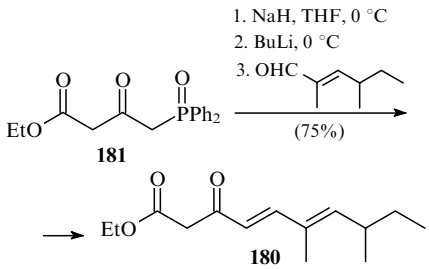

d. Related methods

In conclusion, we shall consider methods of olefination of carbonyl compounds making use of 'non-phosphorus' equivalents of the Wittig reagents based on arsenic **182**,[194,195] antimony **183**[196] and tellurium **184**.[197,198] It should be noted that in the case of complex syntheses, the use of arsonium derivatives has substantial advantages. The advantages and shortcomings involved in the use of antimony and tellurium derivatives have not been adequately elucidated.

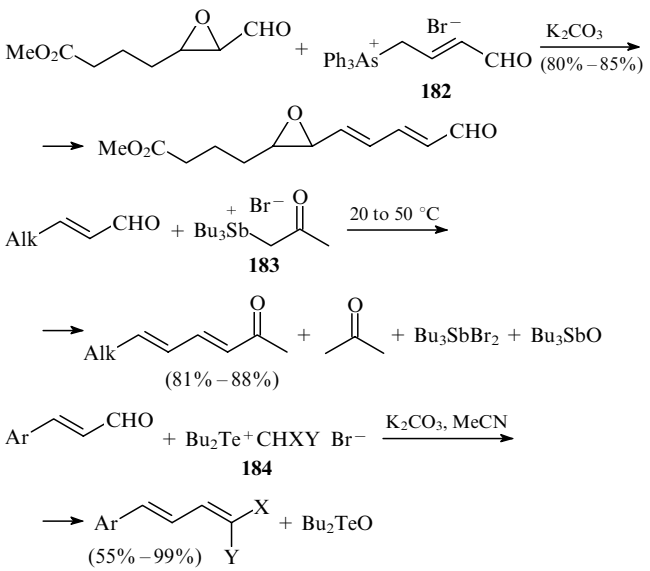

X = CN, CO_2Et; Y = H, Ph.

3. Miscellaneous methods of olefination of carbonyl compounds

a. The Peterson reaction

The Peterson reaction consists in elimination of vicinal silyl and hydroxy groups, resulting in the formation of a double bond (see Section II). Here, we consider the version used to olefinate α,β-unsaturated carbonyl compounds. In this technique, the starting β-hydroxy silanes **185** are formed *in situ* upon the addition of silicon-containing carbanion reagents **186** to the carbonyl compounds **125**.[46,47]

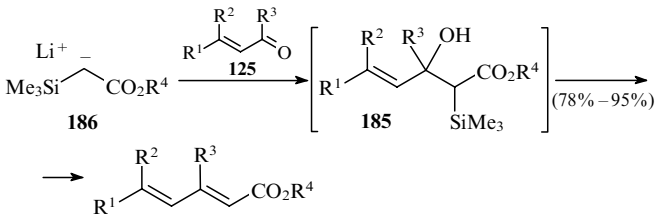

An advantage of this approach is the possibility of using not only α,β-unsaturated aldehydes but also ketones including relatively non-reactive chalcone.[48] An organosilicon reagent should contain a group exhibiting a $-M$-effect. Apart from esters **186**, the acetylene derivative $Me_3SiCH_2C{\equiv}CSiMe_3$ and the nitrile **187**[49] have also been involved in this reaction. Deprotonation is carried out by amides such as LDA; the yields are high in all cases.

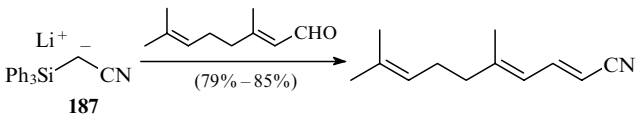

In recent years, a convenient C_2 olefinating synthon **188** has been devised; it contains two geminal silyl groups and is able to react with aldehydes **189** in the presence of Lewis acids under very mild conditions.[199]

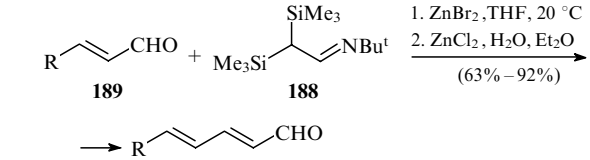

A similar vinylogous C_4 synthon with two silyl groups has not been prepared; however, C_4 olefination can be accomplished under other conditions using monosilyl reagent **190**.[200,201] The

reactions of carbonyl compounds and acetals with cyclic γ-silyl-α,β-enones **191** giving rise to dienones **192** have been described.[202]

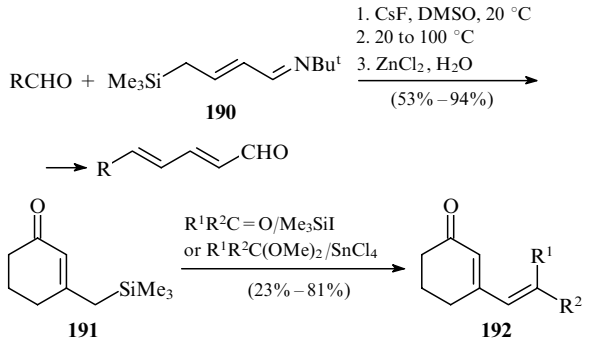

b. The Baudin – Julia method

The Julia method consists in condensation of aryl sulfones with aldehydes followed by reductive elimination of the sulfone group from unsaturated sulfone of the type **64** (see Scheme 2),[78,79] for example, on treatment with $LiAlH_4$. The involvement of unsaturated sulfones **193** in this process should furnish dienes. It has been proposed [203] to use BuMgCl for the reduction of the intermediate *Z*-olefinic sulfones **194** in the reaction catalysed by $Pd(acac)_2$ or $Ni(acac)_2$. The isomeric purity of the products **55** was 93% – 97%; however, the yields were moderate.

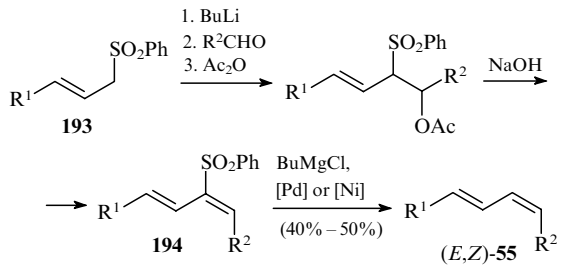

In another study,[204] olefination of α,β-enals with saturated sulfone of the type **195** and olefination of saturated aldehydes with allylic sulfones **196** (Ar = Ph) have been studied in substantial detail with verification of numerous factors. Elimination of vicinal sulfonyl and hydroxy groups was induced by sodium amalgam. The yields of dienes were moderate, despite the efforts made by the authors.

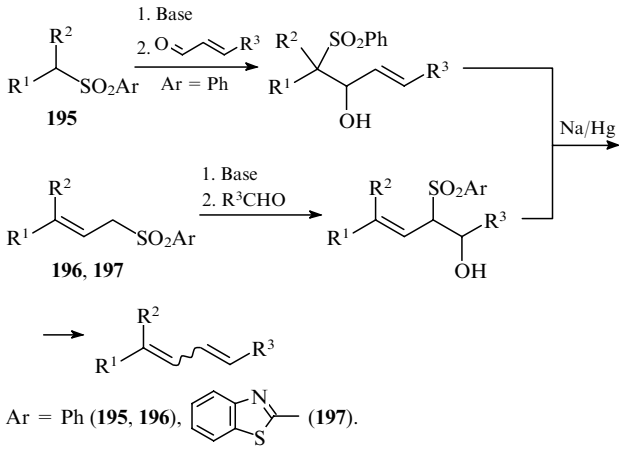

In a perfected method, the phenyl group in the sulfone **196** was replaced by various heterocyclic groups, which resulted in higher product yields, the best results being attained for the 2-benzothiazole substituent (compound **197**).[205–207] This is due to the fact that heteroatoms in the aryl group change the final steps of the olefination mechanism; this influences the product yield, which can reach 86%.

Both reactions — unsaturated sulfone + saturated aldehyde and *vice versa* — are used for the synthesis of dienes. Usually, this gives a mixture of *E,E*- and *E,Z*-isomers, their ratio being dictated by the pattern of substitution at the double bond in the reactants.

c. The Krief reaction and other olefination methods

The ability of selenoacetals **198** to exchange one selenium-containing group for lithium has underlain the new Krief olefination method.[208–210] The reaction of the carbanion formed (stabilised by the remaining selenium atom) with aldehydes or ketones yields β-hydroxy alkyl selenides **199**, which readily form olefins on the subsequent treatment with acidic reagents. In the case of unsaturated aldehydes, the method results in conjugated dienes.[211,212]

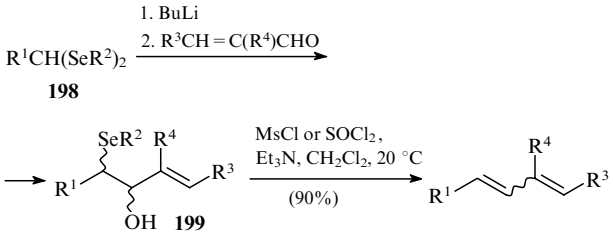

Another variant of organoselenium synthesis of dienes, namely, the reaction of a saturated aldehyde and an unsaturated selenium component, is also possible. Allyl selenides **200**, the CH acidity of which is high enough for hydrogen to be eliminated on treatment with LDA, are possible precursors of this type of selenium component. The resulting carbanion, however, exhibits ambident properties and furnishes mixtures of isomeric products in reactions with electrophiles.[213] To ensure the required regiodirectivity, the reagent is treated with Lewis acids; the ate-complex thus formed reacts with an aldehyde to give the 'normal' product **201**.

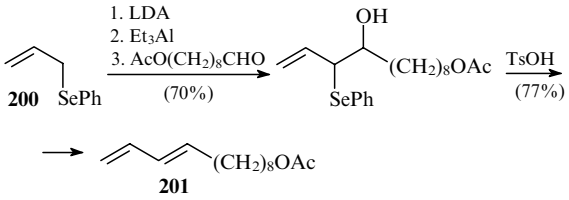

The titanium carbene complex $Cp_2Ti{=}CH_2$ (the Tebbe reagent) is an efficient methylenating agent.[214] It reacts with unsaturated carbonyl compounds giving rise to conjugated dienes including those difficult to prepare by other methods, such as **202**.[215]

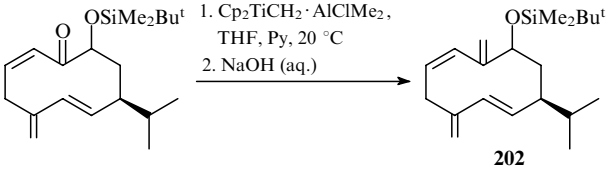

Recently, it has been shown that unsaturated analogues of the Tebbe reagent (**203**) can be prepared from α,β-enal cyclic thioacetals **204** on treatment with a titanocene(II) complex with triethyl phosphite.[216] The reactions of the carbenes **203** with aldehydes, ketones, and even esters (!) result in the formation of a new double bond. Instead of the thioacetals **204**, 1,3-diphenylthioalk-1-enes **205** (R^1 = SPh) [217] can be used in the reaction (they are produced from α,β-enals under conditions of acetalisation with monothiols). In the case of non-branched dienes ($R^2 = R^4 = H$), the proportion of *E,E*-isomer exceeds 87%.

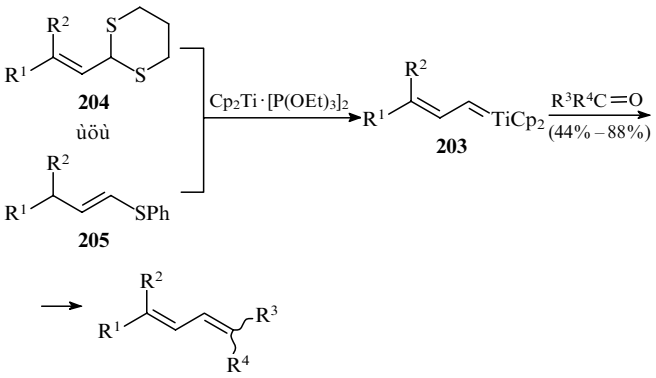

R^3 = Alk; R^4 = H, Alk, Ar, OAlk.

Isocyanides **206** can also serve as olefinating agents;[218] however, in this case, in addition to alkenes **207**, the reaction gives substantial amounts of oxazolines **208**. This route was use to convert cinnamaldehyde into 1-phenylbuta-1,3-diene (R^1 = R^2 = H, R^3 = PhCH=CH) in 28% yield.

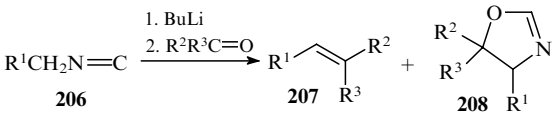

The reaction of aldehydes with diazo esters leading to α,β-unsaturated esters can also be classified as olefination. In the only known example, namely, in the reaction of cinnamaldehyde with diazo ester, the yield of the corresponding conjugated diene is 92%.[219]

IV. Organometallic reactions

1. Cross-coupling of vinylic and/or acetylenic components

Cross-coupling reactions belong to the most advanced methods for the creation of a C−C bond. The thermodynamic factor, which accounts for the occurrence of these reactions, is the formation of a favourable bond between the electropositive element M of reactant **209** and the electronegative element X of reactant **210** (Scheme 7). The reactions of the general form **209** + **210** are usually classified according to the sort of the electropositive element in the reactant **209**, the nature of which governs the mechanism of the process, although the outcome is formally the same.

Scheme 7

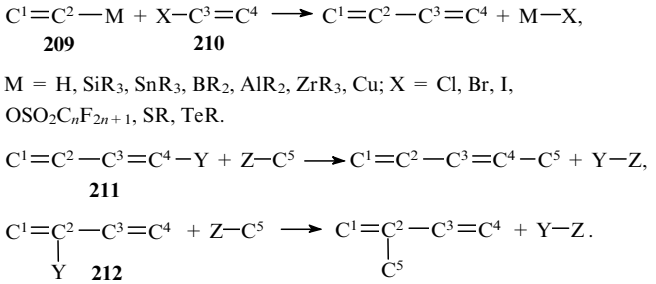

M = H, SiR_3, SnR_3, BR_2, AlR_2, ZrR_3, Cu; X = Cl, Br, I, $OSO_2C_nF_{2n+1}$, SR, TeR.

In the synthesis of carbo-substituted conjugated dienes, cross-coupling of two vinylic components giving rise to the central single bond is used most often. The replacement of the heteroatom in a preformed diene system **211** or **212** by a carbon-centred fragment is used more rarely. A fundamental feature of cross-coupling reactions is retention of the configuration of the reacting centres, which permits one to prepare, as desired, any of the possible isomers of conjugated dienes (*E*,*E*-, *E*,*Z*-, *Z*,*E*- and *Z*,*Z*-isomers).

Cross-coupling can also involve components with triple bonds such as **213**. First, they react with alkenyl reagents to give conjugated enynes **214**. Second, some organometallic reagents of the type **215** or **216** are capable of adding to triple bonds to give

Scheme 8

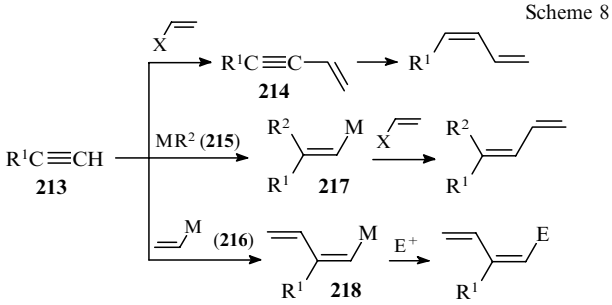

new metal alkenyls, **217** or **218**, respectively. All the compounds obtained can be further converted into dienes (Scheme 8).

The reactions listed above have been thoroughly studied and discussed in numerous publications;[220–227] therefore, in this review, we present only a brief characterisation. There is a fairly detailed list of published data on each type of reaction.[10]

In early examples, cross-coupling has been carried out with stoichiometric amounts of organometallic reagents. The scope of these reactions is limited as they mainly permit the preparation of symmetrical compounds. This is indicated by homodimerisation of alkenylalanes **219** induced by CuCl[228] or of various alkenyl halides **220** in the presence of stoichiometric amounts of nickel complexes such as $Ni(cod)_2$ (cod is cycloocta-1,5-diene)[229] or $Ni(bipy)_n$ prepared *in situ*.[230]

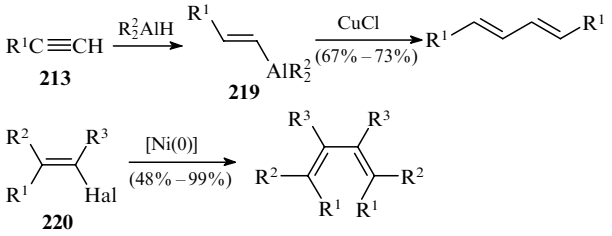

Catalytic cross-coupling protocols are much more efficient. Palladium or nickel complexes are the most popular catalysts of these processes.

a. The Heck reaction and its modifications

The coupling of α-alkenes (**209** with M = H, see reviews[220,221]) with alkenyl or aryl halides catalysed by palladium complexes is called the Heck reaction. Coupling of the vinylic components **221** and **222** affords conjugated dienes **223**.[231]

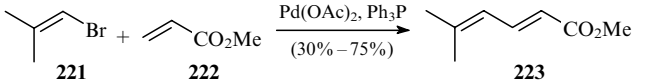

It is advantageous to perform this process in the presence of Ag salts as HHal acceptors;[232,233] in this case, the allylic alcohols **73** can also be introduced in the reaction.

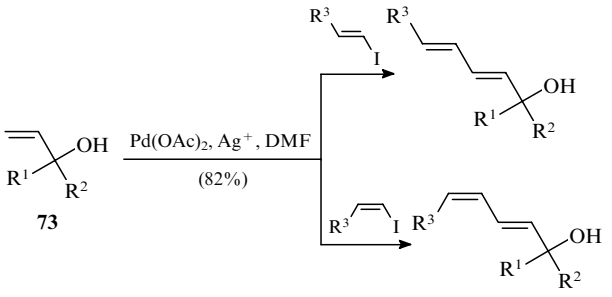

Apart from alkenyl halides, the Heck reaction can be carried out for alkenyl perfluoroalkyl sulfonates,[234,235] alkenylsilanols,[236] alkenylpentafluorosilicates[237] and alkenyl(aryl)iodonium salts.[238] Coupling of alkenyl bromides with potassium but-3-enoate (**224**), similar to the Heck reaction in the outcome but

catalysed by the rhodium complex $RhCl(PPh_3)_2$, has been described.[239]

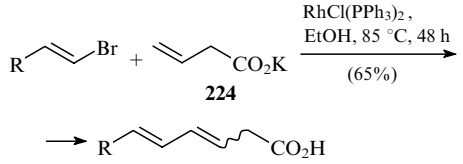

b. The Stille reaction

Coupling of organotin compounds with halides catalysed by palladium complexes has been called the Stille cross-coupling (**209** with M = SnR_3, see reviews [222, 223]). In addition to the synthesis of biaryls, styrenes and enynes, this reaction is also good for the synthesis of various conjugated dienes **225**.[240, 241] The reaction proceeds with full retention of the configurations of the reacting centres; the initial compounds may contain diverse substituents and the product yields are usually high.

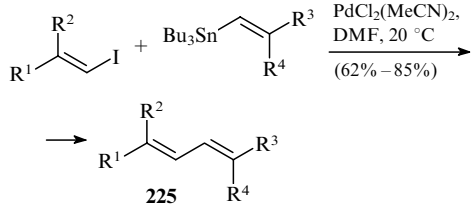

The Stille reaction has been used in the total synthesis of complex natural products, for example, didemnenones **226**, biologically active compounds generated by marine *Tunicata*.[242]

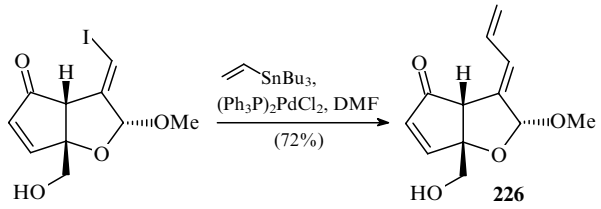

Triflates can be involved in this reaction instead of halides;[243] this has been used in the synthesis of triene **227**, the closest precursor of the C_{16} juvenile hormone (**228**).[244]

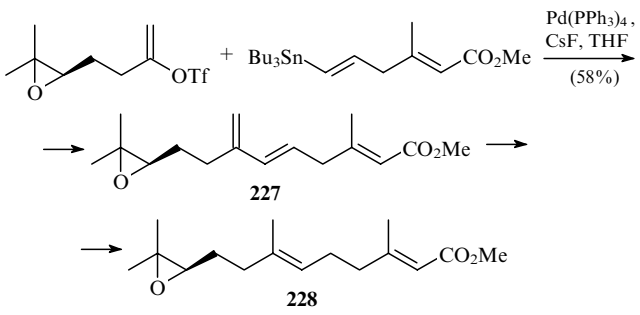

1,1-Dibromoalkenes **229** react with organotin compounds, first of all, at the bromine atom located in the *trans*-position.[245] By varying the order of addition of the alkenyltin and aryltin reagents, either *E*- or *Z*-isomers of 3-aryl-1,3-dienes **230** can be obtained as desired.

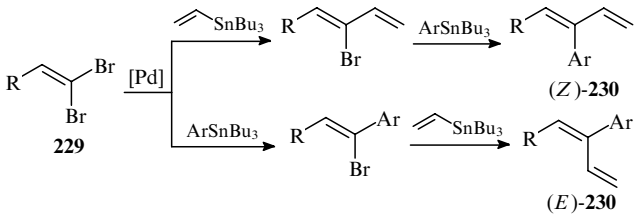

Alkynyltin derivatives **231** can also enter into the Stille cross-coupling. Conjugated enynes **232** thus formed can be reduced selectively yielding *E*,*Z*-dienes.[246]

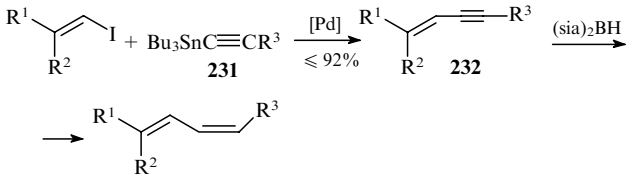

sia is 3-methylbutan-2-yl.

Using this strategy, two pheromones **235** and **236** with similar structures but opposite configurations of the conjugated double bonds have been synthesised from the same initial alkyne **233** and alkynol **234** (Scheme 9).[246]

Direct coupling of tertiary acetylenic alcohols **237** with alkenyl bromides in the presence of stoichiometric amounts of tin hydrides seems to involve the hydrostannylation step, the overall reaction looking like the Stille cross-coupling.[247]

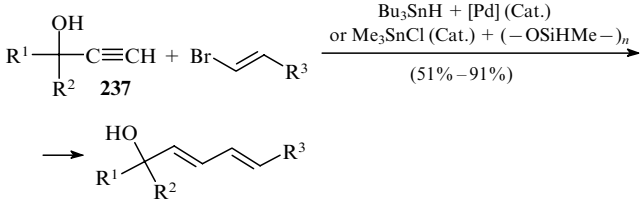

The reaction in question can also involve alkynylamines $R^1R^2C(NH_2)C{\equiv}CH$ and other sterically hindered terminal acetylenes. The same result is attained when catalytic amounts of $(Bu_3Sn)_2O$ [247] or Me_3SnCl,[248] and stoichiometric amounts of polymethylhydrosiloxanes are used instead of tin hydrides as hydride-ion donors. This modification of the Stille reaction opens up prospects for extending the scope of its application because this version implies markedly smaller proportions of tin-containing wastes.

c. The Suzuki reaction and its modifications

Coupling of organoboron compounds with halides or their equivalents (*e.g.*, triflates) catalysed by palladium complexes has been called the Suzuki coupling (**209** with M = BR_n, see reviews [224, 225]). Like the Stille cross-coupling, this reaction can be applied to the synthesis of various types of compound including conjugated dienes. An important feature of the process is that it

Scheme 9

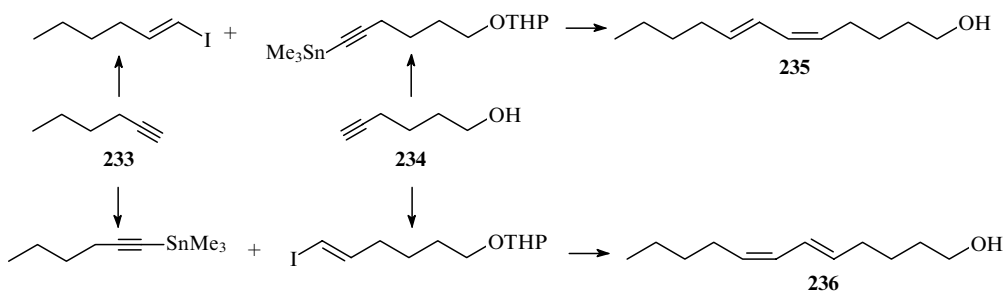

should be carried out in the presence of bases (NaOEt, NaOH, KOH, K_3PO_4, Na_2CO_3, *etc.*): coordination of the anion to the boron atom results in a higher electron density on the reaction centre, which facilitates the replacement of boron by palladium. In the case of sterically hindered alkenyl bromide, methyllithium proved to be a more suitable base.[249] The catalyst used most often is $Pd(PPh_3)_4$.

The organoboron approach is distinguished by versatility — by using specific protocols, both *E*- and *Z*-isomers of both the boron and halogen components can be prepared from terminal alkynes. The subsequent coupling in a required combination provides, at one's discretion, any isomer of the conjugated diene **55**.[222] The initial compounds can contain additional substituents and functional groups.

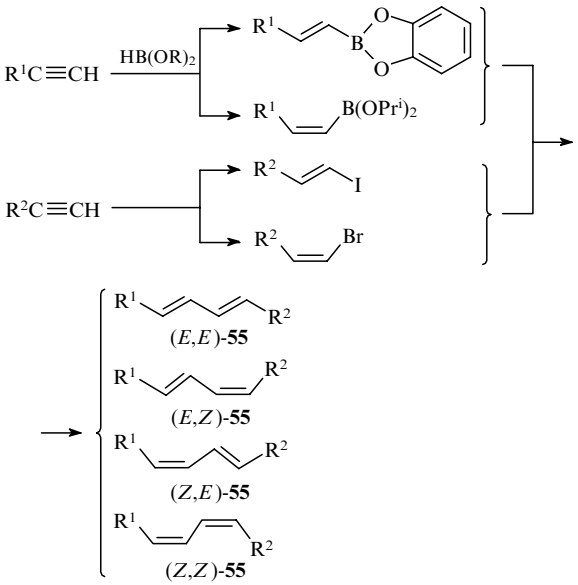

The Suzuki cross-coupling has been used successfully for the stereocontrolled preparation of dienes **238** with a more complex pattern of substitution including cyclic and polyfunctional compounds.[250–254]

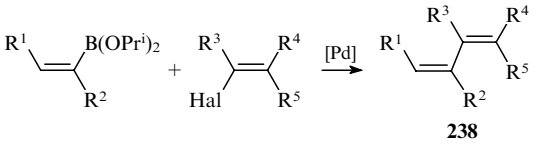

Thus this reaction has been used to prepare hydroprene (**239**) from alkenylboronic acid **240**.[255, 256]

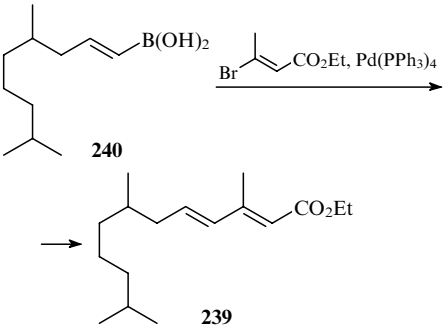

An interesting methodological expedient is to carry out this process in the aqueous acetonitrile medium.[257] The reaction was catalysed by a system comprising $Pd(OAc)_2$ and water-soluble sulfonated triphenylphosphine, $P(C_6H_4SO_3H)_3$. Both compounds subjected to coupling contained functional groups.

The nature of the base in the Suzuki cross-coupling can influence the process regioselectivity. Thus in the presence of triethylamine, catecholboranes **241** are coupled with alkenyl halides (or aryl halides) according to the 'head-to-tail' pattern giving rise to branched dienes **242**, the process regioselectivity being higher than 94%.[258]

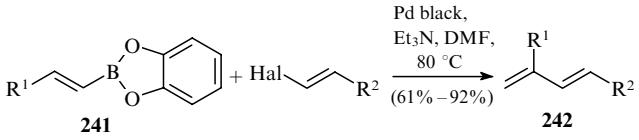

d. Other variants of cross-coupling of vinyl components

Vinyl derivatives of other elements are used somewhat less extensively in the cross-coupling reactions. The use of zinc, magnesium, aluminium and zirconium compounds for this purpose has been surveyed in a review.[224] For example, hydrometallation of terminal alkynes with R_2AlH [259, 260] or Cp_2ZrClH [261] to give the corresponding organometallic intermediates **243** and **244** followed by proper coupling resembles conceptually the Suzuki coupling discussed above.

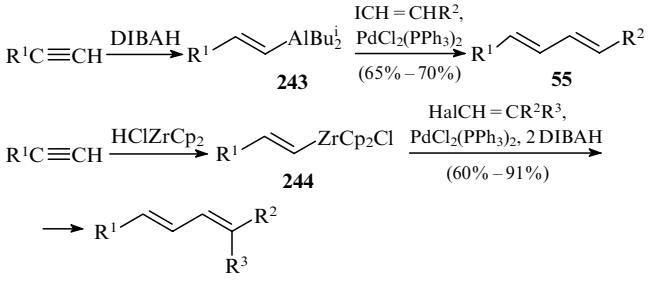

The cross-coupling of vinylcopper reagents with alkenyl halides is also catalysed by palladium or nickel complexes. This reaction had been discovered earlier than the more convenient Stille and Suzuki reactions. Characteristic features of this process have been studied in detail by Normant and Alexakis.[9] The main work rule that ensures high yields and involvement of both alkenyl fragments of the reactants $(RCH=CH)_2CuLi$ is preliminary transmetallation of these compounds carried out by adding equivalent amounts of magnesium and zinc halides to the reaction mixture. Thus it is actually an organozinc compound that enters into the coupling reaction. Cross-coupling of neat organocopper compounds catalysed by nickel or palladium complexes gives products in a yield not exceeding 50%.

The coupling of alkenylmagnesium bromides **245** and **246** with alkenyl bromides **247** and **248** can be induced not only by palladium complexes but also by iron [262] or nickel [263, 264] complexes; in the latter case, thiolate ion can act as the leaving group.

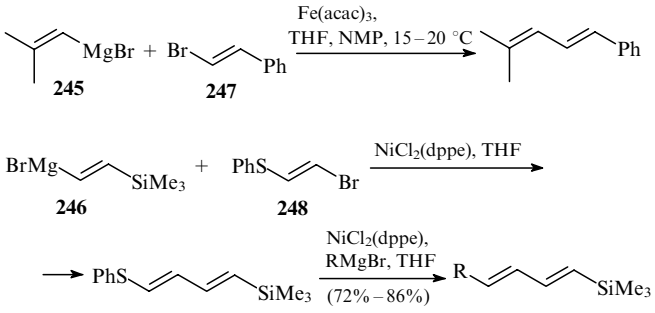

NMP is *N*-methylpyrrolidone.

Vinyl silicon derivatives, unlike similar tin compounds, normally do not enter into the cross-coupling reaction (see reviews [265, 266]). Nevertheless, a particular type of active vinylsilanes containing fluorine atoms at silicon has been identified among them.[267–269] Vinyl iodides and triflates were used as electrophiles; $(\eta^3\text{-}C_3H_5)PdCl_2$ was found to be the best catalyst. The process was carried out in THF at 60 °C in the presence of Bu_4NF.

Dimerisation of alkenylmercury reagents **249** follows the 'head-to-tail' pattern.[270]

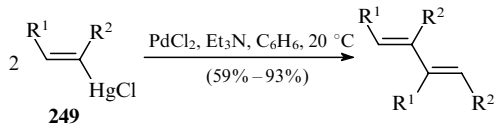

e. Cross-coupling of diene and saturated components

This reaction is used more rarely. Two general cases are known, one with the diene component acting as the nucleophile and the saturated one being the electrophile and *vice versa*. Dienylalane **250** reacts with methoxyethoxymethyl chloride (MEMCl) to give the expected ether **251**.[271] The compound **250** does not react properly with aldehydes and cyanogen; however, the target dienonitriles **252** and dienic alcohols **13** can be prepared from the corresponding ate-complex **253**.[271, 272]

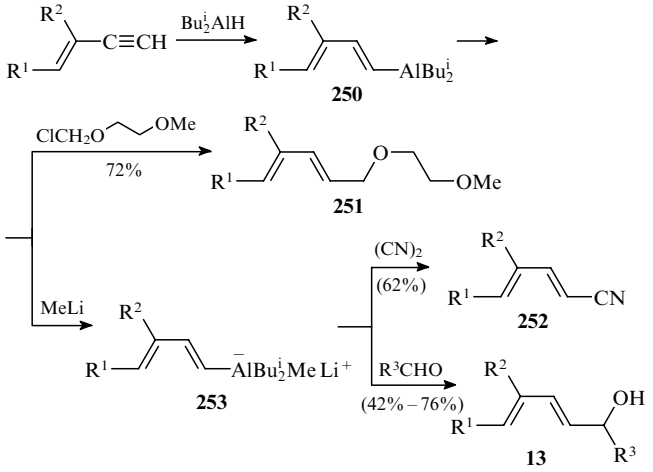

Yet another example of using a 'nucleophilic' diene component is the Heck arylation of the terminal conjugated dienes **38**.[273, 274] The process is carried out in the presence of HHal acceptors such as amines [273] and silver or thallium acetates,[274] the *E*,*E*-isomer of diene **254** being formed predominantly irrespective of the configuration of the initial compound **38**.

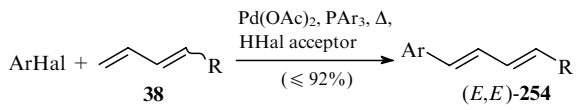

An original synthesis of bombykol **96** can serve as an example of cross-coupling with 'electrophilic' diene component **255** (easily prepared from dibromide **256** formed upon bromination of unsaturated aldehyde **257**) and a 'nucleophilic' saturated component.[275] In this case, the bond configuration at the reaction centre is not violated. This strategy was verified using numerous examples, the yields of *Z*,*E*-dienes ranging from 58% to 85%.[275]

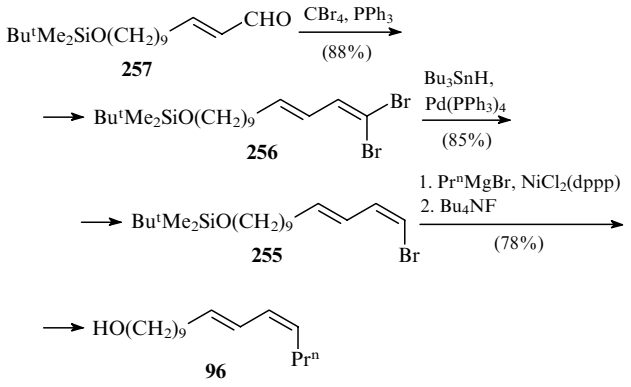

Some examples of using dienyl sulfides **258** (R^3 = Ph, Bu^t) in these reactions are documented;[45, 263, 276] in this case, the thiolate ion is the leaving group (the *tert*-butyl substituent is preferred [45]). The configuration of the products **55** remains the same as in the initial sulfides **258**.

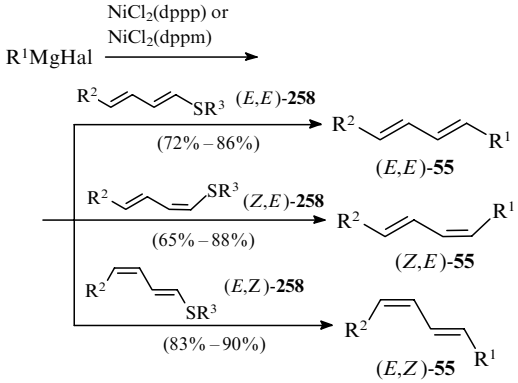

The cross-coupling strategy makes it possible to substitute a nucleofugal group at the 2-position of the diene system; this results in branched derivatives **259** and **260**. Dienol triflates **261** or phosphates **262**, which are easily prepared from the corresponding α,β-enones **263** or **264**, can serve as convenient substrates for this purpose. The cyclic dienol triflates **261** react with the Grignard reagents in the presence of catalytic amounts of CuI,[277] while the acyclic phosphates **262** react in the presence of complex nickel catalysts.[278] The dienes **260** are formed as mixture of geometric isomers. The phosphate strategy is suitable also for the synthesis of cyclic dienes **259**.

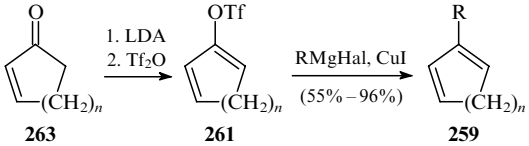

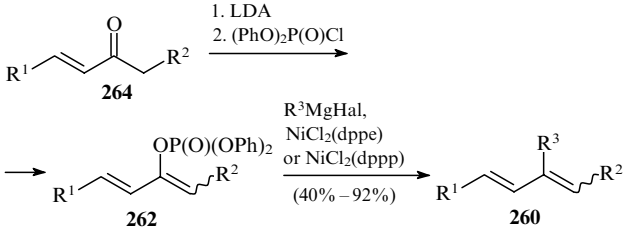

This technique has been used to introduce a methyl group during the synthesis of methoprene (**265**) according to the $C_{10} + C_4 + C_1$ pattern; the substitution of the methyl group for the OAc group in compound **266** occurred with complete retention of the initial configuration.[279]

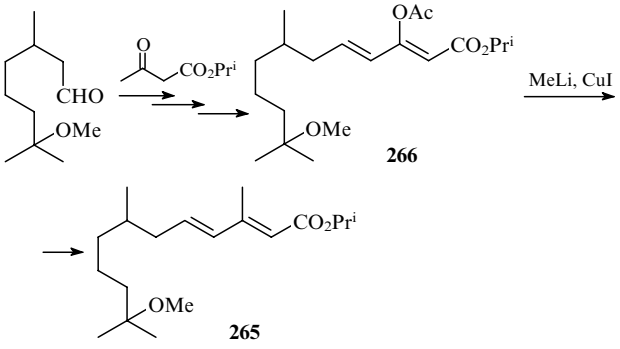

f. Cross-coupling involving 1,2-dihaloethenes

The (*E*)- and (*Z*)-isomers of 1,2-dichloroethene (**267**) can serve as convenient and inexpensive synthons for the preparation of conjugated dienes (as well as styrenes, enynes and so forth) (see a review [280]). By varying the conditions and catalysts, it is possible to perform consecutive coupling of these compounds, first, with a saturated and then, a vinylic component (or *vice versa*),[281] resulting in the formation of the target dienes in high yields and with high isomeric purity. It is of interest that 1,2-dibromoethene is much less effective in this type of process.[280]

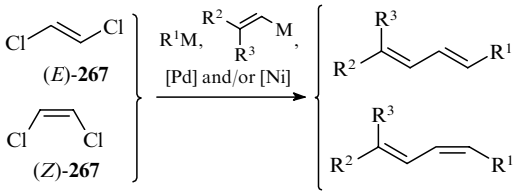

g. Synthesis of 1,3-dienes from alkynes and allenes

As noted above, alkynes can be used in the cross-coupling instead of alkenes. The reactions of terminal alkynes or their metallated derivatives with alkenyl halides (the Sonogashira reaction, see a review,[282] and transformation of **213** into **214** in general Scheme 8) yield conjugated enynes, which can be reduced to dienes (the reduction techniques are described in Section VII). In addition to alkenyl halides, these reactions can be carried out for alkenyl- (**268**) and dienyl tellurides **269**; these afford conjugated enynes **270** and dienynes **271**, respectively.[283]

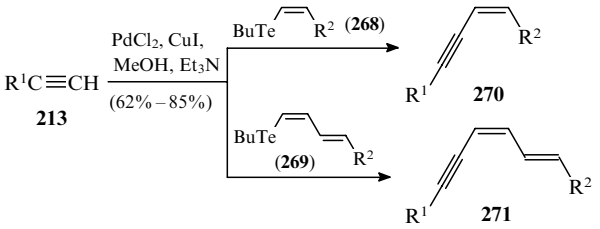

The addition of metal hydrides or organometallic reagents to the triple bond is stereospecific (*cis*-1,2-addition), which permits the preparation of pure isomers. Of relatively early studies, one should note the synthesis of dienonitrile **272** on the basis of hydroalumination of hex-3-yne.[272]

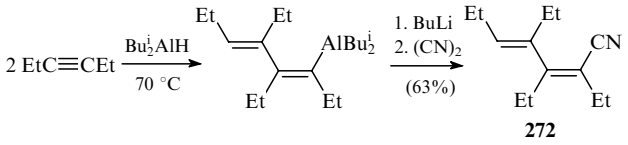

Hydroboration of alkynes resulting in alkenylboranes is the obligatory first stage of the Suzuki cross-coupling (see above). However, other methods of transformation of alkenylboranes **273** into the conjugated dienes **55** are also known, for example, successive hydroborations of chloroalkyne **274** and the alkyne **213** followed by the borotropic rearrangement.[284]

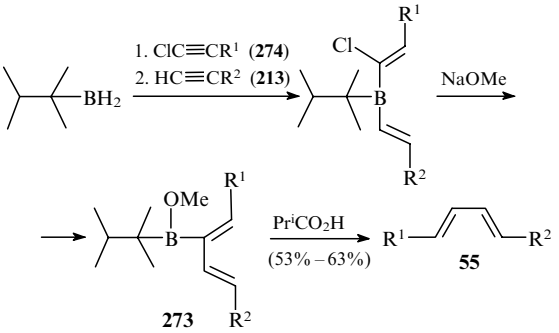

Yet another organoboron method consists in sequential chemoselective coupling of two alkynes (**275** and **276**, the latter as the lithium derivative), which gives conjugated enynes **277**, the immediate precursors of *E*,*Z*-dienes.[285, 286]

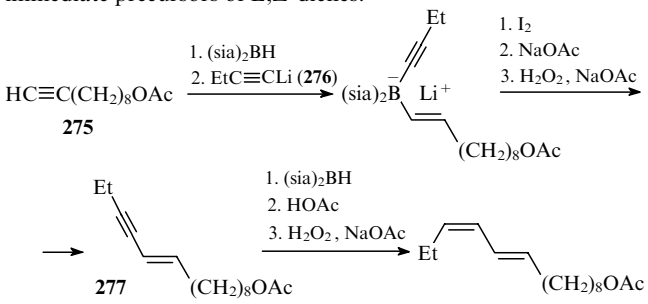

The addition of the cuprate reagents at the triple bond has been studied most comprehensively (see reviews [9, 287]). In early studies,[288, 289] cuprate reagents **278** have been prepared from the corresponding vinyllithium derivatives; their subsequent *syn*-addition to the triple bond in alk-2-ynoates **279** furnished dienoates **280** (pathway *a*). The stereochemical outcome of the reaction is important: the new double bond always has the *E*-configuration and the initial configuration of the vinylcuprate reagent does not change.

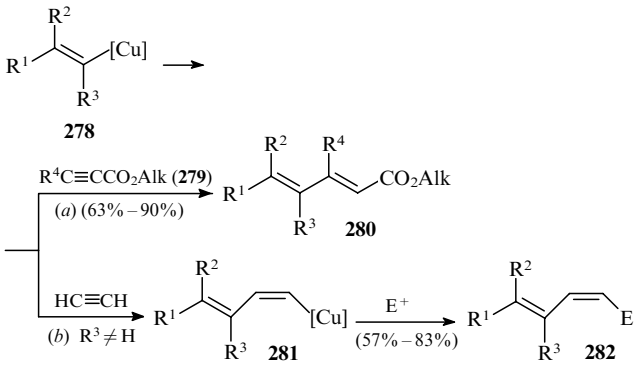

The development of methods for the addition of cuprate reagents to a non-activated triple bond has markedly extended the scope of the synthesis of dienes.[287, 290] Starting from different vinylcuprates **278** ($R^3 \neq H$) and acetylene (pathway *b*), one can obtain diene intermediates **281**, which then react with C-electrophiles (AlkI, CO_2, $PhSCH_2NEt_2$). This affords dienes **282** in which the double bond is *Z*-configured. Simple vinylcuprates **283** are formed from alkylcuprates **284** and acetylene; according to the stereochemistry of this process, this vinylcuprate has a *cis*-configuration.[291 – 293] By varying the natures of the second, acetylenic component and the final electrophile, one can obtain products **285** and **286** with a desired configuration of the second double bond.

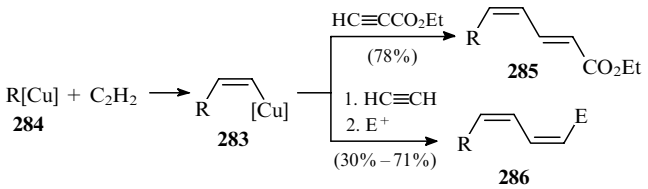

Recently, the organocuprate method has been successfully used for the preparation of dienes of the cyclobutane series of type **287** and **288** using an intramolecular reaction.[294] Fairly stable organotin substrates **289** and **290**, which underwent transmetallation under the reaction conditions, served as the precursors of active species.

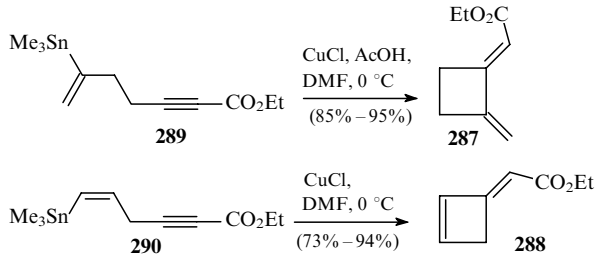

The ability of cuprate reagents to add to the double bond of α,β-enones has been used for the formation of the conjugated diene system in the synthesis of ipsenol **291**. The α-allenyl ketone **292** needed for this purpose was prepared from amide **293** and allene **294**.[295]

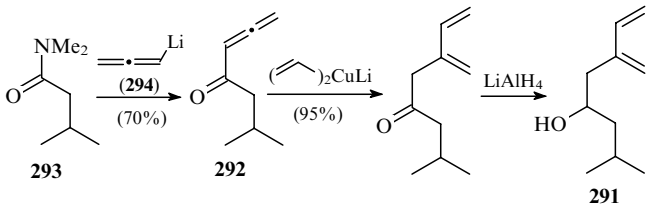

The addition of alkylcuprate reagents at the triple bond of enynes **295** results in the branched conjugated dienes **242** or alka-2,4-dienoic acids **296**.[296]

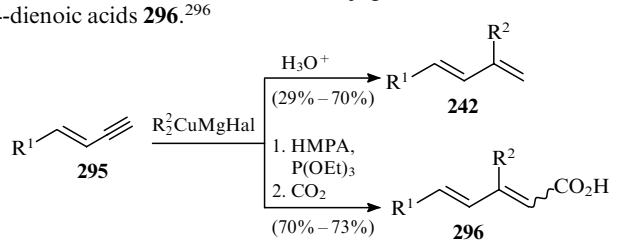

h. Coupling of alkene and alkyne components using ruthenium catalysts

The last decade was marked by enhanced interest in the catalysts based on ruthenium complexes (see a review [297]) which catalyse other types of transformation than palladium, which has become a routine material. These processes include coupling of activated alkenes **297** with alkynes (Scheme 10). This reaction catalysed by the Ru(cod)(cot) complex (cot is cycloocta-1,3,5,7-tetraene) and resulting in conjugated dienes **298** is a stereospecific addition of a terminal alkene to the triple bond.[298] The product yield depends dramatically on the nature of the substituents: in the case of acrylates (X = OAlk), good results were obtained only with diphenylacetylene (R = Ph); on passing to acrylamides (X = NMe_2), the range of possible acetylenic components is broader.

Scheme 10

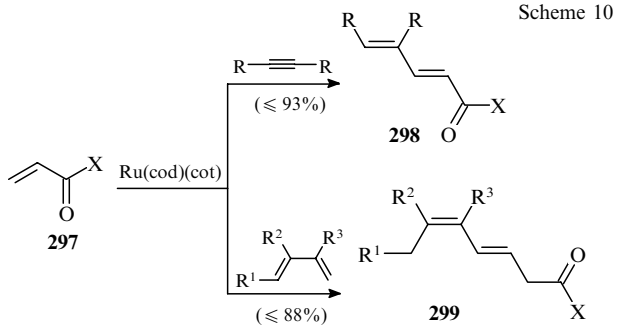

X = OAlk, Alk, $NAlk_2$.

Instead of alkynes, diene hydrocarbons can also been used in this reaction;[299] in this case, incompletely conjugated dienyl carbonyl compounds **299** are formed as the reaction products. This reaction is also sensitive to the type of substitution at the double bonds of the reactants and can result in isomer mixtures.

Coupling of terminal non-activated alkynes **213** with non-activated alkenes **300** takes place on prolonged refluxing in pyridine in the presence of $CpRu(PPh_3)_2Cl$ and $NaPF_6$.[300] The newly formed double bond in the diene **55** always has the *Z*-configuration, the process being accompanied by the formation of noticeable amounts (up to 13%) of non-linear isomers of **242**.

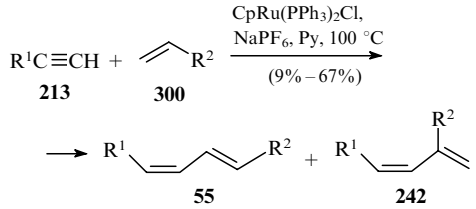

The reactions of alkynes with alkenes catalysed by another ruthenium catalyst, Cp(cod)RuCl, result in 1,4-dienes.[301] This method is suitable for the preparation of conjugated dienones **301** only in the case where the initial acetylene derivative **302** contains a latent carbonyl group. This facilitates isomerisation of the 1,4-diene system to a conjugated one.

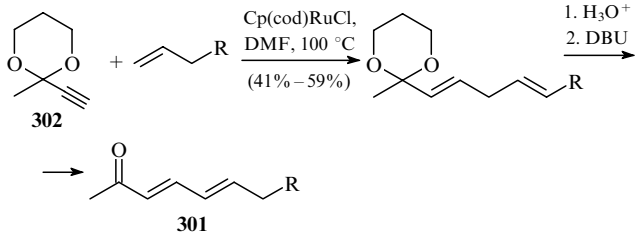

Coupling of two different acetylene derivatives **213** and **304** catalysed by the complex **303**, which gives enynes **305** (potential precursors of dienes), proceeds strictly stereospecifically.[302, 303]

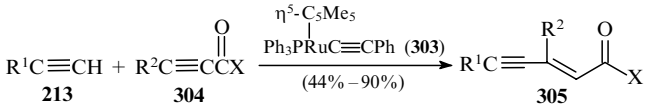

C_5Me_5 is pentamethylcyclopentadienyl.

Intramolecular cyclisation of diterminal diacetylenes of the general type **306** with a relatively long linking chain (which can contain functional groups and even a ferrocene residue) induced by ruthenium complex **307** is accompanied by the formation of enynes of the macrocyclic series **308** (see Ref. 304).

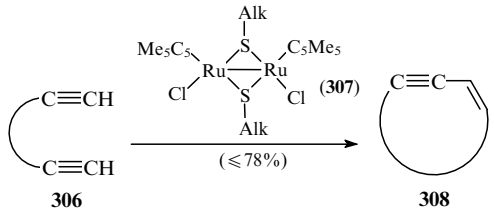

i. Syntheses of exocyclic dienes

In conclusion, mention should be made of several intramolecular cross-coupling reactions of the same type, resulting in five-membered vicinally substituted carbo- or heterocyclic compounds **309**. Of these, cyclisation of 1,6-enynes of the general type **310** has been studied most comprehensively. When catalysed by palladium complexes,[305 – 308] this reaction proceeds smoothly in most cases if the vinyl group of the initial enyne **310** does not contain a substituent (R^2 = H). A single example has been reported [309] where this reaction occurred smoothly in the presence of a substituent in this group, namely, $R^2 = CH_2OR^3$. However, in most cases, mixtures of isomers having the same carbon skeleton

of the type **309** and differing in the position of the double bonds are produced.[310, 311]

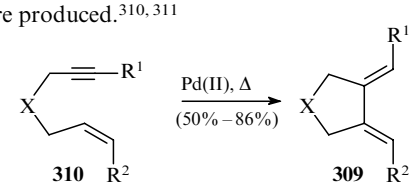

X = CMe_2, $C(CO_2Me)SO_2Ph$, $C(CO_2Me)_2$, NR.

In some cases, this approach can be used to prepare six-membered rings but with some limitations regarding the type of substitution in the initial compounds.[312, 313] Similar regularities have been found for the same transformation catalysed by nickel complexes immobilised on phosphinylated polystyrene.[313]

Ruthenium complexes, for example, $RuCl(cod)(C_5Me_5)$ and $RuClH(CO)(PPh_3)$, are capable of inducing cyclisation of allyl propargyl ethers[314] and derivatives of alk-2-en-7-ynoic acids **311**[315] the products of which are dienes **312** and **313**, respectively. Reactions catalysed by ruthenium complexes are much less sensitive to the nature of substituents than the same reactions catalysed by palladium complexes.

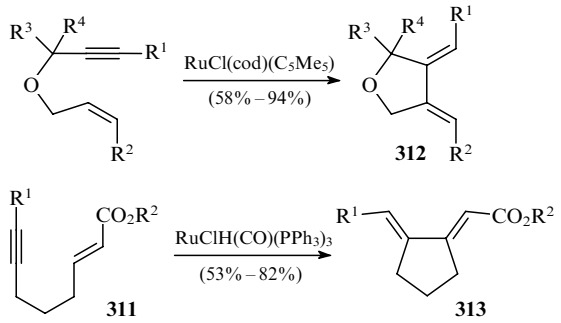

The preparation of vicinal di-*exo*-methylene compounds **314** by intramolecular cyclisation of bromides **315** (process of the Heck reaction type) has been described.[308, 316] The reaction takes place smoothly in the presence of the $Pd(OAc)_2 - PPh_3$ catalytic system[308] or the $RhCl(PPh_3)_4$ catalyst,[316] whereas with the $Pd(PPh_3)_4$ catalyst, the six-membered isomer **316** is the major product.[316] Intramolecular coupling of dibromides **317** affords the dimethylene isomer **314** as the only product; according to the balance, a stoichiometric amount of a reducing agent [Ph_3P or $(p\text{-}MeOC_6H_4)_3P$] is required.[317]

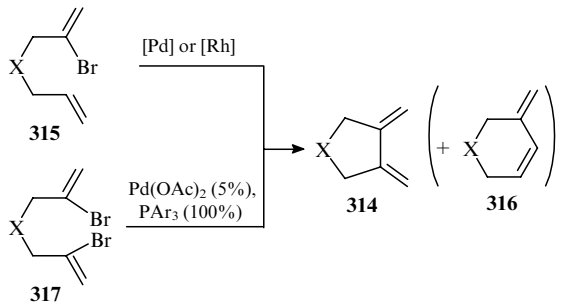

X = $PhCH_2N$, $C(CO_2Et)_2$, $C(COMe)_2$.

1,2-Dialkylidene-substituted cyclic compounds **318** can also be prepared from diacetylene derivatives **319**; this requires participation of a reducing reagent. In one of the procedures, cyclisation is induced by titanocene (Cp_2Ti)[318] or zirconocene (Cp_2Zr) generated *in situ*.[319] In most cases, the use of zirconium is more advantageous than titanium:[320] in the synthesis of four-, five-, six- and seven-membered rings, good yields are obtained even in the case of bulky R^1 and R^2 substituents. However, when $R^1 = R^2 = OEt$, it is necessary to use the titanium reagent.

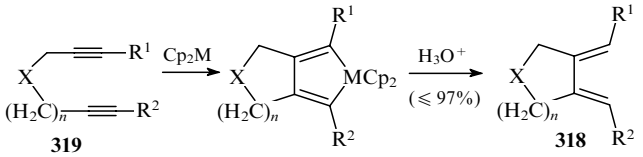

X = CH_2, O; $n = 0-3$; M = Ti, Zr.

The transformation of 1,6-diynes, for example, **320**, into the corresponding exocyclic diene **321** can be carried out with participation of the $(dba)_3Pd_2 \cdot CHCl_3$ palladium catalyst and the Et_3SiH reducing agent (stoichiometric amounts).[321]

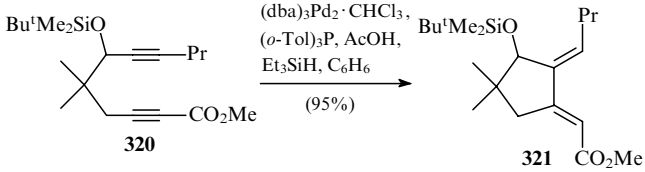

In the case of other substrates of this chemical type, the yields vary in the range of 34% – 95%.

Two cases of cyclisation of compounds **322** and **323** followed by functionalisation are known.[322, 323] The functional groups being introduced occupy the *Z*-position in products **324** and **325**, which is related to the mechanism of intramolecular *syn*-carbometallation at the cyclisation stage.

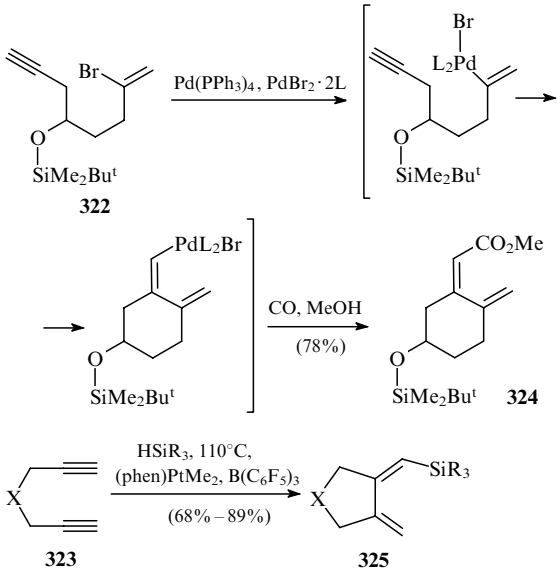

X = $C(CO_2Me)_2$, $C(CH_2OR^1)_2$, $[C(CO_2Et)_2]_2$.

2. Miscellaneous reactions catalysed by organometallic compounds

The reactions considered in this Section are difficult to classify on the basis of a particular feature. Most of them have been discovered in the current decade and it is obvious that these investigations are at the stage of accumulation of facts. Nevertheless, it can be noted that the interest of researchers tends towards reactions catalysed by ruthenium complexes. These complexes are active in transformations differing from those catalysed by Pd and Ni complexes. Some of them (cross-coupling of alkenes and alkynes) were described in the preceding Section.

a. Alkene – alkyne metathesis

Ruthenium carbenoid complexes catalyse an interesting coupling reaction of alkenes with alkynes during which the reactants undergo metathesis to give branched conjugated dienes.[324, 325] One of these complexes, $Cl_2(Cy_3P)_2Ru{=}CHPh$ (**326**, Cy is cyclohexyl), the so-called Grubbs catalyst II, has now become com-

mercially available and has been tested in reactions of ethylene with numerous acetylene derivatives of various structures. Unfortunately, only for dienes of the type **327** and **328**, have preparative yields been attained; esters of propargyl alcohols **329** and *N*-tosylpropargylamines **330** served as the precursors of these products. However, even in these cases, reactions did not proceed to completion, which is in line with the concept of reversibility of metathesis.

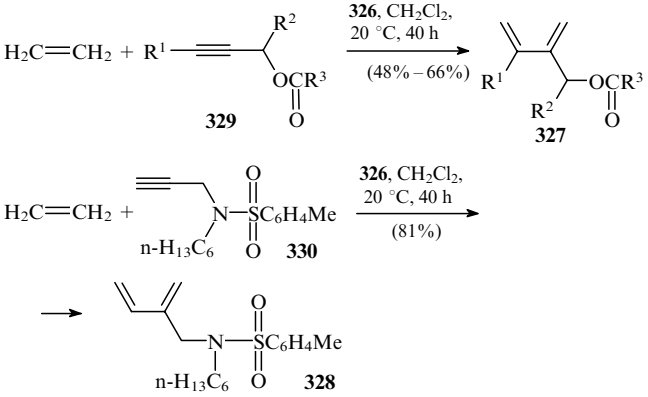

By conducting reactions under a pressure of ethylene (~4 atm), one can shift the equilibrium towards the products (for esters of type **329** with the terminal triple bond, $R^1 = H$, the yields increased to 92%);[326] however, upon further increase in the ethylene pressure, the reactions were retarded due to the degenerate ethylene–ethylene metathesis.[326, 327]

The problem of separation of the initial and final compounds, the polarities of which are close, should also be mentioned. An ingenious solution of this problem has been proposed.[328] The researchers suggested that the initial propargyl alcohol be immobilised on a polymeric support through a linker of an ester structure **331**.[328] In this case, after metathesis, the immobilised product has already the allyl carboxylate structure **332**. The subsequent reaction of the compound **332** with nucleophiles catalysed by palladium complexes results in diene product **333**, which passes to the solution, while the unreacted propargyl derivative **331** remains on the support.

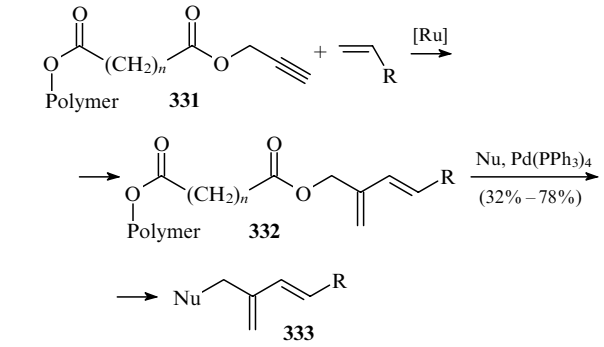

Stable imidazolidinylruthenium complex **334**, obtained recently

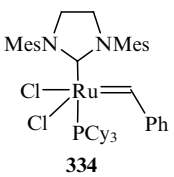

exhibits in many cases a much higher efficiency than the Grubbs catalyst II.[329] In particular, with the assistance of this complex, metathesis can be carried out for alkenes and alkynes characterised by a substantially broader spectrum of functionalisation and substitution [330] (*cf.* data of Refs 325 and 327).

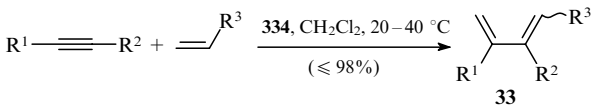

R^1 = $Ph_3CO(CH_2)_2$, Me_3Si, Cy, CO_2Bu^t, CH_2OAc, $CH_2OSiR^4_3$;
R^2 = H, Alk, CH_2OAc; R^3 = CH_2SiMe_3, $CH_2OSiR^4_3$, CH_2CO_2Bn.

The intramolecular alkene–alkyne metathesis of enynes **335**, discovered previously, is much less sensitive to the chemical type of the initial compounds than the intermolecular process because it is accompanied by the formation of favourable cyclic systems **336**.[331, 332] The product yields are very high, except for the case of terminal alkynes (R^1 = H). Later, the problem of low yields from terminal alkynes has been unexpectedly solved: it was found that this process should be carried out under an atmosphere of ethylene.[333] Ethylene does not formally participate in the reaction but it favours catalyst transfer in the form of the carbene $Ru=CH_2$.

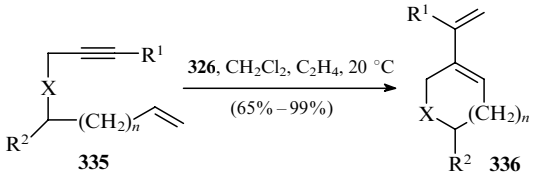

X = O, NR^3, $C(CO_2Et)_2$; R^1 = Me, CH_2OAc, $CH_2OSiMe_2Bu^t$, CO_2Me, H; R^2 = H, Ph; n = 0–2.

A study [334] demonstrating the possibility of involvement of alkynylboronic acids **337** in intramolecular metathesis deserves attention. Under the action of Ru catalyst **326**, they are smoothly converted into boryl-substituted dienes **338**, potential substrates for the Suzuki cross-coupling.[334]

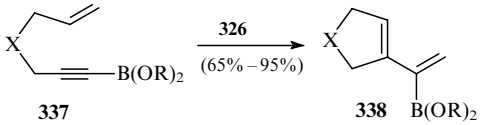

X = CH_2, $(CH_2)_2$, O, TsN, OCH_2O, $C(CO_2Et)_2$.

It is of interest that compounds **339** with an appropriate mutual arrangement of the two double bonds and one triple bond undergo double metathesis catalysed by $Cl_2(Cy_3P)_2Ru=CHCH=CPh_2$ (Grubbs catalyst I) to give bicyclic 1,3-diene structures of the general type **340** (n = 1, 2; m = 0–2).[335] The nature of the substituent R at the triple bond plays a crucial role: high product yields were obtained for R = H, Alk, Ph, CO_2Me, whereas for R = Br, I, Me_3Si or Bu_3Sn, cyclisation did not proceed. When tungsten-based catalysts of metathesis are used, cyclisation of the same substrates involves two double bonds and is accompanied by the ejection of a lower alkene without participation of the acetylene fragment.

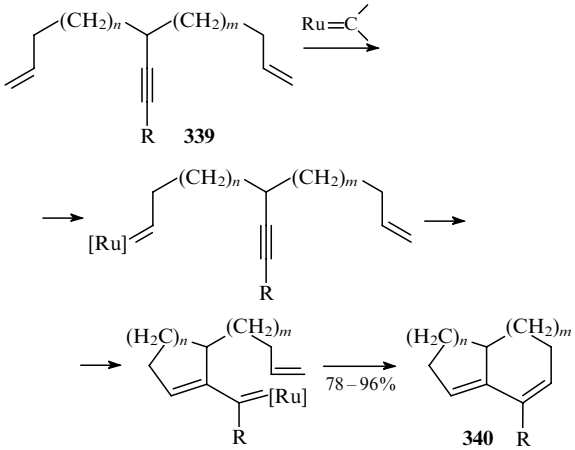

1,6-Enynes **341** are converted in the presence of $[RuCl_2(CO)_3]_2$ to give diene product **342**. The process fits formally the concept of the intramolecular alkene–alkyne metathesis considered above. Nevertheless, the researchers [336] suggest a different reaction mechanism.

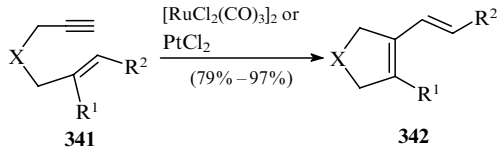

341 **342**

With $PtCl_2$ catalysis, enynes of the type **341** containing electron-withdrawing groups or a cyclic enyne fragment (with a medium or large ring) are also converted into formal metathesis products **342**).[337] Otherwise, they tend to form cyclopropane derivatives **343**.

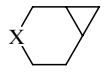

343

b. Synthesis of 1,3-dienes from allene derivatives

Ruthenium complexes catalyse an unusual addition of allenes **344** to activated alkenes **345** giving rise to 1,3-disubstituted conjugated dienes **346**.[338] To activate the catalyst, alkynols are used, the best results being attained with 2,4,7,9-tetramethyldec-5-yne-4,7-diol.

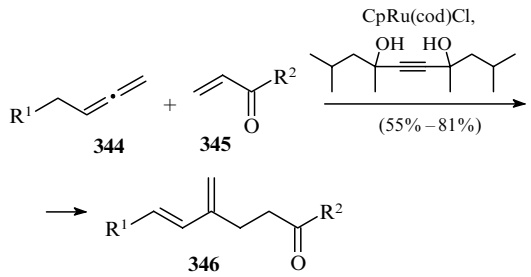

344 **345** **346**

The presence of a nitrile, ester or amide substituent in the side chain of the allene does not influence the course of the reaction. Regarding allene alcohols, a limitation has been found in the study of the mechanism — the number of carbon atoms between the allene system and the hydroxy group should not equal three or four; otherwise, oxygen-containing heterocyclic compounds are formed.[339]

Palladium complexes can catalyse not only cross-coupling of vinylic components but also other types of reaction resulting in conjugated dienes. A series of studies dealing with coupling of vinylic (**347**), allene (**348**) and CH-acidic (**349**) components,[340–344] resulting in branched functionalised dienes of the type **350**, has been reported. Various combinations of three components differing in the nature of the substituents and functional groups have been tested. Thus the vinylic component can be either linear or incorporated in a carbo- or heterocyclic system; the leaving group can be represented by either bromide or triflate. Among C-nucleophiles, Schiff's base $Ph_2C{=}NCH_2{-}\ CO_2Me$ has been studied, apart from the standard β-dicarbonyl compounds. The yields vary over broad limits and can reach 94%.

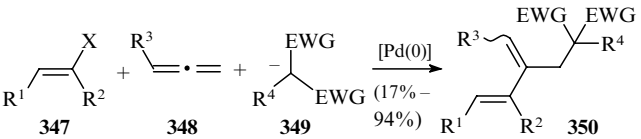

347 **348** **349** **350**

EWG is electron-withdrawing group.

Allene hydrocarbons **351** containing an allylic α-hydrogen atom undergo a $Pd(dba)_2$-catalysed reaction with aryl and alkenyl halides and triflates [345] to give conjugated diene compounds **352**. The highest yields (60% – 94%) were obtained in the case of aryl bromides and iodides.

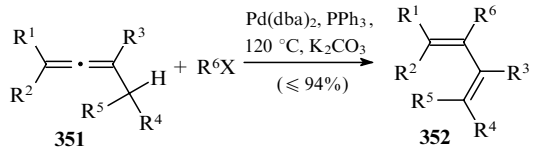

351 **352**

Carbonylation of allenylmethylamines **353** is directed at the allylic position, to the central atom of the allene system. The allylic rearrangement affords conjugated dienes **354** with the amino-carbonyl function at the 2-position.[346]

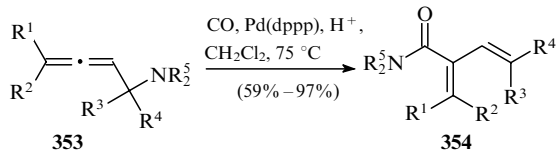

353 **354**

Hydrozirconation of allenylstannane (**355**) yields intermediate **356**, the reaction of which with aldehydes or ketones is accompanied by the allylic rearrangement [347] (the same outcome is provided by the reaction of aldehydes with pinacol 1-trimethylsilylprop-1-ene-3-boronate [43,44]). Decomposition of adduct **357** is accompanied by the formation of conjugated dienes, the proportion of *E*,*E*-isomer being more than 93% in the case of aldehydes (R^2 = H).[347]

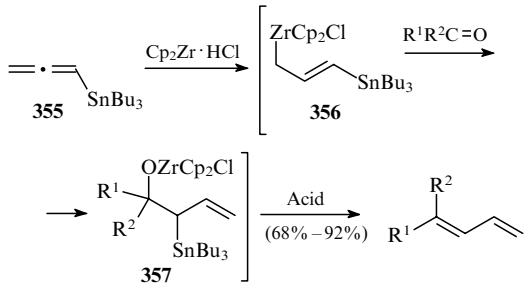

355 **356** **357**

c. Synthesis of 1,3-dienes on the basis of alkynes

Hydroformylation of conjugated enynes **358** in the presence of rhodium complex **359** gives branched dienic aldehydes **360**.[348] A minor admixture of monounsaturated aldehyde is also formed.

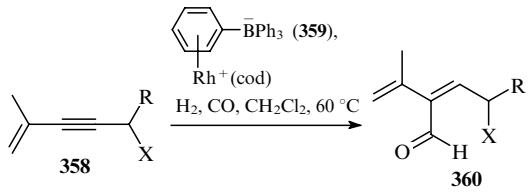

358 **360**

X = H, OAc, OMe.

Diethyl dienedioates **361** are produced upon carbonylation of alkyne-α,α′-diol dicarbonates **362**.[349] The reaction occurs through the intermediate formation of allene derivative **363**. The possibility of preparing dienoates **364** from the corresponding α-allenyl carbonates **365** was also demonstrated.

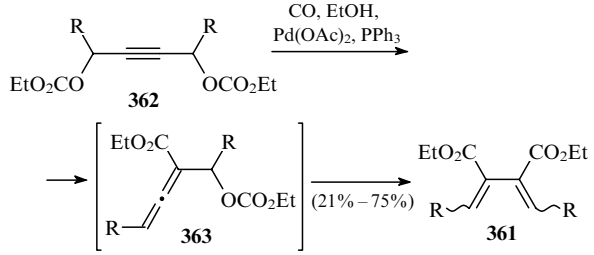

362 **363** **361**

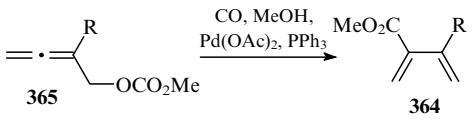

365 **364**

The reaction of propargyl dicarbonates **366a**,**b** with organoboron or -tin compounds catalysed by palladium complexes is accompanied by the double allylic rearrangement, resulting in substituted 1,3-dienes **367a**,**b**.[350]

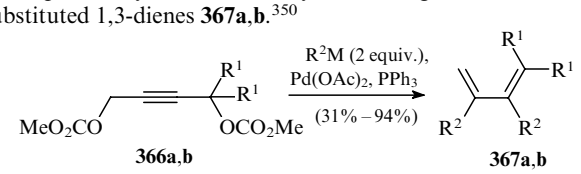

366a,**b** **367a**,**b**

R^1 = H (**a**), Me (**b**); R^2M = $NaBPh_4$, $ArB(OH)_2$, $HetB(OH)_2$, $HetSnBu_3$, $PhC{\equiv}CSnBu_3$.

A reaction with a similar outcome giving rise to similar dienes consists in the interaction of organotin compounds of various structures with α,α′-disubstituted acetylenes **368** (X = Cl, OTs).[351]

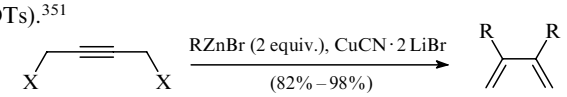

368

In the presence of $Ni(cod)_2$, propargylsilane **369** reacts with aldehydes and organozinc compounds to give the 2,4-disubstituted 1,3-dienes **242**.[352]

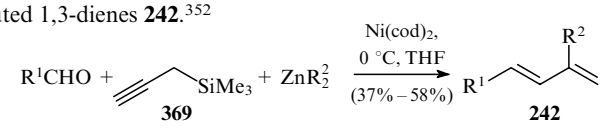

369 **242**

Complex cyanocuprates **370** derived from terminal alkynes add 4 moles of iodomethylzinc iodide (**371**). The subsequent treatment of the addition product with electrophilic reagent **372** furnishes conjugated 2,3-disubstituted diene **373**.[353] The reaction includes the stages of insertion of a carbenoid and two allylic rearrangements. In the case where the cyanocuprate complex **374** contains a fragment of sterically hindered ether and the process is initially carried out in the presence of an electrophile (cyclopentanone), three moles of the reagent **371** are added. This route was used to prepare diene **375**.

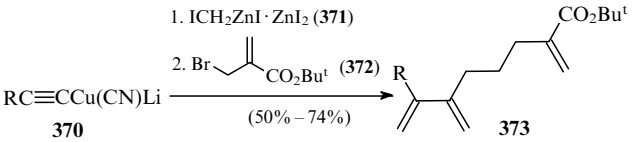

370 **373**

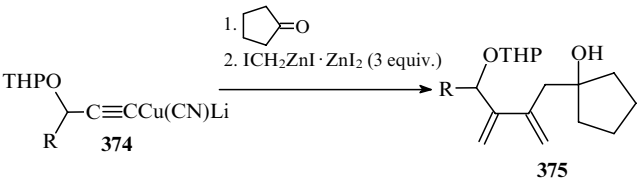

374 **375**

Hydrozirconation of ethoxyacetylene (**117**) and treatment of the resulting zirconium intermediate **376** with α,β-enals affords dienals **377** in a preparative yield.[354] The same products can be obtained using the same reactions but starting from 1-methoxybut-1-en-3-yne and a saturated aldehyde.

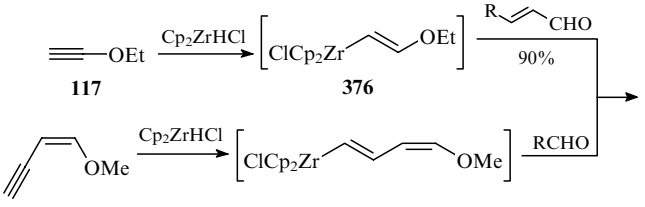

117 **376**

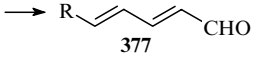

377

Alkenylzirconium compound **378** reacts with lithiated epoxy nitriles **379** to yield nitriles **380**.[355] If pure epoxy nitrile isomers are used, the reaction still gives a mixture of geometric isomers at the cyano-substituted double bond.

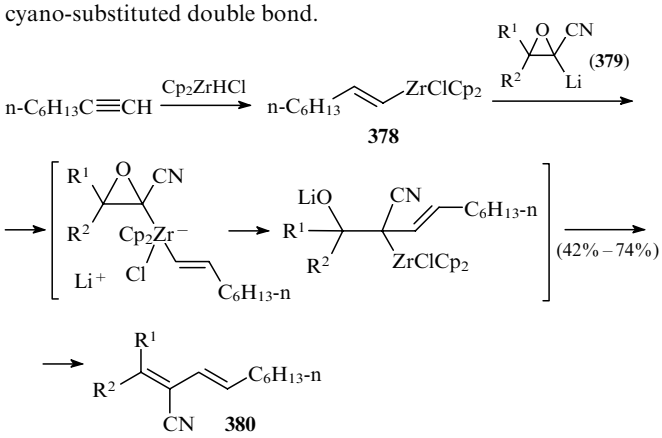

378 **380**

The reaction of disubstituted acetylenes with the carbene derivative of titanocene (the Tebbe reagent) results in a [2 + 2]-addition product, substituted titanacyclobutene **381**.[356] The subsequent regioselective reaction of **381** with carbonyl compounds gives conjugated dienes **382**. In the case of dimethyl- or diethylacetylene (R^1 = Me, Et), various aldehydes and ketones can be used, whereas in the case of tolan (R^1 = Ph), the range of carbonyl compounds is limited to reactive aldehydes (R^2 = H; R^3 = H, Me, Ph).

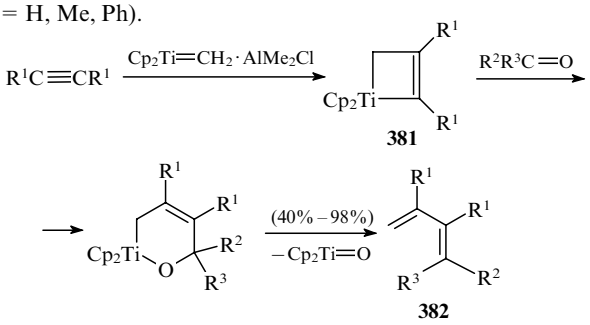

381 **382**

A curious process of acetylene dimerisation in the presence of electron-deficient alkenes makes it possible to prepare bifunctional *Z*,*E*-dienes **383**.[357] Acrolein (Y = CHO), vinyl ketones (Y = COR), nitroethylene (Y = NO_2) and β-substituted crotonaldehyde were tested in this reaction. In the latter case, the product yield was not more than 3%.

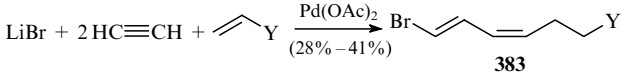

383

The reactions of disubstituted alkynes **384** with niobium pentachloride under reductive conditions gives intermediate **385**, containing the niobiacyclopropene fragment, able to add two equivalents of aldehydes.[358] Finally, conjugated dienes **386** with identical substituents at the ends of the system are produced.

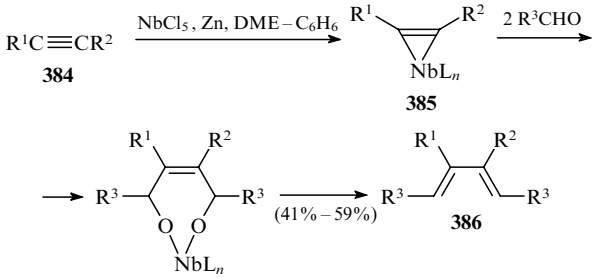

384 **385** **386**

Similar tantalum compounds **387** add a second acetylene molecule; after hydrolysis, the conjugated diene **179** is liberated.[359] The scope and limitations of this method have not been adequately studied.

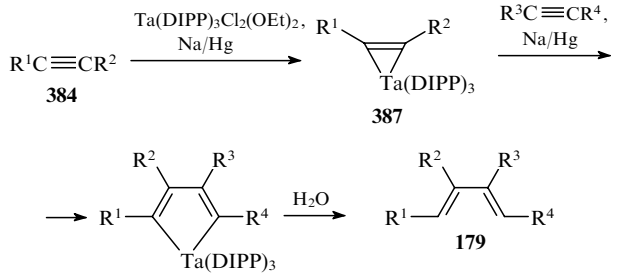

384 **387** **179**

DIPP is 2,6-diisopropylphenoxide.

The reactions of hexacarbonyldicobalt complexes of alkynes **388** with activated alkenes afford conjugated dienes **389** in moderate yields.[360]

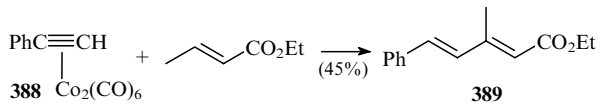

388 **389**

d. Syntheses of conjugated dienes from other dienes

Allylic acetates **390** and **391** react with malonate anions in the presence of palladium catalysts to give products **392** and **393** with a diene system.[361, 362] To ensure the maximum regio- and stereoselectivity, the process should be carried out in the presence of tributylphosphine. When triphenylphosphine is used, the regioselectivity substantially decreases. For example, the transformation of the acetate **391** gives, in addition to the product **393**, 40% of the product of nucleophile addition at the central carbon atom.

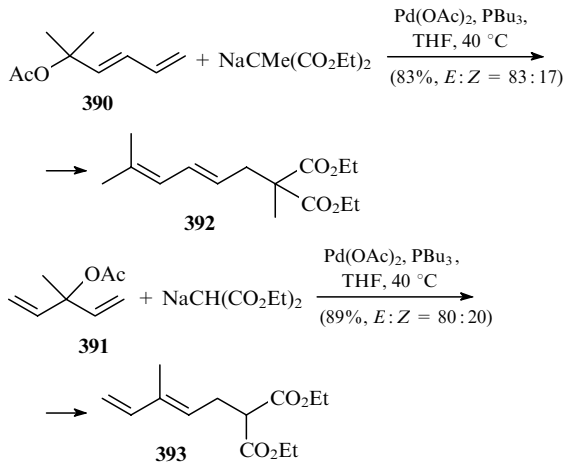

390 **392** **391** **393**

The reaction of allylic carbonates with the dimethyl malonate carbanion catalysed by the $Mo(CO)_3(EtCN)_3$ system with chiral ligand **394**

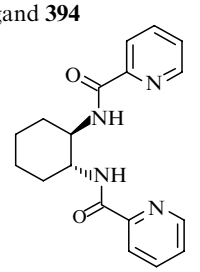

394

is accompanied by allylic rearrangement producing optically active homoconjugated compounds.[363] When triene carbonates **395** are used, the conjugated diene system is retained in the product and is connected to the chiral carbon atom.

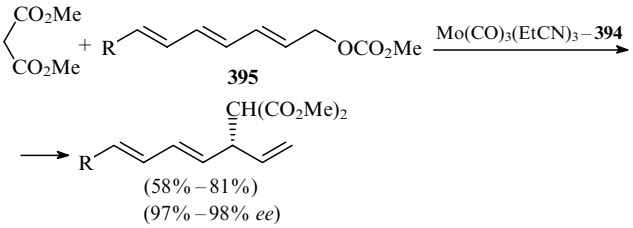

395

The reaction of dienes with electron-deficient alkenes (see Scheme 10)[299] catalysed by ruthenium complexes should also be attributed to this type of reaction.

e. Reactions of iron diene complexes

Conjugated dienes form stable complexes **396** with tricarbonyliron (see a review[364]). The electron-donating properties of $Fe(CO)_3$ facilitate the addition of electrophilic reagents at the termini of the diene system and contribute to the stabilisation of the allylic carbocation; this enables introduction of nucleophilic reagents into this position.

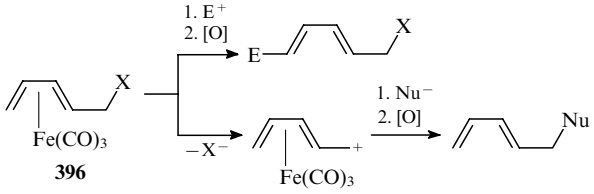

396

It has been proposed to use this type of complexation as a temporary protection of a diene system. The diene regeneration from the complex takes place on treatment with mild oxidants, for example, $(NH_4)_2Ce(NO_3)_6$ or *N*-oxides.

The following examples demonstrate the successfulness of using this strategy in fine organic synthesis. Complexes of terminal dienes can easily be converted into functional derivatives **397** some of which are insect pheromones.[365]

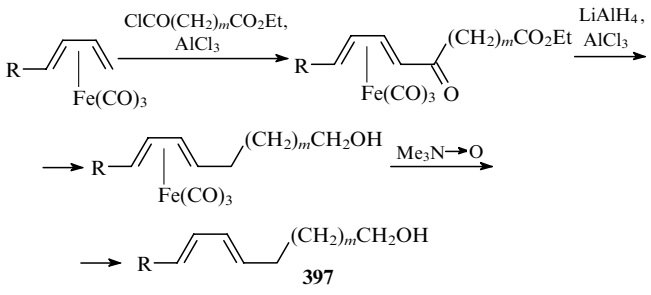

397

The complex of conjugated dienal **398** can react with some C-nucleophiles at the aldehyde group without a catalyst.[366]

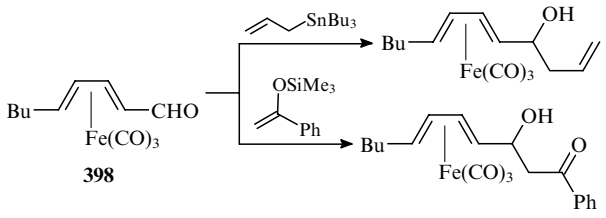

398

The reaction of π-allylcarbene cationic complex of tricarbonyliron **399** with boron ate-complexes of enolates yields η^4-complex derived from conjugated diene **400**.[367] Decomposition of the complex **400** on treatment with Ce(IV) gives rise to diene **401** containing an oxo group in the β-position.

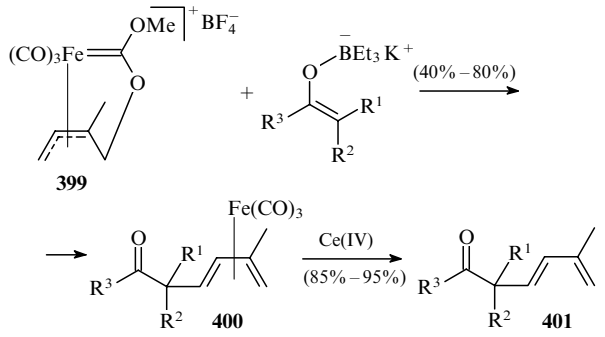

Mention should be made of recent publications [368, 369] describing the synthesis of functional derivatives of diene tricarbonyliron complexes **402** [368] and **403**.[369]

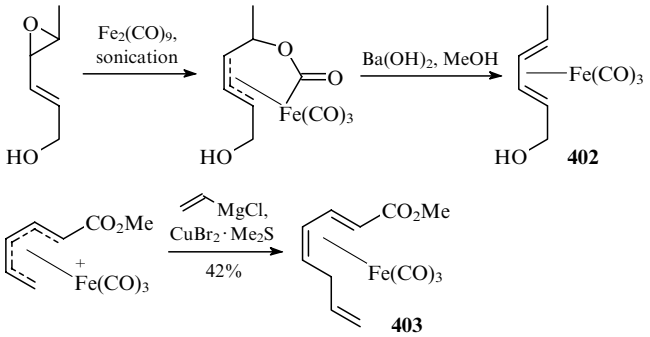

f. Miscellaneous organometallic reactions

The reaction of furans **404** with diazo esters in the presence of $Rh_2(OAc)_4$ affords a product mixture containing, among other compounds, oxodienoate **405**.[370] On treatment with catalytic amounts of iodine, this mixture can be converted into the pure diene (*E*,*E*)-**405** (or a mixture of *E*,*E*- and *E*,*Z*-isomers if $R^2 \neq H$).

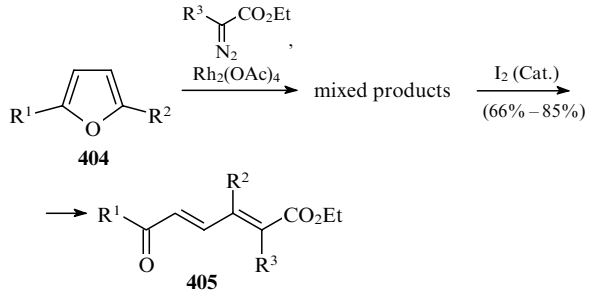

Cyclic thioacetals **406** react with cyclopropyl Grignard reagents **407** in the presence of catalytic amounts of $NiCl_2(PPh_3)_2$ on refluxing in benzene or toluene to give dienes.[371] If the type of substitution in the three-membered ring differs from that in **407**, the reaction gives a mixture of isomers.

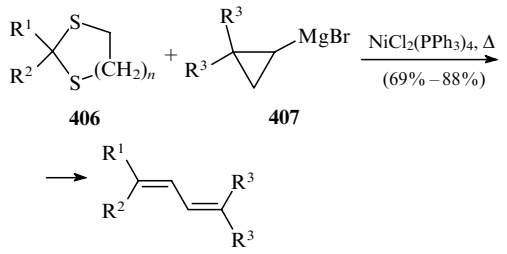

V. The synthon approach to conjugated dienes

Many reactions considered above could have been placed in this Section because versatile reagents can simultaneously be regarded as synthons if they contain fragments incorporated in the product molecule. Below we consider 'synthon syntheses' not included in the preceding Sections. They are arranged according to the type of fragment introduced in the final conjugated diene.

1. The $=CH-CH=CH_2$ (C_3) synthons

The widely known allylic Wittig reagents and their analogues are equivalent to the $=CH-CH=CH_2$ synthon. This type of reagents also includes 1-bromo-3-iodopropene.[372] The reaction of this compound with aldehydes on treatment with tin(II) chloride is accompanied by allylic rearrangement and gives terminal 1,3-dienes **38** in moderate yields.

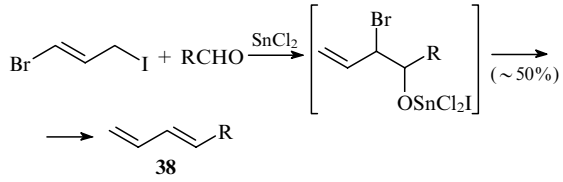

2. The $-CH=CH-CH=CH_2$ (C_4) synthons

In a known four-step procedure for the preparation of butadienyl ketones **408**, 4-phenylthiobutanal (**409**) is used as the source of the diene fragment for 'dienylation' of α-chlorosulfoxides.[373]

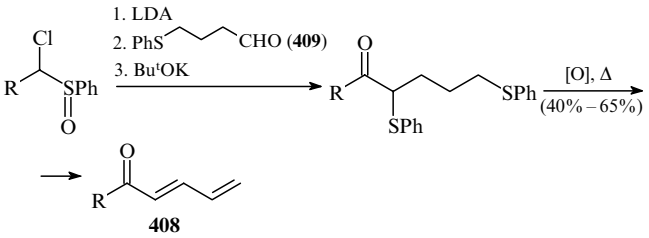

A broader range of compounds of type **410** can be prepared on the basis of 1-phenylsulfo-4-trimethylsilylbut-2-ene (**411**) (pathway *a*).[374] The same products are formed when a more readily available isomer, 1-phenylsulfo-4-trimethylsilylbut-1-ene (**412**) is used instead (pathway *b*).[375]

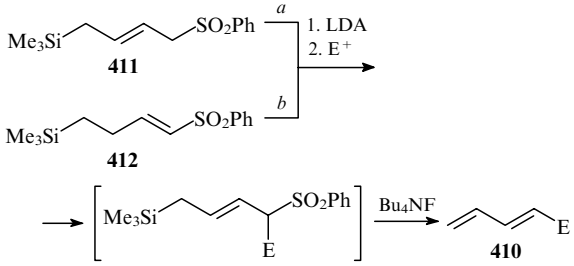

E = Alk, RC(O), , R_3Si, R_3Ge.

3. The $-CH_2-CH=CH-CH=CH_2$ (C_5) synthons and their homologues

The readily available 2,4-dienes of the general formula **413** containing a functional group (for example, a hydroxy group) at the 1-position can serve as the sources of these synthons. The corresponding allyl bromide **414** or acetate **415** acts as an electrophile when treated with Grignard reagents.[376, 377]

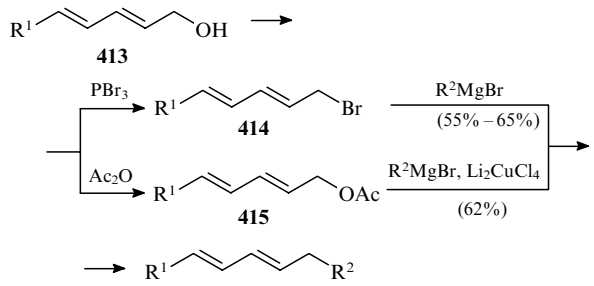

The reaction of pentadiene isomers with lithium followed by treatment with trimethylchlorosilane yields only one product, 1-trimethylsilylpenta-2,4-diene (**416**).[378, 379] This compound reacts with C-electrophiles of various types.

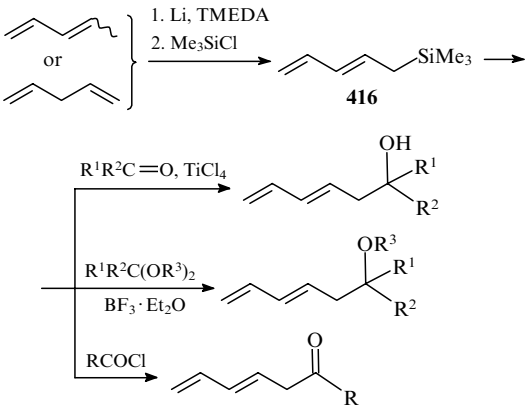

4. The =CH–CH=CH–CHO (C_4) synthons

Many compounds considered in Section III can be considered among the reagents capable of serving as sources of these synthons. Nevertheless, other versatile reagents for such 'dienylation' also do exist. For example, 1,4-heterodisubstituted butadienes **417** or **418** can be easily converted into organolithium derivatives **419** or **420**, which are much more reactive towards aldehydes and ketones than the Wittig–Horner reagents. Final hydrolysis gives rise to dienals **421**, formed predominantly as the *E*,*E*-isomers [380–382] (almost 100% for R^2 = H).

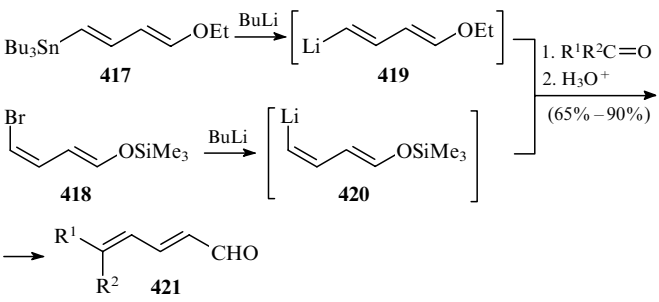

The dienals **377** can also be prepared using 1-methoxybut-1-en-3-yne (**422**) or its homologues.[354, 383, 384]

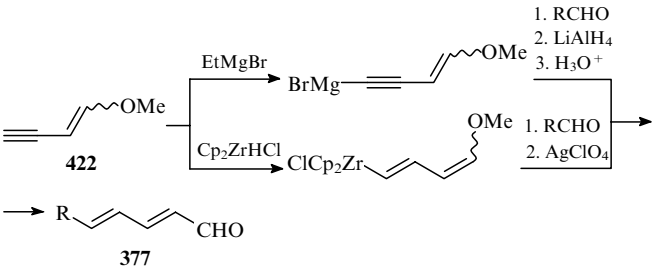

5. The –CH=CH–CH=CHCHO and –CH=CH–CH=CHCO$_2$R (C_5) synthons

Reagent **423**, equivalent to a nucleophilic synthon of the given type, belongs to the class of thiol thiocarbamates. The products of its α-alkylation (**424**) undergo two [3,3]-heterosigmatropic rearrangements giving ultimately linear dienes **425**,[385] which are precursors of the dienals **377**.

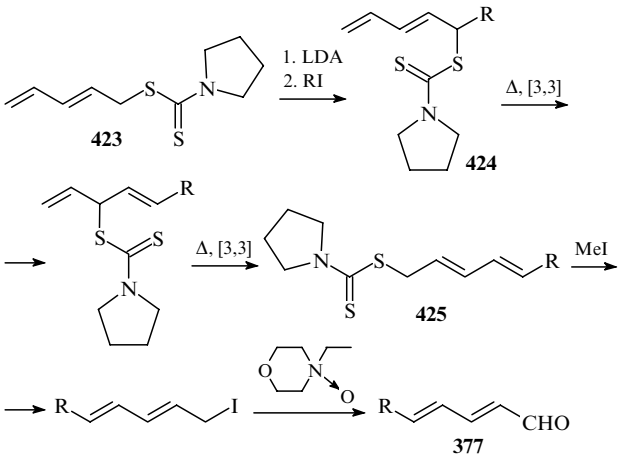

However, the most widely used synthons of this type are electrophilic reagents such as 5-bromopenta-2,4-dienal (**426**),[386, 387] 5-dimethylaminopenta-2,4-dienal (**427**)[388] and ethyl 5-(butyltelluro)penta-2,4-dienoate (**428**).[389] Substitution of alkyl groups for the electronegative elements (Br, NMe_2 and BuTe) in these compounds is accomplished by means of organometallic reagents.

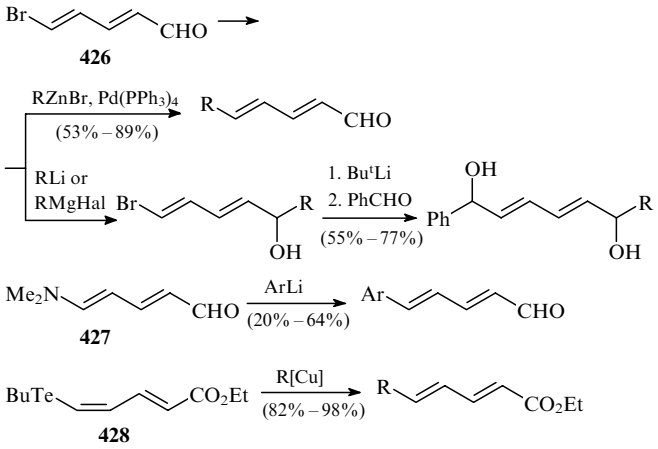

Yet another source of the synthons in question is represented by pyrylium salts **429**.[390, 391] The (*Z*,*E*)-alkadienals **430** formed initially in their alkylation are easily transformed into the *E*,*E*-isomers.

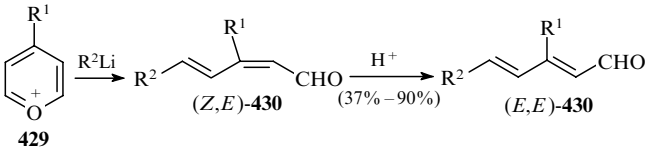

A similar role is played by the potassium derivative of glutacondialdehyde (**431**), which can be easily converted into the dienal **377** upon protection of one of the functional groups, treatment with a Grignard reagent and acid hydrolysis.[392]

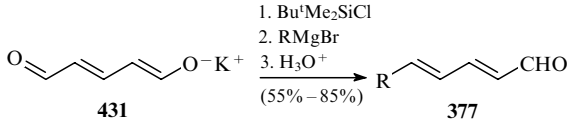

Furfural tosylhydrazone (**432**) can serve as a convenient synthon for the preparation of various 5-arylpenta-2,4-dienals **433**.[393]

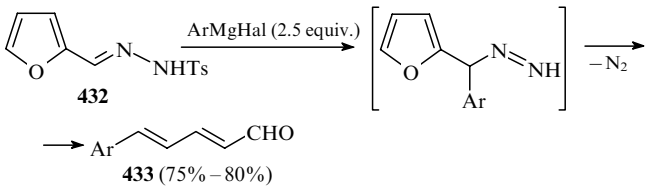

When made to react with alkylmagnesium halides, the same furfural **432** furnishes other products, namely, furan derivatives.

3-Ethynyl-β-propiolactone (**434**) reacts with organomagnesium compounds in the presence of copper(I) salts to give allenic acids **435**, which can be isomerised to dienoic acids.[394]

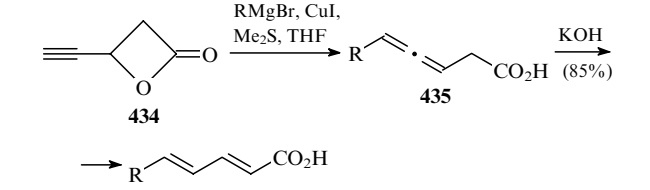

Finally, a three-step procedure for the synthesis of methyl 6-hydroxyalka-2,4-dienoates **436** has been developed; in this method, pent-4-enoic acid (**437**) serves as the source of the diene fragment.[395]

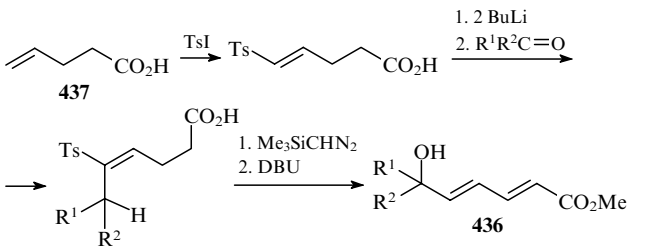

6. The $-C(=CH_2)-CH=CH_2$ (C_4) synthons

The synthon approach has been implemented successfully for the preparation of branched 1,3-dienes with functional substituents at the 2-position. One approach is based on the allylic rearrangement of allylsilanes and allylboranes in the reactions with carbonyl compounds. α-Allene derivatives **438** and **439**, similar to the allylic derivatives of silanes and boranes, react with carbonyl compounds at the *sp*-hybridised carbon atom yielding branched compounds **440**, which contain a conjugated diene fragment.[396, 397] In the case of the silyl derivative **438**, not only aldehydes but also acetals can be used, resulting in the corresponding ethers. The effect of a chiral group present in the electrophilic reagent was studied; after removal of this group, the resulting secondary dienic alcohols had *ee* values of up to 96%.

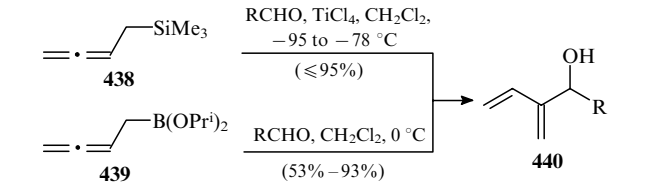

Branched allene silanes **441**, which can be easily prepared from acetylene derivatives **442**, behave in a similar way. They can be used to prepare 2,3-disubstituted butadienes **443**.[398]

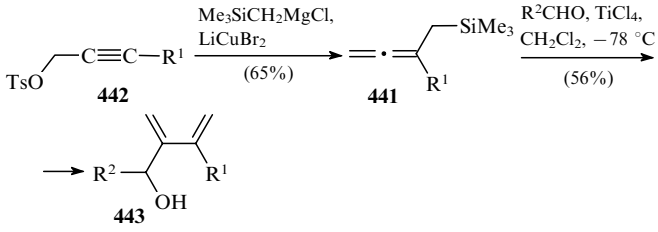

Great synthetic capabilities are provided by the butene derivative **444**, containing benzotriazole and trimethylsilyl vicinal groups.[399] After introduction of a desired fragment, the vicinal groups from the structures **445** and **446** can be eliminated by heating.

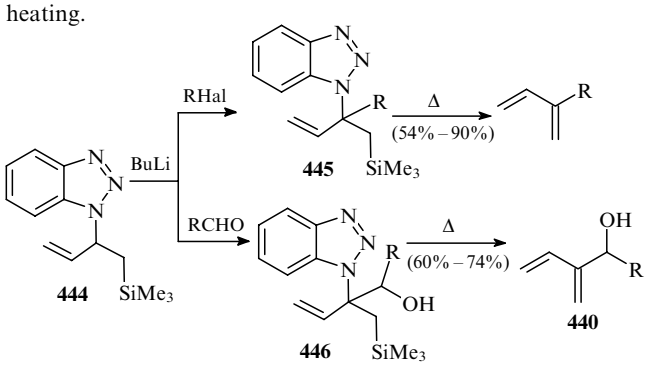

The Grignard reagent **447**, prepared from 2-chlorobuta-1,3-diene (chloroprene), can react with a number of electrophilic reagents, namely, α,β-unsaturated carbonyl compounds,[400] alkyl halides[400, 401] (including various bromoalkanonitriles[401]) and aryl iodides.[402] This is a very simple and versatile approach to the synthesis of 2-substituted 1,3-dienes. In the absence of copper salts, the Grignard reagent **447** can add to ketones; however, this gives about 25% of the rearranged allene-type product.[403]

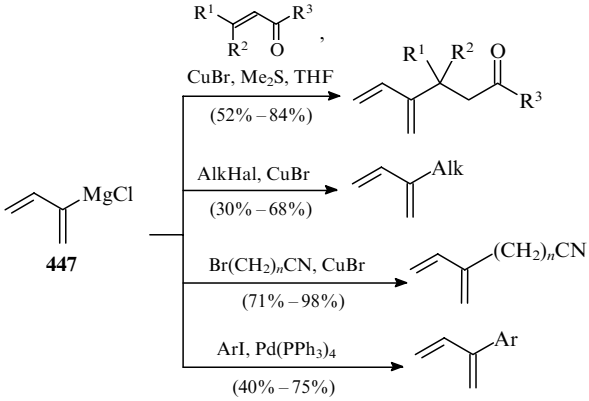

2-Substituted butadienes with a bulky substituent R^1 can be prepared from 1,4-dichlorobut-2-yne (**368**) using hydroboration.[404] The mechanism of this reaction has been studied in detail.[405]

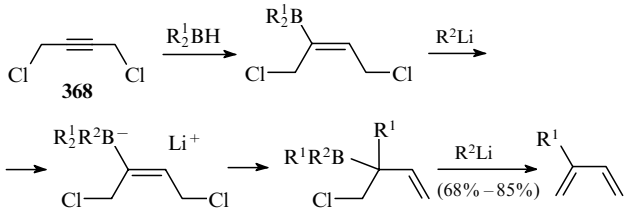

7. The $-CH_2-C(=CH_2)-CH=CH_2$ (C_5) synthons

α-Bromoisoprene (**448**) and organometallic derivatives prepared from it are typical examples of the title synthons. A convenient method has been proposed for the preparation of the corresponding Grignard reagent **449** in two simple steps without isolation of the bromoisoprene **448**.[34] The reaction of the Grignard reagent **449** with isovaleraldehyde results in ipsenol (**291**) (Scheme 11). 1-Methylene-2-(trimethylsilyl)cyclobutane (**450**) can be used instead of the Grignard reagent **449**; the compound **450** reacts with aldehydes with the allylic rearrangement to give a cyclobutene derivative **451**.[406] Pyrolysis of this product furnishes the same diene derivative **291**.

Organotin compound **452** with an isoprene fragment reacts with allylic bromides in the presence of Lewis acids giving rise to

Scheme 11

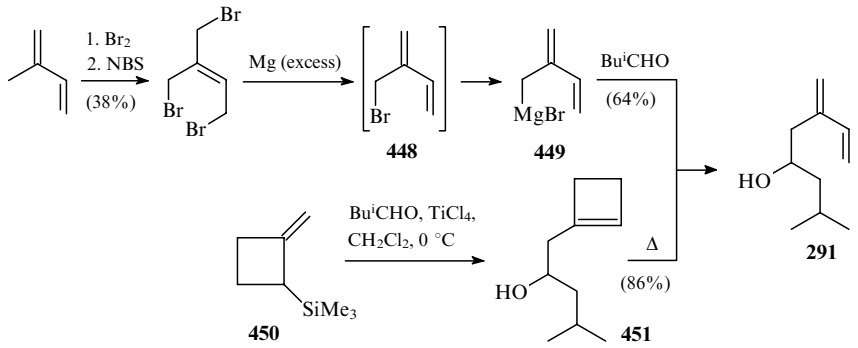

branched 1,3-dienes.[407] This method was tested in the synthesis of the corresponding terpenes **453** — myrcene (R = H) and β-farnesene (R = $Me_2C=CHCH_2$).

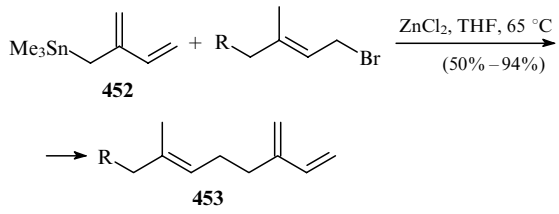

In compound **454**, the allylic chloromethyl group can serve as both an electrophilic and a nucleophilic centre, depending on the reaction conditions.[408] The tosyl and trimethylsilyl vicinal substituents act as a latent double bond, resulting in the vinyl fragment in the final products **455** and **456**.

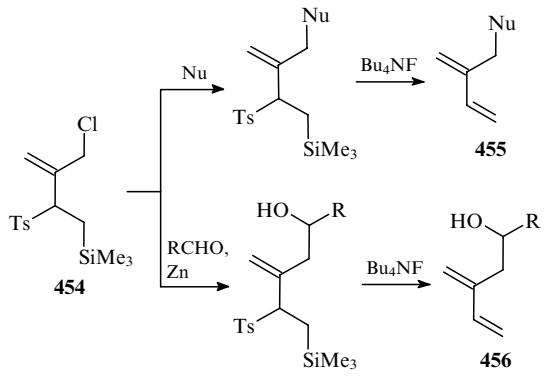

VI. Electrocyclic reactions

1. Thermolysis of cyclobutenes

Two electrocyclic reactions resulting directly in conjugated dienes are known, namely, thermal disrotatory closure of conjugated hexatrienes accompanied by the formation of cyclohexadienes and conrotatory opening of cyclobutenes to give conjugated dienes, occurring at high temperatures. The use of the former reaction for preparative purposes is limited; some publications dealing with this topic are cited in a monograph.[10] The latter reaction has found a more extensive synthetic application. Depending on the nature of substituents in the initial compound, the process can be performed either by heating cyclobutene derivatives having the general formula **457**[409,410] or by passing them through a heated Vigreux column at a reduced pressure.[411]

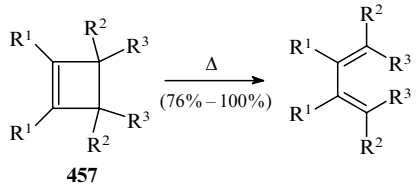

This method has been used in elegant syntheses of ipsenol **291**;[406,412] in one of them, the initial cyclobutene derivative **451** was prepared from the corresponding selenide **458**.

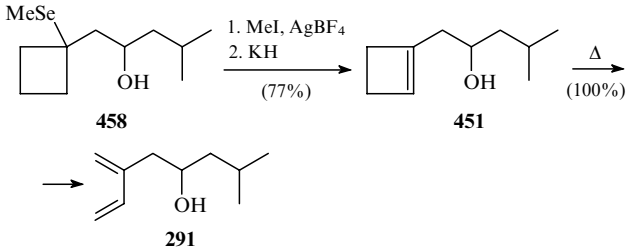

Unlike primary alcohols **459**, 3-formylcyclobutenes **460** undergo ring opening even at low temperatures.[413] The low-temperature Swern oxidation of the alcohol **459** affords the expected *Z*,*E*-isomer **377** (conrotatory ring opening), which is readily transformed into the *E*,*E*-isomer when allowed to stand. Oxidation of the cyclobutenol **459** with pyridinium chlorochromate at room temperature directly affords (*E*,*E*)-**377**.

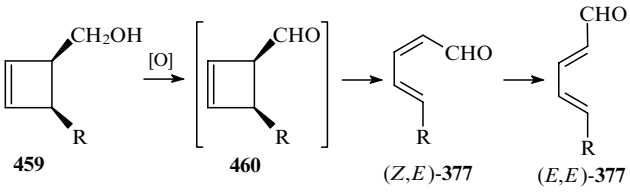

Other electrocyclic reactions are suitable for the synthesis of conjugated dienes only in those cases where the compounds under study contain additional double bonds or functional groups capable of being readily detached to give a double bond.

2. Sigmatropic [3,3]-rearrangements

Sigmatropic [3,3]-rearrangements have been often used for the preparation of conjugated dienes; the variant used most often is the Claisen rearrangement consisting in the thermal transformation of vinyl allyl ethers into Δ^4-unsaturated functional derivatives (see a review[414]).

An example is provided by the syntheses of diene derivatives **461** and **462** by the Claisen rearrangement of vinyl ethers of divinylmethanols **463** and **464**, respectively.[415–417] In the latter case, triethyl orthoacetate serves as an equivalent of the vinyl ether.

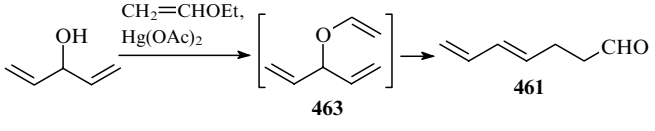

Scheme 12

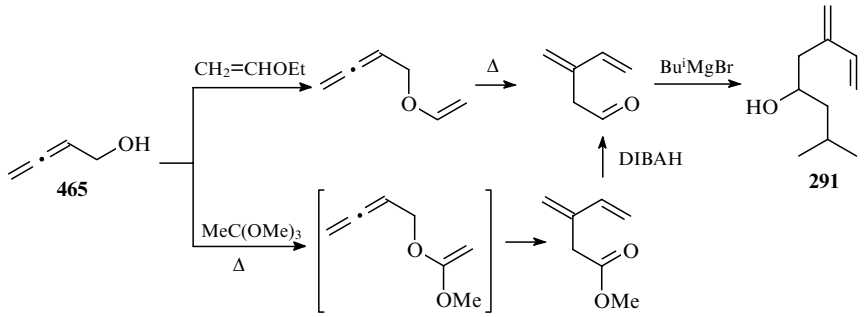

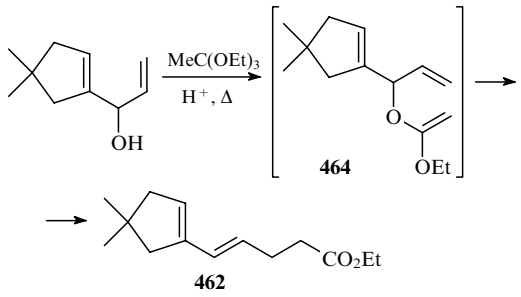

A similar reaction involving buta-2,3-dien-1-ol **465** results in branched conjugated dienes; this was employed in two equivalent syntheses of ipsenol **291** (Scheme 12).[418, 419]

Vinylalkynylmethanols **466** can be used to prepare conjugated enynoates **467** and enynoic acids **468**, which are the closest precursors of dienes.[420, 421]

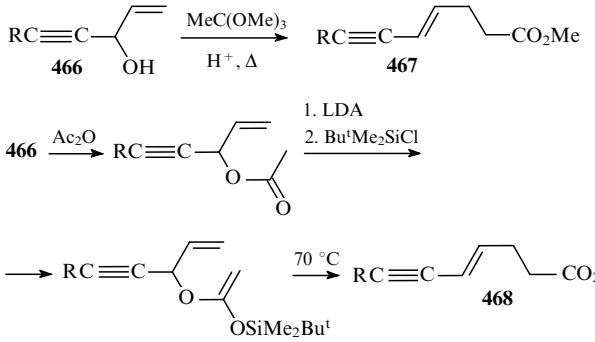

The Claisen rearrangement of propargyl vinyl ethers with the general formula **469** gives rise to β-oxoallene derivatives **470**, which readily isomerise into conjugated diene derivatives **471**. This process became exceptionally important after it had proved to be useful for the synthesis of vitamins A and E and some valuable terpenoids.

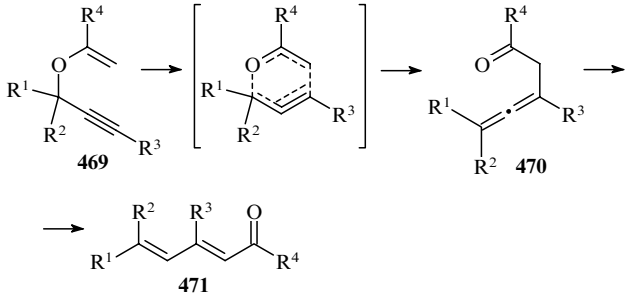

In many cases, there is no need to synthesise these propargyl vinyl ethers because they are formed *in situ* under the reaction conditions from the corresponding propargyl alcohols **237**. Initially, this was attained by either pyrolysis of their acetoacetates or heating with ethyl acetoacetate or diethyl malonate (the product yields were moderate in this case).[422–424] Later, these reactions were substantially updated; more precisely, isopropenyl methyl ether was taken instead of ethyl acetoacetate [425] and orthoesters of carboxylic acids were used in place of diethyl malonate.[426–428] The yields of products **472** and **473** depend markedly on the pattern of substitution in the initial compounds, being very high under favourable circumstances.

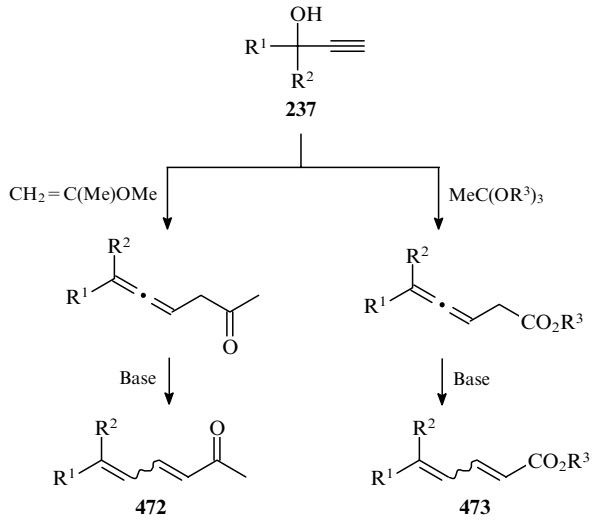

The reaction of propargyl alcohol with ynamine **474** occurs in a similar way, giving rise to *N*,*N*-diethylamides of allenic **475** and dienoic **476** acids.[429]

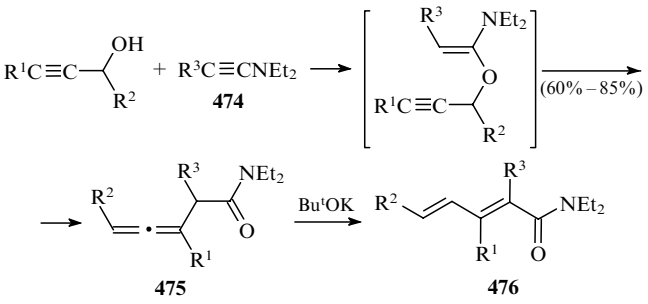

Acetylenic alcohol **477** containing a butenyl fragment reacts with isopropenyl methyl ether to give allene ketone **478**. On treatment with an alkali, this product isomerises in a conventional way to give ketone **479** with a diene fragment.[430] However, on prolonged heating, the ketone **478** can undergo one more [3,3]-sigmatropic rearrangement accompanied by the formation of intermediate **480** and, further, the conjugated dienone **481**.

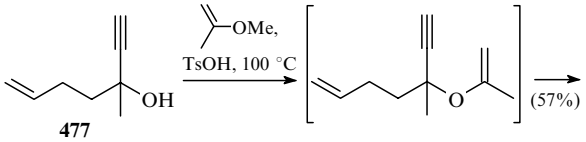

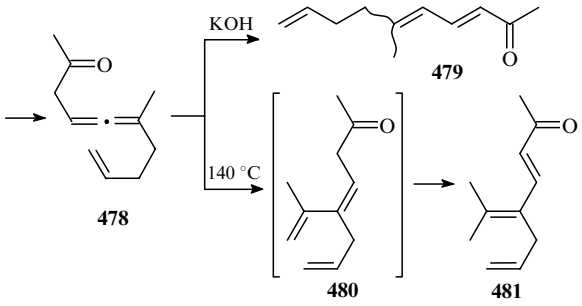

β-Allene acids obtained from ethers of propargyl alcohols upon [3,3]-sigmatropic rearrangement can also be used in another synthesis of dienes; decarboxylation of allene acid **482** is accompanied by the migration of the β,γ-double bond, resulting in the formation of conjugated 3-methylhexa-2,4-diene (**483**).[431]

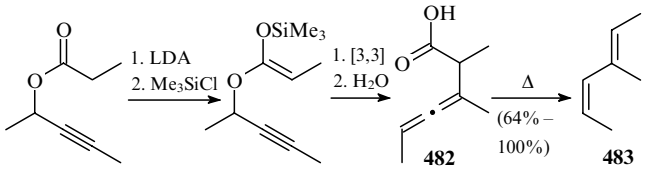

The Claisen rearrangement can also involve allyl vinyl ethers of a more complicated structure. Thus allenyl phenyl sulfoxide **484** reacts with allyl alcohol derivatives to give adduct **485** with a suitable mutual arrangement of the double bonds.[432] The driving force of the rearrangement is transformation of the β-alkoxyvinyl sulfoxide fragment into the α-sulfinyl ketone fragment. Conjugated diene is formed in the subsequent thermal elimination of the sulfoxide group from compound **486**.

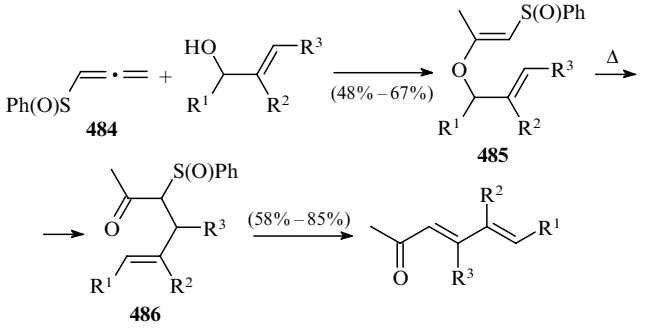

α-Phenylsulfinyl-Δ^4-unsaturated derivatives can be synthesised from allylic alcohols using yet another reagent, *viz*., triethyl phenylsulfinylacetate (**487**). Elimination of the sulfoxide group occurs simultaneously with the sigmatropic rearrangement.[433] This method allows one-step synthesis of not only linear (**488**) but also exocyclic (**489**) conjugated dienes.

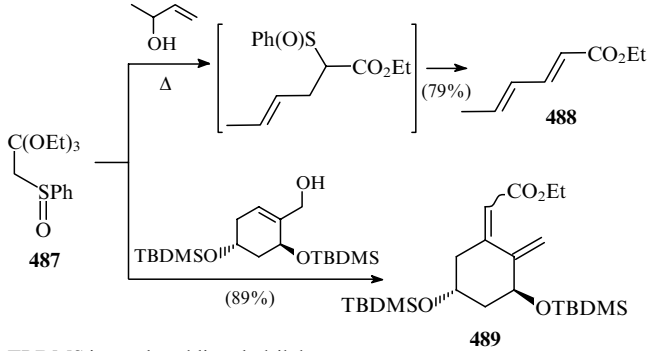

TBDMS is *tert*-butyldimethylsilyl.

Branched dienes of the type **490** are produced in the allene version of the oxy-Cope rearrangement of alcohols **491**.[434, 435]

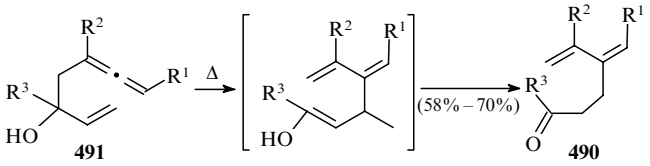

The oxy-Cope [3,3]-rearrangement of 1,5-enyn-4-ols **492** results initially in a compound with incompletely conjugated α,β,δ,ε-dienone fragment (**493**), which can be subsequently isomerised to give compound **494** with a conjugated α,β,γ,δ-dienone fragment.[436] It is convenient to combine isomerisation with the rearrangement by adding inorganic halogen compounds (HCl, HBr, I_2, NH_4Br) to the reaction mixture.[437] The method is applicable for the synthesis of pseudoionone.

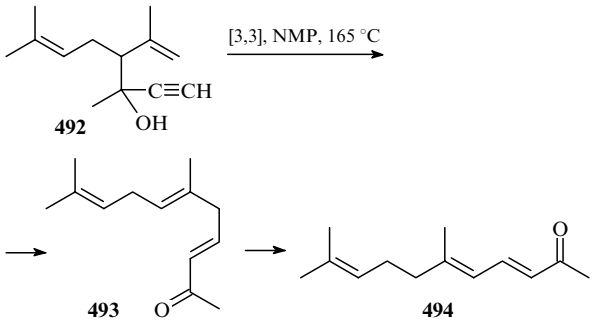

The hydroxy and trimethylsilyl vicinal groups can serve as a source of the double bond (the Peterson reaction). If the molecule of the initial compound **495** is constructed in such a way that, after rearrangement, these substituents in the product **496** occur in the required positions, this may provide a route to the conjugated dienes **67**.[438] The initial compounds **496** were resolved into individual *erythro*- and *threo*-diastereomers, which were convrted into individual *E*,*E*- and *Z*,*E*-isomers of the dienoates **67** by varying the elimination method.

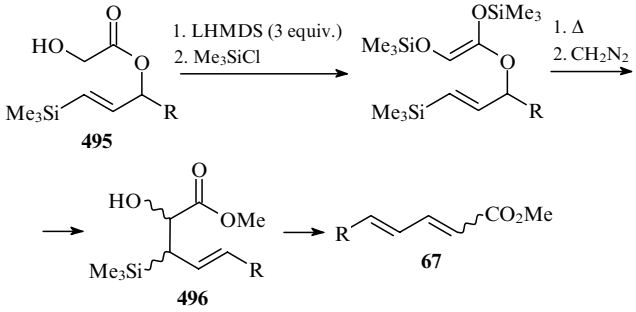

Compound **498**, which contains a trimethylsilyl group and an epoxide ring on different sides of the double bond, is unstable and is easily converted into hydroxy acid **499** with a diene fragment. The compound **498** is formed in the [3,3]-sigmatropic rearrangement of the precursor **500**,[439] which is, in turn, prepared from 2-methylpent-2-enol (**497**).

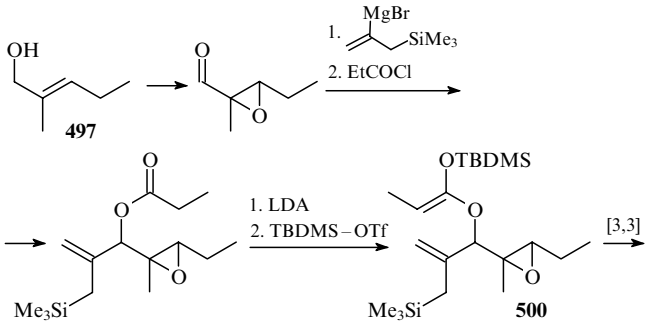

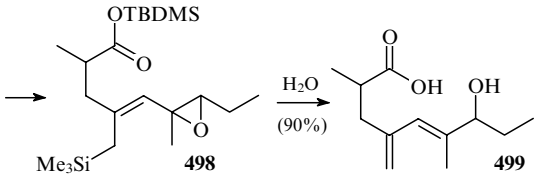

3. The Wittig sigmatropic [2,3]-rearrangement

The Wittig rearrangement of carbanions derived from compounds **501** and **502** has also been used to synthesise conjugated dienes of the type **413** and **503**.[440,441] In both cases, the second double bond was formed upon elimination of the silyl and hydroxy groups from the corresponding alcohols **504** and **505** (the Peterson reaction); in the former case, zirconium served as the counter-cation to ensure the required configuration of alcohol **504** (*cf.* data of Ref. 442).

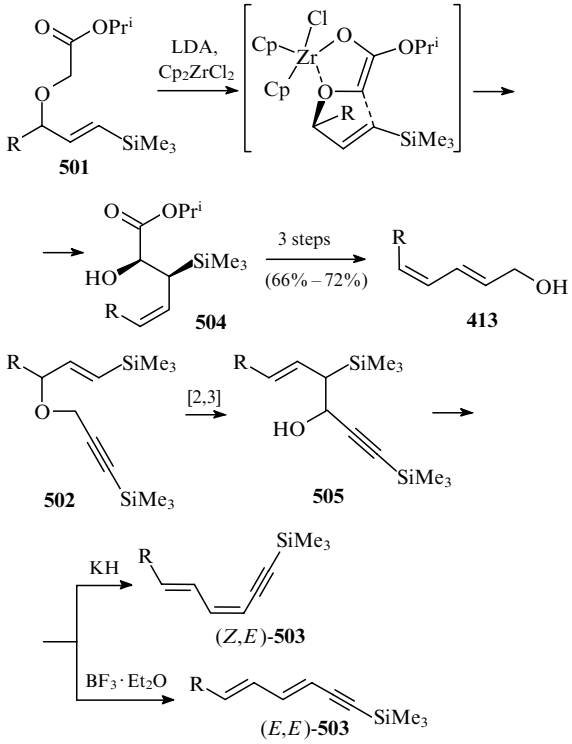

4. Ene reaction

Ene reactions take place between the dienes **506** and reactive aldehydes and afford dienic alcohols **507**.[443] The formation of the compounds **507**, however, can be explained in terms of the Prins reaction mechanism, which is known to be accelerated by acids. On heating without a catalyst, the above-mentioned reactants enter into a [4 + 2]-cycloaddition reaction giving rise to dihydropyrans **508**.

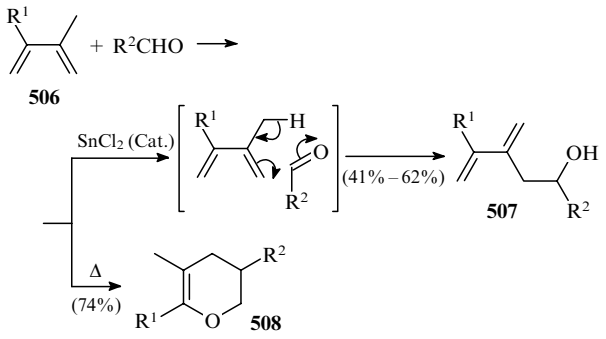

R^1 = H, Me; R^2 = CCl_3, CO_2Bu.

VII. Methods based on migration or reduction of multiple bonds

The strategy for the synthesis of dienes making use of migration and reduction is attractive because a conjugated diene system is formed at the final stage of the synthesis in a molecule which already has the required carbon skeleton and functional groups in the required positions.

1. The migration of multiple bonds

On treatment with bases or some transition metal complexes, non-conjugated dienes are converted into thermodnamically more favourable conjugated isomers. Generally, this reaction is not regioselective, therefore, it has a preparative value for hydrocarbon substrates only in a few cases, for example, in the synthesis of cycloocta-1,3-diene by heating cycloocta-1,5-diene in DMSO in the presence of potassium *tert*-butoxide.[444] However, the situation changes dramatically if the molecule contains a carbonyl group; in this case, the migration of multiple bonds results in an individual product. Examples of isomerisation of 2,5-dien-1-ones and β-allene ketones and esters into 2,4-diene derivatives are considered in Section VI. An organocopper route to the dienes **285** from β-allene esters **509** is also known. Unfortunately, this route is suitable only in the case where sulfonates of secondary acetylenic alcohols and ethyl acetate enolate are used as the initial compounds.[445]

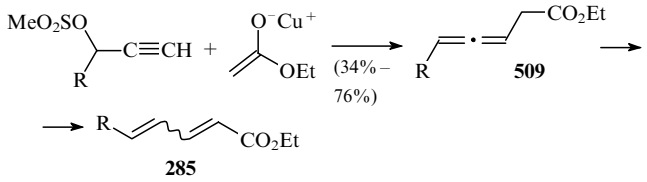

On treatment with strong bases, homoconjugated 1,4-dienes **510** form a delocalised carbanion, which is attacked regioselectively by specific reagents, for example, $BF(OMe)_2$ (**511**).[446] The subsequent treatment of these products with hydrogen peroxide yields primary conjugated dienic alcohols (*E*,*E*)-**413** or (*Z*,*E*)-**413**. Depending on the configuration of the Δ^4-double bond in the initial 1,4-diene **510** and the type of base, definite stereoisomers **413** are produced.

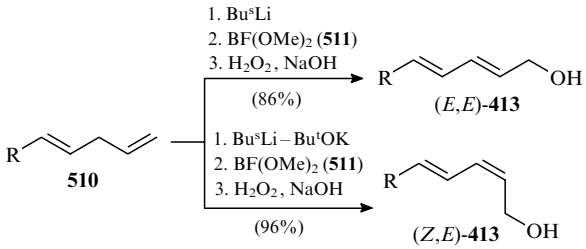

The diene system of alka-2,4-dienoates **512** can be deconjugated from the carbonyl group by treatment with LDA in THF in the presence of HMPTA[162,447] or *N*,*N*′-dimethyl-*N*,*N*′-(1,3-propylene)urea (DMPU).[163] It is of interest that the dienes (2*E*,4*Z*)-**512** are converted into (3*E*,5*E*)-**513**, while (2*E*,4*E*)-**512** are converted into (3*E*,5*Z*)-**513**.[447]

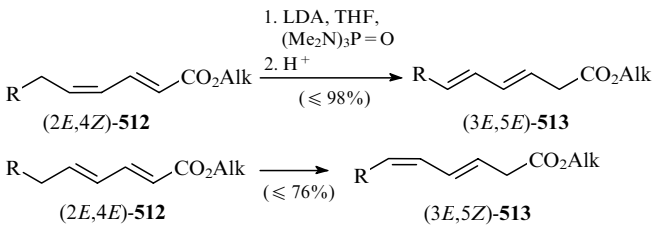

Thus methyl hepta-3,5-dienoate (**514**) can be prepared from incompletely conjugated dienoate **515** on prolonged keeping (12 h) in the presence of Et_3N.[448]

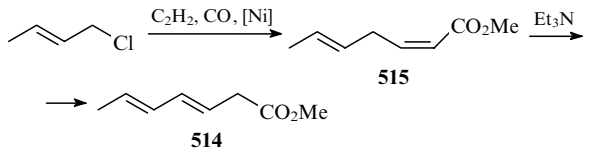

Divinylmethanols and their derivatives are readily isomerised on treatment with acidic reagents to give conjugated diene derivatives. For example, the allylic rearrangement of dialkenylmethyl acetates **516** catalysed by palladium complexes takes place with retention of the configuration of one double bond.[449] It is evident that in the case of non-symmetrical substrates ($R^1 \neq R^2$), the reaction gives rise to a mixture of regioisomers **517**.

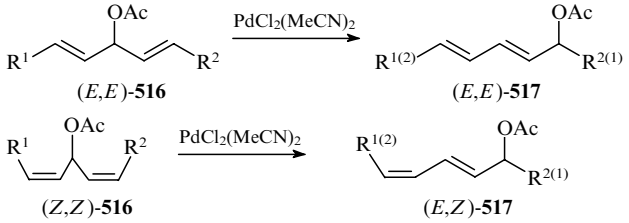

The regiodirectivity of this type of rearrangement can be controlled by introducing a heteroatom into the β-position of one of the vicinal groups. For example, readily available thio derivatives **518** can be smoothly converted into dienals **430**.[450]

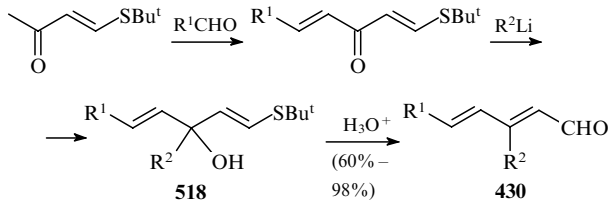

The rearrangement of α-silylallenes **519** into dienes **242** is also regioselective and, in some cases, stereoselective.[451]

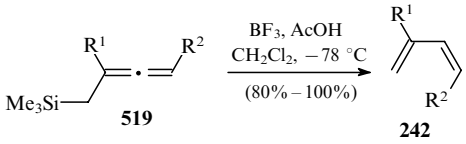

In the last decade, an absolutely new method for the synthesis of conjugated diene derivatives **520** was discovered; this is isomerisation of alkynes **521**, in which the triple bond is located close to an electron-withdrawing group. In the first publication, it was noted that this isomerisation is induced by various palladium catalysts.[452] Similar results have been obtained with ruthenium or iridium complexes,[453, 454] which have also proved suitable for isomerisation of cyclohexene derivatives **522** into the corresponding trienes **523**.

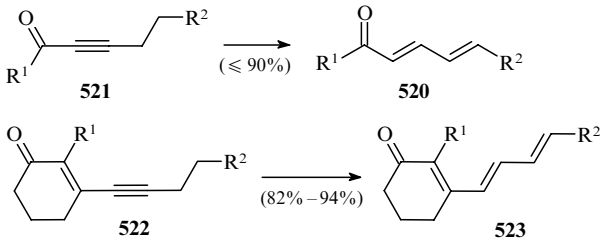

Later, it has been found that the crucial role in the isomerisation is played by the phosphine ligands contained in the catalysts. Indeed, prolonged refluxing of various activated alkynes in toluene in the presence of triphenylphosphine alone also furnishes the diene isomers of type **520** in very good yields.[455] Later, factors influencing the reaction route have been studied in detail

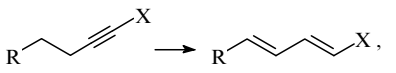

and recommendations for methods have been given. The data are summarised in Table 2. For isomerisation of less reactive amides of alk-2-ynoic acids (X = $C(O)NR_2$) to take place, the process should be carried out at higher temperatures (refluxing in xylene) in the presence of acetic acid. Conversely, more reactive acetylenic ketones [X = C(O)Alk and C(O)Ar] are isomerised even at room temperature on treatment with Ph_3P. For a similar transformation of esters (X = CO_2R) and *N*,*N*-dialkylamides [X = $C(O)NR_2$], tributylphosphine was found to be the reagent of choice.[456]

Table 2. Isomerisation of acetylene derivatives into conjugated dienes.

X	R	Catalyst	Reaction conditions		Yields (%)	Ref.
			T /°C	*t* /h		
$C(O)Bu^t$	Me	$Pd(OAc)_2$, Ph_3P	100	22	73	452
C(O)Cy	H	$Pd(OAc)_2$, dppb	100	21	73	452
C(O)Ph	Et	$Pd(OAc)_2$, dppb	100	0.75	82	452
CO_2Bn	Me	Ph_3P	110	6	75	455
C(O)Ph	Et	Ph_3P	80	4	83	455
C(O)NHPh	Me	Ph_3P, AcOH	140	14	84	455
C(O)Me	C_5H_{11}	Ph_3P	25	34	84	456
CO_2Me	Et	Ph_3P	25	35	0	456
CO_2Me	Et	Bu_3P	110	24	82	456
CO_2All	Me	Bu_3P	25	48	80	456
C(O)N(All)Bn	Me	Bu_3P	110	24	60	456
$CO_2C_6F_5$	Bu	Ph_3P	50	5	96	457, 458
$CO_2C_6F_5$	$HC \equiv C(CH_2)_2$	Ph_3P	50	5	76	457, 458
$(CF_2)_8Cl$	Me	Ph_3P	110	24	0	459
$(CF_2)_8Cl$	Me	$Pd(dba)_2$, Ph_3P, AcOH	110	12	82	459
$(CF_2)_4Cl$	Me	$Pd(dba)_2$, Ph_3P, AcOH	110	12	75	459
CF_3	$(CH_2)_5OH$	$Pd(dba)_2$, Ph_3P, AcOH	110	12	85	459

However, pentafluorophenyl esters (X = $CO_2C_6F_5$), which exhibit strong electron-withdrawing properties, can be isomerised under milder conditions, namely, at 50 °C and in the presence of Ph_3P; if the molecule contains other acetylenic groups, they remain intact.[457, 458] In this connection, an interesting example is the selective transformation of diacetylene **524** into dienyne **525**.

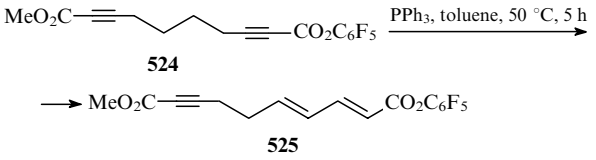

Among acetylene derivatives able to undergo isomerisation, 'non-carbonyl' polyfluoroalkyl compounds proved to be an interesting type of substrates [459] (see Table 2). The transformation of these compounds into dienes requires the presence of palladium catalysts and acetic acid, apart from phosphines.

Two processes, similar at the first glance, are known to form a diene system (for example, in compounds **526** and **520**) from dialkynylmethanols **527**[460] and α-oxo-α′-hydroxyacetylenes **528**.[461] Nevertheless, for balance, the former reaction requires involvement of an oxidising agent, while the latter, of a reducing agent.

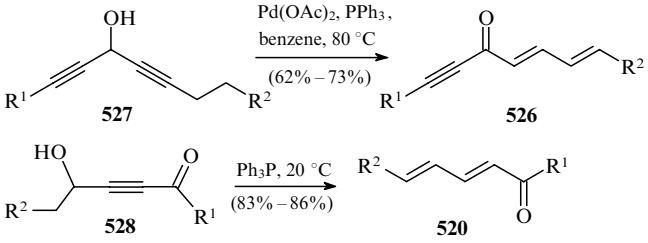

On treatment with superbases, for example, lithium aminoethylamide, internal alkynes are transformed into terminal isomers. It has been shown recently that this process can also be applied successfully to diacetylenes **529**. Since terminal diynes are unstable, it has been suggested that the lithium derivatives formed initially should be quenched immediately with electrophilic reagents; this provides a pathway to diacetylenic alcohols **530** and **531**, which are potential precursors of the corresponding conjugated dienes.[462–464]

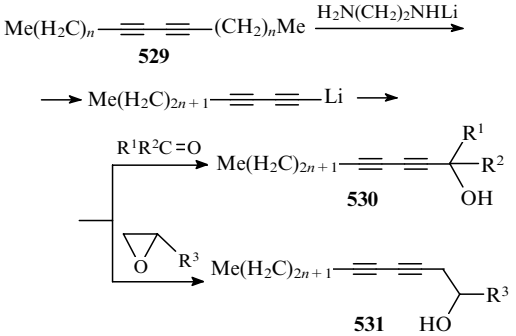

2. Partial reduction of a triple bond in enynes and 1,3-diynes

Incomplete reduction of the conjugated enynes **232** and diynes **532** to the dienes **533** and **55** has been considered comprehensively in the literature;[8, 10, 12] therefore, only the basic principles are discussed here. The transformation of a triple bond into a *Z*-double bond in these systems is accomplished using the same techniques as employed for monoacetylenes. Hydrogenation in the presence of Lindlar-type catalysts ensures, in principle, the required transformation (see, for example, Ref. 465); however, the presence of the second, conjugated bond activates the substrate molecule, resulting in a lower selectivity. Better results are obtained when hydrogen carriers are used; for this purpose, the substrate is refluxed in ethanol-containing solvents with activated zinc.[466–468]

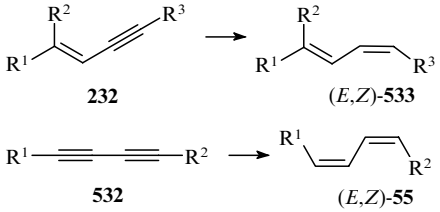

However, hydroboration of the triple bond followed by protolysis of the resulting vinylborane has won the greatest recognition. The hydroborating reagent of choice is di(*sec*-isoamyl)borane $(sia)_2BH$, which is reactive, under the reaction conditions, only towards triple bonds but does not affect double bonds. This method was used to transform enynes and diacetylenes into insect pheromones containing a conjugated diene system in which either one or both double bonds have *Z*-configuration.[246, 420, 469]

Unfortunately, known methods of reduction of alkynes into *E*-alkenes (sodium in liquid ammonia, $LiAlH_4$ with heating) are inapplicable to the reduction of enynes and diynes, because in this case reactions give complex mixtures of products. Exceptions are enynic alcohol **534**[26, 470–472] and diynic alcohol **535** (*n* = 0, 1),[473–475] which are hydrogenated to dienic **536** and enynic **537** alcohols, respectively. In the compound **535**, the triple bond closest to the hydroxy group is reduced fairly smoothly to the *E*-double bond on treatment with $LiAlH_4$ in ether or THF. Hydrogenation products, namely, conjugated *E*-enynic alcohols **537**, can further be converted into *E*,*Z*-dienic alcohols **538**.[475] In the case of propargyl compounds, the desired effect is also attained by transforming the alcohol into alcoholate with the subsequent addition of DIBAH, the reduction taking place within the ate-complex formed.[473] It is noteworthy that careful bromination of the reaction mixture carried out instead of the final hydrolysis in the reduction of the enynic alcohols **534** results in bromo-containing dienic alcohols **539** being formed as the major products; in this case, the configuration of double bonds is disturbed.[476]

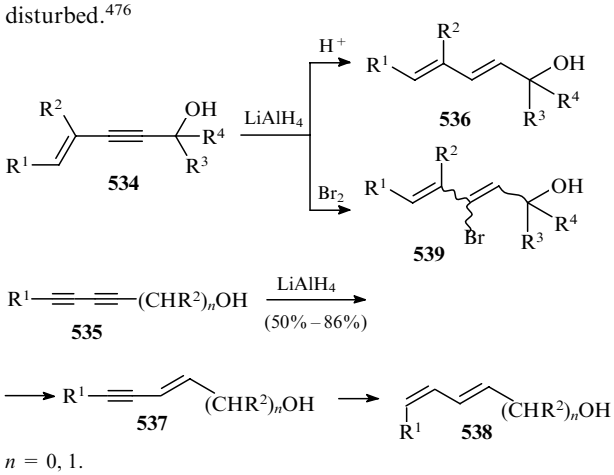

n = 0, 1.

Enynonitriles **540** can undergo similar reduction, the cyano group in products **541** being stable against lithium aluminium hydride under the reaction conditions.[477]

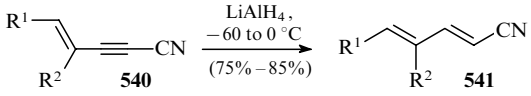

VIII. Miscellaneous methods

The methods discussed in this Section could be assigned, if desired, to one or another type of reactions considered in the preceding Sections. However, these examples are usually single

and have substantial differences from the typical processes; therefore, we consider them separately.

The introduction of double bonds by elimination of vicinal hydrogen atoms finds only limited use. The high-temperature catalytic dehydrogenation occurs selectively only in the preparation of simple dienes, for example, butadiene from butane and butenes or isoprene from isopentane. Of more complex examples, one should note the transformation of α,β-unsaturated oxo compounds **542** (X = Ph, OEt) into the corresponding dienes **543** on treatment with stoichiometric amounts of Na_2PdCl_4 as an oxidant.[478] The yields are moderate in all cases. This method has been used to prepare steroidal dienones with fragment **544** from the corresponding enones **545**.

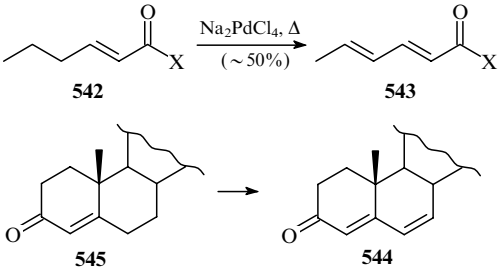

542 **543** **545** **544**

The tetrahydropyranyl derivatives of α-dienic alcohols **546** can react with a number of C-, N-, Si- or Sn-nucleophiles giving rise to dienes **547** with a different arrangement of double bonds.[479] The methoxymethyl derivatives react in a similar way; however, the reaction stereoselectivity is lower.

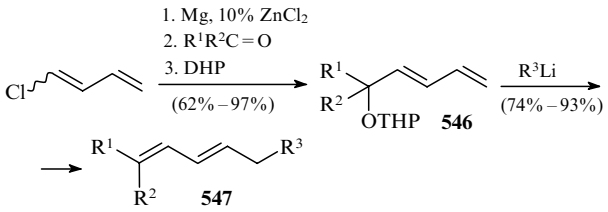

546 **547**

DHP is dihydropyran; R^3 = Alk, NEt_2, $SiMe_2Ph$, $SnMe_3$.

The methoxymethyl ether of the enol **548** can be introduced, after lithiation, into reactions with aldehydes.[480] The resulting dienes **549** contain an oxygen function at the diene system. The presence of this function is necessary for this reaction to take place (chelate control).

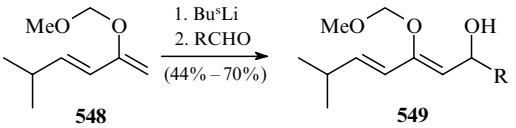

548 **549**

The tertiary analogues of cinnamic alcohols **550** are dehydrated under reaction conditions and the resulting diene is formylated giving rise to dienals **551**.[481]

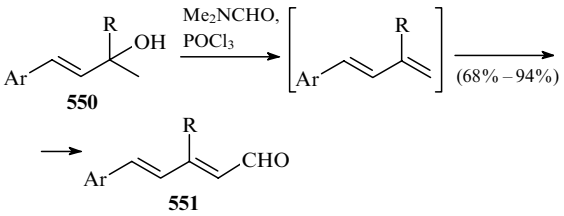

550 **551**

Direct acylation of conjugated dienes **552** has remained problematic until recently. However, development of reactive cationoid reagents has enabled the synthesis of dienones **553** and **554** in reasonable yields.[482–484]

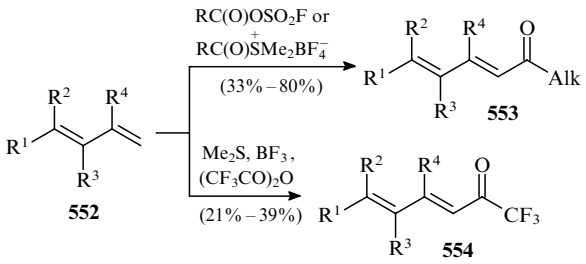

552 **553** **554**

The use of α-allenyl alcohols **555** in the synthesis of alkenes according to the Murahashi method affords the conjugated dienes **242**.[485]

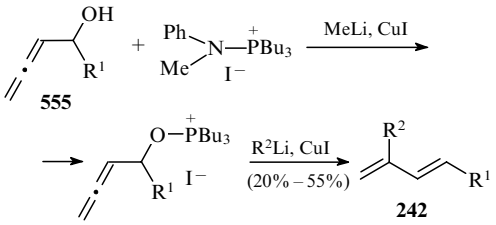

555 **242**

The carbocationic rearrangement of cyclopropylalcohols can proceed smoothly under appropriate conditions to yield homoallyl derivatives. In the case of cyclopropyl(alkenyl)methanols **556**, conjugated diene system **557** is produced.[486–488]

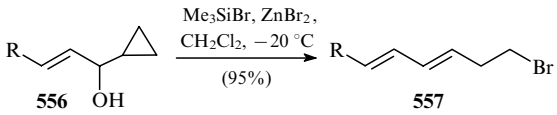

556 **557**

A very simple method for the synthesis of dienes consists in heating of aliphatic α-branched ketones **558** in DMSO with potassium *tert*-butoxide,[489] DMSO serving as the source of a new carbon atom in the molecule of product **559**. Unfortunately, in many instances, these reactions give mixtures of isomers.

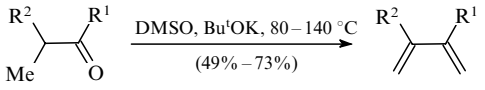

558 **559**

A two-step method for the preparation of dienylstannanes **560** from acetylenic carbonyl compounds **561** is documented.[490] Transmetallation provides a nucleophilic diene equivalent.

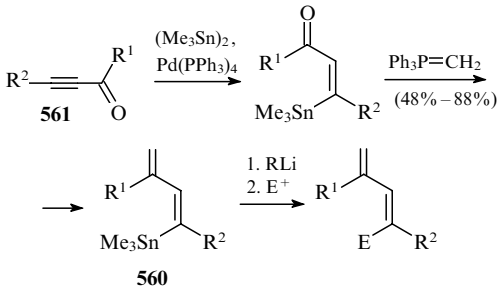

561 **560**

Diketene **562** exposed to UV radiation in a mixture of propan-2-ol and acetone gives adduct **563**, which is a convenient precursor of conjugated dienoate **564**.[491]

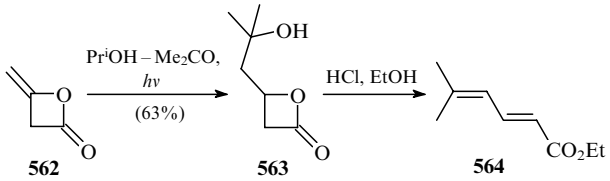

562 **563** **564**

Oxidation of *o*-quinone, pyrocatechol or phenol with ammoniacal copper oxide in pyridine results in *cis,cis*-muconic acid mononitrile (**565**).[492] In the case of substituted compounds, for example, 4-*tert*-butyl-*o*-quinone, a mixture of regioisomers is formed.

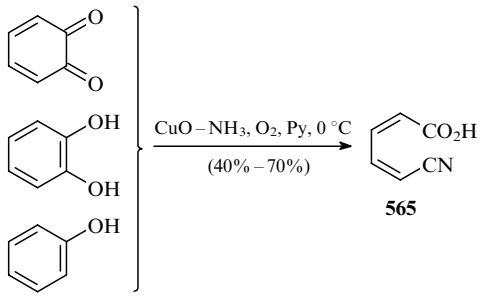

565

The adduct **566** of itaconic anhydride with cyclopentadiene was converted into compound **567**. Pyrolysis of this compound liberates the methylene group, which had initially been protected; this group is found to be conjugated with a new vinyl group,[493] which finally results in ipsenol **291**.

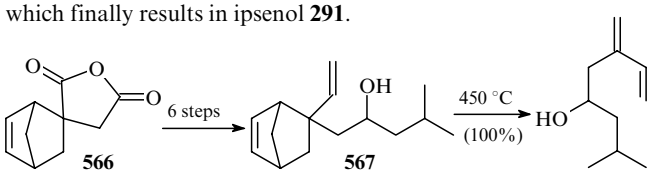

566 **567** **291**

The coupling of two carbonyl compounds by means of the McMurry titanium reagent results in alkenes; if one compound is unsaturated, the expected product is a diene. Thus intramolecular cyclisation of dialdehyde **568** results in diterpene hydrocarbon **569** difficult to prepare by other methods.[494]

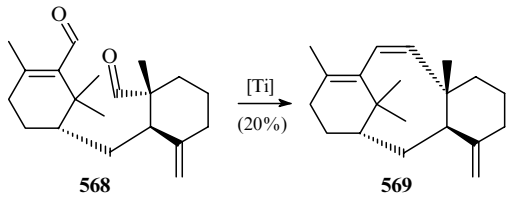

568 **569**

IX. Conclusion

One cannot but note the great diversity of the methods for synthesis of conjugated dienes considered in this review. Nevertheless, despite the wide range of choice, when selecting the method of synthesis of a target object, a researcher would be guided, first of all, by its reliability and simplicity as well as the availability and cost of initial compounds and, strange though it may seem, by the reputation and popularity of the method. Table 3 presents a comparative analysis of the methods considered. It is fairly difficult to evaluate the true 'rating' of each of them because this requires analysis of a different type of literature, namely, the use of these methods in target-directed syntheses of intricate structures in which they are often used only as an episode in a multistep protocol. The more reliable the method, the less the attention researchers draw to it! The popularity of a method can be judged to some extent by the presence of reviews devoted to it, or (less reliably) by mentions of this method in textbooks.

When methods' reputations are equivalent, when planning the synthesis, one should analyse first of all the possibility of performing the task on the basis of standard reactions, *viz*., elimination (the formation of double bonds with a preformed carbon skeleton), olefination of carbonyl compounds (the $C_1 + C_3$ pattern of diene formation with formation of a double bond) and, more rarely, cross-coupling (the $C_2 + C_2$ pattern of diene formation with the formation of the central single bond, or the C_4 + substituent pattern). Each of these general approaches has its own limitations. In particular, alkenyl halides and alkenyl derivatives of elements used in cross-coupling are rather expensive and their synthesis requires high skills. This and other reasons stimulate the search for new, different reactions which would provide an absolutely untrivial approach to the synthesis of conjugated dienes. The progress achieved in the alkene – alkyne metathesis over the last three years can serve as an example. This method, as well as new organometallic reactions, undoubtedly hold great promise because it requires rather simple initial compounds and commercially available metal complex catalysts.

Table 3. Brief characterisation of the most important methods for the preparation of conjugated dienes (from the bibliography of this review).

Reactions	Stereohemical outcome	Features	The range of yields (%)	The number of references (of these, reviews)
Elimination	depends on the method and the substrate	effective methods are expensive	36 – 97	92 (8)
Reduction of enynes and diynes	good for the synthesis of *Z*-isomers, poorer for *E*-isomers	inexpensive method	50 – 86	15
Olefination of carbonyl compounds				118 (9)
condensation	high for linear *E*-dienes	used for the synthesis of α-functionalised dienes	24 – 98	35 (6)
Wittig reactions	depends on the method and the substrate but is controllable	adjustment of details for a particular synthesis is often required	27 – 98	58 (3)
other reactions	depends on the method and the substrate	more reliable than the Wittig olefination	23 – 94	25
Cross-coupling	very high; determined by the reactant structure	high cost of the reactants	30 – 93	104 (16)
Miscellaneous organometallic reactions	depends on the method and the substrate	some procedures are very effective	21 – 99	48 (1)
Electrocyclic reactions	high	industrially feasible	25 – 90	35 (3)
Miscellaneous methods	depends on the method and the substrate	–	20 – 95	75

References

1. Z Rappoport (Ed.) *The Chemistry of Dienes and Polyenes* Vol. I (New York: Wiley-Interscience, 1997)
2. Z Rappoport (Ed.) *The Chemistry of Dienes and Polyenes* Vol. II (Chichester: Wiley-Interscience, 2000)
3. M Sodeoka, M Shibasaki *Synthesis* 643 (1993)
4. A A Vasil'ev, A L Vlasyuk, G D Gamalevich, E P Serebryakov *Bioorg. Med. Chem.* **4** 389 (1996)
5. *Houben-Weyl. Methoden der Organische Chemie* Vol. V/1c, Pt 3 (Stuttgart: Thieme, 1970) p. 2
6. S Coffey (Ed.) *Rodd's Chemistry of Carbon Compounds* Vol. I (Amsterdam: Elsevier, 1964) p. 438
7. C A Buehler, D E Pearson *Survey of Organic Synthesis* (New York: Wiley-Interscience, 1970)
8. G Pattenden, in *Comprehensive Organic Chemistry* Vol. 1 (Eds D Barton, W D Ollis) (Oxford: Pergamon Press, 1979) p. 171
9. J F Normant, A Alexakis, in *Current Trends in Organic Synthesis* (Ed. H Nozaki) (Oxford: Pergamon Press, 1983)
10. R C Larock *Comprehensive Organic Transformations. A Guide to Functional Group Preparations* (New York: VCH, 1989)
11. K Mori, in *The Total Synthesis of Natural Products* Vol. 9 (New York: Wiley, 1992) p. 37
12. G Mehta, H S P Rao, in *The Chemistry of Dienes and Polyenes* Vol. I (Ed. Z Rappoport) (New York: Wiley-Interscience, 1997) p. 359
13. L A Paquette, M Gugelchuk, M L McLaughlin *J. Org. Chem.* **52** 4732 (1987)
14. B M Trost, M Lautens, B Peterson *Tetrahedron Lett.* **24** 4525 (1983)
15. Y Naruta, N Nagai, Y Arita, K Maruyama *J. Org. Chem.* **52** 3956 (1987)
16. P G McDougal, J G Rico *J. Org. Chem.* **52** 4819 (1987)
17. J Tsuji, T Yamakwa, M Kaito, T Mandai *Tetrahedron Lett.* 2075 (1978)
18. F M Hauser, R Tommasi, P Hewawasam, Y S Rho *J. Org. Chem.* **53** 4886 (1988)
19. H Matsushita, E Negishi *J. Org. Chem.* **47** 4161 (1982)
20. M Suzuki, Y Oda, R Noyori *J. Am. Chem. Soc.* **101** 1623 (1979)
21. S-K Kang, D-C Park, C-H Park, R-K Hong *Tetrahedron Lett.* **36** 405 (1995)
22. J B Hendrickson, M A Walker, A Varvak, M S Hussoin *Synlett* 661 (1996)
23. A S Demir *Tetrahedron* **57** 227 (2001)
24. S Tanaka, A Yasuda, H Yamamoto, H Nozaki *J. Am. Chem. Soc.* **97** 3253 (1975)
25. A Yasuda, S Tanaka, H Yamamoto, N Nozaki *Bull. Chem. Soc. Jpn.* **52**1752 (1979)
26. T Laird, W D Ollis, I O Sutherland *J. Chem. Soc., Perkin Trans. 1* 2033 (1980)
27. G Decodts, G Dressaire, Y Langlois *Synthesis* 510 (1979)
28. H M Walborsky, H H Wüst *J. Am. Chem. Soc.* **104** 5807 (1982)
29. A Claesson, C Bogentoft *Acta Chem. Scand.* **26** 2540 (1972)
30. G Solladié, J Hutt *J. Org. Chem.* **52** 3560 (1987)
31. G Solladié, A Girardin, P Metra *Tetrahedron Lett.* **29** 209 (1988)
32. G Solladié, A Girardin *Tetrahedron Lett.* **29** 213 (1988)
33. H R Pfaendler, F K Maier, S Klar *J. Am. Chem. Soc.* **108** 1338 (1986)
34. A G Martinez, J L M Contelles *Synthesis* 742 (1982)
35. L A Paquette, J Dressel, K L Chasey *J. Am. Chem. Soc.* **108** 512 (1986)
36. L Engman, S E Byström *J. Org. Chem.* **50** 3170 (1985)
37. L Crombie, L J Rainbow *J. Chem. Soc., Perkin Trans. 1* 673 (1994)
38. B Barlaam, J Boivin, S Z Zard *Tetrahedron Lett.* **34** 1023 (1993)
39. D J Ager *Synthesis* 384 (1984)
40. P A Brown, R V Bonnert, P R Jenkins, M R Selim *Tetrahedron Lett.* **28** 693 (1987)
41. J A Prieto, G L Larson, R Berrios, A Santiago *Synth. Commun.* **18** 1385 (1988)
42. P A Brown, R V Bonnert, P R Jenkins, N J Lawrence, M R Selim *J. Chem. Soc., Perkin Trans. 1* 1893 (1991)
43. D J S Tsai, D S Matteson *Tetrahedron Lett.* **22** 2751 (1981)
44. D A Smith, K H Houk *Tetrahedron Lett.* **32** 1549 (1991)
45. Y Ikeda, J Ukai, N Ikeda, H Yamamoto *Tetrahedron* **43** 731 (1987)
46. S L Hartzell, D F Sullivan, M W Rathke *Tetrahedron Lett.* 1403 (1974)
47. L Strekowsky, M Visnick, M A Battiste *Tetrahedron Lett.* **25** 5603 (1984)
48. K Shimoji, H Taguchi, K Oshima, H Yamamoto *J. Am. Chem. Soc.* **96** 1620 (1974)
49. Y Yamakado, M Ishiguro, N Ikeda, H Yamamoto *J. Am. Chem. Soc.* **103** 5568 (1981)
50. A G Angoh, D L J Clive *J. Chem. Soc., Chem. Commun.* 534 (1984)
51. R Angell, P J Parsons, A Naylor, E Tyrrell *Synlett* 599 (1992)
52. I Fleming, I T Morgan, A K Sarkar *J. Chem. Soc., Chem. Commun.* 1575 (1990)
53. M Ochiai, S Tada, K Sumi, E Fujita *Tetrahedron Lett.* **23** 2205 (1982)
54. D L G Clive *Tetrahedron* **34** 1049 (1978)
55. K C Nicolaou, N A Petasis *Selenium in Natural Products Synthesis* (Philadelphia: CIS, 1984) p. 66
56. H J Reich *Org. React.* **44** 4 (1993)
57. A Krief, in *Comprehensive Organometallic Chemistry II* Vol. 11 (Oxford: Pergamon Press, 1995) p. 515
58. C C Silveira, M A Araujo, E J Lenardao, A L Braga, M J Dabdoub *Synthesis* 1305 (1995)
59. J Tsuji, K Masaoka, T Takahashi *Tetrahedron Lett.* 2267 (1977)
60. L Lebarillier, F Outurquin, C Paulimier *Tetrahedron* **56** 7483 (2000)
61. P J Kocienski, G Cernigliaro, G Feldstein *J. Org. Chem.* **42** 353 (1997)
62. K Mori, T Nukada, T Ebata *Tetrahedron* **37** 1343 (1981)
63. K Ando, T Yamada, Y Takaishi, M Shibuya *Heterocycles* **29** 1023 (1989)
64. A A Vasil'ev, L Engman, E P Serebryakov *J. Chem. Res.* (*S*) 706 (1998)
65. A A Vasil'ev, L Engman, E P Serebryakov *Acta Chem. Scand.* **53** 611 (1999)
66. H J Reich *J. Org. Chem.* **40** 2570 (1975)
67. D L J Clive, G Chittattu, N J Curtis, S M Menchen *J. Chem. Soc., Chem. Commun.* 770 (1978)
68. H J Reich, I L Reich, S Wollowitz *J. Am. Chem. Soc.* **100** 5981 (1978)
69. T R Hoye, A J Caruso *Tetrahedron Lett.* 4611 (1978)
70. H Ishibashi, H Komatsu, K Maruyama, M Ikeda *Tetrahedron Lett.* **26** 5791 (1985)
71. Y Tamura, H-D Choi, H Maeda, H Ishibashi *Tetrahedron Lett.* **22** 1343 (1981)
72. T Mandai, H Yokoyama, T Miki, H Fukuda, H Kobata, W Kawada, J Otera *Chem. Lett.* 1057 (1980)
73. B M Trost, L Weber, P Strege, T J Fullerton, T J Dietsche *J. Am. Chem. Soc.* **100** 3426 (1978)
74. H J Reich, S Wollowitz *J. Am. Chem. Soc.* **104** 7051 (1982)
75. J H Babler, R A Haack *J. Org. Chem.* **47** 4801 (1982)
76. R Tanikaga, Y Nozaki, M Nishida, A Kaji *Bull. Chem. Soc. Jpn.* **57** 729 (1984)
77. C Herve du Penhoat, M Julia *Tetrahedron* **42** 4807 (1986)
78. M Julia, J-P Stacino *Tetrahedron,* **42** 2469 (1986)
79. M Julia, H Lauron, J-P Stacino, J-N Verpeaux *Tetrahedron* **42** 2475 (1986)
80. T Mandai, T Yanagi, K Araki, Y Morisaki, M Kawada, J Otera *J. Am. Chem. Soc.* **106** 3670 (1984)
81. J Otera, H Misawa, K Sugimoto *J. Org. Chem.* **51** 3830 (1986)
82. T Moriyama, T Mandai, M Kawada, J Otera, B M Trost *J. Org. Chem.* **51** 3896 (1986)
83. T Mandai, T Moriyama, K Tsujimoto, M Kawada, J Otera *Tetrahedron Lett.* **27** 603 (1986)
84. J-E Bäckvall, R Chinchilla, C Najera, M Yus *Chem. Rev.* **98** 2291 (1998)
85. N A Plobeck, J-E Bäckvall *J. Org. Chem.* **56** 4508 (1991)
86. J-E Bäckvall, A M Ericsson, N A Plobeck, S K Juntunen *Tetrahedron Lett.* **33** 131 (1992)
87. J M Clough, in *Comprehensive Organic Syntheses I* Vol. 3 (Eds B M Trost, I Fleming) (Oxford: Pergamon Press, 1991) p. 861
88. E Block, M Aslam *J. Am. Chem. Soc.* **105** 6164 (1983)
89. E Block, M Aslam, V Eswarakrishnan, A Wall *J. Am. Chem. Soc.* **105** 6165 (1983)
90. E Block, M Aslam, V Eswarakrishnan, K Gebreyes, J Hutchinson, R Iyer, J-A Laffitte, A Wall *J. Am. Chem. Soc.* **108** 4568 (1986)
91. P A Grieco, D Boxler *Synth. Commun.* **5** 315 (1975)

92. T E Bezmenova *Khimiya Tiolen-1,1-Dioksidov* (The Chemistry of Thiolene-1,1-Dioxides) (Kiev: Naukova Dumka, 1981)
93. S Yamada, H Ohsawa, T Suzuki, H Takayama *J. Org. Chem.* **51** 4934 (1986)
94. Y Gaoni *Tetrahedron Lett.* 947 (1977)
95. A N Kasatkin, Y A Prokopenko, A M Khabibov, G A Tolstikov *Mendeleev Commun.* 17 (1993)
96. R Bloch, J Abecassis *Tetrahedron Lett.* **23** 3277 (1982)
97. R Bloch, J Abecassis *Tetrahedron Lett.* **24** 1247 (1983)
98. R Bloch, D Hassan-Gonzales *Tetrahedron* **42** 4975 (1986)
99. T Nomoto, H Takayama *J. Chem. Soc., Chem. Commun.* 295 (1989)
100. K Kosugi, A V Anisimov, H Yamamoto, R Yamashiro, K Shirai, T Kumamoto *Chem. Lett.* 1341 (1981)
101. J M McIntosh, R A Sieler *J. Org. Chem.* **43** 4431 (1978)
102. H F Schmitthenner, S M Weinreb *J. Org. Chem.* **45** 3372 (1980)
103. J Mulzer, G Brüntrup, U Kühl, G Hartz *Chem. Ber.* **115** 3453 (1982)
104. B M Trost, J M Fortunak *J. Am. Chem. Soc.* **102** 2841 (1980)
105. A Rüttimann, A Wick, A Eschenmoser *Helv. Chim. Acta* **58** 1450 (1975)
106. G Jones *Org. React.* **15** 204 (1967)
107. O Doebner *Berichte* **33** 2140 (1900)
108. T Lennarts *Berichte* **76** 1006 (1943)
109. M Jacobson *J. Am. Chem. Soc.* **78** 5084 (1956)
110. C F H Allen, J van Allan *Org. Synth., Coll.* **3** 783 (1955)
111. J Klein, E D Bergmann *J. Am. Chem. Soc.* **79** 3452 (1957)
112. J Rodriguez, B Waegell *Synthesis* 534 (1988)
113. N Ragoussis *Tetrahedron Lett.* **28** 93 (1987)
114. G Tetradis, N Ragoussis, in *The 8th International IUPAC Conference on Organic Synthesis (Additional Abstracts), Helsinki, 1990* p. 2-514
115. P F Vlad, M Z Krimer *Org. Prep. Proced. Int.* **30** 657 (1998)
116. C A Henrick, W E Willy, J W Baum, T A Baer, B A Garecia, T A Mastre, S M Chang *J. Org. Chem.* **40** 1 (1975)
117. A T Nielsen *Org. React.* **16** 1 (1968)
118. V S Markevich, S M Markevich *Khim. Promst* 898 (1973)
119. M Mousseron-Canet, C Levallois *Bull. Soc. Chim. Fr.* 993 (1963)
120. V N Belov, N A Daev, S D Kustova, K V Leets, S S Poddubnaya, N I Skvortsova, E I Shepelenkova, A K Shumeiko *Zh. Obshch. Khim.* **27** 1384 (1957) [a]
121. A A Petrov, N A Razumova, M L Genusov *Zh. Obshch. Khim.* **28** 1128 (1958) [a]
122. S A Voitkevich *865 Dushistykh Veshchestv dlya Parfyumerii i Bytovoi Khimii* (865 Perfumes for Perfumery and Household Chemistry) (Moscow: Pishchevaya Promst, 1994) p. 225
123. J Herscovici, L Boumaiza, K Antonakis *Tetrahedron Lett.* **32** 1791 (1991)
124. J Herscovici, S Delatre, K Antonakis *Tetrahedron Lett.* **32** 1183 (1991)
125. E J Corey, D Enders *Tetrahedron Lett.* 11 (1976)
126. S Saito, M Shiozawa, M Ito, H Yamamoto *J. Am. Chem. Soc.* **120** 813 (1998)
127. R Lantzsch, D Arlt *Liebigs Ann. Chem.* 1757 (1976)
128. E J Corey, G Schmidt *Tetrahedron Lett.* 2317 (1979)
129. L A Yanovskaya, in *Reaktsii i Metody Issledovaniya Organicheskikh Soedinenii* (Reactions and Methods of Investigation of Organic Compounds) (Moscow: GNTIKhL, 1962) Vol. 11, p. 321
130. L A Yanovskaya, S S Yufit, V F Kucherov *Khimiya Atsetalei* (The Chemistry of Acetals) (Moscow: Nauka, 1975) p. 222
131. I N Nazarov, Zh A Krasnaya, V P Vinogradov *Zh. Obshch. Khim.* **28** 460 (1958) [a]
132. Zh A Krasnaya, V F Kucherov *Izv. Akad. Nauk SSSR, Otd. Khim. Nauk* 1057 (1962) [b]
133. L A Yanovskaya, G M Zhdankina, G V Kryshtal', E P Serebryakov *Izv. Akad. Nauk SSSR, Ser. Khim.* 2790 (1987) [b]
134. O Isler, M Montavor, R Rüegg *Helv. Chim. Acta* **39** 259 (1956)
135. G Stork, M Tomasz *J. Am. Chem. Soc.* **86** 471 (1964)
136. H J Hagermeyer *Ind. Eng. Chem.* **41** 765 (1949)
137. Braz. P. 7 407 691; *Chem. Abstr.* **86** 105 955 (1977)
138. K Maruoka, A B Conception, H Yamamoto *Synlett* 31 (1992)
139. D G Kubler *J. Org. Chem.* **27** 1435 (1962)
140. O A Shavrygina, S M Makin *Zh. Org. Khim.* **2** 1354 (1966) [c]
141. A Maercker, in *Organic Reactions* Vol. 14 (New York: Wiley, 1965) p. 270
142. B E Maryanoff, A B Reitz *Chem. Rev.* **89** 863 (1989)
143. G V Kryshtal', E P Serebryakov *Izv. Akad. Nauk, Ser. Khim.* 1867 (1995) [b]
144. X Wei, R J K Taylor *J. Org. Chem.* **65** 616 (2000)
145. H J Bestmann, O Vostrowsky, H Paulus, W Billmann, W Stransky *Tetrahedron Lett.* 121 (1977)
146. J Rokach, R N Young, M Kakushima, C-K Lau, R Seguin, R Franette, Y Guindon *Tetrahedron Lett.* **22** 979 (1981)
147. J Rokach, R Zambani, C-K Lau, Y Guindon *Tetrahedron Lett.* **22** 2759 (1981)
148. S R Baker, J R Boot, S E Morgan, D J Osborn, W J Ross, P R Shrubsall *Tetrahedron Lett.* **24** 4469 (1983)
149. I Ernest, A Main, R Menasse *Tetrahedron Lett.* **23** 167 (1982)
150. L Alcaraz, G Macdonald, J Ragot, N J Lewis, R J K Taylor *Tetrahedron* **55** 3707 (1999)
151. Y Guindon, D Delorme, C K Lau, R Zamboni *J. Org. Chem.* **53** 267 (1988)
152. Y Leblanc, B J Fitzsimmons, R Zamboni, J Rokach *J. Org. Chem.* **53** 265 (1988)
153. G M Zhdankina, V I Kadentsev, G V Kryshtal', E P Serebryakov, L A Yanovskaya *Izv. Akad. Nauk SSSR, Ser. Khim.* 1179 (1987) [b]
154. R J K Taylor *Synthesis* 564 (1977)
155. R J K Taylor *Synthesis* 566 (1977)
156. D F Taber, B P Gunn *J. Am. Chem. Soc.* **101** 3992 (1979)
157. M Moreno-Mañas, A Trius *Tetrahedron Lett.* **22** 3109 (1981)
158. M Moreno-Mañas, R M Ortuso, M Prat, M A Galán *Synth. Commun.* **16** 1003 (1986)
159. S W Scheuplein, R Brückner *Chem. Ber.* **124** 1871 (1991)
160. J D White, M S Jensen *Tetahedron Lett.* **33** 577 (1992)
161. Y Shen, T Wang *Tetrahedron Lett.* **32** 4353 (1991)
162. G Vidari, S Ferriño, P A Grieco *J. Am. Chem. Soc.* **106** 3539 (1984)
163. T K M Shing, Y Tang *Tetrahedron* **46** 2187 (1990)
164. J Villieras, M Rambaud *Synthesis* 300 (1983)
165. A A Vasil'ev, L Engman, V M Merkulova *Izv. Akad. Nauk, Ser. Khim.* 1300 (2000) [b]
166. A A Vasil'ev, G V Kryshtal, E P Serebryakov *Mendeleev Commun.* 41 (1995)
167. K Ando *J. Org. Chem.* **63** 8411 (1998)
168. K Ando, T Oishi, M Hirama, H Ohno, T Ibuka *J. Org. Chem.* **65** 4745 (2000)
169. R Liu, M Schlosser *Synlett* 1197 (1996)
170. B S Lee, S Y Lee, D Y Oh *J. Org. Chem.* **65** 4175 (2000)
171. R N Gedye, K C Westaway, P Arora, R Bisson, A H Khalil *Can. J. Chem.* **55** 1218 (1977)
172. D Murali, R G S Krishna Rao *Synthesis* 254 (1987)
173. G V Kryshtal', E P Serebryakov, L M Suslova, L A Yanovskaya *Izv. Akad. Nauk SSSR, Ser. Khim.* 2377 (1988) [b]
174. G V Kryshtal', G M Zhdankina, E P Serebryakov *Izv. Akad. Nauk, Ser. Khim.* 1839 (1997) [b]
175. A A Vasil'ev, A L Vlasyuk, G V Kryshtal', E P Serebryakov *Izv. Akad. Nauk, Ser. Khim.* 2026 (1995) [b]
176. V N Odinokov, V R Akhmetova, R G Savchenko, A A Fatykhov, K I Pashkevich, E P Serebryakov *Izv. Akad. Nauk, Ser. Khim.* 2196 (1995) [b]
177. G V Kryshtal', G M Zhdankina, E P Serebryakov *Izv. Akad. Nauk, Ser. Khim.* 1089 (1993) [b]
178. G V Kryshtal', G M Zhdankina, E P Serebryakov *Izv. Akad. Nauk, Ser. Khim.* 1094 (1993) [b]
179. G V Kryshtal', E P Serebryakov, L M Suslova, L A Yanovskaya *Izv. Akad. Nauk SSSR, Ser. Khim.* 1414 (1990) [b]
180. G V Kryshtal, G M Zhdankina, E P Serebryakov, in *The 11th International Conference on Organic Synthesis (Book of Abstracts), Amsterdam, 1996* p 587
181. D Mead, A E Asato, M Denny, R S H Liu, Y Hanzawa, T Taguchi, A Yamada, N Kobayashi, A Hosoda, Y Kobayashi *Tetrahedron Lett.* **28** 259 (1987)
182. A Trehan, R S H Liu *Tetrahedron Lett.* **29** 419 (1988)
183. W R Roush *J. Am. Chem. Soc.* **100** 3599 (1978)
184. P Bæckström, U Jacobsson, T Norin, C R Unelius *Tetrahedron* **44** 2541 (1988)

185. J M Takacs, M R Jaber, F Clement, C Walters *J. Org. Chem.* **63** 6757 (1998)
186. A A Vasil'ev, E P Serebryakov *Zh. Org. Khim.* **34** 1033 (1998) [c]
187. A Mohamed-Hachi, E About-Jaudet, J-C Combret, N Collignon *Synthesis* 1188 (1999)
188. N Kann, T Rein, B Ekermark, P Helquist *J. Org. Chem.* **55** 5312 (1990)
189. L Dumahel, J Guillemont, Y L Gallc, G Ple, J-M Poirier, Y Ramondenc, P Chabardes *Tetrahedron Lett.* **31** 3129 (1990)
190. J Xiao, Y Feng, C Yuang *J. Chem. Soc., Perkin Trans. 1* 4240 (2000)
191. Y Ikeda, J Ukai, H Yamamoto *Tetrahedron* **43** 723 (1987)
192. A H Davidson, I Fleming, J I Grayson, A Pearce, R L Snowden, S Warren *J. Chem. Soc., Perkin Trans. 1* 550 (1977)
193. J H Rigby, M Qabar *J. Org. Chem.* **54** 5852 (1989)
194. Y Wang, J Li, Y Wu, Y Huang, L Shi, J Yang *Tetrahedron Lett.* **27** 4583 (1986)
195. C Gravier-Pelletier, J Dumas, Y Le Merrer, J C Depezay *Tetrahedron Lett.* **32** 1165 (1991)
196. Y-Z Huang, C Chen, Y Shen *Synth. Commun.* 501 (1989)
197. A Osuka, Y Mori, H Shimizu, H Suzuki *Tetrahedron Lett.* **24** 2599 (1983)
198. Q Zhong, Y L Cheng, J G Shao, C Q Liu *Chin. Chem. Lett.* **2** 51 (1991)
199. M Bellassoued, A Majidi *J. Org. Chem.* **58** 2517 (1993)
200. M Bellassoued, M Salemkour *Tetrahedron Lett.* **34** 5281 (1993)
201. M Bellassoued, M Salemkour *Tetrahedron* **52** 4607 (1996)
202. Y Hatanaka, I Kuwajima *J. Org. Chem.* **51** 1932 (1986)
203. T Cunigny, C Herve du Penhoat, M Julia *Tetrahedron* **43** 859 (1987)
204. P J Kocienski, B Lythgoe, S Ruston *J. Chem. Soc., Perkin Trans. 1* 829 (1978)
205. J B Baudin, G Hareau, S A Julia, O Ruel *Bull. Soc. Chim. Fr.* **130** 336 (1993)
206. J B Baudin, G Hareau, S A Julia, R Lorne, O Ruel *Bull. Soc. Chim. Fr.* **130** 856 (1993)
207. N D Smith, P J Kocienski, S D A Street *Synthesis* 652 (1996)
208. M Clarembeau, A Cravador, W Dumont, L Hevesi, A Krief, J Lucchetti, D van Ende *Tetrahedron* **41** 4793 (1985)
209. A Krief, W Dumont, M Clarembeau, E Badaoui *Tetrahedron* **45** 2023 (1989)
210. H J Reich, F Chow *J. Chem. Soc., Chem. Commun.* 790 (1975)
211. J Remion, A Krief *Tetrahedron Lett.* **41** 3743 (1976)
212. A A Vasil'ev, L Engman, E P Serebryakov *J. Chem. Soc., Perkin Trans. 1* 2211 (2000)
213. Y Yamamoto, H Yatagi, Y Saito, K Maruyama *J. Org. Chem.* **49** 1096 (1984)
214. F N Tebbe, G W Parshall, G S Reddy *J. Am. Chem. Soc.* **100** 3611 (1978)
215. H Hauptmann, G Mühlbauer, H Sass *Tetrahedron Lett.* **27** 6189 (1986)
216. Y Horikawa, M Watanabe, T Fujiwara, T Takeda *J. Am. Chem. Soc.* **119** 1127 (1997)
217. T Takeda, Y Takagi, N Saeki, T Fujiwara *Tetrahedron Lett.* **41** 8377 (2000)
218. U Schöllkopf, F Gerhart *Angew. Chem.* **80** 842 (1968)
219. O Fujimura, T Honma *Tetahedron Lett.* **39** 625 (1998)
220. S Bräse, A de Meijere, in *Metal-Catalyzed Cross-Coupling Reactions* (Eds F Diederich, P Stang) (Weinheim: Wiley-VCH, 1998) p. 99
221. I P Beletskaya, A V Cheprakov *Chem. Rev.* **100** 3009 (2000)
222. T N Mitchell, in *Metal-Catalyzed Cross-Coupling Reactions* (Eds F Diederich, P Stang) (Weinheim: Wiley-VCH, 1998) p. 167
223. V Farina, V Krishnamurthy, W J Scott *The Stille Reaction*. Wiley New York 1998
224. N Miyaura, A Suzuki *Chem. Rev.* **95** 2457 (1995)
225. A Suzuki, in *Metal-Catalyzed Cross-Coupling Reactions* (Eds F Diederich, P Stang) (Weinheim: Wiley-VCH, 1998) p. 49
226. E Negishi, F Liu, in *Metal-Catalyzed Cross-Coupling Reactions* (Eds F Diederich, P Stang) (Weinheim: Wiley-VCH, 1998) p. 1
227. K Ritter *Synthesis* 735 (1993)
228. G Zweifel, R L Miller *J. Am. Chem. Soc.* **92** 6678 (1970)
229. M F Semmelhack, P M Helquist, J D Gorzynski *J. Am. Chem. Soc.* **94** 9234 (1972)
230. R Vanderesse, Y Fort, S Becker, P Caubere *Tetrahedron Lett.* **27** 3517 (1986)
231. H A Dieck, R F Heck *J. Am. Chem. Soc.* **96** 1133 (1974)
232. T Jeffery *J. Chem. Soc., Chem. Commun.* 324 (1991)
233. T Jeffery *Tetrahedron Lett.* **34** 1133 (1993)
234. E Bernocchi, S Cacchi, P G Ciattini, E Morera, G Ortar *Tetrahedron Lett.* **33** 3073 (1992)
235. M Webel, H-U Reissig *Synlett* 1141 (1997)
236. K Hirabayashi, Y Nishihara, A Mori, T Hiyama *Tetrahedron Lett.* **39** 7893 (1998)
237. J Yoshida, K Tamao, H Yamamoto, T Kakui, T Uchida, M Kumada *Organometallics* **1** 542 (1982)
238. R M Moriarty, W R Epa, A K Awasthi *J. Am. Chem. Soc.* **113** 6315 (1991)
239. G P Chuisoli, G Salerno, W Giroldini, L Pallini *J. Organomet. Chem.* **219** C16 (1981)
240. J K Stille, B L Groh *J. Am. Chem. Soc.* **109** 813 (1987)
241. M Abarbi, J-L Parrain, J-C Cintrat, A Duchêne *Synthesis* 82 (1996)
242. C J Forsyth, J Clardy *J. Am. Chem. Soc.* **110** 5911 (1988)
243. H -O Kim, C O Ogbu, S Nelson, M Kahn *Synlett* 1059 (1998)
244. Y Naruse, T Esaki, H Yamamoto *Tetrahedron Lett.* **29** 1417 (1988)
245. W Shen, L Wang *J. Org. Chem.* **64** 8873 (1999)
246. J K Stille, J H Simpson *J. Am. Chem. Soc.* **109** 2138 (1987)
247. R E Maleczka, I Terstiege *J. Org. Chem.* **63** 9622 (1998)
248. R E Malescka Jr, W P Gallagher, I Terstiege *J. Am. Chem. Soc.* **122** 384 (2000)
249. Y Kobayashi, N Nakayama, R Mizojiri *Tetrahedron* **54** 1053 (1998)
250. M Satoh, N Miyaura, A Suzuki *Chem. Lett.* 1329 (1986)
251. I Rivera, J A Soderquist *Tetrahedron Lett.* **32** 2311 (1991)
252. X Chen, J G Millar *Synthesis* 113 (2000)
253. N Miyaura, Y Satoh, S Hara, A Suzuki *Bull. Chem. Soc. Jpn.* **59** 2029 (1986)
254. T Oh-e, N Miyaura, A Suzuki *J. Org. Chem.* **58** 2201 (1993)
255. M V Mavrov, N A Urdaneta, C H Nguyen, E P Serebryakov *Izv. Akad. Nauk SSSR, Ser. Khim.* 2633 (1987) [b]
256. M V Mavrov, N A Urdaneta, E P Serebryakov *Bioorg. Khim.* **16** 711 (1990) [d]
257. J P Genêt, A Linquist, E Blart, V Mouries, M Savignac *Tetrahedron Lett.* **36** 1443 (1995)
258. N Miyaura, A Suzuki *J. Organomet. Chem.* **213** C53 (1981)
259. E Negishi, T Takahashi, S Baba, D E van Horn, N Okukado *J. Am. Chem. Soc.* **109** 2393 (1987)
260. J-E Bäckvall, H E Schink, Z D Renko *J. Org. Chem.* **55** 826 (1990)
261. N Okukado, D E van Horn, W L Klima, E Negishi *Tetrahedron Lett.* 1027 (1978)
262. G Cahiez, H Avedissian *Synthesis* 1199 (1998)
263. V Fiandanese, G Marchese, G Mascolo, F Naso, L Ronzini *Tetrahedron Lett.* **29** 3705 (1988)
264. I D Gridnev, N Miyaura, A Suzuki *J. Org. Chem.* **58** 5351 (1993)
265. T Hiyama, in *Metal-Catalyzed Cross-Coupling Reactions* (Eds F Diederich, P Stang) (New York: Wiley, 1998) p. 421
266. Y Hatanaka, T Hiyama *Synlett* 845 (1991)
267. Y Hatanaka, T Hiyama *J. Org. Chem.* **53** 918 (1988)
268. Y Hatanaka, T Hiyama *J. Org. Chem.* **54** 268 (1989)
269. Y Hatanaka, T Hiyama *Tetrahedron Lett.* **31** 2719 (1990)
270. R C Larock, B Riefling *J. Org. Chem.* **43** 1468 (1976)
271. A P Koziokowski, Y Kitigawa *Tetrahedron Lett.* **23** 2087 (1982)
272. G Zweifel, J T Snow, C C Whitney *J. Am. Chem. Soc.* **90** 7139 (1968)
273. B A Patel, J E Dickerson, R F Heck *J. Org. Chem.* **43** 5018 (1978)
274. T Jeffery *Tetrahedron Lett.* **33** 1989 (1992)
275. J Uenishi, R Kawahama, Y Izaki, O Yonemitsu *Tetrahedron* **56** 3493 (2000)
276. Y Ikeda, J Ukai, N Ikeda, H Yamamoto *Tetrahedron Lett.* **25** 5177 (1984)
277. A S E Karlström, M Rönn, A Thorarensen, J-E Bäckvall *J. Org. Chem.* **63** 2517 (1998)
278. A S E Karlström, K Itami, J-E Bäckvall *J. Org. Chem.* **64** 1745 (1999)
279. L Novak, J Rohaly, P Kolonits, P Fekete, L Varjac, C S Szantay *Liebigs Ann. Chem.* 1173 (1982)
280. M Alami, J-F Peyrat, J-D Brion *Synthesis,* 1499 (2000)

281. V Ratavelomanana, G Linstrumelle *Tetrahedron Lett*. **22** 315 (1982)
282. K Sonogashira, in *Metal-Catalyzed Cross-Coupling Reactions* (Eds F Diederich, P Stang) (New York: Wiley, 1998) p. 203
283. G Zeni, V Comasseto *Tetrahedron Lett*. **40** 4619 (1999)
284. E Negishi, T Yoshida *J. Chem. Soc., Chem. Commun*. 606 (1973)
285. E Negishi, G Lew, T Yoshida *J. Chem. Soc., Chem. Commun*. 874 (1973)
286. E Negishi, A Abramovich *Tetrahedron Lett*. 411 (1977)
287. J F Normant, A Alexakis *Synthesis* 841 (1981)
288. F Näf, P Degen *Helv. Chim. Acta* **54** 1939 (1971)
289. E J Corey, C U Kim, R H K Chen, M Takeda *J. Am. Chem. Soc*. **94** 4395 (1972)
290. A Alexakis, J F Normant *Tetrahedron Lett*. **23** 5151 (1982)
291. A Alexakis, G Cahiez, J F Normant *Tetrahedron* **36** 1961 (1980)
292. M Furber, R J K Taylor, S C Burford *J. Chem. Soc., Perkin Trans. 1* 1809 (1986)
293. M Furber, R J K Taylor, S C Burford *Tetrahedron Lett*. **26** 3285 (1985)
294. E Piers, E M Boehringer, J G K Yee *J. Org. Chem*. **63** 8642 (1998)
295. J C Clenet, G Linstrumelle *Nouv. J. Chim*. **1** 373 (1977)
296. F Scott, G Cahiez, J F Normant, J Villieras *J. Organomet. Chem*. **144** 13 (1978)
297. T Naota, H Takaya, S Murahashi *Chem. Rev*. **98** 2599 (1998)
298. T Mitsudo, S-W Zhang, M Nagao, Y Watanabe *J. Chem. Soc., Chem. Commun*. 598 (1991)
299. T Mitsudo, S-W Zhang, T Kondo, Y Watanabe *Tetrahedron Lett*. **33** 341 (1992)
300. M Murakami, M Ubukata, Y Ito *Tetrahedron Lett*. **39** 7361 (1998)
301. B M Trost, A F Indolese, T J J Müller, B Treptow *J. Am. Chem. Soc*. **117** 615 (1995)
302. C S Yi, N Liu *Organometallics* **17** 3158 (1998)
303. C S Yi, N Liu *Synlett* 281 (1999)
304. Y Nishibayashi, M Yamanashi, I Wakiji, M Hidai *Angew. Chem., Int. Ed. Engl*. **39** 2909 (2000)
305. B M Trost, M Lautens *J. Am. Chem. Soc*. **107** 1781 (1985)
306. B M Trost, S-F Chen *J. Am. Chem. Soc*. **108** 6053 (1986)
307. B M Trost, D T MacPherson *J. Am. Chem. Soc*. **109** 3483 (1987)
308. C M Huwe, S Blechert *Tetrahedron Lett*. **35** 9537 (1994)
309. B M Trost, J Y L Chung *J. Am. Chem. Soc*. **107** 4586 (1985)
310. B M Trost, G J Tanoury, M Lautens, C Chan, D T MacPherson *J. Am. Chem. Soc*. **116** 4255 (1994)
311. B M Trost, M Lautens *Tetrahedron Lett*. **26** 4887 (1985)
312. B M Trost, O J Gelling *Tetrahedron Lett*. **34** 8233 (1993)
313. B M Trost, J M Tour *J. Am. Chem. Soc*. **109** 5268 (1987)
314. J Le Paih, D C Rodriguez, S Dérien, P H Dixneuf *Synlett* 95 (2000)
315. M Nishida, N Adachi, K Onozuka, H Matsumura, M Mori *J. Org. Chem*. **63** 9158 (1998)
316. R Grigg, P Stevenson, T Worakun *Tetrahedron* **44** 2033 (1988)
317. R Grigg, P Stevenson, T Worakun *Tetrahedron* **44** 2049 (1988)
318. W A Nugent, J C Calabrese *J. Am. Chem. Soc*. **106** 6422 (1984)
319. E Negishi, F E Cederbaun, T Takahashi *Tetrahedron Lett*. **27** 2829 (1986).
320. W A Nugent, D L Thorn, R L Harlow *J. Am. Chem. Soc*. **109** 2788 (1987)
321. B M Trost, D C Lee *J. Am. Chem. Soc*. **110** 7255 (1988)
322. J M Nuss, M McMurphy, R A Rennels, M H Heravi, B J Mohr *Tetrahedron Lett*. **34** 3079 (1993)
323. J W Madine, X Wang, R A Widenhoefer *Org. Lett*. **3** 385 (2001)
324. A Kinoshita, N Sakakibara, M Mori *J. Am. Chem. Soc*. **119** 12 388 (1997)
325. A Kinoshita, N Sakakibara, M Mori *Tetrahedron* **55** 8155 (1999)
326. J A Smulik, S T Diver *J. Org. Chem*. **65** 1788 (2000)
327. A A Vasil'ev, L Engman, E P Serebryakov *Mendeleev Commun*. 101 (2000)
328. S C Schörer, S Blechert *Synlett* 166 (1998)
329. L Ackermann, A Förstner, T Weskamp, F J Kohl, W A Herrmann *Tetrahedron Lett*. **40** 4787 (1999)
330. R Stragies, U Voigtmann, S Blechert *Tetrahedron Lett*. **41** 5465 (2000)
331. A Kinoshita, M Mori *Synlett* 1020 (1994)
332. A Kinoshita, M Mori *J. Org. Chem*. **61** 8356 (1996)
333. M Mori, N Sakakibara, A Kinoshita *J. Org. Chem*. **63** 6082 (1998)
334. J Renaud, C-D Graf, L Oberer *Angew. Chem., Int. Ed. Engl*. **39** 3101 (2000)
335. S -H Kim, W J Zuercher, N B Bowden, R H Grubbs *J. Org. Chem*. **61** 1073 (1996)
336. N Chatani, T Morimoto, T Muto, S Murai *J. Am. Chem. Soc*. **116** 6049 (1994)
337. A Fürstner, H Szillat, F Stelzer *J. Am. Chem. Soc*. **122** 6785 (2000)
338. B M Trost, A B Pinkerton *J. Am. Chem. Soc*. **121** 4068 (1999)
339. B M Trost, A B Pinkerton *J. Am. Chem. Soc*. **121** 10842 (1999)
340. B Friess, B Cazes, J Gore *Tetrahedron Lett*. **29** 4089 (1988)
341. N Kopola, B Friess, B Cazes, J Gore *Tetrahedron Lett*. **30** 3963 (1989)
342. V Gauthier, B Cazes, J Gore *Tetrahedron Lett*. **32** 915 (1991)
343. N Chaptal, V Colovray-Gotteland, C Grandjean, B Cazes, J Gore *Tetrahedron Lett*. **32** 1795 (1991)
344. N Vicart, B Cazes, J Gore *Tetrahedron Lett*. **36** 5015 (1995)
345. H-M Chang, C-H Cheng *J. Org. Chem*. **65** 1767 (2000)
346. Y Imada, G Vasapollo, H Alper *J. Org. Chem*. **61** 7982 (1996)
347. H Maeta, T Hasegawa, K Suzuki *Synlett* 341 (1993)
348. B G van den Hoven, H Alper *J. Org. Chem*. **64** 3964 (1999)
349. J Kiji, T Okano, E Fujii, J Tsuji *Synthesis* 869 (1997)
350. J Böhmer, R Grigg *Tetrahedron* **55** 13463 (1999)
351. L Zhu, R D Rieke *Tetrahedron Lett*. **32** 2865 (1991)
352. X Qi, J Montgomery *J. Org. Chem*. **64** 9310 (1999)
353. M J Rozema, P Knochel *Tetrahedron Lett*. **32** 1855 (1991)
354. H Maeta, K Suzuki *Tetrahedron Lett*. **34** 341 (1993)
355. A N Kasatkin, R J Whitby *Tetrahedron Lett*. **41** 6201 (2000)
356. K M Doxsee, J K M Mouser *Tetrahedron Lett*. **32** 1687 (1991)
357. Z Wang, X Lu, A Lei, Z Zhang *J. Org. Chem*. **63** 3806 (1998)
358. Y Kataoka, J Miyai, K Oshima, K Takai, K Utimoto *J. Org. Chem*. **57** 1973 (1992)
359. J R Stricker, P A Wexler, D E Wigley *Organometallics* **10** 118 (1991)
360. I U Khand, P L Pauson *J. Chem. Soc., Chem. Commun*. 379 (1974)
361. P G Andersson, J-E Bäckvall *J. Org. Chem*. **56** 5349 (1991)
362. Y I M Nilsson, P G Andresson, J-E Bäckvall *J. Am. Chem. Soc*. **115** 6609 (1993)
363. B M Trost, S Hildbrand, K Dogra *J. Am. Chem. Soc*. **121** 10416 (1999)
364. R Grée *Synthesis* 341 (1989)
365. G R Knox, I G Thon *J. Chem. Soc., Chem. Commun*. 373 (1981)
366. D F Harvey, V B Selhau *J. Org. Chem*. **65** 2282 (2000)
367. J Böhmer, F Hampel, R Schobert *Synthesis* 661 (1997)
368. C E Anson, G Dave, G R Stephenson *Tetrahedron* **56** 2273 (2000)
369. H Birmann, V Prahlad, C Tao, Y K Yun, Z Wang, W A Donaldson *Tetrahedron* **56** 2283 (2000)
370. E Wenkert, M Guo, R Lavilla, B Porter, K Ramachandran, J-H Sheu *J. Org. Chem*. **55** 6203 (1990)
371. D K P Ng, T-Y Luh *J. Am. Chem. Soc*. **111** 9119 (1989)
372. J Auge, S David *Tetrahedron Lett*. **24** 4009 (1983)
373. T Satoh, S Motohashi, K Yamakawa *Chem. Pharm. Bull*. **36** 1169 (1988)
374. T P Meagher, L Yet, C-N Hsiao, H Shechter *J. Org. Chem*. **63** 4181 (1998)
375. T P Meagher, H Shechter *J. Org. Chem*. **63** 4193 (1998)
376. K Mori *Tetrahedron* **30** 3807 (1974)
377. A Ichihara, N Miki, H Tazaki, S Sakamura *Tetrahedron Lett*. **28** 1175 (1987)
378. I Fleming, A Barbero, D Walter *Chem. Rev*. **97** 2063 (1997)
379. D Seyferth, J Pornet *J. Org. Chem*. **45** 1721 (1980)
380. R H Wollenberg *Tetrahedron Lett*. 717 (1978)
381. E J Corey, D A Clark, G Goto, A Marfat, C Mioskowski, B Samuelsson, S Hammarström *J. Am. Chem. Soc*. **102** 1436 (1980)
382. B Contreras, L Duhamel, G Plé *Synth. Commun*. 2983 (1990)
383. R M Seifert, R G Buttery *J. Agric. Food Chem*. **28** 68 (1980)
384. M S Brouwer, H Hulkenberg, J G J Kok, R van Moorselaar, W R M Overbeek, P G J Wesselman *Recl. Trav. Chim. Pays-Bas* **98** 316 (1979)
385. T Hayashi, K Sasaoka, T Oishi *J. Chem. Soc., Chem. Commun*. 1362 (1990)
386. N Vicart, D Castet-Caillabet, Y van Ramondenc, G Plé, L Duhamel *Synlett* 411 (1998)
387. D Soullez, G Plé, L Duhamel, P Duhamel *J. Chem. Soc., Chem. Commun*. 563 (1995)

388. A C Friedly, E Yang, S R Marder *Tetrahedron* **53** 2717 (1997)
389. Y-Z Huang, X-S Mo, L Wang *Tetrahedron Lett*. **39** 419 (1998)
390. Y Y Belosludtsev, B C Borer, R J K Taylor *Synthesis* 320 (1991)
391. R J K Taylor, K Hemming, E F De Medeiros *J. Chem. Soc., Perkin Trans. 1* 2385 (1995)
392. N Lewis, P W McKen, R J K Taylor *Synlett* 898 (1991)
393. S Chandrasekhar, M V Reddy, K S Reddy, C Ramaro *Tetrahedron Lett*. **41** 2667 (2000)
394. T Fujisawa, N Okada, M Takeuchi, T Sato *Chem. Lett*. 1271 (1983)
395. F Caturla, C Najera, M Varea *Tetrahedron Lett*. **40** 5957 (1999)
396. S Hatakeyama, K Sugawara, M Kawamura, S Takano *Tetrahedron Lett*. **32** 4509 (1991)
397. R Soundararajan, G Li, H C Brown *J. Org. Chem*. **61** 100 (1996)
398. M Montury, B Psaume, J Goré *Tetrahedron Lett*. **21** 163 (1980)
399. A R Katritzky, L Serdyuk, D Toader, X Wang *J. Org. Chem*. **64** 1888 (1999)
400. K J Shea, P Q Phem *Tetrahedron Lett*. **24** 1003 (1983)
401. F F Fleming, T Jiang *J. Org. Chem*. **62** 7890 (1997)
402. S Nunomoto, Y Kawakami, Y Yamashita *Bull. Chem. Soc. Jpn*. **54** 2831 (1981)
403. O Tsuge, E Wada, S Kanemasa, H Sakoh *Chem. Lett*. 469 (1984)
404. A Arase, M Hoshi *J. Chem. Soc., Chem. Commun*. 531 (1987)
405. M Hoshi, Y Masuda, A Arase *J. Chem. Soc., Chem. Commun*. 1629 (1987)
406. R R Wilson, L R Phillips, K J Natalie *J. Am. Chem. Soc*. **101** 3340 (1979)
407. J P Godschalx, J K Stille *Tetrahedron Lett*., **24** 1905 (1983)
408. C Najera, J M Sansano *Tetrahedron* **50** 5829 (1994)
409. G O Schenck, W Hartmann, R Steinmetz *Chem. Ber*. **96** 498 (1963)
410. H -D Scharf, J Mattay *Liebigs Ann. Chem*. 772 (1977)
411. D Bellus, C D Weis *Tetrahedron Lett*. 999 (1973)
412. S Halazy, A Krief *Tetrahedron Lett*. **21** 1997 (1980)
413. S Ingham, R W Turner, T W Wallace *J. Chem. Soc., Chem. Commun*. 1664 (1985)
414. G B Bennett *Synthesis* 589 (1977)
415. S F Reed *J. Org. Chem*. **30** 1663 (1965)
416. S A Bal, P Helquist *Tetrahedron Lett*. **22** 3933 (1981)
417. T Hudlicky, T M Kutchan, S R Wilson, D T Mao *J. Am. Chem. Soc*. **102** 6351 (1980)
418. S Karlsen, P Frøyen, L Skattebøl *Acta Chem. Scand., Ser. B* **30** 664 (1976)
419. M Bertrand, J Viala *Tetrahedron Lett*. 2575 (1978)
420. J N Labovitz, C A Henrick, V L Corbin *Tetrahedron Lett*. 4209 (1975)
421. D Samain, C Descoins *Bull. Soc. Chim. Fr., Pt II* 71 (1979)
422. L A Yanovskaya, in *Reaktsii i Metody Issledovaniya Organicheskikh Soedinenii* (Reactions and Methods of Investigation of Organic Compounds) (Moscow: Khimiya, 1963) Vol. 12, p. 273
423. I N Nazarov, L A Yanovskaya, B P Gusev, S M Makin, I I Nazarova *Dokl. Akad. Nauk SSSR* **114** 1029 (1957) [e]
424. G I Samokhvalov, M A Miropol'skaya, N A Preobrazhenskii *Dokl. Akad. Nauk SSSR* **107** 103 (1956) [e]
425. G Saucy, R Marbet *Helv. Chim. Acta* **50** 1158 (1967)
426. J K Crandall, G L Tindell *J. Chem. Soc., Chem. Commun*. 1411 (1970)
427. C A Henrick, W E Willy, D R McKean, E Baggiolini, J B Siddall *J. Org. Chem*. **40** 8 (1975)
428. S Tsuboi, T Masuda, H Makino, A Takeda *Tetrahedron Lett*. **23** 209 (1982)
429. J Ficini, N Lumbroso-Bader, J Pouliquen *Tetrahedron Lett*. **39** 4139 (1968)
430. B Bowden, R C Cookson, H A Davis *J. Chem. Soc., Perkin Trans. 1* 2634 (1973)
431. J E Baldwin, P A R Bennet, A K Forrest *J. Chem. Soc., Chem. Commun*. 250 (1987)
432. R C Cookson, R Gopalan *J. Chem. Soc., Chem. Commun*. 608 (1978)
433. G H Posner, C M Kinter *J. Org. Chem*. **55** 3967 (1990)
434. A Douthean, G Balme, M Malacria, J Goré *Tetrahedron Lett*. 1803 (1978)
435. A Douthean, G Balme, M Malacria, J Goré *Tetrahedron* **36** 1953 (1980)
436. T Onishi, Y Fujita, T Nishida *Chem. Lett*. 765 (1979)
437. Y Fujita, T Onishi, K Hino, T Nishida *Tetrahedron Lett*. **21** 1347 (1980)
438. T Sato, H Tsunekawa, H Kohama, T Fujisawa *Chem. Lett*. 1553 (1986)
439. J J Eshelby, P J Parsons, N C Sillars, P J Crowley *J. Chem. Soc., Chem. Commun*. 1497 (1995)
440. S Kuroda, T Katsuki, M Yamaguchi *Tetrahedron Lett*. **28** 803 (1987)
441. S Mikami, T Maeda, T Nakai *Tetraheron Lett*. **27** 4189 (1986)
442. M Uchikawa, T Katsuki, M Yamaguchi *Tetrahedron Lett*. **27** 4581 (1986)
443. E I Klimova, E G Treshchova, Yu A Arbuzov *Dokl. Akad. Nauk SSSR* **180** 865 (1968) [e]
444. D Devaprabhakara, C G Cardenas, P D Gardner *J. Am. Chem. Soc*. **85** 1553 (1963)
445. R A Amos, J A Katzenellenbogen *J. Org. Chem*. **43** 555 (1978)
446. H Bosshardt, M Schlosser *Helv. Chim. Acta* **63** 2393 (1980)
447. S Tsuboi, A Kuroda, T Masuda, A Takeda *Chem. Lett*. 1541 (1984)
448. L I Zakharkin, S A Babich *Zh. Org. Khim*. **18** 2261 (1982) [c]
449. B T Golding, G Pierpoint, R Aneja *J. Chem. Soc., Chem. Commun*. 1030 (1981)
450. S Akiyama, S Nakatsuji, T Hamamura *Tetrahedron Lett*. 2809 (1979)
451. B Psaume, M Montury, J Gorè *Synth. Commun*. **12** 409 (1982)
452. B M Trost, T Schmidt *J. Am. Chem. Soc*. **110** 2301 (1988)
453. D Ma, Y Yu, X Lu *J. Org. Chem*. **54** 1105 (1989)
454. X Lu, C Guo, D Ma *Synlett* 357 (1990)
455. B M Trost, U Kazmaier *J. Am. Chem. Soc*. **114** 7933 (1992)
456. C Guo, X Lu *J. Chem. Soc., Perkin Trans. 1* 1921 (1993)
457. U Kazmaier *J. Chem. Soc., Chem. Commun*. 2305 (1997)
458. U Kazmaier *Tetrahedron* **54** 1491 (1998)
459. Z Wang, X Lu *Tetrahedron* **51** 11765 (1995)
460. C Guo, X Lu *Synlett* 405 (1992)
461. C Guo, X Lu *J. Chem. Soc., Chem. Commun*. 394 (1993)
462. I A Balova, L A Remizova, V F Makarycheva, E G Rumyantseva, I A Favorskaya *Zh. Org. Khim*. **27** 64 (1991)
463. I A Balova, S N Morozkina, S V Voskresenskii, L A Remizova *Zh. Org. Khim*. **36** 1466 (2000) [c]
464. I A Balova, I V Zakharova, L A Remizova *Zh. Org. Khim*. **29** 1732 (1993) [c]
465. G Rickards, L Weiler *J. Org. Chem*. **43** 3607 (1978)
466. W-N Chou, D L Clark, J B White *Tetrahedron Lett*. **32** 299 (1991)
467. D Chemin, G Linstrumelle *Synthesis* 377 (1993)
468. U Mäeorg, T Välimäe *Izv. Akad. Nauk Est. SSR. Khim*. **37** 186 (1988)
469. J A Cabezas, A C Oehlschlager *Synthesis* 107 (1999)
470. W Oppolzer, C Fehr, J Warneke *Helv. Chim. Acta* **60** 48 (1977)
471. A P Khrimyan, O A Gharibyan, L Streinz, Z Wimmer, M Romanuk, S O Badanyan *Collect. Czech. Chem. Commun*. **54** 3284 (1989)
472. A P Khrimyan, G M Makaryan, A L Ovanisyan, Z Vimmer, M Romanyuk, L Shtreints, Sh O Badanyan *Khim. Prirod. Soed*. 117 (1991) [f]
473. R E Doolittle *Synthesis* 730 (1984)
474. M V Mavrov, Z G Chrelashvili, E P Serebryakov *Izv. Akad. Nauk, Ser. Khim*. 769 (1993) [b]
475. Z G Chrelashvili, M V Mavrov, A V Dolidze, A O Chizhov, E P Serebryakov *Izv. Akad. Nauk, Ser. Khim*. 1133 (1993) [b]
476. O A Garibyan, G U Palikyan, Sh O Badanyan *Zh. Org. Khim*. **36** 1462 (2000) [c]
477. H Westmijze, H Kleijn, P Vermeer *Synthesis* 430 (1979)
478. R K Haynes, W R Jackson, A Stragalinou *Austr. J. Chem*. **33** 1537 (1980)
479. T Ishii, N Kawamura, S Matsubara, K Utimoto, S Kozima, T Hitomi *J. Org. Chem*. **52** 4416 (1987)
480. P G McDougal, J G Rico, D van Derveer *J. Org. Chem*. **51** 4492 (1986)
481. M P Reddy, G S K Rao *Synthesis* 815 (1980)
482. T N Gavrishova, A V Shastin, E S Balenkova, N A Novikov *Zh. Org. Khim*. **23** 1322 (1987) [c]
483. P V Verteletskii, V G Nenaidenko, E S Balenkova *Vestn. Mosk. Univ., Ser. 2, Khim*. 540 (1996)

484. V G Nenaidenko, A V Sanin, E S Balenkova *Zh. Org. Khim.* **30** 531 (1994) [c]
485. C Fan, B Cazes *Tetrahedron Lett.* **29** 1701 (1988)
486. C Descoins, D Samain, B Lalanne-Cassou, M Gallois *Bull. Soc. Chim. Fr., Pt II* 941 (1977)
487. N M Ivanova, B A Czeskis, A M Moiseenkov, O M Nefedov *Izv. Akad. Nauk SSSR, Ser. Khim.* 2521 (1991) [b]
488. A M Moiseenkov, B A Czeskis, N M Ivanova, O M Nefedov *J. Chem. Soc., Perkin Trans. 1* 2639 (1991).
489. T Arenz, M Vostell, H Frauenrath *Synlett* 23 (1991)
490. E Piers, R D Tillyer *J. Chem. Soc., Perkin Trans. 1* 2124 (1989)
491. T Kato, M Sato, Y Kitagawa, R Sato *Chem. Pharm. Bull.* **29** 1624 (1981)
492. T R Demmin, M M Rogić *J. Org. Chem.* **45** 2737 (1980)
493. J Haslouin, F Rouessac *Bull. Soc. Chim. Fr., Pt II* 1242 (1977)
494. A S Kende, S Johnson, P Sanfilippo, J C Hodges, L N Jungheim *J. Am. Chem. Soc.* **108** 3513 (1986)

[a] — *Russ. J. Gen. Chem. (Engl. Transl.)*
[b] — *Russ. Chem. Bull. (Engl. Transl.)*
[c] — *Russ. J. Org. Chem. (Engl. Transl.)*
[d] — *Russ. J. Biorg. Chem. (Engl. Transl.)*
[e] — *Dokl. Chem. (Engl. Transl.)*
[f] — *Chem. Nat. Compd. (Engl. Transl.)*

Russian Chemical Reviews **70** (9) 777 – 790 (2001) © 2001 Russian Academy of Sciences and Turpion Ltd

DOI 10.1070/RC2001v070n09ABEH000670

Magnetic properties of complex oxides $LiMO_2$ (M = Sc – Ni) with different types of cationic ordering

D G Kellerman

Contents

I.	Introduction	777
II.	Structures of $LiMO_2$ oxides	777
III.	Magnetic properties of $LiMO_2$ oxides	781
IV.	Structure and magnetic properties of $LiM_{1-x}M'_xO_2$ solid solutions	785
V.	Conclusion	788

Abstract. The crystal structures and magnetic properties of complex oxides of the $LiMO_2$ series (M = Sc – Ni) and of solid solutions they form are described. Although the structures of the oxides are all derived from the NaCl structure, their magnetic properties are fairly diverse and depend on the type of cationic ordering. Primary attention is given to the oxides with layered structures in which the degree of ordering is a variable. The bibliography includes 225 references.

I. Introduction

During the past 15 years, compounds with the general formula of $LiMO_2$, where M is a transition 3*d* metal, have actively been explored, and the interest in them is not lost up to date. First of all, this is related to the prospects of considering many $LiMO_2$ complex oxides as promising cathodic materials for chemical power sources.[1–3] These prospects are usually determined by such properties as a high positive potential, small molecular mass and structural stability during electrochemical intercalation and deintercalation

$$LiMO_2 \rightleftharpoons Li_{1-x}MO_2 + x\,Li^+ + x\,e^-.$$

Besides this applied aspect, interesting magnetic properties of $LiMO_2$ complex oxides draw the attention of many theoreticians and researchers.[4] These oxides include antiferromagnetic, ferromagnetic, paramagnetic, diamagnetic, weak ferromagnetic materials, *etc*. The magnetic properties of $LiMO_2$ oxides are largely determined by the type of superstructures they form. The whole spectrum of structures found in $LiMO_2$ is based on the rock-salt structure, the deviations being determined by the way the cations are distributed over the positions of this basal structure. This distribution can either be random or ordered, the latter giving rise to the formation of a superstructure. In solid solutions of complex oxides, the type and the degree of ordering can change depending on the component concentrations. This is why compounds for which the degree of structural ordering (η) varies as a function of synthetic conditions, which entails profound changes in magnetic structures, are of particular interest. In this review, the studies in which the magnetic properties of $LiMO_2$ compounds and solid solutions based on them are correlated with the peculiarities of their crystal structures are analysed. Most of numerous electrochemical studies are beyond the scope of this review, these being surveyed elsewhere.[3–5]

D G Kellerman Institute of Solid State Chemistry, Urals Branch of the Russian Academy of Sciences, ul. Pervomaiskaya 91, 620219 Ekaterinburg, Russian Federation. Fax (7-343) 274 44 95. Tel. (7-343) 249 34 42. E-mail: kellerman@ihim.uran.ru

Received 26 March 2001
Uspekhi Khimii **70** (9) 874 – 889 (2001); translated by T Ya Safonova

II. Structures of $LiMO_2$ oxides

The crystal structures of $LiMO_2$ complex oxides derive from the NaCl structure and differ from one another only in the way the cations of alkali and transition metals are distributed over the planes of the basal cubic lattice. When lithium and transition-metal ions occupy severally the alternating (111) planes of the sodium chloride cubic lattice, layered structures characterised by a high diffusion mobility of alkali-metal atoms are formed. Hence, in such compounds as, *e.g.*, $LiCoO_2$ and $LiNiO_2$, deep and reversible electrochemical intercalation of lithium can occur which attracts the attention of scientists. The quest for a wide array of new compounds with the layered structures favourable for electrochemical processes stimulates the development of the methods for the preparation of metastable $LiMO_2$ modifications. For this purpose, low-temperature methods which involve precursor synthesis and ion-exchange processes, chemical and electrochemical intercalation, etc. are used. Usually, these phases lose their stabilities with an increase in temperature and transform into stable modifications.

The $LiMO_2$ compounds preferentially form three structural types. The first structure represents a disordered cubic lattice of α-$LiFeO_2$ (NaCl), the second structure of the α-$NaFeO_2$ type represents a trigonal superlattice on the basis of the NaCl structure and the third compound represents a spinel in which transition-metal and lithium atoms occupy, correspondingly, the 16*a* and 16*b* positions. The effects of the size and the charge of a transition-metal ion on the formation of a particular lattice type have been discussed.[6] As was shown by calculation, if the ionic radii of alkali and transition metals are close, the random distribution of ions over the positions corresponds to the state with the minimum energy, *viz*., the cubic lattice of α-$LiFeO_2$. With an increase in the differences in the ionic sizes, the probability of formation of the α-$NaFeO_2$-type layered structure also increases, which is favoured by lower charges of transition-metal ions. The low stability of spinel phases (*e.g.*, the low-temperature $LiCoO_2$ phase), which exist only in very narrow temperature and pressure intervals is explained by the fact that their origination is governed by kinetic factors rather than by thermodynamic ones.

$LiScO_2$ represents a nonconducting white powder under ordinary conditions. A review of the structural data one can see in Ref. 4. $LiScO_2$ was first described in 1959 (Ref. 7). X-Ray diffraction studies carried out for both single crystals[8] and powders[9] and Mössbauer studies of Fe^{3+} impurity centres in $LiScO_2$ (see Refs 10, 11) have shown that the perfect ordering of Sc^{3+} and Li^+ cations in the basal NaCl structure produces a superlattice with $I4_1/amd$ symmetry ($a = 4.18$, $c = 9.30$ Å), which is similar to the superlattice of totally ordered γ-$LiFeO_2$ phase. This structure is characterised by the atoms of transition and alkali metals regularly occupying the alternate positions along the tetragonal c axis.

Yet another approach to the description of the $LiScO_2$ structure is known.[12] According to experimental results,[12] the oxygen octahedra which enclose lithium ions are shown to be distorted in a such way as if lithium represented a Jahn–Teller ion (four short and two long Li–O distances). The concept of distorted anatase seems to describe the $LiScO_2$ structure more precisely than the model of a tetragonally ordered NaCl modification.

$LiTiO_2$ has a completely disordered cubic structure of the NaCl type ($a = 4.140$ Å).[13, 14] Extensive information on $LiTiO_2$ is cited in Ref. 4. Low-temperature chemical lithiation of $LiTi_2O_4$ spinel gave rise to a modification of $LiTiO_2$.[15] X-Ray diffraction patterns of this phase virtually did not differ from those of the parent spinel. Using the neutron diffraction technique, it was shown[16] that the formation of $LiTiO_2$ ($Li_2Ti_2O_4$) ($a = 8.3756$ Å) is accompanied by transposition of lithium from tetrahedral sites to octahedral ones unoccupied in the parent spinel. Thus, the titanium and lithium ions in the metastable phase are distributed over the positions 16c and 16d, respectively, of the $Fd3m$ space group, and a superstructure of the atacamite type is formed.[17] Heating above 920 K results in irreversible transition of the $Li_2Ti_2O_4$ spinel into a stable disordered cubic phase of $LiTiO_2$.[15] This transition appears to occur in several steps, because DSC (differential scanning calorimetry) revealed three endothermic effects (in total, 950 cal mol^{-1} were liberated).[18]

$LiVO_2$ represents a black powder. It was described for the first time in 1954 (Ref. 19). This compound is isostructural to the hexagonal α-$NaFeO_2$. Generally, such a structure is typical of this class of compounds (Fig. 1). It is formed by the ions of alkali and transition metals ordered in parallel (111) planes of the NaCl cubic lattice. In the ordered structure, all vanadium ions have six-fold oxygen coordination, the V–O distances are equal to 1.987 Å. At 450 K, a phase transition occurs in $LiVO_2$,[13, 20–22] which is accompanied by pronounced changes in the unit cell volume and interatomic distances [$a = 2.837$, $c = 14.775$, V–O = 1.98, V–V = 2.84 Å at 300 K; $a = 2.913$, $c = 14.640$, V–O = 2.02, V–V = 2.91 Å at 550 K for $Li_{0.7}VO_2$ (see Ref. 23)], although the main structural motif remains unchanged. A substantial temperature hysteresis was observed. During the transition, the enthalpy changed by 50–1000 cal mol^{-1} (see Ref. 22). It was assumed[24] that at room temperature vanadium ions are combined in V_3 trimers which disintegrate during the phase transition. The formation of trimers was confirmed experimentally. Thus, the structure of $Li_{0.8}VO_2$ single crystals prepared by the flux method (see Ref. 26) was analysed in detail using X-ray diffraction and EXAFS techniques.[25] It was shown that vanadium ions are shifted by 0.160 Å from the positions they should occupy in the perfect hexagonal structure. Probably, the symmetry of the low-temperature phase differs from the $R\bar{3}m$ symmetry as followed from the presence of very weak additional reflexes in the X-ray patterns of this phase ($a' = a\sqrt{3}$, $c' = c$).[23]

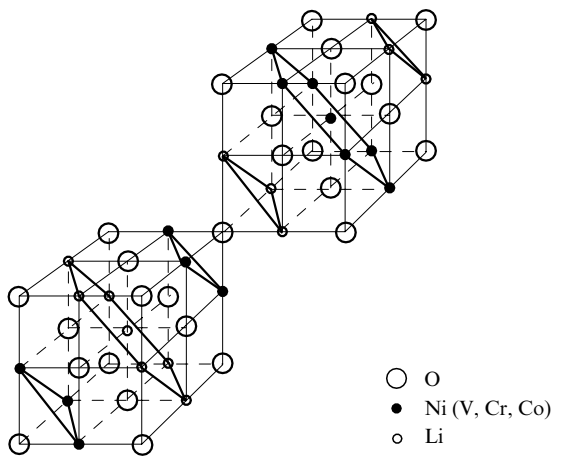

Figure 1. Schematic representation of the formation of layered structures for $LiVO_2$, $LiCrO_2$, $LiCoO_2$ and $LiNiO_2$ as a result of cationic ordering in the NaCl-type cubic lattice.

It was shown that stoichiometric $LiVO_2$ can be transformed into $Li_{1-x}VO_2$ phases by both chemical and electrochemical deintercalation.[27, 28] Studies on the structure of deintercalated vanadates showed that the removal of lithium from the layered structure for $x \geqslant 0.3$ results in redistribution of vanadium ions. For example, in $Li_{0.22}VO_2$, approximately one third of vanadium ions occupy the octahedral positions in Li layers, which favours stabilisation of the cubic structure. With increasing temperature, the $Li_{1-x}VO_2$ phase becomes unstable, and its disproportionation can proceed by two routes[29]

$$Li_{1-x}VO_2 \longrightarrow (1-2x)\,LiVO_2 + x\,LiV_2O_4,$$

$$Li_{1-x}VO_2 \longrightarrow (1-8x)\,LiVO_2 + 8x\,Li_{0.875}VO_2.$$

The coexistence of hexagonal and cubic phases was established.[30]

At high pressures, another polymorphous modification of $LiVO_2$ with a superlattice of the atacamite type was obtained.[31] Heating above 700 K resulted in irreversible transition of this phase into a stable hexagonal form.

$LiCrO_2$ prepared by ceramic technology represents a green powder with a layered trigonal structure of α-$NaFeO_2$ ($a = 2.88$, $c = 14.6$ Å). Like $LiVO_2$, the $LiCrO_2$ oxide was first prepared and described in 1954 (Ref. 19). Single crystals of $LiCrO_2$ were grown by the flux method.[32] In contrast to most $LiMO_2$ compounds, deintercalation of lithium from $LiCrO_2$ is hindered; however, under hydrothermal conditions, the ion-exchange reaction is possible, which results in the formation of an isostructural phase of $HCrO_2$.[33]

$LiMnO_2$ in the form of a brown powder (orthorhombic unit cell) was first synthesised with the aim of studying the $Li_xMn_{1-x}O$ system.[34] The crystal structure of $LiMnO_2$ was studied in more detail for polycrystalline material[35] and single crystals[36], the latter being obtained by the hydrothermal method.[37] A number of structural peculiarities of orthorhombic $LiMnO_2$ compared with other $LiMO_2$ complex oxides[38] are apparently caused by the Jahn–Teller effect.

The orthorhombic lattice of $LiMnO_2$ ($a = 2.805$, $b = 5.757$, $c = 4.527$ Å), $Pmmn$ (see Ref. 36) also represents one of the versions of the NaCl basal structure ordering (Fig. 2). The MnO_6 octahedra are substantially distorted due to the Jahn–Teller effect. Two long distances along the b axis (2.291 Å) and two pairs of almost identical equatorial distances, *viz.*, 1.920 and 1.937 Å, were observed. In each (001) plane, cations of one type are arranged in chains along either ⟨100⟩ (orthorhombic) or ⟨110⟩ (cubic) directions. In alternate (001) planes, the chains retain their orientation with respect to the upper and lower planes, but are shifted forming the ABA packing along the c axis. Compared to the hypothetical cubic lattice with a parameter a', the parameters of the real lattice are as follows: $a = (1/2)\sqrt{2}a'$, $b = \sqrt{2}a'$ and $c = a'$.

Considerable anisotropy of the thermal expansion coefficient was observed[39] at temperatures < 300 K. The thermal expansion coefficient did not exceed 10^{-7} K^{-1} in the directions a and b and was 3.7×10^{-6} K^{-1} in the direction c.

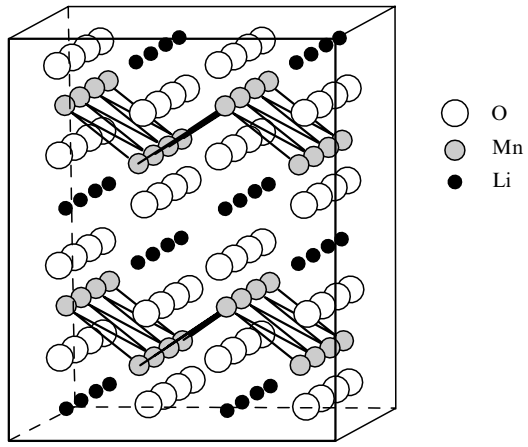

Figure 2. Crystal structure of $LiMnO_2$.

Studies on the morphological peculiarities of orthorhombic $LiMnO_2$ synthesised by a conventional ceramic procedure (sintering of an Mn_2O_3 + LiOH mixture at 1073 K in an inert atmosphere) revealed the presence of certain cationic disordering, namely, the existence of defects of the Li_{Mn} and Mn_{Li} types.[40] The degree of disordering (3% – 12%) was attributed to the preset excess or deficiency of LiOH. Scanning electron microscopy showed that the sizes and shapes of grains also depended on the LiOH content in the reaction mixture. The deficiency of lithium favoured the formation of fine and size-uniform grains, whereas excess of lithium resulted in a wide scatter of the grains both in sizes and shapes. It was the former modification that demonstrated good characteristics in the electrochemical process.[41] The stacking faults in orthorhombic $LiMnO_2$ with a small ($d \approx 0.3$ μm) grain size were studied in detail.[42] It was concluded that these represent monoclinic interstitial layers between the orthorhombic blocks. The portion of such defects was 1% – 6%, which correlated well with the degree of cationic disordering.

The existence of a low-temperature modification of $LiMnO_2$ with a tetragonal structure, which was obtained by chemical lithiation of $LiMn_2O_4$ spinel: $a = 5.662$, $c = 9.274$ Å, $I4_1/amd$, $Z = 8$, was reported.[43,44] Above 500 °C, the tetragonal phase transformed into the stable orthorhombic phase.

Recently, yet another metastable low-temperature modification of $LiMnO_2$ has attracted great interest. This phase was first synthesised in 1996 (Ref. 45). The phase has a monoclinic lattice ($C2/m$, $a = 5.4387$, $b = 2.8086$, $c = 5.3878$ Å, β = 116 °). For its synthesis, the ion-exchange method was applied in which layered α-$NaMnO_2$ was used as the precursor. The product also exhibited a layered structure. In addition, it was noted[46,47] that the ion-exchange reaction can also proceed in a mixture of γ-MnOOH and $LiOH \cdot H_2O$. The lower symmetry of the layered $LiMnO_2$ modification compared, for instance, with layered $LiCoO_2$ was associated with the strong Jahn–Teller effect for Mn^{3+} ions (see Ref. 45). As was shown by the results of X-ray diffraction analysis and neutron diffraction,[45,48,49] the Li-layers of the layered $LiMnO_2$ modification contain 3% – 9% of manganese ions. An electron-diffraction study in a convergent beam[50] have shown that a typical specimen synthesised by the ion-exchange method contains, in addition to layered $LiMnO_2$, an admixture of a tetragonal spinel phase of $Li_2[Mn_2]O_4$ and traces of orthorhombic $LiMnO_2$. The following atomic planes and directions were also shown[50] to be equivalent for the spinel and layered phases:

$$(200)_{lay} \equiv (222)_{sp}$$

$$(020)_{lay} \equiv (4\text{-}40)_{sp}$$

$$[001]_{lay} \equiv [11\text{-}2]_{sp}$$

A comparative analysis of the stability of orthorhombic and monoclinic layered structures of $LiMnO_2$ was carried out.[51] The calculations have shown that the antiferromagnetic exchange coupling of Mn^{3+} ions plays a substantial role in stabilisation of the orthorhombic structure; and, therefore, stabilisation of the layered structure requires that manganese was partly replaced by elements that weaken this interaction. The elements Al, Co, Cr, V, Ti, Mo, Mg, Nb, Zn and Pd can serve as the dopants.

In the Li–Mn–O system, yet another monoclinic phase designated as m-Li_xMnO_2 ($x = 0.2 – 0.3$) was detected and identified.[52] It can be obtained by durable sintering of intimately mixed β-MnO_2 and LiOH at 420 K. According to the results of X-ray diffraction analysis, the new phase has a primitive monoclinic unit cell ($a = 9.38$, $b = 5.65$, $c = 4.906$ Å, β = 102.2 °) and is stable up to 820 K.

In a thermobaric treatment ($P = 6.5$ GPa, $T = 100$ K) of orthorhombic $LiMnO_2$, a totally disordered phase with the rock-salt structure ($a = 4.1658$ Å) was obtained. According to crystallographic data, no structural distortions caused by the Jahn–Teller effect were observed.[4]

$LiFeO_2$ exists in several polymorphous modifications (Fig. 3). A disordered structure of cubic α-$LiFeO_2$ is identical to that of NaCl ($a = 4.158$ Å).[53] The structure of $LiFeO_2$ represents a rare example of structures in which two different cations occupy the same positions.[54,55] The results of electron-microscopic studies have shown[56,57] that the α-$LiFeO_2$ cubic structure involves the elements of the short-range order. For γ-$LiFeO_2$, an ordered tetragonal structure similar to that of $LiScO_2$ is typical ($a = 4.057$, $c = 8.759$ Å).[58] Apparently, the metastable β-$LiFeO_2$ modification is intermediate between α- and γ-phases. Discrepant opinions were advanced on the β-$LiFeO_2$ structure: some authors (see, *e.g.*, Ref. 53) claim the existence of a body-centred tetragonal unit cell, while others believe it to be monoclinic.[59,60] The monoclinic structure of the β-phase was confirmed by electron microscopy[56] ($C2/c$, $a = 8.571$, $b = 11.59$, $c = 5.147$ Å, β = 145.70 °, $Z = 8$). The tetragonal structure exhibits no ordering in the distribution of cations over the positions. In contrast, the monoclinic phase is ordered.

Detailed studies[53,61] have detected the transition of α-$LiFeO_2$ first to β-$LiFeO_2$ at $T > 570$ K and further to the ordered γ-$LiFeO_2$ phase at $T > 870$ K. The latter phase transforms back into the disordered α-modification with further increase in temperature (> 920 K). The transitions proceeded slowly and depended on the sample's prehistory.

Currently, many efforts are concentrated on the synthesis of metastable modifications of $LiFeO_2$ with layered structures. For

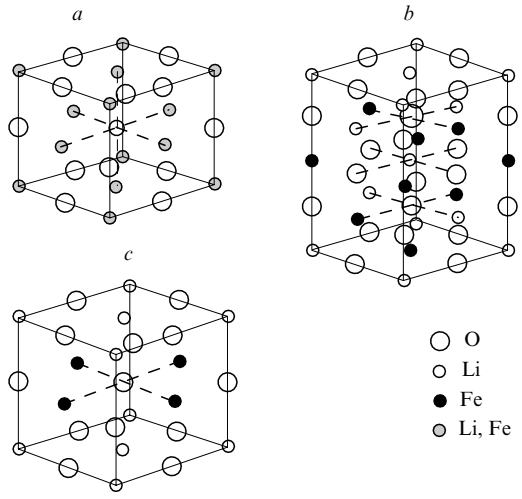

Figure 3. Structural modifications of $LiFeO_2$; (*a*) is the cubic α-phase, (*b*) is the tetragonal β-phase and (*c*) is the tetragonal γ-phase (1/2 of the unit cell is shown).

example, the preparation of $LiFeO_2$, the corrugated layered structure of which is similar to that of a stable orthorhombic modification of $LiMnO_2$, was described.[62] The synthesis involved the ion exchange reaction between γ-FeOOH and $LiOH \cdot H_2O$. The reaction was carried out under hydrothermal conditions at 370 – 520 K. The structure of the phase obtained was noted to resemble very closely that of the original γ-FeOOH. The transition from γ-FeOOH to $LiFeO_2$ presumes a shift of corrugated layers by 1/2 along the *b* direction. According to the X-ray diffraction studies, the lattice parameters of $LiFeO_2$ are $a = 4.0610(5)$, $b = 2.9621(5)$ and $c = 6.0319(11)$ Å. Yet another orthorhombic structure of the goethite type with the parameters $a = 9.677(5)$, $b = 2.934$ and $c = 5.005$ Å, *Pmna* was also synthesised by using an ion-exchange reaction (carried out in an ethanolic solution, in contrast to the previous reaction).[63] It is interesting that at certain Li to Fe ratios, a totally disordered cubic modification of α-$LiFeO_2$ ($a = 4.161$ Å, *Fm3m*) can be obtained by this method,[64] its conventional synthesis requires high temperatures.

The ion-exchange reaction of $NaFeO_2$ in a lithium chloride melt resulted in $LiFeO_2$ with a layered trigonal structure of α-$NaFeO_2$, which is typical of this class of compounds.[65] The degree of cationic ordering was found to depend on the ordering of the precursor phase.

In addition to metastable forms of $LiFeO_2$ discussed above, yet another low-temperature modification, *viz*., a phase with a tunnel structure was documented.[66] However, this has not been described in detail in further publications.

$LiCoO_2$ is usually obtained at 1200 – 1300 K as a black powder from cobalt oxide and lithium carbonate. This phase is referred to as a high-temperature (HT) one. It is thermally stable up to 1120 K.[67] According to results of neutron diffraction studies,[68] HT-$LiCoO_2$ has a perfectly ordered structure of the α-$NaFeO_2$ type ($R\bar{3}m$) with the cell parameters $a = 2.8166$ and $c = 14.052$ Å.[69] The $LiCoO_2$ structure was studied for single crystals obtained by the flux method.[70] The layered structure of HT-$LiCoO_2$ is very stable and, as was shown by calculations,[71] the order – disorder transition can occur only at ~5100 K. This is substantially higher than the melting point, which makes such a transition practically unfeasible. On the other hand, according to calculations,[72] the use of high pressures can stimulate the transition with the formation of a cubic phase.

Synthesis at temperatures below 700 K produces a low-temperature (LT) phase with a structure somewhat different from that of HT-$LiCoO_2$.[73 – 81] According to the results of neutron diffraction analysis,[75] nearly 6% of lithium sites in LT-$LiCoO_2$ are occupied by cobalt. The phase formed upon deintercalation of lithium from LT-$LiCoO_2$ (Li_xCoO_2; $1 \geqslant x \geqslant 0.5$) can be described[77] either as a spinel modification ($Fd\bar{3}m$) in which up to 80% of lithium atoms occupy tetrahedral positions[74] or a phase with the trigonal layered structure ($R\bar{3}m$). NMR studies[82] are in favour of the second version, because the substantial structural disordering observed by this method corresponds to the second co-ordination sphere of lithium. Hence, the nearest neighbouring of lithium remains octahedral so that LT-$LiCoO_2$ may be considered as a partly disordered trigonal structure based on NaCl. A different opinion on this problem has been advanced.[83] Based on the combined use of transmission electron microscopy and X-ray diffraction analysis, it was concluded that the structure of LT-$LiCoO_2$ may be considered as an intermediate between the structures of perfect spinel and the layered modification.

A number of studies dealt with the phase transitions that occur both in HT-[84 – 86] and LT-$LiCoO_2$ [75 – 77] during electrochemical deintercalation of these compounds. The stabilities of the phases obtained were calculated,[87, 88] and the phase diagram of Li_xCoO_2 was constructed.

The completely deintercalated layered phase of CoO_2 ($a = 2.822$, $c = 14.29$ Å) was first isolated and described in 1997 (Ref. 89). Unexpectedly, it was found that despite the structural disordering processes that occur during electrochemical deintercalation the product exhibited a very high degree of structural ordering. Several metastable polymorphous modifications were formed upon electrochemical deintercalation of Li_xCoO_2 [90] synthesised from $Na_{0.7}CoO_2$ by ion-exchange.[91] Depending on the depth of the deintercalation process, the mode of CoO_6 octahedra packing changed.

In studies of phase transitions that occur during the chemical extraction of lithium from $LiCoO_2$ with the formation of $Li_{0.5}CoO_2$ it was found [92] that a common hexagonal structure is retained only up to the $Li_{0.92}CoO_2$ composition. For deeper extraction of lithium, a second, also hexagonal phase appears, which becomes the only phase present starting from the $Li_{0.79}CoO_2$ composition. The hexagonal structures differ in the *c*/*a* ratio, which is substantially higher for the second phase.

$LiNiO_2$ with a structure similar to that of α-$NaFeO_2$ ($a = 2.878$, $c = 14.19$ Å) was described for the first time in 1953 (Ref. 93). This oxide is isostructural to $LiCoO_2$ and $LiVO_2$. The distribution of atoms over the positions is as follows: Ni(3*a*) (0, 0, 0); Li(3*b*) (0, 0, 1/2); O(6*c*) (0, 0, 1/4) (0, 0, −1/4). The ratio $c/a = 4.93$ indicates the presence of an almost perfect face-centred cubic sublattice of oxygen, for which $c/a = 2\sqrt{6} = 4.90$. An EXAFS study of the Jahn – Teller co-operative effect has shown that two long (2.09 Å) and four short (1.91 Å N – O distances are present as a result of local distortion in NiO_6 octahedra.[94 – 95]

The layered $LiNiO_2$ oxide is traditionally considered as an end member of the series of $Li_xNi_{1-x}O$ solid solutions. The cationic ordering that takes place with increasing concentration of lithium in Li_xNiO_2 is well known and was discussed in a number of publications.[96] The disordered phase ($x < 0.56$) is isostructural to NiO (NaCl type), and the formation of a layered structure involves the ordering of ions of transition and alkali metals in alternate (111) planes of the NaCl-type cubic lattice, which is accompanied by lowering of the symmetry to trigonal. Due to the close radii of Ni^{3+} and Li^+ ions, the degree of ordering of cations over the positions in the alternate planes (η) can vary widely even for an invariant transition-to-alkali metal ratio. For example, the synthesis and properties of virtually stoichiometric $LiNiO_2$ with $0 \leqslant \eta \leqslant 1$ were described.[97, 98] The structural order $\eta = 0$ corresponds to cubic $LiNiO_2$ prepared by quenching of $LiNiO_2$ with $\eta = 1$ from a temperature of 1200 K.[97] The quenched phase is metastable; hence, the ordering process can occur at temperatures above 600 K.

The temperature of the order → disorder transition (layered → cubic structure) is 1020 K.[99] The transition proceeds slowly and is not completely reversible.

The difficulties of synthesising the stoichiometric $LiNiO_2$ were associated with the loss of lithium during sintering.[100 – 102] In this case, the parameter of cubic or trigonal cell depended linearly on the value of *x* in $Li_xNi_{1-x}O$.[96] Different versions of the synthesis, which allow one to minimise lithium losses, were described.[103]

It is of note that even upon annealing for a long time at sufficiently high temperatures (1100 K) $Li_xNi_{1-x}O$ is characterised by a heterogeneous bulk composition.[104] The procedure of refining of structural data turned out to be more efficient being carried out within the framework of a multiphase system rather than a 'single-phase' one.

The cationic distribution in nonstoichiometric $Li_{1-x}Ni_{1+x}O_2$ solutions was studied by X-ray diffraction analysis.[105] It was confirmed that, with an increase in *x*, the degrees of occupation of 3*a* and 3*b* positions by lithium (nickel) ions approach one another, which results in their random distribution for $x \geqslant 0.4$.

Two models of cationic distribution in $Li_{1-x}Ni_{1+x}O_2$ exist. According to the first model, superstoichiometric nickel occupies free sites in lithium layers, and the oxide can be described by the formula $[Li_{1-x}Ni_x][Ni]O_2$.[106] The second model assumes partial mixing of cations in both sites; in this case, the oxide has the following formula: $[Li_{1-x-\delta}Ni_{x+\delta}][Ni_{1-\delta}Li_\delta]O_2$.[105, 106] If the oxide composition approaches stoichiometric, then the first model is assumed[107] to be more probable.

It should be noted that the nickel that occupies 3*a* positions in the nickel sublattice of $Li_{1-x}Ni_{1+x}O_2$ corresponds predominantly to the Ni^{3+} state, whereas the lithium sublattice (2*a* positions) mainly involves bivalent nickel ions.[108]

It was shown[106] that the concentration-induced order–disorder transition in $Li_{1-x}Ni_{1+x}O_2$ is well simulated by using the 'lattice gas' concept. The dependences of the ordering parameter on the lithium content were obtained, and $\eta_{max} = 0.96$ was found even for the stoichiometric composition. Moreover, it was shown that even the region of the existence of cubic structures ($x \geqslant 0.4$) is characterised by the effects of the short-range structural order, which were studied in detail by synchrotron X-ray emission.[109] Based on the results obtained, the sizes of short-range order domains were assessed.

A small magnitude of the X-ray scattering factor for lithium makes it impossible to determine the degree of cationic disordering in $Li_{1-x}Ni_{1+x}O_2$ near the stoichiometric composition. For this purpose, other methods, such as ESR[110] or X-ray absorption spectroscopy[111] were used. Thus it was found[111] that two different Ni–O distances (2.07 and 1.94 Å) whose ratio varies with *x* are present.

Three successive first-order transitions which occur during electrochemical extraction of lithium[112,113] (at high potentials, completely deintercalated 'NiO_2' phases can also be obtained[114]) cause the following changes in the $LiNiO_2$ structure: hexagonal → monoclinic → hexagonal′ → hexagonal″. The relationships between the unit cell parameters of monoclinic (*C*2*m*, similar to that observed for $NaNiO_2$) and hexagonal phases are as follows:

$$a_m = \sqrt{3}a_h,$$

$$b_m = a_h,$$

$$c_m = \frac{c_h}{3\sin\beta},$$

$$\beta = 180 - \operatorname{arctg}\frac{c_h}{\sqrt{3}a_h}.$$

It is also important that the monoclinic phase is only formed upon deintercalation of virtually stoichiometric $Li_{1-x}NiO_2$, whereas intercalation of $Li_{1-x}NiO_2$ with $x \geqslant 0.05$ does not affect the symmetry.[115] Stoichiometry of the initial compound also affects the process of chemical deintercalation: with a decrease in the lithium content, extraction of lithium and admixed nickel from lithium layers is supplemented by ion exchange which involves protons.[116]

The presence of nickel in the lithium layers plays a significant role in the stabilisation of the monoclinic phase.[117] Using EXAFS methods, it was shown[118] that the local distortion of NiO_6 octahedra in the monoclinic deintercalated phase of Li_xNiO_2 ($0.5 < x < 0.75$) is substantially weaker compared with the stoichiometric trigonal phase. This was attributed to the electron exchange between Ni^{3+} and Ni^{4+} sites. Also, the results of electron-microscopic studies have shown the monoclinic phase to involve a superstructure formed by partially ordered lithium ions (vacancies in the lithium layers).[119] The deintercalated Li_xNiO_2 phase is thermally unstable, and the layered hexagonal structure gives way to the cubic spinel structure at 453 K, which is accompanied by oxygen loss.[120]

Efforts were undertaken to obtain the $Li_{1+x}NiO_2$ oxide superstoichiometric with respect to lithium.[121,122] For instance, a phase with $x \geqslant 0.3$ having a monoclinic structure was described.[122,123] The latter was formed by closely packed oxygen layers (slightly distorted) which separated purely lithium layers from those filled by 1/3 with lithium ions and by 2/3 with nickel ions.

III. Magnetic properties of $LiMO_2$ oxides

Structural differences in the series of $LiMO_2$ oxides, where M is a transition 3*d* metal, are not significant: the crystal structures differ only in the mode in which the cations of alkali and transition metals are ordered in the planes of the parent cubic lattice. Nonetheless, these compounds exhibit fairly diverse magnetic properties.

$LiVO_2$. Magnetic effects which suggest phase transitions in $LiVO_2$ were first described by Bongers.[13] Heating above 450 K results in a fourfold increase in the magnetic susceptibility (Fig. 4); at higher temperatures, the latter is practically independent of the temperature. To explain the magnetic properties of $LiMO_2$ in the region below the transition temperature, a mechanism of formation of molecular orbitals in the basal plane of the hexagonal $LiVO_2$ structure was proposed.[125] The trigonal V_3 clusters thus obtained are nonmagnetic due to Heisenberg antiferromagnetic exchange coupling, and the phase transition is associated with their decomposition.

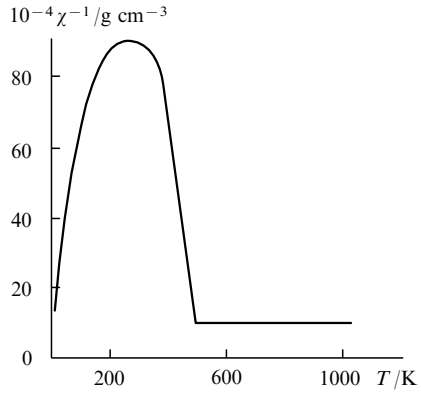

Figure 4. Temperature dependence of the reciprocal magnetic susceptibility of $LiVO_2$.[124]

Another model proposed[4,126] does not imply any changes in the symmetry. This interprets the low-temperature magnetic data in terms of the existence of a two-dimensional 'metal' cluster built by vanadium ions bound by metal–metal bonds. In the high-temperature region, *d* electrons are delocalisated, and $LiVO_2$ becomes a narrow-zone metal. This fact was evidenced by IR spectra, results on electrical conductivity[4] and the data from X-ray absorption spectroscopy.[127] Phase transitions which, as in the above model, were attributed to the changes in the critical M–M distance are typical of many transition-metal simple oxides: V_2O_3, VO_2, V_4O_7, Ti_3O_5, Ti_4O_7.[128–131] The role the structural changes in $LiVO_2$ play in the first-order phase transition from nonmagnetic to magnetic phase was discussed in detail.[132] It has been found that due to the changes in the magnetic energy the high-temperature phase is more stable.

$LiCrO_2$. The studies on the magnetic properties of $LiCrO_2$ as well as of many other oxides were pioneered by Bongers.[13] Magnetic susceptibility data indicated antiferromagnetic ordering to exist below 300 K and the Curie–Weiss paramagnetism with $\Theta = -577$ K and $\mu_{ef} = 3.71\ \mu_B$ to be present above 300 K. These characteristics were refined later: the Néel temperature (T_N) was found to be 56 K[133]; the value of μ_{ef} obtained by ESR technique[134] was 3.8258 μ_B (the deviation from an intrinsic spin value by 0.0529 μ_B was attributed to spin-orbit coupling).

Many studies have been made of the magnetic structure of $LiCrO_2$.[135–137] The structure was assumed[135] to be two-dimensional with an exchange-coupling constant inside the layer of $J = -39 \pm 1$ K. Based on the results of neutron scattering on $LiCrO_2$ single crystals, a magnetic structure with a single propagation vector $\mathbf{k} = [1/3, -2/3, 3/3]$ has been proposed.[137]

The relative orientation of the spins of neighbouring Cr^{3+} ions in the magnetic planes of $LiCrO_2$ was explained by the competition of direct antiferromagnetic interactions and indirect ferromagnetic double exchange coupling.

In many studies (see, *e.g.*, Refs 138, 139), the structure of $LiCrO_2$ was considered as a Heisenberg trigonal lattice. Such compounds attract attention due to the fact that ferromagnetic compounds can involve different magnetic orders compared with the classical Néel order. A joint analysis of the data on susceptibility, neutron scattering and magnetisation have led to the following conclusions:[140] first, during the magnetic phase transition, a 120-degree magnetic structure which involves Cr^{3+} ions is formed in each layer; in the process, the magnetic ordering both in the layers and along the *c* axis occurs at the same Néel temperature; second, the magnetic structure is characterised by two wave vectors $\mathbf{k} = [1/3, 1/3, 0]$ and $[-2/3, 1/3, 1/2]$.

Figure 5 shows the temperature dependence of the magnetic susceptibility of $LiCrO_2$.

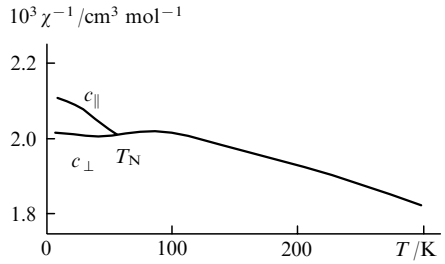

Figure 5. Temperature dependence of the magnetic susceptibility of $LiCrO_2$.[140]

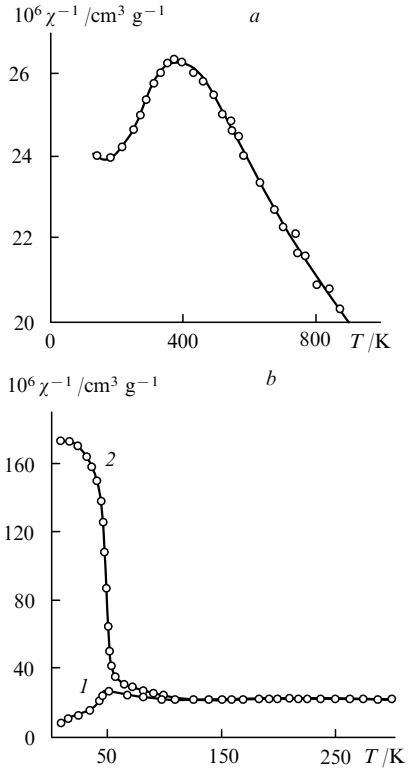

Figure 6. Temperature dependence of the magnetic susceptibility of $LiMnO_2$ in the regions (*a*) 100 – 1000 K and (*b*) 4 – 300 K.[141, 142] (*1*) Cooling in a zero field; (*2*) cooling in a 100-Œ field.

$LiMnO_2$. The first information on the magnetic properties of orthorhombic $LiMnO_2$ can be found in Ref. 13, in which the antiferromagnetic transition at 300 K was deduced. This fact was confirmed by more detailed studies.[39, 141] The magnetic susceptibility variation is characterized by the following features: the paramagnetic behaviour follows the Curie – Weiss law at temperatures above 600 K ($\Theta = -1056$ K, $\mu_{ef} = 4.82\ \mu_B$ per Mn^{3+} ion); the magnetic susceptibility passes a broad maximum at 400 K and its polytherms diverge below 100 K, being measured upon cooling both in the zero field and in the 100-Œ applied field (Fig. 6). Based on the results on neutron scattering, the magnetic structure of $LiMnO_2$ was supposed to have a propagation vector $\mathbf{k} = [1/2, 1/2, 1/2]$ and a magnetic moment equal to 3.69 μ_B per Mn^{3+} ion and preferentially oriented along the *b* axis. The Néel temperature, which characterises a phase with three-dimensional magnetic order, is 261.5 K;[141] above this value, the effects of short-range 2D order are observed.

Yet another magnetic effect observed in $LiMnO_2$ at 50 K was probably the result of weak ferromagnetism.[139, 141] Its magnitude and the temperature of its manifestation depended on the stoichiometry. It was shown [142] that even a small number of structural defects can radically change the magnetic characteristics of $LiMnO_2$ in this region. The magnetic susceptibilities of $Li_{0.99}MnO_2$, $Li_{1.01}MnO_2$ and $LiMnO_{1.99}$ compositions were measured. Presumably, the manganese ions present in lithium sites which serve as the bridges between the double layers of manganese are the most probable reason for the formation of the three-dimensional magnetic structure.[142] This is why $Li_{0.99}MnO_2$ was assumed to be more prone to three-dimensional ordering than $LiMnO_2$. At the same time, the presence of excess lithium in $Li_{1.01}MnO_2$ should apparently hinder the formation of defects of the Mn_{Li} type and, hence, the formation of the three-demensional magnetic structure. The results obtained for defective samples confirmed this assumption: indeed, the appearance of Mn_{Li} defects favoured the formation of the three-dimensional magnetic structure. An analysis of magnetisation curves have shown the spontaneous magnetisation to increase in the sequence $Li_{1.01}MnO_2$, $Li_{0.99}MnO_2$, $LiMnO_{1.99}$ and to be equal to 0.282, 0.333 and 0.421 G cm^3 g^{-1}, respectively. The coercive force increases in the same sequence: 1100, 2651 and 5974 Œ. The fact that the temperature of magnetic ordering is higher for lithium-deficient and oxygen-deficient compositions compared with stoichiometric $LiMnO_2$ also confirms the hypothesis put forward.

A cubic modification of $LiMnO_2$ obtained at high pressure exhibits antiferromagnetic properties with $T_N = 40$ K, $\Theta = -200$ K and $\mu = 4.90\ \mu_B$.[4]

$LiFeO_2$. At low temperatures, all three modifications of $LiFeO_2$ (α, β and γ) are antiferromagnetically ordered (Fig. 7); the Néel temperature is 42 K for α- and β-$LiFeO_2$ and 295 K for γ-$LiFeO_2$. For all three modifications, the temperature dependences of the magnetic susceptibility were shown to deviate in the paramagnetic region from the Curie – Weiss law, which was

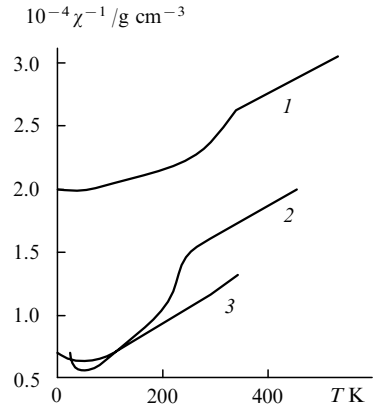

Figure 7. Temperature dependence of the reciprocal magnetic susceptibility of $LiFeO_2$.[57] (*1*) γ- $LiFeO_2$; (*2*) α-$LiFeO_2$: (*3*) β-$LiFeO_2$.

associated with the fact that distributions of iron and lithium ions involve elements of the short-range order. The magnetic structures of α- and γ-$LiFeO_2$ were found [143] in studies on the Mössbauer effect and from the results of neutron scattering. The latter structure is characterised by tetragonal magnetic symmetry with strong antiferromagnetic superexchange coupling of Fe^{3+} ions in (001) planes and much stronger interplane interaction. Magnetic moments of ions are directed along the [001] axis. The magnetic structure of the α-$LiFeO_2$ cubic phase is characterised by ferromagnetically ordered spins inside parallel (111) planes, the latter being antiferromagnetically bound with one another. For this structure to appear, it is necessary that lithium and iron ions are substantially separated in alternate (111) planes. Such a trend was demonstrated by the studies on the Mössbauer effect.

Magnetic properties of a metastable layered modification of $LiFeO_2$ prepared by the hydrothermal method were described.[144, 145] The antiferromagnetic ordering was shown to exist below 20 K. No effects associated with the transition into the spin-glass state typical of the isostructural $LiNiO_2$ phase were observed. It was shown that variations in the degree of cationic ordering affect the Néel temperature.

$LiCoO_2$. Trivalent cobalt in $LiCoO_2$ is in the low-spin state [146] $(t_{2g}^{\alpha})^3 (t_{2g}^{\beta})^3 (e_g)^0$, hence, its magnetic moment is equal to zero. This is why the magnetic susceptibility of $LiCoO_2$ should not depend on the temperature. However, this statement is only true for stoichiometric specimens.[147] The defects present in $LiCoO_{2-x}$ and the attendant paramagnetic centres which are apparently represented by Co^{2+} ions increase the magnetic susceptibility and make it temperature-dependent. This was confirmed by the results of thermogravimetry. The paramagnetic component was also described for $LiCoO_2$ superstoichiometric with respect to lithium.[82]

Above 750 K, the polytherms of magnetic susceptibility of both stoichiometric and defective $LiCoO_2$ were found to ascend reversibly [13, 147] (Fig. 8). Such an increase with the temperature indicated the appearance of paramagnetic centres. The following assumptions on the nature of these centres were drawn.

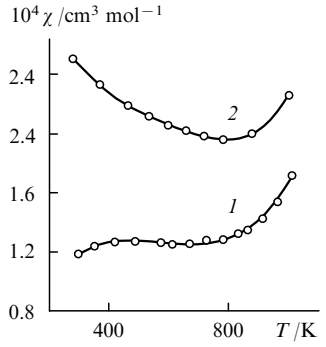

Figure 8. Temperature dependences of the magnetic susceptibility of $LiCoO_2$.[147] (*1*) Synthesis and measurements in an oxygen atmosphere; (*2*) synthesis and measurements under reduced pressure.

1. At temperatures above 750 K, thermally activated centres appear in $LiCoO_2$ as a result of oxygen exchange with the gas phase. The following process of defect formation is possible, which results in the formation of paramagnetic centres Co^{2+} (Co'_{Co}):

$$2Co_{Co} + O_O \longrightarrow (1/2)\,O_2(g) + V_O^{\cdot\cdot} + 2Co'_{Co}\,.$$

The appearance of each oxygen vacancy leads to the formation of two paramagnetic centres.[147]

2. The reason for the increase in the magnetic susceptibility is the transition of Co^{3+} ions to the high-spin state $(t_{2g}^{\alpha})^3 (t_{2g}^{\beta})^1 (e_g)^2$ ($\mu_{ef}^2 = 24\ \mu_B^2$).[13]

The magnetic susceptibility of chemically delithiated $LiCoO_2$ was studied.[92] This was shown to obey the Curie–Weiss law in the temperature interval from 83 to 300 K for all compositions irrespective of the degree of lithium extraction. The values of the effective moment were as follows:

Oxide	$LiCoO_2$	$Li_{0.92}CoO_2$	$Li_{0.76}CoO_2$	$Li_{0.61}CoO_2$
μ_{ef}/μ_B	1.157	1.164	1.731	1.733

The effective magnetic moments of the latter two compositions almost coincided. This was associated with changes in the degree of electron localisation.

$LiNiO_2$. The magnetic properties of layered $LiNiO_2$ depend on both the stoichiometry and the degree of structural order. The results of numerous experiments were often conflicting. This also concerns the manifold interpretations of the data obtained.

Thus it was concluded [96] that magnetic properties of $LiNiO_2$ can adequately be described on an assumption that trivalent nickel ions are in the low-spin state $[(t_{2g}^{\alpha})^3 (t_{2g}^{\beta})^3 (e_g)^1]$. Later, this fact has found an experimental confirmation [148] and was substantiated theoretically.[149] However, in a number of studies (*e.g.*, in Ref. 150), trivalent nickel is assumed to be in the high-spin state $[(t_{2g}^{\alpha})^3 (t_{2g}^{\beta})^2 (e_g)^2]$, which forms a Kramers doublet with $S = 1/2$.

A different viewpoint exists: the magnetic properties of $LiNiO_2$ are determined by the exchange-coupled ($Ni^{2+} - O^{1-}$) pairs.[151] Charge-compensation processes in $LiNiO_2$, which are responsible for the appearance of holes in the oxygen zone, resemble those observed in high-temperature superconductors and were revealed for the first time in the studies of X-ray absorption spectra for the $Li_xNi_{1-x}O$ system.[151] Similar results were obtained in other studies.[152, 153] Calculations [154] confirmed that an electron hole appears in the 2*p* oxygen band rather than in the 3*d* nickel band. However, the fact that such techniques as ^{7}Li NMR and ESR [155] have not confirmed this observation deserves mention.

In a number of studies, the magnetic properties of $LiNiO_2$ were considered in relation to the problem of the ground state of a two-dimensional (2D) triangular lattice antiferromagnet with $S = 1/2$. Thus within the framework of the model of a quantum liquid (resonance valence zone), it was assumed for the first time [156] that the ground state of such systems in the absence of long-range magnetic order has a low energy compared with the classical Néel state. This problem was the subject of wide speculation in the context of the assumption that it is the resonance valence zone that is responsible for high-temperature superconduction in copper complex oxides.[157] The $LiNiO_2$ oxide characterised by $S = 1/2$ and a structure based on face-centred cubic packing of oxygen atoms where nickel and lithium atoms occupy the interstices and form alternate layers (as a result, the interlayer distances substantially exceed those between magnetic atoms inside a layer) can well be described by the aforementioned model.[150, 155, 158, 159]

The magnetic properties of a number of $Li_xNi_{1-x}O$ solid solutions and $LiNiO_2$ as the end member of this series were studied in detail.[96] The main attention was focused on the magnetic transition in the temperature range of 200–300 K (this temperature is usually denoted as T_{N1}), which was claimed to be of the ferromagnetic nature. The dependences of the Curie temperature and magnetisation of $Li_xNi_{1-x}O$ on concentration had maxima at $x = 0.43$ (Fig. 9), and the degree of structural order η [the degree of cationic ordering in (111) alternate planes of the basal NaCl lattice] increased monotonically with an increase in the lithium content and reached a maximum for $LiNiO_2$, which, however, was below 100%. It is the latter observation that explained the fact that magnetic measurements carried out later [97, 98, 160–162] for $LiNiO_2$ samples with a higher degree of structural ordering revealed no magnetic transition described in Ref. 96. Thus, the magnetic ordering is an indicator of $\eta < 1$. The fact that the magnetic properties of $LiNiO_2$ can indicate the structural ordering of a sample stems from the structural peculiarity of perfectly ordered $LiNiO_2$ [namely, the fact that each plane occupied by

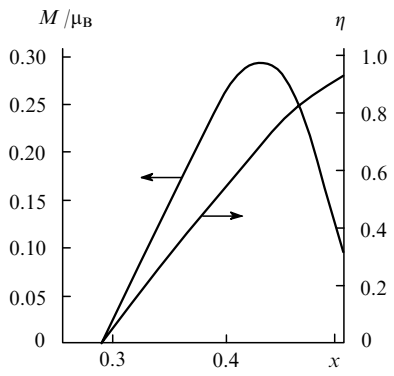

Figure 9. Concentration dependences of magnetisation M and degree of ordering η in $Li_xNi_{1-x}O$.[96]

magnetic ions (Ni^{3+}) is separated from another plane by three nonmagnetic planes (O–Li–O)] and the partial disordering caused by the presence of nickel ions in lithium sites (and *vice versa*).

A complete cationic disordering ($\eta = 0$) is typical of cubic $LiNiO_2$ the magnetic properties of which have been described.[98] The polytherm of its magnetic susceptibility demonstrated an anomalous feature, which allowed the paramagnetic—antiferromagnetic transition at 280 K to be deduced (Fig. 10).

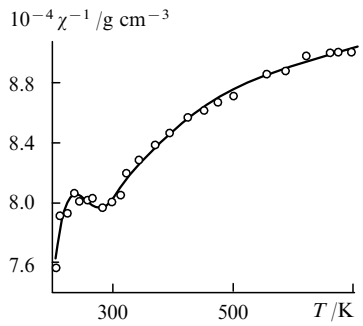

Figure 10. Temperature dependence of the reciprocal magnetic susceptibility of $LiNiO_2$ with the degree of ordering $\eta = 0$.[98]

The magnetic transition occurring in this oxide at 210 K was studied in detail [150, 158, 159]. The magnetic structure of $LiNiO_2$ was simulated on an assumption of a perfect ordering. However, from the synthetic conditions mentioned ($LiOH + Ni_2O_3$; $T = 1100$ K) suggest that the degree of ordering in the samples studied did not exceed $\eta = 0.8$. Below the transition temperature, $LiNiO_2$ was found to exhibit the ferrimagnetic behaviour. However, in contrast to classical ferrimagnetic materials, the field dependence of the magnetisation [$M(H)$] in $LiNiO_2$ was nonlinear below T_{N1}, did not reach saturation and infinitely increased with the field strength according to $M \propto H^{1/\delta}$.

It should be noted that the possibility of assigning the magnetic transition which occurs in $LiNiO_2$ with $\eta < 1$ in the temperature interval of 150–300 K to the ferrimagnetic type [96] was not confirmed later. In neutron diffraction studies,[150, 163] magnetic reflexes were not observed below the transition point even on long-term exposures. The ordering at 240 K was found [161] to be of a ferromagnetic nature. The same conclusion was made in Ref. 98.

In addition to the magnetic transition observed in the region of 150–300 K, the temperature and even the possibility of which depend on the degree of the structural order of $LiNiO_2$, other anomalous magnetic features were observed at lower temperatures. A broad spectrum of mechanisms were invoked for their

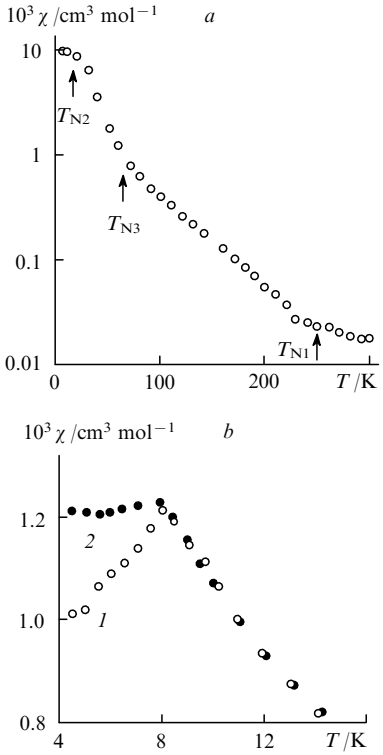

Figure 11. Temperature dependences of the magnetic susceptibility of $LiNiO_2$ measured in an applied field of (*a*) 1000 [165] and (*b*) 10 Œ.[162] (*1*) Cooling in a zero field; (*2*) cooling in a 10-Œ field.

explanation. For example, virtually stoichiometric and perfectly ordered $LiNiO_2$ with Ni–Ni interactions of the 2D type was shown [160, 162, 164] to behave as a typical spin glass. The temperature dependence of the magnetisation measured upon zero-field cooling demonstrated a sharp peak at 9 K (this temperature was denoted as T_{N2}; according to the results of other authors, T_{N2} is 35–50 K, see, *e.g.*, Ref. 165). At the same time, upon cooling in a nonzero field, the magnetic susceptibility increased monotonically (Fig. 11). The frequency dependence of the height and position of the peak, which was obtained by measuring the AC susceptibility, also indicated the attainment of a spin glass state. In certain studies,[159, 166] the state below T_{N2} was considered as the quantum liquid state in which the spins form mobile pairs. The temperature $T_{N2} = 6$ K was claimed [161] to be the Curie temperature for a two-dimensional Ising system. Such a conclusion was drawn by taking into account the fact that the slope of the linear dependence $\ln(M/H)$ *vs.* $\ln(T - T_c)$ was found to be equal to -1.7, which agrees with the critical factor of $-7/4$ for the 2D model of Ising.[167]

The temperature dependence of the magnetic susceptibility of $LiNiO_2$ demonstrated yet another special point in the temperature range from 70 to 80 K, *viz.*, T_{N3}.[165] The values of both T_{N2} and T_{N3} depended on the sample quality.[165] The magnetic behaviour of $LiNiO_2$ at low temperatures can be described as follows.[164]

1. The $T_{N3} < T < T_{N1}$ interval corresponds to nonlinear magnetisation in the external field. The magnetic entropy decreases by 20%. A model of the spin-system inhibition for the antiferromagnetic triangular lattice with the planar short-range order is realised.

2. In the $T_{N2} < T < T_{N3}$ region, magnetisation sharply increases. The magnetic entropy decreases twofold in the absence of any noticeable anomalies which would have indicated the appearance of a long-range magnetic order. The interactions between the layers are assumed to generate the effects of the three-dimensional short-range order.

3. In the $T < T_{N2}$ region, the temperature dependence of the magnetisation tends to saturation. A noticeable residual magnetic

entropy is preserved up to T_{N2}. No anomalies associated with the long-range order are observed. The existence of a frozen spin state somewhat different from that of common spin glasses is assumed. The difference lies in the fact that the temperature dependence of the specific heat is quadratic in the former case and linear in the latter case.

Due to a strong 180-degree aniferromagnetic $Ni_{Li}-O-Ni_{Ni}$ interaction, a ferromagnetic coupling of nickel ions located above and below the Li layer arises, and a small ferromagnetic cluster forms around the Ni_{Li} defect.[168] The existence of such a cluster was proved experimentally by ESR in an applied field of up to 245 GHz.[169] Two types of clusters were observed: those of the first type are formed below 235 K, the other are formed below 120 K. Such a system was proposed to be considered as a superparamagnetic one, *i.e.*, built of separate ferromagnetic domains.[155] The formation of the latter is consistent with the fact that spontaneous magnetisation is suppressed in layered oxides.[170]

Above the temperature of magnetic ordering, the magnetic susceptibility of $LiNiO_2$ is adequately described by the Curie–Weiss law the parameters of which found by different authors differ substantially [μ_{ef} = 1.84 μ_B, Θ = 79.3 K (see Ref. 164); μ_{ef} = 2.2 μ_B, Θ = 2 K (see Ref. 171)]. These parameters also depended on the stoichiometry and the degree of structural order. The temperature dependence of $1/\chi$ in the magnetically disordered region was not smooth and consisted of linear segments.[98] Taking this into account, it was assumed that yet another phase transition takes place in $LiNiO_2$, *viz.*, a paramagnetic–paramagnetic transition. A possible reason for the break observed in $1/\chi$ *vs.* T dependences is the transition of nickel from the low-spin to high-spin state. Table 1 lists the parameters of the Curie–Weiss equation determined for the low-temperature and high-temperature segments of the $1/\chi$ *vs.* T dependences for $LiNiO_2$ samples with different η values. It is noteworthy that the magnetic moments and the Weiss constants of two paramagnetic phases approach one another with an increase in the degree of structural ordering. It appears that these parameters can serve as indicators of the completeness of the cationic ordering in $LiNiO_2$.

Table 1. Magnetic moments and Weiss constants of $LiNiO_2$ with different degrees of structural ordering.[98]

η	T = 200–400 K		T = 600–900 K	
	μ_{ef}/μ_B	Θ /K	μ_{ef}/μ_B	Θ /K
0.67	1.489	185	2.547	−287
0.85	1.751	131	2.201	−87
0.94	1.869	31	2.061	−36
0.98	1.987	33	2.237	−20

It is interesting that $LiNiO_2$, which was shown to be antiferromagnetically ordered in its metastable structurally disordered state and ferromagnetically ordered at sufficiently high degrees of structural ordering [η = 0.6–0.8 (see Ref. 98)], retained its paramagnetic properties up to the liquid helium temperature for the case of perfect ordering. The latter observation can be explained by the fact that, as was shown by de Jongh and Miedema,[172] two-dimensional Heisenberg systems which apparently involve the perfectly ordered $LiNiO_2$ oxide [98] have no long-range magnetic order. The experimentally observed phase transitions in these systems were caused by deviations from the ideal behaviour, which resulted in an interaction arising between the layers. For example, $(C_nH_{2n+1}NH_3)Cu_4Cl_2$ (see Ref. 173) with a small number of nonmagnetic layers separating the magnetic layers has ferromagnetic properties, while the same substance with a greater number of nonmagnetic layers exhibits no ferromagnetism. For $LiNiO_2$, it is those nickel ions which occur in the lithium layers due to partial disordering that are responsible for the interlayer interaction.

In view of the fact that the degree of structural order in $LiNiO_2$ is closely related to stoichiometry, the magnetic properties depend even on small changes in x in $Li_{1-x}Ni_{1+x}O_2$. This was confirmed in a study [160] in which it was shown that samples with $x \leqslant 0.01$ demonstrate a thermomagnetic hysteresis typical of a spin glass at 8 K, whereas samples with $x \approx 0.08$ exhibit spontaneous magnetisation at 5 K, which corresponds to a magnetic moment of ~ 0.3 μ_B/Ni. Similar results were obtained in another study [174]: it was observed that $LiNiO_2$ is a spin glass, in contrast to $Li_{0.93}Ni_{1.07}O_2$.

IV. Structure and magnetic properties of $LiM_{1-x}M'_xO_2$ solid solutions

The $LiMO_2$ oxides under consideration can form solid solutions. The attention paid to solid solutions, first of all, is associated with the prospects of stabilising the structural types which can be used as cathodic materials in electrochemical devices. Moreover, solid solutions formed by compounds with different types of cationic ordering are interesting from the viewpoint of studying the short-range order effect, the three-dimensional–two-dimensional structural transitions and the formation of new superstructures.

$LiNi_{1-x}Co_xO_2$ ($0 \leqslant x \leqslant 1$). Oxides $LiNiO_2$ and $LiCoO_2$ form a continuous series of solid solutions, which, like the original phases, have a trigonal structure with the $R\bar{3}m$ symmetry. With a decrease in the content of cobalt (the ionic radius of which is smaller than that of nickel), the cell parameters a and c decrease monotonically. However, the concentration dependence of the c/a ratio is not monotonic, and for x = 0.3 its slope changes, *i.e.*, the increase in the c/a ratio slows down.[175] This result was reproduced in another study;[176] however, the authors of the latter study have attributed the singular point to the composition with x = 0.5. In their opinion, an increase in c/a from 4.96 (x = 0.5) to 4.99 (x = 1) does not bring about mixing of lithium and nickel ions in the octahedral positions of the hexagonal face-centred lattice. The value c/a = 4.99 corresponds to a perfect hexagonal unit cell. For smaller c/a values and hence for higher nickel concentrations, partial cationic disordering takes place, which results in a deviation of the $LiNi_{1-x}Co_xO_2$ symmetry from the ideal hexagonal towards the parent cubic one. For a perfect close-packed structure of the $Fm\bar{3}m$ symmetry, c/a = 4.90. Based on the results of X-ray diffraction analysis (the Rietveld method), it was found [177] that, at low cobalt contents ($x \leqslant 0.2$), the excessive bivalent nickel ions are always present in solid solutions studied: $Li_{1-z}Ni_{1+z-t}Co_tO_2$ [$t = x(1 + z)$]. An increase in the cobalt content reduces the nonstoichiometry and stabilises the 2D structure.

The stabilising effect cobalt has on the 2D structure of the solid solution also manifests itself in electrochemical intercalation. Phase transitions that take place during electrochemical intercalation of $LiNiO_2$ do not occur in solid solutions.[178] This is explained by the fact that cobalt suppresses the ordering of lithium vacancies. At the same time, it is noteworthy that deep chemical extraction of lithium from solid solutions enriched with nickel results in a monoclinic distortion of the lattice.[179]

To avoid the distortion of the regular layered structure (2D) of $LiNi_{1-x}Co_xO_2$ solid solutions, the low-temperature synthetic methods were applied, using, *e.g.*, β-$Ni_{1-y}Co_yOOH$ [180] or $Ni_{1-y}Co_y(OH)_2$[181] as the starting materials. Solid solutions with minimum cationic disordering were obtained by the sol–gel method [182, 183] (this also refers to pure $LiNiO_2$), pyrolysis [184] and co-precipitation from solutions.[185]

^{6}Li and ^{7}Li NMR studies on $LiNi_{1-x}Co_xO_2$ solid solutions ($0 \leqslant x \leqslant 1$) carried out in both static and dynamic modes [186, 187] have revealed structural microheterogeneities unrelated to the cationic ordering. These microheterogeneities did not cause any phase formation and could not be revealed by the diffraction techniques. They represented clusters of several cobalt atoms.

A magnetic phase diagram (Fig. 12) was constructed based on the results of detailed studies of magnetic properties of $LiNi_{1-x}Co_xO_2$ solid solutions ($0 \leqslant x \leqslant 1$).[188] A model was pro-

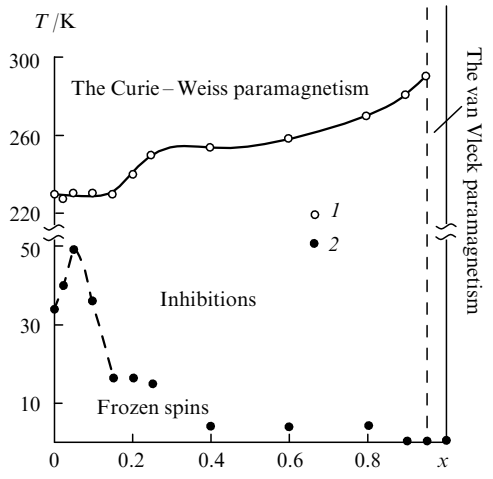

Figure 12. Magnetic phase diagram of $LiNiO_2-LiCoO_2$ system.[188] (*1*) T_{N1}; (*2*) T_{N2}.

posed that described the magnetic properties of both $LiNiO_2$ and $LiNi_{1-x}Co_xO_2$. This model is based on an assumption of an antiferromagnetic interaction within a layer and a weak ferromagnetic bonding between the layers. A conclusion that a system of three sublattices is unstable which was drawn from this model is of prime importance. It is with this conclusion that the absence of magnetic reflexes (1/3 1/3 *n*) is related.

The data on $LiNi_{1-x}Co_xO_2$ solid solutions additionally doped with manganese,[189] magnesium [190] and strontium [191] can be found in the literature.

$LiNi_{1-x}Ti_xO_2$ ($0 \leqslant x \leqslant 0.5$). According to the results of X-ray analysis,[192] the solid solutions with $0 \leqslant x \leqslant 0.3$ are isostructural to the layered $LiNiO_2$. At a higher titanium content, the structure becomes cubic, due to complete cationic disordering. The structural data refined using the Rietveld technique indicated that $LiNi_{0.7}Ti_{0.3}O_2$ also involves a certain number of transition metal ions in the lithium layers; hence, the regular two-dimensional structure is distorted. It is of note that these layers involve bivalent nickel and trivalent titanium. This result was obtained by means of the XPS technique. The authors of this study [192] did not mention the mechanism of the charge compensation in $LiNi_{0.7}Ti_{0.3}O_2$ solid solutions which involve Ni^{2+} ions: whether a certain number of titanium ions appears or the oxygen content changes. It should be noted that the degee of oxidation of Ti (Ti^{3+}) is not typical of titanium compounds synthesised in air at sufficiently high temperatures, *i.e.*, under conditions in which the solid solutions under discussion have been prepared.

$LiNi_{1-x}Mn_xO_2$. Solid solutions isostructural to $LiNiO_2$ were studied.[193–199] Certain cationic disordering was described [197] within the frameworks of the hexagonal structure and later confirmed.[193] To stabilise the trivalent state of nickel ions and thereby stabilise the layered structure, a special procedure of coprecipitation in an oxidative medium was developed.[193] As a result, solid solutions with the composition $LiNi_{1-x}Mn_xO_{2+\delta}$ ($0 \leqslant x \leqslant 0.5$) were obtained. The oxidation states of the transition metals in these solid solutions were determined by measuring the magnetic susceptibilities. It was shown that both transition metals in the sample bulk are in the trivalent state, whereas traces of Mn^{4+} were detected on the surface. All solid solutions studied exhibited a ferromagnetic transition at a temperature (T_C) which increased with the manganese content. The exception was pure $LiNiO_2$, which is characterised by a strong interlayer ferromagnetic interaction of the Ni(3*b*)–O–Ni(3*a*)–O–Ni(3*b*) type responsible for the high T_C. The existence of the ferromagnetic transition both in pure $LiNiO_2$ and $LiNi_{1-x}Mn_xO_{2+\delta}$ solid solutions points to the incomplete cationic ordering and to the presence of transition metal ions in the lithium layers. Table 2 shows the magnetic characteristics of $LiNi_{1-x}Mn_xO_{2+\delta}$ ($0 \leqslant x \leqslant 0.5$).

Table 2. Magnetic characteristics of $LiNi_{1-x}Mn_xO_{2+\delta}$ ($0 \leqslant x \leqslant 0.5$).[193]

x	Θ /K	μ_{ef}/μ_B		T_C /K
		experiment	calculation	
0	162	1.7	1.74	196
0.1	−118	2.1	2.06	39
0.2	−55	2.2	2.37	53
0.4	−96	3.0	3.00	72
0.5	−107	3.3	3.32	88

$LiNi_{1-x}Fe_xO_2$. The $LiNi_{1-x}Fe_xO_2$ system demonstrates two types of solid solution. Compositions with $0 < x < 0.22$ are isostructural to $LiNiO_2$. Their degree of ordering gradually decreases, which manifests itself in weaker X-ray reflections superstructural to those of the sodium chloride cubic lattice. Moreover, cubic solid solutions are formed in the concentration interval of $0.42 < x < 1$. In the intermediate region, two phases are present.[200–202] By studying this systems, one can follow the changes in the magnetic properties that occur with a decrease in the dimensionality from 3D ($LiFeO_2$) to 2D ($LiNiO_2$).

At $T > 300$ K, the magnetic susceptibilities of all $LiNi_{1-x}Fe_xO_2$ compositions obey the Curie–Weiss law. The first group of solid solutions is characterised by a transition to a magnetically ordered phase. The transition temperature and spontaneous magnetisation both increase with the iron content. The presence of magnetic ordering in the interval from 150 to 200 K points to partial cationic disordering, *i.e.*, the presence of a certain amount of transition metal ions in the Li layers. These results were confirmed by crystallographic data.[203] For a composition with 20% iron, the distribution of cations over positions is: $[Li_{0.965}M_{0.035}]_{3b}[M_{0.965}Li_{0.035}]_{3a}O_2$, M = 0.2Fe + 0.8Ni.

The fact that X-ray patterns of the second group of solid solutions involve no lines superstructural with respect to the NaCl lattice unambiguously indicates that the ions of alkali and transition metals are not ordered in the planes, in contrast to $LiNiO_2$. Nonetheless, at $T < 200$ K, the magnetic susceptibility of this solid-solution group depends on the field strength. This dependence becomes more pronounced with an increase in the nickel content, which points to a magnetic ordering.[201] The magnetisation polytherms statistically processed using the technique of thermodynamic coefficients have revealed no spontaneous magnetisation. Hence, the nonlinear variation of magnetisation for structurally disordered samples is a result of the short-range order associated with the trend of nickel ions for aggregation within the framework of this structure. In other words, the exchange couplings, which are the reason for the magnetic ordering, are limited in solid solutions by certain atomic ensembles. In this case, the condition for percolation do not arise. Such a system is considered [201] as a superparamagnetic one. Based on the concepts mentioned, the cluster size was estimated. The volume of magnetic clusters increased with the nickel content in the cubic solid solution phase, and, at a nickel concentration above 43%, the system first became two-phase and then a hexagonal one.

The number of atoms in clusters (*n*) and the mean size (*d*) of the latter for the superparamagnetic region of $LiFe_{1-x}Ni_xO_2$ are as follows:[201]

x	0.1	0.2	0.3	0.4
n	17	28	38	116
d /Å	7	8	9	13

$LiMn_{1-x}Co_xO_2$ ($0 \leqslant x \leqslant 1$). This group of solid solutions was studied by two groups of researchers.[204, 205] The lattice type was found to be determined by the ratio of transition metal

ions;[205] for $x < 0.2$, oxides with trigonal structures are formed, for $0.2 \leqslant x \leqslant 0.7$, cubic structures are realised and, for higher manganese contents, the symmetry of solutions is tetragonal ($I4_1/amd$). It should be noted that, to obtain solid solutions in the $0.2 \leqslant x \leqslant 1$ concentration interval, the synthesis was carried out in a nitrogen atmosphere.

A different way [205] was chosen for synthesising solid solutions of two layered compounds, *viz*., $LiCoO_2$ and Li_2MnO_3. It was shown that in order to prepare a solid solution (rather than a mechanical mixture of the extreme members), the synthesis should be carried out with an excess of lithium. All solid solutions thus obtained had monoclinic structures. The transformation of a trigonal (hexagonal) unit cell of $LiCoO_2$ into a monoclinic one is expressed as follows (for parameter a as an example):

$$a_h = \frac{1}{\sqrt{3}} a_m .$$

The magnetic properties of $LiMn_{1-x}Co_xO_2$ solid solutions ($0 \leqslant x \leqslant 1$) formed by diamagnetic $LiCoO_2$ and antiferromagnetic $LiMnO_2$ [$T_N = 50$ K, $\Theta = -33$ K, $\mu_{ef} = 3.83\ \mu_B$ (see Ref. 206)] change nonmonotonically: the compounds are paramagnetic for $x \leqslant 0.5$ and the antiferromagnetic transition is observed for higher manganese content. The analysis of the concentration dependence of the effective magnetic moment showed that the oxidation state of manganese is Mn^{4+} for the manganese content > 75%, whereas for its content < 75% the presence of trivalent manganese ions may be assumed.

Methods for the synthesis of $LiMn_{1-x}Co_xO_2$ solid solutions and of $LiMn_{1-x}Ni_xO_2$ and $LiMn_{1-x}Fe_xO_2$ solid solutions with layered structures have been discussed.[207]

$LiCr_{1-x}Fe_xO_2$. This system was studied for both polycrystalline specimens and single crystals.[208] Like $LiNi_{1-x}Fe_xO_2$, this system is formed by two phases, one of which has an ordered layered structure and another has a cubic lattice characterised by a random distribution of metal ions over the lattice positions. It was found that the transition from the cubic structure to trigonal one corresponds to the solution with 73% $LiFeO_2$. A somewhat different value ($\sim 85\%$) was found in another study.[209] The magnetic susceptibility of structurally ordered compositions was shown to have anomalies in the vicinity of 50 K. These anomalies seem to indicate the three-dimensional order. Above the mentioned temperature, the magnetic interactions corresponded to two-dimensional interactions. An analysis of the Mössbauer spectra has shown [210] that 2D interactions also play the key role at low temperatures. At temperatures above 400–600 K, the variation of the magnetic susceptibility obeys the Curie–Weiss law. Table 3 shows the magnetic characteristics of the system. Divergence between experimental and calculated values of the magnetic moment was attributed to anisotropy of magnetic interactions.

In order to explain the parabolic shape of the dependence of the Weiss constant (Θ) on the concentration, the exchange-coupling parameters were separated and the intra- (J_1) and interlayer (J_2) exchange-coupling constants were estimated based on the data from the magnetic susceptibility). In addition, the partial values of the Weiss constants related to different types of coupling were obtained. Thus for interlayer interactions, $\Theta_2^{Cr-Cr} = -185$ K, $\Theta_2^{Cr-Fe} = 59$ K and $\Theta_2^{Fe-Fe} = -30$ K.

$LiV_{1-x}Mg_xO_2$ and **$LiV_{1-x}Al_xO_2$**. These systems were synthesised and studied [211] with the aim of following how the partial substitution of vanadium for an ion with a spin $S \neq 1$ in $LiVO_2$ affects the structural and magnetic parameters of the phase transition. It was assumed that the first system involves V^{2+} ions with $S = 3/2$ and the second system involves Al^{3+} with $S = 0$; the solid solutions have sufficiently narrow homogeneity regions, *viz*., $0 \leqslant x \leqslant 0.06$ and $0 \leqslant x \leqslant 0.1$, respectively. In both systems, the phase transition temperatures were lower than those of pure $LiVO_2$. Moreover, a weak but systematic decrease in the Curie constant was observed in the low-temperature region, which indicated that 'triangular' clusters $V^{3+}-V^{2+}-V^{3+}$ with $S = 1/2$ separated by singlet trimers contributed to the overall susceptibility. Based on these studies, it was concluded that the exchange-coupling constant of V^{3+} ions and the transition temperature both depend on the V–V distance and on the shift of vanadium ions from their positions.

Other solid solutions. Information on $LiAl_xNi_{1-x}O_2$ solid solutions ($x \leqslant 0.25$) with the $LiNiO_2$ structure is availiable.[212, 213] With an increase in the aluminium content, the c/a ratio somewhat increases. It is noteworthy that introduction of aluminium in $LiMO_2$ compounds is considered as one of the factors that stabilise the α-$NaFeO_2$-type layered structure, the latter being the most suitable from the electrochemical viewpoint. Calculations of miscibility carried out for eight compositions of the $LiAl_{1-x}M_xO_2$ system have shown [214] that for M = Ti, V, Cr and Mn layered solid solutions are formed at the temperatures of the conventional synthesis. For M = Fe, Co, Ni and Cu, a low temperature region of immiscibility exists. Special attention was given to $LiAl_{1-x}Co_xO_2$ and $LiAl_{1-x}Cr_xO_2$ systems, which, according to calculations, were completely miscible up to 600 °C. Limitations that arose at higher temperatures were associated with the transition of $LiAlO_2$ into a tetragonal γ-modification.[215] It was experimentally shown [216] that the synthesis carried out at 650 K results in an amorphous modification, whereas at 700–900 K a layered hexagonal structure is formed. It is essential that in $LiAl_{1-x}Co_xO_2$ as well as in $LiAl_{1-x}Ni_xO_2$ aluminium can be shifted from octahedral positions.[217] Synthesis of $LiAl_{1-x}Cr_xO_2$ solid solutions ($0 \leqslant x \leqslant 1$) was described.[218]

Solubility of aluminium in $LiMnO_2$ reached a maximum (5%–7%) at 1220 K.[219] As in the previous case, the existence of the maximum was explained by the formation of γ-$LiAlO_2$. Introduction of even minor amounts of aluminium to $LiMnO_2$ gives rise to a layered structure of the $NaFeO_2$ type. The use of chromium as the dopant led to a similar result.[220]

In addition, the possibility of formation of $LiCr_{1-x}Co_xO_2$, $LiCr_{1-x}Ni_xO_2$,[221] $LiFe_{1-x}Co_xO_2$ [222] and $LiNi_{1-x}B_xO_2$ [223] solutions was demonstrated.

Table 3. Magnetic characteristics of $LiCr_{1-x}Fe_xO_2$.[210]

x	The Curie constant /cm^3 K mol^{-1}	μ_{ef}/μ_B		Θ /K	Θ_1 /K	Θ_2 /K	T_N /K	J_1/k /K	J_2/k /K
		experiment	calculation						
0	1.58	3.57	3.87	−570	−472	−98	15	−33	−6.9
0.1	1.98	4.17	4.07	−546	−399	−147	56	−25	−8.5
0.2	1.76	3.77	4.28	−300	−180	−120	40	−17	−4.3
0.3	1.90	3.91	4.49	−204	−138	−66	35	−11	−2.2
0.4	1.81	3.83	4.69	−25	7.5	−32.5	50	−0.70	−1.1
0.5	1.82	3.83	4.90	0	16.3	−16.3	55	0.58	−0.6
0.6	2.40	4.39	5.10	−47	−35.5	−11.5	45	−1.8	−0.7
0.7	2.64	4.65	5.30	−94	−80.5	−13	40	−3.7	−0.6

V. Conclusion

Complex oxides with the general formula $LiMO_2$ where M is a trivalent transition 3*d* metal are considered as inorganic functional materials of a new generation.[224,225] First of all, this is associated with their good electrochemical characteristics. This factor has stimulated numerous studies not only in applied but also in fundamental directions. Of prime importance are structural and magnetic studies, because the layered structure characteristic of many $LiMO_2$ compounds not only provides adequate diffusion of the alkali metal atoms, which is essential for electrochemical processes, but also is of special interest from the viewpoint of studying low-dimensional magnetic interactions.

At present, the crystal structure of $LiMO_2$ is sufficiently thoroughly described for all stable modifications, and efforts are mainly concentrated on the synthesis and structural description of metastable phases preferentially with layered structures of the α-$NaFeO_2$ type.

The results of investigations of the magnetic properties of $LiMO_2$ show that structural defects may often play the key role in the formation of magnetic structures. First of all, this refers to compounds with variable degrees of structural order.

References

1. R B Goldner, F O Arntz, G Berera, T E Haas, G Wei, K K Wong, P C Yu *Solid State Ion.* **53–56** 617 (1992)
2. S Megahed, W Ebner *J. Power Sources* **54** 155 (1995)
3. C Delmas, in *Industrial Chemistry Library. Lithium Batteries. New Materials, Developments and Perspectives* Vol. 5 (Ed. G Pistoia) (Amsterdam; London; New York; Tokyo: Elsevier, 1994) p. 457
4. T A Hewston, B L Chamberland *J. Phys. Chem. Solids* **48** 97 (1987)
5. R Alcantara, P Lavela, J L Tirado, E Zhecheva, R Stoyanova *J. Solid State Electrochem.* **3** 121 (1999)
6. E J Wu, P D Teresch, G Ceder *Philos. Mag. B* **77** 1039 (1998)
7. R Hoppe *Angew. Chem.* **71** 457 (1959)
8. C J M Rooymans *Z. Anorg. Allg. Chem.* **313** 324 (1961)
9. R Hoppe, B Schepers, H Rohrbon, E Vielhaber *Z. Anorg. Allg. Chem.* **339** 130 (1965)
10. T Birchall, A F Reid *J. Solid State. Chem.* **6** 411 (1973)
11. B L Dickson, K K P Srivastava *J. Solid State Chem.* **19** 117 (1976)
12. Y B Kuo, W Scheld, R Hoppe *Z. Kristallogr.* **164** 121 (1983)
13. P F Bongers Ph D Thesis, The University of Leiden, Leiden, 1957
14. A Lecerf *Ann. Chim., Sci. Mater.* **7** 513 (1962)
15. D W Murphy, M Greenblatt, S M Zahurak, R J Cava, J V Waszczak, G W Hull, R S.Hutton. *Rev. Chim. Miner.* **19** 442 (1982)
16. R J Cava, D W Murphy, S Zahurak, A Santoro, R S Roth *J. Solid State Chem.* **53** 64 (1984)
17. A F Wells *Structural Inorganic Chemistry* (Oxford: Clarendon Press, 1984)
18. T A Hewston Ph D Thesis, The University of Connecticut, Storrs, CT, 1985
19. W Rüdorff, H Becker *Z. Naturforsh., B Chem. Sci.* **9** 613 (1954)
20. B Reuter, R Weber, J Jaskowski *Z. Electrochem.* **66** 832 (1962)
21. K Kobayashi, K Kosuge, S Kachi *Mater. Res. Bull.* **4** 95 (1969)
22. T A Hewston, B L Chamberland *J. Solid State Chem.* **65** 100 (1986)
23. L P Cardoso, D E Cox, T A Hewston, B L Chamberland *J. Solid State Chem.* **72** 234 (1988)
24. J B Goodenough, G Dutta, A Manthiram *Phys. Rev. B* **43** 10170 (1992)
25. K Imai, H Sawa, M Koike, M Hasegawa, H Takei *J. Solid State Chem.* **114** 184 (1995)
26. H Takei, M Koike, K Imai, H Sawa, H Kadowaki, Y Iye *Mater. Res. Bull.* **27** 555 (1992)
27. L A Picciotto, M M Thackeray, W I F David, P G Bruce, J B Goodenough *Mater. Res. Bull.* **19** 1497 (1984)
28. L A Picciotto, M M Thackeray *Solid State Ion.* **18–19** 773 (1986)
29. J B Goodenough, A Manthiram, G Dutta *Eur. J. Solid State Inorg. Chem.* **28** 1125 (1991)
30. L A Picciotto, M M Thackeray *Mater. Res. Bull.* **20** 187 (1985)
31. C Chieh, B L Chamberland, A F Wells *Acta Crystallogr., Sect. B* **37** 1813 (1981)
32. C Simo, S L Holt *J. Solid State Chem.* **4** 76 (1972)
33. L Hernan, M Macias, J Morales, C Perez-Vicente, J L Tirado *Mater. Res. Bull.* **24** 781 (1989)
34. W D Johnston, R R Heikes *J. Am. Chem. Soc.* **78** 3255 (1956)
35. G Ditrich, R Hoppe *Z. Anorg. Allg. Chem.* **368** 262 (1969)
36. R Hoppe, G Brachtel, M Jansen *Z. Anorg. Allg. Chem.* **417** 1 (1975)
37. P Strobel, J Levy, J-C Joubert *J. Cryst. Growth* **66** 257 (1984)
38. J D Dunitz, L E Orgel *J. Phys. Chem. Solids* **3** 20; 318 (1957)
39. D G Kellerman, V S Gorshkov, V G Zubkov, V A Perelyaev, V R Galakhov, E Z Kurmaev, St Uhlenbrock, M Noimann *Zh. Neorg. Khim.* **42** 1012 (1997) [a]
40. L Croguennec, P Deniard, R Brec, A Lecerf *J. Mater. Chem.* **5** 1919 (1995)
41. L Croguennec, P Deniard, R Brec, P Biensan, M Broussely *Solid State Ion.* **89** 127 (1996)
42. L Croguennec, P Deniard, R Brec, A Lecerf *J. Mater. Chem.* **7** 511 (1997)
43. M M Thackeray, W I F David, P G Bruce, J B Goodenough *Mater. Res. Bull.* **18** 461 (1983)
44. A Mosbah, A Verbnere, M Tournoux *Mater. Res. Bull.* **18** 1375 (1983)
45. A R Armstrong, P G Bruce *Nature (London)* **381** 499 (1996)
46. J N Reimers, J E W Fuller, E Rossen, J R Dahn *J. Electrochem. Soc.* **140** 3396 (1993)
47. R J Gummow, M M Thackeray *J. Electrochem. Soc.* **141** 1178 (1994)
48. C Delmas, F Capitaine, in *Extended Abstracts II-B-33 of the 8th International Meeting on Lithium Batteries, Nagoya, 1996* p. 470
49. F Capitaine, P Gravereau, C Delmas *Solid State Ion.* **89** 197 (1996)
50. Y Shao-Horn, S A Hackney, A R Armstrong, P G Bruce, R Gitzendanner, C S Johnson, M M Thackeray *J. Electrochem. Soc.* **146** 2404 (1999)
51. G Ceder, S K Mishra. *Electrochem. Solid State Lett.* **2** 550 (1999)
52. F Le Gras, P Strobel, M Anne, D Bloch *J. Mater. Chem.* **7** 2519 (1997)
53. J C Anderson, S M Anderson *J. Phys. Chem. Solids* **25** 961 (1964)
54. E Posnjak, T Barth *Phys. Rev.* **38** 2234 (1931)
55. A Hoffman *Naturwissenschaften* **26** 431 (1938)
56. R Famery, P Bassoul, F Queyroux *J. Solid State Chem.* **57** 178 (1985)
57. J C Anderson, S K Dey, V Halpern *J. Phys. Chem. Solids* **26** 1555 (1965)
58. R W G Wykoff *Crystal Structure* Vol. 2 (New York: Intrscience, 1964) p. 312
59. M Brunel, F de Bergevin *J. Phys. Chem. Solids* **29** 163 (1968)
60. M Brunel, F de Bergevin *J. Phys. Chem. Solids* **30** 2011 (1969)
61. J C Anderson, M Schieber *J. Phys. Chem.* **67** 1838 (1963)
62. R Kanno, T Shirane, Y Kawamoto, Y Takeda, M Takano, M Ohashi, Y Yamaguchi *J. Electrochem. Soc.* **143** 2435 (1996)
63. Y Sakurai, H Arai, S Okada, J Yamaki *J. Power Sources* **68** 711 (1997)
64. Y Sakurai, H Arai, J Yamaki *Solid State Ion.* **113–115** 29 (1998)
65. R Kanno, T Shirane, Y Inaba, Y Kawamoto *J. Power Sources* **68** 145 (1997)
66. Y Inaba, Y Kawamoto, in *Extended Abstracts I-B-04 of the 22nd Symposium on Solid State Ionics, Nagoya, 1996* p. 53
67. E Antolini, M Ferretti *J. Solid State Chem.* **117** 1 (1995)
68. H J Orman, P J Weisman *Acta Crystallogr., Sect. C* **40** 12 (1984).
69. W D Johnston, R R Heikes, D Sestrich *J. Phys. Chem. Solids* **7** 1 (1958).
70. J Akimoto, Y Gotoh, Y Oosawa *J. Solid State Chem.* **141** 298 (1998)
71. C Wolverton, A Zunger *Phys. Rev. B* **57** 2242 (1998)
72. C Wolverton, A Zunger *J. Electrochem. Soc.* **145** 2424 (1998)
73. R J Gummow, M M Thackeray *Solid State Ion.* **53–56** 681 (1992)
74. R J Gummow, M M Thackeray *J. Electrochem. Soc.* **140** 3365 (1993)
75. R J Gummow, D C Liles, M M Thackeray *Mater. Res. Bull.* **28** 235 (1992)
76. R J Gummov, D C Liles, M M Thackeray, W I F David *Mater. Res. Bull.* **28** 1177 (1993)
77. E Rossen, J N Reimers, J R Dahn *Solid State Ion.* **62** 53 (1993)
78. J Morales, R Stoyanova, J L Tirado, E Zhecheva *J. Solid State Chem.* **113** 182 (1994)
79. B Garcia, P Barboux, F Ribot, A Kihn-Hirari, L Mazerolles, N Baffier *Solid State Ion.* **80** 111 (1995)

80. W W Huang, R Frech *Solid State Ion*. **86** – **88** 395 (1996)
81. G G Amatucci, J M Tarascon, D Larcher, L C Klein *Solid State Ion*. **84** 169 (1996)
82. M Carewska, S Scaccia, F Croce, S Arumugam, Y Wang, S Greenbaum *Solid State Ion*. **93** 227 (1997)
83. Y Shao-Horn, S A Hackney, S C Johnson, A J Kahaian, M M Thackeray *J. Solid State Chem*. **140** 116 (1998)
84. J N Reimers, J R Dahn *J. Electrochem. Soc*. **139** 2091 (1992)
85. T Ohzuku, A Ueda *J. Electrochem. Soc*. **141** 2972 (1994)
86. G G Amatucci, J M Tarascon, L C Klein *J. Electrochem. Soc*. **143** 1114 (1996)
87. A van der Ven, M K Aydinol, G Ceder, G Kresse, J Hafner *Phys. Rev. B* **58** 2975 (1998)
88. A van der Ven, M K Aydinol, G Ceder *J. Electrochem. Soc*. **145** 2149 (1998)
89. B Garcia, J Farcy, J P Pereira-Ramos, N Baffier *J. Electrochem. Soc*. **144** 1179 (1997)
90. A Mendiboure, C Delmas, P Hagenmuller *Mater. Res. Bull*. **19** 1383 (1984)
91. C Delmas, J Braconnier, P Hagenmuller *Mater. Res. Bull*. **17** 117 (1982)
92. N Imanishi, M Fujiyoshi, Y Takeda, O Yamamoto, M Tabuchi *Solid State Ion*. **18** 121 (1999)
93. L D Dyer, B S Borie, G P Smith *J. Am. Chem. Soc*. **76** 1499 (1953)
94. A Rougier, C Delmas, A V Chadwick *Solid State Commun*. **94** 121 (1995)
95. A Rougier, A V Chadwick, C Delmas *Nucl. Instum. Methods Phys. Res*. **97** 75 (1995)
96. J B Goodenough, D G Wickham, W J Croft *J. Phys.Chem. Solids* **5** 107 (1958).
97. V S Gorshkov, D G Kellerman, V A Perelyaev, G P Shveikin *Izv. Akad Nauk SSSR, Neorg. Mater*. **27** 1274 (1991) [b]
98. V S Gorshkov, D G Kellerman, V A Perelyaev, G P Shveikin *Zh. Neorg. Khim*. **41** 16 (1996) [a]
99. Z Lu, X Huang, H Huang, L Chen, J Schoonman *Solid State Ion*. **120** 103 (1999)
100. E Antolini *J. Mater. Sci*. **27** 3335 (1992)
101. E Antolini *J. Mater. Sci. Lett*. **13** 1599 (1994)
102. T Sata *Ceram. Int*. **24** 53 (1998)
103. H Arai, S Okada, H Ohtsuka, M Ichimura, J Yamaki *Solid State Ion*. **80** 261 (1995)
104. V Berbenni, V Massarotti, D Capsoni, R Riccardi, A Marini, E Antolini *Solid State Ion*. **48** 101 (1991)
105. J Morales, C Perez-Vicente, J L Tirado *Mater. Res. Bull*. **25** 623 (1990)
106. W Li, J N Reimers, J R Dahn *Phys. Rev. B* **46** 3236 (1992)
107. A Rougier, P Gravereau, C Delmas *J. Electrochem. Soc*. **143** 1168 (1996)
108. I J Pickering, J T Lewandowski, A J Jacobson, A Goldstone *Solid State Ion*. **53** – **56** 405 (1992)
109. J N Reimers, W Li, J R Dahn *Phys. Rev. B* **47** 8486 (1993)
110. R Alcantara, P Lavela, J L Tirado, R Stoyanova, E Kuzmanova, E Zhecheva *Chem. Mater*. **9** 2145 (1997)
111. I J Pickering, G N George, J T Lewandowski, A J Jacobson *J. Am. Chem. Soc*. **115** 4137 (1993)
112. T Ohzuku, A Ueda, M Nagayama *J. Electrochem. Soc*. **140** 1862 (1993)
113. I Nakai, K Takahashi, Y Shiraishi, T Nakagome, F Nishikawa *J. Solid State Chem*. **140** 145 (1998)
114. L Croguennec, C Pouillerie, C Delmas *Solid State Ion*. **135** 259 (2000)
115. A Hirano, R Kanno, Y Kawamoto, Y Takeda, K Yamaura, M Takano, K Ohyama, M Ohashi, Y Yamaguchi *Solid State Ion*. **78** 123 (1995)
116. R Stoyanova, E Zhecheva *J. Solid State Chem*. **108** 211 (1994)
117. A Hirano, R Kanno, Y Kawamoto, K Oikawa, T Kamiyama, F Izumi *Solid State Ion*. **86** – **88** 791 (1996)
118. C Delmas, J P Peres, A Rougier, A Demourgues, F Weill, A V Chadwick, M Broussely, F Perton, P Biensan, P Willmann *J. Power Sources* **68** 120 (1997)
119. J P Peres, F Weill, C Delmas *Solid State Ion*. **116** 19 (1999)
120. H Arai, S Okada, Y Sakurai, J-i Yamaki *Solid State Ion*. **109** 295 (1998)
121. J R Dahn, U von Sacken, C A Michal *Solid State Ion*. **44** 87 (1990)
122. V W Bronger, H Bade, W Klemm *Z. Anorg. Allg. Chem*. **333** 188 (1964)
123. H N Migeon, A Courtois, M Zanne, C Cleitzer *Rev. Chim. Miner*. **13** 1 (1976)
124. P F Bongers, in *Crystal Structure and Chemical Bonding in Inorganic Chemistry* (Eds C J M Rooymans, A Rabenau) (New York: Elsevier, 1975) p. 246
125. J B Goodenough *Magnetism and the Chemical Bond* (New York, London: Wiley-Interscience, 1963)
126. Y Kimishima, M Tsuchiya, K Tomimoto, J Akimitsu *J. Magn. Magn. Mater*. **104** – **107** 779 (1992)
127. H F Pen, L H Tjeng, E Pellegrin, F M F de Groot, G A Sawatsky, M A van Veendaal, C T Chen *Phys. Rev. B* **55** 15500 (1997)
128. N F Mott *Metal-Insulator Transition* (London: Taylor and Francis, 1974)
129. Ya V Vasil'ev, S M Ariya *Izv. Akad. Nauk SSSR, Neorg. Mater*. **1** 347 (1965) [b]
130. A A Bugaev, B P Zakharchenya, F A Chudnovskii *Fazovyi Perekhod Poluprovodnik – Metall i ego Primenenie* (Semiconductor – Metal Phase Transition and Its Application) (Leningrad: Nauka, 1979)
131. D G Kellerman, V S Gorshkov, V A Perelyaev *Izv. Akad. Nauk SSSR, Neorg. Mater*. **24** 1547 (1988) [b]
132. M Onoda, T Inabe *J. Phys. Soc. Jpn*. **62** 2216 (1993)
133. B Laar, D J Ijdo *J. Solid State Chem*. **3** 590 (1971)
134. M Krysowska *Acta Phys. Pol. A* **52** 97 (1977)
135. C Delmas, G Le Flem, C Fouassier, P Hagenmuller *J. Phys. Chem. Solids* **39** 55 (1978)
136. N Kojima, K Ito, I Mogi, M Takeda, G Kido,Y Nakagawa, M Sakai, N Kuroda, Y Nishina *J. Phys. Soc. Jpn*. **62** 4137 (1993)
137. J L Soubeyboux, D Fruchart, J C Marmeggi, W J Fitzgerald, C Delmas, G Le Flem *Phys. Status Solidi A* **67** 633 (1981).
138. M Suzuki, I Yamada, H Kadowaki, F Takei *J. Phys., Condens. Matter* **5** 4225 (1993)
139. Y Ajiro, H Kikuchi, S Sugiyama, T Nakashima, S Shamoto, N Nakayama, M Kiyama, N Yamamoto, Y Oka *J. Phys. Soc. Jpn*. **57** 2268 (1988)
140. H Kadowaki, H Takei, K Motoya *J. Phys., Condens. Matter* **7** 6869 (1995)
141. J E Greedan, N P Raju, I J Davidson *J. Solid State Chem*. **128** 209 (1997)
142. V S Gorshkov, V V Karelina, D G Kellerman, in *Oksidy. Fiziko-Khimicheskie Svoistva i Tekhnologiya (Tez. Dokl. Vserossiiskoi Nauchno-Prakticheskoi Konf.)* [Oxides. Physicochemical Properties and Technology (Abstracts of Reports of the All-Russian Scientific and Practical Conference)] (Ekaterinburg: Ural Branch of the Russian Academy of Sciences, 1999) p. 157
143. D E Cox, G Shirane, P A Flinn, S L Ruby, W J Takei *Phys. Rev., Ser. 2* **132** 1547 (1963)
144. M Tabuchi, K Ado, H Kobayashi, I Matsubara, H Kageyama, M Wakita, S Tsutsui, S Nasu, Y Takeda, C Masquelier, A Hirano, R Kanno *J. Solid State Chem*. **141** 554 (1998)
145. M Tabuchi, S Tsutsui, C Masquelier, R Kanno, K Ado, I Matsubara, S Nasu, H Kageyama *J. Solid State Chem*. **140** 159 (1998)
146. M Oku *J. Solid State Chem*. **23** 177 (1978)
147. V S Gorshkov, D G Kellerman, V V Karelina *Zh. Fiz. Khim*. **73** 1041 (1999) [c]
148. R Stoyanova, E Zhecheva, C Friebel *Solid State Ion*. **73** 1 (1994)
149. G F Dionne *J. Appl. Phys*. **67** 4561 (1990)
150. K Hirakawa, H Kadwaki, K Ubukoshi *J. Phys. Soc. Jpn*. **54** 3256 (1985)
151. P Kuiper, G Kruizinga, J Ghijsen, G A Sawatsky, H Verweij *Phys. Rev. Lett*. **62** 221 (1989)
152. V R Galakhov, E Z Kurmaev, S Uhlenbrock, M Neumann, D G Kellerman, V S Gorshkov *Solid State Commun*. **95** 347 (1995)
153. T Mizokawa, H Namatame, A Fujimori, K Akeyama, H Kondoh, H Kuroda, N Kosugi *Phys. Rev. Lett*. **67** 1638 (1991)
154. J Meng, P Jena, J M Vail *J. Phys., Condens. Matter* **2** 10371 (1990)
155. P Ganguly, V Ramaswamy, I S Mulla, R F Shinde, P P Bakare, S Ganapathy, P R Rajamohanan, N V K Prakash *Phys. Rev. B* **46** 11595 (1992)
156. P W Anderson *Mater. Res. Bull*. **8** 153 (1973)

157. P W Anderson *Science* **235** 1196 (1987)
158. M Itoh, I Yamada, K Ubukoshi, K Hirakawa, H Yasuoka *J. Phys. Soc. Jpn.* **55** 2125 (1986)
159. I Yamada, K Ubukoshi, K Hirakawa *J. Phys. Soc. Jpn.* **54** 3571 (1985)
160. K Yamaura, M Takano, A Hirano, R Kanno *J. Solid State Chem.* **127** 109 (1996)
161. J P Kemp, P A Cox, J W Hodby *J. Phys., Condens. Matter* **2** 6699 (1990)
162. T Shirakami, M Takematsu, A Hirano, R Kanno, K Yamaura, M Takano, T Atake *Mater. Sci. Eng. B* **54** 70 (1998)
163. H Yoshikawa, H Mori, K Hirota, M Ishikawa *J. Phys. Soc. Jpn.* **59** 2631 (1986)
164. K Hirota, Y Nakazawa, M Ishikawa *J. Phys., Condens. Matter* **3** 4721 (1991)
165. K Hirota, Y Nakazawa, M Ishikawa *J. Magn. Magn. Mater.* **90 – 91** 279 (1990)
166. K Hirakawa, H Kadwaki *Physica B* **136** 335 (1986)
167. M E Fisher *Rep. Prog. Phys.* **30** 615 (1967)
168. D Mertz, Y Ksari, J Celestini, J M Debierre, A Stepanov, C Delmas *Phys. Rev. B* **61** 1240 (2000)
169. A-L Barra, G Chouteau, A Stepanov, C Delmas *J. Magn. Magn. Mater.* **177 – 181** 783 (1998)
170. P Ganguly *Proc. Indian Natl. Sci. Acad. A* **52** 13 (1986)
171. J N Reimers, J R Dahn, J E Greedan, C V Stager, G Liu, I Davidson, U von Sacken *J. Solid State Chem.* **102** 542 (1993)
172. L J de Jongh, A R Miedema *Adv. Phys.* **23** 1 (1974)
173. J H P Colpa *Physica B* **57** 347 (1972)
174. R Kanno, H Kubo, Y Kawamoto, T Kamiyama, F Izumi, Y Takeda, M Takano *J. Solid State Chem.* **110** 216 (1994)
175. C Delmas, I Saadoune *Solid State Ion.* **53** 370 (1992)
176. Y-M Choi, S-I Pyun, S-I Moon *Solid State Ion.* **89** 43 (1996)
177. A Rougier, I Saadoune, P Gravereau, P Willmann, C Delmas *Solid State Ion.* **90** 83 (1996)
178. I Saadoune, C Delmas *J. Solid State Chem.* **136** 8 (1998)
179. R Alcantara, J Morales, J L Tirado, R Stayanova, E Zhecheva *J. Electrochem. Soc.* **142** 3997 (1995)
180. Y Fujita, K Amine, J Maruta, H Yasuda *J. Power Sources* **68** 126 (1997)
181. J Cho, G Kim, H S Lim *J. Electrochem. Soc.* **146** 3571 (1999)
182. C-C Chang, N Scarr, P N Kumta *Solid State Ion.* **112** 329 (1998)
183. S Tao, Q Wa, Z Zhan, G Meng *Solid State Ion.* **124** 33 (1999)
184. C Julien, S S Michael, S Ziolkievicz *Int. J. Inorg. Mater.* **1** 29 (1999)
185. D Caurant, N Baffer, B Garcia, J P Pereira-Ramos *Solid State Ion.* **91** 45 (1996)
186. M Menetrier, A Pougier, C Delmas *Solid State Commun.* **90** 439 (1994)
187. C Marichal, J Hirschinger, P Granger, M Menetrier, A Rougier, C Delmas *Inorg. Chem.* **34** 1773 (1995)
188. K Hirota, H Yoshikawa, M Ishikawa *J. Phys., Condens. Matter* **4** 6291 (1992)
189. Z L Liu, A S Yu, J Y Lee *J. Power Sources* **82** 416 (1999)
190. Y Cao, M V Yakovleva, W B Ebner *Electrochem. Solid State Lett.* **1** 117 (1998)
191. H-J Kweon, D G Park *Electrochem. Solid State Lett.* **3** 128 (2000)
192. H S Chang, S-G Kang, S-W Song, J-B Yoon, J-H Choy *Solid State Ion.* **86 – 88** 171 (1996)
193. M E Spahr, P Novak, B Schnayder, O Haas, R Nesper *J. Electrochem. Soc.* **145** 1113 (1998)
194. S Fujiwara, S Yamada, M Kanda, in *Extended Abstracts of the 34th Battery Symposium, Nagoya, 1993* p. 135
195. M Yoshio, K Yamata, J Itoh, H Noguchi, M Okada, T Mouri, in *Rechargeable Lithium and Lithium Ion Batteries* (Eds S Megahed, B M Barnett, L Xie) (Pennington, NJ: Electrochemical Society, 1995) p. 251
196. Y Nitta, K Okamura, K Haraguchi, S Kobayashi, A Ohta *J. Power Sources* **54** 511 (1995)
197. E Rossen, C D W Jones, J R Dahn *Solid State Ion.* **57** 311 (1992)
198. D Caurant, N Baffier, V Bianchi, G Gregoire, S Bach *J. Mater. Chem.* **6** 1149 (1996)
199. J M Paulsen, C L Thomas, J R Dahn *J. Electrochem. Soc.* **147** 861 (2000)
200. D G Kellerman, V S Gorshkov, V A Perelyaev, G P Shveikin *Zh. Neorg. Khim.* **35** 1267 (1990) [b]
201. D G Kellerman, V S Gorshkov, V V Karelina *Zh. Neorg. Khim.* **44** 1078 (1999) [b]
202. C Delmas, G Prado, A Rougier, E Suard, L Fournes *Solid State Ion.* **135** 71 (2000)
203. J N Reimers, E Rossen, C D Jones, J R Dahn *Solid State Ion.* **61** 335 (1993)
204. R Stoyanova, E Zhecheva, L Zarkova *Solid State Ion.* **73** 233 (1994)
205. K Numata, C Sakaki, S Yamanaka *Solid State Ion.* **117** 257 (1999)
206. M Jansen, R Hoppe *Z. Anorg. Allg. Chem.* **397** 279 (1972)
207. F Zang, M S Whittingham *Electrochem. Solid State Lett.* **3** 309 (2000)
208. A Tauber, W M Moller, E Banks *J. Solid State Chem.* **4** 138 (1972)
209. E Kordes, J Petzoldt *Z. Anorg. Allg. Chem.* **335** 138 (1965)
210. C Delmas, F Menil, G Flem, C Fouassier, P Hagenmuller *J. Phys. Chem. Solids* **39** 51 (1978)
211. T Naka, M Onoda, H Nagasawa *Solid State Commun.* **87** 679 (1993)
212. T Ohzuku, T Yanagawa, M Kouguchi, A Ueda *J. Power Sources* **68** 131 (1997)
213. G X Wang, S Zhong, D H Bradhurst, S X Dou, H K Liu *Solid State Ion.* **116** 271 (1999)
214. S Buta, D Morgan, A van der Ven, M K Aydinol, G Ceder *J. Electrochem. Soc.* **146** 4335 (1999)
215. H-A Lehman, H Hesselbarth *Z. Anorg. Allg. Chem.* **313** 117 (1961)
216. G Chen, W Hao, Y Shi, Y Wu, S Perkowitz *J. Mater. Res.* **15** 583 (2000)
217. R Stoyanova, E Zhecheva, E Kuzmanova, R Alcantara, P Lavela, J L Tirado *Solid State Ion.* **128** 1 (2000)
218. K R Poeppelmeier, S H Thong *J. Less-Common Met.* **156** 191 (1989)
219. Y I Jang, Y M Chiang *Solid State Ion.* **130** 53 (2000)
220. B Ammundsen, J Desilvestro, T Groutso, D Hassell, J B Metson, E Regan, R Steiner, P J Pickering *J. Electrochem. Soc.* **147** 4078 (2000)
221. C D W Jones, E Rossen, J R Dahn *Solid State Ion.* **68** 65 (1994)
222. H Kobayashi, H Shigemura, M Tabuchi, H Sakaebe, K Ado, H Kageyama, A Hirano, R Kanno, M Wakita, S Morimoto, S Nasu *J. Electrochem. Soc.* **147** 960 (2000)
223. C Julien, G A Nazri, A Rogier *Solid State Ion.* **135** 121 (2000)
224. Yu D Tret'yakov, O A Brylev *Ros. Khim. Zh.* **44** 10 (2000) [d]
225. C A Vincent *Solid State Ion.* **134** 159 (2000)

[a] — *Russ. J. Inorg. Chem. (Engl. Transl.)*
[b] — *Inorg. Mater. (Engl. Transl.)*
[c] — *Russ. J. Phys. Chem. (Engl. Transl.)*
[d] — *Mendeleev Chem. J. (Engl. Transl.)*

Russian Chemical Reviews **70** (9) 791 – 800 (2001) © 2001 Russian Academy of Sciences and Turpion Ltd

DOI 10.1070/RC2001v070n09ABEH000669

Characteristic features of heterophase polymerisation of styrene with simultaneous formation of surfactants at the interface

N I Prokopov, I A Gritskova

Contents

I. Introduction 791
II. Surface properties of the potassium salts of carboxylic acids with alkyl substituents of different lengths and the composition of styrene emulsions prepared during their formation at the interface 792
III. Bulk properties of the salts of carboxylic acids sparingly soluble or virtually insoluble in water and the composition of styrene emulsions formed in parallel with their synthesis at the interface 794
IV. Synthesis of polystyrene suspensions with a narrow particle size distribution under the conditions of formation of surfactants at the interface 794
V. Conclusion 799

Abstract. Data on the heterophase polymerisation of styrene under conditions of surfactant formation at the monomer – water interface are generalised. A new, in principle, approach is proposed the essence of which is to obtain a monomer emulsion simultaneously with the synthesis of an emulsifier at the monomer – water interface and with initiation of the polymerisation in the interfacial layer. The preparation of surfactants at the interface allows one to control efficiently the degree of dispersion and the stability of the emulsions formed. By varying the nature of the acid and the metal counter-ion used in the surfactant synthesis at the interface, it is possible to change the interfacial tension, to influence the microemulsification, disintegration of the monomer, and the formation of structure of interfacial adsorption layers. The mechanism of formation of polymer-monomeric particles as well as their diameter and size distribution depend substantially on the solubility of the resulting surfactants in water. The bibliography includes 47 references.

I. Introduction

For several decades, researchers' assumptions concerning the compositions of monomer emulsions and the patterns of emulsion polymerisation have been based on the Harkins – Yurzhenko views; these also underlie the only existing quantitative theory (the Smith – Ewart theory).[1–4] However, numerous deviations of experimental data from theoretical predictions have stipulated the search for new approaches to the description of this process. These deviations have been detected even in a study of styrene polymerisation initiated by potassium persulfate carried out in the presence of an ionic emulsifier, which is exactly the reaction that served initially as the basis for the Smith – Ewart theory. The problem of description of emulsion polymerisation became especially topical after the appearance of results which could not be predicted by existing theories. Thus the occurrence of a quasi-spontaneous microemulsification of the monomer at phase interface has been observed;[5,6] polystyrene microbeads with a narrow size distribution have been prepared in the absence of surfactants;[7,8] the governing role of the composition of monomer emulsions in the mechanism of formation of polymer-monomeric particles (PMP) and its influence on the particle size distribution have been established.[9–14]

Detailed study of emulsions of monomers with various natures — styrene, methyl methacrylate, chloroprene, isoprene, mixtures of polar and non-polar monomers (for example, styrene and methacrylic acid) —has shown[15–19] that the emulsion composition and the degree of dispersion can be controllable. For example, the addition of water-insoluble surfactants to the monomer phase of the emulsion or to the other phase gives rise to emulsions consisting mainly of monomer microdroplets. Meanwhile, emulsions prepared in the presence of sodium alkylsulfonate insoluble in the monomer consist of emulsifier micelles and monomer macrodroplets. Thus, the procedure used to prepare the initial emulsion of the monomer (or monomers) can pre-determine the particle diameter in the polymer suspension and the size distribution of particles.

It has been proposed to perform heterophase polymerisation of monomers with simultaneous synthesis of a surfactant at the phase interface in order to control the emulsion composition. This polymerisation method differs essentially from the commonly accepted one,[20–26] as becomes obvious already when the initial monomer emulsion is prepared.

Traditionally, a monomer and an aqueous solution of an emulsifier are stirred at a rotational velocity of 600 – 800 rpm until a uniform emulsion is produced. The size of monomer droplets in this emulsion depends on the rotational velocity, interfacial tension ($\sigma_{1,2}$) and temperature. The size of monomer droplets and the nature of the surfactant influence the emulsion stability. Various stability factors act in the interfacial adsorption layer (IAL). The surfactant concentration in the IAL is determined by the surfactant capability of being adsorbed at the surface of droplets. Since the surfactant concentration is usually higher than the critical micelle concentration (CMC), it is generally accepted that the initial emulsion consists of surfactant micelles, which solubilise the monomer, and of monomer macrodroplets.

The method used to prepare the initial emulsion for polymerisation under conditions of surfactant synthesis at the interface differs in principle from the above-described one. In this case, a long-chain carboxylic acid is dissolved preliminarily in the mono-

N I Prokopov, I A Gritskova M V Lomonosov Moscow State Academy of Fine Chemical Technology, prosp. Vernadskogo 86, 117571 Moscow, Russian Federation. Fax (7-095) 434 87 11. Tel. (7-095) 434 86 44.
E-mail: fun-latex@mtu-net.ru (N I Prokopov).
Tel. (7-095) 247 04 43 (I A Gritskova).

Received 26 March 2001
Uspekhi Khimii **70** (9) 890 – 900 (2001); translated by Z P Bobkova

mer phase, while an alkali is dissolved in the aqueous phase. This procedure gives a fine emulsion of the monomer, owing to the significant decrease in the interfacial tension caused by the fact that the emulsifier formed in the neutralisation reaction is accumulated in the interfacial layer. In this case, the interfacial tension decreases much more significantly than in the case when the same emulsifier is adsorbed on the surface of droplets from the aqueous phase in the conventional preparation of the emulsion (< 1 and ~ 10 mN m^{-1}, respectively).

The degree of dispersion of the resulting emulsion must also depend on the nature of the emulsifier synthesised at the interface. For example, if the emulsifier is soluble both in the monomer and in water, its mass transfer through the interface takes place in conformity with the partition coefficient, the stability of the interfacial boundary is degraded, and the monomer undergoes disintegration and microemulsification. In this case, apart from monomer droplets, the resulting emulsion contains monomer microdroplets and emulsifier micelles if the emulsifier content in the aqueous phase is greater than that required for stabilisation of monomer droplets and microdroplets.

The composition of the monomer emulsion determines the mechanism of formation and the diameter distribution of the PMP. When the PMP are formed from emulsifier micelles and monomer microdroplets, the polymer suspension contains particles of different sizes (with diameters from 0.06 to 0.4 μm) and is characterised by a broad size distribution.

Polymerisation of an emulsion consisting of monomer microdroplets affords a polymer suspension with an average particle diameter of 0.08 to 0.7 μm, depending on the structure and the surface-active properties of the emulsifier synthesised at the interface.

The particle size distribution (PSD) depends on the stability of the PMP during the synthesis. If some factors providing stabilisation of the interfacial adsorption layer arise at initial stages of monomer conversion, the PSD is narrow.

This review describes new approaches to the control of the composition of monomer emulsions. These methods allow the preparation of polymer suspensions with particles of different diameters and with a narrow PSD.

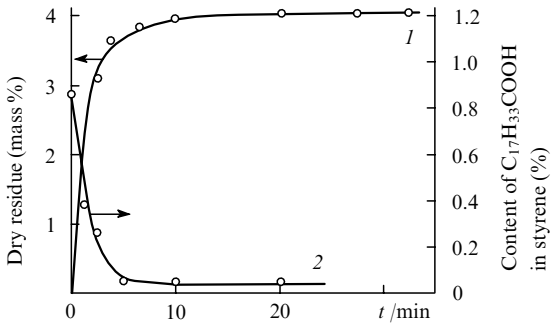

Figure 1. Content of potassium oleate in water (*1*) and oleic acid in styrene (*2*) *vs.* duration of neutralisation.

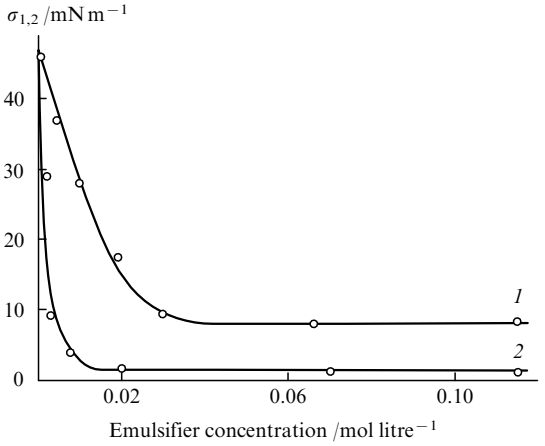

Figure 2. Interfacial tension at the interfaces 'aqueous solution of potassium laurate–styrene' (*1*) and 'aqueous solution of potassium hydroxide–styrene solution of the lauric acid' (*2*) *vs.* emulsifier concentration.

II. Surface properties of the potassium salts of carboxylic acids with alkyl substituents of different lengths and the composition of styrene emulsions prepared during their formation at the interface

In several studies,[20–26] salts of oleic acid, salts of saturated fatty acids with the $C_{11}-C_{25}$ hydrocarbon chains, and the potassium soap from disproportionated rosin have been used as the objects of investigation.

The interfacial tension $\sigma_{1,2}$ at the styrene–water interface decreases from 42.2 to 30.8 mN m^{-1} over the homologous series from lauric to cerotic acid. For none of the acids does the interfacial tension depend on the time the surface has existed, *i.e.*, adsorption of the acid is not the limiting stage of the surfactant formation. However, the interfacial tension sharply decreases with an increase in the alkali concentration to reach ~ 1 mN m^{-1} for an alkali content in water of 10^{-2} mass %.

Figure 1 presents the data on the neutralisation kinetics of oleic acid with potassium hydroxide at the styrene–water interface at a temperature of 20 °C. The data were gained by gravimetry (curve *1*) and refractometry (curve *2*). It can be seen that neutralisation is almost completed over a period of several minutes. After 5–10 min, the concentration of potassium oleate in water becomes ~ 4 mass %.

The substantial difference between the interfacial tension at the interface between styrene solutions of lauric acid of various concentrations and aqueous solutions of alkali in the synthesis of potassium laurate and the interfacial tension for the adsorption of the same emulsifier from the aqueous phase is illustrated in Fig. 2.

When potassium laurate is synthesised at the interface, the interfacial tension is less than 1 mN m^{-1}, whereas this value for the interface between an aqueous solution of potassium laurate, on the one hand, and styrene, on the other hand, is $\sigma_{1,2} = 8$ mN m^{-1}.

The isotherms of interfacial tension were used to calculate the limiting adsorption value (Γ_{max}), the area occupied by one surfactant molecule in a saturated adsorption layer (S_{min}) and the surface activity of the surfactant (G) (Table 1). It can be seen that for the formation of emulsifiers at the interface, the G value markedly increases, Γ_{max} also increases, and S_{min} decreases.

The procedure of formation of emulsions should have a pronounced influence on the formation and properties of the interfacial adsorption layers on the surface of monomer droplets.[27–30] Indeed, when the monomer is emulsified by an aqueous solution of an emulsifier, the interfacial layer is formed by the molecules of a highly ionised carboxylic acid salt adsorbed from the aqueous phase, and when the emulsifier is synthesised at the interface, this layer is formed initially by the adsorbed molecules of the carboxylic acid and after neutralisation, it is formed by salt molecules.

The instability of the phase interface caused by the chemical synthesis of the emulsifier taking place in the boundary layer and the emulsifier mass transfer to the aqueous phase, which are accompanied by the transformation of the chemical reaction energy directly into the surface energy,[31–33] result in effective fragmentation of monomer droplets and monomer microemulsification. This influences, first of all, the average diameter of the droplets of the monomer emulsion. If the emulsion is prepared

Table 1. Surface properties of emulsifiers at the interface.

Emulsifier	The way of introducing the emulsifier [a]	$10^6\Gamma_{max}$ /mol m^{-2}	S_{min} /nm^2	G /mN m^2 mol^{-1}
Potassium laurate	A	4.0	0.41	18
	B	6.4	0.26	84
Potassium myristate	A	3.6	0.45	30
	B	8.4	0.22	67
Potassium palmitate	A	4.8	0.35	44
	B	10.3	0.16	82
Potassium oleate	A	4.0	0.41	27
	B	6.4	0.26	135
Potassium behenoate	A	2.0	0.81	4
	B	13.4	0.12	21
Potassium cerotate	A	2.9	0.58	12
	B	9.6	0.18	33

[a] A — the emulsifier is introduced in the aqueous phase, B — the emulsifier is formed at the interface.

under conditions of synthesis of potassium laurate and the potassium soap from disproportionated rosin at the interface, the average diameter of monomer droplets is $\sim$2 times smaller than that for the case of monomer emulsification by an aqueous solution of the surfactant (10 and 20 μm, respectively).

Study of monomer microemulsification under static conditions has shown [20] that the intensity of this process depends on the method for the preparation of emulsions. In a styrene emulsion prepared with the formation of the emulsifier at the interface, the volume of the microemulsion layer is several times as great as that at the interface between styrene and an aqueous solution of the emulsifier. This can be clearly seen when considering the preparation of styrene emulsions by these methods in the presence of rosin soap (Fig. 3). A large volume of the microemulsion increases the emulsion stability. For example, styrene emulsions prepared with the formation of ionogenic surfactants at the interface are 5–10 times as stable as the emulsions formed upon emulsification of the monomer by an aqueous solution of the emulsifier.

Procedures making use of small-angle X-ray diffraction and electron microscopy of liquid–liquid systems have been developed to study the composition of styrene emulsions. Using these procedures, the degrees of dispersion of liquid–liquid systems can be studied without hardening the monomer phase.[34, 35]

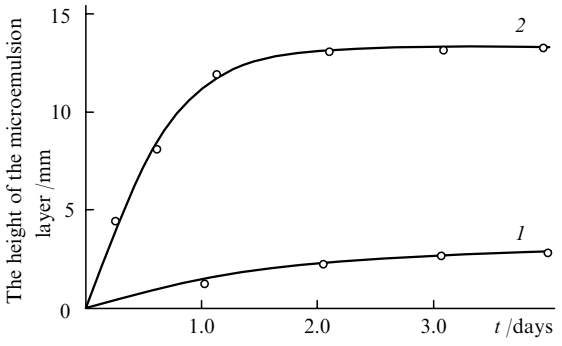

Figure 3. Variation of the height of a microemulsion layer under static conditions at the interfaces 'styrene–aqueous solutions of the rosin soap' (*1*) and 'styrene solution of rosin–an equimolar aqueous solution of KOH' (*2*). Emulsifier concentration is 1.1×10^{-2} mol litre^{-1}, 25 °C.

X-Ray diffraction and electron-microscopic investigations [22, 23] of styrene emulsions prepared with the synthesis of potassium carboxylates at the interface showed that they contain particles of various sizes, namely, monomer macrodroplets with a size of not more than 10 μm, monomer microdroplets 0.03–0.04 μm in diameter, and emulsifier micelles with a size of 0.003–0.005 μm. The surfactant concentration calculated for the aqueous phase equals 2 mass %–5 mass %, which is 50–100 times as high as the CMC.

If the concentration of the emulsifier formed at the interface is decreased to the level sufficient only for stabilisation of monomer microdroplets, the surfactant content in the aqueous phase would be lower than the CMC and the formation of emulsifier micelles would become impossible. In this case, the emulsion would mainly consist of monomer microdroplets. This situation has been realised in the preparation of styrene emulsions under conditions of synthesis of potassium carboxylates at the interface. It can be seen from the data presented in Table 2 that the emulsifier concentration corresponding to the minimum $\sigma_{1,2}$ values in the aqueous phase is several times lower than that corresponding to complete neutralisation of the acid. This means that some of the surfactant is consumed for the formation of the adsorption layer on the surface of monomer droplets and microdroplets.

Table 2. Variation of the emulsifier concentration during neutralisation of the acid under static conditions (25 °C, overall time of reaction 24 h).

Emulsifier	Total emulsifier concentration /mass %	Emulsifier concentration in the aqueous phase at $\sigma_{1,2\,min}$ /mass %
Potassium laurate	0.15	0.08
(CMC 0.22%)	0.25	0.10
	0.50	0.21
	4.00	1.00
Potassium oleate	0.15	0.02
(CMC 0.04%)	0.25	0.04
	0.50	0.12
	4.00	1.50

The critical micelle concentration of the emulsifier in the aqueous phase is attained only in the case where the acid concentration in the monomer phase exceeds 0.5 mass % with respect to styrene.[36] As was to be expected, the lithium salts of acids have lower concentrations in the aqueous phase than the potassium salts.

Since all the salts synthesised at the interface are soluble in water, effective mass transfer of these salts to the aqueous phase takes place as well as quasi-spontaneous emulsification of the monomer and the formation of microemulsions as a quite visible white belt.

Under dynamic conditions, the CMC of the emulsifier in the aqueous phase is attained when the acid concentration in the monomer phase is >1 mass %. This is twice that in the synthesis of surfactants under static conditions; this is explained by the increase in the interfacial area owing to stirring and to the consumption of the emulsifier for the stabilisation of monomer droplets and microdroplets.

Thus, if the concentration of the emulsifiers (potassium carboxylates) formed at the interface is 0.5 mass % relative to the monomer, the initial emulsion of styrene contains only monomer microdroplets because the rest of the emulsifier is spent for their stabilisation. This means that, upon initiation of polymerisation in these emulsions, the polymer-monomeric particles would be formed from monomer droplets and the polymer suspensions would have a narrow particle size distribution.

III. Bulk properties of the salts of carboxylic acids sparingly soluble or virtually insoluble in water and the composition of styrene emulsions formed in parallel with their synthesis at the interface

The solubility of lithium salts of carboxylic acids in water exceeds only slightly the CMC. Thus the solubilities of lithium laurate, stearate and oleate at 50 °C are 0.28 mass %, 0.10 mass % and 0.13 mass %, while the CMC values are 0.25 mass % – 0.30 mass %, 0.07 mass % and 0.12 mass %, respectively.[37] The solubilities of the barium, calcium and zinc salts of the same acids in water do not exceed 0.004 – 0.008 g per 100 g of water. The Li, Ba, Ca and Zn salts are also virtually insoluble in the organic phase, in particular, in styrene.[37]

Analysis of the interfacial tension isotherms shows that the surface tension for the formation of lithium, barium, calcium and zinc myristates at the styrene – water interface is of the order of 21 – 31 mN m^{-1}, whilst potassium myristates decrease the interfacial tension almost to zero (Fig. 4).

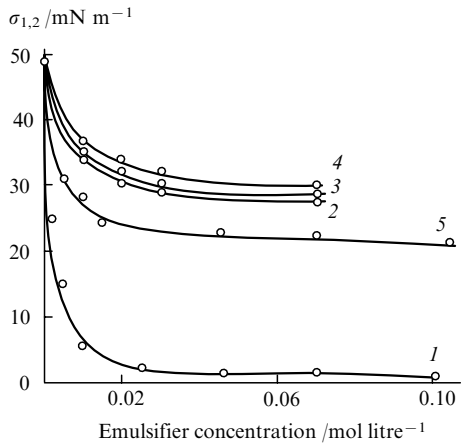

Figure 4. Interfacial tension at the interfaces 'styrene solution of myristic acid – aqueous solution of potassium (*1*), barium (*2*), calcium (*3*), zinc (*4*), or lithium (*5*) hydroxide' *vs*. emulsifier concentration. The time of droplet formation is 20 s, 20 °C.

The surfactants insoluble in both phases exhibit a much lower (by a factor of 10 – 20) surface activities than water-soluble potassium myristate (Table 3). Lithium myristate occupies an intermediate position; its surface activity at the styrene – water interface is 3 – 6 times higher than those of the barium, calcium, and zinc salts but is ~3 times lower than the activity of the potassium salt.

Emulsions prepared under the conditions of formation of potassium myristate at the interface are 2 – 3 times as stable as emulsions prepared in parallel with the synthesis of lithium, barium, calcium and zinc salts (all other conditions being the same), which is due to the formation of microemulsions at the surface of monomer droplets.

Table 3. Surface properties of emulsifiers at the styrene – water interface.

Emulsifier	G /mN m^2 mol^{-1}	$\sigma_{1,2\,min}$ /mN m^{-1}
Potassium myristate	67.0	< 0.5
Lithium myristate	22.5	20.6
Barium myristate	7.3	27.1
Calcium myristate	5.4	28.7
Zinc myristate	3.5	30.2

Table 4. Size of particles in an emulsion of styrene prepared with simultaneous synthesis of surfactants of various natures at the interface (styrene : water volume ratio of the phases 1 : 2, surfactant concentration in the aqueous phase 0.084 mol litre^{-1}).

Surfactant	Method used to determine the particle size [a]	Particle size [b] /nm
Potassium stearate	SAXD	3.5
	SAXD	34
	EM	36
Lithium stearate	LCS	120
	EM	115
Lithium laurate	LCS	210
	EM	200
Barium stearate	LCS	500
Zinc stearate	LCS	490

[a] SAXD is small-angle X-ray diffraction, EM is electron microscopy, LCS is laser correlation spectroscopy; [b] The first line in the column implies the size of surfactant micelles, while the other numbers are the sizes of monomer microdroplets.

It has been shown by electron microscopy and laser correlation spectroscopy that, when poorly water-soluble or virtually water-insoluble surfactants, namely, lithium and barium stearates, are employed, the emulsions formed during their synthesis at the interface consist of macro- and microdroplets of the monomer, the size of the latter ranging from 120 to 500 nm, and no emulsifier micelles are present.

The data on the degree of dispersion of the styrene emulsions prepared simultaneously with the synthesis of various surfactants at the interface are summarised in Table 4. These data indicate that the composition of a styrene emulsion depends substantially on the method of its preparation and that it is much more intricate than it has been considered in the classical works by Smith – Ewart, Yurzenko, and their pupils.[3, 4]

The investigations have shown that the reaction of surfactant formation at an interface affects substantially the surface phenomena in the interfacial adsorption layers and can serve as a powerful factor for controlling the dispersivity of emulsions, and, hence, the mechanism of formation of particles.

IV. Synthesis of polystyrene suspensions with a narrow particle size distribution under the conditions of formation of surfactants at the interface

Research into the synthesis of polymer dispersions with a specified diameter of particles and a narrow particle size distribution has shown that these properties are mainly dictated by the granulometric composition of the initial emulsion of the monomer, the time of formation of the PMP, and the creation of conditions which ensure stability of emulsions in the interfacial layer.[38, 39] These factors depend on many parameters, most of all, on the conditions chosen for the preparation of emulsions and for polymerisation.

The granulometric composition of the initial emulsion of the monomer and, hence, the mechanism of PMP formation can be readily controlled by selecting appropriate surfactants and an appropriate way of introducing them into the system (either as separate solutions in water or in the monomer or as solutions both in water and in the monomer the concentration of which is determined by the surfactant solubility in these phases) and by the synthesis of surfactants at the interface.[14, 18, 26] Any of these methods gives monomer emulsions characterised by different degrees of dispersity due to different concentrations of the surfactant at the interface. Correspondingly, the interfacial tensions also differ significantly.

The time of formation of the PMP is a very important factor which largely determines the diameter and the size distribution of particles; this factor depends considerably on the efficiency of initiation of polymerisation and on the process temperature.

Finally, the stability of the PMP during polymerisation is ensured by the existence of factors of PMP stability acting in the interfacial adsorption layers (electrostatic or structure-mechanical factor or both). These factors also influence the diameter of particles and their size distribution.

The duration of the stage of PMP formation can vary from several minutes to several hours. It depends appreciably on the granulometric composition of the emulsion and the efficiency of initiation. At this stage, particles can coalesce due to instability giving rise to a coagulum. Such a phenomenon has been observed, for example, in suspension polymerisation of styrene in the presence of poly(vinyl alcohol), starch, or gelatin as stabilisers. It is at the stage of PMP formation that the diameter of particles of a polymer suspension can be controlled by affecting their coalescence in one or another way. This process is extremely complex. In order to eliminate the coagulum formation, surfactants are added to the system. They, in turn, can induce the formation of new PMP and extend markedly the size distribution of particles.

When styrene polymerisation is carried out in the presence of organosilicon surfactants, insoluble in water and incompatible with the resulting polymer, this stage occurs in a different way.[40,41] In this case, a strong interfacial layer consisting of the surfactant displaced by the polymer and of the polymer itself is formed on the PMP surface at relatively low degrees of monomer conversion. The diameter of particles in a polymer suspension can be controlled by varying the nature of the surfactant and the temperature.

Performing styrene polymerisation with simultaneous synthesis of a surfactant at the interface ensures, on the one hand, the possibility of realisation of either emulsion or suspension polymerisation mechanism giving rise to polymer suspensions in which the diameter of particles can differ by an order of magnitude and, on the other hand, it ensures stability of these suspensions because the surfactant concentration in the interface is higher than that in the case where the surfactant is adsorbed onto the PMP surface from the aqueous phase. Thus polymerisation can be carried out at lower concentrations of the surfactant and gives polymer suspensions more stable during storage or modification (*e.g.*, by proteins).

The morphology of particles prepared under conditions of surfactant synthesis at the interface should differ essentially from that resulting from conventional synthesis.

When emulsions are prepared under ordinary conditions, the interfacial adsorption layer is formed upon adsorption of the emulsifier from the aqueous phase first on monomer droplets and then on the PMP. When polymerisation is carried out with synthesis of an emulsifier at the interface, the initial monomer emulsion as such does not actually exist. In this case, simultaneously with vigorous disintegration (microemulsification) of monomer droplets, initiation of polymerisation takes place; the resulting microdroplets capture radicals being thus converted into the PMP. In parallel, the interfacial adsorption layers are formed from the acid molecules dissolved in the monomer, the salt molecules resulting from neutralisation of the acid, and polymer molecules (polymerisation occurs in the area of the PMP adsorption layers). The preliminary dissolution of the acid in the monomer ensures the optimal orientation of the acid and salt molecules in the interfacial layer, which gives rise to the electrostatic factor of stabilisation. Due to the high polymer concentration in the interfacial layer, the viscosity of the IAL substantially increases and the structure-mechanical factor of stabilisation also starts to be effective.

The synthesis of water-insoluble surfactants at the interface should yield particles with the 'core–shell' type structure. The formation of these particles is responsible for the specific features of polymerisation kinetics. Even at early stages of the process, the PMP become a sort of microreactors in which polymerisation progresses involving the monomer and the radicals present therein. In this case, the rate of polymerisation and the PMP diameter should not depend on the concentration of the initiator, and an increase in the surfactant concentration would entail an increase in the polymer molecular mass due to the decrease (caused by diffusion restrictions) in the concentration of radicals which enter the PMP at an initial stage of the process.

Thus, by conducting polymerisation of monomers with simultaneous synthesis of surfactants at the interface, one can obtain polymer suspensions which differ not only in the particle diameter and size distribution but also in the morphology of particles. For example, in the case of synthesis of water-soluble sodium or potassium carboxylates, polymeric suspensions with a broad size distribution of particles should be produced because the initial emulsion contains monomer microdroplets and emulsifier micelles from which the PMP are formed.

Preparation of polymer suspensions with a narrow particle size distribution by polymerisation under conditions of the synthesis of water-soluble surfactants at the interface proved possible only when the concentrations of the monomer (volume ratio of the phases) and the surfactant were such that the surfactant being formed was consumed only for stabilisation of the monomer microdroplets and of the PMP formed from them, *i.e.*, when virtually no surfactant micelles were present in the aqueous phase.

The foregoing is illustrated by experimental data. Figure 5 shows the kinetic curves for the emulsion polymerisation of styrene under conditions of formation of potassium salts of carboxylic acids at the interface. In these experiments, aliphatic acids with alkyl substituents from C_{11} (lauric acid) to C_{25} (behenic acid) were used; the conditions of polymerisation were identical. It can be seen that polymerisation occurs without any induction period, which could have corresponded to the stage of formation of polymer-monomeric particles, and the high rate of the process is retained almost to the complete monomer conversion. The reaction system is stable, and the final polymer suspension contains no coagulum. The stability of particles in the suspension is largely ensured by the action of the electrostatic factor of stabilisation, as indicated by the high ξ-potential of particles (Table 5).

It follows from the data given in Table 5 that the polymerisation rate w_p somewhat increases as the alkyl radical of the

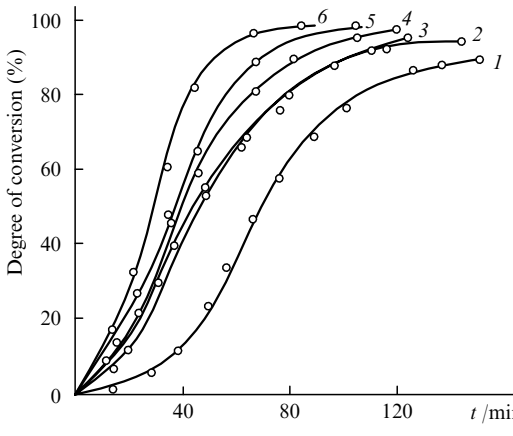

Figure 5. Yield of polymer *vs.* time of styrene polymerisation in the presence of emulsifiers.
Emulsifier: (*1*) potassium laurate; (*2*) potassium myristate; (*3*) potassium palmitate; (*4*) potassium stearate; (*5*) potassium cerotate; (*6*) potassium behenoate. Polymerisation temperature 50 °C, monomer : water = 1 : 2 (by volume), concentration of the initiator (azobisisobutyronitrile) in styrene 5×10^{-2} mol litre^{-1}, emulsifier concentration in the aqueous phase 8.4×10^{-3} mol litre^{-1}.

Table 5. Properties of polymers and polymer suspensions prepared in the polymerisation of styrene with simultaneous formation of the potassium salts of fatty acids at the interface.

Surfactant	w_p (% min^{-1})	10^{-6} MM	d /nm	n	ξ-Potential /mV
Potassium laurate	0.68	2.3	102	1.19	−52
Potassium myristate	0.73	3.3	93	1.22	−47
Potassium palmitate	0.83	3.6	90	1.20	−49
Potassium stearate	0.88	4.0	80	1.20	−50
Potassium cerotate	0.92	4.2	76	1.07	−46
Potassium behenoate	0.94	4.2	70	1.07	−45

Note. Here and in other tables: MM is the viscosity-average molecular mass, d is the average particle diameter, n is the polydispersity coefficient.

surfactant becomes longer; this is due to a slight change in the number of PMP formed.

The molecular mass (MM), equal to $(2.5-4.2)\times10^6$, and the molecular-mass distribution (MMD) of the polymers correspond to known published data on the emulsion polymerisation of styrene initiated by an oil-soluble initiator, namely, azobis(isobutyronitrile)[39] (Fig. 6). For low degrees of monomer conversion (1% and 5%), the MMD curves exhibit two peaks, one at lower and one at higher molecular masses (MM ≈ 100 000 and MM > 1 000 000, respectively). When the degree of monomer conversion increases to 90%, the lower-molecular-mass peak substantially decreases or even disappears. The presence of the lower-molecular-mass peak is due to the fact that polymerisation occurs both in the bulk PMP and in the emulsifier micelles.[13, 39]

As noted above, an increase in the length of the alkyl radical is accompanied by a decrease in the solubility of its salts in the aqueous phase. Whereas potassium laurate, myristate, palmitate, and stearate are soluble in water fairly readily (30 mass % – 70 mass %), potassium cerotate and behenoate are much less soluble (3 mass % – 5 mass %).[24] This should influence the mechanism of PMP formation. In the former case, the particles are formed by a mixed mechanism — both from micelles of the surfactant which solubilises the monomer and from the monomer microdroplets. In the latter case, the particles are mainly formed from monomer microdroplets. Indeed, polymer suspensions formed under conditions of synthesis of potassium laurate at the interface have very broad particle size distributions, whereas suspensions prepared with the synthesis of potassium behenoate are virtually monodisperse (Fig. 7).

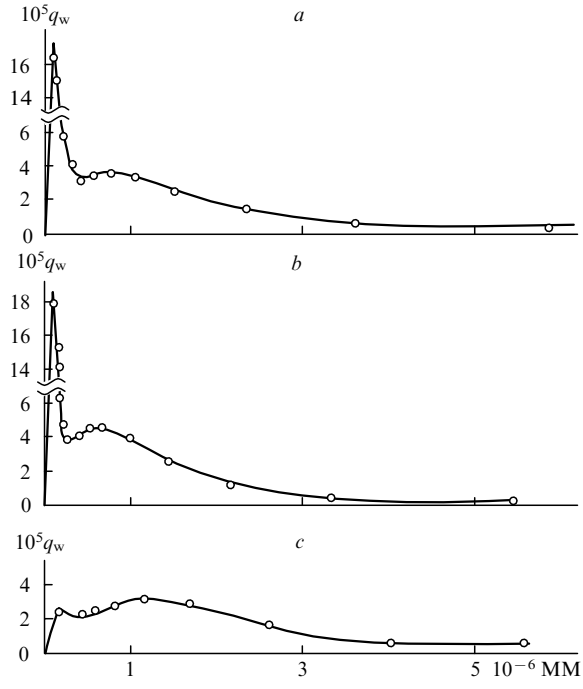

Figure 6. Molecular-mass distribution (q_w) of polystyrene prepared by polymerisation of the monomer under conditions of formation of potassium laurate at the interface for degrees of conversion of (%): (*a*) 1; (*b*) 5, (*c*) 90.

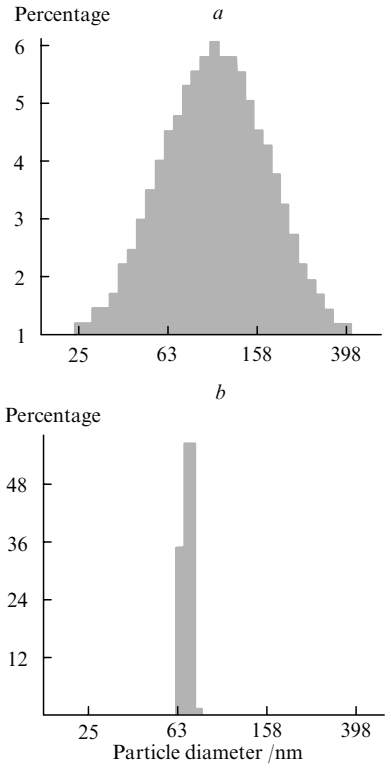

Figure 7. Particle size distribution for a polystyrene suspension prepared with simultaneous formation of potassium laurate (*a*) and potassium behenoate (*b*) at the interface.

If the emulsifier formed at the interface is poorly soluble in water (for example, lithium salts of carboxylic acids), the initial emulsion of styrene, as shown above, contains only microdroplets of the monomer, the emulsifier being spent entirely for their stabilisation.

Polymerisation of styrene under conditions of the synthesis of lithium carboxylates has some distinctive features (Fig. 8), which are due, first of all, to the fact that these salts are less soluble than the potassium salts. Thus the solubility of lithium myristate in water does not exceed 0.28 mass % and the surface activity of this compound is lower. Therefore, when styrene polymerisation is conjugated with the synthesis of lithium salts of fatty acids, the mean diameter of particles of polymer suspensions is 1.5 – 3 times greater than that attained with potassium salts, all other factors being the same (Table 6). The particle size distribution in the 'lithium' suspensions is fairly narrow because all the emulsifier is consumed for the formation of the interfacial adsorption layer of droplets, microdroplets and the polymer-monomeric particles formed from them.

The rate of polymerisation and the molecular mass of the polymer prepared in the presence of lithium myristate are lower than those with lithium laurate because the number of PMP produced in this case is smaller.

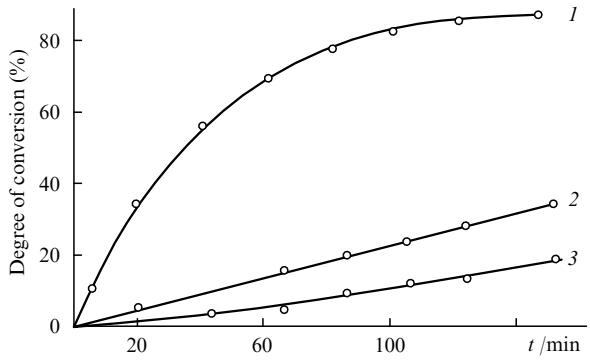

Figure 8. Yield of polymer *vs.* time of styrene polymerisation in the presence of emulsifiers. Emulsifier: (*1*) lithium oleate; (*2*) lithium laurate; (*3*) lithium stearate. The volume phase ratio monomer : water = 1 : 10, initiator concentration in water 0.1 mass %, emulsifier concentration in water 0.5 mass %.

Table 6. Characteristics of the particles of polymer suspensions prepared while performing styrene polymerisation simultaneusly with the synthesis of ionogenic surfactants at the interface (temperature 70 °C, styrene : water phase ratio 1 : 10, initiator concentration 0.1 mass %).

Surfactant	c (mass %) [a]	d /nm	n' (%) (see [b])	ξ-Potential /mV	10^{-6} MM
Lithium laurate	0.25	258	5	−35	1.2
Lithium stearate	0.50	220	6	−34	1.3
Potassium laurate	0.25	193	4	−48	3.8
Potassium stearate	0.50	65	6	−50	4.2

[a] Emulsifier concentration in the aqueous phase; [b] size variation coefficient.

Attempts to synthesise polymer suspensions consisting of larger particles with a narrow size distribution failed: either the reaction system was unstable, resulting in a substantial amount of the coagulum, or the particle size distribution was too broad.

Polymerisation of styrene accompanied by the formation of barium, calcium and zinc salts of carboxylic acids taken in the same concentration occurs in a different way. This was demonstrated in relation to myristates. In this case, the diameter of particles scarcely depends on the metal nature and equals ~800 nm (Table 7). The average diameter of particles also remained nearly constant as the degree of monomer conversion changed, and the polymer suspensions had a narrow distribution

Table 7. Polymerisation of styrene under simultaneous synthesis of myristates at the interface.

Surfactant	$w_p\,10^2$ /mol litre^{-1} s^{-1}	10^{-5} MM	d /nm (see [a])	ξ-Potential /mV
Barium myristate	5.5	6.7	700	−29.5
Calcium myristate	5.4	6.6	800	−25.7
Zinc myristate	4.9	6.2	850	−23.2

Note. Here and in Tables 8, 9 and 11: polymerisation temperature 70 °C, volume ratio of the phases 1 : 10, potassium persulfate concentration in relation to the monomer 1 mass %, emulsifier concentration in the aqueous phase 0.4 mass %.

[a] Stability of all the particles to electrolytes was 0.2 mol litre^{-1}.

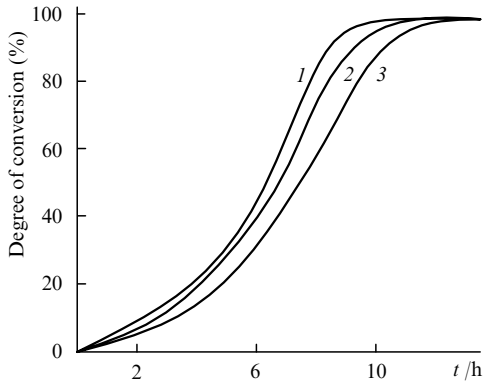

Figure 9. Yield of polymer *vs.* time of styrene polymerisation under conditions of formation of emulsifiers at the interface. Emulsifier: (*1*) barium myristate; (*2*) calcium myristate, (*3*) zinc myristate. Here and in Figure 10: polymerisation temperature 70 °C, monomer : water volume phase ratio 1 : 10, potassium persulfate concentration in relation to the monomer 1 mass %, emulsifier concentration in the aqueous phase 0.4 mass %.

of particles over diameters. This implies that, from the very moment of formation of the polymer-monomeric particles, a strong interfacial layer appears on their surface and protects the particles from coalescence.[42, 43]

The kinetic curves for styrene polymerisation under the conditions of synthesis of barium, calcium and zinc myristate at the interface are presented in Fig. 9. The curves are all S-shaped, which is typical of heterophase polymerisation; the formation of polymer-monomeric particles occurs over a period of 120–240 min, and the time it takes to achieve the complete conversion of styrene is 10–12 h.

It is of interest to compare these data with the results obtained for styrene polymerisation under conditions in which the monomer emulsions were formed *via* emulsification of the monomer with aqueous suspensions of insoluble salts of myristic acid. The resulting polymer suspension had low stability, and the average particle diameter or the size distribution could not be determined due to the high content of coagulum (more than 30%). Thus, polymerisation with the synthesis of surfactant at the interface has certain advantages pointing to good prospects of this method.

As was to be expected, the change in the concentration of the insoluble salt synthesised at the interface (Table 8) barely influences the rate of polymerisation, the particle diameter and the particle size distribution, which remains narrow over the whole range studied. The increase in the polymer molecular mass with an increase in the concentrations of the insoluble salts synthesised at the interface is, apparently, due to the decrease in the concentration of radicals entering the PMP from the aqueous phase, caused by the increase in the thickness and viscosity of the

Table 8. Effect of the emulsifier concentration (barium myristate) on the rate of styrene polymerisation, the size of particles in the polymer suspensions and on the molecular mass of the resulting polymer.

Emulsifier concentration in the aqueous phase (mass %)	$w_p\,10^2$ /mol litre^{-1} s^{-1}	10^{-5} MM	d /nm
0.8	5.5	7.0	695
0.4	5.5	6.7	700
0.1	5.3	6.4	720
0.05	5.2	5.6	780
0.025	4.9	4.4	820
0.0125	4.8	2.0	850
0.00625	4.7	1.5	920

interfacial adsorption layer, resulting in the appearance of diffusion restrictions.

The stability of PMP during polymerisation is ensured by the structure-mechanical and electrostatic factors of stabilisation acing in the interfacial layer. The ξ-potential of the particles in a polymer suspension is -27 mV, which is much lower than that for styrene polymerisation under the same conditions but without an emulsifier (-70 mV).[44] The low ξ-potential can be accounted for by diffusion restrictions arising due to a definite orientation of the functional groups of polymer chains at the interface.

Thus, styrene polymerisation accompanied by the synthesis of salts of myristic acid insoluble in both phases makes it possible to prepare polymer suspensions with a narrow particle size distribution (the particle diameter is 600–900 nm). The conditions of synthesis of these polymer suspensions are technologically simple and the reaction system remains stable during polymerisation.

Due to the low ξ-potentials, the particles of a polystyrene suspension stabilised by barium, calcium and zinc myristates prove unstable during immobilisation of bioligands in an isotonic solution. An increase in the stability of polymer suspensions without substantial change in the particle diameter and without deterioration of the narrow size distribution of particles can be attained by using the synthesis of mixtures of potassium and barium myristates at the interface during polymerisation.[45] When the content of the water-soluble potassium salt in the salt mixture is 6.25 mass % to 12.5 mass %, polymerisation gives rise to stable polymer suspensions with a mean particle diameter of 580–680 nm and a narrow particle size distribution (Table 9). An increase in the stability is explained by an increase in the ξ-potential of the particles to -40 mV.

Table 9. Dependence of the rate of styrene polymerisation, the molecular mass of the polymers and the average diameter of particles in a polymer suspension on the ratio of emulsifiers, barium and potassium myristates (the total concentration of emulsifiers in the aqueous phase was 0.4 mass %).

Emulsifier percentages		$10^2 w_p$ /mol litre^{-1} s^{-1}	10^{-5} MM	d /nm (see [a])
barium myristate	potassium myristate			
50	50	14.4	25	100
62.5	37.5	12.7	19	130
75	25	8.5	14	280
87.5	12.5	5.8	8.5	580
93.75	6.25	5.5	7.8	680

[a] For particles with sizes of 100 and 130 nm, the stability to electrolytes was 0.15 mol litre^{-1}; for other particles, it was 0.20 mol itre^{-1}.

It of interest to compare the properties of the polymer suspensions prepared under conditions of surfactant formation at the interface with the properties of those prepared by conventional polymerisation (*i.e.*, with emulsification of the monomer with an aqueous solution of an emulsifier) as well as the kinetic features of both processes. As an example, we shall consider polymerisation of styrene accompanied by the synthesis of myristic acid salts at the interface.

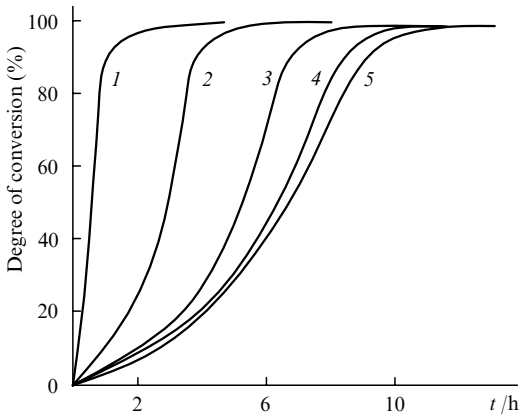

Figure 10. Yield of polymer *vs.* time of styrene polymerisation in the presence of emulsifiers. Emulsifier: (*1*) potassium myristate; (*2*) lithium myristate, (*3*) barium myristate, (*4*) calcium myristate; (*5*) zinc myristate.

The kinetic curves for styrene polymerisation with the synthesis of the myristates under discussion are presented in Fig. 10.

They all have an S-like shape, typical of heterophase polymerisation, and differ from one another in the duration of the non-steady-state stage of the formation of polymer-monomeric particles, the rate of polymerisation, the range of degrees of conversion in which the rate of the process is constant, and in the time required for the full monomer conversion. For example, polymerisation of styrene accompanied by the synthesis of potassium myristate starts almost immediately, while in the case of synthesis of barium, calcium, and zinc salts insoluble both in water and in the monomer, the formation of polymer-monomeric particles requires 120–240 min. The time periods required to attain complete conversion of styrene are also different: in the former case, polymerisation occurs over a period of 2.5–3 h and in the latter case, this takes 10–12 h.

For clarity, we shall compare the processes taking place in the PMP formed in the styrene polymerisation performed simultaneously with the synthesis of soluble and insoluble salts of carboxylic acids (Table 10). The concentration of free radicals during bulk polymerisation is known[46] to be usually about 10^{-7}–10^{-8} mol litre^{-1}, or 10^{12}–10^{13} radical ml^{-1}, *i.e.*, the volume per radical is, on average, 5×10^{-1}–5×10^{-2} μm^3. The microdroplets formed under conditions of synthesis of soluble surfactants at the interface have a volume of 10^{-3}–10^{-4} μm^3, which is much less than the volume per radical for bulk polymerisation. Therefore, each particle does not contain more than one radical; only when the termination rates are very low (for example, when radicals are fixed in the polymeric matrix of the interfacial layers), can a microdroplet contain several radicals. If the concentration of microdroplets in the system is 10^{14} ml^{-1}, the rate of initiation is close to that for bulk polymerisation

Table 10. Characteristics of styrene bulk polymerisation (I) and polymerisation in microdroplets of various sizes (II, III).

Characteristics	I	II [a]	III [b]
The number of particles	–	10^{14}–10^{15}	10^{12}–10^{13}
The number of radicals per particle	–	0.5	5–10
The total number of radicals in 1 ml of the system	10^{12}–10^{13}	0.5×10^{14}–0.5×10^{15}	0.5×10^{13}–0.5×10^{14}
Volume of the monomer per radical /μm^3	10^{-1}–10^{-2}	10^{-3}–10^{-4}	10^{-1}–10^{-3}
Rate of initiation /radical ml^{-1} s^{-1}	10^{12}–10^{13}	10^{12}–10^{13}	10^{12}–10^{13}
Average lifetime of radicals /s	1	10–100	5–10

[a] The size of microdroplets is 0.05–0.1 μm (water-soluble surfactants); [b] the size of microdroplets is 0.4–0.8 μm (water-insoluble surfactants).

($10^{-7}-10^{-8}$ mol litre^{-1} s^{-1}, or $10^{12}-10^{13}$ radical ml^{-1} s^{-1}), and the initiation efficiency is equal to unity, the lifetime of radicals in these particles should be fairly long (10–100 s). With this lifetime, the molecular mass of the polymer is determined by the rate of chain transfer *via* the monomer. In the case of styrene, MM = $1\times10^6-2\times10^6$.

A different situation arises when styrene polymerisation proceeds in the monomer microdroplets formed in the synthesis of water-insoluble surfactants at the interface. Their volume is now $10^{-1}-10^{-3}$ μm^3; therefore, they can accommodate several radicals (5 to 10), the lifetime of which is several seconds, and the polymer molecular mass is up to 10^5.

These differences are consistent with the data on the diameter of the polymer-monomeric particles in which polymerisation proceeds (Table 11). Indeed, in the styrene polymerisation accompanied by synthesis of potassium myristate at the interface, the average diameter of the PMP is 63 nm, while for the synthesis of barium myristate under the same conditions, the diameter is an order of magnitude greater and equals 700 nm.

Table 11. Polymerisation of styrene in the presence of myristates.

Surfactant	$10^2 w_p$ /mol litre s^{-1}	10^{-5} MM	d /nm (see [a])	ξ-Potential /mV
Potassium myristate	15.1	50	65	−52
Lithium myristate	11.3	15	270	−35
Barium myristate	5.5	6.7	700	−29
Calcium myristate	5.4	6.6	800	−26
Zinc myristate	4.9	6.2	850	−23

[a] For particles with sizes of 65 and 270 nm, the stability to electrolytes is 0.15 mol litre^{-1}; for other particles, 0.20 mol litre^{-1}.

In the former case, when small particles contain not more than one radical, emulsion polymerisation of styrene takes place, which is characterised by a high rate and gives polymers with high molecular masses. In this case, the PMP are formed, apparently, both from the monomer microdroplets and from micelles of the emulsifier which solubilises the monomer.

In large particles with an average diameter of about 700 nm, polymerisation follows a suspension mechanism and has a rate close to the rate of suspension polymerisation of styrene in the presence of conventional stabilisers of suspension particles, namely, poly(vinyl alcohol), gelatin, *etc*. However, the molecular masses of the polymers formed in the PMP stabilised by water-insoluble salts of myristic acid are higher than those attained in styrene polymerisation in the presence of standard stabilisers. Presumably, the high viscosity of the interfacial layer creates diffusion restrictions which prevent the penetration of radicals and the monomer into the layer bulk; therefore, only radicals that have entered the PMP during initiation of the polymerisation and the monomer present in the PMP bulk participate in the polymerisation.

V. Conclusion

On the basis of the published data cited and the results of authors' research, a new, in principle, approach to the conduct of heterophase polymerisation has been proposed.[47] The essence of the approach is that monomer emulsions are prepared simultaneously with the synthesis of the emulsifier at the monomer–water interface and with initiation of the polymerisation in the interfacial layer.

For the preparation of emulsions of monomers sparingly soluble in water, the formation of the emulsifier at the monomer–water interface is an efficient way of controlling the stability and the granulometric composition of the emulsions.

The synthesis of emulsifiers at the interface makes it possible to control the interfacial tension, disintegration and microemulsification of the monomer, to form the structure of interfacial adsorption layers of surfactants by an appropriate selection of the carboxylic acid and the counter-ion.

The mechanism of formation of the polymer-monomeric particles and their diameter and size distribution are dictated by the solubility in water of the surfactant formed at the interface. When polymerisation is carried out under conditions of synthesis of a soluble surfactant at the interface, the polymer-monomeric particles are produced from the emulsifier micelles and monomer microdroplets. This ensures the formation of polymer suspensions with a broad particle size distribution. Owing to the low concentration of the resulting surfactant, which is, however, sufficient for providing the stability of polymer-monomeric particles, micelles are excluded from the formation of the PMP, and polymer suspensions with narrow size distributions of particles are formed.

When surfactants poorly soluble or insoluble in water are synthesised at the interface, the PMP are mainly produced from monomer microdroplets, and a narrow size distribution of particles in the resulting suspensions is achieved.

References

1. M S El-Aasser, R M Fitch (Eds) *Future Directions in Polymer Colloids* (Dordrecht: Martinus Nijhoff, 1987)
2. E S Daniels, E D Sudol, M S El-Aasser (Eds) *Polymer Latexes: Preparation, Characterization and Applications* (Dordrecht: Martinus Nijhoff, 1992)
3. R G Gilbert *Emulsion Polymerization: a Mechanistic Approach* (London: Academic Press, 1995)
4. P A Lovell, M S El-Aasser (Eds) *Emulsion Polymerization and Emulsion Polymers* (New York: Wiley, 1997)
5. M A Filatova, S A Nikitina, A B Taubman, P A Rebinder *Dokl. Akad. Nauk SSSR* **140** 874 (1961) [a]
6. V A Spiridonova, S A Nikitina, A B Taubman *Dokl. Akad. Nauk SSSR* **182** 640 (1968) [a]
7. F K Hansen, J Ugelstad *J. Polym. Sci., Polym. Chem. Ed.* **17** 3069 (1979)
8. J Ugelstad, H R Mfutakamba, P C Mørk, T Ellingsen, A Berge, R Smied, L Holm, A Jørgedal, F K Hansen, K Nustad *J. Polym. Sci., Polym. Symp.* **72** 225 (1985)
9. S S Medvedev, in *Kinetika i Mekhanizm Obrazovaniya i Prevrashcheniya Makromolekul* (Kinetics and Mechanism of Formation and Conversion of Macromolecules) (Moscow: Nauka, 1968) p. 5
10. I A Gritskova, L I Sedakova, D S Muradyan, B M Sinekaev, A V Pavlov, A N Pravednikov *Dokl. Akad. Nauk SSSR* **243** 403 (1978) [a]
11. I A Gritskova, L I Sedakova, D S Muradyan, A N Pravednikov *Dokl. Akad. Nauk SSSR* **238** 607 (1978) [a]
12. G A Simakova, V A Kaminskii, I A Gritskova, A N Pravednikov *Dokl. Akad. Nauk SSSR* **276** 151 (1984) [a]
13. S V Zhachenkov, G I Litvinenko, V A Kaminskii, P E Il'menev, A V Pavlov, V V Gur'yanova, I A Gritskova, A N Pravednikov *Vysokomol. Soedin., Ser. A* **27** 1249 (1985) [b]
14. I A Gritskova, S V Zhachenkov, N I Prokopov, P E Il'menev *Vysokomol. Soedin., Ser. A* **33** 1476 (1991) [b]
15. S I Tregubenkov, A A Bryzgachev, L I Sedakova, I A Gritskova, A N Pravednikov *Vysokomol. Soedin., Ser. A* **30** 322 (1988) [b]
16. I M Yakovleva, G A Simakova, I A Gritskova, R A Lyubimskaya, G S Virasuriya, A N Pravednikov *Kolloid. Zh.* **50** 610 (1988) [c]
17. R A Lyubimskaya, G S Virasuriya, I M Yakovleva, G A Simakova, I A Gritskova *Kolloid. Zh.* **50** 562 (1988) [c]
18. G I Litvinenko, M Khaddazh, V A Kaminskii, A V Pavlov, A G Davtyan, I A Gritskova, A N Pravednikov *Vysokomol. Soedin., Ser. B* **26** 683 (1984) [a]
19. G A Simakova, Doctoral Thesis in Chemical Sciences, Moscow Institute of Fine Chemical Technology, Moscow, 1990
20. A N Pravednikov, G A Simakova, I A Gritskova, N I Prokopov *Kolloid. Zh.* **47** 189 (1985) [c]
21. A N Pravednikov, G A Simakova, I A Gritskova, N I Prokopov *Kolloid. Zh.* **47** 192 (1985) [c]

22. N I Prokopov, Candidate Thesis in Chemical Sciences, Moscow Institute of Fine Chemical Technology, Moscow, 1987
23. N I Procopov, G A Simakova, G M Plavnik, A I Koshevnikov, E Ghiva *Polymery* **37** 516 (1992)
24. N I Prokopov, I A Gritskova, Zh V Maksimenko, I Legocka, I Grzywa-Niksinska, E I Grzywa *Polimery* **40** 568 (1995)
25. N I Prokopov, G P Kheinman, I A Gritskova, M V Chirkova *Kolloid. Zh.* **57** 561 (1995) [c]
26. N I Prokopov, I A Gritskova *Kolloid. Zh.* **61** 264 (1999) [a]
27. C A Miller *Colloids Surf.* **29** 89 (1988)
28. M Vermeulen, P Joos *Colloids Surf.* **36** 13 (1989)
29. J Rudin, D T Wasan *Ind. Eng. Chem. Res.* **31** 1899 (1992)
30. J Rudin, C Bernard, D T Wasan *Ind. Eng. Chem. Res.* **31** 1899 (1994)
31. A A Zhukhovitskii, V A Grigoryan, E Mikhalik *Dokl. Akad. Nauk SSSR* **155** 392 (1964) [a]
32. V A Grigoryan, A A Zhukhovitskii, E Mikhalik *Zh. Fiz. Khim.* **39** 1179 (1965) [d]
33. G A Grigor'ev, T V Ingerova *Zh. Fiz. Khim.* **72** 1103 (1998) [d]
34. Y Moroi, R Matuura *J. Phys. Chem.* **89** 2923 (1985)
35. L V Kolpakov, S A Nikitina, A B Taubman, V A Spiridonova, A E Chalykh, N I Puchkov, V A Luk'yanovich *Kolloid. Zh.* **32** 229 (1970) [c]
36. A Rikhavi, Candidate Thesis in Chemical Sciences, Moscow Institute of Fine Chemical Technology, Moscow, 1990
37. W Linke (Ed.) *Solubilities Inorganic and Metalloorganic Compounds* (Washington, DC: American Chemical Society, 1965)
38. I A Gritskova, V A Kaminskii *Zh. Fiz. Khim.* **70** 1516 (1996) [d]
39. P E Il'menev, G I Litvinenko, V A Kaminskii, I A Gritskova, A V Pavlov *Dokl. Akad. Nauk SSSR* **301** 638 (1988) [a]
40. I A Gritskova, A A Zhdanov, O V Chirikova, O I Shchegolikhina *Dokl. Akad. Nauk* **334** 57 (1994) [a]
41. O V Chirikova, Candidate Thesis in Chemical Sciences, Moscow State Academy of Fine Chemical Technology, Moscow, 1994
42. D Yu Mityuk, Candidate Thesis in Chemical Sciences, Moscow Institute of Fine Chemical Technology, Moscow, 1985
43. S Ya Shalyt, Doctoral Thesis in Chemical Sciences, Moscow Institute of Fine Chemical Technology, Moscow, 1987
44. Kh Bakharvand, A A Kapustina, I Gzhiva-Niksin'ska, A A Oganesyan, I A Gritskova, P V Nuss, V N Izmailova *Kolloid. Zh.* **59** 299 (1997) [c]
45. G P Kheinman, Candidate Thesis in Chemical Sciences, Moscow State Academy of Fine Chemical Technology, Moscow, 1999
46. G Odian *Principles of Polymerization* (New York: Wiley-Interscience, 1991)
47. N I Prokopov, Doctoral Thesis in Chemical Sciences, Moscow State Academy of Fine Chemical Technology, Moscow, 1999

[a] — *Dokl. Chem. (Engl. Transl.)*
[b] — *Polym. Sci. (Engl. Transl.)*
[c] — *Colloid J. (Engl. Transl.)*
[d] — *Russ. J. Phys. Chem. (Engl. Transl.)*

Russian Chemical Reviews **70** (9) 801 – 807 (2001) © 2001 Russian Academy of Sciences and Turpion Ltd

DOI 10.1070/RC2001v070n09ABEH000674

Anion-conducting fluoride and oxyfluoride glasses

N I Sorokin

Contents

I.	Introduction	801
II.	Fluoride glasses based on MF_2	802
III.	Fluoride glasses based on MF_3	803
IV.	Fluoride glasses based on MF_4	803
V.	Oxyfluoride glasses	804
VI.	Optimisation of characteristics of fluoride-conducting glasses and prospects of their practical applications	805
VII.	Conclusion	806

Abstract. Main mechanisms of the anion (fluoride ion) transport in fluoride and oxyfluoride glasses are analysed. The variation in the transport number of F^- ions depending on the glass composition is followed. Methods for optimisation of the conductivity characteristics of the glasses in question are considered. The prospects of using fluoride-conducting glasses in electrochemical devices are discussed. The bibliography includes 90 references.

I. Introduction

The discovery [1] of the anionic (fluoride) conductivity of fluoroberyllate glasses of the $BeF_2 + MF$ (M = Na or Cs) type and fluorophosphate glasses of the $Ba(PO_3)_2 + MF_2$ (M = Ca, Sr, Ba or Mg) type and, particularly, the preparation of fluorozirconate glasses in systems involving ZrF_4 and BaF_2 and investigations [2] of their transport properties gave impetus to extensive studies of fluoride transport in glassy materials. Glasses possessing high F^- ionic conductivity constitute a special class of anion-conducting solid electrolytes. Since the glassy state is characterised by a distinctive structural solid-state disordering, one would expect that high anionic conductivity can be achieved in amorphous materials. In addition, fluoride glasses are of practical interest in a search for new solid electrolytes because of their technological effectiveness and cheapness as compared to crystalline materials. A search for glassy solid electrolytes follows two main directions: first, new glass-forming systems are investigated and, second, the electrophysical properties of the known fluoride glasses are modified by doping (by increasing the number of components).

Difficulties encountered in preparing fluoride glasses are associated with their high tendency to crystallisation. With the aim of suppressing this effect, various metal fluorides are introduced as stabilisers, which complicates the glass composition. By varying the composition, one can enhance the chemical stability of glasses, prepare specimens up to ~ 1 cm in thickness,[3] extend the temperature range of their application, reveal the contributions of various components to the dynamics of the ionic conductivities and obtain information on the mobility and concentration of charge carriers.

Problems of the formation and atomic structures of glasses in fluoride systems were surveyed in reviews.[4–9] Structural models are generally constructed based on comparison of the structural data for glassy and crystalline phases with the same chemical composition. Presently, a disordered network is used as the basic model for the glass structure.[10] According to this model, the glass structure represents a disordered (the long-range order is absent) three-dimensional glass-forming network consisting of coordination polyhedra of glass-forming cations, which are linked to each other through shared vertices occupied by bridging F_b^- anions. The cavities of the network are occupied by modifying cations bound to non-bridging F_{nb}^- anions. To gain insight into the glass structure, the reasons for the formation of disordered networks need to be revealed.

The model for a disordered network (the short-range order in the glass structure) is refined taking into account up-to-date experimental data. Among various structural models for fluoride glasses, the cluster (the short-range order and 'medium-range' order in the glass structure) model (see, for example, Ref. 11), which is closely related to the model for the disordered network, is most universally employed.[8] Structures of fluoride crystalline phases, which are chemically close to glasses, contain infinite chains of coordination polyhedra of glass-forming cations linked through F_b^- anions. The chains of the polyhedra, in turn, are linked in a three-dimensional disordered glass-forming network. Large low-charge modifying cations are not involved in this network and give rise to ionic cation – fluoride bonds. The introduction of modifying fluoride ions exhibiting high bond ionicity leads to strengthening of covalent bonds in the glass-forming network through the charge transfer.

The keys to an understanding of the anion transport in fluoride glasses are, apparently, the formation of the F_{nb}^- anions and the variation in the coordination number of glass-forming cations. It is the ability of glass-forming cations to adapt themselves to the change in the coordination number that promotes jumps of mobile anions between the adjacent polyhedra. The results of ^{19}F NMR studies [12–14] and computer simulation [15] demonstrated that it is precisely the F_{nb}^- anions located in the vicinity of the modifying cations that serve as mobile charge carriers. Local motions of F_{nb}^- anions initiate the diffusive motion of fluoride anions (anionic conductivity) through the glass-forming network.

N I Sorokin A V Shubnikov Institute of Crystallography, Russian Academy of Sciences, Leninsky prosp. 59, 119991 Moscow, Russian Federation. Fax (7-095) 135 10 11. Tel. (7-095) 330 78 74.
E-mail: sorokin1@mail.ru

Received 11 April 2001
Uspekhi Khimii **70** (9) 901 – 908 (2001); translated by T N Safonova

Glasses possessing ionic conductivity are characterised by dielectric relaxation associated with the jump migration of charge carriers resulting in the frequency dependence of the ionic conductivity.[16] Ion-conducting glasses follow the universal relationship: the direct-current conductivity σ is directly proportional to the dielectric relaxation frequency ω_m. This universal regularity was explained [17] within the framework of a model for the potential barrier distribution according to which the frequency of the dielectric loss peak is the minimum jump frequency of conducting ions. Hence, the directly proportional dependence of σ on ω_m is physically justified. Within the framework of this approach, the characteristic features of the jump mechanism for electric current carriers in ZrF_4-based fluoride glasses were examined.[18–20] The anionic conductivity in fluoride glasses depends primarily on the activation energy of the ion transport.

Particular mechanisms of the anion transport in glasses remain poorly studied because the available structural data are scarce. A necessary condition for the manifestation of essential anionic conductivity is the existence of glass-forming cations, which adopt high coordination numbers and differ in the form and size of their coordination polyhedra. Low coordination numbers of glass-forming cations (in fluoroberyllate and fluoroaluminate glasses) are responsible for low anionic conductivities.

For cation-conducting glasses, the polycationic (polyalkali) effect is well known. This effect lies in the fact that the replacement of one alkali metal cation by another gives rise to a minimum in the composition dependence of the ionic conductivity. The polycationic effect in fluoride and oxyfluoride glasses is manifested if the cationic conductivity exceeds the fluoride-ionic conductivity.[21–24] In the $Ba(PO_3)_2 + NaX$ (X = F, Cl or I) and $Ba(PO_3)_2 + BaF_2 + BaX_2$ (X = Cl or Br) glasses, the polyanionic effect (which was called by analogy with the polycationic effect) was experimentally observed upon the replacement of one halogen by another.[25,26] The polyanionic effect was confirmed for the $ZrF_4 + BaX_2$ (X = F or Cl) [27] and $30\,SiO_2 \cdot 55\,PbO \cdot 15\,Pb(F_{1-x}Cl_x)_2$ ($0 \leqslant x \leqslant 1$) glasses.[28] The $ZrF_4 + BaF_2 + MX$ (M = Li or Na; X = F or Cl) [29] and $ZrF_4 + BaF_2 + MF_n + LiF$ glasses ($M^{n+} = La^{3+}$ or Th^{4+}, the Li^+ and F^- mobile ions) exhibit the combined effect associated with lowering of the conductivity due to the simultaneous presence of mobile cations and anions.[30]

In the present review, the results of studies of the fluoride-ion transport in glassy solid electrolytes are analysed. Mechanisms of the cation transport in fluoride and oxyfluoride glasses call for a special discussion and are beyond the scope of the present review. The abundant experimental data on fluoride glasses are classified, wherever possible, into groups according to the type of the basis glass-forming fluoride. It should be noted that this classification becomes more difficult as the composition of multicomponent glasses is complicated (the most stable fluoride glasses contain three or more components). Various families of glasses based on MF_2, MF_3 or MF_4 are considered. Recently, glasses based on MF_5, where M = Nb, Ta, V or Mo, have been discovered (the glass transition temperature T_g varies from -45 to -60 °C; the crystallisation temperature T_{cr} ranges from 0 to -10 °C),[31] but their electrophysical properties remain to be explored. The characteristics of the anionic conductivities of some two- and three-component fluoride and oxyfluoride glasses are given in Table 1.

Fluoride glasses attract considerable interest because they are transparent in the IR region and possess low glass transition temperatures as well as because they are promising materials for fibre optics. According to the results of calculations, theoretical losses in the optical transmission of information in these glasses are an order of magnitude smaller than those in traditional oxide (silicate) glasses.

Table 1. Characteristics of the fluoride-ionic conductivity in two- and three-component fluoride and oxyfluoride glasses.

Glass	σ /S m^{-1}	T /°C	E_a /eV	Ref.
Fluoride glasses based on MF_2				
$80\,BeF_2 \cdot 20\,CsF$	6×10^{-11}	150	1.12	32 [a]
$67\,MnF_2 \cdot 33\,BaF_2$	1×10^{-4}	180	0.55	32
$67\,ZnF_2 \cdot 33\,BaF_2$	2×10^{-4}	180	0.59	32
$55\,ZnF_2 \cdot 45\,PbF_2$	4×10^{-4}	180	0.55	32
$30\,ZnF_2 \cdot 25\,AlF_3 \cdot 45\,LiF$	1×10^{-4}	200	0.86	33
$35\,ZnF_2 \cdot 20\,BaF_2 \cdot 45\,LiF$	3×10^{-3}	200	0.85	34
$45\,ZnF_2 \cdot 30\,BaF_2 \cdot 25\,YF_3$	1×10^{-3}	200	0.73	34
Fluoride glasses based on MF_3				
$30\,AlF_3 \cdot 40\,PbF_2 \cdot 30\,ZnF_2$	2×10^{-7}	150	0.79	32
$40\,AlF_3 \cdot 22\,CaF_2 \cdot 38\,YF_3$	5×10^{-9}	150	0.83	32
$40\,AlF_3 \cdot 40\,BaF_2 \cdot 20\,YbF_3$	4×10^{-7}	200	1.13	35
$30\,GaF_3 \cdot 50\,PbF_2 \cdot 20\,MnF_2$	2×10^{-4}	200	0.61	32
$40\,GaF_3 \cdot 40\,BaF_2 \cdot 20\,YbF_3$	1×10^{-5}	200	0.96	35
$40\,ScF_3 \cdot 40\,BaF_2 \cdot 20\,YbF_3$	1×10^{-3}	200	0.75	35
$40\,ScF_3 \cdot 40\,BaF_2 \cdot 20\,YF_3$	1×10^{-3}	200	0.70	12
$54\,InF_3 \cdot 36\,BaF_2 \cdot 10\,LiF$	6×10^{-3}	200	0.64	36
$25\,InF_3 \cdot 45\,PbF_2 \cdot 30\,ZnF_2$	4×10^{-3}	200	0.57	32
$35\,InF_3 \cdot 35\,PbF_2 \cdot 30\,MnF_2$	4×10^{-3}	200	0.56	32
$35\,InF_3 \cdot 35\,PbF_2 \cdot 30\,SnF_2$	2×10^{-3}	150	0.49	32
$40\,InF_3 \cdot 45\,PbF_2 \cdot 15\,BaF_2$	5×10^{-2}	200	0.535	37
$40\,InF_3 \cdot 40\,BaF_2 \cdot 20\,YbF_3$	1×10^{-3}	200	0.78	35
$30\,InF_3 \cdot 35\,BaF_2 \cdot 35\,BiF_3$	3×10^{-2}	200	0.52	38
Fluoride glasses based on MF_4				
$60\,ZrF_4 \cdot 15\,BaF_2 \cdot 25\,CsF$	1×10^{-5}	200	0.74	32
$62\,ZrF_4 \cdot 30\,BaF_2 \cdot 8\,LaF_3$	3×10^{-5}	200	0.79	32
$60\,ZrF_4 \cdot 30\,BaF_2 \cdot 10\,AlF_3$	1×10^{-4}	200	0.77	39
$59\,ZrF_4 \cdot 26\,BaF_2 \cdot 15\,BiF_3$	1×10^{-5}	200	0.73	32
$62.5\,ZrF_4 \cdot 28\,BaF_2 \cdot 9.5\,ThF_4$	3×10^{-5}	200	0.79	32
$59\,ZrF_4 \cdot 26\,BaF_2 \cdot 15\,HfF_4$	2×10^{-5}	200	0.76	32
$60\,ZrF_4 \cdot 33\,ThF_4 \cdot 7\,LaF_3$	3×10^{-6}	200	0.83	32
$70\,HfF_4 \cdot 30\,BaF_2$	8×10^{-5}	200	0.925	35
$55\,HfF_4 \cdot 30\,BaF_2 \cdot 15\,CsF$	2×10^{-5}	200	0.71	32
$62\,HfF_4 \cdot 30\,BaF_2 \cdot 8\,NdF_3$	9×10^{-5}	200	0.88	35
$62\,HfF_4 \cdot 30\,BaF_2 \cdot 8\,YbF_3$	9×10^{-5}	200	0.88	35
Oxyfluoride glasses				
$20\,Al(PO_3)_3 \cdot 80\,PbF_2$	8×10^{-7}	200	1.00	32
$10\,Al(PO_3)_3 \cdot 85\,PbF_2 \cdot 5\,MnF_2$	1×10^{-2}	200	0.63	32
$10\,Pb(PO_3)_2 \cdot 35\,PbF_2 \cdot 55\,MnF_2$	8×10^{-3}	200	0.56	32
$20\,NaPO_3 \cdot 40\,BaF_2 \cdot 40\,MnF_2$	4×10^{-6}	200	1.09	12
$10\,B_2O_3 \cdot 90\,PbF_2$	1×10^{-3}	200	0.91	34
$30\,B_2O_3 \cdot 50\,PbO \cdot 20\,PbF_2$	2×10^{-5}	127	0.55	40
$5\,Bi_2O_3 \cdot 95\,PbF_2$	1×10^{-4}	200	0.85	34
$10\,V_2O_3 \cdot 90\,PbF_2$	5×10^{-7}	200	0.85	34
$10\,SnO_2 \cdot 90\,PbF_2$	2×10^{-4}	200	0.79	34
$10\,GeO_2 \cdot 90\,PbF_2$	3×10^{-5}	200	1.05	34
$15\,GeO_2 \cdot 15\,PbO \cdot 15\,PbF_2$	3×10^{-5}	300	1	41
$10\,GeO_2 \cdot 80\,PbF_2 \cdot 10\,BiF_3$	9×10^{-4}	200	0.80	34
$10\,GeO_2 \cdot 80\,PbF_2 \cdot 10\,PbCl_2$	1×10^{-3}	200	0.84	34
$35\,SiO_2 \cdot 50\,PbO \cdot 15\,PbF_2$	5×10^{-5}	200	0.74	32
$30\,SiO_2 \cdot 30\,PbO \cdot 40\,PbF_2$	6×10^{-4}	200	0.75	42

Note. E_a is the activation energy of the conductivity. Different researchers calculated the E_a values according to the formula: $\sigma T = A\exp(-E_a/kT)$ or $\sigma = A\exp(-E_a/kT)$. The results differ by less than 0.05 eV.

[a] The original studies were cited in Ref. 32.

II. Fluoride glasses based on MF_2

Of simple fluorides MF_n ($n = 1-4$), BeF_2 is the only fluoride compound capable of undergoing a glass transition. The coordination polyhedron of the glass-forming Be^{2+} cation is the $[BeF_4]^{2-}$ tetrahedron (the coordination number is 4). The structural motif of crystalline BeF_2 (isostructural to SiO_2) is based on an ordered three-dimensional framework formed by the $[BeF_4]^{2-}$ tetrahedra, which are linked to each other *via* shared vertices. The transformation of BeF_2 into the glassy state occurs through rotations of the tetrahedra about the bridging $Be-F_b-Be$ bonds accompanied by distortions of the angles in the tetrahedra. As a result, a disordered three-dimensional framework consisting of the distorted $[BeF_4]^{2-}$ tetrahedra is formed. This framework is characterised by the absence of the long-range order. Tetrahedral fluoroberyllate glasses are structural analogues of silicate glasses. The introduction of alkali metal fluorides acting as modifiers leads to the cleavage of the bridging $Be-F_{nb}-M$ bonds and the occurrence of non-bridging fluorine atoms. It was found that the ratio between the cationic and anionic components of the conductivities in alkaline fluoroberyllate glasses is a function of the alkali metal–fluorine bond. Measurements of the transport numbers demonstrated that the $BeF_2 + MF$ and $BeF_2 + MF + M'F$ glasses (M and M′ = Na or Cs) exhibit virtually unipolar anionic conductivities.[1] The mechanism of the anionic conductivity in these glasses is associated with the increase in the amount of mobile non-bridging F^-_{nb} ions as the content of the MF modifying component increases. However, the fluoride-ionic conductivities are low and reach $\sim 10^{-6}$ S m^{-1} at 300 °C.

The electrical properties of multicomponent glasses based on manganese and zinc fluorides in the MnF_2-BaF_2, ZnF_2-MF_2 (M = Ba or Pb), ZnF_2-BaF_2-LiF, $ZnF_2-BaF_2-YF_3$, $ZnF_2-PbF_2-AlF_3-LiF$ and $ZnF_2-BaF_2-InF_3-SrF_2-NdF_3-MF$ systems (M = Li, Na, K or Rb) were studied.[33,34,43,44]. Apparently, crystalline phases formed in the ZnF_2-BaF_2 system, for example $BaZnF_4$, are most similar in structural units to fluorozincate glasses.[45,46] The crystal structure of $BaZnF_4$ consists of the $[ZnF_6]^{4-}$ octahedra linked in chains through shared vertices, whereas the barium atoms are located in the cavities. An analogous motif composed of the $[ZnF_6]^{4-}$ octahedra is observed in the structure of Ba_2ZnF_6. It can be assumed that fluorozincate glasses retain the short-range order of the arrangement of the $[ZnF_6]^{4-}$ octahedra, whereas the Ba^{2+} positions are partially occupied by the modifying Sr^{2+}, Nd^{3+}, Y^{3+}, Li^+, Na^+, K^+ or Rb^+ cations, their arrangement meeting the condition for charge compensation. The indium atoms, which adopt the coordination numbers of 6 and 7 in fluoride structures,[9] are, apparently, incorporated into the glass-forming network. In the octahedral $50\,ZnF_2 \cdot 19.5\,BaF_2 \cdot 10\,InF_3 \cdot 10\,SrF_2 \cdot 0.5\,NdF_3 \cdot 10\,MF$ glasses, the conductivity at 127 °C changes from 5×10^{-6} to 3×10^{-4} S m^{-1} and the activation energy E_a changes from 0.82 to 0.68 eV as the ionic radius of M^+ increases from 0.9 (Li^+) to 1.66 Å (Rb^+)†. In the $30\,ZnF_2 \cdot 25\,AlF_3 \cdot (45-x)\,PbF_2 \cdot x\,LiF$ ($0 \leqslant x \leqslant 20$, T_g = 230–275 °C) glasses, the ZnF_2-AlF_3 group acts as a glass-forming agent, whereas PbF_2 and LiF serve as modifiers. The anionic conductivity (at 200 °C) decreases from 1×10^{-4} to 1×10^{-5} S m^{-1}, whereas the activation energy E_a increases from 0.86 to 1.24 eV as the LiF content increases due to capture of mobile F^- ions by Li^+ cations.

III. Fluoride glasses based on MF_3

Trifluoride-based glasses are formed in systems containing MF_3 (M = Al, Fe, Ga or In) or AF_2 (A = Ba or Pb).[48,49] As for the glass-forming $MF_3 + M'F_2 + M''F_2$ (M = Fe, Ga or In; M′ = Pb or Ba; M″ = Mn, Zn, Cd, Sn or Ba) systems, the most stable glasses appear in the $InF_3-BaF_2-PbF_2$ system (T_g = 250–280 °C, $\Delta T = T_g - T_{cr} \approx 70$ °C). The structures of MF_3-based glasses consist of the $[MF_6]^{3-}$ octahedra linked in zigzag chains through fluorine atoms. The $[AlF_4]^-$ and $[GaF_4]^-$ tetrahedra can be present, but they are not involved in formation of glass networks. The data on the $46.7\,InF_3 \cdot 19\,PbF_2 \cdot 23.8\,BaF_2 \cdot 1.9\,AlF_3 \cdot 4.9\,SrF_2 \cdot 2.8\,YF_3$ glass obtained by Raman spectroscopy, the optical transmission method and magneto-chemistry[50,51] are indicative of octahedral coordination about the small indium ($r_{In^{3+}} = 1.06$ Å) and aluminium ($r_{Al^{3+}} = 0.675$ Å) atoms; whereas the large lead ($r_{Pb^{2+}} = 1.43$ Å) and barium ($r_{Ba^{2+}} = 1.56$ Å) atoms act as modifiers and occupy cavities in the three-dimensional octahedral glass-forming network. Consideration of the structure of this glass from the standpoint of the close packing of fluorine atoms leads to the same conclusion, *viz*., small In^{3+} and Al^{3+} cations occupy octahedral positions in the anionic packing, whereas large Pb^{2+} and Ba^{2+} cations introduce strong disturbance in the packing of fluoride anions.[52] It was assumed that the $[InF_7]^{4-}$ polyhedra are present in the glass-forming networks of indium-containing glasses.[9]

The properties of the $40\,MF_3 \cdot 40\,BaF_2 \cdot 20\,YbF_3$ glasses (M = Al, Ga, Sc or In) whose compositions are determined by the position of a low-melting eutectic in the phase diagrams of the $MF_3-BaF_2-YbF_3$ systems were examined.[35] In the course of formation of these glasses, the MF_3 trifluorides serve as glass-forming agents. The structures of the $40\,ScF_3 \cdot 40\,BaF_2 \cdot 20\,YbF_3$ and $40\,InF_3 \cdot 40\,BaF_2 \cdot 20\,YbF_3$ glasses contain fragments both of two-dimensional networks formed by the seven- and eight-vertex $[MF_n]^{-n+3}$ polyhedra (n = 7 or 8) and chains formed by the $[MF_6]^{3-}$ octahedra. Since the Al^{3+} and Ga^{3+} ions cannot be incorporated in seven-vertex polyhedra, the structure of the glass-forming network changes.[53] These glasses are characterised by a sharp increase (by three orders of magnitude) in the isothermal conductivity as the ionic radius of M^{3+} increases (as the $M^{3+}-F^-$ chemical bond is weakened) due to a linear decrease in the activation energy of the conductivity (see Table 1). The introduction of GaF_3 into the fluoroindate glasses $(40-x)\,InF_3 \cdot x\,GaF_3 \cdot 20\,ZnF_2 \cdot 16\,BaF_2 \cdot 20\,SrF_2 \cdot 2\,GdF_3 \cdot 2\,NaF$ ($0 \leqslant x \leqslant 30$) also leads to a sharp decrease in their conductivities.[54]

The mobility of the fluoride ions and the conductivities of glasses in the $InF_3-BaF_2-PbF_2$, $InF_3-BaF_2-BiF_3$ and $InF_3-BaF_2-PbF_2-AlF_3-LiF$ systems were examined.[36–38,55] The addition of AlF_3 and LiF to the former system promotes the preparation of $InF_3 + BaF_2 + PbF_2$ glasses and allows one to vary their composition over a wider range. Two phases were identified among the crystallisation products obtained in the $InF_3-BaF_2-PbF_2-AlF_3$ system,[56] *viz*., a fluorite-like solid solution based on PbF_2 and BaF_2 and a solid solution based on the high-temperature tetragonal modification of $Ba_3In_2F_{12}$. The conductivities of glasses of the $InF_3-BaF_2-PbF_2-AlF_3-LiF$ system are improved as the PbF_2 content increases, whereas the conductivities are impaired as the AlF_3 content increases. At room temperature, the anionic conductivity of the $20\,InF_3 \cdot 50\,PbF_2 \cdot 10\,BaF_2 \cdot 10\,AlF_3 \cdot 10\,LiF$ glass is 30 times as large as that of the superionic conductor β-PbF_2, which is widely used in scientific and applied studies. This fact underlines the important role of indium and lead fluorides in the preparation of new amorphous superionic conductors.

IV. Fluoride glasses based on MF_4

In the middle 1970s, ZrF_4 and BaF_2-based fluoride glasses were prepared. This result was unexpected because the glass-forming Zr^{4+} cation is characterised by high ($\geqslant 6$) coordination numbers, which is contradictory to the conventional criteria for glass formation. The data of analysis of the shielding tensors and the chemical shifts of the signals in the ^{19}F NMR spectra[14,57] and the results of calculations by the Monte-Carlo method and molecular dynamics[58] demonstrated that the short-range structures in the barium fluorozirconate glasses $50\,ZrF_4 \cdot 50\,BaF_2(BaZrF_6)$ and $60\,ZrF_4 \cdot 40\,BaF_2$ are similar to the structure of crystalline

† The crystal-chemical ionic radii were taken from Ref. 47.

α-$BaZrF_6$ and that the medium-range ordering of the cluster type occurs along with the short-range order. Fluorozirconate glasses can contain Zr polyhedra with the coordination numbers of 6, 7 or 8. The structural networks of the glasses consist predominantly of the $[ZrF_7]^{3-}$ and $[ZrF_8]^{4-}$ polyhedra linked through bridging bonds; BaF_2 acts as a modifier.[59] The glass-forming ability of the ZrF_4-BaF_2 system is insufficient for the preparation of glasses several millimetres in thickness. These glasses can be prepared by introducing additional MF_n components ($n = 1-4$); the number of the components can be 10 or even larger.

The pioneering study on the anionic conductivities of fluorozirconate glasses[2] was concerned with the glasses $ZrF_4 + BaF_2 + ThF_4$ (55 mol.% – 62.5 mol.% ZrF_4, 28 mol.% – 36.3 mol.% BaF_2 and 7.5 mol.% – 13.8 mol.% ThF_4, $T_g \approx 320$ °C), $62\,ZrF_4 \cdot 30\,BaF_2 \cdot 8\,MF_3$ (M = La, Pr or Nd; $T_g = 310$ °C), $60\,ZrF_4 \cdot 33\,ThF_4 \cdot 7\,LaF_3$ ($T_g = 455$ °C) and $60\,ZrF_4 \cdot 25\,BaF_2 \cdot 8\,ThF_4 \cdot 7\,LaF_3$ ($T_g = 320$ °C). Measurements of the transport numbers demonstrated that the glasses possess unipolar fluoride-ionic conductivities (the transport numbers of the electron transport are $< 10^{-3}$). In the $ZrF_4 + BaF_2 + ThF_4$ glasses, the conductivity increases moderately as the content of the BaF_2 modifier increases. On the average, the fluoride-ionic conductivity in these glasses is $\sim 10^{-4}$ S m^{-1} at 200 °C and $E_a \approx 0.8$ eV.

Later on, the electrophysical properties of the multicomponent glasses $ZrF_4 + BaF_2 + AlF_3$,[39] $ZrF_4 + BaF_2 + MF_n$ (M = Li, Na, Rb, Cs, Ca, Sr, Ba, Sb^{3+}, Bi, La, Nd or Hf),[60] $60\,ZrF_4 \cdot 30\,BaF_2 \cdot 10\,LnF_3$ (Ln = La – Lu or Y),[61] $ZrF_4 + M'F_2 + M''F_3$ (M' = Ba or Sn^{2+}; M'' = Ga, La or Nd),[62,63] $ZrF_4 + BaF_2 + AlF_3 + LnF_3$ (Ln = La or Y),[64] $ZrF_4 + BaF_2 + LaF_3 + M'F$ (M' = Na or Li),[19,20] $ZrF_4 + BaF_2 + ThF_4 + LiF$,[20] $ZrF_4 + MF_n + AlF_3 + YF_3 + NaF$ (M = Ba or La),[18,19,65] $ZrF_4 + BaF_2 + LaF_3 + LiF + NaF$[66] and $ZrF_4 + BaF_2 + AlF_3 + YF_3 + ZnF_2 + CdF_2 + LiF$[67] were examined with the aim of improving the anion-transport characteristics. It was found that the anionic conductivity of fluorozirconate glasses depends primarily on the activation energy of the conductivity. The polarisability and the ionic radius of M^{n+} are the major factors influencing the E_a value. The activation energy of the fluoride-ion transport decreases as the ionic radius and the polarisability of the M^{n+} cations increases, which is, apparently, due to weakening of the $M^{n+} - F^-$ bond. The ZrF_4-BaF_2-CsF system exhibits the most promise for preparing glasses possessing high fluoride-ionic conductivity.

According to the ^{19}F NMR data,[12–14,64] the mechanism of the anionic conductivity in fluorozirconate glasses is associated with the non-bridging F^-_{nb} anions localised at the modifying cations. These anions execute local motions ($E_a \approx 0.2$ eV) in the vicinity of the modifying cations and diffusion motions ($E_a \approx 0.6$ eV) between the modifying cations. The fluorine diffusion is limited by the potential barriers between the modifying cations. In the $55\,ZrF_4 \cdot (38.5-x)\,BaF_2 \cdot 4AlF_3 \cdot (2.5+x)\,LaF_3$ ($0 \leqslant x \leqslant 7$) and $55\,ZrF_4 \cdot (37-x)\,BaF_2 \cdot 4\,AlF_3 \cdot (4+x)\,YF_3$ ($0 \leqslant x \leqslant 5$) glasses, the conductivity is enhanced as the BaF_2 content increases.[64]

In lithium fluorozirconate glasses containing less than 20 mol.% of LiF, the conductivities are determined by the Li^+ and F^- ions, whereas the conductivities in the glasses containing more than 20 mol.% of LiF are conditioned only by the Li^+ cations. In the sodium fluorozirconate glasses, the conductivities are governed exclusively by the F^- ions. For the $50\,ZrF_4 \cdot (45-x)\,BaF_2 \cdot 3\,AlF_3 \cdot 2\,YF_3 \cdot x\,NaF$ ($10 \leqslant x \leqslant 40$) and $45\,ZrF_4 \cdot 3\,LaF_3 \cdot 3\,AlF_3 \cdot 4\,YF_3 \cdot 45\,NaF$ glasses, the concentrations of the charge carriers were estimated within the framework of the jump mechanism of the conductivity.[18,19] A small portion of fluoride ions (3% – 5% of their total amount) is responsible for the transport properties of these glasses. The conductivity decreases as the NaF content increases due to a decrease in the mobility of the charge carriers and partial capture of mobile F^- anions by Na^+ cations.

Since zirconium and hafnium tetrafluorides (the ionic radii $r_{Zr^{4+}} = 0.98$ and $r_{Hf^{4+}} = 0.97$ Å) have similar physicochemical and structural characteristics, fluorohafnate glasses are isovalent analogues of fluorozirconate glasses. The electrolytic properties of glasses in the HfF_4-BaF_2 and $HfF_4-BaF_2-MF_3$ systems (M = Nd, Yb or Y) were investigated.[35,68] The parameters of the anion transport in HfF_4-containing glasses are virtually independent of the type and concentration of trifluorides of rare-earth elements, *viz.*, $\sigma \approx 3 \times 10^{-4}$ S m^{-1} at 223 °C and $E_a \approx 0.9$ eV. Trivalent rare-earth cations replace zirconium (hafnium) in glass-forming networks. Apparently, the addition of trifluorides of rare-earth elements with substantially different ionic radii (for example, $r_{Nd^{3+}} = 1.249$ and $r_{Yb^{3+}} = 1.125$ Å) to the glass-forming HfF_4-BaF_2 system has no effect on the surface contour of the potential energy (~ 0.9 eV), where the fluoride ions move. These results of conductometric studies are, apparently, indicative of microheterogeneity of glasses including large (from the viewpoint of the atomic scale) spatial regions free of trifluorides of rare-earth elements.

According to the NMR data,[69] high mobility of the F^- ions is observed in glasses based on tin tetrafluoride, *viz.*, in $SnF_4-BaF_2-MF_3$ (M = Al, Sc or Ga); however, the data on their ionic conductivities are lacking.

V. Oxyfluoride glasses

To prepare glasses, fluorides are added to mixtures of oxides. Thus, no glass was obtained from a mixture of pure oxides SiO_2, Al_2O_3 and BeO, whereas a transparent glass was prepared in the presence of even a small amount (several mass percent) of CaF_2. This is associated with a decrease in viscosity and an increase in mobility of structural units in melts in the presence of fluoride. The properties of these glasses are determined by the influence of fluorides on the structure of the oxide matrix. Glasses possessing unipolar fluoride-ionic conductivities were prepared by introducing fluorides MF_n ($n = 1-3$) into glass-forming oxyphosphate compounds of the $NaPO_3$, $M(PO_3)_2$ (M = Ba, Pb, Sr or Zn) and $Al(PO_3)_3$ types.[1,32,70] In the $Ba(PO_3)_2-MgF_2$ system whose glass-forming region extends to 70 mol.% of MgF_2, as an example, the fluoride-ion transport number reaches 0.98. For the most extensively studied fluorophosphate glasses, the following regularities were revealed:

(1) the fraction of fluoride anions involved in the conductivity increases sharply as the fluoride content in the glass increases;

(2) the F^- transport number is determined by the strength of the metal – fluorine bond;

(3) glasses with a fluoride content higher than 30 mol.% – 50 mol.% (depending on the system) are characterised predominantly by anionic conductivity.

The electrophysical properties of fluorine-containing oxyfluoride glasses were studied in the $Ba(PO_3)_2-AlF_3-MF_2$ (M = Mg, Ca, Sr or Ba; $T_g = 450-550$ °C), $ZnB_2O_4-CdB_2O_4-AlF_3-PbF_2$ ($T_g = 250-500$ °C) and $BaGeO_3-BaAl_2GeO_8(Ca_2Al_2GeO_7, Pb_2GeO_4)-CaF_2-MgF_2$ ($T_g = 550-700$ °C) systems.[71] Fluorine plays a binding role in the construction of the structural networks of glasses. The meta-, pyro- and monofluorophosphate groups and the fluoride fragments coexist in networks of fluorophosphate glasses. In borofluoride glasses, the function of fluorine consists primarily in changing the coordination of the boron atoms. The germanate and fluoride structural fragments coexist in fluorogermanate glasses. At 20 °C, the conductivity of fluorophosphate glasses varies from 10^{-11} to 10^{-6} S m^{-1} and the conductivity of borofluoride glasses ranges from 10^{-11} to 10^{-4} S m^{-1}.

In glassy oxyfluoride systems, fluorine can serve different functions depending on the type of the modifying cation. The structural positions and the dynamics of fluoride ions in glasses of the $Al(PO_3)_3-BaF_2$, $Ba(PO_3)_2-CdF_2$ and $Al(PO_3)_3-BaF_2-AlF_3-MF_n$ systems (M = Li, Na, K, Rb, Cs, Mg, Zn or Cd) were studied by ^{19}F NMR spectroscopy.[72,73] Several structurally

nonequivalent positions of the fluorine atoms involved in the coordination polyhedra about Ba, Al and Cd were found. In glasses of the $Al(PO_3)_3-BaF_2$ system, the F^- anions exhibit high mobility, the most mobile anions being bound to the barium atoms. In glasses of the $Ba(PO_3)_2-CdF_2$ system, no mobility of fluoride ions was observed.

Particular attention was given to PbF_2-containing glasses formed in the $M_nO_m-PbF_2$ ($M_nO_m = B_2O_3$, Bi_2O_3, V_2O_3, SnO_2, GeO_2),[34] $Al(PO_3)_3-PbF_2-MnF_2$,[74] $Pb(PO_3)_2-PbF_2-MnF_2$,[75] $SiO_2-PbO-PbF_2$,[32,42,76,77] $B_2O_3-PbO-PbF_2$ and $B_2O_3-PbO-PbF_2-AlF_3$ systems.[40] For glasses of the $M_nO_m-PbF_2$ systems, the activation energy of the conductivity varies from 0.8 to 1.0 eV and the conductivity at 127 °C ranges from 1×10^{-8} to 1×10^{-5} S m^{-1}. In the $SiO_2-PbO-PbF_2$ system, the F^- transport number increases as the concentration of PbF_2 rises from 0.4 for the $95(2\,PbO:SiO_2)\cdot5\,PbF_2$ glass to 1 for the $80(2\,PbO:SiO_2)\cdot20\,PbF_2$ glass. The change of the proton conductivity exhibited by the above-mentioned oxide glasses to the fluoride-ionic conductivity is attributed to a decrease in the content of structurally bound water as PbF_2 is added. The fluoride-ionic conductivity of the $80(2\,PbO:SiO_2)\cdot20\,PbF_2$ glass is $\sim10^{-4}$ S m^{-1} at 200 °C. The electron transport occurs primarily with the participation of the F^- ions bound to the Pb^{2+} ions. The structures of the $30\,B_2O_3\cdot(70-x)\,PbO\cdot x\,PbF_2$ ($0\leqslant x\leqslant25$) and $10\,B_2O_3\cdot20\,AlF_3\cdot(70-x)\,PbO\cdot x\,PbF_2$ ($0\leqslant x\leqslant60$) glasses are formed by borate groups and aluminium atoms each coordinated by six fluorine atoms. The charge transport involves F^- anions. The conductivity of glasses increases (or decreases) by several orders of magnitude as the concentration of PbF_2 increases (or upon addition of AlF_3).

Therefore, the best characteristics of the fluoride-ionic conductivity were achieved for oxyfluoride glasses with a high PbF_2 content in the $Al(PO_3)_3-PbF_2-MnF_2$ and $Pb(PO_3)_2-PbF_2-MnF_2$ systems. The conductivity of the $Al(PO_3)_3+PbF_2+MnF_2$ glasses containing 70 mol.%–80 mol.% of PbF_2 reaches $\sim10^{-2}$ S m^{-1} at 200 °C, which is comparable with that of the oxide glass $67\,B_2O_3\cdot33\,Na_2O$. A model was proposed for the superionic glass $10\,Al(PO_3)_3\cdot80\,PbF_2\cdot10\,MnF_2$ In the latter case, the glass structure is described by alternating layers of a conductor and an insulator.[78]

VI. Optimisation of characteristics of fluoride-conducting glasses and prospects of their practical applications

In the study,[8] the crystal-chemical concept of isomorphism was extended to the glassy state. Isovalent (in some cases, heterovalent) substitutions can be realised in series of glass-forming cations and/or in series of modifying cations. Cations, which can isomorphically replace each other, must have close sizes, similar bond ionicities and coordination polyhedra of the same type and occupy approximately equal volumes. For fluoride glasses, the following isomorphous series are most important: Li–Na–K–Rb–Cs, Ca–Cd–Sr–Pb–Ba, $Mg-Ni^{2+}-Co^{2+}-Fe^{2+}-Zn-Mn^{2+}$, Ln–Bi–Y–In–Sc, $Al-Ga-V^{3+}-Fe^{3+}-Cr^{3+}-In-Sc$ and Zr–Hf–U–Th.

The possibility of the application of the crystal-chemical concept of isomorphism to the glassy state was experimentally exemplified by the execution of the control over the electrophysical properties of glasses by changing their chemical compositions in the isoconcentration series $55\,ZrF_4\cdot20\,BaF_2\cdot25\,MF$ (the conductivity increases in the series Li < Na < Cs), $59\,ZrF_4\cdot26\,BaF_2\cdot15\,MF$ (Na < Rb < Cs),[60] $50\,ZnF_2\cdot19.5\,BaF_2\cdot10\,InF_3\cdot10\,SrF_2\cdot10\,MF\cdot0.5\,NdF_3$ (Li < Na < K < Rb),[34] $65\,ZrF_4\cdot25\,BaF_2\cdot10\,MF_2$ (Ca < Sr < Ba),[60] $59\,ZrF_4\cdot26\,BaF_2\cdot15\,MF_3$ (Sb < Nb < Bi),[60] $60\,ZrF_4\cdot30\,BaF_2\cdot10\,LnF_3$ (Lu < Gd < La)[61] and $40\,MF_3\cdot40\,BaF_2\cdot20\,YbF_3$ (Al < Ga < Sc < In).[35]

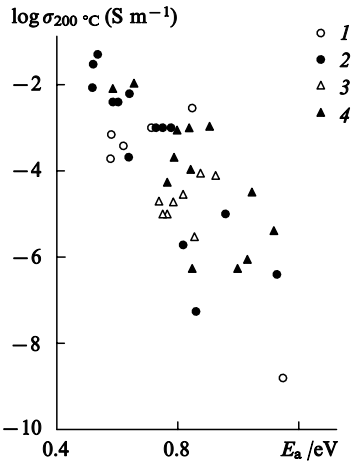

Figure 1. Dependence of $\log\sigma_{200\,^\circ C}$ on the activation energy of the conductivity for various families of fluoride glasses.
(*1*) MF_2-based glasses; (*2*) MF_3-based glasses; (*3*) MF_4-based glasses; (*4*) oxyfluoride glasses. The conductivity was calculated for 200 °C, the activation energy was calculated by the equation $\sigma T = A\exp(-E_a/kT)$.

The dependence of the conductivity on its activation energy for various families of anion-conducting glasses is shown in Fig. 1. It can be seen that the fluoride-ionic conductivity is determined primarily by the activation energy. To perform the directed search for glassy fluoride-conducting solid electrolytes and optimisation of their transport characteristics, it is necessary to reveal the factors responsible for the mechanism of the conductivity. The following facts are evidence for the high fluoride-ionic conductivity in glasses:

(1) the presence of highly coordinated glass-forming cations located in polyhedra of different types and sizes;[12]

(2) high polarisability of the cations;[60]

(3) weak energy of the cation–fluorine bond;[12]

(4) an increase in the molar volume of the glass.[34,35]

From the aforesaid it follows that the Ba^{2+} and Pb^{2+} ions acting as modifiers have the most substantial and yet different effect on the fluoride-ion transport. Taking into account the essential role of the electron shells of the ions in interionic interactions, it can be assumed that this distinction is due to the difference in the configuration of the outer electron shells of the Pb^{2+} ion (Group IV element) and the M^{2+} ions (M = Ca, Sr, Ba and Cd, which are Group II elements). Studies of the mixed $Pb_{1-x}Cd_xF_2$ crystals demonstrated[79,80] that the anionic conductivity in these isovalent solid solutions occurs predominantly with the participation of the fluoride ions whose nearest environment is formed by lead cations. This is confirmed by the fact that the energies of formation of Frenkel defects in the β-PbF_2 and BaF_2 crystals are substantially different (1 and 1.8 eV, respectively[81]). The temperature dependences of the anionic conductivity for fluoride glasses and crystalline conductors based on PbF_2 are shown in Fig. 2. It can be seen that the conductivities of glasses are higher than that of the superionic conductor PbF_2 but lower than those of the fluorite solid solutions $Pb_{0.85}Yb_{0.15}F_{2.15}$ and $Pb_{0.9}In_{0.1}F_{2.1}$.

Presently, problems associated with the environmental protection from various fluorine-containing pollutants gain momentum. The use of fluoride solid electrolytes as functional elements in detectors and chemical current sources is a topical line of investigations in this field.[70,85,86] Let us consider the prospects of the practical use of fluoride-conducting glassy solid electrolytes in electrochemical devices. Since glasses are isotropic and have no grain boundaries (as opposed to ceramics), their conductivities do not decrease as the temperature is lowered due to the blocking effect of grain boundaries. The chemical composition and the structure of glasses can be varied over wide ranges (the composi-

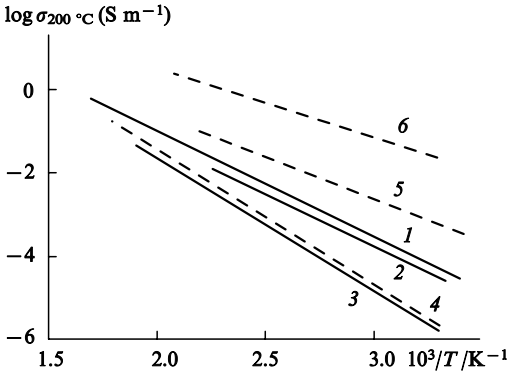

Figure 2. Temperature dependences of the anionic conductivities for glassy and crystalline fluoride solid electrolytes; (*1*) the $40\,InF_3 \cdot 45\,PbF_2 \cdot 15\,BaF_3$ glass,[37] (*2*) the $30\,InF_3 \cdot 35\,BaF_2 \cdot 35\,BiF_3$ glass,[38] (*3*) the $10\,Al(PO_3)_3 \cdot 85\,PbF_2 \cdot 5\,MnF_2$ glass,[32] (*4*) β-PbF_2 single crystal,[82] (*5*) $Pb_{0.85}Yb_{0.15}F_{2.15}$ single crystal,[83] (*6*) $Pb_{0.9}In_{0.1}F_{2.1}$ polycrystal.[84]

tional and structural flexibility), which allows one to optimise the requirements imposed on materials used in devices and ensure a good interface contact between solid electrolytes and electrodes taken in the glassy state, thus eliminating the problems inherent in crystalline systems.

The use of solid electrolytes as active elements of detectors is based on the Nernst equation:

$$E = \frac{RT}{nF} \ln\left(\frac{a'_F}{a''_F}\right),$$

where E is the electromotive force of the electrochemical cell , n is the number of electrons involved in the electrode reaction, F is the Faraday constant, a'_F and a''_F are the activities (in particular cases, the concentrations) of fluorine at two solid electrolyte–electrode interfaces.

The ionic conductivity is responsible for the rate of the establishment of thermodynamic equilibrium between the electrode and the solid electrolyte with respect to the F^- ions (the response speed of the detector). It is generally essential that the anionic conductivity of a solid electrolyte should be higher than 10^{-4} S m^{-1} for it to be used in detectors. This anionic conductivity of a fluoride glass can be achieved by various means.

The construction of chemical current sources based on fluoride solid electrolytes is appealing due to high free energies of the formation of fluorides. Taking into account these values, high calculated electromotive forces (several Volts) were obtained. The fluoride-ionic conductivities of fluoride glasses used presently in chemical current sources are in the range of 10^{-5}–10^{-4} S m^{-1} at room temperature. The internal resistances of these sources are higher than those of traditional cells based on liquid electrolytes. To reduce the internal resistance of a current source, it is necessary to use either high temperature (heating to 150 °C) or a thin-film technology. It should be noted that amorphous solid electrolytes readily form thin films, which do not require high annealing temperatures and are compatible with the silicon technology.

VII. Conclusion

By applying the principles of the isomorphism of atoms to the glassy state, multicomponent glasses possessing the required electrophysical properties can be prepared in the basic glass-transition region of the fluoride system. Isovalent substitutions in the series $Li^+ < Na^+ < K^+ < Rb^+ < Cs^+$, $Ba^{2+} < Pb^{2+}$, $Al^{3+} < Ga^{3+} < Sc^{3+} < In^{3+}$ and $Hf^{4+} < Zr^{4+}$ lead to the enhancement of the ion transport in fluoride glasses. However, it should be noted that the introduction of hygroscopic KF, RbF and CsF or readily hydrolysable PbF_2, InF_3 and BiF_3 leads to a decrease of the chemical stability of glasses.[8]

Compositions of fluoride glasses, which possess high anionic conductivities and can serve as a basis for ion-selective membranes and detectors, have been formulated. An increase in the fluoride-ionic conductivity is associated primarily with a decrease in the activation energy of migration of charge carriers. High conductivities are characteristic of fluoroindate glasses of the $40\,InF_3 \cdot 45\,PbF_2 \cdot 15\,BaF_3$ ($\sigma_{200\,°C} = 5 \times 10^{-2}$ S m^{-1}) and $30\,InF_3 \cdot 35\,BaF_2 \cdot 35\,BiF_3$ ($\sigma_{200\,°C} = 3 \times 10^{-2}$ S m^{-1}) types and also of fluorophosphate glasses of the $10\,Al(PO_3)_3 \cdot 85\,PbF_2 \cdot 5\,MnF_2$ type ($\sigma_{200\,°C} = 1 \times 10^{-2}$ S m^{-1}).

Investigations of the cation (particularly, lithium) transport in fluoride glasses call for special consideration. For example, high lithium-ionic conductivities are manifested by the fluoride and oxyfluoride glasses $50\,LiF \cdot 30\,Li_2O \cdot 20\,Al(PO_3)_3$ ($\sigma_{300\,°C} = 1$ S m^{-1}),[87,88] $80\,LiF \cdot 20\,UF_4$ ($\sigma_{150\,°C} = 1 \times 10^{-1}$ S·m^{-1}), $60\,LiF \cdot 30\,ThF_4 \cdot 10\,BaF_2$ ($\sigma_{170\,°C} = 2 \times 10^{-2}$ S m^{-1}, $E_a = 0.58$ eV), $80\,LiF \cdot 20\,Al(PO_3)_3$ ($\sigma_{200\,°C} = 3 \times 10^{-3}$ S m^{-1}, $E_a = 0.61$ eV),[32] $60\,LiF \cdot 20\,ZrF_4 \cdot 10\,ThF_4 \cdot 10\,BaF_2$ ($\sigma_{175\,°C} = 2 \times 10^{-2}$ S m^{-1});[89] high sodium-ionic conductivities are exhibited by the glasses $80\,NaF \cdot 20\,Al(PO_3)_3$ ($\sigma_{200\,°C} = 2 \times 10^{-3}$ S m^{-1}, $E_a = 0.80$ eV)[23] and $50\,NaF \cdot 50\,B_2O_3$ ($\sigma_{200\,°C} = 2 \times 10^{-5}$ S m^{-1}, $E_a = 0.93$ eV);[90] potassium-ionic conductivity is manifested by the $80\,KF \cdot 20\,Al(PO_3)_3$ glass ($\sigma_{200\,°C} = 4 \times 10^{-6}$ S m^{-1}, $E_a = 0.76$ eV).[23]

Studies of crystallisation of glasses are of interest in connection with the possibility of the construction of nanocrystalline superionic conductors. One of the problems is the design of a microcrystalline structure in an amorphous glass by crystallisation (the preparation of superionic composites); in fluoride systems, the conductivities of partially disordered crystalline phases (solid solutions) are higher than those of glassy phases (see Fig. 2). To produce a microcrystalline structure in a glass, annealing should be carried out in such a way that a large number of crystallisation centres appear and the rate of crystal growth is low. The first stage of crystallisation may involve isolation of small crystals of intermediate metastable phases. It is assumed that the growth of large crystals is retarded by the amorphous phase.

References

1. K K Evstrop'ev, G T Petrovskii *Dokl. Akad. Nauk SSSR* **241** 1334 (1978) [a]
2. D Leroy, J Lucas, M Poulain, D Ravaine *Mater. Res. Bull.* **13** 1125 (1978)
3. E B Merkulov, V K Goncharuk, in *Tezisy Dokladov X Simpoziuma po Khimii Neorganicheskikh Ftoridov, Moskva, 1998* (Abstracts of Reports of the Xth Symposium on the Chemistry of Inorganic Fluorides, Moscow, 1998) p. 106
4. J Videau, J Portier, in *Inorganic Solid Fluorides* (Ed. P Hagenmuller) (New York: Academic Press, 1985) p. 309
5. J Lucas *Mater. Sci.* **24** 1 (1989)
6. V D Khalilev, V L Bogdanov *Zh. Vsesoyuz. Khim. O-va im. D I Mendeleeva* **36** 593 (1991) [b]
7. P P Fedorov *Neorg. Mater.* **33** 1415 (1997) [c]
8. P P Fedorov *Kristallografiya* **42** 1141 (1997) [d]
9. P P Fedorov, R M Zakalyukin, L N Ignat'eva, V M Buznik *Usp. Khim.* **69** 767 (2000) [*Russ. Chem. Rev.* **69** 705 (2000)]
10. A R West *Solid State Chemistry and Its Application* (New York: Wiley, 1984)
11. S G Bakhvalov, E M Petrova, A A Shubin, E A Odintsov *Fiz. Khim. Stekla* **26** 326 (2000) [e]
12. D Ravaine, G Perera, M Poulain *Solid State Ion.* **9–10** 631 (1983)
13. P J Bray, D E Hintenlang, R V Mulkern, S G Greenbaum, D C Tran, M Drexhage *J. Non-Cryst. Solids* **56** 27 (1983)
14. Y Kawamoto, J Fujiwada *Phys. Chem. Glasses* **31** 117 (1990)
15. R Yamamoto, M Kano, Y Kawamoto *J. Phys., Condens. Matter* **9** 5157 (1997)
16. D R Almond, G K Duncan, A R West *Solid State Ion.* **8** 159 (1983)

17. J C Dyre *J. Non-Cryst. Solids* **88** 271 (1986)
18. N F Uvarov, E F Hairetdinov, J M Reau, J M Bobe, J Senegas, M Poulain *Solid State Ion.* **74** 195 (1994)
19. J M Bobe, J M Reau, J Senegas, M Poulain *Solid State Ion.* **82** 39 (1995)
20. J M Bobe, J M Reau, J Senegas, M Poulain *J. Non-Cryst. Solids* **209** 122 (1997)
21. N V Gur'ev, G T Petrovskii, A A Pronkin *Fiz. Khim. Stekla* **26** 623 (2000) [e]
22. I A Sokolov, Yu P Tarlakov, I V Murin, A A Pronkin *Fiz. Khim. Stekla* **25** 96 (1999) [e]
23. I A Sokolov, Yu P Tarlakov, V N Naraev, A A Pronkin *Fiz. Khim. Stekla* **24** 795 (1998) [e]
24. X Zhao, S Sakka *J. Non-Cryst. Solids* **112** 347 (1989)
25. N G Artyushkina, K K Evstrop'ev, A A Pronkin *Fiz. Khim. Stekla* **3** 280 (1977) [e]
26. V N Naraev, A A Pronkin *Fiz. Khim. Stekla* **10** 42 (1984) [e]
27. R M Almeida, J D Mackenzie *J. Mater. Sci.* **17** 2533 (1982)
28. H Kahnt, J M Reau *Phys. Status Solidi A* **121** 73 (1990)
29. M Tatsumisago, Y Akamatsu, T Minami *Solid State Ion.* **31** 41 (1988)
30. J M Reau, H Kahnt, M Poulain *J. Non-Cryst. Solids* **119** 347 (1990)
31. S P Gabuda, V K Goncharuk, E B Merkulov, E I Voit, A V Voit, V Ya Kavun, in *Tezisy Dokladov X Simpoziuma po Khimii Neorganicheskikh Ftoridov, Moskva, 1998* (Abstracts of Reports of the Xth Symposium on the Chemistry of Fluorides, Moscow, 1998) p. 34
32. J M Reau, M Poulain *Mater. Chem. Phys.* **13** 189 (1989)
33. M Sural, A Ghosh *Solid State Ion.* **130** 259 (2000)
34. N I Sorokin, M V Fominykh, A I Boltalin, P P Fedorov, B P Sobolev *Neorg. Mater.* **31** 702 (1995) [c]
35. N I Sorokin, P P Fedorov, B P Sobolev *Kristallografiya* **39** 119 (1994) [d]
36. N I Sorokin, R M Zakalyukin, T Yu Glazunova, A I Boltalin, P P Fedorov, B P Sobolev *Neorg. Mater.* **36** 1008 (2000) [c]
37. N I Sorokin, P P Fedorov, R M Zakalyukin, B P Sobolev, A I Boltalin, M D Val'kovskii *Neorg. Mater.* **35** 88 (1999) [c]
38. V Ya Kavun, N I Sorokin, E B Merkulov, V K Goncharuk *Neorg. Mater.* **37** 613 (2001) [c]
39. V F Ruban, I V Murin, A A Pronkin *Fiz. Khim. Stekla* **10** 112 (1984) [e]
40. Y Wang, A Osaka, Y Miura *J. Non-Cryst. Solids* **112** 323 (1989)
41. R Gopalakrishan, B V R Chowdari, K L Tan *Solid State Ion.* **51** 203 (1992)
42. A A Pronkin, V E Kogan, I A Sokolov, Yu P Tarlakov *Fiz. Khim. Stekla* **21** 496 (1995) [e]
43. G Demortain, J M Reau, G Villeneuve, A Tressaud *J. Fluorine Chem.* **36** 273 (1987)
44. N I Sorokin, M V Fominykh, P P Fedorov, B P Sobolev *Solid State Phenomena* **39 – 40** 293 (1994)
45. H G Schnering, P Bleckmann *Naturwissenschaften* **55** 342 (1968)
46. M Samouel *Rev. Chim. Miner.* **8** 537 (1971)
47. R D Shannon *Acta Crystallogr., Sect. A* **32** 751 (1976)
48. N Auriault, J Guery, A M Mercier, C Jacoboni, R de Pape *Mater. Res. Bull.* **20** 309 (1985)
49. S G Bakhvalov, E M Bayukov, E M Petrova, K A Sablina, V M Buznik, V M Denisov, N A Poddubetskaya *Fiz. Khim. Stekla* **25** 457 (1999) [e]
50. C Jacoboni, A le Bail, R de Pape, J P Renard, in *Studies in Inorganic Chemistry* (Ed. R Metselaar) (Amsterdam: Elsevier, 1983) p. 687
51. B Boulard, C Jacoboni, M Rousseau *J. Solid State Chem.* **80** 17 (1989)
52. M Poulain *Nature (London)* **293** 279 (1981)
53. L N Ignat'eva, T F Antokhina, V Ya Kavun, S A Polishchuk, E A Stremousova, E B Petrova, V M Buznik, S G Bakhvalov *Fiz. Khim. Stekla* **21** 75 (1995) [e]
54. J Kincs, A Soufiane *J. Non-Cryst. Solids* **213 – 214** 388 (1997)
55. V Ya Kavun, E B Merkulov, V K Goncharuk, L N Ignat'eva *Fiz. Khim. Stekla* **26** 287 (2000) [e]
56. R M Zakalyukin, N I Sorokin, P P Fedorov, A I Boltalin, in *Tezisy Dokladov X Simpoziuma po Khimii Neorganicheskikh Ftoridov, Moskva, 1998* (Abstracts of Reports of the Xth Symposium on the Chemistry of Inorganic Fluorides, Moscow, 1998) p. 57
57. S P Gabuda, V K Goncharuk, V Ya Kavun, A P Kulikov, G T Petrovskii *Dokl Akad. Nauk SSSR* **296** 1150 (1987) [a]
58. V A Ignatyuk, R G Lednev, G A Pisarenko *Fiz. Khim. Stekla* **25** 140 (1999) [e]
59. A P Kulikov, L N Ignat'eva, T Nakadzima, E B Merkulov, E I Overchuk *Fiz. Khim. Stekla* **22** 20 (1996) [e]
60. Y Kawamoto, I Nohara *Nippon Kagaku Kaishi* 1783 (1985)
61. A Konishi, H Izumi, R Kanno, Y Kawamoto *J. Mater. Sci.* **29** 1584 (1994)
62. V Ya Kavun, V K Goncharuk, E B Merkulov, V M Buznik, S A Stepanov *Fiz. Khim. Stekla* **20** 221 (1994) [e]
63. V A Ignatyuk, V K Goncharuk, E B Merkulov *Fiz. Khim. Stekla* **20** 529 (1994) [e]
64. J M Bobe, J Senegas, J M Reau, M Poulain *J. Non-Cryst. Solids* **162** 169 (1993)
65. J M Bobe, J M Reau, J Senegas, M Poulain *Phys. Status Solidi A* **139** K87 (1993)
66. J M Reau, H Kahnt, M Poulain, P Hagenmuller *Z. Anorg. Allg. Chem.* **598 – 599** 269 (1991)
67. J M Reau, X Y Jun, J Senegas, C Le Deit, M Poulain *Solid State Ion.* **95** 191 (1997)
68. Y Kawamoto, I Nohara, J Fujiwara, Y Umetani *Solid State Ion.* **24** 327 (1987)
69. V Ya Kavun, G D Lukiyanchuk, V K Goncharuk *Fiz. Khim. Stekla* **23** 466 (1997) [e]
70. I V Murin, A A Pronkin, A A Il'in, I A Sokolov, in *Tezisy Dokladov Vserossiiskoi Konferentsii 'Sensor 2000', S-Peterburg, 2000* (Abstracts of Reports of the All-Russian Conference 'Sensor 2000', St Petersburg, 2000) p. 17
71. Yu G Igitkhanyan, N B Knyazyan, N M Semetskaya, V D Khalilev, in *Tezisy Dokladov V Simpoziuma po Khimii Neorganicheskikh Ftoridov* (Abstracts of Reports of the Vth Symposium on the Chemistry of Inorganic Fluorides) (Moscow: Nauka, 1978) p. 123
72. V A Vopilov, N N Gurova, V M Buznik, L N Urusovskaya *Fiz. Khim. Stekla* **17** 826 (1991) [e]
73. V M Buznik, L N Urusovskaya, V E Galant, V A Vopilov *Fiz. Khim. Stekla* **22** 146 (1996) [e]
74. A R Kulkani, C A Angell *Mater. Res. Bull.* **21** 1115 (1986)
75. A R Kulkani, H G K Sundar, C A Angell *Solid State Ion.* **24** 253 (1987)
76. I A Sokolov, I V Murin, Kh D Viemkhefer, A A Pronkin *Fiz. Khim. Stekla* **24** 175 (1998) [e]
77. I A Sokolov, I V Murin, Kh D Viemkhefer, A A Pronkin *Fiz. Khim. Stekla* **24** 509 (1998) [e]
78. S K Saha, D Chakravorty *J. Non-Cryst. Solids* **167** 89 (1994)
79. M Ya Valakh, I Kosatskii, A P Litvinchuk *Fiz. Tv. Tela* **27** 3667 (1985) [g]
80. M Ya Valakh, I Kosatskii, A P Litvinchuk *Fiz. Tv. Tela* **28** 641 (1986) [g]
81. A V Chadwick *Solid State Ion.* **8** 209 (1983)
82. R W Bonne, J Schoonman *J. Electrochem. Soc.* **124** 28 (1977)
83. N I Sorokin, G A Shchavlinskaya, I I Buchinskaya, B P Sobolev *Elektrokhimiya* **34** 1031 (1998) [f]
84. J M Reau, S Matar, S Kasim, J C Champarnaud-Mesjard, B Frit *Solid State Ion.* **7** 165 (1982)
85. I V Murin, O V Glumov, D B Samusik, V B Bogolyubov, E A Krivandina, B P Sobolev, in *Trudy II Vsesoyuznoi Konferentsii 'Metody i Sredstva Kontrolya Zagryazneniya Atmosfery i Promyshlennykh Vybrosov i ikh Primenenie'* (Proceedings of the Second All-Union Conference 'Methods and Facilities of Control of Atmosphere Pollution and Industrial Wastes and Their Application') (Ed. V I Krasnov) (Leningrad: Gidrometioizdat, 1988) p. 228
86. J W Fergus *Sens. Actuators B, Chem.* **42** 119 (1997)
87. K K Evstrop'ev, G I Veksler, B S Kondrat'eva *Dokl. Akad. Nauk SSSR* **215** 902 (1974) [a]
88. A A Pronkin, K K Evstrop'ev *Fiz. Tv. Tela* **20** 1524 (1978) [g]
89. J Senegas, J M Reau, H Aomi *J. Non-Cryst. Solids* **85** 315 (1986)
90. I A Sokolov, V N Naraev, A N Nosakin, A A Pronkin *Fiz. Khim. Stekla* **26** 848 (2000) [e]

[a] — *Dokl. Chem. (Engl. Transl.)*
[b] — *Mendeleev Chem. J. (Engl. Transl.)*
[c] — *Inorg. Mater. (Engl. Transl.)*
[d] — *Crystallogr. Rep. (Engl. Transl.)*
[e] — *Glass Phys. Chem. (Engl. Transl.)*
[f] — *Russ. J. Electrochem. (Engl. Transl.)*
[g] — *Phys. Solid State (Engl. Transl.)*

Russian Chemical Reviews **70** (10) 809 – 825 (2001) © 2001 Russian Academy of Sciences and Turpion Ltd

DOI 10.1070/RC2001v070n10ABEH000671

Nanochemistry of metals

G B Sergeev

Contents

I.	Introduction	809
II.	Synthesis and chemical reactions of metal nanoparticles	809
III.	Cryonanochemistry of metals	813
IV.	Ensembles involving nanoparticles	815
V.	Photochemistry and nanophotonics	817
VI.	Semiconductors and sensors	818
VII.	Catalysis on nanoparticles	820
VIII.	Nanoparticles in biology and medicine	822
IX.	Conclusion	823

Abstract. The results of studies on the nanochemistry of metals published in recent years are generalised. Primary attention is centred on the methods for the synthesis of nanoparticles and their chemical reactions. The means of stabilisation of nanoparticles which involve individual metals and incorporate atoms of several metals are considered as well as their physicochemical properties. Self-assembling processes of nanoparticles are described. The prospects of using metal nanoparticles in semiconductor devices, catalysis, biology and medicine are discussed. The bibliography includes 165 references.

I. Introduction

The last decade of the XXth century was marked by the increased attention of scientists in the fields of physics, chemistry, materials science, *etc*. devoted to nanoparticles, *viz*., to their synthesis, properties and different reactions. The reason for this lies in the fact that particles of nanometer sizes exhibit peculiar mechanical, optical, electrical and magnetic properties different from those of the corresponding macroparticles. Since 1990, the annual growth in publications devoted to both nanoparticles themselves and the prospects of their application in nanotechnologies has been observed. The methods of synthesis and stabilisation of nanoparticles as well as their optical, magnetic and other properties have already been summarised. In particular, quite a number of books, collections of papers and surveys devoted to metal and semiconductor nanoparticles and materials fabricated on their basis have already been published.[1–15]

At the same time, studies on the chemical reactions that involve nanoparticles are still in their infancy, and even the keyword 'nanochemistry' has appeared in reference journals relatively recently. This review is intended to make up for this gap. It mainly deals with chemical reactions that involve metal nanoparticles; however, a special section is devoted to the synthesis, stabilisation and physicochemical properties of nanoparticles based on individual metals, several metals and metal compounds.

In this review, an attempt is undertaken to follow the main trends in the development of this new scientific field by considering studies published mostly in 2000. Primary attention is given to the use of low temperatures in studies on the activities of metal nanoparticles and size effects. (The question of how the particle size affects its reactivity still remains one of most challenging and stubborn questions of modern chemistry.[16]) Self-assembling of nanoparticles and their application in catalysis and photocatalysis are discussed. Major problems of the chemistry of nanoparticles and nanomaterials are considered and approaches to their solution are suggested.

II. Synthesis and chemical reactions of metal nanoparticles

Until recently, particles with sizes in the range from 1 to 100 nm were assigned to nanoparticles (in certain studies, this interval was even extended to 1000 nm), although, in accordance with the International System of Units (SI) (the prefix nano- is used for fraction units, *viz.,* 10^{-9}), nanoparticles should involve only particles with sizes in the range from 1 to 10 nm, and it is more correct to consider 100-nm particles as ultradispersed ones and the materials based on them as macroscopic materials.

Nanochemistry studies synthetic methods and chemical properties of particles with sizes of 1 – 10 nm. The most interesting problems of nanochemistry are concerned with the reactivity of nanoparticles. For example, chemical properties of 1-nm particles that contain $\sim$10 metal atoms can be changed by introduction of only one atom. This is why, it is important to know and correctly understand the chemical and physical regularities that govern the activities of particles with the sizes of an order of magnitude of 1 nm.

Investigation of the dependence of chemical and physical properties of nanoparticles on the number of constituent metal atoms and the nature of ligands bound to nanoparticles represents a new direction in nanochemistry. At present, this field accumulates the knowledge which will allow one to understand the effects of the geometry, electronic properties and sizes of such systems on their reactivities. Properties of nanoparticles synthesised in the gas

G B Sergeev Department of Chemistry, M V Lomonosov Moscow State University, Leninskie Gory, 119899 Moscow, Russian Federation.
Fax (7-095) 939 02 83. Tel. (7-095) 939 54 42.
E-mail: gbs@kinet.chem.msu.ru

Received 28 March 2001
Uspekhi Khimii **70** (10) 915 – 933 (2001); translated by T Ya Safonova

phase have been studied in more detail. The joint use of a supersonic jet, pulse lasers and mass spectrometry made it possible to obtain, identify and characterise 'free' nanoparticles containing different numbers of metal atoms. The dependence of the chemical activity of nanoparticles in the gas phase on the number of the constituent atoms was studied in detail for niobium [17] and iron [18] particles.

At present, attention is focused on the development of methods for the synthesis and stabilisation of nanoparticles in the liquid phase. Special attention is paid to the preparation of monodispersed particles.

1. Reduction in solution

Methods of chemical reduction play an important role in the solution of the problem of synthesis of monodispersed particles. These methods were mainly used for the synthesis of gold and silver nanoparticles and less often for platinum, cobalt, nickel and copper nanoparticles.

Spherical silver nanoparticles with sizes of 3.3–4.8 nm were synthesised by reduction of silver nitrate by sodium borohydride in the presence of bis[(trimethylammoniodecanoylamino)ethyl] disulfide dibromide as a stabiliser.[19] The particles obtained were characterised by active light absorption in the wavelength range near 400 nm, which corresponded to the silver plasmon peak and indicated the metallic nature of the particles. The environment effect on the stability of silver particles formed showed that the latter form aggregates in the presence of sulfuric and hydrochloric acids. The stability of silver particles was also shown to depend on the pH of the medium; at pH 5–9 in aqueous media, the particles remained stable for a week. Both an increase and a decrease in the pH resulted in fast aggregation and precipitation of silver particles. The effect of the pH on the stability of gold particles was less pronounced compared with silver particles.

Metal nanoparticles of controllable sizes (1–2 nm) were prepared using amphifillic poly(octadecylsiloxane) as a matrix.[20]

Hybrid matrices based on polyelectrolyte gels with oppositely charged surfactants were used as nanostructurised media for the reduction of various platinum salts by sodium borohydride and hydrazine. It was shown that with $NaBH_4$ as the reductant small platinum particles with radii of $\sim$2–3 nm were mainly formed, whereas the use of hydrazine resulted in particles of $\sim$40 nm.[21]

For cobalt nanoparticles in aqueous solutions, the formation mechanism, electronic spectra and reactions were studied.[22] Radiation-induced chemical reduction of cobalt ions from aqueous solutions of $Co(ClO_4)_2$ and HCOONa produced spherical cobalt particles with diameters of 2–4 nm. Sodium polyacrylate with a molecular mass of 2100 was used as a stabiliser. Radiolysis produced solvated electrons e^-_{aq}, hydroxyl radicals, hydrogen atoms and $CO_2^{-\bullet}$ radical ions

$$H_2O \longrightarrow e^-_{aq}, H^\bullet, OH^\bullet,$$

$$OH^\bullet(H^\bullet) + HCO_2^- \longrightarrow H_2O(H_2) + CO_2^{-\bullet}.$$

Hydrated electrons and $CO_2^{-\bullet}$ radical ions reduced Co^{2+} ions producing cobalt nanoparticles which demonstrated an absorption maximum in the 200 nm wavelength range. The use of pulse radiolysis has shown that the reduction of Co^{2+} with the formation of cobalt nanoparticles occurred by an autocatalytic mechanism.

Radiation-induced chemical reduction of Ni^{2+} ions in aqueous solutions of $Ni(ClO_4)_2$ containing propan-2-ol in the presence of polyethylene, polyacrylate and poly(vinyl sulfate) produced metal sols comprising spherical particles with diameters of 2–4 nm. Nickel nanoparticles easily oxidisable by O_2 and H_2O_2 form sufficiently stable Ni–Ag nanosystems in the interaction with silver ions.[23]

Spherical copper particles measuring 20–100 nm were obtained by γ-radiolysis of $KCu(CN)_2$ aqueous solutions in the presence of methanol and propan-2-ol as the acceptors of hydroxyl radicals.[24]

Silver particles were obtained upon γ-radiolysis of solutions of silver nitrate in water, ethanol and 0.01 M $C_{12}H_{25}OSO_3Na$.[25] The fractal dimensions of aggregates were 1.81, 1.73 and 1.70 in water, ethanol and $C_{12}H_{25}OSO_3Na$, respectively.[25] Stable nanoparticles (the average size of 1–2 nm) of platinum, rhodium and ruthenium were prepared in organic media by heating the corresponding colloidal solutions of the metal hydroxides in ethanol.[26]

Silver particles measuring 2–7 nm were obtained by electrochemical dissolution of a metal anode (silver plate) in an aprotic solution of tetrabutylammonium bromide in acetonitrile.[27] This process was shown to depend on such characteristics as the current density and the nature of the cathode material. Thus at high current densities under nonequilibrium conditions, particles of irregular shapes can be formed. In the interval from -1.35 to -6.90 nA cm^{-2}, the particle diameter changed from 6 ± 0.7 to 1.7 ± 0.4 nm. In the reduction of silver ions stabilised by tetrabutylammonium bromide, silver nanoparticles were formed and deposited on cathodes made of either platinum or aluminium (Fig. 1). The use of platinum cathodes resulted mainly in the formation of spherical silver nanoparticles, whereas only films were deposited on aluminium cathodes. An analysis of the optical spectra of nanoparticles measured during their syntheses led to the conclusion that this process includes an autocatalytic stage. It was also shown that the half-width of the surface plasmon peak of a particle linearly depends on $1/R$ (R is the particle radius) and the plasmon band shifts to lower frequencies with a decrease in the particle size.

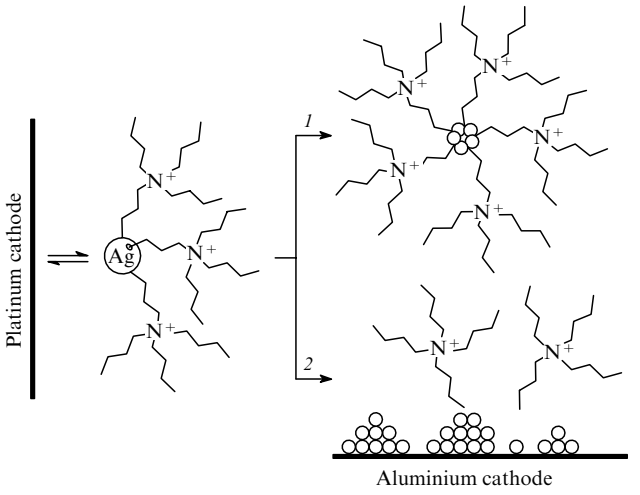

Figure 1. Schematic illustration of the competition between two processes. (*1*) Formation of silver particles and (*2*) deposition of particles and formation of a film.[27]

2. Reactions in micelles, emulsions and dendrimers

Micelles, emulsions and dendrimers,† which can be considered as a sort of nanoreactors, which make it possible to synthesise particles of definite sizes, are used for preparing metal nanoparticles. Crystalline bismuth nanoparticles measuring less than 10 nm were obtained by reduction of aqueous solutions of bismuth salts inside reverse micelles based on sodium diisooctyl sulfosuccinate (usually designated as AOT).[28] Mixing of AOT dissolved in isooctane with a certain volume of an aqueous solution of $BiOClO_4$ resulted in the formation of reverse micelles. The

† A dendrimer represents a highly branched macromolecule which includes a central core, internal repeating units and terminal functional groups. Dendrimers with small numbers of internal units exist in an 'open' form, whereas those involving large number of units form spherical three-dimensional structures. Terminal groups of dendrimers can be modified by hydroxy, carboxy and alkyl groups.

micellar solution of $NaBH_4$ was prepared in the same fashion with the same ratio $w = [H_2O]:[AOT]$. Both solutions were mixed under argon. Bismuth particles precipitated after the mixture was kept for several hours at room temperature. The liquid phase was removed *in vacuo*, and the dry residue was dispersed in toluene. According to X-ray powder diffraction and electron spectroscopy data, a dark solution thus obtained contained bismuth particles measuring 3.2 ± 0.35 nm for $w = 2$ and 6.9 ± 2.2 nm for $w = 3$. When polymers were used for the protection of crystalline bismuth particles, the particle size increased to 20 nm and further.[29]

Reduction of rhodium salts in water in the presence of an amphiphilic block copolymer of styrene with ethylene oxide and an anionic surfactant (sodium dodecyl sulfate) produced rhodium particles with diameters of 2–3 nm stabilised by the block copolymer.[30] Luminescent nanomaterials based on yttrium oxide doped with europium were synthesised using non-ionic reverse microemulsions based on poly(ethylene oxide) and other ethers.[31]

At present, an active search is directed to macromolecules that can be used as matrices in syntheses of nanoparticles. In such methods, the stabiliser molecules interact with the surfaces of metal particles and affect their growth. For example, the reduction of bivalent copper in the presence of poly(*N*-vinylpyrrolidone) produced particles with the diameters of 7 ± 1.5 nm at 11 °C and 10 ± 2 nm at 30 °C.[32] Studies on the temperature effect on the stability of preformed nanoparticles have shown that if copper particles formed at 11 °C were heated to 30 °C, their polymeric shell lost its protective properties, which enhanced aggregation and accelerated oxidation of metal particles. The opposite result was achieved by cooling to 11 °C the system formed at 30 °C. In this case, the particles do not aggregate, their sizes remain unchanged and the resistance to oxidation increases. The competition of different temperature-dependent processes is reflected not only in the stabilities of particles formed but also in their size distribution.

Photochemical reduction of Ag^+ ions in the presence of dendrimers with terminal amino and carboxy groups produced silver particles with an average diameter of ~7 nm.[33] Below, a possible mechanism of particle formation is shown.

$$Ag^+ + [\text{dendrimer}]-CO_2^- \xrightarrow{h\nu} Ag^0 + [\text{dendrimer}]-CO_2^{\bullet} \longrightarrow$$
$$\longrightarrow [\text{dendrimer}]^{\bullet} + CO_2,$$
$$Ag^+ + [\text{dendrimer}]-NH_2 \xrightarrow{h\nu} Ag^0 + [\text{dendrimer}]-NH_2^{+\bullet}.$$

The particle size can be controlled by varying the nature of the dendrimers. Currently, stabilisation of metal nanoparticles is performed in the presence of dendrimers based on polyamidoamines and their derivatives. The use of dendrimers as microreactors for the synthesis of metal nanoparticles was documented in Ref. 34. Monodispersed spherical polyamidoamine dendrimers are permeable to low-molecular reactants. Thus an addition of $HAuCl_4$ to an aqueous solution of a dendrimer with primary and tertiary amino groups results in the appearance of a protonated dendrimer with $AuCl_4^-$ as the counter-ion. Reduction of $AuCl_4^-$ anions by sodium borohydride have produced 1–5-nm gold particles. By varying either the concentration ratio (D) of $AuCl_4^-$ counter-ions to terminal amino groups or the diameter (generation) of the dendrimer, one can control the particle size. Reduction of gold ions in a dendrimer of the ninth generation (G.9) resulted in the formation of spherical gold particles with the sizes of 2.5, 3.3 and 4 nm for $D = 1:4$, $1:2$ and $1:1$, respectively. For $D = 1:1$, gold particles measuring 2, 2.5, 3.2 and 4 nm were formed in dendrimers of the G.6, G.7, G8 and G.9 generations, respectively.

Reduction of gold and silver salts in the presence of modified dendrimers produced particles with an average diameter of 2–6 nm. The autocatalytic mechanism of the reaction has been revealed using spectral methods.[35]

The prospects of using mesopores for the preparation of different nanosize materials were discussed.[36] Nanoparticles of silver and silver sulfide were obtained in nanosize cavities of perfluorinated ionomer membranes.[37] Reduction of metal ions in the presence of aminodextran and styrene resulted in the formation of spherical polystyrene particles with diameters of ~2.0 μm covered with gold and silver islets measuring from 5 to 200 nm.[38]

3. Particles of different shapes and films

The sizes and shapes of particles often depend on the synthetic methods; however, the ratio of nucleation to growth rates of particles is also of great importance. Each of these processes depends in turn on variations in the reaction conditions such as temperature, the nature and concentrations of metal and ligand and the nature of stabiliser and reductant. The problems of nucleation and particle growth are surveyed in detail elsewhere.[15]

The shapes of metal nanoparticles formed in the reduction of metal salts can be controlled using tetra-n-octylammonium carboxylates $(n\text{-}C_8H_{17})_4N^+(RCO_2)^-$ as the reductants and stabilisers (see Ref. 39). Palladium particles measuring 1.9 and 6.2 nm were formed in the reaction

$$Pd(NO_3)_2 + (n\text{-}C_8H_{17})_4N^+(RCO_2)^- \xrightarrow{\text{THF, 66 °C}} \text{Pd particles.}$$

Their sizes and shapes were determined by electron microscopy. It was found that if acetate, dichloroacetate, pivalate or pyruvate anions were used, the particles formed had largely spherical shape. However, if palladium nitrate was treated with an excess of $(n\text{-}C_8H_{17})_4N^+(HOCH_2CO_2)^-$, triangular particles with an average size of 3.6 nm were formed in addition to spherical ones. The shape changes observed were attributed [39] to the presence of the hydroxy group in the anion.

A nickel compound $Ni(COD)_2$ (COD is cycloocta-1,5-diene) was used for elucidating the role (reductant or stabiliser) the glycolic acid residue plays in the reduction.[39] The reaction was as follows:

$$Ni(COD)_2 + (n\text{-}C_8H_{17})_4N^+(HOCH_2CO_2)^- \xrightarrow{H_2,\ 60\ °C} \text{Ni particles.}$$

Inasmuch as nickel in $Ni(COD)_2$ is in its zerovalent state, the glycolate can act only as a stabiliser, whereas it is hydrogen that reduces COD to cyclooctane. By means of electron microscopy it was found that the reaction produces crystalline nickel particles with an average size of 4.5 nm preferentially shaped as triangles. In control experiments using $(n\text{-}C_8H_{17})_4N^+Br^-$ or $(n\text{-}C_8H_{17})_4N^+NO_3^-$ as stabilisers, spherical particles were formed. The triangular shape of particles was additionally confirmed by the results of scanning tunnelling microscopy. The glycolate effect on the morphology of particles formed seems to be associated with the selective adsorption of anions on growing nanocrystals, which can be traced by changes in the absorption spectra. During synthesis of nanoparticles, the band at 1621 cm^{-1} which belongs to dissolved glycolate disappears, and a new band appears at 1604 cm^{-1}, which corresponds to adsorbed glycolate. It is believed [39] that the changes observed in the IR spectra recorded *in situ* agree with the proposed mechanism.

The formation of spherical and cylindrical silver nanoparticles was observed upon photochemical reduction of silver salts in the presence of polyacrylic acid.[40,41] Polyacrylic acid and Ag^+ ions form a complex which, being illuminated, produces silver nanoparticles. According to electron microscopy and sedimentation analysis data, photoreduction of the complex produced spherical silver nanoparticles measuring 1–2 nm. In the presence of a modified (partially decarboxylated) acid, apart from spherical particles, elongated particles (nanorods) with lengths of up to 80 nm characterised by light absorption in the 500–800-nm range were also formed. Apparently, decarboxylation disturbs the cooperative mechanism of the bonding between polyacrylic acid and

silver cations, making the stabilisation of spherical particles less effective and favouring the growth of nanorods.

The sizes of metal particles formed in the presence of macromolecular stabilisers depend on the conditions of formation of the polymeric protective shell. If the polymer involved is an insufficiently effective stabiliser, a particle already bound to the macromolecule may continue to grow. Changing the monomer and the corresponding polymer and varying the polymer concentration in solution, enables one to control the sizes and shapes of particles formed.

An original method of changing the stabilising ability of a polymer was proposed.[42] The authors studied how the conformation of poly(*N*-isopropylacrylamide) affected the shape of platinum nanopartilcles formed upon the reduction of K_2PtCl_4 by hydrogen. This polymer can change its conformation with temperature. Below 306 K, polymer molecules are hydrophilic and represent swelled globules; in this case, up to 60% of platinum nanoparticles formed have irregular shapes. At temperatures above 306 K, polymer molecules are hydrophobic and begin to collapse. The stabilising ability of such molecules decreases. At 313 K, the reduction of platinum ions proceeded on the most active (111) face of the growing nanocrystal, and cubic nanoparticles were preferentially formed (in up to 68% yield). The morphology of the particles also depended on the concentration ratio of platinum salt and polymer in solution (however, to the lesser extent than on the temperature).

The shapes and sizes of silver nanoparticles can be controlled when the methods of pulse sonoelectrochemistry (the use of ultrasound in electrochemistry) were applied.[43,44] Ultrasound allows one to clean and degasify the electrode surface, accelerate mass transfer and increase the reaction rate. Silver particles shaped as spheres, rods and dendrites were obtained by the electrolysis of aqueous solutions of $AgNO_3$ in the presence of $N(CH_2COOH)_3$. These were characterised by electron microscopy, X-ray diffraction and electron spectroscopy. The shapes of particles were found to depend on the reagent concentration. Spherical particles had diameters of $\sim$20 nm. The diameters of rods were 10–20 nm. In certain cases, their surfaces exhibited protrusions which could be developed into dendrites.

An interesting method of successive layer-by-layer deposition of thin (100–300 nm) films incorporating magnetic nanoparticles was considered.[45] Alternating layers of magnetic nanoparticles, *e.g.*, Fe_3O_4, and poly(diallyldimethylammonium bromide) were first deposited on a glass plate covered with paraffin and acetyl cellulose. Upon reaching the desirable film thickness, the cellulose layer was removed, and the whole specimen was dissolved in acetone. The suspension thus obtained could be applied on any porous surfaces and dense supports. It was noted that the films which incorporate uniform magnetic nanoparticles measuring $\sim$10 nm, can be used in memory devices.[46]

At present, the control over the shapes and sizes of nanoparticles seems to be the most important problem of nanochemistry.[47] Synthesis of uniform spherical and rod-like particles of metallic iron have been described.[48] Nanoparticles were prepared by thermal decomposition of iron pentacarbonyl in the presence of stabilisers. Spherical particles measuring 2 nm were uniformly dispersible in solution and formed rods of 2-nm diameters and 11-nm lengths. These particles were amorphous, whereas the rods had the face-centred cubic structure of α-iron.

Different supports with films of 4-mercaptobenzoic acid applied in high vacuum were used for the preparation of thin heterogeneous films with incorporated nanoparticles of gold, silver, and cadmium sulfate. The heterogeneous films were synthesised by successive immersion of supports in the corresponding solutions.[49]

High-resolution electron microscopy has shown that, being encapsulated into micelles, rod-like gold nanoparticles prepared by an electrochemical method grow along the [001] axis. Here, (100) faces of the particles remain stable, whereas (110) faces are unstable.[50]

The possibility of structural changes in platinum nanoparticles supported on silicon and the microcrystalline structure of individual nanoparticles were studied by electron microscopy before and after the system was heated *in vacuo* and in hydrogen and oxygen atmospheres.[51] In all the cases, the mass of particles remained unchanged, but the sizes of constituent crystals increased with temperature. This was attributed to surface fusion and self-diffusion of platinum particles. Studies of adhesion of platinum particles to silica which were carried out using atomic force microscopy have shown that heating changes the crystalline nature of particles and strengthens their adhesion to silica. Moreover, platinum nanoparticles were shown to be stable both under oxidative and reductive conditions.

4. Reactions of oxides

Like metals, oxides also find extensive application in practice. The reactivity of metal oxides is low compared with the corresponding metals; therefore, oxide formation is used for stabilising metal nanoparticles. Recently, metal oxide nanoparticles have been employed in reactions which are of interest for nanochemistry.

An original application of nanocrystalline zinc oxide has been described,[52] where zinc oxide was synthesised by a modified sol–gel method by the reactions

$$ZnEt_2 + 2\,Bu^tOH \longrightarrow Zn(OBu^t)_2 + 2\,C_2H_6,$$

$$Zn(OBu^t)_2 + 2\,H_2O \longrightarrow Zn(OH)_2 + 2\,Bu^tOH,$$

$$Zn(OH)_2 \longrightarrow ZnO + H_2O.$$

The process of ZnO preparation involved three stages: synthesis, isolation and activation. The latter process, in turn, consisted of several successive stages of thermal treatment. First, the powder was slowly heated to 90 °C and kept at this temperature for 15 min. Then, the temperature was gradually increased to 250 °C, held at this level for 15 min and slowly decreased to room temperature. Zinc oxide thus obtained represented crystalline nanoparticles measuring 3–5 nm with a surface area of $\sim$120 $m^2\ g^{-1}$. Nanosize zinc oxide was used in the reaction

$$2\,ZnO + CCl_4 \longrightarrow CO_2 + 2\,ZnCl_2.$$

The process was carried out at 250 °C, and CCl_4 was introduced into the reaction vessel portionwise at 7-min intervals. Carbon dioxide and nonconsumed CCl_4 were quantitated by gas chromatography. Nanocrystalline zinc oxide was shown to be more reactive than common commercial specimens. It was also shown that the adsorption of sulfur dioxide and the destructive adsorption of diethyl 4-nitrophenyl phosphate (a noxious organophosphorus compound) proceed with a higher efficiency on nanocrystalline zinc oxide.[52] In these processes, nanocrystalline ZnO exhibited higher reactivity compared with commercial specimens.

Nanocrystalline oxides of alkali-earth metals were successfully used for deactivation of yperite (mustard gas) and other war gases. Autocatalytic dehydrohalogenation of 2,2′-dichlorodiethyl sulfide on nanocrystalline calcium oxide was studied using NMR technique.[53] The decomposition products of 2,2′-dichlorodiethyl sulfide were found to involve divinyl sulfide ($\sim$80%) and thioglycol and/or a sulfonium ion ($\sim$20%) with a hydroxyalkyl group, which seem to provide its binding to the surface of the alkali-earth metal oxide. In addition to the reaction of CaO with yperite, its reactions with organophosphorus compounds were studied. The kinetics of the reactions of all studied substances with calcium oxide was shown to be characterised by a rapid initial stage followed by a slow diffusion-controlled stage.

An interesting application of transition metal oxides has been discussed.[54] Particles of cobalt, nickel, copper and iron oxides measuring 1–5 nm were used as the electrode materials in lithium power sources (electrochemical capacity of 700 $\mu A\ h\ g^{-1}$). Here, the formation and decomposition of Li_2O and the accompanying reduction and oxidation of nanoparticles occur on electrodes

made of CoO nanoparticles. The scheme of reversible reactions is as follows:

$$2\,Li - 2e^- \rightleftharpoons 2\,Li^+$$
$$CoO + 2\,Li^+ + 2e^- \rightleftharpoons Li_2O + Co$$
$$CoO + 2\,Li \underset{2}{\overset{1}{\rightleftharpoons}} Li_2O + Co$$

The direct reaction (*1*) is possible and thermodynamically permissible. The reverse reaction (*2*) is unusual for electrochemistry, because Li_2O is traditionally considered to be electrochemically inactive. Electrochemical decomposition of Li_2O using mechanically ground Li_2O and CoO powders could not be effected.[54] Thus, the possibility of the reverse reaction is associated with the use of nanoparticles and the increase in their electrochemical activity with a decrease in size.

Currently, great attention has been drawn to the preparation and analysis of physicochemical properties of hybrid nanomaterials of the core–shell type and the particles which involve two and even three different metals.

New nanocrystalline hybrid core–shell materials such as TiO_2-MoO_3 were prepared and studied in detail.[55] The $TiO_2-(MoO_3)_x$ particles were synthesised by co-nucleation of metal oxides on the surfaces of micelles.

In such materials, the photoabsorption energy correlates with the particle size. With a decrease in the sizes of TiO_2-MoO_3 particles from 8 to 4 nm, the absorption energy decreased from 2.9 to 2.6 eV. For comparison, it may be noted that the forbidden gap energies of bulk TiO_2 and α-MoO_3 are 3.2 and 2.9 eV, respectively. Unfortunately, the materials obtained turned out to be less efficient in photocatalysed oxidation of acetaldehyde compared with common titanium dioxide produced by Degussa (France).

To facilitate the electron transport in metal nanoparticles, it was proposed to use the pH-induced changes in the charges of stabilising shells which are bound to the particle surface. Molecules of rigid mercaptophenylacetylenes were shown to bind strongly gold and silver particles.[56] It was found that electron transport in charged gold particles is better described in terms of classical rather than quantum-mechanical concepts.[57]

The use of nanoparticles of metals and their oxides in optical and electronic devices requires that new approaches be found to the solution of such problems as: establishment of reliable electrical contacts between individual nanoparticles; determination of characteristics of electromagnetic interactions between particles in symmetrical well-organised aggregates of nanoparticles; elucidation of how the chemical properties of the surface of nanoparticles depend upon their size and its effect on their optical and electronic properties.[58]

5. Bi- and trimetallic particles

Nanoparticles that involve two or more different metals are of particular interest for the development of materials with novel properties, because at the nanolevel it is possible to synthesise such intermetallic compounds and alloys that can never be formed for bulk specimens.

Nanoparticles involving two[59] and even three[60] different metals were obtained by radiation-induced reduction of salt solutions. A two-step synthesis was used for the preparation of Au–Hg particles. First, radiation-induced reduction produced 46-nm gold particles. Then, $Hg(ClO_4)_2$ and propan-2-ol were added to the gold sol, which resulted in deposition of mercury ions on the gold particles. Finally, mercury ions were reduced by free radicals formed upon radiolysis.

Palladium particles measuring 4 nm with a narrow size distribution were prepared by the reduction of Na_2PdCl_4 by hydrogen in the presence of sodium citrate. The addition of $K_2Au(CN)_2$ to the sol of palladium particles in methanol followed by γ-irradiation resulted in the reduction of gold ions. No individual gold particles were formed: all gold was deposited on palladium particles and formed an outer layer. A silver layer could also be deposited on the Pd–Au particles obtained. These multilayer clusters seem to be of interest for studying rapid (femtosecond) electronic processes.[61,62]

The use of silicates modified by organic compounds as matrices and stabilisers made it possible to synthesise bimetallic nanoparticles, their sols and gels by a single-step method.[63] Scanning tunnelling microscopy studies of Pd–Pt particles have shown the latter to consist of palladium cores covered with platinum shells. Thin silicate films with bimetallic nanoparticles were used in electrocatalytic oxidation of ascorbic acid.

A sonochemical method was applied to produce bimetallic gold–palladium nanoparticles.[64] The particles were synthesised in aqueous solutions of $NaAuCl_4 \cdot 2H_2O$ and $PdCl_2 \cdot 2NaCl \cdot 3H_2O$ with sodium dodecyl sulfate added. The latter functioned as both the stabiliser and the reductant. The bimetallic particles synthesised represented cores of gold atoms surrounded by shells of palladium atoms. The sizes of cores and shells were measured for different gold to palladium ratios using high-resolution electron microscopy. The use of X-ray spectroscopy allowed the gold and palladium contents in the particles to be determined. With the known density, mass and initial ratio, one can estimate the sizes of cores and shells (Table 1). Using the sonochemical synthesis of bimetallic particles, one can control the sizes of cores and shells by varying Au^{3+} and Pd^{2+} concentrations. Bimetallic Au–Pd particles exhibited high catalytic activity in hydrogenation of pent-4-enoic acid.

Table 1. Core diameter (gold) and shell thickness (palladium) in Au–Pd bimetallic nanoparticles.

Au : Pd ratio	Experiment		Estimate	
	core diameter	shell thickness	core diameter	shell thickness
1 : 1	6.0	1.0	6.4	0.8
1 : 4	5.0	1.5	4.8	1.6

A comparative study of gold, nickel and bimetallic Au–Ni nanoparticles on amorphous carbon supports, which were obtained by laser ablation of the corresponding pure metals and the alloy, was carried out.[65] Studies accomplished by different methods have shown the bimetallic particles to have, on average, diameters of 2.5 nm and a narrow size distribution, while their composition was found to correspond to that of the evaporated alloy.

Nanoparticles of FeTiH were prepared by mechanical synthesis from a mixture of iron and titanium hydride.[66] Nanosize iron–tungsten composite particles with a tungsten concentration varying from 2 at.% to 85 at.% were synthesised by coreduction of a mechanical mixture of iron hydroxide ($FeOOH \cdot nH_2O$) and tungstic acid (H_2WO_4) in a flow of hydrogen at 740 °C for 1 h. The particles obtained were studied by X-ray diffraction and Mössbauer spectroscopy.[67]

III. Cryonanochemistry of metals

The presence of stabilisers, the size distribution of nanoparticles, their different shapes and the interactions between nanosize particles and the medium complicate the studies of the reactions involving metal nanoparticles. In addition, high chemical activities of metal atoms and nanoparticles they form require special approaches to their studies to be developed. One of such approaches is isolation of nanoparticles at superlow temperatures (4–10 K) in inert-gas matrices. Co-condensation of a large amount of an inert gas, *e.g.*, argon, and a small number of nanoparticles (more than 1000 inert gas species per metal particle) allows active particles to be effectively isolated from one another,

while low temperatures hinder diffusion of these particles and provide their stabilisation in an inert matrix.

Here, we will not analyse all the studies devoted to reactions of metal atoms and the corresponding nanoparticles at low and superlow temperatures and only consider the results of recent publications.[68–70] The specimens under discussion were prepared by co-condensation of vapours of metals and ligands on surfaces cooled either to 10 or 77 K. In certain experiments, the vapours were diluted by argon. The amount of metal deposited was determined using quartz-crystal microbalances. The co-condensates obtained were studied by spectroscopy in UV, visible and IR ranges. ESR spectroscopy was also used. Table 2 lists the products formed upon reactions of magnesium and samarium particles with different ligands in argon matrices at 10–40 K.[68,69]

Table 2. Reaction products of samarium and magnesium particles with different ligands in an argon matrix at 10–40 K.

Metal	Ligand		
	CO_2	C_2H_4	CH_3X (X = Cl, Br)
Mg	$Mg^+CO_2^-$, upon annealing of the matrix	cyclic $Mg(C_2H_4)_2$ (see Fig. 2 *a*), upon annealing of the matrix	CH_3MgX, upon irradiation ($\lambda > 280$ nm for Mg and $\lambda > 300$ nm for Mg_{2-4} and Mg_x)
Mg_{2-4}	$Mg^+CO_2^-$, upon co-condensation		
Mg_x	$Mg^+CO_2^-$, upon annealing of the matrix		
Sm	$Sm^+CO_2^-$, CO, $SmCO_3$, upon annealing of the matrix	$Sm(C_2H_4)$ and $Sm(C_2H_4)_2$ complexes	methane, upon co-condensation
Sm_2, Sm_x	$Sm^+CO_2^-$, CO, $SmCO_3$, upon co-condensation		

Studies of properties of metal nanoparticles, in particular at low temperatures, face various difficulties. Therefore, theoretical simulation of the structures of metal nanoparticles, their electronic, optical and other properties and the processes of their aggregation is gaining in importance.

In theoretical studies of nanoparticles, valuable results can be obtained by *ab initio* quantum-chemical calculations which use the concepts developed by solid-state physics, and by calculations based on the molecular dynamics approach. At present, the Hartree–Fock method is applied for the determination of properties of atoms and small clusters. Particularly, this method was successfully employed for the calculation of the properties of nickel particles which involved $n = 4$, 6, 8 and 13 atoms.[71] The density functional method is also widely used for the simulation of the behaviour of metal nanoparticles.[13] For example, the latter method was used for studying the structure and properties of Pt_{13} and Pt_{55} species.[72] The results obtained were also compared with those of different *ab initio* and semi-empirical quantum-mechanical methods which are used in calculations of properties of metal nanoparticles. The density functional method was applied[73] for studying the products of carbon monoxide adsorption on palladium particles deposited on magnesium oxide. An extended Hückel method was used for studying bimetallic nanoparticles of Pt–Fe alloys with a number of atoms ranging from 13 to 309.[74]

The *ab initio* quantum-mechanical calculations have shown that the magnesium–carbon dioxide system represents a metastable $Mg^+{}^{\bullet}CO_2^{-\bullet}$ radical-ion pair. According to calculations, this pair is stabilised by the argon matrix. The IR spectrum of the argon–ethylene co-condensate have revealed absorption bands of ethylene dimers. As was shown by calculations, the potential

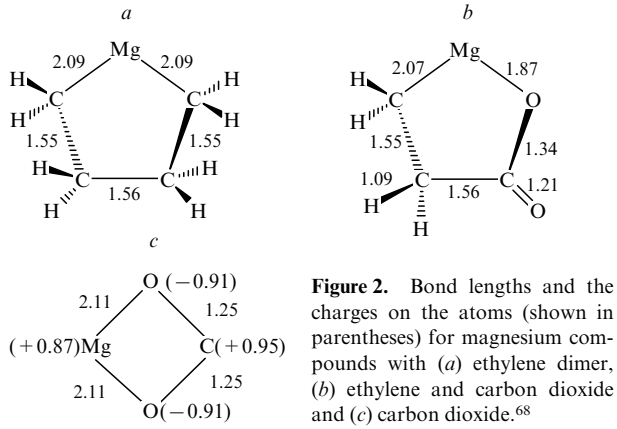

Figure 2. Bond lengths and the charges on the atoms (shown in parentheses) for magnesium compounds with (*a*) ethylene dimer, (*b*) ethylene and carbon dioxide and (*c*) carbon dioxide.[68]

surface of the $Mg \cdot 2C_2H_4$ complex demonstrates no global minimum corresponding to the C_{2v} symmetry. The global minimum can be obtained if only all the restrictions on the system's symmetry are removed. In the Møller–Plessett (MP2) approximation, the minimum corresponded to a cyclic structure which involves an ethylene dimer and a magnesium atom. The interatomic distances in the structures of magnesium complexes with ethylene and carbon dioxide were calculated. Figure 2 shows the structures of these complexes.

Studies of a samarium–carbon dioxide co-condensate have shown that samarium and CO_2 form a complex with an angular structure. In the reaction products, CO and CO_3^{2-} were detected. Radical anions $CO_2^{-\bullet}$ and a samarium carbonyl compound of an uncertain composition were also formed. Figure 3 shows the data on the reaction products identified and on their interconversions. Figure 4 shows the temperature dependence of the relative activity of samarium nanoparticles in the reaction with CO_2. The results

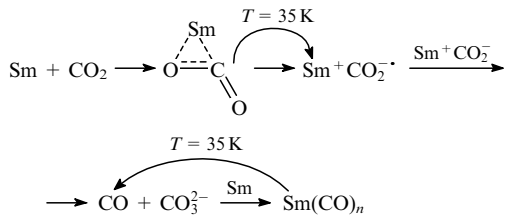

Figure 3. Schematic illustration of the reactions of samarium atoms with carbon dioxide molecules in an argon matrix. Straight arrows are the reactions occurring during co-condensation; curved arrows are the reactions occurring during heating of the co-condensate.[68]

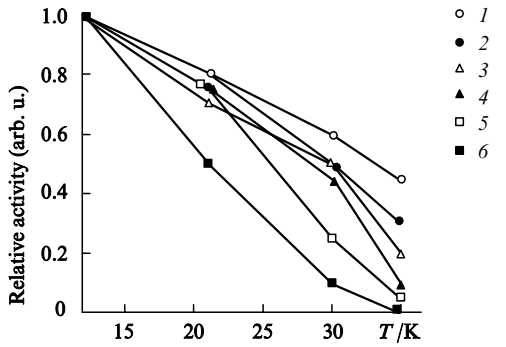

Figure 4. A temperature dependence of the relative activity (in arbitrary units) of samarium atoms and nanoclusters in the reaction with carbon dioxide.[9] (*1*) Sm, $\lambda = 501$ nm; (*2*) Sm, $\lambda = 557$ nm; (*3*) Sm, $\lambda = 520$ nm; (*4*) Sm_x, $\lambda = 641$ nm; (*5*) Sm_x, $\lambda = 600$ nm; (*6*) Sm_2, $\lambda = 541$ nm (λ is the wavelength in the electronic spectrum).

shown suggest a higher activity of samarium nanoparticles compared with samarium atoms. A similar trend was observed for magnesium nanoparticles. According to IR spectroscopic data, in samarium – ethylene co-condensates, 'sandwich' π-complexes of samarium and ethylene SmC_2H_4 and $Sm(C_2H_4)_2$ are formed rather than cyclic compounds typical of magnesium co-condensates.

At ordinary temperatures, the reactions of bulk magnesium and samarium with alkyl halides occur in a similar way to give organometallic compounds. At low temperatures, atoms and small clusters of these metals react with haloalkanes (*e.g.*, with halomethanes) by different routes. Magnesuim inserts into the C – Br and C – Cl bonds with the formation of Grignard reagents, whereas samarium, being more reactive, reduces CH_3Cl and CH_3Br to methane. Thus, on the nanoparticle level, magnesium and samarium behave differently.

Another peculiarity in the behaviour of magnesium and samarium nanoparticles was observed in their reactions with mixtures of two ligands, *viz*., CO_2 and C_2H_4. It was found that under comparable conditions magnesium and samarium react only with CO_2 and do not react with ethylene. The results obtained demonstrate that no unambiguous relationship exists between the activity and selectivity of metal nanoparticles.

The formation of complexes and organometallic nanostructures was studied by an example of film co-condensates of the vapours of metallic silver and mesogenic cyanobiphenyls $C_nH_{2n+1}C_6H_4C_6H_4CN$ ($n = 5$ and 8) and $C_nH_{2n+1}OC_6H_4.C_6H_4CN$ ($n = 8$) in the temperature interval of 80 – 350 K.

Low-temperature co-condensation of silver particles with $C_5H_{11}C_6H_4C_6H_4CN$ and $C_8H_{17}C_6H_4C_6H_4CN$ produced π-complexes stable at low temperature.[68] IR and UV spectroscopic studies have confirmed their formation and revealed their sandwich structures and 1 : 2 composition; 1 : 1 complexes were also detected. The structure of π-complexes determined from IR spectroscopic data was confirmed by model quantum-chemical calculations.[75] Vibrational frequencies of CN groups were also calculated and compared with the experimental ones. Spectral properties of the reaction products of mesogenic cyanobiphenyls with silver particles were discussed in detail elsewhere.[76]

Thermal degradation the complexes undergo on being heated to the room temperature results in the formation of nanosize (15 – 30 nm) silver clusters and their subsequent aggregation with formation of anisotropic particles (more than 200 nm long) stabilised in a liquid-crystal line matrix.[76] An analysis of the ESR spectrum of a co-condensate of silver particles with 4-pentyl-4′-cyanobiphenyl at 90 K has revealed two spectral doublets. The values of the *g*-factor and the hyperfine coupling constant (*a*) for ^{107}Ag and ^{109}Ag are as follows: $g(^{107}Ag) = 2.001$, $a(^{107}Ag) = 48.5$ mT and $g(^{109}Ag) = 2.003$, $a(^{109}Ag) = 72.75$ mT. The occupation degree (ρ_m) of valence *s* orbitals of the metal in the complex was estimated ($\rho_m = 0.77$). The value obtained suggests that electron density is shifted from a silver atom to the π-orbitals of the ligand. The ESR spectrum also revealed a broad anisotropic singlet which was tentatively attributed to zero-valent silver nanoparticles.

Optical spectroscopy in the UV and visible ranges in combination with the dynamic light scattering technique were used for studying the properties of polymer-stabilised silver nanoparticles.[77] Co-condensation of vapours of silver and 2-dimethylaminoethyl metacrylate *in vacuo* occurred on the walls of a glass vessel cooled by liquid nitrogen. According to the electron microscopic data, heating of the co-condensate to room temperature resulted in the formation of polymer-stabilised silver nanoparticles measuring 5 – 12 nm. Dynamic light scattering studies have shown that the size distribution of these particles is bimodal. Such a distribution seems to suggest that both isolated silver particles and their aggregates are simultaneously present in the system. The dependence of the radius of a solvated particle on the nature of the solvent was studied. Among the solvents such as water, toluene and acetone, the latter gave solutions containing silver particles with the smallest radii.[78]

Co-condensation of lead and a monomer polymerisable at low temperatures, *viz*., *p*-xylylene, vapours at 80 K, afforded films with incorporated lead nanoparticles. Conductivity of the films was studied in the course of co-condensation and subsequent heating.[79] The metal – polymer films obtained exhibited satisfactory sensor activity with respect to ammonia in air and ammonia in the presence of water vapour.

Complexes of zero-valent samarium with 1,3,5-tri(*tert*-butyl)-benzene were obtained by co-condensation of metal and ligand vapours at 80 K. Kinetics of thermal decomposition of these complexes was studied.[80,81] Transformations that occur in samarium complexes with mesogenic cyanobiphenyls were also studied at low temperatures.[82] It was shown that the complex with the composition $Sm : C_5H_{11}C_6H_4C_6H_4CN = 1 : 2$ transforms in the temperature range 170 – 210 K into the complex $Sm : C_5H_{11}C_6H_4C_6H_4CN = 1 : 1$; this reaction is characterised by an effective activation energy of 8 kJ mol^{-1}. The reaction of magnesium particles with chloro-, bromo- and iodobutanes at low temperatures was studied.[83] It was shown that the yield of octane (the Würtz reaction product) depends on the amount of magnesium and the carbon – halogen binding energy. The mechanism of the reaction of magnesium with alkyl halides and the earlier data on the cryonanochemistry of metal particles have been discussed elsewhere.[2,3]

IV. Ensembles involving nanoparticles

When metal nanoparticles are synthesised by the condensation method, the process begins with the formation of nanoparticles of individual metal atoms; this may be considered as 'self-assembly' or 'self-organisation'‡ of atoms with the formation of atomic ensembles.

As applied to metal nanoparticles, it is common practice to consider both the ensembles of particles themselves and the ensembles of stabilising protective layers. Prime attention is given to the effect of the chemical nature of stabilisers on self-assembly processes. An analysis of studies devoted to self-assembly and performed before 2000 is given elsewhere.[13] The synthesis of thiol-covered metal particles and their self-assembly into one-, two- and three-dimensional superlattices were surveyed in Ref. 85.

The processes of assembly and self-assembly of nanoparticles were discussed most extensively by the example of silver and gold nanoparticles. Monodispersed silver nanocrystals were stabilised by chemisorption of dodecanethiol on the receptor sites of the crystal surface.[86] The kinetics of aggregation and the structure of the formed ensembles of stabilised particles depend on the number of receptors on the nanocrystal surface.

The formation of alternating positively charged gold particles and negatively charged silver particles and their self-assembly in the presence of 4-mercaptoaniline and 4-mercaptobenzoic acid on a glass surface were described.[87] One-dimensional layers of gold particles on silicon supports were also formed.[88] The latter process was realised using atomic force microscopy (AFM) for surface treatment and chemical deposition of gold particles.

Self-assembly of gold particles measuring 4.6 nm results in aggregates with diameter of ~30 nm.[89] The initial gold particles were prepared by the reduction of $HAuCl_4$ by $NaBH_4$ in the presence of $HSCH_2COONa$. Removal of the excess metal ions from the solution by dialysis resulted in the formation of coarser aggregates. Before the dialysis, the electronic spectra of particles revealed no plasmon peak typical of gold particles.

A method of synthesising materials from 'bricks and mortar' was first described in Ref. 90. Binding between a polymer and

‡ General description of such self-organisation is given in a monograph by Lehn.[84]

thymine-protected gold particles was provided by hydrogen bonds formed. The process of self-association of particles into aggregates, the sizes of the aggregates and their morphology were temperature-controlled. At 23 °C, the initial 2-nm gold nanoparticles formed spherical aggregates with diameter of 97 ± 17 nm. At -20 °C, spherical aggregates with diameter of 0.5 – 1 μm, which in turn comprised finer aggregates as individual subunits, were formed. At 10 °C, ~50-nm-long chains built of spherical nanoparticles were formed. These self-association processes were studied using X-ray small-angle scattering and transmission electron microscopy (TEM). It was assumed that the formation of aggregates at 10 °C is an intermediate stage of the formation of coarser ensembles at -20 °C, and the former aggregates can be used as the precursors of nanoensembles of different shapes and sizes.

Self-assembly of rod-like gold particles with diameter of 12 nm and lengths of 50 – 60 nm was studied using high-resolution electron microscopy.[91] By choosing concentrations of these particles, their size distribution, the conditions of solvent evaporation, its ionic strength and the surfactant concentration, one-, two- and three-dimensional structures can be obtained by electrolysis. A mixture of hexadecyltrimethylammonium bromide and tetraoctylammonium bromide was used as the water-soluble electrolyte. Tetraoctylammonium bromide provided the formation of cylindrical particles, where the ratio of two surfactants determined the diameter to length ratio of the gold nanorods formed. The electrolysis was carried out for 4.5 min. Gold nanorods were formed on a copper wire net partially immersed in solution (on net – solution contacts). Presumably, the following two factors are most important for further self-assembly of the rods, *viz*., the induced convective transfer of particles from the solution to the thin film by evaporation of water and the interaction of particles within the film, which results in the formation of different structures.[91] A possible reason for the parallel arrangement of rod-like particles is associated with capillary forces that act between parallel rods, although more accurate theoretical analysis is required to explain the anisotropy of the rod ensembles observed.

Self-assembly of nanoparticles entails not only the translational ordering but also the orientational one. The orientational ordering is typical of particles with well determined shapes.[92] Structural changes in gold nanorods upon the action of femtosecond and nanosecond laser pulses were studied by high-resolution electron microscopy.[93] The energy of a pulse did not exceed the value necessary for melting the rods but was sufficient for inducing deformational processes which caused changes in the shapes of nanoparticles: a transition of nanorods into nanospheres was observed. The size and shape distributions of nanorods before and after their exposure to a laser beam were statistically analysed.[94]

In connection with the problem of the development of electronic nanodevices, the problem of synthesising nanoparticles protected by monolayers has attracted attention. The methods of preparation of such layers on gold particles by using solutions of hexanethiols and hexanedithiols in organic[95] and aqueous[96] media were developed.

Stable gold films which involved particles measuring ~4 nm were prepared[97] by the reaction of low-molecular-weight ($M \leqslant 4000$) polymers (such as polyethylenimine and poly-L-lysine) with gold particles covered with carboxylic acids. The film morphology was shown to depend on the nature of the acid which covers the particles. The use of mercaptododecanoic and mercaptosuccinic acids has provided films with higher degrees of ordering.

Glass-supported thin porous gold films were prepared using colloidal gold crystals as the templates. These films were studied by scanning tunnelling microscopy.[98, 99]

Microstructures, wettabilities and thermal stabilities of self-assembly manolayers of partially fluorinated alkanethiols of the $F(CF_2)_{10}(CH_2)_nSH$ (n = 2, 6, 11, 17, 33) type on gold particles were studied.[100] Introduction of fluorocarbon chains as the terminal groups into alkanethiols enhanced the stability of self-assembly manolayers (a gold-supported monolayer of non-fluorinated alkanethiols loses its ordering at ~100 °C). Fluorinated compounds with the numbers of methylene groups in a chain n = 11, 17, 33 formed well ordered monolayers. For smaller numbers of methylene units, the degree of ordering decreased. Wettabilities of the layers were also shown to depend on the number of methylene units. Thermal stabilities of self-assembled gold monolayers increased with an increase in n, and for n = 33 the monolayer films formed remained stable in air at 150 °C for 1 h.

The effect of the nature of the support on the morphology of two- and three-dimensional superlattices formed by dodecanethiol-covered silver sulfide nanocrystals of sizes of 5.8 nm were studied.[101] Oriented pyrolylic graphite and molybdenum disulfide were used as the supports. The self-assembly process was monitored by scanning electron microscopy and AFM. It was found that self-assembly into superlattices depends on the nature of the support and is governed, in addition to capillary forces, by van der Waals interactions of the particle – particle and particle – support types.

Self-assembled monolayers of 4′-hydroxy-4-mercaptobiphenyl, 4-(4-mercaptophenyl)pyridine and their mixtures with 4′-methyl-4-mercaptobiphenyl were deposited on the (111) faces of gold crystals and used as the templates for growing glycine crystals.[102] The morphology of glycine crystals obtained depended on the properties of supporting surfaces and was determined by hydrogen bonds formed between glycine molecules in the growing layer and functional groups on the self-assembled monolayer. Hydrogen bonds formed between the CO_2^- and NH_3^+ groups of glycine and a hydroxy group on the surface of a monolayer comprised of $HOC_6H_4C_6H_4SH$ molecules was assumed to be stronger than the interaction between the NH_3^+ group of glycine and the nitrogen atom of pyridine on the surface of a monolayer built of $NC_5H_4C_6H_4SH$ molecules.

As a rule, self-assembly of monolayers of different substances on metal nanoparticles and films was studied using X-ray photoelectron spectroscopy, ellipsometry and diffraction techniques. Electronic spectroscopy was successfully used [103] in studying self-assembly of monolayers of metalloporphyrins and metallophthalocyanines on ultrathin gold films. Gold films 1.3 – 10-nm thick were prepared using high-vacuum evaporation on mica at low temperatures. The deposition rate was varied in the range 0.2 – 0.4 A s^{-1}. The films were annealed at 250 °C for 2.5 – 4 h. The resulting films were studied using scanning atomic force microscopy, electronic spectroscopy and X-ray diffraction techniques. It was shown that isolated structurised islets were formed on the mica surface the sizes and optical properties of which were governed by the conditions of evaporation and subsequent annealing. The electronic spectra of such films demonstrated a peak due to a gold surface plasmon with a wavelength shifting from 606 to 530 nm as the thickness of the film decreased from 10 to 1.3 nm. The kinetic data on the light absorption were used for making semiquantitative estimates of the nature of bonding and chemical and structural properties of the monolayers. It was shown that the absorption in the region of the gold surface plasmon band, which is caused by association of molecules of organometallic compounds on gold films, may be used for monitoring molecules devoid of chromophore groups.

In addition to the sodium salt of AOT, its derivatives with other metals were used as the templates for self-assembly. To correctly interpret the template effect on the self-assembly of metal particles, phase diagrams of such systems are necessary.[104] By the example of the $Cu(AOT)_2 - iso\text{-}C_8H_{18} - H_2O$ system used as a template, it was shown that the shapes of nanocrystalline particles can be dramatically changed under the effect of various salts in small concentrations.[105]

The development of methods for synthesising metal nanoparticles of controllable sizes is of great interest. Apparently, the

majority of studies in this direction employed thiolates and were devoted to the preparation of gold nanoparticles. The use of alkanethiol monolayeres made it possible to synthesise gold particles stable both in solution and in the 'dry' state. Introduction of functional groups in alkanethiols [57] extended the possibilities of such a synthesis.

In the presence of alkanethiols, the formation of gold nanoparticles and the appearance of a protective layer proceed in two steps [106]

$$AuCl_4^- \text{ (in toluene)} + RSH \longrightarrow (Au^ISR)_n \text{ (polymer)},$$

$$(Au^ISR)_n + BH_4^- \longrightarrow Au_x(SR)_y .$$

This reaction combines the processes of nucleation and passivation. An increase in the RSH : Au molar ratio and the addition of the reductant at the earlier stage result, on average, in the formation of particles with smaller metal cores. A short interruption of the reaction favours the formation of thicker coatings with very small cores (< 2 nm).

The dynamics of growth of gold cores in the presence of protective monolayer coatings was studied.[106] The use of transmission electron microscopy made it possible to monitor slow changes in the sizes of gold particle cores which followed the active initial stage of the reaction. Thus it was found that with hexanethiol as the stabilising coating, the core size of a particle based on gold atoms increased to 3 nm during the first 60 h of the reaction and then remained unchanged. The knowledge of the mechanisms of growth and annealing of nanoparticles will allow one to refine the methods for synthesising finer particles with narrower size distributions.

V. Photochemistry and nanophotonics

Recently, studies which deal with kinetics and dynamics of reactions that involve metal nanoparticles have appeared. A photochemical reaction which involves n-dodecanethiol-covered silver nanoparticles dispersed in cyclohexane was studied in a picosecond time interval.[107] Figure 5 schematically shows the photoreaction mechanism.

According to electron microscopic data, the average size of polyhedral $Ag_xSC_{12}H_{25}$ nanoparticles was ~6.2 nm. Under short-term irradiation, the nanoparticles first decomposed to smaller particles (< 2 nm). However, an increase in the irradiation time to 9 min resulted in the appearance of larger (20-nm) particles. Photochemical transformations were detected from the time variations of the intensity and broadness of silver plasmon absorption lines (marked by heavy lines in Fig. 5). It was found that this absorption depends nonlinearly on the light intensity. The kinetics of photolysis of the particles was studied in the nanosecond range, and the corresponding kinetic constants were determined. Changes in the dielectric properties of the environment occurred within 0.5 ns. In response to optical excitation, a part of alkanethiol molecules were split off over the time (3.6 ns) determined by the energy liberated as heat (E_{th}). The proportion of particles with split off thiol groups depended on the excitation-pulse energy. Within 40 ns (recombination time), the thiol-covered particles could also undergo fragmentation. Subsequent exposure to light partially prevented fragmentation of nanoparticles.

In contrast to silver-based nanoparticles, which undergo light-induced chemical transformations, the behaviour of gold-based nanoparticles under similar conditions is characterised by changes in their shapes. Fragmentation of these nanoparticles is dramatically weakened both in polar solvents and with the changes in the length of the alkanethiol chain.[108]

Silver nanoparticles were used for carrying out photochemical transformations of phenazine and acridine.[109] Being adsorbed on the surfaces of silver particles, both molecules were found to decompose under the action of light in a single-photon process with N–C bond cleavage. The reaction rate and the degree of photodecomposition depended on the light wavelength. Being exposed to short-wave laser light, phenazine decomposed with the formation of graphite. The decomposition rate of phenazine was higher compared to acridine, which apparently is due to different orientation of these molecules on the surfaces of silver particles. The reason for the decomposition these molecules undergo on the surfaces of silver nanoparticles remains unclear.[109] The spectra of acridine adsorbed on nanoparticle surfaces revealed two new

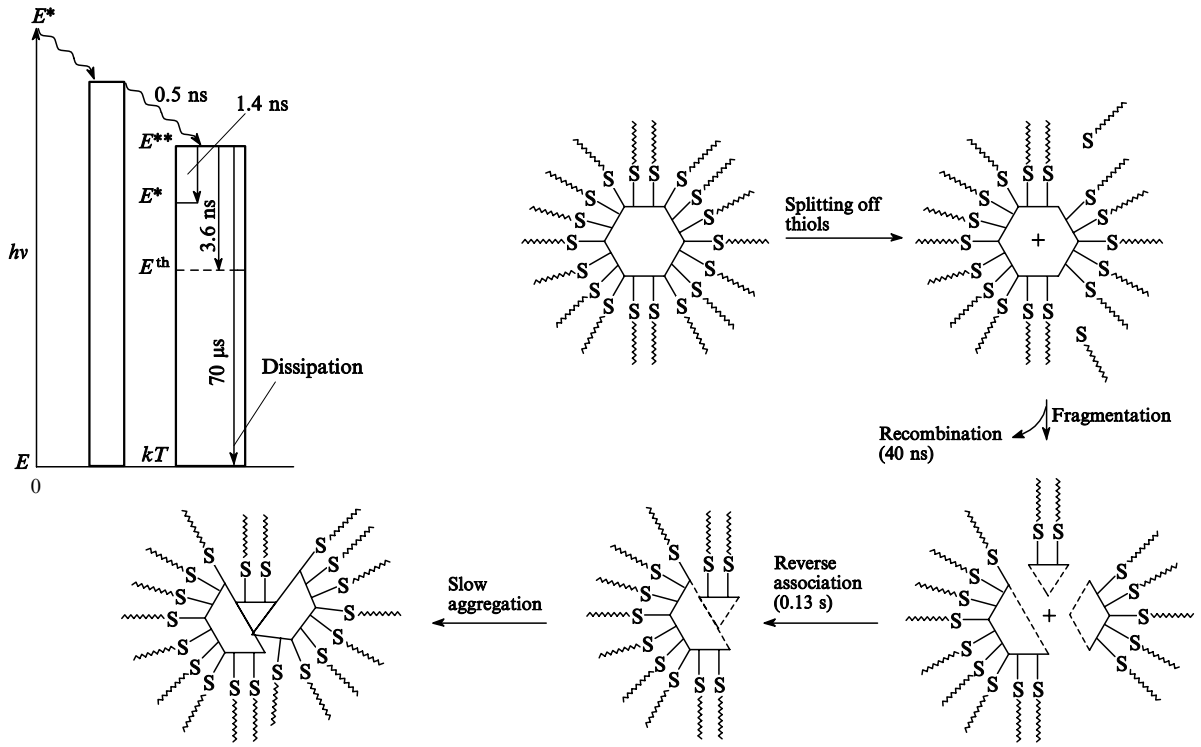

Figure 5. Schematic illustration of the photoreaction involving $Ag_xSC_{12}H_{25}$ dispersed in cyclohexane.[107]

bands at 543 and 619 cm^{-1}, which are close to those observed for quinazoline adsorbed on a silver surface.[110] It was noted that the rate and the extent of photoreactions described are not interrelated. It was assumed that to be decomposed the molecules of phenazine and acridine should either be adsorbed on certain surface sites or form definite geometrical configurations; hence, only a small proportion of molecules can be involved in the reaction.

Optical properties of gold nanoparticles with radii of 2.5, 9 and 15 nm prepared by γ-radiolysis of an aqueous solution of $KAuCl_4$ and stabilised in polyvinyl alcohol were studied.[111] It was found that solutions containing 2.5-nm particles do not attenuate transmitting light, whereas those with larger particles severely decrease the intensity of a laser pulse with a wavelength of 530 nm. The effects observed were attributed to the appearance of a great number of light-diffusion centres formed as a result of evaporation of gold nanoparticles under the laser pulse. Light-diffusion centres were formed in several nanoseconds and largely relaxed to the initial state; upon the next pulse, they partially degraded to small particles.

By means of time-resolved laser measurements, the electron–phonon interactions in metal particles based on Au particles with sizes ranging from 2 to 120 nm and in bimetallic particles based on Au, Ag and Pb were studied. Particles with Au cores and Ag shells and those with Au cores and Pb shells were studied in most details. All the particles were synthesised by radiolysis.[61] It was shown that for Au, in contrast, *e.g.*, to Ag, the time scale of the electron–phonon interaction is independent of the particle size.[112]

Finally, the studies dealing with the prospects of obtaining nanosize quantum dots, quantum wells and quantum wires in inorganic semiconductors [113] should be mentioned, as well as the works on nanophotonics. The latter studies optical properties of objects with much smaller sizes compared with the irradiation wavelength. The efforts were largely focused on investigation of linear optical effects, while the field of non-linear nanoscale optical phenomena is still under way.[114] The problems and prospects of nanophotonics were analysed in Ref. 115.

VI. Semiconductors and sensors

Semiconducting nanoparticles are widely used in heterogeneous catalysis, they are also promising materials for laser engineering, in manufacturing flat displays, light-emitting diodes and sensors. The use of AOT-based reverse micelles for the preparation of ZnSe nanoparticles was first reported in Ref. 116. ZnSe particles measuring 5.7 nm were studied using X-ray diffraction, electronic spectroscopy, light scattering, electron microscopy and luminescence techniques.

A method of stabilisation of nanoparticles of a semiconductor (exemplified by CdS, co-deposition of CdS–ZnS) and a metal (exemplified by gold) was put forward by Japanese scientists.[117] Reverse micelles were prepared and nanoparticles were stabilised by *in situ* polymerisation of (cetyl)dimethyl(*p*-vinylbenzyl)ammonium chloride which was initiated either by light or the addition of azobisisobutyronitrile. The polymer obtained was soluble in polar solvents and formed transparent films with incorporated nanoparticles of cadmium sulfide measuring from 4.7 to 6.3 nm. The proposed method seems to be versatile.

Internal cores of vesicles based on α-phosphatidylcholine can be used as 'nanoreactors' for growing monodispersed (with ~8% deviation) nanocrystals of CaS, ZnS, HgS with definite sizes.[118]

A simple and inexpensive method of synthesising gram quantities of stable water-soluble nanocrystalline powders of zinc sulfide (particles measuring ~6 nm) was put forward.[119] Cysteine-covered ZnS particles were obtained by introduction of sulfide to predissolved zinc salt and cysteine. Following deposition, redissolution and drying, crystalline ZnS powders were obtained, which remained stable for 30 months at 4 °C. Their stability was checked by carrying out catalytic decomposition of *p*-nitrophenol on freshly prepared and aged powders. Upon long-term storage, the optical properties of powders remained unchanged. Highly concentrated aqueous solutions (up to ~100 mmol $litre^{-1}$) of semiconducting particles were used as fluorescent biological labels.

Multilayer films incorporating CdSe nanoparticles were synthesised.[120] The particles measuring 1.7–2.0 nm were obtained from a dimethylformamide solution of cadmium salts and selenium. The films incorporating CdSe particles were prepared by successive formation of layers on quartz or CaF_2 plates. Layers of benzoic acid derivatives and polyvinylpyridine were first applied to the plate surface. The plate thus treated was placed in a dimethylformamide solution of CdSe in order to form a layer containing particles of cadmium selenide. Multilayer (up to five layers) films were obtained by severally adding polyvinylpyridine and cadmium selenide to the solution. Such films are interesting for the development of new types of light-emitting diodes and non-linear optical devices and can serve as conducting films.

Preparation of semiconducting nanowires of definite diameters by using colloidal nanoparticles of metal-catalysts was described.[121–124] As an example, we consider the results of controlled synthesis of GaP nanowires with diameters of 10, 20 and 30 nm and lengths exceeding 10 μm.[124] The wires were obtained by laser ablation of a solid target made of GaP and gold (catalyst). For this purpose, a solution that contained gold particles was applied on a target. The latter was placed in a quartz tube with a solid ZnS target. The tube was located in a blown end of an oven, which was heated to 700 °C and the target was ablated for 10 min by means of an excimer laser. Simultaneous generation of nanoclusters of gold and of GaP semiconductor occurred; the latter particles formed semiconducting nanowires.

Control experiments have shown that in the absence of gold particles no semiconducting wires form. A relationship between the sizes of gold nanoparticles and the diameters of semiconducting GaP wires allowed the authors to conclude that the diameters of the wires obtained can be controlled. A similar method of governing the diameters of silicon nanowires was proposed.[123]

The effect of the size of a semiconducting nanoparticle on its forbidden gap width was studied using CdSe particles measuring from 0.7 to 2 nm as an example.[125,126] All the particles were obtained by using the methods of organometallic chemistry so that their surfaces bore phosphorus atoms and phenyl and propyl groups. For example, the composition of one of the particles studied was $Cd_{10}Se_4(SePh)_{12}(PPr_3)_4$. The atomic structure of the particles was determined using the X-ray diffraction technique. Figure 6 shows the dependence of the forbidden gap width of cadmium selenide nanoparticles on their sizes. It is seen that as the

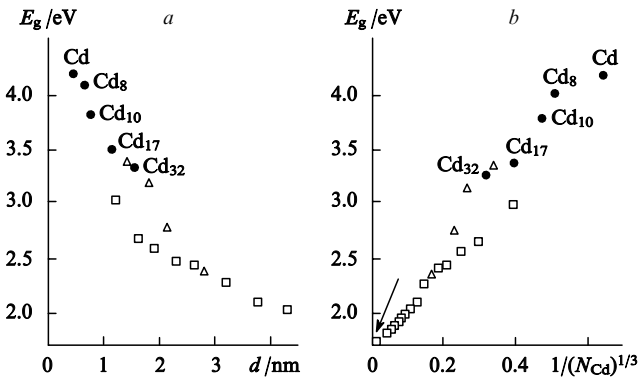

Figure 6. Forbidden gap thickness of CdSe nanoparticles as a function of their (*a*) diameter and (*b*) reciprocal radius.[125] *N* is the number of atoms in a particle. Black points are experimental data, open points are literature data for larger particles (results by different authors). The arrow marks a bulk particle.

nanoparticle size increases the forbidden gap width (E_g) of a particle approaches the E_g value of CdSe bulk samples.

Dynamic properties of charge carriers on the liquid–semiconductor interface are important for photocatalysis, solar energy conversion and photoelectrochemistry. The properties of charge carriers, *viz*., electrons and holes, were studied in a number of semiconducting nanosystems using laser techniques.[127]

Suspensions of cadmium sulfide nanoparticles were used for the initiation of acrylonitrile polymerisation. The polyacrylonitrile (PAN) obtained and the products of its partial hydrolysis were used as the templates which governed the shapes of CdS nanoparticles and CdS/PAN composite nanowires with diameters of 6 nm and lengths varying from 200 nm to 1 μm.[128]

A nanosize electronic switch was built of gold nanoclusters and compounds containing redox groups.[129] Synthesis of *N,N′*-di(10-mercaptodecyl)-4,4′-bipyridinium dibromide containing a bipyridinium fragment as the redox group was described.[130] When gold nanoparticles are bound to the film of bipyridinium dibromide molecules, the reduction of the bipyridinium group on a gold electrode proceeds readily and reversibly.

$$bipy^{2+} + e^- \rightleftharpoons bipy^{+\bullet}.$$

Figure 7 schematically shows an electronic switch measuring less than 10 nm which is controlled by the voltage applied to the STM probe.§ When a molecule involves bipyridinium in a reduced ($bipy^{+\bullet}$) state, a noticeable tunnelling current flows in the nanocluster–molecule–electrode circuit. If a certain threshold voltage is applied to the gold electrode, the tunnelling current decreases. The threshold voltage corresponds to the oxidation of $bipy^{+\bullet}$ to $bipy^{2+}$. At present, such devices operate slowly and require an amplifier. However, they can be used in those fields where amplification is of less importance, *e.g*., as the chemical sensors for detection of single molecules or individual chemical reactions. Moreover, based on these systems, memory devices for computers can be developed.[131]

§ The scheme is taken from Ref. 131, in which the results of another study (Ref. 130) are commented upon. The system shown was assumed [130] to correspond to approximately 60 organic molecules and required no less than 30 electrons to operate.

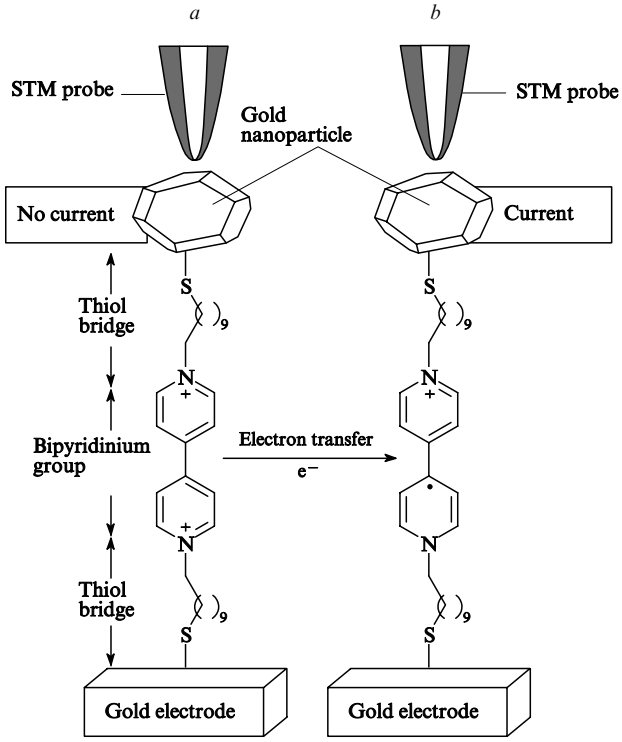

Figure 7. Schematic illustration of the performance of an electronic switch.[131] (*a*) Bipyridinium group is in the oxidised state and no current flows, (*b*) accepting an electron, the bipyridinium group is reduced and a current arises.

New possibilities in designing sensors and optoelectronic devices including those with nanoparticles have been pioneered.[132] It was shown that pore-free crystals of organoplatinum compounds can reversibly absorb and evolve sulfur dioxide without any losses in their crystallinity. Figuratively speaking, the crystals 'breath'. Figure 8 schematically shows the corresponding transitions.

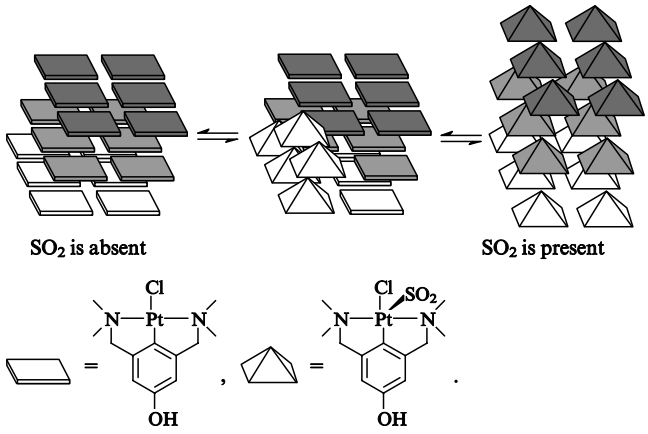

Figure 8. Crystals that reversibly absorb SO_2.[133]

On being exposed to SO_2 for one minute, the crystal acquires an orange colouring. The colour change is accompanied by a transition of planar square platinum complexes into square-pyramidal complexes which involve SO_2 as the fifth ligand. In the process, the crystal increases its volume by 25% but retains the ordered crystal structure. Then, if the crystal is exposed to air, it breathes out SO_2 and relaxes to its initial colourless SO_2-free state. The process can be repeated many times without loss of the crystallinity. It was suggested to use such crystals as optical switches and SO_2-sensors. It is possible that some other similar compounds can reversibly interact with chlorine, CO_2 and other gases. There are strong grounds to believe that substances that bind gases in solution can also bind them in the solid state.

Nanocrystalline films of semiconducting oxides can also be used as the sensitive units of gas sensors. The effects of ethanol and nitrogen dioxide vapours on the properties of SnO_2 nanocrystals applied on single-crystal silicon and of SnO_2 nanocrystals doped by nickel, palladium and copper were studied.[134] Doped SnO_2 nanocrystals were synthesised by pyrolysis of aerosols. According to X-ray diffraction data, their average size was 6–8 nm. It was shown that diffusion of gases affects the voltammetric characteristics of heretostructures, which manifests itself in variations of the potential-barrier height on the heterogeneous boundary and in the changes in the tunnelling processes at the interface.

A new generation of chemical sensors can be synthesised by using non-uniform nanosystems and unusual electronic and physicochemical properties of nanoparticles involved in such systems. In these systems, compact crystalline cores of nanoparticles are surrounded by outer amorphous shells, and the electron transfer induced by adsorbed gas molecules proceeds through the nanoparticles arranged in ensembles and interacting with one another. The sensor properties of non-uniform nanocomposite films were studied[135] for the oxide–oxide (SnO_2–TiO_2), metal–oxide (Cu–SiO_2) and metal–polymer [Cu–poly(*p*-xylylene)] systems. The sensor activities of the specimens with respect to hydrogen, wet air and ammonia were

determined from conductivity variations. All specimens were synthesised under non-equilibrium conditions, which seems to be necessary for the preparation of effective sensor materials.

VII. Catalysis on nanoparticles

The studies devoted to using nanoparticles in the development of novel catalysts which were published before 2000 are surveyed in detail by Bukhtiyarov and Slin'ko.[14] In this section, we consider only the studies published in 2000.

Methane combustion in air proceeds steadily at temperatures above 1300 °C. However, at these temperatures, noxious nitrogen oxides evolve resulting in smog. In this connection, the search for new catalysts of methane combustion is urgent. A new catalyst was synthesised[136] which provided methane combustion at 400 °C. This was prepared using reverse microemulsions based on isooctane, water and surfactants such as the polyethylene oxide–alcohol adducts. Alkoxides $Ba(OC_3H_7)_2$ and $Al(OC_3H_7)_3$ were dissolved in isooctane and mixed with the microemulsion at room temperature: the resulting solid crystalline nanosize barium hexaaluminate exhibited high catalytic activity in CH_4 combustion. The advantage of barium hexaaluminate lies in the fact that the sizes and surfaces of its particles remain unchanged at high temperatures. Moreover, this can be modified by cerium, cobalt, manganese and lanthanum. Modification with cerium oxide produced a composite which enabled methane combustion at temperatures below 400 °C. The history of the search for new methane-combustion catalysts and their characteristics are described elsewhere.[137]

In aqueous AOT–n-heptane buffer microemulsions, a number of reactions were catalysed by palladium nanoparticles. The reaction of *N,N*-dimethyl-*p*-phenylenediamine with $Co(NH_3)_5Cl^{2+}$ catalysed by palladium nanoparticles was described.[138] The catalytic oxidation of *N,N,N′,N′*-tetramethyl-*p*-phenylenediamine by $Co(NH_3)Cl^{2+}$ was also studied in similar microemulsions at pH 5.6.[139] The limiting stage of the reaction was the adsorption of *p*-phenylenediamine on palladium particles of 2.5-nm radii within the microemulsion. This conclusion relies on an observation that the activation energy of the reaction changes from 97 at 15 °C to 39 kJ mol^{-1} at 40 °C and on the results of electrochemical measurements. The specific features of the reaction were discussed in terms of the microreactor model.

Synthesis of platinum, palladium, rhodium and iridium nanoparticles and their use in catalytic hydrogenation of cyclooctene, dodec-1-ene and *o*-chloronitrobenzene were described.[140] Nanoparticles were synthesised by reduction of metal salts by alcohols and stabilised by an amphiphilic copolymer of 1-vinylpyrrolidone with acrylic acid (PVP–AA). The diameters of particles were 0.74 (Ir), 1.93 (Rh), 2.2 (Pd) and 1.2–2.2 nm (Pt), which were determined by electron microscopy.

The introduction of nickel ions into the PVP–AA–Pt catalytic system enhances the effeciency of the latter. Hydrogenation of chloronitrobenzene to chloroaniline at 330 K was carried out with a selectivity of 97.1% and 100% conversion. Introduction of Co^{2+} and Fe^{3+} ions reduced the hydrogenation selectivity to 78.1% and 72.1%, respectively. The analysis of IR spectra have shown that, on being exposed to hydrogen, the ions of nickel, iron and cobalt were not reduced to zero-valent metals. This was explained by the fact that the metal ions interact with two C=O groups in the PVP–AA copolymer and only with a single C=O group in poly(1-vinylpyrrolidone).[141]

The problems of measuring sizes of metal particles applied on supports and size and surface-area distributions for particles with diameters smaller than 2.5 nm were discussed in Ref. 142.

When chemisorption is used for the determination of a catalyst's properties, it is necessary to know how to follow catalyst operation with contaminated surfaces and make an allowance for strong interaction of the metal with the support. A systematic study (in the temperature interval of 573–973 K) of palladium particles of average size ~2 nm applied on activated carbon has been accomplished.[143] The use of two methods, *viz*., X-ray small-angle scattering and transmission electron microscopy allowed the effective sizes of palladium particles to be estimated and the results to be compared with the data obtained in studying CO chemisorption on supported palladium. The agreement between the results of two aforementioned methods was observed for the stoichiometric ratio Pd : CO = 2.

A high catalytic activity of nanoparticles composed of metal cores and outer shells was demonstrated in several studies.[144–147] Gold nanoparticles measuring 2 and 5 nm surrounded by decanethiol molecules were used for electrochemical oxidation of carbon monoxide.[145] Figure 9 schematically shows the electrode reaction. It is noteworthy that the use of thiol-covered gold nanoparticles suggests a co-operative increase in the catalytic activity.

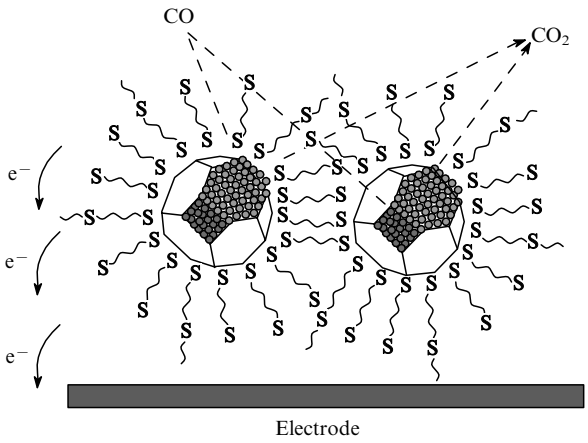

Figure 9. Catalytic oxidation of carbon monoxide on an ensemble of thiol-covered gold nanoparticles on the electrode surface.

The methods of preparation of optimal catalysts may involve varying the shapes of cores, the structures and properties of molecular shells and the types of core–shell bonding. The latter factor affects active sites, defect packing and co-operative electronic properties of nanoparticles.

Platinum nanoparticles were obtained by reducing chloroplatinic acid ($H_2PtCl_6 \cdot 6H_2O$) by ethanol in the presence of poly(*N*-vinylformamide), poly(*N*-vinylacetamide), poly(*N*-isopropylacrylamide) or poly(*N*-vinylpyrrolidone). The particles synthesised had an average diameter of ~2.0–2.5 nm.[148] The effects of additon of KCl and Na_2SO_4 and of temperature variations on the stability of nanoparticles were studied. The particles obtained were used in hydrogenation of allyl alcohol in water and in a salt solution (0.8 M Na_2SO_4). It was shown that catalytic platinum particles are stable in the salt solution and their activity is equal to that in water.

Bimetallic Au–Pt/C(graphite) catalysts were prepared by selective deposition of gold on a platinum film on graphite as a support.[149] The latter monometallic catalyst was obtained by the reduction of H_2PtCl_6 in anhydrous ethanol. The monometallic catalyst was modified by two methods. The first method used platinum as the reagent which reduced $AuCl_4^-$. In the other method, the monodispersed catalyst was first treated with hydrogen and then $HAuCl_4$ was added. At pH 1, bimetallic particles were formed according to the reaction

$$3\,PtH + AuCl_4^- \longrightarrow Pt_3Au + 4\,Cl^- + 3\,H^+.$$

The average size of particles was ~10 nm. The properties of particles and their reactions were studied by several techniques.

Being chemically inactive, gold did not attract much attention as a catalyst until recently. However, gold ions Au^{n+} ($1 \leqslant n \leqslant 3$) in zeolites turned out to be active in the reaction

$$H_2O + CO \longrightarrow H_2 + CO_2$$

at 323 K.[150]

Lithographic systems comprising SiO_2-supported platinum nanoparticles and Al_2O_3-supported silver nanoparticles, which were prepared using electronic beams, were used as model metallic catalysts.[151] The particles with the average sizes of 20–50 nm were spaced at 100–200 nm. The thermal stability of the systems obtained was studied by means of electron microscopy and AFM. The system with platinum particles was stable up to 973 K, whereas the system with silver particles was stable up to 773 K in both vacuum and hydrogen and up to 623 K in oxygen. The catalytic effect of a model catalyst with SiO_2-supported platinum nanoparticles was compared to that of a platinum foil in hydrogenation and dehydrogenation of cyclohexene at 100 °C.[152] The reactivity of a system with platinum particles of 28 nm diameter was shown to be twice as high compared with that of the foil, and its selectivity was higher by a factor of 3.

Isomerisation of dichlorobutanes catalysed by iron-containing nanoparticles stabilised in polymeric matrices was studied.[153] The catalytic activity was shown to depend on the nature of the matrix and the metal content.

Photocatalytic reduction of bis(2-bipyridyl) disulfide (RSSR) to pyridine-2-thiol (RSH) by water selectively proceeded on the surface of titanium dioxide. The reaction rate substantially increased when silver nanoparticles (0.24 mass %) with sizes < 1 nm were applied on TiO_2.[154]

The following mechanism was assumed [154] for this reaction:

$$(1)\ RSSR + 2\,AgTiO_2 \overset{K_a}{\rightleftharpoons} 2\,RSAgTiO_2,$$

$$(2)\ 2\,RSAgTiO_2 \xrightarrow{I\varphi} 2\,RSAgTiO_2(e^- \ldots h^+),$$

$$(3)\ 2\,RSAgTiO_2\,(e^- \ldots h^+) \xrightarrow{k_{d1}} 2\,RSAgTiO_2,$$

$$(4)\ 2\,RSAgTiO_2\,(e^- \ldots h^+) \xrightarrow{k_{cs}} 2\,RSAg(e^-)TiO_2(h^+),$$

$$(5)\ 2\,RSAg(e^-)TiO_2(h^+) \xrightarrow{k_{d2}} 2\,RSAgTiO_2,$$

$$(6)\ 2\,RSAg(e^-)TiO_2(h^+) + H_2O \xrightarrow{k_0} 2\,RSAg(e^-)TiO_2 + 2\,H^+ + \frac{1}{2}O_2,$$

$$(7)\ 2\,RSAg(e^-)TiO_2 + 2H^+ \xrightarrow{k_r} 2\,RSH + AgTiO_2,$$

where K_a is the equilibrium adsorption constant, I is the light intensity, φ is the intensity of light absorption.

In the first stage, the selective adsorption of RSSR on the surfaces of silver nanoparticles is accompanied by the cleavage of the S–S bond. In the second stage, upon the excitation of nanoparticles in the forbidden gap range of TiO_2, an electron (e^-)–hole(h^+) pair is generated. Most of electron–hole pairs recombine (stages *3* and *5*). In stage *4*, charge separation occurs: silver nanoparticles accept electrons, and holes are transferred to the TiO_2 support. The positive potential of a hole is sufficient for water to be oxidised with the formation of H^+ ion and O_2 molecule (stage *6*). In stage *7*, the catalytic system is reduced producing RSH. As a result, the deposited silver nanoparticles seem [154] to cause the following effects:

— acceleration of RSSR adsorption;

— space separation of sites responsible for reduction (silver particles) and oxidation (TiO_2 support), *i.e.*, the effect of charge separation;

— selective adsorption of the substance to be oxidised (RSSR) and the reducing agent (H_2O) in the reduction and oxidation sites, which makes the process highly selective.

Comparison of TiO_2 and $AgTiO_2$ catalytic systems has shown that both systems provide equal activation energies in the photocatalytic reduction (30 ± 1.5 kJ mol^{-1}), which suggests that the multistage process is limited by stage *6* rather than by photocatalysis. Below, the reduction on TiO_2 is shown.

$$2\,RS...TiO_2(e^-) + 2\,H^+ \xrightarrow{k_r} 2\,RSH + TiO_2.$$

In recent years, semiconducting nanoparticles have been actively used in photocatalysis. In this connection, the catalytic activities of nanoparticles of different oxides and sulfides in aqueous and polar (acetonitrile) organic solvents were compared [155] using photooxidation of pentachlorophenol (a toxic compound used as a fungicide and a bactericide and for wood conservation) as an example. Figure 10 shows the relative concentration of pentachlorophenol as a function of the time of its exposure to light in the presence of nanoparticles of different metal sulfides.

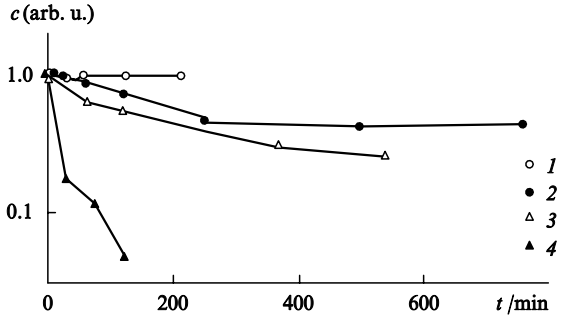

Figure 10. Changes in the relative concentration of pentachlorophenol (c) in water with the time of its exposure to light of the wavelength $400 < \lambda < 700$ nm (*1*) in the absence and (*2–4*) in the presence of catalysts.[155] (*1*) Without catalyst (or TiO_2); (*2*) CdS powder (0.1 mg ml^{-1}), (*3*) MoS_2 particles with diameters of 4.5 nm (0.036 mg ml^{-1}), (*4*) MoS_2 particles with diameters of 3 nm (0.09 mg ml^{-1}).

It is of note that the effect of the nanoparticle size on the reaction rate is extremely strong for MoS_2 particles. This reflects the effect of the forbidden gap width of particles on the reaction and is associated with the corresponding change in the reduction potential. In contrast to a common photocatalyst, *viz.*, titanium oxide, which is active in the UV region, molybdenum disulfide particles measuring 3 nm catalyse the reaction in the visible range. When SnO_2 nanoparticles measuring 26 and 58 nm were used, the nanoparticle size did not significantly affect the photooxidation of pentachlorophenol.

One can predict the development of a new direction of nanochemistry which is associated with realisation of chemical reactions by means of AFM and STM probes. Interesting examples of chemical modification of terminal functional groups in aggregates of organosilicon molecules were carried out by the catalytic action of an AFM probe covered (at open circuit conditions) with palladium.[156]

A minimum effort required for such chemical reactions to occur is ~2.5 μN at a scanning rate below 5 μm s^{-1}. It should be noted that the typical activation energy of the bimolecular reactions shown is ~50 kJ mol^{-1}. At the same time, according to estimates, the energy of surface deformation of an associate formed by organosilicon molecules is ~340 kJ mol^{-1}, which far exceeds the activation energy.

An approach to 'chemical lithography', which consists in chemical modification of functional groups in the molecules arranged along definite preset lines in a sample, was first documented in Ref. 157.

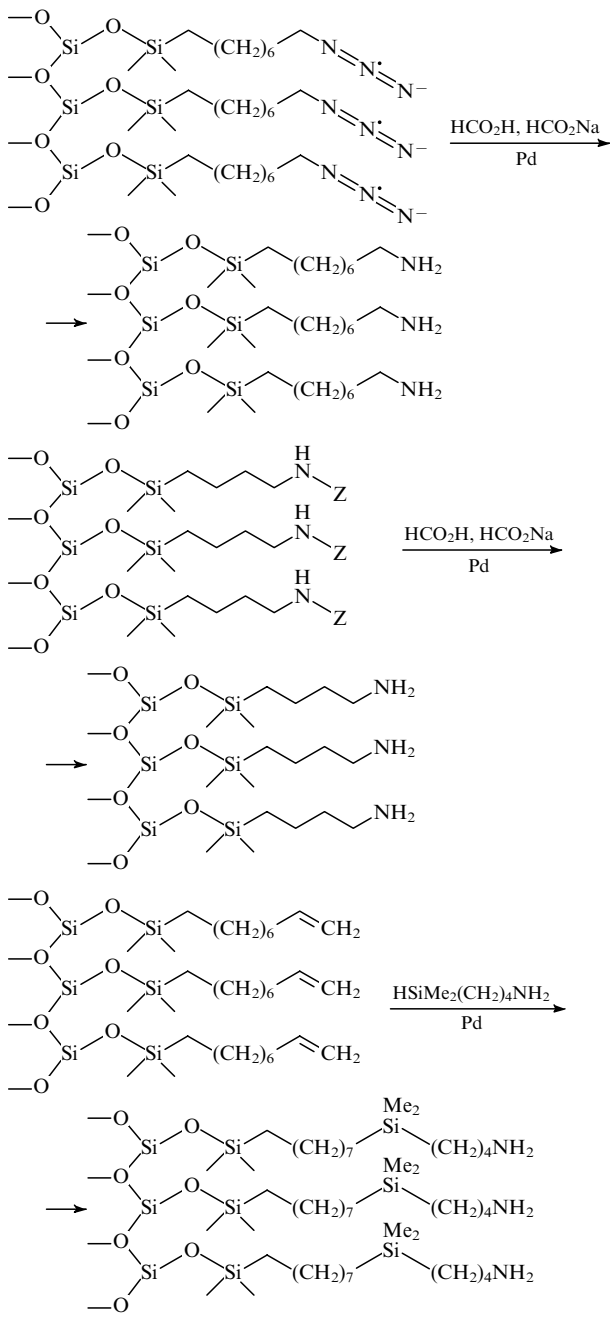

Z is a benzyloxycarbonyl group.

VIII. Nanoparticles in biology and medicine

At present, a new direction of nanochemistry is being developed vigorously. The goal of these studies is the synthesis and application of systems comprising metal nanoparticles (mainly, gold and silver) and various biomolecules: DNA, peptides and oligonucleotides. The optical properties of aggregates of gold nanoparticles bound by DNA fragments containing from 27 to 72 nucleotide pairs were discussed.[158] Alkanethiol-modified gold particles of diameter $\sim$15 nm were used. The effect of the length of an oligonucleotide chain on the optical properties of aggregates obtained was studied, and the position of the metal plasmon peak was found to depend on the chain length. The sizes of nanoparticle aggregates were determined by the kinetic method, because their growth rate depended on the lengths of oligonucleotide chains and on the distances between nanoparticles. Among the factors that affect the growth rate of aggregates, the rate of binding of DNA linkers ¶ with complementary DNA molecules on the surfaces of gold nanoparticles (k_1) and the rate of aggregate growth (k_2) are the most important. Optical changes were also observed upon annealing of structures formed by two longest nucleotides-linkers at temperatures below their melting point. Thus, DNA linkers can be used for kinetic control over aggregate growth.

A new method of introduction of biomaterials into living cells was proposed [159] based on electrospraying of metal particles with large electrical charges and high velocities. If one disperses gene-covered metal particles using the equipment developed, these particles disintegrate in liquid drops under the external non-uniform field. Gene fragments thus obtained have charges of the same sign as the metal particles and are present in high concentrations. Monkey fibroblasts were used as the living cells and either suspensions of plasmids † labelled with fluorescent peptides or plasmids with gold nanoparticles measuring 5–10 nm were used as the biomaterials. UV fluorescent microscopic studies have shown plasmid suspensions with gold particles to penetrate into cells. The fact that gold-free plasmid suspensions also penetrated into the cells and got incorporated into its DNA is of prime importance. This result seems to be most significant, because this allows one to dispense with gold traditionally used for these purposes. It was noted that electrostatic spraying opens up new possibilities for transfection of genes and gene therapy.

Nanoparticles doped with gadolinium ions were proposed for use as new contrast materials for NMR studies in medicine. Such nanoparticles with diameters of 120 nm are sufficiently small to penetrate easily into blood vessels. These have been used for obtaining the images of hearts and gastric channels in rats.[160]

Approaches to using biomolecules for identification of common inorganic materials are being developed. These can be realised by applying the principles of selective binding known from molecular biology. Selective binding of peptides to different semiconductors was proposed as a method of preparation of nanocrystalline ensembles.[161] It was shown that nanocrystalline semiconductors can be used for the isolation of certain peptides which bind specifically to the semiconductor surface. Five different faces of semiconducting single crystals were used, as the substrates, *viz*., GaAs(100), GaAs(111)Ga (with Ga atoms on the surface), GaAs(111)As (with As atoms on the surface), InP(100) and Si(100). Each substrate was found to select and bind certain amino acid sequences from a large number of random peptides. The nanocrystalline ensembles obtained were studied using antibodies labelled with 20-nm gold nanoparticles and the methods of transmission and fluorescent microscopy, photoelectron spectroscopy and atomic-force and scanning tunnelling microscopy.

Figure 11 illustrates two different approaches to the development of biomolecular ensembles on surfaces of inorganic materials.[162] Development of these approaches is a challenge to materials science of the XXIst century.

In this context, attention should be drawn to a study [163] in which the prospects of synthesising two- and three-dimensional nanostructures based on biological principles were considered. It is believed that the strategy of synthesising complex ensembles from simpler ones will be developed in the new century. Biological structures may be used as surface detectors which organise binding of large organic and inorganic building blocks. Indeed, in this approach, the principles developed in the course of evolution for building new functional structures may be used for synthesising new materials.

¶ Linkers are nonhelical segments of a double-stranded DNA which interlink compact DNA segments stabilised by peptides and polyamines.
† Plasmids are extrachromosome formations representing closed circles of double-stranded DNA.

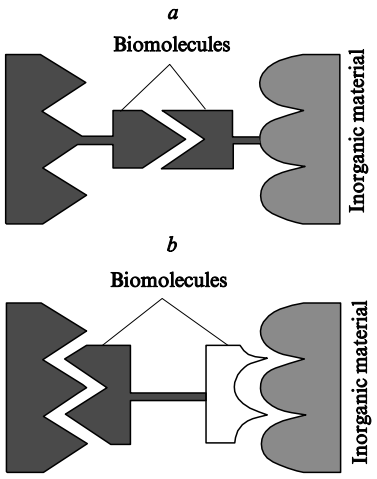

Figure 11. Two approaches to assembly of inorganic materials into complex structures with the use of biological molecules.
(*a*) The use of complementarity of two biomolecules, (*b*) the use of biomolecule interaction with an inorganic material.[162]

IX. Conclusion

The analysis of studies published in recent years shows that many aspects of nanochemistry of metals and semiconductors are gaining importance, and considerable progress has been made towards their solution.

The factors that affect the sizes and shapes of nanoparticles during their synthesis, the processes of self-assembly of both nanoparticles themselves and ligands that stabilise them are being actively studied. The list of polymers, surfactants, reversed micelles and thiols, which are traditionally used for the stabilisation of nanoparticles, was successfully replenished with dendrimers. The use of nanoparticles in catalysis has been extended, as well as the use of semiconducting particles in photocatalysis. The studies in which metal nanoparticles are used in carrying out unusual reactions are conducted more intensively. The problem of synthesising and studying the reactions of non-protected metal nanoparticles becomes increasingly pressing. Interest is shifting to reactions of metal nanoparticles measuring less than 1 nm. In this aspect, the use of inert gas at low and superlow temperatures as the matrices for the synthesis of nanoparticles seems to be very promising.

Yet another challenging direction of nanochemistry may be developed at the boundary of such sciences as biology, organic and inorganic chemistry and materials science. Mutual 'recognition' and joint self-assembly of inorganic and biological molecules are the key problems which being solved, will provide new advanced materials.[164]

At the beginning of 2000, a new programme aimed at the development of fundamental and applied studies in nanotechnology was formulated in the USA.[165] In 2001, this issue is additionally financed by 500 million dollars. The following directions were chosen as the most challenging:

— the use of modern experimental equipment for studying the processes which involve nanoparticles or proceed on the surfaces of nanostructures;

— elucidation of the roles nanoparticles play in such important processes as deposition of proteins, desorption of contaminants, stabilisation of colloidal dispersions, aggregation of micelles and control over microorganism mobility;

— development of experimental techniques and their computerisation for studying the role of nanoparticles in the processes that occur in the atmosphere and water sources;

— the use of mesoporous structures integrated with appropriate microcomponents to provide highly sensitive and highly selective contamination detectors.

In conclusion, it should be stated that at present the studies of nanoparticle properties form an interdisciplinary scientific field which largely determines the development of the other neighbouring fields.

The author is grateful to his co-workers, post-graduate students and students of the Laboratory of Low-Temperature Chemistry for their assistance in the preparation of this review. This review was partially financially supported by the Russian Foundation of Basic Research (Project No. 99-03-32206).

References

1. K J Klabunde *Free Atoms, Clusters and Nanoscale Particles* (San Diego; New York; Boston; London; Sydnay; Tokyo: Academic Press, 1994)
2. G B Sergeev, in *Khimicheskaya Fizika na Poroge XXI v* (Chemical Physics at the Threshold of the XXIst Century) (Moscow: Nauka, 1996) p. 149
3. G B Sergeev, M A Petrukhina *Prog. Solid State Chem.* **24** 183 (1996)
4. A D Pomogailo *Usp. Khim.* **66** 750 (1997) [*Russ. Chem. Rev.* **66** 679 (1997)]
5. R F Khairutdinov *Usp. Khim.* **67** 125 (1998) [*Russ. Chem. Rev.* **67** 109 (1998)]
6. A S Edelstein, R C Cammarata (Eds) *Nanomaterials: Synthesis, Properties and Applications* (Bristol: J N Arrowsmith Ltd, 1998)
7. J H Fendler (Ed.) *Nanoparticles and Nanostructured Films* (New York: Wiley-VCH, 1998)
8. B G Ershov *Izv. Acad. Nauk, Ser. Khim.* 1 (1999) [a]
9. G B Sergeev *Vestn. Mosk. Univ., Ser. 2, Khim.* **40** 312 (1999) [b]
10. A D Pomogailo, A S Rozenberg, I E Uflyand *Nanochastitsy Metallov v Polimerakh* (Metal Nanoparticles in Polymers) (Moscow: Khimiya, 2000)
11. H Gleiter *Acta Mater.* **48** 1 (2000)
12. B D Summ, N I Ivanova *Usp. Khim.* **69** 995 (2000) [*Russ. Chem. Rev.* **69** 911 (2000)]
13. V I Roldughin *Usp. Khim.* **69** 899 (2000) [*Russ. Chem. Rev.* **69** 821 (2000)]
14. V I Bukhtiyarov, M G Slin'ko *Usp. Khim.* **70** 167 (2001) [*Russ. Chem. Rev.* **70** 147 (2001)]
15. I P Suzdalev, P I Suzdalev *Usp. Khim.* **70** 203 (2001) [*Russ. Chem. Rev.* **70** 177 (2001)]
16. A L Buchachenko *Usp. Khim.* **68** 99 (1999) [*Russ. Chem. Rev.* **68** 85 (1999)]
17. M A El-Sayed *J. Phys. Chem.* **95** 3898 (1991)
18. C S Feigerle, S Bililign, J C Miller *J. Nanopart. Res.* **2** 147 (2000)
19. T Yonezawa, S Onoue, N Kimizuka *Langmuir* **16** 5218 (2000)
20. L M Bronstein, D M Chernyshov, P M Valetsky, E A Wilder, R J Spontak *Langmuir* **16** 8221 (2000)
21. D I Svergun, E V Shtykova, M B Kozin, V V Volkov, A T Dembo, E V Shtykova Jr , L M Bronstein, O A Platonova, A N Yakunin, P M Valetsky, A R Khokhlov *J. Phys. Chem. B* **104** 5242 (2000)
22. B G Ershov, N L Sukhov, E Janata *J. Phys. Chem. B* **104** 6138 (2000)
23. B G Ershov *Izv. Akad. Nauk, Ser. Khim.* 1733 (2000) [a]
24. A Henglein *J. Phys. Chem. B* **104** 1206 (2000)
25. S Wang, H Xin *J. Phys. Chem. B* **104** 5681 (2000)
26. Z L Wang *J. Phys. Chem. B* **104** 1153 (2000)
27. L Rodrigues-Sanchez, M L Blanko, M A Lopez-Quintela *J. Phys. Chem. B* **104** 9683 (2000)
28. E E Foos, R M Stroud, A D Berry, A W Snow, J P Armistead *J. Am. Chem. Soc.* **122** 7114 (2000)
29. J Fang, K L Stokes, J Wiemann, W Zhou *Mater. Lett.* **42** 113 (2000)
30. L M Bronstein, D M Chernyshov, G I Timofeeva, L V Dubrovina, P M Valetsky, A R Khokhlov *J. Colloid Interface Sci.* **230** 140 (2000)
31. M-H Lee, S-G Oh, S-C Yi *J. Colloid Interface Sci.* **226** 65 (2000)
32. O E Litmanovich, A A Litmanovich, I M Papisov *Vysokomol. Soedin., Ser. A* **42** 670 (2000) [c]
33. S Keki, J Torok, G Deak, L Daroczi, M Zsuga *J. Colloid Interface Sci.* **229** 550 (2000)

34. F Grohn, B J Bauer, Y A Akpalu, C L Jackson, E J Amis *Macromolecules* **33** 6042 (2000)
35. K Esumi, T Hosoya, A Suzuki, K Torigoe *J. Colloid Interface Sci.* **226** 346 (2000)
36. M Liu, X Yan, H Liu, W Yu *React. Funct. Polym.* **44** 55 (2000)
37. H W Rollins, F Lin, J Johnson, J-J Ma, J-T Liu, M-H Tu, D D DesMarteau, Y-P Sun *Langmuir* **16** 8031 (2000)
38. O Siiman, A Burshteyn *J. Phys. Chem. B* **104** 9795 (2000)
39. J S Bradly, B Tesche, W Busser, M Maase, M T Reetz *J. Am. Chem. Soc.* **122** 4631 (2000)
40. M V Kiryukhin, B M Sergeev, A N Prusov, V G Sergeev *Vysokomol. Soedin., Ser. B* **42** 2171 (2000) [c]
41. M V Kiryukhin, B M Sergeev, A N Prusov, V G Sergeev *Vysokomol. Soedin., Ser. B* **42** 1069 (2000) [c]
42. A Miyazaki, Y Nakano *Langmuir* **16** 7109 (2000)
43. J Zhu, S Liu, O Palchik, Y Koltypin, A Gedanken *Langmuir* **16** 6396 (2000)
44. J Zhu, S T Aruna, Y Koltypin, A Gedanken *Chem. Mater.* **12** 143 (2000)
45. A A Mamedov, N A Kotov *Langmuir* **16** 5530 (2000)
46. S Sun, C B Murray, D Weller, L Folks, A Moser *Science* **287** 1989 (2000)
47. X Peng, L Manna, W Yang, J Wickham, E Scher, A Kadavanich, A P Alivisatos *Nature (London)* **404** 59 (2000)
48. S-J Park, S Kim, S Lee, Z G Khim, K Char, T Hyeon *J. Am. Chem. Soc.* **122** 8581 (2000)
49. M Sastry, A Gole, S R Sainkar *Langmuir* **16** 3553 (2000)
50. Z L Wang, R P Gao, B Nikoobakht, M A El-Sayed *J. Phys. Chem. B* **104** 5417 (2000)
51. A S Eppler, G Rupprechter, E A Anderson, G A Somorjai *J. Phys. Chem. B* **104** 7286 (2000)
52. C L Carnes, K J Klabunde *Langmuir* **16** 3764 (2000)
53. G W Wagner, O B Koper, E Lucas, S Decker, K J Klabunde *J. Phys. Chem. B* **104** 5118 (2000)
54. P Poisot, S Laruelle, S Gruqeon, L Dupont, J-M Tarascon *Nature (London)* **407** 496 (2000)
55. S H Elder, F M Cot, Y Su, S M Heald, A M Tyryshkin, M K Bowman, Y Gao, A G Joly, M L Balmer, A C Kolwaite, K A Magrini, D M Blake *J. Am. Chem. Soc.* **122** 5138 (2000)
56. J P Novak, D L Feldheim *J. Am. Chem. Soc.* **122** 3979 (2000)
57. A C Templeton, W P Wuelfing, R W Murray *Acc. Chem. Res.* **33** 27 (2000)
58. W P McConnell, J P Novak, L C Brousseau III, R R Fuierer, R C Tenent, D L Feldheim *J. Phys. Chem. B* **104** 8925 (2000)
59. A Henglein, M Giersig *J. Phys. Chem. B* **104** 5056 (2000)
60. A Henglein *J. Phys. Chem. B* **104** 6683 (2000)
61. J H Hodak, A Henglein, G V Hartland *J. Phys. Chem. B* **104** 9954 (2000)
62. J H Hodak, A Henglein, G V Hartland *Pure Appl. Chem.* **72** 189 (2000)
63. L D'Souza, S Sampath *Langmuir* **16** 8510 (2000)
64. Y Mizukoshi, T Fujimoto, Y Nagata, R Oshima, Y Maeda *J. Phys. Chem. B* **104** 6028 (2000)
65. J L Rousset, F J C S Aires, B R Sekhar, P Melinon, B Prevel, M Pellarin *J. Phys. Chem. B* **104** 5430 (2000)
66. A A Novakova, O V Agladze, B P Tarasov *Zh. Neorg. Khim.* **45** 1288 (2000) [d]
67. A A Novakova, T Yu Kiseleva, V V Levina *Zh. Neorg. Khim.* **45** 1388 (2000) [d]
68. G B Sergeev, T I Shabatina, V N Soloviev, A V Nemukhin *Spectrochim. Acta, Part A* **56** 2527 (2000)
69. G B Sergeev, T I Shabatina, V N Soloviev, V V Zagorskii *Mol. Cryst. Liq. Cryst.* **356** 111 (2001)
70. T I Shabatina, A V Vlasov, E V Vovk, D J Stufkens, G B Sergeev *Spectrochim. Acta, Part A* **56** 2539 (2000)
71. G L Estiu, M G Gory, M Z Zerner *J. Phys. Chem. A* **104** 233 (2000)
72. E Apra, A Fortunelli *J. Mol. Struct. (Theochem)* **501 – 502** 251 (2000)
73. K M Neyman, N Rosch, G Pacchioni *Appl. Catal. A: General* **191** 3 (2000)
74. A Fortunelli, A M Velasco *J. Mol. Struct. (Theochem)* **528** 1 (2000)
75. E V Polikarpov, T I Shabatina, G B Sergeev, A V Nemukhin *Vestn. Mosk. Univ., Ser. 2, Khim.* **41** 283 (2000) [b]
76. T I Shabatina, E V Vovk, Yu N Morozov, V A Timoshenko, G B Sergeev *Mol. Cryst. Liq. Cryst.* **356** 143 (2001)
77. B M Sergeev, G B Sergeev, V A Kasaikin, E A Litmanovich, A N Prusov *Mol. Cryst. Liq. Cryst.* **356** 121 (2001)
78. B M Sergeev, V A Kasaikin, E A Litmanovich, G B Sergeev, A N Prusov *Khim. Fiz.* **19** 121 (2000) [e]
79. V E Bochenkov, N Stefan, L Brehmer, V V Zagorskii, G B Sergeev *Colloids Surf. A* (2001) (in the press)
80. V E Bochenkov, V V Zagorskii, G B Sergeev *Vestn. Mosk. Univ., Ser. 2, Khim.* **41** 327 (2000) [b]
81. V E Bochenkov, V V Zagorskii, G B Sergeev *Mol. Cryst. Liq. Cryst.* **356** 299 (2001)
82. T I Shabatina, A V Vlasov, G B Sergeev *Mol. Cryst. Liq. Cryst.* **356** 149 (2001)
83. S V Ivashko, V V Zagorskii, G B Sergeev *Mol. Cryst. Liq. Cryst.* **356** 443 (2001)
84. J-M Lehn *Supramolecular Chemistry. Concepts and Perspectives* (Weinheim: VCH, 1995)
85. C N R Rao, G U Kulkarni, P J Thomas, P P Edwards *Chem. Soc. Rev.* **29** 27 (2000)
86. S Fullam, S N Rao, D Fitzmaurice *J. Phys. Chem. B* **104** 6164 (2000)
87. A Kumar, A B Mandale, M Sastry *Langmuir* **16** 6921 (2000)
88. J Zheng, Z Zhu, H Chen, Z Liu *Langmuir* **16** 4409 (2000)
89. E Adachi *Langmuir* **16** 6460 (2000)
90. A K Boal, F Ilhan, J E DeRouchey, T Thurn-Albrecht, T P Russell, V M Rotello *Nature (London)* **404** 746 (2000)
91. B Nikoobakht, Z L Wang, M A El-Sayed *J. Phys. Chem. B* **104** 8635 (2000)
92. Y Wang, J Ren, K Deng, L Gui, Y Tang *Chem. Mater.* **12** 1622 (2000)
93. S Link, Z L Wang, M A El-Sayed *J. Phys. Chem. B* **104** 7867 (2000)
94. S Link, C Burda, B Nikoobakht, M A El-Sayed *J. Phys. Chem. B* **104** 6152 (2000)
95. S Chen *J. Phys. Chem. B* **104** 663 (2000)
96. S Chen *J. Am. Chem. Soc.* **122** 7420 (2000)
97. L Maya, G Muralidharan, T G Thundat, E A Kenik *Langmuir* **16** 9151 (2000)
98. O D Velev, E W Kaler *Adv. Mater.* **12** 531 (2000)
99. P M Tessier, O D Velev, A T Kalambur, J F Rabolt, A M Lenhoff, E W Kaler *J. Am. Chem. Soc.* **122** 9554 (2000)
100. H Fukushima, S Seki, T Nishikawa, H Takiguchi, K Tamada, K Abe, R J Colorado, M Graupe, O E Shmakova, T R Lee *J. Phys. Chem. B* **104** 7417 (2000)
101. L Motte, E Lacaze, M Maillard, M P Pileni *Langmuir* **16** 3803 (2000)
102. J F Kang, J Zaccaro, A Ulman, A Myerson *Langmuir* **16** 3791 (2000)
103. G Kalyuzhny, A Vaskevich, G Ashkenasy, A Shanzer, I Rubinstein *J. Phys. Chem. B* **104** 8238 (2000)
104. P Andre, A Filankembo, I Lisiecki, C Petit, T Gulik-Krzywicki, B W Ninham, M-P Pileni *Adv. Mater.* **12** 119 (2000)
105. A Filankembo, M P-Pileni *J. Phys. Chem. B* **104** 5865 (2000)
106. S Chen, A C Templeton, R W Murray *Langmuir* **16** 3543 (2000)
107. C S Ah, H S Han, K Kim, D-J Jang *J. Phys. Chem. B* **104** 8153 (2000)
108. C S Ah, H S Han, K Kim, D-J Jang *Pure Appl. Chem.* **72** 91 (2000)
109. D H Jeong, J S Suh, M Moskovits *J. Phys. Chem. B* **104** 7462 (2000)
110. D H Jeong, N H Jang, J S Suh, M Moskovits *J. Phys. Chem. B* **104** 3594 (2000)
111. L Francois, M Mostafavi, J Belloni, J-F Delouis, J Delaire, P Feneyrou *J. Phys. Chem. B* **104** 6133 (2000)
112. J H Hodak, A Henglein, G V Hartland *J. Chem. Phys.* **112** 5942 (2000)
113. R Houdre, H Benisty, C Weisbuch *J. Lumin.* **85** 271 (2000)
114. Y Shen, D Jakubczyk, F Xu, J Swiatkiewicz, P N Prasad, B A Reinhardt *Appl. Phys. Lett.* **76** 1 (2000)
115. Y Shen, C S Friend, Y Jiang, D Jakubczyk, J Swiatkiewicz, P N Prasad *J. Phys. Chem. B* **104** 7577 (2000)
116. F T Quinlan, J Kuther, W Tremel, W Knoll, S Risbud, P Stroeve *Langmuir* **16** 4049 (2000)
117. T Hirai, T Watanabe, I Komasawa *J. Phys. Chem. B* **104** 8962 (2000)
118. B A Korgel, H C Monbouquette *Langmuir* **16** 3588 (2000)
119. R Kho, C L Torres-Martinez, R K Mehra *J. Colloid Interface Sci.* **227** 561 (2000)
120. E Hao, T Lian *Langmuir* **16** 7879 (2000)
121. X Duan, C M Lieber *J. Am. Chem. Soc.* **122** 188 (2000)
122. X Duan, C M Lieber *Adv. Mater.* **12** 298 (2000)

123. J D Holmes, K P Johnston, R C Doty, B A Korgel *Science* **287** 1471 (2000)
124. M S Gudiksen, C M Lieber *J. Am. Chem. Soc.* **122** 8801 (2000)
125. V N Soloviev, A Eichhoefer, D Fenske, U Banin *J. Am. Chem. Soc.* **122** 2673 (2000)
126. V N Soloviev, A Eichhoefer, D Fenske, U Banin *J. Am. Chem. Soc.* **123** 2354 (2001)
127. J Z Zhang *J. Phys. Chem. B* **104** 7239 (2000)
128. M Chen, Y Xie, H Chen, Z Qiao, Y Zhu, Y Qian *J. Colloid Interface Sci.* **229** 217 (2000)
129. D I Gittins, D Bethell, D J Schiffrin, R J Nichols *Nature (London)* **408** 67 (2000)
130. D I Gittins, D Bethell, R J Nichols, D J Schiffrin *J. Mater. Chem.* **10** 79 (2000)
131. D Feldheim *Nature (London)* **408** 45 (2000)
132. M Albrecht, M Lutz, A L Spek, G van Koten *Nature (London)* **406** 970 (2000)
133. J W Steed *Nature (London)* **406** 943 (2000)
134. R B Vasil'ev, A M Gas'kov, M N Rumyantseva, A S Ryzhikov, L E Ryabova, B Ya Akimov *Fiz. Tekh. Poluprovod.* **34** 993 (2000) [f]
135. B Sh Galyamov, S A Zav'yalov, L Yu Kupriyanov *Zh. Fiz. Khim.* **74** 459 (2000) [g]
136. A J Zarur, J Y Ying *Nature (London)* **403** 65 (2000)
137. J G McCarty *Nature (London)* **403** 35 (2000)
138. M Spiro, D M De Jesus *Langmuir* **16** 2464 (2000)
139. D M De Jesus, M Spiro *Langmuir* **16** 4896 (2000)
140. W Tu, H Liu, K Y Liew *J. Colloid Interface Sci.* **229** 453 (2000)
141. J Liu, Y Shin, Z Nie, J H Chang, L -Q Wang, G E Fryxell, W D Samuels, G J Exarhos *J. Phys. Chem. A* **104** 8328 (2000)
142. G Fagherazzi, P Canton, P Riello, F Pinna, N Pernicone *Catal. Lett.* **64** 119 (2000)
143. G Fagherazzi, P Canton, P Riello, N Pernicone, F Pinna, M Battagliarin *Langmuir* **16** 4539 (2000)
144. L Wang, M Rocci-Lane, P Brazis, C R Kannewurf, Y-I Kim, W Lee, J-H Choy, M G Kanatzidis *J. Am. Chem. Soc.* **122** 6629 (2000)
145. M M Maye, Y Lou, C-J Zhong *Langmuir* **16** 7520 (2000)
146. M M Maye, W Zheng, F L Leibowitz, N K Ly, C-J Zhong *Langmuir* **16** 490 (2000)
147. M M Maye, C-J Zhong *J. Mater. Chem.* **10** 1895 (2000)
148. C-W Chen, D Tano, M Akashi *J. Colloid Interface Sci.* **225** 349 (2000)
149. P Del Angel, J M Dominguez, G Del Angel, J A Montoya, E Lamy-Pitara, S Labruquere, J Barbier *Langmuir* **16** 7210 (2000)
150. M M Mohamed, T M Salama, M Ichikawa *J. Colloid Interface Sci.* **224** 366 (2000)
151. G Rupprechter, A S Eppler, A Avoyan, G A Somorjai *Stud. Surf. Sci. Catal. A* **130** 215 (2000)
152. A S Eppler, J Zhu, E A Anderson, G A Somorjai *Top. Catal. B* 33 (2000)
153. O V Zagorskaya, V Yu Zufman, T N Rostovshchikova, V V Smirnov, S P Gubin *Izv. Akad. Nauk, Ser. Khim.* 854 (2000) [a]
154. H Tada, K Teranishi, Y Inubushi, S Ito *Langmuir* **16** 3304 (2000)
155. J P Wilcoxon *J. Phys. Chem. B* **104** 7334 (2000)
156. C Blackledge, D A Engebreston, J D McDonald *Langmuir* **16** 8317 (2000)
157. S Hong, C Mirkin *Science* **288** 1808 (2000)
158. J J Storhoff, A A Lazarides, R C Mucic, C A Mirkin, R L Letsinger, G C Schatz *J. Am. Chem. Soc.* **122** 4640 (2000)
159. D-R Chen, C H Wendt, D Y H Pui *J. Nanopart. Res.* **2** 133 (2000)
160. C H Reynolds, N Annan, K Beshah, J H Huber, S H Shaber, R E Lenkinski, J A Wortman *J. Am. Chem. Soc.* **122** 8940 (2000)
161. S R Whaley, D S English, E L Hu, P F Barbara, A M Belcher *Nature (London)* **405** 665 (2000)
162. C A Mirkin, T A Taton *Nature (London)* **405** 626 (2000)
163. C A Mirkin *J. Nanopart. Res.* **2** 121 (2000)
164. P Ball *Nature (London)* **406** 118 (2000)
165. C Macilwain *Nature (London)* **405** 730 (2000)

[a] — *Russ. Chem. Bull. (Engl. Transl.)*
[b] — *Moscow Univ. Bull. (Engl. Transl.)*
[c] — *Polym. Sci. (Engl. Transl.)*
[d] — *Russ. J. Inorg. Chem. (Engl. Transl.)*
[e] — *Chem. Phys. Rep. (Engl. Transl.)*
[f] — *Semiconductors (Engl. Transl.)*
[g] — *Russ. J. Phys. Chem. (Engl. Transl.)*

Russian Chemical Reviews **70** (10) 827 – 863 (2001) © 2001 Russian Academy of Sciences and Turpion Ltd

DOI 10.1070/RC2001v070n10ABEH000660

The chemistry and application of carbon nanotubes

E G Rakov

Contents

I.	Introduction	827
II.	Filling of the inner cavities of carbon nanotubes	828
III.	Functionalisation of carbon nanotubes	832
IV.	Decoration of carbon nanotubes and their use as templates	836
V.	Substitution of the carbon atoms of nanotubes by atoms of other elements	836
VI.	Insertion of 'guest' atoms and molecules into the intertubular space of multi-walled nanotubes and nanotube bundles	837
VII.	Adsorption and storage of gases in carbon nanotubes	839
VIII.	Potential fields of application of carbon nanotubes	840
IX.	Conclusion	854

Abstract. The review concerns the main chemical and physicochemical properties and the methods of modification of carbon nanotubes, a novel promising material. The feasible and potential fields of applications of carbon nanotubes are outlined. The bibliography includes 573 references.

I. Introduction

Nanotubes (nanotubulenes, hereafter NTs) were discovered by Iijima in 1991.[1] A decade has passed since then; however, solid state chemists and physicists as well as materials scientists persist in giving increasing attention to NTs.[2] Moreover, it is NTs that are believed to be a tool for passage from macromolecules to nanotechnology and for transformation of the latter from a scientific concept into reality.

Currently, we cannot say whether these dreams will come true or not. Intensive research into NTs continues to expand, the number of publications increases rapidly;[3] some monographs, books of collected works and a textbook on NTs have been published.[4–10] Unfortunately, only a few out of the dozens of journal reviews concerning NTs were reported in the journals published in the Russian Federation.[11–16] In addition, at present these reviews fail to cover not only some recent advances, but also entire avenues of research into NTs. The author of this review strove to bridge this gap.

The background of the NT problem was briefly outlined recently.[15,16] The structure, some physical properties and methods for the preparation of NTs have also been reviewed.[14,16] To get acquainted with carbon NTs, we can also recommend a visit to the Website of the Michigan State University (USA) at URL http://www.pa.msu.edu/cmp/csc/nanotube.html. Here, it will only be remembered that perfect, defect-free NTs are formed by rolling planar atomic graphite sheets (graphenes) into seamless cylinders. Nanotubes can be multi-walled (MWNTs), comprising several coaxial cylinders, or single-walled (SWNTs). As a rule, the proportion of defects in SWNTs is less than in MWNTs. Moreover, SWNTs can become defect-free after high-temperature annealing in inert media. The structure of NTs affects their electronic, mechanical and chemical properties; because of this, SWNTs and MWNTs behave in fundamentally different manners.

The inner diameters of NTs vary between 0.4 nm and several nanometres. The volume of the inner cavity of NTs is sufficient for the molecules of other substances to occupy the cavity.

Graphene sheets in SWNTs and in each shell of MWNTs can have different orientations of the primitive graphene lattice vectors. This affects the properties of NTs.

The as-prepared NTs are usually closed by hemispherical or conical 'caps' at their ends.

A salient feature of NTs is their aggregation into rather stable bundles (bunches or ropes), which can be either bent or even closed (ring-like structures). The axes of individual NTs in the bundles are parallel to one another. The shortest distance between individual NTs is $\sim$0.32 nm. Nanotube bundles arise due to van der Waals forces. The intertubular space can be filled with 'guest' molecules.

Initially, most of NTs were synthesised by the arc method which involves graphite vaporisation in a dc arc struck between graphite electrodes in an inert gas flow. This technique was replaced by laser-induced thermal synthesis. This technique involves vaporisation of a graphite target under the action of a scanning laser beam in a furnace heated to a particular temperature and has a higher performance. In recent years, increasing attention has been given to pyrolytic synthesis from gaseous hydrocarbons (CH_4, C_2H_2, *etc.*) and CO. Preference is given to the catalytic processes which allow the preparation of not only MWNTs, but also SWNTs in relatively high yields.[16] It is thought that the processes proceeding in the presence of a 'volatile catalyst' introduced into the reaction zone in the form of vapours along with the substances to be decomposed can provide the highest performance.

Nanotubes can be prepared in different forms. Synthesis of NTs can give a tough precipitate of different density, *e.g.*, a rubber-like material consisting of entangled NTs (compact 'nanopaper', 'buckypaper', 'mats'), a web-like material and a textured material comprised of arrays of aligned NTs separated by some distance from one another (nanotube 'forest', nanotube 'towers').

E G Rakov D I Mendeleev Russian University of Chemical Technology, Miusskaya pl. 9, 125047 Moscow, Russian Federation.
Fax (7-095) 490 75 23. Tel. (7-095) 948 54 67. E-mail: rakov@rctu.ru

Received 13 February 2001
Uspekhi Khimii **70** (10) 934 – 973 (2001); translated by A M Raevsky

In addition to hollow cylindrical NTs, conical, helical, horn-like ('nanohorns'), bamboo-like (consisting of individual closed extended sections), different types of alternating conical NTs ('nanobells' and 'fishbone') as well as L-, T- and Y-shaped NTs (both bent and branched) can also be formed.

The synthesis of NTs is often accompanied by the formation of other forms of carbon (*e.g.*, fullerenes, polyhedral particles and amorphous carbon). Therefore, in many instances purification of NTs (removal of side products) is a necessary stage.

Before going to the main body of the text, mention should be made of the term 'carbon nanotube chemistry', which is currently used in a rather broad sense.† Carbon nanotube chemistry covers, first of all, the synthesis and purification of carbon nanotubes and their opening in reactions with various oxidants. In addition, the subject matters of carbon nanotube chemistry are modification of NTs (filling the inner cavity with different reactants, attachment of functional groups to the NT ends and side walls and decoration of these surfaces with particular molecules, replacement of some of the carbon atoms on the NT side walls by atoms of other elements, insertion of 'guest' atoms and molecules into the intertubular space of NT bundles); the use of carbon NTs for template synthesis of nanowires, nanorods and nanotubes made of other substances; adsorption of gases on NTs and NT bundles and physicochemical properties of NTs. Research in the field of carbon nanotube chemistry also includes studies on the effect of the chemical modification on the electronic, magnetic, mechanical and other properties of NTs.

With rare exceptions, in this review we will not dwell on the methods for the preparation and purification of NTs and filling their inner cavities. These problems have been considered in detail recently.[16]

Chemical transformations of fullerenes, graphite and NTs exhibit some common features. Nevertheless, it should be emphasised that nanotube chemistry differs essentially from both fullerene and graphite chemistry. This is due to the unique shape, structural peculiarities and small diameter of NTs. Nanotubes differ from fullerenes in the relatively large volume of the inner cavity (stable fullerene molecules are too small to contain more than three or four atoms of other elements within the inner cavity). Perfect (defect-free) NTs differ from graphite in very low percentage or even the absence of chemically active dangling bonds. A feature of NTs is a variety of specific distances that are due to van der Waals forces (*e.g.*, the separations between individual shells of MWNTs, between individual tubules in NT bundles, *etc.*).

Each fullerene can be considered as a molecule which can form or be a constituent of molecular crystals. Graphite represents a typical layered polymeric crystal. In contrast to them, individual NTs cannot be thought of as individual molecules (SWNTs resemble molecules, while MWNTs are similar to carbon fibres) and NT bundles cannot be classified as conventional three-dimensional crystals (topologically, individual NTs and NT bundles represent one-dimensional and two-dimensional crystals, respectively.[18]).

Graphite, NTs and fullerenes can form intercalation compounds with fundamentally different structures. Graphite forms two-dimensional structures, NTs usually form one-dimensional structures (formation of two-dimensional structures is possible for the rolled-up NTs), whereas fullerenes form [topologically] zero-dimensional structures. In addition, only NTs can form several types of intercalation compounds with different geometries.

Sometimes, NTs exhibit quite unexpected chemical behaviour. For instance, bent NTs contain topological defects (*e.g.*, pairs of carbon pentagons and heptagons) and their reactivity differs from that of straight NTs. Carbon NTs also allow one to study the effect of the radius of curvature of the surface on the strength of the bonding between the substances reacting on the NT surface and the carbon atoms.

Modification of NTs can lead to essential changes in their electronic structure and functional properties and to creation of novel materials including those with unbelievable properties. The possibility of modification of fullerenes and NTs was first predicted theoretically (see, *e.g.*, Refs 19 and 20) and then confirmed experimentally.

This review concerns the chemical properties of NTs and their role in the processes of fabrication of the NT-derived end products. In the largest part of the review (Section VIII), we consider the potential fields of application of NTs. This seems to be of great importance since NTs are no longer 'exotic fruits'.

II. Filling of the inner cavities of carbon nanotubes

The inner cavities of NTs can be filled in the course of synthetic procedures or in a targeted manner after the preparation and purification of NTs. The latter strategy was found to be more versatile and rational.

Targeted filling can be performed with melts, solutions or reactive gases that are either involved in the chemical vapour deposition reactions or form covalent chemical bonds with carbon atoms within the NTs. Filling the NT cavities with gases due to adsorption represents a special case.

1. Nanotube filling in the course of synthetic procedures

Many substances can fill the inner cavities of NTs in the course of synthetic procedures.[16] In this review, we will dwell on the results reported in some of the most recent reviews and original studies.

According to Seraphin,[21] in the case of arc synthesis of NTs the additives (B, Mg, Mn, Fe, Co, Ni, Cu, Y, Nb, Mo and Ta) can be encapsulated into the NTs in the form of carbides. The filling of NTs with Nb, Ta and Mo carbides has been studied in more detail.[22] Nanotubes can also be filled with rare-earth element carbides and, in an H_2 atmosphere, with metallic Cu and Ge which do not tend to form carbides.

Two types of NT filling, a complete and incomplete one, have been described.[23] For instance, Se, Sb, S and Ge fill NTs completely (up to several micrometres long), whereas Bi, B, Al and Te form short particles. No rationalisation was provided to this phenomenon.

Sulfur is thought to play the key role in the formation of filled NTs in arc synthesis.[24] Thorough removal of sulfur from the anodic material reduces the probability of the growth of filled NTs.

The effect of sulfur on the NT growth mechanism in the case of arc synthesis was confirmed by Demoncy *et al.*[25] who found that sulfur added to the anode material favours the filling of NTs with such metals as Co, Ni, Cr and Dy if the content of S is less than 1% of the metal mass.

Boron, a well-known graphitisation catalyst, also has a strong effect on the NT growth mechanism.[26] A theoretical study of the effect of boron on the growth rate and morphology of NTs showed that boron stabilises the zigzag-shaped end of a NT, thus preventing it from 'capping' and favouring the NT filling.[27]

Other substances also can act as promoters. The addition of both a catalyst (2% Co) and promoter (5% Bi) to the anode material (graphite) resulted in an increase in the diameter of the grown SWNTs, namely, nearly 50% of them were found to be 1.5 nm and more in diameter and a large proportion of the SWNTs had a diameter of 2 nm.[28]

It seems to be more interesting to consider the growth of NTs with encapsulated fullerene molecules. In this case, the encapsulated fullerene molecules must affect the properties of composites filled with such NTs, the electronic properties of the NTs and their filling with other substances. Smith *et al.*[29] showed that the molecules of C_{60} and C_{70} and elongated capsules with diameters close to that of C_{60} can exist within NTs. It was also found that the

† This term was first used by the researchers from the Oxford University in 1996.[17] Their communication concerned the synthesis, opening (removal of 'caps'), filling and potential uses of NTs.

encapsulated fullerene molecules can move jumpwise and form pairs.

The assumption of the possibility of filling the NT cavity with C_{60} molecules was first proposed in the study of the products of laser-induced thermal synthesis.[30] After a short time, an experimental confirmation of this hypothesis was obtained, *viz*., nanoscale 'peapod' structures were found among acid treated and *in vacuo* annealed (1100 °C) reaction products.[31] Most of such structures have a NT diameter of 1.4 nm, which is twice as large as that of the C_{60} molecule (0.7 nm). They are characterised by yet another, third, type of specific separation that is due to the van der Waals forces (the above-mentioned two types are characteristic of MWNTs and NT bundles,[32] see also Section I). This separation differs from the interlayer spacing in graphite but is close to this value (the shortest distance between the C_{60} molecule and the NT wall is ~0.35 nm). The fact that the C_{60} molecules form pairs indicates that some other interactions occur in these systems in addition to the van der Waals forces.

Two-walled NTs with the inner diameter equal to that of the C_{60} molecule were found to be less abundant than SWNTs.[29]

It was assumed that C_{60} molecules are formed in the gas phase independently of NTs and enter the NT cavities most likely through defects due to diffusion that occurs in the gas phase (or, which is less probably, due to the diffusion over the NT surface) in the course of *in vacuo* annealing.[33] Then, the defects are 'healed' and the C_{60} molecules self-assemble into chains up to 30 units long and coalesce into interior tubes at temperatures above 1100 °C. There is an optimum temperature for the C_{60} molecules adsorbed on the outer surface to pass inside the NTs. At low temperatures, the saturated vapour pressure of C_{60} is too low and filling the NT cavity takes a long time. At high temperatures, the saturated vapour pressure is, on the contrary, too high and the desorbed fullerene molecules move away from the NTs.

The formation of interior elongated (several nanometres long) capsules was also explained by coalescence of the C_{60} encapsulated within NTs due to electron irradiation. The electron beam also damages the outer NT shell; however, this occurs at a lower rate than the inner coalescence.[34]

To prove that NTs are filed with C_{60} molecules, the NT walls were acid etched and the 'peads' were suspended in toluene.[35] The results of spectral studies of the suspension showed that the sample under study was characterised by a C_{60}-filled tube length fraction of 4.5%. The 'peapod' structures were found to be stable to at least 1200 °C (*cf.* 1000 °C for the transformation of pure cubic solid C_{60} into amorphous carbon).

Initially, it was assumed that nanoscale 'peapods' are solely comprised of NTs 1.3 to 1.4 nm in diameter and C_{60} molecules. More recently, this opinion was rejected. The C_{60} fullerene molecules can also be encapsulated within SWNTs obtained by arc method.[36] In this case, molecular fullerenes were found to be present inside 5% to 10% of all of the observed NTs and to have different chemical compositions spanning the range from C_{36} to C_{120} (C_{60} was the most abundant). A clear correlation was also found between the NT diameter and the encapsulated fullerene size.

Blockage of the filling of fullerene-containing NTs with other substances was observed.[36]

The inner cavities of NTs can be filled with carbides using not only the arc method, but also laser-induced thermal synthesis. The addition of boron to the material of graphite target resulted in the appearance of carbide particles inside the grown NTs near their ends.[37] Filling of NTs also seems not to be improbable in the case of catalytic pyrolysis of hydrocarbons (see, *e.g.*, Ref. 38).

2. 'Targeted' filling of carbon nanotubes

Filling pre-fabricated NTs requires that they be opened (in other words, 'caps' at the NT ends should be removed). Most often, this can be done by selective oxidation, which, therefore, is a necessary stage of the process of 'targeted' filling of NTs.

a. Oxidation of carbon nanotubes

'Caps' at the ends of closed NTs are built of carbon pentagons and hexagons. The former type of polygon is more reactive, which determines the possibility of its selective oxidation. This can be achieved by using gaseous reactants, aqueous solutions or melts. Processes in solutions and melts can be initiated or activated electrochemically. Reactions in gaseous media are sometimes initiated using electric discharge or laser irradiation.

It should be kept in mind that NTs prepared *via* different synthetic routes can exhibit different behaviours in oxidation and other chemical reactions. For instance, the densities of materials produced by electric arc method and by laser-induced thermal synthesis can differ by an order of magnitude. Multi-walled NTs and SWNTs also behave in different manner, the latter being oxidised more readily.

Air, oxygen, CO_2 and oxygen plasma represent conventionally used gaseous oxidants. According to *ab initio* calculations,[39] the oxygen atoms bound to the carbon atoms at the end of an open NT cause its stabilisation. However, the authors of this study [39] believe that the heat of desorption of the CO_2 molecules changes its sign as the NT radius increases, so that an endothermic process is transformed into an exothermic one. Therefore, NTs with relatively large diameters are more prone to 'capping'. An increase in temperature also favours the formation of closed NTs. According to calculations, the oxidation energies of 'caps' and lateral surfaces of NTs differ appreciably.

The oxidation of a SWNT material containing carbonaceous impurities, Ni and Co begins at ~370 °C (Fig. 1), a large fraction of NTs being oxidised along with other forms of carbon at relatively low temperatures [40] {see also information posted at the website of the Rice University (USA) at URL [http://www.ruf.rice.edu/~johnz/researchorig.html]**D**}.‡ Exothermic oxidation of metals and amorphous carbon causes a local increase in temperature, which results in the oxidation of NTs at these 'hot spots'. Noteworthy is the coincidence of the curves shown in Fig. 1 *b* at temperatures above 450 °C. Probably, the conditions for preliminary oxidation in HNO_3 do not affect the amount of NTs consumed. (For unknown reasons, the curve *3* in Fig. 1 *a* and curve *2* in Fig. 1 *b* in the original study differ.)

Intercalation with $CuCl_2$ or Br_2 changes the character of the oxidation of MWNTs and allows their purification with O_2.[41–44] The interaction of Br_2 with unpurified NTs leads to intercalation of bromine molecules into graphite nanoparticles that are 'swelled' due to an increase in the interlayer spacings, which

‡ In most cases, the original research results posted at the Webpages cited in this review are represented in the form of abstracts or in other popular forms. Detailed information can be obtained by visiting the Websites labelled as **D**.

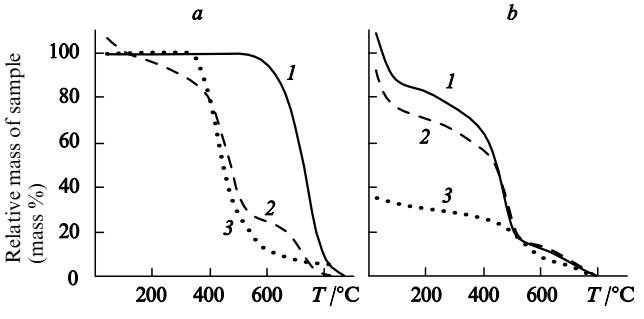

Figure 1. TGA curves for the oxidation of 1–2 mg NT samples in air.[40] The air flow rate was 100 cm^3 min^{-1} and the temperature was raised at a rate of 5 K min^{-1}. The data for the refluxed material was normalised to 100% at 100 °C to compare dry weights; (*a*): purified NTs (*1*), unpurified NTs (*2*) and NTs after a 16 h reflux in 3 M HNO_3 (*3*); (*b*): NTs after a reflux in 3 M HNO_3 for 4 (*1*), 16 (*2*) and 48 h (*3*).

favours a more ready oxidation of the nanoparticles. The reaction with Br_2 is completed after 96 to 240 h while the oxidation (4% O_2 in He, 530 °C) takes a period of 48 to 72 h.[42] The yield of purified NTs is determined by the O_2 flow rate, the sample mass and the conditions for arc synthesis and can reach a value between 10% and 20%. Some of the Br_2 molecules form complexes with the carbon atoms of the NT walls.

Purification of NTs using $CuCl_2$ is carried out as follows:

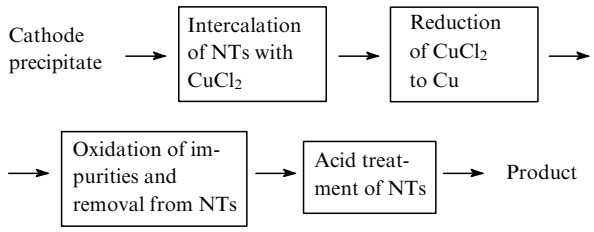

This procedure is inapplicable to SWNTs since the yield of the pure product obtained using the Br_2-O_2 system is very low (only ~3%). This is thought to be related to different curvatures of the MWNT and SWNT surfaces.[45]

Functionalisation of SWNTs reduces the rate of their oxidation. Zimmerman *et al.*[45] studied purification of NTs with moist chlorine and proposed a mechanism which involves the formation of hydroxy- and chloride-functionalised NT 'caps' with the $\rangle C-Cl$ and $\rangle C-OH$ groups that withstand further oxidation. The description of the experimental setup and material of a discussion concerning the purification mechanism can be obtained *via* the Internet [URL http://www.ruf.rice.edu/~johnz/researchorig.html]**D**.

Smith and Luzzi[46] reported the 'closure' of NT ends in inert atmosphere at a very low temperature (~550 °C). This is consistent with the idea of the 'closure' of dangling bonds at the open NT ends in O_2, Cl_2 or H_2 atmospheres.

The selectivity of impurity oxidation in the course of purification of SWNT bundles in a 1% O_2–Ar mixture can be enhanced by using catalysts, *e.g.*, ultrafine gold particles with a diameter of ~20 nm, and benzalkonium chloride as surfactant.[47] (The article contains no information on whether or not the NT opening occurs in the low-temperature oxidation at 350 °C.) After a short time the oxidation conditions were refined and the optimum concentrations were found to be 0.6 at.% for gold particles and 7 g litre^{-1} for benzalkonium chloride.[48] It was also shown that amorphous carbon burns out in the temperature range from 300 to 550 °C, the NT oxidation temperatures span the range from 550 to 750 °C and the residual graphite flakes are oxidised at temperatures above 730 °C. It was suggested that benzalkonium chloride facilitates breakdown of NT bundles.

The list of reactants that can be used in the form of melts is also short. Opening of 'capped' NTs was carried out in air using molten lead at 400 °C (the lead oxide that is formed in the course of the reaction acts as a catalyst).[49,50] The reaction in the presence of molten bismuth in air at 850 °C follows the same pattern (in this case, Bi is oxidised into Bi_2O_3). Experiments on NT opening can also be performed with V_2O_5 (see Ref. 51) and low-melting metal nitrates (see below).

Aqueous solutions were found to be the most appropriate and efficient reagents for NT opening. High yields of open NTs can be achieved by prolonged refluxing of NTs in HNO_3. The efficiency of aqueous solutions of other reagents (*e.g.*, $K_2Cr_2O_7$, $KMnO_4$, H_2O_2, OsO_4, RuO_4, $HClO_4$, H_3IO_5) and various mixtures was also studied. It was shown that treatment with concentrated hydrochloric acid can lead to the opening of NTs.[52] Relatively high yield of the open purified NTs obtained by pyrolytic technique was achieved using a $KMnO_4$ solution in H_2SO_4.[53,54] Experiments with $H_2SO_4-HNO_3$ mixtures were also reported.[55]

The mechanism of the interaction between various oxidants and NTs remains unclear as yet. It is known that NT shells with different chiralities are oxidised at different rates.[56]

Studies on the NT oxidation in the course of their purification were reviewed by Duesberg *et al.*[57]. They pointed out that the results obtained by different authors who used nitric acid treatment of NTs are close despite considerable differences in duration of the acid treatment, the concentration of nitric acid and the operating temperatures. After oxidation, acid-treated NTs are covered by small fragments of carbon particles which should be washed off with alkali solutions. Duesberg *et al.*[57] also described mechanical and physicochemical methods for purification of NTs.

b. Filling of carbon nanotubes from liquid media

General methods of filling carbon NTs from liquid media can be conventionally divided into three groups. These are one-step, two-step and three-step methods. The one-step method uses the interaction of NTs with metal nitrates in the course of nitric acid assisted opening of NTs. Subsequent removal of HNO_3 and thermal decomposition of the nitrates upon calcination of NTs leads to the formation of metal oxide crystallites inside the NTs.[17,58]

The two-step method involves the interaction of pre-opened NTs with concentrated salt solutions. Preference should be given to this method in those cases where fillers are unstable or poorly soluble in acid.[58]

The three-step method involves an intermediate stage between the opening and filling of NTs, namely, *in vacuo* annealing at 2000–2100 °C.[59,60]

Surface tension is an important characteristic of liquids that fill NTs. Only those substances can be soaked in the NT cavities that have a surface tension of at most 150 mN m^{-1} (see Ref. 61). On the other hand, this numerical value is a function of the NT diameter. For instance, the action of capillary forces allows the filling of NTs with a diameter of at least 4 nm for $AgNO_3$ [61] and ~1 nm for PbO and V_2O_5.

In air, NTs can also be filled with PbO_2; *e.g.*, a nanorod with a diameter of 4 nm and a length of more than 400 nm was obtained at 450 °C.[59] Molten V_2O_5, Bi_2O_3, B_2O_3 and MoO_3 also fill the inner cavities of NTs with ease to form continuous crystals along the entire nanotube length.[51,62] If the NT diameter is less than 3 nm, a disordered glassy phase is formed instead of the crystalline phase for unknown reasons.

Filling of SWNTs with a diameter of at most 3.5 nm with bismuth occurs upon heating of mixtures of capped NTs with the metal nanoparticles to 400 °C in air.[28,63] The stability of the filled NTs under conditions of electron irradiation in vacuum was studied.[64]

Kiang *et al.*[63] reported a study on the NT filling with bismuth (i) in the course of the arc synthesis of NTs (equal amounts of Bi and Co were introduced into the graphite anode material), (ii) from melt or vapours (a mixture of NTs and Bi was heated in air) and (iii) from aqueous solutions [boiling in 1 M solution of $Bi(NO_3)_3$ in HNO_3 followed by reduction with H_2]. The abundance of filled NTs was found to be less than 1% for method (i), ~10% for method (ii) and more than 30% for method (iii) provided that the experiments were performed with the same type of NTs.

Since only a few low-melting metal oxides are known, recent studies were carried out using metal halides and nitrates. In particular, NTs were 'doped' with $ZrCl_4$, UCl_4, AgCl, $CdCl_2$, CsCl, AgBr, with AgCl–AgBr mixture and with eutectic mixtures KCl–UCl_4 and KCl–$ThCl_4$.[36,65,66] Filling with uranium tetrachloride was found to occur only in the presence of KCl, since the surface tension of UCl_4 exceeds 370 mN m^{-1} at 900 K. At temperatures above the liquidus temperature, the mixtures with the molar ratios KCl : UCl_4 = 1 : 1 and 2 : 1 are characterised by a surface tension of 120 (750 K) and 68 mN m^{-1} (950 K), respectively. The surface tension of silver chloride is 173 mN m^{-1} (833 K) while that of silver bromide is 151 mN m^{-1} (800 K).

The structure of the metal halide 'dopant' affects the crystal chemistry features of the product (for detailed information, we recommend visiting the Website at URL http://www.cpes/sussex.

ac.uk/nanotec99/present/mlhg.htm). For instance, depending on the NT structure, layered $CdCl_2$ and CdI_2 encapsulated in NTs were found in different polymorphous modifications. Substances that form chain structures can either retain native polyhedral chain patterns ($ZrCl_4$, NbI_4) or change them inside NTs. Bulky chain halides ($ThCl_4$, UCl_4) form one-dimensional structures inside NTs.

A 0.1 nm space resolution study of the structure of an ultra-small single crystal, a KI inclusion into a SWNT, obtained by heating open NTs with molten salt revealed considerable lattice distortion as compared to bulk crystals.[67–69] The cross-section of the KI crystal encapsulated within a 1.6-nm-diameter NT represented a 3×3 atomic array. A longitudinal contraction of the KI crystal by 0.695–0.705 nm along the $\langle 001 \rangle$ axis as compared to the 'bulk' substance was determined. The coordination numbers (CN) of the face and edge atoms were found to be 5 and 4, respectively. Since the proportion of such atoms is rather large, one can expect that differences in the geometry and CN will affect the electronic properties of substances. For instance, typical metals can turn into dielectrics or *vice versa*. This opens up possibilities for the design of new materials.

Even smaller KI single crystal was obtained in an 1.4 nm-diameter NT. The cross-section of this crystal represented a 2×2 atomic array. Each atom was found to have a CN of 4.[68] Compared to the bulk phase, a strong tetrahedral distortion of the cubic crystal lattice was observed and the lattice parameter was found to be more than halved. As in the preceding case, the $\langle 001 \rangle$ direction was parallel to the NT axis.

Lattice distortions and changes in the crystal lattice parameters of the substances encapsulated within NTs were also observed by other authors (see, *e.g.*, Ref. 63); however, detailed study and discussion concerning the prospects for practical implementation of this phenomenon were first undertaken.[67]

Silver, cobalt and copper nitrates have low melting temperatures and their melts are characterised by low surface tension. They are oxidants and can therefore be encapsulated into capped NTs. These compounds were used for the preparation of NTs with encapsulated continuous silver rods 4 nm in diameter and up to 47 nm in length and CoO rods 1.7 nm in diameter and 17 nm long.[59]

Govindaraj *et al.*[70] used metal halide hydrates (in particular $HAuCl_4 \cdot x\,H_2O$) as the reactants for filling open SWNTs and reported the conditions for filling NTs with molten $PdCl_2$.

β-Tin nanowires were obtained by electrolysis of a $LiCl-SnCl_2$ melt using graphite electrodes.[22]

Electrochemical preparation of Sn–Pb nanowires 40 to 90 nm long inside NTs was reported.[71]

Usually, nanowires are 1.0 to 1.4 nm in diameter and up to 90 nm long. In some cases, it has been possible to prepare single-crystalline metal nanowires; however, most often they represent polycrystalline structures.[70] Sometimes, filling of NTs was accompanied by their decoration due to insertion of the metal atoms into the intertubular space of NT bundles.[70] The thickness of the intercalated metal layers was 0.4 to 0.5 nm, which is somewhat larger than the van der Waals separation between individual NTs ($\sim$0.3 nm).

Most often, carbon NTs are filled using aqueous solutions[17] since this method is easy to operate.

The substances encapsulated into NTs can participate in chemical reactions. These are, *e.g.*, thermal decomposition of nitrates resulting in the formation of oxides or metals; reduction of metal chlorides and oxides with hydrogen to obtain NTs filled with Cu,[41] Ni, Fe, Ag, Au, Pd and Rh (see Ref. 58); reactions between chlorides and dioxygen to prepare NTs with encapsulated uranium oxychlorides[65]) and alkali hydrolysis of $SnCl_2$. Kyotani *et al.*[72] studied the filling of carbon NTs with the acid $H_2PtCl_6 \cdot 6\,H_2O$ in solution and reduction of the acid by $NaBH_4$ at room temperature. Sulfidising reactions of NTs with encapsulated CdO or $AuCl_3$ in an H_2S atmosphere to give CdS and AuS_x were investigated.[58] It was found that many substances encapsulated into NTs can be dissolved in HNO_3. Decomposition of silver chloride and silver bromide encapsulated within NTs and then exposed to light or electron beam has been reported.

To prepare NTs with encapsulated SnO, they were opened, washed with HNO_3, placed in a concentrated $SnCl_2$ solution and then the pH value of the suspension was slowly increased to 10.2 using a solution of Na_2CO_3.[73] Encapsulated crystallites were found to have a spherical or ellipsoidal shape and a diameter from 2 to 6 nm.

Successful synthesis[74] of MWNTs with extremely small inner diameter (0.4 nm) opens up the prospects for the preparation of nanowires with uniquely small diameter by encapsulation into such NTs.

c. Filling of carbon nanotubes from gaseous media

Filling the inner cavity of NTs using chemical vapour deposition technique can be performed using, *e.g.*, volatile metal compounds which can decompose on heating to give non-volatile substances. Using this method and $Fe(C_5H_5)_2$, the inner cavities of the NTs grown in the pores of anodised aluminum (Fig. 2) were filled with Fe or Fe_3O_4 nanoparticles.[75] The formation of the oxide inside NTs in the decomposition of ferrocene was explained by partial oxidation of the iron.

A similar process was performed using $Ni(C_5H_5)_2$ at 275 °C.[76] Carbon NTs with the outer diameter of 30 nm were found to be filled with Ni wires 4 nm in diameter and up to 500 nm long. It is noteworthy that no nanowires were formed near the open ends of the NTs; this can hardly be rationalised. It is also unclear why the diameter of the nickel nanowires appeared to be much smaller than the inner diameter of the carbon NTs. Usually, the diameters of the nanowires prepared using other methods were only slightly different from the inner NT diameter (see, *e.g.*, Refs 23 and 50).

Filling of NTs with various compounds was studied by the molecular dynamics method. Simulation was performed assuming that filling occurs due to the capillary forces and that the model NT 2.74 Å in diameter comprised 56 carbon atoms. According to calculations, lead clusters can fill NTs along their entire length, whereas carbon and sulfur clusters are retained near the open ends of the NTs.[77] Carbon NTs can also be filled with molten selenium which forms atomic chains.[78]

Targeted filling without pre-opening the NTs occurs in the course of catalytic pyrolysis of hydrocarbons in porous $AlPO_4$.[79] The porous material is preliminarily filled with cobalt which is then encapsulated into NTs. Experiments with NaY zeolite template also revealed the formation of NTs; however, no filling of the NTs with the catalyst particles was observed due to different character of the interaction between the catalyst and template.

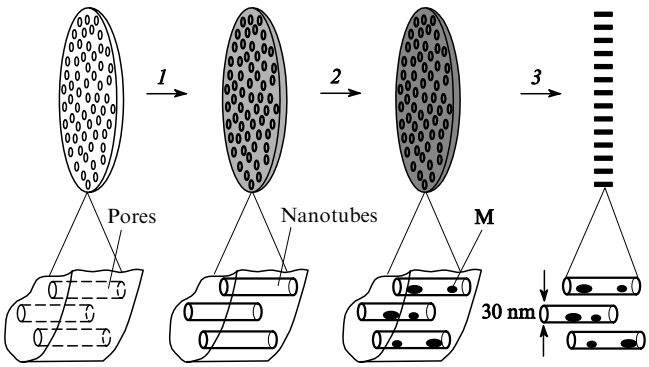

Figure 2. A scheme illustrating the filling of NTs from the gas phase using a porous Al_2O_3 film.[75]
Propylene pyrolysis (*1*), chemical vapour deposition of the metal (*2*) and dissolution of the template in NaOH (*3*). The metal particles are labelled as M.

A short review of recent advances in the field of the preparation of filled NTs and metallic nanowires was reported by Terrones *et al.*[80]

III. Functionalisation of carbon nanotubes

Chemical modification of activated carbons and carbon fibres has been studied in detail. Several methods for attachment of oxygen-containing groups to the NT surfaces have been developed.[81,82]

Cahill and Rohling[83] showed that functional groups can bound to the NT side walls. The oxidised surfaces of NTs were found to be covered by the carboxylic, carbonyl and hydroxyl groups in the approximate ratio 4 : 2 : 1.[53]

The behaviour of acid groups on the surfaces of nitric acid treated NTs was studied by temperature-programmed decomposition and acid-base titration.[84] The concentration of these groups on the NT surfaces was found to be $\sim 1 \times 10^{20}$ g^{-1}, whereas graphite treated under the same conditions showed a lower concentration (5.3×10^{19} g^{-1}). Sonication of NTs prior to the functionalisation in acids increases the concentration of acid groups.

Oxidation of NTs with a $H_2SO_4-HNO_3$ mixture leads to a higher concentration of functional groups on the surface than in the case of treatment with HNO_3.[85] The formation of functional groups and their subsequent bonding to the metal ions can be described by the following mechanism:

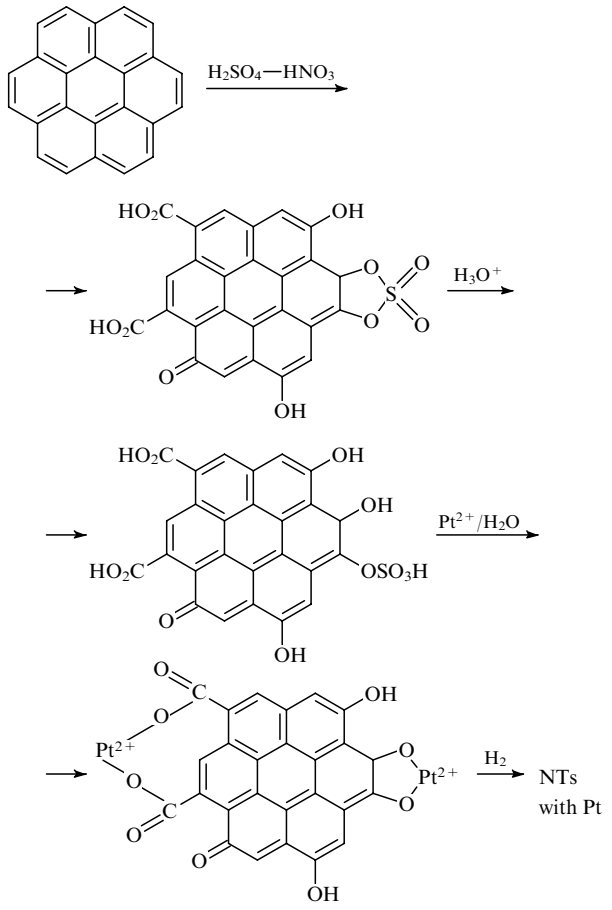

Prolonged acid treatment followed by heating in air is used for purification of SWNTs {see Ref. 40 and material posted at URL [http://www.ruf.rice.edu/~johnz/researchorig.html]**D**}. After a 16 h reflux in 3 M HNO_3 (120°C), washing and drying the mass loss was 18%, of which ~6% were identified as metal impurities. The surfaces of acid treated NTs were found to be uniformly coated with polyaromatic hydrocarbons, which can be removed by oxidation in air at 550 °C for 30 min. The residue (~20% of the initial mass) represented high-purity pristine SWNTs. The impurity content was at most 2%. Oxidation of these NTs begins at 735 °C. This temperature is ~125 °C higher than that reported earlier,[55] which indicates that the NTs are defect-free and contain no dangling bonds.

Long-term acid treatment of NTs leads to changes in the chemical composition of the material. Indeed, the uniform hydrophilic carbonaceous precipitate disappears and NTs randomly coated with both the precipitate 'spots' and particle aggregates appear in addition to the pristine NTs after 48 h with 3 M HNO_3. A large fraction of NTs was found to be damaged and shortened ('cut'). Being oxidised in air, this material behaves in a different manner compared to the material obtained after acid treatment for shorter times (see Fig. 1) and the yield of purified NTs becomes nearly halved.

It should be noted that SWNTs obtained by different methods exhibit different behaviour in the course of acid treatment and subsequent oxidation. Oxidation of nitric acid treated SWNTs with gases results in selective removal of thin NTs.[86]

Functional groups can be removed from the surface of NTs by heating. The process begins at temperatures above 623 K;[87] however, complete removal is observed at 1073 K (higher stability of functional groups up to a temperature of 1173 K was also reported[83]).

The density of oxidised (defect) carbon sites in closed (10,10)-NTs after acid treatment and removal of CO_2 and CO at 1273 K can be determined using ozone titration.[88] The fraction of defect carbon sites was estimated to be 5.5%.

To enhance the possibilities of atomic force microscopes (AFM) with nanotube probe tips, the tip ends are functionalised.[89–91] This can be done with both solutions[89–91] and gases.[92–94] The latter approach is thought to be preferred since it involves a single-step treatment.[92] A schematic representation of the AFM cantilever functionalisation process is shown in Fig. 3. The treatment procedure uses electric discharge in O_2, H_2, N_2 and H_2-N_2 mixtures. Modified probes can be used for studying the surfaces of non-ionisable self-assembled layers terminated in OH

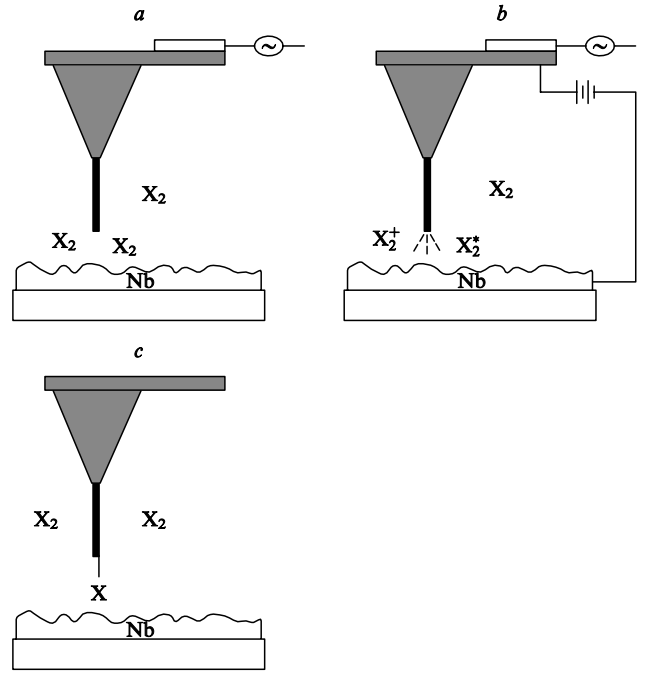

Figure 3. Schematic representation of the AFM cantilever functionalisation process.
Carbon nanotube attached to a cantilever is oscillated above a sputtered niobium surface in the presence of gas, X_2 (*a*); applying a potential produces electric discharge between the oscillating NT and the surface (*b*) and the nanotube probe tip functionalised with X (*c*).

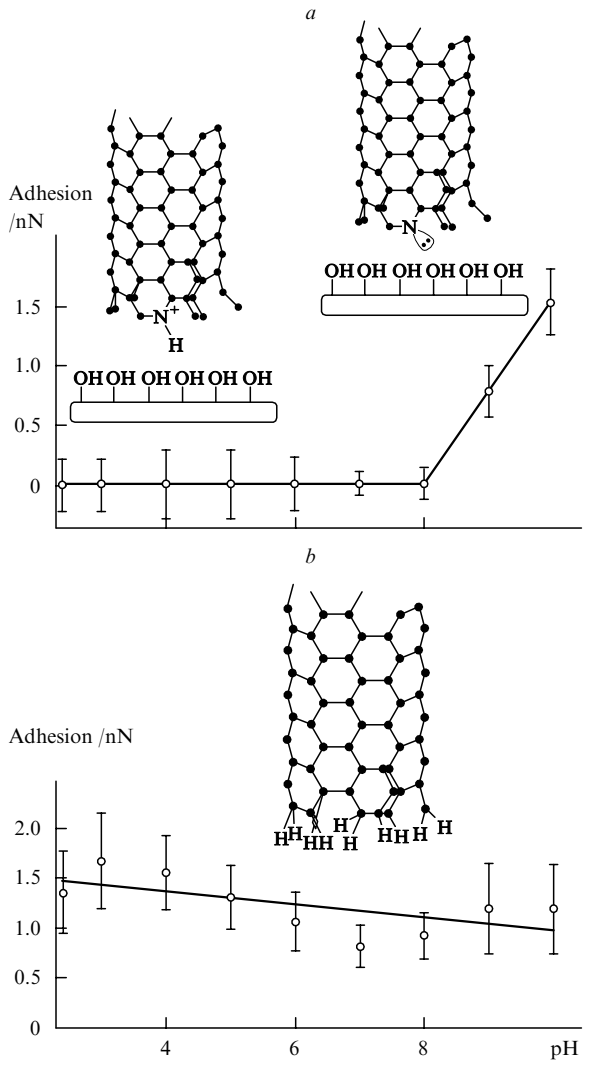

Figure 4. Adhesion of nanotubes to the surface of self-assembling monolayers as a function of pH (measured using an AFM).
A probe with a nanotube tip modified by nitrogen (*a*) and hydrogen (*b*) atoms.[92]

groups. Modification of nanotube tips using a discharge in N_2 atmosphere results in the formation of nitrogen-containing heterocycles at the tip ends. Chemically modified nanotube tips can be used for measuring the pH values of different surfaces (Fig. 4).

High degree of saturation of nanotube tips with functional groups (up to the atomic ratio O : C = 0.2) is achieved by treatment with a low-pressure ammonia plasma followed by oxidation with a $NaClO_3$ solution.[93]

According to calculations, bombardment of SWNT bundles with $CH_3^{\bullet}$ radicals with energies between 10 and 80 eV must result in bonding the radicals or their fragments to the surface.[94]

A theoretical study on the hypothetical structure of NTs 1 nm in diameter and 5 nm long with acid functionalities attached to the outer surface and on the structure of NTs linked through such functional groups has been reported.[95]

a. Fluorination of carbon nanotubes

Fluorination plays a distinctive role in the modification of NTs and functionalisation of NTs.

A review by Touhara and Okino [96] covers the latest studies of researchers from Japan in the field of fluorination of carbon materials. The authors of this review believe that fluorination belongs to the most efficient chemical methods of modification and control of the physicochemical properties of these materials. They constructed a binding energy scale for the C – F bonds and inferred that these bonds can be of different nature and can vary from covalent to semi-ionic and thus be responsible for the variety of properties of fluorinated materials.

Graphite fluorides and intercalation compounds based on them are known to be of paramount importance as compared to other graphite compounds (oxides and salts). They are readily available, exhibit relatively high chemical and thermal stability and are characterised by high energy content, which makes them the subject of great practical interest as promising materials for chemical current sources and components for solid lubricants. Studies on fluorination of NTs have led to some remarkable findings.

Pioneering experiments on the fluorination of MWNTs were carried out by researchers from Japan in 1996.[96,97] It was shown that fluorine is first of all intercalated into the outer layers of NTs. Fluorinated graphene sheets were found to retain their tubular structure on heating up to 300 – 400 °C, the spacing between them being increased to 0.53 and even to 0.65 nm at higher temperatures. As in the case of graphite, nanotube fluorination is accompanied by buckling of graphene sheets and the formation of a polymeric structure 2 to 3 nm thick with covalently bonded fluorine atoms on the surfaces of NTs. By analogy with fluorination of graphite, nanotube fluorination was assumed [97] to proceed as stepwise process. However, this hypothesis was not confirmed more recently.

Experiments on fluorination of MWNTs 20 to 40 μm in diameter and up to 10 μm long obtained by catalytic pyrolysis [98] showed that these NTs are more reactive than graphite but less reactive than C_{60} and C_{70}.[96] The reaction of the NTs with a $F_2 - HF - IF_5$ mixture at room temperature resulted in the formation of a black compound of composition $CF_{0.4}$ (fluorination of graphite under the same conditions resulted in graphite monofluoride). The reaction product was found to represent an intercalate, though no intercalation of IF_5 into the NTs was observed. The product retained the tubular morphology and sp^2-hybridisation of the carbon atoms.

Fluorination of NTs at 500 °C for 4 h resulted in distortion of a regular structure of NT bundles and in the formation of a white compound with a chemical composition close to that of graphite monofluoride (at 600 °C).

Studies of the electrochemical properties of fluorinated NTs [96,99] revealed that the capacity of a nanotube-derived electrode material fluorinated at 480 °C and then used in batteries can be as high as 620 A h kg^{-1}.[96]

The results of earlier studies [98,99] were to some extent confirmed by the results of experiments on the fluorination of 'buckypaper' fabricated from purified SWNTs with dilute F_2 (9% F_2 in He).[100] It was shown that fluorine atoms can be attached to the side walls of NTs.[100] The atomic ratio F : C was found to be merely ~0.1 at 150 °C, ranged between 0.46 and 0.52 at 250 °C and within nearly the same limits at 325 °C and corresponded to the formation of a compound with approximate composition C_2F, which retained its tubular structure. At temperatures above 500 °C most of the NTs were destroyed and the formation of structures similar to MWNTs was observed at 500 °C. Fluorination was found to have a strong effect on the electronic properties of NTs, namely, the untreated NTs were conductors while the fluorinated NTs were insulators.

Surprisingly, fluorination of NTs at $T \leqslant 325$ °C appeared to be reversible. The interaction between fluorinated NTs with a composition close to C_2F and anhydrous hydrazine resulted in removal of the fluorine atoms and in recovery of the initial structure of the NTs. This was accompanied by recovery of many (but not all) initial properties of the NTs. This was associated [100] with the reaction

$$CF_{n\,(NTs)} + \frac{n}{4}\,N_2H_4 \longrightarrow C_{(NTs)} + n\,HF + \frac{n}{4}\,N_2\,.$$

However, no structure recovery was observed if NTs were fluorinated at 400 °C.

'Fluorocarbon' NTs were shown to react with such a strong nucleophile as sodium methoxide to give a relatively stable compound with an approximate composition $C_{4.4}F(OCH_3)_{0.25}$. Sonication of fluorinated NTs in various alcohols leads to solvation of the NTs, the degree of solvation being much higher than that reported by Chen *et al.*[102] Solvated NTs can form solutions, which is of great importance for the development of nanotube chemistry and some technological procedures, *e.g.*, for nanotube sizing and purification.

Mickelson *et al.*[101] studied the fluorination of thoroughly purified NTs primarily with the (10,10) structure. The reaction product consisted of ~70 at.% C and 30 at.% F and corresponded to the empirical formula $C_{2.33}F$. The C–F bond ionicity was found to be much higher than in, *e.g.*, alkyl fluorides. This allowed the preparation of metastable solutions of the NTs in methanol, ethanol, 2,2,2-trifluoroethanol, propan-2-ol, butan-2-ol, n-pentanol, n-hexanol, cyclohexanol and n-heptanol by sonication. These solutions were stable for 24–168 h. Of the solvents used, propan-2-ol and butan-2-ol were found to be the best. The solubility of NTs in butan-2-ol was at least 1 mg ml^{-1}. It was assumed that solvation is accompanied by the formation of hydrogen bonds following the scheme

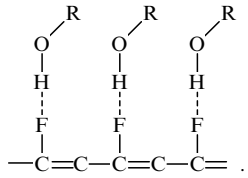

Prolonged sonication of the fluorinated NTs (~10 min and longer) results in removal of some of the fluorine atoms from the surface of NTs.

The solutions of the NTs in chloroform appeared to be much less stable. Attempts at solvating the NTs in perfluorinated liquids, acetic acid and aqueous acetone solutions also failed.

Reactions in solutions also proved the role of hydrazine as defluorinating agent. The structures of the NTs precipitated out of the solution after adding anhydrous hydrazine and characterised by low fluorine content were only slightly different from those of the untreated NTs.

Smalley *et al.*[103] succeeded in replacing the fluorine atoms attached to the side walls of NTs by alkyl groups. Fluorinated NTs of stoichiometry $C_{2.33}F$ were treated with either a solution of alkyllithium in alkane or with Grignard reagents RMgBr (R = Me, Et, Bu, C_6H_{13}, C_8H_{17} or $C_{12}H_{25}$) in THF. The reactions were activated by sonication.

It was found that the NTs alkylated with hexyl groups can be dissolved in chloroform (up to a concentration of ~0.6 g $litre^{-1}$), THF (~0.4 g $litre^{-1}$) and methylene chloride (~0.3 g $litre^{-1}$). No flocculation was observed over a period of several weeks.

Heating of the alkylated NTs in air can lead to recovery of the initial composition the NTs had before fluorination. The hexylated NTs decompose or are oxidised at 250 °C. Judging from the mass loss over a period of 1 h, there are 10 carbon atoms of the outer surface of the NT per hexyl group.

Smalley *et al.*[103] also reported convincing proofs of the chemical nature of the bonding between alkyl groups and the surface of NTs. They also found that alkylated NTs can form true solutions and various complex functional nanostructures linked through the atoms attached to their side walls.

To establish the fluorination and functionalisation mechanisms, Kelly *et al.*[104] studied fluorinated and butylated NTs by scanning tunnelling microscopy (STM) and carried out quantum-chemical calculations of the energies of different isomers. The observed STM images were consistent with the formation of the 1,4-isomer (Fig. 5), though the calculations predict that this isomer is only slightly more stable than the 1,2-isomer. The

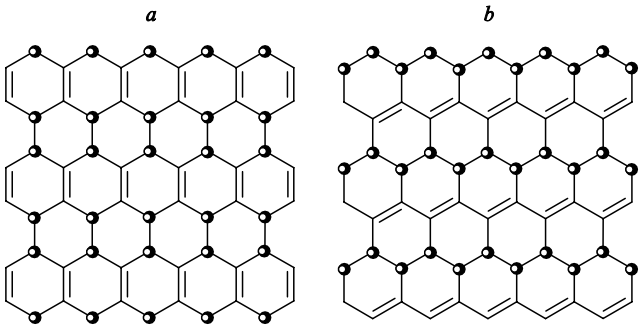

Figure 5. Structure of fluorinated nanotubes. 1,4-isomer (*a*) and 1,2-isomer (*b*).

mechanism of fluorination involves the addition of fluorine atoms to the side walls of NTs around the circumference of the NTs in the intermediate stages.

Fluorination of the external side walls of NTs affects their electronic properties. For instance the conductivity type of NTs can vary from semiconducting to metallic (and *vice versa*).[105]

The binding energies of one, two, three and four fluorine atoms to the side-wall carbon atoms of a (10,0)-NT have been calculated.[106] The sum of the binding energies of two fluorine atoms to the carbon atoms of the NT is much higher than the binding energy in the F_2 molecule.

A group of researchers from Japan studied the process of fluorination of the inner cavity of NTs and the effect of changes in the chemical composition of the NTs on their properties.[107] The starting material, open-end SWNTs, was produced in a porous Al_2O_3 template with a pore diameter of ~30 nm and a pore length of 75 μm. After treatment with F_2 under isothermal conditions at 50 to 200 °C and atmospheric pressure the template was dissolved to separate the fluorinated NTs (Fig. 6). The product was shown to retain the tubular structure.

Fluorinated carbon nanotube membranes are thought to be a perfect material for electrochemical batteries or capacitors.[96]

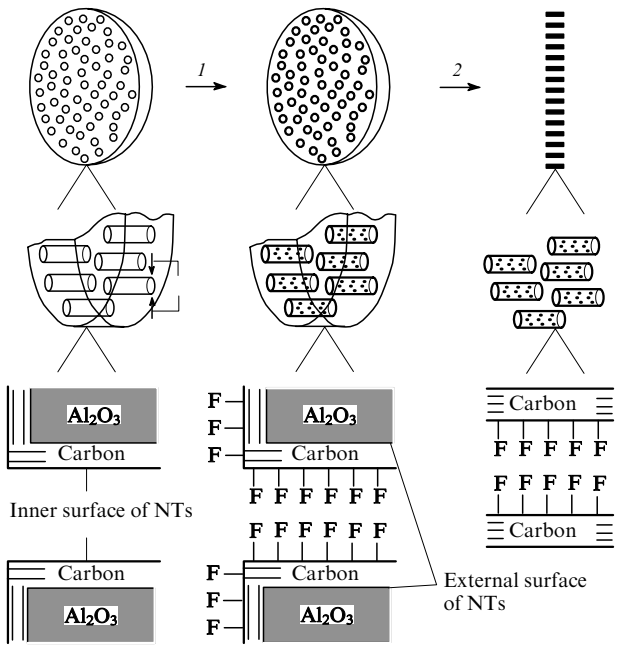

Figure 6. The preparation of nanotubes with fluorinated inner cavity using a porous Al_2O_3 film (deposition of the carbon layer is not shown).[107] Fluorination (*1*) and dissolution in HF (*2*).

Long-term (168 h) fluorination of MWNTs with 'roll' structure and nanoparticles obtained by arc method with BrF_3 vapours at room temperature results in tubular or quasi-spherical C_2F.[108] This is accompanied by corrugation of the external shells of the NTs while the inner shells of the NTs retain the shape of coaxial cylinders. As the depth of fluorination increases, the interlayer spacings and the NT diameter also increase. At a critical fluorination depth (or, in other words, at some critical strain), a number of the outer shells are simultaneously unrolled, thus leading to the formation of multilayered plate-like particles.

This phenomenon was first observed. The interlayer spacing for the untreated NTs was 0.342 nm (by 0.007 nm larger than for graphite), whereas that for the fluorinated NTs was 0.614 nm, which is indicative of a very weak interlayer coupling. However, the role of Br_2 used in the form of (i) vapours to pre-saturate the NTs and (ii) solution to evaporate BrF_3 is still to be clarified.

b. Soluble carbon nanotubes

The ability of NTs to dissolve in various solutions opens new possibilities for their purification, classification (selection of fractions with uniform structure and equal length) and modification.

Pioneering studies on the attachment of organic functional groups to NT bundles by radiation-induced photolabilisation using biradicals and nitrene sources followed by treatment with dichlorocarbene were carried out by Smalley *et al.*[109] They found that the interaction with dichlorocarbene leads to the appearance of chlorine within the NT bundles but failed to determine whether the reactant is attached to the NT walls or to amorphous carbon due to insufficient purity of the starting material. Dichlorocarbene was attached to the double bond of a NT using another reaction, namely, the interaction of NTs with $PhHgCCl_2Br$.[109] The reaction product was found to contain $\sim$2 at.% of chlorine.

Solvation of SWNTs due to the attachment of octadecyl groups has been reported.[102] Single-walled NTs with an average diameter of 1.38 nm were obtained by arc discharge technique, purified, cut to 100 to 300 nm, opened, acid-functionalised (in HCl in the final stage) and treated with $SOCl_2$ containing a small amount of DMF for 24 h at 70 °C. The solid phase was separated from the solution, washed with anhydrous THF, dried and heated with octadecylamine at 90–100 °C for 96 h. The solid residue obtained after removal of excess amine and four-fold washing with ethanol contained up to 60% of NTs that were extracted using a dichloromethane solution. It was found that the functionalised NTs can be dissolved in chloroform, benzene, toluene, chlorobenzene, dichlorobenzene and CS_2. The solubility limit in dichlorobenzene and CS_2 was greater than 1 g litre^{-1}. Dilute solutions were brown while nearly saturated solutions were black.

Functionalisation was accompanied by noticeable swelling of NTs, which was tentatively related to the breakdown of the NT bundles. It should be noted that a $\sim$300-nm (10,10)-NT contains $\sim$50 000 carbon atoms and has a molecular mass of $\sim$600 000 Da.

Solutions of solubilised SWNTs with attached $CONH(CH_2)_{17}CH_3$ groups were studied by IR, Raman and UV spectroscopy[102] and by the ^{1}H NMR (see Ref. 102) and ESR spectroscopy.[110] The ESR signal with the parameters $g = 2.003$ and $\Delta H = 2.1$ G observed by Chen *et al.*[110] is characteristic of the cut NTs. Reactions of NTs with Br_2 and I_2, which can also proceed in solutions, were shown to cause changes in the electronic structure of the NTs.

Dissolution of SWNTs *via* their functionalisation has been studied in detail.[111] The SWNTs were first treated with $SOCl_2$ and then the chloride groups were replaced by amino groups using the reaction with 4-$CH_3(CH_2)_{13}C_6H_4NH_2$. Solution-phase doping of the solubilised NTs with iodine and bromine resulted in pronounced changes in the vibrational spectra of the NTs and served as evidence that the reactions in the solutions do proceed. Compared to the cut NTs, the uncut functionalised NTs were found to be much less soluble. Distinctions between the absorption bands of semiconducting and metallic NTs and better solubility of the NTs of larger diameter (their fraction is small) in pyridine than in THF, CH_2Cl_2 and CS_2 were also pointed out. Dissolution of the amine-functionalised NTs can be achieved using the amines with long alkyl radicals since the interaction with aniline was found to have almost no effect on the solubility of the NTs.

Soluble NTs were also obtained by treating with poly(phenylacetylene).[112] Short NTs helically wrapped by the polymer molecules (the NT content in the composite was 1.9 mass % to 6.0 mass %) were dissolved in THF, toluene, chloroform and 1,4-dioxane.

The addition of poly(*m*-phenylene vinylene-*co*-2,5-dioctyloxy-*p*-phenylene vinylene) to powdered NTs allows their dissolution in standard organic solvents (*e.g.*, toluene) and purification from insoluble particles of turbostratic graphite.[113, 114] The polymer is prone to form helices with a diameter of $\sim$20 nm and a pitch of $\sim$6 nm. The NTs under study were 15 to 20 nm in diameter and 0.5 to 1.5 μm long. Because of the correspondence between the NT diameter and the diameter of the polymer helix, the polymer molecules can wrap the NTs, though in some instances they were found inside the NTs. Noteworthy is that the interaction of bright yellow polymer with black NTs resulted in a dark green composite. The nanotube/polymer suspensions were stable for a period of at least 6 months.

c. Colloidal solutions and dispersions of carbon nanotubes

Solubilisation of NTs can also be achieved by colloid chemistry tools. Functionalised soluble NTs differ from surfactant-coated NTs in strength of the bonds they form (only in the former case these bonds are covalent). Suspensions of NTs are stabilised using common surfactants.[91] Surfactant-stabilised dispersions of MWNTs and SWNTs are convenient for chromatographic purification.[115–117]

The most often used surfactants are DMF and *N*-methylpyrrolidone. Dispersions of NTs in DMF are stable.[103, 118] However, the authors of a more recent study[119] showed that these dispersions tend to aggregate after a period of several days. One can assume that NTs tested by different authors exhibited different properties.

The most stable are dispersions of NTs in strong Lewis bases which do not form hydrogen bonds.[119] These are (in the descending order of the optical density of NT dispersions) *N*-methylpyrrolidone, DMF, hexamethylphosphoric triamide, cyclopentanone, tetramethylenesulfoxide and ε-caprolactam. The optical spectra of NT dispersions in these solvents follow the same pattern. Dispersions of NTs in DMSO, acrylonitrile, 4-chloroanisole and ethylisothiocyanate follow another spectral pattern, while NT dispersions in 1,2-dichlorobenzene, 1,2-dimethylbenzene, bromobenzene, iodobenzene and toluene follow yet another, third, spectral pattern.

The third group of solvents is thought to be the best for C_{60} and C_{70} (see Ref. 120).

Complexation with polyacrylic acid and surfactants allows solubilisation of MWNTs up to several micrometres long.[121]

Exact reproduction of the geometry of NT-derived nanoscale devices required studies on the behaviour of micellar dispersions of NTs on patterned surfaces[122] and preparation of the Langmuir–Blodgett films based on amphiphilic molecules and NTs.[123] Such films were fabricated by dispersion of NTs in aqueous solution of lithium dodecyl sulfate, isolation of the residue by centrifugation and introduction of the residue into the subphase of the aqueous solution of poly(allylamine hydrochloride).

Burghard *et al.*[124] coated electrodes with NTs using surfactant-stabilised NT suspensions or Langmuir–Blodgett films. At low temperatures, SWNT bundles in the Langmuir–Blodgett films exhibit nonlinear current-*vs*.-voltage characteristics.[125]

IV. Decoration of carbon nanotubes and their use as templates

Coating of the side walls of NTs can be achieved *via* their pre-treatment (functionalisation) or without it. The first route implies the chemical interaction as a necessary stage and is often called nanotube decoration. The second route implies that NTs are used only as templates for the deposition of other substances, though in this case the chemical interaction between the NTs and the substance to be deposited cannot often be ruled out.

A clear correlation was established between the amount of adsorbed Pd^{2+} ions and the concentration of acid groups on the surfaces of both closed and open NTs and graphite.[84] Adsorption of Cu^{2+}, Co^{2+}, Fe^{2+}, Ni^{2+}, Pr^{3+} and UO_2^{2+} ions on the surface of functionalised open NTs was also studied. The adsorption capacity was found to range between 0.005 (UO_2^{2+}) and 0.029 (Pd^{2+}) mmol per gramme of carbon. To obtain metallic palladium using NTs, they were first reduced with H_2 at 250 °C.

Coating of acid-treated NTs with platinum clusters has been described.[85]

To show that NTs can be used as a template, they were oxidised in two steps,[124] namely, by long-term (3 h) reflux in HNO_3 followed by short-term treatment with a strongly acidic $KMnO_4$ solution (the oxidant was decomposed after less than 1 min by adding acetic acid). The oxidised NTs acquired the ability to be readily dispersed in water and to attach copolymers with hydrophobic (butyl methacrylate) and hydrophilic (4-vinylpyridine) groups. The external surfaces of the functionalised NTs were then decorated with gold nanoparticles that form a conducting layer.

Copper nanoparticles with narrow particle size distribution can hardly be obtained by conventional techniques; because of this, they were synthesised using NTs as a template.[126] The NTs used in this study were prepared by catalytic pyrolysis of CH_4. Changing the catalyst composition enabled production of NTs with different diameters and narrow diameter distributions (from 5–10 to 25–35 nm). In addition to variation of (i) the copper salt concentration in the aqueous solution and (ii) the initial ratio Cu : NTs, the procedure involved the reduction in H_2 and washing from the template by sonication and resulted in either Cu nanoparticles or nanofibres. The smaller the NT diameter and the lower the salt concentration in the solution, the smaller the diameter of the copper particles (with the smallest particle size between 5 and 10 nm). An increase in the salt concentration in the solution and the Cu : NTs ratio resulted in the formation of copper nanofibres from 100 nm to 5 μm in diameter and up to hundreds of micrometres long.

Decoration of activated NTs with copper and nickel particles in the presence of Pd complexes using one-step and two-step activation-sensitisation has been reported.[127] Both methods imply coverage of the NT surface with Pd or Pd–Sn nuclei followed by the formation of a continuous coating of the NTs with copper and nickel. The coating density was determined by the activation conditions.

The structure of the coating formed on the external surfaces of NTs interacting with molten V_2O_5 was studied and discussed by Ajayan *et al.*[51,62] This coating can be formed due to surface tension and be very thin. Vanadium oxide has a pseudolayered structure with pyramidal VO_5 units held together by bridging oxygen atoms. These layers can uniformly cover the entire surface of NTs and form thin films. Oxidation of such films in air at 650–675 °C resulted in removal of carbon and preparation of V_2O_5 flakes less than 1 nm thick and rod-like V_2O_5.

A topotactic correspondence between the oxide layer and NTs should be pointed out, *viz.*, the *c* axis of the oxide is perpendicular to the NTs axis. Mention was also made of preferred orientation of the crystallites found inside and outside the NTs (see, *e.g.*, Ref. 52).

The possibility of coordinating $Cr(CO)_6$ to NTs has been reported.[128] Molecular dynamics simulations showed that the chromium center of the $Cr(CO)_3$ group is coordinated to the three double bonds of a benzene ring of the NT side wall.

Nickel and cobalt with small additives of P and B can be chemically deposited onto the MWNT 'forest' to form a continuous polycrystalline coating.[129,130] Similar experiments on the deposition of Ni on the NTs that were dispersed in $SnCl_2$ and $PdCl_2$ solutions by sonication and transferred then into the bulk solution were also carried by Li *et al.*[131] who, however, failed to obtain continuous coating. Strong effect of the pH value of the bulk solution on the character of the coating and, in particular, on the degree of aggregation of the nickel particles was pointed out.

Decoration of NTs with complex molecules including DNA is also possible. For instance, long-term storage of the solutions of such compounds with the NTs pre-treated to be covered with acidic centres resulted in immobilisation of 'small proteins' metallothioneine, cytochrome C_3 and β-lactamase I. The fact that most parts of the immobilised proteins remain catalytically active indicates the absence of pronounced conformational changes. The adhesion force between the proteins and the surface is rather strong and the proteins cannot be washed off with water.[132]

Multi-walled NTs coated with a rhodium phosphine complex were prepared.[133]

The use of gel techniques and, in particular, sol-gel process opens considerable opportunities for NT decoration. For instance, coating of NTs with zirconium propoxide followed by calcination and burning out of carbon resulted in zirconia nanotubes.[134] After functionalisation and interaction with $Zr(OPr^n)_4$ the NTs was washed with methanol and dried at 373 K. The gel was then calcinated at 723 K and carbon was burnt out in air at 973 K. The zirconia nanotubes thus obtained were 40 nm in diameter, had the side walls 6 nm thick and represented a mixture of equal amounts of monoclinic and tetragonal zirconia phases.

Fabrication of Y_2O_3-stabilised zirconia NTs *via* gelation of colloidal solutions of $ZrOCl_2$ and $Y(NO_3)_3$ by addition of NH_4OH followed by heat treatment is a considerable step forward. A similar procedure was used for the synthesis of hollow NTs or nanorods from SiO_2, Al_2O_3, V_2O_5, Sb_2O_5, MoO_2, MoO_3, WO_3 and RuO_2.[135,136] Gels were prepared using (i) the vanadium, molybdenum or tungsten acids synthesised from corresponding salts by ion exchange technique and (ii) metal chlorides. TiO_2-Coated NTs were also prepared (this report can be accessed *via* the Internet at URL http://www.fys.kuleuven.ao.be/vsm/spm/Ti_oxidation_fig11.html).

It was established that physically deposited Ti, Ni and Pd coatings cover the surfaces of NTs by continuous or quasi-continuous layers, whereas Al, Au and Fe coatings only form isolated discrete particles on the NTs.[137,138]

Calculations[139] of the adsorption of potassium atoms on the external and internal NT surfaces showed that the process is energetically favourable for small-diameter NTs.

A theoretical study of the interaction of Ni and Ni_2 with graphite and NT side walls[140] revealed considerable differences in bonding sites, magnetic moments and the direction of charge transfer. The effect of the NT surface curvature[§] on the reactivity of graphene sheets has been studied.[141] Some conclusions drawn based on the results of quantum-chemical calculations were confirmed experimentally.

V. Substitution of the carbon atoms of nanotubes by atoms of other elements

The interest in carbon NTs in which some of the carbon atoms are partially or completely replaced by atoms of other elements, as well as the interest in the NTs made of other substances stems from the fact that these NTs can exhibit improved electronic properties as compared to the carbon NTs. For instance, the electronic

§ The study[141] concerns bending of NTs and has a new term in the title, 'Kinky Chemistry'.

characteristics of boron nitride NTs (hereafter, BN-NTs) are known to be independent of their structure.[142] Young's modulus of BN-NTs is ~1.2 TPa, which is a record value for fibrous dielectrics.[143] Therefore, BN-NTs are thought to be the best material for encapsulation of conductors in their inner cavities. This type of NTs is promising for fabrication of low-voltage field emission devices and preparation of composites from coaxial sandwiches of carbon NTs and BN-NTs.[144]

The structure and electronic properties of nitrogen-containing NTs have been studied at different N : C ratios and different structure of isomers.[145] It was found that, depending on the mutual arrangement of nitrogen and carbon atoms, NTs can exhibit either metallic or semiconducting properties with a narrow energy gap.

However, BN-NTs as well as B_xC-NTs or B_xCN_y-NTs are difficult to prepare using the procedures developed for production of carbon NTs. An original method of attacking the problem of preparation of B_xC-NTs involves replacement of the C atoms in carbon NTs by B atoms.[146, 147] Indeed, the oxidation of NTs by B_2O_3 vapours in Ar stream at 1373 K resulted in B_xC-MWNTs ($x \leqslant 0.1$) with the same diameter and length as those of the untreated NTs.

$$x\,B_2O_3 + (2 + 3x)\,C_{(NTs)} \longrightarrow 2\,B_xC_{(NTs)} + 3x\,CO.$$

It was suggested that the low degree of substitution is related to the multi-walled nature of the starting material (the untreated NTs) and that mostly the outer shells were involved in the reaction. In addition to B_xC-NTs, crystalline rod-like nanomaterials of stoichiometry B_4C and $B_{13}C_2$ were found among the reaction products.

Preparation of $(BN)_xC$-NTs from carbon NTs with an average diameter of 10 nm and B_2O_3 powder in N_2 stream at 1573 K has been reported.[148] In this case, the graphite crucible used for the synthesis of B_xC-NTs should be replaced by a BN crucible. Noteworthy, C → B substitution was found to lead to a more ordered NT structure.

The same procedure was also used for the synthesis of BN-SWNTs and carbon NTs doped with boron and nitrogen.[149]

The reaction

$$B_2O_3 + 3\,C_{(NTs)} + N_2 \longrightarrow 2\,BN_{(NTs)} + 3\,CO$$

was conducted in an induction furnace at temperatures between 1523 and 1803 K and resulted in B_xC-NTs, $B_xC_{1-x-y}N$-NTs and BN-NTs. The yield of the BN-NTs increased as the temperature increased. However, not all NTs were involved in the reaction. It is interesting that some of the BN-NTs were filled with octahedral BN particles, which resembles the formation of nanoscale 'pea-pod' structures of carbon NTs.

A more complicated procedure for increasing the yield of substituted NTs consists of MoO_3-promoted synthesis using B_2O_3.[150] The reaction was carried out at the mass ratio $B_2O_3 : MoO_3 : NTs = 5 : 2 : 1$ at 1773 K. The reaction was nearly complete after 30 min due to the stronger oxidative effect of the MoO_3 additive compared to that of B_2O_3 and resulted in the formation of BN-NT bundles up to 1 μm long. The authors of this study [150] suggest that the process begins with the oxidation of NTs following the reaction

$$MoO_3 + 3C_{(NTs)} \longrightarrow Mo + 3\,CO.$$

As a result, the NTs are opened, thus enhancing their reactivity towards B_2O_3 and N_2. The Mo atoms chemisorbed at the NT ends act as catalysts to preclude the formation of 'caps'. This is accompanied by filling the NTs with Mo-containing clusters.

Boron- and nitrogen-doped SWNTs containing up to 10 at.% B and up to 2 at.% N were produced in high yield using substitution reactions.[151] The highest yield was achieved at 1553 K after 30 min synthesis. All the SWNTs synthesised were found to form bundles with an inter-tube spacing of ~0.3 nm.

A multistage substitution reaction was used for the template synthesis of GeO_2 nanorods (NR).[152] A mixture of powdered Ge, Si and SiO_2 with carbon MWNTs 15 nm in diameter was heated in Ar atmosphere at 850 °C for 3–4 h. The overall process is assumed to involve a number of reactions of Ge vapours, *viz.*, partial exchange with SiO_2, a reaction with the carbon atoms on the NT surfaces and oxidation into GeO_2 in the presence of O_2.

$$Ge_{(gas)} + 2\,O_2 + 2\,C_{(NTs)} \longrightarrow GeO_{2(NR)} + 2\,CO.$$

Nanotubes were used for the template synthesis of SiC,[153, 154] TiC, NbC, Fe_3C and BC_x (see Ref. 153); GaN,[155] Si_3N_4 (see Ref. 156) and TaC [157] *via* reactions with volatile oxides (SiO, Ga_2O, B_2O_3), chlorides ($FeCl_3$) and iodides (TiI_x, NbI_x).

Nanotubes can be coated with titanium.[137, 138, 158]

Reactions of the type

$$xC_{(solid)} + M_{(solid,gas)} \longrightarrow MC_{x(solid)}$$

do not belong to but are much the same as substitution reactions. The interaction of SWNTs and SWNT bundles with silicon begins at temperatures above 800 °C and is accompanied by the formation of β-SiC nanorods that retain the morphology of the carbon NT bundles (this holds even for long rods!).[159] The reactions of individual NTs or NT bundles at 970 °C in ultrahigh vacuum resulted in structures with the $Si-SiC_{(NR)}-C_{(NTs)}$ heterojunctions. Similar structures with well-defined carbide–metal interfaces were obtained in reactions of NTs with titanium. A schematic illustration of the method is shown in Fig. 7.

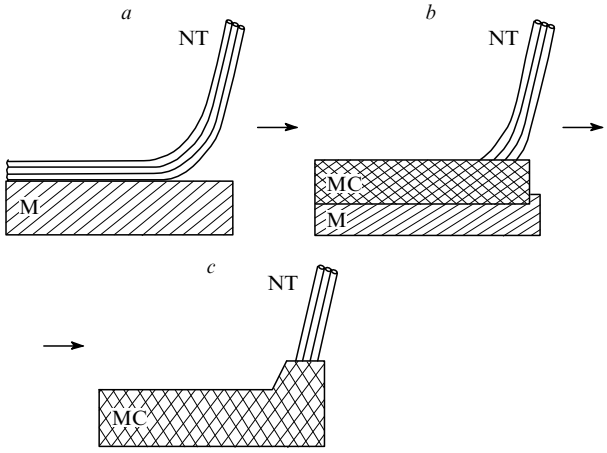

Figure 7. A schematical illustration of the method for fabricating $MC-C_{(NTs)}$ heterojunctions.
Before reaction (*a*), formation of carbide in the reaction of the nanotube with the metal (*b*) and after reaction (*c*).

Preparation of structures with $NbC-C_{(NT)}$ heterojunctions appeared to be a more difficult task due to peeling of NTs from the carbide on cooling. However, the reaction with niobium is convenient for cutting long NTs and making a uniform morphology of NT ends, which is of great importance for fabrication of field emitting devices.[160] To this end, a perforated Nb wafer was coated with a suspension of NTs, the solvent was removed and the NT-coated wafer was kept in $\sim 10^{-8}$ mm Hg vacuum at 950 °C.

VI. Insertion of 'guest' atoms and molecules into the intertubular space of multi-walled nanotubes and nanotube bundles

Intercalation compounds of carbon materials are of considerable interest in many respects. Lithium-intercalated graphite and related substances are commercially used in lithium batteries; the theoretical limit for the specific energy capacity of these materials equals 372 mA h g^{-1} and corresponds to the composition LiC_6 (see Ref. 161). Sometimes, the second electrode in lithium chem-

ical current sources is fabricated from fluorinated graphite (see, *e.g.*, Ref. 162). Fullerenes and NTs can also be used for these purposes.[163] Theoretically, NTs must possess a higher degree of intercalation than fullerenes.

Intercalation of MWNTs and SWNTs are two basically different processes. In the case of MWNTs, the intercalated particles penetrate into the space between the nested shells through topological defects and stay there.[164, 165] Single-walled NTs cannot be intercalated in this manner, but the 'guest' atoms or molecules can penetrate into the intertubular space of the SWNT bundles.

Intercalated NTs are also fundamentally different from fullerene intercalation compounds. For instance, fullerene C_{60} can form charge-transfer complexes only with electron donors.[166, 167] On the other hand, the results obtained by Raman [168] and optical [169] spectroscopy and from conductivity measurements [170] show that SWNT bundles exhibit the double behaviour typical of graphite and can be doped with either electron donors or acceptors. Charge transfer in SWNTs was also observed in many other experimental studies. This is characteristic of both metallic and semiconducting SWNTs.[169] Charge transfer in MWNTs also does occur.

The conductivity temperature coefficient of crystalline bundles of single-walled (10,10)-NTs is positive, thus indicating their metallic properties. Intercalation with Br_2 or K reduces the electrical resistance of the NTs at 300 K by a factor of 30 and extends the temperature range in which the conductivity temperature coefficient is positive. This points to the fact that Br_2- or K-doped NTs ($C_{52}Br_2$ and $C_{116}Br_2$) belong to the synthetic metals.[170]

Intercalates are ionic compounds and intercalation leads to an increase in the charge carrier density. Optical spectrometry studies [171] proved the possibility of controlled shift of the Fermi level of individual SWNTs by doping them with various substances. The results of electrochemical measurements also point to reversible doping of SWNTs ('nanopaper') with Li^+ ions in organic radical anions (naphthalene, benzophenone, fluorenone, anthraquinone and benzoquinone) and to shift of the Fermi level.[20] No intercalation stages typical of graphite intercalation reactions were observed. It was found that the chemical composition of the doped NT samples can be varied smoothly.

Absorption spectra of intercalated SWNTs in the visible region exhibit complex patterns which depend on the dopant concentration.[172]

Conclusions drawn by Iijima *et al.*[173] contradict the known idea that NT intercalation is accompanied by a rather high degree of charge transfer. The results obtained in this study should be more thoroughly analysed because of the high scientific authority of the authors.

1. Intercalation of electron donors

Multi-walled NTs [164, 165] and SWNT bundles [170, 174] are characterised by a different structure of the van der Waals spacings between individual NTs. However, both types of NTs can be intercalated with alkali metal vapours up to the composition MC_8 (M = K, Rb, Cs). The capacity of these materials is comparable to that of graphite which also forms compositions of stoichiometry MC_8 upon intercalation.

Multi-walled NT bundles increase their mass by 33% upon intercalation with potassium and by 260% upon intercalation with $FeCl_3$. The intercalation is accompanied by changes in the NT shape, volume and morphology and by swelling and formation of necks. Intercalation products can be readily hydrolysed; however, subsequent washing leads to recovery of their initial state. Different types of MWNTs (*i.e.*, with the 'Russian doll' and 'roll' structure) are believed to exhibit different intercalation behaviours.[175, 176]

In vacuo intercalation of SWNT bundles with Cs and K vapours at room temperature is reversible and leads to structural disordering of NT bundles.[177] The chemical composition of the intercalation products corresponds to the empirical formulae KC_{24} and CsC_x ($x = 8-24$). Disordered structure of SWNT bundles prevents locating the metal sites.[177] Disordering is due to presence of the metal atoms in the intertubular space rather than filling of individual NTs (the samples used in the experiments were 'capped').

Electrochemical intercalation of SWNTs with alkali metals involves three stages characterised by different rates. These are charge transfer through the macroscopic electrolyte–electrode interface, diffusion through the mesopores of the electrode and diffusion in the NT bundles.[178]

A number of studies [168, 170, 179] were carried out using 'mat'-like SWNT structures. However, NT 'mats' consist of a mixture of metallic and semiconducting NTs and the results obtained appeared to be hardly interpretable.

Chemically doped semiconducting NT bundles change their hole-type conductivity to electron conductivity.[180] A correlation between the concentration of the intercalated potassium and the charge carrier density was found. Typically, the electron density varies between 100 and 1000 μm^{-1}. The effective mobility of electrons was found to be 20 to 60 $cm^2\ V^{-1}\ s^{-1}$, which is in agreement with the corresponding numerical estimate obtained for holes.[181]

Intercalation of SWNTs and SWNT bundles with potassium also changes their transport properties.[182–184] Pichler *et al.*[184] found that at 425 K the C : K ratio in potassium-intercalated NT bundles approaches 7, which corresponds to the formation of a stage-1 intercalation compound, KC_8. According to Pichler *et al.*,[184] intercalation leads to a relatively small increase in the intertubular spacing and the total conductivity of the intercalated bundles is somewhat lower than that of the untreated NT bundles.

Molecular dynamics simulation [185] predicted the most stable structures of K-doped single-walled (10,10)-NTs. These were found to be KC_{16} (filling of the intertubular space) and KC_{10} (filling of both the inner NT cavities and intertubular space). The optimum structure corresponds to the compositions $K_5^{exo}C_{80}$ for the former type of NT filling and $K_5^{exo}K_3^{endo}C_{80}$ for the latter.

2. Intercalation of electron acceptors

As mentioned above, charge transfer occurs between the NTs and intercalated Br_2. Photoelectron spectra [42] point to the formation of surface complexes $C-Br_2$. The nature of the interaction between Br_2 and the NTs was studied by high-resolution transmission electron microscopy.[186] A preferential orientation of the bromine atoms was found, which is consistent with the results obtained in other studies. It appeared quite surprising that the region of Br_2 accumulation in MWNTs extends perpendicular to the NTs axis, which means that the liquid Br_2 behaves to some extent like a solid. The complexes formed were found to be not too stable and Br_2 can be washed off with CCl_4. Br_2-Intercalated NTs retain tubular structure, though the arrangement of the nested carbon shells becomes somewhat disordered (the NTs are 'amorphised'). After removal of Br_2, the NTs were more readily oxidised with oxygen than the unintercalated NTs.¶

The interaction of molten iodine with NT bundles in a sealed ampoule at 140 °C results in disordering within the NT bundles.[187] The two-dimensional crystal lattice of the NT bundles expands (the cross-section area increases).

In the intertubular space the iodine atoms are grouped and form $(I_5)^-$ chains separated by ~2.1 nm at moderate intercalation degrees. Intercalation reduces the electrical resistance and thermal electromotive force (emf) of the NTs. The iodine-doped

¶ A somewhat arbitrary use of the term 'intercalation' for the description of the above-mentioned processes should be pointed out. Strictly speaking, no increase in the interlayer spacing occurs in this case and the crystal lattice parameter increases insignificantly. Liquid Br_2 is adsorbed on the outer surfaces of NTs and is soaked into the inner cavity after opening the NTs due to wetting.

NTs are stable in air. More recently,[188] the poly(iodide) chains formed inside SWNTs were found to have a helical shape.

Bower *et al.*[189] studied the interaction of 70% HNO_3 with SWNT bundles and found that (i) intercalation occurs reversibly and (ii) the intertubular spacing increases upon the insertion of the acid molecules. The starting material was a 'mat'-like substance, or 'nanopaper', with the NT content of about 70%. The intercalation occurred at room temperature and, in contrast to the interaction with graphite, took a rather short time due to the capillary effect of the NT bundles and was accompanied by an increase in the intertubular spacing within the bundles. The crystallinity of the NT bundles remained after intercalation; however, an increase in the lattice parameter from $\sim$1.7 to 2.0 nm was observed. No proton abstraction from the HNO_3 molecule was suggested. The structure of the HNO_3/SWNTs intercalate is shown in Fig. 8. *In vacuo* heating of the samples to 500 K caused the onset of the reverse process. Extention of intercalation time to 12 h and longer times resulted in the loss of order within the NT bundles and in partial or complete breakdown of the NT bundles into individual NTs upon removal of HNO_3.

A study of electrochemical oxidation of SWNT bundles by H_2SO_4 revealed some remarkable features.[190] A spontaneous charge-transfer reaction was observed in the NT bundles. In contrast to the graphite–H_2SO_4 system, this reaction proceeds even before applying the potential difference. On the other hand, both systems share some common features. Under the action of electric current the NT bundles behave similarly to graphite, namely, the reaction

$$H_2SO_4 + \bar{e} \longrightarrow HSO_4^- + \frac{1}{2}H_2$$

proceeds by the 'charge exchange' mechanism and there is an 'overoxidation' regime (irreversible formation of covalent bonds C–O).

$FeCl_3$-Intercalated MWNT bundles exhibit metallic conductivity.[175, 176, 191] The temperature dependence of this parameter was studied by Baxendale and Amaratunga.[192]

Intercalation of NTs with $CuCl_2$ followed by reduction of the chloride to metallic Cu can be used for purification of the NTs.[41]

An interesting reaction was studied by Hsu *et al.*[193] The main goal of the study[193] was to obtain diamond from NTs *via* treatment of potassium-intercalated NTs with CCl_4 to give KCl and excess carbon. This reaction seems to be of no interest for large-scale implementation; however, it opens new prospects for synthetic chemistry. The authors hoped that the reaction

$$4K + CCl_4 \longrightarrow 4KCl + C$$

would result in cross-linking of adjacent graphite basal planes and in replacement of the sp^2-bonds by sp^3-bonds within the intertubular space of the MWNTs. The reaction was carried out in an autoclave at 200 °C; however, no diamond was produced. Analysis of the reaction products revealed the loss of ordering ('amorphisation') of the tubular structure and the formation of KCl crystallites within the space between graphite shells with presumably distorted structure. No KCl crystallites were found (i) within the NTs with the outer diameter of less than 10 nm and (ii) far from the outer surface of the MWNTs.

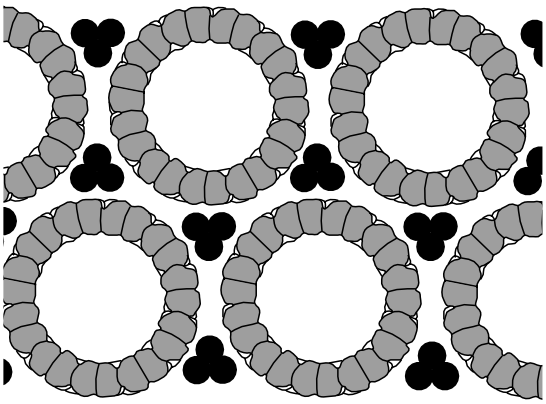

Figure 8. A model of the structure of the HNO_3/SWNTs intercalate. The C–O distance was assumed to be the same as in the case of HNO_3 intercalated graphite, the distance between the centres of the nanotube cross-sections was set to $\sim$2.0 nm.

VII. Adsorption and storage of gases in carbon nanotubes

Nanotubes can adsorb gases at high pressures or under conditions of electrochemical saturation. Adsorption can occur on the internal surfaces of NTs (within the innner cavities), on the external surfaces of free-standing NTs and in the intertubular space of NT bundles.

Pioneering calculations of the adsorption of gases on NTs were carried out by Maddox *et al.*[194]

Model calculations of the sorption of hydrogen, oxygen and chlorine atoms by SWNTs and graphite revealed three types of surface sites and provided an explanation for high efficiency of hydrogen storage in NTs.[195]

Compared to fluorine atoms, attachment of hydrogen atoms to the side walls of NTs is less probable; the attachment of two or four hydrogen atoms to a (10,0)-NT is an endothermic process.[108]

Adsorption of a Lennard-Jones gas mixture on single-walled arm-chair NTs with inner diameters of 6.125, 7.482 and 8.16 Å was theoretically studied by Ayappa.[196, 197] He showed that at $T \geqslant 388.9$ K adsorption of large particles occurs for the most part. These particles interact relatively strongly with the NTs walls. As the temperature decreases, the equilibrium is shifted towards smaller particles which completely replace the large particles at $T \leqslant 303$ K. Condensation of the small particles occurs in pores.

A series of theoretical studies on the adsorption of gases in NTs was carried out by Stan *et al.*[198–204] In the case of adsorption of inert gases on NTs the bonding between the adsorbate and the surface is stronger than in the case of graphite.[198] At low surface coverages, the adsorption strongly depends on the NT structure and size. A salient feature of the process is its one-dimensional character.

Helium and neon readily fill the intertubular space of NT bundles. They are strongly bound to the NT side walls even under those conditions where almost no adsorption occurs on the basal planes of graphite.[200] The condensed phase is strongly anisotropic. Since adsorption leads to the formation of a quasi-one-dimensional system, the properties of this system differ from those of standard systems.[201]

According to calculations, adsorption of small atoms occurs both inside NTs and in the intertubular space of NT bundles, whereas the adsorption of relatively large atoms and molecules with rare exceptions occurs only inside the NTs.[203] Helium atoms are strongly bound to the side walls within the intertubular space of NT bundles. The system can behave like a lattice gas or condensed phase; despite the fact that the content of the adsorbate atoms is at most 2% they contribute much more to the specific heat capacity than the 'host' molecules at low temperatures.[202] In the case of adsorption of a $^3He-^4He$ mixture the partial pressure of each component is determined by the ratio of their concentrations within NT bundles; the situation looks like adsorption is controlled by some rule similar to Raoult's law.[204]

A study on the desorption of ^4He at 14–23 K showed[205, 206] that the process can be described by the equation for one-dimensional adsorption of neutral particles with very high binding energy estimated as 330 K (at 14–16 K), which is very close to the calculated value (340 K).[200] Channels in the intertubular space of NT bundles can be represented by cylinders 0.21 nm in

diameter and their cross-sections can be filled by at most one helium atom. At temperatures above 16 K, the experimental adsorption capacity was higher than the theoretical value for unknown reasons.

The binding energies of other noble gases (neon and xenon) and CH_4 to the external surfaces of closed SWNT bundles are nearly 75% higher than to the flat graphite surface.[207, 208] However, neither of the gases can be adsorbed in the intertubular space of the NT bundles.

Enhanced adsorption of xenon inside SWNTs at 95 K in the presence of defects, especially after removal of carboxylic groups from the NT surface was observed.[87] The experimentally determined activation energy of xenon desorption (26.8 kJ mol^{-1}) was found to be close to the calculated value (22.6 kJ mol^{-1}).[198]

Experimental study of N_2 adsorption on MWNTs that were open at one end, with mesopores of width 4.0 ± 0.8 nm, at 77 K showed [209] that nitrogen molecules are adsorbed on both the external and inner NT surfaces. It was found that adsorption on the external surface is five times greater than that on the inner surface and that the corresponding adsorption isotherms are considerably different. Adsorption in mesopores was described in terms of the classical theory of capillary condensation and the calculated pore diameter was found to be 4.5 nm. The adsorption isotherms exhibited no hysteresis, in stark contrast to the curves reported by Kyotani *et al.*[210] who studied adsorption in mesoporous NTs open at both ends. These differences were rationalised by accessibility of only one NT end.

Single-walled NT bundles also readily adsorb N_2. Unpurified NTs prepared by the arc method were characterised by an inner specific surface of 233 $m^2\ g^{-1}$ and an external specific surface of 143 $m^2\ g^{-1}$ (see Ref. 211). Acid treatment of the NTs resulted in an increase in the total specific surface from 376 $m^2\ g^{-1}$ to 483 (HCl) and 429 $m^2\ g^{-1}$ (HNO_3) and enhanced the adsorption capacity towards benzene and methanol.

Adsorption of gases affects the electronic [212] and emission [213] properties of NTs. The effect of O_2 adsorption on the electronic and magnetic properties of NTs has been studied.[214]

VIII. Potential fields of application of carbon nanotubes

Increasing interest in NTs is due to great potentialities of their efficient use in industry.[2, 18, 215–219] Small size and unique structure of NTs determine their unusual mechanical and electronic properties (these can be controllably varied over a wide range). In contrast to graphite, NTs are free from dangling bonds and are therefore chemically inert. Nanotubes represent a highly rigid and, at the same time, elastic material that exhibits the ability to undergo reversible swelling (buckling up) and folding (compression, flattening).

The fields of application of NTs can be arbitrarily divided into two groups. The first group of applications utilises NTs in the form of relatively large devices or parts (many NTs 'function') such as light, strong, conducting (if necessary) and impact energy absorbing fillers for various composites, materials for chemical current sources and accumulators of gases. The second group of applications uses NTs in mini- and microcomponents and devices (individual NTs 'operate'). These are electronic components and devices including ultrasmall and ultrafast computers, cathodes for electron field emitters, indestructible nanoscale scanning microscope probes, high-frequency resonators, 'nanostraw' and nanopipettes for introduction into living cells to study their chemical nature.

1. Composites

a. Chemical composition and properties

Nanotubes can serve as ideal reinforcing fillers for composite materials with matrices of any chemical nature, *i.e.*, polymeric and inorganic (metals, ceramics). Many characteristics of NT-filled composite materials can reach record values. Of great importance is also the fact that NTs have low density. This allows one to obtain light composite materials. However, it should be kept in mind that the properties of NTs depend on their origin. For instance, the flexural rigidity of graphitised arc-grown NTs is ~ 1 TPa, which is two orders of magnitude higher than that of the NTs synthesised by chemical deposition of hydrocarbons.[220]

Development of methods for obtaining uniformly distributed and oriented fillers is a vital issue in the fabrication of filled composite materials. Nanotubes are characterised by large aspect ratios (1000 and more), which makes possible reinforcement of composite materials. At the same time, NTs are very short and therefore standard equipment for the production of polymers can be utilised. Using conventional long fibres imposes restrictions on the shape of finished products (carbon fibres are brittle). In the case of NTs these restrictions are removed since products of any shape can be produced by moulding.

Nanotubes are known to be highly rigid. They exhibit high axial strength [221] and a record value of Young's modulus, which approaches 1.25 TPa.[144] This value remains unchanged on going from SWNTs to MWNTs, since it is determined by the strength of the C–C bonds in individual shells.[222, 223] Not without reason theoretical estimates of possible mechanical properties of some composite materials were obtained assuming that the Young moduli of SWNTs (along the NTs axis) and diamond are comparable in magnitude.[224]

The tensile strength of MWNTs can be as high as 63 GPa, which is 50 to 60 times greater than that of high-quality steels (this material can be accessed *via* the Internet at URL http://wupa.wustl.edu/record/archive/2000/02-03-00/articles/nanotube.html).

The limiting pressure for NTs approaches 100 GPa. This is two orders of magnitude higher than for other fibres and allows the use of NTs for production of bullet-proof jackets, car and truck bumpers and for construction of earthquake-proof buildings.[225]

According to *ab initio* calculations, NTs can undergo plastic deformation.[226] Experimental studies of NTs confirmed the possibility of creating NT-derived accumulators of mechanical energy.[227] Compression of purified, oriented, highly crystalline SWNTs is accompanied by exceptionally large and reversible volume reduction. The properties of the NTs resemble those of an ideal flat spring. Under load the NT density increases smoothly to reach that of graphite, which was related to compression and flattening of entangled NT bundles. This phenomenon was also observed in studies of MWNTs.

A theoretical study on the strain and bending behaviour of NTs and the influence of defects on their transport properties was reported.[228]

The lack of the filler materials precluded extensive research into reinforcement of polymers by filling them with NTs. Nevertheless, pioneering experiments [229, 230] showed that design of various types of composite materials is possible. Single-walled NTs appeared to be the best fillers, since the inner shells of MWNTs are not involved in reinforcement.[231] Potential advantages and disadvantages of this type of composite materials have been discussed by Ajayan *et al.*[232]

Tensile test of an epoxy resin/MWNTs (5 mass %) composite showed that only the outer MWNT shells were loaded.[233] On the other hand, the results of compression test of the same composite indicated loading of all the MWNT shells.

Mechanical tests of composite materials [234–236] revealed that mechanical strength of the composites filled with MWNTs is an order of magnitude higher than that of materials filled with conventionally used fibres. The ultimate compression strength of NT-filled composite materials was found to be ~ 60 GPa, which is nearly two orders of magnitude higher than that of standard composites.[235]

The bonding between the matrix and filler in composite materials is known to be neither too weak nor too strong. In this respect the situation with NTs was unclear. The effect of the origin and concentration of SWNTs on their interaction with the

polymer matrix was studied taking PMMA-based composites filled with NTs as examples.[237] Mixtures with the NT content ranging from 1 to 20% were also studied.[238] It was found that at low NT concentrations (2.5% and 5%) the NT bundles remain unchanged, though one can assume that they do interact with the matrix since the Raman spectra indicate an increase in the intertubular spacings within the bundles.[238]

One of the nondestructive methods for increasing the surface energy of NTs consists in attachment of functional groups to the NT surfaces.[231] Chen *et al.*[102] studied solubilisation of NTs and showed that they can be dispersed in polymeric matrices without cutting. The bonding between NTs and matrix can also be increased by using defect NTs, though this can lead to some decrease in the strength of the composite material.

Of particular interest are conjugated polymer/NT composites. A salient feature of this class of polymers is the presence of an extended π-electron system that is due to the formation of a specific electronic structure with energy gaps 1.5 to 2.5 eV wide. Usually, these polymers exhibit low hopping conductivity. Introduction of NTs into composites must increase their conductivity, mechanical strength, thermal conductivity and resistance to optical damage. Indeed, a composite material with interesting optoelectronic properties was obtained from electroluminophor poly(*m*-phenylene vinylene-*co*-2,5-dioctyloxy-*p*-phenylene vinylene) and MWNTs.[113,114] The electrical conductivity of this material was measured to be eight orders of magnitude higher than that of the starting polymer. Polymer chains were found to wrap themselves around the NTs, thus making the composite material extremely strong and allowing the NTs to be suspended in the excess polymer solution. Introduction of low concentrations of NTs had little effect on the luminescent properties of the polymer. Moreover, it was found that NTs act as a nanoscale heat sink, thus preventing the composite material from overheating and destruction (under the action of, *e.g.*, laser beams).

Coleman *et al.*[239] studied the properties of poly(*m*-phenylene vinylene-*co*-2,5-dioctyloxy-*p*-phenylene vinylene)/NT composites with the NT content ranging from 0.5% to 36%. It is noteworthy that at low NT concentrations an increase in the NTs content is accompanied by insignificant increase in the conductivity of the composite material. At the NT concentrations in the range between 7% and 10% the conductivity of the material increases jumpwise by ten orders of magnitude and then again increases insignificantly at higher NT content. This behaviour is also typical of composites filled with other carbonaceous materials, *e.g.*, soot. It was found that charge transfer occurs between the polymer and NTs; however, the effective mobility of the charge carriers decreases. A study on the percolation character of the conductivity of composite materials was reported.[240] At low NT concentrations, no aggregation of MWNTs in the polymeric system occurs despite the weak interaction between the polymer and NTs.[241]

Single-walled NTs in conjugated polymers with hole-type conductivity can trap charge carriers.[242] Methods for preparation and fields of application of composite materials comprised of conjugated polymers and C_{60} or NTs were reviewed by Dai.[243]

Wrapping of polymer molecules around NTs was also observed by Seifert *et al.*[105] who polymerised phenylacetylene in the presence of NTs to prepare NTs that could be dissolved in organic solvents. The use of polymers for dissolution of NTs was studied by M in het Panhius *et al.*[244] Nanotube solutions can be used as optical filters while composite materials as converters of light into electricity.[245] Ago *et al.*[246] reported fabrication of photovoltaic devices based on NT-filled composites.

Raman spectroscopy provides the largest body of information in studies of the structure of novel carbon nanomaterials.[247] This method has also been successfully applied to composites. Raman spectroscopy allowed the researchers to follow tension due to load of an epoxy resin/NT composite material and to show that reinforcement with fibrous fillers is usually more pronounced than reinforcement with particles.[248] Wood *et al.*[249] identified the components responsible for the appearance of particular lines in the Raman spectrum of an SWNT-filled polymer, studied the effect of temperature on the spectral patterns, revealed the lines caused by thermal stress and established a stress–strain correlation.

Fragmentation of MWNTs in an urethane–diacrylate polymeric matrix under load has been studied[250] (the content of NTs was not reported).

Composites with NTs can be used for production of aligned NT arrays. By cutting thin slices (50–200 nm) of a composite material based on epoxy resin with random orientation of NTs one can obtain partial alignment of the NTs on the surface of the slice.[229] A more simple and efficient procedure involves the use of composite materials based on thermoplastic polymers. Aligned NT arrays can also be produced by mechanical tension on heated composite material followed by cooling under load.[251] The desired effect was observed only in the experiments with MWNTs.

Nanotube alignment by applying mechanical shear to a composite material sandwiched between two pieces of glass slides was reported by Tang and Xu.[112]

Composite materials based on NTs and polyvinyl alcohol[252] and polypyrrole[253] were prepared. An increase in the NT content to 10 mass % is accompanied by a sharp increase in the electrical conductivity. At higher NT concentrations, the increase in the conductivity is less pronounced.[252] Introduction of 1% MWNTs leads to an increase in the tensile strength and elasticity modulus of the polystyrene films by 36%–42% and ~25%, respectively.[254]

Nanotube fillers can be used for production of high-strength composite fibres, ribbons and coatings with enhanced wear resistance, which can find application in military, aerospace and automotive industries and pharmacy.

For instance, Andrews *et al.*[255] introduced SWNTs (Carbolex, USA) into fibres based on petroleum pitch. The filler was added to a hot pitch solution in quinoline, the solvent was removed and fibres containing 1 mass % or 5 mass % NTs (extrusion at higher NT concentrations becomes difficult) were extruded and carbonised at 1100 °C. Tests showed that the ~18-μm-diameter composite fibres with 5% NTs exhibited improved tensile strength, elasticity modulus and conductivity as compared to those of the unfilled fibres (by 90%, 150% and 340%, respectively).

An original method for fabrication of macroscopic composite fibres and ribbons incorporating flow-aligned SWNTs by forming a net from solution of NTs in a polymer followed by directed alignment was proposed.[256] Such fibres with regularly aligned NTs exhibit an elasticity modulus of 15 GPa, which is lower than that of free-standing NTs but much higher than that of, *e.g.*, 'nanopaper' (1 GPa). The fibres can be bent, crumpled and even knotted.

Reinforced PMMA fibres filled with oriented NTs were prepared.[257]

Two methods for production of composite materials based on commercially sold polymers and NTs have been developed.[258] To synthesise polymer-coated NTs, poly(ethylene glycol), poly(2-vinylpyridine), poly(4-vinylpyridine), poly(4-vinylphenol) or poly(ethylene oxide) were dissolved in DMF and NTs were added. To obtain polymer-grafted NTs, the NTs were mixed with a solution of $SOCl_2$ in C_6H_6, kept in N_2 atmosphere for 120 h, dried *in vacuo* and then triethylamine and poly(ethylene oxide) were added (140 °C, N_2, 48 h). Poly(ethylene oxide) was washed off with DMF. Thin films of the composite materials and NT solutions exhibited remarkable nonlinear optical properties.

Conducting NT-containing composite materials can be used in car body panels to replace metallic car bodies, since they allow spray painting by giving the spray electrostatic charge.[231] In this respect the properties of a composite material based on polyphenylene ether/polyamide mixture containing 10% NTs were found to be quite interesting and useful.[245] The conductivity of the epoxy resin increases by several orders of magnitude upon introduction

of minute amounts of NTs (merely 0.1 vol.%) and becomes higher than that measured after addition of the same amount of soot.[259]

It is assumed that lightweight composite materials will find use in the preparation for human Martian mission.[245]

Nanotubes can be used as additives to polymeric electroluminophors. Colouration of these luminophors occurs by giving them electrostatic charge, which makes possible painting of metallic rather than dielectric surfaces. It is believed that these limitations can be removed by introducing NTs as conductivity-enhancing additives into thermoplastic polymers.[240]

Research efforts aimed at creating chemoresistive sensors based on NT/polymer composites for a multichannel 'electronic nose' are being undertaken.

Sun and Crooks[260] reported the preparation of NT-filled polymeric membranes for sensing large neutral molecules.

Composite materials comprised of a dielectric matrix and conducting filler in the form of small extended particles can be used for electromagnetic shielding, in aerials, waveguides, *etc*. Nanotubes can serve as ideal fillers (http://www.sbirsttr.com/SbirMisc/alld991.htm). The introduction of SWNTs 10 nm in diameter (23 mass %) into ethyl methacrylate matrix leads to a nearly 35-fold increase in the dielectric constant of thick films at 500 MHz.[261]

At low NT concentrations (4% to 7%), composite materials based on NT-filled thermoplastic polymers can exhibit relatively high and uniform electrical conductivity (a short communication was posted in the Internet at URL http://www/rtpcompany.com/news/press/nanotube.htm).

Nanotubes coated with conducting polypyrrole represent a special class of materials.[262] They were prepared by polymerisation of pyrrole immediately on the NT surfaces. No chemical interaction between the polymer and NTs was observed; nevertheless, the modification led to pronounced changes in the properties of the NTs.

Methods for purification of NTs can employ stability of NT solutions in polymers[113,114,263] or the difference in precipitation rates between NTs and impurities in polymer solutions.[264,265] The proportion of short and thin NTs increases upon purification.[263]

A NT/crystalline C_{60} composite was prepared (see Ref. 266).

Research into metal/NT composites has been less intensive compared to studies on polymeric composite materials. Xu *et al*.[267] studied the morphology, mechanical and electric properties of NT/aluminium composites obtained by hot pressing of powder-like mixtures. Introduction of NTs leads to a slight increase in the electrical resistance of aluminium at room temperature and to a sharp drop of the resistance at 80 K. Related composites were prepared and investigated by researchers from Japan (this material can be accessed *via* the Internet at URL http://www.mrs.org/publications/jmr/jmra/1998/sep/013.html). It was found that hot pressing or hot extrusion do not damage NTs and that the NTs do not form products of chemical interaction with aluminium. In contrast to aluminium produced by powder metallurgy, mechanical properties of the aluminium/NT composites remained virtually unchanged upon annealing (873 K).

Introduction of NTs into a titanium matrix substantially increases its hardness.[268]

A composite NTs(3%)/metallic glass $Fe_{82}P_{18}$ was prepared by pressing a mixture of powdered starting components with NTs, melting and quenching of the melt on a copper wheel rotating at a linear speed of 30 m s^{-1}. Composite ribbons 40 μm thick were characterised by uniform distribution of the NTs that retained their initial structure.[269] Some of the NTs 'capped' at both ends were filled with iron alloy.

The number of studies on the composites with ceramic matrices is a little more than those concerning the composites with metallic matrices. Introduction of NTs into composites with $Bi_2Sr_2CaCu_2O_{8-\delta}$ (a Bi-2212 superconductor) has the same effect as irradiation of the Bi-2212 by heavy ions and favours an increase in the current density.[270] Nanotube composites with superconductors of other chemical composition were also studied.[271–273]

To prepare NT/Fe/Al_2O_3 composites, Laurent *et al*.[274–276] calcined amorphous solid solution $Al_{1.8}Fe_{0.2}O_3$ at 1025–1100 °C and then reduced it with a 88% H_2–12% CH_4 mixture at 1050°C. Calcination at 1100 °C resulted in the formation of a solid solution α-$Al_{2-2x}Fe_{2x}O_3$ ($x < 0.1$) and trace amounts of the Fe-enriched phase α-$Al_{2-2y}Fe_{2y}O_3$. Iron particles isolated upon reduction of this phase catalysed the growth of flattened (ribbon-like) arrays of NT bundles. It was found that homogenenous solid solution α-$Al_{1.8}Fe_{0.2}O_3$ with large specific surface area (this favours an increase in the NT yield and improves NT quality) can be obtained only at temperatures between 1025 and 1050 °C. This method results in two-walled NTs with an average inner diameter of ~2 nm as the main product. The proportion of SWNTs was nearly 20%.

The same authors reported the synthesis of powder-like NT/Co/MgO mixtures.[277]

b. Space cable

In 1910 F A Tsander put forward an idea of connecting the Earth and the Moon by a cable. More recently this idea was transformed into the concept of a transport cable connecting the Earth and a geostationary artificial satellite {for references, please visit the Internet Website at URL [http://www.isd.net/anowicki/SPBI120.HTM]**D**}. Conventional space rocket mass transportation systems would travel a predetermined length to transfer cargo and then mass transportation would be performed along the cable due to the action of centrifugal force.

However, no materials suitable for such a cable have been developed as yet. Polymers are vulnerable to space radiation while steel has too high density so a steel cable must have enormous weight. The best commercially available fibrous material based on specially prepared polyethylene fibres, 'Spectra 1000', has a characteristic length of 315 km. (Characteristic length is the maximum length of a cable that can carry its own weight). Recently, NASA's specialists returned to the idea of implementation of a space elevator using a NT-based fibre. The calculated characteristics of this fibre and other materials are listed in Table 1.

Table 1. Properties of particular fibrous materials (http://www.isd.net/anowicki/SPBI1MA.NTsM).

Material	Tensile strength /Pa	Young's modulus /GPa	Density /kg m^{-3}	Longitudinal speed of sound /m s^{-1}
Steel	1–5	200	7900	5000
Beryllium fibre	3.3	310	1870	12870
Boron fibre	3.5	400	2450	12778
Fused silica	–	73	2200	5760
Pyrex glass	–	62	2320	5170
E-Glass fibre	2.4	72.4	2540	5339
S-Glass fibre	4.5	85.5	2490	5860
Kevlar-49 (aramid fibre)	3.6	130	1440	9502
'Spectra 1000'	3.0	170	970	13239
PBO[a]	5.8	365	1580	15199
Carbon fibre	2–5	250–830	1850	11600–21200
Buckytube cable (theoretical data)	150	630	1300	22014

[a] PBO is poly(*p*-phenylene benzobisthiazole), a plastic fibre.

As can be seen, none of the other materials is comparable to the NT cable in tensile strength. The NT cable also must have the greatest characteristic length.

c. Artificial muscles †

As long ago as 1940s it was found that fibres made of polymeric gel-like materials compress in acidic solutions and extend in alkali solutions. The phenomenon can be used in practice by changing the direction of direct electric current. This idea provides the basis for the development of actuators and artificial muscles. For some time, conducting polymers were thought to be the most promising material for electrochemical actuators.[278] However, recent studies [279, 280] revealed that NTs are even more promising.

To function, most of the previously studied materials required application of a voltage of at least 30 V, whereas the operating voltage for 'nanopaper' varies from 1 and 4 V.[279, 280] The new material is characterised by a deformation (changes in linear dimensions) of $\sim 1\%$ and is capable of developing a maximum force of $\sim 3 \times 10^7$ J m^{-3} per cycle, which is about 30 times greater than the characteristics of the best ferroelectric, electrostriction and magnetostriction materials and is even greater than the force developed by human muscles. Schematic representation of the 'nanopaper' test device is shown in Fig. 9 and the relative elongation-*vs*.-voltage curve of this actuator is presented in Fig. 10.

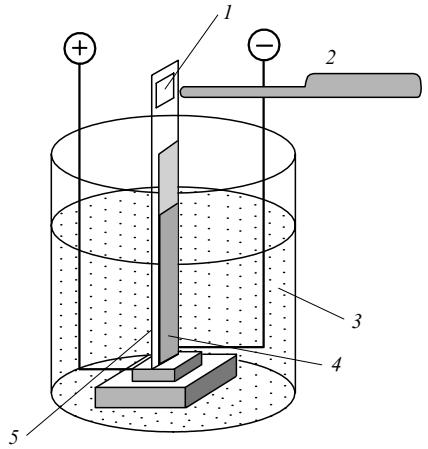

Figure 9. A scheme for a 'nanopaper' test device.
Mirror (*1*), optical sensor (*2*), electrolyte (*3*), 'nanopaper' ribbons (*4*) and insulator, a poly(vinyl chloride) film (*5*).

'Nanopaper' was studied electrochemically.[281] Samples with apparent densities of 0.30 to 0.40 g cm^{-3} containing NT bundles 1.2 to 1.4 nm in diameter were tested in various electrolytes, in the presence of both light and heavy ions, over a wide range of pH values and at different voltage scan rates. It was found that, in contrast to other forms of porous carbon, the capacity of 'nanopaper' depends only slightly on most of the parameters studied (except for the regions characterised by very low and very high pH values). Typically, the 'nanopaper' capacity varies between 18.0 and 40.7 F g^{-1} in 1.0 M NaCl solution at 0.4 V and a scan rate of 50 mV s^{-1}. These results show that pores inside the NT bundles are readily accessible to ions of different size and charge and that, at least for small samples, penetration of the electrolyte into the pores is not controlled by diffusion. The charging mechanism is described by the equation

$$\rangle C{=}O + H^+ + \bar{e} \longrightarrow \rangle COH.$$

The results obtained in these studies are of great importance for further development of not only electromechanical actuators, but also supercapacitors, sensors, *etc*.

† Information presented in this Section does not take into account the results obtained for many new chemical systems that are thought to be potentially used for the creation of artificial muscles.

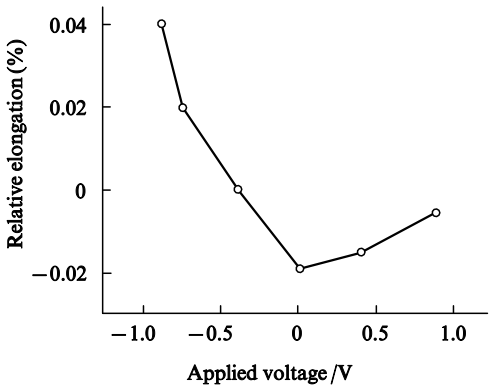

Figure 10. A relative elongation-*vs*.-voltage curve for a 'nanopaper' actuator.[279]

Che *et al*.[282] experimented with an actuator made of a 'nanostructured carbon material' (most likely, NTs).

Potential fields of application of artificial muscles cover a rather wide range from mechanical actuators that operate under severe conditions (as, *e.g*., 'windshield wipers' for space vehicles, in jet engines at 1000 °C, *etc*.) to prostheses, though the last-named task requires considerable research and development efforts and is quite time-consuming. The reverse process, *i.e*., conversion of mechanical energy into electric energy, can draw attention in the context of development of electric generators that use the energy of sea waves.

2. Fields of application of nanotubes in electronics ‡

Miniaturisation (the characteristic size of electronic chips is halved every 3 years) and improvement of performance of silicon-based electronic devices should sooner or later stop (see, *e.g*., Ref. 283). On going from micrometre (0.3 – 1.0 μm) to nanometre scale ($\sim$10 nm) electronics comes into the world of quantum effects and materials change their behaviour. Industry will make this step in the coming decade, this makes research aimed at developing new electronics vitally important.

The use of single molecules or quantum dots as functional devices can be considered the ultimate point of miniaturisation process. However, electrical contacts can hardly be attached to molecules. Therefore, the most promising candidates for practical implementation in molecular electronic devices are NTs, which can serve as the basis for creation of a new generation of integrated circuits (ICs). Search for suitable chemical substances for future electronics has been carried out since the mid-1990s. Recently, research plans were corrected and focussed on NTs.[284 – 287]

Depending on their structure, NTs possess metallic or semiconducting properties (see, *e.g*., Refs 288 and 289). For this reason alone they can be used for fabrication of heterostructures with metal – metal, metal – semiconductor and semiconductor – semiconductor junctions. In this respect particular emphasis is placed on SWNTs.

Nanotube conductivity is of quantum character.[290 – 293] Defect-free metallic NTs appeared to be ballistic conductors of electric current that flows without heat release. The current density can reach a colossal value of 10^7 A cm^{-2} and, were NTs classical conductors, they would be immediately vaporised. Ohm's law is not valid for ideal ballistic conductors, namely, their resistance is independent of length and approaches a theoretical (quantum) limit of 6500 Ω. The conductivity in NTs differs from that in two- and three-dimensional systems and can be described in the framework of the Luttinger liquid theory.[294, 295]

‡ In this Section, we present the results of selected research studies in physics and technology that are of prime interest for chemists.

Nanotube conductivity also differs from conductivity in conducting polymers where free electrons are supplied by dopants. Graphite is characterised by delocalisation of one of the four valence electrons. Graphene is an electronic hybrid; it is neither a dielectric nor a conductor, and also not a metal as well. Rather, it is a zero-gap 'semimetal' or semiconductor. Therefore, the properties of graphene depend on some extra conditions, in particular, the manner of rolling into NTs.

Of course, there is no need to discard silicon-based electronics with billion-dollars investments and start new, NTs-based electronics at the very beginning, the more so as many problems (in particular, high surface resistance of contacts, *etc*.) are still to be solved. On the other hand, production of various devices exploiting unique electronic properties of NTs that will function along with 'old' electronic is thought to be a short distance in the future. This can be a new generation of electronic and logical microchips and mechanical and electromechanical devices. Theoretically, the switching rate of NT-derived electronic devices can be as high as 10 THz. It is believed that the first step of new electronics will be fabrication of hybrid circuits. Therefore, Si-supported NTs have been the subject of intensive studies.

a. Diodes and transistors

Semiconductor diodes (two-electrode elements with one junction) and transistors (three-electrode elements with two of more junctions) are main building blocks of ICs. It is these components that first of all appeared to be the focus of research activity.

Junctions can be formed in several ways, namely, by matching two NTs (in particular, NTs of different diameters) with different electronic properties; by bending NTs; by partial filling of the inner NT cavities with those substances that give the filled parts of the NTs distinct electronic properties; by branching NTs or by making them three-terminal (Y- or T-shaped NTs). Matching two NTs with different structures requires insertion of pair defects (pentagon–heptagon) into their hexagonal atomic sheets. If the pair defects form a 'belt' along the circumference of the junction, the NTs keep their coaxial structure. If the defects are arranged opposite each other, the NTs become bent (Fig. 11). Bent NTs do exist and can be found among products of catalytic pyrolysis of hydrocarbons, as was reported by Han *et al*.[296] who observed NTs bent at angles from 18 to 34 °.

Service *et al*.[297] reported the first, theoretical, study on the subject. Insertion of pair defects into the NT structure was studied [298–302] and their energy characteristics were discussed.[303, 304]

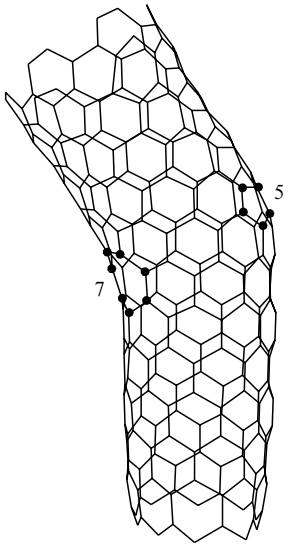

Figure 11. Schematical representation of a bent nanotube with topological defects.

Rectification of alternating electric current by a molecular diode comprised of semiconducting SWNTs and impurity molecules has been studied by Antonov and Johnson.[305] A number of theoretical studies is devoted to the properties of different junctions. [306–309] Nanotube junctions can function as Schottky barriers.

A prototype of single-electron transistor was first fabricated from SWNT bundles.[290] This type of transistor can also be assembled from free-standing NTs.[291, 310] Yao *et al*.[311] found that a bent NT with metal–semiconductor junction functions as diode rectifier. Among a total of nearly 500 NTs they found four nanotubes with one junction and one NT with two junctions and studied their current-*vs*.-voltage characteristics and the temperature dependence of conductivity.

A prototype of single-electron MWNT transistor was fabricated [312] {for references, please visit the Website at URL [http://haithabu.fy.chalmers.se/abstracts/031-html]**D**}. Researchers from Japan reported high operational characteristics of diodes based on NTs with homo- and heterojunctions.[313]

Nanotube-based field effect transistors were called TUBUFETs by analogy with the abbreviation MOSFET (Metal Oxide–Semiconductor Field-Effect Transistor).[314] Characteristics of the TUBUFET transistors fabricated from aligned SWNT arrays approach those of silicon-based MOSFET transistors. IBM Corp. (USA) also reported successful development of SWNT- and MWNT-based field effect transistors (for references, visit IBM 's Website at URL http://www.research.ibm.com/nanoscience/nanotubes.html). Researchers at IBM believe that NT-based transistors will soon be quite competitive with silicon transistors.

Junctions consisting of two crossed SWNTs (a metallic NT and a semiconducting one) were studied experimentally.[315] This type of junction can be readily fabricated and they can serve as the basis for large-scale production of useful devices.

Fabrication of integrated circuits of NTs requires enabling controlled growth and arrangement of NTs in the space between electrodes. A feature article by Dai *et al*.[316] concerns methods for the synthesis of NTs and integrated NT-based devices; particular emphasis was placed on SWNTs. The authors of this study pointed to the fact that, in contrast to traditional architectures of microelectronic devices and ICs based on the 'top–down' fabrication techniques, the methods being developed for NTs are based on the 'bottom–up' approach.

Lefebvre *et al*.[317] briefly outlined different techniques for fabrication of ICs incorporating SWNTs. Using electron beam lithography and nanomanipulation with an AFM, they showed the possibility of fabricating diodes, devices with junctions between matched individual SWNTs, single-electron transistors and field effect transistors. This study seems to be the first communication that concerns the effect of chemical environment, *i.e*., the adsorbate molecules, on the characteristics of electronic devices, since adsorption can change the electronic properties of substances when fabricating nanometre size NT-based devices. Mention was also made of the effect of mechanical deformation on the functional properties of NTs.

Very recently, strong limitations on the use of NTs in electronic devices were found.[318] They are due to specific noise that appears as electric current flows through NTs. Impurities adsorbed on the external surface of NTs are thought to be the source of the noise (or one of the noise sources). If so, NTs will enable production of very sensitive sensors.[319] Noise reduction can be achieved by simply cleaning the NT surfaces.

In a continuation of their research [318] Collins *et al*.[320] studied the effect of O_2 impurity on the electrical conductivity and thermal emf of NT bundles and films. It was found that adsorption of O_2 (i) changes the *n*-type conductivity of the NTs to *p*-type conductivity, (ii) increases the NT conductivity by 10% to 15% as compared to the value in vacuum and (iii) changes the thermal emf from -10 to $+20\,\mathrm{mV\ K^{-1}}$.

Model calculations predict that bonding of O_2 molecules to SWNTs will affect their electronic and magnetic properties.[214]

Electronic devices can be fabricated by controlled deposition of individual SWNTs with attached CO_2H groups through a mask on the surface that was chemically pre-functionalised with NH_2 groups.[118] Another closely related technique [321] involves plasma etching prior to the adsorption of functionalised NTs. Both procedures allow a space resolution of several micrometres.

Schematic representation of a chemical process of fabrication of integrated circuits incorporating nanotubes by pyrolysis of CH_4 on a Fe–Mo catalyst patterned by electron beam lithography is shown in Fig. 12.[322] Recent developments in this field allow fabrication of metal–horizontally aligned NT arrays–metal structures [323] or three-dimensional Si–vertically aligned NT arrays–metal aggregates [324] on silicon substrates using lithography and chemical vapour deposition.

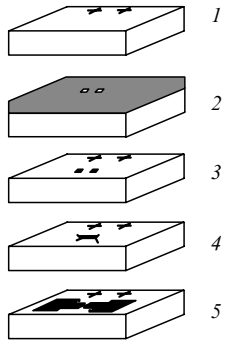

Figure 12. A scheme illustrating the order of operations in the production of integrated circuits with embedded nanotubes.[322]
Patterning with Ti–Al alloy (*1*), coating with PMMA with Petri dishes (*2*), catalyst deposition on the Petri dishes and dissolution of PMMA (*3*), chemical vapour deposition of nanotubes by catalytic pyrolysis of CH_4 (*4*) and coating with metallic electrodes (*5*).

Tests for the best ohmic contact between NTs and metallic electrodes were carried out with Ag, Al, Au, Ca, Cr, Mg, Nb, Ni and Ti.[316] The lowest contact resistance was found for titanium. One can also use Sc and V in addition to Ti, whereas Fe, Co, Ni and Cu exhibit high contact resistance.[325] A procedure for improving the stability of contacts with Ti–Al electrodes involves short-term (30 s) heating at 600–800 °C.[326] Special research into MWNT-based electrical contacts carried out to develop a fabrication procedure resulted in a rather simple method consisting in placing a tungsten wire 4.3 μm in diameter (a shadow mask) crosswise on the MWNTs, deposition of a conducting layer and removal of the wire.[327]

Since chemical methods for fabrication of NT-based devices are currently in a primitive state of development, the problem of manipulating NTs is usually solved by using scanning probe microscopes.[312, 313, 328]

Some rather exotic types of NTs have been studied. Molecular dynamics simulation revealed the possibility of fabricating metal–semiconductor–metal junctions in three-terminal NTs taking T-shaped [329] and Y-shaped [330] NTs as examples. Electronic properties of these systems were also studied theoretically.[331–333]

Branched NTs (a mixture of Y-, T- and L-shaped NTs) were first obtained in low yield by the arc method.[334] Formation of Y-shaped NTs in the course of hot wire activated CVD synthesis of diamond was reported.[335]

Higher yields of this type of NTs can be obtained by other methods, *e.g.*, CVD in the course of pyrolysis of hydrocarbons [336–338] and transition metal catalysed decomposition of C_{60}.[339] Branched NTs were also obtained by pyrolysis of acetylene followed by deposition on an Al_2O_3 template with electrochemically etched, Y-shaped channels, which was dissolved after completion of the process.[336] Microwave plasma enhanced pyrolysis of CH_4 diluted with H_2 was catalysed by nanocrystalline Pd on the surface of porous silicon.[337]

Yet another procedure for the synthesis of Y-shaped NTs involves pyrolysis of a gaseous nickelocene–thiophene mixture at 1000°C.[338] The yield of ~40 nm-diameter, Y-shaped NTs with an angle of nearly 90° between the junctions was as high as 70%. Asymmetry of the current-*vs*.-voltage curves of these NTs with respect to the bias current points to the fact that the NTs function as rectifiers. These synthetic results were found outstanding.[340]

A chlorophyll-containing protein in spinach is capable of not only receiving photons of light, but also transmitting electric signals in one direction at a rate 100 times faster than in silicon photodiodes. A nanodiode 10 nm long was fabricated from the molecules of this protein. Using 2-mercaptoethanol, the protein molecules were oriented perpendicular to the surface of a gold support and then connected by NTs to give a biomolecular device. This biochip was first demonstrated in spring 1999. Illumination by a pulse of light caused the device to conduct an electric current {this material can be accessed *via* the Internet at URL [http://www.ornl.gov/ORNLReview/rev32_3/brave.htm]**D**}.

b. Field emission devices

Cathode-ray tubes (CRT) with hot-cathode electron sources appeared more than 50 years ago. Now it is timely to replace CRT by compact flat panel displays with field (or tunnel) emitters.[341, 342] Field emission, *i.e.*, the emission of electrons from highly curved surfaces (tips, blades, *etc*.) under influence of an applied voltage, is usually observed only in ultrahigh vacuum at high voltages and the emission current is limited to several μA. Fabrication of field emitters is complicated and expensive since tips are made of single-crystalline silicon or diamond pyramids. However, these devices offer some clearly seen advantages over the hot-cathode sources, such as operation in the cold emission regime, small size, small energy expenditure in the operating mode and high density of the emission current. Because of this, field emitters have been the subject of intensive current research. For instance, it was found that ~7 μm-diameter carbon fibres used as field emitters operate under somewhat lower vacuum than other materials do (see, *e.g.*, Ref. 343).

Graphite is characterised by a relatively high work function of electrons (4.4 eV) and many graphite-based materials (in particular, micro-coarse, powder-like, ion-irradiated graphite) can be used for fabrication of field emitter cathodes. However, all of them have a great drawback consisting in rapid degradation under operating conditions. Nanotubes were proposed to be used as field emitters based on similarity of the field emission mechanisms from graphite materials and NTs.[344] Large aspect ratio, small radius of curvature of the NT end, high electrical and thermal conductivity and chemical stability of NTs make them promising for field emission applications. Not only individual NTs, but also NT bundles can serve as field emitters and function in moderate vacuum.

Schematic representation of an NT-based field emitter is shown in Fig. 13.[345]

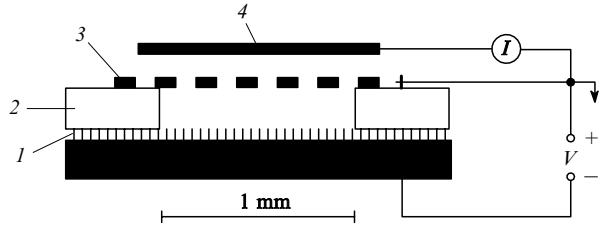

Figure 13. A scheme of a nanotube-based field emitter.
A film comprised of nanotube arrays grown perpendicular to the support surface (*1*), insulator (mica) (*2*), grid (*3*) and anode (*4*).

Let us consider the properties of NTs as field emitters. For purified MWNTs, the work function for electrons is 4.3 eV and increases up to 4.8 eV on oxidation of the NT surface.[346] The work function for NT-containing films is much lower than for graphite, though it depends on the film surface relief.[347]

Pioneering experimental studies of the emission properties of NTs were carried out by Chernozatonskii *et al*.[348] in the Russian Federation and by Ugarte *et al*.[349, 350] (in Western countries) who fabricated NT-based field emitters. An NT-based cathode can have a surface area of up to several hundreds of square centimetres, it is cheap and stable in air. However, the procedure for fabrication of aligned NT arrays (suspension, filtering and fixation of precipitate) proposed by Ugarte *et al*.[349, 350] was found to be too complicated to be used in large-scale production.

Nanotubes are characterised by emission current densities of up to 10 mA cm^{-2} at a rather low gate electric field (0.8 V μm^{-1}).[351, 352] The gate fields for SWNTs are lower than for MWNTs; however, the latter have longer lifetimes.[353]

Both open and closed NTs can emit electrons. The effect of opening of the NT ends on the emission properties has been studied.[354] Free-standing MWNTs 10 to 15 nm in diameter were produced by arc method and opened by oxidation in air at 650 °C or by laser ablation. It was found that (i) opening of NTs enhances field emission and (ii) opening by oxidation in air is more efficient than laser ablation. In their short review Schonenberger and Forro [222] pointed out that closed NTs are more efficient emitters. Theoretically, open NTs must produce higher emission currents than closed NTs; however, impurities (*e.g*., oxygen atoms) attach themselves to the free dangling bonds at the end of the NT and the emission current reduces. Nevertheless, in both cases the emission current reaches colossal values for such small-size emitters. Emitters based on aligned arrays of 'capped' MWNT were found to exhibit the most reproducible properties and the longest lifetimes.

Nanotubes operating in the field electron emission mode emit light.[355, 356] In a dark room, the glow can be seen by the naked eye. This phenomenon is of great importance for understanding the emission mechanism.

Nanotubes produced by different methods and having different structures possess markedly different emission properties (Table 2).[357]

Table 2. Average field amplification coefficients (β), trigger and threshold electric field strengths (E_t and E_{thr} /V μm^{-1}) and average NT lifecycles (τ /h) at a current density of 0.2 mA cm^{-2} for different NT samples.

NT	β	E_t	E_{thr}	τ
Multi-walled nanotubes				
open	1100	4.5	30	20
closed	1600	1.1	2.2	120
catalytic	830	5.6	14	10
Single-walled nanotubes	3400	1.5	3.9	12.9

Kim *et al*.[359] fabricated field emitters with improved characteristics (β = 17 000 – 33 000, $E_t \leqslant 1.0$ V μm^{-1}, the brightness of the green phosphor was 1800 cd m^{-2}) using highly dense (5 – 10 μm^{-1}), well-aligned NT arrays. Diamond-'capped' silicon whiskers are characterised by record values of the turn-on (E_t) and threshold (E_{thr}) fields; however, parameters of the best samples of NT-based field emitters approach them.[358]

Characteristics of field emitters are closely related to the methods and conditions for the synthesis and purification of NTs.[44, 360] Experiments with NTs grown by plasma-assisted CVD showed that the emission current can change by an order of magnitude upon variation of the procedure for coating the catalyst (at different substrate – solution contact times).[361]

Information reported in studies on the field emission from NTs is often contradictory and the mechanism of the process is still to be clarified. The limiting field emission currents differ by orders of magnitude. Some contradictions were eliminated by Dean and Chalamala [213] who showed that saturation of the emission current is due to the presence of adsorbed impurities (the effect of saturation is observed at voltages between 1600 and 1800 V and leads to deviation of the emission currents by 2 to 4 orders of magnitude from that expected from the Fowler – Nordheim theory) . On the one hand, the presence of impurities favours an increase in the emission current. On the other hand, the impurities are removed as the emission current increases and after some time the dependence follows another pattern. Predesorption of impurities by heating samples *in vacuo* eliminates the saturation effect and reduces the emission current.

Electron energy distribution for emitting *n*-Si-supported SWNTs has been studied.[362] The observed current densities were as high as 25 mA cm^{-2}. The emitter appeared to be stable with time and exhibited well-reproducible properties. A similar study on SWNT bundles was carried out.[363]

Emission from NT bundles gives a bright structureless spot on a phosphor screen. Unexpectedly, emission from a free-standing NT with an open end gave a conical spot. The cone angles were estimated at $\sim$0.2 rad for the external and 0.05 rad for the internal parts of the cone.[364, 365]

Field emitters can also be fabricated from entangled NT arrays. The emission current density achieved in experiments with a material incorporating randomly oriented NTs (according to Collins and Zettl,[353] this favours elimination of defects) was as high as 400 mA cm^{-2} at 200 V. Cathodes for field emitters can be fabricated from NTs sintered under mild conditions (2273 K, 25 MPa).[366]

Dai and Mau [367] discussed some of the known methods for fabrication of aligned NTs. These methods can be arbitrarily divided into two groups. The first group comprises two-step procedures that involve individual stages of NT synthesis and alignment , namely, the above-mentioned cutting of thin composite slices,[229, 368] passage of a NT dispersion through a microporous filter [350] and rubbing a NT-coated plastic surface with a thin Teflon plate or Al foil.[349]

The second group comprises one-step methods that involve synthesis-induced alignment of NTs and are of much greater importance. These are template synthesis using microporous substrates and synthesis with patterned catalyst coated on the substrate surface (possible patterns are strips, squares, *etc*). Usually, experiments are carried out using Al_2O_3 membranes with parallel pores obtained by anodisation of Al, mesoporous SiO_2 and porous silicon as microporous substrates. The catalyst is either deposited on the bottom of micropores by CVD or sputtered onto the substrate surfaces that were pre-treated by lithography or programmed etching. Precipitation of catalyst from solutions is also used.

Fabrication of ordered structures from NTs by thermal decomposition of silicon carbide represents a special case.[369, 370]

Nanotube synthesis using porous Al_2O_3 has been described [129, 350, 371 – 375] (some of these studies do not concern fabrication of field emitters). The diameter, length and degree of ordering of NT arrays are completely determined by the properties of the template and can be varied over a rather wide range. Synthesis of NTs using mesoporous SiO_2 has also been reported.[376 – 378]

Fan *et al*.[379] succeeded in growing a 'forest' of NTs with uniform length distribution on the surface of porous n^+-Si substrate with an area of $\sim$4 cm^2 by catalytic pyrolysis of C_2H_4. Catalytic iron particles were deposited on the silicon surface through a shadow mask. It is thought that this method can be applied to larger surface areas (Fig. 14). The MWNT 'forest' was grown perpendicular to the substrate and presented regularly arranged, square (2 × 2 μm) NT arrays, or towers, of the same height varied in the range from 10 to 240 μm. Each of the 15 samples fabricated by the authors of this study [379] exhibited stable low-voltage electron emission. Considerable advantages of

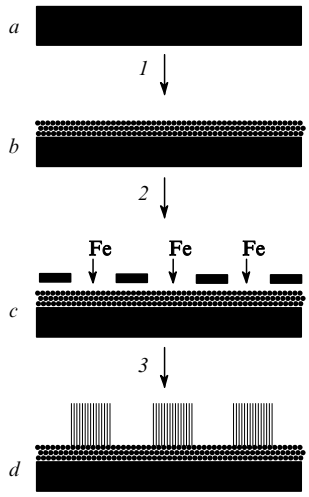

Figure 14. A scheme illustrating the process of fabrication of aligned NT layers on the surface of porous silicon.
Anodisation (*1*), sputtering of iron (*2*) and growth of NTs (*3*); n^+-silicon (*a*), porous silicon (*b*), mask (*c*) and product (*d*).

porous silicon in the synthesis of oriented NTs were pointed out. (A special issue of the journal '*Physica Status Solidi A*'[380] was dedicated to the preparation, properties and applications of porous silicon). The substrate surface can be patterned with the catalyst either lithographically or by vaporising a fraction of pre-coated catalyst.

Fabrication of field emitters from SWNTs is a more complicated problem. Nevertheless, the use of pyrolytic method and substrates patterned with 1 to 5 μm wide catalytic islands resulted in the synthesis of NTs that were 0.7 to 4.0 nm in diameter and bridged adjacent islands.[322, 381, 382] A special procedure was developed for the deposition of NTs on top of Si 'towers' pre-coated with catalyst using a contact printing technique.[383] The NT structures obtained resembled power lines with suspended SWNT bridges.

Related NT structures of some larger size were fabricated by researchers from the Russian Federation. Nanotubes for field emitters were grown by catalytic pyrolysis of acetone or by disproportionation of CO on silicon whiskers.[384]

Enhanced performance of acetylene pyrolysis and an increase in the surface area for NT deposition can be achieved by patterning the substrate with the catalyst using microcontact printing technique.[385] Experiments were carried out using hydrophilised polydimethylsiloxane as 'stamp' and solutions of iron, cobalt and nickel nitrates or their mixtures in ethanol as 'ink'. The method allows one to obtain NT strips $\sim$10 μm wide, grow NTs 5 to 15 μm high and control the NT density on the surfaces.

Fabrication of NT structures by pyrolysis of hydrocarbons in the presence of volatile catalyst or by pyrolysis of the chemical NT precursors containing both the carbon source and metal catalyst [386–390] represents a special case. [To some extent, decomposition of a $Fe(CO)_5-C_2H_2$ mixture [391] also falls in this category].

There are two ways for fabricating NT structures on thermally unstable substrates, in particular, polymeric materials. These are transfer of the precipitate obtained on thermally stable materials to polymer and reduction of the pyrolysis temperature by introducing particular additives into the chemical composition of the starting gas mixture followed by physical activation of the process. For instance, pyrolysis of C_2H_2 in excess NH_3 allowed NT deposition immediately on the low-melting glass.[392, 393]

Polymeric substrates are coated with NT 'forests' using NT deposition on quartz glass followed by dissolution of the substrate and oriented transfer of the precipitate.[321, 388]

Hot filament activated pyrolytic synthesis of NTs on different substrates was developed by researchers from France.[394] By varying the reaction conditions they grew carbon nanostructures with different morphologies and emission characteristics. It was shown that a coral-like material containing NTs and nanoparticles with reasonable emission properties can be deposited immediately on the glass surface.

Catalytic pyrolysis was used for NT deposition from gaseous hydrocarbons and fabrication of field emitters from entangled randomly oriented NTs on large surface areas.[395]

Emission characteristics of oriented NTs grown by glow discharge method from a CH_4-H_2 mixture were studied by researchers from Moscow and Novosibirsk, Russian Federation {this material can be accessed *via* the Internet at URL http://carbon.phys.msu.su/MRS/Mrs.htm]**D**}.

Emission properties of an NT 'forests' grown pyrolytically from C_2H_2 on oxidised Si surfaces coated with nickel, cobalt or a nickel–cobalt alloy were reported.[396–400]

Swiss researchers grew NTs on a silicon substrate and showed that field emission is observed without preliminary treatment of the deposited film and even in the presence of catalyst.[401] The work function for electrons was estimated to be 5.3 eV.

Field emitters are produced in the USA, Japan, Russian Federation, Australia, in EC and South-East Asia. It was shown that NT-based field emitters can exhibit improved technological characteristics (density of emission current, gate voltage, brightness and lifetime) compared to analogous devices made of other materials and hot-cathode emitters. For instance, experiments at the Oak Ridge National Laboratory (USA) showed that NT-based field emitters are 10 times more efficient than diamond ones {this material can be accessed *via* the Internet at URL [http://www.ornl.gov/ORNLReview/rev32_3/brave.htm]**D**}.

MWNT-Based cathode tubes for elements of large-area outdoor displays were produced in Japan.[402–404] The tube diameter and length were 20 and 74 mm, respectively. The devices exhibited stable electron emission and long lifetimes (continuous glow over a period of 3 months). Their brightness was twice as high as that of conventional hot-cathode devices.

The results of research into NT-based field emitters for CRT displays and light sources carried out in Japan were reviewed by Saito and Uemura.[405]

A flat plane display with a brightness of up to 800 cd cm^{-2} at 5 V μm^{-1} was fabricated in Taiwan.[406] A method for fabrication of field emitters from SWNT bundles was developed by researchers from the PR China.[407]

Nanotubes represent a new kind of goods on the world market. The emission properties of commercially sold SWNTs and MWNTs were studied by Monteiro *et al.*[408]

An SWNT-based display 11.4 cm in diagonal with a brightness of 1800 cd cm^{-2} was fabricated (see Ref. 409). In 1998 and 1999, Ulvac Japan Ltd. and ISE Electronics Corp. (both from Japan) and Samsung Corp. (South Korea) demonstrated elements of CRT and prototypes of MWNT-based displays (these materials can be accessed *via* the Internet at URLs http://www.jnmr.com/intro/nanotubes.html and http://www.itron-ise.co.jp/english/nano/). In the late 1999, ISE Electronics Corp. had test-produced these display devices (this material can be accessed *via* the Internet at URL http://www.jnmr.com/intro/nanotubes.html). Research at Samsung Advanced Institute of Technology led to development of an NT-based 9 inch colour flat panel display with a resolution of 576 × 242 lines (this material was presented by J M Kim at the American Physical Society Conference in March 2000 and can also be accessed *via* the Internet at URLs http://www.eps.org/aps/meet/MAR00/baps/abs/S2090003.html and http://fuji.stanford.edu/seminars/spring00/slides/kimSlides.html). Samsung Corp. plans to start commercial production of NT-based colour displays in 2001–2002.

Large-scale industrial production of NT-based displays requires solving two major problems, *viz*., to make NTs cheaper

and to develop methods for fabrication of large-area NT-based emitting surfaces with uniform nanotube characteristics.

Nanotube-based field emitters can find applications not only in flat panel displays, but also in production of light sources, in such devices as vacuum pressure probes, microtriodes, klystrons, *etc*.

c. Memory devices

No NT-based memory devices have been fabricated so far. Nevertheless, some proposals that NTs can be used for this purpose have been made. Such memory elements can consist of, *e.g*., $K@C_{60}^{+}$ complex encapsulated into short, closed 1.4 nm-diameter (10,10)-NTs (any other alkali metal can be used instead of K). The $K@C_{60}^{+}$ 'molecule' can change the equilibrium position from the 'bit 0' to the 'bit 1' ends of the capsule under the action of an electric current. The time taken to reach the opposite end of the NT is only 4 ps, which is ten times shorter than the switching time of conventionally used memory elements.[410] The system resembles a kind of nanoscale 'abacus' or a nanoscale 'shuttle'. The authors of this study[410] have discussed some approaches to large-scale fabrication of these structures; however, solving this problem faces great difficulties at present.

Nanotube structures with encapsulated neutral C_{60} molecules (nanoscale 'peapods')[31] are formed by cyclic raising and lowering the temperature. The yield of these structures can be increased by varying the reaction conditions.[33] It was stated that this method allows mass production of the nanoscale 'peapods'.[34]

Prospects for fabrication of NT-based memory devices for molecular computers have been outlined.[411] Memory arrays built of NTs are expected to store 10 000 to 30 000 times larger amounts of information and operate 1000 to 10 000 times faster than modern memory chips.

d. Nanolithography

Currently, intensive research has been carried out into fabrication of semiconductor devices with a characteristic size of 100 nm and less. Optical lithography using sources of short-wave UV radiation (λ = 193 nm) is limited by the lack of optically transparent materials at wavelengths shorter than 190 nm. This requires development of alternative methods for nanoscopic etching that use, *e.g*., a new type of microscope probes.

The invent of scanning tunnelling microscope (STM) dates back to the early 1980s. The AFM, which is based on measurement of the adhesive force, is known since 1986. Usually, the STMs provide better resolution than the AFMs which are capable of operating without conducting substrate. The invention of the STM and AFM offered the possibility of manipulating individual atoms and molecules and moving them nanometre-scale distances.[412–420] The greatest drawback of both types of instrument consists in frequent metallic probe tip 'crashes' with the surface. The probe lifetime can be extended by using a carbon NT attached to the end of a silicon cantilever as the probe tip.[421]

Molecular dynamics simulations demonstrated that diamond surface can be selectively etched using an NT tip with attached C_2 groups.[422] It was concluded that NTs with the unmodified ends with strong covalent C–C bonds can be used for atomic-scale etching of semiconductor surfaces with relatively weak bonds (*e.g*., Si and Ge). Another simulations performed by the same method revealed the possibility of nanoscale etching and indentation of the Si(001) surface using NT ends (this material can be accessed *via* the Internet at URL http://www.foresight.org/Conferences/MNTs6/Papers/Dzegilenko/).

Local anodisation of hydrogenated Si(100) surface and lithographic transfer of silicon dioxide in the form of lines 10 nm wide at a speed of $\sim$0.5 mm s^{-1} in the experiments with an AFM equipped with a MWNT probe tip were reported.[423] The lithographic writing speed achieved using the MWNT probe tip was 5 times higher than with other probes. It was shown that the NT tips present a solution to the tip-wear problem and are impervious to breakdown in high electric field. Theoretical foundations of the method were considered.

Nanoscale lithography experiments with polysilane films using an STM equipped with an NT probe tip showed that the NT tip provides higher resolution, larger groove depth-to-width ratio at higher scanning speeds and extended tip lifetime than the probe tips made of other materials.[424]

Impressive experiments were carried out on the manipulation and deposition of individual atoms on a surface using the STM probe tip[425,426] and the possibility of atomic-level modification of nanostructures was shown.[415] This gave an impetus to the study by Král and Tománek[427] who tried to eliminate the major drawback of modern STM, that is, manipulation of a single atom. They theoretically substantiated the possibility of design of a 'molecular pump'. Open NTs serve as ideal material for such a 'pump'. The atoms filling the inner cavities of NTs can be pumped through the NTs by irradiating with two pulsed lasers.

New lithographic methods are expected to provide fabrication of ICs with the circuit density 8 times higher and performance 16 times higher than those of the ICs produced using optical lithography technique by 2004.

e. Amplifiers and generators for cell phone communication

Using the ability of NTs to emit electrons upon application of relatively low voltages (this requires small energy expenditures but the current density remains high), researchers from the North Carolina University (USA) developed an NT-based microwave generator.[428] This property of NTs can find applications in wireless communication devices. Usually, cell phones generate weak signals that are amplified at a central office. Unique properties of NTs allow production of the central offices characterised by smaller size and longer service life. A prototype of such central office has been developed.

The property of NTs to change their electric characteristics under the action of mechanical stress was proposed for use in a new generation of phones.[428]

f. Other applications

Tsukagoshi *et al*.[429] obtained rather encouraging results concerning the use of NTs for design of electron spin devices. Injection of spin-polarised electrons into MWNTs resulted in coherent electron spin transport.

Nanotubes have unusually high thermal conductivity which approaches or even reaches some record values.[430–433] This suggests the possibility of using NTs as heat sink for ICs and electric motors (this material can be accessed *via* the Internet at URL http://composite.about.com/industry/composite/library/PR/2000/blupenn1.htm). According to model calculations,[430] individual nanotubes in NT bundles interact with one another rather weakly and thermal vibrations occur solely along the NT axis.

Prospects for design of an NT-based molecular-scale digital computer and a new chemical approach to production of ICs have been discussed (this material can be accessed *via* the Internet at URL http://marble.he.net/~foresite/Conferences/MNT7/Abstracts/Ellenbogen2/index.html).

To reduce the size of electrical contacts in future ultraminiature ICs and electromechanical nanosystems, researchers at ORNL proposed to replace the wires and pins by NTs placed both on and off the chip. It is assumed that carbon NTs outside the chip will communicate with the on-chip NTs through field-emitted electron beams (this material can be accessed *via* the Internet at URL http://www.ornl.gov/ORNLReview/rev32_3/brave.htm).

Nanotube-based electrodes can find efficient application in gas-discharge tube protector units which are used in telecom network interface device boxes and central office switching gears to provide protection from lightning and AC power cross faults. Tests showed that characteristics of experimental NT-based gas-discharge tubes (mean DC breakdown voltage and breakdown

reliability) were better than those of commercial products (this material can be accessed *via* the Internet at URL http://www.eps.org/aps/meet/MAR00/baps/abs/S4890/html; communication M10.003).

3. Fields of application of nanotubes in power engineering

a. Lithium batteries

Research on current sources with high specific (per unit mass and unit volume) energy capacity is an important avenue of development of 'small' power engineering. Here, the most widely used are lithium current sources in which lithium is intercalated into graphite or other carbon materials (see, *e.g.*, Ref. 434). Nearly immediately after their discovery, fullerenes appeared to be the subject of intensive studies in this field. This also holds for NTs. If the capacity of graphite is limited to one lithium atom per six carbon atoms, the capacity of NT bundles must be higher, since lithium atoms can fill both the intertubular space of the NT bundles and the inner cavities of individual NTs. According to *ab initio* calculations, the content of lithium in SWNT bundles can be much higher than in graphite and correspond to the composition LiC_2.[435]

Intercalation of lithium and other alkali metals follows the same pattern and is accompanied by charge transfer without structural distortions. Single-walled NTs recovering their initial structure after de-intercalation similarly to NT bundles seem to be of greatest interest for the use in rechargeable batteries.[174]

Single-walled NT bundles were intercalated with Li not only by vapour transport, but also electrochemically.[178,436] The limiting intercalation degree corresponded to the composition $Li_{1.7}C_6$, which is much higher than the ideal value for graphite and that determined for MWNTs (LiC_6).[437–439] The irreversible specific capacity was as high as 952 mA h g^{-1}. The reversible specific capacity was measured to be 447 mA h g^{-1}; however, it reduced to 237 mA h g^{-1} and lower after fifth charge–discharge cycle. For comparison, the reversible capacity of lithium cells with graphite electrodes lies between 280 and 330 mA h g^{-1} (see Ref. 434).

As a rule, electrochemical intercalation of lithium into SWNT bundles is performed using a pressed NT mat placed on a platinum plate as the working electrode and a 1 M $LiAsF_6$ solution in ethylene carbonate and diethyl carbonate (1 : 1) as electrolyte.

Heat treatment of NTs improves their texture and reduces the oxidation–reduction overvoltage difference but has a drawback consisting in reduction of capacity.

High intercalation degrees (up to $Li_{2.7}C_6$) were achieved using impact grinding pre-treatment of purified SWNTs followed by electrochemical intercalation in 1 M $LiClO_4$ solution in a mixture of ethylene carbonate and dimethyl carbonate taken in equal volumes.[161] Mechanical treatment for some time resulted in the loss of ordering of the NT bundles and in an increase in the average intertubular spacing. However, the mechanism of such a strong enhancement of the NT capacity to lithium remains unclear. Most likely, the metal atoms fill not only the intertubular space, but also the inner cavities of NTs.[161]

The metal content in the product can be increased by increasing pressure.[440] Intercalation of lithium into NTs at high pressures resulted in a material with the atomic ratio Li : C = 2. The NTs retained their structure and the lattice parameter along the *c* axis increased to 0.411 nm.[441]

Another method involves coating of NTs with copper, their oxidation in air for 12 h at 160 °C and subsequent electrochemical intercalation with lithium.[442] Carbon NTs obtained in this manner can reversibly store the amount of lithium (per gramme of carbon) corresponding to a capacity of 700 mA h (*cf.* 268 mA h per gramme of CuO for composites). Intercalation of lithium into and deintercalation from CuO require applying a voltage ranging from 1.7 to 1.0 V and from 2.3 to 2.5 V, respectively (*vs.* lithium electrode). The reactions proceed by the following mechanism

$$CuO + x\bar{e} + x\,Li \longrightarrow CuOLi_x.$$

Yet another, relatively recently proposed route to enhancement of the capacity of lithium current sources consists in the use of membranes with vertically aligned NT arrays as anodes. (The NTs were prepared by template synthesis followed by removal of the template, as shown in Fig. 2). Che *et al.*[374] used a 60 μm thick Al_2O_3 template with 200 nm pores. Nanotubes were deposited within the pores. The NTs were held together by the thin layer of carbon precipitate formed on the external surface of the template. Multistage treatment of the product followed by dissolution of the Al_2O_3 template resulted in a pure carbon NT membrane consisting of the NTs of relatively large diameter which replicated the structure of the template. The inner cavities of this membrane were filled with iron catalyst (from solution), the CVD procedure was repeated to obtain thin helical NTs inside the large-diameter NTs and then the system was electrochemically intercalated with lithium. It was found that the well-developed membrane surface allowed the capacity to lithium to be nearly doubled as compared to that of a membrane without 'internal' NTs.

The use of NTs in lithium current sources is thought to be promising. Recently fabricated SWNT- and MWNT-based Li anodes are characterised by a discharge capacity of 640 and 385 mA h g^{-1}, respectively, which is much higher than the parameters of industrially produced samples.

b. Hydrogen accumulators

The development of lightweight and safe systems for H_2 storage is necessary for wide use of highly efficient H_2–air fuel elements in, *e.g.*, transportation vehicles. According to calculations, for a car with rechargeable hydrogen 'reservoir' to travel 500 km, 3.1 kg of H_2 is required. To this end, the 'reservoir' must have a capacity of 62 kg m^{-3} and the concentration of H_2 in the hydrogen-saturated material must be at least 6.5% (these values represent the U.S. Department of Energy targets for hydrogen storage for fuel cell vehicles). Hydrogen fuel is more environmentally safe than hydrocarbon fuel, since the only combustion products are water vapour. For long, industry looked to hydride-forming metals and alloys as the basis for high-capacity and safe H_2 storage systems.[443] On the other hand, a number of studies on the use of fibrous and tubular forms of carbon and SWNTs has been published recently.[444–449]

The first experimental data on the hydrogen sorption on NTs were reported by Dillon *et al.*[444] in 1997. In studies of temperature-programmed desorption of H_2 from a material containing only 0.1% of SWNTs 1.2 nm in diameter and obtained by arc method in the presence of Co catalyst using the Siverts apparatus, they inferred that the adsorption capacity of nanotubes to hydrogen varies between 5 mass % and 10 mass % or 20 kg m^{-3} at −140 °C and 40 kPa. Since the measurements were performed for unpurified material, the authors had to make a far-reaching extrapolation to NTs of purity 99%, so the results obtained can hardly be considered precise. It was found that the adsorption capacity of NTs 2.0 nm in diameter (up to 50 kg m^{-3}) approaches the desired characteristics (Fig. 15).

Ye *et al.*[450] studied pristine SWNTs and found that hydrogen adsorption on the NTs was 8.25 mass % at 80 K and a pressure of 12 MPa. Single-walled NTs were prepared by laser-induced thermal synthesis in the presence of catalysts. Individual NTs were 1.3 nm while NT bundles were 6 to 12 nm in diameter. The specific surface area of the material was 285 m^2 g^{-1}. At pressures above 4 MPa, the SWNT material undergoes a transition to a new state of hydrogen coverage. Here, adsorption occurs not only on the external surfaces of the NT bundles, but also on the surface of individual NTs (according to calculations, the specific surface area of the NTs was 1600 m^2 g^{-1}). The cohesive energy of the SWNT bundles was estimated at 4.5 meV per carbon atom. The behaviour of sonicated material differs from that of the untreated material.

Bacsa *et al.*[451] prepared NTs with a specific surface area of 790 m^2 g^{-1} and suggested even higher adsorption capacity of their material.

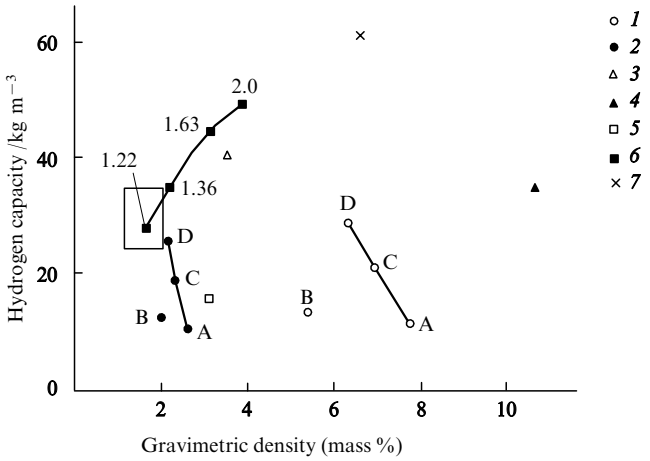

Figure 15. Characteristics of different materials as hydrogen accumulators.[444]
H_2 in the C/polymer composite cylinders at different pressures (*1*), H_2 in the glass fibre/Al composite cylinders at different pressures (*2*), H_2 produced in the reaction of Fe with H_2O (*3*), liquefied H_2 (*4*), H_2 on activated carbon (*5*), H_2 in SWNTs (figures denote the nanotube diameters given in nm) (*6*) and the region of desired parameters (*7*). The region of metal hydrides is shown within a rectangle. Pressure /MPa: 20 (A), 24.8 (B), 40 (C) and 60 (D).

Table 3. H_2 Storage properties of various systems.

Material	Max. mass % H_2	T/K	P /MPa	Ref.
Single-walled NTs (low purity)	5–10	133	0.040	444
Single-walled NTs (high purity)	8.25	80	7.18	450
Single-walled NTs (50% mass pure)	4.2	300	10–12	449
Nanofibres (tubular)	11.25	298	11.35	446
Nanofibres (herringbone)	67.55	298	11.35	446
Nanofibres (platelet)	53.68	298	11.35	446
No structure given	0.4	298–773	0.101	447
Graphite	4.52	298	11.35	446
Li–NTs	20.0	473–673	0.101	447
Li–graphite	14.0	473–673	0.101	447
K–NTs	14.0	<313	0.101	447
K–graphite	5.0	<313	0.101	447
FeTi–H	<2.0	>263	2.5	455
NiMg–H	<4.0	>523	2.5	456
Sorbent saturated at low temperature	~5	~77	2.0	456
Octane gasoline [a]	17.3	>233	0.1	456

[a] Given for comparison.

Single-walled NTs of relatively large diameter (1.85 nm) were synthesised by the arc technique. The reaction was performed in an apparatus with a rotating 400 mm-diameter cylindrical anode with drilled radial openings filled with graphite powder and a catalyst.[448] To obtain cheaper NTs, the synthesis was carried out in a H_2–Ar rather than H_2–He mixture using S-containing additives. Nanotubes were produced at a rate of several grammes per hour.

Specially treated NTs 1.85 nm in diameter can store up to 4.2% of H_2 with respect to their own mass (the atomic ratio H : C = 0.52) at room temperature and a pressure of 10 MPa. It was found that ~80% H_2 can be desorbed and room temperature at atmospheric pressure. Complete desorption of H_2 requires some heating of the material.[449] The samples under study were pre-annealed at 773 K for 2 h, which favoured enhancement of the adsorption capacity. The capacity was nearly unchanged after four charge–discharge cycles. The NT content in the material was varied between 50% and 60%, so its purification was suggested to result in considerable enhancement of the adsorption capacity.

Chen *et al.*[447] reported sensational results, according to which lithium-doped MWNTs can adsorb up to 20% of H_2 with respect to their own mass over a period of 2 h at 380 °C while the adsorption capacity of potassium-doped MWNTs can be as high as 14% at room temperature. According to calculations, a 20% adsorption corresponds to 3 hydrogen atoms per carbon atom while the fuel necessary for a car to travel 500 km can be stored in a 18 litres 'reservoir' of carbon NTs (this material can be accessed *via* the Internet at URL http://www.nus.edu.sg/INTsRO/newsletters/issue_20/CurrRes.htm). The results obtained by Chen *et al.*[447] were considered doubtful.[452] Indeed, attempts at reproducing these results using NTs produced by the same methods inferred that such a large increase in mass was due to the presence of water vapour in H_2.[453] Alkali metals do enhance the adsorption capacity of NTs, but to a much lesser extent than was reported by Chen *et al.*[447]

Great interest was attracted to the study by Rodriguez *et al.*[446] who synthesised graphite fibres capable of storing up to 67% of their own mass of H_2, which corresponds to a H : C ratio of 24. These results met initially with wide spread scepticism, since no experimental details were reported. Park *et al.*[454] to some extent clarified the situation. Unusual behaviour of the fibres was related to their structure with a specific surface area of 1000 $m^2\ g^{-1}$ and specific volumes of microscopic and macroscopic pores of 0.36 and 0.41 $m^2\ g^{-1}$, respectively. However, this issue requires further investigations.

The data listed in Table 3 characterise the hydrogen storage properties of NTs and other hydrogen accumulators and the state-of-the-art in this field.

Hydrogen storage in NTs was reviewed by Fischer[457] and Tarasov *et al.*[458]

Electrochemical storage of hydrogen in unpurified MWNTs 2 to 15 nm in diameter and SWNTs 0.7 to 1.2 nm in diameter was studied.[459] Relatively reliable results were obtained only in the experiments with SWNTs whose specific energy capacity was found to be rather high (110 mA h g^{-1}, or 0.39%). The reaction proceeded reversibly.

Electrodes with open SWNTs provided reversible electrochemical charging of up to 2.9 mass % of hydrogen, which corresponds to a specific energy capacity of up to 800 mA h g^{-1} (see Ref. 460). As the charge current changed from 10 to 100 mA, the capacity changed only by 50 mA h g^{-1}. This differs NTs from metal hydrides whose specific capacities are strongly dependent on the charge current. The maximum specific capacity was achieved after 20 charge–discharge cycles and was kept constant for the next nearly 50 cycles.

A large number of theoretical studies on H_2 adsorption has been published. Most of them were cited by Park *et al.*[454] Pederson and Broughton[461] were the first to propose that NTs can be filled with gas molecules due to the action of capillary forces.

The results of model calculations of H_2 adsorption[199] differ appreciably from experimental data. Insignificance of quantum effects at temperatures above 50 K and low hydrogen coverages of the NT surfaces was pointed out. The calculated storage capacities were found to be lower than those obtained from gravimetric measurements.[462–464]

Hydrogen adsorption in SWNT bundles was calculated.[465] The bundles consisted of square arrays of SWNTs 0.7 to 1.96 nm in diameter with an intertubular spacing of 0.334 nm. The effect of variation of the intertubular spacing on the NT storage capacity was studied taking 1.174-nm-diameter NTs as an example. It was shown that the highest H_2 storage capacity at room temperature

(10.7 kg m^{-3}) is achieved at an intertubular spacing of 0.7 nm. However, the manner in which the intertubular spacing in the NT bundles can be changed remains unclear.

The possibility of electrochemical storage of H_2 in SWNTs was confirmed by Lee *et al.*[466,467] who also performed a theoretical study of the process. Several adsorption sites in and on the SWNTs were found. According to Raman spectroscopy data, the inner NT cavities are filled with H_2 molecules. Molecular dynamics simulations showed that the highest hydrogen storage capacity of (10,10)-NTs is 14.3 mass % (160 kg H_2 m^{-3}) and increases linearly with the NT diameter. Multi-walled NTs exhibit a lower hydrogen storage capacity. In this case, hydrogen is adsorbed on the external MWNT surfaces and their capacity is independent of diameter.

Based on the above-mentioned experimental results, yet another group of theoretical studies was carried out. For instance, it was found that the desired 62 kg m^{-3} capacity (3.1 kg of H_2) of the NT 'reservoir' at 77 K can be achieved using SWNTs 0.6 nm in diameter at an intertubular spacing greater than 1.0 nm. Nanotubes carrying an electric charge were predicted to exhibit an enhanced hydrogen storage capacity (by 10% to 20% at 298 K and by 15% to 30% at 77 K).[468]

Williams and Eklund[469] attempted to bridge the gap between the results of theoretical and experimental studies. They pointed to the fact that all calculations performed so far used a model of infinite three-dimensional SWNT crystal lattice, whereas electron microscopy data show that SWNT bundles form a close-packed triangular 'honeycomb' lattice and have finite diameters and length. Mention was also made of inadequacy of the approach relating enhanced adsorption to arbitrarily changed symmetry or increased intertubular space.

c. Electrolytic capacitors

Thin NT films coated on metallic surfaces are of considerable practical interest for production of supercapacitors characterised by high capacity and the ability to survive a large number of charge–discharge cycles. The capacity of capacitors with an electrical double layer is known to increase linearly with the specific surface area that is rather large in the case of NTs (more than 300 m^2 g^{-1}).[470] In addition, it is important to use low-resistance electrode materials and to know the resistance of the electrolyte in the porous electrode structure. Carbon or graphite provide no possibility for fabrication of highly porous, 'mat'-like electrodes, which is necessary for obtaining an optimum pore structure; however, this can be readily done using NTs. The specific capacitance of catalytically grown NTs of size $\sim$8.0 nm in 38% H_2SO_4 reaches 102 and 49 F g^{-1} at 1 and 100 Hz, respectively. A single cell device had a power density exceeding 8000 W kg^{-1} (see Ref. 471).

Cyclic voltammetry measurements[472] revealed an effective capacitance of 283 F g^{-1} at 0.5 V (*vs.* silver reference electrode), which is twice as large as the maximum value for carbon electrodes in non-aqueous media (120 F g^{-1}). The material was stable on potential cycling and no differences were observed after continuous cycles over 30 min at 50 mV s^{-1}.

Capacitors with NT block electrodes and specific capacitance of 90 F g^{-1} were produced.[473]

Nanotube-derived capacitors can be used for laser power supplies, wrist watches, flash lamps, starters for electric motors, *etc.* They can also find military applications in, *e.g.*, bird- or insect-size reconnaissance airborne vehicles.[470]

4. Fields of application of nanotubes in analytical instruments

a. Sensors

Single-walled NTs are rather sensitive to gas atmosphere and can change their electrical resistance and thermal emf upon adsorption of N_2 or He.[212] This was the starting point for work on an 'electronic nose', or a chemical gas sensor.

SWNT-Based chemical NO_2 and NH_3 sensors are characterised by extremely short response time, thus being different from conventionally used sensors.[474] The sensitivity of the new sensors is three orders of magnitude higher than that of standard solid-state devices. A 0.02% concentration of NO_2 increases the electrical conductivity by 3 orders of magnitude after 10 s exposure, while exposure to 1% NH_3 decreases it by two orders of magnitude after 2 min. To reset the new sensors, they must be heated because of the low relaxation rate at room temperature. These sensors are very small (their size does not exceed several micrometres), simple in design (an NT connecting two conductors), cheap and operate at room temperature. A CO_2 sensor has been developed (this material can be accessed *via* the Internet at URL http://www.newscientist.com/ns/19991225/newsstory13.html). It should be mentioned that providing the possibility of sensing particular gases in complex mixtures selectively remains a moot question.

Nanotubes are thought to be of use for development of miniature sensors that each soldier might carry to detect poison gas or biological weapons (this material can be accessed *via* the Internet at URL http://www.post-gazette.com/healthscience/1999101nanotubes1.asp).

Frequency shift in the Raman spectra upon immersion of SWNTs in various liquids can find practical application in the development of sensors to test liquids. The frequency shift magnitude depends on the surface tension of a particular liquid, which can be used for the determination of its chemical composition.[249,475]

Construction and characteristics of items fabricated from individual MWNTs were reported.[476] Nanotubes 80 to 120 nm in diameter and 15 to 50 μm long were attached to a platinum tip using conducting epoxy resin. The NT side walls were insulated with polyphenol. Cyclic voltammograms measured at different electrode immersion depths in electrolyte solutions were obtained.

Nanotubes can be used as electrode material.[477] Redox-proteins immobilised on the surface and inside NTs exhibited well reproducible cyclic voltammograms. Immobilisation of DNA treated with I_2 and $[Pt(NH_3)_2]^{2+}$ and other proteins on NTs was also carried out.[478]

The possibility of attachment of metal porphyrins (including enzymes) to NTs allows fabrication of biosensors for studying different biomolecules and other biological objects. In particular, a proposal was made that NTs can be used as microelectrodes for the determination of glucose and cholesterol concentrations. The use of NTs can lead to basic change in the blood count procedure, so a drop will be enough to perform complete blood count over a very short time. The results reported by Balavoine *et al.*[479] who obtained ordered helical shells of protein molecules on the NT surfaces can be considered as the first step towards the development of new biosensors.

b. Microscope probes

Usually, STM probes are made of tungsten or platinum while AFM cantilevers are made of silicon or Si_3N_4. Typically, the radius of curvature of the AFM cantilever tips varies between tens and hundreds of Ångström. The use of NTs as probe tips was first reported by Dai *et al.*[421] who attached SWNTs to a pyramidal silicon cantilever, tested the device and obtained encouraging results. The use of chemically inert, conducting, hydrophobic, thin and flexible NTs makes the research process more simple; allows penetration into narrow grooves; improves resolution and provides the possibility of performing non-destructive studies of delicate biological objects.

A detailed instruction for attachment of NTs to commercial STM probes was posted on the Internet at URL {[http://cnst.rice.edu/mount.html]**D**}.

Nanotube growth immediately on commercial STM probes by pyrolysis of hydrocarbons was reported.[480–483] This method is considered to be much more simple than attachment of arc-grown NTs. Yet another technique consists in attachment of NTs in an electric field.[484–486] However, the simplest and most closely related to large-scale production conditions method[487] involves

a combination of (i) CVD of NTs on a special cartridge by catalytic pyrolysis [384] and (ii) transfer of the grown NT from the cartridge to the microscope probe tip in an electric field.

The properties of 'capped' NTs as materials for tunnelling microscope probes have been described by Harrison *et al.*[488] The radius of curvature of an SWNT probe tip is 3 to 6 nm (sometimes, even 0.2 to 0.5 nm), which is several times smaller than for conventional probe tips.[489]

Using an AFM with an NT probe tip, Choi *et al.*[490] obtained images of individual NTs on mica surface, while Zha *et al.*[491] studied chromium-filled NTs with an STM.[491]

Wong *et al.*[89, 90, 92, 492] oxidised NTs in air at 700 °C (98% of the carbon material was burnt out), functionalised their tips with carboxylic groups and obtained world's first chemically sensitive probe microscope capable of analysing different substances at the molecular and atomic levels. Then they performed amino, hydrocarbon and bioactive functionalisation of the carboxy-modified probe tips by the formation of chemical bonds between CO_2^- groups and one of the amino groups of ethylenediamine molecule, amide bonds with benzylamine molecule and amide bonds with biotin derivatives, respectively. The first (carboxy-functionalised), second and third probe tips possessed acidic, basic and hydrophobic properties, respectively. The fourth probe tip was sensitive to streptavidine. In principle, CO_2^- groups can form bonds with a broad spectrum of functional groups, which allows fabrication of probe tips for various applications.

Wong's 'constructions' exhibit some advantages over the previously used probes. The point is that earlier functionalisation of the Si_3N_4 or SiO_2 cantilevers resulted in attachment of functional groups not only to the tip, but also to the side walls, which damaged the objects under study. In contrast to this, no damages were observed in the experiments with NT tips since the functional groups were attached only to the 'cap'. In addition, NT probes are characterised by small effective radius and provide higher resolution. Finally, 1.4-nm-diameter (10,10)-NTs contain only 20 atoms at the open end, so it is an easy matter to choose the conditions for fabrication of a probe tip functionalised with a single group with known structure and orientation even at random distribution of the NTs with different number of carboxylic groups at the end.

Specifically functionalised NT probe tips can be used for selective removal of atoms from the surface.

Probe microscopes were used to obtain the first images of DNA molecules.[489] Microscopes with NT probe tips allow shortening the time taken to analyse large DNA molecules.[493]

Atomic force microscopes with NT probe tips were used for the determination of the structure of protein complexes [494] and for manipulating DNA molecules. At particular voltages, the DNA molecules were adsorbed on NTs and arranged on their surfaces in a predetermined manner (this material can be accessed *via* the Internet at URL http://www.eps.org/aps/meet/MAR00/baps/abs/S4890/html; communication M10.010). A well-resolved image of right-hand helical DNA molecule has been reported.[495]

Nanotube-modified cantilevers allow improving the resolution of electrostatic force microscopes.[496]

Improved AFMs with NT probe tips can be used in studies of both rigid and soft surfaces in aqueous solutions. According to recent predictions, these microscopes will serve as the basis for a breakthrough in biological studies.[497]

Nanotube probe tips can also be used as the 'reading' probes in memory storage devices of supercomputers. A possible candidate would be a system consisting of layering H and F atoms on a diamond surface and a pyridine molecule attached to the probe tip end. Theoretically, the system can store 10^{15} bytes cm^{-3} (this material can be accessed *via* the Internet at URL http://www.msu.edu/~hungerf9/nanotube.html).

5. Nanotubes as catalyst and sorbent supports

The idea of using NTs as catalyst supports was proposed nearly immediately after the discovery of this form of carbon.[498, 499] This application of NTs is based on their chemical stability and well-developed surface. Catalysts can be obtained by the filling of the inner cavities of NTs or in the course of their decoration or, in particular, in the course of the NT synthesis.

Only one study concerning SWNTs was cited in a short review on the application of fullerenes and NTs as catalyst supports.[500] After long-term storage in hydrogen at 673 K a material grown by arc method in the presence of cobalt and platinum exhibited high selectivity in the liquid-phase hydrogenation of cinnamaldehyde.[501]

Multi-walled NTs were also studied as catalyst supports. A Ru catalyst coated on arc-grown MWNTs with a specific surface area of 27 $m^2\ g^{-1}$ allowed an increase in the yield of hydrocinnamic alcohol obtained by hydrogenation of cinnamaldehyde to 80%. It was found that reduction selectivity increased from 30% – 40% to 92%.[502] A nanotube-supported rhodium catalyst was found to be efficient in the thermal decomposition reaction.[503] Complete decomposition of NO occurs at 600 °C on NTs without catalyst, at 450 °C on NTs containing 1 mass % Rh and at 300 °C on the catalyst pre-treated with H_2 at 300 °C or higher temperatures. After 2 h exposure to NO at 500 °C the Al_2O_3 – Rh (1%) catalyst contained rhodium only in the form of Rh_2O_3, while the NTs – Rh catalyst contained metallic Rh (8 nm particles).

The efficiency of different supports was compared taking the reaction of catalytic hydroformylation of propene as an example.[133] It was found that MWNT-supported ruthenium phosphine complex is not only much more active than other supports, but also exhibits high regioselectivity towards butyraldehyde (the reaction product) despite relatively small specific surface areas (155 and 237 $m^2\ g^{-1}$) and pore volume (0.46 and 1.33 $cm^3\ g^{-1}$) and relatively small pore diameter (3.2 – 3.6 and 2.4 – 3.2 nm) of the MWNTs used. Nanotubes were compared with supports characterised by much larger specific surface area (up to 1210 $m^2\ g^{-1}$, a carbon molecular sieve TDX-601), larger pore volume (up to 1.66 $cm^3\ g^{-1}$, a polymeric support GDX-102), and a larger (20 – 100 nm, GDX-102) or smaller pore diameter (1.4 – 2.0 nm, activated carbon).

Efficient catalysts were obtained by filling the inner cavities of the above-mentioned carbon membranes (see Section VIII.3.a) [374] with catalytically active metals. For instance, solution-coated platinum enhanced the rate of electrocatalytic reduction of O_2, while a Pt – Ru mixture enhanced the reduction of CH_3OH, which means that these catalysts are promising to be used for fuel elements. A study of the electrocatalytic reduction of dissolved O_2 using NTs showed that the exchange current density in the H_2SO_4 solution (pH 2) was five times higher than in the reaction carried out on graphite. This suggests possible use of NTs in fuel batteries.[504]

The rates of electrochemical processes occurring at platinum- and ruthenium-coated NT electrodes are higher than at platinated glass electrodes.

'Nanohorns', a recently found kind of NTs, appeared to be an excellent adsorbent of liquid ethanol. (The properties of 'nanohorns' were studied by Murata *et al.*[505]). The oxygen adsorption capacity of 'nanohorns' is 3.5 times higher than that of other forms of carbon with the largest specific surface area.[506] Moreover, 'nanohorns' catalyse oxidation of ethanol into acetaldehyde.

6. Application of nanotubes in optical devices

Molecules with high third-order optical nonlinearity and second-order hyperpolarisability are considered promising for use in photonic devices, *e.g.*, optical switches, data processing systems, optical filters and sensors. However, most of the third-order nonlinear optical materials have low second-order hyperpolarisability. Exotic electronic structure of NTs allowed researchers to hope for their application in nonlinear optical devices.

A theoretical model for SWNTs was proposed by Xie.[507 – 511] who also reported a third-order optical nonlinearity in chiral carbon NTs.[512] Chiral NTs as nonlinear optical materials are

quite competitive with conducting polymers. Large nonlinear optical effects are typical of zigzag and B-(N-)doped NTs.[513]

Second-order hyperpolarisability of NTs was predicted.[514, 515] The optical properties of NTs are strongly affected by the NT symmetry, the presence or absence of the 'cap' and the number of constituent carbon atoms.[516]

A theoretical expression for the third-order nonlinear optical susceptibility of NTs, related to the third harmonic generation, was derived by Margulis *et al.*[517] who pointed out that the resonant optical susceptibility of NTs is several orders of magnitude higher than that of C_{60} or C_{70}.

The properties of SWNTs 1.3 nm in diameter and ~ 160 nm long in a DMF solution were studied.[518] The ultrafast second-order hyperpolarisability was estimated at 2.1×10^{-28} esu.

Absorbing cells filled with a suspension of SWNTs in water were used as protection from laser radiation.[519] The effect of optical limitation was observed at 1064 and 532 nm. It was found that an increase in the radiation intensity by three orders of magnitude can reduce the optical transparency by two orders of magnitude.

Due to their unique properties, SWNTs rank first as nonlinear optical switches among all the materials used in this field, though the mechanism of the phenomenon is still to be clarified. Studies on the optical limitation of SWNT suspensions in water, ethanol and ethylene glycol showed that the magnitude of the effect can differ substantially in different liquids.[520]

Multi-walled NTs also exhibit remarkable nonlinear optical properties[258, 521, 522] that are comparable with those of soot and C_{60} suspensions. This type of NTs combines the advantages of both soot and C_{60}. Similarly to soot particles, NTs are relatively large. Similarly to fullerenes, NTs can be readily modified by, *e.g.*, filling to acquire desired optical properties.

Third-order optical nonlinearity of MWNTs was measured experimentally.[523] However, more recently it was found that incorrect experimental design led to observation of unusually high and unstable nonlinear optical response.

Nanotubes are poorly soluble; however, their composites with polymeric matrices can be used for protection from laser radiation. Laser irradiated solutions of NT solubilised in poly(phenylacetylene) exhibited unusual behaviour, *viz.*, they turned opaque with an increase in the radiation intensity.[112] Nanotube additives preclude optical damage to the polymer even at such high fluences as 10 J cm^{-2}.

Soluble complexes of MWNTs with polyacrylic acid and surfactants exhibit nonlinear optical properties.[121]

Dispersions of NTs in ethanol can be used for alignment of NTs under the action of electric current; they possess anisotropic properties and can change the direction of polarisation of the incident laser beam.[524] Conclusions drawn by the authors of this study deserve further confirmations, since all the measurements were carried out using insufficiently purified material.

Nanotube-containing composites can find application in photoelectric (photovoltaic) devices and light emitting diodes (LEDs).[113, 114, 246] Filling conjugated polymers with fullerenes was shown to be promising in the early 1990s. More recently, NTs became the subject of research. For instance, attempts at fabricating LEDs with microfiltration-aligned NT layer have been undertaken. However, the method involving preparation of an NT film by centrifugation and subsequent coating of the NT film with a poly(*p*-phenylene vinylene) film led to the best results.[246] Multi-walled NTs on the surface of polymer films somewhat reduce photoluminescence. The efficiency of NTs as hole-collecting electrodes of photovoltaic devices appeared to be twice as large as that of standard indium–tin oxide electrodes (the quantum yield at 2.9 to 3.2 eV was 1.8%).

Thin films of this composite can be used as emitting layer of LEDs and glow at lower current densities compared to the untreated polymer.[113]

7. Molecular nanotechnology

Nanotechnology is a field in which unique properties of NTs can best be used. Molecular nanotechnology concerns fabrication of functional structures and devices by atom-by-atom or molecule-by-molecule assembling using programmed robots (assemblers) capable of self-replication. According to calculations, the mass of an assembler equipped with a molecular computer and actuator can be at most 10^9 amu (this material can be accessed *via* the Internet at URL http://www.public.iastate.edu/~bhein/FAQ.html). The assembly will occur consistent with the chemical laws; however, under conditions of 'position' synthesis, where an atom or a molecule is supplied exactly to the place, these laws act in another manner compared to conventional chemical reactions conditions; if necessary, the overcoming of activation barriers can be achieved by consuming mechanical energy supplied from outside.

After the invention of STM and AFM, molecular nanotechnology is no longer only a scientific concept. There remains only some disagreement about how long its development will take {[this material can be accessed *via* the Internet at URLs http://www.nanomedicine.Com/2.1.html]**D**, .../2.2.html]**D**, .../2.3.html]**D** and .../2.4.html]**D**}.

In 1998, Zivex LLC (USA) demonstrated the possibility of three-dimensional manipulating NTs inside a scanning electron microscope with a resolution approaching that of the scanning probe microscopes and near real-time video control. The development of this manipulator and especially its improvement to provide the possibility of simultaneous operation of several independent manipulators inside one microscope is a great stride in the development of nanotechnology.

Probe microscopes allow one to manipulate NTs and move ('push around') molecules over the surface. Using a 'nanoplotter', one can draw lines up to 30 nm wide. However, these devices have a strongly confined action range.

New possibilities for manipulating nanoscale objects and studying their properties are opened after the development of the scanning probe microscope with 'nanotweezers', that is, two tiny plates of gold separated by a thin glass layer and attached to the tips of 100-nm-diameter NTs.[525] By applying an electric field it is possible to close and open the NTs and to grab and move submicrometre-size clusters and nanowires. Nanotubes of smaller diameter should make it possible to manipulate objects only 2 nm in size, *i.e.*, single molecules and structures inside biological cells, thus modifying them.

Initially, the greatest interest of experts in nanotechnology was attracted to various organic substances, especially a number of products of biosynthesis. It is assumed that molecular computers will be the first commercial fruit of the development of nanotechnology {this material can be accessed *via* the Internet at URL [http://www.resonance-pub.com/e-print%201.htm]**D**}. Currently, more definite hopes are associated with fullerenes and especially NTs. In particular, severe requirements imposed on the chemical and thermal stability of structural elements of molecular machines for aerospace industry make the use of NTs for fabrication of these elements justified.

Experts at NASA's Research Center (Ames, USA) also point out that NT-based nanotechnology can provide a way to reduce the cost of space missions.[526–529]

Bearings, springs and gears are important components of future nanomechanical systems. Their development is one of the main research avenues.

In 1992, benzene was found to react with C_{60} by the 2,4-cycloaddition mechanism. According to calculations (1997), such reactions on the external side walls of NTs are possible. That is why one of the pioneering studies on the development of NT-based nanomechanical devices was concerned with molecular dynamics simulation of a NT-based gear with benzene gear teeth {see Ref. 530 and material posted on the Internet at URLs [http://www.nas.nasa.gov/Groups/Nanotechnology/publications/MGMS_EC1/simulation/]**D** and [...MGM_EC1/quantum/index.

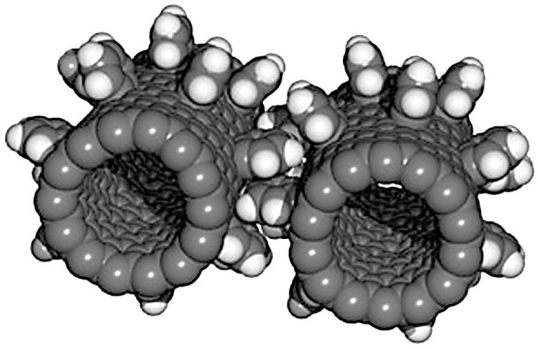

Figure 16. A nanotube gear with attached C_6H_6 molecules.

html]**D**}. Calculations were carried out for systems containing up to 2000 atoms. The angular momentum was transferred *via* two (14,0)-NTs 1.1 nm in diameter (Fig. 16). According to calculations, the gear could operate at frequencies up to 100 GHz *in vacuo* at room temperature. More recently, systems comprised of hundreds of thousands of atoms were calculated.

Other types of molecular gears were also calculated (this material can be accessed *via* the Internet at URLs http://www.nas.nasa.gov/Groups/Nanotechnology/publications/MGMS_EC1/simulation/paper.html and ...MGMS_EC1/index.html) and the behaviour of molecular devices in helium and neon atmosphere was studied. A phenomenological model of a laser-driven molecular motor was studied. The motor supplied power to a nanotube gear.[531]

Several video clips and animations illustrating the operation of various nano-gear devices can be accessed *via* the Internet at URL http://science.nas.nasa.gov/Groups/Nanotechnology/publications/MGMS_EC1/simulation/data/index.html.

Calculations of gears consisting of internal and external NTs were carried out. A concept of fullerene motor consisting of two concentric graphite cylinders (a shaft and a clutch) was proposed.

Possible conditions for coaxial arrangement of two NTs of different diameter (10 carbon atoms around the circumference of the shaft and 30 or 34 atoms around the circumference of the clutch) were calculated.[532]

Pioneering experimental studies attracted considerable attention. A team from the California University at Berkeley (USA) and Lawrence National laboratory (Berkeley, USA) managed to elongate MWNTs by pulling out the inner shells and then to shorten them by reducing the force exerted.[533] No indications of the 'nanospring' fatigue or wear were observed after 10 to 20 in/out cycles. The author of a popular essay on the subject predicts a passage from microelectromechanical systems that are on the scale of a human hair to nanoelectromechanical systems (NEMS) that are so small that 10 000 bearings for such systems can be stretched across the diameter of a human hair (this material can be accessed *via* the Internet at URL http://www.berkeley.edu/news/media/releases/2000/07/27_nano.html). According to expert evaluations, these systems will be developed in the nearest two years. At first, these will be hand-made devices and then some methods for their mass production are expected to be developed.

Based on the results of their studies on the behaviour of MWNTs under load, Yu *et al.*[534–536] pulled out inner shells of MWNT using an AFM and estimated the magnitudes of forces that act in this system. The proposed model of the process included the shear interaction, a specific type of 'capillary' effect (an interaction between two solids) and boundary effect (the influence of dangling bonds at the end of the inner NT 'immersed' in the outer shell).

The development of NT-based nanotechnology is associated with the breakthrough studies on nanolithography,[423] development of 'nano-fountain pen',[427] fabrication of functionalised probe tips and theoretical investigation of selective removal of hydrogen atoms from diamond surface.[422]

A rather large number of communications on NTs were reported at the 8th Conference on molecular nanotechnology held in the USA in November 2000 and called 'foresight'. In particular, new results were obtained on the character of conductivity in the 'arm-chair' NTs (http://www.foresight.org/Conferences/MNTs8/Abstracts/White/index.html); on the possibility of fabricating all-carbon electronic devices (.../Fuhrer/index.html); on the application of SWNTs of different chemical compositions (including metal-doped NTs) for fabrication of ICs (.../Darsey/index.html); on the stability of composite (cluster-type) structural elements made of NTs and diamond; on the possibility of fabricating heterojunctions for nanoscale logical and memory devices and NT-based field emitters 'capped' with diamond (.../Shenderova2/index.html); on theoretically studied gas separation processes using NTs and on the effect of NT filling with gases and C_{60} molecules on the mechanical properties of the NTs (.../Sinnott/index.html); on the thermodynamic properties of polyatomic liquids inside NTs and on the stability of NTs in aqueous solutions (.../Walther/index.html); on the quantum-mechanically studied effect of the surface curvature on the reactivity of NTs and fullerenes (.../Srivastava/index.html).

A recently published short review 'Carbon nanotubes. From macromolecules towards nanotechnology' [537] contains almost no information on applications of NTs in nanotechnology.

IX. Conclusion

Nanotube chemistry becomes a rather large division of general chemistry. Currently, it includes inorganic, colloid, polymer, physical and analytical chemistry of nanotubes (analytical chemistry of NTs also includes sensorics, the subject of which is development of chemical and biochemical sensors). Nanotube chemistry is closely related to nanotube physics, materials science and quantum chemistry. Some problems of NT chemistry are common to electronics and photonics.

Nanotube chemistry is also related to biochemistry. Some of the potential fields of application of NTs in biology were pointed out by Guo *et al.*[478] These are vessels for pharmaceuticals, biomimetic systems, which simulate biological objects and processes, catalysts prepared from immobilised enzymes, sensors, selective electrodes, biomolecule sensors, *etc*.

Studies on NT filling with various compounds can lead to applications of NTs as specific type of chemical reactors. One can expect that chemical reactions in the NT cavities will proceed in a significantly different manner compared to processes that are on different scale, since even such phenomena as melting of crystals and crystallisation of liquids or glasses inside NTs are characterised by some salient features.[538–540]

Nanotube chemistry is expected to become an integral part of nanotechnology which undergoes rapid development. Close relation between methods for fabrication of devices incorporating NT-derived elements and nanotube chemistry is also evident. Many applied research avenues have demands for NTs with uniform structure and size, and require chemical modification of NTs, *etc*.

Nanotubes continue to surprise researchers by their unusual properties. Among new discoveries are, *e.g.*, the superconductor proximity effect (a change in the electronic properties of a conventional conductor in the immediate vicinity of a superconductor);[541] superconductivity in $\sim$1-nm-diameter NTs at 4 K; magnetic flux trapping by a MWNT 'forest';[542] and oriented growth of SWNTs prepared by catalytic pyrolysis of CH_4 on the surface of single-crystalline Si.[543] For instance, NTs grown on the Si surface are oriented parallel to the surface in two perpendicular directions for Si(100) and in three directions at angles of 60° for Si(111). Probably, in the future this discovery will allow simplification of the fabrication process of hybrid NT structures and devices based on them.

However, the period when the results of almost all studies on NTs were considered fundamentally important (or at least of great importance) and when the search for new methods for the NT synthesis and the studies of their properties were the focus of research activity is now over. The focus of current research has been applied studies.

On the other hand, the synthesis of NTs with reproducible properties is still a challenge. For instance, a semi-continuous setup with a rotating anode for the arc synthesis of NTs has been reported;[448] an installation with rotating cathode for preparation of NTs under microgravitation conditions has been developed,[544] a method for continuous preparation of NTs using an arc immersed in liquid nitrogen was proposed,[545] a technique for the preparation of mostly two-walled NTs was developed;[546] and the performance of the setups for production of NTs by laser-induced thermal synthesis was improved and is now as high as 20 g per 24 h.

New synthetic approaches were developed. These are synthesis of NTs under hydrothermal conditions,[547] by exposure of a mixture of graphite and iron nanoparticles to atomic hydrogen,[548] by irradiation of amorphous carbon (fly ash) with Ar ions (this material can be accessed *via* the Internet at URL http://www.jnmr.com/intro/nanotubes.html) and thermal decomposition of aminoazines (in the presence of catalysts)[549] and saccharose.[550] A plasma jet method for the preparation of NTs was tested.[551] A joint team from Osaka Gas Co. (Japan) and Laboratory for New Technology developed a new technique for the synthesis of NTs, based on electron irradiation of a solid residue obtained by decomposition of fluorocarbons. This method allows the obtaining of a product containing $\sim$50% of SWNTs. The process requires the use of powerful electron accelerators and is expected to be readily scaled up (this material can be accessed *via* the Internet at URLs http://www.jnmr.com/intro/nanotubes.html and http://www.kippo.or.jp/news/1998-e/0617.htm).

Researchers from the Russian Federation were involved in the R&D of a method for the preparation of NTs by vaporisation of carbon at gas mixture pressures up to 1300 atm,[552] while researchers from Belorussia undertook considerable efforts aimed at developing the synthesis of NTs at temperatures below room temperature.[553]

However, the greatest advances were made in the preparation of NTs by the pyrolytic method, in particular, by decomposition of CO. The most remarkable is the development of a setup 'Marc II'[554] for production of highly pure SWNTs (up to 99%) by catalytic decomposition of CO. A jet of a mixture of CO and a metal carbonyl flows out of a high-pressure (tens of atmospheres) chamber and is heated to 900–1000 °C using a laser. The performance of the setup is expected to be $\sim$100 g of NTs per 24 h.[554]

A process of catalytic decomposition of CO under pressure (trade mark HiPCO^{TM}) was proposed to be of use for commercial production of SWNTs. It is expected that NTs will be produced at a rate of up to 10 kg per day in 2002 and at rates of hundreds or thousands of kilogrammes per day in 2003–2004 (this material can be accessed *via* the Internet at URL http://www.cnanotech.com; htth://carbonnanotech.com/CNI_ home.html).

A mixture of CO with 25% H_2 and iron carbonyl can be used for the synthesis of SWNTs at atmospheric pressure at 1100 °C (this material can be accessed *via* the Internet at URL http://fy.chalmers.se/f3a/Fullerenes/Nanotubes/projects/Ntproduction.html).

Catalytic pyrolysis of hydrocarbons at temperatures above 1000 °C was proposed to be a method for NT production at a rate of several hundreds of kilogrammes per day. The National Institute of Materials and Chemical Research (JNMR, Japan) and the Showa Denko Co. (Japan) work on a pilot plant since 1999 (this material can be accessed *via* the Internet at URL http://www.jnmr.com/intro/nanotubes.html).

Currently, various MWNT-based products are produced. These are NT powders, 'spaghetti', suspensions in various solvents and substrates covered with NT 'forest' arrays. An industrial process for the preparation of MWNTs of purity 95% is based on pyrolysis of hydrocarbons performed according to the method proposed by Ren *et al.*[392] The assortment of NTs and price lists are available in the Internet at URL http://www.nano-lab.com/SubPages/prices.html. In 1999, the market price was 100 USD per gramme for unpurified NTs and 1400 USD per gramme for purified SWNTs.[245] In March 2001, the price of purified SWNTs was reduced down to 60 to 100 USD per gramme (this material can be accessed *via* the Internet at URL http://www.carbolex.com/).

The pyrolytic method is expected to allow realisation of the idea of NT synthesis (build-up) on a 'seed' (a short NT with particular structure), thus presenting a solution to a complex problem of sorting the synthesised products by structure or shape (this material can be accessed *via* the Internet at URL http://cnst.rice.edu/VARENNA.html).

The idea of existence of a critical size for a catalytic particle is well known. It is believed that the use of catalytic particles of larger size makes preparation of NTs impossible.[555] This gave an impetus to search for novel approaches to development of catalysts. A JNMR's technology for mass production of MWNTs to be used in cathodes of television displays is based on the reversed micelle method. (this material can be accessed *via* the Internet at URL http://www.jnmr.com/dez/online/nlpage1013.html).

Flame preparation of NTs represents a kind of pyrolytic synthesis of NTs.[556–558] This process has much in common to an industrial processes of soot production and can be adapted to large-scale synthesis of NTs. Pyrolysis of sputtered solution of $Fe(C_5H_5)_2$ in C_6H_6 is yet another pyrolytic technique.[557]

In Russian Federation research into NTs are well-based (see, *e.g.*, recently published reviews[559, 560] covering studies in a close field of catalytic pyrolysis of hydrocarbons to prepare carbon filaments). A setup for catalytic decomposition of CO operating at a rate of kilogramme quantities of products per day was tested.

* * *

A number of studies on the subject of this review were published in the course of preparation of the manuscript. The most important and interesting results are outlined below.

A special issue of the journal 'Physics World'[561] dedicated to research into NTs was published.

Hirahara *et al.*[562] reported the synthesis of unique compound, $(Gd@C_{82})_n@$NTs. Structurally, it represents a nanoscale 'peapod' consisting of a SWNT with encapsulated electrically charged C_{82} 'peas' with a Gd atom inside each 'pea'. This 'doubly endohedral' substance was synthesised by the interaction of $Gd@C_{82}$ vapours with pre-open NTs. Electrical resistance measurements revealed electron transfer from the metal atom not only to the C_{82} molecule, but (tentatively) to the NTs. This opens new possibilities for modification of NTs and brings the advent of unique memory devices closer.

Two studies[563, 564] carried out independently concern chemical modification of particular sections of NTs, which can lead to the formation of intramolecular heterojunctions and creation of molecular electronic devices. Researchers from the Stanford University (USA) studied the adsorption of potassium atoms on semiconducting and *p*-type conducting NTs.[564] Theoreticians from the N S Kurnakov Institute of General and Inorganic Chemistry (Moscow, Russian Federation) calculated the properties of fluorinated NTs.[563] Their results are in agreement with those reported by Kelly *et al.*[104] who showed that fluorinated isomers capable of forming ring-like fluorinated sections should be the most stable.

Ouyang *et al.*[565] experimentally and theoretically studied the atomic structure and electronic properties of metal–semiconductor and metal–metal heterojunctions in SWNTs. This appeared

to be a step towards fabrication of intramolecular heterojunctions.

The first biological study of the structure of malaria-infected erythrocytes using an AFM with an NT probe tip was reported by Nagao *et al*.[566] The space resolution obtained using an NT probe tip was four times better than with the Si probe.

Mattson *et al*.[567] proposed the use of functionalised NTs as substrates for neural growth.

Nanotubes appeared to be excellent sorbents for purification of waste gases from low concentrations of highly stable carcinogenic dioxins.[568] In this respect, NTs are more efficient than activated carbon and sorbents based on porous graphite.

New procedures for preparation of NTs at moderate temperatures have been developed. One of them consists in reduction of hexachlorobenzene with potassium in the presence of bimetallic Co – Ni catalyst at 350 °C,[569] while the second involves hydrolysis of $Al(OBu^s)_3$ in the presence of acetylacetone or acetic acid and $Co(NO_3)_2 \cdot 6H_2O$, followed by gelation, drying of the gel and heating to 300 – 400 °C.[570]

A method for quantitative determination of the NT content in the reaction products using conjugated polymer filtration was first developed.[571] The method involves preparation of a NTs – polymer composite dispersion of the composite in toluene and storage until complete precipitation of impurities for at least 48 h.

A method for obtaining stable colloidal solutions of carboxylated SWNTs in water, ethanol, acetone and DMF was proposed[572] and some of their nonlinear optical properties were measured. These solutions were shown to be promising for the use in optical information processing systems.

The synthesis of NTs decorated with hydrated RuO_2 was reported.[573] Using these NTs, the specific capacity of electrochemical capacitors was enhanced up to 560 F g^{-1}.

This review has been written with partial financial support of the Russian Foundation for Basic Research (Project No. 01-03-33225) and the Ministry of Education of the Russian Federation (Grant No. 00-5.0-24).

The author expresses his gratitude to Prof. E V Zharikov for submitting the preprints of the NASA Conference (June 6 – 8, 2000, Hantsville, Alabama, USA) on the materials prepared under microgravitation conditions, to Prof. E I Givargizov, Prof. N A Kiselev, Prof. A V Okotrub and all colleagues who sent him reprints.

References

1. S Iijima *Nature (London)* **354** 56 (1991)
2. R F Service *Science* **281** 940 (1998)
3. T Braun, A P Schubert, R N Kostoff *Chem. Rev*. **100** 23 (2000)
4. M S Dresselhaus, G Dresselhaus, P Eklund (Eds) *Science of Fullerenes and Carbon Nanotubes* (San Diego, CA: Academic Press, 1996)
5. T W Ebbesen (Ed.) *Carbon Nanotubes, Preparation and Properties* (New York: CRC Press, 1996)
6. R Saito, G Dresselhaus, M S Dresselhaus *Physical Properties of Carbon Nanotubes* (London: Imperial College Press, 1998)
7. P J F Harris *Carbon Nanotubes and Related Structures: New Materials for the Twenty-First Century* (Cambridge: Cambridge University Press, 1999)
8. K Tanaka, T Yamabe, K Fukui (Eds) *The Science and Technology of Carbon Nanotubes* (Oxford: Elsevier, 1999)
9. M S Dresselhaus, P C Eklund, G Dresselhaus, in *Carbon Materials in Advances Technol*ogy (Ed. T D Burchell) (Oxford: Pergamon Press, 1999) p. 35
10. P R Birkett *Annu. Rep. Prog. Chem., Sect. A: Inorg. Chem*. **95** 431 (1999); *Chem. Abstr*. **132** 101 851 (2000)
11. V S Kraposhin *Stal* 72 (2000)
12. Yu E Lozovik, A M Popov *Usp. Fiz. Nauk* **167** 751 (1997) [a]
13. A V Eletskii *Usp. Fiz. Nauk* **167** 945 (1997) [a]
14. A L Ivanovskii *Usp. Khim*. **68** 119 (1999) [a]
15. E G Rakov *Zh. Neorg. Khim*. **44** 1827 (1999) [b]
16. E G Rakov *Usp. Khim*. **69** 41 (2000) [*Russ. Chem. Rev*. **69** 35 (2000)]
17. J Cook, J Sloan, M L H Green *Chem. Ind*. 600 (1996)
18. R E Smalley, B I Yakobson *Solid State Commun*. **107** (11) 597 (1998)
19. N Hamada, S Sawada, A Oshiyama. *Phys. Rev. Lett*. **68** 1579 (1992)
20. E Jouguelet, C Mathis, P Petit *Chem. Phys. Lett*. **318** 561 (2000)
21. S Seraphin *J. Electrochem. Soc*. **142** 290 (1995)
22. M Terrones, W K Hsu, A Schilder, H Terrones, N Grobert, J P Hare, Y Q Zhu, A Schwoerer, K Prassides, H W Kroto, D R M Walter *Appl. Phys. A* **66** 307 (1998)
23. A Loiseau, H Pascard *Chem. Phys. Lett*. **256** 246 (1996)
24. N Demoncy, O Stephan, N Brun, C Colliex, A Loiseau, H Pascard *Eur. Phys. J. B* **4** 147 (1998)
25. N Demoncy, O Stephan, N Brun, C Colliex, A Loiseau, H Pascard *Synth. Met*. **103** 2380 (1999)
26. H Lange, A Huczko, P Byszewski, E Mizera, H Shinohara *Chem. Phys. Lett*. **289** 174 (1998)
27. E Hernandes, P Ordejon, I Boustani, A Rubio, J A Alonso *J. Chem. Phys*. **113** 3814 (2000)
28. Chin-hwa Kiang *Carbon* **38** 1699 (2000)
29. B W Smith, M Monthioux, D E Luzzi *Chem. Phys. Lett*. **315** 31 (1999)
30. P Nikolaev, A Thess, A G Rinzler, D T Colbert, R E Smalley *Chem. Phys. Lett*. **266** 422 (1997)
31. B W Smith, M Monthioux, D E Luzzi *Nature (London)* **396** 323 (1998)
32. C-H Kaing, M Endo, P M Ajayan, G Dresselhaus, M S Dresselhaus *Phys. Chem. Lett*. **81** 1869 (1998)
33. B W Smith, D E Luzzi *Chem. Phys. Lett*. **321** 169 (2000)
34. D E Luzzi, B W Smith *Carbon* **38** 1751 (2000)
35. B Burteaux, A Claye, B W Smith, M Monthioux, D E Luzzi, J E Fisher *Chem. Phys. Lett*. **310** 21 (1999)
36. J Sloan, R E Dunin-Borkowski, J L Hutchison, K S Coleman, V C Williams, J B Claridge, A P E York, C Xu, S R Bradley, S Friedrichs, M L H Green *Chem. Phys. Lett*. **316** 191 (2000)
37. K Hirahata, K Suenaga, S Bandow, S Iijima *Chem. Phys. Lett*. **324** 224 (2000)
38. R Sen, A Govindaraj, C N R Rao *Chem. Mater*. **9** 2078 (1997)
39. M S C Mazzoni, H Chacham, P Ordejón, D Sánchez-Portal, J M Soler, E Artacho *Phys. Rev. B* **60** R2208 (1999)
40. A C Dillon, T Gennett, K M Jones, J L Alleman, P A Parilla, M J Heben *Adv. Mater*. **11** 1354 (1999)
41. F Ikazaki, S Ohshima, K Uchida, Y Kuruki, H Hayakawa, M Yumura, K Takahashi, K Tojima *Carbon* **32** 1539 (1994)
42. Y K Chen, M L H Green, J L Griffin, J Hammer, R M Lago, S C Tsang *Adv. Mater*. **8** 1012 (1996)
43. K Morishita, T Takarada *J. Mater. Sci*. **34** 1169 (1999)
44. M Yumura, S Ohsima, K Uchida, Y Tasaka, Y Kuruki, F Ikazaki, Y Saito, S Uemura *Diam. Relat. Mater*. **8** 785 (1999)
45. J L Zimmerman, R K Bradley, C B Huffman, R H Hauge, J L Margrave *Chem. Mater*. **12** 1361 (2000)
46. B W Smith, D E Luzzi *Nanospace 2000. The 3rd International Conference on Integrated Nano/Microtechnology for Space Application, Vol. 1, Houston, TX, 2000* p. 23
47. E Mizoguti, F Nihey, M Yudasaka, S Iijima, T Ichihashi, K Nakamura *Chem. Phys. Lett*. **321** 297 (2000)
48. M Zhang, M Yudasaka, F Nihey, S Iijima *Chem. Phys. Lett*. **328** 350 (2000)
49. P M Ajayan, S Iijima *Nature (London)* **361** 333 (1993)
50. P M Ajayan, T B Ebbesen, T Ichihashi, S Iijima, K Tanigaki, H Hiura *Nature (London)* **362** 522 (1993)
51. P M Ajayan, T B Ebbesen *Rep. Prog. Phys*. **60** 1025 (1997)
52. J Sloan, J Hammer, M Zwiefka-Sibley, M L H Green *Chem. Commun*. 347 (1998)
53. H Hiura, T W Ebbesen, K Tanigaki *Adv. Mater*. **7** 275 (1995)
54. J-F Colomer, P Piedigrosso, A Fonseca, J B Nagy *Synth. Met*. **103** 2482 (1999)
55. A G Rinzler, J Liu, H Dai, P Nikolaev, C B Huffman, F J Rodrigúez-Mactas, P J Boul, A H Hu, D Heymann, D T Colbert, R S Lee, J E Fischer, A M Rao, P C Eklund, R E Smalley *Appl. Phys. A* **67** 29 (1998)
56. N Yao, V Lordi, S X C Ma, E Dujardin, A Krishnan, M M J Treacy, T W Ebbesen *J. Mater. Res*. **13** 2432 (1998)
57. G S Duesberg, J Muster, H J Byrne, S Roth, M Burghard *Appl. Phys. A* **69** 269 (1999)
58. J Cook, J Sloan, M L H Green *Fullerene Sci. Technol*. **5** 695 (1997)

59. D Ugarte, T Stockli, J M Bonard, A Châtelain, W A De Heer *Appl. Phys. A* **67** 101 (1998)
60. D Ugarte, A Châtelain, W A De Heer *Science* **274** 1897 (1994)
61. E Dujardin, T W Ebbesen, A Krishnan, M M J Treacy *Adv. Mater.* **10** 1472 (1998)
62. P M Ajayan, O Stephan, Ph Redlich, C Colliex *Nature (London)* **375** 564 (1995)
63. C-H Kiang, J-H Choi, T Tran, A D Bacher *J. Phys. Chem. B* **103** 7449 (1999)
64. P M Ajayan, V Ravikumar, J-C Charlier *Phys. Rev. Lett.* **81** 1437 (1998)
65. J Sloan, J Cook, A Chu, M Zwiefka-Sibley, M L H Green, J L Hutchison *J. Solid State Chem.* **140** 83 (1998)
66. J Sloan, D M Wright, H-G Woo, S Bailey, G Brown, A P E York, K S Coleman, J L Hutchison, M L H Green *Chem. Commun.* 699 (1999)
67. R R Meyer, J Sloan, R E Dunin-Borkowski, A I Kirkland, M C Novotny, S R Bailey, J L Hutchison, M L H Green *Science* **289** 1324 (2000)
68. J Sloan, M C Novotny, S R Bailey, G Brown, C Xu, V C Williams, S Friedrichs, E Flahaut, R C Callender, A P E York, K S Coleman, M L H Green, R E Dunin-Borkowski, J L Hutchison *Chem. Phys. Lett.* **329** 61 (2000)
69. M Freemantle *Chem. Eng. News* **78** (36) 44 (2000)
70. A Govindaraj, B C Satishkumar, M Nath, C N R Rao *Chem. Mater.* **12** 202 (2000)
71. W K Hsu, S Trasobares, H Terrones, M Terrones, N Grobert, Y Q Zhu, W Z Li, R Escudero, J P Hare, H W Kroto, D R M Walton *Chem. Mater.* **11** 1747 (1999)
72. T Kyotani, L Tsai, A Tomita *Chem. Commun.* 701 (1997)
73. J Sloan, J Cook, J R Heersom, M L H Green, J L Hutchison *J. Cryst. Growth* **173** 81 (1997)
74. H Y Peng, N Wang, Y F Zheng, Y Lifshitz, J Kulik, R Q Zhang, C S Lee, S T Lee *Appl. Phys. Lett.* **77** 2831 (2000)
75. B K Pradhan, T Toda, T Kyotani, A Tomita *Chem. Mater.* **10** 2510 (1998)
76. B K Pradhan, T Kyotani, A Tomita *Chem. Commun.* 1317 (1999)
77. J Wu, M-L Wang, R Lü, W Duan *Int. J. Mod. Phys. B* **12** 1601 (1998)
78. R A Jishi, C T White, J W Mintmire *Int. J. Quantum. Chem.* **80** 480 (2000)
79. A K Sinha, D W Hwang, L-P Hwang *Chem. Phys. Lett.* **332** 455 (2000)
80. M Terrones, N Grobert, W K Hsu, Y Q Zhu, W B Hu, H Terrones, J P Hare, H W Kroto, D R M Walton *MRS Bull.* **24** 43 (1999)
81. H P Boehm *Carbon* **32** 759 (1994)
82. K Esumi, M Ishigami, A Nakajima, K Sawada, H Honda *Carbon* **34** 279 (1996)
83. P A Cahill, C M Rohling *Tetrahedron* **52** 5247 (1996)
84. R M Lago, S C Tsang, K L Liu, Y K Cheng, M L H Green *J. Chem. Soc., Chem. Commun.* 1355 (1995)
85. R Yu, L Chen, Q Lin, J Lin, K-L Tan, S C Ng, H S O Chan, G-Q Xu, T S A Hor *Chem. Mater.* **10** 718 (1998)
86. S Nagasawa, M Yudasaka, K Hirahara, T Ichihashi, S Iijima *Chem. Phys. Lett.* **328** 374 (2000)
87. A Kuznetsova, D B Mawhiney, V Naumenko, J T Yates Jr, J Liu, R E Smalley *Chem. Phys. Lett.* **321** 292 (2000)
88. D B Mawhinney, V Naumenko, A Kuznetsova, J T Yates Jr, J Liu R E Smalley *Chem. Phys. Lett.* **324** 213 (2000)
89. S S Wong, E Joselevich, A T Wooley, C L Cheung, C M Lieber *Nature (London)* **394** 52 (1998)
90. S S Wong, A T Wooley, E Joselevich, C L Cheung, C M Lieber *J. Am. Chem. Soc.* **120** 8557 (1998)
91. J Liu, A G Rinzler, H Dai, J Hafner, R K Bradley, P Boul, A Lu, T Iverson, K Shelimov, C B Huffman, F Rodriguez-Macias, Y-S Shon, T R Lee, D T Colbert, R E Smalley *Science* **280** 1253 (1998)
92. S S Wong, A T Wooley, E Joselevich, C M Lieber *Chem. Phys. Lett.* **306** 219 (1999)
93. S Depleux, K Metenier, R Benoit, F Vivet, L Beufendi, S Bonnamy, F Beguin, in *AIP Conference Proceedings, 1999 (Electronic Properties of Novel Materials — Science and Technology of Molecular Structures)* p. 470; *Chem. Abstr.* **132** 841 34b (2000)
94. B Ni, S B Sinnott *Phys. Rev. B* **61** R16343 (2000)
95. R Sen, B C Satishkumar, G Raina, C N R Rao *Fullerene Sci. Technol.* **5** 489 (1997)
96. H Touhara, F Okino *Carbon* **38** 241 (2000)
97. T Nakajima, S Kasamatsu, Y Matsuo *Eur. J. Solid State Inorg. Chem.* **33** 831 (1996)
98. A Hamwi, H Alvergnat, S Bonnamy, F Beguin *Carbon* **35** 723 (1997)
99. A Hamwi, P Gendraud, H Gaucher, S Bonnamy, F Beguin *Mol. Cryst. Liq. Cryst. Sci. Technol., Sect. A* **310** 185 (1998)
100. E T Mickelson, C B Huffman, A G Rinzler, R E Smalley, J L Margrave *Chem. Phys. Lett.* **296** 188 (1998)
101. E T Mickelson, I W Chiang, J L Zimmerman, P J Boul, J Lozano, J Liu, R E Smalley, R H Hauge, J L Margrave *J. Phys. Chem. B* **103** 4318 (1999)
102. J Chen, M A Hamon, H Hu, Y Chen, A M Rao, P C Eklund, R C Haddon *Science* **282** 95 (1998)
103. P J Boul, J Liu, E T Mickelson, C B Huffman, L M Ericson, I W Chiang, K A Smith, D T Colbert, R G Hauge, J L Margrave, R E Smalley *Chem. Phys. Lett.* **310** 367 (1999)
104. K F Kelly, I W Chiang, E T Mickelson, R G Hauge, J L Margrave, X Wang, G E Scuseria, C Radloff, N J Halas *Chem. Phys. Lett.* **313** 445 (1999)
105. G Seifert, T Kohler, T Frauenheim *Appl. Phys. Lett.* **77** 1313 (2000)
106. C W Bauschlicher Jr *Chem. Phys. Lett.* **322** 237 (2000)
107. Y Hattori, Y Watanabe, S Kawasaki, F Okino, B K Pradhan, T Kyotani, A Tomita, H Touhara *Carbon* **37** 1033 (1999)
108. A V Okotrub, N F Yudanov, A V Chuvilin, I P Asanov, Yu V Shubin, L G Bulusheva, A V Gusel'nikov, I S Fyodorov *Chem. Phys. Lett.* **322** 231 (2000)
109. Y Chen, R C Haddon, S Fang, A M Rao, P C Eklund, W H Lee, E C Dickey, E A Grulke, J C Pendergrass, A Chavan, B S Haley, R E Smalley *J. Mater. Research* **13** 2423 (1998); *Chem. Abstr.* **129** 189 054 (1998)
110. Y Chen, J Chen, H Hu, M A Hamon, M E Itkis, R C Haddon *Chem. Phys. Lett.* **299** 532 (1999)
111. M A Hamon, J Chen, H Hu, Y Chen, M E Itkis, A M Rao, P C Eklund, R C Haddon *Adv. Mater.* **11** 834 (1999)
112. B Z Tang, H Xu *Macromolecules* **32** 2569 (1999)
113. S Curran, P Ajayan, W Blau, D Carroll, J Coleman, A Dalton, A P Davey, B McCarthy, A Stevens *Adv. Mater.* **10** 1091 (1998)
114. S Curran, A P Davey, J Coleman, A Dalton, B McCarthy, S Maier, A Drury, D Gray, M Brennan, K Ryder, M Lamy de la Chapelle, C Journet, P Bernier, H J Byrne, D Carroll, P M Ajayan, S Lefrant, W Blau *Synth. Met.* **103** 2559 (1999)
115. G S Duesberg, M Burghard, J Muster, G Phillipp, S Roth *Chem. Commun.* 453 (1998)
116. G S Duesberg, M Burghard, J Muster, V Krstic, S Roth *Appl. Phys. A* **67** 117 (1998)
117. G S Duesberg, W Blau, H J Byrne, J Muster, M Burghard, M Roth *Synt. Met.* **103** 2484 (1999)
118. J Liu, M J Casavant, M Cox, D A Walters, P Boul, W Lu, A J Rimberg, K A Smith, D T Colberg, R E Smalley *Chem. Phys. Lett.* **303** 125 (1999)
119. K D Ausman, R Piner, O Lourie, R S Ruoff, M Korobov *J. Phys. Chem. B* **104** 8911 (2000)
120. M V Korobov, A L Mirakyan, N V Avramenko, G Olofsson, A L Smith, R S Ruoff *J. Phys. Chem. B* **103** 1339 (1999)
121. Z Jin, L Huang, S H Goh, G Xu, W Ji *Chem. Phys. Lett.* **332** 461 (2000)
122. M Burghard, G S Duesberg, G Philipp, J Muster, S Roth *Adv. Mater.* **10** 584 (1998)
123. V Krstic, G S Duesberg, J Muster, M Burghard, S Roth *Chem. Mater.* **10** 2338 (1998)
124. M Burghard, V Krstic, G S Duesberg, G Philipp, J Muster, S Roth, C Journet, P Bernier *Synth. Met.* **103** 2540 (1999)
125. V Krstic, J Muster, G S Duesberg, G Philipp, M Burghard, S Roth *Synth. Met.* **110** 245 (2000)
126. P Chen, X Wu, J Lin, K L Tan *J. Phys. Chem. B* **103** 4559 (1999)
127. L M Ang, T S A Hor, G Q Xu, C H Tung, S P Zhao, J L S Wang *Carbon* **38** 363 (2000)
128. R Dagani *Chem. Eng. News* **77** (2) 31 (1999)
129. J Li, M Moskovits, T L Haslett *Chem. Mater.* **10** 1963 (1998)

130. J Li, M Moskovits, T L Haslett *Proceedings of Electrochemical Society, 1988 (Recent Advances in the Chemistry and Physics of Fullerene and Related Materials)* p. 822; *Chem. Abstr.* **129** 325 197 (1998)
131. Q Li, S Fan, W Han, C Sun, W Liang *Jpn. J. Appl. Phys.* **36** (4B) L501 (1997)
132. S C Tsang, J J Davis, M L H Green, H A O Hill, Y C Lang, P J Sadler *J. Chem. Soc., Chem. Commun.* 2579 (1995)
133. Y Zhang, H-B Zhang, G-D Lin, P Chen, Y-Z Yuan, K R Tsai *Appl. Catal. A* **187** 213 (1999)
134. C N R Rao, B C Satishkumar, A Govindaraj *Chem. Commun.* 1581 (1997)
135. B C Satishkumar, A Govindaraj, M Nath, C N R Rao *J. Mater. Chem.* **10** 2115 (2000)
136. B C Satishkumar, A Govindaraj, E M Vogl, L Basumalik, C N R Rao *J. Mater. Res.* **12** 604 (1997)
137. Y Zhang, N W Franklin, R J Chen, H Dai *Chem. Phys. Lett.* **331** 35 (2000)
138. Y Zhang, H Dai *Appl. Phys. Lett.* **77** 3015 (2000)
139. Y Miyamoto, A Rubio, X Blase *Phys. Rev. Lett.* **74** 2993 (1995)
140. M Menon, A N Andriotis, G E Froudakis *Chem. Phys. Lett.* **320** 425 (2000)
141. D Srivastava, D W Brenner, J D Schall, K D Ausman, M Yu, R S Ruoff *J. Phys. Chem. B* **103** 4330 (1999)
142. X Blase, A Rubio, S G Louie, M L Cohen *Europhys. Lett.* **28** 335 (1994)
143. N G Chopra, A Zettl *Solid State Commun.* **105** 297 (1998)
144. L Vaccarini, C Goze, L Henrard, E Hernándes, P Bernier, A Rubio *Carbon* **38** 1681 (2000)
145. Y Huang, J Gao, R Liu *Synth. Met.* **113** 251 (2000)
146. W Han, Y Bando, K Kurashima, T Sato *Appl. Phys. Lett.* **73** 3085 (1998)
147. W Han, Y Bando, K Kurashima, T Sato *Chem. Phys. Lett.* **299** 368 (1999)
148. W Han, Y Bando, K Kurashima, T Sato *Jpn. J. Appl. Phys.* **38** Pt. 2 7A L755 (1999)
149. D Golberg, Y Bando, W Han, K Kurashima, T Sato *Chem. Phys. Lett.* **308** 337 (1999)
150. D Golberg, Y Bando, W Han, K Kurashima, T Sato *Chem. Phys. Lett.* **323** 185 (2000)
151. D Golberg, Y Bando, L Bourgeois, K Kurashima, T Sato *Carbon* **38** 2017 (2000)
152. Y Zhang, J Zhu, Q Zhang, Y Yan, N Wang, X Zhang *Chem. Phys. Lett.* **317** 504 (2000)
153. H Dai, E W Wong, Y Z Lu, S Fan, C M Lieber *Nature (London)* **375** 769 (1995)
154. W Han, S Fan, Q Li, W Liang, B Gu, D Yu *Chem. Phys. Lett.* **265** 374 (1997)
155. W Q Han, S Fan, Q Li, Y Hu *Science* **277** 1287 (1997)
156. W Han, S Fan, Q Li, X Zhang, D Yu *Appl. Phys. Lett.* **71** 2271 (1997)
157. A Fukunaga, S Y Chu, M E McHenry *J. Mater. Res.* **13** 2465 (1998)
158. S Motojima, S Yang, X Chen, H Iwanaga *J. Mater. Sci.* **34** 5989 (2000)
159. Y Zhang, T Ichihashi, E Landree, F Niney, S Iijima *Science* **285** 1719 (1999)
160. Y Zhang, S Iijima *Appl. Phys. Lett.* **77** 966 (2000)
161. B Gao, C Bower, J D Lorentzen, L Fleming, A Kleinhammes, X P Tang, L E McNeil, Y Wu, O Zhou *Chem. Phys. Lett.* **327** 69 (2000)
162. N Ishikawa (Ed.), in *Novoe v Tekhnologii Soedinenii Ftora* (Fluorine Compounds. Modern Technology and Application; Translated into Russian from Japanese; Moscow: Mir, 1984) p. 132
163. J C Withers, R O Lotfy, T P Lowe *Fullerene Sci. Technol.* **5** 1 (1997)
164. O Zhou, R M Fleming, D W Murphy, C H Chen, R C Haddon, A P Ramirez, S H Glarum *Science* **263** 1744 (1994)
165. S Suzuki, M Tomita *J. Appl. Phys.* **79** 3739 (1996)
166. V I Sokolov, I V Stankevich *Usp. Khim.* **62** 455 (1993) [*Russ. Chem. Rev.* **62** 419 (1993)]
167. H Werner, M Wesemann, R Schlogl *Eur. Lett.* **20** 107 (1992)
168. A M Rao, P C Eklund, S Bandow, A Thess, R E Smalley *Nature (London)* **388** 257 (1997)
169. S Kazaoui, N Minami, R Jaquemin, H Kataura, Y Achiba *Phys. Rev. B* **60** 13339 (1999)
170. R S Lee, H M Kim, J E Fisher, A Thess, R E Smalley *Nature (London)* **388** 255 (1997)
171. P Petit, C Mathis, C Journet, P Bernier *Chem. Phys. Lett.* **305** 370 (1999)
172. R Jacquemin, S Kazaoui, D Yu, A Hassanien, N Minami, H Kataura, Y Achiba *Synth. Met.* **115** 283 (2000)
173. S Bandow, A M Rao, G U Sumanasekera, P C Eklund, F Kokai, K Takahashi, M Yudasaka, S Iijima *Appl. Phys. A* **71** 561 (2000)
174. C Bower, S Suzuki, K Tanigaki, O Zhou *Appl. Phys. A* **67** 47 (1998)
175. V Z Mordkovich, M Baxendale, S Yoshimura, R P H Chang *Carbon* **34** 1301 (1996)
176. V Z Mordkovich, M Baxendale, M Yudasaka, S Yoshimura, J-Y Daie, R P H Chang *Mol. Cryst. Liq. Cryst. Sci. Technol., Sect. A* **310** 159 (1998); *Chem. Abstr.* **129** 114 120 (1998)
177. S Suzuki, C Bower, O Zhou *Chem. Phys. Lett.* **285** 230 (1998)
178. A Claye, J E Fischer, A Métrot *Chem. Phys. Lett.* **330** 61 (2000)
179. L Grigorian, G U Sumanasekera, A R Loper, S Famg, J L Allen, P C Eklund *Phys. Rev. B* **58** R4194 (1998)
180. M Bockrath, J Hone, A Zettl, P L McEuen, A G Rinzler, R E Smalley *Phys. Rev. B* **61** R10 606 (2000)
181. R Martel, T Schmidt, H R Shea, T Hertel, P Avouris *Appl. Phys. Lett.* **73** 2447 (1998)
182. B Ruzicka, L Degiorgi, R Gaal, L Thien-Nga, J-P Salvetat, L Forró *Phys. Rev. B* **61** R2468 (2000)
183. R S Lee, H J Kim, J E Fisher, J Lefebvre, M Radosavljević, J Hone, A T Johnson *Phys. Rev. B* **61** 4526 (2000)
184. T Pichler, M Knupfer, M S Golden, J Fink, A Rinzler, R E Smalley *Synth. Met.* **103** 2515 (1999)
185. G Gao, T Carin, W A Goddard III *Phys. Rev. Lett.* **80** 5556 (1998)
186. Z-X Jin, D Q Xu, S H Goh *Carbon* **38** 1135 (2000)
187. L Grigorian, K A Williams, S Fang, G U Sumanasekera, A L Lopez, E C Dickey, S J Pennycook, P C Eklund *Phys. Rev. Lett.* **80** 5560 (1998)
188. X Fan, E C Dickey, P C Eklund, K A Williams, L Grigorian, R Buczko, S T Pantelides, S J Pennycook *Phys. Rev. Lett.* **84** 4621 (2000)
189. C Bower, A Kleinhammes, Y Wu, O Zhou *Chem. Phys. Lett.* **288** 481 (1998)
190. G U Sumanasekera, J L Allen, S L Fang, A L Loper, A M Rao, P C Eklund *J. Phys. Chem. B* **103** 4292 (1999)
191. V Z Mordkovich, M Baxendale, R P H Chang, S Yoshimura *Synth. Met.* **86** 2049 (1997)
192. M Baxendale, G A Amaratunga *Synth. Met.* **103** 2496 (1999)
193. W K Hsu, W Z Li, Y Q Zhu, N Grobert, M Terrones, H Terrones, N Yao, J P Zhang, S Firth, R J H Clark, A K Cheetham, J P Hare, H W Kroto, D R M Walton *Chem. Phys. Lett.* **317** 77 (2000)
194. M W Maddox, S L Sowewrs, K E Gubbins *Adsorption* **2** 23 (1996)
195. I V Zaporotskova, F O Litinskii, L A Chernozatonskii *Pis'ma v Zh. Eksp. Teor. Fiz.* **66** 799 (1997)
196. K G Ayappa *Chem. Phys. Lett.* **282** 59 (1998)
197. K G Ayappa *Langmuir* **14** 880 (1998)
198. G Stan, M W Cole *Surf. Sci.* **395** 280 (1998)
199. G Stan, M W Cole *J. Low Temp. Phys.* **110** 539 (1998)
200. G Stan, V H Crespi, M W Cole *J. Low Temp. Phys.* **113** 447 (1998)
201. G Stan, S M Gatica, M Boninsegni, S Curtarolo, M W Cole *Am. J. Phys.* **67** 110 (1999)
202. M W Cole, V H Crespi, G Stan, C Ebner, J M Hartman, S Moroni, M Boninsegni *Phys. Rev. Lett.* **84** 3883 (2000)
203. G Stan, M J Bojan, S Curtarolo, S M Gatica, M W Cole *Phys. Rev. B* **62** 2173 (2000)
204. G Stan, J M Hartman, V H Crespi, S M Gatica, M W Cole *Phys. Rev. B* **61** 7288 (2000)
205. W Teizer, R B Hallock, E Dujardin, T W Ebbesen *Phys. Rev. Lett.* **82** 5305 (1999)
206. W Teizer, R B Hallock, E Dujardin, T W Ebbesen. *Phys. Rev. Lett.* **84** 1844 (2000)
207. S E Weber, S Talapatra, C Journet, A Zambano, A D Migone *Phys. Rev. B* **61** 13150 (2000)
208. S Talapatra, A Z Zambano, S E Weber, A D Migone *Phys. Rev. Lett.* **85** 138 (2000)
209. S Inoue, N Ichikuni, T Suzuki, T Uematsu, T Kaneko *J. Phys. Chem. B* **102** 4689 (1998)
210. T Kyotani, L Tsai, A Tomita *Chem. Mater.* **7** 1427 (1995)

211. M Eswaramoorthy, R Sen, C N R Rao *Chem. Phys. Lett.* **304** 207 (1999)
212. G U Sumanasekera, C K W Adu, S Fang, P C Eklund *Phys. Rev. Lett.* **85** 1096 (2000)
213. K A Dean, B R Chalamala *Appl. Phys. Lett.* **76** 375 (2000)
214. S-H Jhi, S G Louie, M L Cohen *Phys. Rev. Lett.* **85** 1710 (2000)
215. M Terrones, W K Hsu, H W Kroto, D R M Walton, in *Topics on Current Chemistry. Fullerenes and Related Structures* (New York: Springer, 1999) Vol. 199, p. 189
216. S Subramoney *Adv. Mater.* **10** 1157 (1998)
217. P M Ajayan *Chem. Rev.* **99** 1787 (1999)
218. F T Edelman *Angew. Chem., Int. Ed. Engl.* **38** 1381 (1999)
219. T Kuzumaki, K Ito, H Ichinose *Bull. Ceramic Soc. Jpn.* **33** 438 (1998)
220. J-P Salvetat, J-M Bonard, N H Thomson, A J Kulik, L Forro, W Benoit, L Zuppiroli *Appl. Phys. A* **69** 255 (1999)
221. R S Ruoff, D C Lorents *Carbon* **33** 925 (1995)
222. C Schonenberger, L Forro *Phys. Web -Phys. World Magazine* **13** (6) 1 (2000)
223. E W Wong, P E Sheehan, C Lieber *Science* **277** 1971 (1997)
224. S B Sinnott, O A Shenderova, C T White, D W Brenner *Carbon* **36** 1 (1998)
225. C Seife *Mater. Today* **2** (1) 25 (1999)
226. J Bernholc, C Brabec, M Nadelli, M Buongiorno, A Maiti, C Roland, B I Yacobson *Appl. Phys. A* **67** 39 (1998)
227. S A Chesnokov, V A Nalimova, A G Rinzler, R E Smalley, J E Fischer *Phys. Rev. Lett.* **82** 343 (1999)
228. M Buongiorno Nardelli, J-L Fatterberd, D Orlikowski, C Roland, Q Zhao, J Bernholc *Carbon* **38** 1703 (2000)
229. P M Ajayan, O Stephan, C Colliex, D Trauth *Science* **265** 1212 (1994)
230. P M Ajayan, P Redlich, M Ruhle *J. Microscopy* **185** 275 (1997)
231. P Calvert *Nature (London)* **399** 210 (1999)
232. P M Ajayan, L S Schadler, S C Giannaris, A Rubio *Adv. Mater.* **12** 750 (2000)
233. L S Schadler, S C Giannaris, P M Ajayan *Appl. Phys. Lett.* **73** 3842 (1998)
234. O Lourie, H D Wagner *J. Mater. Res.* **13** 2418 (1998)
235. O Lourie, D M Cox, H D Wagner *Phys. Rev. Lett.* **81** 1638 (1998)
236. O Lourie, H D Wagner *Appl. Phys. Lett.* **73** 3527 (1998)
237. M Lamy de la Chapelle, C Stéphan, T P Nguyen, S Lefrant, C Journet, P Bernier, L Alvarez, D Laplaze, E Munoz, A Benito, W K Maser, M T Martinez, G F de la Fuente, T Guillard, G Flamant *Synth. Met.* **103** 2510 (1999)
238. C Stéphan, T P Nguyen, M Lamy de la Chapelle, S Lefrant, C Journet, P Bernier *Synth. Met.* **108** 139 (2000)
239. J N Coleman, S Curran, A B Dalton, A P Davey, B McCarthy, W Blau, R C Barklie *Synth. Met.* **102** 1174 (1999)
240. J N Coleman, S Curran, A B Dalton, A P Davey, B McCarthy, W Blau, R C Barklie *Phys. Rev. B* **58** 7492 (1998)
241. A B Dalton, H J Byrne, J N Coleman, S Curran, A P Davey, B McCarthy, W Blau *Synth. Met.* **102** 1176 (1999)
242. H S Woo, R Czerw, S Webster, D L Carroll, J W Park, J H Lee *Synth. Met.* **116** 369 (2001)
243. L Dai *Polym. Adv. Technol.* **10** 355 (1999)
244. M in het Panhius, R W Munn, W J Blau *Synth. Met.* **121** 1187 (2000)
245. R Dagani *Chem. Eng. News.* **77** (23) 25; 29; 34 (1999)
246. H Ago, K Petritsch, M S P Shaffer, A H Windle, R H Friend *Adv. Mater.* **11** 1281 (1999)
247. E D Obraztsova, J-M Bonard, V L Kuznetsov, V I Zaikovskii, S M Pimenov, A S Pozarov, S V Terekhov, V I Konov, A N Obraztsov, A P Volkov *Nanostruct. Mater.* **12** 567 (1999)
248. C A Cooper, R J Young *J. Raman Spectrosc.* **30** 929 (1999)
249. J R Wood, Q Zhao, M D Frogley, E R Meurs, A D Prins, T Peijs, D J Dustan, H D Wagner *Phys. Rev. B* **62** 7571 (2000)
250. H D Wagner, O Lourie, Y Feldman, R Tenne *Appl. Phys. Lett.* **72** 188 (1998)
251. L Jin, C Bower, O Zhou *Appl. Phys. Lett.* **73** 1197 (1998)
252. M S P Shaffer, A H Windle *Adv. Mater.* **11** 937 (1999)
253. G Z Chen, M S P Shaffer, D Coleby, G Dixon, W Zhou, D J Fray, A H Windle *Adv. Mater.* **12** 522 (2000)
254. D Qian, E C Dickey, R Andrews, T Rantell *Appl. Phys. Lett.* **76** 2868 (2000)
255. R Andrews, D Jacques, A M Rao, T Rantell, F Derbyshire, Y Chen, J Chen, R C Haddon *Appl. Phys. Lett.* **75** 1329 (1999)
256. B Vigolo, A Penicaud, C Coulon, C Sauder, R Pallier, C Journet, P Bernier, P Poulin *Science* **290** 1331 (2000)
257. R Haggenmueller, H H Gommans, A G Rinzler, J E Fisher, K I Winney *Chem. Phys. Lett.* **330** 219 (2000)
258. Z Jin, X Sun, G Xu, S H Goh, W Ji *Chem. Phys. Lett.* **318** 505 (2000)
259. J Sandler, M S P Shaffer, T Prasse, W Bauhofer, K Schulte, A H Windle *Polymer* **40** 5967 (1999)
260. L Sun, R M Crooks *Langmuir* **15** 738 (1999)
261. C A Grimes, C Mungle, D Kouzoudis, S Fang, P C Eklund *Chem. Phys. Lett.* **319** 460 (2000)
262. J Fan, M Wan, D Zhu, B Chang, Z Pan, S Xie *J. Appl. Polym. Sci.* **74** 2605 (1999)
263. M Yudasaka, M Zhang, C Jabs, S Iijima *Appl. Phys. A* **71** 449 (2000)
264. J N Coleman, A B Dalton, S Curran, A Rubio, A P Davey, A Drury, B McCarthy, B Lahr, P M Ajayan, S Roth, R C Barklie, W J Blau *Adv. Mater.* **12** 213 (2000)
265. M Holzinger, A Hirsch, P Bernier, G S Duesberg, M Burghard *Appl. Phys. A* **70** 599 (2000)
266. T Kuzumaki, T Hayashi, K Miyazawa, H Ichinose, K Ito, Y Ishida *Mater. Trans., JIM* **39** 578 (1998)
267. C L Xu, B Q Wei, R Z Ma, J Liang, X K Ma, D H Wu *Carbon* **37** 855 (1999)
268. T Kuzumaki, O Ujiie, H Ichinose, K Ito *Adv. Eng. Mater.* **2** 416 (2000)
269. Y B Li, Q Ya, B Q Wei, J Liang, D H Wu *J. Mater. Sci. Lett.* **17** 607 (1998)
270. S-L Huang, M R Koblischka, K Fossheim, T W Ebbesen, T H Johansen *Physica C* **311** 172 (1999)
271. P Yang, C M Lieber *Science* **273** 1836 (1996)
272. P Yang, C M Lieber *Appl. Phys. Lett.* **70** 3158 (1997)
273. P Yang, C M Lieber *J. Mater. Res.* **12** 2981 (1997)
274. Ch Laurent, A Peigney, A Rousset *J. Mater. Chem.* **8** 1263 (1998)
275. Ch Laurent, A Peigney, O Dumortier, A Rousset *J. Eur. Ceram. Soc.* **18** 2005 (1998); *Chem. Abstr.* **130** 157 064 (1999)
276. Ch Laurent, A Peigney, E Flahaut, A Rousset *Mater. Res. Bull.* **35** 661 (2000)
277. E Flahaut, A Peigney, Ch Laurent, A Rousset. *J. Mater. Chem.* **10** (2) 249 (2000)
278. R H Baughman *Synth. Met.* **78** 339 (1996)
279. R H Baughman, C Cui, A A Zakhidov, Z Iqbal, J N Barisci, G M Spinks, G G Wallace, A Mazzoldi, D De Rossi, A G Rinzler, O Jaschinski, S Roth, M Kertesz *Science* **284** 1340 (1999)
280. R H Baughman, C Cui, A A Zakhidov, Z Iqbal, J N Barisci, G M Spinks, G G Wallace, A Mazzoldi, D De Rossi, A G Rinzler, O Jaschinski, S Roth, M Kertesz, in *The 13th International Winterschool on Electronic Properties of Novel Materials. Sciences and Technology of Molecular Nanostructures (Program and Abstracts), Kirchberg, 1999* p. 17
281. J N Barisci, G G Wallace, R H Baughman *J. Electroanal. Chem.* **488** 92 (2000)
282. C L Che, S A Miller, E R Fisher, C R Martin *Anal. Chem.* **71** 3187 (1999)
283. S Saito *Science* **278** 77 (1997)
284. M Dresselhaus *Phys. World.* 16 (1996)
285. L Kouvenhoven *Science* **275** 1896 (1997)
286. S Roth, M Burghard, G Leising *Curr. Opin. Solid State Mater. Sci.* **3** 209 (1998)
287. C Dekker *Phys. Today* **52** 22 (1999)
288. J W G Wildoer, L C Venema, A G Rinzler, R E Smalley, C Dekker *Nature(London)* **391** 59 (1998)
289. T W Odom, J Huang, P Kim, C M Lieber *Nature (London)* **391** 62 (1998)
290. M Bockrath, D H Cobden, P L McEuen, N G Chopra, A Zettl, A Thess, R E Smalley *Science* **275** 1922 (1997)
291. S J Tans, M H Devoret, H Dai, A Thess, R E Smalley, L J Geerlings, C Dekker *Nature (London)* **386** 474 (1997)
292. S Frank, P Poncharal, Z L Wang, W A de Heer *Science* **280** 1744 (1998)
293. J-C Charlier, J-P Issi *Appl. Phys. A* **67** 79 (1998)

294. P Delaney, H J Choi, J Ihm, S G Louie, M L Cohen *Nature (London)* **391** 466 (1998)
295. M Bockrath, D H Cobden, J Lu, A G Rinzler, R E Smalley, L Balents, P L McEuen *Nature (London)* **397** 598 (1999)
296. J Han, M P Anantram, R Z Jaffe, J Kong, H Dai *Phys. Rev. B* **57** 14983 (1998)
297. R F Service *Science* **271** 1232 (1996)
298. B I Dunlap *Phys. Rev. B* **49** 5643 (1994)
299. L Chico, V H Crespi, L X Benedict, S G Louie *Phys. Rev. Lett.* **76** 971 (1996)
300. L Chico, L X Benedict, S G Louie, S G Louie *Phys. Rev. B* **54** 2600 (1996)
301. J C Charlier, T W Ebbesen, Ph Lambin *Phys. Rev. B* **53** 11108 (1996)
302. G Treboux, P Lapstun, K Silverbrook *J. Phys. Chem. B* **103** 1871 (1999)
303. V Meunier, L Henrard, Ph Lambin *Phys. Rev. B* **57** 2586 (1998)
304. P Lambin, V Meunier *Appl. Phys. A* **68** 263 (1999)
305. R D Antonov, A T Johnson *Phys. Rev. Lett.* **83** 3274 (1999)
306. A A Farajian, K Esfarjani, Y Kawazoe *Phys. Rev. Lett.* **82** 5084 (1999)
307. L Francois, J Tersoff *Phys. Rev. Lett.* **83** 5174 (1999)
308. A A Odintsov *Phys. Rev. Lett.* **85** 150 (2000)
309. A A Odintsov, Y Tokura *J. Low Temp. Phys.* **118** 509 (2000)
310. S J Tans, A R M Versueren, C Dekker *Nature (London)* **393** 49 (1998)
311. Z Yao, H W Ch Postma, L Balents, C Dekker *Nature (London)* **402** 273 (1999)
312. L Roschier, J Penttili, M Martin, P Hakonen, M Paalanen, U Tapper, E I Kauppinen, C Journet, P Bernier *Appl. Phys. Lett.* **75** 728 (1999)
313. H Nishijima, S Akita, Y Nakayama *Jpn. J. Appl. Phys.* **38** Pt. 1 12B 7247 (1999)
314. R Baum, M Rouhi *Chem. Eng. News* 11 (1998)
315. M S Fuhrer, J Nygárd, L Shin, M Forero, Y-G Yoon, M S C Mazzoni, H J Choi, J Ihm, S G Louie, A Zettl, P L McEuen *Science* **288** 494 (2000)
316. H Dai, J Kong, C Zhou, N Franklin, T Tombler, A Cassell, S Fan, M Chapline *J. Phys. Chem. B* **103** 11246 (1999)
317. J Lefebvre, R D Antonov, M Radosavljević, J F Lynch, M Llaguno, A T Johnson *Carbon* **38** 1745 (2000)
318. P G Collins, M S Fuhrer, A Zettl *Appl. Phys. Lett.* **76** 894 (2000)
319. R Service *Science* **285** 2053 (1999)
320. P G Collins, K Bradley, M Ishigani, A Zettl *Science* **287** 1801 (2000)
321. Q Chen, L Dai *Appl. Phys. Lett.* **76** 2719 (2000)
322. H T Soh, C F Quate, A F Morpurgo, C M Marcus, J Kong, H Dai *Appl. Phys. Lett.* **75** 627 (1999)
323. Y Y Wei, G Eres *Nanotechnology* **11** (2) 61 (2000)
324. B Wei, Z J Zhang, G Ramanath, P M Ajayan *Appl. Phys. Lett.* **77** 2985 (2000)
325. A N Andriotis, M Menon, G E Froudakis *Appl. Phys. Lett.* **76** 3890 (2000)
326. J-O Lee, C Park, J-J Kim, J Kim, J Wan, K-H Yoo *J. Phys. D* **33** 1953 (2000)
327. P J de Pablo, E Graugnard, B Walsh, R P Andres, S Datta, R Reifenberger *Appl. Phys. Lett.* **74** 323 (1999)
328. T Hertel, R Martel, P Avouris *J. Phys. Chem. B* **102** 910 (1998)
329. M Menon, D Srivastava *Phys. Rev. Lett.* **79** 4453 (1997)
330. M Menon, D Srivastava, S Saini *Semicond. Sci. Technol. A* **13** 51 (1998)
331. G Treboux *J. Phys. Chem. B* **103** 10378 (1999)
332. G Treboux, P Lapstun, Z H Wu, K Silverbrook *J. Phys. Chem. B* **103** 8671 (1999)
333. G Treboux, P Lapstun, K Silverbrook *Chem. Phys. Lett.* **306** 402 (1999)
334. D Zhou, S Seraphin *Chem. Phys. Lett.* **238** 286 (1995)
335. B Gan, J Ahn, Q Zhang, S F Yoon, Rusli, Q-F Huang, H Yang, M-B Yu, W-Z Li *Diam. Relat. Mater.* **9** 897 (2000)
336. J Li, C Padapopoulos, J Xu *Nature (London)* **402** 253 (1999)
337. S H Tsai, C T Shiu, W J Jong, H C Shin *Carbon* **38** 1899 (2000)
338. B C Satishkumar, P J Thomas, A Govindaraj, C N R Rao *Appl. Phys. Lett.* **77** 2530 (2000)
339. P Nagy, R Ehrlich, L P Biro, J Gyulai *Appl. Phys. A* **70** 481 (2000)
340. L Venema *Nature (London)* **407** 959 (2000)
341. D Normille *Science* **281** 632 (1998)
342. D Temple *Mater. Sci. Eng. Rep.* **24** (5) 185 (1999)
343. Y Chen, S Patel, Y Ye, D T Shaw, L Guo *Appl. Phys. Lett.* **73** 2119 (1998)
344. A N Obraztsov, A P Volkov, I Pavlovsky *Diam. Relat. Mater.* **9** 1190 (2000)
345. R Nesper, H-J Muhr *Chimia* **52** (10) 571 (1998)
346. H Ago, F Cacialli, K Petritsch, R H Friend, Th Kugler, W R Salaneck, Y Ono, T Yamabe, K Tanaka *Synth. Met.* **103** 2494 (1999)
347. Y V Gulyaev, N I Sinitsyn, G V Torgashov, S T Mevlyut, A I Zhbanov, Y F Zakharchenko, Z Y Kosakovskaya, L A Chernozatonskii, O E Glukhova, I G Torgashov *J. Vac. Sci. Technol. B* **15** 422 (1997)
348. L A Chernozatonskii, Yu V Gulyaev, Z Ya Kosakovskaya, N I Sinitsyn, G V Torgashov, Yu F Zakharchenko, E A Fedorov, V P Val'chuk *Chem. Phys. Lett.* **233** 63 (1995)
349. W A de Heer, W S Basca, A Chatelain, T Gerfin, R Humphrey-Baker, L Forro, D Ugarte. *Science* **268** 845 (1995)
350. W A de Heer, A Chatelain, D Ugarte *Science* **270** 1179 (1995)
351. J M Bonard, J P Salvetat, T Stockli, W A de Heer, L Forro, A Chatelain *Appl. Phys. Lett.* **73** 918 (1998)
352. Q H Wang, T D Corrigan, R P H Chang *Appl. Phys. Lett.* **70** 3308 (1997)
353. P G Collins, A Zettl *Appl. Phys. Lett.* **69** 1969 (1996)
354. A G Rinzler, J H Hafner, P Nikolaev, L Lou, S G Kim, D Tomanek, P Nordlander, D T Colbert, R E Smalley *Science* **269** 1550 (1995)
355. J-M Bonard, T Stockli, F Maier, W A de Heer, A Chatelain, J-P Salvetat, L Forru *Phys. Rev. Lett.* **81** 1441 (1998)
356. C Wu *Sci. News* **154** (8) 116 (1998)
357. J-M Bonard, J-P Salvetat, T Stlckli, L Forru, A Câvtelain *Appl. Phys. A* **69** 245 (1999)
358. V V Zhirnov, A B Voronin, E I Givargizov, A L Meshcheryakova *J. Vac. Sci. Technol. B* **14** 2034 (1996)
359. J M Kim, W B Choi, N S Lee, J E Jung *Diam. Relat. Mater.* **9** 1184 (2000)
360. J I Sohn, S Lee, Y-H Song, S-Y Choy, R-I Cho, K-S Nam *Appl. Phys. Lett.* **78** 901 (2001)
361. W-K Hong, H-C Shin, S-H Tdai, F-G Tarntai, H-C Cheng *Jpn. J. Appl. Phys.* **39** Pt. 2 9A/B L925 (2000)
362. R Schlesser, R Collazzo, C Bower, O Zhou, Z Sitar *Diam. Relat. Mater.* **9** 1201 (2000)
363. D Lovall, M Buss, E Graugnard, R P Andres, R Reifenberger *Phys. Rev. B* **61** 5683 (2000)
364. Y Saito, K Hamaguchi, K Hata, K Uchida, Y Tasaka, F Ikazaki, M Yumura, A Kasuya, Y Nishina *Nature (London)* **389** 554 (1997)
365. Y Saito, K Hamaguchi, K Hata, K Tohji, A Kasuya, Y Nishina, K Uchida, Y Tasaka, F Ikazaki, M Yumura *Ultramicroscopy* **73** (1–4) 1 (1998)
366. R Z Ma, C L Xu, B Q Wei, J Liang, D H Wu, D J Li *Mater. Res. Bull.* **34** 741 (1999)
367. L Dai, A W H Mau *J. Phys. Chem. B* **104** 1891 (2000)
368. P M Ajayan *Adv. Mater.* **7** 489 (1995)
369. M Kusunoki, T Suzuki, K Kaneko, M Ito *Philos. Mag. Lett.* **79** (4) 153 (1999)
370. M Kusunoki, M Rokkaku, T Suzuki *Appl. Phys. Lett.* **71** 2620 (1997)
371. R V Parthasarathy, K L N Phani, C R Martin *Adv. Mater.* **7** 896 (1995)
372. T Kyotani, L Tsai, A Tomita *Chem. Mater.* **8** 2190 (1996)
373. G Che, B B Lakshmi, C R Martin, E R Fischer, R S Ruoff *Chem. Mater.* **10** 260 (1998)
374. G Che, B B Lakshmi, E R Fischer, C R Martin *Nature (London)* **393** 346 (1998)
375. J S Suh, J S Lee *Appl. Phys. Lett.* **75** 2047 (1999)
376. W Z Li, S S Xie, L X Qian, B H Chang, B S Zou, W Y Zhou, R A Zhao, G Wang *Science* **274** 1701 (1996)
377. Z W Pan, S S Xie, B H Chang, C Y Wang, L Lu, W Y Zhou, W Z Li, L X Qian *Nature (London)* **394** 631 (1998)
378. Z W Pan, S S Xie, B H Chang, L F Sun, W Y Zhou, G Wang *Chem. Phys. Lett.* **299** 97 (1999)

379. S Fan, M G Chapline, N R Franklin, T W Tombler, A M Cassell, H Dai *Science* **283** 512 (1999)
380. *Phys. Status Solidi A* **182** (1) (2000)
381. J Kong, H Soh, A Cassell, C F Quate, H Dai *Nature (London)* **395** 878 (1998)
382. J Kong, C Zhou, A Morpurgo, H Soh, C Marcus, C Quate, H Dai *Appl. Phys. A* **69** 305 (1999)
383. A Cassell, N R Franklin, T W Tombler, E M Chan, J Han, H Dai *J. Am. Chem. Soc.* **121** 7975 (1999)
384. A N Stepanova, E I Givargizov, V I Muratova, in *9 Natsional'naya Konferentsiya po Rostu Kristallov (Tez. Dokl.)* [The 9th National Conference on Crystal Growth (Abstracts of Reports)] (Moscow: Institute of Cryptography of the Russian Academy of Sciences, 2000) p. 320
385. H Kind, J-M Bonard, C Emmenegger, L-O Nilsson, K Hernadi, E Maillard-Schaller, L Schlapbach, L Forru, K Kern *Adv. Mater.* **11** 1285 (1999)
386. C N R Rao, A Govindaraj, R Sen, B S Satishkumar *Mater. Res. Innovat.* **2** (3) 128 (1998)
387. C N R Rao, R Sen, B S Satishkumar, A Govindaraj *Chem. Commun.* 1525 (1998)
388. S Huang, L Dai, A W H Mau *J. Phys. Chem. B* **103** 4223 (1999)
389. Y Yang, S Huang, H He, A W H Mau, L Dai *J. Am. Chem. Soc.* **121** 10832 (1999)
390. S Huang, A W H Mau, T W Turney, P White, L Dai *J. Phys. Chem. B* **104** 2194 (2000)
391. F Rohmund, L K L Falk, E E B Campbell *Chem. Phys. Lett.* **328** 369 (2000)
392. Z F Ren, Z P Huang, J H Xu, P B Wang, M P Siegal, P N Provencio *Science* **282** 1105 (1998)
393. Z P Huang, J W Xu, Z F Ren, J H Wang, M P Siegal, P N Provencio *Appl. Phys. Lett.* **73** 3845 (1998)
394. A M Bonnot, M N Séméria, J F Boronat, T Fournier, L Pontonnier *Diam. Relat. Mater.* **9** 852 (2000)
395. X Xu, G R Brandes *Appl. Phys. Lett.* **74** 2549 (1999)
396. C J Lee, D W Kim, T J Lee, Y C Choi, Y S Park, W S Kim, Y H Lee, W B Choi, N S Lee, K S Park, J M Kim *Chem. Phys. Lett.* **312** 461 (1999)
397. C J Lee, D W Kim, T J Lee, Y C Choi, Y S Park, W S Kim, Y H Lee, W B Choi, N S Lee, J M Kim, J C Choi, S C Yu *Appl. Phys. Lett.* **75** 1721 (1999)
398. C J Lee, J Park, S Y Kang, J H Lee *Chem. Phys. Lett.* **326** 175 (2000)
399. C J Lee, J H Park, J Park *Chem. Phys. Lett.* **323** 560 (2000)
400. C J Lee, J Park, S Y Kang, J H Lee *Chem. Phys. Lett.* **323** 554 (2000)
401. O M Küttel, O Groening, C Emmenegger, L Schlapbach *Appl. Phys. Lett.* **73** 2113 (1998)
402. Y Saito, S Uemura, K Hamaguchi *Jpn. J. Appl. Phys.* **37** (3B) L346 (1998)
403. Y Saito, K Hamaguchi, S Uemura, K Uchida, Y Tasaka, F Ikazaki, M Yumura, A Kasuya, Y Nishina *Appl. Phys. A* **67** 95 (1998)
404. Y Saito *Bull. Ceramic Soc. Jpn.* **33** 434 (1998)
405. Y Saito, S Uemura *Carbon* **38** 169 (2000)
406. J L Kwo, M Yokoyama, W C Wang, F Y Chuang, I N Li *Diam. Relat. Mater.* **9** 1270 (2000)
407. Y Ding, Q-L Hang, H-Z Zhang, S-Q Feng, Z-G Bai, D-P Yu, Z-X Zhang, Z-Q Xue, Z-J Shi, Y-F Lian, Z-N Gu *Chin. Phys. Lett.* **16** 117 (1999); *Chem. Abstr.* **131** 12 291 (1999)
408. O R Monteiro, V P Mammana, M C Salvadori, J W Ager III, S Dimitrievic *Appl. Phys. A* **71** 121 (2000)
409. W B Choi, Y H Lee, N S Lee, J H Kang, S H Park, H Y Kim, D S Chung, S M Lee, S Y Chung, J M Kim *Jpn. J. Appl. Phys.* **39** Pt.1 5A 2560 (2000)
410. Y-K Kwon, D Tomanek, S Iijima *Phys. Rev. Lett.* **82** 1470 (1999)
411. T Rueckes, K Kim, E Joselevich, G Y Tseng, C-L Cheung, C M Lieber *Science* **289** 94 (2000)
412. J K Gimzewski, T A Jung, M T Cuberes, R R Schlittler *Surf. Sci.* **386** 101 (1997)
413. H Tang, M T Cuberes, C Joachim, J K Gimzewski *Surf. Sci.* **386** 115 (1997)
414. T A Jung, R R Schlittler, J K Gimzewski, H Tang, C Joachim *Science* **271** 181 (1996)
415. M F Crommie, C P Lutz, D M Eigler *Science* **262** 218 (1993)
416. Ph Avouris, I-W Lyo, Y Hasegawa *J. Vac. Sci. Technol. A* **11** 1725 (1993)
417. I-W Lyo, Ph Avouris *Science* **253** 173 (1991)
418. T-C Shen, C Wang, G C Abeln, J R Tucker, J W Lyding, Ph Avouris, R E Walkup *Science* **268** 1590 (1995)
419. D H Huang, M Aono *Surf. Sci.* **386** 166 (1997)
420. T Komeda, R Hasunuma, H Mukaida, H Tokumoto *Surf. Sci.* **377 – 379** 149 (1997)
421. H Dai, J H Hafner, A G Rinzler, D T Colbert, R E Smalley *Nature (London)* **384** 147 (1996)
422. F N Dzegilenko, D Srivastava, S Saini *Nanotechnology* **9** 325 (1998)
423. H Dai, N Franklin, J Han *Appl. Phys. Lett.* **73** 1508 (1998)
424. A Okazaki, S Akita, H Nishijima, Y Nakayama *Jpn. J. Appl. Phys.* **39 B** Pt. 1 6 B 3744 (2000)
425. D M Eigler, E K Schweizer *Nature (London)* **344** 524 (1990)
426. J A Stroscio, D M Eigler *Science* **254** 1319 (1991)
427. P Král, D Tománek *Phys. Rev. Lett.* **82** 5373 (1999)
428. T W Tombler, C Zhou, L Alexseyev, J Kong, H Dai, L Liu, C S Jayanthi, M Tang, S-Y Wu. *Nature (London)* **405** 769 (2000)
429. K Tsukagoshi, B P Alphenaar, H Ago *Nature (London)* **401** 572 (1999)
430. J Hone, B Batlogy, Z Benes, A T Johnson, J E Fisher *Science* **289** 1730 (2000)
431. S Berber, Y-K Kwon, D Tománek *Phys. Rev. Lett.* **84** 4613 (2000)
432. J Hone, A Zettl, M Whitney *Synth. Met.* **103** 2498 (1999)
433. J Hone, M Whitney, C Piskoti, A Zettl *Phys. Rev. B* **59** R2514 (1998)
434. M Endo, C Kim, K Nishimura, T Fujino, K Miyashita *Carbon* **38** 183 (2000)
435. J Zhao, A Buldum, J Han, J P Lu *Phys. Rev. Lett.* **85** 1706 (2000)
436. B Gao, A Kleinhammes, C Bower, L Fleming, Y Wu, O Zhou *Chem. Phys. Lett.* **307** 153 (1999)
437. E Frackowiak, S Gautier, H Gaucher, S Bonnamy, F Beguin *Carbon* **37** 61 (1999)
438. F Leroux, K Metenier, S Gautier, E Frackowiak, S Bonnamy, F Beguin *J. Power Sources* **81 – 82** (1 – 2) 317 (1999)
439. S Gautier, E Frackowiak, S Bonnamy, F Beguin, in *Proceedings of Electrochemical Society, 1998 (Recent Advances in the Chemistry and Physics of Fullerene and Related Materials)* p. 1291; *Chem. Abstr.* **129** 307 743 (1998)
440. V A Nalimova *Mol. Cryst. Liq. Cryst. Sci. Technol., Sect. A* **310** 5 (1998)
441. D E Sklovsky, H Gaucher, G H Bondarenko, S Menu, F Beguin, S Bonnamy, J Conard, V A Nalimova *Mol. Cryst. Liq. Cryst. Sci. Technol., Sect. A* **310** 165 (1998); *Chem. Abstr.* **129** 75 448 (1998)
442. G T Wu, C S Wang, X B Zhang, H S Tang, Z F Qi, W Z Li *J. Power Sources* **75** (1) 175 (1998); *Chem. Abstr.* **129** 218 927 (1998)
443. G Sandrock *J. Alloys Compd.* **293 – 295** 877 (1999)
444. A C Dillon, K M Jones, T A Bekkedahl, C H Kiang, D S Bethune, M J Heben *Nature (London)* **386** 377 (1997)
445. C Journet, W K Maser, P Bernier, A Loiseau, M Lamy de la Chapelle, S Lefrant, P Denierd, R Lee, J E Fischer *Nature (London)* **388** 756 (1997)
446. A Chambers, C Park, R T K Baker, N M Rodriguez *J. Phys. Chem. B* **102** 4253 (1998)
447. P Chen, X Wu, J Lin, K L Tan *Science* **285** 91 (1999)
448. H M Cheng, C Liu, H T Cong, M S Dresselhaus *Carbon* **37** 1649 (1999)
449. C Liu, Y Fan, M Liu, H T Cong, H M Dresselhaus *Science* **286** 1127 (1999)
450. Y Ye, C C Ahn, C Witham, B Fultz, J Liu, A G Rinzler, D Colbert, K A Smith, R E Smalley *Appl. Phys. Lett.* **74** 2307 (1999)
451. R R Bacsa, Ch Laurent, A Peigney, W S Bacsa, Th Vaugien, A Rousset *Chem. Phys. Lett.* **321** 566 (2000)
452. *Chem. Eng. News* **77** (27) 29 (1999)
453. R T Yang *Carbon* **38** 623 (2000)
454. C Park, P E Anderson, A Chambers, C D Tan, R Hidalgo, N M Rodriguez *J. Phys. Chem. B* **103** 10572 (1999)
455. G C Carter, F L Carter, in *Metal-Hydrogen Systems* (Ed. T N Veziroglu) (Oxford: Pergamon Press, 1981) p. 503
456. S Hynek, W Fmller, J Bentley *Int. J. Hydrog. Energy* **22** 601 (1997)

457. J E Fischer *Chem. Innovation* **30** (10) 21 (2000)
458. B P Tarasov, N F Goldshleger, A P Moravsky *Usp. Khim. 70* 149 (2001) [*Russ. Chem. Rev.* **70** 131 (2001)]
459. C Nützenadel, A Züttel, D Chartouni, L Schlapbach *Electrochem. Solid-State Lett.* **2** 30 (1999)
460. N Rajalakshmi, K S Dhathathrevan, A Gavindaraj, B S Satishkumar *Electrochim. Acta* **45** 4511 (2000)
461. M R Pederson, J Q Broughton *Phys. Rev. Lett.* **69** 2689 (1992)
462. M Rzepka, P Lamb, M A de la Casa-Lillo *J. Phys. Chem. B* **102** 10894 (1998)
463. Q Wang, J K Johnson *J. Chem. Phys.* **110** 577 (1999)
464. Q Wang, J K Johnson *J. Phys. Chem. B* **103** 277 (1999)
465. F Darkrim, D Levesque *J. Chem. Phys.* **109** 4981 (1998)
466. S M Lee, K S Park, Y Ch Choi, Y S Park, J M Bok, D J Bae, K S Nahm, Y G Choi, S Ch Yu, N-G Kim, T Frauenheim, Y H Lee *Synth. Met.* **113** 209 (2000)
467. S M Lee, Y H Park *Appl. Phys. Lett.* **76** 2877 (2000)
468. V Simonyan, P Diep, J K Johnson *J. Chem. Phys.* **111** 9778 (1999)
469. K A Williams, P C Eklund *Chem. Phys. Lett.* **320** 352 (2000)
470. R H Baughman *Science* **290** 1310 (2000)
471. C Niu, E K Siche, R Hoch, D Moy, H Tennent *Appl. Phys. Lett.* **70** 1480 (1997)
472. C Liu, A J Bard, F Wudl, I Weitz, J R Heath *Electrochem. Solid State Lett.* **2** 577 (1999)
473. R Ma, J Liang, B Wei, B Jang, C Xu, D Wu *Bull. Chem. Soc. Jpn.* **72** 2563 (1999)
474. J Kong, N R Franklin, C Zhou, M G Chapline, S Peng, K Cho, H Dai *Science* **287** 622 (2000)
475. J R Wood, H H Wagner *Appl. Phys. Lett.* **76** 2883 (2000)
476. J K Campbell, L Sun, R M Crooks *J. Am. Chem. Soc.* **121** 3779 (1999)
477. J-J Davis, R J Coles, H A O Hill *J. Electroanal. Chem.* **440** (1 – 2) 279 (1997); *Chem. Abstr.* **128** 120 894 (1998)
478. Z Guo, P J Sadler, S C Tsang *Adv. Mater.* **10** 701 (1998)
479. F Balavoine, P Schultz, C Richard, V Mallouth, T W Ebbesen, C Mioskowski *Angew. Chem., Int. Engl. Ed.* **38** 1912 (1999)
480. J H Hafner, C L Cheung, C M Lieber *J. Am. Chem. Soc.* **121** 9750 (1999)
481. J H Hafner, C L Cheung, C M Lieber *Nature (London)* **398** 761 (1999)
482. C L Cheung, J H Hafner, C M Lieber *Proc. Natl. Acad. Sci. USA* **97** 3809 (2000)
483. C L Cheung, J H Hafner, T W Odom, K Kim, C M Lieber *Appl. Phys. Lett.* **76** 3136 (2000)
484. H Nishijima, S Kamo, S Akita, Y Nakayama, K I Hohmura, S H Yishimura, K Takahashi *Appl. Phys. Lett.* **74** 4061 (1999)
485. Y Nakayama, H Nishijima, S Akita, K I Hohmura, S H Yoshimura, K Yakeyashi *J. Vac. Sci. Technol. B* **18** 661 (2000)
486. R M D Stevens, N A Frederick, B L Smith, D E Morse, G D Stucky, P K Hansma *Nanotechnology* **11** 1 (2000)
487. R Stevens, C Nguyen, A Cassell, L Delzeit, M Meyyappan, J Han *Appl. Phys. Lett.* **77** 3453 (2000)
488. J A Harrison, S J Stuart, D H Robertson, C T White *J. Phys. Chem. B* **101** 9682 (1997)
489. S S Wong, A T Woolley, T W Odom, J-L Huang, P Kim, D V Vezenov, C M Lieber *Appl. Phys. Lett.* **73** 3465 (1998)
490. N Choi, T Uchihashi, H Nishijima, T Ishida, W Mizutani, M Ishikawa, H Tokumoto *Jpn. J. Appl. Phys. B* **39** Pt.1 6B 3707 (2000)
491. F-X Zha, R Czerw, D L Carroll, Ph Kohler-Redlich, B-Q Wei, A Loiseau, S Roth *Phys. Rev. B* **61** 4884 (2000)
492. S S Wong, J D Harper, P T Lansbury, C M Lieber *J. Am. Chem. Soc.* **120** 603 (1998)
493. A T Woolley, G Guillemette, C L Cheung, D E Housman, C M Lieber *Nat. Biotechnol.* **18** 760 (2000)
494. K I Hohmura, Y Itokazu, S H Yoshimura, G Mizuguchi, Y Masamura, K Takeyasu, Y Shiomi, T Tsurimoto, H Nishijima, S Akita, Y Nakayama *J. Electron. Microscopy* **49** 415 (2000)
495. T Uchihashi, N Choi, M Tanigawa, M Ashino, Y Sugawara, H Nishijima, S Akita, Y Nakayama, H Tokumoto, K Yokoyama, S Morita, M Ishikawa *Jpn. J. Appl. Phys.* **39** Pt. 2 8B L887 (2000)
496. S B Arnason, A G Rinzler, Q Hudspeth, A F Habard *Appl. Phys. Lett.* **75** 2842 (1999)
497. J Li, A M Cassell, H Dai *Surf. Interface Anal.* **28** (1) 8 (1999)
498. T W Ebbesen, P M Ajayan *Nature (London)* **358** 220 (1992)
499. N M Rodriguez, M S Kim, R T Baker *J. Phys. Chem.* **98** 13108 (1994)
500. B Coq, J M Planeix, V Brotons *Appl. Catal. A, Gen.* **173** 175 (1998)
501. V Brotons, B Coq, J M Planeix *J. Mol. Catal. A, Chem.* **116** 397 (1997)
502. J M Planeix, N Coustel, B Coq, V Brotons, P S Kumbhar, R Dutartre, P Geneste, P Bernier, P M Ajayan *J. Am. Chem. Soc.* **116** 7935 (1994)
503. J Z Luo, L Z Gao, Y L Leung, C T Au *Catal. Lett.* **66** (1 – 2) 91 (2000)
504. P J Britto, K S V Santhapam, A Rubio, J A Alonso, P M Ajayan *Adv. Mater.* **11** 154 (1999)
505. K Murata, K Kaneko, F Kokai, K Takahashi, M Yudasaka, S Iijima *Chem. Phys. Lett.* **331** 14 (2000)
506. J A Nisha, M Yudasaka, S Bandow, F Kokai, K Takahashi, S Iijima *Chem. Phys. Lett.* **328** 381 (2000)
507. R-H Xie *Nuovo Cimento D* **19** 1867 (1997)
508. R Xie, J Jiang *J. Appl. Phys.* **83** 3001 (1998)
509. R Xie, J Jiang *Chem. Phys. Lett.* **280** 66 (1997)
510. R Xie, J Jiang *Appl. Phys. Lett.* **71** 1029 (1997)
511. R-H Xie *J. Chem. Phys.* **108** 3626 (1998)
512. R H Xie, Q Rao *Chem. Phys. Lett.* **313** 211 (1999)
513. R H Xie *Chem. Phys. Lett.* **310** 379 (1999)
514. V Margulis, T Sizikova *Physica B* **245** 173 (1998)
515. X Wan, J Dong, D Xing *Phys. Rev. B* **58** 6756 (1998)
516. J Jiang, J Dong, X Wan, D Xing *J. Phys. B, At. Mol. Opt. Phys.* **31** 3079 (1998)
517. Vl A Margulis, E A Gaiduk, E N Zhidkin *Diam. Relat. Mater.* **8** 1240 (1999)
518. S Wang, W Huang, H Yang, Q Gong, Z Shi, X Zhou, D Qiang, Z Gu *Chem. Phys. Lett.* **320** 411 (2000)
519. L Vivien, E Anglaret, D Riehl, F Bacou, C Journet, C Goze, M Andrieux, M Brunet, F Lafonta, P Bernier, F Hache *Chem. Phys. Lett.* **307** 317 (1999)
520. S R Mishra, H S Rawat, S C Mehendale, K C Rustagi, A K Sood, R Bandyopadhyay, A Govindaraj, C N R Rao *Chem. Phys. Lett.* **317** 510 (2000)
521. X Sun, R Q Yu, G Q Xu, T S A Hor, W Ji *Appl. Phys. Lett.* **73** 3632 (1998)
522. P Chen, X Wu, X Sun, J Liu, W Ji, K L Tan *Phys. Rev. Lett.* **82** 2548 (1999)
523. X Liu, J Si, B Chang, G Xu, Q Yang, Z Pan, S Xie, P Ye, J Fan, M Wan *Appl. Phys. Lett.* **74** 164 (1999)
524. K Bubke, H Gnewuch, H Hempstead, J Hammer, M L H Green *Appl. Phys. Lett.* **71** 1906 (1997)
525. P Kim, C M Lieber *Science* **286** 2148 (1999)
526. A Globus, D Bailey, J Han, R Jaffe, C Levit, R Merkle, D Srivastava *J. Br. Interplanet. Soc.* **51** 145 (1998)
527. A Globus, C Bauschlicher, J Han, R Jaffe, C Levit, D Srivastava *Nanotechnology* **9** 192 (1998)
528. B S Files *J. Nanopart. Res.* **1** 507 (1999)
529. B S Files, in *Proceedings of NanoSpace'98, Houston, TX, 1998*
530. J Han, A Globus, R Jaffe, G Deardorff *Nanotechnology* **8** (3) 95 (1997)
531. D Srivastava *Nanotechnology* **8** (4) 186 (1997)
532. R E Tuzun, K Sohlberg, D W Noid, B G Sumpter *Nanotechnology* **9** (1) 37 (1998)
533. J Cumings, A Zettl *Science* **289** 602 (2000)
534. M-F Yu, O Lourie, M J Dyer, K Moloni, T F Kelly, R S Ruoff *Science* **287** 637 (2000)
535. M-F Yu, M J Dyer, G D Skidmore, H W Rhors, X K Lu, K D Ausman, J R V Ehr, R S Ruoff *Nanotechnology* **10** 244 (1999)
536. M-F Yu, B I Yakobson, R S Ruoff *J. Phys. Chem. B* **104** 8764 (2000)
537. P M Ajayan, J-C Charlier, A G Rinzler *Proc. Natl. Acad. Sci. USA* **96** 14199 (1999)
538. Q Jiang, N Aya, F G Shi *Appl. Phys. A* **64** 627 (1997)
539. R Raj *Phys. Status Solidi A* **166** 529 (1998)
540. C Carraro *Phys. Rev. B* **61** R16351 (2000)
541. A F Morpurgo, J Kong, C M Marcus, H Dai *Science* **286** 283 (1999)
542. V I Tsebro, O E Omel'yanovskii *Usp. Fiz. Nauk* **170** 906 (2000) [a]

543. M Su, Y Li, B Maynor, A Buldum, J P Lu, J Liu *J. Phys. Chem. B* **104** 6505 (2000)
544. A K MacKnight, A Zakhidov, R Baughman, M Grac, V Rakov, V Ufimtsev, O Jouravlev *NASA Microgravity. Materials of Scientific Conference, Huntsville, AL, 2000 (Preprint)*
545. M Ishigami, J Cumings, A Zettl, S Chen *Chem. Phys. Lett.* **319** 457 (2000)
546. J L Hutchison, N A Kiselev, E P Krinichnaya, A V Krestinin, R O Loutfy, A P Morawsky, V E Muradyan, E D Obraztsova, J Sloan, S V Terekhov, D N Zakharov *Carbon* **39** 761 (2001)
547. J M Calderon Moreno, S S Swamy, T Fujino, M Yoshimura *Chem. Phys. Lett.* **329** 317 (2000)
548. M L Terranova, S Piccirillo, V Sessa, P Sbornicchia, M Rossi, S Botti, D Manno *Chem. Phys. Lett.* **327** 284 (2000)
549. N Grobert, M Terrones, S Trasobares, K Kondratos, H Terrones, J Olivares, J P Jang, Ph Redlich, W K Hsu, C L Reeves, D J Wallis, Y Q Zhu, J P Hare, A J Pidduck, H W Kroto, D R M Walton *Appl. Phys. A* **70** (2) 175 (2000)
550. A A Setlur, S P Doherty, J Y Dai, R P H Chang *Appl. Phys. Lett.* **76** 3008 (2000)
551. Y Ando, X Zhao, K Hirahata, K Suenaga, S Bandow, S Iijima *Chem. Phys. Lett.* **323** 580 (2000)
552. V D Blank, I G Gorlova, J L Hutchison, N A Kiselev, A B Ormont, E V Polyakov, J Sloan, D N Zakharov, S G Zybtsev *Carbon* **38** 1217 (2000)
553. A T Matveev, D Golberg, V P Novikov, L L Klimkovich, Y Bando *Carbon* **39** 155 (2001)
554. *Chem. Eng. News* **78** (9) 36 (2000)
555. W Z Li, L X Qian, S F Qian, W Y Zhou, G Wang, C S Fu, R A Zhao, S S Xie *Sci. China A* **39** 657 (1996)
556. R L Vander Wal, T M Ticich, V E Curtis *Chem. Phys. Lett.* **323** 217 (2000)
557. R L Vander Wal *Chem. Phys. Lett.* **324** 217 (2000)
558. R Kamalarakan, M Terrones, T Seeger, Ph Kohler-Redlich, M Rmhle, Y A Kim, T Hayashi, M Endo *Appl. Phys. Lett.* **77** 3385 (2000)
559. V V Chesnokov, R A Buyanov *Usp. Khim.* **69** 675 (2000) [*Russ. Chem. Rev.* **69** 623 (2000)]
560. V K Frantsuzov, A P Petrusenko, B V Peshnev, A L Lapidus *Khim. Tv. Topliva* (2) 52 (2000)
561. *Phys. World* **3** 6 (2000)
562. K Hirahara, K Suenaga, S Bandow, H Kato, T Okazaki, H Shinohara, S Iijima *Phys. Rev. Lett.* **85** 5384 (2000)
563. D V Kirin, N N Breslavskaya, P N D'yachkov *Dokl. Akad. Nauk* **374** 68 (2000) [c]
564. C Zhou, J Kong, E Yenilmez, H Dai *Science* **290** 1552 (2000)
565. M Ouyang, J-L Huang, C L Cheung, C M Lieber *Science* **291** 97 (2001)
566. E Nagao, H Nishijima, S Akita, Y Nakayama, J A Dvorak *J. Electron Microscopy* **49** 453 (2000)
567. M P Mattson, R C Haddon, A M Rao *J. Mol. Neurosci.* **14** 175 (2000)
568. R Q Long, R T Yang *J. Am. Chem. Soc.* **123** 2058 (2001)
569. Y Jiang, Y Wu, S Zhang, C Xu, W Yu, Y Xie, Y Qian *J. Am. Chem. Soc.* **122** 12 383 (2000)
570. L Ji, J Lin, H C Zeng *Chem. Mater.* **12** 3466 (2000)
571. J N Coleman, D F O'Brian, A B Dalton, B McCarthy, B Lahr, A Drury, R C Barclie, W J Blau *Chem. Commun.* 2001 (2000)
572. Z Shi, Y Lian, X Zhou, Z Gu, Y Zhang, S Iijima, Q Gong, H Li, S-L Zhang *Chem. Commun.* 461 (2000)
573. R Ma, B-Q Wei, C Xu, J Liang, D Wu *Bull. Chem. Soc. Jpn.* **73** 1813 (2000)

[a] — *Physics-Uspekhi (Engl. Transl.)*
[b] — *Russ. J. Inorg. Chem. (Engl. Transl.)*
[c] — *Dokl. Chem. (Engl. Transl.)*

Russian Chemical Reviews **70** (10) 865 – 884 (2001) © 2001 Russian Academy of Sciences and Turpion Ltd

DOI 10.1070/RC2001v070n10ABEH000646

State-of-the-art coordination chemistry of radioactive elements

B I Kharisov, M A Mendez-Rojas

Contents

I.	Introduction	865
II.	General notion of technetium and actinide complexes	865
III.	Actinide alkoxides and other oxygen-containing complexes and salts	867
IV.	Halide complexes of actinides	869
V.	Actinide π-complexes with allyl, cyclopolyene, arene and related ligands	870
VI.	Hydride and hydroborate complexes of actinides	873
VII.	Actinide complexes with macrocyclic ligands	874
VIII.	Actinide complexes with nitrogen-containing ligands	874
IX.	Complexes with phosphorus-containing ligands	875
X.	Sulfur-containing actinide complexes	876
XI.	Technetium complexes	877

Abstract. Modern procedures for the synthesis of coordination and organometallic compounds of actinides and technetium and the properties of these compounds are surveyed. Experimental techniques, including methods for the synthesis of actinide and technetium complexes from elemental metals (oxidative dissolution and direct electrosynthesis), salts and halide, carbonyl and other complexes are generalised. The bibliography includes 283 references.

I. Introduction

Among compounds of natural and artificial radioactive elements (Tc, Pm, Po, Fr, Ra, Ac and actinides), only organometallic compounds and complexes of technetium and actinides (An) have been well studied. Complexes of these metals attract interest because technetium, which is available in multikilogram quantities, is widely used for medical and technical purposes and actinides find application in nuclear industry and power engineering. Over a period of the last two decades, a large number of experimental studies, reviews and monographs were devoted to Tc and An complexes.[1–16] The aim of the present review is to give a comprehensive survey of modern synthetic procedures for the preparation of coordination and organometallic compounds of radioactive elements. The data are systematised according to the nature of the ligands in these complexes.

B I Kharisov Facultad de Ciencias Quimicas, Universidad Autónoma de Nuevo León, 66450 San Nicolás de los Garza 18-F, Nuevo León, México. Fax (52-8) 374 07 09. Tel. (52-8) 375 30 68.
E-mail: bkhariss@ccr.dsi.uanl.mx
M A Mendez-Rojas Centro de Investigaciones Quimicas, Universidad Autónoma del Estado de Hidalgo, Carretera Pachuca-Tulancingo Km. 4.5, 42073 Pachuca, Hidalgo, México. Fax (52-7) 717 20 00, ext. 5075. Tel. (52-7) 717 20 00, ext. 4881.
E-mail: mmendez@uaeh.reduaeh.mx

Received 22 December 2000
Uspekhi Khimii **70** (10) 974 – 995 (2001); translated by T N Safonova

II. General notion of technetium and actinide complexes

Actinium (atomic number 89) and all elements with atomic numbers from 90 to 103 (actinides) are radioactive.[17] Only four actinides (Th – Np) and actinium by itself were found in nature, whereas the remaining elements were prepared artificially by irradiation of U and other elements with neutrons or by bombardment with heavy atoms. Actinides are analogues of lanthanides. They belong to the same IIIB Group but reside in the next row.

Technetium (atomic number 43) has several isotopes two of which are characterised by large half-lifes (2.12×10^5 and 1.5×10^6 years for ^{99m}Tc and ^{98}Tc, respectively) and is a rhenium analogue.[18]

The electronic states of the actinide atoms and ions differ substantially from those of the lanthanide atoms and ions. In both series, the *f* level is successively filled up to the f^{14} configuration; however, this filling in actinides begins with Th only formally because Th does not bear *f* electrons and is an electronic analogue of hafnium.[16] In contrast to lanthanides, actinides can exist in various oxidation states. Actinides in the oxidation state +3 are analogues of lanthanides, whereas actinides in the oxidation state +4 are analogues of Hf(IV) and Ce(IV).

Actinides produce the An^{m+} ($m = 2-4$) and AnO_2^{m+} ($m = 1$ or 2) ions whose highest occupied level is filled only with *f* electrons. In the series of the An^{3+} anions, the actinide contraction is observed, this contraction changing in parallel with the lanthanide contraction. The 5*f* and 6*d* energy levels of the An^{m+} ions as well as the 4*f* and 5*d* energy levels of the Ln^{m+} ions correlate with each other. The difference in the correlations for the An^{3+} and Ln^{3+} ions leads to the noticeable difference in the magnetic properties and electronic spectra of their compounds.[17] Technetium (the $4s^24p^64d^55s^2$ or $4s^24p^64d^65s^1$ electronic configuration) exists in the oxidation states from +1 to +7, the oxidation states from +4 to +7 being most stable.[18]

Spin – orbit coupling (*J*) in the An^{3+} ions is very strong (2000 – 4000 cm^{-1}) and it is ~1000 cm^{-1} stronger than *J* in the Ln^{3+} ions. In contrast to lanthanides, the splitting due to spin – orbit coupling in actinides is comparable with the crystal field splitting and, hence, the *J* value is no longer a good quantum number. Since the 5*f* and 6*d* orbitals have close energies and the

thermally accessible excited states of actinides are filled, the equation for the effective magnetic moment

$$\mu_e = g[J(J+1)]^{1/2}$$

is less appropriate than in the case of lanthanides.[17, 19]

Actinide organometallic complexes contain actinide–carbon π bonds, actinide–carbon σ bonds or bonds of both types. Organometallic complexes of all early actinide elements from thorium to californium are known.[20] However, most data have been obtained for the chemistry of organometallic compounds of Th and U due to the extremely large half-lifes of natural ^{232}Th and ^{238}U (1.41×10^{10} and 4.468×10^9 years, respectively). The first actinide organometallic compound, *viz*., Cp_3UCl, was isolated by Reynolds and Wilkinson in 1956.[21]

The actinide atoms possess rather large atomic and ionic radii and large (up to 14) coordination numbers.[22] Examples of actinide compounds characterised by various coordination numbers and oxidation states are listed in Table 1.

The maximum coordination numbers were found for polymeric uranium hydroborates, whereas the presence of bulkier ligands, for example, of NPh_2, leads to a decrease of the maximum coordination number to 5 or even to 4.[17] Like lanthanides, the spherical An^{3+} and An^{4+} ions have the highest coordination numbers (generally, 8 or 9) and often form isomorphous complexes in which the polyhedron type is determined by repulsions between the ligands (steric factors) or packing factors rather than by the electronic effects.[23] For example, the square antiprism in the rhodanide complexes $Cs_4An(NCS)_8$ and $U(NCS)_4(Ph_3PO)_4$ is transformed into the dodecahedron in the case of $Th(NCS)_4[(Me_2N)_2CO]_4$ or into the cube in the case of $(NEt_4)_4An(NCS)_8$.[17]

The nature of the bond between the π-donor ligand and the actinide centre has been discussed.[24, 25] The authors emphasised that there is no simple answer to the question as to the nature of the bond in organoactinide complexes. Examples of almost completely ionic binding of the Cp^- anions or cyclooctatetraene (COT) with U^{4+} (see Ref. 26) as well as of covalent binding of the metal atom with the aromatic ring of the ligand in uranocene accompanied by essential ligand-to-metal electron transfer are available in the literature.[24, 27, 28] It was concluded [24, 29] that the

Table 1. Coordination numbers (CN) and coordination polyhedra in actinide compounds.[17]

Oxidation state	CN	Coordination polyhedron	Examples of compounds
+7	6	octahedron	$Li_5(AnO_6)$ (An = Np, Pu)
+6	6	octahedron	$(NEt_4)(PaOCl_5)$, AnF_6 (An = U, Np, Pu), *trans*-$UO_2Cl_2(OPPh_3)_2$
	7	pentagonal bipyramid	$[UO_2Cl_2(acac)_2]\cdot$Hacac, $PuO_2(C_2O_4)\cdot 3H_2O$, $K_3UO_2F_5$
	8	hexagonal bipyramid	$Cs_2[AnO_2(MeCO_2)_3]$ (An = Np, Pu, Am), $(UO_2)(NO_3)_2(H_2O)_2$
+5	6	octahedron	$CsAnF_6$ (An = U, Np, Pu)
	7	pentagonal bipyramid	$PaCl_5$
	8	cube	$Na_3(AnF_8)$ (An = Pa, U, Np)
	9	tricapped trigonal prism	$M_2(PaF_7)$ (M = NH_4, K, Rb, Cs)
+4	4	tetrahedron	$U(OAr)_4\cdot[N(SiMe_3)_2]_3\cdot$THF
	5	trigonal bipyramid	$U_2(NEt_2)_8\cdot[Li(THF)_4]\cdot[U(OAr)_5]$
	6	octahedron	Na_2PuCl_6, *cis*-$UCl_4\cdot 2Ph_3PO$, *trans*-$UBr_4\cdot 2Ph_3PO$, $UCl_4\cdot 2$HMPA
		trigonal prism	$U_4(dmed)_3$
	7	pentagonal bipyramid	UBr_4, K_3UF_7
		monocapped octahedron	$[UCl(TMPO)_6]Cl_3$
	8	dodecahedron	$Np(HCOO)_4$, $Th(tta)_4$, $An(S_2CNEt_2)_4$ (An = Th, U, Np, Pu)
		square antiprism	$K_7Th_6F_3$, $An(acac)_4$ (An = Th, U)
+4	8	cube	$(NEt_4)_4[An(NCS)_8]$ (An = Th, Pa, U, Np)
		bicapped trigonal prism	$Th(acac)_4$
		bicapped octahedron	$[UCl_2(Me_2SO)_6](UCl_6)$
	9	tricapped trigonal prism	$(NH_4)_3(ThF_7)$, $LiUF_5$, $Th(tta)_4\cdot$TOPO
		monocapped square antiprism	Li_3ThF_7, $Th(tfa)_4\cdot 2H_2O$, $[C(NH_2)_3]_5[Th(CO_3)_3F_3]$
	10	bicapped square antiprism	$U(C_2H_3O_2)_4\cdot 2H_2O$, $An(MeCO_2)_4$ (An = Th, U), $Na_6[Th(CO_3)_5]\cdot 2H_2O$
	11	irregular structure	$An(NO_3)_4\cdot 5H_2O$ (An = Th, Pu)
	12	icosahedron	$(PPh_4)[Th(NO_3)_5(OPMe_3)_2]$, $An(BH_4)_4$ (An = Np, Pu)
	14	bicapped hexagonal antiprism	$[An(BH_4)_4]_n$ (An = Th, U)
+3	5	trigonal bipyramid	$[K(THF)_2]_2[U(NHAr)_5]\cdot$THF
	6	octahedron	$[UCl_6]^{3-}$
	8	dodecahedron bicapped trigonal prism	$UCl_3\cdot 3$DMSO $AnBr_3$ (An = Pu, Am, Cm, Bk), AnI_3 (An = Pa, U, Np, Pu)
	9	tricapped trigonal prism	$NaPuF_4$, $AnCl_3$ (An = U, Np, Pu, Am, Cm), $Am(sal)_3\cdot H_2O$
+2	6	framework structure	Th_6Br_{12}
0	8	cube	$U(bipy)_4$

Note: acac is acetylacetonate, Hacac is acetylacetone, HMPA is hexamethylphosphoramide, dmed is *N*,*N*′-dimethylethylenediamine, TMPO is trimethylphosphine oxide, tta is thenoyltrifluoroacetonate, TOPO is tri-n-octylphosphine oxide, tfa is trifluoroacetylacetonate, sal is salicylate, bipy is bipyridyl.

covalent binding of the metal atom with the ligand in $U(COT)_2$ involves primarily the 6*d* orbitals of uranium, while the 5*f* orbitals are of secondary importance.

As mentioned above, actinides show various oxidation states in aqueous solutions. Stable oxidation states vary from +3 for Ac to +6 for U and Np and then gradually decrease to +3 for Am and the following elements, except for No (+2). For Ac, Th, Pa, U, Md and Lr, the maximum oxidation states are stable; Np and Pu can occur in the oxidation state +7; Am can exist in the oxidation state +6; Cm, Bk, Cf, Es and Fm can occur in the oxidation state +4; the oxidation state +3 is possible for No. In aqueous solutions, virtually all actinides can exist in the unstable oxidation state +2.[17] The hydrated An^{2+}, An^{3+}, An^{4+}, AnO^{2+} and AnO_2^{2+} ions behave as Brönsted acids.[30]

$$An^{n+} + H_2O \longrightarrow An(OH)^{(n-1)+} + H^+.$$

The An^{4+} ions are typical of actinides from thorium to californium (however, U^{4+} is readily oxidised). As for Th, only Th^{4+} ions exist in solutions. The acidity decreases in the series $Pa^{4+} \gg U^{4+} > Pu^{4+} > Np^{4+} > Th^{4+}$.[17] Individual ions occur only in very dilute solutions. These ions tend to form polynuclear species as the concentration increases

$$m An^{4+} + n H_2O \rightleftharpoons An_m(OH)_n^{(4m-n)+} + n H^+ .$$

The acidity of the An^{n+} ions depends on their charge and radius. The An^{4+} and AnO_2^{2+} ions are much stronger acids than the An^{3+} and AnO_2^{+} ions, respectively.[17] The redox behaviour of actinides is complicated by their high radioactivity, which, in particular, results in the formation of hydrogen peroxide in aqueous solutions.

The data on the complex formation of the actinide ions An^{3+}, An^{4+}, AnO_2^{+} and AnO_2^{2+} (An = U, Np or Pu) with chlorides were surveyed in several comprehensive reviews.[30–32] The results of recent studies of hydrated and chloride complexes of UO_2^{2+}, NpO^{2+}, Np^{4+}, Pu^{3+}, *etc.* by XAFS (X-ray absorption fine structure) spectroscopy were covered in Refs 33 and 34. In particular, using hydrated ions and fluoride complexes of U(IV) and Th(IV) as examples, it was demonstrated that the coordination number of these hydrated ions is 10 and the M–O distances for U(IV) and Th(IV) are in the ranges of 2.42 ± 0.01 and 2.45 ± 0.01 Å, respectively.[34] The results of physical and chemical studies of hydrated complexes of uranium were published in the literature.[35,36]

Mössbauer spectroscopy is very convenient to use for studying the oxidation states and the symmetry of the ligand environment. The Mössbauer effect is observed for ^{232}Th, ^{231}Pa, ^{238}U, ^{240}Pu, ^{243}Am and, particularly, ^{237}Np generated upon the ^{237}U β^--decay. The maximum isomer shifts (up to -70 mm s^{-1}) are observed for Np(VII) compounds; for Np(III) compounds, these shifts decrease to +30 mm s^{-1} (see Ref. 37).

III. Actinide alkoxides and other oxygen-containing complexes and salts

Uranium alkoxides are similar to alkoxides of transuranium elements. Their chemistry has been surveyed in the recent review.[37] Homoleptic alkoxides $An(OR)_n$ are known for $n = 3$ (U and Pu), 4 (Th, U, Np and Pu), 5 (Pa and U) and 6 (U). A great quantity of such U and Th compounds are available, whereas only a few Pa and Pu complexes were prepared. Alkoxides of uranium in the the oxidation states +3, +4, +5 and +6 are known. Complexes characterised by mixed oxidation states, such as $[U(OPh)_3(THF)]_2[UO_2(THF)_2]_2(\mu\text{-}OPh)_4(\mu_3\text{-}O)_2$, were also prepared.[38] Compounds of U(IV) are analogous to Th(IV) compounds.

Most actinide alkoxides are oligomeric {like $[U_3O(OBu^t)_{10}]$}. However, derivatives of bulky alcohols and 2,6-disubstituted phenols are monomeric,[17] for example, $U(OCHBu^t_2)_4$,[39] $U(OEt)_5$,[37] $U(OMe)_6$, $U_2(OEt)_{10}$, $U(OAr)_4$ and $U(OAr)_3$ (Ar = 2,6-$Bu^tC_6H_3$).[37,40,41] The influence of electronic factors on the structure and stability of complexes of uranium tri-*tert*-butylmethoxide was examined.[42]

Monomeric alkoxides can react with each other[43]

$$U(OEt)_4 + U(OEt)_6 \xrightarrow{C_6H_{14}} U_2(OEt)_{10}.$$

Anionic alkoxide complexes, such as $(Bu^t_4N)[U_2(OBu^t)_9]$ and $[Li(THF)_4][U(OAr)_5]$, were also obtained.[44] Treatment of $[U(COT)(BH_4)_2]$ with alcohols ROH (R = Et, Pr^i or Bu^t) afforded the alkoxide derivatives $[U(COT)(BH_4)(OR)]$.[45]

In a toluene solution of the $Th(OCHPr^i_2)_4$ complex, a monomer–dimer equilibrium occurs; however, only the dimeric form crystallises (with trigonal-bipyramidal geometry).[46]

Actinide alkoxides are very readily hydrolysed[17]

$$3\,U_2(OBu^t)_8(HOBu^t) + 2\,H_2O \xrightarrow{PhMe} 2\,U_3O(OBu^t)_{10} + 7\,HOBu^t.$$

The actinide ions have large radii and, consequently, high coordination numbers, which are often responsible for oligomerisation of homoleptic alkoxide complexes of *f* metals[37,47–49] giving rise to dinuclear (**1**), tetranuclear (**2**, **3**) or higher oligomers.[47]

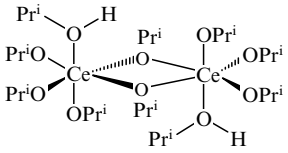

1

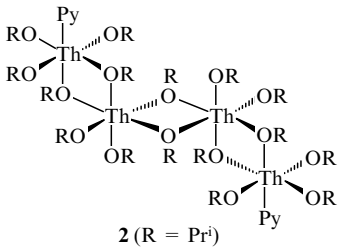

2 (R = Pr^i)

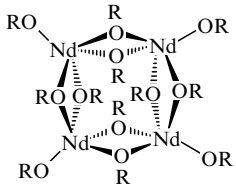

3 (R = CH_2Bu^t)

Dimeric actinide complexes are exemplified by the $\{U[O(2,6\text{-}Pr^i_2C_6H_3)]_3\}_2$ complex (**4**), which contains the unusual π-arene bridge and is sterically hindered due to the presence of the isopropyl groups.[47,49] This complex is stabilised through π-arene interactions both in the solid state and in solution.

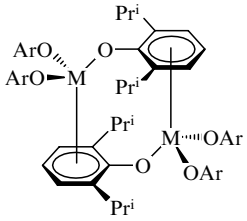

4

Ar = 2,6-$Pr^i_2C_6H_3$; M = La, Nd, Sm, Er, U.

Some actinide complexes can occur both in the monomeric and dimeric forms. Thus treatment of metallacycle **5** with isopropyl alcohol afforded the homoleptic $Th_2(OCHPr^i_2)_8$ complex.

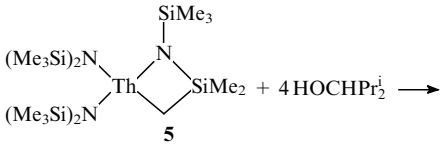

5

$$\longrightarrow 1/2\,Th_2(OCHPr^i_2)_8 + 3\,HN(SiMe_3)_2$$

6

In the solid state, the latter exists as dimer **6** (the coordination number of thorium is 5) consisting of two ThO_5 fragments (with trigonal-bipyramidal geometry), which are linked *via* a shared

axial-equatorial edge.[44] At room temperature, this complex in non-coordinating solvents exists as monomer **7**.[46,47]

$$\underset{\mathbf{6}}{Th_2(OCHPr^i_2)_8} \rightleftharpoons 2\,\underset{\mathbf{7}}{Th(OCHPr^i_2)_4}$$

The dimeric halide-alkoxide complex $Th_2I_4(OPr^i)_4(HOPr^i)_2$ was prepared by the reaction of metallic thorium with 2 equivalents of iodine in isopropyl alcohol.[50] This reaction provides an example of the direct synthesis from elemental metals. The $Th_2I_4(OPr^i)_4(HOPr^i)_2$ complex (the triclinic system, space group $P\bar{1}$) has a bioctahedral structure (the octahedra are linked *via* a shared edge), the isopropyloxy anions occupying the bridging positions. This complex is isostructural to its uranium analogue $U_2I_4(OPr^i)_4(HOPr^i)_2$ (see Ref. 51) and is structurally similar [50] to a number of alkoxide and halide-alkoxide compounds of lanthanides and early transition metals, such as $M_2(OPr^i)_8(HOPr^i)_2$ (M = Zr or Ce) [52] and $Ti_2Cl_4(OR)_4(HOR)_2$ (R = CH_2CH_2Cl).[53] It was assumed that the $[AnI(OPr^i)_2(HOPr^i)_4]I$ intermediates (An = U or Th) were initially formed, which then underwent dimerisation.[50] Other alkoxide complexes of actinides, for example $Th_2(OBu^t)_8(HOBu^t)$,[54] $(TBA)U_2(OBu^t)_9$ (TBA is tetrabutylammonium) and $KU_2(OBu^t)_9$,[55] were also characterised. It was demonstrated that the K^+ cations in the latter complex in solutions remain associated with the dimeric anions, the structures of the molecular unit in the crystalline state and solution being, apparently, identical.

Oxidation of the uranium(III) aryloxide complex $U(OAr)_3$ (**8**) (OAr is 2,6-di-*tert*-butylphenoxide) afforded various oxide and halide-oxide complexes of U(IV).[50]

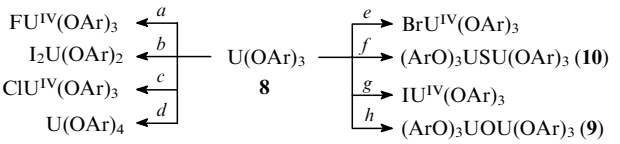

(*a*) $AgBF_4$ or $AgPF_6$; (*b*) CI_4; (*c*) PCl_5; (*d*) O_2; (*e*) AgBr, CBr_4 or PBr_5; (*f*) COS or $Ph_3P=S$; (*h*) N_2O, NO, Me_3NO or pyridine *N*-oxide.

In the presence of an appropriate source of chalcogenide, oxidation gave rise to bridged binuclear uranium(IV) complexes **9** or **10**.[50]

Alkoxide complexes of cyclooctatetraenyluranium(IV) were synthesised by the reactions of cyclooctatetraenyluranium precursors with alcohols.[56]

The unusual monomeric complex $U(OTeF_5)_6$ can be considered as an analogue of metal alkoxides.[57] In spite of the large molecular weight, this complex sublimes at 333 K (1.3 Pa).[57]

Actinide alkoxides are generally prepared from dialkylamides and alcohols.[44] The homoleptic $UX_4(MeCN)_n$ complex can serve as a precursor in the synthesis of mixed halide-alkoxide compounds of uranium. The coordination environment in the reaction product depends on the nature of the halogen. Thus the reaction of $UBr_4(MeCN)_4$ with 2 equivalents of KOAr in THF afforded the $Br_2U(OAr)_2(THF)\cdot 4THF$ complex, whereas UCl_4 produced the anionic $[K(THF)_4][UCl_3(OAr)_2]$ complex. In solution, mixed halide-aryloxide complexes do not undergo ligand exchange. Light halides of uranium(IV) are reagents of choice in the metathesis because $UI_4(MeCN)_4$ is thermally unstable.[58] A series of aryloxides and alkoxides of (triamidoamine)uranium(IV) were described.[59]

One of the approaches to the synthesis of methoxide derivatives of actinides of type **11** involves the reactions of $Cp^*_2MH_2$ (Cp^* is pentamethylcyclopentadienyl; M = U or Th) with trimethyl phosphite in pentane.[60]

$$Cp^*_2ThH_2 \xrightarrow[-H_2]{P(OMe)_3} Cp^*_2Th(OMe)_2 + \underset{\mathbf{11}}{[Cp^*_2Th(OMe)_2](\mu\text{-}PH)}$$

The corresponding thorium derivatives can also be prepared by alcoholysis of alkyl complexes, for example, of $Cp^*_2ThMe_2$, the reactions of $Cp^*_2ThCl_2$ with alkali metal hydroxides, the insertion of ketones at the Th–Alk bond (see the review [37] and references cited therein)

$$Cp^*_2ThCl(Me) + Me_2CO \xrightarrow{PhMe} Cp^*_2ThCl(OCMe_3)\,,$$

and hydrogenation of η^2-acyl complexes [37]

$$Cp^*_2ThCl(\eta^2\text{-}OCCH_2Bu^t) \xrightarrow{H_2} Cp^*_2ThCl(\eta^2\text{-}OCH_2CH_2Bu^t).$$

Crystallisation of a Pu(IV) salt (0.15 mol litre^{-1}) from a solution of Na_2CO_3 (2.6 mol litre^{-1}) afforded single crystals of $[Na_6Pu(CO_3)_5]_2\cdot Na_2CO_3\cdot 33\,H_2O$ (the space group is $P2_1/c$).[61] In the solid state, the asymmetric unit contains a complex framework consisting of $[Pu(CO_3)_5]^{6-}$ anions and Na^+ cations linked through interactions between the CO_3^{2-} ligands and the H_2O molecules. The $[Pu(CO_3)_5]^{6-}$ anion can be considered as a pseudohexagonal bipyramid with three carbonate ligands in the equatorial plane and two carbonate ligands in the axial positions. Its structural unit is very similar to that of the related $[Th(CO_3)_5]^{6-}$ anion involved in the crystal structures of $Na_6[Th(CO_3)_5]\cdot 12\,H_2O$ and $[C(NH_2)_3]_6[Th(CO_3)_5]\cdot 4\,H_2O$ (see Ref. 61 and references cited therein). Clark *et al.*[61] believed that the well-known coordination polyhedron (hexagonal bipyramid) in the $[PuO_2(CO_3)_3]^{4-}$ complex (**12**) [62–64] is analogous to that of the $[Pu(CO_3)_5]^{6-}$ anion (**13**).

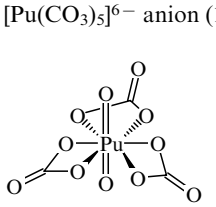

12

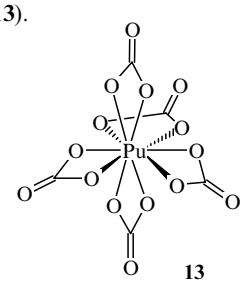

13

The structure of yet another carbonate complex, *viz.*, $(Me_4N)_4[NpO_2(CO_3)_3]\cdot 8\,H_2O$, consists of alternating anionic and cationic layers.[65] The water molecules of crystallisation are involved in the formation of the $\{[NpO_2(CO_3)_3]\cdot 8\,H_2O\}_n^{4n-}$ anionic layers. Analogous uranium and uranyl complex ions in carbonate,[66,67] sulfate,[68] nitrate,[69] phosphate,[70] silicate [70] and citrate complexes [71] as well as in other oxygen-containing compounds were also studied. In particular, the behaviour of carbonate complexes of uranium in $CO_2-HCO_3^-$ solutions of various ionic strengths (I = 0.5, 1.0, 2.0 or 3.0 mol litre^{-1} of $NaClO_4$) at 25 °C was examined by UV/Vis spectrophotometry.[65] The authors believed that tetracarbonate complexes exist in an equilibrium with pentacarbonate complexes

$$[U(CO_3)_4]^{4-} + CO_3^{2-} \rightleftharpoons [U(CO_3)_5]^{6-}\,.$$

Citric acid forms mixed Fe and U complexes analogous to the citrate complex of uranium. The mixed Fe–U citrate complex is stable to biodegradation.[71]

Among other oxygen-containing actinide compounds, uranium peroxo complexes with various ligands, *viz.*, with tri- and tetradentate Schiff's bases,[72] amines or aminocarboxylic acids,[73] were described. The einsteinium(II) complexes with crown ethers $[Es(18\text{-}C\text{-}6)]L_2$ (L = ClO_4^- and BF_4^-, BPh_4^-) were prepared.[74] The behaviour of einsteinium(II) in THF was examined by co-crystallisation. It was found that the coefficients of co-crystallisation of Es(II) with solid $[Sr(18\text{-}C\text{-}6)]I_2$ in THF depend on the ClO_4^- and BF_4^- ions as additives and are independent of the presence of the BPh_4^- ions.

Very stable actinide complexes with β-diketones [for example, with $An(acac)_4$ or $AnO_2(acac)_2$] are used for isolation and separation of actinides by extraction. These complexes are prepared by the reactions of metal or actinyl halides with the

Table 2. Preparation of actinide alkoxides and related oxygen-containing complexes.

Starting compound or metal	Reaction system	Products	Ref.
Synthesis from elemental metals			
U anode	Hbac, O_2 or N_2 (see [a])	$UO_2(bac)_2(Hbac)_{0.5}$, $UO_2(bac)_2$	84
	Hacac, O_2 or N_2 (see [a])	$U(acac)_4$, $UO_2(acac)_2 \cdot Hacac$	84
Synthesis from salts			
$UO_2(MeCO_2)_2$	Hacac Hdbm HBTF in EtOH	$UO_2(Hacac)_2$ $UO_2(Hdbm)_2$ $UO_2(HBTF)_2$	75–77, 85
$ThCl_4$	$NaOPr^i$, $HOPr^i$	$Th(OPr^i)_4(HOPr^i)_x$	37, 38, 86
$PaCl_5$	NaOEt, EtOH	$Pa(OEt)_5$	37, 87
$NpCl_4$	LiOR, ROH (R = Me, Et)	$Np(OR)_4$	37, 88
Synthesis from halide complexes			
$UBr_4(MeCN)_4$	KOAr	$Br_2U(OAr)(THF) \cdot (THF)_4$	89
$ThBr_4(THF)_4$	2,6-$Bu^t_2C_6H_3OK$ (see [b])	$ThBr_2(OAr)_2(THF)_2$	44, 90
Py_2PuCl_6	NH_3, PhH, Pr^iOH [c]	$Pu(OPr^i)_4$, $Pu(OPr^i)_4(Py)$	91
Synthesis from β-diketonates or alkoxides			
$U(OCHBu^t_2)_4$	MeLi	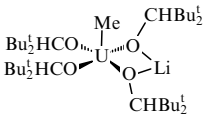	92
$Th(acac)_4$	electrochemical reduction [d]	$[Th(acac)_4]^-$	93
Synthesis from π-complexes			
$(MeCp)_3U(THF)$	alcohols or thiols	$(MeCp)_3UR$ (R = OMe, OPr^i, OPh, SPr^i)	94, 95
Cp^*_3UH	EtOH	Cp^*_3UOEt	96
$HU(C_5H_4Bu^t)_3$	EtOH	$(C_5H_4Bu^t)_3UOEt$	96
$HU(C_5H_4SiMe_3)_3$	EtOH	$(C_5H_4SiMe_3)_3UOEt$	96

[a] Direct electrochemical synthesis; [b] alkylation of the product afforded $Th(OAr)_2(CH_2SiMe_3)_2$; [c] recrystallisation from hot isopropyl alcohol gave rise to $Pu(OPr^i)_4(HOPr^i)$; [d] the product lost acac[7] to form $Th(acac)_3$; the known Th(III) complexes are few in number.

corresponding diketone in the presence of a base. In the case of An(IV) actinides, only fluorine-containing diketonates form complexes with Lewis bases; diketonates of actinyls AnO_2 (An = Np or Pu) generally exhibit the Lewis acid properties and are stabilised through the formation of adducts. The fluorinated complex $UO_2(hfa)_2$ (hfa is hexafluoroacetylacetonate) exhibits pronounced acidic properties and its adducts with water and alcohols can be sublimed without decomposition.[17]

Uranyl acetylacetonate,[75,76] other actinide β-diketonates[77] and uranyl complexes with 2-hydroxy-1-naphthaldehyde (**14**)[78] and 2-hydroxybenzaldehyde[79] were studied in detail by spectroscopic methods. These investigations made it possible to establish the structure of the complex **14** synthesised previously.[80]

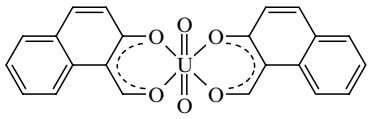

14

Based on the data on the electronegativities obtained earlier (see references cited in the study [78]), the U–O bond orders in the complexes **14**, $UO_2(acac)_2$, $UO_2(Hdbm)_2$ and $UO_2(HBTF)_2$ (Hdbm is dibenzoylmethane, HBTF is 1,1,1-trifluoropentane-2,4-dione) were calculated. The results of the calculations indicated that the equatorially coordinated 2-hydroxy-1-naphthaldehyde ligand exerts a pronounced effect on the oxygen atoms of the UO_2^{2+} anion.[78]

Based on the spectra of neptunium β-diketonates,[77] the Np(IV) complexes with acetylacetonate, dibenzoylmethane, benzoylacetone (Hbac), benzoyltrifluoroacetone (Hbtfa) and thenoyltrifluoroacetone (Htta) can be divided into two groups according to the type of coordination polyhedron about the central atom. In $Np(acac)_4$, $Np(dbm)_4$ and $Np(tta)_4$, the coordination polyhedron is a tetragonal antiprism, whereas $Np(bac)_4$ and $Np(btfa)_4$ (dbm is dibenzoylmethanate, bac is benzoylacetonate and btfa is benzoyltrifluoroacetonate) have bitetrahedral structures. Apparently, when Np(IV) β-diketonates are dissolved in benzene, the bidentate ligands are oriented about the central atom so that the oxygen atoms form the tetragonal-pyramidal coordination.[77]

It should be noted that uranium β-diketonates were also prepared by direct electrochemical synthesis using a dissolving anode. Thus electrochemical oxidation of uranium in the presence of β-diketones afforded chelate complexes of the UL_4 or UO_2L_2 type (L is diketonate).[81–83] The reaction with benzoylacetone gave rise to a compound with composition $UO_2(bac)_2(Hbac)_{0.5}$ along with the above-mentioned complexes.[82] In our opinion, the structure **15**, which was assigned to this compound on the basis of the IR spectroscopic data, needs further investigation.

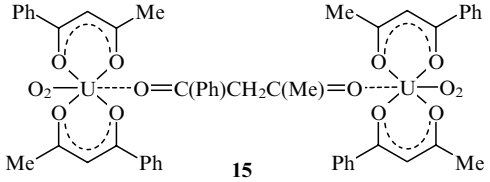

15

Selected methods for the synthesis of actinide alkoxides are listed in Table 2.

IV. Halide complexes of actinides

Light actinides (U, Np and Pu) react with iodine or bromine in donor solvents[97,98] to give complexes of trivalent actinides AnX_3L_4 (X = Br or I).

$$U + 1.5\,I_2 + n\,L \xrightarrow{0\ ^\circ C} UI_3L_n$$

16a–c

$n = 2$, L = DME (**a**); $n = 4$, L = THF (**b**), Py (**c**).

This reaction is a convenient and highly efficient procedure for the preparation of halide complexes of actinides in quantitative yields, which does not require special equipment.

Complexes of uranium triiodide with Lewis bases are used as intermediates in the synthesis of other trivalent uranium compounds. For example, the $UI_3(THF)_4$ adduct (**16b**), which can be prepared in large amounts, is a soluble form of UI_3 convenient for subsequent use in synthesis.[98] Reactions involving solvate complexes of other uranium halides or alkoxides can be complicated, for example, by the formation of mixtures of products.

The mononuclear complex $UI_3(THF)_4$ (**16b**) crystallises in the space group $P2_1/c$. The coordination environment about the central U atom is a pentagonal prism. The complex **16b** is stable up to 75 °C. At a higher temperature, the THF molecules are successively eliminated; at 162 °C, UI_3 is finally formed.

Other adducts of uranium halides UX_3 were also described.[99–103]

Actinide tetrahalides readily react with Lewis bases to give complexes containing two or four donor atoms. The compositions of some resulting products differ from usual $AnCl_4 \cdot 2L$ or $AnCl_4 \cdot 4L$. For example, the $AnCl_4 \cdot nL$ complexes, where $n = 2.5$, 5 [L is *N*,*N*-dimethylacetamide (DMA)] or 6 (L = DMSO or TMPO), were prepared. Complexes with composition $AnCl_4 \cdot 2$ HMPA (An = Th or U) are extremely volatile.[17] The coordination polyhedron typical of the $AnCl_4 \cdot 2L$ complexes is a *trans*-octahedron.[17]

The cationic uranium(IV) complexes $UX_2L_4Y_2$ [X = Cl, Br or I; L is a bulky neutral O-donor ligand, such as tris(pyrrolidin-1-yl)phosphine oxide; Y = ClO_4 or BPh_4] were described.[102]

The reactions of UI_4 with a series of sulfoxide donor ligands in non-aqueous media were investigated. The behaviour of UI_4 was compared with that of UCl_4 and UBr_4 in the presence of the same ligands. It was demonstrated that UI_4 was readily oxidised with dimethyl or diisobutyl sulfoxide at ~20 °C. Only complexes with compositions $UI_4(DMSO)_8$ and $UI_4(DIBSO)_6$ (DIBSO is diisobutyl sulfoxide) appeared to be stable and were isolated.[104]

All actinide halides tend to accept Hal^- ions to form anionic complexes. The stability of the complexes decreases in the series F ≫ Cl > Br ≫ I. Adducts of actinide trihalides are ionised to a large extent. Thus uranium trichloride crystallises from dimethyl sulfoxide as the solvate $UCl_3 \cdot 3$ DMSO. Its structure consists of the dodecahedral $[U(OSMe_2)_8]^+$ cations and the octahedral $[UCl_6]^-$ anions. X-ray diffraction study demonstrated that americium chloride hexahydrate has an ionic structure built of the $[AmCl_2(H_2O)_6]^+$ cations and $[Cl(H_2O)_6]^-$ anions, which are linked *via* hydrogen bridges.[17]

Uranium and protactinium pentahalides generate complexes of the $AnX_5 \cdot L$ type (X = Cl or Br; L = R_3PO or HMPA). Dissolution of UO_3 in thionyl chloride afforded the $UCl_5 \cdot SOCl_2$ adduct, whereas dissolution of Pa(V) hydroxide gave rise to the ionic complex $(SO)(PaCl_6)_2$. Generally, actinide hexahalides do not react with Lewis bases (except for the $UCl_6 \cdot$ bipy complex), whereas actinyl halides readily form complexes with composition $AnO_2X_2 \cdot nL$ ($n = 1$, 1.5, 2, 3 or 4).[17]

Uranium fluorides UF_5 and UF_6 give complexes with 2-fluoropyridine (F-Py) or bipy.[105] Thus UF_6 in CH_2Cl_2 produced the $UF_4 \cdot$(F-Py) and $U_2F_{12} \cdot$ bipy complexes, respectively. However, in the case of the UF_6–bipy system, reduction of UF_6 was the predominating process and the formation of $U_2F_{12} \cdot$ bipy {the authors believed that this complex has the structure $[UF_4(bipy)_2]^{2+} \cdot [UF_7]_2^- \cdot UF_6$} can be considered as the first stage of this reduction.

In the case of UF_5, two products were obtained and structurally characterised. These are the extremely moisture-sensitive $UF_5 \cdot$ bipy and the ionic derivative $[(bipy)_2H]^+[UF_6]^-$.

The $AnX_3(THF)_4$ complexes serve as synthetic precursors of a number of inorganic and organometallic complexes due, in particular, to their high solubility in toluene and THF. The use of $UI_3(THF)_4$ can also provide a convenient approach to the synthesis of many other compounds of trivalent uranium.[97]

Salts of organic ligands with alkali metals react with $AnX_3(THF)_4$ to give the corresponding aryloxides, amides, *etc*. This reaction can serve as a highly efficient procedure for the preparation both of the known and new complexes of trivalent actinides. Thus reduction of uranium tetrachloride with NaH or Na/Hg in THF afforded poorly soluble $UCl_3(THF)_n$.[106] This compound is sometimes used for the synthesis of other uranium complexes. However, this procedure is of limited application due to the formation of by-products. For example, the synthesis of $U[N(SiMe_3)_2]_3$ from $UCl_3(THF)_n$ and $NaN(SiMe_3)_2$ often give rises[97] to a mixture of a U(III) complex and a uranium(IV) derivative, *viz*., the metallacycle $[(Me_3Si)_2N]_2U(CH_2SiMe_2NSiMe_3)$.[107]

Selected procedures for the synthesis of halide complexes of actinides are listed in Table 3.

Table 3. Synthesis of halide complexes of actinides.

Starting compound or metal	Reaction system	Products	Ref.
Synthesis from elemental metals			
U	X_2 (X = Cl, Br, I), THF	$UX_3(THF)_4$	97, 98
Th	X_2 (X = Br, I), THF	$ThX_4(THF)_4$	44
Th anode [a]	Br_2, MeCN	$ThBr_4(MeCN)_4$	108
U	$HgCl_2$, THF	$UCl_4(THF)_3$ (see [b])	109
An (U, Np, Pu)	Br_2 or I_2, THF	$AnX_3(THF)_4$ (see [c])	97
Synthesis from salts or halide complexes			
UI_4	DMSO	$UI_4(DMSO)_n$ ($n = 6, 8$)	104
	DIBSO	$UI_4(DIBSO)_n$ ($n = 6, 8$)	104
UCl_4	NaH	$UCl_3 \cdot n$ THF	44
$ThBr_4(THF)_4$	$KNPh_2$, THF KNMePh, THF	$Th(NPh_2)_4 \cdot$ THF $K[Th(NMePh)_5]$	110
$ThBr_4(THF)_4$	Cp*MgBr(THF)	$Cp^*ThBr_3(THF)_3$	111
$UI_3(THF)_4$	KCp*, THF	$Cp^*UI_2(THF)_3$	20, 98
$AnI_3(THF)_4$ (An = U, Np, Pu)	$NaN(SiMe_3)_2$, THF	$An[N(SiMe_3)_2]_3$	97, 112

[a] Direct electrochemical synthesis; [b] a large amount of a uranium amalgam was obtained as a by-product; [c] air-sensitive.

V. Actinide π-complexes with allyl, cyclopolyene, arene and related ligands

Considerable recent attention has been given to actinide complexes with allyl, cyclopolyene and arene ligands, particularly, with cyclopentadiene and its derivatives (see review [20]).

Allyl complexes can be synthesised from $AnCl_4$ and the Grignard reagent[44]

$$AnCl_4 + AllMgCl \xrightarrow[<0\ ^\circ C]{Et_2O} An(\eta^3\text{-All})_4 .$$

According to the data of low-temperature NMR spectroscopy,[20] the allyl groups in these complexes are η^3-coordinated and can be replaced under the action of HX or alcohols to produce, for example, $U(C_3H_5)_3X$ or $[U(C_3H_5)_3(OR)]_2$.[44] Thus the dimeric *tert*-butyloxyallyl complex $[U(C_3H_5)_3(OR)]_2$ (**17**) was synthesised.[20]

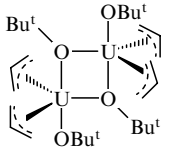

17

Of actinide π-complexes, the uranium(III, IV) and thorium(III, IV) complexes with cyclopentadiene and its derivatives were obtained in the widest range.

Uranium(V, VI) complexes [20] and neptunium(VI) and californium(III) sandwich complexes were also prepared.[44] These complexes can be compositionally divided into the following groups: Cp_nAn (n = 3 or 4), Cp_nAnX (n = 2 or 3), Cp_2AnX_n (n = 1 or 2) and $CpAnX_n$ (n = 2 or 3), X being generally Hal. The corresponding cyclopentadienyl alkyls, carbonyls, alkoxides, *etc*. are also known.[20] All Cp_4An complexes are poorly soluble in organic solvents. The U–C distances in the Cp_4U complex are 2.81(2) Å. The bonds between the An atom and the ligand are covalent in character.[20, 44]

The Cp_3An complexes are strong Lewis acids and form complexes with various Lewis bases (see Ref. 24 and references cited therein).

The Cp_3UCl complex, which was the first synthesised organoactinide compound,[21, 44] serves as a precursor of compounds containing the non-bridging metal–metal bond between, for example, uranium and iron or ruthenium [$Cp_3U-MCp(CO)_2$, M = Fe or Ru] or between uranium and germanium (Cp_3UGePh_3).[20, 113] The first organouranium(III) complexes,[24, 114, 115] *viz*., tris[(cyclopentadienyl)uranium] and some its derivatives of the Cp_3UL type, are also used for the synthesis of bimetallic compounds.[24]

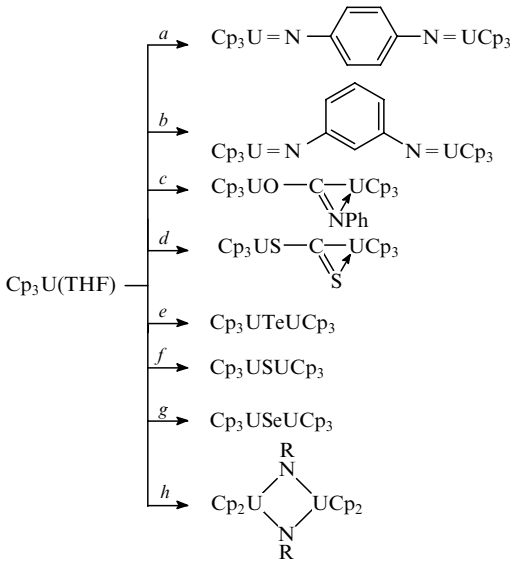

(*a*) 1,4-$(N_3)_2C_6H_4$; (*b*) 1,3-$(N_3)_2C_6H_4$ (*c*) PhNCO; (*d*) CS_2; (*e*) $TePBu_3$; (*f*) COS or $Ph_3P=S$; (*g*) $Ph_3P=Se$; (*h*) $Cp_3U=NR$; R = Ph, $SiMe_3$.

Voltammetric studies [116] demonstrated that oxidation of $(RC_5H_4)_3UCl$ (R = H, Me, Bu^t or Me_3Si) was accompanied by disproportionation. NMR studies revealed electron transfer and ligand exchange in Cp_3UX (X = Hal, BH_4 or Alk).[24, 117]

$$Cp_3UX \underset{-e^-}{\overset{e^-}{\rightleftharpoons}} Cp_3UX^-,$$

$$Cp_3UX + Cp_3U^*(THF) \rightleftharpoons Cp_3U^*(THF) + Cp_3U^*X,$$

$$Cp_3UX^- + Cp_3U^*(THF) \rightleftharpoons Cp_3U^*(THF) + Cp_3U^*X^-.$$

The equilibrium constants of the ligand exchange in complexes with substituted cyclopentadienyl ligands were determined.[24, 118] It was found that binding of ligands with $(MeCp)_3U$ is reduced in the series of the ligands PMe_3 > $P(OMe)_3$ > Py > tetrahydrothiophene > THF > quinuclidine > CO, whereas binding of $(Me_3SiC_5H_4)_3U$ with the EtNC ligand is stronger than with the EtCN ligand, which is indicative of substantial π-back bonding with uranium in the case of π-acceptor ligands.[24] The results of calculations of the electronic structure of the model $Cp_3U(CO)$ complex showed substantial back bonding between the 5*f* orbitals of U and the 2π orbitals of CO, which leads to stabilisation of the 5*f* atomic orbitals of uranium.[20, 119] Some uranium complexes containing carbonyl ligands were described in the study.[120] The relativistic effective core potentials of tris(cyclopentadienyl) actinide complexes were calculated by the *ab initio* quantum-chemical method. These complexes were examined also by gas-phase UV photoelectron spectroscopy.[121, 122]

The Cp_3AnR^1 complexes tend to incorporate the CO, CO_2 and CNR^2 ligands to form η^2-acyl (**18**), η^2-carboxylate (**19**) and η^2-iminoalkyl (**20**) complexes, respectively.[20]

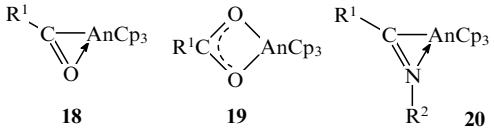

The Cp_3UX compounds containing the U–P, U–N, U–Si, U–Sn or U–Ge bonds were prepared from Cp_3UCl by the replacement of the chloride ligand.[24] In the crystal structures of $Cp_3U(OPh)$ and $Cp_3U(OSiPh_3)$, which were established by X-ray diffraction analysis, the U–O distances are shortened [2.119(7) and 2.135(8) Å, respectively] and the U–O–C and U–O–Si angles are 159.4(5)° and 172.6(6)°, respectively. These geometric parameters are indicative of strong π-bonding between the U and O atoms in oxygen-containing uranium complexes.[24] The bimetallic oxygen-bridged complex, *viz*., μ-*O*-bis[tris(cyclopentadienyl)uranium(IV)] was investigated.[123] The absolute enthalpies of the cleavage of the uranium–ligand bonds in complexes containing the U–S bonds of the L_3U-SR type (L = $C_5H_4Bu^n$, $C_5H_4SiMe_3$ or $C_9H_6SiMe_3$; R = Et or Bu) were determined.[124] The heteroatomic compound $UCp_2(\mu\text{-}Cl)_2Li[(Me_2NCH_2CH_2)_2$. .NMe] containing two chloride bridges provides yet another example of bimetallic complexes.[125]

The electronic structure and configuration of the ground state of the monomeric alkyl uranium(III) complex η^5-$Cp^*_2UCH(SiMe_3)_2$ were studied.[126] The ground state of the molecule is $4A''[(a')^1(a'')^1(a'')^1]$, which corresponds to the $5f^3$ configuration of the uranium atom; its energy is close to that of the higher-lying $4A''(5f^26d^1)$ state. The uranium(III) ions free of ligands can adopt two different electronic configurations, *viz*., $5f^3$ and $5f^2d^1$ (see Ref. 126 and references cited therein). The ground state of the U^{3+} ions in the gaseous phase has the $5f^3$ configuration. According to the results of an EPR study of the Th[η^5-$C_5H_3(SiMe_3)_2]_3$ complex in the gaseous state, Th(III) in the ground state adopts the $6d^1$ configuration, whereas the free ion has the $5f^1$ configuration.[127]

The insertion of CO or CO_2 into the An–R bond in the $Cp^*_2AnR_2$ complexes gave rise to complexes **21**–**23** or carbene-like η^2-acyl complexes $Cp^*_2An(COR)_2$ (**24**, R = Alk).[20, 128–130]

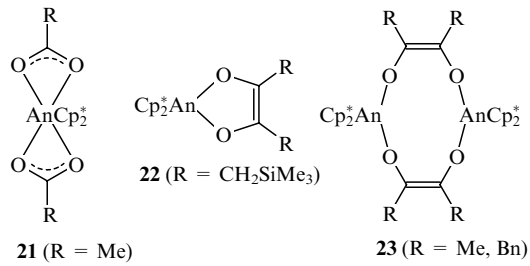

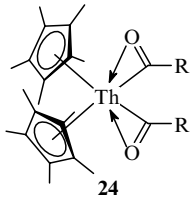

The dynamic behaviour of $CpUCl_3L_2$ in solutions was examined.[24, 131] In toluene, rapid isomerisation and the ligand exchange were observed.[24]

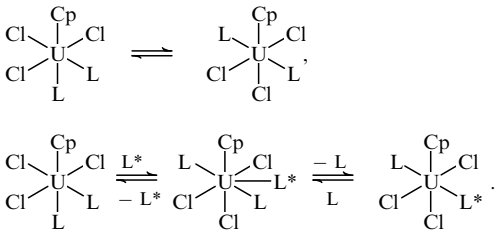

The tribromide complex $Cp^*ThBr_3(THF)_3$ (see Ref. 111 and Table 3) is a convenient compound for studying the chemistry of mono(pentamethylcyclopentadienyl) derivatives of thorium. Treatment of this complex with bases or Grignard reagents afforded aryloxide or alkyl derivatives.[111]

$$Cp^*ThBr_3(THF)_3 + KOAr \xrightarrow[18\ h]{THF} Cp^*ThBr_2(OAr)(THF) + KBr,$$

$$Cp^*ThBr_3(THF)_3 + 2\,KOAr \xrightarrow[18\ h]{THF} Cp^*ThBr_2(OAr)_2 + 2\,KBr,$$

$$Cp^*ThBr_2(OAr)_2 + MeMgBr \longrightarrow Cp^*MeTh(OAr)_2 + MgBr_2.$$

In 1971, the first indenyl derivative of actinides was prepared upon treatment of uranium tetrachloride with indenyl anions.[132] The indenyl uranium(III) complex $U(C_9H_7)_3$ was synthesised from UCl_3 and indenylsodium.[133] Indenyl actinide(IV) complexes **25** were prepared from the corresponding halides and indenylpotassium.[20]

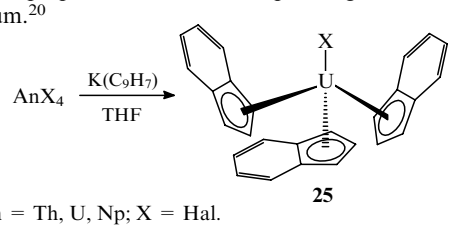

25

An = Th, U, Np; X = Hal.

Uranium complexes **26**–**28** containing phosphacyclopentadienyl ligands were described.[24, 134]

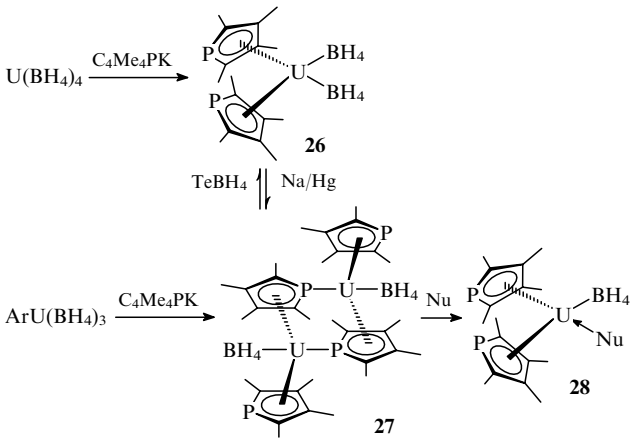

Nu = THF, $OPPh_3$.

The structure of the first cycloheptatrienyl sandwich complex $[K(18\text{-}C\text{-}6)][U(\eta\text{-}C_7H_7)_2]$ was established.[135] The authors believed that the cycloheptatrienyl ligand can be formally considered as $C_7H_7^{3-}$ and the uranium atom occurs in the oxidation state +5.[135, 136] It was demonstrated that the C_7H_7 ligands in this compound are planar and are located parallel to each other and perpendicular to the axis passing through the uranium atom and the centres of the rings.[135]

Generally, cyclooctatetraene complexes of actinides have the composition $(COT)_2An$ or $(COT)AnX_2$ (X = Hal). Compounds of the mixed type (COT)AnCp can also be obtained. Some of these complexes contain solvent molecules, for example, THF.[20] Compounds of this type can be prepared, for example, according to the following procedures:

$$AnCl_4 + 2\,K_2(COT) \longrightarrow An(COT)_2 + 4\,KCl,$$

An = Th, Pa, U, Np;

$$(PyH)_2PuCl_6 + 2\,K_2(COT) \longrightarrow Pu(COT)_2 + 4\,KCl + 2\,PyHCl,$$

$$ThCl_4 + Th(COT)_2 \longrightarrow 2\,(COT)ThCl_2(THF)_2,$$

$$UCl_4 + COT + 2\,NaH \longrightarrow (COT)UCl_2(THF)_2 + 2\,NaCl + H_2.$$

Cyclooctatetraene complexes of uranium, thorium, protactinium, neptunium and plutonium $[(\eta\text{-}COT)An(\mu\text{-}SPr)_2]_2$ with

Table 4. Selected actinide complexes with allyl, cyclopolyene, arene, alkyl and carbonyl ligands.

Starting compound	Reagent	Reaction product	Ref.
Allyl complexes			
$AnCl_4$	C_3H_5MgCl, Et_2O	$An(C_3H_5)_4$	20, 44
$U(C_3H_5)_4$	HOR, Et_2O	$[U(C_3H_5)_2(OR)_2]_2$	20
Cyclopentadienyl complexes			
Cp_3AnCl	$NaC_{10}H_8$, THF or Na/Hg, THF	$Cp_3An(THF)$	24, 140
MX_4 (M = Th, U, Np; X = Cl, Br, I)	M′Cp, DME (M′ = Na, K, Tl)	Cp_3AnX	20, 44, 141
$(MeC_5H_4)_3UBu^t$	C_2H_4 or CO in PhMe	$(MeC_5H_4)_3U(Bu^t)L$ (L = C_2H_4, CO)	142
Cp_3UCl	LiL (L = PPh_2, NEt_2, $SiPh_3$)	Cp_3UL	143–145
Cp_3UX (X = NEt_2, PPh_2, $SiPh_3$)	2,6-$Me_2C_6H_3NC$	$Cp_3U\cdot[\eta^2\text{-}C(X)=N\cdot C_6H_3Me_2\text{-}2,6]$	20, 145, 146
$Cp_3U(NEt_2)$	$HSnPh_3$	$Cp_3U(SnPh_3)$	24
$Cp_3U{=}C(H)PPh_2Me$	HC≡CPh	$Cp_3UC{\equiv}CPh$	24

Starting compound	Reagent	Reaction product	Ref.
Cyclopentadienyl complexes			
$(MeCp)_3U(THF)$	Me_3SiN_3 or PhN_3	$(MeCp)_3U=NR$ (R = Me_3Si, Ph)	20
L_3UH, (L = Cp*, $C_5H_4Bu^t$, $C_5H_4SiMe_3$)	I_2	L_3UI	96
Cp_3AnCl (An = Th,U,Np)	RMgX in THF or RLi in Et_2O	Cp_3AnR	20
Cp_4U, Cp_3UBu^n or Cp_3UBu^i	Bu^nCl, Bu^tCl, BnCl	Cp_3UBu^n, $Cp_3UCH_2CMe_2Cl$, Cp_3UBn, Cp_3UCl or $CpUBn_3$	147
$Cp^*_2ThX_2$ (X = Cl, Br)	$CpRu(CO)_2Na$	$Cp^*_2(X)Th\cdot Ru(Cp)(CO)_2$	24
$Cp^*_2AnCl_2$	LiR, Et_2O	$Cp^*_2AnR_2$ (R = Alk)	20
$(Me_3Si)_2C_5H_3UX_2$	Na/Hg, THF	$(Me_3Si)_2C_5H_3\cdot UX(THF)$	20
$BkCl_3$	Cp_2Be	$[Cp_2BkCl]_2$	20

Table 4 (continued).

Starting compound	Reagent	Reaction product	Ref.	Starting compound	Reagent	Reaction product	Ref.
Arene complexes				Cyclooctatetraene complexes			
UCl_4	C_6Me_6, $AlCl_3$, Al	$[U_3(\mu_3\text{-}Cl)_2(\mu_2\text{-}Cl)_3 \cdot (\mu_1,\eta^2\text{-}AlCl_4)_3 \cdot (\eta^6\text{-}C_6Me_6)_3](AlCl_4)$	24	AnX_3 (An = U, Np, Pu, Am)	$K_2(COT)$, solvent (solv)	$[K(solv)][An(COT)_2]$	152, 153
	Al, $AlCl_3$, PhH	$(PhH)U(AlCl_4)_3$	98	$AnCl_4$ (An = U, Th)	COT, NaH	$(COT)AnCl_2(THF)_2$	24
	Zn, $AlCl_3$, C_6Me_6	$[(C_6Me_6)_2U_2Cl_7]^+ \cdot [AlCl_4]^-$	98	$U(BH_4)_4$	COT	$(COT)U(BH_4)_2$	24
Alkyl complexes				$(PyH)_2PuCl_6$	$K_2(COT)$, THF	$Pu(COT)_2$	20
UCl_4	LiR, L (L = THF, Et_2O)	$Li_2UR_6L_8$	20	$(COT)ThCl_2(THF)_2$	Cp*MgCl(THF), PhMe	(COT)ThCp*Cl(THF)	154
$ThCl_4$	LiMe, TMEDA, Et_2O	$[Li(TMEDA)]_3 \cdot ThMe_7 \cdot TMEDA$ [a]	148	$UI_3(THF)_4$	1) KCp*, THF 2) $K_2(COT)$	Cp*U(COT)(THF)	155
Cycloheptatriene complexes				Carbonyl complexes			
UCl_4	C_7H_8, THF	$[U(\eta\text{-}C_7H_7)_2]^-$	96	U (vapour)	CO, Ar (4 K)	$U(CO)_x$	156
UX_4 (X = NEt_2, BH_4)	$K(C_7H_9)$	$K[X_3U \cdot (\mu\text{-}\eta^7\text{:}\eta^7\text{-}C_7H_7)UX_5]$	149	$[(Me_3Si)_2C_5H_3]U$	CO	$[(Me_3Si)_2C_5H_3]U(CO)$	20
Cyclooctatetraene complexes				Cp_3MR (M = U, Th, Np)	CO	$Cp_3M(CO)R$	44, 157
UCl_4	$K_2(COT)$	$U(COT)_2$	150, 151				

[a] In this complex, six of seven CH_3 groups are involved in coordination to the $Li(TMEDA)^+$ cations, two groups being coordinated to each of the cations; TMEDA is tetramethylenediamine.

mixed ligands were prepared by treatment of $An(COT)(BH_4)$ with thiol.[137] Mono(cyclooctatetraene) amide uranium complexes $K[U(COT)(NEt_2)_2]$ and $U(COT)(NEt_2)_2(THF)$ were synthesised from tetrakis(diethylamine)uranium and bis(cyclooctatetraene)uranium, respectively. Oxidation of these complexes afforded a series of uranium(V) derivatives.[138]

As can be seen from Table 4, actinide π-complexes containing the cyclopolyene or arene ligands (see also Ref. 139) are more abundant than actinide complexes with other ligands.

VI. Hydride and hydroborate complexes of actinides

The first organoactinide hydrides were prepared by hydrogenation of $Cp^*_2AnR_2$.[20]

$$Cp^*_2AnR_2 + H_2 \longrightarrow Cp^*_2AnH_2 + 2\,RH$$

Both monomeric and oligomeric hydride complexes of actinides are available. Generally, these complexes contain OAlk, 1,2-bis(dimethylphosphino)ethane (dmpe) or cyclopentadienyl as additional ligands. Thus uranium and thorium tetrahydroborates are polymeric compounds, whereas neptunium and plutonium tetrahydroborates are monomeric. Methyltrihydroborate derivatives $An(MeBH_3)_4$ always occur as monomers.

$$AnF_4 + 2\,Al(BH_4)_3 \xrightarrow{0\ ^\circ C} An(BH_4)_4 + 2\,AlF_2(BH_4)$$

The volatility of the complexes increases and their stability decreases on going from thorium to plutonium.[17]

Thorium, neptunium, plutonium and protactinium hydroborates and uranium tris(tetrahydroborate) possess similar properties. However, Th, Np, Pu and Pa hydroborates have a number of characteristic structural features.[44] The $UH(BH_4)_3(DME)$ complex contains the U–H bond. The $U(BH_4)_3[Ph_2P(Py)]_2$ complex was also described in the cited study.[44]

Trimeric thorium complex **29** provides a rare example of hydride complexes of early actinides, which are stabilised only by the aryloxide ligands.[90]

$$Th(OAr)_2(CH_2SiMe_3)_2 \xrightarrow[-\,SiMe_4]{H_2,\ PhP,\ 1.5\ atm,\ 7\ days} \longrightarrow$$

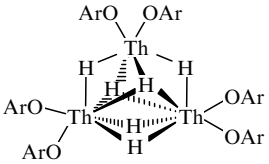

29

Ar = $C_6H_3Bu^t_2$-2,6

The complex **29** exhibits moderate catalytic activity in hydrogenation of hex-1-ene.[158] Alkoxide tetrahydroborate complexes of uranium(IV) were also described.[159]

Organoactinide hydrides are formed from the Ar_nAnR complexes through metathesis of σ-bonds.[20]

$$Ar_nAnR + H_2 \longrightarrow \begin{array}{c} \overset{\delta-}{H}\!-\!\overset{\delta+}{H} \\ Ar_nAn\text{----}R \\ \delta+\quad\ \delta- \end{array} \longrightarrow Ar_nAnH + RH$$

The structure of complex **30** was established.[20] The geometric parameters [the H–Th–Th and Th–H–Th angles are 58(1)° and 122(4)°, respectively; the distance between the thorium atoms is 4.007(8) Å] indicate that the metal–metal interaction in this complex is weak.

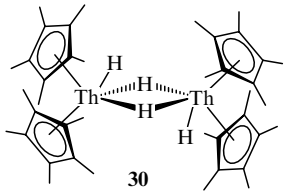

30

The unusual electron-deficient cyclopentadienyl complexes $(C_5H_4PPh_2)_2U(BH_4)_2$ and $(C_5H_4BH_3)_2U(BH_4)_2$ were described.[160]

Other cyclopentadienyl and related hydroborate complexes, for example, $[Na(THF)_6][Cp^*U(BH_4)_3]_2$,[161] were also synthesised.[161,162]

Selected examples of hydride and hydroborate complexes of actinides are listed in Table 5.

Table 5. Selected hydride and hydroborate complexes of actinides.

Starting compound	Reagent	Reaction product	Ref.
UH_3	B_2H_6, THF	$U(BH_4)_3(THF)_3$	44
$U(BH_4)_4$	thermal decomposition in solution	$U(BH_4)_3$	44
	THF	$U(BH_4)_4(THF)_2$	44
	Et_2O	$[U(BH_4)_4(Et_2O)]_\infty$	44
ThX_4 (X = Cl, Br)	$Li_2C_2B_9H_{11}$	$[Li(THF)_4]_2 \cdot Th(\eta^5\text{-}C_2B_9H_{11})_2X_2$	163
$ThBr_4(THF)_4$	CpMgBr(THF)	$CpThBr_3(THF)_3$	164
$Th(OAr)_2 \cdot (CH_2SiMe_3)_2$	H_2	$Th_3(\mu_3\text{-}H)_2(\mu_2\text{-}H)_4 \cdot (OAr)_6$	90
$UBr_4(MeCN)_2$	$Li_2C_2B_9H_{11}$, MeCN	$Li_2[U^{IV}(\eta^5\text{-}C_2B_9H_{11})_2 \cdot Br_2]$	165
$UI_3(THF)_4$	$Li_2C_2B_9H_{11}$, TMEDA	$[Li(TMEDA)] \cdot [U(C_2B_9H_{11})I_2(THF)_2]$	165
$Cp^*_2UH_2$	dmpe	$Cp^*_2U(H)Cl$	20
$(Me_3XC_5H_4)_3UCl$ (X = C, Si)	$KHBEt_3$	$(Me_3XC_5H_4)_3UH$	166
Cp^*_3UH	Ph_3PBH_3	$Cp^*_3UBH_4$	96
$(C_5H_4Bu^t)_3UH$	Ph_3PBH_3	$(C_5H_4Bu^t)_3UBH_4$	96
$(C_5H_4SiMe_3)_3UH$	Ph_3PBH_3	$(C_5H_4SiMe_3)_3UBH_4$	96
$[U(\eta\text{-}C_5Me_5)_2 \cdot Cl(THF)]$ or $[U(\eta\text{-}C_5H_4R)_3Cl]$ (R = H, Bu, $SiMe_3$)	$[K(THF)_2] \cdot [ReH_6(PPh_3)_2]$	$K[Cl(\eta\text{-}C_5Me_5)_2UH_6 \cdot Re(PPh_3)_2]$ or $[U(\eta\text{-}C_5H_4R)_3UH_6 \cdot Re(PPh_3)_2]$	167
Cp_2MR_2 (M = U, Th)	H_2	$Cp_2M(H)(\mu\text{-}H)_2 \cdot M(H)Cp_2$	44
$[(\eta^5\text{-}C_2B_9H_{11})_2 \cdot U^{IV}Br_2] \cdot 2[Li(THF)_4]$	electrochemical reduction and reduction with Na/Hg	$[(\eta^5\text{-}C_2B_9H_{11})_2U^{III}Br \cdot (THF)] \cdot 2[Li(THF)_x]$ ($x = 2-4$)	168

VII. Actinide complexes with macrocyclic ligands

Data on several actinide complexes with crown ethers and other macrocyclic ligands were published in the literature. Thus treatment of uranium and thorium tetrakis(diethylamides) $[An(NEt_2)_4]$ with free porphyrin (TPP) afforded the diporphyrin non-planar sandwich complexes $An(TPP)_2$.[17] Ultrafast electronic deactivation and the vibrational dynamics for the excited states of the uranium(IV) porphyrin sandwich complexes were examined.[169]

General procedures for the preparation of actinide complexes with macrocyclic Schiff's bases involve direct binding of the metal ion with the corresponding ligand and cyclisation in the presence of the metal ion. Thus phthalodinitrile reacted with anhydrous uranyl dichloride in DMF to give a 'superphthalocyanine' uranyl complex. Condensation of ethylenediamine with 2,6-dicarbonylpyridine in the presence of UO_2^{2+} gave rise to a hexaazamacrocyclic complex.[17] When irradiated with neutrons, the phthalocyanine complex $ThPc_2$ (Pc is phthalocyanine) entered into the nuclear reaction to give the corresponding protactinium(IV) complex.[17]

$$^{232}ThPc_2(n,\gamma)^{233}ThPc_2 \longrightarrow {}^{233}PaPc_2$$

The phthalocyanine complexes $AnPc_2$ were described in detail in a number of publications.[170–173]

Complexes with other polydentate ligands, for example, with chelating agents, can be used for efficient binding of actinide ions. These complexes are soluble both in water and organic solvents.[17] The higher the dentation of the ligand the more stable the complex. In the An^{4+}(EDTA) complexes (EDTA is ethylenediaminetetraacetic acid), the ligand is hexadentate and adopts a twist conformation.[17] Binding of plutonium and other radionuclides can be carried out with the use of cyclic and linear catecholamines.[174]

Actinide complexes with crown ethers are generally prepared from actinide salts. Complexes only with tri- and tetravalent actinide ions are known {for example, $[UCl_3(18\text{-}C\text{-}6)]_2 \cdot [UO_2Cl_3(OH)H_2O]$}. The hydrogen bonds between the oxygen atoms of the ether and the water molecules of coordination were found in the UO_2^{2+} complexes.[17] The IR spectra and the isotope effects for uranium complexes with crown ethers and the crystal structures of some of these compounds were published in the literature.[175]

Actinide complexes with crown ethers can be prepared also from organometallic compounds. Thus Cp_3UCl reacted with 18-C-6 in the presence of a sodium amalgam in THF to yield $(Cp_3UCl)[Na(18\text{-}C\text{-}6)]$ (see Ref. 24 and references cited therein).

VIII. Actinide complexes with nitrogen-containing ligands

Most of N-donor bases possess low affinity for actinides and act predominantly as proton acceptors. The An–N bonds with mono- and even bidentate N-donor ligands are rather weak.[17] The complex $UO_2(hfa)_2$ exhibiting high acidity forms a 1:1 complex only with ammonia. Like actinide alkoxides, actinide amides occur generally in the associated form. For example, these compounds react with chelating *N,N′*-dimethylethylenediamine to give the linear trimeric $[U(dmed)_2]_3$ complex and the square tetrameric $[U(dmed)_2]_4$ complex.[17,176] Dialkylamide and related complexes, such as $U[N(SiMe_3)_2]_3$, $[U(NEt_2)_3]BF_4$, $U(NPh_2)_4$, $UO_2[N(SiMe_3)_2]_2 \cdot (OPPh_3)_2$ and $UO_2CrO_4 \cdot 2\,MeCONEt_2$, were described in the literature.[97,177–182]

The structure of the $U[N(SiMe_3)_2\{N(SiMe_3)[SiMe_2-CH_2B(C_6F_5)_3]\}]$ complex was established by X-ray and neutron diffraction analysis. It was demonstrated that the electron deficiency on the uranium atom is effectively compensated by the formation of multicentre bonds between the U atom and the $SiCH_2$ groups of the amine ligands. The X-ray diffraction data are unambiguously indicative of μ^3-coordination of the BH_4 groups.[183] The structure of the unusual uranium(III) complex with a tripodal aromatic amine, *viz.*, tris[(2,2′-bipyridin-6-yl)]amine, was established by X-ray diffraction analysis.[184]

Protolysis of the U–N bond in amide complexes of uranium affords cationic complexes. This procedure was used for the synthesis of compounds containing the cations $[U(\eta\text{-}Cp)_3(THF)]^+$, $[U(\eta\text{-}Cp^*)(NEt_2)_2(THF)_2]^+$, $[(U\text{-}\eta\text{-}C_5R_5)_2 \cdot (NEt_2)(THF)]^+$, $[U(\eta\text{-}C_5R_5)(\eta\text{-}COT)(THF)_2]^+$ (R = H, Me),[185] $[U(NEt_2)_3]^+$, $[U(NEt_2)_2(THF)_3]^{2+}$, *etc.*[177] The resulting Th and U complexes with the silylated $N(CH_2CH_2NSiMe_3)_3$ ligand contain bonds between the metal atoms and the chlorine, carbon, hydrogen or oxygen atoms.[186] Chloro, pentamethylcyclopentadienyl and tetrahydroborate complexes of uranium containing the $N(CH_2CH_2NSiMe_3)_3$ ligand were characterised by the X-ray diffraction method.[186] The reactions of actinide amides were surveyed in a recent review.[187]

Only several imide complexes of actinides are known: $Me_3SiN=U^{V}[N(SiMe_3)_2]_3$, $Me_3SiN=U^{VI}F[N(SiMe_3)_2]_3$, $Cp_2.U(NC_6H_2Bu^t_3\text{-}2,4,6)$ and $U[N(CHMeCH=PPh_2Me)]Cp_3$.[188,189] In complexes of the $(C_5H_4Me)_3U=NR$ type (R = Ph or $SiMe_3$), both lone electron pairs of nitrogen are involved in binding with uranium.[24,190] Of the simplest nitrogen-containing ligands, the azide anion gives very stable complexes with uranium ($K_{diss} = 5\times10^{-3}$). The stabilities of the latter complexes are comparable with those of fluoride complexes.[17] The binuclear (U—Mo) heterocomplexes with N_2 were prepared.[191] IR spectroscopic and quasirelativistic theoretical studies of the coordination and activation of N_2 with the uranium and thorium atoms were carried out virtually at the same time.[192]

The mononuclear $UCp^*_2(NHR)_2$ complexes (R = 2,6-$Me_2C_6H_3$, Et or Bu) were synthesised, their structures were established and these complexes were demonstrated to catalyse hydroamination of terminal alkynes with ammonia.[193] The data on complex formation of uranium(VI) with neutral N-donors in DMSO were reported.[194]

An analogue of the uranyl ion was found in the crystal structure of the red complex $PPh^+_4\{UOCl_4[NP(C_6H_4Me\text{-}3)_3]\}^-$ (**31**).[195] The air-stable complex **31** was prepared from compound **32** by the replacement of the chloride ligand in the $[UOCl_5]^-$ anion accompanied by elimination of Me_3SiCl.

$$PPh^+_4[UOCl_5]^- + Me_3Si[NP(C_6H_4Me\text{-}3)_3] \xrightarrow[-Me_3SiCl]{CH_2Cl_2} PPh^+_4\{UOCl_4[NP(C_6H_4Me\text{-}3)_3]\}^-$$

32 → **31**

According to the data of X-ray diffraction analysis, the $\{UOCl_4[NP(C_6H_4Me\text{-}3)_3]\}^-$ ion contains the linear O=U=N group coordinated by four chlorine atoms.[195] The U—O distance (1.76 Å) is typical of the uranyl ion (see Ref. 195 and references cited therein). The U—N distance (1.90 Å) indicates that the bond order is no less than 2. The U—N—P group is nearly linear (171.9°), which suggests that the π electrons of the nitrogen atom are completely involved in bonding with uranium. The orders of the bonds between the uranium atom and each of the oxygen atoms in the uranyl ion can be equal to 3 due to the fact that the uranium atom bears simultaneously *f* and *d* valence orbitals.[195,196]

Other anionic actinide complexes can be prepared immediately from salts. For example, UF_5 and UF_6 react with nitrogen bases to give molecular or ionic compounds, such as $[(bipy)_2H]^+[UF_6]^-$, $UF_4(2\text{-}FC_5H_4N)$ and $U_2F_{12}(bipy)$.[197]

Thermolysis of the thorium derivative $Th(OSO_2CF_3).[N(SiMe_3)_2]_3$ in the presence of 1 equiv. of pentamethylcyclopentadiene afforded binuclear complex **33**.[111]

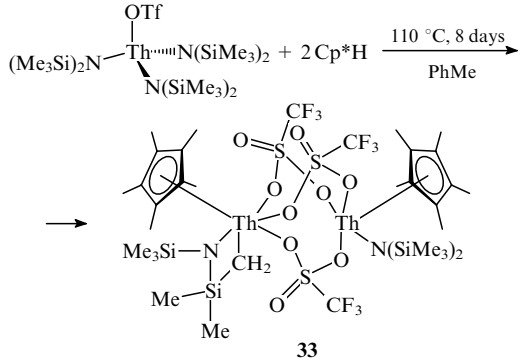

33

The actinide complex with 1,4-di-*tert*-butyl-1,4-diazabutadiene (DAB) **34** was prepared for the first time from the complex containing $N(CH_2CH_2NHSiMe_3)_3$ (tren) as a ligand.[198]

$$[(tren)ThCl]_2 + 2\,Li[Bu^t_2(DAB)_2] \xrightarrow[-80\ ^\circ C]{THF} 2\,(tren)Th[Bu^t_2(DAB)] + 2\,\{Li[Bu^t_2(DAB)]\}Cl$$

34

The complex **34** was obtained as red paramagnetic crystals (monoclinic, the space group is $P2_1/n$). The $N(CH_2CH_2NHSiMe_3)_3$ ligand ensures the optimum spatial environment for stabilisation of this complex. Since thorium(IV) compounds are diamagnetic, the diazabutadiene ligand in the paramagnetic complex **34** is subjected to one-electron reduction, *i.e.*, this ligand is present as the $[Bu^t_2DAB]^{-\bullet}$ radical anion.

The complex formation of neptunium(VI) with 3,3′-bis(diazaridine) derivatives[199] and of uranium(VI) with 8-hydroxyquinoline and its 5-halogen derivatives was studied.[200] In the latter case, the UO_2L and UO_2L_2 complexes (where L is a 8-hydroxyquinoline derivative) were obtained.[200]

Considerable recent attention has been given to uranium complexes with Schiff's bases (see, for example, the review[201]). Uranium(VI) complexes with Schiff's bases are used as organic oxidants (the catalytic modifications of these reactions were also developed).[202] Polystyrene-supported chelating resins incorporating U(VI) complexes with Schiff's bases are available.[203,204] Salicylaldehyde[205] and triethylenetetramine,[203] 3-formylsalicylic acid and *o*-hydroxybenzylamine[204] or salicylaldehyde and 1-amino-2-hydroxynaphthalene-4-sulfonic acid[206] were used as precursors of Schiff's bases. Uranium(VI) complexes with Schiff's bases exhibit photochromic properties. The kinetics and the mechanisms of photochromic conversions were examined.[207]

Examples of actinide complexes with nitrogen-containing ligands are given in Table 6.

Table 6. Selected actinide complexes with nitrogen-containing ligands.

Starting compound	Reagents	Reaction products	Ref.
UO_2Cl_2	$KN(SiMe_3)_2$, THF	$UO_2[N(SiMe_3)_2]_2\cdot(THF)_2$	208
$ThBr_4(THF)_4$	KNR_2	$Th(NPh_2)_4(THF)$ or $K[Th(NMePh_5)]$	44, 110
$UCl_3(THF)_3$	$NaN(SiMe_3)_2$, THF	$U[N(SiMe_3)_2]_3$	112
$U(NPh_2)_4$	L (L = Py, Et_2O, THF, $(EtO)_3PO$)	$U(NPh_2)_4\cdot L$	180
$(NSiMe_2)_2U\cdot CH_2SiMe_2NSiMe_3$	Ph_2NH	$U(NPh_2)_4$	44
UCl_4	$LiNEt_2$	$U(NEt_2)_4$	44
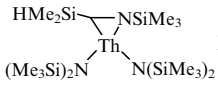	HNMePh	$Th[N(SiMe_3)_2]_2\cdot(NMePh)_2$	110
$(Me_3Si)_2N[ThN\cdot(SiMe_3)\cdot(SiHMe_2CH)]$	1) CF_3SO_3H 2) CpH	$Cp[(Me_3Si)_2N]Th\cdot(\mu_2\text{-}OSO_2CF_3)_3\cdot Th[N(SiMe)_3\cdot(SiHMe_2CH)]Cp$	208
$Cp_3U=C(H)PPh_2Me$	$HNPh_2$	Cp_3UNPh_2	24
$(C_5H_4Me)_3U(THF)$	RN_3 (R = Me_3Si, Ph)	$(C_5H_4Me)_3U=NR$	190
$Cp_2U(NEt_2)_2$	RNC	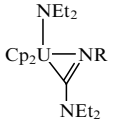	44

IX. Complexes with phosphorus-containing ligands

A large number of actinide complexes, which bear oxygen-containing phosphorus ligands and in which the metal atom is

coordinated by the oxygen atom, are available.[17] Examples of phosphine complexes containing the An–P bond are few in number.[209] Thus thorium(IV) and uranium(IV) tetrahalides react with trimethylphosphine to give the 1 : 2 complexes $MCl_4(PMe_3)_2$ (M = U or Th).[17, 210] The $U[Me_2PCH_2CH_2PMe_2]_4$ complex containing an eight-coordinate uranium atom, which is isostructural to the thorium analogue, was described.[211] Uranium complexes with phosphorus donor ligands, procedures for their synthesis, structures and properties were considered in the study.[212]

Ligands of the phosphacyclopentadienyl type serve as bridges, for example, in the dimeric uranium(III) complex **27**.[24, 134, 213]

The reactions of lithium salts of the potentially tridentate diphosphinoamide ligands $N(CH_2CH_2PR_2)^{2-}$ (R = Et or Pr^i) with uranium or thorium tetrachlorides afforded diphosphinoamide complexes of actinides. Ligands of this type are suitable for the preparation of various complexes of uranium(IV) (for example, $\{UCl_2[N(CH_2CH_2PEt_2)_2]_2\}_2$), uranium(V) and thorium(IV). Depending on the reaction conditions, these ligands can be mono-, bi- and tridentate. The character of the coordination compounds can be radically changed by varying the substituents at the neutral phosphine centre.[214]

Thorium and uranium complexes with diphosphazane dioxides were synthesised.[215] The crystal structure of the $UO_2(NO_3)_2[Ph_2P(O)N(Ph)P(O)Ph_2]$ complex was established. It was demonstrated that the metal atom is coordinated by diphosphazane dioxide in a bidentate fashion. Some other organophosphorus and related compounds of uranium were described in the studies.[216–219]

Actinide complexes containing simultaneously the phosphine and cyclopentadienyl ligands are few in number. Only the $Cp_2ThX_2(Me_2PCH_2CH_2PMe_2)$ complexes (X = Cl, Me or Bn)[179] and monomeric hydride complex of uranium(III) **35** were prepared.[220]

$$Cp^*_2UR_2 + Me_2PCH_2CH_2PMe_2 \xrightarrow[\text{autoclave, } -20\ ^\circ C]{\text{PhMe, } H_2}$$

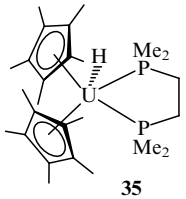

R = Me, CH_2SiMe_3. **35**

The reactions of $U(BH_4)_3(THF)_x$ with some diphosphine ligands afforded the $U(BH_4)_3(L)_2$ complexes [L is dimethylphosphinoethane[221] or 2-(diphenylphosphino)pyridine[222]]. In these compounds, dynamic transformations are observed within the NMR time scale even at low temperature.

Table 7. Selected actinide complexes with phosphorus-containing ligands.

Substrate	Reagent	Product	Ref.
$AnCl_4$	$MP(CH_2CH_2PMe_2)_2$ M = Li, K	$An[P(CH_2CH_2PMe_2)_2]_4$ An = Th, U	211, 214
$ThCl_4$	$[N(CH_2CH_2PPr^i_2)]^{2-} \cdot Li^+_2$	$ThCl_2[NCH_2CH_2PPr^i_{0.5}]_2$	211, 214
UCl_4	$[N(CH_2CH_2PEt_2]^{2-} \cdot Li^+_2$	$\{UCl_2[N(CH_2 \cdot CH_2PEt_2)_2]_2\}_2$	211, 214
$[UOCl_5]^-$	$Me_3Si[NP \cdot (C_6H_4Me\text{-}3)_3]$	$[UOCl_4NP \cdot (C_6H_4Me\text{-}3)_3]^-$ (see [a])	189
$UO_2Cl_2 \cdot (Ph_3PO)_2$	$KOBu^t$	$UO_2(OBu^t)_2 \cdot (Ph_3PO)_2$	181
	$NaN(SiMe_3)_2$	$UO_2[N(SiMe_3)_2]_2 \cdot (Ph_3PO)_2$	181
$Cp^*_2UCl_2$	$HNPPh_3$	$Cp^*_2UCl_2(HNPPh_3)$ [b]	223

[a] The red salt containing the Ph_4P^+ cation is air-stable and is soluble in CH_2Cl_2 and MeCN; [b] the first complex of the *f* element with the phosphineimino ligand.

Examples of actinide complexes with phosphorus-containing ligands are given in Table 7.

X. Sulfur-containing actinide complexes

Being hard acids, actinides usually do not form stable complexes with S-donor ligands, which are soft bases. Only a few examples of complexes with sulfur-containing ligands are available in the literature, *viz*., $UCl_4(dmte)_2$ (dmte is 1,2-dimethylthioethane), $An(S_2CNEt_2)_4$ (An = Th, U, Np or Pu), $(NEt_4)[Np(S_2CNEt_2)_4]$, $(NMe_4)[UO_2(S_2CNEt_2)_3]$,[17] $U(SBu^n)_4$, $[U(SBu^n)_6]^{2-}$ and $[U(SPh)_6]^{2-}$;[224] $[Na(18\text{-}C\text{-}6) \cdot (THF)][U(COT)(C_4H_4S_4)_2]$ is the only known uranium(V) complex containing the metal–sulfur bond.[225] The reaction of UCl_4 with $Li_2(SCH_2CH_2S)$ in dimethoxyethane afforded[226] the first homoleptic dithiolate complex of an *f* element (**36**; the space group is $P2_1/n$).

$$UCl_4 + 4\,Li_2(SCH_2CH_2S) \xrightarrow{DME} [Li(DME)]_4[U(SCH_2CH_2S)_4] \cdot DME$$

36

The nature of the U–S bond in the complex **36** was estimated by the semiempirical Hückel method. It was found that the 6*d*, 7*s* and 7*p* orbitals of uranium are responsible for interactions with sulfur-containing ligands. The involvement of 5*f* orbitals is insignificant, and hence, the π interaction between uranium and sulfur is weak.[226] The authors also gave a brief review of the state of the art in the chemistry of actinide ions with sulfur-containing ligands.[226]

Derivatives of uranium(IV) tetrathiolate were prepared by treatment of $U(NEt_2)_4$, $U(BH_4)_4$ or $U(SBu^n)_4$ with thiols and by oxidation of metallic uranium with disulfides.[227] It was found that the reactions of the $U(SBu^i)_4$ complex with acids, I_2 and CS_2 proceeded at the U–S bond.[227]

The neptunium(V) complex with DMSO with composition $[(NpO_2)_2(DMSO)_7(H_2O)_2](ClO_4)_2 \cdot H_2O$ was structurally characterised.[228] The structure contains the dimeric complex $[(NpO_2)_2(DMSO)_7(H_2O)_2]^+$ cations, perchlorate anions, coordinated water molecules and water molecules of crystallisation. The IR and electronic spectra are indicative of the non-equivalence of the dioxo cations. Thus $Np(1)O_2^+$ acts as a monodentate ligand, whereas $Np(2)O_2^+$ serves as the coordination centre.[228]

Treatment of the $U(COT)(BH_4)_2$ complex with thiols or sodium thiolates (RSH or RSNa, where R = Bu^n, Pr^i or Bu^t) afforded first organouranium compounds containing the bridging disulfide $\{[U(COT)(\mu\text{-}S)_2]_2\}$ and thiolate $\{[U(COT)(\mu\text{-}SR)_2]_2\}$ groups. The structures of these compounds differ from those of their alkoxide analogues, which contain only two bridging OR groups.[229]

The reaction of $U(NEt_2)_4$ with Pr^iSH and $OP(NMe_2)_3$ gave rise to the first structurally characterised tetrathiolate complex of uranium $U(SPr^i)_4[OP(NMe_2)_3]_2$.[229] The uranium sulfur cluster $U_3(\mu_3\text{-}S)(\mu_3\text{-}SBu^t)(\mu_2\text{-}SBu^t)_3(SBu^t)_6$ was also described.[230]

The $Cp^*_2U(dddt)$ complex (dddt is 5,6-dihydro-1,4-dithiin-2,3-dithiolate)[231] and the homoleptic uranium(IV) complexes $(THF)_3Na(\mu\text{-}SR)_3U(\mu\text{-}SR)_3Na(THF)_3$ (R = Bu^t or Ph) were synthesised.[232]

Recently, the first heteroleptic uranium(V) complex **38** was prepared by oxidation of complex **37** with $AgBPh_4$ in THF.[233]

$$(COT)UX_2(THF)_n + Na_2(dddt) \longrightarrow$$

$$\longrightarrow [(COT)U^{IV}(dddt)_2][Na(18\text{-}C\text{-}6)]_2 \xrightarrow[THF]{AgBPh_4}$$

37

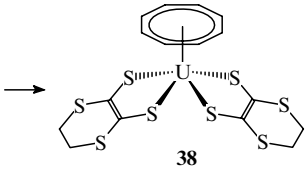

38

X = BH_4, *n* = 0; X = I, *n* = 1.

Notwithstanding the fact that the available sulfur-containing actinide complexes are few in number, these compounds are of great interest in the coordination chemistry [230] and can find use for extraction of actinides.[232]

Examples of sulfur-containing uranium complexes are given in Table 8.

Table 8. Selected sulfur-containing uranium complexes.

Starting compound	Reagents	Product	Ref.
UCl_4 or $U(BH_4)_4$	NaSR (R = Bu^t, Ph), THF	$(THF)_3Na(\mu\text{-}SR)_3U\cdot(\mu\text{-}SR)_3Na(THF)_3$	232
UI_4	DMSO DIBSO	$UI_4(DMSO)_n$ (n = 6, 8) $UI_4(DIBSO)_n$ (n = 6, 8)	104
$Cp^*_2UCl_2$	Na_2(dddt)	Cp^*_2U(dddt)	230
$U(NEt_2)_4$	Pr^iSH, $(Me_2N)_3PO$	$U(SPr^i)_4[OP(NMe_2)_3]_2$	233

XI. Technetium complexes

The chemistry of technetium becomes increasingly important, particularly, due to the fact that the short-lived ($T_{1/2}$ 6.015 h, γ irradiator) nuclide ^{99m}Tc is used in diagnostic medicine. This nuclide has been used over many years in bone scanning. Recently, ^{99m}Tc has found use in the treatment of various diseases of the heart, brain, kidney, liver and other organs as well as of tumour tissues. Technetium complexes are also of interest in the radiopharmaceutical industry.[234] Owing to the ideal energy of γ radiation (140 keV), lack of particulate radiation dose, the small half-life $T_{1/2}$ and the fact that ^{99m}Tc is readily accessible, this isotope is a radionuclide of choice for obtaining images in diagnostic nuclear medicine.[235, 236]

1. Complexes with nitrogen-containing ligands

Complexes of Tc(III), Tc(II) and Tc(I) with pyridine ligands were prepared.[237] The authors were interested to prepare a coordinatively unsaturated low-valence electron-rich Tc metal centre surrounded by very weak π-donor ligands.

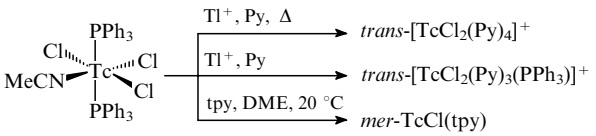

tpy is terpyridine.

The $TcCl_2(Py)_4$, $TcCl_3(PPh_3)_2$(TMEDA), $TcCl_3[Bu^t_3(tpy)]$ and [Tc(tpy)(Py)$_3$]Cl compounds were characterised by electrochemical and spectroscopic methods and by X-ray diffraction analysis.[237] According to the data of this investigation, π-back bonding is observed in the Tc(II) and Tc(I) complexes, unlike the Tc(III) complexes. In particular, the Tc–N bonds in pyridine complexes of Tc(II) are shortened by 0.04–0.06 Å and the Tc–N(internal) bonds in terpyridine complexes of Tc(I) are shortened by 0.09 Å compared to those in the analogous Tc(III) complexes.[237] These effects are favourable for stabilisation of low oxidation states of the metal atoms. The pyridine Tc(III) complexes give Knight-shifted ^{1}H NMR spectra. The visible regions of the spectra show transitions, which were empirically assigned to ligand-to-metal charge transfer transitions; multiple reversible electrochemical redox couples were found.[237]

Reduction of pertechnates (as well as perrhenates or permolybdates) with 2-hydrazinopyridine hydrochloride in methanol afforded complexes containing the M(η^1-$NNC_5H_4NH_x$)(η^2-$HNNH_yC_5H_4N$) core (M = Tc, Re or Mo).[238] In particular, the $TcCl_3(NNC_5H_4NH)(HNNC_5H_4N)$ complex was prepared. The latter was used for the synthesis of the $Tc(C_5H_4NS)_2$.$(NNC_5H_4N)(HNNC_5H_4N)$ complex (C_5H_4NS is pyridine-2-thiolate), which is a precursor of ^{99m}Tc-containing peptide reagents for medical investigations. The bifunctional hydrazine ligands used in the study [238] are efficient and versatile linkers for labelling antibodies and protein fragments. Other organic hydrazine complexes of ^{99m}Tc were also prepared. The reactions of $[TcOCl_4]^-$ with hydrazine hydrochloride (PhMe, 20 °C or CH_2Cl_2, 36 °C) gave rise to $[TcCl_2(C_8H_5N_4)(PPh_3)_2]\cdot 0.75\,PhMe$ and $[TcNCl_2(PPh_3)_2]\cdot 0.25\,CH_2Cl_2$, respectively.[239] The exchange reaction of $Tc(MeCN)(PPh_3)_2Cl_3$ with 2-hydrazinopyridine afforded Tc(III) complex **39**.[240]

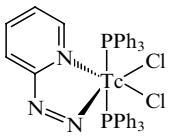

39

Complexes with compositions *mer*-$[Cl_3(pic)_3Tc]$ and *mer*-$[Cl_3(pic)(PMe_2Ph)_2Tc]$ (pic is 4-picoline) were prepared by the reactions of $[TcOCl_4]^-$ with a series of phosphine ligands in 4-picoline. The process was accompanied by the oxygen atom migration. The resulting compounds were characterised by spectroscopic methods and X-ray diffraction analysis.[241]

Complexes of high oxidation state technetium containing the $[Tc\equiv N]^{2+}$ core are more stable than the corresponding complexes of technecyl $[Tc=O]^{3+}$ and their properties resemble those of technecyl derivatives.

The technetium(V) complex $[TcN(L)(H_2O)]\cdot 2\,H_2O$ (L is the tetraazamacrocycle) was prepared by the reaction of $TcNCl_2(PPh_3)_2$ with the tetraazamacrocycle.[242] A complex with the $[Tc\equiv N]^{2+}$ core was synthesised using ancillary polydentate phosphorus- and nitrogen-containing ligands. The reaction of $[TcNBr_4]^-$ with 2,2′-bipyridyl in ethanol afforded the *cis*-octahedral $[TcNBr(bipy)_2]_2(TcBr_4)$ complex with the $[Tc\equiv N]^{2+}$ core containing the tetrahedral tetrabromo technetate(II) cation.[243]

Other chelate nitride complexes of technetium(V) with the N_2S_2 ligand and the $[Tc\equiv N]^{2+}$ core were prepared by the reactions of $TcNCl_2(PPh_3)_2$ with $(HSCR_2CH_2NRCH_2)_2$ (R = Me or Et).[244]

Since the chemical behaviour of the Mo^VO complexes is similar to that of the $Tc^{VI}N$ complexes, pertechnate complexes can be synthesised according to the procedure developed for the preparation of analogous Mo^VO complexes. Thus chelate nitride complexes of technetium(V) with ligands of the N_2S_2 type and the $[Tc\equiv N]^{2+}$ core, *viz*., $[TcN(S_2CNEt_2)]_2(\mu\text{-}O)_2$, $[TcN.(S_2CNC_4H_8)]_2(\mu\text{-}O)_2$, $(AsPh_4)_2\{[TcN(CN)]_2(\mu\text{-}O)_2\}$ and $(AsPh_4)_2.\{[TcN(edt)]_2(\mu\text{-}O)_2\}$ [edt = $S(CH_2)_2S$], were prepared by the reactions of $\{[TcN(OH_2)_3]_2(\mu\text{-}O)_2\}^{2+}$ or $Cs_2(TcNCl_5)$ with precursors of the corresponding ligands in solutions of $Na_4P_2O_7$.[245]

The reaction of $TcNCl_2(PPh_3)_2$ with the piperidinium ferrocenyldithiocarboxylate gave rise to nitride complex **40**. According to the data of cyclic voltammetry,[246] two iron(II) atoms in the complex **40** act as independent redox centres linked through the $[Tc\equiv N]$ core. Chelate complexes **41** and **42** containing the same $[Tc\equiv N]$ core were also synthesised.[247]

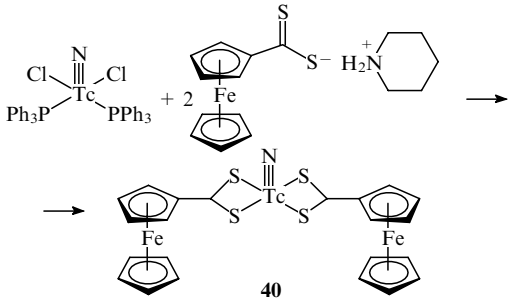

40

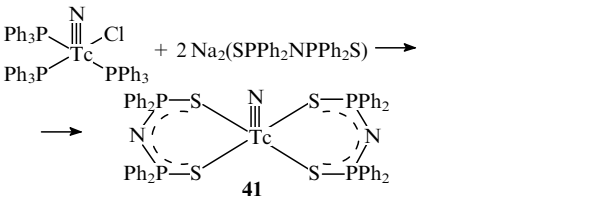

41

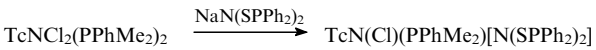

42

The possibility of radiopharmaceutical application of nitride technetium complexes with nitrogen-substituted amino acids, *viz*., derivatives of 2,5-dimethyldithiocarbamic acid, was reported.[248] Complexes with composition $TcN(L^n)(PPh_3)$, where L^n = Z-Gly-dtc (n = 1), Z-Ala-dtc (n = 2), Z-Phe-dtc (n = 3), Z-Val-dtc (n = 4) or Z-Leu-dtc (n = 5), were synthesised. All these complexes were characterised by spectral methods and X-ray diffraction analysis.

Binuclear complexes of Tc(VII) **43** and Tc(VI) **44** were synthesised by reduction of complexes **45** and **46**, respectively, with sodium.[249]

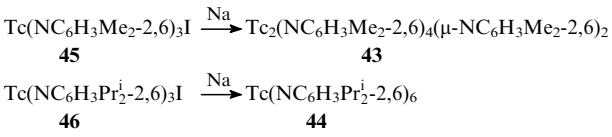

The crystal structure of the complex **43** consists of tetrahedra linked *via* shared edges, whereas the complex **44** has an 'ethylene-like' structure.[249] The reaction of the pertechnate ion with the salt of 3,6-bis(2′-pyridyl-1,2,4,5-tetrazine) (bptz · 2 HCl) in methanol or ethanol afforded binuclear complexes of the general formula $(\mu\text{-bptz})(TcO_3X)_2$ (X = Cl, OMe or OEt) containing Tc(VII), Tc(V) and the bridging bptz ligand. 4-Phenyl-3,6-bis(2′-pyridyl)-pyridazine (pppz) was used as a ligand for the preparation of mononuclear complexes from pertechnate and $TcOCl_4$ in an aqueous-ethanolic solution of HCl.[250] The binuclear polypyridyl oxo-bridged technetium(III) complex $\{(tpy)[Me_2(bipy)]Tc-O-Tc(tpy)[Me_2(bipy)]\}(OTf)_4$ was prepared by the reaction of $TcCl_3(tpy)$ with thallium triflate in the presence of water.[251]

The synthesis of diazene technetium complexes was described.[252] Thus the $TcCl(NNR)_2(PPh_3)_2$ complex (R = C_6H_4Cl-4), which was prepared from $TcOCl_4^-$ and monosubstituted hydrazine $RNHNH_2$ in methanol, reacted with the bidentate S_2CNR_2 ligand and maltol to give $Tc(NNR)L_2(PPh_3)$ and $TcCl(NNR)L(PPh_3)$ (L = S_2CNR_2) in high yields.[252]

The template synthesis from tetrabutylammonium pertechnate $(NBu_4)(TcOCl_4)$ or $(NH_4)_2(TcXO)$ (X = Cl or Br) followed by reduction by divalent tin afforded seven-coordinate Tc(III) complexes, for example, such as the monocapped adduct of boric acid with technetium(III) trisdioximate or $TcX(dioxime)_3BR$ (X = Cl or Br; dioxime = dimethylglyoxime or cyclohexanone dioxime; R = Me or Bu).[253]

A technetium(III) complex containing acetonitrile, *viz*., $TcCl_3(MeCN)(PR_3)_2$ (R = Ph or C_6H_4Me-3), was prepared by reduction of $TcCl_4(PPh_3)_2$ with zinc in acetonitrile in the presence of PPh_3. This complex is a convenient intermediate in the synthesis of other Tc(III) compounds. Its reactions with bipy, 1,10-phenanthroline (phen) and tpy afforded dicationic Tc(III) complexes, *viz*., $[Tc(bipy)_3]^{2+}$, $[Tc(phen)_3]^{2+}$ and $[Tc(tpy)_3]^{2+}$, respectively, as salts with BPh_4^- or PF_6^-.[254]

2. Complexes with sulfur- and oxygen-containing ligands

Reduction of $[Tc(OH)O(dmpe)_2]^{2+}$ in the presence of an excess of toluene-3,4-dithiol (H_2tdt) gave rise to the thiolate Tc(IV) complex $[Tc(tdt)(dmpe)_2](PF_6)$ (tdt = $MeC_6H_3S_2$-3,4).[255] Its structure was established by spectroscopic methods and X-ray diffraction analysis. The coordination polyhedron about technetium is intermediate between the octahedron and the trigonal prism [the Tc–S and Tc–P distances are 2.318(6) Å and 2.902(7) Å, respectively; the S–Tc–S angle is 84.49(4) °].

Refluxing of the salt $(NBu_4)(TcOCl_4)$ in alcoholic solution with dihydrooxazoles and dihydrothiazoles, for example, with 2-(2-hydroxyphenyl)-4,5-dihydrooxazole, 2-(2-hydroxy-3-methylphenyl)-4,5-dihydrooxazole or 2-(2-hydroxyphenyl)-4,5-dihydrothiazole, yielded the six-coordinate complexes $TcOClL_2$ (L is the corresponding (hydroxyphenyl)dihydrooxazole or -thiazole).[256]

The reaction of ammonium pertechnate with 3,5-di-*tert*-butylpyrocatechol (DBCat) in methanol afforded a mixture of the $Tc^{VI}(DBCat)_3$ and $Tc^{VI}(DBCat)_2(DBAP)$ complexes (DBAP is the amidophenoxide ligand).[257] The amidophenoxide ligand is formed through condensation of ammonia (from ammonium pertechnate) with pyrocatechol to give the Schiff's base. According to the data of EPR spectroscopy and X-ray diffraction analysis, technetium in the complex exists in oxidation state +6, which is very untypical. The DBCat ligand serves both as a reducing and chelating agent.

3. Complexes with nitrogen- and sulfur-containing ligands

The $HTcO(cysteine)_2$ complex (**47**) and its barium salt $Ba[TcO(cysteine)_2]_2$ were synthesised.[258] These compounds are of importance in biology and medicine. The properties of these complexes were studied.

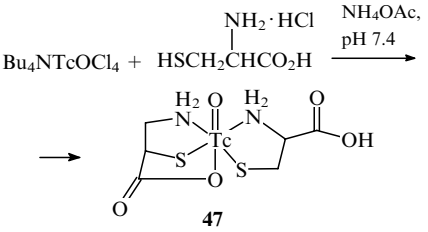

47

The complex **47** can be synthesised starting from ammonium pertechnate and cysteine. All previous attempts to prepare technetium complexes with cysteine afforded products contaminated by polymeric compounds.[258] It was also reported[259–263] that chelation of technetium with polyfunctional ligands was accompanied by the formation of polymeric by-products. It is believed that an excess of the ligand causes decomposition of the initially formed chelate. The use of S-protective groups (for example, benzyl, acetylaminomethyl or benzoylaminomethyl) prevents the formation of undesirable polymeric products.[258]

The technetium (^{99m}Tc) analogue of oxorhenium bis-cysteinate possesses valuable biological properties. In particular, it is accumulated in kidneys,[264] which is useful in diagnostics of the morphological status of this organ.[258]

Potential radiopharmaceuticals for diagnostics of the renal function were synthesised with the use of chelating carboxyl-containing ligands bearing N- and S-centres . The carboxyl groups favour the renal uptake of these compounds.[264] The $^{99}TcO(ECH_3)$ complex was prepared based on the ammonium salt $NH_4(TcOX_4)$ (X = Hal) and (2*R*,7*R*)-2,7-dicarboxy-3,6-diaza-1,8-octanedithiol (ECH_3). In the isostructural rhenium(V) complex, one of the carboxyl groups in the *trans* position with respect to the oxo ligand is coordinated in an unexpected fashion.[265]

The choice of other ligands, *viz*., Schiff's bases, was governed by their tendency to be coordinated to technetium in various unusual oxidation states. The chemistry of technetium(I) complexes is poorly known. Only a few compounds were identified and characterised. The reaction of $(PPh_3)_2(CO)_3Cl$ with the lithium salt of Schiff's base, *viz*., *N-ortho*-hydroxybenzylidene-2-thiazolylimine, in boiling THF gave rise to the Tc(I) complex with composition $Tc(PPh_3)_2(CO)_2[(C_3H_2NS)N=CHC_6H_4O]$. This six-coordinate complex has a distorted octahedral structure with *trans*-PPh_3 and *cis*-CO groups and one chelating bidentate anion.[266]

Complexes containing biologically active molecules, such as peptides, proteins or antibodies, as ligands can be used as unique

target-specific radiopharmaceuticals in diagnostics. The reaction of $[TcO_4]^-$ with $SnCl_2$, sodium gluconate and RP 294 produced the $^{99}Tc(V)$ oxo complex with RP 294, which exists as the *syn* and *anti* isomers. The study of the crystal structure of the isostructural rhenium(V) complex demonstrated that the isomerism results from the positions of the CH_2OH groups in the serine residues. At room temperature, the isomers in solution undergo interconversion. The ^{99m}Tc and rhenium complexes with RP 294 exhibit similar chemical properties.[267]

The ^{99}Tc and ^{99m}Tc complexes with new tetradentate N_2S_2 and NS_2 ligands were prepared by refluxing a methanolic solution of $(TcOCl_4)(NBu_4)$ with the corresponding NS_3H_3 proligands. The technetium(V) complex $[TcO(NS_3)](NBu_4)$ (**48**) was obtained in high yield. However, compounds of this type are unstable and decompose in a matter of several hours or days. By analogy with the crystal structure of the related rhenium oxo complex, these compounds can be considered as square-pyramidal complexes containing the oxygen atom in the apical position.[268]

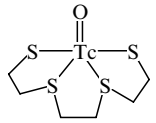

48

4. Complexes with phosphorus-containing ligands

Phosphine ^{99m}Tc-labelled derivatives can be used for obtaining images of internal organs, for example, heart images. Complexes of the $[TcO_2(PR_3)_3](BPh_4)$ (R = Et or Pr) type[234] have distorted trigonal-bipyramidal structures with two oxo ligands located in a single plane. Salts of the $[TcO_2(PR_3)_3]^+$ cations are convenient starting compounds for the synthesis of other complexes with mixed ligands.

$$[TcO_2(PR_3)_2]^+ \xrightarrow[MeOH]{Py} [TcO_2(PR_3)_2(Py)_2]^+$$

The trimethylphosphine derivative $[TcO_2(PMe_3)_2(Py)_2]^+$ can be prepared according to a one-pot procedure directly from pertechnates $[TcO_4]^-$. Apparently, this procedure can be adapted for the preparation of ^{99m}Tc radiopharmaceuticals in hospitals.

$$NH_4(TcO_4) \xrightarrow[MeOH]{Py,\ PMe_3} [TcO_2(PMe_3)_2(Py)_2]^+$$

The $[TcO_2(PR_3)_2(Py)_2]^+$ derivatives are diamagnetic, which is indicative of a noticeable deviation of their geometry from the ideal octahedron.[234]

The reactions of pertechnate with derivatives of phosphinocarboxylic acids afforded the TcL_3 complexes [L is 2-(diphenylphosphino)benzoic acid, 3-(diphenylphosphino)propionic acid or (diphenylphosphino)acetic acid]. According to the results of spectroscopic studies and X-ray diffraction analysis, these complexes possess a distorted octahedral geometry with the *mer* configuration in which the donor atoms of the same type are in *trans* positions with respect to each other and the phosphorus atom is in the *trans* position with respect to the oxygen atom.[269]

Complexes of the short-lived ^{99m}Tc isotope were prepared analogously. Their physical and chemical properties are similar to those of ^{99}Tc complexes. Biological assays revealed significant brain uptake of these compounds.

Chelate technetium(V) complexes with bis(*o*-hydroxyphenyl)-phenylphosphine and (*o*-hydroxyphenyl)diphenylphosphine were prepared by metathesis of the corresponding Tc(V) precursors or by reduction–ligand exchange with ammonium pertechnate.[270] These complexes combine a soft phosphine donor site and two hard phenoxide centres. It was expected that this fact would stabilise technetium in intermediate oxidation states.

The $[Tc(tu\text{-}S)_6]Cl_3 \cdot 4H_2O$ complex (tu-S is thiourea) was used as the precursor of $[Tc(dppe)_2(Bu^tNC)_2](PF_6)$ (dppe is diphenylphosphinoethane).[271] This complex can be prepared by mixing both ligands and a source of technetium(III) in ethanol followed by refluxing of the reaction mixture. This procedure is more convenient than the method involving a sodium amalgam, dppe and $TcCl_4(PPh_3)_2$. In the $[Tc(tu\text{-}S)_6]Cl_3 \cdot 4H_2O$ complex, the coordination polyhedron about the technetium atom is a distorted tetrahedron, the isocyanide ligands being in *trans* positions with respect to each other.

Treatment of $[TcO_4]^-$ with an excess of the corresponding S,P-bidentate phosphinothiolate ligands, such as 2-(diphenylphosphino)ethanedithiolate, 2-(diphenylphosphino)propanethiolate or 2-(diphenylphosphino)thiophenoxide, yielded neutral technetium(III) complexes.[272] These complexes have a trigonal-bipyramidal geometry, two phosphorus donor centres (consisting of two chelate rings) occupying axial positions and being in *trans* positions with respect to each other.

5. Complexes with the metal–metal bond, carbonyl complexes

The data on complexes containing multiple Tc–Tc bonds are scarce. Thus several diamagnetic phosphine ditechnetium(II) complexes of the $Tc_2Cl_4(PR_3)_4$ type (**49**) were described.[160] These complexes contain a triple bond between the metal atoms and provide the first examples of phosphine complexes possessing a multiple technetium–technetium bond.

$$TcCl_4(PR_3)_2 \xrightarrow[PhH,\ PhH,\ utrasonics]{PhMe,\ 50-55\ ^\circ C\ or} \underset{\mathbf{49}\ (>90\%)}{\text{image_ref 2}}$$

PR_3 = PEt_3, PPr^n_3, $PMePh_2$, PMe_2Ph.

The polymeric chain structure of $[Tc_2Cl_6]^{2n-}_n$ also contains triple metal–metal bonds.[273] The triple Tc≡Tc bond was found in the α and β forms of the $Tc_2Cl_4(dppe)_2$ complex.[274] The α isomer **50** adopts an eclipsed conformation; the Tc–Tc distance is 2.15(1) Å. In the β isomer **51**, the twist angle is 35(2)° and the Tc–Tc distance is 2.117(1) Å. These isomeric complexes were prepared by refluxing $Tc_2Cl_4(PR_3)_4$ (PR_3 = PEt_3 or PMe_2Ph) in toluene in the presence or in the absence of an excess of dppe, respectively.

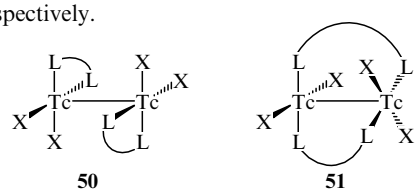

50 **51**

L = dppe, X = Cl.

Complexes containing the multiple Tc–Tc bond of order 3.5 were synthesised in high yields by one-electron chemical oxidation of the $Tc_2Cl_4(PMe_2Ph)_4$ complex with ferrocenium hexafluorophosphate in acetonitrile.[275] In this study, the cationic $[Tc_2Cl_4(PMe_2Ph)_4](PF_6)$ complex was prepared.[275] Oxidation in the presence of bis(triphenylphosphine)iminium produced the neutral $Tc_2Cl_5(PMe_2Ph)_3$ complex.[275] The complexes $Tc_2Cl_4(PR_3)_4$ **49** (PR_3 = PEt_3, $PMePh_2$ or PMe_2Ph) reacted with molten diphenyl- or di-*p*-tolylformamidine to give mixtures of formamidine-bridged complexes of the general formula $Tc_2(L)_4Cl_n$ (n = 1 or 2) in moderate yields.[276] Complexes with the triple Tc≡Tc bond, for example $[Tc_2(MeCN)_{10}](BF_4)_4$,[277] in an acetonitrile solution can undergo photodissociation to give the $[Tc(MeCN)_6]^{2+}$ ions in almost quantitative yields.[278] A decaacetonitrile binuclear complex with the triple Tc≡Tc bond was obtained in good yield by acidification of a solution of $Tc_2Cl_4(PR_3)_4$ in a mixture of acetonitrile and dichloromethane using $HBF_4 \cdot Et_2O$.[277] The $[Tc_2Cl_8]^{n-}$ (n = 2, 3 or 4) and

$[Mo_2Cl_8]^{m-}$ ($m = 4$ or 5) clusters were studied by theoretical methods.[279]

Of other types of Tc complexes, noteworthy are Tc carbonyl derivatives.[280–282] The $Tc(CO)_5I$ complex, which is isostructural to the $Mn(CO)_5I$ complex, exists as orthorhombic crystals. Its crystal structure consists of $Tc(CO)_5I$ molecules. The crystals of $[Tc(CO)_4I]_2$ are monoclinic and are also built of individual $[Tc(CO)_4I]_2$ molecules. Complexes with composition $[M(CO)_4X]_2$ (M = Mn, Tc or Re; X = Cl, Br or I) are isostructural. The main types of technetium complexes are given in Table 9.

* * *

In spite of the difficulties associated with operations with radioactive elements, their complexes are being studied intensively. The development of the coordination chemistry of these compounds, particularly, of those containing radioactive elements in unusual oxidation states,[24] is dictated both by the possibility of their practical use and theoretical interest. Thus considerable recent attention has been given to bimetallic complexes of 5*f* elements in connection with a search for new unusual properties and molecular structures. Investigations and a search for new uranium(V) complexes remain to be of great importance. Information[166,167] on the unique activities of alkylcyclopentadienyl derivatives $Cp^*_2AnR_2$ (An = Th or U; R = H or Alk) as catalysts of alkene hydrogenation and polymerisation gave impetus to studies in this field of chemistry. These compounds proved to be ten times more active than traditional Pt/SiO_2 catalysts. Hence, actinide complexes are of interest from the viewpoint of extension of the scope of their use in catalysis, as the starting compounds in organometallic synthesis[17,24] and for separation and extraction of actinides.[283]

We are grateful to Professor M Ephritikhine (Service de Chimie Moleculaire, France) for permission to reproduce schemes from his articles and Professors A D Garnovskii (Rostov State University, Russia) and S S Berdonosov (Moscow State University, Russian Federation) for valuable advice.

Table 9. Synthesis of technetium complexes with oxygen-, sulfur-, nitrogen- and phosphorus-containing ligands.

Starting compound	Reagent and reaction conditions	Products	Ref.
Complexes with oxygen- and sulfur-containing ligands			
$KTcO_4$	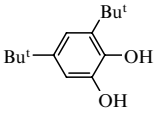	$Tc(DBCat)_3$, $Tc(DBCat)_2(DBAP)$	257
$Tc(PPh_3)_2(CO)_3Cl$	$LiOC_6H_4CH=N(CSNC_3H_2)$, THF	$Tc(PPh_3)_2(CO)_2 \cdot [(C_3H_2NSC)N=CHC_6H_4O]$	266
$Tc(CO)_5X$ (X = Cl, Br, I)	H_2O	$[Tc(CO)_3(H_2O)_3]^+$	282
Complexes with nitrogen-containing ligands			
$Tc_2Cl_4(PR_3)_4$ (PR_3 = PEt_3, PMe_2Ph, $PMePh_2$)	(1) Bu_3SnH or Zn (2) MeCN, HBF_4	$[Tc_2^{II}(MeCN)_{10}](BF_4)_4$ (see [a])	277
$[TcCl_6]^{2-}$	(1) Bu_3SnH or Zn (2) MeCN, HBF_4	$[Tc_2^{II}(MeCN)_{10}](BF_4)_4$	277
$(Bu_4N)(TcOCl_4)$	Cys [b]	$HTcO(Cys)_2$	258
$TcCl_3(PPh_3)_2(MeCN)$	$Bu^t_3(tpy)$, DME	$TcCl_3[Bu^t_3(tpy)]$	237
NH_4TcO_4	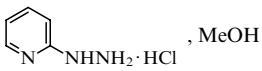 , MeOH	$TcCl_3(\eta^1\text{-}NNC_5H_4NH)(\eta^2\text{-}HNNC_5H_4N)$	238
Complexes with phosphorus-containing ligands			
$Tc_2Cl_4(PMe_2Ph)_4$	$(Cp_2Fe)(PF_6)$	$[Tc_2Cl_4(PMe_2Ph)_4](PF_6)$ [c]	275
$NH_4(TcO_4)$	PR_3, MeOH (R = Et, Pr) (see [d])	$[TcO_2(PR_3)_3]^+$	234
$[TcO_2(PR_3)_3]^+$ (R = Et, Pr)	PR_3, MeOH, Py (R = Et, Pr)	$[TcO_2(PR_3)_3(Py)_2]^+$	234
$TcCl_3(PPh_3)_2(MeCN)$	TMEDA, PhMe, DME	$TcCl_3(PPh_3)_2(TMEDA)$	237
	Py	*mer*-$TcCl_3(Py)_2$	241
$TcCl_4(PPh_3)_2$	PR_3 (R = Et, Pr^n), THF	$TcCl_4(PR_3)_2$	160
$TcCl_4(PEt_3)_2$	Zn, PhH, utrasonics	$Tc_2Cl_4(PEt_3)_4$	160

[a] The yield was 50%, the Tc—Tc multiple bond is present; [b] Cys is an aqueous solution of cysteine chloride monohydrate; [c] the multiple Tc—Tc bond is present; [d] the yield was 60%–70%; a ~10-fold excess of the ligand was used; there was no need for the use of reducing agents; the reaction was accompanied by the formation of NH_3.

References

1. *Metody Elementoorganicheskoi Khimii. Lantanidy i Aktinidy* (Methods of Organoelement Chemistry. Lanthanides and Actinides) (Eds N A Nesmeyanov, K A Kocheshkov) (Moscow: Khimiya, 1974)
2. T J Marks, R D Ernst, in *Comprehensive Organometallic Chemistry* Vol. 3 (Eds D Wilkinson, F G Stone, E W Abel) (Oxford: Pergamon Press, 1982) p. 173
3. T J Marks, V W Day, in *Fundamental and Technological Aspects of Organo-f Element Chemistry* (Eds T J Marks, I L Fragala) (Dordrecht: Reidel, 1985) p. 115
4. J Takats, in *Fundamental and Technological Aspects of Organo-f Element Chemistry* (Eds T J Marks, I L Fragala) (Dordrecht: Reidel, 1985) p. 159
5. I Santos, A Pires de Matos, A G Maddock *Adv. Organomet. Chem.* **34** 65 (1989)
6. B E Bursten, R J Strittmatter *Angew. Chem., Int. Ed. Engl.* **30** 1069 (1991)
7. *NATO ASI Ser., Partnership Sub-Ser. 2, Environ.* **41** (1998)
8. D J Cardin (Ed.) *Organometallic Compounds of the Lanthanides, Actinides, and Early Transition Metals* (London: Chapman and Hall, 1985)
9. D N Suglobov, G V Sidorenko, E K Legin, in *Letuchie Organicheskie i Kompleksnye Soedineniya f-Elementov* (Volatile Organic and Complex Compounds of the f Elements) (Moscow: Energoatomizdat, 1987) p. 208
10. K Schwochau, U Pleger *Radiochim. Acta* **63** 103 (1993)
11. C E Housecroft *Coord. Chem. Rev.* **162** 305 (1997)
12. F S Schoster, S K Zeisler *J. Rad. Nucl. Chem.* **220** 149 (1997)
13. N M Vanlic-Razumenic, T N Maksin, L P Vuksanovic *J. Serb. Chem. Soc.* **60** 641 (1995)
14. C E Housecroft *Coord. Chem. Rev.* **142** 21 (1995)
15. E C Constable, C E Housecroft *Coord. Chem. Rev.* **131** 153 (1994)
16. U Mazzi *Polyhedron* **8** 1683 (1989)
17. G L Soloveichik, in *Encyclopedia of Inorganic Chemistry* Vol. 1 (Ed. R B King) (New York: Wiley, 1994) p. 2
18. An N Nesmeyanov *Radiokhimiya* (Radiation Chemistry) (Moscow: Khimiya, 1978)
19. M S S Brooks, B Johansson, H L Skriver, in *Handbook on the Physics and Chemistry of the Actinides* Vol. 1 (Eds A J Freeman, G H Lander) (Amsterdam: North-Holland, 1984) Pt. 3, p. 153
20. D L Clark, A P Sattelberger, in *Encyclopedia of Inorganic Chemistry* Vol. 1 (Ed. R B King) (New York: Wiley, 1994) p. 19
21. L T Reynolds, G Wilkinson *J. Inorg. Nucl. Chem.* **2** 246 (1956)
22. J H Burns, in *The Chemistry of Actinide Elements* Vol. 2 (Eds J J Katz, G T Seaborg, L R Morris) (London: Chapman and Hall, 1986) p. 1417
23. D Kepert *Inorganic Stereochemistry* (Berlin: Springer, 1982)
24. M Ephritikhine *New J. Chem.* **16** 451 (1992)
25. C J Burns, B E Bursten *Comments Inorg. Chem.* **9** 61 (1989)
26. P Pyykkoe, L L Lohr Jr *Inorg. Chem.* **20** 1950 (1981)
27. N Rösch, A Streitwieser Jr *J. Am. Chem. Soc.* **105** 7237 (1983)
28. N Rösch *Inorg. Chim. Acta.* **94** 297 (1984)
29. A H H Chang, R M Pitzer *J. Am. Chem. Soc.* **111** 2500 (1989)
30. S Ahrland, in *The Chemistry of Actinide Elements* Vol. 2 (Eds J J Katz, G T Seaborg, L R Morris) (London: Chapman and Hall, 1986) p. 1480
31. I Grenthe, J Fuger, R J M Konings, R J Lemire, A B Muller, C Nguyen-Trung, H Wanner, H Forest, in *Chemical Thermodynamics of Uranium* (Eds H Wanner, I Forest) (Amsterdam: Elsevier, 1992) p. 193
32. J Fuger, in *Plutonium Chemistry* (*American Chemical Society, Symposium Series)* (Eds W T Carnall, G R Choppin) Vol. 216; (Washington, DC: American Chemical Society, 1983) p. 74
33. P G Allen, J J Bucher, D K Shuh, N M Edelstein, T Reich *Inorg. Chem.* **36** 4676 (1997)
34. H Moll, M A Denecke, F Jalilehvand, M Sanström, I Grenthe *Inorg. Chem.* **38** 1795 (1999)
35. A Plyasunov, T Fanghanel, I Grenthe *Acta Chem. Scand.* **52** 250 (1998)
36. S Basak, D Banerjea *Indian J. Chem., Sect. A* **32** 129 (1993)
37. W G van der Sluys, A P Sattelberger *Chem. Rev.* **90** 1027 (1990)
38. A J Zozulin, D C Moody, R R Ryan *Inorg. Chem.* **21** 3083 (1981)
39. J L Stewart, R A Andersen *J. Chem. Soc., Chem. Commun.* 1846 (1987)
40. L R Avens, D M Barnhart, C J Burns, S D McKee, W H Smith, *Inorg. Chem.* **33** 4245 (1994)
41. N Edelstein *J. Less-Common Met.* **133** 39 (1987)
42. C Baudin, D Baudry, M Ephritikhine *J. Organomet. Chem.* **415** 59 (1991)
43. R G Jones, E Bindschadler, D Blume, G Karmas, G A Martin Jr, J R Thirtle, F A Yeoman, H Gilman *J. Am. Chem. Soc.* **78** 6030 (1956)
44. F A Cotton, G Wilkinson, C A Murillo, M Bochmann *Advanced Inorganic Chemistry* (New York: Wiley, 1999)
45. T Arliguie, D Baudry, M Ephritikhine, M Nierlich, M Lance, J Vigner *J. Chem. Soc., Dalton Trans.* 1019 (1992)
46. D L Clark, J C Huffman, J G Watkin *J. Chem. Soc., Chem. Commun.* 266 (1992)
47. D M Barnhart, D L Clark, J C Gordon, J C Huffman, J G Watkin, B D Zwick *Inorg. Chem.* **34** 5416 (1995)
48. R C Mehrotra, A Singh, U M Tripathi *Chem. Rev.* **91** 1287 (1991)
49. W G van der Sluys, C J Burns, J C Huffman, A P Sattelberger, *J. Am. Chem. Soc.* **110** 5924 (1988)
50. D M Barnhart, T M Frankcom, P L Gordon, N N Sauer, J A Thompson, J G Watkin *Inorg. Chem.* **34** 4862 (1995)
51. W G van der Sluys, J C Huffman, D S Ehler, N N Sauer *Inorg. Chem.* **31** 1316 (1992)
52. B A Vaartstra, J C Huffman, P S Gradeff, L G Hubert-Pfalzgraf, J-C Daran, S Parraud, K Yunlu, K G Caulton *Inorg. Chem.* **29** 3126 (1990)
53. C H Winter, P H Sheridan, M J Heeg *Inorg. Chem.* **30** 1962 (1991)
54. D L Clark, J G Watkin *Inorg. Chem.* **32** 1766 (1993)
55. J M Berg, A P Sattelberger, D E Morris, W G van der Sluys, P Fleig *Inorg. Chem.* **32** 647 (1993)
56. T Arliguie, D Baudry, J C Berthet *New J. Chem.* **15** 569 (1991)
57. L K Templeton, D H Templeton, N Bartlett, K Seppelt *Inorg. Chem.* **15** 2720 (1976)
58. S D McKee, C J Burns, L R Avens *Inorg. Chem.* **37** 4040 (1998)
59. P Roussel, P B Hitchcock, N D Tinker, P Scott *Inorg. Chem.* **36** 5716 (1997)
60. M R Duttera, V W Day, T J Marks *J. Am. Chem. Soc.* **106** 2907 (1984)
61. D L Clark, S D Conradson, D W Keogh, P D Palmer, B L Scott, C D Tait *Inorg. Chem.* **37** 2893 (1998)
62. A Anderson, C Chieh, D E Irish, J P K Tong *Can. J. Chem.* **58** 1651 (1980)
63. A Coda, A Dell Giusta, V Tazzoli *Acta Crystallogr., Sect. B* **37** 1496 (1981)
64. R Graziani, G Bombieri, E Forsellini *J. Chem. Soc., Dalton Trans.* 2059 (1972)
65. M S Grigor'ev, I G Tananaev, N N Krot, A I Yanovskii, Yu T Struchkov *Radiokhimiya* **39** 325 (1997) [a]
66. J Bruno, I Grenthe, P Robouch *Inorg. Chim. Acta.* **158** 221 (1989)
67. L B Serezhkina, V N Serezhkin *Radiokhimiya* **38** 117 (1996) [a]
68. L B Serezhkina, V N Serezhkin *Zh. Neorg. Khim.* **41** 427 (1996) [b]
69. L B Serezhkina, V N Serezhkin *Zh. Neorg. Khim.* **41** 438 (1996) [b]
70. L B Serezhkina, V N Serezhkin *Koord. Khim.* **22** 786 (1996) [c]
71. C J Dodge, A J Francis *Environ. Sci. Technol.* **31** 3062 (1997)
72. M T H Tarafder, A R Khan *J. Indian Chem. Soc.* **74** 489 (1997)
73. M Bhattacharjee, M K Chaudhuri, R N D Purkoyastha *J. Chem. Soc., Dalton Trans.* 2883 (1990)
74. S A Kulyukhin, N B Mikheev *Radiokhimiya* **39** 127; 130 (1997) [a]
75. C S Tellez, J Gomez-Lara *Spectrochim. Acta.* **51A** 395 (1995)
76. C S Tellez, J Gomez-Lara, M A Mondragdn, V M CastaKho, G R Mena *Vib. Spectrosc.* **9** 279 (1995)
77. I A Charushnikova, A Yu Garnov, V P Perminov, A A Bessonov, N N Krot *Radiokhimiya* **40** 302 (1998) [a]
78. C A Tellez-Sara, J Gomez-Lara *J. Braz. Chem. Soc.* **7** 505 (1996)
79. C A Tellez-Sara, M Arissawa, J Gomez-Lara, M A Mondragdn *Polyhedron* **19** 2353 (2000)
80. J Gomez-Lara, *Bol. Inst. Quim. UNAM* **16** 27 (1964)
81. L Matassa, N Kumar, D G Tuck *Inorg. Chim. Acta.* **109** 19 (1985)
82. N N Kostyuk, T A Kolevich, V L Shirokii, D S Umreiko *Koord. Khim.* **15** 1704 (1989) [c]

83. N N Kostyuk, V L Shirokii, I I Vinokurov, N A Maier *Zh. Obshch. Khim.* **64** 1432 (1994) [d]
84. *Direct Synthesis of Coordination and Organometallic Compounds*. (Eds A D Garnovskii, B I Kharisov) (Amsterdam: Elsevier, 1999)
85. R L Belford, A E Martell, M Calvin *J. Inorg. Nucl. Chem.* **14** 169 (1960)
86. D C Bradley, M A Saad, W Wardlaw *J. Chem. Soc.* 1091 (1954)
87. A G Maddock, A Pires de Matos *Radiochim. Acta.* **18** 71 (1972)
88. E T Samulski, D G Karraker *J. Inorg. Nucl. Chem.* **29** 993 (1967)
89. S D McKee, C J Burns, L R Avens *Inorg. Chem.* **37** 4040 (1998)
90. D L Clark, S K Grumbine, B L Scott, J G Watkin *Organometallics* **15** 949 (1996)
91. D C Bradley, B Harder, F Hudswell *J. Chem. Soc.* 3318 (1957)
92. W G van der Sluys, C J Burns, A P Sattelberger *Organometallics* **8** 855 (1989)
93. A Vallat, E Laviron, A Dormond *J. Chem. Soc., Dalton Trans.* 921 (1990)
94. J G Brennan, R A Andersen, A Zalkin *Inorg. Chem.* **25** 1756 (1986)
95. S D Stults, R A Andersen, A Zalkin *Organometallics* **9** 1623 (1990)
96. J-C J Berthet, J F Le Maréchal, M Lance, M Nierlich, J Vigner, M Ephritikhine *J. Chem. Soc., Dalton Trans.* 1573 (1992)
97. L A Avens, S G Bott, D L Clark, A P Sattelberger, J G Watkin, B D Zwick *Inorg. Chem.* **33** 2248 (1994)
98. D L Clark, A P Sattelberger, S G Bott, R N Vrtis *Inorg. Chem.* **28** 1771 (1989)
99. J Drozdzyuski, J G H Du Preez *Inorg. Chim. Acta.* **218** 203 (1994)
100. L R Avens, D M Barnhart, C J Burns, S D McKee *Inorg. Chem.* **35** 537 (1996)
101. W G van der Sluys, J M Berg, D Barnhardt *Inorg. Chim. Acta.* **204** 251 (1993)
102. J G H Du Preez, L Gouws, H Rohwer, B J A M van Brecht, B Zeelie, U Casellato, R Graziani *J. Chem. Soc., Dalton Trans.* 2585 (1991)
103. J G H Du Preez, H E Rohwer, B J A M van Brecht, H Zeelve, U Casellato, R Graziani *Inorg. Chim. Acta.* **189** 67 (1991)
104. J G H Du Preez, B Zeelie *Inorg. Chim. Acta.* **161** 187 (1989)
105. L Arnaudet, R Bougon, B Buu, M Lance, M Nierlich, J Vinger *Inorg. Chem.* **33** 4510 (1994)
106. D C Moody, J D Odom *J. Inorg. Nucl. Chem.* **41** 533 (1979)
107. S J Simpson, R A Andersen *J. Am. Chem. Soc.* **103** 4063 (1981)
108. N Kumar, D G Tuck *Inorg. Chem.* **22** 1951 (1983)
109. G B Deacon, T D Tuong *Polyhedron* **7** 249 (1988)
110. D M Barnhart, D L Clark, S K Grumbine, J G Watkin *Inorg. Chem.* **34** 1695 (1995)
111. R J Butcher, D L Clark, S K Grumbine, B L Scott, J G Watkin *Organometallics* **15** 1488 (1996)
112. R A Andersen *Inorg. Chem.* **18** 1507 (1979)
113. R S Sternal, T J Marks *Organometallics* **6** 2621 (1987)
114. B Kanellokopulos, E O Fischer, E Dornberger, F Baumgartner *J. Organomet. Chem.* **24** 507 (1970)
115. D Baudry, E Bulot, M Ephritikhine *J. Chem. Soc., Chem. Commun.* 1316 (1989)
116. C Clappe, D Hauchard, G Durand *J. Electroanal. Chem.* **448** 95 (1998)
117. J-F Le Maréchal, C Villers, P Charpin, M Lance, M Nierlich, J Vigner, M Ephritikhine *J. Chem. Soc., Chem. Commun.* 308 (1989)
118. J G Brennan, S D Stults, R A Andersen, A Zalkin *Inorg. Chim. Acta.* **139** 201 (1987)
119. B E Bursten, R J Strittmatter *J. Am. Chem. Soc.* **109** 6606 (1987)
120. J E Ellis, W Beck *Angew. Chem.* **34** 2489 (1995)
121. S Di Bella, A Gulino, G Lanza, I L Fragala *J. Phys. Chem.* **97** 11673 (1993)
122. A C Gulina, S Di Bella *Organometallics* **11** 3248 (1992)
123. M Spirlet, J Rebizant, C Apostolidis, E Dornberger, B Kanellakopulos, B Powietzka *Polyhedron* **15** 1503 (1996)
124. X Jemine, J Goffart, P C Leverd *J. Organomet. Chem.* **469** 55 (1994)
125. P C Blake, M F Lappert, J L Atwood, H Zhang *J. Chem. Soc., Chem. Commun.* 1436 (1988)
126. S Di Bella, G Lanza, I L Fragala, T J Marks *Organometallics* **15** 205 (1996)
127. W K Kot, G V Shalimov, N M Edelshtein, M A Edelman, M F Lappert *J. Am. Chem. Soc.* **110** 986 (1988)
128. K G Moloy, T J Marks *J. Am. Chem. Soc.* **106** 7051 (1984)
129. K G Moloy, T J Marks *Inorg. Chim. Acta.* **110** 127 (1985)
130. K Tatsumi, A Nakamura, P Hoffman, P Stauffert, R Hoffmann *J. Am. Chem. Soc.* **107** 4440 (1985)
131. J-F Le Marechal, M Ephritikhine, G Folcher *J. Organomet. Chem.* **299** 85 (1986)
132. J H Burns, P G Laubereau *Inorg. Chem.* **10** 2789 (1971)
133. J Goffart, S Bettonville *J. Organomet. Chem.* **361** 17 (1989)
134. D Baudry, M Ephritikhine, F Nief, L Ricard, F Mathey *Angew. Chem., Int. Ed. Engl.* **29** 1485 (1990)
135. T Arliguie, M Lance, M Nierlich, J Vigner, M Ephritikhine *J. Chem. Soc., Chem. Commun.* 183 (1995)
136. J C Green, N Kaltsoyannis, K H Sze, M MacDonald *J. Am. Chem. Soc.* **116** 1994 (1994)
137. A R Schake, L R Avens, C J Burns, D L Clark, A P Sattelberger, W H Smith *Organometallics,* **12** 1497 (1993)
138. C Boisson, J C Berthet, M Ephritikhine *J. Chem. Soc., Dalton Trans.* 947 (1996)
139. A F England, C J Burns, S L Buchwald *Organometallics* **13** 3491 (1994)
140. B Kanellakopulos, E Dornberger, F Baumgarther *Inorg. Nucl. Chem. Lett.* **10** 155 (1974)
141. C-H Wong, T Yen, T Lee *Acta Crystallogr.* **18** 340 (1965)
142. M Weydert, J G Brennan, R A Andersen, R G Bergman *Organometallics* **14** 3942 (1995)
143. G Paolucci, G Rosserto, P Zanella, R G Fischer *J. Organomet. Chem.* **284** 213 (1985)
144. F Ossola, G Rosserto, P Zanella, G Paolucci *J. Organomet. Chem.* **309** 55 (1986)
145. M Porchia, N Brianese, U Casellato, F Ossola, G Rosserto, P Zanella, R Graziani *J. Chem. Soc., Dalton Trans.* 677 (1989)
146. P Zanella, N Brianese, U Casellato, F Ossola, M Porchia, G Rossetto, R Graziani *J. Chem. Soc., Dalton Trans.* 2039 (1987)
147. M R Leonov, N I Gramoteeva, V A Il'yushenkov, L A Pogodina *Radiokhimiya* **42** 210 (2000) [a]
148. H Lauke, P N Swepston, T J Marks *J. Am. Chem. Soc.* **106** 6841 (1984)
149. T Arliguie, M Lance, M Ephritikhine *J. Chem. Soc., Dalton Trans.* 2501 (1997)
150. T R Boussie, D C Eisenberg, J Rigsbee, A Streitwieser, A Zalkin *Organometallics* **10** 1922 (1991)
151. A Streitwieser, M T Barros, H K Wang, T R Boussie *Organometallics* **12** 5023 (1993)
152. D G Karraker, A Stone *J. Am. Chem. Soc.* **96** 6885 (1974)
153. D G Karraker *J. Inorg. Nucl. Chem.* **39** 87 (1977)
154. T M Gilbert, R R Ryan, A P Sattelberger *Organometallics* **8** 857 (1989)
155. A R Achake, L R Avens, C J Burns, D L Clark, A P Sattelberger, W H Smith *Organometallics* **12** 1497 (1993)
156. J Ogden, in *Cryochemistry* (Eds M Moskovitz, G A Ozin) (New York: Wiley, 1976) Ch. 7, p. 146
157. C Villiers, M Ephritikhine *J. Chem. Soc., Dalton Trans.* 3397 (1994)
158. B C Ankianies, P E Fanwick, I P Rothwell *J. Am. Chem. Soc.* **113** 4710 (1991)
159. R Adam, C Villiers, M Ephritikhine *New J. Chem.* **17** 455 (1993)
160. A Hafid, A Dormond, D Baudry *New J. Chem.* **18** 557 (1994)
161. R R Ryan *Inorg. Chim. Acta.* **162** 221 (1989)
162. D Baudry, E Bulot, M Ephritikhine *J. Chem. Soc., Chem. Commun.* 1369 (1988)
163. D Rabinovich, R M Chamberlin, B L Scott, J B Nielsen, K D Abney *Inorg. Chem.* **36** 4216 (1997)
164. D L Clark, J G Watkin, S K Grumbine *J. Am. Chem. Soc.* **117** 9089 (1995)
165. D Rabinovitch, C M Haswell, B L Scott, R L Miller, J B Nielsen, K D Abney *Inorg. Chem.* **35** 1425 (1996)
166. J-C Berthet, J-F Le Maréchal, M Ephritikhine *J. Chem. Soc., Chem. Commun.* 360 (1991)
167. S M Cendrowski-Guillaume, M Ephritikhine *J. Chem. Soc., Dalton Trans.* 1487 (1996)
168. F M De Rege, W H Smith, B L Scott, J B Nielsen, K D Abney *Inorg. Chem.* **37** 3664 (1998)
169. O Bilsel, S N Milam, G S Girolami, K S Suslick, D Holten *J. Phys. Chem.* **97** 7216 (1993)

170. B I Kharisov, M A Mendes-Roias, F A Ganich *Koord. Khim.* **26** 323 (2000) [c]
171. M K Engel *Rep. Nakamura Inst. Chem. Res., Vol. Date 1996* **8** 11 (1997)
172. B Nartsissov, US Department of Commerce, Aerospace Technology Division, Library of Congress, Washington, DC, Rep. No AD 629515 (Microfilm) (1966)
173. A L Thomas *Phthalocyanines. Research and Application* (Boca Raton, FL: CRC Press, 1990)
174. K L Raymond, G E Freeman, M J Kappel *Inorg. Chim. Acta* **94** 193 (1984)
175. Y-D Z Han, S-Y Ying-Jie Niu *Sci. China., Ser. B, Chem., Life Sci.* **36** 1061 (1993)
176. M G Lappert, P P Power, A R Sanger, R C Srivastava *Metal and Metalloid Amides* (New York: Wiley, 1980)
177. J C Berthet, C Boisson, M Lance, J Viegner, M Nierlich, M Ephritikhine *J. Chem. Soc., Dalton Trans.* 3019 (1995)
178. P Roussel, P Hitchcock, B P Scott *Inorg. Chem.* **36** 5716 (1997)
179. A Zalkin, J G Brennan, R A Andersen *Acta Crystallogr., Sect. C.* **43** 418; 421 (1987)
180. S E Turman, W G van der Sluys *Polyhedron* **11** 3139 (1992)
181. C J Burns, D C Smith, A P Sattelberger, H B Gray *Inorg. Chem.* **31** 3724 (1992)
182. Yu N Mikhailov, Yu E Gorbunova, V N Serezhkin *Dokl. Akad. Nauk, Ser. Khim.* **358** 360 (1998)
183. M Müller, V C Williams, L H Doerrer, M A Leech, S A Mason, M L H Green, K Prout *Inorg. Chem.* **37** 1315 (1998)
184. R Wietzke, M Mazzanti, J Pecaut *J. Chem. Soc., Dalton Trans.* 4087 (1998)
185. J-C Berthet, Ch Boisson, M Ephritikhine *J. Chem. Soc., Dalton Trans.* 3027 (1995)
186. P Scott, P B Hitchcock *J. Chem. Soc., Dalton Trans.* 603 (1995)
187. J-C Berthet, M Ephritikhine *Coord. Chem. Rev.* **178** 83 (1998)
188. D S J Arney, C J Burns *J. Am. Chem. Soc.* **117** 9448 (1995)
189. R E Cramer, K Panchanatheswaran, J W Gilje *J. Am. Chem. Soc.* **106** 1853 (1984)
190. J G Brennan, R A Andersen *J. Am. Chem. Soc.* **107** 514 (1985)
191. A L Odom, P L Arnold, C C Cummins *J. Am. Chem. Soc.* **120** 5836 (1998)
192. G P Kushto, P F Souter, L Andrews *J. Chem. Phys.* **108** 7121 (1998)
193. T Straub, W Frank, M S Eisen *J. Chem. Soc., Dalton Trans.* 2541 (1996)
194. A Cassol, P Di Bernardo, R Portanova, M Tolazzi, G Tomat, P Zanonato *Inorg. Chem.* **29** 1079 (1990)
195. D R Brown, R G Denning, R H Jones *J. Chem. Soc., Chem. Commun.* 2601 (1994)
196. R G Denning *Struct. Bond.* **79** 215 (1992)
197. L R Morss, W T Carnall, C W Williams *J. Less-Common Met.* **169** 1 (1991)
198. P Scott, P B Hitchcock *J. Chem. Soc., Chem. Commun.* 579 (1995)
199. V S Koltunov, E A Mezhov, S M Baranov *Radiokhimiya* **42** 65 (2000) [a]
200. O V Mikhailov *Radiokhimiya* **40** 316 (1998) [a]
201. M R Maurya, R C Maurya *Rev. Inorg. Chem.* **15** 1 (1995)
202. A M El-Hendawy, A El-Kourashy, M M El-Ghany Shanab *Polyhedron* **11** 523 (1992)
203. A Syamal, M M Singh *Indian J. Chem., Sect. A, Inorg.* **37** 350 (1998)
204. A Syamal, M M Singh *Indian J. Chem., Sect. A, Inorg.* **31** 110 (1992)
205. A H Amrallah *Pak. J. Sci. Ind. Res.* **37** 231 (1994)
206. A Syamal, M M Singh *React. Polym.* **21** 149 (1993)
207. I V Khudyakov, N J Turro, I K Yakushenko *J. Photochem. Photobiol.* **63** 25 (1992)
208. D L Clark, J G Watkin, R J Butcher *Organometallics,* **14** 2799 (1995)
209. M D Fryzuk, T S Haddad, D J Berg *Coord. Chem. Rev.* **99** 137 (1990)
210. P G Edwards, P A Andersen, A Zalkin *J. Am. Chem. Soc.* **103** 7792 (1981)
211. P G Edwards, J S Parry, P W Reed *Organometallics* **14** 3649 (1995)
212. S G Deshpande, S C Jain *Indian J. Chem., Sect. A, Inorg.* **30** 549 (1991)
213. M Nierlich, P Gradoz, M Ephritikhine *J. Organometal. Chem.* **481** 69 (1994)
214. S J Coles, A A Danopoulos, P W Read *J. Chem. Soc., Dalton Trans.* 3401 (1995)
215. K Aparna, S S Krishnamurthy, M Nethaji *J. Chem. Soc., Dalton Trans.* 2991 (1995)
216. A Vasilescu-Saidel, C N Turcanu, R Grosescu *J. Radioanal. Nucl. Chem.* **203** 177 (1996)
217. A Vasilescu-Saidel, C N Turcanu, R Grosescu *J. Radioanal. Nucl. Chem.* **203** 189 (1996)
218. R Arad-Yellin, M Zangen, H Gottlieb *J. Chem. Soc., Dalton Trans.* 2081 (1990)
219. T L Novoderezhkina, A F Borina, B N Kulikovskii *Koord. Khim.* **22** 797 (1996) [c]
220. M R Duttera, P J Fagan, T J Marks, V W Day *J. Am. Chem. Soc.* **104** 865 (1982)
221. H J Wasserman, D C Moody, R R Ryan *J. Chem. Soc., Chem. Commun.* 532 (1984)
222. H J Wasserman, D C Moody, R T Paine, R R Ryan, K V Salazar *J. Chem. Soc., Chem. Commun.* 533 (1984)
223. R E Cramer, S Roth, J W Gilje *Organometallics* **8** 2327 (1989)
224. P C Leverd, M Lance, M Ephritikhine *J. Chem. Soc., Dalton Trans.* 3563 (1994)
225. T Arliguie, M Fourmique, M Ephritikhine *Organometallics* **19** 109 (2000)
226. K Tatsumi, I Matsubara, Y Inoue, A Nakamura, R E Cramer, G J Tagoshi, J A Golen, J W Gilje *Inorg. Chem.* **29** 4928 (1990)
227. P C Leverd, M Lance, M Ephritikhine *J. Chem. Soc., Dalton Trans.* 237 (1995)
228. I A Charushnikova, N N Krot, Z A Starikova *Radiokhimiya* **42** 397 (2000) [a]
229. P C Leverd, T Arliguie, M Lance *J. Chem. Soc., Dalton Trans.* 501 (1994)
230. P C Leverd, T Arliguie, M Ephritikhine *New J. Chem.* **17** 769 (1993)
231. T Arliguie, M Fourmigue, M Ephritikhine *Organometallics* **19** 109 (2000)
232. L Bahadur, J P Pandey *J. Electrochem. Soc.* **137** 3755 (1990)
233. P C Leverd, M Lance, M Nierlich, J Viegner, M Ephritikhine *J. Chem. Soc., Dalton Trans.* 2251 (1993)
234. F D Rochon, R Melanson, P-C Kong *Inorg. Chem.* **37** 87 (1998)
235. S Baum, R Bramlet *Basic Nuclear Medicine* (New York: Appleton-Century-Crofts, 1975)
236. *Radiopharmaceuticals* (Eds G Subramanian, B A Rhodes, J F Cooper, V J Sodd) (New York: The Society of Nuclear Medicine, 1975)
237. J Barrera, A K Burrel, J C Bryan *Inorg. Chem.* **35** 335 (1996)
238. D J Rose, K P Maresca, T Nicholson, A Davison, A G Jones, J Babich, A Fischman, W Graham, J R D DeBord, J Zubieta *Inorg. Chem.* **37** 2701 (1998)
239. M J Abrams, S K Larsen, S N Shalkh, J Zubieta *Inorg. Chim. Acta* **185** 7 (1991)
240. M Hirsch-Kuchma, T Nicholson, A Davison, W M Davis, A G Jones *Inorg. Chem.* **36** 3237 (1997)
241. J Lu, A Yamano, M J Clarke *Inorg. Chem.* **29** 3483 (1990)
242. A Marchi, R Rossi, L Magon, A Duatti, U Casellato, R Graziani, M Vidal, F Riche *J. Chem. Soc., Dalton Trans.* 1935 (1990)
243. C M Archer, J R Dilworth, D V Griffiths, M McPartlin, J D Kelly *J. Chem. Soc., Dalton Trans.* 183 (1992)
244. A Marchi, L Marvelli, R Rossi, L Magon, V Bertolasi, V Ferretti, P Gilli *J. Chem. Soc., Dalton Trans.* 1485 (1992)
245. J Baldas, J F Boas, S F Colmanet, G A Williams *J. Chem. Soc., Dalton Trans.* 2845 (1992)
246. C Bolzati, L Uccelli, A Duatti, M Venturini, C Morin, S Chéradame, F Refosco, F Ossola, F Tisato *Inorg. Chem.* **36** 3582 (1997)
247. U Abram, E S Lang, S Aram, J Wegmann, J R Dilworth, R Kirmse, J D Woollins *J. Chem. Soc., Dalton Trans.* 623 (1997)
248. M Cattabriga, A Marchi, L Marvelli, R Rossi, G Vertuani, R Pecoraro, A Scattarin, V Bertolasi, V Ferretti *J. Chem. Soc., Dalton Trans.* 1453 (1998)
249. A K Burrell, D L Clark, P L Gordon, A P Sattelberger, J C Bryan *J. Am. Chem. Soc.* **116** 3813 (1994)
250. J G Du Preez, T I A Gerber, M L Gibson *J. Coord. Chem.* **22** 33 (1990)
251. J Barrera, J C Bryan *Inorg. Chem.* **35** 1825 (1996)

252. C M Archer, J R Dilworth, P Jobanputra, R M Thompson, M McPartlin, W Hiller *J. Chem. Soc., Dalton Trans*. 897 (1999)
253. E N Treher, L C Francesconi, J Z Gougoutas, M F Malley, A D Nunn *Inorg. Chem*. **28** 3411 (1989)
254. C M Archer, J R Dilworth, R M Thompson, M McPartlin, D C Povey, J D Kelly *J. Chem. Soc., Dalton Trans*. 461 (1993)
255. T Konno, J R Kirchhoff, M J Heeg, W R Heineman, E Deutsch *J. Chem. Soc., Dalton Trans*. 3069 (1992)
256. E Shuter, H R Hoveyda, V Karunaratne, S J Rettig, C Orvig *Inorg. Chem*. **33** 368 (1996)
257. L A de Learie, R C Haltiwangen, C G Pierpont *J. Am. Chem. Soc*. **111** 4324 (1989)
258. M Chatterjee, B Achari, S Das, R Banerjee, C Chakrabarti, J K Dattagupta, S Banerjee *Inorg. Chem*. **37** 5424 (1998)
259. N Bryson, J C Dewan, J Lister-James, A G Jones, A Davison *Inorg. Chem*. **27** 2154 (1988)
260. N Bryson, J Lister-James, A G Jones, W M Davis, A Davison *Inorg. Chem*. **29** 2948 (1990)
261. A Yokoyama, H Saji, H Tanaka, T Odori, R Morita, T Mori, K Torizuka *J. Nucl. Med*. **17** 810 (1976)
262. I Ikeda, O Inoue, K Kurata *J. Nucl. Med*. **18** 1223 (1977)
263. W Brandau, B Bubeck, M Eisenhut, D M Taylor *Appl. Radiat. Isot*. **39** 121 (1988)
264. M Chattopadhyay, K N Jalan, A K Pal, S N Benerjee *Nucl. Med. Biol*. **15** 535 (1988)
265. L G Marzilli, M G Banaszcyk, L Hansen, Z Kuklenyik, R Cini, A Taylor *Inorg. Chem*. **33** 4850 (1994)
266. R Rossi, A Marchi, L Magon, A Duatti, V Casellato, R Graziani *Inorg. Chim. Acta* **160** 23 (1989)
267. E Wong, T Fauconnier, S Bennett, J Valliant, T Nguyen, F Lau, L F L Lu, A Pollak, R A Bell, J R Thornback *Inorg. Chem*. **36** 5799 (1997)
268. C M Archer, J R Dilworth, D V Griffithi, M J Al-Jebbori, J D Kelly, C Lu, M J Rosser, Y Zheng *J. Chem. Soc., Dalton Trans*. 1403 (1997)
269. F Refosco, F Tisato, G Bandoli, E Deutsch *J. Chem. Soc., Dalton Trans*. 2901 (1993)
270. H Luo, I Setyawati, S J Rettig, C Orvig *Inorg. Chem*. **34** 2287 (1995)
271. L Kaden, A J L Pombeiro, Y Wang, U Abram *Inorg. Chim. Acta* **230** 189 (1995)
272. F Tisato, F Refosco, G Bandoli, C Bolzati, A Moresco *J. Chem. Soc., Dalton Trans*. 1453 (1994)
273. F A Cotton, L M Daniels, L R Falvello, M S Grigoriev, S V Kryuchkov *Inorg. Chim. Acta* **189** 53 (1991)
274. F A Cotton, L M Daniels, S C Haefner, A P Sattelberger *Inorg. Chim. Acta* **288** 69 (1999)
275. F A Cotton, S C Haefner, A P Sattelberger *Inorg. Chem*. **35** 1831 (1996)
276. F A Cotton, S C Haefner, A P Sattelberger *Inorg. Chem*. **35** 7350 (1996)
277. J C Bryan, F A Cotton, L M Daniels, S C Haefner, A P Sattelberger *Inorg. Chem*. **34** 1875 (1995)
278. F A Cotton, S C Haefner, A P Sattelberger *J. Am. Chem. Soc*. **118** 5486 (1996)
279. Yu V Plekhanov, S V Kryuchkov *Radiokhimiya* **39** 210 (1997) [a]
280. M S Grigor'ev, A E Miroslavov, G V Sidorenko, D N Suglobov *Radiokhimiya* **39** 204 (1997) [a]
281. M S Grigor'ev, A E Miroslavov, G V Sidorenko, D N Suglobov *Radiokhimiya* **39** 207 (1997) [a]
282. N I Gorshkov, A A Lumpov, A E Miroslavov, D N Suglobov *Radiokhimiya* **42** 213 (2000) [a]
283. S S Travnikov, E V Fedoseev, A V Davydov, B F Myasoedov, in *Teoreticheskaya i Prikladnaya Khimiya β-Diketonatov Metallov* (Theoretical and Applied Chemistry of Metal β-Diketonates) (Eds V I Spitsyn, L I Martynenko) (Moscow: Nauka, 1985) p. 224

[a] — *Radiochemistry (Engl. Transl.)*
[b] — *Russ. J. Inorg. Chem. (Engl. Transl.)*
[c] — *Russ. J. Coord. Chem. (Engl. Transl.)*
[d] — *Russ. J. Gen. Chem. (Engl. Transl.)*
[e] — *Dokl. Chem. (Engl. Transl.)*

Russian Chemical Reviews **70** (10) 885 – 895 (2001) © 2001 Russian Academy of Sciences and Turpion Ltd

DOI 10.1070/RC2001v070n10ABEH000659

Recent trends in the chemistry of sulfur-containing reducing agents

S V Makarov

Contents

I.	Introduction	885
II.	The structure of molecules of sulfur-containing reducing agents	885
III.	Classification of sulfur-containing reducing agents and the fields of their application	886
IV.	Methods of synthesis of sulfur-containing reducing agents	888
V.	The kinetics and mechanisms of reactions involving sulfur-containing reducing agents	888
VI.	Conclusion	893

Abstract. Data on the structure, synthesis, stability and reactivity of sulfur-containing reducing agents with C – S or S – S bonds — sodium dithionite, sodium hydroxymethanesulfinate and thiourea oxides — are surveyed. Reactions of anaerobic and aerobic decomposition of sulfur-containing reducing agents are discussed. The applications of these compounds in the studies of non-linear phenomena in chemical kinetics and in guanidine syntheses are considered. The bibliography includes 165 references.

I. Introduction

Compounds containing an S – S or C – S bond, namely, sodium dithionite, sodium hydroxymethanesulfinate (HMS, commercial name rongalite) and thiourea dioxide (TUDO), have long been used in chemistry and chemical technology as reducing agents. The traditional fields of application including printing and dyeing of textiles,[1] production of synthetic rubber,[2] manufacture of uranium and transuranium element compounds,[3] preparative organic[4] and inorganic[5] chemistry have been covered fairly comprehensively in monographs.[6,7] In recent years, some new fields of application appeared and the above-mentioned fields (mainly, organic synthesis[8,9]) have been further developed. In particular, increasing numbers of publications are devoted to the use of these compounds in biochemistry,[10–12] in organofluorine chemistry,[13] and in investigations of non-linear phenomena in chemical kinetics.[14,15] A promising field of application of thiourea dioxides and the products of their oxidation, trioxides, is the synthesis of guanidines.[16–20] The researchers' interest in the guanidine properties, which has increased in recent years,[21,22] is due to the discovery of an important biological function of nitrogen oxide, the precursor of which in an organism is L-arginine (2-amino-5-guanidinovaleric acid), and to the search for new medical drugs.[18,20] Thus, there is a need for a review that would reflect the state-of-the-art of the chemistry of sulfur-containing reducing agents.

S V Makarov Ivanovo State University of Chemistry and Technology, prosp. F Engelsa 7, 153460 Ivanovo, Russian Federation.
Fax (7-093) 241 79 95. Tel. (7-093) 232 73 97.
E-mail: makarov@icti.ivanovo.su

Received 13 February 2001
Uspekhi Khimii **70** (10) 996 – 1007 (2001); translated by Z P Bobkova

II. The structure of molecules of sulfur-containing reducing agents

The molecular structures of sodium dithionite, HMS and TUDO have been studied in detail by IR and Raman spectroscopy and by X-ray diffraction analysis. The structure of sodium dithionite has aroused the greatest interest. Seemingly, the structure of the $S_2O_4^{2-}$ ion should resemble the structures of well-known sulfur-and-oxygen anions with the S – S bonds, *e.g.*, $S_2O_5^{2-}$ and $S_2O_6^{2-}$ (see Ref. 23). One might expect that $S_2O_4^{2-}$ and $S_2O_6^{2-}$ ions would correspond to D_{3d} and C_{2h} point groups of symmetry, respectively. This prediction came true only for the latter anion, while for sodium dithionite, unexpected results were obtained. According to X-ray diffraction data,[24,25] the $S_2O_4^{2-}$ ion belongs to the C_{2v} point group and contains an abnormally long S – S bond (2.39 Å). Later, it was shown by Raman spectroscopy[26,27] that in aqueous solutions of sodium dithionite, the structure of the $S_2O_4^{2-}$ ion changes, namely, it becomes centrosymmetrical and corresponds to the C_{2h} point group. The influence of the nature of the salt cation on the structure of the dithionite ion has been studied.[23] It was shown that the 'abnormal' eclipsed conformation (C_{2v}) of $S_2O_4^{2-}$ can be found in salts with small cations, for example, with sodium. In the salts with large cations, in particular, in tetraethylammonium dithionite, this anion is centrosymmetrical both in the solid state and in solution. Thus, the abnormal structure of sodium dithionite in the solid phase is due to the influence of the cation and to the associated packing effects[23] rather than to the properties of the $S_2O_4^{2-}$ anion itself. These experimental data were substantiated theoretically by the results of LCAO-X_α density functional calculations.[28] It was shown that the curve for the total energy *vs.* S – S bond length for dithionite ion, unlike these curves for $S_2O_6^{2-}$ or $S_2O_5^{2-}$ ions, has a very broad minimum. This indicates that the S – S bond length in $S_2O_4^{2-}$ depends appreciably on external factors, in particular, on the packing effects in the crystal. It was also found that the barrier to rotation in the dithionite ion is very low. This accounts for the easy dehydration of $Na_2S_2O_4 \cdot 2H_2O$ and the concomitant change in the dithionite structure (for example, the S – S bond length increases from 2.298 Å in the dihydrate to 2.393 Å in the anhydrous salt). Therefore, it can be expected that the properties of solid dithionites should depend on the nature of solvents from which they have been crystallised. Indeed, it has been demonstrated in relation to lithium dithionite[29] that the products isolated from aqueous and tetrahydrofuran solutions have different properties; in particular, the latter is extremely susceptible to oxidation and to self-ignition in air. When lithium dithionite is stored in a sealed capillary, its

crystal lattice is transformed giving rise to defects, and this accelerates solid-phase processes. A similar transformation but taking place at elevated temperatures was observed for the sodium salt. Thus, conditions used to prepare dithionites affect appreciably their properties. A substantial dependence of the stability on the nature of the solvent used for recrystallisation is also typical of solid sodium hydroxymethanesulfinate.[30]

Due to the long and rather weak S–S bond, dithionites tend to undergo homolytic decomposition giving rise to the $SO_2^{-\bullet}$ radical anions. The structural parameters of the $SO_2^{-\bullet}$ radical anion have been determined;[31] the (*r*) S–O distance is 1.523 ± 0.02 Å, the O–S–O angle (α_{O-S-O}) is $115.6 \pm 2.0^\circ$. The structures of the $SO_2^{-\bullet}$ radical anion and the $NaSO_2$ charge transfer complex were also determined by *ab initio* calculations.[32]

According to X-ray diffraction studies,[33] HMS is the sodium salt of hydroxymethanesulfinic acid, $HOCH_2SO_2Na$. The crystal lattice parameters of HMS and the interatomic distances in the $HOCH_2SO_2^-$ anion were determined; the C–S bond was found to be the longest one (1.838 Å).

X-Ray diffraction analysis of TUDO was first performed by Sullivan and Hargreaves;[34] later, the data were refined.[35,36] In the solid phase, TUDO exists as $(NH_2)_2CSO_2$. The CSO_2 group is pyramidal, the S–O and C–N bond lengths are 1.496 and 1.296 Å, respectively, and the C–S bond (1.867 Å) is much longer than this bond in the thiourea (1.716 Å) molecule. The bond lengths in the TUDO molecule found from X-ray diffraction data are in good agreement with the results of *ab initio* calculations.[36] It was suggested that TUDO is a combination of two zwitter-ion forms

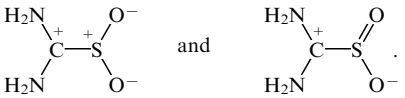

In these ions, the negative charge is concentrated on the oxygen and nitrogen atoms and the positive charge is on the hydrogen, carbon and sulfur atoms, mainly, on sulfur. The results of calculations indicate that nucleophilic attack is directed at the carbon and sulfur atoms. The structure of thiourea dioxide depends substantially on the solvent. It was found[37] that after dissolution of TUDO in water, the acidity increases, a constant pH value being established very slowly. It was found in special experiments that these changes are not related to decomposition of TUDO or to the presence of oxygen. The ^1H NMR spectra of aqueous[38] and dimethyl sulfoxide[39] solutions of TUDO were found to vary with time. The peak observed initially in the TUDO spectrum is rapidly split into a doublet, these changes taking place only in the first minutes after dissolution of thiourea dioxide. Quantum-chemical calculations by the AM1 method for TUDO in the $(NH_2)_2CSO_2$ and $NH_2C(=NH)SO_2H$ (aminoiminomethanesulfinic acid) forms[40] showed that solvation with water or dimethyl sulfoxide decreases substantially the total energy of the system. Note that unlike the gas phase, in aqueous solutions, aminoiminomethanesulfinic acid is the thermodynamically more stable form. Thus, quantum-chemical calculations imply the possibility of TUDO tautomerisation in aqueous solutions. The tautomeric transformations of TUDO in aqueous solutions have been studied theoretically using the method of critical points on the potential energy surface.[41] The most probable mechanism of tautomerisation includes stages of successive intermolecular proton transfer in TUDO oligomers and decomposition of the oligomers to give solvated monomers of aminoiminomethanesulfinic acid.

The structure of thiourea trioxide (TUTO) has also been studied.[42] It was found that the C–N bonds in TUTO are virtually equivalent (1.298 and 1.297 Å) and are much shorter than the typical C–N single bond (1.470 Å), while the C–S bond length (1.815 Å) is slightly greater than the sum of the covalent radii of the S and C atoms (1.790 Å). The tetrahedral S atom forms three nearly equivalent S–O bonds (1.439, 1.431, and 1.446 Å). The structures of thiourea di- and trioxides are stabilised by intermolecular hydrogen bonds.[36,42] The unusually high density calculated[42] for TUTO, 1.948 g cm^{-3} (the density of thiourea dioxide is[36] 1.70 g cm^{-3}) points to a highly efficient packing of $(NH_2)_2CSO_3$ molecules in the crystal lattice. Apparently, the structure of TUTO is similar to that of TUDO.

The research into the structures of sodium dithionite, HMS and TUDO showed that each of these molecules contains an abnormally long bond, which is, hence, highly prone to rupture (S–S bond in the dithionite and C–S bonds in HMS and TUDO). It is this structural feature that accounts for the high reducing activities of these compounds. As will be shown below, the chemical reactivities of dithionites, HMS, TUDO and their analogues are governed by transformations of the same intermediates, namely, sulfoxylic acid H_2SO_2 or its anions and the $SO_2^{-\bullet}$ radical anion. This fact, together with the similarity of methods for the use of these compounds explain why they have been combined in one group.

III. Classification of sulfur-containing reducing agents and the fields of their application

The sulfur-containing reducing agents considered here (Table 1) can be classified into dithionites, α-hydroxyalkanesulfinates, and thiourea dioxides.

Thiourea trioxides are also included in Table 1. Data on α-aminoalkanesulfinates not reflected in the Table can be found in a monograph.[7] Note that the properties of most of compounds listed in Table 1 have been little studied. The only exceptions are sodium dithionite, HMS and TUDO, which have found wide practical use. Sodium dithionite and hydroxymethanesulfinate are used most often for the reduction of vat dyes in textile industry.[1] The processes involving these reducing agents form the basis of all industrial printing and vat dyeing techniques. The textile industry also makes use of zinc hydroxymethanesulfinates, which possess a lower reducing activity than HMS.[6] Conversely, α-hydroxyethanesulfinate is a stronger reducing agent than HMS.[7]

An important application of HMS and TUDO is the manufacture of synthetic rubber.[2] For instance, a mixture of HMS with isopropylbenzene hydroperoxide and ethylenediaminetetraacetatoferrate(III) initiates copolymerisation of butadiene with styrene. The Fe^{2+}–TUDO–H_2O_2 system is used to initiate polymerisation of various vinyl monomers.[59] Other effective initiating systems are TUDO–$KBrO_3$[60] and TUDO–$KMnO_4$.[61] In addition, TUDO is used for waste paper processing[62] and for wool bleaching.[63] Numerous publications have been devoted to the use of the reducing agents in question, mainly sodium dithionite, in biochemistry.[10–12,64–66] Sodium dithionite is used for the reduction of many natural and synthetic electron transfer agents including nicotinic acid derivatives, flavins and cytochromes;[64,65] TUDO is used for reduction of ferredoxin, cytochrome C and other substrates[66] and for inactivation and modification of cytidine triphosphate synthase.[11,12] *N*,*N*′-Dimethylthiourea is a highly efficient antioxidant, which has found wide use in biochemical and medical research.[67] Thus the reaction of hydrogen peroxide with *N*,*N*′-dimethylthiourea, resulting in the dioxide, can be used to determine the content of H_2O_2 in biological systems.[55]

Sulfur-containing reducing agents are widely used in organic synthesis. Thus sodium dithionite serves as the reagent for the reduction of nitro, nitroso, azido and azo compounds, aldehydes, ketones, keto esters, benzyls, quinones, heterocycles, and compounds with double bonds as well as for the synthesis of sulfones.[4] Hydroxymethanesulfinate and thiourea dioxide are used in similar processes, in particular, in the preparation of a light-stabiliser for plastics, Benazol P,[68] a stabiliser for motor oils called Diafen FP[69] and sulfones.[70–74] In recent years, the possibility of using these reducing agents in the chemistry of organofluorine compounds has been studied intensively.[13,75] Thiourea dioxide is also employed to reduce organosulfur compounds (sulfylimines, sulf-

Table 1. Sulfur-containing reducing agents.

Name of compound	Formula	Ref.
Dithionites		
Sodium dithionite	$Na_2S_2O_4$	7
Potassium dithionite	$K_2S_2O_4$	43
Lithium dithionite	$Li_2S_2O_4$	29
Zinc dithionite	ZnS_2O_4	44
Tin dithionite	$Sn(S_2O_4)_2$	25
Tetraethylammonium dithionite	$(Et_4N)_2S_2O_4$	45
α-Hydroxyalkanesulfinates		
Sodium hydroxymethanesulfinate (rongalite)	$HOCH_2SO_2Na$	7
Disodium hydroxymethanesulfinate	$NaOCH_2SO_2Na$	6
Zinc hydroxymethanesulfinate	$(HOCH_2SO_2)_2Zn$	46
Zinc hydroxyl hydroxymethanesulfinate	$HOCH_2SO_2Zn(OH)$	47
Zinc hydroxymethanesulfinate, disubstituted		6
Calcium hydroxymethanesulfinate, disubstituted	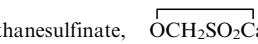	6
Titanium hydroxymethanesulfinate	$(HOCH_2SO_2)_4Ti$	6
Barium hydroxymethanesulfinate, disubstituted	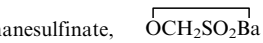	6
Lead(II) hydroxymethanesulfinate, disubstituted	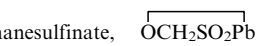	6
Mercury(II) hydroxymethanesulfinate, disubstituted		6
Sodium α-hydroxyethanesulfinate	$MeCH(OH)SO_2Na$	48
Sodium α-hydroxytrifluoroethanesulfinate	$CF_3CH(OH)SO_2Na$	49
Potassium α-hydroxyethanesulfinate	$MeCH(OH)SO_2K$	6
Sodium α-hydroxypropanesulfinate	$EtCH(OH)SO_2Na$	7
Potassium α-hydroxy-2-propanesulfinate	$Me_2C(OH)SO_2K$	6
Sodium α-hydroxy-n-butanesulfinate	$Pr^nCH(OH)SO_2Na$	6
Thiourea dioxides		
Thiourea dioxide	$(NH_2)_2CSO_2$	36
N-Methylthiourea dioxide	$MeNHC(NH_2)SO_2$	50
N-Propylthiourea dioxide	$Pr^nNHC(NH_2)SO_2$	50
N-Isopropylthiourea dioxide	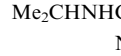	50
N-Butylthiourea dioxide	$Bu^nNHC(NH_2)SO_2$	50
N-But-2-ylthiourea dioxide	$Et(Me)CHNHC(NH_2)SO_2$	50
N-*tert*-Butylthiourea dioxide	$Me_3CNHC(NH_2)SO_2$	50
N-Neopentylthiourea dioxide	$Me_3CCH_2NHC(NH_2)SO_2$	50
N-Hydroxymethylthiourea dioxide	$HOCH_2NHC(NH_2)SO_2$	51
N-Hexylthiourea dioxide	$C_6H_{13}NHC(NH_2)SO_2$	52
N-Dodecylthiourea dioxide	$C_{12}H_{25}NHC(NH_2)SO_2$	52
N-Phenylthiourea dioxide	$PhNHC(NH_2)SO_2$	51
N-*p*-methylphenylthiourea dioxide	p-$MeC_6H_4NHC(NH_2)SO_2$	53
N-*o*-hydroxyphenylthiourea dioxide	o-$HOC_6H_4NHC(NH_2)SO_2$	51
N-*o*-methoxyphenylthiourea dioxide		51
N-2,6-Dimethylphenylthiourea dioxide	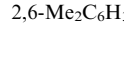	50
Thiourea dioxides		
N-2,6-Diethylphenylthiourea dioxide	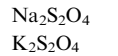	50
N-2,6-Diisopropylphenylthiourea dioxide	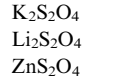	50
N-Guanylthiourea dioxide	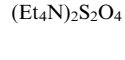	54
N-Diphenylmethylthiourea dioxide	$Ph_2CHNHC(NH_2)SO_2$	50
N-Triphenylmethylthiourea dioxide	$Ph_3CNHC(NH_2)SO_2$	50
N,*N*-Dimethylthiourea dioxide	$Me_2NC(NH_2)SO_2$	50
N,*N*-Dipropylthiourea dioxide	$Pr^n_2NC(NH_2)SO_2$	50
N,*N*-Dibutylthiourea dioxide	$Bu^n_2NC(NH_2)SO_2$	50
N,*N*-Di(2-methylpropyl)thiourea dioxide	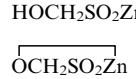	50
N,*N*′-Dimethylthiourea dioxide	$(MeNH)_2CSO_2$	55
N,*N*′-Dibut-2-ylthiourea dioxide	$[Et(Me)CHNH]_2CSO_2$	50
N,*N*′-Diphenylthiourea dioxide	$(PhNH)_2CSO_2$	51
N,*N*′-Di-*o*-methylphenylthiourea dioxide	$(o$-$MeC_6H_4NH)_2CSO_2$	53
N,*N*′-Dicyclohexylthiourea dioxide	$(cyclo$-$C_6H_{11}NH)_2CSO_2$	50
Thiourea trioxides		
Thiourea trioxide	$(NH_2)_2CSO_3$	17
N-Methylthiourea trioxide	$MeNHC(NH_2)SO_3$	56
N-Propylthiourea trioxide	$Pr^nNHC(NH_2)SO_3$	56
N-But-2-ylthiourea trioxide	$Et(Me)CHNHC(NH_2)SO_3$	56
N-*tert*-Butylthiourea trioxide	$Me_3CNHC(NH_2)SO_3$	56
N-Allylthiourea trioxide	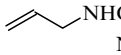	56
N-Phenylthiourea trioxide	$PhNHC(NH_2)SO_3$	56
N-Benzylthiourea trioxide	$PhCH_2NHC(NH_2)SO_3$	56
N-*o*-Methylphenylthiourea trioxide	o-$MeC_6H_4NHC(NH_2)SO_3$	17
N-*o*-Chlorophenylthiourea trioxide	o-$ClC_6H_4NHC(NH_2)SO_3$	17
N-*p*-Fluorophenylthiourea trioxide	p-$FC_6H_4NHC(NH_2)SO_3$	16
N-2-Isopropylphenylthiourea trioxide	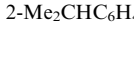	56
N-2,6-Dimethylphenylthiourea trioxide	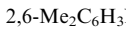	56
N-2,6-Diethylphenylthiourea trioxide	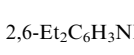	17
N-2,6-Diisopropylphenylthiourea trioxide	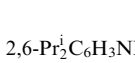	56
N-2,6-Dichlorophenylthiourea trioxide		17
N,*N*-Dimethylthiourea trioxide	$Me_2NC(NH_2)SO_3$	56
N-Ethyl-*N*-phenylthiourea trioxide	$Ph(Et)NC(NH_2)SO_3$	57
N,*N*′-Diethylthiourea trioxide	$(EtNH)_2CSO_3$	57
N,*N*′-Diisopropylthiourea trioxide	$(Me_2CHNH)_2CSO_3$	56
N,*N*′-Dibut-2-ylthiourea trioxide	$[Et(Me)CHNH]_2CSO_3$	56
N,*N*′-Di-*tert*-butylthiourea trioxide	$(Me_3CNH)_2CSO_3$	56
N,*N*′-Dineopentylthiourea trioxide	$(Me_3CCH_2NH)_2CSO_3$	56
N,*N*′-Dicyclohexylthiourea trioxide	$(cyclo$-$C_6H_{11}NH)_2CSO_3$	56
N,*N*′-Diphenylthiourea trioxide	$(PhNH)_2CSO_3$	57
N,*N*′-Dibenzylthiourea trioxide	$(PhCH_2NH)_2CSO_3$	58

oxides, disulfides),[76,77] for the preparation of a number of compounds of selenium and tellurium[78,79] and deoxygenation of various heteroaromatic *N*-oxides;[8] in addition, it serves as a convenient reductant in phase transfer catalysis.[76,80] Sodium hydroxymethanesulfinate is also utilised in the syntheses of various compounds of selenium and tellurium[81,82] and for the preparation of sultins.[9]

An important application of thiourea oxides is the synthesis of guanidines and their derivatives,[16–20,83–85] which consists in the reaction of thiourea oxides with primary[83] or heterocyclic secondary amines, for example, morpholine,[85] or with amino acids[84] and other amino compounds. The reactions of thiourea oxides with amines are carried out in organic solvents (methanol,[83] acetonitrile[85]), while the reactions with amino acids take place in aqueous solutions.[84] The mechanism proposed for this reaction includes the addition of the nucleophile (*i.e.*, amine) to thiourea oxide and decomposition of the intermediate giving rise to guanidine.[85] The use of trioxides is more convenient because it permits the preparation of guanidines[85] and guanidine acids[84] in high yields. Currently, thiourea trioxide is among the most important guanidylating agents used in the syntheses of guanidines with various structures.[18–20,86–98] Unfortunately, the kinetics of the reactions of thiourea oxides with amino compounds has not yet been studied, despite the fact that the interest in guanidines is very high due to the discovery of the crucial role of nitrogen oxide in functioning of the vascular system.[99–101] It was found that it is the guanidine fragment of L-arginine that is oxidised *in vivo* to give citrulline and nitrogen oxide (in a recent publication,[87] the possibility of using thiourea trioxide in the syntheses of L-arginine derivatives is demonstrated). Guanidines have proved efficient in the treatment of cardiovascular diseases.[100] Thus chemists of the Du Pont company have developed the Du P 714 preparation,[18] which prevents thrombus formation; this synthesis was a success only when thiourea dioxide was used to introduce the guanidine group. The attempts to synthesise this preparation using other guanidylating agents failed. Thiourea trioxide[86–98] and *N*-phenylthiourea trioxide[16] have also been employed for the preparation of other medicinal drugs. Thiourea trioxides are the initial compounds in the syntheses of aminoiminoethanenitriles, 5-aminotetrazoles, *N*-cyanoguanidines and *N*-hydroxyguanidines.[57] The reaction of $(NH_2)_2CSO_3$ with methyl anthranylate affords 5*H*-quinazolino[3,2-*a*]quinazoline-5,12(6*H*)-dione.[102]

Numerous studies have been devoted to the use of reduction reactions involving HMS and TUDO to produce metals — silver,[103] cadmium,[104] technetium,[105] nickel,[106] and metallic coatings on fibres.[107]

IV. Methods of synthesis of sulfur-containing reducing agents

Metal dithionites are prepared by the reduction of sulfur dioxide with zinc, sodium formate[44] or borohydrides.[43] A method for the synthesis of extra pure sodium dithionite containing 99% of the required substance has been developed.[108] A procedure for the preparation of tetraethylammonium dithionite using ion exchange resins is documented.[45]

Several methods for the synthesis of sodium hydroxymethanesulfinate are known.[6] The preparation of HMS by the reduction of sodium hydroxymethanesulfonate with disperse zinc is used most often.

Thiourea mono-, di- and trioxides are produced upon the oxidation of thiourea with hydrogen peroxide in a neutral medium.[7] The synthesis of TUDO is performed at 0–5°C. Unlike the dioxide, thiourea monoxide is quite unstable. More stable monoxides are formed from thiourea derivatives containing bulky substituents at the nitrogen atoms. Thus *N*-phenyl- and ethylenethiourea monoxides have been prepared.[109] The formation of these compounds in solution was proved by the test reaction with $FeCl_3$, typical of mono-*S*-oxygenated thioamides and thiocarbamates. Neutral aqueous solutions of the monoxides synthesised are stable over a period of 24 h at 0 °C; however, these compounds are exceptionally unstable in the solid state. *N*-Phenyl-, *N*,*N*′-diphenyl-, *N*-*o*-hydroxyphenyl- and *N*-*o*-methoxyphenylthiourea dioxides have been prepared by using sodium molybdate[51] to catalyse the reaction between the corresponding thiourea derivative and H_2O_2. Dioxides of other *N*-aryl-substituted thioureas have also been prepared.[53] Syntheses of *N*-aryl- and *N*-alkyl-substituted thiourea dioxides in 80%–90% yields without catalysts have been reported.[50,110] In order to prepare *N*-phenylthiourea dioxide containing ~100% of the required substance, the synthesis should be carried out at −7 to 12 °C.[17] An attempt to prepare *N*,*N*′-diphenylthiourea dioxide by a procedure proposed previously[53] failed.[17] Thiourea trioxides can be synthesised by treatment of thioureas or thiourea dioxides with three or one equivalent of peracetic acid, respectively.[56] An electrochemical procedure for the synthesis of thiourea trioxides has been proposed.[111]

The major products formed in the reaction of thiourea with hydrogen peroxide in strongly acidic media and in the presence of metal ions are formamidine disulfide salts.[112] There is no consensus of opinion on the mechanism of the reaction between thiourea and H_2O_2. The kinetics and the mechanism of the reactions of thiourea and *N*,*N*′-dialkylthiourea with hydrogen peroxide in acid media have been studied.[113] Presumably, in this case, these thioureas act as nucleophiles by replacing the peroxide oxygen, *i.e.*, the reaction does not involve free radicals. However, the use of spin traps, namely, *N*-benzylidene-*tert*-*N*-butylamine *N*-oxide and 5,5-dimethyl-1-pyrroline *N*-oxide (DMPO) allowed detection of the carbamidinothiyl radical $NH_2(=NH)CS^{\bullet}$ upon oxidation of thiourea with hydrogen peroxide.[114] The stability of this radical was found to depend substantially on the medium pH, the most intense EPR signal being observed at 2.5–3.0.

V. The kinetics and mechanisms of reactions involving sulfur-containing reducing agents

Decomposition of sulfur-containing reductants and their reactions with oxidants are closely interrelated because they proceed *via* the formation of the same intermediates. Therefore, we shall first consider the results of research into decomposition of sulfur-containing reducing agents. The stability of these compounds in aqueous solutions depends appreciably on the pH. Sodium dithionite and HMS are less stable in acid media.

Oxygen-free decomposition of sodium dithionite in acid solutions has been studied in detail.[115,116] Polarography was used to measure the time variation of the concentrations of dithionite and the products of its decomposition, which include sulfide, sulfite, thiosulfate, and active sulfur (S_a); the term 'active sulfur' implies atomic sulfur, the $S\cdot H_2O$ hydrate, the HSOH thioperoxide, the polymeric biradical and sulfur in a polysulfide chain.

Decomposition was found to be autocatalytic, active sulfur and sulfide functioning as the catalysts. The influence of sulfide, sulfite, thiosulfate and sulfur dichloride additives (and also of mixtures of these compounds) on the rate of dithionite decomposition has been studied.[115] On the basis of the results obtained, it was concluded that the following reactions are responsible for the dithionite decomposition:

— non-catalysed reaction proceeding during the induction period,

$$2\,H_2S_2O_4 \longrightarrow S_a + 3\,SO_2 + 2\,H_2O; \quad (1)$$

— autocatalytic reaction mainly proceeding at the fast decomposition stage,

$$3\,H_2S_2O_4 \longrightarrow H_2S + 5\,SO_2 + 2\,H_2O. \quad (2)$$

Simultaneously, a series of side reactions take place. On the basis of experimental data,[115] a mathematical model of the dithionite decomposition was proposed.[116] Calculations performed in terms of this model made it possible to estimate the

contribution of individual homogeneous reactions and to demonstrate that the proposed two-stage scheme is adequate to describe the real mechanism of decomposition.

Non-catalysed and catalysed decomposition of sodium dithionite in weakly acidic solutions in the presence of sulfur-containing admixtures has been investigated.[117] Particular attention is devoted to the influence of sulfite. In the opinion of the researchers cited,[117] in the case of a high sulfite concentration in the solution, decomposition of $S_2O_4^{2-}$ can follow two mechanisms, a heterolytic and a homolytic one. The former includes the following stages:

$$S_2O_4^{2-} + HSO_3^- \longrightarrow [O_2S(O_2)S-SO_2OH]^{3-}, \quad (3)$$

$$[O_2S(O_2)S-SO_2OH]^{3-} + H^+ \longrightarrow S_3O_6^{2-} + H_2O. \quad (4)$$

In this case, reaction (3) is the rate-determining stage. The trithionate formed in reaction (4) participates, together with the $SO_2^{-\bullet}$ radical ion, in the decomposition by the homolytic mechanism

$$S_2O_4^{2-} \rightleftharpoons 2\,SO_2^{-\bullet}, \quad (5)$$

$$HSO_3^- + SO_2^{-\bullet} \rightleftharpoons S_2O_5H^{2-\bullet}, \quad (6)$$

$$S_2O_5H^{2-\bullet} + S_3O_6^{2-} \longrightarrow SO_2 + HSO_3^- + SO_3^{2-} + S_2O_3^{-\bullet}, \quad (7)$$

$$S_2O_3^{-\bullet} + SO_2^{-\bullet} \longrightarrow S_2O_3^{2-} + SO_2. \quad (8)$$

The reaction between two dianions [reaction (7)] determines the rate of the whole homolytic process.

When the sulfite concentration in the solution is low, the process follows a third pathway

$$S_2O_4^{2-} + HSO_3^- \longrightarrow [O_2S(O_2)S-OSOOH]^{3-}, \quad (9)$$

$$[O_2S(O_2)S-OSOOH]^{3-} \longrightarrow S_2O_5^{2-} + HSO_2^-, \quad (10)$$

$$2\,HSO_2^- \longrightarrow S_2O_3^{2-} + H_2O, \quad (11)$$

$$S_2O_5^{2-} + H_2O \rightleftharpoons 2\,HSO_3^-. \quad (12)$$

Unlike the heterolytic mechanism mentioned above, in this pathway, the initial reaction is the transfer of an oxygen atom from the bisulfite ion to the dithionite sulfur atom.

A serious drawback of the mechanisms proposed by Holman and Bennett [117] [see reactions (3)–(12)] is that nothing is said about the role of sulfur or sulfides in the dithionite decomposition. This is explainable for a large excess of sulfite present because in acid media, HSO_3^- rapidly reacts with sulfur and sulfides, which virtually cancels out their effect on the dithionite decomposition. However, in the case of low initial concentrations of sulfite in the solution, the influence of sulfur or sulfide, which are the main products of dithionite decomposition in acid media, cannot be neglected.

Decomposition of sodium hydroxymethanesulfinate in acid media has been studied.[118, 119] This process is autocatalytic, being accelerated by active sulfur. The catalytic effect of S_a is attributable to its influence on the decomposition of sodium dithionite, which is one of the main intermediate compounds formed upon decomposition of HMS. The following sequence of reactions was proposed as taking place during oxygen-free decomposition of HMS in acidic aqueous solutions:

$$HOCH_2SO_2^- \rightleftharpoons HSO_2^- + CH_2O, \quad (13)$$

$$2\,HSO_2^- \longrightarrow S_2O_3^{2-} + H_2O, \quad (11)$$

$$S_2O_3^{2-} \rightleftharpoons S_a + SO_3^{2-}, \quad (14)$$

$$SO_3^{2-} + H^+ \rightleftharpoons HSO_3^-, \quad (15)$$

$$HSO_2^- + HSO_3^- \rightleftharpoons S_2O_4^{2-} + H_2O, \quad (16)$$

$$S_2O_4^{2-} \rightleftharpoons 2\,SO_2^{-\bullet}. \quad (5)$$

An important role in the mechanisms of decomposition of sodium dithionite as well as HMS and TUDO is played by reaction (5), *i.e.*, the homolytic cleavage of $S_2O_4^{2-}$.

The equilibrium constant of reaction (5) at 298 K is equal to 1.4×10^{-9} mol litre^{-1} (see Ref. 120). Studies of the temperature dependence of this equilibrium constant gave quite contradictory results. Thus it has been found [121] that an increase in the temperature from 298 to 353 K results in a 10-fold increase in the concentration of the $SO_2^{-\bullet}$ radical anion, which entails an increase in the equilibrium constant of reaction (5) by a factor of 10. A similar pattern of dependence of the constant on the temperature was also indicated by other researchers.[122] However, according to some other studies,[120, 123, 124] the increase in the equilibrium constant upon an increase in the temperature is much more gradual.

In view of the inconsistency of the data on the temperature dependence of the equilibrium constant, the thermodynamic characteristics of reaction (5) were determined using other methods.

The standard enthalpies of formation (Δ_fH°) of the $SO_x^{-\bullet}$ ($x = 2-4$) radical anions were calculated.[125] The $\Delta_fH^\circ(SO_x^{-\bullet}, 298)$ values in an aqueous solution were determined on the basis of thermodynamics data for liquid-phase decomposition of ions of the $[R-R]^{2-}$ type including the dithionite ion:

$$[R-R]^{2-} \rightleftharpoons R^{-\bullet} + R^{-\bullet}. \quad (17)$$

The standard enthalpy of formation of the product of this reaction can be estimated using the following relation:

$$\Delta_fH^\circ(R^{-\bullet}, 298) = 0.5\,\{\Delta_rG^\circ(298) + T\Delta_rS^\circ(298) + \Delta_fH^\circ([R-R]^{2-}, 298)\}, \quad (18)$$

where $\Delta_rG^\circ(298)$ and $\Delta_rS^\circ(298)$ are the change in the standard Gibbs energy and the standard entropy in reaction (17) at 298 K, respectively, $\Delta_fH^\circ([R-R]^{2-}, 298)$ is the standard enthalpy of formation of the $[R-R]^{2-}$ ion at 298 K.

The $\Delta_rG^\circ(298)$ (52.3 ± 1.3 kJ mol^{-1}) and $\Delta_fH^\circ(S_2O_4^{2-}, 298)$ (-753.7 kJ mol^{-1}) values for the decomposition of $S_2O_4^{2-}$ are known. The uncertainty in $T\Delta_rS^\circ(298)$ is due to the absence of data on the standard entropy of formation of the $SO_x^{-\bullet}$ anion at 298 K [$S_f^\circ(SO_x^{-\bullet}, 298)$]. These values were estimated using the empirical dependence of the standard entropy of the $[R-R]^{2-}$ oxy anion on its mass (M), charge (Z), the distance between the central atom and the peripheral oxygen atoms (r), and the empirical factor (f) that takes into account the ion geometry

$$S_f^\circ(298) - 6.3\,R(\ln M) = 276 - 338.6\,(Z/\rho), \quad (19)$$

where R is the universal gas constant, ρ is an empirical variable equal to r/f. For $SO_2^{-\bullet}$, the ρ value was found proceeding from the values $r = 0.151$ nm, $f = 0.87 \pm 0.11$. The $S_f^\circ(SO_2^{-\bullet})$ value at 298 K found on the basis of relation (19) amounted to 134 ± 25 J mol^{-1} K^{-1} [for the dithionite ion, $S_f^\circ(S_2O_4^{2-}) = 104.5$ J mol^{-1} K^{-1}]. The $\Delta_rS^\circ(298)$ value for reaction (5) corresponding to these parameters is equal to 163.5 ± 50 J mol^{-1} K^{-1}. The $\Delta_fH^\circ(SO_2^{-\bullet}, 298)$ value determined from Eqn (18) amounts to -326.5 ± 8 kJ mol^{-1}. The researchers cited [125] did not compare the resulting $\Delta_rH^\circ(298)$ (100.7 ± 17 kJ mol^{-1}) with the values found from the temperature dependence of the equilibrium constant of reaction (5). It is noteworthy that this value is close to $\Delta_rH^\circ(298) = 89.1$ kJ mol^{-1}, presented in a publication.[122] Unfortunately, the standard enthalpies and entropies of formation of the sulfoxylate ion SO_2^{2-} have not been determined yet.

Equilibrium (5) in aprotic media has been studied using tetraethylammonium dithionite.[45] It was shown by EPR and UV spectroscopy that the $S_2O_4^{2-}$ dimer dissociates to give the $SO_2^{-\bullet}$ radical anions in DMF, DMSO and acetonitrile, the equilibrium constants in non-aqueous solvents being 10^7 times as high as that in water. Thus, the equilibrium constant for reaction (5) depends appreciably on the nature of the solvent.

Unlike HMS or sodium dithionite, TUDO is much less stable in alkaline solutions than in neutral or acidic solutions.

Comparative investigation of the composition of the products of decomposition of thio- and *N*-phenylthiourea di- and trioxides

and *N*,*N*′-diphenylthiourea trioxide in neutral and alkaline solutions has been carried out.[17] Ureas are the major products of thiourea dioxide decomposition in alkaline media. Conversely, decomposition of thio- and *N*-phenylthiourea trioxides affords mainly cyanamides (pH 13–14) (*N*,*N*′-diphenylthiourea trioxide is mainly converted into *N*,*N*′-diphenylurea). In less alkaline solutions (pH 10), the percentage of ureas in the products of dioxide decomposition decreases, while the content of cyanamides increases. Under similar conditions, thiourea trioxide gives melamine in 52% yield; the formation of cyanoguanidine (dicyanodiamide) was also detected (the formation of substituted triazine related to melamine has been observed previously in the decomposition of *N*-propylaminoiminomethanesulfonic acid in the presence of *tert*-butylamine [16]). Presumably, a product of self-condensation of TUTO is formed intermediately in the reaction of melamine formation.

The essentially different decomposition mechanisms of thiourea dioxides and trioxides and, as a consequence, different compositions of the reaction products have been attributed,[17] first of all, to the different stabilities of $NH_2NHRCSO_2$ and $NH_2NHRCSO_3$ in alkaline media (R = H, Ph). The trioxide is assumed to be much more stable in solution than the dioxide; however no experimental evidence supporting this assumption is available. No data on the sulfur-containing products of decomposition of thiourea oxides are available either.

It has been assumed [126] that an important role in the decomposition of TUDO is played by dithionite ions and the $SO_2^{-\bullet}$ radical anions. The appearance of these species in alkaline solutions of TUDO was detected by polarography and interpreted as being due to the reaction

$$(NH_2)_2CSO_2 + OH^- \longrightarrow HSO_2^- + (NH_2)_2CO, \quad (20)$$

as well as reactions (5) and (16) presented above. Presumably,[126] decomposition of TUDO gives sulfoxylate as the primary product [however, it is not indicated what process is responsible for the formation of sulfite needed for the formation of dithionite by reaction (16)]. Yet another mechanism of TUDO decomposition has also been proposed;[104] according to this mechanism, the strong reducing properties of TUDO in alkaline media are due to the homolytic decomposition of the $H_2N(=NH)CSO_2^-$ anion to give reactive species, $SO_2^{-\bullet}$ and $(NH_2)_2C^{\bullet}OH$. It has also been suggested [127] that the $SO_2^{-\bullet}$ radical anion (in the aqueous alkali–ethanol system) is formed as the primary product of TUDO decomposition.

Unfortunately, in most of the above-mentioned studies, no integrated approach is used to investigate the processes of decomposition of sulfur-containing reducing agents. This is especially true for thiourea oxides. The transformations of their 'sulfur' and 'nitrogen' components have been studied independently by chemists working in different fields. The former, 'sulfur' part has been studied by inorganic chemists and specialists in chemical kinetics, while the latter, 'nitrogen' part has been an object of investigations of organic chemists and biochemists. These investigations have not been connected with one another and, moreover, the results have been published in journals of different disciplines. The fewness of kinetic data concerning the processes of decomposition of sulfur-containing reducing agents also appears surprising. Data on the decomposition mechanisms are fragmentary and often contradictory. Unfortunately, in many publications, no attention is paid to the role of oxygen in the decomposition of the compounds in question. Often, it is even impossible to grasp whether the reaction was carried out in an inert atmosphere or in air (this is especially typical of papers in organic chemistry). It will be shown below that it is the effect of oxygen on the composition of the intermediate and final products in the decomposition of sulfur-containing reducing agents that is the main reason for the contradictions mentioned above.

Let us consider the reactions of sulfur-containing reductants with oxygen. Creutz and Sutin,[128] who confirmed the previously proposed [120] mechanism of the dithionite reaction with oxygen,

$$S_2O_4^{2-} \rightleftharpoons 2\,SO_2^{-\bullet}, \quad (5)$$

$$SO_2^{-\bullet} + O_2 \longrightarrow \text{products}, \quad (21)$$

showed also that the process rate is determined by reaction (5), the rate constant for the forward reaction being virtually independent of the pH: $k = 2.5$ (pH 6.5) and 1.8 s^{-1} (pH 13). The researchers also determined the lower limit for the rate constant for reaction (21): $k_{21} \geqslant 1 \times 10^8$ litre mol^{-1} s^{-1}. Later, the value $k_{21} = 2.4 \times 10^9$ litre mol^{-1} s^{-1} was found.[129]

The kinetics of the reaction of sodium dithionite with hydrogen peroxide has been studied.[128] As in the case of oxygen, the $SO_2^{-\bullet}$ radical anion rather than the $S_2O_4^{2-}$ dithionite ion enters into the reaction with the oxidant. The influence of oxygen on the decomposition of HMS and TUDO has been studied.[119, 130] It was found that in the HMS decomposition under aerobic conditions, the appearance of dithionite is preceded by an induction period, which is missing when the experiment is carried out under an inert atmosphere.[119] Study of decomposition of HMS in the presence of superoxide dismutase, catalase and sodium formate showed that active forms of oxygen (superoxide, peroxide, hydroxyl radicals) have little influence on the rate of dithionite formation. Sulfite additives exert a much more pronounced influence under both anaerobic and aerobic conditions.

Decomposition of air-saturated alkaline solutions of thiourea dioxides is also accompanied by the formation of dithionite, preceded by an induction period.[130] However, unlike HMS, sulfite additives do not affect decomposition of TUDO. In addition, decomposition of thiourea dioxides under anaerobic conditions does not give dithionite. Thus, the $S_2O_4^{2-}$ ion and the $SO_2^{-\bullet}$ radical anion occurring in equilibrium arise upon the reaction of a sulfur-containing product of thiourea dioxide decomposition with oxygen. Apparently,[130] this sulfur-containing product is the sulfoxylate ion SO_2^{2-}. This species reacts with oxygen to give the $SO_2^{-\bullet}$ radical anion, which in turn reacts with oxygen [reaction (23)] and dimerises [back reaction (5)]:

$$SO_2^{2-} + O_2 \longrightarrow SO_2^{-\bullet} + O_2^{-\bullet}, \quad (22)$$

$$SO_2^{-\bullet} + O_2 \longrightarrow SO_2 + O_2^{-\bullet}, \quad (23)$$

$$S_2O_4^{2-} \rightleftharpoons 2\,SO_2^{-\bullet} \quad (5)$$

These reactions occur during the induction period. Since dithionite ion is accumulated after the completion of the induction period, *i.e.*, after oxygen has disappeared, the sulfur-containing species react with superoxide or with the product of its dismutation, peroxide. However, it is known that superoxide is quite stable in strongly alkaline media [131] (most experiments were carried out in a solution of NaOH with a concentration of 0.5 mol $litre^{-1}$) and is unlikely to undergo dismutation over the period of TUDO decomposition. Thus, the peroxide can be formed only upon the reduction of superoxide. This was proved by an independent research of the reaction of TUDO with potassium superoxide in the absence of oxygen. The shape of the resulting kinetic curves was similar to that typical of the curves of TUDO decomposition and dithionite accumulation in the presence of oxygen. The same regularities were also observed in the reaction of TUDO with peroxide under anaerobic conditions; this is due to reactions of the sulfoxylate (arising upon decomposition of TUDO deprotonated in a strongly alkaline medium) and the $SO_2^{-\bullet}$ radical anion with peroxide, giving rise to a hydroxyl radical [represented in Eqns (25) and (26) as the deprotonated form $O^{-\bullet}$]:

$$(NH)_2CSO_2 \longrightarrow SO_2^{2-} + NH{=}C{=}NH, \quad (24)$$

$$SO_2^{2-} + HO_2^- \longrightarrow SO_2^{-\bullet} + O^{-\bullet} + OH^-, \quad (25)$$

$$SO_2^{-\bullet} + HO_2^- \longrightarrow SO_2 + O^{-\bullet} + OH^-, \quad (26)$$

$$S_2O_4^{2-} \rightleftharpoons 2\,SO_2^{-\bullet}, \quad (5)$$

$$NH = C = NH + H_2O \longrightarrow (NH_2)_2CO. \quad (27)$$

Thus, study of the kinetics of reactions of thiourea dioxide with oxygen and its reduced forms made it possible to prove that

the sulfoxylate ion SO_2^{2-} rather than the $SO_2^{-\bullet}$ radical anion, as had been proposed previously,[104] is the primary sulfur-containing product of TUDO decomposition in strongly alkaline media. It is the formation of sulfoxylate that accounts for the strong reducing properties of TUDO in alkaline media.

The aerobic decomposition of *N*-methyl- and *N*,*N*′-dimethylthiourea dioxides follows regularities similar to those considered above for TUDO.[130] *N*,*N*′-Dimethylthiourea dioxide is the most reactive reductant, apparently due to the much higher stability of the intermediate formed primarily in its decomposition, namely, *N*,*N*′-dimethylcarbodiimide, compared to the stabilities of carbodiimide and *N*-methylcarbodiimide.[132] Conversely, the rates of the reactions of oxygen and its reduced forms with *N*-methylthiourea dioxide (MTUDO) are lower than those in the case of TUDO. Among the compounds considered, MTUDO is the most stable. *N*-Phenylthiourea dioxide (PTUDO) also exhibits a higher stability in solutions than TUDO.[133] Data on the reactivity of thiourea dioxides can be important for interpreting the toxicity of thioureas. Many thioureas, especially *N*-substituted ones, are known to be highly toxic. Thus lethal doses of α-naphthyl- and *N*-phenylthioureas amount to 0.5 and 5 mg kg^{-1}, respectively.[17] The toxicity of thioureas is supposed to be due to their oxidation [134–137] and the tendency of the resulting oxides to undergo desulfurisation;[17] the higher this tendency, the more toxic the compound. However, data of some publications [130, 133] are at variance with this conclusion:[17] the rates of desulfurisation of *N*-methyl- and *N*-phenylthiourea dioxides are lower than that of thiourea dioxide; nevertheless, *N*-methyl- and *N*-phenylthioureas are much more toxic than the unsubstituted thiourea. Apparently, there are also other reasons for the high toxicity of *N*-substituted thioureas. Therefore, the formation and the properties of adducts produced by thiourea oxides and proteins are being vigorously studied.[137]

In weakly alkaline solutions of thiourea dioxides, dithionite ions are accumulated much more slowly. Among other reasons, this is due to the sharp increase in the reactivity of hydrogen peroxide upon a decrease in the pH, which results in a change in the mechanism of interaction of H_2O_2 with TUDO. It was found that at pH < 13, TUDO reacts directly with the peroxide to give thiourea dioxide radicals and hydroxyl radicals.[138] The latter have been detected by EPR in the presence of DMPO. Yet another possible reason for the appreciable decrease in the rate of dithionite formation in solutions of thiourea dioxides is a change in the mechanism of their decomposition. To verify this, a comparative kinetic study [138] of the processes of TUDO decomposition and its reactions with oxygen at various pH has been carried out. The rate of the reaction of thiourea dioxide with oxygen at $[TUDO]_0 \gg [O_2]_0$ was found to be described by the equation $v = k[TUDO]$. In nearly neutral and in strongly alkaline media, the rate constants for both processes virtually coincide. However, in the pH range of 9–12, substantial differences are observed: the rate constant for TUDO decomposition increases much more rapidly and reaches a constant level at pH 10, whereas the rate constant for the reaction of thiourea dioxide with O_2 continues to grow even in the pH 10–13.7 range. The non-coincidence of the mechanisms of TUDO decomposition at pH 10 and 13 has been also discovered by other authors. Thus it has been found [139] that the reaction of glycine with TUDO in concentrated ammonium hydroxide solutions affords guanidinoacetic acid in 36% yield. When the reaction is carried out in a solution of K_2CO_3 with a concentration of 1 mol $litre^{-1}$ (pH 10), guanidineacetic acid is not formed.[17] In addition, ammonia was detected upon decomposition of TUDO in this solution [17] (ammonia is also formed when thiourea trioxide decomposes in weakly acidic media [42]). These facts led to the conclusion [138] that decomposition of thiourea dioxide at pH 9–12 follows two pathways. According to one of them, ammonia is eliminated (as this takes place, TUDO loses the guanidylating capacity towards glycine) but the C–S bond is not cleaved, the SO_2^{2-} anion is not formed, and the reaction with oxygen does not occur. Conversely, the second pathway includes a stage of formation of the SO_2^{2-} anion and the C–N bond remains intact; therefore, TUDO actively reacts with oxygen and glycine. It was found[138] that both pathways have a stage of TUDO ionisation. Since the dependence of the rate constant for the reaction of thiourea dioxide on pH is shifted to the region of high pH, the pathway involving the formation of sulfoxylate is assumed to result from decomposition of TUDO dianions. In the TUDO monoanion, the C–N bond is apparently much weaker than the C–S bond; hence, the primary decomposition stage yields ammonia.

In acid media, thiourea dioxide is very stable and barely decomposes at room temperature.[7] On heating in glacial acetic acid, TUDO and some its analogues decompose to give formamidine acetate and sulfur dioxide.[110]

The data presented here indicate that oxygen and active forms of oxygen (AFO) play an important role in the reactions with sulfur-containing reductants. Let us consider published data dealing with the reaction of the TUDO precursor, thiourea, with AFO (oxidation with peroxide has been mentioned above, in the discussion of the methods of synthesis of thiourea oxides). The strongest oxidant among the AFO is the hydroxyl radical.[140] The reaction of thiourea with the $OH^{\bullet}$ radicals proceeds at a very high rate [141] ($k = 1.2 \times 10^{10}$ litre mol^{-1} s^{-1}). The hydroxyl radicals also oxidise very effectively *N*,*N*′-dimethylthiourea [55] and tetramethylthiourea.[141]

The reactivity of the $O_2^{-\bullet}$ superoxide is substantially lower than that of $OH^{\bullet}$ radicals. In aqueous solvents, superoxide reacts with thiourea to give cyanamide.[142] It is assumed that TUDO is formed as an intermediate of this process. The reaction of superoxide with diarylthiourea follows a different pathway [143] giving rise to a substituted guanidine. In nonaqueous solutions, superoxide reduces sulfur dioxide

$$SO_2 + O_2^{-\bullet} \rightleftharpoons SO_2^{-\bullet} + O_2 . \qquad (28)$$

The equilibrium constant for this reaction, calculated on the basis of redox potentials (E°) of the $O_2/O_2^{-\bullet}$ and $SO_2/SO_2^{-\bullet}$ couples, equals 4.8;[144] however, experimental data indicate that reaction (28) proceeds virtually to completion. This is due to the subsequent transformations of the $SO_2^{-\bullet}$ radical anion, namely, dimerisation to give $S_2O_4^{2-}$ and complexation with SO_2. In the aqueous medium, superoxide does not reduce sulfur dioxide: the redox potential of the $O_2/O_2^{-\bullet}$ couple at pH 7 and pH 14 equals −0.16 V; that at pH 0 is +0.12 V;[145] E° of the $SO_2/SO_2^{-\bullet}$ pair is −0.26 V.[146]

In some studies,[147–149] electron transfer reactions in the $O_2/O_2^{-\bullet}$–metal complex systems are considered in terms of the Marcus theory. The equations derived

$$k_{12} = \sqrt{k_{11}k_{22}K_{12}f_{12}} , \qquad (29)$$

$$\log f_{12} = \frac{(\log K_{12})^2}{4\log(k_{11}k_{22}/z^2)} , \qquad (30)$$

where z is a factor taking into account the frequency of collisions of the reacting species in solution, were used to determine the rate constant for the electron exchange in the $O_2/O_2^{-\bullet}$ system (k_{22}) on the basis of known constants for electron exchange in metal complexes (k_{11}) and the experimental rate constants for the reduction of metal complexes by superoxide (k_{12}), for example

$$Co(NH_3)_6^{3+} + O_2^{-\bullet} \longrightarrow Co(NH_3)_6^{2+} + O_2 \qquad (31)$$

[in Eqns (29), (30), K_{12} is the equilibrium constant for reaction of type (31)].

However, the k_{22} values found in these calculations,[147] based on the data on the kinetics of reactions of $O_2^{-\bullet}$ with various metal complexes, varied in the range of 10^{-8}–$10^{5.7}$ litre mol^{-1} s^{-1}. In the opinion of the researchers cited,[145] the unsuitability of the Marcus theory for the calculation of k_{22} was due to the unequal solvations of O_2 and $O_2^{-\bullet}$. Later,[148] a different approach was used to determine the k_{22} values, namely, the kinetics of the reaction of metal complexes with oxygen

$$CrL_3^{2+} + O_2 \longrightarrow CrL_3^{3+} + O_2^{-\bullet}, \quad (32)$$

rather than with superoxide was studied (L is 2,2′-bipyridine, 1,10-phenanthroline and their derivatives).

The use of this approach provided the k_{22} values in the range of 1–10 litre mol^{-1} s^{-1} (in a later review,[150] a value of 10 litre mol^{-1} s^{-1} was recommended). The reasons for the so great difference between the k_{22} values calculated from the data on the kinetics of reduction of complexes with superoxide remain unknown. No corresponding data concerning the superoxide reduction to peroxide can be found from the literature.

Comparison of the rate constants for the reactions of the $O_2^{-\bullet}$ and $SO_2^{-\bullet}$ radical anions with identical oxidants, metal complexes, published in a study is of interest.[149] The ratio of the rate constants for the reactions involving $SO_2^{-\bullet}$ and $O_2^{-\bullet}$ was found to be approximately 10^3; it does not depend on the nature of the oxidant, which is consistent with the Marcus theory and the equation derived from it

$$\frac{k(SO_2^{-\bullet})}{k(O_2^{-\bullet})} = \sqrt{\frac{k(SO_2/SO_2^{-\bullet})}{k(O_2/O_2^{-\bullet})} \cdot 10^{16.9\,\Delta E}}, \quad (33)$$

where $k(SO_2^{-\bullet})$ and $k(O_2^{-\bullet})$ are the rate constants for the reaction of $SO_2^{-\bullet}$ and $O_2^{-\bullet}$ with the same substrate; ΔE is the difference between the reduction potentials of O_2 (−0.16 V) and SO_2 (−0.26 V), and $k(SO_2/SO_2^{-\bullet})$ and $k(O_2/O_2^{-\bullet})$ are the self-exchange rate constants of the $SO_2/SO_2^{-\bullet}$ and $O_2/O_2^{-\bullet}$ systems, respectively.

If we assume that $k(SO_2^{-\bullet})/k(O_2^{-\bullet}) = 10^3$, the $k(SO_2/SO_2^{-\bullet})/k(O_2/O_2^{-\bullet})$ ratio should be equal to $\sim 10^4$.

In most studies devoted to the electron exchange in the $SO_2/SO_2^{-\bullet}$ couple, dithionite served as the source of $SO_2^{-\bullet}$.[149] The $k(SO_2/SO_2^{-\bullet})$ values calculated for the outer-sphere oxidation of CrL_3^{2+} (L is bipyridine, phenanthroline, and their substituted derivatives) with sulfur dioxide were compared with the values determined previously in experiments using $SO_2^{-\bullet}$ as the reagent.[151] It was found that, unlike the $k(O_2/O_2^{-\bullet})$ values, the $k(SO_2/SO_2^{-\bullet})$ constants calculated from the kinetic data for reactions involving SO_2 and $SO_2^{-\bullet}$ are rather close: $k(SO_2/SO_2^{-\bullet}) = (1-18) \times 10^4$ litre mol^{-1} s^{-1} at 298 K. These values are approximately 10^4 times as high as the value $k(O_2/O_2^{-\bullet}) = 10$ litre mol^{-1} s^{-1} reported in a review,[150] which is consistent with the results cited above.[149]

Thus, the published data indicate that the Marcus theory is applicable to the $SO_2/SO_2^{-\bullet}$ and $O_2/O_2^{-\bullet}$ couples. It is noteworthy that the $SO_2^{-\bullet}/SO_2^{2-}$ couple in which $SO_2^{-\bullet}$ is the oxidised form has not been studied. Apparently, this is due to the difficulty of reduction of the $SO_2^{-\bullet}$ radical anion. Oxidation of sulfoxylate would be the preferred variant. The above data indicate that thiourea dioxides can be used as sources of SO_2^{2-}.

Let us consider data on the reactions of thioureas with yet another active form of oxygen, namely, singlet oxygen $^1O_2$. Thus oxidation of thiourea with photochemically generated singlet oxygen has been studied.[152] It was shown previously that solutions of thiourea do not undergo photolysis either in the absence or in the presence of oxygen even on prolonged exposure to UV light. Photooxidation of thioureas was observed when their alcohol solutions containing oxygen and a sensitiser (dye) were exposed to the visible light. The composition of photooxidised products depends on the nature of thiourea and, to a lesser extent, the dye. The major products formed in the reaction of thiourea with $^1O_2$ include SO_2, sulfur and TUDO (the sensitisers used are Methylene Blue or chlorophyll). In the presence of Rose Bengal, the formation of dicyanediamide was also observed.

Photochemical destruction of thiourea was discovered when titanium dioxide was used as the sensitiser.[153] The reaction yields cyanamide and dicyanamide.

The acid HOCl is also an active form of oxygen.[55] The kinetics of reactions of thiourea with oxohalogen compounds draws special attention.[14, 15, 154, 155] Until recently, studies of non-linear phenomena in chemical kinetics have been mainly related to the chemistry of halogens. However, at present, oscillators based on sulfur compounds are becoming more and more important. The combination of halogen and sulfur compounds in one reaction is rather attractive. However, data on the kinetics of such reactions are scarce.

One of the first chemical oscillators based on sulfur-containing compounds[156] is a mixture of sulfide, sulfite, oxygen and the Methylene Blue dye. It has been reported that the reaction between chlorite and thiourea is accompanied by oligo-oscillation.[154] Diverse non-linear effects have been discovered in the reactions of thiourea with iodate, bromate, chlorine dioxide, iodine and bromine.[155, 157, 158] However, the greatest attention of researchers is still attracted by the reaction with chlorite. Nevertheless, there is no consensus of opinion concerning the mechanism of the reaction between thiourea and chlorite. Thus it has been assumed[155] that the protonated form of the chlorite $HClO_2$ is much more reactive than the deprotonated form. However, other researchers[159] hold to the opposite opinion. They proposed a mechanism for the reaction of ClO_2 and $(NH_2)_2CS$, according to which two ClO_2 molecules successively transfer the oxygen atoms to $HOSCNHNH_2$ to give $HO_3SCNHNH_2$. However, other researchers[155] believe that the reaction between ClO_2 and the thiourea monoxide is accompanied by electron transfer giving rise to ClO_2^- and $H_2NNHCSO^\bullet$ (it has been assumed[60] that the reaction of thiourea dioxide with bromate also follows a radical mechanism). It was shown experimentally[155] that the rates of reactions of formamidine disulfide and thiourea dioxide with ClO_2 depend substantially on the time elapsed after the preparation of solutions of the sulfur-containing compounds. This was attributed[155] to accumulation of reactive aminoiminomethanesulfenic acid (thiourea monoxide) in the solution. However, this explanation can hardly be considered to be convincing because thiourea monoxide is exceptionally unstable at 298 K and can hardly be expected to accumulate in solution.

It was shown[158] that, among other reasons, non-coincidence of the kinetic data obtained by different researchers may be due to the influence of impurities of metal compounds, especially copper and iron compounds (Cu and Fe compounds are known to catalyse efficiently the processes of reduction by thiourea). However, the main reason for the inconsistency mentioned above is that no kinetic data concerning individual stages of the multistage reaction between thiourea and oxohalogen compounds have been available until recently. Only in 1993–1995, were reactions between an intermediate of $(NH_2)_2CS$ oxidation, *i.e.* thiourea dioxide, with iodate,[160] bromate[15] and chlorite[14] studied. The kinetic parameters thus found made it possible to correct (in some cases, the corrections were quite significant) the rate constants for the individual stages of thiourea oxidation published previously. However, the reported[14] ratios of the rate constants for reactions of thiourea di- and trioxides with the same oxidants raise doubts. Thus the rate constants for the reactions of TUDO and TUTO with HOCl are nearly equal (9.5×10^3 and 6.5×10^3 litre mol^{-1} s^{-1}) but those for the reaction with ClO_2 differ by a factor of 60 (6×10^2 and 10 litre mol^{-1} s^{-1}, respectively). The reasons for this discrepancy have not been elucidated. The interpretation[161, 162] of the results of kinetic studies of the reactions of hydroxymethanesulfinate with bromate and chlorite in acid media is even more objectionable. Presumably, the reactions of HMS with any oxohalogen compounds either present initially or formed at intermediate stages (BrO_3, $HBrO_2$, HOBr, ClO_2^-, HOCl, ClO_2, Cl_2O_2) afford hydroxymethanesulfonate.[161, 162] As a result of oxidation, this product gives sulfate, *i.e.*, as in the case of reactions involving thiourea, the C–S bond rupture takes place after the appearance of sulfonate. Meanwhile, it is known that hydroxymethanesulfonate is very stable in acid media and does not tend to participate in redox reactions.[7] Conversely, HMS rapidly decomposes in acid solutions, the products of its decomposition exhibiting strong reducing properties. Unfortunately, in the studies cited above,[161, 162] no mention is even made of the HMS decomposition or the role of its products —

sulfoxylate and formaldehyde (later, the same researchers demonstrated [163] that formaldehyde reacts with chlorite at a rather high rate). The results of study of Makarov *et al.*[164] made it possible to introduce substantial changes to the schemes of reactions of halogens and oxohalogen compounds with thiourea, thiourea dioxide and hydroxymethanesulfinate. It was shown [164] that the rates of oxidation of sulfonates (thiourea trioxide and hydroxymethanesulfonate) are much lower than the rates of oxidation of sulfinates (thiourea dioxide and hydroxymethanesulfinate) and even thiourea. Thus, it appears that thiourea trioxide and hydroxymethanesulfonate are not intermediates of the reactions of TUDO, thiourea and HMS with halogens and oxohalogen compounds. During the oxidation of sulfinates, rupture of the C–S bond takes place before the formation of sulfonates.[164] The active reducing agent thus formed, sulfoxylate, is then oxidised to sulfite and sulfate.

VI. Conclusion

The data on the properties of sodium dithionite, sodium hydroxymethanesulfinate and thiourea dioxides considered in the review provide a number of conclusions. An important feature common to these compounds is decomposition in solutions to give strong reducing agents. However, the opposite patterns of dependence of the stability of TUDO and HMS on the pH entail differences between the processes of their decomposition. Indeed, in solutions of HMS, the dithionite ion is formed predominantly according to an 'anaerobic' mechanism, whereas in solutions of TUDO, this occurs by an 'aerobic' mechanism. Sulfur-and-oxygen ions (sulfite, thiosulfate) barely affect the TUDO decomposition, whereas the mechanism of decomposition of hydroxymethanesulfinate largely depends on admixtures. Thus, in the case of HMS decomposition, the subsequent reactions of sulfur-containing compounds are much more significant than in the decomposition of TUDO. Decomposition of HMS is affected most appreciably by dithionite ions. The very low stability of these ions in acid media and the capability of decomposing in aqueous solutions by an autocatalytic mechanism account for the autocatalytic mode of HMS decomposition as a whole. The unique character of dithionite is due to the presence of the very long S–S bond. Therefore, insertion of monoatomic sulfur into the S–S bond becomes possible and, as a consequence, decomposition of dithionite and hydroxymethanesulfinate is accelerated. Conversely, in the thiourea dioxide molecule, direct insertion of sulfur into the shorter C–S bond is difficult. No conjugate pathway for dithionite destruction exists in the decomposition of TUDO (in alkaline solutions of thiourea dioxide under aerobic conditions, dithionite formation does take place but it is much more stable in these media than TUDO).

The following important circumstance should also be mentioned. Thiourea dioxides are the most convenient precursors of the little studied sulfoxylate ion (SO_2^{2-}). This sulfur-and-oxygen ion is quite interesting from both practical and theoretical standpoints. The need to study systematically its properties is due not only to its high reductive activity but also to the fact that sulfoxylate is the possible intermediate in the hydrogen sulfide oxidation.[165] The importance of this process as a part of natural sulfur cycle is beyond doubt.

References

1. R P Yakimchuk, A V Mishchenko, N E Bulusheva *Primenenie Kubovykh Krasitelei* (The use of Vat Dyes) (Moscow: Legprombytizdat, 1985)
2. P N Kirpichnikov, L A Averko-Antonovich, Yu A Averko-Antonovich *Khimiya i Tekhnologiya Sinteticheskogo Kauchuka* (The Chemistry and Technology of Synthetic Caoutchouc) (Leningrad: Khimiya, 1975)
3. B V Gromov *Vvedenie v Khimicheskuyu Tekhnologiyu Urana* (Introduction in the Chemical Technology of Uranium) (Moscow: Atomizdat, 1976)
4. O Louis-Andre, G Gelbard *Bull. Soc. Chim. Fr.* **4** 565 (1986)
5. V Yu Kukushkin, Yu N Kukushkin *Teoriya i Praktika Sinteza Koordinatsionnykh Soedinenii* (The Theory and Practice of the Synthesis of Coordinating Compounds) (Leningrad: Nauka, 1990)
6. V V Budanov *Khimiya i Tekhnologiya Vosstanovitelei na Osnove Sul'foksilovoi Kisloty. Rongalit i Ego Analogi* (The Chemistry and Technology of Reducing Agents Based on Sulfoxylic Acid. Rongalite and Its Analogues) (Moscow: Khimiya, 1984)
7. V V Budanov, S V Makarov *Khimiya Serosoderzhashchikh Vosstanovitelei (Rongalit, Ditionit, Dioksid Tiomocheviny)* [The Chemistry of Sulfur-Containing Reducing Agents (Rongalite, Dithionite, Thiourea Dioxide)] (Moscow: Khimiya, 1994)
8. R Balicki, U Chmielowiec *Monatsh. Chem.* **131** 1105 (2000)
9. J-H Liu, A-T Wu, M-H Huang, C-W Wu, W-S Chung *J. Org. Chem.* **65** 3395 (2000)
10. L Jia, C Bonaventura, J Bonaventura, J S Stamler *Nature (London)* **380** 221 (1996)
11. J G Robertson, L J Sparvero, J J Villafranca *Protein Sci.* **1** 1298 (1992)
12. J G Robertson *Biochemistry* **34** 7533 (1995)
13. G G Furin *Usp. Khim.* **69** 538 (2000) [*Russ. Chem. Rev.* **69** 491 (2000)]
14. J B Jones, C R Chinake, R H Simoyi *J. Phys. Chem.* **99** 1523 (1995)
15. C R Chinake, R H Simoyi, S B Jonnalagadda *J. Phys. Chem.* **98** 545 (1994)
16. C A Maryanoff, R C Stanzione, J N Plampin *Phosphorus Sulfur Relat. Elem.* **27** 221 (1986)
17. A E Miller, J J Bischoff, K Pae *Chem. Res. Toxicol.* **1** 169 (1988)
18. J Witiak, R A Earl, M M Abelman, Y B Bethel, B N Fisher, G S Kauffman, C A Kettner, P Ma, J L McMillan, L J Mersinger, J Pesti, M E Pierce, F W Rankin, R J Chorvat, P N Confalone *J. Org. Chem.* **60** 3717 (1995)
19. R O Dempsy, K A Browne, T C Bruice *J. Am. Chem. Soc.* **117** 6140 (1995)
20. P Mantri, D E Duffy, C A Kettner *J. Org. Chem.* **61** 5690 (1996)
21. L Heys, C G Moore, P J Murphy *Chem. Soc. Rev.* **29** 57 (2000)
22. G S Berlinck *Nat. Prod. Rep.* **16** 339 (1999)
23. W C Hodgeman, J B Weinrach, D W Bennett *Inorg. Chem.* **30** 1611 (1991)
24. J D Dunitz *Acta Crystallogr.* **9** 579 (1956)
25. A Magnusson, L-G Johansson *Acta Chem. Scand., Ser. A* **36** 429 (1982)
26. L Peter, B Meyer *J. Mol. Struct.* **95** 131 (1982)
27. H Takahashi, N Kaneko, K Miwa *Spectrochim. Acta, Part A* **38** 1147 (1982)
28. K L Carter, J B Weinrach, D W Bennett *J. Am. Chem. Soc.* **115** 10981 (1993)
29. S A Chmielewski, J B Weinrach, D W Bennett, W P Kilroy *J. Electrochem. Soc.* **135** 904 (1988)
30. S V Makarov, O N Murav'ev, V V Budanov *Zh. Fiz. Khim.* **70** 1908 (1996) [a]
31. M R Nimlos, G B Ellison *J. Phys. Chem.* **90** 2574 (1986)
32. F Ramondo, L Bencivenni *Mol. Phys.* **67** 707 (1989)
33. M R Truter *J. Chem. Soc.* 3400 (1962)
34. R L Sullivan, A Hargreaves *Acta Crystallogr.* **15** 675 (1962)
35. I-C Chen, Y Wang *Acta Crystallogr., Sect. C, Cryst. Struct. Commun.* **40** 1937 (1984)
36. J S Song , S H Kim, S K Kang, S S Yun, I-H Suh, S-S Choi, S Lee, W P Jensen *Bull. Korean Chem. Soc.* **17** 201 (1996)
37. S M Evdokimova, A N Aleksandrova, S V Makarov, V V Budanov *Izv. Vyssh. Uchebn. Zaved., Khim. Khim. Tekhnol.* **38** (6) 24 (1995)
38. V Lepentsiotis, R van Eldik, D M Stulov, S V Makarov *J. Chem. Soc., Dalton Trans.* 2915 (1998)
39. G Gattow, W Manz *Z. Anorg. Allg. Chem.* **561** 66 (1988)
40. S V Makarov, E V Kudrik, A V Lyubimtsev, D M Stulov *Zh. Obshch. Khim.* **70** 1488 (2000) [b]
41. S V Makarov, E V Kudrik *Izv. Akad. Nauk, Ser. Khim.* 196 (2001) [c]
42. S V Makarov, C Mundoma, J H Penn, J L Petersen, S A Svarovsky, R H Simoyi *Inorg. Chim. Acta* **286** 149 (1999)
43. S A Chmielewski, D W Bennett *Synth. React. Inorg. Metal.-Org. Chem.* **16** 95 (1986)

44. M E Pozin *Tekhnologiya Mineral'nykh Solei* (Technology of Mineral Salts) Vol. 1 (Moscow: Khimiya, 1970)
45. S M Lough, J W McDonald *Inorg. Chem.* **26** 2024 (1987)
46. M Tordeux, B Langlois, C Wakselman *J. Org. Chem.* **54** 2452 (1989)
47. V V Budanov, T V Verina, V P Panov, N F Boleslavskaya *Izv. Vyssh. Uchebn. Zaved., Khim. Khim. Tekhnol.* **18** 920 (1975)
48. S V Makarov, V V Budanov, G V Shalimova *Zh. Prikl. Khim.* **58** 1098 (1985) [d]
49. M Mulliez, C Naudy *Tetrahedron* **49** 2469 (1993)
50. W Walter, G Randau *Liebigs Ann. Chem.* **722** 80 (1969)
51. E Ya Yarovenko, R P Lastovskii *Zh. Org. Khim.* **6** 947 (1970) [e]
52. Jpn. P. 63-243 896; *Ref. Zh. Khim.* 3N 47P (1992)
53. D De Filippo, G Ponticelli, E F Troqu, A Lai *J. Chem. Soc., Perkin Trans. 2* 1500 (1972)
54. M F Kondrashova, E Ya Yarovenko, in *Metody Polucheniya Khimicheskikh Reaktivov i Preparatov* (The Methods for Preparation of Chemical Reagents and Chemicals) (Moscow: Izd. NIITEKHIM, 1969) No. 20, p. 56
55. W E Curtis, M E Muldrow, N B Parker, R Barkley, S L Linas, J E Repine *Proc. Natl. Acad. Sci. USA* **85** 3422 (1988)
56. W Walter, G Randau *Liebigs Ann. Chem.* **722** 98 (1969)
57. A E Miller, D I Feeney, Yan Ma, L Zarcone, M A Aziz, E Magnuson *Synth. Commun.* **20** 217 (1990)
58. W Walter, K-P Ruess *Justus Liebigs Ann. Chem.* 243 (1974)
59. N Y Abou-Zeid, A Waly, A Higazy, A Hebeish *Angew. Makromol. Chem.* **143** 85 (1986)
60. M H El-Rafie, M K Zahran, K F El Tahlawy, A Hebeish *Polym. Degrad. Stab.* **47** 73 (1995)
61. S A Abdel-Hafiz *J. Appl. Polym. Sci.* **58** 2005 (1995)
62. C Daneault, C Leduc *Cellul. Chem. Technol.* **28** 205 (1994)
63. J Gacen, J Cegarra, M Caro *J. Soc. Dyers Colour* **107** 138 (1991)
64. R M S Dawson, D C Elliott, W H Elliott, KM Jones *Date for Biochemical Research* (Oxford: Clarendon Press, 1986)
65. O S Ksenzhek, S A Petrov *Elektrokhimicheskie Svoistva Obratimykh Biologicheskikh Redoks-Sistem* (Electrochemical Properties of Reversible Biological Redox-Systems) (Moscow: Nauka, 1986)
66. V E Shashoua *Biochemistry* **3** 1719 (1964)
67. R C Sprong, C J M Aarsman, J F L M van Oirschot, B S van Asbeck *J. Lab. Clin. Med.* **129** 470 (1997)
68. I N Sokolova, V V Budanov, Yu V Polenov, I R Polyakova *Izv. Vyssh. Uchebn. Zaved., Khim. Khim. Tekhnol.* **26** 822 (1983)
69. Yu V Polenov, V V Budanov *Izv. Vyssh. Uchebn. Zaved., Khim. Khim. Tekhnol.* **31** (4) 40 (1988)
70. R Kerber, J Starnick *Chem. Ber.* **104** 2035 (1971)
71. R Kerber, W Gestrich *Chem. Ber.* **106** 798 (1973)
72. P Messinger, H Greve *Synthesis* 259 (1977)
73. A R Harris *Synth. Commun.* **18** 659 (1988)
74. A Loupy, S Sansoulet, A R Harris *Synth. Commun.* **19** 2939 (1989)
75. W-Y Huang, F-H Hong *Isr. J. Chem.* **39** 167 (1999); *Ref. Zh. Khim.* 24-19 Zh 501 (2000)
76. G Borgogno, S Colonna, R Fornasier *Synthesis* 529 (1975)
77. S Drabowicz, M Mikolajczyk *Synthesis* 542 (1978)
78. E S Lang, J V Comasseto *Synth. Commun.* **18** 301 (1988)
79. J B T Ferreira, A R M de Oliveira, J V Comasseto *Synth. Commun.* **19** 239 (1989)
80. E V Dehmlow, S S Dehmlow *Phase Transfer Catalysis* (Weinheim: Verlag Chemie, 1983)
81. T Junk, G Gritzner, K J Irgolic *Synth. React. Inorg. Metal.-Org. Chem.* **19** 931 (1989)
82. H J Reich, F Chow, S K Shah *J. Am. Chem. Soc.* **101** 6638 (1979)
83. K Kim, Y-T Lin, H S Mosher *Tetrahedron Lett.* **29** 3183 (1988)
84. A E Miller, J J Bischoff *Synthesis* 777 (1986)
85. C A Maryanoff, R C Stanzione, J N Plampin, J E Mills *J. Org. Chem.* **51** 1882 (1986)
86. D R Artis, C Brotherton-Pleiss, J H Pease *Bioorg. Med. Chem. Lett.* **10** 2421 (2000)
87. B O Bachmann, C A Townsend *Biochemistry* **39** 11187 (2000)
88. W Han, J C Pelletier, L J Mersinger *Org. Lett.* **1** 1875 (1999)
89. C Li, L P Budge, C D Driscoll, B M Willardson, G W Allman, P B Savage *J. Am. Chem. Soc.* **121** 931 (1999)
90. S Routier, J-L Bernier, J-P Catteau, J-F Riou, C Bailly *Anti-Cancer Drug Des.* **13** 407 (1998)
91. T Lu, B Tomczuk, C R Illig, R Bone, L Murphy, J Spurlino, F R Salemme, R M Soll *Bioorg. Med. Chem. Lett.* **8** 1595 (1998)
92. P Chand, Y S Babu, S Bantia, N Chu, L B Cole, P L Kotian, W G Laver, J A Montgomery, V P Ved, S L Petty, D P Shrout, D A Walsh, G M Walsh *J. Med. Chem.* **40** 4030 (1997)
93. A P Kozikowski, D S Dodd, J Zaidi, Y-P Pang, B Cusack, E Richelson *J. Chem. Soc., Perkin Trans. 1* 1615 (1995)
94. M von Itzstein, W-Y Wu, B Jin *Carbohydr. Res.* **259** 301 (1994)
95. D J Aitken, D Guillaumne, H P Husson *Tetrahedron* **49** 6375 (1993)
96. L Crombie, S R M Jarrett *J. Chem. Soc., Perkin Trans. 1* 3179 (1992)
97. W R Jackson, F C Copp, J D Cullen, F J Guyett, I D Rae, A J Robinson, H Pothaulackis, A K Serelis, M Wong *Clin. Exp. Pharmacol. Physiol.* **19** 17 (1992); *Chem. Abstr.* **117** 82 892 (1992)
98. U Schmidt, K Mundinger, R Mangold, A Lieberknecht *J. Chem. Soc., Chem. Commun.* 1216 (1990)
99. R J P Williams *Chem. Soc. Rev.* **25** 77 (1996)
100. V G Granik, S Yu Ryabova, N B Grigoriev *Usp. Khim.* **66** 792 (1997) [*Russ. Chem. Rev.* **66** 717 (1997)]
101. R Howlett *Nature (London)* **395** 625 (1998)
102. M Prashad, L Chen, O Repic, T Blacklock *Synth. Commun.* **28** 2125 (1998)
103. A A Ryabukha, L S Zakidysheva, V V Petrochenko *Zh. Neorg. Khim.* **35** 1009 (1990) [f]
104. J E McGill, F Lindstrom *Anal. Chem.* **49** 26 (1977)
105. M Neves, H Ferronha, L Patricio *J. Radioanal. Nucl. Chem.* **132** 241 (1989)
106. S V Ermolina, S V Makarov, I N Terskaya, V V Budanov *Zh. Neorg. Khim.* **40** 1466 (1995) [f]
107. D N Akbarov, L A Samoilova, T N Ovchinnikova *Khim. Volokna* 24 (1987)
108. C E McKenna, W G Gutheil, W Song *Biochim. Biophys. Acta* **1075** 109 (1991)
109. L L Poulsen, R M Hyslop, D M Ziegler *Arch. Biochem. Biophys.* **198** 78 (1979)
110. J J Havel, R Q Kluttz *Synth. Commun.* **4** 389 (1974)
111. W Li, T Nonaka *Electrochim. Acta* **44** 2605 (1999)
112. N V Vorob'ev-Desyatovskii, Yu N Kukushkin, V V Sibirskaya *Koord. Khim.* **11** 1299 (1985) [g]
113. M Hoffmann, J O Edwards *Inorg. Chem.* **16** 3333 (1977)
114. S K Saha, D J Greenslade *Bull. Chem. Soc. Jpn.* **65** 2720 (1992)
115. V Cermak, M Smutek *Coll. Czech. Chem. Commun.* **40** 3241 (1975)
116. M Smutek, V Cermak *Coll. Czech. Chem. Commun.* **40** 3265 (1975)
117. D A Holman, D W Bennett *J. Phys. Chem.* **98** 13300 (1994)
118. S V Makarov, Yu V Polenov, V V Budanov *Zh. Neorg. Khim.* **29** 2456 (1984) [f]
119. S V Makarov, C Mundoma, S A Svarovsky, X Shi, P M Gannett, R H Simoyi *Arch. Biochem. Biophys.* **367** 289 (1999)
120. D O Lambeth, G Palmer *J. Biol. Chem.* **248** 6095 (1973)
121. U Baumgarte *Textilveredlung* **4** 821 (1969)
122. L Burlamacchi, G Casini, C Fagioli *Ric. Sci.* **37** 97 (1967)
123. S Lynn, R G Rinker, W H Corcoran *J. Phys. Chem.* **68** 2363 (1964)
124. R N Mehrotra, R G Wilkins *Inorg. Chem.* **19** 2177 (1980)
125. G A Poskrebyshev *Zh. Fiz. Khim.* **71** 1360 (1997) [a]
126. V V Budanov, I N Sokolova, B N Mel'nikov *Izv. Vyssh. Uchebn. Zaved., Khim. Khim. Tekhnol.* **19** 240 (1976)
127. J F K Wilshire *Austr. J. Chem.* **41** 995 (1988)
128. C Creutz, N Sutin *Inorg. Chem.* **13** 2041 (1974)
129. R E Huie, C L Clifton, N Altstein *Radiat. Phys. Chem.* **33** 361 (1989)
130. S A Svarovsky, R H Simoyi, S V Makarov *J. Chem. Soc., Dalton Trans.* 511 (2000)
131. B H J Bielski, A O Allen *J. Phys. Chem.* **81** 1048 (1977)
132. M Mikolajczyk, P Kielbasinski *Tetrahedron* **37** 233 (1981)
133. K Lekhimena, S V Makarov, V V Budanov *Izv. Vyssh. Uchebn. Zaved., Khim. Khim. Tekhnol.* **34** (8) 122 (1991)
134. C Mitchell, G B Steventon *Sulfur Rep.* **16** 117 (1994)
135. K Ziegler-Skylakakis, S Nill, J F Pan, U Andrae *Environ. Mol. Mutagen.* **31** 362 (1998)
136. T Mizutani, K Yoshida, M Murakami, M Shirai, S Kawazoe *Chem. Res. Toxicol.* **13** 170 (2000)
137. G J Stevens, K Hitchcock, Y K Wang, G M Coppola, R W Versace, J A Chin, M Shapiro, S Suwanrumpha, B L K Mangold *Chem. Res. Toxicol.* **10** 733 (1997)

138. S V Makarov, Doctoral Thesis in Chemical Sciences, Ivanovo State Chemical Technological University, Ivanovo, 2000
139. W Walter *Angew. Chem.* **67** 275 (1955)
140. N A Kuznetsova, O L Kaliya *Zh. Ross. Khim. O-va im. D I Mendeleeva* **62** 36 (1998) [h]
141. W-F Wang, M N Schuchmann, H-P Schuchmann, W Knolle, J von Sonntag, C von Sonntag *J. Am. Chem. Soc.* **121** 238 (1999)
142. G Crank, M I H Makin *J. Chem. Soc., Chem. Commun.* 53 (1984)
143. Y H Kim, G H Yon *J. Chem. Soc., Chem. Commun.* 715 (1983)
144. D Stallings, D T Sawyer *J. Chem. Soc., Chem. Commun.* 340 (1979)
145. D T Sawyer, J S Valentine *Acc. Chem. Res.* **14** 393 (1981)
146. D M Stanbury *Adv. Inorg. Chem.* **33** 69 (1989)
147. S M McDowell, J H Espenson, A Bakac *Inorg. Chem.* **23** 2232 (1984)
148. K Zahir, J H Espenson, A Bakac *J. Am. Chem. Soc.* **110** 5059 (1988)
149. Z Bradic, R G Wilkins *J. Am. Chem. Soc.* **106** 2236 (1984)
150. D M Stanbury, in *Electron Transfer Reactions: Inorganic, Organometallic, and Biological Applications* (Ed. S S Isied) (Washington, DC: American Chemical Society, 1997) p. 165
151. C A Simmons, A Bakac, J H Espenson *Inorg. Chem.* **28** 581 (1989)
152. G Crank, A Mursyidi *J. Photochem. Photobiol. A, Chem.* **64** 263 (1992)
153. E Esqueva, J Garcia, X Domenich, J Peral *Oxid. Commun.* **20** 546 (1997)
154. M Alamgir, I R Epstein *Int. J. Chem. Kinet.* **17** 429 (1985)
155. G Rabai, R T Wang, K Kustin *Int. J. Chem. Kinet.* **25** 53 (1993)
156. M Burger, R J Field *Nature (London)* **307** 720 (1984)
157. R H Simoyi, I R Epstein, K Kustin *J. Phys. Chem.* **98** 551 (1994)
158. C J Doona, D M Stanbury *J. Phys. Chem.* **98** 12630 (1994)
159. I R Epstein, K Kustin, R H Simoyi *J. Phys. Chem.* **96** 5852 (1992)
160. E Mambo, R H Simoyi *J. Phys. Chem.* **97** 13662 (1993)
161. S B Jonnalagadda, C R Chinake, R H Simoyi *J. Phys. Chem.* **99** 10231 (1995)
162. M A Salem, C R Chinake, R H Simoyi *J. Phys. Chem.* **100** 9377 (1996)
163. C R Chinake, O Olojo, R H Simoyi *J. Phys. Chem. A* **102** 606 (1998)
164. S V Makarov, C Mundoma, J H Penn, S A Svarovsky, R H Simoyi *J. Phys. Chem. A* **102** 6786 (1998)
165. J-Z Zhang, F J Millero, in *Environmental Geochemistry of Sulfide Oxidation* (Eds C N Alpers, D W Blowes) (Washington, DC: American Chemical Society, 1992) p. 393

[a] — *Russ. J. Phys. Chem. (Engl. Transl.)*
[b] — *Russ. J. Gen. Chem. (Engl. Transl.)*
[c] — *Russ. Chem. Bull. (Engl. Transl.)*
[d] — *Russ. J. Appl. Chem. (Engl. Transl.)*
[e] — *Russ. J. Org. Chem. (Engl. Transl.)*
[f] — *Russ. J. Inorg. Chem. (Engl. Transl.)*
[g] — *Russ. J. Coord. Chem. (Engl. Transl.)*
[h] — *Mendeleev Chem. J. (Engl. Transl.)*

Russian Chemical Reviews **70** (11) 897 – 920 (2001) © 2001 Russian Academy of Sciences and Turpion Ltd

DOI 10.1070/RC2001v070n11ABEH000593

Rearrangements of sulfoxides and sulfones in the total synthesis of natural compounds †

E N Prilezhaeva

Contents

I.	Introduction	897
II.	Syntheses involving rearrangements of sulfoxides into sulfenates and sulfenates into sulfoxides	897
III.	Syntheses based on the Pummerer reaction	902
IV.	Use of the Ramberg – Bäcklund rearrangement for the insertion of C = C bonds	914
V.	Conclusion	918

Abstract. Data on applications of the most important rearrangements of sulfoxides and sulfones to stereoselective total syntheses of natural compounds are systematised. The bibliography includes 175 references.

I. Introduction

Rearrangements of sulfoxides and sulfones along with other reactions of these compounds (see the review [1]) are widely used in stereospecific total syntheses of natural compounds. The mechanisms of the rearrangements of sulfoxides and sulfones were detailed in the reviews.[2, 3] In the present review, syntheses of natural compounds involving these rearrangements as the key stages are surveyed.

In spite of the fact that the Mislow – Evans rearrangement of sulfoxides can be applied only to the construction of allylic alcohol fragments, whereas the Ramberg – Bäcklund rearrangement can be used only for the formation of C = C bonds, both these reactions are often utilised in the syntheses of complex natural compounds. An important point is that the sulfur-containing group is removed in both processes.

The Pummerer reaction is used much more extensively. This rearrangement was discovered in 1910 [4] and did not come to the attention of chemists for 50 years. Once Horner [5, 6] had demonstrated that this reaction has a general character, the Pummerer rearrangement gained wide acceptance. It should be noted that Pummerer appraised the essence of this reaction quite adequately and related it to the lability of the α-hydrogen atom and generation of the sulfenium cation.[4]

Later on, the assumptions made by Pummerer were supported by the fundamental studies of Oae *et al.*[7, 8] devoted to the mechanism of this process.

Different aspects of the synthetic applications of the Pummerer reaction were considered in many reviews, for example, in the reviews [9 – 13] published in the last decade. However, the data on the use of this reaction as well as of other rearrangements for the preparation of natural compounds have not been systematised. The only exception is the review [14] in which consideration was given to the use of additive Pummerer conversions of enantiomerically pure vinyl sulfoxides in asymmetric syntheses of natural compounds.

E N Prilezhaeva N D Zelinsky Institute of Organic Chemistry, Russian Academy of Sciences, Leninsky prosp. 47, 119991 Moscow, Russian Federation. Fax (7-095) 135 53 28. Tel. (7-095) 938 36 21

Received 29 March 2001
Uspekhi Khimii **70** (11) 1013 – 1038 (2001); translated by T N Safonova

II. Syntheses involving rearrangements of sulfoxides into sulfenates and sulfenates into sulfoxides

The mechanisms of the rearrangements of sulfoxides into sulfenates and sulfenates into sulfoxides and the effects of the structures of the initial compounds and the reaction medium were detailed in a review.[2] Thermal rearrangements of benzyl sulfenates into sulfoxides, which proceed in nonpolar solvents by an ion-pair mechanism, did not find wide use in synthesis. On the contrary, rearrangements of β,γ-unsaturated aliphatic sulfoxides have assumed great importance. This is particularly true for the reversible allyl sulfoxide – allyl sulfenate Mislow – Evans rearrangement and, to a lesser extent, holds for the propargyl sulfenate – allenyl sulfoxide Braverman rearrangement.

1. Syntheses based on the reversible rearrangement of allyl sulfoxides into allyl sulfenates (the Mislow – Evans rearrangement)

a. General observations

The thermal reversible rearrangement of allyl sulfoxides into allyl sulfenates proceeds as a intramolecular process through a five-membered transition state and is accompanied by migration of the double bond. This rearrangement is presently among the best-studied [2,3]-sigmatropic processes. The structure of allyl sulfoxide is thermodynamically more favourable than that of sulfenate due to which the equilibrium in the liquid phase under normal conditions is virtually completely shifted toward sulfoxide. The occurrence of this equilibrium was assumed [15] based on the fact that racemisation of optically active allyl sulfoxides proceeds much more rapidly than racemisation of saturated sulfoxides. This assumption was additionally supported by the fact that the reaction of allylic alcohol with sulfenyl chloride in the presence of a base afforded sulfoxide (rather than sulfenate).

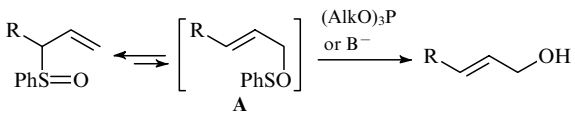

A

† Dedicated to Academician O M Nefedov with appreciation and on the occasion of his seventieth birthday.

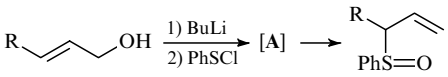

Both reactions proceeded through allyl sulfenate **A**, which is readily isomerised. The mechanism of the intramolecular completely concerted process was proved by kinetic data and by the results of experiments using labelled compounds.[15]

The Mislow–Evans rearrangement is used as a general procedure for the preparation of allylic alcohols.[16] Trimethyl phosphite was proposed as the thiophilic reagent of choice.[16] This reagent moves sulfenate off the equilibrium, which is virtually completely shifted toward allylic alcohol. In some cases, such bases as amines, thiolates or Na_2S are used as thiophiles.

This procedure was later modified[17] so that it involved the one-pot synthesis of allylic alcohol by oxidation of allyl sulfide with 30% H_2O_2 in the presence of a catalytic amount of SeO_2 followed by treatment with 0.1 equiv. of TsOH (alcohols were obtained in ~70% yields).

For this procedure to be successfully employed in the synthesis of complex compounds, it was necessary to find appropriate conditions for α-alkylation of the simplest allyl sulfoxides. Evans and Andrews[16] revealed that selective α-alkylation ($\alpha/\gamma \ll 10$) took place only in the case of allyl sulfoxides that contain the double bond in the ring or bear two terminal alkyl substituents; otherwise noticeable amounts (up to 50%) of γ-alkylated products formed due to which the yield of the target allylic alcohol decreased substantially.

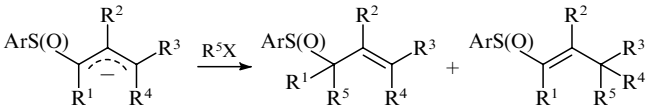

R^1, R^2, R^3, R^4 = H, Alk; R^5 = Alk.

To eliminate this problem, it was suggested[16] that alkylation of allyl sulfides bearing heterocyclic (for example, 2-pyridyl or 2-imidazolyl) substituents at the sulfur atom should be followed by oxidation of the resulting compounds to sulfoxides. These sulfides underwent predominantly α-alkylation due to the chelating effect of the heteroatom.

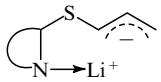

Evans and Andrews[16] also established that deprotonation with alkyllithium in the case of alkylation of allyl sulfoxides with weak electrophiles, such as long-chain halides, must be performed in aprotic solvents at below-zero temperatures.

The advantage of the allyl sulfoxide–allyl sulfenate rearrangement is the stereoselective formation of the (*E*)-C=C bond because the *trans* conformation (according to the nomenclature proposed by Mislow[15]) in the transition state is more favourable. Recently, *ab initio* calculations for 2-methyl-3-phenylsulfinylbut-1-ene confirmed that the formation of the (*E*)-C=C bond is energetically more favourable.[18] However, the difference between the energies of the *trans* and *cis* transition states is small. Hence, isomerisation of sulfoxides can afford up to 10% of the (*Z*)-isomer depending on the character of the substituents. If the double bond is involved in the corresponding ring, the product with the (*Z*) configuration can be obtained in quantitative yield. Recently, it has been demonstrated that distant functional groups exert efficient (*E*)-stereocontrol. Thus the presence of branched groups in the β position[19] or the hydroxy group in the γ position[20] of allyl sulfoxide is favourable for (*E*)-stereoselectivity (80%–99%).

Mislow was the first to note[15] that isomerisation of sulfoxides containing a chiral centre at the C(1) atom is accompanied by migration of this centre to the C(3) atom. The characteristic features of this asymmetric synthesis, which was called self-immolative, and the effects of the bulkiness and the character of the substituents were thoroughly investigated by Hoffmann.[21]

b. Syntheses of natural compounds involving the Mislow–Evans rearrangement

The [2,3]-sigmatropic Mislow–Evans rearrangement was first applied to the syntheses of prostaglandins.[22–27]

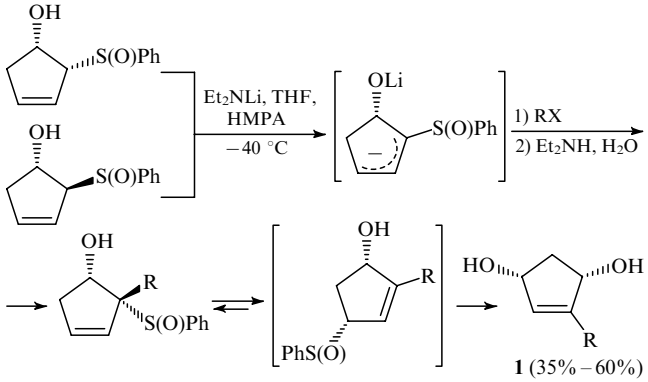

HMPA is hexamethylphosphoramide;

RX = $C_6H_{13}I$, BnBr, $\overline{OCH_2CH_2OCH}(CH_2)_6I$,

$Bu^tCO_2(CH_2)_2C{\equiv}CCH_2Br$, $Bu^tCO_2(CH_2)_6I$, $PhCH{=}CHCH_2Br$.

This procedure was used for the preparation of *cis*-cyclopentene glycols **1**, which are convenient starting compounds for preparing prostaglandins,[22] and the stereocontrolled construction of the chiral centre at the C(15) atom in compound **2** was carried out. The latter compound was utilised in the synthesis of prostaglandin PgA_2.[23]

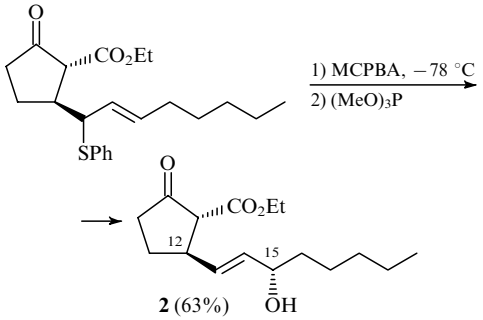

MCPBA is *m*-chloroperbenzoic acid.

This methodology was also employed for the preparation of racemic products: prostaglandin $F_{2\alpha}$ (**3**),[24] methyl ester of 11-deoxyprostaglandin E_1 (**4**)[25] and stable analogues of prostaglandin PgI_2, *viz*., 7-hydroxy- and 7-acetoxy-PgI_2 (**5a**,**b**).[26]

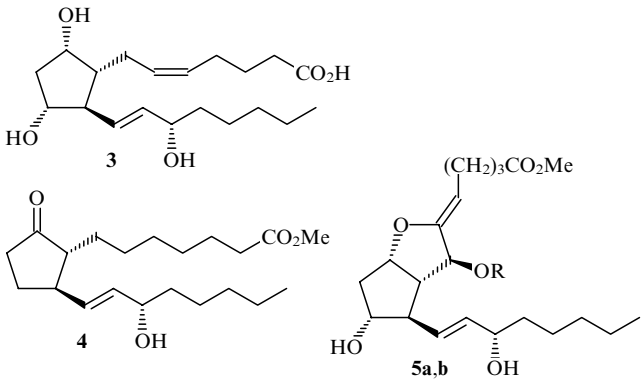

R = H (**a**), Ac (**b**).

Of special interest is the study, which demonstrated high stereo- and enantioselectivity of the sigmatropic process.[27] The methyl ester of *rac*-PgE_1 (**7**), which is completely identical to the natural specimen, was prepared in high yield by a two-step

procedure starting from the readily accessible *rac*-(13*Z*)-prostaglandin (**6**) through unstable sulfenate **8** and sulfoxide **9**. In this study, both directions of the Mislow – Evans rearrangement were utilised.

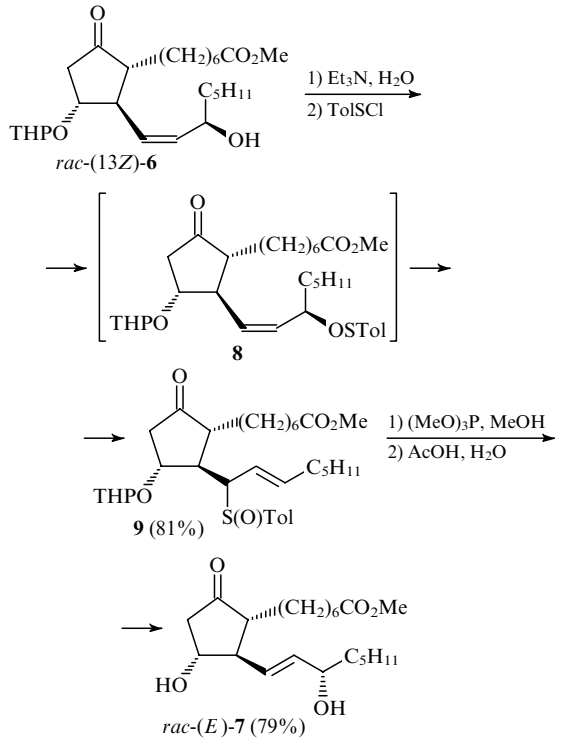

Tol = 4-MeC_6H_4, THP = .

Linear terpenoids and related compounds were synthesised using the above-mentioned alkylation at the stage of allyl sulfide. (*E*)-Nuciferol (**10**) and the terpenoid (*E*)-nuceferal (**11**) were prepared starting from methallyl imidazol-2-yl sulfide (**12**).[16]

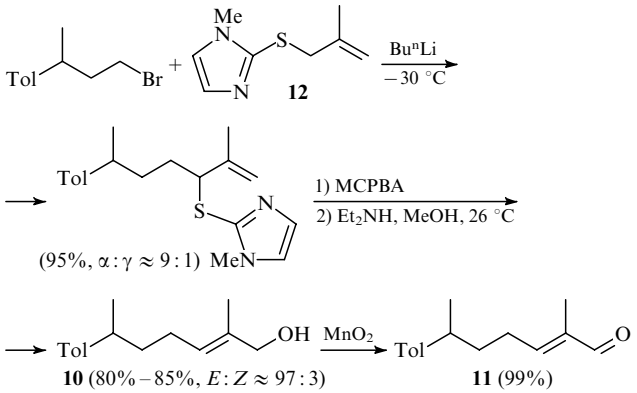

Alcohol (**13**), which is the key compound in the synthesis of the mealybug pheromone, *viz*., (*R*)-2,6-dimethylhepta-1,5-dien-3-ol acetate (**14**), was prepared in four steps starting from methallyl 2-pyridyl sulfide (**15**).[28] After oxidation of intermediate **16** and rearrangement, the alcohol **13** was isolated by chromatography. The pheromone (*R*)-**14** and its (*S*)-enantiomer were prepared in four steps involving asymmetric Sharpless epoxidation. This synthesis allowed the establishment of the absolute configuration of the natural pheromone.

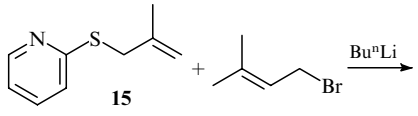

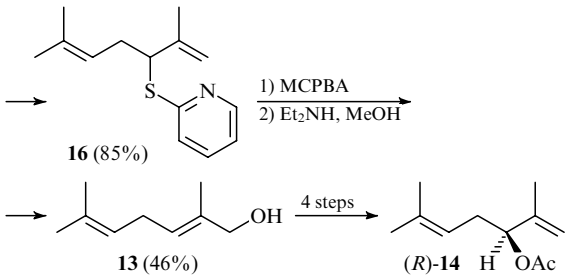

The ingenious short synthesis of yomogi alcohol **17** was carried out starting from sulfide **18**, which was prepared by alkylation of tetramethyldiallyl sulfide **19** with methyl iodide.[16]

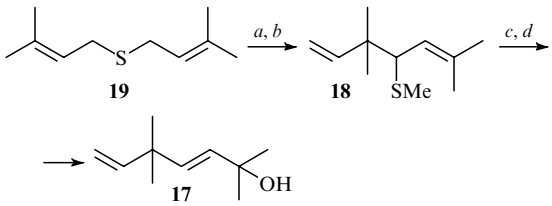

(*a*) Bu^nLi, TMEDA (1,1,4,4-tetramethylethylenediamine); (*b*) MeI; (*c*) $NaIO_4$; (*d*) Et_2NH, MeOH, 25 °C, 24 h.

The sulfoxide – sulfenate rearrangement was also used for the functionalisation of the isopropylidene group of farnesol, related isoprenoids [29, 30] and compounds of the terpene – quinone series.[31]

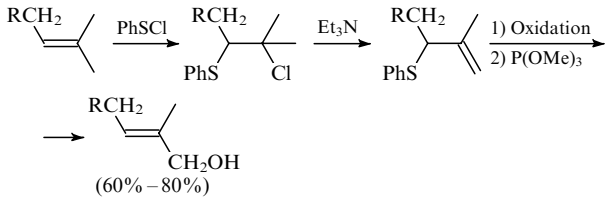

Hence, the sulfoxide-sulfenate rearrangement can be performed as a one-pot procedure after oxidation of allyl sulfide to sulfoxide.

If quinones of the terpene series are used as the starting compounds, the functionalisation products containing ω-hydroxyprenyl or -geranyl chains can serve as convenient building blocks in syntheses of biologically important compounds, such as ubiquinone or vitamins K.[31]

The sulfoxide – sulfenate rearrangement made it possible to perform one-pot epimerisation of 17β-hydroxy-17α-vinylsteroids of type **20** to produce the previously unavailable epimers **21** with the 17α-hydroxy-17β-vinyl group through sulfoxide **22** (the total yield was 88%, the isomer ratio **21** : **20** = 86 : 14).[32]

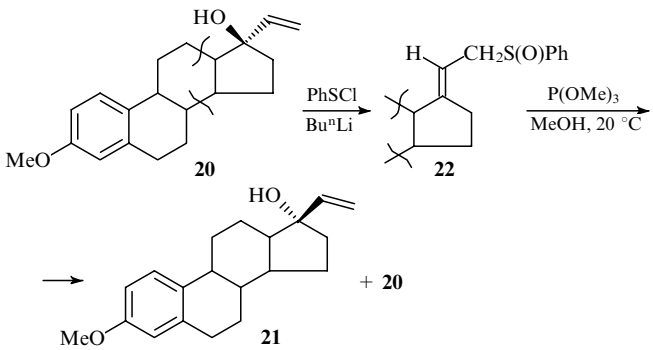

The reaction has a general character and can be applied to steroids containing the *A* rings with different structures.[32]

Tandem processes involving other procedures for the preparation of allyl sulfoxides were also described; among them the so-

called SPAC reaction (Sulfoxide Piperidine and Carbonyl)[33] is noteworthy.

This reaction proceeds under very mild conditions and is typical of sulfoxides containing an electron-withdrawing group in the α position. It is believed that the reactions of the latter compounds with carbonyl groups in the presence of bases proceed according to a cascade mechanism, which involves the Knoevenagel reaction yielding substituted vinyl sulfoxide **A**, its isomerisation to allyl sulfoxide **B** and the subsequent Mislow–Evans rearrangement into sulfenate **C**. In the presence of a base, the latter compound gives the reaction product **D**.

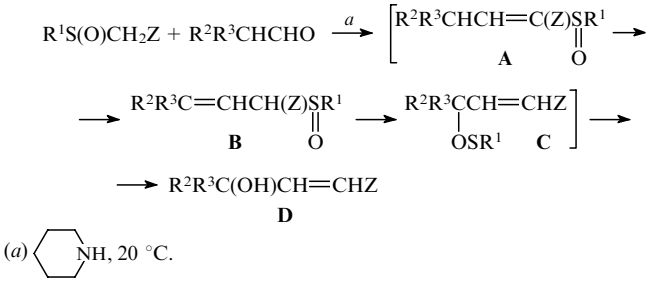

The SPAC reaction and its use in syntheses of natural compounds were considered in detail in a review.[1] This procedure was followed in the preparation of compound **23**, which is a key intermediate in the synthesis of brefeldin A,[34,35] protected seco acid **24**, which is a precursor of (*R*,*R*)-pyrenophorin,[36] and macrocyclic lactones of type **25**.[37]

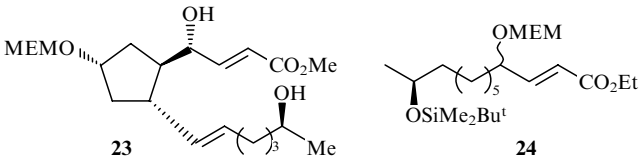

MEM = $MeO(CH_2)_2OCH_2$.

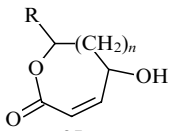

25 (R = H, Me; *n* = 7, 9).

Diene condensations of sulfinyl-substituted 1,3-dienes afford adducts containing the allylsulfinyl fragment due to which they can be used in tandem with the subsequent sulfoxide–sulfenate rearrangement of the adduct (see the review[38]).

The first example of such a tandem process involving the Diels–Alder reaction and the sulfoxide–sulfenate rearrangement has been described in the early study of Evans *et al.*[39] The authors prepared compound **26** with the skeleton of the alkaloid hasubanan by the transformation (without isolation) of adduct **27**, which was synthesised by the stereoselective reaction of 1-phenylsulfinylbuta-1,3-diene (**28**) with tetrahdydrobenzoindole (**29**).

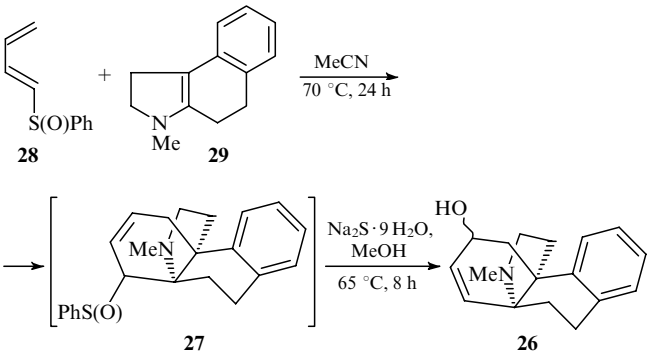

This combination of the reactions offers promise for the synthesis of biologically important substituted cyclohexenols, which cannot be prepared by other procedures.[39] However, this approach has received little use in the synthesis of natural compounds.

There are several examples of the reactions, which do not belong to tandem processes because they involve rearrangements proceeding with the participation of adducts isolated in the pure form.

Thus compound **30**, which is a key intermediate in the total synthesis of chorismic acid, was prepared by the rearrangement of the adduct of 2-(tolylsulfinyl)pyrone with ethyl vinyl sulfide.[40] The rearrangements of the adducts of 2-phenylsulfinylbuta-1,3-diene with 3,3-dimethylcyclopropene or methyl vinyl ketone afforded carenols **31** (a mixture of the α- and β-isomers in a ratio of 7.5 : 1) and a mixture of isomers of 4-acetyl-2-hydroxycyclohexanone (**32**), respectively.[41]

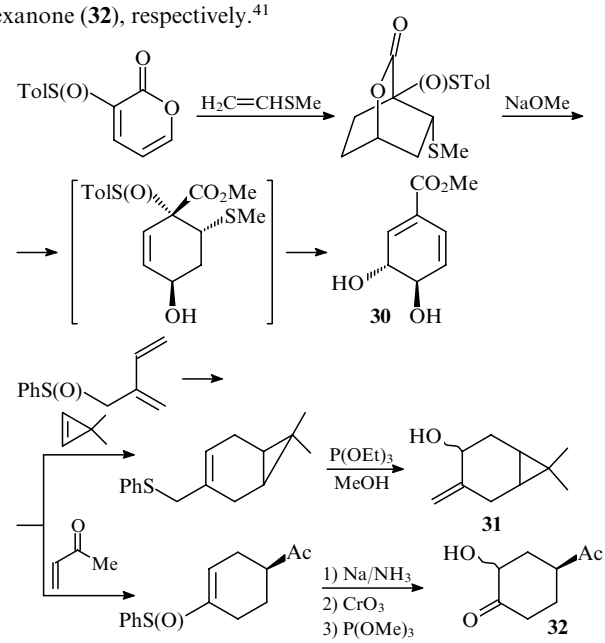

The asymmetric tandem process consisting of the Diels–Alder reaction and the sulfoxide–sulfenate rearrangement can be performed with the use of enantiomerically pure 1-arylsulfinylbuta-1,3-dienes containing an electron-withdrawing substituent at position 4. Thus one-pot thermal reactions of such dienes with an excess of *N*-methylmaleimide gave rise to enantiomerically pure cyclohexene-containing compounds in high yields.[38] This methodology has not been extended to the synthesis of natural compounds. However, the recent study carried out by Carreño *et al.*[42] was devoted to the condensation of [S_R]-1-(1*E*,3*E*)-1-(tolylsulfinyl)penta-1,3-diene (**33**) with 4-methyldihydro-1,2,4-triazole-3,5-dione in the presence of trimethyl phosphite. This reaction proceeded in quantitative yield to form enantiomerically pure compound **34** serving as a key intermediate in the synthesis of optically active β-hydroxy-γ-amino acids.

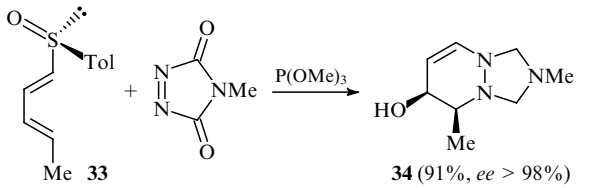

There are also other examples of the use of alcohols, which were prepared by the Mislow–Evans reaction, as key compounds in syntheses of natural products. Thus diol **35** was generated by the rearrangement of an epimeric mixture of sulfoxides, which was obtained by oxidation of sulfide **36**, and served as a key intermediate in the synthesis of cembranoids.[43]

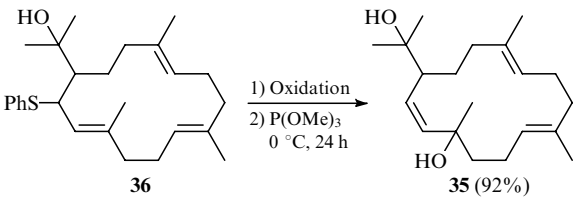

Bicyclic vinyl sulfide **37** was used for the preparation of derivative **38**,[44] which is a key compound in the facile synthesis of the sesquiterpenoid fragment of the active antitumour agent verrucarin. The scheme involves oxidation of the sulfide **37** to vinyl sulfoxide **39** followed by a cascade process consisting in the isomerisation of allyl sulfoxide **40** and the rearrangement of the latter into allylic alcohol **41**, which is spontaneously isomerised with the ring expansion to give the final product.

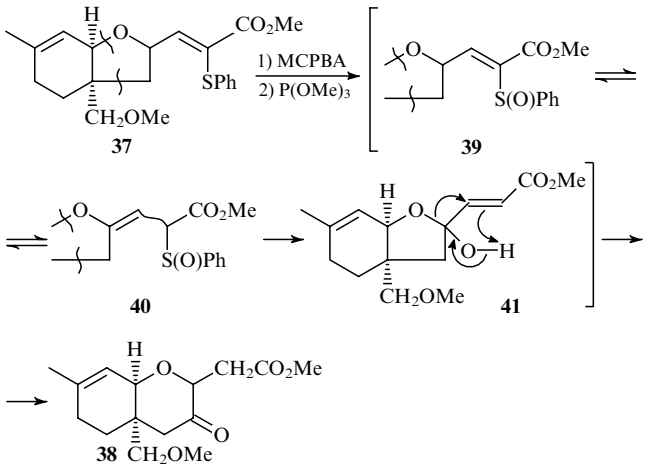

The general procedure for the preparation of β-hydroxy- and β-acetoxy-γ-lactones **42**, which are precursors of compounds possessing allergic action, is based on cyclisation of susbtituted allylic alcohols of type **43**.[45] The latter were prepared by oxidation and the rearrangement of allyl sulfides **4**. This procedure was used in the first synthesis of tuliposide B, which is an agent of allergic dermatitis caused by prolonged contact with tulip bulbs. The precursor of tuliposide B **45** was synthesised starting from allylic alcohol **43a** and acetobromoglucose.

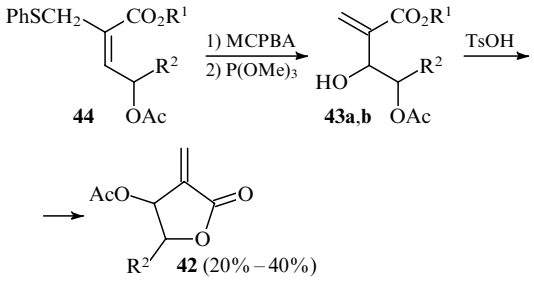

R^1 = Me, Et; R^2 = H (**a**), Alk (**b**).

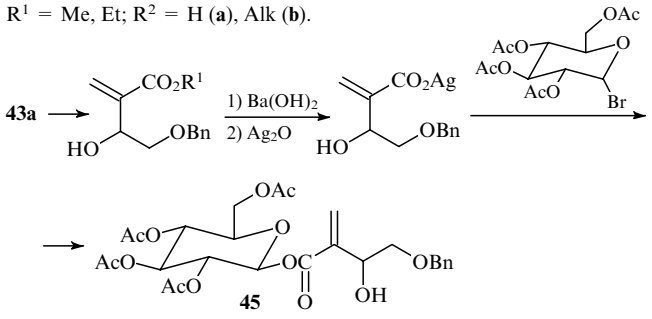

Compound **46**, which is a key intermediate in the route to the synthesis of an active antitumour drug taxol, was prepared starting from allenyl sulfoxide **47**. Its treatment with lithium phenoxide led to the cascade reaction accompanied by cyclisation and the rearrangement of intermediate **48** containing the allyl sulfoxide unit. Oxidation of the resulting tertiary allylic alcohol **49** afforded the target compound **46**.[46] It should be noted that the intermediate **48** was isolated in the reaction of the sulfoxide **47** with less basic nucleophile $PhMe_2Al$.

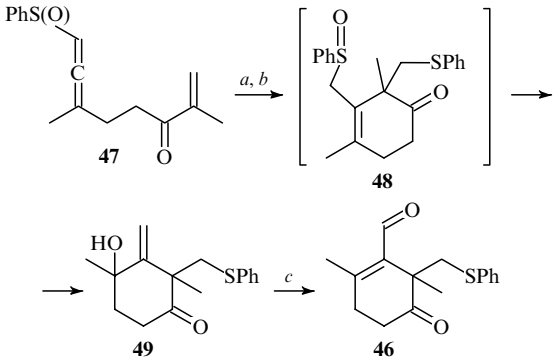

(*a*) LiSPh, THF, 0 °C; (*b*) H_2O; (*c*) Me_2N– 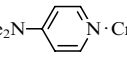 –$N \cdot CrO_3 \cdot HCl$, $ClCH_2CH_2Cl$, 100 °C

2. Syntheses involving the sigmatropic rearrangement of propargyl sulfenates into allenyl sulfoxides

The rearrangement of propargyl sulfenates into allenyl sulfoxides discovered by Braverman (see Ref. 2) has received little use in syntheses of natural compounds as compared to the Mislow – Evans rearrangement. The former rearrangement is a reversible [2,3]-sigmatropic reaction proceeding under mild conditions. This rearrangement is utilised in syntheses of natural products only as a convenient procedure for the preparation of allenyl sulfoxides starting from available propargylic alcohols. Allenyl sulfoxides can, in turn, be converted into substituted allyl sufoxides by the addition of a nucleophile at the activated C = C bond of allenyl sulfoxide.

A procedure was developed[47] for the preparation of the antiinflammatory agent hydrocortisone acetate (**50**) bearing the $COCH_2OH$ group at position 17β, which is typical of corticosteroids.

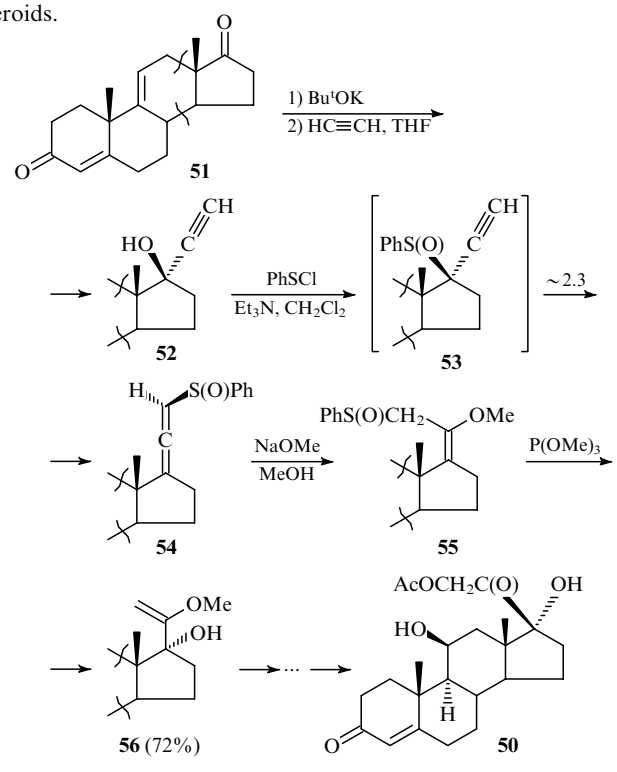

Readily accessible androst-4,9(11)-diene-3,17-dione (**51**) was used as the starting compound. The reaction of alcohol **52**, which was prepared by the selective addition of acetylene to the carbonyl group at position 17 of compound **51**, with $PhSCl-NEt_3$ afforded sulfenate **53**. The latter is stable only below −40 °C and underwent the [2,3]-rearrangement to give allene sulfoxide **54** as a mixture of isomers. The addition of the methoxy group at the double bond of the sulfoxide **54** gave rise to an epimeric mixture of allyl sulfoxides **55**, which were isomerised into allylic alcohol **56** through the Mislow–Evans rearrangement. This process provides the basis for a general method for the conversion of ketosteroids to corticosteroids. The stereochemistry of all stages of this process was investigated.[47]

The addition of the alkyne fragment to the carbonyl group followed by desulfinylation of allenyl sulfoxides under the action of MeLi was used for the preparation of steroids containing allene substituents.[48, 49]

In the study,[50] allenyl sulfoxides were utilised as the starting compounds in the development of a general method for the preparation of 2,5-dihydrofuranones **57** by cyclisation of substituted allylic alcohols **58**, which are products of the [2,3]-rearrangement of allyl sulfoxides **59**. The compounds **59** were prepared by the addition of a sodium derivative of dimethyl malonate to allenyl sulfoxides.

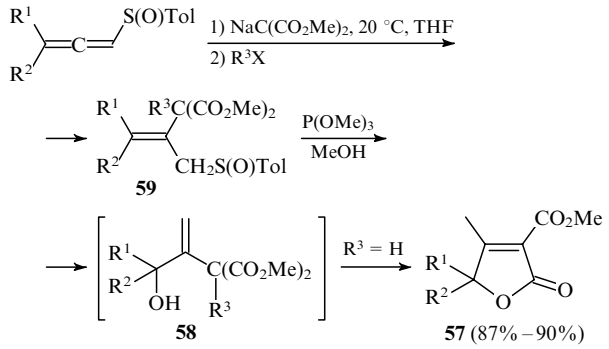

R^1 = H, Me; R^2 = Me; $R^1-R^2 = (CH_2)_5$.

This procedure was also employed for the conversion of mestranol **60** to spiro lactone **61** *via* allenyl sulfoxide **62**.[50]

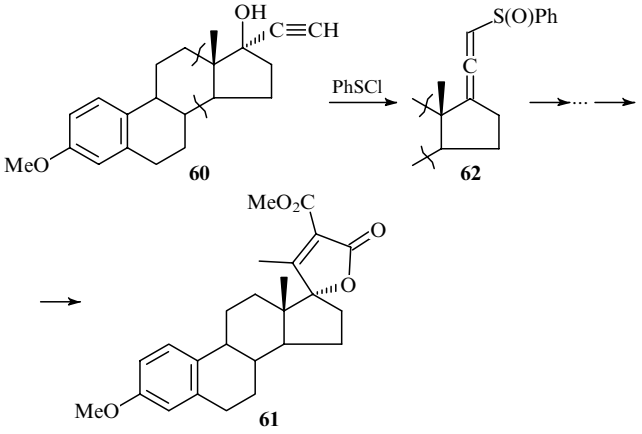

In the synthesis of sesquiterpenoid sterpurene [(+)-**63**], the key tetraene sulfoxide **64** was derived from propargylic alcohol **65**.[51]

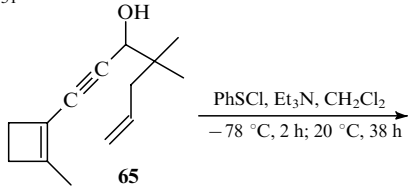

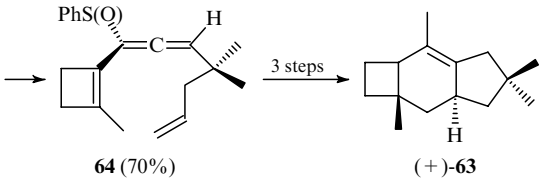

Other examples of the synthetic applications of vinylallenyl-containing sulfoxides prepared in a similar way were presented in a review,[52] which covered the use of vinylallenes in the synthesis of metabolites of vitamin D_3.

III. Syntheses based on the Pummerer reaction

The Pummerer reaction consists in the transformation of sulfoxides bearing at least one α-hydrogen atom under the action of electrophilic reagents. The reactions of saturated sulfoxides resulted in reduction of the sulfinyl group to the sulfide group and oxidation of an α-hydrogen atom. It is believed [7, 8, 11, 53] that the reaction proceeds through successive equilibrium stages of the formation of the acyloxy sulfonium ion **A**, ylide **B** and the sulfenium cation **C**. The reactions ended in the attack of an internal or external nucleophile on the cation **C**.

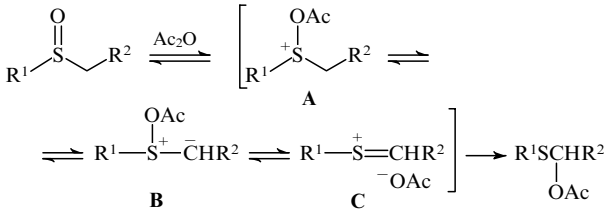

All three main experimental versions of this reaction are employed in syntheses of natural compounds.

The first version is the classical Pummerer reaction in which sulfoxides containing no unsaturated groups in the α,β positions react with acids or their derivatives (most often with anhydrides and sometimes in the presence of bases). As shown in the above scheme, these reactions afford α-acyloxy sulfides as the primary reaction products.

The second version involves the so-called sila-Pummerer reactions. In this case, the substrate or the electrophilic reagent possesses labile Si–X bonds due to which the reactions often proceed under milder conditions (generally at below-zero temperatures). Trimethylchlorosilane [54] or other silicon-containing electrophiles are used as silylating agents.

The third version of the Pummerer reaction consists in additive processes involving vinyl sulfoxides as substrates, which undergo Pummerer-like rearrangements under the action of various inorganic or organic electrophilic reagents.[55] The version proposed by Marino and Neisser [56] is of particular interest. In the latter case, dichloroketene generated *in situ* served as the electrophilic reagent.

Examples of the use of the Pummerer reaction in syntheses of biologically active compounds are systematised below according to the nature of the nucleophilic reagent involved in the reaction with the sulfenium cation.

1. Syntheses based on hydrolytic cleavage of α-acyloxy sulfides

Hydrolysis of α-acyloxy sulfides generated in the course of the classical Pummerer reaction provides a convenient way of transforming sulfoxides into carbonyl compounds. These reactions are generally performed under the action of alkalis with the addition of salts, such as $HgCl_2$ or $CaCl_2$, which promote elimination of the RS group. This section is concerned with examples of the applications of this procedure to the construction of carbonyl groups in natural compounds or key intermediates for their syntheses.

(*R*)-(+)-Perillaldehyde (**66**) was prepared [57] starting from an enantiomeric mixture of optically active sulfoxides **67** [which were synthesised in two steps from (+)-limonene epoxide] by hydrolysis of the Pummerer-reaction product **68** without its isolation. Side chain deacylation of the intermediate **68** afforded vinyl sulfide **69**.

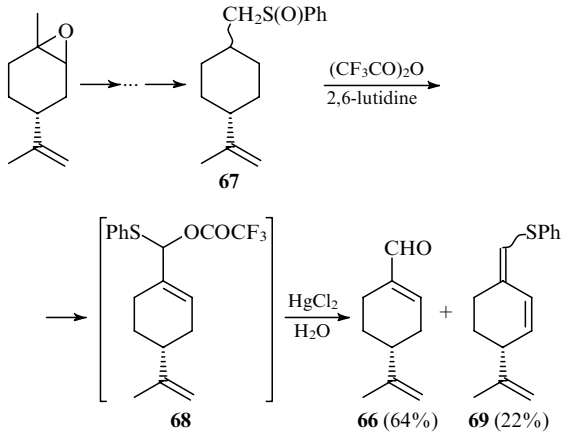

6-Acetoxy-2,5,7,8-tetramethylchroman-2-carbaldehyde (**70**), which is a key starting compound in the total synthesis of α-tocopherol, was derived [58] from sulfoxide **71** by hydrolysis of α-acyloxy sulfide **72** isolated in the individual form.

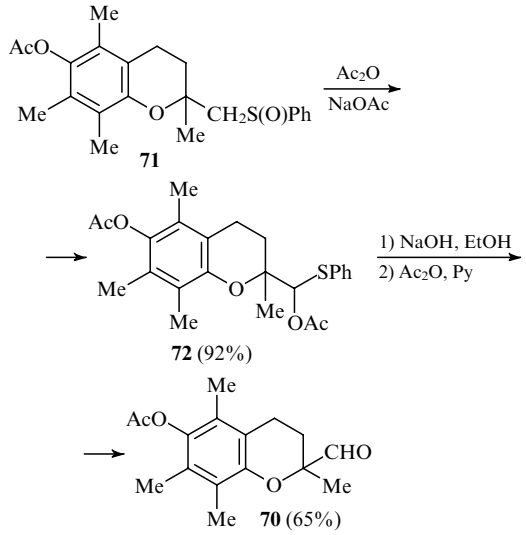

Racemic 5-desoxyleukotriene D [(±)-**73**] was synthesised with the use of aldehyde **74**, which was prepared from sulfoxide **75** without isolation of intermediate acyloxy sulfide. The scheme of the synthesis of the aldehyde **74** involves the reaction of 1-phenylsulfinylpenta-2,4-diene **76** with methyl 5-formylvalerate in the presence of butyllithium followed by migration of the sulfinyl group in benzoyl derivative **77**, which proceeds very readily through a two-step [2,3]-rearrangement.[59]

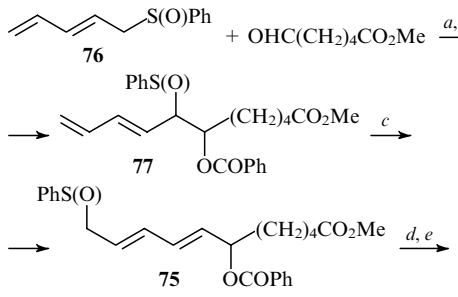

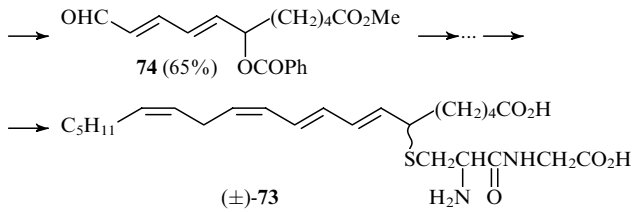

(*a*) Bu^{n}Li; (*b*) PhCOCl, −40 °C; (*c*) 25 °C, 3 h, (*d*) Ac_2O, 2,6-lutidine, $(CF_3CO)_2O$, NaOH; (*e*) $CaCO_3$, $HgCl_2$, MeCN – H_2O.

In the key stage of the total synthesis of asteltoxin [(±-**78**)], aldehyde **79** was generated from sulfoxide **80** also without isolation of intermediate acyloxy sulfoxide.[60]

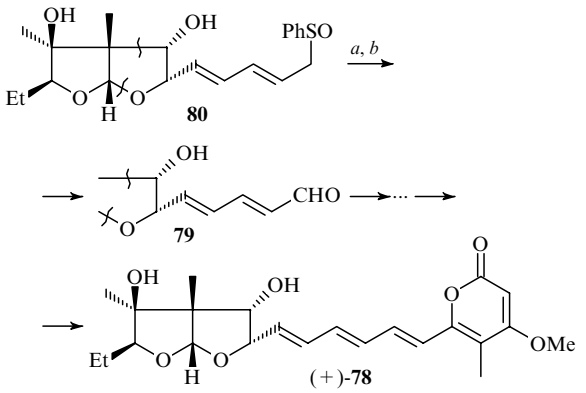

(*a*) $(CF_3CO)_2O$, Ac_2O, 2,6-lutidine; (*b*) $CaCl_2$, $HgCl_2$, MeCN – H_2O.

3-Trichloroacetylaminohex-4-enal (**81**) was synthesised starting from sorbinic alcohol. [61] In this case, acyloxy sulfide **82** was isolated as an intermediate. Hydroxylation of the aldehyde **81** with OsO_4 afforded the *N*-trichloroacetyl derivative of racemic daunosamine (**83**), which is a carbohydrate fragment of the antitumour antibiotic daunorubicin used in clinical practice. Variations of this procedure made it possible to synthesise the related carbohydrates, *viz*., racemic vancosamine and ristosamine.[61]

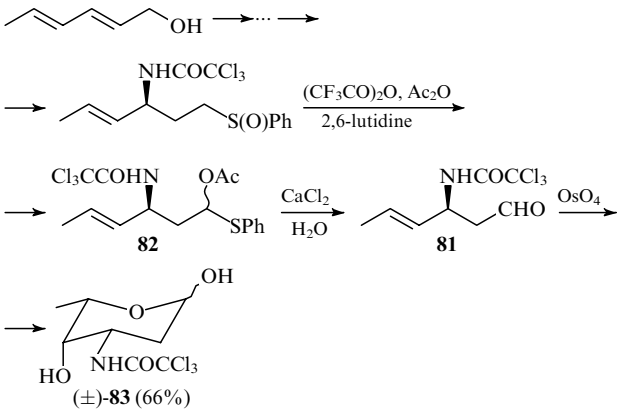

Branched sugar **84** was synthesised [62] in three steps from keto ester **85**. The latter was obtained as the major product of the Pummerer reaction of sulfinyl-substituted ester **86**, which was prepared by diene condensation of menthyl (*S*)-(2-pyridylsulfinyl)acrylate with furan.[63] The Pummerer reaction involving the sulfoxide **86** afforded vinyl sulfide **87** as a by-product. Acid hydrolysis of the latter gave rise to the keto ester **85** in low yield (< 25%).[62]

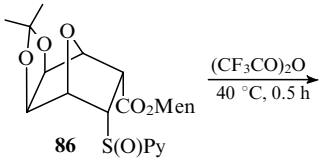

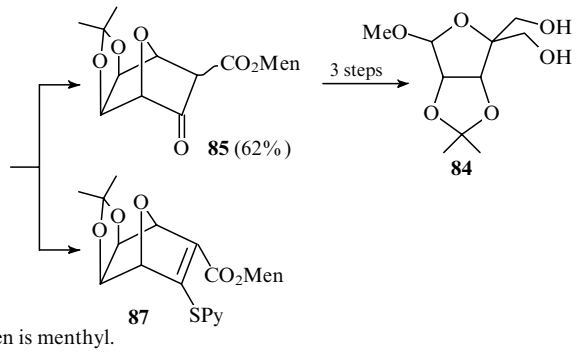

Men is menthyl.

However, some of these reactions proceed readily; examples of such reactions were described in the literature. Thus vinyl sulfide **88**, which was prepared by the Pummerer reaction starting from sulfoxide **89**, was utilised in the synthesis of ketolactone **90**. The latter is the direct precursor in the synthesis of the antitumour agent sarcomycin (**91**).[64]

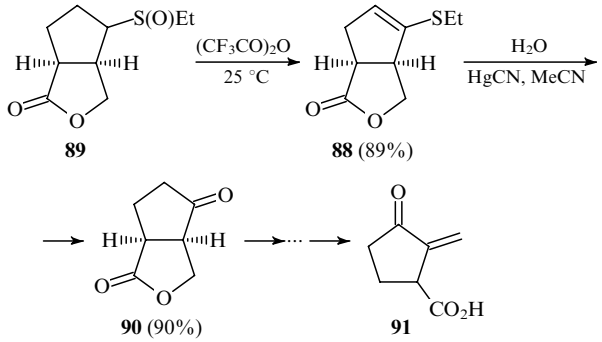

Below is given a scheme illustrating additional potentialities arising from a combination of the classical Pummerer reaction and the subsequent transformation of its products without their isolation. A combination of hydrolysis of acetoxy sulfide and reduction of the intermediate carbonyl compound starting from sulfoxides **92**–**94** made it possible to prepare labile compounds, such as γ-geraniol (**95**),[65] dendrolasin (**96**)[66] and enantiomerically pure penta-*O*-acetyl-L-arabinitol (**97**).[67]

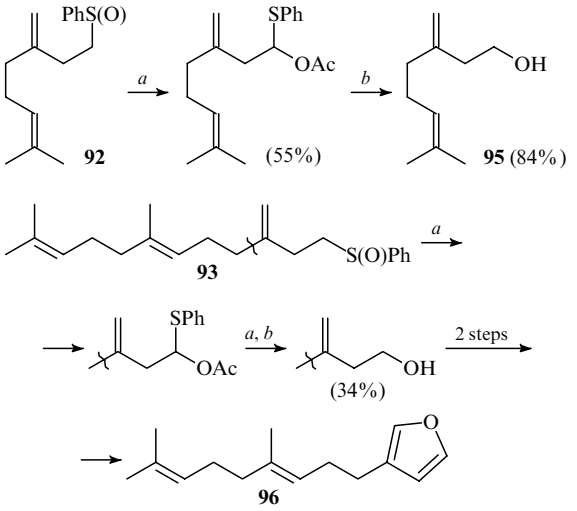

(*a*) Ac_2O, $(CF_3CO)_2O$ (cat); (*b*) $NaBH_4$, EtOH, H_2O.

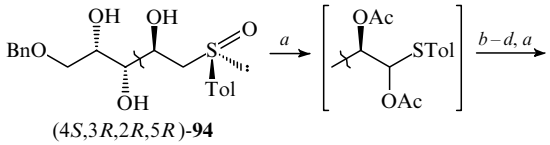

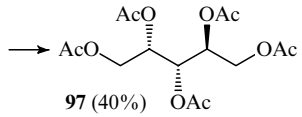

(*a*) Ac_2O, AcONa; (*b*) Bu^i_2AlH; (*c*) Ac_2O; (*d*) Pd/C, C_6H_{10}.

In more recent studies, for example, in the synthesis of 2-deoxy sugars[68] or in the construction of a fragment of the antibiotic nystatin A_1 containing five chiral alcoholic centres, Solladié *et al.*[69] used yet another modification of the acyloxy sulfide group. The Pummerer-reaction product, which was purified only by column chromatography, was immediately subjected to desulfurisation with Raney nickel. This procedure is exemplified by the preparation of derivative **98** of (2-deoxy-D-ribonic acid) starting from sulfoxide **99**.

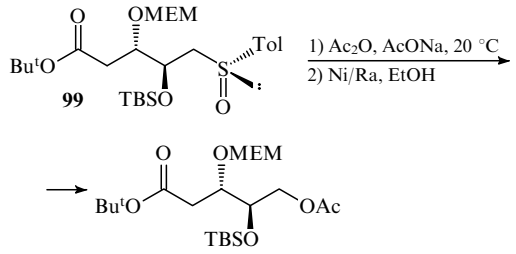

TBS = Bu^tMe_2Si.

The procedure developed for the synthesis of substituted pyridines[70] involves a combination of four reactions, *viz.*, oxidation of sulfide to sulfoxide, the classical Pummerer reaction, hydrolysis of α-acyloxy sulfide and the formation of the pyridine ring by the reaction of ammonia with intermediate 1,5-ketoaldehyde.

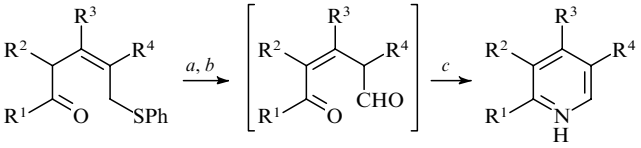

(*a*) $NaIO_4$, MeOH, H_2O; (*b*) $(CF_3CO)_2O$, Py; (*c*) NH_3, MeOH, H_2O.

This procedure made it possible[71] to synthesise natural neurotoxin, *viz.*, acromelic acid A (**101**), starting from phenylthio-substituted pyrrolidine **100**. Isomeric acromelic acid B was prepared analogously.[72] More complex synthetic schemes involving the Pummerer reaction as the key stage are considered at the end of the section.

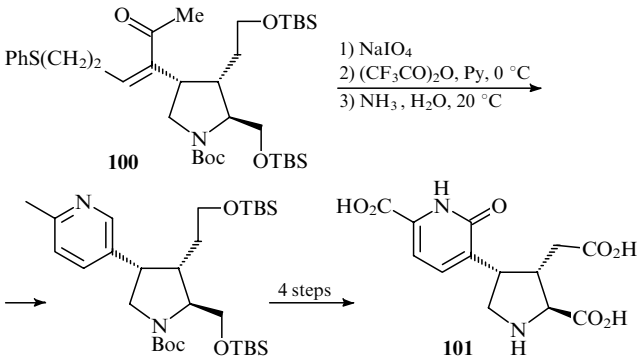

Boc = Bu^tOCO.

2. Syntheses based on intermolecular reactions of sulfenium cations with C = C bonds of alkenes

The sulfenium cation is a highly electrophilic reagent, particularly, if the initial sulfoxide bears activating electron-withdrawing

groups (most often carbonyl groups). This cation can react even with the weakly nucleophilic C=C bond. Analogous intermolecular processes were used in syntheses of predominantly linear unsaturated components of pheromones. In most studies, no consideration has been given to intermediates and hence, the mechanism of this reaction is unknown. Ishibashi and coworkers [73–77] proposed the ene-type mechanism involving the sulfenium cation.

The natural insecticide pellitorine (**102**) was prepared [73] by the reaction of oct-1-ene with the product of the Pummerer rearrangement of (methylsulfinyl)acetamide (**103**). (*E*)-9-Oxodec-2-enoic acid (the queen substance) (**104**) was synthesised analogously from methyl methylsulfinylacetate (**105**) and oct-1-en-7-one.[74] Additional C=C bonds were generated by thermolysis of sulfoxides prepared by oxidation of adducts **106** and **107**.

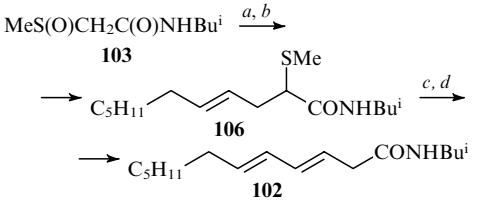

(*a*) $(CF_3CO)_2O$; (*b*) $C_6H_{13}CH=CH_2$; (*c*) $NaIO_4$; (*d*) Δ.

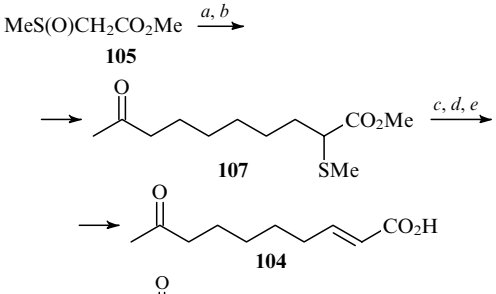

(*a*) $(CF_3CO)_2O$; (*b*) 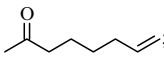 ; (*c*) $NaIO_4$; (*d*) Δ; (*e*) OH^-.

p-Chlorophenylmethyl sulfoxide proved to be a particularly convenient starting compound in such reactions. The Pummerer reaction involving primary product **108** afforded numerous biologically active compounds, for example, the sex pheromone of red cotton moth (**109**) with the ratio of the (*E*)- and (*Z*)-isomers identical to that observed in the natural substance,[75] the pheromone of some tortricids **110** [76] and bicyclic *exo*-brevicomin **111**, which is the aggregation pheromone of fir moth (in a mixture with 11% of the *endo* epimer).[77]

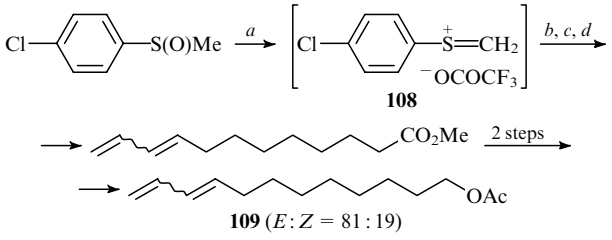

(*a*) $(CF_3CO)_2O$; (*b*) 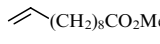 ; (*c*) MCPBA; (*d*) Δ.

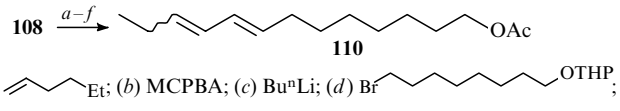

(*a*) 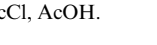 ; (*b*) MCPBA; (*c*) Bu^nLi; (*d*) ;
(*e*) EtNHLi; (*f*) AcCl, AcOH.

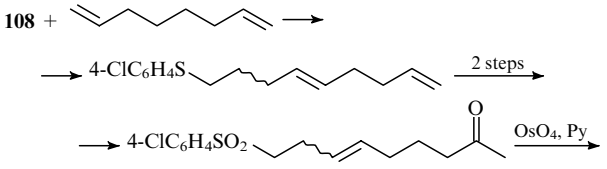

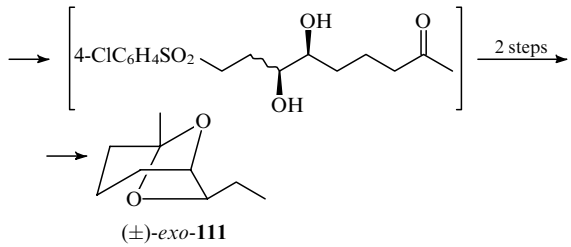

(±)-*exo*-**111**

Trideca-(4*E*,7*Z*)-4,7-dien-1-ol acetate (**112**), which is the potato moth pheromone, was synthesised [78] starting from phosphorus-substituted sulfide **113**. The latter was derived from (methylsulfinyl)phosphonate by the Pummerer reaction followed by the reaction with 5-heptyl acetate. The synthesis ended in oxidation of the sulfur atom in the adduct to the sulfonyl group, chain elongation by the Horner–Wadsworth–Emmons reaction with hexanal and a three-step modification of intermediate **114**.

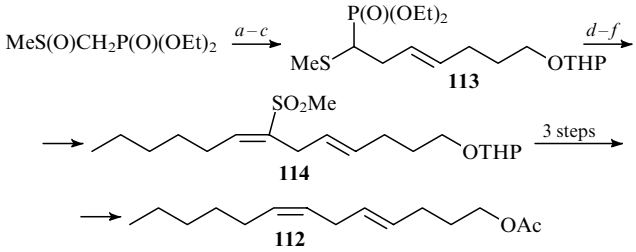

(*a*) $(CF_3CO)_2O$; (*b*) 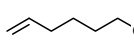 ; (*c*) 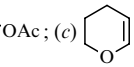 , H^+; (*d*) MCPBA;
(*e*) Bu^nLi; (*f*) 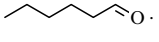 .

3. Cyclisations based on intramolecular reactions of sulfenium cations with C=C bonds

Intramolecular coupling of the Pummerer-reaction products and C=C bonds proved to be much more fruitful. The reaction of the sulfenium cation, which was derived from the sulfinyl fragment of compounds **115a**,**b**, with the C=C bond of the indole fragment was the key step in the synthesis of tetracyclic pyrido[4.3-*b*]carbazole alkaloids olivacine (**114a**) and ellipticine (**114b**). The target alkaloids **114a**,**b** were prepared in rather high yields by ten-step transformations of intermediates **116a**,**b**.[79]

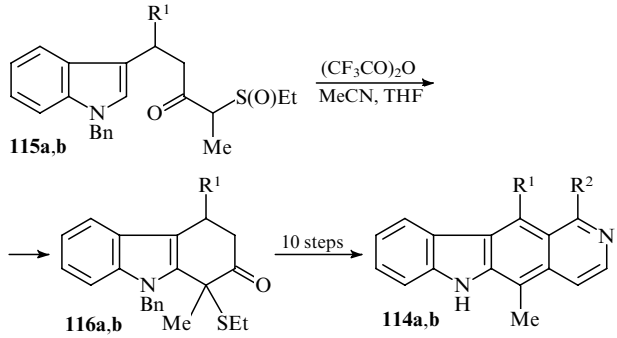

Compound	R^1	R^2	Yield (%)
116a	H		51
116b	Me		55
114a	H	Me	28
114b	Me	H	23

Magnus and coworkers carried out systematic research into the synthesis of polycyclic indole alkaloids (see the review [80]) and devised the [2,3]-quinodimethane strategy for constructing these alkaloids. (±)-Aspidospermidine (**117**), which is the simplest representative of pentacyclic alkaloids from *Aspidosperma sp.* plants, was a convenient compound for the development of the methodology. Gallagher *et al.*[81] synthesised tetracyclic precur-

sors, *viz*., substituted octahydro-7*H*-pyrido[3,2-*c*]carbazole **119** and **120**, starting from nitrogen-protected 3-formyl-2-methylindole (**118**). The compound **119** contains the sulfinyl-substituted exocyclic amide group, whereas the compound **120** bears the endocyclic amide group. Under the conditions of the Pummerer reaction, compounds **119** and **120** very readily undergo cyclisation to compounds **121** and **122** to form the *E* ring (apparently through intermediates **123** and **124**, respectively). After deprotection of the indole nitrogen atom and reductive removal of the carbonyl and sulfide groups, racemic aspidospermidine **117** was obtained through the compounds **119** and **120** in total yields of 6.3% of 11.7%, respectively. Cyclisation proceeded with exceptional stereoselectivity resulting in the natural *cis*-fusion of the rings. Cyclisation proceeded readily due to the close arrangement of the sulfenium cation and the π-electron system of the nucleophilic indole fragment.

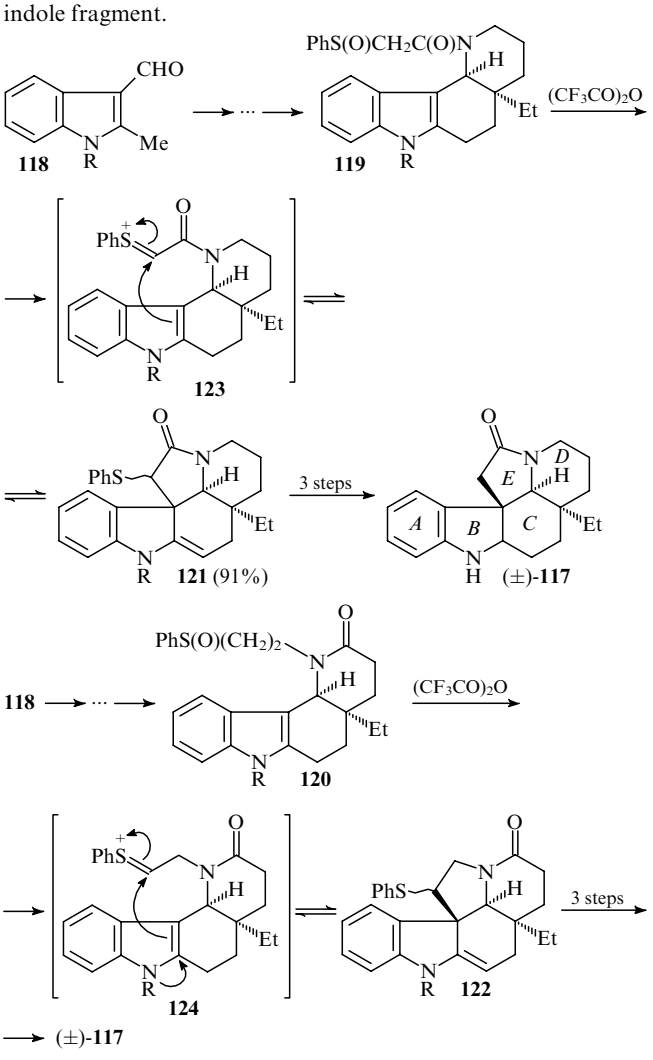

R = $SO_2C_6H_4OMe$-4.

The electronic or steric factors inhibiting the ring formation can (owing to the equilibrium character of this reaction) promote other conversions of a sulfenium-containing intermediate. Thus researchers failed to construct the *E* ring of indole alkaloids of the aspidospermine group under the standard conditions of the Pummerer reaction starting from model compound **125**, which contains the electron-donating methoxy group in the benzene ring typical of alkaloids of the vinblastine and vindoline groups. Cyclisation was successfully performed under the action of trifluoroacetic anhydride in the presence of 2,6-di-*tert*-butyl-4-methylpyridine as a base.[82] After thermolysis, compound **126** was obtained in rather high yield.

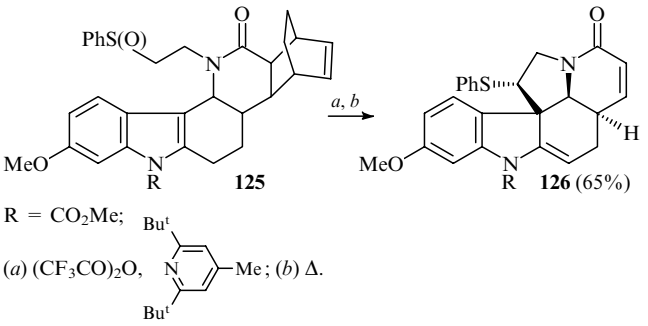

Magnus did not extend this discovery to natural alkaloids of the vinblastine and vindoline series, probably, because Langlois and coworkers [83] have reported an ingenious procedure for their preparation, which was also based on the Pummerer reaction but which utilised β-ketosulfinyl-containing tetrahydroindolo[2,3-*a*]-quinolizidines of type **127** as the starting compounds. Vindoline (**128a**) and vindorosine (**128b**) were prepared from the compounds **127a**,**b** in which the indole nitrogen atom was protected with the methyl group. Under the conditions of the Pummerer reaction, the compounds **128a,b** underwent a retrobiomimetic rearrangement *via* the intermediates **A** → **B** → **C**. The reaction started with the coupling of the sulfenium cation with the indole C=C bond and ended in the construction of the *E* ring in **129a**,**b**, which are key compounds in the synthesis of the target alkaloids. If the indole nitrogen atom is not protected (as in the precursors **127c** or **130a**), the indole C=C bond can couple with the nearby sulfenium cation (*via* the intermediate **D**) under the conditions of the Pummerer

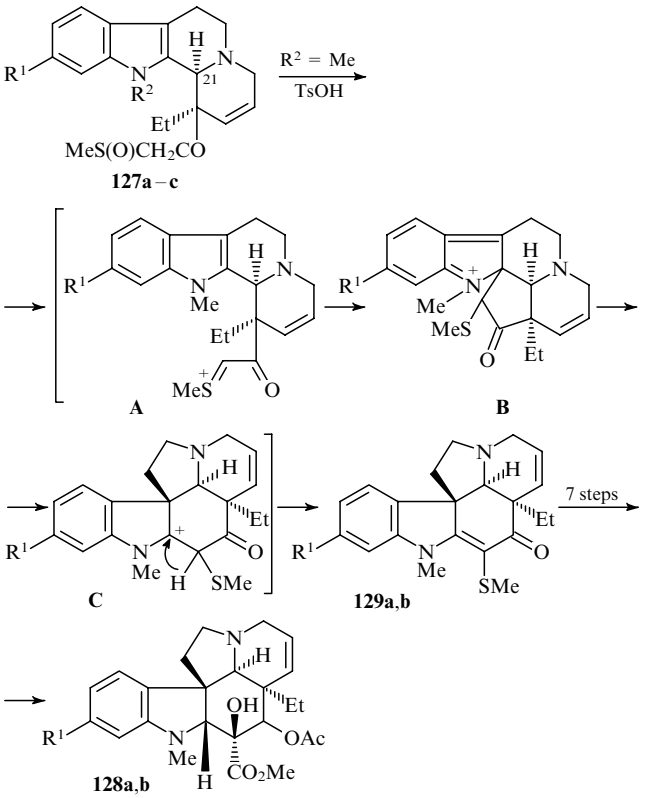

Compound	R^1	R^2	Yield (%)
127a	OMe	Me	–
127b	H	Me	–
127c	H	H	–
128a	OMe		10 (total)
128b	H		–
129a	OMe		73
129b	H		70

reaction giving rise to eburn-type alkaloids, for example, to compound **131**. However, for this reaction pathway to become dominant, the indole C=C bond must be additionally shielded by the β-hydrogen atom at the C(21) atom as in indoloquinolizidine **130a**.[84]

The Pummerer reaction involving the epimeric compound **127c**, which bears an α-hydrogen atom at the C(21) atom, afforded a mixture of aspidospermidine- and eburn-type alkaloids with the former predominating.[85]

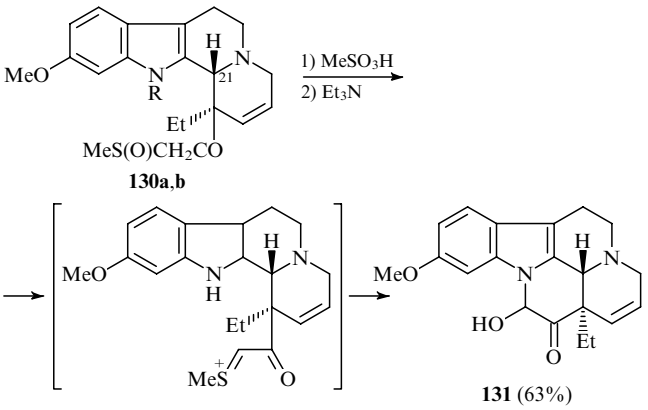

R = H (**a**), Me (**b**).

Vindoline **128a** can be prepared with equal ease from the C(21)-epimeric precursors **127a** or **130b**. It was assumed [84] that the compound **130b** was converted into the compound **127a** due to rapid reversible Mannich-type isomerisation. Apparently, this reversible process is also responsible for racemisation, which was observed in attempting to prepare enantiomerically pure alkaloids of this series from optically pure indoloquinolizidines.[84, 86]

Further progress in studies on the synthesis of alkaloids of the aspidospermine group performed by Magnus and coworkers [87] was achieved owing to the employment of additional functionalisation of pentacyclic thio-containing amides. Thus racemic 8-oxotabersonine (**132**) was prepared [87] from pentacyclic compound **133** in five steps.

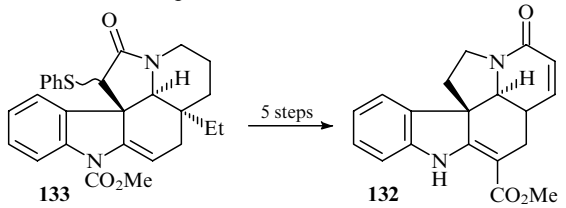

The synthesis of heptacyclic alkaloids of the kopsan series was a more complicated problem. For this purpose, key compound **134a** containing the diene system in the *C* ring was constructed. Under the conditions of the Pummerer reaction, aromatisation of the *C* ring competed with cyclisation due to which the use of the diene precursor **135** did not afford the target compound **134a**. The reaction involving chlorine-containing analogue **136** took the desired path [88] and the intermediate **A** readily underwent dehydrochlorination.

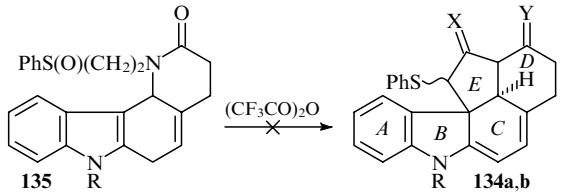

R = $SO_2C_6H_4OMe$-4; X = H, Y = O (**a**); X = O, Y = H (**b**).

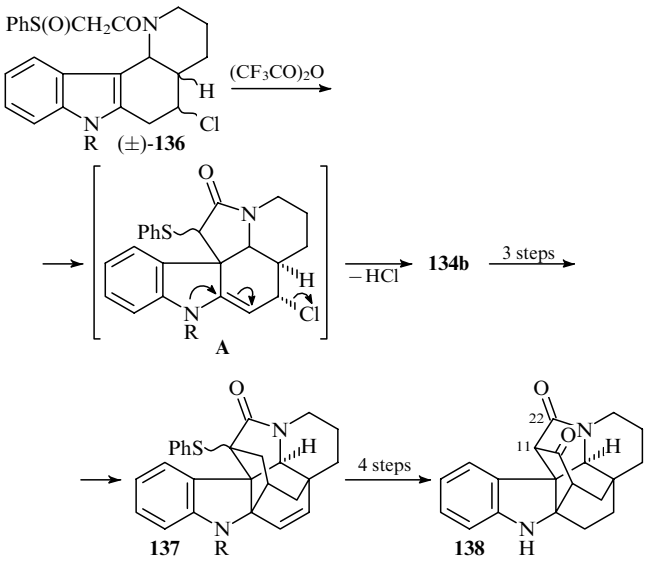

R = $SO_2C_6H_4OMe$-4.

The one-pot synthesis of heptacyclic compound **137** containing all major elements of the kopsan system was carried out with the use of the pentacyclic compound **134b**. For this purpose, the starting compound was allylated at the C(11) atom followed by intramolecular diene condensation involving the diene system of the *C* ring. The key alkaloid of this series, *viz*., (±)-10,22-dioxokopsan (**138**), was synthesised from the compound **137** in four steps [the keto group at the C(22) atom was formed by the Pummerer reaction of the intermediate C(22)-sulfoxide]. C(22)-Oxokopsan and epimeric C(22)-kopsanols were readily derived from the compound **138**.

An analogous procedure was also used [89] for the preparation of optically active (+)-dioxokopsan [(+)-**138**] based on enantiomerically pure (taking into account the sulfinyl group) tetracyclic precursor (+)-**139**. In the cited study,[89] the data on the optical

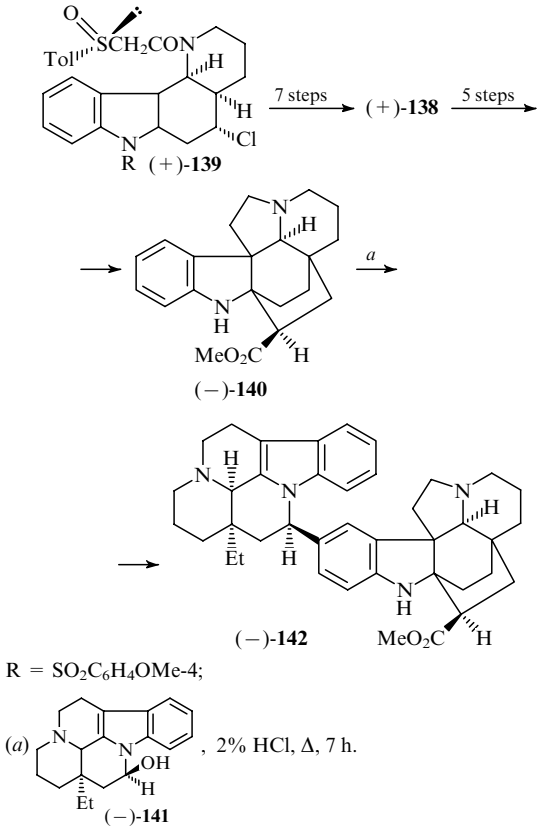

R = $SO_2C_6H_4OMe$-4;

(*a*)

, 2% HCl, Δ, 7 h.

(–)-**141**

purity and absolute configurations of the products are lacking. However, the conversion into (−)-kopsinine (**140**) followed by its condensation with optically pure (−)-eburnamine [(−)-**141**] afforded bis-indole (−)-norpleiomutine [(−)-**142**] characterised by an optical rotation identical to that of the natural alkaloid.

The application of Magnus's procedure to the construction of the fifth ring of the more strained systems of alkaloids from plants of the *Strychnos* family utilising either precursor **143a**, which contains the exocyclic sulfinylamide group, or precursor **143b**, which is an endocyclic amide, has not met with success.[90] In the study of Bosch and coworkers,[91] steric hindrances to the favourable arrangement of the sulfenium ion relative to the indole C=C bond were overcome with the use of the more flexible sulfinylalkylamine group in tetracyclic precursor **143c**. In the latter case, after the standard treatment with trifluoroacetic anhydride, the process was terminated at the stage of formation of α-acyloxy sulfide, which was converted without isolation into cyclisation product **144** under the action of boron trifluoride etherate. The yield was insufficiently high because the undesirable hydration product **145** was simultaneously obtained. However, the cited study[91] can be considered as a facile synthesis of strychnine alkaloids. Compound **146** was obtained in 50% yield. It is a 20-deethylated analogue of the final intermediate (which was prepared previously[92]) in the synthetic pathway of the most important representatives of strychnine alkaloids, *viz*., tubifoline, tubifolidine, *etc*.

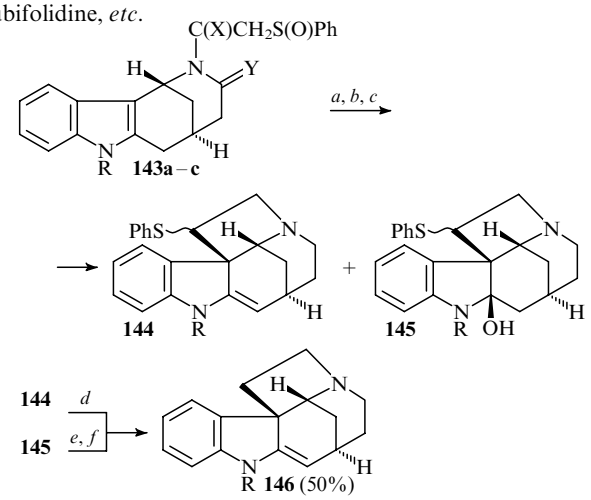

R = CO_2Me; X = O, Y = H_2 (**a**); X = H_2, Y = O (**b**); X = Y = H_2 (**c**); (*a*) X = Y = H_2, $(CF_3CO)_2O$; (*b*) $BF_3 \cdot Et_2O$; (*c*) CH_2Cl_2, Δ, 4 h; (*d*) Ni/Ra; (*e*) TsOH, 20 °C; (*f*) Ni/Ra.

Sulfinylalkylamines were successfully used in syntheses of other groups of alkaloids. (±)-Deethylibophyllidine (**147**) was prepared[93] according to the standard Pummerer reaction from tetracyclic compounds **148** by the construction of the fifth ring.

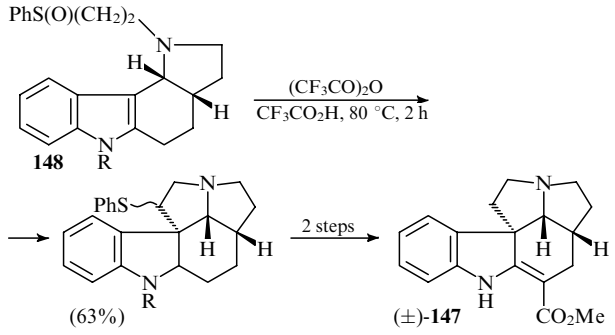

R = CO_2Me.

In the facile synthesis of (±)-geissoschizine (**149**) starting from precursor **150**, the six-membered ring was successfully constructed only under the conditions of the sila-Pummerer reaction.[94] Under the conditions of the classical Pummerer reaction, the unexpected formation of hydroxy sulfide **151** from the compound **150** was observed instead of cyclisation. In a special study,[95] it was demonstrated that such an anomalous Pummerer reaction is typical of C(3)-unsubstituted indole derivatives and is attributable to the prior formation of the seven-membered ring.

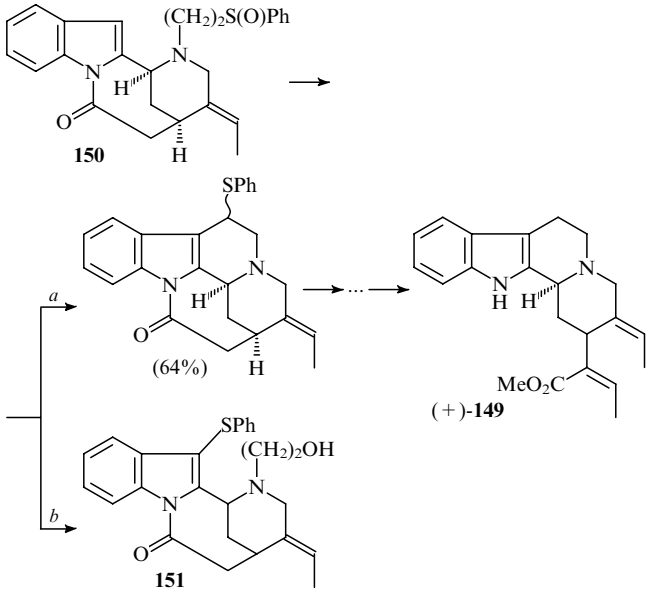

(*a*) Me_3SiOCF_3, 20 °C; (*b*) $(CF_3CO)_2O$, CF_3CO_2H.

This research group[96] carried out the first synthesis of an alkaloid of the 3,4-secoakuammilan series by cyclisation of sulfoxide **152** under the conditions of the Pummerer reaction. In this synthesis, the strongly strained quaternary centre at the C(7) atom was generated through the formation of the eight-membered lactam ring.

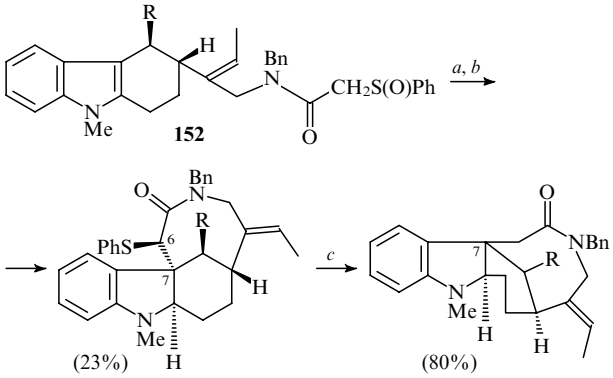

(*a*) $(CF_3CO)_2O$, CH_2Cl_2; (*b*) $NaCNBH_3$; (*c*) Ni/Ra, EtOH.

4. Synthesis of cyclic compounds by intramolecular reactions of sulfenium cations with various nucleophilic traps

The Pummerer reaction is finding increasing use in the construction of various rings, including those present in natural compounds, primarily, of heterocycles (see the review[12]), and, to a lesser extent, of carbocycles. Natural heterocycles are constructed by intramolecular binding of the sulfenium cation to various nucleophilic traps. The C=C bonds other than those present in indoles can serve as nucleophiles as exemplified by the ingenious synthesis of the alkaloid (±)-3-demethoxyerythratidinone (**153**).[97] The latter was prepared starting from substituted sulfinylacetamide **154**, which was subjected to double cyclisation *via* intermediate **A**.

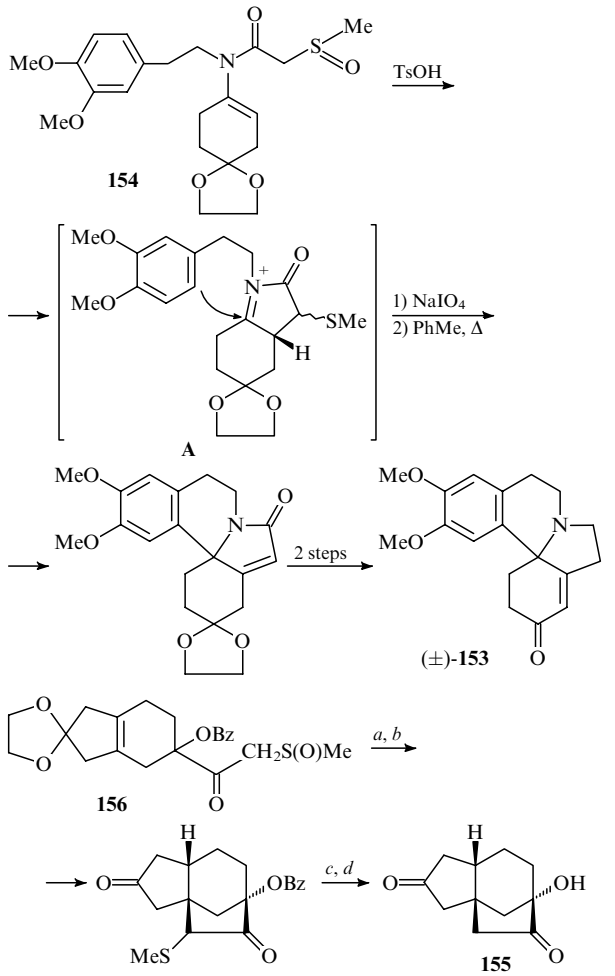

(*a*) $(CF_3CO)_2O$; (*b*) $SnCl_4$; (*c*) Ni/Ra; (*d*) H_2, Pd/C.

In the synthesis of the key starting compound **155** for the preparation of gibberellic acid, cyclisation also proceeded through the intramolecular coupling of the sulfenium cation with the double bond of compound **156**.[98]

Ishibashi and coworkers used the intramolecular coupling of the sulfenium cation with the C=C bond in the development of a general facile procedure for the synthesis of pyrrolizidine alkaloids [99] and in the construction of the optically active (−)-trachelanthamidine (**157**) from precursor **158**.[100]

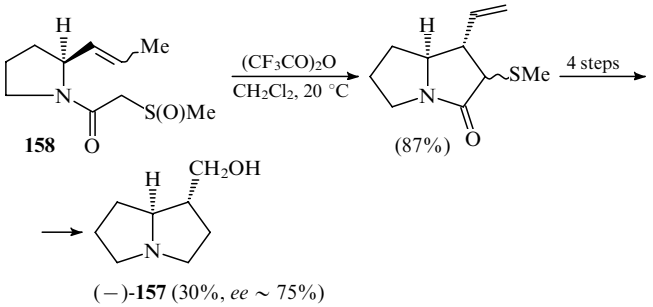

(−)-**157** (30%, *ee* ~ 75%)

Cyclisation can proceed through a Friedel–Crafts-like coupling of the sulfenium cation with the aromatic ring containing activating alkoxy groups. Thus isoquinolone alkaloids, *viz*., dimethoxymethylisocarbostyril (**159a**) and doryanine (**159b**), as well as *N*-methylcorydaldine (**160a**) and oxyhydrastinine (**160b**) were synthesised starting from common precursors **161a**,**b**.[101] The latter were prepared by the reactions of Ac_2O with alkylamides **162a**,**b**. Cyclisation of α-acetoxy sulfides **161a**,**b** under the action of TsOH afforded alkaloids **159a**,**b**, whereas treatment of the compounds **161a**,**b** with CCl_3CO_2H gave rise to intermediates **163a**,**b**, which were subjected to desulfurisation to form the compounds **160a**,**b**.

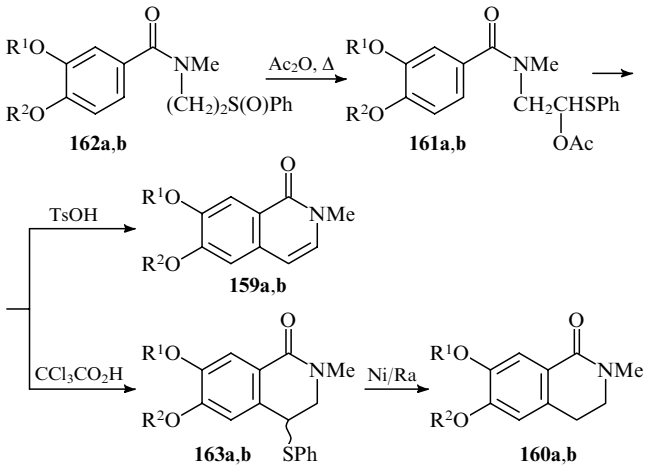

$R^1 = R^2 = Me$ (**a**), $R^1 - R^2 = CH_2$ (**b**).

Analogous procedures were used for the preparation of the tetrahydroisoquinoline alkaloid hydrohydrastinine from the corresponding aromatic amino sulfoxide [102] and for the facile synthesis of the polycyclic alkaloid chilenine (**164**),[103] the seven-membered ring of the latter being constructed upon cyclisation of precursor **165**.

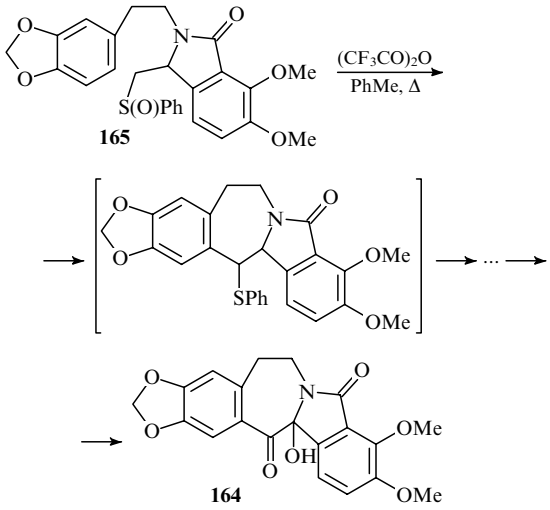

(+)-Aphanorphine (**166**), which exhibited specific optical rotation identical to that of the natural alkaloid, was synthesised [104] from optically active sulfinyl-substituted lactone **167**. The Pummerer reaction was accompanied by cyclisation to yield a

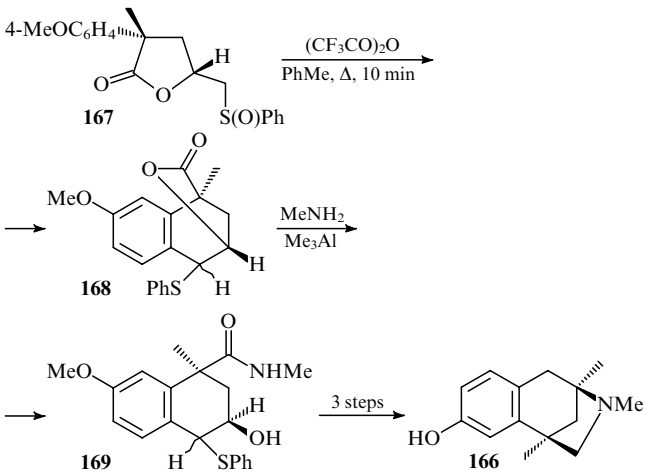

mixture of enantiomeric lactones **168**. The lactone-ring opening was performed under the action of methylamine and the resulting bicyclic intermediate **169** was converted into the target alkaloid **166** in three steps.

The short synthesis of gymnopusin (**170**),[105] which is the first representative of natural phenanthrenes with the oxygen-containing substituent at the C(10) atom, provides yet another example. It should be noted that the results of this synthesis proved the structure of natural gymnopusin.

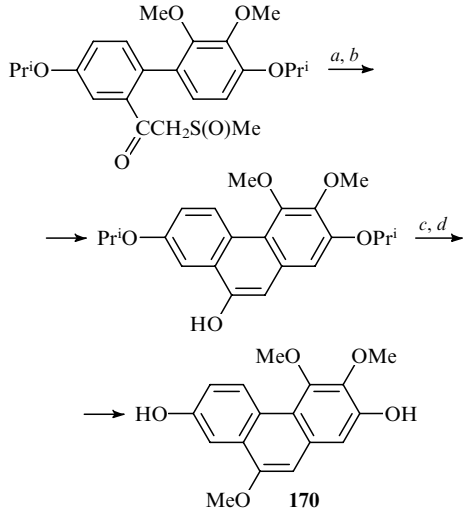

(*a*) $(CF_3CO)_2O$; (*b*) Na/NH_3; (*c*) $(MeO)_2SO_4$, $CaCO_3$; (*d*) BCl_3, CH_2Cl_2.

Oxygen-containing groups can also be involved in intramolecular coupling with the sulfenium cation to form oxacycles. Thus the involvement of the aldehyde group of sulfinyl-substituted α,β-unsaturated aldehyde **171** in cyclisation under the conditions of the Pummerer reaction made it possible to synthesise butenolides isodrimenin (**172**) or confertifolin (**173**) *via* intermediate compounds **174** or **175** containing substituted furan rings.[106, 107] The possible mechanism of this process involves the free (under the action of Ac_2O) or hydrated aldehyde group (upon heating in aqueous dioxane in the presence of K_2CO_3) (transition states **A** and **B**, respectively).

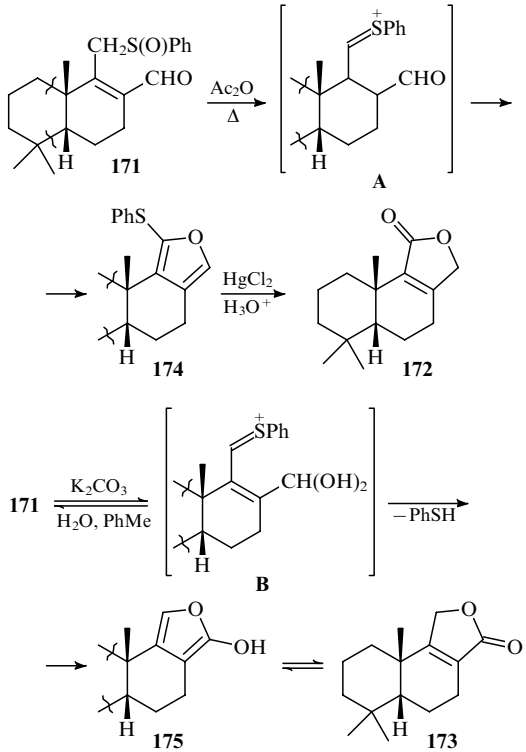

The short one-pot synthesis of furanoterpene perylene (**176**) (a component of insect communication pheromones) was carried out using the sila-Pummerer rearrangement of hydroxy-containing allyl sulfoxide **177**, which was readily derived from the adduct of β-myrcene with benzenesulfinyl chloride.[108] The authors of the cited study believed that the furan ring was generated from intermediate hydroxyaldehyde **178**.

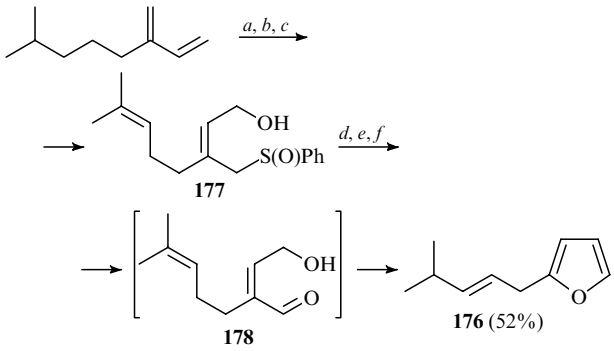

(*a*) PhSOCl, 5 kbar; (*b*) AcOK, AcOH; (*c*) H_2SO_4, MeOH; (*d*) Bu^nLi, −85 °C; (*e*) Me_3SiCl, −85 to 25 °C; (*f*) H_2O, C_5H_{12}.

The synthesis of bicyclic lactones **179a**,**b**, which are 3-normethylene analogues of avenaciolide and isoavenaciolide, respectively, provides an example of the involvement of the ester group in cyclisation of the above-mentioned type.[109] The Pummerer reaction of optically active sulfenyl-substituted ester of tetrahydrofuranocarboxylic acid **180** afforded a mixture of diastereomeric bicyclic compounds **181a**,**b** in a ratio of 5 : 1. Both these compounds were converted into the target compounds **179a**,**b** in four steps.

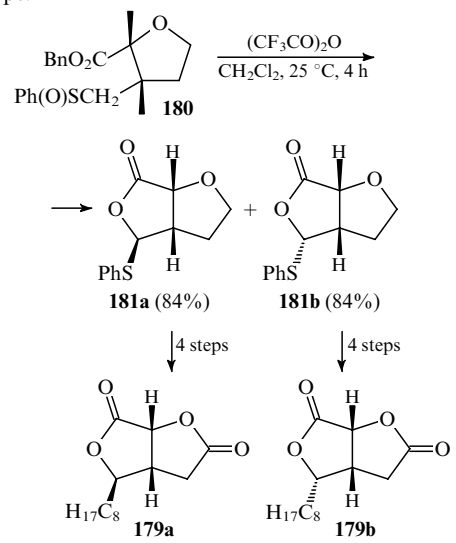

The ring closure can occur with the participation of the OH group. Optically active pyran derivative (+)-**182** serves as the common key intermediate in enantiospecific syntheses of iridoid monoterpenes. This derivative was prepared[110] from bicyclic lactone **183** containing the required chiral centres. The compound **183** was converted into sulfide **184** by reactions in which the latter centres remained intact. Oxidation to sulfoxide and cyclisation, which occurred through the Pummerer reaction involving the enol hydroxy group, gave rise to compound **185** in which the SPh group was replaced by OMe. The methylacetal of iridoid aglycone sweroside **186** was prepared from the compound **182** in six steps.

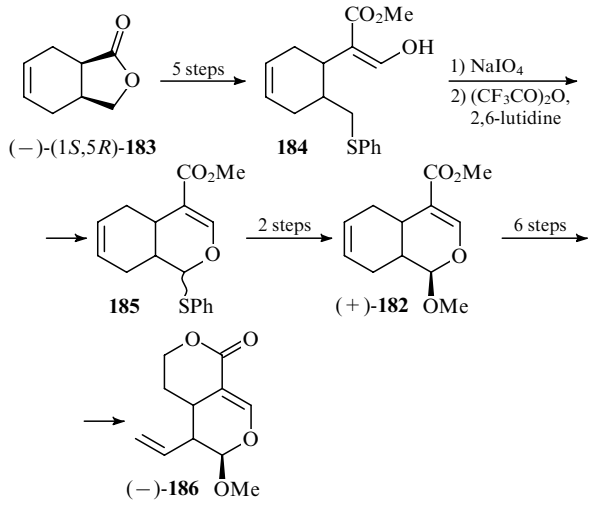

To construct the seven-membered oxathiazepine ring involved in the L-eudistamine molecule (**187**),[111] which shows activity against *Herpes simplex*, the Pummerer reaction was carried out with the use of intermediate **188** in the course of which the sulfenium ion was coupled with the adjacent N—OH group.

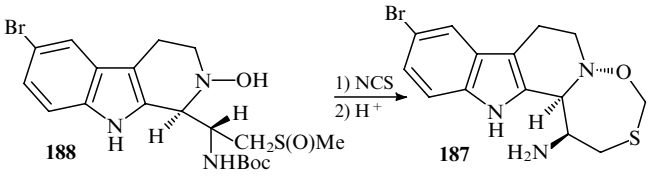

NCS is *N*-chlorosuccinimide.

The Pummerer reaction was used in the chemistry of penicilins and related biologically active lactams. This reaction allows one to convert rather inactive sulfoxides of the penam series into penem derivatives exhibiting high biological activities (see, for example, Refs 112 and 113).

The most interesting results were obtained on cyclisation of β-amido sulfoxides in which intramolecular coupling of the sulfenium cations with the nitrogen atom of the imino group occurred to form substituted lactams. Thus Kaneko [114] was the first to perform intramolecular cyclisation in mild conditions of the sila-Pummerer reaction under the action of silyl trifluoromethanesulfonate on β-amidosulfoxides **189a–d** and obtained 4-arylthio-substituted lactams **190a–d**. Kaneko demonstrated that the compound **189c** containing one β-alkyl substituent produced predominantly *cis*-3,4-disubstituted lactam **190c**, whereas enantiomerically pure precursors, *viz*., (*R*)- or (*S*)-**189d**, yielded optically active (*R*)- or (*S*)-lactams **190d** with *ee* ~ 67% (see Ref. 115).‡ These results provided supporting evidence for the assumption as to the correlation between the mechanism of the

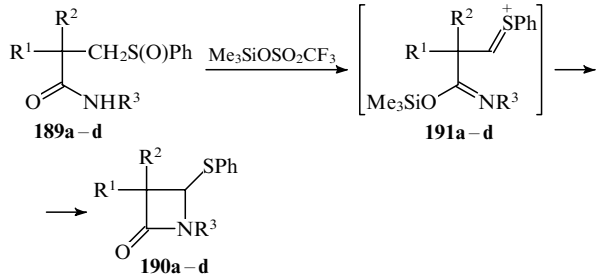

$R^1 = R^2 = Me$, $R^3 = OBn$ (**a**); $R^1 = R^2 = H$, $R^3 = OBn$ (**b**); $R^1 = Me$, $R^2 = R^3 = H$ (**c**); R^1, R^2, $R^3 = H$ (**d**).

‡ Unfortunately, the absolute configurations of the compounds used in the investigation [115] were not established.

Pummerer reaction (involving sulfenium intermediate **191**) and the first stage of the biosynthesis of lactam antibiotics.

Kita and coworkers made a considerable contribution to the solution of the problems associated with the synthesis of β-lactams. The authors demonstrated that nitrogen heterocycles containing the thio group in the α position can be readily synthesised with the use of versatile silylating agents, *viz*., silyl ketene acetals.[116] This methodology was first examined for the Pummerer cyclisation of ω-amido sulfoxides to obtain intermediates utilised in the synthesis of pyrrolizidine and indolizine alkaloids.[117] Later on, this procedure was extended to the synthesis of β-lactam carbapenems starting from ω-amido sulfoxides.[118] 4-(Arylthio)-azetidin-2-ones **192**, which were prepared by the reactions of methyl(trimethylsilyl) ketene acetal with amido sulfoxides **193**, were used as the starting compounds. The compounds **192** were oxidised to sulfoxides **194**. Under the action of the same ketene acetal, the latter compounds were transformed into *trans*-disubstituted azetidin-2-ones containing ester groups at the C(4) atom [**195**, the ratio *trans*:*cis* = (89–95):(5–11)], which are the key precursors in the synthesis of β-lactam antibiotics, carbapenems. This procedure was employed for the preparation of racemic carbapenem PS-5 (**196**)[119] and β-methylcarbapenem.[120] The enantioselective synthesis of thienamycin was carried out starting from enantiomerically pure β-amido sulfoxide of the type **193**.[121]

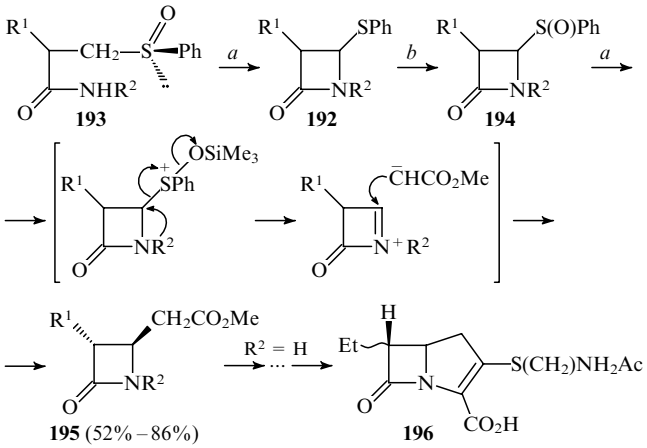

(*a*) 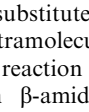 , ZnI_2 (cat), MeCN, 20 °C, (*b*) oxidation.

Kita *et al*.[122] demonstrated that (*S*)-(tolylthio)lactams **198a–d** (*ee* 82%–83%) can be prepared in high yields starting from optically active β-amido sulfoxides, for example, from (*R*)-**197a–d**, whereas the corresponding (*R*)-lactams can be prepared with high enantioselectivity from (*S*)-**197a–d**. Hence, the authors of the cited study not only improved the enantioselectivity of this reaction compared to the method proposed by Kaneko,[114] but also proved unambiguously that cyclisation was accompanied by the transfer of the asymmetric centre from the sulfinyl group to the C(4) atom of the lactam ring.

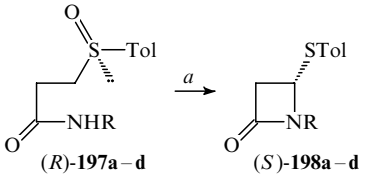

R = MeCHPh (**a**), Bn (**b**), $CHPh_2$ (**c**), 2-$BrC_6H_4CH_2$ (**d**);

(*a*) 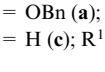 , ZnI_2 (cat), MeCN, 20 °C.

The mechanism of the first stage of the biosynthesis of penicillins consisting in the construction of the *cis*-disubstituted lactam ring by oxidative cyclisation of the tripeptide δ-(L-α-

aminoadipyl)-L-cysteinyl-D-valine (**199**) (LLD-ACV, which was assumed [123] as the direct precursor of isopenicillin N), has long been unknown.

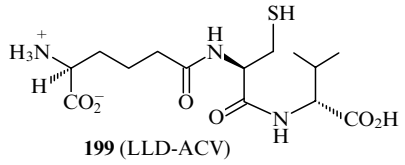

199 (LLD-ACV)

Under the conditions of the sila-Pummerer reaction, amido sulfoxides **200a**,**b**, which contain substituents analogous to those in the compound **199**, were demonstrated [124] to give predominantly *cis*-disubstituted lactams **201a**,**b**. This fact was seemingly evidence in favour of the possible occurrence of the Pummerer sulfenium intermediate in the first stage of the biosynthesis of penicillins.

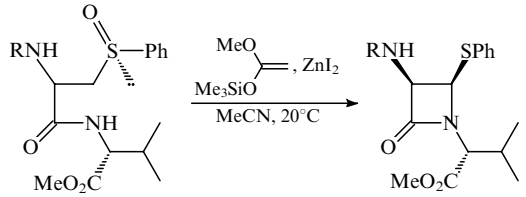

(*R*)-**200a**,**b** *cis*-**201a**,**b**

R = BnO_2C (**a**); BnO_2CHN (**b**).

However, the results of the recent investigation performed by Baldwin and coworkers [125] gave conclusive evidence that the biosynthesis of penicillins takes quite a different path. The key stage of this process involves the attack of the Fe-activated enzyme IPNS on the thiol group of LLD-ACV (**199**). When analysing this problem, Shibata and Kita [126] admitted that their strategy [124] has not elucidated the mechanism of the biosynthesis of penicillins, but led to substantial improvement in Pummerer-type asymmetric cyclisation and in the Pummerer reactions of nonracemic sulfoxides. In earlier studies (see the review [14]), high asymmetric induction was not achieved and *ee* was at most 30%.

5. Syntheses involving additive Pummerer reactions

The most interesting results in the field of the asymmetric synthesis of natural compounds were obtained with the so-called additive Pummerer reaction (primarily using the procedure proposed by Marino). These investigations have been considered in detail in a previous review [14] and hence, they are only briefly outlined in the present review .

The mechanism of the additive Pummerer reaction involves the initial attack of electrophilic dichloroketene, which is prepared *in situ* by the reaction of the zinc–copper pair with trichloroacetyl chloride, on the sulfinyl oxygen atom [127, 128] as exemplified below

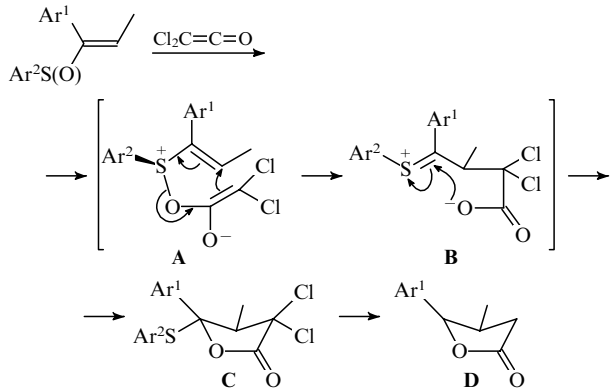

by disubstituted vinyl sulfoxide. Then the zwitterionic intermediate **A** is converted into the Pummerer sulfenium-cationic intermediate **B** through the [3,3]-sigmatropic rearrangement involving the vinyl C=C bond. The intermediate **B** is stabilised through the intramolecular reaction with the carboxylate anion to give 3-arylthio-5,5-dichloro-γ-lactone **C**.

After dechlorination and desulfurisation, 3,4-disubstituted lactone **D** is obtained. The configurations of the chiral centres in the latter compound are completely controlled by the configuration of the chiral sulfinyl group in the initial vinyl sulfoxide. The synthesis of the key precursor of the neolignane porosin **202** starting from (*S*)-(dimethoxyphenyl)prop-1-enyl tolyl sulfoxide (**203**) [128] is an example of the additive Pummerer reaction. Thiosubstituted dichlorolactone **204**, which was obtained in high yield, was dechlorinated with aliminium amalgam to obtain lactone **205**. The latter was desulfurised with freshly prepared Raney nickel at 0 °C. The resulting enantiomerically pure γ-lactone **206** was converted into the target compound (3*S*,4*R*)-**202** in two steps.

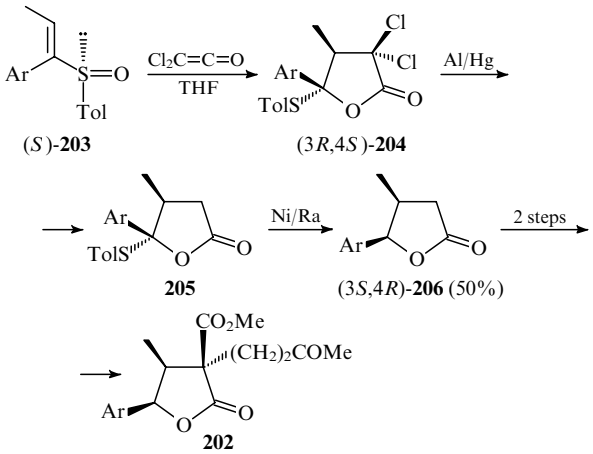

(*S*)-**203** (3*R*,4*S*)-**204**

205 (3*S*,4*R*)-**206** (50%)

202

Ar = 3,4-$(OMe)_2C_6H_3$.

Separation of the dechlorination and desulfation stages is important for a successful synthesis. For example, the synthesis of oak lactones **207** from (*E*,*R*)-3-(tolylsulfinyl)hept-2-ene (**208**),[127] which involved one-step dechlorination–desulfurisation of lactone **209** under the action of tributylstannane, afforded the final product as a mixture of enantiomers.

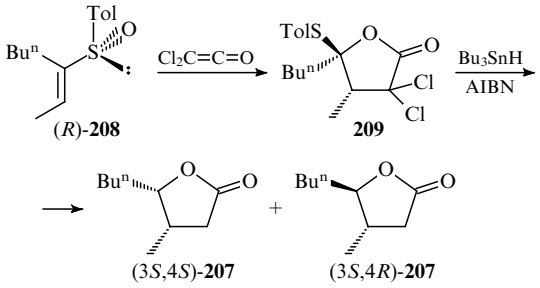

(*R*)-**208** **209**

(3*S*,4*S*)-**207** (3*S*,4*R*)-**207**

AIBN is azodiisobutyronitrile.

The additive Pummerer reactions can be performed with various nonracemic α,β-unsaturated sulfoxides. Thus lactone (+)-(*R*)-**212**, which is the key intermediate in the syntheses of a broad spectrum of lignane lactones, was derived from (*Z*,*R*)-piperonylvinyl sulfoxide (**210**) *via* lactone **211**.[129]

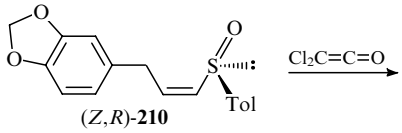

(*Z*,*R*)-**210**

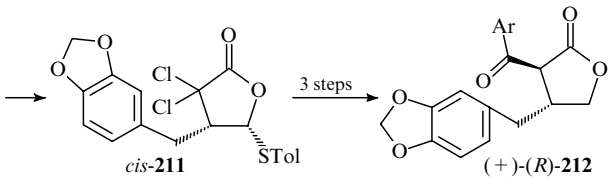

cis-**211** (+)-(*R*)-**212**

Ar = 3,4,5-$(OMe)_3C_6H_2$.

In the synthesis of (−)-physiostigmine (**213**) (the alkaloid used for the treatment of glaucoma), the reaction pathway was found to depend on the electronic and steric characteristics of the sulfinyl group and on the bulkiness of the protecting group at the nitrogen atom of the initial 2-sulfinylindole.[130] 5-Benzyloxy-3-methyl-2-(isopropylsulfinyl)indole [(*S*)-**214**] containing the protecting Boc group at the nitrogen atom proved to be the starting compound of choice. The reaction involving the above reagent proceeded through the tricyclic adduct with dichloroketene **215** to yield (−)-physiostigmine [(−)-**213**] exhibiting specific optical rotation identical to that of the natural compound.

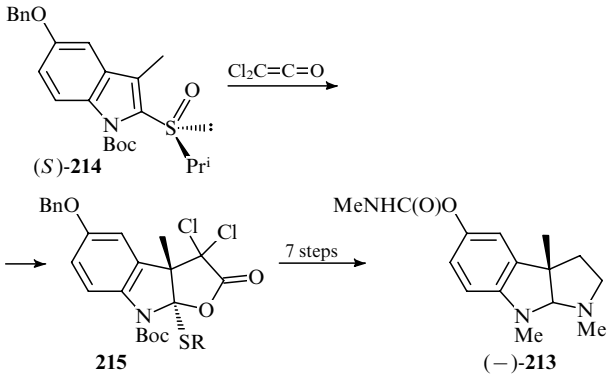

(*S*)-**214** **215** (−)-**213**

Sulfinyl-substituted triene **216** is an example of polyunsaturated sulfinyl precursors. This compound was utilised in the synthesis[131] of drimane-type sesquiterpenoids (+)-fragolide (**217**) and (+)-pereniporin (**218**). The process began with the addition of dichloroketene and the construction of *p*-tolylthiodichloro-γ-lactone fragment in compound **219**. The subsequent multistage transformation involved dechlorination and desulfurisation along with cationic cyclisation with the participation of the vinylsilane group.

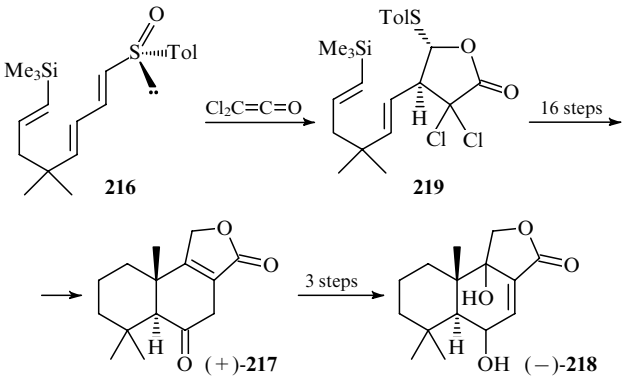

216 **219**

The advantages of the additive Pummerer reaction are the possibile subsequent transformations of primary γ-lactones, which can be used in enantioselective syntheses of compounds with various structures. For example, in the facile synthesis of the pheromone with the linear structure, *viz*., (7)-(4*S*,6*S*,7*S*)-serricornin (**220**),[132] starting from (*E*,*R*)-3-(tolylsulfinyl)pent-2-ene (**221**), γ-lactone **222** was converted into the key intermediate, *viz*., 4,5-disubstituted valerolactone **223**, with retention of the chiral centres.

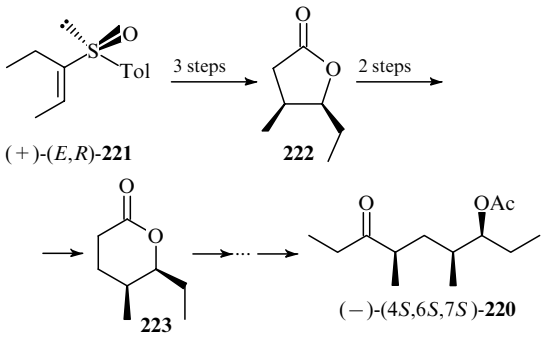

(+)-(*E*,*R*)-**221** **222** **223** (−)-(4*S*,6*S*,7*S*)-**220**

The product of the Pummerer reaction of β,β-disubstituted vinyl disulfoxide (*R*)-**224** with dichloroketene was dechlorinated *in situ* and then converted into 4,4-disubstituted cyclohexenone **225**, which was the key compound in the synthesis of the alkaloid (+)-mesembrin [(+)-**226**].[133]

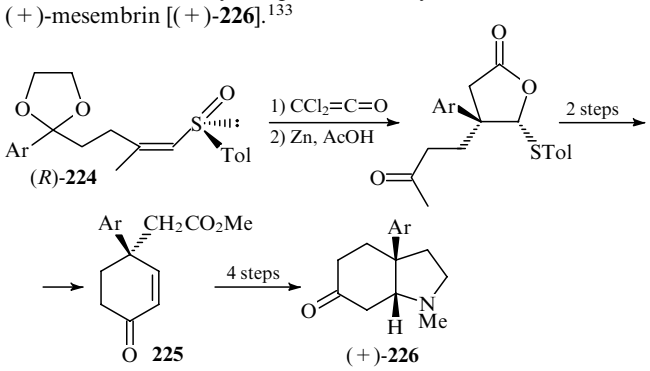

(*R*)-**224** **225** (+)-**226**

Ar = 3,4-$(OMe)_2C_6H_3$.

Marino's procedure does not exhaust the synthetic possibilities of the additive Pummerer reaction. Iwata *et al.*[134] found that α,β-unsaturated sulfoxides, including cyclic sulfoxides, underwent the Pummerer-like reaction under the action of allylmagnesium bromide and applied this reaction to the enantioselective total synthesis of (−)-sibirine (**227**).[135] The monoallylation product **228** of cyclohexene sulfoxide (−)-(*S*)-**229**, which was readily separated from diallylated compound **230**, already contained the chiral quaternary carbon atom characteristic of (−)-sibirine **227**. The latter was prepared by a multistage transformation; its specific optical rotation corresponded to that of the natural alkaloid.

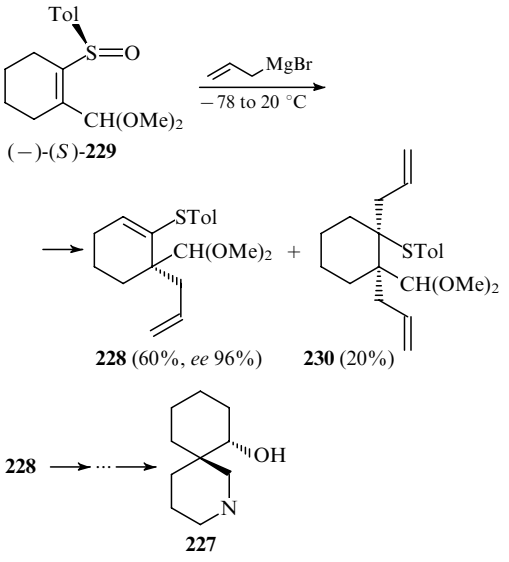

(−)-(*S*)-**229** **228** (60%, *ee* 96%) **230** (20%) **227**

An analogous methodology was employed in the facile synthesis of the spirocyclic alkaloid (−)-perhydrohistrionicotoxin, which also contains the quaternary chiral centre.[136]

6. Syntheses based on cascade processes involving the Pummerer reaction

Examples of application of cascade processes involving the Pummerer reaction to syntheses of natural products were considered above. It should be noted that Padwa and coworkers have obtained particularly impressive results in recent years.[12, 137–139]

The tandem use of the Pummerer and Diels–Alder reactions made it possible to develop a versatile procedure for the construction of polycyclic molecules. Thus treatment of sulfinylmethyl-substituted diaryl ketone **231** with acetic anhydride and then with dimethyl maleate afforded [137] adduct **232** of the initially formed Pummerer-reaction product, *viz*., α-ethylthioisobenzofuran **233**, in high yield. Simple transformations of the adduct **232** gave rise to natural lactones of the naphthalene series, *viz*., taiwanin **234** and justicidin E **235**.

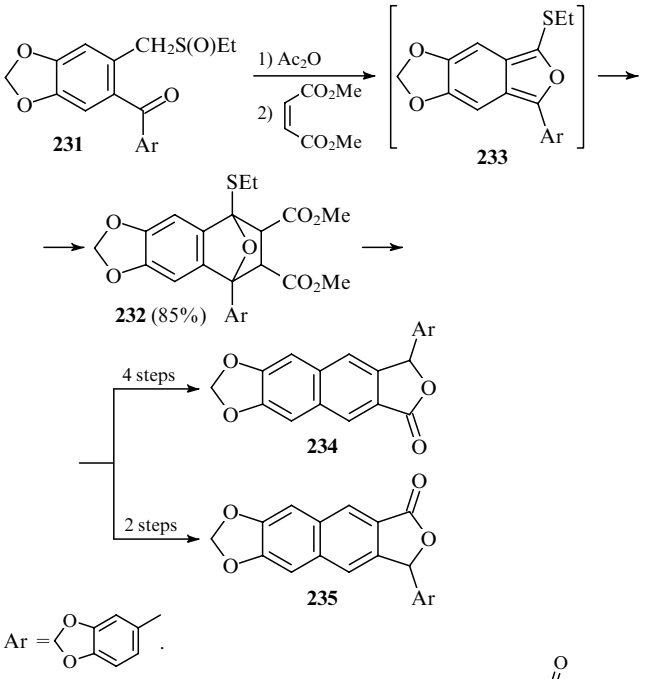

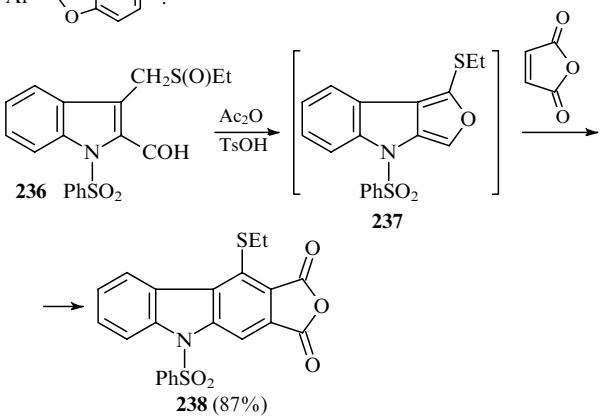

Kappe and Padwa [138] used *o*-formyl-substituted indole sulfoxide **236** as the starting compound. After the Pummerer reaction, the primary cyclisation product **237** was treated (without isolation) with maleic anhydride to obtain carbazole derivative **238** in high yield. This method can be used for the construction of natural carbazoles, for example, of ellipticine.[12]

The one-pot synthesis of the five-membered cyclic skeleton of the alkaloid erythrinane is a particularly elegant cascade procedure.[139] For this purpose, compound **239**, which was derived from polysubstituted aromatic sulfoxide **240** under the action of Ac_2O in the presence of a catalytic amount of TsOH, was heated with an additional amount of TsOH. The process involved an intramolecular Diels–Alder reaction giving rise to adduct **241** followed by the oxabicycle opening yielding product **242** and, finally, cyclisation of the latter involving the *N*-acyliminium ion to give 3,4-benzoerythrinane **243** (the total yield was 70%). Padwa *et al*.[139] noted that the tandem process proceeded more or less readily depending on the reaction conditions. The best results were obtained with the use of Ac_2O in toluene in the presence of catalytic amounts of TsOH, which efficiently suppressed the formation of acetoxy sulfide (a normal product of the Pummerer reaction).

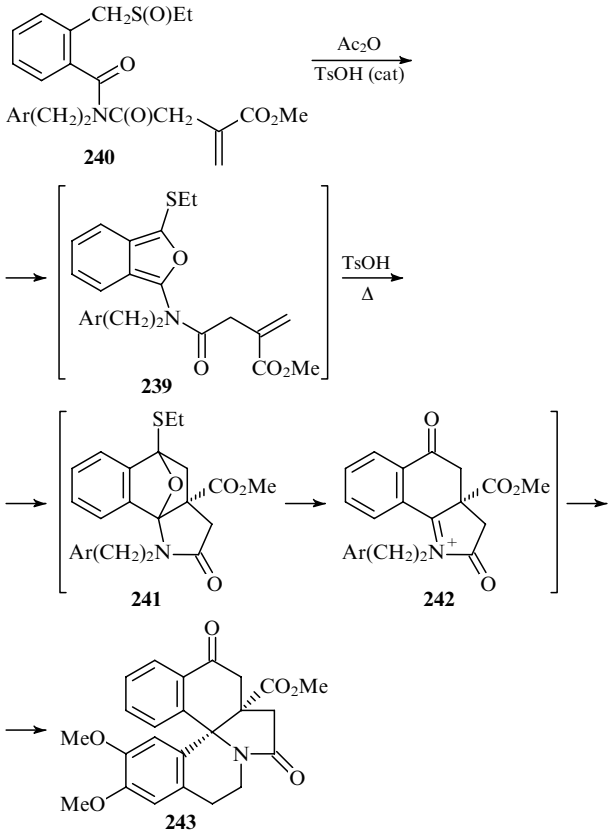

Ar = 3,4-$(MeO)_2C_6H_3$.

IV. Use of the Ramberg–Bäcklund rearrangement for the insertion of C=C bonds

The Ramberg–Bäcklund rearrangement (see the reviews [3, 141, 142]), which is the oldest reaction [140] of all known sulfonyl rearrangements, proceeds with the participation of sulfones of type **244** containing a substituent X in the α position as substrates. The substituent can be readily removed in the anionic form once carbanion **245** is generated through α-deprotonation. The mechanism of the process was confirmed by the results of numerous kinetic studies (see the review [3]).

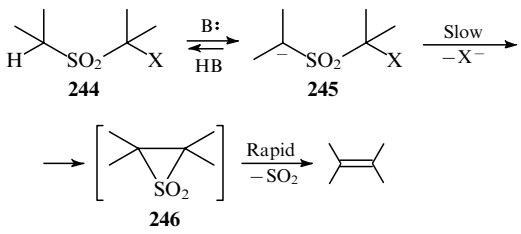

The reaction gives rise to the C=C bond in the strictly fixed site of the molecule through the formation of episulfone **246**, which readily eliminates SO_2. The involvement of the intermediate **246** in the rearrangement was long judged from indirect evidence. Recently, episulfones, which are stable only below −20 °C, were prepared by the reactions of Bu^tOK with some highly reactive α-iodosulfones primarily of the thiolane 1,1-dioxide series.[143]

The Ramberg–Bäcklund reactions are traditionally carried out with the use of α-Cl and α-Br-substituted sulfones as the starting compounds. Halogenation with soft reagents, for example, with *N*-halogenosuccinimides, is often performed at the stage of the initial sulfide before its oxidation to sulfone.

Meyers *et al.*[144] devised a convenient modification of this reaction, which allowed the one-pot preparation of α-chlorosubstituted sulfone and its subsequent rearrangement. In this version, sulfone was treated with powdered KOH in CCl_4–Bu^tOH. Unfortunately, this reaction is sometimes complicated by side processes, such as excessive halogenation or formation of chlorocarbene. To prevent these side reactions, Chen *et al.*[145] used KOH adsorbed on Al_2O_3 in Bu^tOH in the presence of CBr_2F_2, which does not generate carbenes.

The Ramberg–Bäcklund reaction is actually a versatile procedure for the construction of the C=C bond; the configuration of the latter depends both on the structure of the initial sulfone and the reaction medium; in open-chain compounds, the resulting bond generally has the *E* configuration. The synthetic importance and applications of this reaction were covered in reviews.[141, 142, 146] However, the data on use of this process in syntheses of natural compounds is systematised for the first time in the present review.

Examples of the construction of isolated C=C bonds in open-chain natural compounds or in linear fragments of more complex molecules are considered below. Thus the Bu^tOK-induced rearrangement of α-chlorosulfone was used in the highly *E*-stereoselective synthesis of Δ^{22}-unsaturated steroids of types **247a**,**b** starting from sulfides **248a**,**b**, which were prepared based on 3α,5α-cyclo-6β-methoxypregnane.[147] The structure of the compound **247a** was proved by its conversion into the known steroid **249a**. This synthesis was carried out in view of the fact that many exotic steroids from plants and animals contain unsaturated side chains.

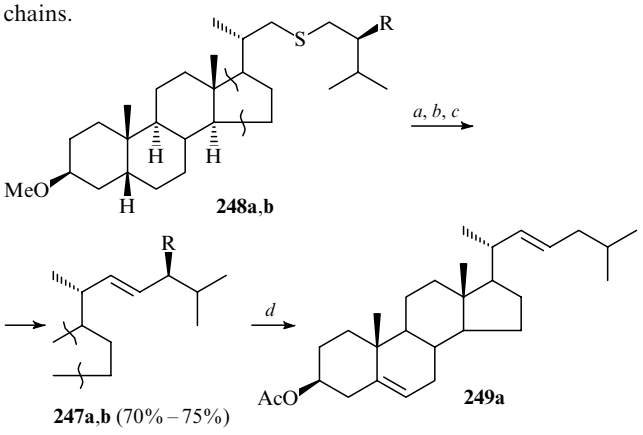

R = H (**a**), Et (**b**); (*a*) NCS, CCl_4; (*b*) MCPBA, $NaHCO_3$; (*c*) 3 equiv. of Bu^tOK; (*d*) R = H, $Zn(OAc)_2$, AcOH.

Non-6-en-1-ol (**250**), which is a pheromone of Mediterranean fruit flies,[148] was synthesised with the use of the rearrangement of linear α-bromosulfone **251**, which was prepared by the reaction of 2-(*n*-propylsulfonyl)cyclohexanone (**252**) with bromine and NaOH. This reaction provided the basis for a general procedure for the synthesis of α-bromosulfones. The scheme of the synthesis ended in reduction of the carboxyl group to the alcoholic group in the initially formed non-6-enoic acid.

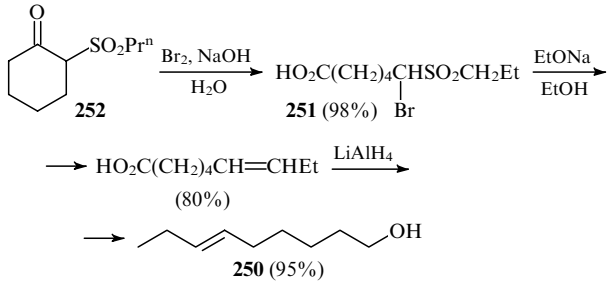

The short synthesis of natural artemisia ketone (**253**) (the total yield was 86%) starting from methyl trifluoromethylsulfonylmethyl sulfone (**254**) demonstrated that the triflate fragment is an excellent leaving group in the Ramberg–Bäcklund reaction. The rearrangement of ketosulfone **255**, which was prepared by alkylation followed by acylation of the sulfone **254**, was carried out at room temperature under conditions of phase transfer catalysis.[149]

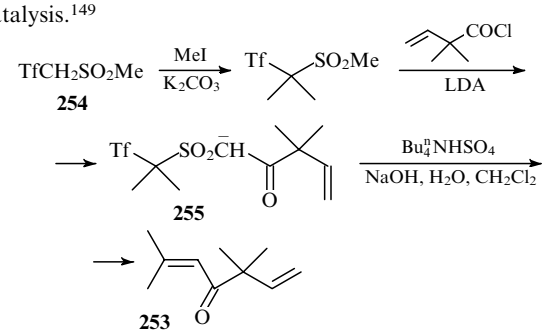

Tf = CF_3SO_2; LDA is lithium diisopropylamide.

Polyenes, including those containing conjugated C=C bonds, can be constructed by the Ramberg–Bäcklund rearrangement starting from substituted diallyl sulfones. In an early study,[150] sulfones **256a**–**d** were used for this purpose. It appeared that treatment of the sulfones **256a**–**c** with KOH and CCl_4 at room temperature afforded mixtures of stereoisomeric polyenes **257a**–**c** in high yields, whereas the retinyl sulfone **256d** did not enter into the reaction under these conditions. To prepare a mixture of polyenes from the latter compound, it was successively treated with butyllithium (it was assumed that dianion **258** was formed) and halogen. Isomerisation of a mixture of the compounds **257d** under the action of iodine or upon heating gave rise to natural all-*trans*-β-carotene (**259**).

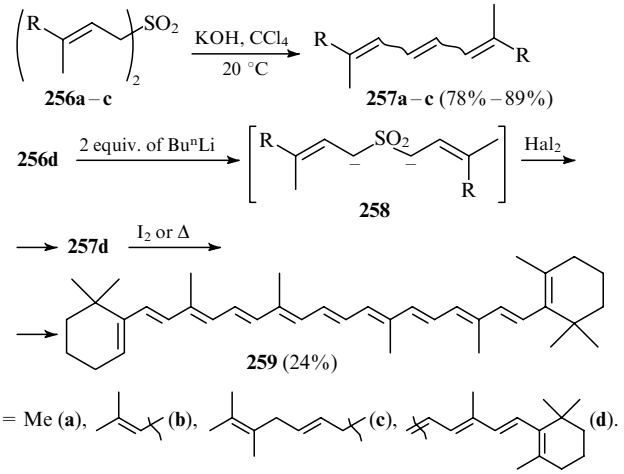

R = Me (**a**), (**b**), (**c**), (**d**).

Later, mixtures of substituted polyisoprenoids **261a**–**c** were obtained from diallyl sulfones **260a**–**c** containing polar substituents Z according to Meyers's procedure.[151]

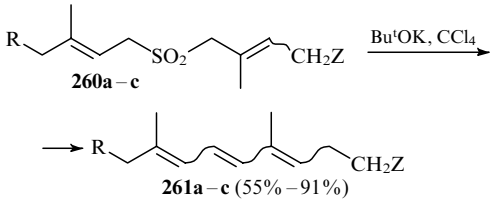

R = H, ; Z = OEt (**a**), CH_2COMe (**b**), $CH_2C(Me)(OH)CH=CH_2$ (**c**).

The synthesis of natural undecatrienes **262** and **263** and undecatetraenes **264** and **265** (the compounds **262** and **263** find use in perfumery) from the corresponding diallyl sulfones according to Meyers's procedure [152] also afforded mixtures of geometric isomers.

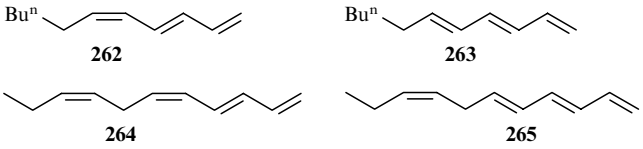

Burger *et al.* [153] failed to elaborate the stereoselective synthesis by decreasing the basicity of the reaction medium through the generation of the required anion by the addition of the sulfinate anion to α-halogenovinyl- (**266**) or butadienyl sulfones **267** [the so-called MIRB process (Michael Induced Ramberg–Bäklund)]. Starting from sulfones **268** and **269**, this procedure also yielded mixtures of stereoisomeric isoprenoinds.[153] The authors of the cited studies [150, 151, 153] did not examine the mechanisms of these processes. Hence, the stage at which *Z*-bonds are formed in the syntheses starting from all-*trans* compounds remains unknown.

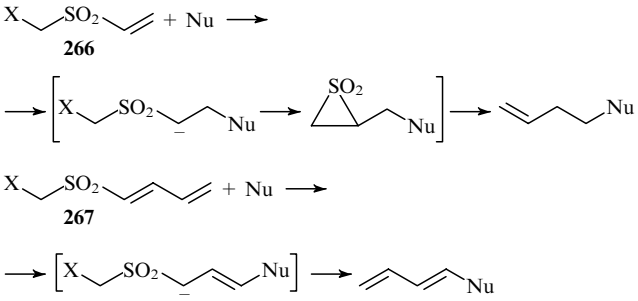

Nu = SO_2Ph; X = Cl, Br.

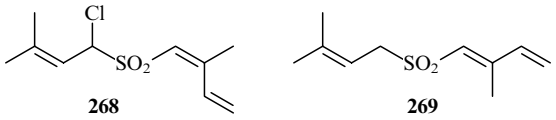

Recently, the problem of the construction of all-*trans*-polyene through the Ramberg–Bäcklund rearrangement has been successfully solved [154] in the synthesis of natural β-carotene **259**, which (along with its analogues) is finding increasing use as a food ingredient possessing simultaneously chemotherapeutic activity against some varieties of cancer. The scheme of the synthesis was based on alkylation of readily accessible sulfone **270** with dichlorodiallyl sulfide, which was prepared from isoprene in four steps. In the alkylation stage, NaI was added to the reaction mixture to form *in situ* more reactive iodide. Then intermediate **271** was converted into sulfone **272** and the latter was subjected to the rearrangement into compound **273** under very mild conditions (oxidation with peroxyphthalic acid formed *in situ* and Meyers's rearrangement under an atmosphere of argon). The sulfonyl groups were removed from the intermediate **273** by reduction. Starting from isoprene, β-carotene **259** (all-*trans*) was obtained in a total yield of 13%. Judging from the results obtained in the cited study, the Ramberg–Bäcklund rearrangement of the sulfone **272** gave rise exclusively to the (*E*)-C=C bond. The presence of sulfonyl groups in the radical R prevents isomerisation of the already existing (*E*)-C=C bonds.

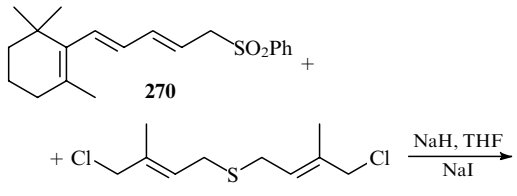

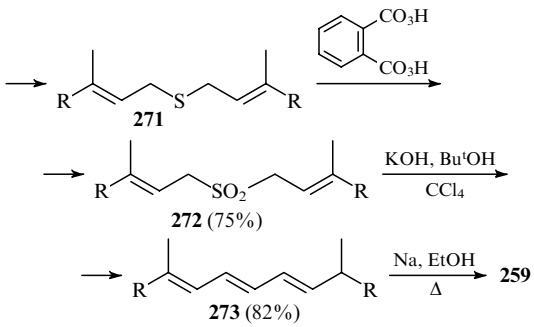

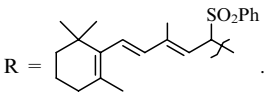

This procedure can also be used for the construction of other natural all-*trans*-polyenes. Thus, this procedure was employed [154] for the preparation of key intermediate **274** in the synthesis of carotenoids by the Wittig method.

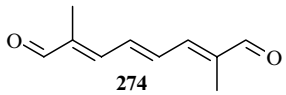

In his review, Paquette [141] emphasised that the construction of unsaturated rings of different sizes is one of the problems, which can be solved by applying the Ramberg–Bäcklund rearrangement. Examples of the use of this rearrangement in the synthesis of natural compounds are the preparation of both unsaturated carbocycles and oxygen-containing heterocycles.

In the study,[155] the cyclopentene ring in steroid **275** was formed starting from tetracyclic α-chloro-substituted sulfone **276**, which was synthesised in two steps from the adduct of diene **277** and 2,3-dihydrothiopyran-4-one *S*,*S*-dioxide (**278**).

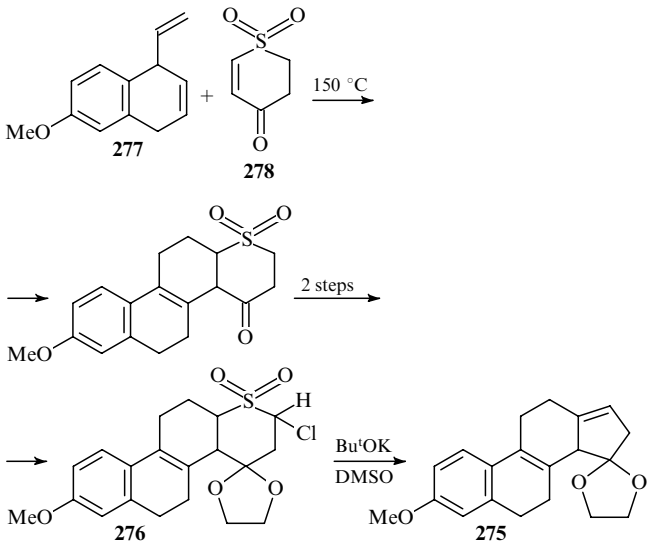

Dehydrojasmone **279** was synthesised starting from (trifluoromethylsulfonylmethyl)sulfone **254**. The latter compound was converted into cyclic ketosulfone **280** containing the triflate group, which was eliminated to give the target product **279**.[156]

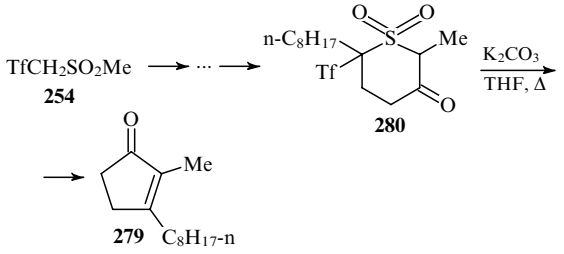

An interesting procedure was developed [157, 158] for the synthesis of enantiomerically pure cyclohexene alcohols of type **281a**–**c**, *viz*., conduritols containing four chiral alcoholic centres. These compounds are inhibitors of glycosidases and also serve as the key compounds in the preparation of agents, which show promise for AIDS treatment. These alcohols were synthesised starting from sugar derivatives containing the required chiral centres. The latter compounds were converted into thiepanes whose oxidation to sulfones followed by the rearrangement under Meyers's conditions gave rise to conduritols in high yields. This procedure was used for the preparation of (−)-conduritol E derivative (**281a**) [157] from Δ-mannitol through thiepane **282** and its sulfone **283**. All reactions proceeded in quantitative yields, the starting chiral centres remaining intact. Later, this procedure was extended [158] to the synthesis of derivatives of (−)-conduritol F (**281b**) and (+)-conduritol B (**281c**) starting from Δ-sorbitol and L-iditol, respectively. Conduritols (−)-F and (−)-E containing four unprotected hydroxy groups were obtained in 83% and 79% total yields, respectively, using readily removable benzyl instead of methyl as protecting groups.[158]

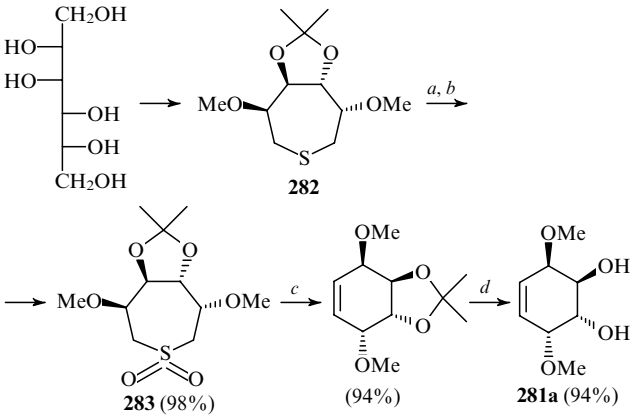

(*a*) MCPBA, 0 °C; (*b*) $Na_2S_2O_5$, CCl_4, 20 °C; (*c*) KOH, Bu^tOH, CCl_4, H_2O, 20 °C; (*d*) 0.1 N H_2SO_4.

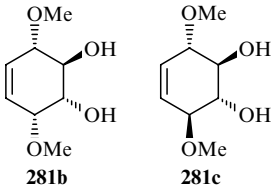

In the synthesis of the strained nine-membered oxygen-containing ring of (+)-eremantholide (**284**), which exhibits antitumour activity *in vitro*, the final stages were carried out with the use of α-chloro-substituted sulfone **285**.[159] The latter was unstable in the presence of strong bases due to which the rearrangement was performed under the action of the weakly basic alkoxide of 3-ethylpentan-3-ol. Under these conditions, intermediate **286** was obtained in quantitative yield and was converted into the final product in one step.

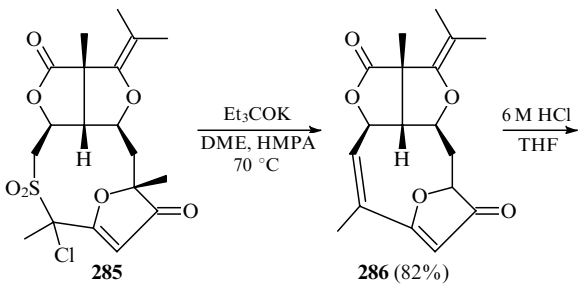

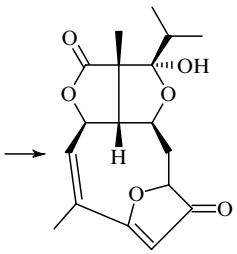

Meyers's method was successfully used [160] for the conversion of 1,4-oxathiane fragment of compound **287** (after oxidation of sulfide sulfur to sulfonyl sulfur) into the dihydrofuran fragment of compound **288**. The latter compound was converted in three steps into acetogenin (+)-solamine (**289**). This procedure is applicable to syntheses of other acetogenins possessing various biological activities.

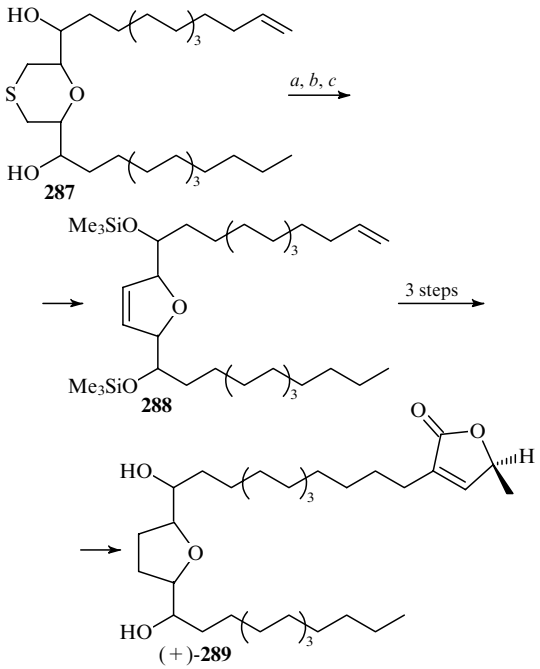

(*a*) MCPBA; (*b*) Me_3SiCl, Et_3N; (*c*) Bu^tOK, Bu^tOH, CCl_4.

In the course of the studies aimed at preparing polycyclic ciguatoxin, an efficient procedure was devised [161] for the preparation of dioxabicyclic systems. For this purpose, *trans*-fused bicyclic intermediates **290a**,**b** and **291a**,**b** generated by thioannelation were successively subjected to α-chlorination, oxidation to sulfones and rearrangement without isolation of intermediates. The resulting oxabicyclic compounds **292a**,**b** and **293a** containing

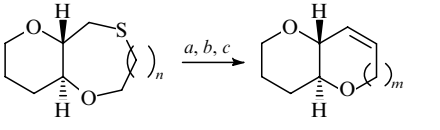

n = 2 (**290a**), 3 (**290b**); m = 1 (**292a**), 2 (**292b**).

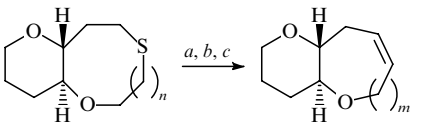

n = 3 (**291a**), 4 (**291b**); m = 2 (**293a**), 3 (**293b**).
(*a*) NCS, CCl_4; (*b*) MCPBA; (*c*) Bu^tOK, THF.

the newly formed six-, seven or eight-membered rings occurred as individual *trans*-fused molecules. Only compound **293b** with the nine-membered ring was obtained as a mixture of *cis* and *trans* isomers.

V. Conclusion

The data surveyed in the present review show that rearrangements of sulfoxides and, to a lesser extent, of sulfones find many varied applications in the total syntheses of natural compounds, including enantioselective processes.

In the coming years, one would expect the wider use of cascade processes involving these rearrangements.

The extension of tandem processes, for example, the Diels–Alder reaction followed by the sulfoxide–sulfenate rearrangement involving enantiomerically pure sulfinyl-substituted dienes, to the synthesis of natural compounds has considerable promise.[162] The SPAC cascade process, which has been developed recently (by two research groups [163, 164] virtually simultaneously) and which provides a route to the synthesis of γ-hydroxy-α,β-unsaturated sulfones, can find application in functionalisation of natural compounds.

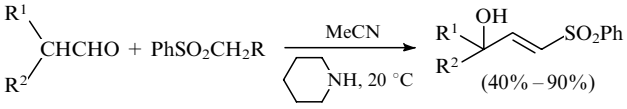

R = 4-MeC_6H_4, 4-ClC_6H_4.

In particular, Trost and Grese [164] demonstrated that this process occurred under very mild conditions, which allow the successful use of even such a labile compound, as galactose derivative **294**, as an aldehyde component.

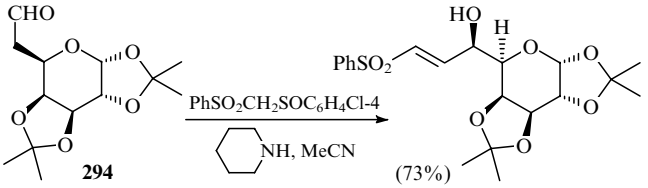

However, the reagents used in a particular stage of the tandem process must be chosen with caution. Thus attempt was made to synthesise the ethyl ester of 15-D_{2c}-isoprostane (**295**) (which belongs to compounds structurally related to prostaglandins) starting from sulfide **296** through the Mislow–Evans rearrangement.[165] Generally (see Refs 23–26), the oxidation–rearrangement tandem processes give rise to the 'lower branch' of the product with correct stereochemistry. However, the last-mentioned process afforded C(12)-,C(15)-epimer **297** rather than isoprostane **295**.

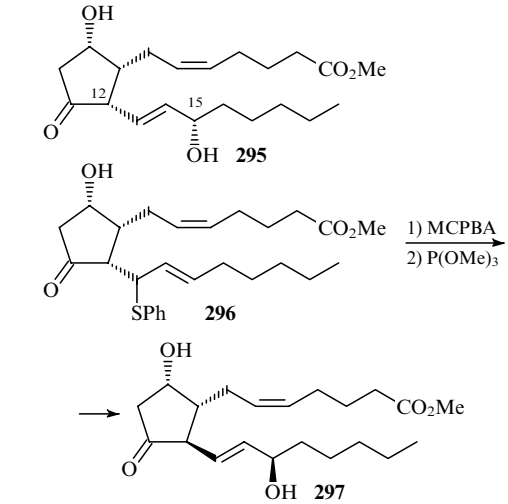

The authors believed that epimerisation was preceded by rearrangement under the action of residual amounts of *m*-chloroperbenzoic acid.

As for the Pummerer reaction, one would expect new examples of its application to the asymmetric synthesis of natural compounds both involving novel efficient inducing agents (for example, vinyl esters containing the ethoxy group in the α position proposed in recent years [166]) and by designing new reagents for the additive Pummerer process. Investigations carried out by Padwa and coworkers with the aim of devising new cascade processes hold much promise. For example, the tandem use of the Pummerer reaction and subsequent intramolecular [3 + 2]-cycloaddition has been applied.[167]

One would expect that the Ramberg–Bäcklund reaction will continue in use for the construction of unsaturated natural cyclic molecules.

It is likely that the recent cascade process,[168] which readily affords benzoannelated polycyclic molecules, will be extended to the synthesis of natural compounds. The process starts with the photochemical [6π + 4π]-cycloaddition of various dienes to the chromium tricarbonyl complex of 1,1-thiepin dioxide (**298**) and ends in the Ramberg–Bäcklund rearrangement of the resulting adduct **299**.

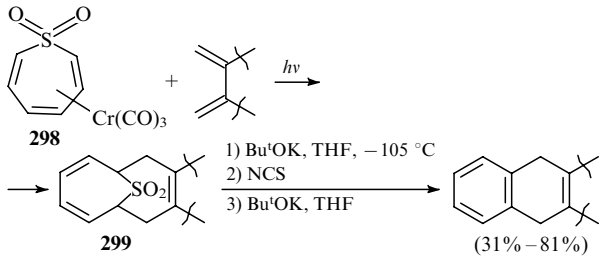

The characteristic feature of this process is that it makes possible both rapid assembly of the final polycyclic product (for example, in the synthesis of compound **300**) and the stereospecific synthesis (for example, in the synthesis of compound **301**) with the use of chiral nonracemic dienes.

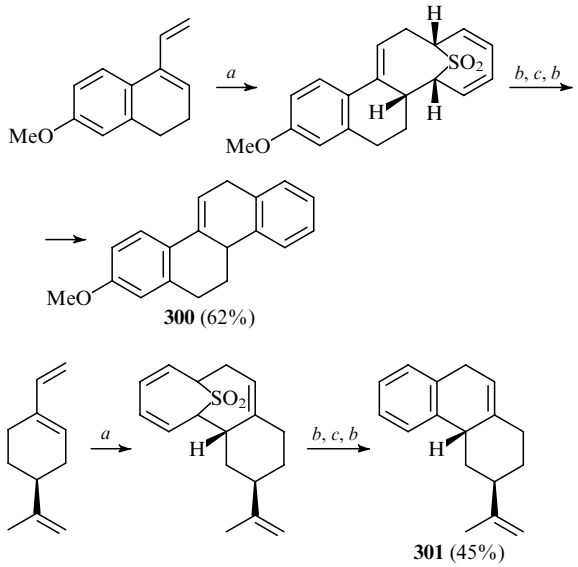

(*a*) **298**, *hv*; (*b*) ButOK, THF, −105 °C; (*c*) *N*-iodosuccinimide, THF.

The investigations published in the very recent past [169–175] (after the present review had already been written) demonstrated that the rearrangements of sulfones and sulfoxides continue in use in syntheses of natural products. The investigations of Padwa and coworkers devoted to the application of cascade Pummerer cyclisation–deprotonation–cycloaddition processes to syntheses of alkaloids were summarised in a review.[169] Intramolecular Pummerer cyclisation was used as the key stage in the synthesis of bicyclic precursors for anthracyclinones.[170] The Pummerer

reaction was employed[171] in the stereoselective synthesis of 4β-thioribonucleosides. The procedure for the construction of the oxathiazepine ring using the modified Pummerer cyclisation[111] was extended to the synthesis of (−)-eudistamines C, E, F, K and L.[172]

Other rearrangements were used more rarely. Thus the Mislow–Evans reaction was employed in the synthesis of enantiomerically pure diastereomers of 8-F_{2t} isoprostane.[173] The Ramberg–Bäcklund reaction was utilised in the syntheses of (+)-estradiol[174] and exocylcic cisoid dienes, which served as the starting compounds for the preparation of natural substances.[175]

In conclusion, it should be emphasised that rearrangements of sulfoxides and sulfones other than the above-considered three processes were also described in the literature (see, for example, the reviews [2, 3]). There is still room for progress in the applications of these reactions to syntheses of natural molecules. This review will hopefully be found interesting and useful by chemists and contribute to progress in this field of chemistry.

References

1. E N Prilezhaeva *Usp. Khim.* **69** 403 (2000) [*Russ. Chem. Rev.* **69** 367 (2000)]
2. S Braverman, in *The Chemistry of Sulfones and Sulfoxides* (Eds S Patai, Z Rappoport, C J M Stirling) (New York: Wiley, 1988) p. 717
3. S Braverman, in *The Chemistry of Sulfones and Sulfoxides* (Eds S Patai, Z Rappoport, C J M Stirling) (New York: Wiley, 1988) p. 665
4. R Pummerer *Berichte* **43** 1401 (1910)
5. L Horner, P Kaiser *Liebigs Ann. Chem.* **626** 19 (1959)
6. L Horner *Liebigs Ann. Chem.* **631** 198 (1960)
7. S Oae, T Numata, in *Isotopes in Organic Chemistry* Vol. 5 (Eds E Bunce, C C Lee) (New York: Elsevier, 1980) p. 45
8. S Oae, T Numata, T Ioshimura *The Chemistry of Sulphonium Group* (Eds C J M Stirling, S Patai) (New York: Wiley, 1981)
9. A M Moiseenkov, V A Dragan, V V Veselovskii *Usp. Khim.* **60** 1255 (1991) [*Russ. Chem. Rev.* **60** 643 (1991)]
10. O De Lucci, U Miotti, G Modena *Org. React.* **40** 147 (1991)
11. D S Grierson, H P Husson, in *Comprehensive Organic Synthesis* Vol. 6 (Eds B M Trost, J E Fleming) (Oxford: Pergamon Press, 1991) p. 910
12. A Padwa, D E Gunn Jr, M H Osterhout *Synthesis* 1353 (1997)
13. E N Prilezhaeva, in *Poluchenie i Svoistva Organicheskikh Soedinenii Sery* (Preparation and Properties of Organic Compounds of Sulfur) (Ed. L I Belen'kii) (Moscow: Khimiya, 1998) p. 209
14. M S Carreño *Chem. Rev.* **95** 1717 (1995)
15. P Bickart, F W Carson, J Jacobus, E G Miller, K Mislow *J. Am. Chem. Soc.* **90** 4869 (1968)
16. D A Evans, G C Andrews *Acc. Chem. Res.* **7** 147 (1974)
17. Y Masaki, K Sakuma, K Kaji *Chem. Pharm. Bull.* **33** 2531 (1985)
18. D K Jones-Hertzog, W L Jorgensen *J. Org. Chem.* **60** 6682 (1995)
19. T Sato, J Otera, H Nozaki *J. Org. Chem.* **54** 2779 (1989)
20. T Sato, J Otera *Tetrahedron Lett.* **35** 6701 (1994)
21. R W Hoffmann *Angew. Chem., Int. Ed. Engl.* **18** 563 (1979)
22. D R Evans, T C Crawford, T T Fujimoto, A C Thomas *J. Org. Chem.* **39** 3176 (1974)
23. D F Taber *J. Am. Chem. Soc.* **99** 3513 (1977)
24. K Kondo, T Umemoto, K Yako, D Tunemoto *Tetrahedron Lett.* 3927 (1978)
25. K Kondo, T Umemoto, Y Takahatake, D Tunemoto *Tetrahedron Lett.* 113 (1977)
26. K Bannai, T Toru, T Oba, T Tanaka, N Okamura, K Watanabe, S Kurozumi *Tetrahedron Lett.* **22** 1417 (1981)
27. J G Miller, W Kurz, K G Untch, G Stork *J. Am. Chem. Soc.* **96** 6774 (1974)
28. K Mori, H Ueda *Tetrahedron* **37** 2581 (1981)
29. Y Masaki, K Hashimoto, K Kaji *Tetrahedron Lett.* 5123 (1978)
30. Y Masaki, K Hashimoto, K Sakuma, K Kaji *Chem. Pharm. Bull.* **32** 3952 (1984)
31. Y Masaki, K Hashimoto, K Kaji *Chem. Pharm. Bull.* **32** 3959 (1984)
32. E Morera, G Octar *J. Org. Chem.* **48** 119 (1983)
33. K Tanikaga, Y Nozaki, T Tamura, A Kaji *Synthesis* 134 (1983)
34. E J Corey, P Carpino *Tetrahedron Lett.* **31** 7555 (1990)
35. J Nokami, M Ohkura, Y Dan-oh, Y Sakamoto *Tetrahedron Lett.* **32** 2409 (1990)
36. G Solladie, C Gerber *Synlett* 449 (1992)
37. J Nokami, T Taniguchi, S Gomyo, T Kakihara *Chem. Lett.* 1103 (1994)
38. K Neuschuetz, J Velker, K Neier *Synthesis* 227 (1998)
39. D A Evans, C A Bryan, C L Sims *J. Am. Chem. Soc.* **94** 2891 (1972)
40. G H Posner, A Haces, W Harrison, C M Kinter *J. Org. Chem.* **52** 4836 (1987)
41. V V Veselovskii, Z G Makarova, A I Lutsenko, N A Shapiro, V M Zhulin, A M Moiseenkov *Izv. Akad Nauk SSSR, Ser. Khim.* 810 (1988) [a]
42. M C Carreño, M B Cid, J L Garcia-Ruano, M Santos *Tetrahedron Lett.* **39** 1405 (1998)
43. M Kodama, K Shimada, S Ito *Tetrahedron Lett.* 2763 (1977)
44. B M Trost, J H Rigby *J. Org. Chem.* **43** 2938 (1978)
45. J-P Corbet, C Bezra *J. Org. Chem.* **46** 1141 (1981)
46. P J Parsons, M Stefinovic *Synlett* 931 (1993)
47. V van Reenen, K P Shephard *J. Org. Chem.* **44** 1582 (1979)
48. G Neef, U Eder, A Seeger *Tetrahedron Lett.* **21** 903 (1980)
49. A Haces, M G A van Kruchten, W H Okamura *Tetrahedron Lett.* **23** 2707 (1982)
50. H J Altenbach, H Soike *Tetrahedron Lett.* **27** 1561 (1986)
51. R A Gibbs, K Bartels, R W K Lee, W H Okamura *J. Am. Chem. Soc.* **111** 3717 (1989)
52. W H Okamura *Acc. Chem. Res.* **16** 81 (1983)
53. T Durst, in *Comprehensive Organic Chemistry* Vol. 3 (Eds D Barton, W D Ollis) (Oxford: Pergamon Press, 1979)
54. S Lane, S J Quick, R J K Taylor *Tetrahedron Lett.* **25** 1039 (1984)
55. D Craig, K Daniels, A R McKenzie *Tetrahedron Lett.* **31** 6441 (1990)
56. J P Marino, M Neisser *J. Am. Chem. Soc.* **103** 7687 (1981)
57. M A Tius, M A Terr *Synth. Commun.* **18** 1905 (1988)
58. J M Akkerman, H de Koning, H O Huisman *J. Chem. Soc., Perkin Trans. 1* 2124 (1979)
59. E J Corey, D J Hoover *Tetrahedron Lett.* **23** 3463 (1982)
60. S L Schrieber, K Satake *J. Am. Chem. Soc.* **106** 4186 (1984)
61. F M Houser, S R Ellenberger, J P Glusker, C J Smart, H L Carrell *J. Org. Chem.* **51** 50 (1986)
62. T Takai, H Kotsubo, T Koizumi *J. Chem. Soc., Perkin Trans. 1* 1667 (1991)
63. H Takayama, A Iyobe, T Koizumi *J. Chem. Soc., Chem. Commun.* 771 (1986)
64. R Baker, R B Keen, M D Morris, R W Turner *J. Chem. Soc., Chem. Commun.* 987 (1984)
65. T Mandai, K Mizobuchi, M Kawada, J Otera *J. Org. Chem.* **49** 3403 (1984)
66. T Mandai, K Kawada, J Otera *J. Org. Chem.* **48** 5183 (1983)
67. G Solladié, J Hutt, C Frechou *Tetrahedron Lett.* **28** 61 (1987)
68. G Solladié, A Almario *Tetrahedron Asymmetry* **5** 1717 (1994)
69. G Solladié, N Wilb, C Bauder, C Bonini, L Viggiani, L Chiummiento *J. Org. Chem.* **64** 5447 (1999)
70. K Konno, K Hashimoto, H Shirahama, T Matsumoto *Tetrahedron Lett.* **27** 3865 (1986)
71. K Konno, K Hashimoto, Y Ohfune, H Shirahama, T Matsumoto *Tetrahedron Lett.* **27** 607 (1986)
72. K Hashimoto, K Konno, H Shirahama, T Matsumoto *Chem. Lett.* 1399 (1986)
73. Y Tamura, H Maeda, H D Choi, H Ishibashi *Synthesis* 56 (1982)
74. H Ishibashi, M Ohnishi, T Senda, M Ikeda *Synth. Commun.* **19** 857 (1989)
75. H Ishibashi, H Komatsu, K Maruyama, M Ikeda *Tetrahedron Lett.* **26** 5791 (1985)
76. H Ishibashi, H Komatsu, M Ikeda *J. Chem. Res. (S)* 296 (1987)
77. H Ishibashi, C Uehara, H Komatsu, M Ikeda *Chem. Pharm. Bull.* **35** 2750 (1987)
78. T H Kim, K M Park *Tetrahedron Lett.* **36** 4833 (1995)
79. Y Oikawa, O Yonemitsu *J. Chem. Soc., Perkin Trans. 1* 1479 (1976)
80. P Magnus, T Gallagher, P Brown, P Pappalardo *Acc. Chem. Res.* **17** 35 (1984)
81. T Gallagher, P Magnus, J C Huffman *J. Am. Chem. Soc.* **105** 4750 (1983)
82. K Cordwell, B Hewitt, P Magnus *Tetrahedron Lett.* **28** 3303 (1987)
83. R Z Andriamialisoa, N Langlois, Y Langlois *J. Org. Chem.* **50** 961 (1985)

84. P L Feldman, H Rapoport *J. Org. Chem.* **51** 3882 (1986)
85. D Genin, R Z Andriamialisoa, N Langlois, Y Langlois *Heterocycles* **26** 377 (1987)
86. M Dardaine, N Langlois *Tetrahedron Lett.* **33** 3641 (1992)
87. M Ladlow, P M Cairns, P Magnus *J. Chem. Soc., Chem. Commun.* 1756 (1986)
88. P Magnus, T Gallagher, P Brown, J C Hoffman *J. Am. Chem. Soc.* **106** 2105 (1984)
89. P Magnus, P Brown *J. Chem. Soc., Chem. Commun.* 184 (1985)
90. P Magnus, N L Sear, C S Kim, N Vicker *J. Org. Chem.* **57** 70 (1992)
91. M Amat, J Bosch *J. Org. Chem.* **57** 5792 (1992)
92. M Amat, A Linares, J Bosch *J. Org. Chem.* **55** 6299 (1990)
93. J Catena, N Valls, J Bosch, J Bonjoch *Tetrahedron Lett.* **35** 4433 (1994)
94. M-L Bannasar, J-M Jimenez, B A Sufi, J Bosch *Tetrahedron Lett.* **37** 9105 (1996)
95. M Amat, M L Bennasar, S Hadida, B A Sufi, E Zulaica, J Bosch *Tetrahedron Lett.* **37** 5217 (1996)
96. M L Bennasar, E Zulaica, A Ramirez, J Bosch *Tetrahedron Lett.* **37** 6611 (1996)
97. H Ishibashi, T Sato, M Takahashi, M Hayashi, M Ikeda *Heterocycles* **27** 2787 (1988)
98. A Barco, S Benetti, A Casolari, S Manfredini, G P Pollini, E Polo, V Zanirato *Tetrahedron* **45** 3935 (1989)
99. H Ishibashi, K Sato, K Maruyama, M Ikeda, Y Tamura *Chem. Pharm. Bull.* **33** 4593 (1985)
100. H Ishibashi, H Ozaki, M Ikeda *J. Chem. Soc., Chem. Commun.* 654 (1986)
101. A W Lee, W H Chan, E T T Chan *J. Chem. Soc., Perkin Trans. 1* 309 (1992)
102. S Takano, H Iida, K Inomata, K Ogasawara *Heterocycles* **35** 47 (1993)
103. H Ishibashi, H Kawanami, H Irigyama, M Ikeda *Tetrahedron Lett.* **36** 6733 (1995)
104. S Takano, K Inomata, T Sato, K Ogasawara *J. Chem. Soc., Chem. Commun.* 1591 (1989)
105. A B Hughes, M V Sargent *J. Chem. Soc., Perkin Tarans. 1* 1787 (1987)
106. A de Groot, B J M Jansen *J. Org. Chem.* **49** 2034 (1984)
107. B J M Jansen, C T Bouwman, A de Groot *Tetrahedron Lett.* **35** 2977 (1994)
108. V V Veselovskii, A I Moiseenkov *Izv. Akad. Nauk, Ser. Khim.* 113 (1993) [a]
109. S D Burke, K W Jung, R E Perri *Tetrahedron Lett.* **35** 5841 (1994)
110. T Ikeda, C R Hutchinson *J. Org. Chem.* **49** 2837 (1984)
111. M Nakagawa, J-J Liu, T Hino *J. Am. Chem. Soc.* **111** 2721 (1989)
112. C U Kim, P F Misco, D N McGregor *J. Org. Chem.* **47** 170 (1982)
113. J E Baldwin, A K Forrest, S Ko, L Sheppard *J. Chem. Soc., Chem. Commun.* 81 (1987)
114. T Kaneko *J. Am. Chem. Soc.* **107** 5490 (1985)
115. T Kaneko, Y Okamoto, K Hatada *J. Chem. Soc., Chem. Commun.* 1511 (1987)
116. Y Kita, H Yasuda, O Tamura, F Itoh, Y Tamura *Tetrahedron Lett.* **25** 4681 (1984)
117. Y Kita, O Tamura, T Miki, Y Tamura *Tetrahedron Lett.* **28** 6479 (1987)
118. Y Kita, N Shibata *Synlett* 289 (1996)
119. Y Kita, N Shibata, O Tamura, T Miki *Chem. Pharm. Bull.* **39** 2225 (1991)
120. Y Kita, N Shibata, T Tojho, N Yoshida *J. Chem. Soc., Perkin Trans. 1* 1795 (1992)
121. Y Kita, N Shibata, T Miki, Y Takemura, O Tamura *Chem. Pharm. Bull.* **40** 12 (1992)
122. Y Kita, N Shibata, N Kawano, T Tohjo, C Fujimori, K Matsumoto *Tetrahedron Lett.* **36** 115 (1995)
123. J E Baldwin, M Bradley *Chem. Rev.* **90** 1079 (1990)
124. Y Kita, N Shibata, N Kawano, T Tohjo, C Fugimori, H Ohishi *J. Am. Chem. Soc.* **116** 5116 (1994)
125. P L Roach, I J Clifton, C M H Hensgens, N Shibata, C Shofield, J Hajdu, J E Baldwin *Nature (London)* **387** 827 (1997)
126. N Shibata, Y Kita *Khim. Geterotsikl. Soedin.* 1463 (1998) [b]
127. J P Marino, R Fernandez de la Pradilla *Tetrahedron Lett.* **26** 5381 (1985)
128. J P Marino, R Fernandez de la Pradilla, E Laborde *Synthesis* 1088 (1987)
129. H Kosugi, K Tagami, A Takahashi, H Kanna, H Uda *J. Chem. Soc., Perkin Trans. 1* 935 (1989)
130. J P Marino, S Bogdan, K Kimura *J. Am. Chem. Soc.* **114** 5566 (1992)
131. S D Burke, K Shankaran, M J Helber *Tetrahedron Lett.* **32** 4655 (1991)
132. J T B Ferreira, J A Marques, J P Marino *Tetrahedron Asymmetry* **5** 641 (1994)
133. H Kosugi, Y Miura, H Kanna, H Uda *Tetrahedron Asymmetry* **4** 1409 (1993)
134. C Iwata, N Maezaki, T Kurumada, H Fukuyama, K Sugiyama, T Imanishi *J. Chem. Soc., Chem. Commun.* 1408 (1991)
135. T Imanishi, T Kurumada, N Maezaki, K Sugiyama, C Iwata *J. Chem. Soc., Chem. Commun.* 1409 (1991)
136. N Maezaki, H Fukuyama, S Yagi, T Tanaka, C Iwata *J. Am. Chem. Soc., Chem. Commun.* 1835 (1994)
137. A Padwa, J E Kochran, C O Kappe *J. Org. Chem.* **61** 3706 (1996)
138. C O Kappe, A Padwa *J. Org. Chem.* **61** 6166 (1996)
139. A Padwa, C O Kappe, T S Reger *J. Org. Chem.* **61** 4888 (1996)
140. L Ramberg, B Bäklund *Arkiv Kemi, Mineral., Geol.* **A13** 27 (1940); *Chem. Abstr.* **34** 4725 (1940)
141. L A Paquette *Org. React.* **25** 1 (1977)
142. J N Clough, in *Comprehensive Organic Synthesis* Vol. 3 (Eds B M Trost, J Fleming, G Pattenden) (New York: Pergamon Press, 1991) p. 861
143. R A Ewin, W A Loughlin, S M Pyke, J C Morales, R J K Taylor *Synlett* 660 (1993)
144. C Y Meyers, A M Malte, W S Matthews *J. Am. Chem. Soc.* **91** 7510 (1969)
145. T L Chen, S Fong, Y Li, C D Poon *J. Chem. Soc., Chem. Commun.* 1771 (1994)
146. J March, in *Advanced Organic Chemistry* (New York: Wiley, 1985) p. 921
147. T Schmittberger, D Uguen *Tetrahedron Lett.* **37** 29 (1996)
148. D Scholz *Liebigs Ann. Chem.* 98 (1983)
149. J B Hendrickson, G J Boudreaux, P S Palumbo *J. Am. Chem. Soc.* **108** 2358 (1986)
150. G Büchi, R M Freidinger *J. Am. Chem. Soc.* **96** 3332 (1974)
151. M Julia, D Lave, M Mulhauser, M Ramirez-Munoz, D Uguen *Tetrahedron Lett.* **24** 1783 (1983)
152. F Nef, R Decorzant, S D Esher *Tetrahedron Lett.* **23** 5043 (1982)
153. J J Burger, T B R A Chen, E R de Waard, H O Huisman *Tetrahedron* **37** 417 (1981)
154. H Choi, M Ji, M Park, I-K Yun, S-S Oh, W Baik, S Koo *J. Org. Chem.* **64** 8051 (1999)
155. J Kattenberg, E R de Waard, H O Huisman *Tetrahedron Lett.* 1173 (1977)
156. J B Hendrickson, P S Palumbo *J. Org. Chem.* **50** 2110 (1985)
157. V Cere, F Peri, S Pollicino *Tetrahedron Lett.* **38** 7797 (1997)
158. V Cere, G Montovani, F Peri, S Pollicino, A Ricci *Tetrahedron* **56** 1225 (2000)
159. R K Boeckman Jr, S K Yoon, D K Heckendorn *J. Am. Chem. Soc.* **113** 9682 (1991)
160. B M Trost, Z Shi *J. Am. Chem. Soc.* **116** 7459 (1994)
161. E Alvarez, M Delgado, M T Diaz, L Hanxing, R Perez, J D Martin *Tetrahedron Lett.* **37** 2865 (1996)
162. E Arce, M C Carreno, M B Cid, J L G Ruano *J. Org. Chem.* **59** 3421 (1994)
163. E Dominguez, J C Carretero *Tetrahedron Lett.* **31** 2487 (1990)
164. B M Trost, T A Grese *J. Org. Chem.* **56** 3189 (1991)
165. D F Taber, K Kanai *J. Org. Chem.* **63** 6607 (1998)
166. N Shibata, M Matsugi, N Kawano, S Fukui, C Fujimori, K Gotanda, K Murata, Y Kita *Tetrahedron Assymetry* **8** 303 (1997)
167. J T Kuethe, A Padwa *J. Org. Chem.* **62** 774 (1997)
168. J H Rigby, N C Warshakoon *J. Org. Chem.* **61** 7644 (1996)
169. A Padwa, T M Heidelbaugh, J T Kuehte *J. Org. Chem.* **65** 2368 (2000)
170. J L G Ruano, C Garcia Peredes *Tetrahedron Lett.* **41** 261 (2000)
171. T Naka, N Minakawa, H Abe, D Kaga, A Matsuda *J. Am. Chem. Soc.* **122** 7233 (2000)
172. J-J Liu, T Hino, A Tsuruoka, N Harada, M Nakagawa *J. Chem. Soc., Perkin Trans. 1* 3487 (2000)
173. D F Taber, Q Jiang *J. Org. Chem.* **66** 1876 (2001)
174. J H Rigby, N C Warshakoon, A J Payen *J. Am. Chem. Soc.* **121** 8237 (1999)
175. C P Raj, T Pichnit, S Braverman *Tetrahedron Lett.* **41** 1501 (2000)

[a] — *Russ. Chem. Bull., Int. Ed. (Engl. Transl.)*
[b] — *Chem. Heterocycl. Compd. (Engl. Transl.)*

Russian Chemical Reviews **70** (11) 921 – 938 (2001) © 2001 Russian Academy of Sciences and Turpion Ltd

DOI 10.1070/RC2001v070n11ABEH000685

(Het)aroylpyruvic acids and their derivatives as promising building blocks for organic synthesis†

S G Perevalov, Ya V Burgart, V I Saloutin, O N Chupakhin

Contents

I.	Introduction	921
II.	Methods of synthesis and tautomerism of (het)aroylpyruvates	921
III.	Chemical properties of (het)aroylpyruvates	923
IV.	Biological activities of (het)aroylpyruvates and the products of their heterocyclisation	935
V.	Conclusion	936

Abstract. Methods of synthesis of (het)aroylpyruvic acids and their acyclic derivatives (esters, amides and hydrazides), and their reactions with various C-, N-, O-, S-nucleophiles are described. Problems of tautomerism and biological activity of (het)aroylpyruvates and products of their transformation are briefly considered. The bibliography includes 191 references.

I. Introduction

(Het)aroylpyruvic acids [(H)APA] and their derivatives, (het)aroylpyruvates, [(H)AP] were discovered back in the XIX century.[1, 2] They proved to be interesting and useful synthons permitting the preparation of a very broad spectrum of products, in particular, diverse heterocyclic compounds many of which possess biological activities. At present, this class of compound still remains attractive for researchers.[3 – 9] The chemistry of (H)AP is fairly extensive but the current state of investigations in this field is not covered in the world literature. This review is meant to fill this gap.

Cyclic APA derivatives, 5-aryl-2,3-dihydrofuran-2,3-diones have been considered in reviews[7, 10] and will not be discussed here in detail. A review has been devoted to the chemistry of perfluoroaroylpyruvates;[3] therefore we note below only specific features of these compounds not found for non-fluorinated analogues.

II. Methods of synthesis and tautomerism of (het)aroylpyruvates

1. Methods of synthesis of (het)aroylpyruvates

The Claisen condensation of the corresponding (het)aryl methyl ketones **1** with dialkyl oxalates in the presence of sodium metal or sodium (potassium) alkoxides is the main and the most convenient method for synthesis of (H)APA esters **2** (Scheme 1). Alcohols, diethyl ether, benzene or toluene are used as solvents.[1, 2, 11 – 23] Pentafluorobenzoylpyruvates are prepared from pentafluoroacetophenone in the presence of lithium hydride.[3, 5, 24, 25] It is convenient to isolate and purify labile AP as their copper(II) chelates **3**.[1, 13, 14, 16] This is especially required in the case of pentafluorobenzoylpyruvates,[5, 24, 25] which cyclise very easily to chromone derivatives due to the presence of *ortho*-fluorine atoms in the benzoyl substituent. Hydrolysis of the esters **2** to the corresponding acids **4** is normally carried out in an acid medium,[1, 23, 26, 27] although examples of alkaline hydrolysis are also documented.[2, 11]

A method for the preparation of ethyl 4-(1,2-diaryl-4-hydroxy-5-oxo-1*H*-pyrrol-3-yl)-2-hydroxy-4-oxobut-2-enoates **5**

Scheme 1

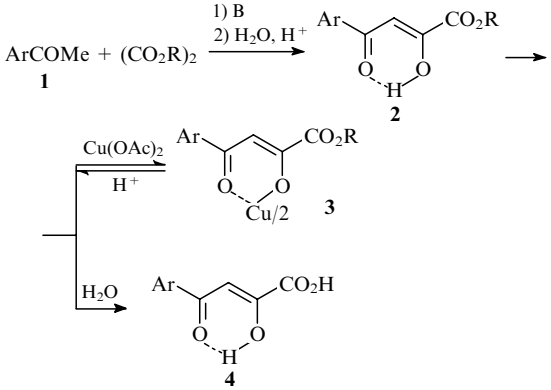

1 – 4: Ar = Ph, 2-XC_6H_4 (X = NO_2, OH), 4-XC_6H_4 (X = NHAc, Br, Cl, Ph, OH, OMe), 2-OH-4-OMe-C_6H_3, 2-OH-4-OEt-C_6H_3, 2,4-$(OEt)_2C_6H_3$, 2,5-$(OEt)_2C_6H_3$, 2,4-$Me_2C_6H_3$, 2,4,6-$(OMe)_3C_6H_2$, 2-OH-4,6-$(OMe)_2C_6H_2$, C_6F_5, 2-naphthyl, 1-hydroxy-2-naphthyl, 3-phenanthryl, 2-pyrrolyl, 2,5-dimethyl-3-pyrrolyl, 2,3-dimethyl-4-pyrrolyl, 2-thienyl, 5-methyl-2-thienyl, methyl(phenyl)-2-thienyls, 2-furyl, Py, 5-X-indol-3-yls (X = H, OMe, Cl), 2-methyl-5-methoxy-3-benzo[*b*]-furyl, substituted 5-oxazolyls, 2,4-dimethyl-5-thiazolyl, 3-X-4-sydnonyls (X = Me, Ph), cymantrenyl.
B = Na, NaOR, KOR, LiH; R = Et, Me, Pr, Ph.

S G Perevalov, Ya V Burgart, V I Saloutin, O N Chupakhin Institute of Organic Synthesis, Ural Branch of the Russian Academy of Sciences, ul. S Kovalevskoi 20, 620219 Ekaterinburg, Russian Federation.
Fax (7-343) 274 59 54. Tel. (7-343) 249 34 91.
E-mail: fc208@ios.uran.ru (S G Perevalov)
Tel. (7-343) 249 34 91. E-mail: burgart@ios.uran.ru (Ya V Burgart)
Tel. (7-343) 249 59 54. E-mail: saloutin@ios.uran.ru (V I Saloutin)
Tel. (7-343) 274 11 89. E-mail: chupakhin@ios.uran.ru (O N Chupakhin)

Received 15 June 2001
Uspekhi Khimii **70** (11) 1039 – 1058 (2001); translated by Z P Bobkova

† Dedicated to Academician O M Nefedov with appreciation and on the occasion of his seventieth birthday.

by the reaction of diethoxalylacetone with diarylazomethines was proposed not long ago.[28]

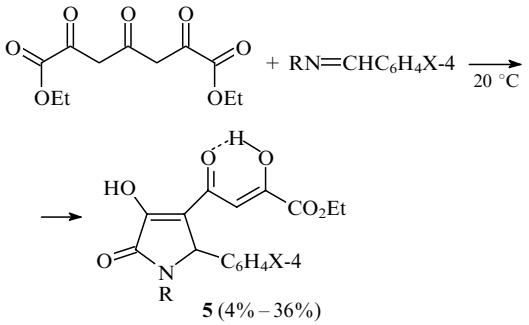

5 (4% – 36%)

R = Me, 4-YC$_6$H$_4$ (Y = H, Me, OMe, Br); X = H, OMe, Br, Cl.

The condensation of acetophenones **1** with esters of oxanilic acids is used for the synthesis of APA amides **6**.[29]

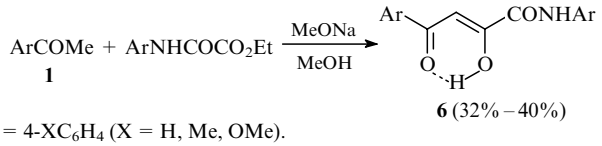

6 (32% – 40%)

Ar = 4-XC$_6$H$_4$ (X = H, Me, OMe).

Preparation of the amides **6** from the APA methyl esters **2** and *N*-phenylethylenediamine[30] or 2-aminopyridine has been described.[31]

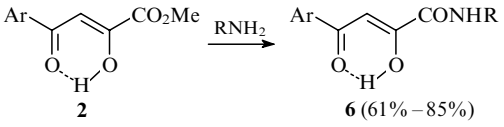

6 (61% – 85%)

Ar = 4-XC$_6$H$_4$ (X = H, Me, OMe, Br); R = (CH$_2$)$_2$NHPh, 2-pyridyl.

Methods for the synthesis of APA **4**,[32] the esters **2**,[32–37] the amides **6**,[30,31,37–64] and hydrazides [65–74] based on the reaction of the corresponding 5-aryl-2,3-dihydrofuran-2,3-diones **7**[38] with diverse nucleophiles have now become significant practically. The range of reagents used includes water,[32] alcohols,[32] oximes [33–36] and amides of 2-hydroxy acids;[37] amines,[30,31,37–39,41–44,48,51–64] 2-aminophenol,[37] ethanolamine,[37] amino acids,[40,49] thiols,[44,45] mercaptoethanolamine,[44] amides of thioacids,[50] acyl- and aroyl-hydrazides,[65,67–69,72,73] hydrazine,[66] and hydrazones.[70,71,74]

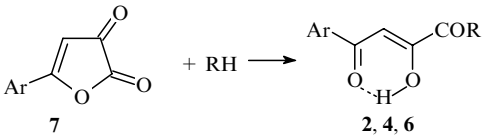

2, **4**, **6**

2: R = OAlk, OPh, ON = CR^1_2; **4**: R = OH;
6: R = NH$_2$, NHAlk, NHAr, NHHet.

The APA amides and hydrazides **6** have been prepared by acid hydrolysis of 5-aryl-2-imino-2,3-dihydrofuran-3-ones **8**.[75–78]

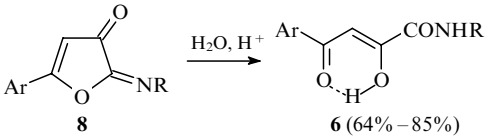

6 (64% – 85%)

Ar = 4-YC$_6$H$_4$ (Y = H, Me, OMe, Cl, Br); R = CH$_2$SO$_2$C$_6$H$_4$Me-4, 1-adamantyl, N = CHCOPh.

Extensive hydrolysis of 1-aryl-4-aroyl-5-methoxycarbonyl-2,3-dihydropyrrole-2,3-diones **9** affords the APA **4**.[79]

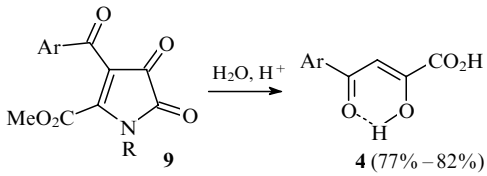

4 (77% – 82%)

Ar = 4-XC$_6$ H$_4$ (X = H, Me, OMe), R = Ar (X = H, Me, OMe, NO$_2$), *etc*.

3-Halogen-substituted esters **10** (R = OEt, OMe) and amides **11** (R = NHPh) of APA are prepared by halogenation of the corresponding AP **2** (see papers [18,80–84]) and **6**[39,85,86] (Scheme 2).

Scheme 2

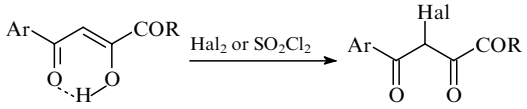

10, **11** (83% – 98%)

Ar = 4-YC$_6$H$_4$ (Y = H, Me, OMe, F, Cl, Br), 2,4,6-Me$_3$C$_6$H$_2$, 2-naphthyl; Hal = Cl, Br; R = OEt, OMe, NHPh.

The amides **11** can also be synthesised from 5-aryl-4-halo-2,3-dihydrofuran-2,3-diones **12** by introducing them into a reaction with diarylazomethines.[87] Hydrolysis of the furandiones **12** readily gives 3-halo-APA **13**.[88]

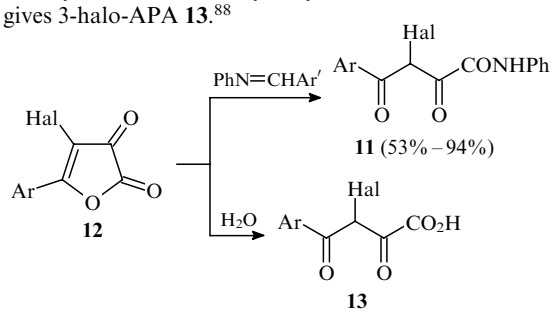

11 (53% – 94%)

13

Hal = Cl, Br; Ar = 4-YC$_6$H$_4$ (Y = H, Me, OMe, Cl).

The reaction of the APA esters **2** and amides **6** with diphenyldiazomethane gives rise to 3-diphenylmethyl-substituted AP **14**[81,89] and **15**.[90] It should be noted that APA **4** are esterified in this reaction to give the esters **2** (Scheme 3).

Scheme 3

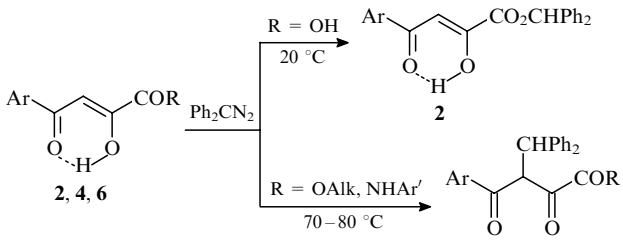

2, **4**, **6**

14, **15** (7% – 87%)

Azo coupling of the APA **4** [91–93] and the esters **2** [94–96] with aryldiazonium salts is used to prepare 3-arylhydrazones of 4-aryl-2,3,4-trioxobutanoic acids **16** and their esters **17** (Scheme 4).

Scheme 4

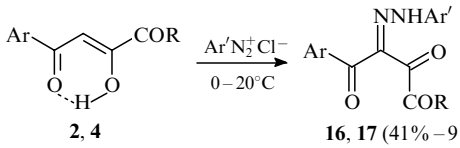

2, **4**

16, **17** (41% – 91%)

2, **17**: R = OMe, OEt; **4**, **16**: R = OH.

The esters **17** are also formed in the alcoholysis of 1-aryl-3-aroyl-4,5-dihydropyrazole-4,5-diones (**18**).[92] Treatment of the

pyrazolediones **18** with amines yields 4-aryl-2,3,4-trioxobutyramide 3-arylhydrazones **19**[97,98] and **20**.[98]

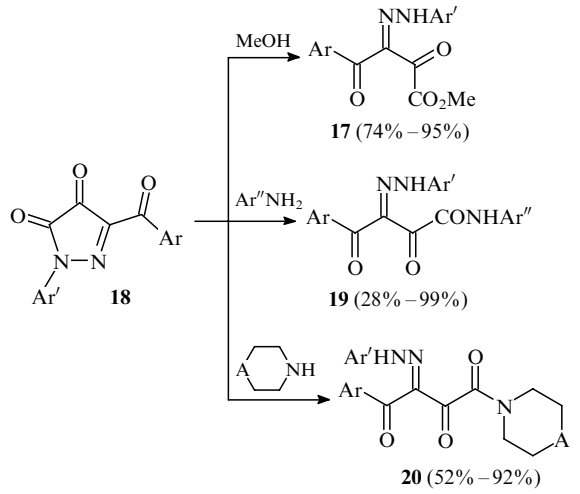

2. Tautomerism of (het)aroylpyruvates

Tautomeric equilibrium has been studied for a series of (H)AP (Scheme 5). According to ^{1}H NMR data, the 3-unsubstituted (H)APA **4**, their esters **2** and amides **6** exist in solution as enols.[81,99,100] The enol structure of the benzoylpyruvic acid **4a** has also been confirmed by X-ray diffraction analysis.[101] Only ethyl 4-(3-indolyl)-2,4-dioxobutanoate in DMF-d_7 is a mixture of ketone and enol tautomers in a ratio of $\sim 1:1$.[20]

Scheme 5

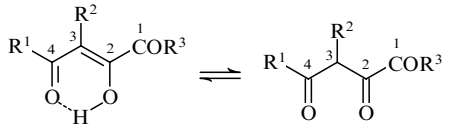

R^1 = Ar, Het; R^2 = H, Cl, Br, N = NAr, Alk, Ar; R^3 = OR^4, NR^4_2, $NR^1NR^4_2$ (R^4 = H, Alk, Ar, COAlk).

In the case of 3-alkyl- and 3-halo-substituted AP **10**, **11**, and **13**–**15**, the ketone form predominates.[102–105] Apparently, the hampered formation and energetic destabilisation of the enol form are caused by the presence of bulky substituents at the 3-position.

The spectral data for the AP **16**, **17**, **19** and **20** available to date indicate that 3-arylhydrazone-substituted acids **16**,[92] esters **17**[92,96] and amides **19** and **20**[97,98] occur as equilibrium mixtures of *Z*- and *E*-tautomers of the ketone form relative to the C = N bond.

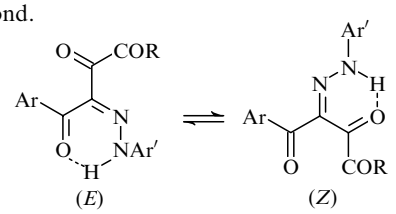

III. Chemical properties of (het)aroylpyruvates

(Het)aroylpyruvates contain three electrophilic centres, namely, the C(1) atom of the ester group and the C(2) and C(4) carbonyl atoms, and one nucleophilic centre, namely, the *meso*-position of the β-dicarbonyl fragment, *i.e.*, the C(3) atom (see Scheme 5). Therefore, the (H)APA **4**, their esters **2** and the amides **6** tend to react with nucleophilic reagents at the C(1), C(2) and C(4) atoms. In addition, (H)AP enter into reactions with electrophiles at the C(3) centre. These transformations are mainly considered in the previous Section concerned with the methods of synthesis of (H)AP (see Schemes 2–4). A typical feature of (H)AP is the susceptibility to thermal transformation. Some (H)AP are able to undergo intramolecular cyclisations.

1. Thermal transformations and intramolecular cyclisations of (het)aroylpyruvates

a. Thermal transformations

Virtually all (H)AP are fairly labile compounds. *O*-Aroylpyruvoyl oximes **21** undergo decarbonylation at 100°C giving rise to *O*-aroylacetyl oximes **22**.[34]

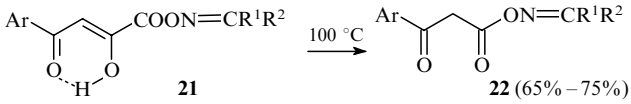

Ar = 4-XC_6H_4 (X = H, Me, Et, Cl); R^1 = H, Me; R^2 = Ph, 2-HOC_6H_4, 1-adamantyl.

Under similar conditions, *O*-aroylpyruvoyl oximes **23**, containing an amino group, cyclise to 3-aryl-5-(3-aroyl-1-hydroxypropenyl)-1,2,4-oxadiazoles **24**.[35]

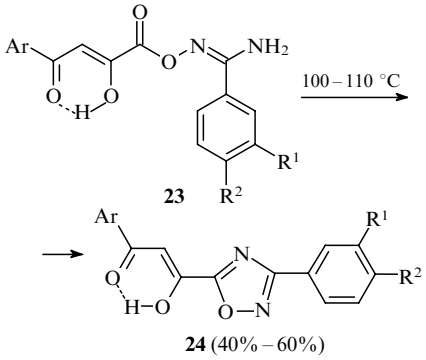

Ar = 4-XC_6H_4 (X = H, Me): R^1 = R^2 = H, OMe; R^1 = H, R^2 = NO_2.

Arylamides of the 3-unsubstituted APA **6** are stable even at 220 °C.[81,106] *N*-(2-Hydroxyphenyl)-3-benzoylpyruvoylamide is an exception; on refluxing in mesitylene, this compound decomposes into acetophenone **1a** and 3,4-dihydro-2*H*-1,4-benzoxazine-2,3-dione (**25**).[37]

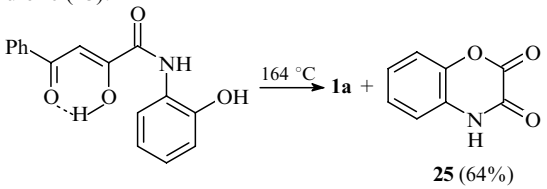

Meanwhile, 3-methyl- (**26**)[106] and 3-diphenylmethyl-substituted (**15**)[90] arylamides are decarbonylated on heating giving rise to *N*-aryl-2-methyl- (**27**) and *N*-aryl-2-diphenylmethyl-3-phenyl-3-oxopropanamides **28**.

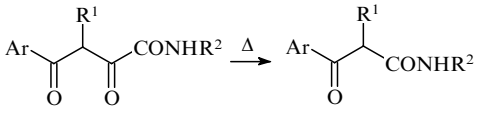

26, **27**: Ar = Ph, R^1 = Me, R^2 = YC_6H_4 (Y = H, 3-OMe, 4-OMe); **15**, **28**: Ar = 4-YC_6H_4 (Y = H, Me); R^1 = $CHPh_2$, R^2 = Ph, 4-$MeOC_6H_4$.

b. Intramolecular cyclisations

On refluxing in aqueous HCl, ethyl aroylpyruvates **29a**–**d**, containing a hydroxy group in the *ortho*-position of the benzene ring cyclise to give 4-oxachromene-2-carboxylic acids **30a**–**d**.[16]

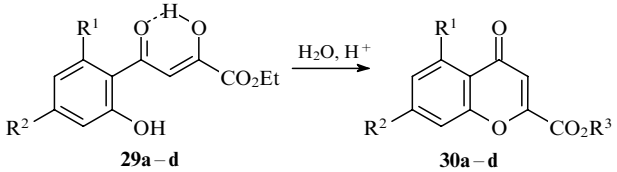

R^3 = Et: R^1 = R^2 = H (**a**), OEt (**b**); R^3 = H, R^1 = H (**c**), OMe (**d**), R^2 = OMe.

Pentafluorobenzoylpyruvates **31a**,**b** cyclise either over a period of one month at 20 °C or rapidly on heating to give 2-alkoxycarbonyl-5,6,7,8-tetrafluoro-4*H*-chromen-4-ones **32a**,**b**.[3, 6, 24] Acid **31c** (R = H) is stable under these conditions.[27] It cyclises to be converted into chromone-2-carboxylic acid (**32c**) only after treatment with anhydrous ammonia or triethylamine in dioxane at 20 °C. The copper(II) chelates **31d**,**e** are also converted into chromones **32a**,**b** on heating in DMSO at 80 – 90 °C[3, 4, 6, 24] (Scheme 6).

Scheme 6

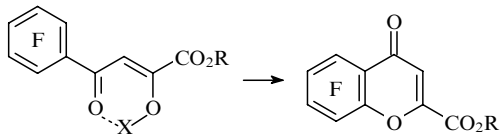

31a – e **32a – e**

31: X = H: R = Et (**a**), Me (**b**), H (**c**); X = Cu/2, R = Et (**d**), Me (**e**);
32: R = Et (**a**), Me (**b**), H (**c**).

Under conditions of acid hydrolysis, the ethyl pyrrolylpyruvates **5** undergo cyclisation which involves the hydroxy group of the pyrrole fragment and gives 5,6-diaryl-2-carboxypyrano[2,3-*c*]pyrrole-4,7(4*H*,5*H*)-diones **33**.[107]

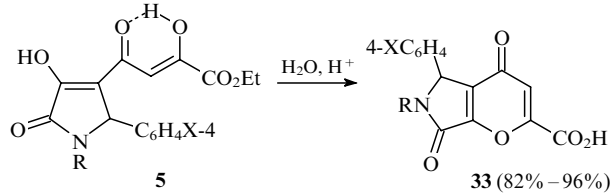

5 **33** (82% – 96%)

R = Me, Ph, 4-MeOC$_6$H$_4$, 4-BrC$_6$H$_4$; X = H, NO$_2$, Br.

Acid hydrolysis of APA *N*-benzoylmethylene- (**34**)[78] and APA *N*-benzimidenehydrazides **35**[108] results in the formation of the same 6-aryl-4-hydroxy-2,3-dihydropyridazin-3-ones **36**.

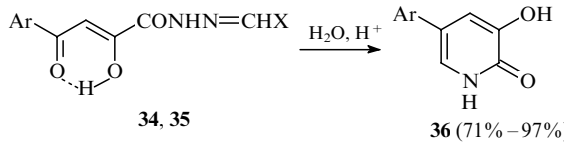

34, **35** **36** (71% – 97%)

Ar = 4-YC$_6$H$_4$ (Y = OMe, Cl, H, Me); X = COPh (**34**), Ph (**35**).

The amides **15** and **26** cyclise in boiling AcOH being thus converted into the corresponding 1,5-diaryl-4-diphenylmethyl-(methyl)-2,3-dihydropyrrole-2,3-diones **37**[90, 109] and **38**[110] (Scheme 7). The compound **37** (X = Me, Ar = R = Ph) recyclises on refluxing in ditolylmethane to afford 4-hydroxy-3-methyl-2-phenylquinoline (**39**).[110]

Scheme 7

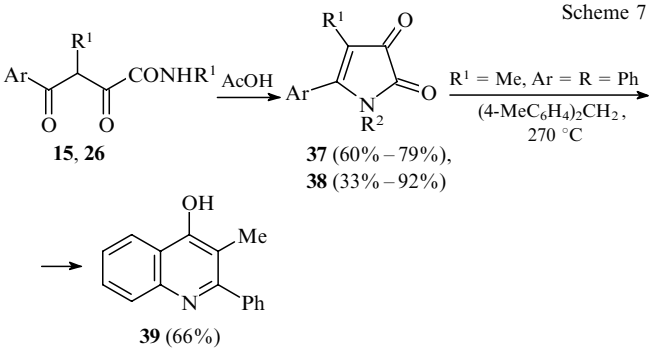

15, **26** **37** (60% – 79%), **38** (33% – 92%) **39** (66%)

15, **37**: Ar = 4-YC$_6$H$_4$ (Y = H, Me), R^1 = CHPh$_2$, R^2 = Ph, 4-MeOC$_6$H$_4$, 4-ClC$_6$H$_4$;
26, **38** : Ar = Ph, R^1 = Me, R^2 = YC$_6$H$_4$ (Y = H, 3-OMe, 4-OMe, 4-Me, 4-OH, 2-OH, 4-Br).

When heated in benzene with thionyl chloride (65 – 70 °C)[38] or acetic anhydride (60 – 70 °C),[111, 112] the acids **4** undergo dehydration to the furandiones **7**. The two methods provide similar yields of the compounds **7**.

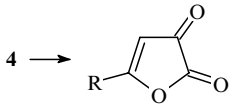

7 (49% – 95%)

R = Ar, Het.

The APA 3-arylhydrazones **16** cyclise on treatment with thionyl chloride to give pyrazolediones **18**.[92, 93] The same compounds are produced on prolonged refluxing of the methyl esters **17** in acetic anhydride.[113]

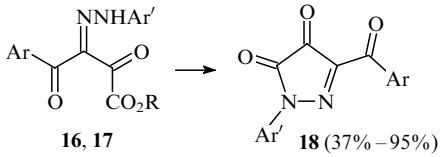

16, **17** **18** (37% – 95%)

Ar = 4-YC$_6$H$_4$ (Y = H, Me, OMe, NO$_2$, Br, Cl); Ar′ = 4-YC$_6$H$_4$ (Y = H, OMe, Cl).

A distinctive feature of pentafluorophenyl-substituted arylhydrazones (**17**, Ar = C$_6$F$_5$) is their ability to undergo cyclisation either on heating with DMSO in the presence of potassium carbonate or in a mixture of triethylamine with chloroform; the reaction furnishes 1-aryl-5,6,7,8-tetrafluoro-3-ethoxalyl-1,4-dihydrocinnolin-4-ones **40**.[95, 96]

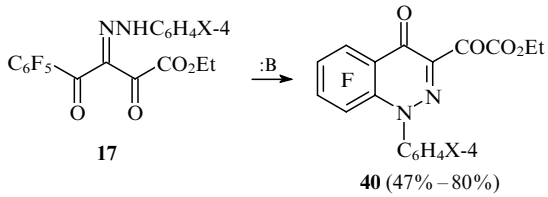

17 **40** (47% – 80%)

X = H, Me, OMe.

Cyclodehydration of APA arylamides **41**[49] and **42**[64] with participation of the amide group capable of enolisation gives benzoxazines **43**, **44**. In the case of the amide **41**, the reaction was carried out by heating the compound in benzene with thionyl chloride (with DMF as the catalyst),[49] and for the compound **42**, it was performed in acetic anhydride.[64]

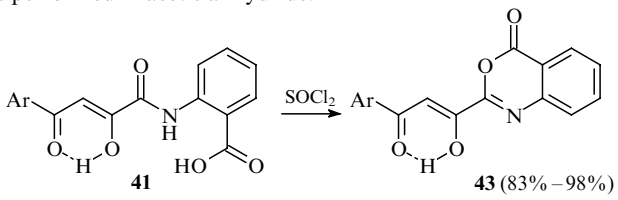

41 **43** (83% – 98%)

Ar = 4-XC$_6$H$_4$ (X = OMe, OEt, Br, Cl).

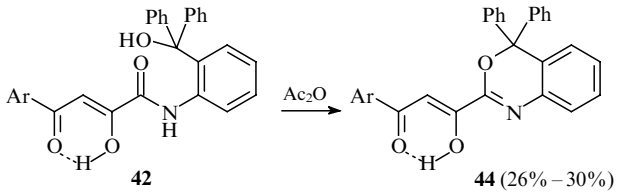

42 **44** (26% – 30%)

Ar = 4-XC$_6$H$_4$ (X = H, Me, OMe).

2. Reactions of (het)aroylpyruvates with mononucleophiles

Reactions with some C-, N- and O-mononucleophiles are known for the (H)APA **4** and their esters **2** and amides **6**.

a. Reactions with C-mononucleophiles

The reported reactions of AP with C-mononucleophiles are few in number because AP tend to decompose under conditions where nucleophiles are generated and/or are sufficiently reactive and heterocyclisation is precluded.

Mention should be made of condensations of **4a** with 2-hydroxyphenylacetic acid in the presence of PBr_3 resulting in the product **45** and with 5-phenyl-2,3-dihydrofuran-2-one in the presence of acetic anhydride to give the compound **46**.[114]

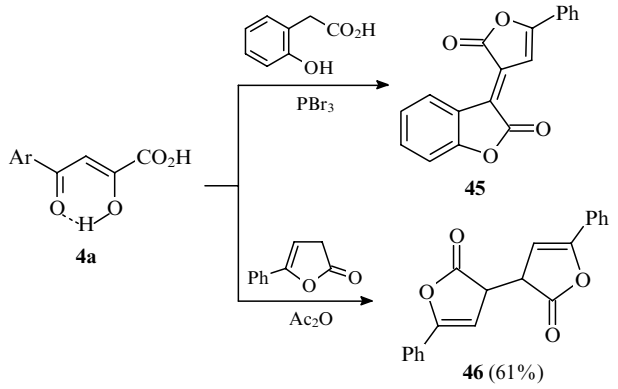

b. Reactions with O-mononucleophiles

Of the transformations of (H)AP in reactions with alcohols, only transesterification of the esters **2** is known. Most of the APA esters **2** (Ar is substituted phenyl) are unstable under conditions of alkaline hydrolysis and decompose yielding the corresponding acetophenone **1**, alcohol and oxalate.[1] The HPA esters **2** are more stable to this cleavage because the acids **4** [Ar = 2-thienyl,[2] 3-(2,4-dimethylpyrrolyl) [11]] can be prepared by alkaline hydrolysis of the corresponding esters **2**. However, ethyl 3-indolyl- and 3-(5-methoxyindolyl)pyruvates are readily cleaved by alkalis and are even partially cleaved during recrystallisation from ethanol.[20] Recently, ethyl pentafluorobenzoylpyruvate copper(II) chelate **31d** was reported to undergo transesterification into the chelate of the methyl ester **31e**. For the free AP **2**, this reaction is unknown.

c. Reactions with N-mononucleophiles

The esters **2** are known [115] to react with ammonium acetate on refluxing in an AcOH – benzene mixture; the reaction involves the carbonyl group at the C(2) atom and gives ethyl 2-amino-4-arylbut-2-en-4-onoates **47** in ~80% yield. Under mild conditions (at 20 – 50 °C), both the (H)APA **4** and their esters **2** add aniline and its derivatives at the carbonyl group giving rise to 2-arylamino-4-aryl-4-oxobut-2-enoates **48** (the yields vary from 9% to 83%).[79, 102, 116] Electron-withdrawing substituents and steric hindrance in the reactants result in lower yields of the products **48**. The structure of the compounds **48**, stabilised by an intramolecular hydrogen bond (IMHB) in the β-amino vinyl ketone fragment, was confirmed by NMR spectroscopy.[117] The APA arylamides **6** behave in a similar way in reactions with aniline, giving rise to arylamides of 4-aryl-4-oxo-2-phenylaminobut-2-enoic acids **49** in 60% – 93% yields.[29, 118]

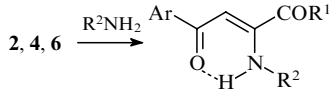

47, **48**, **49**

2, **47**: R^1 = OEt; R^2 = H; **2**, **4**, **48**: R^1 = OH, OMe; R^2 = Ar′; **6**, **49**: R^1 = NHAr′; R^2 = Ph.

The pyrrolylpyruvates **5** are also converted into amino esters **50b – e** when heated with arylamines to 60 °C.[107] However, on stronger heating (150 – 220 °C), these products cyclise to give compounds **51b – e**.[107] The cyclisation is facilitated by electron-withdrawing substituents in the pyrrole ring of **5**. Indeed, 1-methylpyrrolylpyruvate **5a** readily cyclises with aniline at 20 °C giving rise to heterocycle **51a**; the intermediate compound **50a** cannot be isolated.[107]

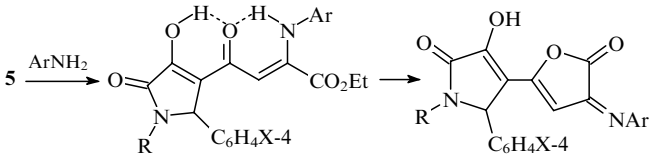

50b – e (87% – 97%) **51a – e** (29% – 58%)

Ar = Ph, R = Me, X = H (**a**); Ar = R = Ph (**b – d**): X = H (**b**), Br (**c**), NO_2 (**d**); Ar = R = 4-BrC_6H_4, X = Br (**e**).

It has been reported that salts decarboxylated on refluxing in mesitylene (164 °C) to give 3-aryl-3-oxopropanal monoanils **52** can be isolated from the products of reaction between the APA **4** and aromatic amines at 20 °C.[119]

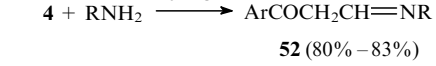

52 (80% – 83%)

Ar = 4-XC_6H_4 (X = H, Me, OMe, Cl, Br); R = 4-XC_6H_4 (X = H, OMe, Cl, Br).

It is of interest that refluxing of methyl aroylpyruvates **2** in benzene with 2-aminopyridine results in APA 2-pyridylamides **53** instead of the 2-amino-derivatives such as **48**, **49**.[31] The unusual pathway of 2-aminopyridine addition to AP is due, apparently, to the fact that in the transition state, the highly basic pyridine nitrogen atom of the nucleophile is coordinated to the C(2) carbonyl atom of the AP and the amino group is coordinated to the C(1) atom.

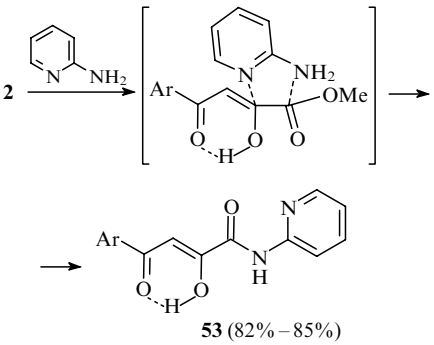

53 (82% – 85%)

Ar = 4-XC_6H_4 (X = H, Me, OMe, Br).

Unlike 3-unsubstituted esters **2**, 3-arylhydrazones **17**, which are efficiently stabilised by an IMHB, react with arylamines on refluxing in benzene; the reaction involves the ester group and gives the arylamides **19**.[98]

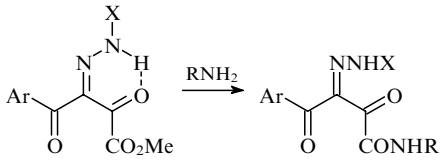

17 **19** (40% – 63%)

Ar = Ph, 4-$EtOC_6H_4$; R = 4-YC_6H_4 (Y = H, Me, Cl); X = Ph.

It is known [120] that APA arylamides containing a bulky group at the 3-position readily cyclise yielding 4-substituted 1,5-diaryl-2,3-dihydropyrrole-2,3-diones **37**, **38** (see Scheme 7).[90, 109, 110] The tendency toward cyclisation is sometimes so pronounced that it is not always possible to isolate arylamides formed in the reaction of APA esters with amines.[121] Indeed, the reaction of ethyl 3-phenylbenzoylpyruvate (**54**) with methyl- or benzylamine in chloroform at 20 °C yields immediately the products of cyclisation of intermediate amides, 1-alkyl-4,5-diphenyl-3,5-dihydroxy-2,5-dihydropyrrol-2-ones **55**. It is noteworthy that in this case, as for arylhydrazones **17**, it is the ester group that is involved in the

reaction with the amine. The products **55** are dehydrated to give 1-alkyl-4,5-diphenyl-2,3-dihydropyrrole-2,3-diones **56**.[103]

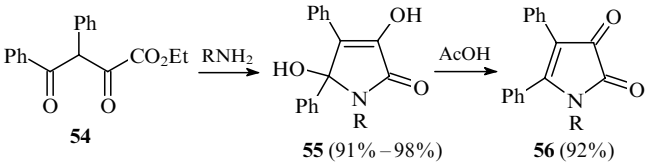

54 **55** (91% – 98%) **56** (92%)

R = Me, CH_2Ph.

Unlike the amides **6**, APA β-aroylhydrazides **57** are cleaved by aromatic amines when fused together (160 – 165 °C); this gives rise to acetophenones **1** and mixed amidohydrazides of oxalic acid **58**.[67] Benzylamine splits the hydrazides **57** even at 60 – 65 °C.

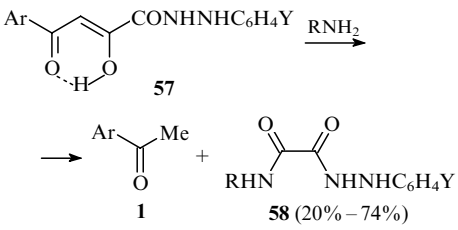

57 **1** **58** (20% – 74%)

Ar = 4-XC_6H_4 (X = H, Me, OMe); R = 4-XC_6H_4 (X = H, Me, OEt), CH_2Ph; Y = H, 3-NO_2, 4-OMe.

Fluorine-containing AP behave quite differently in reactions with amines. Thus the pentafluorobenzoylpyruvates **31a**,**b** rapidly cyclise to the chromones **32a**,**b** when made to react with aqueous ammonia at 20 °C[3, 121] (see Scheme 6); the reaction of the pyruvate **31a** with cyclohexylamine on heating in DMSO does not stop at the cyclisation stage but proceeds as nucleophilic substitution with removal of the fluorine atom at the 7-position of the aromatic ring, thus yielding 5,6,8-trifluoro-7-cyclohexylamino-2-ethoxycarbonylchromen-4(4*H*)-one (**59**).[121]

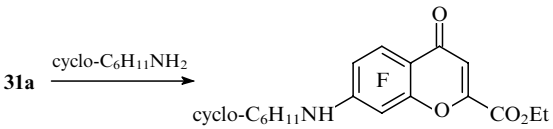

59 (63%)

As noted above, the reaction of pentafluorobenzoylpyruvic acid (**31c**) with anhydrous ammonia or triethylamine in dioxane at 20 °C leads to chromone-2-carboxylic acid (**32c**) (see Scheme 6). Heating of the acid **31c** with aqueous ammonia and primary amines affords 2-(alkyl)amino-4-oxo-4-polyfluoroaryl-2-butenoic acids **60**.[26, 27] The acid **60a** cyclises reversibly into the chromone **32c** on heating in an acid medium. On treatment with aqueous alkali, the acids **60b**,**c** undergo cyclisation to give 1-alkyl-2-carboxy-7-hydroxy-5,6,8-trifluoroquinolin-4(4*H*)-ones **61**.[26, 27] The structure of the quinolone **61b** as DMSO adduct has been determined by X-ray diffraction analysis.[104]

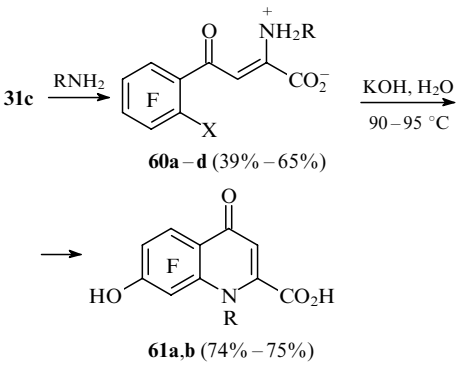

60a – **d** (39% – 65%)

61a,**b** (74% – 75%)

60: X = OH, R = H (**a**); X = F: R = Pr^i (**b**), cyclo-C_6H_{11} (**c**), Ph (**d**); **61**: R = Pr^i (**a**), cyclo-C_6H_{11} (**b**).

Thus, the reactions of APA **4**, their esters **2** and amides **6** with N-mononucleophiles mainly involve the oxo group at the C(2) atom, although in the case of esters having bulky substituents at the 3-position, the ester group becomes more reactive.

3. Reactions of (het)aroylpyruvates with dinucleophiles

The reactions of (H)AP with bifunctional nucleophiles are widely used in organic synthesis to prepare five-, six-, and seven-membered heterocycles and their fused derivatives.

a. Reactions with C,N-dinucleophiles

Reactions with C,C-dinucleophiles are unknown. Of transformations of (H)AP on treatment with C,N-dinucleophiles, the reactions with ethyl 3-aminocrotonate and cyanoacetamide are documented. Under mild conditions (at 20 °C in the absence of bases), the pyruvate **2a** adds ethyl 3-aminocrotonate at the β-diketone fragment to give 3,4-bis(ethoxycarbonyl)-2-methyl-6-phenylpyridine (**62**).[105] The most electrophilic centre of AP [the C(2) atom] reacts with the C-nucleophilic centre of the crotonate and the C(4) atom reacts with the amino group.

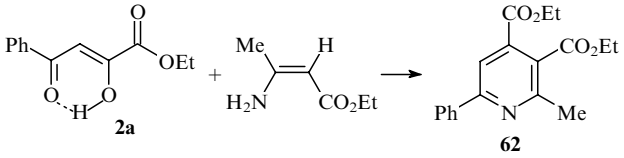

2a **62**

The reaction of the (H)AP **2** with cyanoacetamide proceeds in a similar way giving rise to 6-aryl-3-cyano-4-ethoxycarbonyl-2-pyridones **63**.[13,14, 122] The reaction was carried out by refluxing the reactants in ethanol in the presence of piperidine[122] or diethylamine.[13, 14] The use of *N*-methylcyanoacetamide affords not only 6-aryl-3-cyano-4-ethoxycarbonyl-1-methyl-2-pyridones **64**, but also 6-aryl-3-cyano-4-ethoxycarbonyl-2-methoxypyridines **65** as side products.[13, 14]

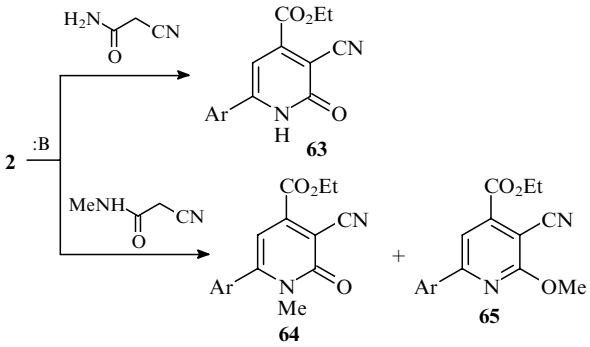

63 **64** **65**

2, **63**: R = Et, Ar = Ph, 2-furyl, 4-diphenylyl; **64**, **65**: Ar = 2-furyl, 4-diphenylyl.

b. Reactions with N,N-dinucleophiles

The reactions of (H)AP with N,N-dinucleophilic reagents possess the highest synthetic value; these reactions have been the best studied.

Reactions with hydrazine and its derivatives. The acids **4**, the esters **2** and the amides **6** react selectively with hydrazine at the β-dicarbonyl fragment [C(2) and C(4) atoms] to give 5-(het)arylpyrazole-3-carboxylic acid derivatives **66** in good yields.[3 – 5, 11, 13, 14, 16, 17, 20, 21, 23, 31, 53, 59, 62, 67, 72, 73, 123 – 126] The solvents used in these reactions are acetic acid, 1,4-dioxane, alcohols or water. The (H)AP **2**, **4** and **6** react with monomethyl and arylhydrazines in a similar way, the reaction proceeding regioselectively to give exclusively 1-methyl-[13, 14] and 1-aryl-5-(hetero)arylpyrazole-3-carboxylic acid derivatives **67**.[1 – 5, 13, 14, 20, 23, 67, 124, 127]

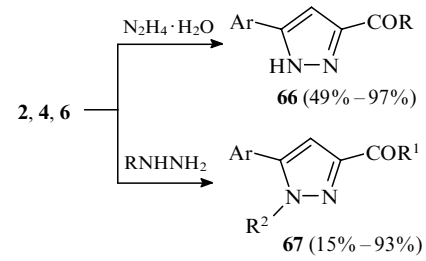

66: Ar = XC_6H_4 (X = H, 4-OH, 4-Me, 4-OMe, 4-OEt, 4-Br, 3-Br, 4-F, 4-Cl), 2,4-$Me_2C_6H_3$, 4-diphenylyl, 3-phenanthryl, C_6F_5, 2-furyl, 3-indolyl, cymantrenyl, 3-methyl-5-phenyl-2-thienyl, 4-methyl-5-oxazolyl, 2,4-dimethyl-5-oxazolyl, 5-(2,4-dimethylthiazolyl); R = OEt, OH, NHPh, $NH(CH_2)_2NHAc$, 2-pyridylamino, 3-pyridylamino, 2-bromo-5-pyridylamino, 2-thiazolylamino, 2-pyrimidylamino, 3-cyano-4,5-tetramethylene-2-thienylamino, NHNHCOAr′ (Ar′ = Ph, 4-$MeOC_6H_4$), NHNHCOCO-CH = PPh_3, $NHNHCOC_6H_4Y$ (Y = 2-methylphenylamino, 2-methyl-4-quinolyl);

67: Ar = Ph, 4-MeC_6H_4, 4-diphenylyl, C_6F_5, 2-pyrrolyl, 2-furyl, 2-thienyl, 5-methyl-2-furyl, 3-methyl-2-phenyl-5-thienyl, 2,4-dimethyl-5-oxazolyl, 2,4-dimethyl-5-thiazolyl, 3-indolyl; R^1 = OH, OEt, OPr^i; 2(3)-pyridylamino, 5-bromo-2-pyridylamino, $NHNHCOC_6H_4Y$-4 (Y = H, OMe); R^2 = Ph, 4-$NO_2C_6H_4$, 2,4-$(NO_2)_2C_6H_3$, Me.

For the synthesis of pyrazoles **66**, the use of equimolar amounts of (H)AP and hydrazine hydrate or dihydrochloride is recommended.[14] Some examples of cleavage of (H)AP upon the use of excess hydrazine have been reported.[13, 20] In addition, under these conditions, the ester group in the final pyrazoles **66** is usually converted into a hydrazide group.[11, 13, 17] Thus the reaction of 2-furoylpyruvate **2c**[13] with excess hydrazine gives 5-(2-furyl)pyrazole-3-carbohydrazide together with the target pyrazole **66** (Ar = 2-furyl, R = OEt) even under mild conditions.

Note that the reaction of phenyl benzoylpyruvate with hydrazine involves both the β-dicarbonyl fragment and the phenoxycarbonyl group, resulting in 5-phenylpyrazole-3-carbohydrazide.[16]

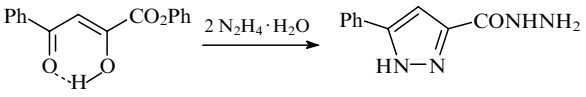

3-Arylhydrazono-APA **16**[128] behave in reactions with hydrazine and phenylhydrazine similarly to 3-unsubstituted analogues giving rise to 4-arylazo-(1-phenyl)-5-arylpyrazole-3-carboxylic acid derivatives **68**.

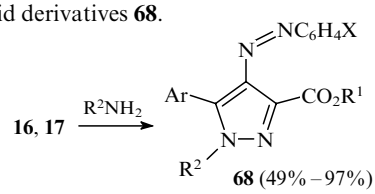

Ar = C_6H_4Y (Y = H, 4-Me, 4-OMe, 4-Cl); R^1 = H, Et; R^2 = H, Ph.

Conversely, the 3-chloroaroylpyruvates **10** are cleaved by hydrazine even under mild conditions without giving pyrazoles.[80]

Reactions of some esters of the (H)APA **2** with arylhydrazines at 20 °C catalysed by AcOH involve the C(2) = O group and result in the corresponding arylhydrazones **69** in good yields (87% for Ar = R^2 = Ph).[127] Upon heating in an acid medium (AcOH, AcOH + HCl), these products cyclise almost quantitatively (93% for Ar = R^2 = Ph)[127] to give pyrazoles **70**.[11, 20, 124, 127]

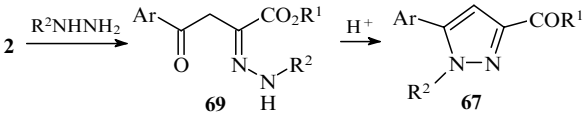

Ar = Ph, 3-indolyl, 2,4-dimethyl-3-pyrrolyl; R^1 = Et, Pr^i; R^2 = 2,4-$(NO_2)_2C_6H_3$, Ph.

The reactions of methyl aroylpyruvates **2** with *N*,*N*-dimethyl-,[129] *N*-alkyl-*N*-arylhydrazines[130] and benzophenone and 9-fluorenone hydrazones[131] involve exclusively the C(2) centre and give AP *N*,*N*-dimethyl- (**70**) and *N*-alkyl-*N*-arylhydrazones **71** and AP *N*-(di)arylmethylenehydrazones **72**, respectively.

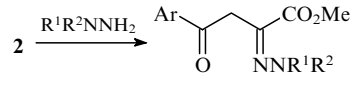

70 – **72** (27% – 69%)

70: Ar = XC_6H_4 (X = H, 4-Me, 4-OMe, 4-Br, 4-Cl, 3-NO_2, 4-NO_2); R^1 = R^2 = Me; **71**: Ar = Ph; R^1 = Me, Et, Pr^i; R^2 = 4-XC_6H_4 (X = OMe, Me, H, Br, NO_2); **72**: Ar = XC_6H_4; R^1 + R^2 = CPh_2, 9-fluorenylidene.

It was shown by ^{1}H NMR spectroscopy[129] that the dimethylhydrazones **70** exist in solutions as equilibrium mixtures of β-ketoimine (*syn*-KI, *anti*-KI) and ketoenamine [(*Z*)-KEA, (*E*)-KEA] tautomers. In low-polarity aprotic solvents, the content of the KEA tautomer is higher. Electron-donating substituents X in the aromatic nucleus of the compounds **70** and an increase in the solvent polarity result in a higher content of the KI forms. The *syn*-KI form predominates in the KI pair, while in the KEA pair, the preferred form is (*Z*)-KEA, which is stabilised by an IMHB. The hydrazone **70** (X = H) was isolated from a solution as a mixture of the *syn*-KI and (*Z*)-KEA isomers, whereas other hydrazones **70** were obtained only as (*Z*)-KEA.

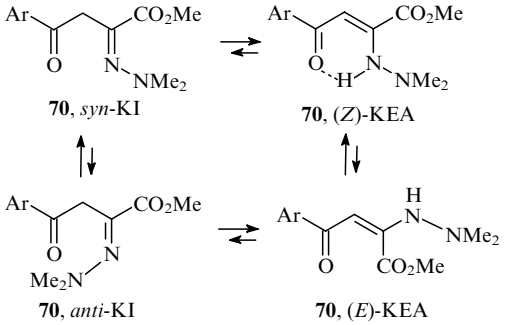

The *N*-alkyl-*N*-arylhydrazones **71** are isolated as the (*Z*)-KEA tautomers. However, they exist in chloroform and pyridine solutions as equilibrium mixtures of the (*Z*)-KEA and *syn*-KI forms.[130] In DMSO, the (*E*)-KEA form was also found. The influence of the nature of the solvent and the substituent X in the R^2 group on the tautomeric equilibria has been elucidated. On passing from chloroform to pyridine, the content of the tautomer (*Z*)-KEA increases, while in DMSO, the total content of the KEA isomers increase, the (*E*)-KEA form being the preferred one. The content of (*Z*)-KEA increases with the enhancement of the −M-effect of the group X on passing from OMe to NO_2.

The AP **2** react with benzoylhydrazine at the α-carbonyl group to give the corresponding hydrazones **73a**–**h**.[132]

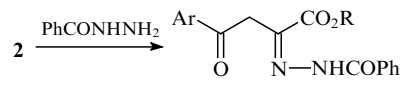

73a–**h** (70% – 86%)

R = Me; Ar = XC_6H_4 (X = H (**a**), 4-Me (**b**), 4-OMe (**c**), 4-NMe_2 (**d**), 4-Cl (**e**), 3-NO_2 (**f**), 4-NO_2 (**g**)); R = Et, Ar = Ph (**h**).

A ^{1}H NMR study of the tautomerism in the series of benzoylhydrazones **73** has shown[133] that these compounds exist in solutions as equilibrium mixtures of three tautomers, namely, *Z*-(**A**) and *E*-(**B**) ketohydrazones and 5-hydroxypyrazoline (**C**). Their proportions depend on the nature of the hydrazone **73** and the solvent. The electron-donating substituent X in the aryl group of the hydrazone **73** promotes an increase in the content of ketohydrazone. In $CDCl_3$, *Z*-form **A** stabilised by IMHB is preferred, while in DMSO-d_6, *E*-form **B** predominates. The

hydrazones **73e–g** with electron-withdrawing groups X predominantly exist in solutions as cyclic form **C**. The content of tautomer **C** is higher in DMSO than in $CDCl_3$. The benzoylhydrazones **73a–d** were isolated from methanol in form **A**, while **73e–g**, in form **C**.

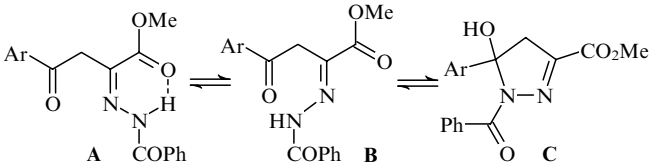

The synthesis of 2-isonicotinoylhydrazone **74** from ethyl 2-furoylpyruvate **2c** and isonicotinic acid hydrazide has been reported.[33]

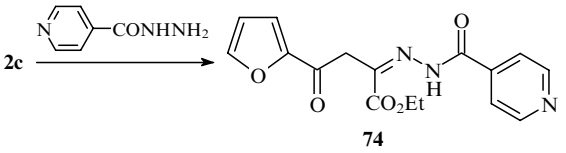

The reaction of the ester (H)AP **2c** [13] and the acid **4a** [134] with semicarbazide or its hydrochloride results in the formation of monosemicarbazones, which have, in our opinion, the structure **75a,b**. These semicarbazones undergo thermal decomposition giving the corresponding pyrazoles **66a,b**. On short-term refluxing in an aqueous solution of potassium carbonate, semicarbazone **75b** is converted into 5-(2-furyl)-3-carboxypyrazole **66b**.[33]

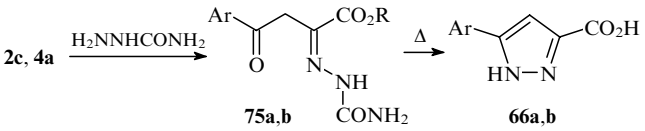

Ar = Ph, R = H (**4a**, **75a**, **66a**); Ar = 2-furyl, R = Et (**2c**, **75b**, **66b**).

The acid **4a** reacts with thiosemicarbazide with participation of both carbonyl groups to give bis(thiosemicarbazone) **76**. The alkaline hydrolysis of this product affords 1,2,4-triazine derivatives **77a,b**.[134]

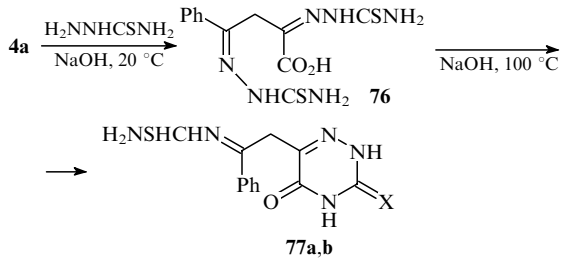

X = S (**a**), O (**b**).

The reaction of the APA **4** and their methyl esters **2** with *S*-methylisothiosemicarbazide hydroiodide involves the α-dicarbonyl fragment and affords 6-aroylmethyl-3-methylthio-1,2,4-triazin-5(2*H*)-ones **78** or 6-aroylmethyl-1,2,4-triazine-3,5(2*H*,4*H*)-diones **79**, depending on the nature of the aryl substituent and the reaction duration.[135, 136] Thus refluxing in ethanol for 2 h gives 3-methylthio-1,2,4-triazinones **78**; when the reaction time increases to 10 h, the products of their hydrolysis, 1,2,4-triazinediones **79**, are formed.[136] The compounds **78** are converted into the triazinediones **79** upon short-term refluxing in aqueous dioxane in the presence of catalytic amounts of HCl. According to the ^1H NMR spectra, the compounds **78** in DMSO-d_6 are mixtures of the imine (**A**) and enamine (**B**) tautomers in 4 : 1 ratio.[135, 136]

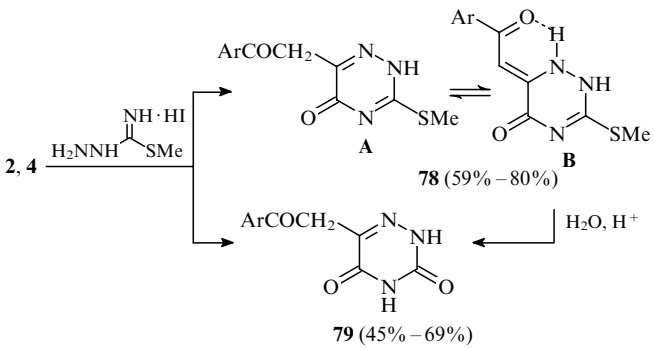

Ar = 4-XC_6H_4 (X = H, Me, OMe, Cl, Br, I, NO_2), 2,4-$Me_2C_6H_3$.

On refluxing in dioxane, the acids **4** add selectively thiocarbohydrazide at the α-ketocarboxyl fragment to give 4-amino-6-aroylmethyl-3-thioxo-2*H*,4*H*-1,2,4-triazin-5-ones **80**.[136]

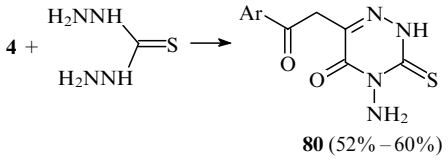

Ar = 4-XC_6H_4 (X = H, Me, Cl).

Reactions with 1,2-diaminoethane and its derivatives. Both the APA **4** [30, 137] and their esters **2** (see [21, 30, 137–141]) add 1,2-diaminoethane [21, 30, 138–140] or its mono-*N*-methyl-,[141] *N*-benzyl- [137] and *N*-phenyl-substituted [30, 141] derivatives in chemo- and regioselective reactions involving the α-dicarbonyl fragment [the C(1) and C(2) atoms] giving rise to 3-aroylmethylidenepiperazin-2-ones **81** or their 1-alkyl(aryl) derivatives **82**. The reactions are normally carried out on heating in toluene, ethanol or acetic acid. The piperazin-2-ones **81** can also be prepared by heating the sodium enolates of H(AP) **2** with 1,2-diaminoethane in glacial AcOH.[140] Under mild conditions (ethanol, 20 °C) the AP **2** and **4** react with *N*-phenyl-1,2-diaminoethane at the α-carbonyl group to give acyclic 4-aryl-4-oxo-2-(2-phenylamino)ethylamino-2-butenoic acids or their esters **83**.

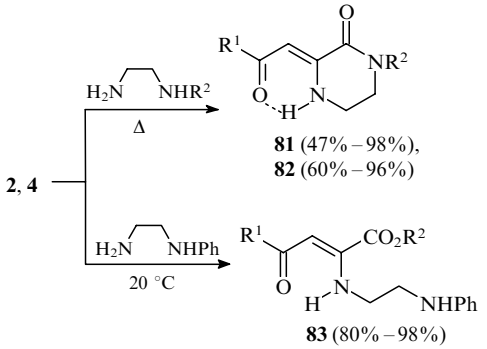

81: R^1 = Ar, Het, ferrocenyl, R^2 = H; **82**: R^1 = Ar, Het, R^2 = Me, Ph, CH_2Ph; **83**: R^1 = Ar, Het, R^2 = H, Me, Et.

However, on refluxing in ethanol, the pyruvate **2b** reacts with *N*-phenyl-1,2-diaminoethane at the ester fragment [the C(1) atom] to give benzoylpyruvic acid 2-phenylaminoethylamide in 61% yield.[30] 1,2-Diphenylaminoethane does not react with AP.[30]

It is noteworthy that the reaction of pentafluorobenzoylpyruvate **31a** with 1,2-diaminoethane gives, depending on the conditions, either 3-pentafluorobenzoyl- (**84a**) or 3-(2-hydroxy-3,4,5,6-tetrafluoro)benzoyl-methylidenepiperazin-2-ones (**84b**).[3, 5] The piperazinone **84a** is formed when the pyruvate **31a** is treated with a large excess of ethylenediamine at 20 °C in a MeOH–AcOH mixture, and the product **84b** is produced on refluxing equimolar amounts of the reactants in methanol.

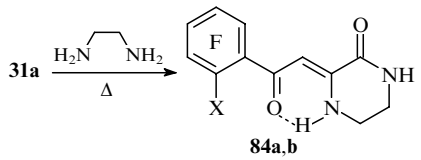

84a,**b**

X = F (**a**, 43%), OH (**b**, 18%).

Non-symmetric 1-methyl- and 1-phenyl-1,2-diaminoethanes have been shown [142] to react selectively with the APA esters **2** on refluxing in an ethanol–acetic acid mixture to give the corresponding 6-methyl- or 6-phenyl-3-aroylmethylenepiperazin-2-one **85** as the only reaction product.

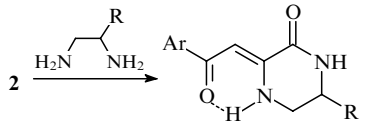

85 (58%–93%)

Reactions with 1,2-phenylenediamine and other arylenediamines. The major process involved in the reaction of the (H)APA **4**, their esters **2**, and the amides **6** with 1,2-phenylenediamine (PDA) is cyclocondensation at the α-dicarbonyl fragment [the C(1) and C(2) atoms] giving rise to the corresponding 3-aroylmethylidene-1,2,3,4-tetrahydroquinoxalin-2-ones (**86**).[3, 5, 8, 12, 21, 44, 46, 58, 62, 67, 107, 115, 123, 126, 143–149]

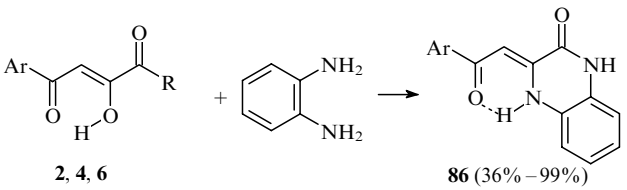

2, **4**, **6** **86** (36%–99%)

Ar = XC_6H_4 (X = H, 4-Me, 4-Et, OH, OMe, 4-Ph, 4-NO_2, 3-NO_2, 4-F, 4-Cl, 4-Br), 2,5-$Me_2C_6H_3$, 2,4,6-$Me_3C_6H_2$, C_6F_5, 1-naphthyl, 3-phenanthryl, 2-furyl, 2-thienyl, 4-pyridyl, 4-hydroxy-5-oxo-1,2-diphenyl-2,5-dihydroxypyrrol-3-yl, cymantrenyl;

2: R = OMe, OEt, OBu^t, SCH_2Ph; **4**: R = OH;

6: R = N(Ar′)C(Ph)=CH_2, NH_2, NHNHAr′, NHAr′, 3-pyridylamino, 2-pyridylamino.

Tautomerism of 2-quinoxalones **86** has been studied by spectroscopy.[145, 146] It was found that these compounds exist as IMHB-stabilised form **A** in the solid state and in solutions in DMSO-d_6. Noticeable amounts of forms **B**–**D** are found only in solutions in CF_3CO_2D.[145]

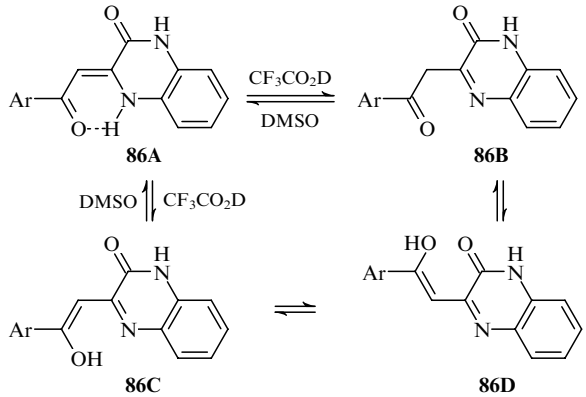

86A **86B** **86C** **86D**

3-Substituted APA and their esters react with PDA similarly to unsubstituted analogues to yield 3-(1-X-aroylmethyl)-1,2-dihydroquinoxalin-2-ones **87**.[80, 83, 89, 147] For instance, the 3-arylhydrazones **16**,[91] **17**[94–96] and 3-alkyl-substituted APA esters **14**[89, 147] readily react with PDA on refluxing in ethanol. The 3-halogen-containing AP **10** are more reactive and are converted into quinoxalinones **87** on treatment with PDA at 20 °C.[80, 83, 147] Heating of the reactants induces resinification [80] or formation of quinoxaline-2,3(1*H*,4*H*)-dione (**88**).[83]

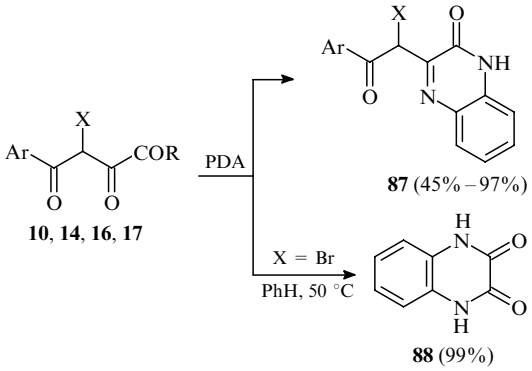

10, **14**, **16**, **17** **87** (45%–97%) **88** (99%)

10: X = Cl, Br; Ar = 4-YC_6H_4 (Y = H, Me, Br, OMe, F, Cl); R = OMe, OEt; **14**: X = Me, Et, $CHPh_2$; Ar = 4-YC_6H_4 (Y = H, Me, Br, Cl, NO_2); R = OMe, OEt; **16**, **17**: X = N = NAr′; R = OMe, OEt, OH; Ar = C_6H_4Y (Y = H, 4-Cl, 4-Br), C_6F_5; **87**: X = Me, Et, $CHPh_2$, Cl, Br, N = NAr′; Ar = 4-YC_6H_4 (Y = H, Me, Br, OMe, F, Cl, NO_2), C_6F_5.

However, prolonged refluxing in ethanol of 3-bromo-substituted ethyl benzoylpyruvate **10a** (Ar = Ph, R = Et, X = Br) with PDA furnishes 3-benzoylmethylidenequinoxalinone **86a** containing no bromine.[150]

When the acid **4a** has been made to react with PDA under mild conditions (Pr^iOH, 20 °C), a labile intermediate, 2-(2-ammoniophenylamino)-4-oxo-4-phenyl-2-butenoate (**89**), has been isolated. On heating, this compound is quantitatively converted into quinoxalinone **86a**.[148]

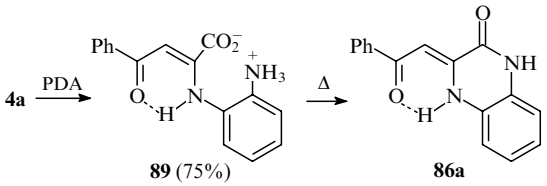

89 (75%) **86a**

It is notable that *tert*-butyl benzoylpyruvate prepared *in situ* from the acid **4a** and isobutylene in the presence of H_2SO_4 reacts with PDA to give, apart from the quinoxalinone **86a**, 2-*tert*-butoxycarbonyl-4-phenylbenzo[*b*]-1,4-diazepine isolated as hydrochloride **90**. The product **90** results from the competing cyclocondensation of PDA at the β-dicarbonyl fragment of the pyruvate **4a**. The diazepine **90** easily recyclises into the quinoxalinone **86a** upon dissolution.[149]

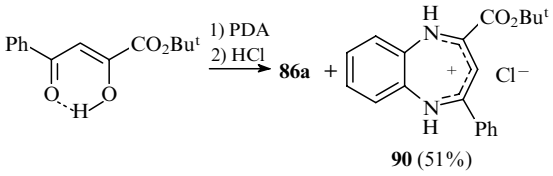

90 (51%)

Unlike the APA **4** and their esters **2**, the APA arylamides **6** react with PDA to give, depending on the reaction conditions, 4-arylbenzo[*b*]-1,4-diazepine-2-carboxylic acid arylamides **91**[29, 151] instead of the expected quinoxalinones **86**,[115] or a mixture of these products.[62, 149] The formation of the quinoxalinones **86** is promoted by performing the reaction in EtOH–AcOH–H_2O–HCl mixtures at pH 2.4–4.6 and temperatures of 20–65 °C.[115] Meanwhile, short-term fusion of the reactants at 115–130 °C furnishes predominantly the benzodiazepines **91**.[29, 115, 149] It was noted that electron-donating substituents in the aryl group of the initial amide **6** lead to higher yields of the benzodiazepines **91**, while electron-withdrawing groups promote the formation of the quinoxalinones **86**.[149] The reaction of the 3-pyridylamide **6b** with PDA on refluxing in a Pr^iOH–AcOH

mixture affords both the quinoxalinone **86a** and the benzodiazepine **91** (R = 3-pyridyl).[62]

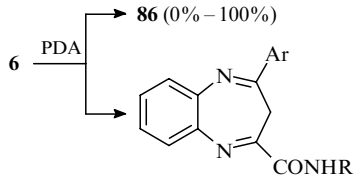

91 (39% – 99%)

86: Ar = XC_6H_4 (X = H, 4-Me, 4-OMe, 4-Cl, 4-Br, 4-NO_2, 3-NO_2);
91: Ar = 4-XC_6H_4 (X = H, Me, OMe, Br); R = 4-YC_6H_4 (Y = H, Me, OMe, Br), 3-pyridyl.

N-Monoalkyl(aryl)-1,2-phenylenediamines react with the AP **2** and **4** similarly to PDA giving rise to 1-alkyl(aryl)-3-aroylmethylidene-1,2,3,4-tetrahydroquinoxalin-2-ones **92** [8, 143, 152, 153] stabilised by an IMHB.[153] Note that these reactions proceed regio- and chemoselectively.

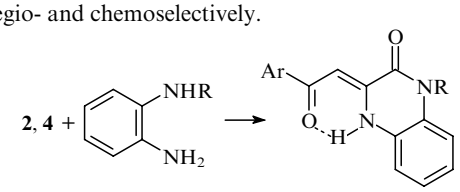

92 (40% – 84%)

Ar = 4-XC_6H_4 (X = H, Cl); R = Me, 4-XC_6H_4 (X = H, Me, OEt, Cl).

Heterocyclisations of the AP **2** with 1,2-phenylenediamines containing various substituents in the benzene ring have been described. The addition pattern depends on the nature of the substituent in the benzene ring of the nucleophile. 1,2-Diamino-chlorobenzene [145] and 1,2-diamino-4-nitrobenzene [8] provide 3-benzoylmethylidene-7-chloro- (**93a**) and 3-benzoylmethylidene-7-nitro-1,2,3,4-tetrahydroquinoxalin-2-ones (**93b**), whereas 3,4-diaminobenzonitrile forms 3-aroylmethylidene-6-cyano-1,2,3,4-tetrahydroquinoxalin-2-ones **94**.[51]

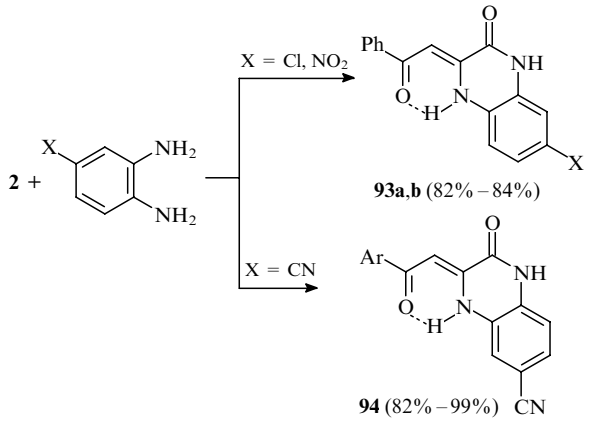

93a,**b** (82% – 84%)

94 (82% – 99%)

X = Cl (**a**), NO_2 (**b**); Ar = 4-YC_6H_4 (Y = H, Me, Cl).

2,3-Diaminonaphthalene reacts with the AP **2a** similarly to PDA to give 3-benzoylmethylene-1,2,3,4-tetrahydrobenzo[*g*]quinoxalin-2-one (**95**).[145]

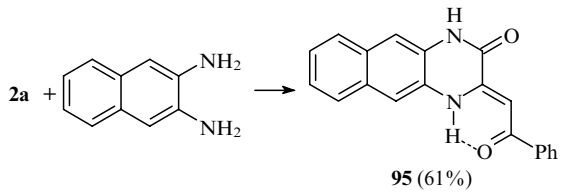

95 (61%)

On treatment with 5,6-diaminoacenaphthene, the AP **2a**,**b** and **4a** are cleaved even under mild conditions (at 18 °C) to give 6,7-ethanoperimidine-2-carboxylic acid **96**.[154]

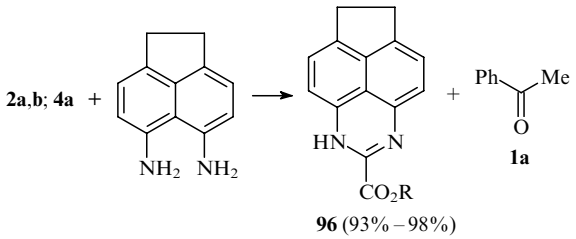

96 (93% – 98%)

R = H, Me, Et.

When the acid **4a** is refluxed with 2(6)-substituted 8-amino-1,2,3,4-tetrahydroquinolines **97a**,**b** in ethanol, 2-benzoylmethyl-4,5,6,7-tetrahydropyrido[1,2,3-*d*,*e*]quinoxalin-3(4*H*)-one derivatives **98a**,**b** are formed.[155]

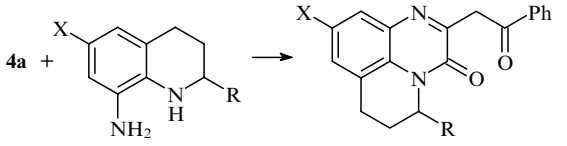

97a,**b** **98a**,**b** (39% – 68%)

R = Me, X = H (**a**); R = H, X = OMe (**b**).

Reactions with heterocyclic diamines. Known reactions of the (H)APA **4** and their esters **2** with heteroaromatic *ortho*-diamines result in the preparation of annelated pyrazin-2-one derivatives [156 – 162] (the products of addition at the α-dicarbonyl fragment of the AP) or [*b*]annelated 1,4-diazepines [160] (the products of cyclocondensation at the β-dicarbonyl part of the AP), depending on the nature of the reactants. In the case of non-symmetric diamines, these reactions proceed regioselectively. Moreover, in some cases, both possible series of regioisomers can be prepared.[157, 162]

It has been reported [156] that refluxing the HPA **4b**,**c** with 2,3-diaminopyridine (DAP) in an AcOH – H_2O mixture results in the formation of (*Z*)-2-heteroaroylmethylidene-1,2,3,4-tetrahydropyrido[2,3-*b*]pyrazin-3-ones **99b**,**c**. The researchers cited [156] confirmed the structure of the heterocycles **99** by converting them into 3-heteroaroyl-1,2,4,5-tetrahydropyrrolo[1,2-*a*]pyrido[2,3-*b*]pyridazine-1,2,4-triones **100** upon condensation with oxalyl chloride.[156]

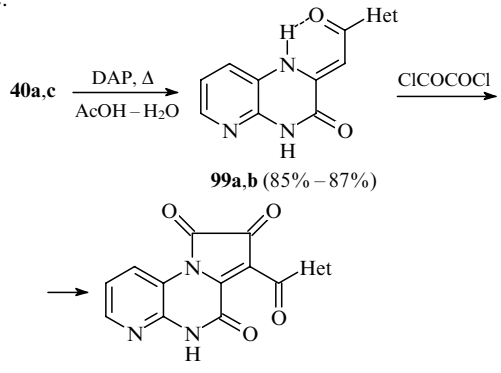

99a,**b** (85% – 87%)

100a,**b** (69% – 72%)

Het = 2-furyl (**4b**, **99a**, **100a**), 5-thiazolyl (**4c**, **99b**, **100b**).

Unlike the APA **4**, the esters **2** can yield two regioisomeric products, depending on the conditions, in the cyclocondensation with DAP. Thus 3-aroylmethylidene-1,2,3,4-tetrahydropyrido[2,3-*b*]pyrazin-2-ones **101** were prepared in an AcOH – EtOH – H_2O solvent mixture, whereas the use of an H_2SO_4 – EtOH – H_2O mixture gave 2-aroylmethylidene-1,2,3,4-tetrahydropyrido[2,3-*b*]pyrazin-3-ones **102**.[157] The structure of the heterocycles **101** and **102** was confirmed by hydrolysis of the compounds **101a** and **102a** followed by reduction to give the known methyltetrahydropyrido[2,3-*b*]pyrazinone **103**, **104** isomers.[163]

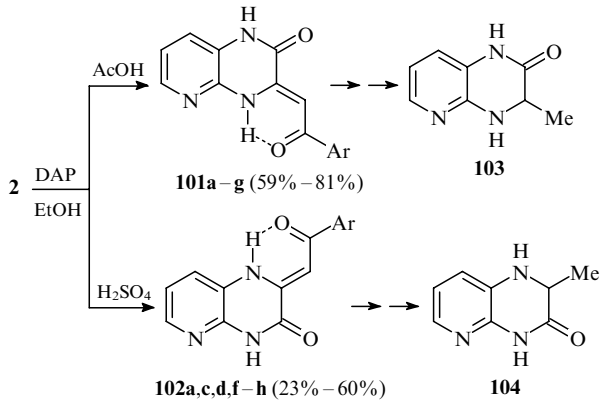

Ar = XC_6H_4 (X = H (**a**), 4-Me (**b**), 4-OMe (**c**), 3-OMe (**d**), 2-OMe (**e**), 4-OH (**f**), 4-Br (**g**), 2-OH (**h**)).

The reaction of the acid **4a** with 4,5-diamino-1-phenyl- (**105a**) and 4-amino-5-methylamino-1-phenyl-1,6-dihydropyridazin-6-ones (**105b**) in boiling ethanol has been described.[158] In the case of the diamine **105a**, the reaction gives the product of cycloaddition at the α-oxocarboxy group of the acid, 3-benzoylmethyl-6-phenyl-1,2,5,6-tetrahydropyrazino[2,3-*d*]pyridazine-2,5-dione (**106**), while the reaction with **105b** gives benzoylpyruvic acid *N*-(5-methylamino-6-oxo-1-phenyl-1,6-dihydropyridazinyl)amide (**107**).[158]

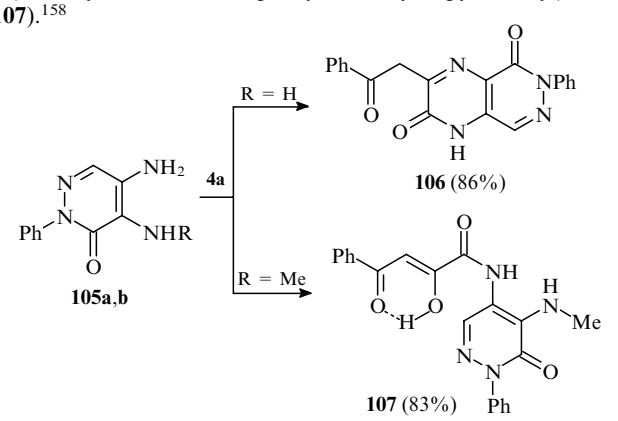

R = H (**a**), Me (**b**).

The reaction of the APA **4** with 1,2-diaminobenzimidazole in boiling AcOH occurs chemo- and regioselectively to yield 2-aroylmethyl-3,4-dihydro-1,2,4-triazino[2,3-*a*]benzimidazol-3-ones **108**.[159] Refluxing of the same reactants in methanol affords salts, which are formed, apparently, at the pyridine N(3) atom of the diamine (yields 80% – 85%). When refluxed in AcOH, the salts cyclise to give heterocycles **108** in 80% – 87% yields.[159]

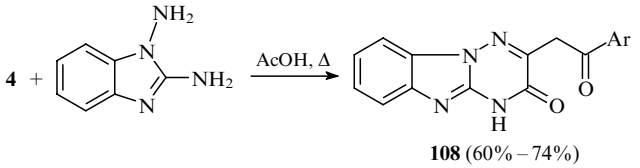

Ar = 4-XC_6H_4 (X = H, Me, OMe, Cl, Br).

The direction of the reactions of the AP **2**, **4** with 4,5-diamino-3-methyl-1-phenylpyrazole (**109**) depends on the conditions and on the nature of the α,β-tricarbonyl compound.[160] At 20 °C in methanol, in the presence of a catalytic amount of HCl, both the APA **4** and their esters **2** add selectively the diamine **109** at the β-dicarbonyl fragment giving rise to 7-aryl-5-carboxy(methoxycarbonyl)-3-methyl-1-phenyl-6*H*-pyrazolo[5,4-*b*]-1,4-diazepines **110**.

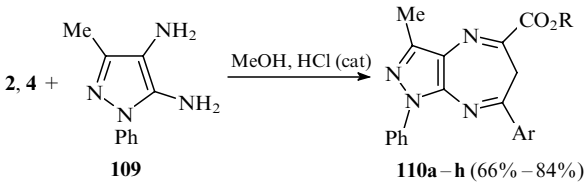

R = H (**a** – **c**), Me (**d** – **h**); Ar = 4-X C_6H_4 [X = H (**a**, **d**), Me (**b**, **e**), Cl (**c**, **f**), NO_2 (**g**)], 2,4-$Me_2C_6H_3$ (**h**).

When the reaction is carried out in benzene at 20 °C, the APA **4a** and diamine **109** form 2-(5-amino-3-methyl-1-phenylpyrazol-4-yl)amino-4-oxo-4-phenylbut-2-enoic acid (**111**), which cyclises to give pyrazolodiazepine **110a** when heated to 50 °C in methanol in the presence of HCl. Unlike the acid **4a**, the methyl ester **2b** adds selectively the diamine **109** at the α-oxoester fragment under similar conditions; this furnishes 5-benzoylmethyl-3-methyl-1-phenyl-6,7-dihydropyrazolo[4,5-*b*]pyrazin-6-one (**112**). The product **112** can also be obtained by heating the acid **111** without a solvent at 130 – 140 °C.[160]

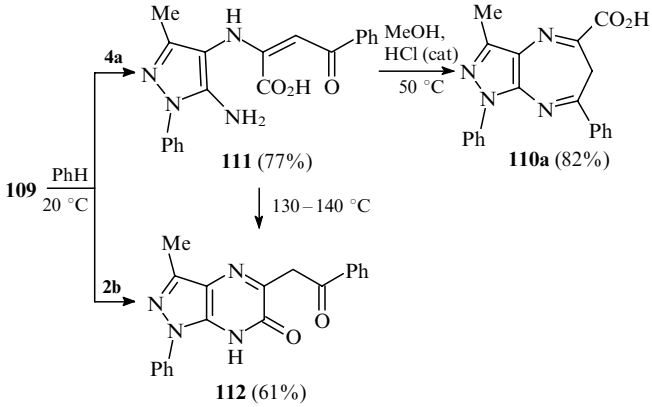

Although cyclocondensation at the α-dicarbonyl fragment is the major process in the reaction of both the APA **4** and the methyl ester **2** with 1,2-diamino-4-methyl-1,6-dihydropyrimidin-6-one on refluxing in AcOH, this process yields different regioisomers for these two types of substrate, namely, 2-aroylmethyl-6-methyl-4,8-dihydro-4*H*-pyrimido[1,2-*b*]-1,2,4-triazine-3,8-diones **113** and (*Z*)-3-aroylmethylidene-6-methyl-2,3,4,8-tetrahydro-1*H*-pyrimido[1,2-*b*]-1,2,4-triazine-2,8-diones **114**, respectively.[161]

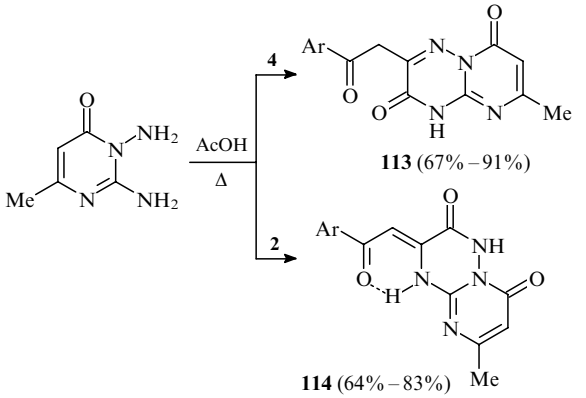

Ar = 4-XC_6H_4 (X = H, Me, OMe, Cl, OEt, Br, NO_2).

Heterocyclic amines such as 2,4,5,6-tetraamino- (**115a**) and 4-hydroxy-2,5,6-triaminopyrimidines (**115b**) condense with the AP **2** similarly to *o*-diamines. When refluxed in a solution of AcOH, both amines react selectively with the AP **2** or with the corresponding sodium enolates at the α-oxoester fragment to give 2,4-diamino-7-aroylmethylidene-5,6,7,8-tetrahydropteridin-6-ones

Scheme 8

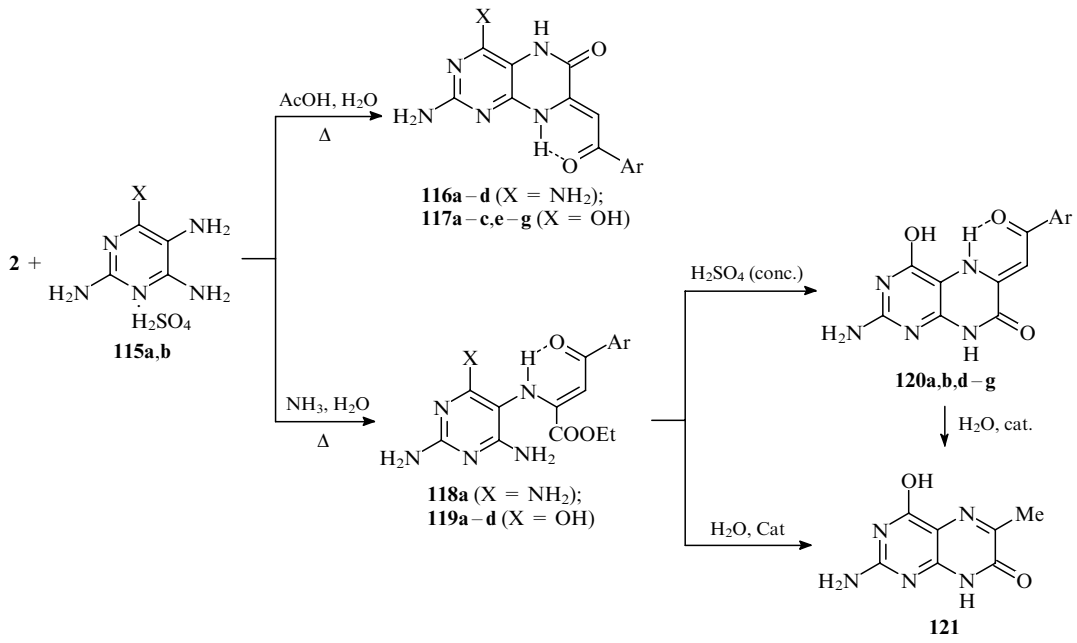

116, **117**, **119**: Ar = 4-YC_6H_4 [Y = H (**a**), Me (**b**), CN (**c**), OH (**d**), Cl (**e**), Br (**f**), CO_2H (**g**)]; **118a**: Ar = 4-OHC_6H_4 .

116 in the case of the amine **115a** or 2-amino-7-aroylmethylidene-4-hydroxy-5,6,7,8-tetrahydropteridin-6-ones **117** in the case of **115b**.[162] When the reaction is conducted in aqueous NH_3 (1 mol litre^{-1}, pH 8), derivatives of 4-aryl-2-(5-heteroaryl)-amino-4-oxobut-2-enoic acids **118a** and **119a–d**, respectively, can be isolated.[162, 164] In concentrated H_2SO_4, the compounds **119** cyclise into 2-amino-6-aroylmethylidene-4-hydroxy-5,6,7,8-tetrahydropteridin-7-ones **120**, which are isomers of the pteridines **117**. The structures of the products **119** and **120** were proved by hydrolysis, which gave rise to known 2-amino-4-hydroxy-6-methyl-7,8-dihydropteridin-7-ones (**121**) and benzoic acids (Scheme 8).[162]

Reactions with urea and sulfamides. The aroylpyruvic acids **4** react with urea at the α-oxocarboxyl fragment on fusion (120–130 °C); this affords 5-aroylmethylidene-2,3,4,5-tetrahydroimidazole-2,4-diones **122**.[165]

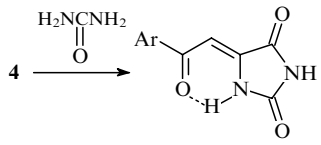

122 (68%–96%)

Ar = 4-XC_6H_4 (X = H, Me, Bu^t, OMe, F, Cl, Br).

The direction of reactions of methyl 3-bromoaroylpyruvates **10** (X = Br) with urea is determined by the reaction conditions. Fusion of equimolar amounts of the reactants for 20–30 min at 105–120 °C results in the formation of 6-aroyl-5-hydroxy-1,2,3,4-tetrahydropyrimidine-2,4-diones **123**, whereas the use of a great excess of urea and a longer reaction time (2 h) gives 5-aryl-4-methoxycarbonyl-2,3-dihydro-1*H*-imidazol-2-ones **124**.[166–168] The researchers proposed a mechanism for the formation of the heterocycles **123** and **124**, according to which the common first stage of the reaction is nucleophilic substitution of urea for the bromine atom in the initial AP **10**.[166]

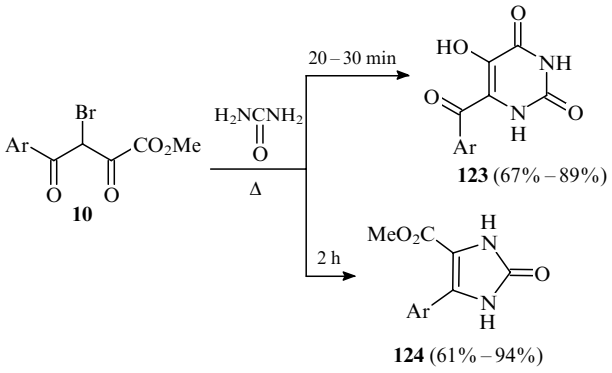

R = Me, X = Br; Ar = 4-YC_6H_4 (Y = H, Me, OMe, F, Cl, Br).

The APA esters **2** react with sulfamide on refluxing in HCl-saturated ethanol at the β-dicarbonyl fragment to give 5-aryl-3-ethoxycarbonyl-2*H*-1,2,6-thiadiazine 1,1-dioxides (**125**).[169] Similarly, *N*-methylsulfamide cyclocondenses selectively with the AP **2** giving rise to only one series of regioisomers, the position of the methyl group in which is not indicated in the study cited.[133] The most probable structure is, apparently, **126**, *i.e.*, the structure of 6-methyl-substituted 1,2,6-thiadiazine dioxides **125**. The products of reactions of the compounds **125**, **126** with ammonia, primary amines and hydrazine possess biological activities.[133, 169]

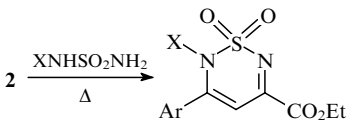

125 (X = H);
126 (X = Me)

Ar = 4-YC_6H_4 (Y = H, Cl, Me).

c. Reactions with N,O-dinucleophiles

Reactions with hydroxylamine. The acids **4** and their esters **2** react with hydroxylamine hydrochloride at the β-dicarbonyl fragment to give isoxazoles of only one of the two possible regioisomer classes — 5-arylisoxazole-3-carboxylic acids **127**. The reactions are usually carried out by refluxing in aqueous ethanol [13–15, 123, 170, 171] or at 20 °C in the presence of Na_2CO_3 with subsequent short-term heating with either strong acids [15] or acetyl chloride.[2] Less reactive arylamides AP **6** are converted into the corresponding amides **127** (R = NHAr) on refluxing with hydroxylamine hydrochloride in ethanol in the presence of KOH,[62] while the AP hydrazides **58** produce hydrazides **127** (R = NHNHAr) in boiling dioxane.[67]

Under mild conditions (EtOH – H_2O, Na_2CO_3, 20 °C), it is sometimes possible to isolate 2-oximes **128** formed as intermediates in the reactions of the (H)AP **2**, **4** with hydroxylamine hydrochloride.[2, 13, 15] The oximes **128** readily cyclise into isoxazoles **127** on heating or on treatment with strong acids [13, 15] or with dehydrating agents such as acetyl chloride.[2] The formation of ethyl 3-pyridoylpyruvate (**128h**) requires more drastic conditions.[17]

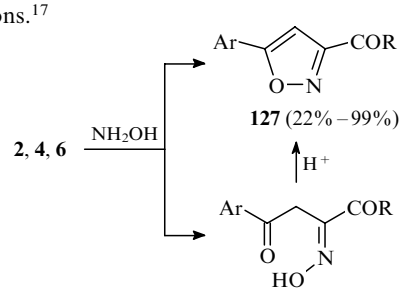

127: Ar = Ph, YC_6H_4 (Y = 4-Me, 4-Cl, 2-OMe, 4-AcNH), C_6F_5, 4-diphenyl, 3-phenanthryl, 2-pyrrolyl, 2-furyl, 2-thienyl, 5-methyl-2-thienyl; R = OH, OEt, 3-pyridylamino, $NHNHCOC_6H_4Z$ (Z = H, 4-OMe);
128: Ar = YC_6H_4 [Y = H (**a**), 2-NO_2 (**b**, **c**), 4-AcNH (**d**)], 2-furyl (**e**), 2-thienyl (**f**), 5-methyl-2-thienyl (**g**), 3-pyridyl (**h**); R = OH (**a**, **b**), OEt (**c** – **g**), OMe (**h**).

Reactions with 2-aminoethanol. The acids **4** add 2-aminoethanol at the α-oxocarboxyl fragment to give oxazine derivatives, the regiodirectivity of the reaction being dependent on the reaction conditions. The refluxing of the APA **4** with potassium 2-aminoethoxide in anhydrous dioxane yields 3-aroylmethylidene-3,4,5,6-tetrahydro-2*H*-1,4-oxazin-2-ones **129**;[172] the reaction in anhydrous ethanol affords 2-aroylmethylidene-3,4,5,6-tetrahydro-2*H*-1,4-oxazin-3-ones **130**.[173]

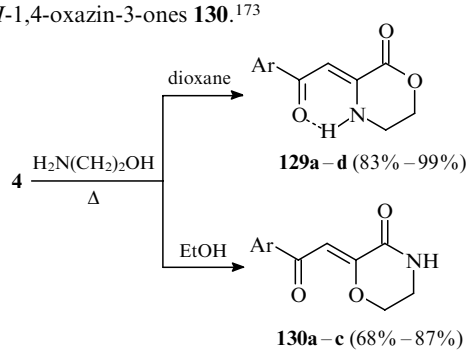

Ar = 4-XC_6H_4 [X = H (**a**), F (**b**), Br (**c**), Cl (**d**)].

The acid **31c** reacts with 2-aminoethanol in boiling dioxane also to give 3-pentafluorobenzoylmethylidene-3,4,5,6-tetrahydro-2*H*-1,4-oxazin-2-one (**129e**). The structure of the compound **129e** was confirmed by the fact that on heating in DMSO, it cyclises to yield 7,8,9,10-tetrafluoro-1,2-dihydro-1,4-oxazino[4,3-*a*]quinoline-4,6(4*H*,6*H*)-dione (**131**). On treatment with aqueous KOH, this product undergoes opening of the lactone ring, which gives potassium 1-(2-hydroxyethyl)-5,6,7,8-tetrafluoro-4-oxo-1,4-dihydroquinoline-2-carboxylate (**132**).[26, 27]

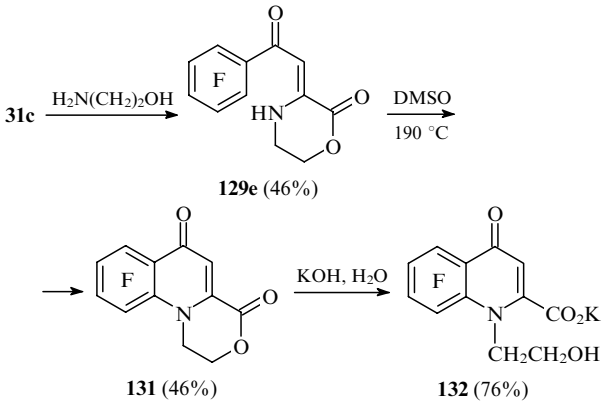

Reactions with 2-aminophenol and its derivatives. The reactions of 2-aminophenol with the APA **4**, their esters **2** and anilides **6** also involve the α-dicarbonyl fragment and give 3-aroylmethylidene-3,4-dihydro-1,4-benzoxazin-2(2*H*)-ones **133**.[3, 5, 9, 21, 29, 37, 44, 45, 53, 174–177]

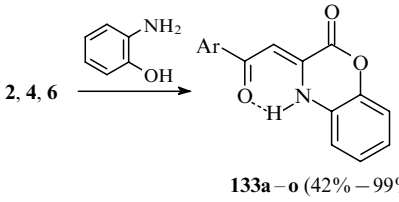

2: R = OMe, OEt; **4**: R = OH; **6**: R = NHPh.
Ar = XC_6H_4 [X = H (**a**), 4-Me (**b**), 4-OMe (**c**), OH (**d** – **f**), 4-F (**g**), 4-Cl (**h**), 4-Br (**i**), 4-NO_2 (**j**)], 2,4,6-$Me_3C_6H_2$ (**k**), 2-furyl (**l**), 2-thienyl (**m**), 4-pyridyl (**n**), cymantrenyl (**o**);

The tautomerism of benzoxazines **133** has been studied by spectroscopy.[145, 146] It was shown that in the solid state and in DMSO-d_6 solutions, they exist as form **A** stabilised by an IMHB. Noticeable amounts of forms **B** – **D** are present only in CF_3CO_2D.[145]

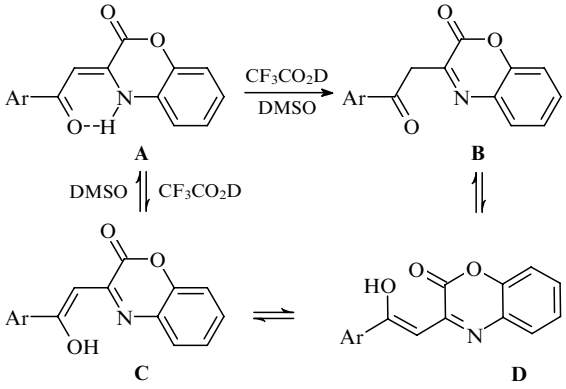

When the reaction of the acid **4a** with 2-aminophenol was carried out under mild conditions (ethanol, 20 °C), a salt was isolated. On heating, this salt readily cyclised to benzoxazin-2-one **133a**.[37] It has been shown [37] that benzoxazinones **133** are thermodynamically less stable than quinoxalones **86**. Thus the compound **133a** is converted into the quinoxalone **86a** almost quantitatively when fused with PDA; in solutions, this transformation occurs even at 20 °C.

Pentafluorobenzoylpyruvate **31a** can react with 2-aminophenol to give, unlike non-fluorinated analogues, not only 3-pentafluorobenzoylmethylidene-3,4-dihydro-1,4-benzoxazin-2(2*H*)-one (**133p**), but also its mixture with 2-hydroxy-3,4,5,6-tetrafluorobenzoylmethylidene-3,4-dihydro-2*H*-1,4-benzoxazin-2-one (**133q**). The compound **133p** is formed under mild conditions (at 20 °C)

in alcohol, while the product mixture is produced when the reactants are refluxed.[3, 5, 176]

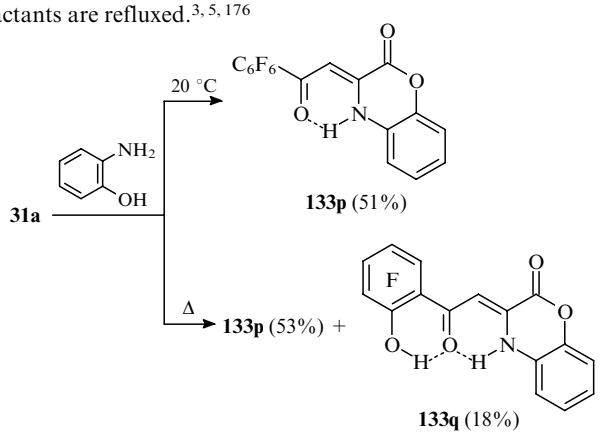

4(5)-Monosubstituted 2-aminophenols and 1-amino-2-naphthol react with the AP **2** similarly to 2-aminophenol yielding 6(7)-derivatives of 3-aroylmethylidene-3,4-dihydro-1,4-benzoxazin-2(2*H*)-ones **134a**–**d** and 3-benzoylmethylidene-3,4-dihydronaphtho[2,1-*b*]-1,4-benzoxazin-2(2*H*)-one (**135**), respectively.[145, 175, 177]

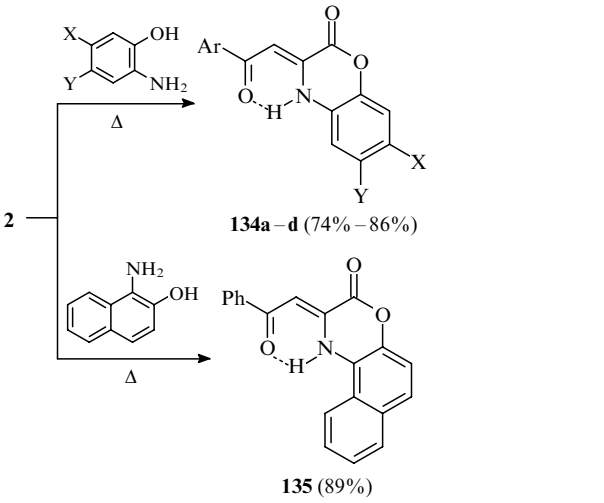

Ar = Ph (**a**–**c**), 4-MeC$_6$H$_4$ (**d**); X = H (**a**–**c**), Me (**d**); Y = Me (**a**), Cl (**b**), NO$_2$ (**c**), H (**d**).

The reaction of the APA **4** with 2-aminobenzyl alcohol carried out by refluxing in toluene gives 4-aroylmethylidene-3,4-dihydro-1*H*,5*H*-benzo[*e*]-1,4-oxazepin-3-one **136**.[178]

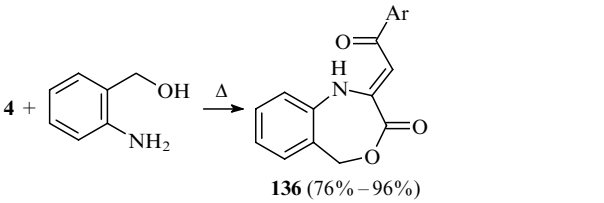

The reactions of the APA **4** and their methyl esters **2** with 2-aminophenyldiphenylmethanol carried out by refluxing in benzene do not result in cyclisation products but give instead 4-aryl-2-[2-(1-hydroxydiphenylmethyl)phenylamino]-4-oxo-4-but-2-enoic acids and their esters **137**. Unlike the ester **137d**, the acids **137a**,**b** cyclise when refluxed in acetic anhydride to 5-acetyl-4-aroylmethylidene-1,1-diphenyl-3,4-dihydro-1*H*,5*H*-benzo[*e*]-1,4-oxazepin-3-ones **138**.[64, 179]

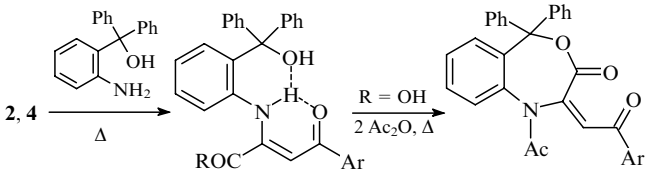

Ar = 4-XC$_6$H$_4$ [X = H (**a**), Me (**b**, **d**), Cl (**c**)]; R = OH (**a**–**c**), OMe (**d**).

d. Reactions with N,S-dinucleophiles

Reaction with 2-mercaptoethylamine. The acids **4** react with 2-mercaptoethylamine in boiling ethanol to give acyclic 4-aryl-2-(2-mercaptoethylamino)-4-oxobut-2-enoic acids **139**, except for the APA having a methoxy group in the aryl substituent. In this case, the reaction yields cyclic 3-(4-methoxybenzoylmethylidene)-2,3,5,6-tetrahydro-1,4-thiazin-2(4*H*)-one (**140**), which is due, apparently, to the strong electron-donating effect of the methoxy group.[44]

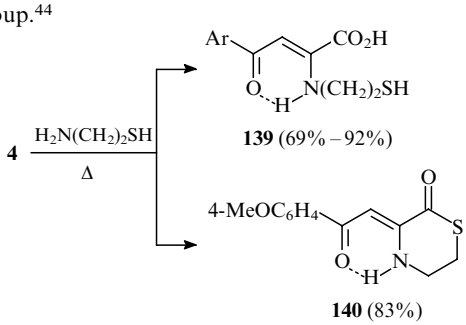

Ar = 4-XC$_6$H$_4$ (X = H, Me, Cl, Br, NO$_2$).

Reaction with 2-mercaptoaniline. The aroylpyruvic acids **4** react with 2-mercaptoaniline on refluxing in toluene; the reaction involves the α -oxocarboxyl fragment and affords 2-aroylmethylidene-3,4-dihydro-1,4-benzothiazin-3(2*H*)-ones **141**.[180] Unlike the acids **4**, their methyl esters **2** react with 2-mercaptoaniline on fusion to give the products of addition at the carbonyl group attached to C(2), *i.e.*, 2-aroylmethyl-2-methoxycarbonyl-2,3-dihydrobenzothiazoles **142**.[180, 181]

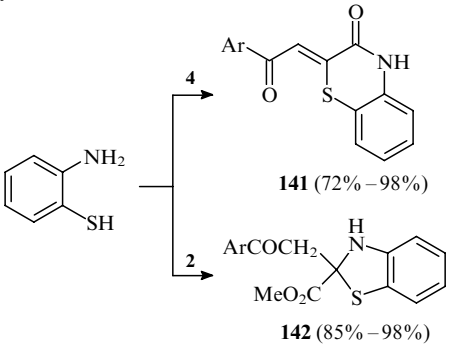

Ar = 4-XC$_6$H$_4$ (X = H, Me, OMe, Cl, Et, F, Br).

It is of interest that pentafluorobenzoylpyruvates **31b**,**d** behave in a different way towards 2-mercaptoaniline. The pyruvate **31b** is cleaved by the nucleophile under mild conditions (methanol, 15–25 °C) to give ultimately 2-[4-(2-aminophenylthio)-2,3,5,6-tetrafluorophenyl]benzothiazole (**143**). Under similar conditions, the copper(II) chelate **31d** reacts with 2-mercaptoaniline hydrochloride to give the product of selective cyclocondensation at the α-oxoester fragment, 3-pentafluorobenzoylmethylidene-3,4-dihydro-1,4-benzothiazin-2(2*H*)-one (**144**).[3, 6]

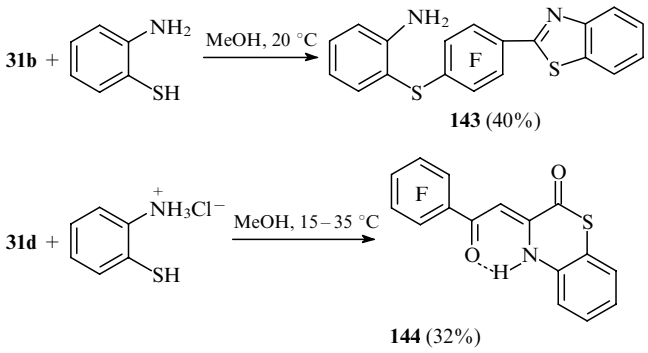

4. Miscellaneous reactions

A specific feature of the APA **4** and their esters **2** in the formation of heterocycles is the ability to react simultaneously at the nucleophilic C(3) atom and one electrophilic center.

Fusion of ethyl benzoylpyruvate **2a** with benzylideneaniline is known [182] to result in the formation of 4-benzoyl-3-hydroxy-1,5-diphenyldihydropyrrol-2(5*H*)-one (**145**, Y = H, Ar = R = Ph). Borsche has shown [183] that the same pyrrol-2-ones **145** can be prepared from the APA **4** if an equimolar mixture of arylamine and aldehyde is used instead of *N*-arylaldimine. In subsequent studies dealing with the synthesis of pyrrolediones **145**, all the three components, namely, (H)AP, aldehydes and amines were varied over wide limits.[13, 184–187] These reactions are usually carried out in alcohol, AcOH or dioxane at 20–60 °C. The yields of the target products **145** can be increased by using an aldehyde – amine mixture, instead of the corresponding aldimine, and in the case where the AP **2**, **4** contain electron-withdrawing substituents. It is of interest that pyrrolediones **145** are easily (AcOH, 20 °C) formed also from benzoylpyruvic acid 2-pyridylamide **6** (Ar = Ph, R = 2-Py) and diarylaldimines.[187]

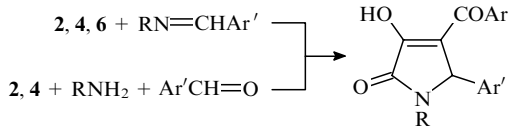

Ar = Ph, 4-XC_6H_4 (X = Me, OMe, OEt, Cl, Br, NO_2), 2-furyl;
R = Ph, 2-naphthyl, 4-MeC_6H_4, CH_2CO_2H, $(CH_2)_2NMe_2$;
Ar′ = C_6H_4Y (Y = H, 4-OMe, 4-I, 4-Cl, 4-Br, 4-OH, 2-OMe, 2-F, 2-Cl).

In the given reactions, the aldimine acts as an N-nucleophile and a C-electrophile with respect to AP. The enolysed structure of **145** has been confirmed by NMR spectroscopy.[184–186]

It is notable that when 2-aminonaphthalene (or the corresponding aldimines) are used as the amine component, the acid **4a** is not converted into pyrrolones **145** in boiling ethanol but forms (according to the Doebner condensation pattern) 2-substituted 3-benzoyl-4-carboxybenzo[*f*]quinolines **146**.[183, 188] In this case, the Schiff base acts as a C-nucleophile [the C(1) atom of the 2-naphthyl group] and a C-electrophile with respect to the AP.

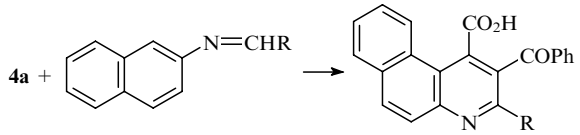

R = H, Me, Ph, 4-$MeOC_6H_4$, piperonyl.

The reaction of ethyl 2-furoylpyruvate **4c** with 2-aminobenzaldehyde gives 3-(2-furoyl)-2-ethoxycarbonylquinoline (**147**).[13]

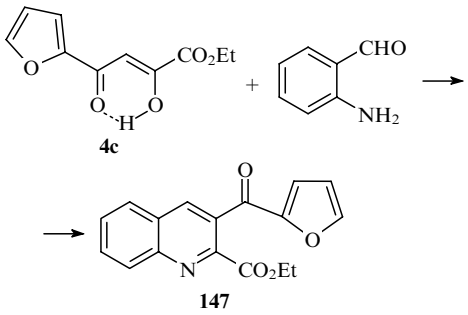

It has been reported [89] that refluxing of ethyl 4-chlorobenzoylpyruvate with diphenyldiazomethane in benzene induces cycloaddition of the ester at the C(2) and C(3) atoms without elimination of nitrogen to give 3,3-diphenyl-5-(4-chlorobenzoyl)-4-ethoxycarbonyl-3*H*-1,2-pyrazole (**148**).

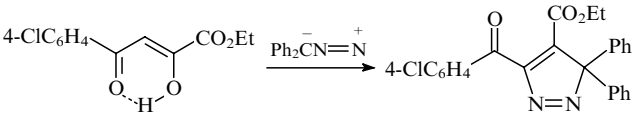

IV. Biological activities of (het)aroylpyruvates and the products of their heterocyclisation

The interest in the (H)AP chemistry is related, first of all, to the broad spectrum of biological activities exhibited by representatives of this group of compounds and the products of their heterocyclisation.

Thus sodium enolates derived from ethylbenzoyl- and 4-chlorobenzoylpyruvates possess an antimicrobial activity *in vitro*.[189] Hetaroylpyruvic acids [23] and their esters [22, 33, 34, 36] have been found to display antiaggregation,[23] antibacterial,[23, 33, 34] antiviral,[22] antiinflammatory [34] and analgesic [36] activities. 3-Halogenated esters of APA showed antibacterial [80, 84] and antifungal [18, 80] effects. The most diverse and the highest biological activities were found for (H)APA amides and hydrazides. Substances with analgesic,[31, 54, 59, 61, 62, 73, 94, 179, 190] antiinflammatory,[31, 42, 50, 54, 57–60, 62, 69, 70, 72, 73, 85, 94, 179] anticonvulsant,[43, 61] antiviral [69–71] and antibacterial [50, 51, 57, 58, 61, 62, 66, 69, 70, 73, 77, 86, 179, 190] activities have been found among this group.

Many heterocyclic compounds obtained from (H)AP possess various types of physiological activities. The pyrazoles **66** (R^1 = NHR^2) exhibit antiinflammatory,[31, 59, 62, 73] analgesic [59, 73] and antibacterial [62, 69, 128] activities with low toxicity. 5-(3-Pyridyl)-3-hydrazinocarbonylpyrazole (**66**, Ar = 3-pyridyl, R = $NHNH_2$) has been patented as an antitumour agent.[17] Antibacterial action has been discovered for a number of 1-phenyl-5-hetarylpyrazole-3-carboxylic acids **67**.[23] 3-Aroylmethylenepiperazin-2-ones **81** [137, 139, 191] and their 1-methyl- and 1-phenyl- **82**[141, 191] or 6-methyl- and 6-phenyl-substituted **85**[142] derivatives show antiinflammatory, anticonvulsant and analgesic activities in combination with low toxicity. Antiinflammatory [94] and analgesic [91, 94] effects of 3-(1-phenylazoaroylmethylene)-1,2,3,4-tetrahydroquinoxalin-2-ones **87** (X = N = NPh) have been reported. *N*-Aryl-4-arylbenzo[b]diazepine-2-carboxamides **91** were patented as analgesics.[151] Antibacterial and antiinflammatory activities have been found for 3-aroylmethylene-6-cyano-2-quinoxalinones **94**.[51] The tetrahydropyridoquinoxalinones **98** exhibited a tuberculostatic activity *in vitro*.[155] It was found that 4-aryl-2-(5-heteroaryl)amino-4-oxobut-2-enoic acid **119** stimulates the cell growth of some microorganisms.[162, 164] Some 5-aroylmethyleneimidazolidine-2,4-diones **122** possess an anticonvulsant activity while having low toxicity; they depress the central nervous system and, possibly, the activity of the microsomal liver enzymes.[165] A series of 5-aryl-1,2,6-thiadiazine-3-

carboxylic acid 1,1-dioxide derivatives **125**, **126** demonstrated antiviral and sedative activities.[133] The benzoxazepinones **136** show antimicrobial action.[178] An antibacterial activity has been noted for 4-aryl-2-[2-(1-hydroxydiphenylmethyl)phenylamino]-4-oxo-4-but-2-enoic acids and their esters **137**.[179] The benzothiazoline **142** (Ar = Ph) has an antiinflammatory activity.[181] In the case of some pyrrolones **145**, antibacterial[185, 186] and nootropic activities have been found.[185]

V. Conclusion

Analysis of the published data demonstrates that (H)AP represent an ample class of organic compounds containing carboxyl, ester, or amide functional groups. An indispensable structural feature of these substances is the presence of the β-dicarbonyl fragment. The structure of (H)AP accounts for their great synthetic potential. The availability of a wide range of (H)AP is ensured by facile and convenient procedures for their preparation, the main of them being the Claisen condensation or hydrolysis (alcoholysis) of 2,3-dihydrofuran-2,3-diones and -pyrrole-2,3-diones.

When comparing the reactivity of the APA **4**, the esters **2** and the amides **6**, one cannot but note that the amides **6** are somewhat less reactive. Indeed, similar reactions require more drastic conditions in the case of the APA amides **6**. In all the (H)AP **2**, **4** and **6**, the C(2) centre, *i.e.*, the α-carbonyl group, is the site of choice for the primary attack in the reactions with both mono- and dinucleophilic reagents (see Scheme 5). However, when a bulky substituent has been introduced at the 3-position of (H)AP, some reactions involve the ester group. The transformations of (H)AP on treatment with dinucleophiles arouse the greatest interest because these reactions serve as the basis for the synthesis of various heterocyclic systems. The reaction can involve either the α- or β-dicarbonyl fragment. In the reactions with α-dinucleophiles (hydrazines, hydroxylamine), the β-dicarbonyl moiety of (H)AP is involved in the process, while for most of other nucleophiles, the addition at the α-dicarbonyl residue is preferred. In the majority of cases, these processes are regio- and chemoselective, which allows (H)AP to be used for targeted synthesis of heterocycles.

Nevertheless, the chemistry of (H)AP is far from being exhausted. Further research into the properties of these compounds and into the prospects for using them in organic synthesis appears quite topical. These may be related, for example, to investigation of fluoro-containing (H)AP the chemistry of which has essential distinctive features. In addition, (H)AP with organometallic aryl groups are still unknown. The authors hope that this review will be favourable for the development of research into the biological activity of (H)AP and their heterocyclic derivatives, which has been studied only cursorily and fragmentarily.

Thus, (H)AP are readily available and convenient building blocks for the design of diverse acyclic and heterocyclic structures. They can be considered to be promising for further investigations in the fields of heterocyclic and medical chemistry.

This review was supported by the Russian Foundation for Basic Research (Project No. 00-03-32767a).

References

1. C Beyer, L Claisen *Berichte* **20** 2178 (1887)
2. S Salvatori *Gazz. Chim. Ital.* **21** (2) 268 (1891)
3. V I Saloutin, Y V Burgart, C O Kappe, O N Chupakhin *Heterocycles* **52** 1411 (2000)
4. V I Saloutin, Ya V Burgart, O N Chupakhin *Usp. Khim.* **68** 227 (1999) [*Russ. Chem. Rev.* **68** 203 (1999)]
5. V I Saloutin, S G Perevalov *J. Fluor. Chem.* **96** 87 (1999)
6. V I Saloutin, S G Perevalov, O N Chupakhin *Zh. Org. Khim.* **36** 727 (2000) [a]
7. D D Nekrasov *Khim. Geterotsikl. Soedin.* 291 (2001) [b]
8. I V Mashevskaya, R R Makhmudov, G A Aleksandrova, O V Golovnina, A V Duvalov, A N Maslivets *Khim.-Farm. Zh.* **35** (4) 20 (2001) [c]
9. I A Tolmacheva, I V Mashevskaya, A N Maslivets *Zh. Org. Khim.* **37** 630 (2001) [a]
10. S N Shurov, Yu S Andreichikov, in *Khimiya Pyatichlennykh 2,3-Dioksogeterotsiklov* (The Chemistry of Five-Membered 2,3-Dioxoheterocycles) (Perm': Perm' State University, 1994) p. 5
11. O Piloty, H Will *Berichte* **46** 2607 (1913)
12. S Fatutta, A Stener *Gazz. Chim. Ital.* **88** 89 (1958)
13. C Musante, S Fatutta *Gazz. Chim. Ital.* **88** 879 (1958)
14. S Fatutta, M Balestra *Gazz. Chim. Ital.* **88** 899 (1958)
15. T S Gardner, E Wenis, J Lee *J. Org. Chem.* **26** 1514 (1961)
16. V A Zagorevskii, D A Zykov *Zh. Obshch. Khim.* **33** 2469 (1963) [d]
17. US P. 3 449 350; *Chem. Abstr.* **71** 70 595 (1969)
18. H A Burch, J E Gray *J. Med. Chem.* **15** 429 (1972)
19. USSR P. 345 134; *Chem. Abstr.* **78** 71 485 (1973)
20. V P Gorbunova, N N Suvorov *Khim. Geterotsikl. Soedin.* 1519 (1973) [b]
21. Yu S Andreichikov, Z D Belykh, E V Kalmykova, M D Reshetova, in *4-ya Vsesoyuznaya Konferentsiya po Metalloorganicheskoi Khimii, Kazan' 1988* (The Fourth All-Union Conference on Organometallic Chemistry, Kazan' 1988) Pt. 1, p. 15
22. Russ. P. 2 032 683; *Chem. Abstr.* **124** 106 627 (1996)
23. T N Yanborisov, I A Zhikina, Yu S Andreichikov, A V Milyutin, A N Plaksina *Khim.-Farm. Zh.* **32** (9) 26 (1998) [c]
24. V I Saloutin, Z E Skryabina, I T Bazyl', O N Chupakhin *Izv. Akad. Nauk, Ser. Khim.* 362 (1993) [e]
25. V I Saloutin, Z E Skryabina, I T Bazyl', O N Chupakhin *J. Fluor. Chem.* **65** 37 (1993)
26. V I Saloutin, I T Bazyl', Z E Skryabina, P N Kondrat'ev, O N Chupakhin *Izv. Akad. Nauk, Ser. Khim.* 299 (1994) [e]
27. V I Saloutin, Z E Skryabina, I T Bazyl', P N Kondrat'ev, O N Chupakhin *J. Fluor. Chem.* **69** 119 (1994)
28. Yu S Andreichikov, V L Gein, L O Kon'shina, N N Shapet'ko *Zh. Org. Khim.* **25** 2494 (1989) [a]
29. Yu S Andreichikov, S P Tendryakova, Yu A Nalimova, S G Pitirimova, L A Voronova *Zh. Org. Khim.* **13** 529 (1977) [a]
30. Yu S Andreichikov, T N Tokmakova, L N Voronova, Yu A Nalimova *Zh. Org. Khim.* **12** 1073 (1976) [a]
31. Yu S Andreichikov, A V Milyutin, I V Krylova, R F Saraeva, E V Dormidontova, L P Drovosekova, F Ya Nazmetdinov, V E Kolla *Khim.-Farm. Zh.* **24** (7) 33 (1990) [c]
32. Yu S Andreichikov, S P Tendryakova, Yu A Nalimova, G D Plakhina *Khim. Geterotsikl. Soedin.* 1030 (1977); [b] USSR P. 740 747; *Chem. Abstr.* **93** 185 976 (1980)
33. Yu S Andreichikov, D D Nekrasov, E A Kolevatova, M A Trushule *Khim.-Farm. Zh.* **24** (12) 33 (1990) [c]
34. D D Nekrasov, V G Chizh, Yu S Andreichikov, R R Makhmudov *Khim.-Farm. Zh.* **28** (4) 30 (1994) [c]
35. D D Nekrasov, V G Chizh, Yu S Andreichikov, G A Tul'bovich *Zh. Org. Khim.* **32** 761 (1996) [a]
36. D D Nekrasov, V G Chizh, Yu S Andreichikov, G A Tul'bovich, G A Aleksandrova *Khim.-Farm. Zh.* **31** (3) 34 (1997) [c]
37. Yu S Andreichikov, L A Voronova, A V Milyutin *Zh. Org. Khim.* **15** 847 (1979) [a]
38. Yu S Andreichikov, Yu A Nalimova, G D Plakhina, R F Saraeva, S P Tendryakova *Khim. Geterotsikl. Soedin.* 1468 (1975); [b] USSR P. 476 254; *Chem. Abstr.* **83** 178 796 (1975)
39. Yu S Andreichikov, Yu A Nalimova, S P Tendryakova, Ya M Vilenchik *Zh. Org. Khim.* **14** 160 (1978) [a]
40. USSR P. 727 633; *Chem. Abstr.* **93** 185 792 (1980)
41. USSR P. 727 632; *Chem. Abstr.* **93** 149 825 (1980)
42. USSR P. 686 308; *Chem. Abstr.* **96** 115 968 (1982)
43. USSR P. 769 992; *Chem. Abstr.* **96** 28 651 (1982)
44. Yu S Andreichikov, S P Tendryakova, Yu A Nalimova, I V Krylova *Zh. Org. Khim.* **18** 193 (1982) [a]
45. USSR P. 630 253; *Chem. Abstr.* **90** 87 078 (1979)
46. Yu S Andreichikov, Yu V Ionov *Zh. Org. Khim.* **18** 2430 (1982) [a]
47. USSR P. 956 462; *Chem. Abstr.* **98** 53 435 (1983)
48. Yu S Andreichikov, D D Nekrasov, M A Rudenko, A Yu Konovalov *Khim. Geterotsikl. Soedin.* 740 (1987) [b]
49. Yu S Andreichikov, I V Krylova *Zh. Org. Khim.* **24** 2212 (1988) [a]

50. Yu S Andreichikov, D D Nekrasov, I V Krylova, V I Bachurina *Khim. Geterotsikl. Soedin.* 1461 (1992) [b]
51. Yu S Andreichikov, D D Nekrasov, S G Pitirimova, A S Zaks, M I Korsheninnikova, P N Plaksina, Z N Semenova, V A Kopeikin *Khim.-Farm. Zh.* **23** 946 (1989) [c]
52. A V Milyutin, Yu S Andreichikov, in *Seminar-Soveshchanie 'Potrebiteli i Proizvoditeli Organicheskikh Reaktivov', Erevan, 1991* (Seminar-Meeting 'Users and Producers of Organic Agents', Erevan, 1991) p. 67
53. D D Nekrasov, S V Kol'tsova, Yu S Andreichikov *Khim. Geterotsikl. Soedin.* 173 (1994) [b]
54. Russ. P. 2 021 262; *Chem. Abstr.* **123** 276 022 (1995)
55. D D Nekrasov, S V Kol'tsova, Yu S Andreichikov, G A Tul'bovich *Zh. Org. Khim.* **31** 907 (1995) [a]
56. Z G Aliev, S N Shurov, E Yu Pavlova, Yu S Andreichikov, L O Atovmyan *Izv. Akad. Nauk, Ser. Khim.* 1552 (1995) [e]
57. T N Yanborisov, N N Kasimova, A V Milyutin, Yu S Andreichikov, I P Rudakova, G N Novoselova, V E Kolla, F Ya Nazmetdinov *Khim.-Farm. Zh.* **29** (8) 29 (1995) [c]
58. A V Milyutin, L R Amirova, F Ya Nazmetdinov, R R Makhmudov, A L Golovanenko, Yu S Andreichikov, V E Kolla *Khim.-Farm. Zh.* **30** (5) 47 (1996) [c]
59. A V Milyutin, R R Makhmudov, Yu S Andreichikov, A F Goleneva, G A Tul'bovich, T I Kovina *Khim.-Farm. Zh.* **30** (6) 20 (1996) [c]
60. Russ. Appl. 94 037 753/04; *Ref. Zh. Khim.* 18 O 97 P (1997)
61. N M Igidov, E N Koz'minykh, A V Milyutin, E S Berezina, G A Shavkunova, I B Yakovlev, S A Shelenkova, V E Kolla, E V Voronina, V O Koz'minykh *Khim.-Farm. Zh.* **30** (11) 21 (1996) [c]
62. A V Milyutin, L R Amirova, I V Krylova, F Ya Nazmetdinov, G N Novoselova, Yu S Andreichikov, V E Kolla *Khim.-Farm. Zh.* **31** (1) 32 (1997) [c]
63. M A Tlekhusezh, Yu S Andreichikov, Z I Tyukhteneva, L A Badovskaya *Khim. Geterotsikl. Soedin.* 1422 (1998) [b]
64. N V Kolotova, V O Koz'minykh, E V Dolbilkina, E N Koz'minykh *Izv. Akad. Nauk, Ser. Khim.* 2317 (1998) [e]
65. USSR P. 785 303; *Chem. Abstr.* **94** 208 569 (1981)
66. USSR P. 782 317; *Chem. Abstr.* **97** 127 273 (1982)
67. A N Maslivets, O P Tarasova, I S Berdinskii, Yu S Andreichikov *Zh. Org. Khim.* **25** 1039 (1989) [a]
68. Yu S Andreichikov, Yu V Ionov, O P Tarasova, A N Maslivets *Khim. Geterotsikl. Soedin.* 846 (1990) [b]
69. V O Koz'minykh, N M Igidov, V I Il'enko, A V Milyutin, V E Kolla, Z N Semenova, Yu S Andreichikov *Khim.-Farm. Zh.* **26** (7–8) 28 (1992) [c]
70. V O Koz'minykh, N V Safonova, A V Milyutin, V G Armaginova, V E Kolla, S A Shelenkova, I V Yakovlev, G N Novoselova, Yu S Andreichikov, V I Il'enko *Khim.-Farm. Zh.* **28** (3) 42 (1994) [c]
71. Russ. P. 1 623 134; *Chem. Abstr.* **126** 70 116 (1997)
72. A V Milyutin, N V Safonova, V P Chesnokov, F Ya Nazmetdinov, E V Voronina, I V Krylova, Yu S Andreichikov, V E Kolla, Yu V Kozhevnikov *Khim.-Farm. Zh.* **30** (5) 26 (1996) [c]
73. A V Milyutin, L R Amirova, V E Kolla, F Ya Nazmetdinov, L P Drovosekova, Yu S Andreichikov *Khim.-Farm. Zh.* **32** (8) 24 (1998) [c]
74. S N Shurov, L N Karpova, E Yu Posyagina, Yu V Ionov, T N Somova, N G Shilova, Yu S Andreichikov *Zh. Org. Khim.* **35** 1232 (1999) [a]
75. Yu S Andreichikov, S N Shurov, V V Zalesov, N N Shapet'ko *Zh. Org. Khim.* **22** 857 (1986) [a]
76. T N Yanborisov, S N Shurov, Yu S Andreichikov, in *3-e Vsesoyuznoe Soveshchanie po Khimicheskim Reaktivam, Ashkhabad, 1989* (The Third All-Union Meeting on Chemical Agents, Ashkhabad, 1989) p. 38
77. T N Yanborisov, S N Shurov, Yu S Andreichikov, I P Rudakova, E N Semenova, G N Novoselova *Khim.-Farm. Zh.* **23** 1470 (1989) [c]
78. V V Zalesov, N A Pulina, Yu S Andreichikov *Zh. Org. Khim.* **25** 1054 (1989) [a]
79. Yu S Andreichikov, A N Maslivets, L I Smirnova, O P Krasnykh, A P Kozlov, L A Perevozchikov *Zh. Org. Khim.* **23** 1534 (1987) [a]
80. Yu S Andreichikov, G D Plakhina, S G Pitirimova, E P Oshchepkova, A N Plaksina *Khim.-Farm. Zh.* **12** (1) 76 (1978) [c]
81. L N Kurkovskaya, N N Shapet'ko, Yu S Andreichikov, V L Gein, G D Plakhina, S P Tendryakova *Zh. Strukt. Khim.* **16** 1070 (1975) [f]
82. USSR P. 466 208; *Chem. Abstr.* **83** 43 070 (1975)
83. Yu S Andreichikov, G D Plakhina, S P Tendryakova, Yu A Nalimova, Z D Belykh, in *Khimiya Elementoorganicheskikh Soedinenii II, IV, V, VI Grupp Periodicheskoi Sistemy* (The Chemistry of Organoelement Compounds of Groups II, IV, V and VI of Periodic System (Perm': Perm' State University, 1978) p. 156
84. USSR P. 650 329; *Chem. Abstr.* **96** 68 617 (1982)
85. USSR P. 623 356; *Chem. Abstr.* **96** 28 650 (1982)
86. USSR P. 750 971; *Chem. Abstr.* **96** 46 260 (1982)
87. L N Karpova, N V Kolotova, S N Shurov, Yu S Andreichikov *Zh. Org. Khim.* **28** 779 (1992) [a]
88. Yu S Andreichikov, N V Gel't, A P Kozlov *Zh. Org. Khim.* **20** 1749 (1984) [a]
89. A L Fridman, Yu S Andreichikov, V L Gein *Zh. Org. Khim.* **13** 1422 (1977) [a]
90. E V Brigadnova, A N Maslivets, Yu S Andreichikov *Zh. Org. Khim.* **26** 327 (1990) [a]
91. USSR P. 505 641; *Chem. Abstr.* **85** 41101 (1976)
92. E V Pimenova, Yu S Andreichikov *Zh. Org. Khim.* **28** 376 (1992) [a]
93. E V Pimenova, A N Maslivets, R A Khamatgaleev, Yu S Andreichikov, in *Karbonil'nye Soedineniya v Sinteze Geterotsiklov* (Carbonyl Compounds in the Synthesis of Heterocycles) (Saratov: Saratov State University, 1996) P. 124
94. Yu S Andreichikov, L F Gein, V L Gein, E L Pidemskii *Khim.-Farm. Zh.* **11** (4) 17 (1977) [c]
95. Y V Burgart, A S Fokin, O G Kuzueva, O N Chupakhin, V I Saloutin *J. Fluor. Chem.* **82** 101 (1998)
96. V I Saloutin, A S Fokin, Ya V Burgart *Zh. Org. Khim.* **35** 309 (1999) [a]
97. E V Pimenova, A N Maslivets, S N Shurov, Yu S Andreichikov *Zh. Org. Khim.* **31** 604 (1995) [a]
98. E V Pimenova, R A Khamatgaleev, E V Voronina, Yu S Andreichikov *Khim.-Farm. Zh.* **33** (8) 22 (1999) [c]
99. P Battesti, O Battesti, M Selim *Bull. Soc. Chim. Fr.* 2214 (1974)
100. L N Kurkovskaya, N N Shapet'ko, Yu S Andreichikov, R F Saraeva *Zh. Strukt. Khim.* **13** 1026 (1972) [f]
101. Z G Aliev, S N Shurov, D D Nekrasov, I B Podvintsev, L O Atovmyan *Zh. Strukt. Khim.* **41** 1255 (2000) [f]
102. A N Maslivets, O P Krasnykh, L I Smirnova, Yu S Andreichikov *Zh. Org. Khim.* **25** 1045 (1989) [a]
103. USSR P. 1 608 186; *Chem. Abstr.* **115** 29 111 (1991)
104. V I Saloutin, I T Bazyl', Z E Skryabina, G G Aleksandrov, O N Chupakhin *Zh. Obshch. Khim.* **64** 2054 (1994) [d]
105. O Mumm, O Böhme *Berichte* **54** 726 (1921)
106. D I Sychev *Zh. Org. Khim.* **25** 1341 (1989) [a]
107. V L Gein, L O Kon'shina, Yu S Andreichikov *Zh. Org. Khim.* **28** 2134 (1992) [a]
108. USSR P. 1 441 735; *Chem. Abstr.* **116** 128 947 (1992)
109. Yu S Andreichikov, V L Gein, O I Ivanenko, E V Brigadnova, A N Maslivets *Zh. Org. Khim.* **24** 1115 (1988) [a]
110. Yu S Andreichikov, D I Sychev *Zh. Org. Khim.* **29** 1085 (1993) [a]
111. N M Igidov, E N Koz'minykh, O A Sof'ina, T M Shironina, V O Koz'minykh *Khim. Geterotsikl. Soedin.* 1466 (1999) [b]
112. S N Shurov, I A Zhikina *Zh. Obshch. Khim.* **70** 1890 (2000) [d]
113. E V Pimenova, Yu S Andreichikov, in *Khimiya Pyatichlennykh 2,3-Dioksogeterotsiklov* (The Chemistry of Five-Membered 2,3-Dioxoheterocycles) (Perm': Perm' State University, 1994) p. 188
114. E Klingsberg *Chem. Rev.* **54** 59 (1954)
115. Yu S Andreichikov, A P Kozlov, L N Kurdina *Zh. Org. Khim.* **20** 826 (1984) [a]
116. A P Kozlov, V V Ryabova, G A Kozlova, Yu S Andreichikov *Zh. Org. Khim.* **33** 406 (1997) [a]
117. L N Kurkovskaya, N N Shapet'ko, Yu S Andreichikov, R F Saraeva *Zh. Strukt. Khim.* **16** 139 (1975) [f]
118. Yu S Andreichikov, A P Kozlov, L N Kudrina *Zh. Org. Khim.* **19** 378 (1983) [a]
119. USSR P. 488 811; *Chem. Abstr.* **84** 16 930 (1976)
120. A N Maslivets, Yu S Andreichikov, in *Khimiya Pyatichlennykh 2,3-Dioksogeterotsiklov* (The Chemistry of Five-Membered 2,3-Dioxoheterocycles) (Perm': Perm' State University, 1994) p. 91
121. V I Saloutin, I T Bazyl', Z E Skryabina, O N Chupakhin *Izv. Akad. Nauk, Ser. Khim.* 904 (1994) [e]

122. D Liberman, N Rist, F Grumbach, S Cals, M Moyeux, A Rouaix *Bull. Soc. Chim. Fr.* 687 (1958)
123. C Musante, S Fatutta *Ann. Chim. (Rome)* **49** 1496 (1959)
124. J Elguero, G Guiraud, R Jacquier *Bull. Soc. Chim. Fr.* 619 (1966)
125. Yu S Andreichikov, A N Maslivets, L I Smirnova *Zh. Org. Khim.* **23** 2254 (1987) [a]
126. V I Saloutin, Z E Skryabina, P N Kondrat'ev, S G Perevalov *Zh. Org. Khim.* **31** 266 (1995) [a]
127. E V Pimenova, R A Khamatgaleev, E V Voronina, Yu S Andreichikov *Khim.-Farm. Zh.* **32** (8) 27 (1998) [c]
128. I I Lapkin, Yu S Andreichikov *Zh. Org. Khim.* **2** 2075 (1966) [a]
129. S I Yakimovich, I V Zerova *Zh. Org. Khim.* **14** 42 (1978) [a]
130. S I Yakimovich, I V Zerova *Zh. Org. Khim.* **16** 1633 (1980) [a]
131. O P Krasnykh, A N Maslivets, V R Stukov, Yu S Andreichikov, in *Khimiya Fiziologicheski Aktivnykh Soedinenii. Vsesoyuznyi Seminar, Chernogolovka, 1989* (The Chemistry of Physiologically Active Compounds. All-Union Seminar, Chernogolovka, 1989) p. 137
132. S I Yakimovich, V N Nikolaev *Zh. Org. Khim.* **17** 284 (1981) [a]
133. US P. 3 223 703; *Chem. Abstr.* **64** 8217 (1966)
134. E Cattelain, P Chabrier *Bull. Soc. Chim. Fr.* 1098 (1947)
135. Z G Aliev, L O Atovmyan, Yu S Andreichikov, S V Kol'tsova, D D Nekrasov *Izv. Akad. Nauk, Ser. Khim.* 704 (1998) [e]
136. Yu S Andreichikov, S V Kol'tsova, I A Zhikina, D D Nekrasov *Zh. Org. Khim.* **35** 1567 (1999) [a]
137. A V Milyutin, N V Safonova, R R Makhmudov, G A Tul'bovich, V A Safin, A F Goleneva, in *8-ya Mezhdunarodnaya Konferentsiya po Khimicheskim Reaktivam, Ufa, 1995* (The Eighth International Conference on Chemical Agents, Ufa, 1995) p. 98
138. Yu S Andreichikov, T N Tokmakova, E L Pidemskii, L A Voronova, Ya M Vilenchik *Khim.-Farm. Zh.* **11** (5) 85 (1977) [c]
139. USSR P. 1 544 773; *Chem. Abstr.* **113** 23 949 (1990)
140. A V Milyutin, N V Safonova, A F Goleneva, Yu S Andreichikov, G A Tul'bovich, R R Makhmudov *Khim.-Farm. Zh.* **28** (12) 37 (1994) [c]
141. A V Milyutin, N V Safonova, R R Makhmudov, G N Novoselova, A F Goleneva, Yu S Andreichikov *Khim.-Farm. Zh.* **30** (3) 42 (1996) [c]
142. A V Milyutin, N V Safonova, R R Makhmudov, Yu S Andreichikov, Z G Aliev *Khim.-Farm. Zh.* **32** (1) 27 (1998) [c]
143. G S Predvoditeleva, T V Kartseva, M N Shchukina, T N Zykova, G N Pershin *Khim.-Farm. Zh.* **2** (11) 19 (1968) [c]
144. Yu S Andreichikov, R F Saraeva, A L Fridman *Khim. Geterotsikl. Soedin.* 259 (1973) [b]
145. Y Iwanami, T Seki, T Inagaki *Bull. Chem. Soc. Jpn.* **44** 1316 (1971)
146. Y Iwanami, T Inagaki *J. Heterocycl. Chem.* **13** 681 (1976)
147. Yu S Andreichikov, S G Pitirimova, R F Saraeva, V L Gein, G D Plakhina, L A Voronova *Khim. Geterotsikl. Soedin.* 407 (1978) [b]
148. A N Maslivets, L I Smirnova, O I Ivanenko, Yu S Andreichikov *Khim. Geterotsikl. Soedin.* 697 (1991) [b]
149. Yu S Andreichikov, S G Pitirimova, S P Tendryakova, R F Saraeva, T N Tokmakova *Zh. Org. Khim.* **14** 169 (1978) [a]
150. E V Brigadnova, Yu S Andreichikov *Zh. Org. Khim.* **25** 1169 (1989) [a]
151. USSR P. 611 421; *Chem. Abstr.* **91** 193 345 (1979)
152. G S Predvoditeleva, T V Kartseva, T N Zykova, M N Shchukina, G N Pershin *Khim.-Farm. Zh.* **6** (10) 3 (1972) [c]
153. A N Maslivets, L I Smirnova, Yu S Andreichikov *Zh. Org. Khim.* **28** 2141 (1992) [a]
154. USSR P. 895 983; *Chem. Abstr.* **97** 92 303 (1982)
155. T V Kartseva, G S Predvoditeleva, V I Shvedov, N B Lapaeva, G N Pershin *Khim.-Farm. Zh.* **12** (7) 89 (1978) [c]
156. I V Mashevskaya, I A Tolmacheva, A N Maslivets *Khim. Geterotsikl. Soedin.* 1277 (2000) [b]
157. T Seki, H Sakata, Y Iwanami *J. Heterocycl. Chem.* **32** 347 (1995)
158. G S Predvoditeleva, T V Kartseva, M N Shchukina *Khim.-Farm. Zh.* **8** (9) 7 (1974) [c]
159. V P Kruglenko, V P Gnidets, N A Klyuev, E V Logachev, M A Klykov, M V Povstyanoi *Khim. Geterotsikl. Soedin.* 1402 (1985) [b]
160. T N Yanborisov, I A Zhikina, O A Yanborisova, S N Shurov, Yu S Andreichikov *Zh. Org. Khim.* **28** 2554 (1992) [a]
161. D D Nekrasov, S N Shurov, O I Ivanenko, Yu S Andreichikov *Zh. Org. Khim.* **30** 126 (1994) [a]
162. Y Iwanami, T Seki *Bull. Chem. Soc. Jpn.* **45** 2829 (1972)
163. T Seki, H Sakata, Y Iwanami *J. Heterocycl. Chem.* **32** 703 (1995)
164. Jpn. P. 72-45 752; *Chem. Abstr.* **78** 97 697 (1973)
165. V S Zalesov, Yu S Andreichikov, Yu A Nalimova, S P Tendryakova, S M Starkova, N A Podushkina *Khim.-Farm. Zh.* **12** (7) 93 (1978) [c]
166. Yu S Andreichikov, G D Plakhina *Zh. Org. Khim.* **23** 872 (1987) [a]
167. USSR P. 674 414; *Chem. Abstr.* **93** 150 271 (1980)
168. USSR P. 794 007; *Chem. Abstr.* **95** 25 060 (1981)
169. J B Wright *J. Org. Chem.* **29** 1905 (1964)
170. P G Baraldi, A Barco, S Benetti, S Manfredini, G P Pollini, D Simoni *Tetrahedron* **43** 235 (1987)
171. P G Baraldi, D Simoni, F Moroder, S Manfredini, L Mucchi, F D Vecchia, P Orsolini *J. Heterocycl. Chem.* **19** 557 (1982)
172. USSR P. 621 676; *Chem. Abstr.* **90** 87 478 (1979)
173. USSR P. 910 627; *Chem. Abstr.* **97** 92 298 (1982)
174. Yu S Andreichikov, L A Voronova, A P Kozlov *Zh. Org. Khim.* **15** 520 (1979) [a]
175. A N Maslivets, I V Mashevskaya, O P Krasnykh, S N Shurov, Yu S Andreichikov *Zh. Org. Khim.* **28** 2545 (1992) [a]
176. V I Saloutin, S G Perevalov, Z E Skryabina *Zh. Org. Khim.* **32** 1386 (1996) [a]
177. Z G Aliev, O P Krasnykh, A N Maslivets, L O Atovmyan *Izv. Akad. Nauk, Ser. Khim.* 2080 (2000) [e]
178. USSR P. 666 799; *Chem. Abstr.* **93** 71 822 (1980)
179. N V Kolotova, V O Koz'minykh, E V Dolbilkina, E N Koz'minykh, V E Kolla, S A Shelenkova *Khim.-Farm. Zh.* **32** (9) 32 (1998) [c]
180. Yu S Andreichikov, S P Tendryakova, Yu A Nalimova, L A Voronova *Khim. Geterotsikl. Soedin.* 755 (1977); [b] USSR P. 615 071; *Chem. Abstr.* **89** 129 528 (1978)
181. USSR P. 625 392; *Chem. Abstr.* **95** 150 646 (1981)
182. R Schiff, L Gigli *Berichte* **31** 1306 (1898)
183. W Borsche *Berichte* **42** 4072 (1909)
184. Yu S Andreichikov, V L Gein, I N Anikina *Zh. Org. Khim.* **22** 1749 (1986) [a]
185. V L Gein, L F Gein, N Yu Porseva, E V Voronina, M I Vakhrin, K D Potemkin, V E Kolla, L P Drovosekova, A V Milyutin, N S Shchuklina, G A Veikhman *Khim.-Farm. Zh.* **32** (9) 23 (1998) [c]
186. V L Gein, N N Kasimova, E V Voronina, L F Gein *Khim.-Farm. Zh.* **35** (3) 31 (2001) [c]
187. A V Milyutin, V L Gein, Yu S Andreichikov *Zh. Obshch. Khim.* **62** 2633 (1992) [d]
188. E A Robinson, M T Bogert *J. Org. Chem.* **1** 65 (1936)
189. H Rinderknecht, J L Ward, F Bergel, A L Morrison *Biochem. J.* **41** 463 (1947)
190. E N Koz'minykh, N M Igidov, E S Berezina, G A Shavkunova, I B Yakovlev, S A Shelenkova, V E Kolla, E V Voronina, V O Koz'minykh *Khim.-Farm. Zh.* **30** (7) 31 (1996) [c]
191. Russ. P. 2 067 579; *Chem. Abstr.* **126** 312 261 (1997)

[a] — *Russ. J. Org. Chem. (Engl. Transl.)*
[b] — *Chem. Heterocycl. Compd. (Engl. Transl.)*
[c] — *Chem.-Pharm. J. (Engl. Transl.)*
[d] — *Russ. J. Gen. Chem. (Engl. Transl.)*
[e] — *Russ. Chem. Bull., Int. Ed. (Engl. Transl.)*
[f] — *J. Struct. Chem. (Engl. Transl.)*

Russian Chemical Reviews **70** (11) 939 – 969 (2001) © 2001 Russian Academy of Sciences and Turpion Ltd

DOI 10.1070/RC2001v070n11ABEH000682

Synthetic molecular systems based on porphyrins as models for the study of energy transfer in photosynthesis

N V Konovalova, R P Evstigneeva, V N Luzgina

Contents

I.	Introduction	939
II.	Porphyrin dimers	940
III.	Multiporphyrin ensembles	954
IV.	Porphyrin – carotenoid compounds	962
V.	Conclusion	967

Abstract. The published data on the synthesis and photochemical properties of porphyrin-based molecular ensembles which represent models of natural photosynthetic light-harvesting complexes are generalised and systematised. The dependence of the transfer of excitation energy on the distance between donor and acceptor components, their mutual arrangement, electronic and environmental factors are discussed. Two mechanisms of energy transfer reactions, *viz*., 'through space' and 'through bond', are considered. The bibliography includes 96 references.

I. Introduction

Absorption of solar energy and its subsequent transformation by cells in the course of photosynthesis is the basis for the energy supply for vital activities of all living organisms. It is therefore not surprising that this problem arouses considerable theoretical and practical interest from investigators.[1–6] Spectroscopic and theoretical studies of photosynthetic processes are mainly focused on the fundamental analysis of photophysical and photochemical characteristics of biological energy-transforming systems and the construction of supramolecular ensembles for molecular photonics and optoelectronics.[7–10]

Chlorophylls and related pigments as well as quinones and carotenoid polyenes are the major components of natural photosynthetic systems. Their interactions are reduced to three basic photochemical processes, *viz*., singlet – singlet energy transfer, triplet – triplet energy transfer and photoinduced electron transfer. For example, antenna systems, which contain chlorophylls, carotenoids and other accessory pigments, collect light and transfer excitation energy to the reaction centres *via* a singlet – singlet energy transfer mechanism.[11,12] Carotenoids are responsible for photoprotection of living organisms from destructive effects of highly reactive singlet oxygen by rapid quenching of the triplet state of chlorophylls *via* a triplet – triplet energy transfer mechanism.[13] The excitation energy derived from antenna complexes is transformed into chemical energy in the course of photoinduced electron transfer mediated by chlorophylls and quinones, which, in turn, generates long-living states with transmembrane separation of charges.[14–16]

Recent studies have led to the synthesis of molecular systems which successfully simulate certain stages of natural conversion of solar energy, particularly, the above-mentioned singlet and triplet energy transfer reactions. The choice of pigments, donors and acceptors for such model systems is based of their spectral properties, which determine the energy characteristics of various excited states. Chromophores related to pigments involved in natural photosynthetic processes are the most promising components for such systems.

The choice of the working principle, which regulates interactions between the individual fragments of a system, is no less important. These interactions, which are controlled by the spatial arrangement of the photosynthetic components and the nature of the separating medium, strongly affect the rates and quantum yields of photochemical processes. The spatial arrangement of pigments, donors and acceptors in natural photosynthetic systems is provided by their interactions with protein subunits. One of the strategies in the construction of artificial photosynthetic systems consists of the substitution of covalent bonds for pigment – protein interactions.[1–3,6] An alternative strategy involves noncovalent assembly of supramolecular complexes, mostly by virtue of the formation of hydrogen and coordination bonds.[17] The construction, in the past few years, of models in which amino acids and peptides are used as connecting bridges (spacers) permitted one to study different regularities of energy and electron transfer in a protein matrix.[18]

The majority of supramolecular model systems described in the literature reproduce the photoinduced electron transfer step. Spectroscopic studies of donor – acceptor model systems have made it possible to establish the dependence of rates of photochemical charge separation reactions on structural factors, such as the distance between the system components and their orientation, on the interactions between the electronic systems of the donor and the acceptor, thermodynamic driving force of the electron transfer and environmental factors.[1–3,6]

Until very recently, much less attention was given to the development of model systems mimicking certain functional steps of light-harvesting antenna complexes.

Light-harvesting antenna complexes inherent in natural photosynthetic systems absorb low-intensity sunlight at wavelengths ~280 – 900 nm (up to 1040 nm in the case of some bacterial complexes) eventually resulting in the transfer of energy to the reaction centres. These complexes contain a large number of chlorophyll or bacteriochlorophyll molecules, carotenoid poly-

N V Konovalova, R P Evstigneeva, V N Luzgina M V Lomonosov Moscow State Academy of Fine Chemical Technology, 117571 Moscow, Prosp. Vernadskogo 86, Russian Federation. Fax (7-095) 434 87 11. Tel. (7-095) 434 85 44. E-mail: httos.mitht@g23.relcom.ru (N V Konovalova)

Received 1 June 2001
Uspekhi Khimii **70** (11) 1059 – 1093 (2001); translated by R L Birnova

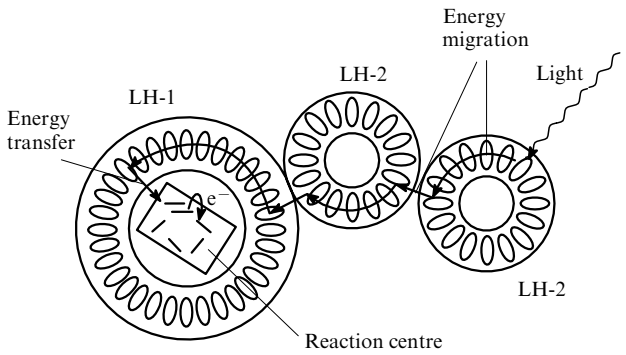

Figure 1. The structures of the bacterial light-harvesting complexes LH-1 and LH-2 responsible for the transfer of absorbed light energy to the reaction centres.[11]

enes and some other accessory pigments held at a small distance from one another by virtue of noncovalent interactions with the protein environment. Absorption of photons by pigments of antenna complexes is followed by migration of excited state energy generated by pigment ensembles until excitation reaches the reaction centre (Fig. 1). The energy can be transferred over sufficiently large distances at record-breaking high speed and with nearly quantitative quantum efficiency (quantum yields).[11, 12]

The complexity of supramolecular pigment–protein structures of natural antenna complexes hinders detailed investigations of light-harvesting reactions at the molecular level and does not provide unambiguous answers to the following questions. How do electronic, photophysical and photochemical properties of pigments influence the efficiency of light-harvesting processes? How does energy migration depend on the three-dimensional configuration of pigments (*viz.*, the distance between the components, their orientation, spatial packing, *etc.*)? What are the mechanisms of electronic interactions between pigments and the role of local environment? What are the effects of these interactions on the synthetic ensembles after substitution of covalent bonds for pigment–protein interactions between the components? What is the mechanism of functioning of the pigments as integral antenna systems within the ensembles and at what distances does energy migrate? Is it possible to increase the efficiency of energy migration in artificial systems by varying the system structure or energy gradients and what are the structural limitations for directional migration of energy? These questions are of crucial importance for the correct understanding of light-harvesting processes occurring in photosynthesising organisms and purposeful utilisation of solar energy. In this context, artificial model systems offer convenient subjects for the study of regularities of energy transfer in natural antenna complexes.

In this review, we consider the main principles of the construction of porphyrin-based model photosynthetic systems and the methods of their synthesis. The applications of these systems in the study of energy transfer in photosynthesis are also discussed.

II. Porphyrin dimers

Porphyrin dimers present special interest for investigation of pairwise interactions between pigments in larger ensembles as the simplest models for energy transfer studies. According to the type of their binding, these compounds can be divided into three groups, *viz.*, covalently bound molecules with hydrocarbon spacers, complexes with amino acid and peptide spacers and systems linked by non-covalent bonds.

1. Porphyrin dimers with hydrocarbon spacers

a. Synthesis

The synthesis of covalently bound pigment ensembles is the most popular approach to the design of bisporphyrin model systems.

Covalently bound π-conjugated donor–acceptor systems are convenient models for the study of regularities of energy transfer at large distances. The polyyne- and polyene-bound bisporphyrins **1a–d** and **2a–d** are examples of such systems.[19] The strength of electron-exchange reactions between the donors and the acceptors in these compounds is largely determined by the 'centre-to-centre' distance between two porphyrin macrocycles. This, in turn, is strictly correlated with the number of unsaturated bonds in polyyne-bound systems and can be measured, with a high degree of precision, for polyene-bound molecules taking account of rotation of porphyrin rings around the single bonds.

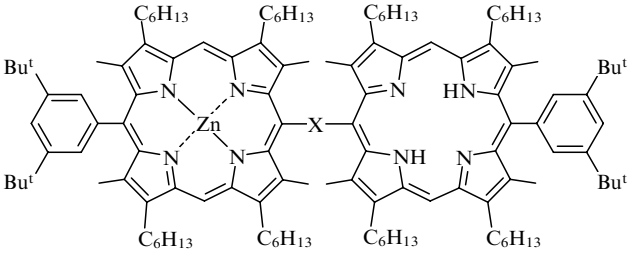

1a–d, **2a–d**, **3a–c**

1: X = *p*-C_6H_4–(–C≡C–)$_n$–C_6H_4-*p*; *n* = 1 (**a**), 2 (**b**), 3 (**c**), 4 (**d**);

2: X = *p*-C_6H_4–(–CH=CH–)$_n$–C_6H_4-*p*; *n* = 1 (**a**), 2 (**b**), 3 (**c**), 4 (**d**);

3: X = *p*-$C_6H_4C{\equiv}C{-}Ar{-}C{\equiv}C\,C_6H_4$-*p*; Ar = 1,2-$C_6H_4$ (**a**), 1,3-C_6H_4 (**b**), 1,4-C_6H_4 (**c**).

The efficiency of intramolecular singlet energy transfer in the dimeric porphyrins **3a–c** and **4a–c** containing bis(phenylethynyl)phenylene bridges is determined by both the distance and mutual arrangement of the pigments.[20, 21]

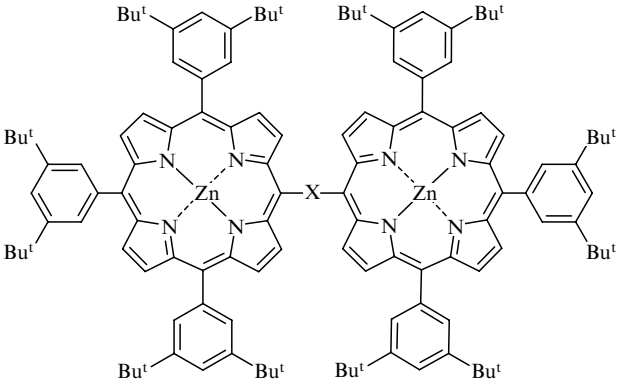

4a–c

X = *p*-$C_6H_4C{\equiv}C-Ar-C{\equiv}CC_6H_4$-*p*; Ar = 1,2-$C_6H_4$ (**a**), 1,3-C_6H_4 (**b**), 1,4-C_6H_4 (**c**).

The polyyne-bound bisporphyrins **1a–d** were obtained by trichloroacetic acid-catalysed condensation of 3,5-di-*tert*-butylbenzaldehyde (**5**), dipyrrolylmethane **6** and dialdehydes **7a–d**

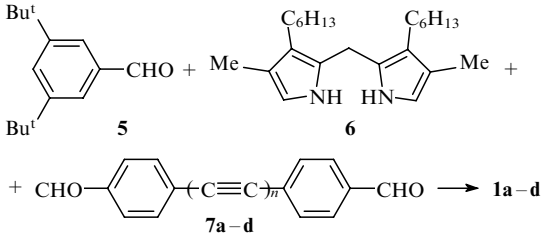

1a–d

n = 1 (**a**), 2 (**b**), 3 (**c**), 4 (**d**).

with subsequent oxidation with *p*-chloranil [22, 23] and metallation of one of the porphyrin rings. The yields of bisporphyrins ranged from 13% to 46%.[19] Similarly, the dimers **2a**,**b** and **3a**,**b** were synthesised by condensation of dialdehydes with compounds **5** and **6**.[19, 20]

This one-pot synthesis of bisporphyrins is both convenient and efficient. The formation of polymeric side products in the condensation is suppressed by a large excess of the terminal monoaldehyde; the polyyne and polyene groups, which are especially acid-sensitive, are not affected, since the reaction is carried out under mild conditions.[22, 23]

An alternative approach, which includes condensation of the formyl-substituted zinc-porphyrin monomer **8** with bisphosphonates **9a**,**b**, was used in the synthesis of bisporphyrins **2c**,**d**.[19]

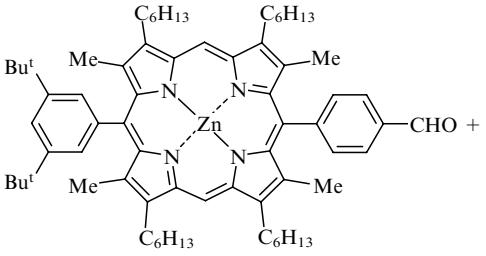

8

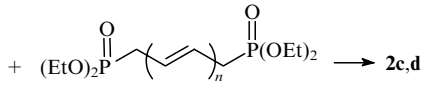

9a,**b** → **2c**,**d**

n = 1 (**a**), 2 (**b**).

Bisporphyrin **3c** was synthesised by palladium-catalysed condensation of ethynylporphyrin **10** [the latter was prepared by the reaction of 4-ethynylbenzaldehyde (**11**) with compounds **5** and **6** with subsequent oxidation by *p*-chloranil] with 1,4-diiodobenzene.[24, 25] The yield of the dimer **3c** was 35%.[20]

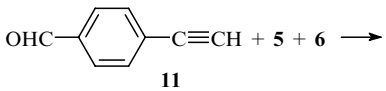

11

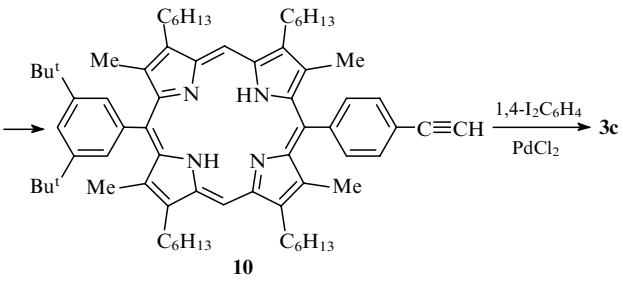

10

Similarly, bisporphyrins **4a**–**c** were synthesised in 49%, 55% and 84% yields, respectively, by the reaction of ethynyl-substituted tetraarylporphyrins with 1,2-, 1,3- and 1,4-diiodobenzene in the presence of tris(dibenzylideneacetone)dipalladium(0) and triphenylarsine.[21]

An approach to the construction of model light-harvesting systems has been developed, which makes use of porphyrin building blocks. Firstly, *meso*-substituted porphyrins are synthesised from aldehyde precursors (containing iodine atoms and ethynyl groups) and pyrrole (or dipyrrolylmethanes) with subsequent palladium-catalysed condensation optimised for mild coupling of the porphyrin building blocks. In this case, spacers between porphyrins are formed directly in the condensation step.[25–27] This block synthesis was used to prepare the dimeric ensembles **12a**–**i**,[27–31] **13a**–**c** [32] and **14a**,**b**.[33] These model systems were employed for the systematic analysis of structural and electronic factors and their effects on the degree of electronic interactions between tetrapyrrole macrocycles as well as for the synthesis of the amphiphilic porphyrin dimers **15a**,**b**.[34] The latter can be incorporated into lipid bilayer membranes for transmembrane energy transfer studies.

Condensation of the iodoporphyrin **16** free base and the zinc ethynylporphyrin complex **17** in the presence of tris(dibenzylideneacetone)dipalladium(0) and triphenylarsine in a 5 : 1 toluene–triethylamine mixture (35 °C) afforded the dimer **12a** with a diphenylethyne linker (yield > 70%).

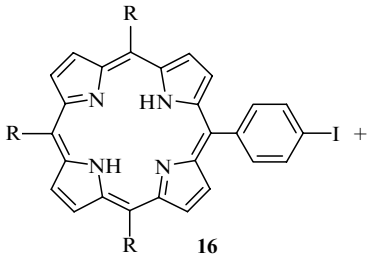

16

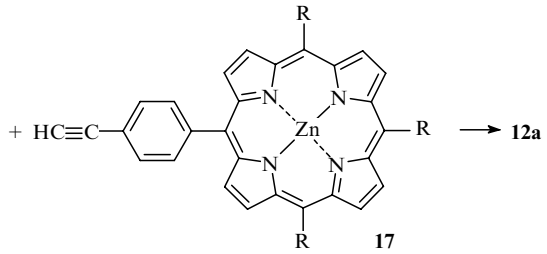

17

R = 2,4,6-$Me_3C_6H_2$.

Bisporphyrins **12b**–**h** were synthesised analogously in 70%–80% yields.[27–31]

Since the palladium catalyst present in the reaction mixture is not involved in undesirable metallation reactions, free porphyrin bases can be used. If the reaction is carried out in neutral and weakly basic solvents at moderate temperatures, neither demetallation of zinc complexes nor oligomerisation of ethynyl-substituted porphyrins take place.[25, 27]

The diphenylethyne linkers in the systems **12a**–**i** ensure a sufficiently large (~20 Å) distance and relatively weak electronic interactions between the pigments, which excludes quenching of the excited state owing to the electron transfer, which competes with the energy transfer. However, in this case it is desirable to reduce the distance between the porphyrin chromophores in order to increase the rate of the energy transfer.

It was shown [35] that the distance between the porphyrin components of a dimer can be reduced to 13 Å if a *para*-phenylene linker is used, which significantly enhances their electronic interactions. Compounds **18a**,**b** were obtained by one-pot condensation of the corresponding aldehyde with terephthalaldehyde and pyrrole using boron trifluoride etherate as a catalyst and oxidation of the resulting product by 2,3-dichloro-5,6-dicyano-1,4-benzoquinone.

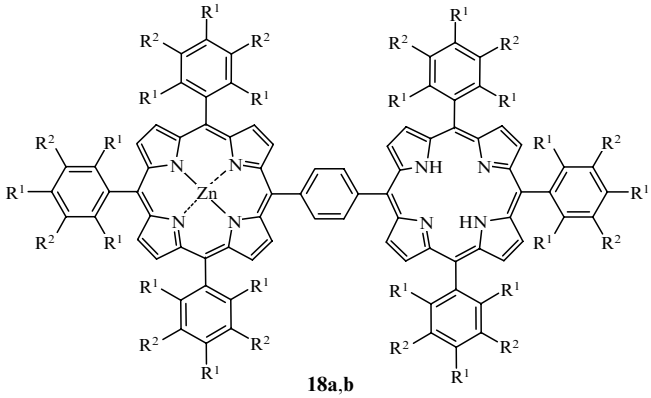

18a,**b**

R^1 = Me, R^2 = H (**a**), R^1 = R^2 = F (**b**).

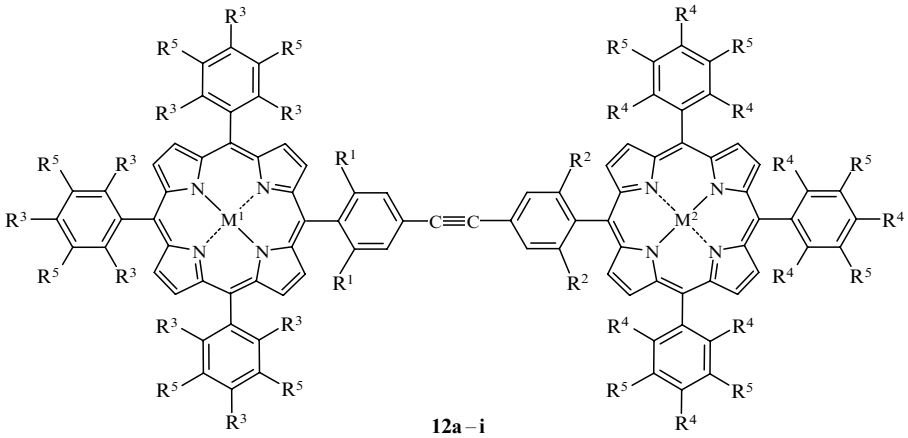

12a–i

Compound **12**	R^1	R^2	R^3	R^4	R^5	M^1	M^2
a	H	H	Me	Me	H	Zn	2 H
b	H	Me	Me	H	H	Zn	2 H
c	Me	H	H	Me	H	Zn	2 H
d	Me	Me	H	H	H	Zn	2 H
e	Cl	Cl	H	H	H	Zn	2 H
f	H	H	F	F	F	Zn	2 H
g	H	H	Me	Me	H	Mg	2 H
h	H	H	Me	Me	H	Cd	2 H
i	H	H	Me	Me	H	Zn	Mg

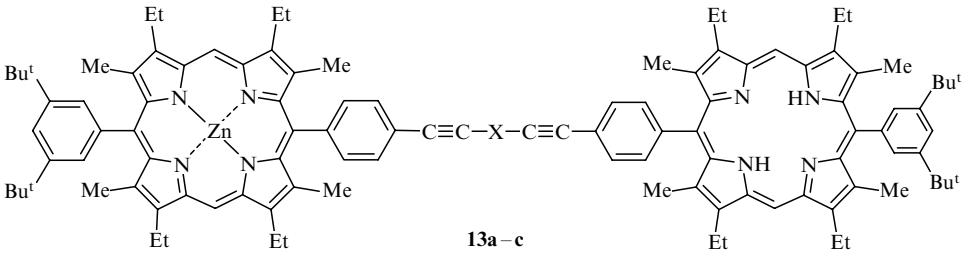

13a–c

X = 1,4-C_6H_4 (**a**), 1,4-naphthylene (**b**), 9,10-anthracenylene (**c**).

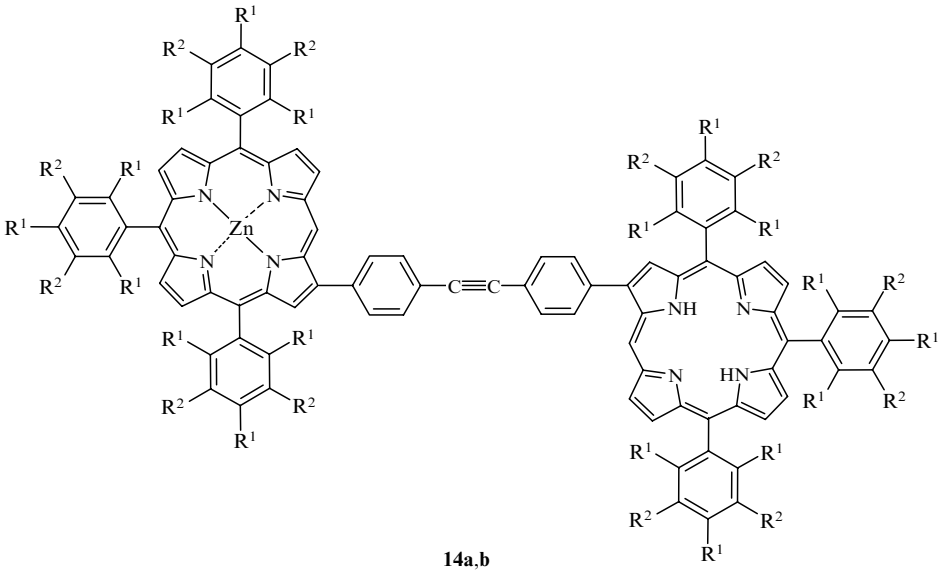

14a,**b**

R^1 = Me, R^2 = H (**a**); R^1 = R^2 = F (**b**).

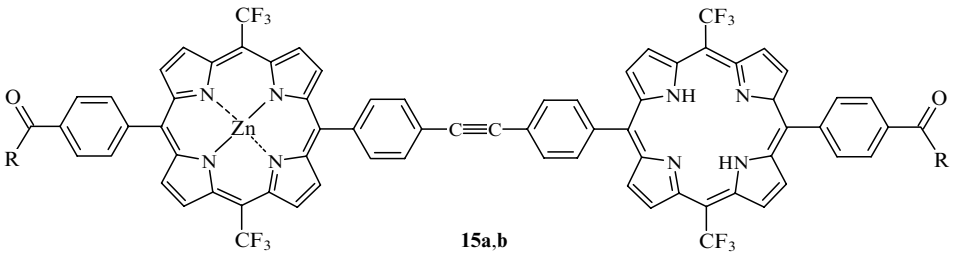

15a,**b**

R = OH (**a**), $N(CH_2)_2SO_3^-Et_3NH^+$ (**b**).

Scheme 1

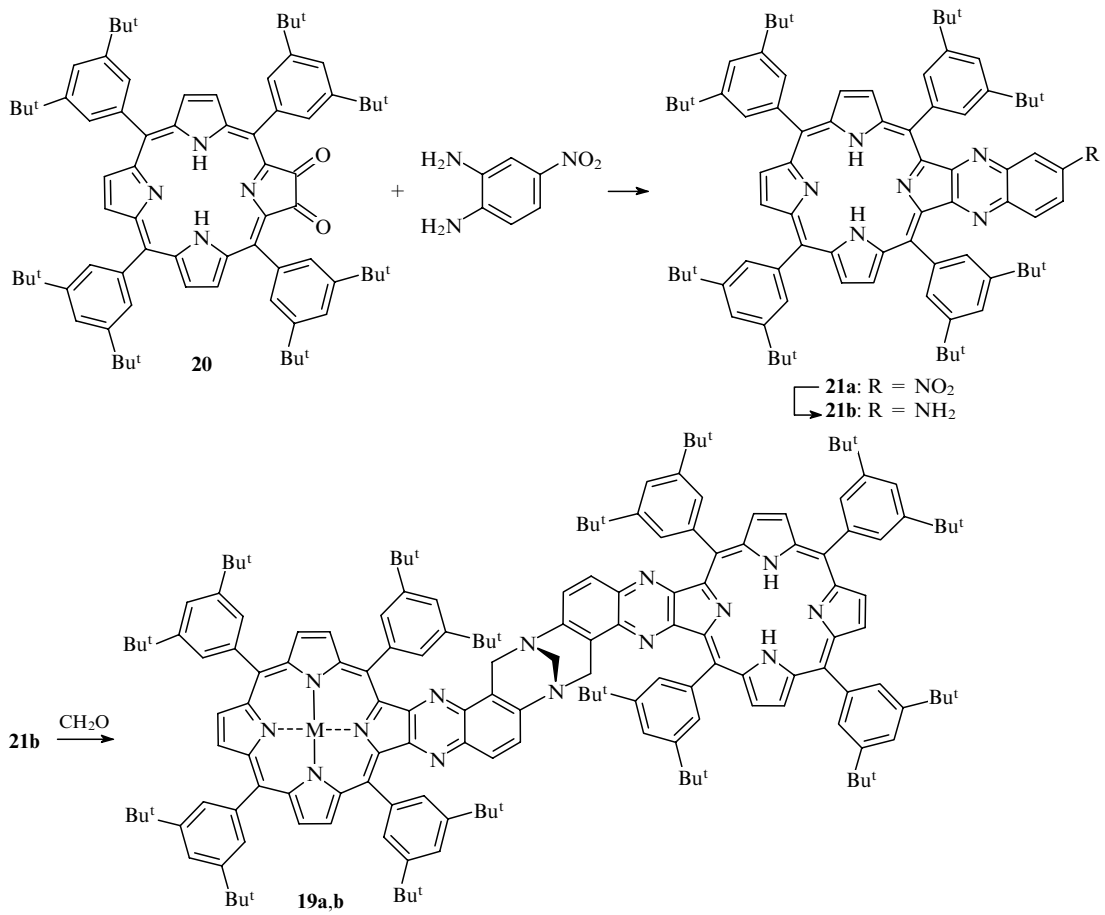

The 'centre-to-centre' distance between two porphyrin fragments in the dimers **19a**,**b** (Scheme 1) is equal to 16.5 Å, whereas their spatial configuration is fixed by two-point addition of each macrocycle to a rigid bridge in such a way that the angle between the planes is 96°. The synthesis of this system includes condensation of porphyrin-2,3-dione **20** with 1,2-diamino-4-nitrobenzene resulting in nitroquinoxalinoporphyrin **21a.** The latter is reduced by tin chloride in hydrochloric acid and the aminoquinoxalinoporpyrin **21b** formed reacts with formaldehyde. The yield of the dimer **19a** is 88%. Compound **19b** was obtained by metallation of bisporphyrin **19a** in 73% yield.[36]

Non-symmetrical porphyrin dimers containing two different macrocycles are promising models for the study of photosynthetic energy transfer. Studies into these compounds provide valuable information about the effects of electronic properties of porphyrin fragments on the yields and the direction of the energy transfer. For example, the covalently linked dimers **22a**,**b** and **23a**,**b** contain tetraphenylporphyrin and octaalkylporphyrin components; their π-systems possess different electronic properties. This allows their selective irradiation and elucidation of pathways of energy transfer following photoexcitation by light with an appropriate wavelength.

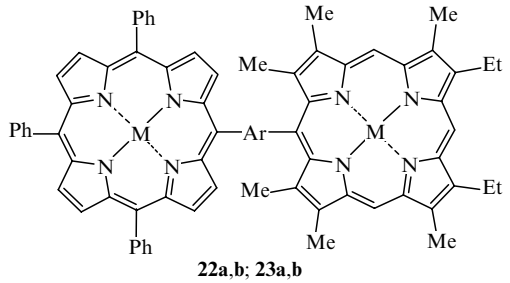

22: Ar = 1,4-C_6H_4; **23**: Ar = 1,3-C_6H_4; M = 2 H (**a**), Zn (**b**).

The non-symmetrical dimers **22a**,**b** and **23a**,**b** were synthesised in the following way. The condensation of 8,12-diethyl-2,3,7,13,17,18-hexamethylbiladiene-*a*,*c* dihydrobromide (**24**) with terephthalaldehyde resulted in porphyrin **25a** with the formyl group in the *para*-position. The reaction of the latter with pyrrole and benzaldehyde gave the dimer **22a**. Similarly, bisporphyrin **23a** was synthesised using isophthalaldehyde in the first step.[37]

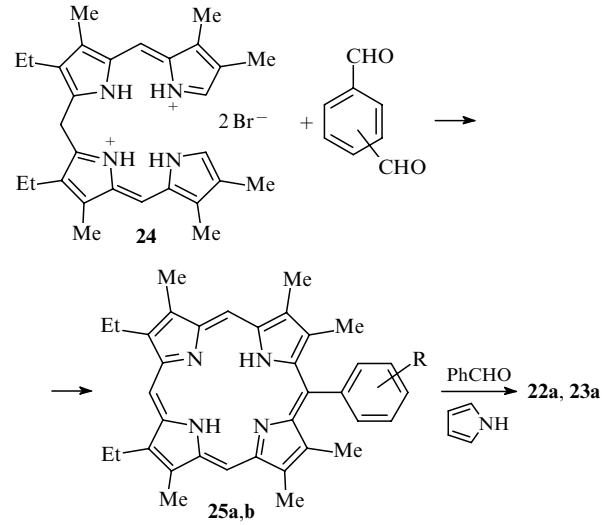

25: R = CHO (**a**), $CH(OEt)_2$ (**b**).

Despite the similarity of many structural, chemical and photophysical characteristics of synthetic porphyrins and natural chlor-

ins, their electronic properties differ considerably because of changes in the symmetry and conjugation pattern in chlorin due to the presence of a reduced pyrrole ring. The main difference between porphyrins and chlorophylls (or bacteriochlorophylls) constituting natural photosynthetic antenna complexes is in that the former absorb light strongly only in the blue region of the solar spectrum, whereas the latter absorb light in both blue and red regions. The orthogonal axes N–N in metalloporphyrins are degenerate (planar oscillator), whereas the dipole moment of the longwave transition in the metal complexes of hydroporphyrins is polarised along one of the N–N axes (linear oscillator), which favours directed transfer of energy. Therefore, the design of chlorin-containing donor–acceptor systems is a promising approach for the modelling of natural light-harvesting complexes.

In the ensembles **26a–c** and **27a,b**, the porphyrin and chlorin macrocycles are linked through rigid aromatic spacers, which fix the macrocycles in parallel planes at a fixed 'centre-to-centre' distance equal to ~12.8 Å.[38,39]

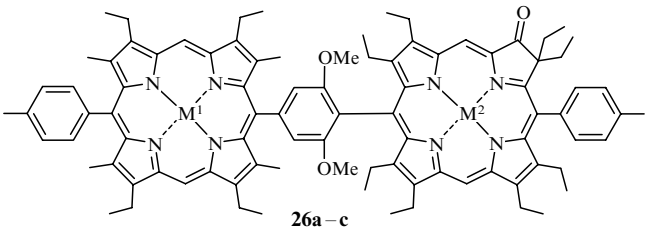

26a–c

$M^1 = M^2 = 2H$ (**a**); M^1 = Zn, $M^2 = 2H$ (**b**); $M^1 = M^2$ = Zn (**c**).

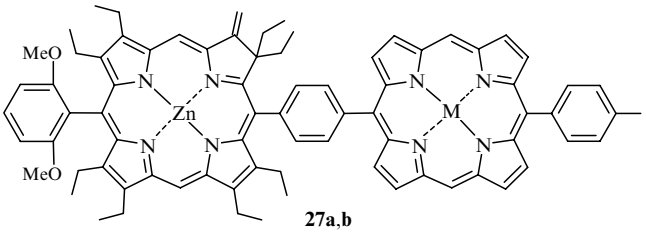

27a,b

M = 2H (**a**), Zn (**b**).

The macrocyclic ensembles **26a–c** were synthesised in the following way. Condensation of the aldehydes **28** and **29** with 3,3′,4,4′-tetraethyldipyrrolylmethane (**30**) resulted in the porphyrin **31**; its hydroxylation with osmium tetroxide and treatment with trifluoroacetic acid gave the oxochlorin **32**. Condensation of compound **32** with *p*-tolualdehyde (**29**) and dipyrrolylmethane (**33**) and subsequent incorporation of zinc resulted in compound **26c** (yield 18%); demetallation of the latter by hydrochloric acid afforded the product **26a** in a quantitative yield. Treatment of the metal-free dimer **26a** with an equimolar amount of zinc acetate resulted in the selectively metallated bisporphyrin **26b** in quantitative yield.[38]

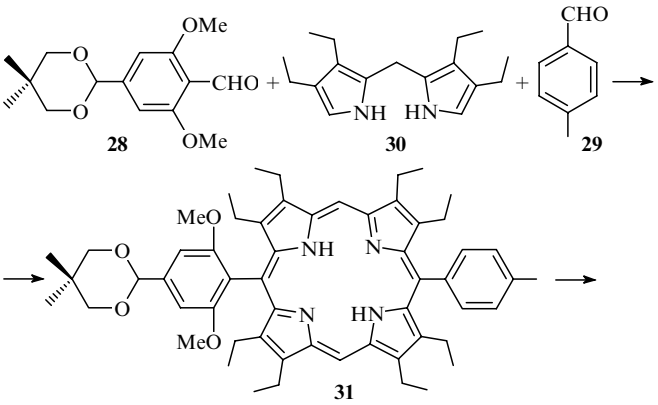

28 **30** **29**

31

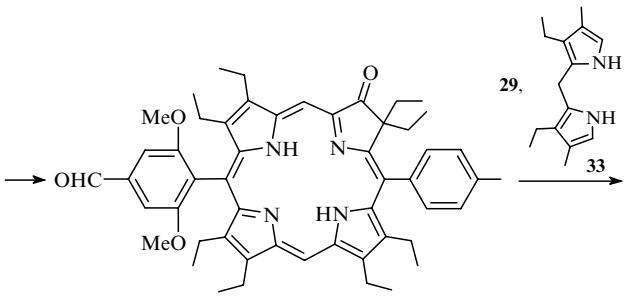

26c → **26a** → **26b**

The dimeric ensembles **27a,b** were synthesised in a similar way. The chlorin component was obtained by condensation of tetraethyldipyrrolylmethane **30** with 2,6-dimethoxybenzaldehyde and 4-(5,5-dimethyl-1,3-dioxan-2-yl)benzaldehyde. The resulting porphyrin was oxidised to oxochlorin, which was further converted into hydroxychlorin by treatment with methyllithium in ether according to Chang. Subsequent dehydration by boiling with trifluoroacetic acid in the presence of 2,2-dimethylpropane-1,3-diol gave methylenechlorin, which was condensed with dipyrrolylmethane and *p*-tolualdehyde following hydrolysis of the protective acetal group. The resulting metal-free dyad reacted with zinc acetate to give a mixture of mono- and dizinc-containing complexes **27a,b** (yields 15% and 30%, respectively).[39]

The porphyrin–chlorin heterodimers **34a,b** containing ether bonds between the macrocycles have also been synthesised. The dimer **34a** was prepared from 2-hydroxy-3,3,7,8,12,13,17,18-octaethyl-22*H*,24*H*-chlorin. This was treated with trifluoroacetic anhydride and the resulting trifluoroacetate reacted with 2-(1-hydroxyethyl)-3,7,8,12,13,17,18-heptaethylporphyrin.[40] The heterodimer **34b** was synthesised by condensation of the trifluoroacetylated porphyrin component with the corresponding hydroxychlorin in the presence of catalytic amounts of 4-dimethylaminopyridine.[41] Data from thin-layer chromatography, ^{1}H NMR spectroscopy and computer modelling studies suggest that these compounds exist as two stable isomers. One of them has a sterically hindered structure due to the spatial proximity of the porphyrin and chlorin macrocycles, while the tetrapyrrole fragments of the other isomer do not virtually overlap.[40–42] The effects of conformational mobility on spectroscopic and photophysical properties of the donor–acceptor systems were studied using the porphyrin–chlorin heterodimer **34a** as an example.

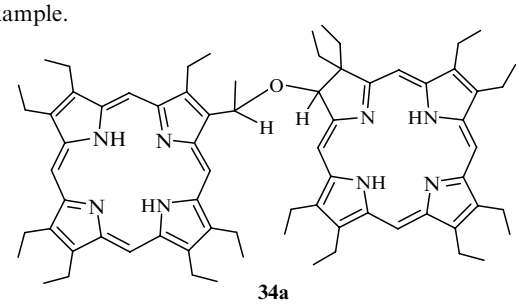

34a

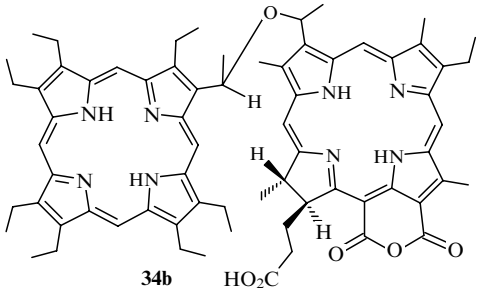

34b HO_2C

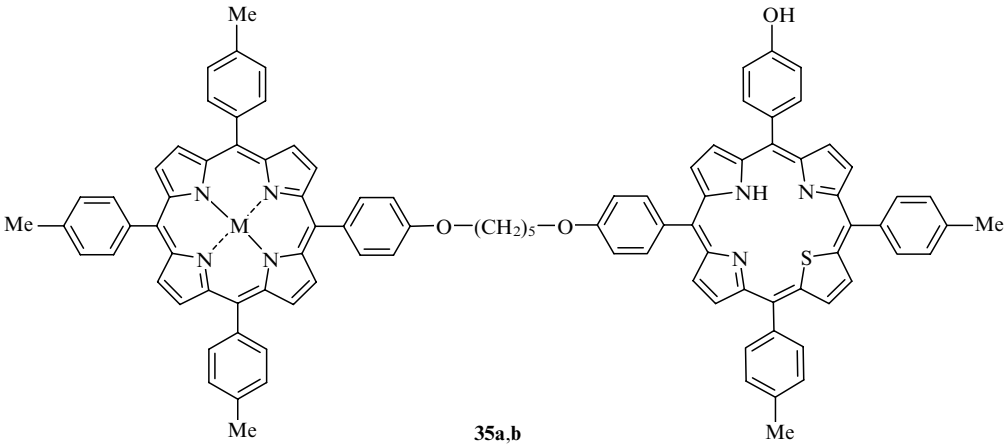

35a,**b**

M = 2 H (**a**), Zn (**b**).

The dimeric ensembles **35a**,**b**, which contain an ordinary porphyrin and thiaporphyrin, have been synthesised.[43] The sulfur atom in one of their macrocycles changes the electronic structure of the porphyrin backbone; therefore, the properties of the tetrapyrrole fragments in the ground and excited states of these systems differ considerably.

The synthesis of the bisporphyrins **35a**,**b** included the preparation of a monomeric thiaporphyrin precursor by condensation of pyrrole and 2,5-bis(*p*-tolylhydroxymethyl)thiophene with *p*-hydroxybenzaldehyde and subsequent reaction of the resulting product with 5-[4-(5-bromopentyloxy)phenyl]-10,15,20-tritolylporphyrin.[43]

The ensembles in which the chromophores are linked through ethylene, ethyne or butadiyne linkers introduced directly into *meso*- or β-positions of the porphyrin macrocycles manifest interesting properties. These systems, in contrast to the above-described systems, are characterised by extraordinarily strong exciton and electronic interactions between the chromophores as can be evidenced from the significant changes in the electronic absorption spectra (splitting of the Soret band, pronounced bathochromic shifts, *etc*.).[8,44–49] As regards photosynthesis, these compounds can serve as spectral models of antenna pigments possessing absorption in the red spectral region.[44] However, dimers with conjugated ethylene, ethyne and butadiyne units between the chromophores are not used for the modelling of energy transfer; therefore, their synthesis and spectroscopic properties are not considered in this review.

b. Photochemical properties

Studies of photochemical properties of model compounds have shed light on the dependences of the rates and efficiencies of energy transfer reactions on the distance between donor and acceptor components,[19–21,35] their mutual arrangement[20,21,37] and extent of electronic interactions.[21,28,29]

Quenching of singlet excited states of porphyrin donors in the absence of acceptors can be effected in several ways (Fig. 2), *viz*., by radiative quenching through fluorescence emission with the rate constant k_F and by non-fluorescent quenching including intersystem transition to the triplet state, inradiative quenching to the ground energy state, *etc*., with the rate constant k_{NF}. For dilution commonly employed in photochemical studies ($\sim 10^{-6}$ mol litre^{-1}), intermolecular quenching can be neglected. Attachment of an acceptor to the porphyrin donor provides an additional route of quenching of its excited state, *viz*., intramolecular singlet energy transfer with the rate constant k_{EN}.[19]

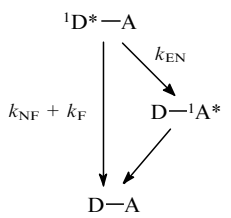

Figure 2. Possible ways of quenching of the singlet excited state of the donor (D, donor, A, acceptor).[19]

Emission spectra provide essential information about photoprocesses occurring in model systems. Quenching of fluorescence of a porphyrin donor concomitant with enhanced fluorescence of the acceptor implies an intramolecular transfer of singlet excitation energy.[19,50,51]

High efficiency of energy transfer is a prerequisite for the normal functioning of natural light-harvesting antenna complexes. The quantum yields (Φ) of the energy transfer can be correctly determined by several methods. One of them includes detailed comparison of steady-state absorption and fluorescence excitation spectra. However, high quantum fluorescence yields, significant overlap of the donor and acceptor fluorescence spectra and the presence of residual amounts of the original monomers do not allow reliable estimation of energy transfer efficiency in molecular ensembles by static measurements alone. An alternative approach consists in comparison of the rates of the energy transfer and competing quenching channels of the donor excitation (see Fig. 2).

The use of this method for the determination of quantum yields of the energy transfer from the zinc-containing porphyrin to the free base in the dimeric ensembles **12a**–**i** has demonstrated extremely high efficiency of this reaction (Φ = 87%–99%)[28–31,51] despite of the large distance (20 Å) and weak interactions between the chromophores. Similar results were obtained in the study of the model systems **18a**,**b** where the quantum yields of the energy transfer were $\geqslant$ 99%.[35] Efficient energy transfer from the octaalkylporphyrin to the tetraphenylporphyrin component was observed for the dimers **22** and **23** (Φ = 79%–99%).[37] Analysis of these systems did not reveal any competitive electron transfer reactions. Thus, the energy transfer is a predominant channel of decay of the excited states of porphyrin donors in these ensembles.

Energy transfer reactions follow two basic mechanisms. The first of them is the Förster 'through-space' mechanism, which is determined by the interactions between transient dipole moments. In this case, the reaction rate depends on the mutual donor and acceptor arrangement, the 'centre-to-centre' distance between them and the integral of spectral overlap of the donor emission and the acceptor absorption. The second route, *viz*., the Dexter 'through-bond' mechanism, is realised in the presence of strong electron-exchange interactions in the case of close contacts between the donor and the acceptor or the presence of a π-conjugated bridge between them.[52]

It was shown that linear π-conjugated polyyne and polyene spacers enhance the 'through-bond' electron-exchange interactions between two porphyrin macrocycles in donor–acceptor bisporphyrin systems.[19]

The values of rate constants for the intramolecular energy transfer in the systems **3b**,**c** containing porphyrin macrocycles in the *meta*- and *para*-positions of the aryl ring, are virtually identical despite the differences in the 'centre-to-centre' distances between the chromophores, which is a clear evidence of electronic 'through-bond' interactions in these compounds. Comparison of the energy transfer rates in the linear dimer **3c** ($k_{EN} = 5.7 \times 10^8$ s^{-1} for the 'centre-to-centre' distance of 26.2 Å) and the diphenylpolyyne-bound bisporphyrin **1d** ($k_{EN} = 1.9 \times 10^9$ s^{-1} for the 'centre-to-centre' distance of 27.0 Å) has demonstrated that the 1,4-bis(phenylethynyl)phenylene bridge is less active in 'through-bond' electronic interactions than diphenylpolyyne spacers of analogous lengths.[19,20]

At the same time, the rates of the energy transfer in the bisporphyrins **13a**,**b**, in which the arrangement of the porphyrin rings and the structures of spacers are similar to those in the dimer **3c**, are comparable with that calculated in the framework of the Förster approximation ($k_{EN} = 4.9 \times 10^8$ s^{-1}). This suggests that the electron energy transfer in these compounds follows the 'through-space' mechanism.[32] Probably, in this case both mechanisms contribute to the interactions between the electronic systems of these pigments.

The energy transfer in the diarylethyne-linked ensembles **12a**–**e** predominantly occurs by the 'through-bond' mechanism mediated by the π-electron system of the linker. This is supported by the fact that the rate constants for the energy transfer for all the dimers of this series (7.5×10^9 s$^{-1} < k < 4.2 \times 10^{10}$ s^{-1}) exceed markedly that predicted by the Förster theory for the 'through-space' mechanism (1.4×10^9 s^{-1}).

In terms of the Lindsey hypothesis, the dihedral angle between the porphyrin ring and the aryl rings of the linker is a critical structural parameter, which determines the possibility of the 'through-bond' energy transfer. Thus steric hindrances created by the introduction of *ortho*-substituents into the linker unit preclude coplanar arrangement of the aryl rings of the linker and the porphyrin rings. This diminishes orbital overlap and decreases fivefold the rate of the 'through-bond' energy transfer. In the dimer **12e**, this effect is predominant over other effects, such as withdrawal of the electron density and interactions of the π-orbitals of *ortho*-chloro-substituents with the *meso*- carbon atoms of porphyrins.[28,51]

Comparison of the rates of singlet–singlet energy transfer in two series of bis(phenylethynyl)phenylene-linked bisporphyrins **3a**–**c** and **4a**–**c** gave similar results. The β-alkyl groups in the dimers **3a**–**c** adjacent to the bridge attachment site hold the bridge in the virtually perpendicular position relative to the porphyrin planes, which minimises the electronic interactions between the porphyrins and the bridge. This conformational restriction is not so severe in the dimers **4a**–**c**, which is a reason for enhanced electronic interactions between porphyrins and increased rates of the 'through-bond' energy transfer in these systems in comparison with the bisporphyrins **3a**–**c**.[21]

The superexchange mechanism, which involves the binding chromophore, is also responsible for increased energy transfer rates in the systems **19a**,**b** characterised by strictly fixed mutual spatial arrangement of the porphyrin macrocycles and the bridge.[53]

At the same time, the decrease in the degree of conjugation between the π-electron systems of the linker and the porphyrins is accompanied by somewhat enhanced contribution of the 'through-space' energy transfer to the overall process. Thus the contribution of this mechanism to the energy transfer in the dimers **12d,e** where the rotation of the linker's aromatic rings is restricted by the substituents, exceeds 10%.[28,51]

The experimental values of the rate constants for the energy transfer for the dimers **22a** (2.4×10^8 s^{-1}), **23a** (8.5×10^8 s^{-1}) and **23b** (2.5×10^{10} s^{-1}) are in good accord with those predicted by the Förster theory. This can apparently be explained by the fact that the macrocycles in the above models cannot lie in the same plane with the binding phenylene groups due to steric hindrances; therefore, direct conjugation between the π-systems of the porphyrins and the linker is excluded while the contribution of the 'through-space' mechanism to the overal energy transfer process increases in accordance with the Lindsey hypothesis.[37]

Energy transfer in natural photosynthetic systems occurs at very fast rates. One of the ways to accelerate this process in synthetic ensembles is to reduce the distance between the porphyrins. Thus the rate constant for the energy transfer in the bisporphyrin **3a** exceeds by about an order of magnitude that in the dimer **3c**, which has an identical spacer, but the distance between chromophores is twice as long.[20] In the case of the dimer **4a** with closely located porphyrin fragments, the energy transfer rate is higher than in the system **4c**, but the effect is far less pronounced.[21]

The rates of the energy transfer in the *p*-phenylene-linked dimers **18a** (2.9×10^{11} s^{-1}) and **18b** (1×10^{11} s^{-1}) are much higher than in structurally similar ensembles containing the diphenylethyne linker, *viz*,. 4.2×10^{11} s^{-1} for **12a** and 4.2×10^9 s^{-1} for **12f**. The observed increase in the reaction rate is mainly due to enhancement of the electronic interactions between the porphyrin components which, in turn, is due to shortening of the distance between the chromophores in the former case.[35]

Analysis of spectral properties of the heterodimer **34a** revealed that the efficiency of the energy transfer in the 'folded' conformer characterised by spatial closeness of the two macrocycles (the 'centre-to-centre' distance determined by computer simulation studies is ~6 Å) is close to 100%. At the same time, the quantum yield of the energy transfer for the isomer having an 'open' conformation of the macrocycles (the distance between the chromophores is > 10 Å) is lower (74%) (see Ref. 54).

It was shown that direct dipole–dipole 'through-space' interactions become predominant in the energy transfer in the ensembles **3a**,[20] **18a**,**b** [35] and **34a** [54,55] with decreased distances between the donor and acceptor components.

Whereas the effects of steric factors on the rates and mechanisms of energy transfer have been studied in sufficiently great detail, the contribution of spacers to the electronic structure of the excited state has been studied to lesser extent. It is known, however, that the strength of the electronic interaction depends not only on structural parameters, such as the distance between the chromophores constituting the system and their mutual arrangement, but also on the relative orbital energies of the donor, the acceptor and the spacer group.

Investigation into the effect of the electronic structures of bridges on the rate of energy transfer has been carried out [32] with the systems **13a**–**c** with identical distances between the macrocycles, well-defined mutual arrangements of two porphyrin ring planes and minimum degree of conjugation between the donor, the bridge and the acceptor, which allowed consideration of the system components as individual chromophores.

Spectral studies of the model bisporphyrins **13a**–**c** revealed the strongest quenching of donor emission in the case of the anthracenylene-linked dimer **13c**, which suggests the higher efficiency of the energy transfer in this compound. Moreover, the rate constant for the energy transfer for the dimer **13c** ($k = 10^9$ s^{-1}) exceeds approximately twofold those for the bisporphyrins **13a**,**b** (5.8×10^8 and 5.4×10^8 s^{-1}, respectively) with phenylene- and naphthylene-containing spacers. These results indicate stronger electronic interactions in the dimer with anthracene-containing spacer, apparently due to the proximity of the energy levels of the lower singlet excited states of the donor, the acceptor and the anthracene chromophore (17 500, 16 000 and 21 600 cm^{-1}, respectively). However, splitting of the energy levels between the donor and the bridge as well as between the bridge and the acceptor is large enough to prevent stepwise energy transfer with the involvement of the intermediate excited state of the binding chromophore.[32]

Comparison of photochemical properties of the dimeric ensemble **12f** containing pentafluorophenyl groups in all the non-binding *meso*-positions of the tetrapyrrole macrocycle and its non-fluorinated analogue **12a** was carried out in order to elucidate the effects of electronic factors on the extent of interactions of the porphyrin components in the ground and excited states. The rate of the energy transfer in the bisporphyrin **12f** was 10 times lower than that in the dimer **12a** despite identical diphenylethyne linker in both compounds. The lower rate of the energy transfer in the former dimer is attributed to weakened electronic interactions between Zn-porphyrin and the free base in the S_1 excited state.

The degree of the 'through-bond' energy transfer between components of dimeric ensembles depends on the electronic and oscillation matrix elements. In the dimers **12a**,**f** possessing identical linkers, oscillator contributions are the same and interactions between the porphyrin components are predominantly determined by electronic factors. Their magnitude depends on the nature and distribution of the electron density of molecular orbitals involved in bonding. In compound **12a**, as in most *meso*-substituted porphyrins, HOMO has the a_{2u} symmetry characterised by considerable electron densities on *meso*-carbon atoms including those attached to the linker. In contrast, the pentafluorophenyl groups in the dimer **12f** stabilise the orbital with the a_{2u} symmetry, which changes the HOMO symmetry to a_{1u}. Such a change in the orbital ordering diminishes the electron density on the peripheral *meso*-atoms of the macrocycle where the linker is attached, and thus reduces the electronic matrix element. Thus, the rate of the energy transfer between the zinc-containing porphyrin and the free base of the dimer decreases. Redistribution of the electron density from the *meso*-carbon atoms of the a_{2u} orbital to the strongly electron-withdrawing pentafluorophenyl rings is yet another factor inducing appreciable decrease in the rate of the energy transfer in the dimer **12f**.[29]

In the case of the fluorine-containing dimer **18b**, a threefold decrease in the rate of the energy transfer was observed in comparison with the non-fluorinated analogue **18a** (1×10^{11} and 2.9×10^{11} s^{-1}, respectively). This effect correlates with the above-described fluorine-induced changes in the orbital characteristics of porphyrin components in the case of *meso*-diarylethyne-linked dimers.[35]

An opposite effect was observed for the β-linked dimers **14a**,**b** in which the presence of pentafluorophenyl groups in the non-binding *meso*-positions promotes stronger electronic interactions. As a result, the rate of the energy transfer in the dimer **14b** ($k = 4.2 \times 10^{10}$ s^{-1}) exceeds more than twofold that in the mesityl-substituted ensemble **14a** ($k = 1.8 \times 10^{10}$ s^{-1}). This, too, is due to enhanced contribution of the a_{1u} orbital characterised by higher electron density on the β-pyrrole atoms, where the linker is attached, to the wave function of the excited electronic state in pentafluorophenyl-substituted dimers.[33]

A 17-fold decrease in the rate of the energy transfer in the *meso*-diphenylethyne-linked β-alkyl-substituted dimer **1a** (see Ref. 19) in comparison with the *meso*-aryl-substituted bisporphyrin **12a** possessing the identical linker is mainly due to the electronic factors determined by the differences in the orbital ordering.[29] In particular, eight β-alkyl substituents and two aryl groups in the *meso*-positions of each porphyrin fragment in the dimer **1a** determined the a_{1u} HOMO symmetry characterised by the absence of electron density on the *meso*-carbon atoms to which the linker is attached. In addition, the steric hindrance due to the β-methyl groups in the pyrrole rings of the porphyrin macrocycle limit the rotation of the aromatic rings of the linker and prevent their coplanarity with the porphyrin macrocycles. This diminishes the conjugation of their π-electron systems and thus makes an additional contribution to the weakening of the electronic interactions between the dimer components.

The enhancement of 'through-bond' electronic interactions and the increase in the rate of singlet energy transfer upon substitution of the tetraarylporphyrin component in the systems **4a**–**c** for the 10,20-diaryloctaalkylporphyrin component in the dimers **3a**–**c** are explained in a similar way.[21]

Thus, the site of attachment of the linker should be chosen with due regard to the general pattern of substitution in the tetrapyrrole macrocycle in order to ensure optimum electronic interactions. For porphyrins with the a_{2u} HOMO symmetry, the strongest electronic interactions are provided by linkers attached to the *meso*-positions of the macrocycles, whereas stronger electronic interactions between the pigments with the a_{1u} HOMO symmetry are provided by spacers introduced into β-pyrrole positions. It should also be considered that the electron densities of the eight β-pyrrole carbon atoms with the a_{1u} orbital symmetry are much lower than those of the four *meso*-atoms with the a_{2u} orbital symmetry. Consequently, the electronic interactions through spacers connecting β-positions of the porphyrin macrocycles should be less efficient than those through spacers connecting *meso*-carbon atoms.[29, 33]

The LUMO characteristics also contribute to linker-mediated electronic interactions between chromophores. The electronic factor is determined by the overlap of the e_g orbitals of porphyrin with the d_π-orbitals of the metal. Thus an increase in the rate of the energy transfer in the cadmium-containing ensemble **12h** ($k = 6.7 \times 10^{10}$ s^{-1}) in comparison with the magnesium-containing dimer **12g** ($k = 3.2 \times 10^{10}$ s^{-1}) reflects the putative role of cadmium *d*-orbitals in the electronic interactions.[31] Stronger 'through-bond' interactions in the zinc-containing diporphyrin **19b** in comparison with its non-metallated analogue **19a** is thought[53] to be due to the interaction of the metal d_π-orbitals with the porphyrin ring, which increases the electron density on the pyrrole carbon atoms bearing the spacer group.[53]

The effect of the bridge topology on the electronic interactions between porphyrins in the ground and excited states was studied in the example of the conjugated dimers **36** and **37**. The energies of absorption maxima in the region of the Q-bands of the β,β-linked ensembles **36a**,**b** are essentially the same as those of the isolated zinc-containing tetraphenylporphyrin complex, which points to weak electronic interactions between the chromophores in the ground and the lowest singlet electron-excited states. Contrariwise, a pronounced bathochromic shift and enhanced low-energy absorption in the region of the Q-bands in the *meso*,*meso*-linked dimer **37** suggest the presence of strong electronic interactions between the porphyrin macrocycles. These data are in good agreement with the order of changes in the strength of the electronic interaction (*meso*,*meso* > *meso*,β > β,β) for *meso*-substituted porphyrins at a fixed twist angle between the tetrapyrrole planes predicted on the basis of the above-described analysis of the electronic structure. Moreover, the rotation barrier around the ethyne linker in the *meso*,*meso*-linked ensemble **37** is a minimum in comparison with β,β-linked dimers. This suggests that the conformers in which the components of the *meso*,*meso*-linked dimer have planar structures and maximum conjugation predominate in solutions at room temperature.[44, 45]

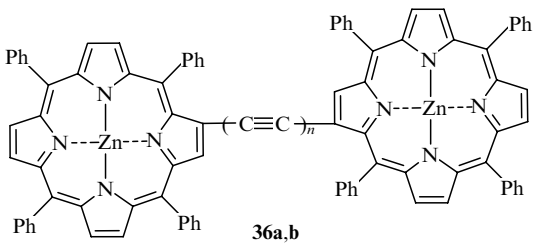

36a,**b**

$n = 1$ (**a**), 2 (**b**).

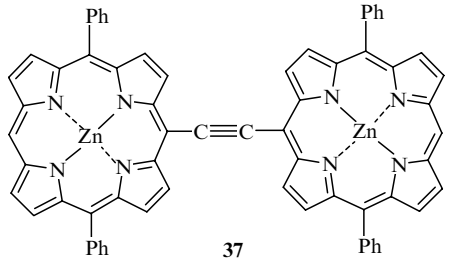

37

These data suggest that the electronic structure together with steric factors are essential for efficient electronic interactions and high rates of the energy transfer in dimeric ensembles.

Zinc-containing porphyrin complexes analogous in structural, chemical and photophysical characteristics to those of chlorophylls and bacteriochlorophylls are widely employed in photosynthetic model systems. However, natural photosynthetic pigments contain magnesium atoms in their chlorin rings. Spectral properties of the ensembles **12a**,**g**,**h**, which contain zinc, magnesium and cadmium in one of their macrocycles, were compared in order to examine the effects of metal substitution on the photodynamic behaviour of bisporphyrins. The rates of the energy transfer for the three dimers were very close, which can be attributed to the similarity of electronic interactions between the chromophores in the magnesium-, zinc- and cadmium-containing bisporphyrins. However, the quantum yield of the energy transfer for the Mg-containing dimer (Φ = 99.7%) is higher than that for the Zn-containing dimer (Φ = 99%) due to the longer lifetime of the excited state of the Mg-porphyrin (10 ns) in comparison with that of the Zn-porphyrin (2 ns). Although this difference is insignificant in the case of the isolated dimer, this may be multiplied in multiporphyrin ensembles, which perform more energy transfer steps.[30] A more significant decrease in the efficiency of the energy transfer in the case of the cadmium-containing dimer (Φ = 87%) is almost exclusively due to the very short ($\sim$ 100 ps) lifetime of the Cd-porphyrin excited state, which, in turn, may be a result of acceleration of the singlet–triplet intersystem transition, which competes with the energy transfer due to the presence of a heavy metal.[31] Moreover, magnesium- and especially cadmium-containing bisporphyrins are more labile with respect to demetallation and photochemical oxidation and are more prone to electron transfer, whereas zinc-containing dimers are rather stable against these side reactions.

These data suggest that synthetic ensembles capable of highly efficient energy transfer may contain both Mg- and Zn-porphyrins; the choice of a metal should be made with due regard to all the factors mentioned above.[30] Moreover, the extremely high rate ($k = 1.1 \times 10^{11}$ s^{-1}) and the nearly quantitative efficiency of the energy transfer in the dimer **12i**, which contains Zn- and Mg-tetraarylporphyrin complexes, confer attractive properties on the combination of these complexes within a single ensemble. At the same time, the use of cadmium complexes in artificial energy-transforming systems is limited due to reduced efficiency of the energy transfer and lability of these compounds.[31]

The effects of environmental factors, such as viscosity, solvent polarity and temperature, on the photodynamic behaviour of the diarylethyne-linked ensembles **12a**–**d** have been discussed.[51] These studies have shown that the rates of energy transfer in viscous media (*e.g.*, castor oil) are 1.3–1.9 times lower than in toluene. This can be explained by the fact that higher viscosity of the medium impedes probably the rotation of the aromatic rings of the linker around a single bond, which prevents their coplanarity with the porphyrins and thus weakens electronic 'through-bond' interactions between the porphyrin macrocycles.

With a decrease in temperature to 150 K, the rates of the energy transfer in these dimers show a slight decrease. Presumably, the mobility of the aromatic group and a concomitant change in the average dihedral angle between the linker and the porphyrin are also decreased due to freezing of the solvent. The degree of thermoinduced conformational changes depends on rotational restrictions of the linker. Therefore, the most appreciable (2.5-fold) decrease in the rate of the energy transfer is observed for the dimer **12a** where a broad range of dihedral angles is possible due to the lack of torsional restrictions. No such changes were observed for the ensemble **12d**.[51]

The dynamics of singlet–singlet energy transfer in the porphyrin–chlorin system **34a** containing ether bond between the macrocycles changes with temperature. At 293 K, the excitation energy migrates repeatedly between the interacting donor and acceptor components over the lifetime of acceptor fluorescence, since the rates of forward and reverse energy transfer reactions exceed the deactivation rates of S_1 states of porphyrin and chlorin by more than an order of magnitude. In contrast, the transfer of excitation energy from porphyrin to chlorin at 77 K is irreversible, for in this case the calculated rate of the reverse transfer is much lower than the deactivation rate of the acceptor S_1 state.[55]

It was shown that the polarity of the solvent affects only slightly the efficiency and rate of energy transfer in diarylethyne-linked dimers. However, significant quenching of fluorescence of the porphyrin free base in the dimers **12a**,**b** observed in polar solvents (*e.g.*, dimethyl sulfoxide) is ascribed to the charge transfer from the neighbouring metal complex.[51] Magnesium-containing ensembles are even more sensitive to this process due to increase in the driving force of the electron transfer process.[30]

Similar photoinduced electron transfer to the excited singlet state has also been observed in the hybrid porphyrin–chlorin dimer **26b** (see Ref. 38) and the bisporphyrins **38a**,**b** (see Ref. 56).

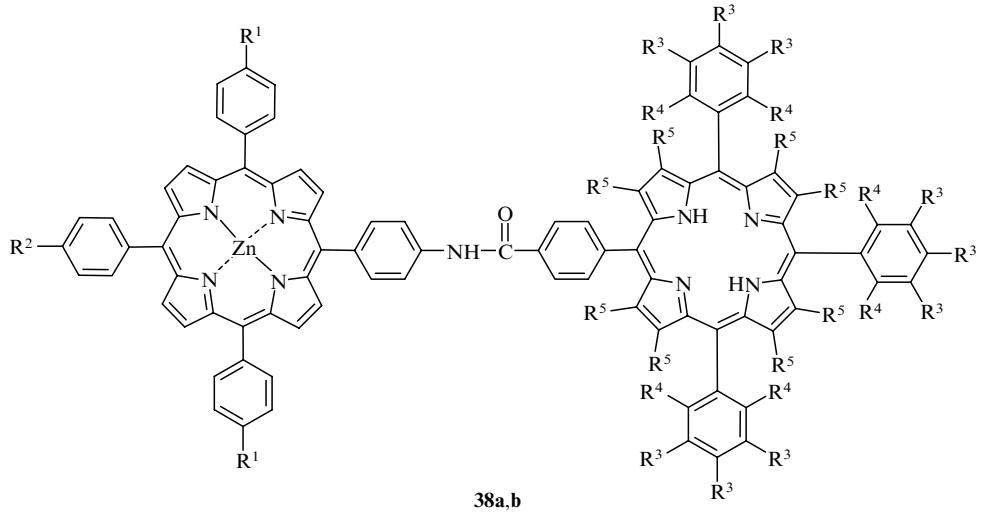

38a,**b**

R^1 = Me, R^2 = NHCOMe, R^3 = H, R^4 = R^5 = Cl (**a**); R^1 = R^2 = NMe_2, R^3 = R^4 = F, R^5 = H (**b**).

It should be emphasised that the charge transfer occurs after the excitation has reached the acceptor and has no appreciable influence on the energy transfer between the donor and acceptor components in the above-described ensembles.[51]

The fluorescence spectra of bisporphyrins linked by flexible hydrocarbon chains can be interpreted by the existence of two conformations, *viz*., the 'open' conformation where quenching of the donor fluorescence is fairly ineffective and the 'folded' conformation characterised by effective quenching of donor emission owing to the transfer of singlet energy to the acceptor.[57–59] Changes in the solvent polarity bring about transition of one form into another. Thus the 'open' conformation is predominant for solutions of bisporphyrins **35** in toluene, whereas in dimethylformamide the 'folded' conformation is preferable in which the 'centre-to-centre' distance between two porphyrin components is 18.7 Å. Such conformational transition results in the enhancement of the efficiencies and rates of energy transfer in polar solvents.[59]

The knowledge of regularities of the energy transfer depending on structural, electronic and environmental factors is useful for the design of more complex model donor–acceptor systems.

2. Porphyrin dimers with peptide spacers

All the bisporphyrins described above contain hydrocarbon spacers. However, chlorophyll and bacteriochlorophyll in photosynthetic antenna systems exist in a protein environment, which affects the photophysical properties.[11, 12, 60] Synthetic porphyrin dimers with the macrocycles linked through amino acid or peptide spacers represent convenient model subjects for the study of intramolecular interactions and energy transfer between tetrapyrrole chromophores within natural pigment–protein complexes.

a. Synthesis

The porphyrin dimers **39a**,**b** and **40a**,**b** linked through amino acid bridges served as models for the studies of spectral properties of chromophores in biological photosynthetic systems.[61] These compounds were synthesised in 10%–15% yields by condensation of 5-*o*-(2-bromoethoxy)phenyl-10,15,20-triphenylporphyrin with glycine or racemic phenylalanine in dimethylformamide in the presence of a phase-transfer catalyst.

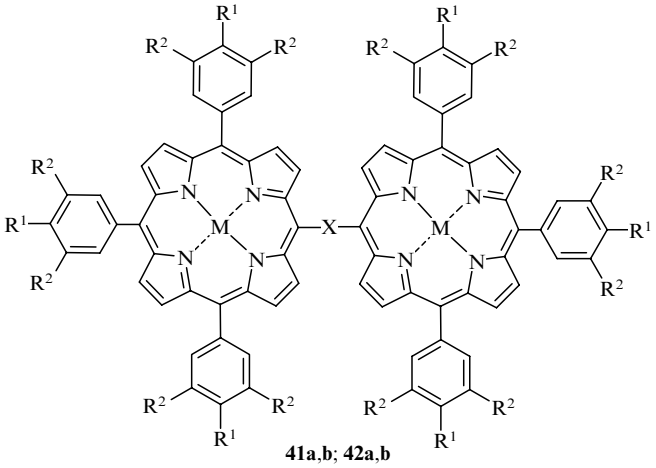

41a,**b**; **42a**,**b**

41: R^1 = Me, R^2 = H; **42**: R^1 = H, R^2 = Bu^t; M = 2H (**a**), Zn (**b**).

D,L-**41**, D,L-**42**: X = 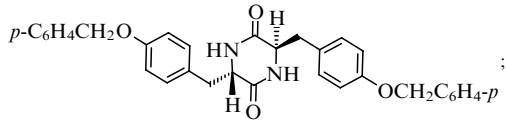 ;

L,L-**41**, L,L-**42**: X = 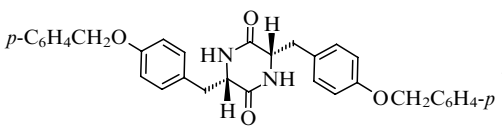 .

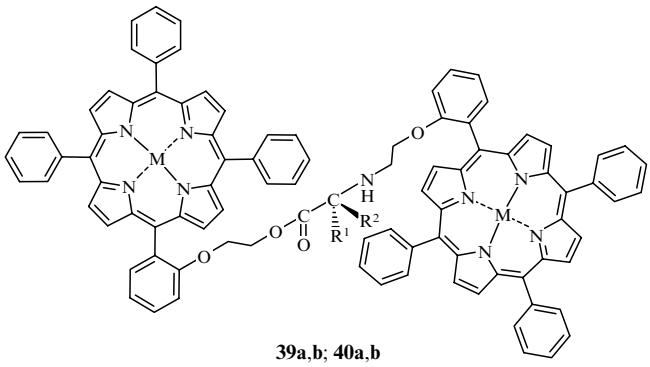

39a,**b**; **40a**,**b**

39: R^1 = R^2 = H; **40**: R^1 = Bn (H), R^2 = H (Bn); M = 2H (**a**), Zn (**b**).

The porphyrin dimers with macrocycles covalently linked through cyclic dipeptides, *viz*., piperazine2,5-diones (compounds **41a**,**b** and **42a**,**b**),[62] β-folded oligopeptides (dimers **43a**,**b**, **44a**–**d**, **45a**,**b**)[63] and the oligo-L-proline spacers **46a**–**i** and **47a**–**i**,[64] were synthesised for studies of intramolecular interactions and energy transfer between the porphyrin components.

In these dimers, two porphyrin rings are held in specific conformations by rigid peptide spacers. Thus rigid β-folded structures of the dipeptides in the molecules **43a**,**b**, **44a**–**d** and **45a**,**b** are determined by the formation of hydrogen bonds between the carbonyl groups of the porphyrins and amino groups of amino acid residues of the peptides.[63] Due to the cyclic side chain, the oligo-L-proline spacers in the dimers **46a**–**i** and **47a**–**i** acquire fairly stable helical conformations provided the number of amino acid residues is no less than four.[18, 64]

The general strategy of the preparation of these compounds is based on the use of standard protocols of the peptide synthesis. The symmetrical bisporphyrins **41a**,**b** and **42a**,**b,** which are covalently linked to tyrosine residues by ether bonds to form piperazine-2,5-dione, were obtained from the zinc-containing porphyrins **48a**,**b**, which in turn were synthesised by the condensation of the corresponding aromatic aldehydes with methoxycarbonylbenzaldehyde and pyrrole followed by reduction of the ester groups to hydroxy groups, substitution of bromine for

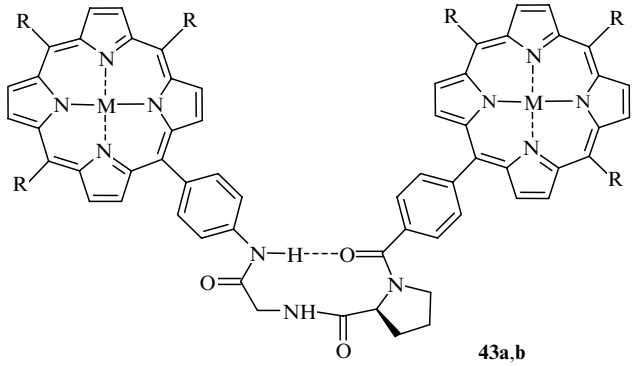

43a,**b**

R = *p*-MeC$_6$H$_4$; M = 2H (**a**), Zn (**b**).

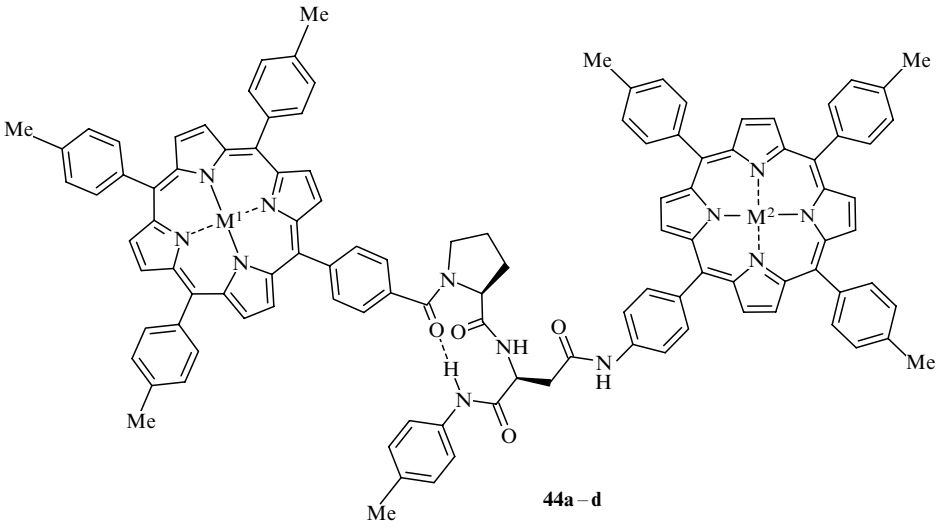

44a–d

$M^1 = M^2 = 2H$ (**a**), Zn (**b**); M^1 = Zn, $M^2 = 2H$ (**c**); $M^1 = 2H$, M^2 = Zn (**d**).

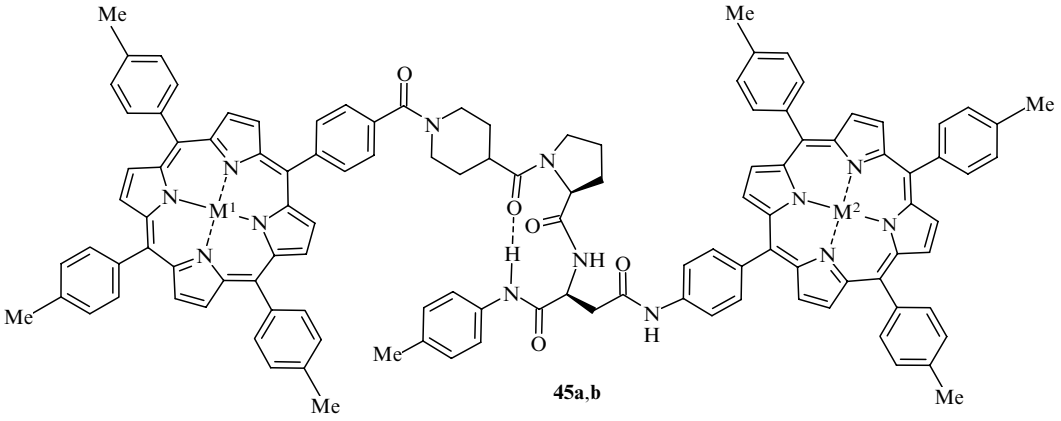

45a,b

$M^1 = 2H$, M^2 = Zn (**a**); M^1 = Zn, $M^2 = 2H$ (**b**).

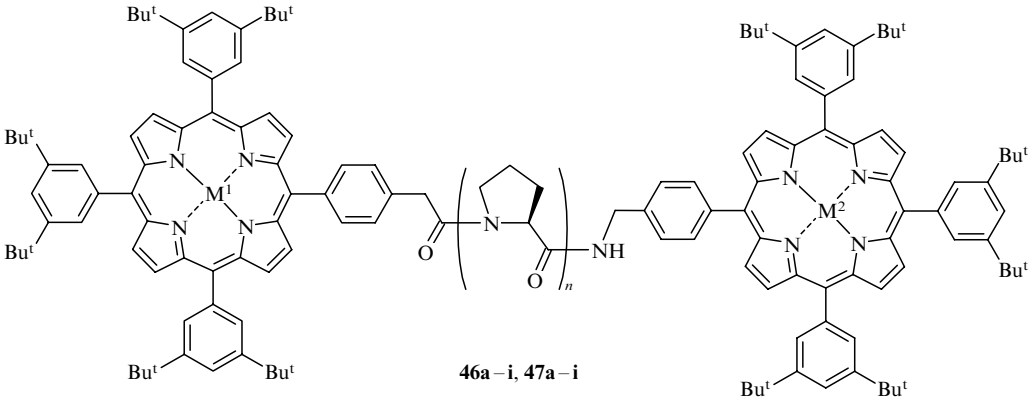

46a–i, 47a–i

46: M^1 = Zn, $M^2 = 2H$; **47**: $M^1 = 2H$, M^2 = Zn; n = 0 (**a**), 1 (**b**), 2 (**c**), 3 (**d**), 4 (**e**), 5 (**f**), 6 (**g**), 7 (**h**), 8 (**i**).

hydroxy groups and introduction of zinc into the porphyrin rings.[62]

Condensation of benzyloxycarbonyl-protected L- or D-tyrosine with L-tyrosine methyl ether afforded dipeptides, which were converted into piperazine-2,5-diones following deprotection. Reactions of the latter with the porphyrins **48a**,**b** afforded the diastereomerically pure zinc-containing dimers **41b** and **42b**; their demetallation resulted in compounds **41a** and **42a**.[62]

An alternative approach was used in the synthesis of the porphyrin dimers **43a**,**b**, **44a–d** and **45a**,**b** linked through β-folded peptides. In this synthesis, 5-(*p*-carboxyphenyl)-10,15,20-tri-*p*-tolylporphyrin (**49**) and 5-(*p*-aminophenyl)-10,15,20-tri-*p*-tolylporphyrin (**50**) were used as the porphyrin components, while

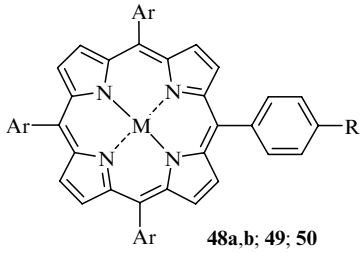

48a,b; **49**; **50**

48: R = CH_2Br, M = Zn, Ar = 4-MeC_6H_4 (**a**), 3,5-$Bu^t_2C_6H_3$ (**b**);
49: R = CO_2H, M = 2H, Ar = 4-MeC_6H_4;
50: R = NH_2, M = 2H, Ar = 4-MeC_6H_4.

the amino acid sequences D-Pro-Gly and D-Pro-L-Asp were used as the β-folded peptide spacers. The acid **49** was converted into its acid chloride, which reacted with D-proline to yield compound **51**.

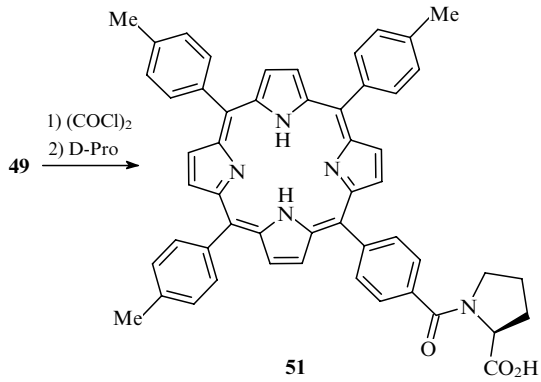

51

The reaction of the amine **50** with *tert*-butoxycarbonylglycine (Boc-Gly) using dicyclohexylcarbodiimide (DCC) as a coupling reagent resulted in the derivative **52a**. The last step included condensation of the acid **51** with the amine **52b** under the action of DCC in the presence of 1-hydroxybenzotriazole. This reaction afforded the porphyrin dimer **43a** linked through a β-folded dipeptide (yield 76%). The bisporphyrin **43a** was easily converted into the dizinc complex **43b** by treatment with an excess of zinc acetate.[63]

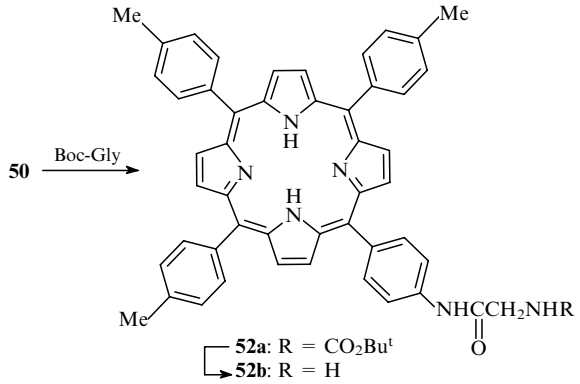

51 + **52b** ⟶ **43a** ⟶ **43b**

The dimers in which both porphyrin residues are linked to aspartic acid were synthesised in the following way. First, the β-carboxy group of Boc-L-Asp(OH)-OH was selectively protected followed by protection of the α-carboxy group. Subsequent hydrolysis of benzyl ester afforded the amino acid derivative **53** with a free β-carboxy group; its reaction with the amino acid component **50** yielded the derivative **54a**. Condensation of the acid **51** with the amine **54b** (obtained in 66% yield by deprotection of compound **54a**) gave the dimer **44a**, which gave further the complex **44b** (yield 58%).

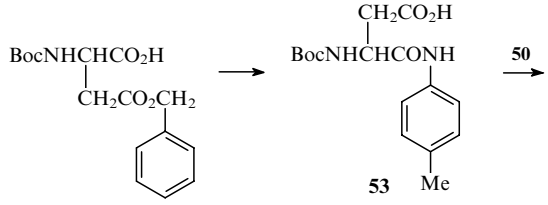

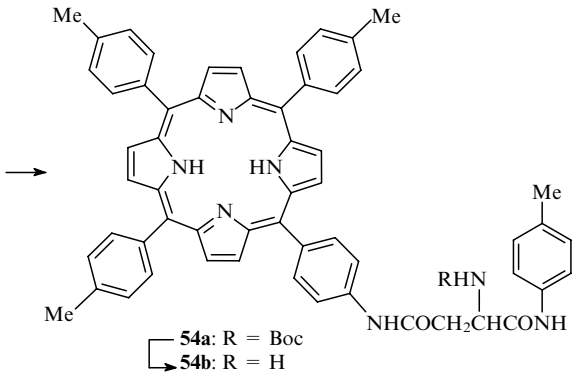

54b + **51** ⟶ **44a** ⟶ **44b**

The selectively metallated dimers **44c**,**d** were synthesised by the condensation of the zinc-containing porphyrin component with the porphyrin free base.[63]

The synthesis of the dimer **45a** included condensation of 5-(*p*-carboxyphenyl)-10,15,20-tri-*p*-tolylporphyrin (**49**) with piperidine-4-carboxylic acid, reaction of the product with D-proline to yield the amino acid derivative **55** and condensation of the latter with the zinc – porphyrin complex **54b** in the presence of DCC.[63]

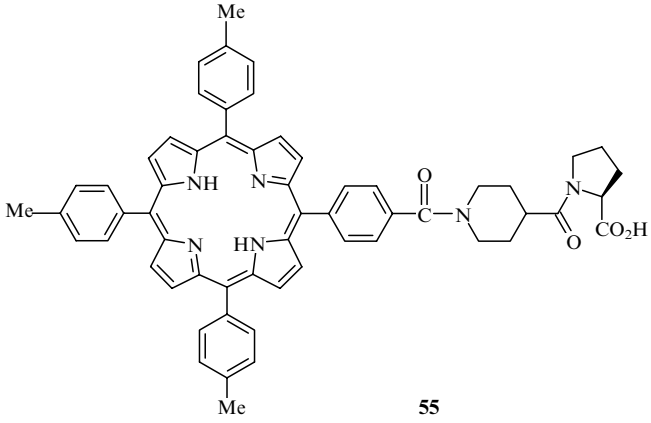

55

The bisporphyrin **45b** was synthesised from the zinc complex of compound **55** and the porphyrin free base **54b** in a similar way.[63] This strategy was also used in the synthesis of the bisporphyrin donor – acceptor model systems **46a** – **i** and **47a** – **i** linked by oligoproline spacers.

Porphyrin components differing in the positions of their functional groups used in the synthesis of peptide-linked bisporphyrins made it possible to obtain *meso*-β-linked ensembles **56a** – **c**.[65,66] An interesting feature of these systems is that their spacers contain an aromatic amino acid, *viz*., phenylalanine. Incorporation of aromatic amino acids into model photosynthetic systems is an important issue, since it was found that such aromatic amino acids as tyrosine and tryptophan mediate interactions between tetrapyrrole chromophores by virtue of electronic coupling of their molecular orbitals. Substitution of aliphatic amino acids for aromatic ones enables one to establish the dependence of the strength of interchromophore interactions and the efficiencies of photoinduced processes on the nature of the amino acid components of the spacers. The bisporphyrins **56a** – **c** were synthesised from the amino acid derivatives of 5-(*p*-aminophenyl)-10,15,20-triphenylporphyrin and 2-(2-carboxy)-vinyl-5,10,15,20-tetraphenylporphyrin using the dicyclohexylcarbodiimide method.

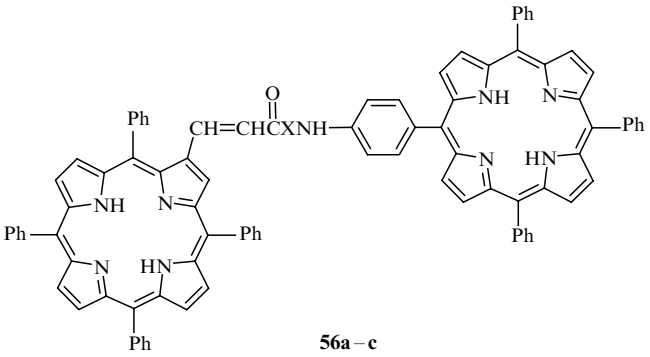

56a–c

X = NHCHCNHCH$_2$CO (**a**), NHCHCNHCH$_2$CO (**b**),
CHMe$_2$ CH$_2$Ph

NHCH$_2$CNHCHCNHCH$_2$CO (**c**).
CH$_2$Ph

The covalently linked mesoporphyrin dimers **57a-g** containing a lysine residue as the spacer were synthesised to study chlorophyll–protein interactions. UV-Vis and circular dichroism spectroscopic studies revealed that these dimers form complexes with polypeptides of natural light-harvesting systems owing to axial coordination of zinc and nickel atoms with histidine and the formation of hydrogen bonds between the ester groups of the dimer and the polar amino acid residues of the peptides. In the synthesis of the dimers **57a–g**, the mesoporphyrin IX monomethyl ester was condensed with Boc-L- or Boc-D-lysine using *N*-hydroxysuccinimide–DCC as the activating reagents. The product formed reacted with the second molecule of the mesoporphyrin monomethyl ester under identical conditions.[67]

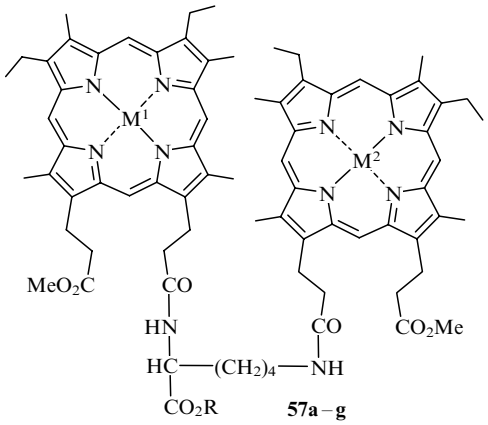

57a–g

Compound **57**	M^1	M^2	R
a	2 H	2 H	H
b	Zn	2 H	H
c	Zn	Zn	H
d	Zn	Zn	H (D-isomer)
e	2 H	2 H	Me
f	Zn	Zn	Me
g	Zn	Ni	H

b. Photochemical properties

Photochemical studies of the piperazine-2,5-dione-linked systems **41a**,**b** and **42a**,**b** revealed that the chromophores of the L,L-dimers **41a**,**b** having *p*-tolyl substituents interact more efficiently than the chromophores of the L,L-dimers **42a**,**b** with 3,5-di-*tert*-butylphenyl substituents. This difference is due to the fact that the bulkier 3,5-di-*tert*-butyl groups in the molecules **42a**,**b** disturb interactions of the porphyrin rings.

It was also found that the porphyrin components in the L,L-dimers **41a**,**b** and **42a**,**b** interact more efficiently in comparison with the D,L-dimers. This can be attributed to the localisation of both tyrosine phenylene groups in L,L-isomers on one side of the piperazine-2,5-dione plane, whereas in D,L-isomers these groups are localised on different sides of this plane. Thus the porphyrin components of the L,L-dimers are closer to each other than in the D,L-dimers. It thus follows that the strength of intramolecular interaction depends on the 'centre-to-centre' distance between the porphyrin rings.[62]

Evidence for the dependence of interactions between chromophores on the 'centre-to-centre' distance was also obtained for the dimers **43a**,**b** and **44a–d**.[63]

The efficiency of intramolecular energy transfer from zinc complexes to porphyrin free bases in the asymmetrical dimers **44c**,**d** (Φ = 86%) and **45a**,**b** (Φ = 76%) depends on the distance between tetrapyrrole components rather than on the nature of the spacer. The efficiency of quenching of the excited states of zinc-containing porphyrin complexes in compounds **46** and **47** decreases with an increase in the number of proline residues, *i.e.*, the average distance between the chromophores, in the course of energy transfer irrespective of its direction. These findings prompted a conclusion that singlet energy transfer in dimers linked by peptide spacers occurs predominantly 'through-space'.[63,64]

The dipole–dipole 'through-space' interaction described by the Förster approximation is the most probable mechanism of energy transfer from the zinc complex to the nickel-containing porphyrin in the dimer **57g**. The most efficient energy transfer was noted between the porphyrin rings that form coordination and hydrogen bonds with polypeptides of natural light-harvesting complexes. This suggests that polypeptides induce efficient intramolecular energy transfer between pigments in model photosynthetic compounds.[67]

3. Non-covalently linked bisporphyrin systems

The above-described methods for the construction of model photosynthetic systems are based on the formation of covalent bonds between chromophores, but they are not always suitable for the synthesis of muticomponent ensembles. An alternative approach consists in the assembly of supramolecular aggregates due to non-covalent interactions, such as the formation of hydrogen bonds, salt bridges and coordination bonds between metals and ligands.[17]

The strategy of synthesis of non-covalently linked ensembles consists first in the synthesis of chromophores possessing specific recognition sites and their subsequent self-assembly into highly ordered multicomponent structures. According to the type of their binding, these model systems resemble those discovered in the light-harvesting antennae.

The design of non-covalently linked supramolecular complexes can be based on pairwise interactions between complementary heterocyclic bases. The complex **58–59**, which is stabilised by hydrogen bonds between guanine and cytosine residues, was among the first ensembles of this kind described in the literature.[68]

However, high flexibility of this first-generation system prevented detailed studies of the energy transfer mechanism observed. The synthesis of the rigid dimeric porphyrin ensemble **60–61** in which the donor and the acceptor are linked directly to guanosine and cytidine residues through phenyl groups has been described.[69] The arrangement of its two porphyrin residues is such that the angle between the planes of their macrocycles is $\sim 90^\circ$ and the 'centre-to-centre' distance was estimated[69] to be ~ 22.5 Å. The porphyrin fragments can rotate by $\sim 45^\circ$ around the C–C bond linking the phenyl ring to the heterocyclic base.

The nucleoside-substituted porphyrin **60** was prepared by the Lindsey condensation of the guanosine-containing benzaldehyde **62** with benzaldehyde and 3,3′-dibutyl-4,4′-dimethyldipyrrolyl-

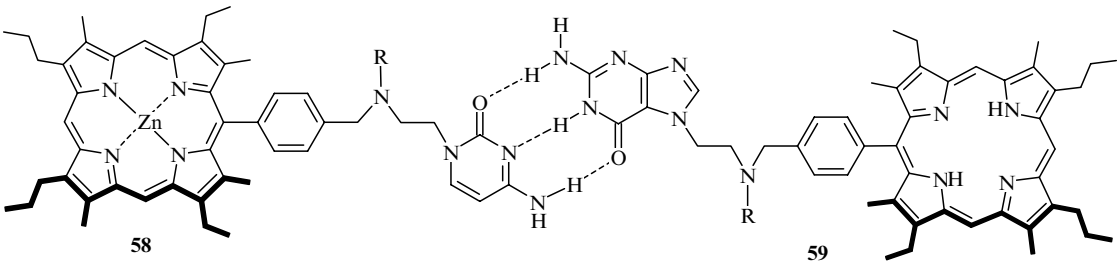

58 **59**

R = $(CH_2)_2O(CH_2)_2OMe$.

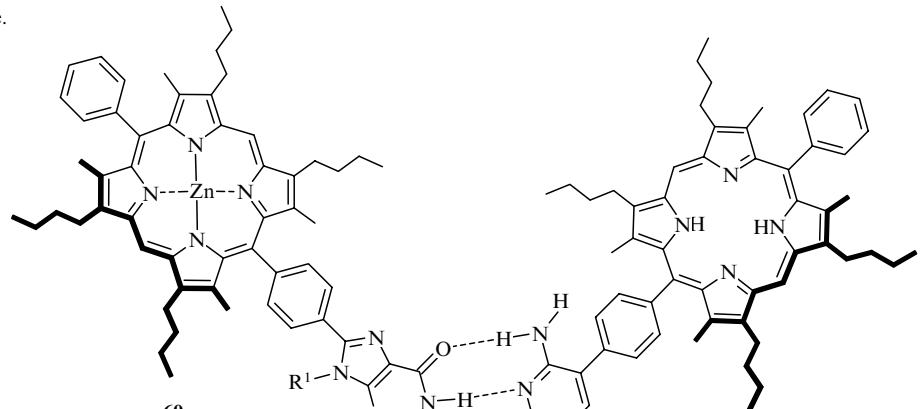

60 **61**

R^1 = 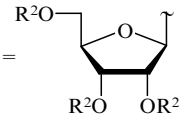 , $R^2 = SiMe_2Bu^t$.

methane (**64**) with subsequent removal of the isobutyryl group, introduction of the *tert*-butyldimethylsilyl group and metallation.

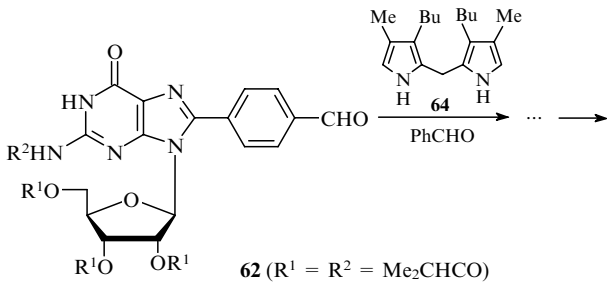

62 ($R^1 = R^2 = Me_2CHCO$)

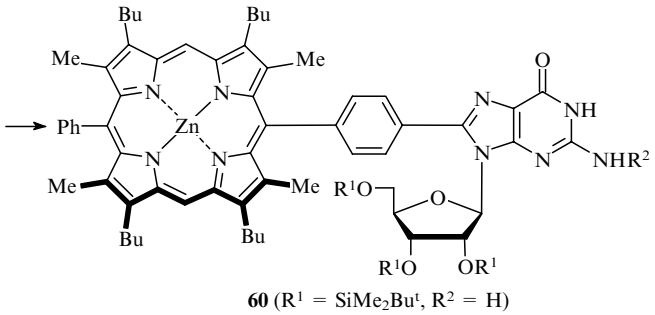

60 ($R^1 = SiMe_2Bu^t$, $R^2 = H$)

The nucleoside-substituted metal-free porphyrin **61** was synthesised in a similar way from the cytidine-containing benzaldehyde **63**.

The reaction of the cytidineporphyrin **61** with the guanosine-containing zinc complex **60** in dichloromethane results in the formation of a three-point hydrogen bond between the complementary bases. According to ^1H NMR spectroscopic data, the binding constants of the guanosine and cytidine derivatives in the ensemble **60**–**61** are equal to $22\,000 \pm 2000$ litre mol^{-1} (see Ref. 69).

The photoactive non-covalent complexes **65**–**66a** and **65**–**66b** (see Ref. 70) were assembled from carboxylate-containing porphyrins and the monoprotonated pentapyrrole chromophore sapphirine through the salt bridge formed. These systems are prepared by mixing porphyrin and sapphirine (in the form of a free acid and a free base) in dichloromethane; their binding constants determined by ^1H NMR spectroscopy are $\sim 10^3$ litre mol^{-1}. The two chromophores in these ensembles are oriented perpendicularly to each other in such a way that porphyrin is localised above the plane of sapphirine, while the 'centre-to-centre' distance between the chromophores is equal to 12.5 Å.

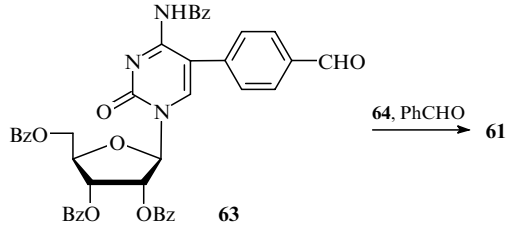

63 **61**

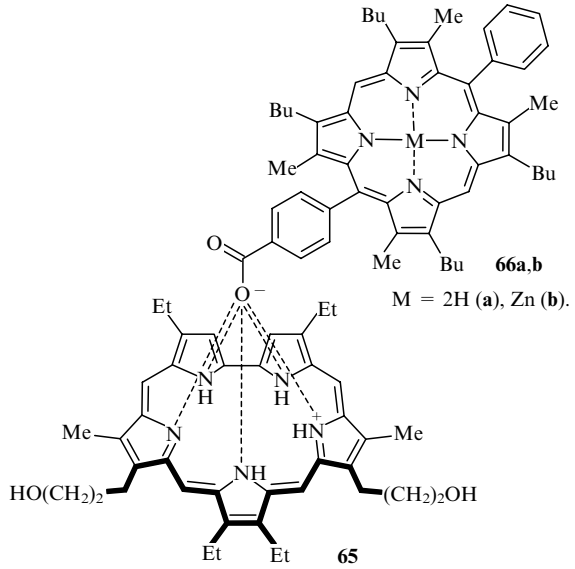

66a,**b**

M = 2H (**a**), Zn (**b**).

65

It was shown [69, 70] that the non-covalently linked bisporphyrin systems described above can be used as models in studies of photoinduced energy transfer between pigments.

The singlet–singlet energy transfer from the zinc complex to the porphyrin free base in the ensemble **60**–**61** is effected to a distance of ~ 22.5 Å and is characterised by the rate constant $k \approx 9.1 \times 10^8$ s^{-1} and 60% efficiency, which is consistent with the parameters calculated on the basis of the Förster approximation. These results suggest that dipole–dipole 'through-space' interactions are the most probable mechanism of singlet energy transfer. In this case, the role of hydrogen bonds between complementary bases is solely to bind chromophores and not to promote singlet energy transfer.

On the other hand, the triplet energy transfer in the ensemble **60**–**61,** which follows from the appearance of an absorption band at 545 nm characteristic of triplet states of metal-free porphyrins, seems to be effected through hydrogen bonds which play in this case a more active mediatory role.[69]

Irradiation of porphyrin subunits in the ensembles **65**–**66a** and **65**–**66b** induces singlet–singlet energy transfer from porphyrin to sapphirine within the complexes; this process is characterised by lower energy of the first excited singlet state. The calculated rate constants for the energy transfer in systems, which utilise metal-free bases and zinc–porphyrin complexes as donors, were equal to 4.3×10^{10} and 1.1×10^{11} s^{-1}, respectively, which is consistent with the Förster mechanism. Rapid energy transfer in the ensembles **65**–**66a** and **65**–**66b** is due to higher values of spectral overlap integrals of porphyrin emission and sapphirine absorption.[70]

The donor–acceptor ensembles described in this Section can be incorporated into more complex multicomponent systems mimicking natural light-harvesting complexes.

III. Multiporphyrin ensembles

Natural photosynthetic light-harvesting complexes contain several hundreds of pigments responsible for the migration and transfer of excitation energy to the reaction centres. Therefore, an ideal model system should include a great and strictly defined number of chromophores with known photophysical properties. The molecular organisation of such a system should allow accurate control over the mutual arrangement of pigments in the integral ensemble. This, in turn, will ensure efficient transfer of excited state energy.

Limited solubility of multiporphyrin ensembles is one of the main difficulties in their design. The approaches to the solution of this problem include incorporation of long alkyl groups into β-pyrrole positions and of alkyl, 3,5-di-*tert*-butylphenyl or *ortho*-disubstituted phenyl groups into more accessible *meso*-positions of terrapyrrole macrocycles. The porphyrins thus substituted are less susceptible to aggregation and, correspondingly, are more readily soluble in organic solvents, which facilitates the synthesis, chemical and spectroscopic analysis of the multiporphyrin ensembles based on them.[27]

Yet another problem is related to the quenching of excited states by photoinduced electron transfer which competes with the energy transfer. One of the ways to limit the energy transfer envisages the design of porphyrin ensembles with sufficiently long fixed 'centre-to-centre' distances where electronic interactions between the pigments are relatively weak.

1. Synthesis

Two promising approaches to the synthesis of multiporphyrin ensembles include building block synthesis of covalently linked systems and self-assembly of pigments possessing special recognition sites. Building block synthesis, which consists in condensation of substituted iodoaryl- and ethynylarylporphyrins under mild conditions in the presence of a palladium catalyst, was used for the preparation of linear trimers **67**[25] and **68**,[27] the linear amphiphilic ensemble **69**[34] and the star-like five-porphyrin ensemble **70**[30, 71] in which the macrocycles were linked through diarylethyne spacers.

The synthesis of a dithiaporphyrin (N_2S_2) block and its further use in the construction of the model light-harvesting system **71** have been reported.[72] The preparation of the N_2S_2-porphyrin includes the reaction of 4-(trimethylsilylethynyl)benzaldehyde (2 equiv.) with dilithiothiophene (1 equiv.), condensation of 2,5-bis[4-(trimethylsilylethynyl)phenyl(hydroxy)methyl]thiophene with pyrrole in the presence of boron trifluoride etherate and removal of trimethylsilyl protective groups. The reaction of the dithiaporphyrin formed with 5-(4-iodophenyl)-10,15,20-tris(3,5-di-*tert*-butylphenyl)porphyrin in the presence of a palladium catalyst and triphenylarsine affords the pentamer **71** in 37% yield.

As mentioned previously, one of the main tasks in photosynthetic modelling is the construction of molecular ensembles which, like natural antenna complexes, are characterised by high molar absorption coefficients in both blue and red regions of the visible spectrum and significant overlap of absorption spectra of the acceptor and emission spectra of the donor. These properties are inherent in systems containing porphyrins and phthalocyanines, which differ in their electronic characteristics. Yet another attractive feature of the combination of porphyrin and phthalocyanine chromophores within a single ensemble is that the energy of the first singlet excited state of phthalocyanine is lower than that for porphyrin.

The light-harvesting complexes **72** and **73** contain four and eight porphyrin components, respectively, which are covalently linked to phthalocyanine to form a star-like structure. The use of a phenylethyne linker between the porphyrin and phthalocyanine components makes it possible to reduce the distance and to enhance interchromophore electronic interactions in the above systems in comparison with their structural analogues, *viz*., the diphenylethyne-linked pentamers **70** and **71**.

The ensembles **72a**,**b** were synthesised in 45% and 15% yields by cyclotetramerisation of ethyne-linked porphyrin–phthalonitrile in pentan-1-ol in the presence of 1,8-diazabicyclo[5.4.0]undec-7-ene and $MgCl_2$ or $Zn(OAc)_2$, respectively. Subsequent selective demetallation and metallation reactions afforded the pentads **72c**–**e**, which contain different metals in their tetrapyrrole macrocycles.[73]

A similar approach was used for the synthesis of the ensembles **73a**–**c**. In this case, cyclotetramerisation was preceded by palladium-catalysed preparation of the porphyrin dimer containing a phthalonitrile fragment.[74]

Miller *et al*.[75] have carried out the synthesis of the linear chromophore ensemble **74**, containing perylene, bisporphyrin and phthalocyanine components, which manifests enhanced light-harvesting properties owing to strong absorption in all the visible region of the spectrum. This system can function as a cascade transferring excitation energy towards the acceptor. The ensemble **74** was synthesised in four steps: (1) synthesis of *trans*-substituted AB_2C-porphyrin building blocks, each possessing only one non-substituted *meso*-position; (2) oxidative *meso,meso*-condensation of the porphyrin monomers to yield the bisporphyrin containing the phthalonitrile and iodophenyl fragments; (3) synthesis of bisporphyrinphthalocyanine ensembles by mixed cyclisation of the bisporphyrin and 4-*tert*-butylphthalonitrile and (4) palladium-catalysed condensation of the resulting product with ethynylperylene.

X-Ray diffraction analysis of antenna complexes of photosynthesising bacteria revealed that these consist of two concentric circular ensembles of bacteriochlorophyll molecules non-covalently bound to apoproteins (see Fig. 1).[11] The planes of overlapping bacteriochlorophyll *a* molecules in the inner ring containing two thirds of all chromophores are perpendicular to the plane of the tylakoid membrane, whereas the planes of chromophores in the outer ring are almost parallel to the membrane surface. Such spatial arrangement ensures the most efficient energy transfer through dipole–dipole resonance interactions between pigments in the photosynthetic subunit.

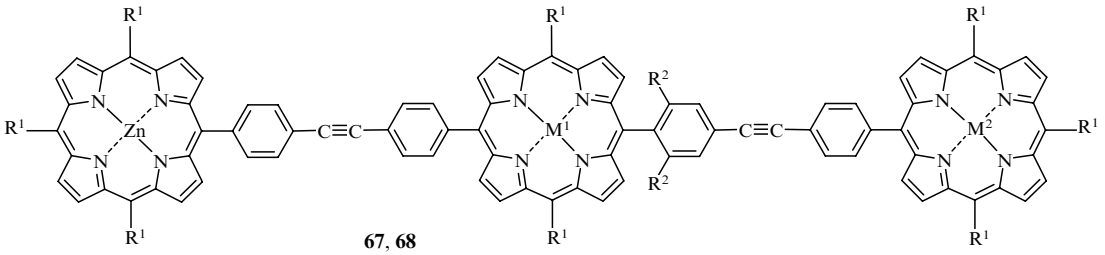

67, **68**

67: R^1 = 2,4,6-$Me_3C_6H_2$, R^2 = H, M^1 = 2 H, M^2 = Zn; **68**: R^1 = 2,4,6-$Me_3C_6H_2$, R^2 = Me, M^1 = Zn, M^2 = 2 H.

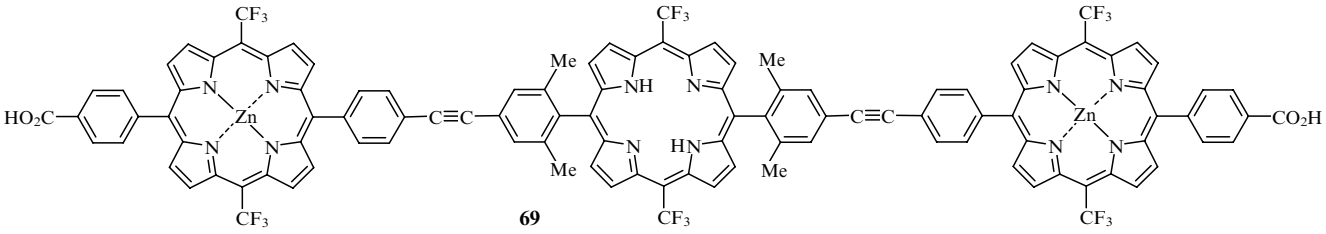

69

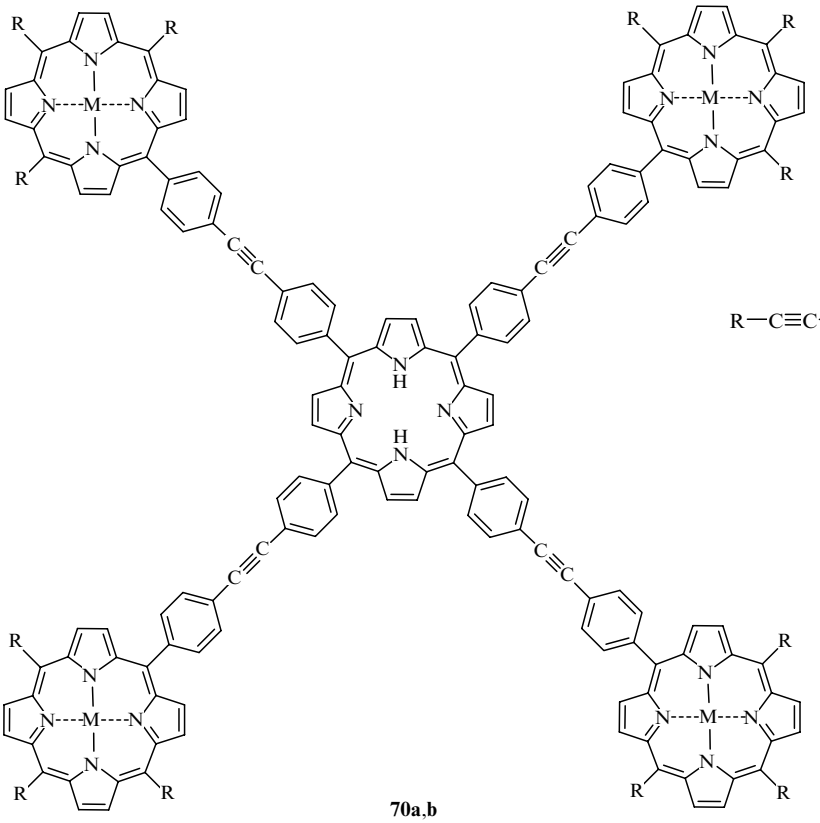

70a,**b**

R = 2,4,6-$Me_3C_6H_2$; M = Zn (**a**), Mg (**b**).

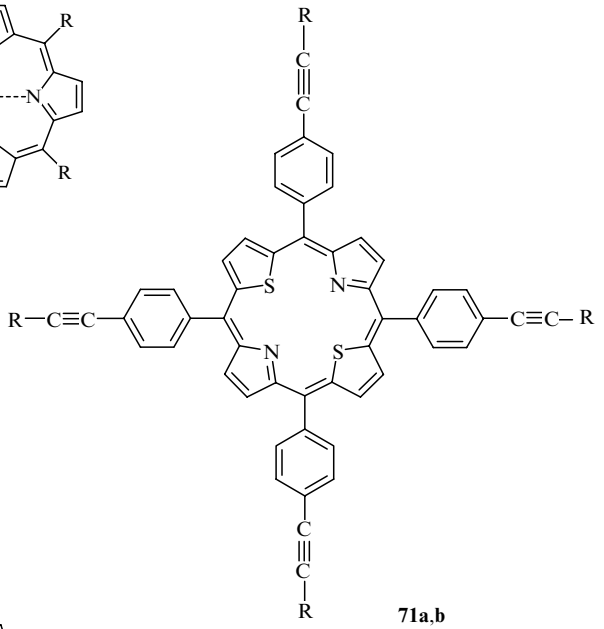

71a,**b**

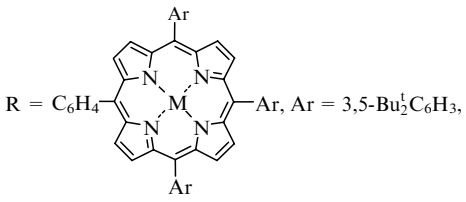

M = 2 H (**a**), Zn (**b**).

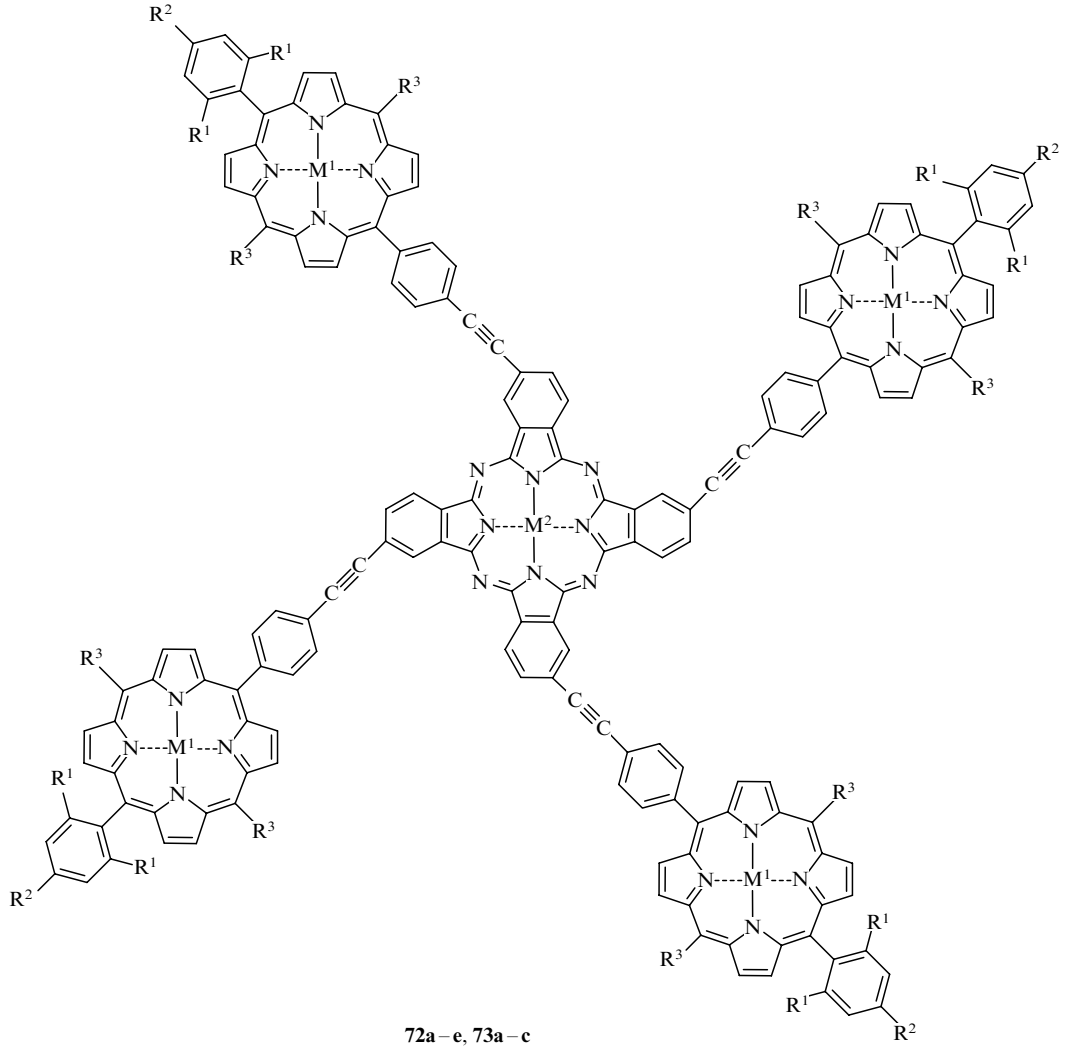

72a–**e**, **73a**–**c**

72: $R^1 = R^2 = Me$, $R^3 = 2,4,6\text{-}Me_3C_6H_2$; **73**: $R^1 = H$, $R^2 =$ 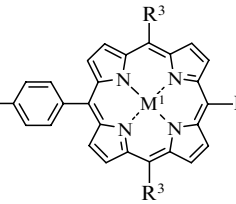 R^3; $R^3 = 2,4,6\text{-}Me_3C_6H_2$;

$M^1 = M^2 = Mg$ (**a**), Zn (**b**), 2 H (**c**), $M^1 = 2\,H$, $M^2 = Mg$ (**d**), $M^1 = Zn$, $M^2 = Mg$ (**e**).

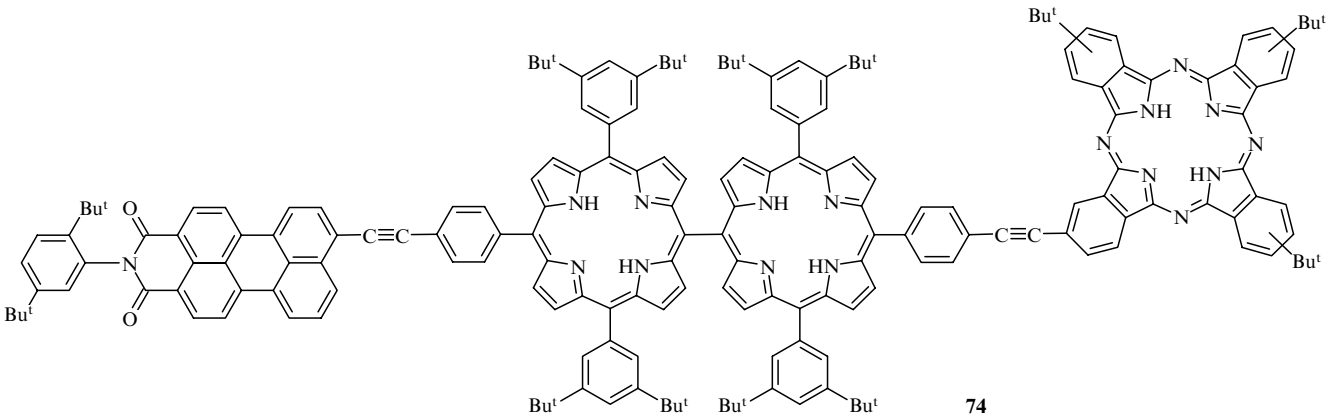

74

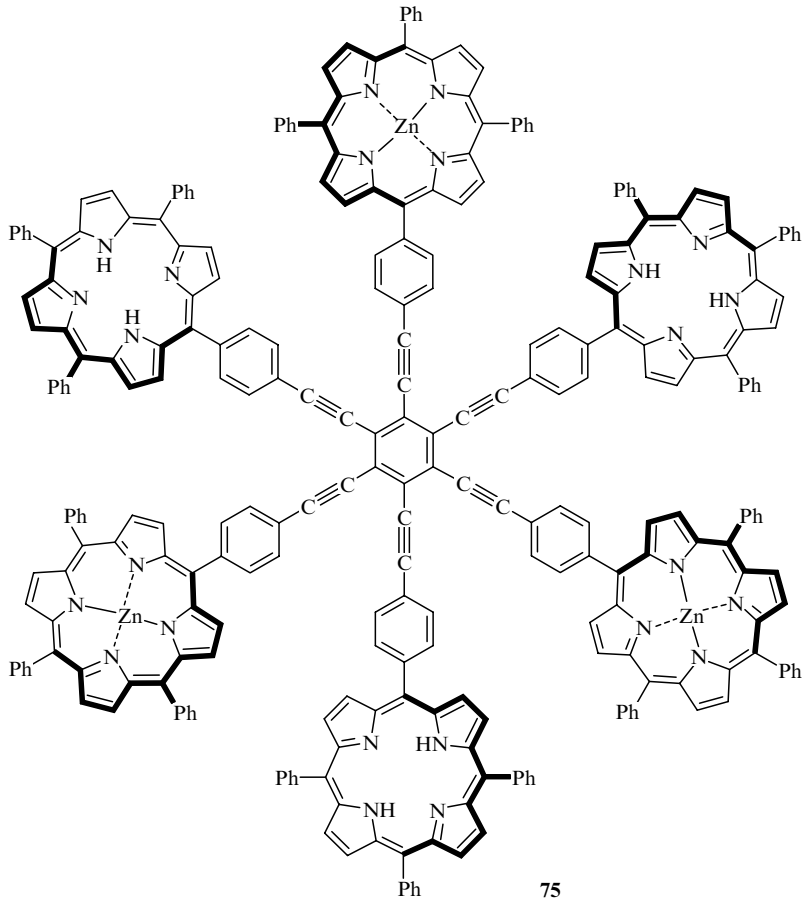

75

The multiporphyrin ensemble **75** was designed for simulation of spatial arrangements of chromophores in the inner rings of natural antenna complexes. In this model, six porphyrin rings are covalently linked through rigid ethynyl linkers to six positions of the benzene ring, which functionally replaces protein matrices of natural complexes. The diameter of the cyclic ensemble **75** is 46.7 Å and the 'centre-to-centre' distance between chromophores is 13.2 Å, *i.e.*, it is higher than the average distance (~9 Å) between magnesium ions of bacteriochlorophylls in natural systems.

The three-step synthesis of the hexaporphyrin ensemble **75** includes reaction of the zinc-containing complex of 5-(4-iodophenyl)-10,15,20-triphenylporphyrin with the 1,3,5-tris(trimethylsilyl) derivative of hexaethynylbenzene in the presence of a palladium catalyst under standard conditions, removal of protective groups and reaction of the star-like trimer formed with a large excess of the metal-free porphyrin. The total yield of the resulting ensemble **75** is 11%.[76]

The hexagonal cyclic ensembles **76a**,**b** have been described[77] in which the six porphyrin rings are linked rigidly through six *meta*-diethynylphenyl bridges to form a cavity with an internal diameter of ~ 46 Å. A multistep synthesis of these ensembles is based on the use of only one building block (**77**) in which two protected, reactive positions, *viz*., the ethynyl group and the carbon atom of the phenyl ring, can be activated selectively (Scheme 2). Cross-condensation of porphyrins **78a** and **79**, which are readily prepared from compound **77** by treatment with methyl iodide or sodium hydroxide, respectively, in the presence of a palladium catalyst results in the bisporphyrin **80a**. Iteration of this three-step reaction sequence yields porphyrin tetramers; their condensation with dimeric fragments and cyclisation result in the formation of the hexameric ensembles **76a**,**b**.

Eight chromophores in the system **81** are linked to the polypeptide chain, which may form a secondary α-helical structure after certain degree of oligomerisation. This conformation is determined by the natural trend of porphyrins for aggregation and is characterised by overlap of the chromophores, which ensures electronic interactions sufficient to enhance migration of excitation energy within the ensemble.

The synthesis of the octamer **81** is based on the use of the L-lysine-containing porphyrin **82**, which was prepared by condensation of carboxy and amino components in the presence of DCC and 1-hydroxybenzotriazole (HOBT) (yield 94%). The strategy of oligomer synthesis involves selective removal of protective *tert*-butoxycarbonyl and allyl groups under mild conditions (Scheme 3). Thus treatment of the porphyrinlysine **82** with a solution (1 mol litre^{-1}) of chlorotrimethylsilane and phenol in dichloromethane results in the removal of the protective Boc group (yield 91%). Removal of the allyl protection from the carboxy group of compound **82** was carried out in a dimethylacetamide–piperidine mixture in the presence of tetrakis(triphenylphosphine)palladium in 84% yield. The dimer **83** was synthesised by condensation of the amine and the acid in the presence of DCC and HOBT. Iteration of this three-step procedure affords the tetramer **84** and the octamer **81** in 86% and 80% yields, respectively.[78]

A strategy based on an ordered assembly of chromophores owing to specific non-covalent interactions, was used in the design of a model photosynthetic system **85**. This is formed as a result of pairwise interactions between complementary heterocyclic bases upon mixing of guanosine and cytidine porphyrin derivatives in dichloromethane.[69]

Scheme 2

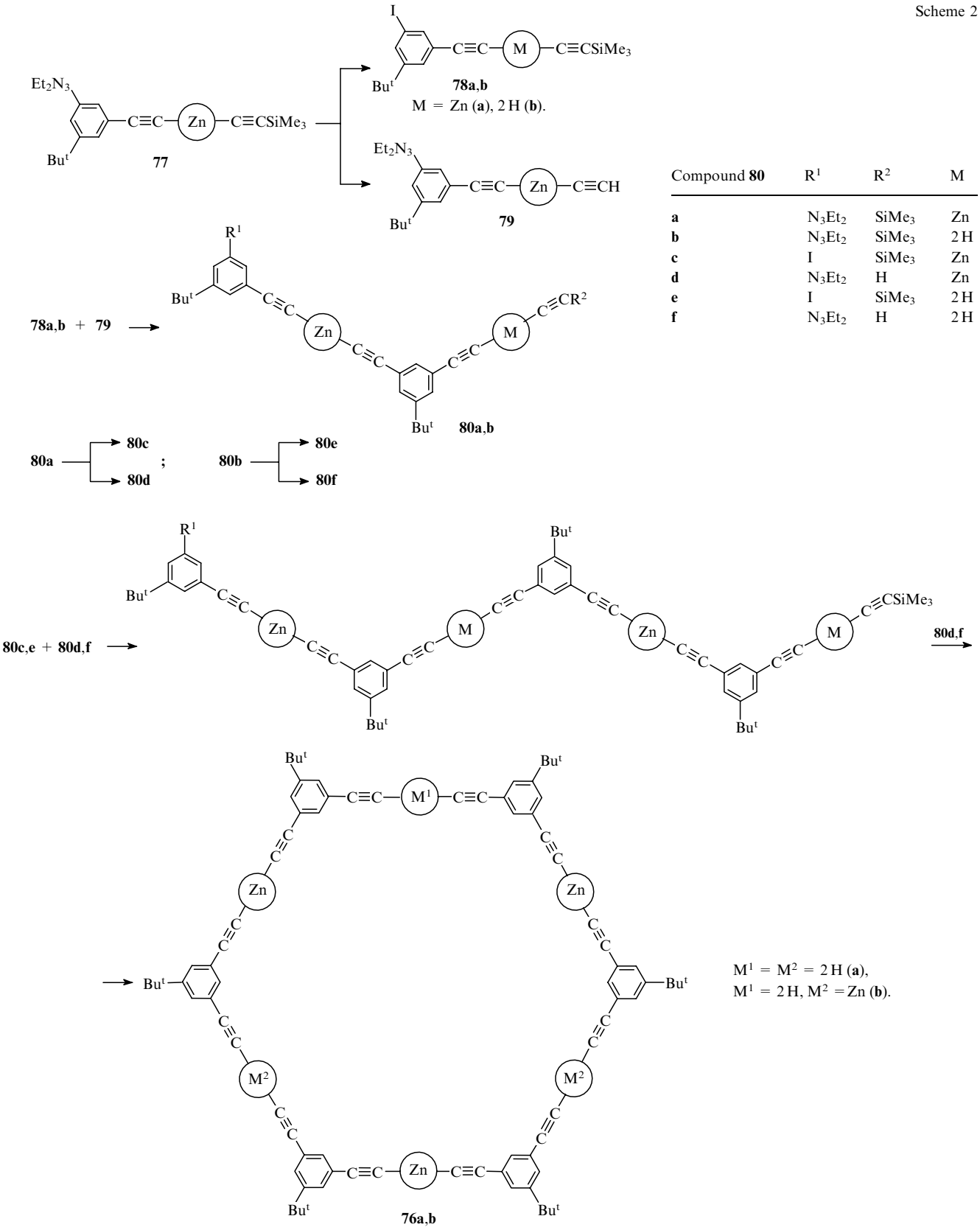

Compound **80**	R^1	R^2	M
a	N_3Et_2	$SiMe_3$	Zn
b	N_3Et_2	$SiMe_3$	2 H
c	I	$SiMe_3$	Zn
d	N_3Et_2	H	Zn
e	I	$SiMe_3$	2 H
f	N_3Et_2	H	2 H

Scheme 3

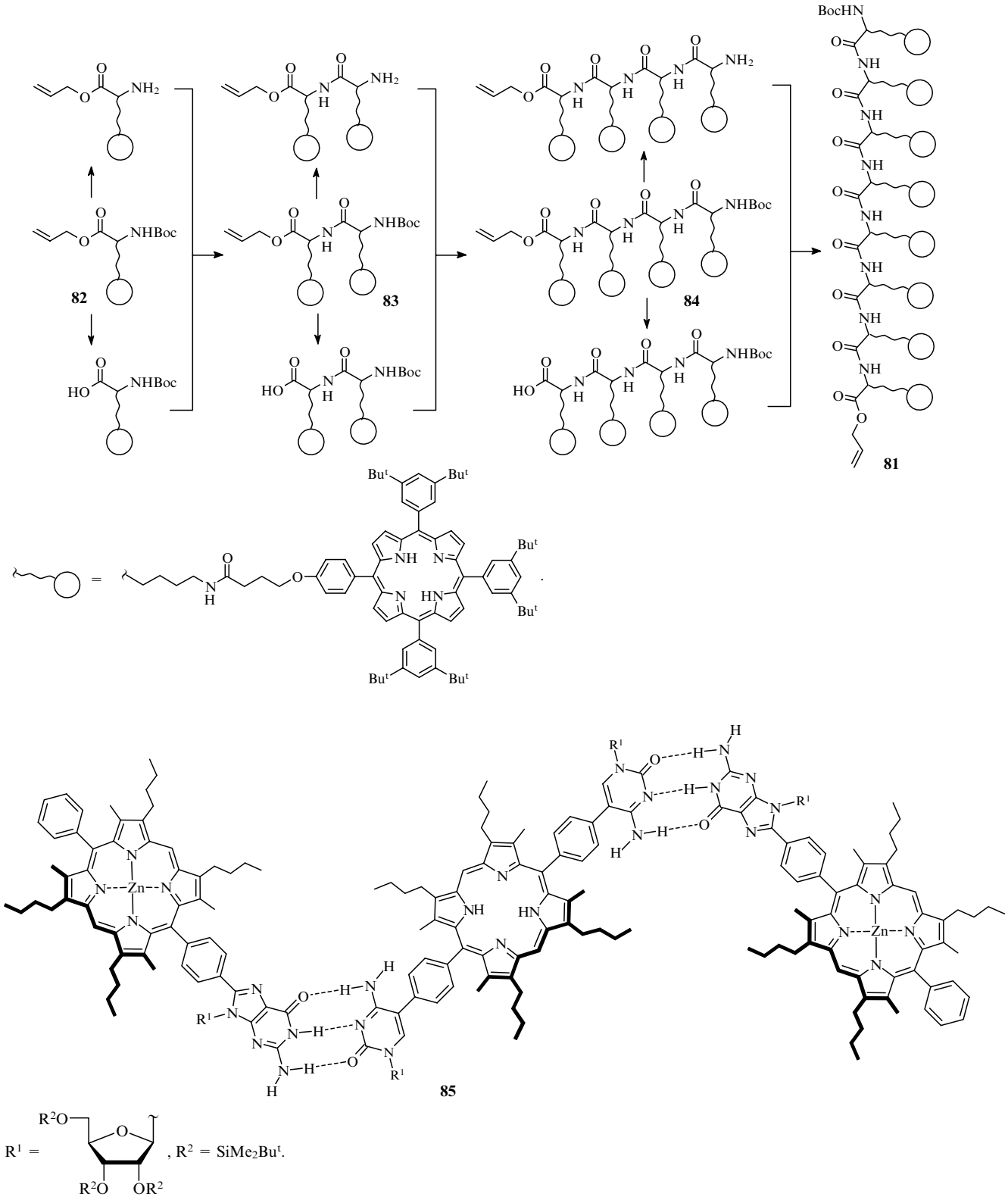

2. Photochemical properties

Photochemical studies of the system **70a** have shown that the emission from the central porphyrin free base predominates in the fluorescence spectrum. The quantum yields of emission of zinc-containing complexes within the ensemble (Φ = 0.38%) were 12-fold smaller than that of the corresponding monomeric zinc-porphyrin complex. At the same time, the presence of four peripheral metal-containing porphyrin fragments virtually did not influence the emission yield of the central porphyrin free base (Φ = 12%). It was noted also that the whole fluorescence excitation spectrum coincided almost completely with the absorption spectrum. Based on these data, the yield of the energy transfer from the peripheral zinc complexes to the porphyrin free base was estimated to be equal to 90%. Thus, the pentamer **70a** can accumulate and concentrate the energy of photons in the centre of the ensemble.[71]

Similar results were obtained for the ensembles **71a**,**b** where the efficient energy transfer occurs from the peripheral porphyrin fragments to the central dithiaporphyrin subunit.[72]

The quantum yields of the energy transfer from the photoexcited porphyrin components to the central phthalocyanine in the model systems **72b**–**e** exceed 99%. However, the efficiency of energy transfer in the ensemble **72a** is decreased by 40%, which is attributed to the contribution of the charge transfer from the excited porphyrin to the ground state of phthalocyanine due to probable easier oxidation of magnesium-containing porphyrins in comparison with zinc-porphyrin complexes and free bases.[73]

An approach to the targeted transfer of energy to the terminal acceptor includes a cascade of energy transfers along the ensemble of pigments linked in succession. Studies of spectral properties of the linear molecular system **74** revealed an ultrafast ($k \geqslant 3.3 \times 10^{11}$ s^{-1}) and nearly quantitative cascade-like energy transfer from perylene to bisporphyrin and further to phthalocyanine. The directional energy transfer in this rigid structure is determined by the nature of the donor and acceptor chromophores, type of spacers and strong electronic interactions between the pigments in the bisporphyrin energy-transferring subunit. In addition, the ensemble **74** is characterised by significant overlap of absorptions of the components in the visible region of the spectrum, which determines its high light-harvesting capacity.[75]

The effective transfer of singlet excitation energy from zinc-containing complexes to porphyrin free bases was observed in the ensembles **75** ($\Phi = 98\%$) and **76a** ($\Phi = 91\%$) in which the spatial configuration of the chromophores mimicks the mutual arrangement of pigments in light-harvesting complexes of natural photosynthesising organisms.[76,77] At the same time, the energy transfer from five zinc-containing chromophores to the single acceptor in the hexamer **76b** occurs with the quantum efficiency of 40%.[77] Such a significant difference is explained by the increase in the number of non-productive stages in the energy transfer between zinc-containing porphyrins in the ensemble **76b**.

In contrast with the above-described systems, the singlet energy transfer in the non-covalently linked ensemble **85** where two zinc complexes and one porphyrin free base are held at a distance of 22.5 Å from one another due to pairwise interactions between guanine and cytosine follows the Förster 'through-space' mechanism ($k \approx 9 \times 10^8$ s^{-1}) with a 60% efficiency. The quantum efficiency of the energy transfer in this system can be optimised by reducing the distance (by ~ 5 Å) between the porphyrin components.[69]

Fast migration of excitation energy between isoenergetic pigments takes place in natural light-harvesting complexes. It was of interest to determine the rate of this process. In an attempt to study the dynamics of this process and the feasibility of a reversible energy transfer, Hsiao *et al.*[51] have performed computer-assisted simulation of the photodynamic behaviour of the trimer **68** with some admissions. First, considering that absorption characteristics of two zinc-containing chromophores are identical, the authors admitted that primary excitation is distributed uniformly between these two porphyrins. Second, it was assumed that the two-photon absorption was negligible under the conditions used. Third, it was suggested that the rate of energy transfer from the terminal zinc porphyrin (ZnP) to the central one (k_1) is equal to that of the reverse process (k_{-1}). And, finally, the rate of the energy transfer between the central zinc-containing complex and the porphyrin free base (H_2P) (k_2) was taken to be equal to the rate measured for the analogous dimer **12c** (Scheme 4).

The temporal evolution of the energy transfer between the chromophores in the trimer is described by a system of differential equations which, for a fixed value of k_1 with a time interval of 0.5 ps, is solved with respect to the concentrations of singlet excited states for each of the three individual chromophores at a given moment of time. The decay curves constructed on the basis of the calculated values should correlate with the experimental monoexponential curves of absorption bleaching of the metal-free

Scheme 4

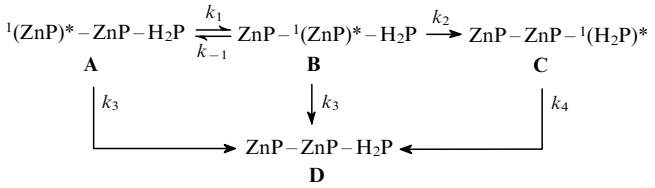

porphyrin in the ground energy state and of decay of the singlet state of zinc-containing porphyrins. The rate constant for the energy transfer between two isoenergetic zinc-containing porphyrins estimated in this way, $k_1 = k_{-1} = (2.2 \pm 0.8) \times 10^{10}$ s^{-1}, is comparable to that for the energy transfer between a zinc-containing complex and the free base.[51]

The total quantum yields of energy transfers in multicomponent porphyrin ensembles are difficult to predict, even if the efficiencies of individual steps of these processes are known. As the synthesis of such ensembles is very time and material consuming, rational design of efficient energy-transmitting molecular structures demands reliable prediction of their properties.

Van Patten *et al.*[79] have developed a general analytical technique for simulation of the kinetics of energy migration in weakly bound multipigment ensembles containing several donors but only one terminal acceptor. This approach is based on the system of differential equations which describe the temporal evolution of the energy transfer between the neighbouring chromophores. Thus in the case of the trimeric porphyrin ensemble **68**, these processes include energy migration between the donors (k_1, k_{-1}), energy transfer to the terminal acceptor (k_2), relaxation of the singlet state of the donors (k_3) and the terminal acceptor (k_4) (see Scheme 4). In this specific case, it is necessary to consider four configurations the interaction of which is described by the following system of differential equations:

$$dA/dt = (-k_1 - k_3)A + (k_{-1})B,$$

$$dB/dt = k_1 A + (-k_{-1} - k_2 - k_3)B,$$

$$dC/dt = k_2 B - k_4 C,$$

$$dD/dt = k_3 A + k_3 B + k_4 C,$$

where $A - D$ are the concentrations of states **A**–**D**, respectively.

In the general case, the energy transfer for a multiporphyrin ensemble $ZnP_{N-1}-H_2P$ can be regarded as an analogous first-order task for a series of reactions with N + 1 configurations. These equations are constructed with allowance for irreversibility of the energy transfer to the acceptor, whereas excitation energy migrates between isoenergetic donors in both directions (see Scheme 4).

By varying the initial conditions for excitation and the empirical data for the rates of energy transfer in all stages, it is possible to find solutions for the given system with respect to the concentrations of singlet excited states for each particular chromophore at a given moment of time. Their subsequent summation in time makes it possible to determine the general quantum efficiency of the energy transfer, *i.e.*, the percentage of ensembles in which the excitation reaches the terminal acceptor. This method allows prediction of the quantum efficiency depending on the rates, lifetimes of excited states and structures of ensembles.

The results of these calculations showed that the quantum efficiency of the energy transfer to the terminal acceptor in linear ensembles during random excitation of isoenergetic donor pigments with fixed rates of the energy transfer in each step decreases rapidly with an increase in the molecule length. The quantum efficiency strongly depends on the changes in the rates of the energy transfer between isoenergetic pigments. For example, the quantum efficiency of excitation capture for a linear twenty-porphyrin ensemble (the rate constant for the energy transfer between its isoenergetic pigments, k_1, is 2×10^{10} s^{-1}) is as low as 35%. However, with an increase in the transfer rate

($k_1 = 1 - 10^{12}\ s^{-1}$) the quantum yield of the energy transfer for this ensemble increases to 70%, whereas that for the linear fifty-porphyrin ensemble is 43%. Thus, the increase in the rate of the energy transfer results in a significant increase in the quantum efficiency.

The energy transfer becomes more efficient provided the migration of energy competes successfully with relaxation of the excited state. With this in mind, van Patten *et al.*[79] have studied the dependence of the efficiency of the energy migration in linear ensembles on the lifetime of the singlet excited states. A comparative study for different rates of competing deactivation has demonstrated that the quantum efficiency increases significantly with an increase in the lifetime (τ) of the excited singlet state of the donor. Calculations have shown that the quantum yields for ten-component linear ensembles containing zinc- and magnesium–porphyrin complexes as donors (τ = 2.4 and 9 ns, respectively) are 62% and 85%, respectively. Qualitatively similar results were obtained in simulation of linear ensembles where the excitation and energy capture occur at different ends of the molecule.

Since the quantum yields are determined by the competition between the energy migration and relaxation of the excited state, the efficiency of the energy transfer increases significantly in cyclic and branched ensembles with the minimum number of non-productive energy transfer steps. For example, the quantum efficiency for a tri-branched ten-component ensemble shown in Fig. 3 *c* (Φ = 91%) is similar to that for a linear tetramer, whereas that for a linear ensemble comprising nine zinc-containing porphyrins and one free base is as low as 63%.[79]

It should be noted that the quantum efficiency estimated for a cyclic porphyrin decamer with an integral acceptor (Φ = 84%, see Fig. 3 *b*) exceeds markedly the experimental value for the hexamer **76b** with an identical structure (Φ = 40%). There are several explanations for this phenomenon: (1) different sizes of the macrocyclic ensembles in theoretical and synthetic models; (2) decreased (in comparison with theoretical value) rate of intramolecular energy transfer in the synthetic ensemble where porphyrin subunits are linked through *meta*-positions of aromatic rings of the linkers; (3) predominant excitation, under the experimental conditions, of only one zinc-containing chromophore in each multiporphyrin ensemble with the resulting loss of excitation energy in the reversible energy transfer between neighbouring zinc porphyrins and (4) possible rotation of porphyrin chromophores in the synthetic hexamer.[77]

Introduction of different types of donors into model systems increases the ratio of rates of forward and reverse energy transfer processes between the donors ($k = k_1/k_{-1} > 1$), which, in turn, leads to a directed energy transfer (Fig. 4) and sharp increase in the quantum efficiency. Modelling of such cascade ensembles demonstrated that a twofold decrease in the rate of the reverse reaction (k = 2) results in an increase in the quantum efficiency which is commensurate with a 50-fold increase in the rate of direct energy transfer in the linear ensemble under conditions of random migration of the excitation energy.[79]

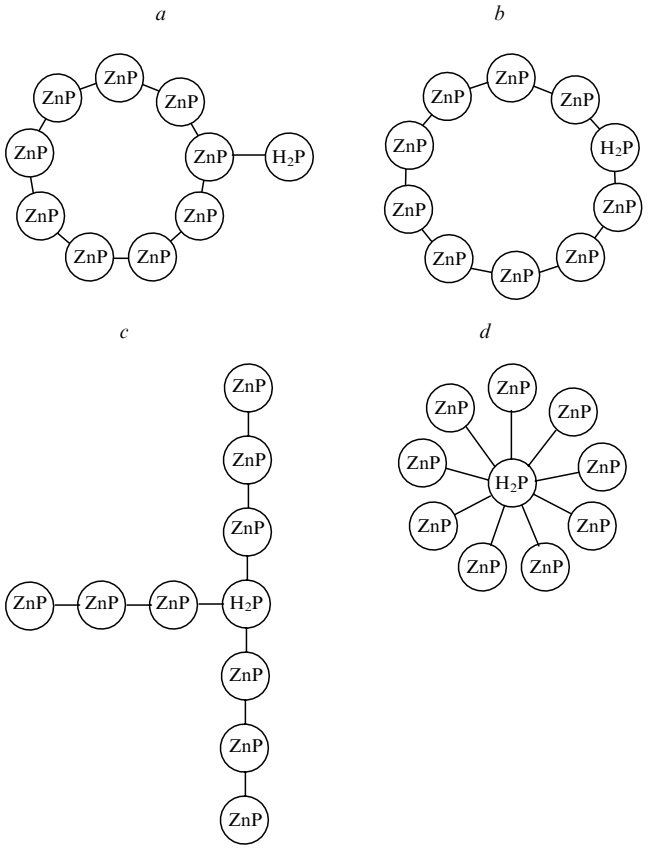

Figure 3. The effect of architecture on the quantum yields (Φ) of energy migration to a single acceptor in cyclic (*a*, *b*) and branched (*c*, *d*) ensembles containing nine donor pigments. All donor pigments have similar absorption patterns: $k_1 = k_{-1} = 2 \times 10^{10}\ s^{-1}$, $k_2 = 2.1 \times 10^{10}\ s^{-1}$, $k_3 = 4.2 \times 10^{8}\ s^{-1}$; Φ = 76% (*a*), 84% (*b*), 91% (*c*), 98% (*d*).[79]

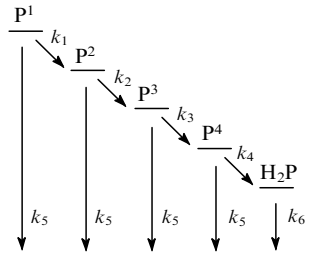

Figure 4. A five-membered cascade ensemble containing several types of donor pigments ($P^1 - P^4$) and an acceptor (H_2P).[79] (Here and in Figs 5 and 6 k_i are the rate constants of the corresponding energy transfer).

An important characteristics of light-harvesting model systems is their antenna effects, which represent products of the number of donor pigments in an ensemble with the quantum efficiency of the energy transfer. For example, the dimer **12a** and the corresponding star-like pentamer **70** have identical quantum efficiencies (98%),[51, 71] but the antenna effect of the former ensemble is 0.98, whereas that of the latter is 3.92, which points to a higher light-harvesting capacity of the pentamer.[79]

The antenna effect provides a possibility for the choice of strategies in the design of multicomponent ensembles. From the standpoint of energy capture by the acceptor, the most efficient architecture of the ensemble is the one which ensures maximum antenna effect. Thus the addition of three donors to a ten-component tri-branched ensemble (see Fig. 3 *c*), which manifests an antenna effect of 8.19 and a quantum efficiency of 91%, can be effected in two ways. Attachment of one zinc-containing porphyrin each to the ends of branches decreases the quantum efficiency to 87%, while the antenna effect increases to 10.44. An alternative route consists in direct addition of the fourth linear ensemble consisting of three zinc-containing porphyrins to a free base resulting in the formation of a symmetrical cross-shaped structure. This procedure does not influence the level of quantum efficiency, since all the four linear branches are independent structures, but enhances the antenna effect to 10.92. These calculations have shown that the appearance of a new individual route for the direct energy transfer from additional donors to the acceptor does not increase the number of non-productive energy transfers in the existing set of donors and is therefore the most efficient way to enhance the light-harvesting properties of the ensemble. Systems with star-like architecture (see Fig. 3 *d*) manifest the best light-harvesting properties, their quantum efficiencies are comparable with those of the corresponding dimer and the

antenna effect depends linearly on the number of the attached donors.

The results of theoretical modelling pave the way to the synthesis of multicomponent ensembles with anticipated high efficiency of the overall energy transfer process.[79]

IV. Porphyrin – carotenoid compounds

Carotenoids (Car) are present in the composition of antenna complexes and reaction centres of natural photosynthetic systems. They function as light-harvesting pigments by absorbing light in the spectral regions where the extinction coefficients of chlorophylls (Chl) and bacteriochlorophylls (BChl) are low and by supplying the excitation energy to these pigments through a fast singlet – singlet transfer.[12, 80–82]

$$Car + h\nu \longrightarrow {}^1Car^*,$$

$${}^1Car^* + Chl\ (BChl) \longrightarrow Car + {}^1Chl^*,$$

$${}^1Chl^* \longrightarrow Chl + h\nu\ (\text{fluorescence}).$$

Contrariwise, in the case of high light intensity carotenoids dissipate excesse energy through singlet energy transfer from chlorophyll to the carotenoid and thus control the intensity of singlet energy flow to photosynthetic reaction centres.[83]

In addition, carotenoids fulfil the photoprotective function. Upon irradiation of photosynthetic complexes with high-intensity light, primary electron donors (special pairs) obtain excitation energy from antenna systems and effect primary electron transfer prior to regeneration of the quinone component of the electron transport chain. Under these conditions, the primary charge-separated state, which involves the radical cation of the special pair and the radical anion of bacteriopheophytin (BPh), is not subject to ordinary conversions and undergoes recombination with the formation of the triplet state of the special pair. Triplet states of chlorophylls are usually long-living and are highly energetic. They can also react with other compounds, particularly, with molecular oxygen to generate singlet oxygen. Sensitisation of singlet oxygen represents an energy transfer from the triplet state of chlorophyll to the ground state of oxygen according to an electron-exchange mechanism.

$$BChl \xrightarrow{h\nu} {}^1BChl^*,$$

$${}^1BChl^* + BPh \longrightarrow BChl^{+\bullet} + BPh^{-\bullet},$$

$$BChl^{+\bullet} + BPh^{-\bullet} \longrightarrow {}^3BChl^* + BPh,$$

$${}^3BChl^* + O_2 \longrightarrow BChl + {}^1O_2^*.$$

Singlet oxygen is known to be extremely reactive and causes the destruction of plant tissues.

Carotenoid polyenes prevent the deleterious effects of singlet oxygen by quenching the triplet states of chlorophylls and bacteriochlorophylls prior to their reaction with oxygen. This represents a triplet – triplet energy transfer and results in the formation of a low-lying triplet state of a carotenoid, which is harmless for plant tissues.

Studies of the temperature dependences of the decay rate of the triplet state of the primary donor and the quantum yield of the triplet carotenoid have led to the discovery of a transient excited state which was attributed to the triplet state of the monomeric bacteriochlorophyll localised on the inactive side of the reaction centre. Thus, the triplet energy is transferred from the special pair to the neighbouring bacteriochlorophyll in a thermally activated step; the triplet state of bacteriochlorophyll generated in this process is rapidly quenched by the carotenoid.[84]

$${}^3(BChl_2)^* + BChl + Q \longrightarrow BChl_2 + {}^3BChl^*,$$

$${}^3BChl^* + Car \longrightarrow BChl + {}^3Car^*,$$

$${}^3Car^* \longrightarrow Car + Q,$$

where Q is heat.

Carotenoids behave also as photoprotectors by directly quenching singlet oxygen.[84, 85]

$$Car + {}^1O_2^* \longrightarrow {}^3Car^* + {}^3O_2,$$

$${}^3Car^* \longrightarrow Car + Q.$$

Biomimetic model compounds containing porphyrin or chlorophyll derivatives covalently linked to carotenoid polyenes have been developed for the study of photochemical characteristics of carotenoids, particularly, their photoprotective and antenna functions.

1. Synthesis

The carotenoid – tetraarylporphyrin dyads **86a**,**b** linked by the ester bond, were described in 1980. With these compounds it was shown for the first time that the efficient intramolecular singlet – singlet energy transfer from carotenoids to porphyrins requires that strict conformational demands be met.[86, 87] The models **86c** – **f** were subsequently prepared for the study of singlet – singlet and triplet – triplet energy transfer between carotenoids and porphyrins.[2, 85]

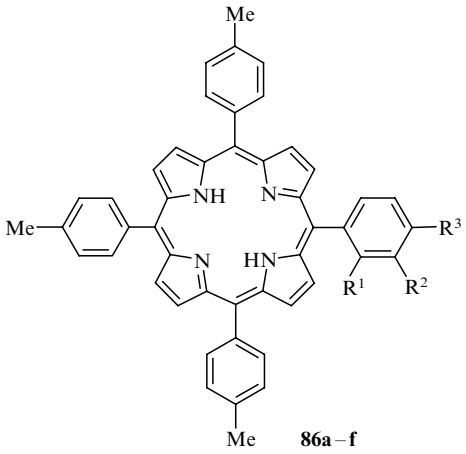

86a – **f**

$R^1 = R^2 = H$, $R^3 = CO_2CH_2X$ (**a**), NHCOX (**c**), $O(CH_2)_3OCOX$ (**f**);
$R^2 = R^3 = H$, $R^1 = CO_2CH_2X$ (**b**), NHCOX (**e**); $R^1 = R^3 = H$,

R^2 = NHCOX (**d**); X = 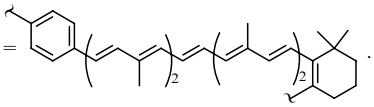

The synthesis and investigation into photodynamic behaviour of the dyads **87a** – **k** and **88a** – **k** in which the carotenoid and the porphyrin are linked through aromatic groups have been reported.[88] Owing to steric repulsion between the *meso*-aryl rings and methyl groups in the adjacent β-pyrrole positions, the aromatic bridge occupies an almost perpendicular position relative to the porphyrin plane and the 'centre-to-centre' distances between the pigments in the majority of models are fixed. These conformational restrictions permit one to establish the dependences of the rates of dynamic processes of the photoexcited state on geometric parameters of the molecules. Yet another essential feature of these models is conjugation of carotenoid and porphyrin π-electronic systems in the systems **87a** – **g** and **88a** – **g** containing phenylene, naphthylene and biphenylene spacers, which help realisation of considerable 'through-bond' electronic interactions between the chromophores.

The dyads **87a** – **k** were prepared by trichloroacetic acid-catalysed condensation of the carotenoid-substituted aromatic aldehydes **89a** – **k**, which in turn were synthesised by the Wittig reaction from the corresponding arylphosphonium salt and β-apo-8′-carotenal, with 4-methoxycarbonylbenzaldehyde (**90**) and dipyrrolylmethane **6** (Scheme 5). Despite the lability of the carotenoids in acidic media, this method afforded carotenoid-linked porphyrins in quite acceptable yields. Metallation of

Scheme 5

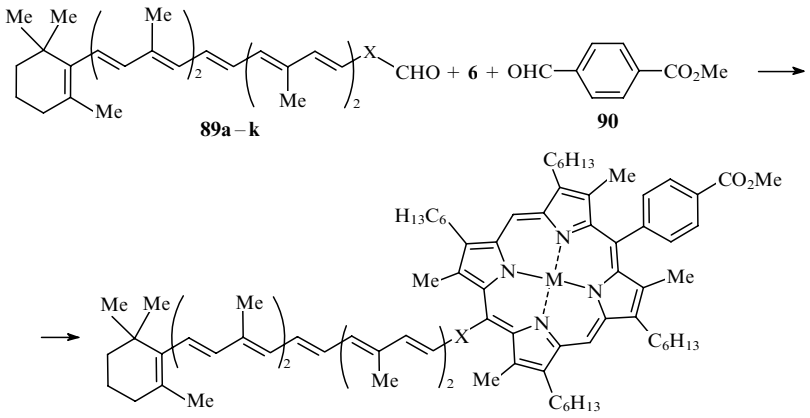

89a–k **90**

87a–k: M = 2 H; **88a–k**: M = Zn

X = 1,4-C_6H_4 (**a**), 1,3-C_6H_4 (**b**), 2,6-naphthylene (**c**), 2,7-naphthylene (**d**), *p*-$C_6H_4-C_6H_4$-*p* (**e**), *m*-$C_6H_4-C_6H_4$-*p* (**f**), *p*-$C_6H_4-C_6H_4$-*m* (**g**),

p-$C_6H_4-CH_2-C_6H_4$-*p* (**h**), 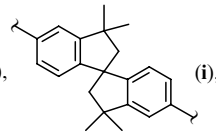 (**i**), 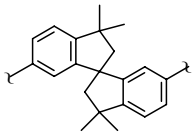 (**j**), *p*-$C_6H_4-CONH-C_6H_4$-*p* (**k**).

compounds **87a–k** by zinc acetate results in the model systems **88a–k**.[88]

The carotenoid–pyropheophorbide dyads **91–95** (see Refs 89–91) were prepared to study the interactions of the carotenoid and chlorophyll in the excited state. The natural carotenoids fucoxanthin and zeaxanthin used in these model studies fulfil different functions in the photosynthetic apparatus. It was found that fucoxanthin transfers energy to chlorophyll *a* in natural systems with high efficiency, whereas zeaxanthin, which is a member of the xanthophyll cycle, quenches excess energy during intense illumination. Studies of electronic interactions of these carotenoids with chlorin-type pigments are important for gaining insight into the mechanisms of photochemical processes underlying biological functions of natural carotenoids. The use of different pyropheophorbide components allows one to vary the energy levels of their S_1 states and the extent of 'through-bond' electronic interactions between the two pigments.

The dyads **91–95** were prepared by the reaction of chlorophyll *a* derivatives with fucoxanthin and zeaxanthin in the presence of 4-dimethylaminopyridine using 2-chloro-1-methylpyridinium iodide as a condensing reagent. These reactions occurred with acceptable yields (15%–30%) without formation of side products and *cis–trans*-isomerisation of the carotenoid component. According to ^{1}H NMR spectroscopic data, these dyad molecules have extended conformations in solution.

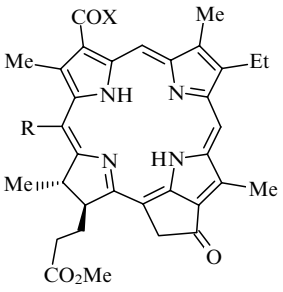

91a,**b**: R = H; **92a**,**b**: R = Cl

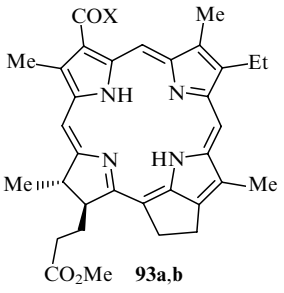

93a,**b**

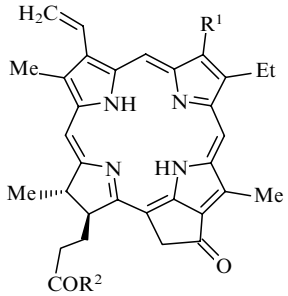

94a,**b**: R^1 = Me, R^2 = X; **95a**,**b**: R^1 = COX, R^2 = OMe.

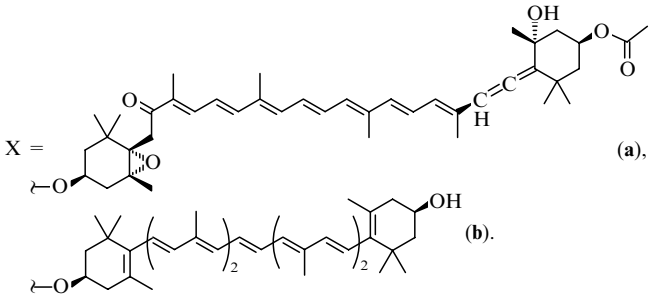

(**a**), (**b**).

2. Singlet–singlet energy transfer

Despite the large number of publications devoted to the studies of light-harvesting function of carotenoids in photosynthesising organisms, the detailed mechanism of the transfer of solar energy to chlorophylls is still obscure. Among a variety of factors hampering the understanding of singlet–singlet energy transfer mechanisms mediated by carotenoids, special mention should be made of the following: (1) experimental problems connected with determination of energy levels of the lowest excited singlet states of carotenoids; (2) fast time scale of the energy transfer; (3) difficulties in estimation of the energy transfer rate constants for individual chromophore pairs within multicomponent ensembles; (4) lack of detailed information about the structures of light-harvesting antenna complexes.

A characteristic feature of carotenoids is the presence of two low-lying singlet excited states. Intense colour of carotenoids, *e.g.*, β-carotene, is due to a strictly allowed electric dipole transition to the second excited singlet state S_2. The radiative rate constant for

this state is rather high, but its lifetime is ~ 200 fs and, correspondingly, the quantum yield of fluorescence is very low. The first excited singlet state S_1 is characterised by a longer lifetime (~ 10 ps), but is strictly forbidden and is seldom detected in ordinary absorption spectra. The radiative rate constant for this state and quantum yield of fluorescence are usually very low.[80] As a consequence, spatial requirements for effective singlet–singlet energy transfer from carotenoids to chlorophylls or porphyrins are very strict, which imposes strong limitations on molecular structures of artificial photosynthetic systems.

The very first studies of energy transfer in porphyrin–carotenoid compounds revealed that sreric factors influence strongly the efficiency of this process. Thus the carotenoid unsaturated chain in the dyad **86a**, which contains tetraarylporphyrin linked to the carotenoid through the *para*-position of the *meso*-aryl ring, is removed from the tetrapyrrole macrocycle as a result of which singlet–singlet energy transfer does not take place. At the same time, the folded carotenoid chain in the *ortho*-isomer **86b** lies above the porphyrin macrocycle with an interchromophore distance of ~ 4 Å and the π-electron systems of the two chromophores are in contact with one another. In this case, the singlet–singlet energy transfer occurs with ~ 25% efficiency (see Refs 2, 86 and 87).

Singlet–singlet transfer of excitation energy from carotenoids to porphyrins can be studied by fluorescence excitation spectroscopy. In these studies, the fluorescence intensity of porphyrin depends on the excitation wavelength. If porphyrin fluorescence is induced by the light absorbed by the carotenoid, the energy transfer from the carotenoid to porphyrin follows the singlet–singlet mechanism.[2] The use of this technique has made it possible to detect this type of intramolecular energy transfer in compounds **87a**–**k**. The efficiency of this process was estimated from the ratio of excitation to absorption spectra and is equal to 9%–35% (see Ref. 88). The energy transfer from the carotenoid to pyropheophorbide in the fucoxanthin-containing compounds **91a**–**95a** occurs with the quantum efficiency of 12%–44% (see Ref. 91).

Elucidation of the mechanism of the singlet–singlet energy transfer from the carotenoid to chlorophyll in photosynthesising organisms is a topical problem in the study of the light-harvesting function of carotenoids. The existence of close orbital contact needed for the singlet–singlet energy transfer in the dyad **86b** calls into question the applicability of the Förster dipole–dipole approximation, which has been formulated for complexes where the distances between chromophores are larger than their sizes. Thus, the probability of energy transfer through electron-exchange interactions which demand orbital overlap becomes higher. In the carotenoid–porphyrin dyad **86c**, the chromophores are linked by a partially conjugated amide bond and the energy transfer yield is ~ 13%. This is rather high, especially with reference to a very short lifetime of the excited singlet state of the carotenoid. Electron-exchange interactions caused by partial overlap of π-electron systems of carotenoid and porphyrin through the amide bond appeared to play a crucial role in the energy transfer in this model system.

Similar results were obtained for the dyads **96a**,**b** in which the carotenoid is linked to the pyropheophorbide derivative. The quantum yield of the energy transfer in compound **96a** is < 5%; the lifetime of the corotenoid singlet state (16 ps) remains unchanged upon attachment of pyropheophorbide. In contrast, the lifetime of the carotenoid S_1 state in the dyad **96b** decreases to 7 ps due to energy transfer to pyropheophorbide which occurs with the quantum efficiency of ~ 50%. These results are interpreted by the fact that in the molecule **96a** saturated carbon atoms separate the π-orbitals of the two chromophores and thus prevent electron-exchange interactions required for effective singlet energy transfer. In the molecule **96b**, partial conjugation of the π-electron systems of the carotenoid and porphyrin through the amide bond ensures electron-exchange interactions; therefore, energy transfer occurs with high efficiency.[2,85]

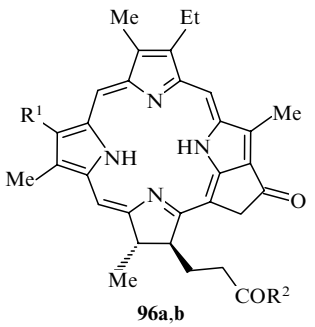

96a,**b**

R^1 = CH=CH_2, R^2 = NHX (**a**), R^1 = CONHX, R^2 = OMe (**b**);

X = 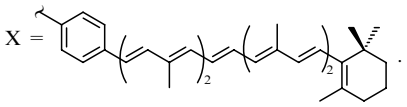

In the model compounds **87a**–**g**, the conjugation of the π-electron system of the carotenoid with the porphyrin macrocycle through the aryl bridge enhances electronic interactions between the chromophores. The rates of singlet–singlet intramolecular energy transfer in these dyads depend on the site of attachment of the carotenoid to the aromatic spacer. Thus comparison of the energy transfer rates in the dyads **87a**,**b** revealed that this process occurs faster in a *para*-linked structure than in the *meta*-isomer ($k = 5 \times 10^{10}$ and 3×10^{10} s^{-1}, respectively). This can be rationalised by stronger electronic interaction between chromophores in the former case due to much greater orbital density in the *para*-position. Analogously, distribution of the electron density on the molecular orbitals of spacers provides an explanation for the observed dependence of the rate of the energy transfer on the carotenoid-binding site in naphthylene- and biphenylene-bound systems. The results obtained suggest that 'through-bond' electronic interactions represent the most essential mechanism of intramolecular singlet–singlet energy transfer. This conclusion is consistent with the dipole-forbidden nature of the carotenoid S_1 state, since energy transfer involving such forbidden states can only be effective in the presence of electron-exchange interactions in the system.[88]

Effective orbital overlap, is possible where chromophores are in van-der-Waals contact. In the case of bound chromophores (see above), orbital overlap occurs in folded conformations, where the π-systems of the donor and the acceptor are in direct contact with one another. The orbitals of the linkers and the environment (*e.g.*, the solvent or a protein) also take part in electron-exchange interactions. Orbital contacts of non-bound pigments in solution require molecular collisions; therefore, the rates of electron-exchange interactions depend directly on the rate of diffusion. However, the lifetime of the S_1 state of carotenoids is so short (tens of picoseconds) that no collisions with the expected energy acceptors (*viz.*, porphyrins or chlorophylls) can take place. It thus follows that carotenoids are inefficient donors of the singlet state energy in non-bound systems in solution.[85]

The results illustrating the necessity of electron exchange for singlet energy transfer from carotenoid pigments are very important for the design of more complex photosynthetic model systems in which chlorophylls and carotenoids are bound to the protein. Functioning of carotenoids as antennae in the transfer of singlet excitation energy to chlorophylls requires that two protein-bound pigments were in a van-der-Waals contact with one another.

Although the predominance of electron-exchange interactions in 'through-bond' singlet energy transfer from the carotenoid to porphyrin has been confirmed experimentally, one should not rule out some contribution of dipole–dipole interactions. The two π-electron systems in the fucoxanthin–pyropheophorbide dyads **91a**–**95a** are separated by at least five saturated carbon atoms and there is no evidence of folded conformation. In this case, direct orbital overlap required for 'through-bond' electron-exchange interactions is insignificant and its contribution to the singlet–

singlet energy transfer observed is very low. However, in non-symmetrical carotenoids, such as fucoxanthin, the S_1 state can 'borrow' oscillating dipole energy from the S_2 state and thus become weakly dipole-allowed. The rate constants and the efficiencies of energy transfer in the dyads **91a**–**95a** estimated with the use of the Förster approximation are in good agreement with the experimental results. These studies suggest that dipole–dipole interactions play a crucial role in the intramolecular singlet–singlet energy transfer from fucoxanthin to pyropheophorbide in these compounds.[89, 91]

According to Sadovnikova *et al.*,[92] the energy transfer in model compounds **97a**,**b** is also described in terms of the Förster theory. The efficiency of energy transfer in these systems varies depending on the lengths of the conjugated bonds in the polyene and changes from 33% to 55% on going from compound **97b** to compound **97a**, apparently due to the increased spectral overlap integral of the donor fluorescence and the acceptor absorption in the latter case.

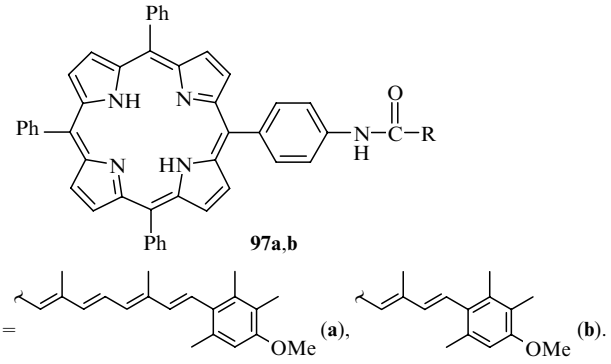

Elucidation of the role of two excited singlet carotenoid states in the energy transfer is yet another important problem, which attracts keen attention of investigators. An analysis of time resolved fluorescence spectra showed that the quenching time of the carotenoid S_1 state in compound **96b** (7 ps) coincides with the time of formation of the singlet state of the pyropheophorbide component.[85] A similar phenomenon was observed for the fucoxanthin-containing dyads **91a**–**95a**. Besides, the decrease in the efficiency of the energy transfer in the series **92a** > **91a** > **93a** is commensurate with the decrease in the spectral overlap between the fluorescence of the S_1 state of fucoxanthin and Q_y-absorption of pyropheophorbide.[88–90] The lifetime of the carotenoid S_2 state does not exceed several hundreds of femtoseconds and therefore cannot contribute to the energy transfer, which proceeds on a picosecond time scale. These findings point to the involvement of the carotenoid S_1 state as an energy donor in the singlet energy transfer.[80, 85, 89]

The energy transfer from the carotenoid S_2 state is also possible as was the case with the light-harvesting antenna complex B800-850 of the purple bacterium *Rhodobacter sphaeroides*; however, in this case the process proceeds on a femtosecond time scale.[80]

The S_1 state of zeaxanthin in the dyads **91b**–**95b** is energetically lower than the singlet state of pyropheophorbide and cannot therefore take part in the energy transfer to pyropheophorbide. An alternative route of the energy transfer from the singlet-excited state to pyropheophorbide is that from the S_2 state of zeaxanthin. This hypothesis is corroborated by the fact that the fluorescence spectrum from the S_2 state of zeaxanthin overlaps with the high-energy absorption Q_x-band of pyropheophorbide. The quantum yields of the energy transfer from the S_2 state of the carotenoid to the S_1 state of pyropheophorbide in compounds **91b**–**95b** do not exceed 15%. The strictly allowed nature of the $S_2 \rightarrow S_0$ transition permits the contribution of dipole–dipole interactions to this mechanism. However, the rate constants for the energy transfer estimated with the use of the Förster model correlate weakly with experimentally determined values. The Förster theory of dipole–dipole interactions assumes that the excitation is followed by oscillatory relaxation of the donor state prior to its deactivation through energy transfer. However, no complete oscillatory equilibrium can be reached in zeaxanthin-containing compounds in which the rapid energy transfer is effected from the short-lived S_2 state. Therefore, the use of the Förster model for the description of the energy transfer mechanism is not correct in this case. It should be noted, however, that the carotenoid and pyropheophorbide components of the dyads **91b**–**95b** are separated by fewer saturated carbon atoms in comparison with the components of the corresponding fucoxanthin-containing compounds **91a**–**95a**. This structural difference can favour somewhat stronger 'through-bond' electronic interactions in those cases where the energy is transferred from zeaxanthin to pyropheophorbide.[89–91]

Thus, highly efficient transfer of excitation energy from carotenoids to chlorophylls can follow several mechanisms. Their detailed study in each concrete case depends on the structures of the carotenoid and chlorophyll and their mutual arrangement in the protein environment.

Efficient singlet–singlet energy transfer is thermodynamically possible in those cases where the singlet state energy of the donor (carotenoid) exceeds that of the acceptor (chlorophyll or bacteriochlorophyll). In the case of partial degeneracy of excited singlet states of the carotenoid and chlorophyll, the overall efficiency of the energy transfer may depend on the lifetimes of their singlet states. The reduction of the lifetime of the S_1 state of chlorophyll in natural photosynthetic systems owing to the fast electron transfer to an additional acceptor, *e.g.*, accessory chlorophyll, can enhance the efficiency of the energy transfer from the carotenoid to chlorophyll. On the other hand, in the absence of additional fast photochemical processes, which quench the singlet state of chlorophyll, the efficiency of the energy transfer from the carotenoid to chlorophyll can be less than optimum.[85]

In addition to the key light-harvesting function discussed above, an opposite process, *viz.*, photochemical quenching of the first excited singlet state of porphyrin or chlorophyll by the carotenoid, was discovered in the studies of carotenoid-containing model compounds. This phenomenon is similar to energy dissipation after excessive irradiation of chlorophylls *in vivo*. A comprehensive analysis of mechanisms of quenching of porphyrin fluorescence by carotenoids will shed additional light on the ability of the latter to control the intensities of singlet energy fluxes to photosynthetic reaction centres.

Spectroscopic studies of the dyads **91b** and **94b** have demonstrated that zeaxanthin diminishes the intensity of pyropheophorbide fluorescence by 20% and 45%, respectively, and noticeably reduces the lifetime of the excited singlet state of pyropheophorbide (5.6 and 3.9 ns, respectively) in comparison with dimethyl esters of free pyropheophorbides (6.8 and 7.8 ns, respectively). This points to the existence of an additional pathway of quenching of the singlet excited state of pyropheophorbide in carotenoid-containing systems.[89] A possible explanation of this phenomenon is electron transfer from the carotenoid to the singlet excited state of pyropheophorbide with subsequent ultrafast recombination of charges.[93] An alternative mechanism of quenching of pyropheophorbide fluorescence consists in reverse singlet–singlet energy transfer from the excited S_1 state of pyropheophorbide to zeaxanthin. This route is thermodynamically allowed, since the S_1 state of zeaxanthin possesses lesser energy than that of pyropheophorbide. The ability of zeaxanthin to quench the singlet excited state of pyropheophorbide corresponds with the role played by this carotenoid in the quenching of excess energy of chlorophyll under conditions of the excess irradiation *in vivo*.[89, 90]

Similar quenching of porphyrin fluorescence by the carotenoid was observed in the dyads **87a**–**k** and **88a**–**k.** Thus the lifetime of porphyrin fluorescence in compound **87a** decreases to 850 ps, *i.e.*, becomes close to the time of formation of the carotenoid S_1 state (930 ps), which reflects the intramolecular energy transfer from the excited singlet state of porphyrin to the carotenoid. The carotenoid S_1 state generated is subjected to reversible energy transfer to porphyrin, which competes with its

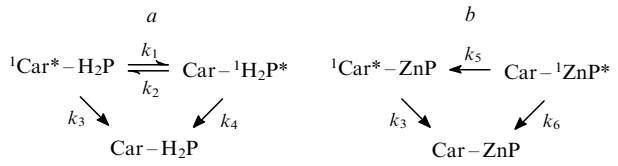

Figure 5. A scheme of singlet energy transfer in the porphyrin – carotenoid compounds **87a** – **k** (*a*) and **88a** – **k** (*b*).[88]

fast internal transition to the ground state. The singlet – singlet energy transfer between the carotenoid and the metal-free porphyrin in compounds **87a** – **k** is reversible (Fig. 5 *a*) assuming that the S_1 states of the two chromophores are nearly isoenergetic. At the same time, the unidirectional singlet – singlet energy transfer from zinc porphyrin to the carotenoid (Fig. 5 *b*) observed in systems **88a** – **k** indicates that the S_1 state of the carotenoid is energetically lower than that of the zinc – porphyrin complex.[88]

The above-described approach, which is based on the changes in positions of the S_1 energy level of porphyrin or chlorophyll induced by chemical modifications, *e.g.*, metallation, introduction of appropriate substituents and changes in the π-electron system, makes it possible to estimate the true localisation of the non-radiative S_1 state of carotenoids provided the lifetime of the singlet excited state is determined exclusively by the intramolecular energy transfer between the carotenoid and the tetrapyrrole pigment.[89]

3. Triplet – triplet energy transfer

Photoprotection of plant tissues from the destructive action of singlet oxygen is provided by quenching of triplet states of chlorophylls through the transfer of energy to carotenoids. In contrast to singlet – singlet energy transfer, triplet – triplet transfer is forbidden as regards the dipole – dipole mechanism and occurs exclusively in the presence of electron-exchange interactions, which demand orbital overlap of the donor and the acceptor.

The triplet – triplet energy transfer in porphyrin – carotenoid dyads can be studied by monitoring the quenching of transient absorption of the triplet state of porphyrin around ~ 440 nm and the concomitant increase in the carotenoid triplet absorption at ~ 550 nm.

The triplet – triplet energy transfer in the isomeric dyads **86c**,**d** in which the carotenoid is linked to porphyrin through the *para*- and *meta*-position of the *meso*-aryl group, respectively, was studied in order to determine structural and photophysical parameters of effective photoprotection. In these systems, electron-exchange interactions are mediated by π-electrons of the amide bonds. The rate constants for the triplet energy transfer in compounds **86d** and **86c** determined by laser-flash spectroscopy for solutions of these compounds in toluene were equal to 2×10^7 and 1×10^8 s^{-1}, respectively. The calculated yield of the singlet oxygen generated by the triplet state of porphyrin in the *meta*-linked dyad **86d** was 30%; singlet oxygen was not formed in the case of the *para*-isomer **86c**. These findings suggest that in the former case the carotenoid fails to entrap the bulk of the singlet oxygen sensitised by the attached porphyrin. As a result, singlet oxygen avoids direct contacts with the quencher even if the former is localised in immediate proximity to the latter. It thus follows that the triplet energy transfer from porphyrin to the carotenoid should proceed at a very fast rate in order to suppress completely the formation of singlet oxygen. Thus the triplet of the special pair of bacteriochlorophyll in the reaction centres of *Rhodobacter sphaeroides* is quenched by the energy transfer to the carotenoid with the rate constant $k > 10^8$ s^{-1}.

In the absence of conjugation between the chromophores, rapid triplet transfer takes place in a molecule with a folded conformation in which all the π-electron systems are in close contact with one another. Fast triplet – triplet energy transfer was observed in the porphyrin – carotenoid system **86b** characterised by good spatial orbital overlap of the two chromophores.[2,85]

The energy transfer from the triplet excited state of pyropheophorbide (Ppd) to the attached carotenoid was observed in model compounds **91a**,**b** and **94a**,**b**. It was found that the rates of energy transfer in these systems did not depend on the type of the carotenoid, but were determined by the flexibility of the bond linking the chromophores. In this case, 'through-bond' electron-exchange interactions are weak due to the presence of saturated carbon atoms between the π-systems of the chromophores and the orbital overlap required for such triplet transfer should be effected 'through-space'. However, according to ^{1}H NMR data the extended conformations of these dyads are the most stable where the carotenoids are spatially separated from pyropheophorbide. Folded conformations may appear exclusively in the case of intramolecular mobility of chromophores in solution. The molecular structures **91a**,**b** are little flexible. To some extent, this restricts their intramolecular movement, which would bring the π-systems of the two chromophores into close contact. Correspondingly, the rates of the triplet – triplet energy transfer in these compounds are lower than those in the more flexible molecules **94a**,**b**.[89]

The triplet – triplet energy transfer mediated by intramolecular movements was also observed in the porphyrin – carotenoid dyad **86f** containing flexible polymethylene spacer between the chromophores.[2] This dynamic process is similar to that observed between non-bound donors and acceptors upon collision in solution.

Fast quenching of the triplet state of the special pair in *Rhodobacter sphaeroides* is a two-step process, which includes a triplet energy transfer from the bacteriochlorophylls of the special pair to the auxiliary bacteriochlorophyll with its subsequent transport to the carotenoid.[84]

The photochemical properties of the molecular triads **98a**,**b** and **99**, which consist of a carotenoid covalently linked to porphyrin, which, in turn, is linked to a pyropheophorbide derivative (Car – P – Ppd) in the system **98** and the fullerene (Car – P – C_{60}) in the system **99**, were studied in order to elucidate the structural and dynamic parameters of multistep triplet energy transfer.[94,95]

The excitation of porphyrin or pyropheophorbide in compound **98a** dissolved in acetone results in the population of the first excited singlet state of pyropheophorbide, which accepts singlet energy from the excited porphyrin with ~ 100% efficiency (Fig. 6). Subsequent intersystem transition gives rise to the triplet state of pyropheophorbide (the quantum yield is ~ 1), which sensitises the formation of singlet oxygen in air ($k \approx 2.5 \times 10^9$ s^{-1}).

The quantum yield of the singlet oxygen in the triad **98a** (Φ = 36%) is much lower than that for the free pyropheophorbide (Φ = 80%), which reflects competitive quenching of the triplet state of pyropheophorbide in the triad by intramolecular energy

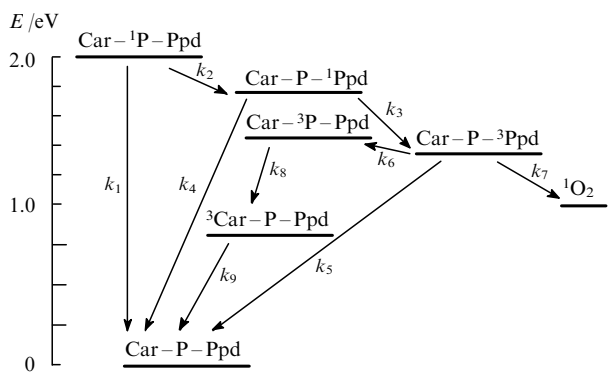

Figure 6. A scheme of energy transfer in the triad Car – P – Ppd.[94]

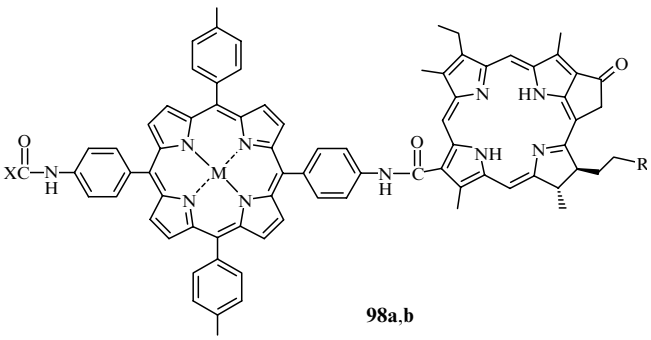

98a,b

M = 2 H (**a**), Zn (**b**); R = CO_2Me;

X =

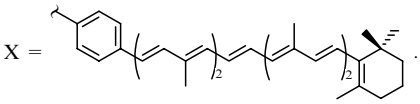

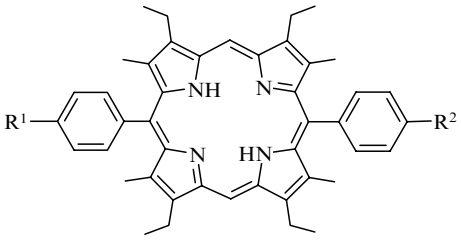

99

R^1 =

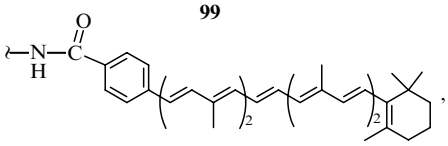

R^2 = Me—N

transfer with the formation of a carotenoid triplet state. The rate constant for this triplet transfer, k_6, is equal to 2.9×10^6 s^{-1}. The linear structure of the triad prevents the appearance of conformations where orbital interactions of the carotenoid with pyropheophorbide required for the triplet–triplet energy transfer are possible. It was suggested[94] that intramolecular triplet energy transfer in compound **98a** is a two-step process. Its first step consists in the energy transfer from the triplet state of pyropheophorbide ($\sim$ 1.33 eV) to the attached porphyrin, while the second step includes fast quenching of the porphyrin triplet state formed (1.44 eV) by the carotenoid ($k_8 > 10^8$ s^{-1}) (see Fig. 6). The rate of the overall process is determined by the endoergic step of the triplet energy transfer from pyropheophorbide to porphyrin.

The temperature dependence of the formation of the carotenoid triplet state was studied in order to gain an insight into the two-step mechanism of triplet energy transfer. No triplet absorption of the carotenoid was observed upon excitation of cooled (to 77 K) solution of compound **98a** in butyronitrile, which points to the lack of the energy transfer. Consequently, this process requires sufficient activation energy for its realisation, which correlates with the putative two-step mechanism of the triplet energy transfer with the first endoergic step.

The height of the potential barrier in such endoergic transfer can be varied by chemical modification of the system. The presence of a zinc atom in the porphyrin macrocycle of the triad **98b** increases the triplet state energy of porphyrin from 1.44 to 1.59 eV with a concomitant increase in the activation energy by 0.15 eV. In this case, the transfer of triplet energy is too slow to compete with sensitisation of singlet oxygen. As a result, the carotenoid loses its ability to afford photoprotection by quenching the triplet state of pyropheophorbide.[85,94]

The quantum yield of singlet oxygen in the triad **98b** is commensurate with that obtained for the corresponding pyropheophorbide–porphyrin dyad. Consequently, in the absence of energy transfer the proximity of the carotenoid to the site of singlet oxygen generation does not provide effective photoprotection. This clearly demonstrates that rapid quenching of the triplet state of the sensitiser is a much more efficient means of photoprotection than deactivation of singlet oxygen that has already formed.[94]

The triplet excitation energy in the fullerene-containing triad **99** is transferred from the fullerene component (Car–P–$^3C_{60}$) to the carotenoid polyene resulting in the generation of state ^{3}Car–P–C_{60}. As in the previous case, the activation energy E_a = 0.17 eV is necessary for the energy transfer, which is consistent with the two-step mechanism where the energy migrates from the excited triplet state of fullerene to porphyrin with the formation of Car–^{3}P–C_{60} in a slow thermally activated step, fast transfer of energy from the porphyrin triplet to the carotenoid culminates in the generation of the terminal state.[95]

Thus, there are several strict structural and energetic limitations for the stepwise triplet energy transfer, *viz*., electronic interactions between the donor chromophore, the intermediate porphyrin and the carotenoid should be sufficiently strong; in addition, the thermodynamic barrier to migration of the triplet energy should not be too high.

In contrast to the triplet state of chlorophyll, the excited triplet state of the carotenoid does not sensitise singlet oxygen, which is a prerequisite for photoprotection. Thermodynamic analysis of this process suggests that the energy of the lower triplet state of a potential sensitiser should exceed that of the singlet oxygen (0.98 eV) for the latter could be formed. The published data on the energy of the triplet states of carotenoids are very scarce, which can be attributed to the difficulties in the detection of phosphorescence of the carotenoid chromophore.

Moore *et al*.[85] have carried out a series of photoacoustic laser-flash experiments using the dyad **86c** as an example and calculated the energy of the lowest triplet state of the carotenoid by measuring heat energy released upon relaxation of ^{3}Car–P into the ground state in solution. The triplet energy of the carotenoid determined in this way (0.64 $\pm$ 0.04 eV) is much lower than that of chlorophyll ($\sim$ 1.3 eV) and bacteriochlorophyll ($\sim$ 1 eV) in photosynthetic reaction centres. This allows directed transfer of triplet energy to the carotenoid trap, which makes the transfer fast and irreversible. Low triplet energy of carotenoids also explains the lack of sensitisation of singlet oxygen by the triplet state of the carotenoids needed for effective functioning of natural photoprotective systems.

V. Conclusion

The porphyrin-containing ensembles described in this review are convenient models for the study of photoinduced energy transfer. These data suggest that optimisation of efficiency of electronic interactions between pigments and the rates of energy transfer in these models should take into account structural characteristics altogether, such as mode and the character of substitution in macrocycles, the type of coordination metal ions, the nature and binding site of the linker, *etc*. By varying these features, it is possible to gain control over electronic and steric factors, which determine various parameters of photodynamic processes and to obtain compounds with predetermined spectral characteristics and energy levels of excited states of pigments. The data on the structure of natural light-harvesting antenna complexes combined with fundamental energy transfer theories provide a basis for the construction and fine tuning of model molecular photosynthetic systems.[2,29,35]

The use of the multistep energy transfer strategy is an efficient approach to the reproduction of natural photosynthetic processes.

The development of novel methods for the synthesis of covalently linked ensembles [27] and the principles of non-covalent self-assembly of pigments [17] has made possible the synthesis of a great variety of multicomponent structures. Preliminary reliable estimation of expected photochemical properties of each target structure allows the design of highly efficient model photosynthetic systems.[79]

The synthesis of multicomponent clusters with several isolated sets of donors which provide independent routes of energy transfer to the terminal acceptor is a promising approach to the modelling of energy transfer. Such systems possess the most efficient light-harvesting properties, although their application is limited for steric reasons. Yet another promising strategy consists in incorporation of several types of donor pigments into a single ensemble, which may lead to directed energy transfer and a sharp increase in the quantum efficiency of energy migration. The construction of such cascade ensembles has become possible owing to fine tuning of energy levels of excited states of pigments. For example, cascade ensembles may include linear compositions of porphyrin, chlorin and bacteriochlorin pigments; their longest wavelength absorption bands are shifted from 646 to 740 nm.[79]

Synthetic light-harvesting complexes reproduce only some of the structural and functional characteristics of natural objects, which opens up new possibilities for their investigation. Further approximation of artificial photosynthetic schemes to biological transmembrane energy-transducing processes is aimed at reaching a definite level of supramolecular organisation of cofactors, which is controlled by polypeptide subunits of natural photosystems. Elucidation of factors providing effective control over the rates and mechanisms of biological energy transfer occurring in the protein matrix still continues to be a central problem. Only a few synthetic models containing peptide-linked chromophores have been designed so far in order to elucidate the effects of protein components on interpigment interactions and regularities of energy transfer processes.[67, 78] However, the usefulness of this approach demands further investigations.

And, finally, it seems very tempting to use multiporphyrin ensembles in non-biological objects, such as molecular photonic and optoelectronic devices. The feasibility of incorporation of such systems into highly ordered structures, *e.g.*, liposomes, micelles, polymers and monolayers deposited onto conducting supports, significantly increases the efficiency of molecular devices due to limited intramolecular migrations of pigments. Multicomponent ensembles able to function as molecular photonic wires and optoelectronic switches have already been devised.[10, 96] Hence, the basic principles of photosynthesis can successfully be employed in the design of synthetic molecular devices. Their versatility and main characteristics are comparable to, and sometimes surpass, those of the natural systems.

This review has been written with financial support of the Russian Foundation for Basic Research (Project Nos 01-03-06155 and 00-15-97866).

References

1. M R Wasielewski *Chem. Rev.* **92** 435 (1992)
2. D Gust, T A Moore, A L Moore *Acc. Chem. Res.* **26** 198 (1993)
3. K Maruyama, A Osuka, N Mataga *Pure Appl. Chem.* **66** 867 (1994)
4. H Kurreck, M Huber *Angew. Chem., Int. Ed. Engl.* **34** 849 (1995)
5. G Steinberg-Yfrach, P A Liddell, S-C Hung, A L Moore, D Gust, T A Moore *Nature (London)* **385** 239 (1997)
6. S E Gribkova, R P Evstigneeva, V N Luzgina *Usp. Khim.* **62** 1020 (1993) [*Russ. Chem. Rev.* **62** 963 (1993)]
7. S M LeCours, H-W Guan, S G DiMagno, C H Wang, M J Therien *J. Am. Chem. Soc.* **118** 1497 (1996)
8. G E O'Keefe, G J Denton, E J Harvey, R T Phillips, R H Friend, H L Anderson *J. Chem. Phys.* **104** 805 (1996)
9. M P Debreczeny, W A Svec, M R Wasielewski *Science* **274** 584 (1996)
10. R W Wagner, J S Lindsey, J Seth, V Palaniappan, D F Bocian *J. Am. Chem. Soc.* **118** 3996 (1996)
11. G McDermott, S M Prince, A A Freer, A M Howthornthwaite-Lawless, M Z Papiz, R J Cogdell, N W Isaacs *Nature (London)* **374** 517 (1995)
12. R van Grondelle, J P Dekker, T Gillbro, V Sundstrom *Biochim. Biophys. Acta* **1187** 1 (1994)
13. R J Cogdell, H A Frank *Biochim. Biophys. Acta* **895** 63 (1987)
14. R K Klayton *Photosynthesis. Physical Patterns and Chemical Models* (Cambridge: Cambridge University Press, 1980)
15. V A Shuvalov *Pervichnoe Preobrazovanie Svetovoi Energii pri Fotosinteze* (Primary Transformation of Light Energy in Photosynthesis) (Moscow: Nauka, 1990)
16. M E van Brederode, J P Ridge, I H M van Stokkum, F van Mourik, M R Jones, R van Grondelle *Photosynth. Res.* **55** 141 (1998)
17. M D Ward *Chem. Soc. Rev.* **26** 365 (1997)
18. S S Isied *Adv. Chem. Ser.* **253** 331 (1997)
19. A Osuka, N Tanabe, S Kawabata, I Yamazaki, Y Nishimura *J. Org. Chem.* **60** 7177 (1995)
20. S Kawabata, I Yamazaki, Y Nishimura, A Osuka *J. Chem. Soc., Perkin Trans. 2* 479 (1997)
21. A Osuka, M Ikeda, H Shiratori, Y Nishimura, I Yamazaki *J. Chem. Soc., Perkin Trans. 2* 1019 (1999)
22. S Kawabata, N Tanabe, A Osuka *Chem. Lett.* 1797 (1994)
23. A Osuka, B-L Liu, K Maruyama *Chem. Lett.* 949 (1993)
24. J S Lindsey, S Prathapan, T E Johnson, R W Wagner *Tetrahedron* **50** 8941 (1994)
25. R W Wagner, T E Johnson, F Li, J S Lindsey *J. Org. Chem.* **60** 5266 (1995)
26. M Ravikanth, J-P Strachan, F Li, J S Lindsey *Tetrahedron* **54** 7721 (1998)
27. R W Wagner, T E Johnson, J S Lindsey *J. Am. Chem. Soc.* **118** 11 166 (1996)
28. J-P Strachan, S Gentemann, J Seth, W A Kalsbeck, J S Lindsey, D Holten, D F Bocian *Inorg. Chem.* **37** 1191 (1998)
29. J-P Strachan, S Gentemann, J Seth, W A Kalsbeck, J S Lindsey, D Holten, D F Bocian *J. Am. Chem. Soc.* **119** 11 191 (1997)
30. F Li, S Gentemann, W A Kalsbeck, J Seth, J S Lindsey, D Holten, D F Bocian *J. Mater. Chem.* **7** 1245 (1997)
31. P Hascoat, S I Yang, R K Lammi, J Alley, D F Bocian, J S Lindsey, D Holten *Inorg. Chem.* **38** 4849 (1999)
32. K K Jensen, S B van Berlekom, J Kajanus, J Martensson, B Albinsson *J. Phys. Chem. A* **101** 2218 (1997)
33. S I Yang, J Seth, T Balasubramanian, D Kim, J S Lindsey, D Holten, D F Bocian *J. Am. Chem. Soc.* **121** 4008 (1999)
34. N Nishino, R W Wagner, J S Lindsey *J. Org. Chem.* **61** 7534 (1996)
35. S I Yang, R K Lammi, J Seth, J A Riggs, T Arai, D Kim, D F Bocian, D Holten, J S Lindsey *J. Phys. Chem. B* **102** 9426 (1998)
36. M J Crossley, A C Try, R Walton *Tetrahedron Lett.* **37** 6807 (1996)
37. K M Kadish, N Guo, E van Caemelbecke, A Froiio, R Paolesse, D Monti, P Tagliatesta, T Boschi, L Prodi, F Bolletta, N Zaccheroni *Inorg. Chem.* **37** 2358 (1998)
38. A Osuka, S Marumo, K Maruyama, N Mataga, Y Tanaka, S Taniguchi, T Okada, I Yamazaki, Y Nishimura *Bull. Chem. Soc. Jpn.* **68** 262 (1995)
39. A Osuka, S Marumo, N Mataga, S Taniguchi, T Okada, I Yamazaki, Y Nishimura, T Ohno, K Nozaki *J. Am. Chem. Soc.* **118** 155 (1996)
40. E G Levinson, A N Nizhnik, A F Mironov *Mendeleev Commun.* 95 (1992)
41. E G Levinson, A F Mironov *Bioorg. Khim.* **21** 230 (1995) [a]
42. D A Ban, A F Mironov *Mendeleev Commun.* 153 (1995)
43. R P Pandian, T K Chandrashekar *Inorg. Chem.* **33** 3317 (1994)
44. V S-Y Lin, S G DiMagno, M J Therien *Science* **264** 1105 (1994)
45. R Kumble, S Palese, V S-Y Lin, M J Therien, R M Hochstrasser *J. Am. Chem. Soc.* **120** 11489 (1998)
46. D P Arnold, D A James *J. Org. Chem.* **62** 3460 (1997)
47. L H Anderson *Inorg. Chem.* **33** 972 (1994)
48. K-i Sugiura, G Ponomarev, S Okubo, A Tajiri, Y Sakata *Bull. Chem. Soc. Jpn.* **70** 1115 (1997)
49. E G Levinson, N A Reztsova, A F Mironov *Mendeleev Commun.* 44 (1995)
50. J A Anton, P A Loach *Photochem. Photobiol.* 235 (1987)

51. J-S Hsiao, B P Krueger, R W Wagner, T E Johnson, J K Delaney, D C Mauzerall, G R Fleming, J S Lindsey, D F Bocian, R J Donohoe *J. Am. Chem. Soc.* **118** 11 181 (1996)
52. S Speiser *Chem. Rev.* **96** 1953 (1996)
53. E K L Yeow, P J Sintic, N M Cabral, J N H Reek, M J Crossley, K P Ghiggino *Phys. Chem. Chem. Phys.* **2** 4281 (2000)
54. O V Lobanov, S Yu Arjantsev, E G Levinson, A F Mironov *Proc. SPIE–Int. Soc. Opt. Eng.* **2078** 179 (1994)
55. E I Zenkevich, V N Knyukshto, A M Shulga, V A Kuzmitsky, V I Gael, E G Levinson, A F Mironov *J. Lumin.* **75** 229 (1997)
56. J M DeGraziano, P A Liddell, L Leggett, A L Moore, T A Moore, D Gust *J. Phys. Chem.* **98** 1758 (1994)
57. A N Kozyrev, A F Mironov *J. Heterocycl. Chem.* **25** 885 (1988)
58. V V Borovkov, J M Lintuluoto, Y Inoue *Helv. Chim. Acta* **82** 919 (1999)
59. M Ravikumar, R P Pandian, T K Chandrashekar *J. Porphyr. Phthalocyan.* **3** 70 (1999)
60. J Barber, E Morris, C Buchel *Biochim. Biophys. Acta, Bioenergetics* **1459** 239 (2000)
61. H-Y Liu, J-W Huang, X Tian, X-M Hu, L-N It *Chem. J. Chin. Univ.* **19** 511 (1998)
62. H Tamiaki, S Suzuki, K Maruyama *Bull. Chem. Soc. Jpn.* **66** 2633 (1993)
63. H Tamiaki, K Nomura, K Maruyama *Bull. Chem. Soc. Jpn.* **66** 3062 (1993)
64. H Tamiaki, K Nomura, K Maruyama *Bull. Chem. Soc. Jpn.* **67** 1863 (1994)
65. R P Evstigneeva, V N Luzgina, H Yu Kiseleva, N V Konovalova, I V Rakitina *Bioorg. Khim.* **24** 229 (1998) [a]
66. N V Konovalova, N A Karavaeva, A A Gribkov, V N Luzgina, R P Evstigneeva *Bioorg. Khim.* **26** 112 (2000) [a]
67. A Kashiwada, Y Takeuchi, H Watanabe, T Mizuno, H Yasue, K Kitagawa, K Iida, Z-Y Wang, T Nozawa, H Kawai, T Nagamura, Y Kurono, M Nango *Tetrahedron Lett.* **41** 2115 (2000)
68. A Harriman, D J Magda, J L Sessler *J. Chem. Soc., Chem. Commun.* 345 (1991)
69. J L Sessler, B Wang, A Harriman *J. Am. Chem. Soc.* **117** 704 (1995)
70. S L Springs, D Gosztola, M R Wasielewski, V Král, A Andrievsky, J L Sessler *J. Am. Chem. Soc.* **121** 2281 (1999)
71. S Prathapan, T E Johnson, J S Lindsey *J. Am. Chem. Soc.* **115** 7519 (1993)
72. M Ravikanth, N Agarwal, D Kumaresan *Chem. Lett.* 836 (2000)
73. J Li, J R Diers, J Seth, S I Yang, D F Bocian, D Holten, J S Lindsey *J. Org. Chem.* **64** 9090 (1999)
74. J Li, J S Lindsey *J. Org. Chem.* **64** 9101 (1999)
75. M A Miller, R K Lammi, S Prathapan, D Holten, J S Lindsey *J. Org. Chem.* **65** 6634 (2000)
76. O Mongin, N Hoyler, A Gossauer *Eur. J. Org. Chem.* 1193 (2000)
77. O Mongin, A Schuwey, M-A Vallot, A Gossauer *Tetrahedron Lett.* **40** 8347 (1999)
78. N Solladie, A Hamel, M Gross *Tetrahedron Lett.* **41** 6075 (2000)
79. P G van Patten, A P Shreve, J S Lindsey, R J Donohoe *J. Phys. Chem. B* **102** 4209 (1998)
80. R J Cogdell, T Gillbro, P O Andersson, R S H Liu, A E Asato *Pure Appl. Chem.* **66** 1041 (1994)
81. H A Frank, R J Cogdell *Photochem. Photobiol.* **63** 257 (1996)
82. Y Koyama, M Kuki, P O Andersson, T Gillbro *Photochem. Photobiol.* **63** 243 (1996)
83. B Demmig-Adams *Biochim. Biophys. Acta* **1020** 1 (1990)
84. A Angerhofer, F Bornhauser, V Aust, G Hartwich, H Scheer *Biochim. Biophys. Acta* **1365** 404 (1998)
85. T A Moore, D Gust, A L Moore *Pure Appl. Chem.* **66** 1033 (1994)
86. G Dirks, A L Moore, T A Moore, D Gust *Photochem. Photobiol.* **32** 277 (1980)
87. A L Moore, G Dirks, D Gust, T A Moore *Photochem. Photobiol.* **32** 691 (1980)
88. A Osuka, H Yamada, K Maruyama, N Mataga, T Asahi, M Ohkouchi, T Okada, I Yamazaki, Y Nishimura *J. Am. Chem. Soc.* **115** 9439 (1993)
89. A Osuka, S Shinoda, S Marumo, H Yamada, T Katoh, I Yamazaki, Y Nishimura, Y Tanaka, S Taniguchi, T Okada, K Nozaki, T Ohno *Bull. Chem. Soc. Jpn.* **68** 3255 (1995)
90. S Shinoda, A Osuka, Y Nishimura, I Yamazaki *Chem. Lett.* 1139 (1995)
91. M P Debreczeny, M R Wasielewski, S Shinoda, A Osuka *J. Am. Chem. Soc.* **119** 6407 (1997)
92. N A Sadovnikova, N D Gudkov, Yu M Stolovitskii, V N Luzgina, E I Fillipovich, R P Evstigneeva *Dokl. Akad. Nauk SSSR* **312** 481 (1990) [b]
93. R M Hermant, P A Liddell, S Lin, R G Alden, H K Kang, A L Moore, T A Moore, D Gust *J. Am. Chem. Soc.* **115** 2080 (1993)
94. D Gust, T A Moore, A L Moore, A A Krasnovsky Jr, P A Liddell, D Nicodem, J M DeGraziano, P Kerrigan, L R Makings, P J Pessiki *J. Am. Chem. Soc.* **115** 5684 (1993)
95. D Gust, T A Moore, A L Moore, D Kuciauskas, P A Liddell, B D Halbert *J. Photochem. Photobiol. B: Biology* **43** 209 (1998)
96. R W Wagner, J S Lindsey *J. Am. Chem. Soc.* **116** 9759 (1994)

[a] — *Russ. J. Bioorg. (Engl. Transl.)*
[b] — *Dokl. Chem. (Engl. Transl.)*

Russian Chemical Reviews **70** (11) 971 – 990 (2001) © 2001 Russian Academy of Sciences and Turpion Ltd

DOI 10.1070/RC2001v070n11ABEH000642

Silica gel in organic synthesis

A K Banerjee, M S Laya Mimó, W J Vera Vegas

Contents

I.	Introduction	971
II.	Cyclisation reactions	971
III.	Rearrangements	978
IV.	Reduction	979
V.	Oxidation	980
VI.	Condensations	981
VII.	Formylation	981
VIII.	Hydration and dehydration reactions	982
IX.	Protection of functional groups	984
X.	Deprotection of functional groups	986
XI.	Miscellaneous reactions	986

Abstract. The data on the use of silica gel in organic synthesis are presented. Some specific features of cyclisation (both intra- and intermolecular) reactions, rearrangements, reduction, oxidation, condensation, formylation, hydration and dehydration, protection of functional groups, *etc*., in the presence of silica gel, are discussed. The bibliography includes 96 references.

I. Introduction

Silica gel represents a uniform, non-deformable, three-dimensional network consisting of densely packed colloidal silicon oxide particles.[1] It contains substantial amounts of water which is retained tenaciously in the gel network even after drying, which points to the presence of hydrates or silicic acids.

Owing to its highly developed surface (5 – 800 $m^2\ g^{-1}$) and high porosity, silica gel is generally used as a sorbent for dehydration of gases and fluids, chromatographic separation of organic compounds, as a catalyst support, an enhancer of thixotropic properties of fluids, *etc*. Various chemical applications of silica gel have been described in the monograph of Vail.[2]

In addition, silica gel plays an important role in fine organic synthesis. Chemical reactions catalysed by silica gel usually proceed under mild conditions and with high chemo-, regio- and stereoselectivities and involve operationally more simple procedures for the isolation of final products in comparison with the corresponding homogeneous reactions.

A vast number of papers published over the past 20 years have been devoted to the use of silica gel in organic synthesis (see, *e.g*., Ref. 3), and their number is steadily increasing. This review is an attempt to generalise the published data. The overwhelming majority of studies in this area were aimed at obtaining maximum yields of target products rather than at elucidating mechanisms underlying catalytic (or any other) effects of silica gel in these reactions.

Although this review does not give an exhaustive account of reactions on silica gel, it sheds more light on its usefulness for organic synthesis.

A K Banerjee, M S Laya Mimó, W J Vera Vegas Centre of Chemistry, Venezuelan Scientific Research Institute, 1020-A Caracas, Apartado 21827, Venezuela. Fax (58-212) 504 13 50.
Tel. (58-212) 504 13 24. E-mail: abanerje@quimica.ivic.ve (A K Banerjee)
Tel. (58-212) 504 13 29. E-mail: mlaya@quimica.ivic.ve (M S Laya Mimó)
Tel. (58-212) 504 13 85. E-mail: wvera@quimica.ivic.ve (W J Vera Vegas)

Received 23 November 2000
Uspekhi Khimii **70** (11) 1094 – 1115 (2001); translated by R L Birnova

II. Cyclisation reactions

Most of the studies published over the past 20 years and devoted to various applications of silica gel in organic synthesis provide a description of various cyclisation reactions. This can be explained by the fact that these reactions have found wide application in the synthesis of diverse physiologically active compounds, particularly, of alkaloids.

1. Intramolecular cyclisation reactions

A simple procedure for the synthesis of isoquinoline and naphthalene fragments of an unusual alkaloid, *viz*., ancistrocladein (**1**), has been proposed by Bringmann.[4]

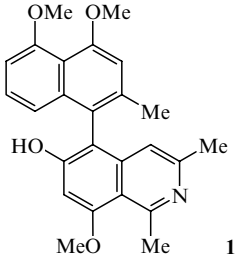

1

This synthesis employed the indan derivatives **2** and **3** as the starting compounds. They were converted into the corresponding polyketones **4** and **5** by mild ozonolysis (in the absence of oxygen) followed by cyclisation into the phenolic derivatives **6** and **7** in the presence of silica gel.†

† The possibility of cyclisation of polyketone **4** under the action of bases was postulated long ago by Birch *et al*.,[5] however, the reaction products have not been studied.

The conversion of phenol **6** into the isoquinoline derivative **8** was carried out by consecutive methylation by dimethyl sulfate and cyclisation by concentrated ammonia in methanol. Selective removal of the 2-hydroxyethyl group afforded 6-hydroxy-8-methoxy-3-methylisoquinoline (**9**). In turn, treatment of the phenol **7** with a base resulted in 1,8-dihydroxy-3-methylnaphthalene (**10**);‡ its methylation by dimethyl sulfate gave the dimethoxy derivative **11**. Further reaction of isoquinoline **9** with naphthalene **11** resulted in ancistrocladein **1**.

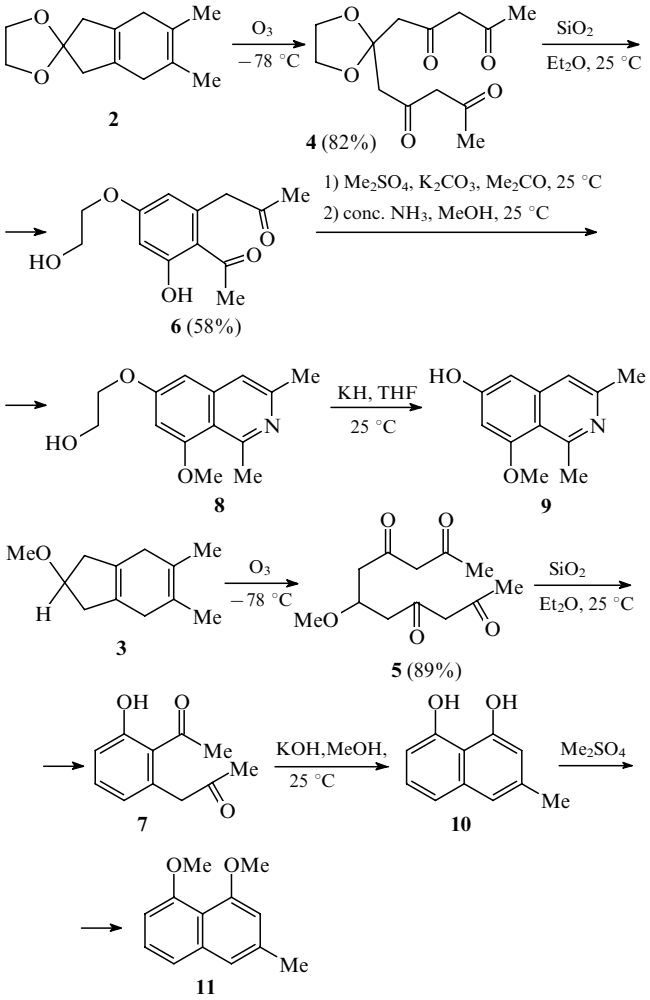

2 **4** (82%) **6** (58%) **8** **9** **3** **5** (89%) **7** **10** **11**

The use of silica gel in the synthesis of the sesquiterpene pallescensin A (**12**) has been described.[6] Trimethylcyclohexanone **13** and furylacetylenide **14** were used as the starting compounds. The addition of acetylenide **14** to cyclohexanone **13** and subsequent dehydration of the reaction product followed by hydrogenation over Lindlar's catalyst yield the derivative **15**; its cyclisation on silica gel affords the *trans*-fused tricyclic product **16**. Selective hydrogenation and desilylation of the product **16** yield pallescensin A (**12**). It is of note that hydrogenation is accompanied by partial reduction of the furan ring.

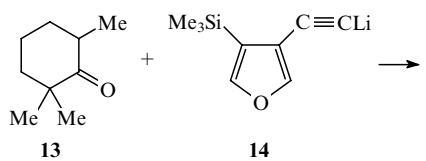

13 **14**

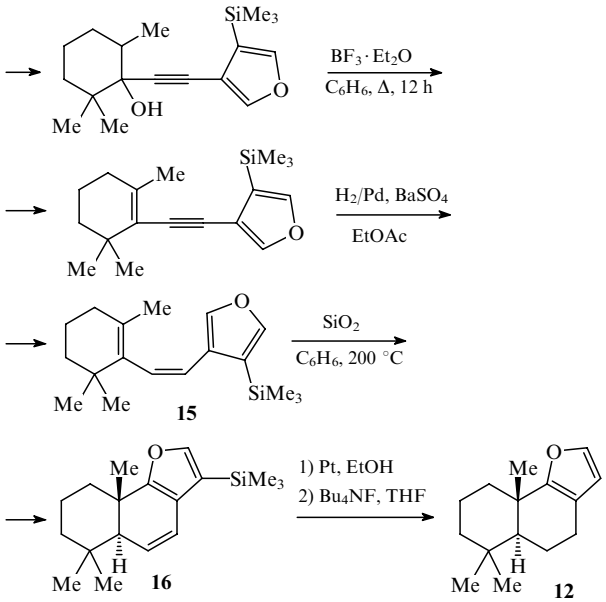

15 **16** **12**

In this reaction, silica gel not only facilitated the cyclisation of the furyl derivative **15** but also ensured control over the stereochemistry of ring fusion, which made this procedure attractive on the whole.

The synthesis of five-membered lactams **17a**–**c** by photocyclisation of *N*,*N*-dibenzyl-2-benzoylcarboxamides **18a**–**c** adsorbed on silica gel has been reported.[7]

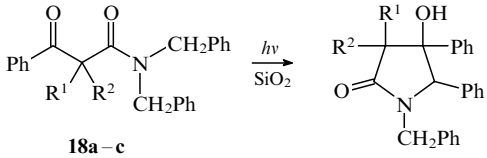

18a–**c** **17a**–**c**

Compound	R^1	R^2	Yield of **17** (%)	
			C_6H_6	SiO_2
a	H	H	80	83
b	Me	H	90	91
c	Me	Me	65	63

It is suggested that this reaction, similar to that performed in solution,[8] occurs as an intramolecular 1,3-hydrogen shift towards the carbonyl oxygen atom.

The rate of consumption of the starting β-oxo amides **18a**–**c** depends on their surface densities, *i.e.*, the amount of β-oxo amide adsorbed per g of silica gel. If solid β-oxo amides are irradiated in the absence of silica gel, the yields of lactams are low.

The use of silica gel as adsorbent in photoconversions of β-oxo amides is very effective, since it ensures uniform distribution of the latter over the whole surface of silica gel. The yields of lactams **17a**–**c** obtained by photocyclisation on silica gel are comparable to those obtained in solutions.[9]

Reductive cyclisation on silica gel of a series of 2-nitro-β-piperidinostyrenes **19a**–**g** prepared§ by condensation of substituted 2-nitrotoluenes **20a**–**g** with tripiperidinomethane has been described.[10] In this study, the Fe–AcOH system was used as the reducing agent and toluene as the solvent. The yields of the reaction products, *viz.*, indoles **21a**–**g**, were 62%–94%.

‡ The derivative **10,** which is extremely sensitive to oxidation, was found in the berries *Diospyros mollis* possessing anti-helminthic activity.

§ This procedure for indole synthesis is a modification of the Leimguber–Batcho method,[11] which includes aminovinylation of 2-nitrotoluenes followed by reductive cyclisation of *trans*-β-dialkylamino-2-nitrostyrenes formed.

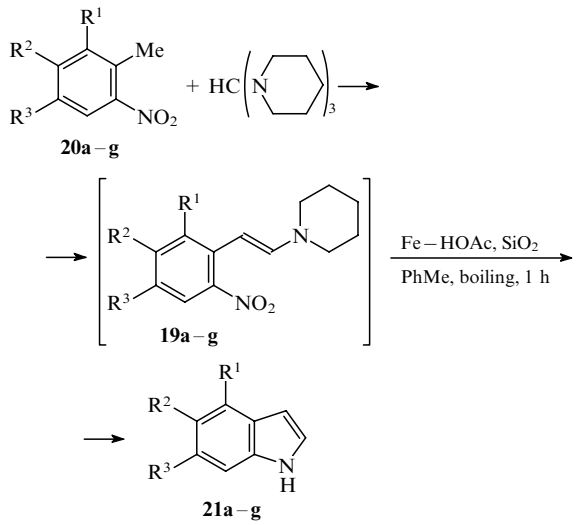

Compound	R^1	R^2	R^3	Yield of **21** (%)
a	H	H	H	82
b	F	H	H	87
c	H	H	Cl	90
d	OMe	H	H	94
e	OCH_2Ph	H	H	85
f	H	H	OMe	81
g	H	OCH_2Ph	OCH_2Ph	62

In the absence of silica gel, the yields of indoles are much lower, which can be ascribed to intramolecular reactions involving β-dialkylamino-2-nitrostyrenes.[12]

This approach was successfully employed in the synthesis of 5,6-bis(benzyloxy)-4-fluoro-, 5,6-bis(benzyloxy)-7-fluoro- and 4,7-difluoro-5,6-diphenylmethylenedioxyindoles (yields 61%, 53% and 53%, respectively); these products are intermediates in the synthesis of halogeno-substituted analogues of pharmaceutically useful neurotoxins, *viz*., 5,6- and 5,7-dihydroxytryptamines. If $TiCl_3$–$AcONH_4$ and Ni-Raney–N_2H_4 are used as reducing agents in the condensation, the yields of indoles are much lower. Thus the yields of 5,6-bis(benzyloxy)-7-fluoroindole were as low as 19% and 23%, respectively, apparently due to side reactions,[13] whereas these undesirable intramolecular reactions are suppressed in the processes carried out in non-polar solvents (*e.g*., toluene) in the presence of silica gel.

It is noteworthy that the use of silica gel together with toluene increases sharply the yields of indoles in reductive cyclisation with Fe–AcOH. Thus the yield of indole **21a** was 82%, while that obtained with the Fe–AcOH system in ethanol was as low as 17%.

The system mentioned (iron + acetic acid, toluene and SiO_2) was used by Corey *et al*.[14] in the synthesis of a substituted tryptamine, a starting compound in the synthesis of the indole alkaloid aspidophytin **22**.

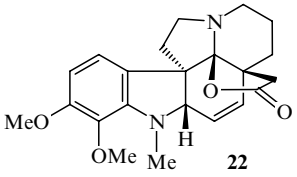

22

Dinitrostyrene **24** was used as the starting compound in the synthesis of tryptamine **23**.

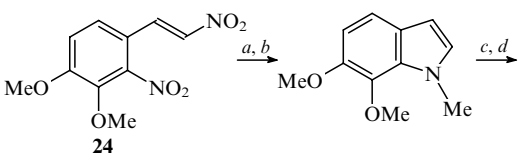

24

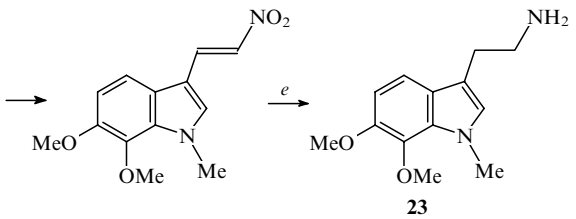

23

(*a*) Fe–HOAc, SiO_2, MePh, Δ; (*b*) MeI, KOH, Bu_4NI, THF, 23 °C; (*c*) $POCl_3$, DMF, 35 °C, 1 h, NaOH(aqueous), Δ; (*d*) $MeNO_2$, NH_2OAc, Δ, 1 h; (*e*) $LiAlH_4$, THF, Δ, 1 h.

The use of silica gel for cyclisation of several ketene acetals resulting in polyfunctional bicyclo[2.2.2]octanones has been described.[15]

Ketene mixed acetals **25a**–**c** were prepared from 3-methoxycyclohex-2-enone (**26a**) and its 6-methyl- (**26b**) and 2,6-dimethyl derivatives (**26c**). To this end, cyclohexenones following treatment with lithium diisopropylamide (LDA) at low temperature reacted with methyl acrylate with subsequent silylation. In this case, the reaction of cyclohexenones with methyl acrylate was stopped in the step of formation of mixed ketene acetals **25a**–**c**; no twofold Michael addition products were detected. The cyclisation of acetals **25a**–**c** was carried out in two ways, *viz*., by passage through a short column packed with silica gel and by treatment with titanium tetrachloride at low temperature. In the former case, the reaction is stereoselective and the yields of the corresponding bicyclo[2.2.2]octanones **27a**–**c** exceed 98%. The yields of reaction products prepared by an alternative route are much lower.

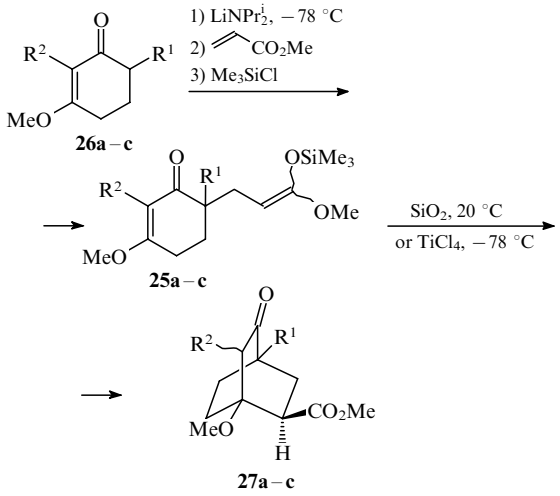

Compound	R^1	R^2	Yield of **27** (%)	
			SiO_2	$TiCl_4$
a	H	H	> 98	72
b	Me	H	> 98	83
c	Me	Me	> 98	54

Bicyclooctanones **27** present certain interest as precursors of cyclic products having several asymmetric centres. To this goal, compounds **27** are converted into lactones **28** by regioselective Baeyer–Villiger oxidation. Opening of the lactone ring affords the cyclic products **29**, which contain three asymmetric centres with defined configurations.

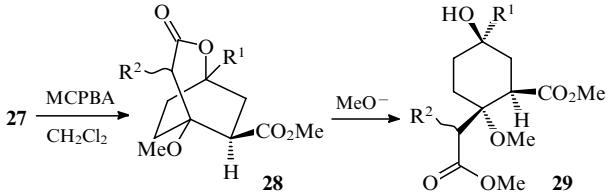

Later, Schinzer and Kalesse[16] used this method to obtain other bicyclo[2.2.2]octanone derivatives. 3-Vinyl- and 3-(*N*-methyl-*N*-tosylamino)-substituted cyclohex-2-enones were used as the starting compounds. It was found that the former derivative reacts with methyl acrylate similarly to the 3-methoxy derivative, *viz*., first, the corresponding ketene acetal is formed, which is then cyclised on silica gel into the final vinyl-substituted bicyclo[2.2.2]octanone. On the other hand, the amino derivative affords directly bicyclooctanone at −78 °C as a result of twofold Michael addition.

Acid-catalysed cyclisation of unsaturated carbonyl compounds in the presence of Lewis acids has been studied in sufficiently great detail (see, *e.g*., the review[17] and references cited therein). This approach is very attractive in the generation of a new C−C bond. However, the use of ordinary Lewis acids does not always ensure high selectivity, the reactions are accompanied by the formation of side products. The use of silica gel as a catalyst for this reaction has been recommended by Marshall *et al*.[18] Thus, silica gel catalyses efficiently the cyclisation of unsaturated aldehydes **30**.[19,20]

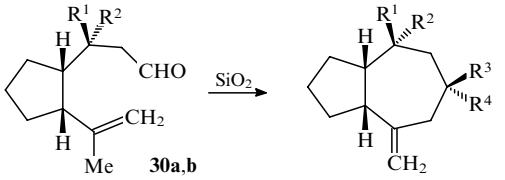

30a: R^1 = Me, R^2 = H, R^3 = H, R^4 = OH (from **30a**),
30b: R^1 = H, R^2 = Me, R^3 = OH, R^4 = H (from **30b**).

The results of studies[21] of different reagents absorbed on silica gel provide convincing evidence that silica gel always contains some amount of bound water molecules, particularly as silicic acid. It is known that high pressure increases the pK_a of acids. Although we still have no direct proof of the effect of high pressure on the acidity of silica gel, it can be assumed, with a high degree of certainty, that the acidity of silica gel will increase with pressure. According to Dauben and Hendricks,[22] oven-dried silica gel efficiently catalyses the cyclisation of various unsaturated carbonyl compounds. Acid-catalysed cyclisation on silica gel as a mild acid catalyst under a pressure of 15 kbar was used in the synthesis of six- and five-membered carbocycles.

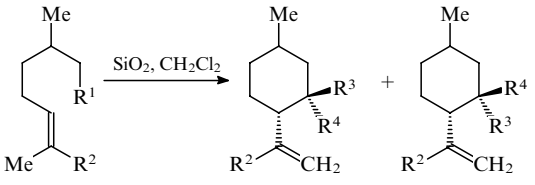

Compound	R^1	R^2	R^3	R^4	Yield (%)	
					32	**33**
a	CHO	Me	OH	H	58	15
b	CHO	H	OH	H	5	20
c	COMe	Me	OH	Me	46	20
d	CH=C$(CO_2Me)_2$	Me	CH$(CO_2Me)_2$	H	66	7

The cyclisation of unsaturated carbonyl compounds **31a**–**d** yields the six-membered stereoisomeric cyclic products **32a**–**d** and **33a**–**d**. The yields of the carbocyclic products from compounds **31a**, **31c** and **31d** on silica gel at 15 kbar are comparable to those obtained previously with Me_2AlCl[23] and $ZnBr_2$.[24,25] In the case of the aldehyde **31b**, the yields of the cyclisation products **32b** and **33b** are low (5% and 20%, respectively), whereas the yield of the product **32b** prepared with Me_2AlCl is 90%. Under normal pressure, compound **31c** is not cyclised on silica gel; compound **31a** is cyclised but the yields of the reaction products are < 10% after 7-day exposure on silica gel. No cyclisation of compounds **31a** and **31d** takes place at 15 kbar in the absence of silica gel.

The unsaturated aldehyde **34** undergoes cyclisation on silica gel at 15 kbar to yield a mixture of five-membered cyclic products **35**–**37**. The methyl ketone homologue of the aldehyde **34** is not cyclised under these conditions.

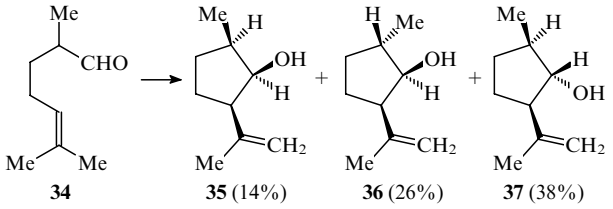

The unsaturated ester **38** yields the cyclic derivatives **39** and **40** under identical conditions.

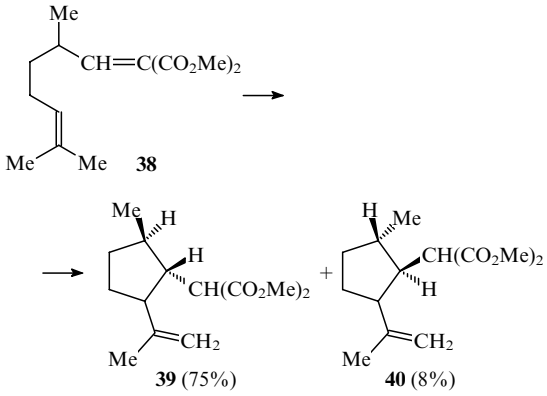

The use of silica gel in combination with a pressure of 15 kbar was also found to be helpful in the cyclisation of the labile vinylcyclopropane-containing aldehyde **41** into compounds **42** and **43**. An attempt to cyclise compound **41** under the action of zinc bromide failed, the products **42** and **43** were detected but in trace amounts.

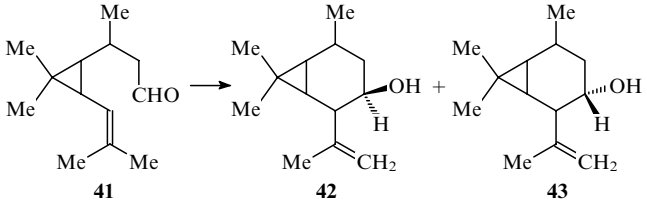

It was shown[22] that the yields and selectivities in ene-type cyclisations on silica gel at 15 kbar are comparable to those obtained by other methods (see, *e.g*., Refs 26 and 27). The conditions mentioned proved to be of choice in certain cases, as in the cyclisation of the aldehyde **41**.

Treatment of γ-halogeno-substituted esters **44a**,**b** and their vinylogues **45** and **46** with silica gel in xylene results in high yields of γ-butyrolactones **47a**,**b**, **48** and **49**, respectively.[28]

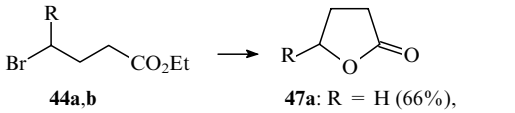

47a: R = H (66%),
47b: R = n-C_6H_{13} (79%).

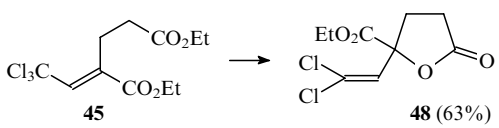

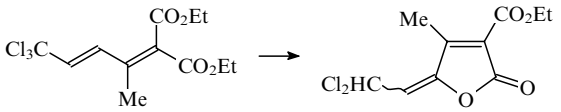

46 **49** (46%)

The silica gel used in this reaction was dried for 3 h at 200–250 °C and 20 Torr. The reactions were performed by heating the substrates with silica gel in xylene for 3–15 h.

The efficacy of silica gel was demonstrated in the conversion of ethyl 4-bromobutyrate (**44a**) as an example. Boiling of compound **44a** in xylene in the presence of SiO_2 results in γ-butyrolactone **47a** in 66% yield, whereas heating of the haloester in xylene in the absence of silica gel affords no lactonisation product.

Acid-catalysed lactonisation of γ-halogeno-substituted carboxylic acids is one of the most attractive methods for the synthesis of γ-butyrolactones. However, this is inapplicable to substrates containing easily hydrolysable functional groups. The use of silica gel not only lifts these restrictions, but also increases the yields of the target products. Previous reports describe moderate yields of γ-butyrolactones prepared upon heating of γ-halogeno esters in the absence of solvents. It is of note that the conditions for this reaction (170–180 °C) are more drastic than those used for the lactonisation on silica gel.

This method was also used in the synthesis of bis-γ-butyrolactones. Thus the triester **50** and the diester **51** are converted into dilactones **52** and **53** in high yields by treatment with silica gel.

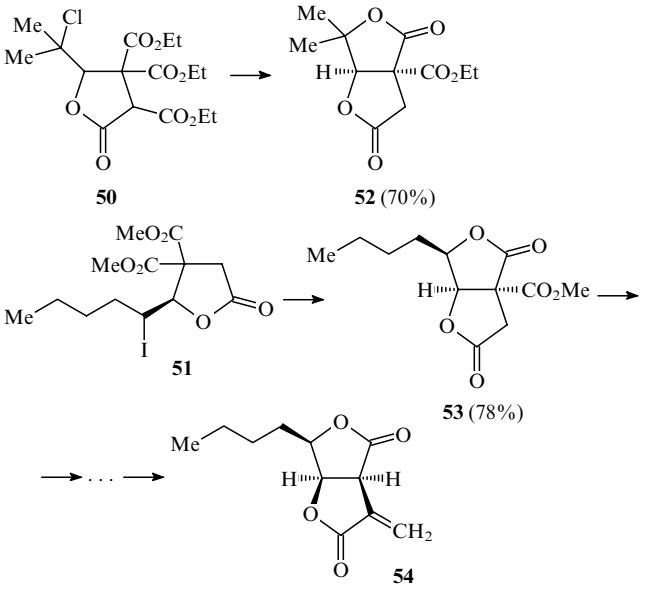

50 **52** (70%) **51** **53** (78%) **54**

Compound **53** is the key intermediate in the synthesis of (+)-canadensolide (**54**), a metabolite isolated from *Penicillium canadense*.

A novel method of the synthesis of γ- (compounds **55a–e**) and δ-lactones (compounds **56a–e**) by conversion of methyl 4-aryl-5-tosyloxyhexanoates **57a–e** in the presence of silica gel in hexane has been reported.[29]

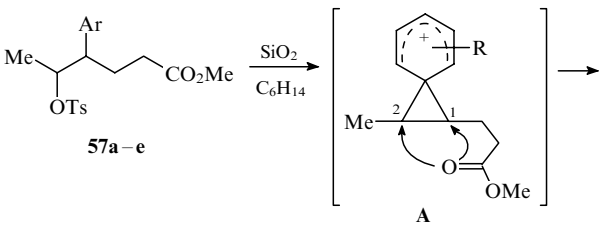

57a–e **A**

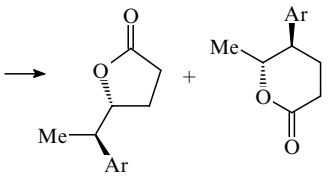

55a–e **56a–e**

Compound	Ar	Yield (%)	
		55	**56**
a	4-$MeOC_6H_4$	30	42
b	2-$MeOC_6H_4$	11	67
c	3,4-$(MeO)_2C_6H_3$	34	36
d	4-MeO-2-MeC_6H_3	7	73
e	2-MeO-4-MeC_6H_3	14	68

The structures of the resulting lactones were determined from spectroscopic data. In all cases studied, the yields of δ-lactones exceeded those of γ-lactones.

The stereochemistry of δ-lactones **56a–e** suggests that these compounds, like γ-lactones **55a–e**, are formed *via* an intermediate phenonium ion (**A**), rather than by direct substitution of the tosyloxy group by the ester group. It was concluded that the regioselectivity of the lactonisation reaction, which proceeds *via* the intermediate phenonium ion (**A**), is controlled by electronic factors. It was also found that the lactonisation of compounds **57a–e** under conditions of thermodynamic control is selective and yields γ-lactones **55a–e**, whereas that under conditions of kinetic control yields predominantly δ-lactones **56a–e**. It should be noted that methyl 4-(4-methyl-2-methoxyphenyl)-5-tosyloxypentanoate (**58**) is converted exclusively into γ-lactone **59** upon lactonisation on silica gel in hexane.

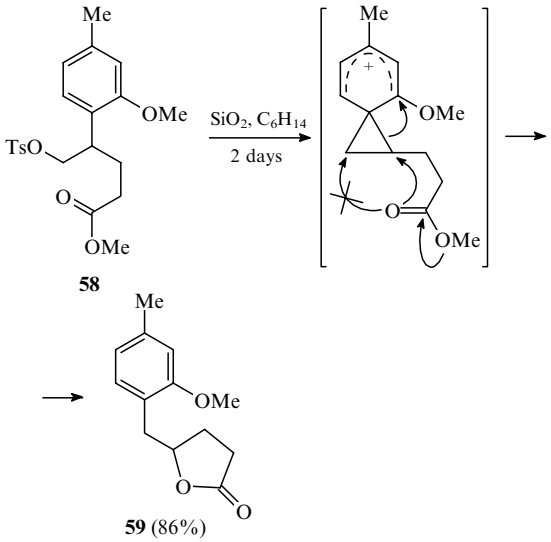

58 **59** (86%)

We believe that lactonisation on silica gel will find broad application in synthetic organic chemistry.

A simple procedure for lactam synthesis, which includes cyclodehydration of the corresponding amino acids by treatment with silica gel in boiling toluene, has been described.[30]

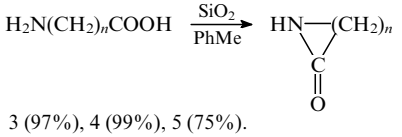

n = 3 (97%), 4 (99%), 5 (75%).

The corresponding lactams are formed in very high yields. This reaction proceeds smoothly on alumina as well.

An efficient procedure for the synthesis of nitrogen heterocycles, which includes cyclisation of *N*-(Δ^4- or Δ^5-alkenyl)carbamates under the action of PhSeCl in the presence of silica gel, has been developed (Table 1).[31] Presumably, this reaction proceeds in two steps, *viz*., initial rapid addition of PhSeCl in CH_2Cl_2 to the double bond of the urethane and subsequent cyclisation of the adduct formed on the surface of silica gel.

The PhSe-groups were removed by treatment of the selenides with triphenyltin hydride in boiling toluene.

It was noted that the ring closure occurs more easily in the presence of predried silica gel (Merck 60 PF-254) and the yield of the target products (the corresponding pyrrole and piperidine derivatives) is increased (Table 1). In the case of *N*-ethoxycarbonyl-2-(3-methylbut-2-enyl)aniline both 5-*exo*- and 6-*endo*-cyclisation products were obtained.[32]

This method provides a reasonable alternative to Hg^{2+}-induced cyclisation commonly used in the synthesis of nitrogen heterocycles and a good supplement to palladium-assisted cyclisation, which affords products at a different level of hydrogenation.

Table 1. Cyclisation of urethanes.

Urethane	Product	Yield (%)	
		in solution	on SiO_2
	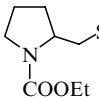	77	93
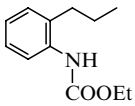	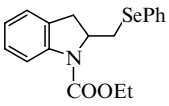	73	85
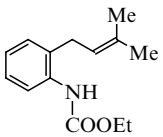	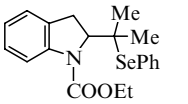 + 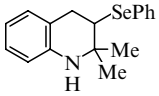	–	76
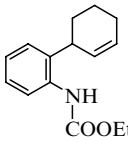	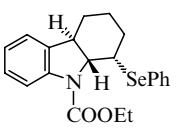	59	82
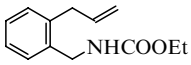	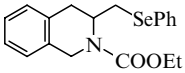	52	87
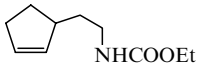	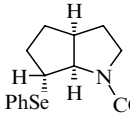	–	94
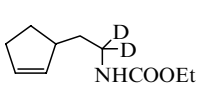	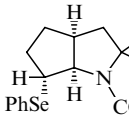	–	83
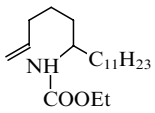	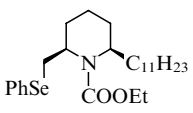	–	84
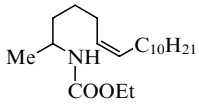	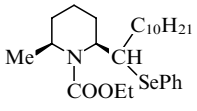	–	35

2. Intermolecular cycloaddition reactions

The efficiency of silica gel in intermolecular cycloaddition reactions has been described in numerous papers (see, *e.g*., reviews [3,21] and references cited therein). Here we shall consider only some of the most interesting studies devoted to [4 + 2]-cycloaddition reactions (the Diels – Alder reaction). A new methodology for [4 + 2]-cycloaddition of dienes **60** to dienophiles **61** on the surface of chromatographic adsorbents (*e.g*., SiO_2, $MgO \cdot SiO_2$, Al_2O_3) under solvent-free conditions has been described.[33,34]

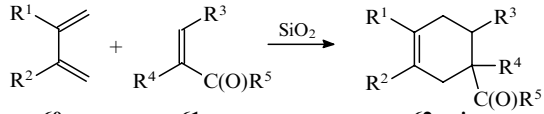

60 **61** **62a – i**

Compound	R^1	R^2	R^3	R^4	R^5	Yield of **62** (%)
a	H	H	H	H	Me	85
b	H	H	H	H	H	67
c	Me	H	H	H	Me	72
d	Me	H	H	H	H	56
e	Me	Me	H	H	Me	92
f	Me	Me	H	Me	H	89
g	Me	Me	Me	H	H	83
h	$(CH_2)_2CH=CMe_2$	H	H	H	Me	73
i	$(CH_2)_2CH=CMe_2$	H	H	H	H	66

With SiO_2, the yields of the [4 + 2]-adducts **62a – i** were 56% – 92%. Condensation of these compounds in the liquid phase in the absence of catalysts usually requires drastic conditions (120 – 160 °C, 3 – 6 h). If the reaction is carried out on SiO_2 without solvents, the temperature can be decreased considerably (*e.g*., by 50 – 100 °C). In some cases, the Diels – Alder diene products are obtained in higher yields. Presumably, the role of silica gel is to ensure polyfunctional catalysis (due to multicentre adsorption), and the absence of a solvent favours formation of pre-reaction complexes due to weak van-der-Waals interactions of adsorbed substrates devoid of shielding solvation shells. If the reaction is carried out on the surface of SiO_2 in the presence of solvents (*e.g*., C_6H_{14}, CH_2Cl_2), the efficiency of cycloaddition decreases considerably, presumably due to partial desorption of the reactants from the surface of SiO_2.

It is suggested that the activity of silica gel depends critically on the water content. The highest yields were obtained with silica gel dried at 200 °C for 6 h in order to remove physically adsorbed water. Florisil ($MgO \cdot SiO_2$, Florisil) tested in this reaction appeared to be less efficient. With $MgO \cdot SiO_2$, the reaction temperature had to be increased by 20 – 30 °C in order to make the yields of [4 + 2]-adducts comparable to those obtained with dried SiO_2.

The main advantage of this method is that cycloaddition reactions on silica gel in the absence of solvents are highly regio- and stereoselective, whereas reactions in liquid media yield mixtures of isomers. Thus the SiO_2-catalysed addition of methyl vinyl ketone and acrolein to cyclopenta- and cyclohexadienes results in the predominant formation of the *endo*-isomers **63**, whereas the liquid-phase reaction involving these substrates yields a mixture of isomers where the *exo*-isomer content is > 20%.

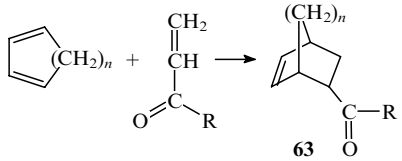

63

R = H, Me.

The reaction of furan (**64a**) and silvane (**64b**) with methyl vinyl ketone occurs differently under these conditions. This reaction is fast, but yields exclusively addition products, *viz*., compounds **65**

and **66**, respectively. This can be attributed to high lability of methyl vinyl ketone on such a sorbent as silica gel. At the same time, the use of florisil ($MgO \cdot SiO_2$) as a sorbent affords the expected [4 + 2]-cycloaddition products **67a**,**b**.

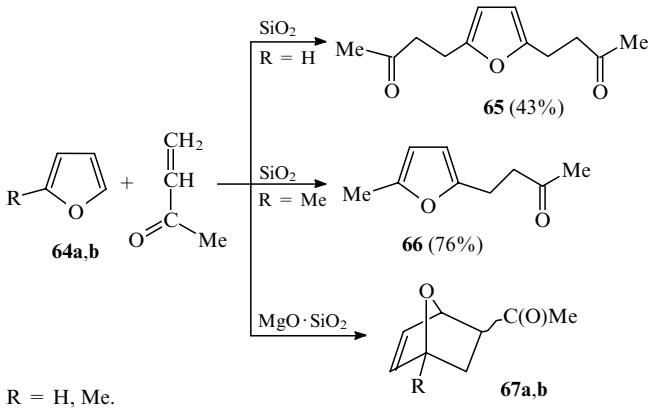

R = H, Me.

An illustrative example of the high efficiency of the dry-adsorption method is provided by the hetero-Diels–Alder synthesis.[35] It was found that the cycloaddition of alkoxyallenes **68** to α,β-enals and α,β-enones **69** results in the [4 + 2]-adducts **70**.

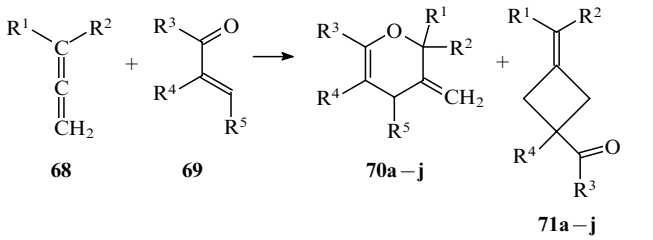

Compound	R^1	R^2	R^3	R^4	R^5	Yield of **70** + **71** (%)
a	EtO	H	H	H	H	71 (with predominance of **70**)
b	EtO	H	Me	H	H	68 (with predominance of **70**)
c	EtO	H	H	Me	H	58 (with predominance of **71**)
d	EtO	H	H	H	Me	< 5
e	MeO	Me_3Si	H	H	H	47 (**70**) + 26 (**71**)
f	MeO	Me_3Si	Me	H	H	47 (with predominance of **70**)
g	MeO	Me_3Si	H	Me	H	38 (**70**) + 43 (**71**)
h	MeO	H	H	H	H	47 (with predominance of **70**)
i	MeO	H	Me	H	H	65 (with predominance of **70**)
j	MeO	H	H	Me	H	82 (1 : 1)

In addition to the dihydropyran derivatives **70**, which represent [4 + 2]-cycloaddition products, this reaction affords a small amount of [2 + 2]-cycloaddition by-products, *viz*., the cyclobutane derivatives **71**.

The highest yields of the [4 + 2]-cycloaddition products were obtained when dried silica gel deactivated with triethylamine (0.2% – 0.5%) was used. It is of note that the acidity of ordinary silica gel is a factor which is responsible for the destruction and polymerisation of cycloaddition products. The use of more basic florisil as a medium for the hetero-Diels–Alder reaction helps avoid undesired side reactions,[34] but the reaction rate decreases. Alumina manifests no catalytic activity in this reaction.

The 2-alkoxy-5-methylidene-3,4-dihydro-2*H*-pyrans **70** formed are the starting products in the synthesis of valuable derivatives of glutaraldehyde.

According to Posner *et al*.,[36] preparative [4 + 2]-cycloaddition of commercial 3-methoxycarbonyl-2-pyrone (**72**) to vinyl ethers **73** and **74** is strongly accelerated under the action of silica gel (EM Science 60) at room temperature, resulting in *endo*-bicyclic products (**75** and **76**) diastereoselectively and in extremely high yields.

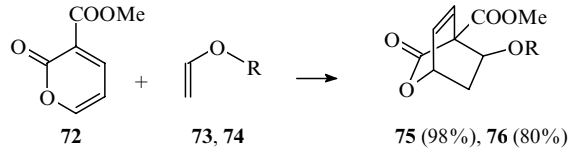

R = Bu^n (**73**, **75**), $PhCH_2$ (**74**, **76**).

The *endo*-adducts **77** (the diastereomer ratio is ~4 : 1) are also formed upon cycloaddition of benzyl vinyl ether (**74**) to the enantiomerically pure (*R*)-methyl pyrone-3-carbonyl lactate **78**. This reaction was carried out on dried (200 °C, 16 h) silica gel (Syloid 221) in toluene.

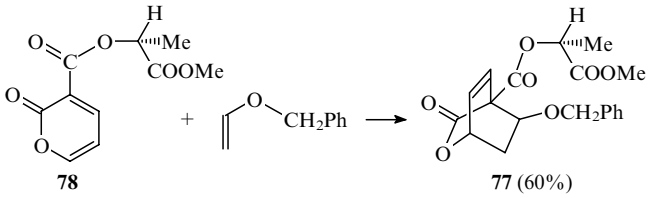

No [4 + 2]-cycloaddition products are formed in the absence of silica gel.

The above-described silica gel-catalysed cycloaddition reactions are operationally simple, stereoselective methods for the synthesis of bicyclic lactones and represent 'atom-economical' procedures[¶] in which all the atoms of both reactants are incorporated into the final products.

Despite the immense diversity of synthetic methods used to obtain nitrogenous heterocycles, the interest of investigators in simple and convenient procedures does not fade, since nitrogenous heterocycles are constituents of many physiologically active compounds. Recently, Ranu *et al*.[37] have developed a simple and efficient method for quinoline synthesis from anilines and alkyl vinyl ketones by treatment with indium(III) chloride on silica gel under microwave irradiation without any solvent.

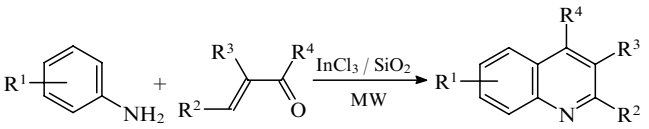

Compound	R^1	R^2	R^3	R^4	Yield of **79** (%)
a	H	H	H	Me	85
b	2-Me	H	H	Me	81
c	3-Me	H	H	Me	84
d	4-Me	H	H	Me	85
e	2-OMe	H	H	Me	80
f	4-OMe	H	H	Me	83
g	3-OH	H	H	Me	81
h	3-Cl	H	H	Me	87
i	4-Cl	H	H	Me	80
j	4-Br	H	H	Me	80
k	2-Me-4-I	H	H	Me	83
l	C_4H_4	H	H	Me	82
m	H	Me	H	*p*-$MeOC_6H_4$	81
n	3-Cl	Me	H	*p*-$MeOC_6H_4$	83
o	H	Pr^n	Et	Me	55

¶ This term was originally suggested by B Trost.

This method allows one to obtain quinolines **79a–o** in high yields irrespective of the nature of substituents in the anilines and alkyl vinyl ketones. This reaction includes the Michael addition of aniline to vinyl ketone followed by cyclisation and aromatisation catalysed by $InCl_3/SiO_2$. When $InCl_3$ is used without silica gel, the reaction is sluggish, while imines are formed on silica gel in the absence of $InCl_3$.

The same authors have developed a convenient one-step method for the synthesis of polysubstituted pyrroles.[38] It was found that the reaction of α,β-unsaturated carbonyl compounds with amines and nitroalkenes on the surface of silica gel (HF 254) under microwave irradiation without any solvent affords various polysubstituted pyrroles **80a–p**.

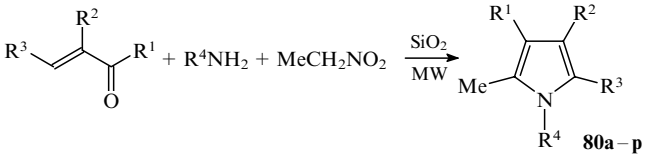

80a–p

Compound	R^1	R^2	R^3	R^4	Yield of **80** (%)	
					SiO_2	THF, Δ
a	Ph	H	H	$PhCH_2$	60	30
b	Ph	H	Ph	$PhCH_2$	65	32
c	Ph	H	Me	$PhCH_2$	64	35
d	H	H	Me	$PhCH_2$	60	31
e	H	H	Me	cyclo-C_6H_{11}	60	32
f	Ph	H	H	C(Ph)HMe	62	33
g	Ph	H	Me	C(Ph)HMe	66	33
h	Ph	H	H	Pr^i	64	35
i		H	Me	Pr^i	68	36
j		H	Me	$PhCH_2$	72	40
k	Pr^n	Et	H	$PhCH_2$	60	28
l	Pr^n	Et	H	cyclo-C_6H_{11}	65	35
m	Ph	H	H	Pr^n	62	31
n	Ph	H	Me	Bu^n	65	40
o	Ph	H	H	Bu^n	61	32
p	$-(CH_2)_4-$		Me	Bu^n	68	40

Heating of mixtures of starting compounds in the absence of silica gel results in resinification. When this reaction is carried out in solution (*e.g.*, boiling in THF), the yields of the reaction products decrease significantly, whereas the reaction time increases.

In our opinion, the one-step syntheses of quinolines and pyrroles from readily available compounds developed by Ranu *et al.*[37,38] are among the best methods presently available. To obvious advantages of these methods one can relate simple procedures, high product yields, high reaction rates and the possibility to obtain a broad array of quinolines and pyrroles.

A convenient procedure for the preparation of quinoxaline di-*N*-oxide derivatives **81a–f** from β-dicarbonyl compounds and benzofuroxan in methanol in the presence of silica gel has been proposed.[39]

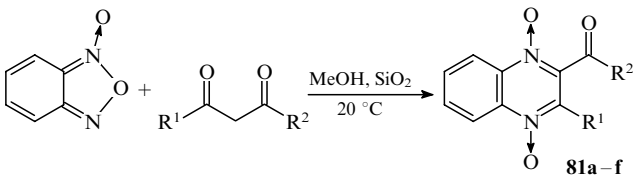

81a–f

Compound	R^1	R^2	Enol content (%)	Yield of **81** (%)
a	OMe	OMe	0	0
b	Me	OMe	12.6	16
c	Ph	OEt	27	63
d	Me	Me	84	58
e	Ph	Ph	90–100	66
f	Me	Ph	94	88

This reaction is carried out as follows. Benzofuroxan and the β-dicarbonyl compound are dissolved in methanol, the solution is mixed with silica gel and concentrated at 20 °C. The resulting mixture containing the adsorbed reagents is kept at room temperature for 1–2 weeks without drying after which the corresponding quinoxaline di-*N*-oxide is isolated. The efficacy of this reaction strongly depends on the type of silica gel used. Convenient gels are Wako gel C-200 (Wako Pure Chemical Industries) and Silica gel 60 (Merck).

It is assumed that the yields of the products **81a–f** correlate with the per cent content of the enol form of the carbonyl compound. When alumina (basic, neutral or acidic) was used instead of silica gel, the yields of quinoxaline di-*N*-oxides **81a–f** were much lower. In all cases studied, the main product appeared to be contaminated with side products.

III. Rearrangements

Many organic compounds undergo diverse molecular rearrangements under the action of acids and bases. The papers published before 1979 provide examples of interesting rearrangements of certain classes of organic compounds, such as aminopyrrolidines,[40] hydroxycyclopropanes,[41] oxazolidines[42] and aldehydes, on silica gel.[18] A great variety of interesting rearrangements induced by silica gel have been described in the review of McKillop and Young,[21] therefore we shall omit them from consideration and shall confine ourselves to a few cases only.[43–45]

Thus multiple passage of addition products of methyl-substituted 1-acetoxybuta-1,3-dienes **82–85** to chlorobenzoquinones **86–89** through a column with silica gel leads to rearrangement and concomitant aromatisation leading to naphthoquinones **90–96**.[43]

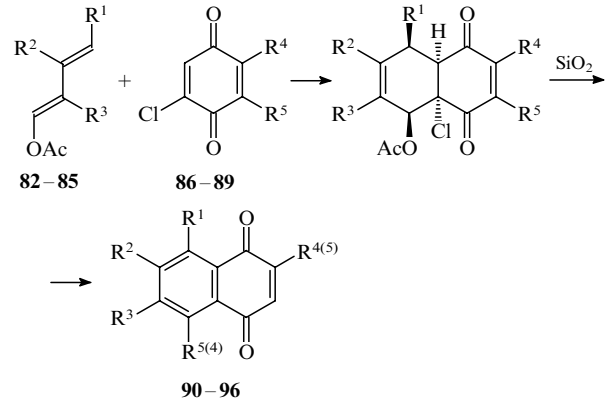

82–85 **86–89**

90–96

Reaction	Product	R^1	R^2	R^3	$R^{4(5)}$	$R^{5(4)}$	Yield (%)
82+**87**	**90**	H	H	H	Cl	H	92
83+**86**	**91**	H	H	Me	Cl	H	79
83+**87**	**92**	H	H	Me	(H)	(Cl)	65
84+**86**	**92**	H	Me	H	Cl	H	88
84+**87**	**91**	H	Me	H	(H)	(Cl)	80

Reaction	Product	R^1	R^2	R^3	$R^{4(5)}$	$R^{5(4)}$	Yield (%)
85 + 86	**93**	Me	H	H	Cl	H	80
85 + 87	**94**	Me	H	H	(H)	Cl	90
84 + 88	**95**	H	Me	H	OMe	H	96
84 + 89	**96**	H	Me	H	(H)	(OMe)	79

This method is especially convenient for the synthesis of substituted naphthoquinones which represent fragments of many natural alkaloids.

Yet another interesting rearrangement coupled with aromatisation has recently been observed in studies of the conversion of ketone **97**.[44] This was first transformed into alkene **98** by the Wittig reaction and then into the target diol **99** by treatment with Woodward's reagent (MeCOOAg, I_2, MeCOOH, H_2O) followed by alkaline hydrolysis. An attempt to purify the diol **99** on a column with silica gel (Silica gel 60, Merck) gave unexpectedly tetralin **100** in 90% yield. Apparently, during its passage through the column diol **99** first undergoes dehydration and then rearrangement.

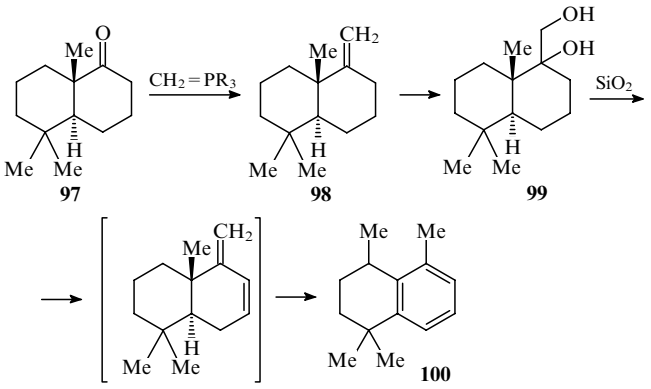

A simple procedure for flavanone synthesis from esters (the Fries rearrangement) has been proposed.[45] This rearrangement is effected by microwave irradiation in the presence of the catalytic system $AlCl_3 - ZnCl_2 - SiO_2$.

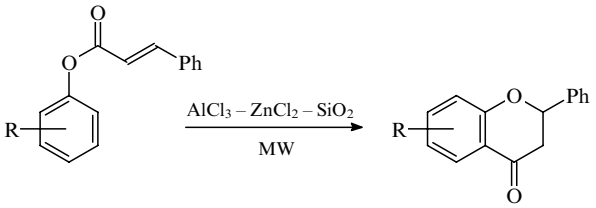

IV. Reduction

Reduction of nitrostyrenes **101a – e** to nitroethylbenzenes **102a – e** was carried out by treatment with sodium borohydride in chloroform – isopropyl alcohol in the presence of silica gel.[46]

$$R^1C_6H_4CH{=}CR^2NO_2 \xrightarrow[SiO_2]{NaBH_4} R^1C_6H_4CH_2CHR^2NO_2$$

101a – e **102a – e**

Compound	R^1	R^2	Yield of **102** (%)
a	H	H	93
b	H	Me	93
c	2-Me	H	99
d	4-Me	H	92
e	3-Me	H	92

The reduction results in highly polar negatively charged intermediates **103**. In the absence of silica gel, such intermediates bind a proton or a second molecule of the original styrene resulting in a mixture of products **102** and **104** in a nearly equal ratio. The formation of the dimer **104a** in solution shown in the scheme below is an example.

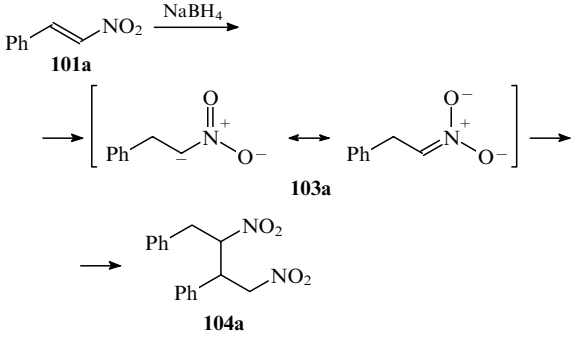

In the presence of silica gel, the intermediates **103** are formed most probably on the surface. In this case, the addition of the second styrene molecule is hindered, and the reaction yields nitroethylbenzenes **102** as the main products.

The use of chloroform as a solvent in this reaction is more preferable than the use of dichloromethane, ether or benzene. The reason is that the dissolution of the intermediate in this solvent is minimal due to the low dielectric permeability of chloroform, whereas its high density favours uniform distribution of silica gel in the reaction mixture.

For the same reasons, the use of isopropyl alcohol is more preferable than the use of methanol and ethanol, for it dissolves sodium borohydride to a lesser extent and, correspondingly, the formation of the dimeric side products **104** is less probable.

The reduction of bicyclic diketones **105** and **106**, tricyclic ketone **107** and several steroidal ketones (5α and 5β-androstane-3,17-diones, methyl esters of di- and trioxocholanoic acids, *etc.*) by treatment with the $BH_3 \cdot NMe_3$ complex has been described.[47] It was shown that the reaction carried out in the presence of silica gel impregnated with $FeCl_3 \cdot 6H_2O$ or $ZnCl_2$ resulted in selective reduction of only one keto group. Thus diketones **105** and **106** are reduced to the corresponding hydroxy ketones **108** and **109** in good yields; this reaction does not require protection of the second carbonyl group.

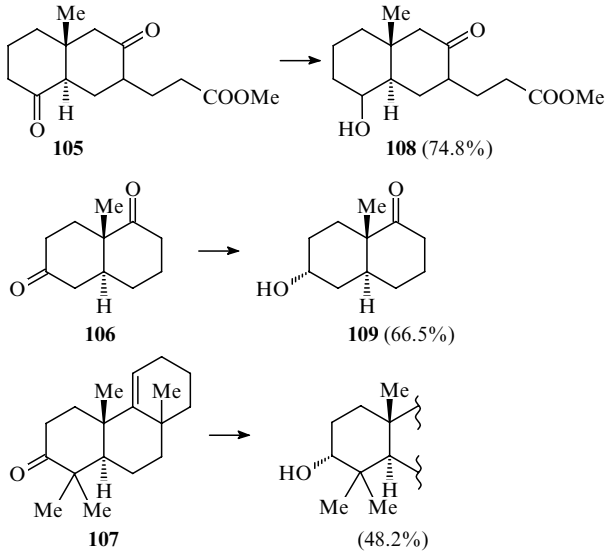

The presence of a small amount of water (5%) in silica gel accelerates the reaction, apparently due to enhanced adsorption of the amine.

Compounds containing several carbonyl groups can be regioselectively adsorbed on silica gel. Thus IR-spectroscopic studies of 5α- and 5β-androstane-3,17-diones revealed that during adsorption of these steroids on silica gel one of the carbonyl groups, *viz.*, C(17)O, forms stronger hydrogen bonds with the OH groups

present on the surface of silica gel in comparison with C(3)O. Thus, the former becomes protected from reduction with the $BH_3 \cdot NMe_3$ complex. In the cases of all steroidal ketones studied, it was the carbonyl group at position 3 that underwent reduction preferentially to the carbonyl groups at positions 7, 12, 17 and 20.

Three catalytic systems, *viz*., $SiO_2 \cdot FeCl_3 - PhH$, $SiO_2 - ZnCl_2 - PhH$ and $ZnCl_2 - PhH$, were tested in the reduction of 5α- and 5β-androstane-3,17-diones with $BH_3 \cdot NH_3$. All these reactions afforded mixtures of 3α- and 3β-hydroxy derivatives. The catalytic system $SiO_2 - FeCl_3 - PhH$ proved to be the best as the reaction was complete within 2 h, whereas reduction in the presence of the other two systems required 18–20 h. It should be noted also that in the absence of silica gel (the third catalytic system) the yields of steroid alcohols were very low.

Ranu and Das[48] have proposed an excellent method for the synthesis of cyclic and acyclic allylic alcohols by reduction of the corresponding conjugated unsaturated ketones and aldehydes by zinc borohydride supported on silica gel. This reaction was carried out with unsaturated aldehydes (crotonic aldehyde, citral, *etc*.) and ketones (substituted 3-methylcyclohex-2-enones, α-ionone, pent-2-enone, *etc*.); in most cases, the yields of the corresponding allylic alcohols were quantitative. Thus the yields of alcohols in the reduction of substituted 3-methylcyclohex-2-enones exceeded 80%.

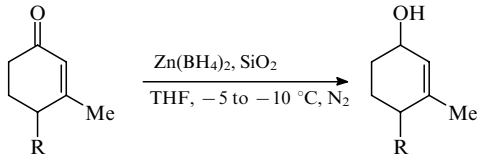

R = H (80%), COOEt (82%), COOMe (85%).

Zinc borohydride manifested high selectivity in hydrogenation, which affected exclusively carbonyl groups, but no double bonds.

Later, Ranu *et al*.[49] recommended this reagent for use in reductive amination of conjugated aldehydes and ketones in the presence of silica gel (substitution of the amino group for the carbonyl group is a very important process in organic synthesis).

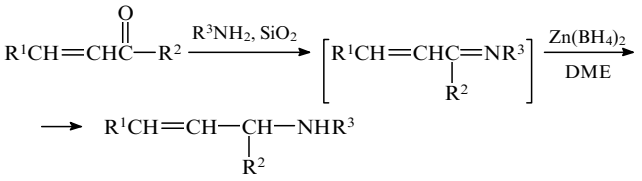

R^1, R^3 = Alk, Ar; R^2 = H, Alk.

Attempts to use other catalysts, *e.g*., $BF_3 \cdot Et_2O$ or $ZnCl_2$, in this reaction were unsuccessful; good yields (75%–90%) of the corresponding imines were obtained only in the case when the reaction was carried out on silica gel.

Among other recent studies devoted to hydrogenation of carbonyl compounds, special mention should be made of the one[50] where the reduction of ketones and aldehydes into the corresponding alcohols was effected with sodium borohydride in the presence of silica gel in an aprotic solvent (hexane). The main advantages of this reaction are easy availability, low cost of reagents and catalysts, mild reaction conditions, ease of isolation of final products and, which is even more important, high yields.

V. Oxidation

The use of inorganic oxidants in organic synthesis is often limited by their poor solubilities in low-polar media. One of the most popular oxidants is ozone. Dry ozonisation in the presence of silica gel for the insertion of oxygen atoms into non-activated C–H bonds has been described in sufficiently great detail by Basyuk;[3] therefore, we shall not discuss this process in this chapter and shall confine ourselves to the consideration of some other inorganic oxidants.

1. Oxidation of alcohols

The use of bis(trimethylsilyl) chromate supported on silica gel for the oxidation of some alcohols to carbonyl compounds has been described.[51] This reaction is initiated by microwave irradiation and takes place in the absence of solvents.

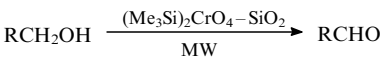

R = *p*-MeC_6H_4 (98%), n-C_7H_{15} (86%).

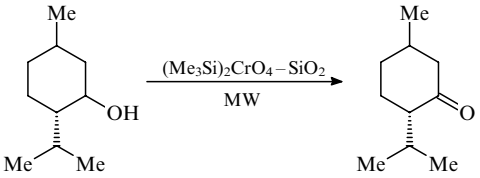

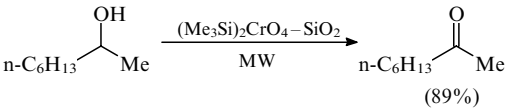

The reaction is complete within a short period of time. High yields of carbonyl compounds, simple methodology, easy isolation of reaction products and stability of the oxidant make this procedure especially attractive for synthetic chemists.

Oxidation of alcohols in CH_2Cl_2 with bis(trimethylsilyl) chromate supported on silica gel had been described earlier.[52]

2. Oxidation of phenols

Despite the great diversity of methods employed in quinone synthesis, studies in this field are currently under way, since many quinones possess biological activities and some of them are valuable semi-products in the synthesis of medicinal drugs. Recently, Hashemi and Bni[53] have proposed a very convenient, from our point of view, procedure for quinone synthesis which consists in oxidation of phenols with oxygen in the presence of a mixture of manganese and cobalt salts of 4-aminobenzoic acid supported on silica gel.

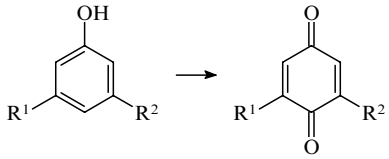

$R^1 = R^2 = H$ (64%); R^1 = Me, R^2 = H (53%); $R^1 = R^2$ = Me (57%)

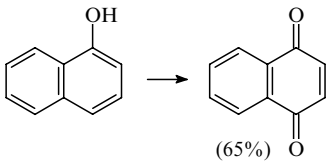

Benzene, toluene and ethylbenzene can be used as solvents in this reaction.

3. Oxidation of silyl ethers

Bis(trimethylsilyl) chromate supported on silica gel was also used for the oxidation of trimethylsilyl ethers of primary and secondary alcohols.[54] This reaction was run in dichloromethane.

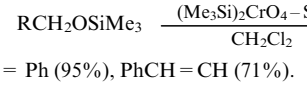

R = Ph (95%), PhCH=CH (71%).

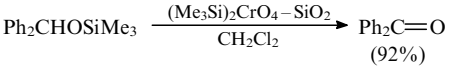

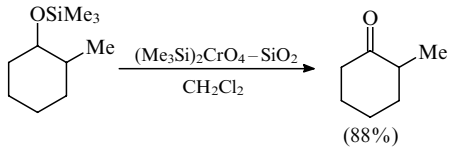

It is worth noting that in addition to the expected cinnamic aldehyde, the oxidation of 3-phenylallyl silyl ether yielded an appreciable amount (28%) of benzaldehyde, which points to the vulnerability of the double bond under these conditions.

Special mention should be made of the oxidation of trimethylsilyl ethers by atmospheric oxygen which is catalysed by manganese and cobalt salts of 4-aminobenzoic acid supported on silica gel.[55] This reagent is also effective in the transformation of acetals and ketals into the corresponding carbonyl compounds.

4. Oxidation of sulfides

An effective procedure for the synthesis of sulfoxides by oxidation of sulfides in the absence of solvents has been developed.[56] The oxidation is carried out with manganese dioxide in the presence of a catalytic system, $H_2SO_4-SiO_2$.

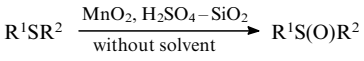

VI. Condensations

Silica gel is an efficient catalyst for the Knoevenagel condensation. The condensation of peptidylacetonitriles derived from *N*-acetyl-L-phenylalanine, *N*-acetyl-L-leucyl-L-phenylalanine and *N*-acetyl-L-leucyl-D-phenylalanyl-L-phenylalanine with aromatic aldehydes and ketones has been described.[57]

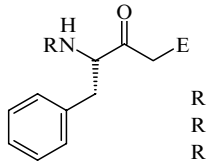

R = Ac: E = CN, CO_2Me, NO_2;
R = *N*-Ac-L-Leu, E = CN;
R = *N*-Ac-L-Leu-D-Phe, E = CN.

When this reaction is performed under homogeneous conditions, it requires weak bases, but even in this case the yields of reaction products are moderate. High yields can be achieved in heterogeneous conditions, *viz*., on silica gel. It is assumed that silica gel, which is acidic, catalyses enolisation of cyanomethyl ketones R^1CH_2CN and activates electrophilic carbonyl compounds.

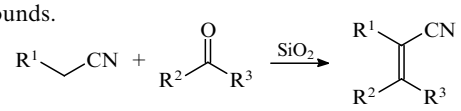

R^1	R^2	R^3	Yield (%)
L-PhCH$_2$CH(NHAc)C(=O)–	H	4-$MeOC_6H_4$	100
	H	Ph	85
	H	4-$Me_2NC_6H_4$	58
	H	4-$O_2NC_6H_4$	37
	H	2-$HO_2CC_6H_4$	97
	H	3-MeO-4-HOC_6H_3	93
	$-(CH_2)_5-$		46
	$-(CH_2)_4-$		35
	Me	Me	44
	$HOCH_2$	Me	80
	MeC(OH)H	Me	61
L-PhCH$_2$CH(NH-*N*-Ac-L-Leu)C(=O)–	H	4-$MeOC_6H_4$	98
L-PhCH$_2$CH(NH-*N*-Ac-L-Leu-D-Phe)C(=O)–	H	4-$MeOC_6H_4$	94

This reaction holds great promise in the synthesis of peptide inhibitors of α-chymotrypsin by virtue of its operational simplicity, high yields of the reaction products and the fact that it is not accompanied by epimerisation. The condensation of (*N*-acetylphenylalanyl)acetonitrile with 2-formylbenzoic acid and vanillin has demonstrated that no preliminary protection of functional groups is necessary when this reaction is performed on silica gel. These data altogether suggest that silica gel is a mild selective acidic catalyst of the Knoevenagel reaction.

In addition to peptidylacetonitriles, other compounds, such as R^1CH_2E (E = CN, CO_2Me, NO_2; R = CN, NO_2, C(O)Ph, CO_2Me, CO_2Et and SO_2Ph) containing activated methylene groups, were tested in this reaction. It was found that the reaction takes place only if compounds with E = CN and R^1 = CN, NO_2 and C(O)Ph are used; compounds with E = CO_2Me and R^1 = CO_2Me, CO_2Et and SO_2Ph do not enter into this reaction, presumably, due to steric hindrances.

The reaction of malonic acid with carbonyl compounds is an important synthetic route to the preparation of valuable unsaturated acids. α,β-Unsaturated acids are formed upon heating of the starting compounds in the presence of bases (pyridine and piperidine). The Knoevenagel condensation catalysed by SiO_2 was recommended for the synthesis of β,γ-unsaturated acids.[58] This reaction was performed under microwave irradiation without any solvent.

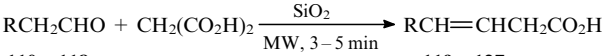

110 – 118 **119 – 127**

R = Et (**110**, **119**, 84%), Pr^n (**111**, **120**, 83%), Bu^n (**112**, **121**, 84%), n-C_5H_{11} (**113**, **122**, 84%), n-C_6H_{13} (**114**, **123**, 88%), n-C_7H_{15} (**115**, **124**, 86%), n-C_8H_{17} (**116**, **125**, 90%), Ph (**117**, **126**, 92%), Bn (**118**, **127**, 89%).

Thus the reactions of aldehydes **110**–**118** with malonic acid afforded unsaturated acids **119**–**127**. The target products are formed in high yields and are stereochemically pure. The method is distinguished by the ease of preparation and rapidity.

VII. Formylation

The Vilsmeier–Haack reaction is widely employed for the introduction of aldehyde groups into aromatic rings. Taking into account the great importance of this reaction in organic synthesis, Paul *et al*.[59] made an attempt to find optimum conditions for its performance. It was found that irradiation in a conventional microwave oven of substituted aromatic compounds and the Vilsmeier–Haack reagent ($POCl_3$–DMF) supported on silica gel affords maximum yields of the corresponding aldehydes and decreases reaction time to 1.5–2.5 min (Table 2).

The amount of the reagent is crucial for achieving maximum yields. For liquid substrates supported on silica gel, the amount of the Vilsmeier-Haack reagent may not exceed 2 equiv., whereas formylation of solid substrates requires no less than 3 equiv. The amount of silica gel pre-irradiated for 5 min at 700 W needed for the formylation also depends on the amount of the reagent. Evidence for the important role of microwave irradiation in this reaction follows from the fact that the yields of aromatic aldehydes formed upon microwave irradiation exceed significantly those obtained upon conventional heating of the reactants at the same temperature.

The use of microwave irradiation in combination with silica gel is an excellent procedure for the rapid (within 1.5–2.5 min) and quantitative Vilsmeier–Haack reaction.

Table 2. The Vilsmeier – Haack reaction.

Starting compound	Product	Yield (%)
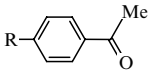	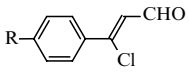	
	R = Cl	79
	R = Br	75
	R = OMe	88
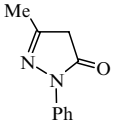	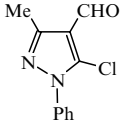	66
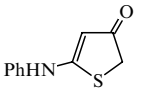	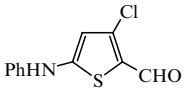	64
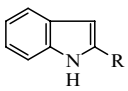	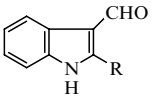	
	R = Ph	71
	R = 4-MeC$_6$H$_4$	68
	R = 4-ClC$_6$H$_4$	75
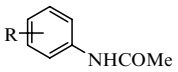	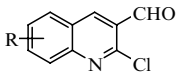	
	R = H	79
	R = 6-OMe	58
	R = 6-Me	65
	R = 8-Me	75
	R = 7-Me	68
	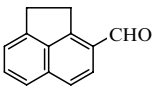	89
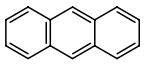	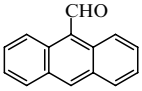	92
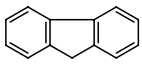	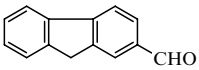	72
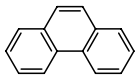	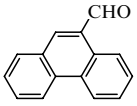	78
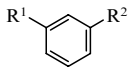	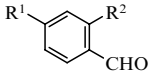	
	R^1 = R^2 = OH	81
	R^1 = R^2 = OMe	85
	R^1 = NMe$_2$, R^2 = H	78

VIII. Hydration and dehydration reactions

Dehydration of alcohols resulting in the formation of alkenes and the inverse reaction, *viz*., hydration of alkenes, are valuable synthetic conversions widely applicable in organic synthesis.

A general method for the selective anti-Markownikoff addition of water to alkenes in the presence of silica gel has been described in detail by Ranu.[60] An alkene supported on preactivated silica gel (200 °C, reduced pressure) was treated with a solution of $Zn(BH_4)_2$ in 1,2-dimethoxyethane (DME) at room temperature and then hydrolysed. This reaction gives good yields of primary and secondary alcohols (Table 3).

Table 3. Anti-Markownikoff addition of water to alkenes.

Starting compound	Product	Yield (%)
$Me(CH_2)_6CH{=}CH_2$	$Me(CH_2)_6CH_2{-}CH_2OH$	95
$Ph{-}CH{=}CH_2$	$Ph{-}CH_2{-}CH_2OH$ + $Ph{-}\underset{\displaystyle OH}{\underset{\vert}{CH}}{-}Me$ (4 : 1)	85
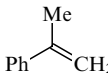	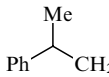	90
	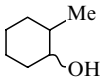	80
	cis : *trans* = 3 : 7	
	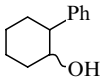	70
	cis : *trans* = 1 : 3	
	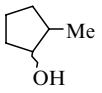	70
	cis : *trans* = 3 : 7	

The obvious advantages of this method include ease of performance, mild conditions, lack of side reactions and high yields of reaction products. The reaction mechanism is not quite clear, but the authors exclude the possibility of conventional hydroboration – oxidation.

The efficiency of silica gel in the dehydration of alcohols is determined by the acidic properties of its surface (SiO_2 is a weak Lewis acid).

Thus application of iron(III) chloride hexahydrate dissolved in a volatile solvent (methanol, ether, *etc*.) onto the surface of commercial silica gel (Kieselgel 60, Merck) and subsequent evaporation of the solvent under high vacuum (0.1 Torr) yield a catalyst for selective dehydration of tertiary, allylic and sterically hindered secondary alcohols.[61] The corresponding alkenes are obtained in quantitative yields (Table 4).

This reaction is carried out under mild conditions using ether and acetone as solvents. The content of water affects the catalytic activity: the addition of H_2O (2 mass %) to the dry catalyst changes only slightly the catalytic activity, whereas at higher water content (> 10%) the activity is completely lost.

The $FeCl_3 \cdot 6H_2O - SiO_2$ system containing 2% of water also catalyses the epoxide ring opening and certain rearrangements (see below):

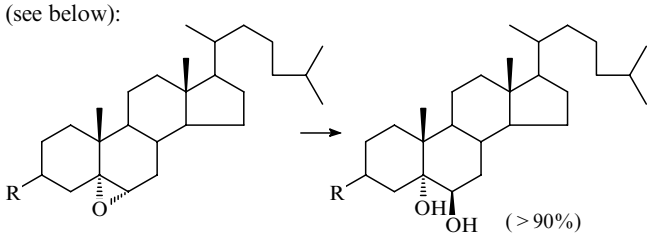

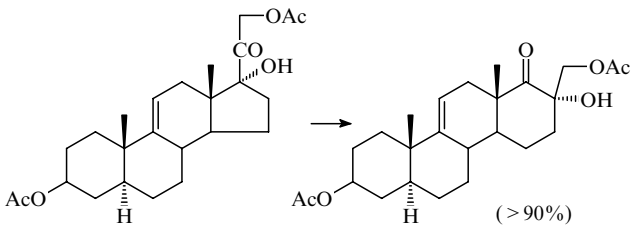

Later, the $FeCl_3 - SiO_2$ system prepared from anhydrous iron chloride by simple grinding of components was recommended for dehydration of alcohols.[62] This system proved to be efficient in

Scheme 1

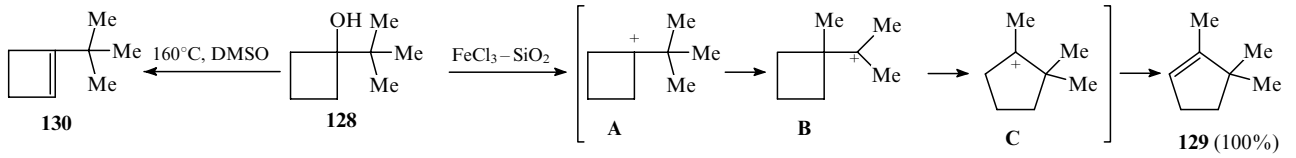

dehydration of tertiary alcohols where the yields of reaction products were quantitative.

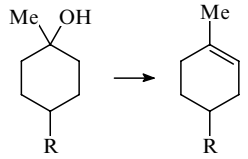

R = Me (95%), Bu^t (91%).

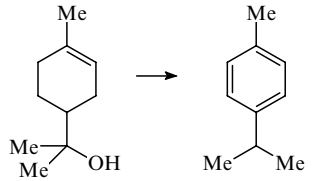

(90%)

The reaction is carried out in the absence of the solvent. 1-*tert*-Butylcyclobutan-1-ol **128** undergoes an interesting rearrangement with ring enlargement and formation of 1,5,5-trimethylcyclopentene (**129**) (Scheme 1). In this case, the dehydration occurs *via* carbocations **A**, **B** and **C**.

If the dehydration of the alcohol **128** is carried out under different conditions, *viz*., by heating in DMSO at 160 °C, compound **129** is formed in low yield (5%), while the yield of the alkene **130** reaches 95%.

Table 4. Selective dehydration of alcohols by iron(III) chloride on silica gel.

Starting compound	Product	Yield (%)
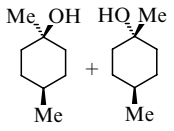	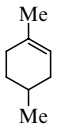	>90
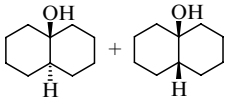	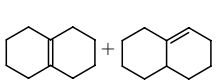	>90
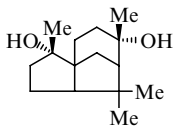	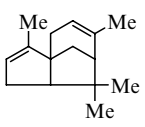	>90
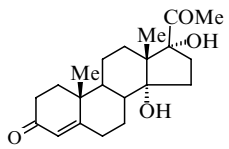	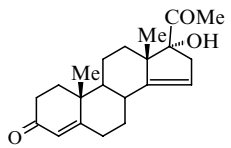	>90
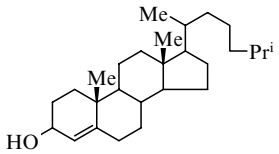	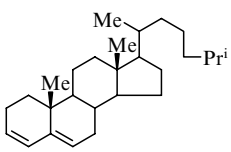	>90

The dehydration of the alcohol **131** in the presence of the $FeCl_3 - SiO_2$ system also proceeds *via* the intermediate cyclopentyl cation **132** and results in the cyclic ether **133**. The same product (**133**) is obtained in good yield upon dehydration of the alcohol **134** under identical conditions.

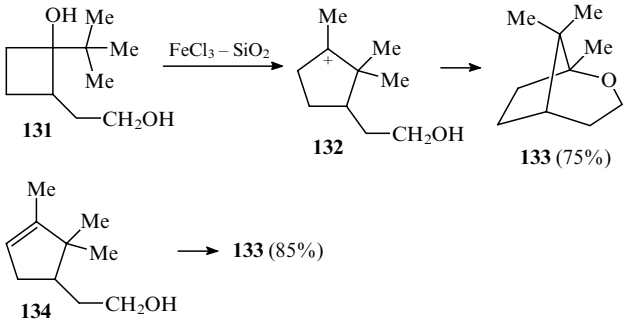

Thus, the $FeCl_3 - SiO_2$ system catalyses efficiently both dehydration reactions and rearrangements including ring enlargement. Some rearrangement products are key precursors in the synthesis of sesquiterpenoids.

Toluene-*p*-sulfonic acid supported on silica gel is an excellent catalyst in dehydration of secondary and tertiary alcohols (primary alcohols do not react under these conditions).[63] Thus alcohols **135** – **138** are converted into alkenes **139** – **142** in high yields.

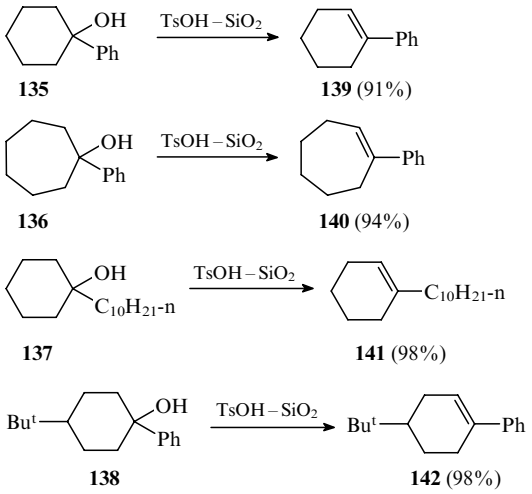

Dehydration of the alcohol **143** gave alkene **144** in somewhat lower yields under identical conditions.†

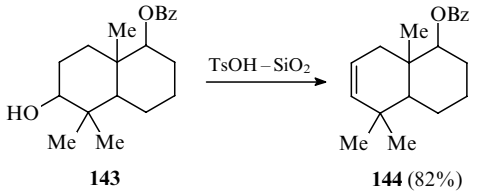

This system was also used for dehydration of 3-hydroxysteroids. The reaction occurred *via* carbocations and resulted in Δ^2-alkenes and $\Delta^{3,5}$-dienes.

† The authors' unpublished data.

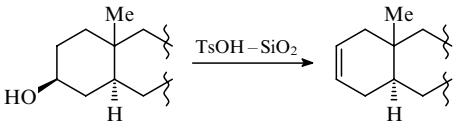

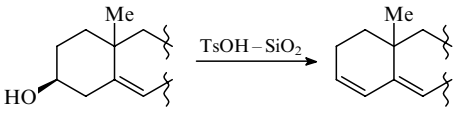

It was found [64] that silica gel-supported copper(II) sulfate is an efficient catalyst in smooth dehydration of secondary and tertiary alcohols into alkenes. The catalyst was prepared by mixing chromatographic silica gel with an aqueous solution of copper(II) sulfate with subsequent evaporation by heating at 2 Torr. The catalytic activity depended on the evaporation time and temperature and was maximum when the catalyst was dried at 200 °C for 3 h or at 240 °C for 1 h. With a further increase in the evaporation temperature (300 °C, 1 h), the catalyst lost its activity completely. The dehydration rate depended on the $SiO_2 : CuSO_4$ ratio (the optimum ratio is 4 : 1). Under these conditions, alcohols **145** – **148** are converted into alkenes **149** – **153** in high yields.

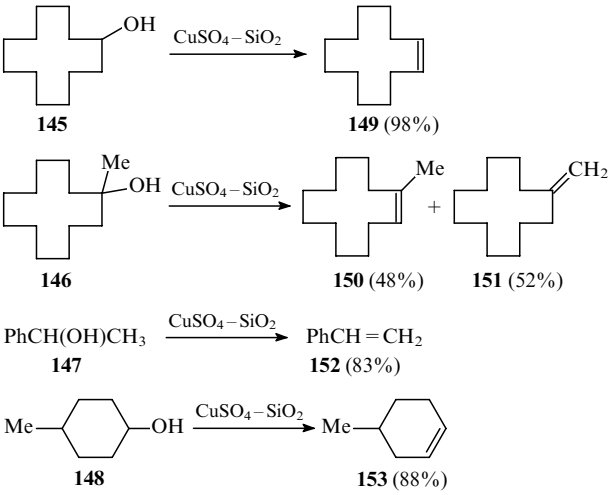

Tertiary alcohols are dehydrated more easily than secondary ones. The mechanism of this reaction is still unclear, but it is reasonable to assume the formation of carbenium cations, since dehydration rates of tertiary alcohols are higher than those of secondary and primary ones. This system can also be used for dehydration of 3-hydroxysteroids.

Special mention should be made of a detailed study [65] of dehydration of various primary, secondary and tertiary alcohols catalysed by transition metal sulfates supported on silica gel. The activities of various brands of silica gel in this reaction have been compared. The highest activity was manifested by Silica gel BW-300 (Fuji-Davidson). The catalytic activities of metal sulfates supported on silica gel decreased in the following order: Fe(III) = Ce(IV) = Ti(IV) > Sn(IV) > Al(III) > Cu(II) > Zn(II) > Co(III) > Ni(II) > Fe(II) > Mn(II) > Cd(II). The optimum conditions (time, temperature) for treatment of catalysts providing maximum yields of dehydration products have been found.[65] The effects of solvents, reagent ratios and reaction conditions on the product yields have been investigated. Some suggestions on the possible mechanism of this reaction have been put forward.

Interesting examples of the preparation of α-methylidenecarbonyl compounds from derivatives of cyclic β-(hydroxyalkyl)-vinyl ethers, β-alkylthio- and β-arylthioacroleins have been described,[66] which involved dehydration of intermediate alcohols in the presence of silica gel as one of the steps. The following catalytic systems, *viz.*, $SiO_2 - H_2O - HOOCCOOH - HgCl_2$, $SiO_2 - H_2O - HOOCCOOH$ and $SiO_2 - H_2O - H_2SO_4$ and dichloromethane as a solvent, were employed.

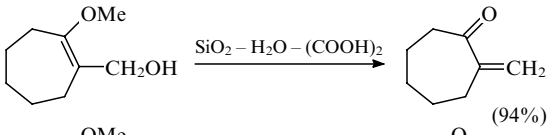

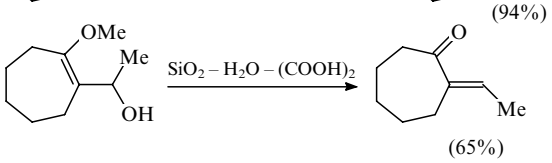

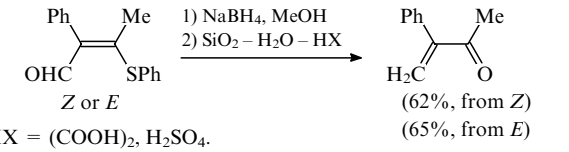

HX = $(COOH)_2$, H_2SO_4.

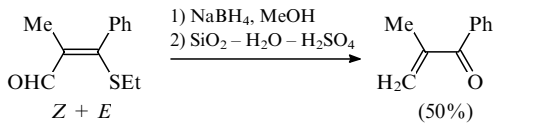

IX. Protection of functional groups

The use of silica gel as a catalyst for introduction of protective groups is a popular procedure in organic synthesis.

1. Tetrahydropyranylation of alcohols

The tetrahydropyran-2-yl group (THP) is one of the most popular groups used for the protection of alcohols and phenols. Many methods have been devised for its introduction.

It has been found [67, 68] that sulfuric acid adsorbed on silica gel can be used as a catalyst in tetrahydropyranylation of alcohols and phenols. Dichloromethane is generally used as a solvent in this reaction.

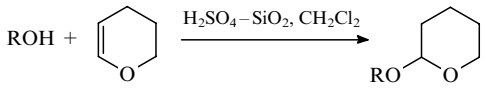

R = Ph (95%), $PhCH_2$ (96%), α-$C_{10}H_7$ (98%), $PhCH{=}CHCH_2$ (96%), $PhOCH_2\underset{|}{C}HC{\equiv}CH$ (94%).

This simple and inexpensive method gives the reaction products, as a rule, in high yields.

Recently, this reaction has been carried out [69] using microwave irradiation in the presence of the same catalyst but without solvent. This permitted one to obtain reaction products in a pure state and in high yields. The absence of solvents makes it possible to run this reaction under mild conditions. Other advantages include short reaction time (10 – 15 min), omission of the aqueous workup and environmental safety.

2. Thioacetalisation and acetalisation

Protection of carbonyl groups as acetals or thioacetals is a common procedure in the synthesis of organic compounds, in particular, of complex polyfunctional compounds. However, protic and Lewis acids and some silicon reagents [70] commonly used in (thio)acetalisation do not afford selective protection of aldehyde groups in the presence of keto groups.

Silica gel treated with thionyl chloride effects their protection. It was found that this silica gel effectively catalyses thioacetalisation ‡ of many aldehydes and ketones by 1,2-ethanedithiol or 1,3-

‡ The inverse reaction occurs upon treatment with sulfuryl chloride in the presence of wet silica gel.

propanedithiol and affords selective protection of aldehyde groups when both these groups are present simultaneously.[71]

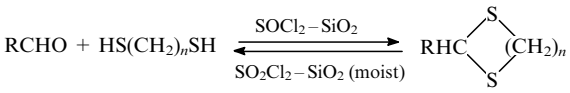

R	*n*	Yield of thioacetal (%)
C_6H_{13}	2	99
	3	99
PhCHMe	2	100
$H_2C=CH(CH_2)_8$	2	100
MeCH=CH	2	100
PhCH=CH	2	97
	3	100
Ph	2	100
	3	97
4-MeC_6H_4	2	98
4-ClC_6H_4	2	99
4-$MeOC_6H_4$	2	98
4-HOC_6H_4	2	88
4-$HO_2CC_6H_4$	2	98
4-$Me_2NC_6H_4$	2	98
2-$O_2NC_6H_4$	2	93

By itself, silica gel (without $SOCl_2$) does not manifest any noticeable catalytic activity in thioacetalisation of aldehydes. Treatment of heptanal with 1,2-ethanediol afforded the corresponding 1,3-dithiolane in as low a yield as 11%.

The reaction with ketones in benzene proceeds very slowly; however, this can be completed within 24 h in boiling toluene.

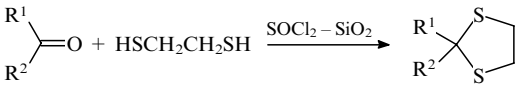

R^1	R^2	Yield (%)
Ph	Me	91
$-(CH_2)_5-$		100
$PhCH_2$	$PhCH_2$	93
Ph	Ph	31

The difference in the rates of thioacetalisation of aldehydes and ketones permits selective protection of aldehydes in the presence of ketones (Table 5) as well as selective thioacetalisation of oxo aldehydes.

Table 5. Thioacetalisation of mixtures of aldehydes and ketones in the presence of $SOCl_2-SiO_2$.

Aldehyde	Ketone	Conversion	
		aldehyde	ketone
PhCHO	PhC(O)Me	100	0
4-ClC_6H_4CHO	PhC(O)Me	96	0
$Bu^n(Et)CHCHO$	$(PhCH_2)_2C=O$	100	0
4-$MeOC_6H_4CHO$	$Bu^i_2C=O$	100	0
Ph(Me)CHCHO	PhCH=CHC(O)Me	83	0
$C_6H_{13}CHO$	PhC(O)C(O)Ph	100	0

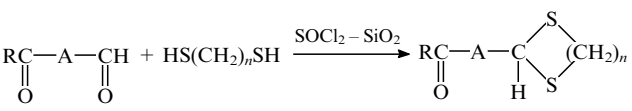

A	R	*n*	Yield (%)
$-C_6H_4-$	Me	2	90
	Me	3	99
	Ph	2	78
$-(CH_2)_3-$	Me	2	89
	Me	3	98
$-CH_2CH(Ph)CH_2-$	Me	2	98
	Me	3	99
$-CHMe-$	Ph	2	92
	Ph	3	92

All these reactions proceed with high selectivity and do not require complex equipment. The unusual chemoselectivity of this method can be attributed to the differences in spatial interactions of the aldehyde and ketone groups with the porous surface of silica gel.

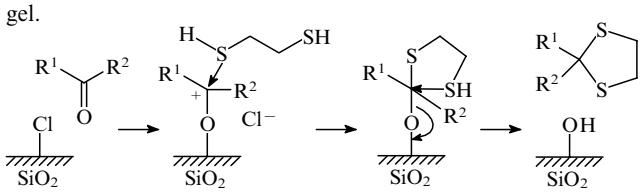

This method holds especially great promise for multistep syntheses of complex molecules.

The synthesis of thioacetals from aldehydes (or ketones) and 1,2-ethanedithiol in the presence of catalytic amounts of copper(II) trifluoromethanesulfonate supported on silica gel in the absence of solvents has been described.[72] All thioacetals were obtained in high yields.

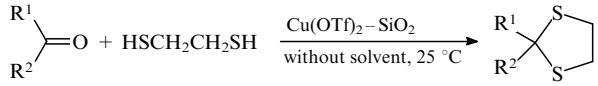

R^1	R^2	Yield (%)
n-C_6H_{13}	H	91
cyclo-C_6H_{11}	H	92
2-Furyl	H	91
2,5-$(MeO)_2C_6H_3$	H	98
PhCH=CH	H	89
2-HOC_6H_4	H	96
2-$O_2NC_6H_4$	H	93
4-ClC_6H_4	H	98
4-MeC_6H_4	H	99
4-$MeOC_6H_4$	H	99
4-HOC_6H_4	H	94
Ph	Me	92
$-CH_2CH_2CHBu^tCH_2CH_2-$		94
$-CH_2CH(CO_2Me)CH(CO_2Me)CH_2-$		93

In most cases, the reactions proceed selectively and at room temperature. This reaction can also be performed in the presence of the $CuCl_2-SiO_2$ system (in the absence of solvent), however, in this case the reaction rate and the product yields are lower.

In addition to thioacetals, cyclic acetals, which are stable in alkaline or weakly acidic media, are used to protect aldehydes and ketones in multistep syntheses.[73] The reaction of aldehydes with ethylene glycol in the presence of strong protic or Lewis acids is a common procedure for their synthesis; however, this method is characterised by low yields and long reaction time. Other methods for acetal synthesis require drastic conditions, the use of expensive or hazardous reagents, sophisticated synthetic and isolation procedures, *etc*.

An efficient method for protection of the aldehyde and ketone groups by treatment with ethylene glycol with microwave irradiation without any solvent has been developed.[74] Here, metal sulfates [$Ce(SO_4)_2$, $MgSO_4$ and $NaHSO_4$] supported on silica gel are used as catalysts.

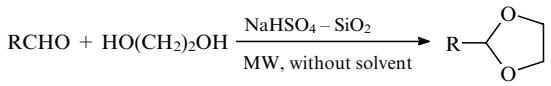

R = Ph (85%), 2-$O_2NC_6H_4$ (98%), 2-$MeOC_6H_4$ (82%), 2-ClC_6H_4 (90%), 3-NCC_6H_4 (97%), 3-$PhOC_6H_4$ (85%), 3-$BnOC_6H_4$ (81%), PhCH(CN) (90%), β-$C_{10}H_7$ (87%), 4-[PhC(O)CH_2O]C_6H_4 (75%),

PhCH=CH (81%), [X = O (94%), S (81%)],

MeCH=CH (82%), MeC(O)CH_2CH_2 (82%), n-C_6H_{13} (90%), n-$C_{10}H_{21}$ (87%), $ClCH_2CH$=CH (78%), $MeO_2C(CH_2)_4$ (85%).

This technique provides selective protection of aldehyde groups in the presence of keto groups (the latter proved to be fairly resistant to microwave irradiation).

X. Deprotection of functional groups

There is a vast body of evidence concerning the use of silica gel as a catalyst in hydrolytic reactions aimed at removal of protective (trityl, ketal, ester, *etc.*) groups.[3,21] Some examples of these reactions will be given below.

Very good yields of carbonyl compounds were obtained upon removal of the thioacetal group by boiling the dithioacetals in organic solvents with silica gel-supported copper(II) sulfate.[75]

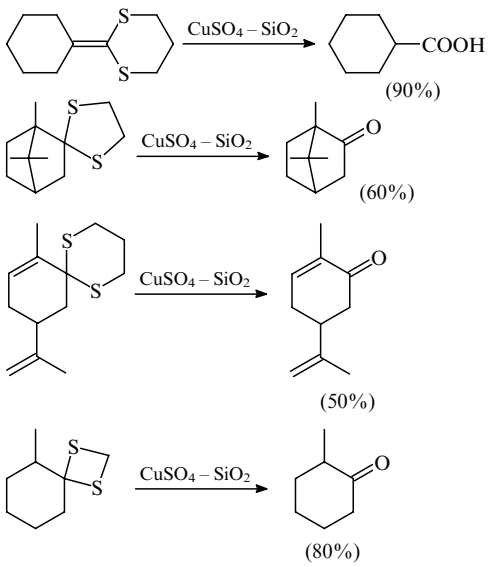

The reaction is generally completed in 2–20 h. Its mechanism is still unclear.

Many oximes are converted into the starting carbonyl compounds under the action of chromium trioxide supported on silica gel.[76] These reactions occur on heating in such solvents as toluene, benzene or ether. Mitra *et al.*[77] have proposed to use sodium bismuthate supported on moist silica gel for removal of the oxime protective group. This reaction is initiated by microwave irradiation.

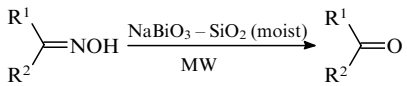

R^1	R^2	Yield (%)
Bu^i	Me	81
$-(CH_2)_5-$		73
Ph	Ph	90
$C_{10}H_7$	Me	90
Ph	Me	89
4-MeC_6H_4	Me	85
4-$MeOC_6H_4$	Me	94
4-$O_2NC_6H_4$	Me	82

This reaction is quantitative and is completed within several minutes at normal pressure.

Later, the same authors used this reagent to convert semicarbazones into the original carbonyl compounds.[78]

Hydrolysis of esters, which is usually carried out by heating in aqueous solutions of acids or bases, is one of the most common reactions in organic synthesis. These conditions can result in hydrolysis of compounds containing acid- or base-sensitive groups. Therefore, studies in this field are aimed at the search for conditions of ester hydrolysis in neutral media. An original procedure for ester hydrolysis by microwave irradiation on moist silica gel impregnated with indium triiodide has been proposed recently.[79] This approach made it possible to hydrolyse various acyclic and carbocyclic esters to the corresponding acids in high yields.

R = $PhCH_2$ (92%), n-$C_{17}H_{35}$ (70%), Ph_2CH (70%).

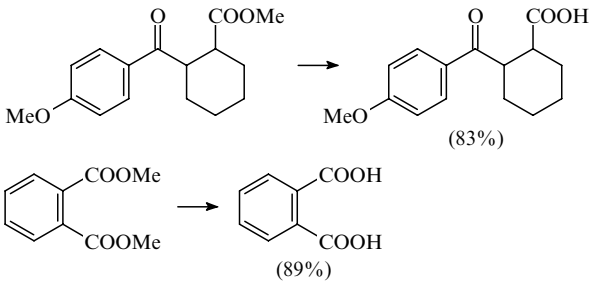

The duration of this reaction was 25–80 min. This reaction proceeded smoothly even in the case of sterically hindered esters and diesters. Mild reaction conditions make this reaction suitable for hydrolysis of compounds containing additional functional groups, *e.g.*, keto and hydroxy groups, as well as C=C bonds.

XI. Miscellaneous reactions

Among other reactions, we shall consider the Nef, Ritter, Wittig and Prins reactions as well as acylation, substitution, halogenation and ring-opening reactions. These types of conversions will be outlined below.

1. The Nef reaction

The use of silica gel in the Nef reaction has been described.[80] Nitroalkanes were converted into the corresponding carbonyl compounds in high yields by treatment with sodium percarbonate in the presence of silica gel in aqueous DMF (40 °C, 1 h).

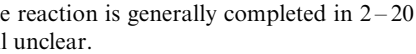

R^1	R^2	Yield (%)
$-(CH_2)_4-$		73
$-(CH_2)_5-$		68
n-C_5H_{11}	H	65
$PhCH_2$	Me	81

In the absence of silica gel, the reaction proceeds at a slow rate (12–15 h). If sodium carbonate is used instead of percarbonate, the reaction does not take place.

2. The Ritter reaction

The Ritter reaction of benzyl alcohols with nitriles initiated by iron(III) chloride supported on silica gel results in the corresponding amides in high yields.[81]

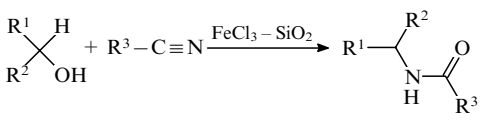

R^1	R^2	R^3	Yield (%)
Ph	Ph	Me	94
Ph	Me	Me	95
Ph	Ph	$PhCH_2$	92
4-$MeOC_6H_4$	H	Me	80
4-ClC_6H_4	H	$ClCH_2$	91
4-$O_2NC_6H_4$	H	Ph	–

This reagent has a number of advantages over concentrated sulfuric acid commonly used in this reaction; it is non-hygroscopic and does not require any special precautions. All reactions were conducted under solvolytic conditions using nitrile as a solvent. The iron salt and the substrate were used in equimolar amounts. *p*-Nitrobenzyl alcohol does not enter into the reaction under these conditions.

3. The Wittig reaction

The Wittig reaction with the use of silica gel[82] allows one to selectively synthesise α,β-unsaturated carbonyl compounds in high yields from stable phosphorylides and aldehydes. Thus irradiation of mixtures of ethoxycarbonylmethylidenetriphenylphosphorane with aldehydes in a microwave oven in the presence of silica gel yielded esters of the corresponding α,β-unsaturated carboxylic acids.

$$RCHO + Ph_3\overset{+}{P}-\overset{-}{C}HCOOMe \xrightarrow[n\text{-}C_6H_{14},\ MW]{SiO_2} RCH{=}CHCOOMe$$

R = Pr^n (87%), Bu^t (78%), cyclo-C_6H_{11} (90%), $MeOCH_2$ (85%).

The use of silica gel not only accelerates the reaction, but also promotes the separation of the triphenylphosphine oxide formed. As a result, target products are formed in high yields and do not contain admixtures. In addition to aldehydes, ketones can also be involved in the reaction.

4. The Prins reaction

The Prins reaction, which includes condensation of alkenes with aldehydes (usually, formaldehyde), affords 1,3-diol derivatives. This reaction is catalysed by mineral acids, soft Lewis acids and solid catalysts, such as ion-exchange resins, zeolites and clays (montmorillonite K-10).

Recently, the Prins reaction has been carried out with microwave irradiation under solvent-free conditions using $TaCl_5$ supported on silica gel as a catalyst.[83] Under these conditions, alkenes were converted into 1,3-diol derivatives in high yields.

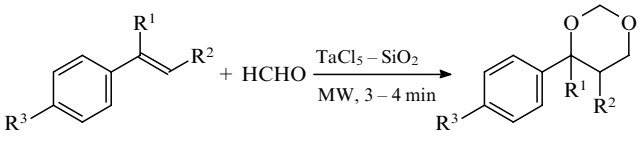

R^1	R^2	R^3	Yield (%)
H	H	H	90
Me	H	H	88
H	Me	H	86
H	H	Me	88
H	H	Cl	85
H	H	NO_2	80
H	Me	Me	90
H	Ph	H	85

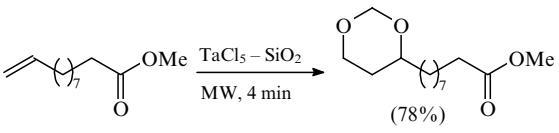

These reactions are usually completed within 3–4 min, whereas under conventional conditions (in dioxane) it takes 10–13 h and the yields do not exceed 80%.

5. Substitution reactions

Thioamides were converted into the corresponding amides under mild conditions by treatment with Caro's acid (peroxymonosulfuric acid) supported on silica gel. The reaction was carried out in acetonitrile at room temperature in air.[84]

$$R^1C(S)NHR^2 \xrightarrow{H_2SO_5-SiO_2} R^1C(O)NHR^2$$

R^1	R^2	Yield (%)
Ph	CH_2Ph	84
4-$O_2NC_6H_4$	CH_2Ph	76
Ph	Bu^n	82
Me	C_6H_4Me	87

This reaction is operationally simple. However, it is not suitable for conversion of primary thioamides which yield a mixture of products difficult to identify. Despite this limitation, Caro's acid supported on silica gel allows mild conversion of secondary and tertiary thioamides into amides in the yields comparable and sometimes exceeding those described previously. This reaction is successfully employed in the chemistry of thio analogues of nucleic acids and nucleosides.[85]

6. Synthesis of nitriles from aldehydes

Nitriles are used as starting components in the synthesis of many biologically active compounds; therefore, elaboration of effective methods of their synthesis is a topical problem. The conversion of aldehydes into the corresponding nitriles represents an important transformation of functional groups. A simple and efficient procedure for the synthesis of nitriles from aldehydes and hydroxylamine using microwave irradiation in the presence of $NaHSO_4$ supported on silica gel has been described.[86]

$$RCHO \xrightarrow[NaHSO_4-SiO_2,\ MW]{NH_2OH-HCl} RCN$$

R = Ph (84%), 4-HOC_6H_4 (90%), 4-$MeOC_6H_4$ (91%), 3-Me-4-HOC_6H_3 (96%), 3-HOC_6H_4 (91%), 3,4-$(MeO)_2C_6H_3$ (97%), 3,4-$(CH_2O_2)C_6H_3$ (95%), PhCH=CH (85%), n-C_7H_{15} (81%), n-C_8H_{17} (80%).

This reaction proceeds very fast (1–3 min) and final products are formed in high yields. Presumably, the aldehyde is converted into the corresponding aldoxime which is immediately dehydrated to yield the nitrile.

7. Acylation, alkylation and esterification

The use of solid adsorbents in organic synthesis provides high selectivity in many chemical reactions including alkylation, acylation, esterification, *etc*. The most essential feature of these reactions is that they can be applied for selective protection of one functional group in bi- and polyfunctional compounds. Thus acetylation of a series of symmetrical 1,*n*-diols adsorbed on silica gel (Wako gel C-200, Wako Pure Chemical Industries) by heating with acetyl chloride in cyclohexane resulted in monoacetyl derivatives in quantitative yields.[87]

$$HO(CH_2)_nOH \xrightarrow[2\text{ h, boiling}]{AcCl,\ cyclo\text{-}C_6H_{12}} AcO(CH_2)_nOH$$

n	Yield on SiO_2 (%)		Yield in the homogeneous reaction (%)
	mono	bis	
4	99.5	0	52.3
6	99.5	0	58.6
8	99.8	0	54.3
10	99.8	0	56.5
12	99.0	1.0	66.5
16	99.9	0	30.2

n	Yield on SiO_2 (%)		Yield in the homogeneous reaction (%)
	mono	bis	
HO—⬡—OH	29.9	40.8	32.6
$HOCH_2$—⬡—CH_2OH	36.0	47.5	52.5

Under identical conditions, cyclic diols [cyclohexane-1,4-diol and 1,4-bis(hydroxymethyl)benzene] yield predominantly diol diacetates. The dependence of reaction selectivity on temperature was studied in the example of cyclohexane-1,4-diol; the yields of monoacetylated and bisacetylated products at 80 °C were 29.9% and 40.8% and at 0 °C, 52.4% and 19.3%.

The silica gel used in this reaction seems to play a protective role for one of hydroxy groups of the diol which is adsorbed on the silica gel surface. It is thought that the diol is adsorbed on the surface of silica gel resulting in the formation of a monomolecular layer, which has been demonstrated in the methylation of alcohols (1-decanol, geraniol and cyclohexanol), phenol, α- and β-naphthols, 2,6-di-*tert*-butylphenol, *etc*., by diazomethane.[88] Presumably,[88] it is alcohols (in the form of alkoxides) adsorbed on the surface of SiO_2 that enter into the reaction. This reaction does not take place in the absence of silica gel. Ogawa *et al*.[88] determined the maximum amount of the alcohol adsorbed on silica gel beyond which the reaction rate does not change further. For 1-decanol, it was equal to 4 mmol g^{-1} SiO_2, which corresponds to the formation of a monomolecular layer of the alcohol molecules on the surface of silica gel. It was found that 2,6-di-*tert*-butylphenol, which cannot be adsorbed on the surface of SiO_2 due to steric hindrances, is not methylated under these conditions.

An alternative procedure[89] for selective monoacylation of diols by reaction with esters (ethyl acetate, ethyl formate, methyl propionate, methyl isobutyrate) has been developed;[89] this reaction is catalysed by metal sulfates [$NaHSO_4$, $Ce(SO_4)_2$] supported on chromatographic silica gel. This method was used to prepare monoesters of ethylene glycol, butane-1,4-diol, pentane-1,5-diol and hexane-1,6- and -2,5-diols.

The reaction occurs in the presence of hexane at the controllable hexane : ester ratio of ~1 : 4. The yields of monoesters decrease with the increase in this ratio. This phenomenon is attributed to the effect of solvent polarity on the adsorption of alcohols and esters. With the above ratio, only alcohols are adsorbed, which are more polar than the monoesters.

A selective procedure for esterification of aliphatic carboxylic acids in the presence of aromatic acids has been developed;[90] an interesting example of selective esterification of dicarboxylic acid **154** into the monoester **155** has been described.

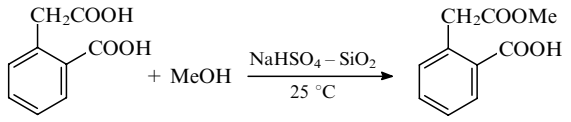

154 **155** (96%)

8. Halogenation of aromatic compounds

Preparation of novel effective reagents for electrophilic chlorination of aromatic compounds has been described.[91] It was found that many chlorine-containing organic compounds acquire strong electrophilic properties in the presence of silica gel, although they differ substantially in reactivities. The systems based on *N*,*N*-dichlorourethane, dichloramine-T and *tert*-butyl hypochlorite appeared to be the most active. They quantitatively chlorinate aromatic compounds under controlled conditions. The *tert*-butyl hypochlorite – chromatographic silica gel (BDH) system proved to be very convenient for monochlorination of some aromatic compounds.[91] In some cases, the yields of *ortho*- and *para*-chlorinated derivatives reached 100%.

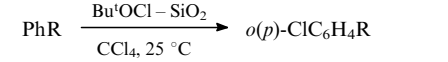

R	Yield (%)	*ortho* : *para* Ratio
Me	100	65 : 35
Et	86	57 : 43
Pr^i	100	44 : 56
Bu^t	70	15 : 85
OMe	100	30 : 70
Ph	70	56 : 44

This reaction has significant advantages over classical electrophilic chlorination reactions involving chlorine and sulfuryl chloride and is characterised by high yields, ease of isolation of reaction products and the absence of HCl. The nature of silica gel is very important for the successful implementation of this reaction. Satisfactory results were obtained exclusively with strongly acidic (pH < 5) chromatographic silica gel dried at 120 °C. The dichlorourethane – silica gel system in acetonitrile was used for chlorination of benzene and the dichloramine – silica gel system in carbon tetrachloride was used for chlorination of toluene.

The addition of silica gel to *N*-bromosuccinimide in carbon tetrachloride resulted in a catalytic system, which allows selective monobromination (presumably, in the *para*-position) of some alkoxybenzenes.[92]

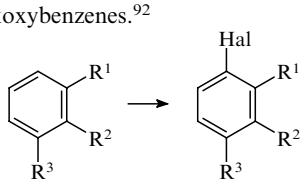

R^1	R^2	R^3	Yield (%)
OMe	H	OMe	99
OMe	OMe	H	98
Me	H	OMe	87
Pr^i	H	OMe	78
Et	H	OMe	90
H	H	OMe	90
H	H	OEt	96

Thus bromination of *m*-alkylmethoxybenzenes (Alk = Me, Et, Pr^i) occurs exclusively in the *para*-position relative to the methoxy group. 4-Bromo-3-*tert*-butyl-1-methoxybenzene is the major product even in the case of *m*-(*tert*-butyl)methoxybenzene. Quite unexpectedly, the ratio of 4-Br- to 6-Br-derivatives was found to be equal to 74 : 26, considering the large size of the *tert*-butyl substituent (bromination of this compound in the presence of Fe-catalysts yields exclusively the 6-Br derivative). The rate of this reaction strongly depends on the amount of silica gel and the mixing rate; this points to the heterogenous character of the reaction. No bromination occurs in the absence of silica gel. Many types of silica gels manifest catalytic activities in this reaction; noteworthy, acidic silica gels are more reactive, whereas neutral and basic ones are more selective. The acidic chromatographic silica gel Microbead 3A (Fuji – Davidson) exhibited the highest efficiency. Availability of the commercial reagent, ease of performance, excellent yields of reaction products and the absence of hydrogen bromide make this method especially attractive.[92]

This reagent has been used in previous studies for the bromination of indoles and benzoimidazoles.[93]

9. Ring opening

A convenient method for the synthesis of high-boiling alkenes (b.p. = 250 °C) from β-lactones by heating the latter in benzene or cyclohexane in the presence of chromatographic silica gel has been proposed.[94]

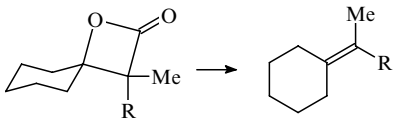

R = H (90%), Me (88%), CO_2Et (97%), CH_2OH (77%).

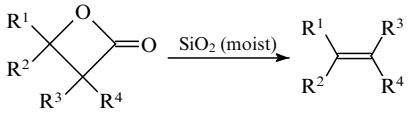

R^1	R^2	R^3	R^4	Yield (%)
Me	$Ph(CH_2)_2$	Me	Me	95
Me	$SiMe_2Bu^t$	H	H	93
Me	cyclo-C_6H_{11}	Me	H	95
Pr^i	H	n-C_7H_{15}	H	75

Distillation of lactones over moist silica gel is the best procedure for the preparation of alkenes with b.ps < 200 °C.[95] Silica gel was used to accelerate the decarboxylation of β-lactones; this is an excellent procedure for stereoselective synthesis of alkenes. Anhydrous silica gel fire-dried *in vacuo* is not always suitable for decarboxylation, since this may cause isomerisation of alkenes formed. In the above-described experiments, silica gel was used in the amount of 10 mass %, since the amount of water released in the course of distillation decreases with the silica gel dose.

Zinc borohydride supported on silica gel proved to be a convenient reagent for the regio- and stereoselective opening of epoxides.[96] The least substituted alcohols are prepared by *anti*-opening of the rings.

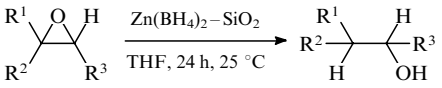

R^1	R^2	R^3	Yield (%)
n-C_7H_{15}	H	H	88
$ClCH_2$	H	H	85
Ph	H	H	90
Ph	Me	H	91
Ph	H	Ph	88

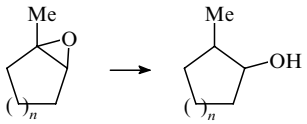

n = 1 (84%), 2 (85%).

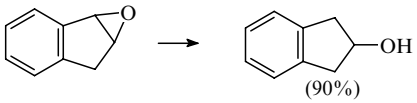

The main advantages of this method include high regioselectivity of epoxide opening, low toxicity and availability of the reagents.

References

1. R K Iler, in *The Chemistry of Silica* (New York: Wiley, 1979) p. 462
2. J G Vail *Soluble Silicates (ACS Monograph Ser.)* Vols 1, 2 (New York: Reinhold, 1952)
3. V A Basyuk *Usp. Khim.* **64** 1073 (1995) [*Russ. Chem. Rev.* **64** 1003 (1995)]
4. G Bringmann *Angew. Chem., Int. Ed. Engl.* **21** 200 (1982)
5. A J Birch, P Fitton, D C C Smith, D E Steere, A R Stelfox *J. Chem. Soc.* 2209 (1963)
6. D Liotta, W Ott *Synth. Commun.* **17** 1655 (1987)
7. T Hasegawa, J Moribe, M Yoshioka *Bull. Chem. Soc. Jpn.* **61** 1437 (1988)
8. T Hasegawa, H Aoyama, Y Omote *J. Chem. Soc., Perkin Trans. 1* 963 (1979)
9. T Hasegawa, H Aoyama, Y Omote *J. Chem. Soc., Perkin Trans. 1* 2054 (1976)
10. M Kawase, A K Sinhababu, R T Borchardt *J. Heterocycl. Chem.* **24** 1499 (1987)
11. A D Batcho, W Leimguber *Org. Synth.* **63** 214 (1985)
12. J Harley-Mason *J. Chem. Soc.* 200 (1953)
13. A K Sinhababu, R T Borchardt *J. Org. Chem.* **48** 3347 (1983)
14. F He, Y Bo, J D Altom, E J Corey *J. Am. Chem. Soc.* **121** 6771 (1999)
15. D Schinzer, M Kalesse, J Kabbara *Tetrahedron Lett.* **29** 5241 (1988)
16. D Schinzer, M Kalesse *Synlett* 34 (1989)
17. B B Snider *Acc. Chem. Res.* **13** 426 (1980)
18. J A Marshall, N H Andersen, P C Johnson *J. Org. Chem.* **35** 186 (1970)
19. N H Andersen, D W Ladner *Synth. Commun.* **8** 449 (1978)
20. J A Marshall *Synthesis* 517 (1972)
21. A McKillop, D W Young *Synthesis* 401 (1979)
22. W G Dauben, R T Hendricks *Tetrahedron Lett.* **33** 603 (1992)
23. B B Snider, M Karras, R T Price, D J Rodini *J. Org. Chem.* **47** 4538 (1982)
24. L F Tietze, U Beifuss *Tetrahedron Lett.* **27** 1767 (1986)
25. L F Tietze, U Beifuss *Liebigs Ann. Chem.* 321 (1988)
26. B B Snider, D J Rodini, M Karras, T C Kirk, E A Deutsch, R Cordova, R T Price *Tetrahedron* **37** 3927 (1981)
27. S Sakane, K Maruoka, H Yamamoto *Tetrahedron* **42** 2203 (1986)
28. S Tsuboi, H Fujita, K Muranaka, K Seko, A Takeda *Chem. Lett.* 1909 (1982)
29. S Nagumo, T Hisano, Y-I Kakimoto, N Kawahara, M Ono, T Furukawa, S Takeda, H Akita *Tetrahedron Lett.* **39** 8109 (1998)
30. A Bladé-Font *Tetrahedron Lett.* **21** 2443 (1980)
31. D L J Clive, V Farina, A Singh, C K Wong, W A Kiel, S M Menchen *J. Org. Chem.* **45** 2120 (1980)
32. J E Baldwin *J. Chem. Soc., Chem. Commun.* 734 (1976)
33. V V Vesselovsky, A S Gybin, A V Lozanova, A M Moiseenkov, W A Smit, R Caple *Tetrahedron Lett.* **29** 175 (1988)
34. V V Veselovsky, A S Gybin, A V Lozanova, A M Moiseenkov, W A Smit *Izv. Akad. Nauk SSSR, Ser. Khim.* 107 (1990) [a]
35. M Conrads, J Mattay *Chem. Ber.* **124** 1425 (1991)
36. G H Posner, J-C Carry, J K Lee, D S Bull, H Dai *Tetrahedron Lett.* **35** 1321 (1994)
37. B C Ranu, A Hajra, U Jana *Tetrahedron Lett.* **41** 531 (2000)
38. B C Ranu, A Hajra, U Jana *Synlett* 75 (2000)
39. M Hasegawa, T Takabatake *Synthesis* 938 (1985)
40. N Viswanathan, A R Sidhaye *Tetrahedron Lett.* 5025 (1979)
41. J A Donnelly, S O'Brien, J O'Grady *J. Chem. Soc., Perkin Trans. 1* 1674 (1974)
42. J F W Keana, T D Lee *J. Am. Chem. Soc.* **97** 1273 (1975)
43. L Boisvert, P Brassard *Tetrahedron Lett.* **24** 2453 (1983)
44. A K Banerjee, V E Khalil, W Vera *Synth. Commun.* **30** 4375 (2000)
45. F M Moghaddam, M Ghaffarzadeh, S H Abdi-Oskoui *J. Chem. Res. (S)* 570 (1999)
46. A K Sinhababu, R T Borchardt *Tetrahedron Lett.* **24** 227 (1983)
47. S-I Gohzu, M Tada *Chem. Lett.* 61 (1986)
48. B C Ranu, A R Das *J. Org. Chem.* **56** 4796 (1991)
49. B C Ranu, A Majee, A Sakhar *J. Org. Chem.* **63** 370 (1998)
50. S Yakabe, M Hirano, T Morimoto *Synth. Commun.* **29** 295 (1999)
51. M M Heravi, D Ajami, K Tabar-Heydar *Synth. Commun.* **29** 163 (1999)
52. J J Lee, J A Lee, S Y Sohn *Synth. Commun.* **26** 543 (1996)
53. M M Hashemi, Y A Bni *J. Chem. Res. (S)* 138 (1998)
54. M M Heravi, D Ajami, K Tabar-Heydar *Synth. Commun.* **29** 1009 (1999)
55. M M Hashemi, F Kalantari *Synth. Commun.* **30** 1857 (2000)
56. H Firouzabadi, M Abbasi *Synth. Commun.* **29** 1485 (1999)
57. D Brillon, G Sauvé *J. Org. Chem.* **57** 1838 (1992)
58. H M Sampath Kumar, B V Subba Reddy, E Jagan Reddy, J S Yadav *Tetrahedron Lett.* **40** 2401 (1999)
59. S Paul, M Gupta, R Gupta *Synlett* 1115 (2000)
60. B C Ranu *Synlett* 885 (1993)
61. E Keinan, Y Mazur *J. Org. Chem.* **43** 1020 (1978)

62. A Fadel, J Salaün *Tetrahedron* **41** 413 (1985)
63. F D'Onofrio, A Scettri *Synthesis* 1159 (1985)
64. T Nishiguchi, N Machida, E Yamamoto *Tetrahedron Lett*. **28** 4565 (1987)
65. T Nishiguchi, C Kamio *J. Chem. Soc., Perkin Trans. 1* 707 (1989)
66. M Pellet, F Huet *Tetrahedron* **44** 4463 (1988)
67. F Chavez, R Gadinez *Synth. Commun*. **22** 159 (1992)
68. M M Heravi, M A Bigdebi, N Nahid, D Ajami *Indian J. Chem*. **38B** 1285 (1999)
69. M M Heravi, D Ajami, M Ghassemzadeh *Synth. Commun*. **29** 1013 (1999)
70. T W Greene, P G M Wuts *Protective Groups in Organic Synthesis* (New York: Wiley, 1973)
71. Y Kamitori, M Hojo, R Masuda, T Kimura, T Yoshida *J. Org. Chem*. **51** 1427 (1986)
72. R V Anand, P Saravanan, V K Singh *Synlett* 415 (1999)
73. P J Kocienski *Protecting Groups* (Stuttgart: Thieme, 1994)
74. J S Yadav, B V Subba Reddy, R Srinivas, T Ramalingam *Synlett* 701 (2000)
75. G M Caballero, E G Gros *J. Chem. Res. (S)* 320 (1989)
76. P M Bendale, B M Khadilkar *Synth. Commun*. **30** 665 (2000)
77. A K Mitra, A De, N Karchaudhuri *Synlett* 1345 (1998)
78. A K Mitra, A De, N Karchaudhuri *J. Chem. Res. (S)* 320 (1999)
79. B C Ranu, P Dutta, A Sarkar *Synth. Commun*. **30** 4167 (2000)
80. C Narayana, N K Reddy, G W Kabalka *Synth. Commun*. **22** 2587 (1992)
81. F Salehi, A R Motlagh *Synth. Commun*. **30** 671 (2000)
82. V J Patil, U Mävers *Tetrahedron Lett*. **37** 1281 (1996)
83. S Chandrasekhar, B V Subba Reddy *Synlett* 851 (1998)
84. B Movassagh, M M Lakouraj, K Ghodrati *Synth. Commun*. **30** 2353 (2000)
85. R H Hall *The Modified Nucleosides in Nucleic Acids* (New York; London: Columbia University Press, 1971)
86. B Das, P Madhusudhan, B Venkataiah *Synlett* 1569 (1999)
87. H Ogawa, M Amano, T Chihara *J. Chem. Soc., Chem. Commun*. 495 (1998)
88. H Ogawa, T Hagiwara, T Chihara, S Teratani, K Taya *Bull. Chem. Soc. Jpn*. **60** 627 (1987)
89. T Nishiguchi, H Taya *J. Am. Chem. Soc*. **111** 9102 (1989)
90. B Das, B Venkataiah, P Madhusudhan *Synlett* 59 (2000)
91. K Smith, M Butters, W E Paget *Synthesis* 1155 (1985)
92. H Konishi, K Aritomi, T Okano, J Kiji *Bull. Chem. Soc. Jpn*. **62** 591 (1989)
93. A G Mistry, K Smith, M R Bye *Tetrahedron Lett*. **27** 1051 (1986)
94. R L Danheiser, J S Nowick *J. Org. Chem*. **56** 1176 (1991)
95. W Adam, L A A Encarnacion *Synthesis* 388 (1979)
96. B C Ranu, A R Das *J. Chem. Soc., Chem. Commun*. 1334 (1990)

[a] — *Russ. Chem. Bull., Int. Ed. (Engl. Transl.)*

Russian Chemical Reviews **70** (12) 991 – 1016 (2001) © 2001 Russian Academy of Sciences and Turpion Ltd

DOI 10.1070/RC2001v070n12ABEH000633

Organic molecules with abnormal geometric parameters

I V Komarov

Contents

I.	Introduction	991
II.	Stability of strained molecules	992
III.	Abnormally long and short C – C bonds	993
IV.	Elongated and shortened C = C bonds	995
V.	Variations of the triple carbon – carbon bond lengths in organic compounds	995
VI.	Distortions of bond angles at the tetrahedral carbon atom	996
VII.	Distortions of bond and torsion angles at the double bond in alkenes	1001
VIII.	Distortions of the bond and torsion angles in the molecules of aromatic compounds	1005
IX.	Distortions of cumulated double bonds	1008
X.	Bending of the $X^1-C\equiv C-X^2$ fragment	1010

Abstract. Organic molecules, the structural parameters of which (carbon – carbon bond lengths, bond and torsion angles) differ appreciably from the typical most frequently encountered values, are discussed. Using many examples of 'record-breaking' molecules, the limits of structural distortions in carbon compounds and their unusual chemical properties are demonstrated. Particular attention is devoted to strained compounds not yet synthesised whose properties have been predicted using quantum-chemical calculations. Factors that ensure the stability of such compounds are outlined. The bibliography includes 358 references.

I. Introduction

The experimentally determined lengths of carbon – carbon bonds of one type in the molecules of various organic compounds are usually very close. Thus the lengths of single and multiple carbon – carbon bonds usually deviate only slightly (as a rule, by less than 0.01 – 0.02 Å) from the values obtained by averaging over a large number of experimentally determined bond lengths. These values are often referred to as 'typical' or 'standard' geometric parameters. Some standard lengths of carbon – carbon bonds determined by X-ray diffraction analysis are listed in Table 1.[1–4] The same is true, although to a lesser extent (due to the smaller values of the corresponding force constants), for the bond angles the departure of which from the standard values is normally several degrees. The torsion angles usually vary over broader limits than bond angles; however, in some cases, in particular, for fragments with multiple bonds, these angles are also characteristic parameters.

The standard molecular geometric parameters are fundamental values used in stereochemistry.[5] The invariance of these parameters underlies various types of molecular models and various methods for structure calculation, in particular, molecular mechanics methods.[6]

I V Komarov Department of Chemistry, Taras Shevchenko Kiev National University, ul. Vladimirskaya 64, 01033 Kiev, Ukraine.
Fax (7-38 044) 226 12 73. E-mail: ik214@mail:yahoo.com

Received 26 October 2000
Uspekhi Khimii **70** (12) 1123 – 1151 (2001); translated by Z P Bobkova

Table 1. Typical (averaged) lengths of some carbon – carbon bonds.

Type of bond	Length /Å
Single bond	
$C(sp^3)-C(sp^3)$	1.53
$C(sp^3)-C(sp^2)$	1.51
$C(sp^3)-C(sp)$	1.47
$C(sp^2)-C(sp^2)$	1.48
$C(sp)-C(sp)$	1.38
Double bond	
$C(sp^2)=C(sp^2)$	1.32
$C(sp^2)=C(sp)$	1.31
$C(sp)=C(sp)$	1.28
Triple bond [a]	
$C(sp)\equiv C(sp)$	1.186

[a] The data of Ref. 4.

Meanwhile, in the molecules of some compounds, the bond (or torsion) angles and the bond lengths sharply deviate from the typical values. The synthesis of such compounds is often stimulated by a chemist's desire to overstep the limits of the existing theoretical views and concepts. A vivid example is the synthesis of four- and three-membered carbocyclic compounds performed successfully by W H Perkin at the end of the XIX century,[7,8] despite the opinion of scholars of authority in those days who considered the synthesis of small rings to be impossible.[9]

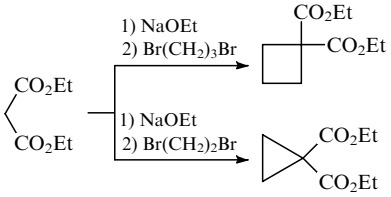

A different tendency has been observed in recent years: one can name a number of compounds with appreciably distorted molecular geometry the successful synthesis of which was pre-

ceded by theoretical predictions of their possible existence and calculations of their spectral properties. In any case, synthesis and study of these compounds were favourable for the accumulation of knowledge on the nature of the chemical bond and mechanistic details for reactions of organic compounds.[10] Research along this line has resulted in the development of new original methods of synthesis and experimental techniques which made an invaluable contribution to modern synthetic organic chemistry.[11,12] The non-trivial syntheses of highly deformed molecules, together with many total syntheses of natural compounds,[13] can be regarded as classical achievements of modern chemical science.

What properties are inherent in substances the molecules of which have highly distorted bond lengths and angles? What is the degree of distortion of the molecular geometry of organic compounds that results in a qualitative (discontinuous) change in their properties? What is the maximum attainable degree of distortion of bond lengths and bond (torsion) angles and do calculations reproduce the observed structural characteristics? In this review, we consider the recent publications concerned with these problems.†

The literature on the synthesis and structural studies of compounds with distorted geometric parameters of molecules is very extensive. This review does not claim to be an exhaustive analysis of all these studies; the author's goal was to illustrate the limits of the possible geometric distortions of organic molecules using a number of interesting examples. Among the vast material, studies devoted to 'record-holder' molecules with the greatest distortions of bond lengths and bond and torsion angles either observed experimentally or calculated are discussed. However, structural chemistry is so rapidly developing that any unusual molecule soon loses the record-breaker title.[18]

The review discusses compounds the molecules of which are stable despite substantial distortions of the molecular geometry. The structures of these compounds are studied by physical methods, most often by X-ray diffraction analysis. Therefore, first, it is pertinent to discuss the specific features of the structures of strained molecules which allow them to reach the stability needed to study them by physical methods.

II. Stability of strained molecules

Organic molecules with abnormal geometric parameters possess increased energy. A usual quantitative characteristic of these molecules is strain energy, which is defined as the difference between the experimental standard enthalpy of formation of the molecule and the enthalpy calculated for the 'strainless' (often hypothetical) molecule containing the same number of atoms and the same sequence of bonds between them but no distortion of bond lengths or bond angles and no non-valence intramolecular interactions (for example, steric repulsion).[19] The concept of molecular strain is widely used in chemistry, although it is not exact because the calculation schemes for the enthalpies of formation of strain-free molecules are arbitrary and often different.[20] Therefore, when comparing strain energies, one has to be sure that they have been calculated by the same methods. Normally, calculations involve summation of the strain increments known for the structural fragments present in the molecule.[19]

Molecules for which this enthalpy difference is great are referred to as strained. It should be noted that the criteria for regarding one or another structure as strained are quite arbitrary. Even the adamantane molecule with a strain energy of 7.6 kcal mol^{-1} can be regarded as 'strained', although its molecular model seems misleadingly unstrained.[14,15] We shall discuss molecules with strain energies many times exceeding that of adamantane. Such molecules are often reactive and susceptible to intra- and intermolecular reactions which are not typical of strainless analogues. The combination of these properties is associated with the qualitative notion of 'instability', while the factors due to which the chemical transformations of strained molecules can be retarded or entirely avoided are associated with 'stability' of the molecules.

Most highly strained 'record-breaker' compounds known to date exist owing to kinetic stability. Despite the substantial strain energy of the molecules of these compounds, their structures correspond to minima on potential energy surfaces (PES),[21] indicating the possibility of preventing decomposition and relaxation of the geometrically distorted fragments to the unstrained state.

The stability against structural changes that bring a fragment with distorted bonds and angles to the 'normal' state is provided most often by the fact that this fragment is incorporated into a ring or a rigid polycyclic cage. Alternatively, steric repulsion of bulky groups, especially *tert*-butyl substituents, also helps to avoid relaxation of a distorted fragment to an unstrained state.[22] The molecules of compounds **1** and **2** with a twisted double bond can serve as examples of strained molecules having a distorted fragment within a polycycle or bulky groups.

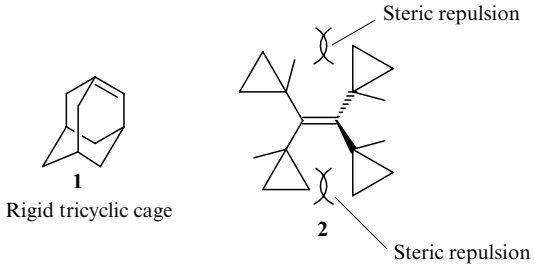

To attain stability of strained molecules, it is necessary to prevent them from entering reactions either with one another (oligomerisation, polymerisation) or with other potential reactants (solvents, oxygen, moisture, *etc.*). These reactions can be prevented by creating steric restrictions around the reaction centres. For example, tetrahedrane **3** is so reactive that it has not been prepared until now, in spite of considerable effort,‡ whereas tetra-*tert*-butyltetrahedrane (**4**), in which the strained C_4 core is shielded, has been isolated and studied, in particular, by X-ray diffraction analysis.

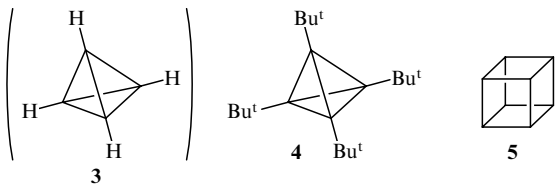

The instability of strained molecules is also related to their tendency to undergo intramolecular rearrangements. Kinetic stability due to electronic factors is an effective method for preventing these rearrangements. A classical example is cubane (**5**) in which the possible rearrangement pathways are forbidden by the orbital symmetry rules. The strain energy of molecule **5** is very high (157 kcal mol^{-1}; determined using data on the heat of

† This review covers studies published before the beginning of 2001. Analysis of publications on this topic up to mid-1970s was carried out by Greenberg and Liebman.[14,15] The publications for this review were collected using the STN electronic databases (Scientific Technical Network,[16] first of all, the REGISTRY database, which contains information on more than 18 000 000 organic and inorganic compounds), *Chemical Abstracts* and *Beilstein* as well as the Cambridge Structural Database (CSDB; the version of April 2001 presents structural information on more than 233 000 compounds).[17]

‡ From here on, the formulae of compounds not obtained experimentally are drawn in parentheses.

combustion of cubane [23]);§ however, cubane does not decompose even at temperatures above the melting point (130–131 °C).[26]

The strain energy of compound **5**, as well as that for other molecules described below, is markedly higher than that required for rupture of the C–C bond. However, the stability of cubane is secured by even distribution of the steric strain over the whole carbon skeleton.

The exceptionally stable C_{60} fullerene (**6**) in the molecule of which strain is uniformly distributed over all the 90 carbon–carbon bonds can serve as yet another example of stable but very strained molecules. The heats of combustion of C_{60} and C_{70} fullerenes and their standard enthalpies of formation, which can be used to estimate the strain energy, have been determined experimentally.[27]

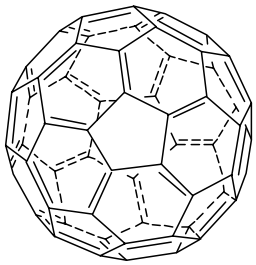

6

In some cases, the concept of thermodynamic stability of strained molecules is discussed but this term is often used improperly. For example, it has been claimed [28] that coordination of a metal atom to a distorted fragment can ensure 'thermodynamic stability' of strained ligands, in particular, *trans*-cycloalkenes. The overlap of molecular π orbitals of a strained alkene with the vacant orbitals of the transition metal and interaction of the occupied *d* orbitals of the metal with the π* orbital of the double bond (dative bond) finally stabilise the complex. However, in our opinion, this is a case of kinetic stability. Thermodynamic stability implies reversible transformations, for example, those between a complex with a ligand containing a distorted structural fragment and a complex with a strain-free analogue of the same ligand. Most transformations of strained molecules are irreversible; therefore, their thermodynamic stability is seldom encountered.

An example is provided by compound **7**, stable in methanol.[29] The driving force of the spontaneous formation of compound **7**, the molecule of which contains a strained twisted amide fragment, in equilibrium with zwitter-ion **8** is the steric strain in the bicyclic system, which decreases upon cyclisation.

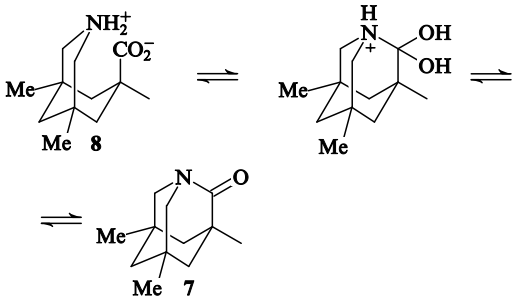

It makes sense to discuss the stability of a compound when conditions for its isolation or investigation are known. For example, a large number of compounds unstable at room temperature have been studied in inert matrices at 4–77 K.[30] Low-temperature isolation in solid matrices of inert gases prevents diffusion and, hence, excludes intermolecular reactions of the compounds under study. Moreover, intramolecular transformations, even those having an energy barrier of only several calories per mole are also retarded.[31]

One more method that provides a sufficient (in particular, for spectroscopic studies at room temperature) lifetime of reactive species should also be mentioned, namely, preparation of these species inside cavities of large macromolecules — carcerands and hemicarcerands. In recent years, several studies have been published (see below) devoted to spectroscopic and chemical properties of compounds the isolation and investigation of which at room temperature could not even be discussed before the advent of this method, for example, cyclobutadiene and dehydrobenzene.[32]

III. Abnormally long and short C–C bonds

The characteristic lengths of C–C, C=C and C≡C bonds (see Table 1) can be regarded as fundamental parameters in chemistry. Deviations from 'normal' values are seldom encountered, and they serve as an indicator for the occurrence of steric or electronic effects.

The quest for the longest $C(sp^3)-C(sp^3)$ bond has been called a 'real Odyssey.' [33] Considerable attention was devoted to hexaalkyl- and hexaarylethanes such as **9**–**11**,[34–36] in the molecules of which the central C–C bond is longer than 1.64 Å.

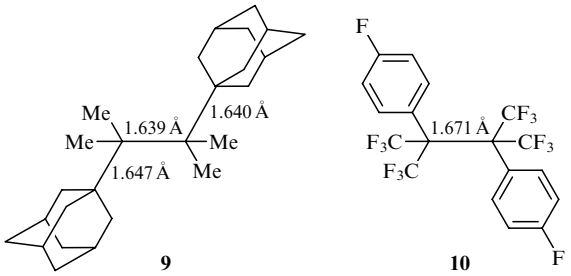

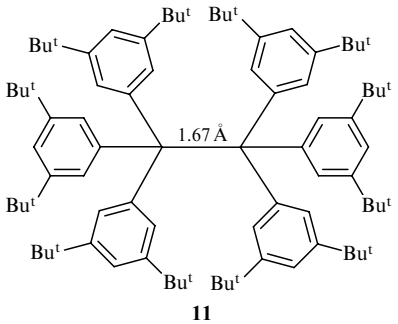

The main cause for bond elongation is steric repulsion between bulky groups. The elongated bonds are weakened, which accounts for the thermal instability of these hydrocarbons.[34] In the case of compound **9**, molecular mechanics (MM2) calculations¶ for the molecular geometry were carried out and good agreement between experimental and calculated values was obtained.

In 1996, Toda *et al.*[37] have reported exceptionally long C–C bonds in two benzocyclobutane derivatives, **12** (1.720 Å) and **13** (1.710 and 1.724 Å).

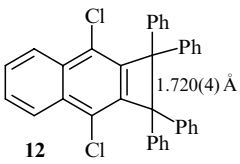

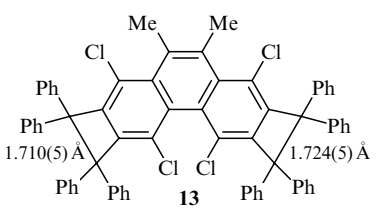

§ These data are somewhat outdated; however, more precise values have not yet been reported. The strain energy of the cubane molecule presented here is consistent with rough values determined from the heats of combustion of various cubane derivatives and with calculated values.[24, 25]

¶ Most of the calculation methods mentioned in the review are described in a book by Jensen.[21]

These values are almost 0.18 Å greater than the standard length of a single carbon–carbon bond; therefore, it is not surprising that some doubts have been cast upon the X-ray diffraction data published. Before the study by Toda *et al.*,[37] examples of compounds with even longer C–C bonds had been reported; however, a thorough verification showed the results of structural studies of these compounds to be incorrect. Thus the lengths of the central bonds in the molecule of compound **14**, a photoisomer of [2.2]tetrabenzoparacyclophane **15**, have been reported [38] to be 1.77 Å. Later, it was found that the measurements were carried out for a mixture of the photoisomers **14** and **15** rather than for a crystal of pure **14**.[39] In subsequent studies of a pure sample of **14** at 170 K, the lengths of the central bonds were found to be 1.648 Å.[40]

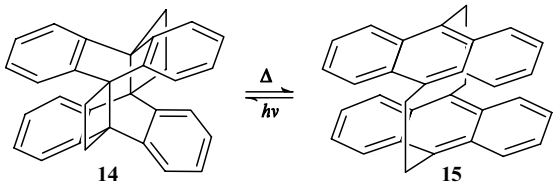

14 **15**

Repeated studies [41] of the compound **12** have confirmed, nevertheless, the validity of the previously obtained data,[37] and quantum-chemical calculations (B3LYP/6-31G*) reproduced them satisfactorily.[42] Model calculations [B3LYP/DZ(2d,p)] for the 1,1,2,2-tetraphenylbenzocyclobutene molecule also provided a Ph_2C-CPh_2 bond length consistent with the value found experimentally [37] in compound **12**. These calculations demonstrated the importance of taking into account the electron correlation in order to obtain correct values for geometric parameters of the strained molecules. It was also shown [41] that satisfactory interpretation of the observed elongation of the C–C bond requires that only steric effects (repulsion between bulky groups) be taken into account without considering hyperconjugation effects.[43] This conclusion is also confirmed by recently published data on the synthesis and X-ray diffraction analysis of the even more sterically hindered compound **16**.[44,45] The C–C bond length in the four-membered ring of **16** equals 1.729 Å, *i.e.*, it is longer than those in the molecules **12** and **13**.

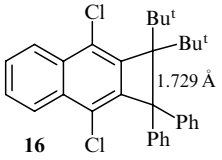

16

The distance between the carbon atoms formally not bound to each other in bicyclo[1.1.1]pentane (**17**) and its derivatives is close to the lengths of the 'stretched' C–C bonds given above. The C(1)–C(3) distance in this simple hydrocarbon measured by electron diffraction [46] is 1.874 Å (or 1.845 Å according to another publication [47]). The search through the CSDB for the shortest C(1)–C(3) distance among the bicyclo[1.1.1]pentane derivatives gave a value of 1.80 Å in bis(3-iodobicyclo[1.1.1]pentan-1-ylpyridinium)iodide triiodide **18**.[48] In this case, the X-ray diffraction data can best be interpreted by assuming that structures containing [1.1.1]propellane contribute to the resonance hybrid. In the molecules of bicyclo[1.1.1]pentane derivatives, the non-bonded bridging carbon atoms are so close to each other that the 'through-space' electronic interaction is clearly identified.[49]

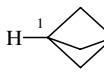

17

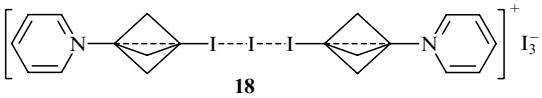

18

The above-mentioned studies raise the question of what is the longest distance between carbon atoms in a molecule that enable the existence of a chemical bond between them.

Proceeding from the empirical definition of the chemical bond † proposed by Pauling [50] without restricting the consideration to saturated systems, one can find examples of structures with formal C–C bonds longer than 1.729 Å, which is the value established for molecule **16**.

For example, a distance between carbon atoms equal to 2.83 Å has been found recently in the crystal of dimer **19**, formed by two tetracyanoethylene radical anions (**20**). Nevertheless, the results of structural, magnetic, and spectroscopic studies are consistent with the existence of a chemical bond between them.[51] This two-electron four-centre bond results from the π–π binding interaction between the radical anions **20** and the Coulomb repulsion between them. It was shown that the dimers are metastable species, *i.e.*, their formation is an endothermic process; in the solid phase, they can be stabilised upon interaction with metal cations.

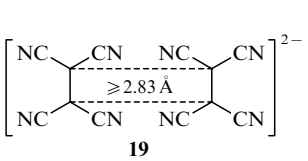

19

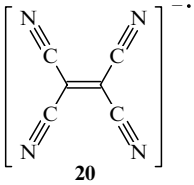

20

Apparently, it is impossible to establish the limiting bond length of any type on the basis of merely geometric criteria such as 'longer (or shorter) than..'; it is necessary to invoke conceptual models of chemical binding including new ones. Some new approaches to the determination of the nature of the chemical bond could be provided by Bader's theory.[52] This theory is based on the mathematical analysis of topological characteristics of the total molecular electron density function either found experimentally or calculated. In terms of this theory, it is possible to give strict criteria for the occurrence of a bonding interaction between a pair of atoms, irrespective of the distance between them.

A number of studies have been devoted to the search for strained molecules with short carbon – carbon single bonds. For example, the length of the exocyclic bond in bicubane **21** was found to be 1.458 Å,[53] which was explained by rehybridisation of the carbon orbitals. The exocyclic bonds in cubane have a greater *s*-character and, therefore, they are shorter than the standard $C(sp^3)-C(sp^3)$ bonds. The steric strain that could result in elongation of the central C–C bond in compound **21** is insignificant, unlike that in the molecule of 1,1′-biadamantane **22** (the length of the central bond in **22** is 1.578 Å [54]).

The central bond in bicubane can be compared with that in butadiene, the length of which is 1.383 Å, according to electron diffraction data;[55] however, in the latter compound, this bond is further shortened due to conjugation.

Schleyer and Bremer [56] not only compared the experimental and calculated (MNDO, MP2/3-21G, 6-31G*) lengths of the central bonds in molecules **23**–**25**, similar to the bicubane molecule, but also carried out model calculations for ethane (MP2/3-21G) with variation of the C–C–H bond angle. It was shown that an increase in this angle to 150° entails energy redistribution between molecular orbitals, resulting in strengthening of the C–C bond. The calculated (MP2/6-31G*) length of the C–C central bond in bitetrahedrane **25** is 1.438 Å. The compound **25** has not yet been synthesised; however, Ermer *et al.*[57] believe that the hexa-*tert*-butyl derivative of this compound could be prepared.

† According to Pauling, '... there is a chemical bond between two atoms or groups of atoms in the case that the forces acting between them are such as to lead to an aggregate with sufficient stability to make it convenient for the chemist to consider it as an independent molecular species.'

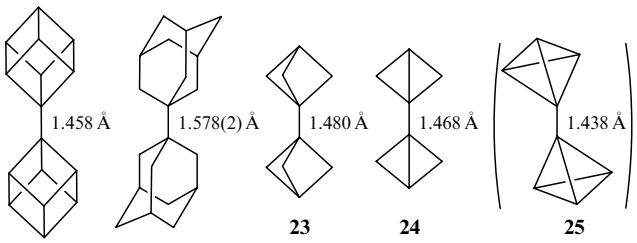

21 **22** **23** **24** **25**

The angle strain in the cyclopropane molecule is known to result in shortening of the formally single C–C bonds (1.499 Å).[58] In the bicyclobutane (**26**) molecule, which is the smallest one among the molecules of bicyclic hydrocarbons, two cyclopropane rings are fused; the central C–C bond exhibits properties of the double bond (for example, electrophilic reagents readily add at this bond to give cyclobutane derivatives) and is abnormally short (1.497 Å). X-Ray diffraction study of bicyclobutane derivatives showed that the length of the central bond depends on the angle between the planes of the three-membered rings. In the compound **26**, this angle is ~122.7°, while in its derivatives **27**, this angle is much smaller (~87°) and the C(1)–C(3) bond is much shortened (1.408 Å), *i.e.*, this is one of the shortest single bonds known to date.[59]

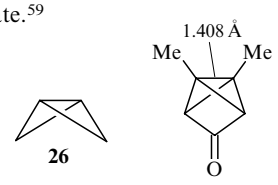

26 **27**

IV. Elongated and shortened C=C bonds

Analysis of the structures deposited in the CSDB shows that abnormally long formally double C=C bonds are found in systems containing long chains of conjugation (see, for example, compound **28**).[60] In aromatic derivatives (see, for example, compound **29**),[61] the C=C bonds can also be elongated. The shortest formally double carbon – carbon bonds have been found in a number of strained molecules (for example, in molecule **30**).[62] Exceptionally long carbon – carbon double bonds have also been found in twisted alkenes. The elongation of these bonds is due to a decrease in the degree of π-bonding.

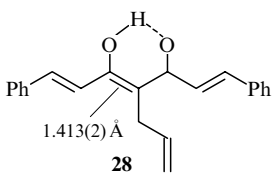

28

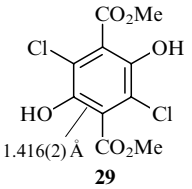

29

Let us consider the compounds the molecules of which incorporate the shortest (**30**) and the longest (**31**)[63] $C(sp^2)=C(sp^2)$ bonds known to date.

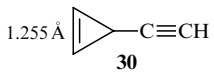

30

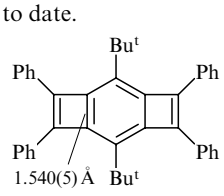

31

The length of the double bond in ethynylcyclopropene **30** is approximately an average between the bond lengths found in strain-free alkene and alkyne molecules — 1.255 Å. Even very high-level calculations provide overestimated lengths for the C=C bond in this molecule.[62]

Ab initio (HF/3-21G, 6-31G*) calculations for benzo[1,2:4,5]-dicyclobutene **32** predicted[64] two types of isomerism, one type being due to different bond lengths (**32a** and **32b**, **32c**) and the other type being due to different positions of the double bonds (**32b** and **32c**). X-Ray diffraction analysis[63] of the compound **31** did not confirm the results of calculations reported earlier.[64] The structural parameters found experimentally for **31** and those determined by quantum-chemical calculations for the hydrocarbon **32** (B3LYP/6-31G*, MP2/6-31G*) correspond to the structure **32d** with elongated bonds in the benzene ring. However, it should be emphasised that in this case, we are dealing with aromatic bonds rather than purely double bonds (as in alkenes).

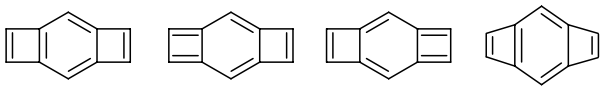

32a **32b** **32c** **32d**

V. Variations of the triple carbon – carbon bond lengths in organic compounds

The deviations of the lengths of triple carbon – carbon bonds in organic compounds from typical values are less pronounced than similar deviations in the case of single or double bonds. For example, according to analysis of the CSDB data,[4] the difference in the C≡C bond lengths in acetylene and its alkyl derivatives is less than 0.05 Å.

It is noteworthy that triple bond lengths determined by electron or neutron diffraction are often greater than those found by the conventional X-ray diffraction technique for the same compound (the difference can reach 0.02 Å or even more). This is due to the fact that X-rays are scattered by the electron density of the object and the electron density maxima (centroids) identified as 'atoms' in the X-ray diffraction method do not always coincide with the positions of the atomic nuclei. The electron density maxima can be displaced towards each other in the case of high concentration of the electron density in the interatomic space, which is often the case for multiple bonds including triple bonds. However, in modern X-ray diffraction software packages, this effect can easily be taken into account. Nevertheless, statistic analysis covering only those parameters in the CSDB which have been determined by electron diffraction in the gas phase results in an even smaller scatter of the C≡C bond lengths, namely, 0.012 Å.[4]

As a rule, elongation or shortening of triple bonds is mainly due to electronic factors. For example, this bond is shorter in the molecules of acetylene derivatives containing electron-withdrawing substituents at the triple bond.[65] (Note that this is equally true for double carbon – carbon bonds.) Elongated C≡C bonds have been found in conjugated systems, for example, in butadiyne[55] [1.2176(6) Å], although the lengths of these bonds in vinylacetylene and propynal molecules exceed only slightly the average value. The steric factors in linear alkynes in which substituents at the C≡C bond are far from each other are minimised.

It can be suggested that the loss of π-bonding caused by bending of the X–C≡C–X fragment (X is any substituent) in cycloalkynes would result in elongation of the triple bond. Nevertheless, in most of the known strained molecules of cycloalkynes, the length of the triple bond is close to the typical value. For example, in compound **33**, despite the substantial bending of the Si–C≡C–Si fragment, the C≡C bond length is equal to 1.22 Å, which virtually coincides with the average value (1.201 Å) for silyl-substituted alkynes.[66]

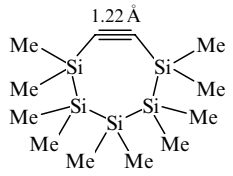

33

VI. Distortions of bond angles at the tetrahedral carbon atom

The modern theory of the structure of carbon compounds is underlain by the hypothesis advanced independently by Van't Hoff [67] and LeBel [68] in 1874 stating that a tetracoordinated carbon atom has a tetrahedral or a nearly tetrahedral configuration. Later, the results of numerous studies including X-ray diffraction analysis have confirmed Van't Hoff's and LeBel's hypothesis based on empirical data, and the sp^3-hybridisation concept has explained simply and conveniently the stability of the tetrahedral configuration. However, as soon as somewhat more than a decade after the publication,[67, 68] Baeyer, who considered distortions of the tetrahedral configuration of the carbon atom, stated the foundations of strain theory.[69]

The types of distortion of bond angles at the sp^3-hybridised carbon atom are illustrated in Fig. 1. First of all, this is a decrease/increase in one bond angle (the angle between the other two bonds usually correspondingly increases/decreases; this is the so-called scissors distortion) as well as distortions leading to flattening of the carbon configuration, *i.e.*, tetrahedral compression and digonal twist. Special mention should be made of configurations in which all atoms attached to a given carbon atom are located on one side of the plane passing through it, namely, inverted and pyramidal configurations to which an umbrella-type distortion leads. Rigorous mathematical analysis of the disortions of the CX_4 fragment has been reported.[70–72]

It should be noted that in experimental or theoretical study of the electron density distribution in the molecules characterised by highly distorted bond angles at carbon atoms, the regions of increased electron density between the atoms ‡ do not lie on the straight lines connecting the atomic nuclei but are displaced from these lines. These bonds have been referred to as curved (banana) bonds; a classic example of these bonds is found in the cyclopropane molecule. The displacement of the maxima of DED (covalent electron density) outwards the ring in cyclopropane derivatives reaches 0.2 Å or more. An even greater shift of the DED maxima away from the internuclear lines, up to 0.5 Å, was found in tetrahedrane derivatives. Banana bonds are found not only in the molecules with small rings but also in highly strained cage systems.[74]

Subsequently, in particular in the analysis of structural data for cyclic and strained cage molecules, the notion of bond path was defined as the interatomic line along which the total electron density is a maximum relative to any 'lateral' displacement and has a minimum in the so-called saddle point.[52, 73–75] A bond path is not necessarily a straight line; the presence of this line implies a chemical bond between the given atoms.[76] These and some other definitions constitute the foundation of the modern quantum theory of interatomic interactions and chemical bonding, developed by Bader.[52]

In Bader's theory, the bond path angle at an atom is determined by the angle between the tangents to two neighbouring bond paths. In strained molecules, the bond paths are curved, as indicated above. In particular, in a cyclopropane molecule, the bond path angle is ~78.8° rather than 60°, which has been confirmed by a number of X-ray diffraction studies of the electron density distribution in this type of system. Therefore, in the case of strained molecules, it would be more appropriate to discuss the bond path angles.

‡ Normally, this is so-called deformation electron density (DED), which characterises the difference between the electron density of the molecule and that calculated as a sum of the electron densities of isolated spherical atoms located at the same distance from each other.[73]

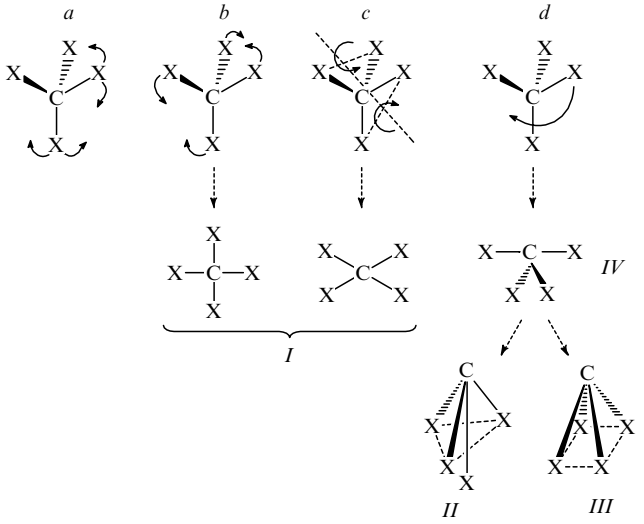

Figure 1. Distortions of bond angles at the tetrahedral carbon atom: scissors (*a*), tetrahedral compression (*b*), digonal twist (*c*), umbrella (*d*). Carbon atom configuration: (*I*) planar, (*II*) inverted, (*III*) pyramidal, (*IV*) intermediate between the tetrahedral and pyramidal.

A number of publications have been devoted to the study of electron density distribution in organic molecules. In these studies, the term 'bond angle' is used to imply the angle between the bond paths and not between the straight lines connecting the atomic nuclei. However, the vast majority of structural studies discuss the angles between the internuclear straight lines. Therefore, in this review, we also consider the latter type of angle unless otherwise indicated.

It should be noted that the Bader's topological approach and definition, in terms of its rigorous theory, of the bond path and some other key concepts of the molecular structure theory are drawing increasing attention of researchers. In particular, the classical term 'bond length' (the distance between the nuclei) is replaced in this theory by the notion of 'bond path length.' In the case of a strained molecule, the bond path length would naturally be longer than the internuclear distance. For example, in the cyclopropane molecule, the distance between the carbon nuclei (bond length) is 1.499 Å,[77] and the bond path length between them is ~1.53 Å, *i.e.*, it is nearly equal to the typical C–C bond length (see Table 1). An even greater inconsistency between the internuclear distances and the bond path lengths is found for cage systems, in particular, for icosahedral carboranes.[78]

1. Scissors type distortion: a decrease in the C–C–C bond angle

A considerable decrease in the C–C–C bond angle is found in molecules of cyclic compounds with small rings. A lot of information on the methods of synthesis and properties of these compounds has been accumulated to date. Many fundamental theoretical concepts, for example, the concept of steric strain and banana bonds, have been developed upon investigations of molecules with three- or four-membered carbocycles.[14, 26, 79–81] We shall consider several prominent examples of research along this line.

In the CSDB, we found eighteen structures with a bond angle at a saturated carbon atom smaller than 50°. The molecules of these compounds contain three-membered rings, and most of them contain multiple bonds in the rings. The smallest A–C–A angles (A is any atom) are typical of compounds with C=N and

N=N bonds in the three-membered rings. In compounds **34**[82] and **35**,[83] the angle at the saturated carbon atom is somewhat smaller than that in cyclopropene derivatives (for example, in compound **36**).[84] This is due to the fact that the C=N or N=N double bonds are shorter than the C=C bond, and the C−N single bonds are longer than the C−C bonds in cyclopropane (the C−C bond length in cyclopropane is 1.499 Å).[77] Both factors result in a decrease in the angle between the single bonds in unsaturated three-membered heterocycles.

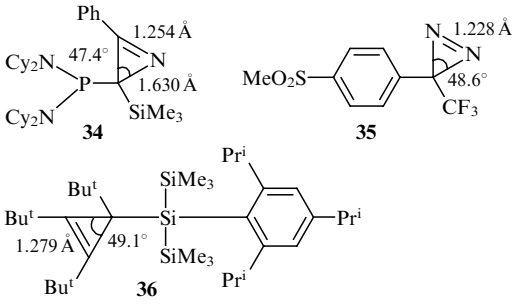

Cy is cyclohexyl.

Among the compounds containing saturated three-membered carbon rings with reduced C−C−C angles, bicyclobutane derivative **37** should be mentioned.[85] In the molecule of this compound, the bond between the bridging carbon atoms is shortened and, therefore, the opposing C−C−C angle in the three-membered rings is reduced.

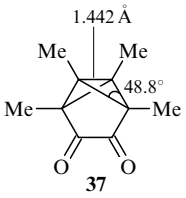

Compounds with reduced bond angles at saturated carbon atoms exhibit unusual reactivity due to the strain in their molecules. As an example, we shall consider derivatives of a hydrocarbon which has not yet been synthesised, tetrahedrane **3**.

Ab initio quantum-chemical calculations of different levels (SCF/4-31G,[86] G2 [87]) give a strain energy of 129–137 kcal mol^{-1} for the unsubstituted tetrahedrane molecule. This value is greater than the dissociation energy of a single C−C bond (72–117 kcal mol^{-1})[88] and exceeds (in relation to one carbon atom) the molecular strain in other hydrocarbons studied to date. It is not surprising that numerous early attempts to synthesise tetrahedrane and its derivatives have failed.[14, 89, 90] Only in 1978, did Maier *et al.*[91] synthesise the first tetrahedrane derivative, tetra-*tert*-butyltetrahedrane **4**, by photochemical transformations of tetra-*tert*-butylcyclopentadienone.

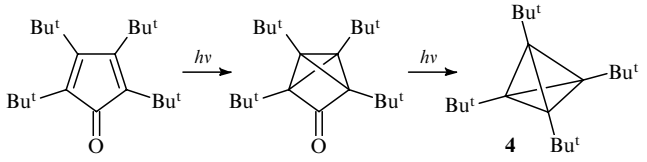

The seeming simplicity of the reaction scheme conceals great efforts of researchers aimed at selecting the optimal conditions for the preparation of a compound the possibility of isolation of which seemed unlikely at that time. The compound **4** is a stable crystalline substance isomerising into tetra-*tert*-butylcyclobutadiene only at 130 °C. Stability is attained owing to the presence of bulky *tert*-butyl substituents, which ensure the steric shielding (so-called 'corset effect') of the central strained fragment of the molecule by shielding it from the attack by reagents and preventing intramolecular rearrangements. The *tert*-butyl groups in the molecule **4** are remote from each other as far as possible but in the transformations of compound **4**, they approach each other, which results inevitably in an increase in the strain energy.

Tri-*tert*-butylisopropyltetrahedrane (**38**) proved to be much less stable than the compound **4**: its thermal isomerisation to cyclobutadiene **39** proceeds over several minutes at 80 °C.[92]

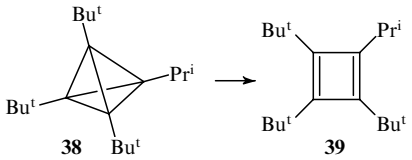

For a long period, researchers did not succeed in preparing other tetrahedrane derivatives.

It was another 10 years after the synthesis of **4** before a new derivative was prepared; this was tri-*tert*-butyl(trimethylsilyl)tetrahedrane (**40**).[93, 94] The approach to substituted cyclopropenyldiazomethane proposed by Masamune *et al.*[95] permitted Maier and co-workers to prepare other silyl- [96] and alkyl-substituted [92] tetrahedranes.

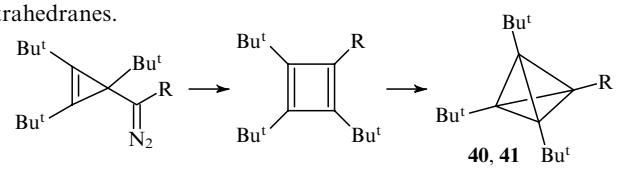

R = $SiMe_3$ (**40**), $SiMe_2OPr^i$ (**41**).

The reaction of compound **41** with the fluoride ion affords highly reactive trisubstituted tetrahedrane **42**.[96]

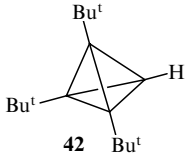

X-Ray diffraction data for the compound **4** showed that the C−C bond length in it (1.485 Å)[97] is shorter than the typical value (1.53 Å) and is even shorter than the C−C bond length in cyclopropane (1.499 Å).[77] This is due to rehybridisation of the cage atoms and bond bending. Early molecular mechanics calculations (MM2) showed that, due to the steric repulsion of the *tert*-butyl groups, the chiral structure (group of symmetry T) is energetically more favourable (by 2–6 kcal mol^{-1}) than the achiral structure (T_d).[98] This conclusion was confirmed by *ab initio* quantum-chemical calculations [B3LYP/6-311+G(d)//B3LYP/6-31G(d)].[99] The difference between the energies of these forms was 0.5–2.0 kcal mol^{-1}. The chemical properties of the compound **4** have also been studied. Besides the above-mentioned thermal rearrangement of the substituted tetrahedrane **4** into tetra-*tert*-butylcyclobutadiene, protonation with gaseous HCl and oxidation into the corresponding radical cation are known.[100]

2. Scissors type distortion: an increase in the C−C−C bond angle

Increased bond angles in the molecules with tetrahedral carbon atoms are observed, naturally, in the same cases where substantially reduced bond angles are found. For example, in the tetra-*tert*-butyltetrahedrane molecule discussed in the preceding Section, the angles between the exocyclic bonds and the bonds in the tetrahedral cage are 144.7 °, according to X-ray diffraction data.[97] A search through the CSDB provided examples of structures with even larger C−C−C angles. The vast majority of these compounds are spiropentane (**43**) or bicyclobutane (**26**) derivatives. According to X-ray diffraction analysis, the bond angles at the spiro carbon atom in the spiropentane molecule amount to 137.6 ° and 136.7 °.[101] The largest C−C−C bond angles were found in bridged derivatives of **43** — molecules **44**–**46** (the greater of the two increased bond angles is given for each molecule).[102]

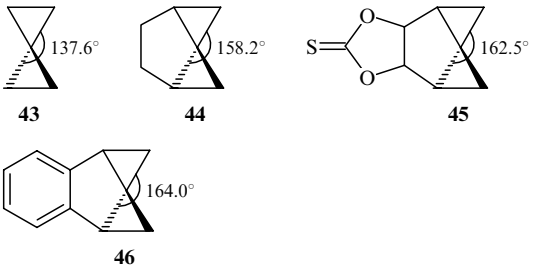

43 **44** **45**

46

Analysis of DED maps for spiropentane and its derivatives has been carried out.[101] In all cases, substantial exocyclic dispacement of DED maxima in the planes of the three-membered rings was found.

An increase in one bond angle at the tetracoordinated carbon atom to 180° would result in a configuration intermediate between the tetrahedral and pyramidal ones (see Fig. 1 *d*). The carbon atoms in dicubane **47** may have a similar configuration. The possibility of synthesis of dicubane has been discussed.[103] The C−C−C bond angle in this molecule was calculated to be ~175°.

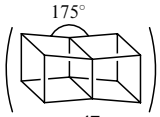

47

According to calculations (MP2/6-31-G*, HF/6-31G*),[104] a carbon configuration with a C(2)−C(1)−C(6) angle of ~180° is also possible in the molecule of compound **48**.

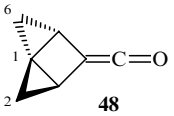

48

This highly reactive tricyclo[3.1.0.0^{1,3}]hexane derivative was detected by IR spectroscopy in an inert matrix at 15 K.[105]

3. Planar configuration of a tetracoordinated carbon atom

In recent years, researchers have devoted particular attention to types of distortion such as tetrahedral compression and digonal twist, resulting in a flattened CX_4 fragment.[106–110]

The search for compounds with such an unusual structure was stimulated by a publication by Hoffmann *et al.*,[111] in which the molecular orbitals in a hypothetical planar methane molecule were analysed and suggestions were made about possible ways of stabilisation of the planar configuration of carbon. According to qualitative analysis of the electronic structure of the planar methane molecule, the carbon atom in this molecule should be sp^2-hybridised. This atom should have two electrons in a non-hybridised *p* orbital and should form two two-electron two-centre C−H bonds and one two-electron three-centre H···C···H bond.

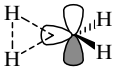

The strain energy of this molecule substantially exceeds the C−H bond dissociation energy; the energy difference (MP2/6-31-G*//6-31G*) between the tetrahedral (T_d) and planar (D_{4h}) methane configurations amounts to 159.7 kcal mol^{-1}. The possibility of existence of the planar structure, even as the transition state in the methane inversion, has been called in question.[112] Calculations[113] [MCSCF/6-31G(d,p), 6-31+G(d,p), TZV++G(d,p)] showed that the planar structure with D_{4h} symmetry does not match any minimum on the PES, whereas the planar structure with C_s symmetry corresponds to a saddle point on the PES. A molecule with this symmetry could represent a transition state formed in the methane inversion: its energy is almost 40 kcal mol^{-1} lower than the energy of the molecule with D_{4h} symmetry (nevertheless, its strain energy is still greater than the energy of C−H bond rupture by 7 kcal mol^{-1}). The same conclusion has also been drawn by other researchers,[114] who used extended basis sets [6-311+G(3df,2p), 6-311G*] to analyse the problem of methane inversion.

Hoffmann *et al.*[111] were the first to consider stabilisation factors of a planar configuration of the formally tetracoordinated carbon atom. One of these factors is electronic stabilisation caused by substituents exhibiting σ-donor and/or π-acceptor properties; the former provide the deficient σ-electron density, while the latter delocalise the increased π-electron density. Delocalisation of the lone electron density of the carbon atom with a planar configuration in the $(4n+2\pi)$-system should also facilitate stabilisation.

The idea of electronic stabilisation has been further extended by Schleyer and coworkers,[115] who found by RHF/STO-3G calculations that the energy of 1,1-dilithiocyclopropane molecule with a planar carbon (**49a**) is lower by 7 kcal mol^{-1} than the energy of the corresponding molecule with the tetrahedral carbon configuration (**49b**).

49a **49b**

Later, Sorger and Schleyer[110] made calculations for a number of molecules that may have a planar configuration of a tetracaroordinated carbon atom stabilised by σ-donor and/or π-acceptor substituents. These include, for example, 1,1- and 1,2-dilithioethylenes (**50** and **51**, respectively) and 3,3-dilithio-1,2-diboracyclopropane (**52**).

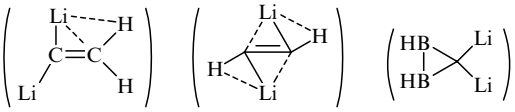

50 **51** **52**

According to calculations (B3LYP/6-31G*), for the last-mentioned compound, the energy of the molecule with a planar carbon configuration is 18.7 kcal mol^{-1} lower than that in the case of tetrahedral configuration.

1,1-Dilithio-2,2,3,3-tetramethylcyclopropane (**53**) has been synthesised;[116] however, its structure has not been determined. The structural studies for this type of compound are complicated by the high degree of aggregation.

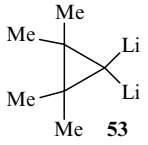

53

Spectroscopic detection of the $[CAl_4]^{2-}$ dianion has been reported.[117] It was suggested that the planar (according to B3LYP/6-311+G* calculations) $[CAl_4]^{2-}$ dianion can be stabilised in the solid phase by an appropriate counter-ion, for example, Na^+.

Organometallic compounds of transition metals the molecules of which contain a tetracoordinated carbon atom with a planar configuration are also known. Complex **54** was the first crystallographically characterised compound of this type.

It is of interest that only two years after the publication of the paper by Cotton and Millar[118] reporting the structural data for complex **54**, Keese *et al.*[119] noticed the unusual planar environment of the carbon atom (marked by an asterisk) in this compound. Quite a few other complexes of this type are also known;[107] however, the mechanisms of stabilisation of the planar configuration of the carbon atom in them are different.[108] In most of the molecules, the carbon atom under interest is a part of an unsaturated (often, aromatic) system, which is an additional stabilising factor. Molecules in which a tetracoordinated carbon

atom with a sum of bond angles equal to ~360° is stabilised only by σ-donor and π-acceptor substituents (as has initially been suggested for planar methane analogues) are found rather rarely; among them, compounds **55**, **56** were the first to be characterised and studied [108] (the carbon atom having a planar configuration is marked by an asterisk).

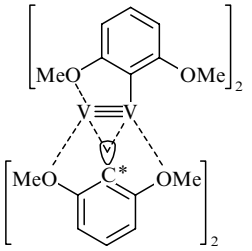

54

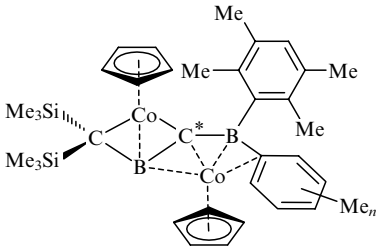

n = 4 (**55**), 3 (**56**)

Stabilisation of a planar methane molecule can be attained by oxidation to give a mono- or di-cation. As shown by calculations [ST4CCD/6-311 + G(2df,2p)],[120] the carbon atom in CH_4^{2+} has a planar environment (the symmetry group is C_{2v} rather than D_{4h}). This cation has been detected experimentally in mass spectra.[121]

The attempts to synthesise compounds in which the carbon atom with a planar configuration would be embedded into a rigid carbon cage have not yet been crowned with success. Hoffmann *et al.*[111] suggested that this type of carbon atom could exist in [*n.n.n.n*]fenestranes

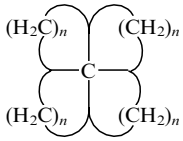

Numerous studies have been devoted to the synthesis of fenestranes; elegant strategies for their synthesis have been developed.[106] However, fenestranes with *trans*-fused five- and four-membered rings (the case in which the greatest distortions of the bond angles at the central carbon atom are expected) have not yet been obtained. Of the fenestranes studied by X-ray diffraction analysis, the greatest distortion has been found in the molecule of [4.4.4.5]fenestrane derivative **57**,[122] in which the opposing bond angles at the central carbon atom are 128° and 129°.

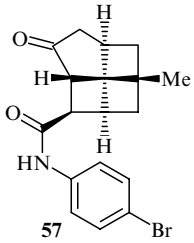

57

A highly distorted tetrahedral, although still not perfectly planar, configuration of the central carbon atom is also expected in the hypothetical structure **58**, which was called bowlane; initially, a pyramidal configuration of the central carbon atom was suggested for this compound.[123]

Ab initio calculations (HF/6-31G*) have shown [124] that the bowlane molecule should have C_{2v} symmetry and a distorted tetrahedral configuration of the central carbon atom with maximum sizes of the opposing angles at this atom of 170.9° and 148.1°. The predicted strain energy of the molecule **58** (RMP2/6-31G*, 166 kcal mol^{-1}) is approximately the same as that found experimentally for cubane (157–181 kcal mol^{-1});[23] therefore, the synthesis of bowlane appears quite possible.[125] However, it is beyond doubt that the reactivity of the distorted CC_4 fragment accessible to attack by reagents from outside would hamper the synthesis. Even in the case of [4.4.4.5]fenestranes (in which the distortion of this fragment is less pronounced), the reactivity is still rather high. Many thermal and photochemical reactions of [4.4.4.5]fenestranes proceed with cleavage of the bonds at the central carbon atom.[126]

The first and not yet synthesised neutral saturated hydrocarbon with a predicted perfectly planar configuration of the carbon atom the structure of which corresponds to a minimum on the PES is dimethanospiro[2.2]octaplane (**59**).

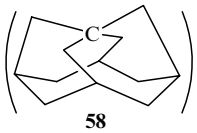

58

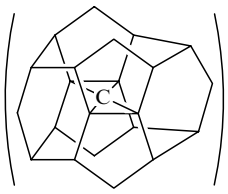

59

The MP2/6-31G(d) calculations predict for the compound **59** a structure with D_{2h} symmetry and a perfect planar configuration of the central carbon atom.[127,128] The highest occupied molecular orbital in **59** is represented by the *p* orbital of the central atom with a lone electron pair. Unusual physical properties of the octaplane **59** were predicted, in particular, a low ionisation potential (~5 eV) comparable with those of alkali metals. In this compound, the planar carbon atom is shielded by the hydrocarbon cage, which may decrease the reactivity.

4. The inverted and pyramidal configurations of the tetracoordinated carbon atom

Now we shall consider examples of molecules containing a carbon atom with bonds located on one side of the plane that passes through this atom (see Fig. 1 *b*,*c*). Inverted and pyramidal configurations should be distinguished.[123,129] The inversion means that one bond of the carbon atom points to a direction opposite to its direction in the tetrahedral configuration, resulting in a fragment with C_{3v} symmetry (see Fig. 1 *b*). In the pyramidal CX_4 fragment, the carbon atom occupies a vertex of a tetragonal pyramid with C_{4v} symmetry (see Fig. 1 *c*).

The existence of inverted configurations was first discussed in relation to propellanes, *i.e.*, structures in which two bonded carbon atoms are additionally connected by three bridges.

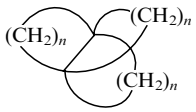

[*n*, *n*, *n*]propellanes

The first representative of small-ring propellanes, [3.2.1]propellane (**60**), was synthesised in 1969.[130] At about the same time, discussion concerning the inverted configuration of the carbon atom was initiated. It was suggested that in small-ring propellanes such as **60**–**63**, unusual configuration of the central atoms is possible. The results of X-ray diffraction analysis of 8,8-dichlorotricyclo[3.2.1.0^{1,5}]octane (**64**) provided the first evidence supporting this hypothesis.[131]

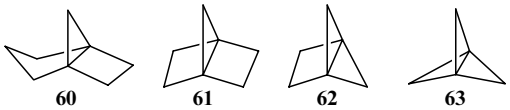

60 **61** **62** **63**

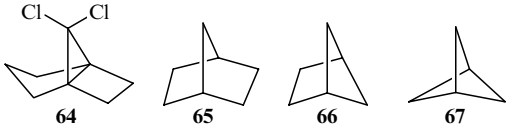

64 **65** **66** **67**

[3.2.1]Propellane **60** proved to be thermally stable but still extremely reactive (it reacts with oxygen and enters into diverse radical addition reactions).[130] An even more strained propellane (**61**) was stabilised only in an argon matrix at 29 K.[132] It appeared that the simplest [1.1.1]propellane **63** could hardly be expected to

be more stable. However, in 1982, Wiberg and Walker [133] predicted theoretically the possibility of synthesis and the highest stability, among the compounds **61**–**63**, for [1.1.1]propellane and later they synthesised it. For the compound **63**, not only the possibility of synthesis and stability were predicted, but also the enthalpy of formation and photoelectron and IR spectra were calculated. The [1.1.1]propellane molecule is the first polyatomic molecule for which correct theoretical predictions preceded the synthesis.[134]

The relative stability of **63** is interpreted in the following way.[134] The molecules **61**–**63** have approximately equal strain, while the strain of the corresponding bicyclic hydrocarbons **65**–**67** with no bond between the central carbon atoms sharply increases on passing from [2.2.1]bicycloheptane (**65**) to [1.1.1]bicyclopentane (**67**).[135] Since the reactions of propellanes include rupture of the bond between the bridging carbon atoms to give species having the skeleton of the corresponding bicyclic hydrocarbons, the energy barrier to the reactions of [1.1.1]propellane is higher than the corresponding values typical of its homologues.

[1.1.1]Propellane was first synthesised from 1,3-dibromobicyclo[1.1.1]pentane, which is difficult to obtain.

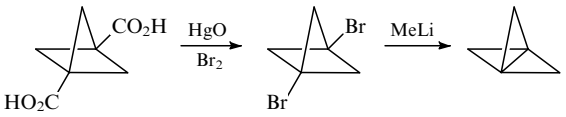

Later, a procedure for the synthesis of the propellane **63** from more easily accessible precursors was developed;[136] this allows the preparation of tens of grams of this compound.

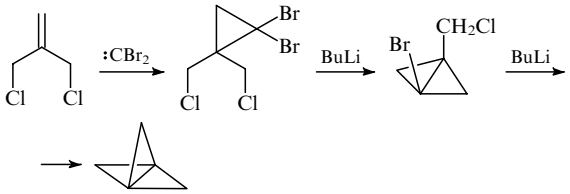

A similar approach has been used to prepare substituted [1.1.1]propellane derivatives.[137] The latest achievements in the synthesis, study of the chemical properties and application of [1.1.1]propellanes are covered in a review.[138]

The structure of [1.1.1]propellane was determined using vibrational spectroscopy,[139] gas-phase electron diffraction [140] and X-ray diffraction analysis.[141] The results of investigations by these methods confirmed the presence of the inverted configuration of the carbon atoms at the bridgehead in the structure of this compound.

The nature of the bond between the central carbon atoms in the compound **63** was the subject of numerous theoretical studies.[134] The energy of this bond was estimated (based on MP2/6-31G* calculations) to be approximately 70% of the energy of a single C–C bond (59 kcal mol^{-1}).[142]

Experimental information on the nature of the central bond in propellanes are provided by studies on the electron density distribution from X-ray diffraction data. Studies of this type have been attempted;[141, 143] however, the accuracy of experimental data proved to be inadequate to draw ultimate conclusions. The most accurate results of X-ray structure determination (at 81 K) and electron density distribution have been reported [143] for two [1.1.1]propellane derivatives, compounds **68** and **69**.

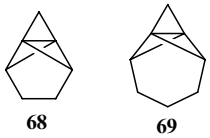

68 **69**

As expected, the DED maxima for non-bridging bonds proved to be concentrated outside the three-membered rings, which is typical of bent (banana) bonds. However, the DED values between the central carbon atoms are negative for both molecules. Nevertheless, this fact alone does not prove the absence of bonds between these atoms and does not contradict the results of the electron density calculation carried out by Wiberg.[144]

The negative DED values on the lines connecting atoms are encountered quite often; this is due to over-subtraction of the electron density of the 'pro-molecule' (combination of spherical non-interacting atoms) from the total density. This is due to the nature of the DED maps — they are differential. Therefore, in investigations of these bonds, a more promising approach includes analysis of the electron distribution topology and construction of non-differential maps, in particular, the Laplacian (the second derivative) of the experimental and theoretical electron density.[75]

The inverted configuration of the bridgehead carbon atoms was also observed in bicyclobutane derivatives (the structure was determined by microwave spectroscopy [145]).

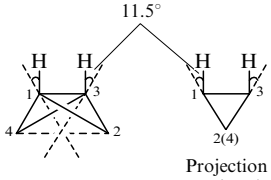

Projection along the straight line passing through C(2) and C(4)

In this molecule, the C(1)–H and C(3)–H bonds form an angle of 11.5° with the plane passing through the C(1), C(2) and C(4) atoms.

X-Ray diffraction data for other bicyclobutane derivatives with inverted configurations of bridgehead carbon atoms have also been published.[146–148]

The Cambridge Database contains also structural data on bicyclobutane heteroanalogues which also incorporate carbon atoms with inverted configurations. Examples are provided by compounds **70**–**72** (the carbon atoms with inverted configurations are marked by asterisks).[149–151]

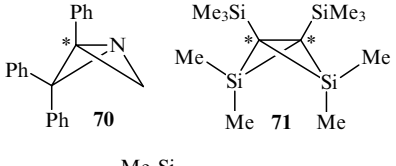

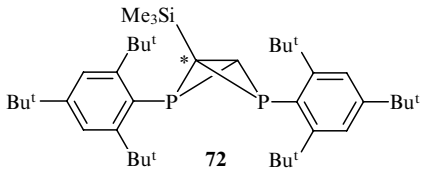

The presence of carbon with inverted configuration in 1,4-dehydrocubane has been doubted based upon the results of theoretical (*ab initio* 6-31G*) and experimental data.[152–154] It is more likely that this highly unstable molecule exists as singlet biradical **73a** and contains no diagonal bond, as shown in **73b**.

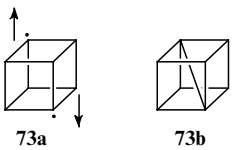

73a **73b**

Theoretical calculations have been performed for the molecules of polycyclic hydrocarbons **74**–**76** [MP2/6-31G(d,p), 6-311++G(d,p), B3LYP/6-31G(d,p)][155] and [2.2.2]propellatriene **77** (CASSCF/6-31G*),[156] in order to find other structure types where existence of 'inverted' carbon atoms is possible.

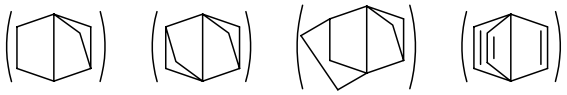

74 **75** **76** **77**

The pyramidal configuration of the carbon atom (see Fig. 1 *d*) is more exotic than the inverted one, and calculation methods still remain the most efficient tool for the investigation of compounds with this type of atom. Noteworthy are studies by Minkin *et al.*,[157, 158] who were the first to demonstrate that among the possible non-tetrahedral configurations of the carbon atom in methane, the pyramidal rather than planar configuration is energetically most favourable. The researchers cited discuss the factors that stabilise the pyramidal configuration; they are similar to those for the planar configuration, namely, the presence of σ-donor or π-acceptor substituents as well as incorporation of a pyramidal carbon atom in a rigid polycyclic cage, especially in small rings.

Known and structurally characterised systems with a pyramidal configuration of carbon (as well as compounds with the planar configuration of carbon) are represented exclusively by organometallic compounds of transition metals. Some of these structures are deposited in the CSDB; most of them are carbido clusters of iron, ruthenium, or osmium in which the carbon atom occupies an open cavity formed by metal atoms. The most frequently encountered types of structures are those present in compounds **78**, **79** (with the so-called butterfly geometry [159, 160]) and compounds **80**, **81**, in which the carbon atom lies below the base of the tetragonal pyramid formed by the metal atoms.[161, 162]

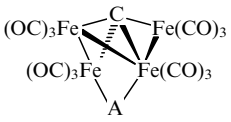

78, **79**

A = H^+ (**78**), CO (**79**)

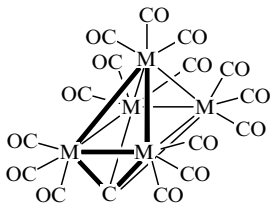

80, **81**

M = Fe (**80**), Ru (**81**)

In recent years, interest in these clusters has substantially increased because they were shown to be the key intermediates in the catalytic reduction of CO with hydrogen to give hydrocarbons, *i.e.*, the Fischer – Tropsch synthesis.[163] The first complex of this type was prepared as a side product of the reaction of $Fe_3(CO)_{12}$ with alkynes;[161] at present, preparative procedures for the synthesis of these compounds in high yields have been developed.[164] The carbon atoms in carbido clusters form σ- and π-bonds involving transition metal *d* orbitals; this stabilises the clusters. Similar complexes containing no carbido (interstitial) ligands are less stable.

Numerous theoretical studies of hypothetical organic molecules having the carbon atoms with pyramidal configuration have been carried out. About 10 years ago, the lack of computer resources and the absence of advanced software did not allow sufficiently accurate and reliable determination of the structural parameters of strained molecules. Many structures calculated at that time have later (according to the results of more advanced methods of calculation) proved unreal, *i.e.*, either not matched by minima on the PES or inaccurate. For example, [1.1.1.1]- and [2.2.2.2]paddlanes (**82**, **83**), which were initially supposed to have pyramidal configurations of carbon atoms, did not correspond to minima on the PES calculated by modern *ab initio* methods.[124]

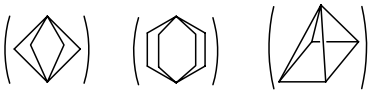

82 **83** **84**

The molecular mechanics calculations for bowlane **58** had also showed the presence of a carbon atom with pyramidal configuration, but *ab initio* calculations carried out later refuted this conclusion.

The C_{4v} structure of pyramidane (**84**) with the pyramidal configuration of a carbon atom corresponds to a local minimum on the PES (MINDO/3,[165] HF/STO-3G [166] and HF/6-31G* [124]).

Rasmussen and Radom [167] have reported results of *ab initio* calculations (B3LYP/6-31G(d)//MP2/6-31G(d)) for hemialkaplane (bowlane **58** is a representative of this class of polycyclic hydrocarbons) and hemispiroalkaplane molecules; according to their data, the central carbon atom has a pyramidal configuration. The general formulae of hemialkaplanes (on the left) and hemispiroalkaplanes (on the right) are shown below:

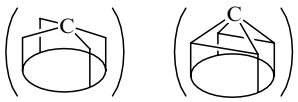

On the basis of calculations of the molecular strain and the so-called apical strain (which characterises the strain of the separate molecular fragment containing the carbon atom with the pyramidal configuration), the researchers concluded that hemispirobioctaplane **85**, hemispirooctaplane **86** and hemispirobinonaplane **87** are the most promising synthetic targets. Analogues of the systems **85** – **87** containing methyl groups (for example, compound **88**) might prove to be easier to prepare because the presence of methyl groups contributes to the kinetic stability of the molecule. The compounds **85** – **88** were predicted to be highly basic.[167]

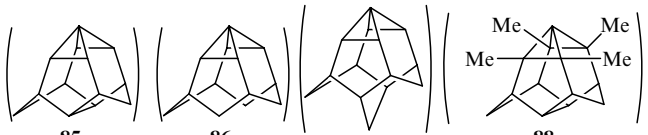

85 **86** **87** **88**

The existence of rigid polycyclic organic molecules, for which the presence of a carbon atom with a pyramidal configuration had been predicted, was later proved experimentally. For example, Wiberg *et al.*[168, 169] have detected one of them, namely, highly reactive tricyclo[2.1.0.$0^{1,3}$]pentane **89**.

89

VII. Distortions of bond and torsion angles at the double bond in alkenes

The research into the distortions of the bond and torsion angles in the molecules of alkenes has a long-standing history. Back in 1890, Baeyer [170] arrived at the conclusion that substantial strain should be expected in the *trans*-cyclohexene molecule and, therefore, isomerisation of *cis*-cyclohexene into the *trans*-isomer is unlikely. Later, when analysing the strain in unsaturated bicyclic molecules, Bredt,[171, 172] formulated a rule according to which the cage of camphane, pinane or other related compounds cannot have a double bond to a bridgehead position. At present, vast theoretical and experimental material on this point has been accumulated and reflected in numerous reviews (see, for example, studies [28, 173 – 176]).

The types of distortion of a planar alkene fragment are illustrated by Fig. 2.

Mathematical analysis of the distortions of the bond and torsion angles in the ethylene molecule has been described in detail in the literature (see, for example, reviews [28, 177]).

Distortions of only one type are seldom encountered in alkene molecules. However, in most cases, the prevailing type of distortion can be distinguished, which determines the total strain of

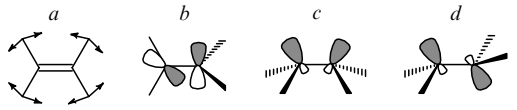

Figure 2. Types of distortion of the planar alkene fragment: (*a*) in-plane distortions; (*b*–*d*) out-of-plane distortions: (*b*) twist, (*c*) *syn*- and (*d*) *anti*-pyramidalisation.

the alkene.[28] Below we consider compounds in which the strain of the molecule is mainly due to the contribution of one type of distortion.

1. In-plane distortions of an sp^2-hybridised carbon atom

The bond angles at the sp^2-hybridised carbon atom can differ appreciably from the ideal value, equal to 120°. Indeed, the internal C–C=C angle in cyclopropene derivatives can be twice as small. The results of a search through the CSDB demonstrated that this angle is about 60° in the molecules of cyclopropene derivatives that also contain an exocyclic double bond (there are 10 structures of this type), for example, **90**, **91**.[178,179]

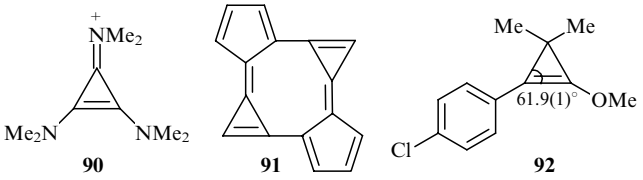

In these molecules, a major contribution to the resonance hybrid is made by canonical forms with the cyclopropenylium cation. In other cyclopropene derivatives, the internal C–C=C angle is close to 60°; for example, in molecule **92** this angle is 61.9°.[180]

The external R–C=C angles in cyclopropene derivatives can be greater than 150° in the case of bulky R substituents, for example, the angle is 155.6° in molecule **93**.[181] Bond angles exceeding 150° have also been found at exocyclic double bonds in compounds with saturated three-membered rings. The deviations of these angles from 150° are caused by steric repulsion of bulky groups (as in compound **94**)[182] or by the fact that double bonds are incorporated in rings (as, for example, in compound **95**).[183]

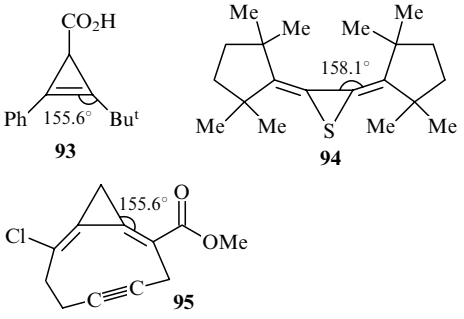

A decrease in the R–C=C angle results in pyramidalisation of the carbon atoms of the double bond. This fact was predicted theoretically:[184] model calculations (RHF/STO-3G) showed that if the H–C=C angles in the planar ethane molecule are less than 100°, pyramidalisation becomes energetically favourable. X-Ray diffraction analysis of compound **96** confirmed this fact experimentally.[185] In molecule **96**, the C–C=C angles in the cyclopropene fragment amount to 64.8° and 65.3°, and the ψ angle characterising pyramidalisation equals 17.6°.

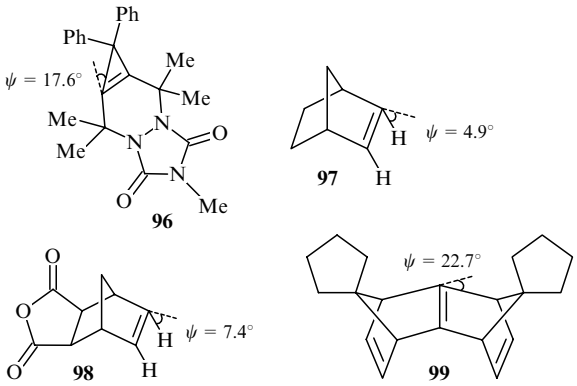

For the norbornene molecule (**97**), pyramidalisation of the carbon atoms of the double bond was predicted theoretically (for example, according to the STO-3G *ab initio* calculations,[186] the hydrogen atoms at the double bond are displaced in the *endo*-direction and the ψ amounts to 4.9°). X-Ray diffraction data for norbornene have not been obtained.

In a norbornene derivative, anhydride of *exo*,*exo*-2,3-norborn-5-enedicarboxylic acid (**98**), the structure of which has been determined by neutron diffraction, the ψ angle proved to be 7.4°.[187] In compound **99**, as shown by X-ray diffraction analysis, the fusion of two norbornyl cages (and, probably, steric repulsion between the cyclopentane rings) accounts for quite a noticeable pyramidalisation: ψ = 22.7°.[188,189]

An exceptionally high pyramidalisation of the carbon atoms at the double bond can be expected, according to calculations (HF, TCSCF, MP2, B3LYP, B3PW91/6-31G*),[190] in compounds **100**–**103**, the synthesis of which has been reported.[191–195]

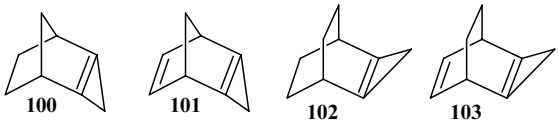

It follows from calculations that each of the tricyclic structures **100**–**103** is matched by two minima on the PES, which correspond to the *endo*- and *exo*-isomers. In the case of the compounds **100** and **101**, a lower energy is found for *endo*-isomers (their energy is 2.2–7.5 kcal mol^{-1} lower than that of the corresponding *exo*-isomers), whereas for the compound **103**, the *exo*-isomer is lower in energy (by 2.2–3.3 kcal mol^{-1}). The carbon atoms of the double bonds in the compounds **100**–**103** should be strongly pyramidalised (ψ > 40°). Experimental verification of these theoretical conclusions would be a complicated task because the strained molecules **100**–**103** are highly reactive (for example, the existence of the compound **103** can only be proved by analysing the products of reactions involving this molecule).[193]

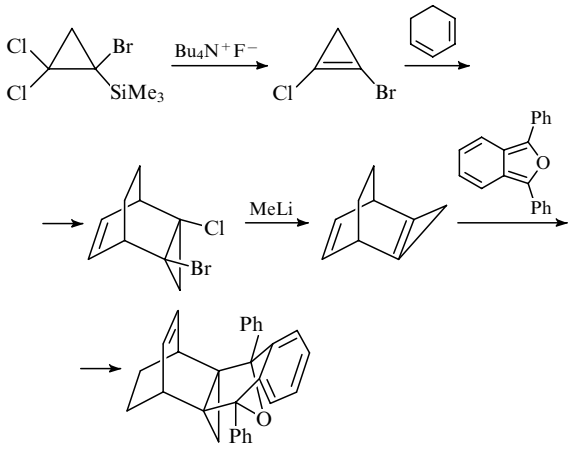

2. Twisting of the double bond

The loss of π-bonding upon distortion of the torsion angles at the double bond (twist) is partially counterbalanced by rehybridisation of carbon atoms, resulting in their pyramidalisation.[196–198] Therefore, when comparing the degree of twisting of double bonds in the molecules of different alkenes, it is not always legitimate to use the dihedral angle between the *a*C(1)*b* and *c*C(2)*d* planes (Fig. 3). Therefore, the so-called twist angle τ was introduced, which is found as the arithmetic mean of the *a*C(1)C(2)*d* and *b*C(1)C(2)*c* dihedral angles.

$$\tau = \frac{a\mathrm{C}(1)\mathrm{C}(2)d + b\mathrm{C}(1)\mathrm{C}(2)c}{2}.$$

This angle is equal to the angle between the *a*C(1)*b* and *c*C(2)*d* planes in the case where no pyramidalisation takes place. The degree of pyramidalisation of the C(1) and C(2) atoms is evaluated from the departure of the *a*C(1)C(2)*c* and *b*C(1)C(2)*d* dihedral angles from 180° and from the pyramidalisation angles $\chi_{C(1)}$ and $\chi_{C(2)}$:

$$\chi_{C(1)} = b\mathrm{C}(1)\mathrm{C}(2)c - b\mathrm{C}(1)\mathrm{C}(2)d + \pi,$$

$$\chi_{C(2)} = a\mathrm{C}(1)\mathrm{C}(2)d - b\mathrm{C}(1)\mathrm{C}(2)d + \pi.$$

The results of theoretical investigations demonstrate that twisting of the molecule of an alkene with all electron-donating or all electron-withdrawing substituents by 90° (τ = 90° or −90°) should give rise to a singlet biradical,[199–201] and the maximum twisting in the molecules of non-symmetrical alkenes (so called push – pull alkenes) yields bipolar species.[202] Twisted systems correspond to the transition state of the *cis–trans*-isomerisation of alkenes. For simple alkenes, the activation free energy of the *cis–trans*-isomerisation found experimentally lies in the range from 51 to 67 kcal mol^{-1} (see Refs 203 – 205). For push – pull alkenes, this barrier is substantially lower.[202] This is why the 'record-holder' molecules in which the τ angle for the C=C bond is close to 90° (or −90°) are represented in the CSDB by push – pull alkenes. For example, according to X-ray diffraction data, in the molecules **104** and **105**, the τ angles are 85.1° and 84.3°, respectively.[206, 207]

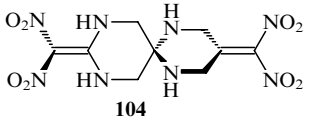

104

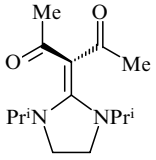

105

When the double bond is conjugated with other π-bonds or aromatic systems, the barrier to the *cis–trans*-isomerisation also decreases. Among the structures of compounds with conjugated double bonds, numerous examples can be found in which the |τ| values are close to 90°. Thus in the octaisopropylcyclooctatetraene molecule (**106**), the τ angles for all multiple bonds exceed 64°.[208]

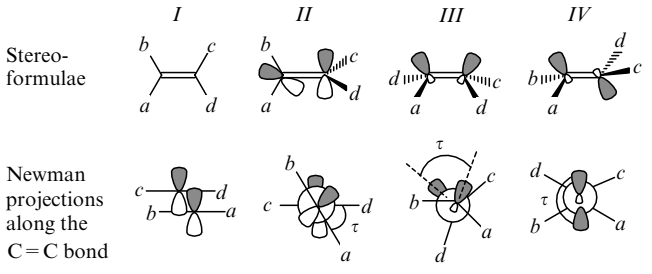

Figure 3. Twist distortion of the C=C bond and definition of the twist angle τ: (*I*) unstrained double bond; (*II*) twisting of double bond without pyramidalisation of the carbon atoms; (*III*, *IV*) twisting + pyramidalisation; *a–d* are substituents.

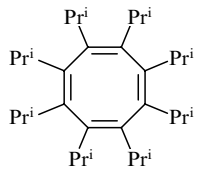

106

If push – pull alkenes and compounds with conjugated double bonds are excluded from consideration, the number of structures with τ angles lying in the range of 20° < |τ| < 90° included in the CSDB sharply decreases. Considerable twist-type distortions of the C=C bond were found both in acyclic and in cyclic or polycyclic compounds.

a. Acyclic twisted alkenes

In acyclic alkenes, twist distortions take place if bulky substituents are present at the double bond. The largest twist of the double bond not incorporated in a ring or a polycyclic system and bearing only hydrocarbon substituents is expected in the tetra-*tert*-butylethylene molecule (**107**). Numerous attempts at synthesising this compound were undertaken; however, they have not yet met with success. *Ab initio* (BLYP/DZd) calculations for the molecule **107** [209] predict a singlet ground state (D_2 symmetry) with τ = 45°, slight pyramidalisation and a strain energy of 93 kcal mol^{-1}. The energy of the triplet state of **107** with τ ≈ 87° would be 12 kcal mol^{-1} higher than the energy of its singlet state.

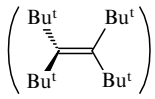

107

The alkenes **2**, **108**, and **109** have been prepared by methods used in the attempts to synthesise the compound **107**. In the molecules of these compounds, as in the molecule of **107**, the quaternary carbon atoms are linked directly to the double bonds. However, the steric repulsion in the molecules **2**, **108** and **119** is weaker than that in tetra-*tert*-butylethylene due to the presence of additional bonds between substituents.[210–213]

Krebs *et al.* [214, 215] approached very closely the synthesis of the compound **107**; they succeeded in synthesising tetrakis(2-formylpropan-2-yl)ethylene (**110**) (τ = 28.6°, according to X-ray diffraction data). However, the formyl groups proved to be so nonreactive that the researchers were unable to reduce them to the methyl groups.

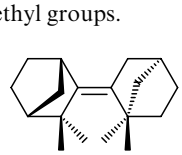

108

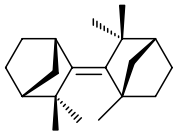

109

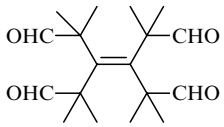

110

The relatively low reactivity of the double bond in the compounds **2** and **108**–**110** should also be mentioned. In all probability, this is due to the shielding of the π-system by bulky substituents. The *cis–trans*-isomerisation of strained alkenes proceeds much more readily than isomerisation of unstrained compounds (the energy barrier can be almost twice as low in the former case). This was used in a study [205] to estimate the energy barrier to the isomerisation of alkenes. Since isomerisation of strained alkenes takes place at relatively low temperatures, side reactions do not complicate the kinetic measurements. The standard enthalpies of formation (with an applied correction for steric effects found by MM2 calculations) of these alkenes were employed to calculate the activatiom barrier to the *cis–trans*-isomerisation (69.5 ± 0.9 kcal mol^{-1}), which does not depend on the nature of substituents at the double bond.

According to the results of a search through the CSDB, the greatest twist distortion of the double bond among acyclic compounds is found in compound **111**.[216]

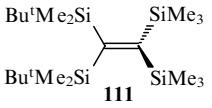

111

In the tetra(trialkylsilyl)ethylene **111**, the τ angle equals 49.6° (note that this value is greater than that predicted for tetra-*tert*-butylethylene **107**), no pyramidalisation of the carbon atoms of the C=C bond takes place, and the double bond length (1.370 Å) exceeds the typical value (1.32 Å).

b. *trans*-Cycloalkenes

Among monocyclic compounds, a substantial distortion of the double bond (mainly twist-type distortion) can be attained in *trans*-cycloalkenes in which the number of carbon atoms in the ring does not exceed nine. *trans*-Cyclooctene (**112**) is the unsubstituted compound with the smallest ring that can be isolated in a pure state at room temperature.[217, 218] The structure of *trans*-cyclooctene was determined by electron diffraction.[219] According to these studies, the C–C=C–C dihedral angle in the molecule **112** amounts to 136°. For a derivative of *trans*-cyclooctene, compound **113**, X-ray diffraction data have been published.[220] The C(8)–C(9)–C(10)–C(11) dihedral angle in the molecule **113** is 139.3°.

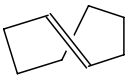

112

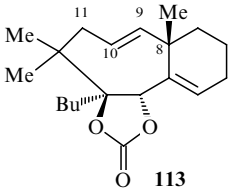

113

Further contraction of the ring containing a *trans*-double bond results in a substantial increase in the reactivity and the tendency for isomerisation to the *cis*-form. *trans*-Cycloheptene (**114**) can be synthesised at low temperatures.[221] Complexes of **114** with transition metals stable at room temperature have also been obtained.[222] Unsubstituted *trans*-cyclohexene (like *trans*-cyclopentene) has not been experimentally detected yet.

Monocyclic compound **115** with the smallest-possible ring containing a *trans*-double bond and stable at room temperature contains a silicon atom in the seven-membered ring and methyl groups in the α-positions relative to the double bond.[223] This compound proved to be sufficiently stable to be studied by X-ray diffraction analysis. The kinetic stability is ensured by the methyl group, while the presence of two C–Si bonds, which are longer than C–C bonds, makes the strain in the molecule **115** lower than that found in *trans*-cycloheptene.

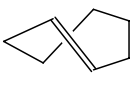

114

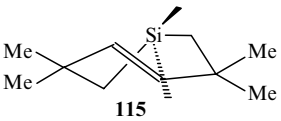

115

A substantial distortion of the double bond in **115** is reflected in the size of the C–C=C–C dihedral angle, which is 130.97°. It is of interest that the H–C=C–H dihedral angle is 173°, and pyramidalisation of the carbon atoms in the molecule **115** is insignificant. The C=C bond length (1.330 Å) deviates only slightly from the typical value, despite the substantial distortion of the dihedral angles. It should be noted that *trans*-cycloalkenes are chiral; the racemic **115** was partially resolved by column chromatography using a chiral adsorbent.

c. Polycyclic compounds with twisted double bonds: anti-Bredt alkenes

Among numerous anti-Bredt alkenes deposited in the CSBD, one can find structures in whose molecules a *trans*-double bond is incorporated into an eight-membered ring. As examples, one can mention compounds **116** and **117** (the molecule of **116** contains also a twisted amide bond [224]).

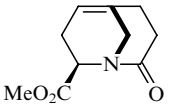

116

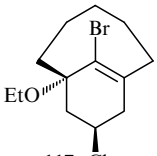

117

The following parameters have been found for the molecule **116**:[225] the angle τ = 10.8°, the average degree of pyramidalisation of the carbon atoms at the double bond χ = 28.45°.

The size of the τ angle attests to an even greater twist distortion of the double bond (τ = 29.3°) in the molecule **117**, although the degree of pyramidalisation in this molecule is lower, χ = 17.1°.[226]

The alkene **117** is very sensitive to moisture and atmospheric oxygen; the compound **116** is less reactive.

Anti-Bredt alkenes with a *trans*-double bond incorporated in rings containing not more than seven carbon atoms are known. The substantial strain in the molecules of these compounds accounts for their enhanced reactivity. The exceptionally reactive alkene **1** contains a *trans*-cyclohexene ring.[227, 228] This compound was stabilised in a solid argon matrix, and the IR absorption frequency for its double bond was determined. The unusually low frequency (1481 cm^{-1}) indicates that the π-bonding has been considerably reduced as a result of angle distortion in the molecule of **1**.

An even more strained molecule of 9-phenyl-1(9)homocubene (**118**) contains a *trans*-'double' bond in the five-membered ring. No spectroscopic or structural characteristics have been obtained so far for this compound because of its high reactivity.[229] The compound **118** rearranges into carbene **119** even at low temperatures.

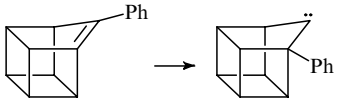

118 **119**

This reaction is uncommon for alkenes (the reverse transformation takes place much more often); the fact that this reaction does proceed implies that the properties of the double bond change substantially upon geometric distortion.

Although the compounds **1** and **118** can be regarded as 'record-breaking twisted alkenes', the *p* orbitals of their 'double' bonds are not orthogonal: the calculated τ values are much smaller than 90° (for example, τ = 64° in the molecule of **1**).[227, 228] Due to the pyramidalisation of non-bridging carbon atoms of the C=C bonds, the orbital overlap is partly restored and the τ value decreases. Perhaps, an ideally orthogonal arrangement of the π orbitals could be realised in 'fixed betweenenes' (or orthogonenes) **120**, **121** (MM2 and semiempirical calculations; no *ab initio* calculations for these structures have been carried out).[230] Tentative results on the synthesis of orthogonenes have been published.[231]

120, **121**

n = 0 (**120**), 1 (**121**).

3. Out-of-plane distortions of angles at the C=C bond: pyramidalisation

It is well-known that alkenes in which the double bond occurs in a non-symmetric environment are often characterised by a pyramidal configuration of the double-bond carbon atoms. This pyramidalisation is slight; the reasons for it are discussed in the

literature (see, for example, the reviews [232, 233]). Pyramidalisation accompanies also in-plane and twist distortion of a double bond (see above). Calculations [234] have shown that *anti*-pyramidalisation of the carbon atoms of the double bond is energetically more favourable than *syn*-pyramidalisation. However, this conclusion requires verification by means of more advanced methods of calculations than those used in the study cited.[234]

In this Section, we consider compounds the structural features of which impose pronounced *syn*-pyramidalisation. As a rule, these compounds contain a rigid polycyclic cage having two mutually perpendicular planes of symmetry one of which accommodates the double bond.[175] Examples of non-symmetric molecules have also been reported.[235] When discussing pyramidalisation in these molecules, in addition to χ, it is convenient to use the angle ϕ

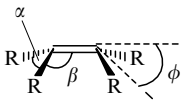

$$\cos\phi = -\frac{\cos\beta}{\cos(0.5\alpha)}$$

The first synthesised compound with a considerable pyramidalisation of the carbon atoms at the double bond (**122**) was reported more than 30 years ago;[236] at present, dozens of compounds of this type are known, for example, **123**,[237, 238] **124**,[239–241] **125**[242] and **126**.

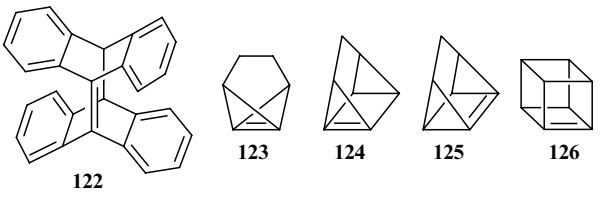

In the cubene molecule (**126**), the angle ϕ, according to the SCF/3-21G calculations, is equal to 84.1°.[243] The possibility of synthesis of the compound **126** was predicted theoretically and then realised in practice.[244] Rough thermodynamic data for cubene [245] and the first results of the study of chemical properties of this highly reactive compound [246] have been published. The calculations showed that, despite the pronounced pyramidalisation of the double-bond carbon atoms, the overlap of the *p* orbitals in the molecule **126** is sufficient for regarding this compound as an alkene rather than a biradical (TCSCF/6-31G* for the singlet state, ROHF/6-31G* for the biradical).[153] This is also indicated by an observed reaction typical of alkenes with highly pyramidalised carbon atoms of the double bond,[247] namely, cubene dimerisation to give the corresponding propellane **127** with subsequent transformation into tetraenes **128** and **129**.

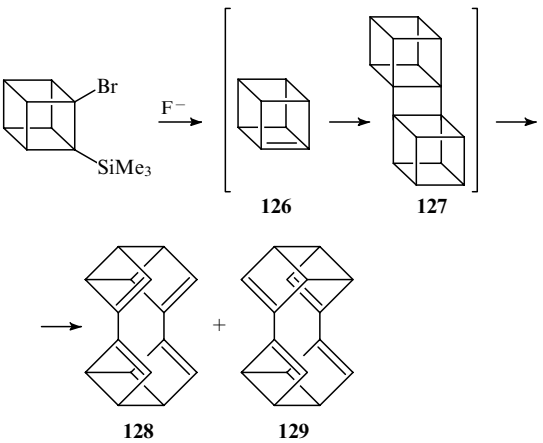

The attempts to synthesise derivatives with even more pyramidalised carbon atoms of the C=C bond, prismene, have so far been unsuccessful.[248] Both prismene isomers, **130** and **131**, have been studied theoretically [HF/6-31G(d), MP2/6-31G(d)].[249] According to calculations, the energy of the molecule **131** is lower than the energy of **130**.

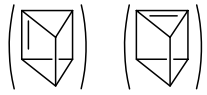

VIII. Distortions of the bond and torsion angles in the molecules of aromatic compounds

Cyclic unstrained aromatic systems are normally planar. The benzene structure,[250] which serves as a sort of standard in discussion of the nature of aromaticity,[251] has been studied in the gas phase (spectroscopic methods and electron diffraction) with high accuracy: the molecule has D_{6h} symmetry, the carbon atoms form a regular hexagon, and the C–C bond length is 1.399 ± 0.001 Å.

The types of distortion investigated for benzene derivatives include changes in the bond angles in the aromatic ring plane and out-of-plane distortions; compounds with 'conformations' similar to those of cyclohexane, *i.e.*, a chair, a boat, and a twist 'conformation,' have been obtained (Fig. 4). Below we consider only benzene derivatives (strained molecules of aromatic heterocyclic compounds have received much less attention in the literature).

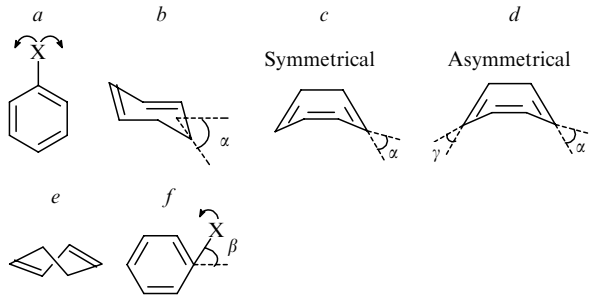

Figure 4. Bond angle distortions in benzene derivatives. (*a*) in the ring plane; (*b*–*f*) out-of-plane distortions: (*b*) chair, (*c*) symmetrical boat, (*d*) asymmetrical boat, (*e*) twist, (*f*) deviations of the C–X bond from the ring plane. The angles characterising the degree of distortion are marked.§

1. Changes in the bond angles in the plane of the benzene ring

The C–C–X bond angles at the carbon atoms of the benzene ring can markedly depart from the ideal value, equal to 120°. These distortions may be caused, in particular, by annelation of small rings to benzene. Mills and Nixon [252] postulated that annelation of cyclopentane to benzene shifts the equilibrium between the two Kekule structures.

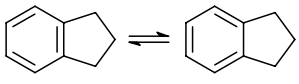

Later, the hypothesis of the existence of an equilibrium between the Kekule structures in benzene derivatives was admitted to be faulty;[50] however, localisation of the double bonds induced by annelation of strained rings was actually discovered.[253] The first experimental proof of this phenomenon was provided by the synthesis of cyclohexatrienes **132** and **133**.[254]

§ These designations of angles are used only in this Section.

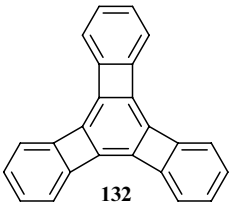

132

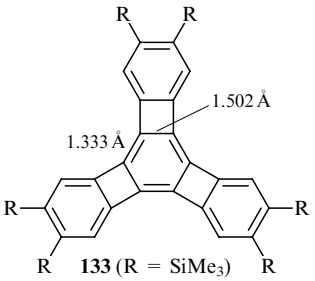

133 (R = $SiMe_3$)

The compound **133** contains, according to X-ray diffraction analysis, noticeably alternating bonds in the central ring. The unusually easy hydrogenation of the central ring in **132** also points indirectly to a substantial localisation of the double bonds.[255] Thermochemical data for this reaction have been published.[256] However, in this type of compound, localisation of the double bonds can be interpreted by assuming a smaller contribution of the structure **134**, with antiaromatic cyclobutadiene rings, to the resonance hybrid. Calculations (B3LYP/6-31G*) demonstrated that it is the bond localisation caused by annelation rather than other π-effects (aromaticity – antiaromaticty) that is responsible for the structure of these compounds.[257]

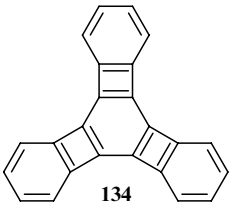

134

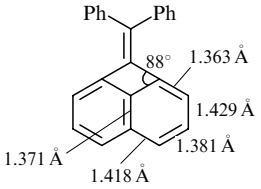

135

The clear-cut bond alternation has been found by X-ray diffraction analysis [258] in the molecules of naphthalene derivative **135**. The bond angles at the carbon atom at the *peri*-positions of the naphthalene ring differ appreciably from 120°.

Alternation of single and double bonds was to be expected in dehydrocyclobuta- and cyclopropabenzenes. It proved to be very difficult to perform the synthesis and X-ray diffraction analysis of strained compounds such as **136**–**143**. However, unexpectedly, no noticeable bond alternation was found in the molecules of these compounds.[259]

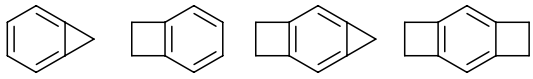

136 **137** **138** **139**

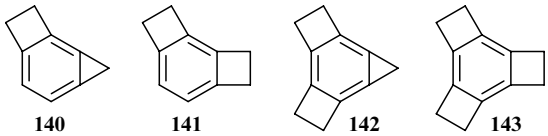

140 **141** **142** **143**

On the one hand, these results are at variance with the calculations (MP2/3-21G, HF/6-31G*) for model systems (benzene molecules with distorted C–C–H bond angles), according to which the decrease in the C–C–H angle to 90° is accompanied by pronounced localisation of the double bonds.[260] However, on the other hand, clear-cut alternation of bonds was found in the benzene ring annelated to bicyclic fragments. In the most strained molecule of this type of compound, tris(tetrahydrobicyclo[2.1.1]-hexa)benzene (**144**), noticeable bond alternation was found, first, by *ab initio* calculations [6-31G(D)(LDF)],[261] [MP2/6-31G(D)],[262] and then by X-ray diffraction analysis.[263] The C–C–C angle in the structure **144** is equal to 102.3° (which is much smaller than 120°). The reason for the observed bond alternation in the structure **144** is currently under discussion.

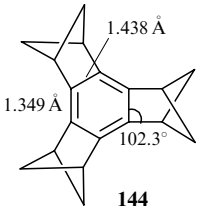

144

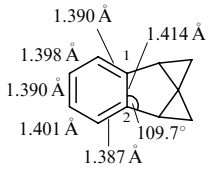

145

The alternation might be caused by the strain in the bicyclic fragments of **144**, which results in elongation of those bonds in the benzene ring at which the bicyclic fragments are annelated. A similar effect was observed for the compound **145**.[101]

2. Out-of-plane distortions of the benzene ring

a. Compounds with benzene rings in the boat 'conformation'

Among the molecules in which the benzene rings are distorted to form a boat 'conformation' typical of the cyclohexane ring, cyclophanes should be mentioned first of all.[264] In recent years, strained molecules of meta-, para- ([*n*]- and [*n.n*]-) cyclophanes have been vigorously studied. The synthesis and properties of these compounds have been considered in detail in reviews.[265–268]

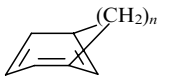

[*n*]metacyclophanes

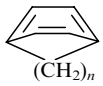

[*n*]paracyclophanes

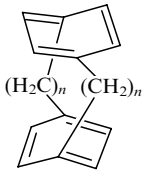

[*n,n*]paracyclophanes

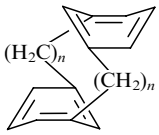

[*n,n*]metacyclophanes

The interest in these compounds, like that in the benzene derivatives **133**–**143** described above (cyclobuta- and cyclopropabenzenes can be treated as [*n*]orthocyclophanes), is related to some extent to the discussion of the nature of aromaticity.

In the case of [*n*]paracyclophanes, the benzene ring is not strained when $n = 9$; however, with a decrease in the bridge length, the ring becomes non-planar; in addition, the exocyclic C–C bonds are also distorted, in particular, they decline from the plane of the two adjacent bonds of the benzene ring (see Fig. 4 for the definition of the α and β angles characterising these distortions). Analogous distortions of the benzene rings in [*n*]metacyclophanes take place when $n \leqslant 7$. In [*n.n*]para- and -metacyclophanes, the benzene rings deviate substantially from the planar configuration at $n \leqslant 3$.

[2.2]Metacyclophane was synthesised in 1899,[269] and [2.2]paracyclophane was prepared in 1949 [270] by closure of the bridge. In the case of homologues with smaller *n* values, [*n*]paracyclophanes with $n \leqslant 7$, or [*n*]metacyclophanes with $n \leqslant 6$, this classical approach is inapplicable. The syntheses of cyclophanes with small *n* values include isomerisation of appropriately substituted valence isomers of benzene as the key stage. Six isomers of this type can be conceived (if only the CH fragments are combined, while charged species are excluded).[267] Different research groups have used four isomers,[271] most often, 3,3′-bicyclopropenyl derivatives.[265]

A decrease in the length of the bridge in cyclophane molecules results in a dramatic increase in their reactivity. The unsubstituted cyclophanes with the smallest *n* (with a saturated bridge) known to date, [4]paracyclophane (**146**) [272,273] and [1.1]paracyclophane (**147**),[274] can be stabilised only in inert matrices at low temperatures, while [4]metacyclophane (**148**) [275] and an extremely unstable [1.1]metacyclophane derivative (compound **149**) [276] were detected as short-lived intermediates.

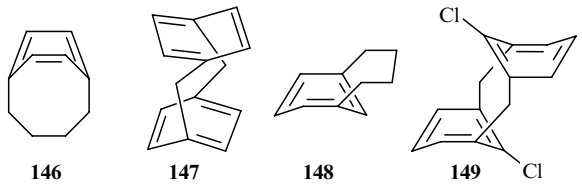

146 **147** **148** **149**

A highly unstable and, apparently, the most strained among the known [*n*]paracyclophanes, bicyclo[4.2.2]decapentaene, has been synthesised.[277] The results of experimental and theoretical studies (MP2, taking account of electron correlation)[278] suggest that the compound has the structure **150a**, which has a lower energy than the other isomer (**150b**).

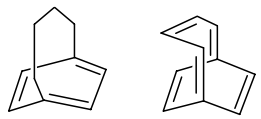

150a **150b**

To study the chemical and spectral properties and the structure of these compounds, it is necessary for them to be stable under experimental conditions. Sufficient stability was attained for strained cyclophanes having electron-withdrawing substituents or bulky groups shielding the most reactive centres, *i.e.*, bridging carbon atoms. Among the known stabilised cyclophane derivatives, the molecules of compounds **151**–**154** contain the most distorted benzene rings.[279–282]

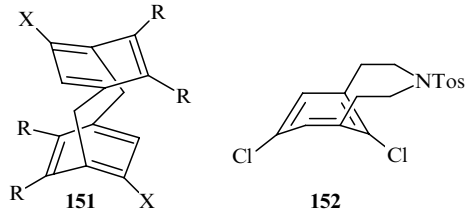

151 **152**

R = CH_2SiMe_3, X = $CONMe_2$, Tos is *p*-toluenesulfonyl.

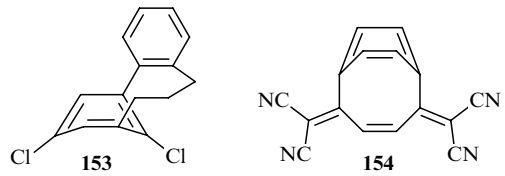

153 **154**

X-Ray diffraction data are available for the compounds **151** and **152**. Appreciable distortion of the benzene ring is indicated by the α and β angles: in the molecule **151**, $\alpha = 25.6°$ and $24.3°$, $\beta = 26.8°$ and $22.9°$, while in the molecule **152**, these parameters are even greater: $\alpha = 27.4°$, $\gamma = 12.3°$, $\beta_{max} = 48.7°$. The distance between the opposing bridging carbon atoms in the cyclophane derivative **151** is equal to 2.376(5) Å. Despite this heavy distortion of the aromatic rings, no bond alternation was detected in the compounds **151** and **152**, and the bond lengths fall in the ranges typical of unstrained benzene derivatives.

The presence of π-electron delocalisation is also indicated by NMR studies of strained cyclophanes including compounds **153** and **154**. The ^1H and ^{13}C NMR signals are exhibited in the chemical shift regions characteristic of aromatic compounds. Thus, despite the substantial distortions, the strained molecules of cyclophanes can still be regarded as aromatic. The system of π-bonds in these molecules is an 'observer' rather than a 'manager' and adapts itself to changes in the σ-core. This was confirmed by *ab initio* calculations for strained [*n*]metacyclophanes.[283] The benzene ring distortion of up to $\alpha = 30°$ is not accompanied by noticeable bond alternation. It may seem that these conclusions contradict the data on the chemical properties of strained cyclophanes, most of all, the data on the ability of these compounds to enter readily into Diels–Alder and nucleophilic substitution reactions.[266] However, one should take into account the fact that the molecules of compounds with non-planar benzene rings possess substantial strain. The reactions of the compounds result in strain relief, which is the driving force of their unusual chemical transformations.[265]

Distorted benzene rings serve as structural blocks of fullerenes; therefore, studies of strained cyclophanes are related to fullerene chemistry. Particular interest was aroused by the synthesis of compounds with fused non-planar aromatic rings, fullerene fragments,[284] for example, of 1,7-dioxa[7](2,7)pyrenophane (**155**).[285] In accordance with X-ray diffraction data, the pyrene residue in this compound is distorted to a greater extent than the similar fragment in C_{70} fullerene; the planes of non-annelated benzene rings make an angle of 109.2°.

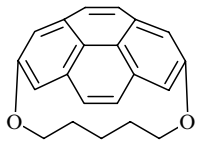

155

In conclusion, it should be noted that distortions of the benzene rings to a boat 'conformation' can be found not only in cyclophanes. In the molecules of 1,2,3-trisubstituted benzene derivatives, this conformation results in a decrease in the steric strain if the substituents are sufficiently bulky. According to analysis of CSDB structures, among benzene derivatives with bulky substituents in the 1,2,3-positions, the molecule **156** has the most distorted benzene ring.[286] The angle values $\alpha = 30.1°$, $\gamma = 11.6°$, and $\beta_{max} = 16.4°$ are comparable with the sizes of these angles in the cyclophane derivative **152**. Nevertheless, in compound **156**, no double bond localisation is found either. The strain in **156** accounts for the unusual reactivity of this compound, first of all, the tendency for isomerisation into prismane **157** [with the intermediate formation of the corresponding derivative of the Dewar benzene (**158**)], in which the steric repulsion between the *tert*-butyl groups is weaker than that in **156**.

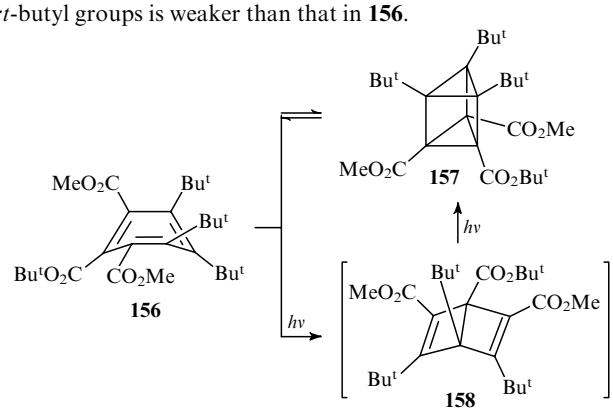

156 **157** **158**

b. Twist and chair 'conformations' of benzene rings

Due to steric repulsion of bulky substituents, the benzene ring can assume twist and chair 'conformations'. According to calculations, the chair 'conformation' can be found in the benzene ring of hexa-*tert*-butylbenzene (**159**).[287] This compound has not been synthesised so far but its less strained silyl-[288] and germyl-containing[287] analogues **160** and **161** are known.

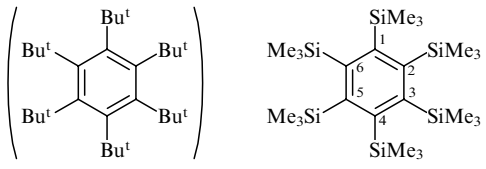

159 **160**

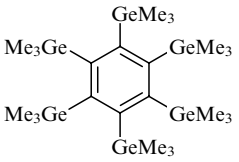

161

X-Ray diffraction analysis of the compound **160** showed that four carbon atoms of the benzene ring [C(1), C(3), C(4), C(6)] are located approximately in one plane, whereas the C(2) atom lies above this plane by ~0.1 Å and the C(5) atom is ~0.1 Å below this plane. The mean value of the C−C−C−C dihedral angle amounts to 9.8° and the C−Si bond deflects from the plane of the benzene-ring bonds adjacent to it by 22.2°. Despite the considerable distortions of the bond angles comparable to the distortions in the molecules **151**–**154**, the bond lengths in the benzene ring are normal for aromatic compounds. Analysis of the spectroscopic properties of the compound **160** shows that the compound can be considered to be aromatic but having an unusually high reactivity. The molecule **160**, similarly to the molecule **156**, is readily rearranged on exposure to radiation giving rise to a Dewar benzene derivative, hexakis(trimethylsilyl)bicyclo[2.2.0]hexa-2,5-diene (further [2 + 2]-cycloaddition to a substituted prismane was not observed). The rearrangement of the compound **160** occurring on heating resulted in benzene ring cleavage; in this case, 1,1,3,4,6,6-hexakis(trimethylsilyl)-1,2,4,5-hexatetraene was isolated. Interestingly, the benzene derivative **162** containing four *tert*-butyl groups in the adjacent positions is thermodynamically less stable than the isomer **163**, which is a Dewar benzene derivative.[289]

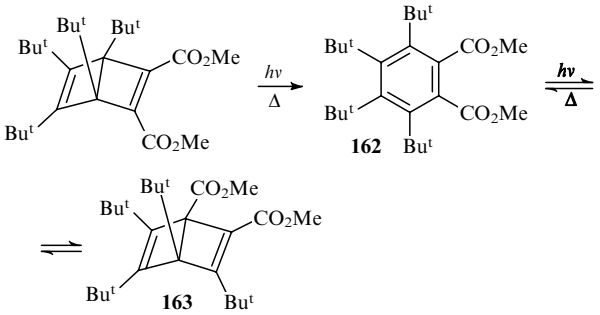

The twist 'conformation' of the benzene ring has been observed in molecules of fused aromatic compounds. Typically, these molecules contain an aromatic polycyclic system twisted to form a helix the axis of which is either perpendicular or parallel to the benzene-ring planes.

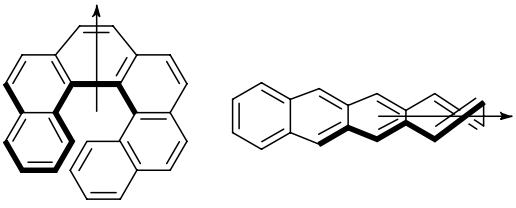

In the molecule **164**, the angle between the terminal bonds of the linear polybenzene system is 105°. Despite the steric strain, the compound **164** is exceptionally stable: it does not decompose on heating to 400 °C.[290]

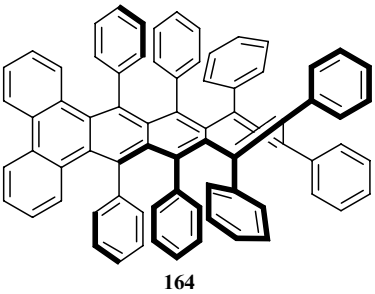

164

IX. Distortions of cumulated double bonds

Cumulenes are hydrocarbons containing two (or more) double bonds with shared carbon atoms. Strain-free cumulene molecules, for example, allene (1,2-propadiene) (**165**), 1,2,3-butatriene (**166**) and 1,2,3,4-pentatetraene (**167**) have a linear carbon skeleton of cumulated double bonds. The four substituents are located either in mutually perpendicular planes (for an even number of cumulated double bonds) or in one plane (for an odd number of these bonds).

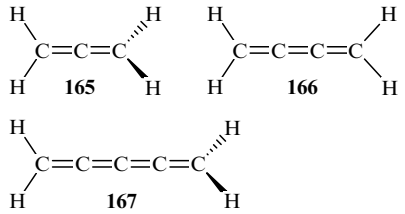

Distortions of cumulenes can include bending and twisting of the linear system of bonds. For allene, these distortions can be represented as follows:

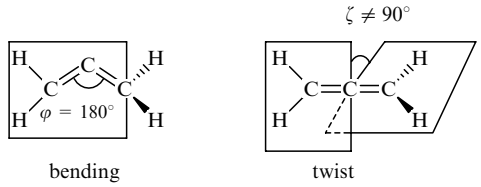

bending twist

Below we consider only allene and 1,2,3-butatriene derivatives in which cumulated double bonds are incorporated in a ring. In the molecules of these compounds, the cumulene fragment is not only bent; twist type distortion is also always observed. The properties of strained cyclic allenes have been analysed in several reviews (see, for example, reviews [291, 292]). Only few publications have been devoted to the study of molecules with predominating twist distortion such as [*n.n*]betweenallenes. In the known betweenallenes, the ζ angle between the planes formed by substituents at the terminal C(sp^2) atoms deviates insignificantly from 90°.[293, 294]

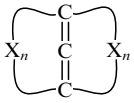

[*n*,*n*]betweenallenes

Even strain-free molecules of cumulenes are highly reactive (reactions involving them readily give stabilised intermediates).[295] Molecular distortions result in a further increase in reactivity and even in a qualitative change in the chemical properties of cumulenes.

1. Strained cyclic allenes

If the allene fragment is incorporated in a carbocycle that consists of not more than ten atoms, it inevitably becomes bent and, in addition, substituents tend to be arranged in one plane, which implies twist distortion. Model calculations showed that bending is always accompanied by twist — optimisation of an artificially bent system of two cumulated double bonds results in a twisted structure.[296] The strain energy of the molecules of cyclic allenes gradually increases up to $\varphi = 20°$ (by ~4 kcal mol^{-1}, according to the SCF/4-31 + G calulations);[297] however, subsequently it rises very steeply.

Even slight angle distortions in allene molecules entail a pronounced increase in the compound reactivity, which is anyway rather high, first of all in the tendency for polymerisation. 1,2-Cyclooctadiene the strain energy of which is calculated to be only

14 kcal mol^{-1}, has not yet been isolated in a pure state.[291] Bulky substituents at double bonds ensure the kinetic stability of allenes; the *tert*-butyl derivative of 1,2-cyclooctadiene **168** represents the smallest-ring carbocyclic allene that has been isolated at room temperature.[298] A cyclic allene with a smaller ring, 1,2-cycloheptadiene, has been stabilised in metal complexes. For compound **169**, X-ray diffraction data have been published,[299] pointing to a substantial distortion (bending and twist) of the allene fragment. Among metal complexes of this type deposited in the CSDB, the most pronounced bending of the allene fragment is found in the molecule of compound **170**, in which the φ angle is 135°.[300]

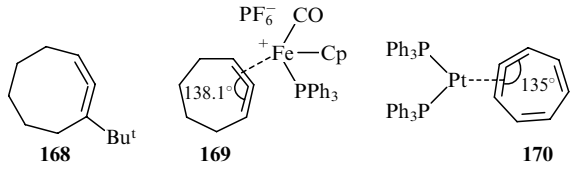

168 **169** **170**

1,2-Cyclohexadiene (**171**) has been known since 1968 when this compound was detected as a short-lived intermediate.[301] Later, it was detected by IR spectroscopy in an argon matrix at 11–170 K.[302] The compound **171** has now been thoroughly studied; according to calculations, the φ angle in this molecule is 138° (MINDO) or 134.8° (HF/6-31G**).[291] The attempts at synthesising 1,2-cyclopentadiene (**172**) have not yet met with success.[303]

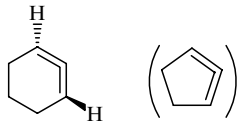

171 **172**

Cyclohexa-1,2,4-triene ('isobenzene') (**173**) has also been studied.[304] There is evidence that deprotonation of the compound **173** gives rise to the phenyl anion (**174**).[305]

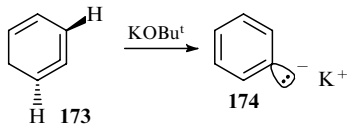

173 **174**

Stable six-membered heterocyclic compounds with a 1,2-diene fragment containing two or three heteroatoms, silicon and phosphorus, have been synthesised. The allene fragment in the cyclic allene **175** is less distorted than that in the six-membered carbocycle **171**; however, the former is stable, which allowed X-ray diffraction analysis of this compound.[306] According to X-ray diffraction data, the allene fragment is bent (φ = 166.4°) and the ζ angle between the Si—C(1)—C(2) and Si—C(3)—C(2) planes is 64.6°. Among stabilised cyclic compounds, the most distorted 1,2-diene group is found in diphosphaisobenzene **176**. A derivative of **176**, compound **177**, has been investigated by X-ray diffraction analysis.[307]

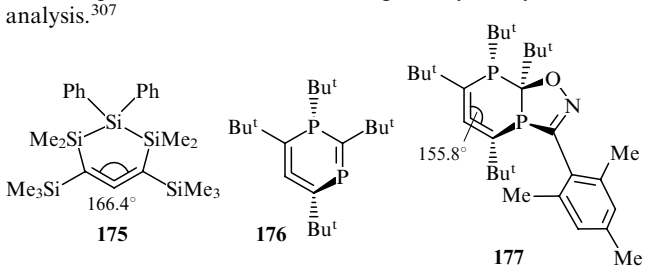

175 **176** **177**

The values for the φ (155.8°) and ζ (40.7°) angles in the molecule **177** significantly depart from the ideal values (180° and 90°, respectively); steric shielding of the central fragment caused by the *tert*-butyl groups is responsible for the rather low reactivity of compound **177**.

The accumulated knowledge makes it possible to form a picture of molecular and electronic structures of highly strained allenes. Several variants of the spatial and electronic structures of these compounds can be suggested. For example, for 1,2-cyclohexadiene, apart from the chiral allene **171**, structures with the planar HC(1)C(2)H fragment and a non-bonding sp^2-hybridised orbital located in the plane of this fragment are also possible, *i.e.*, zwitter-ions **178**, **179**, and singlet (**180**) and triplet (**181**) biradical.

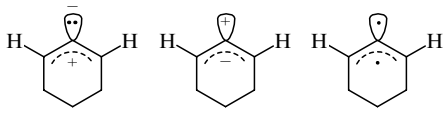

178 **179** S- **180**, T- **181**

The MCSCF/3-21G [308] and HF/6-31G* [309] calculations and experimental data [302, 309, 310] favour a non-planar chiral structure, at least, in 1,2-cycloheptadiene and 1,2-cyclohexadiene. The calculated τ angle at each double bond amounts to ~20°; this is sufficient for effective overlap of *p*-orbitals.[309] In the case of the 1,2-cyclopentadiene **172**, *ab initio* (STO, MP2/3-21G) calculations predict a relatively low energy barrier to racemisation (which might involve the intermediate formation of singlet biradical **182**) — 2–5 kcal mol^{-1} (see Ref. 311). This low value is within the error of the calculation techniques; therefore, experimental data are required to verify the results of theoretical methods.

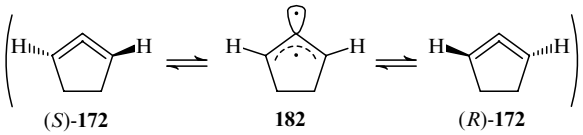

(*S*)-**172** **182** (*R*)-**172**

As regards the chemical properties of cyclic allenes, one should mention their enhanced tendency to enter into cycloaddition reactions, which were used in experiments on trapping short-lived molecules such as 1,2-cyclohexadiene. Strained allenes undergo the Diels–Alder reactions even with dienes having very low reactivity. These reactions are regioselective and *endo*-stereoselective; however, in the case of chiral allenes, no diastereoselectivity was observed. This fact was interpreted using the results of *ab initio* calculations (B3LYP/6-31G*),[312] which showed that in this case, the mechanism involving biradicals is preferred over the synchronous mechanism.

2. Cyclic butatrienes

The unstrained 1,2,3-butatriene fragment can be incorporated into a carbocycle if the number of carbon atoms in it is more than ten. Ring contraction causes bending of the linear C=C=C=C fragment, resulting in rehybridisation of carbon atoms and a substantial increase in the reactivity. Tentative experimental results showed [313] that, among unsubstituted cyclic 1,2,3-butatrienes, the minimum size of the ring which allows isolation of this compound at room temperature, is found in 1,2,3-cyclooctatriene (**183**). Homologues with smaller rings, 1,2,3-cycloheptatriene [314] (**184**) and a benzene isomer, 1,2,3-cyclohexatriene [315] (**185**), are highly reactive short-lived intermediates; only the products of cycloaddition of these species to dienes have been isolated.

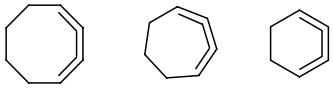

183 **184** **185**

1,2,3-Cyclopentatriene (**186**) has not been prepared to date; however, its heterocyclic analogues, 3,4-didehydrothiophene (**187**) [316] and 1-*tert*-butoxycarbonyl-3,4-didehydro-1*H*-pyrrole (**188**),[317] have been synthesised, and their chemical properties have been studied using trapping reactions.

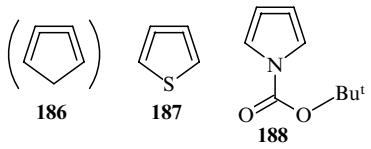

186 **187** **188**

The compound **187** was prepared and identified without substantial difficulties, although it is highly reactive. Meanwhile, the high reactivity of the heterocyclic triene **188** became a serious obstacle in the attempts to prove its existence. Among the strained butatrienes known currently, the geometry of the C=C=C=C system of bonds deviates most appreciably from linearity in the molecule **188**.[317]

Cyclic 1,2,3-butatrienes, like highly strained allenes, readily react with dienes. The high reactivity of the compounds **187** and **188** can be illustrated by their reaction with benzene, which affords cycloadducts **189** and **190**.

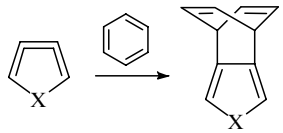

189, **190**

X = S (**189**), NCO_2Bu^t (**190**).

It was suggested that rehybridisation of the carbon atoms of the bent C=C=C=C system of bonds (like pyramidalisation of double bonds, see above) changes the electronic properties of the compounds **187** and **188** so dramatically that they can be regarded as biradicals. To support this, the researchers cited [316] reported the reaction of the heterocyclic triene **187** with tetrahydrofuran.

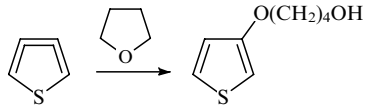

However, an ionic mechanism of this reaction is also possible. It has been shown above in relation to cubene that, even in the case of a very strong pyramidalisation of the carbon atoms of the double bond, alkenes do not exhibit properties of biradicals. Therefore, the conclusion that the compounds **187** and **188** are biradicals appears unlikely and requires further analysis.

Among isolated and structurally characterised cyclic butatrienes, we shall consider metallacyclocumulenes (**191**) with a five-membered ring consisting of a 1,2,3-butatriene fragment and a metal (titanium or zirconium).[318]

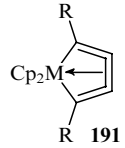

191

M = Ti, R = Bu^t, Ph; M = Zr, R = Bu^t.

The stability of compounds of the type **191** is attributable to the additional stabilisation upon the coordination of the central double bond to the metal. This coordination changes the electronic structure of cumulenes; nevertheless, for some of the complexes **191**, dimerisaition to give radialene (**192**) has been observed.[319]

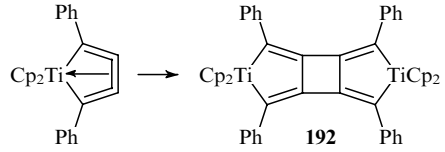

192

This reaction is also characteristic of purely organic strained cumulenes.[320] Metallacyclocumulenes have been investigated by X-ray diffraction analysis. The data obtained indicate that the central double bond is elongated and that the cumulene fragment deviates substantially from the linear geometry: the φ angle varies from 147° to 150°.

X. Bending of the $X^1-C\equiv C-X^2$ fragment

The unstrained $X^1-C\equiv C-X^2$ fragment is linear. The deviations of the bond angles at the carbon atoms from 180° are similar to the analogous deviations found in allene and butatriene molecules. The geometric distortions of the $X^1-C\equiv C-X^2$ fragment can be characterised by variation of the α_1, α_2 and θ angles.

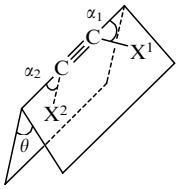

Below, we shall discuss the *cis*- ($\theta = 0°$) and *trans*- ($\theta = 180°$) bendings. Note that it is the *cis*-bending that is found in each organic molecule with a strained triple bond. The calculations showed, however, that *trans*-bending requires less energy than *cis*-bending (in a similar way as *anti*-pyramidalisation of the double bond is energetically more favourable than *syn*-pyramidalisation).[234] Probably, the lower energy of the transition state which contains a *trans*-bent fragment with a triple bond can account for the preferential *trans*-attack of alkyne molecules by nucleophilic reagents. This hypothesis has not been verified experimentally because no organic molecules with a *trans*-bent $X^1-C\equiv C-X^2$ fragment have been synthesised to date.

1. *cis*-Bending

The only known way of realisation of *cis*-bending is incorporation of the $X^1-C\equiv C-X^2$ fragment into a ring or a polycyclic cage.[292, 321] This fragment is bent in carbocyclic alkynes with the number of carbon atoms not exceeding ten. The first strained cyclic alkyne, cyclooctyne (**193**), was synthesised in 1938;[322] later, it was isolated in a pure state.[323]

Cyclooctyne is smallest-ring carbocyclic alkyne stable at room temperature. Cycloheptyne (**194**) polymerises in less than 1 min even at −25 °C in dilute solutions (at −76 °C, it is stable over several hours).[324] Homologues with smaller ring sizes, cyclohexyne (**195**)[325, 326] and cyclopentyne (**196**),[327–333] are highly reactive. They have been detected as intermediates and studied in inert matrices.

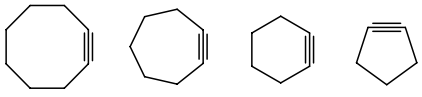

193 **194** **195** **196**

The highly strained molecules **194**–**196** can be prepared using elimination and cycloelimination reactions and by carbene rearrangements.[321] Elimination from appropriate precursors, hypervalent iodine compounds, has proved effective for this purpose.[334] Using this reaction, it was possible to prepare, perhaps, the most strained known (according to MP2/6-31G* calculations) carbocyclic molecule with a bent C−C≡C−C fragment, namely, bicyclo[2.2.1]hept-2-en-5-yne (**197**) molecule.[335]

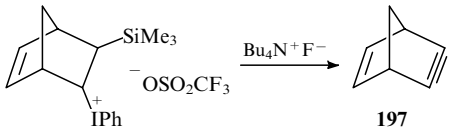

197

Cyclobutyne (**198**) and cyclopropyne (**199**) have not yet been synthesised. The results of calculations (MCSCF(4,4)/6-31G*, MP4/6-31G*//MP2/6-31G*) indicate that the compound **198** is

highly susceptible to a rearrangement to cyclopropylidenemethylene;[336] apparently, this makes this molecule 'elusive'. The existence of perfluorocyclobutyne (**200**) as an intermediate, possibly, more stable than **198**, has now been proven experimentally.[337] Metal complexes with cyclobutyne acting as a two-electron ligand have been prepared; however, cyclobutyne itself was not formed as an intermediate during the synthesis of these complexes.[338, 339]

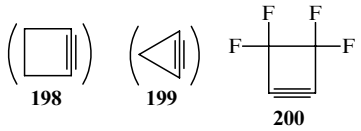

198 **199** **200**

The structure of cyclopropyne (unlike cyclobutyne) does not correspond to a minimum on the PES, even when the PES is calculated using advanced quantum-chemical techniques [such as SCF, TCSCF, CISD, TC-CISD/DZP; CCSD(T)/TZ(2df,2dp)];[340] Cyclopropyne is the only C_3H_2 isomer that has not yet been prepared. The other three isomers — cyclopropenylidene (**201**), propargylene (**202**) and propadienylidene (**203**), have been synthesised and studied in inert matrices.[341] It should be noted that investigation of the potential energy surface of C_3H_2 arouse considerable interest, among other reasons, due to the fact that the molecules **201** [342, 343] and **203** [344] were found in the interstellar space.

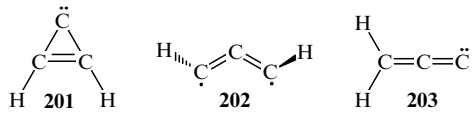

201 **202** **203**

Maier *et al.*[345, 346] synthesised a heteroanalogue of cyclopropyne, silacyclopropyne (**204**).

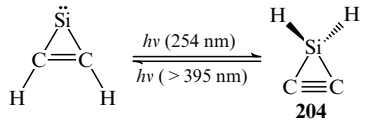

204

The identification of the compound **204** was at variance with the results of SCF/DZ calculations published previously, which indicated that the silacyclopropyne structure has properties of a saddle point rather than a minimum on the PES.[347] Maier *et al.*, who used higher-level calculations (MP2/6-31G**) demonstrated that the structure of **204** still corresponds to a local minimum on the PES; however, the IR frequencies they obtained differed somewhat from those observed experimentally. Only recent calculations [340] have given vibration frequencies on the basis of which the compound **204** was identified. The necessity of using advanced quantum-chemical methods for the prediction of properties of strained molecules such as **204** was demonstrated once again. The difference between the stabilities of cyclopropyne and silacyclopropyne can be explained by the difference between the energies of the carbenes and silapropadienylidenes $^{\cdot\cdot}C=C=XH_2$ (X = C, Si), which are formed presumably upon decomposition of the compound **199** and **204**. The energy of this species with X = Si is higher than the energy of the initial molecule **204**, whereas in the case where X = C, calculations predict the opposite situation.[346]

Cycloalkynes with a bent $X^1-C\equiv C-X^2$ fragment are susceptible to addition reactions with electrophiles, nucleophiles, and radicals.[321] Cycloaddition and oligomerisation also proceed with these molecules much more easily than with strain-free alkynes. Indeed, whereas cyclotrimerisation of strain-free alkynes requires catalysts (transition metal compounds), a similar reaction in the case of cyclic strained alkynes proceeds easily without catalysts. Moreover, the detection of benzene derivatives in the products of elimination reactions of cyclic alkenes can serve as evidence for the formation of highly strained alkynes as intermediates.[348] Trimerisation gave the above-discussed benzene derivative with annelated bicyclic fragments (**144**).

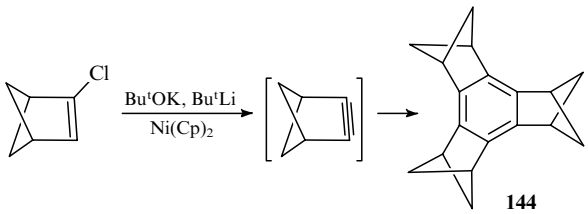

144

Cyclic alkynes stable due to either bulky substituents at the α-position relative to the C≡C bond (for example, as in molecule **205** [292]) or annelation of benzene rings (for example, as in molecule **206** [349]) have been studied by X-ray diffraction analysis. The search through the CSDB showed that in the molecules characterised by the most bent $X^1-C\equiv C-X^2$ fragment, the α_1 and α_2 angles approach ~30°.

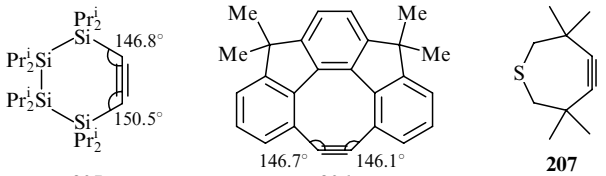

205 **206** **207**

The structure of compound **207** has been studied by electron diffraction in the gas phase.[350–352]

The α_1 and α_2 angles in the molecule **207** are 34.2° and 30.7°, which is somewhat greater than those in **205** or **206**. Despite the pronounced bond angle distortions, the C≡C bond lengths in the compounds **205** and **207** remain within the limits typical of acyclic linear alkynes. Only in some cases (for example, in the molecule **206**), was the triple bond elongated (1.20–1.23 Å).

Finally, we should mention a new, original method of stabilisation of strained molecules and reactive intermediates, which allows one to gain spectroscopic data for these species in solutions at room temperature. The idea of this approach is to generate unstable molecules inside 'molecular vessels' — carcerands and hemicarcerands. Cyclobutadiene [353] and 1,2-dehydrobenzene (**208**) [354, 355] have been fixed in this way. Warmuth [354] has tackled the question whether the molecule **208** should be assigned to strained alkynes or to bent cumulenes. 1,2-Dehydrobenzene was prepared by exposure to UV light of benzocyclobutenedione inside hemicarcerand (**209**). For the compound **208** stabilised in

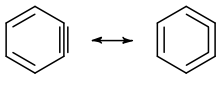

208a **208b**

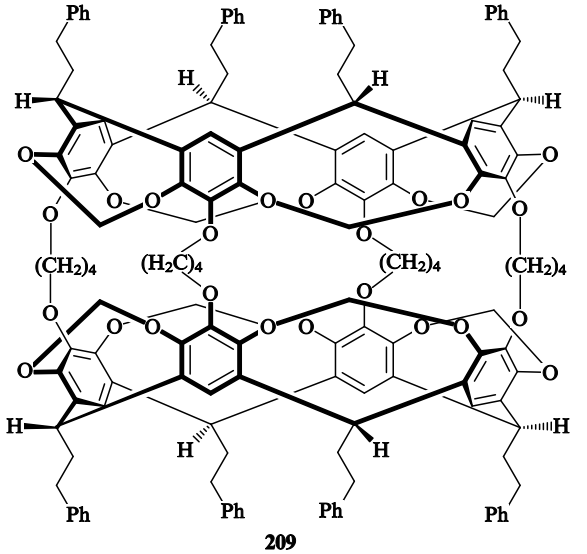

209

this way, it was possible to record the ^{1}H and ^{13}C NMR spectra before the compound has reacted with the host molecule.

Analysis of the NMR spectra led to quite an unexpected conclusion: the spectroscopic data are best described by a hybrid of two contributing structures, **208a** and **208b**, with a predominant contribution of **208b**. This interpretation, however, is inconsistent with the results of other studies (see, for example, Ref. 356).

2. *trans*-Bending

Synthesis of a molecule with a *trans*-bent $X^1-C\equiv C-X^2$ fragment is a difficult task: the shortage of substituents at a triple bond precludes creation of such a bending. However, *trans*-bending of an alkyne ligand can be attained in metal complexes. The first complex of this type **210** was prepared in 1995.[357]

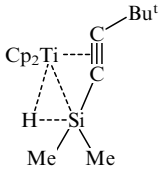

210

A whole series of titanium and zirconium complexes of this type are currently known.[358] In the compound **210**, the agostic Si···H···Ti interaction ensures the *trans*-arrangement of substituents at the C≡C bond coordinated to titanium. The angles $\alpha_1 = 30.5°$ (for Si−C≡C) and $\alpha_2 = 44.8°$ (for C−C≡C) indicate a substantial distortion of bond angles at a triple bond. However, it should be noted that metal coordination also changes substantially the properties of a triple bond, for example, in the complex **210**, the bond length is increased to 1.275(9) Å.

The author is grateful to professors M Yu Kornilov and R R Kostikov, colleagues S P Verevkin, V V Burlakov and V I Tararov for critical remarks, corrections and assistance in preparing the manuscript, and to a colleague, mathematician O B Pikhurko, for consultation and help in the solution of mathematical problems. The author is especially grateful to Corresponding Member of the Russian Academy of Sciences M Yu Antipin for constructive criticism and discussion of the manuscript. This review was written with financial support of the Alexander von Humboldt Foundation (Germany).

References

1. L E Sutton (Ed.) *Tables of Interatomic Distances and Configuration in Molecules and Ions* (London: Chemical Society, 1965)
2. F H Allen, O Kennard, D G Watson, L Brammer, A G Orpen, R Taylor *J. Chem. Soc., Perkin Trans. 2* S1 (1987)
3. E Osawa, in *The Chemistry of Alkanes and Cycloalkanes* (Eds S Patai, Z Rappoport) (New York: Wiley, 1992) p. 79
4. F H Allen, S E Garner, in *The Chemistry of Triple-Bonded Functional Groups* (Ed. S Patai) (New York: Wiley, 1994) p. 4
5. E Eliel, S H Wilen *Stereochemistry of Organic Compounds* (New York: Wiley, 1994)
6. A R Leach *Molecular Modelling. Principles and Applications* (Harlow: Longman, 1996)
7. W H Perkin *Ber. Dtsch. Chem. Ges.* **16** 1787 (1883)
8. W H Perkin *Ber. Dtsch. Chem. Ges.* **17** 54 (1884)
9. V Meyer *Justus Liebigs Ann. Chem.* **180** 192 (1876)
10. M I Page, A Williams *Organic and Bioorganic Mechanisms* (Harlow: Longman, 1997)
11. R R Kostikov *Sovremen. Probl. Org. Khim.* 34 (1987)
12. R S Atkinson, M J Grimshire,B J Kelly *Tetrahedron* **45** 2875 (1989)
13. K C Nicolaou, E J Sorensen *Classics in Total Synthesis* (Weinheim: Wiley-VCH, 1996)
14. J F Liebman, A Greenberg *Chem. Rev.* **76** 311 (1976)
15. A Greenberg, J F Liebman *Strained Organic Molecules* (New York; San Francisco; London: Academic Press, 1978)
16. STNR, http://stn-international.del
17. F H Allen, J E Davies, J J Galloy, O Johnson, O Kennard, C F Macrae, E M Mitchell, G F Mitchell, J M Smith, D G Watson *J. Chem. Inf. Comp. Sci.* **31** 187 (1991)
18. H-J Quadbeck-Seeger, R Faust, G Knaus, A Maelicke, U Siemeling *Chemie Rekorde: Menschen, Märkte, Molecüle* (Weinheim: Wiley-VCH, 1999)
19. P v R Schleyer, J E Williams, K R Blanchard *J. Am. Chem. Soc.* **92** 2377 (1970)
20. K B Wiberg *Angew. Chem.* **98** 312 (1986)
21. F Jensen *Introduction to Computational Chemistry* (Weinheim: Wiley, 1999)
22. T T Tidwell *Tetrahedron* **34** 1855 (1978)
23. B D Kybett, S Carroll, P Natalis, D W Bonnell, J L Margrave, J L Franklin *J. Am. Chem. Soc.* **88** 626 (1966)
24. D R Kirklin, K L Churney, E S Domalski *J. Chem. Thermodyn.* **21** 1105 (1989)
25. V V Avdonin, E P Kirpichev, Yu I Rubtsov, L B Romanova, M E Ivanova, L T Eremenko *Izv. Akad. Nauk, Ser. Khim.* 2472 (1996) [a]
26. P E Eaton *Angew. Chem.* **104** 1447 (1992)
27. H-D Beckhaus, S Verevkin, C Rüchardt, F Diederich, C Thilgen, H-U ter Meer, H Mohn, W Müller *Angew. Chem.* **106** 1033 (1994)
28. W Luef, R Keese *Top. Stereochem.* **20** 231 (1991)
29. A J Kirby, I V Komarov, N Feeder *J. Am. Chem. Soc.* **120** 7101 (1998)
30. W Sander, A Kirschfeld, in *Advances in Strain in Organic Chemistry* Vol. 4 (Ed. B Halton) (London: JAI Press, 1995) p. 1
31. G Maier, H P Reisenauer, T Preiss, H Pacl, D Jürgen, R Tross, S Senger *Pure Appl. Chem.* **69** 113 (1997)
32. R Warmuth *Eur. J. Org. Chem.* 423 (2001)
33. G Kaupp, J Boy *Angew. Chem.* **109** 48 (1997)
34. M A Flamm-ter Meer, H-D Beckhaus, K Peters, H-G von Schnering, C Rüchardt *Chem. Ber.* **118** 4665 (1985)
35. V R Polishchuk, M Yu Antipin, V I Bakhmutov, N N Bubnov, S P Solodovnikov, T V Timofeeva, T Yu Struchkov, B L Tumanskii, I L Knunyants *Dokl. Akad. Nauk SSSR* **249** 1125 (1979) [b]
36. B Kahr, D Van Engen, K Mislow *J. Am. Chem. Soc.* **108** 8305 (1986)
37. F Toda, K Tanaka, Z Stein, I Goldberg *Acta Crystallogr., Sect. C* **52** 177 (1996)
38. M Ehrenberg *Acta Crystallogr.* **20** 183 (1966)
39. G Kaupp *Liebigs Ann. Chem.* 844 (1973)
40. T R Battersby, P Gantzel, K K Baldridge, J S Siegel *Tetrahedron Lett.* **36** 845 (1995)
41. K K Baldridge, Y Kasahara, K Ogawa, J S Siegel, K Tanaka, F Toda *J. Am. Chem. Soc.* **120** 6167 (1998)
42. C H Choi, M Kertesz *Chem. Commun.* 2199 (1997)
43. K K Baldridge, T R Battersby, R VernonClark, J S Siegel *J. Am. Chem. Soc.* **119** 7048 (1997)
44. F Toda, K Tanaka, M Watanabe, K Tamura, I Miyahara, T Nakai, K Hirotsu *J. Org. Chem.* **64** 3102 (1999)
45. F Toda *Eur. J. Org. Chem.* 1377 (2000)
46. A Almenningen, B Andersen, B A Nyhus *Acta Chem. Scand.* **25** 1217 (1971)
47. J F Chiang, S H Bauer *J. Am. Chem. Soc.* **92** 1614 (1970)
48. J L Adcock, A A Gakh, J L Pollitte, C Woods *J. Am. Chem. Soc.* **114** 3980 (1992)
49. W Adcock, A V Blokhin, G M Elsey, N H Head, A R Krstik, M D Levin, J Michl, J Munton, E Pinkhassik, M Robert, J M Savéant, A Shtarev, I Stibor *J. Org. Chem.* **64** 2618 (1999)
50. L Pauling *Nature of the Chemical Bond* (New York: Cornell University Press, 1960)
51. J J Novoa, P Laufente, R E Del Sesto, J S Miller *Angew. Chem.* **113** 2608 (2001)
52. R F W Bader *Atoms in Molecules — a Quantum Theory* (Oxford: Oxford University Press, 1990)
53. R Gilardi, M Maggini, P E Eaton *J. Am. Chem. Soc.* **110** 7232 (1988)
54. R A Alden, J Kraut, T G Traylor *J. Am. Chem. Soc.* **90** 74 (1968)
55. M Tanimoto, K Kuchitsu, Y Morino *Bull. Chem. Soc. Jpn.* **44** 386 (1971)
56. P v R Schleyer, M Bremer *Angew. Chem.* **101** 1264 (1989)
57. O Ermer, P Pell, J Schäfer, G Szeimies *Angew. Chem.* **101** 503 (1989)

58. Z Rappoport *The Chemistry of the Cyclopropyl Group* (New York: Wiley, 1987)
59. H Irngartinger, K L Lukas *Angew. Chem.* **91** 750 (1979)
60. C H Görbitz, A Mostad *Acta Chem. Scand.* **47** 509 (1993)
61. Q-C Yang, M F Richardson, J D Dunitz *Acta Crystallogr., Sect. B* **45** 312 (1989)
62. K K Baldridge, B Biggs, D Bläser, R Boese, R D Gilbertson, M M Haley, A H Maulitz, J S Siegel *Chem. Commun.* 1137 (1998)
63. R Boese, J Benet-Buchholz, A Stanger, K Tanaka, F Toda *Chem. Commun.* 319 (1999)
64. J M Schulman, R L Disch *J. Am. Chem. Soc.* **115** 11153 (1993)
65. J L Hencher, in *The Chemistry of The Carbon*—Carbon Triple Bond (Ed. S Patai) (New York: Wiley, 1978)
66. K S Feldman, C M Kraebel *J. Am. Chem. Soc.* **115** 3846 (1993)
67. J H Van't Hoff *Arch. Neerl. Sci. Exactes Nat.* **9** 445 (1874)
68. J-A LeBel *Bull. Soc. Chim. Fr.* **22** 337 (1874)
69. A Baeyer *Ber. Dtsch. Chem. Ges.* **18** 2269 (1885)
70. P Murray-Rust, H B Bürgi, J D Dunitz *Acta Crystallogr., Sect. B* **34** 1787 (1978)
71. W Luef, R Keese, H-B Bürgi *Helv. Chim. Acta* **70** 534 (1987)
72. W Luef, R Keese *Helv. Chim. Acta* **70** 543 (1987)
73. M A Spackman *Annu. Rep. Progr. Chem.* **94** 117 (1997)
74. R Boese, N Niederprüm, D Bliser, A Maulitz, M Yu Antipin, P R Mallinson *J. Phys. Chem.* **101** 5794 (1997)
75. T S Koritsanszky, P Coppens *Chem. Rev.* **101** 1583 (2001)
76. P Coppens *X-Ray Charge Densities and Chemical Bonding* (Oxford: Oxford University Press, 1977)
77. D Nijveldt, A Vos *Acta Crystallogr., Sect B* **44** 281 (1988)
78. K A Lyssenko, M Yu Antipin *Inorg. Chem.* **37** 5834 (1998)
79. G W Griffin, A P Marchand *Chem. Rev.* **89** 997 (1989)
80. N S Zefirov, T S Kuznetsova, A N Zefirov *Izv. Akad. Nauk, Ser. Khim.* 1613 (1995) [a]
81. A de Meijere, S I Kozhushkov *Chem. Rev.* **100** 93 (2000)
82. G Alcaraz, U Wecker, A Baceiredo, F Dahan, G Bertrand *Angew. Chem.* **107** 1358 (1995)
83. D H R Barton, J Cs Jaszberenyi, E A Theodorakis, J H Reibenspies *J. Am. Chem. Soc.* **115** 8050 (1993)
84. M P Johnson, D B Puranik, M J Fink *Acta Crystallogr., Sect. C* **47** 126 (1991)
85. A L Spek *Acta Crystallogr., Sect. C* **46** 1357 (1990)
86. J M Schulman, T J Venanzi *J. Am. Chem. Soc.* **96** 4739 (1974)
87. M N Glukhovtsev, S Laiter, A Pross *J. Phys. Chem.* **99** 6828 (1995)
88. A J Gordon, R A Ford *The Chemist's Companion* (New York: Wiley-Interscience, 1972)
89. H A Staab, E Wehinger, W Thorwart *Chem. Ber.* **105** 2290 (1972)
90. L T Scott, M Jones *Chem. Rev.* **72** 181 (1972)
91. G Maier, S Pfriem, U Schäfer, R Matusch *Angew. Chem.* **90** 552 (1978)
92. G Maier, F Fleischer, H-O Kalinowski *Liebigs Ann. Chem.* 173 (1995)
93. G Maier, D Born, I Bauer, R Wolf, R Boese, D Cremer *Chem. Ber.* **127** 173 (1994)
94. G Maier, D Born *Angew. Chem.* **101** 1085 (1989)
95. S Masamune, N Nakamura, M Suda, H Ona *J. Am. Chem. Soc.* **95** 8481 (1973)
96. G Maier, R Wolf, H-O Kalinowski, R Boese *Chem. Ber.* **127** 191 (1994)
97. H Irngartinger, A Goldmann, R Jahn, M Nixdorf, H Rodewald, G Maier, K-D Malsch, R Emrich *Angew. Chem.* **96** 967 (1984)
98. W D Hounshell, K Mislow *Tetrahedron Lett.* 1205 (1979)
99. M Balci, M L McKee, P v R Schleyer *J. Phys. Chem. A* **104** 1246 (2000)
100. G Maier, H Rang, R Emrich, S Gries, H Irngartinger *Liebigs Ann. Chem.* 161 (1995)
101. R Boese, D Bläser, K Gomann, U H Brinker *J. Am. Chem. Soc.* **111** 1501 (1989)
102. K B Wiberg, J R Snoonian *J. Org. Chem.* **63** 1402 (1989)
103. E T Seidl, H F Schaefer III *J. Am. Chem. Soc.* **113** 1915 (1991)
104. H Dodziuk, J Leszynski, K S Nowinski *J. Org. Chem.* **60** 6860 (1995)
105. K B Wiberg, J R Snoonian *J. Org. Chem.* **63** 1390 (1998)
106. W Luef, R Keese, in *Advances in Strain in Organic Chemistry* Vol. 3 (Ed. B Halton) (London: JAI Press, 1993) p. 229
107. D Röttger, G Erker *Angew. Chem.* **109** 840 (1997)
108. W Siebert, A Gunale *Chem. Soc. Rev.* **28** 367 **(**1999)
109. W C Agosta, in *The Chemistry of Alkanes and Cycloalkanes* (Eds S Patai, Z Rappoport) (New York: Wiley, 1992) p. 927
110. K Sorger, P v R Schleyer *J. Mol. Struct.* **338** 317 (1995)
111. R Hoffmann, R W Alder, C F Wilcox Jr *J. Am. Chem. Soc.* **92** 4992 (1970)
112. M-B Krogh-Jespersen, J Chandrasekhar, E-U Würtwein, J B Collins, P v R Schleyer *J. Am. Chem. Soc.* **102** 2263 (1980)
113. M S Gordon, M W Schmidt *J. Am. Chem. Soc.* **115** 7486 (1993)
114. M J M Pepper, I Shavitt, P v R Schleyer, M N Glukhovtsev, R Janoschek, M Quack *J. Comput. Chem.* **16** 207 (1995)
115. J B Collins, J D Dill, E D Jemmis, Y Apeloig, P v R Schleyer, R Seeger, J A Pople *J. Am. Chem. Soc.* **98** 5419 (1976)
116. H Kawa, B C Manley, R J Ladow *J. Am. Chem. Soc.* **107** 5313 (1985)
117. X Li, H-F Zhang, L-S Wang, G D Geske, A I Boldyrev *Angew. Chem.* **112** 3776 (2000)
118. F A Cotton, M Millar *J. Am. Chem. Soc.* **99** 7886 (1977)
119. R Keese, A Pfenninger, A Roesle *Helv. Chim. Acta* **62** 326 (1979)
120. M W Wong, L Radom *J. Am. Chem. Soc.* **111** 1155 (1989)
121. D Stahl, F Maquin, T Gäumann, H Schwarz, P-A Carrupt, P Vogel *J. Am. Chem. Soc.* **107** 5049 (1985)
122. V B Rao, C F George, S Wolff, W C Agosta *J. Am. Chem. Soc.* **107** 5732 (1985)
123. H Dodziuk *J. Mol. Struct.* **239** 167 (1990)
124. M P McGrath, L Radom, H F Schaefer III *J. Org. Chem.* **57** 4847 (1992)
125. J M Schulman, R L Disch *J. Am. Chem. Soc.* **107** 5059 (1985)
126. S Wolff, R B Venepalli, C F George, W C Agosta *J. Am. Chem. Soc.* **110** 6785 (1988)
127. D R Rasmussen, L Radom *Angew. Chem.* **111** 3052 (1999)
128. R L Rasmussen *Pure Appl. Chem.* **70** 1977 (1998)
129. K B Wiberg, J E Hiatt, G Burgmaier *Tetrahedron Lett.* 5855 (1968)
130. K B Wiberg, G J Burgmaier *Tetrahedron Lett.* 317 (1969)
131. K B Wiberg, G J Burgmaier, K-W Shen, S J La Placa, W C Hamilton, M D Newton *J. Am. Chem. Soc.* **94** 7402 (1972)
132. F H Walker, K B Wiberg, J Michl *J. Am. Chem. Soc.* **104** 2056 (1982)
133. K B Wiberg, F H Walker *J. Am. Chem. Soc.* **104** 5239 (1982)
134. K B Wiberg *Chem. Rev.* **89** 975 (1989)
135. K B Wiberg, J J Wendoloski *J. Am. Chem. Soc.* **104** 5679 (1982)
136. K Semmler, G Szeimies, J Belzner *J. Am. Chem. Soc.* **107** 6410 (1985)
137. J Belzner, B Gareiß, K Polborn, W Schmid, K Semmler, G Szeimies *Chem. Ber.* **122** 1509 (1989)
138. M D Levin, P Kaszynski, J Michl *Chem. Rev.* **100** 169 (2000)
139. K B Wiberg, W P Dailey, F H Walker, S T Waddell, L S Crocker, M Newton *J. Am. Chem. Soc.* **107** 7247 (1985)
140. L Hedberg, K Hedberg *J. Am. Chem. Soc.* **107** 7257 (1985)
141. P Seiler *Helv. Chim. Acta* **73** 56 (1990)
142. D Feller, E R Davidson *J. Am. Chem. Soc.* **109** 4133 (1987)
143. P Seiler, J Belzner, U Bunz, G Szeimies *Helv. Chim. Acta* **71** 2100 (1988)
144. K B Wiberg, R F W Bader, C D H Lau *J. Am. Chem. Soc.* **109** 985 (1987)
145. K W Cox, M D Harmony, G Nelson, K B Wiberg *J. Chem. Phys.* **50** 1976 (1969)
146. P L Johnson, J P Schaefer *J. Org. Chem.* **37** 2762 (1972)
147. J Z Gougoutas *Acta Crystallogr., Sect. C* **8** 135 (1979)
148. P G Gassman, M J Mullins *Tetrahedron Lett.* 4445 (1979)
149. R Bartnik, Z Cebulska, R Faure *J. Chem. Soc., Chem. Commun.* 148 (1993)
150. G Fritz, S Wartanessian, E Matern, W Honle, H G von Schnering *Z. Anorg. Allg. Chem.* **475** 87 (1981)
151. E Niecke, A Fuchs, M Nieger *Angew. Chem.* **111** 3213 (1999)
152. K Hassenrück, J G Radziszewski, V Balaji, G S Murthy, A J McKinley, D E David, V M Lynch, H-D Martin, J Michl *J. Am. Chem. Soc.* **112** 873 (1990)
153. D A Hrovat, W T Borden *J. Am. Chem. Soc.* **112** 875 (1990)
154. P E Eaton, J Tsanaktsidis *J. Am. Chem. Soc.* **112** 876 (1990)
155. H Dodziuk, J Leszczynski, K Jackowski *J. Org. Chem.* **64** 6177 (1999)
156. E R Davidson *J. Am. Chem. Soc.* **119** 1449 (1997)

157. V I Minkin, R M Minyaev, I I Zakharov *J. Chem. Soc., Chem. Commun*. 213 (1977)
158. V I Minkin, R M Minyaev, I I Zakharov, V I Avdeev *Zh. Org. Khim*. **14** 3 (1978) [c]
159. E M Holt, K H Whitmire, D F Shriver *J. Organomet. Chem*. **213** 125 (1981)
160. J S Bradley, G B Ansell, M E Leonowicz, E W Hill *J. Am. Chem. Soc*. **103** 4968 (1981)
161. E H Braye, L F Dahl, W Hübel, D L Wampler *J. Am. Chem. Soc*. **84** 4633 (1962)
162. D H Farrar, P F Jackson, J Lewis, J N Nicholls *J. Chem. Soc., Chem. Commun*. 415 (1981)
163. E L Muetterties, J Stein *Chem. Rev*. **79** 479 (1979)
164. D H Shriver *The Chemistry of Metal Cluster Complexes* (New York: Wiley, 1990)
165. V I Minkin, R M Minyaev *Zh. Org. Khim*. **15** 225 (1979) [c]
166. V I Minkin, R M Minayev, G V Orlova *J. Mol. Struct*. **110** 241 (1984)
167. D R Rasmussen, L Radom *Chem. Eur. J*. **6** 2470 (2000)
168. K B Wiberg, J V McGlusky *Tetrahedron Lett*. **28** 5411 (1987)
169. K B Wiberg, N McMurdie, J V McGlusky, C M Hadad *J. Am. Chem. Soc*. **115** 10653 (1993)
170. A Baeyer *Liebigs Ann. Chem*. **258** 145 (1890)
171. J Bredt *Liebigs Ann. Chem*. **437** 1 (1924)
172. J Bredt *Ann. Acad. Sci. Fenn*. **29** 1 (1927)
173. G Szeimies, in *Advances in Strain in Organic Chemistry* Vol. 2 (Ed. B Halton) (London: JAI Press, 1992) p. 1
174. W E Billups, M M Haley, G-A Lee *Chem. Rev*. **89** 1147 (1989)
175. W T Borden *Chem. Rev*. **89** 1095 (1989)
176. P M Warner *Chem. Rev*. **89** 1067 (1989)
177. O Ermer *Aspekte von Kraftfeldrechnungen* (München: Verlag Chemie, 1981)
178. T P Radhakrishnan, D Van Engen, Z G Soos *Mol. Cryst. Liq. Cryst*. **150** 473 (1987)
179. S Yoneda, M Shibata, S Kida, Z Yoshida, Y Kai, N Kasai *Angew. Chem*. **96** 75 (1984)
180. I Sotofte, I Crossland *Acta Chem. Scand*. **43** 168 (1989)
181. J Kopf, G Starova, V Plotkin, I Domnin *Acta Crystallogr., Sect. C* **46** 1707 (1990)
182. N Tokitoh, H Hayakawa, M Goto, W Ando *Chem. Lett*. 961 (1988)
183. W Clegg, A R Al Dulayymi, M S Baird *Acta Crystallogr., Sect. C* **52** 3919 (1996)
184. H-U Wagner, G Szeimies, J Ghandrasekhar, P v R Schleyer, J A Pople, J S Binkley *J. Am. Chem. Soc*. **100** 1210 (1978)
185. W Ando, Y Hanyu, T Takata *J. Am. Chem. Soc*. **106** 2216 (1984)
186. N G Rondan, M N Paddon-Row, P Caramella, K N Houk *J. Am. Chem. Soc*. **103** 2436 (1981)
187. O Ermer, P Bell, S A Mason *Angew. Chem*. **101** 1298 (1989)
188. L A Paquette, C-C Shen, J A Krause *J. Am. Chem. Soc*. **111** 2351 (1989)
189. L A Paquette, C-C Shen *J. Am. Chem. Soc*. **112** 1159 (1990)
190. R V Williams, M E Colvin, N Tran, R N Warrener, D Margetic *J. Org. Chem*. **65** 562 (2000)
191. P J Chenier, M J Bauer, C L Hodge *J. Org. Chem*. **57** 5959 (1992)
192. G-A Lee, A N Huang, C-S Chen, Y C Li, Y-C Jann *J. Org. Chem*. **62** 3355 (1997)
193. M Mühlebach, M Neuenschwander *Chimia* **45** 24 (1991)
194. P J Chenier, D A Southard Jr *J. Org. Chem*. **55** 4333 (1990)
195. G-A Lee, Y-H Lin, A N Huang, Y C Li, Y-C Jann, C-S Chen *J. Am. Chem. Soc*. **121** 5328 (1999)
196. N L Allinger *J. Am. Chem. Soc*. **80** 1953 (1958)
197. N L Allinger, J T Sprague *J. Am. Chem. Soc*. **94** 5734 (1972)
198. W L Mock *Tetrahedron Lett*. 475 (1972)
199. J Michl, V Bonacic-Koutecký *Tetrahedron* **44** 7559 (1988)
200. V Bonacic-Koutecký, J Koutecký, J Michl *Angew. Chem*. **99** 216 (1987)
201. O Takahashi, O Kikuchi *Tetrahedron* **46** 3803 (1990)
202. J Sandström *Top. Stereochem*. **14** 83 (1983)
203. J E Douglas, B S Rabinovitch, F S Looney *J. Chem. Phys*. **23** 315 (1955)
204. B S Rabinovitch, K-W Michel *J. Am. Chem. Soc*. **81** 5065 (1959)
205. W v E Doering, W R Roth, F Bauer, R Breuckmann, T Ebbrecht, M Herbold, R Schmidt, H-W Lennartz, D Lenoir, R Boese *Chem. Ber*. **122** 1263 (1989)
206. K Baum, S S Bigelow, N V Nguyen, T G Archibald, R Gilardi, J L Flippen-Anderson, C George *J. Org. Chem*. **57** 235 (1992)
207. R Destro, U Cosentino, G Moro, E Ortoleva, T Pilati *J. Mol. Struct*. **212** 97 (1989)
208. T Takahashi, W-H Sun, K Nakajima *Chem. Commun*. 1595 (1999)
209. H M Sulzbach, E Bolton, D Lenoir, P v R Schleyer, H F Schaefer III *J. Am. Chem. Soc*. **118** 9908 (1996)
210. T Loerzer, R Gerke, W Lüttke *Tetrahedron Lett*. **24** 5861 (1983)
211. P R Brooks, R Bishop, J A Counter, E R T Tiekink *J. Org. Chem*. **59** 1365 (1994)
212. T G Back, D H R Barton, M R Britten-Kelly, F S Guziec *J. Chem. Soc., Perkin Trans. 1* 2079 (1976)
213. T Pilati, M Simonetta *J. Chem. Soc., Perkin Trans. 2* 1435 (1977)
214. A Krebs, W-U Nickel, L Tikwe, J Kopf *Tetrahedron Lett*. **26** 1639 (1985)
215. A Krebs, B Kaletta, W-U Nickel, W Rüger, L Tikwe *Tetrahedron* **42** 1693 (1986)
216. H Sakurai, H Tobita, Y Nakadaira, C Kabuto *J. Am. Chem. Soc*. **104** 4288 (1982)
217. K Ziegler, H Wilms *Justus Liebigs Ann. Chem*. **567** 1 (1950)
218. A C Cope, R A Pike, C F Spencer *J. Am. Chem. Soc*. **75** 3212 (1953)
219. M Traetteberg *Acta Chem. Scand., Ser. B* **29** 29 (1975)
220. D Bourgeois, A Pancrazi, L Richard, J Prunet *Angew. Chem*. **112** 741 (2000)
221. Y Inone, S Takamutu, H Sakurai *J. Chem. Soc., Perkin Trans. 2* 1635 (1977)
222. J T M Evers, A Mackor *Recl. Trav. Chim. Pays-Bas* **98** 423 (1979)
223. A Krebs, K-I Pforr, W Raffay, B Thölke, W A König, I Hardt, R Boese *Angew. Chem*. **109** 159 (1997)
224. A Greenberg, C M Breneman, J F Liebman (Eds) *Amide Linkage* (New York: Wiley, 2000)
225. K J Shea, T G Lease, J W Ziller *J. Am. Chem. Soc*. **112** 8627 (1990)
226. G W Wijsman, W H de Wolf, F Bickelhaupt *J. Am. Chem. Soc*. **114** 9191 (1992)
227. J Michl, J G Radziszewski, J W Downing, J Kopecky, P Kaszynski, R D Miller *Pure Appl. Chem*. **59** 1613 (1987)
228. J Michl, J G Radziszewski, J W Downing, K B Wiberg, F H Walker, R D Miller, P Kovacic, M Jawdosiuk, V Bonacic-Koutecký *Pure Appl. Chem*. **55** 315 (1983)
229. P E Eaton, K-L Hoffmann *J. Am. Chem. Soc*. **109** 5285 (1987)
230. D A Jeffrey, W F Maier *Tetrahedron* **40** 2799 (1984)
231. D A Jeffrey, J M Cogen, W F Maier *J. Org. Chem*. **51** 3206 (1986)
232. K N Houk, N G Rondan, F K Brown *Isr. J. Chem*. **23** 3 (1983)
233. K N Houk, in *Stereochemistry and Reactivity of Systems Containing π Electrons* (Ed. W H Watson) (Deerfield Beach: Verlag Chemie, 1983) p. 1
234. R W Strozier, P Caramella, K N Houk *J. Am. Chem. Soc*. **101** 1340 (1979)
235. A P Marchand, I N N Namboothiri, B Ganguly, W H Watson, S G Bodige *Tetrahedron Lett*. **40** 5105 (1999)
236. N M Weinshenker, F D Greene *J. Am. Chem. Soc*. **90** 506 (1968)
237. U Szeimies-Seebach, J Harnisch, G Szeimies, M Van Meerssche, G Germain, J-P Declerq *Angew. Chem*. **90** 904 (1978)
238. A-D Schlüter, H Harnisch, J Harnisch, U Szeimies-Seebach, G Szeimies *Chem. Ber*. **118** 3513 (1985)
239. J Harnisch, O Baumgärtel, G Szeimies, M Van Meerssche, G Germain, J-P Declerq *J. Am. Chem. Soc*. **101** 3370 (1979)
240. O Baumgärtel, G Szeimies *Chem. Ber*. **116** 2180 (1983)
241. O Baumgärtel, J Harnisch, G Szeimies, M Van Meerssche, G Germain, J-P Declerq *Chem. Ber*. **116** 2205 (1983)
242. J Kenndoff, K Polborn, G Szeimies *J. Am. Chem. Soc*. **112** 6117 (1990)
243. D A Hrovat, W T Borden *J. Am. Chem. Soc*. **110** 4710 (1988)
244. P E Eaton, M Maggini *J. Am. Chem. Soc*. **110** 7230 (1988)
245. P O Staneke, S Ingemann, P Eaton, N M M Nibbering, S R Kass *J. Am. Chem. Soc*. **116** 6445 (1994)
246. K Lukin, P E Eaton *J. Am. Chem. Soc*. **117** 7652 (1995)
247. P Camps, M Font-Bardia, F Pérez, X Solans, S Vázquez *Angew. Chem*. **107** 1101 (1995)
248. R Gleiter, F Ohlbach *J. Org. Chem*. **61** 4929 (1996)

249. V Jonas, G Frenking *J. Org. Chem.* **57** 6085 (1992)
250. K Tamagawa, T Iijima, M Kimura *J. Mol. Struct.* **30** 243 (1976)
251. V I Minkin, M N Glukhovtsev, B Ya Simkin *Aromaticity and Antiaromaticity* (New York: Wiley, 1994)
252. W H Mills, I G Nixon *J. Chem. Soc.* 2510 (1930)
253. J S Siegel *Angew. Chem.* **106** 1808 (1994)
254. R Diercks, K P C Vollhardt *J. Am. Chem. Soc.* **108** 3150 (1986)
255. D L Mohler, K P C Vollhardt, S Wolff *Angew. Chem.* **102** 1200 (1990)
256. H-D Beckhaus, R Faust, A J Matzger, D L Mohler, D W Rogers, C Rüchardt, A K Sawhney, S P Verevkin, K P C Vollhardt, S Wolff *J. Am. Chem. Soc.* **122** 7819 (2000)
257. A Stanger *J. Am. Chem. Soc.* **120** 12034 (1998)
258. A Kumar, F E Friedli, L Hsu, P J Card, N Mathur, H Shechter *J. Org. Chem.* **56** 1663 (1991)
259. R Boese, D Bläser, W E Billups, M M Haley, A H Maulitz, D L Mohler, K P C Vollhardt *Angew. Chem.* **106** 321 (1994)
260. A Stanger *J. Am. Chem. Soc.* **113** 8277 (1991)
261. K K Baldridge, J S Siegel *J. Am. Chem. Soc.* **114** 9583 (1992)
262. N L Frank, K K Baldridge, J S Siegel *J. Am. Chem. Soc.* **117** 2102 (1995)
263. H -B Bürgi, K K Baldridge, K Hardcastle, N L Frank, P Gantzel, J S Siegel, J Ziller *Angew. Chem.* **107** 1575 (1995)
264. F Vögtle *Cyclophane Chemistry* (Chichester: Wiley, 1993)
265. F Bickelhaupt *Pure Appl. Chem.* **62** 373 (1990)
266. F Bickelhaupt, W H de Wolf, in *Advances in Strain in Organic Chemistry* Vol. 3 (Ed. B Halton) (London: JAI Press, 1993) p. 185
267. V V Kane, W H de Wolf, F Bickelhaupt *Tetrahedron* **50** 4575 (1994)
268. F Bickelhaupt, W H de Wolf *J. Phys. Org. Chem.* **11** 362 (1998)
269. M M Pellegrin *Recl. Trav. Chim. Pays-Bas* **18** 457 (1899)
270. C J Brown, A C Farthing *Nature (London)* **164** 915 (1949)
271. *Cyclophanes* (Eds P.M.Keehn S.M.Rosenfeld). Academic Press New York 1983. P. 1
272. G B M Kostermans, M Bobeldijk, W H de Wolf, F Bickelhaupt *J. Am. Chem. Soc.* **109** 2471 (1987)
273. T Tsuji, S Nishida *J. Am. Chem. Soc.* **110** 2157 (1988)
274. T Tsuji, M Ohkita, T Konno, S Nishida *J. Am. Chem. Soc.* **119** 8425 (1997)
275. G B M Kostermans, P van Dansik, W H de Wolf, F Bickelhaupt *J. Am. Chem. Soc.* **109** 7887 (1987)
276. M J van Eis, F J J de Kanter, W H de Wolf, F Bickelhaupt *J. Org. Chem.* **62** 7090 (1997)
277. T Tsuji, S Nishida *J. Am. Chem. Soc.* **111** 368 (1989)
278. T Tsuji, S Nishida, M Okuyama, E Osawa *J. Am. Chem. Soc.* **117** 9804 (1995)
279. H Kawai, T Suzuki, M Ohkita, T Tsuji *Angew. Chem.* **110** 827 (1998)
280. D S van Es, A Egberts, S Nkrumah, H de Nijs, W H de Wolf, F Bickelhaupt *J. Am. Chem. Soc.* **119** 615 (1997)
281. M J van Eis, F J J de Kanter, W H de Wolf, F Bickelhaupt *J. Am. Chem. Soc.* **120** 3371 (1998)
282. M Okuyama, T Tsuji *Angew. Chem.* **109** 1157 (1997)
283. M J van Eis, W H de Wolf, F Bickelhaupt, R Boese *J. Chem. Soc., Perkin Trans. 2* 793 (2000)
284. G Mehta, H S P Rao, in *Advances in Strain in Organic Chemistry* Vol. 6 (Ed. B Halton) (London: JAI Press, 1997) p. 139
285. G J Bodwell, J N Bridson, T J Houghton, J W J Kennedy, M R Mannion *Chem. Eur. J.* **5** 1823 (1999)
286. G Maas, J Fink, H Wingert, K Blatter, M Regitz *Chem. Ber.* **120** 819 (1987)
287. W Weissensteiner, I I Schuster, J F Blount, K Mislow *J. Am. Chem. Soc.* **108** 6664 (1986)
288. H Sakurai, K Ebata, C Kabuto, A Sekiguchi *J. Am. Chem. Soc.* **112** 1799 (1990)
289. G Maier, K-A Schneider *Angew. Chem.* **92** 1056 (1980)
290. X Quiao, D M Ho, R A Pascal *Angew. Chem.* **109** 1588 (1997)
291. R P Johnson *Chem. Rev.* **89** 1111 (1989)
292. F Hojo, W Ando *Synlett* 880 (1995)
293. S A Petrich, Yi Pang, V G Young Jr, T J Barton *J. Am. Chem. Soc.* **115** 1591 (1993)
294. T Shimizu, F Hojo, W Ando *J. Am. Chem. Soc.* **115** 3111 (1993)
295. H F Schuster, G M Coppola, in *Allenes in Organic Synthesis* (New York: Wiley, 1984)
296. R O Angus Jr, PhD Thesis, Iowa State University, USA, 1985
297. J Andrés, R Cardenas, O Tapia *J. Chem. Soc., Perkin Trans. 2* 363 (1985)
298. J D Price, R P Johnson *Tetrahedron Lett.* 4679 (1986)
299. S M Oon, A E Koziol, W M Jones, G I Palenik *J. Chem. Soc., Chem. Commun.* 491 (1987)
300. K A Abboud, Z Lu, W M Jones *Acta Crystallogr., Sect. C* **48** 909 (1992)
301. G Wittig, P Fritze *Liebigs Ann. Chem.* **711** 82 (1968)
302. C Wentrup, G Gross, A Maquestiau, R Flammang *Angew. Chem.* **95** 551 (1983)
303. M Ceylan, H Secen, Y Sütbeyaz *J. Chem. Res. Miniprint* **3** 501 (1997)
304. M Christl, M Braun, in *Strain and Its Implications in Organic Chemistry* (Eds A de Meijere, S Blechert) (Dordrecht: Kluwer, 1989) p. 121
305. M Christl, S Groetsch *Eur. J. Org. Chem.* 1871 (2000)
306. Yi Pang, S A Petrich, V G Young Jr, M S Gordon, T J Barton *J. Am. Chem. Soc.* **115** 2534 (1993)
307. M A Hofmann, U Bergsträßer, G J Reiß, L Nyulászi, M Regitz *Angew. Chem.* **112** 1318 (2000)
308. M W Schmidt, R O Angus Jr, R P Johnson *J. Am. Chem. Soc.* **104** 6838 (1982)
309. N H Werstiuk, C D Roy, J Ma *Can. J. Chem.* **74** 1903 (1996)
310. M Balci, W M Jones *J. Am. Chem. Soc.* **102** 7607 (1980)
311. R O Angus Jr, M W Schmidt, R P Johnson *J. Am. Chem. Soc.* **107** 532 (1985)
312. M Nendel, L M Tolbert, L E Herring, Md N Islam, K N Houk *J. Org. Chem.* **64** 976 (1999)
313. S Hernandez, M M Kirchhoff, S G Swartz Jr, R P Johnson *Tetrahedron Lett.* **37** 4907 (1996)
314. H G Zoch, G Szeimies, R Römer, G Germain, J-P Declercq *Chem. Ber.* **116** 2285 (1983)
315. W C Shakespeare, R P Johnson *J. Am. Chem. Soc.* **112** 8578 (1990)
316. X-S Ye, H N C Wong *J. Org. Chem.* **62** 1940 (1997)
317. J-H Liu, H-W Chan, F Xue, Q-G Wang, T C W Mak, H N C Wong *J. Org. Chem.* **64** 1630 (1999)
318. U Rosenthal, P-M Pellny, F G Kirchbauer, V V Burlakov *Acc. Chem. Res.* **33** 119 (2000)
319. P-M Pellny, V V Burlakov, N Peulecke, W Baumann, A Spannenberg, R Kempe, V Francke, U Rosenthal *J. Organomet. Chem.* **578** 125 (1999)
320. H Hopf, G Maas *Angew. Chem.* **104** 953 (1992)
321. H Meier, in *Advances in Strain in Organic Chemistry* Vol. 1 (Ed. B Halton) (London: JAI Press, 1991) p. 215
322. N A Domnin *Zh. Obshch. Khim.* **8** 851 (1938) [d]
323. A T Blomquist, L H Liu *J. Am. Chem. Soc.* **75** 2153 (1953)
324. G Wittig, J Meske-Schüller *Liebigs Ann. Chem.* **711** 65 (1968)
325. C Wentrup, R Blanch, H Briehl, G Gross *J. Am. Chem. Soc.* **110** 1874 (1988)
326. N Atanes, S Escudero, D Pérez, E Guitián, L Castedo *Tetrahedron Lett.* **39** 3039 (1998)
327. G Wittig, A Krebs, R Pohlke *Angew. Chem.* **72** 324 (1960)
328. G Wittig, R Pohlke *Chem. Ber.* **94** 3276 (1961)
329. G Wittig, J Weinlich, E R Wilson *Chem. Ber.* **98** 458 (1965)
330. K L Erickson, J Wolinsky *J. Am. Chem. Soc.* **87** 1142 (1965)
331. L Fitjer, S Modaressi *Tetrahedron Lett.* **24** 5495 (1983)
332. J C Gilbert, M E Baze *J. Am. Chem. Soc.* **105** 664 (1983)
333. J C Gilbert, M E Baze *J. Am. Chem. Soc.* **106** 1885 (1984)
334. P J Stang, V V Zhdankin *Chem. Rev.* **96** 1123 (1996)
335. T Kitamura, M Kotani, T Yokoyama, Y Fujiwara *J. Org. Chem.* **64** 680 (1999)
336. R P Johnson, K J Daoust *J. Am. Chem. Soc.* **117** 362 (1995)
337. K B Wiberg, M Marquez *Tetrahedron Lett.* **38** 1685 (1997)
338. R D Adams, G Chen, X Qu, W Wu, J H Yamamoto *J. Am. Chem. Soc.* **114** 10977 (1992)
339. R D Adams, X Qu, W Wu *Organometallics* **12** 4117 (1993)
340. C D Sherrill, C G Brandow, W D Allen, H F Schaefer III *J. Am. Chem. Soc.* **118** 7158 (1996)
341. R A Seburg, E V Patterson, J F Stanton, R J McMahon *J. Am. Chem. Soc.* **119** 5847 (1997)
342. H E Mattews, W M Irvine *Astrophys. J.* **298** L61 (1985)
343. P Thaddeus, J M Vrtilek, C A Gottlieb *Astrophys. J.* **299** L63 (1985)

344. J Cernicharo, C A Gottlieb, M Guélin, T C Killian, G Paubert, P Thaddeus, J M Vrtilek *Astrophys. J.* **368** L38 (1991)
345. G Maier, H P Reisenauer, H Pacl *Angew. Chem.* **106** 1347 (1994)
346. G Maier, H Pacl, H P Reisenauer, A Meudt, R Janoschek *J. Am. Chem. Soc.* **117** 12 712 (1995)
347. G Frenking, R B Remington, H F Shaefer III *J. Am. Chem. Soc.* **108** 2169 (1986)
348. P G Gassman, I Gennick *J. Am. Chem. Soc.* **102** 6863 (1980)
349. X-M Wang, R-J Wang, T C W Mak, H N C Wong *J. Am. Chem. Soc.* **112** 7790 (1990)
350. A Krebs, H Kimling *Tetrahedron Lett.* 761 (1970)
351. J Haase, A Krebs *Z. Naturforsch. A* **26** 1190 (1971)
352. H-H Bartsch, H Cobberg, A Krebs *Z. Kristallogr.* **156** 10 (1981)
353. D J Cram, M E Tanner, R Thomas *Angew. Chem.* **103** 1048 (1991)
354. R Warmuth *Angew. Chem.* **109** 1406 (1997)
355. R Warmuth *Chem. Commun.* 59 (1998)
356. A B Whitehill, M George, M L Gross *J. Am. Chem. Soc.* **118** 853 (1996)
357. A Ohff, P Kosse, W Baumann, A Tillak, R Kempe, H Görls, V V Burlakov, U Rosenthal *J. Am. Chem. Soc.* **117** 10 399 (1995)
358. N Peulecke, A Ohff, P Kosse, A Tillak, A Spannenberg, R Kempe, W Baumann, V V Burlakov, U Rosenthal *Chem. Eur. J.* **4** 1852 (1998)

[a] — *Russ. Chem. Bull., Int. Ed. (Engl. Transl.)*
[b] — *Dokl. Chem. (Engl. Transl.)*
[c] — *Russ. J. Org. Chem. (Engl. Transl.)*
[d] — *Russ. J. Gen. Chem. (Engl. Transl.)*

Russian Chemical Reviews **70** (12) 1017 – 1036 (2001) © 2001 Russian Academy of Sciences and Turpion Ltd

DOI 10.1070/RC2001v070n12ABEH000676

Fluorescent and photochromic chemosensors

V A Bren

Contents

I.	Introduction	1017
II.	Fluorescent cation sensors	1018
III.	Fluorescent chemosensors for anions	1026
IV.	Luminescent sensors for molecules	1027
V.	Photochromic chemosensors	1029
VI.	Conclusion	1034

Abstract. Data on organic chemosensors published over recent years are surveyed and described systematically. The bibliography includes 165 references.

I. Introduction

The creation and development of highly sensitive and reliable methods for the quantitation of various elements and their compounds in the environment (atmosphere, hydrosphere and lithosphere) is of current interest in chemistry. Success in solving this task requires that scientific studies be carried out to find the most selective reactions of atoms, ions or molecules which make it possible to determine qualitative and quantitative parameters of an object under study. The search for a selective reaction implies that one needs to find the transformation of the object being studied from a series of other transformations, which converts the substrate into the most convenient form with specific physical characteristics.

Of the many methods used to analyse substrates based on their physical properties (atomic absorption spectroscopy, ion-selective pM-metry (where pM is the negative logarithm of the metal ion concentration), electron microprobe analysis, neutron activation analysis, *etc.*), a special place belongs to electron spectroscopic methods,[1] fluorescence analysis being the most sensitive of these methods.[2]

An organic analytical reagent employed in fluorescence analysis should have a receptor which reacts selectively with the substrate, a signal-generating fragment and a conductor (bridge) between these parts of the molecule.[3] Such a system is called a chemosensor. If a fluorophore is the signal-generating part of a chemosensor, then this is a fluorescent chemosensor. Interaction of the receptor with the substrate followed by transfer of the energy of this interaction through the bridge to the fluorophore changes the spectral signal of the fluorophore, which allows one to make conclusions about the nature of the substrate. It became obvious while developing chemosensors that the set of fluorophores is rather limited, whereas the types of receptor are rather diverse. The most common chemosensors are represented by ionofluorophores; of these, reagents for various cations are used most widely.

Figure 1 shows a schematic diagram of the operating principle of chemosensor for cations.[4] The receptor of such a chemosensor is an electron donor (D), whereas the fluorophore is an electron acceptor.[5,6]

Excitation of the fluorophore results in electron transfer from the highest occupied molecular orbital (HOMO) to the lowest unoccupied molecular orbital (LUMO). This enables electron transfer from the HOMO of the donor (receptor) to the HOMO of the acceptor (fluorophore), thus quenching the fluorescence of the latter. This phenomenon is known as the PET (Photoinduced Electron Transfer).[7] Once a cation (shown as a ball in Fig. 1) has been attached to the receptor, the HOMO energy level of the latter becomes lower than that of the fluorophore, the PET is no longer possible, and the sensor starts to fluoresce.

The majority of fluorescent sensors fit this scheme. However, a different PET mechanism is possible in the case of transition metal cations. In this case, the electron transfer is directed from the fluorophore to the bound metal ion.[8]

If the fluorophore of the sensor incorporates an electron-donor fragment in addition to the electron-withdrawing one, then the so-called PCT mechanism (Photoinduced Charge Transfer) is also observed due to the interaction between the similarly or oppositely charged poles of the fluorophore and the receptor. This effect is observed as a bathochromic or hypsochromic shift of

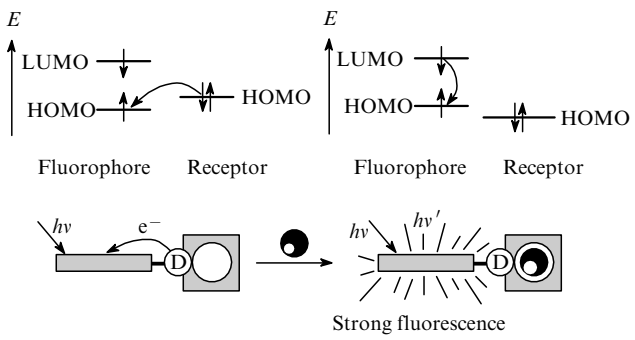

Figure 1. Schematic diagram of cation recognition fluorescent PET sensor.[4]

V A Bren Institute of Physical and Organic Chemistry, Rostov State University, Prosp. Stachki 194/2, 344090 Rostov-on-Don, Russian Federation. Fax (7-863) 243 46 67. Tel. (7-863) 243 47 77. E-mail: bren@ipoc.rsu.ru

Received 12 March 2001
Uspekhi Khimii **70** (12) 1152 – 1174 (2001); translated by S S Veselyi

absorption and emission bands in the spectra, and also as changes in the extinction parameters.[4]

Fluorescence of sensors may get enhanced or quenched if exciplexes † or excimers ‡ appear due to the formation of complexes between the receptor and the substrate.[4]

Fluorescent sensors have certain advantages over other optical chemosensors. The fluorescence method is very sensitive (in certain cases, a few molecules of an object can be detected). These experiments are inexpensive and easy to perform; the method has high resolving power in the wavelength and time measurement scales. Furthermore, luminescence spectra are quite sensitive to both structural changes in the sensor and substrate molecules and the external conditions.[6, 9–12]

Thus, the fluorescence method makes it possible to both solve purely analytical problems and control chemosensor processes.

When Fabbrizzi and Poggi [10] introduced the concept of 'switchable sensors', they distinguished such systems that can be triggered or blocked by changing the pH or the concentration of metal ions in the environment, by applying an external redox potential, *etc*.

The original photo-switching method is based on the photochromism phenomenon. If the sensor is associated with one state of a bistable photochromic device, the sensor function can be reversibly switched on or off by means of a photoreaction.

In this review, recent achievements in the development of organic chemosensor systems are classified and generalised. Fluorescent sensors are considered in the most detail.

II. Fluorescent cation sensors

According to a classification by de Silva,[11, 13] fluorescent cation sensors can be subdivided into four types.

1. Organic molecules that emit light due to the presence of a metal ion.

2. Organometallic complexes containing a metal which emits light.

3. Organometallic complexes which emit light due to interaction with a different metal ion.

4. A complex of two organic compounds which emits light in the presence of an organic 'guest'.

Although this classification of sensors is quite versatile, the need arose recently to expand it and make it more specific, because many new publications have appeared in the field of chemosensors. Detailed reviews have been published in which chemosensors were classified according to the type of interaction between the coordinating, luminescent and conducting parts of the system,[14, 15] as well as reviews dealing with the fundamentals of designing ionofluorophores for general analysis of cations,[4] transition metal ions,[16] anionic substrates,[17, 18] *etc*.

In this review, we have tried to emphasise the role of the receptor as the most functional part of a chemosensor molecule and to show the sensor capacities of various reactive series of compounds containing the same molecular receptors.

1. Azacrown ethers

Chemosensors in which crown ethers serve as receptors belong to the most popular type of cation sensors of various metals. In order to enhance the efficiency of the crown ether receptor, the macrocycle is usually modified by incorporating nitrogen atoms, which are potent complexation centres.

Compound **1a** is the simplest azacrown-containing PET sensor.[19]

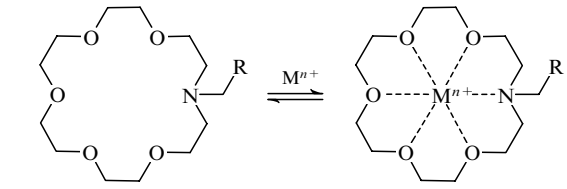

1a–c

R = 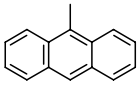 (**a**), 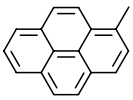 (**b**), (**c**).

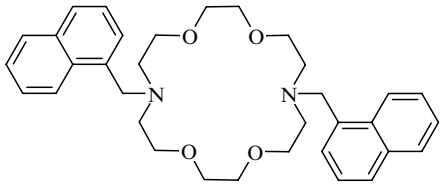

2

For example, if compound **1a** coordinates the K^+ ion, its fluorescence quantum yield in methanolic solutions increases from 0.003 to 0.14. Incorporation of several (more than three) methylene units between the nitrogen atom of the azacrown ether and the aromatic substituent, *i.e*., between the receptor and the fluorophore, results in an abrupt decrease in the PET.[20]

Aza(diaza)-18-crown-6 ethers bound to fluorophores (polynuclear aromatic hydrocarbons) through an *N*-methylene bridge (**1b**,**c** and **2**) were used in order to discriminate between mono- and divalent metal ions.[15, 21] The nature of the solvent and the type of anion in the salt being analysed may affect considerably the character of coordination, and hence the strength of the PET.[22, 23]

The interaction of the sensor **1c** with thiocyanates of mono- and divalent metals can serve as an example; the spectral pattern of this interaction is shown in Fig. 2.[15] Divalent and ammonium cations display the standard PET with luminescence enhancement. Conversely, coordination of monovalent cations results in luminescence quenching. This anomaly can be rationalised by the existence of specific coordination of monovalent cations with the

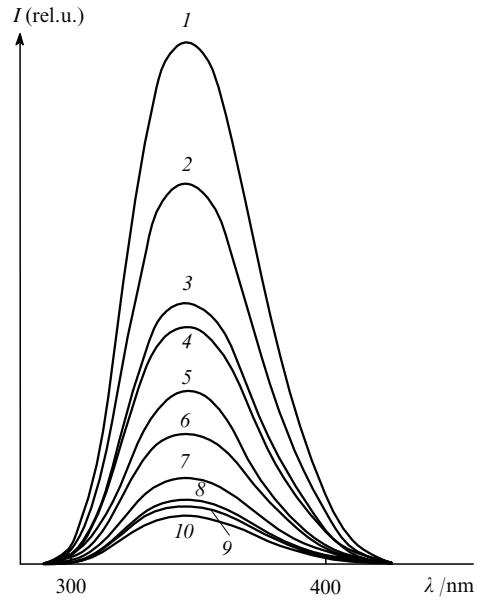

Figure 2. Fluorescence spectra of compound **1c** and its complexes with various metal ions in methanol;[15]
(*1*) Ba^{2+} complex; (*2*) Ca^{2+} complex; (*3*) Zn^{2+} complex; (*4*) NH_4^+ complex; (*5*) Mg^{2+} complex; (*6*) compound **1c**; (*7*) Li^+ complex; (*8*) Na^+ complex; (*9*) Cs^+ or Rb^+ complex; (*10*) K^+ complex.

† An exciplex is an excited molecular complex. It is formed upon association of two molecules (which may be similar or different), one of which is in the ground state while the other is in an excited state.

‡ An excimer (a specific case of an exciplex) is an excited dimer formed from two similar molecules, one of which is in an excited state while the other one is in the ground state.

azacrown ether and the thiocyanate anion, providing additional transfer of electron density from the anion to the naphthalene chromophore.[15]

Using electronic spectra, ^1H and ^{13}C NMR spectra and X-ray diffraction analysis, it was shown that the PET affects the physical characteristics of complexation for a number of sensor series. For example, enhancement of fluorescence in the presence of various 'guest' cations occurs in derivatives of diazacrown ethers containing two, three, or four oxygen atoms in the ring and two fluorescent substituents. There are two reasons that can explain this phenomenon.

1. Quenching of fluorescence in the chemosensor molecules due to intramolecular electron transfer between the fluorescent 'pendants' and two nitrogen atoms of the ring. As a result, coordination of a cation by the crown ether enhances light emission.

2. Coincidence between the steric parameters of the receptor and the substrate and a suitable rate of cation exchange between the free ligand and the complex in the ground state.

It was found[15] that Zn^{2+} ions are coordinated to both nitrogen atoms of the ring, which results in enhancement of luminescence of diaza-12-crown-4 ether **3** by a factor of 182.

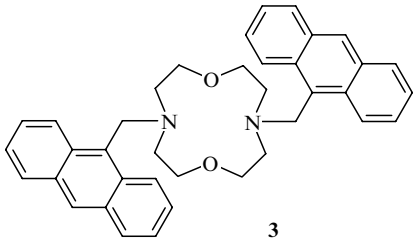

3

It was shown[15] that diaza-18-crown-6, which has two 1-pyrenyl substituents, can be used as a fluorescent sensor for alkali metal ions.

Ionofluorophores **4a**,**b** are suitable for the quantitative determination of Ca^{2+} ions in solutions based on changes in luminescence spectra upon complexation,[24] but they behave differently. For example, the $Ca^{2+} \cdot$ **4a** complex displays an intense fluorescence band, unlike the $Ca^{2+} \cdot$ **4b** complex which is characterised by weak long-wave emission.

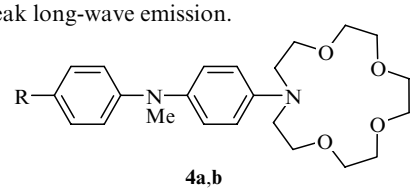

4a,**b**

R = H (**a**), NMe_2 (**b**).

The *N*-aryl receptor of the azacrown sensor **5** with decreased basicity of the nitrogen atom of the crown macrocycle is characterised by strong luminescence enhancement (by a factor of 28) upon interaction with the Ca^{2+} ion in acetonitrile,[25] the fluorescence life time being increased from 0.28 to 3.6 ns.

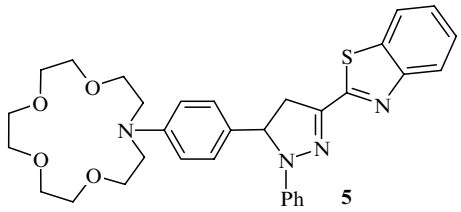

5

The coordination sphere of crown ethers can be expanded by introducing substituents containing additional donors. For example, the sensor **6** is a good fluorescent reagent for 'softer' sodium ions[13] due to involvement of the electron pairs of the *o*-methoxy groups in coordination.

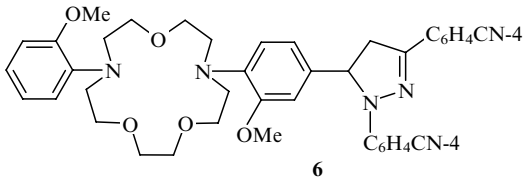

6

Additional coordination sites are also present in compound **7a**, which is a highly selective luminescent sensor for magnesium ions effective in solutions with pH > 6.[26]

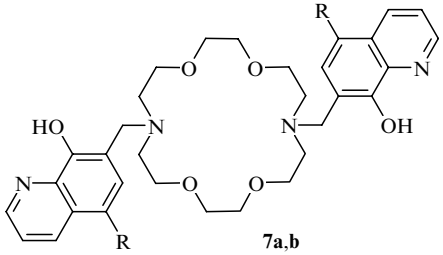

7a,**b**

R = Cl (**a**), NO_2 (**b**).

An analogous ion-selective chemosensor ligand **7b** has high sensitivity and affinity for Hg^{2+} ions over a wide range of pH.[27]

Yet another way to enhance the efficiency of sensors is to incorporate zwitter-ionic fragments. For example, excess electron density on the oxygen atoms of the central zwitter-ionic fragment in the luminescent sensor **8** makes it highly efficient with respect to lithium ions in acetonitrile – dichloromethane system.[28]

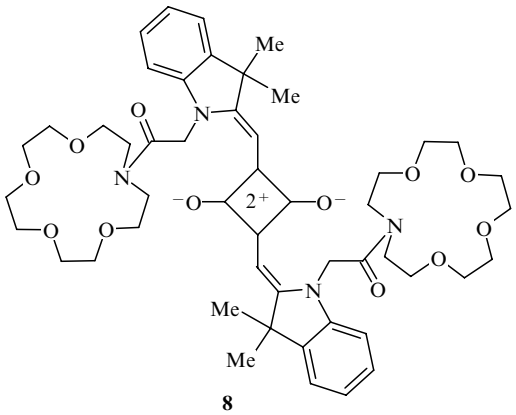

8

Similarly, the efficiency of chemosensors **9a**,**b** for divalent metal ions (Ca^{2+}, Mg^{2+}, Ni^{2+}, Zn^{2+}, Cu^{2+}) can be explained by the presence of a quinolizine and coumarin nuclei in the fluorophore.[29, 30] It was shown[30] that charge transfer from the nitrogen atom of the quinolizine part of the molecule to the carbonyl group of the coumarin part occurs in compounds **9a**,**b**. A strong PCT effect is realised in these molecules, and the electronic spectra manifest bathochromic shifts.[30]

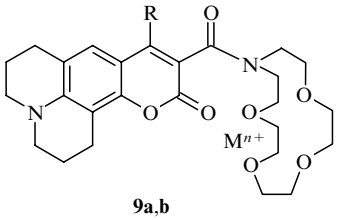

9a,**b**

R = H (**a**), CF_3 (**b**).

Yet another approach to specific chemosensors is the introduction of extra functional groups into the known sensors resulting in alteration of their properties. For example, introduction of carboxyl-containing thiophene derivatives as fluorophores into dipyridino-crown ether makes the resulting caesium tetracarboxylate **10** water-soluble, which is very important for practical use. The fluorescent sensor itself has high selectivity for potassium

ions, because the bulky caesium cations do not compete with potassium ions in solution for the coordination by the cavity of this dipyridinocrown ether.[31]

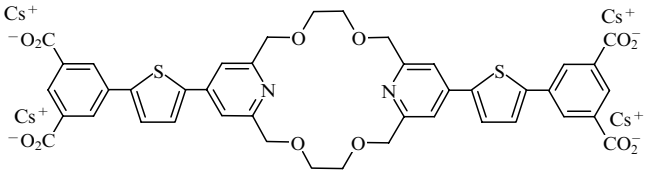

10

Modification of compound **1a** by addition of one more azacrown fragment results in the sensor **11** which can recognise dications. For example, ammonium groups located at α- and ω-carbon atoms of the substrate alkane chains enhance considerably the fluorescence of the sensor **11**; they are probably incorporated into both fragments of the crown ether.[32]

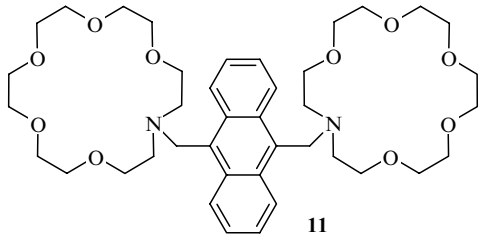

11

Azacrown ethers are characterised by rather a high basicity of the nitrogen atoms. On the one hand, the high basicity of the nitrogen atom increases the chemosensor efficiency and provides a stable PET; on the other hand, undesirable protonation occurs in acidic solutions. Crown-ether ligands are devoid of this drawback.

2. Crown ethers

Benzocrown ether **12a** was one of the first to be suggested as PET sodium ion sensor. When this compound is coordinated by the sodium cation in suitable solvents, fluorescence is enhanced.[33, 34]

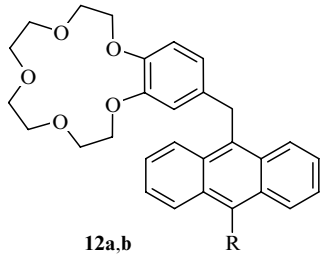

12a,**b** R

R = CN (**a**), CH_2N O (**b**).

Compound **12b** is a so-called 'switchable' fluorescent sensor which operates in acidic media, where the electron-donating morpholine substituent is protonated in the first stage.[35]

Other fluorescent indicators for the Na^+ and K^+ ions based on benzocrown ethers have been synthesised and studied (see Ref. 36).

1,8-Anthraceno-18-crown-5 is a luminescent sensor for ions of alkali and alkaline-earth metals.[37] Fluorometric titration was used to determine the stability constants of its complexes and their dependences on the cation parameters.

Bis(anthracene-9,10-diyl)coronand **13** is a sensor for Na^+ and K^+ ions. It was shown[38, 39] that gradual addition of sodium perchlorate to solutions of compound **13** in methanol or acetonitrile gives a stable excimer complex **14** with the composition 1 : 2, which is the reason for enhancement of the corresponding luminescence. K^+ ions form a 1 : 1 complex.

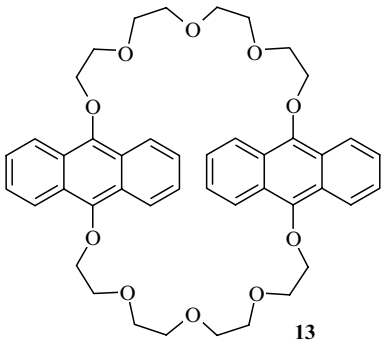

13

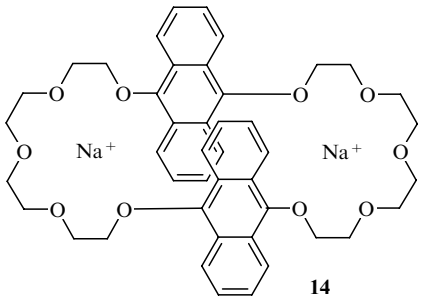

14

Combination of the coumarin fluorophore with benzocrown receptors results in efficient chemosensors. For example, strong substituent polarisation in sensor **15** in an excited state results in additional coordination of alkali and alkaline-earth metal ions with the carbonyl group of the coumarin fragment.

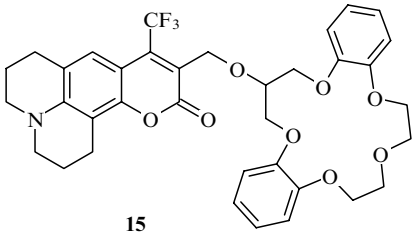

15

This effect is observed in luminescence spectra as a bathochromic shift of the bands (Fig. 3);[4] the strongest quenching is observed in the presence of the Ca^{2+} ion. The selectivity of Ca^{2+}

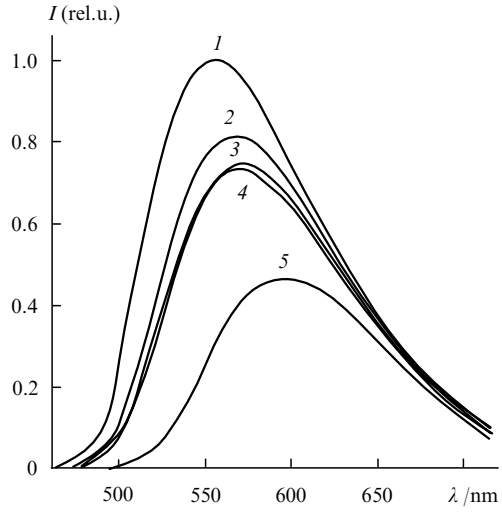

Figure 3. Fluorescence spectra of compound **15** and its complexes with metal ions in acetonitrile;[4]
(*1*) the ligand; (*2*) K^+ complex; (*3*) Na^+ complex; (*4*) Li^+ complex; (*5*) Ca^{2+} complex.

sensor **15** is very high: the ratio of stability constants of the complexes is $k(Ca^{2+}):k(Mg^{2+}) = 12\,500$; $k(Na^{+}):k(K^{+}) = 16$.

A few other sensors containing the coumarin fragment are known. For example, 4-substituted benzo-α-pyronebenzo-12-crown-4, -15-crown-5, and -18-crown-6 in acetonitrile are luminescent sensors for Li^{+}, Na^{+}, K^{+}, and Mg^{2+} ions (see Refs 40 and 41). The effect of the macrocycle size on the extent of fluorescence quenching during the formation of 1 : 1 complexes was studied.[42]

The crown ethers **16** and **17** containing the dihydroxyxanthone fragment have different properties: compound **16** has high affinity for barium ions, whereas the cavity in compound **17** binds selectively potassium ions. In the former case, luminescence is enhanced as the ion concentration increases; in the latter case, it is quenched.[43]

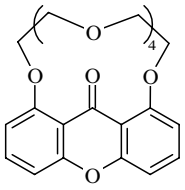

16

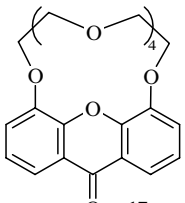

17

Unusual fluorescent sensors, namely, optically active silacrown ethers **18a**,**b** were synthesised.[44] Compound **18a** is a selective reagent for lithium ions and viologen bromide, while compound **18b** reacts with the latter to give rotaxane-like structures.

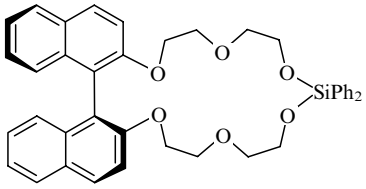

18a

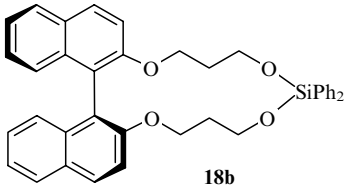

18b

The enantiomerically pure chiral ligand, *viz*., acridinodimethyl-18-crown-6 (**19**), displays high enantioselectivity and gives luminescent complexes with chiral ammonium ions in acetonitrile.[45] The authors of this study give well-reasoned evidence that it is possible to design a series of efficient enantioselective chemosensors for chiral substrates.

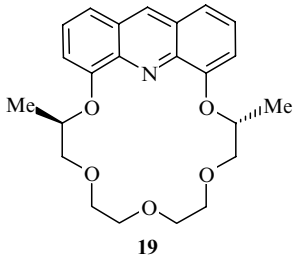

19

Xia *et al.*[46] described the synthesis of the luminescent sensor **20** containing 1,4-di(phenylethynyl)tetramethylbenzene as the chromophore and 18-crown-6 as receptors and discussed its photochemical properties. The chromophore luminescence is considerably quenched only by those lanthanide ions which have large ionic radii and in which *f*–*f* transitions occur (Ce^{3+}, Pr^{3+}, Nd^{3+}). Ions of alkali and alkaline-earth metals, as well as lanthanide ions with smaller radii, do not greatly affect the emission spectra of this sensor.

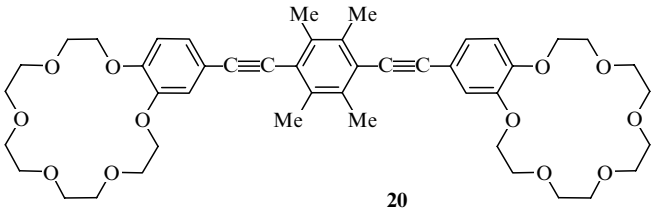

20

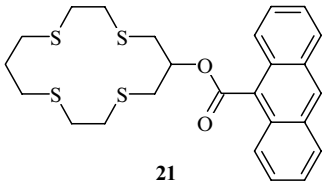

21

Thiacrown ether **21** is selective for Cu^{2+} ions. It is interesting that a 'reverse' PET operates in this complex, and fluorescence quenching occurs due to electron density shift from the anthracene substituent to the copper cation possessing strong oxidising properties.[47]

Thus, depending on the ring size and configuration, crown ethers may be selective for ions of alkali, alkaline-earth, or rare-earth metals.

3. Sensors with polyamine receptors

Even compound **22**, which is a rather simple diamino derivative, can form complexes with Cr^{3+}, Fe^{3+}, Co^{2+}, Ni^{2+}, and Cu^{2+} ions; it manifests the PET and acts as a chemosensor with 30-fold fluorescence enhancement.[48] The sensor **23** acts in a similar way but with higher selectivity for copper ions.[49]

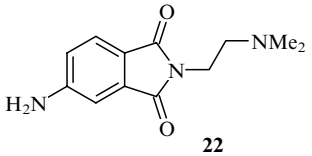

22

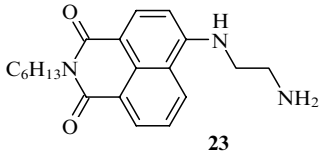

23

The anthracene derivative **24** was the first example of a chemosensor with a short polyalkylamine chain, which forms chelate complexes with transition metal ions.[50] The ligand fluorescence, which is very weak due to the PET process, becomes 1000 times more intense upon addition of zinc chloride in acetonitrile.

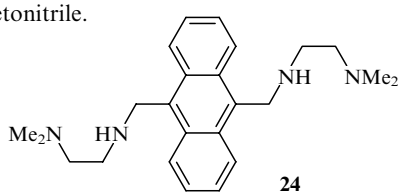

24

The action of chemosensors of the type **25** depends on the nature of the substrate cations and on the acidity of solutions. Coordination of Cu^{2+} and Ni^{2+} ions with compound **25** does not result in intense light emission in weakly acidic and neutral solutions (pH > 4) where the amino groups are not protonated and the PET operates. This results from deactivation of the excited state *via* the energy levels of the metal centre.

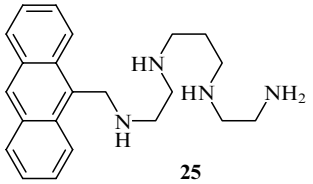

25

On the contrary, a complex of compound **25** with Zn^{2+} luminesces strongly due to the d^{10} configuration of the Zn^{2+} ion and an increase in the oxidation potential of amines.[51]

A large series of open-chain and cyclic *N*-mono- and *N*,*N*-diarylpolyalkylamines has been synthesised and analysed.[52] Compounds **26** are chemosensors for proton and transition metal ions: Co^{2+}, Ni^{2+}, Cd^{2+}, Pb^{2+}, Cu^{2+}, Zn^{2+}. Protonation or coordination of cations change the fluorescence accordingly. Sensors **26** where Ar are terminal anthracene substituents can form excimers.

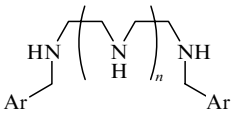

26

$n = 0-4$.

Ligands containing aminoethylamide fragments (*e.g.*, compound **27**) are effective in recognition of Ni^{2+} and Cu^{2+} cations. It is believed that photoexcitation involves electron transfer from the metal ions to the ligand.[53]

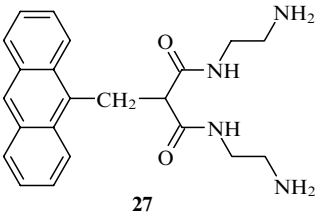

27

Fluorescent complexes with the composition ML_2^{2+} [where L is 6-(9-fluorenyl)-1,4,8,11-tetraazaundecane-5,7-dione and M is a divalent ion of copper, nickel or cobalt] were studied in non-aqueous and aqueous media.[54]

It was found that open-chain polyamines are more efficient sensors than cyclic polyazacyclophanes **28**.[52]

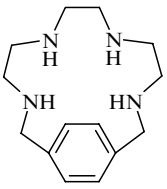

28

In a molecule of compound **28**, the polyamine chain is arranged as a strained arch above the benzene ring plane. As a result, simultaneous coordination of both benzyl nitrogen atoms by a single metal ion becomes impossible. However, the PET can still operate in the complex.

The situation changes if the ring size increases or if additional nucleophilic centers are introduced. For example, macrocyclic ligands **29a**,**b**, in which the receptor ring contains a 1,10-phenanthroline fragment, are chemosensors for hydrogen and zinc cations.[52]

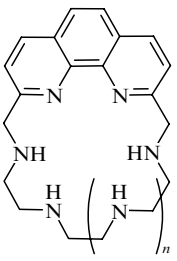

29a,**b**

$n = 1$ (**a**), 2 (**b**).

Compound **29a** forms only a mononuclear complex with zinc, whereas compound **29b** forms both mono- and binuclear complexes. Thus, fluorescence spectra depend on the degree of protonation and complexation.

Rather efficient chemosensors for Zn^{2+}, Cd^{2+}, and Hg^{2+} were obtained based on anthracene-substituted polyazacrown ethers **30** (see Ref. 55).

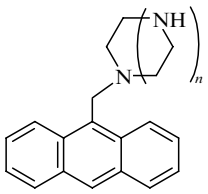

30a–**e**

$n = 1$ (**a**), 2 (**b**), 3 (**c**), 4 (**d**), 5 (**e**).

The luminescence of compounds **30c**,**e** is pH-dependent and increases abruptly upon complexation with Zn^{2+} or Cd^{2+} in water. On the contrary, Hg^{2+} ions quench the residual fluorescence of compounds **30a**–**e**.

The fluorescent properties of macrocyclic ligands **31a**–**d**, containing *N*-(β-naphthylmethyl)amide groups as fluorophores, were studied in water and acetonitrile. All ligands **31** display the typical fluorescence of the naphthalene chromophore (λ_{max} = 337 nm); however, it is weakened due to the PET. The emission spectra of compounds **31b**–**d** contain additional broad bands typical of the naphthalene excimer (λ_{max} = 397–401 nm). The ligands show different luminescent properties in the presence of quenching ions (Pb^{2+}, Ni^{2+}, Cu^{2+}, Eu^{3+}) and ions that cause luminescence enhancement (Zn^{2+}, Cd^{2+}).[56]

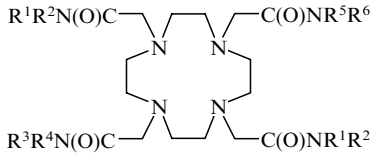

31a–**d**

$R^1 = R^3 = R^5 = H$, $R^2 = R^4 = Me$, $R^6 = 2\text{-}CH_2C_{10}H_7$ (**a**);
$R^1 = R^3 = R^5 = H$, $R^2 = R^4 = R^6 = 2\text{-}CH_2C_{10}H_7$ (**b**);
$R^1 = R^3 = H$, $R^2 = R^4 = Me$, $R^5 = R^6 = 2\text{-}CH_2C_{10}H_7$ (**c**);
$R^1 = H$, $R^2 = Me$, $R^3 = R^4 = R^5 = R^6 = 2\text{-}CH_2C_{10}H_7$ (**d**).

When the ligand **31a** is coordinated with zinc or cadmium ions, the emission intensity increases by a factor of two; addition of Pb^{2+} salts quenches fluorescence by 25% (the heavy atom effect), while addition of Cu^{2+} quenches it by 95%. In the $Tb^{3+}\cdot$**31a** complex, fast deactivation processes predominate, which complicate spectroscopic studies. If Cd^{2+} ions are added, the intensity of the short-wave radiation of protonated sensor **31b** in acetonitrile increases, whereas the excimer band disappears quickly. Similarly, emission is quenched by Pb^{2+} ions. The reason for this is that naphthyl excimers cannot be formed in these complexes because of spatial hindrance. Complexation of the ligand **31c** with metal ions (Zn^{2+}, Cd^{2+}, Pb^{2+}, Ni^{2+}, Cu^{2+}, Eu^{3+}) occurs quickly even in aqueous solutions. Its behaviour in the presence of various ions resembles that of compound **31a**. Coordination of compound **31d** (which is more strained spatially) with metal ions is hindered. The Zn^{2+} and Cd^{2+} ions affect very weakly both the total intensity of fluorescence of the ligand **31d** and the ratio of emission from the monomer and excimer. On the other hand, the Pb^{2+}, Ni^{2+} and Cu^{2+} ions decrease the total emission (by 36%, 37% and 86%, respectively) by affecting considerably the excimer band.

Various physical methods were used to study whether it is possible to determine copper, nickel, zinc, cadmium, mercury, and lead cations using a series of polyaza- and oxazacycloalkanes (14 to 18 units) containing peripheral anthrylmethyl fluorophores. It was found that all metals studied form stable complexes with these ligands in dioxane–water and THF–water media.[57] Copper(II) ions selectively quench the fluorescence of sensors in neutral and acid media; the intensity of luminescence of the 1,4,10-trioxa-7,13-

diazacyclopentadecane ligand increases selectively in the presence of mercury(II) ions in basic medium.

Novel fluorescent chemosensors **32** and **33** for heavy metal ions were suggested.[58] Since the reduced form **33** is readily transformed into the oxidised form **32**, these compounds may be considered as two components of a switchable redox system.

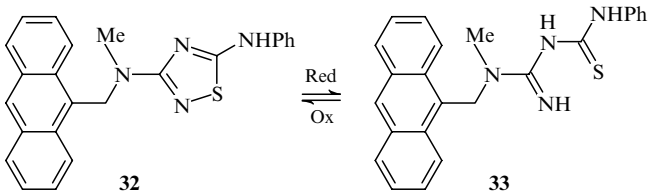

32 **33**

The oxidised form **32** binds mercury ions with a 44-fold increase in fluorescence; the carbamimidoylthiourea fragment of molecule **33** interacts with cadmium ions with a six-fold increase in the fluorescence intensity.

In the majority of fluorescent chemosensors considered above, which incorporate monocyclic or open-chain receptors containing nucleophilic atoms such as O, N, and S, the structures and electronic properties are affected by substrates (in most cases, cations). Nitrogen-containing podands and rings have sensor properties only with respect to hydrogen and transition metal ions. Incorporation of oxygen receptor atoms makes it possible to expand the range of cations that can be analysed (alkali and alkaline-earth metals; rare-earth elements; ammonium ions) and to improve selectivity. The selectivity and sensitivity of chemosensors increase upon transition from two-dimensional molecules to three-dimensional systems that coordinate substrate species in a 'host – guest' fashion in molecular cavities of specific sizes.

4. Tetraaminoalkyl three-dimensional sensors

Some planar chemosensors contain functional substituents which fix a cation or some other substrate outside the plane. As an example, the molecules **6** – **9a**,**b**, **15**, and **31a** – **d** have additional complexation sites located outside the main coordination plane. A tertiary nitrogen atom in a pyramidal configuration often serves as a vertex of a complex molecular frame forming a cavity.

For example, compound **34** containing four nitrogen atoms is a selective sensor for Cu^{2+} and Hg^{2+}. In neutral media, its fluorescence is quenched due to formation of chelates with copper (18-fold) or mercury cations (fourfold).[59]

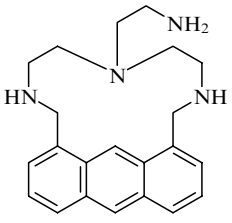

34

The sensor **35a** containing *p*-*N*,*N*-dimethylaminobenzyl fluorophores has an emission band at $\lambda = 360$ nm.[60] The fluorescence of sensor **35a** in solution in the presence of Cu^{2+} ions reaches a maximum at pH 3.8 (protonated form); as the pH is increased and protons are replaced by copper ions, fluorescence is progressively quenched and disappears at pH 5.5. Thus, the system **35a** – Cu^{2+} is an efficient switchable pH-dependent sensor.

The fluorescence of compound **35b**, which contains 5-dimethylaminonaphthalenesulfonyl (dansyl) substituents as chromophores, does not depend on the pH of the medium in the range from 3 to 11. However, complexation with such ions as Cu^{2+}, Co^{2+}, Zn^{2+}, and Cd^{2+} at pH 9.5 affects strongly the luminescence: Cu^{2+} and Co^{2+} quench luminescence, whereas Zn^{2+} and Cd^{2+} enhance it. At pH 6, only Cu^{2+} ions form a complex, which makes compound **35b** a highly selective sensor for copper ions under physiological conditions.[61]

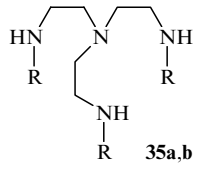

35a,**b**

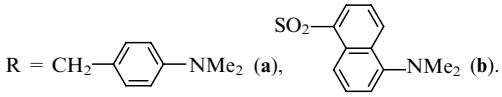

In certain sensors, some of the nitrogen atoms may be involved in heterocycles; for example, this is the case for the sensor **36a** which has high selectivity for zinc ions and may be used to analyse biological objects. Its isomer **36b**, in which the polyamine substituent is at position 6 of the benzene ring, is also highly selective for Zn^{2+} ions. The fluorescence of original starting compounds is almost independent of the medium acidity; it is virtually absent at pH 7.5. However, the fluorescence of compound **36a** becomes 17 times more intense as zinc ions are added, whereas that of the 6-substituted isomer **36b** becomes 51 times more intense.[62]

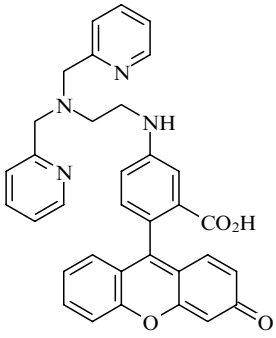

36a

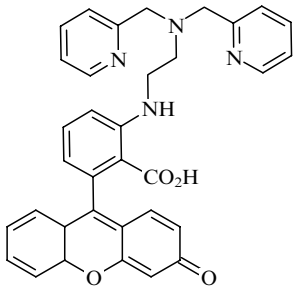

36b

The fluorescence of the sensor **37** is quenched owing to the PET. At appropriate pH values and concentrations of the coordinating Zn^{2+} ions, reversible formation (decomposition) of the exciplex occur because the phenanthroline and anthracene parts of the molecule become closer (or farther, respectively). This allowed Bencini *et al.*[63] to classify this system as a 'molecular machine' controlled by pH and light.

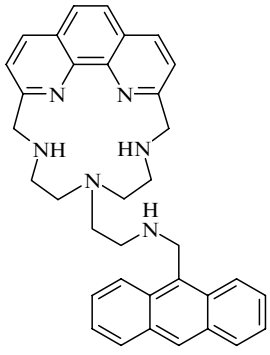

37

Balzani *et al.*[64, 65] used polymeric compositions (dendrimers) based on polypropyleneamine with dansyl end groups (*e.g.*, compound **38**) as luminescent Co^{2+} sensors.

The amine fragments create a polycellular internal cavity which coordinates the cations. The formation of the complex with the Co^{2+} ions does not affect the absorption spectra, but it strongly quenches the radiation from the peripheral fluorophores; one cell of the dendrimer reversibly coordinates one cation. Zinc ions do not affect the properties of dendrimers; in the presence of Cu^{2+} cations, the macromolecule undergoes irreversible changes.

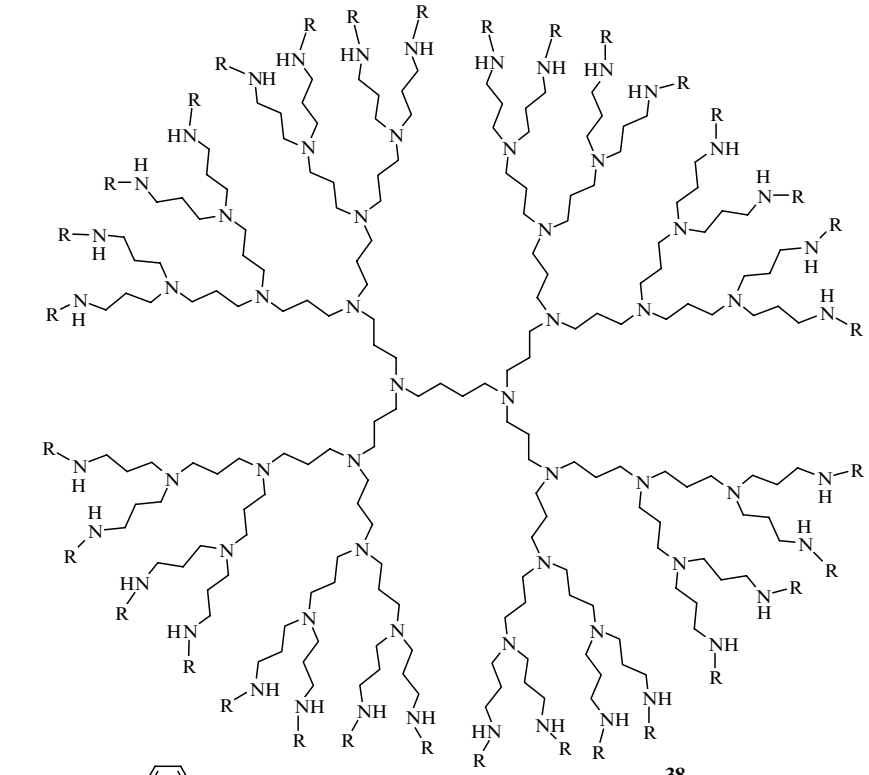

38

R = —SO_2— NMe_2

5. Cryptands

Attachment of an out-of-plane bridge to azacrown ethers results in cryptands, which represent sensors with enhanced receptor capacity.[66] For example, the PET is observed in the molecules of cryptands **39**–**41**. The cavity size in these compounds governs the selectivity: the parameters of the receptors in compounds **39** and **40** match the diameter of the K^+ ion (see Ref. 67), whereas the cavity in compound **41** is suitable for coordinating the sodium cation.[68]

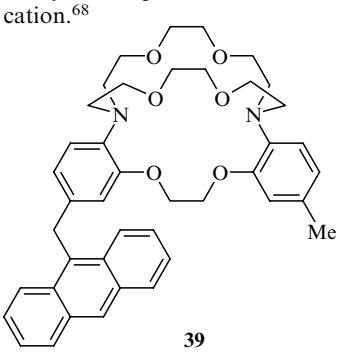

39

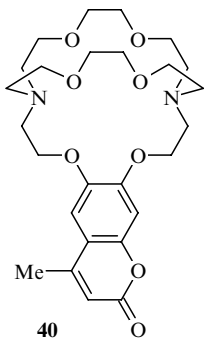

40

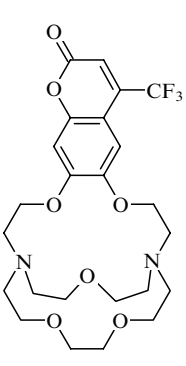

41

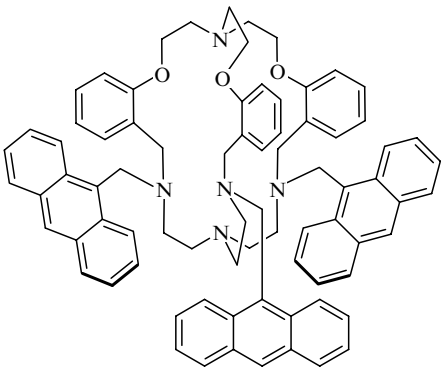

42

In order to determine transition metal ions, it was suggested to use cryptand sensors of the type **42**, which form 1 : 1 adducts with Mn^{2+}, Fe^{3+}, Co^{2+}, Ni^{2+}, Cu^{2+}, Zn^{2+} and Pb^{2+} cations in THF with an accompanying strong increase in the sensor fluorescence.[69] Of these cations, the strongest effect is observed in the case of Zn^{2+}. Silver and mercury ions, which have larger ionic radii, cannot form complexes. The properties of compounds **40**–**42** are strongly pH-affected.[4, 70]

6. Calixarenes

Various calixarene and -hetarene derivatives can also be used as efficient sensor systems. Spatially hindered calixarenes are not very good ligands to form stable complexes; however, they can serve as a supramolecular base for adding diverse receptors and fluorophores. This results in sensors containing cavities with different sizes and properties suitable for several types of 'guest' species.

One of the first simple calix[4]arene systems **43** containing a benzothiazole fluorophore showed selective properties as a sensor for lithium ions.[71] The Li^+ cations replace the phenol proton and coordinate the methoxy groups, thus causing a bathochromic PCT-shift of the fluorescence band. This system shows no response to Na^+ and K^+ ions.

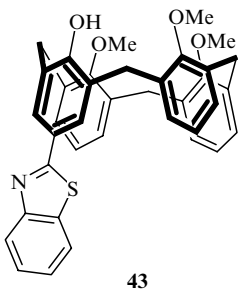

43

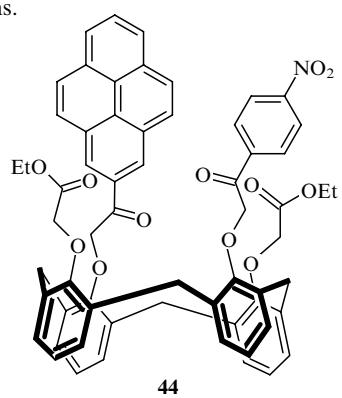

44

The cavity of yet another calix[4]arene sensor **44**, which incorporates ester groups, matches the size of Na^+ (see Ref. 72). Coordination with Na^+ breaks the spatial contact between the pyrene and nitrophenyl rings, which results in disappearance of the PET and enhances fluorescence by a factor of six.

Calixarene **45** is also suitable for the identification of Na^+ (see Ref. 73). Incorporation of the cation into the inner sphere of the sensor prevents the formation of an excimer from the pyrene units; as a result, only the monomer fluorescence remains in the spectrum of the complex. The selectivity factor [the ratio $k(Na^+):k(K^+)$] is 154; the presence of lithium cations does not disturb the system.

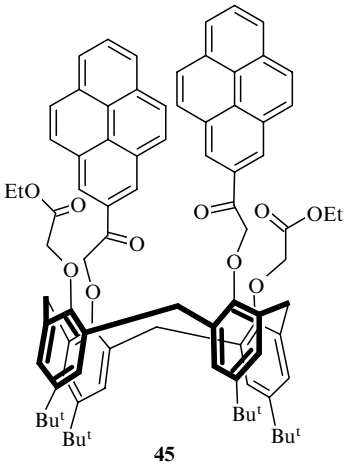

45

Ionophore **45** has recently been modified [74] by introducing a 9-anthroyloxyphenyl fluorophore into the molecule.

The electronic interactions in a series of calix[4]arene crown ethers and their complexes with alkali metal ions were studied. Absorption and emission electron spectroscopies have been used to reveal the effects of π-binding between the cations and the ligand; it was assumed that they have a major effect on the luminescent properties of the fluorophore.[75]

Many calixarene sensors contain crown ether fragments as receptors.

For example, calix[4]crown ether **46** is a strong ionochromophore.[76] If Ca^{2+} ions are added, they enter the cavities and interact with the electrons of the imino, keto, and crown-ether groups; a bathochromic shift occurs, which changes the colour of the compound from blue to green ($\Delta\lambda$ = 112 nm). This phenomenon is not observed in the presence of potassium ions; if the latter are coordinated with compound **46**, the spectrum of the latter is restored due to displacement of calcium ions from the inner sphere.

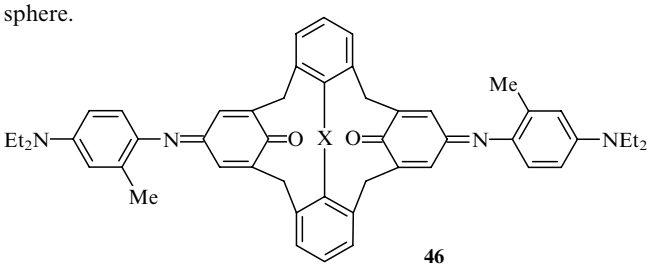

46

X = $OCH_2(CH_2OCH_2)_3CH_2O$.

Alkali metal cations affect strongly the excitation spectra of other calix[4]crown ethers containing two peripheral acetamidoanthraquinone residues.[77]

1,3-Alternating calix[4](9-cyano-10-anthrylmethyl)benzocrown-6 and its dideoxygenated analogue showed high selectivity towards the caesium ion when it was determined in the presence of a tenfold excess of potassium and rubidium cations.[78]

A more complicated calix[4]arene system **47** containing two crown receptors was suggested as an integrated sensor for the determination of potassium cations in alkaline medium and caesium cations in acidic medium.[79] The PET in alkaline solutions results in a very weak residual fluorescence of the anthracene fluorophore. Addition of caesium ions, which are coordinated by the cavity *A*, does not change the spectral characteristics. On the contrary, K^+ cations are incorporated into the cavity *B* of the crown ether, quench the PET and cause a sevenfold increase in fluorescence. In acidic media, where the nitrogen atom of the ring *B* is protonated, the PET is supported by the crown ether fragment *A*, and the fluorescence intensity is low. In this case, the ring *B* cannot coordinate potassium cations. Addition of Cs^+ ions to the solution results in their coordination by the ring *A* and a fourfold increase in fluorophore emission. Li^+ and Na^+ ions do not compete with each other in these processes, but rubidium cations display an effect resembling that of potassium cations in alkaline medium and that of caesium cations in acidic media.

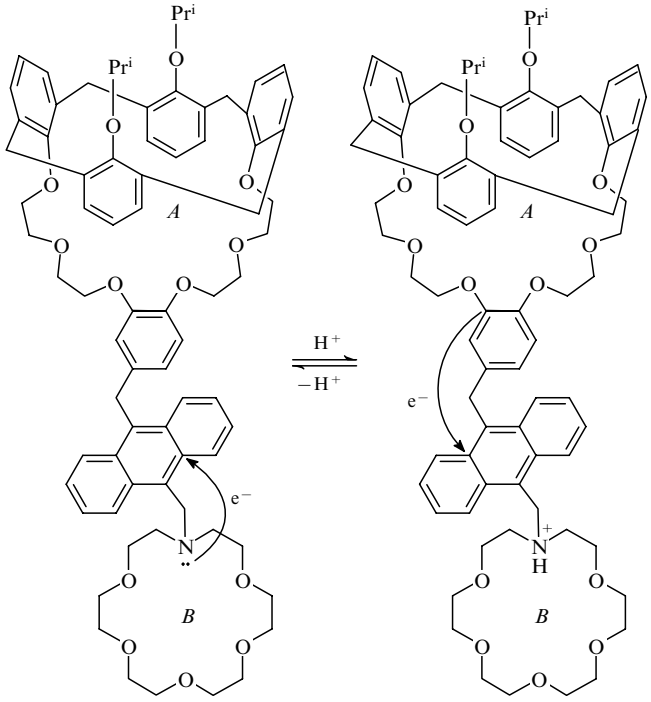

47a **47b**

The range of cations that can be determined by sensors based on calixarenes is rather wide. Such sensors are suitable for analysis of not only alkali but also transition metal cations. For example, the bispyrenyl calix[4]arene **48** with two hydroxamic acid linkers is a good Cu^{2+} and Ni^{2+} sensors (see Ref. 80).

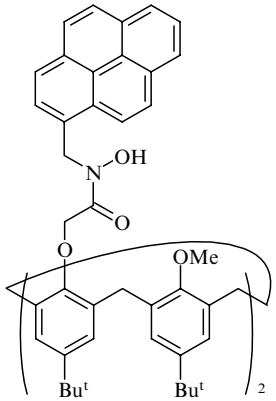

48

In solutions, compound **48** generates a double fluorescence spectrum, which corresponds to the monomeric and excimeric states of the pyrene rings. Addition of copper or nickel salts to the solution quenches abruptly a part of the fluorescent irradiation

depending on the solution acidity. In the opinion of Bodenant *et al.*,[80] the excimer photosensitivity of the ligand makes it possible to consider this system as a new type of chemosensor for the selective determination of transition metal ions in aqueous media.

The selectivity of sensors based on calixarenes may be enhanced by replacing the oxygen atoms in the calixarene skeleton by sulfur atoms. For example, water-soluble thiacalix[4]arenes **49** modified by dansyl fragments were suggested for the first time as fluorescent chemosensors for Co^{2+}, Ni^{2+}, and Cd^{2+}.[81]

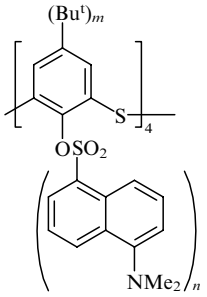

49

$m = 0-4$; $n = 2-4$.

tert-Butyl groups decrease the sensitivity of sensor molecules. The thiacalixarene **49** containing one *tert*-butyl group ($m = 1$) and three dansyl residues ($n = 3$) was found to be the most efficient. The complexation constants of this compound with Co^{2+} and Cd^{2+} are 2380 and 1510, respectively. For comparison, the corresponding constants for the chemosensor **49** containing four *tert*-butyl groups ($m = 4$) and three dansyl residues ($n = 3$) are 130 and 250.

Calix[4]arene systems can be luminescent chemosensors for medium-radius lanthanides.

The recently obtained macrocyclic water-soluble tetra-*p*-sulfonylmethylcalixresorcin[4]arenes coordinated with Nb^{3+} or Eu^{3+} ions show a triplet transition with an analytical frequency of 24 400 cm^{-1} (see Ref. 82). In acetonitrile, the same ions form highly luminescent complexes with calix[4]arene crown ethers containing a 2,2′-bipyridine fragment.[83]

III. Fluorescent chemosensors for anions

The main types of sensor used for the determination of anions have been considered in detail in reviews [17, 18] and in a monograph,[84] hence here it is appropriate to dwell on the general principles for constructing such chemosensors and to discuss recent publications.

Design of luminescent sensors for anions is a more complex task than that for cations, for the following reasons.

1. Anions are usually larger than cations, hence the receptor should have a larger coordination space; in addition, because of a low charge density on the anion, the receptor should form rather strong bonds with the anion (at the hydrogen bond level).

2. Receptors for anions are commonly constructed on the basis of cation receptors by incorporating strong electrophiles (protons, metal cations) enabling reversible coordination of the substrate anion, into the molecule.

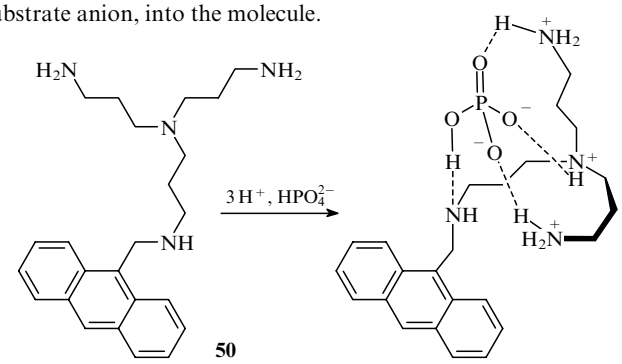

50

The system **50** was the first example of a fluorescent molecular sensor for anions.[85]

In aqueous solutions at pH 6, only three nitrogen atoms are protonated (the nitrogen atom closest to the anthracene fragment remains non-protonated), therefore the PET is effective and emission of the anthracene ring is small. If an HPO_4^{2-} anion is coordinated, the fourth H—N bond appears and fluorescence is enhanced.

Such anions as $H_2PO_4^-$ and HSO_4^- can be detected using the fluorescent system **51**, which incorporates three naphthylurea residues. The sensor **51** forms a 1 : 1 complex with $H_2PO_4^-$ in which the ligand fluorescence is enhanced owing to the PET.[86]

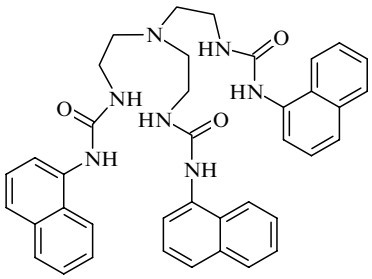

51

Compound **52** is an example of molecular sensor for amino acids.[87] In this compound, the bifunctional receptor is suitable for coordinating a zwitter-ionic amino acid molecule. The fluorescence of the anthracene fragment increases severalfold due to complexation.

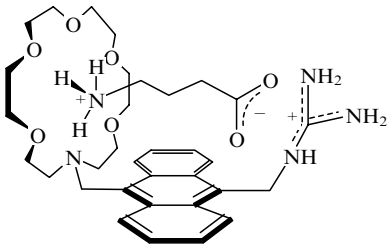

52

Polyazacycles are commonly used as selective sensors for anions. At pH 6, six of the eight nitrogen atoms in the cage of compound **53** are protonated (except the two apical ones). In this case, the fluorescence of the acridine fragment is quenched almost completely. When a dicarboxylate anion of suitable size is incorporated into such a protonated cell, intramolecular isolation

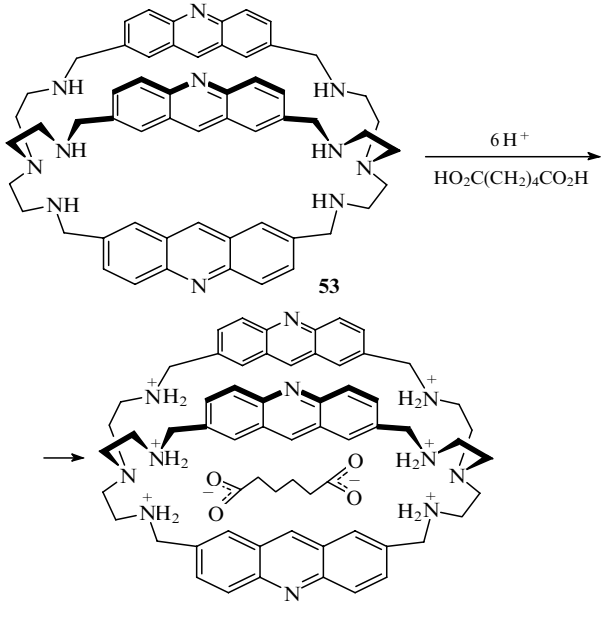

53

of the acridine rings occurs; the latter can no longer form an excimer and hence show strong one-ring fluorescence.[88]

An anion may also be fixed by a cation incorporated into the receptor and capable of coordination. For example, the tetramine **54**, which is a well-known chemosensor for zinc ions, displays secondary sensor capabilities in the presence of aromatic carboxylate anions.[89]

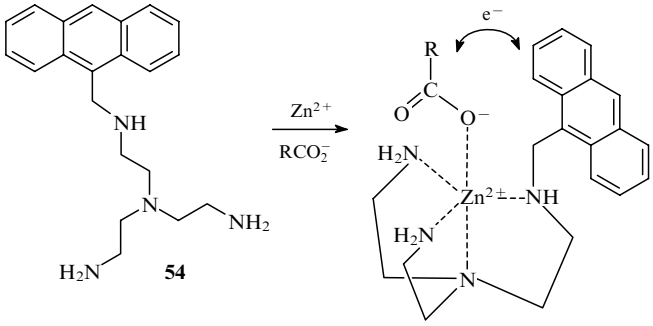

The fluorescence of the excited anthracene fragment is quenched when the carboxylate anion is bound with Zn^{2+}, which is explained [89] by electron transfer between the aromatic moiety of the carboxylic acid and the anthracene fluorophore.

The SO_4^{2-} ions can be determined selectively in acidic aqueous media using a complex of 1,4,8,11-tetrakis(naphthylmethyl)-1,4,8,11-tetraazacyclotetradecane with Cu^{2+}. The fluorescence intensity of this system increases in the presence of sulfate ions.[90]

A number of calix[4]pyrroles bound with anthracene moieties were synthesised and used as fluorescent chemosensors for anions (F^-, Cl^-, $H_2PO_4^-$).[91, 92]

A bulky dizinc octamine complex **55** suitable for the selective determination of a number of anions was synthesised.[93] At pH 8 this complex reacts with ambident anions to give stable 1 : 1 adducts. The cavity of the molecule containing two zinc cations can accommodate linear anions such as N_3^- (2.34 Å), NCO^- (2.42 Å), and (partially) NCS^- (2.75 Å). If any of these anions is added to the sensor, fluorescence of the anthracene moiety is quenched due to electron density transfer.

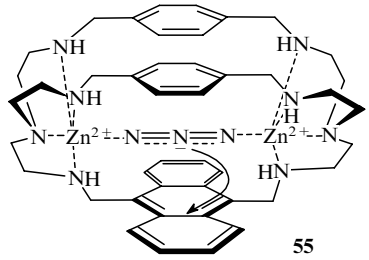

55

Certain other anions, such as NO_3^-, HCO_3^-, SO_4^{2-}, Cl^- and Br^-, do not affect the fluorescence intensity of the anthracene moiety even if they are present in tenfold excess.

Other, less bulky molecular systems can also be effective for the determination of anions. In particular, Sharma and Street [94] reported a fluorescent determination method for nitrate and nitrite ions in water using simple photoreactions resulting in a fluorescent compound with unknown structure. This method is used for monitoring the content of NO_3^- anions in tap water.

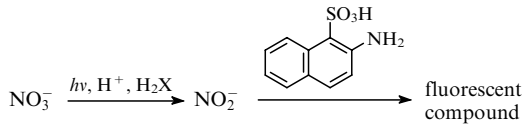

X = S^{2-}, SO_3^{2-}.

A method for the quantitative determination of nitrite ion in water and foodstuffs was elaborated [95] based on quenching of the indole fluorescence upon its interaction with nitrite ions in acidic medium. The detection limit is 2.5 mg per litre of the solution.

IV. Luminescent sensors for molecules

In Section III, we have already considered luminescent sensors for the determination of amino acids in acidic media [87] and dicarboxylic acids in alkaline solutions.[88] Recently, intense development of methods for the analysis of neutral organic molecules belonging to various classes has started. A number of sensors based on cationic and anionic receptors have been created for their determination.

For example, the luminescent sensor **56** has been patented; its non-cyclic analogue **57** has also been synthesised.[96] Complexes of these compounds with lanthanide cations are luminescent; the active cavities and diverse radicals $R^1 - R^{19}$ at the periphery of the macromolecules make it possible to detect a number of organic compounds, including peptides, nucleic acids and enzymes, and also to use these systems as luminescent markers for various purposes.

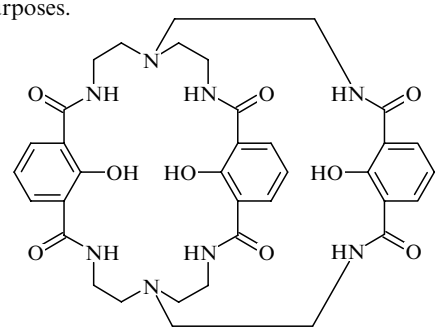

56

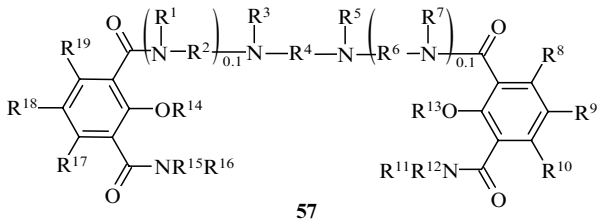

57

The fluorescent monomer **58** has been developed for the selective determination of phenols and anilines in non-polar solvents, even in the presence of aliphatic alcohols and amines, oxygen, and water.[97] The monomer can be involved in copolymerisation.

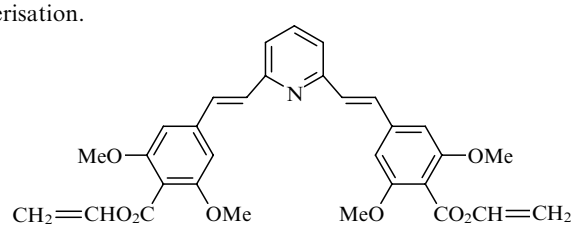

58

A new sensitive fluorimetric method for the determination of formaldehyde is based on the quenching of fluorescence of the aluminium complex of a tetra-substituted aminophthalocyanine in the presence of sulfite and formaldehyde. The latter can be determined at a concentration of 0.040 – 1.19 μg ml^{-1}, the detection limit being 7.5 ng ml^{-1} (see Ref. 98).

In order to determine traces of aldehydes and ketones in water, a fluorescent sensor was suggested, *viz*., 2-aminooxy-*N*-(3-dansylaminopropyl)acetamide.[99] It can be used for identification of formaldehyde, acetaldehyde, acetone, and other aldehydes and ketones at concentrations < 1 μmol $litre^{-1}$. The very low detection threshold makes this method suitable for the analysis of snow, ice and water in clouds for the content of carbonyl compounds.

The content of hydrogen peroxide in snow and ice can be determined with high accuracy using a new chemiluminescent reagent, *viz*., 7-(4,6-dichloro-1,3,5-triazinylamino)-4-methylcoumarin.[100] The chemiluminescence intensity is directly proportional to the concentration of H_2O_2 in the range 1×10^{-1}–4×10^{-4} mol litre^{-1}. The majority of non-transition metals do not interfere with this analysis.

The first fluorescent sensor for the determination of boronic acids based on an anthracene fluorophore was created; a diethanolamine fragment was used as the receptor in this sensor. Complexation increases fluorescence by a factor of 19 due to the PET.[101]

Synthesis of a new water-soluble reagent **59** for carbohydrates based on 3-aminophenylboronic acid and naphthalene-1,8-dicarboxylic anhydride was reported.[102] Naphthalimide is the fluorophore in compound **59**. Significant change in the irradiation intensity ($I/I_0 = 0.25$) makes compound **59** a useful sensor in neutral media.[102]

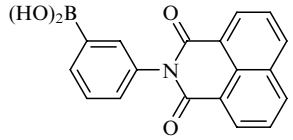

59

The symmetrical molecule **60** with two phenylboronic acid residues allows one to detect carbohydrates in aqueous solutions owing to a considerable enhancement of fluorescence.[103] Its characteristic feature is a low-frequency range; $\lambda_{max} = 645$ nm, with a shoulder at $\lambda = 695$ nm.

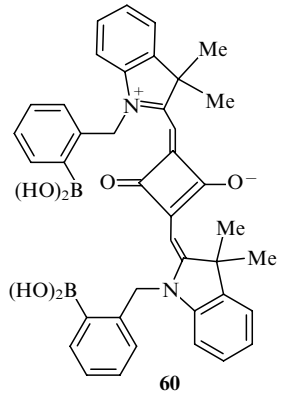

60

A fluorescent sensor for certain choline phospholipids was obtained based on squaramide.[104]

The selective fluorescent sensor **61** for D-glucosamine contains two receptors per molecule: monoaza-18-crown-6 (or monoaza-15-crown-5) and a boronic acid residue.[105]

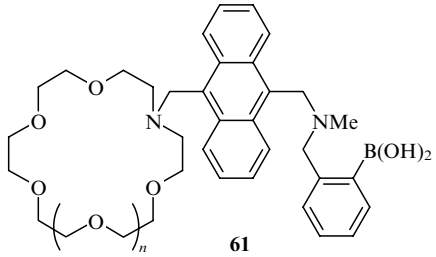

61

$n = 0, 1$.

Fluorescent sensors were found even for such chemically inert organic compounds as hydrocarbons. For example, alkanes increase the fluorescence of berberine sulfate **62** under monochromatic UV irradiation. This effect was explained [106] by ion–dipole interaction of the hydrocarbon with berberine sulfate.

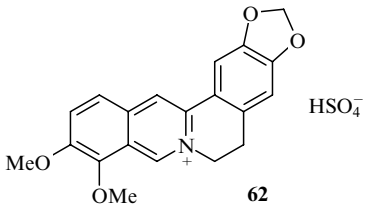

62

A method for selective determination of certain polycyclic aromatic hydrocarbons was suggested, involving the recording of the phosphorescence of sodium dodecyl sulfate micelles in the presence of acridine dyes (as donors of triplet energy) and polycyclic compounds (pyrene, anthracene, *etc*.) as acceptors.[107]

Cyclodextrins (CD) are also of considerable interest as chemosensors. A cavity in a cyclodextrin has low polarity, and its size is suitable for many 'guest' molecules. The properties of the substrate in the complex change considerably; this is reflected in the absorption and emission electronic spectra. Cyclodextrins are valuable sensors, as they often form water-soluble complexes owing to the presence of hydroxy groups; this expands considerably their scope.

More than 30 years ago, an inclusion complex was obtained, consisting of β-cyclodextrin **63** and 8-amino-1-naphthalenesulfonic acid. The molecules of the latter in the bound state showed intense fluorescence.[108] Later, a series of fluorescent sensors were obtained on the basis of this complex.

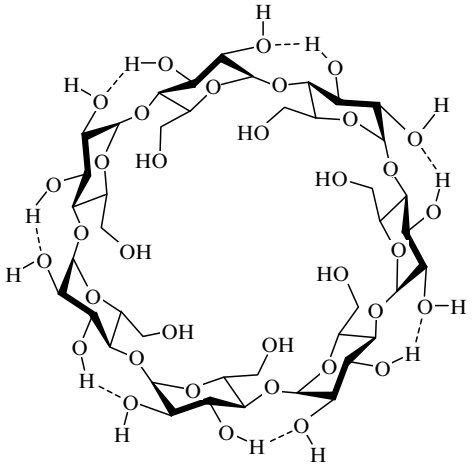

63

Two types of fluorescence, namely, monomer and excimer fluorescence, were studied for inclusion complexes of various naphthalene derivatives with β-CD.[109] Excimer fluorescence predominates for equimolar concentrations of naphthalene and β-CD. Complexes of 2,7-dimethylnaphthalene and 2-benzylnaphthalene with β-CD do not show excimer fluorescence.

Structures of various complexes of β-CD with naphthalene, phenanthrene, fluorene and cyclohexane were studied both by experimental and theoretical methods.[110–112] The complexation energy ranges within 9–12 kcal mol^{-1}.

Long-lived fluorescence at room temperature was found and studied for 2 : 2 complexes of β-CD with naphthalene.[113]

De la Pena *et al*.[114] studied the effect of various factors on the phosphorescence of the complex of α-CD with 6-bromo-2-naphthol in deaerated aqueous solutions at room temperature. Emission maxima were detected at $\lambda = 500$ and 535 nm. The determination threshold of bromonaphthol is 0.26 mg litre^{-1} with a standard deviation of 4%.

It was found subsequently that the addition of small amounts of various non-polar liquids (particularly cyclohexane) results in a very strong enhancement of phosphorescence. However, the presence of reducing agents (sodium sulfite) quenches the signal.[115]

Hydroxypropyl-β-CD in aqueous media forms a supramolecular inclusion compound with 8-anilino-1-naphthalenesulfonic

acid, which results in significant luminescence enhancement of the latter.[116]

Triethylenetetraminebis(β-CD) was synthesised from hydroxypropyl-β-CD and triethylenetetramine; after modification by Cu^{2+} ions, it showed specific luminescence upon interaction with 'guest' molecules, such as 6-(*p*-toluidino)-2-naphthalene- and 8-anilino-1-naphthalenesulfonic acids.[117]

A naphthol-modified β-CD was successfully used as a fluorescent sensor in the determination of trace amounts of CCl_4 and 2-methylisoborneol in water.[118]

β- and γ-Cyclodextrins modified by pyrrolinone residues are fluorescent chemosensors for a number of carboxylic acids, terpenoids and bile acids.[119] The cyclodextrin 'host' has a fluorescence band at $\lambda = 472$ nm, the intensity of which decreases if adamantane-1-carboxylic, *p*-aminobenzoic, benzoic, phthalic or cyclohexenecarboxylic acid is added as the substrate in aqueous medium at pH 5.90. However, if these acids are added in a buffer solution with pH 9.09, fluorescence is enhanced. The same effect is achieved if terpenoids, amino compounds and bile acid salts are added as the 'guests'.

The sensitivity of the cyclodextrin 'host' to the nature of the 'guest' molecules can be varied by changing the cavity size in the 'host'. For example, the terphenyl-substituted β-cyclodextrin **64a**, which has a smaller cycle than the γ-cyclodextrin derivative **64b**, 'recognises' well small terpenoid molecules, especially in the dimethyl sulfoxide–water medium (1 : 9). Bulkier bile acids are detected with lower sensitivity. It is interesting to note that the radiation intensity of cyclodextrin **64a** increases due to interactions with 'hosts', whereas that of compound **64b** decreases.[120]

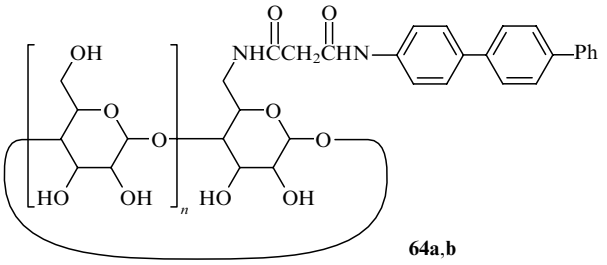

64a,**b**

$n = 6$ (**a**), 7 (**b**).

Dansyl- and tosyl-modified β- and γ-CD are used as chemosensors for bile acids and terpenoids.[121] The luminescence of β-CD is quenched in the presence of 'guest' molecules, while that of γ-CD is enhanced as a result of interactions with monocyclic and non-cyclic molecules. Chenodeoxycholic acid, ursodeoxycholic acid, and (−)-borneol can be recognised with high sensitivity using β-CD, while γ-CD can be used to recognise lithocholic acid and (−)-borneol.

A system comprising a peptide, γ-CD and naphthalene fragments can also respond to the presence of various cholic acids due to the formation of a luminescent excimer.[122]

Mono[6-deoxy-6-(1-methyl-2-pyrrolidinylidenesulfamido)]-β-CD synthesised recently is also a promising sensor.[123]

A highly sensitive water-soluble fluorescent sensor system **65** was obtained; this is a β-CD (receptor) substituted with 2-naphthoic acid (fluorophore).[124]

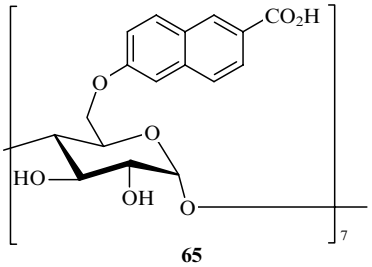

65

The sensor **65** was used to detect surfactants (mostly cations) of the types **66**–**69** with long hydrocarbon chains.

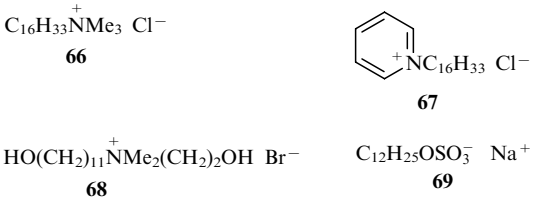

66 **67**

68 **69**

The fluorescence spectra of the sensor **65** undergo specific changes upon micellation or complexation.

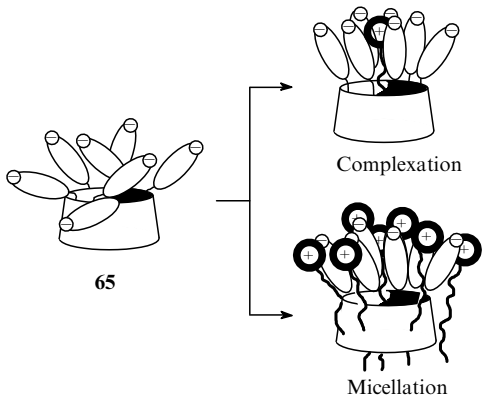

65

The nature of many sensor molecules involves a mechanism to control them, which makes it possible to turn on and off or switch the sensor process. When such systems are exposed to external factors (change in temperature, polarity, pH of the medium, concentration of metal ions, electromagnetic potential, chemical reactions), they undergo intramolecular rearrangements affecting the sensor properties. The following luminescent sensors can serve as examples: pH-controlled ones (azacrown ethers, polyaza compounds), those controlled by redox reactions (compounds **32**, **33**), pK^+- (compound **46**) and pNa^+-dependent (compound **44**).

V. Photochromic chemosensors

New highly sensitive photodynamic fluorescent sensor systems (*i.e.*, those that can be turned on and/or off upon irradiation of a solution) can be created based on photochromic spirocyclic compounds, such as spiropyrans **70a** and spirooxazines **70b**.

The general scheme of these transformations is shown below.

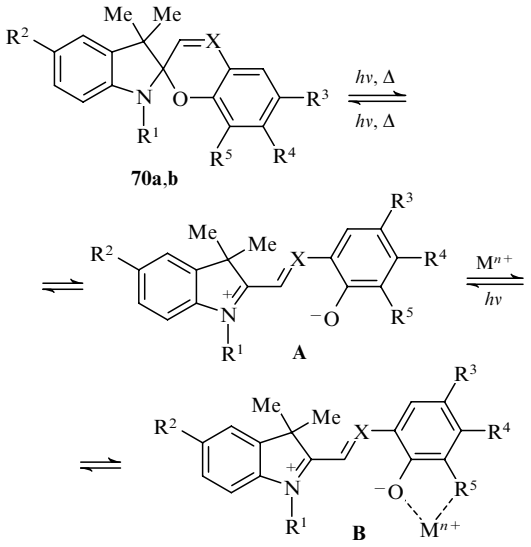

70a,**b** **A** **B**

X = CH (**a**), N (**b**); R^1–R^4 are various substituents, R^5 is complex-forming group.

Exposure of photochromic spirans **70a,b** to short-wave irradiation results in the merocyanine form **A**. The latter can undergo

coordination with metal ions M^{n+} to give the complex **B** having specific absorption and fluorescence spectral characteristics different from those of the form **A**.

Studies of these systems as chemosensors started in the 1960s.[125,126] It was shown that complexes of such ions as Zn^{2+}, Co^{2+}, and Cu^{2+} with the spiropyrans **70a** have characteristic spectral bands in solution and can be used in analytical chemistry.

In 1982–1988, a number of papers were published (see, *e.g.*, Refs 127 and 128) reporting detailed studies on the complexation of various metal ions (Pb^{2+}, Co^{2+}, Ni^{2+}, Zn^{2+}, Cd^{2+}, Cu^{2+}, Ce^{3+}, La^{3+}, *etc.*) with molecules of spiropyrans **70a** (R^1 = Me, R^2 = H, R^3 = H, NO_2, R^4 = H, R^5 = OMe) in organic solvents. The complexes **B** have characteristic bands in the absorption and emission electronic spectra. Certain cations coordinate the oxygen atom of the methoxy group and thus stabilise the open form. The open form **B** is also stabilised for $R^3 = NO_2$.

In solutions of spiropyrans **70a** with $R^1 = (CH_2)_2CO_2^-$ or $(CH_2)_2SO_3^-$, $R^2 = NO_2$, $R^3 = R^4 = R^5 = H$, the merocyanine form **A** is strongly stabilised by divalent metal ions (Zn^{2+}, Ca^{2+}). Specific fluorescence of solutions in acetone was noted.[129] Spiropyrans **70a** with R^1 = Me, R^2 = H, R^3 = H, NO_2, R^4–R^5 = N=CHCH=CH, which form **B**-type strongly fluorescent complexes with Mg^{2+}, Ca^{2+}, Ba^{2+}, Zn^{2+}, Cd^{2+}, Hg^{2+} and other cations, were found to be very sensitive sensors for these cations.

Incorporation of crown ether fragments as receptors into the molecules of spiro compounds changes the properties of these photochromic compounds. For example, nitrobenzospiropyran **71** containing monoazabenzo-15-crown-5 is a good Li^+ and Na^+ sensor with pronounced negative photochromism.[130]

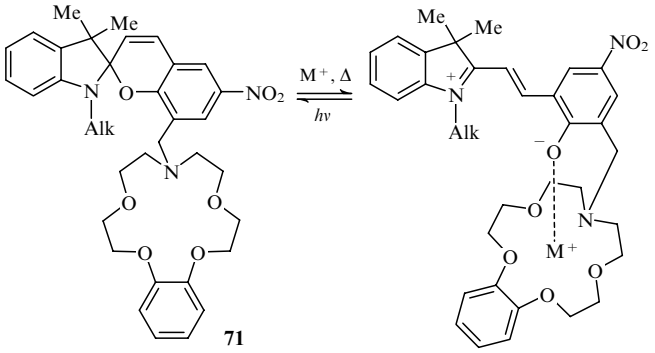

71

M = Li, Na, K.

Spiropyrans **70a** and spirooxazines **70b** with polyfunctional receptors undergo more complex transformations.[131–134] For example, for compounds **72a–c** there are two competing complexation pathways (Scheme 1) involving free alkaline-earth or rare-earth cations (structure **A**) or the same cations bound with the crown ether fragment (structures **B**, **C**). Each type of coordination is characterised by appropriate changes in the electronic spectra.

Complexation can be monitored coulometrically, by femtosecond spectrochromatography,[135] or this monitoring can be combined with mass spectrometric determinations.[136]

Light-sensitive membranes based on polyvinyl chloride with built-in fragments of lipophilic crown-containing spirobenzopyrans were obtained and studied. The photochromic parameters in such systems depend on the pH of the medium and on the concentration of alkali metal ions.[137]

The spirobenzothiapyran **73** containing the aza-12-crown-4 residue can form a complex with Li^+. The coloured photoinduced form of this compound has enhanced thermal stability, partially owing to stabilisation upon complexation.[138,139]

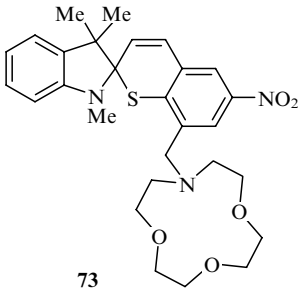

73

Stabilisation of an open merocyanine fragment also accompanies the complexation of Li^+ and especially Ag^+ with analogues of compound **73** containing monoaza-15-crown-5 and -18-crown-6.[139]

The two spirobenzopyran fragments linked with diaza-18-crown-6 (compound **74**) bind the Ca^{2+} ions more strongly than alkali metal cations due to an apical coordination of divalent cations by the anionic oxygen atoms of the ligand. This type of calcium complexation can be controlled by irradiation.[140]

Scheme 1

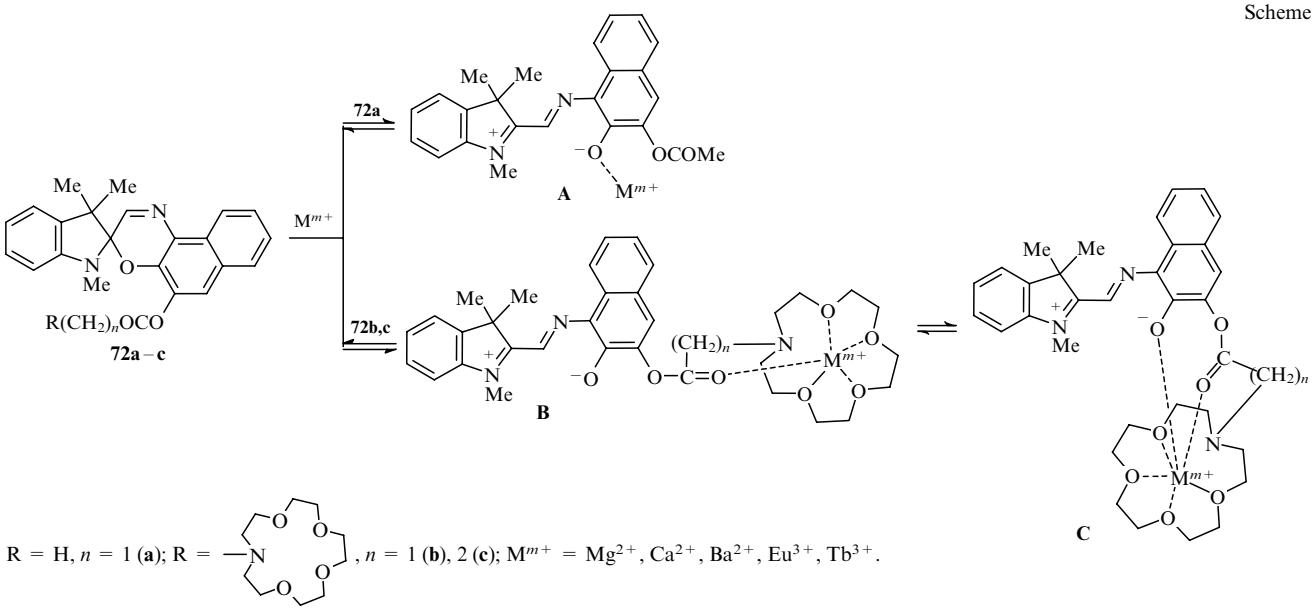

R = H, n = 1 (**a**); R = , n = 1 (**b**), 2 (**c**); M^{m+} = Mg^{2+}, Ca^{2+}, Ba^{2+}, Eu^{3+}, Tb^{3+}.

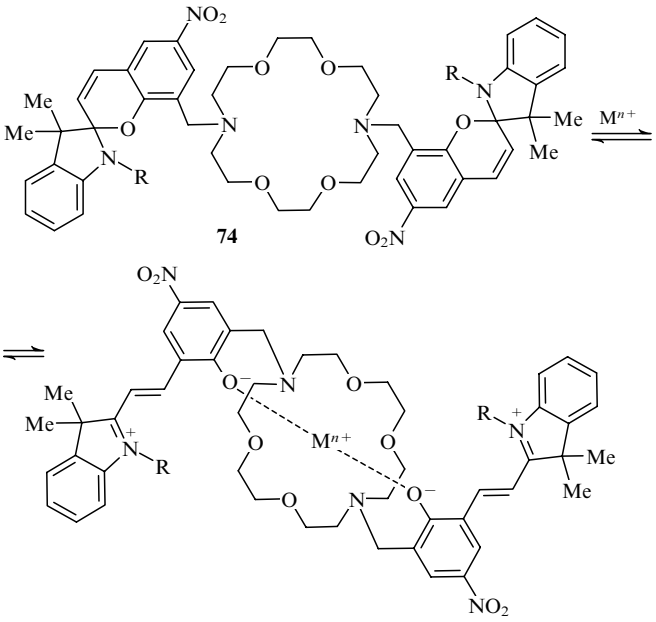

74

Upon complexation with Na^+, K^+ and alkaline-earth metal cations, the shift of the short-wave absorption band of phenylfulgide **75** containing a benzo-15-crown-5 fragment fused to the benzene ring was 28, 12, and > 40 nm, respectively, both in the open and cyclic forms.[141, 142]

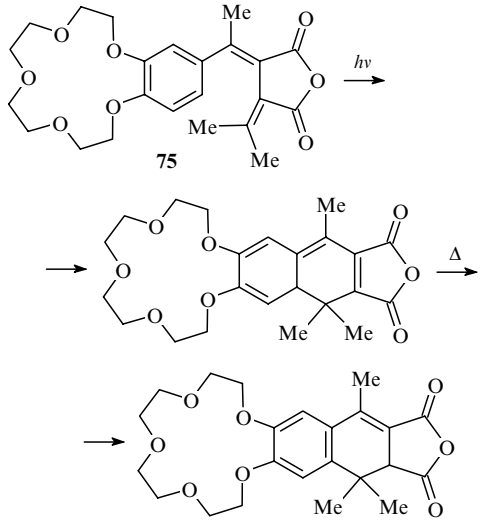

75

Indolylfulgides **76** containing 14-crown-4, 17-crown-5 and 20-crown-6 fragments are sensors for Li^+, Na^+ and K^+, respectively; in this case, both the *E*- and *Z*-isomers of the open forms **76a** are more sensitive for alkali metal ions than the totally cyclic system **76b**.[143]

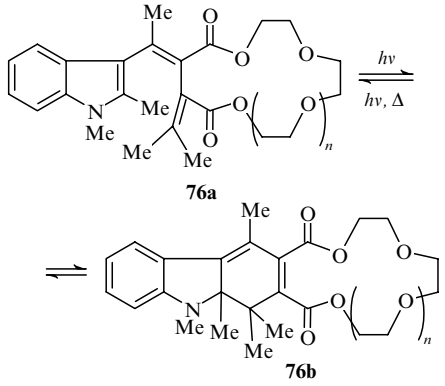

76a

76b

n = 1–3.

Dihetarylcyclopentenes **77** containing crown-ether fragments were synthesised and studied as photochromic sensors. These compounds can decrease considerably the degree of coordination of K^+, Rb^+ and Cs^+ when exposed to UV irradiation at a wavelength of $\lambda = 330 \pm 70$ nm (picrates in aqueous-organic media were analysed).[144–146] This phenomenon was explained by the ability of the original compound **77** to coordinate these cations by both crown-ether fragments simultaneously, whereas the more rigid photoreaction product, *viz*., isomer **A**, is devoid of this ability. The possibility of selective coordination of cations with certain radii is provided by the crown ether ring sizes.

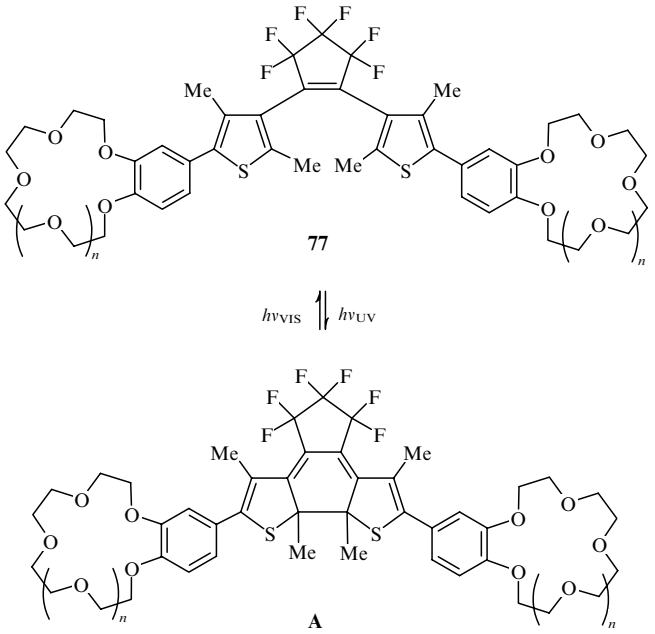

77

A

n = 0–2.

The novel photochromic compound **78a** based on a Malachite Green analogue containing two crown-ether fragments was synthesised.[147] Colourless complexes **78b** with metal cyanides are leuconitriles; their solutions are coloured reversibly under irradiation due to photodissociation.[147] The system **78** is a chemosensor for metal cyanides.

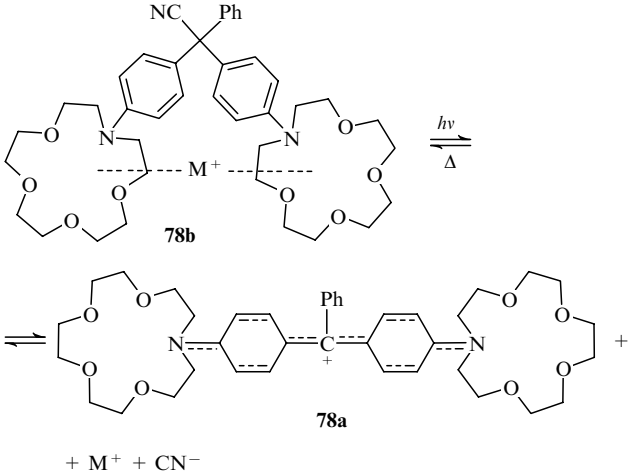

78b

78a

Alfimov *et al.*[148–152] described crown-containing styryl dyes **79**, **80**, which are fluorescent sensors for alkaline-earth metal cations (Mg^{2+}, Ca^{2+}, Ba^{2+}).

Compounds **79b–e** with *trans*-configuration of the double bond

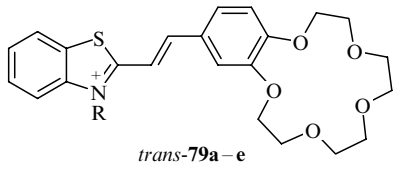

trans-**79a–e**

R = $EtClO_4^-$ (**a**), $(CH_2)_2SO_3^-$ (**b**), $(CH_2)_3SO_3^-$ (**c**), $(CH_2)_4SO_3^-$ (**d**), $CH_2C_6H_4SO_3^-$ (**e**).

form (depending on the type of the substituent R, which serves as a spacer, and the nature of the counter-ion) either monomolecular complexes, in which the metal ion located within the crown is additionally coordinated by the sulfonic group oxygen, or type **A** dimers resulting from reversible [2 + 2]-cycloaddition.[148]

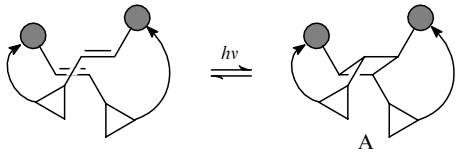

A

● — benzo-15-crown-5 fragment with a metal cation;

△ — benzothiazole residue; ↷ — $(CH_2)_nSO_3^-$ (n = 3, 4).

Illumination with light at a wavelength of 436 nm results in isomerisation of *trans*-complexes **79**·M^{2+} to give *cis*-complexes. The toluenesulfonic acid residue in the complex (*cis*-**79e**)·M^{2+} is arranged above the crown-ether plane to give a molecule 'capped' with the anion.[150]

For dimeric molecules **79f** with a trimethylene bridge connecting the benzothiazole residues, the most stable configuration of the complexes is the structure **79f**·M^{2+} (see Ref. 149).

Quantum-chemical calculations of the energies of ground and excited electronic states of the molecules **79a–f**, their dimers and complexes confirmed the conclusions based on the experimental studies.[151]

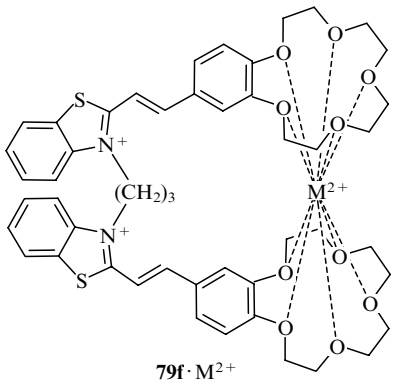

79f·M^{2+}

The *trans*-**80a** dye containing the *N*-phenylaza-15-crown-5 fragment manifests a considerable ionochromic effect registered in electronic spectra (Fig. 4),[148] which, according to the calculated complexation constants, implies the usual complex structure where the Ca^{2+} cation is coordinated in the azacrown fragment.

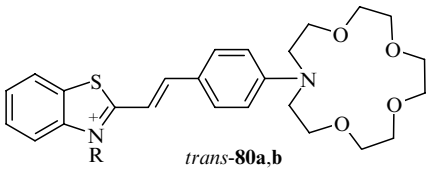

trans-**80a,b**

R = $EtClO_4^-$ (**a**), $(CH_2)_3SO_3^-$ (**b**).

The data obtained for the complexation of compound *trans*-**80b** with Ca^{2+} and Zn^{2+} can be visualised schematically by the following sequence of equilibria

$$S{-}C + M \rightleftharpoons S{-}CM,$$

$$S{-}C + M \rightleftharpoons MS{-}C,$$

$$M(S{-}C)_{n-1} + S{-}C \rightleftharpoons M(S{-}C)_n,$$

$$MS{-}C + M \rightleftharpoons MS{-}CM,$$

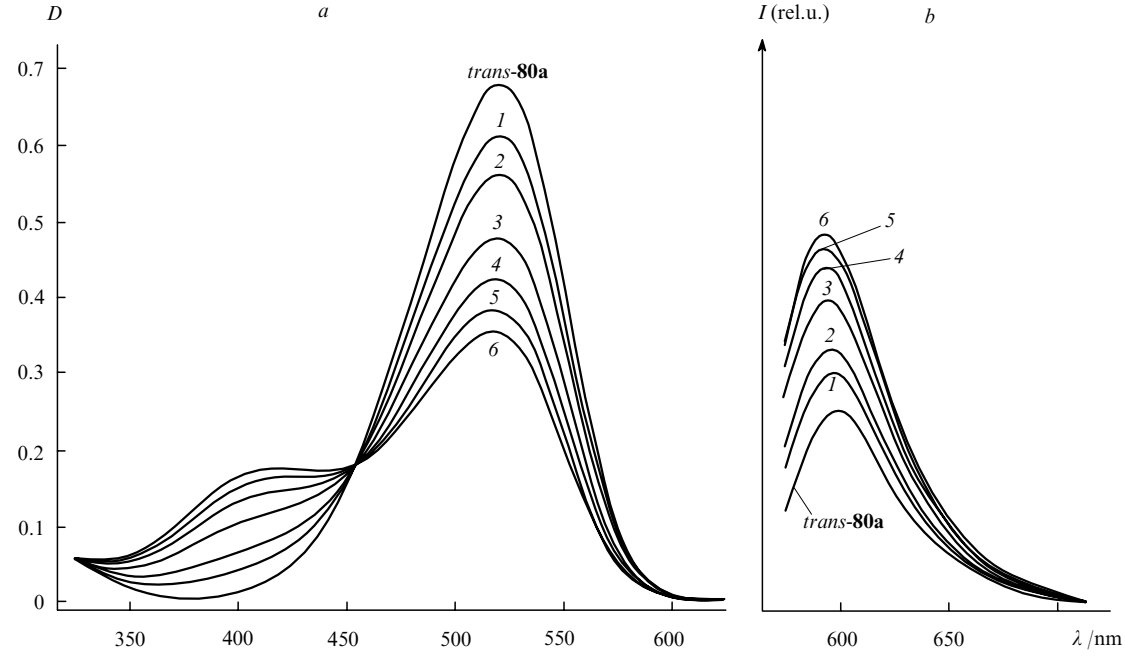

Figure 4. Dependence of absorption spectra (*a*) and fluorescence spectra (*b*) of ligand *trans*-**80a** ($c_{\mathbf{80a}} = 1.0 \times 10^{-5}$ mol litre^{-1}) in MeCN on the Ca^{2+} concentration at a constant concentration of ClO_4^- (0.01 mol litre^{-1});[148]
$c_{Ca2+} : c_{\mathbf{80a}}$ = 50 (*1*), 100 (*2*), 200 (*3*), 300 (*4*), 400 (*5*), 500 (*6*).

where S–C is a *trans*-**80b** molecule (S is a sulfonic group, C is an azacrown ether fragment); M is a metal ion, $n = 2-4$.

This means that, in addition to 1 : 1 complexes, the betaine **80b** forms aggregates comprising four dye molecules and one M^{2+} ion. Probably, the interaction between the metal cations with the sulfonic groups of the molecules makes the major contribution to the stability of these aggregates.[148]

Studies of ion exchange processes involving amphiphilic photochromic compounds **79** in the 'monolayer–aqueous phase' system showed that the Na^+, Ca^{2+} and Mg^{2+} ions increase the strain in the monolayer, whereas the K^+ ions decrease it considerably.[153, 154]

Compound **81**, which comprises thioindigo and dithiocrown-ether fragments, is a novel photochromic sensor for alkali metal cations and Ca^{2+}.[155] It exists as *cis*- and *trans*-isomers, each isomer having characteristic bands in the absorption spectra: $\lambda_{max} = 485$ and 545 nm for *cis*- and *trans*-**81**, respectively. The *trans*-isomer of compound **81**, which has weak coordinating properties, is transformed into the *cis*-isomer upon exposure to light with a wavelength of 550 nm;

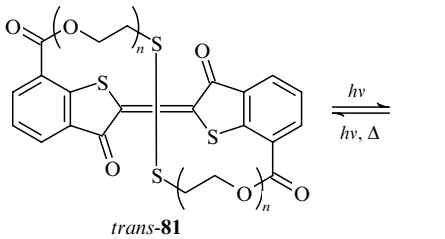

trans-**81**

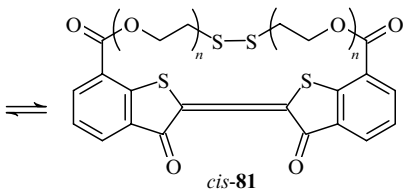

cis-**81**

$n = 2, 3$.

the *cis*-isomer can coordinate a 'guest' cation. The complexation equilibrium constants of metal ions, determined by the extraction method, suggest a high sensitivity of the *cis*-isomer for Na^+, Cs^+ and Ca^{2+}; however, such ions as Hg^{2+}, Cd^{2+}, Cu^{2+}, Co^{2+} and Ag^+ do not form these complexes. The lifetime of the *cis*-isomer is hundreds times longer than that of its analogue (*cis*-thioindigo), even in the absence of metal ions.

We obtained and studied[156, 157] 2-(2-acyloxyphenylamino-methylene)-2,3-dihydrobenzo[*b*]thiophen-3-ones **82a**,**b**. These are solvato- and thermochromic compounds undergoing the following transformations.

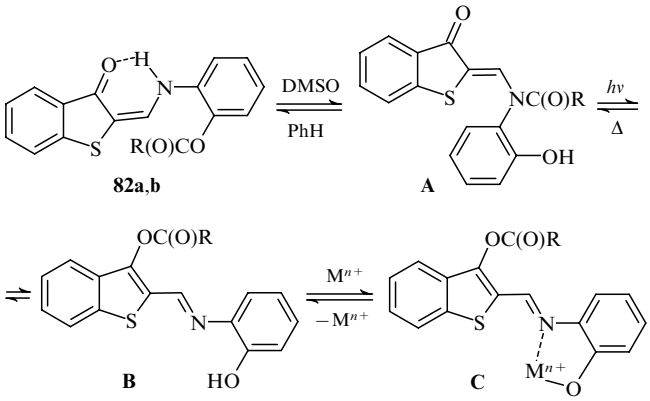

82a,**b** **A** **B** **C**

R = Me (**a**), 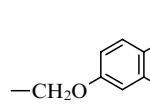 (**b**).

Under irradiation, the form **A** is transformed into the form **B**, thus creating conditions for the formation of the complex **C** with a metal ion; the spectral characteristics of the latter differ from those of compounds **A** and **B**, *i.e.*, the system **82** manifests metal-sensor properties. The acyl moiety can contain a fluorophore group, *e.g.*, the residue of 4-methylcoumarin-7-yloxyacetic acid (compound **82b**). It was shown by ^1H NMR and electronic spectroscopy[158] that an equilibrium is established in solutions between the original compound **82b** and the form **A**; the content of the latter increases with the solvent polarity. Illumination of the equilibrium mixture with light at 436 nm results in transfer of the acyl group from the nitrogen atom to the thiophene fragment. This produces an (*E*)-C=N bond. The absorption spectra of the system **82b** change if the solution contains Ca^{2+}, Mg^{2+}, Zn^{2+} or Ni^{2+} cations. However, the fluorophore residue does not behave as a luminescent indicator, probably because of preferential deactivation of excited molecules.

The system **83** comprising not only a benzothiophene fragment and an *N*-acyl residue but also an annelated crown ether can be used as a photochromic sensor for alkali metal ions.[159]

Illumination of compound **83** and its complexes with alkali metals with light at 436 nm results in migration of the acyl group from the nitrogen atom to the oxygen atom to give *O*-isomers **84** and **85**, respectively. Complexation with lithium ions results in the biggest changes in the absorption spectra.

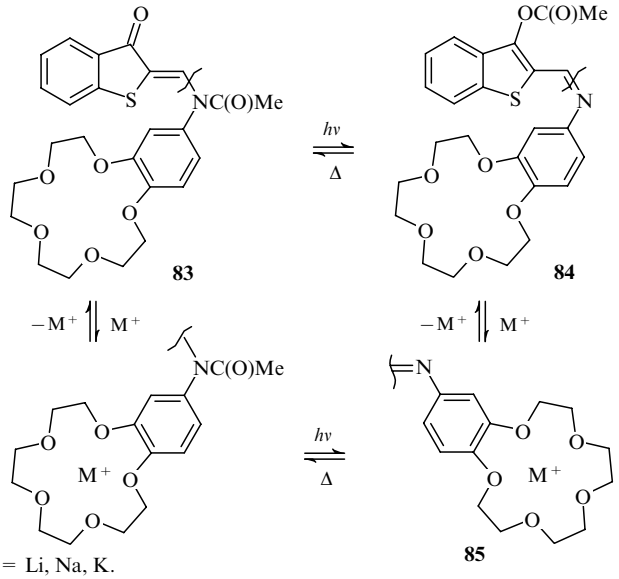

83 **84** **85**

M = Li, Na, K.

Figure 5 shows a plot of the optical density of a solution of the complex **85** *versus* the concentration ratio of LiI and the ligand **84**

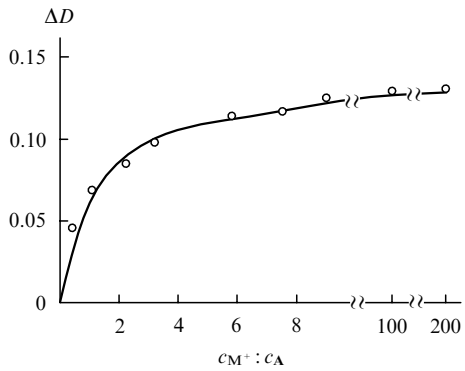

Figure 5. Dependence of the optical density variation (ΔD) of a solution of the complex **85** on the LiI (c_{M^+}) and the ligand **84** (c_A) concentration ratio.[159]

at the absorption wavelength of the complex ($\lambda = 357$ nm) upon addition of lithium iodide to an illuminated solution of the *O*-acetyl form of **85** (at a concentration of 6.55×10^{-5} mol litre^{-1}). The maximum extinction is reached at a tenfold excess of LiI. This specific behaviour of this system and its high sensitivity for Li^+ make it possible to place it among photochromic sensors.[160]

VI. Conclusion

Thus, recent studies demonstrate a considerable interest in the creation of novel chemosensor systems applicable to the analysis of inorganic and organic substrates. Table 1 shows the characteristics of certain organic sensors.

Table 1. Characteristics of certain organic sensors.

Compound	Substrate	Detection threshold /mol litre^{-1}	Analytical fluorescence wavelength /nm	Ref.
1c	Ca^{2+}	1×10^{-6}	333	15
1c	Ba^{2+}	1×10^{-6}	333	15
4a	Ca^{2+}	3×10^{-6}	417	24
4b	Ca^{2+}	3×10^{-6}	404	24
7a	Mg^{2+}	1×10^{-8}	530	27
7b	Hg^{2+}	1×10^{-8}	476	27
20	Ce^{3+}	2×10^{-6}	406	46
20	Nd^{3+}	2×10^{-6}	406	46
30c	Zn^{2+}	1×10^{-6}	416	55
30c	Hg^{2+}	5×10^{-7}	416	55
32	Hg^{2+}	1×10^{-5}	413	58
33	Cd^{2+}	1×10^{-5}	413	58
36a	Zn^{2+}	3×10^{-8}	514	62
36b	Zn^{2+}	1×10^{-8}	514	62
38	Co^{2+}	5×10^{-7}	514	65
40	Ni^{2+}	5×10^{-8}	400	80
45	Na^+	6×10^{-6}	480	74
47a	K^+	1×10^{-6}	427	79
47b	Cs^+	1×10^{-8}	429	79
48	Cu^{2+}, Ni^{2+}	5×10^{-8}	400	80
49 ($m = 4$, $n = 3$)	Cd^{2+}	2×10^{-7}	520	81
	Co^{2+}	1×10^{-7}	520	81
51	$H_2PO_4^-$	2×10^{-6}	377	86
51	HSO_4^-	3×10^{-6}	377	86
59	D-fructose	1×10^{-3}	400	102
84	Li^+	2×10^{-5}	357 [a]	159
Indole	NO_2^-	2.5 [b]	350	95
α-CD	6-bromo-2-naphthol	0.04 [c]	500	115

[a] Absorption band; [b] μg litre^{-1}; [c] mg litre^{-1}.

Currently, diverse types and classes of both organic and inorganic compounds are used as abiotic sensors or substrates. The use of crown-ether compounds as receptors stimulated the creation of chemosensors based on complex three-dimensional systems, including polyamines, dendrimers, calixarenes, cyclodextrins and their combinations.

Fluorescent chemosensors with high sensitivities and selectivities have been synthesised; the action of these sensors is based on specific but reliable intramolecular interaction mechanisms (the PET and PCT effects; excimers and exciplexes). Studies aimed at the external controlling of sensor processes are of current interest. The search for new types of molecular 'switches' is under way. Some chemosensor systems are created using elements of supramolecular chemistry and nanotechnologies; this makes it possible to create sensors with unique capabilities, *e.g.*, properties of molecular machines [52, 161] or artificial memory elements.[14, 52, 79]

The scope of application of fluorescent sensors expands: from routine laboratory reagents for cations and anions, they grow into systems for identifying complex organic molecules, analysing various biological substrates,[35, 55, 61] pesticides,[162] and foodstuffs,[163] monitoring the state of the atmosphere and oceans,[29, 164] *etc*.

Although the theory of chemical sensors has certain achievements,[165] it is developing somewhat more slowly than experimental and applied studies. The general theory of chemosensors requires new data on the mechanisms of intramolecular electronic interactions in the systems receptor – conductor – fluorophore, on the effects of external factors on the properties of sensors, on the nature of complementarity of receptors and substrates, *etc*.

This review has been written with the financial support of the Russian Foundation for Basic Research (Project No. 00-15-97320), the Ministry for Education of the Russian Federation, and CRDF (REC-004).

References

1. *Probe Design and Chemical Sensing. Topics in Fluorescence Spectroscopy* Vol. 4 (Ed. J R Lakowicz) (New York: Plenum, 1994)
2. J D Winefordner (Ed.) *Trace Analysis. Spectroscopic Methods for Elements* (New York: Wiley, 1976)
3. H-G Löhr, F Vögtle *Acc. Chem. Res.* **18** 65 (1985)
4. B Valeur, I Leray *Coord. Chem. Rev.* **205** 3 (2000)
5. A J Bryan, A P de Silva, S A de Silva, R A D D Rupasinghe, K R A S Sandanayake *Biosensors* **4** 169 (1989)
6. A W Czarnik (Ed.) *Fluorescent Chemosensors for Ion and Molecule Recognition (ACS Sym. Ser.)* Vol. 358 (Washington, DC: American Chemical Society, 1993)
7. G J Kavarnos *Fundamentals of Photoinduced Electron Transfer* (Weinheim: VCH, 1993)
8. R Bergonzi, L Fabbrizzi, M Licchelli, C Mangano *Coord. Chem. Rev.* **170** 31 (1998)
9. B Valeur, E Bardez *Chem. Br.* **31** 216 (1995)
10. L Fabbrizzi, A Poggi *Chem. Soc. Rev.* 197 (1995)
11. A P de Silva, H Q N Gunaratne, T Gunnlaugsson, A J M Huxley, C P Mc Coy, J T Rademacher, T E Rice *Chem. Rev.* **97** 1515 (1997)
12. A M Garcia-Campana, W R G Baeyens *Analusis* **28** 686 (2000)
13. A P de Silva, H Q N Gunaratne, T Gunnlaugsson *Chem. Commun.* 1967 (1996)
14. A P de Silva, D B Fox, A J M Huxley, T S Moody *Coord. Chem. Rev.* **205** 41 (2000)
15. K Kubo, T Sakurai *Heterocycles* **52** 945 (2000)
16. L Prodi, F Bolletta, M Montalti, N Zaccheroni *Coord. Chem. Rev.* **205** 59 (2000)
17. L Fabbrizzi, M Licchelli, G Rabaioli, A Taglietti *Coord. Chem. Rev.* **205** 85 (2000)
18. P D Beer, J Cadman *Coord. Chem. Rev.* **205** 131 (2000)
19. A P de Silva, S A de Silva *J. Chem. Soc., Chem. Commun.* 1709 (1986)
20. H-F Ji, R Dabestani, G M Brown, R L Hettich *Photochem. Photobiol.* **69** 513 (1999)
21. K Kubo, R Ishige, J Kubo, T Sakurai *Talanta* **49** 181 (1999)
22. A Yu Tsivadze, A A Varnek, V E Khutorskii *Koordinatsionnye Soedineniya Metallov s Kraun-Ligandami* (Coordination Compounds of Metals with Crown Ligands) (Moscow: Nauka, 1991)
23. A Yu Tsivadze *Ross. Khim. Zh.* **40** 43 (1996) [a]
24. P Crochet, J-P Malval, R Lapouyade *Chem. Commun.* 289 (2000)
25. K Rurack, J L Bricks, A Kachkovski, U Resch *J. Fluoresc.* **7** 63S (1997)
26. L Prodi, F Bolletta, M Montalti, N Zaccheroni *Proc. SPIE – Int. Soc. Opt. Eng.* 202 (1999)
27. L Prodi, C Bargossi, M Montalti, N Zaccheroni, N Su, J S Bradshaw, R M Izatt, P B Savage *J. Am. Chem. Soc.* **122** 6769 (2000)
28. S-H Kim, S-K Han, S-H Park, C-M Yoon, S-R Keum *Dyes Pigments* **43** 21 (1999)
29. J Bourson, F Badaoui, B Valeur. *J. Fluoresc.* **4** 275 (1994)
30. J-L Habib Jiwan, C Branger, J-Ph Soumillion, B Valeur *J. Photochem. Photobiol. A, Chem.* **116** 127 (1998)

31. A Tahri, E Cielen, K J Van Aken, G J Hoornaert, F C De Schryver, N Boens *J. Chem.Soc., Perkin Trans. 2* 1739 (1999)
32. A P de Silva, K R A S Sandanayake *Angew. Chem., Int. Ed. Engl.* **29** 1173 (1990)
33. A P de Silva, K R A S Sandanayake *J. Chem. Soc., Chem. Commun.* 1183 (1989)
34. A P de Silva, K R A S Sandanayake *Tetrahedron Lett.* **32** 421 (1991)
35. A P de Silva, H Q N Gunaratne, C P McCoy *J. Am. Chem. Soc.* **119** 7891 (1997)
36. K V Heyen, E Cielen, A Tahri, A Saleh, N Boens, G J Hoornaert *Tetrahedron* **55** 5207 (1999)
37. H Jiang, H J Xu, P J Xia, Q F Zhou *Chin. Chem. Lett.* **10** 1015 (1999)
38. D Marquis, J-P Desvergne *Chem. Phys. Lett.* **230** 131 (1994)
39. D Marquis, J-P Desvergne, H Bouas-Laurent *J. Org. Chem.* **60** 7984 (1995)
40. C Erk, A Göçmen, M Bulut *Supramol. Chem.* **11** 49 (1999)
41. C Erk, M Bulut, A Göçmen *J. Incl. Phenom. Macrocycl. Chem.* **37** 441 (2000)
42. C Erk, A Göçmen *Talanta* **53** 137 (2000)
43. M Montalti, L Prodi, N Zaccheroni *J. Fluoresc.* **10** 71 (2000)
44. T-J Liu, D Wang, Y-Z Wang, G-Z Xu *Chem. Abstr., Selects: Photochemistry* **14** 9 (2000)
45. L Prodi, F Bolletta, M Montalti, N Zaccheroni, P Huszthy, E Samu, B Vermes *New J. Chem.* **24** 781 (2000)
46. W-S Xia, R H Schmehl, C-J Li *Tetrahedron* **56** 7045 (2000)
47. G De Santis, L Fabbrizzi, M Licchelli, C Mangano, D Sacchi, N Sardone *Inorg. Chim. Acta* **257** 69 (1997)
48. B Ramachandaram, A Samanta *Chem. Commun.* 1037 (1997)
49. K A Mitchell, R G Brown, Y Dongwu, S-C Chang, R E Utecht, D E Lewis *J. Photochem. Photobiol. A, Chem.* **115** 157 (1998)
50. P Nanjappan, A W Czarnik *J. Am. Chem. Soc.* **109** 1826 (1987)
51. L Fabbrizzi, M Licchelli, P Pallavicini, A Perotti, A Taglietti, D Sacchi *Chem. Eur. J.* **2** 75 (1996)
52. F Pina, M A Bernardo, E Garcia-España *Eur. J. Inorg. Chem.* 2143 (2000)
53. L Fabbrizzi, M Licchelli, P Pallavicini, A Perotti, D Sacchi *Angew. Chem., Int. Ed. Engl.* **33** 1975 (1994)
54. L J Jiang, Z L Wang, X Q Jiang, Q H Luo *Chin. Chem. Lett.* **11** 557 (2000)
55. A W Czarnik *Acc. Chem. Res.* **27** 302 (1994)
56. A Beeby, D Parker, J A G Williams *J. Chem. Soc., Perkin Trans. 2* 1565 (1996)
57. Y Al Shihadeh, A Benito, J M Lloris, R Martinez-Manez, T Pardo, J Soto, M D Marcos *J. Chem. Soc., Dalton Trans.* 1199 (2000)
58. G Hennrich, H Sonnenschein, U Resch-Genger. *J. Am. Chem. Soc.* **121** 5073 (1999)
59. J Y N E Ohler, D H Vance, W D Aumiller, A W Czarnik *Tetrahedron Lett.* **38** 3845 (1997)
60. L Fabbrizzi, M Licchelli, L Parodi, A Poggi, A Taglietti *Eur. J. Inorg. Chem.* 35 (1999)
61. L Prodi, F Bolletta, M Montalti, N Zaccheroni *Eur. J. Inorg. Chem.* 455 (1999)
62. T Hirano, K Kikuchi, Y Urano, T Higuchi, T Nagano *J. Am. Chem. Soc.* **122** 12 399 (2000)
63. A Bencini, A Bianchi, C Lodeiro, A Masotti, A J Parola, F Pina, J S de Melo, B Valtancoli *Chem. Commun.* 1639 (2000)
64. V Balzani, P Ceroni, S Gestermann, C Kauffmann, M Gorka, F Vögtle *Chem. Commun.* 853 (2000)
65. F Vögtle, S Gestermann, C Kauffmann, P Ceroni, V Vicinelli, V Balzani *J. Am. Chem. Soc.* **122** 10 398 (2000)
66. J M Lehn *Supramolecular Chemistry* (Weinheim; New York: VCH, 1995)
67. A P de Silva, H Q N Gunaratne, K R A S Sandanayake *Tetrahedron Lett.* **31** 5193 (1990)
68. M Doldda, F Kastenholtz, E Lewitzki, E Grell *J. Fluoresc.* **6** 159 (1996)
69. P Ghosh, P K Bharadwaj, J Roy, S Ghosh *J. Am. Chem. Soc.* **119** 11903 (1997)
70. P Buet, F Kastenholz, E Grell, G Käeb, A Hifner, F W Schneider *J. Phys. Chem. A* **103** 5871 (1999)
71. K Iwamoto, K Araki, H Fujishima, S Shinkai *J. Chem. Soc., Perkin Trans. 1* 1885 (1992)
72. I Aoki, T Sakaki, S Shinkai *J. Chem. Soc., Chem. Commun.* 730 (1992)
73. T Jin, K Ichikawa, T Koyama *J. Chem. Soc., Chem. Commun.* 499 (1992)
74. T Jin *Chem. Commun.* 2491 (1999)
75. L Prodi, F Bolletta, M Montalti, N Zaccheroni, A Casnati, F Sansone, R Ungaro *New J. Chem.* **24** 155 (2000)
76. Y Kubo, S Obara, S Tokita *Chem. Commun.* 2399 (1999)
77. Y-B He, H Huang, L-Z Meng, C-T Wu, T-X Yu *Chem. Lett.* 1329 (1999)
78. H-F Ji, R Dabestani, G M Brown, R A Sachleben *Chem. Commun.* 833 (2000)
79. H-F Ji, R Dabestani, G M Brown *J. Am. Chem. Soc.* **122** 9306 (2000)
80. B Bodenant, T Weil, M Businelli-Pourcel, F Fages, B Barbe, I Pianet, M Laguerre *J. Org. Chem.* **64** 7034 (1999)
81. Y Higuchi, M Narita, T Niimi, N Ogawa, F Hamada, H Kumagai, N Iki, S Miyano, C Kubato *Tetrahedron* **56** 4659 (2000)
82. B Yan, H Zhang, C Xu, T Chen, J Ni *Spectrosc. Lett.* **33** 705 (2000)
83. C Fisher, G Sarti, A Casnati, I Manet, N Sabbatini, R Ungaro *Chem. Eur. J.* **6** 1026 (2000)
84. A Bianchi, K Bowman-James, E Garcia-España *Spectromolecular Chemistry of Anions* (New York: Wiley-VCH, 1997)
85. M E Huston, E U Akkaya, A W Czarnik *J. Am. Chem. Soc.* **111** 8735 (1989)
86. H Xie, S Yi, X Yang, S Wu *New J. Chem.* **23** 1105 (1999)
87. A P de Silva, H Q N Gunaratne, C McVeigh, G E M Maguire, P R S Maxwell, E O'Hanlon *Chem. Commun.* 2191 (1996)
88. M-P Teulade-Fichou, J-P Vigneron, J-M Lehn *J. Chem. Soc., Perkin Trans. 2* 2169 (1996)
89. G de Santis, L Fabbrizzi, M Licchelli, A Poggi, A Taglietti *Angew. Chem., Int. Ed. Engl.* **35** 202 (1996)
90. Y Al Shihadeh, A Benito, J M Lloris, R Martinez-Manez, J Soto, M D Marcos *Inorg. Chem. Commun.* **3** 563 (2000)
91. H Miyaji, P Anzenbacher Jr, J L Sessler, E R Bleasdale, P A Gale *Chem. Commun.* 1723 (1999)
92. J L Sessler, P Anzenbacher Jr, H Miyaji, K Jursikova, E R Bleasdale, P A Gale *Ind. Eng. Chem. Res.* **39** 3471 (2000)
93. L Fabbrizzi, I Faravelli, G Francese, M Licchelli, A Perotti, A Taglietti *Chem. Commun.* 971 (1998)
94. A Sharma, N J Street *Proc. SPIE* 3534 (1999)
95. N Jie, D Yang, Q Jiang, Q Zhang, L Wei. *Microchem. J.* **62** 371 (1999)
96. WO PCT 0 048 990; *Chem. Abstr.* **133** 171 468 (2000)
97. M A Reppy, M E Cooper, J L Smithers, D L Gin *J. Org. Chem.* **64** 4191 (1999)
98. X-Q Zhan, D-H Li, Q-Z Zhu, H Zheng, J-G Xu *Analyst* **125** 2330 (2000)
99. S Houdier, S Perrier, E Defrancq, M Legrand *Anal. Chim. Acta.* **412** 221 (2000)
100. Q Ma, H Ma, Z Wang, M Su, H Xiao, S Liang *Talanta* **53** 983 (2001)
101. W Wang, G Springsteen, S Gao, B Wang *Chem. Commun.* 1283 (2000)
102. D P Adhikiri, M D Heagy *Tetrahedron Lett.* **40** 7893 (1999)
103. B Kukrer, E U Akkaya *Tetrahedron Lett.* **40** 9125 (1999)
104. S Tomás, R Prohens, G Deslongchamps, P Ballester, A Costa *Angew. Chem., Int. Ed. Engl.* **38** 2208 (1999)
105. C R Cooper, T D James *J. Chem. Soc., Perkin Trans. 1* 963 (2000)
106. F P Cossio, A Arrieta, V L Cebolla, L Membrado, J Vela, R Garriga, M P Domingo *Org. Lett.* **2** 2311 (2000)
107. I Yu Goryacheva, G V Mel'nikov, S N Shtykov *J. Anal. Chem.* **55** 874 (2000)
108. F Cramer, W Saenger, H-Ch Spatz *J. Am. Chem. Soc.* **89** 14 (1967)
109. V B Nazarov, V G Avakyan, T G Vershinnikova, M V Alfimov *Izv. Akad. Nauk, Ser. Khim.* 1716 (2000) [b]
110. V B Nazarov, V I Gerko, M V Alfimov *Izv. Akad. Nauk, Ser. Khim.* 2225 (1996) [b]
111. V B Nazarov, V I Gerko, M V Alfimov *Pis'ma Zh. Eksp. Teor. Fiz.* **65** 507 (1997) [c]
112. V G Avakyan, V B Nazarov, M V Alfimov A A Bagatur'yants *Izv. Akad. Nauk, Ser. Khim.* 1857 (1999) [b]

113. V B Nazarov, T G Vershinnikova, M V Alfimov *Izv. Akad. Nauk, Ser. Khim.* 2022 (1999) [b]
114. A Munoz de la Pena, R M Perez, G M Escandar *Talanta* **51** 949 (2000)
115. G M Escandar, M A Boldrini *Talanta* **53** 851 (2001)
116. B D Wagner, P J MacDonald, M Wagner *J. Chem. Educ.* **77** 178 (2000)
117. Y Liu, C-C You, T Wada, Y Inoue *Tetrahedron Lett.* **41** 6869 (2000)
118. J Wang, A Ueno *Macromol. Rapid Commun.* **21** 887 (2000)
119. M Narita, S Koshizaka, F Hamada *J. Inclusion Phenom. Macrocycl. Chem.* **35** 605 (1999)
120. S Ito, M Narita, F Hamada *Int. J. Soc. Mater. Eng. Resour.* **7** 156 (1999)
121. M Narita, F Hamada *J. Chem. Soc., Perkin Trans. 2* 823 (2000)
122. T Toyoda, S Matsumura, H Mihara, A Ueno *Macromol. Rapid Commun.* **21** 485 (2000)
123. L R Reddy, M A Reddy, N Bhanumathi, K R Rao *J. Chem. Res. (S)* 494 (2000)
124. P Choppinet, L Jullien, B Valeur *J. Chem. Soc., Perkin Trans. 2* 249 (1999)
125. J P Phillips, A Mueller, F Przystal *J. Am. Chem. Soc.* **87** 4020 (1965)
126. L D Taylor, J Nickolson, R B Davis *Tetrahedron Lett.* 1585 (1967)
127. L S Atabekyan, G P Roitman, A K Chibisov *Zh. Anal. Khim.* 389 (1982) [d]
128. L S Atabekyan, A K Chibisov *Zh. Anal. Khim.* 1787 (1988) [d]
129. J T C Wojtyk, P M Kazmaier, E Buncel *Chem. Commun.* 1703 (1998)
130. S-H Liu, C-T Wu, in *Proceedings of the 3rd International Symposium on Organic Photochromism, Fukuoka, 1999* p. 92
131. M Tanaka, K Kamada, H Ando, T Kitagaki, Y Shibutani, K Kimura *J. Org. Chem.* **65** 4342 (2000)
132. O A Fedorova, S P Gromov, Yu P Strokach, Yu V Pershina, S A Sergeev, V A Barachevskii, Zh Pepe, A Samat, R Guglielmetti, M V Alfimov *Izv. Akad. Nauk, Ser. Khim.* 1974 (1999) [b]
133. O A Fedorova, S P Gromov, Yu V Pershina, S A Sergeev, Yu P Strokach, V A Barachevsky, M V Alfimov, G Pepe, A Samat, R Guglielmetti *J. Chem. Soc., Perkin Trans. 2* 563 (2000)
134. O A Fedorova, S P Gromov, A V Koshkin, Yu P Strokach, T M Valova, V A Barachevsky, M V Alfimov, V A Lokshin, A Samat, R Guglielmetti, in *Proceedings of the XXth International Conference on Photochemistry, Moscow, 2001* p. 317
135. M V Alfimov, A V Balakin, S P Gromov, Yu V Zaushitsin, O A Fedorova, N I Koroteev, A V Pakulev, A Yu Rosnyanskii, A P Shkurinov *Zh. Fiz. Khim.* **73** 1871 (1999) [e]
136. K Kimura, H Sakamoto, S Kado, R Arakawa, M Yokoyama *Analyst* **125** 1091 (2000)
137. K Kimura, S Kado, H Sakamoto, A Sakai, M Yokoyama, M Tanaka *J. Chem. Soc., Perkin Trans. 2* 2539 (1999)
138. M Tanaka, K Kamada, H Ando, T Kitagaki, Y Shibutani, S Yajima, H Sakamoto, K Kimura *Chem. Commun.* 1453 (1999)
139. M Tanaka, K Kamada, K Kimura *Mol. Cryst. Liq. Cryst. Sci. Technol., Sect. A* **344** 319 (2000)
140. T Teranishi, M Yokoyama, H Sakamoto, K Kimura *Mol. Cryst. Liq. Cryst. Sci. Technol., Sect. A* **344** 271 (2000)
141. Z Guo, G Wang, Y Tang, X Song *Liebigs Ann./Recueil* 941 (1997)
142. Y Yokoyama *Chem. Rev.* **100** 1717 (2000)
143. Y Yokoyama, M Kubo, Y Yokoyama, T Ohmori, T Okuyama, S Uchida, in *Proceedings of the 3rd International Symposium on Organic Photochromism, Fukuoka, 1999* p. 83
144. M Takeshita, M Irie *Tetrahedron Lett.* **39** 613 (1998)
145. M Irie *Chem. Rev.* **100** 1685 (2000)
146. S H Kawai *Tetrahedron Lett.* **39** 4445 (1998)
147. R M Uda, M Yokoyama, K Kimura, in *Proceedings of the 3rd International Symposium on Organic Photochromism, Fukuoka, 1999* p. 55
148. E N Ushakov, S P Gromov, O A Fedorova, M V Alfimov *Izv. Akad. Nauk, Ser. Khim.* 484 (1997) [b]
149. S P Gromov, O A Fedorova, E N Ushakov, A V Buevich, I I Baskin, Yu V Pershina, B Eliasson, U Edlund, M V Alfimov *J. Chem. Soc., Perkin Trans. 2* 1323 (1999)
150. S P Gromov, O A Fedorova, E N Ushakov, I I Baskin, A V Lindeman, E V Malysheva, T A Balashova, A S Arsen'ev, M V Alfimov *Izv. Akad. Nauk, Ser. Khim.* 99 (1998) [b]
151. A Ya Freidzon, I I Baskin, A A Bagatur'yants, S P Gromov, M V Alfimov *Izv. Akad. Nauk, Ser. Khim.* 2185 (1998) [b]
152. S P Gromov, Yu V Fedorov, O A Fedorova, E N Andrioukhina, A I Vedernikov, M V Alfimov, B Eliasson, U Edlund, in *Proceedings of the XXth International Conference on Photochemistry, Moscow, 2001* p. 266
153. S Yu Zaitsev, T I Sergeeva, E A Baryshnikova, W Zeiss, D Mobius, O V Yescheulova, S P Gromov, O A Fedorova, M V Alfimov *Mater. Sci. Eng. C* 469 (1999)
154. T I Sergeeva, E A Baryshnikova, S Yu Zaitsev, O A Fedorova, S P Gromov, M V Alfimov, S Hacke, W Zeiss, D Mobius, in *Proceedings of the XXth International Conference on Photochemistry, Moscow, 2001* p. 480
155. S M Fatah-ur Rahman, K Fukunishi *J. Chem. Soc., Chem. Commun.* 917 (1994)
156. V I Minkin, V A Bren, A E Lyubarskaya, in *Organic Photochromes* (Ed. A El'tsov) (New York: Plenum, 1990) Ch. 5
157. V P Rybalkin, V A Bren, V I Minkin, G D Palui *Zh. Org. Khim.* **28** 2310 (1992) [f]
158. E N Shepelenko, V P Rybalkin, L L Popova, A D Dubonosov, V A Bren, V I Minkin, in *XX Mezhdunar. Chugaevskaya Konf. po Koordinatsionnoi Khimii (Tez. Dokl.), Rostov-na-Donu, 2001* [The XXth International Chugaev Conference on Coordination Chemistry (Abstracts of Reports), Rostov-on-Don, 2001] p. 506
159. V P Rybalkin, A D Dubonosov, E N Shepelenko, L L Popova, V A Bren, V I Minkin *Zh. Org. Khim.* **37** 1083 (2001) [f]
160. V A Bren, in *XX Mezhdunar. Chugaevskaya Konf. po Koordinatsionnoi Khimii (Tez. Dokl.), Rostov-na-Donu, 2001* [The XXth International Chugaev Conference on Coordination Chemistry (Abstracts of Reports), Rostov-on-Don, 2001] p. 107
161. M Venturi, V Balzani, in *Proceedings of the XXth International Conference on Photochemistry, Moscow, 2001* p. 11
162. S Kunsági-Máté, G Nagy, L Kollar *Anal. Chim. Acta* **428** 301 (2001)
163. C L Honeybourne *J. Chem. Educ.* **77** 338 (2000)
164. P J Worsfold, E P Achterberg, A R Bowie, R C Sandford, R F C Mantoura *Ocean Sci. Technol.* **1** 71 (2000)
165. *Coord. Chem. Rev.* **205** (2000)

[a] — *Mendeleev Chem. J. (Engl. Transl.)*
[b] — *Russ. Chem. Bull., Int. Ed. (Engl. Transl.)*
[c] — *J. Exp. Theor. Phys. Lett. (Engl. Transl.)*
[d] — *J. Anal. Chem. (Engl. Transl.)*
[e] — *Russ. J. Phys. Chem. (Engl. Transl.)*
[f] — *Russ. J. Org. Chem. (Engl. Transl.)*

Russian Chemical Reviews **70** (12) 1037 – 1065 (2001) © 2001 Russian Academy of Sciences and Turpion Ltd

DOI 10.1070/RC2001v070n12ABEH000676

Structural and configurational relationships 'metal complex – substrate – product' in asymmetric catalytic hydrogenation, hydrosilylation and cross-coupling reactions

V A Pavlov

Contents

I.	Introduction	1037
II.	Catalyst – substrate structural relationships	1038
III.	Catalyst – product configurational relationships in reactions on C_2-symmetrical chiral metal complexes	1042
IV.	Catalyst – product configurational relationships in reactions on asymmetric metal complexes	1056
V.	The structure of the intermediate complex	1059
VI.	Conclusion	1062

Abstract. The present-day published data on the relationships between the structures of rhodium, iridium, ruthenium, nickel and cobalt catalytic complexes and substrates in homogeneous asymmetric hydrogenation, hydrosilylation and cross-coupling reactions are systematised. The optimum ratio between the number of coordination vacancies in the complex and the number of functional groups of the substrate has been characterised in terms of a criterion of maximum enantioselectivity of the catalytic complex. The relationships between the configurations of the complexes and the products formed in the reactions are analysed. In the case of C_2-symmetrical chiral diphosphine complexes as catalysts (some structural elements of their ligands represent an incomplete turn of a helix surrounding the central metal atoms), substrates of the same kind form the products having definite configurations characteristic of the particular orientation of the helix. For example, rhodium complexes with ligands that form an incomplete *P*-helical turn around metal atoms catalyse the formation of (*R*)-amino acids from the corresponding precursors. If the ligands contain fragments of *M*-helices around rhodium atoms, it is (*S*)-amino acids that are formed. The bibliography includes 234 references.

I. Introduction

Considerable recent interest in asymmetric synthesis is explained not only by the objective logic of organic chemistry, but also by the fact that in the past decade the pharmaceutical industry has largely concentrated on the preparation of drugs in an enantiomerically pure form. Therefore, a search for relatively simple and inexpensive techniques for separation of enantiomers or the synthesis of compounds in the form of individual enantiomers has become a very urgent problem. In this respect, priority is given to asymmetric catalysis, which allows one-step synthesis of products (or intermediates) from prochiral compounds with high enantiomeric excess (*ee*). The latter is expressed in per cent as the ratio of the difference in the yields of two enantiomers to their total yield (the terms 'optical yield' and 'enantiomeric purity' are also used to describe stereoselectivity). The costs of enantiomeric products are sometimes close to those of racemates, since the concentrations of expensive chiral metal complex catalysts in the reaction mixture are usually low and the substrate : catalyst ratios are rather high (up to 70 000).

The progress in asymmetric metal complex catalysis has been documented in numerous publications (see the monographs [1–4] and the reviews [5–19]), and their number is steadily increasing. However, the 'catalyst – substrate – product' structural and configurational relationships remain relatively little-studied. Analysis of these relationships is the first step in the elucidation of the mechanism of a transfer of asymmetry from the catalyst to the reactive substrate, *i.e.*, asymmetric induction.

Most probably, the crucial role in asymmetric induction belongs to chiral ligands of metal complexes. It is these ligands that determine the chiral environment of metal atoms [20] in the catalyst. Therefore, special attention in the analysis of general regularities of 'catalyst – substrate – product' structural and configurational relationships should be given to reactions where the greatest number of different ligands have been used. These reactions include hydrogenation, hydrosilylation and cross-coupling. These were chosen for two additional reasons. First, in these reactions very high enantiomeric excesses of the products have been achieved. Second, this minimum set of reactions allows one to obtain chiral products with the largest number of functional groups (*e.g.*, alcohols, amines, organic acids, amino alcohols, amino acids, hydroxy acids and hydrocarbons), which is of considerable value in the synthesis of drugs and synthons.

By now, a vast variety of ligands, which represent components of C_1- and C_2-symmetrical chiral complexes (see, *e.g.*, reviews [20–32]), have been synthesised and analysed in these and some other reactions. Configurational relationships of chiral complexes having C_2 symmetry axes can be systematised most easily. Complexes with five- and seven-membered chelate cycles formed by bis(diphenylphosphine) ligands (from the simplest [33] to exotic [34, 35]) shown below manifest the highest enantioselectivities.

V A Pavlov N D Zelinsky Institute of Organic Chemistry, Russian Academy of Sciences, Leninsky prosp. 47, 119991 Moscow, Russian Federation. Fax (7-095) 135 53 28. Tel. (7-095) 938 35 02. E-mail: pvlv@cacr.ioc.ac.ru

Received 25 April 2001
Uspekhi Khimii **70** (12) 1175 – 1205 (2001); translated by R L Birnova

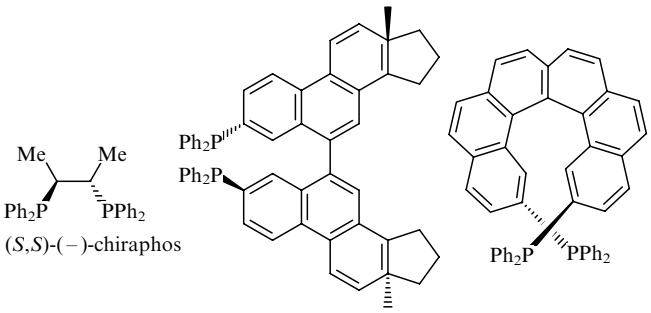

Substrates, such as α-acetamidocinnamic acid, which allow coordination by metals in the catalytic complexes both at the double bonds and at two additional functional groups, are especially suitable for the synthesis of chiral products by hydrogenation. Thus the *ee* of the hydrogenation product reaches 99% (see Ref. 36). The enantioselectivity of this reaction decreases dramatically upon removal of at least one functional group. Ruthenium complexes with atropoisomeric diphosphine ligands of the binap type are most suitable reagents for hydrogenation of such substrates.[37–41]

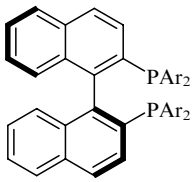

Ar = Ph: (*S*)-binap
Ar = *p*-MeC_6H_4: (*S*)-Tolbinap

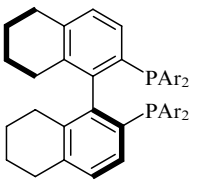

(*S*)-H_8-binap

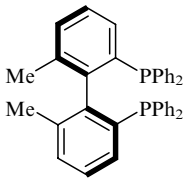

(*S*)-biphemp

In the presence of these complexes, the maximum value of *ee* exceeds 99.5% (see Ref. 40). The enantioselectivity of hydrogenation of substituted ketones in the presence of these complexes is at the same level.[42–50]

Asymmetric hydrosilylation of ketones[3,4]

$$R^1R^2C{=}O + HSiR_3 \xrightarrow{ML_n^*} HR^1R^2COSiR_3 \xrightarrow{H_3O^+} R^1R^2CHOH + HOSiR_3$$

M = Rh, Ir, Ru; L_n^* = P*, ; the chiral fragment or the asymmetric atom is marked with an asterisk

can be regarded as a variant of their asymmetric hydrogenation, since the silyl ether formed can be hydrolysed into an alcohol with retention of the configuration of the asymmetric carbon atom.[51–53] Very often, the same catalysts manifest similar efficiencies in both reactions, which also suggests their similarity.[54] However, specific hydrosilylation catalysts are known[55–57] which result in a maximum *ee* of 97.6% (see Ref. 58).

Asymmetric cross-coupling of organometallic compounds ($R^1M'X$) with alkenyl or aryl halides and related compounds (R^2Y)

$$R^1M'X + R^2Y \xrightarrow{ML_n^*} (R^1{-}R^2)^*$$

M′ = Mg, Zn *etc.*; X = Hal; M = Ni, Pd; Y = Hal, OR, OH, *etc.*;

L_n^* = P*,

results in the formation of a C*−C bond in the product; its enantiomeric purity reaches 95%. In terms of enantioselectivity, this reaction is somewhat inferior to hydrogenation and hydrosilylation, however, cross-coupling combined with allylic alkylation arouses considerable interest,[59–63] since it gives rise to chiral hydrocarbons.

II. Catalyst–substrate structural relationships

In a search for the most suitable substrates for performing their conversions on metal complexes containing structurally different ligands, enantiomeric purity of the product serves usually as the main criterion. Asymmetric hydrogenation on rhodium–phosphine complexes is certainly one of the most extensively studied reactions of this kind.

The *ee* values of hydrogenation products of various substrates depending on the structures of the ligands of the catalytic complexes are listed in Table 1. As can be seen from these examples, any substitution of the alkyl radical for the coordination-active substituent at the double bond results in a drastic decrease in the reaction enantioselectivity. Hence, the double bond should contain at least two groups of the type NHCOR or CO_2R. However, if a catalytic complex contains the bppm ligand, which can be coordinated by three groups (also in the presence of Et_3N), replacement of the acetamido group in the substrate by a group with weaker coordination ability has a smaller effect on the enantioselectivity in comparison with reactions catalysed by complexes with bidentate ligands. Similarly, the number of coordination-active groups in the substrate can be reduced to one (with the exception of C=C) on going from the planar Rh(I) complexes to the octahedral Ru(II) complexes containing ligands of the binap type (Scheme 1).†

† Hereinafter we give the best or close to best parameters cited in the relevant publications.

Scheme 1

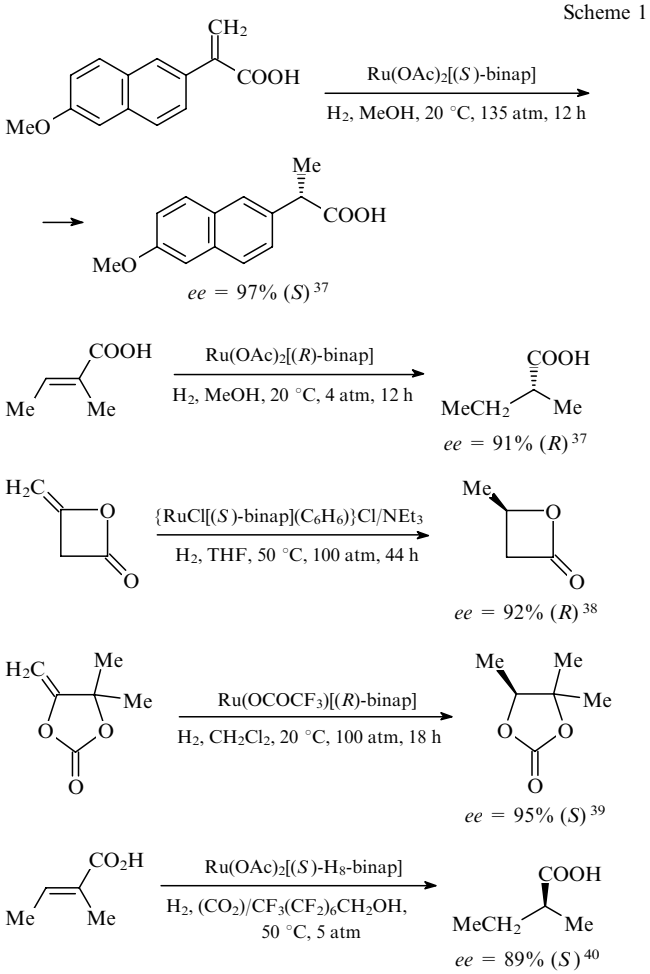

(CO2) is supercritical CO_2, T_c = 31.0 °C, p_c = 72.9 atm,

Table 1. The dependence of enantiomeric excesses of hydrogenation products of various substrates on the ligand structure of the catalytic complex.

Ligand	R^1	R^2	R^3	*ee* (%)	Ref.
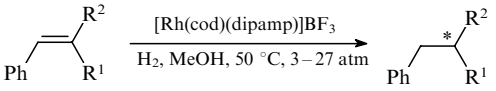					
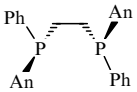 dipamp	NHCOMe	CO_2H		94 (*S*)	64
	CO_2H	NHCOMe		47 (*S*)	64
	NHCOMe	CO_2Me		96 (*S*)	64
	CO_2Me	NHCOMe		23 (*S*)	64
	NHCOPh	CO_2H		93 (*S*)	64
	CO_2H	NHCOPh		39 (*S*)	64
	NHCOPh	CN		89 (*S*)	64
	NHCOMe	Me		51 (*R*)	64
	Me	NHCOMe		9 (*R*)	64
	Me	CO_2H		1 (*R*)	64
	CO_2H	Me		< 1 (*R*)	64
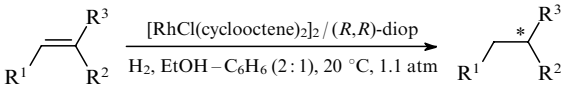					
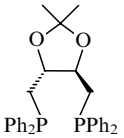 (*R*,*R*)-diop	H	NHCOMe	CO_2H	73 (*R*)	65
	Ph	NHCOMe	CO_2H	82 (*R*)	66
	Pr^i	NHCOMe	CO_2H	22 (*R*)	65
	H	Ph	CO_2H	63 (*S*)	67
	H	Ph	Et	24.5 (*S*)	67
	H	OAc	CO_2Et	27 (*R*)	68
	H	OAc	CF_3	0	68
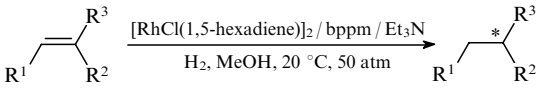					
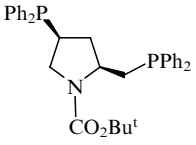 bppm	Ph	NHCOMe	CO_2H	83 (*R*)	69
	H	OAc	CO_2Et	67 (*R*)	68
	H	CF_3	CO_2Et	10 (*S*)	68

Note. Hereinafter, hydrogen pressure (pH_2) is included, among other factors, into the description of reaction conditions. Abbreviations: cod is cycloocta-1,5-diene; An is *o*-$MeOC_6H_4$.

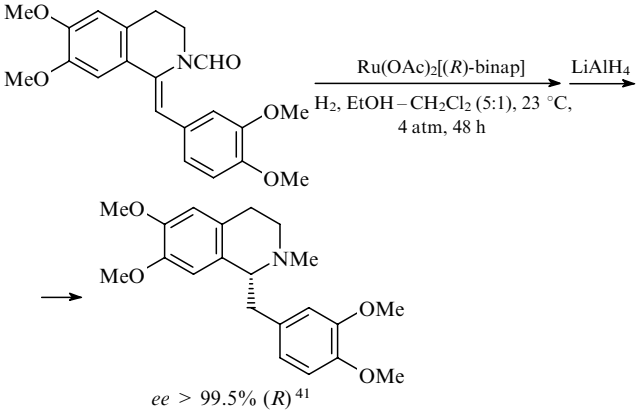

ee > 99.5% (*R*) [41]

These and some other data [70–73] suggest that high enantioselectivity of hydrogenation of substrates, such as tiglic acid in the presence of complexes of the $Ru(OAc)_2$[binap] type is provided by only one coordination group, which is located in the α-position relative to the double bond. Interestingly, hydrogenation of α-acetamidocinnamic acid on such catalysts is less enantioselective than that in the presence of rhodium complexes with binap ligands.[74] Thus for ruthenium complexes, the presence of two coordination-active groups at the double bond of the substrate is excessive and does not favour maximum enantioselectivity.

Simple ketones R^1COR^2 (R^1 = Ar, Alk, R^2 = Alk) are hydrogenated on chiral rhodium diphosphine complexes with low enantioselectivities. This can be improved by addition of an acid or a base to complexes which have proved to be efficient in asymmetric hydrogenation of enamide substrates. Thus in the presence of Rh/camp/Pr^iCO_2H, where camp is the ligand synthesised from camphor, *ee* = 12% (*R*) (see Ref. 75) and in the presence of Rh/(*S*,*S*)-diop/Et_3N, *ee* = 68% (*R*) (see Ref. 76). An alternative approach to increase enantioselectivity consists in the introduction of groups into α- or β-positions of ketones which can coordinate the metal. For example, hydrogenation of the ketone $ArCOCH_2NEt_2$ proceeds with high enantioselectivity without any base [in the presence of Rh/(*S*,*S*)-diop, *ee* = 93% (see Ref. 77)].

Presumably, complexes with bidentate diphosphine ligands (or diamino ligands in hydrogen-transfer hydrogenation reactions) do not provide a sufficiently high level of 'chiral recognition' of simple ketones due to small molecular sizes of the latter, nor do they favour their enantioselective hydrogenation. The results of hydrogenation of various ketones on such complexes

Table 2. Asymmetric hydrogenation of simple and β-substituted ketones on chiral diphosphine and diimine metal complexes.

Catalyst	Ph(C=O)Me		Ph(C=O)CH$_2$NBu^t		Ph(C=O)CH$_2$NR^2		R(C=O)CH$_2$(C=O)OEt	
	ee (%)	Ref.	*ee* (%)	Ref.	*ee* (%)	Ref.	*ee* (%)	Ref.
Rh-(*S*,*S*)-diop	3 – 54 (*R*)	78 – 82	35 (*R*)	83	93(+) (R = Et)	77	–	–
Rh-(*R*)-binap	–	–	6 (*R*)	83	–	–	–	–
Ru-(*R*)-binap	30 – 74 (*S*)	42	78 (*R*)[a]	–	–	–	85 (*S*) (R = Ph)	45
Ru-(*S*)-binap	–	–	–	–	95 (*S*) (R = Me)	42	–	–
Ru(OAc)$_2$[(*R*)-binap]	–	–	–	–	–	–	4 (*S*) (R = Me)	45
RuCl$_2$[(*R*)-binap]	–	–	–	–	–	–	99 (*R*) (R = Me)	45
RuCl$_2$(C$_6$H$_6$)/[(*S*)-binap]	–	–	–	–	–	–	99 (*R*) (R = CH$_2$Cl$_2$)	84
RuCl$_2$(C$_6$H$_6$)/[(*R*)-binap]	–	–	–	–	–	–	99 (*S*) (R = CH$_2$Cl$_2$)	84
Rh-(1*R*,2*R*)-*N*,*N*′-dibenzylidene-1,2-diaminocyclohexane	48 (*S*)	85	–	–	–	–	–	–
Ir-(1*S*,2*S*)-*N*,*N*′-dibenzylidene-1,2-diaminocyclohexane	55 (*R*)	85	–	–	–	–	–	–

[a] Our data obtained with {Ru$_2$Cl$_4$[(*R*)-binap]$_2$}NEt$_3$.

are presented in Table 2. It can be seen that the enantioselectivity increases considerably with an increase in the size of the fragment of the substrate involved in coordination. If an additional coordination-active group of a ketone is blocked by a bulky substituent, *e.g.*, NHBu^t, or cannot compete with an achiral ligand of the catalytic complex for vacancies (*e.g.*, in the presence of the β-ester group in the substrate and the carboxyl ligand in the Ru(AcO)$_2$. .[binap] complex), the enantioselectivity of this reaction at room temperature approximates a level characteristic of unsubstituted ketones [*ee* = 4% (*S*)]; however, at high temperatures the situation is different.[48] The introduction of an additional coordination-active group into a ketone can change both the value and the sign of enantioselectivity (as in reactions of ruthenium catalysts with the binap ligands (see Table 2), which points to the change in the mechanism of asymmetric induction.

Enantioselectivity can be increased by using complexes with ligands coordinated to metals by three groups.[86]

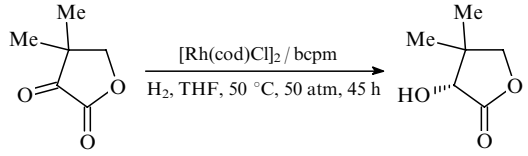

ee = 92% (*R*),[86]

bcpm = 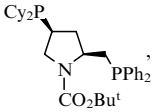

, Cy is cyclohexyl.

And, finally, the maximum enantioselectivity is achieved through a combined use of all the methods described above.

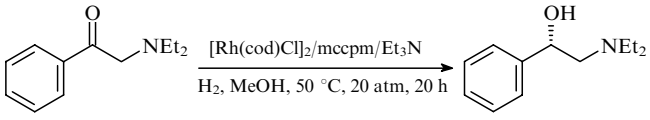

ee = 97% (*S*),[87]

mccpm = 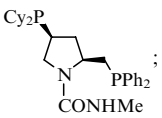

;

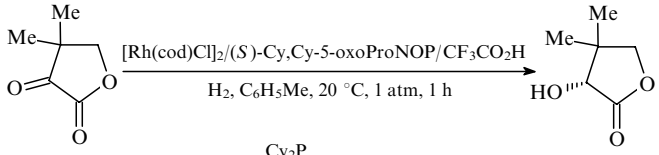

ee = 97.7% (*R*),[88]

(*S*)-Cy,Cy-5-oxoProNOP = 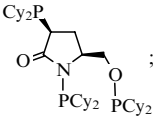

;

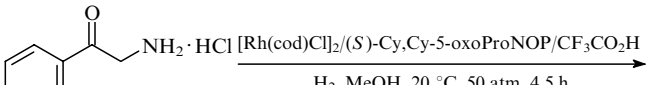

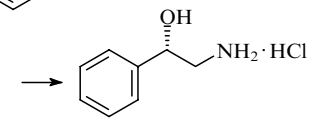

ee = 93% (*S*);[88]

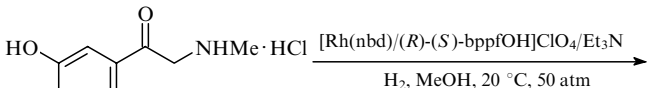

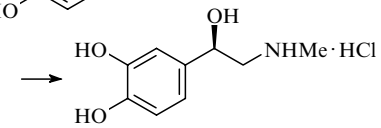

ee = 95% (*R*),[89]

nbd is norbornadiene, (*R*)-(*S*)-bppfOH = 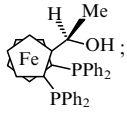

;

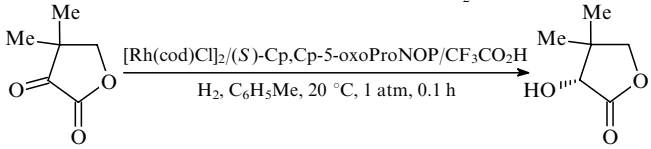

ee = 98.7% (*R*),[88]

(*S*)-Cp,Cp-5-oxoProNOP = 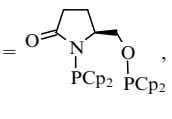

, Cp is cyclopentyl;

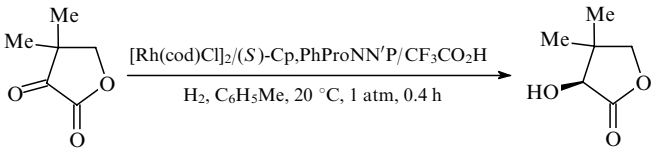

ee = 83% (*S*),[90]

(*S*)-Cp,PhProNN′P = 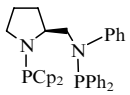

As in the hydrogenation of substrates containing C = C bonds, the use of octahedral ruthenium complexes with such ligands as binap, biphemp, *etc*., is advantageous for an increase in the enantioselectivity of hydrogenation of ketones possessing coordination-active groups in the β-positions relative to carbonyl group.

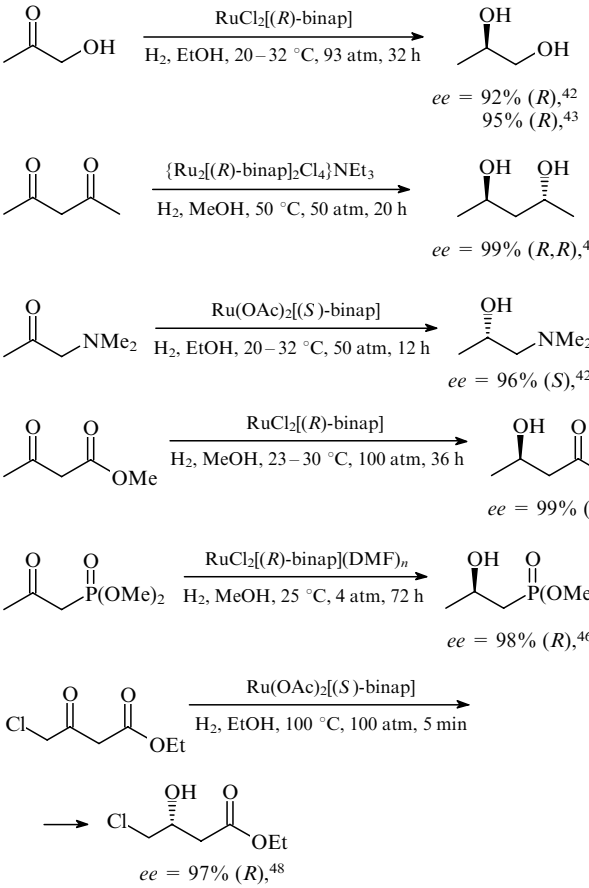

ee = 92% (*R*),[42] 95% (*R*),[43]

ee = 99% (*R*,*R*),[44]

ee = 96% (*S*),[42]

ee = 99% (*R*),[45]

ee = 98% (*R*),[46]

ee = 97% (*R*),[48]

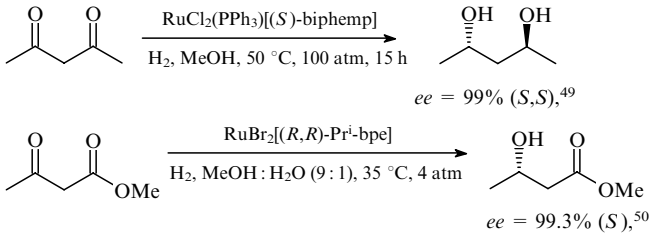

ee = 99% (*S*,*S*),[49]

ee = 99.3% (*S*),[50]

bpe is bis(phospholano)ethane.

Special mention should be made of a group of highly enantioselective catalytic complexes, which are active at atmospheric pressure of H_2. These complexes have the *in situ* composition $\{RuCl_2[binap(or\ biphemp)]\}_2 \cdot MeCOMe$ and are used for hydrogenation of β-oxo esters,[91] β-oxo phosphonates, β-oxo thiophosphonates[92] and phenylthio ketones.[93] Other catalytic complexes of this kind are also known.[34, 94 – 100] The hydrogenation of α- and γ-substituted ketones occurs less enantioselectively.[101 – 103]

Ruthenium complexes with tri- and tetradentate ligands, such as the ligands **1** – **8** and the complex **9**, are used as catalysts for increasing the enantioselectivity of hydrogen-transfer hydrogenation of simple ketones.

The effects of these complexes on the enantioselectivities of different hydrogenation reactions are demonstrated in Table 3 in the example of acetophenone.

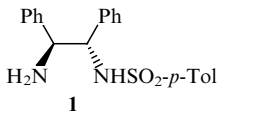

1

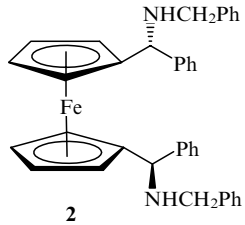

2

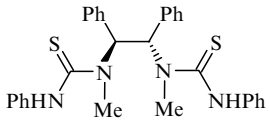

3

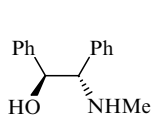

4

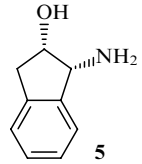

5

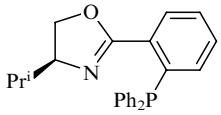

6

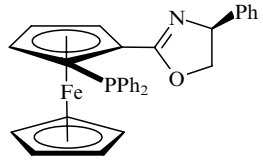

7

Table 3. Hydrogen-transfer hydrogenation of acetophenone on chiral ruthenium complexes.

Precursor of the complex or the complex	Ligand	Base	*T* /°C	Conversion (%)	*ee* (%)	Ref.
$[RuCl_2(1,3,5\text{-}Me_3C_6H_3)]_2$	**1**	KOH	20	95	97 (*S*)	104
$[RuCl_2(1\text{-}Me\text{-}4\text{-}Pr^iC_6H_4)]_2$ (see [a])	**2**	KOH	−30	91	90 (*R*)	105
$[RuCl_2(1\text{-}Me\text{-}4\text{-}Pr^iC_6H_4)]_2$	**3**	Bu^tOK	–	98	87 (*S*)	106
$[RuCl_2(\eta^6\text{-}C_6Me_6)]_2$	**4**	KOH	28	94	92 (*S*)	107
$[RuCl_2(1\text{-}Me\text{-}4\text{-}Pr^iC_6H_4)]_2$	**5**	KOH	20	70	91 (*S*)	108
$RuCl_2(PPh_3)_3$	**6**	NaOH	82	24	94 (*R*) [b]	109
	6	NaOH	82	83	73 (*R*) [c]	109
$RuCl_2(PPh_3)_3$	**7**	Pr^iOK	28	80	97 (*R*)	110
	7	Me_2CHOK	80	87	88 (*R*) [c]	110
$[RuCl_2(C_6H_6)]_2$	**8**	NaOH	80	72	79 (*R*)	111
9		Me_2CHOK		93	97 (*R*)	112

[a] 1-Acetylnaphthalene was used as a substrate. [b] The reaction time was 5 min. [c] The decrease in *ee* at higher levels of conversion is attributed to the reversibility of the hydrogen transfer reaction.[113]

Table 4. Hydrosilylation of acetophenone on chiral rhodium complexes.

Complex precursor	Chiral ligand (L)	L : Rh	Achiral ligand	Solvent	T /°C	Yield (%)	*ee* (%)	Ref.
$[Rh(cod)Cl]_2$	**10**	5	–	–	0	83	48.1(*R*)	114
	11	8	–	CCl_4	−5	90	64.0 (*R*)	115
	12	8	–	CCl_4	−5	84	65.0 (*R*)	115
	13	9	–	–	−15	98	86.7 (*R*)	116
	14	13	–	–	−20	99	97.6 (*R*)	58
	14	2	–	–	0	–	75.6 (*R*)	58
$RhCl_3$	**15**	4	$2AgBF_4$	–	0	94	95.0 (*S*)	117, 118
	16	4	$AgBF_4$	THF	5	98	90.0 (*S*)	119

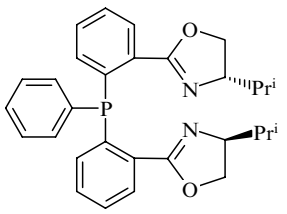

8

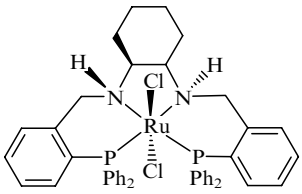

9

In order to achieve maximum enantioselectivity of hydrosilylation, bi-, tri- or tetradentate ligands should be taken in 2–13-fold excess with respect to the metal. This is sufficient to provide the substitution of at least four coordination vacancies in a catalytic complex. But even in this case achiral ligands should sometimes be added. The necessary ratios of the chiral ligands **10**–**16** to rhodium in catalysts for acetophenone hydrosilylation are shown in Table 4.

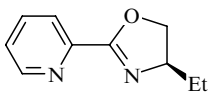

10

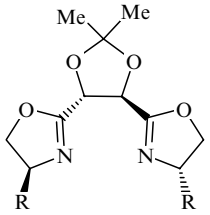

11: R = Pr^i
12: R = Bu^t

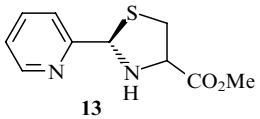

13

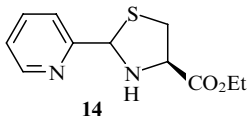

14

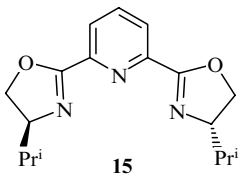

15

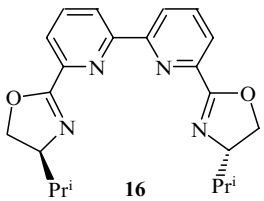

16

Thus, the maximum enantioselectivity will be provided by catalysts which ensure the minimum degree of freedom in the coordination of substrates in the intermediate complexes.

The dependence of enantioselectivity on the ligand structures of catalytic complexes is well studied and is not considered in this review. Until very recently, most of the studies devoted to asymmetric metal complex catalysis were aimed at obtaining maximum enantiomeric excesses of reaction products by simple search for all possible variants of ligand structures. A great body of evidence has been accumulated in this field, the effect of such structural parameter of a complex as symmetry deserves special mentioning.

Apparently, it is the difference in the symmetries of structurally related complexes, *viz*., {Rh[(*S,S*)-chiraphos](nbd)}ClO_4 (**I**) and {Rh[(*R*)-prophos](nbd)}ClO_4 (**II**), that can explain different enantioselectivities of hydrogenation in the presence of these catalysts (Table 5).

Table 5. The enantiomeric excess of the product in asymmetric hydrogenation of enamides on complexes (**I**) and (**II**).[33, 120, 121]

Substrate (S)	**I** (S : Rh = 100)		**II** (S : Rh = 250)	
	THF	EtOH	THF	EtOH
AcΔPhe	74 (*R*)	89 (*R*)	91 (*S*)	90 (*S*)
AcΔTyr	80 (*R*)	88 (*R*)	92 (*S*)	89 (*S*)
AcΔDOPA	80 (*R*)	83 (*R*)	89 (*S*)	87 (*S*)
AcΔLeu	100 (*R*)	93 (*R*)	87 (*S*)	87 (*S*)
BzΔPhe	99 (*R*)	95 (*R*)	93 (*S*)	91 (*S*)
BzΔLeu	87 (*R*)	72 (*R*)	87 (*S*)	87 (*S*)

Note. Hereinafter, the following designations were used: AcΔPhe is (*Z*)-α-acetylaminocinnamic acid; BzΔPhe is (*Z*)-α-benzoylaminocinnamic acid; AcΔTyr is *N*-acetyldehydrotyrosine; AcΔDOPA is 2-*N*-acetyl-β-(4-hydroxy-3-methoxyphenyl)-α-dehydroalanine; AcΔLeu is *N*-acetyldehydroleucine; BzΔLeu is *N*-benzoyldehydroleucine.

As can be seen from the table, the enantioselectivities achieved with the asymmetric complex **II** are less prone to variation than with the C_2-symmetrical chiral complex **I**. The *ee* value in the reactions catalysed by the former is virtually independent of the solvent or the nature of the substituent in the substrate.

III. Catalyst – product configurational relationships in reactions on C_2-symmetrical chiral metal complexes

A search for relationships between configurations of catalytic complexes and products of asymmetric reactions is best carried out for complexes with ligands of the same type. Chiral bis(diphenylphosphine) ligands which form C_2-symmetrical complexes or C_2-symmetrical chelate rings (without substituents) meet these requirements.

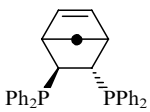

(*S,S*)-norphos

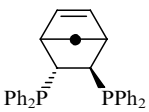

(*R,R*)-norphos

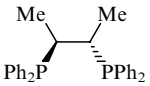

(*S,S*)-chiraphos

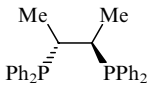

(*R,R*)-chiraphos

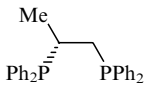

(*R*)-prophos

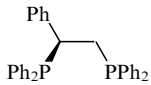

(*S*)-phenphos

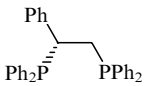

(*R*)-phenphos

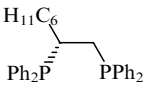

(*R*)-cycphos

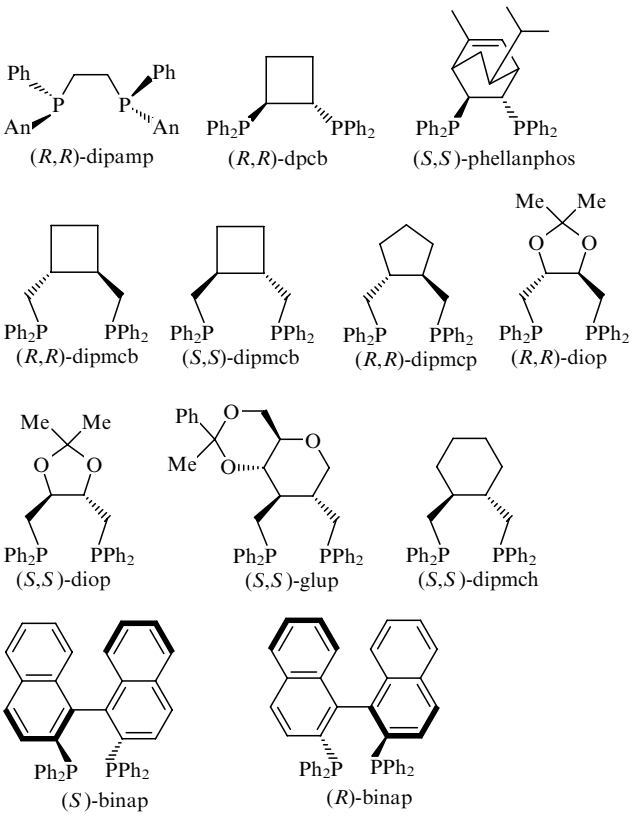

Regular relationships between the configurations of products and catalytic complexes in hydrogenation reactions on rhodium – phosphine catalysts have been established only for complexes with C_2-symmetrical chelate rings. Formal configurational relationships between catalysts and products are not always related to concrete reaction mechanism. A mnemonic dependence was proposed by Knowles in 1983.[122]

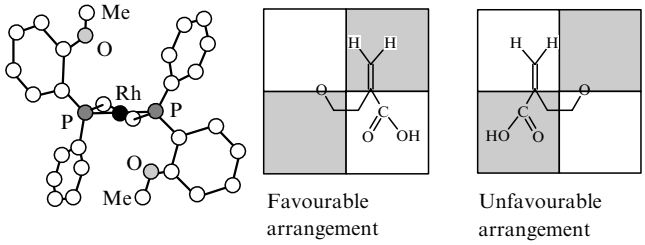

This dependence follows the 'quadrant rule' ‡ which relates the structure of the rhodium complex containing the dipamp ligand to the orientation (or coordination) of the substrate in the intermediate complex. It is assumed that the substituents occupying the hatched quadrants (*i.e.*, those blocked by the phenyl groups edge facing the viewer; the metal atom is located in the centre of the coordinates), experience larger steric hindrances. Therefore, the bulky carboxy group occupies preferably the unhatched quadrant. It is in this orientation that the formation of a particular enantiomer is experimentally observed. These graphical representations were used to describe the enantioselective behaviour of binap [14] and duphos [bis(phospholano)benzene] [124] complexes in asymmetric hydrogenation reactions.

The use of such graphical representations implies that the asymmetric induction step coincides with the coordination of the substrate in the intermediate complex. However, this conclusion demands further verification. The scheme proposed for the description of catalyst – product configurational relationships in the hydrogenation of α-, β- and γ-substituted ketones on ruthenium complexes containing binap ligands is even more formal. The configuration of the product depends exclusively on the configuration of the complex, rather than on the position of the functional group in the ketone.[14]

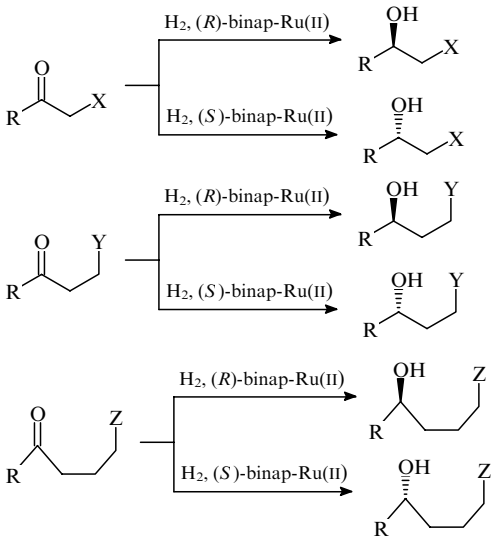

where X, Y, Z are N, O or Hal.

This has led to the development of a formal scheme for the formation of an intermediate complex using hydrogenation of a β-oxo ester as an example (Scheme 2).

A similar scheme of configurational relationships has been proposed for hydrogenation of substituted β-oxo esters.[125] The configuration of the product does not depend on the nature of the substituent at the carbonyl group, whereas the change in the order of priority changes the configuration symbol.

Scheme 2

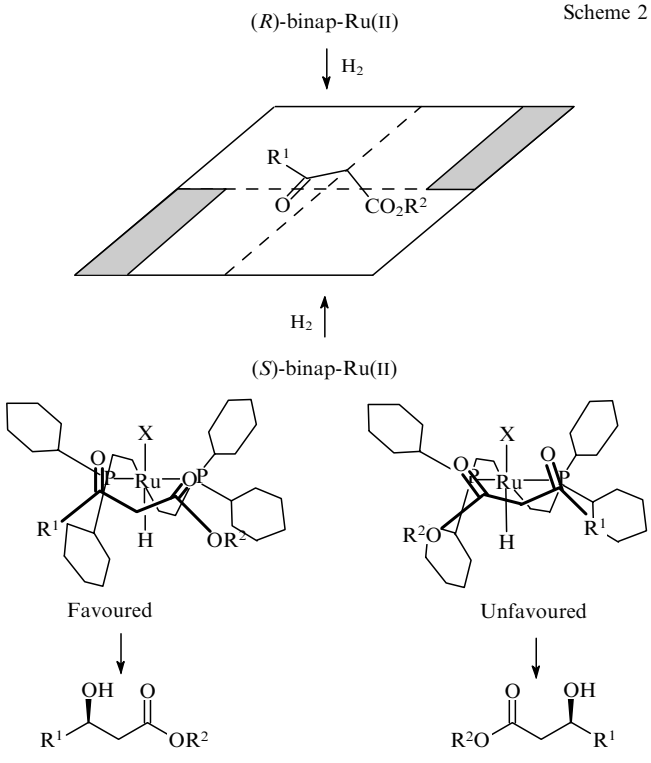

X = Hal.

‡ For the first time, this structural approach in the form of the 'octant rule' has been used to describe the chiral environment of carbonyl groups in steroids.[123]

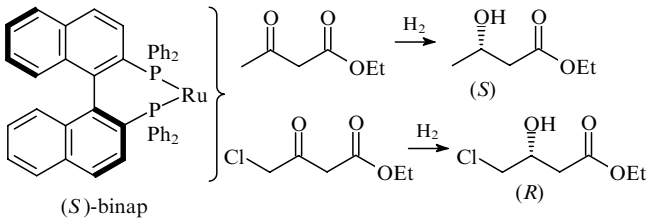

A large body of evidence has been gained concerning the application of rhodium complexes with these ligands as catalysts in hydrogenation of the same kind of substrates, *viz*., α-acetamidocinnamic acid derivatives.

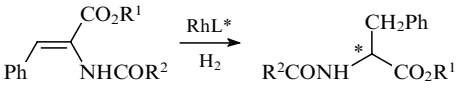

L* = 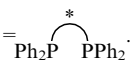

Earlier, it was suggested that enantioselective effects of such complexes are related to chiral arrangements of the phosphine phenyl groups.[120] We suppose that the arrangement of phenyl groups forming the chiral environment of the metal atoms can be related to the sign of helicity or the conformation of the chelate complex (Scheme 3) (view from the side of the metal atom; the chelate complex without substituents is shown by a dotted line). The schematic representations of the helix turns are shown in the right part of the Scheme, where the *P*-helix moves off clockwise, while the *M*-helix moves off anti-clockwise.

The analysis of molecular models has demonstrated that the conformations of λ- or δ-five-membered chelate complexes can be distorted to some extent, but their interconversions are either impossible (*e.g*., for chelates based on cyclic 1,2-diphosphines, such as norphos, phellanphos, dpcb, *etc*.) or result in the formation of chelate complexes with unfavourable axial positions of substituents [126–128] (*e.g*., prophos, chiraphos, cycphos, phenphos, *etc*.). In the case of seven-membered chelate complexes, a change in the sign of chirality in the orientation of the phenyl groups is also accompanied by the transition from the favourable chair-λ (or -δ) conformation to the unfavourable boat-δ (or -λ) conformation. However, in this case the advantage is less apparent.

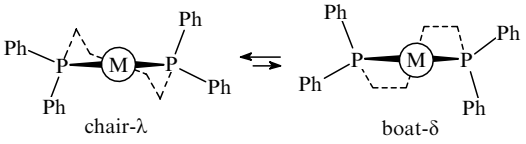

A correlation between the conformations of five-membered chelate rings of rhodium catalytic complexes with bis(diphenylphosphine) ligands and the configurations of the hydrogenation products of acetamidocinnamic acid and its derivatives was found in 1982 simultaneously and independently by two groups of authors (see Refs 129–131 and 132).§ The λ-conformation of the chelate complex determines the formation of (*S*)-, whereas the δ-conformation determines the formation of (*R*)-products. Quite naturally, this effect is directly related to the chiral positions of the phosphine phenyl groups corresponding to these conformations rather than to the conformations themselves. The conformations and the conformational rigidities of chelate rings in catalytic complexes play a crucial role in stabilisation of chiral positions or helical chiralities of the phosphine phenyl groups.

In a simplified form, this regularity may be described by the formula: λ-(*S*), δ-(*R*).[140,141] Another representation of this rule appears to be more complete:

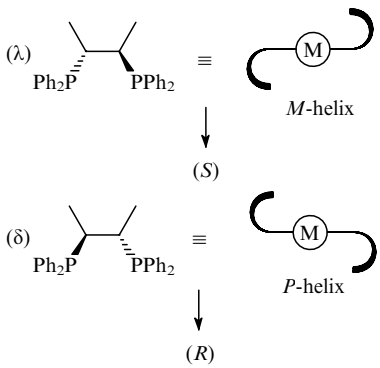

Some known ligands of rhodium complexes and the results of hydrogenation of α-acetylamidocinnamic acid derivatives in the presence of these complexes are shown in Table 6.

As can be seen, the results of hydrogenation in the presence of five-membered chelate rhodium complexes obey the λ-(*S*), δ-(*R*) rule [140,141] irrespective of whether the C_2 symmetry axis is inherent

Five-membered chelate complexes Scheme 3

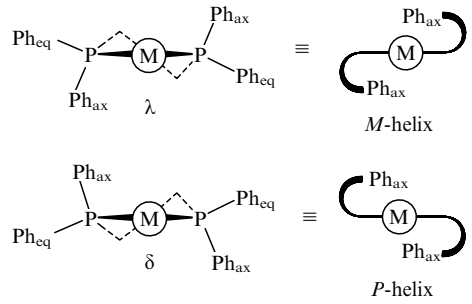

Seven-membered chelate complexes

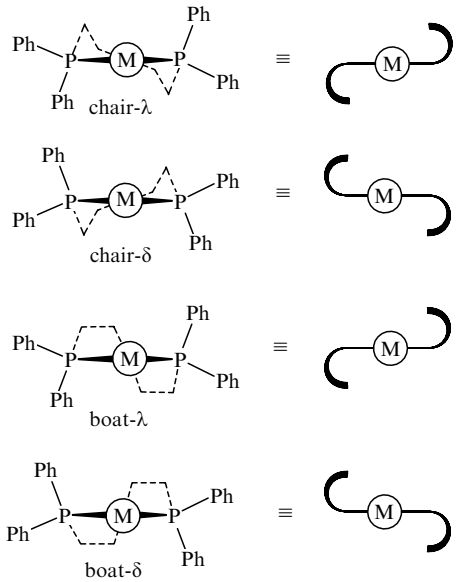

§ There are many examples of simultaneous publications by different research groups of experimental results concerning asymmetric hydrogenation on rhodium phosphine catalysts in which the same catalyst (ligand) was used or, as in our case, the same regularity of the reaction was established (see, *e.g*., Refs 133 and 134; 135,136 and 137; 138 and 139, *etc*.).

Table 6. Arylphosphine ligands forming five-membered rhodium chelate complexes and hydrogenation of α-acetylaminocinnamic acid and its derivatives in the presence of these complexes.

Ligand	Conformation (helix)	Substrate	*ee* (%)	Type of the catalytic complex	Solvent	*T* /°C	p_{H_2} /atm	Ref.
Ligands forming chiral C_2-symmetrical complexes								
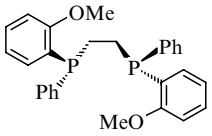 (*R*,*R*)-(−)-dipamp	λ (*M*)	AcΔAla	90 (*S*)	C	M	50	3	142
		AcΔPhe	94 (*S*)	C	M or E	50	3	64,[a] 143
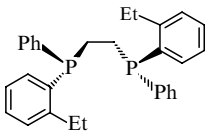	δ (*P*)	AcΔAla	93 (*R*)	C	E	50	3	144 [a]
		AcΔPhe	90 (*R*)	C	Pr^i	50	3	144 [a]
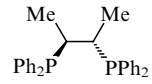 (*S*,*S*)-(−)-chiraphos	δ (*P*)	AcΔAla	91 (*R*)	C	E	20	1	33
		AcΔPhe	89 (*R*)	C	E	20	1	33
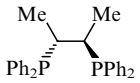 (*R*,*R*)-(+)-chiraphos	λ (*M*)	AcΔAla	91 (*S*)	C	E	20	1–4	145
		AcΔPhe	88 (*S*)	C	E	20	1–4	145
		BzΔPhe	94 (*S*)	C	E	20	1–4	145
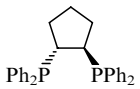 (*R*,*R*)-(+)-dpcp	λ (*M*)	AcΔPhe	91 (*S*)	N	M – B	30	1	125
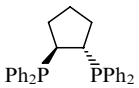 (*S*,*S*)-(−)-dpcp	δ (*P*)	AcΔPhe	90 (*R*)	N	M – B	30	1	125
		BzΔPhe	98 – 100	N	M – B	30	1	146
		BzΔPheOMe	98 – 100	N	M – B	30	1	146
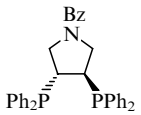	λ (*M*)	AcΔPhe	99 (*S*)	C	M	20	40	36
Ligands forming chiral C_2-symmetrical complexes (without substituents in the chelate rings)								
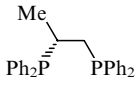 (*R*)-(+)-prophos	λ (*M*)	AcΔPhe	90 (*S*)	C	E	25	1	120
		BzΔPhe	91 (*S*)	C	E	25	1	120
		AcΔPhe	83 (*S*)	N	M	20	1	147
		BzΔPhe	88 (*S*)	N	M	20	1	147
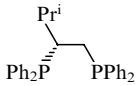 (*R*)-(+)-valphos	λ (*M*)	BzΔPhe	95 (*S*)	N	E	20	1	148
		AcΔAla	88.6 (*S*)	N	E	20	1	148
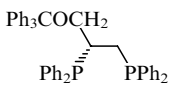	λ (*M*)	AcΔPhe	85 (*S*)	C	E	20	1	149
		AcΔAla	78 (*S*)	C	E	20	1	149
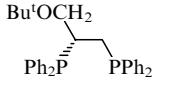	λ (*M*)	AcΔPhe	86 (*S*)	C	E	20	1	150
		AcΔAla	92 (*S*)	C	E	20	1	150
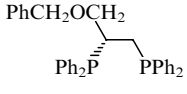	λ (*M*)	AcΔPhe	87 (*S*)	C	E	20	1	150
		AcΔAla	91 (*S*)	C	E	20	1	150
		AcΔPhe	86 (*S*)	C	E	20	1	149
		AcΔAla	75 (*S*)	C	E	20	1	149
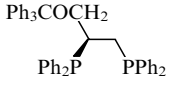	δ (*P*)	AcΔAla	78 (*R*)	C	E	20	1	149

Table 6 (continued).

Ligand	Conformation (helix)	Substrate	*ee* (%)	Type of the catalytic complex	Solvent	T /°C	p_{H_2} /atm	Ref.
Ligands forming chiral C_2-symmetrical complexes (without substituents in the chelate rings)								
cyclo-Hex 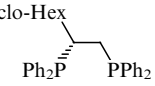 (*R*)-(+)-cycphos	λ (*M*)	AcΔPhe	84 (*S*)	N	M	20	1	147
		AcΔAla	93 (*S*)	N	M	20	1	147
		BzΔPhe	90 (*S*)	N	M	20	1	147
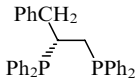 (*R*)-(+)-phephos	λ (*M*)	AcΔPhe	99 (*S*)	C	E – B (2 : 1)	20	20	148
		AcΔAla	84.5 (*S*)	C	E – B (2 : 1)	20	20	148
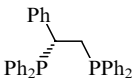 (*R*)-(–)-phephos	λ (*M*)	AcΔPhe	79 (*S*)	N	M	20	1	147
		AcΔPheOMe	88 (*S*)	N	M	20	1	147
		AcΔAla	82 (*S*)	N	M	20	1	147
		BzΔPhe	84 (*S*)	N	M	20	1	147
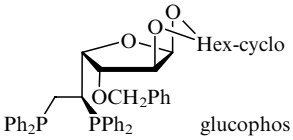 glucophos	λ (*M*)	AcΔPhe	54 (*S*)	C	T	20	1	151
		AcΔPheOMe	41 (*S*)	C	T	20	1	151
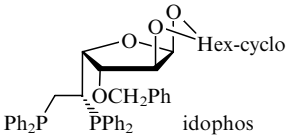 idophos	δ (*P*)	AcΔPhe	56 (*R*)	C	T	20	1	151
		AcΔPheOMe	27 (*R*)	C	T	20	1	151
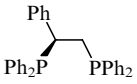 (*S*)-(+)-phenphos	δ (*P*)	AcΔPhe	78 (*R*)	C	T	30	1	152
		AcΔPhe	82 (*R*)	C	T	30	1	152
		AcΔPheOMe	8 (*R*)	C	T	30	1	152
		BzΔPhe	84 (*R*)	C	T	30	1	152
		BzΔPhe	76 (*R*)	C	T	30	1	152
		AcΔPheOMe	76 (*R*)	C	T	30	1	152
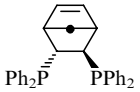 (*R*,*R*)-(–)-norphos	λ (*M*)	AcΔPhe	95 (*S*)	C	E	20	1	153 [a]
		AcΔAla	90 (*S*)	C	E	20	1	153 [a]
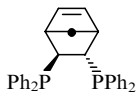 (*S*,*S*)-(+)-norphos	δ (*P*)	AcΔPhe	97 (*R*)	C	M	20	1	153
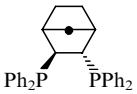 (+)-renophos	δ (*P*)	AcΔPhe	95 (*R*)	C	M	20	1	154
		AcΔAla	95 (*R*)	C	M	20	1	154
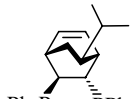 (*S*,*S*)-phellanphos	δ (*P*)	AcΔPhe	95 (*R*)	C	E	25	1	155, 156
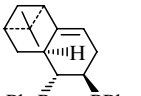 (*R*,*R*)-nopaphos	λ (*M*)	AcΔPhe	80 (*S*)	C	E	25	15	155
		AcΔAla	81 (*S*)	C	E	25	15	155

Note. Hereinafter, the following designations are used. For the substrate: AcΔPheOMe is (*Z*)-α-acetylaminocinnamic acid methyl ester; AcΔAla is α-acetylaminoacrylic acid; for the type of the catalytic complex: N is neutral including that formed *in situ*; C is cationic; for the solvent: M is methanol; E is ethanol; B is benzene; T is tetrahydrofuran.

[a] Data from X-ray diffraction analysis.

in the whole complex or in its chelate ring without substituents. The implementation of this rule is not influenced by the nature of substituents and experimental conditions. The situation is more complicated in the case of seven-membered ¶ chelate rhodium complexes in which the conformational transitions chair-λ – boat-δ and chair-δ – boat-λ are possible (other intermediate conformations have also been described [158]). Such transitions change the helicity sign of the phosphine phenyl groups, as a result of which the configuration of the product also changes. Unfortunately, X-ray diffraction analysis does not provide any unambiguous information about the conformations of the corresponding molecules in solution and especially in the intermediate catalytic complex, since the factors involved in crystal formation are stronger than those inducing conformational changes. Indeed, the conformations acquired by the diop ligand in Ir[(*S*,*S*)-(+)-diop](cod)Cl [159] and [(*R*,*R*)(−)-diop]$NiCl_2$ [160] crystals differ from the more favourable ideal conformations chair-λ and chair-δ. In the case of [(*R*,*R*)(−)-diop]$NiCl_2$, the distortions are so great that the position of the phenyl groups relative to the metal becomes close to symmetrical. If such conformations were maintained in solution, this would contradict the Curie – Pasteur principle ('there is no asymmetry without asymmetry') and would be in conflict with the very logic of asymmetric catalysis. The same complex, *viz*., [(*R*,*R*)-(−)-diop]$NiCl_2$, manifests high enantioselectivity in various cross-coupling reactions;[161] hence, its phenyl groups occupy chiral positions relative to the metal.

Therefore, the opposite statement, *viz*., if the λ-(*S*), δ-(*R*) rule is observed, the true conformations of the ligands in the complexes are close to the predictable chair conformation, seems to be more applicable to seven-membered chelate rhodium complexes.

Some examples of fulfilment of the chair-δ-(*R*), chair-λ-(*S*) rule are given in Table 7,[130, 140] *viz*.:

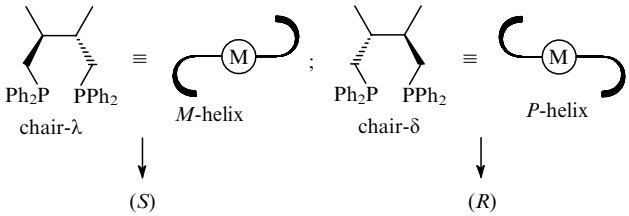

It is easy to ascertain that in the case of both seven-membered chelate complexes with second-order symmetry axes and complexes where only chelate rings without substituents possess C_2 symmetry the chair-λ-(*S*), chair-δ-(*R*) rule [or the boat-λ-(*S*),

¶ Six-membered chelate complexes have been studied relatively little, apparently due to their low efficiencies in asymmetric reactions resulting from conformational labilities of six-membered compounds. However, one such complex, *viz*., Rh(*S*,*S*)-skewphos [skewphos is 2,4-bis(diphenylphosphino)pentane], manifests high enantioselectivity [AcΔPhe, 93% (R)].[157]

Table 7. Arylphosphine ligands forming seven-membered rhodium complexes for which the chair-λ-(*S*), chair-δ-(*R*) rule holds.

Ligand	Conformation (helix)	Substrate	*ee* (%)	Type of the catalytic complex	Solvent	*T* /°C	p_{H_2} /atm	Ref.
Ligands forming chiral C_2-symmetrical complexes								
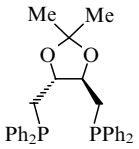	chair-δ (*P*)	AcΔPhe	82 (*R*)	N	E – B (2 : 1)	20	1.1	65, 66
		*Ac*ΔAla	73 (*R*)	N	E – B (2 : 1)	20	1.1	65, 66, 159 [a]
Ph_2P PPh_2								
(*R*,*R*)-(−)-diop								
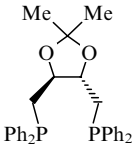	chair-λ (*M*)	AcΔPhe	81 (*S*)	N	E – B (2 : 1)	20	1.0	162, 163
Ph_2P PPh_2								
(*S*,*S*)-(+)-diop								
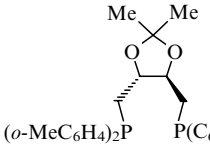	chair-δ (*P*)	AcΔPhe	27 (*R*)	N	E – B (2 : 1)	20	1.0	164
$(o\text{-}MeC_6H_4)_2P$ $P(C_6H_4Me\text{-}o)_2$								
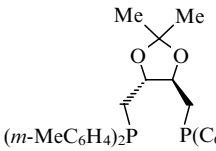	chair-δ (*P*)	AcΔPhe	87 (*R*)	N	E – B (2 : 1)	20	1.1	164
$(m\text{-}MeC_6H_4)_2P$ $P(C_6H_4Me\text{-}m)_2$								
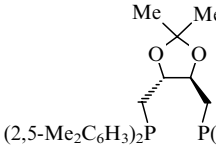	chair-δ (*P*)	AcΔPhe	44 (*R*)	N	E – B (2 : 1)	20	1.1	164
$(2,5\text{-}Me_2C_6H_3)_2P$ $P(C_6H_3Me_2\text{-}2,5)_2$								

Table 7 (continued).

Ligand	Conformation (helix)	Substrate	*ee* (%)	Type of the catalytic complex	Solvent	*T* /°C	p_{H_2} /atm	Ref.
Ligands forming chiral C_2-symmetrical complexes								
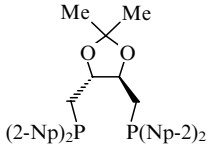 (2-Np)$_2$P P(Np-2)$_2$	chair-δ (*P*)	AcΔPhe	83 (*R*)	N	E–B (2 : 1)	20	1.1	164
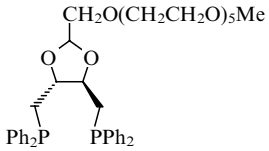 Ph$_2$P PPh$_2$	chair-δ (*P*)	AcΔPhe	64 (*R*)	C	E	25	1.1	165
cyclo-Hex 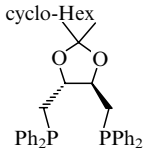 Ph$_2$P PPh$_2$	chair-δ (*P*)	AcΔPhe	77.5 (*R*)	N	E–B (1 : 2)	20	1.1	164
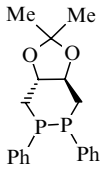	chair-δ (*P*)	AcΔPhe	71 (*R*)	N	E–B (1 : 2)	20	1.1	166
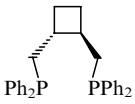 Ph$_2$P PPh$_2$ (*R*,*R*)-(−)-dipmcb	chair-δ (*P*)	AcΔPhe AcΔAla AcΔPhe	86 (*R*) 72 (*R*) 91 (*R*)	N N N	E – B (2 : 3) E – B (2 : 3) E – B (1 : 2)	25 25 25	1.0 1.0 1.1	167 167 168
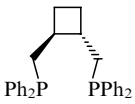 Ph$_2$P PPh$_2$ (*S*,*S*)-(+)-dipmcb	chair-λ (*M*)	AcΔPhe	87 (*S*)	C	E – B (1 : 1)	20	1.0	169
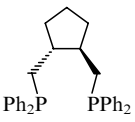 Ph$_2$P PPh$_2$ (*R*,*R*)-(−)-dipmcp	chair-δ (*P*)	AcΔPhe AcΔAla	63 (*R*) 72 (*R*)	N N	E – B (1 : 2.3) E – B (1 : 2.3)	25 25	1.0 1.0	167 167
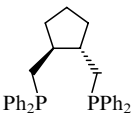 Ph$_2$P PPh$_2$ (*S*,*S*)-(+)-dipmcp	chair-λ (*M*)	AcΔPhe AcΔAla	73 (*S*) 68 (*S*)	N N	E – B (2 : 1) E – B (2 : 1)	25 25	1.0 1.0	168 168
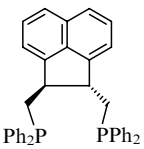 Ph$_2$P PPh$_2$	chair-λ (*M*)	AcΔPhe AcΔAla	81 (*S*) 52 (*S*)	N N	E – B (2 : 1) E – B (2 : 1)	25 25	1.0 1.0	168 168
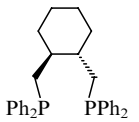 Ph$_2$P PPh$_2$	chair-λ (*M*)	AcΔPhe	35 (*S*)	N	E – B (1 : 2.3)	25	1.0	170

Table 7 (continued).

Ligand	Conformation (helix)	Substrate	*ee* (%)	Type of the catalytic complex	Solvent	T /°C	p_{H_2} /atm	Ref.
Ligands forming chiral C_2-symmetrical complexes								
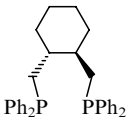	chair-δ (*P*)	AcΔPhe	36 (*R*)	N	E – B (2 : 1)	25	1.0	168
		AcΔAla	39 (*R*)	N	E – B (2 : 1)	25	1.0	168
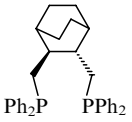	chair-λ (*M*)	AcΔPhe	81 (*S*)	N	E – B (2 : 1)	25	1.0	168
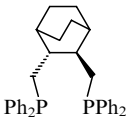	chair-δ (*P*)	AcΔAla	74 (*R*)	N	E – B (2 : 1)	–	1.0	169
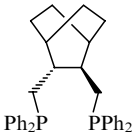	chair-δ (*P*)	AcΔPhe	79.5 (*R*)	N	E – B (2 : 1)	20	1.1	171
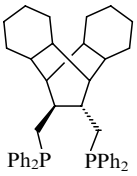	chair-λ (*M*)	AcΔPhe	35 (*S*)	N	E	25	1.0	171
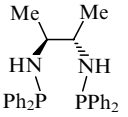	chair-λ (*M*)	AcΔPhe	45 (*S*)	C	E	20	1.0	137, 172
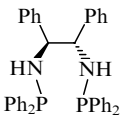	chair-λ (*M*)	AcΔPhe	93.8 (*S*)	C	E	25	1.0	173
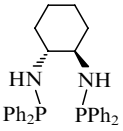	chair-δ (*P*)	AcΔPhe	49 (*R*)	C	E	20	1.0	136
		AcΔPhe	41 (*R*)	C	E	20	1.0	137
		AcΔPhe	47 (*R*)	C	E	20	1.0	135
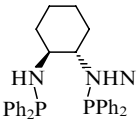	chair-λ (*M*)	AcΔPhe	41 (*S*)	C	E	20	8.0	137
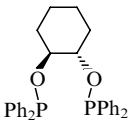	chair-λ (*M*)	AcΔPhe	68 (*S*)	N	E	20	50	174
		AcΔAla	79 (*S*)	N	E	20	50	174
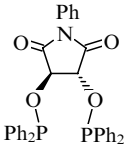	chair-λ (*M*)	AcΔPhe	36 (*S*)	N	M	20	50	175

Table 7 (continued).

Ligand	Conformation (helix)	Substrate	*ee* (%)	Type of the catalytic complex	Solvent	T /°C	p_{H_2} /atm	Ref.
Ligands forming chiral C_2-symmetrical complexes								
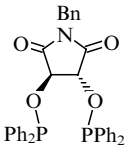	chair-λ (*M*)	AcΔPhe	16 (*S*)	N	M	20	1.0	176
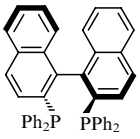 (*R*)-(+)-binap	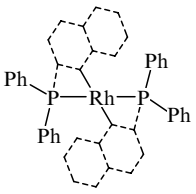 boat-λ (*M*)	BzΔPhe	100 (*S*)	C	E	20	3–4	175
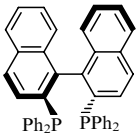 (*S*)-(−)-binap	boat-δ (*P*)	AcΔPhe	84 (*R*)	C	E	20	3–4	178
		AcΔAla	67 (*R*)	C	E	20	3–4	177
		AcΔPhe	84 (*R*)	C	E	20	3–4	177
		BzΔPhe	96 (*R*)	C	E	20	3–4	177
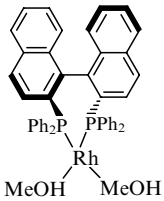	boat-δ (*P*)	BzΔPhe	98 (*R*)	C	E	20	1.0	179
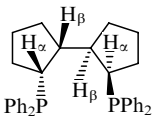 (*R*,*R*)-bicp	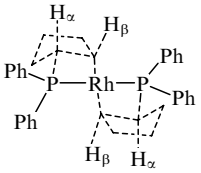 boat-λ, favourable conformation (*M*)	AcΔPhe	89 (*S*)	C	T	20	1.0	180
		BzΔPhe	99 (*S*)	C	T	20	1.0	180
	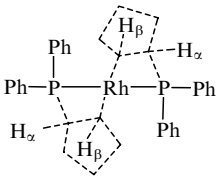 boat-δ, unfavourable conformation (see [b])							
Ligands forming chiral C_2-symmetrical complexes (without substituents in the chelate rings)								
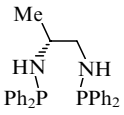	chair-δ (*P*)	AcΔPhe	28 (*R*)	C	E	20	1.0	136
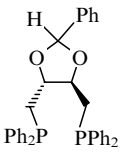	chair-δ (*P*)	AcΔPhe	79.5 (*R*)	N	B–E	20	1.0	163

Table 7 (continued).

Ligand	Conformation (helix)	Substrate	*ee* (%)	Type of the catalytic complex	Solvent	T /°C	p_{H_2} /atm	Ref.
Ligands forming chiral C_2-symmetrical complexes (without substituents in the chelate rings)								
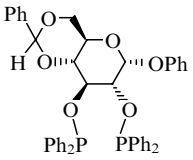 Ph-α-glup	chair-λ (*M*)	AcΔPhe	54 (*S*)	C	M	25	1.0	181
		AcΔPhe	60.5 (*S*)	N	M	25	1.0	181
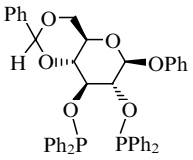 Ph-β-glup	chair-λ (*M*)	AcΔPhe	96 (*S*)	C	M	25	1.0	181
		AcΔPhe	87 (*S*)	N	M	25	1.0	181
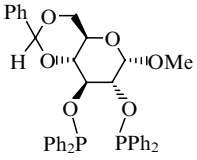	chair-λ (*M*)	AcΔPhe	61 (*S*)	C	E	25	1.0	182
		AcΔPhe	73 (*S*)	C	M	25	1.0	181
		AcΔPhe	75 (*S*)	C	E	0	1.0	183
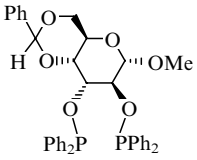	chair-δ (*P*)	AcΔPhe	70 (*R*)	C	E	0	1.0	182
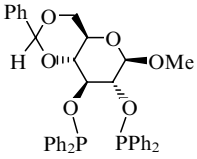	chair-λ (*M*)	AcΔPhe	91 (*S*)	N	E	30	1.0	184
		AcΔAla	91 (*S*)	N	E	30	1.0	184
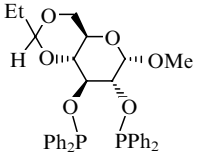	chair-λ (*M*)	AcΔPhe	80 (*S*)	N	M	−25	50	185
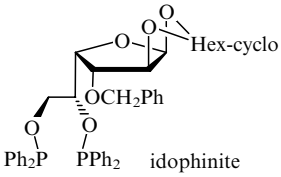 idophinite	chair-λ (*M*)	AcΔPhe	54 (*S*)	C	T	20	1.0	151
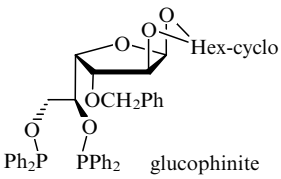 glucophinite	chair-δ (*P*)	AcΔPhe	40 (*R*)	C	T	25	1.0	151

[a] Data from X-ray diffraction analysis. [b] The positions of the phosphine phenyl groups characteristic of the boat-δ conformation (in this case, boat-λ and boat-δ cannot be mutually interconverted without the bond cleavage) is associated with considerable steric hindrances.

boat-δ-(*R*) for the atropoisomeric binap ligands] is obeyed.[140, 141] Thus, the intermediate catalytic complexes have predominantly the chair-λ and chair-δ conformations in solution. In the chelate complexes, the atropoisomeric ligands binap exist in the only possible boat-λ, boat-δ conformation.

The ligands which form complexes with seven-membered chelate rings, but do not formally follow the chair-λ-(*S*), chair-δ-(*R*) rule are shown in Table 8.

Let us consider molecular models. In the ligands based on *trans*-disubstituted cyclopropane, the α-angles between the planes of the rings and the substituents are close to 123°.

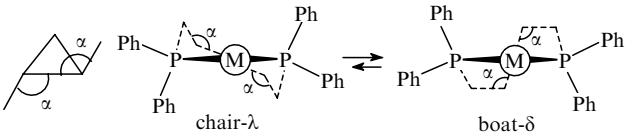

The boat-δ conformation of the chelate ring based on this ligand is preferable to the chair-λ conformation, since the α-angles are closer to 123°, and the λ-(*S*), δ-(*R*) rule is not violated in this case. The structures of the following four ligands, *viz*.:

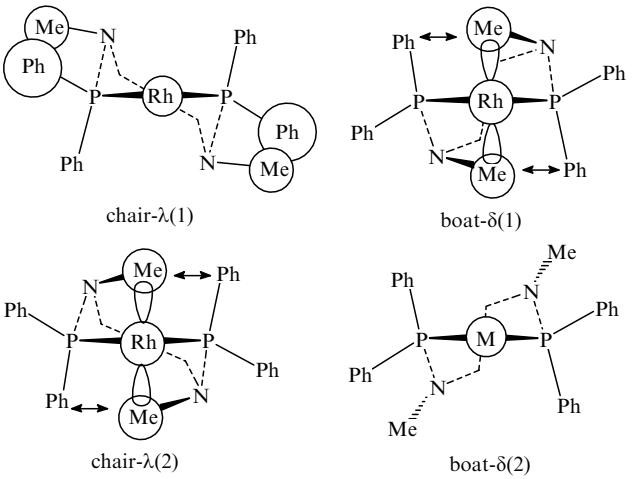

are of the same kind. In our opinion,[140] these ligands can theoretically have four conformers, *viz*., chair-λ(1), boat-δ(1), chair-λ(2) and boat-δ(2), owing to the well-known ability of pyramidal nitrogen atoms to invert.

Of the four possible conformers of the ligand (*S*,*S*)-Mediop(N), the boat-δ(2) conformer is the most sterically favourable. The chair-λ(1) conformation is characterised by spatial proximity of the Ph and Me groups, whereas in the chair-λ(2) and boat-δ(1) conformations non-bonding interactions of the methyl groups with the apical orbitals of rhodium atoms in planar-square complexes are observed.

Another disadvantage of the chair-λ(2) and boat-δ(1) conformations is the interaction of Me and Ph groups (they are marked by bidirectional arrows). We have carried out a series of non-empirical quantum-chemical calculations for the interactions of isolated fragments of these structures.[140] It was found that the boat-δ(2) conformation (or its mirror-opposite boat-λ(2) conformation) is more favourable for NMe-ligands taking into account the interaction between the Me and Ph groups. In the presence of complexes with these conformations of ligands, the reaction should proceed according to the δ-(*R*) [or λ-(*S*)] rule as is actually the case in experiment.

Formally, the *o*-$MeOC_6H_4$-phosphine diop analogue does not conform to this rule, which can also be explained by stabilisation of the 'unfavourable' conformation. The conformational equilibrium in complexes containing this ligand seems to be shifted towards the boat conformation due to the interactions of the electron pairs of the methoxy group oxygens with the apical orbitals of the rhodium atoms.

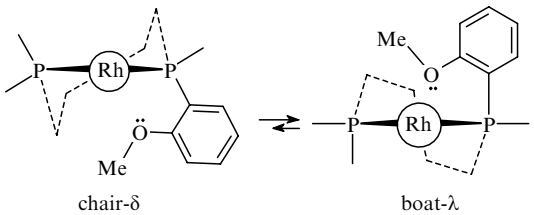

The existence of similar coordination bonds between the *o*-$MeOC_6H_4$ groups and rhodium atoms in complexes with dipamp ligands has been confirmed by X-ray diffraction analysis.[64] The boat-λ conformation is geometrically more fit for the formation of such bonds than the chair-δ conformation. It can therefore be assumed that the λ-(*S*), δ-(*R*) rule is also applicable to the rhodium complex with this ligand. The catalytic system containing the phosphinite ligand $[Rh(nbd)_2]ClO_4/CuCl$ (see Table 8) cannot be considered as an exception to this rule, since it is possible that it is a bimetallic cluster or a complex where the necessary stereochemistry that manifests the catalytic activity under the reaction conditions is violated.

Examination of molecular models of the other two ligands leads to a conclusion that only the boat-λ conformation in the strained bridged structure of 9,10-dihydro-9,10-ethanoanthracene enables the formation of seven-membered chelate complexes with a metal, *viz*., in this case, the λ-(*S*) rule is fulfilled. In the case of 1,4-bisdiphenylphosphino-(2*S*,3*S*)-diphenylbutane, the boat-δ conformation of the chelate complexes, in which both phenyl rings occupy equatorial positions and thus give an additional gain in energy, is more favourable.[127] Therefore, the λ-(S), δ-(R) rule holds true for complexes containing this ligand.

Five-membered chelate rhodium complexes based on alkylphosphine ligands with second-order symmetry axes (Table 9), conform also to this rule,† however, in its basic 'helical' form.

It is impossible to isolate the helical component of the rhodium complex with the (***S***,*S*)-Pr^i-cnrphos ligand without recourse to X-ray diffraction analysis. However, the *P*-helical structure can be predicted from the configuration of the hydrogenation product.

The data presented in Table 9 suggest that the product configuration is determined by the helical component present in all complexes with alkylphosphine ligands.

Sometimes, the enantioselectivity of reactions in the presence of bisdiphenylphosphine complexes is associated with chirality, which is determined by a definite inclination of the planes of the phenyl groups relative to one another.[194] However, the values and the signs of enantioselectivity in complexes with alkylphosphine ligands,[124, 191–193] cyclodiop [166] and Cydiop,[195] which are devoid of such chirality, do not differ from the corresponding parameters of complexes with bisdiphenylphosphine ligands. Therefore, the helical component makes the main contribution.

An experimental proof of the effect of the helical component on enantioselectivity follows from the enantioselective properties of the complex the achiral ligands in which form helices around the metal ions.[196]

The ligands forming eight- and nine-membered chelate complexes with C_2 symmetry axes (with the exception of atropoisomeric non-substituted aminophosphines [197–200]) are not very effective in the majority of asymmetric hydrogenation reactions. Enantioselectivity can be increased either through the use of bimetallic complexes or through a decrease in reaction temperature.

There is no reason to suppose that the above-considered rule concerning the conformation of five- or seven-membered bis(diphenylphosphine) chelate complexes with the C_2 symmetry axes is only applicable to hydrogenation reactions. Presumably, similar rules exist for other reactions, too. Indeed, the hydrosilylation of acetophenone by diphenylsilane in the presence of rhodium complexes proceeds in accordance with the λ-(*S*), δ-(*R*) rule (Table 10).

† In our opinion, the critical attitude [190] to the conformational expression of this rule, *viz*., λ-(*S*), δ-(*R*), is too formal.

Table 8. Arylphosphine rhodium complexes with seven-membered chelate rings which do not formally obey the chair-δ(*S*), chair-δ(*R*) rule.

Ligand	Conformation [a] (helix)	Substrate	*ee* (%)	Type of the catalytic complex	Solvent	*T* /°C	p_{H_2} /atm	Ref.
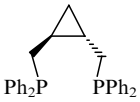	boat-δ (*P*)	AcΔPhe AcΔAla	15 (*R*) 23 (*R*)	N N	E – B (2 : 1) E – B (2 : 1)	25 25	1.0 1	167 167
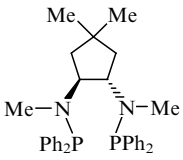 (*S*,*S*)-Mediop(N)	boat-δ(2) (*P*)	AcΔPhe	30 (*R*)	C	E – B	20	1	186
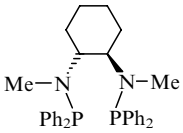	boat-λ(2) (*M*)	AcΔPhe AcΔAla	92 (*S*) 89 (*S*)	C C	E E	25 20	1 1	187 136
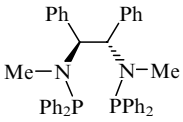	boat-δ(2) (*P*)	AcΔPhe AcΔAla	68.4 (*R*) 86.3 (*R*)	C C	E E	25 25	5 5	135, 173 135, 173
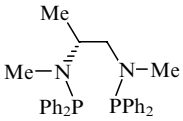	boat-λ(2) (*M*)	AcΔPhe	70 (*S*)	C	E	20	1	136
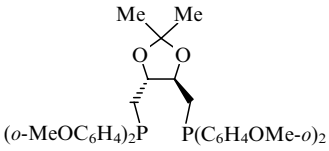	boat-λ (*M*)	AcΔPhe AcΔPheOMe AcΔAla	31 (*S*) 71 (*S*) 8 (*S*)	C C C	M M M	20 20 20	1 1 1	188 188 188
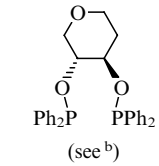 (see [b])	–	AcΔPhe	90 (*S*)	C	E – B	−15	1.48	189
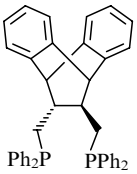	boat-λ (*M*)	AcΔPhe	50 (*S*)	N	E	25	1	171
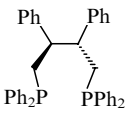	boat-δ (*P*)	AcΔPhe AcΔAla	54 (*R*) 61 (*R*)	C C	E E	25 25	1 1	173 173

[a] The favourable conformation is indicated (see text). [b] The catalytic system $[Rh(nbd)_2]ClO_4$/CuCl was studied using this ligand.

Table 9. Alkylphosphine ligands forming five-membered chelate rhodium complexes and hydrogenation of α-acetylaminocinnamic acid and its derivatives in the presence of these complexes.

Ligand	Conformation (helix)	Substrate	*ee* (%)	Type of the catalytic complex	Solvent	*T* /°C	p_{H_2} /atm	Ref.
P-helix								
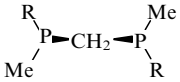 (*R*,*R*)-miniphos	Bu^t	AcΔPhe	97 (*R*)	C	M	20	1	191
	Bu^t	AcΔAla	> 99.9 (*R*)	C	M	20	1	191
	cyclo-C_6H_{11}	AcΔAla	99.1 (*R*)	C	M	20	1	191
	Pr^i	AcΔAla	98 (*R*)	C	M	20	1	191
	Ph	AcΔAla	26 (*R*)	C	M	20	1	191 [a]
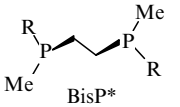 BisP*	Bu^t	AcΔPhe	98.4 (*R*)	C	M	20	2	192
	Et_3C	AcΔPheOMe	94.7 (*R*)	C	M	20	2	192
	1-Adamantyl	AcΔPheOMe	99.9 (*R*)	C	M	20	2	192
	cyclo-C_5H_9	AcΔPheOMe	43.0 (*R*)	C	M	20	2	192
	cyclo-C_6H_{11}	AcΔPheOMe	47.1 (*R*)	C	M	20	2	192 [a]
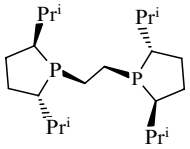 (*R*,*R*)-Pr^i-bpe	–	AcΔPheOMe	93 (*R*)	C	M	20	2	124
	–	AcΔAlaOMe	96.4 (*R*)	C	M	20	2	124 [a]
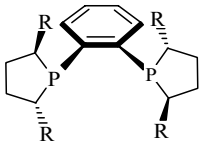 (*S*,*S*)-R-duphos	Me	AcΔPheOMe	98 (*R*)	C	M	20	2	124
	Me	AcΔAlaOMe	99 (*R*)	C	M	20	2	124
	Et	AcΔPheOMe	99 (*R*)	C	M	20	2	124
	Et	AcΔAlaOMe	99.4 (*R*)	C	M	20	2	124
	Pr^n	AcΔPheOMe	> 99 (*R*)	C	M	20	2	124
	Pr^n	AcΔAlaOMe	99.8 (*R*)	C	M	20	2	124
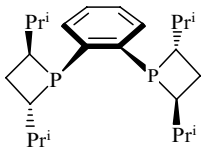 (*S*,*S*)-Pr^i-cnrphos	–	AcΔPheOMe	74 (*R*)	–	–	–	–	193
M-helix								
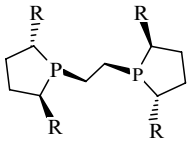	Me	AcΔPheOMe	85 (*S*)	C	M	20	2	124
	Me	AcΔAlaOMe	91.4 (*S*)	C	M	20	2	124
	Et	AcΔPheOMe	93 (*S*)	C	M	20	2	124
	Et	AcΔAlaOMe	98.1 (*S*)	C	M	20	2	124
	Pr^n	AcΔPheOMe	92 (*S*)	C	M	20	2	124
	Pr^n	AcΔAlaOMe	97.7 (*S*)	C	M	20	2	124
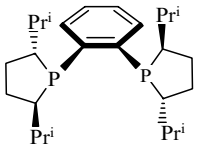 (*R*,*R*)-Pr^i-duphos	–	AcΔPheOMe	87 (*S*)	C	M	20	2	124
	–	AcΔPheOMe	95.4 (*S*)	C	M	20	2	124

[a] Data from X-ray diffraction analysis.

The cross-coupling reaction has been most studied for secondary alkyl or arylalkyl Grignard reagents which react in the following way:[59]

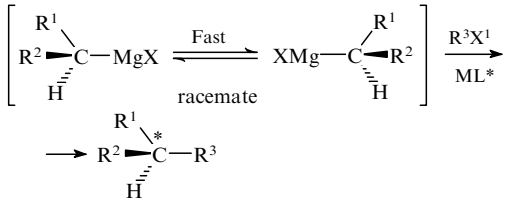

(1)

The cross-coupling of Bu^{s}MgX with PhY in the presence of bis(diphenylphosphine) nickel complexes:

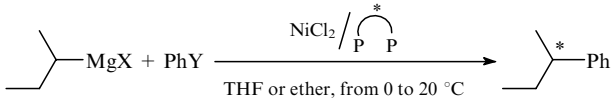

obeys the rule λ-(*R*), δ-(*S*) (Table 11).

Table 10. Hydrosilylation of acetophenone by diphenylsilane on chiral rhodium complexes.

Catalytic system	Conformation of the complex	Ref.	Enantiomeric excess	
			ee (%)	Ref.
$[Rh(cod)Cl]_2$/(*S*,*S*)-norphos	δ	153	15 (*R*)	201
$[Rh(cod)Cl]_2$/(*S*,*S*)-chiraphos	δ	202, 203	3 (*R*) (see [a])	53
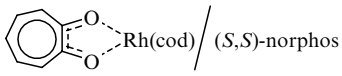 (*S*,*S*)-norphos	δ	153	5.4 (*R*)	204
$[Rh(cod)Cl]_2$/(*S*,*S*)-diop	chair-λ	159, 176	28 (*S*)	52
			23 (*S*)	53
$[Rh(cod)Cl]_2$/(*R*,*R*)-diop	chair-δ	159, 176	31 (*R*)	205
			22.5 (*R*)	206
			55 (*R*) (see [b])	51
$[Rh(cod)Cl]_2$/(*S*,*S*)-glup	chair-λ	159, 176, 200	47 (*S*)	207
$[Rh(cod)Cl]_2$/(*S*,*S*)-cyclo-Hex·diop	chair-δ	159, 176	24 (*R*)	208
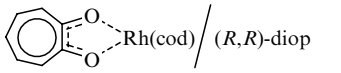 (*R*,*R*)-diop	chair-δ	159, 176	32.7 (*R*)	204

[a] Hydrosilylation of propiophenone. [b] Hydrosilylation with α-$NpPhSiH_2$.

Table 11. The optical yields of asymmetric cross-coupling products of Bu^sMgX with PhY in the presence of nickel complexes.

($NiCl_2$/).

	Conformation of the complex	Ref.	Optical yield (%)		
			X = Y = Cl	X = Y = Br	Ref.
(*R*,*R*)-dipamp	λ	34	4.5 (*R*)	4.2 (*R*)	209
(*R*)-prophos	λ	210	14.4 (*R*)	39.9 (*R*)	209
	λ	210	21.0 (*S*) [a]	44.0 (*R*)	212
(*R*)-cycphos	λ	213	14.4 (*R*)	45.8 (*R*)	209
(*R*)-phenphos	λ	214	18.5 (*R*)	50.0 (*R*)	209
(*S*,*S*)-chiraphos	δ	213, 215	14.5 (*S*)	43.1 (*S*)	209
(*R*,*R*)-norphos	λ	216	26.7 (*R*)	50.7 (*R*)	209
(*R*,*R*)-(−)-diop	chair-δ	214, 217	10.9 (*R*)	–	161
	chair-δ	214, 217	–	17.0 (*R*) [b]	218

[a] Presumably, the (*S*) conformation is indicated erroneously, since more recent studies by the same authors [209, 211] suggest the formation of (*R*)-products in analogous experiments. [b] In this case, X = Br, Y = Cl.

The following catalytic reactions also represent cross-coupling:

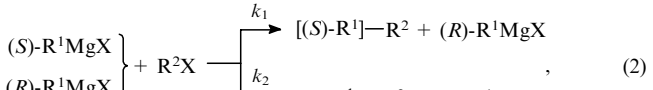

(*S*)-R^1MgX / (*R*)-R^1MgX + R^2X → (k_1) [(*S*)-R^1]—R^2 + (*R*)-R^1MgX; (k_2) [(*R*)-R^1]—R^2 + (*S*)-R^1MgX, (2)

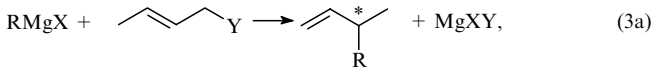

RMgX + + MgXY, (3a)

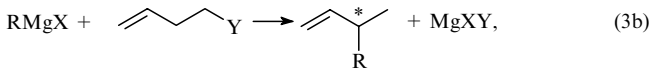

RMgX + + MgXY, (3b)

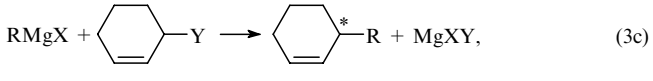

RMgX + + MgXY, (3c)

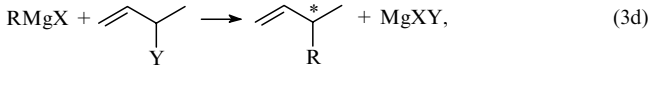

RMgX + + MgXY, (3d)

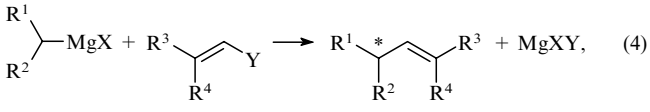

$R^1R^2CHMgX + R^3CH=CHCH_2Y \rightarrow R^1R^2C^*CH=CHR^3 + MgXY$, (4)

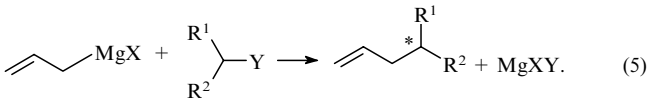

$CH_2=CHCH_2MgX + R^1R^2CHY \rightarrow CH_2=CHC^*R^1R^2 + MgXY$. (5)

The reaction of a vinyl halide with a non-racemisable Grignard reagent also belong to the type of reaction (2).[218–220] In this case, the resolution of the racemic Grignard reagent occurs due to different reactivities of the enantiomers of the racemate in the presence of chiral catalysts (kinetic resolution). This enantioselective reaction results in the enrichment of the non-consumed Grignard reagent with one of the enantiomers.

The results obtained in the study of reaction (3c) are given in Table 12. The data concerning reactions (3a), (3b) and (3d) (Table 13) illustrate the applicability of this rule:

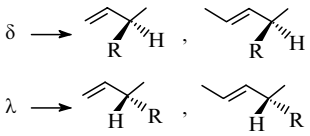

δ →

λ →

Table 12. The optical yields of 2-ethylcyclohexane in asymmetric cross-coupling of EtMgBr with cyclohexene derivatives in the presence of bisdiphenylphosphine nickel complexes.

($NiCl_2$/).[211]

	Conformation of the complex	Substituent in cyclohexene	Optical yield (%)
(*R*)-phephos	λ	OH	28.4 (*S*)
(*S*,*S*)-chiraphos	δ	OH	49.5 (*R*)
(*R*)-phephos	λ	OPh	26.5 (*S*)
(*S*,*S*)-chiraphos	δ	OPh	51.2 (*R*)
(*R*)-prophos	λ	OPh	29.7 (*S*)
(*R*)-cycphos	λ	OPh	16.2 (*S*)
(*R*,*R*)-norphos	λ	OPh	48.1 (*S*)
(*R*,*R*)-dipamp	λ	OPh	11.2 (*R*)

Table 13. Asymmetric cross-coupling of Grignard reagents (R^1MgX) with allylic alcohols, ethers and esters (R^2Y) on chiral nickel complexes at room temperature.

R^2Y	R^1MgX	Complex	Conformation	Product	Optical yield (%)	Ref.
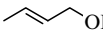	EtMgBr	$NiCl_2$/(*S*,*S*)-chiraphos	δ		22 (*S*)	221
	PhMgBr	$NiCl_2$/(*S*,*S*)-chiraphos	δ		58 (*R*)	221
	EtMgBr	$NiCl_2$/(*S*,*S*)-chiraphos	δ		17 (*S*)	221
	PhMgBr	$NiCl_2$/(*S*,*S*)-chiraphos	δ		58 (*R*)	221
	MeMgBr	$NiCl_2$/(*R*,*R*)-diop	chair-δ	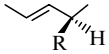	15 (*R*)	222
	MeMgBr	$NiCl_2$/(*R*,*R*)-diop	chair-δ	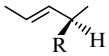	8.5 (*R*)	222
	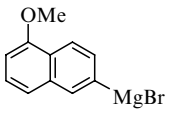	$NiCl_2$/(*S*,*S*)-chiraphos	δ	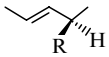	68 (*R*)	223
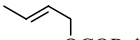	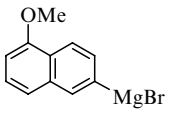	$NiCl_2$/(*S*,*S*)-chiraphos	δ		89 (*R*)	223
	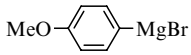	$NiCl_2$/(*S*,*S*)-chiraphos	δ		68 (*R*)	223
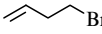	PhMgBr	$NiCl_2$/(*R*,*R*)-diop	chair-δ		6 (*R*)	224
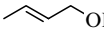	PhMgBr	$NiBr_2$[(*R*,*R*)-dpcp]	λ		41 (*S*)	225
	PhMgBr	$NiBr_2$[(*R*,*R*)-dpcp]	λ		53 (*S*)	225
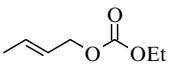	PhMgBr	$NiBr_2$[(*R*,*R*)-dpcp]	λ		52 (*S*)	225
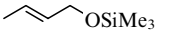	PhMgBr	$NiBr_2$[(*R*,*R*)-dpcp]	λ		67 (*S*)	225

Tables 11 and 12 each contain one entry where the λ-(*S*){(*R*)}, δ-(*R*){(*S*)} regularities are not fulfilled. These examples may be regarded as the exceptions that corroborate the rule.

More generally, if we consider the helical structure of a ligand around the central metal atom rather than the conformation of the chelate complex, this rule can be formulated as follows.[125] In homogeneous asymmetric catalytic hydrogenation, hydrosilylation and cross-coupling reactions C_2-symmetrical chiral complexes with ligands in the form of an incomplete turn of a helix around the central metal atom catalyse, from the same kind of substrates, the formation of products having strictly specific configurations characteristic of this particular helicity sign, the metal and the reaction. For example, (*R*)-amino acids are the products of hydrogenation of amino acid precursors on rhodium complexes in which the ligands form incomplete turns of *P*-helices around the rhodium atoms. If the ligands in such complexes form a part of *M*-helices around the rhodium atoms, (*S*)-amino acids are formed.

IV. Catalyst – product configurational relationships in reactions on asymmetric metal complexes

With respect to asymmetric catalytic reactions catalysed by chiral complexes devoid of any symmetry elements (with the exception of C_1), the regular catalyst – product configurational relationships have been gained exclusively in the cross-coupling reactions catalysed by nickel ($NiCl_2$/L*) and palladium ($PdCl_2$/L*) complexes with ferrocene-based (amino)diphenylphosphine ligands (L). The structural formulae of such complexes are given below.

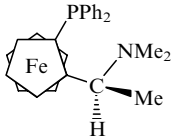
(*S*)-(*R*)-ppfa (**17**)

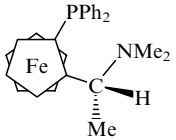
(*R*)-(*R*)-ppfa (**18**)

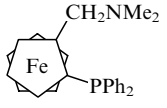
(*S*)-fcpn (**19**)

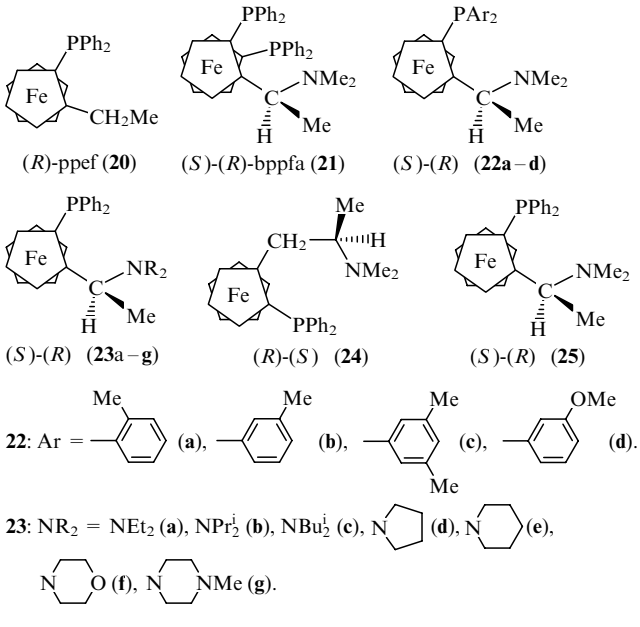

Examination of the cross-coupling reaction (1) (Table 14) demonstrates that the configurations of the products obtained on nickel and palladium complexes containing the same ligand are identical. Moreover, even the value of enantioselectivity virtually does not change. The introduction of *ortho*-substituted aryl radicals at the phosphorus atoms into the ligands decreases the enantioselectivity in comparison with complexes with non-substituted (phenyl) or *meta*-substituted radicals. The absence of amino groups in the ligands, the introduction of bulkier (in comparison with methyl) substituents at the nitrogen atoms and removal of the amino functional groups at a distance of one CH_2 group from the ferrocenyl ring decrease drastically the optical yields of the target products. Therefore, any disturbances in the optimum structures of ligands in catalytic complexes have negative effects on the enantioselectivity of the reaction.

Table 14. Asymmetric cross-coupling of 1-PhEtMgCl with vinyl bromide on chiral nickel and palladium complexes.[226–228]

Ligand	Yield (%)	*ee* (%)	Ligand	Yield (%)	*ee* (%)
(*S*)-(*R*)-ppfa	>95	61 (*R*)	**22c**	90	65 (*R*)
(*R*)-(*S*)–ppfa	>95	68 (*S*)	**22d**	>95	57 (*R*)
17	62	52 (*R*)	**23a**	65	35 (*R*)
17 (Pd)	82	61 (*R*)	**23b**	49	7 (*S*)
18	>95	54 (*R*)	**23c**	50	15 (*S*)
19	>95	65 (*S*)	**23d**	>95	62 (*R*)
20	86	5 (*S*)	**23e**	43	42 (*S*)
21	73	65 (*R*)	**23f**	68	17 (*R*)
21 (Pd)	93	61 (*R*)	**23g**	>95	65 (*R*)
22a	79	33 (*R*)	**24**	88	15 (*S*)
22b	>95	65 (*R*)	**25**	95	57 (*R*)

Reaction (4), which proceeds in the presence of (amino)-diphenylphosphine nickel and palladium complexes, is a somewhat more complicated version of reaction (1). The corresponding experimental data ‡ are presented in Table 15. The coincidence of configurations and optical yields of reaction

‡ The catalyst – product configurational relationships have not been analysed in Refs 219, 220, 227–231.

Table 15. Cross-coupling reactions catalysed by nickel and palladium complexes with ferrocene-based ligands ($0 < T < 25$ °C).

Entry	Ligand	Grignard reagent	Alkenyl (alkynyl) halide	Configuration of the product	Optical yield (%)	Ref.
Nickel complexes						
1	(*S*)-(*R*)- ppfa	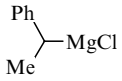	$CH_2=CHBr$	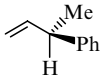	66 (*R*) (see [a])	228
2	(*R*)-(*S*)-ppfa	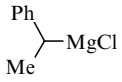	$CH_2=CHBr$	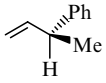	68 (*S*) (see [a])	228
3	(*S*)-(*R*)-ppfa	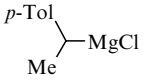	$CH_2=CHBr$	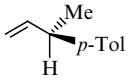	66 (*R*)	219, 220
4	(*S*)-(*R*)-ppfa	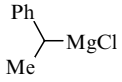	$CH_2=CHBr$	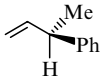	61 (*R*)	227
Palladium complexes						
5	(*S*)-(*R*)-ppfa	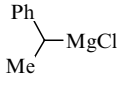	$CH_2=CHBr$	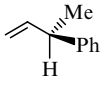	61 (*R*)	227
6	(*S*)-(*R*)-bppfa	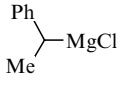	$CH_2=CHBr$	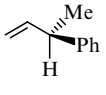	61 (*R*)	227
7	(*R*)-(*S*)-ppfa	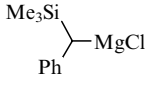	$CH_2=CHBr$	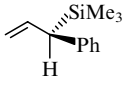	56 (*R*) (see [b])	219, 220, 229
8	(*R*)-(*S*)-bppfa	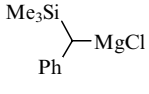	$CH_2=CHBr$	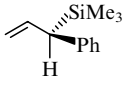	21 (*R*) (see [b])	219, 220, 229

Table 15 (continued).

Entry	Ligand	Grignard reagent	Alkenyl (alkynyl) halide	Configuration of the product	Optical yield (%)	Ref.
9	(*R*)-(*S*)-ppfa	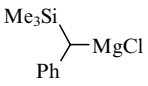	$CH_2=CHBr$	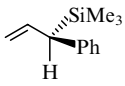	95 (*R*)	219, 220, 229
10	(*R*)-(*S*)-ppfa	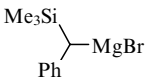	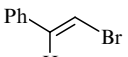	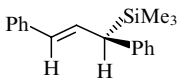	95 (*R*)	219, 220, 229
11	(*R*)-(*S*)-ppfa	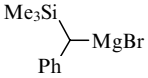	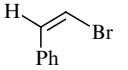	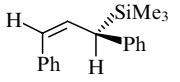	13 (*R*)	219, 220, 229
12	(*R*)-(*S*)-ppfa	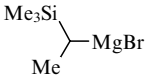	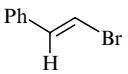	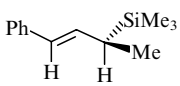	71 (*S*)	219, 220, 229
13	(*R*)-(*S*)-ppfa	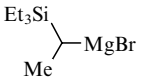	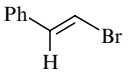	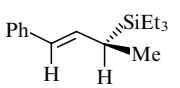	93 (*S*)	219, 220, 229
14	(*R*)-(*S*)-ppfa	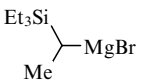	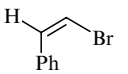	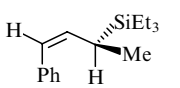	14 (*S*)	219, 220, 229
15	(*R*)-(*S*)-ppfa	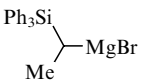	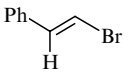	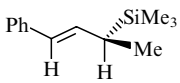	36 (*S*)	219, 220, 229
16	(*R*)-(*S*)-ppfa	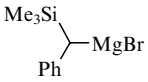	$Ph-C\equiv C-Br$	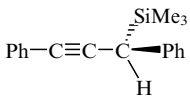	18 (*S*)	230
17	(*R*)-(*S*)-ppfa	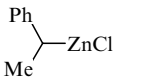	$CH_2=CHBr$	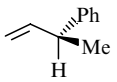	85 (*S*)	231

[a] At −20 °C. [b] At 50 °C.

products in the presence of catalytic complexes $NiCl_2$/(*S*)-(*R*)-ppfa and $PdCl_2$/(*S*)-(*R*)-ppfa (entries 4 and 5), $PdCl_2$/(*S*)-(*R*)-ppfa and $PdCl_2$/(*S*)-(*R*)-bppfa (entries 5 and 6) as well as $NiCl_2$/(*S*)-(*R*)-ppfa (entries 1 and 3), prompt a conclusion about the same type of their structures. Thus the bppfa ligand is coordinated through a metal atom (Ni, Pd) to the PPh_2 and NMe_2 groups belonging to the same five-membered ring of ferrocene (the second PPh_2 group in bppfa is hardly involved in coordination). The palladium catalyst $PdCl_2$/(*R*)-(*S*)-ppfa can be used for the synthesis of optically active allylsilanes (entries 7–15), being much more enantioselective than the $PdCl_2$/(*R*)-(*S*)-bppfa complex (entry 8). In the presence of $PdCl_2$/(*R*)-(*S*)-ppfa, the (*E*)-isomers of alkenyl bromides generate products of higher optical purity than the (*Z*)-isomers (entries 10, 11, 13 and 14). Substitution of the phenyl group for the methyl group in the Grignard reagent $Me_3Si(PhCH)MgBr$ (entries 7–11 and 12–15) has no effect on the configuration of the product, since substitution of the (*S*) symbol for the (*R*) symbol reflects the changes in the order of priority of the substituents only.

The actual configurations of products do not change in reactions involving vinyl bromide and phenylethynyl bromide (entries 7 and 16). The substitution of zinc for magnesium in the Grignard reagent does not affect the product configuration either (entries 2 and 17).

The analysis of configurational relationships between the catalytic complex and the product (Table 16) shows that the Ni- and Pd-complexes with ferrocenyl(amino)diphenylphosphine ligands belonging to the (*S*)-(*R*) and (*R*)-(*S*) configurational series catalyse the formation of enantiomeric products or products with different actual configurations in reactions (3) and (4).

Table 16. Catalyst–product configurational relationships in cross-coupling reactions catalysed by ferrocenyl nickel and palladium complexes.[219, 220, 224, 227–231]

Configuration of the ligand	Configuration of the product [a]	Configuration of the ligand	Configuration of the product
Reaction (3b)		Reaction (4)	
(*S*)-(*R*)	(*S*)	(*S*)-(*R*)	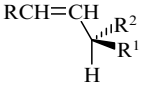
(*R*)-(*S*)	(*R*)	(*R*)-(*S*)	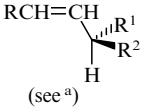 (see [a])

[a] One of the experiments yielded 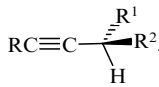 .

Table 17. Enantioselectivity of the cross-coupling reaction catalysed by nickel complexes with aminophosphine ligands prepared from amino acids.

Ligand	R	*ee* (%)
(*S*)-alaphos	Me	38 (*S*)
(*S*)-leuphos	Bu^i	57 (*S*)
(*S*)-phephos	Bn	71 (*S*)
(*R*)-phglyphos	Ph	70 (*R*)
(*S*)-valphos	Pr^i	81 (*S*)
(*S*)-ilephos	Bu^i	81 (*S*)
(*R*)-chglyphos	cyclo-Hex	77 (*R*)
(*R*)-*t*-leuphos	Bu^t	83 (*R*)
		94 (*R*) [a]

[a] The optical yield is adjusted for the optical purity of the ligand.

Reaction (5) has been studied relatively little. In this reaction, asymmetric catalytic effects are produced by complexes (*R*)-(*S*)-$C_5H_5FeC_5H_3(CHMeNMe_2)$·(SR)$PdCl_2$, where R = Me, Pr^i, Ph, *p*-Tol, 4-ClC_6H_4. The optical purity of the product does not depend on the nature of the radical R (*S*-configuration, *ee* = 26%, 22%, 18%, 25% and 16%, respectively).[232]

Interesting relationships were found between the configurations of the metal complexes and the products as well as between the enantioselectivities and the structures of complexes for cross-coupling under the action of chiral nickel complexes with aminophosphine ligands based on amino acids (Table 17).[233, 234]

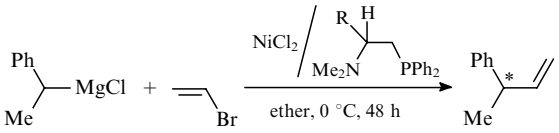

In this reaction, the configurations of the products depend on the configuration of the ligand. Special mention should be made of the stable tendency of enantioselectivity to increase with an increase in the molecular size of the radical R in the ligand.

Reaction (2) of a vinyl halide with a non-racemisable Grignard reagent proceeds with low enantioselectivity [218–221, 234] and does not present special interest from the standpoint of configurational relationships.

V. The structure of the intermediate complex

Knowing the configurations of the catalytic complexes and the products in cross-coupling reactions of Grignard reagents with allylic derivatives, one can conjecture upon the structure of the intermediate complex.[125]

Cross-coupling of Grignard reagents with allyl phenyl ethers gives rise to an intermediate compound.[221]

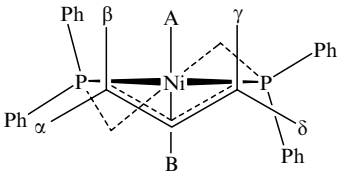

Figure 1. The intermediate compound in the cross-coupling reaction (see Scheme 4), a view from the side of the coordinated allylic group.

Scheme 4

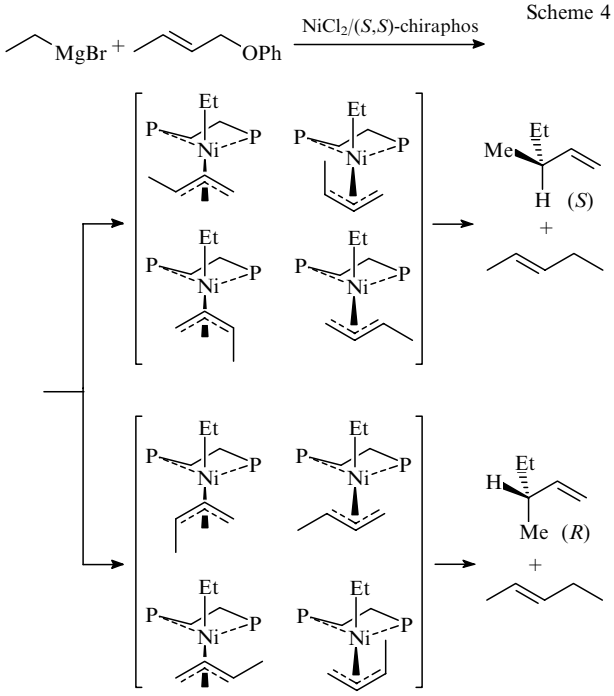

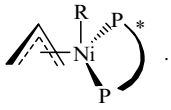

Thus the formation of eight intermediates may be expected resulting in two enantiomers of the product (Scheme 4).

Figure 1 shows a structural scheme for the intermediate compound with a fixed position of the allylic fragment (a view from the side of the coordinated η^3-allylic group). The four positions of the methyl substituent in the allyl group are marked by the letters α, β, γ and δ, whereas the two positions of the apical radical at the nickel atom are designated by the letters A and B (in total, eight possible intermediates).

All these variants as applied to different reactions of the same kind and analysed in terms of their stereochemical properties have been compared with the known experimental data. The α-position of the Me group is unfavourable at any position of the apical substituent at the nickel atom (A and B), because of the unfavourable ('eclipsed') position of this radical relative to the phosphine equatorial phenyl group. Position β is also unfavourable due to the spatial proximity of the Me group to the phosphine axial phenyl group; if a radical of the Grignard reagent occupies position A, this is proximal to the Me group, too. Position γ is unfavourable only in the case where the apical substituent at the nickel atom occupies position A. And, finally, position δ is favourable at any position (A or B) of the apical radical. Thus only three out of eight intermediates are theoretically more or less preferred. An attack of the radical R(Et) from A or B at the nickel atom on the prochiral allylic carbon atom results in the formation of products with (*S*)-, or (*R*)- and (*S*)-configurations, respectively. In general, a small preference (2/3) goes to the (*S*)-configuration, which is consistent with the experimental data.[221] This simple analysis demonstrates a good coincidence with experimental results, which, in turn, corroborates the correctness of the statement about the structure of the intermediate complex (*cf.* Table 18).

Table 18. Relationships between the experimentally determined product configurations of cross-coupling reaction of alkyl (aryl) Grignard reagents with allylic compounds and those predicted from stereochemical models.

Experimental results							Preferential intermediates and configurations of reaction products predicted using the model shown in Fig. 1							
Alkene	Grignard reagent	Catalytic system	Conformation of the complex	Product	*ee* (%)	Ref.	A	B	α	β	γ	δ	C	PC
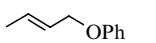	EtMgBr	$NiCl_2$/(*S*,*S*)-chiraphos	δ		22 (*S*)	221	Et	–	H	H	H	Me	*S*	*S*
							–	Et	H	H	Me	H	*R*	
							–	Et	H	H	H	Me	*S*	
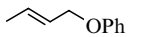	PhMgBr	$NiCl_2$/(*S*,*S*)-chiraphos	δ		58 (*R*)	221	Ph	–	H	H	H	Me	*R*	*R*
							–	Ph	H	H	Me	H	*S*	
							–	Ph	H	H	H	Me	*R*	
	EtMgBr	$NiCl_2$/(*S*,*S*)-chiraphos	δ		17 (*S*)	221	Et	–	H	H	H	Me	*S*	*S*
							–	Et	H	H	Me	H	*R*	
							–	Et	H	H	H	Me	*S*	
	PhMgBr	$NiCl_2$/(*S*,*S*)-chiraphos	δ		58 (*R*)	221	Ph	–	H	H	H	Me	*R*	*R*
							–	Ph	H	H	Me	H	*S*	
							–	Ph	H	H	H	Me	*R*	
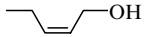	MeMgBr	$NiCl_2$/(*R*,*R*)-diop	chair-δ	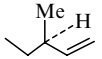	15 (*R*)	222	Me	–	H	H	H	Et	*R*	*R*
							–	Me	H	H	Et	H	*S*	
							–	Me	H	H	H	Et	*R*	
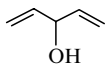	MeMgBr	$NiCl_2$/(*R*,*R*)-diop	chair-δ	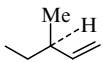	8.5(*R*)	223	Me	–	H	H	H	Et	*R*	*R*
							–	Me	H	H	Et	H	*S*	
							–	Me	H	H	H	Et	*R*	
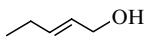	MeMgBr	$NiCl_2$/(*R*,*R*)-diop	chair-δ	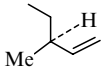	1 (*S*)	223	Me	–	H	H	H	Et	*R*	*R*
							–	Me	H	H	Et	H	*S*	
							–	Me	H	H	H	Et	*R*	
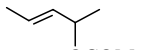	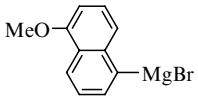	$NiCl_2$/(*S*,*S*)-chiraphos	δ		68 (*R*)	223	Ar	–	Me	H	H	Me	*R*[a]	*R*
							–	Ar	Me	H	H	Me	*R*[a]	
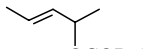	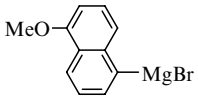	$NiCl_2$/(*S*,*S*)-chiraphos	δ	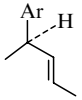	67 (*R*)	223	Ar	–	Me	H	H	Me	*R*[a]	*R*
							–	Ar	Me	H	H	Me	*R*[a]	
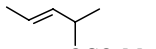	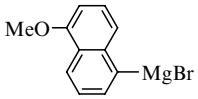	$NiCl_2$/(*S*,*S*)-chiraphos	δ		41 (*R*)	223	Ar	–	Me	H	H	Me	*R*[a]	*R*
							–	Ar	Me	H	H	Me	*R*[a]	

Table 18 (continued).

Experimental results							Preferential intermediates and configurations of reaction products predicted using the model shown in Fig. 1							
Alkene	Grignard reagent	Catalytic system	Conformation of the complex	Product	*ee* (%)	Ref.	A	B	α	β	γ	δ	C	PC
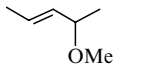	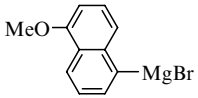	$NiCl_2$/(*S*,*S*)-chiraphos	δ	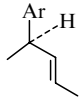	58 (*R*)	223	Ar	–	Me	H	H	Me	*R* [a]	*R*
							–	Ar	Me	H	H	Me	*R* [a]	
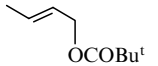	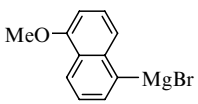	$NiCl_2$/(*S*,*S*)-chiraphos	δ		89 (*R*)	223	Ar	–	H	H	H	Me	*R*	*R*
							–	Ar	H	H	Me	H	*S*	
							–	Ar	H	H	H	Me	*R*	
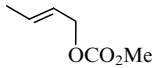	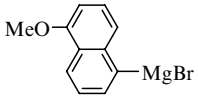	$NiCl_2$/(*S*,*S*)-chiraphos	δ		64 (*R*)	223	Ar	–	H	H	H	Me	*R*	*R*
							–	Ar	H	H	Me	H	*S*	
							–	Ar	H	H	H	Me	*R*	
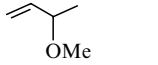	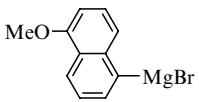	$NiCl_2$/(*S*,*S*)-chiraphos	δ		67 (*R*)	223	Ar	–	H	H	H	Me	*R*	*R*
							–	Ar	H	H	Me	H	*S*	
							–	Ar	H	H	H	Me	*R*	
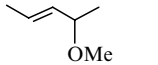	PhMgBr	$NiCl_2$/(*S*,*S*)-chiraphos	δ		47 (*R*)	223	Ph	–	Me	H	H	Me	*R* [a]	*R*
							–	Ph	Me	H	H	Me	*R* [a]	
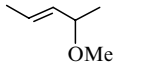	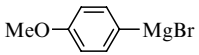	$NiCl_2$/(*S*,*S*)-chiraphos	δ		30 (*R*)	223	Ar	–	Me	H	H	Me	*R* [a]	*R*
							–	Ar	Me	H	H	Me	*R* [a]	
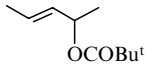	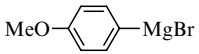	$NiCl_2$/(*S*,*S*)-chiraphos	δ	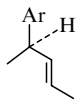	68 (*R*)	223	Ar	–	Me	H	H	Me	*R* [a]	*R*
							–	Ar	Me	H	H	Me	*R* [a]	
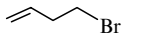	PhMgBr	$NiCl_2$/(*R*,*R*)-diop	chair-δ		6 (*R*)	224	Ph	–	H	H	H	Me	*R*	*R*
							–	Ph	H	H	Me	H	*S*	
							–	Ph	H	H	H	Me	*R*	

Note. Designations: C is configuration of the product formed from the intermediate (Fig. 1); PC is predicted preferential configuration of the product.

[a] The introduction of Ar into the allylic positions (α,β) is less favourable, being sterically more hindered than that into positions (γ,δ) [eclipsed conformation of the C(α,β) – Ar and the P – Ph bonds of the ligand].

VI. Conclusion

The analysis of experimental data presented in this review suggests that the highest enantiomeric excess of the target product can be reached if an optimum correlation is established between the number of coordination vacancies on the metal complex catalyst accessible to the substrate and the number of coordination-active functional groups of the substrate.

Presumably, the nature of asymmetric catalysis is such that high enantioselectivity is ensured with the minimum degree of freedom of the substrate where the latter is coordinated to the catalyst through all of its functional groups. For example, high enantioselectivity in asymmetric hydrogenation of acetamidocinnamic acid, which contains coordination-active groups in addition to the double bond, is attained with rhodium catalytic complexes with bidentate ligands. In hydrogenation of simple ketones, which are coordinated exclusively through one carbonyl group, this is insufficient and catalytic systems with tridentate ligands should be used which produce a chiral catalytic complex devoid of any symmetry elements other than C_1, where one of the vacancies is additionally blocked by an achiral monodentate ligand (*e.g.*, Et_3N, CF_3CO_2H, $PriCO_2H$, *etc.*). But even in such complicated catalytic systems, the most enantioselective hydrogenation is observed for ketones possessing additional coordination-active groups in the α- or, which is better, the β-position relative to the carbonyl.

The ratios of coordinating and coordination-active vacancies of the catalyst and the substrate should be an optimum. For example, substrates of the tiglic acid type, which contain only one coordination-active group (in addition to C=C), are hydrogenated with much higher enantioselectivity on $Ru(OAc)_2$[binap] complexes than on Rh complexes containing the binap ligand. Contrariwise, the hydrogenation of α-acetamidocinnamic acid occurs with higher enantioselectively in the presence of rhodium complexes. If the hydrogenation is carried out on octahedral ruthenium complexes with the binap ligand, substrates with two coordination-active groups seem to be less optimal as regards enantioselectivity than those with only one coordination-active group.

A similar situation is observed in hydrosilylation reactions where rhodium complexes with tri- and tetradentate ligands manifest the maximum enantioselectivity in hydrosilylation of simple ketones.

Simple graphical dependences between the structures of catalytic complexes and the configurations of the reaction products can be useful for predicting the configurations of reaction products at the design stage of asymmetric catalytic synthesis. The relationships between the configurations of reaction products and the signs of the helical components of the complexes seem to suggest the similarity of asymmetric induction mechanisms of all reactions which obey these regularities.

The analysis of putative structures of intermediate complexes based on stereochemical concepts further corroborates the similarity of asymmetric induction mechanisms of certain reactions. This approach, which enables one to predict the configuration of the product, differs from the graphical plots mentioned above. In this case, we deal with the actual structures of the intermediates.

The analysis of stereochemical relationships between chiral metal complex catalysts, substrates and products in asymmetric homogeneous catalytic hydrogenation, hydrosilylation and cross-coupling reactions illustrates the important role of steric factors in asymmetric catalysis. Additional evidence for the extreme importance of asymmetric catalysis can be derived from the fact that the three leading specialists in asymmetric homogeneous catalysis, *viz.*, W S Knowles, K B Sharpless and R Noyori, were awarded the Nobel Prize for Chemistry in 2001.

References

1. E N Jacobsen, A Pfaltz, H Yamamoto (Eds) *Comprehensive Asymmetric Catalysis* Vols 1–3 (Berlin: Springer, 1999)
2. R Noyori *Asymmetric Catalysis in Organic Synthesis* (New York: Wiley, 1994)
3. H Brunner, W Zettlmeier *Handbook of Enantioselective Catalysis with Transition Metal Complexes* Vols 1, 2 (Weinheim: VCH, 1993)
4. I Ojima (Ed.) *Catalytic Asymmetric Synthesis* (New York: VCH, 1993)
5. L Haughton, J M J Williams *J. Chem. Soc., Perkin Trans. 1* 3335 (2000)
6. K Muniz, C Bolm *Chem. Eur. J.* **6** 2309 (2000)
7. M J Palmer, M Wills *Tetrahedron Asymmetry* **10** 2045 (1999)
8. T Naota, H Takaya, S I Murahashi *Chem. Rev.* **98** 2599 (1998)
9. U Nagel, A Judith *Top. Catal.* **5** 3 (1988)
10. O Piccolo *Chim. Ind. (Milan)* **80** 1177 (1998)
11. D J Ager, S A Laneman *Tetrahedron Asymmetry* **8** 3327 (1997)
12. M Wills, in *The Chemistry of Double-Bonded Functional Groups* (Ed. S Patai) (New York: Wiley, 1997) p. 781
13. R Noyori, S Hashiguchi *Acc. Chem. Res.* **30** 97 (1997)
14. R Noyori *Acta Chem. Scand.* **50** 380 (1996)
15. F Agbossou, J-F Carpenter, A Mortreux *Chem. Rev.* **95** 2485 (1995)
16. M J Burk, F Bienewald, in *Transition Metals for Organic Synthesis; Building Blocks and Fine Chemicals* Vol. 2 (Eds M Beller, C Bolm) (Basel: Wiley-VCH, 1994) p. 13
17. V V Dunina, I P Beletskaya *Zh. Org. Khim.* **28** 1929 (1992) [a]
18. V V Dunina, I P Beletskaya *Zh. Org. Khim.* **28** 2368 (1992) [a]
19. V V Dunina, I P Beletskaya *Zh. Org. Khim.* **29** 806 (1993) [a]
20. S T Handy *Curr. Org. Chem.* **4** 363 (2000)
21. M J Burk *Acc. Chem. Res.* **33** 363 (2000)
22. T Hayashi *Acc. Chem. Res.* **33** 354 (2000)
23. F Fache, E Schulz, L Tommasino, M Lemaire *Chem. Rev.* **100** 2159 (2000)
24. G Helmchen, A Pfaltz *Acc. Chem. Res.* **33** 336 (2000)
25. B L Feringa *Acc. Chem. Res.* **33** 346 (2000)
26. D G I Petra, C J Paul, A L Spek, H E Schoemaker, P W N M Van Leeuwen *J. Org. Chem.* **65** 3010 (2000)
27. D A Alonso, S J M Nordin, P Roth, T Tarnai, P G Andersson, M Thommen, U Pittelkow *J. Org. Chem.* **65** 3116 (2000)
28. M T Reetz, A Gosberg *Tetrahedron Asymmetry* **10** 2129 (1999)
29. X Li, R Lou, C-H Yeung, A S C Chan, W K Wong *Tetrahedron Asymmetry* **11** 2077 (2000)
30. N Derrien, C B Dousson, S M Roberts, M J Burk, M Ohff *Tetrahedron Asymmetry*. **10** 3341 (1999)
31. M McCarthy, R Goddard, P J Guiry *Tetrahedron Asymmetry* **10** 2797 (1999)
32. G Bringmann, A Wuzik, M Breuning, P Henschel, K Peters, E-M Peters *Tetrahedron Asymmetry* **10** 3025 (1999)
33. M D Fryzuk, B Bosnich *J. Am. Chem. Soc.* **99** 6262 (1977)
34. V Enev, Ch L J Ewers, M Haare, K Nickisch, J T Mohr *J. Org. Chem.* **62** 7092 (1997)
35. M T Reetz, E W Beuttenmuller, R Goddard *Tetrahedron Lett.* **38** 3211 (1997)
36. U Nagel *Angew. Chem.* **96** 425 (1984)
37. T Ohta, H Takaya, M Kitamura, K Nagai, R Noyori *J. Org. Chem.* **52** 3174 (1987)
38. T Ohta, T Miyake, H Takaya *J. Chem. Soc., Chem. Commun.* 1725 (1992)
39. P Le Gendre, T Braun, C Brauneau, P H Dixneuf *J. Org. Chem.* **61** 8453 (1996)
40. T Xiao, S C A Nefkens, P G Jessop, T Ikariya, R Noyori *Tetrahedron Lett.* **37** 2813 (1996)
41. R Noyori, M Ohta, Yi Hsiao, M Kitamura, T Ohta, H Takaya *J. Am. Chem. Soc.* **108** 7117 (1986)
42. M Kitamura, T Ohkuma, S Inoue, N Sayo, H Kumobayashi, S Akutagawa, T Ohta, H Takaya, R Noyori *J. Am. Chem. Soc.* **110** 629 (1988)
43. H-P Buser, F Spindler *Tetrahedron Asymmetry* **4** 2451 (1993)
44. H Kawano, Y Ishii, M Saburi, S Uchida *J. Chem. Soc., Chem. Commun.* 87 (1988)
45. R Noyori, T Ohkuma, M Kitamura, H Takaya, N Sayo, H Kumobayashi, S Akutagawa *J. Am. Chem. Soc.* **109** 5856 (1987)

46. M Kitamura, M Tokunaga, R Noyori *J. Am. Chem. Soc.* **117** 2931 (1995)
47. A B Charette, A Giroux *Tetrahedron Lett.* **37** 6669 (1996)
48. M Kitamura, T Ohkuma, H Takaya, R Noyori *Tetrahedron Lett.* **29** 1555 (1988)
49. A Mezzetti, G Consiglio *J. Chem. Soc., Chem. Commun.* 1675 (1991)
50. M J Burk, T G P Harper, C S Kalbern *J. Am. Chem. Soc.* **117** 4423 (1995)
51. R J P Curriu, J J E Moreau *J. Organomet. Chem.* **85** 19 (1975)
52. W Dumont, J C Poulin, T P Dang, H B Kagan *J. Am. Chem. Soc.* **95** 8295 (1973)
53. N C Payne, D W Stephan *Inorg. Chem.* **21** 182 (1982)
54. I Ojima, K Hirai, in *Asymmetric Synthesis* Vol. 5 (Ed. J D Morrison) (New York: Academic Press, 1985) p. 103
55. Y Nishibayashi, I Takei *Organometallics* **17** 3420 (1998)
56. M B Carter, B Schiott, A Gutierrez, S L Buchwald *J. Am. Chem. Soc.* **116** 11 667 (1994)
57. G Zhu, M Terry, X Zhang *J. Organomet. Chem.* **547** 97 (1997)
58. H Brunner, R Becker, G Riepl *Organometallics* **3** 1354 (1984)
59. T Hayashi, M Kumada, in *Asymmetric Synthesis* Vol. 5 (Ed. J D Morrison) (New York: Academic Press, 1985) p. 147
60. P W Jolly, in *Comprehensive Organometallic Chemistry* Vol. 8 (Eds G Wilkinson, F G A Stone, E W Abel) (Oxford: Pergamon Press, 1982) p. 713
61. G C Lloyd-Jones, C P Butts *Tetrahedron* **54** 901 (1998)
62. U Nagel, H G Nedden *Inorg. Chim. Acta* **34** 269 (1998)
63. U Nagel, H G Nedden *Chem. Ber.* **130** 535 (1997)
64. B D Vineyard, W S Knowles, M J Sabacky, G L Bachman, D J Weinkauff *J. Am. Chem. Soc.* **99** 5946 (1977)
65. H B Kagan, T P Dang *J. Am. Chem. Soc.* **94** 6429 (1972)
66. H B Kagan *Pure Appl. Chem.* **34** 401 (1975)
67. H Hayashi, M Tanaka, I Ogata *Tetrahedron Lett.* 295 (1977)
68. K E Koenig, G L Bachman, B D Vineyard *J. Org. Chem.* **45** 2362 (1980)
69. K Achiwa *J. Am. Chem. Soc.* **98** 8265 (1976)
70. T Kariya, Y Ishii, H Kawano, T Arai, M Saburi, S Yoshikawa, S Akutagawa *J. Chem. Soc., Chem. Commun.* 922 (1985)
71. H Kawano, Y Ishii, T Ikariya, M Saburi, S Yoshikawa, Y Uchida, H Kumobayashi *Tetrahedron Lett.* **28** 1905 (1987)
72. T Manimaran, T-C Wu, W D Klobucar, C H Kolich, G P Stahly, F R Fronczek, S E Watkins *Organometallics* **12** 1467 (1993)
73. X Zhang, T Uemura, K Matsumura, N Sayo, H Kumobayashi, H Takaya *Synlett* 501 (1994)
74. R Noyori *Tetrahedron* **50** 4259 (1994)
75. J S Solodar *Chem. Technol.* 421 (1975)
76. S Toros, B Heil, L Kollar, L Marko *J. Organomet. Chem.* **197** 85 (1980)
77. S Toros, L Kollar, B Heil, L Marko *J. Organomet. Chem.* **232** C17 (1982)
78. A Levi, G Modena, G Scorano *J. Chem. Soc., Chem. Commun.* 6 (1975)
79. B Heil, S Toros, S Vastag *J. Organomet. Chem.* **94** C47 (1975)
80. S Toros, B Heil, L Marko *J. Organomet. Chem.* **159** 401 (1978)
81. C Botteghi, M Bianchi, E Benedetti, U Matteoli *Chimia* **29** 256 (1975)
82. U Matteoli, P Frediami, M Bianchi *J. Mol. Catal.* **12** 256 (1981)
83. V A Pavlov, E V Starodubtseva, M G Vinogradov, E A Mistryukov, V A Ferapontov, G V Dorochin, in *The Second Conference 'Modern Trends in Chemical Kinetics and Catalysis' (Abstracts of Reports), Novosibirsk, 1995* Part 2, p. 331
84. V A Pavlov, E V Starodubtseva, M G Vinogradov, V A Ferapontov, O R Malyshev, G L Kheis *Izv. Akad. Nauk, Ser. Khim.* 725 (2000) [b]
85. V A Pavlov, M G Vinogradov, E V Starodubtseva, G V Chel'tsova, V A Ferapontov, O R Malyshev, G L Kheis *Izv. Akad. Nauk, Ser. Khim.* 704 (2001) [b]
86. H Takahashi, M Hattori, M Chiba, T Morimoto, K Achiwa *Tetrahedron Lett.* **27** 4477 (1986)
87. H Takeda, T Tachinami, M Aburatani, H Takahashi, T Morimoto, K Achiwa *Tetrahedron Lett.* **30** 363 (1989)
88. A Rucoux, M Devocelle, J-F Carpenter, F Agbossou, A Mortreux *Synlett* 358 (1995)
89. T Hayashi, A Katsumura, M Konishi, M Kumada *Tetrahedron Lett.* 425 (1979)
90. A Rucoux, I Suisse, M Devocelle, J-F Carpenter, F Agbossou, A Mortreux *Tetrahedron Asymmetry* **7** 379 (1996)
91. J P Genet, C Pinel, V Ratovelomanana-Vidal, M C Cano de Andrade, X Pfister, P Guerreiro, J Y Lenoir *Tetrahedron Lett.* **36** 4801 (1995)
92. I Gautier, V Ratovelomanana-Vidal, P Savignac, J P Genet *Tetrahedron Lett.* **37** 7721 (1996)
93. J P Tranchier, V Ratovelomanana-Vidal, J P Genet, S Tong, T Cohen *Tetrahedron Lett.* **38** 2951 (1997)
94. M Kitamura, M Tokunaga, T Ohkuma, R Noyori *Tetrahedron Lett.* **32** 4163 (1991)
95. D F Taber, L J Silverberg *Tetrahedron Lett.* **32** 4227 (1991)
96. J B Hoke, L S Hollis, E W Stern *J. Organomet. Chem.* **455** 193 (1993)
97. T Ohta, T Miyake, N Seido, H Kumobayashi, H Takaya *J. Org. Chem.* **60** 357 (1995)
98. J P Genet, M C Cano de Andrade, V Ratovelomanana-Vidal *Tetrahedron Lett.* **36** 2063 (1995)
99. B Heiser, E A Broger, Y Crameri *Tetrahedron Asymmetry* **2** 51 (1991)
100. D Blanc, J C Henry, V Ratovelomanana-Vidal, J P Genet *Tetrahedron Lett.* **38** 6603 (1997)
101. F Hapiot, F Agbossou, A Mortreux *Tetrahedron Asymmetry* **6** 11 (1995)
102. K Mashima, K Kusano, N Sato, Y Matsumura, K Nozaki, H Kumobayashi, H Sayo, Y Hori, T Ishizaki, S Akutagawa, H Takaya *J. Org. Chem.* **59** 3064 (1994)
103. J F Carpenter, A Mortreux *Tetrahedron Asymmetry* **8** 1083 (1997)
104. S Hashiguchi, A Fujii, J Takehara, T Ikariya, R Noyori *J. Am. Chem. Soc.* **117** 7562 (1995)
105. K Puntener, L Schwink, R Knochel *Tetrahedron Lett.* **37** 8165 (1996)
106. F Touchard, P Gamez, F Fache, M Lemaire *Tetrahedron Lett.* **38** 2275 (1997)
107. J Takehara, S Hashiguchi, A Fujii, S Inoue, T Ikariya, R Noyori *Chem. Commun.* 233 (1996)
108. M Palmer, T Walsgrove, M Wills *J. Org. Chem.* **62** 5226 (1997)
109. T Langer, G Helmchen *Tetrahedron Lett.* **37** 1381 (1996)
110. T Sammakia, E L Stangeland *J. Org. Chem.* **62** 6104 (1997)
111. Y Jiang, Q Jiang, G Zhu, X Zhang *Tetrahedron Lett.* **38** 215 (1997)
112. J X Gao, T Ikariya, R Noyori *Organometallics* **15** 1087 (1996)
113. C Bianchini, E Farnetti, L Glendenning, M Graziani, G Nardini, M Peruzzini E Rocchini, F Zanobini *Organometallics* **14** 1489 (1995)
114. H Brunner, P Brandl *J. Organomet. Chem.* **390** C81 (1990)
115. I Imai, W Zhang, T Kida, Y Nakatsuji, I Ikeda *Tetrahedron Asymmetry* **7** 2453 (1996)
116. H Brunner, G Riepl, H Weitzer *Angew. Chem.* **95** 326 (1983)
117. H Nishiyama, M Kondo, T Nakamura, K Hoh *Organometallics* **10** 500 (1991)
118. H Nishiyama, S B Park, K Itoh *Tetrahedron Asymmetry* **3** 1029 (1992)
119. H Nishiyama, S Yamaguchi, S B Park, K Itoh *Tetrahedron Asymmetry* **4** 143 (1993)
120. M D Fryzuk, B Bosnich *J. Am. Chem. Soc.* **100** 5491 (1978)
121. B Bosnich, N K Roberts *Adv. Chem. Ser.* 196 337 (1982)
122. W S Knowles *Acc. Chem. Res.* **16** 106 (1983)
123. W Moffitt, R B Woodward, A Moscowitz, W Klyne, C Djerassi *J. Am. Chem. Soc.* **83** 4013 (1961)
124. M J Burk, J E Feaster, W A Nugent, R L Harlow *J. Am. Chem. Soc.* **115** 10 125 (1993)
125. V A Pavlov, Doctoral Thesis in Chemical Sciences, Institute of Organic Chemistry, Russian Academy of Sciences, Moscow, 2000
126. M Nogradi *Stereochemistry* (Budapest: Akademiai Kiado, 1981)
127. E J Corey, J C Bailar *J. Am. Chem. Soc.* **81** 2620 (1959)
128. C J Hawkins *Absolute Configuration of Metal Complexes* (New York: Wiley, 1971)
129. V A Pavlov, in *Koordinatsionnoe Soveshchanie po Asimmetricheskomu Katalizu (Tez. Dokl.), Borzhomi, 1982* [Coordination Meeting on Asymmetric Catalysis (Abstracts of Reports), Borzhomi, 1982] p. 31
130. V A Pavlov, E I Klabunovsky *Dokl. Akad. Nauk SSSR* **269** 856 (1983) [c]
131. V A Pavlov, E I Klabunovsky *Izv. Akad. Nauk SSSR, Ser. Khim.* 2015 (1983) [b]
132. H B Kagan, in *Comprehensive Organometallic Chemistry* Vol. 8 (Eds G Wilkinson, F G A Stone, E W Abel) (Oxford: Pergamon Press, 1982) p. 463
133. W S Knowles, M J Sabacky *J. Chem. Soc., Chem. Commun.* 1445 (1968)

134. L Horner, H Siegel, H Buthe *Angew. Chem., Int. Ed. Engl.* **7** 942 (1968)
135. M Fioroni, G M Giongo *J. Mol. Catal.* **5** 303 (1979)
136. K Kashiwabara, K Hanaki, J Fujita *Bull. Chem. Soc. Jpn.* **53** 2275 (1980)
137. K Onuma, T Ito, A Nakamura *Bull. Chem. Soc. Jpn.* **53** 2016 (1980)
138. V A Pavlov, A A Voloboev, L S Gorshkova, E I Klabunovsky, in *The 4th International Symposium on Homogeneous Catalysis (Abstracts of Reports), Leningrad, 1984* Book 1, p. 290
139. P Denis, A Mortreux, F Petit, G Biono, G Peiffer, in *The 4th International Symposium on Homogeneous Catalysis (Abstracts of Reports), Leningrad, 1984* Book 1, p. 221
140. V A Pavlov, A A Bagatur'yants, V B Kazanskii, E I Klabunovsky *Izv. Akad. Nauk SSSR, Ser. Khim.* 508 (1987) [b]
141. V A Pavlov, E I Klabunovsky, in *Vtoroe Respublikanskoe Soveshchanie po Asimmetricheskim Reaktsiyam (Tez. Dokl.), Telavi, 1989* [The Second Republican Meeting on Asymmetric Reactions (Abstracts of Reports), Telavi, 1989] p. 29
142. B D Vineyard, W S Knowles, M J Sabacky *J. Mol. Catal.* **19**159 (1983)
143. W S Knowles, M J Sabacky, B D Vineyard, D J Weinkauff *J. Am. Chem. Soc.* **97** 2567 (1975)
144. T Imamoto, H Tsuruta, Y Wada, H Masuda, K Yamaguchi *Tetrahedron Lett.* **45** 8271 (1995)
145. J Kottner, G Greber *Chem. Ber.* **113** 2323 (1980)
146. D L Allen, V C Gibson, M L H Green, J F Skinner, J Bashkin, P D Grebenik *J. Chem. Soc., Chem. Commun.* **16** 895 (1983)
147. J M Brown, B A Murrer *J. Chem. Soc., Perkin Trans 2* 489 (1982)
148. W Bergstein, A Kleemann, J Mertens *Synthesis* 76 (1981)
149. D Lafont, D Sinou, G Descotes *J. Chem. Res. (S)* **117** 1401 (1982)
150. J Padmakumari Amma, J K Stille *J. Org. Chem.* **47** 468 (1982)
151. T H Johnson, G Rangarajan *J. Org. Chem.* **45** 62 (1980)
152. R B King, J Bakos, C D Hoff, L Marko *J. Org. Chem.* **44** 1729 (1979)
153. H Brunner, W Pieronczyk, B Schohammer, K Sterng, I Bernal, J Korp *Chem. Ber.* **114** 1137 (1981)
154. E P Kyba, R E Davis, P N Juri, K S Sirley *Inorg. Chem.* **20** 3616 (1981)
155. M Lauer, O Samuel, H B Kagan *J. Organomet. Chem.* **177** 309 (1979)
156. O Samuel, R Couffignal, M Lauer, S Y Zhang, H B Kagan *Nouv. J. Chem.* **5** 15 (1981)
157. P A MacNeil, N K Roberts, B Bosnich *J. Am. Chem. Soc.* **103** 2273 (1981)
158. J M Brown, P A Chaloner *J. Am. Chem. Soc.* **100** 4307 (1978)
159. S Brunie, J Mazan, N Langlois, H B Kagan *J. Organomet. Chem.* **114** 225 (1976)
160. V Gramlich, C Salomon *J. Organomet. Chem.* **73** C61 (1974)
161. Y Kiso, K Tamao, N Miyake, K Yamamoto, M Kumada *Tetrahedron Lett.* 3 (1974)
162. G Gelbard, H B Kagan, R Stern *Tetrahedron* **32** 233 (1976)
163. D Sinou, H B Kagan *J. Organomet. Chem.* **114** 325 (1976)
164. T P Dang, J C Poulin, H B Kagan *J. Organomet. Chem.* **91** 105 (1975)
165. Y Amrani, D Sinou *J. Mol. Catal.* **24** 231 (1984)
166. S Y Zhang, S Yemul, H B Kagan, R Stern, D Commereue, Y Chauvin *Tetrahedron Lett.* **22** 3955 (1981)
167. R Glazer, M Twaik, S Geresh, J Blumenfeld *Tetrahedron Lett.* 4635 (1977)
168. P Aviron-Violet, Y Colleuille, J Varagarnat *J. Mol. Catal.* **5** 41 (1979)
169. B D Vineyard, W S Knowles, M J Sabacky *J. Mol. Catal.* **19** 159 (1983)
170. R Glazer, S Geresh, J Blumenfeld, M Twaik *Tetrahedron* **34** 2405 (1978)
171. H J Kreuzfeld, C Dobler *React. Kinet. Catal. Lett.* **24** 153 (1984)
172. K Onuma, T Ito, A Nakamura *Chem. Lett.* 905 (1979)
173. M Fiorini, G M Giongo *J. Mol. Catal.* **7** 411 (1980)
174. M Tanaka, J Ogata *J. Chem. Soc., Chem. Commun.* 735 (1975)
175. J Bourson, L Oliveros *J. Organomet. Chem.* **229** 77 (1982)
176. V A Pavlov, E I Klabunovsky, Yu T Struchkov, A A Voloboev, A I Yanovsky *J. Mol. Catal.* **44** 217 (1988)
177. A Miyashita, H Takaya, T Souchi, R Noyori *Tetrahedron* **40** 1245 (1984)
178. A Miyashita, A Yasuda, H Takaya, K Toriumi, T Ito, T Souchi, R Noyori *J. Am. Chem. Soc.* **102** 7932 (1980)
179. A Miyashita, H Takaya, R Noyori *ACS Symp Ser.* **185** 274 (1982)
180. G Zhu, P Cao, Q Jiang, X Zhang *J. Am. Chem. Soc.* **119** 1799 (1997)
181. R Selke, H Pracejus *J. Mol. Catal.* **37** 213 (1986)
182. R Sinou, G Descotes *React. Kinet. Catal. Lett.* **14** 463 (1980)
183. W R Cullen, Y Sugi *Tetrahedron Lett.* 1635 (1978)
184. Y Sugi, W R Cullen *Chem. Lett.* 39 (1979)
185. R Jackson, D J Thompson *J. Organomet. Chem.* **159** C29 (1978)
186. H B Kagan, J C Fiaud, C Hoornaert, D Meyer, J C Poulin *Bull. Soc. Chim. Belg.* **88** 923 (1979)
187. Y Ohgo, Y Natori, S Takenchi, J Yoshimura *Chem. Lett.* 709 (1974)
188. J M Brown, B A Murrer *Tetrahedron Lett.* **21** 581 (1980)
189. I Habus, Z Raza, V Sunjic *J. Mol. Catal.* **42** 173 (1987)
190. I D Gridnev, N Higashi, K Asakura, T Imamoto *J. Am. Chem. Soc.* **122** 7183 (2000)
191. Y Yamanoi, T Imamoto *J. Org. Chem.* **64** 2988 (1999)
192. T Imamoto, J Watanabe, Y Wada, H Masuda, H Yamada, H Tsuruta, S Matsukawa, K Yamaguchi *J. Am. Chem. Soc.* **120** 1635 (1998)
193. A Marinetti, S Jus, J-P Genet *Tetrahedron Lett.* **40** 8365 (1999)
194. L O Nindakova, B A Shainyan, A I Albanov, M V Ustinov *Zh. Org. Khim.* **36** 1660 (2000) [a]
195. M Chiba, H Takahashi, H Takahashi, T Morimoto, K Achiwa *Tetrahedron Lett.* **28** 3675 (1987)
196. R S Vagg *J. Proc. R. Soc. N. S. W.* **117** 99 (1985)
197. J Bakos, I Toth, B Heil *Tetrahedron Lett.* **25** 4965 (1984)
198. K Tamao, H Yamamoto, H Matsumoto, N Miyake, T Hayashi, M Kumada *Tetrahedron Lett.* 1389 (1977)
199. S Miyano, M Nawa, A Mori, H Hashimoto *Bull. Soc. Chim. Belg.* **57** 2171 (1984)
200. A Uehara, T Kubota, R Tsuchiya *Chem. Lett.* 441 (1983)
201. H Brunner, W Miehling *J. Organomet. Chem.* **275** C17 (1984)
202. G R Ball, N C Payne *Inorg. Chem.* **16** 1187 (1977)
203. J D Oliver, D P Riley *Organometallics* **2** 1032 (1983)
204. H Brunner, A Knott, R Benn, A Rufinska *J. Organomet. Chem.* **295** 211 (1985)
205. T Hayashi, K Yamamoto, K Kasuga, H Omizu, M Kumada *J. Organomet. Chem.* **113** 127 (1976)
206. J Benes, J Helflejs, in *The 6th International Congress on Catalysis, London, 1976* Paper B, p. 42
207. M Capka, J Hetflejs, R Selke *React. Kinet. Catal. Lett.* **10** 225 (1979)
208. J Benes, J Hetflejs *Collect. Czech. Chem. Commun.* **41** 2264 (1976)
209. G Consiglio, F Morandini, O Piccolo *Tetrahedron* **39** 2699 (1983)
210. W S Knowles, M J Sabacky, B D Vineyard *J. Chem. Soc., Chem. Commun.* 10 (1972)
211. G Consiglio, O Piccolo, L Roncetti, F Morandini *Tetrahedron* **42** 2043 (1986)
212. G Consiglio, O Piccolo, F Morandini *J. Organomet. Chem.* **177** C13 (1979)
213. US P. 4 005 127; *Chem. Abstr.* **86** 190 463 (1977)
214. W S Knowles, W C Christopfel, K E Koenig, C F Hobbs *Adv. Chem. Ser. 196* 325 (1982)
215. W S Knowles, M J Sabacky, B D Vineyard *Chem. Technol.* 590 (1972)
216. W S Knowles, M J Sabacky, B D Vineyard *Ann. N.Y. Acad. Sci.* **214** 119 (1973)
217. W S Knowles, M J Sabacky, B D Vineyard *Adv. Chem. Ser. 132* 274 (1974)
218. G Consiglio, C Botteghi *Helv. Chim. Acta* **56** 460 (1973)
219. K Tamao, T Hayashi, H Matsumoto H Yamamoto, M Kumada *Tetrahedron Lett.* **23** 2155 (1979)
220. T Hayashi, K Kanehira, T Hioki, M Kumada *Tetrahedron Lett.* **22** 137 (1981)
221. G Consiglio, F Morandini, O Piccolo *J. Chem. Soc., Chem. Commun.* 112 (1983)
222. M Cherest, H Felkin, J D Umpleby, S G Davies *J. Chem. Soc., Chem. Commun.* 681 (1981)
223. T Hiyama, N Wakasa *Tetrahedron Lett.* **26** 3259 (1985)
224. M Zembayashi, K Tamao, T Hayashi, T Mise, M Kumada *Tetrahedron Lett.* 1799 (1977)
225. V A Pavlov, E A Mistryukov, H Duddeck, M G Vinogradov, G Snatzke *J. Mol. Catal.* **79** 55 (1993)
226. T Hayashi, M Tajika, K Tamao, M Kumada *J. Am. Chem. Soc.* **98** 3718 (1976)
227. T Hayashi, M Konishi, M Fukushima, T Mise, M Kagotani, M Tajika, M Kumada *J. Am. Chem. Soc.* **104** 180 (1982)

228. T Hayashi, M Konishi, T Hioki, M Kumada, A Ratajczak, H Niedbala *Bull. Chem. Soc. Jpn.* **54** 3615 (1981)
229. T Hayashi, M Konishi, H Ito, M Kumada *J. Am. Chem. Soc.* **104** 4962 (1982)
230. T Hayashi, Y Okamoto, T Hioki, M Kumada *Tetrahedron. Lett.* **24** 807 (1983)
231. T Hayashi, T Hagihara, Y Katsuro, M Kumada *Bull. Chem. Soc. Jpn.* **56** 363 (1983)
232. M O Okoroafor, D L Ward, C H Brubaker Jr. *Organometallics* **7** 1504 (1988)
233. T Hayashi, M Fukushima, M Konishi, M Kumada *Tetrahedron Lett.* **21** 79 (1980)
234. T Hayashi, M Konishi, M Fukushima, K Kanehira, T Hioki, M Kumada *J. Org. Chem.* **48** 2195 (1983)

[a] — *Russ. J. Org. Chem. (Engl. Transl.)*
[b] — *Russ. Chem. Bull., Int. Ed. (Engl. Transl.)*
[c] — *Dokl. Chem. (Engl. Transl.)*